JOURNAL OF AGRICULTURAL AND FOOD CHEMISTRY

Article

pubs.acs.org/JAFC

# Transamination Governs Nitrogen Isotope Heterogeneity of Amino Acids in Rats

Alexander Braun,[†] Armin Vikari,[‡] Wilhelm Windisch,[‡] and Karl Auerswald*[,†]

[†]Lehrstuhl für Grünlandlehre, Department of Plant Science and [‡]Fachgebiet für Tierernährung und Leistungsphysiologie, Technische Universität München, D-85350 Freising, Germany

**ABSTRACT:** The nitrogen isotope composition ($\delta^{15}N$) of different amino acids carries different dietary information. We hypothesized that transamination and de novo synthesis create three groups that largely explain their dietary information. Rats were fed with $^{15}N$-labeled amino acids. The redistribution of the dietary $^{15}N$ labels among the muscular amino acids was analyzed. Subsequently, the labeling was changed and the nitrogen isotope turnover was analyzed. The amino acids had a common nitrogen half-life of ∼20 d, but differed in $\delta^{15}N$. Nontransaminating and essential amino acids largely conserved the $\delta^{15}N$ of the source and, hence, trace the origin in heterogeneous diets. Nonessential and nontransaminating amino acids showed a nitrogen isotope composition between their dietary composition and that of their de novo synthesis pool, likely indicating their fraction of de novo synthesis. The bulk of amino acids, which are transaminating, derived their N from a common N pool and hence their $\delta^{15}N$ was similar.

**KEYWORDS:** *amino acid, $^{15}N$, transamination, isotopic scrambling*

## INTRODUCTION

The nitrogen isotope composition ($\delta^{15}N$) of organisms provides information on trophic systems.[1,2] While the bulk $\delta^{15}N$ of tissues indicates the trophic position of organisms,[3,4] the $\delta^{15}N$ of specific compounds has the potential to provide more detailed insights, because different compounds differ in biosynthetic pathways and thus may reveal isotope information from different (dietary) sources.[5] This is particularly true for amino acids, as they provide the main nitrogen reservoir of bulk materials, but have individual biosynthetic pathways.[6] Thus, alanine, aspartic acid, and glutamic acid (among others) reflect a similar trophic position as bulk tissues, whereas glycine and phenylalanine provide an accurate determination of the $\delta^{15}N$ at the base of the food web,[2,7] although reasons for this grouping, as well as the information that can be obtained from other amino acids, remain unknown. Understanding how the major biochemical mechanisms that govern nitrogen input and distribution, namely de novo synthesis and transamination, affect the $\delta^{15}N$ of amino acids would shed light on these knowledge gaps. Additionally, the time window through which such isotope information in amino acids is retained in organisms and differences between amino acids in such time windows are worthy of investigation.

For carbon isotope composition ($\delta^{13}C$), the amino acids' ability for de novo synthesis largely explained the information that can be retrieved from their $\delta^{13}C$.[2,7] Essential amino acids remain biochemically unmodified from diet to consumer and thus represent the $\delta^{13}C$ of the amino acids in the diet. For example, leucine (essential) was not enriched in $^{13}C$ between diet and consumer, whereas glutamic acid (nonessential) became enriched in $^{13}C$. Remarkably, both amino acids were enriched in $^{15}N$,[7] indicating that the classification into essential/nonessential only applies for the carbon backbone but not for $\delta^{15}N$, because a biochemical process interfered that regulates nitrogen exchange beyond de novo synthesis and thus alters the $\delta^{15}N$ even of (at least some) essential amino acids.

Transamination by aminotransferase transfers the amino nitrogen between an amino acid and an $\alpha$-keto acid; in turn, the $\alpha$-keto acid becomes an amino acid and vice versa.[6] Since most transamination reactions have equilibrium constants close to 1, the direction of a transamination reaction proceeds in large part as a function of the intracellular concentrations of the reactants.[8] Transaminations can also be chained, providing a "nitrogen shuttle" even between amino acids of different functional groups (e.g., essential and nonessential).[9,10] For example, L-serine:glyoxylate aminotransferase (transamination enzyme, EC 2.6.1.45) catalyzes the reversible amino transfer from serine to glycine and glycine:2-oxoglutarate aminotransferase (EC 2.6.1.4) catalyzes the reversible amino transfer from glycine to glutamate (Figure 1A). Glutamate, as the central amino acid in metabolism,[6] is in turn linked to other transamination chains, like the branched-chain amino acid metabolism that links the essential amino acids leucine, isoleucine, and valine.[12] Such chains provide continuous redistribution of amino nitrogen among transaminating amino acids beyond de novo synthesis.[8] Hence, amino acids, which are subject to transamination and which we term transaminating amino acids, virtually share one common amino nitrogen pool.[13] This should lead to a reduced heterogeneity in $\delta^{15}N$ among transaminating amino acids when the $\delta^{15}N$ of the diet is heterogeneous. However, since transamination implies an isotope effect, the $\delta^{15}N$ of transaminating amino acids is not completely equal.[14]

Received: May 16, 2014
Revised: July 16, 2014
Accepted: July 18, 2014
Published: July 18, 2014

 © 2014 American Chemical Society 

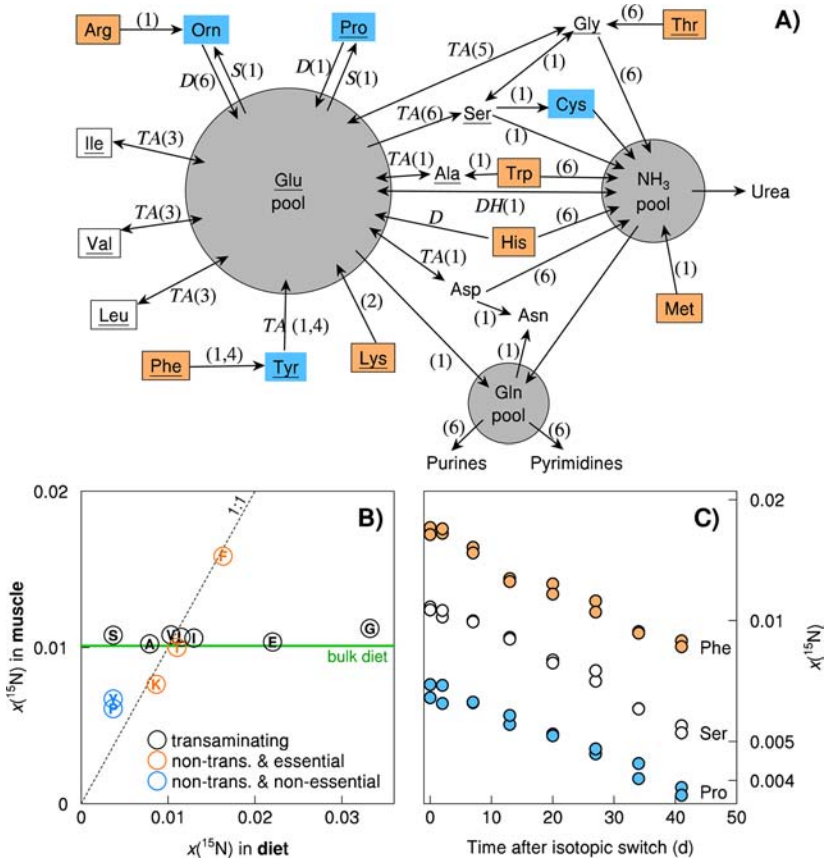


**Figure 1.** (A) Amino acid nitrogen pools and transfers in mammal metabolism. Amino acids (AAs) are given in the standard three-letter code (see Table 1); essential AAs are in boxes, and AAs analyzed in this study are underlined. A colored background, orange for essential and blue for nonessential AAs, means no transamination. The reactions are indicated in italics; they are succeeded by a number in parentheses indicating the reference (1, Berg et al.;[6] 2, Tomé and Bos;[16] 3, Hutson et al.;[12] 4, Matthews;[15] 5, Nakada;[10] 6, Voet and Voet[11]); TA = transamination (aminotransferation with $\alpha$KA = $\alpha$-keto acid) after AA1 + $\alpha$KA2 ↔ $\alpha$KA1 + AA2, in most cases dealing with Glu and $\alpha$-ketoglutaric acid; the double arrows indicate reversibility exclusively for this reaction. In this case, "equilibration" with the Glu pool is faster than any other reaction of the AAs or the $\alpha$KAs. Irreversible TAs, indicated by a one-pointed arrow, may occur, when the $\alpha$KA is rapidly further converted (Tyr) or when the TA does not concern the AS/$\alpha$KA itself but a derivative (Lys and Ser). D = degradation to Glu, S = synthesis from Glu (via different pathways), DH = Glu dehydrogenase. (B) The atom fraction $x(^{15}N)$ of amino acids in diet and in muscle before diet switch. Amino acids are indicated by their one-letter code (see Table 1). The 95% confidence intervals had a similar size as the markers. Note the different ranges of $x$ and $y$ axes. (C) Reaction progress of the atom fraction $x(^{15}N)$ for the amino acids phenylalanine (Phe), serine (Ser), and proline (Pro) after the diet switch. Each of these amino acids belongs to one of the three hypothesized groups (panel A). Since the $y$-axis is logarithmic, similar linear slopes indicate similar turnover rates.

Some amino acids differ in their ability to be transaminated. In mammals, tyrosine can be degraded but not synthesized by transamination, because the equivalent $\alpha$-keto acid that would accept nitrogen and turn into tyrosine is unavailable.[15] Hence, tyrosine can only be a nitrogen donor to the common nitrogen pool. The amino acids lysine,[16] threonine,[17] proline,[18] and phenylalanine (except for the dysfunction phenylkentonuria[6]) do not transaminate at all. Due to their disability of bidirectional transamination, these amino acids are termed "non-transaminating" in this study.

Since many diet reconstruction studies based on isotopes focus on feeding generalists (e.g., refs 2, 13) and feeding generalists likely have an isotopically heterogeneous diet, it should be investigated how the $\delta^{15}N$ of isotopically heterogeneous amino acids changes from diet to consumer, after nitrogen redistribution by de novo synthesis and transamination. We hypothesize that the joint consideration of transamination and de novo synthesis can largely explain the variation in $\delta^{15}N$ among amino acids in consumers. Since transamination is the final step in de novo synthesis, its effect on $\delta^{15}N$ of amino acids should be of a major priority, and hence, amino acids should in the present context be divided into three groups: (i) transaminating amino acids should eventually reach a rather homogeneous $\delta^{15}N$ irrespective of their isotope composition in the diet, because their amino nitrogen is exchanged with that of other transaminating amino acids (a common nitrogen pool); (ii) nontransaminating and essential amino acids should retain their $\delta^{15}N$ from diet, because nitrogen is not exchanged; and (iii) nontransaminating and nonessential amino acids should have a $\delta^{15}N$ that ranges between that of their dietary $\delta^{15}N$ and that of the $\delta^{15}N$ of the nitrogen donor pool that supplies de novo synthesis.

The exchange rate by transamination could determine the nitrogen isotope turnover and thus the time window through which isotope information can be perceived. If this were the case, the nitrogen isotope turnover must differ between amino acids, in particular between transaminating and nontransaminating amino acids. The effect of transamination on nitrogen isotope turnover could, however, be superimposed by the continuous release of amino acids from protein turnover, in particular by the degradation of proteins by proteolysis. In that


dx.doi.org/10.1021/jf502295f | J. Agric. Food Chem. 2014, 62, 8008−8013

case the nitrogen isotope turnover should be similar among all amino acids.

In order to examine the effect of dietary heterogeneity in $\delta^{15}N$ of amino acids on the $\delta^{15}N$ of amino acids in the consumer involving the nitrogen isotope turnover of amino acids, we fed rats a diet with $^{15}N$-labeled amino acids and analyzed the $\delta^{15}N$ of amino acids in muscle protein. Subsequently, we switched the $\delta^{15}N$ of the amino acids in the diet to quantify their nitrogen isotope turnover rate. This was necessary to evaluate potential differences in half-lives among amino acids that could induce differences in $\delta^{15}N$ due to different levels of labeling.

## MATERIALS AND METHODS

**Animals and $^{15}N$ Labeling.** Eighteen juvenile female Sprague–Dawley rats (*Rattus norvegicus*, Berkenhout) were assigned to cages and maintained at 25 °C ambient temperature, 60% relative humidity, and a 12 h day–12 h night cycle for 13 weeks. All rats had ad libitum access to deionized water supplemented with 0.014% NaCl and received a diet of 8 g $d^{-1}$ (dry mass), consisting of 2.2 g of sucrose, 0.6 g of coconut fat, 0.3 g of minerals, 0.2 g of cellulose, 0.1 g of sunflower oil, 0.02 g of vitamins, and 0.02 g of DL-methionine. Diets were supplemented with starch and casein depending on the nutritional requirements of the juvenile rats. During the first 7 weeks, termed the "isotope equilibration period", the supplement was 3.2 g $d^{-1}$ (days 1–17), 3.5 g $d^{-1}$ (days 18–34), and 3.7 g $d^{-1}$ (days 35–49) starch and 1.3, 1.0, and 0.8 g $d^{-1}$ casein, respectively. Digestibility of casein in young rats is close to 100%.[19] A mixture of 12 L-amino acids that was similar to the amino acid profile of casein but highly enriched in $^{15}N$ (atom fraction 0.95 or 0.99) was added, approximately at a ratio 1:100 to casein, which remained constant over time (Table 1). All amino acids were supplied by Chemotrade Chemiehandelsgesellschaft mbH, Leipzig, Germany, except for threonine, which was supplied by Campro Scientific, Veenendaal, The Netherlands. However, in the mixture, aspartic acid and serine were substituted isonitrogenously by glycine, cysteine was substituted by methionine, and tyrosine was substituted by phenylalanine. Proline was not added as a $^{15}N$-enriched amino acid. These modifications led to a large variation in labeling of the individual amino acids in the diet, with the atom fractions of $^{15}N$ ranging from 0.004 to 0.033 (Table 1). This pronounced labeling was chosen because any fractionation by the metabolism will be much smaller and can thus be neglected. For example, biosynthesis of glutamic acid by N transfer from aspartic acid to $\alpha$-keto glutaric acid is accompanied by N isotope fractionation,[14] but this will lower the atomic fraction only by ~0.004 and thus does not interfere with the labeling, which caused an atom fraction in the labeled diet of 0.022.

**Table 1. Amino Acid Profile in Dietary Casein and in the L-Amino Acid Labeling Mixture and Resulting Atom Fraction of $^{15}N$ [$x(^{15}N)$] in the Bulk Diet[a]**

| amino acid | | | content in bulk diet (g/100 g) | | |
|---|---|---|---|---|---|
| | | | from casein | from label mixture | $x(^{15}N)$ |
| alanine | Ala | A | 5 | 0.02 | 0.008 |
| arginine | Arg | R | 2.5 | 0.01 | 0.007 |
| asparagine | Asn | N | 4.1 | 0 | 0.004 |
| aspartic acid | Asp | D | 2.2 | 0 | 0.004 |
| cysteine | Cys | C | 0.8 | 0 | 0.004 |
| glutamine | Gln | Q | 7.7 | 0 | 0.004 |
| glutamic acid | Glu | E | 9.3 | 0.18 | 0.022 |
| glycine | Gly | G | 2.2 | 0.07 | 0.033 |
| histidine[b] | His | H | 1.9 | 0.03 | 0.016 |
| isoleucine[b] | Ile | I | 5.7 | 0.05 | 0.012 |
| leucine[b] | Leu | L | 9.1 | 0.08 | 0.012 |
| lysine[b] | Lys | K | 7.2 | 0.04 | 0.009 |
| methionine[b] | Met | M | 3.8 | 0.05 | 0.020 |
| phenylalanine[b] | Phe | F | 3.9 | 0.05 | 0.016 |
| proline | Pro | P | 9.8 | 0 | 0.004 |
| serine | Ser | S | 7.4 | 0 | 0.004 |
| threonine[b] | Thr | T | 5.7 | 0.05 | 0.011 |
| tryptophan[b] | Trp | W | 0.7 | 0.01 | 0.017 |
| tyrosine | Tyr | Y | 4.2 | 0 | 0.004 |
| valine[b] | Val | V | 7.3 | 0.06 | 0.011 |

[a]The $x(^{15}N)$ of amino acids in the bulk diet is calculated from mass balance and a $x(^{15}N)$ of 0.004 for casein and 0.950 for the enriched amino acids except for Tyr and Try, for which $x(^{15}N)$ was 0.990. The name of the amino acids is followed by their three and one letter codes, respectively. [b]This amino acid is essential for rats and most other mammals.

At day 50, the six-week "chase period" started and supplementation of the $^{15}N$-enriched amino acids was stopped in order to induce an exponential reaction progress in nitrogen isotope composition in the animals. To achieve reaction progress in less time, the protein content was increased to 2.4 g $d^{-1}$ (while starch was accordingly decreased to 2.1 g $d^{-1}$ [20]).

All procedures and protocols were approved by the Animal Care and Use Committee of Technische Universität München.

**Sampling.** Rats were sacrificed by decapitation under anesthesia (diethyl ether) in groups of four rats at day 39 of the equilibration period and on days 2, 7, 13, 20, 34, and 41 during the chase period to investigate the reaction progress of the isotope composition following the diet switch (Figure 1C). The animals were dissected to provide muscle tissue (musculus femoris and musculus quadriceps). The muscles were combined, homogenized with an Ultra-Turrax (IKA-Labortechnik Jahnke & Kunkel GmbH & Co KG, Staufen i. Br., Germany), rinsed with a solution of Hexane–2-propanol (3:2) to eliminate lipids, and filtrated. The fat-free muscle material was dried for 12 h at 70 °C and stored at −80 °C. The diet was collected daily, starting 5 days before the chase period to day 7 of the chase period and additionally on days 10, 13, 17, 22, 27, 34, and 41 of the chase period. For more details on the keeping and sampling, see the work of Braun et al.[20]

**Isotope Analyses of Amino Acids.** Isotope analysis was carried out at the Leibniz-Institut für Nutztierbiologie, Dummerstorf, Germany, following the method of Metges and Petzke.[21] In brief, samples of 2.5–3.5 mg of muscle lyophilizate were double-washed with 10% trichloroacetic acid, acetone, and ether. Washed samples were hydrolyzed for 24 h with 2 mL of 6 N HCl at 110 °C and derivatized to their N-pivaloyl-isopropyl esters. To this end, 2 mL of $CH_2Cl_2$ was added to 3–8 $\mu$mol of amino acids, and the solution was dried and solved in 100 $\mu$L of pyridine. An aliquot of 100 $\mu$L of pivalochloride was added, the solution was acetylated (30 min, 60 °C) and cooled, and 2 mL of $CH_2Cl_2$ was added. The mixture was then passed through a 4 cm silica gel (silica gel 60, 200–400 mesh) column (4 mm i.d.) and the filtrate was dried under a stream of $N_2$ before adding 100 $\mu$L of ethyl acetate. The samples were then analyzed for nitrogen isotope composition on a gas-chromatograph (HP 5890, Waldbronn, Deutschland), connected to a gas-isotope-ratio-mass spectrometer (Finnigan MAT, Bremen, Deutschland), via a GC combustion interface. The interface comprised a combustion furnace reactor filled with copper and nickel oxide and platinum (980 °C) and a reduction furnace filled with elemental copper (600 °C).

**Calculation of $x(^{15}N)$ of Dietary Amino Acids.** In the following, we denote isotope composition as the atom fraction [$x(^{15}N)$], because its use is preferred over the use of $\delta$ values for tracer and mixing calculations:[22]

$$x(^{15}N) = n(^{15}N)/(n(^{14}N) + n(^{15}N)) \quad (1)$$

where $n(^{14}N)$ and $n(^{15}N)$ are the amounts of isotope $^{14}N$ and $^{15}N$ of element N, respectively.

The $x(^{15}N)$ of the amino acids in the bulk diet was calculated according to the mass balance of an amino acid provided by casein and provided by the enriched amino acids of the labeling mixture as

$$x(^{15}N) = (m_{cas}x(^{15}N)_{cas} + m_{label}x(^{15}N)_{label})/(m_{cas} + m_{label}) \quad (2)$$

where $m_{cas}$ and $m_{label}$ are the masses of the specific amino acid provided by casein and by the labeled amino acid mixture, respectively, while $x(^{15}N)_{cas}$ and $x(^{15}N)_{label}$ are the corresponding $x(^{15}N)$ values.

**Turnover Estimation and Statistical Evaluation.** Turnover as quantified herein only applies for nitrogen but not for the carbon skeletons of the amino acids, which follow different pathways of recycling, degradation, and synthesis. A previous study that used the same animals had shown that the reaction progress of all organs including the muscle exhibited a common delay of 0.5 d following a diet switch, which likely was caused by the transit time in the digestive tract.[20] Since neglecting a delay would lead to an underestimate in isotope turnover, the delay (0.5 d) was subtracted from the sampling times to provide a delay-corrected reaction progress.

Since growth affects the apparent reaction progress[20,23] and the muscle from which the amino acids were sampled had a growth rate of ~0.7 g $d^{-1}$,[20] the effects of growth and turnover rate were disentangled from the delay-corrected reaction progress by fitting the function

$$x(^{15}N)_t = x(^{15}N)_\infty - (x(^{15}N)_\infty - x(^{15}N)_0)(1 - \Delta w/w_t)^{(1+r/g)} \quad (3)$$

where $x(^{15}N)_t$ is the atom fraction at time $t$, $x(^{15}N)_\infty$ is the atom fraction of the asymptote at the end of the reaction progress, and $x(^{15}N)_0$ is the atom fraction at time zero (time of isotope switch plus delay). The parameter $w_t$ is the dry mass of an amino acid at time $t$ and $\Delta w$ is $w_t - w_0$, where the subscript 0 denotes time zero. The growth rate constant is denoted $g$ and estimated for each amino acid specifically as $0.7/\gamma$ g $d^{-1}$, where $\gamma$ was the ratio of the mass of a specific amino acid to the mass of all amino acids in the muscle (0.7 g $d^{-1}$ was the growth rate of the entire muscle; see above and in Braun et al.[20]). The ratio $r/g$ gives the relative contribution of isotope turnover ($r$) and growth ($g$) to the apparent reaction progress. The half-life ($t_{1/2}$) is then given by $\ln(2)/r$. The parameter $x(^{15}N)_0$ was obtained by measuring the isotope composition at the end of the "equilibration period" (as described above), as this value characterizes the constant isotope composition during the delay and simultaneously the intercept of the following reaction progress model when delay time is subtracted. The standard errors of the fitting function for $x(^{15}N)_0$ and $t_{1/2}$ were then converted to confidence intervals for $p = 0.05$ and a two-sided error. All data analyses were done in R 2.15.1.

## RESULTS

**$x(^{15}N)$ of Amino Acids.** At the end of the equilibration period, the $x(^{15}N)$ of amino acids varied by about a factor of 2 in muscle tissue, ranging from 0.0067 in tyrosine to 0.0158 in phenylalanine. The $x(^{15}N)$ of dietary amino acids did not correlate significantly with the $x(^{15}N)$ of muscular amino acids ($p > 0.05$, $r^2 = 0.29$), but the following pattern was apparent (Figure 1B):

(i) The transaminating amino acids alanine, glutamic acid, glycine, isoleucine, leucine, serine, and valine had a common $x(^{15}N)$ of 0.0108 (SD 0.0007), which was not statistically different from the mean $x(^{15}N)$ of the diet (0.0101 ± 0.0001). Hence, their $x(^{15}N)$ had changed substantially, including depletion and enrichment in $^{15}N$. The change ranged from −0.0211 in glycine to 0.0071 in serine.

(ii) The $x(^{15}N)$ of nontransaminating and essential amino acids lysine, threonine, and phenylalanine was quite similar in diet and muscle; hence, they appeared on the 1:1 line (Figure 1 B).

(iii) The nontransaminating and nonessential amino acids proline and tyrosine had a $x(^{15}N)$ between their initial (dietary) $x(^{15}N)$ and the $x(^{15}N)$ of their specific nitrogen donor pools, glutamine and phenylanaline, respectively. The coefficient of variation was small among replicates for all amino acids (~2% of the respective mean), indicating equal labeling among rats.

**Turnover of Amino Acid $^{15}N$.** After the diet switch the $x(^{15}N)$ of all amino acids exponentially approached the $x(^{15}N)$ of the unlabeled diet (Figure 2). The mean half-life of the nitrogen in amino acids was 20 d (13−27 d), and the nitrogen half-lives were not significantly different among amino acids, and they were not statistically different from the nitrogen half-life of the entire muscle. In particular, turnover was not different for essential/nonessential and transaminating/nontransaminating amino acids (Figure 1C).

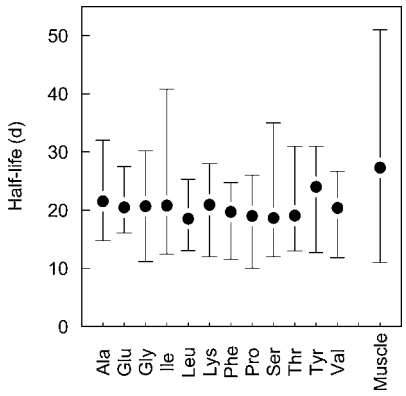


**Figure 2.** Half-lives of nitrogen in amino acids (quantified herein) and in muscle tissue (quantified in Braun et al.[20]), obtained from the same animals. The error bars indicate the 95% confidence intervals.

## DISCUSSION

We hypothesized that the joint consideration of transamination and de novo synthesis divides amino acids into three groups that largely explain the variation in $x(^{15}N)$ among amino acids in animals: (i) transaminating, (ii) nontransaminating and essential, and (iii) and nontransaminating and nonessential amino acids.

Transaminating amino acids had a homogeneous $x(^{15}N)$ value in consumer tissues, despite their $x(^{15}N)$ value in the diet varying by an order of magnitude (Figure 1B). For example, serine was not provided by the labeled amino acid mixture but had the same $x(^{15}N)$ value in the muscle tissue as the labeled amino acids (Table 1). The $x(^{15}N)$ value of transaminating amino acids was similar to the $x(^{15}N)$ of the bulk diet (plus an expectable isotope enrichment[24]), and it was similar to the mean of $x(^{15}N)$ of transaminating amino acids in the diet. This indicated that complete redistribution of amino nitrogen among transaminating amino acids in consumer tissues can be expected, because transamination is the most common reaction involving free amino acids.[17] However, the transaminations cause isotope fractionation[25,26] that appears herein only as minor variation around the homogenized $x(^{15}N)$, because of the very high labeling. Future research should gain detailed knowledge on the isotope fractionations of the specific transamination enzymes.

The harmonization of nitrogen isotope composition of transaminating amino acids seems to be consistent across trophic levels, environments, and diets, as similar nitrogen isotope compositions can be found for transaminating amino acids within herbivores, e.g., pig, and terrestrial and marine carnivores, e.g., lion and whale (see results of Hare et al.[13]). Thus, our results would be applicable to the many studies using

$^{15}N$ in mammals.[27−30] This finding is, however, in contrast to $x(^{15}N)$ values in a zooplankter,[7] indicating that the ability of transamination may differ between organisms that are more remote in their evolution and which do not share conserved biochemical pathways. This calls for the need to repeat such investigations in other animal groups that are in the focus of isotope animal ecology, e.g., birds or insects.

Homogeneous $x(^{15}N)$ in consumer but varying $x(^{15}N)$ in diet implies variation in trophic shifts among transaminating amino acids, including enrichment and depletion in $^{15}N$, as found herein (Figure 1B) and in other studies.[5,31] Amino acids become enriched in $^{15}N$ when their dietary $x(^{15}N)$ is below the homogenized $x(^{15}N)$ and vice versa; the height of the trophic shift will be defined by the difference between isotope composition of an amino acid and the homogenized $x(^{15}N)$. Hence, the trophic shift of a transaminating amino acid cannot indicate the trophic position of the consumer.

Nontransaminating and nonessential amino acids changed their $x(^{15}N)$ from diet to consumer to less extent. Considering their biochemical pathways, each amino acid of this group in consumer is either derived from its dietary amino acid pool (without nitrogen exchange by transamination) or synthesized de novo by the organism. Hence, the change in $x(^{15}N)$ should be a function of their dietary $x(^{15}N)$, the $x(^{15}N)$ of the donor pool supplying de novo synthesis, the fraction of de novo synthesized amino acids, and isotope fractionation during de novo synthesis:[14] Principally, the $x(^{15}N)$ of these amino acids may retain their dietary $x(^{15}N)$ in the case of no de novo synthesis (e.g., when dietary supply exceeds the need); the $x(^{15}N)$ of these amino acids should be equal to the $x(^{15}N)$ of the precursor pool (±isotope fractionation) in the case of the fraction of de novo synthesis being 100%; in cases where the fraction of de novo synthesis is between 0 and 100%, the $x(^{15}N)$ of the amino acid should be between the dietary $x(^{15}N)$ and $x(^{15}N)$ of the de novo synthesis pool (±isotope fractionation). When neglecting the relatively small isotope fractionation compared to the high labeling herein, the de novo synthesis fraction as calculated by mass balance was 25% for tyrosine and 40% for proline, despite their near identical $x(^{15}N)$ in consumer. This contrast resulted from differing nitrogen donor pools (tyrosine is supplied by phenylalanine, whereas proline is supplied by the common nitrogen pool, as glutamic acid is the precursor[32]) that also differed in $x(^{15}N)$ from the common nitrogen pool.

Nontransaminating and essential amino acids almost retained their dietary $x(^{15}N)$ value and hence provide highly conserved isotope information from the base of the food web. However, minor changes in isotope compositions might occur (e.g., small deviations from the 1:1 line in Figure 1B) due to isotope fractionation, e.g., caused by the deamination of threonine.[13]

The half-lives were rather constant among amino acids (Figure 2), indicating that the differences in $x(^{15}N)$ values among amino acids were not influenced by differences in isotope turnover rates that determine the kinetics of label incorporation. This also indicated that the common turnover was not an effect of transamination that differed between amino acids, but rather an effect of proteolysis that governs the degradation of whole proteins and thus affects nearly all amino acids at once. This is not surprising, as transamination is a kinetically perfect reaction, which is so efficient that it is only controlled by the provision of the substrate.

Amino acids had shorter half-lives than their bulk muscle tissue,[20] although statistically indistinguishable. This might result from the slower turnover of other nitrogen-containing components in bulk muscle, like nucleic acids.[33]

## AUTHOR INFORMATION


### Corresponding Author

*E-mail: Auerswald@wzw.tum.de. Phone: +49 (0)8161 713965. Fax: +49 (0)8161 713243.


### Author Contributions

W.W. designed the feeding experiment, A.V. carried out the feeding experiment, K.A. designed data analysis, A.B. analyzed the data, and A.B and K.A. wrote the manuscript. All authors read and approved the final manuscript.


### Funding

The "Deutsche Forschungsgemeinschaft" (grant number AU 183/3-1) is thanked for supporting this project.


### Notes

The authors declare no competing financial interest.

## ACKNOWLEDGMENTS


The authors acknowledge the valuable discussions with Hans Schnyder on experimental design and with Hanns-Ludwig Schmidt on biochemical pathways. Alan Hopkins provided linguistic support.


## ABBREVIATIONS USED

$^{13}C$, stable isotope of carbon with isotopic mass 13 u; $\delta^{13}C$, carbon isotope composition in permil; $^{15}N$, stable isotope of nitrogen with isotopic mass 15 u; $\delta^{15}N$, nitrogen isotope composition in permil; $x(^{15}N)$ nitrogen isotope composition in atom fraction; EC, enzyme commission number; SD, standard deviation.

## REFERENCES


(1) Peterson, B. J.; Fry, B. Stable isotopes in ecosystem studies. *Annu. Rev. Ecol. Syst.* **1987**, *18*, 293−320.

(2) Popp, B. N.; Graham, B. S.; Olson, R. J.; Hannides, C. C. S.; Lott, M. J.; Lopez-Ibarra, G. A.; Galvan-Magana, F.; Fry, B. Insight into the trophic ecology of yellowfin tuna, *Thunnus albacares*, from compound-specific nitrogen isotope analysis of pronteinaceous amino acids. In *Stable Isotopes as Indicators of Ecological Change*; Dawson, T. E., Siegwolf, R. T. W., Eds.; Academic Press: Waltham, MA, 2007; Vol. *1*, p 173 ff.

(3) Minagawa, M.; Wada, E. Stepwise enrichment of $^{15}N$ along food chains: Further evidence and the relation between $^{15}N$ and animal age. *Geochim. Cosmochim. Acta* **1984**, *48*, 1135−1140.

(4) Schmidt, K.; McClelland, J. W.; Mente, E.; Montoya, J. P.; Atkinson, A.; Voss, M. Trophic-level interpretation based on $\delta^{15}N$ values: Implications of tissue-specific fractionation and amino acid composition. *Mar. Ecol.: Prog. Ser.* **2004**, *266*, 43−58.

(5) McMahon, K. W.; Fogel, M. L.; Elsdon, T. S.; Thorrold, S. R. Carbon isotope fractionation of amino acids in fish muscle reflects biosynthesis and isotopic routing from dietary protein. *J. Anim. Ecol.* **2010**, *79*, 1132−1141.

(6) Berg, J. M.; Tymoczko, J. L.; Stryer, L. *Biochemistry*, 5th ed.; W. H. Freeman: New York, 2002; 992 pp.

(7) McClelland, J. W.; Montoya, J. P. Trophic relationships and the nitrogen isotopic composition of amino acids in plankton. *Ecology.* **2002**, *83*, 2173−2180.

(8) Mathews, C. K.; van Holde, K. E.; Ahern, K. G. *Biochemistry*, 4th ed.; Addison Wesley: Boston, MA, 1999; 1200 pp.

(9) Kalhan, S. C.; Parimi, P. S. Transamination of leucine and nitrogen accretion in human pregnancy and the newborn infant. *J. Nutr.* **2006**, *136*, 2815−2875.

(10) Nakada, H. I. Glutamic-glycine transaminase from rat liver. *J. Biol. Chem.* **1964**, *239*, 468−471.

(11) Voet, D.; Voet, J. G. *Biochemie*; VCH Verlagsgesellschaft mbH: Weinheim, Germany, 1992.
(12) Hutson, S. M.; Sweatt, A. J.; LaNoue, K. F. Branched-chain amino acids metabolism: Implications for establishing safe intakes. *J. Nutr.* **2005**, *135*, 1557−1564.
(13) Hare, P. E.; Fogel, M. L.; Stafford, T. W., Jr.; Mitchell, A. D.; Hoering, T. C. The isotopic composition of carbon and nitrogen in individual amino acids isolated from modern and fossil proteins. *J. Archaeol. Sci.* **1991**, *18*, 277−292.
(14) Macko, S. A.; Fogel, M. L.; Hare, P. E.; Hoering, T. C. Isotopic fractionation of nitrogen and carbon in the synthesis of amino acids by microorganisms. *Chem. Geol.* **1987**, *65*, 79−92.
(15) Matthews, D. E. An overview of phenylalanine and tyrosine kinetics in humans. *J. Nutr.* **2007**, *137*, 1549−1555.
(16) Tomé, D.; Bos, C. Lysine requirement through the human life cycle. *J. Nutr.* **2007**, *137*, 1642−1645.
(17) Devlin, M. *Textbook of Biochemistry with Clinical Correlations*, 7th ed.; John Wiley: Hoboken, NJ, 2010; 1240 pp.
(18) Murray, R. K.; Granner, D. K.; Mayes, P. A.; Rodwell, V. W. *Harper's Illustrated Biochemistry*; McGraw-Hill Medical: New York, 2010; 693 pp.
(19) Gilani, G. S.; Sepehr, E. Protein digestibility and quality in products containing antinutritional factors are adversely affected by old age in rats. *J. Nutr.* **2003**, *133*, 220−225.
(20) Braun, A.; Auerswald, K.; Vikari, A.; Schnyder, H. Dietary protein content affects carbon and nitrogen turnover. *Rapid Commun. Mass Spectrom.* **2013**, *27*, 2676−2684.
(21) Metges, C. C.; Petzke, K. Measurement of $^{15}N/^{14}N$ isotopic composition in individual plasma free amino acids of human adults at natural abundance by gas chromatography−combustion isotope ratio mass spectrometry. *Anal. Biochem.* **1997**, *247*, 158−164.
(22) Coplen, T. B. Guidelines and recommended terms for expression of stable-isotope-ratio and gas-ratio measurement results. *Rapid Commun. Mass Spectrom.* **2011**, *25*, 2538−2560.
(23) Carleton, S. A.; del Rio, C. M. Growth and catabolism in isotopic incorporation: A new formulation and experimental data. *Funct. Ecol.* **2010**, *24*, 805−812.
(24) DeNiro, M. J.; Epstein, S. Influence of diet on the distribution of nitrogen isotopes in animals. *Geochim. Cosmochim. Acta* **1981**, *37*, 703−724.
(25) Macko, S. A.; Fogel, M. L.; Engel, M. H.; Hare, P. E. Kinetic fractionation of stable nitrogen isotopes during amino acid transamination. *Geochim. Cosmochim. Acta* **1986**, *50*, 2143−2146.
(26) Tcherkez, G. Natural $^{15}N/^{14}N$ isotope composition in C3 leaves: Are enzymatic isotope effects informative for predicting the $^{15}N$-abundance in key metabolites. *Funct. Plant Biol.* **2011**, *38*, 1−12.
(27) Baroni, M. V.; Podio, N. S.; Badini, R. G.; Inga, M.; Ostera, H. A.; Cagnoni, M.; Gallegos, E.; Gautier, E.; Peral-García, P.; Hoogewerff, J.; Wunderlin, D. A. How much do soil and water contribute to the composition of meat? A case study: Meat from three areas of Argentina. *J. Agric. Food Chem.* **2011**, *59*, 11117−11128.
(28) Osorio, M. T.; Moloney, A. P.; Schmidt, O.; Monahan, F. J. Beef authentication and retrospective dietary verification using stable isotope ratio analysis of bovine muscle and tail hair. *J. Agric. Food Chem.* **2011**, *59*, 3295−3305.
(29) Osorio, M. T.; Moloney, A. P.; Schmidt, O.; Monahan, F. J. Multielement isotope analysis of bovine muscle for determination of international geographical origin of meat. *J. Agric. Food Chem.* **2011**, *59*, 3285−3294.
(30) Scampicchio, M.; Mimmo, T.; Capici, C.; Huck, C.; Innocente, N.; Drusch, S.; Cesco, S. Identification of milk origin and process-induced changes in milk by stable isotope ratio mass spectrometry. *J. Agric. Food Chem.* **2012**, *60*, 11268−11273.
(31) Bloomfield, A. L.; Elsdon, T. S.; Walther, B. D.; Gier, E. J.; Gillanders, B. M. Temperature and diet affect carbon and nitrogen isotopes of fish muscle: Can amino acid nitrogen explain effects? *J. Exp. Mar. Biol. Ecol.* **2011**, *399*, 48−59.
(32) Jones, M. E. Conversion of glutamate to ornithine and proline: Pyrroline-5-carboxylate, a possible modulator of arginine requirements. *J. Nutr.* **1985**, *115*, 509−515.
(33) Halvorson, H. Intracellular protein and nucleic acid turnover in resting yeast cells. *Biochim. Biophys. Acta* **1958**, *27*, 255−266.

JOURNAL OF AGRICULTURAL AND FOOD CHEMISTRY

Article

pubs.acs.org/JAFC

# Evolution of Volatile Compounds and Biogenic Amines throughout the Shelf Life of Marinated and Salted Anchovies (*Engraulis encrasicolus*)

Alexandre Dehaut,[†] Charlotte Himber,[†] Véronique Mulak,[§] Thierry Grard,[#] Frédéric Krzewinski,[⊥] Bruno Le Fur,[§] and Guillaume Duflos*[,†]

[†]Département des Produits de la Pêche et de l'Aquaculture, Laboratoire de Sécurité des Aliments, ANSES, Boulevard du Bassin Napoléon, 62200 Boulogne-sur-Mer, France

[§]Plate-forme d'Innovation Nouvelles Vagues, 15−17 Rue Magenta, 62200 Boulogne-sur-Mer, France

[#]Unité Biochimie des Produits Aquatiques − Université du Littoral-Côte d'Opale, Boulevard du Bassin Napoléon, 62200 Boulogne-sur-Mer, France

[⊥]Unité de Glycobiologie Structurale et Fonctionnelle − UGSF, Université de Lille I, Bâtiment C9 − Cité Scientifique, 59650 Villeneuve d'Ascq, France

**ABSTRACT:** Producers of processed anchovies have developed hazard analysis and critical control points (HACCP) to guarantee the quality of their products. Nonetheless there is a lack of objective data to determine products' shelf life. The quality of a product is usually established on the basis of its safety and organoleptic properties. These parameters were assessed by monitoring the profiles of volatile compounds and quantitating six biogenic amines in samples of two types of processed anchovies during their shelf life. With regard to biogenic amines, quantities were below the regulatory limits throughout shelf life, except when a temperature abuse was applied for marinated samples. Moreover, this work highlights an optimum volatile profile at 5 and 6 months of storage for salted and marinated anchovies, respectively. This is the result of a higher content of six aldehyde and nine ketone compounds, mainly from lipid oxidation.

**KEYWORDS:** *anchovies, shelf life assessment, volatile compounds, biogenic amines, SPME-GC-MS*

## INTRODUCTION

Anchovies are one of the most caught fish species in the world with an estimated 3.5 million tons landed in 2010[1] and quantities consumed estimated at 369,000 tons in 2008. Anchovies can be processed using a wide range of techniques, such as salt ripening or marination in vinegar. Consumers are more and more aware of food quality and food safety. To manage such issues, the European Union has encouraged the application of good manufacturing practices and the development of hazard analysis and critical control points (HACCP). This approach has been developed in industry with specific applications for salted and marinated anchovies.

After their catch, anchovies can be ripened in salt or marinated in vinegar for a specified period and preserved until consumption. The shelf life of processed anchovies has only been empirically estimated, and there is a real lack of objective information on how the properties of products change during storage. The assessment of optimal shelf life will ensure consumers a safe product with good quality.

Numerous studies have described the microbial flora present in salted and marinated anchovies. *Lactobacillus* and *Micrococcus* genera have been identified as the main bacteria present in processed marinated anchovies,[2] and the presence of Enterobacteriaceae was also demonstrated.[3,4] In salted anchovies, potential histaminogenic floras, such as Enterobacteriaceae and *Staphylococcus*, have been reported.[3−5] In a study on brined anchovies,[6] halophilic and psychrophilic floras increased respectively at room temperature and in chilled conditions for samples conserved in low NaCl concentrations brines. A consensus is observed from previous authors to conclude that hygiene management provides a better control of these bacteria. In addition, a study on the ingredients added during the marination process showed that they have no impact on microbiological quality.[7]

Histamine is a biogenic amine resulting from the enzymatic decarboxylation of histidine. This molecule is responsible for many cases of food poisoning, with various symptoms.[8] Due to the high histidine content in their flesh, numerous fish families (Scombridae, Clupeidae, or Engraulidae) show a high histamine risk. This is the major food safety risk encountered in such products. European regulations (Commission Regulation (EC) No. 1441/2007 and Commission Regulation (EC) No. 1019/2013) have defined a limit of 400 mg $kg^{-1}$ of histamine for a single product having undergone enzymatic maturation treatment in brine.[9,10] Other biogenic amines have been reported, especially tyramine, putrescine, cadaverine, spermine, and spermidine.[11−13] Studies tracing biogenic amines during the storage period indicate changes in tyramine, histamine, and tryptamine.[11,13,14] Very few studies have been carried out on the storage of marinated samples and focus mainly on the marination step itself.[2,12] Furthermore, refrigeration limits the

Received: February 4, 2014
Revised: July 15, 2014
Accepted: July 26, 2014
Published: July 26, 2014

ACS Publications © 2014 American Chemical Society



dx.doi.org/10.1021/jf5021736 | J. Agric. Food Chem. 2014, 62, 8014−8022

biogenic amine content.[6,13,14] Analysis of volatile compounds in different food matrices has been increasing over the past decade.[15−17] The volatilome of a matrix can be analyzed by trapping volatiles on a solid phase microextraction (SPME) fiber, in the headspace of a vial.[18] Finally, volatiles can be quantitated thanks to a GC-MS device. To date, most studies on the volatile compounds of processed anchovies have been carried out to assess the maturation step of salted anchovies. Thus, indicators of maturation have been defined for salted anchovies as aldehydes, alkadienals, alcohols, and ketones.[19,20] Acetaldehyde, 2-methylbutanal, and 3-methylpropanal have been described as the most abundant odorant compounds in ripened anchovies.[21] On the basis of sensory analysis, the optimal maturation of salted anchovies has been estimated at close to 160 days.[22]

As anchovy processing is well documented, the goal of this study was focused on the less studied shelf life assessment of processed anchovies. To this end, both salt-ripened and marinated anchovies stored in different conditions, with and without temperature change, were studied. The first half of the study was focused on volatilome monitoring throughout storage, whereas the other half dealt with safety issues by quantitating biogenic amines.

## MATERIALS AND METHODS

**Chemicals.** NaCl used for the headspace analysis was obtained from Oxoid (Dardilly, France). An *n*-paraffin mix, $C_5$−$C_{15}$, used for the calculation of the linear retention index (LRI), was acquired from Sigma-Aldrich (St-Quentin-Fallavier, France). All pure compounds used to improve identification reliability including ethanol, dimethyl sulfide, 2-methylpropanal, 2,3-butanedione, butanal, 3-methylbutanal, 2-methylbutanal, 1-penten-3-ol, 2-ethylfuran, 1-pentanol, 2,3-hexanedione, hexanal, heptanal, benzaldehyde, 1-octen-3-ol, (*E*,*E*)-2,4-heptadienal, octanal, benzeneacetaldehyde, nonanal, (*E*,*Z*)-2,6-nonadienal, and decanal were purchased from Sigma-Aldrich. All chemicals used for quantitating biogenic amines were obtained from Sigma-Aldrich except perchloric acid, which was purchased from Carlo Erba (Val-de-Reuil, France), and toluene and acetonitrile, which were purchased from VWR (Fontenay-sous-Bois, France).

**Anchovy Processing and Preservation.** Samples of anchovies were provided by the Association of French Fish Processing Industries (*Confédération des Industries de Traitement des Produits de la Pêche Maritimes* (CITPPM − Paris)) and held at the innovation platform *PFI-Nouvelles Vagues* (Boulogne-sur-Mer, France). Samples of anchovy fillets (*Engraulis encrasicolus*) consisted of salted or marinated anchovies having been processed and packed.

For salted anchovies, samples were prepared by immersion in brine. Fish were gutted and beheaded and then transferred to vats, with alternating layers of salt and anchovies. Saturated brine was then added. Vats were covered, and pressure was applied to the lids to remove trapped air. Anchovies were ripened at room temperature for several months (a minimum of 3 months). After ripening, samples were packed in glass jars.

Marinated fish samples were produced from fresh anchovies that were cleaned, beheaded, gutted, and filleted. After 24 h of freezing to manage parasite risk, anchovies were then immersed in a vinegar solution. A marination period of a few days (with a minimum of 24 h) under refrigeration was carried out. Anchovies were then covered with oil and vacuum packed.

All storage times applied in this study were set to exceed the shelf life advocated by the guide to good hygiene practices. Two types of temperature of storage were applied to samples: with (wR) or without rupture (w/oR). Concerning marinated samples, storage without any change of temperature consisted of incubation at 4 °C. Storage with breaks in the temperature conditions consisted of one-third of the time at 4 °C and the remaining two-thirds at 8 °C. For the salted anchovies, storage without any change of temperature consisted of incubation at 15 °C, to ensure their inherent shelf stability. Rupture applied in the temperature conditions consisted of two-thirds of the time at 15 °C and the remaining one-third at 22 °C.

**Analysis of the Headspace by SPME-GC-MS.** Analysis of the headspace of vials containing anchovy samples was carried out as described by Duflos et al.[17] Briefly, 50 g of flesh was added to 100 mL of NaCl solution in ultrapure water at 300 g $kg^{-1}$ and then ground with a stomacher at 300 rpm for 2 min. Then, 45 g of filtrate was centrifuged at 10000*g* for 10 min at 4 °C. The supernatant (11 mL) was then distributed in 20 mL SPME vials and tightly sealed. SPME vials were placed at 4 °C on a refrigerated tray. The vials were handled using a combiPAL autosampler (CTC Analytics, Zwingen, Switzerland). The vial was placed for 10 min at 50 °C and shaken at 500 rpm. A 75 μm CAR/PDMS fiber (Supelco, Lyon, France) was introduced into the headspace of the vial to collect volatile compounds for 40 min at 50 °C under the same conditions. The fiber was then removed and placed for 1 min in splitless mode in a Merlin Microseal injector (at 250 °C) of a gas chromatograph GC-2010 equipped with a QP2010 Plus mass spectrometer (Shimadzu, Kyoto, Japan). The GC was equipped with an SLB-5 MS capillary column (60 m × 0.25 mm × 0.25 μm) from Supelco (St-Quentin-Fallavier, France), and helium was used as carrier gas at a flow of 1.78 mL/min. The temperature conditions applied in the oven were as follows: 5 min at 35 °C, increased to 100 °C at a rate of 10 °C/min, then increased to 280 °C at a rate of 20 °C/min, and maintained for 5 min. Spectrometric analysis was performed with the following conditions: interface temperature at 280 °C, ionization voltage at 70 eV, mass range from $m/z$ 33 to 200, and a scan frequency of 500 Hz. After each injection, the fiber was reconditioned at 300 °C with helium flow for 10 min. Volatile compounds were automatically integrated by GC-MS postrun analysis (Shimadzu), with a given retention time, a target ion, and reference ions for each volatile compound (Table 1). A normalization of each area (i.e., division of the area by the sum of areas of all compounds) was realized. Compounds were identified by comparing them with mass spectra in the NIST 08 library database and with LRI found in the literature,[23] calculated using the equation in van den Dool and Kratz.[24] The headspace analysis was performed in duplicate for all samples.

**Separation and Quantitation of Biogenic Amines.** Quantitative assay of biogenic amines was carried out using the method recommended by Commission Regulation (EC) No. 1441/2007 with high-performance liquid chromatography (HPLC).[25,26] Briefly, to extract biogenic amines, 5 g of anchovies was added to 100 μL of 1,3-diaminopropane used as internal standard and 10 mL of 0.2 M perchloric acid. The mix was blended with an Ultraturrax homogenizer and centrifuged at 7000*g* for 5 min at 4 °C. Then, 100 μL of supernatant was transferred in 300 μL of sodium carbonate and 400 μL of dansyl chloride, homogenized, and kept in the dark at 60 °C for 5 min. After derivatization, 100 μL of L-proline was added to remove excess dansyl chloride and kept in the dark at room temperature for 15 min. Then, 500 μL of toluene was added; after settling, the aqueous phase was frozen and the organic phase containing dansyl derivates was specifically recovered and evaporated under nitrogen flow for 5 min. The dry residue was dissolved in 200 μL of acetonitrile and then filtered at 0.2 μm and injected in a high-performance liquid chromatograph. Biogenic amines were separated on a Kromasil C18 reverse phase column (250 mm × 4.6 mm × 5 μm) from Alltech (Deerfield, IL, USA) with a water/acetonitrile gradient and a flow of 1 mL/min. After 30 min of separation, the chromatogram showed the peaks of the six biogenic amines, putrescine, cadaverine, histamine, tyramine, spermidine, and spermine, and the internal standard (1,3-diaminopropane). Quantitation of biogenic amines was performed by calculating each response factor against 1,3-diaminopropane and using a calibration curve.

**Experimental Design and Statistical Analysis.** For the analysis of volatile compounds, marinated samples were studied for 9 months and salted samples for 18 months, to reach or exceed the shelf life recommended by good manufacturing practices. Samples were irregularly supplied by producers, but a minimum of two samples was analyzed in duplicate each month for the duration of the tested

**Table 1. Settings Used To Perform Automatic Integration of the Chromatograms**

| compound[a] | LRI[d] | reliability[e] | ions used for integration $(m/z)$[f] |
|---|---|---|---|
| ethanol[c] | 477 | MS, LRI, Std | **45** (46, 43) |
| dimethyl sulfide | 516 | MS, LRI, Std | **62** (47, 45, 46, 61) |
| trimethylamine[c] | 522 | tentative | **58** (59, 42) |
| 2-methylpropanal[c] | 549 | MS, LRI, Std | **43** (41, 72) |
| 2,3-butanedione[c] | 586 | MS, LRI, Std | **43** (86) |
| butanal | 591 | MS, LRI, Std | **44** (43, 72, 57, 41) |
| 2-butanone[b,c] | 595 | Tentative | **43** (72, 57) |
| 3-methylbutanal[c] | 652 | MS, LRI, Std | **41** (44, 58, 43, 39) |
| 2-methylbutanal[c] | 662 | MS, LRI, Std | **41** (57, 58, 39) |
| 1-penten-3-ol[c] | 684 | MS, LRI, Std | **57** (41, 43, 39, 58) |
| 2,3-pentanedione | 697 | Tentative | **43** (57, 100) |
| 2-ethylfuran[b,c] | 700 | MS, LRI, Std | **81** (96, 53) |
| 3-methyl-1-butanol | 753 | Tentative | **55** (42, 43, 70) |
| (*E*)-2-pentenal[b,c] | 755 | Tentative | **55** (84, 83, 41) |
| 1-pentanol | 768 | MS, LRI, Std | **42** (55, 41, 70) |
| 2,3-hexanedione | 785 | MS, LRI, Std | **43** (41, 71, 57) |
| hexanal[b,c] | 799 | MS, LRI, Std | **44** (56, 41, 43, 72, 82) |
| (*E*)-2-hexenal[b,c] | 855 | Tentative | **41** (42, 39, 83, 69) |
| (*Z*)-4-heptenal[c] | 898 | Tentative | **41** (68, 55, 84, 43) |
| heptanal[b,c] | 900 | MS, LRI, Std | **70** (41, 55, 57, 81, 44) |
| 6-methyl-2-heptanone | 956 | Tentative | **43** (58, 71, 95, 110, 41) |
| (*E*)-2-heptenal[b,c] | 960 | MS, LRI, Std | **41** (68, 55, 84, 43) |
| benzaldehyde[b,c] | 970 | MS, LRI, Std | **77** (106, 105, 51) |
| 1-octen-3-ol | 981 | MS, LRI, Std | **57** (43, 72, 55, 85) |
| 2,3-octanedione[b,c] | 983 | Tentative | **43** (71, 99) |
| (*E*,*E*)-2,4-heptadienal [1][b,c] | 997 | MS, LRI, Std | **81** (110, 53, 41, 67, 79) |
| octanal | 1002 | MS, LRI, Std | **43** (44, 56, 84, 69, 100) |
| (*E*,*E*)-2,4-heptadienal [2][b,c] | 1014 | tentative | **81** (110, 53, 41, 67, 79) |
| benzeneacetaldehyde[b,c] | 1053 | MS, LRI, Std | **91** (120, 92, 65) |
| (*E*)-2-octenal | 1064 | Tentative | **70** (55, 41, 83, 57, 69) |
| (*E*,*E*)-3,5-octadien-2-one [1][c] | 1073 | tentative | **95** (43, 81, 109, 124) |
| 2-nonanone[c] | 1091 | Tentative | **43** (58, 71, 57, 41) |
| (*E*,*E*)-3,5-octadien-2-one [2][c] | 1096 | Tentative | **95** (43, 81, 109, 124) |
| nonanal | 1106 | MS, LRI, Std | **57** (41, 56, 70, 82, 98) |
| (*E*,*Z*)-2,6-nonadienal[b,c] | 1159 | MS, LRI, Std | **41** (69, 70, 53) |
| decanal | 1224 | MS, LRI, Std | **43** (57, 70, 82, 95, 112) |

[a]Numbers in brackets correspond to identifiers of peaks when a double peak is recorded on chromatograms for one identified compound. [b]Compounds used for multivariate analysis of marinated samples. [c]Compounds used for multivariate analysis of salted samples. [d]Linear retention index. [e]MS, LRI, Std, identification confirmed by mass spectrometry, LRI, and pure standard; Tentative, tentative identification by mass spectrometry, and LRI; tentative, tentatively identified compounds by mass spectrometry only. [f]Boldface number, target ion for the method; numbers in parentheses, ions of reference to improve the integration process.

shelf life. A principal component analysis (PCA) was carried out on the data using open-source data-mining software Tanagra 1.4.[27] For each PCA, the two first principal components (PCs) were retained for interpretations. Correlations with PCs resulting from analysis determined which volatile compounds best characterized each group, as visualized by PCA.

Experiments on biogenic amines were designed as follows: for each pair of parameters (methods of preparation and storage conditions), five samples were taken for initial measurements (M0) and three samples for remaining months. Samples were analyzed every 2 months for 8 months (marinated samples) and 14 months (salted anchovies). For each analysis, measures were performed in duplicate. Comparisons of average results of assays, for biogenic amines, were carried out using nonparametric Kruskal–Wallis tests and post hoc pairwise Wilcoxon rank sum tests because the results did not follow a normal distribution and there was not homoscedasticity of variances. The tests were performed using the package "stats" from R software version 3.0.0. Kruskal–Wallis tests leading to significant results ($p$ value < 0.05) indicated that significant differences were observed for the concentration of the biogenic amines with respect to storage time. Pairwise Wilcoxon rank sum tests with $p$ values < 0.05 indicated that the two compared means were significantly different.

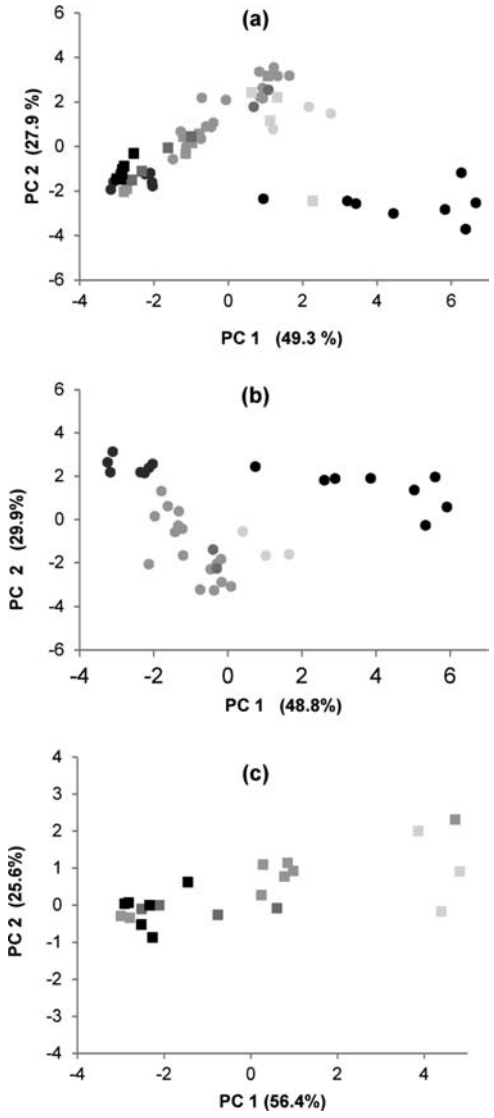


**Figure 1.** PCA obtained on the marinated anchovy samples for the whole data set (a), from the preoptimal phase (b), and from the postoptimal phase (c). Symbols indicate the tested month (M) of storage: M0, lightest gray circles; M2, medium gray circles; M3, dark gray circles; M4, darkest gray circles; M5, black circles; M6, lightest gray squares; M7, medium gray squares; M8, dark gray squares; M9, black squares.

## RESULTS

**Selection of the Volatile Compounds for PCA.** From the whole data set obtained by chromatogram integration, 36 compounds were selected as useful for our analysis (Table 1). These mostly included aldehydes, ketones, and alcohols and three compounds that do not belong to these chemical classes: 2-ethylfuran (furan), dimethyl sulfide (organosulfur), and trimethylamine (TMA) (amine).


dx.doi.org/10.1021/jf5021736 | J. Agric. Food Chem. 2014, 62, 8014–8022

**Table 2. Correlation Coefficients between Chemical Compounds and the Two First Axes Determined by PCA[a]**

| | whole data set | preoptimum phase | postoptimum phase |
|---|---|---|---|
| | | **Marinated Anchovies** | |
| PC 1 | benzaldehyde (**0.93**)[b] | benzaldehyde (**0.95**) | (*E,E*)-2,4-heptadienal [2] (**0.96**) |
| | 2,3-octanedione (**0.88**) | (*E*)-2-heptenal (**0.93**) | heptanal (**0.95**) |
| | (*E,E*)-2,4-heptadienal [2][c] (**0.86**) | 2,3-octanedione (**0.9**) | hexanal (**0.83**) |
| | (*E*)-2-heptenal (**0.85**) | (*E,Z*)-2,6-nonadienal (**0.86**) | (*E*)-2-heptenal (**0.83**) |
| | benzeneacetaldehyde (**0.83**) | (*E,E*)-2,4-heptadienal [2] (**0.81**) | (*E*)-2-hexenal (**0.83**) |
| | heptanal (**0.82**) | benzeneacetaldehyde (**0.78**) | (*E*)-2-pentenal (**0.8**) |
| | (*E,Z*)-2,6-nonadienal (**0.75**) | (*E,E*)-2,4-heptadienal [1] (**0.75**) | 2,3-octanedione (**0.76**) |
| | hexanal (**0.71**) | | 2-ethylfuran (**0.74**) |
| | | | benzaldehyde (**0.71**) |
| | | | (*E,E*)-2,4-heptadienal [1] (**0.74**) |
| *(inertia)* | *(49.3%)*[d] | *(48.8%)* | *(56.4%)* |
| PC 2 | (*E*)-2-pentenal (**0.92**) | (*E*)-2-hexenal (**−0.95**) | (*E,Z*)-2,6-nonadienal (**−0.9**) |
| | 2-ethylfuran (**0.92**) | (*E*)-2-pentenal (**−0.91**) | |
| | (*E*)-2-hexenal (**0.84**) | 2-ethylfuran (**−0.9**) | |
| *(inertia)* | *(27.9%)* | *(29.9%)* | *(25.6%)* |
| | | **Salted Anchovies** | |
| PC 1 | (*E,E*)-3,5-octadien-2-one [1] (**0.97**) | (*E,E*)-3,5-octadien-2-one [1] (**0.98**) | (*E,E*)-3,5-octadien-2-one [2] (**0.95**) |
| | (*Z*)-4-heptenal (**0.96**) | heptanal (**0.97**) | (*E,E*)-3,5-octadien-2-one [1] (**0.93**) |
| | (*E,E*)-3,5-octadien-2-one [2] (**0.95**) | 2-nonanone (**0.97**) | (*E,E*)-2,4-heptadienal [1] (**0.91**) |
| | heptanal (**0.95**) | (*Z*)-4-heptenal (**0.97**) | (*E,E*)-2,4-heptadienal [2] (**0.91**) |
| | (*E*)-2-heptenal (**0.94**) | (*E,E*)-3,5-octadien-2-one [2] (**0.97**) | (*Z*)-4-heptenal (**0.89**) |
| | hexanal (**0.94**) | (*E*)-2-heptenal (**0.95**) | (*E*)-2-heptenal (**0.85**) |
| | 2-nonanone (**0.92**) | hexanal (**0.95**) | (*E*)-2-pentenal (**0.82**) |
| | (*E,E*)-2,4-heptadienal [2] (**0.92**) | benzaldehyde (**0.92**) | benzeneacetaldehyde (**0.78**) |
| | 2,3-octanedione (**0.87**) | (*E,E*)-2,4-heptadienal [2] (**0.9**) | hexanal (**0.75**) |
| | benzaldehyde (**0.85**) | benzeneacetaldehyde (**0.9**) | heptanal (**0.73**) |
| | (*E,E*)-2,4-heptadienal [1] (**0.79**) | 2,3-octanedione (**0.87**) | 2,3-octanedione (**0.71**) |
| | benzeneacetaldehyde (**0.77**) | (*E,E*)-2,4-heptadienal [1] (**0.72**) | trimethylamine (**-0.84**) |
| | | 1-penten-3-ol (**−0.7**) | |
| *(inertia)* | *(52.9%)* | *(57.7%)* | *(45.4%)* |
| PC 2 | (*E*)-2-pentenal (**−0.83**) | 3-methylbutanal (**−0.78**) | 3-methylbutanal (**0.85**) |
| | | 2-methyl-butanal (**-0.74**) | 2-nonanone (**0.76**) |
| | | (*E*)-2-hexenal (**−0.72**) | 2-methylbutanal (**0.73**) |
| *(inertia)* | *(12.0%)* | *(15.2%)* | *(18.2%)* |

[a]Three PCAs were carried out per maturation process. [b]Coefficient in parentheses corresponds to the correlation of the volatile compound with the PC concerned (row) for a given PCA (column). [c]Numbers in brackets correspond to identifiers of peaks when a double peak is recorded on chromatograms for one identified compound. [d]Percentage in parentheses corresponds to the inertia harbored by the PC concerned for a given PCA (e.g., 49.3% means that PC1 harbored 49.3% of the data set inertia in the PCA achieved on the marinated anchovies whole data set).

Among the compounds selected for statistical analysis, none allowed differentiation of storage conditions with or without rupture (data not shown). This study thus focused on the change in the volatilome with regard to each method of anchovy preparation.

**Volatile Compounds in Marinated Samples.** Integration failed to retrieve all of the volatile compounds for each sample. Compounds or sample duplicates with missing values were removed from the data set. Thus, of the 36 compounds, only 13 were analyzed, as shown in Table 1. Among the samples, only one sample was completely removed (i.e., both duplicates), a sample preserved for 9 months without any change in storage temperature. For the remaining samples, only four samples had data from only one duplicate.

Figure 1 illustrates the results of the PCA according to storage time. The global analysis (Figure 1a) showed that samples were relatively homogeneous, especially in the first months of storage (from M0 to M4). Groups of sample storage were differentiated primarily along the *x*-axis. The composition of volatile compounds appeared to change during the first 5 months of preservation, and the product appeared to stabilize in the following months. Table 2 shows that the samples of the fifth month stand out from the other months with higher proportions of (*E,E*)-2,4-heptadienal, (*E,Z*)-2,6-nonadienal, 2,3-octanedione, (*E*)-2-heptenal, hexanal, heptanal, benzeneacetaldehyde, and benzaldehyde. The fifth month may be designated as the month when the volatile compounds reach their optimum with regard to the storage of marinated anchovies.

On the basis of this 5 month optimum, the data set was then split into a preoptimal phase and a postoptimal phase. The preoptimal phase (Figure 1b) shows that months 0−4 are characterized by smaller proportions in the above-mentioned compounds compared to the fifth month, except for hexanal and


dx.doi.org/10.1021/jf5021736 | J. Agric. Food Chem. 2014, 62, 8014−8022

heptanal. Moreover, months 4 and 5 have higher proportions of 2-ethylfuran, (*E*)-2-hexenal, and (*E*)-2-pentenal than the other months. In the postoptimal phase (Figure 1c), groups were differentiated only along the *x*-axis. Thus, from month 6 to month 9, proportions of 2,3-octanedione, (*E*,*E*)-2,4-heptadienal, 2-ethylfuran, (*E*)-2-hexenal, (*E*)-2-pentenal, (*E*)-2-heptenal, hexanal, heptanal, and benzeneacetaldehyde decreased.

Splitting the data set into two phases according to this putative month 5 optimum showed an overall decrease in the proportions of 2-ethylfuran, (*E*)-2-hexenal, and (*E*)-2-pentenal throughout the study. However, for some compounds, proportions increased up until month 5 before decreasing, for example, 2,3-octanedione, 2,4-heptadienal, (*E*)-2-heptenal, and benzeneacetaldehyde.

**Volatile Compounds in Salted Samples.** For these samples also, integration failed to retrieve all of the volatile compounds for each duplicate. Samples with missing values were discarded. Ultimately, data from 24 compounds of the 36 were analyzed as shown in Table 1. Five duplicates were discarded due to missing data.

Figure 2 shows the results according to storage time. The storage month groups were differentiated mainly along the *x*-axis (Figure 2a). Groups were relatively homogeneous, especially during the first months of storage (from M0 to M4). This can be observed, in particular, for samples analyzed at the initial stage. A change in the profile of volatile compounds was recorded at 6 months. Month 6 thus appeared to correspond to the volatile compound optimum for salted anchovies. Table 2 shows that samples from month 2 stand out with higher proportions of 2-pentenal. Samples from month 6 differ from the other groups, probably due to higher relative quantities in the following compounds: (*E*,*E*)-2,4-heptadienal, (*Z*)-4-heptenal, (*E*)-2-heptenal, benzeneacetaldehyde, 2-nonanone, (*E*,*E*)-3,5-octadien-2-one, heptanal, hexanal, 2,3-octanedione, and benzaldehyde. Finally, samples corresponding to the last few months (10, 16, and 18) do not appear different from each other.

According to this putative optimum, the data set was divided into two phases, a preoptimal phase and a postoptimal phase. The PCA of the preoptimal phase (Figure 2b) shows that months 0, 2, and 6 were characterized by higher proportions of (*E*)-2-hexenal, 2-methylbutanal, and 3-methylbutanal compared to month 4. In the same phase, month 6 differs from the other months, showing higher levels for the compounds described for the overall data set and lower proportions of 1-penten-3-ol. The PCA of the postoptimal phase (Figure 2c) shows that month 8 stands out due to higher levels of 2,3-octanedione, (*E*,*E*)-2,4-heptadienal, (*E*)-2-pentenal, (*E*,*E*)-3,5-octadien-2-one, (*Z*)-4-heptenal, (*E*)-2-heptenal, benzeneacetaldehyde, heptanal, and hexanal. Moreover, months 10−16 show higher relative quantities in TMA. Lastly, there seem to be no differences between month 16 and month 18: they both show higher proportions of 2-methylbutanal, 3-methylbutanal, and 2-nonanone compared to previous months.

During the two phases, relative quantities of 2,3-octanedione, (*E*,*E*)-2,4-heptadienal, (*Z*)-4-heptenal, (*E*)-2-heptenal, (*E*,*E*)-3,5-octadien-2-one, hexanal, heptanal, and benzeneacetaldehyde appeared to increase until reaching the optimum level before decreasing. During the same period, a continuous increase of 2-nonanone was recorded.

**Changes in Biogenic Amines.** The overall results are summarized in Table 3. In the large majority of cases, no samples ever exceeded the limit defined by the regulation (Commission Regulation (EC) No. 1441/2007 and Commission

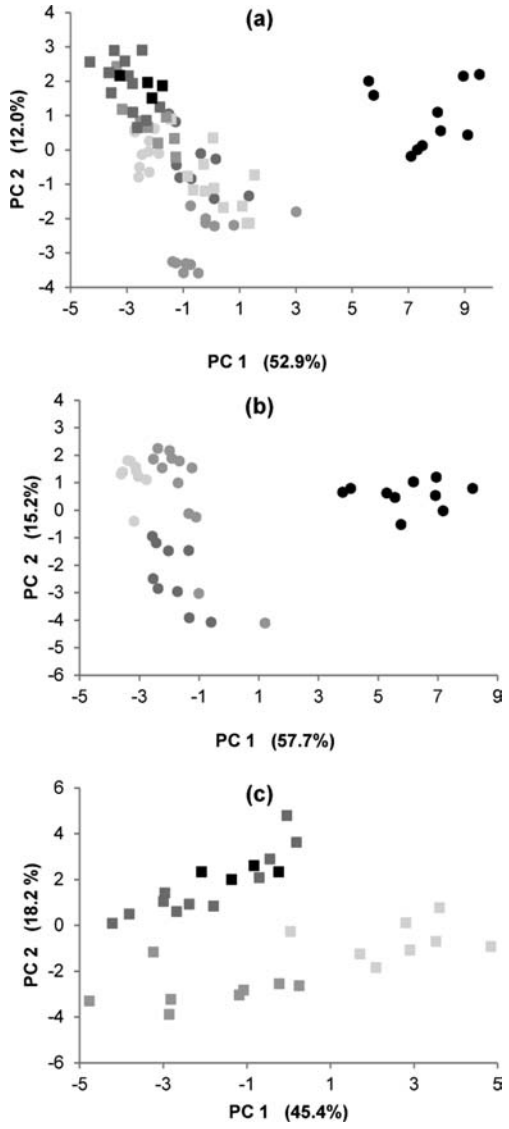


**Figure 2.** PCA obtained on the salted samples for the whole data set (a), from the preoptimal phase (b), and from the postoptimal phase (c). Symbols indicate the tested month (M) of storage: M0, light gray circles; M2, medium gray circles; M4, dark gray circles; M6, black circles; M8, light gray squares; M10, medium gray squares; M16, dark gray squares; M18, black squares.

Regulation (EC) No. 1019/2013) during the study. Only marinated anchovies that underwent a break in the cold chain showed a significant change ($p$ value < 0.001) in the quantity of histamine, exceeding the prescribed limit from month 6. With regard to putrescine, cadaverine, and tyramine, a significant change ($p$ value ≤ 0.003) was also demonstrated with a maximum concentration of nearly 50 mg kg$^{-1}$ between months 4 and 6. Finally, a significant change ($p$ value < 0.001) in the concentrations of spermidine and spermine was recorded, although levels remained low, near 20 mg kg$^{-1}$. The experiment carried out on samples that did not undergo a break in the cold chain shows similar patterns, although all of the amine concentrations were lower. Thus, the concentrations of histamine, putrescine, cadaverine, tyramine, spermidine, and spermine did not exceed the threshold values of 40 mg kg$^{-1}$.

With regard to the salted anchovies, although significant changes were recorded throughout the storage of samples, the

**Table 3. Changes in the Concentrations of Biogenic Amines Throughout a Shelf-Life of 14 Months[a]**

| | histamine[b] (mg kg$^{-1}$) | | | | putrescine (mg kg$^{-1}$) | | | |
|---|---|---|---|---|---|---|---|---|
| | marinated | | salted | | marinated | | salted | |
| | wR | w/oR | wR | w/oR | wR | w/oR | wR | w/oR |
| M0 | 4 ± 1 a | 4 ± 1 a | 1 ± 1 a | 1 ± 1 | 4 ± 1 a | 4 ± 1 a | 3 ± 1 a | 3 ± 1 a |
| M2 | 11 ± 2 b | 6 ± 1 a | nd[d] | 2 ± 2 | 4 ± 0 a | 3 ± 1 a | 2 ± 2 a | 3 ± 2 ab |
| M4 | 28 ± 15 b | 21 ± 11 b | 1 ± 2 a | 1 ± 2 | 25 ± 14 b | 17 ± 8 b | 3 ± 1 a | 2 ± 0 ab |
| M6 | 2826 ± 2356 c | 4 ± 2 a | nd | nd | 48 ± 13 b | 4 ± 0 a | 7 ± 1 b | 7 ± 1 b |
| M8 | 369 ± 269 c | 7 ± 4 ab | nd | nd | 21 ± 6 b | 4 ± 1 a | 3 ± 1 a | 4 ± 0 b |
| M10 | | | nd | nd | | | 6 ± 4 ab | 5 ± 1 ab |
| M12 | | | 1 ± 1 a | nd | | | 8 ± 1 b | 6 ± 1 b |
| M14 | | | 1 ± 1 a | nd | | | 4 ± 0 a | 4 ± 1 ab |
| $p$[c] | <0.001 | 0.003 | 0.007 | 0.291 | <0.001 | 0.002 | <0.001 | <0.001 |

| | tyramine (mg kg$^{-1}$) | | | | cadaverine (mg kg$^{-1}$) | | | |
|---|---|---|---|---|---|---|---|---|
| | marinated | | salted | | marinated | | salted | |
| | wR | w/oR | wR | w/oR | wR | w/oR | wR | w/oR |
| M0 | 14 ± 3 a | 14 ± 3 a | 7 ± 2 a | 7 ± 2 a | 15 ± 2 a | 15 ± 2 a | 12 ± 2 a | 12 ± 2 a |
| M2 | 4 ± 0 b | 5 ± 2 b | 7 ± 1 a | 7 ± 1 a | nd | 12 ± 1 a | 2 ± 1 b | 2 ± 2 ab |
| M4 | 38 ± 25 a | 20 ± 11 b | 4 ± 1 a | 3 ± 1 a | 48 ± 23 b | 36 ± 13 b | 3 ± 0 b | 4 ± 1 ab |
| M6 | 6 ± 3 b | 2 ± 1 a | 10 ± 1 a | 9 ± 1 a | 36 ± 8 b | 38 ± 1 b | 7 ± 1 ab | 8 ± 1 ab |
| M8 | 10 ± 9 ab | 3 ± 2 b | 5 ± 1 a | 4 ± 0 a | 14 ± 4 a | 14 ± 1 a | 4 ± 1 b | 3 ± 0 b |
| M10 | | | 8 ± 2 a | 5 ± 1 a | | | 7 ± 2 ab | 5 ± 1 ab |
| M12 | | | 10 ± 2 a | 5 ± 0 a | | | 6 ± 1 ab | 4 ± 1 b |
| M14 | | | 5 ± 0 a | 4 ± 0 a | | | 4 ± 0 ab | 3 ± 0 b |
| $p$ | 0.003 | <0.001 | <0.001 | <0.001 | <0.001 | <0.001 | <0.001 | <0.001 |

| | spermidine (mg kg$^{-1}$) | | | | spermine (mg kg$^{-1}$) | | | |
|---|---|---|---|---|---|---|---|---|
| | marinated | | salted | | marinated | | salted | |
| | wR | w/oR | wR | w/oR | wR | w/oR | wR | w/oR |
| M0 | 10 ± 3 a | 10 ± 3 a | 18 ± 3 a | 18 ± 3 a | 2 ± 1 a | 2 ± 1 a | 4 ± 1 a | 4 ± 1 a |
| M2 | 22 ± 2 b | 20 ± 5 b | 15 ± 4 ab | 14 ± 3 ab | 13 ± 2 b | 12 ± 4 b | 11 ± 4 ab | 11 ± 3 b |
| M4 | 8 ± 3 a | 13 ± 4 ab | 9 ± 4 ab | 13 ± 1 ab | 6 ± 3 ab | 8 ± 2 b | 3 ± 0 ab | 2 ± 1 ab |
| M6 | 7 ± 3 a | 10 ± 1 a | 8 ± 1 b | 8 ± 1 b | nd | 1 ± 1 a | nd | nd |
| M8 | 15 ± 3 ab | 11 ± 1 a | 8 ± 1 b | 7 ± 1 b | 1 ± 1 a | 5 ± 2 b | 2 ± 2 b | 4 ± 1 ab |
| M10 | | | 11 ± 2 ab | 9 ± 1 ab | | | nd | nd |
| M12 | | | 9 ± 2 b | 8 ± 0 b | | | nd | 2 ± 1 ab |
| M14 | | | 8 ± 0 b | 7 ± 2 b | | | 3 ± 0 b | 4 ± 0 ab |
| $p$ | <0.001 | 0.013 | <0.001 | <0.001 | <0.001 | <0.001 | <0.001 | <0.001 |

[a]Values are listed according to curing method and storage conditions with (wR) or without (w/oR) rupture in the temperature of storage. Means with different letters are significantly different ($p < 0.05$) throughout the tested period. [b]Means of the concentrations ±2 standard error of the mean (95% confidence interval). [c]$p$ value calculated with the Kruskal–Wallis test. [d]nd, value below the limit of quantitation.

threshold of 20 mg kg$^{-1}$ was never reached for any amine at any storage time or either storage condition.

## DISCUSSION

Principal component analysis helped to visualize a significant proportion of the variance contained in the data sets analyzed. For each analysis, principal components explained at least 64% of the variability in the whole data set, which is an acceptable level (Figures 1 and 2).

In these analyses, a difference in the volatile profile between marinated and salted samples was observed. Generally, it was found that the marinated samples did not show as many compounds as those identified for salted anchovy samples. As a result, multivariate statistical analysis could not be carried out on the same number of compounds for both types of processing methods. A significant amount of acetic acid in the headspace of marinated samples may explain the lower number of compounds recovered, possibly due to saturation of the SPME fiber.

With regard to the nature of compounds allowing the discrimination among samples, a large majority originated from the degradation of fatty acids of the $\omega$-3 and $\omega$-6 series (Table 4). This origin is consistent with observations of increased levels of free fatty acids throughout the maturation process of anchovies.[3,28] The presence of products of the catabolism of amino acids was also recorded as well as some products such as TMA or 2-ethylfuran, which are frequently observed in fish matrices. All compounds selected for the analysis of marinated samples were used in the statistical analysis of salted anchovy data set. Among the compounds included in the analysis of salted samples, five come from the degradation of fatty acids, three from the catabolism of amino acids, two from sugar degradation, and one from the degradation of trimethylamine *N*-oxide (TMAO) (Table 4).

The PCA traced the changes in the composition of the headspace over time. From those analyses, volatilome optima appear to occur at 6 months for salted anchovies and at 5 months for marinated anchovies. Only a small change in the

**Table 4. Compounds Used in the Multivariate Statistical Analysis of Anchovies and Their Assumed Origins**

| compound | assumed origin |
|---|---|
| ethanol | fermentation of sugar |
| trimethylamine | trimethylamine *N*-oxide (TMAO) reduction, degradation of choline[36] |
| 2-methylpropanal | amino acid catabolism (L-valine)[37] |
| 2,3-butanedione | fermentation of sugar[38,39] |
| 2-butanone | degradation of 2,3-butanedione[40] |
| 3-methylbutanal | amino acid catabolism (L-leucine)[37] |
| 2-methylbutanal | amino acid catabolism[41] |
| 1-penten-3-ol | eicosapentaenoic acid (EPA) (ω-3) oxidation[42] |
| (*E*)-2-pentenal | α-linolenic acid (ALA) (ω-3) oxidation[43] |
| hexanal | linoleic acid (LA) (ω-6) oxidation and 2,4-decadienal degradation[43−45] |
| 2-ethylfuran | ω-3 fatty acid oxidation (ALA, EPA, docosahexaenoic acid (DHA))[46] |
| (*E*)-2-hexenal | EPA (ω-3) oxidation[42] |
| (*Z*)-4-heptenal | EPA (ω-3) oxidation[42] |
| (*E*)-2-heptenal | linoleic acid (LA) (ω-6) oxidation[47] |
| heptanal | autoxidation of MUFA and PUFA (ω-6)[36,48] |
| benzaldehyde | amino acid catabolism[37,40] |
| 2,3-octanedione | lipid oxidation[49] |
| (*E*,*E*)-2,4-heptadienal | EPA and ALA (ω-3) oxidation[42,50] |
| benzeneacetaldehyde | amino acid catabolism[40] |
| 2-nonanone | lipid autoxidation |
| (*E*,*E*)-3,5-octadien-2-one | EPA (ω-3) autoxidation[42] |
| (*E*,*Z*)-2,6-nonadienal | ω-3 fatty acid oxidation (ALA, EPA, DHA)[51] |

composition of volatile compounds was recorded after this period of storage.

The results of salted samples corroborate those of a study carried out on the selection of sensory attributes for the evaluation of the maturation of processed anchovies: the smell of Iberian ham is a reliable marker of maturation of salted anchovies.[22] SPME-GC-MS studies have specifically shown the presence of heptanal, with a maximum at the sixth month of storage. This compound is described in the literature as having a characteristic odor of ham, fat, even rancidity.[29,30] Moreover, higher proportions of 2,3-octanedione, 2-nonanone, (*Z*)-4-heptenal, (*E*)-2-heptenal, benzaldehyde, hexanal, benzeneacetaldehyde, (*E*,*E*)-2,4-heptadienal, and (*E*,*E*)-3,5-octadien-2-one were recorded for these samples. After 6 months, the proportions of all compounds decreased except for benzaldehyde. Among the above-mentioned compounds, only 2,3-octanedione and 2-nonanone have never been described in the total volatile profile in previous studies on ripened anchovy maturation.[19−21] On the basis of the aromatic qualifiers defined by Leduc et al.,[16] odors can be divided into the following classes: earthy/woody smell, vegetable odor, and floral smell.[30−32] Moreover, anchovy samples from the 10th to 18th months are characterized by higher proportions of TMA compared to the 8th month. This suggests that the increase in total volatile basic nitrogen (TVB-N), the chemical class to which TMA belongs,[33] recorded during the anchovy maturation process[3] continues during storage.

For marinated anchovies, the fifth month appears to mark the volatilome optimum of the product. These samples were characterized by a high proportion of benzeneacetaldehyde, (*E*,*E*)-2,4-heptadienal, (*E*)-2-heptenal, benzaldehyde, (*E*,*Z*)-2,6-nonadienal, and 2,3-octanedione compared with other months. Only 2,3-octanedione has never been described in other studies on salted anchovies[19−21] (there are no published studies on the volatilome of marinated anchovies). The proportion of the above-mentioned compounds decreased except benzaldehyde. These compounds are characterized by respective odors of moss/solvent,[32] fat/soap,[34,35] cardboard/fat,[30,31] almond/woody[29,30] and cucumber for the latter two.[31,34]

Five compounds were present in maximum amounts at the volatilome optimum of processed anchovies, whatever the method of preparation: (*E*,*E*)-2,4-heptadienal, benzeneacetaldehyde, (*E*)-2-heptenal, benzaldehyde, and 2,3-octanedione. To our knowledge, this is the first time that the latter compound has been identified, only by MS and LRI, as a component of volatile compounds in anchovies. 2-Nonanone, hexanal, and (*E*,*E*)-3,5-octadien-2-one appeared to be more specific to salt-ripened anchovies.

Analysis of biogenic amines showed high variability in quantities in similar samples principally in marinated anchovies stored with rupture in the temperature conditions. This probably reflects the heterogeneity of the fish that make up the samples. The initial microbiological load of the product, hygiene measures, and the presence of bruises are all factors that may influence the degradation of anchovies. Despite the high variability of two samples with rupture in the storage conditions, the lower quantities observed exceeded 50 mg $kg^{-1}$, the concentration at which the first allergic symptoms could be observed.

The type of anchovy processing has an impact on the quantity of biogenic amines, because marinated samples had higher concentrations of histamine, cadaverine, putrescine, and tyramine than salted anchovies. This fact can be explained by the bacteriostatic action of salt ripening, whereas the development of lactic flora, potential producers of biogenic amines, is still possible in acidic conditions.[2]

The major factor that determines the production of biogenic amines, as highlighted in our study and previous papers,[6,13,14] is storage temperature. If the cold chain is broken during storage of marinated anchovies, the regulatory threshold of 400 mg $kg^{-1}$ is exceeded. However, it should be noted that the producing process, mainly in salt-ripening treatment, limits the bacterial development at the origin of histamine production.[52]

The present work helps to visualize the changes in the profile of volatile compounds and safety for both types of anchovy processing techniques. It was shown that irregularities in temperatures of storage lead to the development of biogenic amines in marinated samples, whereas no risk was observed in salted samples. In contrast, the modification of temperature conditions did not affect the volatile profile of marinated or salted samples for which the volatilome optimum is respectively reached after 5 and 6 months. None of these results lead to the conclusion of a food safety risk caused by biogenic amines when anchovies are stored in good temperature conditions. However, the study of volatilomes suggests that marinated and salted anchovies should be consumed within 5−6 months after maturation, respectively, so as to guarantee a product with optimal flavor for consumers.

## AUTHOR INFORMATION

### Corresponding Author

*(G.D.) E-mail: guillaume.duflos@anses.fr. Phone: +33 321 992 500. Fax: +33 321 991 725.

### Funding

Funds for this study, for which the CITPPM was project leader, were provided by FranceAgriMer, run by the French Ministry of Agriculture, as part of the program "*Soutien à l'innovation dans la filière des produits de la pêche et de l'aquaculture − Edition 2010*". A.D. is grateful to the Nord-Pas de Calais Regional

Council (France) and ANSES for providing financial support for his Ph.D. studies.

### Notes

The authors declare no competing financial interest.

## ■ ACKNOWLEDGMENTS

We thank Assi N'Guessan, Ossarath Kol, and Philippe Droin for their critical reviews of the manuscript and Ophélie Frottier and Paul Morieux for their kind technical assistance.

## ■ ABBREVIATIONS USED

ALA, $\alpha$-linolenic acid; CAR/PDMS, carboxen/polydimethylsiloxane; DHA, docosahexaenoic acid; EPA, eicosapentaenoic acid; GC, gaa chromatography; HACCP, hazard analysis critical control point; HPLC, high-performance liquid chromatography; LA, linoleic acid; LRI, linear retention index; MS, mass spectrometry; MUFA, monounsaturated fatty acid; PCA, principal component analysis; PUFA, polyunsaturated fatty acid; SPME, solid phase microextraction; TMA, trimethylamine; TMAO, trimethylamine *N*-oxide; TVB-N, total volatile basic nitrogen; wR, with rupture; w/oR, without rupture

## ■ REFERENCES

(1) FAO. The state of world fisheries and aquaculture 2012. In *Food and Agriculture Organization*; FAO: Rome, Italy, 2012; p 24.

(2) Fuselli, S.; Casales, M.; Fritz, R.; Yeannes, M. Microbiology of the marination process used in anchovy (*Engraulis anchoita*) production. *LWT—Food Sci. Technol.* **1994**, *27*, 214−218.

(3) Hernández-Herrero, M. M.; Roig-Sagués, A. X.; López, S. E. I.; Rodríguez-Jerez, J. J.; Mora-Ventura, M. T. Total volatile basic nitrogen and other physico-chemical and microbiological characteristics as related to ripening of salted anchovies. *J. Food Sci.* **1999**, *64*, 344−347.

(4) El-Filali, F.; Hanoune, S.; Khbaya, B.; M'Handi, N.; Kaaya, A. In *Histamine and Microbiological Change during the Storage of Semi-Preserved Anchovies*, 2nd workshop on fish technology, utilization and quality assurance in Africa, Agadir, Morocco, Nov 24−28, 2008; Food and Agriculture Organization of the United Nations (FAO): Rome, Italy, 2009; pp 133−137.

(5) Rodriguez-Jerez, J.; Lopez-Sabater, E.; Hernandez-Herrero, M.; Mora-Ventura, M. Histamine, putrescine and cadaverine formation in Spanish semipreserved anchovies as affected by time/temperature. *J. Food Sci.* **1994**, *59*, 993−997.

(6) Karaçam, H.; Kutlu, S.; Köse, S. Effect of salt concentrations and temperature on the quality and shelf-life of brined anchovies. *Int. J. Food Sci. Technol.* **2002**, *37*, 19−28.

(7) Sen, M.; Temelli, S. Microbiological and chemical qualities of marinated anchovy prepared with different vegetable additives and sauce. *Rev. Med. Vet.* **2003**, *154*, 703−708.

(8) EFSA. Panel on Biological Hazards (BIOHAZ), Scientific opinion on risk based control of biogenic amine formation in fermented foods. *EFSA J.* **2011**, *9*, 2393.

(9) Commission Regulation (EC) No. 1441/2007 of 5 December 2007 amending Regulation (EC) No. 2073/2005 on microbiological criteria for foodstuffs. *Off. J. Eur. Union* **2007**, *322*, 1−18.

(10) Commission Regulation (EC) No. 1019/2013 of 23 October 2013 amending Annex I to Regulation (EC) No. 2073/2005 as regards histamine in fishery products. *Off. J. Eur. Union* **2013**, *282*, 46−47.

(11) Pons-Sanchez-Cascado, S.; Veciana-Nogues, M.; Bover-Cid, S.; Marine-Font, A.; Vidal-Carouu, M. Volatile and biogenic amines, microbiological counts, and bacterial amino acid decarboxylase activity throughout the salt-ripening process of anchovies (*Engraulis encrasicholus*). *J. Food Prot.* **2005**, *68*, 1683−1689.

(12) Pons-Sanchez-Cascado, S.; Vidal-Carou, M. C.; Marine-Font, A.; Veciana-Nogues, M. T. Influence of the freshness grade of raw fish on the formation of volatile and biogenic amines during the manufacture and storage of vinegar-marinated anchovies. *J. Agric. Food Chem.* **2005**, *53*, 8586−8592.

(13) Veciana-Nogues, M.; Marine-Font, A.; Vidal-Carou, M. Changes in biogenic amines during the storage of Mediterranean anchovies immersed in oil. *J. Agric. Food Chem.* **1997**, *45*, 1385−1389.

(14) Veciana-Nogues, M.; Vidal-Carou, M.; Marine-Font, A. Histamine and tyramine in preserved and semi-preserved fish products. *J. Food Sci.* **1989**, *54*, 1653−1655.

(15) Béné, A.; Hayman, A.; Reynard, E.; Luisier, J. L.; Villettaz, J. C. A new method for the rapid determination of volatile substances: the SPME-direct method: Part II. Determination of the freshness of fish. *Sensors Actuat: B−Chem.* **2001**, *72*, 204−207.

(16) Leduc, F.; Tournayre, P.; Kondjoyan, N.; Mercier, F.; Malle, P.; Kol, O.; Berdagué, J. L.; Duflos, G. Evolution of volatile odorous compounds during the storage of European seabass (*Dicentrarchus labrax*). *Food Chem.* **2012**, *131*, 1304−1311.

(17) Duflos, G.; Leduc, F.; N'Guessan, A.; Krzewinski, F.; Kol, O.; Malle, P. Freshness characterisation of whiting (*Merlangius merlangus*) using an SPME/GC/MS method and a statistical multivariate approach. *J. Sci. Food Agric.* **2010**, *90*, 2568−2575.

(18) Leduc, F.; Krzewinski, F.; Le Fur, B.; N'Guessan, A.; Malle, P.; Kol, O.; Duflos, G. Differentiation of fresh and frozen/thawed fish, European sea bass (*Dicentrarchus labrax*), gilthead seabream (*Sparus aurata*), cod (*Gadus morhua*) and salmon (*Salmo salar*), using volatile compounds by SPME/GC/MS. *J. Sci. Food Agric.* **2012**, *92*, 2560−2568.

(19) Triqui, R.; Reineccius, G. A. Changes in flavor profiles with ripening of anchovy (*Engraulis encrasicholus*). *J. Agric. Food Chem.* **1995**, *43*, 1883−1889.

(20) Triqui, R.; Reineccius, G. A. Flavor development in the ripening of anchovy (*Engraulis encrasicholus* L.). *J. Agric. Food Chem.* **1995**, *43*, 453−458.

(21) Triqui, R.; Guth, H. Determination of potent odorants in ripened anchovy (*Engraulis encrasicholus* L) by aroma extract dilution analysis and by gas chromatography-olfactometry of headspace samples. In *Flavor and Lipid Chemistry of Seafoods*; American Chemical Society: Washington, DC, USA, 1997; Vol. 674, pp 31−38.

(22) Besteiro, I.; Rodriguez, C. J.; Tilve-Jar, C.; Pascual, C. Selection of attributes for the sensory evaluation of anchovies during the ripening process. *J. Sens. Stud.* **2000**, *15*, 65−77.

(23) Kondjoyan, N.; Berdagué, J.-L. *A Compilation of Relative Retention Indices for the Analysis of Aromatic Compounds*; du Laboratoire Flaveur: Saint Genes Champanelle, France, 1996.

(24) Van den Dool, H.; Dec Kratz, P. A generalization of the retention index system including linear temperature programmed gas—liquid partition chromatography. *J. Chromatogr., A* **1963**, *11*, 463−471.

(25) Malle, P.; Valle, M.; Bouquelet, S. Assay of biogenic amines involved in fish decomposition. *J. AOAC Int.* **1995**, *79*, 43−49.

(26) Duflos, G.; Dervin, C.; Malle, P.; Bouquelet, S. Relevance of matrix effect in determination of biogenic amines in plaice (*Pleuronectes platessa*) and whiting (*Merlangus merlangus*). *J. AOAC Int.* **1999**, *82*, 1097−1101.

(27) Rakotomalala, R., TANAGRA: un logiciel gratuit pour l'enseignement et la recherche. In *Extraction et Gestion des Connaissances EGC 2005*; Cépaduès-Editions: Toulouse, France, 2005; Vol. 2, pp 697−702.

(28) Roldan, H. A.; Barassi, C. A.; Trucco, R. E. Increase on free fatty acids during ripening of anchovies (*Engraulis anchoíta*). *Int. J. Food Sci. Technol.* **1985**, *20*, 581−585.

(29) García-González, D. L.; Tena, N.; Aparicio-Ruiz, R.; Morales, M. T. Relationship between sensory attributes and volatile compounds qualifying dry-cured hams. *Meat Sci.* **2008**, *80*, 315−325.

(30) Giri, A.; Osako, K.; Okamoto, A.; Ohshima, T. Olfactometric characterization of aroma active compounds in fermented fish paste in comparison with fish sauce, fermented soy paste and sauce products. *Food Res. Int.* **2010**, *43*, 1027−1040.

(31) Ólafsdóttir, G.; Fleurence, J. Evaluation of fish freshness using volatile compounds − classification of volatile compounds in fish. In

*Methods to Determine the Freshness of Fish in Research and Industries*, Proceedings of the Final Meeting of the Concerted Action (Evaluation of Fish Freshness), Nantes, France, Nov 12−14 1997; Institue International du Froid Publication: Paris, France, 1997.
(32) Varlet, V.; Knockaert, C.; Prost, C.; Serot, T. Comparison of odor-active volatile compounds of fresh and smoked salmon. *J. Agric. Food Chem.* **2006**, *54*, 3391−3401.
(33) Gill, T. A. Objective analysis of seafood quality. *Food Rev. Int.* **1990**, *6*, 681−714.
(34) Triqui, R.; Bouchriti, N. Freshness assessments of moroccan sardine (*Sardina pilchardus*): comparison of overall sensory changes to instrumentally determined volatiles. *J. Agric. Food Chem.* **2003**, *51*, 7540−7546.
(35) Jónsdóttir, R. S.; Sveinsdóttir, K. N.; Magnússon, H.; Arason, S. N.; Lauritzsen, K.; Thorarinsdottir, K. A. Flavor and quality characteristics of salted and desalted cod (*Gadus morhua*) produced by different salting methods. *J. Agric. Food Chem.* **2011**, *59*, 3893−3904.
(36) Duflos, G.; Coin, V. M.; Cornu, M.; Antinelli, J.-F.; Malle, P. Determination of volatile compounds to characterize fish spoilage using headspace/mass spectrometry and solid-phase microextraction/gas chromatography/mass spectrometry. *J. Sci. Food Agric.* **2006**, *86*, 600−611.
(37) Sinz, Q.; Schwab, W. Metabolism of amino acids, dipeptides and tetrapeptides by *Lactobacillus sakei*. *Food Microbiol.* **2012**, *29*, 215−223.
(38) Yaylayan, V. A.; Keyhani, A. Origin of 2,3-pentanedione and 2,3-butanedione in D-glucose/L-alanine Maillard model systems. *J. Agric. Food Chem.* **1999**, *47*, 3280−3284.
(39) Álvarez-Martín, P.; Belén Flórez, A.; Hernández-Barranco, A.; Mayo, B. Interaction between dairy yeasts and lactic acid bacteria strains during milk fermentation. *Food Control* **2008**, *19*, 62−70.
(40) McSweeney, P. L. H.; Sousa, M. J. Biochemical pathways for the production of flavour compounds in cheeses during ripening: a review. *Lait* **2000**, *80*, 293−324.
(41) Jaffrès, E.; Lalanne, V.; Macé, S.; Cornet, J.; Cardinal, M.; Sérot, T.; Dousset, X.; Joffraud, J.-J. Sensory characteristics of spoilage and volatile compounds associated with bacteria isolated from cooked and peeled tropical shrimps using SPME−GC−MS analysis. *Int. J. Food Microbiol.* **2011**, *147*, 195−202.
(42) Kawai, T.; Sakaguchi, M. Fish flavor. *Crit. Rev. Food Sci. Nutr.* **1996**, *36*, 257−298.
(43) Hseih, R. J.; Kinsella, J. E. *Oxidation of Polyunsaturated Fatty Acids: Mechanisms, Products, And Inhibition with Emphasis on Fish*; Academic Press: New York, 1989; Vol. 33, p 109.
(44) Josephson, D. B.; Lindsay, R. C. Retro-aldol related degradations of 2,4-decadienal in the development of staling flavors in fried foods. *J. Food Sci.* **1987**, *52*, 1186−1190.
(45) Iglesias, J.; Medina, I. Solid-phase microextraction method for the determination of volatile compounds associated to oxidation of fish muscle. *J. Chromatogr., A* **2008**, *1192*, 9−16.
(46) Medina, I.; Satué-Gracia, M.; Frankel, E. Static headspace gas chromatographic analyses to determine oxidation of fish muscle lipids during thermal processing. *J. Am. Oil Chem. Soc.* **1999**, *76*, 231−236.
(47) Grosch, W. Reactions of hydroperoxides − products of low molecular weight. In *Autoxidation of Unsaturated Lipids*; Chan, H. W. S., Ed.; Academic Press: London, UK, 1987; pp 95−139.
(48) Meynier, A.; Genot, C.; Gandemer, G. Volatile compounds of oxidized pork phospholipids. *J. Am. Oil Chem. Soc.* **1998**, *75*, 1−7.
(49) Young, O. A.; Berdagué, J. L.; Viallon, C.; Rousset-Akrim, S.; Theriez, M. Fat-borne volatiles and sheepmeat odour. *Meat Sci.* **1997**, *45*, 183−200.
(50) Frankel, E. N. Volatile lipid oxidation products. *Prog. Lipid Res.* **1983**, *22*, 1−33.
(51) Frankel, E. *Lipid Oxidation*, 2nd ed.; The Oily Press Lipid Library: Dundee, Scotland, 2005; Vol. 18, p 470.
(52) Nei, D. Evaluation of non-bacterial factors contributing to histamine accumulation in fish fillets. *Food Control* **2014**, *35*, 142−145.

JOURNAL OF AGRICULTURAL AND FOOD CHEMISTRY

Article

pubs.acs.org/JAFC

# Control of Maillard-Type Off-Flavor Development in Ultrahigh-Temperature-Processed Bovine Milk by Phenolic Chemistry

Smaro Kokkinidou and Devin G. Peterson*

Department of Food Science and Nutrition, Food Science and Nutrition Building, 1334 Eckles Avenue, University of Minnesota, St. Paul, Minnesota 55108, United States

**ABSTRACT:** The application of phenolic compounds to suppress Maillard chemistry and off-flavor development in ultrahigh-termperature (UHT)-processed milk during processing and storage was investigated. Five phenolic compounds were examined for structure−reactivity relationships (catechin, genistein, daidzein, 1,2,3-trihydroxybenzene, and 1,3,5-trihydroxybenzene). The levels of key transient Maillard reaction (MR) intermediates (reactive carbonyl species) and select off-flavor markers (methional, 2-acetyl-2-thiazoline, 2-acetyl-1-pyrroline) were quantified by LC-MS/MS and GC-MS/ToF, respectively. The addition of phenolic compounds prior to UHT processing significantly reduced the concentration of MR intermediates and related off-flavor compounds compared to a control sample ($p < 0.05$). All phenolic compounds demonstrated unique structure reactivity and, notably, those with a more activated A-ring for aromatic electrophilic substitution (catechin, genistein, and 1,3,5-trihydroxybenzene) showed the strongest suppression effect on the off-flavor markers and reactive carbonyl species. Sensory studies were in agreement with the analytical data. The cooked flavor intensity was rated lower for the recombination model samples of the catechin-treated UHT milk compared to the control UHT milk. Additionally, consumer acceptability studies showed catechin-treated UHT milk to have significantly higher liking scores when compared the control sample (Fisher's LSD = 0.728).

**KEYWORDS:** *Maillard reaction, phenolic chemistry, reactive carbonyls species, thermal processing, UHT milk, off-flavor inhibition*

## INTRODUCTION

Milk, like many foods and commodities, is mandated to undergo thermal processing during production as stated in the Code of Federal Regulations[1] to improve microbial safety. Additional benefits of thermal processing are enhanced product stability and shelf life, which facilitates distribution and storage. For milk, a number of different pasteurization methods are available such as high temperature−short time (HTST), extended shelf life processing, and ultrahigh temperature (UHT) processing, each technology utilizing different time−temperature profiles. Aseptic UHT processing of milk yields a commercially sterile product, with the longest shelf life of 6 months to 1 year. It also allows for nonrefrigerated storage and transportation, widening distribution opportunities and reducing potential energy requirements. Despite the significant benefits of UHT products, high-temperature treatment also yields a product with reduced flavor and nutritional quality as well as undesirable color development, creating a barrier to consumer acceptance.[2−4] Pasteurized milk (typically consumed in the U.S. market) has as a slightly sweet flavor, weak aroma attributes, and a pleasant mouthfeel and aftertaste.[5] Any alteration to this "clean" flavor profile is considered a product defect. Research performed at Cornell University showed a direct correlation between the flavor quality of milk and the level of consumption.[6] Blake et al.[7] also reported UHT milk had a lower consumer liking compared to other less severe thermally processed samples (i.e., pasteurized milk).

The negative flavor changes in UHT milk previously reported to develop during heat treatment and ambient storage have been associated with the Maillard reaction (MR) and lipid oxidation (LO).[8,9] Recent work by Colahan-Sederstrom and Peterson[2] identified three important Maillard-derived off-flavor compounds that contributed to the "cooked" off-flavor of UHT milk, indicating that the MR is an important pathway of off-flavor development during thermal processing and a point of control to develop flavor improvement strategies for UHT milk and milk-based beverages. The MR is well-known to affect food flavor, color, toxicity, and nutritional value.[10−16] Additionally, it is known to play an important role in regulatory biology, diabetes, and cardiovascular and age-related pathology.[11,17] Therefore, a better understanding of the mechanisms that influence Maillard reaction product (MRP) generation in processed food systems would provide the food industry with the ability to more effectively control quality and also potentially improve the nutritional attributes of food.

Phenolic compounds have been previously shown to inhibit Maillard-type flavor generation pathways and reduce off-flavors.[2] Totlani and Peterson[18] have shown that flavan-3-ols function as trapping agents (via electrophilic aromatic substitution reactions, primarily on the A-ring) of key transient Maillard precursors (reactive carbonyl species (RCSs) C2, C3, C4, and C6 sugar fragments) and consequently suppress the generation of MRPs. Flavanols such as catechin are found in several plant products, most notably in tea, cocoa, and wine, and their antioxidant capacity has been extensively studied. High consumption of those phenols has been associated with decreased risk of cardiovascular disease and cancer, as well as metabolic regulation and weight loss.[19−24] Their use to control reactions that

Received: April 23, 2014
Revised: July 10, 2014
Accepted: July 26, 2014
Published: July 26, 2014

ACS Publications © 2014 American Chemical Society

negatively affect flavor and nutrition would additionally benefit the food industry as consumers are increasingly aware of food labels and there is a greater demand for natural products.

The objective of this study was to investigate phenolic structure−reactivity relationships on the mechanisms of off-flavor development in 1% UHT milk.

## MATERIALS AND METHODS

**Chemicals.** The following chemicals were obtained from the sources given: (+)-catechin ≥97% (TCI America); genistein ≥98% (Shaanxi Schipar Biotechnology Co. Ltd., China); daidzein ≥98% (Shaanxi Schipar Biotechnology Co. Ltd., China); phloroglucinol 97% (1,3,5-trihydroxybenzene) (Aldrich, St. Louis, MO, USA); pyrogallol (Fluka, St. Louis, MO); acetoin ≥96% FCC, food grade (FG) (Aldrich); acetol 90% (Aldrich); 2,3-butanedione 97% (Aldrich); 3-deoxyglucosone (TRC, Toronto Research Chemicals, Ontario, Canada); glyoxal 40% solution in water (Sigma, St. Louis, MO, USA); methylglyoxal 40% solution in water (Sigma); methional 97% FG (Aldrich); 2-acetyl-2-thiazoline ≥96% FG (Aldrich); *o*-phenylenediamine 99.5% (Aldrich); *o*-ethylhydroxylamine hydrochloride (Aldrich); and 99.9+% anhydrous diethyl ether (Fisher Chemicals). 2-Acetyl-1-pyrroline was not commercially available but was extracted from pandan leaves (*Pandanus amaryllifolius* Roxb.), obtained from a local market. The purification procedure is described below.

*Pilot Plant Scale UHT Milk Processing.* Raw skim and whole milk were obtained from the University of Minnesota Joseph Warthesen Food Processing Center (St. Paul, MN, USA) and mixed to yield raw milk with 1% fat content. Samples underwent aseptic UHT processing using a MicroThermics HTST/UHT Indirect Tubular Processing System with water final heat (DIP-W), a homogenizer, and aseptic filling station. Processing conditions were as follows: the unit was first sanitized while passing through a chlorine solution (100 ppm, sodium hypochlorite at pH 7.00) for 1 h at 40 °C followed by a clean water wash at 121.1 °C for 1 h. The milk was homogenized, then processed at final temperature of 140 °C, holding for 6 s to ensure commercial sterilization, immediately cooled to 15 °C, and filled in a sterilized laminar flow hood into previously sterilized 1 L amber bottles.

*Small-Scale Benchtop Simulated UHT Processing.* A simulated UHT method reported by Kokkinidou and Peterson[25] was used to process milk, utilizing small sample volumes for cost and time efficiency to monitor the development of off-flavor compounds in milk spiked with RCSs (Figure 9). Briefly, 5 mL of 1% raw milk in headspace vials was placed in a cooling vial holder held at 8 °C. Vials were transferred to an agitator (150 °C) and held for 265 s to allow the sample to reach a final temperature of 140−141 °C for 6 s and subsequently returned to the cooler.

*Characterization of Off-Flavor Generation in UHT Processed Milk.* Identification and quantitation of MR precursors methylglyoxal, glyoxal, 3-deoxyglucosone, and diacetyl (dicarbonyls) as well as glycolaldehyde, acetoin, and acetol (hydroxycarbonyls) were performed using the synthesized stable isotopes [$^{13}C_4$]-acetoin and [$^{13}C_4$]-diacetyl[26] as internal standards. Each internal standard (0.5 mM) was added to 5 mL of milk, followed by 500 μL of 10% trichloroacetic acid. The samples were then vortexed for 1 min and centrifuged at 3904*g* for 20 min at 4 °C (Beckman Coulter, Allegra X-22R), and the supernatant was collected. A solid phase extraction (SPE) method was used to isolate the compounds of interest and avoid interference from phenolic compounds and adducts according to the method of Kokkinidou and Peterson.[25] A derivatization method followed, and samples were analyzed using an Acquity UPLC system coupled with a Quattro Premier XE micromass mass spectrometer (Waters Co. Milford, MA, USA). An Acquity UPLC 2.1 × 100 mm BEH Phenyl 1.7 μm column with a VanGuard 2.1 × 5 mm BEH Phenyl 1.7 μm precolumn was used for separation, and all experiments were performed in triplicate. Analytes were detected using electrospray positive ionization−multiple reaction monitoring (MRM) using methods previously developed and reported by Kokkinidou and Peterson.[25]

*Generation of Phenolic−RCS Adduct Standards.* Model reactions were used to generate standards of Maillard−phenolic products as previously described by Totlani and Peterson.[27] A 50 mL saline phosphate buffer (pH 7.4, 137 mM NaCl, 2.7 mM KCl, 10 mM $Na_2HPO_4$, and 1.8 mM $KH_2PO_4$) reaction system containing 10 mM catechin and methylglyoxal, glyoxal, or 3-deoxyglucosone was incubated in a shaking water bath at 37 °C for 1 h. After incubation, 5 mL of the reaction mixture was spiked with an internal standard (5 μL of 2% solution of butyl paraben in methanol) and an SPE clean up and concentration step followed (DSC-18 cartridge; Supelco, Bellefonte, PA, USA).

Isolates were then purified using a 2D-RP-HPLC/MS-ESI fraction collection system coupled with a Varian Dynamax Pursuit 5 Diphenyl (250 × 10.0 mm) and a Dynamax Pursuit 5 C18 (250 × 10.0 mm). Chromatography was performed with a flow rate of 3.7 mL/min with the following linear gradient conditions (solvent A, 1 mM ammonium acetate, pH 5; solvent B, methanol): solvent B at 20% (0−15 min), increased to 55% (15−61 min), then to 80% (61−66 min), then to 100% (66−72 min), and finally reduced to 20% (72−81 min). Target analytes were collected by MS guided fractionation (*m*/*z* reported in Table 1).

**Table 1. Mass Fragmentation Ions of Main Detected Adducts between Catechin (CAT) and Glyoxal (GO), Methylglyoxal (MGO), and 3-Deoxyglucosone (3DG) in Model Systems[a]**

| adduct/phenolic | parent ion (*m*/*z*) | cone voltage (V) | collision energy (V) | daughter ion (*m*/*z*) |
|---|---|---|---|---|
| CAT−GO | 347 | 35 | 21 | 167 |
| $CAT_2$−GO | 619 | 35 | 20 | 329 |
| CAT−MGO | 361 | 35 | 20 | 181 |
| CAT−$MGO_2$ | 433 | 35 | 27 | 235 |
| CAT−3DG | 451 | 32 | 22 | 289 |

[a]Optimum multiple-reaction monitoring (MRM) conditions used for their identification based on Mass Lynx (Waters, Milford, MA, USA).

Fragmentation spectra of the purified analytes were determined by LC-MS/MS techniques and are shown in Table 1. Fragmentation spectra were obtained to monitor these analytes in milk by MRM methods as well as to support the hypothesized structures of these adducts.

*Isolation and Quantitation of Off-Flavor Compounds in Milk.* Three off-flavor compounds previously identified in UHT milk[2] were monitored and included methional, 2-acetyl-2-thiazoline (2A2T), and 2-acetyl-1-pyrroline (2AP). Quantitation was conducted by stable isotope surrogate standards of each compound. The labeled compounds were synthesized as previously described [$^2H_3$]-methional,[28] [$^2H_3$]-2-acetyl-1-pyrroline,[29] and [$^2H_4$]-2-acetyl-2-thiazoline.[30] The identity and purity of each labeled standard were confirmed by MS analysis in both electron impact (EI, 70 eV) and chemical ionization (CI, at 115 eV with isobutane as reagent gas), analyzed with a Hewlett-Packard GC (HP 5890 series II) coupled with an MS detector (HP 5972). The concentration of each labeled standard was determined based on GC analysis in comparison to authentic compounds.

*Solvent-Assisted Flavor Evaporation.* Volatile isolates of the samples were prepared by solvent extraction that was adapted from the method of Colahan-Sederstrom and Peterson.[2] Prior to extraction [$^2H_4$]-2A2T, [$^2H_3$]-2AP, and [$^2H_3$]-methional were added as internal standards at levels of 5 μg standard/kg milk. The concentrated extract was then subjected to high-vacuum distillation using a solvent-assisted flavor evaporation (SAFE) apparatus.[31] The isolate was further fractionated into an acidic (A) and a neutral/basic (N/B) fraction as described by Colahan-Sederstrom.[2] The N/B fraction was prepared and stored at −80 °C prior to analysis by an Agilent 7890A GC (Agilent Technologies, Inc., Wilmington, DE, USA) coupled with a TruTOF HT time-of-flight mass spectrometer (Leco Co., St. Joseph, MI, USA) and a DB-5MS column (30 m × 0.250 mm × 0.25 μm, Agilent Technologies). The column heating profile was at 40 °C for 2.00 min, then ramped to 160 °C at 3 °C/min and ramped to 250 °C at 30 °C/min, and held for 5 min. Injection mode was splitless, and temperature was 250 °C.

*Dynamic Headspace GC-MS.* Off-flavor analysis of the milk samples spiked with RCSs (Figure 9) was performed using a 6890 GC coupled with a DB-5MS (30 m × 0.250 mm × 0.25 μm, Agilent Technologies)

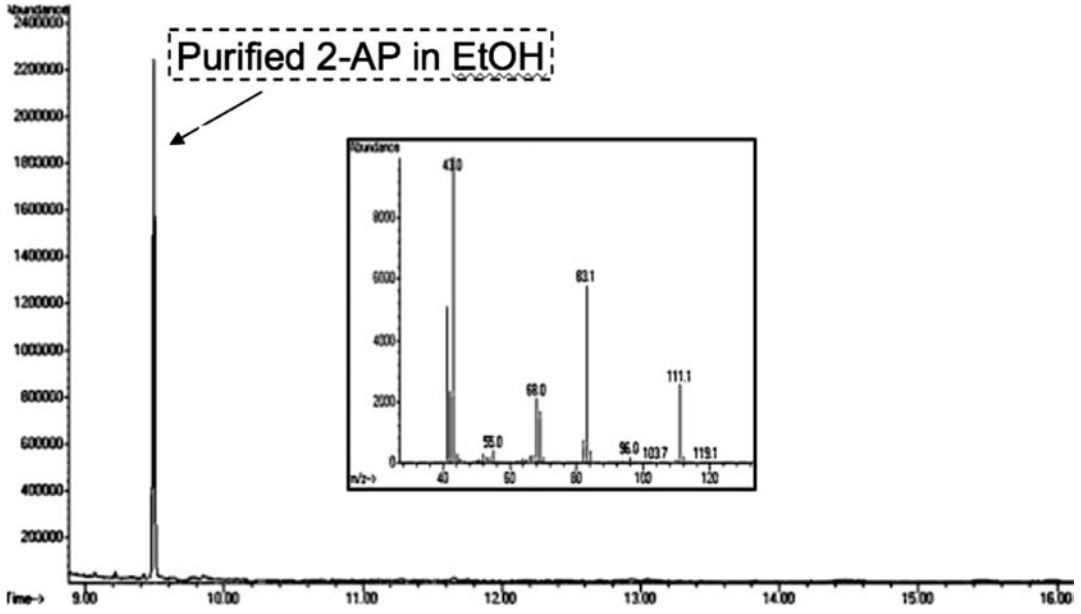


**Figure 1.** Example chromatogram and MS spectra of purified 2AP isolated from pandan leaf extract after multidimensional chromatography, heart-cutting, and fraction collection.

column and equipped with a 5973 mass selective detector (Agilent Technologies), thermal desorption unit (TDU, Gerstel), PTV inlet (CIS 3, Gerstel), and MPS 2 with headspace and dynamic headspace (DHS) option (Gerstel). Briefly, 5 mL of UHT processed milk was placed in headspace vials (20 mL) along with 1 mL of nanopure water and sodium chloride (1 M). Prior to dynamic headspace analysis, [$^2H_4$]-2A2T, [$^2H_3$]-2AP, and [$^2H_3$]-methional were added as internal standards at levels of 5 $\mu$g standard/kg milk. The headspace vials were then incubated at 40 °C for 10 min and subsequently purged with nitrogen at a rate of 40 mL/min for a total time of 12.5 min while agitated at 500 rpm to increase volatility. The trap (Tenax TA) was then dry purged for 4 min at a rate of 30 mL/min and transferred to a thermal desorption unit. The trapped volatiles were then desorbed, cryofocused at −125 °C, and injected in solvent vent mode. The column heating profile was at 40 °C for 2.00 min, ramped to 160 °C at 3 °C/min, then ramped to 250 °C at 30 °C/min, and held for 5 min.

*Identification of Odorants.* Positive identifications were made by linear retention indices (LRI) and mass spectra compared to authentic compounds analyzed under identical conditions.

*Generation of 2-Acetyl-1-pyrroline Standard.* A 2AP standard was prepared from an extract of pandan leaves (*P. amaryllifolius* Roxb.) as previously described by Colahan-Sederstrom and Peterson.[2] The reference compound was further purified using a two-dimensional GC system coupled with a fraction collector.

The analytical system consisted of an Agilent 6890N GC equipped with two Dean switch devices, two Gerstel modular accelerated column heaters (MACH), and an Agilent 7683 autosampler and injector and was additionally coupled with an Agilent 5973N MSD and a Gerstel preparative fraction collector (PFC). An RTX-5S ILMS (30 m × 0.25 mm × 0.25 $\mu$m) was used as a primary column, and a DB-Wax (30 m × 0.25 mm × 0.25 $\mu$m) was used as a secondary column. GC conditions for all runs were as follows: inlet temperature, 200 °C; 10 $\mu$L of sample injected in solvent vent mode (0 kPa, 0.15 min); helium carrier gas ramp pressure mode (initial pressure or 357 kPa held for 7.1 min and then ramped to 10 Pa at 999 kPa/min); and a total flow of 3.9 mL/min with a split 1:4 to MSD and 3:4 to PFC. MSD conditions were as follows: capillary direct interface temperature, 250 °C; mass range, 35−300 amu; The MACH heating profile for the RTX-5S ILMS capillary column was 40 °C for 1 min, then ramped to 280 °C at 10 °C/min, and held for 2.35 min, whereas for the DB-Wax the oven profile was 40 °C for 7.60 min, ramped to 230 °C at 10 °C/min, and held for 2 min. The valve-switching program for heart-cutting and isolation of 2AP was as follows: valve 1 switched on at 6.29 min, directing the flow to the secondary column, and switched off at 7.10 min; then valve two switched on at 15.4 min directing the flow to cryotrap of PFC for 2AP collection and switched off at 15.75 min. The PFC switching device was operated at 250 °C, and the trap was kept at −70 °C. 2AP was extracted from the trap using food grade ethanol and further quantified using vinylpyrrolidine as a standard using an HP 5890 series II GC coupled with an FID. An example chromatogram of 2AP is presented in Figure 1.

*Sensory Analysis of UHT Milk Samples.* Both consumer acceptability and descriptive analysis including off-flavor recombination models were conducted. For the consumer acceptability test, 49 panelists were recruited on the basis of regular milk consumption. Aseptically processed UHT milk samples with and without added 1.7 mM catechin and a commercial UHT milk (Parmalat, Agropur Inc., Division Natrel, USA) were evaluated for acceptability after storage at 30 °C for 1 month. The samples were presented at room temperature in coded 3 oz cups in randomized order. The panelists were asked to rate them on a nine-point hedonic scale (ranging from dislike extremely to like extremely). Differences among treatments were evaluated by analysis of variance (ANOVA) followed by Tukey's HSD pairwise comparison. All analyses were performed with Statistix software (version 9). Significance was established at $p < 0.05$.

For the descriptive analysis trained panelists evaluated the intensity of cooked off-flavor in milk samples. Seven graduate students from the Department of Food Science and Nutrition at the University of Minnesota were recruited for the analysis and were selected on the basis of availability and willingness to participate. They received eight 1 h training sessions focused on the cooked attribute of the milk samples. A cooked reference was prepared by heating 1% milk (Schroder Milk Co.) to 90 °C and holding for 45 min. This cooked reference was mixed with various amounts of pasteurized milk to create a range of cooked intensities. The panel agreed to use the following intensities as references: 100% cooked = 15; 75% cooked/25% pasteurized = 8; 50% cooked/50% pasteurized = 4; 30% cooked/70% pasteurized = 2. Samples were evaluated on a 15-point intensity scale, anchored on the left with "none" and on the right with "extreme".

Panelists participated in three evaluation sessions, occurring over the period of 1 day. The four samples were evaluated in triplicate in a randomized block design. The four samples evaluated were (1) pasteurized 1% milk (Schroder Milk Co.); (2) commercial 1% UHT milk (Parmalat); (3) off-flavor recombination model for simulation of control UHT milk prepared using pasteurized 1% milk (Schroder Milk Co.) spiked with 2AP (1.35 $\mu$g/kg), 2A2T (0.95 $\mu$g/kg), and methional (4.05 $\mu$g/kg); and (4) off-flavor recombination model for simulation of

UHT milk with added catechin prepared using pasteurized 1% milk (Schroder Milk Co.) spiked with 2A2T (0.41 μg/kg) and methional (0.88 μg/kg) to simulate UHT milk (Figure 3) . The spiked levels of off-flavor markers in recombination models were determined after quantitation in pasteurized 1% milk (Schroder Milk Co.) and addition of appropriate amounts for simulation of UHT processed milk samples.

Differences among treatments were evaluated by analysis of variance (ANOVA) followed by Tukey's HSD pairwise comparison. ANOVA was also used to monitor panelist performance. All analyses were performed with Statistix Software (version 9). Significance was established at $p < 0.05$.

*Microbial Testing.* Microbial analysis was conducted on both control and treatment samples using 3 M Petrifilm aerobic count (AC) plates and coliform count (CC) plates (3M Co., St. Paul, MN, USA) according to protocol. For counts in 3M AC and CC plates, 1 mL of each dilution 1:10, 1:100, and 1:1000 of milk samples was plated using phosphate buffer, $KH_2PO_4$ (0.0425 g/L, adjusted to pH 7.2, Butterfield's buffer; Weber Scientific, Hamilton, NJ, USA). Colonies were enumerated after incubation at 37 °C for 24 h for coliforms and at 35 °C after 48 h for aerobic bacteria.

## RESULTS AND DISCUSSION

Milk with 1% fat content was selected for evaluation, as it is the most consumed fluid milk product in the United States. Although overall fluid milk consumption has steadily decreased over the past three decades, consumption of low-fat milk has increased (in comparison to whole milk) as consumers become more aware of caloric intake and negative effects of saturated fat intake.[32] As previously reported[6,7] UHT milk receives significantly lower liking scores than pasteurized milk or other less severely thermally processed milk samples in the domestic marketplace. Consequently, the negative flavor attributes of aseptic UHT milk are a hurdle to utilization and product acceptability. Colahan-Sederstrom and Peterson[2] had previously reported the addition of a phenolic compound prior to UHT processing reduced the cooked flavor intensity of UHT milk suggesting an improved product quality. Therefore as an initial step, a consumer acceptability study was performed to assess the effectiveness of phenolic compound addition on consumer liking. UHT milk samples with and without catechin were stored at 30 °C for 30 days, for accelerated aging (estimated 2−3 months at ambient storage conditions), prior to evaluation. A commercial UHT sample was also included as an internal anchor. The results of the consumer panel are presented in Table 2. The UHT milk with catechin added prior to processing received a significantly higher liking score then both the control and commercial UHT milk samples, demonstrating the application of phenolic compounds to improve UHT milk quality.

**Table 2. Consumer Acceptability Rating of 1% UHT Milk Manufactured with and without Catechin Plus a Commercial UHT Sample**

| sample | mean liking (9-point hedonic scale) |
|---|---|
| 1% UHT-catechin containing (1.72 mM)[a] | 6.04a |
| 1% UHT milk[a] | 5.12b |
| commercial UHT (Parmalot) | 4.73b |

[a]Samples prepared and produced at University of Minnesota Joseph Warthensen Processing Center facilities (processed to 140 °C for 6 s) and stored at 30 °C for 1 month. Different letters indicate statistically significant differences. Fisher's LSD = 0.728 (5% significance level).

**Phenolic Structure Reactivity.** A mechanistic understanding of the reactivity of phenolic chemistry related to off-flavor suppression would be beneficial for the optimization of the dose response. For example, select phenolic structures might be more reactive (effective in suppressing off-flavor) during thermal processing (ca. 140 °C), whereas others could be more reactive during ambient storage.

Five phenolic compounds (see Figure 2) were selected to examine phenolic structure function reactivity on the MR pathways and off-flavor development in UHT processed milk, and the effectiveness of each structure on off-flavor suppression was evaluated immediately after processing as well as after storage. Three common food phenolic compounds, catechin (flavanol), genistein, and daidzein (isoflavones), along with two simple phenols, 1,2,3-trihydroxybenzene and 1,3,5-trihydroxybenzene, were selected.

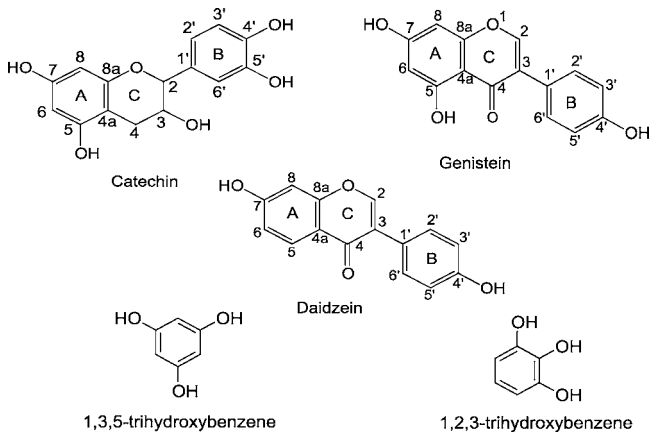


**Figure 2.** Select phenolic compounds evaluated in UHT milk.

The food phenolic compounds differ in the degree and position of hydroxyl substitution on rings A and B as well as the presence of a keto group on the C-ring (isoflavones). The simple phenols were used to simulate different ring chemistry, more redox reactive (123THB) or more "trapping" reactive of carbonyl compounds by electrophilic aromatic substitution reactions (135THB) to investigate the mechanisms by which phenolic compounds alter MR pathways. Among the food-derived phenolic compounds, catechin would have the highest trapping reactivity, followed by genistein and then daidzein, based on the position of the hydroxyl groups on the A-ring and electron-withdrawing groups on the neighboring C-ring (keto group). Phenolic compounds were added at dose levels of 1.7 mM, which was selected as this amount of epicatechin was reported[2] to be effective in suppressing off-flavor development and not result in a detectable bitterness (a sensory attribute associated with polyphenols).

**Sensory Recombination Analysis: Markers of UHT Cooked Flavor.** To quantitatively monitor off-flavor progression in UHT milk, the off-flavor compounds as well as reaction intermediates of these compounds were targeted. For target off-flavor compounds, Colahan-Sederstrom and Peterson[2] identified three Maillard-type reaction products related to the cooked off-flavor profile of 1% UHT milk. These included methional, 2-acetyl-1-pyrroline (2AP) and 2-acetyl-2-thiazoline (2A2T). In the current study the contribution of these off-flavor compounds to the "cooked" off-flavor attributes of UHT milk was further defined by sensory recombination analysis in milk systems.

The concentrations of methional, 2AP, and 2A2T were determined after 30 days of storage at 30 °C in UHT milk as well as in the UHT milk with catechin (see Figure 3). On the basis of

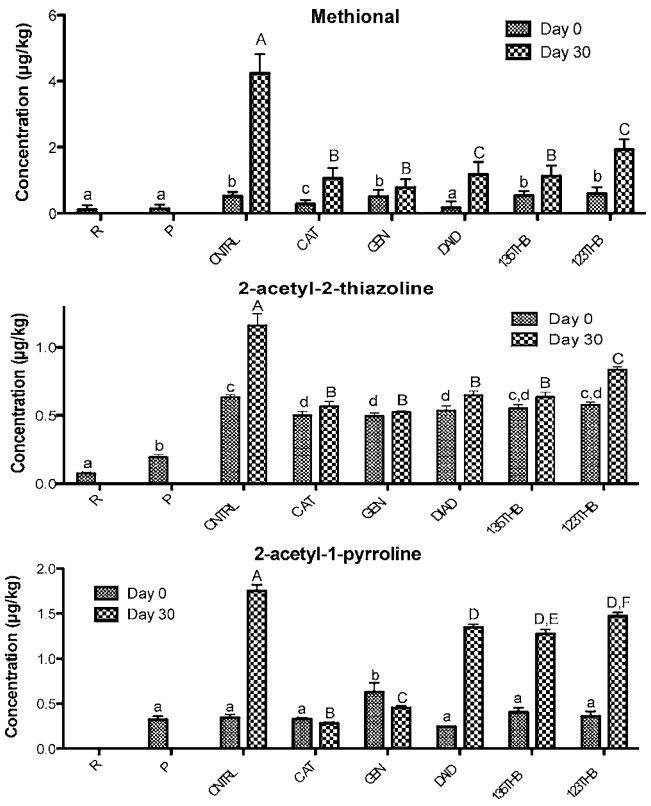


**Figure 3.** Concentration of off-flavor markers 2-acetyl-1-pyrroline (2AP), methional, and 2-acetyl-2-thiazoline (2A2T) in raw (R), pasteurized (P), control UHT milk (CNTRL), and UHT milk with added catechin (CAT), genistein (GEN), daidzein (DAID), 1,3,5-trihydroxybenzene (135THB), and 1,2,3-trihydroxybenzene (123THB) as determined right after UHT processing (day 0) and after 30 days of storage in 30 °C (day 30). The same letters indicate no statistical significant differences ($p < 0.05$). Lower case letters correspond to day 0 treatments, and upper case letters correspond to day 30 treatments.

these quantitative off-flavor fingerprints, the corresponding aroma recombination models of UHT and UHT with catechin samples were made in pasteurized (HTST) milk and evaluated for the cooked flavor intensity (see Table 3). The UHT aroma recombination model was not significantly different in cooked flavor intensity in comparison to commercial UHT milk and was significantly higher in cooked flavor intensity compared to both commercially pasteurized (HTST) milk and the model UHT milk that contained catechin. Overall these findings supported the utilization of these three Maillard-type off-flavor compounds as predictive chemical markers of cooked off-flavor associated with UHT processed milk.

**Table 3. Average Cooked Flavor Intensity of Commercial Milk and Off-Flavor Recombination Model Systems**

| sample | mean rating | homogenous groups[a] |
|---|---|---|
| commercial 1% UHT milk (Parmalat) | 5.5 | A |
| off-flavor recombination model of 1% UHT milk | 5.3 | A |
| commercial 1% pasteurized milk | 1.1 | B |
| off-flavor recombination model of UHT-catechin containing (1.72 mM) | 0.8 | B |

[a]Fisher's LSD = 0.319 (5% significance level), $n = 8$ in duplicate.

**Effect of Phenolic Compounds on Levels of Off-Flavor Markers.** The influence of different phenolic structures on the generation of cooked off-flavor both during thermal treatment (day 0) and after storage (30 days at 30 °C) is further illustrated in Figure 3; the concentration in the raw milk prior to UHT processing was also included for comparison. Overall, the concentration of all three marker compounds (methional, 2AP, and 2A2T) increased during UHT processing and storage at 30 °C in direct comparison to raw and pasteurized milk (Figure 3). Further comparison of the influence of phenolic addition on the suppression of off-flavor compounds indicated the effects reported were variable and dependent on the type of off-flavor compounds, the phenolic structure added, and the temperature of the system (UHT processing temperature, 140 °C, versus storage, 30 °C). For example, catechin and daidzein slightly inhibited the amount of methional generated during UHT processing, whereas the other three phenolics had no substantial effect. However, during storage, all phenolic compounds were reported to suppress its generation, with genistein and catechin being more effective, reducing methional by 80 and 75%, respectively. This observation indicated that catechin was more effective for suppressing the generation of methional during both processing and storage. However, for methional, daidzein is more reactive during processing, whereas genistein was more reactive during storage conditions.

For 2A2T, the addition of phenolic compounds had little impact on off-flavor development during processing temperatures as compared to control UHT, but all effectively suppressed generation during storage. Addition of catechin, genistein, or daidzein resulted in concentrations of 2A2T after storage 42–53% lower than the control, notably at concentrations below the odor threshold of this compound (1 µg/kg). Genistein was the most reactive phenolic compound for off-flavor suppression under storage conditions.

Finally for 2AP, most phenolic compounds had negligible influence on off-flavor development during processing. However, during storage, genistein and catechin were the most reactive and effective in suppressing off-flavor generation, whereas daidzein, 123THB, and 135THB had negligible effects.

In general 135THB, which is more activated toward aromatic electrophilic substitution, was more effective in reducing the concentration of off-flavor markers as compared to 123THB, supporting the idea that one of the mechanisms by which phenolic compounds inhibit MR pathways and off-flavor generation is reactive carbonyl trapping. On the basis of the observed unique structure reactivity of these phenolic compounds, utilizing mixtures of phenolic compounds as an off-flavor inhibition strategy was subsequently investigated in a further study.[25]

**Effect of Phenolic Compounds on RCS Levels.** To further elucidate the influence of the phenolic structure reactivity on the generation of the Maillard-type off-flavor compounds, the RCSs (key transient sugar fragments) were also quantified. The concentrations of dicarbonyl and hydroxycarbonyl sugar fragments as influenced by UHT processing, phenolic addition, and storage are illustrated in Figures 4 and 5, respectively. Overall, UHT processing resulted in increased concentrations of RCSs when compared to both raw and pasteurized milk. This was expected, as the UHT conditions would catalyze the MR and subsequently the generation of MR intermediates such as RCSs. Examination of the sugar fragments in the control UHT sample

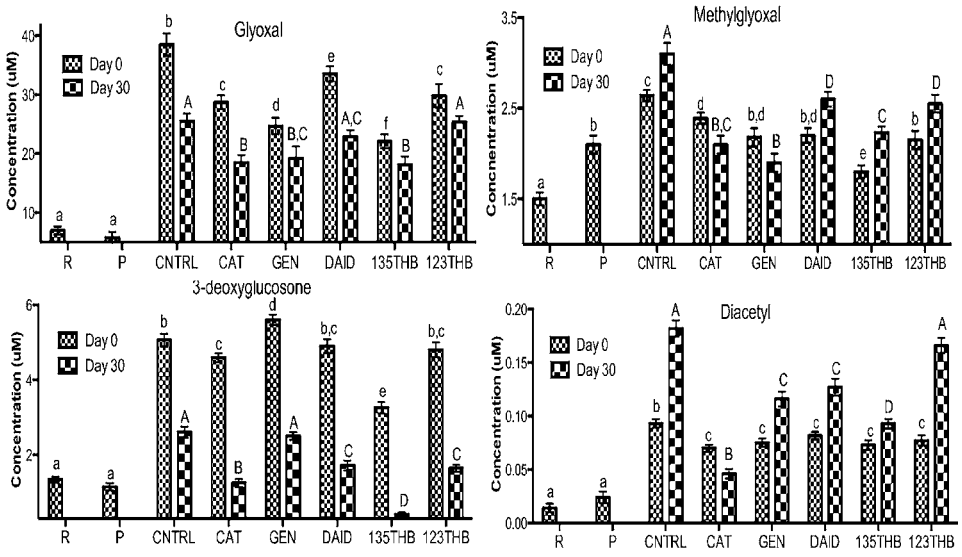


**Figure 4.** Concentrations of $\alpha$-diacarbonyls (glyoxal, methylglyoxal, 3-deoxyglucosone, and diacetyl) in raw (R), pasteurized (P), control UHT milk (CNTRL), and UHT milk with added catechin (CAT), genistein (GEN), daidzein (DAID), 1,3,5-trihydroxybenzene (135THB), and 1,2,3-trihydroxybenzene (123THB), as determined immediately after UHT processing (day 0) and after 30 days of storage in 30 °C (day 30). Each compound was monitored as quinoxaline derivatives and run in triplicate. The same letters indicate no statistical significant differences ($p < 0.05$)). Lower case letters correspond to day 0 treatments, and upper case letters correspond to day 30 treatments. All treatments were significantly different at day 30 when compared to day 0 ($p < 0.05$).

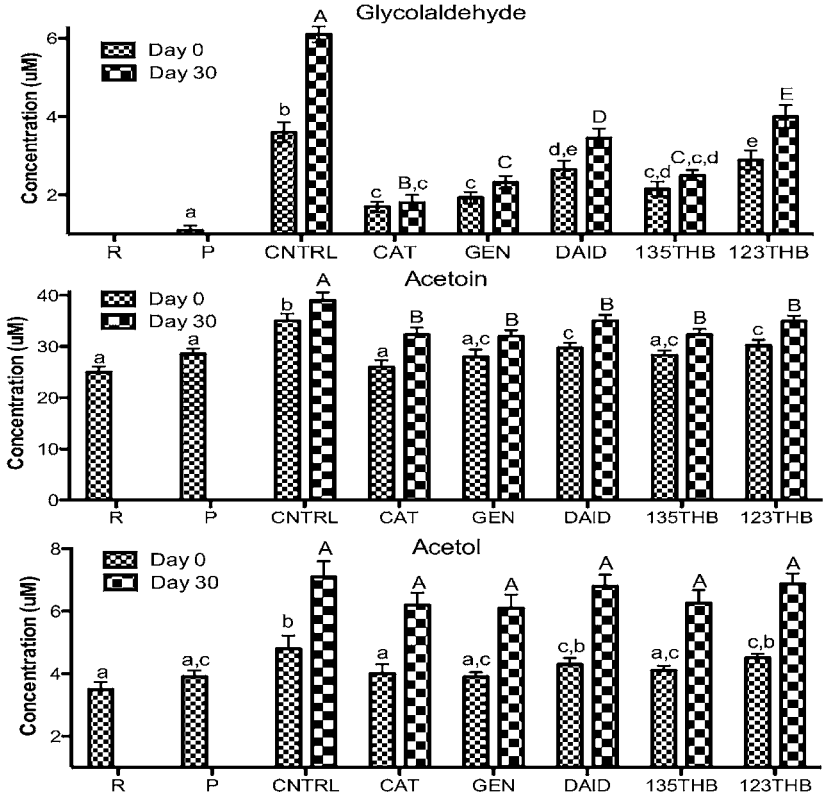


**Figure 5.** Concentration of $\alpha$-hydroxycarbonyls (glycolaldehyde, acetol, and acetoin) in raw (R), pasteurized (P), control UHT milk (CNTRL), and UHT milk with added catechin (CAT), genistein (GEN), daidzein (DAID), 1,3,5-trihydroxybenzene (135THB), and 1,2,3-trihydroxybenzene (123THB), as determined immediately after UHT processing (day 0) and after 30 days of storage in 30 °C (day 30). Each compound was monitored as ethoxylamine derivatives and run in triplicates. The same letters indicate no statistical significant differences ($p < 0.05$). Lower case letters correspond to day 0 treatments, and upper case letters correspond to day 30 treatments. Unless otherwise indicated, all treatments were significantly different at day 30 when compared to day 0 ($p < 0.05$).

after storage indicated that two of the dicarbonyl compounds, namely, methylglyoxal and diacetyl, increased, whereas glyoxal and 3-deoxylglucosone decreased; all hydroxylcarbonyls increased (glycolaldehyde and acetol) or maintained similar levels (acetoin). The observed reduction in the concentration of glyoxal and 3-deoxyglucosone could be indicative of the high


dx.doi.org/10.1021/jf501919y | J. Agric. Food Chem. 2014, 62, 8023−8033

reactivity of glyoxal entering several reaction pathways leading to off-flavor formation, and for 3-deoxyglucosone its further fragmentation to shorter chain sugar fragments further contributed to MRP generation.

In general, the addition of phenolic compounds prior to UHT processing resulted in reduced levels of these MR precursors (RCSs) compared to the control UHT milk samples. The influence of phenolic compounds on the reduction of RCSs indicated that the different structures have unique reactivity and was dependent on the structure of the dicarbonyl or hydroxycarbonyl compound, as well as on the temperature of the system (UHT processing temperature, 140 °C, or storage, 30 °C).

*Dicarbonyls.* Overall, all of the food phenolic compounds (catechin, genistein, and daidzein) reported a significant effect ($p < 0.05$) compared to control UHT milk on the levels of dicarbonyl compounds during processing and storage. Catechin, genistein, and 135THB were the most effective phenolic treatments in reducing the concentration of glyoxal after 30 days of storage followed by diadzein. These observations were expected on the basis of the reactivity of the phenolic structures toward aromatic electrophilic substitution (Figure 2). Genistein and 135THB were the most reactive phenolic compounds during UHT processing, demonstrating the highest reduction of glyoxal as compared to control UHT milk.

Similarly for methylglyoxal, addition of catechin, genistein, or 135THB significantly reduced the concentration of this RCS after 30 days of storage. Additionally, both catechin and genistein were effective in reducing the concentration of methylglyoxal during storage to concentrations lower than observed right after processing (day 0), and it is noteworthy these levels are not significantly different from concentrations found in pasteurized milk demonstrating unique reactivity as compared to other phenolic treatments. The most reactive phenolic compound for suppressing the levels of methylgloxyal during UHT processing was 135THB.

Similarly, 135THB was also the most reactive phenolic treatment in reducing the concentration of 3-deoxyglucosone during both UHT processing and storage, followed by catechin. Notably, these two phenolic treatments resulted in 3-deoxyglucosone levels that were not significantly different from or lower than those found in pasteurized and raw milk. The increased reactivity of 135THB as compared to catechin could also be explained by reduced steric hindrances. Overall, genistein had reduced reactivity toward C6 sugar fragments. The reduced reactivity of both genistein and diadzein as compared to catechin and 135THB was expected due to the presence of a keto group at the C-5 position on ring C that can decrease nucleophilicity of the activated ortho positions of ring A (C-8 and C-6) (Figure 2) and thus its sugar fragment trapping reactivity. The increased reactivity of daidzein as compared to genistein could potentially be attributed to reduced steric hindrance due to the absence of the hydroxyl group at the C-5 position of the A-ring (Figure 2).

Diacetyl was effectively reduced during UHT processing by all phenolic treatments except diadzein, which was not significantly different from the control UHT milk demonstrating negligible reactivity for this C4 sugar fragment. Catechin was the most reactive phenolic treatment in reducing the concentration of diacetyl during storage to levels below those observed at day 0. Findings again demonstrate unique phenolic structure reactivity. For all other phenolic treatments, the concentration of diacetyl continued to increase during storage, albeit at reduced rates when compared to the control.

*Hydroxycarbonyls.* The effect of phenolic treatment on the levels of hydroxycarbonyl compounds also reported unique structure reactivity, but the observed suppression effects were not as pronounced. All phenolic compounds significantly ($p < 0.05$) reduced the levels of glycolaldehyde with the more reactive phenols being catechin, genistein, and 1,3,5-trihydroxybenzene. Only catechin, genistein, and 1,3,5-trihydroxybenzene significantly reduced acetoin, and for acetol no significant ($p > 0.05$) changes were observed for the phenolic treatments when compared to control UHT milk. The overall noted reduction in phenolic reactivity for the hydroxycarbonyl compounds was anticipated. Hydroxylcarbonyl compounds are relatively weaker electrophiles and, thus, are less likely to be trapped by phenolic compounds. From the three hydroxycarbonyls investigated, glycolaldehyde is the most electrophilic and, as predicted, was the most influenced by phenolic addition.

**Phenolic Trapping Reactivity.** Overall, on the basis of the predicted reactivity of the selected phenolic compounds toward aromatic electrophilic substitution reactions and RCS trapping, catechin, as a flavanol, was expected to be significantly more reactive as compared to isoflavones such as genistein and daidzein. However, due to the complexity of food systems, phenolic-carbonyl reactions are anticipated to be influenced by multiple factors such as phenolic stability and competing reactions and hence why this general trend (based on aromatic electrophilic substitution reactions) was not always observed. In this study, genistein demonstrated overall similar reactivity toward trapping RCSs as compared to catechin. This observation could potentially be explained by the increased autoxidation reactivity of catechin resulting in the formation of quinones, thus leading to greater reactivity with milk proteins and other milk constituents and reduced RCS trapping reactivity.

Among the simple phenolic compounds, 135THB was more effective in reducing the levels of RCSs, which is in agreement with previously findings.[33] 1,3,5-Trihydroxybenzene would be expected to be a more reactive trapping agent of sugar fragments than 123THB on the basis of the polyhydroxyl ring configuration. 135THB has three electron-donating hydroxyl groups in the meta configuration on a benzene ring, which activate the ortho and para positions for electrophilic aromatic substitution reactions at the three substituted carbon sites (e.g., RCSs). Consequently, the noted higher reactivity of 135THB suggests that one of the mechanisms by which phenolic compounds alter the flavor generation pathways in UHT milk is the formation of adducts with these precursors as previously hypothesized by Totlani and Peterson.[34] In general, the observed reduction in the concentration of RCSs correlated with both analytical and sensorial data regarding the inhibition of off-flavor generation in UHT milk as influenced by the addition of phenolic compounds when compared with traditional UHT milk.

The noted improvement in the consumer acceptability of UHT milk treated with phenolic compounds (catechin) could also be due to, in part, the reduction in the concentrations of the RCS. Many of the RCS have unique (off)-flavor attributes. Diacetyl has been identified as a contributor to the heated, cooked, and fermented notes of UHT milk with a flavor threshold of 12 ppb (0.14 $\mu$M),[35−37] and notably diacetyl concentration in control UHT milk after 30 days of storage was above this flavor threshold value. Glyoxal and methyglyoxal have mild sour, pungent, and slightly nutty aromas. Acetol is characterized as sweet and roasted or as having a yogurt-like flavor in emulsions, and acetoin has a sweet, buttery, creamy aroma.[38−41]

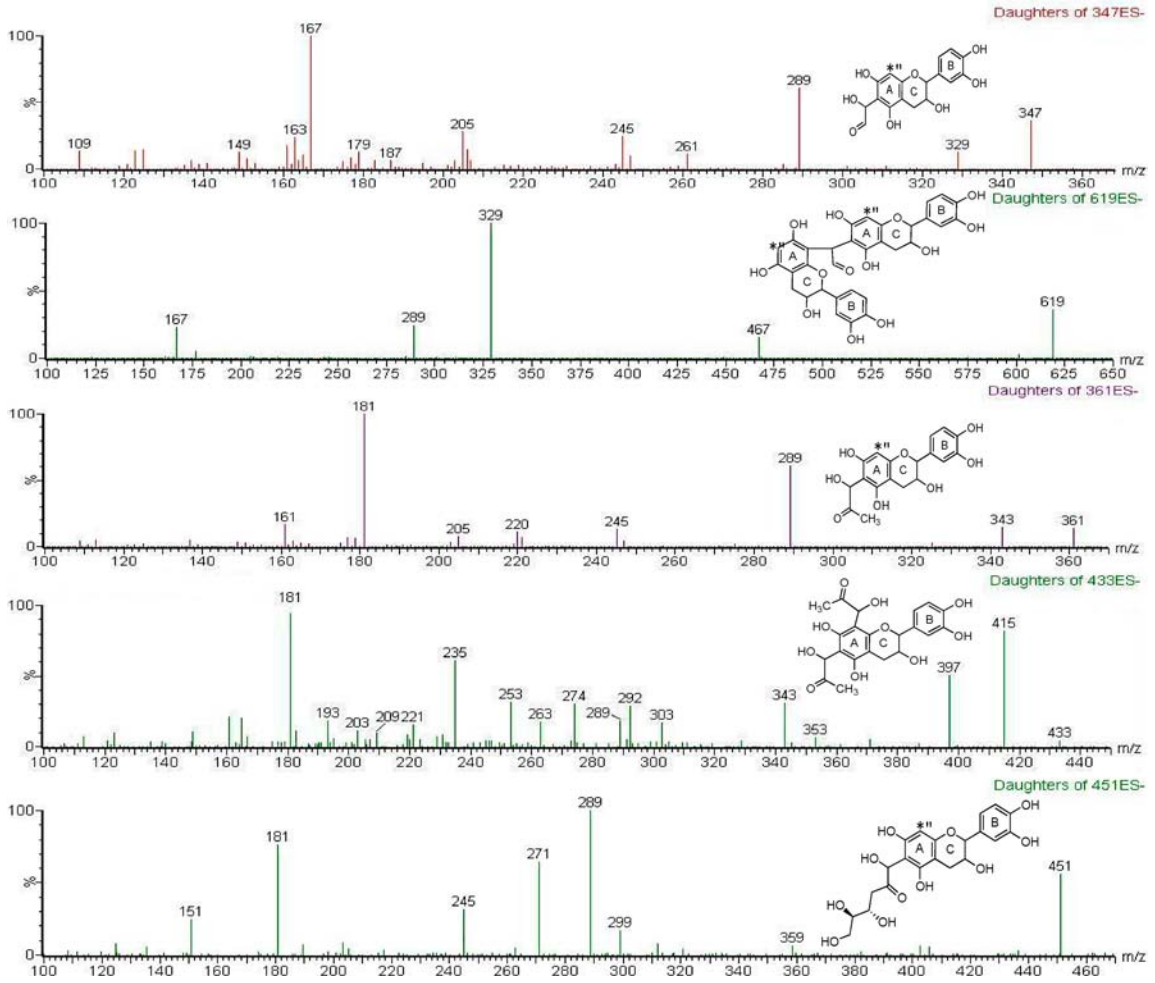


**Figure 6.** MS/MS fragmentation spectra for catechin−sugar fragment adduct reaction products. Spectra correspond to catechin−glyoxal, catechin−glyoxal−catechin, catechin−methylglyoxal, methylglyoxal−catechin−methylglyoxal, and catechin−3-deoxyglucosone adducts from top to bottom. ∗ denotes alternative position activated for aromatic electrophilic substitution. RCSs substitution can occur at either the C-6 or C-8 position of the A-ring. Only one structure is presented for simplicity.

**Phenolics−RCSs Adducts.** To further support the hypothesis of adduct formation as a mechanism for off-flavor inhibition, model reaction systems were prepared and adducts between catechin and glyoxal, methylglyoxal, and 3-deoxyglucosone were purified to develop analytical methods for their identification in UHT milk with added catechin. The most prominent products of these reactions were identified as catechin−glyoxal, catechin−glyoxal−catechin, catechin−methylglyoxal, methylglyoxal−catechin−methylglyoxal, and catechin−3-deoxyglucose adducts. The proposed reaction product structures shown in Figure 7 were based on prior literature[27,42,43] and MS/MS fragmentation patterns (Figure 6). The parent ions of all purified products/adducts generated daughter ions of $m/z$ 289, which corresponds to a catechin moiety along with fragments of $m/z$ 245, 205, and 179, which are characteristic daughter ions of catechin fragmentation[44] confirming its presence in these products. The $m/z$ 245 fragment may be generated after a neutral loss of $CO_2$, characteristic of negative ionization mode.[45] The $m/z$ 205 fragment is most likely generated by loss of rings B and C,[46] and $m/z$ 179 is produced after an A-ring loss. This particular fragmentation pattern (loss of A-ring) supports the adduct formation between catechin and RCSs via electrophilic aromatic substitution at C-8 or C-6 of ring A as well as the proposed adduct structures because fragments that correspond to a loss of ring A with RCS moieties were detected for all adducts. Namely, $m/z$ 167 (A-ring−glyoxal), $m/z$ 181 (A-ring−methylglyoxal), $m/z$ 253 (A-ring−methylglyoxal$_2$), and $m/z$ 271 (A-ring−3-deoxyglucosone) were detected as daughter ions of catechin−glyoxal and catechin−glyoxal−catechin, catechin−methylglyoxal, methylglyoxal−catechin−methylglyoxal, and catechin−3-deoxyglucosone adducts, respectively. MRM methods were developed, and the detection of all adducts in aseptically processed UHT milk with added catechin was achieved. An example chromatogram of the detection of catechin−glyoxal and catechin−methylglyoxal adducts is shown in Figure 8. Multiple peaks in chromatograms were anticipated to be due to four diastereoisomers of catechin forming during thermal processing reacting with RCSs. Catechin−methylglyoxal adducts resulted in more than four peaks as the addition of methylglyoxal added another chiral center to the molecule, thus increasing the number of possible products.

**RCSs and Off-Flavor Causality.** To demonstrate causality between increased levels of RCSs and off-flavor generation, RCSs were additionally added to milk prior to UHT processing and the levels of off-flavor volatiles were monitored. More specifically, pasteurized milk (control) and pasteurized milk spiked with levels of RCSs reported in UHT milk glyoxal (GO) 60 $\mu$M, methylglyoxal (MGO) 20 $\mu$M, diacetyl 0.4 $\mu$M, and 3-


dx.doi.org/10.1021/jf501919y | J. Agric. Food Chem. 2014, 62, 8023−8033

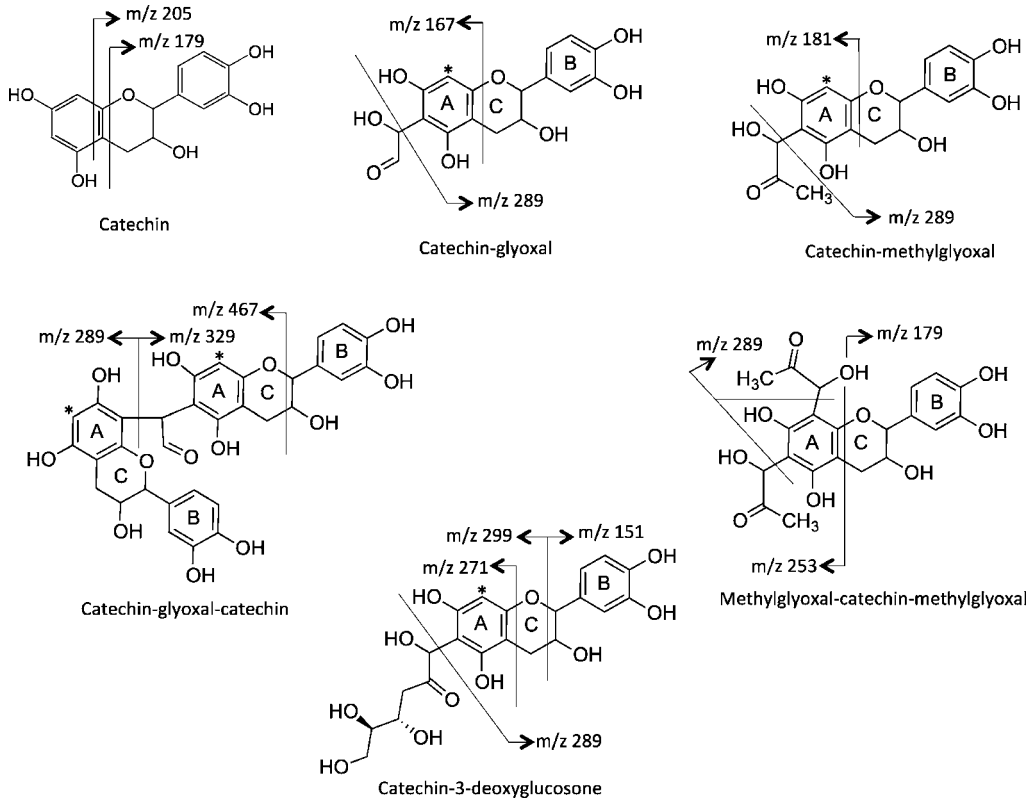


**Figure 7.** Hypothesized MS/MS fragmentation pattern of adducts between catechin and glyoxal, methylglyoxal, and 3-deoxyglucosone. ∗ denotes predicted main alternative position for aromatic electrophilic substitution based on prior literature.[27,42,43] RCSs substitution can occur at either the C-6 or C-8 position of the A-ring. Only one structure is presented for simplicity.

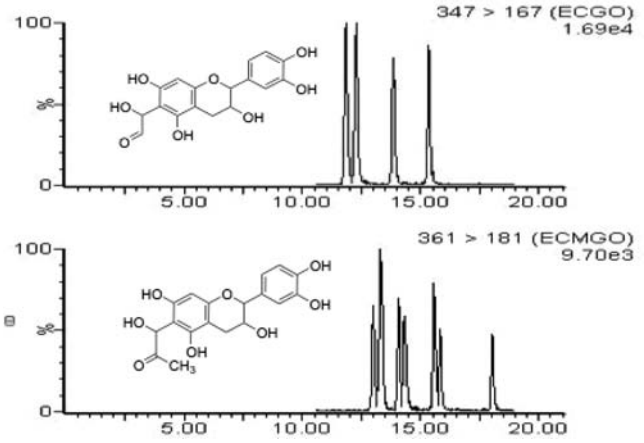


**Figure 8.** LC-MS/MS (ESI negative mode) chromatograms of detection catechin adducts with glyoxal (top,$m/z$ 347 → 167) and methylglyoxal (bottom, $m/z$ 361 → 181) in UHT milk with catechin. A suggested reaction product is illustrated.

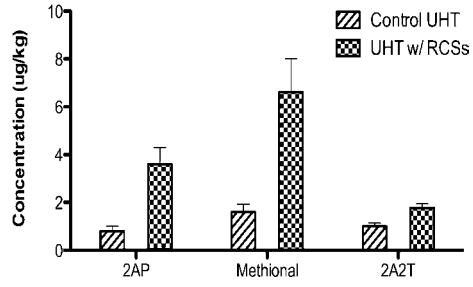


**Figure 9.** Concentration of off-flavor markers 2-acetyl-1-pyrroline (2AP), methional, and 2-acetyl-2-thiazoline (2A2T) in control UHT milk and UHT milk with added glyoxal (65 $\mu$M), methylglyoxal (20 $\mu$M), diacetyl (0.4 $\mu$M), and 3-deoxyglucosone (12 $\mu$M), as determined right after UHT processing (day 0).

deoxyglucosone (3DG) 10 $\mu$M) were subsequently UHT processed, and the concentrations of the selected off flavor markers were determined immediately after processing. The results are shown in Figure 9 and demonstrate that increased levels of RCSs resulted in significantly higher levels of off-flavor markers, as compared to the control. More specifically, 2AP, methional, and 2A2T were increased by 77.5, 74.2, and 42.1%, respectively, when milk was spiked with RCSs prior to UHT processing, thus demonstrating causality and further supporting the formation of phenolic−RCS adducts as one of the main mechanisms of phenolic off-flavor inhibition.

In summary, phenolic compounds were reported to significantly suppress MR off-flavor pathways in UHT milk during thermal processing and storage, resulting in a product with increased consumer acceptability. Furthermore, the results of this study support phenolic trapping reactions of Maillard-generated sugar fragments as an important mechanism of off-flavor suppression. This work further defined the interplay between phenolic chemistry and the mechanisms of the MR in foodstuffs. Unique phenolic−structure reactivity was also reported for the suppression of Maillard chemistry in UHT milk; different phenolic structures were more reactive during thermal processing versus storage in reducing both RCSs and off-flavor markers. Overall, these results support the potential of phenolic compound mixtures or food extracts rich in phenolic compounds (e.g., cocoa, tea, coffee, grape, soy) as treatments to


dx.doi.org/10.1021/jf501919y | J. Agric. Food Chem. 2014, 62, 8023−8033

improve the flavor stability and nutritional value of thermally processed foods and in this case milk and milk-based beverages. Self-affirmed generally regarded as safe (GRAS) phenolic ingredients such as Teavigo (flavanol) and geniVida (isoflavone) are currently commercially available (DSM, NL).

## AUTHOR INFORMATION


### Corresponding Author

*(D.G.P.) E-mail: dgp@umn.edu. Phone: (612) 624-3201. Fax: (612) 625-5272.



### Funding

This work was supported in part by Dairy Management, Inc., as managed by Dairy Research Institute (Rosemount, IL, USA).


### Notes

The authors declare no competing financial interest.

## REFERENCES


(1) 21CFR131.110. Requirements for Specific Standardized Milk Food and Drugs. Code of Federal Regulations, 2005.

(2) Colahan-Sederstrom, P. M.; Peterson, D. G. Inhibition of key aroma compound generated during ultrahigh-temperature processing of bovine milk via epicatechin addition. *J. Agric. Food Chem.* **2005**, *53*, 398−402.

(3) Perkins, M. L.; Deeth, H. C. A survey of Australian consumers' attitudes towards UHT milk. *Aust. J. Dairy Technol.* **2001**, *56*, 28−34.

(4) Zadow, J.; Britwistle, R. The effect of dissolved O2 on the changes occuring in the flavour of ultra-high-temperature milk during storage. *J. Dairy Res.* **1973**, *40*, 169−177.

(5) Thomas, E. L. Trends in milk flavor. *J. Dairy Res.* **1981**, 285−295.

(6) Bandler, D. K. Rancidity: an icreasingly common milk flavor problem. *Dairy Food Sanit.* **1982**, *2*, 312−315.

(7) Blake, M. R.; Weimer, B. C.; Mcmahon, D. J.; Savello, P. A. Sensory and microbial quality of milk processed for extended shelf life by direct steam injection. *J. Food Prot.* **1995**, *58*, 1007−1013.

(8) Simon, M.; Hansen, A. P.; Young, C. T. Effect of various dairy packaging materials on the headspace analysis of ultrapasteurized milk. *J. Dairy Sci.* **2001**, *84*, 774−783.

(9) Thomas, E. L.; Burton, H. J.; Ford, E.; Perkin, A. G. The effect of oxygen content on flavour and chemical changes during aseptic storage of whole milk after ultra-high-temperature processing. *J. Dairy Res.* **1975**, 285−295.

(10) Ames, J. The Maillard reaction in foods. In *Biochemistry of Food Proteins*; Hudson, B. J. F., Ed.; Springer: New York, 1992; pp 95−153.

(11) Baynes, J. W.; et al. The Maillard reaction in food and biological sciences. *Ann. N.Y. Acad. Sci.* **2005**, 1043.

(12) Burton, H. *Ultra-High-Temperature Processing of Milk and Milk Products*; Springer: New York, 1988.

(13) Ikan, R. *Maillard Reaction − Consequences for the Chemical and Life Sciences*; Wiley: Hoboken, NJ, USA, 1996.

(14) Patton, S. Browning and associated changes in milk and its products: a review. *J. Dairy Sci.* **1955**, *38*, 457−478.

(15) Schneeman, B. O.; Dunaif, G. Nutritional and gastrointestinal response to heated non fat dry milk. *J. Agric. Food Chem.* **1984**, *32*, 477−480.

(16) Steinhart, H. The Maillard reaction. Chemistry, biochemistry and implications. *Angew. Chem. Int. Ed.* **2005**, *44*, 7503−7504.

(17) Wells-Knecht, K. J.; Brinkmann, E.; Wells-Knecht, M. C.; Litchfield, J. E.; Ahmed, M. U.; Reddy, S.; Zyzak, D. V.; Thorpe, S. R.; Baynes, J. W. New biomarkers of Maillard reaction damage to proteins. *Nephrol. Dial. Transplant.* **1996**, *1*, 41−47.

(18) Totlani, V. M.; Peterson, D. G. Reactivity of epicatechin in aqueous glycine and glucose Maillard reaction models: quenching of C2, C3, and C4 sugar fragments. *J. Agric. Food Chem.* **2005**, *53*, 4130−4135.

(19) Velayutham, P.; Babu, A.; Liu, D. Green tea catechins and cardiovascular health: an update. *Curr. Med. Chem.* **2008**, *15*, 1840−1850.

(20) Hasan, M.; Nihal, A. Tea polyphenols: prevention of cancer and optimizing health. *Am. J. Clin. Nutr.* **2000**, *71*, 1698−1702.

(21) Maki, K. C.; Reeves, M. S.; Farmer, M.; Yasunaga, K.; Matsuo, N.; Katsuragi, Y.; Komikado, M.; Tokimitsu, I.; Wilder, D.; Jones, F.; Blumberg, J. B.; Cartwright, Y. Green tea catechin consumption enhances exercise-induced abdominal fat loss in overweight and obese adults. *J. Nutr.* **2009**, *139*, 264−270.

(22) Murase, T.; Nagasawa, a; Suzuki, J.; Hase, T.; Tokimitsu, I. Beneficial effects of tea catechins on diet-induced obesity: stimulation of lipid catabolism in the liver. *Int. J. Obesity* **2002**, *26*, 1459−1464.

(23) Nurulain, T. Z. Green tea and its polyphenolic catechins: medicinal uses in cancer and noncancer applications. *Life Sci.* **2006**, *78*, 1073−2080.

(24) Yang, S. C.; Wang, X.; Lu, G.; Pinich, C. S. Cancer prevention by tea: animal studies, molecular mechanisms and human relevance. *Nat. Rev. Cancer* **2009**, *9*, 429−439.

(25) Kokkinidou, S.; Peterson, D. G. Response surface methodology as optimization strategy for reduction of reactive carbonyl species in heat-processed foods by means of phenolic chemistry. *Food Funct.* **2013**, *4* (7), 1093−1004.

(26) Schieberle, P.; Hofmann, T. Evaluation of the character impact odorants in fresh strawberry juice by quantitative measurements and sensory studies on model mixtures. *J. Agric. Food Chem.* **1997**, *45*, 227−232.

(27) Totlani, V. M.; Peterson, D. G. Epicatechin carbonyl-trapping reactions in aqueous maillard systems: identification and structural elucidation. *J. Agric. Food Chem.* **2006**, *54*, 7311−7318.

(28) Sen, A.; Grosch, W. Original paper Synthesis of six deuterated sulfur containing odorants to be used as internal standards in quantification assays. *Z. Lebensm.-Unters. -Forsch.* **1991**, *192*, 541−547.

(29) De Kimpe, N. G.; Stevens, C. V.; Keppens, M. A. Synthesis of 2-acetyl-1-pyrroline, the principal rice flavor component. *J. Agric. Food Chem.* **1993**, *41*, 1458−1461.

(30) Cerny, C.; Grosch, W. Quantification of character-impact odour compounds of roasted beef. *Z. Lebensm.-Unters. -Forsch.* **1993**, *196*, 417−422.

(31) Engel, W.; Bahr, W.; Schieberle, P. Solvent assisted flavour evaporation − a new and versatile technique for the careful and direct isolation of aroma compounds from complex food matrices. *Eur. Food Res. Technol.* **1999**, *209*, 237−241.

(32) USDA/ERS. Livestock, Dairy and Poultry Outlook, 2010.

(33) Noda, Y.; Peterson, D. G. Structure-reactivity relationships of flavan-3-ols on product generation in aqueous glucose/glycine model systems. *J. Agric. Food Chem.* **2007**, *55*, 3686−3691.

(34) Totlani, V. M.; Peterson, D. G. Influence of epicatechin reactions on the mechanisms of Maillard product formation in low moisture model systems. *J. Agric. Food Chem.* **2007**, *55*, 414−420.

(35) Jeon, I. J. Undesirable flavors in dairy products. In *Food Taints and Off-Flavours*; Saxby, M. J., Ed.; Chapman and Hall: London, UK, 1996; pp 139−167

(36) Scanlan, R.; Lindsay, R.; Libbey, L.; Day, E. Heat-induced volatile compounds in milk. *J. Dairy Sci.* **1968**, *51*, 1001−1007.

(37) Shibamoto, T.; Mihara, S.; Nishimura, O.; Kamiya, Y.; Aitoku, A.; Hayashi, J. Flavor volatiles formed by heated milk. In *The Analysis and Control of Less Desirable Flavors in Foods and Beverages*; Charalambous, G., Ed.; Elsevier: Amsterdam, The Netherlands, 1980; pp 241−265

(38) http://www.thegoodscentscompany.com/data/rw1034251.html, organoleptic properties of methylglyoxal (accessed June 23, 2014).

(39) http://www.thegoodscentscompany.com/data/rw1248641.html, organoleptic properties of glyoxal (accessed June 23, 2014).

(40) http://www.thegoodscentscompany.com/data/rw1007331.html, organoleptic properties of acetoin (accessed June 23, 2014).

(41) http://www.thegoodscentscompany.com/data/rw1132561.html, organoleptic properties of acetol (accessed June 23, 2014).

(42) Es-Safi, N. E.; Fulcrand, H.; Cheynier, V.; Moutounet, M. Competition between (+)-catechin and (−)-epicatechin in acetaldehyde-induced polymerization of flavanols. *J. Agric. Food Chem.* **1999**, *47*, 2088−2095.

(43) Lo, C. Y.; Li, S.; Tan, D.; Pan, M. H.; Sang, S.; Ho, C. T. Trapping reactions of reactive carbonyl species with tea polyphenols in simulated phisiological conditions. *Mol. Nutr. Food Res.* **2006**, *50*, 1118−1128.
(44) Sun, J.; Liang, F.; Bin, Y.; Li, P.; Duan, C. Screening non-colored phenolics in red wines using liquid chromatography/ultraviolet and mass spectrometry/mass spectrometry libraries. *Molecules (Basel, Switzerland)* **2007**, *12*, 679−693.
(45) Fabre, N.; Rustan, I.; de Hoffmann, E.; Quetin-Leclercq, J. Determination of flavone, flavonol, and flavanone aglycones by negative ion liquid chromatography electrospray ion trap mass spectrometry. *J. Am. Soc. Mass Spectrom.* **2001**, *12*, 707−715.
(46) Stöggl, W. M.; Huck, C. W.; Bonn, G. K. Structural elucidation of catechin and epicatechin in sorrel leaf extracts using liquid-chromatography coupled to diode array-, fluorescence-, and mass spectrometric detection. *J. Sep. Sci.* **2004**, *27*, 524−528.

JOURNAL OF AGRICULTURAL AND FOOD CHEMISTRY

Article

pubs.acs.org/JAFC

# Identification of Bitter Peptides in Aged Cheddar Cheese

Konstantinia Karametsi, Smaro Kokkinidou, Ian Ronningen, and Devin G. Peterson*

Department of Food Science and Nutrition, University of Minnesota, 145 FScN Building, St. Paul, Minnesota 55108, United States

**ABSTRACT:** The compounds responsible for the bitter taste of aged "sharp" Cheddar cheese were characterized. Sensory-guided fractionation techniques using gel permeation chromatography and multi-dimension semi-preparative reversed-phase high-performance liquid chromatography revealed the presence of multiple bitter compounds. The compounds with the highest perceived bitterness intensity were identified by tandem mass spectrometry *de novo* peptide sequencing as GPVRGPFPIIV, YQEPVLGPVRGPFPI, MPFPKYPVEP, MAPKHKEMPFPKYPVEPF, and APHGKEMPFPKYPVEPF; all originated from *β*-casein. Subsequent quantitative liquid chromatography−tandem mass spectrometry analysis reported that the concentrations of GPVRGPFPIIV, YQEPVLGPVRGPFPI, and MPFPKYPVEP increased during maturation by 28.7-, 3.1-, and 1.8-fold, respectively. When directly compared to young "mild" Cheddar, APHGKEMPFPKYPVEPF was reported only in the sharp Cheddar cheese, whereas the concentration of MAPKHKEMPFPKYPVEPF did not change. Further taste re-engineering sensory experiments confirmed the importance of the identified peptides to the bitterness of sharp Cheddar. The bitter intensity of the aged "sharp" Cheddar model (mild Cheddar with equivalent concentrations of the five bitter peptides in the sharp sample) was rated as not significantly different from the authentic sharp Cheddar cheese. Among the five peptides, GPVRGPFPIIV was reported to be the main contributor to the bitterness intensity of sharp Cheddar. Furthermore, a difference from control sensory test also confirmed the significance of the bitter taste to the overall perception of aged Cheddar flavor. The sharp Cheddar model was reported to be significantly more similar to aged "sharp" Cheddar in comparison to the young "mild" Cheddar cheese sample.

**KEYWORDS:** *Cheddar cheese, aged, bitterness, peptides*

## INTRODUCTION

The chemical stimuli that invoke food flavor can be simplistically defined as a combination of aroma, taste, and chemesthetic compounds. Aroma compounds are volatile and perceived by the olfactory system, while taste compounds can be volatile or non-volatile and are detected by the gustatory system. Chemesthetic compounds are irritants of the pain nerves in the oral cavity. Historically, researchers have looked at food flavor as predominately being influenced by volatile aroma compounds, with minor contributions from taste. This assumption has turned out to be an oversimplification. Understanding the flavor compounds that contribute to the desirable flavor properties of foods provides a basis to develop manufacturing strategies to improve the acceptability of healthier options, such as reduced fat or salt.

Taste stimuli have been recognized as key aspects of the flavor properties of cheese.[1] A number of researchers have characterized the volatile flavor compounds from Cheddar cheese, resulting in an extensive list including a wide variety of compounds, such as acids, alcohols, esters, aldehydes, ketones, sulfur-containing compounds, and phenolics. On the contrary, only limited information is available on the characterization of the taste of most cheese varieties,[1−10] and none is characterized sufficiently to permit duplication of its complete flavor by mixtures of pure compounds.[11]

The degree of ripening of Cheddar cheese is known to affect the development of all aspects of flavor (taste, aroma, and texture). With regard to taste, over time, characteristic bitterness develops that has been associated with hydrophobic peptides. Although some bitterness is considered a normal component of Cheddar cheese taste and contributes to the desirable flavor of mature Cheddar,[12] excessive bitterness is generally regarded as a defect[2,13] and may limit consumer acceptance.

The development of bitterness during the maturation of Cheddar cheese is considered to be the result of the accumulation of hydrophobic peptides that consist of 2−23 amino acid residues in the molecular mass range of 500−3000 Da.[2,12,13] The isolation and characterization of the compounds that are responsible for bitterness in foodstuffs have been the subject of numerous studies over the years. Gouda has been analyzed by sensory-guided fractionation techniques, and 12 peptides were found to contribute to bitterness[8,9] as well as in whey protein and whey protein hydrolysates[14,15] and various kinds of cheeses.[3−5]

Very limited information is available about the taste active compounds in Cheddar cheese. Broadbent et al.[13] used two peptides [*β*-casein (*β*-CN) (f193−f209) and *α*(S1)-casein (*α*(S1)-CN) (f1−f9)] as indicators of excessive bitter development in Cheddar and model systems. However these peptides, or their breakdown products, have not been adequately characterized for their contribution to bitterness perception limiting the application of these data to better understand Cheddar flavor.

The goal of this study was therefore to identify bitter peptides in Cheddar cheese and characterize their sensory contribution to improve our understanding of Cheddar flavor.

**Received:** April 30, 2014
**Revised:** July 10, 2014
**Accepted:** July 14, 2014
**Published:** July 30, 2014

ACS Publications © 2014 American Chemical Society



dx.doi.org/10.1021/jf5020654 | *J. Agric. Food Chem.* 2014, 62, 8034−8041

The chemical nature of the identified taste compounds will provide insight as to whether the flavor compounds are produced during processing or during aging and will afford a basis to better understand flavor generation (precursors involved) and, thus, facilitate the development of strategies for control in related products for flavor improvement.

## MATERIALS AND METHODS

**Samples.** Sharp and mild Cheddar cheese samples were obtained from a local grocery store (Archer Farms, Target, Minneapolis, MN) and stored at −20 °C prior to analysis. Sharp Cheddar is representative of an aged cheese of 9−12 months, whereas mild Cheddar is representative of a young cheese of 2−3 months.

**Chemicals.** Trifluoroacetic acid, formic acid, and high-performance liquid chromatography (HPLC)-grade solvents were obtained from Sigma-Aldrich Co. Synthetic peptides YQEPVLGPVRGPFP, GPVRGPFPIIV, MAPKHKEMPFPKYPVEPF, QEPVLGPVREGPFP, APKHKEMPFPKYPVEPF, YQEPVLGPVRGPFPI, EPVLGPVRGPFP, QEPVLGPVRGPFPI, EMPFPKYPVEPF, LGPVRGPFP, PVLGPVRGPFP, and MPFPKYPVEPF were obtained from EZBiolab, Inc. at a purity of 98%.

**Preparation of the Methanol-Soluble Extract from Cheddar Cheese.** A total of 60 g of Cheddar cheese and 240 mL of water were homogenized for 5 min and, subsequently, centrifuged at 4000*g* for 20 min at 4 °C. The protein pellet as well as the fat layer were collected and re-extracted with 240 mL of methanol (overall analytical scheme is shown in Figure 1). The methanol layer was removed, filtered, and concentrated using a rotary evaporator. The resulting residue was subsequently diluted in water and freeze-dried twice to obtain the methanol-soluble extract (MSE), which was stored at −20 °C prior to further analysis.

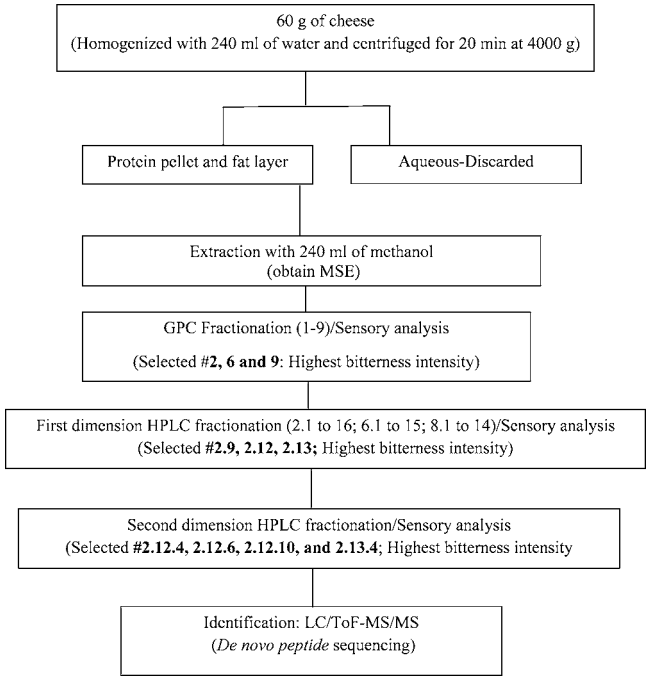


**Figure 1.** Sample preparation scheme and analytical techniques employed for identification of bitter peptides from Cheddar cheese.

**Gel Permeation Chromatography (GPC) Fractionation.** A total of 1 g of MSE was dissolved in 10 mL of nanopure water/methanol (1:1) and separated by size-extrusion gel permeation chromatography (100 × 2.6 cm). The GPC system consisted of a binary solvent delivery system (Shimadzu, LC-8A), a manual injector (SIL-10vp), a variable-wavelength ultraviolet−visible (UV−vis) detector (Shimadzu, SPD-10A), and a Sephadex G-15. Chromatographic separation was performed using isocratic elution, with a mobile phase comprising of 1:1 (50/50%) water and methanol and a flow rate of 5 mL/min. The effluent was collected into nine fractions, and the corresponding fractions (termed 1−9) obtained from several runs were pooled and liberated from solvent (freeze-dried 2×). The resulting residues obtained were then dissolved in water (10 mL) and evaluated for bitterness intensity by sensory analysis.

**First-Dimensional (1D) HPLC Fractionation.** Bitter fractions 2, 6, and 8 identified after the sensory screening of GPC isolates were selected and underwent further separation using a HPLC system coupled with a semi-preparative diphenyl column (250 × 10 mm, pursuit 5, Varian, Palo Alto, CA). The mobile phase comprised of water with 0.1% formic acid at pH 2.5 (A) and methanol (B) at a flow rate of 3 mL/min. The employed linear gradient was as follows: starting at 10% B in A (0−15 min), increasing to 20% B in A (15−25 min), increasing to 70% for 5 min (25−35 min), increasing to 100%, held for 5 min (35−40 min), and back to initial conditions. Total subfractions collected for fraction 2 were 16 (2.1−16); total subfractions collected for fraction 6 were 15 (6.1−15); and total subfractions collected for fraction 8 were 14 (8.1−14). All subfractions were liberated from solvent (freeze-dried 2×) and dissolved in distilled water (10 mL) for subsequent sensory analysis.

**Second-Dimensional (2D) HPLC Fractionation.** Bitter fractions 2.9, 2.12, and 2.13 were selected (had the highest perceived bitterness intensity from first-dimension HPLC fractionation) and were subjected to additional chromatography using a reverse-phase C18 column (250 × 10 mm, pursuit 5, Varian, Palo Alto, CA). The mobile phase was monitored at 220 nm and consisted of a series of linear gradients of solvent A (water with 0.1% formic acid) and solvent B (methanol) starting at 10% B (0−15 min), increasing to 20% B (15−25 min), increasing to 100% B (25−35 min), held for 5 min, and back to initial conditions. Total subfractions collected for 2.9 were 14 (2.9.1−2.9.14); total subfractions collected for 2.12 were 14 (2.12.1−2.12.14); and total subfractions collected for 2.13 were 14 (2.13.1−2.13.14). All subfractions were liberated from solvent (freeze-dried 2×) and dissolved in distilled water (10 mL) for subsequent sensory analysis.

**Liquid Chromatography−Mass Spectrometry/Quadrupole Time-of-Flight−Electrospray Ionization (LC−MS/Q-TOF−ESI) (*De Novo* Peptide Sequencing).** Peptide sequences were analyzed using an Acquity ultra-performance liquid chromatography (UPLC) system coupled with a Waters Q-TOF G2 mass spectrometer equipped with an ESI probe, run in positive mode. The UPLC system consisted of a degasser, binary pumping system, autosampler, column heater, and a reverse-phase C18 column (XBridge RP18 column, 2.5 $\mu$m, 50 × 2.1 mm). Mass spectrometric ionization conditions were as follows: desolvation temperature, 400 °C; source temperature, 120 °C; and capillary voltage, 3 kV. For scan mode, the range of $m/z$ was 100−2300, and for daughter ion analysis, a collision energy ramp was used, ramping from 40 to 120 eV.

**Purification of Synthetic Peptides.** Purchased synthetic peptides were purified prior to use for sensory analysis. The individual peptides were dissolved in water and purified by preparative HPLC. The preparative HPLC system (Shimadzu, Baltimore, MD) consisted of a binary solvent delivery system (LC-8A), a manual injector, and a variable-wavelength UV−vis detector (SPD-10A) coupled with a preparative reverse-phase C18 column (250 × 21.2 mm, pursuit 5, Varian, Palo Alto, CA). The mobile phase was monitored at 220 nm and consisted of a series of linear gradients of solvent A (water) and solvent B (methanol), starting at 10% B (0−5 min), increasing to 95% B (5−25 min), increasing to 100% B (25−26 min), held for 5 min, and back to initial conditions. The purified peptides were freeze-dried twice to remove all traces of solvent prior to use.

**Quantification of Peptides in Mild and Sharp Cheddar Cheese.** Analysis was performed on mild and sharp Cheddar cheese. The cheese sample (30 g) was combined with water (120 mL), and leucine enkephalin was added (5 mg/kg of cheese) as the internal standard (IS). The mixture was homogenized for 5 min and then centrifuged at 10000*g* for 20 min. The supernatant was collected, and the pH was adjusted by formic acid addition (pH ≤ 4.6). The sample


dx.doi.org/10.1021/jf5020654 | J. Agric. Food Chem. 2014, 62, 8034−8041

was recentrifuged at 10000*g* for 20 min, and the supernatant was again collected, pooled, and filtered through a paper filter (Whatman No. 4, Whatman, Ltd., Pittsburgh, PA). The filtrate was then concentrated and desalinized by solid-phase extraction prior to quantification. Briefly, 6 mL of extract was loaded onto a pre-conditioned C-18 SPE cartridge (500 mg of DSC-18 Supelco). The cartridge was then washed with 4 mL of a 98% water, 2% acetonitrile, and 0.1% formic acid solution to remove salt, and the peptides were then eluted using 1 mL of a 40% water, 60% acetonitrile, and 0.1% formic acid solution. Recovery studies were also performed to test the efficiency of the extraction protocol. Target peptides (YQEPVLGPVRGPFPI, GPVRGPFPIIV, MPFPKYPVEPF, PVLGPVRGPFP, MAPKHKEMPFPKYPVEPF, and APHGKEMPFPKYPVEPF) were added in cheese at appropriate concentrations along with water and an IS solution prior to homogenization, and the same extraction procedure was followed. Recovery extractions were performed in triplicate for each sample.

For quantification, the mass spectrometer was operated in positive-ion mode and the spectra were collected by multiple reaction monitoring (MRM). Six-point calibration curves (0.5−200 mg/L) were constructed from corresponding ion transitions of each peptide. Leucine enkephalin was used as an IS and monitored at an ion transition of 556 → 136. Quantitative analysis was performed in triplicate. MRM analysis was performed with Waters Acquity UPLC (column oven, binary solvent manager, sample manager, and a RP-C18 Acquity UPLC HSS T3 1.8 $\mu$m, 2.1 × 100 mm column) coupled with Waters triple-quadruple mass spectrometer (Quattro Premier XE) equipped with an ESI probe. Mass spectrometric ionization conditions were as follows: desolvation temperature, 350 °C; source temperature, 120 °C; and capillary voltage, 3 kV. MRM ion transitions were optimized for each peptide and were as follows: YQEPVLGPVRGPFPI, 835.10 → 136.04; GPVRGPFPIIV, 577.12 → 462.04; MPFPKYPVEPF, 677.05 → 263.31; PVLGPVRGPFP, 569.10 → 169.04; MAPKHKEMPFPKYPVEPF, 726.06 → 263.32; and APHGKEMPFPKYPVEPF, 658.72 → 263.32.

*Precaution Taken for Sensory Analysis of Food Fractions and Taste Compounds.* To remove solvent and buffer compound traces from all fractions isolated from Maillard−catechin reaction models and cocoa, prior to sensory testing, volatiles in each fraction were removed by rotary evaporation and, subsequently, freeze-dried twice. Gas chromatography/mass spectrometry (GC/MS), proton nuclear magnetic resonance ($^1$H NMR), and high-performance ion chromatography revealed that fractions treated by the above protocol are free of solvents and buffer compounds and suitable for sensory analysis.

*Sensory Analysis: Bitterness Intensity of Chromatographic Fractions (GPC, 1D HPLC, and 2D HPLC).* Panelists (five healthy adults, with no history of tasting problems) evaluated the bitterness of the fractions. Bitterness was rated on a 15-point line scale. Four references were provided to panelists [0.03, 0.08, and 0.15% (w/v) caffeine in water], corresponding to bitterness intensity ratings of 2, 5, and 10, respectively. Panelists were asked to avoid eating or drinking 2 h before sensory evaluation. Samples were presented in a randomized order at room temperature in coded 1 oz cups.

*Sensory Analysis: Cheese Samples and Taste Recombination Models.* A trained sensory panel consisting of eight panelists (ages 22−34) evaluated the bitterness intensity of mild and sharp commercial Cheddar cheese samples as well as a recombination "sharp Cheddar model" consisting of mild Cheddar with added purified peptides at levels quantified in sharp Cheddar cheese.

Cheddar cheese was weighted, cubed, and added to a food processor. The food processor was pulsed until cheese pieces were pea-sized. Water (control samples) or peptide solution was added at 1 mL/29 g of cheese, to make a 30 g sample. Cheese and water were mixed until the sample was homogeneous and smooth. A total of 5 g (±0.2) of this cheese was weighed and rolled into a ball, put into a coded sample cup, and covered immediately. All evaluations were conducted with nose clips. Panelists were trained to evaluate bitter taste intensity using caffeine solutions as references. Two reference levels were provided to panelists [0.05 and 0.08% (w/w) of caffeine in water], corresponding to bitterness intensity ratings of 2 and 5, respectively. The performance of a panelist was evaluated by analysis of variation (ANOVA, Statistix 9.0, Analytical Software, Tallahassee, FL). The bitterness and astringency intensity of each individual peptide and a peptide mixture were also evaluated at the corresponding concentrations in water solutions.

*Sensory Analysis: Difference from the Control.* Eight experienced sensory panelists, who regularly consumed Cheddar cheese, were asked to evaluate the size of the overall sensory difference between the commercial sharp Cheddar (control) compared to the sharp model and mild Cheddar cheese. The samples were evaluated in duplicate on a 15-point line scale anchored with "no difference" and "extremely different". The three sample evaluated were (1) the recombination "sharp Cheddar model" consisting of mild Cheddar with added purified peptides at levels quantified in sharp Cheddar cheese, (2) mild Cheddar cheese, and (3) blind control (sharp Cheddar). A Dunnett's test for multiple comparisons with a control was applied to the sample means. Statistix 9.0 (Analytical Software, Tallahassee, FL) was used for analysis.

## RESULTS AND DISCUSSION

A number of extraction protocols have been developed for the analysis of tastants and more specifically for extraction of bitter peptides from cheese matrixes,[1,6,8,9] with water being the most common solvent used. In the current study, the initial water-soluble extract obtained from sharp Cheddar cheese was excessively salty, thus masking the bitter taste attributes. Hence, an alternative extraction method using methanol was developed and implemented (Figure 1) to facilitate initial sensory screening and determine the bitterness profile of mild and sharp Cheddar cheese samples.

The MSE of Cheddar cheese was freeze-dried twice, redissolved at 10% (w/v), and then evaluated for bitterness by trained panelists. The mean bitterness rating of the MSE was 6 (slightly higher than a 0.08% caffeine solution). The MSE was subsequently separated by GPC (see Figure 2). Nine distinct

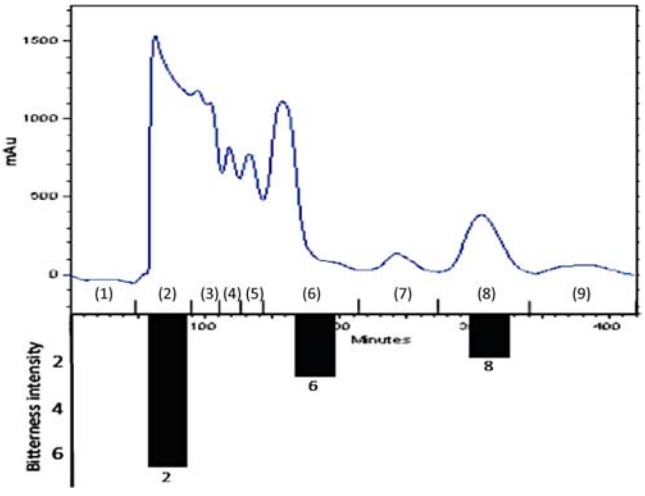


**Figure 2.** GPC chromatogram of Cheddar cheese isolate and the taste intensity chromatogram. Nine fractions were collected (shown in brackets); the fractions with the highest perceived bitter intensity (2, 6, and 8) are illustrated and selected for further investigation.

fractions were obtained and evaluated by a sensory panel. Fractions 2, 6, and 8 were identified as bitter, with average intensity ratings of 6, 2.5, and 1.5 and yields of 8, 12.5, and 15.8%, respectively (Figure 2). On the basis of the intensity of bitterness ratings of these fractions, fraction 2 was selected for further investigation.


dx.doi.org/10.1021/jf5020654 | J. Agric. Food Chem. 2014, 62, 8034−8041

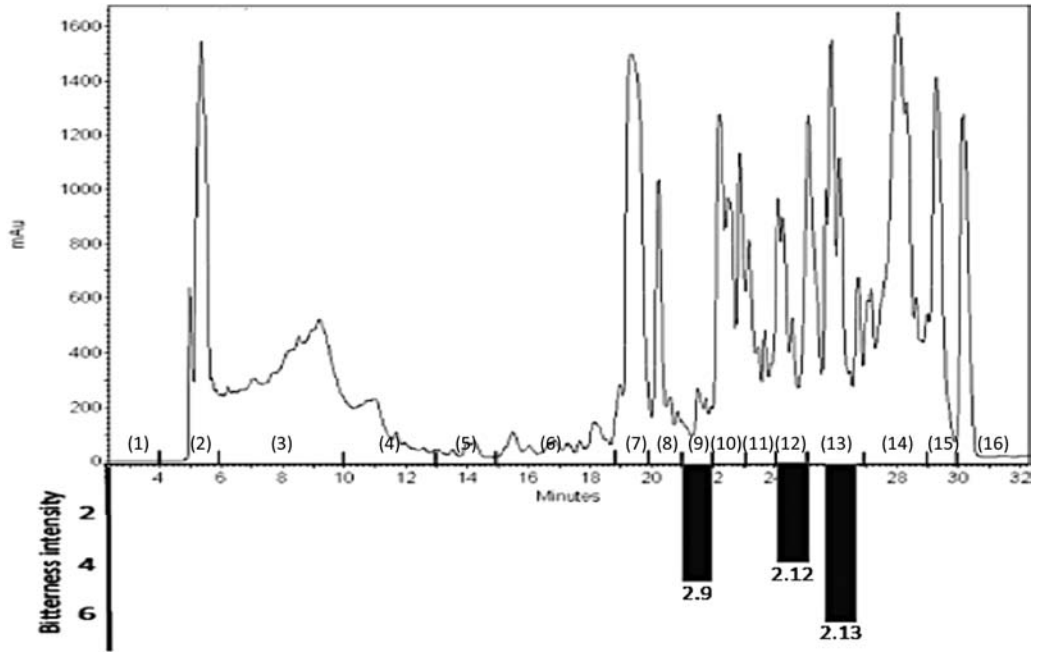


**Figure 3.** HPLC second-dimension chromatogram of fraction 2 obtained from GPC. A total of 16 subfractions of fraction 2 were collected (shown in parentheses); the fractions with the highest perceived bitter intensity (2.9, 2.12, and 2.13) are illustrated and selected for further investigation.

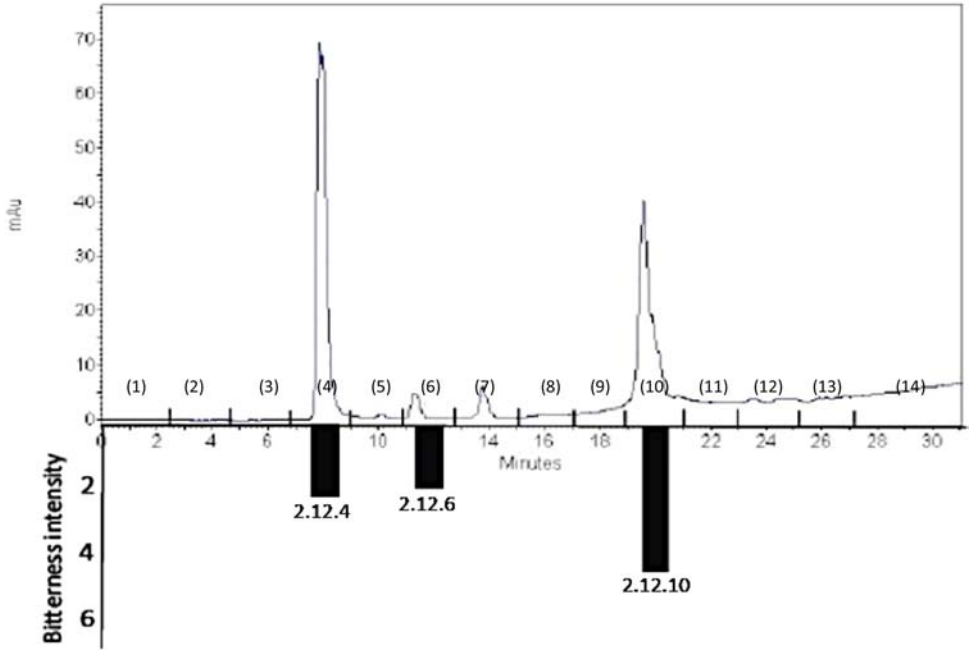


**Figure 4.** Third-dimension HPLC chromatogram of fraction 2.12 obtained from HPLC second-dimension chromatogram. A total of 14 subfractions of fraction 2.12 were collected (shown in parentheses); the fractions with the highest perceived bitter intensity (2.12.4, 2.12.6, and 2.12.10) are illustrated and selected for further investigation.

To decrease the complexity of the GPC isolated bitter-tasting fractions and facilitate identification of the underlying bitter compounds, fraction 2 was further separated using a HPLC system coupled with a diphenyl preparative column in 16 subfractions (see Figure 3). Six of the isolates (2.4, 2.9, 2.11, 2.12, 2.13, and 2.14) were identified as bitter. The fractions with the highest bitter intensity were 2.9, 2.12, and 2.13, corresponding to mean ratings of 4.5, 4, and 6. The remaining fractions (2.14, 2.11, and 2.4) were rated at 0.5 or threshold bitterness and, thus, were not selected for further investigation.

The three main bitter subfractions (2.9, 2.12, and 2.13) were subsequently analyzed by LC−MS, which revealed that more than one predominate peptide was present in each of the selected fractions. Consequently, the fractions were further purified by HPLC using a C-18 semi-preparative column. From this second HPLC separation, 16 fractions were obtained from fraction 2.9 (2.9.1−16) and 2 fractions were reported to be bitter (2.9.9 and 2.9.12). Similarly, 13 fractions were obtained from fraction 2.12 (2.12.1−13), and 12 fractions were obtained from 2.13 (2.13.1−12). Of those, 5 fractions (2.12.4, 2.12.5,


dx.doi.org/10.1021/jf5020654 | J. Agric. Food Chem. 2014, 62, 8034−8041

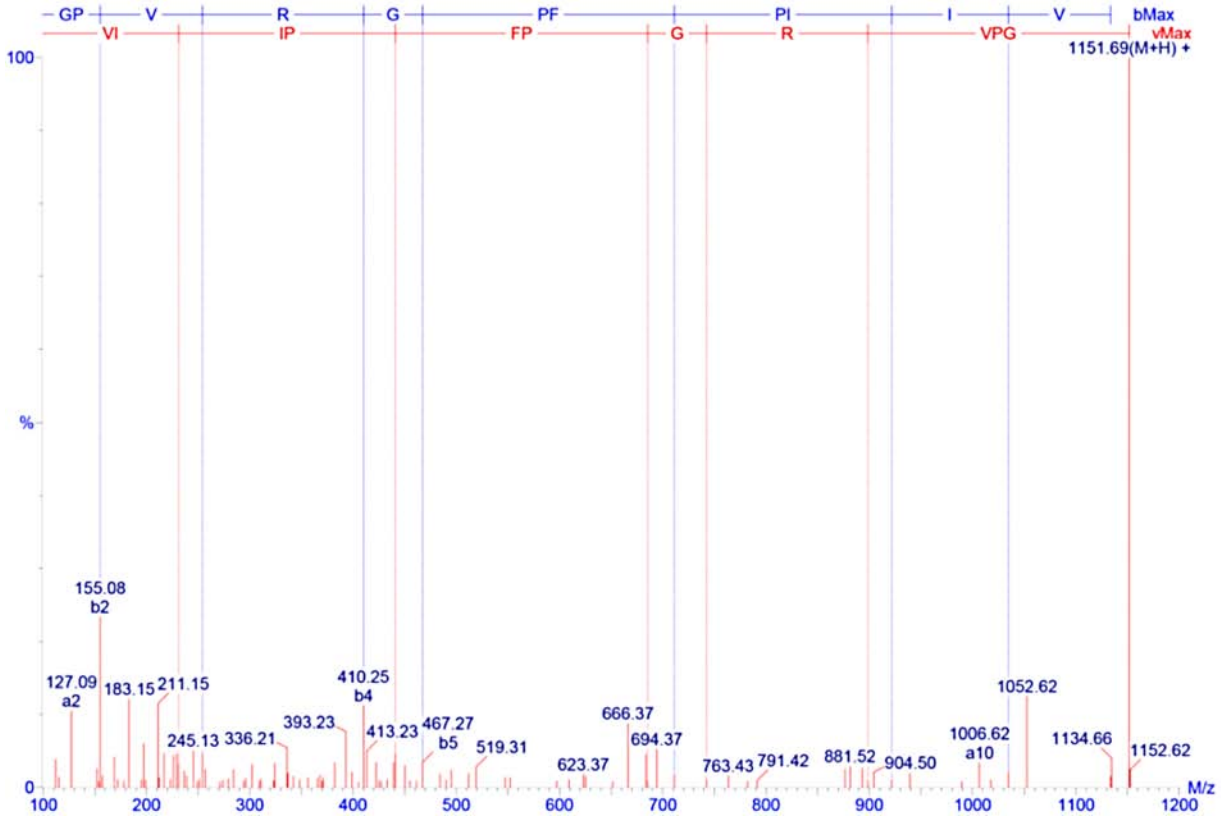


**Figure 5.** MS/MS ESI$^+$ spectra for *de novo* sequence determination of bitter peptide GPVRGPFPIIV.

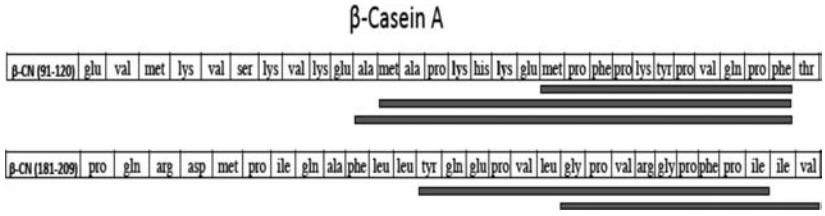


**Figure 6.** $\beta$-CN(91−120) and $\beta$-CN(181−209) sequences of bovine $\beta$-CN and assignment of bitter peptides (black lines) identified in sharp Cheddar cheese.

2.12.6, 2.12.9, and 2.12.10) and 4 fractions (2.13.3, 2.13.4, 2.13.8, and 2.13.9) were found to be bitter, respectively. An example chromatogram of fraction 2.12 is presented in Figure 4. The bitter intensity of the collective resultant fractions ranged from 4 to 0.5, with the highest ratings reported for 2.12.4, 2.12.6, 2.12.10, and 2.13.4.

These four fractions were subsequently analyzed by *de novo* peptide sequencing techniques by time-of-flight tandem mass spectrometry (TOF MS/MS). A total of 12 main peptide candidates were identified as YQEPVLGPVRGPFP, GPVRGPFPIIV, MAPKHKEMPFPKYPVEPF, QEPVLGPVREGPFP, APKHKEMPFPKYPVEPF, YQEPVLGPVRGPFPI, EPVLGPVRGPFP, QEPVLGPVRGPFPI, EMPFPKYPVEPF, LGPVRGPFP, PVLGPVRGPFP, and MPFPKYPVEPF. An example of MS/MS ESI$^+$ spectra of peptide GPVRGPFPIIV is shown in Figure 5. The sequence alignment of the above peptides identified in this study revealed that they originate from $\beta$-CN, as showed in Figure 6, which is in agreement with previous studies.[4,5,12]

Initial sensory screening of synthetic purified peptides revealed that GPVRGPFPIIV, YQEPVLGPVRGPFPI, MPFPKYPVEP, MAPKHKEMPFPKYPVEPF, and APHGKEMPFPKYPVEPF were bitter and, thus, were selected for further examination and taste recombination experiments to determine their overall sensory impact in Cheddar cheese. The five identified bitter peptides are hydrolysis products derived from the $\beta$-CN(91−120) and $\beta$-CN(181−209) sequence regions of bovine $\beta$-CN. Peptides YQEPVLGPVRGPFPI and GPVRGPFPIIV correspond to the following $\beta$-CN sequences, $\beta$-CN(193−207) and $\beta$-CN(199−209), and they are similar to bitter peptides previously identified in Gouda cheese.[8,9] The formation of $\beta$-CN(193−209) can be assigned to the hydrolytic action of chymosin that is responsible for the initial hydrolyisis of $\beta$-CN, yielding three peptides, $\beta$-I, $\beta$-II, and $\beta$-III, produced by cleavage of bonds 192−193 and/or 189−190, 163−164, and/or 165−166, and/or 167−168 and 139−140, respectively.[16−18] In addition to chymosin action, which mainly takes place during the initial stages of cheesemaking, the generation of $\beta$-CN(193−209) can be attributed to the hydrolytic action of the cell envelope proteinase (CEP) of *Lactobacillus* sp. because Leu192−Tyr193 is a known cleavage site of CEP in Cheddar cheese.[19] This peptide [$\beta$-CN(193−209)] has been


dx.doi.org/10.1021/jf5020654 | J. Agric. Food Chem. 2014, 62, 8034−8041

**Table 1. Mean Percent Recovery of Identified Bitter Peptides When Using a Water Extraction Protocol, for Both Mild and Sharp Cheddar Cheese Samples[a]**

| peptide | mild Cheddar (percent recovery ± error) | sharp Cheddar (percent recovery ± error) |
|---|---|---|
| MPFPKYPVEPF | 55.1 ± 7.4 | 56.2 ± 6.1 |
| GPVRGPFPIIV | 60.1 ± 8.1 | 49.1 ± 9.6 |
| MAPKHKEMPFPKYPVEPF | 63.1 ± 7.0 | 63.6 ± 8.0 |
| APHGKEMPFPKYPVEPF | ND | 70.4 ± 8.1 |
| YQEPVLGPVRGPFPI | 67.1 ± 9.4 | 70.6 ± 9.5 |

[a]Analysis conducted in triplicate; mean recovery ± standard error.

**Table 2. Mean Concentration of Select Bitter Peptides in Mild and Sharp Cheddar Cheese[a]**

| peptide | mild Cheddar (concentration ± error) (mg/kg) | sharp Cheddar (concentration ± error) (mg/kg) |
|---|---|---|
| MPFPKYPVEPF | 38.6 ± 2.9 | 69.8 ± 4.3 |
| GPVRGPFPIIV | 5.1 ± 0.4 | 146.4 ± 14.1 |
| MAPKHKEMPFPKYPVEPF | 37.9 ± 2.7 | 33.8 ± 2.7 |
| APHGKEMPFPKYPVEPF | ND | 1.7 ± 0.1 |
| YQEPVLGPVRGPFPI | 1.9 ± 0.2 | 5.8 ± 0.6 |

[a]Analysis conducted in triplicate; mean recovery ± standard error.

previously classified as extremely bitter, and studies have shown that fragments within that sequence exert significant bitterness as well. For example, fragment β-CN(202−209) has been reported to have a low bitterness threshold. Our findings support the contribution of the β-CN(193−209) region to perceived bitterness in aged Cheddar cheese. The formation of peptides MAPKHKEMPFPKYPVEPF [β-CN(102−119)] and APHGKEMPFPKYPVEPF [β-CN(103−119)] can likewise be attributed to chymosin action as well as the CEP of *Lactobacillus* sp. because $Ala^{101}$−$Met^{102}$ is a known cleavage site.[19] Moreover, peptide MPFPKYPVEPF [β-CN(109−119)] has also been previously identified in Gouda cheese,[20] and its formation can be attributed to plasmin, because $Lys^{108}$−$Gly^{109}$ has been identified as a cleavage site of this enzyme.[21]

For quantification, LC−MS/MS−ESI methods were developed for each peptide and ion transitions, and optimized conditions of MRM methods were determined. Six-point calibration curves for each peptide were constructed, exhibiting good linearity within a concentration range of 0.5−200 mg/kg and regression coefficients ranging from 0.960 to 0.999. On the basis of previous reports,[6,22] water extracts have typically been used for isolation and identification of taste components from Cheddar cheese. Thus, an aqueous extraction protocol was developed, and its efficiency was evaluated by performing recovery experiments. Results obtained from peptide spiking experiments and subsequent water extraction demonstrated that mean recovery was between 49.1 and 70.6% (±6.1−9.6%) depending upon the peptide (Table 1), suggesting that water extraction is not a quantitative method of extraction and can lead to underestimation of the levels of peptides present in cheese samples if percent recovery is not considered with the quantification method. Such an underestimation can lead to inaccurate construction of recombination models as well as incorrect conclusions regarding the sensory impact of identified taste active compounds.

The concentrations of the five bitter peptides were determined for both mild and sharp Cheddar cheese and are shown in Table 2. Overall results correlated well with the observed taste profile differences between mild and sharp Cheddar cheese (Table 2). Sharp Cheddar was rated as significantly higher in bitterness compared to mild Cheddar. That was depicted in the concentration of bitter peptides, as GPVRGPFPIIV, YQEPVLGPVRGPFPI, and MPFPKYPVEP increased during maturation by 28.7-, 3.1-, and 1.8-fold, respectively. Additionally, peptide APHGKEMPFPKYPVEPF was only found in quantifiable concentrations in the sharp Cheddar cheese sample, confirming that it was generated during the maturation process. The concentration of peptide MAPKHKEMPFPKYPVEPF was not statistically different between the two samples, indicating that maturation is not responsible for the generation of this bitter compound (Table 2).

To correlate analytical results with sensory impact of identified bitter peptides, taste re-engineering experiments were performed. A model sharp Cheddar was made by spiking appropriate concentrations of the identified peptides in mild Cheddar cheese, and a descriptive analysis study of the bitterness intensity of the samples was conducted. The results confirmed that the perceived bitterness of the sharp Cheddar recombination model was not significantly different [least significant difference (LSD) all-pairwise comparison of 0.46 at 5% significance level] when compared to a commercial sharp Cheddar sample with mean ratings of 1.89 and 1.58, respectively (Table 3). For comparison, the bitterness of the mild Cheddar was reported to be significantly lower than the sharp Cheddar as expected and indicated the importance of aging for the development of this taste attribute.

**Table 3. Mean Bitterness Intensity of Sharp and Mild Cheddar Cheese and a Sharp Cheddar Model Cheese[a]**

| sample | mean rating |
|---|---|
| sharp Cheddar (6 months) | 1.89 a |
| sharp Cheddar model | 1.58 a |
| mild Cheddar (3 months) | 1.07 b |

[a]Eight panelists in duplicate. Samples with different letters within a column are significantly different at $p < 0.05$.

To further evaluate the contribution of the individual peptides to the overall bitterness perception, the bitterness intensity of each peptide as well as a peptide mixture at levels found in sharp Cheddar were determined in water solutions (Table 4). Overall, each of the five peptides was reported to be above the bitter recognition taste threshold values. Peptide

**Table 4. Mean Bitterness Intensity of Each Peptide and the Peptide Mixture Dissolved in Water at Levels Quantified in Sharp Cheddar Cheese[a]**

| peptide | bitterness rating sharp |
|---|---|
| MPFPKYPVEPF | 0.5 ± 0.13 |
| GPVRGPFPIIV | 4.5 ± 0.61 |
| MAPKHKEMPFPKYPVEPF | 0.9 ± 0.20 |
| APHGKEMPFPKYPVEPF | 0.3 ± 0.23 |
| YQEPVLGPVRGPFPI | 0.5 ± 0.15 |

[a]Five panelists in duplicate; mean ± standard error.

GPVRGPFPIIV had the highest contribution to the bitter taste profile of sharp Cheddar cheese, with a mean bitter intensity rating of 4.5. Furthermore, the peptide mixture had a bitterness rating of 5.4 and accounted for 90% of the bitterness intensity of the initial methanol extract of sharp Cheddar. These findings support the relevance of the identified and characterized bitter peptides in the sharp Cheddar sample. This peptide (GPVRGPFPIIV) also provides a more targeted region to monitor bitterness development in Cheddar than the prior used sequences [$\beta$-CN (f193−f209) and $\alpha$(S1)-CN (f1−f9)].[13]

The role of the identified bitter peptides on the overall flavor profile of the sharp Cheddar cheese was also examined using a difference from the control test (see Table 5). The flavor of the

**Table 5. Difference from the Control Test Indicating the Overall Sensory Difference between the Commercial Sharp Cheddar (Control) Compared to the Sharp Cheddar Model (Mild Cheddar Spiked with Appropriate Levels of Bitter Peptides as Sharp Cheese) and Mild Cheddar Cheese[a]**

| sample | mean rating | difference from the control |
|---|---|---|
| sharp Cheddar (blind control) | 3.0 | |
| sharp Cheddar model | 6.2 | 3.3[b] |
| mild Cheddar | 9.4 | 6.5[b] |

[a]Eight panelist in duplicate rated the difference from the control using a 15-point line scale. Data were analyzed by ANOVA, followed by Dunnett's multiple comparisons to the control. [b]Significance at $p < 0.05$.

re-engineered sharp Cheddar cheese model (mild Cheddar cheese spiked with appropriate levels of bitter peptides) was reported to be significantly more similar to commercial sharp Cheddar than it was to mild Cheddar. This observation also indicated the importance of taste and, in this case, bitterness to recognize the characteristic flavor of an aged Cheddar cheese.

Interestingly, the peptides identified in the current study, such as GPVRGPFPIIV, YQEPVLGPVRGPFPI, and MPFPKYPVEPF, have been previously reported to have positive health bioactivities. Peptides GPVRGPFPIIV,[23,24] MPFPKYPVEPF,[20] and YQEPVLGPVRGPFPI[25,26] were found to have antihypertensive actions, with the later also exhibiting antimicrobial activity. This observation is another example of the interplay between bitter taste and beneficial bioactivity.

In summary, bitter peptides in Cheddar were identified and related to the flavor attributes of an aged product. Understanding the molecular drivers of flavor quality provides a basis to develop improved processing technology for flavor optimization.

## AUTHOR INFORMATION


### Corresponding Author

*Telephone: 612-624-3201. Fax: 612-625-5272. E-mail: dgp@umn.edu.



### Funding

This project was partially supported by the Dairy Research Institute, USA.


### Notes

The authors declare no competing financial interest.

## REFERENCES


(1) Soeryapranata, E.; et al. Relationship between MALDI−TOF analysis of $\beta$-CN f193−209 concentration and sensory evaluation of bitterness intensity of aged Cheddar cheese. *J. Agric. Food Chem.* **2002**, *50* (17), 4900−4905.

(2) Broadbent, J. R.; Steele, J. L. Proteolytic enzymes of lactic acid bacteria and their influence on bitterness in bacterial-ripened cheeses. In *Flavor of Dairy Products*; Cadwallader, K. R., Drake, M. A., McGorrin, R. J., Eds.; American Chemical Society (ACS): Washington, D.C., 2007; ACS Symposium Series, Vol. *971*, Chapter 11, pp 193−203.

(3) Engel, E.; et al. Taste active compounds in a goat cheese water-soluble extract. 2. Determination of the relative impact of water-soluble extract components on its taste using omission tests. *J. Agric. Food Chem.* **2000**, *48* (9), 4260−4267.

(4) Engel, E.; et al. Determination of taste-active compounds of a bitter Camembert cheese by omission tests. *J. Dairy Res.* **2001**, *68* (4), 675−688.

(5) Fallico, V.; et al. Evaluation of bitterness in Ragusano cheese. *J. Dairy Sci.* **2005**, *88* (4), 1288−1300.

(6) Lee, K.-P. D.; Warthesen, J. J. Preparative methods of isolating bitter peptides from Cheddar cheese. *J. Agric. Food Chem.* **1996**, *44* (4), 1058−1063.

(7) Singh, T. K.; et al. Production and sensory characterization of a bitter peptide from $\beta$-casein. *J. Agric. Food Chem.* **2005**, *53* (4), 1185−1189.

(8) Toelstede, S.; Dunkel, A.; Hofmann, T. A series of kokumi peptides impart the long-lasting mouthfulness of matured Gouda cheese. *J. Agric. Food Chem.* **2009**, *57* (4), 1440−1448.

(9) Toelstede, S.; Hofmann, T. Quantitative studies and taste re-engineering experiments toward the decoding of the nonvolatile sensometabolome of Gouda cheese. *J. Agric. Food Chem.* **2008**, *56* (13), 5299−5307.

(10) Visser, S. Proteolytic enzymes and their relation to cheese ripening and flavor: An overview. *J. Dairy Sci.* **1993**, *76* (1), 329−350.

(11) Singh, T. K.; Drake, M. A.; Cadwallader, K. R. Flavor of Cheddar cheese: A chemical and sensory perspective. *Compr. Rev. Food Sci. Food Saf.* **2003**, *2*, 166−189.

(12) Maehashi, K.; Huang, L. Bitter peptides and bitter taste receptors. *Cell. Mol. Life Sci.* **2009**, *66* (10), 1661−1671.

(13) Broadbent, J. R.; et al. Contribution of *Lactococcus lactis* cell envelope proteinase specificity to peptide accumulation and bitterness in reduced-fat Cheddar cheese. *Appl. Environ. Microbiol.* **2002**, *68* (4), 1778−1785.

(14) Leksrisompong, P. P.; Miracle, R. E.; Drake, M. Characterization of flavor of whey protein hydrolysates. *J. Agric. Food Chem.* **2010**, *58* (10), 6318−6327.

(15) Liu, X.; Jiang, D.; Peterson, D. Identification of bitter peptides in whey protein hydrolysate. *J. Agric. Food Chem.* **2014**, *62* (25), 5719−5725.

(16) Caries, C.; Ribadeau-Dumas, B. Kinetics of action of chymosin (rennin) on some peptide bonds of bovine $\beta$-casein. *Biochemistry* **1984**, *23*, 6839−6843.

(17) Pakhala, E.; et al. Decomposition of milk proteins during the ripening of cheese. 2. Enzymatic hydrolysis of $\beta$-casein. *Meijeritiet. Aikak.* **1989**, *47*, 63−70.

(18) Visser, S.; Slangen, K. J. On the specificity of chymosin (rennin) in its action on bovine β-casein. *Neth. Milk Dairy J.* **1977**, No. 31, 16−30.
(19) Sighn, T. K.; Fox, P.; Healy, I. Isolation and identification of further peptides in the diafiltration retentate of the water-soluble fraction of Cheddar cheese. *J. Dairy Res.* **1997**, No. 64, 433−443.
(20) Saito, T.; et al. Isolation and structural analysis of antihypertensive peptides that exist naturally in Gouda cheese. *J. Dairy Sci.* **2000**, *83* (7), 1434−1440.
(21) Gallagher, D. P.; Singh, T. K.; Mulvihill, D. M. Hydrolysis of porcine β-casein by bovine plasmin and bovine chymosin. *Z. Lebensm.-Unters. -Forsch. A* **1999**, *208* (2), 83−89.
(22) Yang, B. I. N.; Vickers, Z. Taste components of Cheddar cheese: Fractionation and optimization of Cheddar cheese taste in water. *J. Sens. Stud.* **2004**, *19* (6), 546−559.
(23) Contreras, M. M.; et al. Novel casein-derived peptides with antihypertensive activity. *Int. Dairy J.* **2009**, *19* (10), 566−573.
(24) Hayes, M.; et al. Casein fermentate of *Lactobacillus animalis* DPC6134 contains a range of novel propeptide angiotensin-converting enzyme inhibitors. *Appl. Environ. Microbiol.* **2007**, *73*, 4658−4667.
(25) Birkemo, G. A.; et al. Antimicrobial activity of two peptides casecidin 15 and 17, found naturally in bovine colostrum. *J. Appl. Microbiol.* **2009**, *106* (1), 233−240.
(26) Torres-Llanez, M. J.; et al. Angiotensin-converting enzyme inhibitory activity in Mexican Fresco cheese. *J. Dairy Sci.* **2011**, *94* (8), 3794−3800.

JOURNAL OF AGRICULTURAL AND FOOD CHEMISTRY

Article

pubs.acs.org/JAFC

# Occurrence of Glycosidically Conjugated 1-Phenylethanol and Its Hydrolase β-Primeverosidase in Tea (*Camellia sinensis*) Flowers

Ying Zhou,[†,∥] Fang Dong,[‡,∥] Aiko Kunimasa,[§] Yuqian Zhang,[†] Sihua Cheng,[†] Jiamin Lu,[†] Ling Zhang,[†] Ariaki Murata,[⊗] Frank Mayer,[⊥] Peter Fleischmann,[⊥] Naoharu Watanabe,[#] and Ziyin Yang*[,†]

[†]Key Laboratory of Plant Resource Conservation and Sustainable Utilization, South China Botanical Garden, Chinese Academy of Sciences, Xingke Road 723, Tianhe District, Guangzhou 510650, China

[‡]Guangdong Food and Drug Vocational College, Longdongbei Road 321, Tianhe District, Guangzhou 510520, China

[§]Graduate School of Agriculture and [⊗]Graduate School of Science and Technology, Shizuoka University, 836 Ohya, Suruga-ku, Shizuoka 422-8529, Japan

[⊥]Institute of Food Chemistry, Technische Universität Braunschweig, Schleinitzstrasse 20, DE-38106 Braunschweig, Germany

[#]Graduate School of Science and Technology, Shizuoka University, 3-5-1 Johoku, Naka-ku, Hamamatsu 432-8561, Japan

Supporting Information

**ABSTRACT:** A previous study found that 1-phenylethanol (1PE) was a major endogenous volatile compound in tea (*Camellia sinensis*) flowers and can be transformed to glycosically conjugated 1PE (1PE-Gly). However, occurrences of 1PE-Gly in plants remain unknown. In this study, four 1PE-Glys have been isolated from tea flowers. Three of them were determined as (*R*)-1PE β-D-glucopyranoside ((*R*)-1PE-Glu), (*S*)-1PE-Glu, and (*S*)-1PE β-primeveroside ((*S*)-1PE-Pri), respectively, on the basis of NMR, MS, LC-MS, and GC-MS evidence. The other one was identified as (*R*)-1PE-Pri on the basis of LC-MS and GC-MS data. Moreover, these 1PE-Glys were chemically synthesized as the authentic standards to further confirm their occurrences in tea flowers. 1PE-Glu had a higher molar concentration than 1PE-Pri in each floral stage and organ. The ratio of (*R*) to (*S*) differed between 1PE-Glu and 1PE-Pri. In addition, a 1PE-Gly hydrolase β-primeverosidase recombinant protein produced in *Escherichia coli* exhibited high hydrolysis activity toward (*R*)-1PE-Pri. However, β-primeverosidase transcript level was not highly expressed in the anther part, which accumulated the highest contents of 1PE-Gly and 1PE. This suggests that 1PE-Gly may not be easily hydrolyzed to liberate 1PE in tea flowers. This study provides evidence of occurrences of 1PE-Glys in plants for the first time.

**KEYWORDS:** *glucopyranoside, 1-phenylethanol, primeveroside, primeverosidase, stereochemistry, tea flower*

## INTRODUCTION

Plants synthesize and emit a large variety of volatile organic compounds, which possess extremely important ecological functions. The volatile compounds can also be converted from free forms to glycosidically bound forms, which are more water-soluble and less reactive than their free aglycone counterparts.[1] Many glycosylated volatile compounds have been isolated and identified in various plant species or plant-derived foods. In many cases, alcoholic volatiles such as benzyl alcohol, 2-phenylethanol, methyl salicylate, (*Z*)-3-hexenol, linalool, linalool oxides, and geraniol can be transformed to glycosidically bound form.[2−6] Besides alcoholic volatile compounds, some nonalcoholic volatile compounds such as benzaldehyde, coumarin, and damascenone were found to occur as glycosidically bound form, and these glycosidically bound volatile compounds take more steps than the glycosidically bound alcoholic volatiles to release free volatile compounds.[7−9] The glycosylated volatile compounds are involved in diverse events in plants. For example, when plants are exposed to stresses or affected by environmental factors, the glycosylated volatile compounds can be hydrolyzed to release free volatile compounds, which are involved in the plant defense system.[10] Another example is that the glycosylated volatile compounds are related to regulation of emission of floral volatiles.[11] In our previous study, we found that 1-phenylethanol (1PE) was a major endogenous volatile compound in tea (*Camellia sinensis*) flowers, whereas only a little 1PE was emitted from the flowers.[12] This may be because 1PE was transformed to glycosically conjugated 1PE (1PE-Gly). However, occurrences of 1PE-Gly in plants remain unknown.

There is extensive literature on human health benefits of tea leaves and their bioactive compounds. Recently, tea flowers have attracted increasing interest of researchers. One reason is that tea flowers are an abundant and nonutilized resource; for example, over 1.8 billion kilograms of tea flowers are available annually in China.[13] Another reason is that tea flowers contain many bioactive compounds including catechins, caffeine,[14] floratheasaponins,[15−17] flavonol glycosides,[18] polysaccharides,[19] amino acids,[20] spermidine derivatives,[21] and volatile compounds.[12,22] In the present study, four glycosylated volatile compounds including (*R*)-1PE-β-D-glucopyranoside ((*R*)-1PE-Glu), (*S*)-1PE-Glu, (*R*)-1PE-β-primeveroside ((*R*)-1PE-Pri), and (*S*)-1PE-Pri were first identified in tea flowers. Moreover, the four 1PE-Glys were chemically synthesized for the first time to further confirm their occurrences in tea flowers, although the

Received: May 13, 2014
Revised: July 10, 2014
Accepted: July 26, 2014
Published: July 28, 2014

ACS Publications © 2014 American Chemical Society



dx.doi.org/10.1021/jf5022658 | J. Agric. Food Chem. 2014, 62, 8042−8050

enzymatic syntheses of 1PE-Gly by cultured plant cells have been reported previously.[23−25] In addition, β-primeverosidase, one of 1PE-Gly hydrolases, transcript level was not highly expressed in the anther part, which accumulated the highest contents of 1PE-Gly and 1PE. This suggests that 1PE-Gly may not be easily hydrolyzed to liberate 1PE in tea flowers.

## MATERIALS AND METHODS

**Chemicals.** D-Xylose and triphenylmethyl chloride were purchased from Tokyo Chemical Industries Co., Ltd., Japan. Ethyl *n*-decanoate, $CDCl_3$ (99.8 atom % D + 0.03% v/v tetramethylsilane (TMS)), and organic solvents used for chemical synthesis were purchased from Kanto Chemical Co. Inc., Japan. *N*-Methyl-*N*-(trimethylsilyl)-trifluoroacetamide (MSTFA) was purchased from Regis Chemical Co., USA. (*R*)-1PE, (*S*)-1PE, $CD_3OD$ (99.8 atom % D + 0.05% v/v TMS), $CD_3COCD_3$ (99.9 atom % D + 0.05% v/v TMS), and reagents used for chromatography analysis and chemical synthesis were purchased from Wako Pure Chemical Industries Ltd., Japan. Polyvinylpolypyrrolidone (PVPP), XAD-2, isopropyl-β-D-thiogalactopyranoside (IPTG), HBr/AcOH, β-glucosidase, and Spectrum Plant Total RNA Kit were purchased from Sigma-Aldrich Co. Ltd., USA. β-Primeverosidase was purchased from Amano Enzyme Inc., Japan. ODS-C18 was purchased from Chemco Scientific Co., Ltd., Japan. Sep-PakVac 6 $cm^3$ was purchased from Waters Corp., USA. Coomassie Blue R250, 30% acrylamide/Bis solution, *N*,*N*,*N*′,*N*′-tetramethylethylenediamine (TMEMD), sodium dodecyl sulfate (SDS), and 2× SYBR Green Universal PCR Mastermix were purchased from Bio-Rad Laboratories, USA. Ni-NTA resin was purchased from Qiagen Inc., USA. Enterokinase was purchased from Novagen, MERCK Eurolab, Germany. Quick RNA Isolation Kit was purchased from Huayueyang Biotechnology Co., Ltd., China. PD-10 desalting column was purchased from GE Healthcare Life Sciences, USA.

**Plant Materials.** The flowers of *C. sinensis* var. Jinxuan were obtained from tea fields at the South China Agricultural University (Guangzhou, China) between October and November 2012 and 2013. As described in our previous study,[12] flower development was divided into three stages: at stage 1 the flower buds are closed, at stage 2 the flower is half open, and at stage 3 the flower is fully open. In addition, the flowers at stage 3 were divided into four parts including petals, filaments, anthers, and other parts. The "other parts" comprise a mixture of carpels, receptacles, sepals, and pedicels.

**Isolation and Purification of 1PE-Gly from Tea Flowers.** Figure S1 (Supporting Information) shows a brief flowchart of the isolation and purification of 1PE-Gly from tea flowers. Eight hundred grams (fresh weight) of the flowers was extracted with 3 L of 80% ethanol overnight at 4 °C and then centrifuged at 17000*g* and 4 °C for 20 min. The supernatant was filtered, and the filtrate was concentrated to 500 mL by a rotary evaporation. Forty grams of PVPP was added to the concentrated filtrate to remove polyphenols. The mixture was stirred at 4 °C for 60 min and then centrifuged at 17000*g* and 4 °C for 20 min. Twenty grams PVPP was added to the supernatant, stirred at 4 °C for 30 min, and then centrifuged again at 17000*g* and 4 °C for 20 min. The resultant supernatant was extracted with 300 mL of $CHCl_3$ three times. The aqueous fraction was evaporated to remove $CHCl_3$ residue and diluted with Milli-Q water to 600 mL. The diluted solution was passed through an XAD-2 column (about 600 mL, i.d. 6 cm × 21 cm) and then eluted with 3 L of Milli-Q water and 3 L of methanol, successively. The methanolic eluate was concentrated to dryness and dissolved in 120 mL of 5% methanol. The 5% methanol-soluble solution was passed through an ODS-C18 open column (60 mL, i.d. 2.4 cm × 13.3 cm) and eluted with 120 mL of 25% methanol, 120 mL of 50% methanol, and 120 mL of 100% methanol, successively. The 50% MeOH/methanolic eluate was concentrated to dryness, dissolved in 1.5 mL of 16% MeCN, and then subjected to the first preparative HPLC (LC pump, Jasco PU-980; detector, 875-UV; solvent mixing module, Jasco LG-1580-02; degasser, Jasco DG-1580-53; column oven, Jasco CO-965; Jasco, Tokyo, Japan) isolation. The first preparative HPLC used a Capcell Pak C18 reversed-phase column (20 mm × 250 mm, 5 μm particle size, Shiseido Co. Ltd., Japan) with 16% MeCN as mobile phase, at 254 nm and a flow rate of 10 mL/min. The injection volume was 100 μL/isolation. Each collection volume was 10 mL/fraction. The obtained fractions 14 and 15 (RT 18−20 min) were subjected to the second preparative HPLC isolation, for which conditions were the same as for the first preparative HPLC isolation. The obtained fraction 6 (RT 17−18 min) was subjected to the third preparative HPLC isolation. The third preparative HPLC used a Capcell Pak C18 reversed-phase column (10 mm × 250 mm, 5 μm particle size, Shiseido Co. Ltd., Japan) with 16% MeCN as mobile phase, at 254 nm and a flow rate of 2.5 mL/min. The injection volume was 50 μL/isolation. The collection volume was 1.25 mL/fraction. The obtained fractions 4−8 were identified to have 1PE-Gly (Figure S2). Fractions 4 and 5 (RT 18.0−19.0 min) and fraction 6 (RT 19.0−19.5 min) were subjected to the recycle HPLC (LC pump, Jasco PU-9986; detector, Jasco 875-UV; Jasco) isolation, respectively. The recycle HPLC used a Capcell Pak C18 reversed-phase column (10 mm × 250 mm, 5 μm particle size, Shiseido Co. Ltd., Japan) with 18% MeCN as mobile phase, at 210 nm and a flow rate of 4.0 mL/min. The injection volume was 50 μL/isolation. Purified disaccharide of (*S*)-1PE and monosaccharide of (*S*)-1PE were obtained from fractions 4 and 5. The disaccharide of (*S*)-1PE and monosaccharide of (*R*)-1PE were obtained from fraction 6. Fractions 7 and 8 (RT 19.5−20.5 min) were subjected to the further preparative HPLC isolation to obtain the purified monosaccharide of (*R*)-1PE. The HPLC used a Capcell Pak C18 reversed-phase column (10 mm × 250 mm, 5 μm particle size, Shiseido Co. Ltd., Japan) with 18% MeCN as mobile phase, at 210 nm and a flow rate of 2.5 mL/min. The injection volume was 50 μL/isolation.

**Determination of 1PE-Gly Isolated from Tea Flowers.** *Determination of 1PE-Gly by Enzymatic Hydrolysis Combined with GC-MS Analysis during the Isolation.* The enzymatic hydrolysis combined with GC-MS analysis method is the same as described by Dong et al.[12] The isolated fraction (50 μL) as shown above was concentrated in a vacuum, dried under nitrogen gas, redissolved in 0.4 mL of 50 mM citric acid buffer (pH 6.0) containing 10 mg of β-primeverosidase (1.12 unit) and 0.6 mg β-glucosidase (from almonds, 3.12 unit), and allowed to react at 37 °C for 14 h. Sodium chloride (144 mg) was added to the reaction solution, which was allowed to stand for 15 min. Afterward, 5 nmol of ethyl *n*-decanoate as an internal standard was added. The solution was extracted with 0.4 mL of hexane/ethyl acetate (1:1) and centrifuged (16400*g*, 4 °C, 3 min), and the supernatant was dried over anhydrous sodium sulfate. The samples were then analyzed by GC-MS QP5000 (Shimadzu Corp.), which was controlled by a Class-5000 workstation. The temperature of the injector was 230 °C. The GC was equipped with a capillary SUPELCOWAX 10 column (30 m × 0.25 mm i.d., and 0.25 μm film thickness, Supelco Inc., Bellefonte, PA, USA). Helium was used as the carrier gas at a flow rate of 1.6 mL/min. The GC temperature was 60 °C for 3 min, ramped at 40 °C/min to 180 °C followed by 10 °C/min to 240 °C, and then held at 240 °C for 3 min. MS was performed in full scan mode (mass range $m/z$ 70−200).

*Determination of 1PE-Gly by LC-MS Analysis during the Isolation.* To further investigate the molecular weight of the isolated fractions containing 1PE-Gly, the isolated fractions were analyzed by a LCMS-2010 A system (Shimadzu Corp.) equipped with a UG120 C-18 reversed-phase column (2.0 mm × 150 mm i.d., 5 μm particle size, Shiseido Co. Ltd., Japan) with solvent A ($HCOOH/H_2O$, 0.05:99.95, v/v) and solvent B (MeCN), at a flow rate of 0.2 mL/min at 40 °C. A total of 5 μL of the sample solutions was analyzed using a gradient elution. Elution was started under isocratic conditions of 16% of solvent B for 5 min and followed by a linear increase of solvent B to 90% at 10 min and subsequently brought back within 0.5 min to 16% of solvent B and held for another 7.5 min to allow for column equilibration. UV−vis spectra were recorded between 190 and 370 nm for each chromatographic peak. Optimized electrospray operating conditions were as follows: dry gas, 1.5 L/min; capillary voltage, 1.5 kV; dry temperature, 250 °C. MS was performed in full scan mode (mass range $m/z$ 100−500) and SIM mode ($m/z$ 283, 329, 415, and 461).

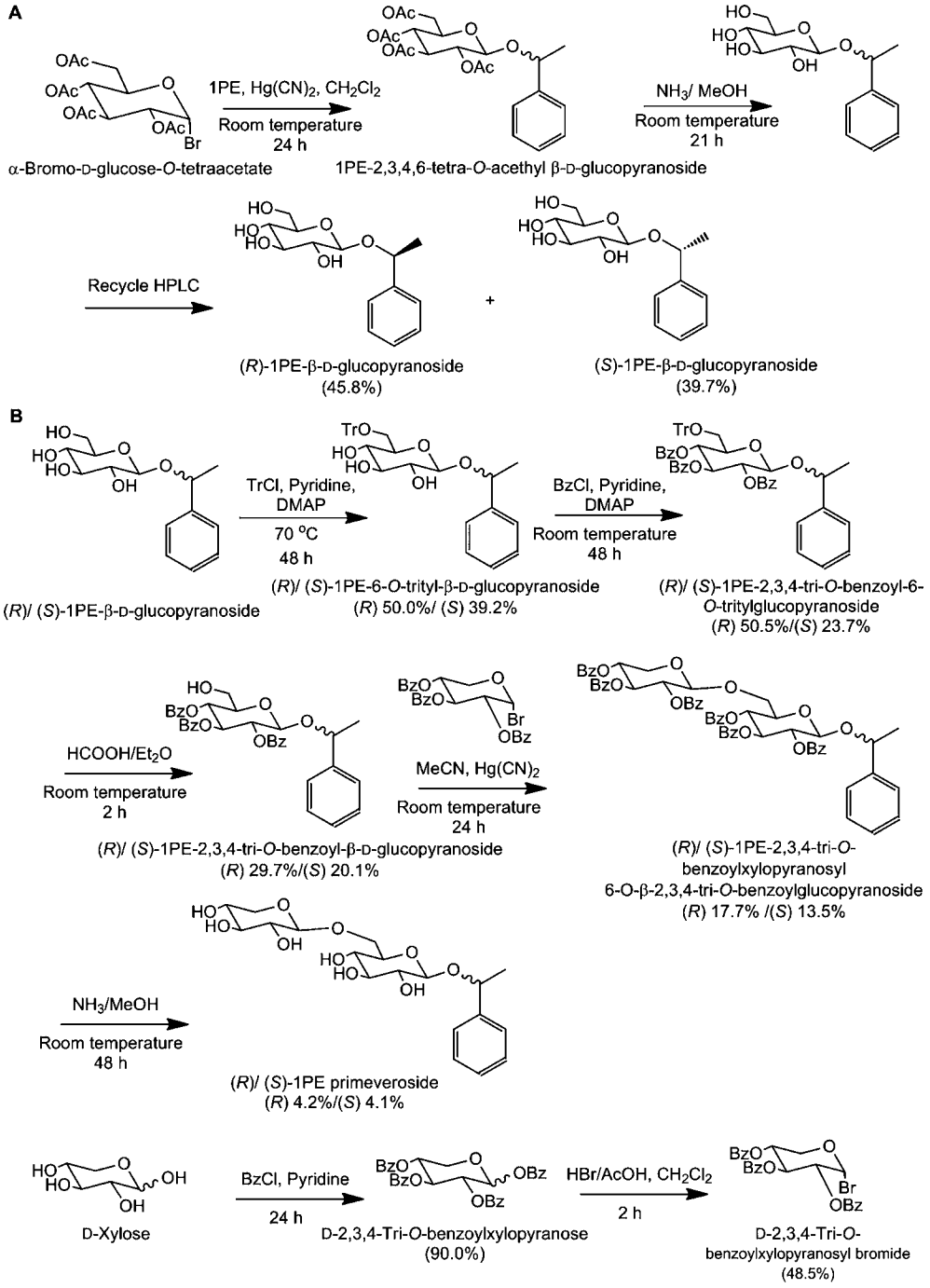


**Figure 1.** Schemes of chemical synthesis of (*R*)/(*S*)-1PE-Glu (A) and (*R*)/(*S*)-1PE-Pri (B).

*Determination of Stereochemistry of 1PE-Gly by LC-MS and GC-MS Analyses.* To determine the stereochemistry of 1PE-Gly, LC-MS was employed to analyze the 1PE-Gly in the crude extract of tea flowers (Supporting Information Figure S3) by comparison with the chemically synthesized authentic standards as shown below. The protocol of LC-MS analysis is shown under Quantitative Analysis of 1PE-Gly. Furthermore, the (*R*)- and (*S*)-1PE obtained from the enzymatic hydrolysis of the isolated fractions containing 1PE-Gly as described above were analyzed by using a GC-MS QP5000 (Shimadzu) equipped with an InertCap CHIRAMIX (30 m × 0.25 mm × 0.25 μm, GL Sciences, Inc., Torrence, CA, USA). Helium was used as the carrier gas at a flow rate of 1.8 mL/min. The temperatures were 40 °C for 5 min, a ramp of 3 °C/min to 180 °C, and then held at 180 °C for 10 min. MS was performed in full scan mode (mass range *m*/*z* 70−200) and SIM mode (*m*/*z* 77, 79, 107 and 122).

*Determination of Chemical Structures of 1PE-Gly by High-Resolution Mass Spectra (HRMS) and NMR.* The purified 1PE-Glys were identified by HRMS (JMS-T100LC AccuTOF mass spectrometer, JEOL, Tokyo, Japan) using polypropylene glycol as an internal standard and NMR (JNM-LA 500 FT-NMR, JEOL, Tokyo, Japan) using $^{1}H$, $^{13}C$, COSY, HSQC, and HMBC with TMS as an internal standard. The MS conditions were as follows: ionization, ESI (positive mode); scan at *m*/*z* 50−550.

As some $^{1}H$ NMR signals of the sugar moiety of the purified 1PE-Gly were overlapped, an acetylation reaction was employed to assign the $^{1}H$ NMR signal. One milligram of the purified 1PE-Gly was dissolved in 100 μL of dehydrated pyridine and 200 μL of dehydrated acetic anhydride. The solution was stirred for 17 h at room temperature. Afterward, toluene was added and then concentrated to


dx.doi.org/10.1021/jf5022658 | J. Agric. Food Chem. 2014, 62, 8042−8050

dryness. The acetylated product was dissolved in $CD_3OD$, and analyzed by $^1H$ NMR (500 MHz).

**Chemical Synthesis of 1PE-Gly.** To further confirm the chemical structures of the isolated 1PE-Gly, we chemically synthesized the (*R*)-1PE-Glu, (*S*)-1PE-Glu, (*R*)-1PE-Pri, and (*S*)-1PE-Pri as authentic standards, on the basis of the method described by Ma et al.[26] The schemes of chemical synthesis of these 1PE-Glys are shown in Figure 1. The detailed chemical synthesis protocol is described in the Supporting Information. The optical rotation of each compound is shown as (*R*)-1PE-Glu $[\alpha]^{29}_D$ +1.00° (*c* 1.0, $CH_3OH$), (*S*)-1PE-Glu $[\alpha]^{29}_D$ −18.01° (*c* 1.1, $CH_3OH$), (*R*)-1PE-Pri $[\alpha]^{21}_D$ −4.24° (*c* 1.3, $CH_3OH$), and (*S*)-1PE-Pri $[\alpha]^{21}_D$ −4.35° (*c* 0.2, $CH_3OH$). Figure S4 shows the UV spectra and HR-MS data.

**Quantitative Analysis of 1PE-Gly.** *Relative Quantitative Analysis of 1PE-Gly by MSTFA Derivatization and GC-MS Analysis.* The crude extract of 1PE-Gly was prepared by using the method described in refs 6 and 12 with a slight modification. Five hundred milligrams (fresh weight, finely powdered) of plant tissues was extracted with 2 mL of cold methanol by vortexing for 2 min followed by ultrasonic extraction in ice-cold water for 10 min. The extracts were mixed with 2 mL of cold chloroform and 0.8 mL of cold water for phase separation, and the resulting upper layer was dried and redissolved in 1 mL of water. The resulting solution was mixed with 30 mg of PVPP, allowed to stand for 90 min, and centrifuged (16400*g*, 4 °C, 10 min). The resultant supernatant was loaded on an Amberlite XAD-2 column and eluted successively with 3 mL of water, 3 mL of pentane/dichloromethane (2:1), and 5 mL of methanol. The methanol eluate was concentrated in a vacuum, dried under nitrogen gas, derivatized with 70 μL of MSTFA and 70 μL of pyridine at 37 °C for 60 min, and then centrifuged. The MSTFA derivates were then analyzed by a GC-MS QP2010 SE (Shimadzu Corp.) equipped with an HP-5 column (30 m × 0.25 mm × 0.25 μm, Agilent Technologies, Germany). The injector temperature was 240 °C, splitless mode was used with a splitless time of 1 min, and helium was the carrier gas with a velocity 1.0 mL/min. The GC temperatures were 80 °C for 2 min, ramp of 15 °C/min to 300 °C, then held at 300 °C for 10 min. The mass spectrometry was operated with full scan mode and SIM mode (see Table S1 in the Supporting Information). *m*/*z* 259 was used as quantifier ion.

*Quantitative Analysis of 1PE-Gly by LC-MS Analysis.* Two grams (fresh weight, finely powdered) of tea flowers at each stage was extracted with 36 mL of methanol containing 5 nmol of *p*-nitrophenyl-Glu (*p*NP-Glu) and 5 nmol of *p*NP-Pri as internal standards. Nine milliliters of methanol extracts was dried and redissolved in 4 mL of water. The solution was loaded on a Sep-PakVac 6 $cm^3$ (1 g) column and eluted successively with 20 mL of water, 60 mL of 25% methanol (in water), and 20 mL of methanol. The 25% methanol eluate was concentrated in a vacuum and dissolved in 500 μL of water. The resultant solution was analyzed by a LCMS-2010 A system (Shimadzu Corp.) equipped with a UG120 C-18 reversed-phase column (2.0 mm × 150 mm i.d., 5 μm particle size, Shiseido Co. Ltd., Japan) with solvent A ($HCOOH.H_2O$, 0.05:99.95, v/v) and solvent B (MeCN) at a flow rate of 0.2 mL/min at 40 °C. A total of 5 μL of the sample solution was analyzed using a gradient elution. Elution was started from a linear increase of solvent B from 5 to 7% at 60 min and held at 7% of solvent B for 15 min. MS was performed in SIM mode (*m*/*z* 329 and 461 for $[M + HCOOH]^-$ of 1PE-Glu and 1PE-Pri, respectively, and *m*/*z* 346 and 478 for $[M + HCOOH]^-$ of *p*NP-Glu and *p*NP-Pri, respectively) (Supporting Information Figure S3).

**Gene Cloning and Recombinant Protein Expression of β-Primeverosidase in *Escherichia coli*.** Finely powdered tea floral tissues (100 mg) were used to isolate RNA, and total RNA was isolated using a Spectrum Plant Total RNA Kit. The first-strand cDNA was synthesized using a Reverse Transcription System (Promega, Madison, WI, USA). The GenBank accession number of β-primeverosidase is AB088027.1. The cDNA coding was amplified by PCR with forward primer 5′-GATATCGCTCAAATCTCCTCCTTC-AAC-3′, containing an *Eco*RV site, and reverse primer 5′-GTCGAC-CTACTTGAGGAGGAATTTCTT-3′, containing a *Sal*I site.[27] The PCR conditions were adjusted as follows: denaturation at 94 °C for 5 min, followed by 35 cycles of 98 °C for 15 s, 54 °C for 15 s, 72 °C for 1 min 30 s, and a final extension at 72 °C for 10 min. The resulting PCR product was purified and subcloned into the pGEM-T vector (Promega) and sequenced to confirm the correctness of ORF. To obtain the mature form of a recombinant protein, the correct ORF was subcloned into pET32a vector (Novagen, Madison, WI, USA) to obtain the expression constructor (pET32a/PRD). After verification by sequencing, the expression constructor was transformed into *E. coli* Rosetta (Novagen) for inducible His-tagged protein expression. Freshly transformed Rosetta cells harboring pET32a/PRD vector were grown at 37 °C to an $OD_{600}$ = 0.6. After the addition of 0.05 mM IPTG, the cultures were grown at 20 °C for another 16 h to produce recombinant His-tagged protein. The cells were harvested at 4000*g* for 10 min and then disrupted by sonication in a 50 mM $NaH_2PO_4$ (pH 8.0) buffer containing 300 mM NaCl and 10 mM imidazole. After centrifugation at 10000*g* for 20 min, the supernatant was collected and purified by using affinity binding on Ni-NTA resin according to the manufacturer's instruction. The partially purified protein was passed through a PD-10 desalting column for further enzyme activity assay.

**SDS-PAGE Analysis.** The *E. coli*-expressed proteins were subjected to SDS-PAGE with the use of a separation gel (2.4 mL of 30% acrylamide/bis(acrylamide), 1.8 mL of Tris-HCl (pH 8.8), 0.07 mL of 10% SDS, 0.07 mL of 10% ammonium persulfate, 2.7 mL of $ddH_2O$, 0.003 mL of TMEMD) and a concentration gel (0.34 mL of 30% acrylamide/bis(acrylamide), 0.25 mL of Tris-HCl (pH 6.8), 0.02 mL of 10% SDS, 0.02 mL of 10% ammonium persulfate, 1.4 mL of $ddH_2O$, 0.002 mL of TMEMD). After completion of electrophoresis, the proteins were stained with Coomassie Blue R250 for at least 3 h and then decolored three times.

***E. coli*-Expressed β-Primeverosidase Assay.** To identify the *E. coli*-expressed β-primeverosidase activity, (*R*)-1PE-Glu, (*S*)-1PE-Glu, (*R*)-1PE-Pri, and (*S*)-1PE-Pri were selected as substrates. The reaction mixture contained 5 μg of substrate, 350 μL of 20 mM sodium citrate buffer (pH 5.0), and 10 μg of partially purified protein. The reactions were incubated at 37 °C for 10 h. After cooling to room temperature, the reaction mixture was extracted with 400 μL of hexane/ethyl acetate (1:1). The upper phase was dried over anhydrous sodium sulfate, and 1 μL of the extract was subjected to GC-MS analysis. Samples were analyzed using a GC-MS QP2010 SE (Shimadzu Corp.) equipped with a SUPELCOWAX 10 column (30 m × 0.25 mm × 0.25 μm, Supelco Inc.). The injector temperature was 240 °C, splitless mode was used with a splitless time of 1 min, and helium was the carrier gas with a velocity 1.0 mL/min. The GC temperatures were 60 °C for 3 min, ramp of 40 °C/min to 180 °C followed by 10 °C/min to 240 °C, and then held 240 °C for 5 min. The mass spectrometer was operated with SIM mode (*m*/*z* 77, 79, 107, 122). 1PE was identified by comparing its retention times and mass spectra with those of authentic compound.

**Transcript Expression Analysis of β-Primeverosidase.** Total RNA was isolated immediately after dissection (Fast Plant Total RNA Kit). Ten times-diluted reverse-transcribed cDNA was subjected to qRT-PCR analysis. The qPCR primers for β-primeverosidase were 5′-TGCCTCTTCTGCCTACC-3′ (sense) and 5′-TGTTCACTCCTC-CGCTAA-3′ (antisense). The qPCR primers for internal standard β-actin were 5′-GCCATATTTGATTGGAATGG-3′ and 5′-GGTGCC-ACAACCTTGATCTT-3′.[28] Each qPCR reaction (20 μL) was assembled in a 0.2 mL microtube by adding iTaq Universal SYBR Green Supermix (10 μL) (Bio-Rad, Hercules, CA, USA), 300 nM of each primer, 10 times-diluted cDNA (2 μL), and $ddH_2O$ (6 μL). The qRT-PCR was carried out on a Roach LightCycle 480 (Roach Applied Science, Mannheim, Germany) under conditions of one cycle of 95 °C for 60 s, 40 cycles of 95 °C for 15 s, and 60 °C for 30 s. A melt curve was performed at the end of each reaction to verify PCR product specificity. The $2^{-\Delta\Delta ct}$ method was used to calculate the relative expression level.[29] β-Actin was used as an internal reference. Change in mRNA level of β-primeverosidase for each treatment was normalized to that of β-actin.

## RESULTS AND DISCUSSION

**1PE-Glys in Tea Flowers Were Determined as (*R*)/(*S*)-1PE-Glu and 1PE-Pri.** 1PE-Gly may be involved in regulating the emission of 1PE from tea flowers.[12] To investigate the occurrence of 1PE-Gly in tea flowers, the 1PE-Gly compounds **1**, **2**, and **3** were isolated (Figure 2). On the basis of HR-MS

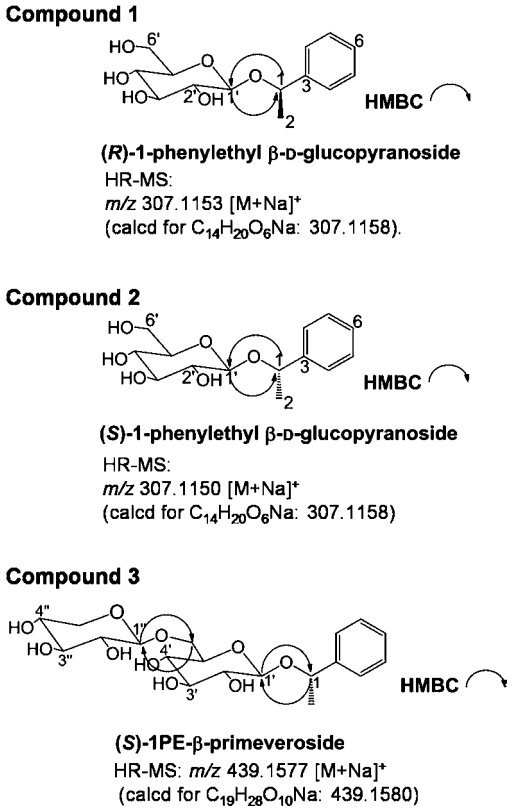


**Figure 2.** HR-MS data and chemical structures of 1PE-monosaccharides (compounds **1** and **2**) and 1PE-disaccharide (compound **3**) isolated from tea flowers.

data, the isolated compounds **1** and **2** are proposed as diastereomeric isomers of monoglycoside of 1PE (Figure 2). The $^{13}$C NMR data show that compounds **1** and **2** have 14 carbon signals (Supporting Information Table S2). $^{1}$H NMR showed that both compounds **1** and **2** have anomeric protons with $J$ = 7−8 Hz (Table S3). Moreover, the $\beta$-glucosidase could hydrolyze the glycoside to release 1PE (data not shown). These suggest that the glycoside moieties of compounds **1** and **2** have $\beta$-connectivity. The $^{1}$H chemical shifts of H-1′ significantly differ between (*R*)- and (*S*)-1PE glucopyranoside, and that of the (*R*) type is generally higher than that of the (*S*) type (Table S3). Moreover, after enzymatic hydrolysis, compounds **1** and **2** were hydrolyzed to release (*R*)-1PE and (*S*)-1PE, respectively. These indicate that compound **1** is (*R*) type and compound **2** is (*S*) type. The peracetate of compound **1** was obtained, and the structure of its glycosidic part was analyzed on the basis of the coupling patterns of each proton. As shown in Figure S5, from H-1′ to H-5′ all of the protons are *trans*-diaxial, suggesting that the C6 sugar moiety is $\beta$-glucopyranose. Therefore, compounds **1** and **2** were proposed as $\beta$-glucopyranose of (*R*)-1PE and (*S*)-1PE, respectively. On the HMBC, cross peaks between H-1′/C-1 and H-1/C-1′ revealed their connection between the aglycone and the sugar residue (Figure 2). To further confirm the proposed structures, $\beta$-D-glucopyranosides of (*R*)-1PE and (*S*)-1PE were chemically synthesized (Figure 1A and Supporting Information). On the basis of the $^{13}$C NMR data, the synthetic (*R*)-1PE and (*S*)-1PE $\beta$-D-glucopyranosides were coincided with those of compounds **1** and **2** (Table S2). The differences between (*R*)-1PE and (*S*)-1PE $\beta$-D-glucopyranosides were observed in the chemical shifts of C-1, C-2, C-1′, and C-3 (Table S2). On the basis of the above observations, compound **1** is identified as (*R*)-1PE-Glu and compound **2** as (*S*)-1PE-Glu.

On the basis of the HR-MS data and enzymatic hydrolysis to form (*S*)-1PE, compound **3** was proposed as a disaccharide of (*S*)-1PE, which has one additional $C_5$ sugar (Figure 2). The $^{1}$H NMR signal of H-1″ is 4.36 with $J$ = 7.6 Hz, suggesting that the sugar moiety with $C_5$ must be a pyranose form not in furanose form (5.10, $J$ = 6.0 Hz) (Supporting Information Table S4). We also need to determine if the disaccharide moiety is primeveroside or vicianoside. The differences between primeveroside and vicianoside are OH orientation at H-4″ (Figure S6A). Due to the differences, the coupling pattern for H-3″ should be different. The signal for H-3″ of primeveroside should have coupling with the same/similar values with H-2″ and H-4″, whereas the signal for H-3″ of vicianoside should have different coupling constants between H-2″ and H-4″ due to the *J*ax-ax and *J*ax-eq (Figure S6A). As the H-3″ $^{1}$H NMR signals were overlapped, we carried out acylated reaction of compound **3** and then analyzed its $^{1}$H NMR. We found that the $J$ H-3″ was a triplet with $J$ = 9.5 Hz (Figure S6B). To further confirm the proposed structures, $\beta$-primeverosides of (*R*)-1PE and (*S*)-1PE were chemically synthesized (Figure 1B and Supporting Information). The $^{13}$C NMR data of the synthetic (*S*)-1PE-Pri (Table S5) coincided with those of compound **3** (Table S4). On the basis of the above observations, compound **3** is identified as (*S*)-1PE-Pri. We did not obtain a sufficient purified amount for NMR identification of (*R*)-1PE-Pri. On the basis of LC-MS data on a column of ODS and the GC-MS equipped with a CHIRAMIX column after enzymatic hydrolysis (Figure S2), (*R*)-1PE-Pri was tentatively identified in tea flowers. By comparison with the GC-MS chromatogram of the MSTFA-derived product of synthesized (*R*)-1PE-Pri, tea flowers indeed contained (*R*)-1PE-Pri (Figure S7D). Moreover, LC-MS analysis by comparison with the chemically synthesized authentic standards also provided evidence that four 1PE-Glys, including (*R*)/(*S*)-1PE-Glu and (*R*)/(*S*)-1PE-Pri, occurred in the tea flowers at stages 1, 2, and 3 (Figure S3). In addition, the NMR data of the four 1PE-Glys from either tea flowers or chemical synthesis coincided with those from enzymatic syntheses by cultured plant cells that were reported previously.[23−25]

**1PE-Glu Was the Major 1PE-Gly Occurring in Tea Flowers.** To further characterize the occurrence of each 1PE-Gly, we quantified each 1PE-Gly in different floral stages and organs. MSTFA derivatization and GC-MS were employed to analyze the relative content of each 1PE-Gly. Figure S7 in the Supporting Information shows mass spectra and chromatograms of MSTFA-derived products of authentic 1PE-Gly standards and crude 1PE-Gly extract from tea flowers, suggesting the presences of the four 1PE-Glys in tea flowers. Table S1 shows the characteristic ions of MSTFA-derived products of each 1PE-Gly based on GC-MS and GC-TOFMS analyses. Relative quantitation results show that 1PE-Glu had higher molar concentration than 1PE-Pri in each floral stage and organ (Figure 3A,B). On the basis of the calculation of the


dx.doi.org/10.1021/jf5022658 | J. Agric. Food Chem. 2014, 62, 8042−8050

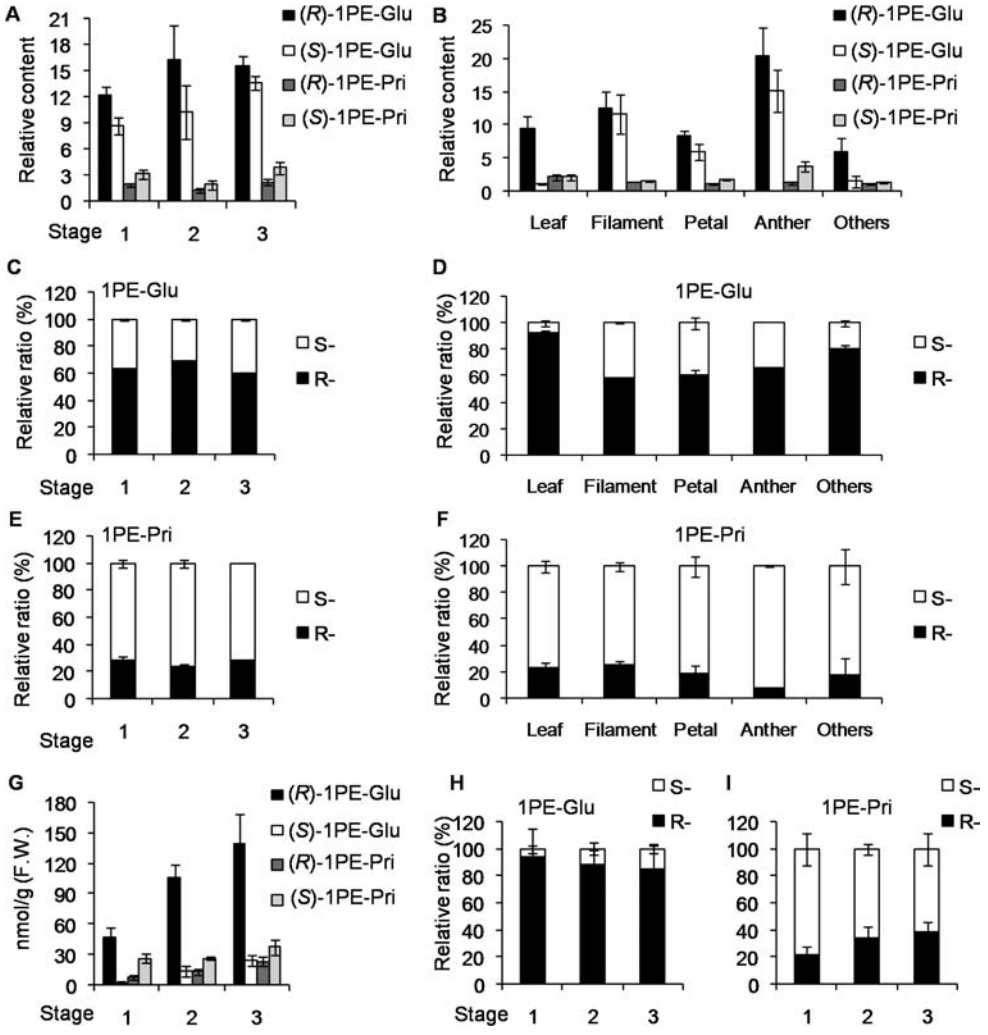


**Figure 3.** Distributions of 1PE-Gly in each floral stages and organ. (A, B) The relative quantitations of (*R*)-1PE-Glu, (*S*)-1PE-Glu, (*R*)-1PE-Pri, and (*S*)-1PE-Pri were performed using MSTFA derivatization and GC-MS. "Others" is a mixture of carpels, receptacles, sepals, and pedicels. (C–F) The relative ratio (%) of (*R*) and (*S*) was calculated on the basis of the peak area of characteristic ion *m*/*z* 259 from the MSTFA derivatization and GC-MS analysis. (G–I) The quantitations of (*R*)-1PE-Glu, (*S*)-1PE-Glu, (*R*)-1PE-Pri, and (*S*)-1PE-Pri were performed using LC-MS.

peak area of the characteristic ion *m*/*z* 259 (Table S1 and Figure S7), the relative ratio of (*R*) type of 1PE-Glu was higher than that of (*S*) type (Figure 3C,D), whereas the relative ratio of the (*S*) type of 1PE-Pri was higher than that of the (*R*) type (Figure 3E,F). Considering the possible effects of MSTFA derivatization reaction on the quantitation, we applied LC-MS to directly quantitate the content of each 1PE-Gly (Figure S3). The LC-MS analytical results (Figure 3H,I) show similar trends of ratio of *R* to *S* of 1PE-Gly with the GC-MS analytical results (Figure 3C,E), although concentrations of 1PE-Gly analyzed by LC-MS (Figure 3G) were higher than those analyzed by MSTFA derivatization and GC-MS (Figure 3A). In many cases, glycosylated alcoholic volatiles are found in tea leaves as $\beta$-primeverosides or glucopyranoside, and the $\beta$-primeverosides occur primarily in the glycosidically bound form.[30,31] Glucopyranoside was a major form of 1PE-Gly, although both glycosidic forms of 1PE were identified in tea flowers. Interestingly, the ratio of (*R*) to (*S*) differed between the 1PE-Glu and the 1PE-Pri. In our previous study, we used exogenous glycoside hydrolases to liberate free 1PE from the crude 1PE glycoside extract of tea flowers[12] and found that (*R*) type was the major hydrolyzed 1PE. In this study, we further demonstrated that (*R*)-1PE-Glu is the major 1PE-Gly in tea flowers.

**1PE-Gly Hydrolase $\beta$-Primeverosidase Transcript Level Was Not Highly Expressed in Floral Tissue.** To further clarify the hydrolysis of 1PE-Gly to liberate 1PE, we investigated the 1PE-Gly hydrolase $\beta$-primeverosidase. The recombinant $\beta$-primeverosidase expressed in *E. coli* (Figure S8 in the Supporting Information and Figure 4A,B) displayed strong enantioselectivity. Compared with (*S*)-1PE-Pri, the hydrolysis ability of $\beta$-primeverosidase toward (*R*)-1PE-Pri was significantly higher (Figure 4). On the other hand, neither (*S*)-1PE-Glu nor (*R*)-1PE-Glu was found to be hydrolyzed by $\beta$-primeverosidase. We attempted to express recombinant $\beta$-glucosidase in *E. coli* to verify its function. *E. coli* itself contained a high amount of its own $\beta$-glucosidase, which could hydrolyze 1PE-Glu to liberate 1PE. In contrast to the $\beta$-glucosidase occurring in *E. coli*, the expressed target $\beta$-glucosidase was very low. Therefore, it was very hard to distinguish if the expressed target $\beta$-glucosidase has a hydrolysis function of 1PE-Gly to form 1PE.

$\beta$-Primeverosidase transcript level showed a slight but nonsignificant decrease trend during floral development


dx.doi.org/10.1021/jf5022658 | J. Agric. Food Chem. 2014, 62, 8042–8050

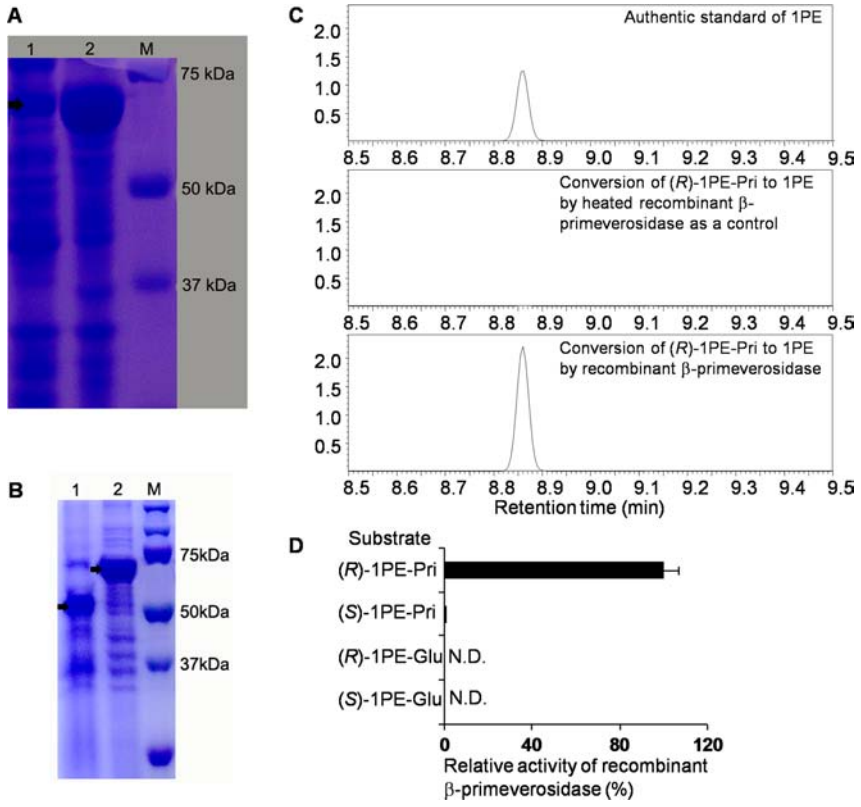


**Figure 4.** SDS-PAGE analysis of recombinant *β*-primeverosidase (A, B) and GC-MS identifications of formation of 1PE from (*R*)-1PE-Pri under the action of recombinant *β*-primeverosidase (C) and relative activities of recombinant *β*-primeverosidase toward different substrates (D). (A) Arrows indicate target protein. Proteins were resolved by SDS-PAGE on polyacrylamide gel and stained with Coomassie brilliant blue. Lanes: M, protein marker; 1, supernatant of crude extracts from *E. coli* cells with expression of vector pET32a/PRD; 2, pellet of crude extracts from *E. coli* cells with expression of vector pET32a/PRD. (B) Arrows indicate target protein. Lanes: M, protein marker; 1, enterokinase digested recombinant *β*-primeverosidase; 2, recombinant protein purified with Ni-NTA agarose from the supernatant of crude *E. coli* extracts. (C) 1PE product was identified by GC-MS. Total mass chromatography of characteristic ions of 1PE (*m*/*z* 77, 79, 107, and 122) is shown. (D) Activity toward (*R*)-1PE-Pri was highest and set as 100%. The activity toward other substrate was expressed as percent of maximum activity. N.D., not detected, which indicates that there were no differences between enzymatic reaction and control. The heated enzyme reaction was used as a control to exclude the possible effects of autodegradation of 1PE-Gly.

(Figure 5A). *β*-Primeverosidase was highly expressed in leaves, whereas it was not accumulated in floral tissues (Figure 5B). Furthermore, *β*-primeverosidase was lowly expressed in anthers, which accumulated the highest amounts of 1PE-Gly and 1PE (Figure 3B and ref 12). *β*-Primeverosidase has been purified from tea leaves, and its full amino acid sequence and function have been characterized.[27,32] *β*-Glucosidase was only partially characterized in tea leaves.[33] However, full the amino acid sequence of *β*-glucosidase has not been characterized, and its function has not been verified yet. In contrast to *β*-glucosidase, *β*-primeverosidase showed more involvement in the hydrolysis of glycosidically bound volatile compounds in tea leaves, because the *β*-primeverosides occur primarily in the glycosidically bound form.[27] The glycosidically bound volatile compounds occur in vacuoles. However, *β*-primeverosidase was observed to be localized in cell walls and the cavity areas among cells.[27] This compartmentation of substrates and enzymes in plant cells leads to the rare available evidence of hydrolysis of glycosidically bound volatile compounds in intact tea leaves.[34] In contrast, such enzymatic hydrolysis has mostly been investigated during the manufacturing process of tea leaves, which can have interactions between the enzyme and the substrate.[35,36] Investigations in flowers indicate that there is still evidence that the glycoconjugated volatile compounds can be hydrolyzed by endogenous glycosidases to liberate the volatile compounds from the plant. In *Rosa damascena* flowers, 2-phenylethanol is released from its precursor 2-phenylethyl *β*-D-glucoside during or after flower opening.[37] During flower development in *R. damascena*, *β*-glucosidase activity increases 5 times,[38] and *β*-glucosidase was suggested to be partly responsible for controlling the diurnal emission of 2-phenylethanol.[39] In *Gardenia jasmonoides* flowers, the formation of flower fragrance compounds was attributed to a glycosidase activity, reaching a maximum level at the flower opening stage.[40] In our present study, *β*-primeverosidase did not show an increase trend during the tea flower development and was relatively lowly expressed in tea flowers, suggesting that 1PE-Gly may not be easily hydrolyzed to liberate 1PE and be considered as transportable storage compounds.

Our previous study showed that tea flowers contained a high amount of endogenous 1PE.[12] 1PE is used as a fragrance in the food flavor and cosmetics industries because of its mild floral odor and as an intermediate in the pharmaceutical industry. This study provides detailed chemical evidence of occurrences of glycosidically conjugated 1PE in tea flowers for the first time. These results would contribute to our understanding of the formation of 1PE and provide essential information for future potential application of tea flowers in the food flavor and cosmetics industries.

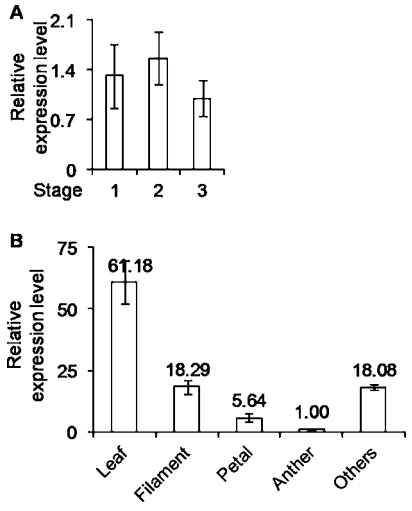


**Figure 5.** Stage-specific (A) and tissue-specific (B) expression profiles of $\beta$-primeverosidase. Transcript abundance was calculated on the basis of the difference in cycle threshold (Ct) values between $\beta$-primeverosidase and $\beta$-actin transcripts by the normalized relative quantitation $2^{-\Delta\Delta Ct}$ method. Data represent the mean value ± standard deviation of three independent experiments performed in triplicate. (B) Leaves were the first to third leaves. The fully open flowers were divided into four parts including petals, filaments, anthers, and other parts. "Others" is a mixture of carpels, receptacles, sepals, and pedicels.

## ■ ASSOCIATED CONTENT

### Ⓢ Supporting Information

Additional experimental details, Figures S1−S8, and Tables S1−S5. This material is available free of charge via the Internet at http://pubs.acs.org.

## ■ AUTHOR INFORMATION

### Corresponding Author

*(Z.Y.) Phone: +86-20-38072989. E-mail: zyyang@scbg.ac.cn.

### Author Contributions

‖Ying Zhou and Fang Dong equally contributed to this work.

### Notes

The authors declare no competing financial interest.

## ■ ACKNOWLEDGMENTS

This study was supported by "100 Talents Programme of the Chinese Academy of Sciences" (Y321011001 and 201209), the Foundation of Key Laboratory of Plant Resources Conservation and Sustainable Utilization, South China Botanical Garden, Chinese Academy of Sciences, the Foundation of Guangdong Food and Drug Vocational College (2013YZ003), and the Japanese Society for the Promotion of Science (P10101). We also thank technical support of Mr. Totsuka for this research.

## ■ ABBREVIATIONS USED

HRMS, high-resolution mass spectra; IPTG, isopropyl-$\beta$-D-thiogalactopyranoside; MSTFA, *N*-methyl-*N*-(trimethylsilyl)-trifluoroacetamide; 1PE, 1-phenylethanol; 1PE-Gly, glycosically conjugated 1PE; 1PE-Glu, 1PE $\beta$-D-glucopyranoside; 1PE-Pri, 1PE $\beta$-primeveroside; *p*NP-Glu, *p*-nitrophenyl-$\beta$-D-glucopyranoside; *p*NP-Pri, *p*-nitrophenyl-$\beta$-primeveroside; PVPP, polyvinylpolypyrrolidone; SDS, sodium dodecyl sulfate; TMEMD, *N*,*N*,*N*′,*N*′-tetramethylethylenediamine; TMS, tetramethylsilane

## ■ REFERENCES

(1) Winterhalter, P.; Skouroumounis, G. K. Glycoconjugated aroma compounds: occurrence, role and biotechnological transformation. In *Advances in Biochemical Engineering/Biotechnology, Vol. 55 Biotechnology of Aroma Compounds*; Berger, R. G., Ed.; Springer: Berlin, Germany, 1997; pp 73−105.

(2) Nishikitani, M.; Kubota, K.; Kobayashi, A.; Sugawara, F. Geranyl 6-*O*-$\alpha$-L-arabinopyranosyl-$\beta$-D-glucopyranoside isolated as an aroma precursor from leaves of a green tea cultivar. *Biosci., Biotechnol., Biochem.* **1996**, *60*, 929−931.

(3) Nishikitani, M.; Wang, D.; Kubota, K.; Kobayashi, A.; Sugawara, F. (*Z*)-3-Hexenyl and *trans*-linalool 3,7-oxide $\beta$-primeverosides isolated as aroma precursors from leaves of a green tea cultivar. *Biosci., Biotechnol., Biochem.* **1999**, *63*, 1631−1633.

(4) Guo, W.; Hosoi, R.; Sakata, K.; Watanabe, N.; Yagi, A.; Ina, K.; Luo, S. (*S*)-Linalyl, 2-phenylethyl, and benzyl disaccharide glycosides isolated as aroma precursors from oolong tea leaves. *Biosci., Biotechnol., Biochem.* **1994**, *58*, 1532−1534.

(5) Guo, W.; Sakata, K.; Watanabe, N.; Nakajima, R.; Yagi, A.; Ina, K.; Luo, S. Geranyl 6-*O*-$\beta$-D-xylopyranosyl-$\beta$-D-glucopyranoside isolated as an aroma precursor from tea leaves for oolong tea. *Phytochemistry* **1993**, *33*, 1373−1375.

(6) Wang, D. M.; Yoshimura, T.; Kubota, K.; Kobayashi, A. Analysis of glycosidically bound aroma precursors in tea leaves. 1. Qualitative and quantitative analyses of glycosides with aglycons as aroma compounds. *J. Agric. Food Chem.* **2000**, *48*, 5411−5418.

(7) Guo, W.; Sasaki, N.; Fukuda, M.; Yagi, A.; Watanabe, N.; Sakata, K. Isolation of an aroma precursor of benzaldehyde from tea leaves (*Camellia sinensis* var. *sinensis* cv. Yabukita). *Biosci., Biotechnol., Biochem.* **1998**, *62*, 2052−2054.

(8) Yang, Z. Y.; Kinoshita, T.; Tanida, A.; Sayama, H.; Morita, A.; Watanabe, N. Analysis of coumarin and its glycosidically bound precursor in Japanese green tea having sweet-herbaceous odour. *Food Chem.* **2009**, *114*, 289−294.

(9) Kinoshita, T.; Hirata, S.; Yang, Z. Y.; Baldermann, S.; Kitayama, E.; Matsumoto, S.; Suzuki, M.; Fleischmann, P.; Winterhalter, P.; Watanabe, N. Formation of damascenone derived from glycosidically bound precursors in green tea infusions. *Food Chem.* **2010**, *123*, 601−606.

(10) Mattiacci, L.; Dicke, M.; Posthumus, M. A. $\beta$-Glucosidase: an elicitor of herbivore-induced plant odor that attracts host-searching parasitic wasps. *Proc. Natl. Acad. Sci. U.S.A.* **1995**, *92*, 2036−2040.

(11) Picone, J. M.; Clery, R. A.; Watanabe, N.; MacTavish, H. S.; Turnbull, C. G. N. Rhythmic emission of floral volatiles from *Rosa damascena semperflorens* cv. 'Quatre Saisons'. *Planta* **2004**, *219*, 468−478.

(12) Dong, F.; Yang, Z. Y.; Baldermann, S.; Kajitani, Y.; Ota, S.; Kasuga, H.; Imazeki, Y.; Ohnishi, T.; Watanabe, N. Characterization of L-phenylalanine metabolism to acetophenone and 1-phenylethanol in the flowers of *Camellia sinensis* using stable isotope labeling. *J. Plant Physiol.* **2012**, *169*, 217−225.

(13) Chen, X. P.; Zhang, W. M.; Shi, J. S.; Gu, G. P. Tea flowers' value in use and the comprehensive exploitation of the products (in Chinese). *Modern Agric. Technol.* **2007**, *3*, 97−98.

(14) Lin, Y. S.; Wu, S. S.; Lin, J. K. Determination of tea polyphenols and caffeine in tea flowers (*Camellia sinensis*) and their hydroxyl radical scavenging and nitric oxide suppressing effects. *J. Agric. Food Chem.* **2003**, *51*, 975−978.

(15) Yoshikawa, M.; Morikawa, T.; Yamamoto, K.; Kato, Y.; Nagatomo, A.; Matsuda, H. Floratheasaponins A-C, acylated oleanane-type triterpene oligoglycosides with anti-hyperlipidemic activities from flowers of the tea plant (*Camellia sinensis*). *J. Nat. Prod.* **2005**, *68*, 1360−1365.

(16) Yoshikawa, M.; Nakamura, S.; Kato, Y.; Matsuhira, K.; Matsuda, H. Medicinal flowers. XIV. New acylated oleanane-type triterpene oligoglycosides with antiallergic activity from flower buds of Chinese tea plant (*Camellia sinensis*). *Chem. Pharm. Bull.* **2007**, *55*, 598−605.

(17) Morikawa, T.; Miyake, S.; Miki, Y.; Ninomiya, K.; Yoshikawa, M.; Muraoka, O. Quantitative analysis of acylated oleanane-type

triterpene saponins, chakasaponins I-III and floratheasaponins A-F, in the flower buds of *Camellia sinensis* from different regional origins. *J. Nat. Med.* **2012**, *66*, 608−613.
(18) Yang, Z. Y.; Tu, Y. Y.; Baldermann, S.; Dong, F.; Xu, Y.; Watanabe, N. Isolation and identification of compounds from the ethanolic extract of flowers of the tea (*Camellia sinensis*) plant and their contribution to the antioxidant capacity. *LWT−Food Sci. Technol.* **2009**, *42*, 1439−1443.
(19) Wang, Y.; Yang, Z.; Wei, X. Sugar compositions, α-glucosidase inhibitory and amylase inhibitory activities of polysaccharides from leaves and flowers of *Camellia sinensis* obtained by different extraction methods. *Int. J. Biol. Macromol.* **2010**, *47*, 534−539.
(20) Wang, L.; Xu, R.; Hu, B.; Li, W.; Sun, Y.; Tu, Y.; Zeng, X. Analysis of free amino acids in Chinese teas and flower of tea plant by high performance liquid chromatography combined with solid-phase extraction. *Food Chem.* **2010**, *123*, 1259−1266.
(21) Yang, Z. Y.; Dong, F.; Baldermann, S.; Murata, A.; Tu, Y. Y.; Asai, T.; Watanabe, N. Isolation and identification of spermidine derivatives in tea (*Camellia sinensis*) flowers and their distribution in floral organs. *J. Sci. Food Agric.* **2012**, *92*, 2128−2132.
(22) Joshi, R.; Poonam; Saini, R.; Guleria, S.; Babu, G. D.; Kumari, M.; Gulati, A. Characterization of volatile components of tea flowers (*Camellia sinensis*) growing in Kangra by GC/MS. *Nat. Prod. Commun.* **2011**, *6*, 1155−1158.
(23) Hirata, T.; Koya, K.; Sarfo, K. J.; Shimoda, K.; Ito, D. I.; Izumi, S.; Ohta, S.; Lee, Y. S. Glucosylation of benzyl alcohols by the cultured suspension cells of *Nicotiana tabacum* and *Catharanthus roseus*. *J. Mol. Catal. B: Enzym.* **1999**, *6*, 67−73.
(24) Hirata, T.; Shimoda, K.; Fujino, T.; Yamane, S. Y.; Ohta, S. Diastereoselective formation of disaccharides from (*RS*)-1-phenylethanol by cultured cells of *Catharanthus roseus*. *Bull. Chem. Soc. Jpn.* **2001**, *74*, 539−542.
(25) Shimoda, K.; Katsuragi, H. Enzymatic resolution of (*RS*)-1-phenylalkyl β-D-glucosides to (*R*)-1-phenylalkyl β-primeverosides and (*S*)-1-phenylalkyl β-D-glucosides via plant xylosyltransferase. *Tetrahedron: Asymmetry* **2010**, *21*, 2060−2065.
(26) Ma, S. J.; Mizutani, M.; Hiratake, J.; Hayashi, K.; Yagi, K.; Watanabe, N.; Sakata, K. Substrate specificity of β-primeverosidase, a key enzyme in aroma formation during oolong tea and black tea manufacturing. *Biosci., Biotechnol., Biochem.* **2001**, *65*, 2719−2729.
(27) Mizutani, M.; Nakanishi, H.; Ema, J.; Ma, S. J.; Noguchi, E.; Inohara-Ochiai, M.; Fukuchi-Mizutani, M.; Nakao, M.; Sakata, K. Cloning of β-primeverosidase from tea leaves, a key enzyme in tea aroma formation. *Plant Physiol.* **2002**, *130*, 2164−2176.
(28) Shi, C.; Yang, H.; Wei, C.; Yu, O.; Zhang, Z.; Jiang, C.; Sun, J.; Li, Y.; Chen, Q.; Xia, T.; Wan, X. Deep sequencing of the *Camellia sinensis* transcriptome revealed candidate genes for major metabolic pathways of tea-specific compounds. *BMC Genomics* **2011**, *12*, 131−149.
(29) Livak, K. J.; Schmittgen, T. D. Analysis of relative gene expression data using real time quantitative PCR and $2^{-\Delta\Delta ct}$ method. *Methods* **2001**, *25*, 402−408.
(30) Sakata, K.; Mizutani, M.; Cho, J. Y.; Kinoshita, T.; Shimizu, B. Improvement of flavour quality of black tea using molecular basis of aroma formation in oolong tea. In *Economic Crisis in Tea Industry*; Jain, N. K., Rahamn, F., Baker, P., Eds.; Studium Press: New Delhi, India, 2008; pp 212−225.
(31) Yang, Z. Y.; Baldermann, S.; Watanabe, N. Recent studies of the volatile compounds in tea. *Food Res. Int.* **2013**, *53*, 585−599.
(32) Ma, S. J.; Mizutani, M.; Hiratake, J.; Hayashi, K.; Yagi, K.; Watanabe, N.; Sakata, K. Substrate specificity of β-primeverosidase, a key enzyme in aroma formation during oolong tea and black tea manufacturing. *Biosci., Biotechnol., Biochem.* **2001**, *65*, 2719−2729.
(33) Li, Y. Y.; Jiang, C. J.; Wan, X. C.; Zhang, Z. Z.; Li, D. X. Purification and partial characterization of β-glucosidase from fresh leaves of tea plants (*Camellia sinensis* (L.) O. Kuntze). *Acta. Biochim. Biophys. Sin.* **2005**, *37*, 363−370.
(34) Sarry, J. E.; Günata, Z. Plant and microbial glycoside hydrolases: volatile release from glycosidic aroma precursors. *Food Chem.* **2004**, *87*, 509−521.
(35) Wang, D. M.; Kurasawa, E.; Yamaguchi, Y.; Kubota, K.; Kobayashi, A. Analysis of glycosidically bound aroma precursors in tea leaves. 2. Changes in glycoside contents and glycosidase activities in tea leaves during the black tea manufacturing process. *J. Agric. Food Chem.* **2001**, *49*, 1900−1903.
(36) Wang, D. M.; Kubota, K.; Kobayashi, A.; Juan, I. M. Analysis of glycosidically bound aroma precursors in tea leaves. 3. Changes in glycoside contents during the oolong tea manufacturing process. *J. Agric. Food Chem.* **2001**, *49*, 5391−5396.
(37) Watanabe, S.; Hashimoto, I.; Hayashi, K.; Yagi, K.; Asai, T.; Knapp, H.; Straubinger, M.; Winterhalter, P.; Watanabe, N. Isolation and identification of 2-phenylethyl disaccharide glycosides and mono glycosides from rose flowers, and their potential role in scent formation. *Biosci., Biotechnol., Biochem.* **2001**, *65*, 442−445.
(38) Oka, N.; Ohishi, T.; Hatano, T.; Hornberger, M.; Sakata, K.; Watanabe, N. Aroma evolution during flower opening in *Rosa damascena* Mill. *Z. Naturforsch.* **1999**, *54C*, 889−895.
(39) Hayashi, S.; Yagi, K.; Ishikawa, T.; Kawasaki, M.; Asai, T.; Picone, J.; Turnbull, C.; Hiratake, J.; Sakata, K.; Takada, M.; Ogawa, K.; Watanabe, N. Emission of 2-phenylethanol from its β-D-glucopyranoside and the biogenesis of these compounds from [$^2H_8$]-L-phenylalanine in rose flowers. *Tetrahedron* **2004**, *60*, 7005−7013.
(40) Nakajima, R.; Moon, J. H.; Shimokihara, K.; Watanabe, N.; Watanabe, S.; Inagaki, J.; Etoh, H.; Asai, T.; Sakata, K.; Ina, K. Formation of flower fragrance compounds from their precursors by enzymatic action during flower opening. *Biosci., Biotechnol., Biochem.* **1993**, *57*, 1101−11106.

JOURNAL OF AGRICULTURAL AND FOOD CHEMISTRY

Article

pubs.acs.org/JAFC

# Eggshell Membrane-Based Biotemplating of Mixed Hemimicelle/Admicelle as a Solid-Phase Extraction Adsorbent for Carcinogenic Polycyclic Aromatic Hydrocarbons

Weidong Wang,[†,‡] Bo Chen,[†] and Yuming Huang*[,†]

[†]Key Laboratory of Luminescent and Real-Time Analytical Chemistry, Ministry of Education; College of Chemistry and Chemical Engineering, Southwest University, Chongqing 400715, China

[‡]Basic Department of Rongchang Campus, Southwest University, Chongqing 402460, China

Supporting Information

**ABSTRACT:** A new solid-phase extraction (SPE) format was demonstrated, based on eggshell membrane (ESM) templating of the mixed hemimicelle/admicelle of linear alkylbenzenesulfonates (LAS) as an adsorbent for the enrichment of carcinogenic polycyclic aromatic hydrocarbons (PAHs) in environmental aqueous samples. The LAS mixed hemimicelle/admicelle formation and SPE of the target PAHs were conducted simultaneously by adding the organic target and LAS through a column filled with 500 mg of ESM. The effect of various factors, including LAS concentration, solution pH, ionic strength, and humic acid concentration on the recoveries of PAHs were investigated and optimized. The results showed that LAS concentration and solution pH had obvious effect on extraction of PAHs, and the recoveries of PAHs compounds decreased in the presence of salt and humic acid. Under the optimized analytical conditions, the present method could respond down to 0.1−8.6 ng/L PAHs with a linear calibration ranging from 0.02 to 10 μg/L, showing a good PAHs enrichment ability with high sensitivity. The developed method was used satisfactorily for the detection of PAHs in environmental water samples. The mixed hemimicelle/admicelle adsorbent exhibited high extraction efficiency to PAHs and good selectivity with respect to natural organic matter and was advantageous over commercial $C_{18}$ adsorbent, for example, high extraction yield, high breakthrough volume, and easy regeneration.

**KEYWORDS:** *biomaterials, eggshell membrane, mixed hemimicelles, solid-phase extraction, polycyclic aromatic hydrocarbons*

## INTRODUCTION

Because of very low concentrations of the organic pollutants in the environment, it is in urgent need of an extraction procedure to enrich these targets before analysis. Among a great diversity of sample pretreatment methods, solid-phase extraction (SPE) is less time-consuming and solvent-consuming than liquid−liquid extraction. Nowadays, SPE has been widely applied in enrichment of various organic pollutants at trace level.[1−3] Although the commercial adsorbents including $C_8$, $C_{18}$, or Oasis HLB as SPE adsorbents have been widely utilized for sample pretreatment in environmental analysis,[4,5] the search for new extraction materials for SPE is still highly needed. This is because the silica-based materials present some shortcomings, such as pH instability and the possibility of discrepant results because of the unrestrained existence of free silanol groups.[6] In the past few years, a liquid−solid extraction system, based on hemimicelles (monolayers of the adsorbed surfactant aggregates at the solid−liquid interface) and admicelles (bilayers of the adsorbed surfactant aggregates at the solid−liquid interface), has been developed to extract organic pollutants from various environmental matrices.[7−11] The process of extracting analytes in hemimicelles and admicelles is defined as "adsolubilization", and it is suggested that both hemimicelles and admicelles regions are desirable for the SPE method.[7] Unlike the commercial adsorbents such as $C_8$, $C_{18}$, or Oasis HLB that can be directly used for extraction of analytes, in the SPE method based on hemimicelles and admicelles, the adsorbents are generated by the adsorption of ionic surfactants on the solid surface of mineral oxides.[7−13] Until now, almost all studies concentrated on the adsolubilization behavior of target analytes in the hemimicelle/admicelle aggregates formed on the surface of chemical structures, such as alumina, ferric oxyhydroxides, silica, and titanium dioxide.[7−18] There is no work yet on the hemimicelle/admicelle aggregates formation on the surface of biological material.

Eggshell membrane (ESM), existing between the egg white and the inner surface of the eggshell, is a worthless biomaterial after the production of egg derivatives in food industry. Its main components are biological molecules and protein fibers. ESM promises very good gas and water permeability and biocompatibility. Recently, ESM has been investigated as an efficient carrier of active components due to its cavity microstructure.[19] Importantly, due to the presence of amines, amides, and carboxylic groups on the surface of ESM,[20,21] ESM has been widely used in the removal of various pollutants, material preparation, catalysis, and organic synthesis.[22−25] On the basis of the principle of hard and soft acids and bases, hard-base groups such as amino groups and carboxylic groups on ESM favor binding to hard acid, such as $H^+$, through strong

Received: January 1, 2014
Revised: July 9, 2014
Accepted: July 15, 2014
Published: July 15, 2014

ACS Publications © 2014 American Chemical Society



dx.doi.org/10.1021/jf501877k | J. Agric. Food Chem. 2014, 62, 8051−8059

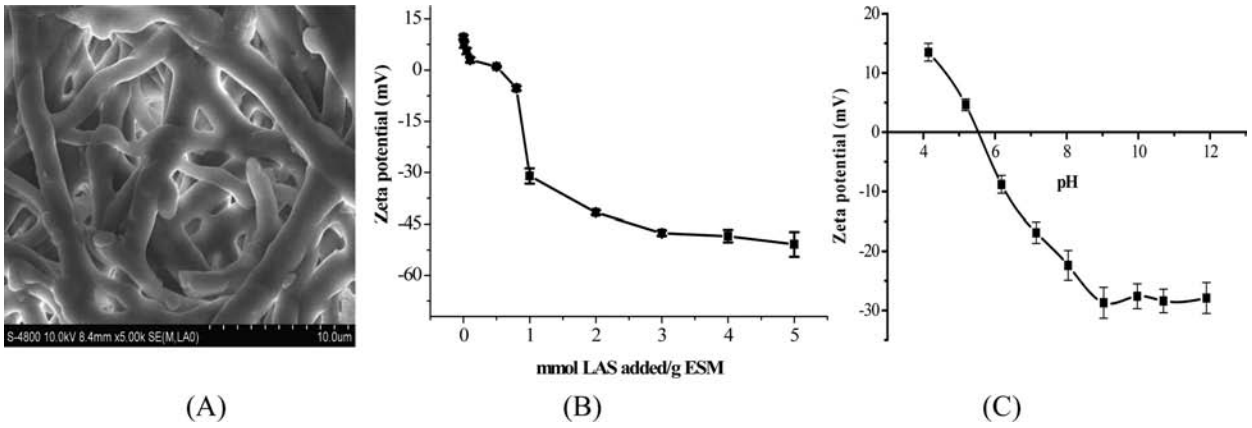


**Figure 1.** (A) Scanning electron microscopy image of the ESM. (B) $\zeta$ potential of ESM by adsorption of LAS at pH 4.97. (C) Effect of solution pH values on the $\zeta$ potential of ESM. Error bars denote standard deviations based on three measurements.

ionic interactions in solution, making ESM surface positively charged under acidic condition. If an anionic surfactant, such as linear alkylbenzenesulfonates (LAS), is added to ESM, the interaction via electrostatic attraction between negatively charged basic sulfonate groups of LAS and the positively charged acidic surface of ESM, results in the formation of hemimicelle/admicelle aggregates on the ESM, which can be used as adsorbents for the enrichment of polycyclic aromatic hydrocarbons (PAHs). On this basis, a new kind of adsorbents, namely, the biotemplating of hemimicelle/admicelle, is obtained. Hence, the objectives of this study were (1) to study the LAS surfactant adsorption onto ESM and mixed hemimicelle/admicelle formation on ESM biomaterial; (2) to investigate the feasibility of using ESM templating of the mixed hemimicelle/admicelle of LAS as new SPE adsorbent for the extraction of 10 PAHs, namely, naphthalene (Nap), acenaphthylene (Acy), fluorene (Flo), phenanthrene (Ph), anthracene (An), fluoranthene (Fl), pyrene (Py), benz[*a*]anthracene (BaA), benzo[*b*]fluoranthene (BbF), and benzo[*k*]fluoranthene (BkF), from environmental water samples. These target PAHs were considered because they are ubiquitous in our environment and are frequently found in rivers and wastewaters.[26,27] Thus, they always were chosen as the target PAH compounds in the analysis of environmental water samples;[26−30] (3) to optimize the predominant factors affecting the enrichment efficiency of this novel adsorbent for PAH target compounds.

## EXPERIMENTAL PROCEDURES

**Reagents and Chemicals.** The ESM was obtained from the eggshells of boiled eggs, which were provided by the local supermarket. After the obtained ESM was treated by 0.5% diluted hydrochloric acid[20] for 30 min, it was rinsed with proper ultrapure water, dried at 80 °C, and stored at 4 °C until use. Ten PAH standards of Nap, Acy, Flo, Ph, An, Fl, Py, BaA, BbF, and BkF were provided by Sigma−Aldrich (Shanghai, China). The stock PAH standard mixture was prepared in methanol media. The working solution of 10 PAHs was prepared every day by proper dilution of stock PAH solution using ultrapure water. Commercial LAS was supplied by Fluka Corporation, in a mixture containing a proportional composition of the different homologues as follows: $C_{10}$, 14.56%; $C_{11}$, 38.00%; $C_{12}$, 30.19%; and $C_{13}$, 17.25%. Acetonitrile and methanol (high-performance liquid chromatography (HPLC) grade) were purchased from Scharlau Chemie S.A. (Scharlau Chemie S.A., Spain). All other solvents and reagents were of analytical reagent grade and provided by the Chongqing Taixin Chemical Co. Ltd. (Beibei, Chongqing). The ultrapure water was used throughout.

**LAS Adsorption onto ESM.** To obtain the adsorption isotherm of LAS on ESM, a series of 100 mL of 0.05−50 mmol/L LAS aqueous solutions (pH 5.0) was prepared and transferred into conical flasks containing 100 mg of ESM. Then, all flasks were placed vertically on a flat surface in a water bath at 25 °C and shaken at 100 rpm for 1 h to ensure the equilibrium between LAS aqueous solution and ESM. The free LAS concentration in solution was analyzed by HPLC−UV (see the Supporting Information).

**SPE Procedure.** Before adsorption of LAS, ESM was cut into small pieces (about 0.5 mm × 0.5 mm). An ESM-packed cartridge was organized by amending a $C_{18}$ cartridge (1 g, 6 mL, polypropylene) from SUPELCO Corporation, USA. The 500 mg of the as-prepared ESM was filled into the emptied cartridge. Because ESM is a complex biomaterial probably containing various impurities such as inorganic cations and organic matters,[22,31] in order to remove these possible impurities, the homemade ESM column was washed consecutively with $CH_2Cl_2$, hexane, $CH_3OH$, $CH_3CN$, and ultrapure water, 5 mL for each. Before sample loading, the ESM-packed column was pretreated by 5 mL of acetone and 5 mL of ultrapure water. Extraction of 10 PAHs was fulfilled by passing 500 mL of the PAH standard solution in water or 100−500 mL of the different water samples (500 mL for the tap water sample, the Jialingjiang water sample and the Changjiang water sample, 100 mL for wastewater from the effluent of a constructed wetland treatment system) containing LAS surfactants (the amount of LAS added was kept 0.5 mmol/g ESM) through the 0.5 g ESM-packed cartridge (for 500 mL sample) or 0.1 g ESM-packed cartridge (for 100 mL sample) at 6 mL/min flow rate. After extraction, 10 mL of ultrapure water was used to wash the homemade ESM column. Then, the column was dried under the negative pressure of 20 mmHg for 15 min, and the enriched 10 PAHs were eluted with 5 mL of acetone. Finally, a volume of 20 $\mu$L was used for HPLC−UV analysis of 10 PAHs. The recovery of the target PAHs was used as the criterion for optimizing the parameter for the proposed SPE method, which was obtained based on the ratio of the obtained content of PAHs to the expected content of PAHs, displayed as a percentage.

**Instrumental Analysis.** The HPLC instrument (JASCO Corporation, Japan) consisted of two inert pumps, a column thermostat, and a UV detector. The PAHs were separated on a $C_{18}$ column (250 mm × 4.6 mm, 5 $\mu$m). The mobile phase was a mixture of acetonitrile and water at a ratio of 80−20% (v/v), and its flow rate was set at 1 mL/min. The column temperature was 25 °C. The chromatographic data were recorded at the wavelength of 254 nm. The HPLC−UV system was controlled by the JASCO Chrompass (JASCO Corporation, Japan). Analytical method for LAS determination was based our previous work,[32] and the detailed procedure is provided in the Supporting Information under "LAS Determination by HPLC−UV" (see the Supporting Information). The $\zeta$ potential was measured on a Zetasizer Nano ZS90 apparatus (Malvern, U.K.).

**Analysis of Environmental Water Samples and Comparative Study.** In this study, river water, tap water, and wastewater samples

were used for the detection of 10 PAHs by the proposed method. The river water samples were collected from the Chongqing sections of the Jialingjiang River (Beibei, Chongqing, China) and the Changjiang River (Jiulongpo, Chongqing, China), respectively. Tap water and wastewater samples were sampled from our lab and an effluent of a wastewater treatment system in Yongchuan (Chongqing, China). Prior to sample pretreatment, all of the aqueous samples were filtered through a 0.45 μm mixed fiber membrane (Shanghai Xinya Purification Device Factory, Shanghai, China); then, the pH value of the resulting filtrate was regulated to 5.0 by dilute HCl.

For a comparison, water sample preconcentration by $C_{18}$ was conducted following the published procedures.[33,34] Briefly, the $C_{18}$ SPE cartridge (0.5 g, 3 mL, polypropylene, SUPELCO Corporation, USA) was preconditioned by 5 mL of methanol and 5 mL of ultrapure water. Then, 100−500 mL of water sample spiked with the target PAHs was pumped through the cartridge at 6 mL/min, followed by a rinsing procedure by 10 mL of ultrapure water. After the column was dried for 15 min, the enriched 10 PAHs were eluted with 5 mL of acetonitrile. Finally, 20 μL of the obtained acetonitrile solution was used for HPLC−UV analysis of 10 PAHs.

## RESULTS AND DISCUSSION

**LAS Adsorption on ESM.** It is essential to obtain the adsorption isotherms of LAS on ESM because this is important to locating the ranges where different aggregates form and to interpreting the SPE behavior of the selected analytes when using the mixed hemimicelle/admicelle-based SPE.[13,17] The Fourier transform (FT) IR spectrum of ESM exhibits significant peaks at 3300−3500 $cm^{-1}$ (ascribed to N−H stretching mode), 1630 $cm^{-1}$ (ascribed to N−H bending mode), and 1350−1385 $cm^{-1}$ (ascribed to C−N stretching mode) (see Figure S1, Supporting Information), proving the presence of amines and amides in ESM.[21] In addition, ESM contains macroporous network structure (Figure 1A), consisting of highly cross-linked protein fibers (about 1−3 μm in diameter). The presence of macropores benefits mass transfer as an adsorbent. Figure 1B depicts the ζ potential change of ESM by adsorption of LAS at pH 4.97. The isotherm is similar to those in previous works.[8,17] Generally, the ionic surfactant adsorption isotherms can be classified into three areas, namely, hemimicelles, mixed hemimicelles, and admicelles.[35,36] In the first area, the ζ potential of ESM at pH 4.97 (below the point of zero charge of ESM, about 5.50, see Figure 1C) is positive, and LAS anionic surfactants are sparsely adsorbed onto the positively charged ESM surface. In such a case, adsorption of surfactants occurs primarily via the electrostatic attraction between the positive surface charges of ESM and the negative sulfonate surfactant head groups, resulting in a single-layer coverage (hemimicelles). Hence, the ζ potential decreased from positive to zero. In the area of the mixed hemimicelles, with increase in the amount of LAS, the surface charge of ESM turned to negative due to charge neutralization. For example, the ζ potential gradually decreased from about 1.0 to −41.7 mV when the amount of LAS added increased from 0.5 to 2.0 mmol/g ESM (Figure 1B). This is because the lateral hydrophobic interactions among surfactant tails results in the aggregation of the surfactant molecules at the solid−liquid interface, leading to the formation of bilayers called admicelles. Both hemimicelles and admicelles areas are suitable for the SPE method.[7,17] From the ξ potential isotherm (Figure 1B), the range 0.1−0.8 mmol/g ESM is in the mixed hemimicelles regions, which is suitable for SPE. In the third region, further increases in the amount of LAS caused no obvious change of the surface charge; thus, the ζ potential of ESM remained almost constant. For example, the ζ potential shifted from −47.6 to −50.9 mV when the amount of LAS added increased from 3.0 to 5.0 mmol/g ESM. This suggests that additional increase in the amount of surfactant did not significantly increase LAS adsorption on ESM. In such a case, the LAS surfactant begins to form micelles in solution, and the aqueous LAS micelles are in equilibrium with LAS admicelles. This results in a distribution of target analytes in two kinds of LAS aggregates, which is unsuitable for SPE application.[17] In a word, previous works proved that adsorption of surfactant on inorganic oxides resulted in formation of hemimicelle, hemimicelle/admicelle mixture, as well as admicelle.[7−9,11,12,15] Similarly, the adsorption phenomenon of LAS on ESM under acidic conditions also led to formation of hemimicelle, hemimicelle/admicelle mixture, as well as admicelle.

Figure S2 (Supporting Information) depicts the adsorption isotherms of LAS homologues on ESM. As can be seen, the $C_{10}$ to $C_{13}$ LAS isotherms showed a similar trend (see Figure S2, Supporting Information). The representative fitting parameters by Langmuir[37] and Freundlich[38] adsorption equations proved that the Langmuir equation ideally described the adsorption data ($r^2$ > 0.99, see Table S1, Supporting Information), suggesting the Langmuir isotherm as a better fit with the experimental data than the Freundlich isotherm. This confirms the monolayer adsorption of LAS onto ESM surface.

**Optimization of SPE Procedure for PAHs Extraction.** *Effect of the Amount of LAS Surfactant.* The extraction performance of the mixed hemimicell/admicelle adsorbent to PAHs was investigated, and a HPLC−UV instrument was used for the detection of 10 PAHs in aqueous samples after preconentration by the adsorbent. During the extraction process, the amount of LAS is one of the important factors in the present method because the formation of the mixed hemimicelle/admicelle depends on this condition directly.[7,11,17,18] Thus, the effect of the LAS amount on extraction of 10 PAH compounds was investigated in detail. As shown in Figure 2, when there was no LAS in aqueous solution, the recoveries of 10 PAHs were rather low, showing that PAHs in aqueous media were hardly adsorbed on ESM in the absence of LAS. With increase in the amount of LAS, the recoveries of PAHs increased. This indicated that the mixed hemimicelle/

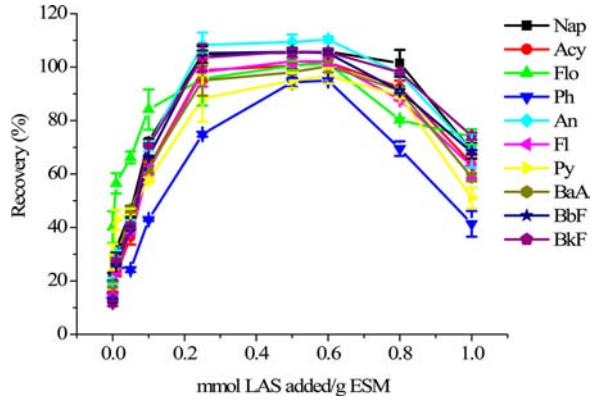


**Figure 2.** Effect of the amount of LAS on recoveries of PAHs. Concentration of sample solution: Nap, 2 μg/L; Acy, 4 μg/L; Flo, 0.4 μg/L; Ph, 0.2 μg/L; An, 0.2 μg/L; Fl, 0.4 μg/L; Py, 0.2 μg/L; BaA, 0.2 μg/L; BbF, 0.4 μg/L; BkF, 0.2 μg/L; SPE column packed with 500 mg of ESM; flow rate of sample solution: 4 mL/min; eluent: 5 mL acetone; pH of sample solution: 5.0; volume of sample solution: 500 mL. Error bars denote standard deviations based on three measurements.


dx.doi.org/10.1021/jf501877k | J. Agric. Food Chem. 2014, 62, 8051−8059

admicelle began to form on the surface of ESM in the presence of LAS, which obviously enhanced the retention of the target PAH compounds. The PAH adsolubilization increased with the amount of LAS surfactants rising up to 0.50 mmol/g ESM, then remained stable until 0.60 mmol/g ESM, and decreased above 0.60 mmol/g ESM. Hence, 0.50 mmol of LAS/g ESM was selected as the optimal addition of surfactant in this investigation, corresponding to 0.5 mmol/L LAS concentration in aqueous solution. This concentration was lower than the critical micelle concentration (CMC) of LAS ranging from 1.8 to 4 mmol/L depending on the solution chemistry and homologues.[39,40] This interesting phenomenon suggested that this novel hemimicelle could occupy the highest adsorptive capacity for PAHs when LAS was self-organized on ESM in a specified pattern of saturated monolayer. The formation of anionic hemimicellar/admicelles was conductive to the generation of analyte−adsorbent mixed aggregates. As expected, the adsolubilization of PAHs gradually reduced for free LAS concentrations close to critical micelle concentration.

*Desorption Condition.* Several organic solvents ($CH_3CN$ and $CH_3OH$, acetone, $CH_2Cl_2$ and hexane) were selected for elution of analytes from ESM templating of hemimicelle/admicelle adsorbents. The effects of the kind and the volume of eluent on desorption were further investigated from 1 to 5 mL. The obtained results proved that desorption ability of acetone was better than that of $CH_3CN$, $CH_3OH$, hexane and $CH_2Cl_2$ (see the Figure S3 of the Supporting Information). Hence, acetone was selected in this work. The effect of volume of acetone as an eluent was investigated in the range of 1−5 mL. The results demonstrated that the recoveries of PAHs increased with volume of acetone as an eluent to 4 mL and then remained stable ranging from 93.8 to 116.9%. Finally, 5 mL of acetone was chosen as an optimized eluent to get the quantitative results.

*Effect of Sample pH and Ion Strength.* The influence of solution pH in extraction of PAHs was examined in the range from 1.0 to 9.0. The retention of all analytes on ESM showed no significant change with solution pH from 1.0 to 5.0 (Figure 3). It is interesting that, for the studied analytes, the adsorption decreased sharply when solution pH was above 5.0. Thus, for practical aqueous samples, pH adjustment is necessary to guarantee quantitative retention of the target PAHs on ESM. This is because solution pH determines both the surface charge of ESM and the existing state of LAS surfactant in aqueous solution. Finally, pH of 5.0 was adopted in this work. The pH effect can be attributed to the fact that ESM contains some functional groups such as $-NH_2$, $-CONH_2$, and $-COOH$ groups, which can be protonated or deprotonated relying on pH value of the sample solution.[35,41] As indicated previously, the $pH_{pzc}$ of ESM is about 5.5 (Figure 1C). Hence, the positively charged sites would form on the ESM surface under acidic media. In the acidic solution ($pH \leq 5.5$), the quantitative recoveries of PAHs were obtained (Figure 3), suggesting that the electrostatic attraction may play a key role in hemimicellar/admicelle formation derived from LAS retained on ESM. At a pH greater than 5.5, the ESM surface became neutral or negatively charged, leading to the decrease of LAS assembled onto ESM and finally leading to the decrease of the target PAH recoveries. The LAS retention decreased at a pH of above 5. This may be caused by the competition effect between the hydroxyl group and the sulfonic group at the identical sorption site of ESM. In fact, it has been found that the adsorption of anions on the positively charged surface decreased by increasing solution pH.[42] In addition, the electrostatic repulsion between the negatively charged ESM surface and the negatively charged sulfonic groups will increase at higher pH. Figure 1C shows that the surface potential of ESM was negatively charged at higher pH values. It became more negative at pH from about 5.5 to 9.0, making electrostatic repulsion between the negatively charged basic sulfonic groups of LAS and ESM stronger at higher pH values than that at more acid pH values. Thus, the LAS adsorption on the surface of ESM decreased at higher pH values, leading to low recoveries of PAHs. The result further indicated the importance of the mixed hemimicelle/admicelle formation arising from LAS for the extraction of PAHs.

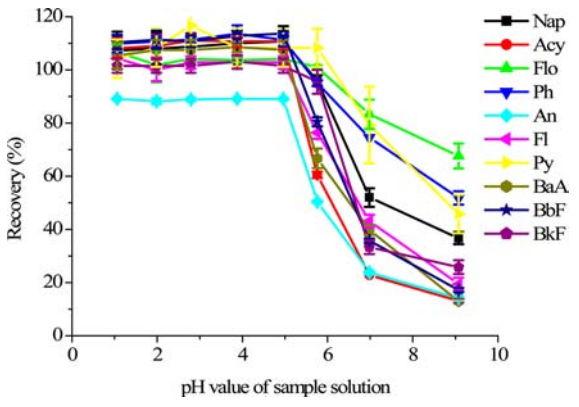


**Figure 3.** Effect of solution pH on recoveries of PAHs. The amount of LAS: 0.5 mmol/g ESM; other conditions were the same as those in Figure 2. Error bars denote standard deviations based on three measurements.

Another experiment was performed to examine the influence of ionic strength on the extraction of PAHs in the presence of sodium chloride. The experimental results indicated that the addition of NaCl reduced the retention of 10 PAH compounds on ESM templating of hemimicelle/admicelle adsorbents (see Figure S4, Supporting Information). For example, the recoveries of 10 PAHs decreased by about 10% to about 25%, as the NaCl was increased from 0% to 2.0% (w/v). A similar result has been observed in the literatures on the solvent microextraction of nitroaromatic explosives in water samples[43] and ion-pair hollow fiber-protected liquid-phase microextraction of acidic herbicides.[44] However, it is noteworthy that the quantitative recovery (recovery >95%) of the target PAHs could be obtained when NaCl concentration was ≤1.0% (w/v). This suggested that the fresh water matrix had a minor effect on extraction of 10 PAH compounds in terms of ion strength. In general, the addition can cause a decrease in the solubility of analytes in an aqueous media,[45] which benefits the extraction of target analytes. However, in our case, the recovery of 10 PAHs decreased in the presence of salt. One possible reason for this finding is the reduced electrostatic pull between negatively charged LAS and the positively charged surface of ESM. In order to confirm this hypothesis, the effect of NaCl addition on the $\zeta$ potential of LAS solution was studied. It is evident that the $\zeta$ potential of LAS solution increased with an increasing concentration of NaCl (see Figure S5, Supporting Information). This would lead to the reduced sorption affinity between negatively charged LAS and the positively charged surface of ESM, which would cause a reduced sorption of PAHs and hence a decrease in recovery. On the basis of the above result,

NaCl was not used in the coming experiments. In addition, in order to clarify the effect of water-structure making or water-structure breaking characters of the added salts on the extraction of 10 PAHs, the effects of KCl and KSCN as water-structure breaking salts[23] on the extraction of PAHs were examined. On the basis of the results shown in Figure S4 (Supporting Information), similar variation trends could be observed for KCl and KSCN, namely, the recoveries of 10 PAHs declined as concentrations of KCl and KSCN increased. Also, they showed a similar trend with NaCl as water-structure making salt[23] (see Figure S4, Supporting Information). The result indicated that both water-structure making salt and water-structure breaking salt had similar effect on the adsorption of PAHs. This is probably because PAHs are hydrophobic compounds; the hydrogen bonds in water have little influence on the solvation pattern of 10 PAHs. Hence, the water-structure making or water-structure breaking characters of the added salts had minor effect on the interaction between ESM and PAHs.

*Breaking through Volume and Flow Rate.* In the present study, LAS hemimicelle/admicelle formation and the target extraction occurred simultaneously. Thus, experiments for determining the sample breaking through volume were realized by passing sample solution through a column filled with 500 mg of ESM. The volume of the aqueous sample was varied from 100 to 1000 mL with the spiked concentration of a 0.2−4 μg/L for the PAH aqueous solution, in which the amount of LAS added was kept 0.25 mmol. The experimental results are shown in Figure 4. As can be seen, when the sample solution volume

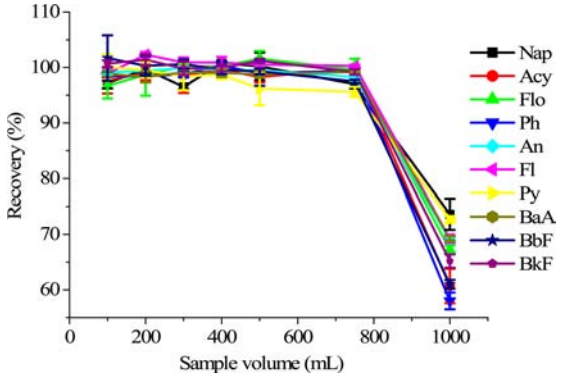


**Figure 4.** Effect of sample volume on recoveries of PAHs. The amount of LAS: 0.5 mmol/g ESM; other conditions were the same as those in Figure 2. Error bars denote standard deviations based on three measurements.

increased from 100 to 750 mL, the quantitative recoveries of PAHs were obtained. Whereas, as the volume of sample solution was increased to 1000 mL, the recoveries of the 10 PAHs decreased. Finally, the sample volume of 500 mL was adopted for further study. It should be indicated that additional experiments were also performed to determine the sample breaking through volume by a common way to work with hemimicelles and/or admicelles. In order to do this, first, 0.25 mmol of LAS in 50 mL of water solution was loaded to 0.5 g of ESM-packed cartridge, then 100−1000 mL of sample solutions spiked with a 0.2−4 μg/L PAH standard solution was loaded to the cartridge. The results demonstrated that, when the sample solution volume increased from 100 to 750 mL, the quantitative recoveries of PAHs were obtained (see Figure S6, Supporting Information). However, the recoveries of the BbF and BkF (86% and 89%, respectively) at 750 mL of sample volume were a little bit lower than those in Figure 4. This indicated that, if the amount of LAS interacting with the ESM adsorbent was kept constant and large enough (0.5 mmol/g ESM in present study) to form the mixed hemimicelle/admicelle onto ESM, the manner for loading LAS surfactant had no obvious effect on the enrichment ability of the mixed hemimicelles/admicelles-based adsorbent for PAHs. However, direct addition of LAS into the water sample before SPE adopted in our study can simplify the experimental separation procedure as compared to a common way to work with hemimicelles and/or admicelles.

The effect of the sample flow rate was studied in the 3−10 mL/min range. The satisfactory recoveries of PAHs (82.4−116.7%) were obtained in the studied range of flow rate, thus allowing the fast pretreatment of the practical samples. Finally, 6 mL/min was chosen for further experiment.

*Effect of Humic Acid.* The natural organic matter (NOM) in the aqueous samples may cause a matrix interference with extraction of the organic pollutants (e.g., PAHs). In this work, the influence of NOM on the extraction of PAHs was studied by using humic acid (HA) as a model of NOM. As shown in Figure S7 (Supporting Information), the recoveries of PAH compounds reduced in the presence of HA. However, HA did not cause obvious effect on the extraction of 10 PAHs when the concentration of HA changed from 0 to 10 mg/L dissolved total organic carbon (TOC). This can be explained based on the property of HA. HA is a weak acid and contains phenolic and carboxylic groups in its structure.[46] The p$K_a$ values of humic substances range from 3 to 7.[46] At pH 5.0, a portion of −COOH groups is deprotonated via ionization of HA. The degree of HA ionization increased with the increasing of HA concentration, leading to the competitive adsorption between LAS and HA on ESM. This phenomenon could result in the decline of recoveries of 10 PAHs by weakening the formation of hemimicelle and admicelle on the surface of ESM, which was further confirmed by the significant reduction of extraction recoveries of 10 PAH compounds at a concentration of HA above 10 mg/L. The concentration of TOC in river water samples used in this work ranges from 3.44 to 3.50 mg/L. Thus, it can be concluded that HA had minor effect on the detection of PAHs in river water. This suggested that the proposed SPE format showed good selectivity with respect to natural organic matter.

*Analytical Performance.* The above-selected experimental conditions were employed to measure the analytical performance, in order to determine whether the developed method could be used to the analysis of PAHs in aqueous samples. The analytical data, including linear range, correlation coefficients, detection limits, and precision, are shown in Table 1. As can be seen, good linear relationships could be obtained for different analytes in the 0.02−10 μg/L range. Detection limits (S/N = 3) of 10 PAH compounds were in the range 0.1−8.6 ng/L under the above-mentioned extraction conditions, proving that the developed method was highly sensitive for the detection of PAHs. The relative standard deviations (RSDs) were from 1.3% to 3.8% ($n$ = 6) for 10 PAHs at concentration levels of 0.2−2 μg/L on the same column on the same day. In addition, the RSD of intercolumn and intracolumn was below 9% ($n$ = 3, Table 2), showing that the reproducibility among the ESM cartridges was desirable.

*Analysis of Environmental Water Samples and Comparative Study.* The developed method was applied to detecting PAHs in several aqueous samples. Also, a comparison of the

**Table 1. Linear Range, Correlation Coefficients, Limits of Detection (LOD), and Relative Standard Deviation (RSD) Using ESM Templating of the Mixed Hemimicelle/Admicelle as SPE**

| analyte | linear range ($\mu$g/L) | correlation coefficient | RSD (%) ($n$ = 6) | LOD (ng/L) |
|---|---|---|---|---|
| Nap | 0.2−10 | 0.9983 | 3.8 | 8.6 |
| Acy | 0.2−10 | 0.9928 | 3.2 | 7.1 |
| Flo | 0.05−2.5 | 0.9941 | 0.6 | 0.3 |
| Ph | 0.02−1.0 | 0.9947 | 2.8 | 0.1 |
| An | 0.025−1.25 | 0.9907 | 3.6 | 0.6 |
| Fl | 0.02−5 | 0.9929 | 1.3 | 1.0 |
| Py | 0.02−5 | 0.9726 | 2.5 | 1.8 |
| BaA | 0.02−5 | 0.9865 | 2.3 | 0.9 |
| BbF | 0.05−2.5 | 0.9893 | 2.0 | 1.2 |
| BkF | 0.02−5 | 0.9836 | 1.3 | 1.3 |

**Table 2. Reproducibility among Home-Made SPE Columns**

| | | RSD (%, $n$ = 3) (for single column) | | | |
|---|---|---|---|---|---|
| analyte | concentration level ($\mu$g/L) | column 1 | column 2 | column 3 | RSD (%, $n$ = 3) (among columns) |
| Nap | 2 | 2.4 | 4.8 | 3.1 | 8.4 |
| Acy | 2 | 6.3 | 1.5 | 4.2 | 0.9 |
| Flo | 0.5 | 1.2 | 2.0 | 2.0 | 7.8 |
| Ph | 0.2 | 5.2 | 4.0 | 1.5 | 5.7 |
| Ant | 0.25 | 1.2 | 2.2 | 0.4 | 3.6 |
| Fl | 1 | 0.8 | 4.4 | 1.6 | 4.5 |
| Py | 1 | 2.3 | 3.9 | 2.0 | 6.7 |
| BaA | 1 | 0.9 | 1.8 | 0.8 | 5.3 |
| BbF | 0.5 | 2.6 | 1.3 | 1.5 | 2.5 |
| BkF | 1 | 0.7 | 1.6 | 3.0 | 3.9 |

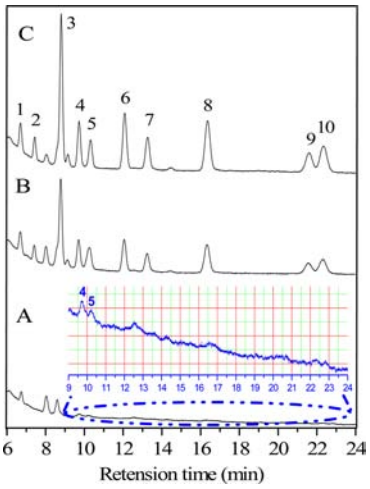


**Figure 5.** HPLC−UV chromatograms of PAHs from (A) 500 mL of the Changjiang River sample; (B) 500 mL of the Changjiang River sample spiked with 0.40 $\mu$g/L Nap, 0.80 $\mu$g/L Acy, 0.08 $\mu$g/L Flo, 0.04 $\mu$g/L Ph, 0.04 $\mu$g/L An, 0.04 $\mu$g/L Fl, 0.04 $\mu$g/L Py, 0.04 $\mu$g/L BaA, 0.08 $\mu$g/L BbF, and 0.04 $\mu$g/L BkF; (C) 500 mL of the ultrapure water spiked with 2 $\mu$g/L Nap, 4 $\mu$g/L Acy, 0.4 $\mu$g/L Flo, 0.2 $\mu$g/L Ph, 0.2 $\mu$g/L An, 0.4 $\mu$g/L Fl, 0.2 $\mu$g/L Py, 0.2 $\mu$g/L BaA, 0.4 $\mu$g/L BbF, 0.2 $\mu$g/L BkF after preconcentrated by ESM templating of the mixed hemimicelle/admicelle as SPE adsorbent. The amount of LAS: 0.5 mmol/g ESM; flow rate of sample solution: 6 mL/min; other conditions were the same as those in Figure 2. Peak identifications: (1) Nap; (2) Acy; (3) Flo; (4) Ph; (5) An; (6) Fl; (7) Py; (8) BaA; (9) BbF; (10) BkF.

mixed hemimicelle/admicelle-based SPE adsorbent and conventional SPE $C_{18}$ adsorbent for the extraction of 10 PAH compounds was made. Figure 5 and Figure S8 (Supporting Information) present the chromatograms of the Changjiang River water sample, wastewater sample, PAH-spiked ultrapure water, PAH-spiked Changjiang River water sample, and PAH-spiked wastewater sample, enriched using LAS hemimicelle/admicelle as adsorbent. The satisfactory recoveries of PAHs were obtained (77.8−112.7%) for all the tested water samples (see Table 3 and Table S2, Supporting Information), although the relatively low recoveries of PAHs were obtained for the wastewater sample (77.8−95.7%) (see Table S2, Supporting Information). This suggests that competitive adsorption processes might occur between the wastewater sample matrix and LAS onto ESM. This may be due to the enhancement of the coextraction of humic substances in the present study. In fact, we determined TOC content in the studied water samples in this work, and the concentration levels (mg/L) are as follows: 3.44−3.50 for river water samples, and 12.04 for the constructed wetland water sample. The NOM in the wastewater was 3 times higher than that in the river water sample. Higher TOC content would cause lower recovery, which was consistent with the result in Figure S7 (Supporting Information). The comparative experiments were performed to obtain comprehensive data of $C_{18}$ and hemimicelle/admicelle adsorbent, using several practical aqueous samples such as tap water, river water, and wastewater. The experiments on water sample preconcentration by $C_{18}$ were conducted following published procedures.[33,34] For $C_{18}$ SPE adsorbent, the recoveries of 10 PAHs varied from 45.6% to 101.0% for tap water and river water (Table 3 and Table S2, Supporting Information), and the recoveries of 10 PAHs varied from 50.8% to 75.2% for wastewater (see Table S2, Supporting Information). Hence, compared with traditional $C_{18}$ SPE adsorbents, LAS hemimicelle/admicelle adsorbent exhibited higher extraction recoveries for PAHs in various aqueous samples.

In conclusion, this work has well illustrated the potential of ESM templating of the mixed hemimicelle/admicelle as a novel SPE adsorbent for the preconcentration of PAHs in environmental aqueous samples. This method provided highly sensitive analysis of PAHs with a LOD of 0.1−8.6 ng/L, linearity of the response from 0.02 to 10 $\mu$g/L, and good selectivity with respect to NOM. The proposed SPE protocol was effective for the concentration of trace PAHs in environmental water sample before HPLC−UV analysis. Compared with commercially available $C_{18}$ materials, the design of ESM templated hemimicelle/admicelle adsorbent for PAHs extraction has advantages as follows: (1) ESM is a biocompatible material and ESM degrades readily; thus, it can be used as a green biomaterial with little secondary contamination; (2) the peculiar macroporous network of eggshell membrane consisting of cross-linking protein fibers benefits mass transfer as a adsorbent; (3) ESM is low-cost and can be obtained in a massive amount as an waste product of food industry. It is believed that the ESM templating of the mixed hemimicelle/admicelle may be a valuable adsorbent for other micropollutants.

**Table 3. Determination Results and Recoveries of 10 PAHs in Water Samples**

| analyte | spiked (μg/L) | found (μg/L) proposed adsorbent | found (μg/L) $C_{18}$ | recovery (%) proposed adsorbent | recovery (%) $C_{18}$ |
|---|---|---|---|---|---|
| Tap Water Sample | | | | | |
| Nap | 0.00 | – | – | | |
| | 0.40 | 0.40 | 0.38 | 99.2 ± 1.4 | 93.9 ± 3.0 |
| | 2.00 | 1.90 | 1.50 | 94.9 ± 2.2 | 75.2 ± 4.0 |
| Acy | 0.00 | – | – | | |
| | 0.80 | 0.89 | 0.74 | 111.1 ± 2.8 | 92.2 ± 2.7 |
| | 4.00 | 3.87 | 2.77 | 96.7 ± 2.7 | 69.3 ± 1.3 |
| Flo | 0.00 | – | – | | |
| | 0.08 | 0.08 | 0.08 | 98.2 ± 3.1 | 98.0 ± 1.7 |
| | 0.40 | 0.38 | 0.18 | 96.1 ± 3.4 | 45.6 ± 2.8 |
| Ph | 0.00 | – | – | | |
| | 0.04 | 0.04 | 0.03 | 109.0 ± 1.6 | 71.6 ± 2.1 |
| | 0.20 | 0.20 | 0.13 | 99.6 ± 0.7 | 64.3 ± 4.1 |
| An | 0.00 | – | – | | |
| | 0.04 | 0.04 | 0.04 | 107.9 ± 3.9 | 91.4 ± 3.5 |
| | 0.20 | 0.20 | 0.14 | 97.7 ± 1.6 | 71.0 ± 1.4 |
| Fl | 0.00 | – | – | | |
| | 0.04 | 0.04 | 0.04 | 97.9 ± 3.6 | 84.1 ± 5.5 |
| | 0.20 | 0.19 | 0.14 | 96.2 ± 3.7 | 68.5 ± 1.6 |
| Py | 0.00 | – | – | | |
| | 0.08 | 0.08 | 0.07 | 107.7 ± 7.7 | 93.3 ± 5.8 |
| | 0.40 | 0.38 | 0.27 | 97.4 ± 2.2 | 68.7 ± 1.7 |
| BaA | 0.00 | – | – | | |
| | 0.04 | 0.05 | 0.03 | 112.7 ± 2.7 | 78.8 ± 2.6 |
| | 0.20 | 0.19 | 0.14 | 94.6 ± 0.7 | 69.1 ± 1.4 |
| BbF | 0.00 | – | – | | |
| | 0.08 | 0.08 | 0.07 | 100.0 ± 8.1 | 88.9 ± 9.6 |
| | 0.40 | 0.39 | 0.28 | 97.5 ± 0.6 | 68.9 ± 1.2 |
| BkF | 0.00 | – | – | | |
| | 0.04 | 0.04 | 0.03 | 97.4 ± 8.9 | 70.4 ± 6.4 |
| | 0.20 | 0.20 | 0.10 | 101.1 ± 1.0 | 50.3 ± 0.9 |
| Changjiang Water Sample | | | | | |
| Nap | 0.00 | 0.01 | 0.01 | | |
| | 0.40 | 0.38 | 0.39 | 93.3 ± 7.6 | 94.7 ± 4.6 |
| | 2.00 | 1.91 | 1.35 | 95.2 ± 0.9 | 67.2 ± 2.2 |
| Acy | 0.00 | – | – | | |
| | 0.80 | 0.77 | 0.72 | 96.3 ± 1.6 | 89.9 ± 2.7 |
| | 4.00 | 3.88 | 2.75 | 97.1 ± 1.0 | 68.7 ± 2.3 |
| Flo | 0.00 | 0.01 | – | | |
| | 0.08 | 0.09 | 0.08 | 92.7 ± 6.3 | 98.0 ± 1.7 |
| | 0.40 | 0.39 | 0.32 | 94.8 ± 2.3 | 80.0 ± 2.8 |
| Ph | 0.00 | – | – | | |
| | 0.04 | 0.04 | 0.03 | 98.2 ± 10.9 | 75.3 ± 2.1 |
| | 0.20 | 0.19 | 0.13 | 94.2 ± 1.1 | 62.6 ± 2.0 |
| An | 0.00 | 0.12 | 0.01 | | |
| | 0.04 | 0.16 | 0.05 | 96.8 ± 0.6 | 84.8 ± 2.6 |
| | 0.20 | 0.30 | 0.14 | 94.7 ± 1.0 | 66.0 ± 0.8 |
| Fl | 0.00 | – | – | | |
| | 0.04 | 0.04 | 0.36 | 102.1 ± 7.2 | 88.9 ± 5.5 |
| | 0.20 | 0.19 | 0.13 | 96.2 ± 0.9 | 66.7 ± 2.4 |
| Py | 0.00 | 0.03 | – | | |
| | 0.08 | 0.11 | 0.07 | 97.4 ± 4.4 | 83.3 ± 5.8 |
| | 0.40 | 0.40 | 0.30 | 92.3 ± 3.8 | 74.7 ± 1.7 |
| BaA | 0.00 | – | – | | |
| | 0.04 | 0.04 | 0.03 | 98.4 ± 2.7 | 80.3 ± 5.2 |
| | 0.20 | 0.19 | 0.15 | 96.7 ± 2.6 | 76.3 ± 1.4 |
| BbF | 0.00 | – | – | | |
| | 0.08 | 0.08 | 0.07 | 94.6 ± 2.7 | 86.8 ± 5.4 |
| | 0.40 | 0.40 | 0.30 | 99.8 ± 2.7 | 74.2 ± 1.8 |
| BkF | 0.00 | – | – | | |
| | 0.04 | 0.04 | 0.03 | 102.6 ± 11.8 | 66.7 ± 9.6 |
| | 0.20 | 0.19 | 0.10 | 97.2 ± 3.5 | 49.7 ± 0.9 |

## ■ ASSOCIATED CONTENT

### Supporting Information

The values of the parameters of the Langmuir and Freundlich equations and the values of the linear regression coefficients (Table S1); determination results and recoveries of PAHs in water samples (Table S2); FT−IR spectrum of ESM (Figure S1); adsorption isotherms, Langmuir isotherms, and Freundlich isotherms for the adsorption of four LAS homologues on ESM (Figure S2); effect of eluent solvent on extraction efficiency of PAHs (Figure S3); effects of NaCl content, KCl content, and KSCN content on recoveries of PAHs (Figure S4); effect of NaCl content on the ζ potential of 0.5 mM LAS solution (Figure S5); effect of sample volume on recoveries of PAHs based on a common way to work with hemimicelles and/or admicelles (Figure S6); effect of HA concentration on recoveries of PAHs (Figure S7); and HPLC−UV chromatograms of wastewater sample from the effluent of a constructed wetland treatment system after preconcentration by ESM templating of the mixed hemimicelle/admicelle as SPE adsorbent (Figure S8). This material is available free of charge via the Internet at http://pubs.acs.org.

## ■ AUTHOR INFORMATION


### Corresponding Author

*Phone/fax: +86 23 68254843; e-mail: yuminghuang2000@yahoo.com.



### Funding

Financial supports by the National Natural Science Foundation of China (21277111), the Fundamental Research Funds for the Central Universities (XDJK2010C043), and the Doctor Foundation of Southwest University (2010BSr07) are gratefully acknowledged.


### Notes

The authors declare no competing financial interest.

## ■ REFERENCES


(1) Zhang, X.; Niu, H.; Li, W.; Shia, Y.; Cai, Y. A core−shell magnetic mesoporous silica sorbent for organic targets with high extraction performance and anti-interference ability. *Chem. Commun.* **2011**, *47*, 4454−4456.

(2) Mozaz, S. R.; Lopez de Alda, M. J.; Barceló, D. Advantages and limitations of on-line solid phase extraction coupled to liquid chromatography−mass spectrometry technologies versus biosensors for monitoring of emerging contaminants in water. *J. Chromatogr. A* **2007**, *1152*, 97−115.

(3) Batt, A. L.; Kostich, M. S.; Lazorchak, J. M. Analysis of ecologically relevant pharmaceuticals in wastewater and surface water using selective solid-phase extraction and UPLC−MS/MS. *Anal. Chem.* **2008**, *80*, 5021−5030.

(4) Sabik, H.; Jeannot, R.; Rondeau, B. Multiresidue methods using solid-phase extraction techniques for monitoring priority pesticides, including triazines and degradation products, in ground and surface waters. *J. Chromatogr. A* **2000**, *885*, 217−236.

(5) Richardson, S. D. Environmental mass spectrometry: Emerging contaminants and current issues. *Anal. Chem.* **2008**, *80*, 4373−4402.
(6) Quintana, M. C.; Ramos, L. Sample preparation for the determination of chlorophenols. *Trends Anal. Chem.* **2008**, *27*, 418−436.
(7) Merino, F.; Rubio, S.; Pérez-Bendito, D. Solid-phase extraction of amphiphiles based on mixed hemimicelle/admicelle formation: Application to the concentration of benzalkonium surfactants in sewage and river water. *Anal. Chem.* **2003**, *75*, 6799−6806.
(8) Zhao, X.; Li, J.; Shi, Y.; Cai, Y.; Mou, S.; Jiang, G. Determination of perfluorinated compounds in wastewater and river water samples by mixed hemimicelle-based solid-phase extraction before liquid chromatography−electrospray tandem mass spectrometry detection. *J. Chromatogr. A* **2007**, *1154*, 52−59.
(9) Li, J.; Cai, Y.; Shi, Y.; Mou, S.; Jiang, G. Determination of sulfonamide compounds in sewage and river by mixed hemimicelles solid-phase extraction prior to liquid chromatography−spectrophotometry. *J. Chromatogr. A* **2007**, *1139*, 178−184.
(10) García-Prieto, A.; Lunar, L.; Rubio, S.; Pérez-Bendito, D. Study of the influence of water matrix components on admicellar sorbents. *Anal. Bioanal. Chem.* **2007**, *388*, 1823−1830.
(11) Moral, A.; Sicilia, M. D.; Rubio, S.; Pérez-Bendito, D. Sodium dodecyl sulphate-coated alumina for the extraction/preconcentration of benzimidazolic fungicides from natural waters prior to their quantification by liquid chromatography/fluorimetry. *Anal. Chim. Acta* **2006**, *569*, 132−138.
(12) Merino, F.; Rubio, S.; Pérez-Bendito, D. Evaluation and optimization of an on-line admicelle-based extraction-liquid chromatography approach for the analysis of ionic organic compounds. *Anal. Chem.* **2004**, *76*, 3878−3886.
(13) García-Prieto, A.; Lunar, L.; Rubio, S.; Pérez-Bendito, D. Hemimicelle-based solid-phase extraction of estrogens from environmental water samples. *Analyst* **2006**, *131*, 407−414.
(14) Moral, A.; Sicilia, M. D.; Rubio, S.; Pérez-Bendito, D. Multifunctional sorbents for the extraction of pesticide multiresidues from natural waters. *Anal. Chim. Acta* **2008**, *608*, 61−72.
(15) Saitoh, T.; Matsushima, S.; Hiraide, M. Concentration of polyaromatic hydrocarbons in water to sodium dodecyl sulfate-$\gamma$-alumina admicelle. *J. Chromatogr. A* **2005**, *1069*, 271−274.
(16) Saitoh, T.; Kondo, T.; Hiraide, M. Concentration of chlorophenols in water to dialkyated catinonic surfactant−silica gel admicelles. *J. Chromatogr. A* **2007**, *1164*, 40−47.
(17) Zhao, X.; Shi, Y.; Cai, Y.; Mou, S. Cetyltrimethylammonium bromide-coated magnetic nanoparticles for the preconcentration of phenolic compounds from environmental water samples. *Environ. Sci. Technol.* **2008**, *42*, 1201−1206.
(18) Li, J.; Zhao, X.; Shi, Y.; Cai, Y.; Mou, S.; Jiang, G. Mixed hemimicelles solid-phase extraction based on cetyltrimethylammonium bromide-coated nano-magnets $Fe_3O_4$ for the determination of chlorophenols in environmental water samples coupled with liquid chromatography/spectrophotometry detection. *J. Chromatogr. A* **2008**, *1180*, 24−31.
(19) Chai, Z.; Li, Y.; Liu, F.; Du, B.; Jiao, T.; Zhang, C.; Leng, X. Outer eggshell membrane as delivery vehicle for polysaccharide/protein microcapsules incorporated with vitamin E. *J. Agric. Food Chem.* **2013**, *61*, 589−595.
(20) Yang, D.; Qi, L.; Ma, J. Hierarchically ordered networks comprising crystalline $ZrO_2$ tubes through sol−gel mineralization of eggshell membranes. *J. Mater. Chem.* **2003**, *13*, 1119−1123.
(21) Tsai, W. T.; Yang, J. M.; Lai, C. W.; Cheng, Y. H.; Lin, C. C.; Yeh, C. W. Characterization and adsorption properties of eggshells and eggshell membrane. *Bioresour. Technol.* **2006**, *97*, 488−493.
(22) Guru, P. S.; Dash, S. Sorption on eggshell waste−A review on ultrastructure, biomineralization and other applications. *Adv. Colloid Interface Sci.* **2014**, *209*, 49−67.
(23) Guru, P. S.; Dash, S. Eggshell particles (ESP) as potential adsorbent for styryl pyridinium dyes−A kinetic and thermodynamic study. *J. Dispersion Sci. Technol.* **2012**, *33*, 1012−1020.
(24) Guru, P. S.; Dash, S. Amino acid modified eggshell powder (AA-ESP)−A novel bio-solid scaffold for adsorption of some styrylpyridinium dyes. *J. Dispersion Sci. Technol.* **2013**, *34*, 1099−1112.
(25) Guru, P. S.; Dash, S. Adsorption of some tailor-made styrylpyridinium dyes on sodium dodecylsulphate-treated eggshell particles (SDS-ESP): Impact of dye chain-length and substituent. *J. Dispersion Sci. Technol.* **2013**, *34*, 898−907.
(26) Djozan, Dj.; Assadi, Y. Monitoring of polycyclic aromatic hydrocarbons in water using headspace solid-phase microextraction and capillary gas chromatography. *Microchem. J.* **1999**, *63*, 276−284.
(27) Zou, Y.; Chen, Y.; Yan, Z.; Chen, C.; Wang, J.; Yao, S. Magnetic solid-phase extraction based on tetrabenzyl modified $Fe_3O_4$ nanoparticles for the analysis of trace polycyclic aromatic hydrocarbons in environmental water samples. *Analyst* **2013**, *138*, 5904−5912.
(28) Es-haghi, A.; Hosseininasab, V.; Bagheri, H. Preparation, characterization, and applications of a novel solid-phase microextraction fiber by sol-gel technology on the surface of stainless steel wire for determination of poly cyclic aromatic hydrocarbons in aquatic environmental samples. *Anal. Chim. Acta* **2014**, *813*, 48−55.
(29) Yang, J.; Li, J.; Qiao, J.; Lian, H.; Chen, H. Solid phase extraction of magnetic carbon doped $Fe_3O_4$ nanoparticles. *J. Chromatogr. A* **2014**, *1325*, 8−15.
(30) Tseng, W.; Chen, P.; Huang, S. Optimization of two different dispersive liquid−liquid microextraction methods followed by gas chromatography−mass spectrometry determination for polycyclic aromatic hydrocarbons (PAHs) analysis in water. *Talanta* **2014**, *120*, 425−432.
(31) Stadelman, W. J. Eggs and egg products. In *Wiley Encyclopedia of Food Science and Technology*, 2nd ed.; Francis, F. J., Ed.; John Wiley & Sons: New York, 1999; pp 593−599.
(32) Wang, W.; Chen, B.; Huang, Y.; Cao, J. Evaluation of eggshell membrane-based bio-adsorbent for solid-phase extraction of linear alkylbenzene sulfonates coupled with high-performance liquid chromatography. *J. Chromatogr. A* **2010**, *1217*, 5659−5664.
(33) Titato, G. M.; Lanças, F. M. Optimization and validation of HPLC−UV−DAD and HPLC−APCI−MS methodologies for the determination of selected PAHs in water samples. *J. Chromatogr. Sci.* **2006**, *44*, 35−40.
(34) Wang, W.; Huang, Y.; Shu, W.; Cao, J. Multiwalled carbon nanotubes as adsorbents of solid-phase extraction for determination of polycyclic aromatic hydrocarbons in environmental waters coupled with high-performance liquid chromatography. *J. Chromatogr. A* **2007**, *1173*, 27−36.
(35) Alila, S.; Boufi, S.; Belgacem, N.; Beneventi, D. Adsorption of a cationic surfactant onto cellulosic fibers I. Surface charge effects. *Langmuir* **2005**, *21*, 8106−8113.
(36) Alila, S.; Aloulou, F.; Beneventi, D.; Boufi, S. Self-aggregation of cationic surfactants onto oxidized cellulose fibers and coadsorption of organic compounds. *Langmuir* **2007**, *23*, 3723−3731.
(37) Peng, X.; Zhong, L.; Ren, J.; Sun, R. Highly effective adsorption of heavy metal ions from aqueous solutions by macroporous xylan-rich hemicelluloses-based hydrogel. *J. Agric. Food Chem.* **2012**, *60*, 3909−3916.
(38) Marín-Benito, J. M.; Sánchez-Martín, M. J.; Andrades, M. S.; Pérez-Clavijo, M.; Rodríguez-Cruz, M. S. Effect of spent mushroom substrate amendment of vineyard soils on the behavior of fungicides: 1. Adsorption-desorption of penconazole and metalaxyl by soils and subsoils. *J. Agric. Food Chem.* **2009**, *57*, 9634−9642.
(39) Conrad, A.; Cadoret, A.; Corteel, P.; Leroy, P.; Block, J. C. Adsorption/desorption of linear alkylbenzenesulfonate (LAS) and azoproteins by/from activated sludge flocs. *Chemosphere* **2006**, *62*, 53−60.
(40) Goon, P.; Manohar, C.; Kumar, V. V. Determination of critical micelle concentration of anionic surfactants: Comparison of internal and external fluorescent probes. *J. Colloid Interface Sci.* **1997**, *189*, 177−180.
(41) Yi, F.; Guo, Z.; Zhang, L.; Yu, J.; Li, Q. Soluble eggshell membrane protein: Preparation, characterization and biocompatibility. *Biomaterials* **2004**, *25*, 4591−4599.

(42) Chen, J. P.; Lin, M. Surface charge and metal ion adsorption on an H-type activated carbon: Experimental observation and modeling simulation by the surface complex formation approach. *Carbon* **2001**, *39*, 1491−1504.
(43) Psillakis, E.; Kalogerakis, N. Application of solvent microextraction to the analysis of nitroaromatic explosives in water samples. *J. Chromatogr. A* **2001**, *907*, 211−219.
(44) Wu, J.; Lee, H. K. Injection port derivatization following ion-pair hollow fiber-protected liquid-phase microextraction for determining acidic herbicides by gas chromatography/mass spectrometry. *Anal. Chem.* **2006**, *78*, 7292−7301.
(45) Zhang, Z.; Duan, H.; Zhang, L.; Chen, X.; Liu, W.; Chen, G. Direct determination of anabolic steroids in pig urine by a new SPME−GC−MS method. *Talanta* **2009**, *78*, 1083−1089.
(46) Karanfil, T.; Kilduff, J. E.; Schlautman, M. A. Adsorption of organic macromolecules by granular activated carbon. 1. Influence of molecular properties under anoxic solution conditions. *Environ. Sci. Technol.* **1996**, *30*, 2187−2194.

JOURNAL OF AGRICULTURAL AND FOOD CHEMISTRY

Article

pubs.acs.org/JAFC

Open Access on 07/10/2015

# Characterization of Near-Infrared Spectral Variance in the Authentication of Skim and Nonfat Dry Milk Powder Collection Using ANOVA-PCA, Pooled-ANOVA, and Partial Least-Squares Regression

James M. Harnly,*[,†] Peter B. Harrington,*[,‡] Lucy L. Botros,[§] Joseph Jablonski,[∥] Claire Chang,[∥] Marti Mamula Bergana,[⊥] Paul Wehling,[#] Gerard Downey,[▽] Alan R. Potts,[§] and Jeffrey C. Moore[§]

[†]Agricultural Research Service, Beltsville Human Nutrition Research Center, Food Composition and Methods Development Laboratory, U.S. Department of Agriculture, Building 161, BARC-East, Beltsville, Maryland 20817, United States

[‡]Center for Intelligent Chemical Instrumentation, Department of Chemistry and Biochemistry, Ohio University, Clippinger Laboratories, Athens, Ohio 45701-2979, United States

[§]U.S. Pharmacopeial Convention, 12601 Twinbrook Parkway, Rockville, Maryland 20852-1790, United States

[∥]Center for Food Safety and Applied Nutrition, Division of Food Processing Science and Technology, U.S. Food and Drug Administration, 6502 South Archer Road, Bedford Park, Illinois 60501, United States

[⊥]Abbott Nutrition, Division of Abbott Laboratories, 3300 Stelzer Road, Columbus, Ohio 43219, United States

[#]General Mills, Inc., 330 University Avenue SE, Minneapolis, Minnesota 55414, United States

[▽]Teagasc Food Research Centre Ashtown, Ashtown, Dublin 15, Ireland

Supporting Information

**ABSTRACT:** Forty-one samples of skim milk powder (SMP) and nonfat dry milk (NFDM) from 8 suppliers, 13 production sites, and 3 processing temperatures were analyzed by NIR diffuse reflectance spectrometry over a period of 3 days. NIR reflectance spectra (1700−2500 nm) were converted to pseudoabsorbance and examined using (a) analysis of variance-principal component analysis (ANOVA-PCA), (b) pooled-ANOVA based on data submatrices, and (c) partial least-squares regression (PLSR) coupled with pooled-ANOVA. ANOVA-PCA score plots showed clear separation of the samples with respect to milk class (SMP or NFDM), day of analysis, production site, processing temperature, and individual samples. Pooled-ANOVA provided statistical levels of significance for the separation of the averages, some of which were many orders of magnitude below $10^{-3}$. PLSR showed that the correlation with Certificate of Analysis (COA) concentrations varied from a weak coefficient of determination ($R^2$) of 0.32 for moisture to moderate $R^2$ values of 0.61 for fat and 0.78 for protein for this multinational study. In this study, pooled-ANOVA was applied for the first time to PLS modeling and demonstrated that even though the calibration models may not be precise, the contribution of the protein peaks in the NIR spectra accounted for the largest proportion of the variation despite the inherent imprecision of the COA values.

**KEYWORDS:** *pooled-ANOVA, milk powder, near-infrared spectroscopy, partial least-squares regression, ANOVA-PCA*

## INTRODUCTION

Skim milk powder (SMP) and nonfat dry milk (NFDM) are important foods/ingredients in the international food supply.[1] In 2011, the United States Pharmacopeial Convention (USP) initiated a project to characterize compositional and functional variations of these powders and develop nontargeted methods for detection of adulteration. One phase of this project analyzed 41 samples collected from 8 national and 3 international suppliers at 13 production sites (Table 1) using diffuse reflectance NIR.[1] The variance of the data was initially characterized using principal component analysis and varimax rotation[2] of the principal components. This Article provides the second step of the analysis by characterizing the NIR variance using analysis of variance-principal components analysis (ANOVA-PCA),[3] pooled-ANOVA,[4,5] and partial least-squares regression (PLSR).[6]

It has become customary to use chemometric methods to simplify and glean information from complex data sets. However, classical statistical methods, such as ANOVA, can also be applied to complex data. ANOVA can be used to compare the difference among the means of multiple groups, and in a factorial mode to isolate and quantify the variance associated with different experimental factors and their interactions. Pooled-ANOVA extends ANOVA from a single dependent variable to a pooled set of multiple variables.[4,5] Thus, ANOVA tests the differences of means among groups, and pooled-ANOVA tests the differences among two or more vectors of means by comparing the pooled variance of the variables.

Harrington et al.[3] used ANOVA to decompose the original sample matrix of mass spectrometry (MS) data into a series of

Received: March 27, 2014
Revised: June 26, 2014
Accepted: July 10, 2014
Published: July 10, 2014

ACS Publications © 2014 American Chemical Society



dx.doi.org/10.1021/jf5013727 | J. Agric. Food Chem. 2014, 62, 8060−8067

**Table 1. Sample Provenance**

| | | | | | | | | | | | | | |
|---|---|---|---|---|---|---|---|---|---|---|---|---|---|
| supplier[a] | 1 | 1 | 1 | 2 | 2 | 2 | 2 | 3 | 4 | 5 | 6 | 7 | 8 |
| prod. site[b] | US1 | US2 | US2 | US3 | US4 | US5 | US6 | I1 | I2 | I3 | US7 | ? | US8 |
| milk class[c] | N | N | S | S | S | S | S | S | S | S | N | N | N |
| samples[d] | 5 | 10 | 2 | 3 | 3 | 4 | 2 | 2 | 1 | 2 | 2 | 2 | 3 |
| proc. type[e] | L,H | L,M | L,? | L,M | L,M | L,H | M | M | M | M | L,H | ? | L |
| no. of analyses[f] | 30 | 60 | 12 | 18 | 18 | 24 | 12 | 12 | 6 | 12 | 12 | 12 | 18 |

[a]Eight suppliers. [b]Production site per supplier in the United States (US), internationally (I), or unknown (?). [c]N = nonfat dry milk and S = skim milk powder. [d]Number of samples collected from each production site. [e]Process type: L = low, M = medium, H = high, or ? = unknown heat. [f]Six subsamples per sample (two subsamples/sample/day for 3 days).

submatrices, each associated with the means of different experimental factors. The final residual matrix was then added to each means matrix and analyzed by principal component analysis (PCA). This combined approach of ANOVA-PCA provides a scores plot for each experimental factor. The separation of scores of the different levels of the factor indicates significance. The separations are defined by 95% confidence ellipses derived from the Hotelling $T^2$ statistic. ANOVA-PCA provides information about the separation of the groups of objects with respect to the experimental factors.

Harnly[4,5] showed that the sum of the squared residuals of the variables of these submatrices derived from ANOVA-PCA could be pooled into a single scalar value and the mean squared statistic could be tested as it is done with ANOVA. The submatrices allowed computation of the percentage of the total variance for each experimental factor, the level of significance of the variance, and the variance associated with the interaction of the factors. The number of variables is omitted from calculation because it is difficult to determine the true rank or degrees of freedom from underdetermined data sets. Thus, the sum of squares across the number of variables is treated as a single squared variable, and the F statistic will underestimate significant differences. If a significant difference is observed, it will indeed be significant. Pooled-ANOVA provides a conservative test for differences among the level averages for each factor.

In this study, the previously reported NIR data for SMP and NFDM[1] are subjected to analysis by ANOVA-PCA, pooled-ANOVA, and PLSR coupled with pooled-ANOVA. The percentages of the total variance according to day of analysis, supplier, production site, milk class, process type, between sample variation, and instrumental variation were determined. A third aspect of the study examined the correlation of the NIR spectra with the protein, moisture, and fat content of the samples. Because this study was large with milk powders collected from many sources, it was difficult to achieve a balanced experimental design, and some of the data with respect to the experimental factors were missing, which prevented interaction from being studied for several factors. A more systematic study would attempt to collect an equal number of milk samples with respect to each experimental factor. Collecting milk powders from different sources produced on the same date and using the same process may be impossible because of limitations of the facility and production schedule.

## MATERIALS AND METHODS

**Milk Powders.** As previously reported,[1] 41 milk powders (19 skim milk and 22 nonfat dry milk) produced between August 2008 and May 2012 were acquired from eight suppliers. Certificates of analysis (COA) indicated product origin details including production sites, lot numbers, process type (labeled as high, medium, and low heat), and weight/weight concentrations of moisture, fat, and protein. The sample information is summarized in Table 1.

The data were analyzed with respect to four sample variables, that is, sample class, production site, process type, and individual samples. The supplier was not treated as a variable because the majority of the suppliers (6 out of 8) only had one production site. A fifth instrumental variable was the day of analysis because the samples were each analyzed on three different days.

**NIR Analysis.** The NIR analysis methodology was previously reported.[1] In brief, Fourier transform (FT) near-infrared spectra were acquired at the U.S. Food and Drug Administration (Center for Food Safety and Applied Nutrition, Division of Food Processing Science and Technology) with a PerkinElmer Frontier FT-NIR system (Waltham, MA) fitted with the NIRA reflectance accessory. Data were acquired from 4000 to 10 000 $cm^{-1}$ (1000−2500 nm). A 99% Spectralon diffuse reflectance standard (Labsphere, cat. no. AS-01160-060, North Sutton, NH) was used to acquire 84 background scans throughout the experiment. NIR spectra of six subsamples for each of the 41 milk powder samples were acquired in a randomized order on three consecutive days of analysis with two subsamples per milk powder being acquired on each day. In addition, on each day of analysis, six replicate measurements were acquired for randomly selected subsamples with the sample remaining on the sampling interface between replicates. Thus, spectral acquisition included 246 unique subsample spectra, 105 additional replicate spectra, and 84 background spectra, yielding a total of 435 spectra.

**Data Processing.** Raw data files consisted of 6001 reflected intensities (1000−2500 nm) for each of the 435 samples. As previously described,[1] the 84 spectra of the diffuse reflectance standard were used to convert reflectance intensities of the samples to pseudoabsorbance ($A_s$):

$$A_s = \log_{10}(I_{standard}/I_{sample}) \quad (1)$$

for which $I_{sample}$ is the diffuse reflectance intensity of the samples, and $I_{standard}$ is the reflected intensity of the 99% reflectance standard. In the current study, only 228 of the 246 unique subsample spectra were used. The 105 replicate spectra were not included, and another 18 spectra (3 samples) were omitted due to provision of incomplete information, that is, missing information regarding process type (Table 1). Initial analysis by PCA showed little variation for the variable loadings of the first and second principal components in the region between 1000 and 1700 nm.[1] Consequently, only the region from 1700 to 2500 nm was used in this study.

Preprocessing of the pseudoabsorbance data prior to PCA transformed the data to the first derivative using a cubic polynomial fit of 35 points followed by standard normal variate (SNV) correction. The 20 points from the 2500 nm end of the wavelength range were removed so that the spectra would range from 1700 to 2480 nm. The derivative was calculated before the shorter wavelengths were excised from the data set so that no points were lost from the shorter wavelength ends of the derivatized spectra. Each derivatized spectrum comprised 1850 data points.

Outliers were detected by calculating the residual data matrix produced by subtracting the sample means from the corresponding spectra. Using a confidence interval defined by the Hotelling distribution at a 99.99% confidence interval applied to the $T^2$ statistic obtained from the first 10 principal component scores, three spectra


dx.doi.org/10.1021/jf5013727 | J. Agric. Food Chem. 2014, 62, 8060−8067

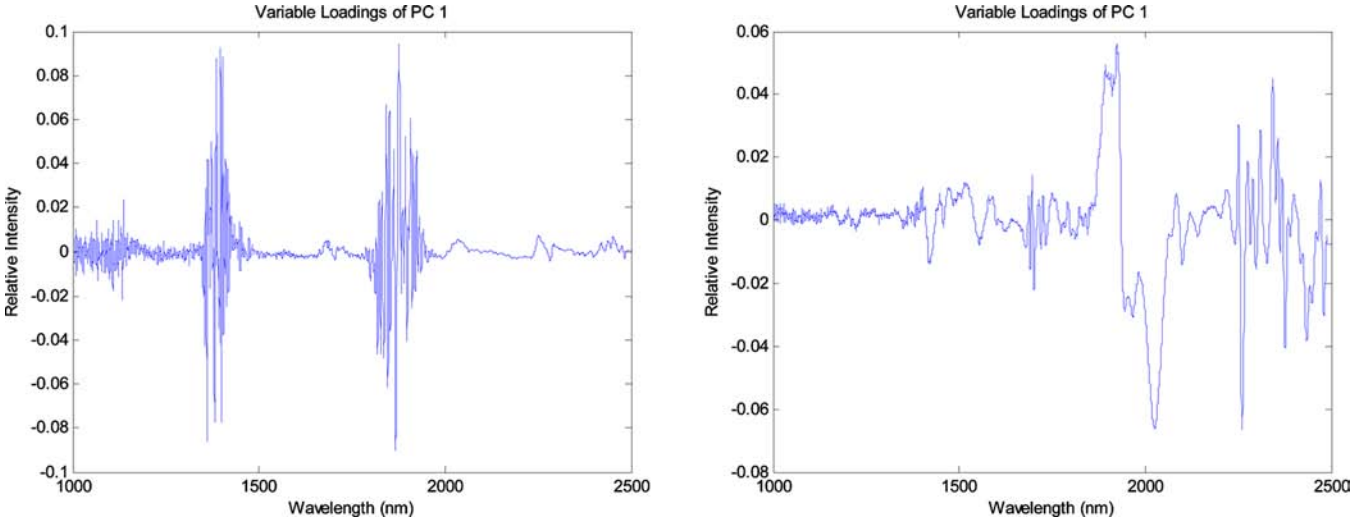


**Figure 1.** First principal component variable loadings of the SNV corrected first derivative spectra obtained from the single beam spectra (left) and pseudoabsorbance spectra (right).

were rejected because they had scores outside this interval. The number of spectra was reduced using this method from 228 to 225. Consequently, the derivatized and SNV corrected data matrix for the current study consisted of 1850 variables (1700−2480 nm) for 225 spectra (6 subsamples of 38 samples less the 3 outlier spectra). These 225 spectra were subjected to ANOVA-PCA, pooled-ANOVA, and PLSR.

PLSR used the NIPALS algorithm implemented in PLS2 mode (i.e., three dependent variables, moisture, fat, and protein). PLSR used a data set further reduced in size because some of the spectra were incomplete with respect to the COA for moisture, fat, and protein. This data set comprised 144 spectra from 24 samples and 7 production sites.

**ANOVA-PCA and Pooled-ANOVA.** Both approaches have been previously described.[2−5] In summary, submatrices are constructed for each experimental factor, for experimental factor interaction, and for the factor residuals. For ANOVA-PCA, the final residual matrix is added back to the means matrices for each factor and then subjected to PCA. For pooled-ANOVA, the residuals matrix for each factor and factor interaction is squared and summed to provide a pooled variance. A more detailed description of the calculation is given in Supporting Information Appendix A.

**PLSR for Protein, Moisture, and Fat.** COA concentrations for moisture, fat, and protein were only available for 24 of the 41 samples, which yielded 144 spectra. The data were preprocessed as described in the Materials and Methods, although it is worthwhile noting that the spectra without numerical derivatization yielded better PLSR prediction results. These results are not included. The PLS-2 nonlinear iterative partial least-squares (NIPALS) algorithm was used as described.[6] The optimum number of principal components was determined by the leave-one-spectrum-out cross validation and the minimum total sum of squared prediction error. Note that the 6 replicates per sample were run at two different times for three sequential days of analysis, so the replicates characterize uncontrolled sources of variation (e.g., instrumental drift with time).

**Pooled-ANOVA PLS Regression.** The pooled-ANOVA can be applied to the PLS calibration to determine the contribution to the X-block (NIR spectra) of each Y-block property (concentration of moisture, fat, and protein). The procedure is quite simple. For each latent variable or component, the pooled sum of squares for the NIR block of the PLS calculation was apportioned by the squared values of the concentration loadings vector (usually designated as $\boldsymbol{q}$). This calculation allows the variation contributions of each property (i.e., moisture, fat, and protein concentration) to be attributed to the NIR spectra.

A PLS model comprises a set of components that span the covariance of the X- and Y-blocks of data. Prediction is accomplished by iteratively removing the contribution of each PLS component or latent variable to the X-block and adding the contribution to the Y-block for the number of components chosen in the model.

$$t_{i,j} = \boldsymbol{x_{i,j-1}} \boldsymbol{w_j} \tag{2}$$

for which $x_{i,j}$ is the NIR spectrum of object $i$ that has been centered with respect to the mean of the calibration set of data. The spectrum is modified for each iteration $j$ of the PLS calculation, and $\boldsymbol{w}_j$ is the $j$th PLS component. The contribution to the NIR spectrum is calculated as

$$\hat{\boldsymbol{x}}_{i,j} = t_{i,j} \boldsymbol{p_j} \tag{3}$$

for which $\hat{\boldsymbol{x}}_{i,j}$ is a component of the reconstructed NIR spectrum $i$ and $p_j$ is a row vector from the PLS regression for component $j$. This contribution is iteratively removed or peeled from the NIR spectrum as follows.

$$\boldsymbol{x_{i,j}} = \boldsymbol{x_{i,j-1}} - \hat{\mathbf{x}}_{i,j} \tag{4}$$

The properties are iteratively estimated as

$$\hat{\boldsymbol{y}}_{i,j} = \hat{\boldsymbol{y}}_{i,j-1} + t_{i,j} b_j \boldsymbol{q_j} \tag{5}$$

for $\hat{\boldsymbol{y}}_{i,0}$ is the average of the properties and the estimate is built up with respect to PLS component number. The $b_j$ is the inner relation, which can be considered a correlation coefficient between the X- and Y-blocks for each component. The property loadings $\boldsymbol{q}_j$ for component $j$ are a row vector.

The pooled sums of squares of the X-block or NIR spectra with respect to the properties of the Y-block or concentrations are calculated as follows:

$$\boldsymbol{ss_{x_{i,j}}} = \boldsymbol{q_j^2} \sum_{k=1}^{n} \hat{\mathrm{x}}_{i,j,k}{}^2 \tag{6}$$

The sum of squares for the reconstructed component is calculated across the $n$ variables of the spectrum or object $i$. The $\boldsymbol{ss}_{\boldsymbol{x}_{i,j}}$ is a row vector that contains the sums of squares of the X-block variance with respect to the PLS component $j$ and the properties for the calibration, in this case, the concentrations of moisture, fat, and protein.

$$\boldsymbol{SS_x} = \sum_{i=1}^{m} \sum_{j=1}^{r} \boldsymbol{ss_{x_{i,j}}} \tag{7}$$


dx.doi.org/10.1021/jf5013727 | J. Agric. Food Chem. 2014, 62, 8060−8067

**Table 2. Pooled-ANOVA of NIR Pseudo-Absorbance Data**

| treatment | df | SS | MS | F | *p*-value | RSS |
|---|---|---|---|---|---|---|
| milk class | 1 | 221 | 221 | 130 | $\ll 10^{-3}$ | 8.7% |
| day | 2 | 21 | 11 | 6.2 | $3 \times 10^{-3}$ | 0.8% |
| processing type | 2 | 223 | 111 | 65 | $\ll 10^{-3}$ | 8.8% |
| production site | 10 | 980 | 98.0 | 57 | $\ll 10^{-3}$ | 38.8% |
| sample | 37 | 665 | 18.0 | 10 | $\ll 10^{-3}$ | 26.3% |
| milk × processing | 2 | 108 | 54.2 | 31 | $\ll 10^{-3}$ | 4.3% |
| processing × day | 4 | 5 | 1 | 0.7 | 0.59 | 0.2% |
| milk × day | 2 | 2 | 1 | 0.7 | 0.51 | 0.1% |
| site × day | 20 | 53 | 2.7 | 1.5 | 0.07 | 2.1% |
| residual error | 144 | 247 | 1.7 | 9.8% | | |

The $ss_{x_{i,j}}$ is summed across the $m$ objects and $r$ PLS components that were used for calibration, and then the pooled-ANOVA is applied to the total $ss_x$ as described previously.

## RESULTS AND DISCUSSION

**Selection of Spectral Region.** The SNV corrected spectra, first derivative with SNV spectra, and variable loadings of the first principal component for both diffuse reflectance and pseudoabsorbance modes are given in Figure 1S of the Supporting Information. Figure 1 gives the variable loadings obtained from the diffuse reflectance spectra, which have two major water bands at 1340−1440 and 1800−1950 nm. The variable loadings obtained from the pseudoabsorbance spectra are given on the right. The water bands of these variable loadings are attenuated when compared to those of the diffuse reflectance spectra. However, the pseudoabsorbance calculation did not completely remove the moisture bands as will become apparent later in the subsequent results. The reference standards were only run every sixth analysis and did not account for any moisture in the milk powder but only for ambient moisture in the NIR beam path. There was no attempt to interpolate a reference spectrum for the spectra acquired between the two reference spectra. Thus, depending on the direction of the drift, the reference standards may have over- or under-corrected the sample pseudoabsorbance spectra.

**Pooled-ANOVA.** Table 2 reports the pooled-ANOVA results for the analysis of the NIR pseudoabsorbance data matrix comprising 38 samples (i.e., 225 spectra) each with 1850 variables (1700−2500 nm). The residuals matrix for each experimental factor and factor interaction were squared to provide the factor variance (see Supporting Information Appendix A). Numbers in bold designate cases associated with significant differences (i.e., less than $10^{-2}$ of a type I error). In other words, bold designees indicate if the average levels of the experimental factors came from the same distribution, which is the Null Hypothesis. The likelihood of obtaining this result would be equal to or less than the corresponding *p*-value. The relative sum of squares (RSS) gives the relative contribution of each factor with respect to the total sum of squares. The sample residuals account for 10% of the RSS as indicated by the residual error (bottom row) of Table 2. The sum of the pairwise factor interactions accounted for less than 7% of the RSS. Rows 6−9 of Table 2 list the interactions between pairs of factors.

At the 99% confidence level, there are significant differences for milk class, day of analysis, production site, process type, and samples (Table 2). It should be noted that pooled-ANOVA, and ANOVA in general, tests for a difference among the averages of each level. Thus, significant differences for factors reported in Table 2 do not indicate that all of these averages are different, but that at least one average of a level differs from the other averages. Further matrix calculations can provide information for specific levels. However, visual methods such as ANOVA-PCA are easier to interpret.

**ANOVA-PCA.** The submatrices used for the pooled-ANOVA calculations in the previous section were also used to compute reconstituted matrices for each factor prior to PCA (see Appendix A in the Supporting Information). The same experimental factors evaluated by pooled-ANOVA in Table 2 are described by ANOVA-PCA in the PCA scores and variable loadings given in Figure 2. However, pooled-ANOVA takes advantage of the power of the Central Limit Theorem to determine if the average spectra are varying, while ANOVA-PCA compares the separation of data points with respect to the individual spectra.

In the top row of Figure 2, the effect of milk class is clearly significant. Skim milk powder (SMP) is compared to nonfat dry milk (NFDM). The RSS reported in Table 2 for milk type accounted for 8.7% of the variation in the data set. The two milk types were significantly different (i.e., *p*-value $\ll 10^{-3}$), and this estimate underestimates the significance because the degrees of freedom from the 1850 NIR spectral variables are neglected.

The second row of Figure 2 gives plots for the effect of the day to day variation. In the score plots, the 95% confidence ellipses for the 3 days of the analysis all overlap with respect to the residual error. However, the third day of analysis, C, clearly has a different mean that is characterized by a shift with respect to the second principal component. The variable loadings for this component indicate that moisture peaks are primarily responsible for the difference. The pooled-ANOVA result (Table 2) is at a level of significance of 0.003, indicating that the averages are different even though the fraction of variance explained by the RSS is a relatively small 0.8%.

The third row corresponds to the three process types labeled as low (LH), medium (MH), and high (HH) heat. The medium and high temperature processes are more different from each other with the low temperature appearing between the two. This trend can be explained by the process differences that arise in milk condensation and dehydration. The pooled-ANOVA results indicate a RSS of 8.8% and similar *p*-value that was far below $10^{-3}$.

The fourth row corresponds to the production site's geographical location, which accounts for the largest source of variation with an RSS of 38.8% and a *p*-value also far less than $10^{-3}$. The score plots indicate that the production sites form nicely defined clusters in the data space.

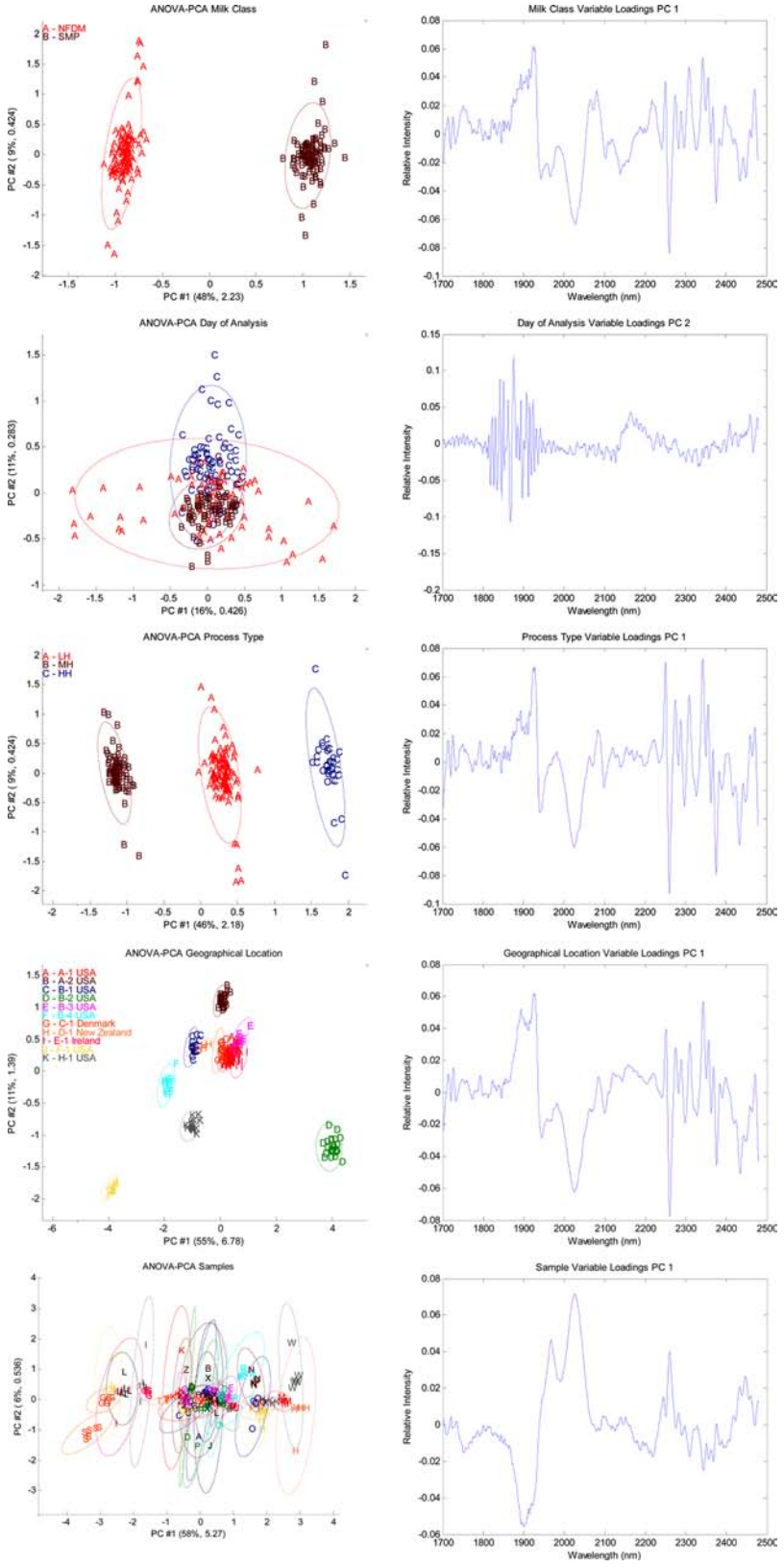


**Figure 2.** (Left) ANOVA-PCA score plots with 95% confidence ellipses. (Right) Corresponding variable loadings. (Row 1) Skim milk (SMP) and nonfat dry milk (NFDM). (Row 2) Day of analysis; for this case, the variable loading for the second principal component is plotted. (Row 3) Low, medium, and high processing temperatures. (Row 4) Production site of milk supplier. (Row 5) Thirty-eight samples.

Each sample was taken from a different lot of milk powders. The fifth row of Figure 2 corresponds to the individual sample level, and, according to its RSS, the samples contribute 26.3% of the variance in the data set, making it the second largest contributor. The sample scores that form tight clusters indicate that NIR spectroscopy of the dried milk powders has the


dx.doi.org/10.1021/jf5013727 | J. Agric. Food Chem. 2014, 62, 8060−8067

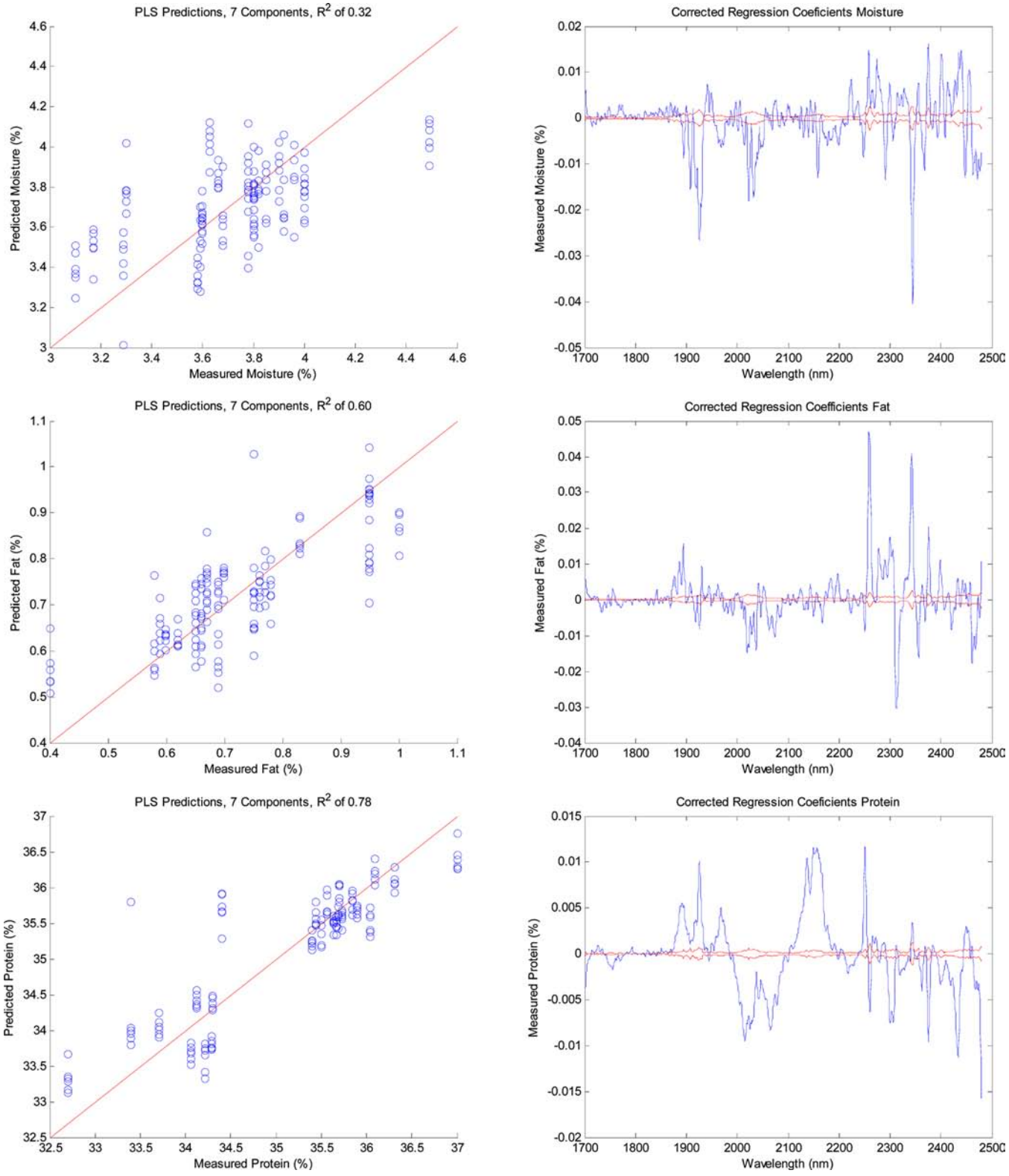


**Figure 3.** Partial least-squares regression cross-validation prediction results using seven latent variables (left). The corresponding corrected average regression coefficients and their 95% confidence intervals (right) for moisture (top), fat (middle), and protein (bottom).

potential to discriminate among the different lots of milk powders.

Interaction between factors was also examined; the figures are available in the Supporting Information (Figure 2S). However, not all interactions could be studied because the experimental design had confounded some of these factors. When plotting the interaction scores, the main effect averages were added back to the data as well as the interaction means for the ANOVA-PCA. The addition of the main effect averages to the interaction averages allows the interplay of factors to be displayed in Supporting Information Figure 2S. The top row/left side of Supporting Information Figure 2S gives the scores


dx.doi.org/10.1021/jf5013727 | J. Agric. Food Chem. 2014, 62, 8060−8067

for the interaction of process type with milk class. One can see that six subgroups are all resolved. On the right side of the top row, the variable loadings for the first principal component are given, which indicate the features of the NIR spectrum that are prominent for this interaction.

However, for the pooled-ANOVA results reported in Table 2, the main effect averages were not included in the sum of squares calculation. The RSS is smaller than those of the main effects with a value of 4.3%; yet this interaction is significant with a $p$-value far less than $10^{-3}$. This result is expected because the process type should affect the milk classes differently since the milk classes differ in chemical and physical composition. NIR spectrometry is affected by the powder morphology, particle size, and chemical composition, all of which may differ among the milk classes, processes, and production sites.

The interactions between milk class and process type with the day of analysis are illustrated by the ANOVA-PCA score plots in the second row of Supporting Information Figure 2S. The confidence intervals of the days are not resolved, although we can see the third day is shifted a bit off center. The respective RSS values for the interaction between day and milk class and between day and process type are 0.2% and 0.1%, respectively. For these cases, the pooled-ANOVA did not detect a significant difference among the means as reported in Table 2.

The bottom row of Supporting Information Figure 2S gives the ANOVA-PCA score plots of the interaction of production site with day of analysis. Because of the large number ($3 \times 11$) of labels for this interaction, the same set of scores is plotted with the day label (left) and the production site label (right). In Table 2, the corresponding RSS is 2.1%, which was not significant at a 95% level of confidence. For this interaction term, the $p$-value was 7%. This result occurs because different samples may have various interactions with moisture because of their varied chemical and physical compositions.

**Influence of Fat, Protein, and Moisture.** An earlier report by this team of investigators implicated the involvement of fats, proteins, and moisture as an influence on the sample variability.[1] Varimax rotations provided variable loadings that correlated with the bands of all three families of compounds. For the partial least-squares regression (PLSR) study, spectra from the 24 samples that had complete COA concentrations for moisture, fat, and protein were used. The concentrations were weight to weight percentages. No spectra from this set of samples were detected as outliers using the same method that was applied to the ANOVA-PCA, so 144 spectra (24 samples × 6 replicates) were available for calibration by PLS regression. Because the two replicates on each day of analysis were blocked with respect to time, a leave one spectrum out cross-validation was used for model building. Each replicate characterized variations with respect to time and sampling by the NIR spectrometer. The squared prediction errors were summed across the fat, moisture, and protein concentrations and plotted with respect to the number of latent variables used by the PLS model. A minimum total prediction error was obtained with seven latent variables or PLS components, so this model was used for the subsequent calculations and figures. Data are not shown.

The prediction results using cross validation of the seven-component PLS model are given in Figure 3. During the cross-validation procedure, each PLS model was converted to a linear set of regression coefficients. These regression coefficients were stored and used to calculate average regression coefficients with 95% confidence intervals that are also given in Figure 3. The coefficient of determination ($R^2$) values were calculated with respect to the cross-validated prediction results and are included with each figure along with a red reference line indicating ideal behavior.

Table 3 reports the pooled-ANOVA results derived from the PLS model. The sum of squares for the NIR (X-Block) are calculated for each component as described by eqs 2−7. From the PLS calibration, the contributions of each concentration can be calculated as a sum of squares for the NIR spectra. In addition, the residual sum of squares (i.e., variation that is not accounted for by the calibration model) can also be calculated for in the spectra. These sums of squares were totaled for the seven components to furnish the top half of Table 3.

**Table 3. Pooled-ANOVA Partial Least-Squares Regression Analysis**

| Near-Infrared Spectra Block | | | | | | | |
|---|---|---|---|---|---|---|---|
| treatment | df | SS | MS | F | $p$-value | | RSS |
| moisture | 6 | 438 | 72.7 | 52 | $\ll 10^{-3}$ | | 25.7% |
| fat | 6 | 178 | 29.7 | 21 | $\ll 10^{-3}$ | | 10.5% |
| protein | 6 | 897 | 149.5 | 107 | $\ll 10^{-3}$ | | 52.6% |
| residuals | 137 | 192 | 1.4 | | | | 11.2% |
| Concentration Block | | | | | | | |
| treatment | df | SS | MS | F | $p$-value | RMSEP | $R^2$ |
| moisture | 6 | 46 | 17.7 | 10.8 | $\ll 10^{-3}$ | 0.24% | 0.32 |
| residual | 137 | 97 | 0.7 | | | | |
| fat | 6 | 87 | 14.4 | 35.0 | $\ll 10^{-3}$ | 0.09% | 0.61 |
| residual | 137 | 97 | 0.4 | | | | |
| protein | 6 | 112 | 18.7 | 82.2 | $\ll 10^{-3}$ | 0.48% | 0.78 |
| residual | 137 | 97 | 0.2 | | | | |

The lower half of Table 3 was obtained from the moisture, fat, and protein concentration predictions using the leave-one-spectrum-out cross validation. The sum of squares of the regression was obtained by subtracting the sum of the squared errors from the sum of the squared mean-centered measured concentrations for moisture, fat, or protein.

Although the coefficients of variation ($R^2$) are not large, it is important to remember that the calibration did not comprise prepared standards over a wide range of concentrations; instead, the concentration ranges used for the calibration were those that were measured from each lot of milk powder, which happened to vary over a narrow range.

Note that, although the contribution to the NIR data for moisture is relatively large as compared to fat, the $R^2$ value of 0.32 is quite low. This trend indicates that the moisture bands in the spectra do not correlate well with the COA moisture concentrations. The samples were stored under ambient conditions, and the moisture content most likely varied during storage. In addition, the COA moisture concentration was measured for the lot of milk powder and not for the individual sample. Last, the range of moisture values was relatively small at 1.8−4.5%, which typically can result in smaller coefficients of determination. NIR spectrometry is sensitive to moisture, and variations of ambient moisture during the measurement may not have been sufficiently corrected by the reference spectrum. According to the RSS, moisture was responsible for one-quarter of the total variation of the NIR spectral data. However, it is important to remember that these data were obtained from a multinational study of many diverse milk powder samples, so the lack of correlation with the moisture concentrations could

be attributed to the different chemical and physical properties of this diverse set of samples.

Fat had the smallest contribution to the NIR data, but its $R^2$ of 0.61 is more than twice that of the moisture. The range of fat concentrations was 0.01−1.05%. The RSS of fat was 10.5%, which indicates that, although the concentration of fat was less than moisture, it still contributed a significant source of variation to the NIR spectra. Although fat is nonvolatile and fairly inert, it could also be affected by ambient storage; for example, lipid oxidation may alter the spectral profile.

Protein was the largest contributor to the variation of the NIR data and gave the best $R^2$ of 0.78. The COA protein concentration range was 32.7−37.0%. The results were encouraging when one considers the wide range of milk powder samples and that the concentration values were determined by lot and not by sample. Typically, calibration models would be devised from a single milk source across a controlled range of concentrations.

Supporting Information Figure 3S gives the production sites with respect to the predicted fat and protein concentrations. These predictions are from the cross-validation of the seven-component PLS regression model. This plot suggests that milk samples processed in the different production sites have different fat and protein concentrations. The 95% confidence ellipses indicate that some sites are statistically different.

In this study, the 38 samples analyzed by NIR showed statistically significant variability with respect to the day of analysis, production site, milk class, process type, and individual samples. NIR spectrometry is very sensitive to chemical composition and physical properties of milk powder products and is an excellent tool for judging the quality of product. The lot to lot variation was not studied. However, the individual samples were precisely determined, which indicates that for targeted or untargeted analysis of milk powders, the models would have to be specific for each sample or lot of milk. Perhaps a future study will examine the lot to lot variations of the milk powders.

Significant correlations were found with the COA concentration values even though some of the coefficients of determination $R^2$ indicated rather weak predictability of models. Many effects could be responsible for the weak PLS models. The range of concentrations was relatively narrow because the observed concentration range was used as opposed to using a standard range of concentrations that would presumably be wider. In addition, the concentrations of fat, moisture, and protein may have changed during storage of the samples. Because these concentrations are relative to the total weight, a change in any one component could also affect the concentration of the others; for example, the adsorption of moisture by the dried milk sample would lower its relative concentrations of protein and fat.

Pooled-ANOVA was combined with PLS regression for the first time. Although the PLS calibration models were not impressively accurate, the pooled-ANOVA applied to PLS regression models demonstrated that the correlated peaks of the NIR spectra were important contributors to the variances of the data set with the protein bands accounting for more than the majority and the moisture bands one-quarter of the total variation of the data set.

This study indicates that for targeted or untargeted analysis of adulterants in milk powders by near-infrared spectrometry, a global model will probably not succeed because the variations arising from milk class, process type, and production site were all significant. Instead localized models that are specific for milk class, process type, and production site would be expected to have a better opportunity for success. Furthermore, local standardization of moisture, fat, and protein would improve calibration models for these important properties. The significance of the variation with respect to the day of analysis indicates that a better approach for collecting reference spectra may be beneficial, especially with respect to controlling variations that arise from ambient moisture.

## ■ ASSOCIATED CONTENT

### Supporting Information

Implementation of pooled-ANOVA in Excel, and additional figures. This material is available free of charge via the Internet at http://pubs.acs.org.

## ■ AUTHOR INFORMATION

### Corresponding Authors

*Tel.: (301) 504-8569. E-mail: james.harnly@ars.usda.gov.
*Tel.: (740) 994-0265. E-mail: peter.harrington@ohio.edu.

### Notes

The authors declare no competing financial interest.

## ■ ACKNOWLEDGMENTS

Walter Hauck and Markus Lipp from USP are thanked for their valuable comments. One of the authors (JMH) acknowledges support or the Agricultural Research Service of the U.S. Department of Agriculture and the Office of Dietary Supplements of the National Institutes of Health.

## ■ REFERENCES

(1) Botros, L. L.; Jablonski, J.; Chang, C.; Bergana, M. M.; Wehling, P.; Harnly, J. M.; Downey, G.; Harrington, P.; Potts, A. R.; Moore, J. C. Exploring authentic skim and nonfat dry milk powder variance for the development of nontargeted adulterant detection methods using near-infrared spectroscopy and chemometrics. *J. Agric. Food Chem.* **2013**, *61*, 9810−9818.

(2) Kaiser, H. F. The Varimax criterion for analytic rotation in factor analysis. *Psychometrika* **1958**, *23*, 187−200.

(3) Harrington, P. D.; Vieira, N. E.; Espinoza, J.; Nien, J. K.; Romero, R.; Yergey, A. L. Analysis of variance-principal component analysis: A soft tool for proteomic discovery. *Anal. Chim. Acta* **2005**, *544*, 118−127.

(4) Luthria, D. L.; Lin, L. Z.; Robbins, R. J.; Finley, J. W.; Banuelos, G. S.; Harnly, J. M. Discriminating between cultivars and treatments of broccoli using mass spectral fingerprinting and analysis of variance-principal component analysis. *J. Agric. Food Chem.* **2008**, *56*, 9819−9827.

(5) Luthria, D. L.; Mukhopadhyay, S.; Robbins, R. J.; Finley, J. W.; Banuelos, G. S.; Harnly, J. A. UV spectral fingerprinting and analysis of variance-principal component analysis: a useful tool for characterizing sources of variance in plant materials. *J. Agric. Food Chem.* **2008**, *56*, 5457−5462.

(6) Geladi, P.; Kowalski, B. R. Partial least-squares regression: A tutorial. *Anal. Chim. Acta* **1986**, *185*, 1−17.

JOURNAL OF AGRICULTURAL AND FOOD CHEMISTRY

Article

pubs.acs.org/JAFC

# Determination of Saffron Quality by High-Performance Liquid Chromatography

M. Valle García-Rodríguez,[†] Jéssica Serrano-Díaz,[†,‡] Petros A. Tarantilis,[§] Horacio López-Córcoles,[∥] Manuel Carmona,[†,⊥] and Gonzalo L. Alonso*[,†]

[†]Cátedra de Química Agrícola, Escuela Técnica Superior de Ingenieros (ETSI) Agrónomos, Universidad de Castilla-La Mancha, Campus Universitario, 02071 Albacete, Spain

[‡]Department of Food Technology, Nutrition and Food Science, Regional Campus of International Excellence "Campus Mare Nostrum", Murcia University, CIBERobn, ISCIII, 30100 Murcia, Spain

[§]Laboratory of Chemistry, Department of Food Science and Human Nutrition, School of Food, Biotechnology and Development, Agricultural University of Athens, Iera Odos 75, Athens 11855, Greece

[∥]Instituto Técnico Agronómico Provincial (ITAP), S.A., Avenida Gregorio Arcos, s/n, 02006 Albacete, Spain

[⊥]Albacete Science and Technology Park, Paseo de la Innovación 1, 02006 Albacete, Spain

**ABSTRACT:** The aim of this work was to propose a high-performance liquid chromatography with diode array detection (HPLC−DAD) method for determining the three main compounds responsible for determining the quality of saffron (crocetin esters, picrocrocin, and safranal) by preparing an aqueous extract according to the ISO 3632 standard to solve the difficulty that this standard has for aroma and taste determination by ultraviolet−visible spectroscopy. Toward this aim, laboratory-isolated picrocrocin, a safranal standard with a purity of ≥88%, *trans*-crocetin di(β-D-gentiobiosyl) ester (*trans*-4-GG) and *trans*-crocetin (β-D-glucosyl)-(β-D-gentiobiosyl) ester (*trans*-3-Gg) standards, both with a purity of ≥99%, and 50 different saffron spice samples from Italy, Iran, Greece, and Spain were used in the intralaboratory validation of the HPLC method. The analytical method proposed was adequate in terms of linearity, selectivity, sensitivity, and accuracy for determining the three foremost parameters that define the quality of saffron using only a saffron solution prepared according to the ISO 3632 standard.

**KEYWORDS:** *Crocus sativus L., aqueous extract, trans-4-GG, trans-3-Gg, picrocrocin, safranal, HPLC−DAD*

## INTRODUCTION

Few spices are able to provide the combination of color, taste, and aroma to the foods and beverages to which they are added. The most popular of these is saffron.[1,2] To hydrophilic foods, saffron leads to a yellow color because of its high crocin content (also called crocetin esters, which are glycosylated carotenoids derived from crocetin), bitter taste because of picrocrocin, and pleasant and unmistakable aroma owing to safranal.

The first reference to crocin [crocetin di(β-gentiobiosyl) ester] was made in 1818 by Aschoff,[3] who gave it its name. Pfander et al.[4] were the first to isolate six glycosides of crocetin in saffron. In 1984, Speranza et al.[5] identified their *trans* and *cis* isomers by high-performance liquid chromatography with ultraviolet−visible spectroscopy (HPLC−UV−vis). Tarantilis et al.[6] identified a greater number of crocetin esters and their *trans* and *cis* isomers by high-performance liquid chromatography with diode array detection and mass spectrometry (HPLC−DAD−MS), and Carmona et al.[7] identified four more by HPLC−DAD−MS. Thus far, the quantification of crocetin esters by HPLC has been carried out without high precision,[8−10] and the use of commercial standards in calibration curves gives low correlation coefficients, owing to the phenomenon of aggregation that some authors have demonstrated that happens in highly concentrated aqueous solutions of crocetin esters.[11,12] The kinetics of individual crocetin ester degradation in aqueous extracts of saffron were studied by Sánchez et al.[8] to determine their stability.

Picrocrocin [4-(β-D-glucopyranosyloxy)-2,6,6-trimethyl-1-cyclohexene-1-carboxaldehyde] has been identified only in the genus *Crocus*, of which the only edible species is *Crocus sativus* L. For this reason, picrocrocin is a molecular marker of this spice that is able to give a unique taste that cannot be imitated from other spices or seasonings. This compound was isolated for the first time in the stigmas of *C. sativus* by Winterstein et al.[13] Its molecular structure was defined in 1934 by Kuhn et al.[14] Glycosidic compounds that are structurally related to picrocrocin have been identified. Tarantilis et al.[6] identified three glycosidic compounds in 1995; the Winterhalter group[15,16] recognized eight other glycosidic compounds between 1997 and 1998; and Carmona et al.[17] identified four more by HPLC−DAD−MS in 2006, which were found in considerably lower amounts than picrocrocin. The picrocrocin stability was determined by Sánchez et al.,[18] and picrocrocin is more stable than the crocetin esters.

More than 40 related compounds with a saffron aroma have been identified,[19−24] with the major aromatic compound being safranal (2,6,6-trimethyl-1,3-cyclohexadiene-1- carboxaldehyde). In the saffron with the highest quality in the world "Azafrán de La Mancha", safranal represents over 65% of the

Received: April 28, 2014
Revised: July 18, 2014
Accepted: July 30, 2014
Published: July 30, 2014

ACS Publications © 2014 American Chemical Society



dx.doi.org/10.1021/jf5019356 | J. Agric. Food Chem. 2014, 62, 8068−8074

total aroma, as determined by gas chromatography (GC).[25] Safranal is a nonpolar compound, but its solubility in water has not been studied. Different analytical techniques have been developed for its quantification, such as gas chromatography−olfactometry (GC−O),[26] gas chromatography/mass spectrometry (GC/MS),[27] high-performance liquid chromatography (HPLC),[28] or ultrasound-assisted extraction/ultraviolet−visible spectroscopy (USAE/UV−vis).[29] The results obtained are quite different between these various methods.

The first references related to the use of saffron regarded their therapeutic properties.[30] In the first century, Dioscórides described a great number of therapeutic properties;[30] in the tenth century, new properties were described by Avicena.[31] The therapeutic uses of saffron declined greatly over the past decade. However, saffron has received much attention by scientists in recent years.[32] Most of these properties are ascribed to the *trans* isomers[33−35] and safranal.[36−38]

The quality of saffron in international commercial agreements is determined according to the ISO 3632[39] standard, which classifies it into three categories depending upon their physical and chemical characteristics. The three foremost parameters used to define the quality of saffron are color, taste, and aroma.[17,28] These parameters are determined by UV−vis based on the study by Corradi et al.,[40] that is, the $E^{1\%}_{1\ cm}$ at 440 nm (coloring strength), the $E^{1\%}_{1\ cm}$ at 257 nm (the wavelength of picrocrocin maximum absorbance), and the $E^{1\%}_{1\ cm}$ at 330 nm (the wavelength of safranal maximum absorbance). While the $E^{1\%}_{1\ cm}$ at 440 nm is directly correlated with the ability to transmit color to foodstuffs to which it is added, the $E^{1\%}_{1\ cm}$ at 257 nm and $E^{1\%}_{1\ cm}$ at 330 nm do not give an accurate measurement of picrocrocin and safranal because the *trans* isomers of the crocetin esters also absorb at 250 nm and the *cis* isomers of the crocetin esters absorb at 250 and 330 nm as well, causing interference in the measurements.[7,28] Moreover, the UV−vis spectrophotometry does not provide the ratio between the *trans* and *cis* isomers of crocetin esters, which is important for their therapeutic use.[33−35]

Therefore, the purpose of this work was to validate a HPLC method for the independent determination of the crocetin esters, picrocrocin, and safranal using only a saffron solution prepared according to the ISO 3632.[39]

## MATERIALS AND METHODS

**Samples and Reagents.** *Samples.* A total of 50 samples of saffron from different countries were used during the same year of their harvest. These were obtained directly from the producers and packers with a guarantee of their origin and freedom from fraud. The samples were from Italy, Iran, Greece, and Spain. All of the samples were of Category I according to ISO 3632.[39]

*Standards.* Safranal with a purity of ≥88% was obtained from Sigma-Aldrich (Madrid, Spain), and crocetin esters, *trans*-crocetin di(β-D-gentiobiosyl) ester (*trans*-4-GG) and *trans*-crocetin (β-D-glucosyl)-(β-D-gentiobiosyl) ester (*trans*-3-Gg), with a purity of ≥99%, were obtained from Phytolab GmbH & Co. KG (Vestenbergsgreuth, Bavaria, Germany).

*Solvents.* Acetonitrile was obtained from Panreac (Barcelona, Spain), while water was purified through a Milli-Q system (Millipore, Bedford, MA).

**Safranal Water Solubility.** To prepare a saturated safranal aqueous solution, increasing aliquots of safranal standard were added to a known volume of water until it was observed that the aqueous solution was saturated with safranal. A volume of 20 μL of the safranal standard in 10 mL of Milli-Q water was enough to obtain a saturated safranal aqueous solution. This solution was stirred using a magnetic stir bar at 1000 rpm for 1 h while being kept away from light. Then, it was allowed to stand to separate the aqueous phase from the safranal, with the saturated aqueous solution of safranal on top of the flask. An aliquot of this saturated solution was taken, *s*, and five dilutions were carried out: *s*/2, *s*/4, *s*/8, *s*/16, and *s*/32. These were then analyzed by UV−vis. The water solubility was calculated as the mean of the concentration values at which the absorbance obeyed the Lambert−Beer law. These analyses were carried out in triplicate at 20 ± 2 °C.

The safranal standard solutions were monitored by scanning from 200 to 400 nm using a PerkinElmer Lambda 25 spectrophotometer (Norwalk, CT) with UV WinLab 2.85.04 software (PerkinElmer). Their absorbance was determined at 330 nm. For the safranal quantification, two series of safranal standard solutions in water with concentrations of 3, 10, 20, 30, and 32 mg/L were prepared and analyzed in duplicate by UV−vis. A calibration curve was constructed for the safranal concentration, *c* (mg/L) as a function of its absorbance *a*, at 440 nm with the equation $c = 22.899a - 0.3027$ and a $R$ value = 0.999.

**Saffron Extract Preparation.** The saffron aqueous extracts were prepared according to ISO 3632.[39] A total of 500 mg of powdered saffron, previously passed through a sieve of 0.5 mm pore diameter, was placed in a 1 L volumetric flask, and 900 mL of Milli-Q water as added. The solution was stirred using a magnetic stir bar at 1000 rpm for 1 h while being kept away from light. The flask was filled to the 1 L mark, and the solution was homogenized through agitation. The solution was filtered through a filter made of hydrophilic polytetrafluoroethylene (PTFE) with a pore size of 0.45 μm (Millipore, Bedford, MA). It was then transferred into a vial for HPLC−DAD analysis. The saffron extraction was checked by doing a second extraction of the vegetable material obtained by filtration of the first extraction of three different saffron extracts prepared according to ISO 3632.[39]

**HPLC−DAD Analysis.** A total of 20 μL of each sample (saffron aqueous extracts) were injected into an Agilent 1200 HPLC chromatograph (Palo Alto, CA) equipped with a 150 × 4.6 mm inner diameter, 5 μm Phenomenex (Le Pecq Cedex, France) Luna $C_{18}$ column that was equilibrated at 30 °C. The eluents were water (A) and acetonitrile (B) with the following gradient: 20% B, 0−5 min; 20−80% B, 5−15 min; and 80% B, 15−20 min. The flow rate was 0.8 mL/min. The DAD detector (Hewlett-Packard, Waldbronn, Germany) was set at 250, 330, and 440 nm for picrocrocin, safranal, and crocetin ester detection, respectively. All of the analyses were performed in duplicate, and two measurements were taken for each replicate.

The identifications of *trans*-4-GG and *trans*-3-Gg were carried out using the UV−vis spectrum, and the retention time was carried out by the HPLC−DAD method at 440 nm and the parameter %III/II[41] of their standards. Their quantification was based on calibration curves.

With the aim of avoiding the phenomenon of aggregation that some authors have described in carotenoids, such as crocetin,[12,42] *trans*-4-GG, and *trans*-3-Gg standard solutions, 10, 20, 30, 40, 50, 60 and 70% acetonitrile/water (v/v) solutions were prepared and analyzed in duplicate by UV−vis at 440 nm.

Two series of *trans*-4-GG standard solutions in water and two other series in 50% acetonitrile/water (v/v) with concentrations of 100, 50, 25, 12.5, 6.25, 3.125, 1.6, and 0.8 mg/L were prepared and analyzed in duplicate by HPLC−DAD.

Two series of *trans*-3-Gg standard solutions in water and two other series in 50% acetonitrile/water (v/v) with concentrations of 50, 25, 12.5, 6.25, 3.125, 1.6, and 0.8 mg/L concentration were prepared and analyzed in duplicate by HPLC−DAD.

Isomeric standards for the *cis*-crocetin esters are not available on the market; therefore, they were identified using the UV−vis spectrum. The retention time by HPLC−DAD−MS at 440 nm was determined by this group[7] and in other works by the parameter %III/II.[41] Isomeric *cis*-crocetin ester quantification was performed by the molecular coefficient absorbance value (63 350), obtained by Speranza et al.[5]

Picrocrocin identification was carried out by combination of its UV−vis spectrum and its retention time by HPLC−DAD at 250 nm. For its quantification, picrocrocin was isolated as described by Sánchez et al.[8] Two series of isolated picrocrocin solutions in water from 2 to 315 mg/L were prepared and analyzed in duplicate by HPLC−DAD.


dx.doi.org/10.1021/jf5019356 | J. Agric. Food Chem. 2014, 62, 8068−8074

Safranal identification was carried out using the UV−vis spectrum and the retention time of the safranal standard by HPLC−DAD at 330 nm. Two series of safranal standard solutions in water with concentrations of 4, 2, 1, 0.5, 0.25, 0.125, 0.06, and 0.03 mg/L were prepared and analyzed in duplicate by HPLC−DAD.

**Ultrasound-Assisted Extraction Followed by Gas Chromatography/Mass Spectrometry (USAE/GC/MS).** Safranal determination by USAE/GC/MS was carried out as described by Maggi et al.[27] USAE was performed in a Super RK 255H ultrasound water bath (Sonorex, Berlin, Germany) at a fixed frequency of 35 kHz. The temperature of the sonicated water bath was 25 °C. The sample flask was charged with 4 g of saffron. The solvent system extractant was 40 mL of diethyl ether. Each saffron sample was sonicated twice for 15 min (two fractions per saffron sample). For each sonication, a new volume of the solvent system extractant was added to the sample flask. The organic extract (80 mL) was concentrated using a Laborata 4000 efficient rotary evaporator (Heidolph Instruments GmbH & Co. KG, Schwabach, Germany). The volume of the final aromatic extract in diethyl ether was 4 mL. The collected diethyl ether was analyzed by GC to check if there was a loss of saffron volatiles during the evaporation procedure, but no saffron volatiles were detected. A HP 5890 series II chromatograph (Hewlett-Packard, Palo Alto, CA) equipped with a HP 5972 mass-selective detector in electron impact mode (70 eV) and a HP-5 MSM capillary column (30 m, 0.25 mm inner diameter, and 0.25 $\mu$m film thickness) with helium as the carrier gas at a flow rate of 1 mL/min was used for the analysis of safranal. The column temperature was initially held for 3 min at 50 °C, then increased to 180 °C at a rate of 3 °C $min^{-1}$, and finally increased to 250 °C at a rate of 15 °C $min^{-1}$. The injector and detector temperatures were set at 200 and 290 °C, respectively. Aliquots of 1 $\mu$L were manually injected in the splitless mode. For the safranal quantification, the external standard method was applied. The calibration curve was established for the series of safranal standard solutions in diethyl ether, with eq 1.

$$\text{mg of safranal/kg of saffron} = 86.6\text{area}_{\text{safranal}} \quad (R = 0.999) \qquad (1)$$

**Analytical Method Validation.** An intralaboratory method validation was carried out according to the Eurachem guideline.[43] For the linearity study, calibration graphs were performed by injecting standard solutions of saffron components (*trans*-4-GG, *trans*-3-Gg, picrocrocin, and safranal) at different concentrations. Each level of concentration was analyzed in duplicate, and two measurements for each one were carried out, with a total of four replicates.

The selectivity was determined by comparing the chromatograms obtained from the saffron samples to those of the standard solutions analyzed by HPLC−DAD.

The sensitivity of the method was determined with regard to the limit of detection (LOD) and limit of quantification (LOQ), comparing the height of a sample peak and the height of a noise peak. The LOD was reached at a signal-to-noise ratio greater than 3, and the LOQ was reached at a signal-to-noise ratio greater than 10.[44] The detection and quantification limits were determined by the empirical examination of the chromatograms from 50 saffron samples.

The accuracy of the method was evaluated with the 50 samples of saffron from different countries. Each sample was analyzed in duplicate, and two measurements were also taken for each replicate. The standard deviation (square root of the arithmetic mean of the variances) was calculated to obtain the repeatability [percent relative standard deviation (% RSD)]. The standard deviation multiplied by the square root of 3 was taken as the reproducibility value if this value was higher than the repeatability. If not, this last value was also taken as the reproducibility.[45]

## RESULTS AND DISCUSSION

**Safranal Water Solubility.** Saffron contains metabolites of different polarity because crocetin esters and picrocrocin are highly water-soluble polar compounds and safranal is a nonpolar constituent that has low solubility in polar solvents. The solubility of safranal in water has not been determined previously.

The water solubility of safranal was calculated from the saturated safranal aqueous solutions and was found to be 673.07 ± 0.01 mg/L at 20 ± 2 °C. An aqueous extract prepared according to ISO 3632[39] contains 500 mg of saffron dissolved in 1 L of water, and its safranal content will be less than the solubility (673.07 mg/L); hence, safranal will be completely dissolved. This result suggests that a saffron aqueous extract according to ISO 3632[39] could be used for safranal determination by HPLC, with the same solution used for determining the crocetin esters and picrocrocin. GC−O,[26] GC/MS,[27] HPLC,[28] or USAE/UV−vis[29] have been used to quantify safranal, with the results between these methods being quite different. HPLC is considered the most efficient analytical technique for the analysis of sensitive compounds in complex extracts of natural products.[46] Some authors have used HPLC for determining safranal,[47−49] but these authors carried out the extraction with organic solvents, such as ethanol or methanol, because of the nonpolar character of safranal and the ignorance of its water solubility.

**Calibration Graphs.** Table 1 shows the calibration curves of the saffron components (*trans*-4-GG, *trans*-3-Gg, picrocrocin, and safranal) calculated by the least-squares method.

**Table 1. Linearity Data for Analysis by HPLC−DAD of *trans*-4-GG, *trans*-3-Gg, Picrocrocin, and Safranal**

| | linear range of concentration (mg/L) | slope | intercept | correlation coefficient ($R^2$) |
|---|---|---|---|---|
| *trans*-4-GG | 0.8−100 | 0.0094 | 2.4861 | 0.976 |
| *trans*-3-Gg | 0.8−50 | 0.0079 | 0.6682 | 0.996 |
| picrocrocin | 2−315 | 0.0290 | 0.5194 | 0.999 |
| safranal | 0.03−4 | 0.0323 | 0.0510 | 0.998 |

The absorbance at 440 nm of the *trans*-4-GG and *trans*-3-Gg standard solutions at different percentages of acetonitrile/water (v/v) increased until a ratio of 40% acetonitrile/water (v/v). From a ratio of 50% acetonitrile/water (v/v) and greater, the absorbance at 440 nm of the *trans*-4-GG and *trans*-3-Gg standard solutions remained stable. This result suggests that, in highly concentrated aqueous solutions of *trans*-4-GG and *trans*-3-Gg standard in 40−50% acetonitrile/water (v/v) or greater, molecular aggregation does not occur.

The calibration curves of *trans*-4-GG and *trans*-3-Gg in water gave correlation coefficients lower than those of the calibration curves of *trans*-4-GG and *trans*-3-Gg in 50% acetonitrile/water (v/v), probably because of the phenomenon of aggregation;[12,42] hence, the calibration curves in 50% acetonitrile/water (v/v) were used. The chromatographic purity of the *trans*-4-GG was 99.43%. The calibration curve for the concentration of *trans*-4-GG, $d$ (mg/L), as a function of its HPLC peak area, $b$, exhibited good linear regression in the range from 0.8 to 50 mg/L with the equation $d = 0.0075b - 0.008$ and a $R$ value = 0.999 for a total of seven data points. The calibration curve of the *trans*-3-Gg concentration, $f$ (mg/L), as a function of its HPLC peak area, $g$, showed good linear regression in the range from 0.8 to 25 mg/L with the equation $f = 0.0071g - 0.0047$ and a $R$ value = 0.999 for a total of six data points. Its chromatographic purity was 99.19%.

The molecular coefficient absorbance values for *trans*-4-GG and *trans*-3-Gg in 50% acetonitrile/water (v/v) were 106


dx.doi.org/10.1021/jf5019356 | J. Agric. Food Chem. 2014, 62, 8068−8074

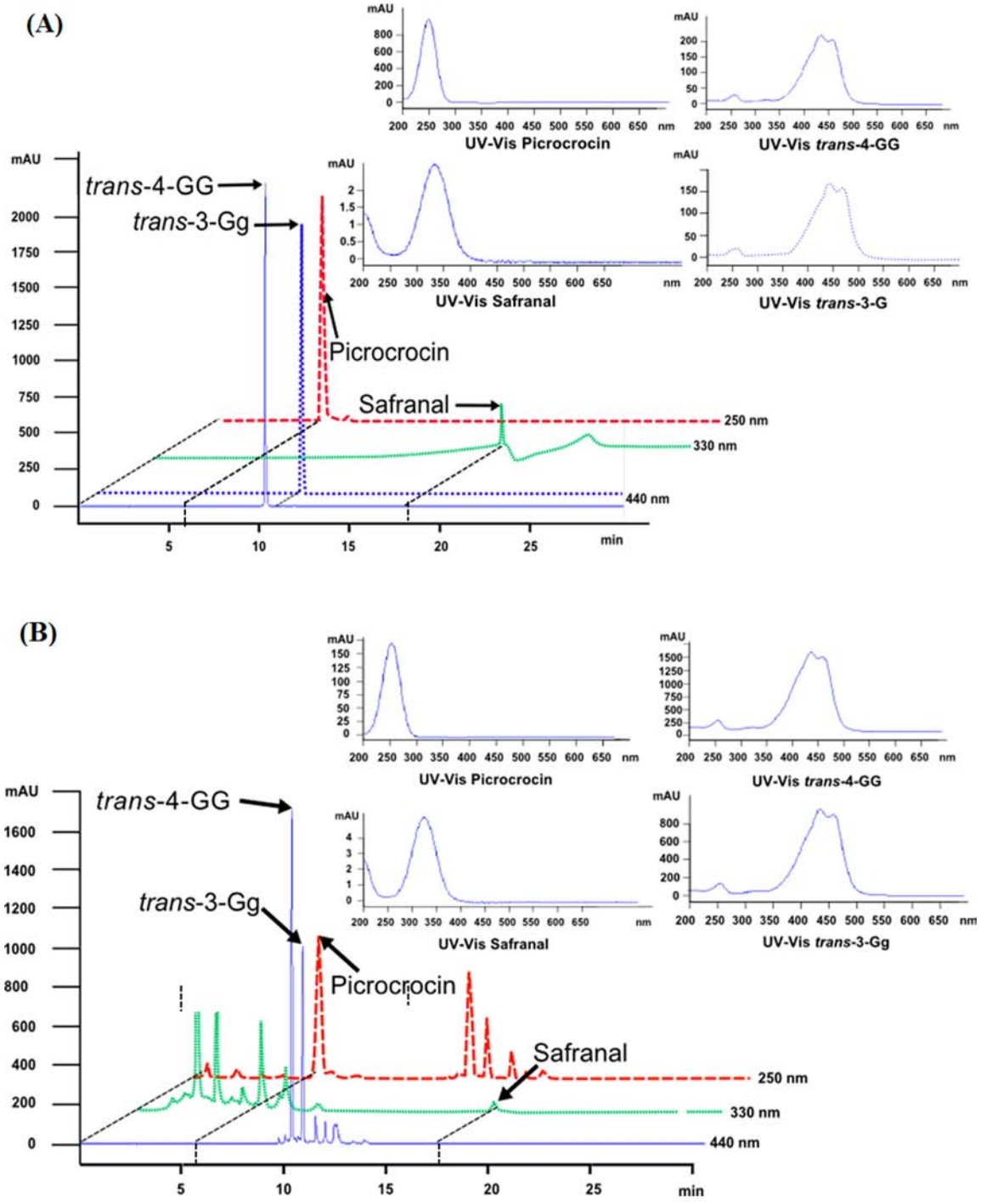


**Figure 1.** (A) Chromatograms of the commercial *trans*-4-GG (440 nm), *trans*-3-Gg (440 nm), and safranal (330 nm) standards and the laboratory-isolated picrocrocina (250 nm) and their UV−vis spectrum. (B) Chromatograms of the saffron sample (440, 330, and 250 nm) and their UV−vis spectrum.

922.75 and 92 781.76 $M^{-1}$ $cm^{-1}$ (440 nm), respectively, which were close to the values obtained by other authors for *trans*-4-GG: 89 000 $M^{-1}$ $cm^{-1}$,[5] 132 200 $M^{-1}$ $cm^{-1}$,[50] 133 750 $M^{-1}$ $cm^{-1}$,[51] and 133 500 $M^{-1}$ $cm^{-1}$;[52] these differences may be due to the use of different solvents. The quantification of the *cis* isomers was based on eq 2

$$C_{cis} = \left(m_{trans} \times \frac{\epsilon cis}{\epsilon trans}\right)\text{area}_{cis} + \left(n_{trans} \times \frac{\epsilon cis}{\epsilon trans}\right) \quad (2)$$

where $C_{cis}$ is the concentration of the *cis*-crocetin esters in mg/L, $m_{trans}$ is the slope of the *trans*-crocetin ester, $\epsilon cis/\epsilon trans$ is the ratio *cis*/*trans* obtained by Speranza et al.,[5] $\text{area}_{cis}$ is the *cis*-crocetin ester peak area, and $n_{trans}$ is the intercept of the *trans*-crocetin ester.

The calibration curve of the picrocrocin concentration, $j$ (mg/L), as a function of the picrocrocin peak area, $k$, showed good linear regression in the range from 2 to 315 mg/L with the equation $j = 0.0290k + 0.5194$ and a $R$ value = 0.999 for a total of six data points. Its chromatographic purity was 96%.


dx.doi.org/10.1021/jf5019356 | J. Agric. Food Chem. 2014, 62, 8068−8074

The chromatographic purity of safranal was 92.99%. The calibration curve of the safranal concentration, $h$ (mg/L), as a function of the peak area for safranal, $i$, revealed good linear regression in the range from 0.03 to 4 mg/L with the equation $h = 0.0323i + 0.051$ and a $R$ value = 0.998 for a total of eight data points.

**Saffron Extraction Conditions.** Saffron extraction was carried out according to ISO 3632.[39] Other authors[40] showed that this method is suitable. In this work, these extraction conditions were checked again, and the results showed that the coloring strength in the second extraction was less than 2%; therefore, it is an efficient and eco-friendly extraction method.

**HPLC−DAD Conditions.** For the HPLC method, we relied on the method proposed by the identification and quantification of the crocetin esters and picrocrocin.[8,53] This method had not been validated previously. For the crocetin ester quantification, an approximate equation was used[8,53] on the basis of the molecular weight of the crocetin ester, the coloring strength of the sample determined by UV−vis according to ISO 3632,[39] the percentage peak area of the crocetin ester by HPLC−DAD at 440 nm, and the molecular coefficient absorbance value determined by Speranza et al.[5] In this work, the quantification of the crocetin esters was carried out using the calibration curves of the standards of *trans*-4-GG and *trans*-3-Gg. Figure 2 represents the comparison of the *trans*-4-GG and *trans*-3-Gg contents, respectively, obtained for 50 saffron samples using the approximate equation[8] and their respective calibration curves. Pearson's correlation ($r$) was 0.953 for *trans*-4-GG and 0.766 for *trans*-3-Gg; thus, in both cases, there was a positive correlation between both methods. The *trans*-3-Gg correlation is lower, possibly because of the use in the approximate equation of the molecular coefficient absorbance value calculated by Speranza et al.[5] for *trans*-4-GG. In this work, we have demonstrated that there is a difference between the molecular absorbance coefficients for *trans*-4-GG and *trans*-3-Gg.

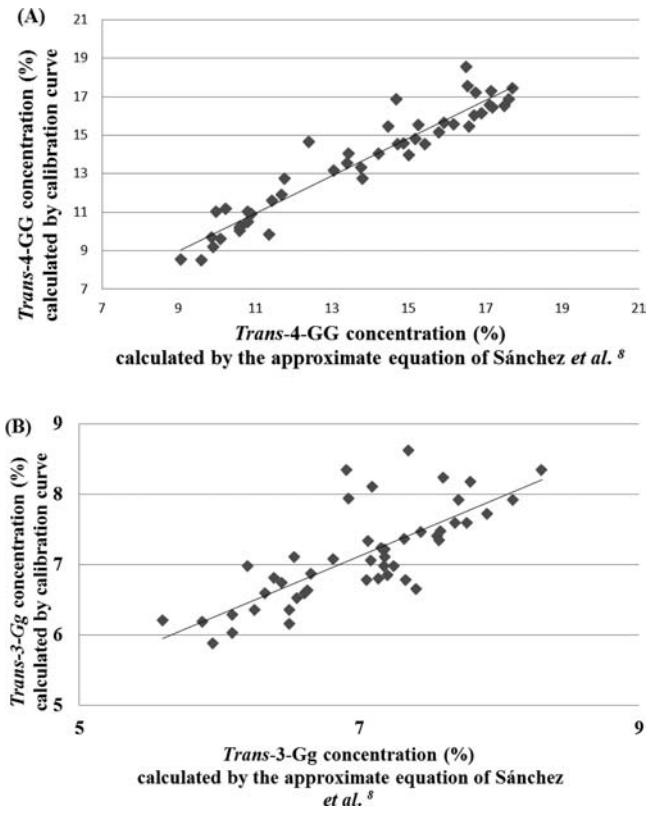


**Figure 2.** Graphical representation of the (A) *trans*-4-GG and (B) *trans*-3-Gg concentrations calculated by the approximate equation of Sánchez et al.[8] versus the (A) *trans*-4-GG and (B) *trans*-3-Gg concentrations calculated by the calibration curve for 50 saffron samples.

In summary, 50 saffron samples were analyzed by HPLC. The values obtained ranged from 182.648 to 82.827 g of *trans*-4-GG/kg of saffron, from 84.093 to 58.819 g of *trans*-3-Gg/kg of saffron, from 73.501 to 36.802 g of picrocrocin/kg of saffron, and from 1.142 to 4.346 g of safranal/kg of saffron.

The evaluation of the method, described in terms of its linearity, selectivity, sensitivity, and accuracy, showed that it was adequate for our objectives. In Table 1, we can see the linearity of the proposed method by means of the calibration graphs for the saffron components *trans*-4-GG, *trans*-3-Gg, picrocrocin, and safranal. The excellent linearity of this HPLC method is demonstrated by taking into account that the correlation coefficients were higher than 0.99 in the majority of the cases.

The proposed method showed a good selectivity because the retention times of their corresponding peaks were practically the same for the standards and the saffron samples analyzed (Figure 1).

The values of the detection and quantification limits, calculated as the concentration, gave a peak height 3 or 10 times the signal-to-noise ratio, as shown in Table 2.

The accuracy of the experimental procedure was also evaluated by studying the reproducibility and repeatability (% RSD). To consider the reproducibility of a method to be acceptable, its value should be lower than 20%. As seen in the results, summarized in Table 2, this parameter ranged from 0.06% (safranal) to 3.33% (*trans*-3-Gg). The same limit (20%) was taken to represent good repeatability, which, in this case, ranged from 0.04% (safranal) to 1.93% (*trans*-3-Gg). Therefore, the method proposed showed very good repeatability and reproducibility parameters.

**Comparison of HPLC−DAD and USAE/GC/MS Methods for Determining Safranal.** The safranal content of the 50 saffron samples was determined by USAE/GC/MS and HPLC−DAD from an aqueous extract to compare the results obtained with both analytical techniques. USAE/GC/MS is a method that has already been validated and published. The values obtained with this method were from 2.367 to 4.945 g of safranal/kg of saffron. The same sample analyzed by HPLC from a saffron aqueous extract gave values from 1.142 to 4.346 g of safranal/kg of saffron. The graph shown in Figure 3 represents the comparison of the safranal content obtained for the 50 saffron samples using HPLC−DAD and USAE/GC/MS. Pearson's correlation coefficient ($r$) was 0.788, showing a positive correlation between both methods.

In conclusion, the proposed HPLC−DAD method allows for the quantification of the three main compounds of saffron in an easy and fast way, using only a water solution,[39] with good linearity, selectivity, sensitivity, and accuracy. This methodology is adequate for determining the three foremost parameters that define the quality of saffron by preparing an aqueous extract according to ISO 3632.[39] Because HPLC−DAD is common in laboratories certified for the quality control of saffron, this method could even be included in the present ISO 3632.[39]

Table 2. Precision of the Experimental Procedure for Analysis by HPLC−DAD of *trans*-4-GG, *trans*-3-Gg, Picrocrocin, and Safranal ($n$ = 4)

| | LOD (g/kg of saffron) | LOQ (g/kg of saffron) | reproducibility (%) | RSD (%) |
|---|---|---|---|---|
| *trans*-4-GG | 0.33 | 0.95 | 3.07 | 1.77 |
| *trans*-3-Gg | 0.38 | 1.02 | 3.33 | 1.93 |
| picrocrocin | 0.60 | 1.01 | 1.34 | 0.77 |
| safranal | 0.105 | 0.28 | 0.06 | 0.04 |

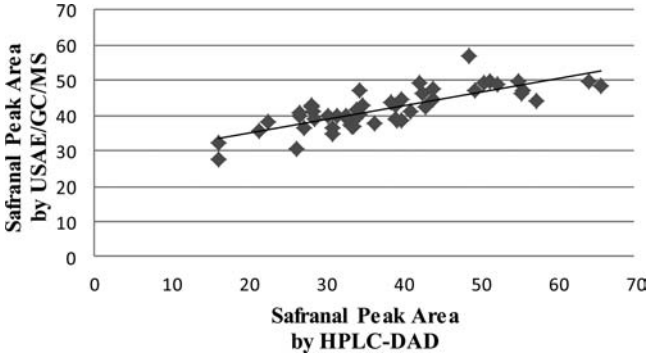


Figure 3. Graphical representation of the safranal content obtained by HPLC−DAD versus the safranal content obtained by USAE/GC/MS for 50 saffron samples.

## AUTHOR INFORMATION

### Corresponding Author

*Telephone: +34-967-599310. Fax: +34-967-599238. E-mail: gonzalo.alonso@uclm.es.

### Funding

The authors thank the Verdú Cantó Saffron Spain S.L. Company (Novelda, Spain) for this collaboration.

### Notes

The authors declare no competing financial interest.

## ACKNOWLEDGMENTS

The authors thank Marco A. García for technical assistance.

## REFERENCES

(1) Peter, K. V. *Handbook of Herbs and Spices*, 2nd ed.; Peter, K. V., Ed.; Woodhead Publishing: Cambridge, U.K., 2012; Vol. *1*, pp 449−491.

(2) Franco Martínez, T. *Manual para Especias*; AMV Ediciones: Madrid, Spain, 2013.

(3) Aschoff, S. Beiträge sur kenntnis des safrans. *Berl. Jb. Pharm.* **1818**, *19*, 142−157.

(4) Pfander, H.; Schurtenberger, H. Bisynthesis of $C_{20}$-carotenoids in *Crocus sativus* L. *Phytochemistry* **1982**, *21* (5), 1039−1042.

(5) Speranza, G.; Dada, G.; Manitto, P.; Monti, D.; Grammatica, P. 13-*cis*-Crocin: A new crocinoid of saffron. *Gazz. Chim. Ital.* **1984**, *114*, 189−192.

(6) Tarantilis, P. A.; Tsoupras, G.; Polissiou, M. Determination of saffron (*Crocus sativus* L.) components in crude plant extract using high-performance liquid chromatography−UV−visible photodiode-array detection−mass spectrometry. *J. Chromatogr. A* **1995**, *699*, 107−118.

(7) Carmona, M.; Zalacain, A.; Sanchez, A. M.; Novella, J. L.; Alonso, G. L. Crocetin esters, picrocrocin and its related compounds present in *Crocus sativus* stigmas and *Gardenia jasminoides* fruits. Tentative identification of seven new compounds by LC−ESI−MS. *J. Agric. Food Chem.* **2006**, *54*, 973−979.

(8) Sánchez, A. M.; Carmona, M.; Ordoudi, S. A.; Tsimidou, M. Z.; Alonso, G. L. Kinetics of individual crocetin ester degradation in aqueous extracts of saffron (*Crocus sativus* L.) upon thermal treatment in the dark. *J. Agric. Food Chem.* **2008**, *56*, 1627−1637.

(9) Ordoudi, S. A.; De Los Mozos Pascual, M.; Tsimidou, M. Z. On the quality control of traded saffron by means of transmission Fourier-transform mid-infrared (FT-MIR) spectroscopy and chemometrics. *Food Chem.* **2014**, *150*, 414−421.

(10) Anastasaki, E. G.; Kanakis, C. D.; Pappas, C.; Maggi, L.; Zalacain, A.; Carmona, M.; Alonso, G. L.; Polissiou, M. G. Quantification of crocetin esters in saffron (*Crocus sativus* L.) using Raman spectroscopy and chemometrics. *J. Agric. Food Chem.* **2010**, *58*, 6011−6017.

(11) Breukers, S.; Opstad, C. L.; Sliwka, H. R.; Partali, V. Hydrophilic carotenoids: Surface properties and aggregation behavior of the potassium salt of the highly unsaturated diacid norbixin. *Helv. Chim. Acta* **2009**, *92*, 1741−1747.

(12) Serrano-Díaz, J.; Sánchez, A. M.; Maggi, L.; Carmona, M.; Alonso, G. L. Synergic effect of water-soluble components on the coloring strength of saffron spice. *J. Food Compos. Anal.* **2011**, *24*, 873−879.

(13) Winterstein, E.; Teleczky, J. Constituents of the saffron. I. Pricrocrocin. *Helv. Chim. Acta* **1922**, *5*, 376−400.

(14) Kuhn, R.; Winterstein, E. Die dihydroverbindung der isomeren bixine und die elektronen-konfiguration der polyene. *Ber. Deustsch. Chem. Ges.* **1934**, *67*, 344−347.

(15) Straubinger, M.; Jezussek, M.; Waibel, R.; Winterhalter, P. Novel glyeosidic constituents from saffron. *J. Agric. Food Chem.* **1997**, *45*, 1678−1681.

(16) Straubinger, M.; Bau, B.; Eckstein, S.; Fink, M.; Winterhalter, P. Identification of novel glycosidic aroma precursors in saffron (*Crocus sativus* L.). *J. Agric. Food Chem.* **1998**, *46*, 3238−3243.

(17) Carmona, M.; Zalacain, A.; Alonso, G. L. *The Chemical Composition of Saffron: Color, Taste and Aroma*; Ed.ial Bomarzo S.L.: Albacete, Spain, 2006.

(18) Sánchez, A. M.; Carmona, M.; Jarén-Galán, M.; Mínguez Mosquera, M. I.; Alonso, G. L. Picrocrocin kinetics in aqueous saffron spice extracts (*Crocus sativus* L.) upon thermal treatment. *J. Agric. Food Chem.* **2011**, *59*, 249−255.

(19) Zarghami, N. S.; Heinz, D. E. Monoterpene aldehydes and isophoronerelated compounds of saffron. *Phytochemistry* **1971**, *10*, 2755−2761.

(20) Zarghami, N. S.; Heinz, D. E. The volatile constituents of saffron (*Crocus sativus* L.). *Lebensm.-Wiss. Technol.* **1971**, *4*, 43−45.

(21) Rödel, W.; Petrizka, M. Analysis of volatile components of saffron. *J. High Resolut. Chromatogr.* **1991**, *14*, 771−774.

(22) Semiond, D.; Dautraix, S.; Desage, M.; Majdalani, R.; Casabianca, H.; Brazier, J. L. Identification and isotopic analysis of safranal from supercritical fluid extraction and alcoholic extracts of saffron. *Anal. Lett.* **1996**, *29*, 1027−1039.

(23) Tarantilis, P. A.; Polissiou, M. G. Isolation and identification of the aroma components from saffron (*Crocus sativus*). *J. Agric. Food Chem.* **1997**, *45*, 459−462.

(24) Cadwallader, K. R.; Baek, H. H.; Cai, M. Characterization of saffron flavor by aroma extract dilution analysis. In *Spices: Flavor Chemistry and Antioxidant Properties*; Riach, S. J., Ho, C. T., Eds.; American Chemical Society (ACS): Washington, D.C., 1997; ACS Symposium Series, Vol. *660*, Chapter 7, p 66−79.

(25) DOCE. *Reglamento n° 378/99 de la Comisión Europea*; DOCE: Spain, Feb 20, 1999; Vol. *L 46 de 20.9.1999*, p 13.

(26) Cullere, L.; San-Juan, F.; Cacho, J. Characterisation of aroma active compounds of Spanish saffron by gas chromatography−

olfactometry: Quantitative evaluation of the most relevant aromatic compounds. *Food Chem.* **2011**, *127*, 1866−1871.
(27) Maggi, L.; Carmona, M.; del Campo, C. P.; Kanakis, C. D.; Anastasaki, E.; Tarantilis, P. A.; Polissiou, M. G.; Alonso, G. L. Worldwide market screening of saffron volatile composition. *J. Sci. Food Agric.* **2009**, *89*, 1950−1954.
(28) Tarantilis, P. A.; Polissiou, M.; Manfait, M. Separation of picrocrocin, *cis*−*trans*-crocins and safranal of saffron using high-performance liquid chromatography with photodiode-array detection. *J. Chromatogr. A* **1994**, *664*, 55−61.
(29) Maggi, L.; Sanchez, A. M.; Carmona, M.; Kanakis, C. D.; Anastasaki, E.; Tarantilis, P. A.; Polissiou, M. G.; Alonso, G. L. Rapid determination of safranal in the quality control of saffron spice (*Crocus sativus* L.). *Food Chem.* **2011**, *127*, 369−373.
(30) de Laguna, A. *Pedacio Dioscorides Anazarbeo. Acerca de la Maeteria Medicinal y de los Venenos Mortíferos*; M.R.A. Creación y Realización Ed.ial S.L.: Barcelona, Spain, 1994; Vol. *I*, pp 31−32.
(31) Hosseinzadeh, H.; Nassiri-Asl, M. Avicenna's (Ibn Sina) the canon of medicine and saffron (*Crocus sativus*): A review. *Phytother. Res.* **2013**, *27*, 475−483.
(32) Licón, C.; Carmona, M.; Llorens, S.; Berruga, M. I.; Alonso, G. L. Potential healthy effects of saffron spice (*Crocus sativus* L. stigmas) consumption. In *Saffron. Functional Plant Science and Biotechnology*; Husaini, A. M., Ed.; Global Science Books, Ltd.: Japan, 2010; Vol. *4*, Special Issue 2, pp 64−73.
(33) Papandreou, M. A.; Kanakis, C. D.; Polissiou, M. G.; Efthimiopoulos, S.; Cordopatis, P.; Margarity, M.; Lamari, F. N. Inhibitory activity on amyloid-$\beta$ aggregation and antioxidant properties of *Crocus sativus* stigmas extract and its crocin constituents. *J. Agric. Food. Chem.* **2006**, *54*, 8762−8768.
(34) Hosseinzadeh, H.; Abootorabi, A.; Sadeghnia, H. R. Protective effect of *Crocus sativus* stigma extract and crocin (*trans*-crocin 4) on methyl methanesulfonate-induced DNA damage in mice organs. *DNA Cell Biol.* **2008**, *27*, 657−664.
(35) Ghadrdoost, B.; Vafaei, A. A.; Rashidy-Pour, A.; Hajisoltani, R.; Bandegi, A. R.; Motamedi, F.; Haghighi, S.; Sameni, H. R.; Pahlvan, S. Protective effects of saffron extract and its active constituent crocin against oxidative stress and spatial learning and memory deficits induced by chronic stress in rats. *Eur. J. Pharmacol.* **2011**, *667*, 222−229.
(36) Hosseinzadeh, H.; Karimi, G.; Niapoor, M. Antidepressant effect of *Crocus sativus* L. stigma extracts and their constituents, crocin and safranal, in mice. *Proceedings of the 1st International Symposium on Saffron Biology and Biotechnolgy*; Albacete, Spain, Oct 22−25, 2003; pp 435−445.
(37) Hosseinzadeh, H.; Talebzadeh, F. Anticonvulsant evaluation of safranal and crocin from *Crocus sativus* in mice. *Fitoterapia* **2005**, *76*, 722−724.
(38) Hosseinzadeh, H.; Sadeghnia, H. R. Safranal, a constituent of *Crocus sativus* (saffron), attenuated cerebral ischemia induced oxidative damage in rat hippocampus. *J. Pharm. Pharm. Sci.* **2005**, *8*, 394−399.
(39) International Organization for Standarization (ISO). *ISO 3632-1, Technical Specification. Saffron (Crocus sativus L.). Part 1 (Specification) and Part 2 (Test Methods)*; ISO: Geneva, Switzerland, 2011.
(40) Corradi, C.; Micheli, G. Determinazione spettrofotometrica del potere colorante, amaricante ed odoroso dello zafferano. *Boll. Chim. Farm.* **1979**, *118*, 553−562.
(41) Mínguez Mosquera, M. I. *Clorofilas y Carotenoides en Tecnología de los Alimentos*; Mínguez Mosquera, M. I., Ed.; Universidad de Sevilla: Sevilla, Spain, 1997; pp 43−60.
(42) Breukers, S.; Opstad, C. L.; Sliwka, H. R.; Partali, V. Hydrophilic carotenoids: Surface properties and aggregation behavior of the potassium salt of the highly unsaturated diacid norbixin. *Helv. Chim. Acta* **2009**, *92*, 1741−1747.
(43) EURACHEM Working Group. *The Fitness for Purpose of Analytical Methods. A Laboratory Guide to Method Validation and Related Topics*; EURACHEM Working Group: Teddington, U.K., 1998; www.eurachem.org.
(44) International Conference on Harmonization (IHC). Harmonized tripartite guideline validation on analytical procedures: Text and methodology. In *International Conference on Harmonization Q2(R1)*; IHC: Geneva, Switzerland, 2005.
(45) Ortega, C.; Lopez, R.; Cacho, J.; Ferreira, V. Fast analysis of important wine volatile compounds Development and validation of a new method based on gas chromatographic−flame ionisation detection analysis of dichloromethane microextracts. *J. Chromatogr. A* **2001**, *923*, 205−214.
(46) Alonso, G. L.; Salinas, M. R.; Garijo, J.; Sanchez-Fernandez, M. A. Composition of crocins and picrocrocin from Spanish saffron (*Crocus sativus* L.). *J. Food Qual.* **2001**, *24*, 219−233.
(47) Loskutov, A. V.; Beninger, C. W.; Hosfield, G. L.; Sink, K. C. Development of an improved procedure for extraction and quantitation of safranal in stigmas of *Crocus sativus* L. using high-performance liquid chromatography. *Food Chem.* **2000**, *69*, 87−95.
(48) Lozano, P.; Delgado, D.; Gomez, D.; Rubio, M.; Iborra, J. L. A non-destructive method to determine the safranal content of saffron (*Crocus sativus* L.) by supercritical carbon dioxide extraction combined with high-performance liquid chromatography and gas chromatography. *J. Biochem. Biophys. Methods* **2000**, *43*, 367−378.
(49) Lage, M.; Cantrell, C. L. Quantification of saffron (*Crocus sativus* L.) metabolites crocins, picrocrocin and safranal for quality determination of the spice grown under different environmental Moroccan conditions. *Sci. Hortic.* **2009**, *121*, 366−373.
(50) Basker, D.; Negbi, M. Crocetin equivalent of saffron extracts. Comparison of three extraction methods. *J. Assoc. Public Anal.* **1985**, *23*, 65.
(51) Friend, J.; Mayer, A. M. The enzymic destruction of carotenoids by isolated chloroplasts. *Biochim. Biophys. Acta* **1960**, *41*, 422.
(52) Weber, F.; Laskawy, G.; Grosch, W. Co-oxidation of carotene and crocin by soybean lipoxygenase iso-enzymes. *Z. Lebensm.-Unters. Forsch.* **1974**, *155*, 142.
(53) Sanchez, A. M.; Carmona, M.; Jaren-Galan, M.; Mosquera, M. I. M.; Alonso, G. L. Picrocrocin kinetics in aqueous saffron spice extracts (*Crocus sativus* L.) upon thermal treatment. *J. Agric. Food Chem.* **2011**, *59*, 249−255.

JOURNAL OF AGRICULTURAL AND FOOD CHEMISTRY

Article

pubs.acs.org/JAFC

# Differentiating Organically and Conventionally Grown Oregano Using Ultraperformance Liquid Chromatography Mass Spectrometry (UPLC-MS), Headspace Gas Chromatography with Flame Ionization Detection (Headspace-GC-FID), and Flow Injection Mass Spectrum (FIMS) Fingerprints Combined with Multivariate Data Analysis

Boyan Gao,[†,§] Fang Qin,[†] Tingting Ding,[†] Yineng Chen,[†] Weiying Lu,*[,†] and Liangli (Lucy) Yu*[,†,§]

[†]Institute of Food and Nutraceutical Science, School of Agriculture and Biology, Shanghai Jiao Tong University, Shanghai, China

[§]Department of Nutrition and Food Science, University of Maryland, College Park, Maryland 20742, United States

**ABSTRACT:** Ultraperformance liquid chromatography mass spectrometry (UPLC-MS), flow injection mass spectrometry (FIMS), and headspace gas chromatography (headspace-GC) combined with multivariate data analysis techniques were examined and compared in differentiating organically grown oregano from that grown conventionally. It is the first time that headspace-GC fingerprinting technology is reported in differentiating organically and conventionally grown spice samples. The results also indicated that UPLC-MS, FIMS, and headspace-GC-FID fingerprints with OPLS-DA were able to effectively distinguish oreganos under different growing conditions, whereas with PCA, only FIMS fingerprint could differentiate the organically and conventionally grown oregano samples. UPLC fingerprinting provided detailed information about the chemical composition of oregano with a longer analysis time, whereas FIMS finished a sample analysis within 1 min. On the other hand, headspace GC-FID fingerprinting required no sample pretreatment, suggesting its potential as a high-throughput method in distinguishing organically and conventionally grown oregano samples. In addition, chemical components in oregano were identified by their molecular weight using QTOF-MS and headspace-GC-MS.

**KEYWORDS:** *UPLC-MS, QTOF-MS, headspace-GC, multivariate data analysis, oregano (Origanum vulgare)*

## INTRODUCTION

Organic food has attracted more consumers in the past decades, especially in the past 5 years. A survey indicated that in 2012, U.S. consumers spent $31.5 billion on organic food, with an annual growth of 10.3% compared with that in 2011.[1] The survey also indicated that private label and contract manufacturing keep increasing in the organic field, which results in a higher demand for analytical technologies to differentiate organic foods from conventionally grown foods. The development of novel methods might prevent food adulteration and protect both consumers and the organic food market.

Oregano (*Origanum vulgare*) is a widely used culinary spice. Besides daily use as a cooking spice, oregano may also be recognized as a functional food because of its bioactivities.[2−19] Previous research indicated that oregano extracts have many beneficial effects, including anti-inflammatory,[2] antibacterial,[3] lipid oxidation reducing,[4,5] antimalarial,[6] antimicrobial,[7−10] and antioxidant[10−19] activities. Both conventional and organic oreganos are commercially available and differ significantly in their prices. Therefore, analytical methods for differentiating oregano samples from different growing conditions are in high demand to detect possible adulteration.

Previous research indicated that both LC-UV and flow injection electrospray ionization with ion trap mass spectrometry (FIMS) fingerprints are effective in differentiating organically and conventionally grown spices.[20−23] Since 2012, conventionally and organically grown peppermint, sage, and basil samples have been differentiated using both HPLC-UV and flow injection electrospray ionization with ion trap mass spectrometry (FIMS) fingerprinting techniques combined with principal component analysis (PCA) in our laboratory.[22−24] As a continuation of our effort in detecting food adulteration, this study examined whether headspace-GC, UPLC-MS, and FIMS fingerprinting combined with statistical approaches could effectively differentiate organically and conventionally grown oregano samples. This was the first effort to distinguish organically and conventionally grown spices by headspace-GC fingerprints of the nonpolar volatile components.

## MATERIALS AND METHODS

**Standard Compounds and Other Chemicals.** LC-MS grade acetonitrile, methanol, and formic acid were purchased from Sigma-Aldrich (St. Louis, MO, USA). LC-MS grade water was obtained from a Milli-Q 10 ultrapure water system (Billerica, MA, USA). All other chemical reagents were of analytical grade purchased from Sigma-Aldrich (St. Louis, MO, USA) and used without further purification.

**Plant Materials and Sample Preparation.** Ten USDA certified organic oregano leaf samples and 10 conventional oregano leaf samples were gifts from the Frontier Natural Products Co-op (Norway, IA, USA). Dry botanical samples were ground to 20 mesh powder using an IKA A11 laboratory grinder (IKA, Staufen, Baden-

Received: May 23, 2014
Revised: July 18, 2014
Accepted: July 22, 2014
Published: July 22, 2014

ACS Publications © 2014 American Chemical Society

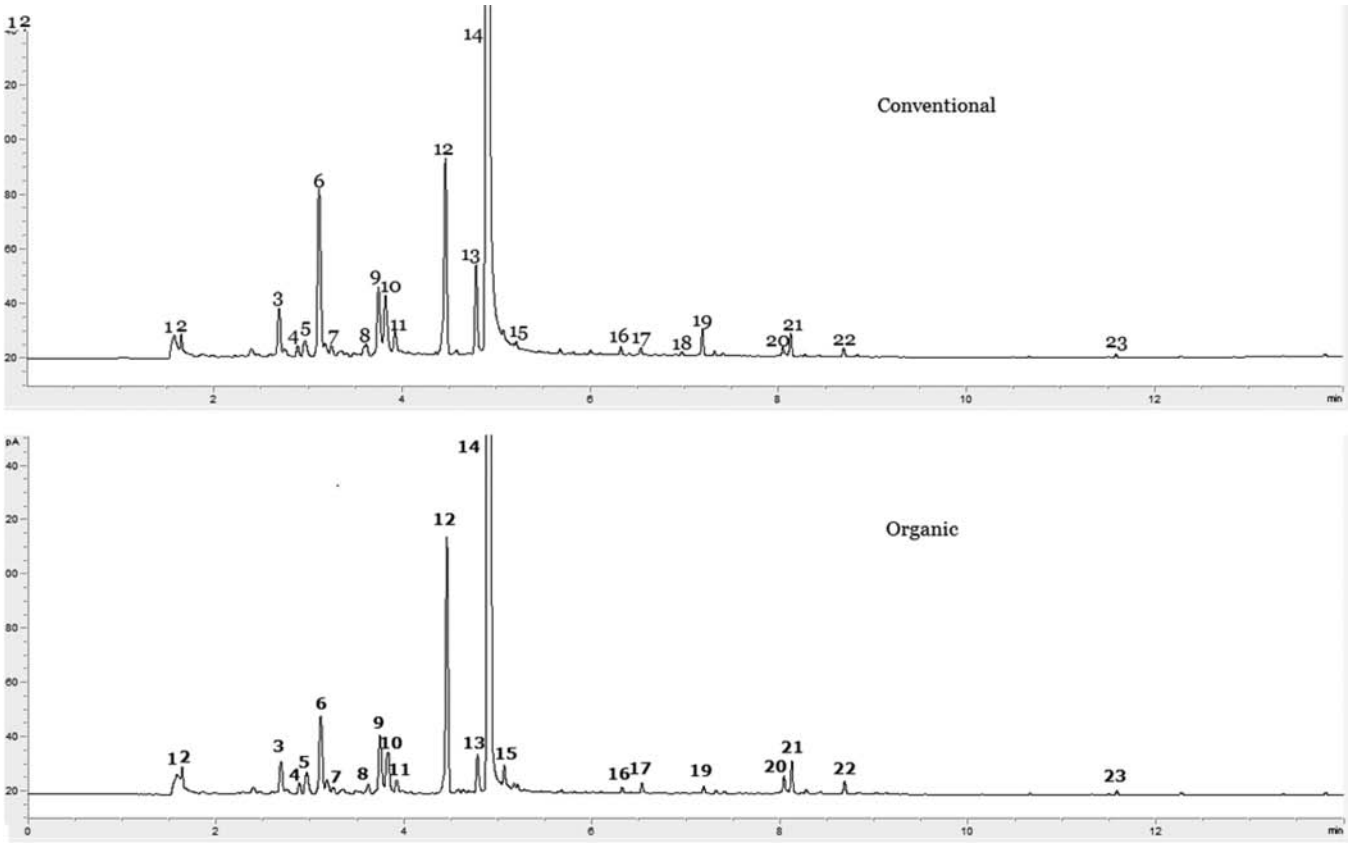


**Figure 1.** Representative headspace-GC fingerprints for commercial conventional and organic oregano samples.

Württemberg, Germany) and stored at −20 °C before analysis. One hundred milligrams of every sample powder was accurately weighed and extracted with 10 mL of water/MeOH (1:1, v/v) with ultrasonication at ambient temperature for 30 min. The extracts were filtered with a 0.22 μm GHP syringe filter (Waters, Milford, MA, USA) and ready for LC-MS and FIMS fingerprinting analyses. One hundred milligrams of oregano samples was accurately weighed and directly sealed into headspace sample bottles and ready for GC analyses. Each sample was analyzed in triplicate.

**Headspace GC and GC-MS Conditions.** An Agilent 7890A GC with an Agilent 7697A headspace sampler and an FID was used for GC fingerprinting analysis (Agilent, Loveland, CO, USA). Carrier gas was helium at a flow rate of 2.5 mL/min. An HP-5 phenyl methyl siloxane column (30 m × 320 μm with a 0.25 μm film thickness) from Agilent was used. The injection volume was 1 μL at a split ratio of 10/1. FID temperature was 300 °C. The initial oven temperature was 100 °C, which was increased at 10 °C/min to 250 °C and held for 5 min. Headspace oven, loop, and transfer line temperatures were 100, 110, and 120 °C, respectively.

An Agilent 7890A/5973N headspace-GC−single-quadruple MS system was selected for the identification of volatile substances. The temperature programming was the same as that for headspace-GC fingerprinting. Quadruple temperature was 150 °C, source temperature was 230 °C, and cone voltage was 70 eV. The mass range was set from 30 to 450 Da.

Individual substances were tentatively identified through the molecular weight of substances and the material information in the database. Quantification was based on the area under each substance peak as absolute peak area, and peak area was compared to the reference peak (peak 14) as relative peak area.

**UPLC-MS and FIMS Conditions.** A Waters Acuity UPLC-Xevo G2 QTOF MS system was selected for both UPLC-MS and FIMS analyses. Mobile phase A consisted of 0.1% formic acid in water, and mobile phase B consisted of 0.1% formic acid in acetonitrile for both UPLC-MS and FIMS analyses. For UPLC-MS, a Waters BEH C18 column (2.1 mm i.d. × 100 mm, 1.7 μm) was used at 40 °C; the elution gradient started with 5% phase B, changed linearly to 50% in 10 min, increased linearly to 90% B at 15 min, was maintained for 2 min and then returned to its initial conditions for 2 min to re-equilibrate the column for the next injection. The flow rate was 0.4 mL/min with an injection volume of 2 μL. The MS detector conditions were as follows: capillary voltage, 2.50 kV; sampling cone voltage, 60 V; extraction cone voltage, 4.0 V; source temperature, 120 °C; and desolvation temperature, 450 °C. The cone gas flow rate was 100 L/h, and the desolvation gas was 800 L/h. An $MS^E$ method was used with a mass range from $m/z$ 100 to 1000 in ESI negative mode, scan time was 0.3 s, and the ramp collision energy was 30 eV.

For FIMS, the mobile phase of methanol/water in a ratio of 1:1 (v/v) was used, and the flow rate was 0.2 mL/min. Oregano extracts were diluted 10 times before injection, and the injection volume was 2 μL. MS spectra were collected from 0.05 to 0.55 min, and MS conditions were the same as those used in UPLC-MS analysis. Masslynx 4.1 software (Waters) was used for alignment of peaks and accurate mass weight calculation and identification.

**Data Processing.** Thirty-seven major chromatographic peaks were detected in the UPLC-MS fingerprints in both organically and conventionally grown oregano samples. Their absolute and relative peak areas were used for orthogonal partial least-squares discriminant analysis (OPLS-DA). For absolute peak area analyses, 37 peak areas in all of the UPLC-MS chromatograms were analyzed with OPLS-DA directly. For relative peak area analyses, peak 36 was selected as a reference peak, and other peak areas were divided to the reference peak in each chromatogram to obtain the relative peak area. Peaks with areas of >5% of the reference peak area were recognized as major peaks and taken into account for calculation. For FIMS fingerprints, one-dimensional spectra ranging from $m/z$ 100 to 1000 were collected for analysis. For headspace-GC fingerprints, both absolute and relative peak areas were selected for analyses. Peak 14, as the largest peak in headspace-GC, was selected as a reference peak, and other peak areas were divided by the reference peak area in each chromatogram to

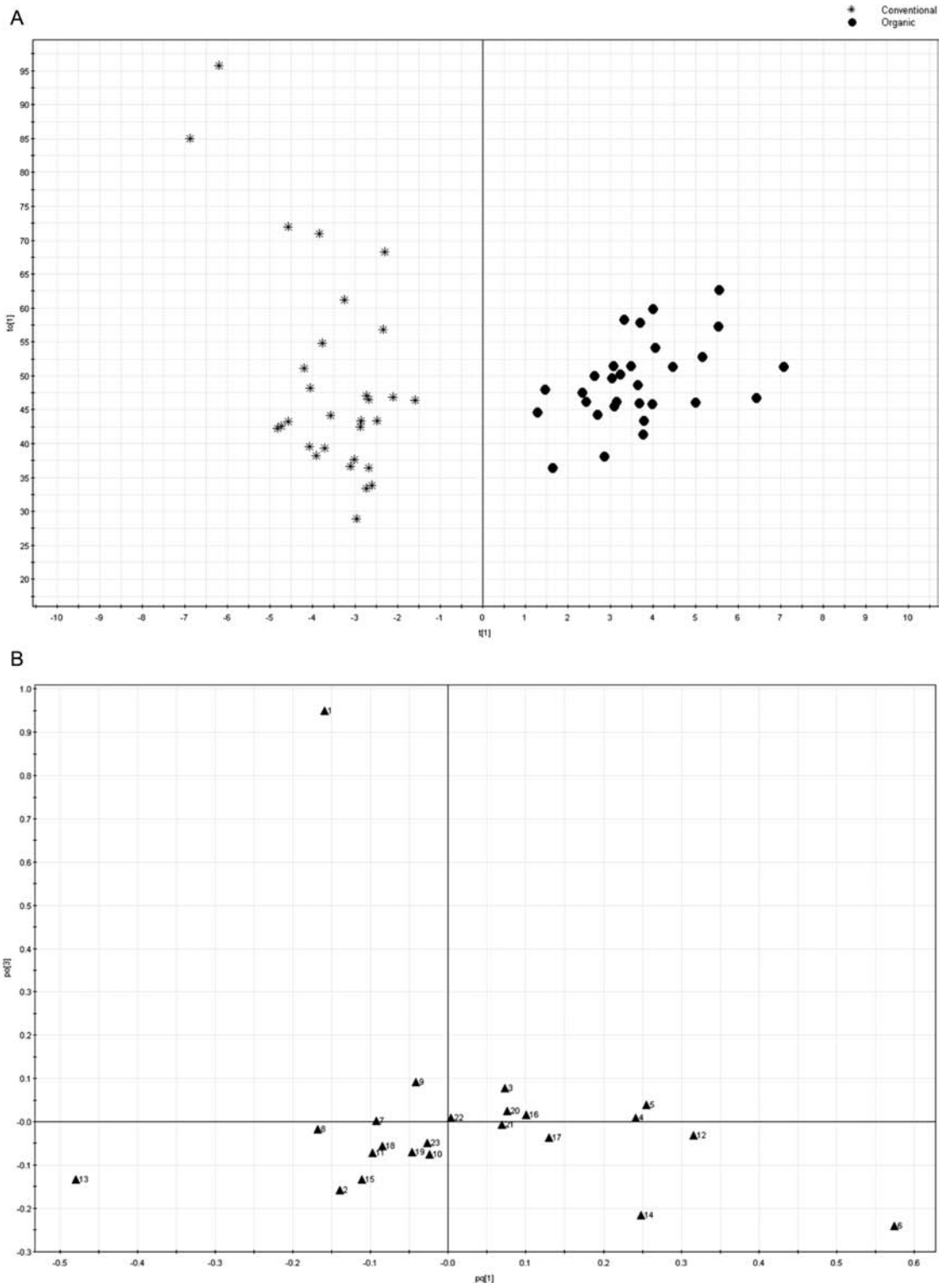


**Figure 2.** Orthogonal partial least-squares discriminant analysis (OPLS-DA) (A) scores plot and (B) loading plot for headspace-GC absolute peak areas of the organically and conventionally grown oregano samples.

obtain the relative peak area. PCA and OPLS-DA were performed using SIMCA-P software (Umetrics, Malmo, Skånelän, Sweden) to analyze all of the data: containing 37 absolute peak areas in all 60 chromatograms and 36 relative peak areas in all 60 chromatograms (20 samples with triplicate analyses each) in UPLC-MS fingerprints; 23 absolute peak areas in all 60 chromatograms and 22 relative peak areas in all 60 chromatograms in headspace-GC fingerprints. PCA was also performed for one-dimensional FIMS fingerprints obtained from $m/z$ 100 to 1000 using the Markerlynx software (Waters).

## RESULTS AND DISCUSSION

**Headspace-GC Fingerprinting Analysis.** This was the first time that headspace-GC fingerprints were examined for their possible application to differentiate organically and


dx.doi.org/10.1021/jf502419y | J. Agric. Food Chem. 2014, 62, 8075−8084

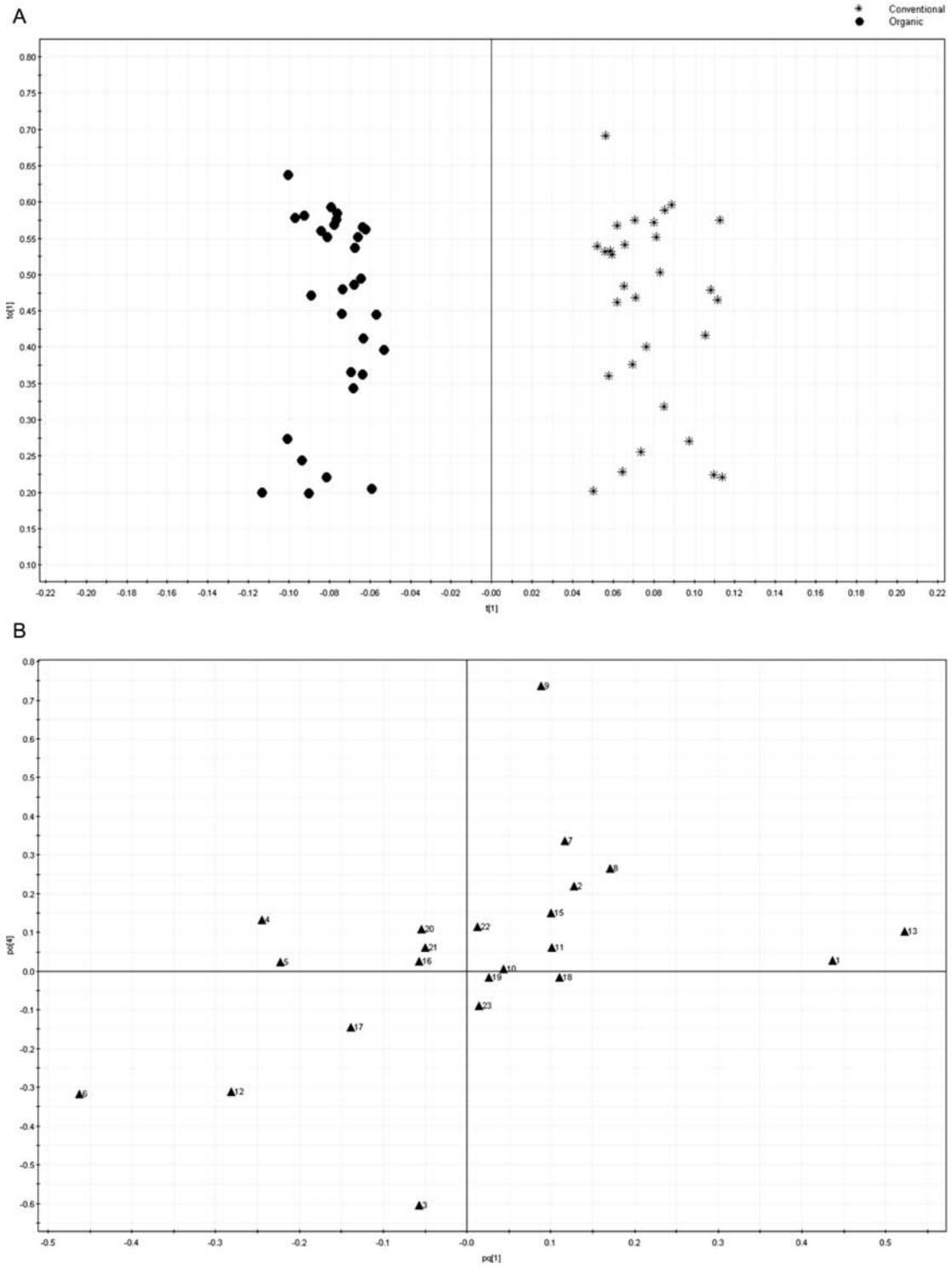


**Figure 3.** Orthogonal partial least-squares discriminant analysis (OPLS-DA) (A) scores plot and (B) loading plot for headspace-GC relative peak areas of the organically and conventionally grown oregano samples. All peak areas were divided by the area of peak 14 in each sample, and the results were used for OPLS-DA.

conventionally grown spices. A total of 23 peaks were detected in a gas chromatograph (Figure 1). As shown in Figure 1, there was no characteristic component or deterministic large peak to separate the conventional and organic oregano samples by manual observation.

OPLS-DA is a statistical method that finds a linear regression model by projecting the predictor and observation variables to a new space. It can be used to find the fundamental relationships between two matrices to model the covariance structures in these two spaces. Headspace-GC fingerprinting is an effective method in the analysis of volatiles. It has been widely used because it requires less sample pretreatment and has high sensitivity. The OPLS-DA scores plot and loading plot of the headspace-GC fingerprints for absolute peak area are provided in panels A and B, respectively, of Figure 2. As shown in Figure 2A, the conventional oregano samples are all on the left side of


dx.doi.org/10.1021/jf502419y | J. Agric. Food Chem. 2014, 62, 8075−8084

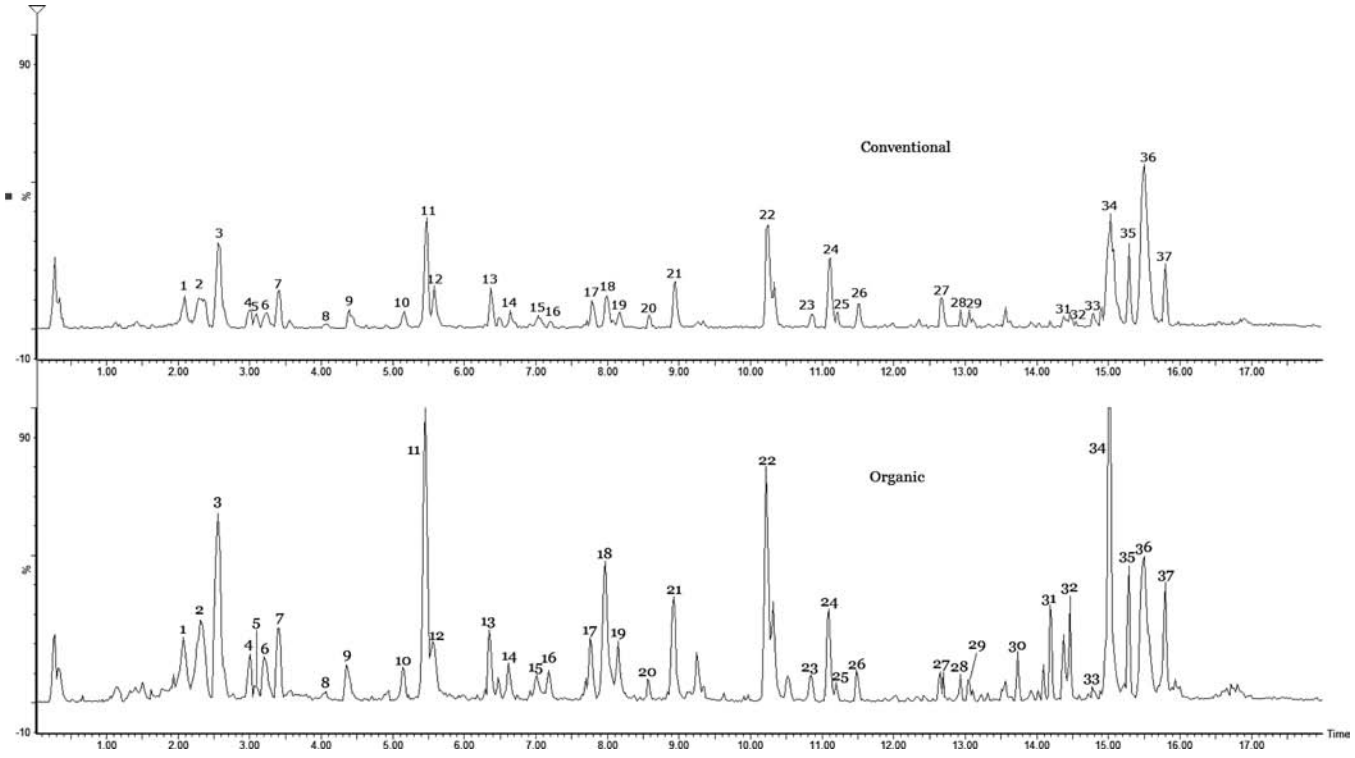


**Figure 4.** Representative UPLC-MS fingerprints for commercial conventionally and organically grown oregano samples.

the scores of latent variable (LV) 1, whereas all of the organic samples are located on the right. The scores plot indicated that headspace-GC combined with OPLS-DA could effectively differentiate the organically and conventionally grown oregano samples by determining their volatile components. This is the first report on the potential application of headspace-GC fingerprints combined with OPLS-DA in differentiating commercial organically and conventionally grown botanicals.

In the loading plot of the headspace-GC absolute peak areas (Figure 2B), peaks 13, 1, and 8 contributed significantly to the separation of conventional samples, whereas peaks 6, 12, 5, and 4 contributed significantly to the separation of organic oregano samples (Figure 2B). In addition, GC-MS analysis was performed, and 10 compounds were tentatively characterized by comparing their MS result with that in the database, including *p*-cymene (peak 3), $\gamma$-terpinene (peak 5), 3,7-dimethyl-1,6-octadien-3-ol (peak 6), 5-methyl-2-(1-methylethyl)cyclohexanone (peak 8), isoborneol (peak 9), thymoquinone (peak 12), thymol (peak 13), 1-(*N*-methylcarbamate), 3-methyl-5-(1-methylethyl)phenol (peak 14), caryophyllene (peak 19), and $\beta$-bisabolene (peak 21).

Relative peak area represents the relative amount of each component against a selected base peak. Previous studies showed the different degrees of effectiveness in differentiating organically and conventionally grown botanicals using the absolute peak area and the relative peak area.[22,23] Therefore, the relative peak areas for the headspace-GC fingerprints were also analyzed using OPLS-DA in the present study, and Figure 3 shows the scores plot and loading plot of the relative peak areas for the organic and conventional oreganos. Among the 23 peaks, peak 14 showed the highest peak area and was selected as the reference peak (RP) for calculating the relative peak area. Other major peaks were defined as at least 1% of the area of the RP. In Figure 3A, all of the conventional oregano samples are clustered on the right side of the OPLS-DA scores plot, whereas all of the organic samples are located on the left side of the scores plot, separating well the LV1. In the loading plot for the headspace-GC relative peak areas (Figure 3B), peaks 13 (thymol) and 1 were on the right side of loading scatter plot, indicating that these two substances had higher concentrations in the conventional oregano samples, and peaks 6 (3,7-dimethyl-1,6-octadien-3-ol), 12 (thymoquinone), 4, and 5 ($\gamma$-terpinene) were greater in the organic oregano samples. Because peak 14 was the RP, the results indicated that the levels of peak 13 (thymol), 6 (3,7-dimethyl-1,6-octadien-3-ol), 12 (thymoquinone), 4, and 5 ($\gamma$-terpinene) might be important in determining if an oregano sample was organically or conventionally produced according to its headspace-GC fingerprints.

**LC-MS Fingerprinting Analysis.** The 50% MeOH extract of oregano samples were analyzed with UPLC-QTOF-MS. As shown in Figure 4, organic oregano samples had the same peak numbers as their conventional counterparts, but relative peak areas were visually different in these two groups, especially for peaks 3, 11, 22, and 34. The OPLS-DA scores plot and loading plot of the UPLC-MS chromatographic absolute peak areas are provided in Figure 5, panels A and B, respectively. The conventional oregano samples are all on the left side of the OPLS-DA scores plot, whereas all of the organic oregano samples are located on the right side. OPLS-DA in LC fingerprints was able to visualize the results and made the comparison of the chromatographic fingerprints easy to read and understand without subjective decisions.

In the loading plot of the OPLS-DA absolute peak areas (Figure 5B), peak 34 (ursolic acid) contributed most to separate the organic samples from their conventional counterparts, followed by peaks 11 (catechin 7-xyloside), 18 (luteolin), 32 (6-methylscutellarein), and 3 (baicalin). On the other hand, peaks 36 (methylgalangin) and 23 (thymol) showed significant contribution to the separation of conventional oregano


dx.doi.org/10.1021/jf502419y | J. Agric. Food Chem. 2014, 62, 8075−8084

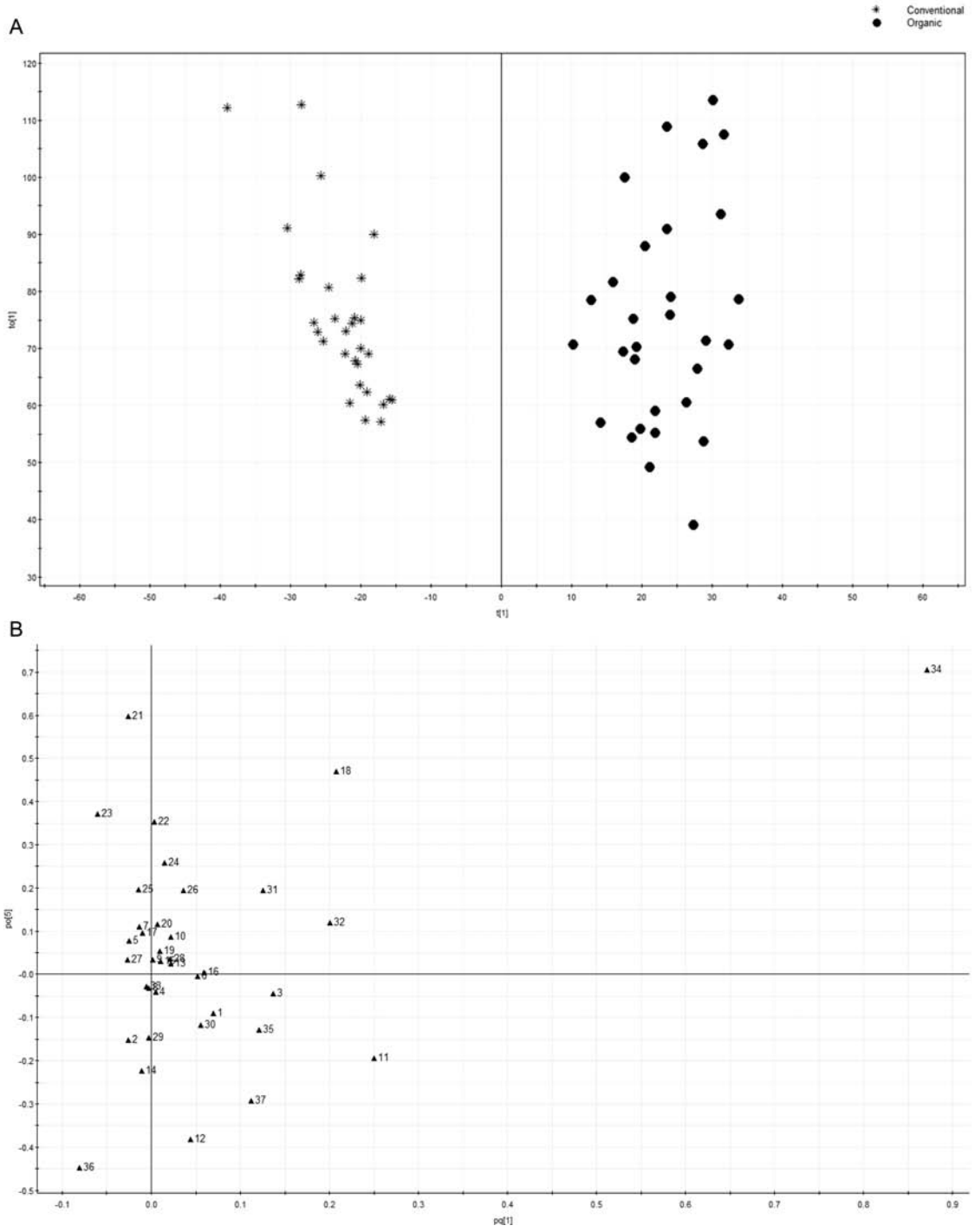


**Figure 5.** Orthogonal partial least-squares discriminant analysis (OPLS-DA) (A) scores plot and (B) loading plot for UPLC-MS absolute peak areas of the organically and conventionally grown oregano samples.

samples. With the UPLC-MS chromatographic fingerprint taken into account, the result also confirmed the fact that organic oregano samples contained higher levels of ursolic acid, catechin 7-xyloside, luteloin, and 6-methylscutellarein. Including the peaks mentioned above, there were a total of 33 identified substances in oregano according to their accurate mass weight and previous research results.[25−28] Peaks were identified as scutellarein (peak 1), baicalin (peak 3), catechin 7-xyloside isomer (peak 4), catechin 7-xyloside isomer (peak 5), catechin 7-xyloside isomer (peak 7), acacetin (peak 9), aromadendrin/eriodictyol (peak 10), catechin 7-xyloside (peak 11), luteolin-7-*O*-glucoside (peak 12), apigenin-7-*O*-glucoside (peak 13), thujene (peak 14), kaempferol 3-xyloside (peak 15), kaempferol 3-*O*-(*β*-D-xylopyranosyl-(1→2)-*α*-D-ribopyranoside) (peak 16), apigenin (peak 17), luteolin (peak 18), fortunellin (peak 19), cassiaoccidentalin B (peak 21), rehin (peak 22), thymol (peak 23), 6,7-dimethylscutellarein (peak 24), 3,3′,4-tri-omethlellagic acid (peak 25), acacetin isomer (peak 26), tricalysioside I (peak 27), hederagenin isomer (peak 28), hederagenin isomer (peak 29), hederagenin (peak 30), 6-methylscutellarein isomer (peak 31), 6-methylscutellarein (peak 32), oleanolic acid (peak 33), ursolic acid (peak 34),


dx.doi.org/10.1021/jf502419y | J. Agric. Food Chem. 2014, 62, 8075−8084

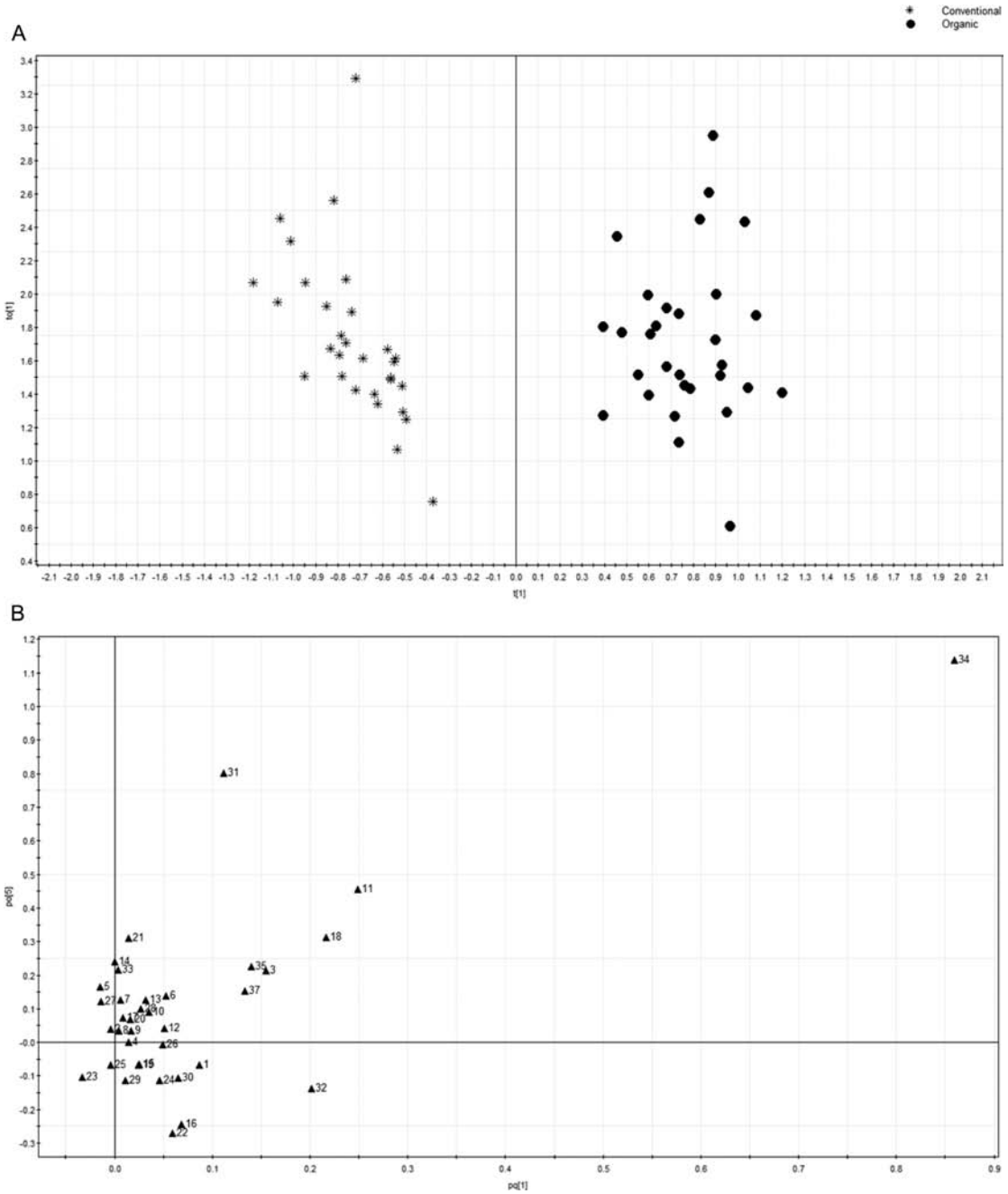


**Figure 6.** Orthogonal partial least-squares discriminant analysis (OPLS-DA) (A) scores plot and (B) loading plot for UPLC-MS relative peak areas of the organically and conventionally grown oregano samples. All peak areas were divided by the area of peak 36 in each sample, and the results were used for OPLS-DA.

pinocembrin (peak 35), methylgalangin (peak 36), and methylgalangin isomer (peak 37). The major peaks that have been detected and identified in oregano by UPLC-MS were flavonoids, flavonoid glycosides, and pentacyclic triterpene acids. The results also confirmed the fact that UPLC-MS is an effective tool in analyzing the polar components in botanicals.

The OPLS-DA scores plots of the relative UPLC-MS peak areas for the organic and conventional oreganos are shown in Figure 6, panels A and B, respectively. In all 37 chromatographic peaks, all of the other 36 peaks were taken into OPLS-DA analysis except peak 36 (methylgalangin) was selected as the reference peak (RP) for calculating the relative peak area. As shown in Figure 6A, the conventional oregano samples are located on the left side of the scores plot, whereas the organic oregano samples are all on the right side of the scores plot. The same trend of scores plot between the absolute peak areas and relative peak areas indicated that all of the oregano samples had a uniformal chemical profile regardless of their growing condition. In the loading plot of UPLC-MS relative peak areas (Figure 6B), the same trend was observed in both organically and conventionally oregano samples. Peak 36 was selected as RP and not taken into account, and peak 23 (thymol) was on the left side of loading scatter plot, indicating that the relative area of thymol was greater in conventional samples, whereas peaks 34 (ursolic acid), 11 (catechin 7-xyloside), 18 (luteolin), 32 (6-methylscutellarein), and 3


dx.doi.org/10.1021/jf502419y | J. Agric. Food Chem. 2014, 62, 8075−8084

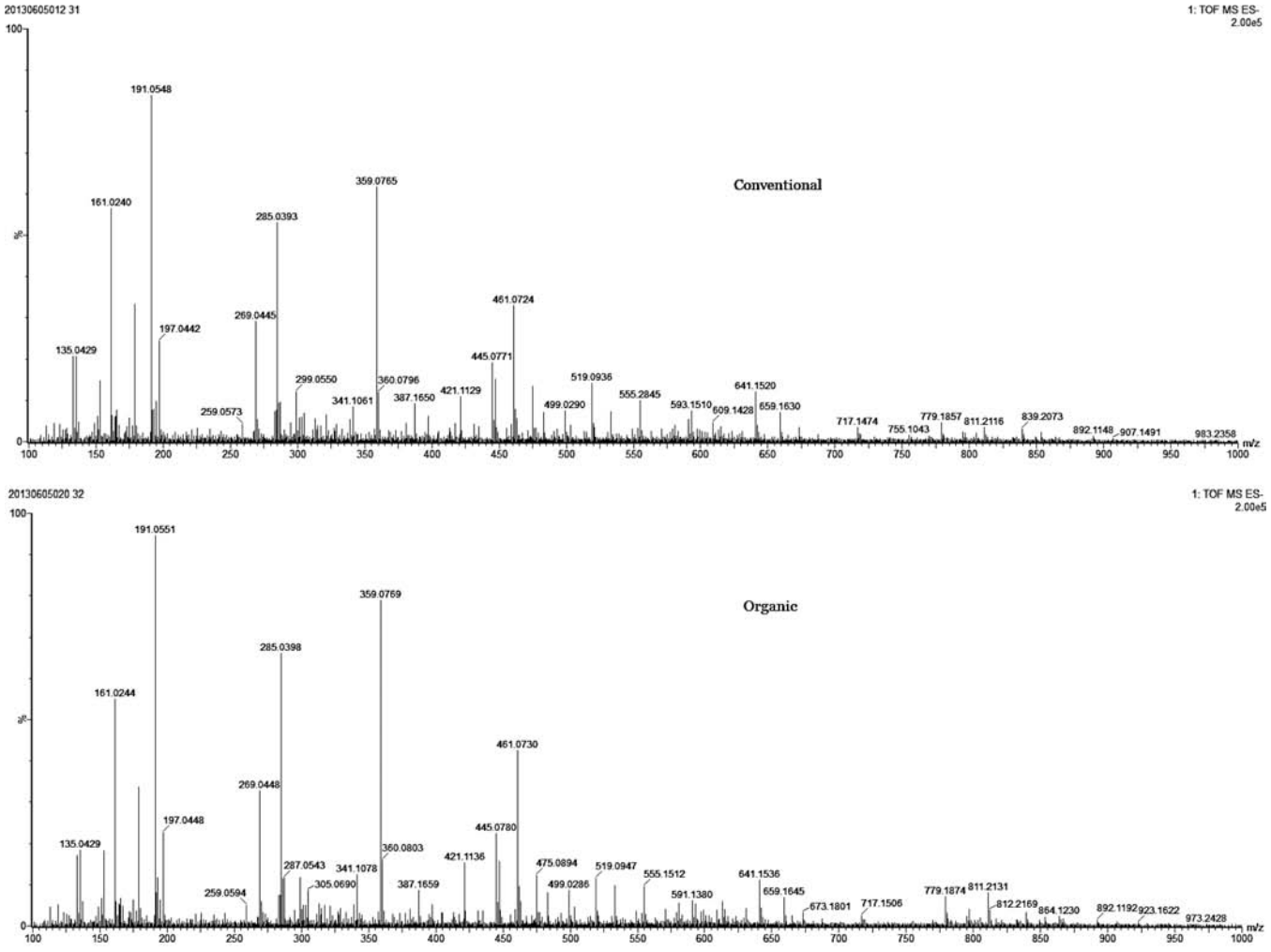


**Figure 7.** Representative FIMS fingerprints for commercial conventionally and organically grown oregano samples.

(baicalin) showed higher relative peak areas in organic oregano samples and are located on the right side of the loading scatter plot.

**FIMS Fingerprint Analysis.** Typical FIMS fingerprints for both organically and conventionally grown oregano samples are shown in Figure 7. The highest natural abundant peak in both conventional and organic oregano spectra is $m/z$ 191.0548, followed by $m/z$ 359.0765, 161.0240, 285.0393, and 461.0724. All of these peaks are not the molecular ion peaks of chemical substances identified in oregano, indicating that these spectral peaks might be the major fragment ion peaks.

The FIMS PCA scores plot and loading plot are shown in Figure 8. As one of the most widely used data analysis methods, PCA is a mathematical approach transforming a large number of correlated variables into a small group of uncorrelated variables, the principal components (PCs). In the PCA scores plot of oregano FIMS fingerprints, all of the conventional samples were on the lower side, whereas all of the organic samples were on the upper side (Figure 8A). The scores plot indicated that FIMS fingerprints could effectively differentiate conventionally and organically grown oregano samples in a 1 min analytical time.

In the loading plot of FIMS fingerprints (Figure 8B), most of the ions were clustered near the abscissa, but there were still a few ions dispersed far away from the center, indicating that these ions and their natural abundance might be more important in differentiating the growth conditions of oregano. In the upper side of the loading plot, ions $m/z$ 200.9919, 127.9888, 290.0744, 230.9881, 199.9843, 154.9736, and 156.9659 yielded higher scores and would lead to positions in the upper side of the PCA scores plot. On the other hand, the most important ions that contributed positively to conventional oregano samples were ions at $m/z$ 867.1962, 614.1596, 798.1968, and 572.1494. All of the ions mentioned above were not the major chemical substances detected in UPLC-MS analysis, indicating that some trace chemical materials or the fragment ions of major chemical materials played the most important role in differentiating organic oreganos from conventional ones in FIMS fingerprints.

In conclusion, headspace-GC, UPLC-MS, and FIMS fingerprints combined with multivariate data analysis tools may have potential application in effectively differentiating commercial organically and conventionally grown oregano and other botanical samples. This was the first study in which headspace-GC fingerprinting showed potential in rapidly differentiating organically and conventionally grown oregano samples. UPLC-MS fingerprinting may obtain detailed chemical composition information about the samples, but requires a longer analysis time. FIMS fingerprinting may provide a rapid and accurate test and has the potential for high-throughput applications. In addition, the results from UPLC-MS fingerprints and GC-MS analyses suggested that thymol might play

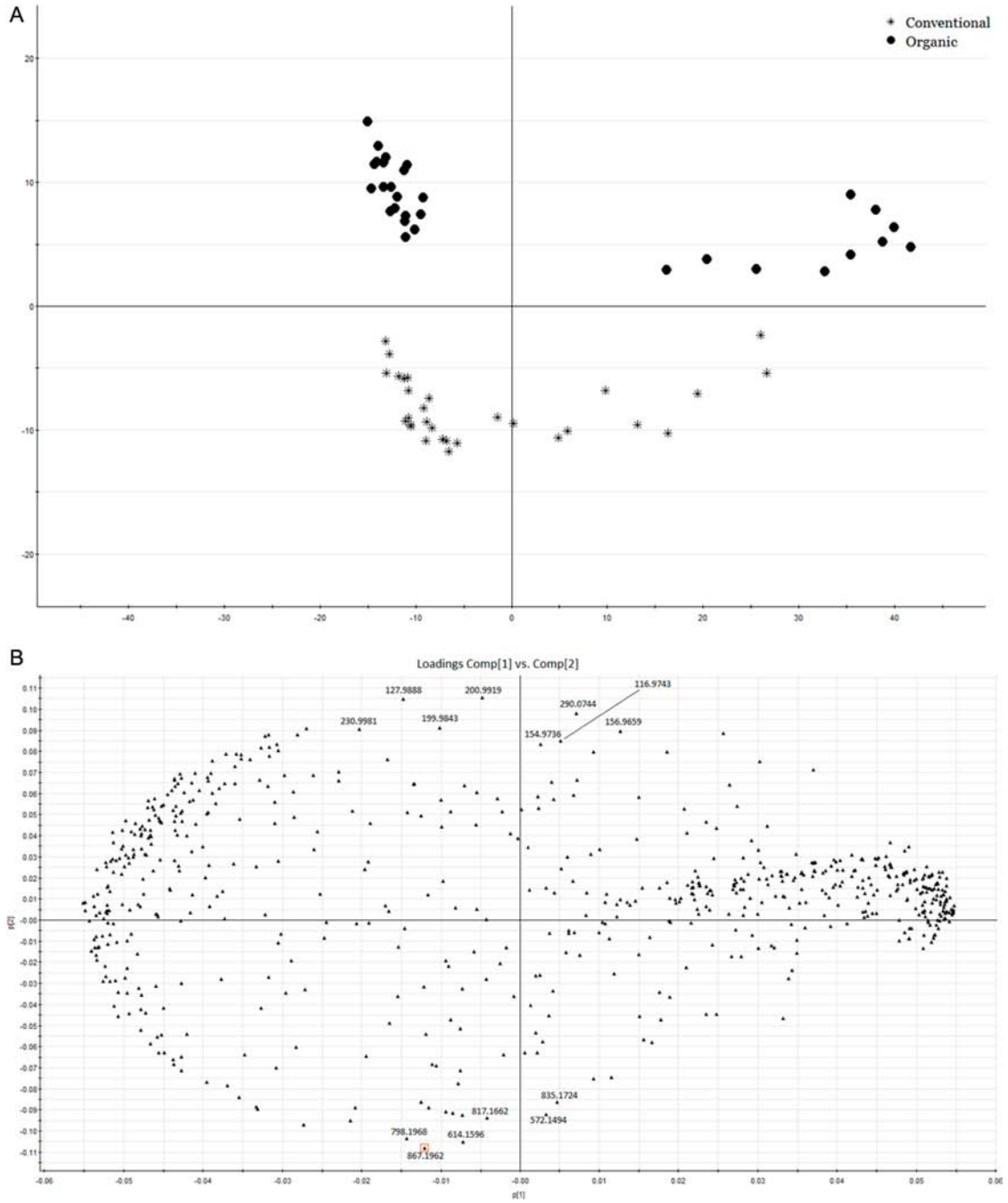


**Figure 8.** Principal component analysis (PCA) (A) scores plot and (B) loading plot for FIMS fingerprints of the organically and conventionally grown oregano samples.

the most important role in separating the conventionally grown oregano samples from the organically grown ones, and the concentration difference of thymol might be due to the different growth condition, genotype, and the interactions between genotype and growing environment. In practical application, headspace-GC fingerprints and FIMS combined with multivariate data analysis may be selected first for unknown spice samples, and additional UPLC-MS and GC-MS identifications may be performed if necessary. Besides, the results also indicated that, compared with PCA, other multivariate data analysis methods such as OPLS-DA may also be utilized for differentiating organically and conventionally grown oregano samples. These data analysis methods and chemical analysis techniques might be used in combination for distinguishing botanical samples.

## AUTHOR INFORMATION

### Corresponding Authors

*(W.L.) E-mail: weiying.lu@sjtu.edu.cn.

*(L.Y.) Mail: Department of Nutrition and Food Science, University of Maryland, College Park, MD 20742, USA. Phone: (301) 314-3313. E-mail: lyu5@umd.edu.

### Funding

This research was supported by two grants from the National High Technology Research and Development Program of China (Grants 2013AA102202 and 2013AA102207), a special

fund for Agro-scientific Research in the Public Interest (Grant 201203069), the SJTU startup fund for young talent (Grant 13X100040047), and the SJTU 985-III disciplines platform and talent fund (Grants TS0414115001 and TS0320215001).

### Notes

The authors declare no competing financial interest.

## REFERENCES

(1) The organic trade association's 2013 organic industry survey. March 10, 2014; http://www.thepacker.com/fruit-vegetable-news/222580921.html.

(2) Shen, D.; Pan, M. H.; Wu, Q. L.; Park, C. H.; Juliani, H. R.; Ho, C. T.; Simon, J. E. LC-MS method for the simultaneous quantitation of the anti-inflammatory constituents in oregano (*Origanum* species). *J. Agric. Food Chem.* **2010**, *58*, 7119−7125.

(3) Dadalioglu, I.; Evrendilek, G. A. Chemical compositions and antibacterial effects of essential oils of Turkish oregano (*Origanum minutiflorum*), bay laurel (*Laurus nobilis*), Spanish lavender (*Lavandula stoechas* L.), and fennel (*Foeniculum vulgare*) on common foodborne pathogens. *J. Agric. Food Chem.* **2004**, *52*, 8255−8260.

(4) Botsoglou, N. A.; Florou-Paneri, P.; Christaki, E.; Fletouris, D. J.; Spais, A. B. Effect of dietary oregano essential oil on performance of chickens and on iron-induced lipid oxidation of breast, thigh and abdominal fat tissues. *Br. Poult. Sci.* **2002**, *43*, 223−230.

(5) Vekiari, S. A.; Oreopoulou, V.; Tzia, C.; Thomopoulos, C. D. Oregano flavonoids as lipid antioxidants. *J. Am. Oil Chem. Soc.* **1993**, *70*, 483−487.

(6) Babili, F. E.; Bouajila, J.; Souchard, J. P.; Bertrand, C. e.; Bellvert, F.; Fouraste, I.; Moulis, C.; Valentin, A. Oregano: chemical analysis and evaluation of its antimalarial, antioxidant, and cytotoxic activities. *J. Food Sci.* **2011**, *76*, 512−518.

(7) Lambert, R. J.; Skandamis, P. N.; Coote, P. J.; Nychas, G. J. A study of the minimum inhibitory concentration and mode of action of oregano essential oil, thymol and carvacrol. *J. Appl. Microbiol.* **2001**, *91*, 453−462.

(8) Becerril, R.; Gomez-Lus, R.; Goni, P.; Lopez, P.; Nerin, C. Combination of analytical and microbiological techniques to study the antimicrobial activity of a new active food packaging containing cinnamon or oregano against *E. coli* and *S. aureus*. *Anal. Bioanal. Chem.* **2007**, *388*, 1003−1011.

(9) Skandamis, P.; Tsigarida, E.; Nychas, G.-J. E. The effect of oregano essential oil on survival/death of *Salmonella* typhimuriumin meat stored at 51C under aerobic,VP/MAP conditions. *Food Microbiol.* **2001**, *19*, 97−103.

(10) Tiziana Baratta, M.; Damien Dorman, H. J.; Deans, S. G.; Biond, D. M.; Ruberto, G. Chemical composition, antimicrobial and antioxidative activity of laurel, sage, rosemary, oregano and coriander essential oils. *J. Essent. Oil Res.* **1998**, *10*, 618−627.

(11) Exarchou, V.; Nenadis, N.; Tsimidou, M.; Gerothanassis, I. P.; Troganis, A.; Boskou, D. Antioxidant activities and phenolic composition of extracts from Greek oregano, Greek sage, and summer savory. *J. Agric. Food Chem.* **2002**, *50*, 5294−5299.

(12) Pizzale, L.; Bortolomeazzi, R.; Vichi, S.; Beregger, E. U.; Conte, L. S. Antioxidant activity of sage (*Salvia officinalis* and *S. fruticosa*) and oregano (*Origanum onites* and *O. indercedens*) extracts related to their phenolic compound content. *J. Sci. Food Agric.* **2002**, *82*, 1645−1651.

(13) Quiroga, P. R.; Grosso, N. R.; Nepote, V. Antioxidant effect of poleo and oregano essential oil on roasted sunflower seeds. *J. Food Sci.* **2013**, *78*, S1904−S1912.

(14) Milos, M.; Mastelic, J.; Jerkovic, I. Chemical composition and antioxidant effect of glycosidically bound volatile compounds from oregano (*Origanum vulgare* L. ssp. *hirtum*). *Food Chem.* **2000**, *71*, 79−83.

(15) Puertas-Mejía, M.; Hillebrand, S.; Stashenko, E.; Winterhalter, P. In vitro radical scavenging activity of essential oils from Columbian plants and fractions from oregano (*Origanum vulgare* L.) essential oil. *Flavour Fragrance J.* **2002**, *17*, 380−384.

(16) Rababah, T. M.; Banat, F.; Rababah, A.; Ereifej, K.; Yang, W. Optimization of extraction conditions of total phenolics, antioxidant activities, and anthocyanin of oregano, thyme, terebinth, and pomegranate. *J. Food Sci.* **2010**, *75*, C626−C632.

(17) Rodriguez-Meizoso, I.; Marin, F. R.; Herrero, M.; Senorans, F. J.; Reglero, G.; Cifuentes, A.; Ibanez, E. Subcritical water extraction of nutraceuticals with antioxidant activity from oregano. Chemical and functional characterization. *J. Pharm. Biomed.* **2006**, *41*, 1560−1565.

(18) Ozkan, G.; Baydar, H.; Erbas, S. The influence of harvest time on essential oil composition, phenolic constituents and antioxidant properties of Turkish oregano (*Origanum onites* L.). *J. Sci. Food Agric.* **2010**, *90*, 205−209.

(19) Kulisic, T.; Radonic, A.; Katalinic, V.; Milos, M. Use of different methods for testing antioxidative activity of oregano essential oil. *Food Chem.* **2004**, *85*, 633−640.

(20) Xie, Z.; Zhao, Y.; Chen, P.; Jing, P.; Yue, J.; Yu, L. L. Chromatographic fingerprint analysis and rutin and quercetin compositions in the leaf and whole-plant samples of di- and tetraploid *Gynostemma pentaphyllum*. *J. Agric. Food Chem.* **2011**, *59*, 3042−3049.

(21) Zhao, Y.; Xie, Z.; Niu, Y.; Shi, H.; Chen, P.; Yu, L. Chemical compositions, UPLC/MS fingerprinting profiles and radical scavenging properties of commercial *Gynostemma pentaphyllum* (Thunb.) Makino samples. *Food Chem.* **2012**, *134*, 180−188.

(22) Gao, B.; Lu, Y.; Sheng, Y.; Chen, P.; Yu, L. Differentiating organic and conventional sage by chromatographic and mass spectrometry flow injection fingerprints combined with principal component analysis. *J. Agric. Food Chem.* **2013**, *61*, 2957−2963.

(23) Gao, B.; Lu, Y.; Qin, F.; Chen, P.; Shi, H.; Charles, D.; Yu, L. Differentiating organic from conventional peppermints using chromatographic and flow-injection mass spectrometric (FIMS) Fingerprints. *J. Agric. Food Chem.* **2012**, *60*, 11987−11994.

(24) Lu, Y.; Gao, B.; Chen, P.; Charles, D.; Yu, L. Characterisation of organic and conventional sweet basil leaves using chromatographic and flow-injection mass spectrometric (FIMS) fingerprints combined with principal component analysis. *Food Chem.* **2014**, *154*, 262−268.

(25) Cavero, S.; Garcıa-Risco, M. R.; Marın, F. R.; Jaime, L.; Santoyo, S.; Senorans, F. J.; Reglero, G.; Ibanez, E. Supercritical fluid extraction of antioxidant compounds from oregano chemical and functional characterization via LC−MS and in vitro assays. *J. Supercrit. Fluids* **2006**, *38*, 62−69.

(26) Lin, L. Z.; Mukhopadhyay, S.; Robbins, R. J.; Harnly, J. M. Identification and quantification of flavonoids of Mexican oregano (*Lippia graveolens*) by LC-DAD-ESI/MS analysis. *J. Food Compos. Anal.* **2007**, *20*, 361−369.

(27) Shen, D.; Pan, M. H.; Wu, Q. L.; Park, C. H.; Juliani, H. R.; Ho, C. T.; Simon, J. E. LC-MS method for the simultaneous quantitation of the anti-inflammatory constituents in oregano (*Origanum* species). *J. Agric. Food Chem.* **2010**, *58*, 7119−7125.

(28) Exarchou, V.; Godejohann, M.; van Beek, T. A.; Gerothanassis, I. P.; Vervoort, J. LC-UV-solid-phase extraction-NMR-MS combined with a cryogenic folw probe and its application to the identification of compounds present in greek oregano. *Anal. Chem.* **2003**, *75*, 6288−6294.

JOURNAL OF AGRICULTURAL AND FOOD CHEMISTRY

Article

pubs.acs.org/JAFC

# Zinc Ionophore Activity of Quercetin and Epigallocatechin-gallate: From Hepa 1-6 Cells to a Liposome Model

Husam Dabbagh-Bazarbachi,[†,⊥] Gael Clergeaud,[‡,⊥] Isabel M. Quesada,[§] Mayreli Ortiz,[‡] Ciara K. O'Sullivan,*[,‡,∥] and Juan B. Fernández-Larrea*[,†]

[†]Nutrigenomics Research Group, Department of Biochemistry and Biotechnology, and [‡]Nanobiotechnology & Bioanalysis Group, Department of Chemical Engineering, Universitat Rovira i Virgili, 43007 Tarragona, Spain

[§]Vascular Biology Laboratory, IMBECU-CONICET, Facultad de Ciencias Médicas, Universidad Nacional de Cuyo, 5500 Mendoza, Argentina

[∥]Institució Catalana de Recerca i Estudis Avançats, 08010 Barcelona, Spain

**ABSTRACT:** Labile zinc, a tiny fraction of total intracellular zinc that is loosely bound to proteins and easily interchangeable, modulates the activity of numerous signaling and metabolic pathways. Dietary plant polyphenols such as the flavonoids quercetin (QCT) and epigallocatechin-gallate act as antioxidants and as signaling molecules. Remarkably, the activities of numerous enzymes that are targeted by polyphenols are dependent on zinc. We have previously shown that these polyphenols chelate zinc cations and hypothesized that these flavonoids might be also acting as zinc ionophores, transporting zinc cations through the plasma membrane. To prove this hypothesis, herein, we have demonstrated the capacity of QCT and epigallocatechin-gallate to rapidly increase labile zinc in mouse hepatocarcinoma Hepa 1-6 cells as well as, for the first time, in liposomes. In order to confirm that the polyphenols transport zinc cations across the plasma membrane independently of plasma membrane zinc transporters, QCT, epigallocatechin-gallate, or clioquinol (CQ), alone and combined with zinc, were added to unilamellar dipalmitoylphosphocholine/cholesterol liposomes loaded with membrane-impermeant FluoZin-3. Only the combinations of the chelators with zinc triggered a rapid increase of FluoZin-3 fluorescence within the liposomes, thus demonstrating the ionophore action of QCT, epigallocatechin-gallate, and CQ on lipid membrane systems. The ionophore activity of dietary polyphenols may underlay the raising of labile zinc levels triggered in cells by polyphenols and thus many of their biological actions.

**KEYWORDS:** *clioquinol, epigallocatechin-gallate, flavonoids, liposomes, quercetin, zinc ionophores*

## 1. INTRODUCTION

Quercetin (QCT), a water-insoluble flavonoid present in onions, nuts, and many other vegetables, and epigallocatechin-3-gallate (EGCG), a water-soluble flavonoid present in green tea, are among the most consumed and most studied polyphenols present in the human diet.[1] Flavonoids are considered bioactive micronutrients whose regular consumption, either as food components, or as dietary supplements and nutraceuticals,[2] entails benefits for human health, including prevention and amelioration of cancers,[3] diabetes, and cardiovascular[4] and neurodegenerative[5] diseases. Many of the health benefits of flavonoids have historically been ascribed to their antioxidant activity, which they exert directly by scavenging reactive oxygen species (ROS) and by chelating the redox-active transition metals iron and copper, which may act as ROS generators in biological systems.[6] Flavonoids also act as antioxidants indirectly by inhibiting redox-sensitive transcription factors and pro-oxidant enzymes as well as through induction of phase II and antioxidant enzymes.[7] However, it is currently believed that the levels of polyphenols achieved through ingestion are not enough to justify their wide array of biological actions. Beyond their antioxidant actions, flavonoids are also known to act as signaling molecules that, either directly or indirectly, interact with proteins and nucleic acids, thus modulating multiple cell signaling pathways, gene transcription, metabolic fluxes, and cell fate including apoptosis.[8,9]

Diverse polyphenols have been shown able to form complexes with the redox-inactive transition metal zinc.[10] Zinc is an essential micronutrient for humans, the deficiency of which causes multiple dysfunctions, including alterations of glucidic and lipidic metabolisms.[11] Within cells, the vast majority of zinc cations (in concentrations usually ranging from 100 to 300 $\mu$M for most cells) are tightly bound to proteins, functioning as a catalytic or structural component of an estimated 3000 mammalian proteins involved in virtually all cellular processes.[12] A minor fraction of intracellular zinc, termed labile zinc, exists in its free ionic form (picomolar concentrations) or loosely bound to proteins (in nanomolar concentrations). This pool of zinc is detectable by specific fluorophores with very high affinities for zinc cations at neutral pH such as Zinquin and FluoZin-3. Zinc ionophores such as pyrithione and clioquinol (CQ) have been used to increment labile zinc within cells and determine the fundamental roles that this zinc pool plays in cellular biology. Thus, free and labile zinc acts as second messenger molecule, which modulates the

Received: April 1, 2014
Revised: July 22, 2014
Accepted: July 22, 2014
Published: July 22, 2014

 © 2014 American Chemical Society  dx.doi.org/10.1021/jf5014633 | J. Agric. Food Chem. 2014, 62, 8085−8093

activity of many enzymes and thus signaling and metabolic pathways and cellular processes, including cell fate and apoptosis.[13,14] While many enzymes are inhibited by small elevations of zinc concentrations, others are activated.[15,16] Mammalian cells tightly control the subcellular distribution of zinc cations and the levels of labile zinc through the coordinated action of dedicated transmembrane zinc transporters and zinc-chelating metallothioneins.

Zinc from the extracellular milieu and from intracellular compartments enters the cytoplasm through 14 specialized transmembrane proteins of the ZIP/SLC39 family, whereas cytoplasmic extrusion of zinc toward organelles or the extracellular environment is performed by 10 transporters of the ZnT/SLC30 family, being ZnT1, located at the plasma membrane, the main regulator of cellular zinc efflux and export of excess zinc in most cells.[17] Within the cytoplasm, zinc may bind to metal free apo-metallothionein (apo-MT) to generate Zn−MT complexes. The apo-MT/Zn−MT ratio controls free and labile zinc concentrations. MT also serves as a ROS scavenger and heavy metal chelator, and the transcription of MT responds, in addition to zinc, to stress stimuli such as ROS, heavy metals, and proinflammatory cytokines.[18] In response to elevations of intracellular zinc, the zinc-sensor transcription factor MTF1 coordinately upregulates the expression of MT and ZnT1,[19] thus keeping zinc levels within a functional range. Excessively high levels of labile zinc are associated with cellular death through apoptosis.[20] Dysfunctions of MT and zinc transporters are promoting factors in cardiovascular diseases,[21] diabetes,[22] Alzheimer's disease,[23] and cancer.[24]

Several studies have shown that flavonoids affect zinc metabolism. For instance, rats fed during long periods with bicalain and rutin showed reduced hepatic levels of total zinc, as well as iron and copper, implying that flavonoids may sequester these metals and render them unavailable for absorption in a similar way as phytate.[25] Consistent with this, feeding obese rats with proanthocyanidins reverse dyslipidemia and lower protein levels of ZnT1 in the liver, reflecting lower levels of hepatic zinc.[26] Early in vitro studies showed that, in human intestinal Caco-2 cells, genistein enhanced the expression of MT, here regarded as an antioxidant enzyme,[27] while QCT increased the copper-induced expression of MT.[28] More recently, QCT was shown to enhance zinc uptake by Caco-2 cells, increasing total zinc accumulation and MT expression.[29] In contrast, grape seed flavonoids, produced a reduction in apical zinc uptake in Caco-2 cells, similar to that produced by phytate, whereas EGCG did not alter zinc absorption.[30] In prostate cancer cells, EGCG accelerated the accumulation of total zinc in the cytosol and mitochondria.[31] Two reports have shown that polyphenols may produce an increase of intracellular labile zinc. A water-soluble glycoside of the isoflavone genistin enhanced MT expression in human hepatocarcinoma HepG2 cells concomitantly increasing labile zinc and cellular death.[32] Furthermore, the stilbene resveratrol was shown to enhance total and labile zinc in normal human prostate epithelial cells, while not significantly affecting MT expression, and this was accompanied by increased cellular death. These authors suggested that the increment of labile zinc elicited by resveratrol might be due to the uptake of resveratrol−zinc complexes, followed by the dissociation of the complexes in the cytoplasm.[33]

Conversely, zinc may affect the bioactivity of flavonoids, as detailed in a few reports, including one that outlines the stimulating effect of zinc on the apoptotic effect of genistein in osteoclastic cells.[34] Zinc also yields EGCG effective in protecting cultured rat hepatocytes against hepatotoxin-induced cell injury[35] and enhances the antiproliferative, proapoptotic effects of EGCG on various lines of prostate cancer cells.[36] Zinc was also shown to affect the uptake of EGCG by prostate carcinoma cells, where Zn−EGCG chelates were less internalized by cells than EGCG alone, while mixtures of EGCG with zinc enhanced the transport of EGCG into the cells. These authors also showed that zinc enhances the incorporation of EGCG into liposomes.[37]

We have previously reported that the water-soluble flavonoid EGCG and the water-insoluble flavonoid QCT profoundly alter zinc homeostasis in cultured human and mouse hepatocarcinoma cells. Whereas EGCG reduced the levels of total intracellular zinc and the expression of MT and ZnT1,[38] QCT enhanced total zinc accumulation as well as MT and ZnT1 expression (M. Bustos, personal communication, 2011, Universitat Rovira i Virgili). However, both QCT and EGCG dose-dependently prevented zinc-induced toxicity, suggesting that most zinc cations in the culture medium are rendered unavailable to cells due to their chelation by flavonoids and the formation of flavonoid−zinc concatemers, as shown for iron and copper complexed with diverse polyphenols.[39] In addition, both polyphenols enhanced cytoplasmic levels of Zinquin-detectable labile zinc, suggesting that a fraction of the flavonoid molecules in the culture medium formed complexes with zinc that cross the plasma membrane; that is, the flavonoids may also act as zinc ionophores, transporting zinc cations across the plasma membrane independently from zinc transporters.

The aim of this work was to evaluate the capacity of QCT and EGCG to act as zinc ionophores. Clioquinol (CQ) was also tested in this study as it is a synthetic antitumor drug recently reported to induce apoptosis in diverse cells lines by enhancing intracellular labile zinc and therefore inferred to act as a water-soluble zinc ionophore.[40] We evaluated the ability of QCT, EGCG, and CQ to chelate zinc cations and the subsequent formation of a complex with FluoZin-3, a fluorophore that displays a very high affinity for zinc cations ($K_d$ = 15 nM).[41] The uptake of zinc by mouse hepatocarcinoma cells was measured fluorescently using FluoZin-3 in the presence and absence of QCT, EGCG, and CQ. This study was repeated using unilamellar liposomes with encapsulated FluoZin-3 to investigate whether the transport of the zinc cations across the cytoplasmic membrane to form a complex with FluoZin-3 was indeed enhanced by the presence of QCT, EGCG, or CQ or was simply due to the activity of cellular zinc transporters.

## 2. MATERIALS AND METHODS

**2.1. Chemicals.** The lipid 1,2-dipalmitoyl-*sn*-glycero-3-phosphocholine (DPPC), cholesterol, zinc chloride ($ZnCl_2$), QCT, EGCG, CQ, dimethyl sulfoxide (DMSO), ethanol, and phosphate-buffered saline (0.01 M PBS, pH 7.4) were bought from Sigma−Aldrich. Cell-impermeant FluoZin-3 tetrapotassium salt and cell permeant FluoZin-3 AM were bought from Molecular Probes. A Simplicity 185 Millipore water system was used to obtain Milli-Q water (18.2 mΩ·cm$^{-1}$) for the preparation of buffers and liposomes. The compounds QCT, EGCG, and CQ were dissolved as 100 μM solutions in 100% DMSO, aliquoted, and stored at −20 °C. $ZnCl_2$ was stored as 1 M solution in ethanol/PBS (50%/50% v/v). FluoZin-3 indicators were used at 10 μM in 100% DMSO.

**2.2. Cell Cultures and Treatments.** The mouse hepatoma cell line Hepa 1-6 was obtained from the European Collection of Cell Cultures (BW7756 ECACC) and propagated in Dulbecco's Modified Eagle medium (DMEM; BioWittaker) supplemented with 10% fetal

bovine serum (BioWittaker), 2 mM glutamine in 0.85% NaCl, 1000 U/mL penicillin/streptomycin, and 1.25 M HEPES. This medium contains 4.9 ± 0.2 $\mu$M zinc, as determined by flame atomic absorption spectroscopy (FAAS). Cells were cultured at 37 °C in a humidified, 5% $CO_2$-enriched atmosphere and routinely split every 3−4 days at a 1:5 ratio upon reaching approximately 80% confluence. For treatments, cells at 80% confluence were detached with Accutase (Sigma−Aldrich) and resuspended at a density of $5 \times 10^5$ cells/mL; 500 $\mu$L of this cell suspension ($25 \times 10^4$ cells) was then seeded per well in 24-well plates (Orange Scientific). Twenty four hours after plating, medium was removed, and the cells were treated by adding 100 $\mu$L of fresh medium containing either 50 $\mu$M $ZnCl_2$, 100 $\mu$M QCT, 100 $\mu$M EGCG, 100 $\mu$M CQ, or the combination of 50 $\mu$M $ZnCl_2$ with each chelator for 1 and 4 h, respectively. As a control experiment, untreated cells were incubated just with medium and vehicle (final 0.1% DMSO and 0.05% ethanol).

**2.3. Measurements of Cytoplasmic Labile Zinc in Hepa 1-6 Cells.** The intracellular levels of free and labile zinc cations were measured as the fluorescence emission of cells upon loading them with the membrane-permeant zinc specific detector FluoZin-3, using fluorescence microscopy as described.[42] Briefly, following cell treatment (Section 2.2), culture media were replaced with a fresh one containing 1.5 $\mu$M FluoZin-3 (AM, cell permeant) and incubated for 30 min at 37 °C. This medium was then removed, and the cells were washed three times with PBS, and the zinc-dependent FluoZin-3 fluorescence within cells was measured using a Nikon Eclipse TE2000-S microscope, with excitation set at 494 nm and emission at 516 nm. Fluorescent intensities were quantified using the NIS-Elements AR software (Nikon Instruments) and the software ImageJ, a Java-based image processing program developed at the NIH (National Institutes of Health).[43]

**2.4. Liposomes as Cell Membrane Models.** Homogeneous populations of liposomes were prepared using a previously reported method.[44] FluoZin-3 in a final concentration of 3 $\mu$M was mixed with 5 mL of PBS (0.01 M, pH 7.4) in a glass reactor protected from light-induced degradation, under stirring conditions and a blanket of argon gas. After 15 min, a mixture of DPPC and cholesterol (9:1 molar ratio) was added and maintained under stirring conditions and argon at 25 °C for another 15 min. The homogeneous mixture was then treated with a rapid pH jump from pH 7.4 to pH 11 and then back to pH 7.4 within a 3 s frame, followed by an equilibration step of 25 min where lipid clusters curl into FluoZin-3 encapsulating liposomes. The resulting FluoZin-3-loaded liposomes were purified using a Sephadex G-100 size-separation column and used immediately.

Liposomes with encapsulated FluoZin-3 were separately incubated with 10 $\mu$M QCT, EGCG, or CQ, in the presence and absence of 10 $\mu$M $ZnCl_2$. All the solutions were allowed to incubate at 25 °C for 30 min before measuring their fluorescence. For the kinetic experiment, liposomes loaded with FluoZin-3 were added to three different cuvettes, the fluorescence was measured for 15 min, followed by addition of $ZnCl_2$ (final 10 $\mu$M) to each cuvette, and the fluorescence emission was measured for another 15 min. Finally, QCT, EGCG, or CQ was added (final 10 $\mu$M) to each sample, and fluorescence emission was monitored over the duration of 1 h until the fluorescent intensity reached a plateau.

## 3. RESULTS

**3.1. QCT, EGCG, and CQ Increase the Cytoplasmic Labile Zinc in Hepa 1-6 Cells.** The increase of cytoplasmic labile zinc is modulated by the cellular zinc transporters, where the zinc ions are transported to the cytoplasm through specific channels of the ZIP family, bound to ionophore molecules that independently cross the lipid bilayer, or liberated from zinc-binding proteins such as metallothioneins (Figure 1).

In order to assess the effect of QCT, EGCG, CQ and zinc on cytoplasmic labile zinc, Hepa 1-6 cells were treated for 1 and 4 h with the chelators and supplemental zinc, and variations in the intracellular levels of labile zinc were measured as changes

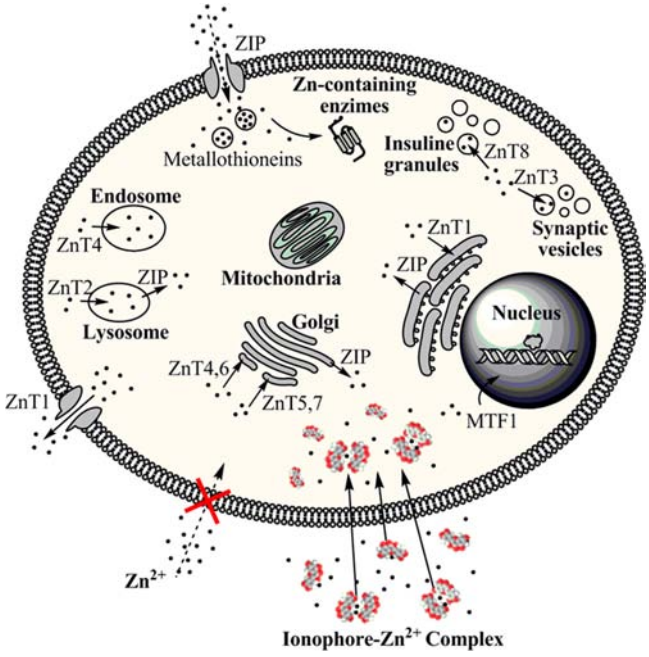


**Figure 1.** Schematic representation of zinc homeostasis. Intracellular labile zinc is modulated by the coordinated activity of a large family of zinc transporters (ZnT and ZIP) and zinc-binding proteins, such as metallothionein or ionophore molecules.

in the FluoZin-3 fluorescence intensity as described in Section 2.3. Figure 2 shows the fluorescent images of the Hepa 1-6 cells after 1 and 4 h of treatment. No significant increase in fluorescence was obtained when QCT or EGCG were added to the culture medium without additional zinc. Only CQ insignificantly enhanced the fluorescence in these conditions, that is, with basal zinc concentration in the culture medium, which is roughly 5 $\mu$M.

However, when 50 $\mu$M $ZnCl_2$ was added, both QCT and EGCG doubled the amount of FluoZin-3-detectable zinc after 1 h, and CQ increased this pool of zinc 10-fold with respect to the control (50 $\mu$M $ZnCl_2$ in the absence of any of QCT, EGCG, or CQ) (Figure 3), suggesting a slower ionophore action of the flavonoids as compared to CQ. After 4 h treatment with additional 50 $\mu$M $ZnCl_2$, all treatments triggered a significant increase in fluorescence intensity. In the case of the control, the increase of the cytoplasmic labile zinc is associated with the plasma membrane ZIP transporters, whereby zinc ions are transported into the cell. QCT doubled the amount of labile zinc attained with only 50 $\mu$M zinc, EGCG quadrupled this value, and CQ increased it 7-fold.

A closer view of intracellular distribution of FluoZin-3 fluorescence (Figure 4) after 4 h of treatment shows a similar punctuated pattern of labile zinc for CQ, EGCG, and QCT, suggesting similar ways of action for the three compounds.

**3.2. Zinc Ionophore Activity of QCT, EGCG, and CQ Using Liposomes as Membrane Models.** Increases of cytoplasmic labile zinc levels triggered by CQ and pyrithione in a variety of cell lines have been attributed to their ionophore activity, that is, to the capacity of CQ−zinc and pyrithione−zinc complexes to cross the plasma membrane. To our knowledge, however, the classification of CQ and pyrithione as zinc ionophores is based on their functional effect in cells, that is, the rapid increase in Zinquin-detectable or Fluozin-3-detectable intracellular zinc, but no direct biochemical assay has

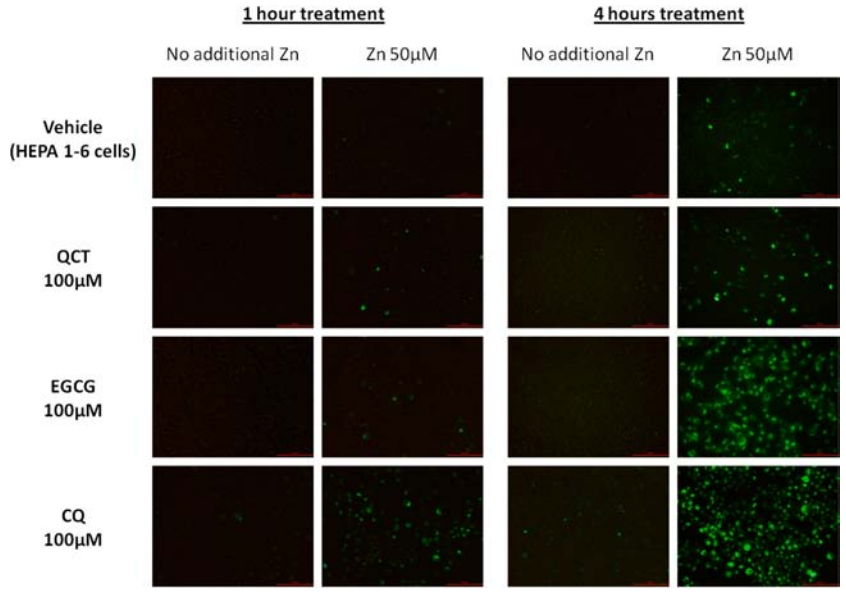


**Figure 2.** Effect of QCT, EGCG, and CQ on the cytoplasmic pool of labile zinc in Hepa 1-6 cells. Hepa 1-6 cells were first treated with 100 $\mu$M QCT, EGCG, or CQ, in the presence or absence of 50 $\mu$M $ZnCl_2$ for 1 and 4 h. The medium was then removed, and 3 $\mu$M FluoZin-3 (AM, cell permeant) was added. After 30 min incubation, cells were washed and examined using a confocal fluorescence microscope. Control cells were treated with vehicle (final 0.05% ethanol, 0.1% DMSO). Scale bars are 50 $\mu$m.

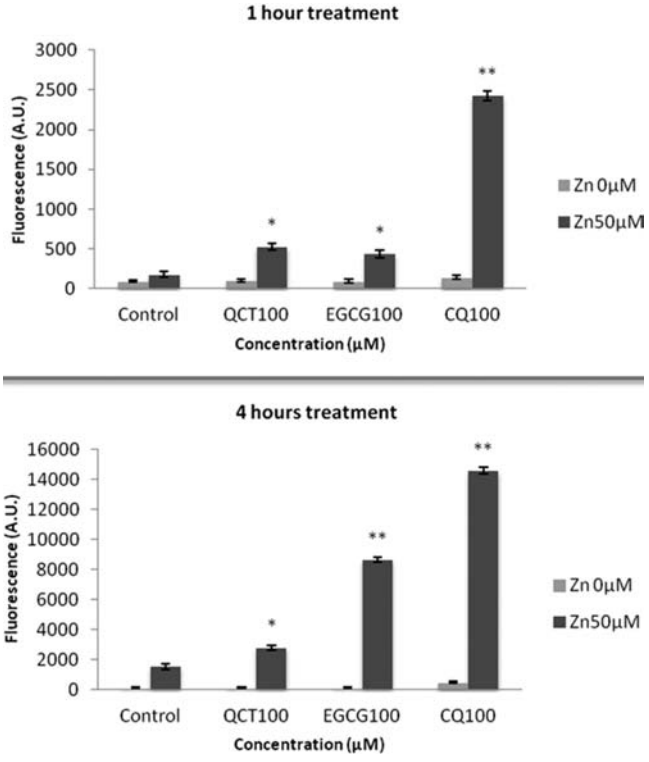


**Figure 3.** Intensity of FluoZin-3 fluorescence signal from images in Figure 2 was quantified using quanta program and considering an equal number of cells in each field. All values are mean ± SEM of three independent experiments. Significant differences between treatments were determined using one-way ANOVA (Tukey test). *$P \leq 0.05$; **$P \leq 0.01$.

been performed to discard the involvement of plasma membrane zinc importers or the origin of labile zinc from intracellular components on this effect. Furthermore, there is no report confirming that polyphenols are able to transport zinc across the plasma membrane independently of cell transport mechanisms, such as zinc transporters or endocytosis. To directly prove the ionophore action of the flavonoids and CQ, we tested their capacity to transport zinc cations across the lipid bilayer of protein-free liposomes as a model system that mimics a cell membrane devoid of protein and polysaccharide fractions. Taking advantage of our previously reported method for the rapid preparation of liposomes,[44] 3 $\mu$M concentration of cell-impermeant FluoZin-3 was encapsulated within unilamellar liposomes composed of DPPC/cholesterol in a 9:1 molar ratio. The resulting FluoZin-3-loaded liposomes were purified by passing the sample through a Sephadex G-100 size-separation column to remove the unencapsulated FluoZin-3 molecules. Dynamic light scattering (DLS) and $\zeta$ potential analysis were performed to clearly confirm the presence of stable liposomes within a size range 1−2 $\mu$m and surface charge around zero (Table 1).

The zinc ionophore activity of polyphenols was then tested as their capacity to transport zinc cations into the liposome cavity, interacting with the encapsulated zinc-dependent FluoZin-3 and consequently increasing the fluorescence signal within the liposomes (Figure 5). $ZnCl_2$ (10 $\mu$M) was added to the liposomal suspension in the absence and presence of 10 $\mu$M QCT, EGCG, and CQ, respectively, and zinc-dependent fluorescence intensity was measured over time. Following the addition of QCT, EGCG, or CQ, the Zn−polyphenol chelation complex is formed and transported across the bilayer, followed by interaction with the encapsulated FluoZin-3 probe, resulting in a significant and immediate increase in the fluorescence intensity.

Following the addition of 10 $\mu$M $ZnCl_2$ to the liposomes, a very small increase in the fluorescence appears due to the presence of a few free FluoZin-3 molecules that were not removed during the purification process and represent the background fluorescent signal. Even so, the fluorescent signal remains very low as zinc ions alone cannot cross the liposome membrane. The results from the kinetic experiment demon-


dx.doi.org/10.1021/jf5014633 | J. Agric. Food Chem. 2014, 62, 8085−8093

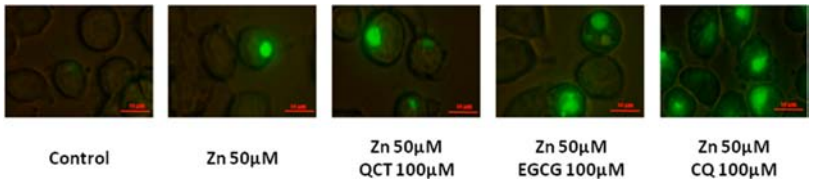


**Figure 4.** Subcellular localization of FluoZin-3 detectable zinc in Hepa 1-6 cells after 4 h treatment in the same samples as in Figure 2 showed at a greater magnification. Scale bars are 10 $\mu$m.

**Table 1. Dynamic Light Scattering and $\zeta$ Potential Measurements of Liposomes Loaded with FluoZin-3 before and after Treatments with 10 $\mu$M Quercetin (QCT10), 10 $\mu$M Epigallocatechin-3-gallate (EGCG10), or 10 $\mu$M Clioquinol (CQ10) in the Presence and Absence of 10 $\mu$M Zinc Chloride (Zn10)[a]**

| sample | size average ($\mu$m) | $\zeta$ potential (mV) |
|---|---|---|
| FluoZin-3-loaded liposomes | 1.4 ± 0.3 | −4.7 ± 2.5 |
| FluoZin-3-loaded liposomes + Zn10 | 1.1 ± 0.7 | −5.0 ± 5.9 |
| FluoZin-3-loaded liposomes + QCT10 | 1.2 ± 0.5 | −1.9 ± 4.1 |
| FluoZin-3-loaded liposomes + EGCG10 | 1.5 ± 0.4 | −6.9 ± 7.6 |
| FluoZin-3-loaded liposomes + CQ10 | 1.4 ± 0.2 | −3.0 ± 3.7 |
| FluoZin-3-loaded liposomes + Zn10 + QCT10 | 1.8 ± 0.2 | −1.2 ± 2.5 |
| FluoZin-3-loaded liposomes + Zn10 + EGCG10 | 1.6 ± 0.3 | −3.5 ± 3.2 |
| FluoZin-3-loaded liposomes + Zn10 + CQ10 | 1.4 ± 0.2 | −9.0 ± 2.7 |

[a]Final concentrations of solvents in the samples were 0.05% ethanol and 0.1% DMSO. Standard deviations were calculated from the mean data of a series of experiments ($n \geq 3$).

strate that QCT, EGCG, and CQ present different ionophore properties. CQ showed the strongest ionophore activity, producing a 35-fold increase in the zinc-dependent FluoZin-3 fluorescence intensity. Moreover, the maximum fluorescence is achieved rapidly after reaching the equilibrium in less than 15 min. QCT and EGCG also display a high ionophore activity in the system, although to a lesser extent as compared to the strong ionophore CQ, with 8- and 16-fold increases in fluorescence signal observed for QCT and EGCG, respectively. It can also be observed that both QCT and EGCG required more time (>60 min) to achieve the plateau phase, displaying slower chelation and transport kinetics (Figure 6).

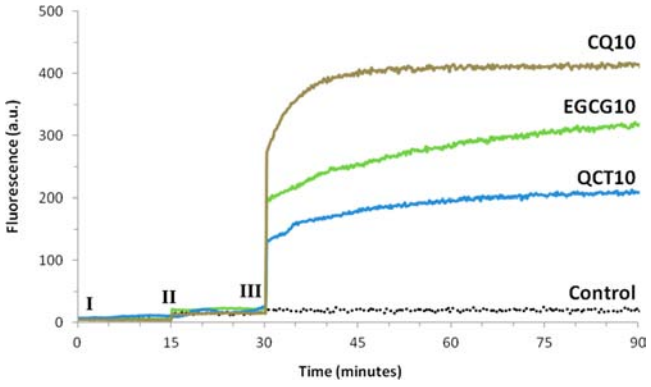


**Figure 6.** Effect of QCT, EGCG, and CQ on the uptake of zinc cations by liposomes. Zinc-dependent fluorescence emission of FluoZin-3 encapsulated within liposomes treated with zinc cations, polyphenols, and CQ. The fluorescence emission ($\lambda_{ex}$ = 494 nm; $\lambda_{em}$ = 516 nm) of purified FluoZin-3-loaded liposomes was recorded continuously. Background fluorescence (0−15 min) was negligible (I). Upon the addition of 10 $\mu$M $ZnCl_2$ to the liposomal suspensions (II), a small fluorescence signal was detected, presumably due to the presence of trace amounts of unencapsulated FluoZin-3 in the liposomal solutions. At time point 30 min, 10 $\mu$M quercetin (QCT10), epigallocatechin-3-gallate (EGCG10), clioquinol (CQ10), or vehicle (control, final 0.1% DMSO) were added to the liposomal solutions, and the fluorescence was monitored for one additional hour (III).

Confocal microscopy analysis was also performed in order to visualize and corroborate that the fluorescence produced by the interaction between zinc and FluoZin-3 was atributable to fluorescence in the inner part of the liposomes. As can be seen in Figure 7, fluorescence is only observed when the combination of $ZnCl_2$ with QCT, EGCG, or CQ is present, and the fluorescent signal comes from the inside part of the liposomes and not from the lipid membrane or the background

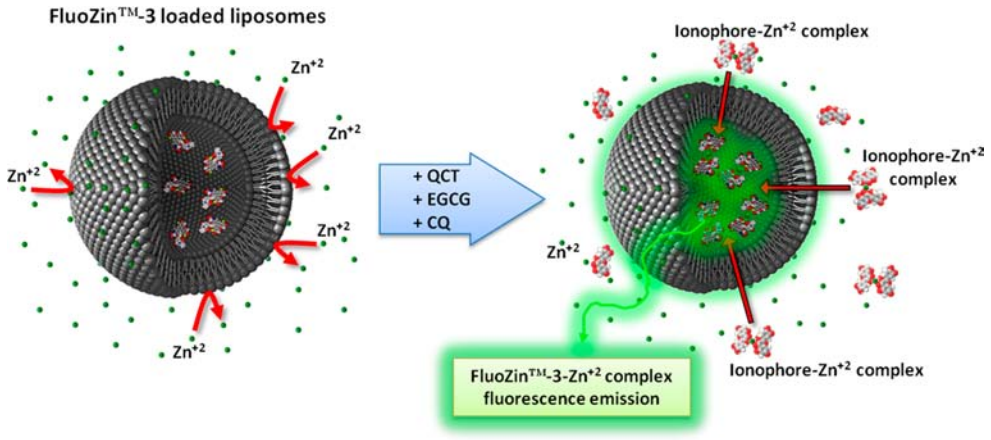


**Figure 5.** Schematic design of the FluoZin-3-loaded liposomes and the ionophore-like effect interpretation.


dx.doi.org/10.1021/jf5014633 | J. Agric. Food Chem. 2014, 62, 8085−8093

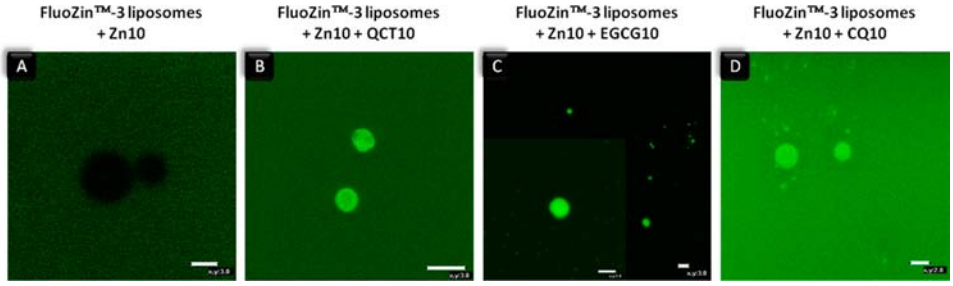


**Figure 7.** Effect of QCT, EGCG, and CQ on the uptake of zinc cations by liposomes. Three-dimensional confocal microscopy images of zinc-dependent fluorescence emission of FluoZin-3 loaded within liposomes treated with zinc cations, polyphenols, and CQ.

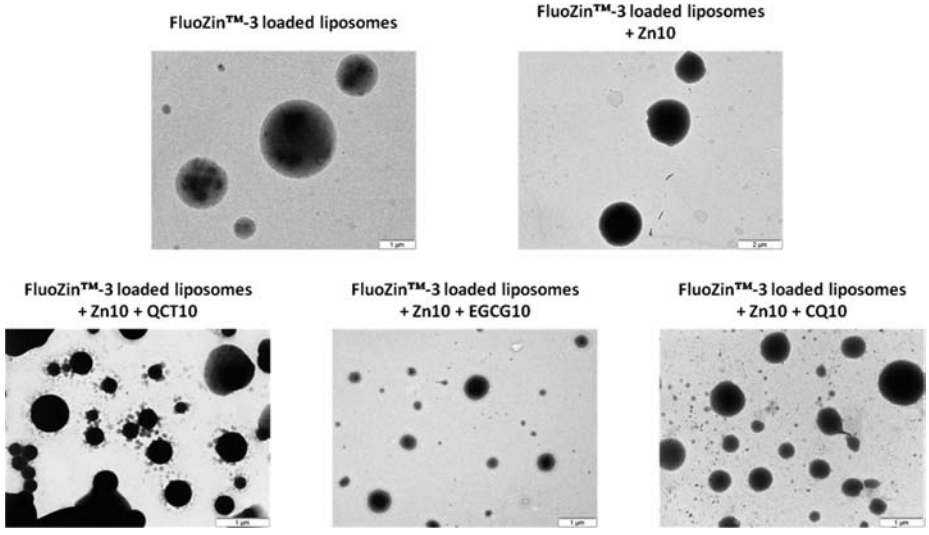


**Figure 8.** Effect of QCT, EGCG, and CQ on the uptake of zinc cations by liposomes. Transmission electron micrographs of liposomes with encapsulated FluoZin-3 after treatment with $ZnCl_2$, QCT, EGCG, and CQ.

solution. To further support this, stability studies were carried out in order to check whether the QCT, EGCG, or CQ can destabilize and break the lipid vesicles. All the liposomes were characterized using transmission electron microscopy (TEM), DLS, and $\zeta$ potential to check that their stability was maintained following exposure.

As shown in Figure 8, TEM images of the liposomes before and after treatments clearly demonstrate that liposome stability was not affected with the morphology and mean size (1−2 $\mu$m) being maintained. Moreover, the DLS and $\zeta$ potential results presented in Table 1, confirmed that the size of the liposomes and their surface charge were not significantly affected by the addition of zinc and/or the ionophores, thus demonstrating that FluoZin-3-loaded liposomes were not destabilized and their around-zero charge, due to the zwitterionic nature of main lipid component DPPC, was maintained, thus confirming that the fluorescence signal is due to transport of the Zn−QCT/EGCG/CQ complex across the lipid membrane.

## 4. DISCUSSION

The consequences that zinc chelation by flavonoids may have on zinc availability to the cells may in principle be dual: sequestering or ionophore, as shown for other well-characterized zinc-binding compounds.[45] On the one hand, the formation of zinc−flavonoid complexes may render zinc unavailable for cells, as do other dietary phytochemicals such as phytatesc[46] and zinc-chelator drugs such as TPEN that induce zinc deficiency in vitro and in vivo.[47] Metal chelating therapy using CQ has been proposed for neurodegenerative disorders that course with high levels of metal accumulation such as Alzheimer's and Parkinson.[48] On the other hand, flavonoids may form water-insoluble membrane-permeant complexes with zinc that cross the plasma membrane, and thereby act as zinc ionophores. The ionophore effect of zinc-binding compounds has been characterized for pyrithione and CQ. Both drugs chelate zinc cations and, when applied to cells, trigger a rapid increase of the intracellular pool of zinc that is detectable with different fluorophores such as Zinquin or FluoZin-3. Thereafter, it is assumed that these chelators form membrane-permeable complexes that are transported into the cell and that, once within the cell, chelator−zinc complexes dissociate into the single compounds due to the low concentration of intracellular free and labile zinc, thus providing labile zinc cations. Although FluoZin-3 has been widely accepted as a fluorophore that specifically interacts with zinc,[49−52] a recent report has indicated that this marker may in fact suffer from a lack of specificity.[53] However, this has no impact on the proof-of-concept study reported here as zinc is the only ion present and studied and thus no interfering effect from other ions will occur. We have shown here that treatment of Hepa1-6 cells with zinc together with QCT, EGCG, or CQ elicits a rapid and drastic increase in FluoZin-3-detectable intracellular zinc. The same effect was previously observed using Zinquin upon treatments of HepG2 cells with combinations of zinc and EGCG or zinc and QCT.[38] In these cells, the upregulation of MT and ZnT1 by zinc was


dx.doi.org/10.1021/jf5014633 | J. Agric. Food Chem. 2014, 62, 8085−8093

enhanced by QCT. In contrast, EGCG decreased the intracellular zinc accumulation. Similar to QCT, the stilbene resveratrol efficiently chelates zinc in solution and enhances total and Zinquin-detectable cytoplasmic zinc in cultured human prostate epithelial cells, and this correlated with the antiproliferative action of resveratrol on cells.[33]

While an increasing effort has been made to understand the interaction of flavonoids with lipid bilayers,[54] no report has been published reporting the use of liposomes to demonstrate the zinc ionophore activity of polyphenols. Liposomes have been widely used as the simplest cell membrane systems in order to study the ionophore activity of molecules across the lipidic bilayer.[55] We have herein used a liposomal system to prove that zinc can transverse lipid bilayers when combined with flavonoids. It is not necessary to evoke the intervention of zinc transporters in the plasma membrane or the mobilization of zinc from intracellular compartments to account for the elevation of intracellular zinc levels in cells treated with flavonoids. The flavonoid-dependent transport of zinc cations into the liposomal cavity also implies that polyphenols may cross biological membranes when conjugated with metal cations. The mechanisms by which polyphenols enter the cells are largely unknown, but our results imply that complexation with metals may increase the bioavailability of polyphenols to cells.

There are several reports that strongly suggest that the demonstrated zinc ionophore effect on polyphenols will be observed in real physiological conditions if studied in vivo. Lee et al.[56] in 2002 has reported that a minor part of the EGCG found in plasma conserved its native form, and it has also been reported that the polyphenol metabolites still maintain their ability to chelate and form complexes with metal ions[30] and furthermore that nanomolar concentrations of polyphenols or their metabolites are able to modulate some metabolic pathways,[5,57,58] as does labile zinc in a picomolar to nanomolar concentration range.[14] While all these reports point toward the same ionophore effect being observed under physiological conditions, in a recent report by Oyama et al.,[59] the authors suggest the dual effect of CQ depending on the extracellular zinc concentration, where the known ionophore effect of CQ was only observed when extracellular zinc was available, and when zinc was not available in the extracellular environment, CQ could cross the membrane and chelate the intracellular zinc ions. To this end, ongoing work is looking at extending the proof-of-concept reported and demonstrated here with both liposomes and cellular models to true physiological conditions exploring the interactions between a range of polyphenols and polyphenol metabolites and zinc in a lower concentration range of picomolar to micromolar.

In conclusion, we have demonstrated that QCT, EGCG, and CQ rapidly increase intracellular labile zinc in Hepa 1-6 cells and that they function as ionophores for zinc in a liposomal system. Thus, natural flavonoids can be added to an arsenal of drugs that may be used to modulate zinc homeostasis and regulate zinc-dependent biological pathways.

## AUTHOR INFORMATION


### Corresponding Authors

*E-mail: ciara.osullivan@urv.cat.

*E-mail: juanbautista.fernandez@urv.cat.

### Author Contributions

[⊥]Husam Dabbagh-Bazarbachi and Gael Clergeaud contributed equally to this work.



### Funding

This work was supported by grant AGL2008-00387 from the Spanish Ministry of Education and Science. H.D. was granted a predoctoral grant from the University Rovira i Virgili.

### Notes

The authors declare no competing financial interest.


## ABBREVIATIONS USED

DPPC, 1,2-dipalmitoyl-*sn*-glycero-3-phosphocholine; EGCG, (−)-epigallocatechin-3-gallate; FluoZin-3, 2-[2-[2-[2-[bis(carboxylatomethyl)amino]-5-methoxyphenoxy]ethoxy]-4-(2,7-difluoro-3-oxido-6-oxo-4*a*,9*a*-dihydroxanthen-9-yl)-anilino]acetate; MRE, metal response element; MT, metallothionein; MTF-1, MRE-binding transcription factor-1; TPEN, *N*,*N*,*N*′,*N*′-tetrakis(2-phridylmethyl) ethylenediamine; Zinquin, ethyl (2-methyl-8-*p*-toluenesulfonamido-6-quinolyloxy); ZIP, ZRT/IRT related protein (SLC39 family of zinc transporters); ZnT, zinc transporter (SLC30 family of zinc transporters)

## REFERENCES


(1) Aron, P. M.; Kennedy, J. A. Flavan-3-ols: Nature, occurrence and biological activity. *Mol. Nutr. Food Res.* **2008**, *52*, 79−104.

(2) Egert, S.; Rimbach, G. Which sources of flavonoids: Complex diets or dietary supplements? *Adv. Nutr.* **2011**, *2*, 8−14.

(3) Ramos, S. Cancer chemoprevention and chemotherapy: Dietary polyphenols and signalling pathways. *Mol. Nutr. Food Res.* **2008**, *52*, 507−526.

(4) Jagtap, S.; Meganathan, K.; Wagh, V.; Winkler, J.; Hescheler, J.; Sachinidis, A. Chemoprotective mechanism of the natural compounds, epigallocatechin-3-O-gallate, quercetin and curcumin against cancer and cardiovascular diseases. *Curr. Med. Chem.* **2009**, *16*, 1451−1462.

(5) Williams, R. J.; Spencer, J. P. E. Flavonoids, cognition, and dementia: Actions, mechanisms, and potential therapeutic utility for Alzheimer disease. *Free Radical Biol. Med.* **2012**, *52*, 35−45.

(6) Selvaraj, S.; Krishnaswamy, S.; Devashya, V.; Sethuraman, S.; Krishnan, U. M. Flavonoid−metal ion complexes: A novel class of therapeutic agents. *Med. Res. Rev.* **2014**, *34*, 677−702.

(7) Na, H.-K.; Surh, Y.-J. Modulation of Nrf2-mediated antioxidant and detoxifying enzyme induction by the green tea polyphenol EGCG. *Food Chem. Toxicol.* **2008**, *46*, 1271−1278.

(8) Williams, R. J.; Spencer, J. P. E.; Rice-Evans, C. Flavonoids: Antioxidants or signalling molecules? *Free Radical Biol. Med.* **2004**, *36*, 838−849.

(9) Ramos, S. Effects of dietary flavonoids on apoptotic pathways related to cancer chemoprevention. *J. Nutr. Biochem.* **2007**, *18*, 427−442.

(10) Le Nest, G.; Caille, O.; Woudstra, M.; Roche, S.; Burlat, B.; Belle, V.; Guigliarelli, B.; Lexa, D. Zn−polyphenol chelation: Complexes with quercetin, (+)-catechin, and derivatives: II Electrochemical and EPR studies. *Inorg. Chim. Acta* **2004**, *357*, 2027−2037.

(11) Prasad, A. S. Discovery of human zinc deficiency: 50 years later. *J. Trace Elem. Med. Biol.* **2012**, *26*, 66−69.

(12) Maret, W. Zinc biochemistry: From a single zinc enzyme to a key element of life. *Adv. Nutr.* **2013**, *4*, 82−91.

(13) Fukada, T.; Yamasaki, S.; Nishida, K.; Murakami, M.; Hirano, T. Zinc homeostasis and signaling in health and diseases. *J. Biol. Inorg. Chem.* **2011**, *16*, 1123−1134.

(14) Maret, W. Metals on the move: Zinc ions in cellular regulation and in the coordination dynamics of zinc proteins. *Biometals* **2011**, *24*, 411−418.

(15) Wilson, M.; Hogstrand, C.; Maret, W. Picomolar concentrations of free zinc(II) ions regulate receptor protein-tyrosine phosphatase $\beta$ activity. *J. Biol. Chem.* **2012**, *287*, 9322−9326.

(16) Maret, W. Inhibitory zinc sites in enzymes. *Biometals* **2013**, *26*, 197−204.

(17) Cousins, R. J.; Liuzzi, J. P.; Lichten, L. A. Mammalian zinc transport, trafficking, and signals. *J. Biol. Chem.* **2006**, *281*, 24085−24089.
(18) Krężel, A.; Maret, W. Thionein/metallothionein control Zn(II) availability and the activity of enzymes. *J. Biol. Inorg. Chem.* **2008**, *13*, 401−409.
(19) Laity, J. H.; Andrews, G. K. Understanding the mechanisms of zinc-sensing by metal-response element binding transcription factor-1 (MTF-1). *Arch. Biochem. Biophys.* **2007**, *463*, 201−210.
(20) Truong-Tran, A. Q.; Ho, L. H.; Chai, F.; Zalewski, P. D. Cellular zinc fluxes and the regulation of apoptosis/gene-directed cell death. *J. Nutr.* **2000**, *130*, 1459S−1466S.
(21) Little, P. J.; Bhattacharya, R.; Moreyra, A. E.; Korichneva, I. L. Zinc and cardiovascular disease. *Nutrition* **2010**, *26*, 1050−1057.
(22) Myers, S. A.; Nield, A.; Myers, M. Zinc transporters, mechanisms of action and therapeutic utility: Implications for type 2 diabetes mellitus. *J. Nutr. Metab.* **2012**, *2012*, 173712.
(23) Watt, N. T.; Whitehouse, I. J.; Hooper, N. M. The role of zinc in Alzheimer's disease. *Int. J. Alzheimer's Dis.* **2010**, *2011*, 971021.
(24) Hogstrand, C.; Kille, P.; Nicholson, R. I.; Taylor, K. M. Zinc transporters and cancer: A potential role for ZIP7 as a hub for tyrosine kinase activation. *Trends Mol. Med.* **2009**, *15*, 101−111.
(25) Gao, Z.; Xu, H.; Chen, X.; Chen, H. Antioxidant status and mineral contents in tissues of rutin and baicalin fed rats. *Life Sci.* **2003**, *73*, 1599−1607.
(26) Baiges, I.; Palmfeldt, J.; Blade, C.; Gregersen, N.; Arola, L. Lipogenesis is decreased by grape seed proanthocyanidins according to liver proteomics of rats fed a high fat diet. *Mol. Cell Proteomics* **2010**, *9*, 1499−513.
(27) Kuo, S.-M.; Leavitt, P. S. Genistein increases metallothionein expression in human intestinal cells, Caco-2. *Biochem. Cell Biol.* **1999**, *77*, 79−88.
(28) Kuo, S.-M.; Huang, C.-T.; Blum, P.; Chang, C. Quercetin cumulatively enhances copper induction of metallothionein in intestinal cells. *Biol. Trace Elem. Res.* **2001**, *84*, 1−10.
(29) Sreenivasulu, K.; Raghu, P.; Nair, K. M. Polyphenol-rich beverages enhance zinc uptake and metallothionein expression in Caco-2 cells. *J. Food Sci.* **2010**, *75*, H123−H128.
(30) Kim, E.-Y.; Pai, T.-K.; Han, O. Effect of bioactive dietary polyphenols on zinc transport across the intestinal Caco-2 cell monolayers. *J. Agric. Food Chem.* **2011**, *59*, 3606−3612.
(31) Yang, J.; Yu, H.; Sun, S.; Zhang, L.; Das, U.; Ruan, H.; He, G.; Shen, S. Mechanism of free Zn(2+) enhancing inhibitory effects of EGCG on the growth of PC-3 cells: Interactions with mitochondria. *Biol. Trace Elem. Res.* **2009**, *131*, 298−310.
(32) Chung, M. J.; Kang, A.-Y.; Lee, K. M.; Oh, E.; Jun, H.-J.; Kim, S.-Y.; Auh, J. H.; Moon, T.-W.; Lee, S.-J.; Park, K.-H. Water-soluble genistin glycoside isoflavones Up-regulate antioxidant metallothionein expression and scavenge free radicals. *J. Agric. Food Chem.* **2006**, *54*, 3819−3826.
(33) Zhang, J. J.; Wu, M.; Schoene, N. W.; Cheng, W.-H.; Wang, T. T. Y.; Alshatwi, A. A.; Alsaif, M.; Lei, K. Y. Effect of resveratrol and zinc on intracellular zinc status in normal human prostate epithelial cells. *Am. J. Physiol.: Cell Physiol.* **2009**, *297*, C632−C644.
(34) Uchiyama, S.; Yamaguchi, M. Genistein and zinc synergistically stimulate apoptotic cell death and suppress RANKL signaling-related gene expression in osteoclastic cells. *J. Cell. Biochem.* **2007**, *101*, 529−542.
(35) Kagaya, N.; Kawase, M.; Maeda, H.; Tagawa, Y.-i.; Nagashima, H.; Ohmori, H.; Yagi, K. Enhancing effect of zinc on hepatoprotectivity of epigallocatechin gallate in isolated rat hepatocytes. *Biol. Pharm. Bull.* **2002**, *25*, 1156−1160.
(36) Sun, S.-l.; He, G.-q.; Yu, H.-n.; Yang, J.-g.; Borthakur, D.; Zhang, L.-c.; Shen, S.-r.; Das, U. N. Free $Zn^{2+}$ enhances inhibitory effects of EGCG on the growth of PC-3 cells. *Mol. Nutr. Food Res.* **2008**, *52*, 465−471.
(37) Yang, J. G.; Yu, H. N.; Sun, S. L.; Zhang, L. C.; He, G. Q.; Das, U. N.; Ruan, H.; Shen, S. R. Epigallocatechin-3-gallate affects the growth of LNCaP cells via membrane fluidity and distribution of cellular zinc. *J. Zhejiang Univ., Sci., B* **2009**, *10*, 411−21.
(38) Quesada, I. M.; Bustos, M.; Blay, M.; Pujadas, G.; Ardèvol, A.; Salvadó, M. J.; Bladé, C.; Arola, L.; Fernández-Larrea, J. Dietary catechins and procyanidins modulate zinc homeostasis in human HepG2 cells. *J. Nutr. Biochem.* **2011**, *22*, 153−163.
(39) Hider, R. C.; Liu, Z. D.; Khodr, H. H. Metal chelation of polyphenols. In *Methods in Enzymology*; Lester, P., Ed.; Academic Press: Waltham, MA, 2001; Vol. 335, pp 190−203.
(40) Ding, W.-Q.; Liu, B.; Vaught, J. L.; Yamauchi, H.; Lind, S. E. Anticancer activity of the antibiotic clioquinol. *Cancer Res.* **2005**, *65*, 3389−3395.
(41) Li, Y.-M.; Shi, J.; Wu, X.; Luo, Z.-F.; Wang, F.-L.; Guo, Q.-X. Tracing of intracellular zinc(II) fluorescence flux to monitor cell apoptosis by using FluoZin-3AM. *Cell Biochem. Funct.* **2009**, *27*, 417−423.
(42) Yu, H.; Zhou, Y.; Lind, S. E.; Ding, W.-Q. Clioquinol targets zinc to lysosomes in human cancer cells. *Biochem. J.* **2009**, *417*, 133−139.
(43) Collins, T. J. ImageJ for microscopy. *Biotechniques* **2007**, *43*, 25−30.
(44) Genç, R. k.; Ortiz, M.; O'Sullivan, C. K. Curvature-tuned preparation of nanoliposomes. *Langmuir* **2009**, *25*, 12604−12613.
(45) Ding, W.-Q.; Yu, H.-J.; Lind, S. E. Zinc-binding compounds induce cancer cell death via distinct modes of action. *Cancer Lett.* **2008**, *271*, 251−259.
(46) Wise, A. Phytate and zinc bioavailability. *Int. J. Food Sci. Nutr.* **1995**, *46*, 53−63.
(47) Li, B.; Tan, Y.; Sun, W.; Fu, Y.; Miao, L.; Cai, L. The role of zinc in the prevention of diabetic cardiomyopathy and nephropathy. *Toxicol. Mech. Methods* **2013**, *23*, 27−33.
(48) Bareggi, S. R.; Cornelli, U. Clioquinol: Review of its mechanisms of action and clinical uses in neurodegenerative disorders. *CNS Neurosci. Ther.* **2012**, *18*, 41−46.
(49) Muylle, F. R.; Adriaensen, D.; Coen, W.; Timmermans, J.-P.; Blust, R. Tracing of labile zinc in live fish hepatocytes using FluoZin-3. *Biometals* **2006**, *19*, 437−450.
(50) Wessels, I.; Haase, H.; Engelhardt, G.; Rink, L.; Uciechowski, P. Zinc deficiency induces production of the proinflammatory cytokines IL-1$\beta$ and TNF$\alpha$ in promyeloid cells via epigenetic and redox-dependent mechanisms. *J. Nutr. Biochem.* **2013**, *24*, 289−297.
(51) Kim, J.-H.; Jeon, J.; Shin, M.; Won, Y.; Lee, M.; Kwak, J.-S.; Lee, G.; Rhee, J.; Ryu, J.-H.; Chun, C.-H.; Chun, J.-S. Regulation of the catabolic cascade in osteoarthritis by the zinc-ZIP8-MTF1 axis. *Cell* **2014**, *156*, 730−743.
(52) Chevallet, M.; Jarvis, L.; Harel, A.; Luche, S.; Degot, S.; Chapuis, V.; Boulay, G.; Rabilloud, T.; Bouron, A. Functional consequences of the over-expression of TRPC6 channels in HEK cells: Impact on the homeostasis of zinc. *Metallomics* **2014**, *6*, 1269−1276.
(53) Landero Figueroa, J. A.; Subramanian Vignesh, K.; Deepe, G. S., Jr.; Caruso, J. Selectivity and specificity of small molecule fluorescent dyes/probes used for the detection of $Zn^{2+}$ and $Ca^{2+}$ in cells. *Metallomics* **2014**, *6*, 301−315.
(54) Efimova, S. S.; Ostroumova, O. S. Effect of dipole modifiers on the magnitude of the dipole potential of sterol-containing bilayers. *Langmuir* **2012**, *28*, 9908−9914.
(55) Sankaram, M. B.; Shastri, B. P.; Easwaran, K. R. K. Interaction of carrier ionophores with phospholipid vesicles. *Biochemistry* **1987**, *26*, 4936−4941.
(56) Lee, M.-J.; Maliakal, P.; Chen, L.; Meng, X.; Bondoc, F. Y.; Prabhu, S.; Lambert, G.; Mohr, S.; Yang, C. S. Pharmacokinetics of tea catechins after ingestion of green tea and (−)-epigallocatechin-3-gallate by humans: Formation of different metabolites and individual variability. *Cancer Epidemiol., Biomarkers Prev.* **2002**, *11*, 1025−1032.
(57) Schroeter, H.; Bahia, P.; Spencer, J. P. E.; Sheppard, O.; Rattray, M.; Cadenas, E.; Rice-Evans, C.; Williams, R. J. (−)Epicatechin stimulates ERK-dependent cyclic AMP response element activity and up-regulates GluR2 in cortical neurons. *J. Neurochem.* **2007**, *101*, 1596−1606.

(58) Vauzour, D.; Vafeiadou, K.; Rice-Evans, C.; Williams, R. J.; Spencer, J. P. E. Activation of pro-survival Akt and ERK1/2 signalling pathways underlie the anti-apoptotic effects of flavanones in cortical neurons. *J. Neurochem.* **2007**, *103*, 1355−1367.
(59) Oyama, T. M.; Ishida, S.; Okano, Y.; Seo, H.; Oyama, Y. Clioquinol-induced increase and decrease in the intracellular $Zn^{2+}$ level in rat thymocytes. *Life Sci.* **2012**, *91*, 1216−1220.

JOURNAL OF AGRICULTURAL AND FOOD CHEMISTRY

Article

pubs.acs.org/JAFC

# Total Myrosinase Activity Estimates in Brassica Vegetable Produce

Edward B. Dosz,[†] Kang-Mo Ku,[‡,§] John A. Juvik,[‡] and Elizabeth H. Jeffery*[,†]

[†]Department of Food Science and Human Nutrition and [‡]Department of Crop Sciences, University of Illinois at Urbana−Champaign, Urbana, Illinois 61801-3838, United States

Supporting Information

**ABSTRACT:** Isothiocyanates, generated from the hydrolysis of glucosinolates in plants of the Brassicaceae family, promote health, including anticancer bioactivity. Hydrolysis requires the plant enzyme myrosinase, giving myrosinase a key role in health promotion by brassica vegetables. Myrosinase measurement typically involves isolating crude protein, potentially underestimating activity in whole foods. Myrosinase activity was estimated using unextracted fresh tissues of five broccoli and three kale cultivars, measuring the formation of allyl isothiocyanate (AITC) and/or glucose from exogenous sinigrin. A correlation between AITC and glucose formation was found, although activity was substantially lower measured as glucose release. Using exogenous sinigrin or endogenous glucoraphanin, concentrations of the hydrolysis products AITC and sulforaphane correlated ($r$ = 0.859; $p$ = 0.006), suggesting that broccoli shows no myrosinase selectivity among sinigrin and glucoraphanin. Measurement of AITC formation provides a novel, reliable estimation of myrosinase-dependent isothiocyanate formation suitable for use with whole vegetable food samples.

**KEYWORDS:** *broccoli, kale, myrosinase activity, sulforaphane, isothiocyanates*

## INTRODUCTION

Brassica vegetable crops contain diverse health-promoting compounds including glucosinolates (GSL), flavonoids, carotenoids, and vitamins. Glucosinolates themselves are not bioactive but are converted into multiple hydrolysis products, including isothiocyanates and nitriles, through the action of the endogenous enzyme myrosinase.[1] The health benefits of broccoli are strongly associated with isothiocyanates including sulforaphane (SF), phenethyl isothiocyanate (PEITC), and allyl isothiocyanate (AITC). The chemical structure of hydrolysis products depends on the structure of the GSL side chain and reaction conditions, including the presence of myrosinase cofactors such as epithiospecifier protein (ESP). Abundance of ESP favors formation of nitriles, which not only lack anticancer activity, but are alternative hydrolysis products to bioactive isothiocyanates, thus lowering isothiocyanate levels.[1,2]

Recent studies report that destruction of myrosinase during processing of commercially available frozen broccoli products was the probable cause for little to no formation of the anticancer compound SF upon crushing the material.[3,4] We and others find that in the absence of myrosinase, only about 10% of the glucoraphanin present in a supplement or processed broccoli product appears as SF and its metabolites in plasma and urine.[5,6] A larger study found that SF absorption from a broccoli product lacking myrosinase may vary between <1% and approximately 40% of the starting dose of glucoraphanin.[7] Therefore, if consumers are to gain the full health benefit of brassica foods, research is needed to find ways to enhance GSL hydrolysis in brassica vegetable produce. A first step in such an endeavor is the accurate measurement of myrosinase activity contained within a whole brassica vegetable sample.

There are many excellent studies of myrosinase focused on the biochemistry of the purified or semipurified enzyme, rather than measurement in unextracted food samples.[1] Current methods for analyzing myrosinase activity measure either substrate disappearance or product (glucose) formation, following addition of an exogenous substrate, sinigrin. A less common measure of myrosinase activity is by the measurement of the acid release rate, by titrating the sample with 1 mM NaOH, using a dedicated pH meter coupled with a dispenser in a thermostatically controlled cell.[8]

Myrosinase activity is typically reported in terms of the hydrolysis of sinigrin, for which a unit of activity is defined as that which hydrolyzes 1 $\mu$mol of sinigrin per minute, and is measured by either sinigrin disappearance or glucose release. Each has benefits as well as limitations, affecting the calculated enzymatic activity. Disappearance of exogenous sinigrin, measured at 227 nm, suffers from interference from other components in the plant sample, including ascorbic acid, endogenous GSL, and proteins.[9] Quantitative analysis of glucosinolates is most commonly carried out by HPLC-UV detection following stabilization by desulfation; indole glucosinolates such as desulfo-neoglucobrassicin are found to have very different response factors compared to desulfo-sinigrin: 0.2 compared to 1, when measured at 227 nm.[10] It is likely that complete, sulfated, glucosinolates will also vary in their molar absorption at 227 nm. Concern for interference from endogenous GSL with differing absorbances has been overcome by hydrolysis of endogenous GSL prior to HPLC measurement of exogenous sinigrin disappearance.[11] A second and major advantage of endogenous GSL hydrolysis followed by HPLC for sinigrin disappearance is the lack of dependence on real-time enzyme analysis using spectrophotometry and, thus, the ability to measure activity in a whole homogenate rather than a clear solution.[11] Glucose release during GSL

Received: April 9, 2014
Revised: June 20, 2014
Accepted: July 3, 2014
Published: July 22, 2014

ACS Publications © 2014 American Chemical Society

hydrolysis is typically measured as a coupled enzyme assay, either glucose oxidase-peroxidase with a chromophore such as 2,2′-azinobis(3-ethylbenzothiazoline-6-sulfonic acid) (ABTS) and 4-hydroxybenzoic acid or hexokinase-glucose-6-phosphate dehydrogenase measuring NADPH at 340 nm. Whereas the glucose release method is sensitive and reliably measures myrosinase activity in a purified system, in the whole vegetable matrix it can suffer from interference from endogenous glucose and antioxidant compounds including ascorbic acid and polyphenolics.[9,12] Hexokinase-glucose-6-phosphate dehydrogenase similarly suffers from interference by endogenous glucose, flavonoids, and decomposition products of ascorbate.[9,12]

To overcome interference, endogenous glucose and GSL are typically removed by aqueous extraction, followed by semi-purification of the crude myrosinase protein, which is time-consuming and alters the protein content and, thus, the reported myrosinase specific activity. Additionally, myrosinase exists in both soluble and insoluble forms in plant material, so extraction could lead to loss of insoluble myrosinase, due to the pellet being discarded following aqueous extraction, and even loss of some soluble myrosinase, due to multiple rinses.[13,14] Therefore, it appears that the myrosinase activity estimated in purified protein, although useful for mechanistic studies, may not directly reflect the myrosinase present in unextracted brassica vegetable tissue samples.

There is only one reported method for myrosinase activity, developed using red cabbage and since applied to other vegetables, which uses a whole vegetable homogenate.[11] The homogenate is sieved to remove larger particles and then incubated for 2 h to hydrolyze potentially interfering GSL and estimates myrosinase as the disappearance of exogenous sinigrin using HPLC.[11,15] This paper offers an alternative method to evaluate total myrosinase activity in whole brassica vegetable homogenates, on the basis of isothiocyanate formation, and compares this to measures of myrosinase activity using a modified glucose release assay.

## MATERIALS AND METHODS

**Sample Collection and Preparation.** Broccoli florets, leaves, and roots (*Brassica oleracea* L. cv. 'Sultan', 'Marathon', 'Patron', 'Pirate', 'Maximo') and kale leaves and roots (*B. oleracea* L. cv. 'Red Winter', 'Red Russian', 'Dwarf Blue Curled Vates') were grown at the University of Illinois in 2013, harvested at commercial maturity, frozen in the field using liquid nitrogen, and transported to the laboratory on dry ice for further processing. Samples were freeze-dried for later analysis of myrosinase activity. In previous work, freeze-drying was shown not to affect the content of glucosinolates or sulforaphane formation during hydrolysis.[16] GSL were measured as previously described.[17]

**Myrosinase Activity Using Allyl Isothiocyanate and Sulforaphane Formation.** Myrosinase activity is traditionally measured as sinigrin hydrolysis.[18] However, broccoli contains little or no sinigrin,[17,19] so we developed an assay that could compare the hydrolysis of exogenous sinigrin with that of endogenous glucoraphanin, by monitoring the concomitant formation of AITC and SF. Myrosinase activity was initiated by the addition of sinigrin (final concentration = 2 mM; Sigma, St. Louis, MO, USA) to 100 mg of freeze-dried broccoli or kale tissue in 5.0 mL of water followed by incubation at 25 °C. Samples (0.5 mL) were removed at 5 min, spiked with an internal standard of benzyl isothiocyanate (Sigma), then immediately extracted into dichloromethane (0.5 mL), centrifuged for 1 min at 16000*g*, and analyzed for AITC and SF content (see below). In later studies, samples were removed from the incubation at different times, as shown in the figures. For calculation of myrosinase activity, the first 3 min was used on the basis of the linearity of isothiocyanate generation.

**Allyl Isothiocyanate and Sulforaphane Measurement.** Using an Agilent model 7683B series autosampler, 1 μL of dichloromethane extract was injected onto an Agilent 6890N gas chromatography system equipped with a single flame ionization detector (Agilent Technologies, Santa Clara, CA, USA). Samples were separated using a 30 m × 0.32 mm J&W HP-5 capillary column (Agilent Technologies). After an initial hold at 40 °C for 2 min, the oven temperature was increased by 10 °C/min to 260 °C and held for 10 min. Injector temperature was 200 °C; detector temperature was 280 °C. Helium carrier gas flow rate was 25 mL/min. Results were quantitated against standards of SF (LKT Laboratories, St. Paul, MN, USA) and AITC (Sigma).

**Determination of Myrosinase Activity Using Glucose Release.** The glucose release assay has traditionally utilized an aqueous extract of plant material. Because we were interested in the activity in the whole food, we chose to run the assay using freeze-dried plant material, which was subjected to extraction only after the hydrolysis was complete. In other aspects, the assay was similar to published methods.[18,20] Briefly, freeze-dried, powdered plant material (50 mg) was weighed in duplicate into 2 mL tubes, and 1 mL of sinigrin (10 mM) was added to each tube. After 10 s of vigorous vortexing, one of the paired samples was put directly into a heating block (95 °C) for 10 min to inactivate the myrosinase enzyme (zero time blank). The second sample was incubated at 40 °C for 30 min and then inactivated as outlined above. After inactivation, samples were cooled on ice for 5 min and then centrifuged at 16000*g* for 2 min. The supernatants were diluted 96-fold, and aliquots (30 μL) or glucose standard was added in a 96-well plate, followed by the addition of 200 μL of an ABTS−glucose solution [2.7 mM ABTS, 1000 units of peroxidase (Type VI-A, Sigma), and 1000 units of glucose oxidase in 100 mL] and incubation for 20 min; absorbance was measured at 630 nm in a μQuant plate reader (Bio-Tek instruments, Winooski, VT, USA). Myrosinase activity was also measured for different incubation times, as shown in the figures. In another study, myrosinase activity was measured by adding water in place of sinigrin to compare myrosinase activity in the presence of exogenous GSL (sinigrin) and endogenous GSL.

**Soluble and Insoluble Myrosinase Activity.** Because we chose to measure myrosinase activity in unextracted plant material, we were interested in comparing myrosinase activity between freeze-dried brassica vegetable tissue and a crude protein plant extract more typical of published measurements: aqueous extracts were generated by extracting plant material into solutions containing ice-cold 10 mM sinigrin, followed by centrifugation at 16000*g* for 1 min. Supernatants containing soluble myrosinase were transferred to new tubes, brought to a final volume of 1 mL using sinigrin in water (10 mM), and either immediately heated (zero time blank) or incubated at 40 °C for 30 min. The myrosinase activity of the centrifugal pellet after crude protein extraction containing insoluble or bound myrosinase was also evaluated by adding 1 mL of 10 mM sinigrin, vortexing, and then heating immediately (zero time blank) or incubating at 40 °C for 30 min and then heating.

**Determination of Interference by Antioxidant Compounds in the Glucose Assay.** To measure interference to the ABTS−glucose assay by endogenous antioxidant compounds from plant samples, eight different concentrations of gallic acid ranging from 1.17 to 150 μM were incubated with glucose (5 μg fixed concentration), and the ABTS−glucose assay was conducted. Interference of glucose measurement by endogenous antioxidant compounds in the plant extracts ('Marathon' root, leaf, or floret) was also measured using the ABTS antioxidant assay.[21] Briefly, plant tissue extracts (30 μL of 50 mg/mL or 96-fold diluted samples) were added to 200 μL of ABTS in 96-well plates (absorption at 630 nm = 1.0), and absorbance was measured after 6 min.

**Statistical Analysis.** Statistical analysis was conducted using JMP 10 software (SAS Institute Inc., Cary, NC, USA). Student's *t* tests were used for comparing treatment groups. Fisher's least significant difference (LSD) test was conducted to compare means; $p < 0.05$

was accepted as significant. Pearson's correlation was conducted whereby pairs of myrosinase activities were compared.

## RESULTS AND DISCUSSION

As shown in Figure 1, myrosinase activity of whole freeze-dried broccoli floret tissue, measured as glucose release, is 63%

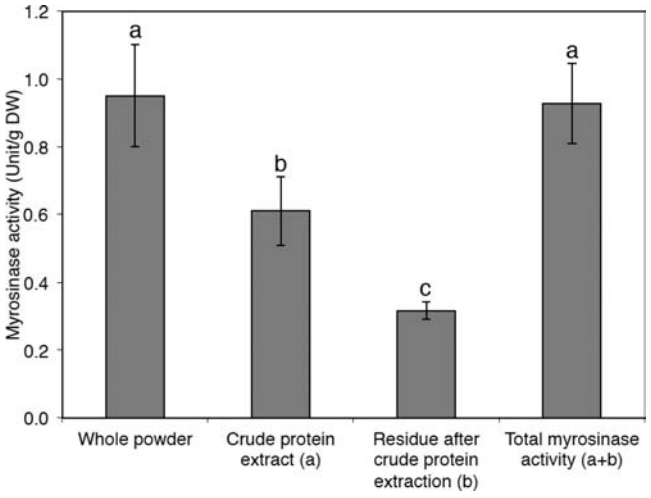


**Figure 1.** Myrosinase activity in whole freeze-dried 'Marathon' broccoli floret samples, crude protein extract (soluble myrosinase), centrifugal pellet after crude protein extraction (insoluble myrosinase), and total myrosinase activity (soluble + insoluble measures), measured as glucose appearance after 30 min of incubation. Mean ± SD ($n$ = 3). Different letters indicate significantly different values based on LSD test ($p < 0.05$). A unit is defined here as 1 $\mu$mol of glucose formed per minute, using 10 mM sinigrin as substrate.

greater than that of the corresponding aqueous extract. The freeze-dried broccoli floret powder best represents total myrosinase activity in a serving of broccoli. Interestingly, when the value for the crude protein extract (soluble myrosinase) was added to the value for myrosinase remaining in the pellet (insoluble myrosinase), this equaled the value obtained for the unextracted plant tissue, suggesting that this was a reasonable measure of soluble plus insoluble myrosinase activity. In a previous study measuring insoluble myrosinase from *Sinapis alba* seeds, the authors found that after three extractions, when the centrifugal pellet was resuspended and assayed for activity, it was highly active, in agreement with our present results for floret tissue.[14] This suggests that measurement of myrosinase activity in an aqueous extract could greatly underestimate the activity of whole, unextracted tissues.

Aqueous extraction can be expected to affect myrosinase activity measurement in several additional ways. For example, isolating crude protein is often preceded by defatting, which could alter myrosinase activity by changing its structure.[22] Protein extraction buffers often contain EDTA, which is known to chelate iron, as well as many other cations. In the simplified matrix of an extract, the iron at the active center of ESP was found to be relatively labile, such that EDTA treatment completely inhibited ESP-dependent nitrile formation in favor of the generation of isothiocyanate.[23] Whereas redirecting away from nitrile formation would not alter measurement of myrosinase activity by sinigrin disappearance or glucose appearance, a drawback of the use of AITC as a measurement of myrosinase activity is that nitriles are alternative products to isothiocyanates, and any nitrile formed would detract from total myrosinase activity measured as AITC formation. Yet because isothiocyanate formation relates directly to any health impact, the measurement of myrosinase-dependent isothiocynate formation may be of significant interest. Inhibition of nitrile production would be expected to increase isothiocyanate production.[24] It would be interesting to include EDTA in our system to determine if so doing increased myrosinase activity measured as isothiocyanate appearance. Furthermore, use of a buffer with or without EDTA, rather than water, to form the homogenate might improve the stability of the enzyme in our system.

Endogenous ascorbic acid and magnesium chloride may be removed during extraction, particularly if extraction is followed by fractionation for semipurification of the enzyme away from endogenous glucose.[18] The use of unextracted plant tissue when total myrosinase activity is measured reduces the risk of excluding insoluble myrosinase and of discarding important cofactors. Alternatively, methods that use semipurified myrosinase often add cofactors at levels chosen to optimize activity, rather than to reflect the content of the food.[13,25]

The results shown in Table 1 are comparisons of myrosinase activity in five broccoli and three kale varieties measured

**Table 1. Comparison of Myrosinase Activity Assays**

| cultivar | tissue | glucose assay, mean ± SD (units/g DW) | AITC assay, mean ± SD (units/g DW) |
|---|---|---|---|
| Sultan | floret | 1.75 ± 0.08 | 15.62 ± 2.43 |
| Sultan | root | 0.83 ± 0.05 | 4.44 ± 0.53 |
| Sultan | leaf | 1.85 ± 0.11 | 20.60 ± 2.27 |
| Marathon | floret | 0.69 ± 0.12 | 13.64 ± 1.25 |
| Marathon | root | 0.73 ± 0.01 | 10.68 ± 0.44 |
| Marathon | leaf | 1.53 ± 0.12 | 19.01 ± 1.94 |
| Patron | floret | 2.04 ± 0.16 | 13.31 ± 1.49 |
| Patron | root | 0.86 ± 0.08 | 9.13 ± 0.25 |
| Patron | leaf | 1.27 ± 0.11 | 15.49 ± 2.68 |
| Pirate | floret | 1.63 ± 0.24 | 14.46 ± 1.10 |
| Pirate | root | 0.56 ± 0.03 | 3.62 ± 0.20 |
| Pirate | leaf | 1.66 ± 0.11 | 14.72 ± 2.39 |
| Maximo | floret | 1.77 ± 0.19 | 13.08 ± 1.41 |
| Maximo | root | 0.80 ± 0.03 | 9.00 ± 1.29 |
| Maximo | leaf | 1.38 ± 0.05 | 17.87 ± 1.74 |
| Red Russian | root | 1.68 ± 0.02 | 9.94 ± 0.32 |
| Red Russian | leaf | 1.96 ± 0.05 | 6.87 ± 0.96 |
| Red Winter | root | 1.09 ± 0.05 | 6.37 ± 0.58 |
| Red Winter | leaf | 2.21 ± 0.24 | 13.04 ± 0.46 |
| Dwarf Blue Curled Vates | root | 1.47 ± 0.07 | 15.30 ± 0.69 |
| Dwarf Blue Curled Vates | leaf | 2.39 ± 0.14 | 14.70 ± 0.94 |

independently using either glucose release or the proposed method of AITC formation. The myrosinase activities from the glucose release assay are much lower values than those from the AITC formation-based assay. Furthermore, although the two assays were in relatively good agreement in ranking activity across plant parts (leaf, floret, root) within a cultivar, there were several striking inconsistencies between assays. For example, 'Red Russian' kale root tissue had only 85% of the activity found in the leaf tissue as measured by the glucose assay, although the same kale root tissue had 145% of the activity found in leaves when measured by the AITC assay. Conversely, for 'Red Winter' kale, root tissue had only 50% of the activity of

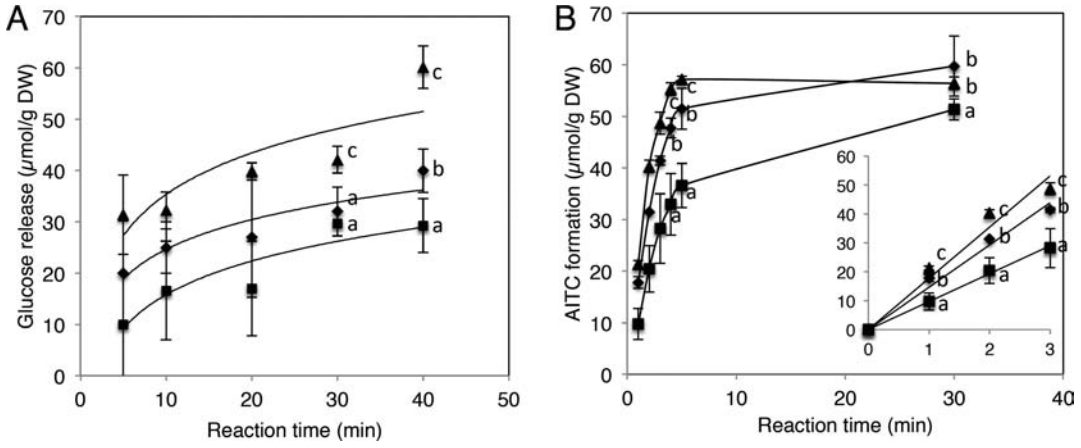


**Figure 2.** Glucose and allyl isothiocyanate (AITC) time-dependent formation from 'Marathon' broccoli floret (solid diamond), root (solid square), or leaf (solid triangle) tissue samples supplemented with sinigrin: (A) glucose release; (B) AITC formation (inset, early time points of AITC formation used for myrosinase activity calculations). Values are means ± SD ($n$ = 3). Different letters indicate significantly different values based on LSD test for the same time point ($p < 0.05$).

leaf samples, measured by either glucose or AITC assays. In all, when myrosinase activity from all tissues was compared across the two assays, although it was not strong, there was a significant, positive correlation between glucose appearance and AITC formation ($r$ = 0.488, $n$ = 21, $p$ = 0.0252). This suggests that the two assays measure the same activity, although not optimally. Therefore, we chose to determine if data were more similar between the two assays at earlier time points.

In reviewing change in enzyme rates over time, Figure 2 shows that rates were initially linear, but no longer linear by 5 min, whether using appearance of glucose (Figure 2A) or formation of AITC (Figure 2B). Background glucose levels are low in semipurified myrosinse preparations but greatly confounded the glucose appearance assay in homogenates at short time points (Figure 2A). For example, at 5 min, there was insufficient glucose formed to differentiate glucose production from background glucose present in the whole tissue sample, causing great variability in repeat measures (Figure 2A). Thus, it was not until 30 min that leaf samples showed significantly greater activity than root samples, and not until 40 min that floret samples showed significantly greater activity than root samples (Figure 2A). Both assays identified leaf as having the greatest myrosinase activity per gram DW of tissue and root the least, even though *under the conditions used*, linearity was possibly only present for the first 3 min of incubation. In leaf tissue, neither glucose nor AITC appearance at 5 min was significantly different from their appearance at 30 min, showing that the reaction had almost stopped by 5 min under these conditions.

In the literature the glucose release or sinigrin disappearance assays are often run for 5 min or more[9,11,18,20,23] and assume linearity of glucose formation during the entire assay,[18] which is likely true for these simplified systems using extracted myrosinase but could greatly underestimate myrosinase activity and not accurately reflect the real-time activity of myrosinase if the reaction slows as we observed in the unextracted tissue. We considered the possibility that substrate loss, when sinigrin is converted to hydrolysis products, could be responsible in part for the change seen in linearity of myrosinase activity. However, on the basis of product formation at 30 min, >40% substrate remained in samples from the AITC method. A previous study suggested that AITC can react with protein, resulting in inhibition of enzymatic activity due to modification of amino acid profile.[26] This could also explain part of the decrease in myrosinase activity that occurred over the 30 min measurement period. We further considered whether the steep decline in rate from 5 to 30 min for the AITC assay (Figure 2B) could be due to reaching the limit of water solubility for AITC. However, AITC solubility is 1.3 mg/mL, and the 30 min values for AITC were an order of magnitude less than this (0.118 mg/mL).[27]

Use of the AITC formation assay (Figure 2B) gave a value closer to linear, particularly when shorter incubation times were used (3 min), an option that is not possible for the glucose appearance assay, if using unextracted plant tissue samples, because of variation due to the high glucose background interference (Figure 2A). However, use of AITC formation could also underestimate myrosinase activity by ignoring nitriles formed due to the presence of ESP.[1] The inclusion of EDTA in the reaction solution could possibly prevent the formation of nitriles, channeling hydrolysis toward isothiocyanate formation.[23] However, this would actually overestimate the formation of isothiocyanates during food consumption, which is important when the role for myrosinase-dependent isothiocyanate release in health-promoting bioactivity is considered.

We considered that antioxidant compounds naturally present in plant tissues might also interfere with glucose estimation in the glucose appearance assay[9,12] because the ABTS-glucose assay is dependent on the oxidation of ABTS (Figure 3). When increasing concentrations of gallic acid were added to the assay medium in the presence of 5 μg of glucose, the appearance of oxidized ABTS was inhibited in a dose-dependent manner, with 150 μM gallic acid causing a >93% inhibition (Figure 4A). To avoid this interference for the ABTS-glucose assay, after

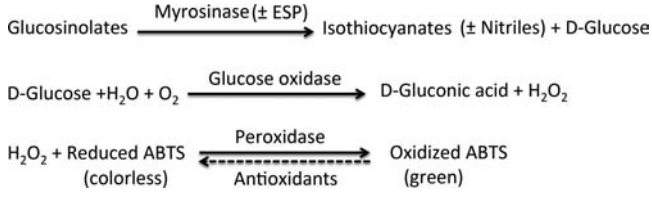


**Figure 3.** Scheme of ABTS-glucose assay showing site of potential risk of antioxidant interference.


dx.doi.org/10.1021/jf501692c | J. Agric. Food Chem. 2014, 62, 8094−8100

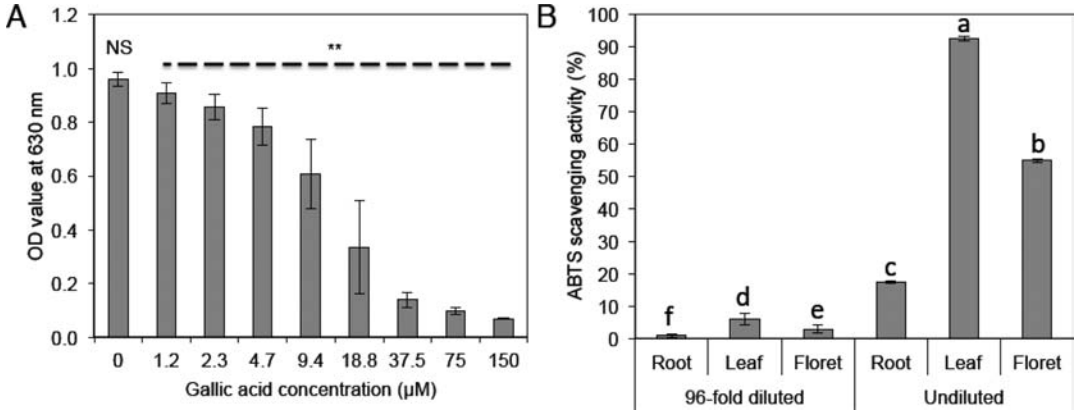


**Figure 4.** Endogenous antioxidant interference of glucose measurement, when using the ABTS-glucose assay: (A) interference of gallic acid (1.17−150 $\mu$M) on measurement of glucose (fixed at 5 $\mu$g); (B) percent interference by endogenous antioxidant compounds in 'Marathon' root, leaf, or floret broccoli tissues. Extracts generated following incubation were either undiluted or diluted 96-fold. Values are means ± SD ($n$ = 3). (**) Significantly different from no gallic acid, $p < 0.01$. Different letters indicate significantly different values based on LSD test ($p < 0.05$).

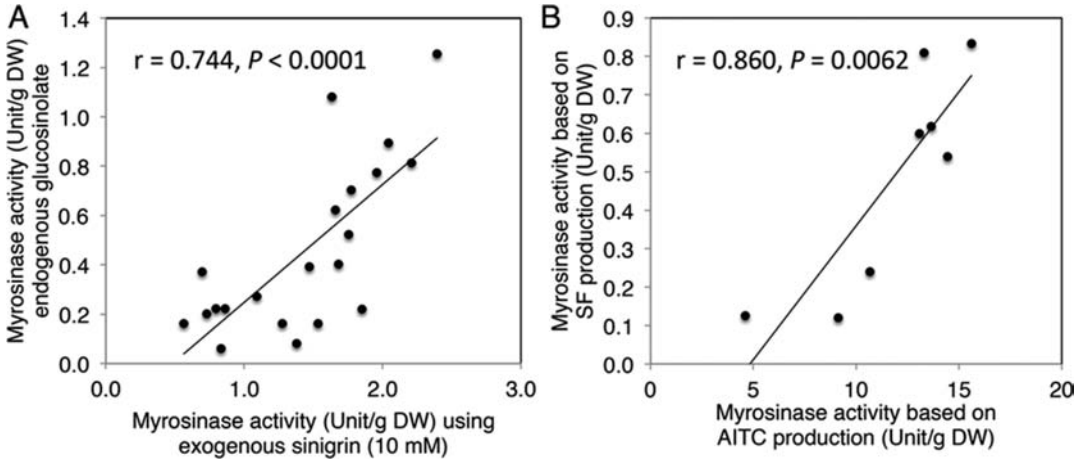


**Figure 5.** Correlation between myrosinase measurements using exogenous (singirin) or endogenous glucosinolate in 21 broccoli and kale tissue samples: (A) sinigrin (10 mM) or no glucosinolate addition, glucose assay; (B) sinigrin (2 mM) or no glucosinolate addition, AITC and SF assay. Pearson's correlation was calculated on the basis of the mean activity for each assay; $n$ = 3.

myrosinase-dependent glucose formation was complete, we evaluated the use of 96-fold diluted sample extracts to estimate glucose. At this dilution, plant endogenous antioxidant compounds interfered with glucose generation less than 1, 6, and 3% for root, leaf, and floret tissues, respectively (Figure 4B). This dilution not only allows us to minimize the potential interference from antioxidant compounds but also to decrease the concentration of endogenous glucose within the capacity range of the ABTS-glucose assay.

Published myrosinase activity assays typically use the addition of excess exogenous GSL; in most cases sinigrin is used and activity is reported in terms of sinigrin hydrolysis.[23] Often, however, myrosinase activity is being measured in samples in which other GSL or isothiocyanates are the compounds of interest. The use of a GSL not endogenous or not found in high concentrations in a cruciferous vegetable may skew results, particularly if substrate specificity exists between myrosinase and endogenous GSL, as previously shown for *Crambe abyssinica* seeds.[28] In this respect we hypothesized that using endogenous GSL to measure myrosinase activity should also be possible if the sample contains sufficient endogenous substrate to ensure that myrosinase (and not substrate) is rate limiting. Hydrolysis of endogenous GSL was measured as the appearance of glucose in 21 test samples. The tissue total GSL concentrations ranged from 1.86 to 70.9 $\mu$mol/g (concentration during the assay, 0.093−3.54 mM, Supporting Information Table S1). There was a highly significant correlation between myrosinase activity using endogenous GSL and exogenous GSL (10 mM sinigrin) measured as glucose appearance ($r$ = 0.744, $n$ = 21, $p < 0.0001$; Figure 5A). This shows that myrosinase activity can be measured using endogenous GSL over this naturally occurring GSL concentration range. The GSL concentration varied significantly from tissue to tissue; averaged values of total broccoli floret and root GSL concentration from five cultivars were 16.2 and 14.8 $\mu$mol/g DW, respectively which were considerably higher concentrations than those observed in leaf tissue (4.0 $\mu$mol/g DW, Supporting Information). Averaged values of kale root and leaf tissue GSL concentrations were 44.3 and 10.0 $\mu$mol/g DW, respectively (Supporting Information). However, this method is only feasible to use for short time measurements and for screening plant tissues that contain sufficient GSL. Because glucoraphanin is usually the predominant GSL found in broccoli, we hypothesized that its hydrolysis would correlate to the myrosinase activity determined previously. We found myrosinase activity using the formation of either AITC or SF to

be significantly correlated ($r = 0.860$, $n = 8$, $p = 0.0062$; Figure 5B). This suggests that the ITC formation-based myrosinase assay described here can be utilized to measure myrosinase activity using endogenous, as well as exogenous, GSL. For example, myrosinase activity in broccoli, watercress, and horseradish might be measured by SF, PEITC, and AITC formation, respectively. However, it is necessary to remember that whereas this may provide an accurate measure for ingested foods, the presence of ESP, and possibly other myrosinase protein cofactors, will cause underestimation of absolute myrosinase activity. Because in vivo formation and bioavailability of ITC from GSL in broccoli is affected by processing conditions,[29] more study should be conducted using foods after the cooking process.

In conclusion, evaluating myrosinase activity from multiple broccoli varieties, we find that leaf and floret tissues have relatively greater activity than root tissue, on a per gram DW basis. Kale varieties exhibited the same trend, with leaf tissues possessing greater myrosinase activity than root. Myrosinase activity based on the formation of AITC can be useful in determining short-term enzymatic rates of myrosinase, with incubation times limited to 1−3 min. Samples can be run and hydrolysis products extracted rapidly, allowing a quick turnaround time for a few activity estimations. When using brassica vegetable tissues, the glucose release assay cannot be run for such short times, due to high baseline interference by endogenous glucose: on average, 30 min was required to reliably measure glucose formation. For limited sampling, the glucose assay also takes longer to perform, with multiple steps and incubations. However, if there are a large number of samples, performance time per sample is reduced radically, making glucose release a better high-throughput method, as long as samples are prepared in such a way that background glucose does not interfere, such as the use of a crude protein extract in place of tissue samples. However, we found that up to 36% of myrosinase activity was discarded in the pellet during generation of the crude protein extract. Whether soluble and insoluble myrosinases are similar with regard to activity or even substrate specificity is not known, although we found that changing substrates from sinigrin to the endogenous substrate glucoraphanin did not alter myrosinase measurements using the AITC method.

The proposed AITC formation assay can measure activity during the short-term linear phase of total myrosinase activity (~3 min) when used for whole brassica vegetable samples. It also has the capacity to evaluate hydrolysis of endogenous glucoraphanin. Whereas this assay appears most relevant for estimating myrosinase activity in terms of food consumption, further studies are needed to understand the impact of cooking on myrosinase activity in whole homogenates, particularly to determine how soluble and insoluble myrosinase enzymes are affected by postharvest processing.

## ■ ASSOCIATED CONTENT

### Supporting Information

Table S1 (glucosinolate concentrations of broccoli and kale cultivars). This material is available free of charge via the Internet at http://pubs.acs.org.

## ■ AUTHOR INFORMATION


### Corresponding Author

*(E.H.J.) Mail: Department of Food Science and Human Nutrition, University of Illinois at Urbana−Champaign, 905 S. Goodwin Ave., Room 467, Urbana, IL 61801-3838, USA. Phone: (217) 333-3820. E-mail: ejeffery@illinois.edu.

### Author Contributions

§K.-M. K. contributed equally to this work.



### Funding

Our thanks to Sakata Seed Co. for their support of E.J. and E.D. and for USDA/NIFA 2010-65200-20398 to E.J.

### Notes

The authors declare no competing financial interest.


## ■ ABBREVIATIONS USED

ABTS, 2,2′-azinobis(3-ethylbenzothiazoline-6-sulfonic acid); AITC, allyl isothiocyanate; ESP, epithiospecifier protein; GSL, glucosinolate; PEITC, phenethyl isothiocyanate; SF, sulforaphane

## ■ REFERENCES


(1) Bones, A. M.; Rossiter, J. T. The myrosinase-glucosinolate system, its organisation and biochemistry. *Physiol. Plant.* **1996**, *97*, 194−208.

(2) Matusheski, N. V.; Swarup, R.; Juvik, J. A.; Mithen, R.; Bennett, M.; Jeffery, E. H. Epithiospecifier protein from broccoli (*Brassica oleracea* L. ssp. *italica*) inhibits formation of the anticancer agent sulforaphane. *J. Agric. Food Chem.* **2006**, *54*, 2069−2076.

(3) Dosz, E. B.; Jeffery, E. H. Commercially produced frozen broccoli lacks the ability to form sulforaphane. *J. Funct. Foods* **2013**, *5*, 987−990.

(4) Dosz, E. B.; Jeffery, E. H. Modifying the processing and handling of frozen broccoli for increased sulforaphane rormation. *J. Food Sci.* **2013**, *78*, H1459−H1463.

(5) Clarke, J. D.; Hsu, A.; Riedl, K.; Bella, D.; Schwartz, S. J.; Stevens, J. F.; Ho, E. Bioavailability and inter-conversion of sulforaphane and erucin in human subjects consuming broccoli sprouts or broccoli supplement in a cross-over study design. *Pharmacol. Res.* **2011**, *64*, 456−463.

(6) Cramer, J. M.; Teran-Garcia, M.; Jeffery, E. H. Enhancing sulforaphane absorption and excretion in healthy men through the combined consumption of fresh broccoli sprouts and a glucoraphanin-rich powder. *Br. J. Nutr.* **2012**, *107*, 1333−1338.

(7) Fahey, J. W.; Wehage, S. L.; Holtzclaw, W. D.; Kensler, T. W.; Egner, P. A.; Shapiro, T. A.; Talalay, P. Protection of humans by plant glucosinolates: efficiency of conversion of glucosinolates to isothiocyanates by the gastrointestinal microflora. *Cancer Prev. Res.* **2012**, *5*, 603−611.

(8) Palmieri, S.; Iori, R.; Leoni, O. Comparison of methods for determining myrosinase activity. *J. Agric. Food Chem.* **1987**, *35*, 617−621.

(9) Kleinwachter, M.; Selmar, D. A novel approach for reliable activity determination of ascorbic acid depending myrosinases. *J. Biochem. Biophys. Methods* **2004**, *59*, 253−265.

(10) Wathelet, J. P.; Marlier, M.; Severin, M.; Boenke, A.; Wagstaffe, P. J. Measurement of glucosinolates in rapeseeds. *Natural Toxins* **1995**, *3*, 299−304.

(11) Verkerk, R.; Dekker, M. Glucosinolates and myrosinase activity in red cabbage (*Brassica oleracea* L. var. Capitata f. rubra DC.) after various microwave treatments. *J. Agric. Food Chem.* **2004**, *52*, 7318−7323.

(12) Travers-Martin, N.; Kuhlmann, F.; Muller, C. Revised determination of free and complexed myrosinase activities in plant extracts. *Plant Physiol. Biochem.* **2008**, *46*, 506−516.

(13) Van Eylen, D.; Oey, I.; Hendrickx, M.; Van Loey, A. Kinetics of the stability of broccoli (*Brassica oleracea* cv. Italica) myrosinase and isothiocyanates in broccoli juice during pressure/temperature treatments. *J. Agric. Food Chem.* **2007**, *55*, 2163−2170.

(14) Eriksson, S.; Ek, B.; Xue, J.; Rask, L.; Meijer, J. Identification and characterization of soluble and insoluble myrosinase isoenzymes in different organs of *Sinapis alba*. *Physiol. Plant.* **2001**, *111*, 353−364.
(15) Yábar, E.; Pedreschi, R.; Chirinos, R.; Campos, D. Glucosinolate content and myrosinase activity evolution in three maca (*Lepidium meyenii* Walp.) ecotypes during preharvest, harvest and postharvest drying. *Food Chem.* **2011**, *127*, 1576−1583.
(16) Keck, A. S.; Qiao, Q.; Jeffery, E. H. Food matrix effects on bioactivity of broccoli-derived sulforaphane in liver and colon of F344 rats. *J. Agric. Food Chem.* **2003**, *51*, 3320−3327.
(17) Ku, K. M.; Jeffery, E. H.; Juvik, J. A. Influence of seasonal variation and methyl jasmonate mediated induction of glucosinolate biosynthesis on quinone reductase activity in broccoli florets. *J. Agric. Food Chem.* **2013**, *61*, 9623−9631.
(18) Ludikhuyze, L.; Rodrigo, L.; Hendrickx, M. The activity of myrosinase from broccoli (*Brassica oleracea* L. cv. Italica): influence of intrinsic and extrinsic factors. *J. Food Prot.* **2000**, *63*, 400−403.
(19) Kushad, M. M.; Brown, A. F.; Kurilich, A. C.; Juvik, J. A.; Klein, B. P.; Wallig, M. A.; Jeffery, E. H. Variation of glucosinolates in vegetable crops of *Brassica oleracea*. *J. Agric. Food Chem.* **1999**, *47*, 1541−1548.
(20) Ku, K. M.; Choi, J. H.; Kim, H. S.; Kushad, M. M.; Jeffery, E. H.; Juvik, J. A. Methyl jasmonate and 1-methylcyclopropene treatment effects on quinone reductase inducing activity and post-harvest quality of broccoli. *PLoS One* **2013**, *8*, No. e77127.
(21) Ku, K. M.; Kim, J.; Park, H. J.; Liu, K. H.; Lee, C. H. Application of metabolomics in the analysis of manufacturing type of pu-erh tea and composition changes with different postfermentation year. *J. Agric. Food Chem.* **2010**, *58*, 345−352.
(22) Dong, A.; Meyer, J. D.; Kendrick, B. S.; Manning, M. C.; Carpenter, J. F. Effect of secondary structure on the activity of enzymes suspended in organic solvents. *Arch. Biochem. Biophys.* **1996**, *334*, 406−414.
(23) Burow, M.; Markert, J.; Gershenzon, J.; Wittstock, U. Comparative biochemical characterization of nitrile-forming proteins from plants and insects that alter myrosinase-catalysed hydrolysis of glucosinolates. *FEBS J.* **2006**, *273*, 2432−2446.
(24) Matusheski, N. V.; Juvik, J. A.; Jeffery, E. H. Heating decreases epithiospecifier protein activity and increases sulforaphane formation in broccoli. *Phytochemistry* **2004**, *65*, 1273−1281.
(25) Burmeister, W. P.; Cottaz, S.; Rollin, P.; Vasella, A.; Henrissat, B. High resolution x-ray crystallography shows that ascorbate is a cofactor for myrosinase and substitutes for the function of the catalytic base. *J. Biol. Chem.* **2000**, *275*, 39385−39393.
(26) Kawakishi, S.; Kaneko, T. Interaction of proteins with allyl isothiocyanate. *J. Agric. Food Chem.* **1987**, *35*, 85−88.
(27) Wilson, E. A.; Ennahar, S.; Marchioni, E.; Bergaentzlé, M.; Bindler, F. Improvement in determination of isothiocyanates using high-temperature reversed-phase HPLC. *J. Sep. Sci.* **2012**, *35*, 2026−2031.
(28) Bernardi, R.; Finiguerra, M. G.; Rossi, A. A.; Palmieri, S. Isolation and biochemical characterization of a basic myrosinase from ripe *Crambe abyssinica* seeds, highly specific for epi-progoitrin. *J. Agric. Food Chem.* **2003**, *51*, 2737−2744.
(29) Oliviero, T.; Verkerk, R.; Vermeulen, M.; Dekker, M. In vivo formation and bioavailability of isothiocyanates from glucosinolates in broccoli as affected by processing conditions. *Mol. Nutr. Food Res.* **2014**, *58*, 1447−1456.

JOURNAL OF AGRICULTURAL AND FOOD CHEMISTRY

Article

pubs.acs.org/JAFC

# Finding of Synergistic and Cancel Effects on the Aroxyl Radical-Scavenging Rate and Suppression of Prooxidant Effect for Coexistence of α-Tocopherol with β-, γ-, and δ-Tocopherols (or -Tocotrienols)

Aya Ouchi,[†] Shin-ichi Nagaoka,[†] Tomomi Suzuki,[‡] Katsuhiro Izumisawa,[‡] Taisuke Koike,[§] and Kazuo Mukai*,[†]

[†]Department of Chemistry, Faculty of Science, Ehime University, Matsuyama 790-8577, Japan

[‡]Eisai Company, Ltd., Koishikawa 5-5-5, Bunkyo-ku, Tokyo 112-8088, Japan

[§]Eisai Food & Chemical Company, Ltd., Nihonbashi 2-13-10, Chuo-ku, Tokyo 103-0027, Japan

Supporting Information

**ABSTRACT:** Measurements of aroxyl radical (ArO•)-scavenging rate constants ($k_s^{AOH}$) of antioxidants (AOHs) [α-, β-, γ-, and δ-tocopherols (TocHs) and -tocotrienols (Toc-3Hs)] were performed in ethanol solution via stopped-flow spectrophotometry. $k_s^{AOH}$ values of α-, β-, γ-, and δ-Toc-3Hs showed good agreement with those of the corresponding α-, β-, γ-, and δ- TocHs. $k_s^{AOH}$ values were measured not only for each antioxidant but also for mixtures of two antioxidants: (i) α-TocH with β-, γ-, or δ-TocH and (ii) α-TocH with α-, β-, γ-, or δ-Toc-3H. A synergistic effect in which the $k_s^{AOH}$ value increases by 12% for γ-TocH (or by 12% for γ-Toc-3H) was observed for solutions including α-TocH and γ-TocH (or γ-Toc-3H). On the other hand, a cancel effect in which the $k_s^{AOH}$ value decreases (a) by 7% for β-TocH (or 11% for β-Toc-3H) and (b) by 24% for δ-TocH (or 25% for δ-Toc-3H) was observed for solutions including two kinds of antioxidants. However, only a synergistic effect may function in edible oils, because contents of β- and δ-TocHs (and β- and δ-Toc-3Hs) are much less than those of α- and γ-TocHs (and α- and γ-Toc-3Hs) in many edible oils. UV−vis absorption of α-Toc•, which was produced by reaction of α-TocH with ArO•, decreased remarkably for coexistence of α-TocH with β-, γ-, or δ-TocH (or β-, γ-, or δ-Toc-3H), indicating that the prooxidant effect of α-Toc• is suppressed by the coexistence of other TocHs and Toc-3Hs.

**KEYWORDS:** *free radicals, vitamin E, tocopherols, tocotrienols, antioxidant activity, reaction rate, stopped-flow spectrophotometry, coexistence of antioixidants, synergistic and cancel effects*

## INTRODUCTION

α-Tocopherol (α-TocH) is well-known as one of the most important lipophilic antioxidants (AOHs) in foods and biological systems.[1−3] The antioxidant action of α-TocH has been ascribed to the scavenging reaction of lipid peroxyl (LOO•) radical, producing the corresponding α-tocopheroxyl (α-Toc•) radical (reaction 1).[1] On the other hand, if α-TocH exists in edible oils and biomembranes, α-Toc• radicals may react with unsaturated lipids (LHs) (reaction 2). Reaction 2 is known as a prooxidant reaction, which induces degradation of unsaturated lipids.[4−8]

$$\text{LOO}^\bullet + \text{α-TocH} \xrightarrow{k_{inh}} \text{LOOH} + \text{α-Toc}^\bullet \quad (1)$$

$$\text{α-Toc}^\bullet + \text{LH} \xrightarrow{k_p} \text{α-TocH} + \text{L}^\bullet \quad (2)$$

Ubiquinol-10 ($UQ_{10}H_2$) is also well-known as a representative lipophilic antioxidant.[9,10] $UQ_{10}H_2$ functions as an antioxidant by (i) scavenging LOO• (reaction 3) and (ii) regenerating α-Toc• to α-TocH (reaction 4):[1,9,10]

$$\text{LOO}^\bullet + UQ_{10}H_2 \xrightarrow{k_{inh}} \text{LOOH} + UQ_{10}H^\bullet \quad (3)$$

$$\text{α-Toc}^\bullet + UQ_{10}H_2 \xrightarrow{k_r} \text{α-TocH} + UQ_{10}H^\bullet \quad (4)$$

where $UQ_{10}H^\bullet$ denotes the ubisemiquinone radical. The results of kinetic studies for reactions 3 and 4 indicated that both reactions are important for the antioxidant actions of $UQ_{10}H_2$.[11−15]

On the other hand, vitamin C (ascorbate monoanion, $AsH^-$) is a representative water-soluble antioxidant. Hydrophilic $AsH^-$ also enhances the antioxidant activity of α-TocH by regenerating α-Toc• to α-TocH (reaction 5):[15−18]

$$\text{α-Toc}^\bullet + \text{AsH}^- \xrightarrow{k_r} \text{α-TocH} + \text{As}^{-\bullet} \quad (5)$$

where $As^{-\bullet}$ is an ascorbate free radical. As described above, α-Toc• is an important key radical, which appears in the process of antioxidant and prooxidant actions of α-TocH (see reactions 1, 2, 4, and 5).

In previous works, we measured the second-order reaction rates ($k_s^{AOH}$) of many kinds of natural antioxidants, such as α-, β-, γ-, and δ-TocHs,[19,20] biological hydroquinones including $UQ_{10}H_2$,[20] vitamin C (or sodium ascorbate),[21] and many polyphenols including catechins and flavone derivatives,[21,22]

Received: April 30, 2014
Revised: July 10, 2014
Accepted: July 22, 2014
Published: July 22, 2014

ACS Publications © 2014 American Chemical Society

with 2,6-di-*t*-butyl-4-(4-methoxyphenyl)phenoxyl (aroxyl, ArO•) (see Figure 1) in ethanol (reaction 6), by use of

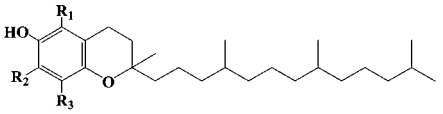


TocH

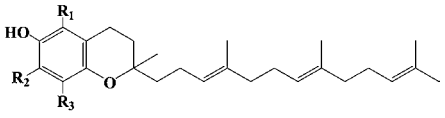


Toc-3H

| | $R_1$ | $R_2$ | $R_3$ |
|---|---|---|---|
| α | $CH_3$ | $CH_3$ | $CH_3$ |
| β | $CH_3$ | H | $CH_3$ |
| γ | H | $CH_3$ | $CH_3$ |
| δ | H | H | $CH_3$ |

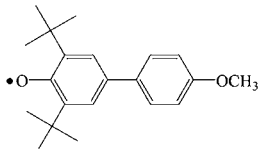


ArO•

**Figure 1.** Molecular structures of *α*-, *β*-, *γ*-, and *δ*-tocopherols (TocHs); *α*-, *β*-, *γ*-, and *δ*-tocotrienols (Toc-3Hs); and aroxyl radical (ArO•).

stopped-flow spectrophotometry. ArO• can be regarded as a model for active oxygen radicals (LOO• and others) in biological systems, as described in previous works.[19,20,23]

$$\mathrm{ArO^{\bullet}} + \mathrm{AOH} \xrightarrow{k_s^{\mathrm{AOH}}} \mathrm{ArOH} + \mathrm{AO^{\bullet}} \quad (6)$$

As described above, *α*-TocH, $UQ_{10}H_2$, and vitamin C are the most important natural antioxidants in biological systems. These antioxidants coexist in relatively high concentrations in human (and rat) plasma and various tissues.[24−27] Furthermore, it is well-known that various antioxidants coexist in many foods.[2] However, a detailed kinetic study has not been performed for mixtures of these antioxidants.

Therefore, recently, measurements of ArO•-scavenging rate constants ($k_s^{\mathrm{AOH}}$) of antioxidants [*α*-TocH, $UQ_{10}H_2$, and sodium ascorbate ($Na^+AsH^-$)] were performed in 2-propanol/water (5/1 v/v) solution by stopped-flow spectrophotometry. $k_s^{\mathrm{AOH}}$ values were measured not only for each antioxidant but also for mixtures of two antioxidants: (i) *α*-TocH with $UQ_{10}H_2$ and (ii) *α*-TocH with $Na^+AsH^-$.[28] A notable synergistic effect in which $k_s^{\mathrm{AOH}}$ values increase 1.6, 2.5, and 6.8 times for *α*-TocH, $UQ_{10}H_2$, and $Na^+AsH^-$, respectively, was observed for solutions including two kinds of antioxidants. Furthermore, formation of *α*-Toc• radical was suppressed remarkably for coexistence of *α*-TocH with $UQ_{10}H_2$ (or $Na^+AsH^-$). The result suggests that the prooxidant effect induced by the reaction between *α*-Toc• radical and LH (reaction 2) may be suppressed by the coexistence of *α*-TocH with $UQ_{10}H_2$ (or $Na^+AsH^-$).

*α*-, *β*-, *γ*-, and *δ*-Tocopherols and -tocotrienols (*α*-, *β*-, *γ*-, and *δ*-TocH and -Toc-3H; see Figure 1) are well-known as vitamin E homologues. As described above, ArO•-scavenging rates ($k_s^{\mathrm{AOH}}$) of *α*-, *β*-, *γ*-, and *δ*-tocopherols have been investigated in previous works.[19,20] However, a detailed kinetic study has not been performed for *α*-, *β*-, *γ*-, and *δ*-tocotrienols, as far as we know.

In the present work, first, measurements of the rate constants ($k_s^{\mathrm{AOH}}$) were performed for eight vitamin E homologues in ethanol solution at 25 °C by stopped-flow spectrophotometry, to investigate the effect of alkyl side chain of *α*-, *β*-, *γ*-, and *δ*-TocHs and -Toc-3Hs on the scavenging rate. Second, measurements of the $k_s^{\mathrm{AOH}}$ value were performed for solutions including two kinds of antioxidants, (i) *α*-TocH with *β*-, *γ*-, and *δ*-TocHs and (ii) *α*-TocH with *α*-, *β*-, *γ*-, and *δ*-Toc-3Hs, to investigate the synergistic and cancel effects of antioxidants on the ArO•-scavenging rate. Third, the effect of coexistence of *α*-TocH and other TocHs (or Toc-3Hs) on the prooxidant action of *α*-TocH has been studied. Vitamin E homologues are included in many kinds of edible oils such as rapeseed, soybean, peanut, rice bran, palm oils, etc.[29−33] Consequently, it will be of interest to study the effect of coexistence of *α*-TocH with other TocHs (or Toc-3Hs) on the antioxidant and prooxidant actions of *α*-TocH.

## MATERIALS AND METHODS

**Materials.** D-*α*-, *β*-, *γ*-, and *δ*-Tocopherols and -tocotrienols were kindly supplied from Eisai Food & Chemical, Co. Ltd., Japan. The purities of tocopherols and tocotrienols used were as follows; *α*-, *β*-, *γ*-, and *δ*-TocHs (99.9%, 99.8%, 100.0%, and 99.5%) and *α*-, *β*-, *γ*-, and *δ*-Toc-3Hs (99.4%, 99.4%, 98.7%, and 98.7%), respectively. ArO• radical was prepared according to the method of Rieker and Scheffler.[34]

**Measurements.** Measurement of the second-order rate constant ($k_s^{\mathrm{AOH}}$) for reaction of ArO• with AOH (reaction 6) was performed on a Unisoku single-mixing stopped-flow spectrophotometer (Model RSP-1000) by mixing equal volumes of ethanol solutions of ArO• and AOH under nitrogen atmosphere.[20,21] The time between mixing the two solutions and recording the first data point (that is, dead time) was 10−20 ms. The reaction was monitored with either single-wavelength detection (Figure 2B) or photodiode-array detection (Figure 2A) attached to the stopped-flow spectrophotometer. All measurements were performed at 25.0 ± 0.5 °C. Experimental errors in the rate constants ($k_s^{\mathrm{AOH}}$) were estimated to be about 5% in ethanol solution.

## RESULTS

**Measurements of Aroxyl Radical-Scavenging Rates for *α*-, *β*-, *γ*-, and *δ*-Tocopherols and -Tocotrienols in Ethanol Solution.** Measurement of the rate constant ($k_s^{\alpha\text{-TocH}}$) for reaction of ArO• radical with *α*-TocH was performed in ethanol solution (reaction 6). Upon reaction of *α*-TocH with ArO• radical, the absorbance at 376 and 580 nm of ArO• decreases and the absorbance at 428 nm of *α*-Toc• radical increases, as shown in Figure 2A. The scavenging rate of ArO• was measured by following the decrease in absorbance at 376 or 580 nm of the ArO• radical, as shown in Figure 2B.[28] The pseudo-first-order rate constants ($k_{obsd}$) at 376 or 580 nm were linearly dependent on the concentration of *α*-TocH [*α*-TocH], and thus, the rate equation is expressed as

$$-\mathrm{d}[\mathrm{ArO^{\bullet}}]/\mathrm{d}t = k_{\mathrm{obsd}}[\mathrm{ArO^{\bullet}}] = k_s^{\alpha\text{-TocH}}[\alpha\text{-TocH}][\mathrm{ArO^{\bullet}}] \quad (7)$$

where $k_s^{\alpha\text{-TocH}}$ is the second-order rate constant for oxidation of *α*-TocH by ArO• radical. $k_s^{\alpha\text{-TocH}}$ was obtained by plotting $k_{obsd}$ against [*α*-TocH], as shown in Figure 2C. The $k_s^{\alpha\text{-TocH}}$(alone) value obtained is $5.14 \times 10^3$ $M^{-1}\cdot s^{-1}$ (see Table 1), where $k_s^{\alpha\text{-TocH}}$(alone) means the ArO• radical-scavenging rate constant obtained in solution including only one antioxidant (*α*-TocH). As described above, upon reaction of *α*-TocH with ArO• in

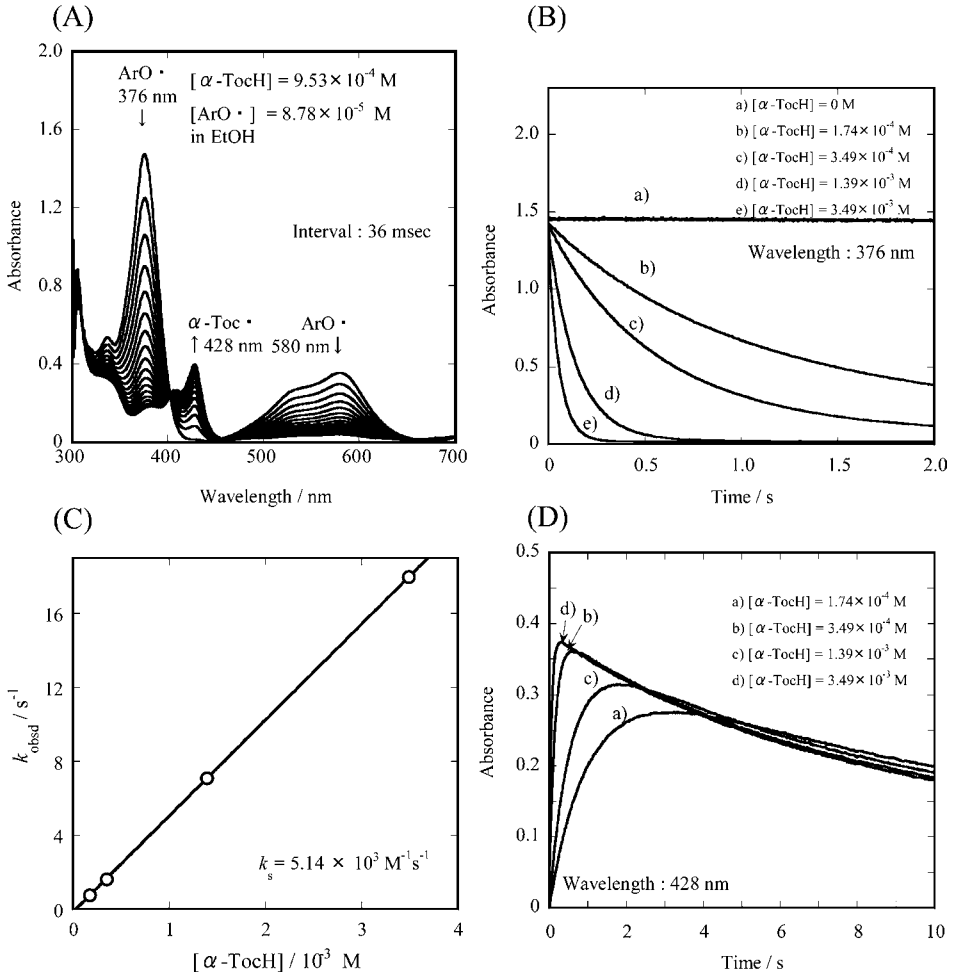


**Figure 2.** (A) Change in electronic absorption spectra of ArO• and α-Toc• radicals during reaction of ArO• with α-TocH in ethanol solution at 25.0 °C. Initial concentrations were $[ArO^{\bullet}] = 8.78 \times 10^{-5}$ M and $[\alpha\text{-TocH}] = 9.53 \times 10^{-4}$ M. Spectra were recorded at 36 ms intervals. Arrow indicates a decrease (ArO•) and an increase (α-Toc•) in absorbance with time. Also shown is the time dependence of absorbance of (B) ArO• radical (at 376 nm) and (D) α-Toc• radical (at 428 nm) in solutions including five and four different concentrations of α-TocH at 25.0 °C, respectively. (C) Pseudo-first-order rate constant ($k_{obsd}$) versus [α-TocH] plot.

ethanol, α-Toc• is produced rapidly. α-Toc• is unstable at 25.0 °C and its absorption peak decreases gradually after passing through the maximum (see Figure 2D).[28,35]

Similar measurements were performed for reaction of ArO• with β-, γ-, and δ-tocopherols and -tocotrienols in ethanol solution. For example, the result obtained for γ-TocH is shown in Figure 3. Upon reaction of γ-TocH with ArO• radical, the absorbance at 376 nm of ArO• decreases rapidly, and an absorption spectrum due to γ-Toc• radical appears at $\lambda_{max}$ = 432 nm, as shown in Figure 3A. However, the absorption observed for γ-Toc• is very weak; its absorption peak (at 432 nm) decreases rapidly after passing through the maximum and disappears almost at 10 s, differing from the case of α-Toc• (see Figures 2D and 3D).[35] The rate constant, $k_s^{\gamma\text{-TocH}}$(alone), was obtained by plotting $k_{obsd}$ against [γ-TocH] (see Figure 3C).

In the present work, measurements of $k_s^{AOH}$(alone) values were repeated three or four times for each α-, β-, γ-, and δ-TocH and -Toc-3H to obtain reliable $k_s^{AOH}$(alone) values, to compare the values of α-, β-, γ-, and δ-tocotrienols with those of α-, β-, γ-, and δ-tocopherols. Each measured $k_s^{AOH}$(alone) value and the average $k_s^{AOH}$(alone) values obtained are summarized in Table 1. As is clear from the $k_s^{AOH}$(alone) values listed in Table 1, the ArO•-scavenging activity in ethanol increases in the order shown in eq 8:

$$\begin{aligned} &\delta\text{-TocH} \sim \delta\text{-Toc-3H} \\ &< \gamma\text{-TocH} \sim \gamma\text{-Toc-3H} \sim \beta\text{-TocH} \sim \beta\text{-Toc-3H} \\ &< \alpha\text{-TocH} \sim \alpha\text{-Toc-3H} \end{aligned} \quad (8)$$

**Measurements of Aroxyl Radical-Scavenging Rates ($k_s^{AOH}$) for Mixtures of α-Tocopherol with β-, γ-, or δ-Tocopherol in Ethanol.** Measurements of $k_s^{\beta,\gamma,\delta\text{-TocH}}$(+α-TocH) values were performed for solutions including α-TocH and β-, γ-, or δ-TocH, respectively. The notation $k_s^{\beta,\gamma,\delta\text{-TocH}}$(+α-TocH) indicates the rate constant obtained in solution including two tocopherol components. First, measurement of $k_s^{\gamma\text{-TocH}}$(+α-TocH) was performed by keeping [α-TocH] constant at 2.88 × $10^{-4}$ M and varying [γ-TocH] from 0 to 1.21 × $10^{-3}$ M (denoted measurement 1 in Table 2).

Upon mixing the solution of ArO• radical with the solution including α-TocH and γ-TocH, absorption of the ArO• at 376 and 580 nm decreases rapidly, as shown in Figure 4. Absorption due to α-Toc• and γ-Toc• was observed at 428 nm, but absorption intensity decreased with increasing [γ-TocH]. By


dx.doi.org/10.1021/jf502049k | J. Agric. Food Chem. 2014, 62, 8101−8113

**Table 1. Second-Order Rate Constants for Reactions of Antioxidants with ArO• Radical, Average Values, and Relative Rate Constants in Ethanol Solution at 25.0 °C**

| antioxidant | meas $k_s^{AOH}$(alone), $M^{-1}\cdot s^{-1}$ | avg $k_s^{AOH}$(alone), $M^{-1}\cdot s^{-1}$ | $k_s^{AOH}$(alone)/$k_s^{\alpha\text{-TocH}}$(alone) |
|---|---|---|---|
| α-TocH | $5.12 \times 10^3$ [a] | avg $5.12 \times 10^3$ | 1.00 |
| α-Toc-3H | $4.76 \times 10^3$ | avg $4.97 \times 10^3$ | avg 0.971 |
| | $4.97 \times 10^3$ | | |
| | $5.19 \times 10^3$ | | |
| β-TocH | $2.74 \times 10^3$ | avg $2.77 \times 10^3$ | avg 0.541 |
| | $2.70 \times 10^3$ | | |
| | $2.86 \times 10^3$ | | |
| β-Toc-3H | $3.11 \times 10^3$ | avg $3.04 \times 10^4$ | avg 0.594 |
| | $2.96 \times 10^3$ | | |
| γ-TocH | $2.85 \times 10^3$ | avg $2.82 \times 10^3$ | avg 0.551 |
| | $2.78 \times 10^3$ | | |
| γ-Toc-3H | $2.89 \times 10^3$ | avg $2.76 \times 10^3$ | avg 0.539 |
| | $2.64 \times 10^3$ | | |
| | $2.76 \times 10^3$ | | |
| δ-TocH | $1.00 \times 10^3$ | avg $1.02 \times 10^3$ | avg 0.199 |
| | $1.02 \times 10^3$ | | |
| | $1.02 \times 10^3$ | | |
| | $1.02 \times 10^3$ | | |
| δ-Toc-3H | $1.08 \times 10^3$ | avg $1.09 \times 10^3$ | avg 0.213 |
| | $1.09 \times 10^3$ | | |

[a]Measurement of $k_s^{\alpha\text{-TocH}}$(alone) for α-TocH was performed many times in ethanol. Average value is $5.12 \times 10^3$ $M^{-1}\cdot s^{-1}$.

analyzing the decay curves of ArO• at 376 nm, $k_{obsd}$ values were determined. Figure 5B (●) shows the $k_{obsd}$ versus [γ-TocH] plot.

If α-TocH and γ-TocH coexist in solution, reactions 9 and 10 will occur competitively in solution, because the difference in $k_s^{\alpha\text{-TocH}}$(alone) and $k_s^{\gamma\text{-TocH}}$(alone) values is not too large, as listed in Table 1.

$$\text{ArO}^\bullet + \alpha\text{-TocH} + \gamma\text{-TocH} \xrightarrow{k_s^{\alpha\text{-TocH}}} \text{ArOH} + \alpha\text{-Toc}^\bullet + \gamma\text{-TocH} \quad (9)$$

$$\text{ArO}^\bullet + \alpha\text{-TocH} + \gamma\text{-TocH} \xrightarrow{k_s^{\gamma\text{-TocH}}} \text{ArOH} + \alpha\text{-TocH} + \gamma\text{-Toc}^\bullet \quad (10)$$

In such a case, we can expect that the $k_{obsd}$ value depends on eq 11, if the interaction among α-TocH, γ-TocH, and their radicals is negligible.

$$k_{obsd} = k_s^{\alpha\text{-TocH}}(\text{alone})[\alpha\text{-TocH}] + k_s^{\gamma\text{-TocH}}(\text{alone})[\gamma\text{-TocH}] \quad (11)$$

Next we will assume that a synergistic effect is present. By substituting $k_s^{\alpha\text{-TocH}}$(alone) and $k_s^{\gamma\text{-TocH}}$(alone) values and the value of [α-TocH] ($2.88 \times 10^{-4}$ M) used for measurement 1 (see Table 2) into eq 11, $k_{obsd}$ was plotted against [γ-TocH] (see dotted line in Figure 5B). Furthermore, the result of the $k_{obsd}$ versus [γ-TocH] plot (○) obtained for the solution including only γ-TocH (see eq 7) is also shown in Figure 5B. As described above, measurement 1 was performed by keeping α-TocH at a constant concentration and varying [γ-TocH]. Consequently, the $k_s^{\gamma\text{-TocH}}$(+α-TocH) value was determined from the gradient of the $k_{obsd}$ versus [γ-TocH] plot (●) in Figure 5B, by use of eq 12:

$$k_{obsd} = k_s^{\alpha\text{-TocH}}(\text{alone})[\alpha\text{-TocH}] + k_s^{\gamma\text{-TocH}}(+\alpha\text{-TocH})[\gamma\text{-TocH}] \quad (12)$$

As expected from the gradient in Figure 5B, the $k_s^{\gamma\text{-TocH}}$(+α-TocH) value ($3.25 \times 10^3$ $M^{-1}\cdot s^{-1}$) is 1.15 times larger than $k_s^{\gamma\text{-TocH}}$(alone) (average $2.82 \times 10^3$ $M^{-1}\cdot s^{-1}$) obtained for the solution including only γ-TocH. A synergistic effect due to the coexistence of α-TocH and γ-TocH in solution was observed for the rate constant $k_s^{\gamma\text{-TocH}}$(+α-TocH). Measurement was repeated twice to ascertain the result obtained above (see measurement 2 in Table 2). The $k_s^{\gamma\text{-TocH}}$(+α-TocH) value ($3.08 \times 10^3$ $M^{-1}\cdot s^{-1}$) obtained showed good agreement with that ($3.25 \times 10^3$ $M^{-1}\cdot s^{-1}$) for measurement 1, indicating a similar synergistic effect.

As an effect of the coexistence of α-TocH and γ-TocH was observed for the rate constants $k_s^{\gamma\text{-TocH}}$(+α-TocH), similar measurements were performed for the solutions including α-TocH and β-TocH (or δ-TocH), by keeping [α-TocH] constant and varying [β-TocH] (or [δ-TocH]) (see measurements 1 and 2 in Table 2), respectively. Figure 5A,C shows the plots for $k_{obsd}$ versus [β-TocH] and [δ-TocH], respectively. As we may see clearly from the above plots (●), both the rate constants$k_s^{\beta\text{-TocH}}$(+α-TocH) and $k_s^{\delta\text{-TocH}}$(+α-TocH) decrease by 11% and 24% compared with the corresponding values of $k_s^{\beta\text{-TocH}}$(alone) and $k_s^{\delta\text{-TocH}}$(alone). Measurements were repeated twice to ascertain the results obtained above (see measurements 1 and 2 in Table 2). The average rate constants are listed in Table 2, indicating a cancel effect due to the coexistence of α-TocH and β-TocH (or δ-TocH).

As observed for the reaction of the solution of ArO• with the solution including α-TocH and γ-TocH (see Figure 4A–C), the absorption due to α-Toc• and β-Toc• (or δ-Toc•) at 428 nm decreased with increasing concentration of β-TocH (or δ-TocH), as shown in Figure 6A,C. The reason will be discussed in the Discussion section.

**Measurements of Aroxyl Radical-Scavenging Rates ($k_s^{AOH}$) for Mixtures of α-Tocopherol with α-, β-, γ-, or δ-Tocotrienol in Ethanol.** As a clear effect of the coexistence of α-TocH and β-, γ-, or δ-TocH was observed for rate constants $k_s^{\beta,\gamma,\delta\text{-TocH}}$(+α-TocH), similar measurements were performed for solutions including α-TocH and α-, β-, γ-, or δ-Toc-3H by

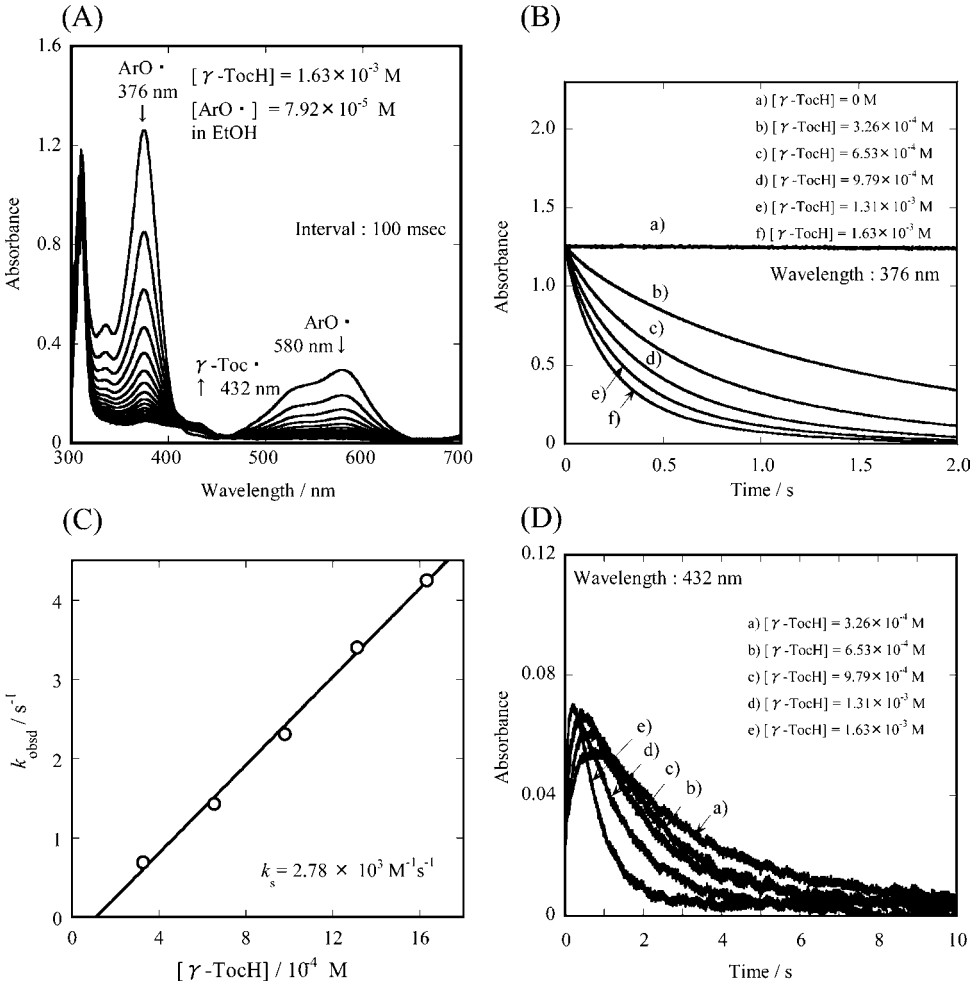


**Figure 3.** (A) Change in electronic absorption spectra of ArO$^{\bullet}$ and $\gamma$-Toc$^{\bullet}$ radicals during reaction of ArO$^{\bullet}$ with $\gamma$-TocH in ethanol solution at 25.0 °C. Initial concentrations were [ArO$^{\bullet}$] = 7.92 × 10$^{-5}$ M and [$\gamma$-TocH] = 1.63 × 10$^{-3}$ M. Spectra were recorded at 100 ms intervals. Arrow indicates a decrease (ArO$^{\bullet}$) and an increase ($\gamma$-Toc$^{\bullet}$) in absorbance with time. Also shown is time dependence of the absorbance of (B) ArO$^{\bullet}$ radical (at 376 nm) and (D) $\gamma$-Toc$^{\bullet}$ radical (at 432 nm) in solutions including six and five different concentrations of $\gamma$-TocH at 25.0 °C, respectively. (C) Plot of $k_{obsd}$ versus [$\gamma$-TocH].

**Table 2. Second-Order Rate Constants Obtained for Mixtures of $\alpha$-Tocopherol with Different Concentrations of $\beta$-, $\gamma$-, or $\delta$-Tocopherol**

| measurement[a] | [$\alpha$-TocH], M | [TocH], M | $k_s^{TocH}$($+\alpha$-TocH), M$^{-1}$·s$^{-1}$ | ratio $k_s^{TocH}$($+\alpha$-TocH)/$k_s^{TocH}$(alone) |
|---|---|---|---|---|
| | | Mixture of $\alpha$-TocH + $\beta$-TocH | | |
| 1 | 2.71 × 10$^{-4}$ | (0−1.04) × 10$^{-3}$ | 2.47 × 10$^{3}$ | 0.892 |
| 2 | 2.95 × 10$^{-4}$ | (0−1.17) × 10$^{-3}$ | 2.65 × 10$^{3}$ | 0.967 |
| avg | | | 2.56 × 10$^{3}$ | 0.930 |
| | | Mixture of $\alpha$-TocH + $\gamma$-TocH | | |
| 1 | 2.88 × 10$^{-4}$ | (0−1.21) × 10$^{-3}$ | 3.25 × 10$^{3}$ | 1.15 |
| 2 | 2.99 × 10$^{-4}$ | (0−1.31) × 10$^{-3}$ | 3.08 × 10$^{3}$ | 1.09 |
| avg | | | 3.17 × 10$^{3}$ | 1.12 |
| | | Mixture of $\alpha$-TocH + $\delta$-TocH | | |
| 1 | 2.63 × 10$^{-4}$ | (0−2.16) × 10$^{-3}$ | 7.43 × 10$^{2}$ | 0.728 |
| 2 | 3.01 × 10$^{-4}$ | (0−2.52) × 10$^{-3}$ | 8.02 × 10$^{2}$ | 0.786 |
| avg | | | 7.73 × 10$^{3}$ | 0.757 |

[a]Measurements were performed by keeping [$\alpha$-TocH] constant and varying [TocH] and were repeated twice to ascertain the results.

keeping [$\alpha$-TocH] constant and varying the concentration of $\alpha$-, $\beta$-, $\gamma$-, or $\delta$-Toc-3H. The $k_{obsd}$ versus [Toc-3H] plots (●) for $\alpha$-, $\beta$-, $\gamma$-, and $\delta$-Toc-3H, respectively, are shown in Figure S1A−D, Supporting Information. Analysis of the rate constant $k_s^{\alpha,\beta,\gamma,\delta\text{-Toc-3H}}$($+\alpha$-TocH) was performed by use of eq 12. The $k_s^{\alpha,\beta,\gamma,\delta\text{-Toc-3H}}$($+\alpha$-TocH) values and ratios of the rate constants $k_s^{\alpha,\beta,\gamma,\delta\text{-Toc-3H}}$($+\alpha$-TocH)/$k_s^{\alpha,\beta,\gamma,\delta\text{-Toc-3H}}$(alone) obtained are listed in Table 3.

To investigate the effect of concentration of $\alpha$-, $\beta$-, $\gamma$-, and $\delta$-Toc-3Hs on the reaction rates $k_s^{\alpha,\beta,\gamma,\delta\text{-Toc-3H}}$($+\alpha$-TocH), similar


dx.doi.org/10.1021/jf502049k | J. Agric. Food Chem. 2014, 62, 8101−8113

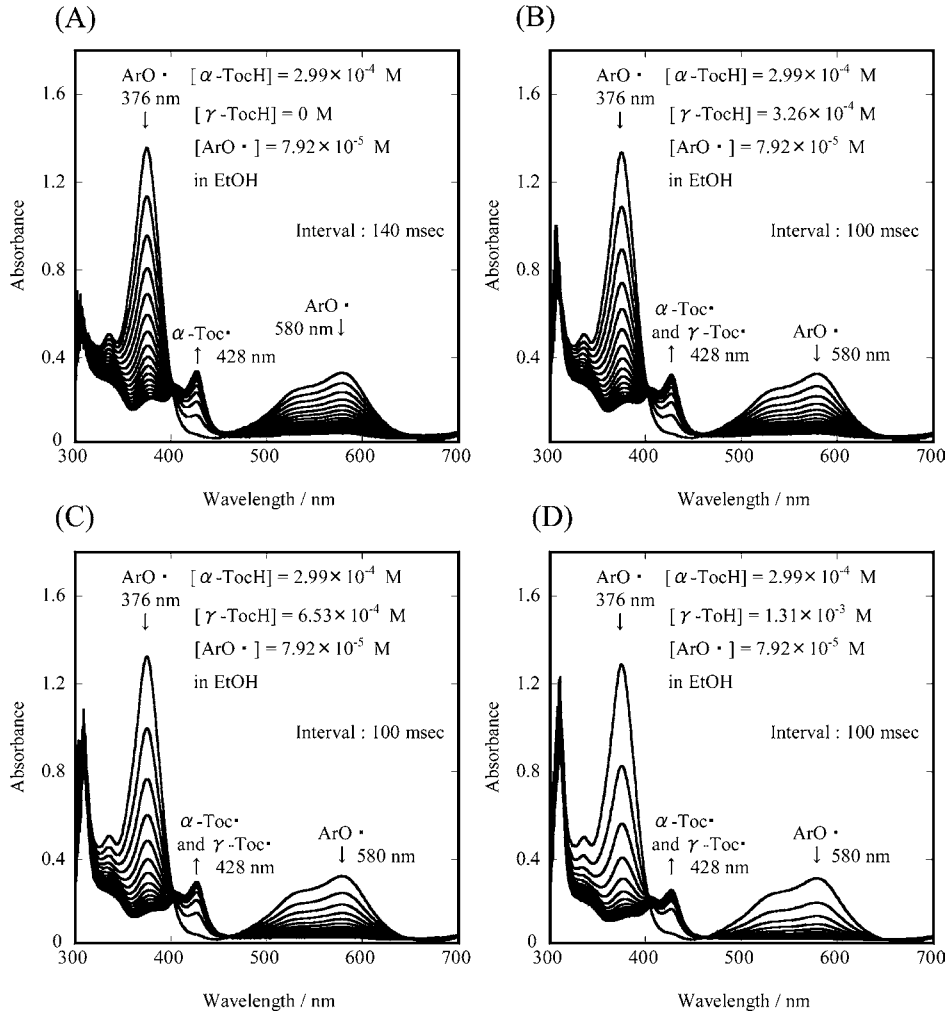


**Figure 4.** Change in electronic absorption spectra of ArO$^\bullet$ and $\alpha$-Toc$^\bullet$ (and $\gamma$-Toc$^\bullet$) radicals during reaction of ArO$^\bullet$ with a mixture of $\alpha$-TocH and $\gamma$-TocH in ethanol at 25.0 °C. [ArO$^\bullet$] = $7.92 \times 10^{-5}$ and [$\alpha$-TocH] = $2.99 \times 10^{-4}$ M. Spectra were recorded at 140 or 100 ms intervals. Absorption of $\alpha$-Toc$^\bullet$ (and $\gamma$-Toc$^\bullet$) decreased with increasing concentrations of $\gamma$-TocH. [$\gamma$-TocH] = (A) 0 M, (B) $3.26 \times 10^{-4}$ M, (C) $6.53 \times 10^{-4}$ M, and (D) $1.31 \times 10^{-3}$ M.

measurements were repeated for the mixture including different concentrations of $\alpha$-, $\beta$-, $\gamma$-, and $\delta$-Toc-3H. $k_s^{\alpha,\beta,\gamma,\delta\text{-Toc-3H}}$(+$\alpha$-TocH) values for measurements 1, 2, and 3 and average values are also summarized in Table 3. As listed in Table 3, $k_s^{\gamma\text{-Toc-3H}}$(+$\alpha$-TocH) values obtained for measurements 1, 2, and 3 showed good accordance with each other. Similar results were obtained for $\alpha$-, $\beta$-, and $\delta$-Toc-3Hs.

As listed in Table 3, a synergistic effect was observed for $\gamma$-Toc-3H, and a cancel effect was observed for $\beta$- and $\delta$-Toc-3H. Furthermore, the degree of increase (average +12%) of the rate constant $k_s^{\gamma\text{-Toc-3H}}$(+$\alpha$-TocH) is similar to that (average +12%) of $k_s^{\gamma\text{-TocH}}$(+$\alpha$-TocH). The degrees of decrease (average −13% and −25%) of $k_s^{\beta\text{-Toc-3H}}$(+$\alpha$-TocH) and $k_s^{\delta\text{-Toc-3H}}$(+$\alpha$-TocH) are also similar to those (average −7% and −24%) of $k_s^{\beta\text{-TocH}}$(+$\alpha$-TocH) and $k_s^{\delta\text{-TocH}}$(+$\alpha$-TocH), respectively.

Similar measurements were performed for solutions including $\alpha$-TocH and $\alpha$-, $\beta$-, $\gamma$-, or $\delta$-Toc-3H by keeping the concentration of $\alpha$-, $\beta$-, $\gamma$-, or $\delta$-Toc-3H constant and varying [$\alpha$-TocH] (see Table 4). The $k_{obsd}$ versus [$\alpha$-TocH] plots (for constant concentrations of $\alpha$-, $\beta$-, $\gamma$-, or $\delta$-Toc-3H) are shown in Figure S2A−D in Supporting Information. The rate constants $k_s^{\alpha\text{-TocH}}$(+$\alpha$-, $\beta$-, $\gamma$-, and $\delta$-Toc-3H) obtained are summarized in Table 4. Although a synergistic effect was observed for $\gamma$-Toc-3H and a cancel effect was observed for $\beta$- and $\delta$-Toc-3H, effects of the coexistence were smaller: 7% increase for $\gamma$-Toc-3H, 6% decrease for $\beta$-Toc-3H, and 7% decrease for $\delta$-Toc-3H. Effect of the coexistence of $\alpha$-TocH and $\alpha$-Toc-3H was small and negligible.

**UV−Visible Absorption Spectra of $\alpha$-, $\beta$-, $\gamma$-, and $\delta$-Tocopheroxyl and -Tocotrienoxyl Radicals in Ethanol Solution.** Measurements of wavelengths of absorption maxima ($\lambda_{max}$) and molar extinction coefficients ($\varepsilon_{max}$) were performed for $\alpha$-, $\beta$-, $\gamma$-, and $\delta$-Toc$^\bullet$ radicals in ethanol in a previous work.[35] By reacting ArO$^\bullet$ with $\alpha$-TocH in ethanol, absorption of $\alpha$-Toc$^\bullet$ is observed, as shown in Figure 2A. $\lambda_{max}^{\ i}$ ($i$ = 1−4) values of $\alpha$-Toc$^\bullet$ are easily determined from absorption peaks of the spectrum. The example for $\gamma$-Toc$^\bullet$ is also shown in Figure 3A. As the stability of $\gamma$-Toc$^\bullet$ is low compared to that of $\alpha$-Toc$^\bullet$, weak absorption was observed. Similarly, $\lambda_{max}^{\ i}$ values for $\alpha$-, $\beta$-, and $\gamma$-Toc-3$^\bullet$ were determined. However, as $\delta$-Toc-3$^\bullet$ is unstable, we could not observe absorption, even if we use high concentration of $\delta$-Toc-3H. The results obtained are summarized in Table 5.

As described above, upon reaction of $\alpha$-TocH with ArO$^\bullet$ in ethanol, $\alpha$-Toc$^\bullet$ is produced rapidly. $\alpha$-Toc$^\bullet$ is unstable at 25.0 °C; its absorption peak decreases gradually after passing through


dx.doi.org/10.1021/jf502049k | J. Agric. Food Chem. 2014, 62, 8101−8113

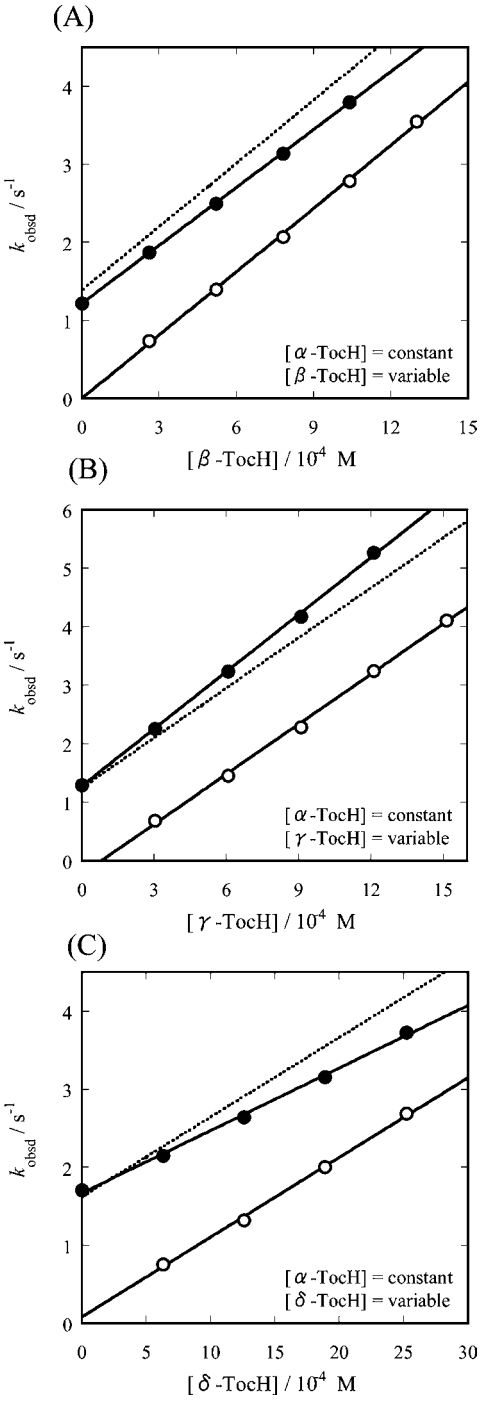


**Figure 5.** Plots of $k_{obsd}$ versus [AOH] for reactions of ArO• radical with (i) AOH only (○) and (ii) mixture of α-TocH and AOH (●). AOH = (A) β-TocH (measurement 1), (B) γ-TocH (measurement 1), and (C) δ-TocH (measurement 2) (see Table 2 and text). Dotted lines show the plots for which any synergistic effect is absent between α-TocH and β-, γ-, or δ-TocHs.

the maximum and disappears by a bimolecular reaction (reaction 13).[15,35]

$$\text{α-Toc}^{\bullet} + \text{α-Toc}^{\bullet} \xrightarrow{2k_d} \text{nonradical products (NRP)} \qquad (13)$$

As shown in Figure 2D, the maximum absorbance (that is, the concentration) of α-Toc• observed at $t_{max}$ increases with increasing [α-TocH] and approaches a constant value, because at high [α-TocH], α-Toc• appears rapidly and the decay of α-Toc• is very small and negligible. Therefore, we can estimate the $\varepsilon_1$ value of α-Toc• radical at $\lambda_{max}^{1}$ = 428 nm by use of the relationship Abs(α-Toc• at $t_{max}$) = $\varepsilon_1$[ArO•]$_{t=0}$, as reported in a previous work.[35] The $\varepsilon_1$ value of α-Toc• radical obtained was 4370 $M^{-1}\cdot cm^{-1}$ in ethanol solution.

Similarly, upon reaction of γ-TocH with ArO• in ethanol, γ-Toc• is produced, and its absorption peak decreases rapidly after passing through the maximum (see Figure 3D). As shown in Figure 3D, the maximum absorbance at 432 nm of γ-Toc• observed at $t_{max}$ increases with increasing [γ-TocH] and approaches a constant value. Therefore, we can tentatively estimate the $\varepsilon_1$ value of γ-Toc• radical at $\lambda_{max}^{1}$ = 432 nm, by use of the relationship Abs(γ-Toc• at $t_{max}$) = $\varepsilon_1$[ArO•]$_{t=0}$.[35] The $\varepsilon_1$ value of γ-Toc• radical obtained was 820 $M^{-1}\cdot cm^{-1}$ in ethanol solution. Similarly, the $\varepsilon_1$ values of β- and δ-Toc• and α-, β-, and γ-Toc-3• radicals were determined (see Table 5).

The $\lambda_{max}^{1}$ and $\varepsilon_1$ values for α-, β-, and γ-Toc-3• show good agreement with those of the corresponding α-, β-, and γ-Toc• in ethanol. The $\lambda_{max}^{1}$ value increases in the order α- < β- ≤ γ- < δ-Toc• (and α- < β- ≤ γ-Toc-3•), although the difference in $\lambda_{max}^{1}$ value among α-, β-, γ-, and δ-Toc• (and -Toc-3•) is comparatively small. On the other hand, the $\varepsilon_1$ value decreases remarkably in the order α- > β- > γ- > δ-Toc• (and α- > β- > γ- > δ-Toc-3•) in ethanol. The reason will be discussed in the Discussion section.

**Decrease in UV−Visible Absorption of α-Tocopheroxyl Radical for Coexistence of α-Tocopherol with β-, γ-, or δ-Tocopherol (or -Tocotrienol).** Upon reaction of ArO• radical with α-TocH, absorption of α-Toc• radical at $\lambda_{max}^{1}$ (= 428 nm) appears rapidly and decreases gradually, as shown in Figure 2D. The concentration of α-Toc• radical produced by reaction with ArO• ([ArO•] = 8.78 × $10^{-5}$ M) is similar to that of ArO• if a high concentration of α-TocH is used for the reaction, as described in a previous section.[35]

On the other hand, if γ-TocH coexists in the above solution, absorption of α-Toc• radical (for [γ-TocH] = 0 M) decreases with increasing [γ-TocH], as shown in Figure 4. The time dependence of absorption observed at 428 nm is shown in Figure 6C, where absorption at 428 nm is due to the sum of α-Toc• and γ-Toc•, although the contribution of the latter is much smaller than that of the former (see Figures 2A and 3A and Table 5). The contribution of γ-Toc• is almost negligible at 10 s, as shown in Figure 3D. Consequently, [α-Toc•] at 10 s was calculated from absorbance of α-Toc•, by use of the relationship Abs = $\varepsilon_1$[α-Toc•], where $\varepsilon_1$ = 4370 $M^{-1}\cdot cm^{-1}$). Figure 6D shows the plot of [α-Toc•], at 10 s (●) in Figure 6C, versus [γ-TocH]. The [α-Toc•] decreases remarkably with increasing [γ-TocH], suggesting that the prooxidant effect induced by α-Toc• is suppressed by the coexistence of γ-TocH. The reason for the decrease of [α-Toc•] due to the coexistence of γ-TocH will be discussed in the Discussion section.

Similar measurements were performed for solutions including α-TocH and β-TocH (or δ-TocH). The time dependence of absorption observed at 428 nm for the coexistence of (i) α-TocH and β-TocH and (ii) α-TocH and δ-TocH is shown in Figure 6A,E, indicating that absorption of Toc• radicals at 428 nm decreases with increasing [β-TocH] or [δ-TocH]. In the case of δ-TocH, δ-Toc• is very unstable, and the contribution of δ-Toc• to absorption is almost negligible at 10 s. The plot of [α-Toc•], at 10 s in Figure 6E, versus [δ-TocH] is shown in Figure 6F. On the other hand, β-Toc• is not so unstable, and its absorption overlaps with that of α-Toc• at the first stage of reactions 9 and 10.

The decrease of [α-Toc•] (at 10 s) due to the coexistence of β-, γ-, or δ-TocH—that is, the ratio of [α-Toc•] with β-, γ-, or δ-


dx.doi.org/10.1021/jf502049k | J. Agric. Food Chem. 2014, 62, 8101−8113

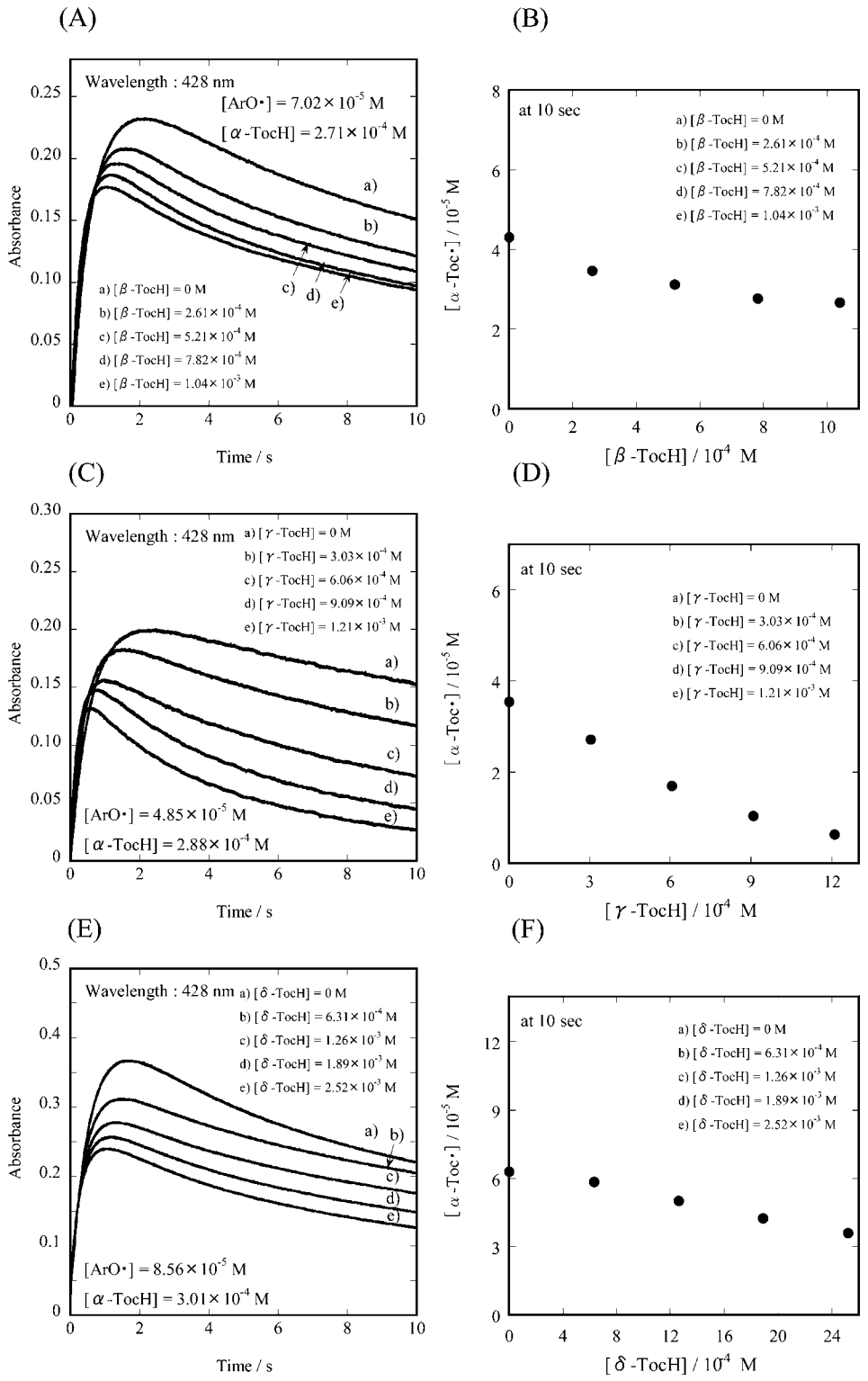


**Figure 6.** (Left panels) Time dependence of absorbance of Toc• radicals (at 428 nm) in ethanol solutions including five different concentrations of (A) $\beta$-, (C) $\gamma$-, and (E) $\delta$-TocH at 25.0 °C. (Right panels) Plots of [$\alpha$-Toc•], at 10 s in corresponding left panels, versus (B) [$\beta$-TocH], (D) [$\gamma$-TocH], and (F) [$\delta$-TocH].

TocH to [$\alpha$-Toc•] without $\beta$-, $\gamma$-, or $\delta$-TocHs—is 0.62 at [$\beta$-TocH] = $1.04 \times 10^{-3}$, 0.18 at [$\gamma$-TocH] = $1.21 \times 10^{-3}$, and 0.57 at [$\delta$-TocH] = $2.52 \times 10^{-3}$ M, which are the maximum concentrations of $\beta$-, $\gamma$-, and $\delta$-TocHs used for measurements.

Similar measurements were performed for solutions including $\alpha$-TocH and $\alpha$-, $\beta$-, $\gamma$-, or $\delta$-Toc-3H. The time dependence of absorption observed at 428 nm for the coexistence of $\alpha$-TocH and $\beta$-, $\gamma$-, or $\delta$-Toc-3H is shown in Figure 7panels A, C, and E, respectively. The decrease of [$\alpha$-Toc•] (at 10 s)—that is, the ratio of [$\alpha$-Toc•] (with $\beta$-, $\gamma$-, or $\delta$-Toc-3H) to [$\alpha$-Toc•] without $\beta$-, $\gamma$-, or $\delta$-Toc-3Hs—is 0.74 at [$\beta$-Toc-3H] = $1.28 \times 10^{-4}$, 0.16 at [$\gamma$-Toc-3H] = $1.45 \times 10^{-3}$, and 0.55 at [$\delta$-Toc-3H] = $2.37 \times$


dx.doi.org/10.1021/jf502049k | J. Agric. Food Chem. 2014, 62, 8101−8113

**Table 3. Second-Order Rate Constants Obtained for Mixtures of α-Tocopherol with Different Concentrations of α-, β-, γ-, or δ-Tocotrienol**

| measurement[a] | [α-TocH], M | [Toc-3H], M | $k_s^{Toc\text{-}3H}$(+α-TocH), $M^{-1}\cdot s^{-1}$ | ratio $k_s^{Toc\text{-}3H}$(+α-TocH)/$k_s^{Toc\text{-}3H}$(alone) |
|---|---|---|---|---|
| | | Mixture of α-TocH + α-Toc-3H | | |
| 1 | $2.82 \times 10^{-4}$ | $(0-2.95) \times 10^{-4}$ | $5.32 \times 10^3$ | 1.07 |
| 2 | $3.09 \times 10^{-4}$ | $(0-9.65) \times 10^{-4}$ | $5.21 \times 10^3$ | 1.05 |
| 3 | $2.83 \times 10^{-4}$ | $(0-1.03) \times 10^{-3}$ | $5.07 \times 10^3$ | 1.02 |
| avg | | | $5.20 \times 10^3$ | 1.05 |
| | | Mixture of α-TocH + β-Toc-3H | | |
| 1 | $2.63 \times 10^{-4}$ | $(0-4.32) \times 10^{-4}$ | $2.70 \times 10^3$ | 0.868 |
| 2 | $3.02 \times 10^{-4}$ | $(0-1.28) \times 10^{-3}$ | $2.69 \times 10^3$ | 0.865 |
| avg | | | $2.70 \times 10^3$ | 0.867 |
| | | Mixture of α-TocH + γ-Toc-3H | | |
| 1 | $3.00 \times 10^{-4}$ | $(0-4.43) \times 10^{-4}$ | $2.98 \times 10^3$ | 1.08 |
| 2 | $2.96 \times 10^{-4}$ | $(0-1.15) \times 10^{-3}$ | $3.21 \times 10^3$ | 1.16 |
| 3 | $3.17 \times 10^{-4}$ | $(0-1.45) \times 10^{-3}$ | $3.08 \times 10^3$ | 1.12 |
| avg | | | $3.09 \times 10^3$ | 1.12 |
| | | Mixture of α-TocH + δ-Toc-3H | | |
| 1 | $2.37 \times 10^{-4}$ | $(0-8.37) \times 10^{-4}$ | $8.22 \times 10^2$ | 0.754 |
| 2 | $3.01 \times 10^{-4}$ | $(0-2.37) \times 10^{-3}$ | $8.55 \times 10^2$ | 0.784 |
| 3 | $2.88 \times 10^{-4}$ | $(0-2.39) \times 10^{-3}$ | $7.94 \times 10^2$ | 0.728 |
| avg | | | $8.24 \times 10^2$ | 0.755 |

[a]Measurements were performed by keeping [α-TocH] constant and varying [TocH] and were repeated two or three times to ascertain the results.

**Table 4. Second-Order Rate Constants Obtained for Mixtures of Different Concentrations of α-Tocopherol with α-, β-, γ-, or δ-Tocotrienol[a]**

| tocotrienol | [Toc-3H], M | [α-TocH], M | $k_s^{\alpha\text{-}TocH}$(+Toc-3H), $M^{-1}\cdot s^{-1}$ | ratio $k_s^{\alpha\text{-}TocH}$(+Toc-3H)/$k_s^{\alpha\text{-}TocH}$(alone) |
|---|---|---|---|---|
| α-Toc-3H | $2.15 \times 10^{-4}$ | $(0-7.51) \times 10^{-4}$ | $5.27 \times 10^3$ | 1.03 |
| β-Toc-3H | $4.99 \times 10^{-4}$ | $(0-7.51) \times 10^{-4}$ | $4.84 \times 10^3$ | 0.945 |
| γ-Toc-3H | $5.02 \times 10^{-4}$ | $(0-8.32) \times 10^{-4}$ | $5.48 \times 10^3$ | 1.07 |
| δ-Toc-3H | $1.10 \times 10^{-3}$ | $(0-7.51) \times 10^{-4}$ | $4.74 \times 10^4$ | 0.926 |

[a]Measurements were performed by keeping the concentration of α-, β-, γ-, or δ-Toc-3H constant and varying [α-TocH].

**Table 5. Values of UV−Visible Absorption Maxima and Molar Extinction Coefficients of α-, β-, γ-, and δ-Tocopheroxyls and -Tocotrienoxyls in Ethanol**

| $Toc^•$ or Toc-$3^•$ | $\lambda_{max}{}^1$, nm ($\varepsilon_1$, $M^{-1}\cdot cm^{-1}$) | $\lambda_{max}{}^2$, nm ($\varepsilon_2$, $M^{-1}\cdot cm^{-1}$) | $\lambda_{max}{}^3$, nm ($\varepsilon_3$, $M^{-1}\cdot cm^{-1}$) | $\lambda_{max}{}^4$, nm ($\varepsilon_4$, $M^{-1}\cdot cm^{-1}$) |
|---|---|---|---|---|
| α-$Toc^•$ | 428 (4370)[a] | 408 (3010) | 387 sh[b] (1630) | 340 sh (3790) |
| α-Toc-$3^•$ | 428 (4280) | 407 (3220) | 387 sh (2120) | 340 sh (3720) |
| β-$Toc^•$ | 431 (1500)[a] | 409 (1200) | | |
| β-Toc-$3^•$ | 430 (1620) | | | |
| γ-$Toc^•$ | 432 (820)[a] | | | |
| γ-Toc-$3^•$ | 432 (745) | | | |
| δ- $Toc^•$ | 434 (380)[a] | | | |
| δ- Toc-$3^•$ | | | | |

[a]See ref 35. [b]Shoulder.

$10^{-3}$ M. The decrease of [α-$Toc^•$] (+[α-Toc-$3^•$]) due to coexistence of α-TocH and α-Toc-3H was negligible, as expected (data not shown). The degree of decrease of [α-$Toc^•$] (at 10 s) increases in the order shown in eq 14:

$$\begin{aligned} \text{α-Toc-3H} &\ll \text{β-TocH} \sim \text{β-Toc-3H} \\ &< \text{δ-TocH} \sim \text{δ-Toc-3H} \\ &< \text{γ-TocH} \sim \text{γ-Toc-3H} \end{aligned} \quad (14)$$

As described above, [α-$Toc^•$] decreases notably with increasing concentration of β-, γ-, or δ-TocH. This result suggests that the prooxidant effect induced by α-$Toc^•$ may be suppressed by the coexistence of β-, γ-, or δ-TocH (or β-, γ-, or δ-Toc-3H). The reason will be discussed in the Discussion section.

## DISCUSSION

**Comparison of Aroxyl Radical-Scavenging Rates ($k_s^{AOH}$) of Tocotrienols with Those of Tocopherols in Ethanol Solution.** α-, β-, γ-, and δ-TocHs and -Toc-3Hs are well-known as vitamin E homologues. Toc-3Hs have received much attention in recent years.[36] Yoshida et al.[37] reported that the reactivities of α-, β-, γ-, and δ-Toc-3Hs toward peroxyl radicals are the same as those of the corresponding α-, β-, γ-, and δ-TocHs in acetonitrile solution. On the other hand, Serbinova et al.[38] reported that α-Toc-3H has more potent antioxidant activity than α-TocH for lipid peroxidation in rat liver microsomal membranes. Moreover, some biological functions such as cholesterol-lowering,[39−41] anti-cancer,[42,43] anti-inflammatory,[44,45] anti-angiogenic,[46,47] and neuroprotection[48] effects

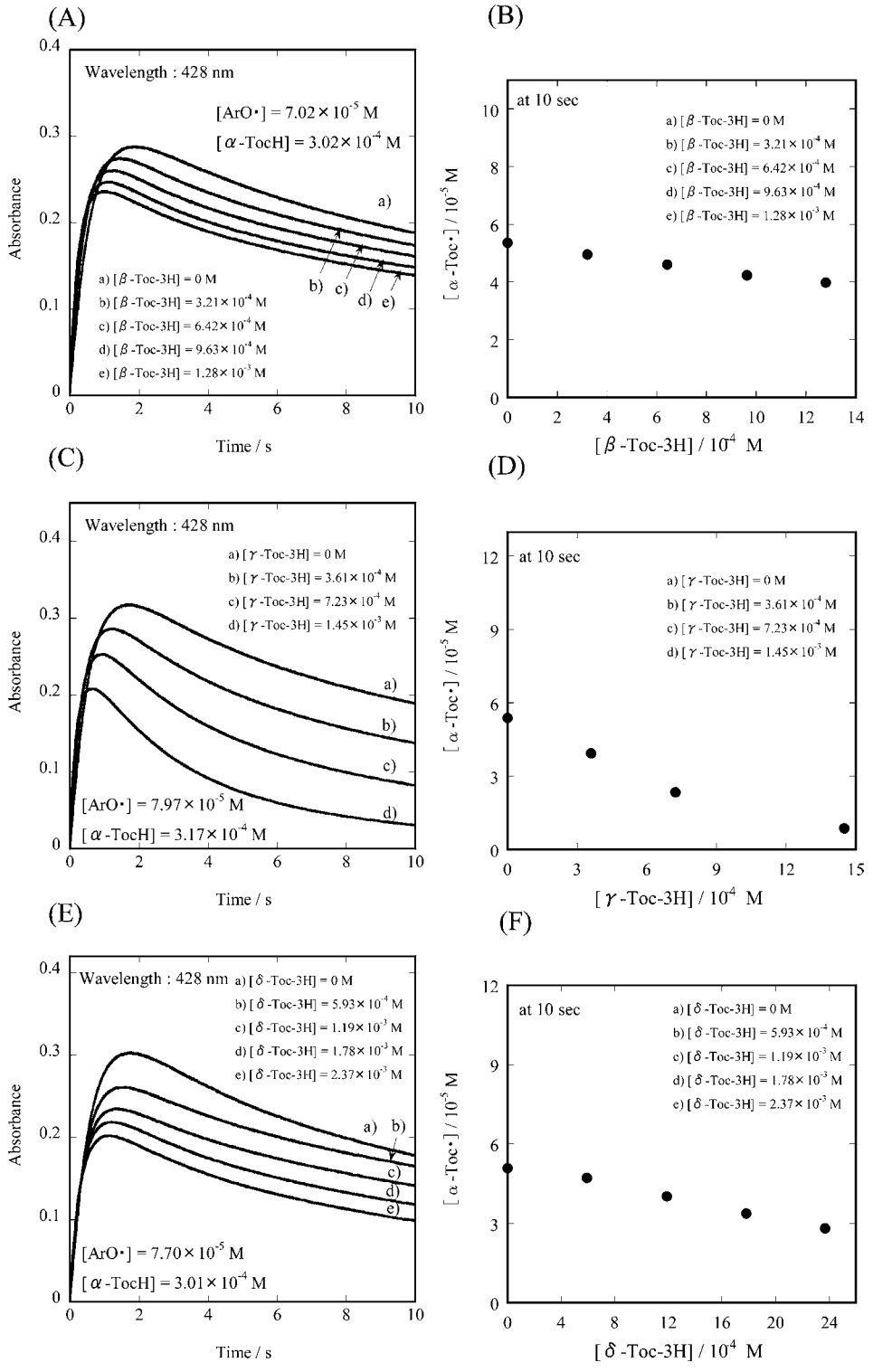


**Figure 7.** (Left panels) Time dependence of absorbance of Toc• radicals (at 428 nm) in ethanol solutions including five (or four) different concentrations of (A) $\beta$-, (C) $\gamma$-, and (E) $\delta$-Toc-3H at 25.0 °C. (Right panels) Plots of [$\alpha$-Toc•], at 10 s in corresponding left panels, versus (B) [$\beta$-Toc-3H], (D) [$\gamma$-Toc-3H], and (F) [$\delta$-Toc-3H].

have been reported for Toc-3Hs. These findings suggest that Toc-3Hs have a wide variety of health benefits.

In the present work, measurements of ArO•-scavenging rate constants, $k_s^{AOH}$(alone), of antioxidants ($\alpha$-, $\beta$-, $\gamma$-, and $\delta$-TocHs and -Toc-3Hs) were performed in ethanol solution via stopped-flow spectrophotometry. As listed in Table 1, the $k_s^{AOH}$(alone) values of $\alpha$-, $\beta$-, $\gamma$-, and $\delta$-Toc-3Hs show good agreement with those of the corresponding TocHs in ethanol, indicating that the difference of the alkyl side chains in tocopherols and tocotrienols does not have a significant effect on the reaction rates. Furthermore, $\lambda_{max}^1$ and $\varepsilon_1$ values of $\alpha$-, $\beta$-, $\gamma$-, and $\delta$-Toc-3• radicals also agree well with the corresponding values of $\alpha$-, $\beta$-, $\gamma$-, and $\delta$-Toc• radicals in ethanol (see Table 5). The result also indicates that the electronic states of the chroman ring in $\alpha$-, $\beta$-,


dx.doi.org/10.1021/jf502049k | J. Agric. Food Chem. 2014, 62, 8101−8113

γ-, and δ-Toc$^{\bullet}$ and -Toc-3$^{\bullet}$ radicals are similar to one another, being independent of the difference in alkyl side chain.

**Finding of Synergistic and Cancel Effects on the Aroxyl Radical-Scavenging Rates ($k_s$) for the Coexistence of α-Tocopherol with β-, γ-, or δ-Tocopherol (or -Tocotrienol.).** It is well-known that various antioxidants coexist in many foods and plants[2] and biological systems.[24−27] However, examples of measurement of free radical-scavenging rates for the coexistence of two antioxidants are very limited.[49] Recently, it has been found that the ArO$^{\bullet}$ radical-scavenging rates ($k_s^{AOH}$) increase notably for the coexistence of two antioxidants, (i) α-TocH and vitamin C and (ii) α-TocH and $UQ_{10}H_2$, in 2-propanol/water (5:1 v/v) solution.[28]

In the present work, measurements of $k_s^{AOH}$ for α-, β-, γ-, δ-TocHs and -Toc-3Hs were performed in ethanol solution. The $k_s^{AOH}$ values were measured not only for each antioxidant but also for the mixtures of two antioxidants, (i) α-TocH and β-, γ-, or δ-TocH and (ii) α-TocH and α-, β-, γ-, or δ-Toc-3H. A clear synergistic effect in which $k_s^{\gamma\text{-TocH}}$(+α-TocH) values increase by 12% was observed for solutions including α-TocH and γ-TocH. On the other hand, a cancel effect in which (i) $k_s^{\beta\text{-TocH}}$(+α-TocH) and (ii) $k_s^{\delta\text{-TocH}}$(+α-TocH) decrease by 7% and 24%, respectively, was observed for the solutions including (i) α-TocH with β-TocH and (ii) α-TocH with δ-TocH. Similar results were observed for the solutions including two kinds of antioxidants (α-TocH with β-, γ-, or δ-Toc-3H).

It is important to know the concentrations of α-, β-, γ-, and δ-TocHs and -Toc-3Hs included in foods and plants (especially in edible oils). The contents of α-, β-, γ-, and δ-TocHs in rapeseed, soybean, peanut, pumpkin, sunflower, canola, corn, wheat germ, and almond oils have been determined by an HPLC method, showing that α- and γ-TocHs are mainly included in edible oils.[29−31] For example, the contents in edible oils are as follows: (i) in peanut oil, concentrations of α-, β-, γ-, and δ-TocH = 73.2, nd, 312.0, and 13.4 mg/kg, respectively; (ii) in sunflower oil, concentrations are 494.2, nd, 131.0, and 9.2 mg/kg, respectively; and (iii) in rapeseed oil, concentrations are 90.9, nd, 527.6, and 6.1 mg/kg, respectively, as reported by Tuberoso et al.[30] Here, nd denotes not detected. Contents of β- and δ-TocHs are much less than those of α- and γ-TocHs. The result suggests that a synergistic effect observed for the reaction rate constant $k_s^{\gamma\text{-TocH}}$(+α-TocH) for the coexistence of α- and γ-TocHs functions mainly in edible oils, to protect the degradation of edible oils. Furthermore, high concentrations of α- and γ-TocHs and -Toc-3Hs are included in rice bran and palm oil.[32,33] Contents of β- and δ-TocHs (and -Toc-3Hs) are much less than those of α- and γ-TocHs (and -TocH-3s), suggesting that a synergistic effect functions in rice bran and palm oils. However, the reason why a synergistic effect functions between α- and γ-TocHs (or γ-TocH-3s) and a cancel effect functions between (i) α-TocH and β-TocH (or β-Toc-3H) and (ii) α-TocH and δ-TocH (or δ-Toc-3H) is not clear at present.

**Scheme for Suppression of Prooxidant Effect of α-Tocopherol for Coexistence of α-Tocopherol with β-, γ-, or δ-Tocopherol (or -Tocotrienol).** As described in the Introduction, α-Toc$^{\bullet}$ is an important key radical, which appears in the process of antioxidant and prooxidant actions of α-TocH. As shown in Figures 4, 6, and 7, we could directly ascertain that the [α-Toc$^{\bullet}$] produced by the reaction with ArO$^{\bullet}$ radical decreases remarkably with the coexistence of β-, γ-, or δ-TocH (or -Toc-3H), by observing the decrease of UV−vis absorption of α-Toc$^{\bullet}$ radical. The result clearly indicates that the prooxidant effect of α-Toc$^{\bullet}$ (see reaction 2) may be suppressed by the coexistence of α-TocH and another TocH (or Toc-3H).

In previous studies, the scheme of the decay reaction of α-, β-, γ-, and δ- Toc$^{\bullet}$ radicals in organic solvents has been investigated.[15,35] In polar ethanol, acetonitrile, and chloroform solvents, α-Toc$^{\bullet}$ decays by a simple bimolecular reaction without dimer formation, suggesting the production of α-TocH and α-tocopherol-*o*-quinonemethide (α-Toc-QM) by disproportionation (reaction 15):

$$\text{α-Toc}^{\bullet} + \text{α-Toc}^{\bullet} \xrightarrow{2k_d} \text{α-TocH} + \text{α-Toc-QM} \quad (15)$$

On the other hand, in nonpolar *n*-hexane, *n*-heptane, and diethyl ether solvents, bimolecular radical decay of α-Toc$^{\bullet}$ radical involves dimerization (recombination) and disproportionation (reaction 16):[35]

$$\text{dimer (α-Toc} - \text{α-Toc)} \underset{2k_{16}}{\overset{2k_{-16}}{\rightleftharpoons}} \text{α-Toc}^{\bullet} + \text{α-Toc}^{\bullet} \xrightarrow{2k_d} \text{α-TocH} + \text{α-Toc-QM} \quad (16)$$

where dimer is quinol ether (see Figure 9d in ref 35), although it is unstable and has not been isolated. $k_{16}$ and $k_{-16}$ represent the rate constants for formation and breakdown of dimer, respectively. Dimerization reactions of phenoxyl radicals (including α-Toc$^{\bullet}$) are fast reactions and are characterized by large rate constants ($k \approx 10^7-10^9$ $M^{-1}\cdot s^{-1}$) in nonviscous solvents at room temperature.[50]

As described in the Results section, the absorbances of α-, β-, γ-, and δ-Toc$^{\bullet}$ radicals produced by reaction with ArO$^{\bullet}$ decrease remarkably in the order α-Toc$^{\bullet}$ > β-Toc$^{\bullet}$ > γ-Toc$^{\bullet}$ > δ-Toc$^{\bullet}$ in ethanol solvent. The smaller absorbance obtained for β-, γ-, and δ-Toc$^{\bullet}$ radicals will be due to the fast formation of dimer (fast equilibrium with the dimer) (reaction 17) in these Toc$^{\bullet}$ radical molecules. The steric repulsion due to two ortho-methyl groups on the α-Toc$^{\bullet}$ radical molecule will hinder the formation of quinol-ether-type dimer in polar ethanol solvent. However, dimer formation will become easier with decreasing number of ortho-methyl groups.

$$\text{dimer (γ-Toc} - \text{γ-Toc)} \underset{2k_{17}}{\overset{2k_{-17}}{\rightleftharpoons}} \text{γ-Toc}^{\bullet} + \text{γ-Toc}^{\bullet} \xrightarrow{2k_d} \text{γ-TocH} + \text{γ-Toc-QM} \quad (17)$$

As described above, if α-TocH and γ-TocH coexist in ethanol and react with ArO$^{\bullet}$, reactions 9 and 10 will occur competitively. The α-Toc$^{\bullet}$ and γ-Toc$^{\bullet}$ radicals produced will disappear following reactions 15 and 17 in ethanol, respectively. In addition to these reactions, α-Toc$^{\bullet}$ radical will react with γ-Toc$^{\bullet}$ and disappear following reactions 18a and 18b:

$$\text{dimer (α-Toc} - \text{γ-Toc)} \underset{2k_{18}}{\overset{2k_{-18}}{\rightleftharpoons}} \text{α-Toc}^{\bullet} + \text{γ-Toc}^{\bullet} \quad (18a)$$

$$2\text{α-Toc}^{\bullet} + 2\text{γ-Toc}^{\bullet} \xrightarrow{2k_d} \text{α-TocH} + \text{γ-Toc-QM} + \text{γ-TocH} + \text{α-Toc-QM} \quad (18b)$$

where $2k_d$ includes three types of bimolecular reaction rates between (i) α-Toc$^{\bullet}$ + α-Toc$^{\bullet}$, (ii) γ-Toc$^{\bullet}$ + γ-Toc$^{\bullet}$, and (iii) α-

Toc$^{\bullet}$ + $\gamma$-Toc$^{\bullet}$, and the reaction produces four kinds of products ($\alpha$-TocH, $\alpha$-Toc-QM, $\gamma$-TocH, and $\gamma$-Toc-QM). Formation of dimer ($\alpha$-Toc−$\gamma$-Toc) will proceed rapidly, because steric hindrance for the reaction between $\alpha$-Toc$^{\bullet}$ and $\gamma$-Toc$^{\bullet}$ is smaller than that between $\alpha$-Toc$^{\bullet}$ and $\alpha$-Toc$^{\bullet}$.

As the electron-donating character of $\alpha$-TocH is larger than that of $\beta$-, $\gamma$-, and $\delta$-TocHs, we may expect that reaction 19 will proceed if $\alpha$-TocH coexists with $\beta$-, $\gamma$-, or $\delta$-Toc$^{\bullet}$ in solution.[19] In fact, Niki et al.[51] ascertained that $\alpha$-TocH reacts quite rapidly with $\beta$-, $\gamma$-, and $\delta$-Toc$^{\bullet}$ radicals to give $\alpha$-Toc$^{\bullet}$ radical and $\beta$-, $\gamma$-, and $\delta$-TocHs, respectively, by electron spin resonance (ESR) measurement.

$$\alpha\text{-TocH} + \beta\text{-, }\gamma\text{-, or }\delta\text{-Toc}^{\bullet} \xrightarrow{k_{19}} \alpha\text{-Toc}^{\bullet} + \beta\text{-, }\gamma\text{-, or }\delta\text{-TocH} \quad (19)$$

Consequently, if ArO$^{\bullet}$ radical reacts with $\alpha$-TocH and $\gamma$-TocH in a solution, $\alpha$-Toc$^{\bullet}$ and $\gamma$-Toc$^{\bullet}$ are produced, and reactions 15, 17, 18a, 18b, and 19 proceed competitively in the solution. On the other hand, even if ArO$^{\bullet}$ radical reacts with $\alpha$-TocH and $\delta$-TocH in a solution, dimer ($\alpha$-Toc−$\delta$-Toc) formation between $\alpha$-Toc$^{\bullet}$ and $\delta$-Toc$^{\bullet}$ (see reactions 18a and 18b) does not occur, because $\delta$-Toc$^{\bullet}$ produced is very unstable and disappears rapidly by forming the dimer $\delta$-Toc−$\delta$-Toc. Consequently, only $\alpha$-Toc$^{\bullet}$ remains in solution and disappears gradually, as shown in Figure 6E. This will be a reason why larger [$\alpha$-Toc$^{\bullet}$] remains in solution at 10 s, compared to the case of coexistence of $\alpha$-TocH and $\gamma$-TocH. In the case of coexistence of $\alpha$-TocH and $\beta$-TocH, reactions 15, 17, 18a, and 18b will proceed competitively in solution. Furthermore, as $\beta$-Toc$^{\bullet}$ is comparatively stable, $\beta$-Toc$^{\bullet}$ disappears and $\alpha$-Toc$^{\bullet}$ is formed by reaction 19, and the $\alpha$-Toc$^{\bullet}$ produced disappears gradually (see Figure 6A) as observed for the case of coexistence of $\alpha$-TocH and $\delta$-TocH.

Similar results were obtained for solution including $\alpha$-TocH and $\beta$-, $\gamma$-, or $\delta$-Toc-3H, as shown in Figure 7, indicating that the difference in alkyl side chain does not have a significant effect on the bimolecular radical decay of Toc$^{\bullet}$ and Toc-3$^{\bullet}$ radical.

As described above, $\alpha$-TocH and the other TocHs and Toc-3Hs (especially $\gamma$-TocH and $\gamma$-Toc-3H) coexist in edible oils.[29−33] Consequently, the above synergistic effect—that is, suppression of the prooxidant reaction— may function in edible oils.

In the present work, a kinetic study of the ArO$^{\bullet}$ radical-scavenging activity of eight vitamin E homologues ($\alpha$-, $\beta$-, $\gamma$-, and $\delta$-tocopherols and -tocotrienols) has been performed in ethanol solution, by use of stopped-flow spectrophotometry. The ArO$^{\bullet}$ radical-scavenging rates ($k_s^{AOH}$) of $\alpha$-, $\beta$-, $\gamma$-, and $\delta$-Toc-3Hs showed good agreement with those of the corresponding $\alpha$-, $\beta$-, $\gamma$-, and $\delta$-TocHs, indicating that the difference of the alkyl side chains in tocopherols and tocotrienols does not have a significant effect on the reaction rates. The $k_s^{AOH}$ values were measured not only for each antioxidant but also for mixtures of two antioxidants: (i) $\alpha$-TocH with $\beta$-, $\gamma$-, or $\delta$-TocH and (ii) $\alpha$-TocH with $\alpha$-, $\beta$-, $\gamma$-, or $\delta$-Toc-3H. Synergistic and cancel effects in which the $k_s^{AOH}$ values increase by 12% and decrease by 7% (or 24%) were observed for the solutions including two kinds of antioxidants, (i) $\alpha$-TocH and $\gamma$-TocH and (ii) $\alpha$-TocH and $\beta$-TocH (or $\alpha$-TocH and $\delta$-TocH). As contents of $\alpha$- and $\gamma$-TocHs included in general edible oils are much higher than those of $\beta$- and $\delta$-TocHs, only a synergistic effect may function in edible oils. Furthermore, UV−vis absorption of $\alpha$-Toc$^{\bullet}$ (at $\lambda_{max}$ = 428 nm), which had been produced by reaction of $\alpha$-TocH with ArO$^{\bullet}$, decreased remarkably for coexistence of $\alpha$-TocH with $\beta$-, $\gamma$-, or $\delta$-TocH (or -Toc-3H). This result indicates that the prooxidant effect of $\alpha$-Toc$^{\bullet}$ may be suppressed by coexistence with another TocH or Toc-3H. The scheme for the decrease of [$\alpha$-Toc$^{\bullet}$] due to coexistence of $\alpha$-TocH with another TocH (or Toc-3H) was discussed on the basis of the results obtained.

## ■ ASSOCIATED CONTENT

### Ⓢ Supporting Information

Two figures showing plots of $k_{obsd}$ vs [AOH] and $k_{obsd}$ vs [$\alpha$-TocH] for reactions of ArO$^{\bullet}$ radical with AOH only and with a mixture of $\alpha$-TocH and AOH. This material is available free of charge via the Internet at http://pubs.acs.org.

## ■ AUTHOR INFORMATION


### Corresponding Author

*Telephone 81-89-927-9588; fax 81-89-927-9590; e-mail mukai-k@dpc.ehime-u.ac.jp.



### Funding

This work was partly supported by a Grant-in-Aid for Challenging Exploratory Research (24658123) from Japan Society for the Promotion of Science.


### Notes

The authors declare no competing financial interest.

## ■ ACKNOWLEDGMENTS


We are very grateful to Dr. Koichi Abe of Eisai Food & Chemical Co., Ltd. for helpful discussion.


## ■ REFERENCES


(1) Niki, E. Assessment of antioxidant capacity in vitro and in vivo. *Free Radical Biol. Med.* **2010**, *49*, 503−515.

(2) Finley, J. W.; Kong, A.-N.; Hintze, K. J.; Jeffery, E. H.; Ji, L. L.; Lei, X. G. Antioxidants in foods: State of the science important to the food industry. *J. Agric. Food Chem.* **2011**, *59*, 6837−6846.

(3) Esterbauer, H.; Dieber-Rotheneder, M.; Striegl, G.; Waeg, G. Role of vitamin E in preventing the oxidation of low-density lipoprotein. *Am. J. Clin. Nutr.* **1991**, *53*, 314S−321S.

(4) Cillard, J.; Cillard, P.; Cormier, M. Effect of experimental factors on the prooxidant behavior of $\alpha$-tocopherol. *J. Am. Oil Chem. Soc.* **1980**, *57*, 255−261.

(5) Terao, J.; Matsushita, S. The peroxidizing effect of $\alpha$-tocopherol on autoxidation of methyl linoleate in bulk phase. *Lipids* **1986**, *21*, 255−260.

(6) Bowry, V. W.; Stocker, R. Tocopherol-mediated peroxidation: The prooxidant effect of vitamin E on the radical-initiated oxidation of human low-density lipoprotein. *J. Am. Chem. Soc.* **1993**, *115*, 6029−6044.

(7) Mukai, K.; Noborio, S.; Nagaoka, S. Why is the order reversed ? Peroxyl-scavenging activity and fats-and-oils protecting activity of vitamin E. *Int. J. Chem. Kinet.* **2005**, *37*, 605−610.

(8) Ouchi, A.; Ishikura, M.; Konishi, K.; Nagaoka, S.; Mukai, K. Kinetic study of the prooxidant effect of $\alpha$-tocopherol: Hydrogen abstraction from lipids by $\alpha$-tocopheroxyl radical. *Lipids* **2009**, *44*, 935−943.

(9) Ernster, L.; Dallner, G. Biochemical, physiological and medical aspects of ubiquinone function. *Biochim. Biophys. Acta* **1995**, *1271*, 195−204.

(10) *Coenzyme Q: Molecular Mechanisms in Health and Disease*; Kagan, V. E.; , Quinn, P. J., Eds.; CRC Press: Boca Raton, FL, 2001.

(11) Naumov, V. V.; Khrapova, N. G. Study of the interaction of ubiquinone and ubiquinol with peroxide radicals by the chemiluminescent method. *Biophysics (Engl. Transl. Biofizika)* **1983**, *28*, 774−780.

(12) Mukai, K.; Kikuchi, S.; Urano, S. Stopped-flow kinetic study of the regeneration reaction of tocopheroxyl radical by reduced ubiquinone-10 in solution. *Biochim. Biophys. Acta* **1990**, *1035*, 77−82.

(13) Barclay, L. R. C.; Vinqvist, M. R.; Mukai, K.; Itoh, S.; Morimoto, H. Chain-breaking phenolic antioxidants: Steric and electronic effects in

polyalkylchromanols, tocopherol analogs, hydroquinones, and superior antioxidants of the polyalkylbenzochromanol and naphthofuran class. *J. Org. Chem.* **1993**, *58*, 7416−7420.
(14) Ouchi, A.; Nagaoka, S.; Mukai, K. Tunneling effect in regeneration reaction of vitamin E by ubiquinol. *J. Phys. Chem. B* **2010**, *114*, 6601−6607.
(15) Gregor, W.; Grabner, G.; Adelwöhrer, C.; Rosenau, T.; Gille, L. Antioxidant properties of natural and synthetic chromanol derivatives: Study by fast kinetics and electron spin resonance spectroscopy. *J. Org. Chem.* **2005**, *70*, 3472−3483.
(16) Packer, J. E.; Slater, T. F.; Willson, R. L. Direct observation of a free radical interaction between vitamin E and vitamin C. *Nature* **1979**, *278*, 737−738.
(17) Mukai, K.; Nishimura, M.; Kikuchi, S. Stopped-flow investigation of the reaction of vitamin C with tocopheroxyl radical in aqueous Triton X-100 micellar solutions. *J. Biol. Chem.* **1991**, *266*, 274−278.
(18) Bisby, R. H.; Parker, A. W. Reaction of ascorbate with the α-tocopheroxyl radical in micellar and bilayer membrane systems. *Arch. Biochem. Biophys.* **1995**, *317*, 170−178.
(19) Nagaoka, S.; Kuranaka, A.; Tsuboi, H.; Nagashima, U.; Mukai, K. Mechanism of antioxidant reaction of vitamin E: Charge transfer and tunneling effect in proton-transfer reaction. *J. Phys. Chem.* **1992**, *96*, 2754−2761.
(20) Mukai, K.; Tokunaga, A.; Itoh, S.; Kanesaki, Y.; Ohara, K.; Nagaoka, S.; Abe, K. Strucure-activity relationship of the free-radical-scavenging reaction by vitamin E (α-, β-, γ-, δ-tocopherols) and ubiquinol-10: pH dependence of the reaction rates. *J. Phys. Chem. B* **2007**, *111*, 652−662 and references cited therein..
(21) Mitani, S.; Ouchi, A.; Watanabe, E.; Kanesaki, Y.; Nagaoka, S.; Mukai, K. Stopped-flow kinetic study of the aroxyl radical-scavenging action of catechins and vitamin C in ethanol and micellar solutions. *J. Agric. Food Chem.* **2008**, *56*, 4406−4417.
(22) Mukai, K.; Oka, W.; Watanabe, K.; Egawa, Y.; Nagaoka, S.; Terao, J. Kinetic study of free-radical-scavenging action of flavonoids in homogeneous and aqueous Triton X-100 micellar solutions. *J. Phys. Chem. A* **1997**, *101*, 3746−3753.
(23) Traber, M. G.; Atkinson, J. Vitamin E, antioxidant and nothing more. *Free Radical Biol. Med.* **2007**, *43*, 4−15.
(24) Homma, Y.; Kondo, Y.; Kaneko, M.; Kitamura, T.; Nyou, W. T.; Yanagisawa, M.; Yamamoto, Y.; Kakizoe, T. Promotion of carcinogenesis and oxidative stress by dietary cholesterol in rat prostate. *Carcinogenesis* **2004**, *25*, 1011−1014.
(25) Lass, A.; Forster, M. J.; Sohal, R. S. Effects of coenzyme $Q_{10}$ and α-tocopherol administration on their tissue levels in the mouse: Elevation of mitochondrial α-tocopherol by coenzyme $Q_{10}$. *Free Radical Biol. Med.* **1999**, *26*, 1375−1382.
(26) Podda, M.; Weber, C.; Traber, M. G.; Packer, L. Simultaneous determination of tissue tocopherols, tocotrienols, ubiquinols, and ubiquinones. *J. Lipid Res.* **1996**, *37*, 893−901.
(27) Colome, C.; Artuch, R.; Vilaseca, M.-A.; Sierra, C.; Brandi, N.; Lambruschini, N.; Cambra, F. J.; Campistol, J. Lipophilic antioxidants in patients with phenylketonuria. *Am. J. Clin. Nutr.* **2003**, *77*, 185−188.
(28) Mukai, K.; Ouchi, A.; Nakaya, S.; Nagaoka, S. Aroxyl-radical-scavenging rate increases remarkably under the coexistence of α-tocopherol and ubiquinol-10 (or vitamin C): Finding of synergistic effect on the reaction rate. *J. Phys. Chem. B* **2013**, *117*, 8378−8391.
(29) Kajimoto, G.; Yoshida, H.; Shibahara, A. Changes in ratio of α-tocopherol to polyunsaturated fatty acid in oil by heating, and α-tocopherol contents in tissue of rats fed with thermally oxidized oil. *Nippon Eiyo Shokuryo Gakkaishi (J. Jpn. Soc. Nutr. Food Sci.)* **1984**, *37*, 37−43.
(30) Tuberoso, C. I. G.; Kowalczyk, A.; Sarritzu, E.; Cabras, P. Determination of antioxidant compounds and antioxidant activity in commercial oilseeds for food use. *Food Chem.* **2007**, *103*, 1494−1501.
(31) Hu, J.-N.; Zhu, X.-M.; Adhikari, P.; Li, D.; Kim, I.-H.; Lee, K.-T. Determination of tocopherol contents in refined edible oils using an HPLC method. *J. Food Sci. Nutr.* **2009**, *14*, 260−264.
(32) Sookwong, P.; Nakagawa, K.; Murata, K.; Kojima, Y.; Miyazawa, T. Quantitation of tocotrienol and tocopherol in various rice brans. *J. Agric. Food Chem.* **2007**, *55*, 461−466.
(33) *Palm Oil Information Series*; Malaysian Palm Oil Promotion Council: Selangor, Malaysia, 1995; pp 18−19.
(34) Rieker, A.; Scheffler, K. Die beteiligung von phenylresten an der aroxylmesomerie. *Liebigs Ann. Chem.* **1965**, *689*, 78−92.
(35) Mukai, K.; Ouchi, A.; Mitarai, A.; Ohara, K.; Matsuoka, C. Formation and decay dynamics of vitamin E radical in the antioxidant reaction of vitamin E. *Bull. Chem. Soc. Jpn.* **2009**, *82*, 494−503.
(36) Niki, E. *Tocotrienols: Vitamin E beyond tocopherols*, 2nd ed; Tan, B., Watson, R., Preedy, V., Eds.; CRC/AOCS Press: Boca Raton, FL, 2012, and references cited therein.
(37) Yoshida, Y.; Niki, E.; Noguchi, N. Comparative study on the action of tocopherols and tocotrienols as antioxidant: Chemical and physical effects. *Chem. Phys. Lipids* **2003**, *123*, 63−75.
(38) Serbinoba, E.; Kagan, V.; Han, D.; Packer, L. Free radical recycling and intramembrane mobility in the antioxidant properties of α-tocopherol and α-tocotrienol. *Free Radical Biol. Med.* **1991**, *10*, 263−275.
(39) Parker, R. A.; Pearce, B. C.; Clark, R. W.; Gordon, D. A.; Wright, J. J. K. Tocotrienols regulate cholesterol production in mammalian cells by post-transcriptional suppression of 3-hydroxy-3-methylglutaryl-coenzyme A reductase. *J. Biol. Chem.* **1993**, *268*, 11230−11238.
(40) Black, T. M.; Wang, P.; Maeda, N.; Coleman, R. A. Palm tocotrienols protect ApoE ± mice from diet-induced atheroma formation. *J. Nutr.* **2000**, *130*, 2420−2426.
(41) Qureshi, A. A.; Sami, S. A.; Salser, W. A.; Khan, F. A. Dose-dependent suppression of serum cholesterol by tocotrienol-rich fraction ($TRF_{25}$) of rice bran in hypercholesterolemic humans. *Atherosclerosis* **2002**, *161*, 199−207.
(42) Sakai, M.; Okabe, M.; Tachibana, H.; Yamada, K. Apoptosis induction by γ-tocotrienol in human hepatoma Hep3B cells. *J. Nutr. Biochem.* **2006**, *17*, 672−676.
(43) Eitsuka, T.; Nakagawa, K.; Miyazawa, T. Down-regulation of telomerase activity in DLD-1 human colorectal adenocarcinoma cells by tocotrienol. *Biochem. Biophys. Res. Commun.* **2006**, *348*, 170−175.
(44) Nesaretnam, K.; Meganathan, P. Tocotrienols: Inflammation and cancer. *Ann. N. Y. Acad. Sci.* **2011**, *1229*, 18−22.
(45) Shibata, A.; Nakagawa, K.; Kawakami, Y.; Tsuzuki, T.; Miyazawa, T. Suppression of γ-tocotrienol on UVB induced inflammation in HaCaT keratinocytes and HR-1 hairless mice via inflammatory mediators multiple signaling. *J. Agric. Food Chem.* **2010**, *58*, 7013−7020.
(46) Nakagawa, K.; Shibata, A.; Yamashita, S.; Tsuzuki, T.; Kariya, J.; Oikawa, S.; Miyazawa, T. In vivo angiogenesis is suppressed by unsaturated vitamin E, tocotrienol. *J. Nutr.* **2007**, *137*, 1938−1943.
(47) Shibata, A.; Nakagawa, K.; Sookwong, P.; Tsuduki, T.; Tomita, S.; Shirakawa, H.; Komai, M.; Miyazawa, T. Tocotrienol inhibits secretion of angiogenic factors from human colorectal adenocarcinoma cells by suppressing hypoxia-inducible factor-1α. *J. Nutr.* **2008**, *138*, 2136−2142.
(48) Khanna, S.; Roy, S.; Slivka, A.; Craft, T. K. S.; Chaki, S.; Rink, C.; Notestine, M. A.; DeVries, A. C.; Parinandi, N. L.; Sen, C. K. Neuroprotective properties of the natural vitamin E α-tocotrienol. *Stroke* **2005**, *36*, 2258−2264.
(49) Niki, E.; Saito, T.; Kawakami, A.; Kamiya, Y. Inhibition of oxidation of methyl linoleate in solution by vitamin E and vitamin C. *J. Biol. Chem.* **1984**, *259*, 4177−4182.
(50) Denisov, E. T.; Khudyakov, I. V. Mechanisms of action and reactivities of the free radicals of inhibitors. *Chem. Rev.* **1987**, *87*, 1313−1357.
(51) Niki, E.; Tsuchiya, J.; Yoshikawa, Y.; Yamamoto, Y.; Kamiya, Y. Oxidation of lipids. XIII. Antioxidant activities of α-, β-, γ-, and δ-tocopherols. *Bull. Chem. Soc. Jpn.* **1986**, *59*, 497−501.

JOURNAL OF AGRICULTURAL AND FOOD CHEMISTRY

Article

pubs.acs.org/JAFC

# Effects of Granule Swelling on Starch Saccharification by Granular Starch Hydrolyzing Enzyme

Zhaofeng Li,[‡] Liming Cai,[†] Zhengbiao Gu,[‡] and Yong-Cheng Shi*,[†]

[†]Department of Grain Science and Industry, Kansas State University, Manhattan, Kansas 66506, United States

[‡]School of Food Science and Technology, Jiangnan University, Wuxi 214122, People's Republic of China

**ABSTRACT:** The effects of granule swelling on enzymatic saccharification of normal corn starch by granular starch hydrolyzing enzyme were investigated. After swelling, $K_m$ values for the saccharification of granular starch decreased compared with native granular starch, indicating that granule swelling caused granular starch hydrolyzing enzyme to have higher affinity for starch granules. The partial swelling of starch granules enhanced starch saccharification. Furthermore, the enhancement at an earlier stage of enzymatic reaction was much more significant than that at later stages. For granular starch pretreated at 67.5 °C for 30 min, conversions to glucose after incubation with the enzyme at 32 °C for 4 and 24 h were approximately 3-fold and 26% higher than for native granular starch, respectively. As a result, proper heat pretreatment of granular starch before simultaneous saccharification and fermentation has great potential to facilitate industrial production of ethanol by use of granular starch hydrolyzing enzyme.

**KEYWORDS:** *corn starch, granule swelling, granular starch hydrolyzing enzyme, saccharification, enhancement*

## INTRODUCTION

Ethanol is the primary renewable liquid transportation fuel, with a long history of good performance, and it can be used in over 80% of automobiles and other light-duty transportation vehicles.[1] The basic procedures for large-scale production of fuel ethanol from starch are enzymatic conversion of starch into fermentable sugars, microbial fermentation of sugars to ethanol, distillation, dehydration, and denaturing (optional).[2] The conventional process for enzymatic hydrolysis of starch into sugars prior to fermentation is to cook a starch slurry of approximately 30% (w/v) in the presence of thermostable α-amylase at above 100 °C, hold it at 90 °C for 1−3 h, and then cool it further to 60 °C with added glucoamylase.[3] This process has considerable economic drawbacks, mainly due to high energy-consuming cooking and liquefaction steps.[4]

An alternative process in which granular starch hydrolyzing enzymes are applied to convert granular or uncooked starch to glucose and other fermentable sugars has been suggested.[5−7] This process does not require high temperatures during cooking and liquefaction, which could reduce the energy requirements of ethanol production[3] and decrease the formation of undesirable byproducts of the Maillard reaction.[8] In addition, the process could simplify the operation and eliminate the cooking and cooling equipment required to handle high-viscosity starch slurries. Granular starch hydrolyzing enzymes are commercially available and have been applied in a simultaneous saccharification and fermentation process for ethanol production.[9−11]

Enzymatic hydrolysis of granular starch is a solid-solution two-phase reaction in which the enzymes need to first diffuse toward and bind to the solid substrate and then cleave the glycosidic linkages.[12] Enzyme adsorption onto starch granules is the initial stage for enzymatic hydrolysis of granular starch;[13−15] consequently, the initial rate of granular starch hydrolysis is related to the morphology, porosity, particle size, and surface area of the starch granules.[15−19] α-Amylase and glucoamylase are relatively large, several nanometers in size.[20−22] Because of their relatively large size, these enzymes have limited access to starch granules. Granule swelling could increase the specific surface area of starch granules (surface area per unit mass of of dry starch) and open up the surface. We postulated that even slight granule swelling would have a great positive impact on enzymatic hydrolysis of granular starch. Thus, the objective of this study was to determine the effects of granule swelling of normal corn starch, the most commonly used starch material in ethanol production, on enzymatic saccharification by a granular starch hydrolyzing enzyme.

## MATERIALS AND METHODS

**Materials.** Normal corn starch was obtained from National Starch LLC (Bridgewater, NJ). Stargen 001, a granular starch hydrolyzing enzyme, was obtained from Genencor International (Palo Alto, CA). Blue dextran, which was prepared from dextran with an average molecular weight of approximately $2.0 \times 10^6$, was purchased from Sigma (St. Louis, MO). Other chemicals were purchased from Fisher Scientific (Santa Clara, CA).

**Determination of Swelling Factor.** The swelling factor of the starches was measured according to the blue dextran dye exclusion method of Tester and Morrison.[23] Normal corn starch (100 mg, dry basis) was weighed into a 10 mL screw-cap tube, 5.0 mL of water was added, and the sealed tubes were incubated with constant shaking in a water bath at a specific temperature for 30 min. Then 0.5 mL of blue dextran solution (5 mg/mL) was added, and the contents were mixed by gently inverting the closed tubes several times. After centrifugation at 5000*g* for 5 min, the absorbance of the supernatant was measured at 620 nm. The absorbance of reference tubes that contained no starch

Received: February 16, 2014
Revised: July 12, 2014
Accepted: July 20, 2014
Published: July 20, 2014

ACS Publications © 2014 American Chemical Society

was also measured. The swelling factor was reported as a ratio of the volume of swollen granules to the volume of dry starch.

**Light Microscopy.** Normal corn starch (100 mg, dry basis) was slurried in water (1.0 mL) and heated in a water bath at a specific temperature for 30 min with constant shaking. The starch slurry without heat pretreatment was used as a control. Starch samples were promptly viewed with an optical microscope with a digital camera (Model BX51, Olympus Co., Japan) and observed under normal visible light by use of a 40× objective.

**Assay for Glucose-Forming Activity.** Glucose-forming activity was measured by incubating 0.05 mL of 100-fold diluted enzyme with 0.95 mL of 1% (dry basis, w/v) normal corn starch slurry in 50 mM citrate buffer (pH 4.2) at 32 °C for 10 min. The reaction was stopped by boiling the mixture for 10 min. Glucose released was measured by high-performance anionic-exchange chromatography (HPAEC) on a Dionex ICS 3000 system equipped with a CarboPac PA-1 column and pulse amperometric detector (PAD, Dionex, Sunnyvale, CA). The mobile phase was 150 mM NaOH at a flow rate of 1 mL/min. One unit of activity was defined as the amount of enzyme that released 1 μmol of glucose/min. Enzyme activity was expressed as units per milliliter of enzyme solution.

**Enzyme Kinetic Studies.** First, normal corn starch slurry in 50 mM citrate buffer (pH 4.2) was heated in a water bath at a specific temperature for 30 min with constant shaking. The starch slurry without heat pretreatment was used as a control. Then 0.05 mL of 100-fold diluted enzyme (Stargen 001) was incubated with 0.95 mL of the preheated starch slurry at 32 °C for 10 min. Kinetic studies were performed by measuring the initial rate of glucose formation at normal corn starch concentrations ranging from 0.05% to 1.0%. The SigmaPlot program (Systat Software Inc., version 10.0 for Windows) was used for curve-fitting of the data to the standard Michaelis–Menten formula: $v = V_{max}[S]/(K_m + [S])$, where $v$ is the rate of glucose formation, $[S]$ is the substrate concentration, $V_{max}$ is the maximal velocity of the reaction, and $K_m$ is the Michaelis–Menten constant.

**Saccharification Process of Granular Starch.** Before enzymatic saccharification, normal corn starch slurry (30%, dry basis, w/v) in 50 mM citrate buffer (pH 4.2) was heated in a water bath at a specific temperature for 30 min with constant shaking. The starch slurry (30%, dry basis, w/v) without heat pretreatment was used as a control. The starch slurry was incubated with Stargen 001 (2.5 units/g dry starch) at 32 °C for 72 h. At regular time intervals, samples were taken and boiled for 10 min to terminate the reaction. Glucose released was measured by HPAEC-PAD.

**Morphology of the Starch Granule.** Starch granule morphology was studied by scanning electron microscopy (SEM). Normal corn starch slurry (30%, dry basis, w/v) in 50 mM citrate buffer (pH 4.2) was heated at 55 or 65 °C for 30 min with constant shaking. The starch slurry (30%, dry basis, w/v) without heat pretreatment was used as a control. Then the above starch slurries were incubated with Stargen 001 (2.5 units/g dry starch) at 32 °C. After 0, 4, or 24 h of incubation, samples were taken, washed with anhydrous ethanol, and dried in a forced-air oven at 30 °C for 24 h. The dried samples were coated with gold–palladium by a sputter coater (Denton Vacuum, LLC, Moorestown, NJ) and viewed at 2000× magnification by SEM (S-3500N, Hitachi Science Systems, Ltd., Japan) operating at an accelerating voltage of 20 kV.

**Statistical Analysis.** Experiments were conducted in triplicate, and average values are reported. Statistical analyses were carried out by SPSS software (SPSS Inc., Chicago, IL). Significant differences ($p < 0.05$) between means were identified by one-way analysis of variance (ANOVA) using the Student–Newman–Keuls (SNK) procedure.

## RESULTS AND DISCUSSION

**Swelling of Starch Granules.** The swelling factors of normal corn starch granules were investigated in the 40–90 °C temperature range. Very little swelling was observed from 40 to 50 °C; the swelling factor increased only slightly at 50–60 °C but greatly at temperatures above 60 °C (Figure 1). It is known

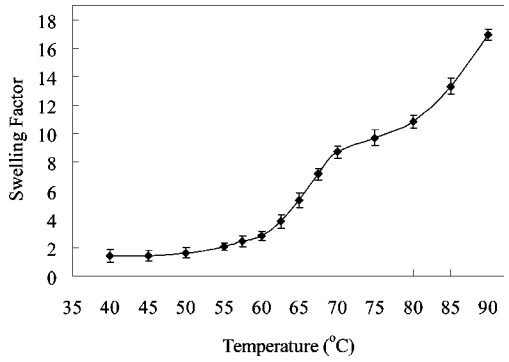


**Figure 1.** Swelling curve of normal corn starch granules heated at different temperatures. Each value represents the mean of three independent measurements.

that normal corn starch has an onset gelatinization temperature of about 58 °C.[17] Starch granules swell significantly above that temperature, resulting in the loss of crystalline order and birefringence. The swelling factor curve reached a plateau value at 70–80 °C with a swelling factor of 9–11. The swelling factor further increased significantly at temperatures above 80 °C and reached approximately 17 at 90 °C. A similar trend has been observed for waxy corn starch at temperatures below 80 °C; compared with normal corn starch, waxy corn starch showed a higher swelling curve.[23,24] The swelling factors of waxy corn starch granules at 75–80 °C reached above 30, which was approximately 2-fold higher than normal corn starch. Previous studies have also shown that the other waxy cereal starches had higher swelling capacities than corresponding normal starches.[23,25] The main reason might be that amylose–lipid complexes in normal starches inhibit granule swelling.[23] Swelling of starch granules is mainly a property of amylopectin.

In addition, when normal corn starch was incubated at 65 or 70 °C for various durations, the period of rapid swelling lasted approximately 10 min (Figure 2). After that, the swelling factor almost plateaued. Thus, incubation at a specific temperature for 30 min could reach a steady state for the swelling of starch granule.

The size and shape of normal corn starch with or without heat pretreatment at a specific temperature for 30 min are shown in Figure 3. Normal corn starch granules without heat pretreatment had polygonal and round shapes. After treatment

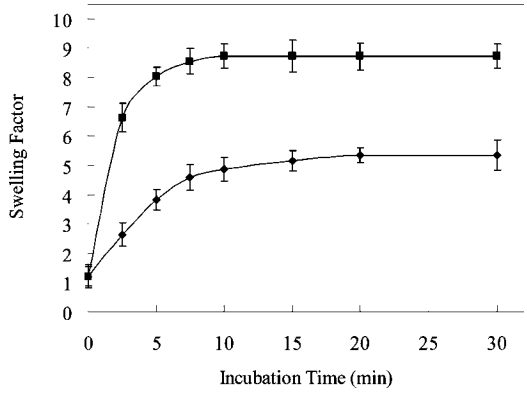


**Figure 2.** Effects of different incubation time durations on granule swelling of normal corn starch (2% solids) preheated in a water bath at (◆) 65 or (■) 70 °C with constant shaking. Each value represents the mean of three independent measurements.


dx.doi.org/10.1021/jf500814g | J. Agric. Food Chem. 2014, 62, 8114–8119

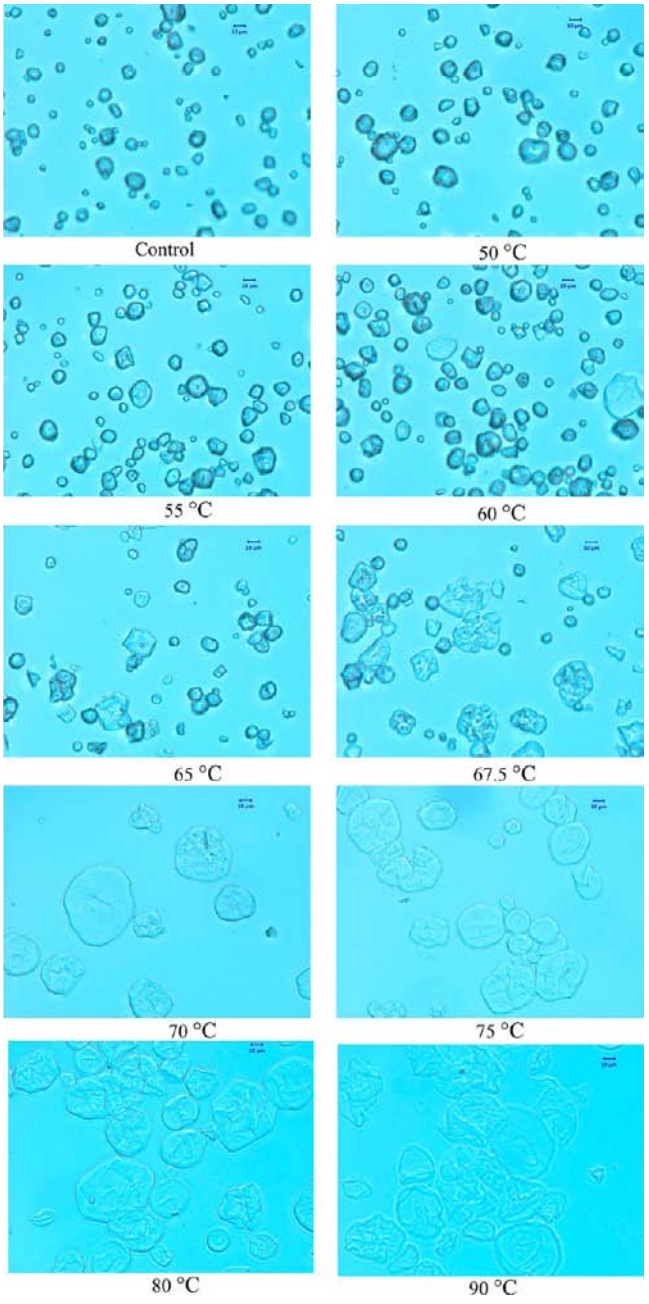


**Figure 3.** Light microscopic images of normal corn starch granules heat-treated at a specific temperature for 30 min with constant shaking. The number below each panel represents the treatment temperature. Starch granules without heat pretreatment were used as a control. Starch samples were observed under normal visible light by use of a 40× objective.

at 50−60 °C, the granules began to swell slightly, whereas granule swelling was obvious only at temperatures above 60 °C. Large starch granules appeared to swell first at around 50−60 °C; small granules did not begin to swell obviously until 65 °C. Few starch granules began to be disrupted at 65 or 67.5 °C. More starch granules were disrupted, and the rest swelled at 70−80 °C, indicating partial gelatinization of starch samples. Almost all granules were irreversibly disrupted at 90 °C, indicating complete gelatinization of starch samples. The swelling trend of normal corn starch granules obtained by optical microscopy agreed with results of swelling factors of normal corn starch granules (Figure 2).

**Kinetic Parameters.** Heat pretreatment of normal corn starch granules at different temperatures greatly affected the kinetic properties of the granular starch hydrolyzing enzyme. After heat pretreatment, $K_m$ values for the saccharification of granular starch decreased compared with those for granular starch without heat pretreatment (Table 1), indicating that granule swelling resulted in higher affinity of the granular starch hydrolyzing enzyme for starch granules. Furthermore, the significant decrease in $K_m$ value was not observed until starch granules swelled almost completely, at 70 °C or above (Figure 3). On the other hand, after heat pretreatment at 50−60 °C, $V_{max}$ values for the saccharification of granular starch increased only slightly compared with those for granular starch without heat pretreatment (Table 1). After the starch granules began to swell at temperatures above 60 °C, however, the increase in $V_{max}$ was significant. Even if the starch granules were pretreated only at 65 or 67.5 °C, at which temperature the starch granules were partly swollen, $V_{max}$ values were more than 1.5-fold higher than those of granular starch without heat pretreatment.

Catalytic efficiency as expressed by $k_{cat}/K_m$ ratios (Table 1) indicated that granular corn starch with heat pretreatment was a better substrate than that without heat pretreatment. It is noteworthy that $k_{cat}/K_m$ values for granular starch preheated at temperatures above 60 °C were much higher than those for granular starch without heat pretreatment (Table 1). For granular starch preheated at 65 or 67.5 °C, the value was more than 2-fold higher than for granular starch without heat pretreatment.

**Saccharification Process of Granular Starch.** Because heat pretreatment of 30% normal corn starch slurry (dry basis, w/v) at 70 °C or above resulted in a high slurry viscosity, temperatures below 70 °C (50−67.5 °C) were chosen to treat the normal corn starch granules before enzymatic saccharification. The pretreatment of normal corn starch granules at 50−67.5 °C enhanced starch saccharification by granular starch hydrolyzing enzyme under conditions resembling the industrial yeast fermentation process for ethanol production (Figure 4). The higher the pretreatment temperature, the more significantly starch saccharification was enhanced. In addition, enhancement of starch saccharification at an earlier stage of the enzymatic reaction was much more significant than at later stages. For granular corn starch pretreated at 65 or 67.5 °C before enzymatic saccharification, conversion to glucose after incubation with the enzyme at 32 °C for 4 h was approximately 2- or 3-fold higher, respectively, than for granular starch without heat pretreatment (Figure 4). In contrast, after incubation for 24 h, pretreatment at 65 or 67.5 °C resulted in approximately 18% or 26% increases in starch conversion into glucose, respectively (Figure 4).

The significant enhancement in saccharification of heat-pretreated granular corn starch at earlier stages might be attributed to the looser surface structure and higher specific surface area of partially swelled starch granules, which give the enzyme greater access to the substrate and allow the enzyme to degrade granular starch more easily and extensively.[26] As the sizes of active α-amylase and glucoamylase are several nanometers,[20−22] the enzymes can enter into the interior of native starch granule only through the limited number of pores to degrade starch, but granule swelling provides greater enzyme access to the granule interior. However, at later stages of the enzymatic reaction, reduced availability of starch to the enzyme


dx.doi.org/10.1021/jf500814g | J. Agric. Food Chem. 2014, 62, 8114−8119

**Table 1. Kinetic Parameters for Granular Starch Hydrolyzing Enzyme Acting on Normal Corn Starch Granules Heat-Treated at a Specific Temperature for 30 Min with Constant Shaking[a,b]**

| temp (°C) | $V_{max}$[c] ($\mu$M/min) | $K_m$[c] (%) | $k_{cat}$[c] ( × $10^5$) | $k_{cat}/K_m$ ( × $10^5$) |
|---|---|---|---|---|
| native starch | 104.2 ± 3.5 a | 0.292 ± 0.012 d | 0.135 ± 0.004 a | 0.462 |
| 50 | 119.1 ± 3.8 b | 0.286 ± 0.014 d | 0.154 ± 0.007 ab | 0.538 |
| 55 | 126.6 ± 4.5 b | 0.241 ± 0.011 c | 0.164 ± 0.008 ab | 0.680 |
| 60 | 138.9 ± 4.3 c | 0.236 ± 0.009 c | 0.180 ± 0.007 b | 0.763 |
| 65 | 256.4 ± 5.1 d | 0.231 ± 0.01 c | 0.333 ± 0.012 c | 1.442 |
| 67.5 | 285.7 ± 5.0 e | 0.229 ± 0.014 c | 0.371 ± 0.014 d | 1.620 |
| 70 | 322.6 ± 6.2 f | 0.129 ± 0.01 b | 0.419 ± 0.016 e | 3.248 |
| 75 | 347.2 ± 7.5 g | 0.056 ± 0.006 a | 0.451 ± 0.018 f | 8.054 |
| 80 | 355.9 ± 6.5 g | 0.053 ± 0.005 a | 0.462 ± 0.021 f | 8.717 |
| 90 | 409.8 ± 6.8 h | 0.052 ± 0.005 a | 0.532 ± 0.025 g | 10.231 |

[a]The starch concentration in reaction mixtures ranged from 0.05% to 1.0%. Stargen 001 concentration [$E_0$] was expressed as enzyme activity units per milliliter of reaction mixture. Stargen 001 was included in reaction mixtures at a constant concentration of 0.077 unit/mL. [b]Kinetic parameters plus standard errors were obtained from fitting of the experimental data to the standard Michaelis−Menten formula by the SigmaPlot program. [c]Means with different letters within the same column are significantly different ($p < 0.05$).

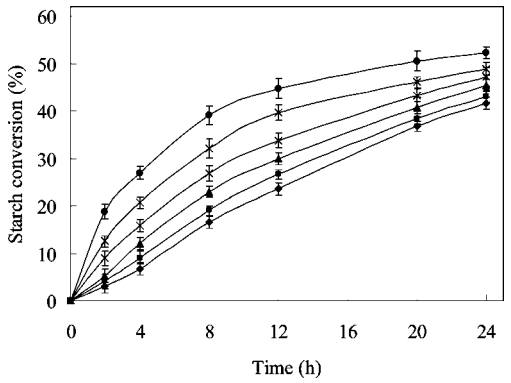


**Figure 4.** Production of glucose under process conditions resembling the industrial yeast fermentation process for ethanol production. Before enzymatic saccharification, normal corn starch slurry (30%, dry basis, w/v) in 50 mM citrate buffer (pH 4.2) was heated in a water bath at (■) 50, (▲) 55, (×) 60, (*) 65, or (●) 67.5 °C for 30 min with constant shaking. The starch slurry without heat pretreatment (◆) was used as a control. During enzymatic saccharification, the formation of glucose was measured by incubation of Stargen 001 (2.5 units/g dry starch) with a starch sample at 32 °C for 24 h and expressed as starch conversion (percent, dry basis). Each value represents the mean of three independent measurements.

might result in a decreased glucose formation rate, especially in the rigid or tight crystalline region of the starch. Because $\alpha$-amylase binds more slowly to crystalline material,[27] the residual starch granules with high crystallinity were resistant to enzymatic hydrolysis. After pretreatment of normal corn starch granules at 55−67.5 °C, which was close to or above the gelatinization temperature, a small portion of the semicrystalline region would be converted into amorphous material,[28,29] which is more readily hydrolyzed,[30] but the crystalline portion of the starch would not be significantly changed. Thus, partial swelling of starch granules would not significantly enhance starch saccharification at later stages of the enzymatic reaction.

During the simultaneous saccharification and fermentation process for ethanol production, improved saccharification of heat-pretreated granular corn starch could reduce the necessary amount of granular starch hydrolyzing enzyme. Granular starch hydrolyzing enzyme is more expensive than conventional enzymes,[31] so the amount of granular starch hydrolyzing enzyme is an important factor in the economics of ethanol production. Although heat pretreatment of granular corn starch resulted in consumption of a small amount of energy, a reduction in the amount of granular starch hydrolyzing enzyme might significantly lower the production cost of ethanol. Heat pretreatment could also result in significant enhancement of the conversion of granular starch into glucose at earlier stages of the enzymatic reaction, which might be beneficial to yeast fermentation for ethanol production because the rapid growth of yeast at the early stage of fermentation (especially the logarithmic growth phase) needs much more glucose as a carbon source than at the later stage of fermentation.

**Morphology of Starch Granules.** During enzymatic saccharification, the morphology of granular corn starch with or without heat pretreatment was observed by SEM (Figure 5A−C). Changes in morphology of normal corn starch before and after digestion by $\alpha$-amylase alone, glucoamylase alone, and a mixture of $\alpha$-amylase and glucoamylase have been reported.[17] In this study, normal corn starch granules pretreated at 55 or 65 °C were larger and had more irregular shapes and rougher surfaces than starch granules without heat pretreatment (Figure 5A−C), further confirming that larger particle size and corresponding higher specific surface area resulted from heat pretreatment. Enzymatic erosion occurred mainly at the surface of starch granules at earlier stages of the enzymatic reaction (Figure 5D−F). After incubation with granular starch hydrolyzing enzyme at 32 °C for 4 h, the surface of starch granules pretreated at 55 °C, especially relatively large granules (Figure 5E), appeared to have a greater number of small pores than granules without heat pretreatment, which could permit more enzyme penetration.[32] As a result, when the external part of the granule was corroded, the enzyme could more easily act internally.[33] For starch granules pretreated at a higher temperature (65 °C), many granules swelled to a higher degree. As a result, starches in external parts of the granule could be corroded more easily by the enzyme, and even internal parts of the granule were hydrolyzed and removed (Figure 5F). In contrast, for the normal corn starch granules without pretreatment, only micropores were observed but not the interior of the granules (Figure 5D). After incubation for 24 h, starch granules without heat pretreatment showed more large pores in the surface than those incubated for 4 h, and the internal part of some granules was corroded (Figure 5G). The greater portion of many starch granules, however, was still not hydrolyzed, and some small granules were almost intact. In contrast, starch granules subjected to heat pretreatment

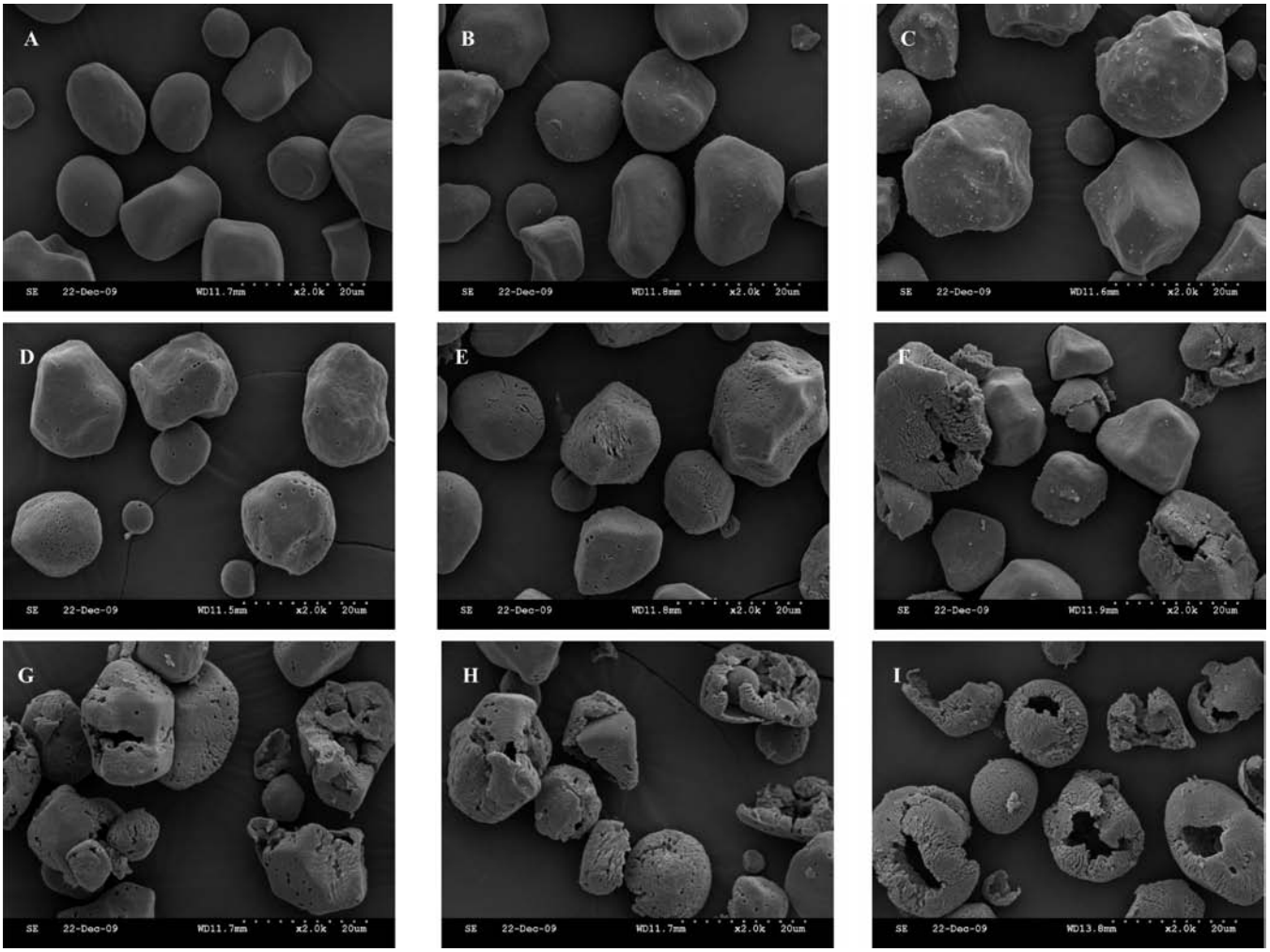


**Figure 5.** Scanning electron micrographs of normal corn starch granules during enzymatic saccharification. Normal corn starch slurry (30%, dry basis, w/v) without heat pretreatment or pretreated at 55 or 65 °C for 30 min was incubated with Stargen 001 (2.5 units/g dry starch) at 32 °C for (A–C) 0, (D–F) 4, or (G–I) 24 h, respectively.

exhibited a higher degree of external and internal starch hydrolysis that resulted in the almost complete collapse of large starch granules (Figure 5H,I). For starch granules heat-pretreated at 65 °C, the residual portion of large granules was very small, and even small ones were also corroded, resulting in a rough porous surface or collapse of the granule (Figure 5I). Both $\alpha$-amylase and glucoamylase are able to hydrolyze crystalline as well as amorphous regions of normal corn starch granules, and a synergetic action was observed when both enzymes were used together.[17] A side-by-side mechanism has been proposed to explain the enzymatic digestion of amylose and amylopectin, as well as crystalline and amorphous regions in normal corn starch granules.[19]

In conclusion, the partial swelling of normal corn starch granules greatly enhanced starch saccharification by granular starch hydrolyzing enzymes. Furthermore, enhancement of starch saccharification at an earlier stage of the enzymatic reaction was much more significant than at later stages. Thus, proper heat pretreatment of granular starch before simultaneous saccharification and fermentation has great potential to facilitate industrial production of ethanol by use of granular starch hydrolyzing enzyme.

## AUTHOR INFORMATION

### Corresponding Author

*Telephone: 785-532-6771; fax 785-532-7010; e-mail ycshi@ksu.edu.

### Notes

The authors declare no competing financial interest.

## ACKNOWLEDGMENTS

This is contribution no. 14-137-J from the Kansas Agricultural Experiment Station.

## REFERENCES

(1) Datta, R.; Maher, M. A.; Jones, C.; Brinker, R. W. Ethanol—the primary renewable liquid fuel. *J. Chem. Technol. Biotechnol.* **2011**, *86*, 473–480.

(2) Casey, L. R. Ethanol plant process. U.S. Patent US20090166172, 2009.

(3) Robertson, G. H.; Wong, D. W.; Lee, C. C.; Wagschal, K.; Smith, M. R.; Orts, W. J. Native or raw starch digestion: A key step in energy efficient biorefining of grain. *J. Agric. Food Chem.* **2006**, *54*, 353–365.

(4) Gibreel, A.; Sandercock, J. R.; Lan, J.; Goonewardene, L. A.; Zijlstra, R. T.; Curtis, J. M.; Bressler, D. C. Fermentation of barley by using *Saccharomyces cerevisiae*: examination of barley as a feedstock for

bioethanol production and value-added products. *Appl. Environ. Microbiol.* **2009**, *75*, 1363−1372.
(5) Uthumporn, U.; Shariffa, Y. N.; Karim, A. A. Hydrolysis of native and heat-treated starches at sub-gelatinization temperature using granular starch hydrolyzing enzyme. *Appl. Biochem. Biotechnol.* **2012**, *166*, 1167−1182.
(6) Sarian, F. D.; van der Kaaij, R. M.; Kralj, S.; Wijbenga, D. J.; Binnema, D. J.; van der Maarel, M. J.; Dijkhuizen, L. Enzymatic degradation of granular potato starch by *Microbacterium aurum* strain B8.A. *Appl. Microbiol. Biotechnol.* **2012**, *93*, 645−654.
(7) Bialas, W.; Szymanowska, D.; Grajek, W. Fuel ethanol production from granular corn starch using *Saccharomyces cerevisiae* in a long term repeated SSF process with full stillage recycling. *Bioresour. Technol.* **2010**, *101*, 3126−3131.
(8) Galvez, A. Analyzing cold enzyme starch hydrolysis technology in new ethanol plant design. *Ethanol Prod.* **2005**, *11*, 58−60.
(9) Wang, P.; Singh, V.; Xu, L.; Johnston, D. B.; Rausch, K. D.; Tumbleson, M. E. Comparison of enzymatic (E-Mill) and conventional dry-grind corn processes using a granular starch hydrolyzing enzyme. *Cereal Chem.* **2005**, *82*, 734−738.
(10) Wang, P.; Singh, V.; Xue, H.; Johnston, D. B.; Rausch, K. D.; Tumbleson, M. E. Comparison of raw starch hydrolyzing enzyme with conventional liquefaction and saccharification enzymes in dry-grind corn processing. *Cereal Chem.* **2007**, *84*, 10−14.
(11) Gibreel, A.; Sandercock, J. R.; Lan, J.; Goonewardene, L. A.; Scott, A. C.; Zijlstra, R. T.; Curtis, J. M.; Bressler, D. C. Evaluation of value-added components of dried distiller's grain with solubles from triticale and wheat. *Bioresour. Technol.* **2011**, *102*, 6920−6927.
(12) Zhang, G. Y.; Venkatachalam, M.; Hamaker, B. R. Structural basis for the slow digestion property of native cereal starches. *Biomacromolecules* **2006**, *7*, 3259−3266.
(13) Leloup, V. M.; Colonna, P.; Ring, S. G. $\alpha$-Amylase adsorption on starch crystallites. *Biotechnol. Bioeng.* **1991**, *38*, 127−134.
(14) Kong, B. W.; Kim, J. I.; Kim, M. J.; Kim, J. C. Porcine pancreatic $\alpha$-amylase hydrolysis of native starch granules as a function of granule surface area. *Biotechnol. Prog.* **2003**, *19*, 1162−1166.
(15) Kim, J. C.; Kong, B. W.; Kim, M. J.; Lee, S. H. Amylolytic hydrolysis of native starch granules affected by granule surface area. *J. Food Sci.* **2008**, *73*, C621−624.
(16) Warren, F. J.; Royall, P. G.; Gaisford, S.; Butterworth, P. J.; Ellis, P. R. Binding interactions of $\alpha$-amylase with starch granules: The influence of supramolecular structure and surface area. *Carbohydr. Polym.* **2011**, *86*, 1038−1047.
(17) Brewer, L. R.; Cai, L.; Shi, Y. C. Mechanism and enzymatic contribution to *in vitro* test method of digestion for maize starches differing in amylose content. *J. Agric. Food Chem.* **2012**, *60*, 4379−4387.
(18) Shrestha, A. K.; Blazek, J.; Flanagan, B. M.; Dhital, S.; Larroque, O.; Morell, M. K.; Gilbert, E. P.; Gidley, M. J. Molecular, mesoscopic and microscopic structure evolution during amylase digestion of maize starch granules. *Carbohydr. Polym.* **2012**, *90*, 23−33.
(19) Zhang, G.; Ao, Z.; Hamaker, B. R. Slow digestion property of native cereal starches. *Biomacromolecules* **2006**, *7*, 3252−3258.
(20) Strobl, S.; Maskos, K.; Betz, M.; Wiegand, G.; Huber, R.; Gomis-Ruth, F. X.; Glockshuber, R. Crystal structure of yellow meal worm $\alpha$-amylase at 1.64 A resolution. *J. Mol. Biol.* **1998**, *278*, 617−628.
(21) Gunning, A. P.; Morris, V. J.; Williamson, G.; Belshaw, N. J.; Kramer, G. F. H.; Kanning, M. W. Imaging glucoamylase by scanning-tunneling-microscopy. *Analyst* **1994**, *119*, 1939−1942.
(22) Pandya, P. H.; Jasra, R. V.; Newalkar, B. L.; Bhatt, P. N. Studies on the activity and stability of immobilized $\alpha$-amylase in ordered mesoporous silicas. *Microporous Mesoporous Mater.* **2005**, *77*, 67−77.
(23) Tester, R. F.; Morrison, W. R. Swelling and gelatinization of cereal starches. I. Effects of amylopectin, amylose, and lipids. *Cereal Chem.* **1990**, *67*, 551−557.
(24) Miao, M.; Zhang, T.; Mu, W. M.; Jiang, B. Effect of controlled gelatinization in excess water on digestibility of waxy maize starch. *Food Chem.* **2010**, *119*, 41−48.
(25) Sasaki, T.; Matsuki, J. Effect of wheat starch structure on swelling power. *Cereal Chem.* **1998**, *75*, 525−529.
(26) Shariffa, Y. N.; Karim, A. A.; Fazilah, A.; Zaidul, I. S. M. Enzymatic hydrolysis of granular native and mildly heat-treated tapioca and sweet potato starches at sub-gelatinization temperature. *Food Hydrocolloids* **2009**, *23*, 434−440.
(27) Warren, F. J.; Butterworth, P. J.; Ellis, P. R. The surface structure of a complex substrate revealed by enzyme kinetics and Freundlich constants for $\alpha$-amylase interaction with the surface of starch. *Biochim. Biophys. Acta, Gen. Subj.* **2013**, *1830*, 3095−3101.
(28) Shi, Y. C. Two- and multi-step annealing of cereal starches in relation to gelatinization. *J. Agric. Food Chem.* **2008**, *56*, 1097−1104.
(29) Shi, Y. C.; Seib, P. A. The structure of four waxy starches related to gelatinization and retrogradation. *Carbohydr. Res.* **1992**, *227*, 131−145.
(30) Tester, R. F.; Morrison, W. R. Properties of damaged starch granules. V. Composition and swelling of fractions of wheat starch in water at various temperatures. *J. Cereal Sci.* **1994**, *20*, 175−181.
(31) Wang, P.; Johnston, D. B.; Rausch, K. D.; Schmidt, S. J.; Tumbleson, M. E.; Singh, V. Effects of protease and urea on a granular starch hydrolyzing process for corn ethanol production. *Cereal Chem.* **2009**, *86*, 319−322.
(32) Kurakake, M.; Tachibana, Y.; Masaki, K.; Komaki, T. Adsorption of $\alpha$-amylase on heat-moisture treated starch. *J. Cereal Sci.* **1996**, *23*, 163−168.
(33) Aggarwal, P.; Dollimore, D. A thermal analysis investigation of partially hydrolyzed starch. *Thermochim. Acta* **1998**, *319*, 17−25.

JOURNAL OF AGRICULTURAL AND FOOD CHEMISTRY

Article

pubs.acs.org/JAFC

# Structural Elucidation of Sorghum Lignins from an Integrated Biorefinery Process Based on Hydrothermal and Alkaline Treatments

Shao-Long Sun,[†] Jia-Long Wen,[†] Ming-Guo Ma,[†] and Run-Cang Sun*[,†,‡]

[†]Beijing Key Laboratory of Lignocellulosic Chemistry, Beijing Forestry University, Beijing 100083, China

[‡]State Key Laboratory of Pulp and Paper Engineering, South China University of Technology, Guangzhou 510640, China

**ABSTRACT:** An integrated process based on hydrothermal pretreatment (HTP) (i.e., 110−230 °C, 0.5−2.0 h) and alkaline post-treatment (2% NaOH at 90 °C for 2.0 h) has been performed for the production of xylooligosaccharide, lignin, and digestible substrate from sweet sorghum stems. The yield, purity, dissociation mechanisms, structural features, and structural transformations of alkali lignins obtained from the integrated process were investigated. It was found that the HTP process facilitated the subsequent alkaline delignification, releasing lignin with the highest yield (79.3%) and purity from the HTP residue obtained at 190 °C for 0.5 h. All of the results indicated that the cleavage of the *β*-*O*-4 linkages and degradation of *β*-*β* and *β*-5 linkages occurred under the harsh HTP conditions. Depolymerization and condensation reactions simultaneously occurred at higher temperatures (≥170 °C). Moreover, the thermostability of lignin was positively related to its molecular weight, but was also affected by the inherent structures, such as *β*-*O*-4 linkages and condensed units. These findings will enhance the understanding of structural transformations of the lignins during the integrated process and maximize the potential utilizations of the lignins in a current biorefinery process.

**KEYWORDS:** *sweet sorghum stem, hydrothermal pretreatment, alkaline treatment, lignin, structural feature, nuclear magnetic resonance (NMR)*

## INTRODUCTION

The ultimate goal of lignocellulosic biomass separation according to the biorefinery was to attain the fractionation of the three primary components (cellulose, hemicelluloses, and lignin) via an effective method, in which the fractions obtained can be converted into different biobased products. Currently, most research has focused on the applications of cellulose in biomass, such as papermaking and cellulosic ethanol production. However, research and development activities directed toward commercial production of cellulosic ethanol have created the opportunity to dramatically increase the transformation of lignin to value-added products.[1] Meanwhile, to maximize the utilization of underlying values of lignocelluloses, it is very important to fractionate them into their main compositions and then transform them into value-added products.[2]

To investigate the utilization of potential values of lignocelluloses, a series of lignocellulosic biorefinery technologies including steam explosion, extrusion process, dilute acid, and hydrothermal treatment have been investigated.[3−6] Among them, hydrothermal pretreatment, a process that disposes of lignocelluloses in a chemical-free, water-only medium, provides a low-cost, handy, and environmentally friendly biorefinery technology.[6] Moreover, physical changes induced by hydrothermal pretreatment that improve enzymatic hydrolysis of cellulose are well-known and include an increase in pore size to enhance enzyme penetration and an increase in accessible cellulose by decreasing its crystallinity and association with lignin.[7,8] Simultaneously, a hydrothermal pretreatment process can produce some chemicals, such as oligosaccharides, furfural, formic acid, acetic acid, and levulinic acid.[9] More importantly, hydrothermal pretreatment accelerates the subsequent delignification. For instance, it has been demonstrated that hydrothermal pretreatment facilitated kraft pulping of hardwood and the subsequent alkaline extraction of lignin.[10] Some integrated biorefinery technologies based on liquid hot water and $H_2SO_4$ catalysis were also proposed.[11] These technologies cause structural changes of lignin and cellulose as well as solubilization of hemicellulose, which in turn contribute to the reduction of biomass recalcitrance. However, the delignification in this process was performed under acidic conditions, which normally needs appropriate acid-resistant equipment. This undoubtedly increases the cost of the entire process.

Sweet sorghum is considered a potential renewable source of energy for economic development and environmental sustainability, owing to its wide adaptability and high photosynthesis.[10] On the basis of previous investigations,[11,12] a combination of hydrothermal pretreatment (i.e., 110−230 °C, 0.5−2.0 h) and sodium hydroxide delignification was proposed in this study. In this integrated process, alkaline treatment has been implemented to disrupt the dense cellular structure in lignocelluloses.[13] It contains many types of chemical reactions in the complex network of lignocelluloses, such as cleavage of ether linkages in lignin units along with peeling reaction of carbohydrates.[14] As a biorefinery process, lignin should receive wide attention due to its potential value in developing biobased materials and chemicals. Although the lignin polymers formed during the hydrothermal pretreatment process were structurally

Received: April 8, 2014
Revised: July 29, 2014
Accepted: July 29, 2014
Published: July 29, 2014

ACS Publications © 2014 American Chemical Society

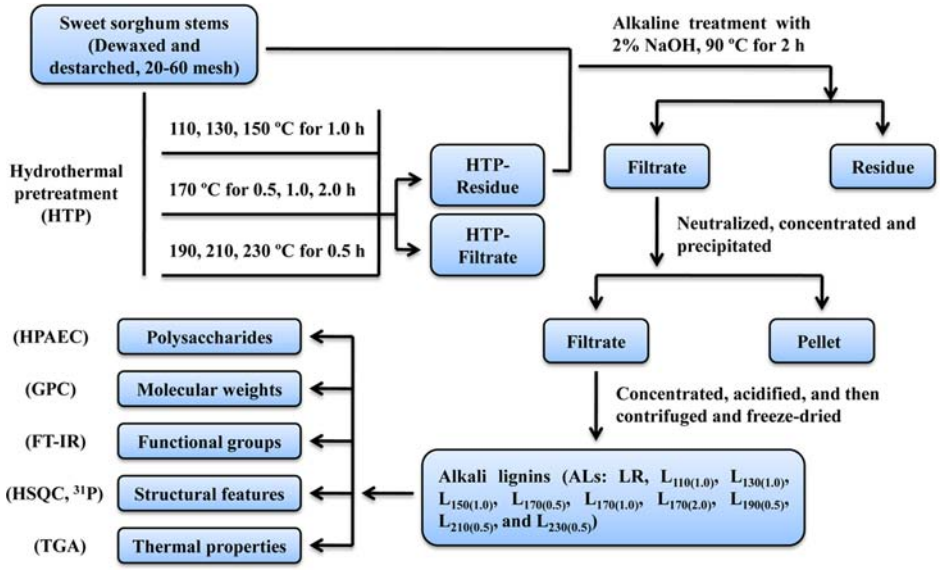


**Figure 1.** Schematic diagram of the lignin extracted from the integrated process.

analyzed previously, some aspects about lignin yield, purity, dissociation mechanisms, and structural features as well as the structural changes during the integrated process should be clarified in the current integrated process.[15] Moreover, these aspects will be conducive for developing renewability, availability, and value-added lignin-based products, such as sustainable construction materials for replacing petroleum-based products.[16−18]

In the present study, the structural features and chemical reactivity of the lignin fractions obtained from the integrated process were thoroughly investigated by high-performance anion exchange chromatography (HPAEC), gel permeation chromatography (GPC), and Fourier transform infrared (FT-IR), quantitative two-dimensional heteronuclear single-quantum coherence (2D-HSQC), and $^{31}$P NMR spectroscopy. In addition, to unveil the relationship between structural features and thermal behaviors, thermogravimetric analysis (TGA) was also performed. It is believed that all of the investigations will increase the availability of these integrated techniques in the current biorefinery industry.

## MATERIALS AND METHODS

**Materials.** Sweet sorghum stems (SSS) were obtained from the experimental farm of the North-Western University of Agricultural and Forest Sciences and Technology (Yangling, People's Republic of China). The dried SSS were cut into small pieces and then ground, and the fractions passing 20−60 mesh were collected. The powder was extracted with toluene/ethanol (2:1, v/v) in a Soxhlet instrument for 6 h, followed by a hot water treatment at 80 °C for 2 h to remove starch. The composition of SSS was 2.3% arabinan, 0.7% galactan, 41.1% glucan, 25.9% xylan, and 21.4% lignin (19.5% Klason lignin and 1.9% acid-soluble lignin), which was determined by using National Renewable Energy Laboratory's (NREL) standard analytical procedure.[19] All experiments were performed in duplicate under the same conditions.

**Hydrothermal Pretreatment (HTP).** The HTP processes were implemented in a 1000 mL stainless steel autoclave (Parr, USA) with a magnetic stirrer at a solid to liquid ratio of 1:10 (g/mL) by a PID controller (Parr 4848, USA). A total of 15.0 g of raw material was mixed with 150 mL of deionized water and then heated at 110, 130, and 150 °C for 1.0 h, at 170 °C for 0.5, 1.0, and 2.0 h, and at 190, 210, and 230 °C for 0.5 h, respectively. At the end of HTP, the mixtures were cooled to room temperature. The solid residues were collected with a Buchner funnel, washed thoroughly with distilled water, and further dried in an oven at 60 °C for 16 h.

**Alkaline Post-treatment.** The unpretreated and hydrothermally pretreated SSS meal was utilized as starting material for the fractionation process (Figure 1). Specifically, the fractionation (5.0 g HTP residue) was operated in 2% NaOH aqueous solution at 90 °C for 2 h under a solid to liquid ratio of 1:20 (g/mL). The collected liquid fractions were neutralized to pH 5.5−6.0 with 6 M HCl and were further concentrated to 40 mL under vacuum. Subsequently, each concentrated solution was poured into 95% ethanol (120 mL) with vigorous stirring, and the hemicellulosic pellet was obtained by filtering, washing with 70% aqueous ethanol, and freeze-drying. The residual supernatants were concentrated to 30 mL and poured in 150 mL of acidic water (pH 2.0, adjusted by HCl) to precipitate the lignins (i.e., alkali lignins, ALs). The notation of the nine ALs ($L_{110(1.0)}$, $L_{130(1.0)}$, $L_{150(1.0)}$, $L_{170(0.5)}$, $L_{170(1.0)}$, $L_{170(2.0)}$, $L_{190(0.5)}$, $L_{210(0.5)}$, and $L_{230(0.5)}$) was according to the increasing pretreatment conditions (i.e., 110−230 °C, 0.5−2.0 h). Raw lignin (LR) was also separated from the unpretreated SSS under the same alkaline treatment condition.

**Analysis Procedures.** The associated polysaccharides in the ALs were calculated by using HPAEC as reported previously.[20] Molecular weights of the ALs were determined by GPC with an ultraviolet detector (UV) at 240 nm. The column used was a PL-gel 10 mm mixed-B 7.5 mm i.d. column, which was calibrated with PL polystyrene standards. Four milligrams of the ALs was dissolved in 2 mL of tetrahydrofuran (THF), and 20 $\mu$L lignin solutions were injected. The column was operated at ambient temperature and eluted with THF at a flow rate of 1.0 mL/min. FT-IR spectra of the ALs were recorded on a Bruker spectrophotometer in the range of 800−2000 cm$^{-1}$ with a resolution of 4 cm$^{-1}$. A KBr disk containing 1% finely ground ALs was used for determination. The solution-state NMR spectra of the ALs were acquired on a Bruker AVIII 400 MHz spectrometer at 25 °C. For 2D HSQC spectroscopic experiments, the data were acquired in HSQC experiment mode using 60 mg of lignin in 0.5 mL of DMSO-$d_6$. Functional groups (phenolic hydroxyl, aliphatic hydroxyl, and carboxyl groups) of the ALs were determined by $^{31}$P NMR spectra according to recent publications.[21,22] Thermal properties of the ALs were measured by using TGA and differential thermogravimetric (DTG) analysis on a simultaneous thermal analyzer (TGA Q500, USA). About 4−8 mg of the AL samples was heated in a platinum crucible from room temperature to 700 °C at a heating rate of 20 °C/min under nitrogen atmosphere. Provision was made for electronic differentiation of the weight signal to give the rate of weight loss.[20]

**Table 1. Solid Yields, Yields, and Contents of Associated Polysaccharides of the Alkali Lignins Obtained from the Integrated Process under Various Processing Conditions**

| temperature (°C)−time (h) | solid yield (%) | lignin fraction | total sugars[a] | arabinose | galactose | glucose | xylose | yield[b] |
|---|---|---|---|---|---|---|---|---|
| control | 100 | LR[c] | 2.9 | 0.7 | 0.3 | 0.3 | 1.6 | 30.7 |
| 110−1.0 | 92.4 | $L_{110(1.0)}$ | 1.3 | 0.3 | ND[d] | 0.2 | 0.8 | 52.3 |
| 130−1.0 | 88.1 | $L_{130(1.0)}$ | 1.8 | 0.3 | 0.2 | 0.2 | 1.1 | 53.4 |
| 150−1.0 | 77.3 | $L_{150(1.0)}$ | 1.4 | 0.4 | ND | 0.2 | 1.2 | 54.9 |
| 170−0.5 | 68.6 | $L_{170(0.5)}$ | 1.7 | 0.1 | ND | 0.2 | 1.4 | 59.6 |
| 170−1.0 | 64.6 | $L_{170(1.0)}$ | 1.2 | ND | ND | 0.1 | 1.1 | 64.7 |
| 170−2.0 | 61.9 | $L_{170(2.0)}$ | 0.8 | ND | ND | 0.1 | 0.7 | 61.6 |
| 190−0.5 | 60.3 | $L_{190(0.5)}$ | 1.2 | ND | ND | 0.1 | 1.1 | 79.3 |
| 210−0.5 | 58.5 | $L_{210(0.5)}$ | ND | ND | ND | ND | ND | 54.8 |
| 230−0.5 | 51.5 | $L_{230(0.5)}$ | ND | ND | ND | ND | ND | 39.9 |

[a]Based on the dry mass of lignin (%, w/w). [b]Based on the Klason lignin content in the corresponding SSS (%, w/w). [c]$L_{110(1.0)}$, $L_{130(1.0)}$, $L_{150(1.0)}$, $L_{170(0.5)}$, $L_{170(1.0)}$, $L_{170(2.0)}$, $L_{190(0.5)}$, $L_{210(0.5)}$, and $L_{230(0.5)}$ represent the lignin fractions isolated by extraction with 2.0% NaOH aqueous solution at 90 °C for 2 h corresponding to the hydrothermal pretreatment temperature−time at 110 °C−1.0 h, 130 °C−1.0 h, 150 °C−1.0 h, 170 °C−0.5 h, 170 °C−1.0 h, 170 °C−2.0 h, 190 °C−0.5 h, 210 °C−0.5 h, and 230 °C−0.5 h, respectively. LR was also fractionated from the unpretreated SSS under the same alkaline treatment condition. [d]ND, not detectable.

**Table 2. Weight-Average ($M_w$) and Number-Average ($M_n$) Molecular Weights and Polydispersities ($M_w/M_n$) of the Alkali Lignins Obtained from the Integrated Process under Various Processing Conditions**

| | LR | $L_{110(1.0)}$ | $L_{130(1.0)}$ | $L_{150(1.0)}$ | $L_{170(0.5)}$ | $L_{170(1.0)}$ | $L_{170(2.0)}$ | $L_{190(0.5)}$ | $L_{210(0.5)}$ | $L_{230(0.5)}$ |
|---|---|---|---|---|---|---|---|---|---|---|
| $M_w$ | 1360 | 1320 | 1300 | 1280 | 1100 | 1030 | 790 | 720 | 600 | 530 |
| $M_n$ | 1100 | 1020 | 950 | 880 | 730 | 720 | 570 | 490 | 380 | 340 |
| $M_w/M_n$ | 1.24 | 1.29 | 1.37 | 1.45 | 1.51 | 1.43 | 1.39 | 1.47 | 1.58 | 1.56 |

## RESULTS AND DISCUSSION

**Solid Yields, Yields, and Associated Polysaccharides of the Lignins.** Table 1 shows that the solid yields decreased from 92.4 to 51.5 g/100 g oven-dried SSS as the pretreatment severity increased. This is mainly due to the degradation and solubilization of hemicelluloses. According to the NREL procedure, the Klason lignin contents in respective HTP residues obtained from the different pretreatment conditions (110, 130, 150 °C for 1.0 h; 170 °C for 0.5, 1.0, 2.0 h; and 190, 210, 230 °C for 0.5 h) were 16.5, 19.2, 20.7, 24.1, 24.7, 25.7, 28.0, 33.6, and 43.9%, respectively. The yields of the ALs were calculated on the basis of the Klason lignin in respective SSS and are shown in Table1. In the integrated process, the yields of the ALs were 52.3, 53.4, 54.9, 59.6, 64.7, 61.6, 79.3, 54.8, and 39.9%, corresponding to the HTP conditions at 110, 130, 150 °C for 1.0 h; 170 °C for 0.5, 1.0, 2.0 h; and 190, 210, 230 °C for 0.5 h, respectively. Particularly, only 30.7% of the alkali lignin (LR) from the unpretreated SSS was obtained. All data indicated that the HTP process facilitated more original lignin (40.9−68.6%) release with alkaline treatment as compared with direct alkaline delignification (30.7%) without the HTP process. In other words, the HTP was a promising pretreatment for efficiently loosening the tight cell wall structure and then facilitating the release of lignin from the plant cell wall with the assist of alkaline treatment. Apparently, the increase of pretreatment temperature from 110 to 170 °C for 1.0 h resulted in a notable increase of the AL yield from 52.3 to 64.7%. The increasing trend was probably related to the HTP process, which cleaved the chemical bonds between lignin and hemicelluloses to some extent (e.g., ester and ether bonds).[23] The partly dissociated components facilitated the following alkaline extraction under the conditions given. However, when the pretreatment temperature was further increased to 230 °C, the yield of the AL distinctly decreased to 39.9%. Meanwhile, when the pretreatment period was further prolonged from 1.0 to 2.0 h at 170 °C, the yields of the ALs decreased from 64.7 to 61.6%. The reduced yield was due to the fact that the lignin content in the HTP residues was overestimated by the klason method because the HTP process under the harsh conditions induced some recondensation reactions between polysaccharides (or polysaccharide degradation products) and lignin, which was also called "'pseudolignin"'.[24] Interestingly, the yield of the AL reached a plateau ($L_{190(0.5)}$, 79.3%) at the pretreatment condition of 190 °C for 0.5 h, demonstrating that the optimized condition for isolating lignin was achieved at this HTP condition. To verify the purity of the extracted ALs, the associated polysaccharides of the ALs were detected by HPAEC (Table 1). As can be seen, all of the ALs contained a rather low amount of associated polysaccharides (<1.80%). In detail, xylose was the major monosaccharide in the ALs, suggesting that the associated polysaccharides in the ALs originated from xylans. Especially, polysaccharides were not detected in $L_{210(0.5)}$ and $L_{230(0.5)}$, suggesting that the hemicellulosic polymer was thoroughly destroyed and degraded under the harsh conditions.

**Molecular Weight Determination.** Changes in molecular weights of the ALs indirectly provided valuable insights into lignin's fragmentation and recondensation reactions during the HTP process. To determine the effect of the HTP on the molecular weight of the ALs obtained, the LR and pretreated lignin fractions ($L_{110(1.0)}$−$L_{230(0.5)}$) were analyzed by GPC. Table 2 lists the changes in molecular weight of the ALs with respect to the HTP temperature and time. As shown in Table 2, the molecular weight ($M_w$) of LR was 1360 g $mol^{-1}$, and its polydispersity ($M_w/M_n$) was 1.24. After the HTP, it was observed that the $M_w$ of the ALs decreased (530−1320 g $mol^{-1}$) as compared to LR. This suggested that the ALs underwent depolymerization with increasing HTP temperature and time.[23,25] It was noted that the depolymerization reaction became more evident under the harsh pretreatment conditions (HTP temperature was higher than 170 °C and/or time exceeded 1.0 h at 170 °C), which resulted in a reduced $M_w$ of


dx.doi.org/10.1021/jf501669r | J. Agric. Food Chem. 2014, 62, 8120−8128

the ALs ($L_{170(2.0)}$, $L_{190(0.5)}$, $L_{210(0.5)}$, and $L_{230(0.5)}$). Furthermore, the content of $\beta$-*O*-4 was positively related to the $M_w$ of the lignin under the conditions given.[26] Especially, the higher the $\beta$-*O*-4 content, the higher the molecular weight of the lignin, which was further confirmed by the subsequent quantitative 2D-HSQC results. Moreover, the polydispersity index of LR obtained from the unpretreated material was 1.24. After the HTP under various processing conditions, the polydispersity indices of the ALs were slightly increased (1.29−1.58) to some extent, suggesting that some inhomogeneous lignin fragments, which were probably originated from HTP and alkaline treatments, occurred and collected after the integrated process.

**FT-IR Spectral Analysis.** Figure 2 exhibits the fingerprint region of FT-IR spectra of the ALs obtained from the integrated process, and the bands were assigned according to the literature.[20,27,28] Specifically, the 1701 $cm^{-1}$ band is attributed to the conjugated/unconjugated carboxyl acid/ester groups or unconjugated $\beta$-ketone carbonyl groups. The bands at 1630−1649 $cm^{-1}$ originate from stretching of conjugated C═O groups, which were prominent in the LR, $L_{110(1.0)}$, and $L_{130(1.0)}$, suggesting that more conjugated C═O appeared at the mild conditions (below 150 °C). The intense bands at 1605, 1514, and 1427 $cm^{-1}$ correspond to aromatic skeletal vibrations and the C−H deformation combined with aromatic ring vibration at 1462 $cm^{-1}$. This suggested that the increase of the pretreatment temperature from 110 to 230 °C and/or time from 0.5 to 2.0 h at 170 °C had no evident influence on the basic lignin structure. A small band at 1153 $cm^{-1}$ (antisymmetric C−O stretching of ester groups) was observed in the spectra of the ALs (LR-$L_{190(0.5)}$), implying that some ester bonds remained under the condition given. However, this band was inconspicuous in the ALs ($L_{210(0.5)}$ and $L_{230(0.5)}$), suggesting that the ester bonds in the lignin macromolecules were significantly cleaved when the HTP temperature reached 210 and 230 °C. The intensity of bands at 1329, 1269, and 1032 $cm^{-1}$ decreased with increasing pretreatment severity, and the bands are assigned to the characteristic of syringyl and condensed guaiacyl units, the ring breathing with C−O stretching in uncondensed guaiacyl units, and aromatic C−H in-plane deformation, respectively. The 1217 $cm^{-1}$ band originates from the C—C, C—O, and C═O stretching. In addition, the band at 1117 $cm^{-1}$, which was ascribed to aromatic C−H in-plane deformation (typical for S units), decreased in $L_{210(0.5)}$ and $L_{230(0.5)}$, suggesting that the proportion of S-type lignin units was decreased as a result of demethoxylation reactions under the harsh pretreatment conditions.[27,29]

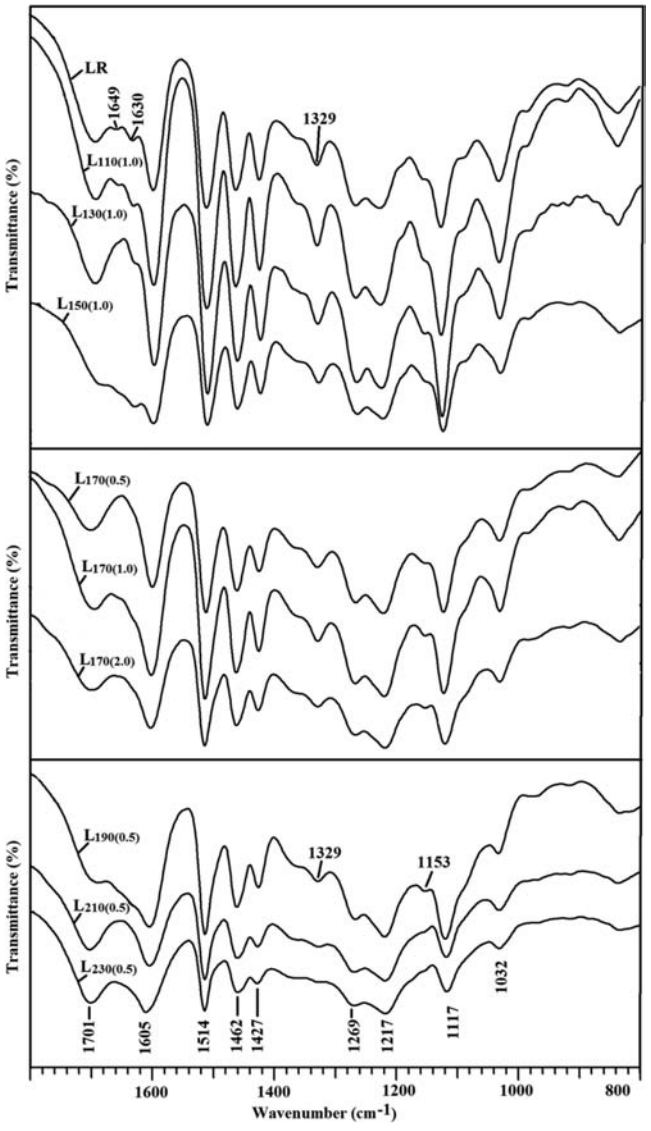


**Figure 2.** FT-IR spectra of the lignins obtained from the integrated process under various processing conditions.

**2D-HSQC NMR Spectral Analysis.** 2D-HSQC NMR was used to obtain important structural information on the ALs to accelerate the understanding of the fundamental chemistry of the ALs obtained from the integrated process. The 2D-HSQC spectra and main linkages of these ALs are shown in Figures 3 and 4, and the signals were assigned (Table 3) on the basis of previous literature.[20,21,23,28−38] In the side-chain region of the AL spectra (Figure 3), cross-peaks of different interunit linkages of the ALs were identified, such as $\beta$-aryl-ether ($\beta$-*O*-4, A), resinol ($\beta$-$\beta$, B), phenylcoumaran ($\beta$-5, C), $\alpha$,$\beta$-diaryl ethers (E), and *p*-hydroxycinnamyl alcohol end groups (F). As can be seen, the cross-peaks of methoxy groups (−$OCH_3$, $\delta_C/\delta_H$ 55.7/3.74) and side chains in $\beta$-*O*-4 substructures (A/A′) were the main substructures. In the integrated process, the relative content of different linkages was changed. For instance, the content of $\beta$-*O*-4 linkages was decreased, whereas the content of $\beta$-5 linkages was increased, suggesting that the $\beta$-*O*-4 linkages were cleaved as a result of the HTP process. In addition, the cleaved $\beta$-*O*-4 linkages were probably recondensed to form $\beta$-5 linkages. Furthermore, it was also noted that lignin−carbohydrate complex (LCC), such as benzyl ether (BE) structure, occurred in the ALs at HTP temperature below 210 °C, implying that the BE structure was more stable during the integrated delignification process. However, no signal of the BE was detected in the $L_{210(0.5)}$ and $L_{230(0.5)}$, implying that the BE was completely cleaved when the HTP temperature was >190 °C.[29]

In the aromatic region of 2D-HSQC spectra (Figure 4) of the ALs, the correlated signals of the ALs from syringyl (S/S′), guaiacyl (G/G′), and *p*-hydroxyphenyl (H) units clearly appeared. Specifically, the S and the $C_\alpha$-oxidized S units (S′) signals for $C_{2,6}$−$H_{2,6}$ correlation were observed at $\delta_C/\delta_H$ 104.1/6.72 and 106.2/7.26, respectively. The G units showed various correlations for $C_2$−$H_2$ ($\delta_C/\delta_H$ 110.8/6.99), $C_5$−$H_5$ ($\delta_C/\delta_H$ 114.9/6.71), and $C_6$−$H_6$ ($\delta_C/\delta_H$ 119.1/6.82), respectively. Moreover, the oxidized G units with a $C_\alpha$ ketone (G′) exhibited


dx.doi.org/10.1021/jf501669r | J. Agric. Food Chem. 2014, 62, 8120−8128

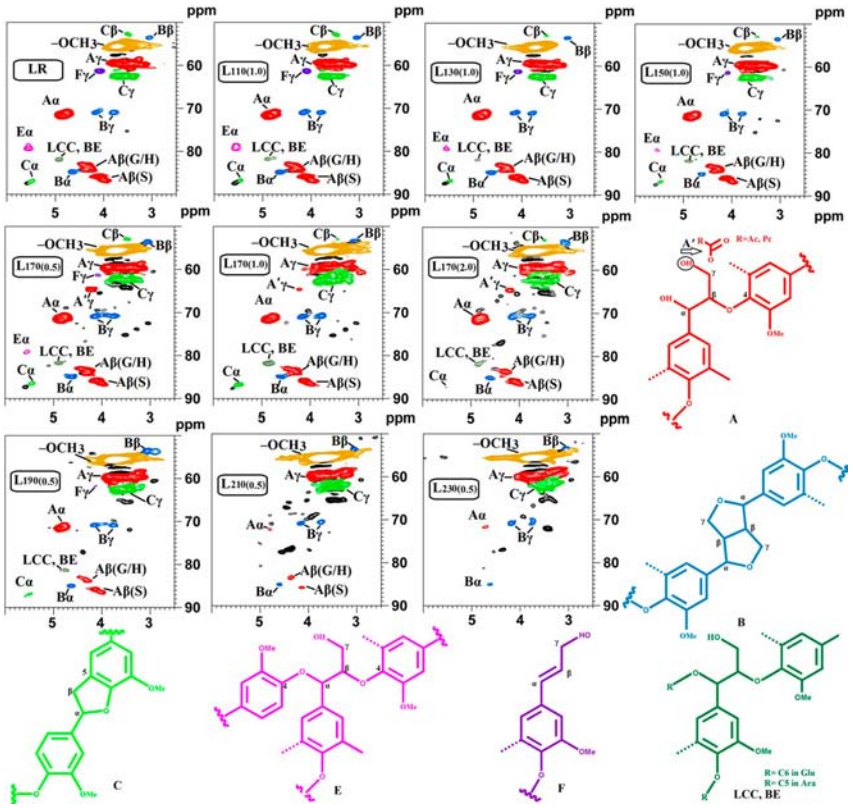


**Figure 3.** 2D-HSQC spectra and the main structures of the lignins obtained from the integrated process under various processing conditions (side-chain region): (A) *β*-aryl-ether units (*β*-*O*-4); (A′) *β*-*O*-4 alkyl-aryl ethers with acylated *γ*-OH with *p*-coumaric acid; (B) resinol substructures (*β*-*β*); (C) phenylcoumaran substructures (*β*-5); (E) *α*,*β*-diaryl ethers (*α*-*O*-4/*β*-*O*-4). Possible lignin−carbohydrate linkages: (BE) benzyl ether.

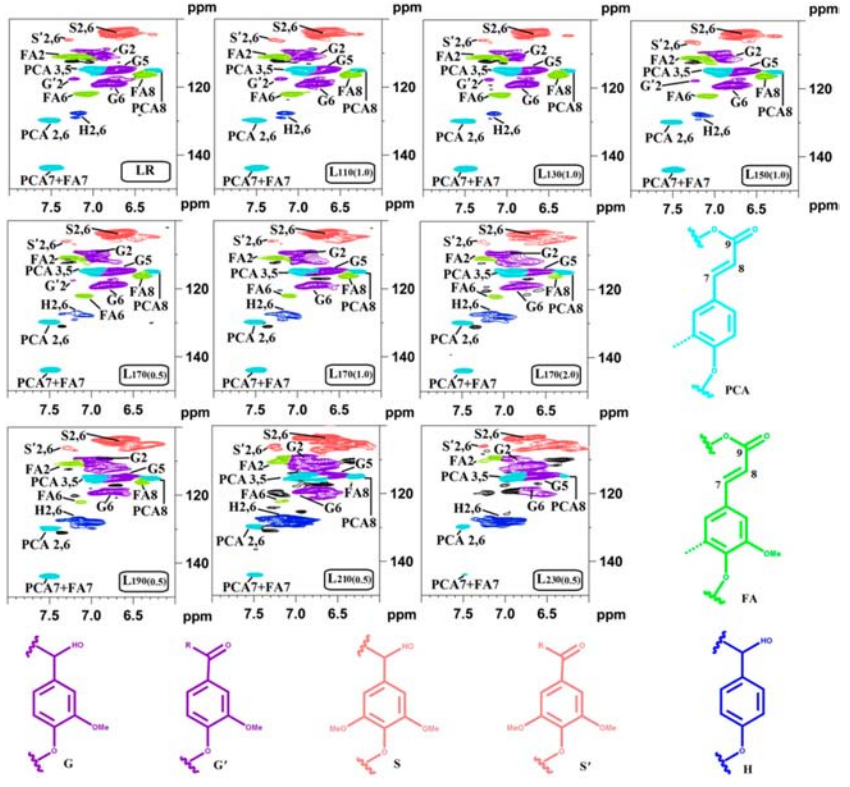


**Figure 4.** 2D-HSQC spectra and the main structures of the lignin polymers obtained from the integrated process under various processing conditions (aromatic region): (PCA) free *p*-coumaric acid; (FA) ferulate; (H) *p*-hydroxyphenyl units; (G) guaiacyl units; (G′) oxidized guaiacyl units with a $C_\alpha$ ketone; (S) syringyl units; (S′) oxidized syringyl units bearing a carbonyl at $C_\alpha$.


dx.doi.org/10.1021/jf501669r | J. Agric. Food Chem. 2014, 62, 8120−8128

**Table 3. Assignments of $^{13}C-^{1}H$ Cross-Peaks in HSQC Spectra of the Alkali Lignins from the Integrated Process under Various Processing Conditions**

| label | $\delta_C/\delta_H$ (ppm) | assignment |
|---|---|---|
| $C_\beta$ | 52.8/3.48 | $C_\beta-H_\beta$ in phenylcoumaran substructures (C) |
| $B_\beta$ | 53.5/3.05 | $C_\beta-H_\beta$ in $\beta$-$\beta$ (resinol) substructures (B) |
| $-OCH_3$ | 55.7/3.74 | C−H in methoxyls |
| $A_\gamma$ | 59.7/3.62 | $C_\gamma-H_\gamma$ in $\beta$-$O$-4 substructures (A) |
| $F_\gamma$ | 61.3/4.09 | $C_\gamma-H_\gamma$ in $p$-hydroxycinnamyl alcohol end groups (F) |
| $C_\gamma$ | 62.4/3.71 | $C_\gamma-H_\gamma$ in phenylcoumaran substructures (C) |
| $B_\gamma$ | 71.0/3.79−4.16 | $C_\gamma-H_\gamma$ in $\beta$-$\beta$ resinol substructures (B) |
| $A_{\alpha(S)}$ | 71.6/4.83 | $C_\alpha-H_\alpha$ in $\beta$-$O$-4 linked to a S unit (A) |
| $E_\alpha$ | 78.9/5.55 | $C_\alpha-H_\alpha$ in $\alpha,\beta$-diaryl ethers (E) |
| LCC, BE | 81.3/4.74 | benzyl ether LCC structures |
| $A_{\beta(G/H)}$ | 83.8/4.27 | $C_\beta-H_\beta$ in $\beta$-$O$-4 linked to G/H unit (A) |
| $B_\alpha$ | 84.8/4.63 | $C_\alpha-H_\alpha$ in $\beta$-$\beta$ resinol substructures (B) |
| $A_{\beta(S)}$ | 85.9/4.10 | $C_\beta-H_\beta$ in $\beta$-$O$-4 linked to a S unit (A) |
| $C_\alpha$ | 87.4/5.56 | $C_\alpha-H_\alpha$ in phenylcoumaran substructures (C) |
| $S_{2,6}$ | 104.1/6.72 | $C_{2,6}-H_{2,6}$ in syringyl units (S) |
| $S'_{2,6}$ | 106.2/7.26 | $C_{2,6}-H_{2,6}$ in oxidized S units (S′) |
| $G_2$ | 110.8/6.99 | $C_2-H_2$ in guaiacyl units (G) |
| $G'_2$ | 117.6/7.22 | $C_2-H_2$ in oxidized G units (G′) |
| $G_5$ | 114.9/6.71 | $C_5-H_5$ in guaiacyl units (G) |
| $G_6$ | 119.1/6.82 | $C_6-H_6$ in guaiacyl units (G) |
| $H_{2,6}$ | 127.7/7.17 | $C_{2,6}-H_{2,6}$ in H units (H) |
| $PCA_{3,5}$ | 115.2/6.92 | $C_{3,5}-H_{3,5}$ in $p$-coumaric acid (PCA) |
| $PCA_{2,6}$ | 129.8/7.51 | $C_{2,6}-H_{2,6}$ in $p$-coumaric acid (PCA) |
| $PCA_7$ | 143.9/7.48 | $C_7-H_7$ in $p$-coumaric acid (PCA) |
| $PCA_8$ | 115.2/6.29 | $C_8-H_8$ in $p$-coumaric acid (PCA) |
| $FA_2$ | 110.9/7.23 | $C_2-H_2$ in ferulic acid (FA) |
| $FA_6$ | 122.1/7.09 | $C_6-H_6$ in ferulic acid (FA) |
| $FA_7$ | 143.9/7.48 | $C_7-H_7$ in ferulic acid (FA) |
| $FA_8$ | 116.5/6.39 | $C_8-H_8$ in ferulic acid (FA) |

correlation for $C_2-H_2$ ($\delta_C/\delta_H$ 117.6/7.22) when the HTP temperature was <170 °C or the HTP time was <1.0 h at 170 °C. However, with further increase of the pretreatment temperature from 170 to 230 °C or increase of the pretreatment time from 1.0 to 2.0 h at 170 °C, no signal of G′ was detected in these corresponding ALs, implying the oxidized G units occurred in a relatively low temperature and time. Furthermore, the $C_{2,6}-H_{2,6}$ correlation signal from H units was found at $\delta_C/\delta_H$ 127.7/7.17. As the temperature increased, the content of H units increased in the ALs, which was mainly as a result of the demethoxylation reactions occurring in G and/or S units, especially at higher temperatures. Besides the normal signals for aromatic rings of the ALs, some condensed S and G units occurred in the 2D HSQC spectra of the ALs.[36] Increasing the pretreatment temperature from 170 to 230 °C or prolonging the pretreatment time from 0.5 to 2.0 h at 170 °C resulted in an obvious increase of the contents of condensed S and G units. The ALs obtained from these processes appeared to contain large amounts of $p$-hydroxycinnamates (PCA and FA). After the same alkaline post-treatment, the lignin obtained (LR-$L_{230(0.5)}$) presented obvious signals of free $p$-coumaric acid correlations ($PCA_8$, $\delta_C/\delta_H$ 115.2/6.29) but not for $PCA_8$ ($\delta_C/\delta_H$ 113.5/6.24), suggesting that the acylated $p$-coumarate (PCE) were significantly cleaved, appeared as free PCA, and coprecipitated with the alkali lignins, which has been discussed in detail in a previous publication.[26] The PCA was characterized by relatively intense correlations at $\delta_C/\delta_H$ 129.8/7.51 ($PCA_{2,6}$), 115.2/6.92 ($PCA_{3,5}$), 115.2/6.29 ($PCA_8$), and 143.9/7.48 ($PCA_7$), whereas ferulic acid (FA) was found at $\delta_C/\delta_H$ 110.9/7.23 ($FA_2$), 122.1/7.09 ($FA_6$), and 116.5/6.39 ($FA_8$).

**Quantitative Analysis of Lignin Structures Based on 2D-HSQC Spectra.** The 2D-HSQC spectra of the pretreated lignins illustrated the relative degradation of the lignin side chains and the aromatic units with increasing pretreatment temperature and time as compared to that of the LR. According to the computing method of the literature,[34,37] the different linkages could be expressed by a comparative mode (Table 4).

**Table 4. Quantification of the Alkali Lignins Obtained from the Integrated Process under Various Processing Conditions by Quantitative 2D-HSQC NMR**

| | $\beta$-$O$-4[a] | $\beta$-$\beta$ | $\beta$-5 | $\alpha$-$O$-4/$\beta$-$O$-4 | S/G[b] | PCA/FA[c] |
|---|---|---|---|---|---|---|
| LR | 54.3 | 3.2 | 2.7 | 3.4 | 1.16 | 0.81 |
| $L_{110(1.0)}$ | 56.5 | 7.7 | 3.4 | 4.8 | 1.13 | 0.71 |
| $L_{130(1.0)}$ | 57.5 | 5.6 | 3.3 | 1.8 | 1.14 | 1.16 |
| $L_{150(1.0)}$ | 47.4 | 3.6 | 3.3 | 1.7 | 1.36 | 1.30 |
| $L_{170(0.5)}$ | 32.0 | 5.8 | 5.7 | Tr[d] | 1.87 | 1.78 |
| $L_{170(1.0)}$ | 25.6 | 2.6 | 3.6 | ND[e] | 3.13 | 4.08 |
| $L_{170(2.0)}$ | 21.4 | 3.7 | ND | ND | 3.76 | 4.53 |
| $L_{190(0.5)}$ | 7.6 | 1.4 | ND | ND | 2.87 | 1.49 |
| $L_{210(0.5)}$ | Tr | Tr | ND | ND | 1.81 | 0.57 |
| $L_{230(0.5)}$ | Tr | Tr | ND | ND | 1.19 | Tr |

[a]Results expressed per 100 Ar based on quantitative 2D-HSQC spectra. [b]S/G ratio obtained by the equation S/G ratio = $0.5IS_{2,6}/IG_2$. [c]PCA/FA ratio obtained by the equation PCA/FA ratio = $0.5IPCA_{2,6}/IFA_2$. [d]Tr, trace. [e]ND, not detectable.

The content of $\beta$-$O$-4 aryl ether in the ALs obtained at the mild conditions was higher than that of the LR, suggesting that some condensed reactions rather than depolymerization reactions occurred under the mild conditions. The condensation reactions led to the decrease of the protonated aromatic carbon and the elevation the content of $\beta$-$O$-4.[29] However, as the pretreatment temperature further increased (150−230 °C), the content of $\beta$-$O$-4 aryl ether in the ALs was sharply decreased, suggesting that the cleavage of $\beta$-$O$-4 aryl ether (depolymerization) was the predominant reaction during the HTP at higher temperatures.

Besides $\beta$-$O$-4 aryl ether linkage cleavage and carbon−carbon linkage degradation or condensation, changes of the S/G and PCA/FA ratios in the ALs were also prominent structural alterations observed after HTP.[29,38] The S/G and PCA/FA ratios in the ALs had no obvious changes ($L_{110(1.0)}$ and $L_{130(1.0)}$) at pretreatment temperature <150 °C as compared to that of the LR. The S/G and PCA/FA ratios gradually increased as the pretreatment temperature rose and time prolonged and reached a maximum ratio (S/G = 3.76; PCA/FA = 4.53) in $L_{170(2.0)}$. The increased S/G ratio suggested that the G-type lignin was more easily degraded during the HTP process, in agreement with a previous study.[29] Meanwhile, the increased PCA/FA ratio suggested that most of the etherified FA was removed during the HTP process. However, with the pretreatment temperature further increased from 190 to 230 °C, the S/G and PCA/FA ratios gradually decreased (S/G = 1.19; PCA/FA = 0.94) at the same time in $L_{230(0.5)}$.


dx.doi.org/10.1021/jf501669r | J. Agric. Food Chem. 2014, 62, 8120−8128

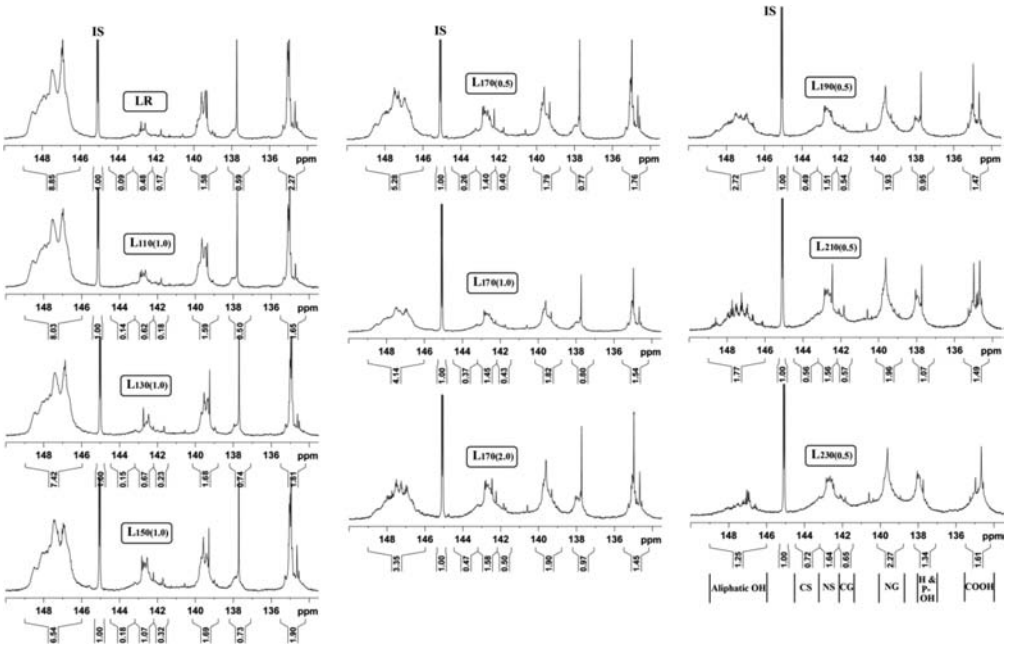


**Figure 5.** $^{31}$P NMR spectra of the lignins obtained from the integrated process under various processing conditions.

**Table 5. Quantification of Functional Groups (mmol/g) in Alkali Lignins Obtained from the Integrated Process under Various Processing Conditions by a Quantitative $^{31}$P NMR Method[a]**

| | | syringyl OH | | guaiacyl OH | | | | |
|---|---|---|---|---|---|---|---|---|
| lignins | aliphtic OH | C | NC | C | NC | *p*-hydroxyphenyl OH + PCA-OH | carboxylic group | total phenolic OH |
| LR | 4.79 | 0.05 | 0.26 | 0.09 | 0.86 | 0.32 | 1.23 | 1.58 |
| $L_{110(1.0)}$ | 4.35 | 0.08 | 0.34 | 0.10 | 0.86 | 0.27 | 0.89 | 1.65 |
| $L_{130(1.0)}$ | 4.02 | 0.08 | 0.36 | 0.12 | 0.92 | 0.40 | 0.98 | 1.88 |
| $L_{150(1.0)}$ | 3.54 | 0.10 | 0.58 | 0.17 | 0.92 | 0.40 | 1.03 | 2.17 |
| $L_{170(0.5)}$ | 2.86 | 0.14 | 0.76 | 0.22 | 0.97 | 0.42 | 0.95 | 2.51 |
| $L_{170(1.0)}$ | 2.24 | 0.20 | 0.79 | 0.23 | 0.99 | 0.43 | 0.83 | 2.64 |
| $L_{170(2.0)}$ | 1.81 | 0.25 | 0.86 | 0.27 | 1.03 | 0.53 | 0.79 | 2.94 |
| $L_{190(0.5)}$ | 1.47 | 0.27 | 0.82 | 0.29 | 1.05 | 0.51 | 0.80 | 2.94 |
| $L_{210(0.5)}$ | 0.96 | 0.30 | 0.84 | 0.31 | 1.06 | 0.58 | 0.81 | 3.09 |
| $L_{230(0.5)}$ | 0.68 | 0.39 | 0.89 | 0.35 | 1.23 | 0.73 | 0.87 | 3.59 |

[a]C, condensed; NC, noncondensed; PCA-OH, free *p*-coumaric acid.

**$^{31}$P NMR Spectral Analysis.** To further investigate the fundamental chemistry of the ALs obtained from the integrated process, a quantitative $^{31}$P NMR technique was also applied (Figure 5).[39,40] Table 5 shows the quantitative data on the distribution of the different OH groups of the ALs. The content of aliphatic OH of the ALs gradually reduced as the pretreatment temperature and time increased during the integrated process, suggesting that the aliphatic OH groups were gradually oxidized and modified under the harsh conditions.[29] The contents of S- and G-type phenolic OH groups were greatly increased from LR to $L_{230(0.5)}$ as a result of the cleavage of the *β*-*O*-4 aryl ether linkages, and the increasing rate of S-type lignin was faster than that of the corresponding G units. Additionally, the gradually increased condensed S and G phenolic OH implied that increasing the pretreatment temperature and time also resulted in more condensation reactions during the HTP process, as shown in the 2D HSQC NMR section aforementioned. The total content of PCA and *p*-hydroxyphenyl OH (H-type lignin unit) could be also revealed by $^{31}$P NMR spectra. The total content in LR was 0.32 mmol/g, whereas it decreased to 0.27 mmol/g in $L_{110(1.0)}$ and it increased from 0.32 to 0.73 mmol/g in the ALs ($L_{130(1.0)}$–$L_{230(0.5)}$) as the pretreatment temperature increased from 130 to 230 °C, suggesting that the demethoxylation reactions probably occurred at G and/or S units, especially at higher temperatures, as revealed by the intensive signals of H units in the 2D HSQC spectra.

**Thermal Analysis.** The thermal behaviors of lignin are extremely important for its utilization in thermochemical conversion into energy and chemicals, for example, thermolysis. The decomposition of lignin is a complex reaction and occurred by diverse bond fissions within the lignin macromolecule. The maximum decomposition temperature ($T_M$) is the corresponding temperature of the maximum decomposition rate ($V_M$).[41] In principle, the different thermal behaviors are not only influenced by the inherent structures and different functional groups of lignin molecule but condensation of the lignin macromolecule also associated with specific chemical features. To investigate the potential relationship between structural features and thermal behaviors, the TGA of the ALs (A, LR and $L_{150(1.0)}$; B, $L_{170(0.5)}$ and $L_{170(2.0)}$; C, $L_{190(0.5)}$ and $L_{230(0.5)}$) were comparatively investigated in this experiment (Figure 6).


dx.doi.org/10.1021/jf501669r | J. Agric. Food Chem. 2014, 62, 8120−8128

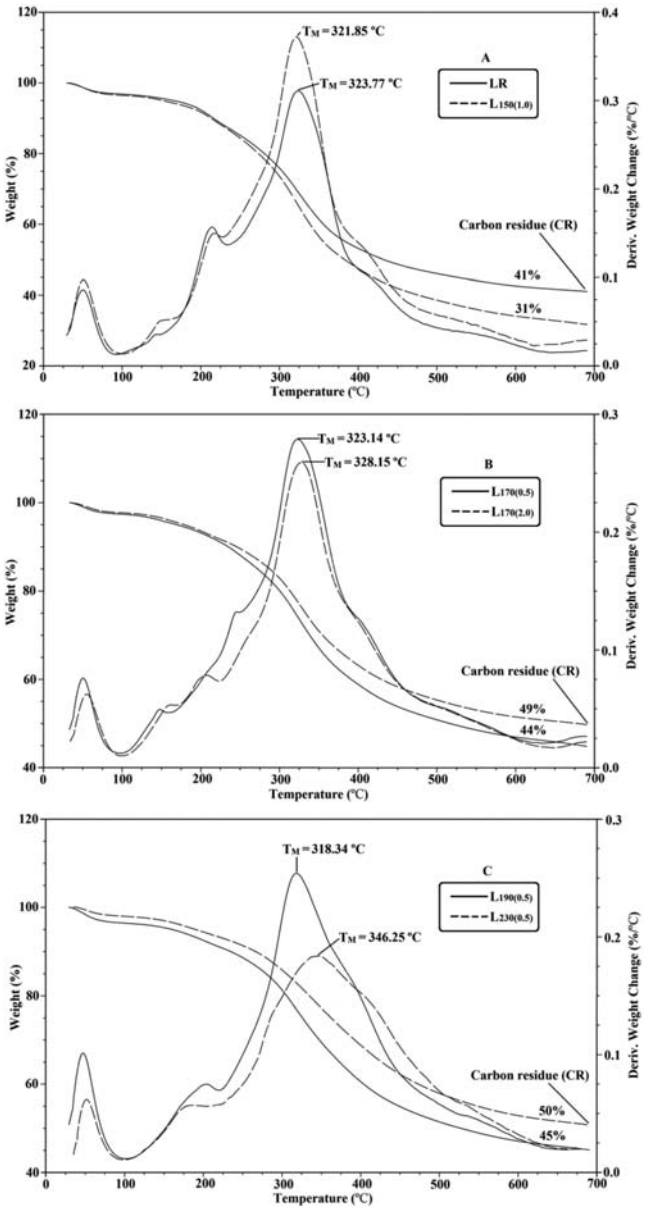


**Figure 6.** Thermogram of the lignins obtained from the integrated process under various processing conditions.

The $T_M$ of the six ALs obtained from the integrated process existed in the higher $T_M$ range from 318.34 to 346.25 °C. A previous study demonstrated that the $T_M$ is positively correlated with the corresponding molecular weight, suggesting that the initial reaction contained the deformation of the weaker C−O bond in the *β-O*-4 unit during the lignin decomposition.[42] In this study, the relationship between $T_M$ and molecular weight reflected only in the ALs extracted from the HTP residue at the mild conditions; however, when the HTP condition became harsh, the lignin extracted contained more condensed units, which in turn affected the corresponding $T_M$. In addition, "condensed lignin" was also reported to be correlated to "carbon residue (CR)".[36] As shown in Figure 6, the CRs were 44% for $L_{170(0.5)}$ and 49% for $L_{170(2.0)}$ at 700 °C as the HTP time increased from 0.5 to 2.0 h at 170 °C (Figure 6B). Similarly, when the HTP temperature further increased from 190 to 230 °C for 0.5 h (Figure 6C), the higher CR was found in $L_{230(0.5)}$ (50%) than in $L_{190(0.5)}$ (45%). That is, the CR was positively related to the "condensed lignin" of the ALs, which was revealed by the $^{31}$P NMR results aforementioned. These facts suggested that lignin with high CR was produced at the harsh HTP conditions.[36] However, only a small amount of condensed structures was observed in the ALs at the mild conditions (HTP temperature <170 °C). Therefore, besides the factor of "condensed structures", the CR in LR was also affected by other factors, such as ash and inorganic salt in plant cell wall.[43] This was why the CR in the LR was higher than that of $L_{150(1.0)}$, which even contained a slightly high content of condensed structures.

In summary, the present study demonstrated that the hydrothermally pretreated conditions had significant effects on the subsequent alkali lignin isolation and their chemical structures and properties. It was found that the alkali lignin with a high yield and purity could be obtained from the HTP residue under a high temperature and a short time (190 °C, 0.5 h). Meanwhile, NMR and molecular weight analysis suggested that the cleavage of the *β-O*-4 linkages and the degradation of *β-β* and *β*-5 linkages occurred during the integrated process, especially at the harsh conditions. Depolymerization and condensation reactions mainly occurred at higher temperatures. In addition, the thermostability was positively related to its molecular weight but also affected by the inherent structures, such as *β-O*-4 linkages and condensed units. However, as an integrated biorefinery process for XOS, high-purity lignin, and bioethanol, the optimal condition for the integrated process should be balanced along with some other aspects, such as cost, operability, and target product, to achieve overall goals. In short, an enhanced understanding of lignin structure features during the integrated process will be beneficial to value-added applications of abundant lignin fractions in a biorefinery process.

## AUTHOR INFORMATION

### Corresponding Author

*(R.-C.S.) Phone: +86 10 62336903. Fax: +86 10 62336903. E-mail: rcsun3@bjfu.edu.cn.

### Funding

We are extremely grateful for financial support from the State Forestry Administration (201204803), Major State Basic Research Projects of China (973-2010CB732204/3, 973-2012CB215302), and 863-project (2012AA023204).

### Notes

The authors declare no competing financial interest.

## REFERENCES

(1) Ragauskas, A. J.; Beckham, G. T.; Biddy, M. J.; Chandra, R.; Chen, F.; Davis, M. F. et al. Lignin valorization: improving lignin processing in the biorefinery. *Science* **2014**, *344*, DOI: 10.1126/science.1246843.

(2) Liu, S.; Lu, H.; Hu, R.; Shupe, A.; Lin, L.; Liang, B. A sustainable woody biomass biorefinery. *Biotechnol. Adv.* **2012**, *30*, 785−810.

(3) Alfani, F.; Gallifuoco, A.; Saporosi, A.; Spera, A.; Cantarella, M. J. Comparison of SHF and SSF processes for the bioconversion of steam-exploded wheat straw. *J. Ind. Microbiol. Biotechnol.* **2000**, *25*, 184−192.

(4) Liu, C.; van der Heide, E.; Wang, H.; Li, B.; Yu, G.; Mu, X. Alkaline twin-screw extrusion pretreatment for fermentable sugar production. *Biotechnol. Biofuels* **2013**, *6*, 97.

(5) Ishizawa, C. I.; Davis, M. F.; Schell, D. F.; Johnson, D. K. Porosity and its effect on the digestibility of dilute sulfuric acid pretreated corn stover. *J. Agric. Food Chem.* **2007**, *55*, 2575−2581.

(6) Karagöz, S.; Bhaskar, T.; Muto, A.; Sakata, Y. Comparative studies of oil compositions produced from sawdust, rice husk, lignin and cellulose by hydrothermal treatment. *Fuel* **2005**, *84*, 875−884.
(7) Walch, E.; Zemann, A.; Schinner, F.; Bonn, G.; Bobleter, O. Enzymatic saccharification of hemicellulose obtained from hydrothermally pretreated sugar cane bagasse and beech bark. *Bioresour. Technol.* **1992**, *39*, 173−177.
(8) Cybulska, I.; Lei, H.; Julson, J. Hydrothermal pretreatment and enzymatic hydrolysis of prairie cord grass. *Energy Fuels* **2009**, *24*, 718−727.
(9) Pronyk, C.; Mazza, G.; Tamaki, Y. Production of carbohydrates, lignins, and minor components from triticale straw by hydrothermal treatment. *J. Agric. Food Chem.* **2011**, *59*, 3788−3796.
(10) Prakasham, R. S.; Nagaiah, D.; Vinutha, K. S.; Uma, A.; Chiranjeevi, T.; Umakanth, A. V.; et al. Sorghum biomass: a novel renewable carbon source for industrial bioproducts. *Biofuels* **2014**, *5*, 159−174.
(11) Lu, H.; Hu, R.; Ward, A.; Amidon, T. E.; Liang, B.; Liu, S. Hot-water extraction and its effect on soda pulping of aspen woodchips. *Biomass Bioenergy* **2012**, *39*, 5−13.
(12) Lu, X.; Zhang, Y.; Angelidaki, I. Optimization of $H_2SO_4$-catalyzed hydrothermal pretreatment of rapeseed straw for bioconversion to ethanol: focusing on pretreatment at high solids content. *Bioresour. Technol.* **2009**, *100*, 3048−3053.
(13) Gould, J. M. Alkaline peroxide delignification of agricultural residues to enhance enzymatic saccharification. *Biotechnol. Bioeng.* **1984**, *26*, 46−52.
(14) Dang, V. Q.; Nguyen, K. L. A universal kinetic equation for characterising the fractal nature of delignification of lignocellulosic materials. *Cellulose* **2007**, *14*, 153−160.
(15) Kaparaju, P.; Felby, C. Characterization of lignin during oxidative and hydrothermal pre-treatment processes of wheat straw and corn stover. *Bioresour. Technol.* **2010**, *101*, 3175−3181.
(16) Doherty, W. O.; Mousavioun, P.; Fellows, C. M. Value-adding to cellulosic ethanol: lignin polymers. *Ind. Crops Prod.* **2011**, *33*, 259−276.
(17) Zhao, J.; Wilkins, R. M. Controlled release of the herbicide, fluometuron, from matrix granules based on fractionated organosolv lignins. *J. Agric. Food Chem.* **2003**, *51*, 4023−4028.
(18) Zhang, X.; Tu, M.; Paice, M. G. Routes to potential bioproducts from lignocellulosic biomass lignin and hemicelluloses. *Bioenergy Res.* **2011**, *4*, 246−257.
(19) Sluiter, A.; Hames, B.; Ruiz, R.; Scarlata, C.; Sluiter, J.; Templeton, D.; Crocker, D. *Determination of Structural Carbohydrates and Lignin in Biomass*; Technical Report NREL/TP-510-42618; National Renewable Energy Laboratory: Golden, CO, USA, 2008.
(20) Sun, S. L.; Wen, J. L.; Ma, M. G.; Li, M. F.; Sun, R. C. Revealing the structural inhomogeneity of lignins from sweet sorghum stem by successive alkali extractions. *J. Agric. Food Chem.* **2013**, *61*, 4226−4235.
(21) Granata, A.; Argyropoulos, D. S. 2-Chloro-4,4,5,5-tetramethyl-1,3,2-dioxaphospholane, a reagent for the accurate determination of the uncondensed and condensed phenolic moieties in lignins. *J. Agric. Food Chem.* **1995**, *43*, 1538−1544.
(22) Wen, J. L.; Sun, S. L.; Yuan, T. Q.; Xu, F.; Sun, R. C. Structural elucidation of lignin polymers of eucalyptus chips during organosolv pretreatment and extended delignification. *J. Agric. Food Chem.* **2013**, *61*, 11067−11075.
(23) Samuel, R.; Cao, S.; Das, B. K.; Hu, F.; Pu, Y.; Ragauskas, A. J. Investigation of the fate of poplar lignin during autohydrolysis pretreatment to understand the biomass recalcitrance. *RSC Adv.* **2013**, *3*, 5305−5309.
(24) Sannigrahi, P.; Kim, D.-H.; Jung, S.; Ragauskas, A. Pseudo-lignin and pretreatment chemistry. *Energy Environ. Sci.* **2011**, *4*, 1306−1310.
(25) Leschinsky, M.; Zuckerstätter, G.; Weber, H. K.; Patt, R.; Sixta, H. Effect of autohydrolysis of Eucalyptus globulus wood on lignin structure. Part 1: comparison of different lignin fractions formed during water prehydrolysis. *Holzforschung* **2008**, *62*, 645−652.
(26) Wen, J. L.; Xue, B. L.; Xu, F.; Sun, R. C.; Pinkert, A. Unmasking the structural features and property of lignin from bamboo. *Ind. Crops Prod.* **2013**, *42*, 332−343.
(27) Faix, O. Classification of lignins from different botanical origins by FT-IR spectroscopy. *Holzforschung* **1991**, *45*, 21−28.
(28) Sun, S. L.; Wen, J. L.; Ma, M. G.; Sun, R. C.; Jones, G. L. Structural features and antioxidant activities of degraded lignins from steam exploded bamboo stem. *Ind. Crops Prod.* **2014**, *56*, 128−136.
(29) Wen, J. L.; Sun, S. N.; Yuan, T. Q.; Xu, F.; Sun, R. C. Fractionation of bamboo culms by autohydrolysis, organosolv delignification and extended delignification: understanding the fundamental chemistry of the lignin during the integrated process. *Bioresour. Technol.* **2013**, *150*, 278−286.
(30) Del Río, J. C.; Rencoret, J.; Prinsen, P.; Martínez, A. N. T.; Ralph, J.; Gutiérrez, A. Structural characterization of wheat straw lignin as revealed by analytical pyrolysis, 2D-NMR, and reductive cleavage methods. *J. Agric. Food Chem.* **2012**, *60*, 5922−5935.
(31) Martínez, Á. T.; Rencoret, J.; Marques, G.; Gutiérrez, A.; Ibarra, D.; Jiménez-Barbero, J.; Del Río, J. C. Monolignol acylation and lignin structure in some nonwoody plants: a 2D NMR study. *Phytochemistry* **2008**, *69*, 2831−2843.
(32) Ralph, J.; Lundquist, K.; Brunow, G.; Lu, F.; Kim, H.; Schatz, P. F.; et al. Lignins: natural polymers from oxidative coupling of 4-hydroxyphenyl-propanoids. *Phytochem. Rev.* **2004**, *3*, 29−60.
(33) Sun, S. N.; Cao, X. F.; Xu, F.; Sun, R. C.; Jones, G. L. Structural features and antioxidant activities of lignins from steam exploded bamboo (*Phyllostachys pubescens*). *J. Agric. Food Chem.* **2014**, *62*, 5939−5947.
(34) Wen, J. L.; Sun, S. L.; Xue, B. L.; Sun, R. C. Recent advances in characterization of lignin polymer by solution-state nuclear magnetic resonance (NMR) methodology. *Materials* **2013**, *6*, 359−391.
(35) Wen, J. L.; Xue, B. L.; Xu, F.; Sun, R. C. Quantitative structural characterization of the lignins from the stem and pith of bamboo (*Phyllostachys pubescens*). *Holzforschung* **2013**, *67*, 613−627.
(36) Wen, J. L.; Sun, S. L.; Xue, B. L.; Sun, R. C. Quantitative structures and thermal properties of birch lignins after ionic liquid pretreatment. *J. Agric. Food Chem.* **2013**, *61*, 635−645.
(37) Sette, M.; Wechselberger, R.; Crestini, C. Elucidation of lignin structure by quantitative 2D NMR. *Chem.−Eur. J.* **2011**, *17*, 9529−9535.
(38) El Hage, R.; Chrusciel, L.; Desharnais, L.; Brosse, N. Effect of autohydrolysis of *Miscanthus* × *giganteus* on lignin structure and organosolv delignification. *Bioresour. Technol.* **2010**, *101*, 9321−9329.
(39) Pu, Y. Q.; Cao, S. L.; Ragauskas, A. Application of quantitative $^{31}P$ NMR in biomass lignin and biofuel precursors characterization. *J. Energy Environ. Sci.* **2011**, *4*, 3154−3166.
(40) Crestini, C.; Argyropoulos, D. S. Structural analysis of wheat straw lignin by quantitative $^{31}P$ and 2D NMR spectroscopy. The occurrence of ester bonds and $\alpha$-*O*-4 substructures. *J. Agric. Food Chem.* **1997**, *45*, 1212−1219.
(41) Hodgson, E.; Nowakowski, D.; Shield, I.; Riche, A.; Bridgwater, A. V.; Clifton-Brown, J. C.; et al. Variation in *Miscanthus* chemical composition and implications for conversion by pyrolysis and thermochemical bio-refining for fuels and chemicals. *Bioresour. Technol.* **2011**, *102*, 3411−3418.
(42) Sun, R. C.; Tomkinson, J.; Jones, G. J. Fractional characterization of ash-AQ lignin by successive extraction with organic solvents from oil palm EFB fibre. *Polym. Degrad. Stab.* **2000**, *68*, 111−119.
(43) Raveendran, K.; Ganesh, A.; Khilar, K. C. Influence of mineral matter on biomass pyrolysis characteristics. *Fuel* **1995**, *74*, 1812−1822.

JOURNAL OF AGRICULTURAL AND FOOD CHEMISTRY

Article

pubs.acs.org/JAFC

# Quantitation of Sugar Content in Pyrolysis Liquids after Acid Hydrolysis Using High-Performance Liquid Chromatography without Neutralization

Patrick A. Johnston[†] and Robert C. Brown*[,†,‡]

[†]Bioeconomy Institute and [‡]Department of Mechanical Engineering, Iowa State University, Ames, Iowa 50011, United States

**ABSTRACT:** A rapid method for the quantitation of total sugars in pyrolysis liquids using high-performance liquid chromatography (HPLC) was developed. The method avoids the tedious and time-consuming sample preparation required by current analytical methods. It is possible to directly analyze hydrolyzed pyrolysis liquids, bypassing the neutralization step usually required in determination of total sugars. A comparison with traditional methods was used to determine the validity of the results. The calibration curve coefficient of determination on all standard compounds was >0.999 using a refractive index detector. The relative standard deviation for the new method was 1.13%. The spiked sugar recoveries on the pyrolysis liquid samples were between 104 and 105%. The research demonstrates that it is possible to obtain excellent accuracy and efficiency using HPLC to quantitate glucose after acid hydrolysis of polymeric and oligomeric sugars found in fast pyrolysis bio-oils without neutralization.

**KEYWORDS:** *HPLC, biomass, bio-oil, acid hydrolysis, levoglucosan, fast pyrolysis, carbohydrates*

## INTRODUCTION

Direct liquefaction is the thermal decomposition of solid organic material into condensable vapors, liquids, or solutions of organic compounds. Examples include fast pyrolysis, solvent liquefaction, and hydrothermal processing. Under appropriate conditions, direct liquefaction can depolymerize lignocellulosic biomass into monosaccharides or disaccharides.[1] Sugars have not received much attention because they have not traditionally been thought to be an important product of direct liquefaction and the difficulty of measuring them in the complex matrix of the liquid products of direct liquefaction.

We are developing analytical methods for measuring sugars in the products of direct liquefaction with a particular focus on bio-oil, the liquid product from the fast pyrolysis of lignocellulosic biomass. Fast pyrolysis is the thermal decomposition of organic compounds in the absence of oxygen at temperatures in the range of 400−600 °C.[2,3] Products include liquids (55−60 wt %), gases (12−22 wt %), and char (16−20 wt %).[4−6] The liquids are a complex mixture of organic acids, alcohols, aldehydes, ketones, phenols, carbohydrates, esters, lignin oligomers, and water.[3] The carbohydrates include monosaccharides and anhydrosugars, most prominently levoglucosan. Usually the yield of levoglucosan from the pyrolysis of lignocellulosic biomass is only a few percent, but Kuzhiyil et al.[1] found that infusing biomass with a weak mineral acid solution prior to pyrolysis increased levoglucosan yields from the cellulose fraction to as much as 59 wt %. These sugars can be upgraded into transportation fuels and chemicals via fermentation to alcohols, catalytic synthesis to hydrocarbons, dehydration to heterocyclic aldehydes (furfurals) and aromatics (furans), and aqueous-phase re-forming to produce alkanes as building blocks of gasoline.[3,7]

Analytical techniques such as high-performance liquid chromatography (HPLC) are commonly used to identify and quantitate sugar concentrations by hydrolyzing oligosaccharides and levoglucosan to glucose.[8,9] However, these traditional HPLC methods can be cumbersome. Methods such as ASTM E1758 "Standard Method for the Determination of Carbohydrates by HPLC" and the National Renewable Energy Laboratory's (NREL) "Determination of Structural Carbohydrates in Biomass" require a neutralization step after hydrolyzing polysaccharides and oligosaccharides to glucose.[10,11] Researchers analyzing wood sugar using other liquid chromatography techniques have been successful in performing analysis without neutralization. Petterson et al.[12] performed wood sugar analysis using anion-exchange chromatography with a pulsed amperometric detector (PAD) after hydrolysis without neutralization. The main problem with the conventional methods of analysis using neutralization is the loss of sugars if the pH is not carefully monitored. The NREL methodology states: "Samples should never be allowed to exceed a pH of 9, as this will result in a loss of sugars".[10] Miller[13] showed spectrophotometer evidence that a significant reduction of glucose was observed with increasing concentrations of sodium hydroxide. Rover et al.[14] determined that a 7% decrease of sugar was observed when the pH was increased to 11. A new HPLC method recently established at Iowa State University (ISU) enables researchers to avoid the neutralization step. Hence, total sugar in lignocellulosic fast pyrolysis oils can be analyzed more rapidly. The new method also helps to prevent degradation and loss of sugars that can sometimes result from neutralization if the pH is not carefully monitored.[10]

**Received:** May 14, 2014
**Revised:** July 28, 2014
**Accepted:** July 30, 2014
**Published:** July 30, 2014

ACS Publications © 2014 American Chemical Society



dx.doi.org/10.1021/jf502250n | *J. Agric. Food Chem.* 2014, 62, 8129−8133

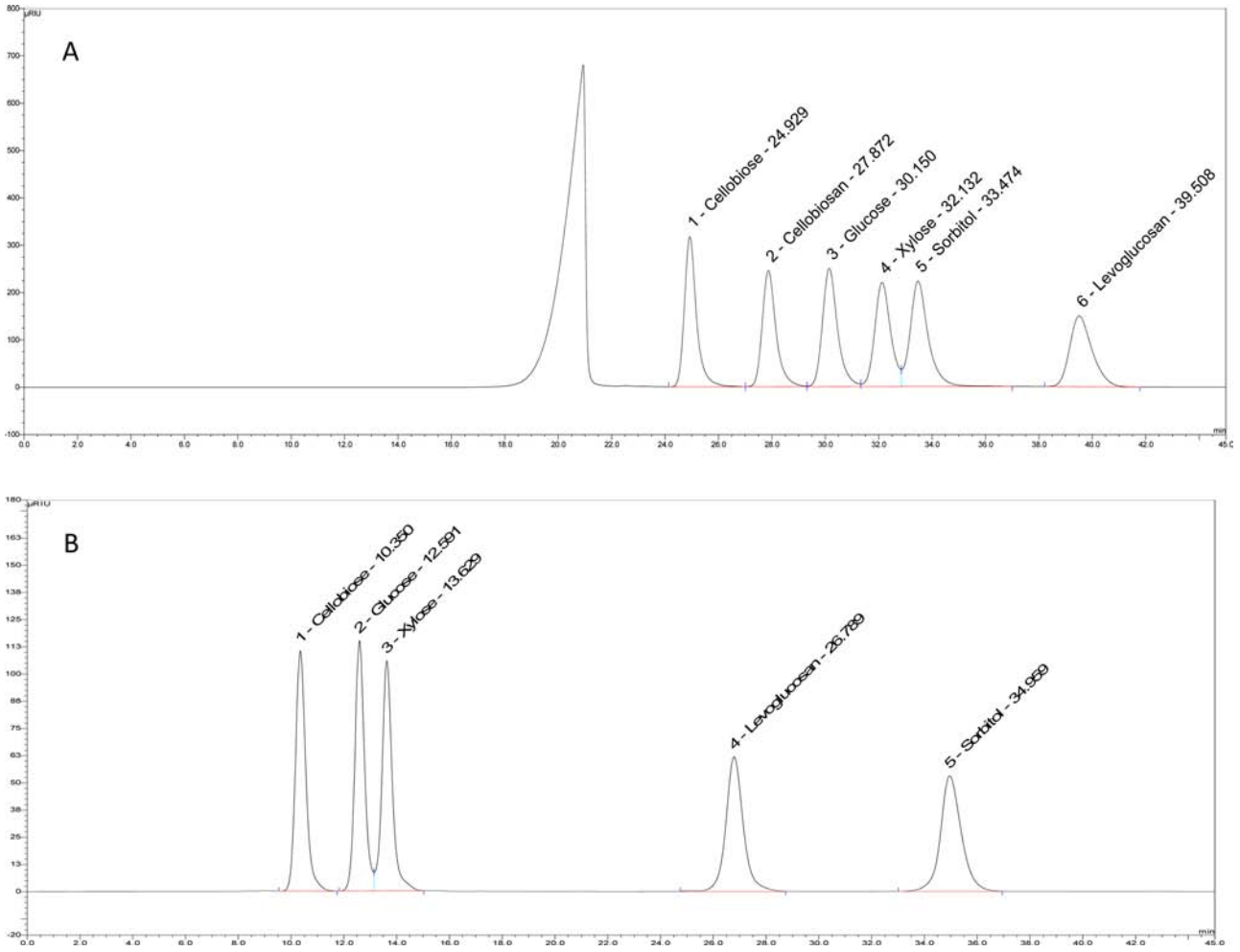


**Figure 1.** Comparison of standard compounds using HPLC: (A) acidic hydrolysate (new method); (B) neutralized hydrolysate (traditional method).

## MATERIALS AND METHODS

**Reagents and Standards.** Levoglucosan and cellobiosan were purchased from Carbosynth (Compton, Berkshire, UK) and had purities of ≥99.0%. Glucose and xylose were purchased from Thermo Fisher Scientific (Waltham, MA, USA) and had purities ≥98.0%. Cellobiose and sorbitol were purchased from Acrōs Organics (Thermo Fisher Scientific) and had purities of ≥99.0 and ≥98.5%, respectively. All samples and standards solutions were prepared using ultrapure 18.2 MΩ deionized water from a Barnstead E-Pure system (Thermo Fisher Scientific). The sulfuric acid used in all experiments was certified 10 N with an assay of 9.95−10.05 (Thermo Fisher Scientific).

**Pyrolysis Liquid Samples.** The pyrolysis liquid used in this study was produced using a fast pyrolysis auger reactor and switchgrass feedstock.[15,16] The reactor was a benchtop 2 kg/h screw (auger) type fast pyrolysis reactor. The feedstock is first mixed with the heat carrier media in the reactor. After the biomass has been thermochemically processed, the particulate matter (char) is removed from the gas by two cyclones. In the final stages the gases are condensed out at different temperatures to produce four fractions of bio-oil. The polysaccharide-rich portion was found mainly in the first two condensers and electrostatic precipitator (ESP) stage fractions.

**Acid Hydrolysis of Bio-Oil Samples.** The anhydro and other polymeric/oligomeric sugars in the fast pyrolysis bio-oil were acid hydrolyzed with 400 mM $H_2SO_4$ at 125 °C for 44 min to glucose.[17] Hydrolysis conditions were based on the previous work of Bennett et al.[17] Aliquots of 6 mL of 400 mM $H_2SO_4$ and 60 mg of bio-oil were added to sealed glass vials. Pure compounds of levoglucosan and cellobiosan were used as check standards to determine complete hydrolysis. These standards were hydrolyzed under the same conditions as the samples to establish complete hydrolysis to glucose and used as reference standards. The reference standards had purities of ≥99.0%. After hydrolysis, all samples were filtered with a 0.45 μm glass microfiber (GMF) syringe filter (Whatman, Pittsburgh, PA, USA) before HPLC analysis. With the traditional method an extra neutralization step was completed before the filtration. The neutralization step was completed as per ASTM E1748 by adding calcium carbonate slowly until a pH of between 5 and 6 was attained. The samples were filtered with a 0.45 μm GMF syringe filter before HPLC analysis.

**Instrumentation.** The HPLC system used for the experiments was a Dionex Ultimate 3000 LC system (Sunnyvale, CA, USA) with a quaternary analytical pump and a Shodex refractive index (RI) detector (New York, NY, USA). Two different types of columns were used in the experiments. The analytical columns used were either a 300 mm × 7.7 mm i.d, 8 μm, HyperRez XP Carbohydrate (Thermo Fisher Scientific) or a 300 mm × 7.8 mm i.d., 9 μm, Aminex 87P (Bio-Rad, Hercules, CA, USA). The guard column for the Aminex was a Micro-Guard de-ashing cartridge with a de-ashing holder (Bio-Rad). The guard column for the HyperRez was a Carbohydrate $H^+$ cartridge with a guard holder (Thermo Fisher Scientific). The guard columns were used to eliminate possible interferences caused by anions and cations. The instrument parameters for the HyperRez were as follows: The mobile phase was ultrapure 18.2 MΩ deionized water with a flow rate of 0.2 mL/min, and the column temperature was set at 55 °C. The instrument parameters for the Aminex column were as follows: The mobile phase was ultrapure 18.2 MΩ deionized water with a flow rate of 0.6 mL/min, and the column temperature was set at 80 °C. The


dx.doi.org/10.1021/jf502250n | J. Agric. Food Chem. 2014, 62, 8129−8133

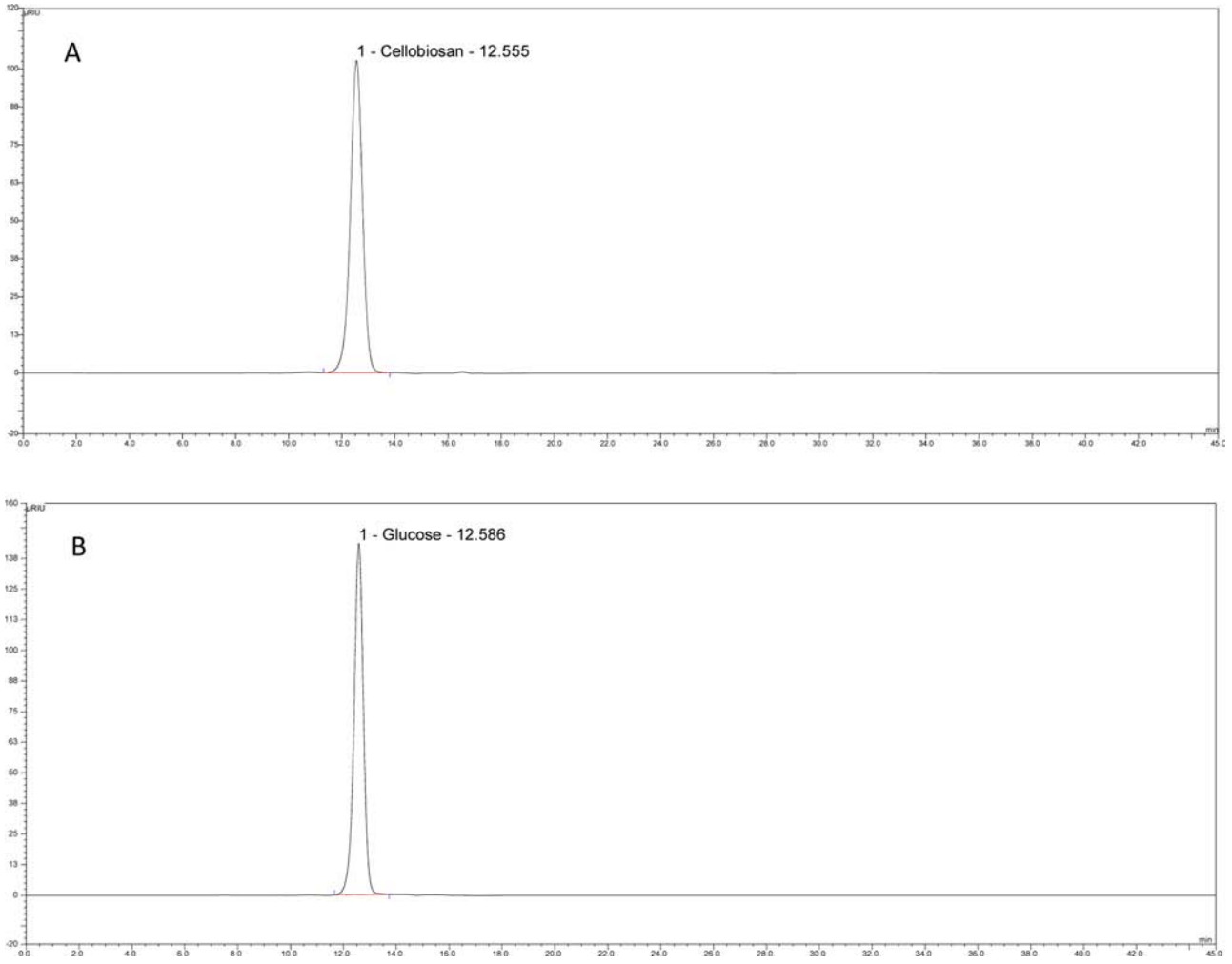


**Figure 2.** Comparison of equivalent retention times of standard compounds (A) cellobiosan and (B) glucose with the traditional method.

injection amount for the HyperRez column was 25 $\mu$L and the Aminex column was 20 $\mu$L.

## RESULTS AND DISCUSSION

A comparison of glucose, cellobiosan, cellobiose, levoglucosan, sorbitol, and xylose standard compounds using both the Aminex 87P and the HyperRez columns is displayed in Figure 1. The concentration of the standard was approximately 10 mg/mL.

A complete set of calibration standards using glucose, cellobiosan, cellobiose, levoglucosan, sorbitol, and xylose was performed in duplicate on the HPLC using the HyperRez column. The same sugars, with the exception of cellobiosan, were measured on HPLC with the Aminex column. Cellobiosan has almost the exact same retention time as glucose (Figure 2). Because the acid hydrolysis reaction will convert the cellobiosan to glucose, this compound is not necessarily needed in the calibration standard. Its absence would, however, be an issue with the conventional column because incomplete hydrolysis of cellobiosan could give falsely high readings for glucose. The calibration curves had 12 points (same concentration in duplicate) in the range of approximately 0.5−10 mg/mL. The coefficient of determination for all standard compounds on both the HyperRez and Aminex columns was >0.999. Check standards were tested after each set of samples was complete. All samples were hydrolyzed in duplicate, and triplicate injections were performed on each sample. The results displayed are based on total polymeric/oligomeric sugars that are converted to glucose after acid hydrolysis. Figure 3 displays the sample chromatograms for both methods after hydrolysis. The sugar yield in milligrams per milliliter was calculated as percent (w/w) using the density of the solution used in the sample preparation. The result for the traditional method was 11.3% (w/w) and that for the new method was 11.2% (w/w). The two methods displayed equivalent results.

Verification standards were tested before and after each set of tests. Reference standards of pure levoglucosan and cellobiosan were hydrolyzed with each set of samples to ensure complete hydrolysis conditions. All samples were tested in duplicate with triplicate injections. The percent RSD for the Aminex column was 1.03% and that for the HyperRez column was 1.13%.

Levoglucosan was added to each bio-oil sample and hydrolyzed in duplicate and analyzed in triplicate. The average recovery yields of the two levoglucosan-spiked samples with a 95% confidence interval were 105 ± 0.20 and 104 ± 0.49%. Levoglucosan recovery yields were very representative of the total amount of sample spiked in the solution.

Both columns had very good linearity and were able to resolve and separate the compounds of interest in the bio-oil samples. The new method produced total sugar results comparable to the traditional method. The HyperRez column,


dx.doi.org/10.1021/jf502250n | J. Agric. Food Chem. 2014, 62, 8129−8133

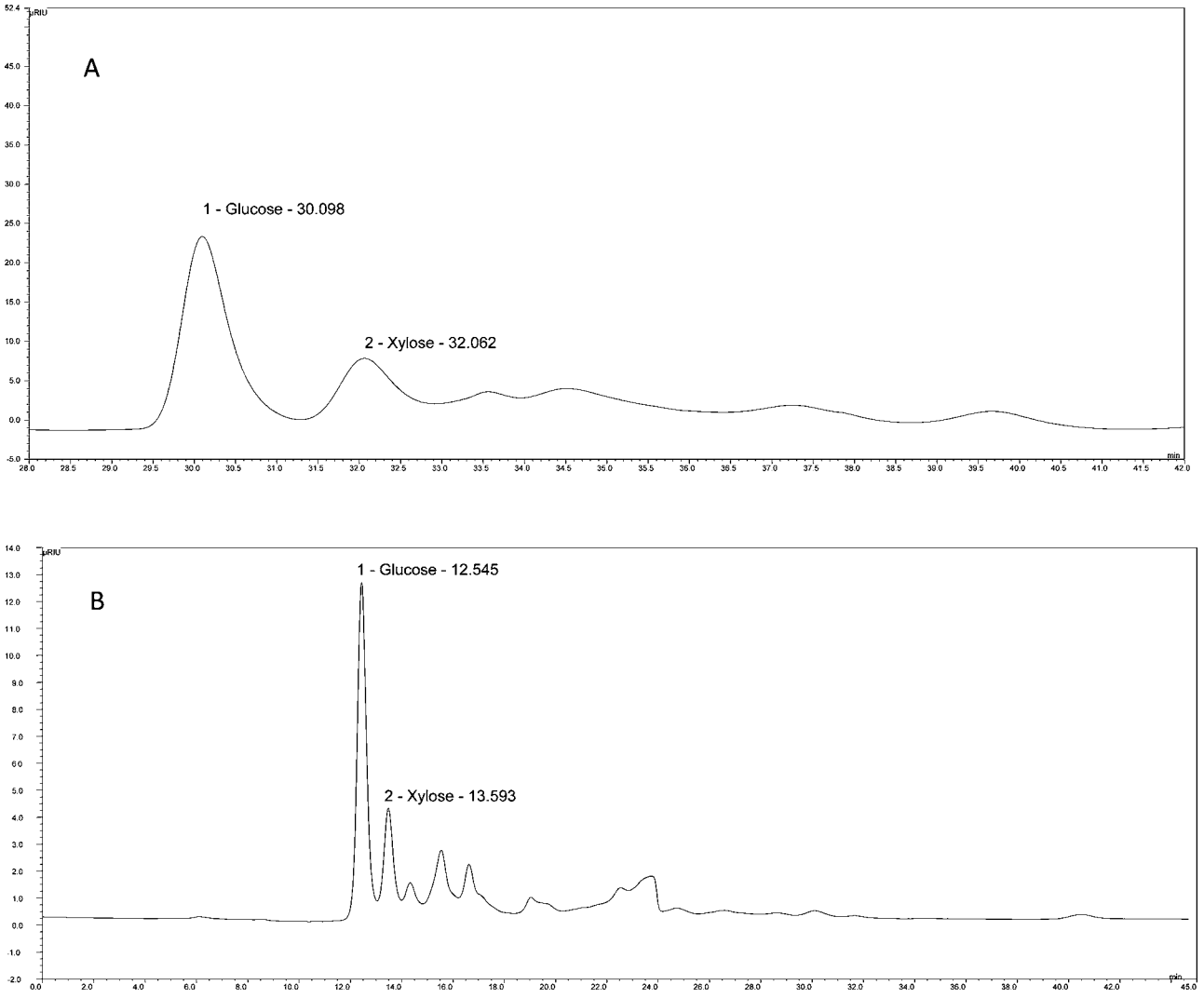


**Figure 3.** Comparison of samples using HPLC: (A) acidic hydrolysate (new method); (B) neutralized hydrolysate (traditional method).

however, offers two distinct advantages. It enables researchers and refineries to quickly analyze hydrolyzed sugar samples, bypassing the time-consuming and tedious neutralization step. The HyperRez column also eliminates possible degradation of sugars that can occur during the conventional neutralization step if pH levels are not closely monitored. Our research demonstrated that it is possible to obtain excellent accuracy and efficiency using HPLC to quantitate glucose after acid hydrolysis of polymeric and oligomeric sugars found in fast pyrolysis bio-oils without neutralization.

## AUTHOR INFORMATION

### Corresponding Author

*(R.C.B.) Phone: (515) 294-7934. Fax: (515) 294-3091. E-mail: rcbrown3@iastate.edu.

### Funding

We acknowledge Phillips 66 Co. for financial support of this project.

### Notes

The authors declare no competing financial interest.

## ACKNOWLEDGMENTS

We thank Marjorie Rover for helpful discussions in the subject area, Dustin Dalluge for producing the pyrolysis liquids, and Nick Jaegers for assisting with laboratory experiments.

## REFERENCES

(1) Kuzhiyil, N.; Dalluge, D.; Bai, X.; Kim, K. H.; Brown, R. C. Pyrolytic sugars from cellulosic biomass. *ChemSusChem* **2012**, *5*, 2228−2236.

(2) Bridgwater, A. V. An introduction to fast pyrolysis of biomass for fuels and chemicals. In *Fast Pyrolysis of Biomass: A Handbook*; CPL Press: Newbury, UK, 1999; pp 1−15.

(3) Brown, R. C. Introduction to thermochemical processing of biomass into fuels, chemicals, and power. In *Thermochemical Processing of Biomass Conversion into Fuels, Chemicals, and Power*; Brown, R. C., Ed.; Wiley: Chichester, UK, 2011; p 330.

(4) Mullen, C. A.; Boateng, A. A.; Goldberg, N. M.; Lima, I. M.; Laird, D. A.; Hicks, K. B. Bio-oil and bio-char production from corn cobs and stover by fast pyrolysis. *Biomass Bioener.* **2010**, *34*, 67−74.

(5) Agblevor, F. A.; Besler, S.; Wiselogel, A. E. Fast pyrolysis of stored biomass feedstocks. *Energy Fuels* **1995**, *9*, 635−640.

(6) Wright, M. M.; Daugaard, D. E.; Satrio, J. A.; Brown, R. C. Techno-economic analysis of biomass fast pyrolysis to transportation fuels. *Fuel* **2010**, *89*, S2−S10.

(7) Lewkowski, J. Synthesis, chemistry and applications of 5-hydroxymethylfurfural and its derivatives. *ARKIVOC* **2001**, 17−54.
(8) Yu, Z.; Zhang, H. Pretreatments of cellulose pyrolysate for ethanol production by *Saccharomyces cerevisiae*, *Pichia* sp. YZ-1 and *Zymomonas mobilis*. *Biomass Bioenergy* **2003**, *24*, 257−262.
(9) Helle, S.; Bennett, N. M.; Lau, K.; Matsui, J. H.; Duff, S. J. A kinetic model for production of glucose by hydrolysis of levoglucosan and cellobiosan from pyrolysis oil. *Carbohydr. Res.* **2007**, *342*, 2365−2370.
(10) Sluiter, A.; Hames, B.; Ruiz, R.; Scarlata, C.; Sluiter, J.; Templeton, D.; Crocker, D. *Determination of Structural Carbohydrates and Lignin in Biomass*; National Renewable Energy Laboratory: Golden, CO, USA, 2008 (revised 2012); http://www.nrel.gov/docs/gen/fy13/42618.pdf.
(11) ASTM. Standard test method for determination of carbohydrates in biomass by high performance liquid chromatography. In *Book of Standards*; ASTM: Philadelphia, PA, USA, 2007; Vol. 11.06, ASTM E1859.
(12) Pettersen, R. C.; Schwandt, V. H. Wood sugar analysis by anion chromatography. *J. Wood Chem. Technol.* **1991**, *11*, 495−501.
(13) Miller, G. L. Use of dinitrosalicylic acid reagent for determination of reducing sugar. *Anal. Chem.* **1959**, *31*, 426−428.
(14) Rover, M. R.; Johnston, P. A.; Jin, T.; Smith, R. G.; Brown, R. C.; Jarboe, L. Production of clean pyrolytic sugars for fermentation. *ChemSusChem* **2014**, *7*, 1662−1668.
(15) Brown, J. N.; Brown, R. C. Process optimization of an auger pyrolyzer with heat carrier using response surface methodology. *Bioresour. Technol.* **2012**, *103*, 405−414.
(16) Brown, J. N. *Development of a Lab-Scale Auger Reactor for Biomass Fast Pyrolysis and Process Optimization Using Response Surface Methodology*; Iowa State University: Ames, IA, USA, 2009.
(17) Bennett, N. M.; Helle, S. S.; Duff, S. J. Extraction and hydrolysis of levoglucosan from pyrolysis oil. *Bioresour. Technol.* **2009**, *100*, 6059−6063.

JOURNAL OF AGRICULTURAL AND FOOD CHEMISTRY

Article

pubs.acs.org/JAFC

# Characterization of Glyphosate Resistance in *Amaranthus tuberculatus* Populations

Lothar Lorentz,[†,§] Todd A. Gaines,[†,#] Scott J. Nissen,[#] Philip Westra,[#] Harry J. Strek,[†] Heinz W. Dehne,[§] Juan Pedro Ruiz-Santaella,[†] and Roland Beffa*[,†]

[†]Bayer CropScience, Industriepark Hoechst, Building H872, 65926 Frankfurt am Main, Germany

[§]INRES-Phytomedicinem University of Bonn, Nußallee 9, 53115 Bonn, Germany

[#]Department of Bioagricultural Sciences and Pest Management, Colorado State University, 1177 Campus Delivery, Fort Collins, Colorado 80523, United States

Supporting Information

**ABSTRACT:** The evolution of glyphosate-resistant weeds has recently increased dramatically. Six suspected glyphosate-resistant *Amaranthus tuberculatus* populations were studied to confirm resistance and determine the resistance mechanism. Resistance was confirmed in greenhouse for all six populations with glyphosate resistance factors (R/S) between 5.2 and 7.5. No difference in glyphosate absorption or translocation was observed between resistant and susceptible individuals. No mutation at amino acid positions G101, T102, or P106 was detected in the *EPSPS* gene coding sequence, the target enzyme of glyphosate. Analysis of *EPSPS* gene copy number revealed that all glyphosate-resistant populations possessed increased *EPSPS* gene copy number, and this correlated with increased expression at both RNA and protein levels. EPSPS $V_{max}$ and $K_{cat}$ values were more than doubled in resistant plants, indicating higher levels of catalytically active expressed EPSPS protein. *EPSPS* gene amplification is the main mechanism contributing to glyphosate resistance in the *A. tuberculatus* populations analyzed.

**KEYWORDS:** *glyphosate absorption, glyphosate translocation, EPSPS gene amplification, EPSPS gene expression, gene duplication, EPSPS enzyme activity, herbicide resistance*

## INTRODUCTION

*Amaranthus tuberculatus* (Moq.) Sauer var. *rudis* (Sauer) Costea & Tardif (common waterhemp) is a dioecious C4 weed that can grow up to 3 m in height with roots reaching a depth of 70 cm. It can occupy a radial area of 2 m with a growing rate of 0.11−0.16 cm per growing degree day.[1−3] The reported growth rate of *A. tuberculatus* is less than that for *Amaranthus palmeri*, but still higher than the values reported for other *Amaranthus* species.[4] The female plant can produce between 35,000 and 1,200,000 seeds during the growing season.[5] It prefers well-drained and nutrient-rich soils also well suited for agricultural production. Therefore, *A. tuberculatus* is an important weed, especially under drought stress conditions, and can vigorously compete with corn and soybean for water and nitrogen.[5,6] *A. tuberculatus* has also evolved resistance to several herbicide modes of action either separately or in combination, including inhibitors of (1) aromatic amino acid biosynthesis, (2) photosystem II, (3) branched-chain amino acid biosynthesis, (4) chlorophyll biosynthesis, and (5) carotenoid biosynthesis.[7−13]

Glyphosate, a broad-spectrum herbicide, acts on enolpyruvyl-5-shikimate-3-phosphate-synthase (EPSPS), the sixth enzyme in the plant shikimic acid pathway. It converts shikimate-3-phosphate (S-3-P) together with phosphoenolpyruvate (PEP) into enolpyruvalshikimate-3-phosphate (EPSP), a precursor in the formation of aromatic amino acids and many secondary aromatic plant metabolites.[14−16] Due to a missing feedback inhibition at this step, the S-3-P concentration in plants increases continuously after glyphosate treatment.[17] With its high-energy bonds, the phosphate group of S-3-P is unstable in plant cells and degrades into shikimic acid, which can be used as an early indicator of the inhibitory activity of glyphosate in plants.[18−21] EPSPS is most active in young, actively growing plant tissue; therefore, the highest shikimic acid can be measured in these tissues, and particularly in the meristems, after glyphosate treatment.[22,23]

Both target- and non-target-site-based resistance mechanisms are responsible for glyphosate resistance.[24] Alterations in the *EPSPS* gene sequence, specifically at the amino acid P106, have been reported in several glyphosate-resistant weeds, including *Eleusine indica* and *Lolium rigidum*.[25,26] Differences in glyphosate translocation have been found in other populations of *L. rigidum* and in *Lolium multiflorum*, *Sorghum halepense*, and *Conyza canadensis*.[27−30] Glyphosate translocation in these populations is mostly restricted within the treated leaves, resulting in significantly less translocation throughout the whole plant. In *C. canadensis* the reduced translocation is based on rapid glyphosate sequestration into vacuoles.[31] In a population of *L. multiflorum* found in Chile, the resistance is based on differences in the spray solution retention and foliar absorption.[32] Both a P106S mutation and reduced translocation were identified in a glyphosate-resistant *A. tuberculatus* population from Mississippi.[13]

Received: February 28, 2014
Revised: June 11, 2014
Accepted: June 23, 2014
Published: June 23, 2014

 © 2014 American Chemical Society 

Although many different glyphosate resistance mechanisms have been reported, new mechanisms continue to be identified, such as the *EPSPS* gene amplification in *A. palmeri* populations from Georgia and Mississippi, USA.[33−35] In these plants the *EPSPS* gene was amplified from 40- to >100-fold. The importance of gene amplification in conferring, for example, insecticide resistance has been well established;[36] however, the amplification of the *EPSPS* gene in a single *A. palmeri* population was the first case of herbicide resistance induced by this mechanism.[34] The *EPSPS* transcript abundance in untreated resistant plants was positively correlated with the genomic *EPSPS* gene copy number, suggesting no significant gene silencing of amplified genes. Amplified *EPSPS* genes were also translated into higher enzyme content.[34,35] Glyphosate resistance based on gene amplification or increased EPSPS activity in vitro also occurred in cell cultures reared on glyphosate containing media, in *Daucus carota* L., *Petunia hybrida*, *Nicotiana tabacum*, *Glycine max*, *Corydalis sempervirens*, and *Medicago sativa*.[37−41] However, plants derived from these cell cultures did not ultimately yield field-level glyphosate resistance.

The scope of the present work is to characterize the glyphosate resistance mechanism(s) in *A. tuberculatus* and compare the role of gene amplification between two related species, *A. tuberculatus* and *A. palmeri*. Populations collected from the field and described as being either susceptible or resistant to glyphosate were characterized without further inbreeding of resistance using biological (greenhouse dose response), physiological (glyphosate absorption and translocation), biochemical (shikimic acid content and EPSPS enzyme activity), and molecular (EPSPS gene copy number and expression) analyses to determine the glyphosate resistance mechanism.

## MATERIALS AND METHODS

Six different and still segregating *A. tuberculatus* populations collected between 2005 and 2009 from different fields in Missouri (MO) and Illinois (IL) (Supporting Information Table SI1) were assessed for their response to glyphosate. Previous results and the glyphosate resistance status of the field populations are described in Table SI1 of the Supporting Information. Six populations (IL-R, MO-R1, MO-R2, MO-R3, MO-R4, and MO-R5) were difficult to control in field, whereas the susceptible population, MO-S, was controlled by the recommended field rate of glyphosate.

The *A. tuberculatus* populations were sown in Petri dishes containing 0.7% agar type A (Sigma-Aldrich Inc., St. Louis, MO, USA). The plates were stored in the dark for 2 days at 4 °C to induce germination and were then transferred to the greenhouse at a photoperiod of 16 h light, 28 °C/8 h dark, 15 °C. At the cotyledon developmental stage, single seedlings were transplanted into a 2 cm diameter pot system and grown for about 3 weeks, before 200−250 uniform plants from each population were transplanted as single plants into 8 cm diameter plastic pots containing a peat/vermiculite mixture (Fafard 2B Mix, Agawam MA, USA). *A. tuberculatus* used for all further experiments was similarly cultivated using 4.5 cm Fertilpots containing a peat/loam 1:1 soil mixture. Plants were grown in the greenhouse at a photoperiod of 16 h light, 22 °C/8 h dark, 14 °C, with a light intensity of at least 220 $\mu$mol $m^{-2}$ $s^{-1}$ (Phillips Son-T AGRO). Watering and fertilization with 0.4% Wuxal Super solution (Wilhelm Haug GmbH & Co. KG, Ammerbuch, Germany) were performed as necessary to maintain vigorous plant growth.

**Response to Glyphosate.** A dose response study was performed to verify the previous reports of glyphosate resistance of the different *A. tuberculatus* populations. The dose response relationship was established according to described methods.[42−45] For each population plants of uniform size and appearance were selected, and nine plants were treated with each glyphosate dose. All populations were treated together when they reached the growth stage defined as BBCH 16[46] to allow unbiased comparisons. Thirteen increasing doses of glyphosate [0, 22.5, 45, 90, 180, 360, 540, 720, 1080, 1440, 2880, 5760, 11520 g ae $ha^{-1}$ formulated as Roundup Weathermax, 660 g ae $L^{-1}$ glyphosate (Monsanto Co., St. Louis, MO, USA)] containing additional nonionic surfactant (0.5% v/v Activator 90, Loveland Industries Inc., Greeley, CO, USA) were applied using a stationary sprayer outfitted with Teejet 8001 nozzles at 280 kPa and a spray volume of 200 L $ha^{-1}$. The fresh weight of the above-ground plant material of each plant was determined 19 days after treatment (DAT).

Dose response curves based on fresh weight and shikimic acid assays were determined using the statistical program R and the drc package to calculate the four-parameter sigmoidal log−logistic dose−response model.[42,47] The calculated upper and lower limits were used in a second step to normalize raw data, allowing unbiased comparisons of dose response curves. The doses causing 50 and 90% effect on fresh weight reduction ($ED_{50}$ and $ED_{90}$, respectively) were calculated for each population. The resistance factor (R/S) for each population was calculated as the ratio between $ED_{50}$ value of the putative resistant population and the susceptible *A. tuberculatus* control population.

Shikimic acid content after glyphosate treatment is an early indicator for glyphosate-mediated plant injury,[17,23] so a shikimic acid accumulation dose response model was evaluated as a potential method to characterize the *A. tuberculatus* populations. Therefore, shikimic acid accumulation was determined 4 DAT in leaf disks from plants used to establish the glyphosate dose response experiments. Four 0.4 cm diameter leaf disks of the youngest fully expanded leaf of each plant were harvested, except for plants treated with 11520 g ae $ha^{-1}$ as these were severely stunted. The color reaction was measured at 380 nm on a 96-well plate reader (Biotek Synergy 4, Winooski, VT, USA) using previously described methods.[18,19]

**Glyphosate Absorption and Translocation.** Alterations in glyphosate absorption and translocation were evaluated in nine plants per population and time point in the *A. tuberculatus* populations MO-S, MO-R1, and IL-R. The application solution was adjusted to a final rate of 720 g ae $ha^{-1}$ glyphosate (Roundup Ultramax; 450 g ae $L^{-1}$ glyphosate; Monsanto Co., St. Louis, MO, USA) and radiolabeled glyphosate (phosphonomethyl-[$^{14}$C]) solution (50 mCi $mmol^{-1}$, American Radiolabeled Chemicals, St. Louis, MO, USA). Twelve 0.5 $\mu$L droplets, each containing 1000 Bq $\mu L^{-1}$, were spotted onto the youngest fully expanded leaf. The treated plants were moved to a growth chamber (model 1401, Rubarth Apparate GmbH, Laatzen, Germany) with a photoperiod of 16 h light and a light intensity of 120 $\mu$mol $m^{-2}$ $s^{-1}$ (Iwasaki Eye MT150D, Middlesex, UK) at a temperature of 25/18 °C day/night and a constant relative humidity of 70%.

To determine the glyphosate absorption, treated leaves were removed from the plant 0, 8, 24, 48, 72, and 96 h after treatment (HAT). They were rinsed for 20 s in 3 mL of 0.1% Triton X-100 and 4% methanol, and radioactivity was measured using a scintillation counter (the scintillation liquid was Rotiszint Eco Plus, Carl Roth GmbH + Co. KG, Karlsruhe, Germany; the scintillation counter was a Packard 2000CA TriCarb Liquid Scintilation counter, Downers Grove, IL, USA).

Glyphosate translocation was quantitatively measured by combusting different plant parts. The harvest time points were set at 0, 8, 24, 48, 72, and 96 HAT for the populations MO-S and MO-R1. The IL-R population had the same harvest time points except for 96 HAT, which could not be collected due to technical problems. Soil was washed off the roots at harvest, and plants were sectioned into roots, shoot above treated leaf, treated leaf, and remaining shoot material. The sectioned plant material was dried at 60 °C and oxidized using a biological sample oxidizer (OX-500, R. J. Harvey Instrument Corp., Hillsdale, NJ, USA) and released $^{14}CO_2$ was determined (Packard 2000CA TriCarb liquid scintillation counter). Values for absorption and translocation were calculated as percent of total applied radioactivity. Glyphosate absorption and translocation were analyzed using nonlinear regression in the R statistical program.[48]

Table 1. $ED_{50}$ and $ED_{90}$ Values and R/S Ratios of *A. tuberculatus* Populations ($n$ = 9) to Glyphosate; Dose Response Relationship in Shikimic Acid Concentration 4 DAT and Fresh Weight Assessment 19 DAT[a]

| | shikimate accumulation, 4 DAT | | fresh weight, 19 DAT | | | |
|---|---|---|---|---|---|---|
| population ratio | $ED_{50}$ (g ae $ha^{-1}$) | R/S ratio | $ED_{50}$ (g ae $ha^{-1}$) | 95% confidence interval | R/S ratio | $ED_{90}$ (g ae $ha^{-1}$) |
| IL-R | 192 | 2.8 a | 420 | 349−491 | 6.8 a | 1363 |
| MO-R1 | 419 | 6.2 b | 317 | 234−399 | 5.2 a | 1728 |
| MO-R2 | 224 | 3.3 ab | 410 | 313−506 | 6.7 a | 1096 |
| MO-R3 | 393 | 5.8 b | 411 | 294−524 | 6.7 a | 2021 |
| MO-R4 | 419 | 6.2 b | 405 | 306−503 | 6.7 a | 1420 |
| MO-R5 | 310 | 4.6 ab | 460 | 335−584 | 7.5 a | 2969 |
| MO-S | 68 | 1 c | 61 | 46−76 | 1 b | 291 |

[a]Means with the same letter are not statistically different ($P$ = 0.05).

To visualize differences in glyphosate transport, autoradiographs were obtained at 8, 18, 48, and 96 HAT. Treated plants of each population and at each time point including the washed leaf and rinsed root were fixed on a paper sheet (20 × 40 cm) and pressed until complete dryness. The dry plants were exposed to a phosphoimaging film (Fujifilm BAS-MS-2040) for 48 h before image detection (BAS-reader 1000, Fujix, Japan). Background reduction and image evaluation were performed with AIDA Image Analyzer software 4.19 (Raytest, Germany).

***EPSPS* Target-Site Detection.** Pyrosequencing was used to detect target-site mutations at G101, T102, or P106 in the *A. tuberculatus* *EPSPS* gene sequence with modifications.[49] The DNA was purified with the Qiagen DNeasy Plant mini kit in eight biological and three technical replicates each. For the sequencing reactions a 195 bp long DNA fragment was amplified using the forward primer gly.a.3f (5′ ATGTTGGACGCTCTCAGAACTCTTGGT 3′) and the 5′-biotinylated reverse primer gly.a.4r (BT - 5′ TGAATTTCCTCCAGCAACGGCAA 3′) in a polymerase chain reaction (PCR). The PCR conditions were 15 min of preincubation at 95 °C, followed by 45 cycles at 94 °C denaturating step (30 s), 55 °C annealing temperature (40 s), 70 °C elongation (40 s)m and a final extension step for 10 min at 70 °C (Eppendorf Mastercycler ep Thermal Cyclers, Hamburg, Germany). The primer gly.pyro.a1.1 (5′ GGAAATGC(AT)GGAACAGCGATGCG 3′) was used to sequence the coding sites G101 and T102, whereas the primer gly.pyro.a1.2 (5′ CAACTTTT(CT)CTTGGAAATGC 3′) was used to sequence the coding site P106 in a Pyromark PSQ 96 device. Evaluation was in all cases done with the manufacturer's software (Qiagen, Hilden, Germany).

**Relative Genomic *EPSPS* Gene Copy Number.** The *EPSPS* gene copy number in the *A. tuberculatus* genomic DNA was determined as previously described with minor modifications.[34] Due to the high homology of *EPSPS* and *ALS* genes of both closely related species, the same quantitative PCR (qPCR) method was used to determine the relative *EPSPS* gene copy number in 16 *A. tuberculatus* plants of each population. The DNA was purified using the Promega Wizard Magnetic 96 DNA Plant system kit (Madison, WI, USA) according to manufacturer's instructions. The comparison was done at a level of 12 times the standard deviation of the background by using the model of crossing points with the manufacturer's software (Roche LightCycler 480 1.5, Mannheim, Germany). The difference between the *ALS* gene and the *EPSPS* gene was expressed as relative *EPSPS* gene amount in relation to the *ALS* reference gene ($2^{\Delta Cp}$).[34,50,51] A calibration curve was performed using increasing DNA concentrations to determine the amplification efficacy of each primer combination.

***EPSPS* Expression Characteristics.** Plants at four-leaf stage, BBCH 14, were sprayed with 720 g ae $ha^{-1}$ glyphosate (Roundup Ultramax, 450 g ae $L^{-1}$ glyphosate) using a single-nozzle overhead track sprayer outfitted with Teejet 8001 nozzle at 280 kPA and a spray volume of 200 L $ha^{-1}$. Plant samples from the shoot tip were taken directly before treatment and at 4, 8, 24, and 48 HAT from both treated and untreated plants maintained under identical conditions.[52] RNA was purified with a RNeasy mini kit (Qiagen, Hilden, Germany) according to the manufacturer's instruction, followed by DNase I (Invitrogen, Carlsbad, CA, USA) treatment. The cDNA synthesis was performed using the Superscript kit (Invitrogen). The expression of *EPSPS* and *ALS* mRNA was determined using the previously described method.[34] A 242 bp long fragment from the *Actin* gene was used as an additional reference gene. The *Actin* gene fragment was amplified with the primer pair act.a.1f (5′ GACTCTGGTGATGGTGTGAGTC 3′) and act.a.2r (5′ GAGCTGCTCTTGGCAGTCTC 3′). Evaluation was done as previously described with the manufacturer's software (Roche LightCycler 480 1.5). The obtained crossing points of the *Actin* fragment were tested for statistical differences in all time points with a $t$ test ($P$ = 0.05) for the populations MO-S, MO-R1, and IL-R and for all time points. Because no changes in expression were observed, the *Actin* gene was used as a stably expressed reference gene. The values obtained for the *Actin* gene were tested for their homogeneity by ANOVA ($t$ test). The relative expression values of the *EPSPS* and *ALS* genes were given by the ratio of their respective absolute values with those obtained for the *Actin* gene. Significant differences between the relative *ALS* and *EPSPS* gene expression values at different time points were tested by ANOVA at a probability value of $P$ = 0.05 (Sigmaplot 11.0, Erkrath, Germany).

**EPSPS Enzyme Activity.** The EPSPS enzyme activity was measured in crude extracts prepared from the youngest leaves and shoot tip of actively growing plants according to previously described methods with minor modifications.[53] The final extract was mixed with 20% glycerol (v/v) and stored at −20 °C. The protein concentration was determined in a Bradford assay (Bio-Rad, Hercules, CA, USA), and bovine serum albumin (BSA) (Sigma-Aldrich Inc., St. Louis, MO, USA) was used to establish the calibration curve.[54] Results are given as micrograms of BSA equivalent protein. The EPSPS activity was measured by monitoring the $P_i$ release of the crude protein extract.[34] The color reaction was continuously measured at 360 nm in a Fluostar Optima 96-well plate reader to determine EPSPS enzyme parameters. The S-3-P concentration was held constant at 0.5 mM while the PEP concentration was varied (0, 0.016, 0.031, 0.0625, 0.125, 0.25, and 0.5 mM PEP). The experiments were conducted with two technical and at least two biological replicates of each population (IL-R and MO-S). A calibration curve was used to express the enzyme activity as micromoles $P_i$ released. Enzyme kinetic parameters were determined using the linear Lineweaver−Burk model[55] and Sigmaplot 11.0. A probability value of $P < 0.05$ was chosen to determine significant differences in a $t$ test between populations (SigmaPlot 11.0).

## RESULTS

**Response to Glyphosate.** The fresh weight of treated plants of *A. tuberculatus* populations IL-R, MO-R1, MO-R2, MO-R3, MO-R4, and MO-R5 assessed 19 DAT (Supporting Information Figure SI1) showed $ED_{50}$ values between 317 and 460 g ae $ha^{-1}$, whereas the $ED_{50}$ of the susceptible population MO-S was 61 g ae $ha^{-1}$ (Table 1). None of the susceptible plants would survive labeled glyphosate rates, as their $ED_{90}$ values were below 300 g ae $ha^{-1}$ glyphosate (Table 1). The resistant populations were clustered together with average $ED_{50}$ values of 396 g ae $ha^{-1}$ and a resistance factor of >5-fold. Some

Table 2. Maximum Glyphosate Foliar Absorption and Translocation ($A_{max}$) in Percentage of Applied Radioactivity and Time Required To Reach 50% of the $A_{max}$ Value ($T_{50}$) in the Different Plant Tissues Assessed in the *A. tuberculatus* Populations MO-S, MO-R1, and IL-R ($n$ = 9; Standard Errors in Parentheses)[a]

| | IL-R | | | | MO-R1 | | | | MO-S | |
|---|---|---|---|---|---|---|---|---|---|---|
| | $A_{max}$ | | $T_{50}$ (h) | | $A_{max}$ | | $T_{50}$ (h) | | $A_{max}$ | $T_{50}$ (h) |
| **Glyphosate Absorption of Treated Leaf** | | | | | | | | | | |
| absorption | 58.2 (3.17) | ns | 28.2 (9) | ns | 69.1 (4) | ns | 60.8 (14.2) | ns | 59.4 (3.8) | 51.9 (14.8) |
| **Glyphosate Translocation Throughout Plant** | | | | | | | | | | |
| applied leaf | 33.6 (3.4) | ns | 29.2 (15.6) | ns | 46.3 (3.6) | ns | 68.4 (20.9) | ns | 37.4 (3.1) | 47 (18.2) |
| shoot | 3.8 (0.9) | ns | 57.8 (49.3) | ns | 4.3 (0.8) | ns | 87.1 (55.2) | ns | 6 (1.6) | 158.3 (121.3) |
| root | 0.6 (0.2) | ns | 0.5 (14.6) | ns | 0.7 (0.1) | ns | 0.6 (10.8) | ns | 0.6 (0.1) | 0.5 (13.3) |
| shoot tip | 5.1 (3) | ns | 447.9 (405.7) | ns | 5.4 (NA) | NA | 549.3 (NA) | NA | 1.6 (0.3) | 74 (54.6) |

[a]Data fitted to the rectangular hyperbolic model. No significant statistical differences (ns) were observed between MO-R1 and IL-R compared to MO-S. NA = not applicable.

plants within these populations survived dose rates of 720 g ae $ha^{-1}$ glyphosate, as their $ED_{90}$ values were between 1350 and 3000 g ae $ha^{-1}$ glyphosate.

**Glyphosate Absorption and Translocation.** Total average recovery of applied radioactivity was 90% in the glyphosate absorption and translocation experiments. Approximately 62.2 ± 2.2% of the total applied radioactivity was the maximum absorption of the *A. tuberculatus* populations MO-S, MO-R1, and IL-R (Table 2; Supporting Information Figure SI2). On average 46.4 ± 7.5 h was necessary to absorb 50% of the maximum amount of radioactivity. No significant differences in absorption were observed between glyphosate-susceptible and -resistant populations at any time points analyzed.

Radioactivity was detected in all plant parts 8 HAT, and concentration increased with time (Supporting Information Figure SI3). Translocation occurred at a nearly constant rate over the 96 h time frame, especially into the root. There were no differences between populations in total amount of glyphosate translocated to the different plant tissues among the investigated populations MO-S, MO-R1, and IL-R (Table 2; Supporting Information Figure SI3). The average maximum amounts of translocation into the root, shoot, and shoot tip and in the applied leaf were 0.65 ± 0.1, 4.8 ± 0.6, 3.1 ± 0.7, and 40 ± 2.1% of total applied radioactivity, respectively. There were also no significant differences in the rate of translocation. The times to reach 50% of the maximum amount of radioactivity ($T_{50}$) in the root, shoot, shoot tip, and applied leaf were 0.55 ± 7.1, 104 ± 43, 242 ± 113.3, and 52 ± 11.7 h after application, respectively. Significant differences among populations were solely obtained from the calculation of the time needed to reach 90% of the maximum translocated amount ($T_{90}$) in the shoot tip. The glyphosate-resistant populations MO-R1 and IL-R absorbed significantly more radioactivity in the shoot tip 72 HAT (2.6 ± 0.6 and 2.3 ± 0.3%, respectively) than the glyphosate-susceptible population MO-S (1.5 ± 0.4%). At $T_{50}$ no significant differences between resistant and susceptible populations were found in translocation to the shoot tip (Table 2).

The autoradiographs in Figure 1 revealed no differences in the translocation of $^{14}$C-labeled glyphosate throughout susceptible and resistant plants. Radioactivity was distributed throughout the plant by 8 HAT, with the highest radioactivity found in the youngest and most actively growing plant parts. The amount of radioactivity in older and less active plant parts and the overall amount in each tissue increased with time. Additionally, no localized differences in directed translocation into leaf margins or into any specific plant organs were observed in these glyphosate-resistant *A. tuberculatus* populations.

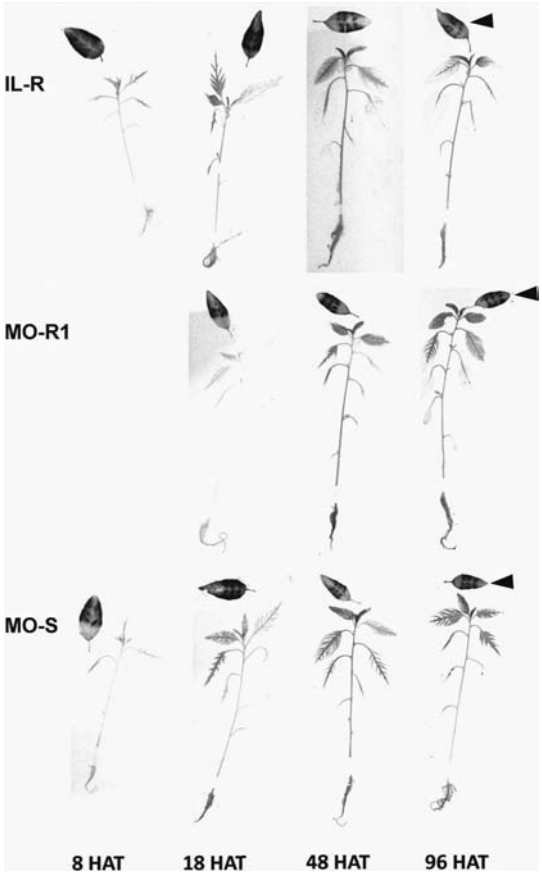


**Figure 1.** Phosphorimaging visualization of $^{14}$C-glyphosate translocation in *A. tuberculatus* populations IL-R, MO-R1, and MO-S at 8, 18, 48, and 96 HAT. Arrow heads indicate the treated leaves at 96 HAT, rinsed at harvest time and dried separately. Each plant is representative of five plants tested at each time point. Increasing color intensity indicates a higher amount of radioactivity within the plant material.

**Mutations in the *EPSPS* Coding Sequence.** Using pyrosequencing to genotype multiple individuals from each glyphosate-resistant *A. tuberculatus* population, no DNA sequence mutations were found in any individual that altered the predicted EPSPS amino acid sequence at position G101, T102, or P106 (data not shown).

***EPSPS* Gene Amplification.** Comparable amounts of *EPSPS* and *ALS* genes in the genome of the susceptible *A. tuberculatus* population MO-S were measured with 1.1 ± 0.4 relative *EPSPS* gene copies (Figure 2). The glyphosate-resistant plants had on average a higher amount of *EPSPS* genes in their genome, from 2- to 8-fold (Figure 2). IL-R had the highest *EPSPS* gene amplification with on average 7.1 ± 0.84 relative *EPSPS* genes. The populations collected in Missouri had on average 2.4 ± 0.11 relative *EPSPS* genes in the genome. The highest gene amplification found in a single resistant plant of the Missouri populations was 6 times the *ALS* gene, but each population also contained some individuals bearing an equal *EPSPS* and *ALS* copy number.

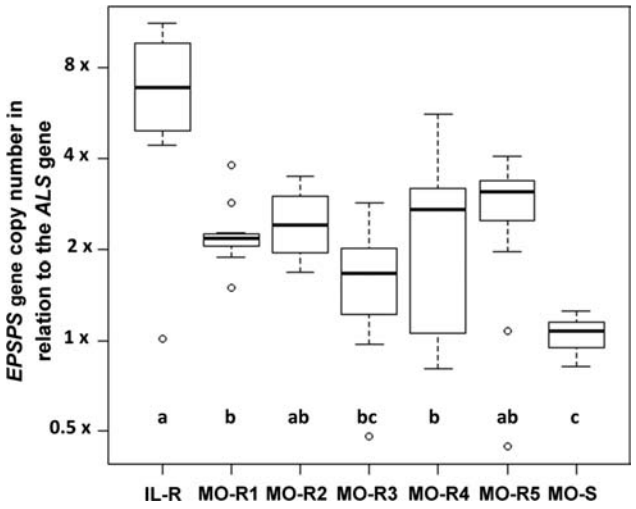


**Figure 2.** Genomic *EPSPS* gene copy number in *A. tuberculatus* populations IL-R, MO-R1, MO-R2, MO-R3, MO-R4, MO-R5, and MO-S relative to the *ALS* gene. Individual plants were not selected for their glyphosate resistance before *EPSPS* gene copy number measurement ($n$ = 16); IL-R = 7.1 ± 0.84 relative *EPSPS* genes; MO-R1 = 2.3 ± 0.15; MO-R2 = 2.5 ± 17; MO-R3 = 1.7 ± 0.15; MO-R4 = 2.7 ± 0.4; MO-R5 = 2.9 ± 0.23; and MO-S = 1.1 ± 0.04. Different letters indicate significant differences among populations ($P$ = 0.05).

To study whether amplified *EPSPS* genes were expressed differently after glyphosate application, the *EPSPS* mRNA expression in untreated plants was compared to those of plants treated with the recommended field rate of 720 g ae ha$^{-1}$ glyphosate. The *Actin* gene and the *ALS* gene were tested for their stable expression among time points and individual plants and found to be suitable as stably expressed reference genes. The *EPSPS* mRNA expression was significantly higher in both *A. tuberculatus* populations MO-R1 and IL-R compared to MO-S ($P$ = 0.05), but there were no significant *EPSPS* expression changes at any time point within a population (Table 3).

**EPSPS Enzyme Activity.** The EPSPS $K_m$ (app) (PEP) values of MO-S and IL-R were 58.49 and 59.92 μM PEP, respectively (Table 4). The lack of difference suggests that no alterations in the EPSPS amino acid sequence influencing the enzyme activity occur in the IL-R population. Significant differences were found in the $V_{max}$ values with a 2.4 times higher $P_i$ release in IL-R ($V_{max}$ of 0.15 μmol $P_i$ s$^{-1}$) than in MO-S ($V_{max}$ of 0.64 μmol $P_i$ s$^{-1}$). Differences were also obtained in the total EPSPS activity per equivalent total protein present in crude extracts. The $K_{cat}$ value of the resistant population IL-R was 3.7 times higher than the $K_{cat}$ value of the susceptible population MO-S, whereas the $K_{cat}$ values of MO-R1, MO-R3, and MO-R4 were about 2 times higher (Table 4). These differences are due to the higher EPSPS enzyme quantity present in the total extract.

## DISCUSSION

**Glyphosate Resistance of the *A. tuberculatus* Populations.** Glyphosate resistance was confirmed in the tested *A. tuberculatus* populations IL-R, MO-R1, MO-R2, MO-R3, MO-R4, and MO-R5 with an average RF of 6.5 ± 0.33, which is at a lower level than found in other glyphosate-resistant *A. tuberculatus* or *A. palmeri* populations.[10,13,33] The 2-fold higher sensitivity of the susceptible population MO-S in comparison to previous results for the same population[10] might explain part of this difference and shows also the impact of environmental conditions on plant susceptibility to herbicides, including glyphosate. Nevertheless, with an $ED_{90}$ value of 1096−2969 g ae ha$^{-1}$ several plants of the populations MO-R1, MO-R2, MO-R3, MO-R4, MO-R5, and IL-R will survive the recommended field rate of 720 g ae ha$^{-1}$ glyphosate and will be able to set viable seeds. Ongoing glyphosate selection pressure will most probably enable the further evolution of higher resistance factors in *A. tuberculatus*.

The accumulation of shikimic acid in plant tissue after glyphosate treatment can be used for an early determination of glyphosate efficacy.[17,23] In the present work shikimic acid content indicated the populations could be grouped according to their response to glyphosate into two different groups. The susceptible and resistant populations were clearly separated by the $ED_{50}$ values, with all resistant populations at least 2.8-fold more resistant than the susceptible population MO-S. This method is suitable to distinguish between resistant and susceptible plants. Also, the $ED_{50}$ values and the R/S factors calculated from the shikimic acid levels of the population MO-S and the different MO-R populations provide a reasonable correlation with the fresh weight data assessed 19 DAT. In comparison, the weaker correlation between the shikimic acid response after glyphosate treatment and the fresh weight data

**Table 3. *EPSPS* Gene Expression Expressed as Fold-Change Relative to the *ALS* Gene (Standard Error in Parentheses) in Individuals ($n$ = 4) of the *A. tuberculatus* Populations IL-R, MO-R1, and MO-S at Different Time Points after Glyphosate Treatment (720 g ae ha$^{-1}$)[a]**

| | 0 HAT | 4 HAT | | 8 HAT | | 24 HAT | | 48 HAT | |
|---|---|---|---|---|---|---|---|---|---|
| | untreated | untreated | treated | untreated | treated | untreated | treated | untreated | treated |
| IL-R | 5.5 (1.3) | 4.3 (0.7) | 4.7 (0.73) | 6.2 (0.42) | 5.6 (1.4) | 6.8 (0.79) | 6.6 (0.78) | 7.7 (1.46) | 7.9 (1.61) |
| MO-S | 1.0 (0.08) | 1.0 (0.09) | 1.0 (0.13) | 1.0 (0.08) | 1.0 (0.04) | 1.0 (0.04) | 1.1 (0.18) | 1.0 (0.12) | 1.0 (0.17) |
| MO-R1 | 4.5 (0.6) | 2.1 (0.14) | 2.7 (0.4) | 2.6 (0.23) | 2.2 (0.37) | 2.4 (0.3) | 3.6 (1.2) | 3.5 (0.49) | 2.7 (0.53) |

[a]Individuals were not selected for glyphosate resistance prior to *EPSPS* expression measurement.

Table 4. Native EPSPS Protein Activity of Plants of the *A. tuberculatus* Populations MO-S, IL-R, MO-R1, MO-R3, and MO-R4[a]

| | MO-S | IL-R | MO-R1 | MO-R3 | MO-R4 |
|---|---|---|---|---|---|
| $K_M$(app) (PEP) ($\mu$M) | 58.49 ns | 59.92 ns | nd | nd | nd |
| $V_{max}$($\mu$mol $P_i$ $s^{-1}$) | 0.064 a | 0.15 b | nd | nd | nd |
| $K_{cat}$ ($\mu$mol $P_i$ $\mu g^{-1}$ protein) | 11.43 a | 41.25 b | 22.5 c | 22.75 c | 21.75 c |

[a]Plants used for the enzyme extraction were not selected for their glyphosate resistance. Values are the mean of two biological replications with two technical replicates each. Samples with different letters are significantly different ($P = 0.05$); ns, not significant; nd, not determined. Crude protein is given in $\mu$g BSA equivalent.

for the IL-R population is probably reflecting bigger genetic differences to the susceptible population MO-S. Determining shikimic acid levels using a dose response provides an early separation of resistant and susceptible individuals, but this approach is not suitable for early and exact prediction of $ED_{50}$ values or of R/S ratios between different resistant *A. tuberculatus* populations. The exact accumulation of shikimate is known to vary between species and populations with different resistance mechanisms.[13,56,57]

**Absorption and Translocation of $^{14}$C-Glyphosate.** Because altered glyphosate translocation is a common glyphosate resistance mechanism in some weeds, translocation patterns were evaluated to clarify whether this mechanism contributes to glyphosate resistance of *A. tuberculatus* populations.[58] No spatial or temporal differences in glyphosate translocation were observed in the *A. tuberculatus* populations analyzed. Slightly higher glyphosate translocation to the shoot tip occurred in glyphosate-resistant populations; however, the higher translocation is likely due to herbicide injury in the susceptible biotype, resulting in what is known as self-limiting translocation.[59] Previous research reported similar absorption during the first 50 HAT in a glyphosate-susceptible *A. tuberculatus* population,[60] which is comparable to data reported here. Glyphosate absorption is within the common range for other species, such as *C. canadensis*.[61] Glyphosate translocation observed in these *A. tuberculatus* populations was similar to more typical patterns of glyphosate translocation,[22,60,62] and differences in absorption or translocation like those described in glyphosate-resistant *C. canadensis*, *S. halepense*, *L. multiflorum*, and *L. rigidum* populations were not found.[26−30] Although reduced translocation has been reported in an *A. tuberculatus* population from Mississippi,[13] our data clearly demonstrated that glyphosate resistance in these *A. tuberculatus* populations is not based on reduced absorption. This diversity in resistance mechanisms among different populations of the same species has been frequently described.[24]

***EPSPS* Gene Amplification.** The *A. tuberculatus* populations MO-R1, MO-R2, MO-R3, MO-R4, MO-R5, and IL-R were resistant to glyphosate in the dose response study; however, on the basis of R/S values resistance was lower than the glyphosate-resistant *A. palmeri* population from Georgia, USA.[33,63] Because *A. palmeri* and *A. tuberculatus* are closely related species and are able to produce fertile crosses, *EPSPS* gene amplification was also evaluated in these populations.[64−66] We found evidence that the glyphosate-resistant *A. tuberculatus* populations evolved *EPSPS* gene amplification, similar to previous reports for multiple species with *EPSPS* gene copy increases from 2−10-fold up to 40−100-fold.[3,34,35,57,67−69] Despite differences in *EPSPS* copy number, all glyphosate-resistant *A. tuberculatus* populations had similar glyphosate resistance based on fresh weight assessment 19 DAT. *EPSPS* expression in IL-R, MO-R1, or MO-S was not induced or silenced by glyphosate treatment, but the *EPSPS* transcript levels showed the same differences between the resistant and susceptible populations as found in genomic DNA. A previous paper hypothesized that glyphosate resistance in *A. tuberculatus* could be determined by a polygenic event.[70] A positive correlation between *EPSPS* gene copy number and increasing glyphosate resistance level has been reported in *A. palmeri*[35,71] and *L. multiflorum*,[57] consistent with the current results showing gene dosage effects of additional *EPSPS* gene copies.

***EPSPS* Enzyme Kinetics.** Previous results showed higher EPSPS protein content in a glyphosate-resistant *A. palmeri* population by immunoblotting and a higher EPSPS activity during the determination of $IC_{50}$ values for glyphosate.[34,35] The EPSPS enzyme activity was measured to test resistant *A. tuberculatus* plants for a higher EPSPS enzyme content relative to susceptible. Glyphosate inhibits EPSPS as a competitive inhibitor of PEP.[72] Higher $K_m$(app) (PEP) values indicate a lower enzyme affinity to its substrate PEP and decreases EPSPS activity at lower PEP concentrations.[72] Glyphosate-resistant plant EPSPS enzymes with target-site mutations typically have increased $K_m$(app) (PEP) values in comparison to wild-type enzymes.[72] The $K_m$(app) (PEP) values were determined in the *A. tuberculatus* populations MO-S and IL-R. The values, although measured in a crude enzyme extract, are comparable to published values (e.g., *Corydalis sempervirens* and *Zea mays*).[41,73] They are about 10-fold higher than those published for *Sorghum bicolor*, *Escherichia coli*, and *Pseudomonas aeruginosa* and also for the EPSPS of *Eleusine indica* and *Zea mays* expressed in *E. coli*.[25,74,75] As the $K_m$ values between the protein extracts IL-R and MO-S plants were not significantly different, it can be hypothesized that the EPSPS enzyme sequence therefore contained no mutations influencing affinity to PEP, the competitive substrate of glyphosate. In addition, no known resistance-endowing EPSPS mutations[76] were found using pyrosequencing. A different *A. tuberculatus* population was reported with a P106S mutation,[13] again demonstrating that different populations of the same species may have different resistance mechanisms.[24]

Whereas no significant differences were obtained between the $K_m$(app) (PEP) values between resistant and susceptible populations, the $V_{max}$ and $K_{cat}$ values were significantly different between resistant and susceptible individuals. Because the $V_{max}$ and $K_{cat}$ values were measured at an equal protein concentration, but not at an equal EPSPS concentration, among populations, the higher $V_{max}$ and $K_{cat}$ values indicate a higher proportion of EPSPS in the protein pool of resistant plants. Increases of 2.3 and 3.7 times in $V_{max}$ and $K_{cat}$ values, respectively, were measured between resistant and susceptible *A. tuberculatus* plants. These values, from a naturally evolved plant population, are lower than those reported for the same mechanism selected in cell culture experiments, for example, a 40-fold increase in EPSPS activity in *C. sempervirens*.[41] However, the obtained values are already high enough to mediate plant glyphosate resistance in the field. The R/S ratio

of $V_{max}$ and $K_{cat}$ values is slightly lower than the R/S ratio of *EPSPS* gene expression results. This slight reduction could be caused by regulatory mechanisms of protein translation or turnover.

In plants, the variability of protein levels in relation to the genome or the transcriptome is unknown.[77,78] In mouse cells, mRNA levels can explain about 40% of the variability in the protein level.[77] In *A. tuberculatus* this relationship is unknown. Nevertheless, the different $V_{max}$ and $K_{cat}$ values indicate an increased amount of active EPSPS in the protein pool of resistant plants and emphasize gene amplification as the glyphosate resistance mechanism in *A. tuberculatus* populations. The results of this work strongly suggest that *EPSPS* gene amplification and the higher content and activity of the EPSPS enzyme in glyphosate-resistant plants are the main mechanisms involved in the glyphosate resistance in the tested *A. tuberculatus* populations.

In conclusion, we have compared glyphosate susceptibility of several *A. tuberculatus* populations from Missouri and Illinois, USA. Glyphosate resistance was observed in each population, either confirming previous reports[10] or reported for the first time. Physiological, biochemical, and molecular approaches showed that the resistance mechanisms of altered glyphosate absorption and translocation and target-site mutations in the *EPSPS* coding sequence could be excluded as the cause of the observed glyphosate resistance in these populations. We showed that *EPSPS* gene amplification occurred in several of these *A. tuberculatus* populations from the areas most affected by resistance, and the amplified *EPSPS* genes resulted in higher *EPSPS* mRNA expression and higher EPSPS protein activity. On the basis of these results we propose that glyphosate resistance in these *A. tuberculatus* populations is mainly based on amplification of the *EPSPS* gene.

## ■ ASSOCIATED CONTENT

### Supporting Information

Name, origin, and year of collection for *A. tuberculatus* populations; glyphosate dose response data; glyphosate absorption and translocation data. This material is available free of charge via the Internet at http://pubs.acs.org.

## ■ AUTHOR INFORMATION


### Corresponding Author

*(R.B.) Phone: +49 69 305 14887. Fax: +49 69 305 34676. E-mail: roland.beffa@bayer.com.


### Notes

The authors declare no competing financial interest.

## ■ ACKNOWLEDGMENTS

The seeds of the different *A. tuberculatus* populations were kindly provided by B. Young, A. Hager, A. York, and K. Bradley for further work.

## ■ REFERENCES


(1) Costea, M.; DeMason, D. A. Stem morphology and anatomy in *Amaranthus* L. (Amaranthaceae) − taxonomic significance. *J. Torrey Bot. Soc.* **2001**, *128*, 254−281.

(2) Horak, M. J.; Loughin, T. M. Growth analysis of four *Amaranthus* species. *Weed Sci.* **2000**, *48*, 347−355.

(3) Tranel, P. J.; Riggins, C. W.; Bell, M. S.; Hager, A. G. Herbicide resistances in *Amaranthus tuberculatus*: a call for new options. *J. Agric. Food Chem.* **2011**, *59*, 5808−5812.

(4) Sellers, B. A.; Smeda, R. J.; Johnson, W. G.; Kendig, J. A.; Ellersieck, M. R. Comparative growth of six *Amaranthus* species in Missouri. *Weed Sci.* **2003**, *51*, 329−333.

(5) Costea, M.; Weaver, S. E.; Tardif, F. J. The biology of invasive alien plants in Canada. 3. *Amaranthus tuberculatus* (Moq.) Sauer var. *rudis* (Sauer) Costea & Tardif. *Can. J. Plant Sci.* **2005**, *85*, 507−522.

(6) Steckel, L. E.; Sprague, C. L. Common waterhemp (*Amaranthus rudis*) interference in corn. *Weed Sci.* **2004**, *52*, 359−364.

(7) Bell, M. S.; Hager, A. G.; Tranel, P. J. Multiple resistance to herbicides from four site-of-action groups in waterhemp (*Amaranthus tuberculatus*). *Weed Sci.* **2013**, *61*, 460−468.

(8) Foes, M. J.; Liu, L. X.; Tranel, P. J.; Wax, L. M.; Stoller, E. W. A biotype of common waterhemp (*Amaranthus rudis*) resistant to triazine and ALS herbicides. *Weed Sci.* **1998**, *46*, 514−520.

(9) Heap, I. The International Survey of Herbicide Resistant Weeds; available at www.weedscience.com (accessed May 14, 2013).

(10) Legleiter, T. R.; Bradley, K. W. Glyphosate and multiple herbicide resistance in waterhemp (*Amaranthus rudis*) populations from Missouri. *Weed Sci.* **2008**, *56*, 582−587.

(11) Sprague, C. L.; Stoller, E. W.; Wax, L. M.; Horak, M. J. Palmer amaranth (*Amaranthus palmeri*) and common waterhemp (*Amaranthus rudis*) resistance to selected ALS-inhibiting herbicides. *Weed Sci.* **1997**, *45*, 192−197.

(12) Ma, R.; Kaundun, S. S.; Tranel, P. J.; Riggins, C. W.; McGinness, D. L.; Hager, A. G.; Hawkes, T.; McIndoe, E.; Riechers, D. E. Distinct detoxification mechanisms confer resistance to mesotrione and atrazine in a population of waterhemp. *Plant Physiol.* **2013**, *163*, 363−377.

(13) Nandula, V. K.; Ray, J. D.; Ribeiro, D. N.; Pan, Z.; Reddy, K. N. Glyphosate resistance in tall waterhemp (*Amaranthus tuberculatus*) from Mississippi is due to both altered target-site and nontarget-site mechanisms. *Weed Sci.* **2013**, *61*, 374−383.

(14) McCue, K. F.; Conn, E. E. Induction of shikimic acid pathway enzymes by light in suspension cultured cells of parsley (*Petroselinum crispum*). *Plant Physiol.* **1990**, *94*, 507−510.

(15) Weaver, L. M.; Herrmann, K. M. Dynamics of the shikimate pathway in plants. *Trends Plant Sci.* **1997**, *2*, 346−351.

(16) Herrmann, K. M.; Weaver, L. M. The shikimate pathway. *Annu. Rev. Plant Physiol. Plant Mol. Biol.* **1999**, *50*, 473−503.

(17) Harring, T.; Streibig, J. C.; Husted, S. Accumulation of shikimic acid: a technique for screening glyphosate efficacy. *J. Agric. Food Chem.* **1998**, *46*, 4406−4412.

(18) Cromartie, T. H.; Polge, N. D. An improved assay for shikimic acid and its use as a monitor for the activity of sulfosate. *Proc. Weed Sci. Soc. Am.* **2000**, *40*, 291.

(19) Koger, C. H.; Shaner, D. L.; Henry, W. B.; Nadler-Hassar, T.; Thomas, W. E.; Wilcut, J. W. Assessment of two nondestructive assays for detecting glyphosate resistance in horseweed (*Conyza canadensis*). *Weed Sci.* **2005**, *53*, 438−445.

(20) Pline, W. A.; Wilcut, J. W.; Duke, S. O.; Edmisten, K. L.; Wells, R. Tolerance and accumulation of shikimic acid in response to glyphosate applications in glyphosate-resistant and nonglyphosate-resistant cotton (*Gossypium hirsutum* L.). *J. Agric. Food Chem.* **2002**, *50*, 506−512.

(21) Singh, B. K.; Shaner, D. L. Rapid determination of glyphosate injury to plants and identification of glyphosate-resistant plants. *Weed Technol.* **1998**, *12*, 527−530.

(22) Lorentz, L.; Beffa, R.; Kraehmer, H. Recovery of plants and histological observations on advanced weed stages after glyphosate treatment. *Weed Res.* **2011**, *51*, 333−343.

(23) Shaner, D. L.; Nadler-Hassar, T.; Henry, W. B.; Koger, C. H. A rapid in vivo shikimate accumulation assay with excised leaf discs. *Weed Sci.* **2005**, *53*, 769−774.

(24) Powles, S. B.; Yu, Q. Evolution in action: plants resistant to herbicides. *Annu. Rev. Plant Biol.* **2010**, *61*, 317−347.

(25) Baerson, S. R.; Rodriguez, D. J.; Tran, M.; Feng, Y. M.; Biest, N. A.; Dill, G. M. Glyphosate-resistant goosegrass. Identification of a mutation in the target enzyme 5-enolpyruvylshikimate-3-phosphate synthase. *Plant Physiol.* **2002**, *129*, 1265−1275.

(26) Wakelin, A. M.; Preston, C. A target-site mutation is present in a glyphosate-resistant *Lolium rigidum* population. *Weed Res.* **2006**, *46*, 432−440.
(27) Lorraine-Colwill, D. F.; Powles, S. B.; Hawkes, T. R.; Hollinshead, P. H.; Warner, S. A. J.; Preston, C. Investigations into the mechanism of glyphosate resistance in *Lolium rigidum*. *Pestic. Biochem. Physiol.* **2002**, *74*, 62−72.
(28) Riar, D. S.; Norsworthy, J. K.; Johnson, D. B.; Scott, R. C.; Bagavathiannan, M. Glyphosate resistance in a Johnsongrass (*Sorghum halepense*) biotype from Arkansas. *Weed Sci.* **2011**, *59*, 299−304.
(29) Perez-Jones, A.; Park, K.-W.; Polge, N.; Colquhoun, J.; Mallory-Smith, C. A. Investigating the mechanisms of glyphosate resistance in *Lolium multiflorum*. *Planta* **2007**, *226*, 395−404.
(30) Feng, P. C. C.; Tran, M.; Chiu, T.; Sammons, R. D.; Heck, G. R.; CaJacob, C. A. Investigations into glyphosate-resistant horseweed (*Conyza canadensis*): retention, uptake, translocation, and metabolism. *Weed Sci.* **2004**, *52*, 498−505.
(31) Ge, X.; d'Avignon, D. A.; Ackerman, J. J. H.; Sammons, R. D. Rapid vacuolar sequestration: the horseweed glyphosate resistance mechanism. *Pest Manag. Sci.* **2010**, *66*, 345−348.
(32) Michitte, P.; De Prado, R.; Espinoza, N.; Ruiz-Santaella, J. P.; Gauvrit, C. Mechanisms of resistance to glyphosate in a ryegrass (*Lolium multiflorum*) biotype from Chile. *Weed Sci.* **2007**, *55*, 435−440.
(33) Culpepper, A. S.; Grey, T. L.; Vencill, W. K.; Kichler, J. M.; Webster, T. M.; Brown, S. M.; York, A. C.; Davis, J. W.; Hanna, W. W. Glyphosate-resistant Palmer amaranth (*Amaranthus palmeri*) confirmed in Georgia. *Weed Sci.* **2006**, *54*, 620−626.
(34) Gaines, T. A.; Zhang, W.; Wang, D.; Bukun, B.; Chisholm, S. T.; Shaner, D. L.; Nissen, S. J.; Patzoldt, W. L.; Tranel, P. J.; Culpepper, A. S.; Grey, T. L.; Webster, T. M.; Vencill, W. K.; Sammons, R. D.; Jiang, J. M.; Preston, C.; Leach, J. E.; Westra, P. Gene amplification confers glyphosate resistance in *Amaranthus palmeri*. *Proc. Natl. Acad. Sci. U.S.A.* **2010**, *107*, 1029−1034.
(35) Ribeiro, D. N.; Pan, Z.; Duke, S. O.; Nandula, V. K.; Baldwin, B. S.; Shaw, D. R.; Dayan, F. E. Involvement of facultative apomixis in inheritance of *EPSPS* gene amplification in glyphosate-resistant *Amaranthus palmeri*. *Planta* **2014**, *239*, 199−212.
(36) Bass, C.; Field, L. M. Gene amplification and insecticide resistance. *Pest Manag. Sci.* **2011**, *67*, 886−890.
(37) Goldsbrough, P. B.; Hatch, E. M.; Huang, B.; Kosinski, W. G.; Dyer, W. E.; Herrmann, K. M.; Weller, S. C. Gene amplification in glyphosate tolerant tobacco cells. *Plant Sci.* **1990**, *72*, 53−62.
(38) Shah, D. M.; Horsch, R. B.; Klee, H. J.; Kishore, G. M.; Winter, J. A.; Tumer, N. E.; Hironaka, C. M.; Sanders, P. R.; Gasser, C. S.; Aykent, S.; Siegel, N. R.; Rogers, S. G.; Fraley, R. T. Engineering herbicide tolerance in transgenic plants. *Science* **1986**, *233*, 478−481.
(39) Widholm, J. M.; Chinnala, A. R.; Ryu, J. H.; Song, H. S.; Eggett, T.; Brotherton, J. E. Glyphosate selection of gene amplification in suspension cultures of 3 plant species. *Physiol. Plant.* **2001**, *112*, 540−545.
(40) Nafziger, E. D.; Widholm, J. M.; Steinrucken, H. C.; Killmer, J. L. Selection and characterization of a carrot cell-line tolerant to glyphosate. *Plant Physiol.* **1984**, *76*, 571−574.
(41) Smart, C. C.; Johanning, D.; Muller, G.; Amrhein, N. Selective overproduction of 5-enol-pyruvylshikimic acid 3-phosphate synthase in a plant-cell culture which tolerates high-doses of the herbicide glyphosate. *J. Biol. Chem.* **1985**, *260*, 6338−6346.
(42) Knezevic, S. Z.; Streibig, J. C.; Ritz, C. Utilizing R software package for dose-response studies: the concept and data analysis. *Weed Technol.* **2007**, *21*, 840−848.
(43) Michel, A.; Peterson, J.; Dogan, M. N.; Ernst, V. Anleitung zur Anlage und Auswertung von Versuchen zur Erstellung quantitativer Dosis-Wirkungsbeziehungen am Beispiel der Wirksamkeit von Herbiziden. *Gesunde Pflanzen* **1999**, *51*, 10−19.
(44) Seefeldt, S. S.; Jensen, J. E.; Fuerst, E. P. Log-logistic analysis of herbicide dose-response relationships. *Weed Technol.* **1995**, *9*, 218−227.
(45) Ritz, C.; Streibig, J. C. Bioassay analysis using R. *J. Statist. Software* **2005**, *12*.
(46) Hess, M.; Barralis, G.; Bleiholder, H.; Buhr, L.; Eggers, T.; Hack, H.; Stauss, R. Use of the extended BBCH scale − general for the descriptions of the growth stages of mono- and dicotyledonous weed species. *Weed Res.* **1997**, *37*, 433−441.
(47) R Development Core Team (2012). *R: A Language and Environment for Statistical Computing*, version 2.15.0; R Foundation for Statistical Computing: Vienna, Austria, 2012; ISBN 3-900051-07-0, http://www.R-project.org.
(48) Kniss, A. R.; Vassios, J. D.; Nissen, S. J.; Ritz, C. Nonlinear regression analysis of herbicide absorption studies. *Weed Sci.* **2011**, *59*, 601−610.
(49) Beffa, R.; Figge, A.; Lorentz, L.; Hess, M.; Laber, B.; Ruiz-Santaella, J. P. Weed resistance diagnostic technologies to detect herbicide resistance in cereal growing areas. A review (25th German Conference on Weed Biology and Weed Control). *Julius-Kühn-Arch.* **2012**, *434*, 75.
(50) Larionov, A.; Krause, A.; Miller, W. A standard curve based method for relative real time PCR data processing. *BMC Bioinf.* **2005**, *6*, 62.
(51) Livak, K. J.; Schmittgen, T. D. Analysis of relative gene expression data using real-time quantitative PCR and the $2^{-\Delta\Delta Ct}$ method. *Methods* **2001**, *25*, 402−408.
(52) Zhu, J.; Patzoldt, W. L.; Shealy, R. T.; Vodkin, L. O.; Clough, S. J.; Tranel, P. J. Transcriptome response to glyphosate in sensitive and resistant soybean. *J. Agric. Food Chem.* **2008**, *56*, 6355−6363.
(53) Arnaud, L.; Sailland, A.; Lebrun, M.; Pallett, K.; Ravanel, P.; Nurit, F.; Tissut, M. Physiological behavior of two tobacco lines expressing EPSP synthase resistant to glyphosate. *Pestic. Biochem. Physiol.* **1998**, *62*, 27−39.
(54) Bradford, M. M. Rapid and sensitive method for quantitation of microgram quantities of protein utilizing principle of protein-dye binding. *Anal. Biochem.* **1976**, *72*, 248−254.
(55) Lineweaver, H.; Burk, D. The determination of enzyme dissociation constants. *J. Am. Chem. Soc.* **1934**, *56*, 658−666.
(56) Culpepper, A. S.; Grey, T. L.; Vencill, W. K.; Kichler, J. M.; Webster, T. M.; Brown, S. M.; York, A. C.; Davis, J. W.; Hanna, W. W. Glyphosate-resistant Palmer amaranth (*Amaranthus palmeri*) confirmed in Georgia. *Weed Sci.* **2006**, *54*, 620−626.
(57) Salas, R. A.; Dayan, F. E.; Pan, Z.; Watson, S. B.; Dickson, J. W.; Scott, R. C.; Burgos, N. R. *EPSPS* gene amplification in glyphosate-resistant Italian ryegrass (*Lolium perenne* ssp. *multiflorum*) from Arkansas. *Pest Manag. Sci.* **2012**, *68*, 1223−1230.
(58) Shaner, D. L. Role of translocation as a mechanism of resistance to glyphosate. *Weed Sci.* **2009**, *57*, 118−123.
(59) Geiger, D. R.; Bestman, H. D. Self-limitation of herbicide mobility by phytotoxic action. *Weed Sci.* **1990**, *38*, 324−329.
(60) Li, J. M.; Smeda, R. J.; Sellers, B. A.; Johnson, W. G. Influence of formulation and glyphosate salt on absorption and translocation in three annual weeds. *Weed Sci.* **2005**, *53*, 153−159.
(61) Koger, C. H.; Reddy, K. N. Role of absorption and translocation in the mechanism of glyphosate resistance in horseweed (*Conyza canadensis*). *Weed Sci.* **2005**, *53*, 84−89.
(62) Cruz-Hipolito, H.; Osuna, M. D.; Heredia, A.; Ruiz-Santaella, J. P.; De Prado, R. Nontarget mechanisms involved in glyphosate tolerance found in *Canavalia ensiformis* plants. *J. Agric. Food Chem.* **2009**, *57*, 4844−4848.
(63) Gaines, T. A.; Shaner, D. L.; Ward, S. M.; Leach, J. E.; Preston, C.; Westra, P. Mechanism of resistance of evolved glyphosate-resistant Palmer amaranth (*Amaranthus palmeri*). *J. Agric. Food Chem.* **2011**, *59*, 5886−5889.
(64) Franssen, A. S.; Skinner, D. Z.; Al-Khatib, K.; Horak, M. J.; Kulakow, P. A. Interspecific hybridization and gene flow of ALS resistance in *Amaranthus* species. *Weed Sci.* **2001**, *49*, 598−606.
(65) Gaines, T. A.; Ward, S. M.; Bukun, B.; Preston, C.; Leach, J. E.; Westra, P. Interspecific hybridization transfers a previously unknown glyphosate resistance mechanism in *Amaranthus* species. *Evol. Appl.* **2012**, *5*, 29−38.

(66) Steinau, A. N.; Skinner, D. Z.; Steinau, M. Mechanism of extreme genetic recombination in weedy *Amaranthus* hybrids. *Weed Sci.* **2003**, *51*, 696−701.
(67) Chandi, A.; Milla-Lewis, S. R.; Giacomini, D.; Westra, P.; Preston, C.; Jordan, D. L.; York, A. C.; Burton, J. D.; Whitaker, J. R. Inheritance of evolved glyphosate resistance in a North Carolina Palmer amaranth (*Amaranthus palmeri*) biotype. *Int. J. Agron.* **2012**, DOI: 10.1155/2012/176108.
(68) Mohseni-Moghadam, M.; Schroeder, J.; Ashigh, J. Mechanism of resistance and inheritance in glyphosate resistant Palmer amaranth (*Amaranthus palmeri*) populations from New Mexico, USA. *Weed Sci.* **2013**, *61*, 517−525.
(69) Nandula, V. K.; Wright, A.; Molin, W.; Ray, J.; Bond, J.; Eubank, T. *EPSPS* amplification in glyphosate-resistant spiny amaranth (*Amaranthus spinosus*): a case of gene transfer via interspecific hybridization from glyphosate-resistant Palmer amaranth (*Amaranthus palmeri*). *Pest Manag. Sci.* **2014**, DOI: 10.1002/ps.3754.
(70) Zelaya, I. A.; Owen, M. D. K. Differential response of *Amaranthus tuberculatus* (Moq ex DC) JD Sauer to glyphosate. *Pest Manag. Sci.* **2005**, *61*, 936−950.
(71) Vila-Aiub, M. M.; Goh, S. S.; Gaines, T. A.; Han, H.; Busi, R.; Yu, Q.; Powles, S. B. No fitness cost of glyphosate resistance endowed by massive *EPSPS* gene amplification in *Amaranthus palmeri*. *Planta* **2014**, *239*, 793−801.
(72) Pline-Srnic, W. Physiological mechanisms of glyphosate resistance. *Weed Technol.* **2006**, *20*, 290−300.
(73) Forlani, G.; Parisi, B.; Nielsen, E. 5-Enol-pyruvyl-shikimate-3-phosphate synthase from *Zea mays* cultured cells. *Plant Physiol.* **1994**, *105*, 1107−1114.
(74) Ream, J. E.; Steinrucken, H. C.; Porter, C. A.; Sikorski, J. A. Purification and properties of 5-enolpyruvylshikimate-3-phosphate synthase from dark-grown seedlings of *Sorghum bicolor*. *Plant Physiol.* **1988**, *87*, 232−238.
(75) Vaithanomsat, P.; Brown, K. A. Isolation and mutation of recombinant EPSP synthase from pathogenic bacteria *Pseudomonas aeruginosa*. *Process Biochem.* **2007**, *42*, 592−598.
(76) Sammons, D. R.; Gaines, T. A. Glyphosate resistance: state of knowledge. *Pest Manag. Sci.* **2014**, *70*, 1367−1377.
(77) Schwanhaeusser, B.; Busse, D.; Li, N.; Dittmar, G.; Schuchhardt, J.; Wolf, J.; Chen, W.; Selbach, M. Global quantification of mammalian gene expression control. *Nature* **2011**, *473*, 337−342.
(78) Muers, M. Gene expression: transcriptome to proteome and back to genome. *Nat. Rev. Genet.* **2011**, *12*, 518−518.

JOURNAL OF AGRICULTURAL AND FOOD CHEMISTRY

Article

pubs.acs.org/JAFC

# Hormones, Polyamines, and Cell Wall Metabolism during Oil Palm Fruit Mesocarp Development and Ripening

Huey Fang Teh, Bee Keat Neoh, Yick Ching Wong, Qi Bin Kwong, Tony Eng Keong Ooi, Theresa Lee Mei Ng, Soon Huat Tiong, Jaime Yoke Sum Low, Asma Dazni Danial, Mohd. Amiron Ersad, Harikrishna Kulaveerasingam, and David R. Appleton*

Sime Darby Technology Centre Sdn Bhd, First Floor, Block B, UPM-MTDC Technology Centre III, Universiti Putra Malaysia, Serdang, 43400 Selangor, Malaysia

Supporting Information

**ABSTRACT:** Oil palm is one of the most productive oil-producing crops and can store up to 90% oil in its fruit mesocarp. Oil palm fruit is a sessile drupe consisting of a fleshy mesocarp from which palm oil is extracted. Biochemical changes in the mesocarp cell walls, polyamines, and hormones at different ripening stages of oil palm fruits were studied, and the relationship between the structural and the biochemical metabolism of oil palm fruits during ripening is discussed. Time-course analysis of the changes in expression of polyamines, hormones, and cell-wall-related genes and metabolites provided insights into the complex processes and interactions involved in fruit development. Overall, a strong reduction in auxin-responsive gene expression was observed from 18 to 22 weeks after pollination. High polyamine concentrations coincided with fruit enlargement during lipid accumulation and latter stages of maturation. The trend of abscisic acid (ABA) concentration was concordant with $GA_4$ but opposite to the $GA_3$ profile such that as ABA levels increase the resulting elevated $ABA/GA_3$ ratio clearly coincides with maturation. Polygalacturonase, expansin, and actin gene expressions were also observed to increase during fruit maturation. The identification of the master regulators of these coordinated processes may allow screening for oil palm variants with altered ripening profiles.

**KEYWORDS:** *oil palm, Elaeis guineensis, polyamines, hormones, cell wall metabolism*

## INTRODUCTION

Fruit development is a complex process, being a combination of events in physiology, gene and protein expression, and biochemical changes toward maturation. To date, metabolite profiling of soft fleshy fruits such as strawberry,[1] peach,[2] and tomatoes[3] during ripening is more widely studied compared to oil fruits such as olive, avocado, and oil palm. This is partly because soft fruits are metabolite rich but also because of their importance to the human diet.[1−3] Studies reported on soft fruit start from the fertilized ovary through to the mature fruit stage. These studies have suggested cross-talk between hormones, polyamines, and cell wall metabolism in fruits during development and ripening.[4] The fruit of the oil palm (*Elaeis guineensis* Jacq.) is a source of two edible oils and is currently the most productive oil crop with average annual yields above 4 ton/ha. Unlike most temperate oil-bearing crops where oil is stored in the seed, the majority of palm oil is produced in the fleshy mesocarp of the fruit, with relatively less as kernel oil. The oil palm fruit consists of the exocarp-outer skin, mesocarp-outer oily fibrous layer, the endocarp layer covering the kernel seed, and the kernel itself. During the later phase of fruit development, most fruit will accumulate high levels of carbohydrates in the form of starch or sugars, whereas oil palm fruits accumulate oil, almost exclusively. Oil palm fruit is considered to be nonclimacteric since no significant ethylene synthesis occurs during the fruit ripening period, i.e., from about 120 to about 150 days post pollination.[5] The study of metabolites involved in ripening, such as phytohormones, polyamines, as well as cell wall metabolism in oil palm mesocarp, may provide useful insights into why it is so productive and lead to the development of varieties that ripen faster through the identification of key controlling genes.

Plant hormones are key regulators of many seed processes, including TAG accumulation. It is known that plant phytohormones are also involved in the control of fruit growth, which is demonstrated by the fact that these chemical compounds help to enhance cell division and promote cell expansion or enlargement during different stages of development. Fruit size is due more to cell division than cell enlargement, hence any factors that contribute to cell division will have an influence on fruit growth and final fruit size.[6] Many recent studies have shown that the phytohormone abscisic acid (ABA) plays an important role in the regulation of fruit development and ripening,[7] and gibberellic acid ($GA_3$) has been proposed as a possible trigger to increase fruit set and fruit size of numerous vine and fruit crops.[8] To date in oil palm, hormone analysis has been reported in sap exudate from stumps of preanthesis inflorescences,[9] wild-type and truncated leaves,[10] and fruit mesocarp.[11] In addition to plant hormones, other natural substances, such as the polyamines (PAs), may be involved in controlling fruit growth and ripening. Spermidine

Received: March 2, 2014
Revised: May 22, 2014
Accepted: July 17, 2014
Published: July 17, 2014

ACS Publications © 2014 American Chemical Society



dx.doi.org/10.1021/jf500975h | J. Agric. Food Chem. 2014, 62, 8143−8152

(Spd), spermine (Spm), putrescine (Put), and ornithine are the most commonly found polyamines in plants with several studies reported on tomatoes,[12] mango,[13] strawberry,[14] and peach.[15] Exogenous applications of PAs have also been reported to increase the endogenous levels of PAs and fruit size.[16] However, biosynthesis and distribution of PAs in relation to oil palm fruit mesocarp growth and development have not been reported to date.

In the context of studying fruit maturation and ripening, hormones, polyamines, and cell wall metabolism have interrelated roles. Mesocarp tissue is composed of thin-walled storage parenchymatous cells that are characterized by a prominent cell wall consisting of a complex network of polysaccharides and proteins giving mechanical strength to the tissues. A wide range of hydrolases that catalyze the process of softening are activated at transcriptional and translational levels. Softening is further enhanced by expansins that break down the multiple polysaccharide networks, thus increasing the accessibility of hydrolases, such as polygalacturonase (PG) or cellulase, to the cell wall polymers.[17] Tomato PG has been the most widely studied cell wall hydrolase in relation to ripening, while pectin degradation during ripening has been reported in avocado mesocarp.[18] We were also interested in studying hormone levels since they are well-known to play important roles in lipid biosynthesis regulation.[19] On the basis of our previous work,[20] we had identified several key biosynthetic pathways that are important to the synthesis of lipids and that the study of hormones may provide insights into the regulation of these networks.

For this study, hormones and polyamines in oil palm mesocarp were analyzed from 12 to 22 weeks after pollination, representing the main stages of lipid accumulation and ripening. Tandem HPLC and mass spectrometry (MS) with multiple reaction monitoring (MRM) were used, in which several plant hormones (IAA, CKs, ABA, and their metabolites) were quantified using deuterated internal standards. We also extracted RNA from mesocarp tissue to determine gene expression changes during ripening. Transcript levels of the cell wall metabolism genes, pectin, polygalacturonase, cellulose, and expansin, were analyzed using an oil palm mesocarp transcriptome microarray. Further understanding of the biological and physiological mechanisms underlying oil palm fruit ripening may be useful for optimizing harvesting as well as lead to the breeding of palms with improved ripening profiles.

## MATERIALS AND METHODS

**Plant Material.** Oil palm fruits were derived from commercial crosses of Serdang Avenue dura and AVROS pisifera to yield hybrid tenera progeny. The fruit bunches were sampled from a commercial estate in Carey Island, Malaysia, at different developmental stages preceding, during, and after the major oil biosynthesis period, namely, 12, 14, 16, 18, 20, and 22 WAP. All fruitlets were separated from the bunches, and then 20 were randomly selected from each without bias to location in the bunch. Mesocarp tissues were harvested and snap frozen in liquid $N_2$ to quench the metabolism of the plant tissues and enzyme activity and then stored in the dark at −80 °C for metabolite analysis and mRNA extraction. Prior to extraction, plant material (100 mg) was ground to a fine powder using a pestle and mortar under liquid nitrogen.

**Chemicals.** Zeatin, gibberellins ($GA_3$ and $GA_4$), ICA, IAA, BA, ABA, MeIAA, SA, CA, MeBA, IBA, JA, MeSA, MeCA, MeJA, and OPDA were purchased from either Aldrich or Sigma Chemical Co. (St Louis, USA). Isotopically labeled internal standards including [$^2H_5$]IAA and [$^2H_6$]ABA and [$^2H_5$] *trans*-zeatin riboside were purchased from OlChemim Ltd. (Olomouc, Czech Republic).

**Metabolite Extraction.** The extraction of polar and lipid metabolites from oil palm tissues was carried out in a single integrated procedure according to a previously published method.[20a] For hormone extraction, ground tissue (100 mg) was extracted with a mixture of 1-propanol:$H_2O$:conc HCl (2:1:0.002, v/v; 500 μL) with internal standards, [$^2H_5$]ABA and [$^2H_5$] *trans*-zeatin riboside (50 ng), added, followed by agitation for 30 min at 4 °C. $CH_2Cl_2$ (1 mL) was then added, followed by agitation for another 30 min and then centrifugation for 5 min at 4 °C, 13 000*g*. After centrifugation, two phases formed with plant debris suspended between the layers. An aliquot of the lower layer (1 mL) was concentrated and resolubilized in MeOH for analysis. All extracts were kept dry at −80 °C until further use. The analysis was comprised of targeted and untargeted LC-MS, GC-MS, and CE-MS analysis.

**Analysis Methods.** *Targeted Profiling of Hormone Metabolites Using LC-MS.* LC-MS data were acquired using UPLC-triplequad MS (Waters, USA). The Waters Acquity UPLC system (Waters Corporation, Milford, MA) was run in gradient mode, as per a previously published method.[21] The column used was reversed-phase C18 (1.8 μm, 2.1 × 100 mm; Waters) set at 30 °C. Solvent A was $H_2O$ (0.1% formic acid v/v), and solvent B was MeOH (0.1% formic acid v/v); the flow rate was 0.3 mL/min. The gradient was as follows: 30% B (0−2.0 min), linearly increased to 100% B at 20 min. The autosampler temperature was set at 4 °C with a 3.0 μL injection volume. MS analysis was performed on a Xevo TQs triple quadrupole mass spectrometer (Waters Corporation, Milford, MA). MS analysis was carried out in positive and negative ion electrospray ionization (ESI) modes of detection. The electrospray ionization capillary voltage on both modes was set at 2.5 kV, with the cone gas flow set at 150 L/h, and desolvation temperature of 350 °C. The collision gas flow was set at 0.15 mL/min. The MRM settings in the MS/MS function with corresponding cone voltage and collision energy were optimized for each standard compound. The total acquisition duration for both UPLC and MS was set at 15 and 5 min, respectively. Data were acquired and processed using MassLynx V4.1 and TargetLynx, respectively. [$^2H_5$] *trans*-zeatin riboside was used as an internal standard for positive mode and [$^2H_6$] ABA for negative mode.

*Targeted Profiling of Polyamine Metabolites Using CE-MS.* Targeted profiling of 108 primary metabolites using CE-MS was carried out by Human Metabolome Technologies, Inc. (HMT), Japan, as per a previously published method.[22]

**RNA Extraction.** Total RNA was extracted according to the San et al. method.[23] The extraction buffer contained 0.1 M Tris-HCl, pH 7.6, 0.1 M NaCl, 6% *p*-aminosalicylic acid, 1% SDS, 0.35% β-mercaptoethanol, and 5% phenol. The buffer was added at a rate of 4 mL/g of plant tissue, vortexed, and extracted with phenol:chloroform. The supernatant was precipitated twice using 3 M LiCl followed by ethanol precipitation. The pellet was then redissolved in DEPC-treated distilled water and again precipitated with 3 M LiCl followed by ethanol. The precipitate was finally dissolved in DEPC-treated distilled water and stored at −80 °C.

**Synthesis of cRNA, Microarray Hybridization, and Scanning.** Expression microarray analysis was performed using Agilent's one color method (Agilent Technologies, Palo Alto, CA, USA).[24] Total RNA samples from mesocarp were individually treated and labeled with a one-color Cy3 dye according to the Low Input Quick Amp Labeling protocol version 6.0, December 2009, provided by Agilent. Briefly, a total of 100 ng of total RNA was used to synthesize cRNA labeled with Cy3 dye. Labeled cRNAs were then purified using Qiagen's RNeasy mini kit as recommended by the manufacturer, and quality and quantity were assessed using the Spectrophotometer ND-1000(NanoDrop). The purified labeled cRNA was hybridized onto the *Arabidopsis*, rice, and custom oil palm mesocarp array at 65 °C for 16 h. After hybridization, 2 steps of washing were performed with wash buffer 1 and 2 for 1 min each. The array was then air-dried for a few seconds before proceeding with image scanning using the Agilent microarray slide scanner (SG11350602). A blank control without RNA, put through the entire hybridization and scanning processes, was also used to provide an estimate of the array background noise when no labeled probe is present.

**Data Extraction, Normalization, and Comparisons.** Raw microarray data were extracted from scanned images by using the Feature Extraction software (version 10.7.31; Agilent). The extracted microarray data were normalized using the Quantile normalization algorithm and analyzed using R (version 2.13.1). After normalization, comparisons of selected candidates between oil palm mesocarp microarray were carried out based on the normalized signal intensity produced.

## RESULTS AND DISCUSSION

**Hormone Metabolism during Oil Palm Development.** Fruit ripening in oil palm is accompanied by lipid and carotenoid accumulation along with chlorophyll degradation.[25] To determine the association of specific hormones with the timing of key ripening events, the major classes of plant hormones (ABA, auxins, cytokinins, and GA) in the mesocarp were profiled during the final stages of fruit development. Endogenous phytohormones occur only in a trace amount in plants. Consequently, for their analysis, sensitive mass spectrometric methods were combined with chromatographic separation techniques such as gas chromatography and high performance liquid chromatography. Unigenes also known to be involved in metabolism and response of multiple hormones including auxin, ethylene, gibberellins (GA), brassinosteroid (BR), jasmonic acid (JA), abscisic acid (ABA), and cytokinins (CK) were identified during mesocarp maturation from microarray expression data. Oil palm mesocarp tissue also had detectable levels of IAA, *trans*-zeatin, *trans*-zeatin glucoside, $GA_3$, $GA_4$, ABA, MeJA, and cinnamic acid. Changes in endogenous concentrations of GA, ABA, and cinnamic acid in mesocarp tissues during fruit growth and development are shown in Figure 1.

**Gibberellins.** Gibberellins (GAs) are plant growth regulators that are known to stimulate physiological responses during plant development, such as shoot growth, flower development, dormancy release, and seed germination, as well as alter the source−sink metabolism through their effect on photosynthesis and sink formation.[26] GA is also important in controlling seed maturation, germination, and seedling growth. While only trace amounts of $GA_3$ were detected, interestingly $GA_3$ and $GA_4$ exhibited clear opposite trends during oil palm mesocarp development. $GA_3$ appeared to be higher at Week 12 and decreased to almost undetectable levels at ripening.[11] However, $GA_4$ exhibited an opposite trend to $GA_3$ as its concentration increased during fruit development and peaked at Week 18, followed by a gradual decline to Week 22. $GA_4$ is the main bioactive hormone in cucumber[27] and *Arabidopsis*[28] and is also clearly important in oil palm fruit ripening. Several unigenes with annotated functions in gibberellin biosynthesis and responses were identified in the oil palm mesocarp transcriptome. Three genes that encode "DELLA proteins", the repressor of GA responses, were identified and showed down-regulated expression patterns toward maturation (Figure 2A). Unigenes encoding proteins homologous to GA20ox and GA3ox that convert the inactive precursors to bioactive GAs also showed mostly down-regulated expression patterns in mesocarp during fruit development after peaking at 18 WAP, concordant with the peak concentration of $GA_4$ observed followed by a decline (Figure 1A in the Supporting Information). In particular, GA20ox exhibited much lower expression at 22 WAP. Interestingly GA2ox, which is involved in the catabolic pathway of $GA_4$, exhibits a similar expression trend, peaking at 14−18 WAP and declining thereafter,

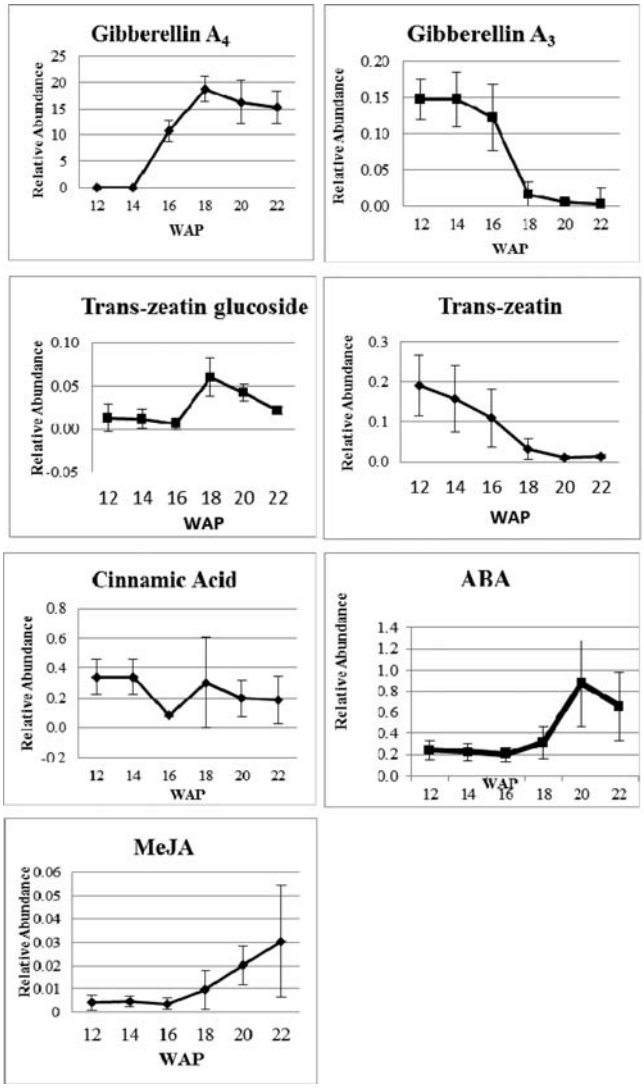


**Figure 1.** Hormone profiles during mesocarp development.

concordant with the lower levels of $GA_3$ observed. The combination of lower expression of GA20ox and GA3ox resulting in less provision of $GA_4$, combined with lower expression of GA2ox after week 18, may contribute to the dramatic lowering of $GA_3$ concentrations at the last stage of ripening.

**Abscisic Acid.** Liu et al. reported that high levels of endogenous ABA occur concurrently with rapid increases in the rate of fresh and dry weight accumulation in soybean seeds and coincide with the maximum rate of cell division.[29] Several studies report an increase in free ABA levels during grape ripening concomitant with sugar accumulation and color changes.[30] In oil palm, mesocarp also contained higher levels of ABA as lipid accumulated during ripening. ABA has been proposed as a possible trigger of ripening in some fruits as well.[31] The specific role of ABA during fruit ripening remains obscure although ABA accumulation appears to be critical and participates in the regulation of ripening of both climacteric and nonclimacteric fruit. Transcription levels of 9-*cis*-epoxycarotenoid dioxygenase 1 gene, *NCED1*, in oil palm mesocarp were also found to be congruent with ABA content clearly indicating its importance to the ripening process of oil palm (Figure 1 and Figure 2B). It was previously observed by Chernys et al. that


dx.doi.org/10.1021/jf500975h | J. Agric. Food Chem. 2014, 62, 8143−8152

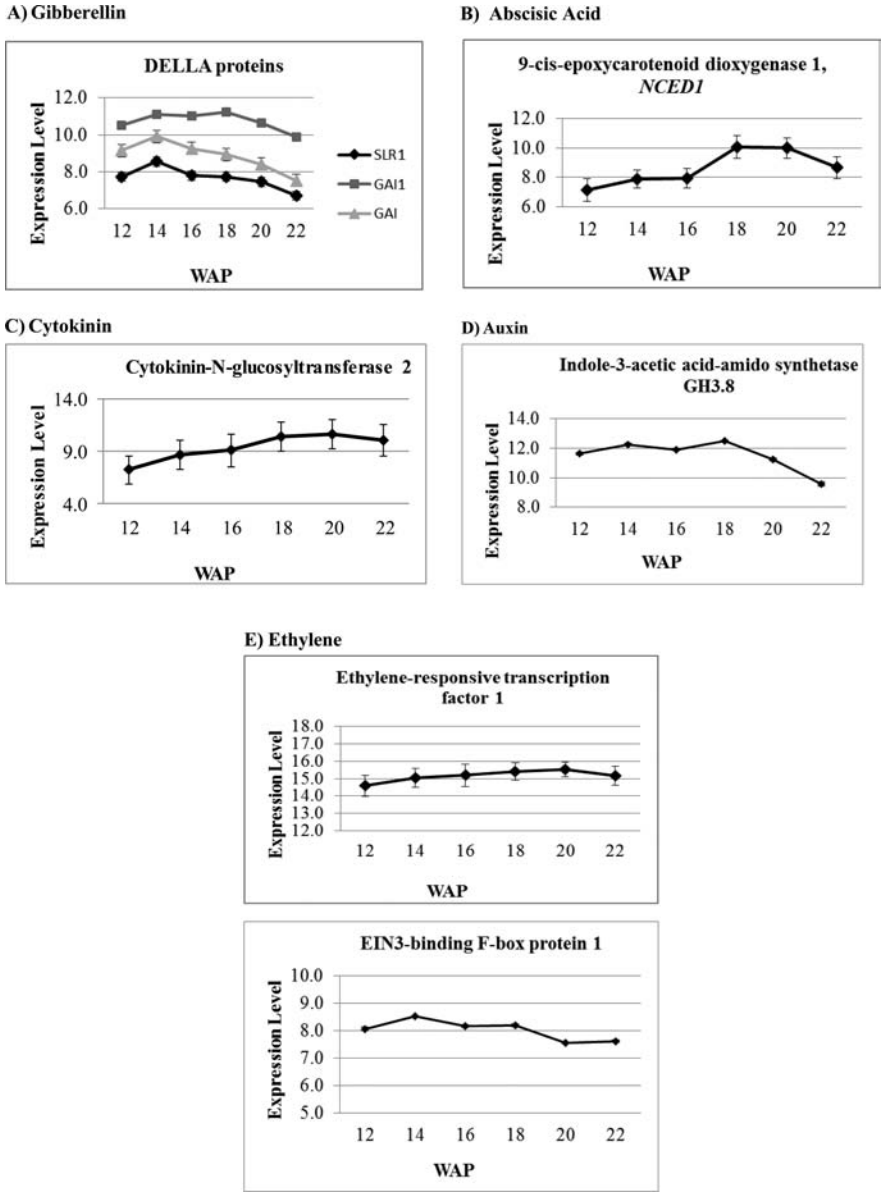


**Figure 2.** (A) Gibberellin, (B) abscisic acid, (C) cytokinin, (D) auxin, (E) ethylene.

*NCED1*, a key enzyme involved in ABA biosynthesis, is up-regulated during the ripening of several fruits, including avocado.[32] In addition, two unigenes for 'abscisic acid 8'-hydroxylase were clearly down-regulated in mesocarp at 20−22 weeks, possibly leading to a decrease in ABA degradation (Supporting Information) allowing accumulation.

The interaction between GA and ABA can have antagonistic effects according to Gao et al.[33] Seed maturation and germination are not determined by ABA alone but instead by the ABA/GA ratio. ABA content increases in *Arabidopsis* seed as the embryo enters the maturation stage, and the resulting high ABA/GA ratio promotes maturation, induces dormancy, and inhibits cell-cycle progression, embryo growth, and germination.[34] While in maize, it also appears to be the ABA/GA ratio and not the absolute hormone concentration that controls germination.[35] For oil palm mesocarp, at the beginning of the maturation phase, ABA levels increase in fruits, while $GA_3$ decreases, the resulting elevated ABA/$GA_3$ ratio clearly coinciding with maturation (Figure 3).

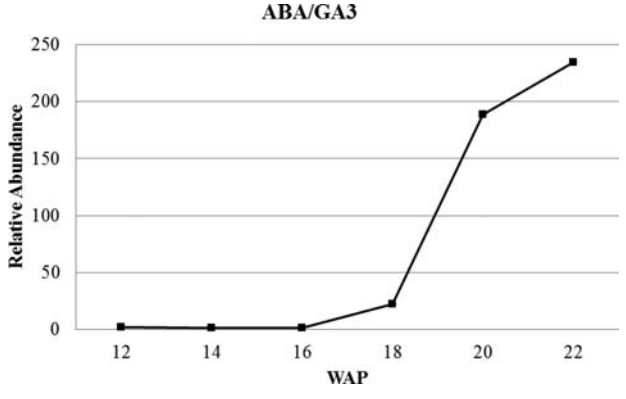


**Figure 3.** ABA/$GA_3$ ratio of palm mesocarp samples during 12−22 WAP. Data obtained from LC-MS-triplequad analysis.

**Cytokinins.** Cytokinins also have an important regulatory role in plant development and growth. They improve seed germination, release bud from apical dominance, and stimulate

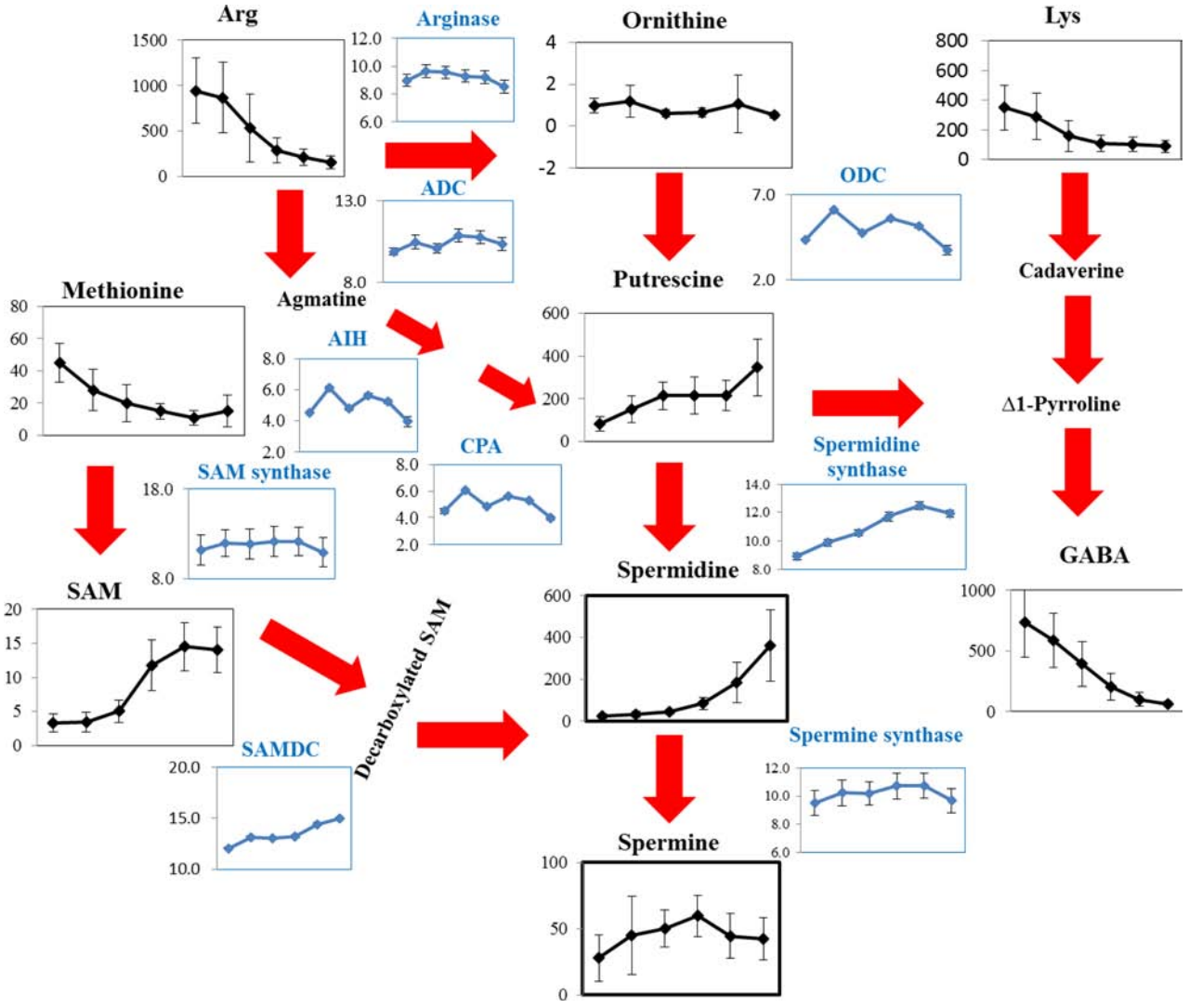


**Figure 4.** Changes in polyamine levels and transcript expression in mesocarp across 6 time points.

leaf expansion and development of reproductive organs and retardation of senescence.[36] Cytokinins have been reported to increase the number of pods/plant and seed weight in soybean. *trans*-Zeatin was the predominant cytokinin detected in oil palm mesocarp, followed by *trans*-zeatin glucoside. Contrary to ABA, the levels of *trans*-zeatin are high early in fruit development but decrease to very low or undetectable levels at maturation (Figure 1). *trans*-Zeatin glucoside exhibited different behavior, being detected at low concentration at weeks 12−16, peaking at week 18, followed by a decline until week 22 (Figure 1). Cytokinins are thought to be involved in berry set and in growth promotion and tend to inhibit fruit ripening.[37] The levels of zeatin are high early in grape development but decrease rapidly to be low at around the time of ripening.[37] Three unigenes encoding proteins homologous to "cytokinin dehydrogenase" and three unigenes for cytokinin-*N*-(or *O*-)glucosyltransferase, which regulate homeostasis by deactivating cytokinin were identified in mesocarp. Of these, only cytokinin-*N*-glucosyltransferase 2 exhibited increased expression towards ripening (Figure 2). Hormonal analysis by Habib et al. revealed that various cytokinin derivatives such as *trans*-zeatin, *trans*-zeatin riboside, *trans*-zeatin *O*-glucoside, and *trans*-zeatin riboside 5′-monophosphate were significantly higher in truncated oil palm leaf syndrome leaves compared to wild-type oil palm leaves.[38]

**Jasmonic Acid.** Jasmonic acid (JA) has been demonstrated to be involved in cross talk with ethylene signaling components in *Arabidopsis* and has been associated with fruit maturation. In climacteric and nonclimacteric fruits, jasmonate levels increase during early fruit developmental stages, suggesting that jasmonate could be involved in cell division and other early fruit expansion processes. Generally, jasmonates and salicylates contribute to local and systemic defenses against pathogens, wounding, and stress responses and are involved in pollen and embryo development, seed germination, senescence, fruit ripening, and allelopathy.[39] To our knowledge jasmonate has not been previously reported in the context of oil fruit ripening. Methyl jasmonic acid (MeJA) was found to increase after oil biosynthesis commences until ripeness in oil palm (Figure 1). JA and MeJA have been reported to retard cell division in soybean callus [*Glycine max* (L.) Merr.].[40] We observed that 12-oxophytodienoate reductase 3, lipoxygenase 7, jasmonate-induced protein, and allene oxide synthase 1 and 2 are expressed at a higher level as compared to other jasmonic acid biosynthesis genes (Figure 1D in the Supporting Information).


dx.doi.org/10.1021/jf500975h | *J. Agric. Food Chem.* 2014, 62, 8143−8152

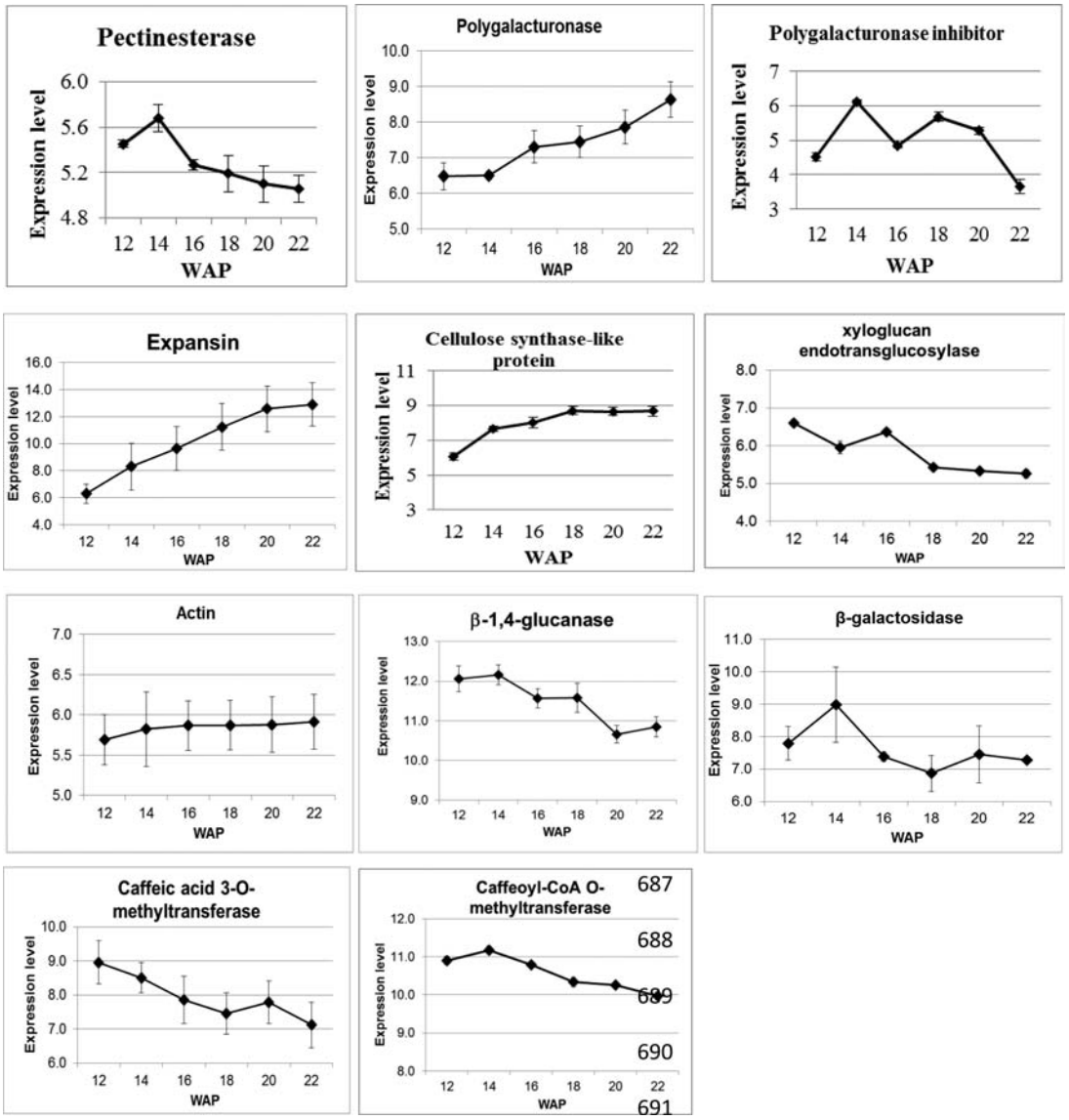


**Figure 5.** Expression microarray data for genes which are involved in cell wall metabolism.

**Auxin.** In oil palm mesocarp it was reported that indole-3-acetic acid (IAA) levels peak after pollination and then decline to very low levels in the ripe fruit.[11] IAA was also found to be undetectable in this study of mesocarp after week 12. However, auxin biosynthesis genes were detected using expression microarray. A gene coding for an indole-3-acetic acid-amido synthetase GH3.8 exhibited the highest expression at week 18 but declined in expression toward ripeness (Figure 2D). Many genes coding for auxin and IAA proteins were down-regulated at week 22 suggesting that auxin levels are indeed lowered toward ripening. A transcript encoding IAA-amino acid hydrolase 1 (ILR1, 5, 6, and 7), which is putatively involved in IAA homeostasis, was down-regulated during fruit development (S1E). Auxin-response factors bind auxin-response elements of auxin-responsive genes and thus seem to act as regulators of gene transcription.[41] In this study, several auxin response factors (ARFs 1, 2, 4, 6, 7, 9, 11, 12, 15, 16, 18, 19, 23) were down-regulated during the maturation stages except ARF 7, 17, and 23 (Figure 1E in the Supporting Information). The majority of transcripts related to auxin transport and perception displayed decreased abundance in mesocarp (Supporting Information).

**Ethylene.** Consistent with the critical roles of ethylene during fruit maturation and ripening, the majority of unigenes related to ethylene functions showed up-regulated expression patterns as maturation progressed. We found that one unigene encoding the EIN3-binding F-box protein in oil palm mesocarp samples, a negative regulator of ethylene action, exhibited down-regulated expression patterns (Figure 2E) along with up-regulated expression patterns for most ethylene function related unigenes. Ethylene-responsive transcription factor 1 is found to be expressed highest among other genes related to ethylene pathways. Recent research reported by Tranbarger et al. shows that oil palm mesocarp exhibits characteristics of a climacteric fruit with an autocatalytic burst of ethylene coordinated transcriptional activity.[11]

**Brassinosteroids.** Lastly, brassinosteroids also regulate various aspects of plant growth and development, including cell elongation, photomorphogenesis, xylem differentiation, and seed germination as well as adaptation to abiotic and biotic environmental stresses.[42] Brassinosteroid insentive 1-associated

receptor kinase 1, brassinosteroid-regulated protein, and brassinosteroid LRR receptor kinase genes were detected in oil palm mesocarp (Figure 1F in the Supporting Information) and decreased from week 12 to 22.

**Polyamine Metabolism during Oil Palm Development.** Polyamines, generally putrescine (Put), spermidine (Spd), and spermine (Spm), are polycationic compounds of low molecular weight that are present in living organisms. In plants, polyamines are present from micromolar (~10 $\mu$M) to millimolar concentrations.[43] They distribute differently among tissues and developmental stages, with Put and Spd being more abundant than Spm and cadeverine (Cad). Plant polyamines are considered as growth regulators, as they play fundamental roles in a wide range of growth, differentiation, and morphogenetic processes during the course of plant ontogeny. They have been shown to be involved in fruit enlargement, maturation, and ripening.[15] Thus, the changes in endogenous free polyamines (Put, Spd, Spm, and ornithine) were monitored to examine their role during mesocarp development. Figure 4 shows the changes in polyamine levels and related gene expression in the oil palm mesocarp across the six time points. The concentrations of both ornithine and Spm remained relatively low compared to Spd and Put. Spd was higher than Put across time points, both increasing toward ripeness. Spermidine synthase (SpdSyn) is a key enzyme in polyamine biosynthesis and is responsible for Spd accumulation as also seen in Figure 4. The concentration profile of Spm also followed the expression levels of spermine synthase (SpmSyn). Along with accumulation of polyamines, arginine showed steady consumption after week 12. The pathway to Spd from methionine also revealed similar coordination with ripening. The increase in polyamines during oil palm fruit ripening suggests that endogenous polyamines may be involved in response to ethylene production.[13] Quinet et al. found that a high level of Put concentration played an active role in triggering biosynthesis of ethylene.[44] For oil palm mesocarp, Put, Spd, and Spm concentrations increased toward maturation along with ethylene.[11] Contrary to oil palm, higher levels of polyamines are found in the initial fruit growth period, progressively declining toward maturation in several fruits including apple,[16] grapes,[45] tomato,[12] mango,[13] and peach.[46] Polyamines are reported to be abundant during the cell division stage and decrease during the subsequent cell enlargement phase, ripening, and postharvest.[47] However, the opposite trend seen in oil palm fruit in this study has been reported in mandarins and rambutans.[48] In addition, Maria et al. recently reviewed that mature olive fruit abscission is associated with up-regulation of polyamine metabolism.[49]

**Cell Wall Metabolism.** Plant cell wall metabolism, particularly cell wall degradation and modification, has long been associated with fruit ripening and softening. The complexity of the cell wall is encoded by multigene families that likely contribute to fruit cell wall metabolism including multiple steps such as substrate generation, synthesis and glycosyl transferase activities, secretory pathways, wall assembly, wall dynamics, and wall disassembly. Genes encoding for cell wall metabolism have been studied for their potential roles in fruit ripening and postharvest fruit softening. During oil palm mesocarp development, the cells continue to grow as they accumulate lipid.[50] Actin gene expression seemed to increase between week 12 and week 14, remaining high thereafter (Figure 5). This may be related to cell expansion during lipid accumulation as actin is involved in a number of cellular processes such as cytoplasmic streaming, cell shape determination, organelle movement, and extension growth.[51] We have also noted that amino acid levels are increased in high yielding fruits at weeks 12−14.[20a]

Identified unigenes with annotated functions in cell wall metabolism represent another major transcriptomics change during mesocarp maturation. Fruit softening during ripening is associated with depolymerization and solubilization of cellulose microfibrils, hemicellulose, and pectins in the cell wall.[52] Fruit softening during ripening results from the hydrolytic breakdown of cell wall polymers (e.g., celluloses, hemicelluloses, pectins) by hydrolases (e.g., polygalacturonase [PG], pectin methyl esterase, pectate lyase, rhamnogalacturonase, $\beta$-galactosidase).[53] Pectolytic enzymes constitute a unique group of enzymes that are responsible for the degradation of pectin and pectic substances in plant cell walls. In peach, high levels of polygalacturonase and low levels of cellulose have been reported for the fruit ripening stage.[54] Much research has focused on pectin degradation, resulting from the action of the ripening-related enzyme polygalacturonase, as the key element underlying the softening process. Expansin gene A-8, cellulose synthase-like protein, and polygalacturonase genes have the similar pattern of gene expression level in mesocarp fruits across the six time points in oil palm mesocarp (Figure 5). Our results also showed that the expression level of polygalacturonase inhibitor transcript exhibited an opposite trend to polygalacturonase. Polygalacturonase gene family members have been studied in fleshy oil palm fruit ripening and abscission recently by Roongsattham et al.[55] They identified the expression level of five transcripts that encode PGs increased during ethylene treatments that induce cell separation. During avocado ripening the amount of high and intermediate sized polymers in the pectin fraction have been reported to decrease.[18] $\beta$-Galactosidase expression decreased during ripening in oil palm mesocarp (Figure 5). $\beta$-Galactosidase may be involved in releasing stored energy for rapid growth, degrading cell wall components during senescence, and releasing free galactose during metabolic recycling of galactolipids, glycoproteins, and cell wall components.[56] Caffeic acid 3-*O*-methyltransferase (COMT) decreased gradually from week 12 to 22 (Figure 5). Caffeoyl CoA 3-*O*-methyltransferase (CCOMT) also peaked at week 14 and decreased gradually thereafter (Figure 5). Strong down-regulation of COMT and CCOMT has been shown to result in decreased lignin content.[57]

Expansins are plant cell wall proteins proposed to disrupt hydrogen bonds within the cell wall polymer matrix so that cell wall hydrolase enzymes can access, thus enhancing softening of, tissues.[58] Expansins are encoded by a super family of genes that are divided into four families, namely, expansin A, expansin B, expansin like A, and expansin like B.[58,59] Expression of specific expansin genes has been observed in tomato (*Lycopersicon esculentum*) meristems, expanding tissues, and ripening fruit. It has been proposed that a tomato-ripening-regulated expansin might contribute to cell wall polymer disassembly and fruit softening by increasing the accessibility of specific cell wall polymers to hydrolase action. We found nine forms of expansin genes expressed during oil palm mesocarp development (Expansin B5, A2, A7, A8, A10, A15, like-A1, like-A2, and like-B1). In particular, expression levels of expansin gene-A8 increased significantly (Figure 5). Xie et al. found that expression and enzyme activity of cell wall hydrolases including

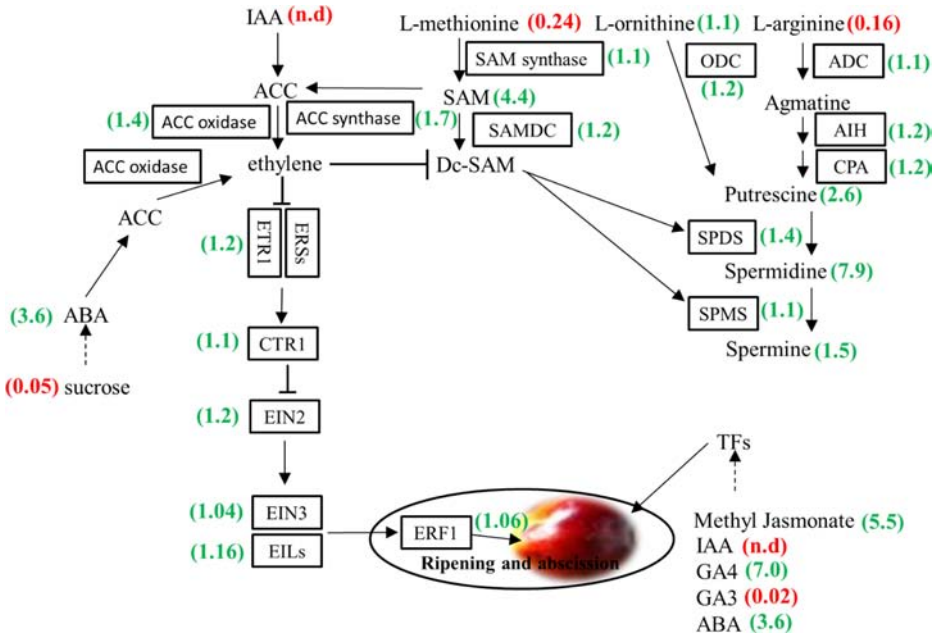


**Figure 6.** Schematic representation of the integration of polyamines, hormones, and their respective genes in mesocarp fruit ripening and abscission events. The numbers between brackets correspond to a gene/metabolite expression ratio of week 20 to week 12. Abbreviations: SAMDC, *S*-adenosylmethionine decarboxylase; SPDS, spermindine synthase; SPMS, spermine synthase; ODC, ornithine decarboxylase; AIH, agmatine iminohydrolase; ADC, arginine decarboxylase; CPA, *N*-carbamoylputrescine amidohydrolase; ACC, 1-aminocyclopropane-1-carboxylic acid; Dc-SAM, decarboxylated *S*-adenosyl methionine; ROS, reactive oxygen species; TFs, transcription factors; EIN, ethylene-insensitive; ERF, ethylene-responsive transcription factor; EIL, EIN3-Like.

expansin and polygalacturonase were increased during the final stages of fruit development and abscission.[4]

Figure 6 shows the temporal expression patterns of hormones and polyamines between weeks 12 and 20. Almost all the polyamines and hormones exhibited increased expression, except $GA_3$, sucrose, arginine, and L-methionine. The ratio of genes coordinated in regulation of these hormones and polyamines was found to be concordant with the ratio value of their metabolites in most cases. Among the hormones and polyamines metabolites, a few were evident as the most critical for ripening in oil palm: Spd (7.9) (driven by SAM (4.4)) and $GA_4$ (7.0) showing the most differential, followed by methyl jasmonate (5.5) and ABA (3.6). As discussed earlier, the effect of ABA may be more pronounced by its ratio with $GA_3$ increasing even more markedly at 20 WAP. Xie et al. reported cross-talk among the hormones, saccharides, and polyamines in apple, mango, and citrus.[4] It can be seen that their levels in oil palm can be related to lipid biosynthesis commencement first and later to fruit maturation (softening and abscsission).

In summary, this work describes the combined analysis of transcripts and metabolites contributing to the involvement of hormones, polyamines, and cell wall metabolism during oil palm fruit ripening from 12 weeks after pollination (WAP). Figure 7 summarizes the changes in total oil content, amino acids, organic acids, polyamines, and hormones in the three main stages of development: lag phase (12−14 WAP), maturation (16−18 WAP), and finally ripening (20−22 WAP). Lag phase (12−14 WAP) occurs after cell division and cell expansion, where peak lipid biosynthesis starts during maturation (16−18 WAP), reaching maximum lipid concentrations at ripening (20−22 WAP). Figure 7 clearly shows the key developmental changes related to oil biosynthesis at weeks 14−16 and then ripening at weeks 20−22 and indicates how hormones and polyamines are coordinated. Some are

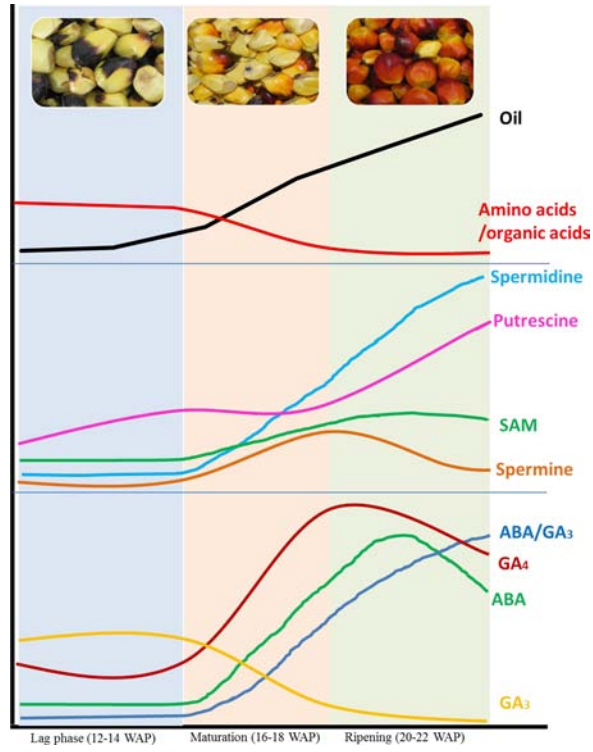


**Figure 7.** Summary of total oil, amino acids, organic acids, polyamines, and hormones in the mesocarp tissue during oil palm fruit development.

concordant with the onset of lipid biosynthesis at 16 WAP, such as $GA_4$ concentration, while others are concordant with the final stages of ripening (fruit softening and abscission), most notably ABA and the ABA/$GA_3$ ratio as well as


dx.doi.org/10.1021/jf500975h | J. Agric. Food Chem. 2014, 62, 8143−8152

polyamines. These results provide a valuable contribution for the understanding of key genes and expression timing changes related to the regulation of the complex process of mesocarp ripening, in particular the initiation of peak oil biosynthesis and final ripening before harvesting. In summary, we conclude that (1) high polyamine concentrations coincide with lipid accumulation and maturation; (2) ABA is concordant with $GA_4$ but not $GA_3$ during fruit development, and the resulting elevated ABA/$GA_3$ ratio appears to promote maturation; (3) ethylene-responsive transcription factor 1,9-*cis*-epoxycarotenoid dioxygenase 1 (NCED1), cytokinin-*N*-glucosyltransferase 2, and ethylene-responsive transcription factor 1 were all expressed higher in up-related pattern until week 20; (4) polygalacturonase, expansin A-8, cellulose synthase-like protein, and actin genes clearly increase toward ripening. The elucidation of the specific promoter binding sites and transcription factors that are in common between genes that exhibit related expression profiles during ripening or transcription factors modulated by hormone concentrations may lead to the identification of important timing regulators of oil biosynthesis and ripening. These will in turn assist in the development of fruit that ripens faster and/or produces more oil.

## ■ ASSOCIATED CONTENT

### Supporting Information

Expression microarray data for hormone genes in developing oil palm fruit. This material is available free of charge via the Internet at http://pubs.acs.org.

## ■ AUTHOR INFORMATION

### Corresponding Author

*E-mail: david.ross.appleton@simedarby.com. Telephone: +603-89422641. Fax: +603- 89431867.

### Notes

The authors declare no competing financial interest.

## ■ ACKNOWLEDGMENTS

The authors would like to thank their colleagues in SDRC for their valued input and discussions, especially the Breeding group and the harvesting team (SDRC). We also thank Human Metabolome Technologies (Japan) for CE-MS analysis.

## ■ REFERENCES

(1) Zhang, J.; Wang, X.; Yu, O.; Tang, J.; Gu, X.; Wan, X.; Fang, C. Metabolic profiling of strawberry (Fragaria x ananassa Duch.) during fruit development and maturation. *J. Exp. Bot.* **2011**, *62* (3), 1103−18.

(2) Lombardo, V. A.; Osorio, S.; Borsani, J.; Lauxmann, M. A.; Bustamante, C. A.; Budde, C. O.; Andreo, C. S.; Lara, M. V.; Fernie, A. R.; Drincovich, M. F. Metabolic profiling during peach fruit development and ripening reveals the metabolic networks which underpin each developmental stage. *Plant Physiol.* **2011**, *157*, 1696−1710.

(3) Carrari, F.; Fernie, A. R. Metabolic regulation underlying tomato fruit development. *J. Exp. Bot.* **2006**, *57* (9), 1883−97.

(4) Xie, R. J.; Deng, L.; Jing, L.; He, S. L.; Ma, Y. T.; Yi, S. L.; Zheng, Y. Q.; Zheng, L. Recent advances in molecular events of fruit abscission. *Biol. Plant* **2013**, *57* (2), 201−209.

(5) Henderson, J.; Osborne, D. J. Inter-tissue 7. *J. Exp. Bot.* **1994**, *45* (7), 943−951.

(6) Cowan, A. K.; Cripps, R. F.; Richings, E. W.; Taylor, N. J. Fruit size: Towards an understanding of the metabolic control of fruit growth using avocado as a model system. *Physiol. Plant.* **2001**, *111* (2), 127−136.

(7) Hauser, F.; Waadt, R.; Schroeder, J. I. Evolution of Abscisic Acid Synthesis and Signaling Mechanisms. *Curr. Biol.* **2011**, *21* (9), R346−55.

(8) Chao, C.-C. T.; Khuong, T.; Zheng, Y.; Lovatt, C. J. Response of evergreen perennial tree crops to gibberellic acid is crop load-dependent. I: GA3 increases the yield of commercially valuable 'Nules' Clementine Mandarin fruit only in the off-crop year of an alternate bearing orchard. *Sci. Hortic. (Amsterdam, Neth.)* **2011**, *130* (4), 743−752.

(9) Huntley, R. P.; Jones, L. H.; Hanke, D. E. Cytokinins and gibberellins in sap exudate of the oil palm. *Phytochemistry* **2002**, *60* (2), 117−27.

(10) Habib, S.; Ooi, S. E.; Novák, O.; Tarkowská, D.; Rolčík, J.; Doležal, K.; Syed-Alwee, S.; Ho, C. L.; Namasivayam, P. Comparative mineral and hormonal analyses of wild type and TLS somaclonal variant derived from oil palm (*Elaeis guineensis* Jacq. var. tenera) tissue culture. *Plant Growth Regul.* **2012**, *68*, 313−317.

(11) Tranbarger, T. J.; Dussert, S.; Joet, T.; Argout, X.; Summo, M.; Champion, A.; Cros, D.; Omore, A.; Nouy, B.; Morcillo, F. Regulatory mechanisms underlying oil palm fruit mesocarp maturation, ripening, and functional specialization in lipid and carotenoid metabolism. *Plant Physiol.* **2011**, *156* (2), 564−84.

(12) Morilla, A.; García, J. M.; Albi, M. A. Free Polyamine Contents and Decarboxylase Activities during Tomato Development and Ripening. *J. Agric. Food Chem.* **1996**, *44* (9), 2608−2611.

(13) Malik, A. U.; Singh, Z. Endogenous Free Polyamines of Mangos in Relation to Development and Ripening. *J. Am. Soc. Hortic. Sci.* **2004**, *129* (3), 280−286.

(14) Ponappa, T.; Miller, A. R. Polyamines in normal and auxin-induced strawberry fruit development. *Physiol. Plant.* **1996**, *98* (3), 447−454.

(15) Liu, J.; Nada, K.; Pang, X.; Honda, C.; Kitashiba, H.; Moriguchi, T. Role of polyamines in peach fruit development and storage. *Tree Physiol.* **2006**, *26* (6), 791−8.

(16) Biasi, R.; Bagni, N.; Costa, G. Endogenous polyamines in apple and their relationship to fruit set and fruit growth. *Physiol. Plant.* **1988**, *73* (2), 201−205.

(17) Payasi, A.; Mishra, N.; Chaves, A.; Singh, R. Biochemistry of fruit softening: an overview. *Physiol. Mol. Biol. Plants* **2009**, *15* (2), 103−113.

(18) Sakurai, N.; Nevins, D. J. Relationship between Fruit Softening and Wall Polysaccharides in Avocado (Persea americana Mill) Mesocarp Tissues. *Plant Cell Physiol.* **1997**, *38* (5), 603−610.

(19) (a) Sharma, N.; Anderson, M.; Kumar, A.; Zhang, Y.; Giblin, E. M.; Abrams, S. R.; Zaharia, L. I.; Taylor, D. C.; Fobert, P. R. Transgenic increases in seed oil content are associated with the differential expression of novel Brassica-specific transcripts. *BMC Genomics* **2008**, *9*, 619. (b) Jadhav, A. S.; Taylor, D. C.; Giblin, M.; Ferrie, A. M.; Ambrose, S. J.; Ross, A. R.; Nelson, K. M.; Irina Zaharia, L.; Sharma, N.; Anderson, M.; Fobert, P. R.; Abrams, S. R. Hormonal regulation of oil accumulation in Brassica seeds: metabolism and biological activity of ABA, 7′-, 8′- and 9′-hydroxy ABA in microspore derived embryos of B. napus. *Phytochemistry* **2008**, *69* (15), 2678−88. (c) Gutierrez, L.; Van Wuytswinkel, O.; Castelain, M.; Bellini, C. Combined networks regulating seed maturation. *Trends Plant Sci.* **2007**, *12* (7), 294−300.

(20) (a) Teh, H. F.; Neoh, B. K.; Hong, M. P.; Low, J. Y.; Ng, T. L.; Ithnin, N.; Thang, Y. M.; Mohamed, M.; Chew, F. T.; Yusof, H. M.; Kulaveerasingam, H.; Appleton, D. R. Differential metabolite profiles during fruit development in high-yielding oil palm mesocarp. *PLoS One* **2013**, *8* (4), e61344. (b) Loei, H.; Lim, J.; Tan, M.; Lim, T. K.; Lin, Q. S.; Chew, F. T.; Kulaveerasingam, H.; Chung, M. C. Proteomic analysis of the oil palm fruit mesocarp reveals elevated oxidative phosphorylation activity is critical for increased storage oil production. *J. Proteome Res.* **2013**, *12* (11), 5096−109.

(21) Pan, X.; Welti, R.; Wang, X. Simultaneous quantification of major phytohormones and related compounds in crude plant extracts by liquid chromatography-electrospray tandem mass spectrometry. *Phytochemistry* **2008**, *69* (8), 1773−81.

(22) Soga, T. Capillary electrophoresis-mass spectrometry for metabolomics. *Methods Mol. Biol. (Clifton, N.J.)* **2007**, *358*, 129−37.
(23) San, C. T.; Shah, F. H. Differential gene expression and characterization of tissue-specific cDNA clones in oil palm using mRNA differential display. *Mol. Biol. Rep.* **2005**, *32* (4), 227−35.
(24) Oberthuer, A.; Juraeva, D.; Li, L.; Kahlert, Y.; Westermann, F.; Eils, R.; Berthold, F.; Shi, L.; Wolfinger, R. D.; Fischer, M.; Brors, B. Comparison of performance of one-color and two-color gene-expression analyses in predicting clinical endpoints of neuroblastoma patients. *Pharmacogenomics J.* **2010**, *10* (4), 258−66.
(25) Sambanthamurthi, R.; Sundram, K.; Tan, Y. Chemistry and biochemistry of palm oil. *Prog. Lipid Res.* **2000**, *39* (6), 507−58.
(26) (a) Yamaguchi, S. Gibberellin metabolism and its regulation. *Ann. Rev. Plant Biol.* **2008**, *59*, 225−51. (b) Serrani, J. C.; Sanjuan, R.; Ruiz-Rivero, O.; Fos, M.; Garcia-Martinez, J. L. Gibberellin regulation of fruit set and growth in tomato. *Plant Physiol.* **2007**, *145* (1), 246−57.
(27) Nakayama, M.; Yamane, H.; Murofushi, N.; Takahashi, N.; Mander, L.; Seto, H. Gibberellin biosynthetic pathway and the physiologically active gibberellin in the shoot of *Cucumis sativus L. J. Plant Growth Regul.* **1991**, *10* (1), 115−119.
(28) Cowling, R. J.; Kamiya, Y.; Seto, H.; Harberd, N. P. Gibberellin dose-response regulation of GA4 gene transcript levels in Arabidopsis. *Plant Physiol.* **1998**, *117* (4), 1195−203.
(29) Liu, X. H. S. J.; Baath, K.; Hashemi, A. M. Soybean (Glycine max) seed growth characteristics in response to light enrichment and shading. *Plant Soil Environ.* **2006**, *52*, 178−185.
(30) Fortes, A. M.; Agudelo-Romero, P.; Silva, M. S.; Ali, K.; Sousa, L.; Maltese, F.; Choi, Y. H.; Grimplet, J.; Martinez-Zapater, J. M.; Verpoorte, R.; Pais, M. S. Transcript and metabolite analysis in Trincadeira cultivar reveals novel information regarding the dynamics of grape ripening. *BMC Plant Biol.* **2011**, *11*, 149.
(31) Zhang, M.; Yuan, B.; Leng, P. The role of ABA in triggering ethylene biosynthesis and ripening of tomato fruit. *J. Exp. Bot.* **2009**, *60* (6), 1579−88.
(32) Chernys, J. T.; Zeevaart, J. A. Characterization of the 9-cis-epoxycarotenoid dioxygenase gene family and the regulation of abscisic acid biosynthesis in avocado. *Plant Physiol.* **2000**, *124* (1), 343−53.
(33) Gao, Y.; Zhao, Y.; Li, T.; Liu, Y.; Ren, C.; Wang, M. Molecular cloning and expression analysis of an F-box protein gene responsive to plant hormones in Brassica napus. *Mol. Biol. Rep.* **2010**, *37* (2), 1037−44.
(34) Finkelstein, R. R.; Gampala, S. S. L.; Rock, C. D. Abscisic Acid Signaling in Seeds and Seedlings. *Plant Cell Online* **2002**, *14* (suppl 1), S15−S45.
(35) White, C. N.; Proebsting, W. M.; Hedden, P.; Rivin, C. J. Gibberellins and Seed Development in Maize. I. Evidence That Gibberellin/Abscisic Acid Balance Governs Germination versus Maturation Pathways. *Plant Physiol.* **2000**, *122* (4), 1081−1088.
(36) Werner, T.; Motyka, V.; Strnad, M.; Schmülling, T. Regulation of plant growth by cytokinin. *Proc. Natl. Acad. Sci. U.S.A.* **2001**, *98* (18), 10487−10492.
(37) Davies, C.; Böttcher, C. *Hormonal Control of Grape Berry Ripening Grapevine Molecular Physiology & Biotechnology*; Roubelakis-Angelakis, K. A., Ed.; Springer: Netherlands, 2009; pp 229−261.
(38) Habib, S. H.; Ooi, S. E.; Novák, O.; Tarkowská, D.; Rolčík, J.; Doležal, K.; Syed-Alwee, S. S. R.; Ho, C. L.; Namasivayam, P. Comparative mineral and hormonal analyses of wild type and TLS somaclonal variant derived from oil palm (Elaeis guineensis Jacq. var. tenera) tissue culture. *Plant Growth Regul.* **2012**, 1−5.
(39) Delker, C.; Stenzel, I.; Hause, B.; Miersch, O.; Feussner, I.; Wasternack, C. Jasmonate biosynthesis in Arabidopsis thaliana–enzymes, products, regulation. *Plant Biol. (Stuttgart, Germany)* **2006**, *8* (3), 297−306.
(40) Ueda, J.; Kato, J. Inhibition of cytokinin-induced plant growth by jasmonic acid and its methyl ester. *Physiol. Plant.* **1982**, *54* (3), 249−252.
(41) Woodward, A. W.; Bartel, B. Auxin: regulation, action, and interaction. *Ann. Bot.* **2005**, *95* (5), 707−35.
(42) Sasse, J. M. Physiological Actions of Brassinosteroids: An Update. *J. Plant Growth Regul.* **2003**, *22* (4), 276−288.
(43) Galston, A. W.; Sawhney, R. K. Polyamines in plant physiology. *Plant Physiol.* **1990**, *94* (2), 406−10.
(44) Quinet, M.; Ndayiragije, A.; Lefèvre, I.; Lambillotte, B.; Dupont-Gillain, C. C.; Lutts, S. Putrescine differently influences the effect of salt stress on polyamine metabolism and ethylene synthesis in rice cultivars differing in salt resistance. *J. Exp. Bot.* **2010**, *61* (10), 2719−33.
(45) Geny, L.; Broquedis, M.; Martin-Tanguy, J.; Bouard, J. Free, Conjugated, and Wall-Bound Polyamines in Various Organs of Fruiting Cuttings of Vitis vinifera L. cv. Cabernet Sauvignon. *Am. J. Enol. Vitic.* **1997**, *48* (1), 80−84.
(46) Liu, J.; Nada, K.; Pang, X.; Honda, C.; Kitashiba, H.; Moriguchi, T. Role of polyamines in peach fruit development and storage. *Tree Physiol.* **2006**, *26* (6), 791−798.
(47) Kakkar, R. K.; Rai, V. K. Plant polyamines in flowering and fruit ripening. *Phytochemistry* **1993**, *33* (6), 1281−1288.
(48) Kondo, S.; Posuya, P.; Kanlayanarat, S. Changes in physical characteristics and polyamines during maturation and storage of rambutans. *Sci. Hortic.* **2001**, *91* (1−2), 101−109.
(49) Gomez-Jimenez, M. C.; Paredes, M. A.; Gallardo, M.; Sanchez-Calle, I. M. Mature fruit abscission is associated with up-regulation of polyamine metabolism in the olive abscission zone. *J. Plant Physiol.* **2010**, *167* (17), 1432−41.
(50) Oo, K.-C.; Teh, S.-K.; Khor, H.-T.; Ong, A. H. Fatty acid synthesis in the oil palm (Elaeis guineensis): Incorporation of acetate by tissue slices of the developing fruit. *Lipids* **1985**, *20* (4), 205−210.
(51) Gallardo, K.; Le Signor, C.; Vandekerckhove, J.; Thompson, R. D.; Burstin, J. Proteomics of Medicago truncatula seed development establishes the time frame of diverse metabolic processes related to reserve accumulation. *Plant Physiol.* **2003**, *133* (2), 664−82.
(52) Prasanna, V.; Prabha, T. N.; Tharanathan, R. N. Fruit ripening phenomena–an overview. *Crit. Rev. Food Sci. Nutrition* **2007**, *47* (1), 1−19.
(53) Coombe, B. G. The Development of Fleshy Fruits. *Ann. Rev. Plant Physiol.* **1976**, *27* (1), 207−228.
(54) Bonghi, C.; Rascio, N.; Ramina, A.; Casadoro, G. Cellulase and polygalacturonase involvement in the abscission of leaf and fruit explants of peach. *Plant Mol. Biol.* **1992**, *20* (5), 839−48.
(55) Roongsattham, P.; Morcillo, F.; Jantasuriyarat, C.; Pizot, M.; Moussu, S.; Jayaweera, D.; Collin, M.; Gonzalez-Carranza, Z.; Amblard, P.; Tregear, J.; Tragoonrung, S.; Verdeil, J.-L.; Tranbarger, T. Temporal and spatial expression of polygalacturonase gene family members reveals divergent regulation during fleshy fruit ripening and abscission in the monocot species oil palm. *BMC Plant Biol.* **2012**, *12* (1), 150.
(56) Smith, D. L.; Starrett, D. A.; Gross, K. C. A gene coding for tomato fruit beta-galactosidase II is expressed during fruit ripening. Cloning, characterization, and expression pattern. *Plant Physiol.* **1998**, *117* (2), 417−23.
(57) Guo, D.; Chen, F.; Inoue, K.; Blount, J. W.; Dixon, R. A. Downregulation of Caffeic Acid 3-O-Methyltransferase and Caffeoyl CoA 3-O-Methyltransferase in Transgenic Alfalfa: Impacts on Lignin Structure and Implications for the Biosynthesis of G and S Lignin. *Plant Cell Online* **2001**, *13* (1), 73−88.
(58) Choi, D.; Cho, H.-T.; Lee, Y. Expansins: expanding importance in plant growth and development. *Physiol. Plant.* **2006**, *126* (4), 511−518.
(59) (a) Li, Y.; Darley, C. P.; Ongaro, V.; Fleming, A.; Schipper, O.; Baldauf, S. L.; McQueen-Mason, S. J. Plant Expansins Are a Complex Multigene Family with an Ancient Evolutionary Origin. *Plant Physiol.* **2002**, *128* (3), 854−864. (b) Sampedro, J.; Cosgrove, D. J. The expansin superfamily. *Genome Biol.* **2005**, *6* (12), 242.

JOURNAL OF AGRICULTURAL AND FOOD CHEMISTRY

Article

pubs.acs.org/JAFC

# Lentinan Degradation in the *Lentinula edodes* Fruiting Body during Postharvest Preservation Is Reduced by Downregulation of the *exo*-*β*-1,3-Glucanase EXG2

Naotake Konno,*[,†,‡] Keiko Nakade,[†] Yosuke Nishitani,[§] Masashi Mizuno,[§] and Yuichi Sakamoto*[,†]

[†]Iwate Biotechnology Research Center, 22-174-4 Narita, Kitakami-shi, Iwate 024-0003, Japan

[‡]Department of Applied Biological Chemistry, Utsunomiya University, 350 mine-machi, Utsunomiya, Tochigi 321-8505, Japan

[§]Department of Agrobioscience, Graduate School of Agricultural Science, Kobe University, 1-1, Rokkodai-cho, Nada-ku, Kobe 657-8501, Japan

Supporting Information

**ABSTRACT:** Lentinan from *Lentinula edodes* fruiting bodies (shiitake mushrooms) is a valuable *β*-glucan for medical purposes based on its anticancer activity and immunomodulating activity. However, lentinan content in fruiting bodies decreases after harvesting and storage due to an increase in glucanase activity. In this study, we downregulated the expression of an *exo*-*β*-1,3-glucanase, *exg2*, in *L. edodes* using RNA interference. In the wild-type strain, *β*-1,3-glucanase activity in fruiting bodies remarkably increased after harvesting, and 41.7% of the lentinan content was lost after 4 days of preservation. The EXG2 downregulated strain showed significantly lower lentinan degrading activity (60−70% of the wild-type strain) in the fruiting bodies 2−4 days after harvesting. The lentinan content of fresh fruiting bodies was similar in the wild-type and EXG2 downregulated strains, but in the downregulated strain, only 25.4% of the lentinan was lost after 4 days, indicating that downregulation of EXG2 enables keeping the lentinan content high longer.

**KEYWORDS:** *shiitake mushroom, lentinan, β-glucan, β-glucanase*

## INTRODUCTION

The cell wall of fungi is typically composed of chitin, *β*-1,3-, and *β*-1,6-glucans. Among these cell-wall polysaccharides, several *β*-glucans from basidiomycetes have been reported to possess physiological activities.[1−3] *Lentinula edodes* (shiitake mushroom) is one of the most widely cultivated edible mushrooms and is highly valued for its medical applications. The water-soluble *β*-1,3-/1,6-glucans from *L. edodes* fruiting bodies are called lentinan[4] and have been reported to have anticancer and immunomodulating activity.[5−8] Lentinan is used clinically as an antitumor and antiallergy agent. Lentinan has a high molecular weight (degree of polymerization range 5400−8900) and a chemical structure of linear *β*-1,3-glucans with two *β*-1,6-glucosyl side chains every five residues.[9,10] It has been suggested that these features of lentinan, the main chain length and the extent of side chains, contribute to its physiological activities.[11]

Basidiomycetes such as *L. edodes* form fruiting bodies for sporulation, and the cell wall components of fruiting bodies undergo autolysis after sporulation or artificial harvesting.[12−15] Although lentinan can be purified from fresh *L. edodes* fruiting bodies, it is rapidly degraded during storage as a result of an increase in glucanase activity.[16,17] Minato et al. (1999) have reported that lentinan content decreases to less than half of the original during 5 days of storage at 20 °C. Previously, we isolated four *β*-glucanases, an *exo*-*β*-1,3-glucanase, EXG2, an *endo*-*β*-1,3-glucanase, TLG1, an *endo*-*β*-1,3-glucanase, GLU1, and an *endo*-*β*-1,6-glucanase, LePus30A, from *L. edodes* fruiting bodies 4 days after harvest.[13,18−20] These enzymes are produced in particular during fruiting body senescence and have the ability to degrade the cell-wall *β*-glucans in *L. edodes* fruiting bodies, suggesting they are involved in fruiting body autolysis.[14]

Among these *β*-glucanases, EXG2 shows the highest activity in vitro toward lentinan in reaction tests.[13] The complementary DNA of EXG2, *exg2*, includes an open reading frame of 2343 bp encoding a 21 amino acid signal peptide and a 759 amino acid mature protein. Sequence analysis indicated that EXG2 is a member of glycoside hydrolase (GH) family 55, and GH 55 *exo*-*β*-1,3-glucanases are found only in filamentous fungi (CAZy: http://www.cazy.org). The expression of *exg2* increases after harvesting, and this pattern correlates with a decrease in lentinan in *L. edodes* fruiting bodies. From these characteristics of EXG2, we deduced that the enzyme strongly enhances lentinan degradation in *L. edodes* fruiting bodies after harvesting.

Downregulation of gene expression in fruiting bodies has been reported in some basidiomycetes such as *Agaricus bisporus* and *Pleurotus ostreatus*.[21,22] Previously, we showed that RNA interference (RNAi) could be used for gene silencing in *L. edodes*.[23] RNAi is a post-transcriptional gene silencing phenomenon in which double-stranded RNA (dsRNA) triggers degradation of cognate mRNA in a sequence-specific manner. In this study, we downregulated the expression of the *exg2* gene in an *L. edodes* strain using RNAi and raised fruiting bodies of the *exg2* downregulated transformant (ivr-exg2#51). Analysis of

Received: April 7, 2014
Accepted: July 10, 2014
Published: July 17, 2014

 © 2014 American Chemical Society 

the phenotype of ivr-exg2#51 indicated that EXG2 is a key enzyme in lentinan degradation in *L. edodes* fruiting bodies after harvest.

## MATERIALS AND METHODS

**Strains and Culture Conditions.** A dikaryotic strain of *L. edodes* SR-1 was used as the recipient host in all transformation experiments. Mycelia were maintained on 0.25 × MYPG medium containing 0.25% Bacto malt extract (Difco, Detroit, MI, USA), 0.1% Bacto yeast extract (Difco), 0.1% tryptone peptone (Difco), and 0.5% glucose.

For postharvest preservation, fruiting bodies were prepared following a previously described method.[13] The harvested mature fruiting bodies were immediately transferred to a room at 25 °C with 80% humidity.[24] After harvest, fruiting bodies were sampled every day for 4 days, with day 0 being defined as corresponding to a fresh mature fruiting body just prior to postharvest preservation. After postharvest preservation, stipes were removed from samples and then immediately frozen in liquid nitrogen. For following enzymatic activity and lentinan content assays, three separate samples were prepared per data.

**Construction of the pChG′ and pChG′-ivrexg2 Vectors.** The pChG′-Gateway vector containing a multicloning site was constructed by Nakade et al. from vector pChG.[23,25] pChG′ was digested by *EheI*, and the Gateway cassette (Gateway Vector Conversion System; Invitrogen, CA, USA) was ligated into the digested pChG′ vector (pChG′-Gateway), then used to transform *Escherichia coli* competent cells (One Shot ccdB Survival cells, Invitrogen).

To construct the RNAi vectors, we synthesized the 250-bp short homologous hairpin dsRNA sequences of the *exg2*,[13] separated by a 60-bp spacer sequence of *lcc1* intron 2 (Figure S1, Supporting Information) (MediBIC Group, Co., Ltd., Tokyo, Japan). Synthesized DNA was inserted into vector pDONR221 (Invitrogen) and then transformed into pChG′-Gateway by an LR reaction (Invitrogen).

***L. edodes* Transformation.** The SR-1 strain was transformed with 2.5 μg of DNA of the above vectors by the restriction enzyme-mediated integration (REMI) method using 5.0 U *SphI*.[26] Transformants were selected on 0.25 × MYPG containing 20 μg mL$^{-1}$ of hygromycin B.

**Protein Extraction.** The frozen pileus and gill parts of the fruiting bodies (0−4 days after harvest, 2 g) were suspended in 0.5 mL of 100 mM sodium acetate buffer (pH 4.2) and mixed for 60 min at room temperature. The extracts containing protein were collected by centrifugation (10 000*g*, 20 min) and filtration (Ultrafree MC HV 0.45 μm filter, Merck Millipore, Darmstadt, Germany). The extracts were desalted and concentrated using an Amicon Ultra 10,000 NMWL filter (Merck Millipore), and 2 μg of the samples was used for Western blotting as described below.

**Protein Assays.** Protein concentration was measured by the Bradford method using the Bio-Rad Protein Assay kit (Bio-Rad Laboratory, CA USA) with a bovine serum albumin (BSA) (Pierce, Rockford, IL, USA) standard. Protein concentration was monitored by absorbance at 595 nm.

**Western Blotting.** For Western blot analysis, fruiting bodies after postharvest preservation and aging fruiting bodies were sampled as described above. Samples were frozen and crushed in liquid nitrogen, suspended in extraction buffer (200 mM sodium acetate, pH 4.2), and incubated by rotation for 15 min at room temperature. Electrophoresis and blotting were performed as described previously.[24] For Western blot analysis, EXG2 antiserum was used as the primary antibody, and antirabbit Ig conjugated with horseradish peroxidase was used as the secondary antibody. ECL detection reagents were used for detection (GE Healthcare, Little Chalfont, UK).[13]

**Measurement of Enzymatic Activity.** To measure enzymatic activity in the fruiting bodies, extracts prepared as above were assayed using lentinan (0.5%), pustulan (0.5%), Curdlan (1%), and *p*-nitrophenyl-*N*-acetyl-β-D-glucosaminide (pNP-GlcNAc, 0.5 mM, Sigma-Aldrich Inc., St. Louis, MO, USA) as substrates in 50 mM sodium acetate buffer (pH 4.2) at 37 °C. Reducing sugars liberated from lentinan, pustulan, and Curdlan were analyzed according to the Somogyi−Nelson method.[27] To assay pNP-GlcNAc, the amount of pNP was determined spectrophotometrically at 405 nm. The extinction coefficient of pNP was assumed to be 17 100 M$^{-1}$ cm$^{-1}$.[28] One unit (U) of enzyme activity was defined as the amount of enzyme that produces 1 μmol of reducing sugar per minute.

**Measurement of Lentinan Content in Fruiting Bodies.** The *L. edodes* fruiting body samples prepared as above (approximately 15 g) were freeze-dried and crushed. A water-soluble cell wall polysaccharide mixture was extracted by autoclaving in 20 mL of water (120 °C, 20 min). The hot-water extract was recovered from the supernatant by ethanol precipitation, and the dried precipitate was used for measurement of lentinan content. The lentinan content of the samples was determined by an ELISA inhibition assay with antilentinan antibodies prepared previously.[16,29]

## RESULTS AND DISCUSSION

**Constructing Downregulated Transformants of *exg2*.** An *exg2* homologous hairpin dsRNA expression vector (pChG′-ivr-exg2) was constructed (Figure S1, Supporting Information) and introduced to *L. edodes* using REMI-based transformation, allowing integration in the genome.[23,26] We obtained 67 transformants of pChG′-ivr-exg2; 6 transformants were selected and tested for EXG2 expression after harvesting of fruiting bodies. Expression of EXG2 in wild type increased after harvesting.[13] Expression of EXG2 in ivr-exg2#7 was higher, but its expression in #26, #39, and #51 was significantly suppressed (Figure 1). Expression of the β-glucanase TLG1

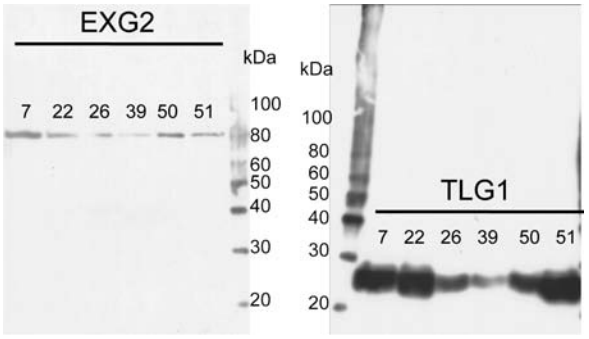


**Figure 1.** Western blot analysis of the crude enzyme from fruiting bodies 4 days after harvest. Selected transformants of pChG′-ivr-exg2 (ivr-exg2 #7, #22, #26, #39,#50, #51) were tested. Western blot analysis was performed using (A) EXG2 antiserum and (B) TLG1 antiserum.

was also suppressed in #26 and #39 for unknown reasons but was similar to wild-type levels in #51.[18] These results suggest that expression of *exg2* is specifically suppressed in ivr-exg2#51.

**Analyzing the Phenotype of ivr-exg2#51.** Fruiting bodies of the EXG2 downregulated transformant (ivr-exg2#51), the pChG′ vector transformant (pChG′), and the control (SR-1) were cultivated, harvested, and preserved for 4 days (Figure S2, Supporting Information). As shown in Figure 2, EXG2 production of ivr-exg2#51 in fruiting bodies preserved for 2−4 days was significantly suppressed compared to pChG′ and SR-1. The EXG2 suppression was also observed in the transcription level (Figure S3, Supporting Information).

Sakamoto et al. reported that EXG2 is involved in self-degradation of cell-wall β-1,3-glucans, causing lentinan degradation during postharvest preservation.[13] To analyze enzyme activity in the fruiting bodies after harvest, crude enzymes were extracted from fruiting bodies and tested for activity on substrates related to fungal cell-wall components. As shown in Figure 3A and 3B, β-1,3-glucanase activities of pChG′

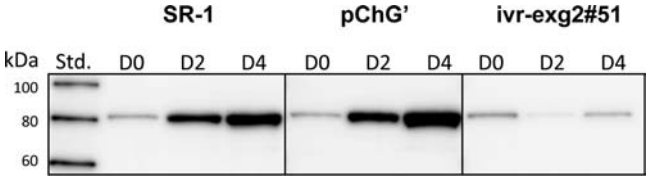


**Figure 2.** Western blotting pattern of extracts from the fruiting bodies of SR-1 (original strain), PchG′ (control strain), and an EXG2 downregulated strain (ivr-exg2#51) using EXG2 antibody. Fruiting bodies were preserved for 0−4 days after harvesting, and the extracts (2 $\mu$g of protein) were separated by SDS-PAGE.

and SR-1 remarkably increased after harvesting of fruiting bodies, whereas the activity of ivr-exg2#51 toward a water-soluble $\beta$-1,3/1,6-glucan (lentinan) was approximately 60−70% lower than that of pChG′ and SR-1. Moreover, the enzymatic activity against a water-insoluble $\beta$-1,3-glucan (Curdlan) was also decreased in the EXG2 downregulated strain; the activity of ivr-exg2#51 at day 2 was approximately 80% lower than that of SR-1 and pChG′, and the activity at day 4 was approximately 60−75% lower (Figure 3B). When $\beta$-1,6-glucan (pustulan) and artificial chitin oligosaccharide (pNP-GlcNAc) were used as substrates, no significant difference was observed in enzymatic activity (Figure 3C and 3D). These results indicate that downregulation of EXG2 specifically caused the reduction of $\beta$-1,3-glucanase activity in the fruiting bodies after harvest.

The lentinan content of hot-water extracts prepared from *L. edodes* fruiting bodies was determined using antibody-based detection.[16,29] The lentinan content of fresh fruiting bodies (D0) was almost similar, 4.1−5.5 mg/g dry weight (dw) in SR-1, pChG′, and ivr-exg2#51. Table 1 shows the changes in lentinan content in the fruiting bodies after harvest; 60.6% of the lentinan content was lost in SR-1, and 61.9% was lost in pChG′ after 4 days of preservation. However, the loss in lentinan content of ivr-exg2#51 after 4 days of preservation was only 27.5%, demonstrating that ivr-exg2#51 preserves the lentinan content over a longer time than the original strain.

**Table 1. Changes in Lentinan Content in the Fruiting Bodies of SR-1 (Original Strain), pChG′ (Control Strain), and an EXG2 Downregulated Strain (ivr-exg2#51) after Harvesting[a]**

| | D0 (mg/g dw) | D4 (mg/g dw) | residual ratio (%) |
|---|---|---|---|
| SR-1 | 4.16 ± 0.69 | 1.64 ± 1.07 | 39.4 |
| pChG′ | 4.70 ± 0.89 | 1.80 ± 1.00 | 38.1 |
| ivr-exg2#51 | 5.45 ± 0.35 | 3.95 ± 1.30 | 72.5 |

[a]The data indicate means ± SD ($n$ = 3 samples).

Previously, we purified two other $\beta$-1,3-glucanases, TLG1 and GLU1, next to EXG2 from harvested *L. edodes* fruiting bodies.[18,19] These two enzymes are also expressed in fruiting bodies after harvest, suggesting that they are involved in fruiting body senescence. The $\beta$-1,3-glucanase activity and the decrease in lentinan content in harvested ivr-exg2#51 fruiting bodies might be caused primarily by the actions of TLG1 and GLU1. However, their $\beta$-1,3-glucanase activities are weaker than that of EXG2. Moreover, TLG1 and GLU1 have been suggested to have strict substrate specificity for $\beta$-1,3-glucan polymers; $\beta$-1,6-linkages within $\beta$-1,3/1,6-glucan would prevent hydrolysis of the $\beta$-1,3-linkages, and the enzymes showed low activity toward $\beta$-1,3-glucan oligomers. Therefore, TLG1 and GLU1 might only perform a partial degradation of cell-wall $\beta$-1,3-glucans at the fruiting body senescence stage. On the other hand, EXG2 can cleave almost all $\beta$-1,3-linkages within $\beta$-1,3-glucans and $\beta$-1,3/1,6-glucans regardless of their length and branching structure.[30] Indeed, lentinan is completely degraded to glucose and gentiobiose by the exotype manner of action of EXG2.[15] EXG2 belongs to GH 55, and the crystal structure of a GH 55 *exo*-$\beta$-1,3-glucanase from the basidiomycete *Phanerochaete chrysosporium*, homologous to EXG2 from *L. edodes*, has been reported.[30] This *P. chrysosporium* enzyme appears to be able to accept a gentiobiose unit in the cleavage site owing to its substrate-binding pocket structure, suggesting that GH 55 *exo*-

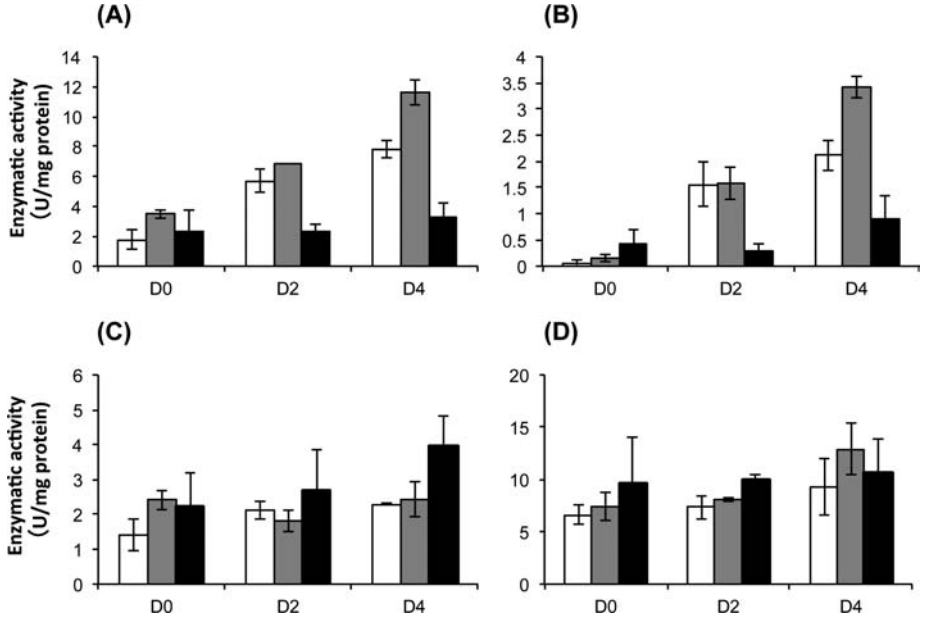


**Figure 3.** Changes in enzymatic activities in the fruiting bodies of SR-1 (original strain, white), pChG′ (control strain, gray), and an EXG2 downregulated strain (ivr-exg2#51, black) after harvesting. Lentinan (A), Curdlan (B), pustulan (C), and pNP-GlcNAc (D) were used as substrates. The data indicate means ± SD ($n$ = 3 samples).


dx.doi.org/10.1021/jf501578w | J. Agric. Food Chem. 2014, 62, 8153−8157

$\beta$-1,3-glucanases can bypass the $\beta$-1,6-glucosyl side chains in lentinan. In this study, approximately 75% of the lentinan content in *L. edodes* was preserved for 4 days by the downregulation of only EXG2. This suggests that EXG2 is the most effective $\beta$-1,3-glucanase in cell-wall autolysis of fruiting bodies after artificial harvesting. Lentinan from *L. edodes* fruiting bodies is a very valuable polysaccharide for medical applications because of its anticancer activity and immunomodulating activity. Lentinan is obtained only from fresh fruiting bodies and decreases rapidly during postharvest storage due to the actions of $\beta$-1,3-glucanases. This study indicates that a knockout or downregulation of EXG2 in *L. edodes* enables a significantly more stable supply of lentinan.

## ■ ASSOCIATED CONTENT

### Supporting Information

Construction of a RNAi vector pChG′-ivr-exg2 (Figure S1). Pictures of fruiting body of the EXG2 downregulated transformant (Figure S2). Analysis of the transcription level of the exg2 gene in the fruiting bodies of SR-1 (original strain), pChG′ (control strain), and an EXG2 downregulated strain (ivr-exg2#51) after harvesting. This material is available free of charge via the Internet at http://pubs.acs.org.

## ■ AUTHOR INFORMATION


### Corresponding Authors

*Tel.: +81-197-68-2911. Fax: +81-197-68-3881. E-mail: sakamoto@ibrc.or.jp (Y. Sakamoto).

*E-mail: konno@cc.utsunomiya-u.ac.jp (N. Konno).



### Funding

This research was supported by a Grant-in-Aid for Scientific Research to N.K. (no. 2510648) from the Japan Society for the Promotion of Science (JSPS), by grants for project research (Development of fundamental technology for analysis and evaluation of functional agricultural products and functional foods), and by the Japan Science and Technology Agency (JST).


### Notes

The authors declare no competing financial interest.

## ■ ACKNOWLEDGMENTS


We thank Akiko Uchidate, Miyuki Ito, Ayumi Obara, Junko Kawaguchi, and Shiho Sato for their help with experiments. We are grateful to Dr. Arend F. van Peer for his suggestions and comments.


## ■ REFERENCES


(1) Bottom, C. B.; Sierhr, D. J. Structure of an alkali-soluble polysaccharide from the hyphal wall of the basidiomycete *Coprinus macrorhizus* var. *microsporus*. *Carbohydr. Res.* **1979**, *77*, 169−181.

(2) Mol, P. C.; Wessels, J. G. H. Differences in wall structure between substrate hyphae and hyphae of fruit body stipes in *Agarucus bisporus*. *Mycol. Res.* **1990**, *94*, 472−479.

(3) Wessels, J. G. H.; Kreger, D. R.; Marchant, R.; Regensburg, B. A.; De Vries, O. M. Chemical and morphological characterization of the hyphal wall surface of the basidiomycete *Schizophyllum commune*. *Biochim. Biophys. Acta* **1972**, *273*, 346−358.

(4) Shida, M.; Ushioda, Y.; Nakajima, T.; Matsuda, K. Structure of the alkali-insoluble skeltetal glucan of *Lentinus edodes*. *J. Biochem.* **1981**, *90*, 1093−1100.

(5) Chihara, G.; Maeda, Y.; Hamuro, J.; Sasaki, T.; Fukuoka, F. Inhibition of mouse srcoma 180 by polysaccharides from *Lentinus edodes* (Berk.) Sing. *Nature* **1969**, *222*, 687−688.

(6) Mizuno, M.; Nishitani, Y.; Hashimoto, T.; Kanazawa, K. Different suppressive effects of fucoidan and lentinan on IL-8 mRNA expression in in vitro gut inflammation. *Biosci. Biotechnol. Biochem.* **2009**, *73*, 2324−2325.

(7) Xu, X.; Pan, C.; Zhang, L.; Ashida, H. Immunomodulatory $\beta$-glucan from *Lentinus edodes* activates mitogen-activated protein kinases and nuclear factor-kappaB in murine RAW 264.7 macrophages. *J. Biol. Chem.* **2011**, *286*, 31194−31198.

(8) Xu, X.; Yasuda, M.; Nakamura-Tsuruta, S.; Mizuno, M.; Ashida, H. $\beta$-Glucan from *Lentinus edodes* inhibits nitric oxide and tumor necrosis factor-$\alpha$ production and phosphorylation of mitogen-activated protein kinases in lipopolysaccharide-stimulated murine RAW 264.7 macrophages. *J. Biol. Chem.* **2012**, *287*, 871−878.

(9) Chizhov, A. O.; Dell, A.; Morris, H. R.; Reason, A. J.; Haslam, S. M.; McDowell, R. A.; Chizhov, O. S.; Usov, A. I. Structural analysis of laminarans by MALDI and FAB mass spectrometry. *Carbohydr. Res.* **1998**, *310*, 203−210.

(10) Kim, Y. T.; Kim, E. H.; Cheong, C.; Williams, D. L.; Kim, C. W.; Lim, S. T. Structural characterization of $\beta$-D-(1−>3, 1−>6)-linked glucans using NMR spectroscopy. *Carbohydr. Res.* **2000**, *328*, 31−41.

(11) Adams, E. L.; Rice, P. J.; Graves, B.; Ensley, H. E.; Yu, H.; Brown, G. D.; Gordon, S.; Monteiro, M. A.; Papp-Szabo, E.; Lowman, D. W.; Power, T. D.; Wempe, M. F.; Williams, D. L. Differential high-affinity interaction of dectin-1 with natural or synthetic glucans is dependent upon primary structure and is influenced by polymer chain length and side-chain branching. *J. Pharmacol. Exp. Ther.* **2008**, *325*, 115−123.

(12) Kües, U. Life history and developmental processes in the basidiomycete *Coprinus cinereus*. *Microbiol. Mol. Biol. Rev.* **2000**, *64*, 316−353.

(13) Sakamoto, Y.; Minato, K.; Nagai, M.; Kawakami, S.; Mizuno, M.; Sato, T. Characterization of the *Lentinula edodes exg2* gene encoding a lentinan-degrading exo-$\beta$-1,3-glucanase. *Curr. Genet.* **2005**, *48*, 195−203.

(14) Sakamoto, Y.; Nakade, K.; Sato, T. Characterization of the post-harvest changes in gene transcription in the gill of the *Lentinula edodes* fruiting body. *Curr. Genet.* **2009**, *55*, 409−423.

(15) Sakamoto, Y.; Nakade, K.; Konno, N.; Sato, T. Senescence of the *Lentinula edodes* fruiting body after harvesting. *Food Quality*; 2012; Chapter 6, pp 83−110, ISBN: 978-953-51-0560-2.

(16) Minato, K.; Mizuno, M.; Terai, H.; Tsuchida, H. Autolysis of lentinan, an antitumor polysaccharide, during storage of *Lentinus edodes*, Shiitake mushroom. *J. Agric. Food Chem.* **1999**, *47*, 1530−1532.

(17) Minato, K.; Kakawami, S.; Nomura, K.; Tsuchida, H.; Mizuno, M. An exo-$\beta$-1,3 glucanase synthesized de novo dgrades lentinan during storage of *Lentinula edodes* and diminishes immunomodulationg activity of the mushroom. *Carbohydr. Polym.* **2004**, *56*, 279−286.

(18) Sakamoto, Y.; Watanabe, H.; Nagai, M.; Nakade, K.; Takahashi, M.; Sato, T. *Lentinula edodes tlg1* encodes a thaumatin-like protein that is involved in lentinan degradation and fruiting body senescence. *Plant Physiol.* **2006**, *141*, 793−801.

(19) Sakamoto, Y.; Nakade, K.; Konno, N. Endo-$\beta$-1,3-glucanase GLU1, from the fruiting body of *Lentinula edodes*, belongs to a new glycoside hydrolase family. *Appl. Environ. Microbiol.* **2011**, *77*, 8350−8354.

(20) Konno, N.; Sakamoto, Y. An endo-$\beta$-1,6-glucanase involved in *Lentinula edodes* fruiting body autolysis. *Appl. Microbiol. Biotechnol.* **2011**, *91*, 1365−1373.

(21) Eastwood, D. C.; Challen, M. P.; Zhang, C.; Jenkins, H.; Henderson, J.; Burton, K. S. Hairpin-mediated down-regulation of the urea cycle enzyme argininosuccinate lyase in *Agaricus bisporus*. *Mycol. Res.* **2008**, *112*, 708−716.

(22) Salame, T. M.; Knop, D.; Tal, D.; Levinson, D.; Yarden, O.; Hadar, Y. Predominance of a versatile-peroxidase-encoding gene, mnp4, as demonstrated by gene replacement via a gene targeting system for *Pleurotus ostreatus*. *Appl. Environ. Microbiol.* **2012**, *78*, 5341−5352.

(23) Nakade, K.; Watanabe, H.; Sakamoto, Y.; Sato, T. Gene silencing of the *Lentinula edodes* lcc1 gene by expression of a

homologous inverted repeat sequence. *Microbiol. Res.* **2011**, *166*, 484−493.
(24) Sakamoto, Y.; Irie, T.; Sato, T. Isolation and characterization of a fruiting body-specific exo-β-1,3-glucanase-encoding gene, *exg1*, from *Lentinula edodes*. *Curr. Genet.* **2005**, *47*, 244−252.
(25) Sato, T.; Okawa, K.; Hirano, T. Construction of novel vectors for transformation of *Lentinula edodes* using a chitin synthase gene promoter. *J. Biosci. Bioeng.* **2011**, *111*, 117−120.
(26) Sato, T.; Yaegashi, K.; Ishii, S.; Hirano, T.; Kajiwara, S.; Shishido, K.; Enei, H. Transformation of the edible basidiomycete *Lentinus edodes* by restriction enzyme-mediated integration of plasmid DNA. *Biosci. Biotechnol. Biochem.* **1998**, *62*, 2346−2350.
(27) Somogyi, M. Notes on sugar determination. *J. Biol. Chem.* **1952**, *195*, 19−23.
(28) Konno, N.; Takahashi, H.; Nakajima, M.; Takeda, T.; Sakamoto, Y. Characterization of β-N-acetylhexosaminidase (LeHex20A), a member of glycoside hydrolase family 20, from *Lentinula edodes* (shiitake mushroom). *AMB Express* **2012**, *2*, 29.
(29) Mizuno, M.; Minato, K.; Tsuchida, H. Preparation and specificity of antibodies to an anti-tumor β-glucan, lentinan. Biochem. *Mol. Biol. Int.* **1996**, *39*, 679−685.
(30) Ishida, T.; Fushinobu, S.; Kawai, R.; Kitaoka, M.; Igarashi, K.; Samejima, M. Crystal structure of glycoside hydrolase family 55 β-1,3-glucanase from the basidiomycete *Phanerochaete chrysosporium*. *J. Biol. Chem.* **2009**, *284*, 10100−10109.

JOURNAL OF AGRICULTURAL AND FOOD CHEMISTRY

Article

pubs.acs.org/JAFC

# Evaluation of Unintended Effects in the Composition of Tomatoes Expressing a Human Immunoglobulin A against Rotavirus

Paloma Juarez, Asun Fernandez-del-Carmen, Jose L. Rambla, Silvia Presa, Amparo Mico, Antonio Granell, and Diego Orzaez*

Instituto de Biología Molecular y Celular de Plantas, Consejo Superior de Investigaciones Científicas, Universidad Politécnica de Valencia, Camino de Vera s/n, 46022 Valencia, Spain

Supporting Information

**ABSTRACT:** The production of neutralizing immunoglobulin A (IgA) in edible fruits as a means of oral passive immunization is a promising strategy for the inexpensive treatment of mucosal diseases. This approach is based on the assumption that the edible status remains unaltered in the immunoglobulin-expressing fruit, and therefore extensive purification is not required for mucosal delivery. However, unintended effects associated with IgA expression such as toxic secondary metabolites and protein allergens cannot be dismissed a priori and need to be investigated. This paper describes a collection of independent transgenic tomato lines expressing a neutralizing human IgA against rotavirus, a mucosal pathogen producing severe diarrhea episodes. This collection was used to evaluate possible unintended effects associated with recombinant IgA expression. A comparative analysis of protein and secondary metabolite profiles using wild type lines and other commercial varieties failed to find unsafe features significantly associated with IgA expression. Preliminary, the data indicate that formulations derived from IgA tomatoes are as safe for consumption as equivalent formulations derived from wild type tomatoes.

**KEYWORDS:** *tomato, IgA, antibody, rotavirus, unintended effects, metabolomics, proteomics*

## INTRODUCTION

Antibody-based treatments for mucosal passive immunization (MPI) have great potential in human and veterinary medicine for the prevention of infection diseases. MPI is particularly advantageous for the treatment of enteric diseases.[1−3] Generally, passive antibody-based treatments require large amounts of antibodies to be delivered to the target mucosa to ensure protection.[4] The high specificity of recombinant monoclonal antibodies makes them excellent candidates for MPI; however, the increasing costs of producing recombinant antibodies in the preferred mammalian cell platforms has hampered their use in MPI.

As an alternative, neutralizing recombinant antibodies aimed at MPI can be inexpensively produced in edible plant organs. Many seeds, fruits, leaves, tubers, and roots are considered safe and palatable for human consumption in minimally processed formulations without heat treatment;[5] therefore, it has been proposed that antibodies produced in plant organs with generally regarded as safe (GRAS) status could be delivered as dose-controlled ingredients in partially processed formulations without the need for exhaustive purification.[4] This would certainly reduce the manufacturing costs, as plant platforms are reportedly easier to scale up than other platforms, for example, those based on fermentation.[5]

The lack of exhaustive purification can, on the other hand, become a drawback when the composition of the final product ultimately results from an event of genetic modification. It could be argued that, besides producing a recombinant antibody, transgenesis could eventually lead to unintended effects in the final fruit composition.[6,7] Such unintended effects could be derived from the integration of the transgene, from biological interactions caused by transgene-encoding proteins, or from spurious somaclonal mutations. Unintended effects have become one of the most controversial issues in biological safety debates.[8] Despite the evidence accumulated during the past 20 years indicating that transgenesis could be even less disruptive of food composition than traditional breeding,[8−10] the absence of unintended, deleterious effects in the composition of genetically modified edible plants organs expressing recombinant antibodies has never been assessed.

Recently, our group reported a model human immunoglobulin A (IgA) for passive protection against the enteric pathogen rotavirus, produced in transgenic tomato fruits. Dry formulations suitable for oral intake and compatible with long-term storage presented a high concentration of active antibodies (≈0.7 mg/g DW), which were shown to inhibit virus infections in an in vitro virus neutralization assay. Thus, minimally processed fruit-derived formulations containing recombinant IgA were proposed as potential vehicles for low-cost MPI treatments.[11] The availability of IgA-producing fruits provides an opportunity to test for the possible unintended effects that the expression of a human antibody could have on the final composition of the fruit and to infer the possible deleterious effects on human health that such unintended effects could have.

Safety concerns in tomato fruit composition arise fundamentally from two sources: proteins (allergens) and secondary metabolites (toxicants). So far, only three tomato protein allergens, Lyc e 1 (profilin), Lyc e 2 (invertase), and Lyc e 3

Received: May 16, 2014
Revised: July 18, 2014
Accepted: July 27, 2014
Published: July 28, 2014

ACS Publications © 2014 American Chemical Society

(nonspecific lipid transfer protein), are listed in the official International Union of Immunological Societies (IUIS) allergen database, although additional potential allergens have been reported.[12−16] To investigate the changes in the fruit protein profile associated with the overexpression of recombinant proteins, a proteomic analysis is required. Proteomics is a powerful nontargeted tool that can be used to detect unintended differences derived from genetic manipulation. Proteomics-based approaches have been used a number of times to compare protein profiles of transgenic maize,[17] tomato,[18] or potato[19,20] with their nontransgenic counterparts.[8]

A second possible source of concern is the presence of toxic metabolites. Fruits are rich in chemically diverse compounds, which can be present in a wide range of different concentrations. The most important toxicants in tomatoes are the steroidal glycoalkaloids $\alpha$-tomatine and dehydrotomatine. Tomato glycoalkaloids are synthesized in tomato fruits during early development and then degraded during fruit maturation.[21−24] There is no analytical method capable of extracting and detecting all metabolites; however, in the past two decades, several methods have been established for large-scale analysis and comparison of metabolites in plant extracts.[8,25] Among them, ultraperformance liquid chromatography−mass spectrometry (UPLC-MS) specifically allows the detection and quantification of semipolar secondary metabolites, which is the major source of potential toxicants.

The goal of this work was to examine a broad set of components in the fruit to search for unintended effects produced by the expression of a human IgA, which could eventually affect the safety of minimally processed formulations derived from IgA tomatoes. First, a protein profile analysis was performed to detect possible changes associated with the production of human IgA in the fruit. Next, the metabolomic profile of IgA tomatoes was compared to that of nontransgenic tomatoes to detect possible unintended effects in the semipolar secondary metabolite pool.

## MATERIALS AND METHODS

**Plant Material.** Seven transgenic lines (A, B, D, F, G, H, and I) of tomato (*Solanum lycopersicum* cv. Moneymaker) expressing human IgA were used in this study along with the parental line, K, used for genetic transformation. Lines A, B, and D were obtained by *Agrobacterium*-mediated transformation of a plasmid carrying the heavy (HC) and light chains (LC) of human IgA under the cauliflower mosaic virus 35s constitutive promoter and the tomato NH fruit promoter,[26] respectively. Lines F, G, H, and I were obtained by cotransformation with two *Agrobacterium* cultures, one carrying a plasmid with the 35s:IgA_HC and the second carrying a plasmid with the 35s:IgA_LC construct. A detailed description of the generation of these transgenic lines can be found in Juarez et al.[11] Additionally, two nullizygote segregant lines, C and E, from the 35S:IgA_HC/NH:IgA_LC transformation, and one wild type moneymaker line, J, obtained from a different laboratory were also included as additional controls. Finally, fruits from three widely consumed tomato varieties, plum (L), round (M), and cherry (N), purchased from a local grocery completed the experimental data set. Tomato seeds (excluding commercial lines L, M, and N) were grown in pots in a greenhouse with a light/dark cycle of 16/8 h. Fruits were harvested 15 days postbreaker. Five independent samples from each plant line were collected. After removal of the gel and seeds, tomato pericarp (with the peel) was ground to a fine powder in liquid nitrogen and stored at −80 °C for further analysis.

**Protein Analysis.** For antibody analysis, frozen tomato powder samples from each group were pooled together. Total soluble protein (TSP) extraction, Western blots, and ELISA tests for IgA quantification were developed as previously described.[11] Proteomic profiling, protein precipitation, fluorescent labeling, 2D electrophoresis, and protein identification by mass spectrometry (MALDI, LC-MS/MS) were developed as previously described.[27] To identify differentially regulated proteins, each 2D gel was loaded with three samples: a transgenic line, a nontransgenic line, and an internal standard (Figure 2a, blue). The internal standard was composed of a pool of all the transgenic and nontransgenic samples used in the analysis. Each of the three samples in a gel was labeled with a different CyDye (Cy2, Cy3, and Cy5). 2D gels were scanned using a Typhoon Trio (GE Healthcare). The three different images corresponding to each fluorophore were overlapped, and the spots from the different gels were matched. Gel image analysis was performed with DeCyder 2D software v. 6.5. Principal component analysis (PCA) was performed with the software package SIMCA-P 11 (Umetrics, Sweden). Sample J was not included in the PCA plot to improve visualization. The PCA plot with the complete set of samples is shown in Supplementay Figure 1 in the Supporting Information.

**UPLC-QTOF and Data Processing.** Ultraperformance liquid chromatography−quadrupole time of flight (UPLC-QTOF) analysis of tomato powder was performed as previously described,[28] with minor modifications. Following extraction in 3 volumes of cold (−20 °C) methanol acidified with 0.125% formic acid, the supernatant was dried (in two separate 750 $\mu$L aliquots) in a Speed-Vac and stored at −80 °C. Prior to analysis, dry extracts were solubilized in 150 $\mu$L of methanol−0.1% formic acid and filtered through a 0.2 $\mu$m Anotop 10 membrane filter (Whatman, Kent, UK). Samples were analyzed by UPLC-MS using an ACQUITYUPLC-PDA system coupled to a Q-Tof micro mass spectrometer (Waters Corp., Milford, MA, USA).[28] Mass spectrometry analysis was performed by electrospray ionization (ESI) in positive and negative modes (using one of the extract aliquots for each ionization mode). A reference sample (made by pooling equal amounts of all biological samples) was injected four times (at regular intervals) in each injection series. MassLynx raw files converted to netCDF format with DataBridge (Waters Corp.) were processed with XCMS package v. 1.34.0 (http://bioc.ism.ac.jp/2.11/bioc/html/xcms.html) run under R v. 2.15.2 (http://www.r-project.org/). The centWave algorithm[29] was used for feature detection; peak grouping and retention time correction were performed with the density and peakgroups algorithms,[30] respectively. Mass features were grouped using the CAMERA algorithm.[31] The area of each extracted mass feature was first normalized to the total chromatogram area; the reference sample was then used to normalize the data between different runs (for each mass feature, the test sample area is divided by the mean area of the reference samples included in that run). Preprocessing of the data generated two discrete data files, one for each ionization mode: ESI− (electrospray ionization in negative mode) and ESI+ (electrospray ionization in positive mode). The ESI− data set contained 386 mass variables, whereas 835 peaks were initially identified in the ESI+ mass profile. To remove low-quality data, a first filtering step was done by imposing two different conditions: (i) a mass feature should be detectable in a minimum of three biological replicates in at least one of the tomato lines, and (ii) the average-day coefficient of variation for the reference sample (computed on normalized data) should not be greater than 40%. Mass peaks that did not fulfill these requirements were considered unreliable and were excluded from the study. A second filtering step was accomplished by removing the redundant isotopic features, which were identified by the package CAMERA (a collection of algorithms for metabolite profile annotation with the primary purpose of annotation and evaluation of isotope peaks, adducts, and fragments in peak lists).[31] The final ESI− and ESI+ data sets, with 107 and 246 peaks, respectively, were joined together in a single matrix for further analysis.

**Statistical Data Analysis.** PCA and OPLS-DA of the protein and metabolite profiles of tomato fruits were performed with the software package SIMCA-P 11 (Umetrics). Variables were log-transformed, mean centered, and scaled to unit variance prior to analysis. Two-sample *t* tests on log transform data were performed using MeV v4.9 (http://www.tm4.org/mev.html), an application of the TM4Microarray Software Suite.[32] Safety thresholds in the proof-of-safety analysis

were defined by the symmetric maximum boundaries of the nonparametric 90% confidence intervals for the ratio to WT of the commercial variety farthest away from the WT. Safety was concluded when the confidence intervals for the ratio to control of the transgenic lines were within the safety limits. For the calculations of the confidence intervals the R package pairwise CI was used.

## RESULTS

**Evaluation of IgA Content in the Fruit.** To detect unintended changes in fruit composition, two types of IgA-producing plants were selected for analysis. The first group was generated in cotransformation experiments (referred to as 35S_IgA) in which tomato explants were simultaneously cotransformed with two *Agrobacterium* cultures carrying HC and LC antibody chains, respectively, both of them expressed under the control of constitutive 35S promoter. In the second group (referred to as NH_IgA), both HC and LC were linked in the same T-DNA, with LC placed under the control of the tomato NH promoter.[26] In the second generation (T2), different segregating lines were obtained. Some NH_IgA segregant lines lacking the transgene (nullizygotes) were selected to serve as appropriate negative controls in subsequent assays. All cotransformed 35s-IgA segregants showed at least one of the two antibody chains. As a consequence, no 35S_IgA nullizygote could be included in the analysis. In total, seven independent transgenic lines from both groups (NH_IgA and 35s_IgA) showing a broad range of IgA levels were used in the different comparative analyses (see Table 1). This includes an

**Table 1. IgA Levels Referred to Fresh Weight (FW) and to Total Soluble Protein (TSP) in Tomato Fruit in All Lines**

| ID | line | total IgA ($\mu$g/gFW) | total IgA (% TPS) |
|---|---|---|---|
| A | NH-IgA | 2.5 ± 0.3 | 0.2 ± 0.1 |
| B | NH-IgA | 5.7 ± 1.6 | 0.4 ± 0.1 |
| C | NH-IgA nullizygote | 0 | 0 |
| D | NH-IgA | 1.9 ± 0.3 | 0.2 ± 0.1 |
| E | NH-IgA nullizygote | 0 | 0 |
| F | 35s_IgA | 13.0 ± 2.2 | 1.0 ± 0.2 |
| G | 35s_IgA | 25.5 ± 6.5 | 2.0 ± 0.5 |
| H | 35s_IgA | 20.9 ± 5.2 | 1.6 ± 0.4 |
| I | 35s_IgA homozygous | 37.5 ± 5.2 | 2.9 ± 0.4 |
| J | Moneymaker seed batch 1 | 0 | 0 |
| K | Moneymaker seed batch 2 | 0 | 0 |
| L | plum | 0 | 0 |
| M | round | 0 | 0 |
| N | cherry | 0 | 0 |

"elite" T4 homozygous IgA line (line I) previously selected from the 35S_IgA group for its high antibody levels. A number of IgA-free control lines were also included, which comprised (i) the above-mentioned nullizygote plants from the segregating NH_IgA lines, (ii) two wild type Moneymaker lines from different seed batches, and (iii) three commercial tomato varieties purchased from a local supermarket (L, M, and N).

Tomato plants of all noncommercial lines were grown in the same greenhouse conditions. Fruits were collected 15 days after breaker stage, and frozen tomato powder of each fruit was prepared. The first analytical step consisted on the determination of the antibody content of the different lines. For this, frozen tomato powder samples were extracted in PBS buffer, and the IgA content in the resulting crude extracts was quantified by means of ELISA. As expected, the "elite" homozygous 35S_IgA line (line I) showed the highest IgA levels, with an average content of 37.5 $\mu$g/g FW. The IgA content of the remaining transgenic lines ranged from 25.5 to 1.9 $\mu$g IgA/g FW (see Table 1). To check the integrity of the IgA in the powder samples, 20 transgenic fruits (4 pools of 5 fruits) were analyzed by Western blot. As expected, specific bands corresponding to the HC (55 kDa) and the LC (28 kDa) were detected in all of the transgenic samples analyzed. A major degradation HC fragment band of 28 kDa HC was also observed in blots developed with anti-HC antibody. This degradation corresponds to the HC domains of reduced fragment antigen-binding (Fab) fragments and was earlier characterized by Juarez et al.[11] In all cases the relative expression levels observed in Western blots were consistent with the ELISA quantification. Neither HC nor LC bands were detected in nontransgenic control samples (Figure 1).

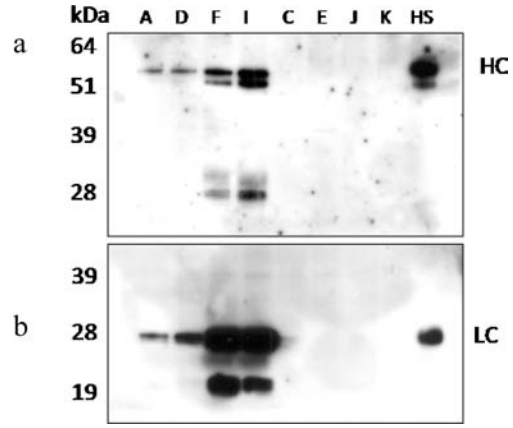


**Figure 1.** Western blot analysis of IgA expression in tomato fruit: (a) Western blot under reducing conditions, developed with anti-heavy chain antibody (HC); (b) Western blot under reducing conditions developed with anti-light chain antibody (LC). Lanes: A and D, NH_IgA lines; F and I, 35S_IgA lines; C and E, nullizygote; J and K, wild type Moneymaker samples from two different seed batches; HS, human serum sample.

**Identification of Differentially Expressed Proteins in IgA Tomatoes by 2D-DIGE and LC-MSMS.** The first assessment of the fruit content was directed to the analysis of the protein composition by 2D-DIGE. A total of eight tomato lines were included in the analysis: four selected IgA lines covering the whole IgA expression range were paired with samples from four nontransgenic lines, which included two in-house-grown Moneymaker plants as well as two NH_IgA nullizygote plants. The NH_IgA tomato samples (A and D from Table 1) were paired with their corresponding nullizygote samples (C and E), in two gels. The other two gels were loaded with 35s_IgA samples (F and I), each one in combination with a different wild type sample (J and K). A total of 1001 spots were located in the four gels. Differential proteins are shown as green spots (with higher levels in transgenic line) or red spots (with higher levels in the control line) (Figure 2). All spots were quantified, and the resulting data were used for the comparative analysis between the composition of the different samples.

A principal component analysis (PCA) was performed with the quantitative data extracted from the quantification of protein spots in the gels (Figure 3). The first two principal components of this PCA model explain 28 and 23% of the total


dx.doi.org/10.1021/jf502292g | J. Agric. Food Chem. 2014, 62, 8158−8168

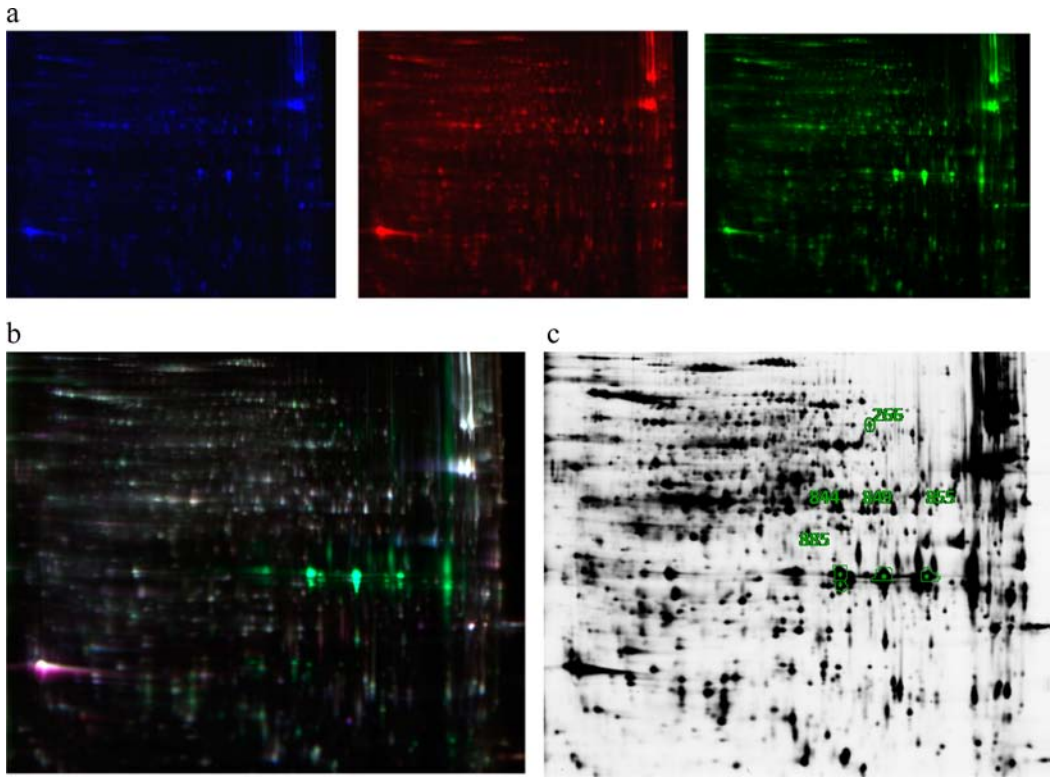


**Figure 2.** Representative 2D DIGE gel of tomato fruit proteins: (a) fluorescence images of gel loaded with equal amounts (50 $\mu$g) of the reference sample (Cy2-labeled, blue), nontransgenic samples (Cy5-labeled, red), and transgenic samples (Cy3-labeled, green); (b) overlay of the three fluorescence images (differential proteins appear in green or red; unaffected proteins appear in white); (c) silver-stained 2D DIGE gel (spots showing significant differences between transgenic and nontransgenic samples are outlined in green).

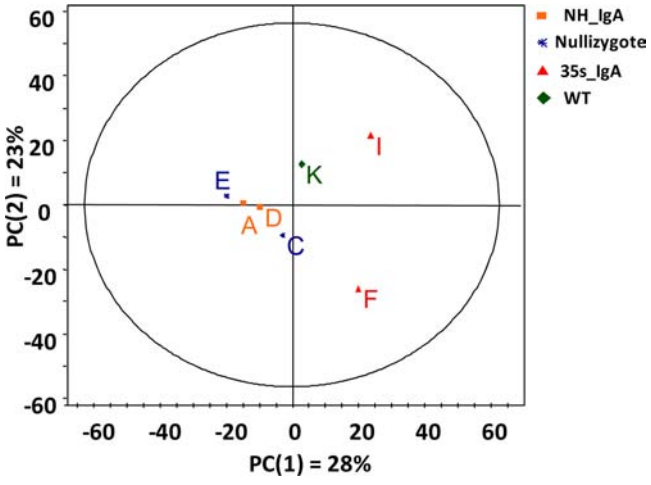


**Figure 3.** PCA of proteomic data of transgenic and nontransgenic tomato lines. Capital letters represent the different tomato lines as described in Table 1. Sample J, which behaves as an outlier, is not included in the plot to improve visualization.

variance, respectively. PC1 slightly separates 35s_IgA lines (F and I) from the rest of the group, which remain together in the scores space. PC2 further discriminates between both 35s_IgA lines (F and I). Interestingly, all samples derived from NH_IgA transformation events (both transgenic and nullizygote) remain closely grouped in the PCA model.

To identify those spots that are the main contributors for class separation, a quantitative comparison between transgenic and nontransgenic lines was performed. From a total of 37 spots showing average ratio higher than 2 (|ratio| > 2), only 19 of them showed an increase in both 35s_IgA and NH_IgA lines when considered separately, and only 5 of these 19 were found statistically significant ($P < 0.05$) (Figure 2c, outlined in green). The identification of all 19 selected spots by LC-MS/MS is shown in Table 2. All spots were identified as HC or LC with the exception of spot 783, which corresponded to a mix of human HC and tomato ACC oxidase.

**Metabolic Profiling by UPLC-MS for the Evaluation of Unintended GM Effects.** Unintended effects on the metabolome of transgenic tomato fruits generated by the expression of human IgA were also evaluated by nontargeted metabolomics. Tomato methanol extracts were used for the analysis, which was carried out by means of reverse-phase UPLC coupled to mass spectrometry (UPLC-QTOF). This technology is especially suited for the detection of semipolar secondary metabolites, primarily tomato polyphenols and alkaloids.[33] Four or five ripe fruits from seven transgenic lines containing different levels of IgA, two nullizygote plants, two wild type Moneymaker lines, and three commercial varieties (L, M, and N) were analyzed.

The mass profile obtained was first processed with XCMS, an integrated metabolomics analysis platform for the determination of metabolic profile differences and metabolite identification.[30] Data processing and filtering generated a total of 356 reliable peaks, which were introduced in a single matrix for analysis. A PCA was performed as the first step in data exploration to examine the relationship between the different sample classes. The first two components of the PCA model explained 30 and 17% of the total variance, respectively. As can be seen in the scores scatter plot depicted in Figure 4a,


dx.doi.org/10.1021/jf502292g | J. Agric. Food Chem. 2014, 62, 8158−8168

**Table 2. Identified Proteins with Ratio >2**

| spot $P < 0.05$ | Paragon score | % cov | accession | name | species | peptides (95%) |
|---|---|---|---|---|---|---|
| 266 | 17.6 | 29.8 | Sp\|P01876\|IGHA1_HUMAN | Ig $\alpha$-1 chain C region | human | 9 |
| 844 | 22.5 | 41.1 | Sp\|B9A064\|IGLL5_HUMAN | immunoglobulin $\lambda$-like polypeptide 5 | human | 30 |
| 885 | 6.1 | 19.2 | Sp\|B9A064\|IGLL5_HUMAN | immunoglobulin $\lambda$-like polypeptide 5 | human | 3 |
| 849 | 12.6 | 42 | LV301_HUMAN | Ig $\lambda$ chain V−III region SH | human | 4 |
| 855 | 14.7 | 39.7 | Sp\|B9A064\|IGLL5_HUMAN | immunoglobulin $\lambda$-like polypeptide 5 | human | 18 |
| spot $P > 0.05$ | Paragon score | % cov | accession | name | species | peptides (95%) |
| 843 | 6.3 | 34.3 | sp\|P01714\|LV301_HUMAN | Ig $\lambda$ chain V−III region SH | human | 4 |
| 896 | 6.2 | 22.4 | sp\|P01876\|IGHA1_HUMAN | Ig $\alpha$-1 chain C region OS=*Homo sapiens* | human | 6 |
| 783 | 2 | 52.3 | sp\|P10967\|ACCH3_SOLLC | 1-aminocyclopropane-1-carboxylate oxidase | *Solanum lycopersicum* | 1 |
|  | 1.7 | 10.5 | sp\|P01876\|IGHA1_HUMAN | Ig $\alpha$-1 chain C region | human | 1 |
| 792 | 9.0 | 17.9 | gi\|46561796 | rpL23−ScFv fusion protein |  | 4 |
| 797 | 2.4 | 10.5 | sp\|P01876\|IGHA1_HUMAN | Ig $\alpha$-1 chain C region | human | 1 |
| 852 | 8.1 | 45.3 | sp\|P0CG04\|LAC1_HUMAN | Ig $\lambda$-1 chain C regions | human | 4 |
| 868 | 9.3 | 45.3 | sp\|P0CG04\|LAC1_HUMAN | Ig $\lambda$-1 chain C regions | human | 4 |
| 869 | 3.6 | 23.6 | sp\|P0CG04\|LAC1_HUMAN | Ig $\lambda$-1 chain C regions | human | 2 |
| 875 | 2.0 | 17.0 | sp\|P0CG04\|LAC1_HUMAN | Ig $\lambda$-1 chain C regions | human | 1 |
| 886 | 10.1 | 38.0 | gi\|21669631 | immunoglobulin $\lambda$ light chain VLJ region | human | 5 |
| 899 | 2 | 10.5 | sp\|P01876\|IGHA1_HUMAN | Ig $\alpha$-1 chain C region | human | 1 |
| 956 | 2.37 | 10.5 | sp\|P01876\|IGHA1_HUMAN | Ig $\alpha$-1 chain C region | human | 1 |
| 1186 | 2 | 15.5 | gi\|7438718 | Ig $\lambda$a chain NIG250 precursor | human | 1 |
| 1169 | 1.82 | 23.6 | sp\|P0CG04\|LAC1_HUMAN | Ig $\lambda$-1 chain C regions | human | 1 |

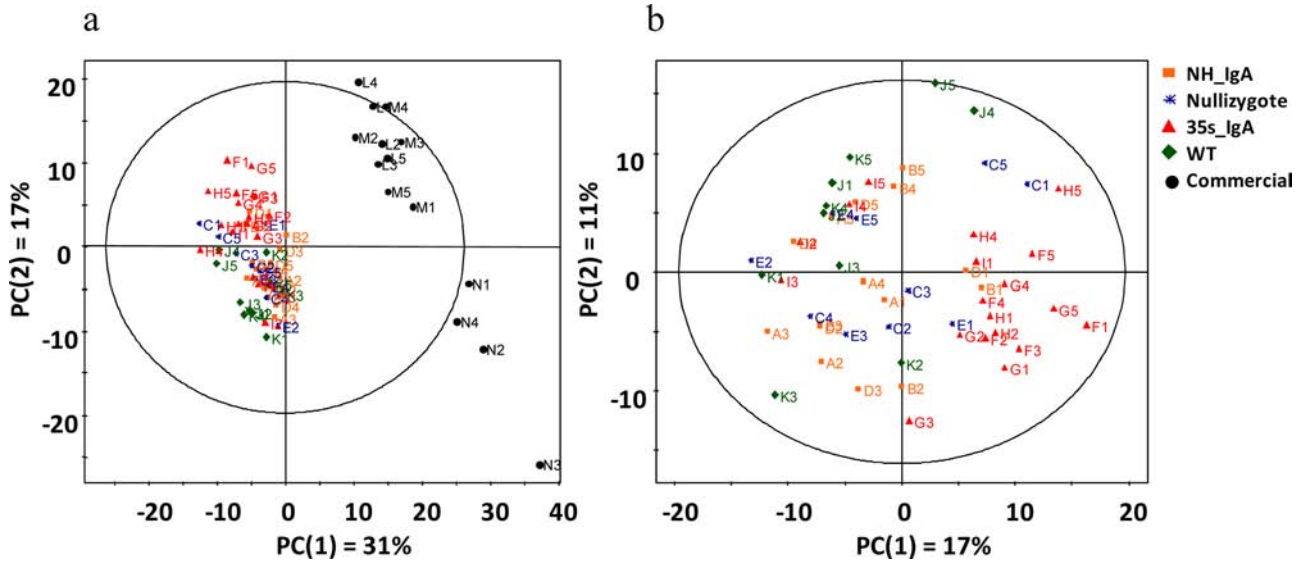


**Figure 4.** PCA scores plots of LC-MS spectra: (a) complete data set of tomato cultivars including transgenic lines expressing IgA, nullizygote lines, wild type lines, and commercial lines; (b) PCA including only Moneymaker lines grown in-house. Each point represents a biological replicate (pool of two to three different fruits). Capital letters represent the different tomato lines as described in Table 1.

PC1 clearly separated the commercial varieties from the remaining samples, whereas PC2 allowed further discrimination within the commercial group between N and L and M lines. The samples from IgA-producing lines and control nullizygote and Moneymaker wild type lines, however, grouped together in the scores space, not being separated by any of the components of the PCA model. As the largest variance in the data set was observed between commercial lines purchased in a supermarket and Moneymaker lines, a new PCA was performed in which commercial lines were excluded from the analysis to thus better explore the differences associated with IgA production. The obtained PCA model (Figure 4b) did not reveal any clear group structure in the data set; only 35S_IgA lines F, G, and H slightly separated from the remaining samples, whereas significant confusion occurred between the homozygous 35S_IgA line I, NH_IgA lines, and the control lines.

To directly search for specific metabolites that discriminate between IgA and control lines, an orthogonal partial least-squares discriminate analysis (OPLS-DA) was set. OPLS-DA makes use of a priori information on class membership (e.g., IgA content) to extract class-related variance in a predictive component and class-uncorrelated variation in one or more orthogonal components. Thus, even in the presence of uncontrolled covariates, OPLS-DA allows a direct identification of class-discriminant variables. As 35s_IgA lines and NH_IgA lines contain very different IgA levels,[11] they were treated separately so that each transgenic group could be compared with its closest control (non-IgA) group. Thus, three separate

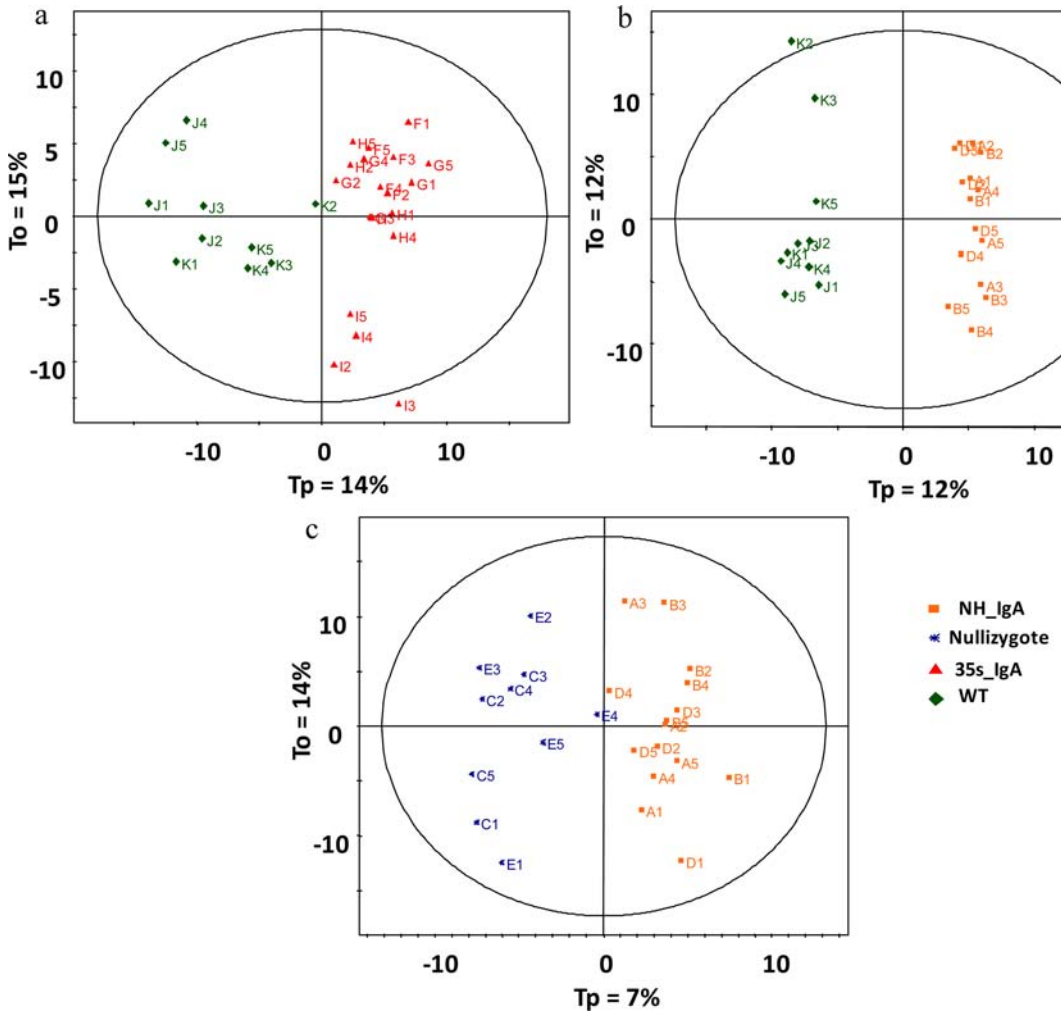


**Figure 5.** OPLS-DA score plots of LC-MS spectra: (a) 35S_IgA versus WT; (b) NH_IgA versus WT; (c) NH_IgA versus nullizygote. Each point represents a biological replicate (pool of two to three different fruits). Capital letters represent the different tomato lines as described in Table 1.

comparisons were made involving 35s_IgA versus WT, NH_IgA versus WT, and NH_IgA versus nullizygote lines (Figure 5). The fitted models comprised one predictive (IgA content) plus one, two, and one orthogonal components, respectively. The variance related to class separation explained by the models was 82, 98, and 84% with a cross-validated predictive ability $Q^2(Y)$ = 0.31, 0.84, and 0.40, indicating a higher uncertainty in the 35s_IgA versus WT and NH_IgA versus nullizygote models regarding class separation. The homozygous line I formed a separate subgroup within the 35s lines as revealed by the first orthogonal component of the model.

The most relevant metabolite ions for class discrimination were selected, according to the following rules: the selected ions should present a high variable influence on projection (VIP ≥ 1), a high correlation with IgA content ($|p(\text{corr})| \geq 0.5$), and narrow jack-knifed 95% confidence intervals of the variable coefficient (confidence interval not crossing zero). Totals of 41, 39, and 27 discriminating mass peaks (counting 91 different masses) were chosen according to these criteria from the 35s_IgA versus WT, NH_IgA versus WT, and NH_IgA versus nullizygote models, respectively. A large proportion of these peaks, however, showed a very modest variation between the transgenic lines and their counterpart controls with <50%, 42 masses, reaching fold ratios ≥2. The complete list of 91 masses is provided in Table S1 as Supporting Information. The three models were then compared by means of shared and unique structures (SUS) plots, an analysis that combines the $p$(corr) profiles from two models, constructed with all of the selected variables (Figure 6). The first SUS plot showed the correlation between models 35s_IgA versus WT and NH_IgA versus WT (Figure 6a). The second SUS plot correlated models 35s_IgA versus WT and NH_IgA versus nullizygote (Figure 6b). The last SUS plot showed the correlation between models NH_IgA versus WT and NH_IgA versus nullizygote (Figure 6c). Only two discriminating ion masses were shared by the three models, namely, masses Mp232 and Mn44. In general, there was little overlap between the 35s_IgA versus WT and NH_IgA versus nullizygote models, except the two mentioned masses, Mp232 and Mn44, sharing high correlation loadings and covariance. Comparison of 35s_IgA versus WT/NH_IgA versus WT and NH_IgA versus WT/NH_IgA versus nullizygote demonstrated greater correspondence, with nine and six common discriminating features, respectively (Figure 6d).

To determine the statistical significance of the differences in the metabolic profiles observed in the OPLS-DA, a univariate analysis was also carried out. A $t$ test was performed for the comparison between NH_IgA versus WT, NH_IgA versus nullizygote, and 35s_IgA versus WT. Seventeen masses, 4.8%


dx.doi.org/10.1021/jf502292g | J. Agric. Food Chem. 2014, 62, 8158−8168

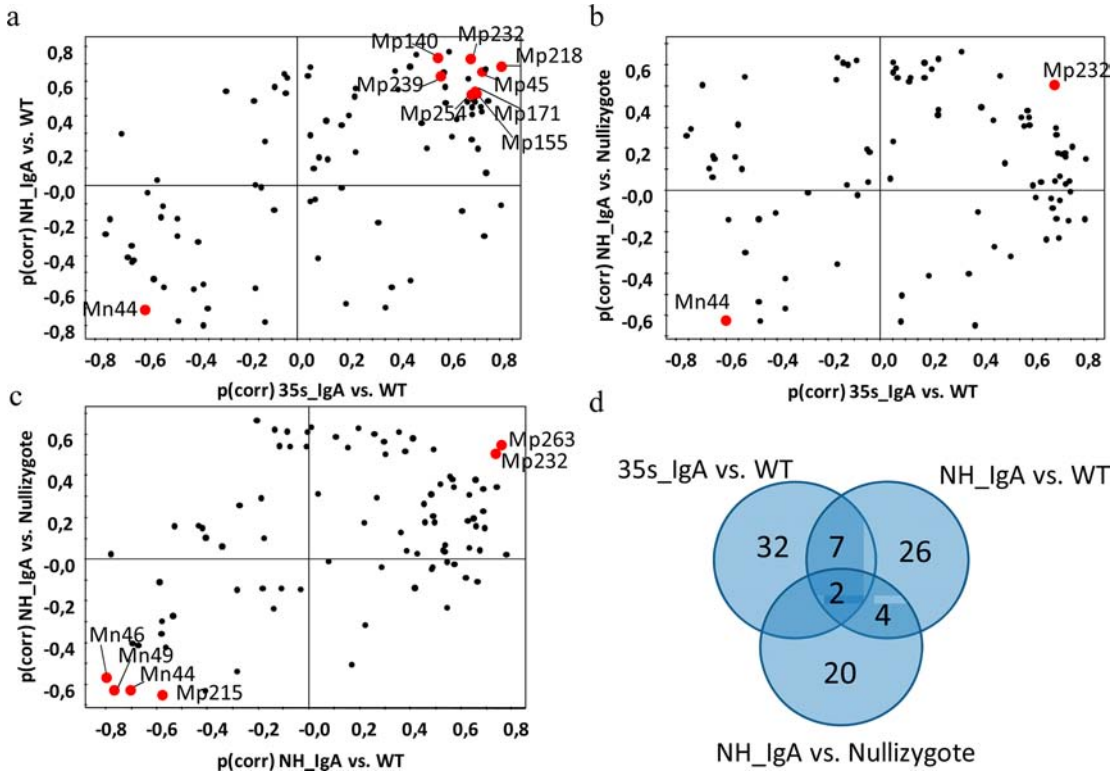


**Figure 6.** SUS plots: (a) between 35S_IgA versus WT and NH_IgA versus WT; (b) between 35S_IgA versus WT and NH_IgA versus nullizygote; (c) between NH_IgA versus WT and NH_IgA versus nullizygote models. Common features are marked in red. Only masses selected as potentially important for class separation in any of the three models were plotted. (d) Venn diagram showing the number of unique and overlapping discriminating mass features.

**Table 3. Significantly Different Mass Features ($t$ Test, FDR < 0.05)[a]**

| | | | fold change | | | |
|---|---|---|---|---|---|---|
| mass ID[b] | $m/z$ | $t_R$[c] (min) | 35S/WT | NH/WT | NH/nullizygote | nullizygote/WT |
| **Mp30** | 385.0445 | 0.85 | 0.97 | 0.38* | 0.91 | 0.42 |
| **Mp46** | 218.1005 | 0.87 | 0.78 | 0.22* | 0.45 | 0.50 |
| Mp140 | 284.1009 | 1.32 | **1.48** | **1.61*** | **1.18** | **1.37** |
| Mp148 | 278.1484 | 1.34 | **2.04*** | **1.60** | **0.94** | **1.70** |
| Mp157 | 316.1386 | 1.44 | **2.13*** | **1.80** | **0.91** | **1.97** |
| Mp171 | 303.1081 | 1.74 | **1.86*** | **1.54** | **0.79** | **1.95** |
| Mp173 | 538.1281 | 1.75 | **1.89*** | **1.18** | **0.65** | **1.83** |
| Mp232 | 287.1153 | 7.36 | **1.96** | **3.38*** | **1.57** | **2.16** |
| Mp241 | 497.1543 | 9.26 | **2.26** | **3.21*** | **1.67** | **1.92** |
| **Mp245** | 425.1431 | 10.58 | 0.85 | 0.40* | 0.76 | 0.52 |
| Mp263 | 359.1337 | 21.05 | **2.68** | **3.19*** | **2.07** | **1.54** |
| **Mp335** | 666.3875 | 30.90 | 0.34* | 0.78 | 1.51 | 0.51 |
| **Mp350** | 415.3230 | 33.79 | 0.56* | 1.18 | 1.44 | 0.82 |
| **Mn44** | 386.9989 | 4.06 | 0.52 | 0.37* | 0.53 | 0.70 |
| **Mn49** | 285.05766 | 4.54 | 0.66 | 0.23* | 0.48 | 0.48 |
| Mn84 | 1430.6555 | 27.99 | **1.79** | **2.23*** | **0.99** | **2.24** |
| **Mn97** | 1120.5295 | 30.87 | 0.38* | 0.89 | 1.44 | 0.62 |

[a]Comparisons in which each mass is significant (FDR < 0.05) are indicated with an asterisk. Mass features showing an uptrend in the transgenic lines are in bold. Contribution to class separation in an OPLS-DA model is indicated by an underscore. [b]Mp, mass detected in ESI+ mode; Mn, mass detected in ESI− mode. [c]$t_R$, retention time.

of the total number of variables, proved to be significant (FDR < 0.05) in at least one of the comparisons (Table 3). All of these metabolic features, which included the ion masses Mp232 and Mn44 above-mentioned, were among the 91 masses selected as major contributors to class separation in the OPLS-DA model. Among the 17 masses, only nine peaks showed an uptrend in the transgenic lines when compared to the WT, which could represent a potential concern regarding the safety of the final product (Supporting Information Supplementary Table 1). These nine mass features, with an average fold variation ranging from 1.6 to 3.4, showed similar tendency in both 35s and NH lines, with the only exception of Mp173,


dx.doi.org/10.1021/jf502292g | J. Agric. Food Chem. 2014, 62, 8158−8168

which remained unaltered in NH lines. However, in all nine cases the same uptrend was observed for the nullizygote lines when compared to the WT. It is also worth noting that no significant differences between the NH_IgA lines and their nullizygote controls were found.

In addition to the assessment of the statistical significance of the differences in the metabolic profiles between the transgenic lines and their counterpart control lines (proof of difference), the safety of the metabolic changes in IgA-producing fruits was also evaluated following a proof-of-safety approach. According to this test, differences will be regarded as safe if the metabolite levels fall within an established safety range.[10,34] When a priori defined safety thresholds are not available, as is necessarily the case for untargeted metabolomic studies, these can be derived from the metabolite levels found in commercial varieties. Thus, following the approach of Kusano et al.,[10] symmetric safety limits were defined as the 90% confidence interval for the ratio to control (WT) of the commercial variety farthest away from the WT. When, for any given metabolite, the confidence interval for the ratio of the transgenic fruits to the WT control is within this safety range, the levels of the metabolite can be regarded as safe. This analysis was performed following three different approaches: in the first one, all 35s lines were analyzed as a group; in the second one, all NH lines were analyzed as a group; and in the third one, the homozygous line was analyzed separately. When these analyses were performed, a single mass, Mn52, showed a ratio to WT outside the acceptable limits in the 35s group. No mass was found to exceed the upper boundary of the safety range in the NH group and, most importantly, all metabolites showed confidence intervals within the acceptable limits when the homozygous line was evaluated separately (Supporting Information Supplementary Table 2). Moreover, it should be noted that Mn52 also exceeds the upper boundary of the safety range when the nullizygote group is analyzed (data not shown).

## DISCUSSION

Plant organs are considered GRAS when at their ripe stage they contain no toxicants, allergens, or antinutrients that could be harmful for the consumer. It is expected that recombinant production of IgA in edible tomatoes does not compromise fruit composition and, consequently, its edibility. However, this hypothesis had never been corroborated experimentally before; the most important compounds concerning edibility in tomato are proteins (allergens) and secondary metabolites (alkaloids).[13] Here, we analyzed proteomic and metabolomic profiles of IgA tomatoes and compared them with those of nontransgenic fruits as a way to evaluate the changes in tomato composition introduced by IgA production. The whole proteome was analyzed by means of 2D-DIGE gels, and UPLC-qTOF was used to analyze secondary metabolites. The changes or similarities are taken as an indication of the safety of minimally processed IgA tomato products.

Four representative transgenic lines paired with four nontransgenic lines were chosen for the proteomic analysis by means of 2D-DIGE. These included NH_IgA compared with their corresponding nullizygote fruits as well as 35s_IgA paired with WT samples. To quantify the magnitude of the changes between transgenic and nontransgenic groups, mean ratios were calculated for each spot between IgA and non-IgA samples. In a first arbitrary cut only spots with ratio >2.0 were selected, as only a high increase in the abundance of a protein can be considered a potential thread. As a result, a total of 19 protein spots were selected for identification by LC-MS/MS, with only 5 of them showing significant increase in a *t* test analysis ($P$ value <0.05). All of the sequenced proteins matched human IgA chains except for spot 783, which showed an overlap between human IgA HC and tomato ACC oxidase, an ethylene-forming enzyme involved in climacteric fruit ripening.[35] ACC oxidase is a common enzyme in climacteric fruits with no allergenic properties reported; thus, a slight increase in this protein probably does not represent a threat for human consumption. Therefore, it can be deduced from this analysis that no other protein apart from IgA is substantially changing the composition of the transgenic tomato.

With regard to the analysis of secondary metabolites, PCA including the commercial varieties L, M, and N showed a clear separation between them and the Moneymaker samples collected from the laboratory greenhouse. This separation could be due to several reasons. It is possible that inherent variety differences are sufficient to separate the samples, but other possible explanations are the cultivation conditions of each tomato batch and the postharvesting conditions to which they have been subjected, for example, refrigeration.[36] These variables seem to mask any differences in semipolar compound levels that could be generated by the production of an immunoglobulin. For this reason, another PCA was made after removal of the commercial samples from the data set. This second PCA showed no separation between IgA lines and IgA-free lines. Both groups showed a similar distribution, meaning that any environmental effect on metabolite composition seems more relevant than putative differences generated by the production of IgA.

Subsequently, OPLS-DA models were set to search for specific unintended effects between transgenic and nontransgenic lines directly related with IgA production. As NH_IgA lines and 35s_IgA lines presented strong differences in IgA levels, they were treated separately. All three OPLS-DA models were able to separate transgenic and nontransgenic lines. However, with the exception of the model set for NH_IgA versus WT comparison, they presented a low predictive power with values of $Q^2 < 0.5$.

In principle, the masses correlating with IgA levels that are common within the three models are expected to be truly related with the IgA production. Only two masses, namely, Mn44 and Mp232, were found to fulfill this criterion. In addition, only Mp232 showed an uptrend in transgenic lines, although this uptrend was significant only when NH_IgA samples were compared with WT but not in the two remaining comparisons. The fact that the Mp232 uptrend is significant in only one of the group comparisons indicates that it has only minor effects in fruit composition. Moreover, the average increase ratio is 3.38-fold, an increase that would be a concern only if high daily doses of tomato-derived products were required. An additional proof-of-safety approach was performed according to the method of Kusano et al.[10] to evaluate if the levels of Mn232 fell outside the safety limits defined by the variability observed among commercial cultivars. In this analysis, all of the measured variables fell within the acceptable limits except for Mn52, which fell outside the safety range when the 35s group was analyzed. However, this mass remained in acceptable safety limits when the NH group and the homozygous line itself were analyzed. It should also be noted that the levels of Mn52 also fell outside the safety range when the nullizygote group was analyzed. These observations, together with the fact that Mn52 was not among the masses

which significantly separated the transgenic from the nontransgenic lines in the OPLS-DA analysis, suggests a lack of association with the IgA production. Most importantly, the levels of mass Mn232 remained within the safety limits in all three approaches. Taken together, these results suggest that no substantial differences beyond natural variation associated with IgA production are found in IgA tomatoes.

It is a common mistake to expect that the composition of a transgenic crop is identical to that of its nontransgenic reference.[37−40] As shown here in PCA and OPLS-DA models, IgA expression leaves an associated footprint in the fruit composition, which can be detected and partially described using proteomic and metabolomic profiling. Similarly, a metabolic signature introduced by the recombinant overexpression of the taste-modifying protein miraculin was found before in tomato fruits using a multiplatform approach, in the context of a substantial equivalence assessment.[10] Other examples pointing out the necessity of assessing the unintended effects in transgenic crops are the transgenic rice lines expressing *sck* and *cry1Ac* genes for insect resistance, which presented slight changes in metabolite concentrations that were caused by gene modification,[41] or the proteome changes found in tomato lines transformed with phytoene synthase-1.[42] There are also a number of remarkable works which point out that transgenesis does not significantly change the metabolic composition of crops.[43−45] As an example, a hierarchical metabolomics approach showed that metabolic changes caused through conventional breeding techniques were at least of a magnitude comparable to those resulting as an unintended effect of genetically modified potato lines expressing inulins.[43] However, to our knowledge, the metabolic signature of a therapeutic protein produced in an edible plant organ was not analyzed before. The overexpression of xenoproteins in the plant cell can induce sequence-specific responses in the host, which range from the suppression of the expression of the foreign gene via post-transcriptional gene silencing to the triggering of a general stress response or the induction of a program of cell death (see Orzaez et al.[46] and references cited therein). Therefore, the accumulation of harmful compounds in response to IgA expression in fruits could not be initially dismissed. By incorporating several independent transformation events leading to different IgA expression levels, this work aimed at evaluating unintended effects associated with producing IgA-based preparations in tomato. However, this work alone cannot rule out the possibility of harmful unintended effects associated with any strategy involving IgA production in fruits. At least three potential sources of uncertainty remain. First, the unexpected accumulation of harmful compounds other than the proteins and semipolar secondary metabolites cannot be dismissed with the methodology used here. A single method enabling complete metabolome analysis does not exist, and therefore additional comprehensive profiling methods should be considered.[7] Second, any new transgenic event involving IgA production in fruits should evaluate possible unintended effects associated specifically with the site of insertion, which can only be evaluated on a case-by-case basis. Finally, as observed in the protein profile, the antibody itself accumulates in the form of different polypeptides with distinct electrophoretic mobilities, probably arising from partial proteolytic degradation and/or different glycosylation patterns. Certainly, the pool of IgA-related polypeptides present in the fruit is different from that occurring in a natural oral passive immunization (OPI), and therefore the safety of the plant-made IgA itself and in the context of the fruit matrix needs to be thoroughly evaluated. All in all, the data shown here constitute a first step for confirming the safety of fruit-based IgA production strategy.

## ■ ASSOCIATED CONTENT

### Ⓢ Supporting Information

Supplementary Figure 1 and Supplementary Tables 1 and 2. This material is available free of charge via the Internet at http://pubs.acs.org.

## ■ AUTHOR INFORMATION

### Corresponding Author

*(D.O.) Phone: +34 963879933. E-mail: dorzaez@ibmcp.upv.es.

### Funding

This work has been funded by Grant BIO2010-15384 from Plan Nacional I + D of the Spanish Ministry of Science. P.Juarez is the recipient of a FPU fellowship.

### Notes

The authors declare no competing financial interest.

## ■ ACKNOWLEDGMENTS

The proteomic analysis was carried out in the Proteomics facility of IBMCP (Instituto de Biologia Molecular y Celular de Plantas UPV-CSIC) and the protein identification was performed in the SCSIE_university of Valencia Proteomics Unit, a member of ISCIII ProteoRed Proteomics Platform. The metabolomic analysis was carried out in the Metabolomics facility of IBMCP. Finally, we thank Vicente Monedero in IATA for kindly providing scFv clone.

## ■ ABBREVIATIONS USED

IgA, immunoglobulin A; MPI, mucosal passive immunization; GRAS, generally regarded as safe; DW, dry weight; HC, heavy chain; LC, light chain; TSP, total soluble protein; ESI, electrospray ionization; PCA, principal component analysis; OPLS-DA, orthogonal partial least-squares discriminate analysis; FDR, false discovery rate

## ■ REFERENCES

(1) Monger, W.; Alamillo, J. M.; Sola, I.; Perrin, Y.; Bestagno, M.; Burrone, O. R.; Sabella, P.; Plana-Duran, J.; Enjuanes, L.; Garcia, J. A.; Lomonossoff, G. P. An antibody derivative expressed from viral vectors passively immunizes pigs against transmissible gastroenteritis virus infection when supplied orally in crude plant extracts. *Plant Biotechnol. J.* **2006**, *4*, 623−631.

(2) Zimmermann, J.; Saalbach, I.; Jahn, D.; Giersberg, M.; Haehnel, S.; Wedel, J.; Macek, J.; Zoufal, K.; Glunder, G.; Falkenburg, D.; Kipriyanov, S. Antibody expressing pea seeds as fodder for prevention of gastrointestinal parasitic infections in chickens. *BMC Biotechnol.* **2009**, *9*, 79−101.

(3) Virdi, V.; Coddens, A.; De Buck, S.; Millet, S.; Goddeeris, B. M.; Cox, E.; De Greve, H.; Depicker, A. Orally fed seeds producing designer IgAs protect weaned piglets against enterotoxigenic *Escherichia coli* infection. *Proc. Natl. Acad. Sci. U.S.A.* **2013**, *110* (29), 11809−11814.

(4) Virdi, V.; Depicker, A. Role of plant expression systems in antibody production for passive immunization. *Int. J. Dev. Biol.* **2013**, *57*, 587−593.

(5) Tokuhara, D.; Alvarez, B.; Mejima, M.; Hiroiwa, T.; Takahashi, Y.; Kurokawa, S.; Kuroda, M.; Oyama, M.; Kozuka-Hata, H.; Nochi, T.; Sagara, H.; Aladin, F.; Marcotte, H.; Frenken, L. G.; Iturriza-Gomara, M.; Kiyono, H.; Hammarstrom, L.; Yuki, Y. Rice-based oral

antibody fragment prophylaxis and therapy against rotavirus infection. *J. Clin. Invest.* **2013**, *123*, 3829−3838.
(6) Gong, C. Y.; Wang, T. Proteomic evaluation of genetically modified crops: current status and challenges. *Front. Plant Sci.* **2013**, *4* (41), 1−8.
(7) Rischer, H.; Oksman-Caldentey, K. M. Unintended effects in genetically modified crops: revealed by metabolomics? *Trends Biotechnol.* **2006**, *24*, 102−104.
(8) Herman, R. A.; Price, W. D. Unintended compositional changes in genetically modified (GM) crops: 20 years of research. *J. Agric. Food Chem.* **2013**, *61* (48), 11695−11701.
(9) Di Carli, M.; Villani, M. E.; Renzone, G.; Nardi, L.; Pasquo, A.; Franconi, R.; Scaloni, A.; Benvenuto, E.; Desiderio, A. Leaf proteome analysis of transgenic plants expressing antiviral antibodies. *J. Proteome Res.* **2009**, *8*, 838−848.
(10) Kusano, M.; Redestig, H.; Hirai, T.; Oikawa, A.; Matsuda, F.; Fukushima, A.; Arita, M.; Watanabe, S.; Yano, M.; Hiwasa-Tanase, K.; Ezura, H.; Saito, K. Covering chemical diversity of genetically-modified tomatoes using metabolomics for objective substantial equivalence assessment. *PLoS One* **2011**, *6* (2), No. e16989.
(11) Juarez, P.; Presa, S.; Espi, J.; Pineda, B.; Anton, M. T.; Moreno, V.; Buesa, J.; Granell, A.; Orzaez, D. Neutralizing antibodies against rotavirus produced in transgenically labelled purple tomatoes. *Plant Biotechnol. J.* **2012**, *10*, 341−352.
(12) Asero, R.; Mistrello, G.; Roncarolo, D.; de Vries, S. C.; Gautier, M. F.; Ciurana, C. L.; Verbeek, E.; Mohammadi, T.; Knul-Brettlova, V.; Akkerdaas, J. H.; Bulder, I.; Aalberse, R. C.; van Ree, R. Lipid transfer protein: a pan-allergen in plant-derived foods that is highly resistant to pepsin digestion. *Int. Arch. Allergy Immunol.* **2000**, *122*, 20−32.
(13) OECD. Consensus document on compositional considerations for new varieties of tomato: key food and feed nutrients, toxicants and allergens. ENV/JM/MONO(2008)26, 2008.
(14) Westphal, S.; Kempf, W.; Foetisch, K.; Retzek, M.; Vieths, S.; Scheurer, S. Tomato profilin Lyc e 1: IgE cross-reactivity and allergenic potency. *Allergy* **2004**, *59*, 526−532.
(15) Westphal, S.; Kolarich, D.; Foetisch, K.; Lauer, I.; Altmann, F.; Conti, A.; Crespo, J. F.; Rodriguez, J.; Enrique, E.; Vieths, S.; Scheurer, S. Molecular characterization and allergenic activity of Lyc e 2 (β-fructofuranosidase), a glycosylated allergen of tomato. *Eur. J. Biochem.* **2003**, *270*, 1327−1337.
(16) Welter, S.; Lehmann, K.; Dolle, S.; Schwarz, D.; Weckwerth, W.; Scheler, C.; Worm, M.; Franken, P. Identification of putative new tomato allergens and differential interaction with IgEs of tomato allergic subjects. *Clin. Exp. Allergy* **2013**, *43*, 1419−1427.
(17) Coll, A.; Nadal, A.; Rossignol, M.; Puigdomenech, P.; Pla, M. Proteomic analysis of MON810 and comparable non-GM maize varieties grown in agricultural fields. *Transgenic Res.* **2011**, *20*, 939−949.
(18) Corpillo, D.; Gardini, G.; Vaira, A. M.; Basso, M.; Aime, S.; Accotto, G. P.; Fasano, M. Proteomics as a tool to improve investigation of substantial equivalence in genetically modified organisms: the case of a virus-resistant tomato. *Proteomics* **2004**, *4*, 193−200.
(19) Khalf, M.; Goulet, C.; Vorster, J.; Brunelle, F.; Anguenot, R.; Fliss, I.; Michaud, D. Tubers from potato lines expressing a tomato Kunitz protease inhibitor are substantially equivalent to parental and transgenic controls. *Plant Biotechnol. J.* **2010**, *8*, 155−169.
(20) Lehesranta, S. J.; Davies, H. V.; Shepherd, L. V.; Nunan, N.; McNicol, J. W.; Auriola, S.; Koistinen, K. M.; Suomalainen, S.; Kokko, H. I.; Karenlampi, S. O. Comparison of tuber proteomes of potato varieties, landraces, and genetically modified lines. *Plant Physiol.* **2005**, *138*, 1690−1699.
(21) Eltayeb, E. A.; Roddick, J. G. Changes in the alkaloid content of developing fruits of tomato (*Lycopersicon esculentum* Mill.). I. Analyses of cultivars and mutants with different ripening characteristics. *J. Exp. Bot.* **1984**, *35*, 252−260.
(22) Eltayeb, E. A.; Roddick, J. G. Biosynthesis and degradation of alpha-tomaine in developing tomato fruits. *Phytochemistry* **1985**, *24*, 253−257.
(23) Friedman, M.; Levin, C. E. *R*-Tomatine content in tomato and tomato products determined by HPLC with pulsed amperometric detection. *J. Agric. Food Chem.* **1995**, *43*, 1507−1511.
(24) Kozuke, N.; Kozuke, E.; Yamashita, H.; Fujii, S. Alpha-tomatine purification and quantification in tomatoes by HPLC. *J. Food Sci.* **1994**, *59*, 1211−1212.
(25) De Vos, R. C.; Moco, S.; Lommen, A.; Keurentjes, J. J.; Bino, R. J.; Hall, R. D. Untargeted large-scale plant metabolomics using liquid chromatography coupled to mass spectrometry. *Nat. Protoc.* **2007**, *2*, 778−791.
(26) Estornell, L. H.; Orzaez, D.; Lopez-Pena, L.; Pineda, B.; Anton, M. T.; Moreno, V.; Granell, A. A multisite gateway-based toolkit for targeted gene expression and hairpin RNA silencing in tomato fruits. *Plant Biotechnol. J.* **2009**, *7*, 298−309.
(27) Munoz-Fambuena, N.; Mesejo, C.; Agusti, M.; Tarraga, S.; Iglesias, D. J.; Primo-Millo, E.; Gonzalez-Mas, M. C. Proteomic analysis of "Moncada" mandarin leaves with contrasting fruit load. *Plant Physiol. Biochem.* **2013**, *62*, 95−106.
(28) Orzaez, D.; Medina, A.; Torre, S.; Fernandez-Moreno, J. P.; Rambla, J. L.; Fernandez-Del-Carmen, A.; Butelli, E.; Martin, C.; Granell, A. A visual reporter system for virus-induced gene silencing in tomato fruit based on anthocyanin accumulation. *Plant Physiol.* **2009**, *150*, 1122−1134.
(29) Tautenhahn, R.; Bottcher, C.; Neumann, S. Highly sensitive feature detection for high resolution LC/MS. *BMC Bioinformatics* **2008**, *9* (504), 1−16.
(30) Smith, C. A.; Want, E. J.; O'Maille, G.; Abagyan, R.; Siuzdak, G. XCMS: processing mass spectrometry data for metabolite profiling using nonlinear peak alignment, matching, and identification. *Anal. Chem.* **2006**, *78*, 779−787.
(31) Kuhl, C.; Tautenhahn, R.; Bottcher, C.; Larson, T. R.; Neumann, S. CAMERA: an integrated strategy for compound spectra extraction and annotation of liquid chromatography/mass spectrometry data sets. *Anal. Chem.* **2012**, *84*, 283−289.
(32) Saeed, A. I.; Sharov, V.; White, J.; Li, J.; Liang, W.; Bhagabati, N.; Braisted, J.; Klapa, M.; Currier, T.; Thiagarajan, M.; Sturn, A.; Snuffin, M.; Rezantsev, A.; Popov, D.; Ryltsov, A.; Kostukovich, E.; Borisovsky, I.; Liu, Z.; Vinsavich, A.; Trush, V.; Quackenbush, J. TM4: a free, open-source system for microarray data management and analysis. *Biotechniques* **2003**, *34*, 374−378.
(33) Moco, S.; Bino, R. J.; Vorst, O.; Verhoeven, H. A.; de Groot, J.; van Beek, T. A.; Vervoort, J.; de Vos, C. H. A liquid chromatography-mass spectrometry-based metabolome database for tomato. *Plant Physiol.* **2006**, *141*, 1205−1218.
(34) Hothorn, L. A.; Oberdoerfer, R. Statistical analysis used in the nutritional assessment of novel food using the proof of safety. *Regul. Toxicol. Pharmacol.: RTP* **2006**, *44*, 125−135.
(35) Penarrubia, L.; Aguilar, M.; Margossian, L.; Fischer, R. L. An antisense gene stimulates ethylene hormone production during tomato fruit ripening. *Plant Cell* **1992**, *4*, 681−687.
(36) Shepherd, L. V.; Fraser, P.; Stewart, D. Metabolomics: a second-generation platform for crop and food analysis. *Bioanalysis* **2011**, *3*, 1143−1159.
(37) Garcia-Canas, V.; Simo, C.; Leon, C.; Ibanez, E.; Cifuentes, A. MS-based analytical methodologies to characterize genetically modified crops. *Mass Spectrom. Rev.* **2011**, *30*, 396−416.
(38) Iwaki, T.; Guo, L.; Ryals, J. A.; Yasuda, S.; Shimazaki, T.; Kikuchi, A.; Watanabe, K. N.; Kasuga, M.; Yamaguchi-Shinozaki, K.; Ogawa, T.; Ohta, D. Metabolic profiling of transgenic potato tubers expressing *Arabidopsis* dehydration response element-binding protein 1A (DREB1A). *J. Agric. Food Chem.* **2013**, *61*, 893−900.
(39) Mehrotra, S.; Goyal, V. Evaluation of designer crops for biosafety − a scientist's perspective. *Gene* **2013**, *515*, 241−248.
(40) Zeng, W.; Hazebroek, J.; Beatty, M.; Hayes, K.; Ponte, C.; Maxwell, C.; Zhong, C. X. Analytical method evaluation and discovery of variation within maize varieties in the context of food safety:

transcript profiling and metabolomics. *J. Agric. Food Chem.* **2014**, *62*, 2997−3009.
(41) Chang, Y.; Zhao, C.; Zhu, Z.; Wu, Z.; Zhou, J.; Zhao, Y.; Lu, X.; Xu, G. Metabolic profiling based on LC/MS to evaluate unintended effects of transgenic rice with cry1Ac and sck genes. *Plant Mol. Biol.* **2012**, *78*, 477−487.
(42) Robertson, F. P.; Koistinen, P. K.; Gerrish, C.; Halket, J. M.; Patel, R. K.; Fraser, P. D.; Bramley, P. M. Proteome changes in tomato lines transformed with phytoene synthase-1 in the sense and antisense orientations. *J. Exp. Bot.* **2012**, *63*, 6035−6043.
(43) Catchpole, G. S.; Beckmann, M.; Enot, D. P.; Mondhe, M.; Zywicki, B.; Taylor, J.; Hardy, N.; Smith, A.; King, R. D.; Kell, D. B.; Fiehn, O.; Draper, J. Hierarchical metabolomics demonstrates substantial compositional similarity between genetically modified and conventional potato crops. *Proc. Natl. Acad. Sci. U.S.A.* **2005**, *102*, 14458−14462.
(44) Shepherd, L. V.; McNicol, J. W.; Razzo, R.; Taylor, M. A.; Davies, H. V. Assessing the potential for unintended effects in genetically modified potatoes perturbed in metabolic and developmental processes. Targeted analysis of key nutrients and anti-nutrients. *Transgenic Res.* **2006**, *15*, 409−425.
(45) Zhao, Y.; Li, Y. Y. [Unintended effects assessment of genetically modified crops using omics techniques]. *Yi Chuan* **2013**, *35*, 1360−1367.
(46) Orzaez, D.; Granell, A.; Blazquez, M. A. Manufacturing antibodies in the plant cell. *Biotechnol. J.* **2009**, *4*, 1712−1724.

JOURNAL OF AGRICULTURAL AND FOOD CHEMISTRY

Article

pubs.acs.org/JAFC

# Cereal Byproducts Have Prebiotic Potential in Mice Fed a High-Fat Diet

Karin Berger,[†] Peter Falck,[‡] Caroline Linninge,[§] Ulf Nilsson,[§] Ulrika Axling,[†] Carl Grey,[‡] Henrik Stålbrand,[∥] Eva Nordberg Karlsson,[‡] Margareta Nyman,[§] Cecilia Holm,[†] and Patrick Adlercreutz*[,‡]

[†]Biomedical Center, Department of Experimental Medical Science, Lund University, BMC C11, Lund SE-22184, Sweden

[‡]Biotechnology, Department of Chemistry, [§]Applied Nutrition and Food Chemistry, Department of Food Technology, Engineering and Nutrition, [∥]Biochemistry and Structural Biology, Department of Chemistry, Lund University P.O. Box 124, Lund SE-22100, Sweden

Supporting Information

**ABSTRACT:** Barley husks, rye bran, and a fiber residue from oat milk production were processed by heat pretreatment, various separation steps, and treatment with an endoxylanase in order to improve the prebiotic potential of these cereal byproducts. Metabolic functions were intended to improve along with improved microbial activity. The products obtained were included in a high-fat mouse diet so that all diets contained 5% dietary fiber. In addition, high-fat and low-fat controls as well as partially hydrolyzed guar gum were included in the study. The soluble fiber product obtained from rye bran caused a significant increase in the bifidobacteria (log copies of 16S rRNA genes; median (25−75 percentile): 6.38 (6.04−6.66) and 7.47 (7.30−7.74), respectively; $p < 0.001$) in parallel with a tendency of increased production of propionic acid and indications of improved metabolic function compared with high-fat fed control mice. The oat-derived product caused an increase in the pool of cecal propionic (from 0.62 ± 0.12 to 0.94 ± 0.08) and butyric acid (from 0.38 ± 0.04 to 0.60 ± 0.04) compared with the high-fat control, and it caused a significant increase in lactobacilli (log copies of 16S rRNA genes; median (25−75 percentile): 6.83 (6.65−7.53) and 8.04 (7.86−8.33), respectively; $p < 0.01$) in the cecal mucosa. However, no changes in measured metabolic parameters were observed by either oat or barley products.

**KEYWORDS:** *dietary fiber, xylanase, gut microbiota, short-chain fatty acids, C57BL/6 mice*

## INTRODUCTION

Dietary fiber is a collective term for carbohydrates in plants with three or more monomeric units that are resistant to digestion by human gastrointestinal enzymes. Health benefits of dietary fiber in the human diet, such as reduced risk for developing obesity, diabetes, coronary heart disease, hypertension, and gastrointestinal disorders such as colorectal cancer are well-known.[1,2] In this respect, the viscosity of the dietary fiber seems to play an important role and the higher the viscosity the higher the beneficial effect.[3] However, in recent years, the effect of short-chain fatty acids (SCFA), produced from soluble fiber during colonic fermentation, has been more emphasized. This means that also nonviscous indigestible carbohydrates of lower molecular weight may contribute to reduce the risk of cardiovascular disease and type 2-diabetes.

Cereals such as wheat, rye, barley, and oats are important sources of dietary fiber in the human diet. The hemicelluloses, which have structural functions in the plant cell walls, constitute major components in the fiber fraction. Cereals contain a variety of hemicelluloses with arabinoxylan as an important example. In obese mice, wheat arabinoxylan has been shown to counteract the high-fat-induced change of the gut microbiota in parallel with decreased body weight gain and insulin resistance.[4]

Dietary fiber, which is fermented by the colonic microorganisms, may be an important modulator of the gut microbiota, which in turn is essential for the metabolic function of the host. A beneficial microbiota may inhibit pathogen colonization, modulate the immune system, and metabolize otherwise indigestible carbohydrates.[5] Indigestible carbohydrates can be regarded as prebiotic if they selectively stimulate the growth and activity of intestinal bacteria with health promoting effects for the host. Mostly oligosaccharides such as fructo-oligosaccharides and galacto-oligosaccharides are included in this concept, but in fact all dietary fiber that are fermented in the colon are potential prebiotic components.[6] Also the formation of bacterial metabolites, formed as a consequence of oligosaccharide fermentation, such as SCFA, may be important. Of the SCFA, propionic acid and butyric acid have mostly been associated with beneficial metabolic effects.[7] Interestingly, the monomeric composition and chain length of the oligosaccharides are of utmost importance in this respect. Thus, FOS of higher chain length gave higher formation of propionic acid in rats than FOS of lower chain length, which instead gave higher amounts of butyric acid.[8]

In addition to FOS, several other types of oligosaccharides have promising properties. These include mannooligosaccharides (MOS), xylooligosaccharides (XOS), and arabinoxylooli-

Received: November 29, 2013
Revised: July 16, 2014
Accepted: July 19, 2014
Published: July 19, 2014

ACS Publications © 2014 American Chemical Society

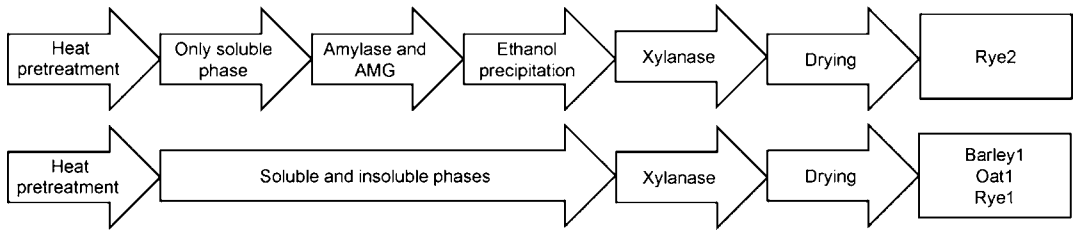


**Figure 1.** Schematic flowchart of the processes used to produce the different products. AMG = amyloglucosidase.

gosaccharides (AXOS). MOS produced from guar gum has been shown to increase the number of bifidobacteria in faeces of humans when incorporated into biscuits.[9] Furthermore, there is now overwhelming evidence that XOS and AXOS are prebiotics.[10] XOS have been shown to be fermented by certain groups of lactobacilli and bifidobacteria present in the human gut microbiota[11,12] XOS have been shown to be fermented by certain strains of the genus *Weissella*, which are putative probiotic bacteria.[13] FOS and XOS were found to stimulate bifidobacteria and lactobacilli, but the stimulation pattern was different.[14]

It should be emphasized that the size and structure of the oligosaccharides are important for their properties in general and for their digestibility by bacteria. Short AXOS have been shown to stimulate digestion by bifidobacteria, while longer ones were shown to decrease protein fermentation (branched SCFA), and it has been suggested that an average degree of polymerization of 5 was optimal for the overall effect on gut health characteristics.[15] It has also been shown that the selectivity for lactobacilli and bifidobacteria, i.e., the prebiotic effect, increased with decreasing size of wheat arabinoxylan.[16]

In the present study, byproducts from industrially processed barley, oats, and rye were treated in different ways, including selective hydrolysis catalyzed by a xylanase for the generation of XOS and AXOS, in order to improve the products' prebiotic potential. The products were evaluated in high-fat fed C57BL/6 mice, a model of obesity and insulin resistance associated with microbial dysbiosis,[17] with special attention on effects on the gut microbiota and generation of SCFA as an improved gut microbial activity was hypothesized to improve metabolic functions of the host. This model was chosen rather than healthy animals in order to get faster effects on physiological parameters and gut microbiota.

## MATERIALS AND METHODS

**Chemicals.** Thermostable amylase (*Bacillus licheniformis*) and amyloglucosidase (*Aspergillus niger*) were purchased from Megazyme (Wicklow, Ireland). Xylanase was from the thermophilic bacterium *Rhodothermus marinus* (*Rm*Xyn10A, catalytic domain[18]) and was produced and purified in-house as described elsewhere.[19] All other chemicals were of analytical grade unless stated otherwise.

**Materials.** Milled barley husks (Lyckeby Stärkelsen, Kristianstad, Sweden), oat fiber residue (Oatly, Landskrona, Sweden), and rye bran (Farina, Kävlinge, Sweden) were included in the study. Partially hydrolyzed guar gum (Guar) was obtained under the trade name Sunfiber R (lot no. 002141) (Taiyo Lucid Pvt. Ltd., Mumbai, India). The Sunfiber has been shown to be polydispersed with an average weight of 20 kDa.[20]

**Processing Steps.** *Heat Pretreatment.* The products Barley1, Oat1, and Rye1 were made from 150 g of dry barley husks (Barley0), oat fiber residue (Oat0), and rye bran (Rye0), respectively (Figure 1). The more refined product Rye2 was made from 1.62 kg of rye bran (Rye0) (Figure 1). The products were mixed with deionized water with a weight ratio of 1:9 and autoclaved in glass bottles at 121 °C for 15 h.

*Treatments of Products Barley1, Oat1, and Rye1.* The autoclaved products were adjusted to pH 6 using NaOH and then heated under stirring to 70 °C. Thereafter, 900 U of the thermostable xylanase was added to the samples. The reaction mixture was maintained at 70 °C for 23 h under constant stirring, and the reaction was terminated by autoclaving at 121 °C for 15 min and the product was freeze-dried (Figure 1).

*Treatments of Soluble Fibers for Product Rye2.* After heat pretreatment of rye bran, the extract was first filtered through a textile cloth and then the filtrate was centrifuged at 10 000 rpm for 30 min to separate the soluble extract from insoluble particles. The soluble extract was concentrated by vacuum evaporation down to 4 L. The extract was treated with 15 kU of amylase at 85 °C. The extract was cooled to 50 °C, 33 kU amyloglucosidase was added, and the reaction mixture was stirred for 60 min. The extract was then precipitated under stirring with ethanol to a final concentration of 80% (v/v), and the precipitate was collected by filtration and air-dried (Figure 1).

The ethanol precipitate was dissolved in 3 L of deionized water and heated under stirring to 70 °C, and the pH was adjusted to 6.5. Then 1.2 kU of xylanase was added. The reaction mixture was maintained at 70 °C for 7 h under stirring, and the reaction was stopped by boiling for 20 min and thereafter the product was freeze-dried.

**Analysis of Final Products.** Protein was analyzed according to Kjeldahl on a FIASTAR 5000 system (FOSS TECATOR). Available starch and total starch contents were analyzed as previously described.[21,22]

Monosaccharide analysis of starting materials and final products was done using a 10 mg sample with 5 mL of 4% sulfuric acid at 100 °C for 3 h according to a modified method by Sluiter et al.[23] After hydrolysis, the hydrolysate was neutralized with 0.1 M $Ba(OH)_2$. Released monosaccharides were analyzed by high-performance anion exchange chromatography with pulsed amperiometric detection (HPAEC-PAD) (DIONEX, California, USA) using a 250 mm × 4 mm i.d., 8.5 $\mu$m CarboPac PA10 column and guard column 50 mm × 4 mm of the same material and an isocratic mobile phase of 1 mM NaOH at 1 mL/min.

Oligosaccharides present in the final products were analyzed using a 250 mm × 3 mm i.d., 5.5 $\mu$m CarboPac PA200 and a guard column 50 mm × 3 mm of the same material and a mobile phase of 100 mM NaOH and a gradient of sodium acetate of 0−50 mM between 0−20 min at 0.5 mL/min.

Dietary fibers were analyzed according to Asp.[24] The fat content was determined using the Schmid−Bondzynsky−Ratzlaff method (SBR) (NMKL Method no. 88, 1974). The water content of the samples was analyzed by NREL/TP-510-42621 and ash by NREL/TP-510-42622 (http://www.nrel.gov/publications/).

**Mouse Study Procedure.** Male 4 week old C57BL/6JBomTac mice (Taconic, Skensved, Denmark) were housed 10 mice per cage in 10 cages from arrival throughout the study. During acclimatization, they were all fed the low-fat diet (LFD) for 12 days. The animals were maintained in a temperature-controlled room with 12 h light−dark cycle. The study was approved by the local animal ethics committee (M185-11, Lund, Sweden), and the principles of laboratory animal care were followed.[46] After acclimatization, the mice were fed either one of the eight experimental diets with supplement or a control diet without supplement. The mice were fed the different diets ad libitum

Table 1. Composition of Fiber Rich Products Used in the Study (%)[a]

| | Oat0 | Oat1 | Barley0 | Barley1 | Rye0 | Rye1 | Rye2 | Guar |
|---|---|---|---|---|---|---|---|---|
| starch and maltodextrin | 5 | 5 | 8 | 6 | 15 | 15 | 0 | |
| monosaccharides and maltose | 5[b] | 3[b] | 1 | 2 | 4 | 10 | 6[c] | |
| dietary fiber | 38 | 38 | 65 | 67 | 41 | 46 | 71 | 80 |
| protein | 30 | 29 | 10 | 10 | 16 | 18 | 4 | 0.6 |
| fat | 13 | 13 | 3 | 3 | 4 | 5 | 1 | |
| ash | 6 | 6 | 7 | 7 | 5 | 5 | 13 | 1 |
| water | 2 | 4 | 6 | 3 | 13 | 3 | 5 | 5 |

[a]Oat: fiber rich residue from oat milk production. Barley: barley husks. Rye: rye bran. Guar: partly hydrolyzed guar gum. 0 = unmodified starting material; 1 = product obtained without separation steps, contains insoluble and soluble material; 2 = soluble product. [b]Mainly maltose. [c]Mainly glucose.

with free access to drinking water for 5 weeks. Body weight and food intake were registered once a week. At the time of sacrifice, mice were fasted for 4 h and thereafter anesthetized with an intraperitoneal injection of midazolam (Midazolam Panpharma 5 mg/mL, Panpharma SA, France) and a mixture of fluanison 10 mg/mL and fentanyl citrate 0.315 mg/mL (Hypnorm, VetPharma, U.K). The mice were weighed, and body fat content and lean body mass were analyzed using dual-energy X-ray absorptiometry (DEXA) technique with a Lunar PIXImus densitometer (GE Medical Systems). Blood was drawn by intraorbital puncture followed by cervical dislocation. The ceca were weighed, content collected and snap frozen for SCFA analysis, and the cecum tissues were rinsed in sterile phosphate buffered saline (PBS; Oxoid, England) and weighed, liquid was thoroughly soaked up by sterile compress, and tissues were snap frozen. All samples were stored at −80 °C until analysis.

*Experimental Diets.* The supplemented cereal byproducts were prepared as described above and analyzed for nutritional content (Table 1). In the eight experimental diets and the high-fat control diet (HFD), 60% of the energy originated from fat while the energy from fat was 10% in the low-fat control diet (LFD). All diets were manufactured by Research Diets (NB, USA). The supplemented products were included in levels so that each product contributed with 5 g/100 g dietary fiber (dry weight basis, dwb, Supporting Information, Table S1), i.e., cellulose was only added in the control HFD and LFD (5 g/100 g, dwb). One of the diets contained guar gum and used as a positive control. All high-fat diets were balanced to contain equal amounts of protein, carbohydrates (starch, maltodextrin, and mono/disaccharides), and fat.

*Plasma Samples.* Blood samples were drawn by intraorbital puncture using an EDTA-coated glass pipet. After immediate centrifugation plasma was collected and stored at −20 °C until analysis. Glucose, total cholesterol, triglycerides, HDL (all from Infinity, Thermo Electron Melbourne, Australia), fructosamine (VetSpec, Catachem Inc., Oxford, CT, USA), and alanine aminotransferase (ALT) (DiscretePak, Catachem Inc.) were measured enzymatically with colorimetric methods. LDL was calculated using Freiwalds formula: LDL = total cholesterol − (triglycerides/2.2 + HDL).[25] Insulin was measured with ELISA (Mercodia, Uppsala, Sweden).

*DNA Extraction from Cecum Tissue.* DNA from cecum tissue was isolated and purified in BioRobot EZ1 (EZ1 DNA Tissue Kit and tissue card; Qiagen, Hilden, Germany). Tissue samples were incubated with 380 μL of Buffer G2 and 30 μL of Proteinase K (Qiagen, Germany) in 56 °C for 6 h. Then 12 glass beads (2 mm in diameter) were added to each sample, which were shaken at 4 °C for 45 min to disintegrate the bacterial cell walls. Then 100 μL of the supernatant and 100 μL sterile PBS were used for extraction in the BioRobot EZ1.

*Microbial Analyses.* The amount of 16S rRNA genes of bacteria belonging to *Lactobacillus*, *Bifidobacterium*, *Enterobacteriaceae*, and *Clostridium leptum* groups and *Akkermansia muciniphila*-like bacteria were estimated using separate quantitative real-time PCR (qPCR) assays as previously described,[26] with previously published primers.[26−28] Detection limit was $10^2$ genes/reaction for *Lactobacillus*, *Bifidobacterium*, and *A. muciniphila*-like bacteria, while the limit for the *Enterobacteriaceae* assay was $10^4$ genes/reaction. For standard curves, 10-fold dilution series of the target DNA were made in TE buffer (10 mM Tris, 1 mM EDTA, pH 8.0). Number of bacteria was expressed as log 16S rRNA genes/g cecum tissue.

*SCFA in Cecum.* The SCFA (acetic, propionic, iso-butyric, butyric, iso-valeric, valeric, caproic, and heptanoic acids) in cecum were analyzed using a GLC method.[29] The intestinal content was homogenized with an Ultra Turrax T25 basic (IKA-Werke, Staufen, Germany) after adding hydrochloric acid (to protonise the SCFA) and 2-ethylbutyric acid (internal standard). The samples were centrifuged (MSE Super Minor, Hugo Tillquist AB, Solna, Sweden) and the supernatant injected on to a fused-silica capillary column with a free fatty acid phase (DB-FFAP 125-3237; J&W Scientific, Agilent Technologies Inc., Folsom, CA, USA). GC ChemStation software (Agilent Technologies Inc., Wilmington, DE, USA) was used for the evaluation. The concentration of each SCFA (μmol/g) was multiplied by the amount of cecal content to obtain the cecal pool (μmol).

**Statistics.** All groups were compared with HFD control. One-way analysis of variance (ANOVA) with Dunnet's multiple comparison post-test was used when the data was Gaussian distributed according to D'Agostino and Pearson omnibus normality test. When not normally distributed, Kruskal−Wallis nonparametric test with Dunn's multiple comparison post-test was used (GraphPad Prism 6.0, GraphPad Software, San Diego, CA, USA or Minitab software, release 16). To find significances between the different oat products and also the three rye products, the general linear model of ANOVA followed by Tukey's procedure was used. These data are not shown in any table but reported in the text under Results and Discussion.

**Principal Component Analysis.** Principal component analysis (PCA) was performed using the software SIMCA (version 13.0.3, Umetrics, Umeå, Sweden) to visualize the relationship between the analyzed bacterial groups, cecal SCFA production, and some physiological parameters in relation to each other and to the various diets.

## RESULTS AND DISCUSSION

In the present study, processed cereal byproducts were used as dietary fiber additives in a high-fat diet (HFD) and their affects were evaluated in a mouse model for human obesity and prediabetes. Three byproducts from industrials processing of cereals were used as raw materials: a fiber-rich residue from the production of oat milk, barley husks, and rye bran. The materials are rich sources of dietary fiber, antioxidants, and possibly also other potentially health-promoting substances. In an attempt to improve their health promoting properties further, the materials were subjected to selective hydrolysis by a thermostable xylanase to generate xylooligosaccharides (XOS) and arabinoxylooligosaccharides (AXOS). A heat pretreatment step was used as pretreatment to solubilize the fibers and make the materials more accessible to the enzymes.

Because no separation steps were included in the processing of three of the four products, the starting materials (Oat0, Barley0, and Rye0) and the xylanase-treated products (Oat1,

Barley1, and Rye1) had similar overall chemical composition (Tables 1 and 2).

**Table 2. Content of Carbohydrates of the Barley, Oat and Rye Products**

| | sugars[a] (mg/g dry weight material) | | | | |
|---|---|---|---|---|---|
| products | Ara | Gal | Glc | Xyl | total |
| Oats0 | 41 | 4 | 190 | 70 | 300 |
| Oats1 | 31 | 4 | 150 | 60 | 240 |
| Barley0 | 35 | 10 | 300 | 180 | 530 |
| Barley1 | 29 | 7 | 280 | 180 | 500 |
| Rye0 | 64 | 9 | 270 | 150 | 490 |
| Rye1 | 54 | 8 | 270 | 140 | 470 |
| Rye2 | 85 | 9 | 240 | 280 | 610 |

[a]Fructose is not included in the analysis because it is degraded to a large extent by sulfuric acid. Values are means, $n$ = 3. SD not more than 3%.

Rye bran was selected as starting material for production of the fourth product (Rye2, Tables 1 and 2), which is a material rich in XOS and AXOS. After heat pretreatment, only the soluble fraction was recovered and further processed. To improve the purity, starch was degraded enzymatically using a combination of $\alpha$-amylase and amyloglucosidase. Precipitation of soluble oligo- and polysaccharides to remove glucose and other small molecular impurities was carried out using ethanol. After redissolving the precipitate, xylanase-catalyzed hydrolysis was carried out. The resulting product (Rye2) had a dietary fiber content of 71% (Table 1) and high amounts of polymeric xylose and arabinose (Table 2). Similar processing has successfully been done with wheat bran to make short chain XOS and AXOS.[30]

The xylanase treatment produced xylobiose from all three tested raw materials, and in most cases longer XOS were formed as well (Figure 2). The xylanase is expected to produce XOS from xylan and from parts of AX without arabinose substituents, and it is thus less efficient in hydrolyzing highly substituted AX.[19] The smallest amount of xylobiose was found in Barley1, although Barley0 was the starting material having the highest content of xylose (Table 2). The main reason was probably the tough, highly cross-linked structure of the barley husk material. In Rye1, the distribution of different XOS was shifted toward the shorter ones, mainly xylobiose and xylotriose, which indicates that the xylanase-catalyzed hydrolysis had proceeded further in this case than in the preparation of Rye2. It has previously been shown that relatively short XOS are efficiently consumed by bifidobacteria and some strains of *Lactobacillus* in vitro.[19] More complex oligosaccharides, tentatively identified as AXOS, were detected in Oat1, Rye1, and in the highest amounts in Rye2.

To assess the effects of the different products in vivo, C57BL/6 mice were fed high-fat diets supplemented with the cereal byproducts. The different diets were evaluated for their effect on metabolic parameters, abundance of selected bacterial groups in the intestinal microbiota, and production of SCFA. The mean body weight of the test diet groups did not differ compared with the HFD control. There were no differences in energy intake, weight gain per energy intake, or body fat mass between the mice fed HFD with or without cereal supplementation. In addition, the measured plasma parameters glucose, insulin, triglycerides, total cholesterol, HDL cholesterol, LDL cholesterol, as well as HOMA-IR did not differ

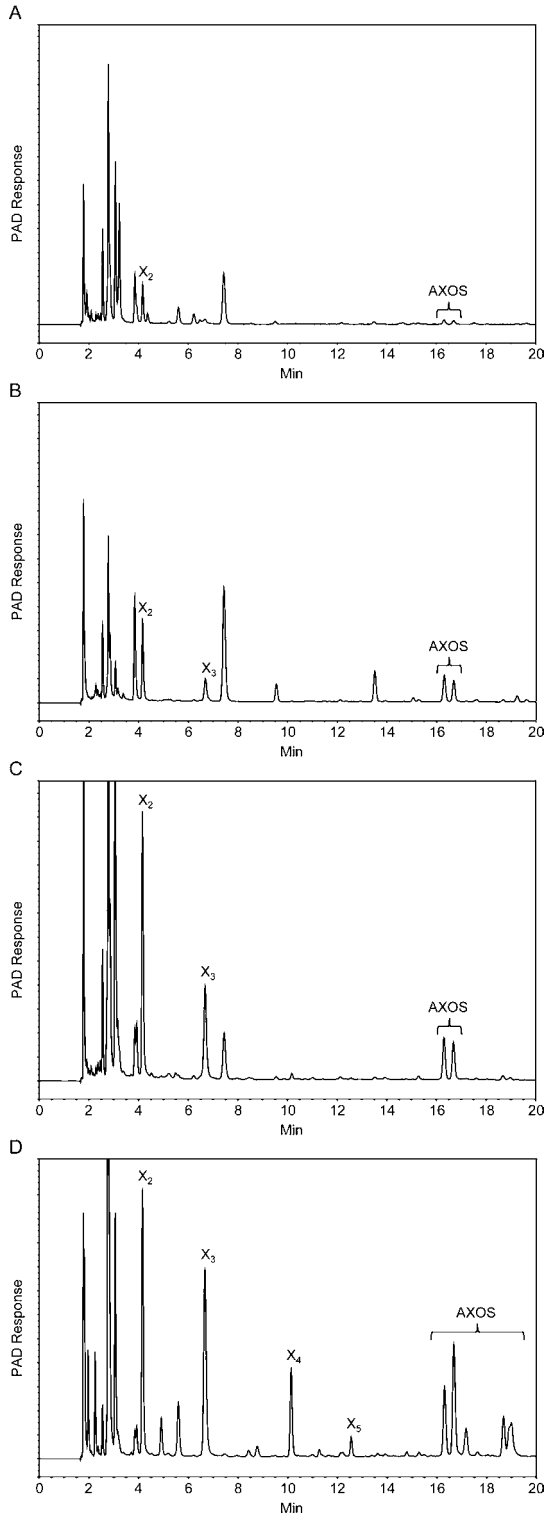


**Figure 2.** HPAEC-PAD analysis of oligosaccharides present in fiber products (A) Barley1, (B) Oat1, (C) Rye1, and (D) Rye2. $M_2$ = maltose; $X_n$ = XOS having $n$ xylose residues.

significantly between the groups fed with fiber-supplemented high-fat diet, compared with the HFD control (Table 4). Mice receiving a diet supplemented with guar gum hydrolysate (Guar, positive control[31]) showed reduced body weight after 5 weeks compared with the HFD control mice group (Table 3). Some minor metabolic changes were observed in mice fed the Rye2 diet. In plasma from Rye2-fed mice, the level of alanine


dx.doi.org/10.1021/jf502343v | J. Agric. Food Chem. 2014, 62, 8169−8178

Table 3. Body Weight and Body Composition after 5 Weeks of Different Diets[a]

| | HFD | Oat0 | Oat1 | Barley0 | Barley1 | Rye0 | Rye1 | Rye2 | Guar | LFD |
|---|---|---|---|---|---|---|---|---|---|---|
| body weight (g) | 30.0 ± 0.8 | 28.9 ± 0.5 | 28.3 ± 0.5 | 31.7 ± 1.3 | 28.2 ± 0.7 | 29.1 ± 0.9 | 28.4 ± 0.5 | 27.6 ± 1.0 | 26.5 ± 0.9[b] | 23.5 ± 0.8[c] |
| body weight gain/feed intake (mg/kcal) | 28.5 ± 2.7 | 30.4 ± 2.5 | 28.6 ± 1.5 | 31.6 ± 4.0 | 26.4 ± 2.1 | 24.6 ± 3.3 | 26.0 ± 1.4 | 24.6 ± 3.5 | 27.2 ± 1.9 | 18.4 ± 4.2 |
| body fat (%) | 28.8 ± 1.7 | 24.1 ± 1.1 | 25.4 ± 2.0 | 27.1 ± 1.6 | 26.4 ± 1.1 | 28.4 ± 1.1 | 27.5 ± 1.0 | 27.7 ± 2.2 | 24.1 ± 1.3 | 18.6 ± 0.7[c] |
| lean body mass (g) | 22.6 ± 10.5 | 23.0 ± 0.4 | 22.6 ± 0.5 | 24.1 ± 0.5 | 22.4 ± 0.4 | 22.2 ± 0.5 | 22.1 ± 0.4 | 21.1 ± 0.5 | 22.2 ± 0.6 | 20.5 ± 0.7 |

[a]Values are means ± SEM, $n = 10$. [b]Indicating significant difference ($p < 0.05$) compared to HFD. [c]$p < 0.001$.

aminotransferase (ALT) was decreased ($p = 0.006$) compared with the HFD control (Table 4), which indicates that Rye2 can counteract HFD-induced liver dysfunction. Also, the Rye2 group had a tendency of lower fructosamine ($p = 0.13$ using ANOVA multiple comparison test and $p = 0.012$ using unpaired $t$ test), which mirrors the blood glucose over the last 2 weeks, indicating an improved glucose control compared to HFD control. As expected, mice fed a low-fat diet (LFD), which was used as an additional control, showed reduced body weight ($p < 0.001$), energy intake ($p < 0.001$), and adiposity ($p < 0.001$) compared with the HFD control.

In a previous study in rats fed a high-fat diet, inclusion of XOS was shown to reduce blood glucose significantly.[32] A few of the differences compared to the present study were that the rat study was somewhat longer (6 weeks), used a pure XOS preparation (obtained from wheat bran), and that the XOS replaced corn starch in the diet, which made the dietary fiber content different in the different groups. In a human study, 4 g/day of XOS for 8 weeks reduced glucose, HbA1c, fructosamine, and blood lipids in type 2 diabetic patients.[33] With these results in mind, there seems to be good reasons to study antidiabetic effects of cereal byproducts enriched in XOS further, although no effects on some of the risk parameters could be seen, and it seems likely that both the dosage and the length of the intake period influence the observed response.

Propionic acid and butyric acid, formed from microbial fermentation of dietary fiber in colon, have been suggested to have positive metabolic effects due to their capacity to modulate pro- and anti-inflammatory markers present in the gut.[3] With this background, it is interesting to see that the cecal amount of SCFA in the mice decreased to almost the half when fed the HFD diet compared with the LFD. When the cellulose in the HFD was replaced by the dietary fiber in the different diets, the cecal amount of total SCFA formed increased in the mice, but it was only significant in mice fed the diet with Oat0 ($p < 0.01$) and guar gum ($p < 0.05$) (Table 5). More significance was seen with the individual SCFA. Guar gum, which was used as a positive control in the experiment, more than doubled the yield of propionic ($p < 0.001$) and butyric acids ($p < 0.01$) compared with the HFD control. Increased amounts of propionic ($p < 0.01$) and butyric ($p < 0.001$) acids could be seen as an effect of Oat0 and Oat1. Interestingly, if comparing the butyric acid formation before and after enzymatic treatment of oats (Oat0 with Oat1) and rye (Rye0 with Rye 1 and Rye2, respectively) there was a lower formation ($p < 0.01$–$p < 0.05$) of butyric acid after enzymatic treatment. However, Rye0 increased the amount of butyric acid ($p < 0.05$) in the cecum of mice compared with the HFD. Enzymatic treatment caused changes in the physicochemical properties of the products. When the insoluble fibers were removed (Rye2), there was an increase of propionic acid in the cecum of mice ($p < 0.05$) compared with Rye0. Similar findings, with an increased amount of propionic acid, have been seen in wheat enzyme-treated in a similar way.[34] None of the barley products had any effects on the amounts of SCFA formed in the cecum of mice compared with the HFD, and the specific SCFA formed were very similar to those formed with the high-fat control diet. The SCFA usually detected in rather low amounts; valeric, iso-valeric, and iso-butyric acid were significantly higher in mice fed the two oat products (Oat0, $p < 0.05$, and Oat1, $p < 0.001$) and with guar gum ($p < 0.001$) compared with the HFD control. Iso-valeric acid was also significantly higher ($p < 0.01$) with Rye2. The physiological impact of this is not known, but higher

**Table 4. Plasma Parameters after 5 Weeks of Different Diets[a]**

| | HFD | Oat0 | Oat1 | Barley0 | Barley1 | Rye0 | Rye1 | Rye2 | Guar | LFD |
|---|---|---|---|---|---|---|---|---|---|---|
| glucose (mM) | 6.5 ± 0.3 | 6.1 ± 0.2 | 6.1 ± 0.3 | 6.3 ± 0.4 | 6.9 ± 0.3 | 7.2 ± 0.2 | 6.6 ± 0.3 | 6.0 ± 0.2 | 6.0 ± 0.3 | 5.4 ± 0.3 |
| insulin (pM) | 272 ± 39 | 188 ± 30 | 222 ± 46 | 370 ± 58 | 294 ± 54 | 280 ± 36 | 267 ± 38 | 257 ± 42 | 316 ± 31 | 119 ± 12[b] |
| HOMA-IR | 11.2 ± 1.9 | 7.2 ± 1.2 | 8.9 ± 2.3 | 14.0 ± 2.1 | 12.9 ± 2.9 | 12.5 ± 1.7 | 11.1 ± 1.6 | 9.7 ± 1.7 | 11.8 ± 1.4 | 5.8 ± 1.9[b] |
| fructosamine ($\mu$M) | 505 ± 17 | 450 ± 9 | 515 ± 25 | 528 ± 21 | 470 ± 11 | 470 ± 16 | 523 ± 25 | 435 ± 18 | 497 ± 40 | 535 ± 14 |
| cholesterol (mM) | 4.4 ± 0.1 | 4.3 ± 0.1 | 4.4 ± 0.2 | 4.2 ± 0.2 | 4.9 ± 0.1 | 4.6 ± 0.2 | 5.1 ± 0.2 | 4.6 ± 0.3 | 4.5 ± 0.1 | 3.4 ± 0.2[b] |
| HDL (mM) | 1.4 ± 0.04 | 1.4 ± 0.03 | 1.5 ± 0.06 | 1.5 ± 0.04 | 1.6 ± 0.04 | 1.5 ± 0.04 | 1.6 ± 0.04 | 1.5 ± 0.06 | 1.4 ± 0.03 | 1.1 ± 0.03[b] |
| LDL (mM) | 2.6 ± 0.1 | 2.5 ± 0.1 | 2.5 ± 0.2 | 2.3 ± 0.2 | 2.9 ± 0.1 | 2.7 ± 0.1 | 3.1 ± 0.2 | 2.7 ± 0.2 | 2.7 ± 0.1 | 1.8 ± 0.1[c] |
| LDL/HDL | 1.9 ± 0.03 | 1.8 ± 0.1 | 1.7 ± 0.1 | 1.5 ± 0.2 | 1.8 ± 0.1 | 1.8 ± 0.1 | 2.0 ± 0.1 | 1.8 ± 0.1 | 1.9 ± 0.1 | 1.5 ± 0.1[b] |
| TAG (mM) | 0.9 ± 0.03 | 1.1 ± 0.05 | 0.9 ± 0.04 | 1.1 ± 0.06 | 1.0 ± 0.05 | 1.0 ± 0.03 | 0.9 ± 0.02 | 0.9 ± 0.04 | 0.9 ± 0.06 | 1.1 ± 0.06 |
| ALT (U/L) | 4.4 ± 0.4 | 4.3 ± 0.4 | 5.8 ± 0.9 | 6.4 ± 1.1 | 4.0 ± 0.3 | 3.1 ± 0.4 | 3.4 ± 0.5 | 1.4 ± 0.2[d] | 2.3 ± 0.4 | 2.9 ± 0.2 |

[a]HFD: high-fat diet. LFD: low-fat diet. HOMA-IR: homeostatic model assessment of insulin resistance. HDL: high-density lipoprotein. LDL: low-density lipoprotein. TAG: triacylglycerol. ALT: alanin aminotransferase. Values are mean ± SEM, $n = 10$. [b]Indicating significant difference ($p < 0.05$) compared to HFD. [c]$p < 0.01$. [d]$p < 0.001$.

**Table 5. Pools of SCFA ($\mu$mol) in Cecum of Mice[a]**

| | HFD | Oat0 | Oat1 | Barley0 | Barley1 | Rye0 | Rye1 | Rye2 | Guar | LFD |
|---|---|---|---|---|---|---|---|---|---|---|
| acetic | 3.06 ± 0.44 | 4.75 ± 0.51 | 4.51 ± 0.51 | 3.38 ± 0.35 | 3.23 ± 0.48 | 2.76 ± 0.17 | 2.53 ± 0.2 | 3.28 ± 0.44 | 5.05 ± 0.69 | 5.85 ± 0.88[c] |
| propionic | 0.62 ± 0.12 | 1.03 ± 0.10[c] | 0.94 ± 0.08[b] | 0.69 ± 0.06 | 0.76 ± 0.10 | 0.55 ± 0.03 | 0.60 ± 0.1 | 0.86 ± 0.13 | 1.62 ± 0.21[d] | 1.17 ± 0.16[c] |
| iso-butyric | 0.05 ± 0.01 | 0.10 ± 0.01[b] | 0.13 ± 0.02[d] | 0.08 ± 0.01 | 0.09 ± 0.01 | 0.05 ± 0.01 | 0.06 ± 0.0 | 0.09 ± 0.02 | 0.16 ± 0.02[d] | 0.12 ± 0.02[c] |
| butyric | 0.38 ± 0.04 | 0.83 ± 0.07[d] | 0.60 ± 0.04[b] | 0.46 ± 0.04 | 0.34 ± 0.04 | 0.68 ± 0.08[b] | 0.36 ± 0.0 | 0.50 ± 0.06 | 0.81 ± 0.13[c] | 0.62 ± 0.08[b] |
| iso-valeric | 0.07 ± 0.01 | 0.11 ± 0.01[b] | 0.16 ± 0.02[d] | 0.09 ± 0.01 | 0.11 ± 0.01 | 0.08 ± 0.01 | 0.09 ± 0.0 | 0.13 ± 0.03[c] | 0.22 ± 0.03[d] | 0.13 ± 0.02[c] |
| valeric | 0.06 ± 0.01 | 0.10 ± 0.01[b] | 0.12 ± 0.01[d] | 0.08 ± 0.01 | 0.07 ± 0.01 | 0.06 ± 0.00 | 0.07 ± 0.0 | 0.07 ± 0.01 | 0.13 ± 0.02[d] | 0.10 ± 0.02[b] |
| caproic[e] | | | | | | | | | | |
| heptanoic[f] | | | | | | | | | | |
| total | 4.25 ± 0.58 | 6.93 ± 069[b] | 6.45 ± 0.64 | 4.77 ± 0.46 | 4.61 ± 0.64 | 4.18 ± 0.25 | 3.73 ± 0.3 | 4.94 ± 0.67 | 7.98 ± 1.07[c] | 8.01 ± 1.17[c] |

[a]Values are means ± SEM, $n = 10$. Indicating significant difference ($p < 0.05$) from HFD. [b]$p < 0.05$. [c]$p < 0.01$. [d]$p < 0.001$. [e]Values were less than 0.01 $\mu$mol. [f]Values were less than 0.004 $\mu$mol.



dx.doi.org/10.1021/jf502343v | J. Agric. Food Chem. 2014, 62, 8169−8178

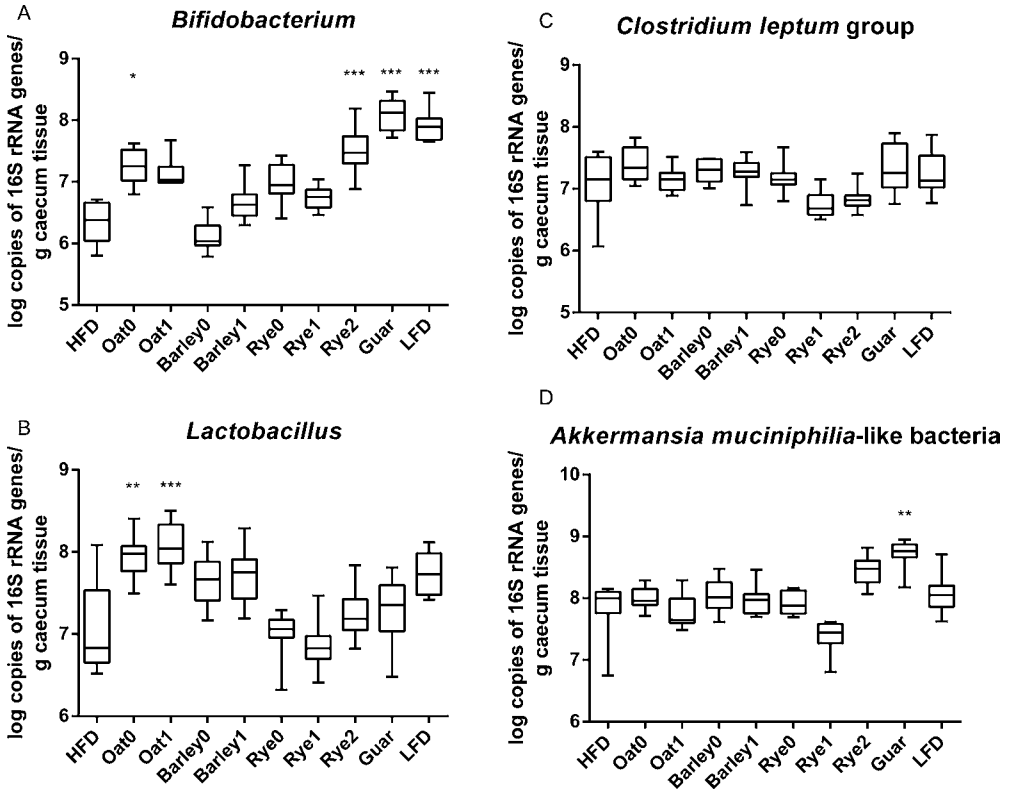


**Figure 3.** Box plots presenting the median, 10th, 25th, 75th, and 90th percentiles of the concentrations of 16S rRNA genes from (A) *Bifidobacterium*, (B) *Lactobacillus*, (C) *Clostridium leptum* group, and (D) *Akkermansia muciniphila*-like bacteria in the cecum tissue of mice on the test diets ($n$ = 7–10 animals/group, * $p < 0.05$, ** $p < 0.01$, *** $p < 0.001$).

amounts of valeric acid in blood have been seen in microscopic colitis patients, who usually have a low dietary fiber intake compared with healthy controls.[35]

*Lactobacillus* and *Bifidobacterium* are bacterial genera considered beneficial for host health.

The abundance of *Lactobacillus* and *Bifidobacterium* was assumed to be stimulated by the supplemented nondigestible carbohydrates that were used in the diets of the present experimental study. Members of the *C. leptum* group are abundant in the gastrointestinal tract and known to contribute to the intestinal butyrate production and so of interest in the present study.[36] *Akkermansia* is a commensal bacterial genus known to degrade mucin and is commonly found in the gastrointestinal tract and has been negatively correlated to obesity and metabolic disorders.[37,38] *Enterobacteriaceae* is a Gram-negative family with pro-inflammatory lipopolysaccharides in its outer cell membrane. Abundance of *Enterobacteriaceae* can be regarded as an indicator if the microbiota is in balance or if dysbiosis occurs.

In the experimental data, prebiotic potential was shown by diets LFD, Oat0, Rye2, and guar gum because animals on these diets had increased amount of *Bifidobacterium* in cecum mucosa compared to animals on HFD ($p < 0.001$, 0.05, 0.001, and 0.001, respectively) (Figure 3A). Furthermore, the number of 16S rRNA genes of *Lactobacillus* were significantly higher in animals on diets Oat0 and Oat1 compared with HFD ($p < 0.01$ and <0.001, respectively) (Figure 3B). The number of 16S rRNA genes from the *C. leptum* group did not differ significantly between the groups (Figure 3C). The number of 16S rRNA genes corresponding to *Akkermansia muciniphila*-like bacteria was increased in animals on a diet supplemented with guar gum compared to animals on HFD ($p < 0.01$) (Figure 3D), possibly indicating a prebiotic potential by enhancing the gut integrity through mucin production.[37] The amount of *Enterobacteriaceae* was below detection limit for all diet groups, so no significant differences between the diet groups could be obtained.

It is obvious that the different diets produced quite different effects on the mucosal bacterial groups quantified in this study. Because the total content of dietary fiber was the same in all cases, it seems that the composition of the fiber had a major influence although other components of the products likely contributed to the observed effects. However, Rye2 and guar gum contained mainly oligosaccharides, so at least in these cases those can be expected to have been of major importance.

The stimulation of bifidobacteria by Rye2 was likely due to its content of XOS and AXOS, which have been shown to have this effect in several other studies. For example, it has been reported that 10% XOS in the diet caused the most efficient stimulation of bifidobacteria in streptozotocin induced diabetic rats.[39] Likewise, XOS caused an increase in bifidobacteria in rats given a Western human diet.[15] In vitro experiments have also shown that XOS are indeed fermented by many intestinal bifidobacteria.[40] The mechanism for XOS utilization has been studied in the strain *Bifidobacterium animalis* subsp. *lactis* BB-12.[41] XOS/AXOS are supposed to be transported into the bacterial cells using an ABC transporter, and they are subsequently degraded intracellularly by xylanolytic enzymes. It is likely that rye fructooligosaccharides also contributed to the stimulation of bifidobacteria, as observed previously.[42] The positive effect of Oat0 on bifidobacteria agrees with previous observations of bifidobacteria stimulation by oat-based


dx.doi.org/10.1021/jf502343v | J. Agric. Food Chem. 2014, 62, 8169–8178

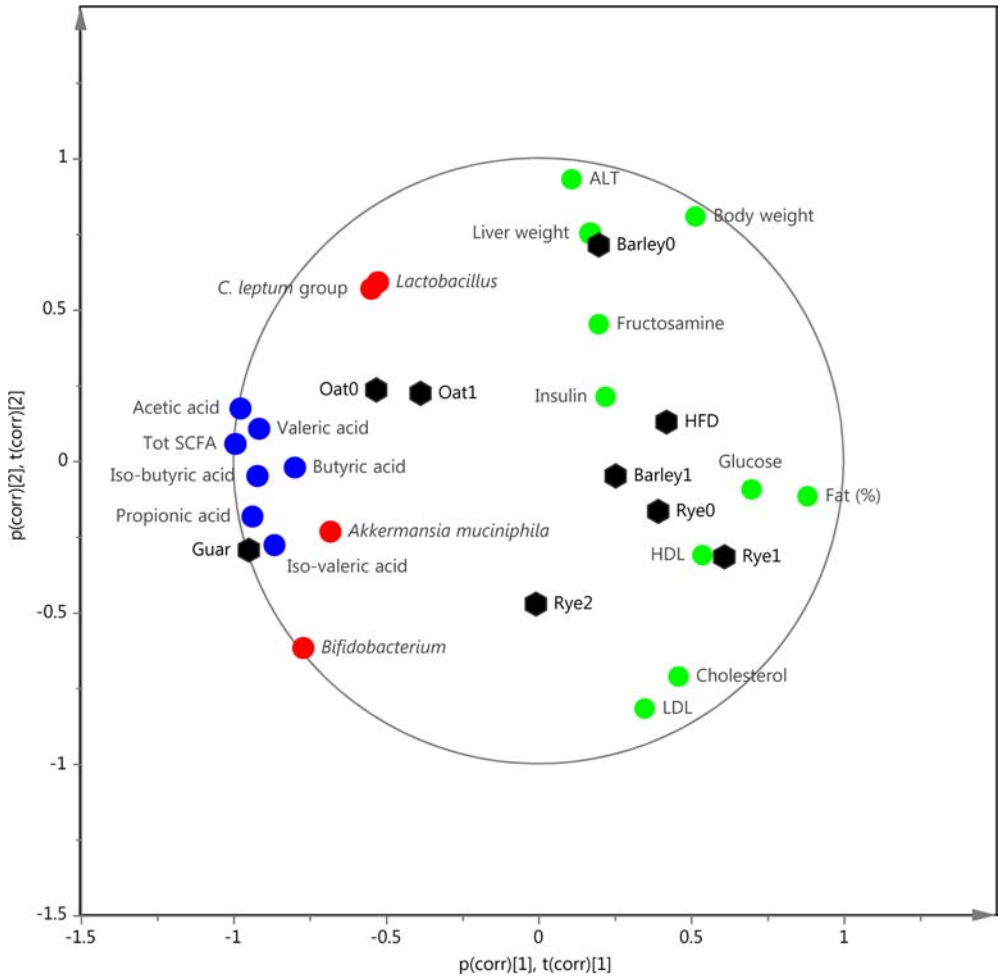


**Figure 4.** To visualize patterns and relationship in the data, a PCA was performed. Data is displayed in a biplot of analyzed bacterial groups, SCFAs, and some physiological parameters in relation to the diet groups. PC1 explained 46.6% and PC2 23.3% of the variation. Blue dots represent mean of cecal pool of analyzed SCFA or total SCFA, red dots represent the mean of the 16S rRNA expression of the analyzed microbial groups, green dots represent mean of the physiological parameters, and black hexagons represent the different diets.

products.[43] It has been reported that $\beta$-glucans from both oats and barley stimulate growth of lactobacilli and bifidobacteria,[44] so that might be at least part of the reason. The third product that caused a significant increase in bifidobacteria compared to HFD was the guar hydrolysate, which is in agreement with results reported by Giannini and co-workers.[45]

The best stimulation of lactobacilli was achieved with the oat-based products. As in the case with bifidobacteria, the stimulation was probably partly due to $\beta$-glucans,[44] but at least some lactobacilli (e.g., *L. brevis* and *L. fermentum*) grow very well on XOS as well.[40] It is interesting that the products composed mainly of oligosaccharides (Rye2 and Guar) favored bifidobacteria, while those based on oats were more efficient for lactobacilli. Notably, the abundance of the *C. leptum* group appeared similar, indicating no major change in this group of butyrate producing bacteria, although some changes of butyrate concentration in cecum content was observed in mice on different diets. Everard et al.[37] suggested *Akkermansia muciniphila* to have extensive prebiotic effects. In the present study, animals on the Guar diet was the only group with significantly higher abundance of *Akkermansia muciniphila*-like bacteria compared to HFD. The Guar group had lower body weight, but no changes of other metabolic parameters could be observed.

Multivariate statistical analysis was performed using PCA to visualize the relationship between SCFA, analyzed microbial groups, and some metabolic parameters (Figure 4). In a biplot, PC1 and PC2 were shown to explain 46.6% and 23.3% of the variation, respectively. The PCA biplot illustrates the fact that the diets supplemented with Guar and Oats (Oat0 and Oat1) cluster with the beneficial bacterial groups and SCFA in cecum but have inverse impact on, for example, body weight, body fat, and blood glucose (Figure 4).

In conclusion, the diet supplemented with Rye2, containing the highest amount of XOS and AXOS, induced bifidobacteria and there was also a tendency to an increased amount of propionic acid in the cecum as compared with the HFD control, indicating a prebiotic effect. Rye2 also significantly reduced the plasma concentration of ALT, indicating that the altered microbiota, with higher amounts of bifidobacteria, had beneficial effects on liver function. In addition, a tendency of reduced fructosamine was observed in the Rye2 group, indicative of improved glucose control compared to HFD control. The lack of other statistically proven beneficial metabolic changes might be due to the relatively short duration of the study. Also, both fractions of oat were shown to increase the amount of lactobacilli and the amounts of propionic and butyric acids in cecum, however, only the nonhydrolyzed Oat0-


dx.doi.org/10.1021/jf502343v | J. Agric. Food Chem. 2014, 62, 8169−8178

supplement increased the bifidobacteria. The present study demonstrated that underutilized byproducts from industrial processing of cereals have a potential to be used as raw materials for production of valuable prebiotic food ingredients.

## ■ ASSOCIATED CONTENT

### Ⓢ Supporting Information

Composition of experimental diets. This material is available free of charge via the Internet at http://pubs.acs.org.

## ■ AUTHOR INFORMATION


### Corresponding Author

*Phone: +46 462224842. Fax: +46 462224713. E-mail: Patrick.Adlercreutz@biotek.lu.se.



### Funding

This study was supported by the Lund University Antidiabetic Food Center, a VINNOVA VINN Excellence center at Lund University, Crafoord Foundation (K.B.), Royal Physiographic Society in Lund (K.B.), A. Påhlsson Foundation (K.B., C.H.), Swedish Research Council (C.H.), Swedish Diabetes Association (C.H.) and Dr. P. Håkansson's Foundation, Eslöv, Sweden (C.L.).


### Notes

The authors declare no competing financial interest.

## ■ ACKNOWLEDGMENTS


We acknowledge Sara Larsson, Lovisa Heyman, and Venkatachalam Narayanan for excellent technical assistance. We also thank Olof Rosén at Umetrics (Malmö, Sweden) for help with PCA and supply of the software SIMCA.


## ■ ABBREVIATIONS USED

SCFA, short-chain fatty acids; GOS, galactooligosaccharides; FOS, fructooligosaccharides; MOS, mannooligosaccharides; XOS, xylooligosaccharides; AXOS, arabinoxylooligosaccharides; HPAEC-PAD, high-performance anion exchange chromatography with pulsed amperiometric detection; HFD, high-fat diet; LFD, low-fat diet; HOMA-IR, homeostatic model assessment of insulin resistance; HDL, high-density lipoprotein; LDL, low-density lipoprotein; TAG, triacylglycerol; ALT, alanine aminotransferase

## ■ REFERENCES


(1) Anderson, J. W.; Baird, P.; Davis, R. H.; Ferreri, S.; Knudtson, M.; Koraym, A.; Waters, V.; Williams, C. L. Health benefits of dietary fiber. *Nutr. Rev.* **2009**, *67*, 188−205.

(2) Aune, D.; Chan, D. S. M.; Lau, R.; Vieira, R.; Greenwood, D. C.; Kampman, E.; Norat, T. Dietary fibre, whole grains, and risk of colorectal cancer: systematic review and dose−response meta-analysis of prospective studies. *Br. Med. J.* **2011**, *343*, 6617.

(3) Galisteo, M.; Duarte, J.; Zarzuelo, A. Effects of dietary fibers on disturbances clustered in the metabolic syndrome. *J. Nutr. Biochem.* **2008**, *19*, 71−84.

(4) Neyrinck, A. M.; Possemiers, S.; Druart, C.; van de Wiele, T.; De Backer, F.; Cani, P. D.; Larondelle, Y.; Delzenne, N. M. Prebiotic Effects of Wheat Arabinoxylan Related to the Increase in Bifidobacteria, Roseburia and Bacteroides/Prevotella in Diet-Induced Obese Mice. *PLoS One* **2011**, 6.

(5) Sekirov, I.; Russell, S. L.; Antunes, L. C. M.; Finlay, B. B. Gut Microbiota in Health and Disease. *Physiol. Rev.* **2010**, *90*, 859−904.

(6) Roberfroid, M. Prebiotics: The concept revisited. *J. Nutr.* **2007**, *137*, 830S−837S.

(7) Delzenne, N. M.; Neyrinck, A. M.; Cani, P. D. Gut microbiota and metabolic disorders: how prebiotic can work? *Br. J. Nutr.* **2013**, *109*, S81−S85.

(8) Nilsson, U.; Nyman, M. Short-chain fatty acid formation in the hindgut of rats fed oligosaccharides varying in monomeric composition, degree of polymerisation and solubility. *Br. J. Nutr.* **2005**, *94*, 705−713.

(9) Tuohy, K. M.; Kolida, S.; Lustenberger, A. M.; Gibson, G. R. The prebiotic effects of biscuits containing partially hydrolysed guar gum and fructo-oligosaccharides—a human volunteer study. *Br. J. Nutr.* **2001**, *86*, 341−348.

(10) Broekaert, W. F.; Courtin, C. M.; Verbeke, K.; Van de Wiele, T.; Verstraete, W.; Delcour, J. A. Prebiotic and Other Health-Related Effects of Cereal-Derived Arabinoxylans, Arabinoxylan-Oligosaccharides, and Xylooligosaccharides. *Crit. Rev. Food Sci. Nutr.* **2011**, *51*, 178−194.

(11) Van Laere, K. M. J.; Hartemink, R.; Bosveld, M.; Schols, H. A.; Voragen, A. G. J. Fermentation of plant cell wall derived polysaccharides and their corresponding oligosaccharides by intestinal bacteria. *J. Agric. Food Chem.* **2000**, *48*, 1644−1652.

(12) Grootaert, C.; Delcour, J. A.; Courtin, C. M.; Broekaert, W. F.; Verstraete, W.; Van de Wiele, T. Microbial metabolism and prebiotic potency of arabinoxylan oligosaccharides in the human intestine. *Trends Food Sci. Technol.* **2007**, *18*, 64−71.

(13) Patel, A.; Falck, P.; Shah, N.; Immerzeel, P.; Adlercreutz, P.; Staalbrand, H.; Prajapati, J. B.; Holst, O.; Karlsson, E. N. Evidence for xylooligosaccharide utilization in Weissella strains isolated from Indian fermented foods and vegetables. *FEMS Microbiol. Lett.* **2013**, *346*, 20−28.

(14) Fooks, L. J.; Gibson, G. R. In vitro investigations of the effect of probiotics and prebiotics on selected human intestinal pathogens. *FEMS Microbiol. Ecol.* **2002**, *39*, 67−75.

(15) Van Craeyveld, V.; Swennen, K.; Dornez, E.; Van de Wiele, T.; Marzorati, M.; Verstraete, W.; Delaedt, Y.; Onagbesan, O.; Decuypere, E.; Buyse, J.; De Ketelaere, B.; Broekaert, W. F.; Delcour, J. A.; Courtin, C. M. Structurally Different Wheat-Derived Arabinoxylooligosaccharides Have Different Prebiotic and Fermentation Properties in Rats. *J. Nutr.* **2008**, *138*, 2348−2355.

(16) Hughes, S. A.; Shewry, P. R.; Li, L.; Gibson, G. R.; Sanz, M. L.; Rastall, R. A. In vitro fermentation by human fecal microflora of wheat arabinoxylans. *J. Agric. Food Chem.* **2007**, *55*, 4589−4595.

(17) Cani, P. D.; Bibiloni, R.; Knauf, C.; Waget, A.; Neyrinck, A. M.; Delzenne, N. M.; Burcelin, R. Changes in Gut Microbiota Control Metabolic Endotoxemia-Induced Inflammation in High-Fat Diet-Induced Obesity and Diabetes in Mice. *Diabetes* **2008**, *57*, 1470−1481.

(18) Abou-Hachem, M.; Olsson, F.; Williamson, M. P.; Hreggvidsson, G. O.; Kristjansson, J. K.; Karlsson, E. N. The modular organisation and stability of a thermostable family 10 xylanase. *Biocatal. Biotransform.* **2003**, *21*, 253−260.

(19) Falck, P.; Precha-Atsawanan, S.; Grey, C.; Immerzeel, P.; Staalbrand, H.; Adlercreutz, P.; Nordberg Karlsson, E. Xylooligosaccharides from Hardwood and Cereal Xylans Produced by a Thermostable Xylanase as Carbon Sources for *Lactobacillus brevis* and *Bifidobacterium adolescentis*. *J. Agric. Food Chem.* **2013**, *61*, 7333−7340.

(20) Yoon, S. J.; Chu, D. C.; Juneja, L. R. Chemical and physical properties, safety and application of partially hydrolized guar gum as dietary fiber. *J. Clin. Biochem. Nutr.* **2008**, *42*, 1−7.

(21) Holm, J.; Bjoerck, I.; Drews, A.; Asp, N. G. A rapid method for the analysis of starch. *Starch/Staerke* **1986**, *38*, 224−226.

(22) Bjorck, I. M. E.; Siljestrom, M. A. In vivo and in vitro digestibility of starch in autoclaved pea and potato products. *J. Sci. Food Agric.* **1992**, *58*, 541−553.

(23) Sluiter, A.; Hames, B.; Ruiz, R.; Scarlata, C.; Sluiter, J.; Templeton, D.; D, C. *Determination of Structural Carbohydrates and Lignin in Biomass: Laboratory Analytical Procedure (LAP)*; Technical Report NREL/TP-510-42618; National Renewable Energy Laboratory: Golden, CO, 2008; http://www.nrel.gov/docs/gen/fy13/42618.pdf.

(24) Asp, N. G.; Johansson, C. G.; Hallmer, H.; Siljestrom, M. Rapid enzymatic assay of insoluble and soluble dietary fiber. *J. Agric. Food Chem.* **1983**, *31*, 476−482.
(25) Friedewald, W.; Fredrick, Ds; Levy, R. I. Estimation of concentration of low-density lipoprotein cholesterol in plasma, without use of preparative ultracentrifuge. *Clin. Chem.* **1972**, *18*, 499−502.
(26) Axling, U.; Olsson, C.; Xu, J.; Fernandez, C.; Larsson, S.; Strom, K.; Ahrne, S.; Holm, C.; Molin, G.; Berger, K. Green tea powder and *Lactobacillus plantarum* affect gut microbiota, lipid metabolism and inflammation in high-fat fed C57BL/6J mice. *Nutr. Metab.* **2012**, *9*, 105.
(27) Rinttilä, T.; Kassinen, A.; Malinen, E.; Krogius, L.; Palva, A. Development of an extensive set of 16S rDNA-targeted primers for quantification of pathogenic and indigenous bacteria in faecal samples by real-time PCR. *J. Appl. Microbiol.* **2004**, *97*, 1166−1177.
(28) Matsuki, T.; Watanabe, K.; Fujimoto, J.; Takada, T.; Tanaka, R. Use of 16S rRNA Gene-Targeted Group-Specific Primers for Real-Time PCR Analysis of Predominant Bacteria in Human Feces. *Appl. Environ. Microbiol.* **2004**, *70*, 7220−7228.
(29) Zhao, G. H.; Nyman, M.; Jonsson, J. A. Rapid determination of short-chain fatty acids in colonic contents and faeces of humans and rats by acidified water-extraction and direct-injection gas chromatography. *Biomed. Chromatogr.* **2006**, *20*, 674−682.
(30) Immerzeel, P.; Falck, P.; Galbe, M.; Adlercreutz, P.; Nordberg Karlsson, E.; Stålbrand, H. Extraction of water-soluble xylan from wheat bran and utilization of enzymatically produced xylooligosaccharides by Lactobacillus, Bifidobacterium and Weissella spp. *LWT—Food Sci. Technol.* **2014**, *56*, 321−327.
(31) Linetzky Waitzberg, D.; Alves Pereira, C. C.; Logullo, L.; Manzoni Jacintho, T.; Almeida, D.; Teixeira da Silva, M. L.; Matos de Miranda Torrinhas, R. S. Microbiota benefits after inulin and partially hydrolized guar gum supplementation: a randomized clinical trial in constipated women. *Nutr. Hosp.* **2012**, *27*, 123−129.
(32) Wang, J.; Cao, Y. P.; Wang, C. T.; Sun, B. G. Wheat bran xylooligosaccharides improve blood lipid metabolism and antioxidant status in rats fed a high-fat diet. *Carbohydr. Polym.* **2011**, *86*, 1192−1197.
(33) Sheu, W. H. H.; Lee, I. T.; Chen, W.; Chan, Y. C. Effects of Xylooligosaccharides in Type 2 Diabetes Mellitus. *J. Nutr. Sci. Vitaminol.* **2008**, *54*, 396−401.
(34) Haska, L.; Andersson, R.; Nyman, M. A water-soluble fraction from a by-product of wheat increases the formation of propionic acid in rats compared with diets based on other by-product fractions and oligofructose. *Food Nutr. Res.* **2011**, *55*, 1−11.
(35) Jakobsdottir, G.; Bjerregaard, J. H.; Skovbjerg, H.; Nyman, M. Fasting serum concentration of short-chain fatty acids in subjects with microscopic colitis and celiac disease: no difference compared with controls, but between genders. *Scand J. Gastroenterol.* **2013**, *48*, 696−701.
(36) Duncan, S. H.; Belenguer, A.; Holtrop, G.; Johnstone, A. M.; Flint, H. J.; Lobley, G. E. Reduced Dietary Intake of Carbohydrates by Obese Subjects Results in Decreased Concentrations of Butyrate and Butyrate-Producing Bacteria in Feces. *Appl. Environ. Microbiol.* **2007**, *73*, 1073−1078.
(37) Everard, A.; Belzer, C.; Geurts, L.; Ouwerkerk, J. P.; Druart, C.; Bindels, L. B.; Guiot, Y.; Derrien, M.; Muccioli, G. G.; Delzenne, N. M.; de Vos, W. M.; Cani, P. D. Cross-talk between *Akkermansia muciniphila* and intestinal epithelium controls diet-induced obesity. *Proc. Natl. Acad. Sci. U. S. A.*. **2013**.
(38) Derrien, M.; Vaughan, E. E.; Plugge, C. M.; de Vos, W. M. *Akkermansia muciniphila* gen. nov., sp nov., a human intestinal mucin-degrading bacterium. *Int. J. Syst. Evol. Microbiol.* **2004**, *54*, 1469−1476.
(39) Gobinath, D.; Madhu, A. N.; Prashant, G.; Srinivasan, K.; Prapulla, S. G. Beneficial effect of xylo-oligosaccharides and fructo-oligosaccharides in streptozotocin-induced diabetic rats. *Br. J. Nutr.* **2010**, *104*, 40−47.
(40) Crittenden, R.; Karppinen, S.; Ojanen, S.; Tenkanen, M.; Fagerstrom, R.; Matto, J.; Saarela, M.; Mattila-Sandholm, T.; Poutanen, K. In vitro fermentation of cereal dietary fibre carbohydrates by probiotic and intestinal bacteria. *J. Sci. Food Agric.* **2002**, *82*, 781−789.
(41) Gilad, O.; Jacobsen, S.; Stuer-Lauridsen, B.; Pedersen, M. B.; Garrigues, C.; Svensson, B. Combined transcriptome and proteome analysis of *Bifidobacterium animalis* subsp. lactis BB-12 grown on xylo-oligosaccharides and a model of their utilization. *Appl. Environ. Microbiol.* **2010**, *76*, 7285−7291.
(42) Mei, G. Y.; Carey, C. M.; Tosh, S.; Kostrzynska, M. Utilization of different types of dietary fibres by protential probiotics. *Can. J. Microbiol.* **2011**, *57*, 857−865.
(43) Martensson, O.; Biorklund, M.; Lambo, A. M.; Duenas-Chasco, M.; Irastorza, A.; Holst, O.; Norin, E.; Welling, G.; Oste, R.; Onning, G. Fermented, ropy, oat-based products reduce cholesterol levels and stimulate the bifidobacteria flora in humans. *Nutr. Res. (N. Y.)* **2005**, *25*, 429−442.
(44) Shen, R.-L.; Dang, X.-Y.; Dong, J.-L.; Hu, X.-Z. Effects of Oat $\beta$-Glucan and Barley $\beta$-Glucan on Fecal Characteristics, Intestinal Microflora, and Intestinal Bacterial Metabolites in Rats. *J. Agric. Food Chem.* **2012**, *60*, 11301−11308.
(45) Giannini, E. G.; Mansi, C.; Dulbecco, P.; Savarino, V. Role of partially hydrolyzed guar gum in the treatment of irritable bowel syndrome. *Nutrition* **2006**, *22*, 334−342.
(46) Institute for Laboratory Animal Research, National Research Council. *Guide for the Care and Use of Laboratory Animals*; National Academy Press: Washington, DC, 1996.

## NOTE ADDED AFTER ASAP PUBLICATION

This article published July 29, 2014 with a typo in the fourth paragraph of the Introduction section, errors in Figure 4, and an incorrect initial designation in the Funding statement. The correct version published August 13, 2014.

JOURNAL OF AGRICULTURAL AND FOOD CHEMISTRY

Article

pubs.acs.org/JAFC

# Inert and Oxidative Subcritical Water Hydrolysis of Insoluble Egg Yolk Granular Protein, Functional Properties, and Comparison to Enzymatic Hydrolysis

Ismael Marcet, Carlos Álvarez, Benjamín Paredes, and Mario Díaz*

Department of Chemical and Environmental Engineering, University of Oviedo, C/Julián Clavería 8, 33006 Oviedo, Spain

**ABSTRACT:** The use of enzymes to recover soluble peptides with functional properties from insoluble proteins could prove to be very expensive, implying high reaction times and low yields. In this study, the insoluble granular protein, previously delipidated, was hydrolyzed using enzymes (trypsin) as a comparison to the proposed alternative method: subcritical water hydrolysis (SWH) using both nitrogen and oxygen streams. The result of the hydrolysis was characterized in terms of the yield and peptide size distribution as well as different functional properties. The SWH of the delipidated granules resulted in a higher recovery yield than that obtained by enzymatic hydrolysis in half of the time. The foaming capacity of the peptides obtained by SWH was higher than that obtained by trypsin hydrolysis, although the foam stability was lower. Slight differences were detected between these peptides in terms of their emulsifying properties.

**KEYWORDS:** *egg yolk, functional properties, insoluble protein, subcritical water hydrolysis, trypsin hydrolysis*

## 1. INTRODUCTION

The use of proteins in the food industry is important, not only because of their nutritional value but also because proteins are capable of interacting among themselves and with other biopolymers in the food matrix, altering their organoleptic and functional properties.

Proteins used in the preparation of a food product can be from animal sources, such as the albumen of egg white, milk casein, or gelatin obtained from the connective tissue of cows and pigs. Vegetable proteins, such as soy protein, are used as well.

While all of these proteins are used to alter the features of food, their resultant peptides can extend these protein-dependent properties or produce other alterations that may be useful and profitable for the food industry. Protein hydrolysis has been broadly studied by Adler-Nissen,[1] and an extensive bibliography on a great variety of proteins has been published. Changes in the functional properties, protein recovery from food industry wastes, and others have been documented.[2−6] The main advantage of enzymatic over non-enzymatic hydrolysis is that the enzymatic reactions require mild conditions that prevent chemical alterations in the processed proteins. Furthermore, the size of the peptides can be adjusted by taking into account the hydrolysis time. This is important because the average size of the peptides is related to their functional properties. However, enzyme use can be considered expensive, and the targeted proteins must be accessible to enzymatic action.

In addition to enzymatic hydrolysis, other hydrolysis reactions can be considered, such as water hydrolysis under subcritical conditions. Water is considered to be subcritical when its temperature varies in the range from 100 to 370 °C, and it is maintained in a liquid state by application of high pressures. In this state, noticeable changes occur in its properties, increasing the ion concentration product ($K_w$) at 250 °C to $10^{-11}$, as well as its decreasing dielectric constant at elevated temperatures, thereby exhibiting higher solvation behavior.[7] In fact, subcritical water has been used previously to recover phenolic compounds[8] and amino acids from biomass discards.[9−11] Furthermore, this method can be used in the hydrolysis of soluble proteins, allowing, with adjustment of the treatment parameters, the control of the end products.[12]

Egg yolk can be easily separated into plasma and granular fractions. The first one is the lipid-rich fraction, and it is mainly composed of lipoproteins. It has been described as having emulsion[13] and gelation properties,[14,15] similar to those found in the whole egg yolk. On the other hand, the second one is the protein-rich fraction, and it requires an ionic strength ≥0.3 M NaCl to solubilize its protein constituent. Below 0.3 M NaCl, the granules from egg yolk show a low solubility[16] and, therefore, decreased functional properties, which reduces their applications.

In this work, the hydrolysis of non-soluble egg yolk proteins has been studied using enzymes and the subcritical water method. For that purpose and because it has a high protein content and limited utility, the egg yolk granular fraction was obtained, delipidated, and hydrolyzed. The hydrolysis yield, average size of the peptides, and their functional properties were evaluated and compared in this study.

## 2. MATERIALS AND METHODS

**2.1. Production of Delipidated Granules.** The egg yolk granules were obtained using the Laca et al.[17] method. Egg yolk was separated from the albumen manually, and the vitelline membrane was discarded using tweezers. The egg yolk was diluted (1:1.5, v/v) with water, and the pH was adjusted to 7. Finally, the diluted egg yolk was kept overnight at 4 °C and centrifuged at 4 °C and 10000*g* for 45 min to obtain the granules in the sediment. Granules were lyophilized and mixed with ethanol (96%, 1:12.5, w/v) at 40 °C for 2 h with gentle agitation. Finally, the granules were recovered using a vacuum pump and Whatman No. 1

Received: December 17, 2013
Revised: July 17, 2014
Accepted: July 17, 2014
Published: July 17, 2014

ACS Publications © 2014 American Chemical Society

filter paper. The delipidated egg yolk granules were then washed with 200 mL of fresh ethanol and dried overnight in a heater at 50 °C to obtain a dehydrated and ethanol-free powder.

**2.2. Enzymatic Hydrolysis.** The hydrolysis was carried out in a 400 mL bioreactor with a pH-STAT automatic titration (pH-Buret 24 2S, Crison) connected to an isothermal shaker. Delipidated egg yolk granules were mixed with water (1:20, w/v) and preheated at 90 °C for 7 min to enhance the dispersion of the granules. Two enzyme−substrate ratios were tested, 1:50 and 1:25, using trypsin from porcine pancreas EC 3.4.21.4 (93610, Sigma-Aldrich), 18 136 U/mg. The dispersed granules were heated at 37 °C, and the pH was adjusted to 7.5 using 0.1 M sodium hydroxide solution. Finally, the enzyme was added to the reactor, and after 6 h, the enzymatic reaction was stopped by heating the hydrolysate for 15 min in a water bath at 90 °C.

The degree of hydrolysis (DH) was evaluated using the pH-STAT method according to Adler-Nissen.[1] In this method, the amount of base solution consumed along the reaction is proportional to the amino groups liberated during the enzymatic hydrolysis. The DH was calculated using the Adler-Nissen equation (eq 1)

$$\mathrm{DH}\ (\%) = \frac{100 V_B N_B}{\alpha M_p h_{tot}} \tag{1}$$

where $\alpha$ is the degree of dissociation of the $\alpha$ amino group calculated by following eq 2, $M_p$ is the amount of protein in the assay (g), and $h_{tot}$ is the total number of peptide bonds in the protein (mequiv $g^{-1}$ of protein). The value of $h_{tot}$ for egg yolk protein was assumed to be 8 based on a suggestion found in ref 18, which perfectly fits with the $h_{tot}$ values reported by Nielsen et al. for raw materials.[19] $V_B$ is the volume (mL) of the base (NaOH) added during the course of the enzymatic reaction, and $N_B$ is the normality of the base.

$$\alpha = \frac{10^{\mathrm{pH}-\mathrm{p}K}}{1 + 10^{\mathrm{pH}-\mathrm{p}K}} \tag{2}$$

The p$K$ value used for the hydrolysis procedure is calculated approximately using the equation by Guadix et al.[20] (eq 3).

$$\mathrm{p}K = 3.80 + 0.45\mathrm{pH} \tag{3}$$

*2.2.1. Subcritical Water Hydrolysis (SWH).* The delipidated granules were dispersed in water (1:20, w/v) to obtain 400 mL of solution and placed in the jacketed reactor shown in Figure 1. Different hydrolysis temperatures were tested, and the lowest temperature tested with a good peptide recovery in 4 h was 180 °C. At each tested temperature, a pressure of 40 bar was achieved using a non-reactive (nitrogen) or an oxidizing (oxygen) gas stream of 1 L/min. A back-pressure valve (Brooks mass flow controller 5850) allowed for pressure control in the system. The injected gas was previously saturated with water to avoid sample evaporation and heated to keep the reactor temperature constant. In this study, the reaction time specified in each case includes the heating time. This heating time was short in each case; therefore, its influence on the overall process is negligible.

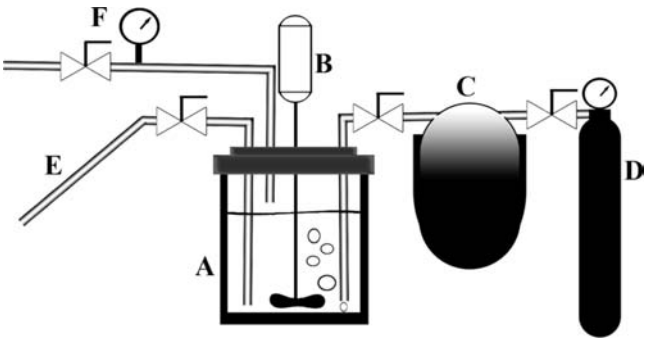


**Figure 1.** Setup of the SWH reactor: (A) pressure reactor, (B) agitation, (C) humidifier, (D) nitrogen or oxygen gas bottle, (E) sample taker, and (F) back-pressure valve.

**2.3. Size-Exclusion Chromatography.** An AKTA fast protein liquid chromatography (FPLC) system (GE Healthcare, Sweden) was employed to determine the peptide size distribution using a size-exclusion column (Superdex Peptide 10/300 GL), which can separate peptides from 100 to 7000 Da. The buffer used was composed of 0.1 M Tris at pH 7.6. The elution flow was adjusted to 1 mL/min. The FPLC system used was dotted with an ultraviolet (UV) detector, and the wavelength employed was 214 nm. Previously, the column was calibrated with weight markers supplied by Sigma-Aldrich: lysozyme (14 307 Da), cytochrome *c* (12 384 Da), aprotinin (6512 Da), cianocobalamin (1355 Da), and tryptophan (204 Da) ($R^2$ = 0.99). The molecular size distribution and the average molecular size of the obtained peptides were analyzed to determine the total concentration. Subsequently, the area of the chromatograms obtained was divided into ranges of molecular size, according to previous calibration. The area of each zone was measured, employing the Unicorn 5.1 analysis software, and transformed into protein concentration. The frequency of each molecular weight range was calculated with regard to the total amount of soluble peptides.

**2.4. Amino Acid Quantification.** The amounts of amino acids produced during the SWH and the enzymatic hydrolysis were calculated by the Rosen method.[21] This method is based on the interaction of ninhydrin with the amino groups, resulting in a colored compound.

**2.5. Functional Properties.** To test the functional properties, after the hydrolysis processes, the solutions were centrifuged at 10000*g* for 30 min. After that, the supernatants were separated from the sediments by decantation. Immediately, the supernatants were lyophilized, and the sediments were discarded. The protein content of the lyophilized product was determined using the Dumas combustion method.[22] For that purpose, the nitrogen content was calculated using a CNHS/O Elementar Vario EL analyzer (Elementar, Germany). The conversion factor employed was 6.25 mg of protein/mg of N.

*2.5.1. Solubility.* The solubility of the hydrolyzed and non-hydrolyzed delipidated egg yolk granules was determined using a modified method by Wang et al.[18] Briefly, they were diluted in distilled water to obtain a protein concentration of 1 mg/mL. The pH of these solutions was adjusted with 1 N HCl or 1 N NaOH and equilibrated at room temperature for 60 min. The pH values were readjusted at 30 and 60 min to correct possible variations. Finally, the diluted samples were centrifuged at 10000*g* and 30 min, and the sediment was discarded. The protein content of the samples was determined according to Markwell et al.,[23] both before centrifugation and in the resulting supernatant. A calibration curve was carried out using bovine serum albumin. The protein solubility was calculated using the following equation:

$$\mathrm{PS}\ (\%) = \frac{\text{protein in supernatant (mg)}}{\text{protein in the initial solution (mg)}} \times 100 \tag{4}$$

*2.5.2. Foaming Capacity (FC) and Foam Stability (FS).* FC and FS were determined according to ref 24, with slight modifications. Peptide solutions of 5 mg/mL protein in water were prepared, and the pH was adjusted to 7 using 1 N NaOH or 1 N HCl. After 30 min of equilibration at room temperature, 30 mL of the solutions were taken and stirred at 15 000 rpm using a Heidolph SilentCrusher for 1 min. The volume of the foam formed was immediately calculated using a cylinder measure, and the FC was determined. To calculate the FS, foam volume changes in the cylinder measure were recorded at 30 min of storage.

$$\mathrm{FC}\ (\%) = \frac{\text{foam volume after whipping (mL)}}{\text{initial liquid volume (mL)}} \times 100 \tag{5}$$

$$\mathrm{FS}\ (\%) = \frac{\text{foam volume after 30 min(mL)}}{\text{foam volume after whipping (mL)}} \times 100 \tag{6}$$

*2.5.3. Emulsifying Properties.* Emulsifying properties were measured according to the study by Pinciroli et al.[25], with slight modifications. Peptides were diluted in a NaCl solution (0.075%, w/v) to obtain a final concentration of 10 mg/mL protein. The pH of these solutions was adjusted to pH 7 using 1 N HCl or 1 N NaOH and equilibrated for 30 min with continuous stirring at room temperature. A total of 15 mL of these solutions were mixed with 10 mL of cottonseed oil at 15 000 rpm

using a Heidolph SilentCrusher (Heidolph, Germany). Immediately, the emulsions were put into a glass measurement cell, and the stability against creaming was measured using a Turbiscan apparatus (Formulaction, France). Backscattered light was monitored every 2 min for 1 h as a function of the sample height. Clarification was measured at the bottom of the measured cell from 0 to 25 mm ($B\%_{0-25\ mm}$), and creaming was determined at the top of the cell ($B\%_{25-40\ mm}$). Furthermore, the initial backscattering value in the medium zone of the measurement cell ($B\%_{ini}$), stability parameter ($t_{0.1}$), and kinetic constant ($K_{0.1}$) were determined too. The stability parameter $t_{0.1}$ was calculated as the time in which the backscattering in the bottom of the measured cell decreased to 10% of its initial value. The kinetic constant $K_{0.1}$ was calculated according to the following equation:

$$K_{0.1}\ (h^{-1}) = (B\%_{ini,0-25\ mm} t_{0.1})^{-1} \quad (7)$$

**2.6. Statistical Analysis.** The assays shown in this work were carried out in triplicate. Mean and standard deviation are shown in each case.

## 3. RESULTS AND DISCUSSION

**3.1. Enzymatic Hydrolysis Characterization.** The DH is a parameter used with respect to enzymatic hydrolysis that is frequently referred to in the literature.[26−29] The DH is directly related to the solubility of the peptides obtained from the insoluble proteins.[30] Figure 2 shows DH versus enzymatic reaction time. It can be seen that, as one would expect, an increase in the hydrolysis time and enzyme concentration lead to an increase in the DH.

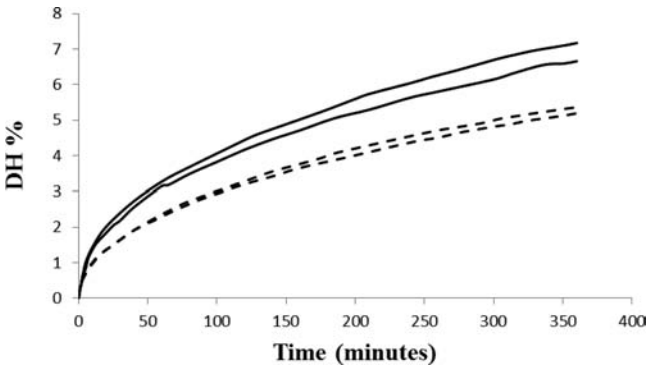


**Figure 2.** DH (%) of delipidated egg yolk granules treated with trypsin. Continuous lines correspond to a 1:25 enzyme/substrate ratio, and discontinuous lines correspond to a 1:50 enzyme/substrate ratio. Reproducibility is shown in each case.

As expected, the low solubility of the delipidated egg yolk granules at any pH impedes the cleavage of the peptide bond by the enzyme. This can be observed in Figure 2, where after 360 min of operation, the DH values reached 5.2 ± 0.12% (enzyme/substrate ratio of 1:50) and 6.9 ± 0.3% (enzyme/substrate ratio of 1:25).

According to the hydrolysis time, these DH values can be considered low compared to others found in the bibliography. In previous studies,[3] the non-delipidated granules were dissolved in a 0.55 M NaCl solution. In this NaCl solution, the phosphocalcic bridges between the granular proteins are disrupted and these proteins became soluble. In this case, the enzyme can interact with the peptide bonds efficiently and the DH increases to 12.0 ± 0.5% after 90 min. In other studies and using different enzymes, the hydrolysis of ethanol-delipidated whole egg yolk resulted in a DH of 6% in 80 or 100 min as a function of the enzyme tested.[18] However, the comparison of the results presented in this work to those obtained by these authors is difficult given the methodology differences. In any case, the trypsin hydrolysis of delipidated egg yolk granules resulted in a significantly longer reaction time compared to those reported by other authors.

The DH is an indication of the peptide sizes obtained; therefore, the higher the DH, the lower the size of these peptides. To calculate their average size with more precision, aliquots obtained at different times during the enzymatic hydrolysis were analyzed by size-exclusion chromatography (SEC). The chromatogram is shown in Figure 3A, and the peaks identified in this figure are detailed in Table 1.

In the hydrolysis using trypsin, five peaks were detected (Figure 3A), which maintain their relative importance during the period of hydrolysis. The main peak identified is number 4, which corresponds to peptides with an average size of 3500 Da (Table 1). Furthermore, in Table 2, the peptides were analyzed according to their size at each hydrolysis time. In enzymatic hydrolysis, the average peptide size was similar at each time tested, with no significant variations during the process.

**3.2. SWH.** In the SWH method, the aliquots obtained at different times were analyzed by SEC. In these non-enzymatic hydrolyses, the peptide size profiles vary according to the reaction time, with their sizes decreasing progressively from 23 000 Da in the initial stages to around 1000 Da at longer times. This can be observed in panels B and C of Figure 3, where at short reaction times, the main peak obtained is the number 1, while at longer reaction times, the SEC chromatograms obtained were progressively moving to the right, with the main peak appearing around the 1000 Da in these cases (peak numbers 3 and 4 in panels B and C of Figure 3). Therefore, in this type of hydrolysis, the temperature and reaction time that are chosen are important to obtain the greatest amount of soluble peptides, because the reaction progression leads to full protein breakdown. According to Abdelmoez et al.,[31] some amino acids are sensitive to temperatures around 230 °C. This can be observed in Table 2, where in both nitrogen and oxygen SWH, the population of peptides of more than 6 kDa decreases with the time of hydrolysis and those peptides of less than 6 kDa increase in a similar way.

**3.3. Process Yield.** The process yield in each case was calculated and shown in Figure 4. For enzymatic hydrolysis, the yield obtained rises with the reaction time. After 360 min of operation, the recovery of soluble peptides corresponds to 50% of the original protein when an enzyme−substrate ratio of 1:25 is used.

In the SWH under nitrogen stream, the maximum yield was obtained at 240 min. After that, the yield decreased slowly until it reached 70% at 580 min. According to ref 32, some additives, such as sodium bicarbonate, can be used to enhance the protein hydrolysis, although it produces a decrement in the molecular weight of final peptides. With regard to the SWH under oxygen stream, the yield rose quickly until 120 min and then decreased quickly too. Using these gas streams, the yield obtained was around 95%, almost doubling the value obtained by the enzymatic hydrolysis and with significantly shorter operation times as well. Between the nitrogen and oxygen treatments, the latter was more efficient, reaching the maximum recovery rate in half of the time required to achieve that value in the hydrolysis under a nitrogen stream. This is because, in the SWH under nitrogen stream, the non-reactive nitrogen has no effect on peptide breakdown, with hydrolysis being possible thanks to the increase in the amount of hydrogen and hydroxide ions in the subcritical water. However, using oxygen, in addition to the

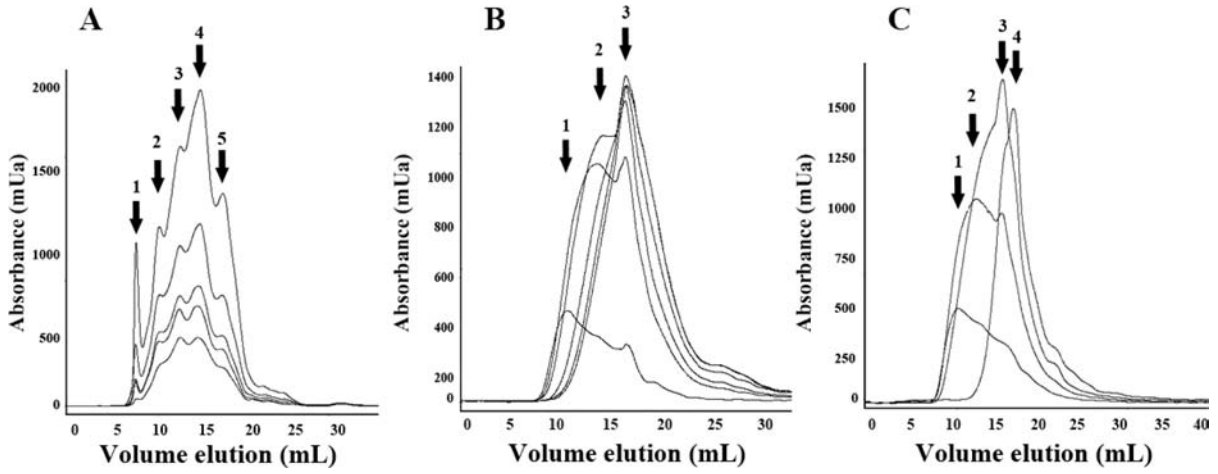


**Figure 3.** SEC chromatograms of the peptides obtained during hydrolysis: (A) peptides obtained from enzymatic hydrolysis, (B) peptides obtained from SWH under nitrogen stream, and (C) peptides obtained from SWH under oxygen stream.

**Table 1. Size of the Main Peaks Detected in Figure 3**

| | trypsin | | nitrogen | | oxygen | |
|---|---|---|---|---|---|---|
| | volume elution (mL) | size (Da) | volume elution (mL) | size (Da) | volume elution (mL) | size (Da) |
| 1 | 7.98 | 112171 | 10.97 | 23836 | 11.03 | 23106 |
| 2 | 10.39 | 32189 | 13.96 | 5065 | 13.98 | 5012 |
| 3 | 12.49 | 10846 | 16.86 | 1127 | 16.8 | 1163 |
| 4 | 14.68 | 3488 | | | 17.95 | 641 |
| 5 | 17.06 | 1016 | | | | |

increase in the ion concentration product of the water, the dissolved oxygen produces a rise in the oxidization of the organic matter. According to the study by Kelvin et al.,[33] the exposure of proteins to the hydroxyl radical and the superoxide anion radical promotes changes in their structure. This could increase their susceptibility to proteolytic action and lead to the rise in peptide bond cleavage that was detected.

During the SWH reaction, loss of protein in the form of amino acids, ammonium compounds, and other volatile products was expected.[34] Amino acids are considered to be the main decomposition compound in both enzymatic and SWH. For this reason, amino acids were measured in the reaction medium at each hydrolysis time (Figure 5). In the enzymatic hydrolysis (Figure 5A), the production of amino acids was the lowest, and after 360 min of reaction, the loss of protein was around 2% (w/w). In the SWH under nitrogen stream, the rise in amino acid production was more noticeable and continuous as the reaction proceeded. However, at the minute of optimum peptide yield (240 min), the loss of protein was 6%, owing to the formation of amino acids. The progression was similar in the SWH under oxygen stream, but because of the fact that the maximum yield was obtained at 120 min, the production of amino acids was reduced to 3%. According to these results, in every hydrolysis method, the loss of protein in the form of amino acids and in the maximum yield times was not relevant.

**3.4. Functional Properties.** For the functional properties assays, the highest yields in each case were chosen according to section 3.3.

*3.4.1. Solubility Profile.* The solubility profiles of the peptides obtained by hydrolysis are shown in Figure 6. The ethanol-delipidated egg yolk granules were used as a reference for the improvement in solubility obtained. Solubility could be considered as the most important functional property of proteins, because other functional properties, such as, for example, their water holding, gelling, foaming, and emulsifying capacities, are dependent upon it.

The low solubility of the delipidated egg yolk granules at any tested pH was expected because of the ethanol treatment that they had undergone, which produces the protein denaturation. In food proteins, denaturation is usually associated with protein insolubilization and loss of other functional properties.[35] An increase in the solubility properties of the resultant peptides is expected after the hydrolysis process.[27,36]

In the case of the enzymatic hydrolysis, the peptides obtained were highly soluble. However, in this type of hydrolysis, it is very difficult to recover all of the initial insoluble protein in the form of soluble peptides. In previous studies using soy protein, a DH of 8% or higher was required and the 100% conversion from protein to soluble peptides was not achieved.[37] As previously commented, in this work, a DH of 7% was obtained and only 50% of the protein was recovered as soluble peptides. This is explained by the remaining hydrophobic protein aggregations that cannot be hydrolyzed by the enzymes.

In nitrogen and oxygen SWH and also in the enzymatic hydrolysis, in the tested pH range, the isoelectric point of the peptides was not detected and their solubility maintains a relative flat profile, instead of the characteristic U-shaped profile expected. In the two SWH tested, in addition to the high solubility of the peptides obtained, 95% of the protein was recovered.

*3.4.2. Foaming Properties.* The FC of the peptides is shown in Figure 7. The FC of the delipidated egg yolk granules was tested too, and it was considered to be 0 because of their low solubility.

As observed in Figure 7, all of the peptides showed foaming properties but differences in the FC and FS were found. Peptides obtained by enzymatic hydrolysis had the lowest values for FC, but their FS was the highest. In comparison, the peptides obtained by SWH under nitrogen and oxygen streams showed a higher FC, but their FS was poor compared to that obtained with the peptides derived from enzymatic hydrolysis.

These differences could be explained by the differences in the average size of the peptides that have been described previously. According to Sijtsma et al.[38] and Addler-Nilsen and Olsen,[37] the optimum peptide size varies from 1650 to 3850 Da. In enzymatic

Table 2. Peptide Size Distribution Obtained from Figure 3[a]

| | trypsin | | | | | nitrogen | | | | | oxygen | | | | |
|---|---|---|---|---|---|---|---|---|---|---|---|---|---|---|---|
| | 20 min | 40 min | 60 min | 120 min | 240 min | 360 min | 120 min | 180 min | 240 min | 300 min | 420 min | 480 min | 60 min | 90 min | 120 min | 150 min | 180 min | 240 min |
| >10 kDa (%) | 30.1 | 36.6 | 32.7 | 33.3 | 32.8 | 31 | 15.7 | 15.1 | 11.3 | 9.58 | 7.17 | 5.01 | 35.8 | 23.4 | 9.8 | 35 | 2.67 | 0.81 |
| 10−6 kDa (%) | 11.9 | 12.7 | 12.9 | 13.2 | 12.0 | 12.2 | 9.54 | 10.0 | 8.61 | 8.06 | 6.41 | 5.56 | 10.7 | 17.5 | 7.84 | 4.36 | 2.77 | 1.17 |
| 6−1 kDa (%) | 39.2 | 39.4 | 40.6 | 40.3 | 41.2 | 42 | 39.7 | 41.8 | 43.6 | 43.8 | 44.8 | 42.3 | 32.8 | 44.0 | 47.1 | 46.8 | 44.7 | 36.6 |
| <1 kDa (%) | 16.2 | 12.3 | 13.5 | 13.6 | 14.0 | 13.8 | 37.0 | 34.3 | 36.8 | 38.3 | 43.4 | 47.4 | 20.5 | 21.7 | 35.7 | 45 | 49.8 | 63.3 |
| average size (kDa) | 7 | 7.9 | 7.4 | 7.5 | 7.4 | 7.1 | 4.6 | 4.7 | 4.1 | 3.8 | 3.37 | 2.9 | 6.4 | 6.5 | 3.9 | 2.8 | 2.4 | 1.8 |

[a]Standard deviations were lower than 10% in each case.

hydrolysis, the average peptide size obtained was around 7 kDa, while in SWH, the average size was around 4 kDa. In this case, it is likely that the lower size peptides obtained by SWH diffuse rapidly and adsorb at the interface.[39] However, the number of interactions at the air−water interface will be larger in the case of bigger proteins, and therefore, although SWH leads to more FC, the bigger size of the peptides derived from enzymatic hydrolysis gives greater FS.[40]

In addition to the peptide size, the adequate distribution of the hydrophobic groups and the charged nuclei in the peptide structure are another important feature for obtaining good interfacial qualities.[35] They are important for creating interactions with the interface and providing the electrostatic repulsions that give FS. The size distribution of the peptides obtained by SWH in oxygen and nitrogen was similar; however, the FC and FS were higher in the peptides obtained under the nitrogen stream than those obtained in the oxygen stream. This could be because, although the oxygen promotes protein hydrolysis, the oxidizing conditions provided could be altering the amino acid residues. According to Stadtman and Levine,[41] the oxidation of proteins leads to the hydroxylation of aromatic groups and aliphatic amino acid side chains, nitration of aromatic amino acid residues, nitrosylation of sulfydryl groups, sulfoxidation of methionine residues, chlorination of aromatic groups and primary amino groups, and conversion of some amino acid residues to carbonyl derivates. It could be interesting to further investigate if these amino acid residue modifications affect the ability of the peptides to interact with the air−water interface and, in particular, to stabilize the foams produced.

*3.4.3. Emulsifying Properties.* The emulsifying properties of the peptides obtained are shown in Figure 8. Figure 8A shows the variation in backscattering at the bottom of the measurement cell, which was measured to study the emulsion creaming. The peptides obtained by enzymatic hydrolysis showed a lower decrease in emulsion backscattering with time when compared to the values obtained for the SWH peptides. In fact, according to the values shown in Table 3, enzymatic hydrolysis produced the peptides whose emulsions were the most stable, with the highest $t_{0.1}$ and the lowest $K_{0.1}$ values. Peptides obtained by SWH under a nitrogen stream showed values closer to those found in the enzymatic hydrolysis, although their creaming was more noticeable. On the other hand, peptides obtained by SWH under an oxygen stream showed the poorest emulsifying properties.

This was confirmed by the $B\%_{ini}$ values. Higher initial values of backscattering are related to emulsions that contain a high number of oil droplets and low size. Therefore, a high value in this parameter is considered indicative of good emulsifying properties.

With regard to stabilization in the cream phase (Figure 8B), the decrease in the backscattering profile detected in the emulsions elaborated using peptides from the two SWH processes showed that coalescence is the main component in the destabilization, reversing the expected rise in backscattering caused by the creaming process.[25] However, the emulsion elaborated using peptides from enzymatic hydrolysis was more stable, which indicates that it is likely that coalescence is not the main cause of emulsion destabilization in this case.

According to the study by Wang et al.,[18] hydrolyzed ethanol-delipidated whole egg yolk protein resulted in improved emulsifying capacity and stability, in particular with the hydrolysates obtained at the highest DH tested (DH = 6%). In our study for delipidated egg yolk granular protein, the

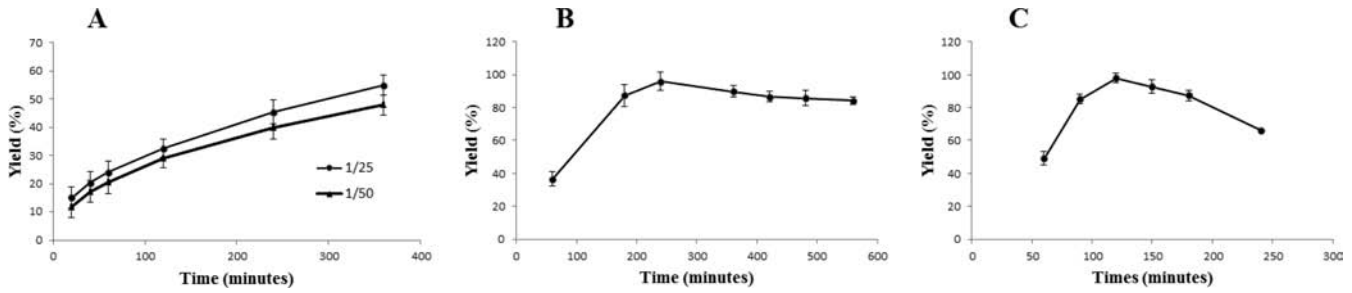


**Figure 4.** Yield of the hydrolysis process against the reaction time: (A) enzymatic hydrolysis process, (B) SWH under nitrogen stream, and (C) SWH under oxygen stream.

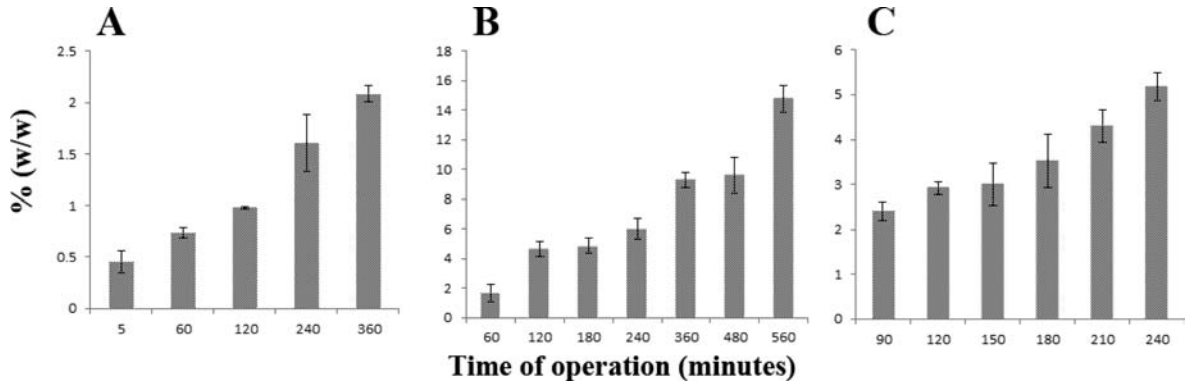


**Figure 5.** Amino acid residue production during the hydrolysis processes: (A) enzymatic hydrolysis process, (B) SWH under nitrogen stream, and (C) SWH under oxygen stream.

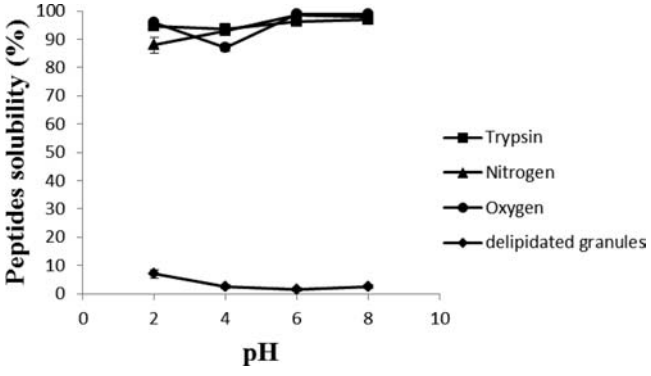


**Figure 6.** Solubility of delipidated granules and peptides at different pH values.

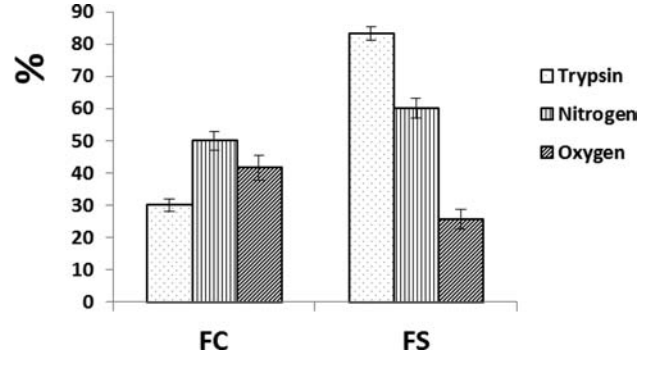


**Figure 7.** FC and FS of the peptides.

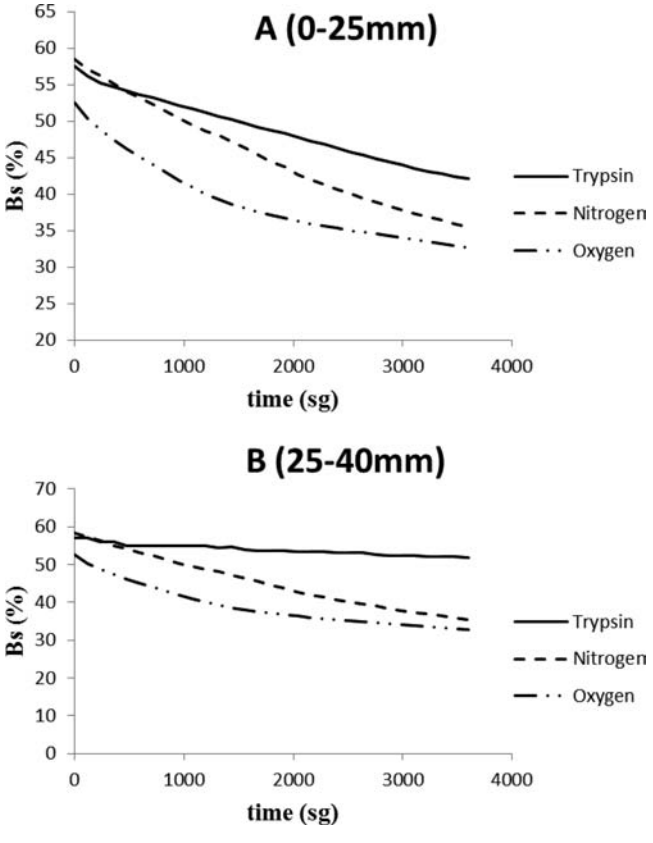


**Figure 8.** Variations in backscattering over 60 min in the emulsions elaborated using the peptides obtained by different means: (A) backscattering measured at the bottom of the cell and (B) backscattering measured in the upper part of the cell.

hydrolysates obtained after the enzymatic hydrolysis, with DH of 7%, had the better emulsifying properties. The SWH method


dx.doi.org/10.1021/jf405575c | J. Agric. Food Chem. 2014, 62, 8179−8186

**Table 3. Parameters Obtained from the Backscattering Variations Shown in Figure 8**

| | trypsin | SWH nitrogen | SWH oxygen |
|---|---|---|---|
| $t_{0.1}$ (min) | 17.5 ± 0.6 | 12.25 ± 0.4 | 5.9 ± 0.11 |
| $K_{0.1}$ ($h^{-1}$) | 0.06 ± 0.002 | 0.08 ± 0.002 | 0.19 ± 0.003 |
| $B\%_{ini}$ | 57 ± 1.5 | 58.3 ± 2 | 52 ± 1 |

resulted in significantly smaller peptides, and they gave less stable emulsions. Therefore, as with foaming properties, the emulsifying properties were highly dependent upon the peptide size. This result is consistent with another study, which suggest that extensive hydrolysis of whey proteins reduces the emulsifying activity of the obtained products.[39]

Finally, the results suggest that the modifications caused by SWH under an oxygen stream had a negative effect on the interfacial properties of the peptides, while SWH under a nitrogen stream resulted in hydrolysates with foaming and emulsifying properties close to those obtained by enzymatic hydrolysis.

In conclusion, the delipidated and non-hydrolyzed egg yolk granular protein used as a control was highly insoluble at any tested pH. Using enzymatic hydrolysis (trypsin), 50% of the initial protein content was recovered in the form of soluble peptides in 360 min of reaction. However, using the SWH method, the yield increased until 95% and the reaction time decreased significantly. The functional properties of the peptides obtained using trypsin and those using SWH under a nitrogen stream showed slight differences in their foam and emulsifying capacities. Furthermore, when a SWH under oxygen pressure was carried out, probably because of the protein modifications caused by the oxidizing gas stream, a decrement in the functional properties of the peptides was detected.

According to these results, the use of SWH to obtain peptides from insoluble proteins can be considered as a good alternative to the enzymatic hydrolysis, being a faster and reactive-free method.

## AUTHOR INFORMATION


### Corresponding Author

*Telephone: +34-985103439. Fax: +34-985103434. E-mail: mariodiaz@uniovi.es.



### Funding

Ismael Marcet acknowledges receipt of a graduate fellowship from the Severo Ochoa Program (Principado de Asturias, Spain).


### Notes

The authors declare no competing financial interest.

## REFERENCES


(1) Adler-Nissen, J. *Enzymic Hydrolysis of Food Proteins*; Elsevier Applied Science Publishers: New York, 1986.

(2) Chang, C.-Y.; Wu, K.-C.; Chiang, S.-H. Antioxidant properties and protein compositions of porcine haemoglobin hydrolysates. *Food Chem.* **2007**, *100*, 1537−1543.

(3) Orcajo, J.; Marcet, I.; Paredes, B.; Díaz, M. Egg yolk hydrolysed granules: Characteristics, rheological properties and applications. *Food Bioprod. Process.* **2013**, *91*, 457−463.

(4) Hasanov, H.; Zakirova, M.; Boboev, A.; Akbarova, N. Enzymatic hydrolysis of various proteins of wheat in heterogeneous conditions. *Int. J. BIOautom.* **2010**, *14*, 197−202.

(5) Nguyen, H. T. M.; Sylla, K. S. B.; Randriamahatody, Z.; Donnay-Moreno, C.; Moreau, J.; Tran, L. T.; Bergé, J. P. Enzymatic hydrolysis of yellowfin tuna (*Thunnus albacares*) by-products using protamex protease. *Food Technol. Biotechnol.* **2011**, *49*, 48−55.

(6) Wu, H.-C.; Chen, H.-M.; Shiau, C.-Y. Free amino acids and peptides as related to antioxidant properties in protein hydrolysates of mackerel (*Scomber austriasicus*). *Food Res. Int.* **2003**, *36*, 949−957.

(7) Miller, D. J.; Hawthorne, S. B. Solubility of liquid organic flavor and fragrance compounds in subcritical (hot/liquid) water from 298 to 473 K. *J. Chem. Eng. Data* **2000**, *45*, 315−318.

(8) Pourali, O.; Asghari, F. S.; Yoshida, H. Production of phenolic compounds from rice bran biomass under subcritical water conditions. *Chem. Eng. J.* **2010**, *160*, 259−266.

(9) Esteban, M.; García, A.; Ramos, P.; Márquez, M. Sub-critical water hydrolysis of hog hair for amino acid production. *Bioresour. Technol.* **2010**, *101*, 2472−2476.

(10) Sereewatthanawut, I.; Prapintip, S.; Watchiraruji, K.; Goto, M.; Sasaki, M.; Shotipruk, A. Extraction of protein and amino acids from deoiled rice bran by subcritical water hydrolysis. *Bioresour. Technol.* **2008**, *99*, 555−561.

(11) Zhu, X.; Zhu, C.; Zhao, L.; Cheng, H. Amino acids production from fish proteins hydrolysis in subcritical water. *Chin. J. Chem. Eng.* **2008**, *16*, 456−460.

(12) Espinoza, A. D.; Morawicki, R. O.; Hager, T. Hydrolysis of whey protein isolate using subcritical water. *J. Food Sci.* **2012**, *77*, C20−C26.

(13) Le Denmat, M.; Anton, M.; Beaumal, V. Characterisation of emulsion properties and of interface composition in O/W emulsions prepared with hen egg yolk, plasma and granules. *Food Hydrocolloids* **2000**, *14*, 539−549.

(14) Anton, M.; Le Denmat, M.; Beaumal, V.; Pilet, P. Filler effects of oil droplets on the rheology of heat-set emulsion gels prepared with egg yolk and egg yolk fractions. *Colloids Surf., B* **2001**, *21*, 137−147.

(15) Kiosseoglou, V.; Paraskevopoulou, A. Molecular interactions in gels prepared with egg yolk and its fractions. *Food Hydrocolloids* **2005**, *19*, 527−532.

(16) Causeret, D.; Matringe, E.; Lorient, D. Ionic strength and pH effects on composition and microstructure of yolk granules. *J. Food Sci.* **1991**, *56*, 1532−1536.

(17) Laca, A.; Paredes, B.; Díaz, M. A method of egg yolk fractionation. Characterization of fractions. *Food Hydrocolloids* **2010**, *24*, 434−443.

(18) Wang, G.; Wang, T. Egg yolk protein modification by controlled enzymatic hydrolysis for improved functionalities. *Int. J. Food Sci. Technol.* **2009**, *44*, 763−769.

(19) Nielsen, P.; Petersen, D.; Dambmann, C. Improved method for determining food protein degree of hydrolysis. *J. Food Sci.* **2001**, *66*, 642−646.

(20) Guadix, A.; Guadix, E. M.; Páex-Dueñas, M. P.; González-Tello, P.; Camacho, F. Technological processes and methods of control in the hydrolysis of proteins. *Ars Pharm.* **2000**, *41*, 79−89.

(21) Rosen, H. A modified ninhydrin colorimetric analysis for amino acids. *Arch. Biochem. Biophys.* **1957**, *67*, 10−15.

(22) Etheridge, R.; Pesti, G.; Foster, E. A comparison of nitrogen values obtained utilizing the Kjeldahl nitrogen and Dumas combustion methodologies (Leco CNS 2000) on samples typical of an animal nutrition analytical laboratory. *Anim. Feed Sci. Technol.* **1998**, *73*, 21−28.

(23) Markwell, M. A. K.; Haas, S. M.; Bieber, L.; Tolbert, N. A modification of the Lowry procedure to simplify protein determination in membrane and lipoprotein samples. *Anal. Biochem.* **1978**, *87*, 206−210.

(24) Deng, Q.; Wang, L.; Wei, F.; Xie, B.; Huang, F.; Huang, W.; Shi, J.; Huang, Q.; Tian, B.; Xue, S. Functional properties of protein isolates, globulin and albumin extracted from *Ginkgo biloba* seeds. *Food Chem.* **2011**, *124*, 1458−1465.

(25) Pinciroli, M.; Vidal, A. A.; Añón, M. C.; Martínez, E. N. Comparison between protein functional properties of two rice cultivars. *LWT—Food Sci. Technol.* **2009**, *42*, 1605−1610.

(26) Tanzadehpanah, H.; Asoodeh, A.; Chamani, J. An antioxidant peptide derived from ostrich (*Struthio camelus*) egg white protein hydrolysates. *Food Res. Int.* **2012**, *49*, 105−111.

(27) Pokora, M.; Eckert, E.; Zambrowicz, A.; Bobak, Ł.; Szołtysik, M.; Dąbrowska, A.; Chrzanowska, J.; Polanowski, A.; Trziszka, T. Biological and functional properties of proteolytic enzyme-modified egg protein by-products. *Food Sci. Nutr.* **2013**, *1*, 184−195.

(28) Graszkiewicz, A.; Żelazko, M.; Trziszka, T. Application of pancreatic enzymes in hydrolysis of egg-white proteins. *Pol. J. Food Nutr. Sci.* **2010**, *60*, 57−61.
(29) Chay Pak Ting, B. P.; Mine, Y.; Juneja, L. R.; Okubo, T.; Gauthier, S. F.; Pouliot, Y. Comparative composition and antioxidant activity of peptide fractions obtained by ultrafiltration of egg yolk protein enzymatic hydrolysates. *Membranes* **2011**, *1*, 149−161.
(30) Soral-Śmietana, M.; Świgoń, A.; Amarowicz, R.; Sijtsma, L. The solubility of trypsin pea protein hydrolysates. *Nahrung* **1998**, *42*, 217−218.
(31) Abdelmoez, W.; Nakahasi, T.; Yoshida, H. Amino acid transformation and decomposition in saturated subcritical water conditions. *Ind. Eng. Chem. Res.* **2007**, *46*, 5286−5294.
(32) Espinoza, A. D.; Morawicki, R. O. Effect of additives on subcritical water hydrolysis of whey protein isolate. *J. Agric. Food Chem.* **2012**, *60*, 5250−5256.
(33) Davies, K. J. Protein damage and degradation by oxygen radicals. I. General aspects. *J. Biol. Chem.* **1987**, *262*, 9895−9901.
(34) Rogalinski, T.; Herrmann, S.; Brunner, G. Production of amino acids from bovine serum albumin by continuous sub-critical water hydrolysis. *J. Supercrit. Fluids* **2005**, *36*, 49−58.
(35) Damodaran, S. Amino acids, peptides, and proteins. In *Food Chemistry*, 3rd ed.; Fennema, O. R., Ed.; Marcel Dekker, Inc.: New York, 1996; pp 322−425.
(36) Panyam, D.; Kilara, A. Enhancing the functionality of food proteins by enzymatic modification. *Trends Food Sci. Technol.* **1996**, *7*, 120−125.
(37) Adler-Nissen, J.; Olsen, H. S. The influence of peptide chain length on taste and functional properties of enzymatically modified soy protein. In *Functionality and Protein Structure*; Pour-El, A., Ed.; American Chemical Society (ACS): Washington, D.C., 1979; ACS Symposium Series, Vol. 92, Chapter 7, pp 125−146.
(38) Sijtsma, L.; Tezera, D.; Hustinx, J.; Vereijken, J. Improvement of pea protein quality by enzymatic modification. *Nahrung* **1998**, *42*, 215−216.
(39) Turgeon, S. L.; Gauthier, S. F.; Paquin, P. Interfacial and emulsifying properties of whey peptide fractions obtained with a two-step ultrafiltration process. *J. Agric. Food Chem.* **1991**, *39*, 673−676.
(40) Kunst, T. Protein modification to optimize functionality: Protein hydrolysates. In *Handbook of Food Enzymology*, Whitaker, J. R., Voragen, A. G. J., Wong, D. W. S., Eds.; Marcel Dekker, Inc.: New York, 2003; pp 221−236.
(41) Stadtman, E.; Levine, R. Free radical-mediated oxidation of free amino acids and amino acid residues in proteins. *Amino Acids* **2003**, *25*, 207−218.

JOURNAL OF AGRICULTURAL AND FOOD CHEMISTRY

Article

pubs.acs.org/JAFC

# Effect of Cooking on Meat Proteins: Mapping Hydrothermal Protein Modification as a Potential Indicator of Bioavailability

Santanu Deb-Choudhury,*[,†] Stephen Haines,[†] Duane Harland,[†] Stefan Clerens,[†] Chikako van Koten,[‡] and Jolon Dyer[†,§]

[†]Food & Bio-based Products and [‡]Knowledge & Analytics, AgResearch Lincoln Research Centre, Christchurch 8140, New Zealand

[§]Biomolecular Interaction Center, University of Canterbury, Christchurch 8140, New Zealand

Supporting Information

**ABSTRACT:** Thermal treatment of meat proteins induces a range of observable and molecular-level changes. In order to understand and track these heat-induced modifications at the amino acid level, various analytical techniques were used. Changes were observed both in the soluble and in the insoluble fractions after hydrothermal treatment of minced beef samples. Redox proteomics clearly indicated increasing oxidative modification of proteins with increased heat exposure. Collagens in the soluble fraction and myosin in the insoluble fraction were found to be highly susceptible to such modifications. Maillard reaction products in the insoluble and pyrrolidone formation in the soluble fraction steadily increased with increased heat exposure. Fluorescence studies indicated a rapid increase in fluorescence with heat, suggesting the formation of advanced glycation end products. Overall these results provide a deeper understanding of the effect of cooking on meat proteins and the possible relationship to processing conditions in meat-derived food.

**KEYWORDS:** *meat proteins, amino acids, heat-induced modifications, microspectroscopy, fluorescence*

## INTRODUCTION

Cooking or hydrothermal treatment of food proteins induces a range of changes observable both at the whole food level (for example color, taste, tenderness, and moisture holding capacity) and at the molecular level, such as changes in the amino acid profile. This is a particularly important consideration for meat-based foods, which generally have some form of heat treatment prior to consumption. To understand and control the properties of meat-derived products, it is essential to understand and map these modifications.

Cooking causes a cascade of chemical reactions; some of these are beneficial while others have undesirable effects on meat proteins. Cooking-induced changes in protein composition and functional properties affect the sensory, textural, and the nutritional quality of meat products.[1,2]

One of the determining factors of nutritional quality is the bioavailability of proteins. The quality of proteins may be compromised if there are modifications to essential amino acids when food is cooked. For example, heat treatment of food may cause the formation of cross-linked amino acids such as lysinoalanine, lanthionine, and histidinoalanines. Bioavailability is also linked to digestibility, and food processing using heat and alkali treatment either reduces or increases the digestibility of proteins.[3−6] Alkaline treatment in the presence of heat may contribute to reduced nutritive quality of proteins due to amino acid racemization. Bioavailability of the amino acid lysine is reported to be reduced as a result of lysinoalanine formation, under such conditions.[7] Digestibility is aided by the hydrolysis of proteins into amino acids and peptides which is an essential step for absorption of food proteins by enterocytes.[8,9] Reduced bioavailability due to the destruction of arginine and lysine (which are proteolytic enzyme substrates) and also due to racemization of L-amino acids to their less utilizable D-form has been reported earlier.[10,11] Enhanced bioavailability on the other hand, is brought about by the inactivation of tannins, phytates, and protease inhibitors and from the release of bound vitamins.[12] It is a complex trade-off, of which a full understanding can only be gained through tracking of modifications to proteins. Unfortunately tracking residue-level modification is particularly difficult due to the complex nature of food which is confounded by various processing conditions. However, understanding these changes can lead to process improvements resulting in improvements in the final product.

Since cooked meat is composed primarily of protein, its functional properties are influenced by changes to constituent amino acids. Oxidative modification can reduce the bioavailability of basic and aromatic amino acids.[13] Oxidation of basic amino acids often leads to the formation of highly reactive carbonyl groups resulting in protein cross-links.[14] Free radicals produced during meat cooking reduces bioavailability of amino acids such as cysteines and tyrosines by the formation of disulfides and dityrosine bridges, respectively.[15] These cross-links may form protein aggregates, which are substrates for proteases, reducing digestibility and nutritional quality. Subsequent fermentation by the colonic microflora of non-hydrolyzed proteins can then lead to the formation of mutagenic products, resulting in detrimental effects on human health.[16] Changes in color, flavor, digestibility, and nutritional value of food, as a result of cooking, are partly due to

Received: March 3, 2014
Revised: July 17, 2014
Accepted: July 17, 2014
Published: July 17, 2014

ACS Publications © 2014 American Chemical Society

the Maillard reaction, a form of nonenzymatic browning. Maillard chemistry encompasses a complex array of reactions starting with the glycation of proteins and progressing to sugar-derived protein adducts and cross-links also known as advanced glycation end products (AGEs). Impaired nutritional value as a result of changes in protein integrity and function through protein cross-linking mediated by AGEs is an undesirable effect of Maillard reactions.[17] On the positive side, an increased antioxidant activity in food has also been attributed to these reactions.[18] Maillard reaction also remains a major contributor toward the development of the most recognized flavor compounds during the process of cooking meat.[19] Prolonged cooking time and high temperature have been shown to produce high levels of heterocyclic aromatic amines (HAA), which are mutagenic in nature.[20,21] HAA formation in meat during heat exposure has been previously demonstrated to be dependent on the type of meat and the cooking method used.[21]

The challenging task of detecting modifications of proteins and peptides in food substrates and tracking molecular changes is possible using advanced proteomic techniques, including mass spectrometry combined with bioinformatics. The evaluation of protein modification pathways is now possible and can provide valuable information on food processing conditions.[22] The aim of this study was to use several different approaches to profile protein modifications introduced during cooking of meat. We were able to identify the level and sites of amino acid modifications which has provided a deeper understanding of the factors affecting heat-induced changes in meat proteins.

## MATERIALS AND METHODS

**Materials.** TPCK-trypsin was obtained from Promega Corp. (Madison, WI, USA). Tris(2-carboxyethyl)phosphine (TCEP) was obtained from Fluka Chemie (Buchs, Germany). Acetonitrile (ACN) and HPLC grade water were obtained from Mallinckrodt (Phillipsburg, NJ, USA). Tris, dithiothreitol (DTT), and formic acid (FA) were obtained from Merck (Darmstadt, Germany). *o*-Phthalaldehyde (OPA) and triethylamine were obtained from Sigma-Aldrich (St. Louis, MO, USA)

**Methods.** *Sample Preparation.* A 500 g amount of beef sample (biceps femoris), obtained from an animal aged 18 months at the time of slaughter, was minced for 2 min. Subsamples (15 g wet weight) were individually weighed out in round-bottomed flasks and dispersed in water at a meat to water ratio of 1:3. An equilibration time of 20 min each was given before the individual samples were boiled under reflux for 0, 15, 30, 60, or 240 min. Samples were constantly stirred for even heat distribution. Afterward, flasks were immediately cooled in an ice bath for 5 min. Samples were centrifuged (Avanti J-30 I, Beckman) at 38400*g* for 10 min at 4 °C to obtain soluble and insoluble fractions. These were individually freeze-dried (Dura-Dry $\mu$P freeze-dryer, FTS Systems) and stored at −80 °C until analyzed.

*Total Fat Analysis.* Approximately 5 g of raw meat sample was finely minced and boiled gently for 30 min using 50 mL of 6 M hydrochloric acid. The hydrolyzate was then filtered using a Whatman 54 filter paper and the residue rinsed with water until a neutral pH was reached. The filter paper containing the residue was then dried and Soxhlet extracted to determine the total fat content.[23] The total fat content was determined to be 2.8%.

*Determination of pH.* The pH of the raw meat was measured using a pH meter (Mettler-Toledo, Columbus, OH, USA) at ambient temperature. The pH was determined to be 5.58.

*OPA Assay.* Free amines were quantified in the soluble fractions from all time points using an OPA assay.[24] Approximately 10 mg of each lyophilized soluble fraction was dissolved in 1 mL of double distilled water which was then further diluted 2-fold. A 100 $\mu$L aliquot of the diluted sample solution was added to 1 mL of OPA reagent prepared as described,[24] briefly vortexed, incubated for 2 min, and the absorbance measured at 340 nm using an Ultrospec II spectrophotometer (LKB, GE Healthcare, Cleveland, OH, USA). Absorbance readings, averaged from three technical repeats, were compared to the serine standard (1.367 mequiv/L) to determine the $\alpha$-$NH_2$ equivalents generated during hydrolysis. The degree of hydrolysis (DH) was calculated according to the method described by Nielsen et al.[24]

*Amino Acid Analysis.* The lyophilized soluble and insoluble fractions were subjected to amino acid analysis after hydrolysis using HCl vapor at 110 °C for 24 h followed by phenylisothiocyanate derivatization.[25]

An Ultimate 3000 HPLC system (Dionex, Thermo Fisher Scientific Inc., Sunnyvale, CA, USA) was used. A 10 mm aliquot of each derivatized sample was injected onto a Zorbax SB-C18, 5 $\mu$m, 250 × 4.6 $mm^2$ column (Agilent Technologies, Santa Clara, CA, USA) protected with a C18 guard column. The separation was performed at 40 °C using a gradient from 2 to 40% mobile phase B over 31 min. Mobile phase A contained sodium acetate (140 mM), sodium azide (7.5 mM), disodium ethylenediaminetetraacetic acid (EDTA; 0.26 mM) and triethylamine (20 mM) in water and was titrated to pH 5.9 with acetic acid. Mobile phase B was 100% acetonitrile. The eluting peaks were monitored at 254 nm using a photodiode array detector (Ultimate 3000 PDA). At the end of each run the column was washed with 100% B for 10 min followed by reequilibration with 1% B for 20 min.

The level of tryptophan, which is also an essential amino acid, cannot be determined by this method because the indole ring of this amino acid is highly sensitive to the acidic conditions. Cysteines and methionines were quantified using performic acid oxidation followed by HCl vapor hydrolysis.

*Gel Filtration Chromatography.* Gel filtration chromatography was performed on a HPLC system (Knauer, Berlin, Germany) equipped with an A 3800 auto sampler and a S 2600 photodiode array detector.

The soluble fraction from each sample was lyophilized, dissolved in HPLC grade water at 5 mg/mL, and injected (50 $\mu$L) onto a Superdex Peptide HR 10/30 column (GE Healthcare), having an exclusion limit of 20000 Da and optimum separation range of 100−7000 Da. Elution was performed at a flow rate of 0.75 mL/min with 0.05 M phosphate buffer (pH 6.9) containing 0.3 M sodium chloride as the mobile phase. Under these conditions, carbonic anhydrase (29 kDa) eluted at 10.0 min, cytochrome C (12.4 kDa) at 11.3 min, aprotinin (6.5 kDa) at 13.3 min, and sodium azide at 28.2 min. A standard curve was established from the elution times of these standards. The column eluate was monitored at 230, 260, and 280 nm.

*LC-MS/MS Analysis.* The freeze-dried samples from the insoluble fractions, approximately 10 mg in weight, were extracted in a buffer consisting of 7 M urea, 2 M thiourea, and 50 mM DTT, at a ratio of 1:2 (w/v). The proteins were then precipitated using methanol/chloroform precipitation.[26] Proteins from both the insoluble and the soluble fractions were reduced with 50 mM TCEP, alkylated with 360 mM acrylamide, and finally digested with sequencing grade trypsin.

Nanoflow LC-MS/MS was performed on a LC-Packings (Amsterdam, Holland) HPLC, consisting of a Famos autosampler, a Switchos column-switching module, and an Ultimate nanoflow pump. Samples were loaded at 8 $\mu$L/min onto a 0.5 cm × 300 $\mu$m trap column (Varian MicroSorb C18, 5 $\mu$m, 300 Å) which was then switched in-line with 20 cm × 75 $\mu$m analytical column (Varian MicroSorb C18, 5 $\mu$m, 300 Å). Both the trap column and the analytical column were packed in-house. Elution was performed at 150 nL/min, using a linear gradient from 5% to 70% acetonitrile (with 0.2% FA) over 45 min. The column outlet was directly interfaced to a QSTAR Pulsar *i* mass spectrometer (AB Sciex) using a stainless steel electrospray needle (Proxeon, Thermo Fisher). Automated information-dependent acquisition (IDA) was performed using Analyst QS 1.1 software, with a MS survey scan over the range $m/z$ 400−1200 followed by three MS/MS spectra from $m/z$ 40−1600 accumulating three cycles, each with 1.3 s duration.

*Data Analysis.* After each LC-MS/MS run, the raw data file was submitted to Mascot Daemon software (Matrix Science, London, U.K.) for peak list extraction. Peak lists were queried against *Bos taurus*

**Table 1. List of Target Amino Acids Used for Heat-Induced Modification Searches**

| | modification | Unimod accession no. | target amino acids | position | formula |
|---|---|---|---|---|---|
| 1 | oxidation | 35 | CMFHPWY | any | O(1) |
| 2 | dioxidation | 425 | CMFHPWY | any | O(2) |
| 3 | trioxidation | 345 | CFHWY | any | O(3) |
| 4 | nitration | 354 | FHWY | any | H(−1)N(1)O(2) |
| 5 | kynurenin | 351 | W | any | C(−1)O(1) |
| 6 | hydroxykynurenine | 350 | W | any | C(−1)O(2) |
| 7 | quinone | 392 | YW | any | H(−2)O(2) |
| 8 | carbamylation | 5 | any | N-terminal | H(1)C(1)N(1)O(1) |
| 9 | deamidation | 7 | NQ | any | H(−1)N(−1)O(1) |
| 10 | dehydration | 23 | S | any | H(−2)O(−1) |
| 11 | didehydro | 401 | T | any | H(−2) |
| 12 | dehydroalanine | 400 | Y | any | H(−6)C(−6)O(−1) |
| 13 | dehydroalanine | 368 | C | any | H(−2)S(−1) |
| 14 | pyro-glu | 27 | E | N-terminal | H(−2)O(−1) |
| 15 | pyro-glu | 28 | Q | N-terminal | H(−3)N(−1) |
| 16 | hex(2) | 512 | KR | any | C(12)H(20)O(10) |
| 17 | carboxymethylation | 6 | K | any | H(2)C(2)O(2) |

sequences in the NCBInr database (release date, Sept. 14, 2011) using the Mascot search engine (v2.2.03, Matrix Science) maintained on an in-house server. The following Mascot search parameters were used: "semitrypsin" as the proteolytic enzyme with two missed cleavages permitted; 200 ppm error tolerance for MS and 0.3 Da for MS/MS. Search results were compiled and analyzed using ProteinScape 2.1 (Bruker) using the ProteinExtractor function. At least one peptide with a score indicating identity, calculated by the search engine, was required for protein identification and results assessed as true matches were used for further analysis.

For the evaluation of heat-induced peptide modifications, Mascot searches were conducted using a combination of up to four of the target modifications listed in Table 1 as variable amino acid modifications at any given time. Error-tolerant searches were performed to account for combinations of modifications that are not in the same group. There were no additional meaningful combinations of modifications found using error-tolerant searches that were not included in the combinations reported.

Modifications between samples were compared using an in-house-developed scoring system. For each modification, the score was calculated by dividing the number of amino acids bearing the modification by the total number of susceptible amino acids in the identified peptides. Modifications 1−7 were categorized as oxidative, 8−15 as other modifications ,and 16−17 as Maillard modifications (Table 1).

For the oxidative modifications, the scores were multiplied by weighing factors associated with damage hierarchies that reflected the relative severities of the modifications relative to the native unmodified amino acid residue.[27] A total oxidative weighted score was then obtained by summing the individual weighted modification scores as shown in the following equation:

$$S_w = \sum_{n}^{i=1} \left( \frac{aa_{mod_i}}{aa_{tot_i}} f_{mod_i} \right)$$

where $S_w$ = total weighted modification score, $aa_{mod_i}$ = count of amino acids affected by the $i$th modification, $aa_{tot_i}$ = total number of amino acids that could be affected by the $i$th modification, and $f_{mod_i}$ = the weighing factor for the $i$th modification.

A similar approach was used for calculating the total scores for Maillard and other heat-induced modifications, but without any weighting factors.

*Microspectroscopic and Fluorescence Studies.* Lyophilized fractions, resuspended in water (15 μL), were transferred by micropipette into 96-well plates for examination (bright field or fluorescence) using a Leica DM6000B microscope (Leica, Wetzlar, Germany) with 200 W Hg lamp. Soluble fractions were examined with UV (340−380 nm)/blue (>425 nm long pass) and blue (450−490 nm)/green (>515 nm long pass) filter sets. Reproducibility (sample transfer accuracy and sample homogeneity) was validated using replicates.

Samples in wells were centered on the microscope stage to standardize the fluid volume being imaged. Microscope and camera (DC500, Leica) settings were standardized to prevent overexposure at the highest sample brightness. Black standard (with shutter in place) and white standard (ultrapure water in well plates) images were taken just before imaging. All images were in sRGB color space and stored as 8 and 16 bit per channel RGB TIFF files.

Mean red, green, and blue values were measured from a central line across each image (AnalySIS 5.0, Olympus, Tokyo, Japan), and these data (900 samples per channel) were transferred to a spreadsheet for analysis. Conversion from sRGB to CIEXYZ and xyY space was achieved by a matrix transform to a 2° Observer, D65 illumination standard.

Insoluble fractions were observed by bright field and fluorescence. In addition to the filters described previously, a multispectral band-pass filter (Leica B/G/R) was used with excitation regions in UV (420 ± 30 nm), blue (495 ± 15 nm), and green/yellow (570 ± 20 nm), and emission in blue (465 ± 20 nm), green (530 ± 30 nm) and red (640 ± 40 nm).

**Statistical Analysis.** All values are reported as the mean ± standard error of the mean from three individual measurements for the OPA and amino acid analysis.

In order to assess the effect of heat exposure time, heat-induced weighted modification scores (oxidative or other) were analyzed using one-sample $t$ test (Minitab v. 16). The first $t$ test compared the oxidative scores of heat-exposed samples ($n$ = 4; i.e., samples with exposure times of 15, 30, 60, and 240 min combined) in the insoluble fraction against the score of the baseline sample (i.e., sample with exposure time of 0 min). The second $t$ test similarly compared the oxidative scores of heat-exposed samples ($n$ = 4) in the soluble fraction against the baseline score. These two $t$ tests were then repeated on the scores other than oxidative ($n$ = 4 each in insoluble or soluble fraction). The statistical significance was set at $p < 0.05$.

## RESULTS

Minced beef samples were exposed to boiling water under reflux for various time periods. Minced meat was used to increase the meat surface area of exposure to the designated temperature as quickly as possible without the formation of a temperature gradient from the surface to the core, as would be expected if bigger meat pieces are used. Individual samples were

then centrifuged to obtain a soluble and an insoluble fraction and subsequently investigated for protein denaturation and amino acid modifications.

**OPA Assay.** Figure 1 shows the amount of free amino groups present in the soluble fraction obtained from the various

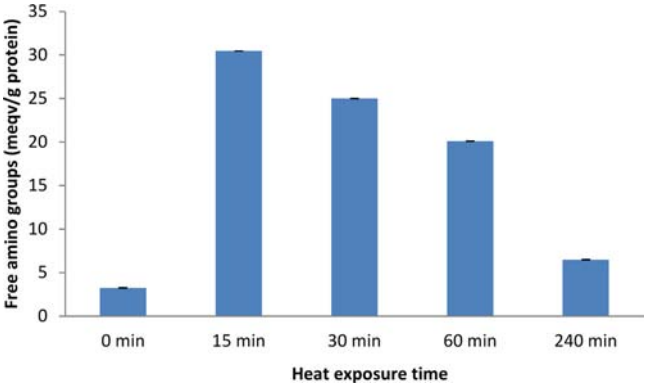


**Figure 1.** Amount of free amines expressed as milliequivalents per gram of protein in the soluble fraction after 0, 15, 30, 60, and 240 min exposure to heat. The error bars represent standard errors of the means.

heat exposure time points. There was an 8-fold increase in the level of free amines within the first 15 min of heat exposure followed by a steady reduction to about double the starting amount on further exposure to heat over the following 210 min.

**Amino Acid Analysis.** The weights of the individual freeze-dried soluble and of the insoluble fractions and their total protein contents at each time point, as determined by quantitative amino acid analysis, are shown in Table 2.

The amount of protein in the soluble fraction was highest in the baseline sample before exposure to heat and was then markedly reduced in the 15, 30, and 60 min samples before being partially restored in the final sample after 240 min heat treatment. In the insoluble fractions, little variation was observed in the protein content. The levels of essential amino acids, expressed as percentages of the total protein amounts in the soluble fractions and in the insoluble fractions, are shown in Figures 2 and 3, respectively.

In the soluble fractions all the essential amino acids, except methionine and histidine, were determined to be highest in the baseline (0 min) fraction. These levels decreased by about half after 15 min heat exposure after which they were relatively stable. The level of methionine however increased to a plateau between 15 and 30 min but then decreased progressively upon longer heat exposure. The level of histidine in the soluble fraction was the lowest as compared to the rest of the essential amino acids. There was no definite trend observed in the changes in histidine level even after 240 min heat exposure.

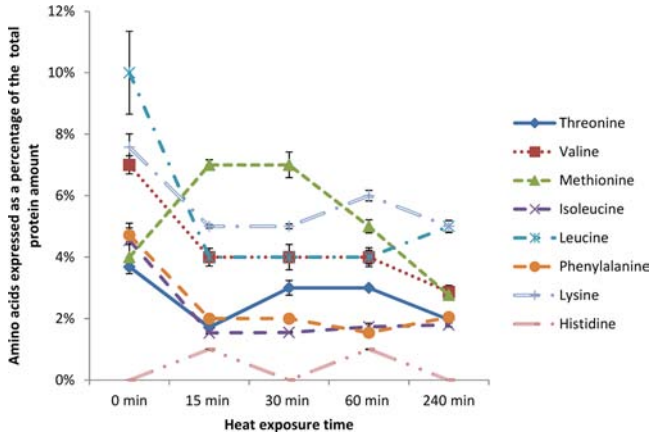


**Figure 2.** Essential amino acids of the soluble fractions after 0, 15, 30, 60, and 240 min exposure to heat, expressed as percentages of the total protein contents. The error bars represent standard errors of the means.

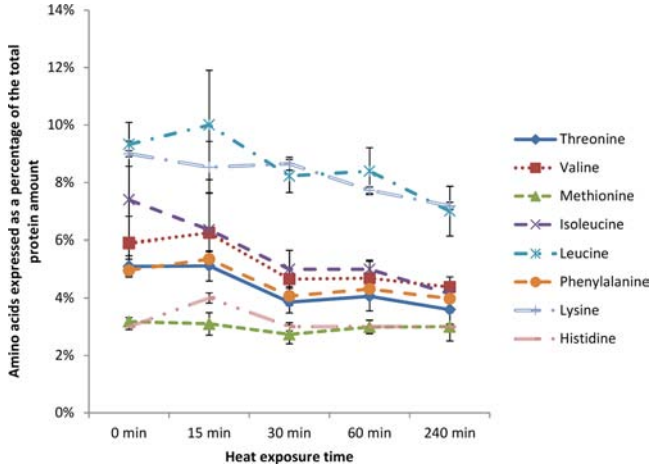


**Figure 3.** Essential amino acids of the total protein contents of the insoluble fractions after 0, 15, 30, 60, and 240 min exposure to heat, expressed as percentages. The error bars represent standard errors of the means.

In the insoluble fraction, the levels of all of the essential amino acids were stable up to 15 min heat exposure. None of the essential amino acids, except isoleucine, showed any marked changes beyond the 15 min exposure time, although slight decreases in the levels of a number of them, in particular leucine, lysine, isoleucine, valine, phenylalanine, and threonine, were observed. The isoleucine level decreased progressively with increased heat exposure time up to 30 min after which it stabilized.

**Gel Filtration Chromatography.** Protein profiling by gel filtration chromatography (GFC) provided an indication of the

**Table 2. Weight and the Total Protein Contents of the Soluble Fractions and of the Insoluble Fractions after 0, 15, 30, 60, and 240 min Exposure to Heat, As Determined by Quantitative Amino Acid Analysis[a]**

| | soluble fraction | | | | | insoluble fraction | | | | |
|---|---|---|---|---|---|---|---|---|---|---|
| heat exposure (min) | 0 | 15 | 30 | 60 | 240 | 0 | 15 | 30 | 60 | 240 |
| weight of freeze-dried sample (mg) | 990 | 496 | 344 | 430 | 541 | 4490 | 4744 | 5061 | 4891 | 4707 |
| amount of protein (mg) | 377.2 | 48.6 | 37.2 | 47.3 | 121.7 | 2488 | 2719 | 2991 | 2944 | 2772 |
| % of protein in freeze-dried sample | 38.1 | 9.8 | 10.8 | 11 | 22.5 | 55.4 | 55.2 | 59.1 | 60.2 | 58.9 |

[a]These values are based on averages of three technical repeats.


dx.doi.org/10.1021/jf502668w | J. Agric. Food Chem. 2014, 62, 8187−8196

molecular mass distribution of proteins and polypeptides in the soluble fraction and also revealed the presence of highly hydrophobic peptides that were retained on the column for longer than expected based on their molecular weights (Figure 4). The distribution of peptides and proteins across the high

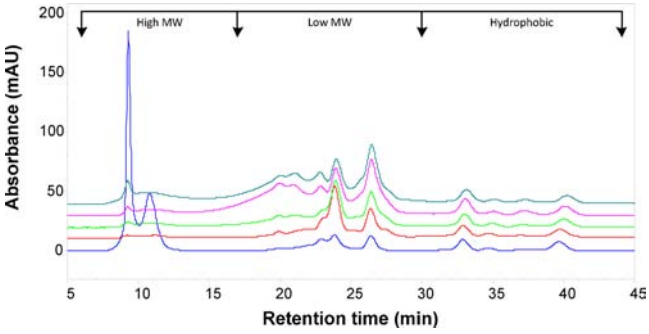


**Figure 4.** Overlaid GFC profiles of the soluble fractions after 0, 15, 30, 60, and 240 min exposure to heat, from bottom to top, respectively.

molecular weight (greater than 2.2 kDa), low molecular weight (less than 2.2 kDa), and the hydrophobic (eluting after the position of the salt peak) ranges is given in Figure 5.

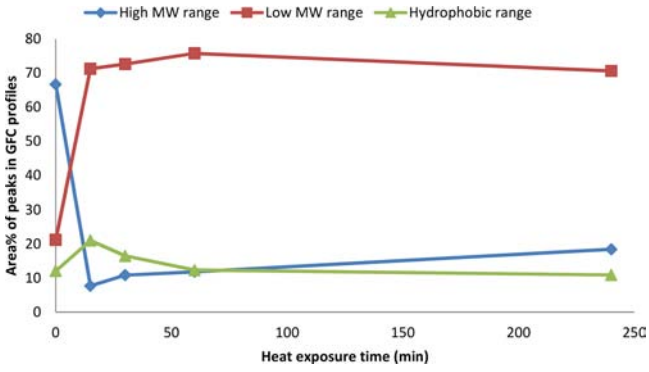


**Figure 5.** Peak area percentages of the high and low molecular weight peptides and hydrophobic peptides in the GFC profiles of the soluble fractions after 0, 15, 30, 60, and 240 min exposure to heat.

A 9-fold decrease in the percentage peak areas of the high molecular weight compounds was observed shortly after 15 min heat exposure. However, with increased heat exposure a gradual increase was noticed, with the 240 min heat-exposed sample showing only a 4-fold decrease in these compounds from the unexposed sample. A 3-fold increase in the area percentage of low molecular weight peaks was obtained after 15 min, the level of which remained constant in the remaining samples up to 240 min. The percentage peak areas of hydrophobic peptides increased 2-fold after 15 min but gradually decreased to slightly less than starting level with increased heat exposure time (Figure 5).

**LC-MS/MS Analysis and Heat-Induced Modification Scoring.** The total number of proteins identified in each fraction, along with the total number of identified peptides, based on the search criteria is listed in Table 3.

The relative scores for oxidative and other heat-induced modifications were calculated using a redox proteomic approach.

Oxidative modifications were observed and scored in the insoluble fraction of the sample without any heat exposure.

**Table 3. List Showing the Number of Proteins Identified from Each Sample and the Total Number of MS/MS Spectra along with the Number of Identified Peptides**

| sample | proteins identified | total no. of MS/MS spectra | total no. of identified peptides |
|---|---|---|---|
| supernatant 0 min | 9 | 595 | 15 |
| supernatant 15 min | 61 | 711 | 219 |
| supernatant 30 min | 63 | 737 | 237 |
| supernatant 60 min | 61 | 979 | 191 |
| supernatant 240 min | 55 | 991 | 172 |
| pellet 0 min | 46 | 764 | 226 |
| pellet 15 min | 33 | 647 | 176 |
| pellet 30 min | 31 | 713 | 120 |
| pellet 60 min | 32 | 645 | 91 |
| pellet 240 min | 22 | 649 | 68 |

These scores gradually showed a slight increase through the exposure times, such that there was an approximate 1.4-fold increase between the 0 and 240 min samples. In contrast, no modifications were detected in the soluble fraction without heat exposure. However, a steep increase of almost 4-fold in the modification score was observed from 30 to 240 min of heat exposure (Figure 6a).

Heat-induced modifications, other than oxidative (Table 1), were also monitored in both the insoluble and the soluble fractions. Here too, a baseline level of these modifications was observed only in the insoluble fraction. A 1.5-fold increase in the score of the insoluble fraction and a slightly higher increase in that of the soluble fraction were detectable from 15 to 240 min heat exposure (Figure 6b). Maillard modifications, monitored separately, could not be initially detected in the soluble fraction. However, after 15 min heat exposure the formation of these products could be detected that remained constant for up to 60 min but decreased thereafter. In the insoluble fraction, a baseline level of these modifications was seen that showed a steady increase with longer heat exposure time (Figure 6c).

The detailed database search results are provided as Supporting Information (Table 1s).

One-sample *t* tests were used to assess the statistical significance of the differences between the baseline sample scores and heat-exposed sample scores (i.e., 15, 30, 60, and 240 min samples combined), for each combination of modification score (oxidative or other) and sample type (insoluble fraction or soluble fraction).

The mean oxidative modification scores of the four heat-treated insoluble fractions (0.16) and of the four heat-treated soluble fractions (0.13) were both significantly higher than their respective baseline scores of 0.13 and 0.00. The scores for the insoluble fraction and the soluble fraction were not significantly different from baseline scores but tended to be higher than their respective unexposed control scores. The mean scores for modifications other than oxidative, in the insoluble fractions, although tending to be higher than the baseline score, were not significantly different. In contrast, in the soluble fractions, the mean score for these modifications was significantly lower for the four samples (0.80) than for the baseline sample (1.28).

**Microspectroscopic and Fluorescence Studies.** A distinct color change was observed in the soluble fraction


dx.doi.org/10.1021/jf502668w | J. Agric. Food Chem. 2014, 62, 8187−8196

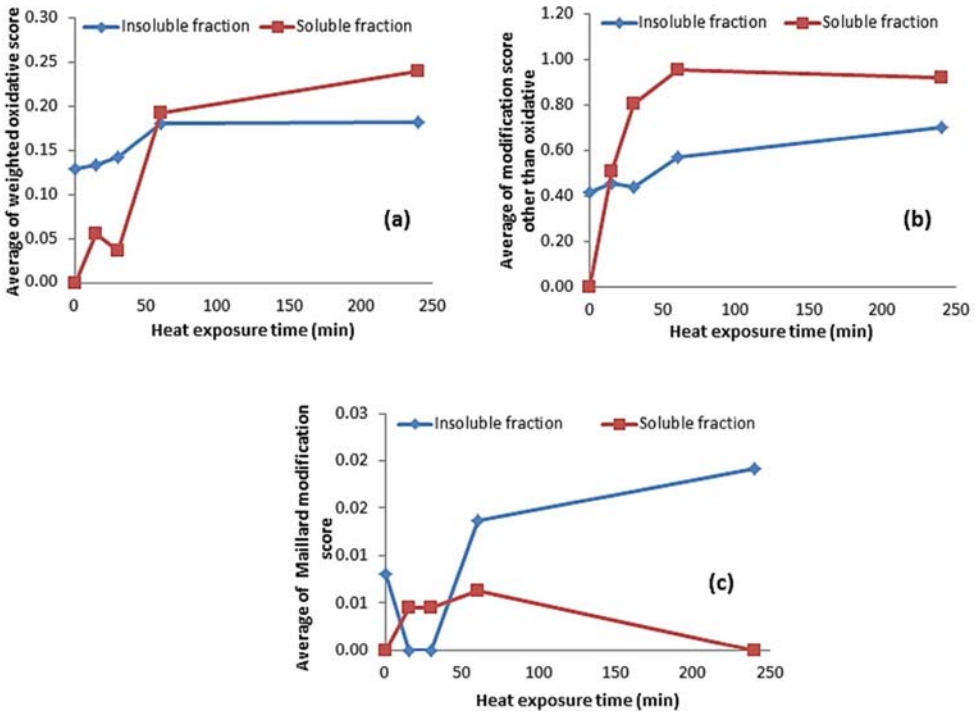


**Figure 6.** (a) Averages of weighted oxidative scores in the insoluble and the soluble fractions after 0, 15, 30, 60, and 240 min exposure to heat. (b) Average of other heat-induced modification scores in the insoluble and the soluble fractions after 0, 15, 30, 60, and 240 min exposure to heat. (c) Average of Maillard modification scores, in the insoluble and the soluble fractions after 0, 15, 30, 60, and 240 min exposure to heat.

from pink to clear to brown during the first 15 min of cooking, as reflected in measurements of hue (Figure 7a). No further large changes in hue were observed, but there was a clear and prospectively linear decrease in the luminosity of the sample (Figure 7b). This rapid initial change, followed by a smaller change during the last 180 min of cooking, was also seen with fluorescence studies with filter sets chosen to fit with expected AGEs (advanced glycation end products) excitation and emission wavelengths (Figure 7c). A similar pattern of events was observed in bright-field and fluorescence micrographs of the insoluble fraction (Figure 8). Color changes and gradual darkening of solid material were observed in bright field, while fluorescence microscopy using UV excitation revealed gradual increases in fluorescence as cooking progressed. However, we also observed a nonhomogeneous increase in red fluorescence during cooking that included excitation well outside that previously reported for AGEs.

## DISCUSSION

In order to minimize nutritional loss during cooking of meat, reliable monitoring parameters are required to check the severity of hydrothermal exposure.[28] Changes in the functional attributes of food proteins can be inferred from information on site specificity and the extent of amino acid modification. Heat induces oxidative modifications in muscle foods, which is of major concern as it contributes to loss of nutritional quality and changes to sensory perceptions. Models that mimic the protein composition in meat and their physicochemical state have been used in previous studies to eliminate the effect of biological variability in meat samples. Models are also useful to independently assess the effect of various processing parameters.[29] However, in meat, the complex nature of heat-induced oxidative changes at the molecular level, the interdependence of the various oxidation pathways, and their effect on bioavailability require further investigations. Once profiled, these changes can ultimately be correlated to information on the nutritional quality as well as functionality of muscle foods.[30]

**Amino Acid Analysis.** Modifications induced at the amino acid level can influence the shelf life, digestibility, and the nutritional value of food proteins.[31,32] Amino acid analysis showed that the percentages of essential amino acids determined in the soluble fraction, except methionine and histidine, decreased with an increase in heat exposure time. Most of the decreases in these levels were evident after 15 min heat exposure, beyond which the changes were minimal. Phenylalanine and tyrosine have previously been reported to be highly sensitive to the oxidative process.[33] Also, model studies on free amino acid oxidation revealed that the aromatic amino acids were most susceptible to oxidation in solution.[34] These amino acids are essential for humans, although tyrosine is not always directly required from the diet. Since tyrosine is synthesized in the body from phenylalanine, deficiency of phenylalanine in the diet can affect the levels of tyrosine. The decrease in the proportions of the essential amino acids, except methionine, in the soluble fraction observed after just 15 min of heat exposure could also be due to heat-induced protein aggregation and the subsequent removal of the precipitated proteins from the solution. In contrast to the soluble fraction, amino acid analysis of the insoluble fraction did not reveal any marked changes with increased exposure to heat. A slight and gradual decrease after 15 min heat exposure indicated a higher stability of the amino acids in the insoluble fraction to heat. A contributory factor to this apparent stability could be due to protein aggregation, leading to a protective effect. A rapid decrease in the total protein content was observed in the soluble fraction with increased heat exposure time, possibly due to an increase in protein aggregation with increasing heat, whereas no such changes were detected in the insoluble

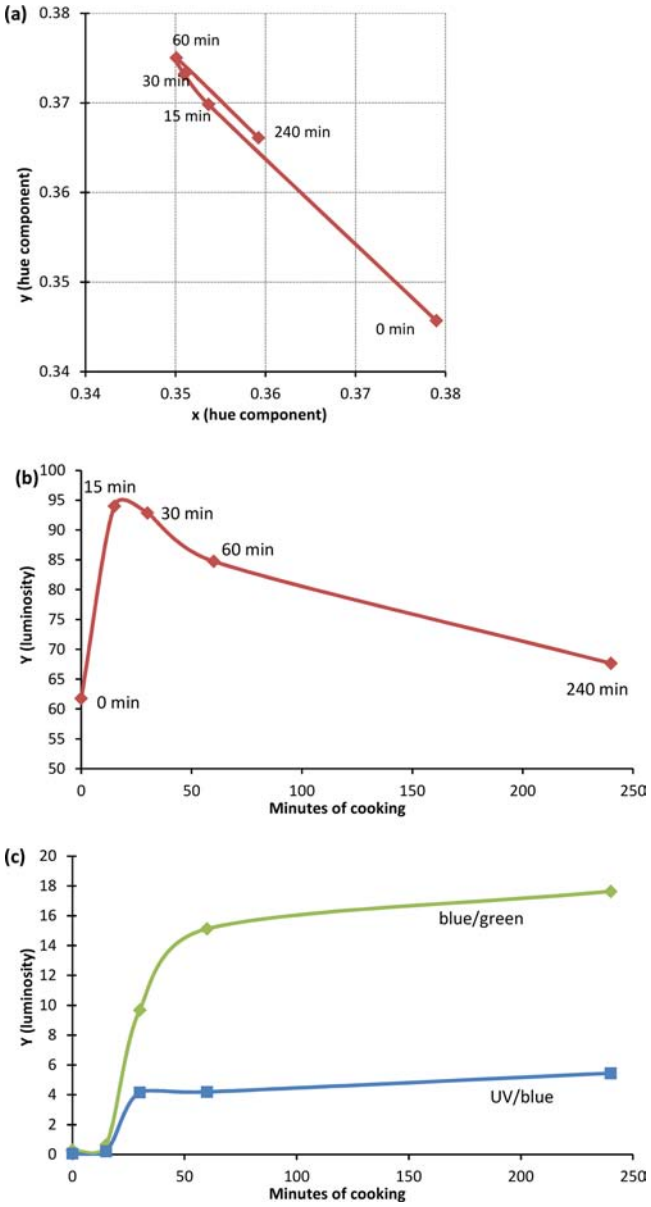


**Figure 7.** Color measurements showing the changes in (a) hue, (b) luminosity, and (c) fluorescence in the soluble fraction after 0, 15, 30, 60, and 240 min exposure to heat. See text for details.

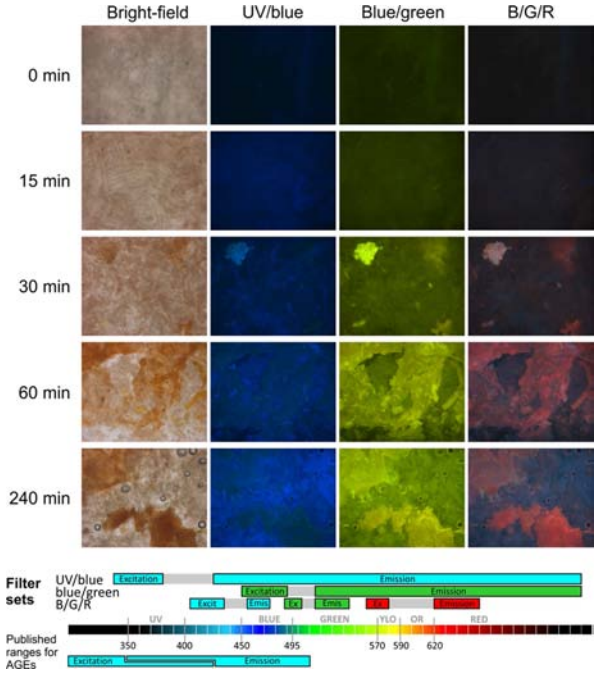


**Figure 8.** Bright-field and fluorescence micrographs of insoluble fractions after 0, 15, 30, 60, and 240 min exposure to heat. Ranges for AGEs fluorescence from refs 48 and 49.

fraction. Thus, it is apparent that the bioavailability of the essential amino acids especially in the soluble fraction is highly dependent on the duration of heat exposure, whereas in the insoluble fraction which contained the bulk of the protein, the effect of heat on these amino acids is reduced.

Cross-linking reactions between amino acid side chains may be a consequence of heat exposure, the most common being the formation of lysinoalanine and lanthionine. Cysteine can degrade in the presence of heat to form dehydroalanine, probably through a $\beta$-elimination reaction, which can then react with the $\varepsilon$-amino group of lysine to form lysinoalanine or with the thiol group of cysteine to form lanthionine. Both lysinoalanine and lanthionine can introduce enzyme-resistant cross-links in proteins, reducing bioavailability of these proteins. Lysinoalanine has been implicated in renal toxicity in rats and is found both in home-cooked as well as commercially processed foods. Although lysinoalanine is usually observed following alkali treatment of food, it is now reported to be present in nonalkali-treated food as well.[35] In the present study, lysinoalanine and lanthionine formation were found to be negligible in both the insoluble fraction as well as in the soluble fraction, suggesting that such cross-links may not be easily formed even after extensive boiling of meat. Determining the cooking temperatures and conditions under which these cross-links form would be a fruitful area for further study.

**Peptide Molecular Weight Profiling.** Peptide molecular weight profiling can provide a useful way of determining the amount of degradation and aggregation of meat peptides and also the generation of peptides with hydrophobic characteristics. From the GFC profiles of the soluble fractions, it was evident that the peptides in the low molecular mass range increased as a result of exposure to heat. A shift from the high molecular weight proteins, seen in the baseline sample, to the low molecular mass region within 15 min heat exposure is indicative of a combination of both hydrolysis and aggregation. Heat-induced hydrolysis of proteins generating a mixture of peptides would contribute to an increase in low molecular weight compounds whereas the formation of heat-induced insoluble protein aggregates would result in an overall decrease in the levels of high molecular weight compounds. Peptides eluting from the Superdex column between 22 and 24 min would be expected to have molecular weights around 1 kDa as determined by a standard curve generated using pure proteins. The size of these peptides provides them with the ability to aggregate in the presence of heat. The results from the OPA assay provided some evidence supporting this hypothesis because, after a substantial initial increase in the free amines, a progressive decrease is noticed with increased heat exposure time. We suspect that this decrease in the amount of free amines is due to an aggregation of peptides which prevents the free amines from the lysine side chains or from the free amino termini of peptides from reacting with the OPA reagent. Although results from the amino acid analysis showed an initial


dx.doi.org/10.1021/jf502668w | J. Agric. Food Chem. 2014, 62, 8187−8196

decrease in the level of lysine residues, after 15 min heat exposure these changes were minimal. These results further indicate that this decrease in free amines, as seen with the OPA assay, were not due to the loss of lysine residues but possibly due to aggregation.

Peaks in the GFC profiles that eluted after 29 min were suggestive of the presence of highly hydrophobic peptides in the hydrolyzates, which were not fully separated based on their molecular size but were selectively retained by hydrophobic interactions with the chromatography matrix.[36] Hydrophobicity in protein hydrolyzates, along with several other factors such as size, primary sequence, and spatial structure of peptides can contribute toward the perception of bitter taste thus affecting product quality.[37] Peptides with hydrophobic characteristics were seen in all the samples including the sample without any heat exposure. An initial increase in the peak areas in this region of the chromatogram followed by a steady decline suggested that hydrophobic peptides initially formed were destroyed or aggregated with other peptides as a consequence of prolonged heat exposure.

**Tracking and Scoring Heat-Induced Damage in Meat Proteins.** We have reported here an advanced application of a scoring system that can be used to characterize oxidative and other heat-induced modifications occurring in meat during cooking. Using this scoring system, we measured a steady increase in the oxidative modification score in both the insoluble fraction and in the soluble fraction with increased heat exposure time. From the results (Table 3) it was evident that the number of proteins identified in the soluble fractions increased almost 7-fold after just 15 min of heat exposure, compared to the unexposed sample. A slight decrease in this number was noticed in the soluble fraction of the sample exposed to heat for the longest period (240 min), possibly due to protein aggregation. A steady decrease in the number of identified proteins in the insoluble fractions was seen with increasing time of heat exposure (Table 3), again possibly due to aggregation. Analysis of the peptides modified by heat indicated that oxidized aromatic amino acids made major contributions to the overall oxidative damage scores (Supporting Information Table 1s). Aromatic amino acids are well-distributed in meat proteins but are also particularly prone to oxidative damage during the cooking process.[15] An increase in the levels of phenylalanine oxidation and the formation of quinone from tyrosine with increasing heat were the major contributors. We suspect that the cause of the measured oxidation lies in another effect; cooking also disrupts muscle tissue releasing iron from the heme molecule. The iron from the heme and nonheme pigments aids in the formation of free radicals which can then react with aromatic amino acid rings forming hydroxylation products.[38−41] Superoxide radicals formed during the cooking process due to autooxidation of myoglobin can attack the aromatic rings of tryptophan forming *N*-formylkynurenine. Oxidation of phenylalanine can form *o*- or *m*-tyrosine and dimers of hydroxylated aromatic amino acids, and tyrosine oxidation can lead to dihydroxyphenylalanine and trihydroxyphenylalanine formation.[42,43]

The results clearly indicated that the proteins extracted in the soluble fraction were more susceptible to heat-induced modifications. Theory would suggest that hydrophilic proteins should be more susceptible to modifications due to their increased solubility and that in meat many of these proteins would be collagens. Our results have confirmed this, and the identities of scored peptides confirm that collagens make up the majority of hydrophilic peptides.

Scores for modifications other than oxidative showed a similar trend. Further study with a larger sample size may resolve further details of these trends. An increase in Maillard reaction products was detected in the insoluble fraction just after 30 min heat exposure. Such an increase was however not observed in the soluble fraction. Myosin was found to be the protein most susceptible to Maillard reactions. Previous reports have shown that a clear correlation exists between decreased rehydrability and protein extractability from freeze-dried meat due to glucose-mediated cross-linking between the heavy chains of myosin through a Maillard type reaction.[44] Our results clearly indicate that myosin is prone to reactions with reducing sugars in the presence of heat.

An interesting observation within the heat-induced modifications other than oxidative was the formation of pyroglutamic acid. A significant increase in the pyroglutamic acid content in the soluble fraction was observed with increased heat exposure. Pyroglutamic acid formation is not related to glycation or oxidation of proteins but is hypothesized to be a heat-induced nonenzymatic cyclization reaction in which the free amino group of glutamic acid or glutamine forms a lactam. This type of modification has been previously reported to increase in milk proteins such as $\alpha$-lactalbumin exposed to heat.[45] Bitterness resulting from the formation of pyrrolidone carboxylic acid at the N-terminus of hydrophobic peptides, during proteolysis of casein, has also been reported.[46] An overall increase in the level of pyrrolidone formation in the soluble fraction with increasing heat exposure indicated that meat proteins/peptides in their soluble form were more susceptible to such modifications. A possible explanation for this could be that hydrolysis of soluble proteins during the cooking process produces an increasing number of peptides with glutamine or glutamic acid residues at their N-termini. These are then readily available for the cyclization process forming pyrrolidones. However, it is also possible that this increase could result due to the method used for sample preparation for the LC-MS studies. Particularly during the trypsin hydrolysis step, an alkaline pH and an elevated temperature of 37 °C may favor the decomposition of the glutamine/glutamic acid residue to pyrrolidone-carboxylic acid,[47] if the tryptic peptide had a glutamine/glutamic acid preceded by a lysine or an arginine residue. A steady increase in the levels of longer peptides with a trypsin cleavage site adjacent to a glutamic acid or glutamine residue was observed in the soluble fraction with increasing heat exposure.

**Microspectroscopic and Fluorescence Studies.** Spectral changes in meat hydrolyzates were of two distinct types: color changes during the first 15 min of cooking, after which the hue remained similar; and reducing luminosity over the following hours. Together with the GFC and oxidative damage data, this suggests a considerable diversity in the processes, substrates, and end products occurring during the initial few minutes of cooking, followed by a less-diverse buildup of particular types of product subsequently.

Fluorescence data clarify these visual color changes in terms of chemistry because we have chosen filter sets with excitation and emission wavelength ranges that cover the spectrum previously published for AGEs.[48,49] Results from the UV/blue and blue/green filter sets suggest that changes in the sample following the first 60 min of cooking are probably gradual and approximately linear. We interpret this as resulting from the

initial formation of condensation products of sugar- and lysine-derived amino acids, during the first 15 min, followed by a gradual build-up over an extended period of heat exposure.

Our microscopy method allowed for direct comparison of the spectral and fluorescence characteristics of both the soluble fraction and the insoluble fraction under the same conditions. We conclude that the changes in the soluble fraction are generally also seen in the insoluble fraction. However, within the insoluble fraction there is considerable spatial variation in buildup of product with some structures showing higher fluorescence than others. While the fluorescence seen with UV and blue light excitation (assumed AGEs) increased in a way similar to that of the soluble fraction, there were also additional fluorescent species that increased in abundance in the later stages of cooking which were excited by longer wavelengths (e.g., yellow/green) and fluoresced red with a multispectral band-pass filter. These appeared to mostly be associated with dense regions of structure that appeared the deepest brown in the visible spectrum. Whether this heterogeneity is due to the difference in the rate of AGE formation is yet to be determined. AGEs have been reported earlier to be dynamic in nature and constantly undergoing rearrangements as they continue to cross-link with other proteins.[49]

Overall the results from amino acid analysis, modification scoring, protein/peptide profiling, and microscopic and fluorescence studies provided a deeper understanding of the changes at the amino acid levels of meat proteins brought about though a series of reactions aided by heat. Essential amino acids were determined to be more susceptible to heat in their soluble form, although heat-induced cross-links such as the formation of lanthionine and lysinoalanine were not detected even after prolonged heat exposure. Meat proteins were also found to be susceptible to aggregation in their soluble form. An increase in the amino acid oxidative modifications was seen especially in the soluble collagen proteins, whereas myosin in the insoluble fraction was most susceptible to other heat-induced modifications such as Maillard reactions. Also most of these changes at the amino acid level were determined to take place quite rapidly in the presence of heat. Further work will however help to elucidate the functional importance and potential effects on bioavailability of these cooking-induced changes.

## ■ ASSOCIATED CONTENT

### Supporting Information

Table listing etailed database search results. This material is available free of charge via the Internet at http://pubs.acs.org.

## ■ AUTHOR INFORMATION

### Corresponding Author

*Tel.: +64-3-321-8758. Fax: +64-3-321-8811. E-mail: santanu.deb-choudhury@agresearch.co.nz.

### Funding

We gratefully acknowledge funding from the New Zealand Ministry of Business, Innovation and Employment (MBIE) via the AgResearch core-funded Red Meat Combifoods Programme (Contract No. ex-FRST/MSI C10X1005).

### Notes

The authors declare no competing financial interest.

## ■ ABBREVIATIONS USED

GFC, gel filtration chromatography; AGEs, advanced glycation end products.

## ■ REFERENCES

(1) Visessanguan, W.; Benjakul, S.; Riebroy, S.; Thepkasikul, P. Changes in composition and functional properties of proteins and their contributions to Nham characteristics. *Meat Sci.* **2004**, *66*, 579−588.

(2) Byrne, D. V.; Bredie, W. L. P.; Bak, L. S.; Bertelsen, G.; Martens, H.; Martens, M. Sensory and chemical analysis of cooked porcine meat patties in relation to warmed-over flavour and pre-slaughter stress. *Meat Sci.* **2001**, *59*, 229−249.

(3) Chung, S. Y.; Swaisgood, H. E.; Catignani, G. L. Effects of alkali treatment and heat treatment in the presence of fructose on digestibility of food proteins as determined by an immobilized digestive enzyme assay (IDEA). *J. Agric. Food Chem.* **1986**, *34*, 579−584.

(4) Gilani, G. S.; Xiao, C. W.; Cockell, K. A. Impact of antinutritional factors in food proteins on the digestibility of protein and the bioavailability of amino acids and on protein quality. *Br. J. Nutr.* **2012**, *108* (Suppl. 2), S315−S332.

(5) Sarwar, G.; L'Abbé, M. R.; Trick, K.; Botting, H. G.; Ma, C. Y., Influence of feeding alkaline/heat processed proteins on growth and protein and mineral status of rats. In *Impact of Processing on Food Safety*; Jackson, L. S., Knize, M. G., Morgan, J. N., Eds.; Kluwer Academic/Plenum: New York, NY, USA, 1999; Vol. *459*, pp 161−177.

(6) Piva, G.; Moschini, M.; Fiorentini, L.; Masoero, F. Effect of temperature, pressure and alkaline treatments on meat meal quality. *Anim. Feed Sci. Technol.* **2001**, *89*, 59−68.

(7) Piva, G.; Moschini, M.; Fiorentini, L.; Masoero, F. Effect of temperature, pressure and alkaline treatments on meat meal quality. *Anim. Feed Sci. Technol.* **2001**, *89*, 59−68.

(8) Gilbert, E. R.; Wong, E. A.; Webb, K. E. BOARD-INVITED REVIEW: Peptide absorption and utilization: Implications for animal nutrition and health. *J. Anim. Sci.* **2008**, *86*, 2135−2155.

(9) Webb, K. E. Intestinal absorption of protein hydrolysis products: A review. *J. Anim. Sci.* **1990**, *68*, 3011−3022.

(10) Bjarnason, J.; Carpenter, K. J. Mechanisms of heat damage in proteins. *Br. J. Nutr.* **1970**, *24*, 313.

(11) Friedman, M. Origin, microbiology, nutrition, and pharmacology of D-amino acids. *Chem. Biodiversity* **2010**, *7*, 1419−1530.

(12) Singh, S.; Gamlath, S.; Wakeling, L. Nutritional aspects of food extrusion: A review. *Int. J. Food Sci. Technol.* **2007**, *42*, 916−929.

(13) Rémond, D.; Savary-Auzeloux, I.; Gatellier, P.; Santé-Lhoutellier, V. Nutritional properties of meat peptides and proteins: Impact of processing. *Sci. Aliments* **2008**, *28*, 389−401.

(14) Promeyrat, A.; Sayd, T.; Laville, E.; Chambon, C.; Lebret, B.; Gatellier, P. Early post-mortem sarcoplasmic proteome of porcine muscle related to protein oxidation. *Food Chem.* **2011**, *127*, 1097−1104.

(15) Promeyrat, A.; Gatellier, P.; Lebret, B.; Kajak-Siemaszko, K.; Aubry, L.; Santé-Lhoutellier, V. Evaluation of protein aggregation in cooked meat. *Food Chem.* **2010**, *121*, 412−417.

(16) Evenepoel, P.; Claus, D.; Geypens, B.; Maes, B.; Hiele, M.; Rutgeerts, P.; Ghoos, Y. Evidence for impaired assimilation and increased colonic fermentation of protein, related to gastric acid suppression therapy. *Aliment. Pharmacol. Ther.* **1998**, *12*, 1011−1019.

(17) Ames, J. M. Dietary Maillard reaction products: Implications for human health and disease. *Czech J. Food Sci.* **2009**, *27* (Special Issue), S66−S69.

(18) van Boekel, M.; Fogliano, V.; Pellegrini, N.; Stanton, C.; Scholz, G.; Lalljie, S.; Somoza, V.; Knorr, D.; Jasti, P. R.; Eisenbrand, G. A review on the beneficial aspects of food processing. *Mol. Nutr. Food Res.* **2010**, *54*, 1215−1247.

(19) Bailey, M. E. Maillard reactions and meat flavour development. In *Flavor of Meat and Meat Products*; Shahidi, F., Ed.; Springer: Dordrecht, The Netherlands, 1994; pp 153−173.

(20) Alaejos, M. S.; Afonso, A. M. Factors that affect the content of heterocyclic aromatic amines in foods. *Compr. Rev. Food Sci. Food Saf.* **2011**, *10*, 52−108.

(21) Liao, G. Z.; Wang, G. Y.; Xu, X. L.; Zhou, G. H. Effect of cooking methods on the formation of heterocyclic aromatic amines in chicken and duck breast. *Meat Sci.* **2010**, *85*, 149−154.
(22) Davis, P. J.; Williams, S. C. Protein modification by thermal processing. *Allergy* **1998**, *53*, 102−105.
(23) Egan, H.; Kirk, R. S.; Sawyer, R.; Pearson, D. *Pearson's chemical analysis of foods*; Churchill Livingstone: Edinburgh, Scotland; New York, NY, USA, 1981.
(24) Nielsen, P. M.; Petersen, D.; Dambmann, C. Improved method for determining food protein degree of hydrolysis. *J. Food Sci.* **2001**, *66*, 642−646.
(25) Cohen, S. A.; Strydom, D. J. Amino acid analysis utilizing phenylisothiocyanate derivatives. *Anal. Biochem.* **1988**, *174*, 1−16.
(26) Wessel, D.; Flügge, U. I. A method for the quantitative recovery of protein in dilute solution in the presence of detergents and lipids. *Anal. Biochem.* **1984**, *138*, 141−143.
(27) Dyer, J. M.; Plowman, J.; Krsinic, G.; Deb-Choudhury, S.; Koehn, H.; Millington, K.; Clerens, S. Proteomic evaluation and location of UVB-induced photomodification in wool. *Photochem. Photobiol., B* **2010**, *98*, 118−127.
(28) Santé-Lhoutellier, V.; Astruc, T.; Marinova, P.; Greve, E.; Gatellier, P. Effect of meat cooking on physicochemical state and in vitro digestibility of myofibrillar proteins. *J. Agric. Food Chem.* **2008**, *56*, 1488−1494.
(29) Promeyrat, A.; Le Louët, L.; Kondjoyan, A.; Astruc, T.; Santé-Lhoutellier, V.; Gatellier, P.; Daudin, J. D. Combined effect of meat composition and heating parameters on the physicochemical state of proteins. *Procedia Food Sci.* **2011**, *1*, 1118−1125.
(30) Villaverde, A.; Estévez, M. Carbonylation of myofibrillar proteins through the Maillard pathway: Effect of reducing sugars and reaction temperature. *J. Agric. Food Chem.* **2013**, *61*, 3140−3147.
(31) Schwass, D. E.; Finley, J. W. Heat and alkaline damage to proteins: Racemization and lysinoalanine formation. *J. Agric. Food Chem.* **1984**, *32*, 1377−1382.
(32) Friedman, M. Dietary impact of food processing. *Annu. Rev. Nutr.* **1992**, *12*, 119−137.
(33) Davies, K. J.; Delsignore, M. E.; Lin, S. W. Protein damage and degradation by oxygen radicals. II. Modification of amino acids. *J. Biol. Chem.* **1987**, *262*, 9902−9907.
(34) Berlett, B. S.; Stadtman, E. R. Protein oxidation in aging, disease, and oxidative stress. *J. Biol. Chem.* **1997**, *272*, 20313−20316.
(35) Sternberg, M.; Kim, C. Y.; Schwende, F. J. Lysinoalanine: Presence in foods and food ingredients. *Science* **1975**, *190*, 992−994.
(36) Aubes-Dufau, I.; Capdevielle, J.; Seris, J. L.; Combes, D. Bitter peptide from hemoglobin hydrolysate: Isolation and characterization. *FEBS Lett.* **1995**, *364*, 115−119.
(37) Spanier, A. M.; Edwards, J. V. Chromatographic isolation of presumptive peptide flavor principles from red meat. *J. Liq. Chromatogr.* **1987**, *10*, 2745−2758.
(38) Ganhao, R.; Morcuende, D.; Estevez, M. Tryptophan depletion and formation of $\alpha$-aminoadipic and $\gamma$-glutamic semialdehydes in porcine burger patties with added phenolic-rich fruit extracts. *J. Agric. Food Chem.* **2010**, *58*, 3541−3548.
(39) Chen, C. C.; Pearson, A. M.; Gray, J. I.; Fooladi, M. H.; Ku, P. K. Some factors influencing the nonheme iron content of meat and its implications in oxidation. *J. Food Sci.* **1984**, *49*, 581−584.
(40) Purchas, R. W.; Busboom, J. R.; Wilkinson, B. H. P. Changes in the forms of iron and in concentrations of taurine, carnosine, coenzyme Q10, and creatine in beef longissimus muscle with cooking and simulated stomach and duodenal digestion. *Meat Sci.* **2006**, *74*, 443−449.
(41) Garcia, M. N.; Martinez-Torres, C.; Leets, I.; Tropper, E.; Ramirez, J.; Layrisse, M. Heat treatment on heme iron and iron-containing proteins in meat: Iron absorption in humans from diets containing cooked meat fractions. *J. Nutr. Biochem.* **1996**, *7*, 49−54.
(42) Żegota, H.; Kołodziejczyk, K.; Król, M.; Król, B. *o*-Tyrosine hydroxylation by $OH^{\bullet}$ radicals.2,3-DOPA and 2,5-DOPA formation in $\gamma$-irradiated aqueous solution. *Radiat. Phys. Chem.* **2005**, *72*, 25−33.
(43) Dyer, J. M.; Bringans, S. D.; Bryson, W. G. Determination of photo-oxidation products within photoyellowed bleached wool proteins. *Photochem. Photobiol.* **2006**, *82*, 551−557.
(44) Kim, H. J.; Loveridge, V. A.; Taub, I. A. Myosin cross-linking in freeze-dried meat. *J. Food Sci.* **1984**, *49*, 699−702.
(45) Meltretter, J.; Pischetsrieder, M. Application of mass spectrometry for the detection of glycation and oxidation products in milk proteins. *Ann. N. Y. Acad. Sci.* **2008**, *1126*, 134−140.
(46) Lemieux, L.; Simrad, R. E. Bitter flavour in dairy products. I. A review of the factors likely to influence its development, mainly in cheese manufacture. *Lait* **1991**, *71*, 599−636.
(47) Tritsch, G. L.; Moore, G. E. Spontaneous decomposition of glutamine in cell culture media. *Exp. Cell Res.* **1962**, *28*, 360−364.
(48) Pongor, S.; Ulrich, C.; Bencsath, F. A.; Cerami, A. Aging of proteins: Isolation and identification of a fluorescent chromophore from the reaction of polypeptides with glucose. *Proc. Natl. Acad. Sci.* **1984**, *81*, 2684−2688.
(49) Wu, J. T.; Tu, M.-C.; Zhung, P. Advanced glycation end product (AGE): Characterization of the products from the reaction between D-glucose and serum albumin. *J. Clin. Lab. Anal.* **1996**, *10*, 21−34.

JOURNAL OF AGRICULTURAL AND FOOD CHEMISTRY

Article

pubs.acs.org/JAFC

# Stable Isotope Ratio Analysis for Verifying the Authenticity of Balsamic and Wine Vinegar

M. Perini,[†] M. Paolini,[†] M. Simoni,[†] L. Bontempo,[†] U. Vrhovsek,[†] M. Sacco,[‡] F. Thomas,[§] E. Jamin,[§] A. Hermann,[∥] and F. Camin*[,†]

[†]Fondazione Edmund Mach (FEM), Via E. Mach 1, 38010 San Michele all'Adige, Trento, Italy

[‡]PONTI S.p.a., Via E. Ferrari 7, 28074 Ghemme, Novara, Italy

[§]Eurofins Analytics France, Rue Pierre Adolphe Bobierre, B.P. 42301, F-44323 Nantes Cedex 3, France

[∥]Landesuntersuchungsamt, Institut für Lebensmittelchemie und Arzneimittelprüfung, Emy-Roeder-Straße 1, 55129 Mainz, Germany

Supporting Information

**ABSTRACT:** In this paper, we investigate whether the analysis of stable isotope ratios D/H and $^{13}C/^{12}C$ in ethanol and acetic acid and of $^{18}O/^{16}O$ in water can be applied to the ingredients of "aceto balsamico di Modena IGP" (ABM) to evaluate their authenticity. We found that impurities in the extraction solution do not affect the $^{13}C/^{12}C$ of acetic acid and the D/H values of acetic acid are not affected under a composite NMR experiment. The standard deviation of repeatability and standard deviation of reproducibility are comparable in wine vinegar and ABM and generally lower than those quoted in the official methods. This means that the validation parameters quoted in the official methods can also be applied to the ingredients of ABM. In addition, we found no changes in the isotopic values from wine to vinegar and to ABM, and from the original must to the ABM must, providing experimental evidence that reference data from wine databanks can also be used to evaluate the authenticity of vinegar and ABM.

**KEYWORDS:** *D/H, $\delta^{13}C$, $\delta^{18}O$, isotope ratio mass spectrometry, SNIF-NMR, vinegar authenticity*

## INTRODUCTION

Wine vinegar is defined by EC Regulations 479/2008 (Annex IV, sections 1 and 17) as a product obtained from the acetous fermentation of wine, which is in turn defined as a product obtained exclusively from the alcoholic fermentation of fresh grapes, whether crushed or not, or from grape must. According to this definition, wine vinegar cannot contain acetic acids obtained from either petroleum derivatives or pyrolysis of wood (synthetic acetic acid) or from the fermentation of nongrape sugars (e.g., from beet or cane). Moreover, wine and wine vinegar cannot be produced from dried grapes diluted with water; therefore, the so-called "raisin vinegar", commonly produced in some Mediterranean countries by fermenting dried grapes and rehydrating with tap water, cannot be considered wine vinegar.[1]

This also applies to "aceto balsamico di Modena IGP" (ABM), a PGI (Protected Geographical Indication) vinegar now renowned throughout the world, obtained from cooked and/or concentrated grape must (at least 20% of the volume), with the addition of at least 10% of wine vinegar and a maximum 2% of caramel for color stability (EU Reg. 583/2009). The geographical origin of ABM ingredients is not specified.

In the case of must and wine, since 1991 the addition of water and exogenous sugars has been detected by analyzing the isotopic ratios of hydrogen (D/H) and carbon ($^{13}C/^{12}C$) in ethanol and of oxygen ($^{18}O/^{16}O$) in water. OIV (International Organization of Vine and Wine) methods are currently adopted: OIV-MA-AS311-05 for site-specific analysis of the D/H ratio using $^{2}H$-site-specific natural isotope fractionation NMR ($^{2}H$-SNIF-NMR), OIV-MA-AS312-06 for analysis of the $^{13}C/^{12}C$ ratio (expressed as $\delta^{13}C$ ‰) using isotope ratio mass spectrometry (IRMS), OIV-MA-AS2-12 for analysis of the $^{18}O/^{16}O$ ratio (expressed as $\delta^{18}O$ ‰) using IRMS. Addition is detected by comparing the results against an appropriate databank, such as the official databank set up in 1991 (EU Regulations 2347 and 2348/91) by the European Union for all wine-producing countries within its territory. According to current regulations (EU Regulation 555/2008), a number of samples representing the wine production of each member state are officially collected every year and analyzed using the above-mentioned OIV methods. The isotope data bank makes available reference data on a yearly basis, thus allowing legal limits to be defined on the basis of isotopic data for each country, each subarea (e.g., region), and each protected denomination (PDO-IGP), as well as general limits[2] when origin and year of production are not declared.

Very recently, isotopic methods have been recognized by the European Committee for Standardization (CEN) and in part by OIV as a means of detecting the presence of exogenous acetic acid and tap water in wine vinegar. The methods are EN 16466-1 for D/H in the methyl site of acetic acid using $^{2}H$-SNIF-NMR, EN 16466-2 and OIV 510/2013 for analysis of $^{13}C/^{12}C$ in acetic acid using IRMS, and EN 16466-3 and OIV 511/2013 for analysis of $^{18}O/^{16}O$ in water using IRMS.

Received: March 19, 2014
Revised: July 2, 2014
Accepted: July 7, 2014
Published: July 7, 2014

ACS Publications © 2014 American Chemical Society



dx.doi.org/10.1021/jf5013538 | J. Agric. Food Chem. 2014, 62, 8197−8203

Moreover, a recent paper[1] showed that the legal limits set on the basis of the wine isotope databank can be used as reference for $\delta^{18}O$ analysis to detect the authenticity of wine vinegar.

As yet, no studies have investigated application of these techniques to the ingredients of ABM (wine vinegar and must) or the possibility of using the wine databank as reference for vinegar and ABM for the isotopic ratios D/H and $\delta^{13}C$.

In this work, we aim to fill these gaps by investigating whether official isotopic methods recognized by OIV and CEN for must and wine vinegar can be used to analyze ABM. To do this, we verified and quantified the presence of impurities in solutions extracted from wine vinegar and ABM, determined the validation parameters of the methods applied to the ingredients of AMB, and compared them with those quoted in the CEN and OIV standards. We also evaluated the variation of D/H and $^{13}C/^{12}C$ between wine ethanol and acetic acid in wine vinegar and ABM in order to determine whether the wine isotope databank can also be used as reference for D/H and $\delta^{13}C$ of acetic acid in order to monitor the authenticity of vinegar and ABM.

## MATERIALS AND METHODS

**Samples.** To assess variation in isotopic parameters along the production chain (Table 1), 13 production chains were considered (Table 1). Nine of them consisted of wine, the corresponding wine vinegar, grape must (100% concentrated must or 100% cooked must or mixtures of the two types), and the corresponding ABM. The other four were obtained directly from vinegar rather than starting from wine. Cane sugar acetic acid was added to two of these vinegar samples (chains 11 and 12).

Table 1. Summary of the Production Chain Samples[a]

| chain | wine | vinegar | cooked must | concentrated must | ABM |
|---|---|---|---|---|---|
| 1 | × | × | × (100%) | | × |
| 2 | × | × | × (52%) | × (48%) | × |
| 3 | × | × | × (20%) | × (80%) | × |
| 4 | × | × | × (20%) | × (80%) | × |
| 5 | × | × | × (50%) | × (50%) | × |
| 6 | × | × | × (50%) | × (50%) | × |
| 7 | × | × | × (50%) | × (50%) | × |
| 8 | × | × | | × (100%) | × |
| 9 | × | × | | × (100%) | × |
| 10 | | × | × (54%) | × (46%) | × |
| 11 | | × | × (50%) | × (50%) | × |
| 12 | | × | × (50%) | × (50%) | × |
| 13 | | × | | × (100%) | × |

[a]Crosses indicate samples from each chain. The first nine chains were started from wine, the other four from vinegar. Cooked grape must or concentrated must or a mixture of the two in different percentages (in parentheses) were used to produce the ABM.

To evaluate the effects of adulteration with exogenous sugars, one sample of wine was divided into seven parts to which were added increasing percentages of alcohol from cane sugar (from 0% to 42%) before being fermented into vinegar. Two of these vinegars (with 10% and 42% cane alcohol added) were used to make ABMs. In addition, two samples of ABM were adulterated with different percentages of synthetic vinegar (20% and 40%).

In the production of ABM, a maximum 2% of caramel can be added for color stability, tangential filtering is usual, and the product may be concentrated to increase its density. To evaluate the effects of these processes, one sample of vinegar was divided into three parts: one was used to produce ABM without filtration, another underwent tangential filtration but no caramel was added, while the third underwent filtration and addition of caramel (1.79%). Another sample of vinegar was divided into three parts, and ABM was produced without concentration from one subsample, and at two different degrees of concentration (45°Brix and 57°Brix) from the other subsamples.

**Pilot Production of Vinegar and ABM.** Wines were transformed into vinegars using a couple of fully automated pilot fermenters (each with a capacity of 8 L) and a continuous fermentation process (at least 10 days per sample) identical to the industrial process with respect to time, temperature, and concentration of alcohol and acetic acid (40 h to entirely transform the alcohol into acetic acid, 34−36 °C, 10.0−10.4% of alcohol in wine, transformation efficiency 95−97%). Oxidation of ethanol was performed by means of *Acetobacter* spp. bacteria.

The ABM was produced according to EU Reg. 583/2009.

When evaluating the effects of adulteration with exogenous sugars, in order to correctly measure the percentages of the different raw materials in each fermentation process, lithium (30 ppm) was added to the wine as a marker; the concentration of each new raw material was calculated on the basis of the lithium concentration in the product (measured using atomic absorption spectrometry).

Tangential filtration was carried out by passing the vinegar through a polysulphone membrane with a porosity of 0.6 $\mu$m; the maximum temperature throughout the process was below 37 °C.

ABM concentration was carried out in batches using pilot vacuum equipment normally used for jam production. The samples were collected at different times during a single concentration process.

**Methods of Isotopic Analysis.** Ethanol was distilled from wine samples following the official OIV method (MA-AS-311-05). Acetic acid was extracted from the vinegars and ABMs according to OIV method 510/2013. Briefly, acetic acid was extracted with diethyl ether or *tert*-butyl methyl ether by liquid−liquid extraction for at least 5 h, and the solvent was then eliminated by distillation using a column that prevents isotopic fractionation of acetic acid. The samples of must and of ABM residue after acetic acid extraction underwent alcoholic fermentation. Before fermentation, the ABM residue was heated to 40° for at least 6 h to remove residual ether. Each sample was inoculated with a fresh culture of *Saccharomyces cerevisiae* (strain ATCC 9763) without added water. Fermentation was carried out in glass bottles with a bubbler valve in the cap; each bottle contained 0.7 L of sample, and the temperature was adjusted to 25 °C. At the end of fermentation, the ethanol was extracted by distillation, according to the procedure described in the OIV MA-AS-311-05 method. The Brix degree of must was measured following the OIV-MA-AS2−02 R2009 method.

**SNIF-NMR Analysis.** The D/H of ethanol from wine and must fermentation (cooked and concentrated as well as the ABM residue after acetic acid extraction) and of acetic acid from vinegar and ABM was determined by SNIF-NMR (FT-NMR AVANCE III 400, Bruker BioSpin GmbH, Karlsruhe, Germany). An NMR spectrometer fitted with a selective 10 mm "deuterium" probe tuned to a frequency Vo characteristic of channel Bo (e.g., Bo = 9.4 T, $\nu o$ = 61.4 MHz) with a decoupling channel (B2) and a field-frequency stabilization channel (lock) at the fluorine frequency. The second channel B2 was also used in the $^1H$ NMR experiment for acetic acid analysis. The resolution measured on the $^2H$-SNIF-NMR spectrum, transformed without exponential multiplication (i.e., LB = 0) and expressed by the width at the half-height of the methyl signal of acetic acid and the methyl signal of TMU (see below for definition) was less than 0.5 Hz. Sensitivity (signal-to-noise ratio) measured when the FID was exponentially weighted by a factor equal to 2 Hz line B broadening (LB), was greater than or equal to 150 for the methyl signal of acetic acid containing less than 25% of water.

Site-specific D/H values were measured in the methyl and methylene sites of ethanol ($(D/H)_I$ or $(D/H)_{CH3}$ and $(D/H)_{II}$) and in the methyl site of acetic acid ($(D/H)_{CH3}$) and expressed in parts per million (ppm). The method described in OIV MA-AS-311-05 was used for wine and must, while for vinegar, we followed the method described in EN 16466-1 with certain modifications that took into account the fact that impurities can be extracted at the organic phase together with acetic acid (see the Results and Discussion section).

3.25 gr of the extract containing acetic acid after filtration was placed in a 10 mm NMR tube together with 1.1 g of the internal standard tetramethylurea (TMU, certified reference material, STA-003m, EC-JRC, Geel, Belgium), as described in EN 16466-1, and a sufficient quantity of lock substance (for example: 50 $\mu$L of hexafluorobenzene or 150 $\mu$L of a homogenized mixture of hexafluorobenzene ($C_6F_6$)/trifluoroacetic acid (TFA) 90/10 v/v). This sample was then measured in the NMR tube by $^1$H NMR and $^2$H-SNIF-NMR by means of a composite NMR experiment.[3,4]

Typical conditions for obtaining $^2$H-SNIF-NMR spectra are as follows: constant probe temperature (e.g., 303 K); rotation of the sample (e.g., 15−20 Hz); acquisition time of at least 5.5 s for 1200 Hz spectral width (i.e., about 20 × $10^{-6}$ at 46.1 MHz); 90° pulse; quadrature detection, fix the offset O1 between the OD and $CH_2D$ reference signals for acetic acid; and determination of the value of the decoupling offset O2 from the $^1$H NMR spectrum measured by the decoupling coil on the same tube. Good decoupling is obtained when O2 is located in the middle of the frequency interval lying between the $CH_3$ and TMU groups. Use of broad band decoupling sequence WALTZ-16.

Typical conditions for obtaining $^1$H NMR spectra are as follows: constant probe temperature (e.g., 303 K); rotation of the sample (e.g., 15−20 Hz); acquisition time of at least 4.1 s for 8000 Hz spectral width (i.e., about 20 × 10−6 at 400 MHz); 30° pulse or less; D1 = 7s at least; parabolic detection, fix the offset O1 between the OH and $CH_3$ reference signals for acetic acid; and no decoupling.

For each spectrum, a number of accumulations sufficient to obtain the signal-to-noise ratio given above were carried out.

Appropriate software based on a complex least-squares curve fitting algorithm should be used to determine the signal area (first-order phasing and baseline correction are sensitive parameters for the proper evaluation of signal areas and have to be correctly adjusted). When larger errors in phasing and baseline distortions can safely be excluded (e.g., by applying suitable spectrometer routines for phasing and baseline correction) software based on the real part of the complex NMR data can be used instead.

For each $^1$H NMR spectrum, we calculated the ratio $S_{TMU}/S_{acetic\ acid}$, where $S$ is the $^1$H NMR signal area, integrated by data processing software after Fourier transform of the free induction decay, with an appropriate line-broadening factor of 0.5 Hz.

For each $^2$H-SNIF-NMR spectrum, we calculated the ratio $S'_{acetic\ acid}/S'_{TMU}$, where $S'$ is the $^2$H NMR signal area, integrated by data processing software after Fourier transform of the free induction decay, with a line-broadening factor of 2 Hz.

The ratio $(D/H)_{CH3}$ is calculated as follows:

$$(D/H)_{CH3} = S'_{acetic\ acid}/S'_{TMU} \times S_{TMU}/S_{acetic\ acid} \times (D/H)_{TMU}$$

where $(D/H)_{TMU}$ is the certified deuterium content in parts per million of the TMU provided by the supplier of the reference product.

Appropriate software enabled these three successive calculations to be made.

The standard deviation of repeatability (sr) of $(D/H)_{CH3}$ quoted in the methods (OIV AS311-05, EN 16466-1) is 0.3 for wine and must and 0.6 ppm for vinegar, whereas the standard deviation of reproducibility (sR) is 0.4 for wine and must and 0.6 ppm for vinegar.

**IRMS Analysis.** The $^{13}C/^{12}C$ of ethanol and acetic acid was measured using IRMS (SIRA II-VG ISOGAS, FISIONS, Rodano, Milano, Italy, or DELTA V, Thermo Scientific, Germany) interfaced with an elemental analyzer (Flash 1112, Carlo Erba, Milano, Italy, or EA Flash 1112, Thermo Scientific), according to the procedures described in OIV-MA-AS312-06, OIV 510/2013 and EN 16466-2.

To evaluate the impact of the impurities present in the extraction solution of acetic acid, we measured the $^{13}C/^{12}C$ in pure acetic acid using gas chromatography combustion (GC-C; Trace GC Ultra, Thermo Scientific) interfaced with an IRMS (DELTA V, Thermo Scientific) through an open split interface. A ZB-FFAP capillary column (30 m × 0.25 mm i.d. × 0.25 $\mu$m film thickness; Phenomenex) with He as carrier gas (at a flow rate of 2.7 mL/min) was used. A volume of 1.5 $\mu$L of a solution of acetic acid/diethyl ether (1:5) was injected in split mode by an autosampler (Triplus, Thermo Scientific). The injector temperature was set at 250 °C, and the oven temperature of the GC set at an initial 50 °C where it was held for 2.5 min before heating at 70 °C/min to 150 °C and held for 20 min. The eluted compound was combusted into $CO_2$ and $H_2O$ in a combustion furnace reactor at 1000 °C and composed of a ceramic tube (320 mm in length) containing an NiO tube in combination with NiO and CuO wires (0.125 mm diameter, 240 mm identical length) braided and centered end-to-end within the tube. Water vapor was removed with a water-removing trap consisting of a Nafion membrane.

The $^{18}O/^{16}O$ analyses of wine, must, vinegar, and ABM were performed using an isotope ratio mass spectrometer (SIRA II, VG Fisons, Middlewich, UK, or Isoprime, Cheadle, UK) connected to a water/$CO_2$ equilibration system (Isoprep 18, VG Fisons or Isoprime Multiflow) according to the procedures described in the OIV-MA-AS2-12, OIV 511/2013, and EN 16466-3 methods for wine, must, and vinegar.

The $^{13}C/^{12}C$ and $^{18}O/^{16}O$ values are expressed on the $\delta$ ‰ scale against international standards V-PDB (Vienna-Pee Dee Belemnite, IAEA, Vienna) and V-SMOW (Vienna-Standard Mean Ocean Water) normalized to the VSMOW−SLAP (Standard Light Antarctic Precipitation) scale, respectively, according to the equation: $\delta‰ = ((R_{sample} - R_{standard})/(R_{standard}))\cdot 1000$ where $R$ is the ratio of the heavy to light stable isotope in the sample ($R_{sample}$) and the international reference material ($R_{standard}$).

The sr of $\delta^{18}O$ quoted in the OIV and EN methods is 0.1 ‰ for wine, must, and vinegar, while the sr of $\delta^{13}C$ is 0.1 ‰ for wine and must and 0.2 ‰ for vinegar. The sR of $\delta^{18}O$ is 0.2 ‰ for wine, must, and vinegar, while the sR of $\delta^{13}C$ is 0.2 ‰ for wine and must and 0.3 ‰ for vinegar.

**GC-MS/MS Analysis.** The solutions after vinegar and ABM vinegar extraction were filtrated with a 0.22 $\mu$m filter and then diluted 5 times with 80% acetic acid (LC/MS grade), and for analysis of acetic acid, 2000 times with water (Milli-Q).

GC analysis was performed using a Trace GC Ultra gas chromatograph coupled with a TSQ Quantum tandem mass spectrometer upgraded to the XLS configuration. A DuraBrite IRIS ion source with prefilter was installed to improve performance of the spectrometer. The system was fitted with a Triplus autosampler (Thermo Electron Corporation, Waltham, MA, USA). The injection volume was 1 $\mu$L, postinjection dwell time was 4 s, and tray temperature was 5 °C. GC separation was performed on a 30 m VF-WAXms capillary column with an internal diameter of 0.25 mm and a film thickness of 0.25 $\mu$m (Varian, Inc., Palo Alto, CA, USA). The temperature program was as follows: 40 °C hold for 2 min after injection, 10 °C/min up to 50 °C, 1.4 °C/min up to 60 °C, hold for 2 min, 1.6 °C/min up to 70 °C, hold for 1 min, 2.2 °C/min up to 100 °C, hold for 0.5 min, 3.1 °C/min up to 140 °C, 4.4 °C/min up to 200 °C, 12 °C/min up to 250 °C, hold for 6 min. Injection parameters were as follows: split injection, split ratio 150 (split flow 120 mL/min), inlet temperature 250 °C, carrier gas was helium 5.5, programmed flow: 0.8 mL/min hold for 62.50 min, 0.8 mL/min up to 1.2 mL/min in 0.5 min, hold for 7 min. The mass spectrometer was operated in electron impact (EI) ionization mode at 70 eV. The temperature of the transfer line was 220 °C. Mass spectrometer parameters were EI ionization mode at 70 eV. Full scan acquisition from $m/z$ 40 to $m/z$ 400 using the third quadripole with a scan time of 0.200 s. Source temperature was 250 °C, and filament emission current was 50 $\mu$A. The mass spectrometer was tuned and calibrated using FC-43 (perfluorotributylamine (PFTBA)). Data acquisition and analyses were performed using Xcalibur Workstation software supplied by the manufacturer. Quantification was performed using Trace finder EFS 3.0 software (Thermo Scientific).

**Statistical Analysis.** The data were analyzed using Statistica v.9 software (StatSoft Italia srl, Padua, Italy). A paired $t$-test was carried out on the data set to identify differences between samples within the production chains.

ANOVA, honestly significant difference (HSD) Tukey, Kruskall−Wallis, and U-Mann−Whitney tests were carried out on the data set to identify differences between the various groups.

Table 2. Mean % of Volatile Compounds in the Extraction Solutions of Vinegar and ABM

| | | vinegar ($n$ = 10) | | | | ABM ($n$ = 11) | | | |
|---|---|---|---|---|---|---|---|---|---|
| compd | confirmed by[a] | mean | std dev | min | max | media | std dev | min | max |
| ethyl ether | STD MS | 0.459 | 0.543 | 0.010 | 1.560 | 0.274 | 0.353 | 0.024 | 0.921 |
| methyl acetate | RI MS | 0.006 | 0.007 | 0.000 | 0.024 | 0.006 | 0.005 | 0.002 | 0.015 |
| ethyl acetate | STD MS | 0.843 | 0.756 | 0.087 | 2.677 | 1.631 | 1.829 | 0.072 | 5.867 |
| 2,3-butanedione | STD MS | 0.043 | 0.048 | 0.001 | 0.163 | 0.045 | 0.050 | 0.002 | 0.147 |
| isobutyl acetate | STD MS | 0.024 | 0.032 | 0.003 | 0.100 | 0.033 | 0.038 | 0.003 | 0.127 |
| acetoin | STD MS | 0.550 | 0.570 | 0.018 | 1.752 | 0.588 | 0.469 | 0.048 | 1.358 |
| ethyl lactate | STD MS | 0.023 | 0.038 | 0.000 | 0.120 | 0.037 | 0.043 | 0.000 | 0.120 |
| ethanol, 2,2′-oxybis-, diacetate | RI MS | 0.226 | 0.194 | 0.009 | 0.644 | 0.243 | 0.223 | 0.018 | 0.714 |
| acetic acid | STD MS | 96.072 | 3.292 | 88.053 | 98.571 | 94.207 | 4.136 | 87.096 | 97.901 |
| 1,2-propanediol, diacetate | RI MS | 0.013 | 0.007 | 0.000 | 0.021 | 0.033 | 0.018 | 0.016 | 0.075 |
| propanoic acid | STD MS | 0.128 | 0.093 | 0.056 | 0.308 | 0.137 | 0.068 | 0.047 | 0.244 |
| butanoic acid, 3-hydroxy-, ethyl ester | RI MS | 0.340 | 0.276 | 0.024 | 0.944 | 0.439 | 0.296 | 0.114 | 0.848 |
| 1-methoxy-2-propyl acetate | RI MS | 0.140 | 0.127 | 0.009 | 0.406 | 0.229 | 0.138 | 0.098 | 0.452 |
| butanoic acid | STD MS | 0.008 | 0.023 | 0.000 | 0.075 | 0.006 | 0.019 | 0.000 | 0.062 |
| 1,3-propanediol, diacetate | RI MS | 0.179 | 0.245 | 0.010 | 0.735 | 0.252 | 0.434 | 0.028 | 1.424 |
| isovaleric acid | STD MS | 0.005 | 0.006 | 0.000 | 0.017 | 0.006 | 0.007 | 0.000 | 0.017 |
| diethyl succinate | RI MS | 0.019 | 0.026 | 0.000 | 0.083 | 0.027 | 0.029 | 0.000 | 0.073 |
| benzyl acetate | STD MS | 0.008 | 0.008 | 0.000 | 0.023 | 0.009 | 0.011 | 0.000 | 0.037 |
| phenethyl acetate | STD MS | 0.123 | 0.109 | 0.002 | 0.296 | 0.157 | 0.135 | 0.015 | 0.364 |
| phenethyl alcohol | STD MS | 0.009 | 0.011 | 0.000 | 0.036 | 0.012 | 0.016 | 0.000 | 0.057 |
| butylated hydroxytoluene | STD MS | 0.025 | 0.032 | 0.000 | 0.080 | 0.060 | 0.046 | 0.011 | 0.142 |
| glycerol 1,2-diacetate* | MS | 0.026 | 0.017 | 0.000 | 0.048 | 0.047 | 0.034 | 0.013 | 0.113 |
| 5-acetoxymethyl-2-furaldehyde | RI MS | 0.001 | 0.001 | 0.000 | 0.003 | 0.323 | 0.257 | 0.035 | 0.742 |
| 1,2,3-propanetriol, 1-acetate* | MS | 0.074 | 0.051 | 0.001 | 0.161 | 0.134 | 0.080 | 0.062 | 0.273 |
| triacetin* | MS | 0.016 | 0.010 | 0.000 | 0.027 | 0.036 | 0.022 | 0.017 | 0.074 |
| 1,1-ethanediol, diacetate* | MS | 0.022 | 0.032 | 0.000 | 0.095 | 0.032 | 0.031 | 0.000 | 0.104 |
| levulinic acid | RI MS | 0.000 | 0.000 | 0.000 | 0.000 | 0.095 | 0.061 | 0.000 | 0.220 |
| ethyl hydrogen succinate | RI MS | 0.122 | 0.149 | 0.000 | 0.458 | 0.186 | 0.203 | 0.011 | 0.649 |
| 5-hydroxymethylfurfural | STD MS | 0.000 | 0.000 | 0.000 | 0.000 | 0.087 | 0.061 | 0.028 | 0.217 |
| *N*-acetyltyramine* | MS | 0.015 | 0.015 | 0.000 | 0.048 | 0.022 | 0.019 | 0.000 | 0.053 |
| 2,3-butanedioldiacetate | RI MS | 0.150 | 0.133 | 0.011 | 0.477 | 0.194 | 0.161 | 0.063 | 0.490 |
| 2,3-butanediol | STD MS | 0.079 | 0.119 | 0.003 | 0.404 | 0.134 | 0.195 | 0.017 | 0.707 |
| isoamyl acetate | STD MS | 0.187 | 0.247 | 0.004 | 0.740 | 0.200 | 0.232 | 0.029 | 0.649 |

[a]STD: standard; MS: mass spectra; RI: retention index; * tentative identification.

## RESULTS AND DISCUSSION

**Impurities in the Extraction Solution from Wine Vinegar and ABM.** First of all, we checked for the presence of impurities in the solution extracted by diethyl ether along with acetic acid from wine vinegar and ABM and whether they affect the isotopic data of acetic acid. We analyzed 11 samples of ABM and 10 of wine vinegar and used GC-MS/MS for quantification (Table 2).

The percentage of impurities was found to be on average 6% in the extraction solution of ABM and 4% in that of wine vinegar. The main impurities (higher than 1%) are the extraction solvent, ethyl acetate, acetoin (= 3-hydroxybutanone) and butanoic acid. Comparison of the ABM and vinegar solutions showed 5-acetoxymethyl-2-furaldehyde (= 5-formylfurfuryl acetate), levulinic acid, and 5-(hydroxymethyl)furfural (= 5-hydroxymethyl-2-furaldehyde), mostly originating from the heating of the grape must and caramel, to be significantly higher in ABM ($p$ < 0.001, Tukey, Kruskall–Wallis and U-Mann–Whitney tests).

In the case of D/H analysis, the presence of impurities was overcome by carrying out a composite NMR experiment on acetic acid, as described in the Materials and Methods section. As for $\delta^{13}C$, we compared the values obtained for the extracted purified solution using EA-IRMS with those for pure acetic acid analyzed by GC/c-IRMS. We did not find any significant differences ($p$ < 0.001) in the 18 vinegar and 21 ABM samples, the mean difference being 0.06 ‰ and the maximum difference 0.3 ‰.

We can conclude that, even if impurities are extracted along with acetic acid from wine vinegar and ABM, the isotopic data of acetic acid are not affected when the methods here described are adopted.

**Validation of the Isotopic Methods for ABM.** There exist official validated isotopic methods for acetic acid and water in wine vinegar and for ethanol in grape must. To ascertain whether the same methods can also be used for analyzing the ingredients of AMB, we assessed the repeatability and reproducibility of SNIF-NMR and IRMS analyses of acetic acid, ethanol, and water in ABM and compared these values with those obtained in vinegar and must and with those reported in the corresponding official methods.

To assess repeatability, we analyzed the same vinegar and ABM samples 10 times. The repeatability values (sr < 0.4 ppm) for $(D/H)_{CH3}$ are comparable for vinegar and ABM and are lower than the repeatability mean value of the EN 16466-1 method (sr = 0.6 ppm). The sr for $\delta^{13}C$ and $\delta^{18}O$ for both vinegar and ABM (≤0.2 ‰) are consistent with those for


dx.doi.org/10.1021/jf5013538 | J. Agric. Food Chem. 2014, 62, 8197–8203

**Table 3. Standard Deviations of Repeatability and Reproducibility (sr, sR) and of Repeatability and Reproducibility Limits (r, R): Comparison of the Values Found in This Study with Those Using OIV and EN Methods**

| | $(D/H)_{CH3}$ (ppm) | | | | $\delta^{13}C$/‰ | | | | $\delta^{18}O$/‰ | | | |
|---|---|---|---|---|---|---|---|---|---|---|---|---|
| | sr | r (2.8 × sr) | sR | R (2.8 × sR) | sr | r (2.8 × sr) | sR | R (2.8 × sR) | sr | r (2.8 × sr) | sR | R (2.8 × sR) |
| wine-must (ethanol, OIV) | 0.3 | 0.8 | 0.4 | 1.1 | 0.1 | 0.3 | 0.2 | 0.6 | 0.1 | 0.3 | 0.2 | 0.6 |
| vinegar (acetic acid, OIV, EN) | 0.6 | 1.7 | 0.6 | 1.7 | 0.2 | 0.6 | 0.3 | 0.8 | 0.1 | 0.3 | 0.2 | 0.6 |
| vinegar (acetic acid, this study) | 0.4 | 1.1 | 0.5 | 1.4 | 0.1 | 0.3 | | <0.4[a] | 0.1 | 0.3 | | <0.4[a] |
| ABM (acetic acid, this study) | 0.2 | 0.6 | 0.4 | 1.1 | 0.2 | 0.6 | | <0.4[a] | 0.1 | 0.3 | | <0.5[a] |
| ABM (ethanol, this study) | 0.5 | 1.4 | | <0.8[a] | 0.2 | 0.6 | | <0.3[a] | | | | |

[a]Maximum difference between laboratories found in this study.

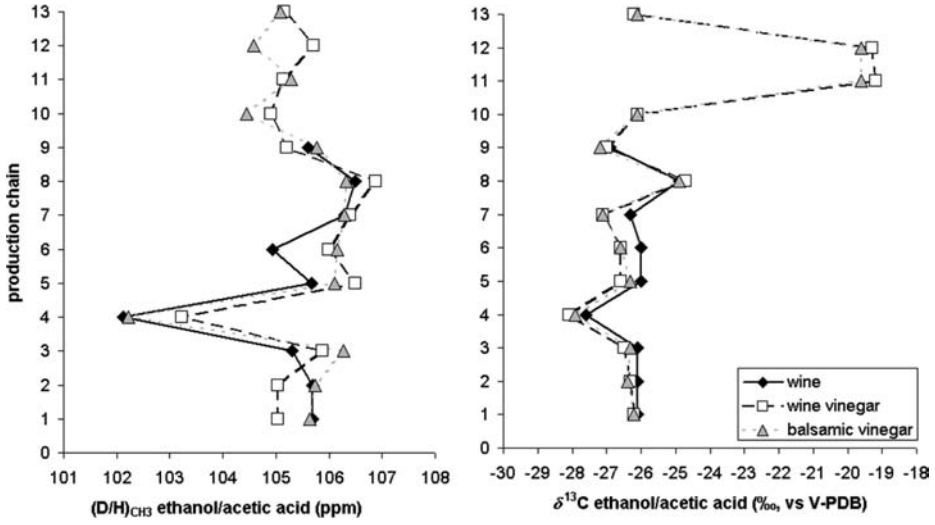


**Figure 1.** Variations in ethanol/acetic acid $(D/H)_I$ and $\delta^{13}C$ values between wine, wine vinegar, and ABM.

vinegar reported in the OIV and EN methods (≤0.2 ‰). The sr for $(D/H)_{CH3}$ (0.5 ppm) and $\delta^{13}C$ (0.2 ‰) of alcohol from must contained in the ABM (residue after acetic acid extraction) are also comparable to those of the OIV-MA-AS311-05 (average sr = 0.3 ppm) and OIV-MA-AS312-06 (average sr = 0.2 ‰) methods, although they were slightly higher for $(D/H)_{CH3}$.

To determine method reproducibility, 10 samples of vinegar (cane sugar acetic acid was added to some of the samples) and 5 of ABM were analyzed in 3 different laboratories, which used as solvent, diethyl ether or tert-butyl methyl ether and as lock substance, $C_6H_6$ or TFA. Table 3 reports a summary of the sr and sR values of the OIV and EN methods compared with those found in this study. Also shown is the repeatability limit (r), that is, the value less than or equal to which the absolute difference between two results obtained under repeatability conditions may be expected to be with a probability of 95% (calculated as 2.8 × sr)[5], and the reproducibility limit (R), that is, the value less than or equal to which the absolute difference between two results obtained under reproducibility conditions may be expected to be with a probability of 95% (2.8 × sR)[5]. The reproducibility values for $(D/H)_{CH3}$ for vinegar and ABM are comparable to each other and to the values of the EN 16466-1 method. The sR values of authentic and adulterated samples are not different. The same was found with $\delta^{13}C$ of acetic acid and $\delta^{18}O$ of water and with $(D/H)_{CH3}$ and $\delta^{13}C$ of ethanol from ABM must fermentation, which were measured only in two laboratories, the differences being always lower than the reproducibility limits for all the isotopic parameters (Table 3).

We conclude that the isotopic methods for analyzing $(D/H)_{CH3}$, $\delta^{13}C$, and $\delta^{18}O$ in grape must and vinegar can also be applied to the ingredients of ABM. The same validation data apply, except for the repeatability values of ethanol $(D/H)_{CH3}$, which are here slightly higher.

**Variations between $(D/H)_{CH3}$ and $\delta^{13}C$ Values in Wine and Must and Those in the Ingredients of ABM.** Figure 1 reports the $(D/H)_{CH3}$ and $\delta^{13}C$ values of ethanol obtained from wine (solid black diamonds connected by black lines), acetic acid extracted from vinegar (open squares connected by dashed lines), and balsamic vinegar (solid gray triangles connected by dotted lines) for the 13 chains, reported along the *y* axis. The mean difference for $(D/H)_{CH3}$ between wine and both vinegar and ABM was +0.3 ppm with a range of −0.7 to 1.1 ppm and therefore below the repeatability limits of the official methods reported in Table 3. The difference was not significant according to a paired *t*-test ($p < 0.001$), in line with previous findings.[6] The wine samples had different $(D/H)_I$ values, ranging from 102.1 to 106.3 ppm, and covered a large part of the typical variability of a grape product.[2]

The $\delta^{13}C$ of ethanol obtained from wine also appears not to differ from that of acetic acid after extraction from both vinegar and ABM (Figure 1), in line with previous findings.[6] The mean differences between wine and vinegar and wine and ABM are 0.4 ‰ and 0.3 ‰, respectively, with a range of −0.8 to 0.2 ‰, averagely lower than the official repeatability limits shown in Table 3. Moreover, the differences were not significant according to a paired *t*-test ($p < 0.001$). The $\delta^{13}C$ values of chains 11 and 12 for both products are very high (on average


dx.doi.org/10.1021/jf5013538 | J. Agric. Food Chem. 2014, 62, 8197−8203

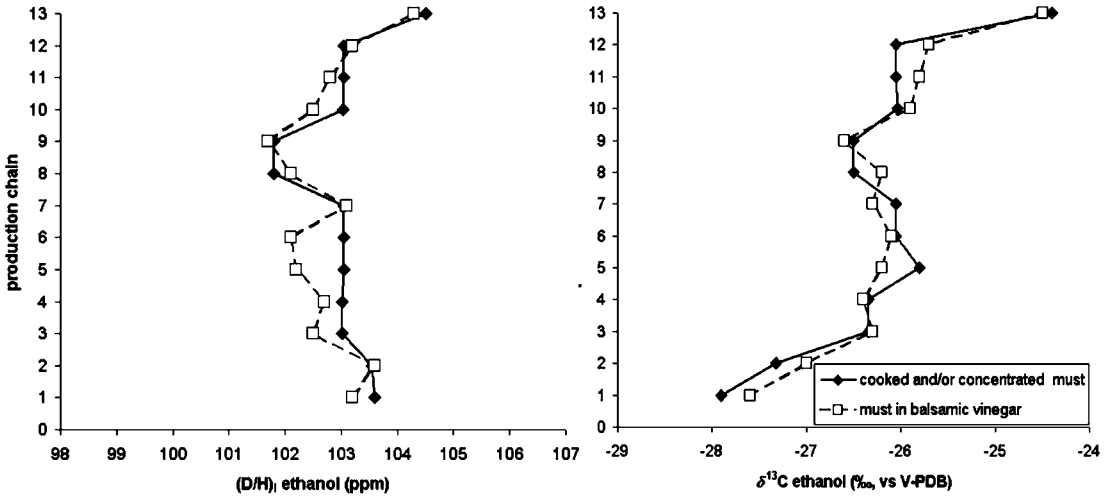


**Figure 2.** Variations in ethanol $(D/H)_I$ and $\delta^{13}C$ between the mixtures of concentrated and cooked must (calculated values) and the corresponding mixture in the ABM.

**Table 4. Effects of Filtration, Concentration, and Addition of Caramel on the Isotopic Values of Acetic Acid and Ethanol of ABM**

| | | | acetic acid fraction | | must fraction | |
|---|---|---|---|---|---|---|
| | density | acidity (g/100 mL) | $(D/H)_{CH3}$ (ppm) | $\delta^{13}C$/‰ vs V-PDB | $(D/H)_I$ (ppm) | $\delta^{13}C$/‰ vs V-PDB |
| concentrated grape must | | | | | 102.9 | −25.9 |
| cooked grape must | | | | | 103.2 | −26.2 |
| expected value of mix | | | | | 103.0 | −26.0 |
| white wine vinegar | | | 104.9 | −26.1 | | |
| ABM (not filtered) | | | 104.5 | −26.1 | 102.6 | −25.9 |
| ABM (tangentially filtered) | | | 104.3 | −26.0 | 102.8 | −26.0 |
| ABM (with 1.79% caramel) | | | 104.1 | −26.0 | 102.7 | −25.9 |
| white wine vinegar | | 11.11 | 105.2 | −26.2 | | |
| ABM (not concentrated) | 1.169 46 | 6.31 | 105.1 | −26.1 | | |
| ABM (45°Brix) | 1.206 38 | 6.31 | 105.3 | −26.1 | | |
| ABM (57°Brix) | 1.278 19 | 5.71 | 105.6 | −26.1 | | |

−19.5 ‰) due to the addition of cane sugar acetic acid to the vinegar.

ABM is made with a mix of concentrated and cooked grape must. In this work, we produced ABM with different percentages of these two ingredients (Table 1). We analyzed the raw must and calculated the values of ethanol $(D/H)_I$ and $\delta^{13}C$ for each mix containing different quantities of concentrated and cooked must (see Table 1). Figure 2 shows a comparison between these values and the values for the ethanol obtained from fermentation of the residual solution of the corresponding ABM after acetic acid extraction. The mean differences were 0.3 ppm for $(D/H)_I$ and 0.1 ‰ for $\delta^{13}C$, ranging from −0.3 to 1 ppm and from −0.4 to +0.4 ‰, respectively. In both cases, the mean values are below the official limits of repeatability (Table 3).

Effects of technological processing stages, such as addition of caramel, tangential filtration, and concentration, were found to be nonsignificant for isotopic ratios of both acetic acid and must ethanol (Table 4): indeed, the maximum difference between values from the same experiment was always below the corresponding repeatability limit (Table 3). As for caramel, we have found by experiment that it does not ferment in the conditions adopted here, which is why its presence does not affect the isotopic values of ethanol. Anyway its low presence (maximum addition allowed 2%) should not influence the data.

The absence of any effect of concentration is not consistent with what is found in the literature,[8] where it has been shown that concentration under vacuum evaporation, as in this case, can change significantly the $\delta^{18}O$ of must water, the $(D/H)_{II}$ of must ethanol and also, but to a lesser extent, $(D/H)_I$.

We conclude that there are no changes in isotopic values $(D/H)_I$ and $\delta^{13}C$ from wine to vinegar and to ABM and from the original must to ABM must, independently of concentration, filtration, and addition of caramel. This supports the suggestion that the methods recognized for vinegar and must using a composite NMR experiment for D/H can also be adopted for analysis of the ingredients in ABM. Moreover, it provides experimental evidence that the reference data of wine databanks can also be used to evaluate the authenticity of vinegar and ABM.

**Detection of Adulteration of Vinegar and ABM.** Previous studies have shown that C and H stable isotope ratios have a marked capacity to identify synthetic vinegars and distinguish C3 and C4 derived products, allowing the adulteration of vinegars with raw fermentation materials cheaper than those declared on the label to be detected.[9−11] Here, we investigated the ability of isotopic analysis to detect the fraudulent addition of increasing percentages of cane sugar ethanol to wine from which vinegar is derived and of synthetic vinegar to ABM. The general reference of wine, as reported by


dx.doi.org/10.1021/jf5013538 | J. Agric. Food Chem. 2014, 62, 8197−8203

Dordevic et al. (98.8 to 106 ppm for $(D/H)_{CH3}$ and −29.3 ‰ to −24.3 ‰),[2] can be adopted for products such as vinegar and ABM, where origin and year of production are generally not known.

Table 5 shows that the addition of more than 20% of cane sugar ethanol to the source wine can be detected because the

**Table 5. Isotopic Values of Nonauthentic Vinegar and ABM**

| | % grape | % cane | $(D/H)_{CH3}$ | $\delta^{13}C/‰$ |
|---|---|---|---|---|
| vinegar 1 | 90% | 10% | 106.7 | −25.3 |
| vinegar 2 | 86% | 14% | 107.3 | −24.1 |
| vinegar 3 | 80% | 20% | 107.0 | −24.2 |
| vinegar 4 | 67% | 33% | 108.5 | −22.6 |
| vinegar 5 | 60% | 40% | 109.3 | −21.5 |
| vinegar 6 | 58% | 42% | 109.1 | −21.2 |
| ABM from vinegar 1 | 90% | 10% | 106.9 | −25.1 |
| ABM from vinegar 6 | 58% | 42% | 108.3 | −21.3 |
| | % grape | % synthetic | $(D/H)_{CH3}$ | $\delta^{13}C/‰$ |
| ABM 1 | 60% | 40% | 112.4 | −27.8 |
| ABM 2 | 80% | 20% | 110.7 | −27.3 |

isotopic parameters fall outside of the limits, taking into account the measurement uncertainty. In addition, the presence of 20% of synthetic acetic acid (and potentially less, since the synthetic sources cover a very wide range)[7] can be detected. In all cases, the actual detection limit depends on the isotopic values of the starting materials (wine vinegar and added substitutes).[2,12] Moreover, detection of adulteration is more efficient if the exact origin of the grapes is known, because the limits are more narrow.

## ■ ASSOCIATED CONTENT

### Supporting Information

Single data of the studies for determining repeatability and reproducibility. This material is available free of charge via the Internet at http://pubs.acs.org.

## ■ AUTHOR INFORMATION


### Corresponding Author

*Phone: +39 0461 615149; fax: +39 0461 615200; e-mail: federica.camin@fmach.it.



### Funding

We extend our grateful thanks to the Italian producers of ABM who funded this work.


### Notes

The authors declare no competing financial interest.

## ■ ACKNOWLEDGMENTS

We thank Cesare Lotti for technical support in the GC-MS analysis.

## ■ REFERENCES


(1) Camin, F.; Bontempo, L.; Perini, M.; Tonon, A.; Breas, O.; Guillou, C.; Moreno-Rojas, J. M.; Gagliano, G. Control of wine vinegar authenticity through $\delta^{18}O$ analysis. *Food Control* **2013**, *29*, 107−111.

(2) Dordevic, N.; Camin, F.; Marianella, R. M.; Postma, G. J.; Buydens, L. M. C.; Wehrens, R. Detecting the addition of sugar and water to wine. *Aust. J. Grape Wine Res.* **2013**, *19*, 324−330.

(3) Hermann, A. Determination of D/H isotope ratio in acetic acid from vinegars and pickled products by $^2H$-NMR-spectroscopy. *Eur. Food Res. Technol.* **2001**, *212*, 683−686.

(4) Fauhl, C.; Wittkowski, R. On-line $^1H$-NMR to facilitate tube preparation in SNIF-NMR analysis. *Z. Lebensm.-Unters. Forsch.* **1996**, 541−545.

(5) Horwitz, W. Protocol for the design, conduct and interpretation of method-performance studies. *Pure Appl. Chem.* **1995**, *67*, 331−343.

(6) Remaud, G.; Guillou, C.; Vallet, C.; Martin, G. J. A coupled NMR and MS isotopic method for the authentication of natural vinegars. *Fresenius' J. Anal. Chem.* **1992**, *342*, 457−461.

(7) Grégrová, A.; Cizkova, H.; Mazac, J.; Voldrich, M. Authenticity and quality of spirit vinegar: Methods for detection of synthetic acetic acid addition. *J. Food Nutr. Res.* **2012**, *51*−*3*, 123−131.

(8) Guyon, F.; Douet, C.; Colas, S.; Salagoity, M. H.; Medina, B. Effects of must concentration techniques on wine isotopic parameters. *J. Agric. Food Chem.* **2006**, *54*−*26*, 9918−9923.

(9) Krueger, D. A. Stable carbon isotope ratio method for detection of corn-derived acetic-acid in apple cider vinegar: Collaborative study. *J. AOAC Int.* **1991**, *75*, 725−728.

(10) Remaud, G.; Guillou, C.; Vallet, C.; Martin, G. J. A coupled NMR and MS isotopic method for the authentication of natural vinegars. *Fresenius' J. Anal. Chem.* **1992**, *3/42*, 457−461.

(11) Thomas, F.; Jamin, E. $^2H$ NMR and $^{13}C$-IRMS analyses of acetic acid from vinegar, $^{18}O$-IRMS analysis of water in vinegar: International collaborative study report. *Anal. Chim. Acta* **2009**, *649*, 98−105.

(12) Dordevic, N.; Wehrens, R.; Postma, G. J.; Buydens, L. M. C.; Camin, F. Statistical methods for improving verification of claims of origin for Italian wines based on stable isotope ratios. *Anal. Chim. Acta* **2012**, *757*, 19−25.

JOURNAL OF AGRICULTURAL AND FOOD CHEMISTRY

Article

pubs.acs.org/JAFC

# Synergy of Licorice Extract and Pea Protein Hydrolysate for Oxidative Stability of Soybean Oil-in-Water Emulsions

Xin Zhang,[†] Youling L. Xiong,*[,‡] Jie Chen,[†] and Lirong Zhou[§]

[†]State Key Laboratory of Food Science and Technology and School of Food Science and Technology, Jiangnan University, Wuxi, Jiangsu 214122, China

[‡]Department of Animal and Food Sciences, University of Kentucky, Lexington, Kentucky 40546, United States

[§]ICL Performance Products LP, St. Louis, Missouri 63141, United States

**ABSTRACT:** Previously developed radical-scavenging pea protein hydrolysates (PPHs) prepared with Flavourzyme (Fla-PPH) and Protamex (Pro-PPH) were used as cosurfactants with Tween 20 to produce soybean oil-in-water (O/W) emulsions, and the suppression of lipid oxidation was investigated. Both PPHs significantly retarded oxidation ($P < 0.05$) of the emulsions when stored at 37 °C for 14 days. Electron microscopy revealed an interfacial peptidyl membrane around oil droplets, which afforded steric restrictions to oxidation initiators. When licorice extract (LE) was also used in emulsion preparation, a remarkable synergistic oxidation inhibition was observed with both PPHs. LE adsorbed onto oil droplets either directly or through associating with PPH to produce a thick and compact interfacial membrane enabling the defense against oxygen species. Liquiritin apioside, neolicuroside, glabrene, and 18$\beta$-glycyrrhetic acid were the predominant phenolic derivatives partitioning at the interface and most likely the major contributors to the notable synergistic antioxidant activity when coupled with PPHs.

**KEYWORDS:** *antioxidant, pea protein hydrolysate, licorice extract, emulsion, oxidative stability, synergism*

## INTRODUCTION

A wide array of natural and processed foods exist as emulsions, such as milk, cream, mayonnaise, and salad dressings. Due to the large contact surface between oxidizable fatty acids and water-soluble oxidants (oxygen and transition metal ions), emulsified oil is much more susceptible to oxidation than bulk oil.[1] Peptides and protein hydrolysates as potential alternatives to traditional antioxidants have been widely reported to be inhibitory of lipid oxidation in biphasic (O/W) systems through scavenging free radicals, sequestrating pro-oxidative metal ions, or forming physical (shielding) barrier around oil droplets.[2−4] Unlike small-molecule antioxidants, protein hydrolysates may also act as stabilizing agents to improve the physical stability of emulsion systems.[5,6]

Phenolic compounds extracted from plants and spices are also recognized for their strong antioxidant activity in food systems due to radical-scavenging activity and chelation of transition metal ions.[7,8] Many polyphenols and their plant extracts are effective against both lipid peroxidation and protein oxidative changes in model systems and in complex food matrices, such as processed meats.[9,10]

The effectiveness of an antioxidant in retarding lipid oxidation in food emulsions depends not only on its chemical reactivity with oxidation initiators and propagators but also on its location, which is dictated by its polarity and affinity for other constituents.[11,12] Due to the size reduction and increased charges, peptides are distributed preferentially in the aqueous phase and can partition at the oil−water interface, thereby preventing the initiation of lipid oxidation induced by water-soluble oxidants. On the other hand, as polyhydroxyl phenol derivatives with both polar and nonpolar moieties, phenolic compounds have the propensity to concentrate at the oil−water interface and are dispersible in the lipid phase (where hydroperoxides and peroxide radicals are generated) to curtail the propagation of lipid radical chain reactions.

Because of their complementary processes in inhibiting lipid oxidation, peptides (protein) and phenolic compounds when used in combination have been found to function synergistically in several biphasic systems, such as O/W emulsions[7,13,14] and a liposome suspension.[15] However, it should be noted that similar to Tween, Span, and monoglycerides, phenolic molecules as surface active compounds might influence the adsorption of peptides at the interface either indirectly by competing for the oil droplets or directly by binding to peptides through hydrophobic interaction and hydrogen bonds.[16] Therefore, the existence of phenolics in a peptide-stabilized emulsion can affect the overall oxidative stability, and possibly also the physical stability, of the emulsion system. Indeed, there have been reports that peptides could suppress the antioxidative action of phenolic compounds.[17,18]

In our previous study, we have reported that radical-scavenging pea protein hydrolysates (PPHs) prepared with Flavourzyme (Fla-PPH) and Protamex (Pro-PPH) exhibit remarkable synergistic antioxidative effect with licorice extract (LE) (an ethanol extract from the herb *Glycyrrhiza glabra*) in a liposomal model system.[15] However, it is not known whether there exists a similar cooperative inhibitory effect of PPH with LE on lipid oxidation in an O/W emulsion and, if so, how they would partition and interact at the oil−water interface. Therefore, the present study was conducted to investigate the influence of LE on the antioxidant activity of Fla-PPH and Pro-

Received: April 4, 2014
Revised: July 23, 2014
Accepted: July 24, 2014
Published: July 24, 2014

ACS Publications © 2014 American Chemical Society



dx.doi.org/10.1021/jf5016126 | J. Agric. Food Chem. 2014, 62, 8204−8213

PPH in a soybean O/W emulsion. To elucidate the reaction mechanism, the adsorption of PPH and LE at the emulsion interface and the interfacial properties were examined.

## MATERIALS AND METHODS

**Materials.** Pea protein isolate (PPI) was extracted from pulverized yellow peas (*Pisum sativum* L.) using the isoelectric precipitation method that involved initial extraction at pH 8.0 followed by precipitation at pH 4.5.[19] After neutralization (pH 7.0), the PPI suspension was lyophilized to yield a dry powder with 92% protein. Flavourzyme and Protamex were donated by Novozymes North America Inc. (Franklinton, NC, USA). Soybean oil was purchased from a local supermarket (Lexington, KY, USA). Licresse, a licorice (*G. glabra*) root ethanol extract (LE) powder with a 23% total phenolic content and <1% glycyrrhizic acid, was obtained from ICL Performance Products LP (St. Louis, MO, USA). All other chemicals were purchased from Fisher Scientific (Fair Lawn, NJ, USA). Nanopure deionized water was used for the preparation of all solutions.

**PPH Preparation.** Antioxidative pea protein hydrolysates Fla-PPH and Pro-PPH were prepared with Flavourzyme and Protamex, respectively, as described previously.[15] Briefly, a preheated (90 °C, 5 min) 2% (w/v) protein solution of PPI was hydrolyzed for 0.5 h with Flavourzyme and Protamex at 50 °C. The enzyme−protein ratio was 1/100, and the hydrolysis pH was 6.0. After inactivating proteases (80 °C, 15 min), solutions were neutralized to pH 7.0, followed by centrifugation at 9000*g* for 10 min to remove insoluble particles. Samples were freeze-dried and stored at 4 °C before use. This hydrolysis condition was found to produce antioxidative Fla-PPH and Pro-PPH that, when combined with LE, also acted concertedly to inhibit lipid oxidation in a liposome suspension.[15] Therefore, it was used in the present study to produce the protein hydrolysates for the testing of synergism with LE in O/W emulsions.

**Emulsion Preparation.** The O/W emulsions were prepared by homogenizing 10% (w/w) soybean oil and 90% (w/w) aqueous phase (10 mM phosphate buffer, pH 7.0) containing different emulsifiers. For emulsifying capacity tests, different concentrations of PPHs (2.5, 5, 10, or 20 mg/mL, final concentrations) were added to the aqueous phase before blending with soybean oil using an Ultra-Turrax homogenizer (Ika T18 Basic, Staufen, Germany) at 13500 rpm for 2 min, followed by passage through a two-stage high-pressure homogenizer (ATS Engineering Inc., Shanghai, China) at a pressure of 30 MPa for two cycles. To investigate the influence of LE on the antioxidant activity of PPHs in emulsion systems, the same ingredient composition and homogenization conditions as mentioned above were used except that 10 mg/mL Tween 20 and different levels of LE (0, 50, 100, and 200 $\mu$g/mL, final concentrations) were added prior to blending. These concentration levels of LE were chosen on the basis of our previous study in which the antiradical activity of LE against $^{\bullet}$OH was found to increase rapidly until about 200 $\mu$g/mL.[20] For comparison, a control emulsion consisting of 10 mg/mL Tween 20 was prepared using the same emulsifying conditions as given above. To prevent microbial growth, 3 mM sodium azide was added to all emulsions.

**Emulsifying Capacity of PPH.** Freshly prepared emulsions were immediately transferred into 25 mL beakers and allowed to stand at room temperature for 1 min (for emulsifying activity testing) and 12 h (for emulsion stability testing). Emulsifying activity index (EAI) and emulsion stability index (ESI) were measured according to the turbidometric method of Pearce and Kinsella.[21] The emulsions were also placed in tightly sealed screw-cap test tubes and set at room temperature for 5 days to monitor their physical stability during storage.

**Emulsion Oxidative Stability.** To evaluate oxidative stability, emulsions were placed in tightly sealed screw-cap test tubes and incubated at 37 °C in the dark for up to 14 days to allow lipid autoxidation. Peroxide values (POVs) and 2-thiobarbituric acid-reactive substances (TBARS) were used to assess the degree of lipid oxidation. POVs were determined according to the AOCS[22] standard procedure using sodium thiosulfate ($Na_2S_2O_3$) titration. TBARS were tested according to the method of Mei et al.[23] and calculated from the standard curve prepared by 1,1,3,3-tetraethoxypropane. Synergism of PPHs and LE in inhibiting peroxides or TBARS formation was expressed and calculated as

$$\text{synergism (\%)} = \frac{(C - M) - [(C - H) + (C - L)]}{C - M} \times 100$$

where *C*, *H*, *L*, and *M* represent the formation of peroxides or TBARS in emulsions containing no antioxidant (control), PPH, LE, and mixed PPH and LE, respectively.

**Partition Coefficient of PPH in the O/W Emulsions.** Partitioning of Fla-PPH and Pro-PPH in the aqueous phase and at the oil−water interface of the emulsions was estimated according to the method of Huang et al.[11] as detailed by Cheng et al.[4] Protein concentrations in the aqueous phases were determined using the Bradford method.[24] The partition coefficient (PC) for PPH in the aqueous phase was calculated as

$$\text{PC} = \frac{V_w}{V_l} \times \left(\frac{W_t}{W_w} - 1\right)$$

where $V_w$ is the volume of the aqueous phase, $V_l$ is the volume of the oil phase, $W_t$ is the total amount of protein, and $W_w$ is the amount of protein in the aqueous phase. The density (g/mL) of oil used for calculating its volume was 0.922. Percentage of PPH in the aqueous phase was calculated as $(W_w/W_t) \times 100$, and that at the interface was calculated by subtraction.

**Characteristics of Emulsion Droplets.** Transmission electron microscopy (TEM) was used to visualize the microstructure of emulsion droplets, which were of different interfacial compositions. Emulsion samples were diluted (1:10, v/v) with 10 mM phosphate buffer (pH 7.0). One drop of the dilute samples and one drop of staining solution (2% phosphotungstic acid, v/v) were applied onto a copper grid with 200 meshes and allowed to stabilize for 10 min to dry out. Images of emulsion droplets were captured using an ES500W Erlangshen CCD camera (Gatan, Inc., Pleasanton, CA, USA) mounted to a JEM-2100 electron microscope (JEOL, Tokyo, Japan).

Zeta-potential and size distribution of emulsion droplets were also determined. The emulsions were diluted to an oil droplet concentration of approximately 0.05% (w/w) using 10 mM phosphate buffer (pH 7.0) and stirred continuously to ensure the samples were homogeneous. The zeta-potential of diluted oil droplets was examined using a particle electrophoresis instrument (Nanosizer, Malvern Instruments, Worcestershire, UK) and reported as the average and standard deviation of measurements. Droplet size distribution of the emulsions was measured using a dynamic light scattering instrument (Nanosizer, Malvern Instruments). The measured droplet sizes were expressed as the *Z*-average diameter and standard deviation of measurements.

**Separation and Characterization of Peptides at the Oil−Water Interface and in the Aqueous Phase.** The emulsions prepared with both PPH and LE were centrifuged at 15000*g* for 30 min to create a cream layer and a serum layer.[4] The cream layer was washed with 10 mM phosphate buffer (pH 7.0), followed by centrifugation at the same condition. After washing for a total of three times, the resultant cream was mixed with chloroform/methanol (2:1, v/v) to eliminate the interference of lipid. The mixture was centrifuged at 10000*g* for 10 min, and the upper methanol phase, which contained interface-located peptides, was subjected to a rotary evaporator to remove the solvent. The recovered cream phase peptide samples were stored at 4 °C before analysis. To recover peptides from the aqueous phase, the serum layer was centrifuged at 15000*g* for 30 min, then filtered through a 0.22 $\mu$m filter membrane, and stored at 4 °C before use. To collect a sufficient amount of peptide samples, a total of 50 mL of emulsions was used. Sodium dodecyl sulfate−polyacrylamide gel electrophoresis (SDS-PAGE) was conducted as described by Liu et al.[25] under nonreducing conditions to characterize the peptide samples.

**Isolation and Identification of LE Compounds at the Oil–Water Interface and in the Aqueous Phase.** The upper methanol phase obtained from the above interfacial peptide recovery step contained both peptides and LE compounds. The peptides were removed by precipitation with 4 volumes of cold acetone added to the methanol extract, and the mixture was stored at −20 °C overnight. After centrifugation at 10000*g* for 10 min at 4 °C, the supernatant (containing LE compounds only) was saved, and the precipitate was washed two times with cold acetone to recover additional LE compounds. The supernatants were combined and then concentrated by rotary evaporation. The recovered cream phase LE compounds were redissolved in methanol and stored at 4 °C before analysis.

To recover LE compounds remaining in the aqueous phase, 4 volumes of cold acetone was added to a portion of the final serum layer collected from the above peptide preparation step. The mixture was kept at −20 °C overnight and then centrifuged at 10000*g* for 10 min at 4 °C. The supernatant was saved, and the precipitate was washed two times with cold acetone. The supernatants were combined, and the solvents were removed by a rotary evaporator. The recovered LE compounds were redissolved in methanol and stored at 4 °C before use. Compound identification was carried out using LC-MS as described previously.[15]

**Statistical Analysis.** All experiments were repeated three times each with a freshly prepared emulsion. Data were expressed as mean ± standard deviation and processed using the general linear model procedure of the Statistix software 9.0 (Analytical Software, Tallahassee, FL, USA). Significant differences ($P < 0.05$) between means were identified by the least significance difference (LSD) procedure.

## RESULTS AND DISCUSSION

**Emulsion Properties.** The emulsifying activity (EAI) of the protein hydrolysates increased in a concentration-dependent manner (Figure 1), suggesting that within the tested protein concentration range (2.5–20 mg/mL), the surface coverage of oil droplets by peptides and the resulting interfacial tension reduction were more effective at high protein concentration levels. Indeed, preliminary interfacial tension measurement revealed a slight drop of the value from 12.3 to 10.1 mN/m ($P < 0.05$) with increasing hydrolysate concentration from 2.5 to 10 mg/mL. The emulsion stability was improved with increasing protein concentrations due to greater interfacial coating and possibly increased viscosity; yet, none of the emulsions was considered stable because the ESI values were well below 100% (Figure 1, inset), reflecting an overall weak surface tension reduction capability of the PPH. This was particularly true for the emulsions prepared with Fla-PPH. After 5 days of storage at room temperature, all Fla-PPH emulsions were separated into two phases, whereas creaming was less obvious for emulsions prepared with ≥5 mg/mL Pro-PPH (data not shown).

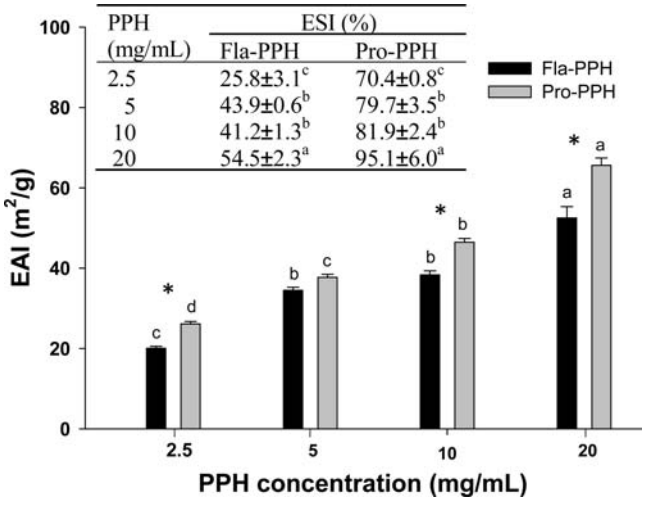


**Figure 1.** Emulsifying capacity of Fla-PPH and Pro-PPH (2.5, 5, 10, and 20 mg/mL) in soybean O/W emulsions. The inset table shows the emulsion stability. Means ± standard deviations ($n = 3$) for the same emulsion type without a common letter differ significantly ($P < 0.05$). (*) Significant difference ($P < 0.05$) between emulsion types at the same protein concentration.

Because PPH alone could not produce a satisfactorily stable O/W emulsion, the subsequent evaluation of antioxidant efficacy of PPH was carried out with emulsions costabilized by Tween 20 (10 mg/mL) and PPH. The strong surface activity of Tween 20 provided a reasonable justification for its use in the PPH emulsion system. For example, under the present experimental conditions, 10 mg/mL Tween 20 had an interfacial tension of 2.7 mN/m, and the Tween 20–5 mg/mL PPH blend had an interfacial tension of 4.7 mN/m, a substantial reduction ($P < 0.05$) from the PPH alone (11.5 mN/m). The Tween 20–PPH costabilized emulsions were remarkably stable and remained homogeneous even after 14 days when stored at room temperature or at 37 °C (data not shown).

**Oxidative Stability.** The efficacy of PPH in inhibiting lipid autoxidation in the Tween 20-aided O/W emulsions was evaluated by means of POV and TBARS analyses. Results showed a remarkable suppression of both primary (peroxides) and secondary (TBARS) product formation upon storage at 37 °C, namely, reductions up to 56 and 62% from the control ($P < 0.05$), respectively, by day 14 (Figure 2). However, the degree of POV or TBARS inhibition was independent of protein concentration, and the percentage of TBARS reduction was more pronounced with increasing storage time. Hence, both PPHs were effective antioxidants even at low concentrations, and peptides present in the continuous phase appeared to play a dominant role in deterring reactive oxygen species.

The oxidation inhibitory effect can be attributed to strong radical-scavenging activity of pea peptides and their affinity for oxidized lipids. As reported previously, peptides present in PPHs that are rich in leucine, lysine, glutamic acid, glutamine, valine, and proline are mostly responsible for the antioxidative protection of liposomes.[15] Ten peptides had been identified by mass spectrometry, of which, LQEEDNVISQ (Leu-Gln-Glu-Glu-Asp-Asn-Val-Ile-Ser-Gln), ITPERTLQLQDLDIFVN (Ile-Thr-Pro-Glu-Arg-Thr-Leu-Gln-Leu-Gln-Asp-Leu-Asp-Ile-Phe-Val-Asn), and LANRDDNEDLVGVL (Leu-Ala-Asn-Arg-Asp-Asp-Asn-Glu-Asp-Leu-Val-Gly-Val-Leu) matched the sequence of pea vicilin. On the other hand, steric hindrances of adsorbed interfacial proteins at low concentrations (e.g., 50 mg/m$^2$ of interfacial protein coverage) can reinforce the oxidative protection of O/W emulsions.[26] Because the greatest oxidation inhibition was already achieved at 5 mg/mL PPH, this dosage was chosen for the subsequent investigation of cooperative effects of PPH and LE for the inhibition of lipid oxidation in O/W emulsions during storage.

The results presented in Figure 3 display stronger suppressions of oxidation with the inclusion of LE than with PPHs alone. As widely reported, LE is capable of stabilizing oxidants due to the presence of radical-scavenging phenolic compounds in the herb extract.[15,27] When PPH and LE were applied together, a remarkable synergistic effect was observed,

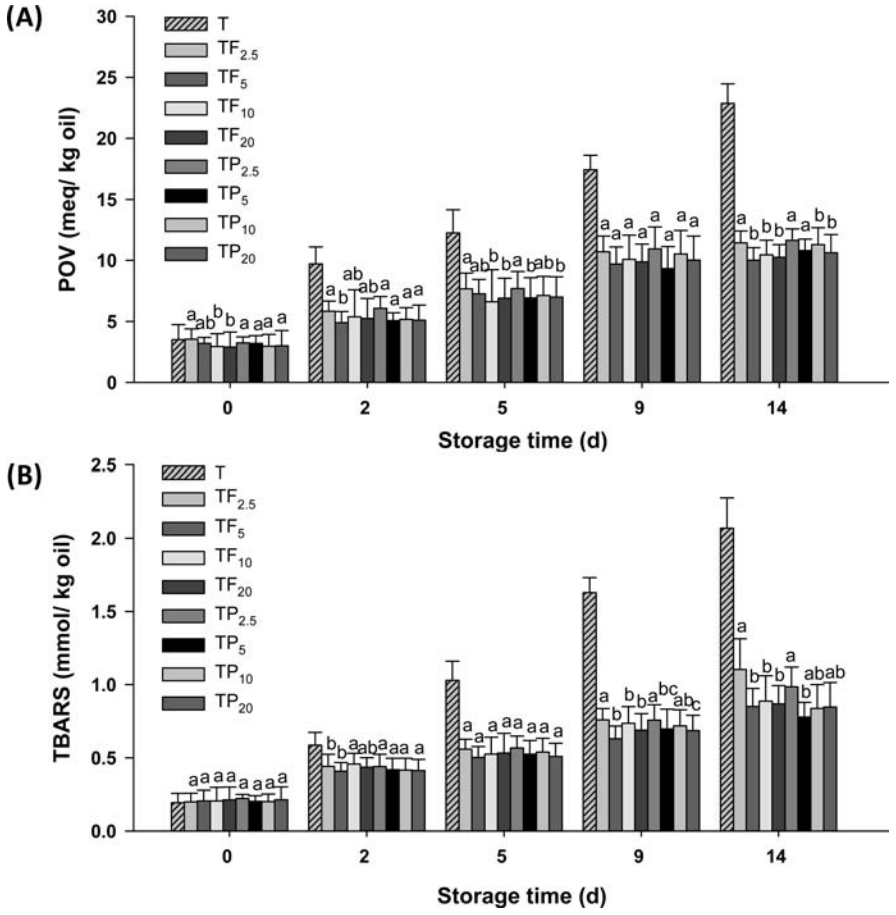


**Figure 2.** Formation of peroxides (A) and TBARS (B) during storage (37 °C) of soybean O/W emulsions prepared with Tween 20 + Fla-PPH (or + Pro-PPH) at various concentrations. T, $TF_x$ (or $TP_x$): emulsions prepared with Tween 20 and with Tween 20 + Fla-PPH (or + Pro-PPH) at the indicated concentrations (mg/mL). Tween 20: 10 mg/mL. Means ± standard deviations ($n$ = 3) for the same emulsion parameter with different letters differ significantly ($P$ < 0.05).

most notably for the inhibition of TBARS. The finding was consistent with our previous result that, when used in combination with LE, PPH provided superior protection of phospholipid-based liposome against radical-initiated oxidation over their separate uses.[15]

From day 9 to day 14, there was a slight reduction in the synergy (Table 1), which could be caused by the consumption of antioxidants or the gradual desorption of antioxidants from the interface during storage.[28] The synergy declined with increasing LE from 100 to 200 μg/mL. This may be explained by the accumulation of LE at the interface that can induce bridging association through phenolic compounds adsorbed onto neighboring oil droplets,[7] thereby promoting droplet aggregation and lipid radical chain propagation. The most remarkable synergy was displayed by Pro-PPH when used together with 100 μg/mL LE, up to 30.9 and 40.8%, for POV and TBARS, respectively. It should be noted that the extent of synergistic inhibition by PPH and LE on lipid oxidation in O/W emulsions was less than that in liposomal model systems.[15] A similar finding has been reported by Medina et al.[29] This result could be due to the differences in lipid chemical structure and interfacial chemical composition, which apparently favored phenolic antioxidant association with phospholipids (liposomes) over that with triacylglycerols (O/W emulsions).

**Distribution of PPH and LE in O/W Emulsions.** The specific location of antioxidants in an O/W emulsion is believed to affect the rate of lipid oxidation.[11] As indicated in Table 2, the bulk of PPH was present in the aqueous phase, and <15% was distributed at the interface. The percentage of interfacial PPH tended to decrease with the addition of LE, although such numerical differences were nonsignificant. It seems reasonable to suggest that LE and PPH adsorbed onto oil droplets in a competitive manner; driven by the concentration gradient, previously adsorbed peptides might be partially displaced by high-concentration LE. Alternatively, LE could bind to PPH through noncovalent interaction to participate in the interfacial layer indirectly. This latter contribution is in line with the finding that BSA and phenols could form protein−phenol "complexes" that accumulate at the oil−water interface due to the surface-active nature of the protein.[14]

A large variety of peptides in the aqueous phase are capable of scavenging free radicals, hence, neutralizing water-soluble oxidants.[2,30] Although much less abundant (<15%) at the interface, PPH located on or immediately above the emulsion droplets would play a crucial role in inhibiting lipid oxidation. In O/W emulsions, the oxidation reaction occurs principally at the oil−water interface.[2] Moreover, the generated lipid hydroperoxides and peroxide radicals are preferentially concentrated at the interface.[1] Furthermore, peptides that accumulate at the interface and phenolics that partition both at the interface and in the interior of oil droplets can reduce the mobility of lipid molecules and the diffusion of radicals within


dx.doi.org/10.1021/jf5016126 | J. Agric. Food Chem. 2014, 62, 8204−8213

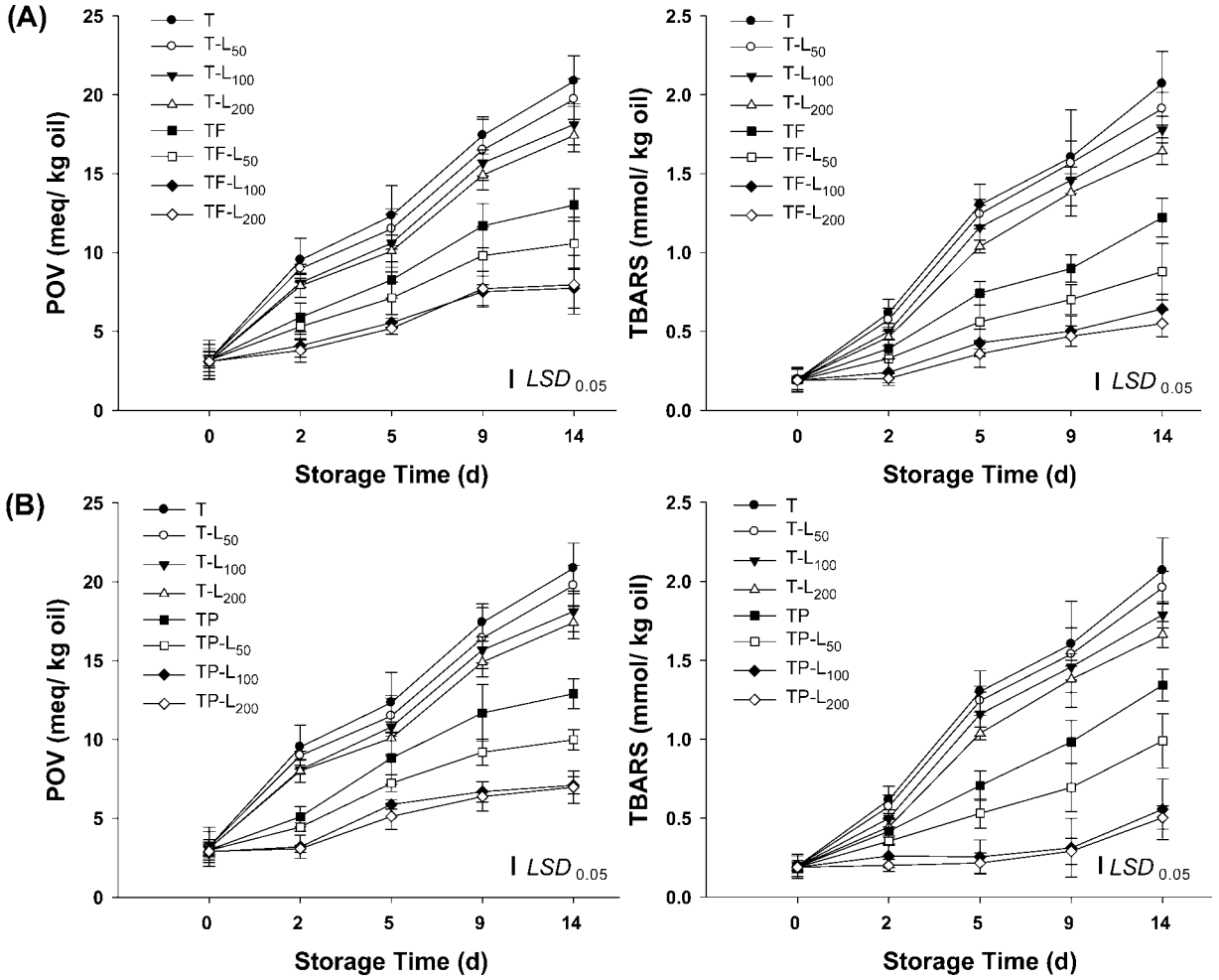


**Figure 3.** Formation of peroxides and TBARS during storage (37 °C) of emulsions prepared with Tween 20 + Fla-PPH (A) or + Pro-PPH (B) coupled with licorice extract (LE) ($n$ = 3). T, T-$L_x$, TF (or TP), TF-$L_x$ (or TP-$L_x$): emulsions prepared with Tween 20, Tween 20 + LE, Tween 20 + Fla-PPH (or + Pro-PPH), and Tween 20 + Fla-PPH (or + Pro-PPH) + LE, respectively. $L_x$: three levels of LE (50, 100, 200 $\mu$g/mL). PPH: 5 mg/mL. Tween 20: 10 mg/mL.

**Table 1. Synergism of PPHs and LE in Inhibiting Peroxides or TBARS Formation in Soybean O/W Emulsions Co-stabilized by Tween 20**

| | POV | | | | TBARS | | | |
|---|---|---|---|---|---|---|---|---|
| synergism[a] (%) | 2 days | 5 days | 9 days | 14 days | 2 days | 5 days | 9 days | 14 days |
| TF-$L_{50}$ | 1.3 | 5.9 | 12.6 | 12.5 | 7.2 | 16.6 | 17.7 | 15.5 |
| TF-$L_{100}$ | 6.6 | 14.3 | 24.6 | 19.3 | 8.4 | 19.7 | 22.8 | 20.2 |
| TF-$L_{200}$ | 8.0 | 11.7 | 15.1 | 12.5 | 8.7 | 12.7 | 18.1 | 16.2 |
| TP-$L_{50}$ | 7.3 | 14.7 | 18.2 | 16.7 | 7.6 | 15.3 | 24.8 | 22.7 |
| TP-$L_{100}$ | 7.4 | 21.8 | 30.9 | 24.3 | 10.6 | 29.5 | 40.8 | 33.5 |
| TP-$L_{200}$ | 8.1 | 20.1 | 25.9 | 20.7 | 10.2 | 24.6 | 35.8 | 29.7 |

[a]For definition of "synergism", see Materials and Methods. TF-$L_x$ (or TP-$L_x$): emulsions prepared with Tween 20 + Fla-PPH (or + Pro-PPH) with LE at the indicated concentrations ($\mu$g/mL). PPH: 5 mg/mL. Tween 20: 10 mg/mL.

the lipid phase.[31] In particular, the physical location and effective concentration of LE at the oil−water interface played a concerted role with PPH to curtail lipid oxidation and produce the observed synergistic antioxidative actions.

Interestingly, if LE was added to PPH emulsions immediately after homogenization instead of during homogenization, it elicited negligible protection of the emulsions (data not shown). Due to different affinities of peptides and phenolics for oil droplets, the combination of PPH and LE not only delayed the initiation but also suppressed the propagation of lipid radical chain reactions, consequently providing the superior antioxidative protection. It has been shown that the synergism observed between some natural phenolic compounds and antioxidative lactoferrin lies in their different affinities toward O/W emulsions.[29] Besides, the association of PPH and LE at the oil−water interface would generate a structural barrier around the oil droplet to hinder the penetration and diffusion


dx.doi.org/10.1021/jf5016126 | J. Agric. Food Chem. 2014, 62, 8204−8213

**Table 2. Partitioning of PPH in the Aqueous Phase versus at the Oil–Water Interface of Soybean O/W Emulsions Prepared with Tween 20 and Fla-PPH or Pro-PPH Coupled with Licorice Extract**

| | PPH in aqueous phase[a] (%) | PPH at interface[a] (%) | partition coefficient (aqueous) |
|---|---|---|---|
| TF | 89.5 ± 0.8 | 10.5 ± 0.6 | 1.05 |
| TF-$L_{50}$ | 90.4 ± 1.8 | 9.6 ± 1.2 | 0.94 |
| TF-$L_{100}$ | 92.8 ± 4.0 | 7.2 ± 2.8 | 0.70 |
| TF-$L_{200}$ | 91.9 ± 0.3 | 8.1 ± 0.3 | 0.80 |
| TP | 85.1 ± 4.2 | 14.9 ± 3.0 | 1.58 |
| TP-$L_{50}$ | 85.3 ± 0.0 | 14.7 ± 0.0 | 1.55 |
| TP-$L_{100}$ | 88.3 ± 6.0 | 11.8 ± 4.2 | 1.20 |
| TP-$L_{200}$ | 89.3 ± 1.2 | 10.7 ± 0.8 | 1.08 |

[a]Means ± standard deviations ($n$ = 3) in the same column do not differ statistically ($P$ > 0.05). TF (or TP) and TF-$L_x$ (or TP-$L_x$): emulsions prepared with Tween 20 + Fla-PPH (or + Pro-PPH) without or with LE at the indicated concentrations ($\mu$g/mL). PPH: 5 mg/mL. Tween 20: 10 mg/mL.

of lipid oxidation initiators, thereby providing the observed synergistic effects beyond their individual actions.

It is noteworthy that small surfactants, such as Tween and sucrose ester micelles, can potentially influence the physical location of antioxidants in O/W emulsions by promoting the solubilization of lipophilic antioxidants in the aqueous phase.[32,33] Therefore, phenolic compounds in LE, which are less polar and have the propensity to accumulate at the interface, are likely to be removed from the oil droplets by Tween 20 micelles, resulting in a reduced antioxidative efficiency. This premise can be applied to explain the unexpected decrease of synergism between PPH and the high-concentration LE (200 $\mu$g/mL) (Table 1). Phenolic antioxidants that reside in the Tween 20 micelles would still be effective because they can scavenge radicals present in the aqueous phase.

**Microstructure of Emulsion Droplets.** The biophysical properties of the oil droplet interface can significantly influence the rate of lipid oxidation due to the nature of the interface that connects two immiscible phases and closely contacts antioxidants, pro-oxidants, and oxidizable substrates.[34] Apart from the aforementioned interfacial composition, the morphology, thickness, and rheology of the interfacial structure are important for the oxidative stability of O/W emulsions.[26,35]

TEM, by virtue of its high resolution, was applied to visualize the interfacial structure of emulsion droplets, and the micrographs are displayed in Figure 4. Emulsion droplets stabilized by Tween 20 did not show a typical definitive membrane structure but, rather, small spherical micelles adsorbing onto the surface (A). In comparison, an interfacial membrane made up of peptides was formed around oil droplets in the emulsion containing PPH (B). Nevertheless, the membrane appeared to be thin and discontinuous, which may arise from the loose and unfolded structure of the peptides and the competitive adsorption of Tween 20, which breaks down protein–protein interactions at the interfacial layer.[36] As a result, the oxidative process was difficult to avoid. On the other hand, when PPH and LE were homogenized together, a thick and compact interfacial membrane was observed (C), which corresponded to the lowest lipid oxidation rate (or the highest synergism). The enhanced steric restrictions of the interface enabled a strong defense mechanism against oxygen species.

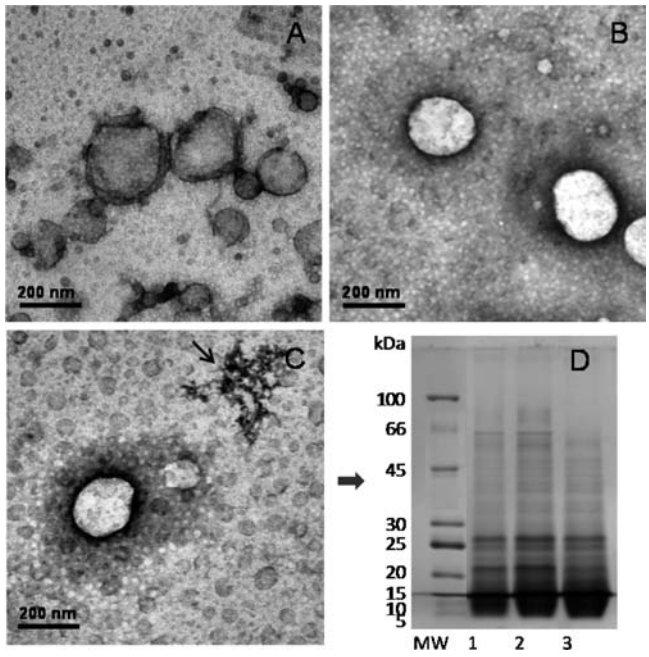


**Figure 4.** TEM micrographs of soybean O/W emulsions prepared with Tween 20 (A), Tween 20 + Pro-PPH (B), and Tween 20 + Pro-PPH + LE (C). SDS-PAGE (D) shows the peptides extracted from different regions of the emulsion prepared with (C), namely, lane 1, native Pro-PPH; lane 2, peptides distributed in the aqueous phase; and lane 3, peptides partitioning at the oil–water interface. MW: molecular weight marker. Tween 20: 10 mg/mL. PPH and LE concentrations were 5 mg/mL and 100 $\mu$g/mL, respectively. Arrow in (C) points to large networks of Pro-PPH and LE.

The complementary chemical and physical mechanisms exerted by PPH and LE for the antioxidative protection of O/W emulsions support the findings of Jiang et al.[26] that steric deterrence is a critical contributor to an emulsion's oxidative stability. Hu et al.[37] and Ogawa et al.[38] also stated the critical role of interfacial membrane thickness in maintaining the oxidative stability of O/W emulsions.

The cooperativity of PPH and LE at the oil–water interface was a primary reason for the formation of a thick and compact interfacial membrane. Atarés et al.[39] reported that the adsorbed layer of rutin molecules can aid in the formation of a thicker droplet interface in emulsions stabilized by whey protein. Moreover, phenolic compounds could modify the structure of polypeptides to a more unfolded and unordered state,[40] allowing a fast adsorption and tight packing of these molecules onto the droplet surface. Meanwhile, as a result of structural changes, reactive amino acid side-chain groups that are capable of neutralizing radicals are increasingly exposed, leading to an increase in the antioxidative protection.[41] Besides, phenolic compounds could act as cross-linkers of these adsorbed peptides, thereby enhancing the protein–protein interaction at the interfacial layer.[36]

The association of PPH with LE could be another important reason for the formation of thick interfacial membranes as proteins and phenolics can attach to each other through noncovalent interactions.[17] Such "complexes" might possess greater interfacial activity and a balanced hydrophilicity–hydrophobicity as well as an increased size relative to individual molecules.[7] Consequently, there is an increased affinity for the interface, and higher amounts of PPH and LE would accumulate at the oil–water boundary to produce a thick and

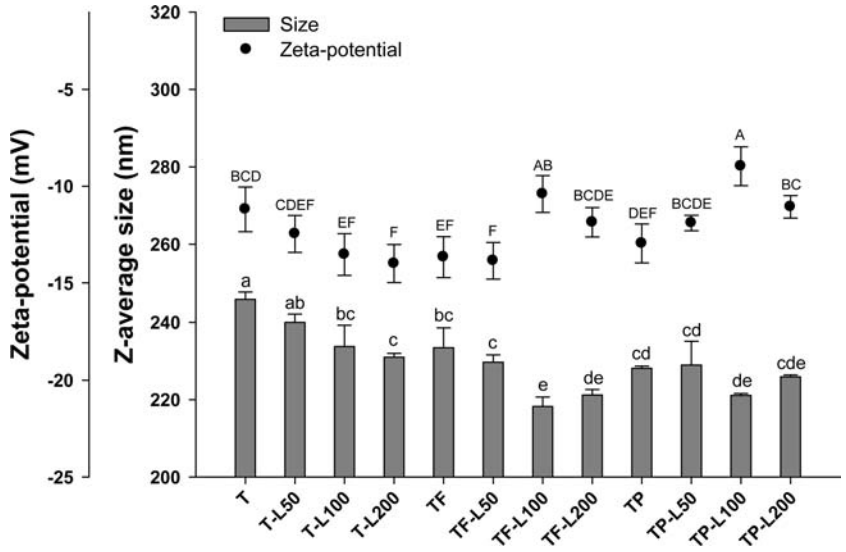


**Figure 5.** Zeta-potential and *Z*-average size of emulsions prepared with Tween 20 + Fla-PPH (or + Pro-PPH) coupled with licorice extract (LE). T, T-Lx, TF (or TP), TF-Lx (or TP-Lx): emulsions prepared with Tween 20, Tween 20 + LE, Tween 20 + Fla-PPH (or + Pro-PPH), and Tween 20 + Fla-PPH (or + Pro-PPH) + LE, respectively. $L_x$: three levels of LE (50, 100, 200 $\mu$g/mL). Tween 20: 10 mg/mL. PPH: 5 mg/mL. Means ± standard deviations ($n$ = 3) for the same emulsion parameter with different letters differ significantly ($P < 0.05$).

compact interfacial membrane. It is noteworthy that PPH can form a self-assembled network.[15] Such a structure may be triggered by $\beta$-sheet conformation transition[42] that provides a solid support for the formation of more interactive PPH−LE units conducive to the thickness and the compactness of droplet interface. The physical filling effect of LE or LE aggregates by self-association[17] can also be a contributor to the enhancement of the membrane thickness and firmness.

Hence, the presence of LE modified the peptidyl interfacial membrane from a mobile and heterogeneous unit into a steady and homogeneous entity. With this resistant interfacial membrane, it was difficult for water-soluble oxidants (e.g., $^{\bullet}$OH) to gain access to the oil droplets to initiate and accelerate lipid peroxidation. Meanwhile, the mobility and diffusion of hydroperoxides and peroxide radicals within oil droplets were restricted, so that they could not easily transfer to other droplets to sustain the radical chain reactions. It should be taken into account that the complexes present in the aqueous phase can associate with each other and finally form large networks (one was captured in Figure 4C and is indicated by an arrow), and they can act as free radical scavengers as well as stabilizers, contributing to the oxidative stability.

The electrophoretic pattern shown in Figure 4 supports the notion that PPH−LE "complexes" were formed as intensive and broad peptide bands were observed in lane 2 (peptides in the aqueous phase) and lane 3 (peptides at the interface) when compared to native PPH (lane 1), indicating the migration of LE into the gel by associating with PPH. Newly formed high-molecular-weight bands ranging from 60 to 80 kDa are visible in lane 2, yet some high-molecular-weight bands were missing in lane 3, which might be due to the loose attraction of these large molecules to the interface so that they were separated and not retained in the prepared interfacial protein samples. It is also plausible that these large peptides were firmly anchored into the lipid phase and remained in the chloroform phase after extraction with methanol.

**Zeta-Potential and Size Distribution.** Measurement of electrical charges on the droplet surface can provide valuable information about interactions between ionizable surfactants and emulsion droplets.[43] As shown in Figure 5, emulsion droplets stabilized by Tween 20 carried negative charges (about −11.5 mV), which can be ascribed to phosphate (buffer). The addition of LE increased the negative potential, indicating the accumulation of negatively charged compounds such as 18$\beta$-glycyrrhetic acid onto the surface of oil droplets.

When LE was incorporated into emulsions containing PPH, the zeta-potential increased to a less negative value, suggesting the displacement of peptides from the interface or the interaction of PPH, and LE shielded the charged groups in peptides that oriented toward the outer layer of the droplet surface.[38] When a droplet surface has a low net charge, there will be less electrostatic repulsion between the interfacial layer and a more compact interfacial membrane tends to be formed. Hence, the reduced surface charge on oil droplets caused by the combination of PPH and LE also favored the formation of a thick and continuous interfacial membrane and contributed to the remarkable synergistic inhibition. The lowest surface potential was displayed at 100 $\mu$g/mL LE, indicating the highest amount of LE being involved at the interface, which correlated well with the greatest synergism. On the other hand, the relatively weak synergism observed at 200 $\mu$g/mL LE was ostensibly due to insufficient adsorption at the interface, which might be caused by the solubilization by Tween 20 micelles or the bridging flocculation.

The combination of PPH and LE also endowed the emulsion with small size distribution, which could be interpreted as an increased coverage of surface active compounds and the enhanced steric hindrance between oil droplets.[7,39] It has been reported that oxidative stability increased with decreasing oil droplet size as on an oil volume basis more emulsifiers were adsorbed onto the droplet surface.[26] Moreover, the "wedge effect" of hydrophobic portion of emulsifiers can more efficiently suppress the mobility of lipid molecules and radicals in small droplets than in large droplets.[44] Hence, the effect of the combination of PPH and LE on decreasing the size distribution of emulsion droplets also contributed to the notable synergistic oxidation inhibition.

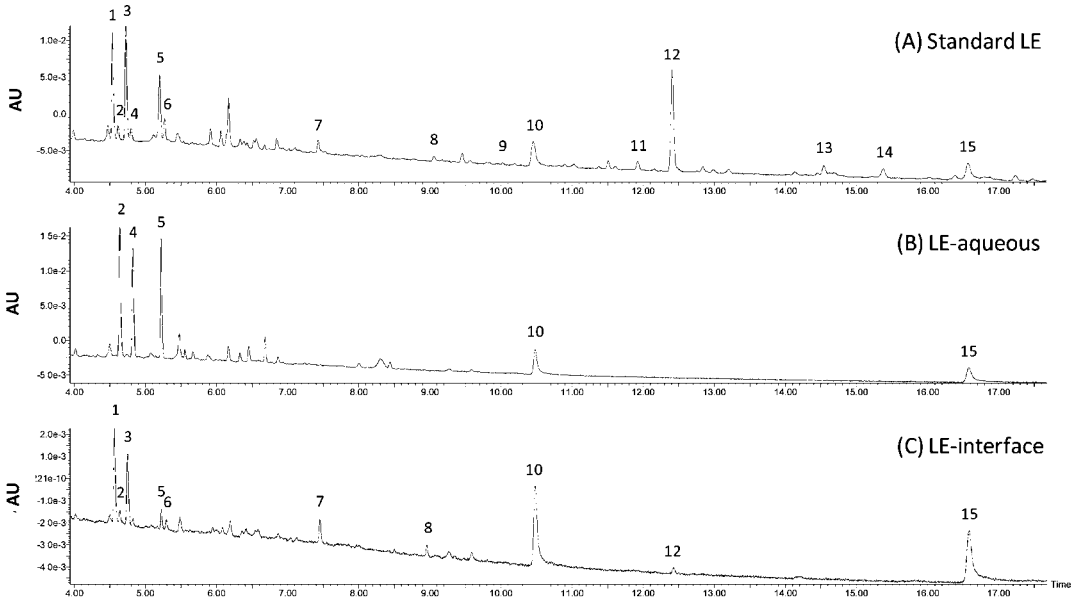


| peak no. | compounds | class | $[M-H]^-$ *(m/z)* |
|---|---|---|---|
| (1) | Liquiritin apioside | Flavanone | 549 |
| (2) | Unknown | | 497 |
| (3) | Neolicuroside | Chalcone | 549 |
| (4) | Isoliquiritin | Chalcone | 417 |
| (5) | Unknown | | 542 |
| (6) | Unknown | | 565 |
| (7) | Licorice glycoside A | Chalcone | 725 |
| (8) | Liquiritigenin | Flavanone | 255 |
| (9) | Glycyrrhizic acid | Triterpene | 821 |
| (10) | Glabrene | Isoflavene | 321 |
| (11) | Neoglycyrol | Coumarin | 365 |
| (12) | Glabridin | Isoflavan | 323 |
| (13) | Glabrol | Isoflavan | 391 |
| (14) | Unknown | | 337 |
| (15) | 18$\beta$-Glycyrrhetic acid | Triterpene | 469 |

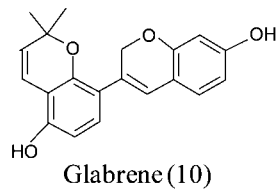


Glabrene (10)

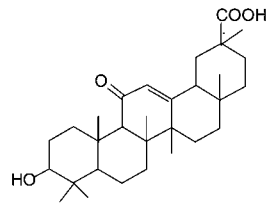


18$\beta$-Glycyrrhetic acid (15)

**Figure 6.** UPLC profiles of licorice extract (LE) by photodiode array and ESI-MS detectors: (A) standard LE; (B) compounds in LE present in the aqueous phase of the emulsion prepared with Tween 20 + Pro-PPH + LE; (C) compounds in LE partitioning at the oil−water interface of the same emulsion, and compounds identified in standard LE (lower table). Tween 20: 10 mg/mL. PPH and LE concentrations were 5 mg/mL and 100 $\mu$g/mL, respectively. The structures of major active compounds partitioning at the oil−water interface are shown on the right.

**Identification of Active Compounds in LE at the Oil−Water Interface.** As displayed in Figure 6, 15 compounds were identified in LE, which were predominantly flavonoids. Most of these compounds were detected at the oil−water interface (C) but with different proportions when compared to standard LE (A). As expected, the amount of glycyrrhic acid was negligible because the LE was prepared to remove this compound. Liquiritin apioside, neolicuroside, glabrene, and 18$\beta$-glycyrrhetic acid were the predominant compounds in LE partitioning at the interface and were likely responsible for the strong antioxidant activity of LE in O/W emulsions and the notable synergism when coupled with PPH.

18$\beta$-Glycyrrhetic acid is known as one of the most effective antioxidants in licorice extract.[45] Glabrene, having a strong conjugation of double bonds in hydroperoxides, can produce a more stable phenoxyl radical formation after the donation of an electron and, therefore, effectively suppresses the oxidative process.[46] Glabridin, the most abundant compound in LE, barely adsorbed at the interface, which can be interpreted as its having a strong affinity for the lipid molecules and dispersing into the interior of oil droplets, so that methanol cannot extract it from the chloroform phase after centrifugation. However, it has to be taken into consideration that both the competitive adsorption and the formation of PPH−LE "complexes" might weaken the partitioning of LE at the oil−water interface. There are also some compounds present in the aqueous phase (B). Some of them can be the detached molecules from the interface due to the loose attraction, and some can be ascribed to the solubilization by Tween 20 micelle from the oil droplets. This result is consistent with that in SDS-PAGE (Figure 4D), as some high-molecular-weight bands were missing from the interface (lane 3).

In conclusion, pea protein hydrolysates prepared with Flavourzyme and Protamex, when used in combination with


dx.doi.org/10.1021/jf5016126 | J. Agric. Food Chem. 2014, 62, 8204−8213

licorice extract, produced a synergistic inhibition on lipid oxidation in soybean O/W emulsions. The physical location and effective concentration of LE at the oil−water interface determined the degree of synergism. The combination of PPH and LE, on the one hand, allowed the efficient removal of radicals in both aqueous and lipid phases and, on the other hand, reduced the surface charge and particle size of oil droplets, thereby facilitating the formation of a thick and compact interfacial membrane, which offered superior defense against oxidative stress. Liquiritin apioside, neolicuroside, glabrene, and 18$\beta$-glycyrrhetic acid were the predominant compounds in LE partitioning at the oil−water interface and were likely responsible for the strong antioxidant activity of LE in O/W emulsions and the notable synergism when coupled with PPHs. Hence, enzymatic pea protein hydrolysates and licorice extract when applied together could help maximize the stability of emulsion-type food products, both physically and chemically.

## AUTHOR INFORMATION


### Corresponding Author

*(Y.L.X.) Phone: (859) 257-3822. Fax: (859) 257-5318. E-mail: ylxiong@uky.edu.



### Funding

X.Z. was supported by an Oversea Study Fellowship from the China Scholarship Council. The study was funded, in part, by the National Natural Science Foundation, China (Grant 31301497). Approved for publication as journal article 14-07-020 by the Director of the Kentucky Agricultural Experiment Station.


### Notes

The authors declare no competing financial interest.

## REFERENCES


(1) McClements, D. J.; Decker, E. A. Lipid oxidation in oil-in-water emulsions: impact of molecular environment on chemical reactions in heterogeneous food systems. *J. Food Sci.* **2000**, *65*, 1270−1282.

(2) Elias, R. J.; Bridgewater, J. D.; Vachet, R. W.; Waraho, T.; McClements, D. J.; Decker, E. A. Antioxidant mechanisms of enzymatic hydrolysates of $\beta$-lactoglobulin in food lipid dispersions. *J. Agric. Food Chem.* **2006**, *54*, 9565−9572.

(3) Kong, B.; Xiong, Y. L. Antioxidant activity of zein hydrolysates in a liposome system and the possible mode of action. *J. Agric. Food Chem.* **2006**, *54*, 6059−6068.

(4) Cheng, Y.; Xiong, Y. L.; Chen, J. Antioxidant and emulsifying properties of potato protein hydrolysate in soybean oil-in-water emulsions. *Food Chem.* **2010**, *120*, 101−108.

(5) Christiansen, K. F.; Vegarud, G.; Langsrud, T.; Ellekjaer, M. R.; Egelandsdal, B. Hydrolyzed whey proteins as emulsifiers and stabilizers in high-pressure processed dressings. *Food Hydrocolloids* **2004**, *18*, 757−767.

(6) Chen, L.; Chen, J.; Ren, J.; Zhao, M. Effects of ultrasound pretreatment on the enzymatic hydrolysis of soy protein isolates and on the emulsifying properties of hydrolysates. *J. Agric. Food Chem.* **2011**, *59*, 2600−2609.

(7) Di Mattia, C. D.; Sacchetti, G.; Mastrocola, D.; Sarker, D. K.; Pittia, P. Surface properties of phenolic compounds and their influence on the dispersion degree and oxidative stability of olive oil O/W emulsions. *Food Hydrocolloids* **2010**, *24*, 652−658.

(8) Maqsood, S.; Benjakul, S. Comparative studies of four different phenolic compounds on *in vitro* antioxidative activity and the preventive effect on lipid oxidation of fish oil emulsion and fish mince. *Food Chem.* **2010**, *119*, 123−132.

(9) Viljanen, K.; Kylli, P.; Kivikari, R.; Heinonen, M. Inhibition of protein and lipid oxidation in liposomes by berry phenolics. *J. Agric. Food Chem.* **2004**, *52*, 7419−7424.

(10) Kong, B.; Zhang, H.; Xiong, Y. L. Antioxidant activity of spice extracts in a liposome system and in cooked pork patties and the possible mode of action. *Meat Sci.* **2010**, *85*, 772−778.

(11) Huang, S.; Frankel, E. N.; Aeschbach, R.; German, J. B. Partition of selected antioxidants in corn oil−water model systems. *J. Agric. Food Chem.* **1997**, *45*, 1991−1994.

(12) Richards, M. P.; Chaiyasit, W.; McClements, D. J.; Decker, E. A. Ability of surfactant micelles to alter the partitioning of phenolic antioxidants in oil-in-water emulsions. *J. Agric. Food Chem.* **2002**, *50*, 1254−1259.

(13) Bishov, S. J.; Henick, A. S. Antioxidant effect of protein hydrolysates in freeze-dried model systems. Synergistic action with a series of phenolic antioxidants. *J. Food Sci.* **1975**, *40*, 345−348.

(14) Almajano, M. P.; Gordon, M. H. Synergistic effect of BSA on antioxidant activities in model food emulsions. *J. Am. Oil Chem. Soc.* **2004**, *81*, 275−280.

(15) Zhang, X.; Xiong, Y. L.; Chen, J.; Zhou, L. Synergistic inhibition of lipid oxidation by pea protein hydrolysate coupled with licorice extract in a liposomal model system. *J. Agric. Food Chem.* **2013**, *61*, 8452−8461.

(16) Chen, J.; Dickinson, E. Protein/surfactant interracial interactions. Part 3. Competitive adsorption of protein+surfactant in emulsions. *Colloids Surf. A: Physicochem. Eng. Asp.* **1995**, *101*, 77−85.

(17) Charlton, A. J.; Baxter, N. J.; Khan, M. L.; Moir, A. J. G.; Haslam, E.; Davies, A. P.; Williamson, M. P. Polyphenol/peptide binding and precipitation. *J. Agric. Food Chem.* **2002**, *50*, 1593−1601.

(18) Ozdal, T.; Capanoglu, E.; Altay, F. A review on protein−phenolic interactions and associated changes. *Food Res. Int.* **2013**, *51*, 954−970.

(19) Jiang, J.; Chen, J.; Xiong, Y. L. Structural and emulsifying properties of soy protein isolate subjected to acid and alkaline pH-shifting processes. *J. Agric. Food Chem.* **2009**, *57*, 7576−7583.

(20) Jiang, J.; Zhang, X.; True, A. D.; Zhou, L.; Xiong, Y. L. Inhibition of lipid oxidation and rancidity in precooked pork patties by radical-scavenging licorice (*Glycyrrhiza glabra*) extract. *J. Food Sci.* **2013**, *78* (11), C1686−C1694.

(21) Pearce, K. N.; Kinsella, J. E. Emulsifying properties of proteins: evaluation of a turbidimetric technique. *J. Agric. Food Chem.* **1978**, *26*, 716−723.

(22) AOCS. AOCS Official Method Cd 8-53: Peroxide value − acetic acid−chloroform method. *Official Methods and Recommended Practices of the American Oil Chemists' Society*, 5th ed.; AOCS: Champaign, IL, USA, 1998.

(23) Mei, L.; McClements, D. J.; Wu, J.; Decker, E. A. Iron-catalyzed lipid oxidation in emulsion as affected by surfactant, pH and NaCl. *Food Chem.* **1998**, *61*, 307−312.

(24) Bradford, M. M. A rapid and sensitive method for the quantitation of microgram quantities of protein utilizing the principle of protein-dye binding. *Anal. Biochem.* **1976**, *72*, 248−254.

(25) Liu, G.; Xiong, Y. L. Electrophoretic pattern, thermal denaturation, and in vitro digestibility of oxidized myosin. *J. Agric. Food Chem.* **2000**, *48*, 624−630.

(26) Jiang, J.; Zhu, B.; Liu, Y.; Xiong, Y. L. Interfacial structural role of pH-shifting processed pea protein in the oxidative stability of oil/water emulsions. *J. Agric. Food Chem.* **2014**, *62*, 1683−1691.

(27) Cheel, J.; Antwerpen, P. V.; Tůmová, L.; Onofre, G.; Vokurková, D.; Zouaoui-Boudjeltia, K.; Vanhaeverbeek, M.; Nève, J. Free radical-scavenging, antioxidant and immunostimulating effects of a licorice infusion (*Glycyrrhiza glabra* L.). *Food Chem.* **2010**, *122*, 508−517.

(28) Berton, C.; Genot, C.; Ropers, M. Quantification of unadsorbed protein and surfactant emulsifiers in oil-in-water emulsions. *J. Colloid Interface Sci.* **2011**, *354*, 739−748.

(29) Medina, I.; Tombo, I.; Satué-Gracia, M. T.; German, J. B.; Frankel, E. N. Effects of natural phenolic compounds on the antioxidant activity of lactoferrin in liposomes and oil-in-water emulsions. *J. Agric. Food Chem.* **2002**, *50*, 2392−2399.

(30) Zhao, J.; Xiong, Y. L.; McNear, D. H. Changes in structural characteristics of antioxidative soy protein hydrolysates resulting from scavenging of hydroxyl radicals. *J. Food Sci.* **2013**, *78*, C152−C159.
(31) Arora, A.; Byrem, T. M.; Nair, M. G.; Strasburg, G. M. Modulation of liposomal membrane fluidity by flavonoids and isoflavonoids. *Arch. Biochem. Biophys.* **2000**, *373*, 102−109.
(32) McClements, D. J.; Dungan, S. R. Light scattering study of solubilization of emulsion droplets by non-ionic surfactant solutions. *Colloids Surf. A: Physicochem. Eng. Asp.* **1995**, *104*, 127−135.
(33) Toro, C.; Sanchez, S. A.; Zanocco, A.; Lemp, E.; Gratton, E.; Gunther, G. Solubilization of lipid bilayers by myristyl sucrose ester: effect of cholesterol and phospholipid head group size. *Chem. Phys. Lipids* **2009**, *157*, 104−112.
(34) Frankel, E. N.; Huang, S.; Kanner, J.; German, J. B. Interfacial phenomena in the evaluation of antioxidants: bulk oils *vs* emulsions. *J. Agric. Food Chem.* **1994**, *42*, 1054−1059.
(35) McClements, D. J. Interfacial properties and their characterization. In *Food Emulsions: Principles, Practice, and Techniques*, 2nd ed.; CRC: Boca Raton, FL, USA, 2005.
(36) Sarker, D. K.; Wilde, P. J.; Clark, D. C. Control of surfactant-induced destabilization of foams through polyphenol-mediated protein−protein interactions. *J. Agric. Food Chem.* **1995**, *43*, 295−300.
(37) Hu, M.; McClements, D. J.; Decker, E. A. Lipid oxidation in corn oil-in-water emulsions stabilized by casein, whey protein isolate, and soy protein isolate. *J. Agric. Food Chem.* **2003**, *51* (6), 1696−1700.
(38) Ogawa, S.; Decker, E. A.; McClements, D. J. Production and characterization of O/W emulsions containing droplets stabilized by lecithin−chitosan−pectin mutilayered membranes. *J. Agric. Food Chem.* **2004**, *52*, 3595−3600.
(39) Atarés, L.; Marshall, L. J.; Akhtar, M.; Murray, B. S. Structure and oxidative stability of oil in water emulsions as affected by rutin and homogenization procedure. *Food Chem.* **2012**, *134*, 1418−1424.
(40) Ali, M.; Homann, T.; Khalil, M.; Kruse, H.; Rawel, H. Milk whey protein modification by coffee-specific phenolics: effect on structural and functional properties. *J. Agric. Food Chem.* **2013**, *61*, 6911−6920.
(41) Aluko, R. E. Bioactive peptides. In *Functional Foods and Nutraceuticals*; Springer: New York, 2012; pp 37−61.
(42) Lamm, M. S.; Rajagopal, K.; Schneider, J. P.; Pochan, D. J. Laminated morphology of nontwisting $\beta$-sheet fribrils constructed via peptide self-assembly. *J. Am. Chem. Soc.* **2005**, *127*, 16692−16700.
(43) Mei, L.; Decker, E. A.; McClements, D. J. Evidence of iron association with emulsion droplets and its impact on lipid oxidation. *J. Agric. Food Chem.* **1998**, *46*, 5072−5077.
(44) Nakaya, K.; Ushio, H.; Matsukawa, S.; Shimizu, M.; Ohshima, T. Effects of droplet size on the oxidative stability of oil-in-water emulsions. *Lipids* **2005**, *40*, 501−507.
(45) Zhang, Q.; Ye, M. Chemical analysis of the Chinese herbal medicine Gan-Cao (licorice). *J. Chromatogr., A* **2009**, *1216*, 1954−1969.
(46) Belinky, P. A.; Aviram, M.; Mahmood, S.; Vaya, J. Structural aspects of the inhibitory effect of glabridin on LDL oxidation. *Free Radical Biol. Med.* **1998**, *24*, 1419−1429.

JOURNAL OF AGRICULTURAL AND FOOD CHEMISTRY

Article

pubs.acs.org/JAFC

# Preparation of Starch Nanoparticles in a Water-in-Ionic Liquid Microemulsion System and Their Drug Loading and Releasing Properties

Gang Zhou, Zhigang Luo,* and Xiong Fu*

Carbohydrate Laboratory, College of Light Industry and Food Science, South China University of Technology, Guangzhou 510640, China

**ABSTRACT:** An ionic liquid microemulsion consisting of 1-butyl-3-methylimidazolium hexafluorophosphate ([Bmim]$PF_6$), surfactant TX-100, 1-butanol, and water was prepared. The water-in-[Bmim]$PF_6$ (W/IL), bicontinuous, and [Bmim]$PF_6$-in-water (IL/W) microregions of the microemulsion were identified by conductivity measurements. Starch nanoparticles with a mean diameter of 91.4 nm were synthesized with epichlorohydrin as cross-linker through W/IL microemulsion cross-linking reaction at 50 °C for 4 h. Fourier transform infrared spectroscopy (FTIR) data demonstrated the formation of cross-linking bonds in starch molecules. Scanning electron microscopy (SEM) revealed that starch nanoparticles were spherical and that some particles showed aggregation formation. Furthermore, drug loading and releasing properties of starch nanoparticles were investigated with mitoxantrone hydrochloride as a drug model. This work provides an efficient and environmentally friendly approach for the preparation of starch nanoparticles, which is beneficial to their further application.

**KEYWORDS:** *ionic liquid microemulsion, cross-linking, starch nanoparticles, drug loading, drug release*

## INTRODUCTION

Starch, one of the most abundant natural polymers, is renewable, biodegradable, and modifiable. However, native starches have limitations such as poor processability and solubility, which limit their industrial application. Therefore, starches have been modified for many years through physical, chemical, or enzymatic processes to improve their properties.[1,2] Among various modifications, cross-linked starch microspheres show good properties, such as high stability toward swelling, high shear, high temperature, and acidic conditions.[3] Besides, cross-linked starch microspheres possess good performance in biodegradability, nontoxicity, stability during storage, and cost-effectiveness as well as simple fabrication method.[4] In view of the good properties, cross-linked starch microspheres can be used in many areas, especially in drug delivery systems as a drug carrier.[5] Several years ago, Malafaya et al.[6] prepared cross-linked starch microspheres and studied their loading properties to biologically active agents. Some researchers found that cross-linked starch microspheres are promising vehicles in the intranasal drug delivery system.[7,8] In addition, starch microspheres have also been used as drug carriers for the treatment of liver cancer or arterial embolism via parenteral route.[9−12] As we know, the applications of starch microspheres in drug delivery systems are influenced by their particle size and administration route. However, the literature about the preparation of cross-linked starch microspheres shows that they possess relatively large size and broad size distribution.[13] Therefore, the quality of starch microspheres is desperately expected to be improved for better application.

Starch microspheres have been synthesized through several approaches, among which the water-in-oil (W/O) emulsion cross-linking technique has been widely used because of the defined and simple preparation steps with mild processing conditions.[14] However, the W/O emulsion cross-linking technique requires a lot of toxic organic reagents, which will influence the quality of starch microspheres and lead to pollution, and starch microspheres obtained from this approach still appear relatively big in size and have a wide size distribution range.[15] Heretofore, there are few reports of the synthesis of starch nanoparticles by the emulsion cross-linking method. Shi et al.[14] prepared starch nanoparticles in a traditional W/O microemulsion system with a volume ratio of oil to water at 15:2. In view of the fact that a lot of toxic organic reagents are used in this traditional microemulsion, it is essential to develop an environmentally friendly emulsion cross-linking method for the synthesis of starch nanoparticles.

Room temperature ionic liquids (ILs) have become more and more important as desirable green solvents and reaction media due to their recyclability and designability.[16] Recently, many documents have shown that ILs can substitute polar phase, nonpolar phase, or surfactant to prepare ionic liquid microemulsions, and some inorganic nanomaterials can be prepared in this kind of system.[17−21] However, only Zhou et al.[22] performed the synthesis of starch nanoparticles through an ionic liquid-in-oil (IL/O) microemulsion technique, and the achieved starch nanoparticles possessed an average diameter of 96.9 nm. In this paper, ionic liquid 1-octyl-3-methylimidazolium acetate substituted for the water phase and cyclohexane served as oil phase. Therefore, this IL/O microemulsion system was not environmentally friendly because of the use of toxic organic reagents such as cyclohexane.

To explore an efficient and environmentally friendly approach for the preparation of starch nanoparticles, we

Received: April 18, 2014
Revised: July 27, 2014
Accepted: July 28, 2014
Published: July 29, 2014

ACS Publications © 2014 American Chemical Society



dx.doi.org/10.1021/jf5018725 | J. Agric. Food Chem. 2014, 62, 8214−8220

substituted the oil phase with [Bmim]$PF_6$ and prepared a water-in-ionic liquid (W/IL) microemulsion. Furthermore, the oil phase substituted by [Bmim]$PF_6$ in the W/IL microemulsion was much less than that in the W/O microemulsion and IL/O microemulsion, suggesting that the W/IL microemulsion was a green system. In this work, we investigated the synthesis of starch nanoparticles in a W/IL microemulsion system. Starch nanoparticles with small size and narrow size distribution were successfully obtained and characterized by Fourier transform infrared spectroscopy (FTIR), scanning electron microscopy (SEM), and dynamic light scattering (DLS). Moreover, drug loading and releasing properties of starch nanoparticles were investigated with mitoxantrone hydrochloride as a drug model. This work provided an efficient and environmentally friendly approach for the preparation of starch nanoparticles and may be beneficial to the further applications of starch nanoparticles in many fields.

## MATERIALS AND METHODS

**Materials.** Acid-treated granular starch was obtained from Guangzhou Chemical Reagent Factory (Guangzhou, China). 1-Butyl-3-methylimidazolium hexafluorophosphate ([Bmim]$PF_6$, >99%) was purchased from Lanzhou Institute of Chemical Physics (Lanzhou, China). Mitoxantrone hydrochloride was provided by Hubei Jianyuan Chemical Co., Ltd. (Wuhan, China). All other chemicals were of analytical grade.

**Preparation of Ionic Liquid Microemulsions.** The preparation of a water/Triton X-100 (TX-100) + 1-butanol/[Bmim]$PF_6$ system was conducted by direct visual observation. First, certain amounts of water and [Bmim]$PF_6$ were added into a small beaker, and their masses were determined by an FA1104N analytical balance (Shanghai Balance Instrument Co., Shanghai, China) with a resolution of 0.0001 g. The temperature was controlled by a DF-II thermostatic magnetic stirring apparatus (Shanghai Yuzheng Instrument Co., Shanghai, China). After thermal equilibrium, the mixture of TX-100 and 1-butanol with the mass ratio of TX-100 to 1-butanol at 3:1 was added into the solution until the hierarchical and hazy liquid solution became transparent, which was indicative of the formation of the single phase.

**Phase Diagram Determination.** The pseudoternary phase diagram of the microemulsion was determined at 25 °C as described above. A series of microemulsions were prepared through changing the mass ratio of [Bmim]$PF_6$/water at 9:1, 8:2, 7:3, 6:4, 5:5, 4:6, 3:7, 2:8, and 1:9, respectively. The corresponding composition of the solution was noted as the phase boundary.

**Conductivity Measurements.** Conductivity measurements were taken with a model DDSJ-308A conductometer (Shanghai Precision Scientific Instrument Co., Shanghai, China) at 1 kHz using a dip-type cell of cell constant 0.971 $cm^{-1}$. The errors in the conductance measurements were ±0.5%. The water was progressively added to the mixture of [Bmim]$PF_6$, TX-100, and 1-butanol, and the conductance was measured after thorough mixing and temperature equilibration.

**Dynamic Light Scattering.** DLS is used to determine the size distribution of microemulsions and further demonstrate the formation of W/IL microemulsions. Measurements were conducted using a Malvern Nano-Zetasizer particle size analyzer (Malvern Instrument Ltd., Worcestershire, UK) at a wavelength of 633 nm. The scattering angle was set at 90°. Samples were maintained at 25.0 °C during the experiments.

**Preparation of Starch Nanoparticles.** Starch nanoparticles were prepared according to the W/IL microemulsion cross-linking method with epichlorohydrin as a cross-linker. This method combined the ionic liquid microemulsion with cross-linking reaction of starch nanoparticles. The solidification of the starch molecules and cross-linking reaction took place during the stable W/IL microemulsion. The reaction scheme for cross-linked starch nanoparticles is depicted in Figure 1. First, the aqueous phase was prepared by dissolving acid-treated granular starch (0.5 g) in 9.5 g of NaOH solution (NaOH/$H_2O$ = 1:50, w/w) and then poured into [Bmim]$PF_6$ (40 g) to form

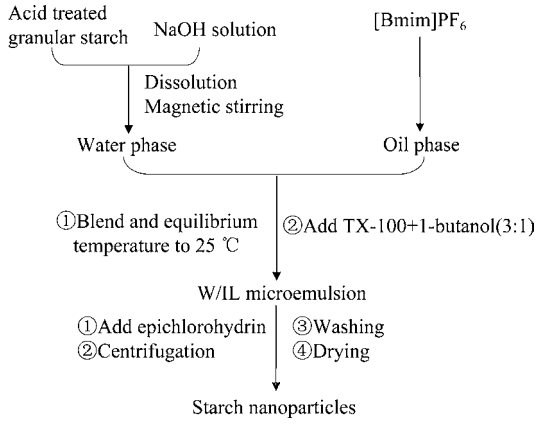


**Figure 1.** Scheme of microemulsion cross-linking reaction of starch.

the W/IL microemulsion with the aid of 40 g of a mixture of surfactant TX-100 and cosurfactant 1-butanol (TX-100/1-butanol = 3:1, w/w). After several minutes of magnetic stirring, epichlorohydrin (1.84 g) was added to the above microemulsion as a cross-linker. In this stage, the mixture was stirred by a DF-II thermostatic magnetic stirring apparatus at the speed of 1200 rpm at 50 °C for 4 h. Subsequently, the reaction solution was cooled to room temperature, and starch nanoparticles were precipitated with methanol under vigorous stirring followed by centrifugation. The precipitate was washed thoroughly with sufficient methanol and ethanol to eliminate [Bmim]$PF_6$, unreacted epichlorohydrin, 1-butanol, and TX-100. Finally, the solid was centrifuged and dried in a vacuum at 45 °C for 24 h.

**Characterization of Starch Nanoparticles.** The structure character of acid-treated granular starch and starch nanoparticles was analyzed by a Nicolet 510 spectrophotometer (Thermo Electron Corp., Waltham, MA, USA) using the KBr disk technique. For FTIR measurement, the samples were mixed with anhydrous KBr and then compressed into thin disk-shaped pellets. The spectra were obtained with a resolution of 2 $cm^{-1}$ over a wavenumber range of 400−4000 $cm^{-1}$. SEM images of acid-treated granular starch and starch nanoparticles were examined by means of a model 430 scanning electron microscope (FEI Corp., Hillsboro, OR, USA). The samples were mounted on an aluminum stub with double sticky tape, followed by coating with gold in a vacuum before examination. The accelerating voltage was 5 kV. The size distribution of starch nanoparticles was determined by DLS. Before measuring, 0.1 g of starch nanoparticles was added to 100 mL of distilled water and treated by ultrasound for 30 min to disperse sufficiently.

**Standard Curves of Mitoxantrone Hydrochloride.** Standard curves of mitoxantrone hydrochloride in phosphate-buffered saline (PBS, 0.2 mol/L, pH 7.4) were obtained using the following approaches: 0.01 mg/mL of mitoxantrone hydrochloride in PBS solution was scanned at wavelengths between 360 and 760 nm with a model TU-1810 ultraviolet−visible spectrophotometer (Beijing Puxi General Apparatus Co., Ltd., Shanghai, China). The wavelength at which mitoxantrone hydrochloride absorbed the most was selected as the testing wavelength for later experiments. Then, 0.0025, 0.005, 0.01, 0.02, 0.03, and 0.04 mg/mL of mitoxantrone hydrochloride in PBS solution were measured at the corresponding testing wavelengths to obtain the standard curve of mitoxantrone hydrochloride absorbance to concentration.

**Drug Loading Analysis.** About 50 mg of starch nanoparticles with diameters of 64, 176, and 255 nm were weighed and suspended in 10 mL of PBS solution with 0.0221, 0.0442, 0.0884, and 0.1326 mg/mL mitoxantrone hydrochloride each. The resulting suspensions were gently stirred at the desired temperature of 17, 27, 37, and 47 °C for 0.5, 1, 1.5, 2, 2.5, and 3 h. Subsequently, the solutions were centrifuged, and each supernatant was extracted to determine the drug loading and encapsulation efficiency with an ultraviolet−visible spectrophotometer according to the standard curve of mitoxantrone hydrochloride absorbance to concentration. The drug loading ($A$) and


dx.doi.org/10.1021/jf5018725 | J. Agric. Food Chem. 2014, 62, 8214−8220

encapsulation efficiency ($B$) were calculated with eqs 1 and 2, respectively.

$$A = (C_0 - nC_1)V_0/W \quad (1)$$

$$B = C_0 - nC_1/C_0 \quad (2)$$

$C_0$ means initial concentration of mitoxantrone hydrochloride in PBS, $C_1$ means diluted concentration of mitoxantrone hydrochloride in PBS, $n$ means dilution multiple of extracted supernatant, $V_0$ means initial volume of mitoxantrone hydrochloride in PBS, and $W$ means the weight of starch nanoparticles dissolved in PBS.

**Drug Release Analysis.** About 90 mg of drug-loaded starch nanoparticles that possess the most drug loading (1.5587 mg/g) under the experimental conditions above was weighed and added to the dialysis tube. Then, 10 mL of PBS solution was added to the dialysis tube. Subsequently, the drug-loaded starch nanoparticles and dialysis tube were placed in a beaker containing 80 mL of PBS solution and slowly stirred in magnetic stirring apparatus at 37 °C. At appropriate time intervals, 5 mL of solution was taken out and replaced by the same volume of fresh PBS solution. The cumulative release rate was determined according to the standard curve of mitoxantrone hydrochloride absorbance to concentration and eq 3.

$$R = M_1/M_0 \quad (3)$$

$M_1$ is the cumulative mass of mitoxantrone hydrochloride released from drug-loaded starch nanoparticles at a given time, and $M_0$ is the total drug loading in starch nanoparticles.

## RESULTS AND DISCUSSION

**Phase Diagram.** A phase diagram is useful for further characterizing the microemulsions and choosing the proper cross-linking reaction system. The phase diagram of the water/TX-100 + 1-butanol/[Bmim]$PF_6$ system at room temperature is shown in Figure 2. Apparently, two different regions, a two-phase region and a one-phase region, could be observed. A continuous stable single-phase microemulsion region could always be observed in the range of the water or [Bmim]$PF_6$ content from 0 to 100% (wt). It could be seen that the phase behavior of the water/TX-100 + 1-butanol/[Bmim]$PF_6$ system was similar to that of the traditional W/O microemulsions and the IL microemulsions reported recently.[23]

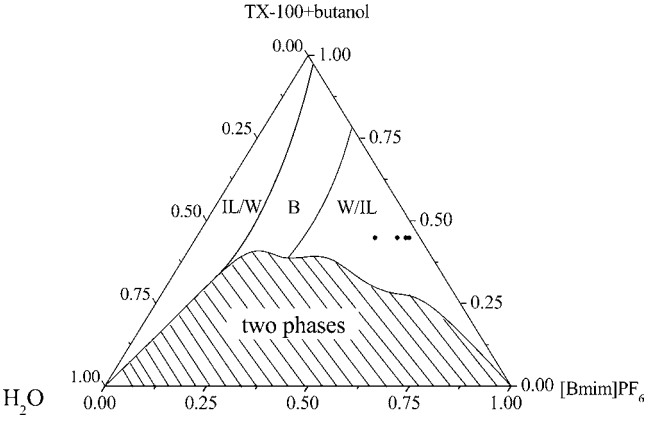


**Figure 2.** Phase diagram of the water/TX-100 + 1-butanol/[Bmim]$PF_6$ (in weight fraction) at 25 °C.

**Conductivity.** Conductivity is frequently used to investigate the structural changes in microemulsions and can provide a basis for the determination of the cross-linking reaction system.[19] The one-phase region could be divided into different subregions, such as the water-in-IL (or oil) microemulsion region, the IL (or oil)-in-water microemulsion region, and the bicontinuous region.[17,24] In our research, the W/IL microemulsion was chosen as the cross-linking reaction system. Therefore, it is essential to investigate the structure of this kind of microemulsion. Conductivity measurement is commonly used to locate the subregions of microemulsions.[24] Figure 3 illustrates the dependence of the conductivity on the weight fraction of water with the mass ratio of [Bmim]$PF_6$ to TX-100 + 1-butanol at 1:4. Obviously, it could be seen that the conductivity increased first and then decreased with an increase in water content, representing the subregion structure transition from W/IL to IL/W after passing through a bicontinuous region (B), indicative of the existence of three subregions. A similar phenomenon could also be seen in ethylene glycol/TX-100/[Bmim]$PF_6$ microemulsions.[25]

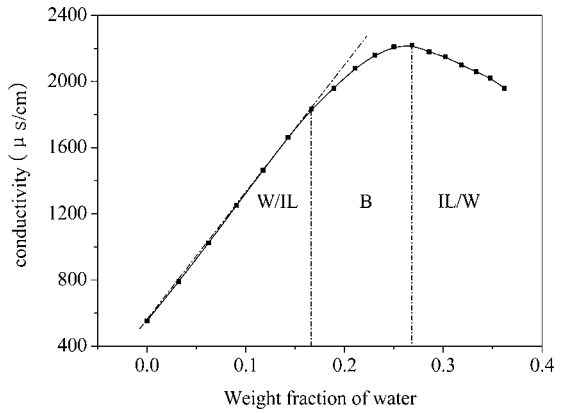


**Figure 3.** Conductivity as a function of weight fraction of water in the microemulsions at 25 °C with the mass ratio of [Bmim]$PF_6$ to TX-100 + 1-butanol at 1:4.

**Size Distribution of Microemulsions.** The size distribution of the droplets in the W/IL microemulsions was characterized by DLS. In this work, several kinds of W/IL microemulsions were chosen for DLS analysis because of their applications in the preparation of starch nanoparticles. The compositions of selected microemulsions are as follows: the weight fraction of mixture of TX-100 and 1-butanol in the microemulsions was 0.45, and the mass ratios of [Bmim]$PF_6$ to water ($R$) are 4:1, 9:1, 15:1, and 20:1, respectively. As shown in Figure 4, the sizes of microemulsions increased from about

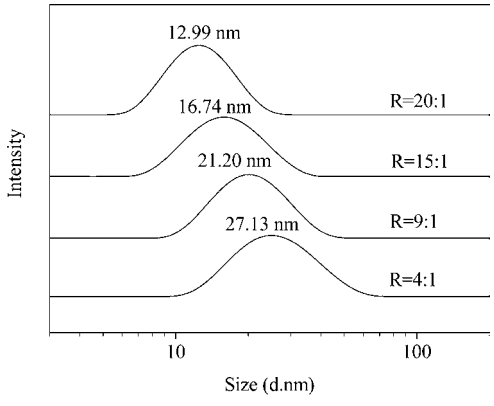


**Figure 4.** Size distribution of the droplets in the water/TX-100 + 1-butanol/[Bmim]$PF_6$ microemulsions at 25.0 °C. $R$ represents the mass ratio of [Bmim]$PF_6$ to water.


dx.doi.org/10.1021/jf5018725 | J. Agric. Food Chem. 2014, 62, 8214−8220

12.99 to 27.13 nm with the increase of water. The microemulsions showed regular swelling behavior with the addition of water, which demonstrated the formation of W/IL microemulsion according to the study by Pramanik et al.[26]

**FTIR Analysis of Acid-Treated Granular Starch and Starch Nanoparticles.** Figure 5 shows the comparative FTIR spectra of acid-treated granular starch (Figure 5a) and starch nanoparticles (Figure 5b). In the case of acid-treated granular starch, the O−H stretching and the C−H stretching vibration give strong signalsat 3389 and 2928 $cm^{-1}$, respectively.[27] The absorption peak at 1651 $cm^{-1}$ belonged to O−H bending vibration.[28] The bands at 1160, 1084, and 1024 $cm^{-1}$ were due to C−O stretching vibrations.[29] In comparison with acid-treated granular starch, FTIR spectra of starch nanoparticles showed some difference. The absorption peaks at 3389 nd 1651 $cm^{-1}$ clearly became narrowed and weaker than that of acid-treated granular starch,which demonstrates the occurrence of cross-linking reaction. The band shape between 900 and 1160 $cm^{-1}$ in starch nanoparticles had changed, and the band intensity became a little stronger compared with acid-treated granular starch. The results suggested that a cross-linking reaction took place between starch molecules. Similar results were also observed in previous literature.[4,29]

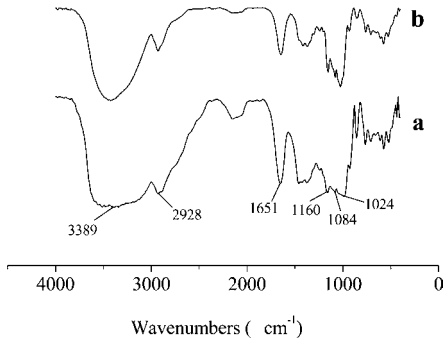


**Figure 5.** FTIR spectra of acid-treated granular starch (a) and starch nanoparticles (b).

**SEM Analysis of Acid-Treated Granular Starch and Starch Nanoparticles.** SEM was used to investigate the morphology of acid-treated granular starch and starch nanoparticles. As shown in Figure 6, acid-treated granular starch showed round or oval shapes with various sizes ranging from about 10 to 30 $\mu$m. In comparison with the acid-treated granular starch, starch nanoparticles exhibited good sphericity and particle sizes ranged from about 100 to 300 nm, but some of the particles showed aggregation formation mainly due to strong van der Waals force and electrostatic attraction.[22]

**Size Distribution of Starch Nanoparticles.** The size distribution of starch nanoparticles was measured using DLS. As observed in Figure 7, the result showed that the size distribution of starch nanoparticles was relatively concentrated, and the mean diameter was 91.4 nm, which is much smaller than that of starch microspheres prepared by the traditional W/O emulsion cross-linking method.[30] From the result, it could be concluded that starch nanoparticles with a relatively concentrated size distribution could be obtained by using the W/IL microemulsion cross-linking approach.

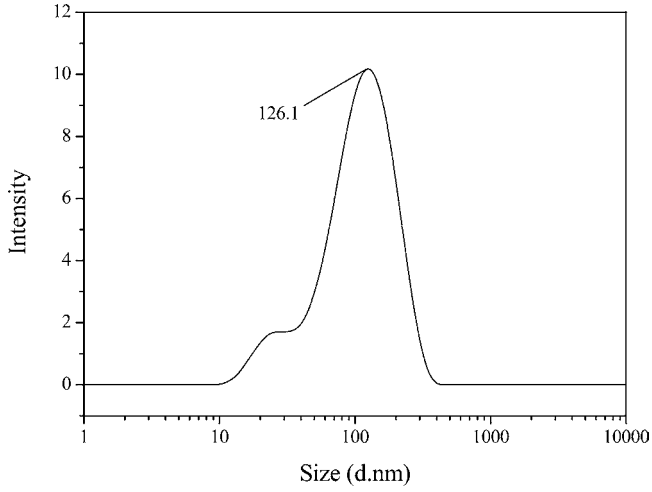


**Figure 7.** Size distribution of starch nanoparticles.

**Drug Loading Analysis.** According to the scanning result, the testing wavelength of PBS solution containing mitoxantrone hydrochloride was 608 nm. Besides, the standard curve of mitoxantrone hydrochloride absorbance to concentration (from 0.0025 to 0.04 mg/mL) was $A = 0.0424 + 24.38C$ ($R^2$ = 0.9982).

The influence of loading time on drug loading property is shown in Figure 8A. The drug loading and encapsulation efficiency increased first and then decreased as time went on. To be exact, the drug loading increased from 0.5102 to 0.7317 mg/g as the time was prolonged from 0.5 to 1.5 h and then decreased to 0.5513 mg/g when the time was extended to 3 h. The encapsulation efficiency increased from 11.54 to 16.55% and then reduced to 12.47% correspondingly. From the result, it could be concluded that the drug loading and encapsulation

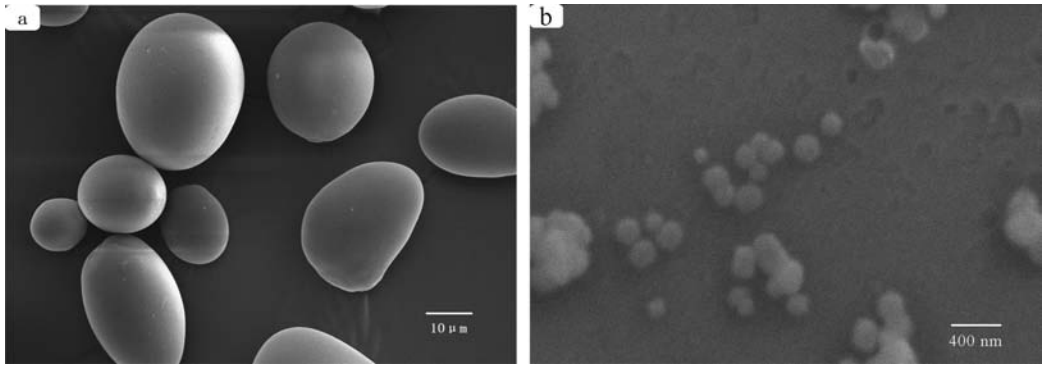


**Figure 6.** SEM images of acid-treated granular starch (a) and starch nanoparticles (b).


dx.doi.org/10.1021/jf5018725 | J. Agric. Food Chem. 2014, 62, 8214−8220

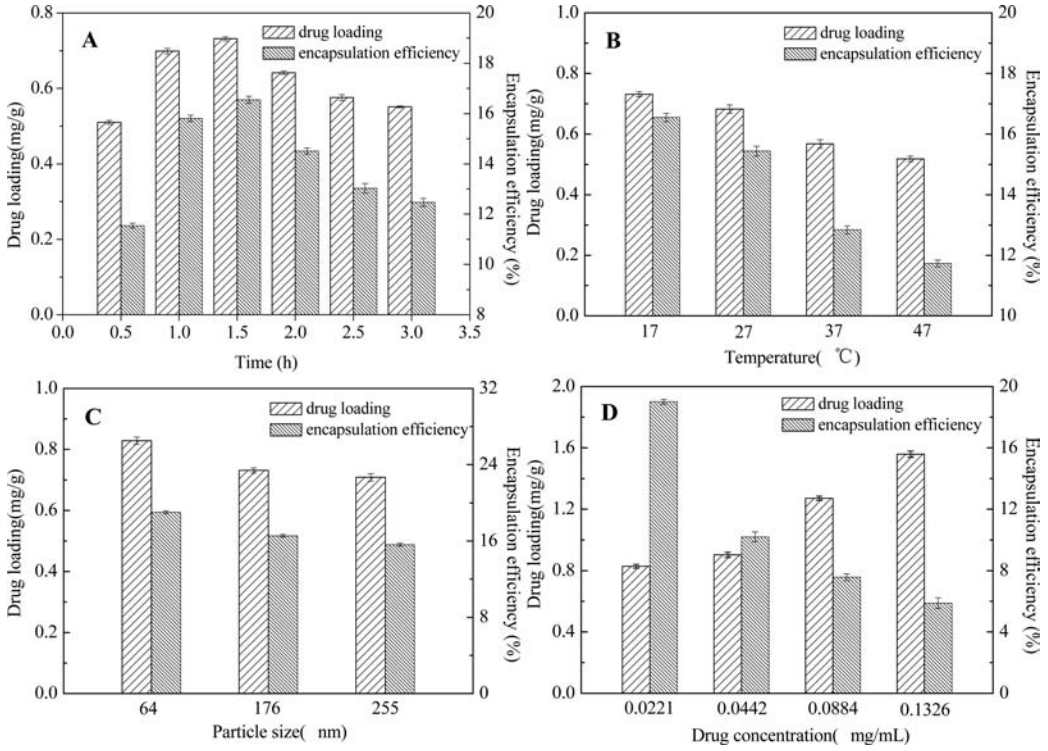


**Figure 8.** Effect of loading time (A), loading temperature (B), particle size (C), and drug concentration (D) on drug loading property. Other conditions: (A) loading temperature, 17 °C; particle size, 176 nm; drug concentration, 0.0221 mg/mL. (B) loading time, 1.5 h; particle size, 176 nm; drug concentration, 0.0221 mg/mL. (C) loading time, 1.5 h; loading temperature, 17 °C; drug concentration, 0.0221 mg/mL; (D) loading time, 1.5 h; loading temperature, 17 °C; particle size, 64 nm.

efficiency of starch nanoparticles on mitoxantrone hydrochloride presented an appropriate time value.

The effect of temperature on drug loading property is observed in Figure 8B. It was obvious that different loading temperatures resulted in significant changes in drug loading and encapsulation efficiency. At a temperature of 17 °C, starch nanoparticles loaded with more mitoxantrone hydrochloride, and encapsulation efficiency showed the same trend. The reason for this phenomenon may be that the adsorption of mitoxantrone hydrochloride was mainly attributed to the existence of opposite charges and high affinity. This adsorption process would be hindered by high temperature; thus, the drug loading reduced at higher temperature.[15]

Starch nanoparticles with different particle sizes (64, 176, and 255 nm) were obtained through changing the reaction conditions such as reaction time, reaction temperature, and starch concentration to investigate the effect of particle size on drug loading property. As shown in Figure 8C, drug loading and encapsulation efficiency decreased with increasing particle size of starch nanoparticles. The reason for this phenomenon may be that starch nanoparticles of smaller particle size have greater specific surface area and stronger adhesion ability.

As shown in Figure 8D, drug loading ascended significantly from 0.7317 to 1.5587 mg/g as the concentration of mitoxantrone hydrochloride rose from 0.0221 to 0.1326 mg/mL. However, the increase of drug concentration caused a decline in encapsulation efficiency. Therefore, higher drug concentration does not necessarily result in better drug loading property.

**Drug Release Analysis.** Drug release experiments were performed in PBS solution. As presented in Figure 9, an initial burst release was observed in the first hour after the drug-loaded starch nanoparticles were immersed into release medium. The high release rate of 32.15% in the first hour was associated with the immediate dispersion of the mitoxantrone hydrochloride close to the surfaces of starch nanoparticles. In the following 9 h, the starch nanoparticles presented a swelling-controlled and sustained release, in which the release rate tailed off, and 79.95% of mitoxantrone hydrochloride contained in the starch nanoparticles was released in the 10th hour. This may be explained by increasing swelling causing a great number of mitoxantrone hydrochloride molecules to diffuse out of the starch nanoparticles and pass into the release medium. This observed phenomenon was consistent with the results of Fang et al.[15]

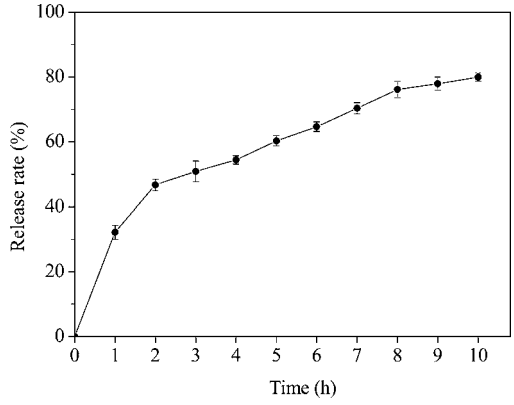


**Figure 9.** Mitoxantrone hydrochloride release of starch nanoparticles in PBS solution.

This paper describes an exploratory study on the preparation of starch nanoparticles by a novel ionic liquid microemulsion


dx.doi.org/10.1021/jf5018725 | J. Agric. Food Chem. 2014, 62, 8214−8220

and drug loading and releasing properties of starch nanoparticles. Water/TX-100 + 1-butanol/[Bmim]$PF_6$ microemulsions were prepared, and the pseudoternary phase diagram was drawn to investigate the phase behavior. The W/IL, bicontinuous, and IL/W microregions of the microemulsions were identified by conductivity measurements. DLS analysis of microemulsions demonstrated the formation of a W/IL microemulsion. Cross-linked starch nanoparticles were prepared with epichlorohydrin as cross-linker through a W/IL microemulsion cross-linking approach. The formation of cross-linking bonds in starch molecules was demonstrated by FTIR spectra. SEM and DLS of starch nanoparticles intuitively suggested the formation of starch nanoparticles. In terms of drug loading property of starch nanoparticles, it was found that the drug loading and encapsulation efficiency were influenced by loading time, loading temperature, and particle size as well as drug concentration. The release curve of drug-loaded starch nanoparticles contained two phases: an initial burst release phase and a sustained release phase depending on the swelling and degradation of starch nanoparticles.

## AUTHOR INFORMATION


### Corresponding Authors

*(Z.L.) Phone: +86-20-87113845. Fax: +86-20-87113848. E-mail: zhgluo@scut.edu.cn.

*(X.F.) Phone: +86-20-87113845. E-mail: lfxfu@scut.edu.cn.



### Funding

This research was supported by the National Natural Science Foundation of China (21376097, 21004023), the program for New Century Excellent Talents in University (NCET-13-0212), the Guangdong Natural Science Foundation (S2013010012318), the Key Project of Science and Technology of Guangdong Province (2012B091100443, 2012B091100047), and the Fundamental Research Funds for the Central Universities, SCUT (2013ZZ0070).


### Notes

The authors declare no competing financial interest.

## ABBREVIATIONS USED

W/IL, water-in-ionic liquid; TX-100, Triton X-100; [Bmim]-$PF_6$, 1-butyl-3-methylimidazolium hexafluorophosphate; DLS, dynamic light scattering; FTIR, Fourier transform infrared spectroscopy; SEM, scanning electron microscopy; IL/W, ionic liquid-in-water; W/O, water-in-oil; ILs, ionic liquids

## REFERENCES


(1) Jobling, S. Improving starch for food and industrial applications. *Curr. Opin. Plant Biol.* **2004**, *7*, 210−218.

(2) Raina, C. S.; Singh, S.; Bawa, A. S.; Saxena, D. C. A comparative study of Indian rice starches using different modification model solutions. *Food Sci. Technol.* **2007**, *40*, 885−892.

(3) Kim, M.; Lee, S. J. Characteristics of crosslinked potato starch and starch-filled linear low-density polyethylene films. *Carbohydr. Polym.* **2002**, *50*, 331−337.

(4) Mundargi, R. C.; Shelke, N. B.; Rokhade, A. P.; Patil, S. A.; Aminabhavi, T. M. Formulation and in-vitro evaluation of novel starch-based tableted microspheres for controlled release of ampicillin. *Carbohydr. Polym.* **2007**, *71*, 42−53.

(5) Stertman, L.; Lundgren, E.; Sjöholm, I. Starch microparticles as a vaccine adjuvant: only uptake in Peyer's patches decides the profile of the immune response. *Vaccine* **2006**, *24*, 3661−3668.

(6) Malafaya, P. B.; Stappers, F.; Reis, R. L. Starch-based microspheres produced by emulsion crosslinking with a potential media dependent responsive behavior to be used as drug delivery carriers. *J. Mater. Sci. Mater. Med.* **2006**, *17*, 371−377.

(7) Mao, S. R.; Chen, Z. M.; Wei, Z. P.; Liu, H.; Bi, D. Z. Intranasal administration of melatonin starch microspheres. *Int. J. Pharm.* **2004**, *272*, 37−43.

(8) Bjork, E.; Edman, P. Characterization of degradable starch microspheres as a nasal delivery system for drugs. *Int. J. Pharm.* **1990**, *62*, 187−192.

(9) Hamdi, G.; Ponchel, G. Enzymatic degradation of epichlorohydrin crosslinked starch microspheres by $\alpha$-amylase. *Pharm. Res.* **1999**, *16*, 867−875.

(10) Gyves, J. W.; Ensminger, W. D.; VanHarken, D.; Niederhuber, J.; Stetson, P.; Walker, S. Improved regional selectivity of hepatic arterial mitomycin by starch microspheres. *Clin. Pharmacol. Ther.* **1983**, *34*, 259−265.

(11) Ishida, K.; Hirooka, M.; Hiraoka, A.; Kumagi, T.; Uehara, T.; Hiasa, Y. Treatment of hepatocellular carcinoma using arterial chemoembolization with degradable starch microspheres and continuous arterial infusion of 5-fluorouracil. *Jpn. J. Clin. Onol.* **2008**, *38*, 596−603.

(12) Kim, D. K.; Mikhaylova, M.; Wang, F. H.; Kehr, J.; Bjelke, B.; Zhang, Y. Starch-coated superparamagnetic nanoparticles as MR contrast agents. *Chem. Mater.* **2003**, *1*, 4343−4351.

(13) Franssen, O.; Hennink, W. E. A novel preparation method for polymeric microparticles without the use of organic solvents. *Int. J. Pharm.* **1998**, *168*, 1−7.

(14) Shi, A. M.; Li, D.; Wang, L. J.; Li, B. Z.; Adhikaric, B. Preparation of starch-based nanoparticles through high-pressure homogenization and miniemulsion cross-linking: influence of various process parameters on particle size and stability. *Carbohydr. Polym.* **2011**, *83*, 1604−1610.

(15) Fang, Y. Y.; Wang, L. J.; Li, D.; Li, B. Z.; Bhandari, B.; Chen, X. D.; Mao, Z. H. Preparation of crosslinked starch microspheres and their drug loading and releasing properties. *Carbohydr. Polym.* **2008**, *74*, 379−384.

(16) Welton, T. Room-temperature ionic liquids: solvents for synthesis and catalysis. *Chem. Rev.* **1999**, *99*, 2071−2083.

(17) Cheng, S. Q.; Fu, X. G.; Liu, J. H.; Zhang, J. L.; Zhang, Z. F.; Wei, Y. L. Study of ethylene glycol/TX-100/ionic liquid microemulsions. *Colloids Surf., A* **2007**, *302*, 211−215.

(18) Cheng, S. Q.; Han, F.; Wang, Y. R.; Yan, J. F. Effect of cosurfactant on ionic liquid solubilization capacity in cyclohexane/TX-100/1-butyl-3-methylimidazolium tetrafluoroborate microemulsions. *Colloids Surf., A* **2008**, *317*, 457−461.

(19) Gao, H. X.; Li, J. C.; Han, B. X.; Chen, W. N.; Zhang, J. L.; Zhang, R.; Yan, Y. D. Microemulsions with ionic liquid polar domains. *Phys. Chem. Chem. Phys.* **2004**, *6*, 2914−2916.

(20) Yan, F.; Texter, J. Surfactant ionic liquid-based microemulsions for polymerization. *Chem. Commun.* **2006**, *25*, 2696−2698.

(21) Zhang, G. P.; Kuang, Y. F.; An, C. L.; Liu, D.; Huang, Z. Y.; Kuang, Y. F. Bimetallic palladium-gold nanoparticles synthesized in ionic liquid microemulsion. *Colloid Polym. Sci.* **2012**, *290*, 1435−1441.

(22) Zhou, G.; Luo, Z. G.; Fu, X. Preparation and characterization of starch nanoparticles in ionic liquid-in-oil microemulsions system. *Ind. Crops Prod.* **2014**, *52*, 105−110.

(23) Najjar, R.; Stubenrauch, C. Phase diagrams of microemulsions containing reducing agents and metal salts as bases for the synthesis of metallic nanoparticles. *J. Colloid Interface Sci.* **2009**, *331*, 214−220.

(24) Gao, Y.; Han, S.; Han, B.; Li, G.; Shen, D.; Li, Z.; Du, J.; Hou, W.; Zhang, G. TX-100/water/1-butyl-3-methylimidazolium 322 hexafluorophosphate microemulsions. *Langmuir* **2005**, *21*, 5681−5684.

(25) Cheng, S. Q.; Fu, X. G.; Liu, J. H.; Zhang, J. L.; Zhang, Z. F.; Wei, Y. L. Study of ethylene glycol/TX-100/ionic liquid microemulsions. *Colloids Surf., A* **2007**, *302*, 211−215.

(26) Pramanik, R.; Ghatak, C.; Rao, V. G.; Sarkar, S.; Sarkar, N. J. Room temperature ionic liquid in confined media: a temperature dependence solvation study in [bmim][BF4]/BHDC/benzene reverse micelles. *J. Phys. Chem. B* **2011**, *115*, 5971−5979.

(27) Kacurakova, M.; Wilson, R. H. Developments in mid-infrared FTIR spectroscopy of selected carbohydrates. *Carbohydr. Polym.* **2001**, *44*, 291−303.
(28) Mano, J. F.; Koniarova, D.; Reis, R. L. Thermal properties of thermoplastic starch/synthetic polymer blends with potential biomedical applicability. *J. Mater. Sci. Mater. Med.* **2003**, *14*, 127−135.
(29) Li, B. Z.; Wang, L. J.; Li, D.; Adhikari, B.; Mao, Z. H. Preparation and characterization of crosslinked starch microspheres using a two-stage water-in-water emulsion method. *Carbohydr. Polym.* **2012**, *88*, 912−916.
(30) Zhao, X. F.; Li, Z. J.; Wang, L.; Lai, X. J. Synthesis, characterization, and adsorption capacity of crosslinked starch microspheres with *N*,*N*′-methylene bisacrylamide. *J. Appl. Polym. Sci.* **2008**, *109*, 2571−2575.

JOURNAL OF AGRICULTURAL AND FOOD CHEMISTRY

Article

pubs.acs.org/JAFC

# Efficient Determination of Protocatechuic Acid in Fruit Juices by Selective and Rapid Magnetic Molecular Imprinted Solid Phase Extraction Coupled with HPLC

Lianwu Xie,*[,†,‡] Junfang Guo,[‡] Yuping Zhang,[‡] and Shuyun Shi*[,‡]

[†]College of Sciences, Central South University of Forestry and Technology, Changsha 410004, People's Republic of China

[‡]College of Chemistry and Chemical Engineering, Central South University, Changsha 410083, Poeple's Republic of China

**ABSTRACT:** Magnetic molecular imprinted polymers (MMIPs) have been prepared as solid phase material to selectively extract protocatechuic acid (PCA) from fruit juices with high capacity and fast binding kinetics. The resulting MMIPs were characterized by TEM, FT-IR, TGA, and VSM. The adsorption process between PCA and MMIPs followed Langumuir adsorption isotherm with maximum adsorption capacity at 7.5 mg/g and pseudo-second-order reaction kinetics with fast binding kinetics (equilibrium time at 40 min). In addition, the prepared MMIPs showed rapid magnetic separation (10 s) and reusability (retained 94.9% after six cycles). Subsequently, MMIPs were successfully applied for selective enrichment and determination of PCA from fruit juices (0.45 $\mu$g/mL in grape juice but not detected in apple juice, pineapple juice, orange juice, and peach juice) with satisfactory recoveries (92−107%). The results indicated that synthesized MMIPs can be used for efficient and selective extraction of PCA from complex matrices.

**KEYWORDS:** *protocatechuic acid, fruit juice, molecular imprinted polymer, magnetic solid phase extraction, HPLC analysis*

## INTRODUCTION

Protocatechuic acid (PCA), a phenolic compound, is widely distributed in commonly consumed foods, fruits, juices, and traditional Chinese medicine. At the same time, PCA is the major human metabolite of cyanidin-glucosides, flavonoids widely existing in fruit.[1,2] Pharmaceutical investigations indicate that PCA exhibits a wide variety of bioactivities, such as strong antioxidant,[3] wide anticancer,[4,5] anti-inflammatory,[6] and anticarcinogenic[7] properties. Moreover, PCA has been studied in ongoing clinical trials.[8] Nowadays, PCA has attracted increasing interest as a dietary supplement in an expanding health food market. However, the qualitative and quantitative analyses of polar PCA in a complex matrix (e.g., fruit juice, food, natural product, and biological sample) are difficult because of the low concentration of PCA (e.g., <1 $\mu$g/mL in fruit juices) and the coelution with some other polar interferences in usual high-performance liquid chromatography (HPLC) analysis.[9] Therefore, it is necessary to develop an efficient and selective extraction method for the recovery and purification of PCA from complex matrices.

Molecularly imprinted polymers (MIPs) are selective materials that contain specific recognition sites in synthesized polymers with the memory of templates and their analogues due to shape, size, and functionality recognition.[10,11] Other powerful features of MIPs are mechanical/chemical stability, low cost, easy preparation, and reversible adsorption/desorption procedure, as indicated by Haupt and Mosbach in a review.[12] Recently, it has attracted wide attention and attained significant application in effective and selective separation/determination of small bioactive components or macromolecules (e.g., proteins) from real complex samples.[13−16]

In most cases, MIPs show specific adsorption of target components at very low concentrations.[13−16] However, MIPs prepared by conventional method, such as bulk polymerization and precipitation polymerization, embed most binding sites, which leads to poor binding capacities and low binding kinetics of templates on MIPs.[17] Karasová et al. prepared PCA-imprinted polymers by bulk polymerization, and the best specific binding capacity of MIPs for PCA was found in porogen solvent; however, it was just 34.7 $\mu$g/g.[18] After that, Chen and co-workers declared that they achieved PCA-imprinted polymers with good adsorption capacity by conventional precipitation polymerization, whereas the binding capacity of MIPs for PCA was only about 0.16 mg/g.[19] Recently, various forms of surface-imprinting techniques, imprinting MIPs on the surface of nano/micro solid supports (e.g., silica,[20] carbon nanotube,[21] polymer support,[22] and magnetic nanoparticle[10,11]), have been successfully and widely used with promising results to address this problem. The results suggest that the surface-imprinted MIPs increase binding capacity obviously because of the high surface area of solid support, leading to more imprinted cavities within the polymer network, and shorten equilibrium time largely from 12−24 h in conventional MIPs to <2 h for the surface recognition sites.[10,11] Notably, magnetic solid supports (e.g, $Fe_3O_4$) have been considered as ideal ones and received increasing attention because they possess significant advantages including but not limited to unique magnetic property for easy and rapid separation from the matrix under external magnetic field after adsorption, which will avoid the column-packing procedure or centrifugation procedure, and then make the pretreatment step

Received: May 9, 2014
Revised: July 23, 2014
Accepted: July 30, 2014
Published: July 30, 2014

ACS Publications © 2014 American Chemical Society



dx.doi.org/10.1021/jf5021895 | J. Agric. Food Chem. 2014, 62, 8221−8228

simple.[10,11,23] However, to our best knowledge, no paper has reported the preparation of magnetic MIPs (MMIPs) using PCA as template to efficiently and selectively extract and determine PCA from complex matrices.

Herein, we attempted to prepare and characterize MMIPs using PCA as template and investigate adsorption isotherms and kinetics, competitive adsorption, reusability analysis, and application in selective extraction and determination of PCA in fruit juices. The results suggested that the prepared MMIPs possessed high binding capacity, fast binding kinetics, excellent selectivity, quick separation ability, and good reusability because of the combination of the advantage of surface-imprinted MIPs and magnetic $Fe_3O_4$.

## MATERIALS AND METHODS

**Chemicals and Reagents.** Iron(III) chloride hexahydrate ($FeCl_3 \cdot 6H_2O$), polyethylene glycol 6000 (PEG 6000), 2,2-azobis-(isobutyronitrile) (AIBN), tetraethyl orthosilicate (TEOS), and HPLC grade methanol were obtained from Sinopharm Chemical Reagent Co., Ltd. (Shanghai, China). Ethylene glycol dimethacrylate (EGDMA), 4-vinylpyridine (4-VP), acrylamide (AM), methacrylamide (MAM), and 3-(trimethoxysilyl)propyl methacrylate (MPS) were acquired from Shaen Chemical Technology Co., Ltd. (Shanghai, China). 4-Hydroxybenzoic acid (4-HBA), salicylic acid (SA), caffeic acid (CA), gallic acid (GA), and PCA with purities >99% were purchased from National Institute for the Control of Pharmaceutical and Biological Products (Beijing, China). Ultrapure water was collected from a Milli-Q gradient ultrapure water system (Millipore, MA, USA). The other reagents were of analytical grade and supplied from Kemiou Chemical Reagent Co., Ltd. (Tianjin, China).

**Procedures for Preparation of MMIPs.** PCA-imprinted polymers were prepared by a surface-imprinted polymerization method using magnetic microparticles as solid support according to our previous work with minor modifications.[10,11] At first, $Fe_3O_4$ microspheres were synthesized by solvothermal reaction as previously reported.[24,25] Then, $Fe_3O_4$ microspheres were coated with a $SiO_2$ layer by hydrolysis of TEOS catalyzed by NaOH.[26] Typically, as-prepared $Fe_3O_4$ microspheres (50.0 mg) were dispersed in deionized water and ultrasonicated for 30 min. Then the resultant homogeneous solution was diluted with 1.0 mM NaOH aqueous solution (450.0 mL) and ultrasonically treated for another 5 min. Subsequently, the obtained basic dispersion was mechanically stirred at 60 °C for 30 min and injected with TEOS/ethanol (1:4, v/v) solution (2.5 mL) for stirring about 1 min and then allowed to stand for 12 h. The $Fe_3O_4$@$SiO_2$ microspheres were collected magnetically, repeatedly washed by deionized water, and dried in a vacuum. After that, $Fe_3O_4$@$SiO_2$ was modified by vinyl groups. Briefly, $Fe_3O_4$@$SiO_2$ (250.0 mg) was dissolved in MPS solution (150.0 μL of MPS dispersed in 40.0 mL of water containing 10% acetic acid). After stirring for 5 h at 60 °C, the vinyl-modified $Fe_3O_4$@$SiO_2$ was magnetically gathered, repeatedly washed with water, and dried in a vacuum.[10,11] Finally, MMIPs were prepared in anhydrous acetonitrile via the surface-imprinted polymerization method. PCA (0.25 mmol) and 4-VP (1.0 mmol) were dissolved in anhydrous acetonitrile (6.0 mL), purged with $N_2$, and then stored in a refrigerator at 4 °C for 12 h to prepare preassembly solution. Then, vinyl-modified $Fe_3O_4$@$SiO_2$ (50.0 mg), EGDMA (5.0 mmol), and AIBN (20.0 mg) were dissolved in acetonitrile (15.0 mL) and added into the above solution, purged with $N_2$ on ice, and then allowed to proceed for 24 h at 60 °C under constant stirring. After polymerization, MMIPs were collected magnetically, rinsed with acetonitrile until the supernatant was clear, and then eluted with methanol/acetic acid (9:1, v/v) to remove the template absolutely, which was monitored by HPLC. Finally, the MMIPs were washed with methanol to neutral pH and dried overnight under vacuum at 50 °C.

As a control, the same procedures were applied for the preparation of magnetic nonmolecularly imprinted polymers (MNIPs) in the absence of PCA.

**Characterization.** The morphology of microspheres was observed by transmission electron microscopy (TEM) (JEM-2100F, JEOL, Japan). The infrared spectra (4000−400 $cm^{-1}$) were recorded on a Fourier transform infrared spectrometer (FT-IR) (Nicolet 6700, Thermo Nicolet Co., Waltham, MA, USA). The encapsulation efficiency of microspheres was determined by thermogravimetric analysis (TGA SDTQ600, TA, USA). Magnetization was measured at room temperature in a vibration sample magnetometer (VSM7407, Lake Shore Cryotronics, Westerville, OH, USA).

**HPLC Analysis.** Chromatographic separation was performed on a Zorbax SB-$C_{18}$ column (150 mm × 4.6 mm, 5 μm, Agilent, Santa Clara, CA, USA) in tandem with a Phenomenex $C_{18}$ guard cartridge (4.0 mm × 3.0 mm, Phenomenex, Torrance, CA, USA). The eluent was delivered from an Agilent 1260 HPLC quaternary pump (Agilent Technologies) equipped with an online vacuum degasser, an autosampler, a thermostated column compartment, and a diode array detector. The mobile phase consisted of A (0.4% acetic acid in water) and B (0.4% acetic acid in methanol), which was programmed as follows: 0−30 min, 20−50% B. The flow rate was 0.8 mL/min, the temperature was controlled at 25 °C, and UV detection was operated at 260 nm.

**Adsorption Experiments.** For equilibrium experiments, 10.0 mg of MMIPs/MNIPs was suspended in 3.0 mL of a series of PCA acetonitrile solutions with initial concentrations ranging from 0.05 to 6.0 mg/mL. The series of mixtures were shaken for 40 min at 298, 308, and 318 K, and then the equilibrium concentrations of PCA were detected by HPLC. The equilibrium adsorption capacity $Q_e$ (mg/g) was calculated according to the equation

$$Q_e = (C_0 - C_e)V/m \quad (1a)$$

where $C_0$ (μg/mL) represents the initial concentration of PCA and $C_e$ (μg/mL) is the equilibrium concentrations of PCA. $V$ (mL) is the volume of PCA solution, whereas $m$ means the mass of MMIPs/MNIPs (g).

Similarly, for kinetic experiments, 10.0 mg of MMIPs/MNIPs was suspended in 3.0 mL of a 1.0 mg/mL PCA acetonitrile solution. The mixtures were then continuously shaken at 298 K, and the concentrations of PCA in the supernatant at certain intervals (5, 10, 20, 30, 40, 50, 70, 100, 140, 180, and 220 min) were analyzed by HPLC; then the adsorption capacity $Q_t$ (μg/g) at different contact times $t$ was calculated as

$$Q_t = (C_0 - C_t)V/m \quad (1)$$

where $C_t$ (mg/mL) is the concentration of PCA at different contact times.

Selectivity adsorption was performed using PCA and its four structurally similar compounds (4-HBA, SA, CA,and GA) in individual standard solutions with the same initial concentrations of 1 mg/mL.

**Regeneration and Reuse Experiments.** MMIPs with loaded PCA were separated magnetically, rinsed with acetonitrile to reduce the nonspecific adsorption, and then eluted with 1.0 mL of methanol/cetic acid (9:1, v/v) for 30 min for PCA desorption, and then the regenerated MMIPs were reused for the next adsorption experiment.

**Extraction and Determination of PCA in Fruit Juices.** Grape juice, apple juice, pineapple juice, orange juice, and peach juice (Huiyuan Juice, Beijing Huiyuan Beverage and Food Co., Ltd., China) were purchased from a local market in Changsha. All kinds of fruit juices (50 mL) were first centrifugated at 8000 rpm for 20 min, and then the supernatants were adjusted to pH 7.0 by 1.0 mM NaOH aqueous solution and submitted to liquid−liquid extraction twice using an equivalent volume of ethyl acetate. The ethyl acetate extraction was concentrated on a rotary evaporator (Shanghai Yarong Biochemical Instrument Factory, Shanghai, China) under reduced pressure at 40 °C to yield dried residue. The residue was dissolved in 10 mL of acetonitrile and stored at 4 °C for further experiments.

MMIPs/MNIPs (10.0 mg) were suspended in 3.0 mL of fruit juice extract. After 40 min of shaking at 298 K, MMIPs/MNIPs were collected by a magnet and then washed with acetonitrile followed by

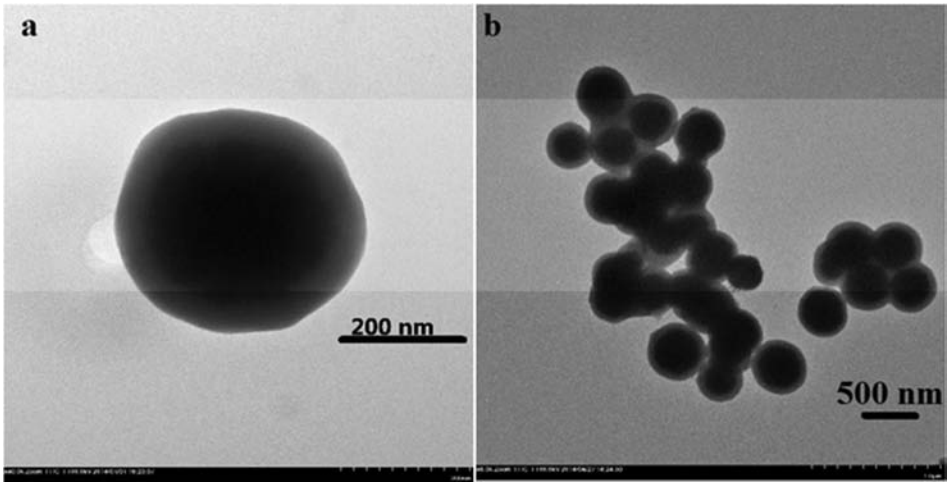


**Figure 1.** TEM images of $Fe_3O_4$@$SiO_2$ (a) and MMIPs (b).

3.0 mL of methanol/acetic acid (9:1, v/v) at 298 K for 30 min to release PCA. The eluates were analyzed by HPLC.

## RESULTS AND DISCUSSION

**Preparation of MMIPs.** MMIPs are prepared by surface-imprinted polymerization technology. The micro size of solid support has a large surface to volume ratio to provide abundant reaction sites for surface imprinting. Furthermore, the thin layer of MIPs is prepared on the surface of the solid support, which benefits the complete removal of template and the enhancement of mass transfer.[27] At the beginning, $Fe_3O_4$ microspheres were synthesized by solvothermal reaction, which have higher magnetic response than those prepared by coprecipitation method.[10,11] Then, well-dispersed $Fe_3O_4$@$SiO_2$ microparticles with magnetic core and silica shell were synthesized. Notably, our previous research indicated that the encapsulation of $Fe_3O_4$ with $SiO_2$ will improve their dispersion in water, reduce agglomeration phenomenon in repetitious magnetic separation, and then increase their reusability.[28] Moreover, a silica-like surface is easily modified with various groups through covalent reaction. After that, vinyl groups were introduced onto the surface of $Fe_3O_4$@$SiO_2$ with MPS for reaction with EDGMA to initiate the copolymerization of 4-VP and PCA in the presence of AIBN. Finally, MMIPs with surface binding sites were achieved by removal of templates.

The binding properties of MMIPs depend on various factors. To achieve high adsorption capacity with efficient recognition, some essential factors were investigated during the preparation procedures. Functional monomer is a key factor for the powerful molecular recognition of MIPs because the molecular recognition is based on the intermolecular interaction between the template and the functional monomer.[29] Templates containing phenolic substructures have been templated in the past, using both acidic and basic functional monomers; however, basic functional monomers associate more strongly with phenol derivatives, through hydrogen bonding between the basic nitrogen atom of the monomer and the phenolic proton.[30] Previous papers have reported the preparation of MIPs for PCA by bulk/precipitation polymerization, and basic AM has been selected as functional monomer.[18,19] Here, three kinds of basic functional monomers (4-VP, AM, and MAM) were selected to evaluate the specific recognition ability of MMIPs for PCA. Finally, 4-VP was considered as the optimum functional monomer because of the existence of strong electrostatic bonds and hydrogen-bonding interactions between pyridyl group of 4-VP and PCA as well as of the $\pi-\pi$ interactions between aromatic rings.[31] Thus, a more stable template−monomer complex between PCA and 4-VP can be formed in the imprinting process, which will lead to the formation of well-defined specific binding sites in MMIPs for high selectivity. Acetonitrile was selected as porogen, in which PCA and 4-VP was dissolved well. Moreover, the weak polarity solvent of acetonitrile was suitable for noncovalent molecular recognition of MIPs for strong polar molecule without any hydrophobic functional group.[32] The molar ratio of template−functional monomer−cross-linker was a critical factor in a successful imprinting protocol due to their effect on the number of recognition sites in synthesized MIPs and the quality of MIPs. Then different molar ratios of template−functional monomer−cross-linker (1:3:20, 1:4:20, 1:5:20, 1:4:16, 1:4:30, and 1:5:30) were evaluated and optimized. The results indicated that PCA−4-VP−EDGMA at 1:4:20 achieved highest adsorption capacity and molecular recognition ability of MMIPs. In addition, there is a competition between surface and bulk polymerization, which could affect the homogeneity of the MIP coating and then affect the binding capacity of MMIPs. Different quantities of $Fe_3O_4$@$SiO_2$ (25, 50, 75, and 100 mg) were used when the concentration of PCA was set at 0.25 mmol. Eventually, 50 mg of $Fe_3O_4$@$SiO_2$ was evaluated as the best choice.

**Characterization of MMIPs.** The particle size and morphology of $Fe_3O_4$@$SiO_2$ and MMIPs can be obviously observed by TEM (Figure 1). It can be seen that the core−shell structure of $Fe_3O_4$@$SiO_2$ microspheres with diameters of approximately at 400 nm were successfully prepared with regular spherical shape, relatively narrow size distribution, and good dispersity. About 50 nm thick $SiO_2$ shell was clearly seen to be uniformly coated on $Fe_3O_4$ dark core (Figure 1a). After the imprinting process, an external imprinted polymer layer of about 40 nm was clearly observed around $Fe_3O_4$@$SiO_2$ microparticles (Figure 1b), which suggested that the MIP layer had been successfully grafted on the surface of $Fe_3O_4$@$SiO_2$ microparticles. There were hardly any free $Fe_3O_4$, $SiO_2$, and MIPs microspheres in the TEM view. It was noted that the surface recognition sites could improve the mass transfer rate for adsorption and desorption of the template quickly.

In FT-IR spectra, the strong absorption peak at about 580 $cm^{-1}$ was characteristic of Fe−O vibration (Figure 2a), and the

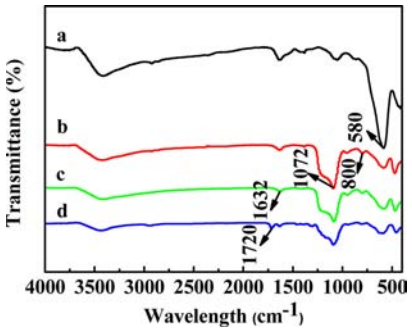


**Figure 2.** FT-IR spectra of $Fe_3O_4$ (a), $Fe_3O_4$@$SiO_2$ (b), vinyl-modified $Fe_3O_4$@$SiO_2$ (c), and MMIPs (d).

strong peaks around 1072 $cm^{-1}$ (Si−O asymmetric strenching vibration) and 800 $cm^{-1}$ (Si−O symmetric strenching vibration) displayed that $SiO_2$ was successfully encapsulated onto the surface of $Fe_3O_4$ microspheres (Figure 2b). The stretching vibration of C═C bonds at 1632 $cm^{-1}$ was attributed to the successful functionalization with vinyl groups (Figure 2c). The new adsorption peak of the C═O stretching band at 1720 $cm^{-1}$ for EDGMA showed that the MIPs were successfully coated on the surface of $Fe_3O_4$@$SiO_2$. The existence of C═C vibration indicated that not all of the EDGMA was cross-linked.[33]

TGA was performed to quantify the encapsulation. As shown in Figure 3, the small weight loss of about 5% at a temperature

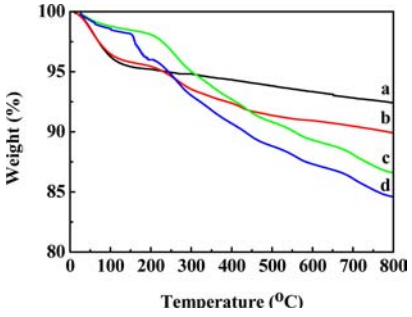


**Figure 3.** TGA curves of $Fe_3O_4$@$SiO_2$ (a), vinyl-modified $Fe_3O_4$@$SiO_2$ (b), MMIPs (c), and MNIPs (d).

of <200 °C was attributed to the elimination of water in samples. After that, $Fe_3O_4$@$SiO_2$ showed a weight loss of about 2% when heated to 800 °C, probably due to some contaminations. About 4% more weight loss was observed for vinyl-modified $Fe_3O_4$@$SiO_2$ because of the decomposition of grafted MPS. Significant weight loss of MMIPs (11%) and MNIPs (14%) could be observed. The slight difference may be come from the different grafting density caused by the template.

The magnetic saturation of MMIPs was about 20 emu/g, which was lower than that of $Fe_3O_4$ microspheres (56 emu/g) (Figure 4). This might be related to the magnetic inactive layer containing $SiO_2$ and imprinted polymer layers. However, the decrease did not seriously affect the magnetic separation of MMIPs, and they remained strongly magnetic and could be accumulated within 10 s in solution under a conventional magnet and dispersed quickly with a slight shake once the magnetic field was removed, which indicated that MMIPs were successfully synthesized with high magnetic responsivity. No

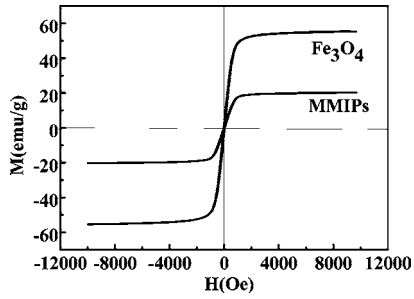


**Figure 4.** Magnetization curves of $Fe_3O_4$ and MMIPs.

remanence was detected after removal of the applied magnetic field, revealing that MMIPs was superparamagnetic.

**Adsorption Isotherms.** Figure 5a shows characteristic adsorption isotherms at 298 K. It was obvious that the equilibrium adsorption capacity of PCA on MMIPs/MNIPs increased first and then became saturated when the concentration reached 0.4 mg/mL. The equilibrium adsorption capacity of PCA on MMIPs was 7.5 mg/g, 1.5 times that on MNIPs (5.3 mg/g), which might result from the imprinting effect. That is to say, MMIPs had a significantly specific adsorption to PCA for the existence of imprinting phenomenon, and MNIPs showed low adsorption ability because of the randomly distributed functional groups on the surface. Therefore, MMIPs can selectively extract PCA from complex matrices. It was noted that equilibrium adsorption capacity of PCA on MMIPs (calculated to be 68.7 mg/(g, MIPs)) was largely higher than that for previously reported traditional MIPs (34.7 $\mu$g/g and 0.16 mg/g).[18,19] We have previously prepared MMIPs using benzoic acid/4-HBA as template, 4-VP as functional monomer, and acetonitrile as porogenic solvent;[10] their equilibrium adsorption capacities of PCA were a little lower (<65 mg/(g, MIPs)) because of the complementary specific sites for template. Clearly, MIPs grafted on microparticles can take measure to ensure almost all of the imprinting sites on surface and then increase the accessibility of template to the recognition sites for high binding capacity.

Figure 5b shows adsorption isotherms of PCA on MMIPs with the temperature at 298, 308, and 318 K. The equilibrium adsorption capacities of PCA increased with the increment of temperature, which corresponded with previous investigation that MIPs prepared at higher temperature tend to work better at higher temperature because of the similar 3D structures.[34] Moreover, lower viscosity and surface tension of the solvent at higher temperature improved wetting of the MMIPs, which was then to a certain extent led to higher binding capacity. To further estimate the binding properties of MMIPs and MNIPs, two classical isotherm models, Langmuir and Freundlich equations, were selected to fit the experimental data. The Langmuir equation $[1/Q_e = 1/(K_L C_e Q_m) + 1/Q_m$, where $Q_m$ is the maximum adsorption capacity (mg/g) and $K_L$ is a characteristic constant (mL/mg)] can be used to describe a monolayer adsorption, whereas the Freundlich equation $[\log Q_e = (\log C_e)/n + \log K_F$, where $n$ and $K_F$ are Freundlich constants] can be used to describe a monolayer adsorption as well as a multilayer adsorption. Table 1 summarizes the fitted parameters $Q_m$, $K_L$, $K_F$, $n$, and $R^2$ (correlation coefficient), which revealed that the Langmuir equation with $R^2 > 0.99$ was found to better fit the isotherm data. Moreover, the saturated adsorption capacities of MMIPs for PCA at different temperatures were


dx.doi.org/10.1021/jf5021895 | J. Agric. Food Chem. 2014, 62, 8221−8228

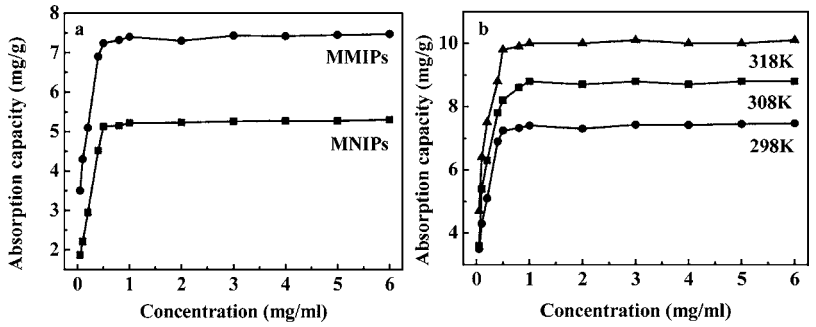


**Figure 5.** Equilibrium adsorption curves of MMIPs/MNIPs for PCA at 298 K (a), and equilibrium adsorption isotherms of MMIPs for PCA with the temperature at 298, 308, and 318 K (b).

**Table 1. Adsorption Isotherm Constants for the Langmuir and Freundlich Equations**

| | | Langmuir | | | Freundlich | | |
|---|---|---|---|---|---|---|---|
| | $T$ (K) | $K_L$ (mL/mg) | $Q_m$ (mL/mg) | $R^2$ | $n$ | $K_F$ | $R^2$ |
| MMIPs | 298 | 4.03 | 8.40 | 0.992 | 3.22 | 9.20 | 0.983 |
| | 308 | 4.49 | 9.82 | 0.999 | 2.81 | 5.28 | 0.981 |
| | 318 | 5.29 | 10.8 | 0.999 | 2.71 | 6.46 | 0.926 |
| MNIPs | 298 | 1.78 | 6.41 | 0.996 | 2.31 | 6.59 | 0.966 |
| | 308 | 1.97 | 7.05 | 0.998 | 1.86 | 3.54 | 0.984 |
| | 318 | 2.39 | 7.75 | 0.995 | 2.14 | 4.02 | 0.971 |

greatly higher than those of MNIPs, which indicated that MMIPs showed higher binding affinity for PCA than MNIPs.

**Adsorption Kinetics.** The kinetic curves of PCA adsorption on MMIPs/MNIPs at 298 K are illustrated in Figure 6. As we can see, the adsorption capacity of PCA

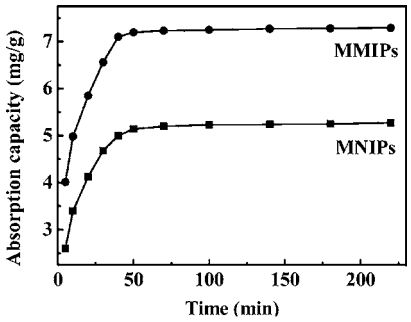


**Figure 6.** Kinetic adsorption curves of MMIPs/MNIPs for PCA at 298 K.

increased with the increment of adsorption time. The adsorption of PCA on MMIPs reached adsorption equilibrium at 40 min, suggesting that the adsorption is a fast process, and then 40 min was chosen as optimal extraction time. In comparison, traditionally imprinted materials would take 12–24 h to reach adsorption equilibrium.[17] Therefore, surface imprinting technology provided binding sites at the surface of microparticles, which then showed the advantage of faster mass transfer and binding kinetics.

The Lagergren pseudo-first-order equation [$\ln(Q_e - Q_t) = \ln Q_e - K_1 t$), where $K_1$ is the pseudo-first-order rate constant ($min^{-1}$)] and pseudo-second-order equation [$t/Q_t = t/Q_e + 1/(Q_e^2 K_2)$, where $K_2$ is the pseudo-second-order rate constant] were used to analyze the kinetic data according to our previous report to determine the rate-controlling and mass transfer mechanisms.[10] The corresponding parameters by two kinetic models were calculated and are displayed in Table 2. It could be concluded that the pseudo-second-order rate equation was considered as the better-fit model from high $R^2$ (>0.99) and close data between calculated $Q_e$ and experimental data suggested. Similar results were reported for adsorption of hydrobenzoic acids on MMIPs.[10]

**Selectivity Adsorption for PCA.** Molecular recognition ability of MMIPs was mainly dependent on the bonding between MMIPs and adsorbed components, and then the binding ability was related to similarity between template and adsorbed components in functional groups, size, and shape. It is obvious in Figure 7 that adsorption capacities of five components (PCA, 4-HBA, SA, GA, and CA) on MNIPs (nonspecific adsorption) had no significant difference. In comparison, the adsorption capacities of five selected components on MMIPs were much higher than those on MNIPs. The difference results illustrated the success of the imprinting process. Although five selected components had close structural homology, the adsorption capacity of PCA was about 1.21, 1.79, 1.48, and 1.81 times that for 4-HBA, SA, GA,

**Table 2. Kinetic Constants for Pseudo-First-Order Rate and Pseudo-Second-Order Rate Equations**

| | | pseudo-first-order | | | pseudo-second-order | | |
|---|---|---|---|---|---|---|---|
| | $Q_{e(exptl)}$ (mg/g) | $R^2$ | $K_1$ ($min^{-1}$) | $Q_{e(calcd)}$ (mg/g) | $R^2$ | $K_2$ (g/mg·min) | $Q_{e(calcd)}$ (mg/g) |
| MMIPs | 7.29 | 0.980 | 0.078 | 5.562 | 0.997 | 0.020 | 8.065 |
| NNIPs | 5.27 | 0.992 | 0.065 | 3.951 | 0.998 | 0.024 | 5.848 |


dx.doi.org/10.1021/jf5021895 | J. Agric. Food Chem. 2014, 62, 8221–8228

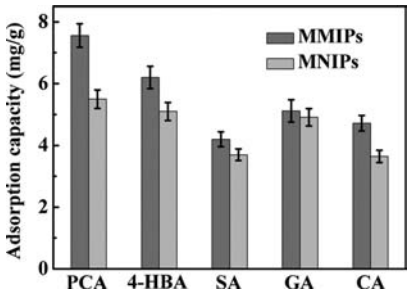


**Figure 7.** Adsorption capacities of PCA, 4-HBA, SA, GA, and CA on MMIPs/MNIPs.

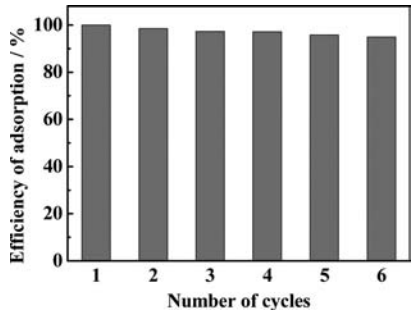


**Figure 8.** Reusability of MMIPs (mean values of five batch samples).

and CA, which was because the specific sites in MMIPs were complementary in shape, size, and spatial distribution to match PCA. The selectivity of MMIPs was further evaluated using three parameters: the distribution coefficient ($K_d$), selectivity coefficient ($K$), and relative selectivity coefficient ($K'$). As shown in Table 3, $K'$ values were >1, which showed a higher binding selectivity of MMIPs than MNIPs for PCA than other tested similar compounds. However, in our previously prepared MMIPs using benzoic acid/4-HBA as template, the $K'$ values ($K' = K_{MMIPs}/K_{MNIPs}$, $K' = K_{d(template)}/K_{d(PCA)}$) for PCA were <1.[10] This could be attributed to the imprinting effect. The comparison result of the adsorption capacity was attributed to the molecular analogue degree of detected compounds to the template molecule. Although 4-HBA, SA, and GA had close structural homology with PCA, except for the numbers and positions of phenolic hydroxyl groups, the lower adsorption capacity was probably because there were no specific imprinted sites for compounds with different molecular size and stereochemistry. For CA, the steric effect of the acrylic group presumably prevented it from entering into the binding cavities, and as a result, weak binding capacity was detected. These data indicated the imprinting effect of MMIPs could make sense for selective extraction of PCA from real complex samples, so the characteristics of MMIPs were superior to those of traditional inefficient selective adsorbents.

**Reusability of MMIPs.** Our previous paper indicated that methanol/acetic acid (9:1, v/v) could weaken the noncovalent interactions between hydroxybenzoic acids and MIPs and then was considered as the optimum desorption solvent to recover template and regenerate MIPs.[11] The optimum desorption time was selected as 30 min according to the desorption ratio (about 96%). The reusability of MMIPs was investigated by monitoring the efficiency of adsorption of five batch samples for great cost benefit on extending its applications. As shown in Figure 8, after six consecutive adsorption−desorption cycles under the same conditions, the efficiency of adsorption was still as high as 94.9% of the first one. The results manifested that MMIPs were stable and six cycles had little influence on its efficiency of adsorption.

**Method Validation.** The MMIPs as adsorbent for extraction and enrichment of PCA and the HPLC-UV method for analysis of PCA had been established. Then the application of the method was evaluated by determining its performance characteristics regarding linearity, reproducibility, accuracy, precision, limit of detection, ruggedness, and robustness. Using the standard curve based method, the ratios of the HPLC peak areas ($A$) with respect to the corresponding concentrations of PCA ($C$) were found to be linear from 1 to 100 $\mu$g/mL with $R^2$ value at 0.9996. The regression equation was $A = 62.6C + 22.7$. The limit of detection (S/N = 3) for PCA was 0.5 $\mu$g/mL, which was sufficient for PCA determination in real samples.

The intraday and interday precisions were investigated by extraction and analysis of PCA-spiked reference standard in grape juice at low, medium, and high concentration levels five times per day and for six consecutive days. The RSD values of intraday precisions ranged from 1.0 to 5.0% ($n = 6$), which were indicative of high reproducibility, and the RSD values of interday precisions over a six-day span were all <6.0%. Indeed, acceptable recovery values, ranging from 92 to 107% with RSD <5%, were obtained for PCA. The results showed that the proposed MMIP extraction and HPLC analysis method was sufficiently accurate, selective, and practical for the determination of PCA from complex matrices.

**Analysis of Fruit Juices.** Fruit juices produced from fruit are very complex matrices, which subsequently can cause matrix effects during the extraction process. For this reason, it was necessary to apply a selective pretreatment step to isolate target components from complex matrices before HPLC analysis. PCA is a polar component with retention time at 5.60 min, and from 3D UV−vis spectra, we can see interferences that had almost the same retention time as PCA in grape juice (Figure

**Table 3. Selectivity Parameters of MMIPs/MNIPs[a] ($n = 3$)**

| | | PCA | 4-HBA | SA | GA | CA |
|---|---|---|---|---|---|---|
| MMIPs | Q (mg/g) | 7.56 ± 0.5 | 6.23 ± 0.4 | 4.22 ± 0.3 | 5.12 ± 0.4 | 4.17 ± 0.2 |
| | $K_d$ (mL/g) | 7.71 | 6.32 | 4.25 | 5.19 | 4.18 |
| | $K$ | | 1.22 | 1.81 | 1.48 | 1.84 |
| MNIPs | Q (mg/g) | 5.22 ± 0.3 | 4.92 ± 0.4 | 3.11 ± 0.2 | 4.31 ± 0.3 | 3.18 ± 0.2 |
| | $K_d$ (mL/g) | 5.29 | 4.98 | 3.23 | 4.37 | 3.21 |
| | $K$ | | 1.06 | 1.64 | 1.21 | 1.65 |
| | $K'$ | | 1.15 | 1.10 | 1.22 | 1.11 |

[a] $K_d$ = binding amount/equilibrium concentration, $K = K_{d(PCA)}/K_{d(similar\ components)}$, $K' = K_{MMIPs}/K_{MNIPs}$.


dx.doi.org/10.1021/jf5021895 | J. Agric. Food Chem. 2014, 62, 8221−8228

9a). Therefore, quantitative analysis results of PCA in grape juice by HPLC-UV method without selective pretreatment

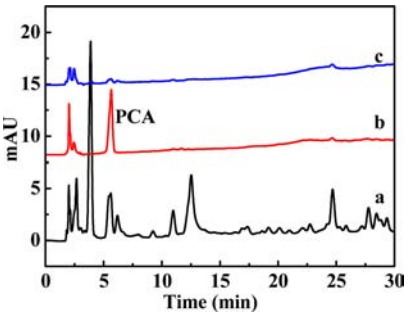


**Figure 9.** Chromatograms of grape juice (a) and the elutions with methanol/acetic acid (9:1, v/v) from MMIPs (b) and MNIPs (c).

process were sometimes imprecise. PCA was then selectively adsorbed and enriched onto MMIPs (Figure 9b), and the peak of PCA appeared distinctly, whereas no obvious PCA peak was observed in the eluted solution MNIPs (Figure 9c), which also demonstrated the selectivity of MMIPs. Therefore, the content of PCA in grape juice was easily found to be 0.45 $\mu$g/mL. However, PCA was not detected in apple juice, pineapple juice, orange juice, and peach juice, which agreed well with values reported in the literature.[35] The results indicated that the prepared MMIPs were very suitable to be directly exploited in efficient and selective enrichment and determination of trace PCA in complex matrices (e.g., juices, foods, natural products, biological samples).

## AUTHOR INFORMATION

### Corresponding Authors

*(L.X.) Phone: +86 731 88879616. E-mail: xiecsu@126.com.
*(S.S.) E-mail: shuyshi@gmail.com.

### Funding

This work was sponsored by the National Natural Science Foundation of China (21275163), the China Postdoctoral Science Foundation (2013M531787, 2014M550426), the Science and Technology Program of Hunan Province, China (2012FJ2006, 2013RS4035, 2014RS4004), the Postdoctoral Science Foundation of Central South University, and the Shenghua Yuying project of Central South University.

### Notes

The authors declare no competing financial interest.

## REFERENCES

(1) Duthie, G. Protocatechuic acid: the missing human cyanidins' metabolite-answer. *Mol. Nutr. Food Res.* **2008**, *53*, 388−388.
(2) Vitaglione, P.; Donnarumma, G.; Napolitano, A.; Galvano, F.; Gallo, A.; Scalfi, L.; Fogliano, V. Protocatechuic acid is the major human metabolite of cyanidin-glucosides. *J. Nutr.* **2007**, *137*, 2043−2048.
(3) Palafox-Carlos, H.; Gil-Chavez, J.; Sotelo-Mundo, R. R.; Namiesnik, J.; Gorinstein, S.; Gonzalez-Aguilar, G. A. Antioxidant interactions between major phenolic compounds found in 'Ataulfo' mango pulp: chlorogenic, gallic, protocatechuic and vanillic acids. *Molecules* **2012**, *17*, 12657−12664.
(4) Tseng, T. H.; Kao, T. W.; Chu, C. Y.; Chou, F. P.; Lin, W. L.; Wang, C. J. Induction of apoptosis by hibiscus protocatechuic acid in human leukemia cells via reduction of retinoblastoma (RB) phosphorylation and Bcl-2 expression. *Biochem. Pharmacol.* **2000**, *60*, 307−315.
(5) Yin, M. C.; Lin, C. C.; Wu, H. C.; Tsao, S. M.; Hsu, C. K. Apoptotic effects of protocatechuic acid in human breast, lung, liver, cervix, and prostate cancer cells: potential mechanisms of action. *J. Agric. Food Chem.* **2009**, *57*, 6468−6473.
(6) Cornò, M. D.; Varano, B.; Scazzocchio, B.; Filesi, C.; Masella, R.; Gessani, S. Protocatechuic acid inhibits human dendritic cell functional activation: role of PPARγ up-modulation. *Immunobiology* **2014**, *219*, 416−424.
(7) Arce, L.; Ríos, A.; Valcárcel, M. Determination of anti-carcinogenic polyphenols present in green tea using capillary electrophoresis coupled to a flow injection system. *J. Chromatogr., A* **1998**, *827*, 113−120.
(8) Yang, Y. C.; Wei, M. C.; Huang, T. C.; Lee, S. Z. Extraction of protocatechuic acid from *Scutellaria barbata* D. Don using supercritical carbon dioxide. *J. Supercrit. Fluids* **2013**, *81*, 55−66.
(9) Kelebek, H.; Selli, S.; Canbas, A.; Cabaroglu, T. HPLC determination of organic acids, sugars, phenolic compositions and antioxidant capacity of orange juice and orange wine made from a Turkish cv. Kozan. *Microchem. J.* **2009**, *91*, 187−192.
(10) Shi, S. Y.; Guo, J. F.; You, Q. P.; Chen, X. Q.; Zhang, Y. P. Selective and simultaneous extraction and determination of hydroxybenzoic acids in acqueous solution by magnetic molecularly imprinted polymers. *Chem. Eng. J.* **2014**, *243*, 485−493.
(11) You, Q. P.; Peng, M. J.; Zhang, Y. P.; Guo, J. F.; Shi, S. Y. Preparation of magnetic dummy molecularly imprinted polymers for selective extraction and analysis of salicyclic acid in *Actinidia chinensis*. *Anal. Bioanal. Chem.* **2014**, *406*, 831−839.
(12) Haupt, K.; Mosbach, K. Molecularly imprinted polymers and their use in biomimetic sensors. *Chem. Rev.* **2000**, *100*, 2495−2504.
(13) Yan, H. Y.; Cheng, X. L.; Sun, N. Synthesis of multi-core-shell magnetic molecularly imprinted microspheres for rapid recognition of dicofol in tea. *J. Agric. Food Chem.* **2013**, *61*, 2896−2901.
(14) Euterpio, M. A.; Pagano, I.; Piccinelli, A. L.; Rastrelli, L.; Crescenzi, C. Development and validation of a method for the determination of (*E*)-resveratrol and related phenolic compounds in beverages using molecularly imprinted solid phase extraction. *J. Agric. Food Chem.* **2013**, *61*, 1640−1645.
(15) Schwarz, L. J.; Danylec, B.; Yang, Y. Z.; Harris, S. J.; Boysen, R. I.; Hearn, M. T. W. Enrichment of (*E*)-resveratrol from peanut byproduct with molecularly imprinted polymers. *J. Agric. Food Chem.* **2011**, *59*, 3539−3543.
(16) You, Q. P.; Zhang, Y. P.; Zhang, Q. W.; Guo, J. F.; Huang, W. H.; Shi, S. Y.; Chen, X. Q. High-capacity thermo-responsive magnetic molecularly imprinted polymers for selective extraction of curcuminoids. *J. Chromatogr., A* **2014**, *1354*, 1−8.
(17) Cheong, W. J.; Yang, S. H.; Ali, F. Molecular imprinted polymers for separation science: a review of reviews. *J. Sep. Sci.* **2013**, *36*, 609−628.
(18) Karasová, G.; lehotay, J.; Sádecká, J.; Skačáni, I.; Lachová, M. Selective extraction of derivates of *p*-hydroxybenzoic acid from plant material by using a molecularly imprinted polymer. *J. Sep. Sci.* **2005**, *28*, 2468−2476.
(19) Chen, F. F.; Wang, G. Y.; Shi, Y. P. Molecularly imprinted polymer microspheres for solid-phase extraction of protocatechuic acid in *Rhizoma homalomenae*. *J. Sep. Sci.* **2011**, *34*, 2602−2610.
(20) Zhou, H.; Xu, Y. P.; Tong, H. W.; Liu, Y. X.; Han, F. Direct synthesis of surface molecularly imprinted polymers based on vinyl-$SiO_2$ nanospheres for recognition of bisphenol A. *J. Appl. Polym. Sci.* **2013**, *128*, 3846−3852.
(21) Anirudhan, T. S.; Alexander, S. Multiwalled carbon nanotubes based molecular imprinted polymer for trace setermination of 2,4-dichlorophenoxyaceticacid in natural water samples using a potentiometric method. *Appl. Surf. Sci.* **2014**, *303*, 180−186.
(22) Guo, M. J.; Hu, X.; Fan, Z.; Liu, J.; Wang, X. C.; Wang, Y.; Mi, H. F. Imprinted polymers with cyclodextrin pseudo-polyrotaxanes as pseudo-supports for protein recognition. *Talanta* **2013**, *105*, 409−416.
(23) Yan, H. Y.; Cheng, X. L.; Sun, N. Synthesis of multi-core−shell magnetic molecularly imprinted microspheres for rapid recognition of dicofol in tea. *J. Agric. Food Chem.* **2013**, *61*, 2896−2901.

(24) Zhang, Y. P.; Shi, S. Y.; Chen, X. Q.; Peng, M. J. Functionalized magnetic nanoparticles coupled with mass spectrometry for screening and identification of cyclooxygenase-1 inhibitors from natural products. *J. Chromatogr., B* **2014**, *960*, 126−132.
(25) Zhang, Y. P.; Nie, M. K.; Shi, S. Y.; You, Q. P.; Guo, J. F.; Liu, L. L. Integration of magnetic solid phase fishing and off-line two-dimensional high-performance liquid chromatography-diode array detector-mass spectrometry for screening and identification of human serum albumin binders from Radix Astragali. *Food Chem.* **2014**, *146*, 56−64.
(26) Deng, Y. H.; Qi, D. W.; Deng, C. H.; Zhang, X. M.; Zhao, D. Y. Superparamagnetic high-magnetization microspheres with an $Fe_3O_4$@$SiO_2$ core and perpendicularly aligned mesoporous $SiO_2$ shell for removal of microcystins. *J. Am. Chem. Soc.* **2008**, *130*, 28−29.
(27) Xie, C. G.; Zhang, Z. P.; Wang, D. P.; Gao, G. M.; Liu, J. H. Surface molecular self-assembly strategy for TNT imprinting of polymer nanowire/nanotube arrays. *Anal. Chem.* **2006**, *78*, 8339−8346.
(28) Liu, L. L.; Shi, S. Y.; Zhao, H. D.; Yu, J. G.; Jiang, X. Y.; Chen, X. Q. Selective fishing and analysis of xanthine oxidase binders from two Fabaceae species by coupling enzyme functionalized core-shell magnetic nanoparticles with HPLC-MS. *J. Chromatogr., B* **2014**, *945−946*, 163−170.
(29) Sun, Z.; Schussler, W.; Sengl, M.; Niessner, R.; Knopp, D. Selective trace analysis of diclofenac in surface and wastewater samples using solid-phase extraction with a new molecularly imprinted polymer. *Anal. Chim. Acta* **2008**, *620*, 73−81.
(30) Tsermentseli, S. K.; Manesiotis, P.; Assimopoulou, A. N.; Papageorgiou, V. P. Molecularly imprinted polymers for the isolation of bioactive naphthoquinones from plant extracts. *J. Chromatogr., A* **2013**, *1315*, 15−20.
(31) Haupt, K.; Dzgoev, A.; Mosbach, K. Assay system for the herbicide 2,4-dichlorophenoxyacetic acid using a molecularly imprinted polymer as an artificial recognition element. *Anal. Chem.* **1998**, *70*, 628−631.
(32) Chen, F. F.; Xie, X. Y.; Shi, Y. P. Preparation of magnetic molecularly imprinted polymer for selective recognition of resveratrol in wine. *J. Chromatogr., A* **2013**, *1300*, 112−118.
(33) Gam-Derouich, S.; Nguyen, M. N.; Madani, A.; Maouche, N.; Lang, P.; Perruchot, C.; Chehmi, M. M. Aryl diazonium salt surface chemistry and ATRP for the preparation of molecularly imprinted polymer grafts on gold substrates. *Surf. Interface Anal.* **2010**, *42*, 1050−1056.
(34) Kong, X.; Gao, R. X.; He, X. W.; Chen, L. X.; Zhang, Y. K. Synthesis and characterization of the core−shell magnetic molecularly imprinted polymers ($Fe_3O_4$@MIPs) adsorbents for effective extraction and determination of sulfonamides in the poultry feed. *J. Chromatogr., A* **2012**, *1245*, 8−16.
(35) de Simón, B. F.; Pérez-Ilzarbe, J.; Hernández, T.; Gómez-Cordovés, C.; Estrella, I. Importance of phenolic compounds for the characterization of fruit juices. *J. Agric. Food Chem.* **1992**, *40*, 1531−1535.

JOURNAL OF AGRICULTURAL AND FOOD CHEMISTRY

Article

pubs.acs.org/JAFC

# Lipases in Wheat Breadmaking: Analysis and Functional Effects of Lipid Reaction Products

Monika Schaffarczyk,[†] Henrik Østdal,[‡] and Peter Koehler*[,†]

[†]Deutsche Forschungsanstalt für Lebensmittelchemie, Leibniz Institut, Lise-Meitner-Straße 34, 85354 Freising, Germany

[‡]Novozymes A/S, Krogshoejvej 36, 2880 Bagsvaerd, Denmark

Supporting Information

**ABSTRACT:** The baking activity of two different lipases was evaluated by a microbaking test on a 10 g flour basis, and the altered lipid composition of lipase-treated wheat lipids was quantitated. To identify and quantitate the various lipid classes, pure glycolipids and phospholipids were isolated from a wheat flour lipid extract by a silica gel batch procedure and silica gel column chromatography. These reference compounds were used to establish a high-performance liquid chromatographic method with evaporative light scattering detection, which was able to separate all of the wheat lipid classes and lipase reaction products. Wheat lipids, dough lipids, and dough lipids after lipase addition were quantitated using cholesterol as an internal standard. Especially digalactosyl diglycerides (−0.9 mmol/kg flour), monogalactosyl diglycerides (−0.4 mmol/kg), and *N*-acyl-phosphatidyl ethanolamine (−0.3 mmol/kg) were hydrolyzed, and a concomitant formation of digalactosyl monoglycerides (+0.6 mmol/kg), monogalactosyl monoglycerides (+0.6 mmol/kg), and *N*-acyl-lysophosphatidyl ethanolamine (+0.5 mmol/kg) was found. The lipase-induced changes of the lipid fraction caused increases in bread volume of 56−58%, depending on the type and concentration of the added lipase. The current results confirm the important relationship between the lipid fraction composition and the baking performance of flour.

**KEYWORDS:** *lipase, wheat lipids, HPLC-ELSD, microbaking test*

## INTRODUCTION

The lipid content of wheat is considered of utmost importance for the baking performance of wheat flour. Wheat grain usually contains 3−4% lipid depending on genetics and growth conditions, while wheat flour contains 1−2.5% lipid depending on the raw materials and milling conditions. Wheat flour lipids are divided into two major groups based on their location and functionality. Two-thirds are nonstarch-bound lipids and one-third is starch-bound lipids.[1] Starch lipids are primarily composed of lysophospholipids, which form inclusion complexes with amylose helices in native starch.[2] Only the nonstarch lipids are considered to be active in baking.[3] Nonstarch lipids are extractable at room temperature (RT) and can be further subdivided into free and bound lipids according to the solvent used for their extraction.

Although lipids are present in wheat in considerably lower levels than are starch and protein, they exhibit important functional properties in breadmaking. Several studies have examined the functionality of endogenous wheat flour lipids in breadmaking based on fractionation and reconstitution methods, as reviewed in detail by Pareyt et al.[4] It was also shown that the improved bread properties were mainly due to the polar wheat lipids,[5,6] and glycolipids are considered more active than phospholipids as suggested by De Stefanis and Ponte.[7]

In the past few decades, demands for consistent quality in baked goods led to the application of a wide range of additives in the baking industry. Beside synthetic emulsifiers such as diacetyl tartaric esters of mono- and diglycerides (DATEM) or sodium stearoyl-2-lactylate (SSL), lipases along with other enzymes are being used to improve the baking quality of wheat flour. Currently available lipases for baking applications hydrolyze a number of different lipid structures in flour and lead to improved surface activity of these endogenous lipids, thus resulting in the significant increase in bread volume after baking.[10] The specific improving effect of individual lipases is mainly considered to be due to their preference for certain lipid classes, resulting in the formation of a lipase-specific range of products.[8] In particular, this has been shown by Gerits et al.,[9,10] who also suggested theories on the mechanism of action. Altogether, information about lipase-generated lipids is known to some extent for single components, but in-depth understanding of lipase-mediated reaction products is missing, and especially information regarding the function of lipid mixtures generated by the action of lipases is still very scarce.

The aim of this study was to quantitate lipids from wheat flour and wheat dough after the addition of two different commercial lipases. Therefore, the generation of lipase reaction products and the consumption of the lipase substrates were quantitatively analyzed. Different lipase concentrations as well as two different lipid extraction procedures were used. The functional effects of lipases in baking were demonstrated by microscale baking tests using 10 g of flour, and classical surfactants such as DATEM and SSL were used as benchmarks. Quantitation of wheat lipids required obtaining reference compounds either by isolation from wheat lipids or by lipase-aided hydrolysis from isolated compounds and fractions. High

Received: May 12, 2014
Revised: July 16, 2014
Accepted: July 17, 2014
Published: July 17, 2014

ACS Publications © 2014 American Chemical Society

performance liquid chromatography coupled to an evaporative light scattering detector (HPLC-ELSD) based on a method published by Gerits et al.[9,10] was applied for lipid analysis with the aim to separate all polar and nonpolar wheat lipid classes, as well as the lipase reaction products, in a single HPLC run. In contrast to Gerits et al.,[10] absolute concentrations of lipid classes were determined.

## MATERIALS AND METHODS

**Wheat Flour.** 'Kolibri' flour, a commercial flour obtained from a mixture of wheat cultivars (Meneba, Rotterdam, The Netherlands, 2012 harvest), was characterized as follows. The moisture and ash contents of the flour were determined according to ICC Standards 110[12] and 104,[13] respectively. Nitrogen contents were determined by means of the method of Dumas on a TruSpec N nitrogen analyzer (Leco, Kirchheim, Germany). A conversion factor of 5.7 was used to calculate the crude protein content from the nitrogen content. Analytical characteristics of the flour were 13.3% moisture, 10.7% protein (dry mass), and 0.52% ash (dry mass).

**Chemicals and Reagents.** Fresh baker's yeast was obtained from Wieninger GmbH (Passau, Germany). All solvents used were HPLC or LC−MS grade and from Sigma-Aldrich (Steinheim, Germany). The following reagents were purchased from the sources given in squared brackets: L-α-phosphatidic acid sodium salt from chicken egg (PA), L-α-phosphatidyl ethanolamine from chicken egg (PE), L-α-phosphatidyl choline (95%) from chicken egg (PC), L-α-phosphatidyl serine sodium salt from soy (PS), L-α-phosphatidyl inositol sodium salt from soy (PI), monogalactosyl diglyceride (MGDG), digalactosyl diglyceride (DGDG), 1-oleoyl-2-hydroxy-*sn*-glycero-3-phosphate sodium salt (LPA), L-α-lysophosphatidyl choline from soy (LPC), 1-oleoyl-2-hydroxy-*sn*-glycero-3-phospho ethanolamine (LPE), L-α-phosphatidyl glycerol sodium salt from soy (PG), 1-oleoyl-2-hydroxy-*sn*-glycero-3-phospho-(1′-rac-glycerol) sodium salt (LPG), 1-oleoyl-2-hydroxy-*sn*-glycero-3-phospho-L-serine sodium salt (LPS), L-α-lysophosphatidyl inositol sodium salt from soy (LPI) [Avanti Polar Lipid through Otto Nordwald GmbH, Hamburg, Germany]; steryl glucosides (SG), acylated steryl glucosides (ASG), ceramides (*N*-acyl-sphingosine) (CER), glucocerebrosides (cerebroside) (CBR) [Matreya LLC through Bio Trend, Cologne, Germany]; Monomuls 90−35 (monoglycerides containing 75% stearic and 35% palmitic acid, monoglyceride content 90%), Lametop 300 (80% DATEM, 20% calcium carbonate as anticaking reagent); Prefera SSL 6000 [BASF, Illertissen, Germany]; glyceryl-1,3-distearate, glyceryl trioleate, ethanolamine (>99%), acetic acid eluent additive for LC−MS [Sigma-Aldrich, Steinheim, Germany]; silica gel G 60 (0.04−0.063 mm), silica gel (0.063−0.200 mm), concentrating zone-high performance thin layer chromatography (HPTLC) plates (20 × 10 $cm^2$) coated with silica gel G 60 on glass, concentrating zone-HPTLC plates (20 × 20 $cm^2$) coated with silica gel G 60 on glass [VWR Merck, Darmstadt, Germany]; commercial enzyme granulate Lipopan F-BG (25.0 KLU/g), commercial enzyme granulate Lipopan Xtra-BG (7.2 KLU/g) [Novozymes A/S, Bagsvaerd, Denmark]. *N*-acyl phosphatidyl ethanolamine and monogalactosyl monoglyceride were obtained from Novozymes (Bagsvaerd, Denmark).

**Lipid Extraction from Flour.** Two different lipid extraction methods were compared regarding the extracted lipid composition. Lipids were extracted from flour using water-saturated 1-butanol (WSB) or 2-propanol at 75 °C. WSB was obtained when HCl (1 L; 80 mmol/L) and 1-butanol (2.5 L) were stirred for 15 min. Subsequently, the water phase was removed using a separating funnel. For each extraction, flour (1000 g) and WSB (3.5 L) were stirred at RT for 16 h. After centrifugation (20 min, 4 °C, 3550 g), the solvent was removed and collected by filtration on a glass filter (porosity 3, pore size 16−40 μm). The combined extracts were evaporated to dryness on a rotary evaporator (Büchi, Rotavapor R-210). The defatted flour was spread out on a flat glass tray in a fume hood for one week. The second extraction method used 2-propanol at 75 °C as the extraction solvent according to Chung et al.[14] The defatted flour was dried as described for the WSB-defatted flour.

**Lipid Extraction from Dough.** The dough was prepared from 50 g of flour by upscaling the recipe for 10 g of flour used by Köhler and Grosch.[15] The ingredients were as follows: flour (50 g), water (27.2 mL), NaCl (1.0 g), sucrose (0.5 g), fresh baker's yeast (3.5 g), L-*threo* ascorbic acid (20 mg/kg flour), and lipase (0−170 mg/kg flour; Lipopan F-BG or Lipopan Xtra-BG, Novozymes, Bagsvaerd, Denmark). The flour, NaCl, sucrose, baker's yeast, and lipase were premixed dry for 1 min in a Farinograph (50 g Z-blade mixer, Brabender, Duisburg, Germany) at 22 °C. Ascorbic acid solution (1.5 mL, 0.67 g/L) and water (27.2 mL) were added within 25 s and mixing was continued until the optimum consistency of the dough (550 Brabender units at 7 min) was reached. The dough was divided into two equal pieces, one was immediately frozen with liquid $N_2$, and the other one was allowed to rest (20 min, 30 °C, water-saturated atmosphere). The dough was then reshaped on a dough rounder (Type 440, Brabender, Duisburg, Germany) for 10 cycles, and the resulting spherical dough piece was rolled (PTFE cylinder; diameter, 5 cm; length, 30 cm) to yield an oval dough piece of 5 mm thickness. The dough piece was folded twice to $^1/_4$ of its original size and was reshaped on the dough rounder for 20 cycles. After proofing (30 °C, water-saturated atmosphere, 38 min), the dough was also frozen in liquid $N_2$. Both dough pieces were freeze-dried and milled using an ultracentrifugal mill ZM 200 (200 μm mesh size, Retsch, Haan, Germany).

Lipids were extracted from the freeze-dried dough powder (10.0 g) by the powder being stirred with WSB (40 mL, 16 h, RT) or 2-propanol (80 mL, 2 h, 75 °C). After centrifugation (5 min, 4 °C, 3550 g), the supernatant was filtered (0.45 μm), and the solvent was evaporated to dryness using a rotational vacuum concentrator (Christ, Osterode, Germany) and stored under an Ar atmosphere at −75 °C until further analysis.

**Isolation of Lipid Reference Compounds.** Reference compounds for the identification and quantitation of lipid classes by HPTLC and HPLC-ELSD were isolated from wheat flour by WSB-extraction. The lipids (6 g) were prefractionated using a preparative solid-phase extraction protocol for complex lipid mixtures ("batch procedure") according to Selmair and Koehler,[6] and all batches were examined by thin layer chromatography.[6] A crude glycolipid fraction was obtained, which was further separated by column chromatography to obtain three pure glycolipid classes, ASG, MGDG, and DGDG, as reported by Selmair and Koehler[6] and three further fractions containing mixtures of lipid classes. The latter three fractions (mixtures of SG/MGDG, NAPE/DGDG, and NAPE/NALPE/PC/DGMG) were further purified by column chromatography. The separation of the fraction containing SG and MGDG was performed by column chromatography using activated silica gel. The silica gel (G 60, 0.040−0.063 mm) was activated as follows: 200 g of silica gel were dried overnight at 105 °C and left to cool in a desiccator. After the addition of water (10 mL), the material was shaken for 20 min. The activated silica gel was dispersed in dichloromethane/acetone/2-propanol (60/39/1, v/v/v), poured into a glass column, and packed to a height of 38 cm (diameter 2 cm). The sample was dissolved in 2 mL of chloroform and applied to the column. The lipids were eluted with 1 L of dichloromethane/acetone/2-propanol (60/39/1, v/v/v). Each fraction was evaporated and examined by HPTLC (see above). Fractions comprising the same pure lipid class were recombined, evaporated to dryness, and weighed.

The fraction containing NAPE and DGDG was separated by silica gel chromatography (35 × 2 $cm^2$) in the same manner as described above using the eluent dichloromethane/methanol (87/13, v/v; 600 mL) and dichloromethane/methanol (83/17, v/v; 400 mL).

To obtain pure NALPE, the fraction containing NAPE, NALPE, PC, and DGMG was separated using column chromatography in the same manner as described above. The eluents were dichloromethane/methanol (87/13, v/v; 1 L), dichloromethane/methanol (80/20, v/v; 500 mL), and methanol (200 mL).

**Synthesis of Digalactosyl Monoglyceride (DGMG).** Isolated DGDG (105 mg) was emulsified in phosphate buffer (5 mL, pH 6.9, 50 mmol/L) with a T8 Ultra-Turrax (IKA Labortechnik, Staufen) and Lipopan F (5.0 mg) was added. The suspension was incubated for 2 h


dx.doi.org/10.1021/jf5022434 | J. Agric. Food Chem. 2014, 62, 8229−8237

at 30 °C in a thermo shaker (HLC BioTech, Bovenden, Germany). The lipids were extracted with chloroform (4 × 5 mL) and separated by activated silica gel column chromatography (3 × 27 $cm^2$) using dichloromethane/methanol (500 mL 84/16, v/v; 500 mL 82/18, v/v; 500 mL 77/23, v/v; 200 mL methanol) as the mobile phase. Each fraction was evaporated and examined by HPTLC (see above). Fractions containing DGMG were combined and evaporated to dryness.

**Nuclear Magnetic Resonance (NMR) Spectroscopy.** The $^1H$ and two-dimensional NMR spectra ($^1H$, COSY ($^1H^1H$, correlated spectroscopy), HMQC ($^1H^{13}C$, heteronuclear multiple quantum coherence), and HMBC ($^1H^{13}C$, heteronuclear multiple bond correlation)) of NALPE and DGMG were recorded on a Bruker AMX 400 II Ultrashield spectrometer (400 MHz, Bruker Biospin, Rheinstetten, Germany) and the $^{13}C$ NMR spectra were recorded on a Bruker AMX 360 spectrometer (360 MHz, Bruker Biospin, Rheinstetten, Germany). All of the experiments were conducted at a temperature of 25 °C. Chemical shift values $\delta$ (in ppm) are given relative to the signal for internal tetramethylsilane (TMS, $\delta = 0$). The values for coupling constants $J$ are given in Hz (see Supporting Information).

**HPLC-ELSD Analysis of Lipid Mixtures.** A HPLC-ELSD analysis was conducted on a 100 × 2 mm Chromolith Performance Si column with a 5 × 4.6 mm security guard Chromolith precolumn (Merck, Darmstadt, Germany). A Jasco HPLC (PU-1580; Gross-Umstadt, Germany) was used in combination with a Jasco autosampler (AS-2057 Plus), a Jasco HPLC Pump (PU-1580), a Jasco Ternary Gradient Unit (LG-1580−02), and a ThermaSphere TS-130 column oven (Phenomenex, Aschaffenburg, Germany) set at 40 °C. The detector was a Sedex 85 ELSD (Sedere, Alfortville, France). The carrier gas used was compressed air with a pressure of 0.35 MPa. The evaporation chamber was kept at 40 °C, the gain was set at 3 or 8, and for the computerized analysis, the software KromaSystem 2000 (Version 1.60) was used.

The gradient of the HPLC solvent was based on the method of Graeve and Janssen[11] for marine lipids. Gerits et al.[9] adapted the procedure for wheat flour lipids to improve the separation of the polar lipid classes; however, further optimization was carried out to separate all wheat flour lipids and lipase reaction products. Table 1 lists the mobile phase solvent gradient. The composition of the three solvent mixtures and the gradient were adapted to improve the separation of glycolipids and phospholipids since not all lipid classes were separated with the gradient of Gertis et al.[9] With the optimized procedure, all nonpolar lipids, glycolipids, and phospholipids were separated in one single run, but for quantitation, two runs at different gain settings were necessary to get signals suitable for calculation. Calibration curves were generated from the isolated or purchased lipid reference compounds, respectively. Two standard mixtures with concentrations of 0.05 μg/μL, 0.1 μg/μL, 0.2 μg/μL, and 0.3 μg/μL of each reference compound were prepared. The solvent was chloroform/methanol (50/50, v/v) containing cholesterol as the internal standard (250 mg/L) as suggested by Gerits et al.[10] The first standard mixture consisted of FFA, MG, CER, SG, NAPE, NALPE, and DGMG; the second mixture contained DG, CBR, ASG, MGDG, MGMG, PC, and LPC. The calibration curves for the lipid classes were obtained by injecting the standard mixtures (10 μL) and monitoring the ELSD-signal at gain 8. The calibration curves of TG and DGDG, which were present in high concentrations, were acquired at a low sensitivity (gain 3) with absolute amounts of TG and DGDG of 5, 10, 15, and 20 μg. The calibration curves were plotted as the peak area ratio (sample/cholesterol) versus the amount of each sample. In all of the calibration and quantitative separations, the inject volume was 10 μL, thus cholesterol was always present in the same amount while the amounts of the analytes varied.

The extracted lipids from flour or dough were dissolved (5 mg lipid extract/mL) in chloroform/methanol (50/50, v/v) containing cholesterol as an internal standard (0.25 mg/mL). The samples (10 μL) were injected into the HPLC column (10 μL) and analyzed by HPLC-ELSD. The ELSD-signal was monitored at gain 3 for TG and DGDG and at gain 8 for all other lipid classes (one run per gain setting).

**Microbaking Test (MBT).** The microbaking test using 10 g of flour was conducted as described by Köhler and Grosch.[15] The appropriate amount of water was determined by a modification of the ICC standard procedure 115 (22 °C instead of 30 °C).[16] Flour (10 g), NaCl (0.2 g), sucrose (0.1 g), baker's yeast (0.7 g), and different amounts of lipases (30−170 mg/kg) or surfactants (0.2−0.8%) were premixed dry for 1 min in a microfarinograph (10 g Z-blade mixer, Brabender, Duisburg, Germany) at 22 °C. An L-*threo*-ascorbic acid solution (0.3 mL, 0.67 g/L) and water (5.44 mL) were added within 25 s and the mixing was continued until the optimum consistency of the dough (550 BU at 7 min) was reached. After removal from the mixer, the dough was fermented (20 min, 30 °C, water-saturated atmosphere). The dough was then reshaped on a dough rounder (custom-made) for 10 cycles. The resulting dough ball passed through the rolls (3 mm roll-gap) of an AMPIA-pasta machine (model 150 mm—Deluxe, Marcato, Italy) to form an oval dough piece. This piece was folded twice to $^1/_4$ of its original size and reshaped on the dough rounder for 20 cycles. The dough was then proofed (30 °C, water-saturated atmosphere, 38 min) and baked (180 °C increasing to 250 °C, 10 min) on an automatic proofing−baking line.[5] The volume of the bread was determined using a benchtop laser-based device (VolScan Profiler, Stable Micro Systems, Godalming, U.K.).

**Micro-Rapid-Mix Test (MRMT).** The dough was microbaked with 10 g of flour and mixed at high-speed for 1 min according to Köhler and Grosch[15] except that the proofing and baking was done in-line with an automatic proofing-baking device. The recipe and additives were the same as described for the MBT.

**Statistical Analysis.** Triplicate determinations were carried out for each control bread and each concentration of additive. The data was statistically evaluated using Microsoft Office Excel 2010 (Microsoft Corporation, Seattle, WA). The following values were used to rate the levels of significance: $p > 0.05$, not significant; $p < 0.05$, statistically significant; $p < 0.01$, significant; and $p < 0.001$, highly significant. The statistical evaluation of all quantitative data was carried out via one-way analysis of variance (ANOVA) using the software Sigma Plot 11.0 (Systat, San José, CA).

**Table 1. Ternary Gradient of Mobile Phase Used for the HPLC Separation of Lipid Classes from Wheat**

| | | % solvent | | |
|---|---|---|---|---|
| time (min) | flow rate (mL/min) | A[a] | B[a] | C[a] |
| 0.0 | 1.4 | 100 | 0 | 0 |
| 1.6 | 1.4 | 98 | 2 | 0 |
| 4.5 | 1.4 | 96 | 4 | 0 |
| 8.0 | 1.4 | 80 | 10 | 0 |
| 14.0 | 1.4 | 65 | 15 | 20 |
| 14.1 | 1.4 | 55 | 25 | 20 |
| 19.0 | 1.4 | 70 | 0 | 30 |
| 27.0 | 1.4 | 65 | 0 | 35 |
| 27.1 | 3.0 | 0 | 100 | 0 |
| 28.5[b] | 3.0 | 0 | 100 | 0 |
| 30.0 | 3.0 | 100 | 0 | 0 |
| 32.0 | 3.0 | 100 | 0 | 0 |
| 34.0 | 1.4 | 100 | 0 | 0 |
| 35.0 | 1.4 | 100 | 0 | 0 |

[a]A, isooctane; B, acetone/ethyl acetate/2-propanol (54/38/8, v/v/v) containing 0.02% (v/v) acetic acid; C, 2-propanol/water (85/15, v/v) containing 0.02% (v/v) acetic acid and 0.05% (v/v) ethanolamine. [b]End of analysis, start of the column wash.

## RESULTS AND DISCUSSION

**Reference Compounds for the Quantitation of Wheat Lipid Classes.** Quantitative methods require reference


dx.doi.org/10.1021/jf5022434 | J. Agric. Food Chem. 2014, 62, 8229−8237

compounds for calibration and all relevant lipid classes from wheat are to be available. For this purpose, pure lipid classes were isolated from wheat flour lipids to obtain reference compounds for HPLC-ELSD analysis. WSB-extracted wheat lipids were prefractionated by a batch procedure into a nonpolar lipid fraction and two polar fractions.[6] The latter were a crude glycolipid and a phospholipid fraction. The glycolipid fraction was further separated by column chromatography into pure fractions of ASG (yield: 4.7%, 103 mg), MGDG (yield: 8.3%, 182 mg), and DGDG (yield: 29%, 650 mg). However, further fractions contained mixtures of lipid classes; therefore, SG, CBR, MGMG, NAPE, NALPE, and DGMG could not be isolated with this column. Thus, mixtures of these compounds had to be further purified by column chromatography.

Nonstarch wheat lipids contain an average of 3% DGMG, but the isolated amount was not sufficient for subsequent purification. Hence, the isolated DGDG was hydrolyzed to DGMG by incubation with Lipopan F at 30 °C in a phosphate buffer. After purification by silica gel column chromatography, DGMG was obtained in a yield of 30% (32 mg). The byproduct MGMG was also isolated with a yield of 8% (9 mg) because impurities of MGDG present in the initial DGDG-fraction were also hydrolyzed by the lipase. These pure glycolipid classes were identified by HPTLC[5] and HPLC-ELSD having used authentic reference compounds commercially available in small amounts. The identity of DGMG and NALPE were verified by NMR because no reference compounds were commercially available. NMR data and structures of DGMG and NALPE are given in the Supporting Information.

**HPLC-ELSD Method to Quantitate Wheat Lipid Classes.** For wheat lipid analysis, an optimized HPLC-ELSD procedure with a ternary gradient of the mobile phase was used. The gradient was optimized in numerous steps to be able to separate all relevant lipid classes that were considered (Table 1). A typical chromatogram of wheat lipids is shown in Figure 1. Only the separation of LPC was complicated because of the irregular baseline at this part of the chromatogram. This affected the accuracy of the quantitative determination of this compound. Table 2 shows the retention times of the 27 reference compounds that were separated in one single run. The different classes of wheat lipids were present in a wide range of concentrations (e.g., ~40% TG vs ~3% PC based on total wheat lipids) so that two different sensitivities of the ELSD (separate runs for gain 3 and gain 8) were necessary to get peaks suitable for quantitation of all of the wheat lipid classes. The relative responses (i.e., signal intensity per mass unit of lipid) of the different lipid classes varied according to the lipid type and the injected amount so that nonlinear relationships between the ratio of the signal intensities (sample/internal standard) and the ratio of the quantities (sample/internal standard) were obtained. Depending on the lipid class, different polynomial calibration curves were fitted from as many calibrators as possible (0.5–3.0 $\mu$g (gain 8), 5–20 $\mu$g (gain 3)).

**Lipid Composition of Flour and Dough Lipids without Lipase Addition.** Table 3 shows the quantitated lipid classes of wheat lipids extracted from 'Kolibri' flour and fermented dough as affected by the solvent used for lipid isolation. On one hand, wheat flour lipids were extracted using 2-propanol at 75 °C (yield: 1.57 ± 0.03% dm) to minimize flour damage and to maximize lipid extraction. On the other hand, WSB was used at RT with a yield of 1.67 ± 0.05% dm. The quantitated lipid composition of wheat flour is in accordance with the literature,[1,17] with TG as the major component of nonpolar

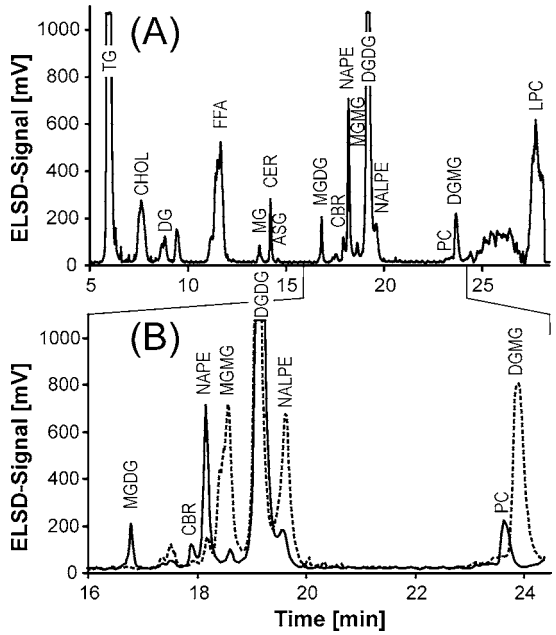


**Figure 1.** HPLC chromatograms of wheat flour lipids (solid line) and dough lipids after mixing and fermentation in the presence of lipase (Lipopan Xtra 130 mg/kg) (dashed line). (A) Retention time of 5–29 min and (B) retention time of 16–24.5 min with details of the relevant lipid classes. Lipid classes are designated as defined in Table 2. Lipids were extracted with WSB at RT.

**Table 2. Retention Times of Lipid Classes from Wheat after Separation by HPLC**

| abbreviation | lipid class | retention time (min) |
|---|---|---|
| TG | triglycerides | 5.1 |
| CHOL | cholesterol | 7.6 |
| DG | diglycerides | 8.6 |
| FFA | free fatty acids | 11.4 |
| MG | monoglycerides | 13.5 |
| CER | ceramides | 13.7 |
| ASG | acylated sterol glucosides | 14.5 |
| SG | sterol glucosides | 16.6 |
| MGDG | monoglactosyl diglycerides | 16.8 |
| CBR | cerebrosides | 17.5 |
| NAPE | *N*-acyl phosphatidyl ethanolamine | 18.1 |
| MGMG | monogalactosyl monoglycerides | 18.5 |
| DGDG | digalactosyl diglycerides | 19.1 |
| PE | phosphatidyl ethanolamine | 19.5 |
| NALPE | *N*-acyl lysophosphatidyl ethanolamine | 19.6 |
| PG | phosphadyl glycerol | 20.0 |
| PA | phosphatidic acid | 21.7 |
| PI | phosphatidyl inositol | 22.9 |
| PS | phosphatidyl serine | 23.3 |
| PC | phosphatidyl choline | 23.4 |
| DGMG | digalactosyl monoglycerides | 23.8 |
| LPE | lysophosphatidyl ethanolamine | 24.0 |
| LPI | lysophosphatidyl inositol | 24.3 |
| LPG | lysophosphatidyl glycerol | 24.6 |
| LPS | lysophosphatidyl serine | 24.9 |
| LPA | lysophosphatidic acid | 25.3 |
| LPC | lysophosphatidyl choline | 28.3 |


dx.doi.org/10.1021/jf5022434 | J. Agric. Food Chem. 2014, 62, 8229–8237

**Table 3. Concentration of Lipids from Wheat Flour and Wheat Dough after Proofing (58 min) as Affected by the Addition of the Lipase Lipopan F and the Solvent Used for Lipid Extraction[a]**

| | concentration (mg/kg dry matter) | | | | |
|---|---|---|---|---|---|
| | | dough lipids with lipase added (mg/kg flour) | | | |
| lipid class[b] | flour lipids | 0 | 30 | 70 | 110 |
| | | Lipid Extraction Using 2-Propanol (75 °C) | | | |
| TG | $5391^{A} \pm 14$ | $2948^{B} \pm 219$ | $3043^{B} \pm 100$ | $3040^{B} \pm 160$ | $2649^{BC} \pm 140$ |
| FFA | $1910^{A} \pm 416$ | $1046^{B} \pm 187$ | $1189^{B} \pm 152$ | $1570^{A} \pm 90$ | $1591^{A} \pm 118$ |
| DG | $458^{A} \pm 27$ | $283^{B} \pm 39$ | $203^{B} \pm 23$ | $203^{B} \pm 11$ | $181^{BC} \pm 2$ |
| MG | $179^{A} \pm 13$ | $90^{B} \pm 15$ | $83^{B} \pm 7$ | $85^{B} \pm 15$ | $83^{B} \pm 11$ |
| ASG | $89^{A} \pm 7$ | $73^{A} \pm 7$ | $74^{A} \pm 5$ | $102^{B} \pm 3$ | $100^{B} \pm 11$ |
| SG | $26^{A} \pm 10$ | $16^{A} \pm 4$ | $19^{A} \pm 4$ | $33^{A} \pm 9$ | $18^{A} \pm 7$ |
| CBR | $278^{A} \pm 4$ | $170^{B} \pm 5$ | $204^{B} \pm 20$ | $240^{B} \pm 20$ | $219^{AB} \pm 42$ |
| DGDG | $1929^{A} \pm 40$ | $1370^{B} \pm 282$ | $1356^{B} \pm 14$ | $1209^{C} \pm 110$ | $970^{C} \pm 39$ |
| DGMG | $157^{A} \pm 24$ | $177^{A} \pm 11$ | $132^{A} \pm 22$ | $337^{B} \pm 14$ | $312^{B} \pm 64$ |
| MGDG | $529^{A} \pm 55$ | $373^{A} \pm 96$ | $207^{B} \pm 49$ | $171^{B} \pm 42$ | $87^{B} \pm 71$ |
| MGMG | $180^{A} \pm 4$ | $103^{A} \pm 66$ | $194^{A} \pm 53$ | $520^{B} \pm 41$ | $399^{B} \pm 10$ |
| NAPE | $779^{A} \pm 35$ | $578^{A} \pm 120$ | $393^{B} \pm 58$ | $342^{B} \pm 29$ | $207^{C} \pm 29$ |
| NALPE | $443^{A} \pm 35$ | $426^{A} \pm 18$ | $500^{A} \pm 91$ | $602^{B} \pm 59$ | $651^{B} \pm 66$ |
| PC | $153^{A} \pm 32$ | $145^{A} \pm 34$ | $219^{A} \pm 61$ | $164^{A} \pm 80$ | $144^{A} \pm 44$ |
| LPC | $245^{A} \pm 70$ | $340^{A} \pm 190$ | $822^{A} \pm 313$ | $830^{A} \pm 250$ | $907^{A} \pm 350$ |
| | | Lipid Extraction Using Water-Saturated 1-Butanol (20 °C) | | | |
| TG | $5383^{A} \pm 150$ | $4248^{B} \pm 118$ | $3945^{C} \pm 33$ | $3108^{D} \pm 187$ | $4266^{BD} \pm 231$ |
| FFA | $1979^{A} \pm 90$ | $1512^{B} \pm 117$ | $1915^{A} \pm 104$ | $2250^{A} \pm 195$ | $2791^{AC} \pm 100$ |
| DG | $444^{A} \pm 30$ | $426^{A} \pm 40$ | $263^{B} \pm 5$ | $185^{B} \pm 3$ | $226^{B} \pm 27$ |
| MG | $165^{A} \pm 20$ | $168^{A} \pm 30$ | $159^{A} \pm 14$ | $107^{A} \pm 6$ | $120^{A} \pm 42$ |
| ASG | $79^{A} \pm 4$ | $78^{A} \pm 28$ | $79^{A} \pm 31$ | $62^{A} \pm 2$ | $86^{A} \pm 27$ |
| SG | $28^{A} \pm 12$ | $18^{A} \pm 6$ | $19^{A} \pm 6$ | $34^{A} \pm 6$ | $33^{A} \pm 6$ |
| CBR | $284^{A} \pm 11$ | $283^{A} \pm 12$ | $294^{A} \pm 17$ | $264^{A} \pm 17$ | $224^{A} \pm 32$ |
| DGDG | $2143^{A} \pm 160$ | $2043^{A} \pm 320$ | $1949^{A} \pm 207$ | $1209^{B} \pm 40$ | $1148^{B} \pm 91$ |
| DGMG | $234^{A} \pm 20$ | $180^{A} \pm 10$ | $295^{A} \pm 72$ | $487^{B} \pm 120$ | $540^{B} \pm 116$ |
| MGDG | $501^{A} \pm 20$ | $498^{A} \pm 25$ | $271^{B} \pm 40$ | $144^{C} \pm 3$ | $158^{C} \pm 18$ |
| MGMG | $304^{A} \pm 11$ | $328^{A} \pm 14$ | $623^{B} \pm 83$ | $563^{B} \pm 1$ | $663^{B} \pm 18$ |
| NAPE | $1071^{A} \pm 30$ | $1013^{A} \pm 3$ | $950^{A} \pm 128$ | $729^{B} \pm 4$ | $742^{B} \pm 53$ |
| NALPE | $561^{A} \pm 30$ | $524^{A} \pm 74$ | $884^{B} \pm 43$ | $851^{B} \pm 6$ | $841^{B} \pm 59$ |
| PC | $190^{A} \pm 90$ | $244^{A} \pm 148$ | $205^{A} \pm 11$ | $191^{A} \pm 135$ | $210^{A} \pm 27$ |
| LPC | $400^{A} \pm 180$ | $520^{A} \pm 250$ | $842^{A} \pm 261$ | $936^{A} \pm 350$ | $950^{A} \pm 223$ |

[a]Mean values ± standard deviations of triplicate determinations. Mean values associated with different capital letters are significantly different within each lipid class (one-way ANOVA, Tukey test, $p \leq 0.05$) [b]Lipid classes are designated as defined in Table 2.

lipids, DGDG of glycolipids, and NAPE of phospholipids. As mentioned before, natural fluctuations of the lipid composition of wheat depend on the individual genetic predisposition (cultivar), the agricultural practices used during cultivation, the environmental effects to which the plant was exposed, and the age of the milled flour.

The lipid compositions per kilogram of dry flour extracted with different solvents differed mainly in the polar lipid composition. More glycolipids and phospholipids were extracted using WSB than using 2-propanol (75 °C). It is known that beside free lipids, bound lipids are also extracted almost completely with WSB,[4] which is possibly due to the "bipolar" character of this solvent. WSB is a combination of a nonpolar and a very polar compound, which is more similar to polar lipids than it is to (water-free) 2-propanol, and thus, dissolves these compounds more effectively. This might explain the higher polar lipid portion in the WSB compared to the 2-propanol-extracted lipids, because bound lipids are more efficiently detached from their binding sites.[4,9] The amount of each lipid class was lower in the dough lipids than in the flour lipids when 2-propanol was used as the extraction solvent. In contrast, the compositions of flour and dough lipids were not significantly different in the lipid extracts obtained with WSB. Our results are in line with the phenomenon of "lipid binding".[4,14] This means that when flour is wetted and mixed into dough, around 70% of the total flour lipids become bound to or are entrapped by the gluten network.[9] Because of the binding of lipids during mixing, fewer lipids were extracted with 2-propanol from dough than were extracted from flour. These results suggest WSB as the preferred solvent for total lipid extraction from wheat flour and dough.

**Baking Performance as Affected by the Addition of Lipase.** To reveal the maximum bread volume increase caused by the addition of lipases and their dose/volume increase dependency, two versions of a microscale baking test based on 10 g of flour differing in the time and intensity of mixing were applied.[18] In the micro-rapid-mix test (MRMT), the dough was mixed for 2 min with a high-speed mixer (1250 rpm), whereas in the microbaking test (MBT), the dough was mixed in a Microfarinograph (63 rpm) until the optimum consistency of the dough was reached (7 min). All other steps were identical. To take dough losses during breadmaking into account, the loaf volumes were based on the dough weight (mL/g dough) before the second proofing session. The bread volume was expressed


dx.doi.org/10.1021/jf5022434 | J. Agric. Food Chem. 2014, 62, 8229−8237

in relation to the respective mean value of the control breads in the individual test series, taking into account both climatic and technical fluctuations.

The breads were baked using the MRMT to study the lipase-dependent volume increase after the addition of Lipopan Xtra (10−70 mg/kg). The lipase was applied as a solid or as a watery suspension; the latter procedure was used to get a more homogeneous distribution of the enzyme. However, both application forms did not cause a significant increase of the bread volume. Even after the application of 700 and 1400 mg of Lipopan Xtra per kilogram of flour, no volume increase was obtained. Similar results were obtained for Lipopan F (50 and 500 mg/kg). Also, for the Lipopan F addition, no significant increase in the loaf volume was obtained after the proofing time was extended from 37 to 54 min. Recent studies[8,19] show that Lipopan F and Lipopan Xtra caused a significant volume increase when a normal scale baking test (300 g of flour) with dough mixing in the Farinograph was used. Consequently, the MBT was used to demonstrate the effect of added lipases. It is known that a rather high-volume increase is typical of the microscale setup when compared to conventional baking. Previous studies on the effect of DATEM have shown that the volume increases were higher in the microscale baking test (40−60% volume increase) than in a normal-scale test with 300 g of flour (10−20% volume increase).[20] However, the correlation between the micro- and normal-scale baking tests was high because the same trend of the loaf volumes was obtained with both setups.[18,20] As shown in Figure 2, significant

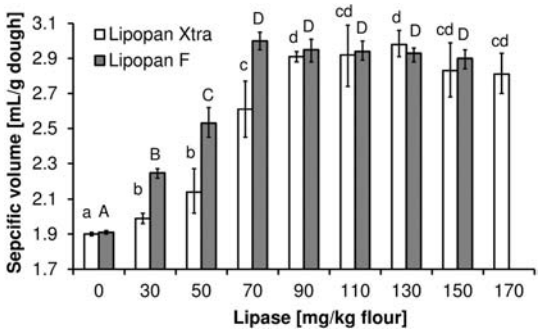


**Figure 2.** MBTs with 10 g of flour. Change of the bread volume as affected by the increasing concentrations of the lipases Lipopan Xtra and Lipopan F. Error bars represent the mean standard deviations of triplicate determinations. Mean values associated with different letters are significantly different within each lipase concentration (one-way ANOVA, Tukey test, $p \leq 0.05$).

volume increases were obtained for both Lipopan Xtra and Lipopan F. The volume increase was found to correlate to the enzyme dosage until a plateau was reached. Lipopan F was found to reach a plateau at a lower dosage (70 mg granulate/kg flour) than did Lipopan Xtra (90 mg granulate/kg flour). A further increase in the enzyme dosage did not cause statistically significant differences in the obtained bread volumes.

These results strongly suggest the MBT as the preferred test to assess the effects of lipase addition. It can only be speculated as to why the MRMT was not suited to study the functional effect of lipases. One explanation would be that the enzymes were shear sensitive and were inactivated by the high mechanical input during mixing.

The commercial synthetic surfactants DATEM and SSL were chosen as reference surfactants to evaluate the potential of lipases and lipase-treated lipids in breadmaking. To determine the concentration of surfactants for a maximum increase in the bread volume, concentrations of 0.2−0.8% were applied. DATEM was applied as a solid or as a watery suspension. There were no significant differences between the two application forms, and a maximum volume increase of 58% at a concentration of 0.6% was obtained. The typical plateau phase was seen at DATEM concentrations between 0.4 and 0.8%, comparable with the plateau phase after lipase application. SSL showed the same phenomenon and caused a maximum bread volume increase of 47% at a concentration of 0.4%. In summary, the functional effects of lipases (volume increase of 56−58%) were comparable to those of DATEM (58%) and superior to those of SSL (47%). Furthermore, the amount of commercial lipase product added, concentration of lipase required for this effect, was approximately 1/50 of the amount of surfactants added.

**Changes of Lipid Composition as Affected by Lipase Addition.** Figure 1 shows an overlay of the chromatograms of the wheat flour lipids and lipase-treated dough lipids. It can be clearly seen that especially certain polar lipid classes (retention time 15−25 min) were hydrolyzed after lipase addition. The quantitative data of the lipase-treated dough lipids are given in Tables 3 and 4. In the following sections, the lipid classes TG, DGDG, NAPE, and DGMG are used as examples to discuss the effect of lipases in more detail. Lipase-treated (Lipopan F and Lipopan Xtra) dough lipids differed significantly from the untreated dough lipids and the flour lipids. The results also confirmed that WSB was more effective in extracting the relevant lipid classes than was 2-propanol. With an increase in the amount of lipases, a decrease of TG, DGDG, NAPE, and MGDG occurred, in particular after proofing. This went hand in hand with the increased concentrations of the hydrolysis products FFA, MGMG, NALPE, and DGMG.

Upon review of the composition of WSB extracted lipids, TG were hydrolyzed by lower concentrations of Lipopan F than of Lipopon Xtra, and the concomitant formation of FFA was observed. This corresponds to Lipopan Xtra having a higher affinity toward phospholipids than does Lipopan F. Furthermore, a larger decrease of DGDG (2043 → 1148 mg/kg flour) and the corresponding increase of DGMG (180 → 540 mg/kg) were detected after proofing with Lipopan F than with Lipopan Xtra (DGDG, 2043 → 1350 mg/kg; DGMG, 180 → 265 mg/kg). However, the changes of the DGDG and DGMG concentrations (Tables 3 and 4) revealed that the formation of DGMG did not compensate for the decrease of the DGDG concentration. An explanation could be that DGMG is a transient intermediate and is subjected to further hydrolysis by the lipase. In contrast to DGDG, the addition of Lipopan Xtra resulted in a significantly stronger hydrolysis of MGDG (498 → 26 mg/kg) and NAPE (1013 → 661 mg/kg) after proofing than did the addition of Lipopan F (MGDG, 498 → 158 mg/kg; NAPE, 1013 → 742 mg/kg). Lipid concentrations before fermentation are given in the Supporting Information (Tables S3 and S4) and show the same trends as the concentrations after proofing.

To get a closer overview of the degradation and formation of lipase substrates and products, mass concentrations were converted into molar concentrations. This was done exemplarily for the addition of Lipopan F and for WSB as a lipid extraction solvent (Table 3). Molar masses of the lipid classes were calculated by the use of linoleic acid ($M$ = 280.5 g/mol) as the default fatty acid. The results for the relevant lipid classes

**Table 4. Concentration of Lipids from Wheat Flour and Wheat Dough after Proofing (58 min) As Affected by the Addition of the Lipase Lipopan Xtra and the Solvent Used for Lipid Extraction[a]**

| | concentration (mg/kg dry matter) | | | | |
|---|---|---|---|---|---|
| | | dough lipids with lipase added (mg/kg flour) | | | |
| lipid class[b] | flour lipids | 0 | 90 | 130 | 170 |
| | | Lipid Extraction Using 2-Propanol (75 °C) | | | |
| TG | $5391^{A} \pm 14$ | $2948^{B} \pm 219$ | $2548^{B} \pm 300$ | $3044^{B} \pm 269$ | $2893^{B} \pm 122$ |
| FFA | $1910^{A} \pm 416$ | $1046^{B} \pm 187$ | $1184^{B} \pm 31$ | $1613^{AC} \pm 51$ | $1626^{AC} \pm 18$ |
| DG | $458^{A} \pm 27$ | $283^{B} \pm 39$ | $226^{B} \pm 46$ | $209^{B} \pm 19$ | $196^{B} \pm 16$ |
| MG | $179^{A} \pm 13$ | $90^{B} \pm 15$ | $93^{B} \pm 24$ | $79^{B} \pm 3$ | $92^{B} \pm 1$ |
| ASG | $89^{A} \pm 7$ | $73^{A} \pm 7$ | $75^{A} \pm 33$ | $54^{A} \pm 16$ | $68^{A} \pm 12$ |
| SG | $26^{A} \pm 10$ | $16^{A} \pm 4$ | $12^{A} \pm 1$ | $18^{A} \pm 3$ | $16^{A} \pm 3$ |
| CBR | $278^{A} \pm 4$ | $170^{B} \pm 5$ | $195^{B} \pm 17$ | $204^{B} \pm 6$ | $213^{B} \pm 31$ |
| DGDG | $1929^{A} \pm 40$ | $1370^{B} \pm 282$ | $1372^{B} \pm 80$ | $1129^{C} \pm 71$ | $1051^{C} \pm 42$ |
| DGMG | $157^{A} \pm 24$ | $177^{A} \pm 11$ | $170^{A} \pm 3$ | $195^{A} \pm 79$ | $307^{B} \pm 64$ |
| MGDG | $529^{A} \pm 55$ | $373^{A} \pm 96$ | $55^{B} \pm 15$ | $14^{B} \pm 1$ | $19^{B} \pm 15$ |
| MGMG | $180^{A} \pm 4$ | $103^{A} \pm 66$ | $276^{B} \pm 14$ | $372^{C} \pm 8$ | $412^{D} \pm 12$ |
| NAPE | $779^{A} \pm 35$ | $578^{A} \pm 120$ | $227^{B} \pm 77$ | $156^{B} \pm 4$ | $224^{B} \pm 43$ |
| NALPE | $443^{A} \pm 35$ | $426^{A} \pm 18$ | $576^{B} \pm 82$ | $569^{B} \pm 7$ | $685^{C} \pm 65$ |
| PC | $153^{A} \pm 32$ | $145^{A} \pm 34$ | $206^{B} \pm 10$ | $190^{B} \pm 32$ | $187^{B} \pm 30$ |
| LPC | $245^{A} \pm 70$ | $340^{A} \pm 190$ | $361^{A} \pm 135$ | $644^{A} \pm 221$ | $762^{AB} \pm 70$ |
| | | Lipid Extraction Using Water-Saturated 1-Butanol (20 °C) | | | |
| TG | $5383^{A} \pm 150$ | $4248^{B} \pm 118$ | $3191^{C} \pm 360$ | $3619^{C} \pm 214$ | $3750^{C} \pm 58$ |
| FFA | $1979^{A} \pm 90$ | $1512^{B} \pm 117$ | $1827^{B} \pm 70$ | $1826^{B} \pm 90$ | $2635^{C} \pm 120$ |
| DG | $444^{A} \pm 30$ | $426^{A} \pm 40$ | $258^{B} \pm 36$ | $245^{B} \pm 41$ | $282^{B} \pm 28$ |
| MG | $165^{A} \pm 20$ | $168^{A} \pm 30$ | $170^{A} \pm 55$ | $153^{A} \pm 10$ | $164^{A} \pm 29$ |
| ASG | $79^{A} \pm 4$ | $78^{A} \pm 28$ | $69^{A} \pm 5$ | $117^{A} \pm 31$ | $106^{A} \pm 33$ |
| SG | $28^{A} \pm 12$ | $18^{A} \pm 6$ | $29^{A} \pm 11$ | $30^{A} \pm 2$ | $35^{A} \pm 1$ |
| CBR | $284^{A} \pm 11$ | $283^{A} \pm 12$ | $249^{A} \pm 11$ | $237^{A} \pm 15$ | $252^{A} \pm 33$ |
| DGDG | $2143^{A} \pm 160$ | $2043^{A} \pm 320$ | $1441^{B} \pm 70$ | $1526^{B} \pm 200$ | $1350^{B} \pm 67$ |
| DGMG | $234^{A} \pm 20$ | $180^{A} \pm 10$ | $170^{AB} \pm 55$ | $140^{AB} \pm 20$ | $265^{B} \pm 108$ |
| MGDG | $501^{A} \pm 20$ | $498^{A} \pm 25$ | $168^{B} \pm 16$ | $42^{C} \pm 41$ | $26^{C} \pm 88$ |
| MGMG | $304^{A} \pm 11$ | $328^{A} \pm 14$ | $639^{B} \pm 5$ | $620^{B} \pm 45$ | $657^{B} \pm 98$ |
| NAPE | $1071^{A} \pm 30$ | $1013^{A} \pm 3$ | $711^{B} \pm 154$ | $609^{B} \pm 125$ | $661^{B} \pm 54$ |
| NALPE | $561^{A} \pm 30$ | $524^{A} \pm 74$ | $807^{B} \pm 7$ | $781^{B} \pm 60$ | $902^{B} \pm 92$ |
| PC | $190^{A} \pm 90$ | $244^{A} \pm 148$ | $184^{A} \pm 52$ | $239^{A} \pm 22$ | $199^{A} \pm 30$ |
| LPC | $400^{A} \pm 180$ | $520^{A} \pm 250$ | $831^{AB} \pm 64$ | $938^{B} \pm 58$ | $990^{AB} \pm 350$ |

[a]Mean values ± standard deviations of triplicate determinations. Mean values associated with different capital letters are significantly different within each lipid class (one-way ANOVA, Tukey test, $p \leq 0.05$). [b]Lipid classes are designated as defined in Table 2.

are shown in Figure 3. The dough without added lipase contained almost equal molar concentrations of TG and FFA (5.5−6 mmol/kg flour). Upon the addition of Lipopan F, TG decreased by 2.5 mmol/kg flour to a minimum value of 3.5 mmol/kg flour (Figure 3A). The corresponding product FFA strongly increased by 4.5 mmol/kg flour to a final concentration of 10 mmol/kg flour as the lipase concentration increased. Thus, hydrolysis of TG only explained 56% of the FFA formation, clearly showing that other substrates such as glyco- and phospho-lipids also contributed to FFA formation.[10] The hydrolysis of NAPE and the concurrent formation of NALPE (Figure 3B) were approximately in the same range (−0.3 vs +0.5 mmol/kg flour, respectively). Comparable results were obtained from the hydrolysis of MGDG (−0.4 mmol/kg flour) and the formation of MGMG (+0.6 mmol/kg flour) (Figure 3D). The situation was somewhat different for DGDG and DGMG (Figure 3C). The decrease of DGDG (−1 mmol/kg flour) was twice as high as the increase of DGMG (+0.5 mmol/kg flour). A possible reason was given above. The calculation of the balance of the reactions on a molar basis showed that the total increase of FFA after lipase addition (+4.5 mmol/kg flour) was almost equaled by the decreases of the lipase substrates DGDG, MGDG, NAPE, and TG. Hydrolysis of these substrates explained 93% of the lipase-mediated formation of FFA (4.2 of 4.5 mmol/kg flour).

**Relevance of the Modified Lipid Composition for the Baking Performance.** Nonpolar lipids and NAPE have a negative influence on baking performance, whereas all glycolipids show positive baking potential.[6] Consequently, the hydrolysis of NAPE to NALPE can be regarded as positive for the baking performance. The formation of MGMG from MGDG is also desirable because it was found that the latter has the proper ratio between hydrophilic and lipophilic moieties in the molecular structure to yield good functionality.[6]

Glycoglycerolipids containing two carbohydrate moieties show different behavior compared to one carbohydrate moiety glycoglycerolipids. Previous studies have shown that DGDG and MGMG have comparable positive effects in baking.[6] Thus, the second acyl residue in DGDG must be essential for a high functionality of this lipid class in baking, while a weaker effect has been shown for purified DGMG.[6] Moreover, these studies have shown that DGDG had the best functional effects of all glycolipids. As a consequence, the degradation of DGDG found here (Tables 3 and 4) can be considered unfavorable because


dx.doi.org/10.1021/jf5022434 | J. Agric. Food Chem. 2014, 62, 8229−8237

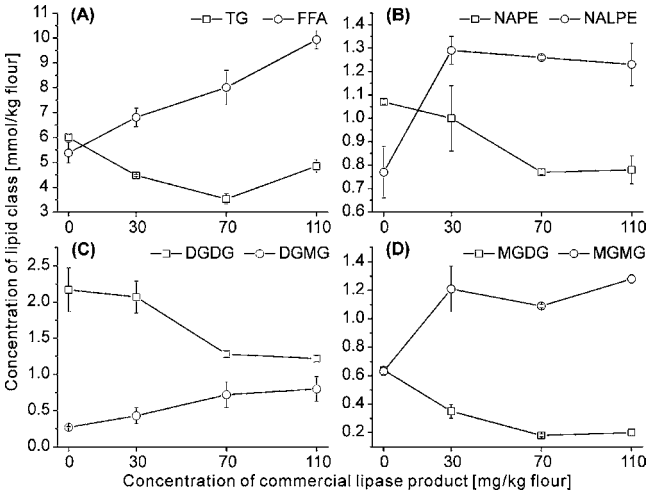


**Figure 3.** Decrease of selected lipase substrates and increase of the corresponding products as affected by the addition of Lipopan F. Mass concentrations given in Table 3 were converted into molar concentrations [mmol/kg flour] using linoleic acid as the default fatty acid. Lipid classes are designated as defined in Table 2. Lipids were extracted with WSB at RT.

the functional effects of DGDG are much stronger than those of DGMG. Generally, the increased concentration of FFA from lipolytic action is considered to decrease the positive effect of the addition of lipases. Experiments in which free linoleic acid (0.1%, 3.6 mmol/kg) was added, show a considerable decrease in the loaf volume (data not shown).

A comparison of the quantitative data of the lipase-modified lipids (Tables 3 and 4) with bread volumes (Figure 2) as affected by lipases shows that the highest amount of polar hydrolysis products obtained at the highest levels of Lipopan F (110 mg/kg) and Lipopan Xtra (170 mg/kg) did not match the concentrations that caused maximum bread volumes (70 and 130 mg/kg, respectively). Accordingly, a higher concentration of polar lipids did not automatically cause a higher bread volume, although the bread volume remained on a high level compared to the bread volume obtained without the addition of lipase. This effect can be explained by the increased amounts of FFA and DGMG, which have a negative (FFA) or at least a less positive effect (DGMG) on the baking performance. Therefore, the type and concentration of the added lipase appears to be of major importance. Evidence for this hypothesis is given in the work of Gerits et al.,[10] who showed that the specificity of the added lipase clearly affects its technological effect.

Finally, synergistic effects between glycolipids and phospholipids must also be considered. Tables 3 and 4 as well as Figure 2 show that PC was also hydrolyzed to LPC. It is generally accepted that lysophospholipids exhibit stronger functional effects than do phospholipids.[21,22] Furthermore, Wilde et al.[23] indicated that the complex of LPC with the lipid-binding protein puroindoline A is more surface active than is LPC or puroindoline A alone, suggesting a synergistic effect in breadmaking. In addition, already very low concentrations of glycolipids are able to enhance the functionality of phospholipids significantly. Selmair[24] showed that a small amount of MGMG added to the phospholipids of lecithin resulted in an improved baking performance of the flour.

## ■ ASSOCIATED CONTENT

### Supporting Information

NMR data and structures of DGMG and NALPE. Quantitative data of lipid classes present in dough lipids after mixing (without fermentation). This material is available free of charge via the Internet at http://pubs.acs.org.

## ■ AUTHOR INFORMATION

### Corresponding Author

*Phone: +49 8161 712928. Fax: +49 8161 712970. E-mail: peter.koehler@tum.de.

### Notes

The authors declare no competing financial interest.

## ■ ACKNOWLEDGMENTS

The authors wish to thank Katharina Schiesser for the excellent technical assistance.

## ■ ABBREVIATIONS USED

ASG, acylated sterol glucosides; BU, Brabender Units; CBR, cerebrosides; CER, ceramides; DG, diglycerides; DATEM, diacetyl tartaric acid ester of mono- and diglycerides; DGDG, digalactosyl diglycerides; DGMG, digalactosyl monoglycerides; dm, dry matter; FFA, free fatty acids; HPLC-ELSD, high performance liquid chromatography coupled with an evaporative light scattering detector; HPTLC, high performance thin layer chromatography; KLU, kilo-lipase-units; LPA, lysophosphatidic acid; LPC, lysophosphatidyl choline; LPE, lysophosphatidyl ethanolamine; LPI, lysophosphatidyl inositol; LPS, lysophosphatidyl serine; MBT, microbaking test; MG, monoglycerides; MGDG, monogalactosyl diglycerides; MGMG, monogalactosyl monoglycerides; MRMT, microrapid-mix-test; NALPE, N-acyl-lysophosphatidyl ethanolamine; NAPE, N-acyl-phosphatidyl ethanolamine; NMR, nuclear magnetic resonance spectroscopy; PA, phosphatidic acid; PC, phosphatidyl choline; PE, phosphatidyl ethanolamine; PI, phosphatidyl inositol; PS, phosphatidyl serine; SD, standard deviation; SG, sterol glucosides; TG, triglycerides; WSB, water-saturated 1-butanol

## ■ REFERENCES

(1) Morrison, W. R.; Mann, D. L.; Coventry, W. S. A. M. Selective extraction and quantitative analysis of non-starch and starch lipids from wheat flour. *J. Sci. Food Agric.* **1975**, *26*, 507−521.

(2) Morrison, W. R.; Law, R. V.; Snape, C. E. Evidence for inclusion complexes of lipids with v-amylose in maize, rice, and oat starches. *J. Cereal Sci.* **1993**, *18*, 107−109.

(3) MacRitchie, F. Flour lipids: Theoretical aspects and functional properties. *Cereal Chem.* **1981**, *58*, 156−158.

(4) Pareyt, B.; Finnie, S. M.; Putseys, J. A.; Delcour, J. A. Lipids in bread making: Sources, interactions, and impact on bread quality. *J. Cereal Sci.* **2011**, *54*, 266−279.

(5) Selmair, P. L.; Koehler, P. Baking performance of synthetic glycolipids in comparison to commercial surfactants. *J. Agric. Food Chem.* **2008**, *56*, 6691−6700.

(6) Selmair, P. L.; Koehler, P. Molecular structure and baking performance of individual glycolipid classes from lecithins. *J. Agric. Food Chem.* **2009**, *57*, 5597−5609.

(7) De Stefanis, V. A.; Ponte, J. G., Jr. Studies on the breadmaking properties of wheat-flour nonpolar lipids. *Cereal Chem.* **1976**, *53*, 636−642.

(8) Moayedallaie, S.; Mirzaei, M.; Paterson, J. Bread improvers: Comparison of a range of lipases with a traditional emulsifier. *Food Chem.* **2010**, *122*, 495−499.

(9) Gerits, L. R.; Pareyt, B.; Delcour, J. A. Single run HPLC separation coupled to evaporative light scattering detection unravels wheat flour endogenous lipid redistribution during bread dough making. *LWT—Food Sci. Technol.* **2013**, *53*, 426−433.
(10) Gerits, L. R.; Pareyt, B.; Delcour, J. A. A lipase based approach for studying the role of wheat lipids in bread making. *Food Chem.* **2014**, *156*, 190−196.
(11) Graeve, M.; Janssen, D. Improved separation and quantification of neutral and polar lipid classes by HPLC−ELSD using a monolithic silica phase: Application to exceptional marine lipids. *J. Chromatogr., B* **2009**, *877*, 1815−1819.
(12) International Association for Cereal Science and Technology. Method 104/1: Determination of ash in cereals and cereal products. In *Methods. In ICCs Standards*, 7th Suppl. ed.; Verlag Moritz Schäfer: Detmold, Germany, 2004.
(13) International Association for Cereal Science and Technology. Determination of the moisture content of cereals and cereal products (practical method). In *Methods. In ICCs Standards*, 7th Suppl. ed.; Verlag Moritz Schäfer: Detmold, Germany, 2004.
(14) Chung, O. K.; Pomeranz, Y.; Finney, K. F.; Shogren, M. D. Defatted and reconstituted wheat flours. II. Effects of solvent type and extracting conditions on flours varying in breadmaking quality. *Cereal Chem.* **1977**, *54*, 484−495.
(15) Köhler, P.; Grosch, W. Study of the effect of DATEM. 1. Influence of fatty acid chain length on rheology and baking. *J. Agric. Food Chem.* **1999**, *47*, 1863−1869.
(16) International Association for Cereal Science and Technology. Method for using the Brabender farinograph. In *Methods. In ICCs Standards*, 7th Suppl. ed.; Verlag Moritz Schäfer: Detmold, Germany, 2004.
(17) Macmurray, T. A.; Morrison, W. R. Composition of wheat-flour lipids. *J. Sci. Food Agric* **1970**, *21*, 520−528.
(18) Kieffer, R.; Wieser, H.; Henderson, M. H.; Graveland, A. Correlations of the breadmaking performance of wheat flour with rheological measurements on a micro-scale. *J. Cereal Sci.* **1998**, *27*, 53−60.
(19) Colakoglu, A. S.; Özkaya, H. Potential use of exogenous lipases for DATEM replacement to modify the rheological and thermal properties of wheat flour dough. *J. Cereal Sci.* **2012**, *55*, 397−404.
(20) Köhler, P. Study of the effect of DATEM. 3: Synthesis and characterization of DATEM components. *LWT—Food Sci. Technol.* **2001**, *34*, 359−366.
(21) Helmerich, G.; Köhler, P. Structure−activity relationships of phospholipids in baked goods. *Getreide, Mehl Brot* **2003**, *57*, 270−273.
(22) Helmerich, G.; Koehler, P. Functional properties of individual classes of phospholipids in breadmaking. *J. Cereal Sci.* **2005**, *42*, 233−241.
(23) Wilde, P. J.; Clark, D. C.; Marion, D. Influence of competitive adsorption of a lysopalmitoylphosphatidylcholine on the functional properties of puroindoline, a lipid-binding protein isolated from wheat flour. *J. Agric. Food Chem.* **1993**, *41*, 1570−1576.
(24) Selmair, P. L. *Structure−function relationship of glycolipids in breadmaking*. Ph.D. Thesis, Deutsche. Forschungsanstalt für Lebensmittelchemie, Garching, Germany, 2010, pp 148−150, ISBN 978-3-938896-32-7.

JOURNAL OF AGRICULTURAL AND FOOD CHEMISTRY

Article

pubs.acs.org/JAFC

# Controlled Release Properties of Zein−Fatty Acid Blend Films for Multiple Bioactive Compounds

Iskender Arcan and Ahmet Yemenicioğlu*

Department of Food Engineering, Faculty of Engineering, Izmir Institute of Technology, 35430, Gülbahçe Köyü, Urla, Izmir, Turkey

Supporting Information

**ABSTRACT:** To develop edible films having controlled release properties for multiple bioactive compounds, hydrophobicity and morphology of zein films were modified by blending zein with oleic ($C_{18:1}$)$\Delta^9$, linoleic ($C_{18:2}$)$\Delta^{9,12}$, or lauric ($C_{12}$) acids in the presence of lecithin. The blend zein films showed 2−8.5- and 1.6−2.9-fold lower initial release rates for the model active compounds, lysozyme (LYS) and (+)-catechin (CAT), than the zein control films, respectively. The change of fatty acid chain length affected both CAT and LYS release rates while the change of fatty acid double bond number affected only the CAT release rate. The film morphologies suggested that the blend films owe their controlled release properties mainly to the microspheres formed within their matrix and encapsulation of active compounds. The blend films showed antilisterial activity and antioxidant activity up to 81 $\mu$mol Trolox/cm$^2$. The controlled release of multiple bioactive compounds from a single film showed the possibility of combining application of active and bioactive packaging technologies and improving not only safety and quality but also health benefits of packed food.

**KEYWORDS:** *active packaging, bioactive packaging, edible film, blend film, lysozyme, CAT*

## INTRODUCTION

In recent years, continuous efforts have been spent to improve safety and quality of food or to increase their shelf life by using novel packaging technologies. Active packaging containing antimicrobials (antimicrobial packaging) or antioxidants (antioxidant packaging) is among the most promising packaging technologies, since its application can inhibit pathogenic and spoilage microorganisms and lipid oxidation in food, respectively.[1] The addition of bioactive compounds into packaging materials has also initiated bioactive packaging, a novel packaging concept that targets enriching packed food with bioactive compounds and improving their potential health benefits.[2]

Because of the health concerns of the consumers and environmental problems, there is an increasing trend to use natural active compounds and edible films in active packaging. Therefore, antimicrobial enzymes including lysozyme (LYS), lactoperoxidase and glucose oxidase, bacteriocins, and natural antimicrobial and antioxidants such as plant phenolics and essential oils have been extensively tested in different edible packaging materials.[3−5] The use of natural phenolic compounds in active packaging attracts a particular interest, since these compounds show antimicrobial and antioxidant activity in food systems and increase health benefits of food because of their potential bioactive effects.[2,6] (+)-Catechins (CATs), a group of flavonoids ($C_6C_3C_6$), are frequently employed in foods, since it is economically feasible to extract these compounds from abundant sources such as green tea[7] and they show well documented bioactive effects such as antioxidant, anticancerogenic, antidiabetic, and antihypertensive activities.[8] LYS obtained from hen egg white is also among the most potential candidates for antimicrobial packaging, since it has a GRAS status and it shows good stability and activity in different films and food systems under refrigerated storage temperature.[9,10] This enzyme is effective mainly on Gram-positive bacteria and shows its antimicrobial activity by splitting the bonds between *N*-acetylmuramic acid and *N*-acetylglucosamine of the peptidoglycan layer in the bacterial cell wall. Thus, the application of LYS in active packaging targets mainly inhibition of critical Gram-positive pathogenic bacteria such as *Listeria monocytogenes* that might cause deadly infections.[10−12] LYS has recently been tested extensively in different plastic materials such as cellulose acetate, nylon, and PVOH[4,13] and biopolymeric materials from zein, soy protein, carrageenan, whey protein, chitosan, alginate, and pullulan[4,14] to develop antimicrobial packaging materials.

Antioxidant and antimicrobial packaging targets mainly the food surface on which oxidative and microbiological changes occur most intensively.[15] A sufficient preservation effect could not be achieved unless the release rate of active compounds from the packaging materials to the food surface is adjusted considering the physical and chemical properties of food, lipid oxidation rate, growth kinetics of target pathogenic or spoilage microorganisms, and expected food shelf life.[15,16] Different studies have been conducted to control the release rate of LYS in different plastic films from cellulose acetate, poly(vinyl alcohol), and glycerol/poly butylenes trephthalate and in different edible films from caseinate, zein, and chitosan.[13,17−20] On the other hand, although the controlled release of CAT had been studied from polypropylene films,[21,22] no studies are determined related to controlled release of CAT from edible films.

Received: February 11, 2014
Revised: July 10, 2014
Accepted: July 15, 2014
Published: July 15, 2014

ACS Publications © 2014 American Chemical Society



dx.doi.org/10.1021/jf500666w | J. Agric. Food Chem. 2014, 62, 8238−8246

The incorporation of LYS into zein films or zein particles has recently gained an increasing interest, since (1) zein is the major coproduct of the oil and rapidly growing bioethanol industries, (2) it is one of the rare film forming proteins soluble in various organic solvents including ethanol, and (3) it provides an effective delivery system for LYS.[9,23−29] The effectiveness of zein-based LYS delivery systems is due to the highly hydrophobic nature of the zein film matrix that contains very limited charges to cause binding and immobilization of LYS that is positively charged in food systems due to its high pI at 11.35.[30] The LYS activity is also highly stable during zein film making and during cold storage of precast zein films.[9] Moreover, LYS release profiles of zein films could be changed effectively by modifying film morphology and hydrophobicity using composite and blend film making technologies. Gucbilmez et al.[23] sustained LYS release from zein films by forming composites of these films with chickpea proteins. Arcan and Yemenicioğlu[24] controlled LYS release from zein films by preparing composites of zein with different waxes. These authors reported that the LYS release profiles of zein−wax composites could be effectively modified by using different types of waxes that create different film morphologies and increase film tortuosity depending on their melting points. Ünalan et al.[15] employed LYS with a mixture of CAT and gallic acid and showed the benefits of using controlled release technology in zein−wax composites applied for antimicrobial and antioxidant packaging of cheese. Not only composite films, but also blend films of zein prepared by forming emulsions of zein with the fatty acid oleic acid (OLE) in the presence of lecithin (LEC) have also been applied for controlled release of LYS.[24] The preparation of zein blend films with OLE causes the formation of microspheres within the film matrix, and this increases barriers against diffusion of encapsulated LYS.[24] The aim of the current work is to investigate the effects of using different fatty acids, OLE ($C_{18:1}$)Δ,[9] linoleic (LIN) ($C_{18:2}$)Δ,[9,12] and lauric (LAU) ($C_{12}$), in zein blend film making to obtain different release profiles for LYS and CAT at the same film system. It was proposed that the use of fatty acids with different chain length, conformation, and saturation level could create different types of zein microspheres and morphologies and this could be exploited to obtain films with different release profiles for LYS and CAT. The use of LAU in blend film making could contribute not only to the controlled release properties of active compounds, but it could also provide an additional antimicrobial effect to films, since it is an active fatty acid with potent antimicrobial activity.[31] This is one of the first studies that aimed in developing a scientific basis for edible packaging materials having controlled release properties for multiple active compounds capable of showing antimicrobial and antioxidant effects not only in packed food (active packaging) but also in the human physiological system after consumption of the enriched packed food (bioactive packaging).

## MATERIALS AND METHODS

**Materials.** Maize zein (batch number: 058 K0093), (+)-CAT hydrate (≥98%), *Micrococcus lysodeikticus*, OLE (tech. 90%), LIN (minimum 99%), and LAU (≥98%) were from Sigma−Aldrich Chem. Co. (St. Louis, MO, USA). Soybean L-α-LEC and glycerol were from Merck (Darmsdadt, Germany). All other chemicals were reagent grade. Fresh hen eggs used in production of LYS were obtained from a supermarket in Izmir (Turkey).

**LYSs Used in the Study.** The partially pure (PP) LYS was produced by the selective precipitation of egg white proteins other than this enzyme according to the method described by Mecitoglu et al.[9] The enzyme was lyophilized by using a freeze drier (Labconco, FreeZone, 6 L, Kansas City, MO, USA) and stored at −18 °C until it was used in film-making. The pure commercial (PC) LYS (protein and specific activity values specified in the manual are ≥90% and ≥40 000 units/mg protein, respectively) was obtained from Sigma−Aldrich Chem. Co. (St. Louis, MO, USA). The specific activities of PP LYS and PC LYS determined by the method described in this study were 40477 and 78984 U/mg protein, respectively. The protein content of the LYS preparations was tested by the classical Bradford method by using bovine serum albumin as the standard. The impurities in the PP LYS and the purity of PC LYS were tested by sodium dodecyl sulfate polyacrylamide gel electrophoresis (SDS-PAGE) according to the method of Laemmli[32] using a 12% separating gel and a 4% stacking gel. Proteins bands were stained with silver salts described by Blum et al.[33]

**Preparations of Zein Films.** The films were produced by modifying the methods described in Padgett et al.[34] and Arcan and Yemenicioglu.[33] Briefly, 1.4 g of zein was dissolved with 8.1 mL of ethanol (96%) by mixing slowly with a magnetic stirrer for 25 min, and 0.4 mL of glycerol was then added to the medium as plasticizer. The mixture was then heated under continuous mixing until it started to boil. The boiling was conducted for 5 min, and the film-making solution was cooled to room temperature. CAT (100 mg/g film-forming solution) and PC LYS (Sigma−Aldrich Chem. Co.) or PP LYS obtained according to Mecitoglu et al.[9] were then added into film-forming solutions. PC LYS (78984 U/mg protein) and PP LYS (40477 U/mg protein) were used at the concentrations of 11.7 and 23.4 mg lyophilized powder/g of film-forming solution, respectively (the final PC LYS, PP LYS, and CAT concentrations in cast and dried films were 0.7, 1.4, and 6 mg/cm$^2$, respectively). The PP LYS concentration used in film making is 2-fold higher than that used in zein films successfully applied to control microbial development in actively packed ground beef patties.[10] After addition of CAT and LYS, the mixtures were homogenized (Heidolph, Germany, rotor Φ = 6.6 mm tip) at 10 000 rpm for 4 min. Then, 4.3 g portions of the homogenized film-forming solutions were cast into the glass templates (W × L × H: 8.5 × 8.5 × 0.4 cm$^3$) and dried for 19 ± 2 h at 25 °C in an incubator unless otherwise was stated. This homogenization and casting procedure was also used to obtain zein−fatty acid blend films by adding fatty acids (LAU, OLE, and LIN) and emulsifier LEC into film-forming solutions at 5−20% (w/w) and 10% (w/w) of zein, respectively. The fatty acids and LEC were added after the boiling step following cooling of zein film-forming solution to room temperature.

**LYS Release Profiles of Films.** For the release tests, film samples (4.5 × 4.5 cm$^2$) were placed between two glass frames (dimensions: inside, 4 × 4 cm$^2$; outside, 6 × 6 cm$^2$). The edges of the glass frames were carefully sealed with paraffin film, and the glass apparatus containing the film was placed horizontally at the bottom of a 500 mL glass beaker containing 150 mL of distilled water at 4 °C. Four 0.5 cm diameter glass rods were placed below the frame at the corners to increase water circulation, and the overall apparatus (the 500 mL beaker) was placed onto an orbital shaker working at 80 rpm in an incubator at 4 °C. The LYS activity released from the films was monitored by taking 0.25 mL (×3) aliquots from the release test solution at different time intervals. The release tests were conducted until equilibrium was reached for release of LYS or an insignificant increase was observed in the activity of released LYS. The LYS activities of collected aliquots were determined spectrophotometrically at 660 nm by using a Shimadzu spectrophotometer (Model 2450, Tokyo, Japan) equipped with a constant temperature cell holder working at 30 °C. The *Micrococcus lysodeikticus* solution prepared in 0.05 M, pH 7.0 Na phosphate buffer (0.26 mg/mL) was used as substrate during activity determination. The reaction mixture was formed by mixing 0.1 or 0.25 mL of release test medium (depending on LYS activity) and 2.4 or 2.25 mL of substrate solution to reach a final reaction volume of 2.5 mL. The enzyme activities were calculated from the slopes of initial linear portions of absorbance versus time curves and were expressed as unit (U) that was defined as the number of 0.001 changes in absorbance in 1 min. All calculations were corrected by considering the activity removed by collected aliquots

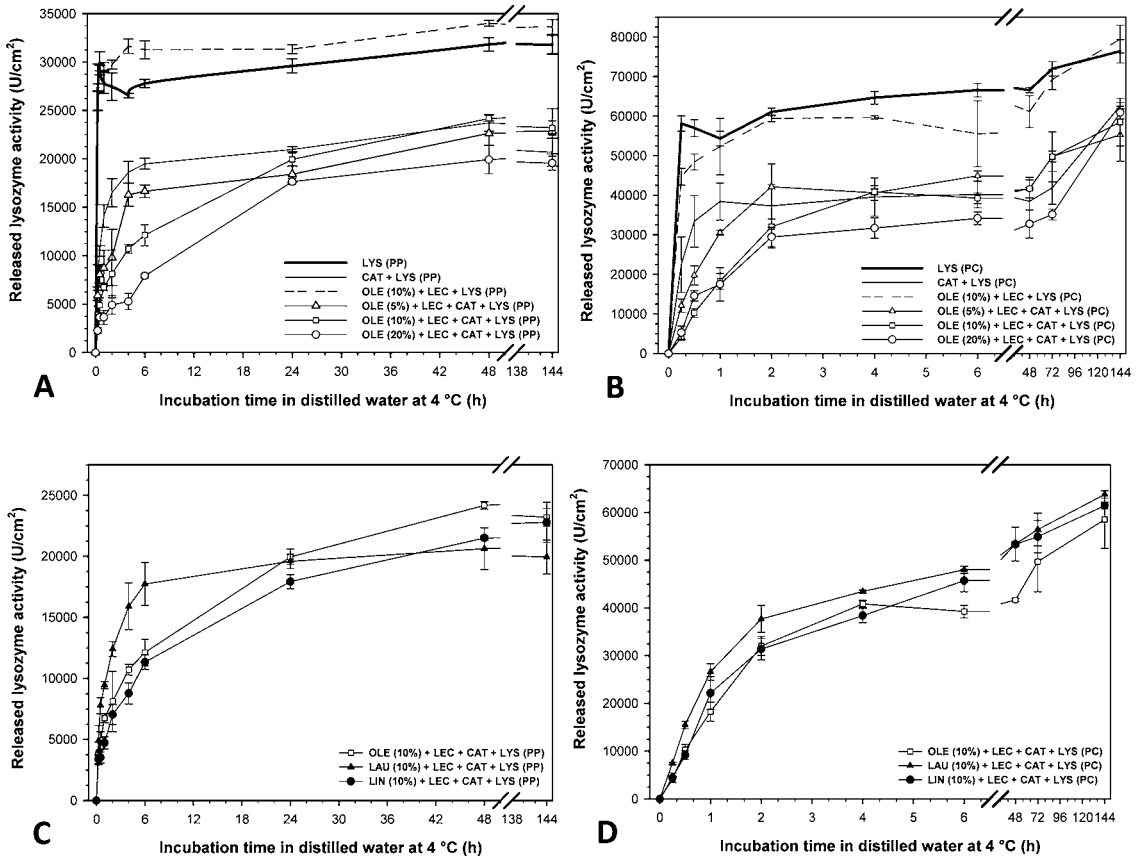


**Figure 1.** Effect of CAT and blend film making on release profiles of (A, C) PP LYS and (B, D) PC LYS. CAT: catechin; LYS: lysozyme; OLE: oleic acid; LAU: lauric acid; LIN: linoleic acid; LEC: lecithin.

during sampling. The total LYS activity released from each film corresponded to maximum units released per centimeter squared of the films (U/cm$^2$) at the equilibrium. All activity measurements were conducted three times. The release curves were formed by plotting calculated released activities (U/cm$^2$) versus incubation time (h). The initial release rates of LYS were determined from the slope of the initial linear portion of the release curve. The release rates were expressed as units per centimeters squared per hour (U/(cm$^2$ h)).

**CAT Release Profiles and Antioxidant Capacity of Films.** To determine the CAT release profiles of films, the release tests were conducted in water as described in the LYS Release Profiles of Films section. The soluble CAT content of the collected samples was determined spectrophotometerically at 510 nm according to the colorimetric method of Meyers et al.[35] used for quantification of flavonoids. The total soluble CAT contents released from the films were expressed as milligrams of CAT per centimeter squared of the films (mg/cm$^2$) using the calibration curve prepared by CAT. All concentration measurements were conducted three times. The release curves were formed by plotting the calculated released phenolic contents (mg/cm$^2$) versus time (h). The initial CAT release rates were determined from the slope of the initial linear portion of release curve. The release rates were expressed as milligrams per centimeter squared per hour (mg/(cm$^2$ h)). The antioxidant capacity of the films was based on calculating the Trolox equivalent antioxidant capacity (TEAC) of their total released CAT content at the equilibrium. The percentage of free soluble CAT in the films was determined by the formula of (total released CAT/initial CAT added) × 100. The TEAC of CAT was determined by using the spectrophotometric ABTS radical cation decolourization assay conducted at 734 nm.[36] The results were expressed as micromoles of Trolox equivalents released per centimeter squared of films ($\mu$mol Trolox/cm$^2$).

**Antimicrobial Potential of Films.** The antimicrobial potentials of films were tested by using *Listeria innocua* (NRRL B-33314; supplied from USDA, Microbial Genomics and Bioprocessing Research Unit, Peoria, IL, USA) as a test microorganism. During antimicrobial tests, 18 discs (1.3 cm in diameter) were prepared from each film by a cork borer. Total of 15 discs were selected randomly, and 3 discs were placed into each Petri dish containing nutrient agar previously inoculated with 0.1 mL of bacterial culture. The inocula were prepared in peptone water (0.1%) by using 48 h culture grown in nutrient agar. The cell concentration was set to 1.0 McFarland unit that corresponded to 13 × 10$^7$ CFU/mL. The Petri dishes containing discs of films were incubated first at 4 °C for 4 h to prevent rapid diffusion of the LYS, and then, second they were incubated at 37 °C for 36 h for microbial growth. The diameter of the zones formed around the discs was measured by using a calliper, and the results were expressed as average zone areas (mm$^2$).

**Scanning Electron Microscopy (SEM) of Films.** The cross sections and surfaces of selected films were monitored by using SEM (Philips XL 30S FEG, FEI Company, Netherlands) under high vacuum mode at an operating voltage at 3 kV. The film cross sections were obtained by crushing films following freezing in liquid nitrogen. The samples were then gold coated with a sputter coater (Emitech K550X, Quorum Technologies Inc., UK) under 15 mA for 60 s. The thickness of the films was measured from SEM cross-sectional views of films by using Scandium software (Olympus Soft Imaging Solutions GmbH, Münster, Germany).

**Mechanical Properties of Films.** Tensile strength at break, elongation at break, and elastic modulus were determined using a Texture Analyzer TA-XT2 (Stable Microsystems, Godalming, UK) according to ASTM standard method D 882-02.[37] The films used in mechanical tests were conditioned by extending the standard drying period from 19 to 48 h at 25 °C and conducting drying at 50% RH using a controlled test cabinet (TK 120, Nüve, Turkey). Films were cut into 5 mm wide and 80 mm length strips, initial grip distance was


dx.doi.org/10.1021/jf500666w | J. Agric. Food Chem. 2014, 62, 8238−8246

Table 1. Some Kinetic Parameters Determined from Release Curves of LYS and Antilisterial Potential of Films

| film composition | | | | | |
|---|---|---|---|---|---|
| CAT (mg/cm$^2$) | fatty acid[a] (%) | LEC[a] (%) | initial LYS release rate[b] (U/(cm$^2$ h)) | total released LYS activity (U/cm$^2$) | antimicrobial activity (zone area as mm$^2$) |
| – | – | – | – | – | no zone formation |
| PP LYS (1.4 mg/cm$^2$) | | | | | |
| – | – | – | 67 472[bc] | 32 501 ± 723a[d] | 65 ± 10a,AB |
| – | 10(OLE) | 10 | 71 152 | 34 002 ± 294a | – |
| 6.0 | – | – | 23 124 | 23 725 ± 867bc | 55 ± 26ab,ABC |
| 6.0 | 5(OLE) | 10 | 17 623 | 22 861 ± 2337bc | – |
| 6.0 | 10(OLE) | 10 | 10 944 | 25 011 ± 1718b | 35 ± 4b,C |
| 6.0 | 20(OLE) | 10 | 7632 | 20 972 ± 886c | – |
| 6.0 | 10(LAU) | 10 | 16 387 | 20 941 ± 1301c | 537 ± 52[e] |
| 6.0 | 10(LIN) | 10 | 8346 | 22 789 ± 1632bc | 34 ± 7b,C |
| PC LYS (0.7 mg/cm$^2$) | | | | | |
| – | – | – | 137 648 | 76 408 ± 2987a | 73 ± 26a,A |
| – | 10(OLE) | 10 | 113 245 | 79 468 ± 3524a | – |
| 6.0 | – | – | 71 418 | 62 576 ± 810b | 38 ± 7b,C |
| 6.0 | 5(OLE) | 10 | 41 314 | 55 255 ± 6622b | – |
| 6.0 | 10(OLE) | 10 | 19 762 | 58 513 ± 6041b | 43 ± 10b,BC |
| 6.0 | 20(OLE) | 10 | 19 863 | 60 868 ± 1608b | – |
| 6.0 | 10(LAU) | 10 | 30 798 | 63 786 ± 749b | 506 ± 7[e] |
| 6.0 | 10(LIN) | 10 | 18 249 | 61 427 ± 696b | 46 ± 7ab,ABC |

[a]Concentrations of fatty acids and LEC as % of zein (w/w). [b]Determined from the slope of the initial linear portion of release curves. [c]Time periods of data used in best fitting curves were between 0 and 0.5 h. $r^2$ values of curves were between 0.6825−0.9994. [d]Different letters (a−c; A−C) in each column show the significant difference at $P < 0.05$. Small letters indicate the differences within each enzyme type. Capital letters indicate the differences within all given results at the column. [e]Not included in statistical analysis.

50 mm, and crosshead speed was 50 mm/min. At least seven replicates of each film were tested.

**Statistical Analysis.** For the determination of effects of film compositions on antimicrobial potentials and mechanical properties of films analysis of variance (ANOVA) was applied using Minitab 15 (Minitab Inc., State College, PA, USA). Multiple comparisons of means were performed using Fisher's least significant difference (LSD) method with a significance threshold of $P < 0.05$.

## RESULTS AND DISCUSSION

**Effect of CAT and Blend Film Making with OLE on LYS Release Profiles.** In the zein film system, the phenolic compounds including CAT not only serve as an active component but they also affect film morphology, since they interact with the film matrix via hydrogen bonding to available zein carbonyl groups.[24] The morphological changes in zein films caused by CAT are particularly important, since they affect the film porosity, thus the controlled release properties of films.[24,38] Arcan and Yemenicioğlu[24] clearly showed the concentration-dependent contribution of CAT in sustained release of LYS form zein and zein−carnauba wax composite films. In the current work, the contribution of CAT in LYS release properties of zein films and zein−OLE (10%) blend films are seen in Figure 1A, B. The control zein films and control zein−OLE (10%) blend films lacking CAT showed 2.9- and 8.5-fold higher release rates for PP LYS, and 1.9- and 7.5-fold higher release rates for PC LYS than CAT-containing zein films and zein−OLE (10%) blend films, respectively (Table 1). The SEM photos for cross sections (Figure 2A−D) and surfaces (Supporting Information, Figure S1) of zein films and zein−OLE (10%) blend films containing and lacking CAT clearly showed the reduced film porosity by incorporation of CAT into films. Thus, it is clear that the CAT used as active compound also contributed to the sustained LYS release rates of zein films. On the other hand, the 2.1- and 3.6-fold lower release rates of CAT-containing zein−OLE (10%) blend films for PP and PC LYS than CAT-containing zein films could be related with the differences in morphological properties of these films. The morphological changes of zein film structure when it is mixed with OLE without use of an emulsifier was recently explained by Wang et al.[39] According to these authors, the morphological changes in the zein−OLE film system occurred at three steps: (1) formation of large numbers of OLE-coated zein microspheres, (2) partial melting of the microspheres by means of OLE, and (3) transformation of a sponge-like morphology by interconnection of microspheres with channels and tunnels. Arcan and Yemenicioğlu[24] who employed the zein−OLE blend films for controlled release of LYS also reported the presence of microspheres within the zein−OLE films and attributed the sustained release properties of these blend films to encapsulation of LYS within the microspheres. However, different from Wang et al.,[39] these workers conducted the blending process by using LEC emulsifier, and they did not observe the presence of interconnections among the formed self-standing microspheres. In this work, the presence of self-standing microspheres was also observed in the SEM photos of both CAT-containing and -lacking zein−OLE blend films that were prepared by using emulsifier LEC (Figure 2C, D). These results suggest that the repulsion formed by negative charges of LEC that interacted with the OLE-coating formed around zein microspheres. This might prevent the interaction and melting down of the microspheres and enables the formation of self-standing microspheres different from the spongelike structure observed by Wang et al.[39] It is also worth to note that the CAT reduced the sizes of microspheres and caused an increase in the number of microspheres. On the other hand, it is important to report that the total released PC or PP LYS activity from CAT-containing zein and zein−OLE (10%) films at the equilibrium

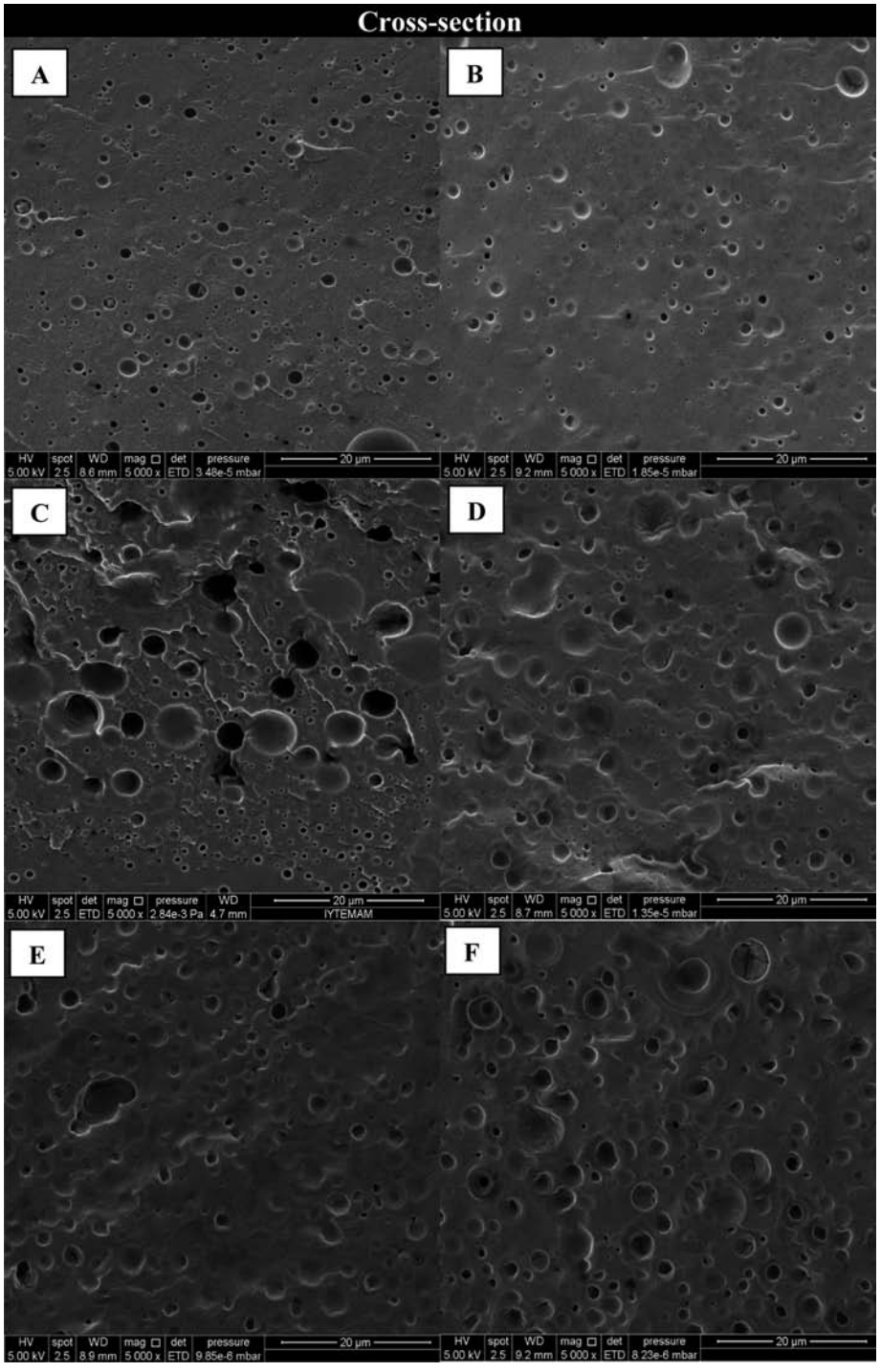


**Figure 2.** Cross-sectional SEM images of developed films: (A) zein film containing PP LYS (1.4 mg/cm$^2$); (B) zein film containing CAT (6 mg/cm$^2$) and PP LYS (1.4 mg/cm$^2$); (C) blend film containing OLE (10%) and PP LYS (1.4 mg/cm$^2$); (D) blend film containing OLE (10%), CAT (6 mg/cm$^2$), and PP LYS (1.4 mg/cm$^2$); (E) blend film containing LAU (10%), CAT (6 mg/cm$^2$), and PP LYS (1.4 mg/cm$^2$); (F) blend film containing LIN (10%), CAT (6 mg/cm$^2$), and PP LYS (1.4 mg/cm$^2$). CAT: catechin; LYS: lysozyme; OLE: oleic acid; LAU: lauric acid; LIN: linoleic acid; LEC: lecithin.

is 18−27% lower than those of their CAT-lacking controls. This result suggests the trapping or immobilization of part of LYS within zein and zein−OLE (10%) films when CAT was incorporated into films. On the other hand, there are no significant differences in total released PC or PP LYS activities from control zein films and zein−OLE (10%) films lacking CAT ($P > 0.05$). Thus, it also appeared that the blend film making with OLE and the formation of microspheres within films did not cause considerable LYS trapping and immobilization.

**Effect of OLE Concentration on LYS Release Profiles of Blend Films.** In order to determine the effect of fatty acid concentration in release profiles of blend films, the OLE concentration of 10% was changed as 5% and 20% (Figure 1A, B). The results clearly showed that the increase of OLE fraction within blend films caused a reduction in release rates for both

Table 2. Some Kinetic Parameters Determined from Release Curves of CAT and Antioxidant Activity of Films

| film composition | | | | | |
|---|---|---|---|---|---|
| CAT (mg/cm$^2$) | fatty acid[a] (%) | LEC[a] (%) | initial CAT release rate (mg/(cm$^2$ h)) | total released CAT (mg/cm$^2$) | antioxidant activity ($\mu$mol Trolox/cm$^2$) |
| PP LYS (1.4 mg/cm$^2$) | | | | | |
| 6.0 | – | – | 1.76[b] | 4.8 ± 0.2a[c] | 77.1 ± 3.0a |
| 6.0 | 10(OLE) | 10 | 0.61 | 4.3 ± 0.1b | 69.3 ± 1.7b |
| 6.0 | 10(LAU) | 10 | 1.10 | 4.7 ± 0.1a | 76.4 ± 1.5a |
| 6.0 | 10(LIN) | 10 | 0.77 | 5.0 ± 0.1a | 80.7 ± 1.6a |

[a]Concentrations of fatty acids and LEC as % of zein (w/w). [b]Time periods (h) of data used in best fitting curves were between 0 and 1 h. $r^2$ values of curves were between 0.6110 and 0.7491. [c]Different letters in each column show significant difference $P < 0.05$.

PC and PP LYS. The initial release rate of PP LYS reduced 1.4- to 1.6-fold as a concentration-dependent manner when OLE concentration in blend films increased between 5% and 20%. On the other hand, the increase of OLE concentration within blend films from 5% to 10% caused almost 2-fold reduction in initial release rate of PC LYS, but further increase of OLE concentration did not affect the initial release rate of PC LYS (Table 1). These results clearly showed the possibility of controlling LYS release rate of CAT-containing zein−OLE blend films by changing fatty acid concentration within the films.

**Effect of Different Fatty Acids on LYS Release Profiles of Blend Films.** To determine the effects of different fatty acids on LYS release profiles of CAT-containing blend films, LIN and LAU at 10% (w/w) of zein were also used in film making. The selected fatty acids enabled determining the possible effects of carbon chain length ($C_{12}$ or $C_{18}$), number of double bonds ($C_{18:1}$ or $C_{18:2}$), and fatty acid tail conformation (LIN has more bent tail than OLE) in LYS release properties (Supporting Information, Figure S2). The LYS release curves of films clearly showed the more different release profiles of LAU-containing blend films than LIN- and OLE-containing blend films (Figure 1C, D). In fact, the initial PP LYS and PC LYS release rates of LAU-containing blend films were 1.6- to 2.0-fold higher than those of OLE- and LIN-containing blend films (Table 1). These results clearly showed the reduced diffusion barriers for LYS when fatty acid chain length was reduced from $C_{18}$ to $C_{12}$. On the other hand, the similar release profiles of LIN- and OLE-containing blend films also showed that the presence of one or two double bonds and the resulting conformational differences at the fatty acid aliphatic tails has no contribution in LYS release properties of blend films. The SEM photos of blend films obtained with LIN and LAU also showed the presence of self-standing microspheres in these films (Figure 2E, F). Thus, it is once more conformed that different fatty acids emulsified with LEC in the zein film system caused self-standing microspheres within the blend films. Moreover, it was also observed that microspheres in OLE- and LIN-containing blend films were larger and more intensive than those observed for LAU-containing films. Thus, it appeared that the higher LYS release rate of zein−LAU blend films than zein−OLE and zein−LIN films is related with the reduced fraction of LYS encapsulated within the microspheres. This result supported our hypothesis that the microspheres formed in zein−fatty acid blend films play a very important role in controlling LYS release rates.

**Effect of Enzyme Purity on LYS Release Profiles of Zein and Blend Films.** In this work, the use of LYS preparations at different purities aimed to test the magnitude of potential variations in the effectiveness of formed controlled release mechanisms. The comparison of the overall results for release tests clearly showed the higher release rates obtained for PC LYS than PP LYS. Almost 2-fold (78984 U/mg PC protein/40477 U/mg PP protein = 1.95) higher purity of PC LYS than PP LYS resulted with 1.6−3-fold higher release rates of PC LYS than the PP LYS from similar films. The results of SDS-PAGE clearly showed the quite similar moleculare weights (MWs) of PP and PC LYS centered around 12 kDa (Supporting Information, Figure S3). The SDS-PAGE profiles of PC LYS did not indicate any considerable protein impurities within this preparation except a thin band appeared at 11 kDa. On the other hand, as expected, the electrophoresis results showed the presence of different protein impurities in the PP LYS. The protein bands observed as impurities in PP LYS between 43 and 65 kDa concentrate around 46−47 kDa that might correspond to the ovalbumin fraction reported to have a MW of 45 kDa.[40] Dense bands observed in PP LYS between 34 and 43 kDa might be ovoglobulins ($G_2$ and $G_3$) and flavoprotein that have reported MWs between 30 and 45 kDa[41] while the dense band centered at 26 kDa might be ovomucoid and ovoglycoproteins that have reported MWs at 28 and 24 kDa, respectively.[41] Thus, it is possible that the PP LYS might form complexes with the impurities present in egg white, and this affected its release profiles. The interaction of PP LYS with egg white protein impurities might modify its diffusion properties due to changes in its molecular weight and affinity (by hydrophobic or charge−charge interactions) to film matrix. However, the results of this work clearly showed the possibility of controlling release rates of LYS at different purities by using blend film technology in the presence of CAT.

**CAT Release Profiles and Antioxidant Potential of Blend Films.** The results of release tests conducted to determine release profiles of CAT showed that 72−84% of CAT existed in soluble form in films (Table 2) while remaining CAT was bound by the film matrix, since this phenolic compound is capable to form H bonds with zein film matrix.[42] Thus, the soluble CAT in films formed a significant antioxidant potential that varies between 69 and 81 $\mu$mol Trolox/cm$^2$. On the other hand, the release curves clearly showed the effectiveness of the formed blend film structures to reduce release rates of CAT (Figure 3). The zein−fatty acid blend films showed 1.6−2.9-fold lower initial CAT release rates than the control zein film. The highest CAT release rate among blend films was observed for that of zein−LAU films while zein−OLE blend films had the lowest CAT release rates and zein−LIN blend films had intermediate CAT release rates. These results clearly proved that the change of chain length of fatty acids during blend film making could be employed as a highly effective tool to control release rates of both CAT and LYS. Moreover, it is also evident that the $C_{18}$ fatty acids' number of double bonds and tail conformation (LIN has more bent tail than OLE) that did not affect release rates of LYS is


dx.doi.org/10.1021/jf500666w | J. Agric. Food Chem. 2014, 62, 8238−8246

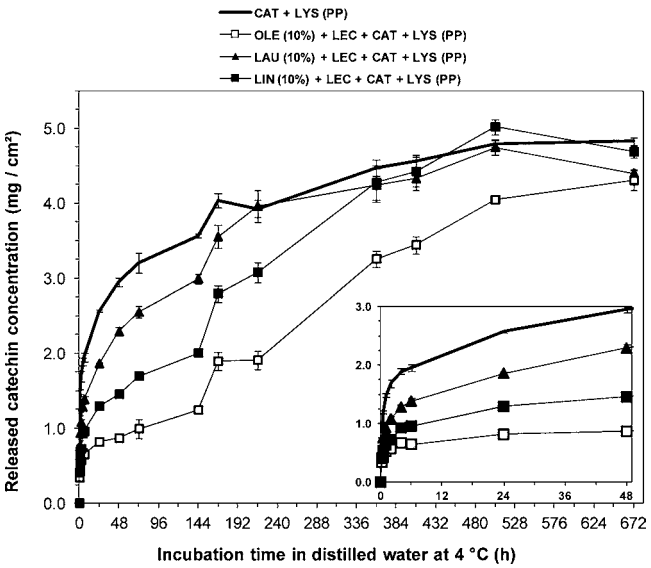


**Figure 3.** Release profiles of CAT from zein-based films containing PP LYS. CAT: catechin; LYS: lysozyme; OLE: oleic acid; LAU: lauric acid; LIN: linoleic acid; LEC: lecithin.

effective on release rates of CAT. The CAT has a significantly lower molecular weight (MW: 290.3 g/mol) than LYS (MW: 14 300 g/mol). However, it is an amphiphilic molecule, and its diffusion properties might change due to its hydrophobic affinity on the aliphatic chains of fatty acids. It appeared that the CAT showed higher hydrophobic affinity to microspheres formed by single double bonded OLE that has a slightly bent tail than those microspheres of double bonded LIN that has an apparently bent tail. In contrast, LYS is a hydrophilic protein, and this might limit its interactions with the hydrophobic tails of fatty acids. These results proved that the developed controlled release mechanism by blend film formation could be employed for delivery of multiple active compounds. Moreover, it is once more proved that the use of fatty acids having different molecular properties could be employed as an effective tool in controlling release profiles of blend films.

**Antimicrobial Potential of Films.** The results of antimicrobial tests on *L. innocua* are given in Table 1. The control zein film without LYS and CAT did not form any inhibition zones. In contrast, all other films containing PC or PP LYS showed antimicrobial effect on *L. innocua* and formed clear zones. Although PC LYS preparation has higher enzyme activity than the PP LYS preparation, there are no significant differences among the clear zone sizes of control zein films containing these enzymes ($P > 0.05$). However, the addition of CAT into films and reduction in their LYS release rate decreased the antimicrobial activity of PC LYS-containing zein control films significantly ($P < 0.05$) while this caused only an insignificant reduction in antimicrobial activity of PP LYS-containing zein control films ($P > 0.05$). Although the CAT-containing blend films with OLE and LIN showed lower LYS release rates than CAT-containing zein control films, there are no significant differences among the antimicrobial activities of these films containing CAT and PC or PP LYS ($P > 0.05$). On the other hand, the CAT-containing zein−OLE and zein−LIN films with sustained LYS release rates had significantly lower antimicrobial activity than PC or PP LYS-containing, but CAT-lacking zein control films showed the highest LYS release rates. In contrast, blend film making with the potent antimicrobial fatty acid LAU gave films with the highest antimicrobial activity. This result was quite expected, since Hoffman et al.[43] previously showed the high antimicrobial activity of LAU-containing zein films against *L. monocytogenes.* Although the results of this work did not indicate antilisterial activity originated from OLE and LIN in zein films, the OLE and LIN solubilized properly in broth medium were reported to have a limited antimicrobial activity on *L. monocytogenes*.[44] However, LAU has reported to have a 6-fold lower minimum inhibitory concentration on *L. monocytogenes* than OLE and LIN solubilized in broth medium.[44] The overall results of antimicrobial tests conducted with the classical zone inhibition test could not reflect the effectiveness of developed films in a food system, but they clearly showed the presence of in vitro antimicrobial activity of blend films with sustained LYS release rates and beneficial effects of using antimicrobial fatty acid LAU in blend film making.

**Mechanical Properties of Films.** In order to analyze their mechanical properties, tensile strength at break, elongation at break, and Young's modulus values of films were determined (Table 3). The control zein films lacking LYS were quite brittle and showed the lowest elongation, but the average tensile strength of these films (17.67 MPa) was significantly higher

**Table 3. Mechanical Properties of Zein-Based Blend Films**

| film composition | | | | | | |
|---|---|---|---|---|---|---|
| CAT (mg/cm$^2$) | fatty acid[a] (%) | LEC[a] (%) | tensile strength at break (MPa) | elongation at break (%) | Young's modulus (MPa) | film thickness ($\mu$m) |
| – | – | – | 17.67 ± 0.93a[b] | 4 ± 1a | 775 ± 44a | 113 ± 1 |
| | | | PP LYS (1.4 mg/cm$^2$) | | | |
| – | – | – | 10.98 ± 0.96b | 3 ± 1a | 530 ± 32c | 143 ± 1 |
| 6.0 | – | – | 0.98 ± 0.14c | 61 ± 18b | 55 ± 12d | 167 ± 1 |
| 6.0 | 10(OLE) | 10 | 1.17 ± 0.26c | 53 ± 9b | 55 ± 19d | 160 ± 2 |
| 6.0 | 10(LAU) | 10 | 0.88 ± 0.10c | 70 ± 10b | 37 ± 9d | 159 ± 2 |
| 6.0 | 10(LIN) | 10 | 1.23 ± 0.10c | 71 ± 15b | 63 ± 9d | 192 ± 5 |
| | | | PC LYS (0.7 mg/cm$^2$) | | | |
| – | – | – | 11.02 ± 0.67b | 3 ± 1a | 611 ± 22b | 119 ± 3 |
| 6.0 | – | – | 0.61 ± 0.06c | 161 ± 18c | 28 ± 5d | 160 ± 5 |
| 6.0 | 10(OLE) | 10 | 0.52 ± 0.02c | 164 ± 17c | 23 ± 4d | 162 ± 8 |
| 6.0 | 10(LAU) | 10 | 0.45 ± 0.04c | 166 ± 10c | 22 ± 4d | 184 ± 12 |
| 6.0 | 10(LIN) | 10 | 0.49 ± 0.08c | 131 ± 25c | 22 ± 6d | 173 ± 2 |

[a]Concentrations of fatty acids and LEC as % of zein (w/w). [b]Different letters in each column show significant difference at $P < 0.05$.

than those of the CAT-containing zein films (0.61−0.98 MPa) and zein−fatty acid blend films (0.45−1.23 MPa) ($P < 0.05$). The addition of LYS reduced the tensile strength and Young's modulus of zein films significantly ($P < 0.05$), but it did not cause any significant change in film elongation ($P > 0.05$). In contrast, the addition of CAT effectively plasticized the zein films and increased their elongation 20−50-fold of that for controls depending on the use of PC or PP LYS. The use of PC or PP LYS did not considerably affect the tensile strength and Young's modulus values of films, but CAT- and PC LYS-containing films showed significantly higher elongation than those containing CAT and PP LYS ($P < 0.05$). The negative effects of PP LYS in flexibility of the plasticized films could be due to its protein impurities that could bind part of the CAT or could cause some local disruptions within the film matrix. However, the CAT-containing films containing PP LYS were not brittle, and they are still much more flexible than the PP LYS-containing but CAT-lacking zein control films. On the other hand, the results of mechanical tests clearly showed that, in the presence of CAT, the blend film making with fatty acids had no considerable additional effect on mechanical properties of films. This result contradicts with those of Santosa and Padua[45] who reported the plasticizing effects of OLE and LIN on zein. However, these workers produced films from zein−fatty acid resins aggregated in cold water and used OLE and LIN in film composition at 50−100% (w/w) of zein.

The factors causing the classical brittleness and flexibility problems of zein films and possibility of using phenolic compounds including CAT in zein film plasticization has been studied recently. Zein films consist of a meshwork that is composed of doughnut structures formed by asymmetric rods joined to each other.[46] The hydrophobic interactions among asymmetric rods is the primary force that keeps them together and maintains the film integrity,[46] but these interactions are also responsible for the brittleness and lack of flexibility in zein films. It was recently shown that the phenolic compounds such as CAT and gallic acid could be used effectively for plasticization of zein films and zein-based films such as zein−wax composite and zein−fatty acid blend films.[24,38,47] It was reported that the zein plasticizing effect of phenolic compounds is due to the formation of H bonds between the hydroxyl groups of phenolic compounds and the carbonyl group of zein as well as the increased hydrophilicity of films due to increased number of −OH groups.[24,47] However, further characterization studies are needed to understand the exact factors effective on mechanical properties and morphologies of zein films.

This work clearly showed the possibility of controlling release rates of both LYS and CAT by using the blend film making technique. The sustained LYS and CAT release mechanisms of developed films were attributed to the encapsulation of a fraction of active compound in microspheres formed within the zein film matrix by blend film making, reduced film porosity caused by CAT and changed affinities of active compounds to modified hydrophilic/hydrophobic balance of film matrix. It was clearly shown that the LYS and CAT release rates of blend films could be changed by changing type and concentration of fatty acid used in blend films. The increase in fatty acid concentration of blend films reduces the LYS release rates. The increased fatty acid chain length is a highly effective factor causing sustained release of both LYS and CAT form the blend films. The formation of blends with $C_{18:1}$ more effectively sustained release rates of CAT than blends formed by $C_{18:2}$. The release tests also showed the presence of differences in LYS release profiles depending on the purity of the enzyme used in film making. The use of antimicrobial fatty acids like LAU in blend film making served not only to improve the controlled release properties of films but also to support the antimicrobial effect of films. This work showed the possibility of obtaining flexible edible films for controlled release of multiple active compounds. The use of LYS and CAT as active compounds could provide highly functional edible films suitable both for active (antimicrobial and antioxidant) packaging and bioactive packaging. Thus, it is possible to employ such multifunctional films not only to increase safety and quality of food but also to improve the potential health benefits of food.

## ■ ASSOCIATED CONTENT

### Ⓢ Supporting Information

Surface SEM images of developed films (Figure S1); chemical structures of OLE, LIN, and LAU (Figure S2); and SDS-PAGE profiles of increasing concentrations of PC and PP LYS (Figure S3). This material is available free of charge via the Internet at http://pubs.acs.org.

## ■ AUTHOR INFORMATION

### Corresponding Author

*Phone: +90 232 7506292; fax: +90 232 7506196; e-mail: ahmetyemenicioglu@iyte.edu.tr.

### Funding

This work (no. 108M353) was funded by The Scientific and Technical Research Council of Turkey (TÜBİTAK).

### Notes

The authors declare no competing financial interest.

## ■ ACKNOWLEDGMENTS

We thank the Materials Research Center and Biotechnology and Bioengineering Research and Applications Center in Izmir Institute of Technology for the generous use of their facilities.

## ■ REFERENCES

(1) Lee, D. S. Antioxidative packaging system. In *Innovations in Food Packaging*, 2nd ed.; Jung, H. H., Ed.; Academic Press: London, 2013; pp 111−132.

(2) Lopez-Rubio, A.; Gavara, R.; Lagaron, J. M. Bioactive packaging: Turning foods into healthier foods through biomaterials. *Trends Food Sci. Technol.* **2006**, *17* (10), 567−575.

(3) Appendini, P.; Hotchkiss, J. H. Review of antimicrobial food packaging. *Innovative Food Sci. Emerging Technol.* **2002**, *3* (2), 113−126.

(4) Joerger, R. D. Antimicrobial films for food applications: A quantitative analysis of their effectiveness. *Packag. Technol. Sci.* **2007**, *20* (4), 231−273.

(5) Mastromatteo, M.; Mastromatteo, M.; Conte, A.; Del Nobile, M. A. Advances in controlled release devices for food packaging applications. *Trends Food Sci. Technol.* **2010**, *21* (12), 591−598.

(6) Wang, S.; Marcone, M. F.; Barbut, S.; Lim, L.-T. Fortification of dietary biopolymers-based packaging material with bioactive plant extracts. *Food Res. Int.* **2012**, *49* (1), 80−91.

(7) Vuong, Q. V.; Stathopoulos, C. E.; Nguyen, M. H.; Golding, J. B.; Roach, P. D. Isolation of green tea catechins and their utilization in the food industry. *Food Rev. Int.* **2011**, *27* (3), 227−247.

(8) Braicu, C.; Ladomery, M. R.; Chedea, V. S.; Irimie, A.; Berindan-Neagoe, I. The relationship between the structure and biological actions of green tea catechins. *Food Chem.* **2013**, *141* (3), 3282−3289.

(9) Mecitoglu, Ç.; Yemenicioglu, A.; Arslanoglu, A.; ElmacI, Z. S.; Korel, F.; Çetin, A. E. Incorporation of partially purified hen egg white lysozyme into zein films for antimicrobial food packaging. *Food Res. Int.* **2006**, *39* (1), 12−21.

(10) Ünalan, İ. U.; Korel, F.; Yemenicioğlu, A. Active packaging of ground beef patties by edible zein films incorporated with partially purified lysozyme and $Na_2EDTA$. *Int. J. Food Sci. Technol.* **2011**, *46* (6), 1289−1295.
(11) Duan, J.; Park, S. L.; Daeschel, M. A.; Zhao, Y. Antimicrobial chitosan-lysozyme (CL) films and coatings for enhancing microbial safety of mozzarella cheese. *J. Food Sci.* **2007**, *72* (9), M355−M362.
(12) Min, S.; Harris, L. J.; Han, J. H.; Krochta, J. M. *Listeria monocytogenes* inhibition by whey protein films and coatings incorporating lysozyme. *J. Food Prot.* **2005**, *68* (11), 2317−2325.
(13) Gemili, S.; Yemenicioglu, A.; Altinkaya, S. A. Development of cellulose acetate based antimicrobial food packaging materials for controlled release of lysozyme. *J. Food Eng.* **2009**, *90* (4), 453−462.
(14) Mendes de Souza, P.; Fernández, A.; López-Carballo, G.; Gavara, R.; Hernández-Muñoz, P. Modified sodium caseinate films as releasing carriers of lysozyme. *Food Hydrocolloids* **2010**, *24* (4), 300−306.
(15) Ünalan, İ. U.; Arcan, I.; Korel, F.; Yemenicioğlu, A. Application of active zein based films with controlled release properties to control *Listeria monocytogenes* growth and lipid oxidation in fresh Kashar cheese. *Innovative Food Sci. Emerging Technol.* **2013**, *20*, 208−214.
(16) Han, J. H. Antimicrobial packaging systems. In *Innovations in Food Packaging*; Jung, H. H., Ed.; Academic Press: London, 2005; pp 80−108.
(17) Buonocore, G. G.; Conte, A.; Corbo, M. R.; Sinigaglia, M.; Del Nobile, M. A. Mono- and multilaver active films containing lysozyme as antimicrobial agent. *Innovative Food Sci. Emerging Technol.* **2005**, *6* (4), 459−464.
(18) Bezemer, J. M.; Radersma, R.; Grijpma, D. W.; Dijkstra, P. J.; Feijen, J.; van Blitterswijk, C. A. Zero-order release of lysozyme from poly(ethylene glycol) poly(butylene terephthalate) matrices. *J. Controlled Release* **2000**, *64* (1−3), 179−192.
(19) de Souza, P. M.; Fernandez, A.; Lopez-Carballo, G.; Gavara, R.; Hernandez-Munoz, P. Modified sodium caseinate films as releasing carriers of lysozyme. *Food Hydrocolloids* **2010**, *24* (4), 300−306.
(20) Park, S. I.; Daeschel, M. A.; Zhao, Y. Functional properties of antimicrobial lysozyme-chitosan composite films. *J. Food Sci.* **2004**, *69* (8), M215−M221.
(21) López de Dicastillo, C.; Castro-López, M. d. M.; López-Vilariño, J. M.; González-Rodríguez, M. V. Immobilization of green tea extract on polypropylene films to control the antioxidant activity in food packaging. *Food Res. Int.* **2013**, *53* (1), 522−528.
(22) López de Dicastillo, C.; Castro-López, M. d. M.; Lasagabaster, A.; López-Vilariño, J. M.; González-Rodríguez, M. V. Interaction and release of catechin from anhydride maleic-grafted polypropylene films. *ACS Appl. Mater. Interfaces* **2013**, *5* (8), 3281−3289.
(23) Gucbilmez, C. M.; Yemenicioglu, A.; Arslanoglu, A. Antimicrobial and antioxidant activity of edible zein films incorporated with lysozyme, albumin proteins and disodium EDTA. *Food Res. Int.* **2007**, *40* (1), 80−91.
(24) Arcan, I.; Yemenicioğlu, A. Development of flexible zein−wax composite and zein−fatty acid blend films for controlled release of lysozyme. *Food Res. Int.* **2013**, *51* (1), 208−216.
(25) Manley, R. H.; Evans, C. D. Binary solvents for zein. *Ind. Eng. Chem.* **1943**, *35* (6), 661−665.
(26) Selling, G. W.; Woods, K. K.; Sessa, D.; Biswas, A. Electrospun zein fibers using glutaraldehyde as the crosslinking reagent: Effect of time and temperature. *Macromol. Chem. Phys.* **2008**, *209* (10), 1003−1011.
(27) Shukla, R.; Cheryan, M. Zein: The industrial protein from corn. *Ind. Crops Prod.* **2001**, *13* (3), 171−192.
(28) Wang, H.-J.; Gong, S.-J.; Lin, Z.-X.; Fu, J.-X.; Xue, S.-T.; Huang, J.-C.; Wang, J.-Y. In vivo biocompatibility and mechanical properties of porous zein scaffolds. *Biomaterials* **2007**, *28* (27), 3952−3964.
(29) Zhang, B.; Luo, Y.; Wang, Q. Effect of acid and base treatments on structural, rheological, and antioxidant properties of α-zein. *Food Chem.* **2011**, *124* (1), 210−220.
(30) Wetter, L. R.; Deutsch, H. F. Immunological studies on egg white proteins: IV. Immunochemical and physical studies of lysozyme. *J. Biol. Chem.* **1951**, *192* (1), 237−242.
(31) Kabara, J. J.; Swieczkowski, D. M.; Conley, A. J.; Truant, J. P. Fatty acids and derivatives as antimicrobial agents. *Antimicrob. Agents Chemother.* **1972**, *2* (1), 23−28.
(32) Laemmli, U. K. Cleavage of structural proteins during the assembly of the head of bacteriophage T4. *Nature* **1970**, *227*, 680−685.
(33) Blum, H.; Beier, H.; Gross, H. J. Improved silver staining of plant proteins, RNA and DNA in polyacrylamide gels. *Electrophoresis* **1987**, *8* (2), 93−99.
(34) Padgett, T.; Han, I. Y.; Dawson, P. L. Incorporation of food-grade antimicrobial compounds into biodegradable packaging films. *J. Food Prot.* **1998**, *61*, 1330−1335.
(35) Meyers, K. J.; Watkins, C. B.; Pritts, M. P.; Liu, R. H. Antioxidant and antiproliferative activities of strawberries. *J. Agric. Food Chem.* **2003**, *51* (23), 6887−92.
(36) Re, R.; Pellegrini, N.; Proteggente, A.; Pannala, A.; Yang, M.; Rice-Evans, C. Antioxidant activity applying an improved ABTS radical cation decolorization assay. *Free Radical Biol. Med.* **1999**, *26* (9−10), 1231−1237.
(37) ASTM. Standard test method for tensile properties of thin plastic sheeting D882-02. In *Annual Book of American Standard Testing Methods*; ASTM: Philadelphia, PA, 2002.
(38) Arcan, I.; Yemenicioğlu, A. Incorporating phenolic compounds opens a new perspective to use zein films as flexible bioactive packaging materials. *Food Res. Int.* **2011**, *44*, 550−556.
(39) Wang, Q.; Yin, L. L.; Padua, G. W. Effect of hydrophilic and lipophilic compounds on zein microstructures. *Food Biophys.* **2008**, *3* (2), 174−181.
(40) Sugimoto, Y.; Sanuki, S.; Ohsako, S.; Higashimoto, Y.; Kondo, M.; Kurawaki, J.; Ibrahim, H. R.; Aoki, T.; Kusakabe, T.; Koga, K. Ovalbumin in developing chicken eggs migrates from egg white to embryonic organs while changing its conformation and thermal stability. *J. Biol. Chem.* **1999**, *274* (16), 11030−11037.
(41) Belitz, H. D.; Grosch, W.; Schieberle, P. *Food Chemistry*, 3rd ed.; Springer: Berlin, Germany, 2004; p 553.
(42) Damodaran, S. Amino acids, peptides and proteins. In *Food Chemistry*, 4th ed.; Fennema, O., Ed.; CRC Press: New York, 1996; pp 217−330.
(43) Hoffman, K. L.; Han, I. Y.; Dawson, P. L. Antimicrobial effects of corn zein films impregnated with nisin, lauric acid, and EDTA. *J. Food Prot.* **2001**, *64* (6), 885−889.
(44) Mbandi, E.; Brywig, M.; Shelef, L. A. Antilisterial effects of free fatty acids and monolaurin in beef emulsions and hot dogs. *Food Microbiol.* **2004**, *21* (6), 815−818.
(45) Santosa, F. X. B.; Padua, G. W. Tensile properties and water absorption of zein sheets plasticized with oleic and linoleic acids. *J. Agric. Food Chem.* **1999**, *47* (5), 2070−2074.
(46) Guo, Y. C.; Liu, Z. D.; An, H. J.; Li, M. Q.; Hu, J. Nano-structure and properties of maize zein studied by atomic force microscopy. *J. Cereal Sci.* **2005**, *41* (3), 277−281.
(47) Alkan, D.; Aydemir, L. Y.; Arcan, I.; Yavuzdurmaz, H.; Atabay, H. I.; Ceylan, C.; Yemenicioğlu, A. Development of flexible antimicrobial packaging materials against *Campylobacter jejuni* by incorporation of gallic acid into zein-based films. *J. Agric. Food Chem.* **2011**, *59* (20), 11003−11010.

JOURNAL OF AGRICULTURAL AND FOOD CHEMISTRY

Review

pubs.acs.org/JAFC

# Biological Functionality of Soyasaponins and Soyasapogenols

Cuie Guang,*[,†] Jie Chen,[†] Shangyuan Sang,[†] and Shuiyuan Cheng*[,§]

[†]State Key Laboratory of Food Science and Technology, Jiangnan University, 1800 Lihu Avenue, Wuxi, Jiangsu 214122, People's Republic of China

[§]Hubei Key Laboratory of Economic Forest Germplasm Improvement and Resources Comprehensive Utilization, Huanggang Normal University, Huanggang, Hubei 438000, People's Republic of China

**ABSTRACT:** Soyasaponins are a group of structurally complex oleanane triterpenoids primarily found in soybeans and have diverse biological properties. The recent investigations and findings (since 2000) regarding the biological functions of soyasaponins and their aglycones, including their anti-inflammatory, antimutagenic, anticarcinogenic, antimicrobial, and hepato- and cardiovascular-protective activities, are herein summarized. The primary conclusion is that the use of soyasaponins and soyasapogenols in functional foods should be considered.

**KEYWORDS:** *soyasaponin, soyasapogenol, anti-inflammatory, anticarcinogenic, hepatoprotective, cardiovascular*

## INTRODUCTION

Soyasaponins are found in soybeans (*Glycine max*) and other legumes, such as lentils (*Lens culinaris*) and green peas (*Pisum sativum* L). Soyasaponins are amphiphilic oleanane triterpenoid glycosides with polar sugar chains conjugated to a nonpolar pentacyclic ring[1] and are generally classified into four major groups according to their aglycones (soyasapogenols): groups A, B, E, and DDMP (2,3-dihydro-2,5-dihydroxy-6-methyl-4*H*-pyran-4-one). Group A soyasaponins are characterized as having a hydroxyl group at C-21 and two sugar moieties separately attached at the C-3 and C-22 positions of soyasapogenol A,[2] with an exceptional compound, A3, that contains one sugar moiety at C-3.[3] In addition to a starting glucoronyl residue, the C-3 side chain has one or two more sugar residues, and the C-22 sugar moiety contains two sugar residues: a starting arabinosyl and an ending xylosyl or glycosyl residue.[4] Group A soyasaponins can be further grouped into acetylated and deacetylated forms.[1] Group B soyasaponins differ from those in group A by the presence of a hydrogen atom at C-21 and only one sugar moiety at the C-3 position of soyasapogenol B,[2] with the exception of three soyasaponins that, in addition to the C-3 sugar chain, contain a sugar moiety at C-22.[5,6] Additionally, soyasaponin Bh, which has a unique five-membered ring exhibiting hemiacetal activity, has been identified.[7] With a DDMP group connected to group B at C-22, DDMP soyasaponins are sometimes categorized as B-type soyasaponins.[1] Unlike DDMP soyasaponins, group E soyasaponins have a carbonyl group at C-22 that may be produced by the photo-oxidation of group B. Approximately 36 soyasaponins have been found in soybean.[2,4] As aglycones of soyasaponins, soyasapogenols A, B, and E do not occur in soybean naturally but can be formed by the acid or alkaline hydrolysis of soyasaponins and therefore may exist in processed soy products. Soyasapogenols C and D may result from the acid hydrolysis of soyasapogenol B and are not genuine aglycones of soyasaponins.[2,4]

The physiological effects of soyasaponins are dependent on their metabolism and absorption.[8] The anaerobic incubation of soyasaponin Ab with human fecal specimens produced two main metabolites, soyasapogenol A and soyasapogenol A 3-$\beta$-D-glucuronide, despite the different metabolic activities and pathways among individuals.[9] When group B soyasaponins were digested by healthy women, the metabolite was soyasapogenol B and was excreted in the feces.[10] In particular, soyasaponin I was metabolized to soyasapogenol B by human fecal microorganisms via soyasaponin III or, alternatively, via soyasaponin III and soyasapogenol B 3-$\beta$-D-glucuronide with apparent first-order kinetics.[8,11] The transepithelial transfer of soyasaponin I across a human colon cancer Caco-2 cell monolayer was concentration independent and saturable with an intermediate apparent permeability coefficient ($P_{app}$) of $(0.9-3.6) \times 10^{-6}$ cm/s, whereas soyasapogenol B was transported across Caco-2 cells in a concentration-dependent manner with a low $P_{app}$ of $(0.3-0.6) \times 10^{-6}$ cm/s.[10] Due to its tighter paracellular route, the Caco-2 model often underestimates the permeability of compounds in the human intestine.[12]

With diverse chemical structures, soyasaponins and soyasapogenols have been reported to possess a wide range of health benefits, including anticancer, antivirus, and antioxidant activities, as well as hepatoprotective and cardiovascular-protective effects.[2,4] In this review, recent studies (since 2000) concerning the biological functions of these compounds have been summarized (Table 1).

## ANTI-INFLAMMATORY EFFECTS

A crude extract of soyasaponins significantly inhibited the production of the pro-inflammatory cytokine tumor necrosis factor (TNF)-$\alpha$ and chemokine monocyte chemoattractant protein (MCP)-1, the inflammatory mediators prostaglandin E2 (PGE2) and nitric oxide (NO), and the inflammatory enzymes cyclooxygenase (COX)-2 and inducible nitric oxide

Received: December 30, 2013
Revised: July 25, 2014
Accepted: July 29, 2014
Published: July 29, 2014

ACS Publications © 2014 American Chemical Society

**Table 1. Biological Effects of Soyasaponins and Soyasapogenols**

| material | effect | in vitro/in vivo | mechanism | ref |
|---|---|---|---|---|
| total soyasaponins | anti-inflammatory | LPS-stimulated macrophages | inhibit TNF-$\alpha$, MCP-1, PGE2, NO, COX-2, and iNOS production and I$\kappa$B-$\alpha$ degradation | 13 |
| | | helper T cells | increase $p27^{KIP1}$ expression and stability; inhibit cyclin D and cyclin E expression, cell cycle transition and proliferation, and secretion of IL-2 and IFN-$\gamma$ | 17 |
| | antimutagenic | *S. typhimurium* | inhibit aflatoxin $B_1$-induced mutagenicity by scavenging electrophiles | 20 |
| | | Hep-G2 cells | inhibit the formation of aflatoxin $B_1$-induced DNA adducts by changing membrane permeability | 20 |
| | anticarcinogenic | colon cancer HT-29 cells | alter membrane structure; inhibit cell growth and migration, I$\kappa$B-$\alpha$ degradation, COX-2 and PKC expressions, and PKC activity; increase AP activity and CEA levels; induce autophagic death | 22−25 |
| | | colon cancer DLD-1 cells | elicit cell cycle arrest at the G2 phase along with early apoptosis | 27 |
| | | mice injected with colon carcinoma CT-26 cells | decrease the incidence of metastatic tumor colonization in lungs | 23 |
| | | fibrosarcoma HT-1080 cells | inhibit the expression and secretion of MMP-2 and MMP-9; increase TIMP-2 secretion; suppress cell migration | 23 |
| | hepatoprotective | mice | decrease lipid peroxidation in the liver by increasing the secretion of thyroid hormones | 44 |
| | | mice with acute alcohol-induced liver damage | protect plasma membrane integrity; increase liver regenerative capacity; decrease serum levels of hepatic marker enzymes and hepatic TG, TC, and MDA contents; activate the hepatic antioxidant system; prevent hepatic steatosis necrosis, inflammation, and swelling | 45 |
| | lung-protective | rats with silicotic pulmonary fibrosis | decrease serum NO and ROS contents and pulmonary MDA level; increase serum SOD level; inhibit Fas/FasL expression and lung cell apoptosis | 59, 60 |
| soyasaponins with no soyasapogenols | anticarcinogenic | hepatocarcinoma Hep-G2 cells | inhibit proliferation; induce a sub-G1 buildup of apoptotic cells and morphological changes | 33 |
| soyasaponins $A_2$ + I + II + III + V + Be | anticarcinogenic | cervical carcinoma HeLa cells | cytotoxic; change cell cycle distribution; increase NO content, the activities of NOS, and iNOS and intracellular $Ca^{2+}$ levels; cause a loss of mitochondrial transmembrane potential; induce apoptosis | 34, 35 |
| soyasaponin Ab | anti-inflammatory | LPS-stimulated macrophages | inhibit TNF-$\alpha$, PGE2, NO, and IL-1$\beta$ production, I$\kappa$B-$\alpha$ degradation and binding of LPS to TLR4 | 14 |
| | | TNBS-induced colitic mice | inhibit colon shortening, myeloperoxidase activity, the expression of TNF-$\alpha$, IL-1$\beta$, COX-2, iNOS and TLR4, and the phosphorylation of IRAK1, IKK-$\beta$ and p65; increase IL-10 expression | 14 |
| soyasaponin $A_1$/ soyasaponin $A_2$ | anti-inflammatory | LPS-stimulated macrophages | inhibit TNF-$\alpha$, NO. and iNOS production, iNOS enzyme activity and NF-$\kappa$B activity | 15 |
| | hepatoprotective | mice | decrease lipid peroxidation in the liver | 44 |
| | adjuvant | mice | stimulate antiovalbumin total-IgG and IgG1 antibody responses | 62 |
| soyasaponin $A_3$ | anti-inflammatory | THP-1 monocytic leukemia cells | inhibit the TNF-$\alpha$-induced expression of ICAM-1 | 18 |
| soyasapogenol A | anticarcinogenic | HT-29 cells | inhibit growth | 26 |
| | | Hep-G2 cells | inhibit proliferation; induce a sub-G1 buildup of apoptotic cells and morphological changes | 32 |
| | | breast cancer MDA-MB-231 cells | inhibit growth | 39 |
| | | breast cancer MCF-7 cells | estrogen-like activity | 39 |
| | hepatoprotective | Hep-G2 cells | protect against aflatoxin $B_1$-induced cytotoxicity | 43 |
| | | mice injected with Con A | reduce the number of infiltrating inflammatory cells in the liver and apoptotic bodies in the liver parenchymal cells, plasma TNF-$\alpha$ level and ALT activity | 46 |
| | antiviral | Vero cells | anti-HSV-1 activity | 57 |
| soyasaponins B + E + DDMP | antimutagenic | Chinese hamster ovary cells | inhibit 2AAAF-induced DNA damage by interception of reactive molecules | 21 |



dx.doi.org/10.1021/jf503047a | J. Agric. Food Chem. 2014, 62, 8247−8255

**Table 1. continued**

| material | effect | in vitro/in vivo | mechanism | ref |
|---|---|---|---|---|
| group B soyasaponins | anticarcinogenic | colon cancer HCT-15 cells | increase $p27^{KIP1}$ content; decrease CDK-2 activity; inhibit cell cycle transition and proliferation; suppress Akt activity; activate ERK 1/2; induce macroautophagy | 28, 29 |
| | | Hep-G2 cells | cytotoxic; induce a significant accumulation of sub-G1 apoptotic cells | 31 |
| | | glioblastoma SNB19 cells | inhibit growth and invasion; decrease S phase; cause loss of mitochondrial transmembrane potential, release of mitochondrial cytochrome *c* into the cytosol, up-regulation of Apaf-1, activation of caspase-9 and caspase-3, and cleavage of polyADP-ribose polymerase and apoptosis | 36 |
| | cardiovascular protective | in vitro | inhibit $\alpha$-glucosidase | 48 |
| | | hamsters | increase the fecal excretion of total bile acid and neutral sterols; lower the TC, non-HDLC, and TG concentrations and the TC-to-HDLC ratio | 53 |
| soyasaponins I + III | anticarcinogenic | Hep-G2 cells | inhibit growth; induce apoptosis | 32 |
| soyasaponin I | anti-inflammatory | LPS-stimulated macrophages | inhibit TNF-$\alpha$, IL-1$\beta$, PGE2, NO, COX-2, and iNOS productions, I$\kappa$B-$\alpha$ phosphorylation, NF-$\kappa$B activity, and iNOS enzyme activity | 15, 16 |
| | | in vitro | anticomplementary activity | 19 |
| | | TNBS-induced colitic mice | inhibit colon shortening, myeloperoxidase activity, the expression of TNF-$\alpha$, IL-1$\beta$, COX-2, iNOS, PGE2, and IL-6; and the activation of NF-$\kappa$B and lipid peroxides; increase the glutathione content and SOD and catalase activities | 16 |
| | anticarcinogenic | MCF-7 cells | inhibit $\alpha$2,3-sialyltransferase activity, ST3Gal IV sialyltransferase expression and the secretion of cell surface $\alpha$2,3-sialic acids; stimulate cell adhesion | 38 |
| | | MDA-MB-231 cells | decrease migration ability | 38 |
| | | melanoma B16F10 cells | inhibit the expression of $\alpha$2,3-sialic acids; increase cell adhesion; reduce cell migration | 40 |
| | | mice injected with B16F10 cells | decrease ability to grow into tumors in lungs | 40 |
| | hepatoprotective | cultured rat hepatocytes | protect against immunological liver injury | 41 |
| | | mice | decrease lipid peroxidation in the liver by increasing secretion of thyroid hormones | 41 |
| | cardiovascular protective | in vitro | inhibit renin activity | 49, 51 |
| | | SHRs | reduce blood pressure, plasma levels of LDLC, AST, ALT, and blood urea nitrogen | 54 |
| | antimicrobial | *E. coli* and *C. albicans* | inhibit growth | 55 |
| | antioxidative | in vitro | scavenge DPPH radicals; inhibit lipid peroxidation in liposomes | 16 |
| | adjuvant | mice | stimulate antiovalbumin total-IgG and IgG1 antibody responses | 62 |
| | kidney protective | mice with PKD | reduce kidney weight, water content, and plasma creatinine and urea levels; impede kidney enlargement and cyst growth | 63 |
| soyasaponin II | hepatoprotective | mice | decrease lipid peroxidation in the liver by increasing secretion of thyroid hormones | 44 |
| | cardiovascular protective | in vitro | inhibit renin activity | 51 |
| | antiviral | Vero cells | anti-HSV-1 activity | 56 |
| | adjuvant | mice | stimulate antiovalbumin total-IgG and IgG1 antibody responses | 62 |
| soyasaponin III | anti-inflammatory | in vitro | anticomplementary activity | 19 |
| | anticarcinogenic | HT-29 cells | inhibit growth | 26 |
| | hepato-protective | mice | decrease lipid peroxidation in the liver by increasing the secretion of thyroid hormones | 44 |
| | adjuvant | mice | stimulate antiovalbumin total-IgG and IgG1 antibody responses | 62 |
| soyasapogenol B | anti-inflammatory | THP-1 monocytic leukemia cells | inhibit the TNF-$\alpha$-induced expression of ICAM-1 | 18 |
| | antimutagenic | Chinese hamster ovary cells | inhibit 2AAAF-induced DNA damage by intercepting reactive molecules | 21 |



dx.doi.org/10.1021/jf503047a | J. Agric. Food Chem. 2014, 62, 8247−8255

**Table 1. continued**

| material | effect | in vitro/in vivo | mechanism | ref |
|---|---|---|---|---|
| | anticarcinogenic | HT-29 cells | inhibit growth | 26 |
| | | Caco-2 cells | inhibit proliferation and reduce viability | 10, 30 |
| | | Hep-G2 cells | inhibit proliferation; induce a sub-G1 buildup of apoptotic cells and morphological changes | 8, 33 |
| | | HeLa and lung cancer A549 cells | cytotoxic | 8 |
| | | MDA-MB-231 and MCF-7 cells | inhibit proliferation | 8, 39 |
| | hepatoprotective | Hep-G2 cells | protect against aflatoxin $B_1$-induced cytotoxicity and actinomycin D-TNF-$\alpha$-induced apoptosis; increase MLR | 43 |
| | | mice injected with Con A | lower plasma ALT level | 47 |
| | antiviral | Vero cells | anti-HSV-1 activity | 56, 57 |
| soyasapogenol C | anti-inflammatory | THP-1 monocytic leukemia cells | inhibit TNF-$\alpha$-induced expression of ICAM-1 | 18 |
| | antiviral | Vero cells | anti-HSV-1 activity | 57 |
| group E soyasaponins | cardiovascular protective | in vitro | inhibit $\alpha$-glucosidase | 48 |
| soyasapogenol E | antiviral | Vero cells | anti-HSV-1 activity | 56 |
| DDMP soyasaponins | anticarcinogenic | Hep-G2 cells | induce differentiation and morphological changes | 31 |
| soyasaponin $\beta$g | antioxidative | in vitro | scavenge $O_2^-$ and DPPH radicals | 58 |



dx.doi.org/10.1021/jf503047a | J. Agric. Food Chem. 2014, 62, 8247−8255

synthase (iNOS) and the degradation of IκB-α, an inhibitor of nuclear transcription factor kappa B (NF-κB), in lipopolysaccharide (LPS)-stimulated macrophages.[13] The phosphorylation and degradation of IκB-α allowed NF-κB to translocate to the nucleus, bind to specific promoter sequences, and induce the expression of inflammatory genes. Thus, it may be through the inhibition of NF-κB activation that soyasaponins exert their anti-inflammatory effects. Soyasaponins Ab, $A_1$, $A_2$, and I were confirmed to contribute to these anti-inflammatory properties.[14−16] Furthermore, soyasaponins $A_1$, $A_2$, and I were found to inhibit iNOS enzyme activity and NF-κB transcriptional activity in LPS-stimulated murine RAW 264.7 macrophages.[15] Soyasaponins Ab and I also suppressed the release of the pro-inflammatory cytokine interleukin (IL)-1β in LPS-stimulated mouse peritoneal macrophages.[14,16] The $IC_{50}$ values of soyasaponin Ab for inhibiting the production of PGE2 and NO and the expression of TNF-α and IL-1β were 2.0 ng/mL, 1.6 μM, 1.3 ng/mL, and 1.5 pg/mL, respectively. In addition, soyasaponin Ab prevented the binding of LPS and Alexa-Fluor-594-conjugated LPS to Toll-like receptor 4 (TLR4),[14] a receptor on macrophages that is linked to the NF-κB pathway via IL-1 receptor-associated kinases (IRAKs) and that recognizes pathogen-associated molecular patterns such as LPS. In contrast to soyasaponins $A_1$, $A_2$, and I, soyasapogenols A and B exhibited no inhibitory effect on the production of NO, iNOS, and TNF-α or on the iNOS enzyme activity in LPS-stimulated macrophages,[15] indicating that the sugar chains in the structures of soyasaponins are critical to their anti-inflammatory activities. Excessive helper T (Th) cell activity occurs during severe inflammation. Soyasaponins were found to enhance the expression and increase the stability of the negative regulator of cyclin-dependent kinases (CDKs) $p27^{KIP1}$ and to decrease the expression of the positive CDK regulators cyclin D and cyclin E in Th cells. CDKs are key molecules for cell cycle progression. Soyasaponins were thus confirmed to block the G1-to-S phase cell cycle transition and inhibit the proliferation of Th cells, leading to the decreased mRNA transcription and secretion of cytokine IL-2 and interferon (IFN)-γ in Th cells.[17] As a member of the immunoglobulin family of adhesion molecules, intercellular adhesion molecule (ICAM)-1 appears to cause acute and chronic inflammatory disease. Soyasaponin $A_3$ mildly inhibited the TNF-α-induced expression of ICAM-1 on THP-1 human monocytic leukemia cells, soyasapogenols B and C exhibited strong inhibitory activities, and soyasapogenol A slightly activated ICAM-1 expression. These results indicate that the hydroxyl group at C-21 and the glycosyl group at C-3 influence the inhibition of ICAM-1.[18] The excessively activated complement system acts fatally on organ transplantation, and its modulation is important in the treatment of inflammatory diseases. Soyasaponin III showed a stronger anticomplementary activity than did soyasaponin I, and their activities were influenced by the nature of glucuronic acid; the free acid forms (−COOH) displayed much more potent activity than did the sodium salt forms ($-COO-Na^+$), methyl ester forms ($-COOCH_3$), or reduced forms ($-CH_2OH$).[19]

In addition to down-regulating the expression of TNF-α, IL-1β, COX-2, and iNOS, orally administered soyasaponins Ab and I potently ameliorated body weight reduction, colon shortening, macroscopic score, and myeloperoxidase activity in the colon of 2,4,6-trinitrobenzenesulfonic acid (TNBS)-induced colitic mice.[14,16] Soyasaponin I also suppressed the expression of PGE2 and another potent pleiotropic inflammatory cytokine, IL-6, and suppressed the activation of NF-κB, reducing the levels of the lipid peroxides malondialdehyde (MDA) and 4-hydroxy-2-nonenal and increasing the glutathione content as well as the superoxide dismutase (SOD) and catalase activities.[16] These results indicate that soyasaponin I may ameliorate colitis by inhibiting NF-κB activation and consequently diminishing its ability to scavenge the lipid peroxides produced by TNBS. Soyasaponin Ab increased the expression of IL-10, an immunosuppressive and anti-inflammatory cytokine that inhibits NF-κB activation and consequently suppresses the production of pro-inflammatory cytokines. Soyasaponin Ab also inhibited the expression of TLR4 and the phosphorylation of IRAK1, the inhibitor of NF-κB kinase (IKK)-β, and the NF-κB subunit p65 in the colon of TNBS-induced colitic mice.[14] Phosphorylated IRAK1 activates a multimeric protein complex, and the activated subunit, transforming growth factor-β activated kinase-1, phosphorylates IKKs. IKKs phosphorylate IκB-α, leading to its ubiquitination and subsequent degradation by the proteasome.[14]

## ANTI-MUTAGENIC AND ANTI-CARCINOGENIC EFFECTS

Crude soyasaponins strongly inhibited aflatoxin $B_1$-induced mutagenicity and blocked the initiation step of carcinogenesis by inhibiting the formation of aflatoxin $B_1$-induced DNA adducts.[20] Additionally, an ethanol extract consisting of group B, E, and DDMP soyasaponins, as well as the purified soyasapogenol B, both repressed 2-acetoxyacetylaminofluorene (2AAAF)-induced DNA damage in Chinese hamster ovary cells and thus exhibited antigenotoxic activity against 2AAAF.[21]

Crude soyasaponins changed the membrane structure and inhibited the growth of WiDr human colon cancer cells (the same cell line as HT-29) by reducing the activity of protein kinase C (PKC) while increasing the activity of alkaline phosphatase (AP) at lower concentrations or by inducing autophagic death at higher concentrations.[22] PKC activity increases as cells undergo the proliferation process, and AP activity is a marker of cell differentiation. For the HT-29 cell line, crude soyasaponins were additionally found to inhibit cell migration and increase the level of another differentiation marker, carcinoembryonic antigen (CEA).[23,24] In addition, crude soyasaponins suppressed the degradation of IκB-α and down-regulated the expression of COX-2 and PKC in HT-29 cells,[25] indicating that the anti-inflammatory activity of soyasaponins is involved in their anticarcinogenic function. Soyasapogenols A and B were found to inhibit the growth of HT-29 cells more strongly than did soyasaponin III.[26] For DLD-1 colon cancer cells, treatment with soyasaponins also elicited cell cycle arrest at the G2 phase and early apoptosis.[27] Group B soyasaponins, at physiologically relevant doses, increased the protein content of the CDK inhibitor $p27^{KIP1}$ and the inhibitory phosphorylation of CDK-2 at $Tyr^{15}$ and decreased the activity of CDK-2, leading to an accumulation of HCT-15 colon cancer cells in S phase and, through this delay, suppressed cell proliferation. Group B soyasaponins also induced type II nonapoptotic programmed cell death or macroautophagy in the HCT-15 cell line, as indicated by the elevated concentration of microtubule-associated protein light chain-3 I and II, by the increased incorporation of monodansylcadaverine into autophagic vacuoles, and by morphological alterations, including reduced cytoplasmic density and prominent vacuolization.[28] The autophagy-inducing action in HCT-15 cells was due to the suppression of Akt activity by reducing the Akt phosphorylation at $Ser^{473}$


dx.doi.org/10.1021/jf503047a | J. Agric. Food Chem. 2014, 62, 8247−8255

and the activation of ERK 1/2, in part modulated by enhanced raf-1 activity.[29] Soyasapogenol B was found to inhibit the proliferation and reduce the viability of Caco-2 cells.[10,30] Feeding with dietary soyasaponins also decreased the incidence of metastatic tumor colonization in the lungs of mice injected with colon carcinoma CT-26 cells.[23]

A reflux extract consisting of group B soyasaponins was cytotoxic to hepatocarcinoma Hep-G2 cells with an $LC_{50}$ value of 0.55 mg/mL and produced a significant accumulation of sub-G1 apoptotic cells, and a room temperature extract containing a greater amount of DDMP soyasaponins induced differentiation and morphological changes.[31] Another extract containing a majority of soyasaponins I and III inhibited Hep-G2 growth with an $LC_{50}$ value of 0.39 mg/mL. The significant accumulation of sub-G1 cells, mid- and late-apoptotic cells, and dead cells confirmed the apoptosis-inducing effects of soyasaponins I and III, with the cellular protein expression of the caspase family of enzymes being a main trigger of the apoptotic pathway.[32] Soyasapogenols A and B more strongly inhibited Hep-G2 proliferation than did a soyasaponin extract containing no soyasapogenols, with $LC_{50}$ values of 0.052, 0.128, and 0.594 mg/mL, respectively, and induced a greater sub-G1 buildup of apoptotic cells.[8,33] All three compounds also induced morphological changes in Hep-G2 cells, such as nuclear condensation and fragmentation.[33]

The treatment of human fibrosarcoma HT-1080 cells with crude soyasaponins inhibited the mRNA expression and secretion of matrix metalloproteinase (MMP)-2 and MMP-9, increased the secretion of tissue inhibitor of metalloproteinase (TIMP)-2, and reduced cell migration.[23] TIMP-2 contributes to the inhibition of pro-MMP-2 and acts as a specific inhibitor of MMP-2, and MMP-2 and MMP-9 degrade extracellular matrix components and contribute to the invasion and metastasis of cancer cells.

A mixture containing soyasaponins $A_2$, I, II, III, V, and Be had obvious cytotoxic effects on human cervical carcinoma HeLa cells, changing the cell cycle distribution and inducing apoptotic features, including nuclear fragmentation, cytoplasm shrinkage, and decreased cell volume.[34] The apoptosis of HeLa cells might be due to the increased NO content and the activities of NOS and iNOS, the loss of mitochondrial transmembrane potential, or the increase in intracellular $Ca^{2+}$ induced by the fraction released through the mitochondrial pathway.[35] Soyasapogenol B also inhibited the proliferation of HeLa cells.[8]

For the SNB19 human glioblastoma cell line, group B soyasaponins inhibited cell growth and invasion and decreased the S phase of the cell cycle with a concomitant increase in the G0/G1 phase. The apoptosis of SNB19 cells induced by group B soyasaponins was due to the loss of mitochondrial transmembrane potential, the release of mitochondrial cytochrome *c* into the cytosol, and the subsequent up-regulation of Apaf-1, the activation of caspase-9 and caspase-3, and the specific cleavage of poly-ADP-ribose polymerase.[36]

Sialyltransferases catalyze the transfer of sialic acids to the nonreducing terminal positions on the sugar chains of glycoconjugates, and the increased sialylation is associated with oncogenic transformation and metastasis. Soyasaponin I, a sialyltransferase inhibitor,[37] was predicted to inhibit the $\alpha$2,3-sialyltransferase activity of nonmetastatic MCF-7 breast cancer cells and depressed the mRNA expression of ST3Gal IV sialyltransferase and the secretion of cell surface $\alpha$2,3-sialic acids. Soyasaponin I also stimulated MCF-7 cell adhesion to collagen I and the Matrigel matrix. Soyasaponin I showed no effect on the migration of MCF-7, but it did significantly decrease the migration ability of highly metastatic MDA-MB-231 breast cancer cells.[38] Soyasapogenol B reduced the proliferation of both estrogen-responsive MCF-7 cells[8,39] and estrogen-insensitive MDA-MB-231, and soyasapogenol A inhibited the growth of MDA-MB-231 but stimulated MCF-7 cell proliferation. Soyasapogenol A also increased estrogen-induced pS2 mRNA expression and activated the estrogen receptor in MCF-7 cells,[39] indicating an estrogen-like activity of soyasapogenol A that might have the same in vivo anticarcinogenic and health-promoting functions as those reported for the soybean phytoestrogen genistein.

Soyasaponin I inhibited the expression of $\alpha$2,3-sialic acids on the surface of highly metastatic B16F10 melanoma cells; increased cell adhesion to the extracellular matrix proteins collagen IV, fibronectin, and laminin; and reduced cell migration. Additionally, soyasaponin I-treated B16F10 cells showed a markedly decreased ability to grow into tumors in the lungs of experimental mice that had harbored the cells for a 2 week period after tail-vein delivery.[40] Soyasapogenol B exhibited potent cytotoxicity against A549 lung cancer cells.[8]

## HEPATOPROTECTIVE EFFECTS

Soyasaponin I exhibited protective activity toward immunological liver injury in primary cultured rat hepatocytes as measured by the reduced alanine aminotransferase (ALT) activity in the medium.[41] The immunological liver injury was considered to be caused by complement-mediated cell damage.[19] Soyasaponin III and soyasapogenol B exerted weak protective effects against the cytotoxicity of *tert*-butyl hydroperoxide to human liver-derived cells.[42] Soyasapogenols A and B were found to protect against aflatoxin $B_1$-induced cytotoxicity to liver cells and, furthermore, soyasapogenol B protected against actinomycin D-TNF-$\alpha$-induced apoptosis and increased the mixed lymphocyte reaction (MLR) in cultured cells. The marked decrease in MLR is proportional to the decrease in immune system function in patients and therefore increases the chance of infectious diseases; thus, soyasapogenol B may be a candidate therapeutic agent for chronic hepatitis.[43]

When total soyasaponins were administered to mice orally and intraperitoneally, significantly decreased lipid peroxidation was observed in the liver, with the effect of the intraperitoneally injected soyasaponins being comparable to that of $\alpha$-tocopherol. Soyasaponins increased the levels of serum thyroid hormones, which then restrained NADPH-dependent lipid peroxidation in vitro in liver microsomes more strongly than did $\alpha$-tocopherol. Propylthiouracil, an antithyroid drug, decreased the effect of the soyasaponins, suggesting that the in vivo inhibition of lipid peroxidation by soyasaponins might be mediated through the secretion of thyroid hormones. Constituent group B soyasaponins (I, II, and III) showed much stronger in vivo reducing effects on hepatic lipid peroxidation than did group A soyasaponins ($A_1$ and $A_2$), and only group B soyasaponins induced a significant increase in thyroid hormones.[44] The administration of crude soyasaponins in mice with acute alcohol-induced liver damage decreased the serum levels of the hepatic marker enzymes aspartate transaminase (AST), ALT, AP, and lactate dehydrogenase by stabilizing the plasma membrane and repairing the hepatic tissue damage as well as the hepatic triglyceride (TG), total cholesterol (TC), and MDA contents. A better profile of the antioxidant system with normal SOD, glutathione *S*-transferase,

and glutathione peroxidase activities was also observed, which was associated with an increase in the hepatic glutathione level. In addition, crude soyasaponins prevented hepatic steatosis necrosis, inflammation, and swelling in acutely alcohol-treated mice.[45] Concanavalin (Con) A injection into mice can lead to autoimmune or viral hepatitis. Soyasapogenol A reduced the number of infiltrating inflammatory cells in the liver and the elevated level of plasma TNF-$\alpha$ and then reduced the elevated plasma ALT activity and the number of apoptotic bodies in the liver parenchymal cells, resulting in the prevention of liver damage in the Con A-induced hepatitis mouse model.[46] Similarly, soyasapogenol B lowered the elevated plasma ALT level in a mouse model, with two hydroxyl groups on the A ring of soyasapogenol B required for the amelioration.[47]

## CARDIOVASCULAR PROTECTIVE EFFECTS

$\alpha$-Glucosidase is involved in the development of diabetes. Group B, E, and DDMP soyasaponins showed strong inhibitory activities against this enzyme in vitro, with $IC_{50}$ values of 10−40 $\mu$M.[48] Renin is the rate-limiting enzyme in the renin−angiotensin system, and its overactivation leads to hypertension. A soybean embryo extract showed approximately 3-fold higher human renin inhibitory activity than did a soybean cotyledon extract, and the active compound was shown to be soyasaponin I. Kinetic analysis indicated partial noncompetitive inhibition, with a $K_i$ value comparable to that of synthetic tetradecanoyl acetal sodium sulfate, an analogue of sodium houttuynin.[49,50] Following a simple structure and activity analysis of 14 saponins and sapogenols, the 3-*O*-$\beta$-D-glucopyranosiduronic moiety in saponins was found to be essential for renin inhibition. In addition to soyasaponin I, soyasaponin II contains such a structure and has a similar human renin inhibitory activity.[51]

Due to the bile acid- or cholesterol-binding ability in the digestive tract,[52] group B soyasaponins increased the fecal excretion of total bile acid, primarily including cholic acid, and neutral sterols, including cholestane, coprostanol, lathosterol, and campesterol, and therefore improved the plasma cholesterol status by lowering the TC, non-high-density-lipoprotein cholesterol (HDLC), and TG concentrations as well as the TC-to-HDLC ratio in hamsters. Greater production of group B soyasaponin metabolites was associated with better plasma cholesterol status in hamsters, indicating that gut microbial variation in soyasaponin metabolism influences the health effect of group B soyasaponins.[53] The oral administration of commercially purified soyasaponin I in spontaneously hypertensive rats (SHRs) significantly decreased their blood pressure and led to reductions in the plasma levels of low-density lipoprotein cholesterol (LDLC), AST, ALT, and blood urea nitrogen, indicating that soyasaponin I may exert its liver and kidney protective functions by lowering blood pressure.[54]

## ANTIMICROBIAL AND ANTIVIRAL EFFECTS

Soyasaponin I was found to have moderate activities against *Escherichia coli* and *Candida albicans*, whereas soyasaponin III showed only weak activity against *E. coli*.[55] Soyasaponin II showed much higher in vitro anti-herpes simplex virus type I (HSV-1) activity than did soyasaponin I, indicating the contribution of the glucosyl unit in the central sugar moiety to the antiviral activity.[56] The activities of soyasapogenols A and E were less than $^1/_{20}$ and $^1/_{10}$ that of soyasapogenol B, respectively; thus, the hydroxyl group at C-21 and the carbonyl group at C-22 seem to reduce anti-HSV-1 activity; soyasapogenol C, with a double bond at C-21 and C-22 instead of the hydroxyl group in soyasapogenol A, showed moderate anti-HSV-1 activity.[56,57]

## ADDITIONAL EFFECTS

Soyasaponin I showed 1,1-diphenyl-2-picrylhydrazyl (DPPH) radical-scavenging activity with a 50% inhibitory concentration of 70.2 $\mu$M, which is comparable to that of $\alpha$-tocopherol ($IC_{50}$ = 52.1 $\mu$M). Soyasaponin I also suppressed lipid peroxidation in liposomes prepared from L-$\alpha$-phosphatidylcholine, with an $IC_{50}$ of 19.5 $\mu$M.[16] Soyasaponin $\beta$g at 1 mM showed an 8% $O_2^-$ scavenging activity and at 25 $\mu$M exhibited a 20.9% DPPH radical-scavenging activity ($IC_{50}$ = 63.8 $\mu$M), which is comparable to that of *tert*-butylhydroxytoluene (21%; $IC_{50}$ = 67.5 $\mu$M). When a low concentration of gallic acid was added, a synergistic effect was observed, with an unpaired electron located on the carbons at C-4 and C-6 and on the ketone group at C-4 of the DDMP moiety of soyasaponin $\beta$g and a two-electron reduction from gallic acid related to the synergistic scavenging action toward $O_2^-$ and DPPH radicals.[58]

The treatment of rats with silicotic pulmonary fibrosis with soyasaponins decreased the serum NO and reactive oxygen species (ROS) contents as well as the MDA level in pulmonary tissue, increased the serum SOD level, and inhibited the expression of Fas and FasL and the apoptosis of lung cells, which thus retarded the progress of $SiO_2$-induced pulmonary fibrosis.[59,60] Soyasaponins bearing sugar chain(s) showed strong adjuvant activities and stimulated anti-chicken ovalbumin total-IgG and IgG1 antibody responses in mice.[61] Among the bisdesmosidic soyasaponins, soyasaponin $A_1$, with a long sugar side chain, induced stronger total IgG and IgG1 antibody responses than did soyasaponin $A_2$. For the monodesmosidic soyasaponins, the antibody response decreased in the order soyasaponin I > II > III. The adjuvant activity of these soyasaponins increased with the ratio of hydrophilic sugar side chain(s) to lipophilic aglycone (HLB). Therefore, the number, length, and composition of sugar side chains affecting the HLB value would indicate the overall conformation of each saponin molecule, and the amphipathic structure would define the fundamental adjuvanticity of soyasaponins.[62] Soyasaponin I also impeded kidney enlargement and cyst growth in the *pyc* mouse model of polycystic kidney disease (PKD), as indicated by the reduced kidney weight, water content, and plasma creatinine and urea levels.[63]

Human beings have consumed soybeans as a source of high-quality protein and other nutrients for hundreds of years. This review summarizes recent findings regarding the health effects of soyasaponins and soyasapogenols. Clearly, the biological functionality of these compounds largely depends on the testing materials, methodology, and dose. Before they are used as components of functional foods, further studies of the in vivo and clinical effects of soyasaponins and soyasapogenols are necessary.

## AUTHOR INFORMATION

### Corresponding Authors

*(C.G.) E-mail: guang1226@hotmail.com. Phone: 86-510-85197883.
*(S.C.) E-mail: s_y_cheng@sina.com. Phone: 86-713-8833866

### Funding

This work was supported by the National Natural Science Foundation of China (Project 31201289), the Research Programs of the State Key Laboratory of Food Science and Technology (Jiangnan University, No. SKLF-ZZB-201208), and the Hubei Key Laboratory of Economic Forest Germplasm Improvement and Resources Comprehensive Utilization (No. 2011BLKF241).

### Notes

The authors declare no competing financial interest.

## ■ ACKNOWLEDGMENTS

We thank Dr. Robert Phillips of the University of Georgia, Griffin, GA, USA, for his helpful comments.

## ■ ABBREVIATIONS USED

DDMP, 2,3-dihydro-2,5-dihydroxy-6-methyl-4*H*-pyran-4-one; TNF, tumor necrosis factor; MCP, monocyte chemoattractant protein; PGE2, prostaglandin E2; NO, nitric oxide; COX, cyclooxygenase; iNOS, inducible nitric oxide synthase; NF-κB, nuclear transcription factor kappa B; IκB, inhibitor of NF-κB; LPS, lipopolysaccharides; IL, interleukin; TLR4, Toll-like receptor 4; IRAKs, IL-1 receptor-associated kinases; Th, helper T; CDKs, cyclin-dependent kinases; IFN, interferon; ICAM, intercellular adhesion molecule; TNBS, 2,4,6-trinitrobenzene-sulfonic acid; MDA, malondialdehyde; SOD, superoxide dismutase; IKK, inhibitor of NF-κB kinase; 2AAAF, 2-acetoxyacetylaminofluorene; PKC, protein kinase C; AP, alkaline phosphatase; CEA, carcinoembryonic antigen; MMP, matrix metalloproteinase; TIMP, tissue inhibitor of metal-loproteinase; ALT, alanine aminotransferase; MLR, mixed lymphocyte reaction; AST, aspartate transaminase; TG, triglyceride; TC, total cholesterol; Con, concanavalin; H(L)-DLC, high (low)-density lipoprotein cholesterol; SHRs, spontaneously hypertensive rats; HSV-1, herpes simplex virus type I; DPPH, 1,1-diphenyl-2-picrylhydrazyl; ROS; reactive oxygen species; PKD, polycystic kidney disease

## ■ REFERENCES

(1) Zhang, W.; Popovich, D. G. Chemical and biological characterization of oleanane triterpenoids from soy. *Molecules* **2009**, *14*, 2959−2975.

(2) Wu, X.; Kang, J. Phytochemicals in soy and their health effects. In *Phytochemicals − Bioactivities and Impact on Health*; Rasooli, I., Ed.; InTech: Rijeka, Croatia, 2011; pp 43−76, ISBN 978-953-307-424-5.

(3) Curl, C. L.; Price, K. R.; Fenwick, G. R. Soyasaponin A3, a new monodesmosidic saponin isolated from the seeds of *Glycine max*. *J. Nat. Prod.* **1988**, *51*, 122−124.

(4) Kang, J.; Badger, T. M.; Ronis, M. J. J.; Wu, X. Non-isoflavone phytochemicals in soy and their health effects. *J. Agric. Food Chem.* **2010**, *58*, 8119−8133.

(5) Hosny, M.; Rosazza, J. P. N. Novel isoflavone, cinnamic acid, and triterpenoid glycosides in soybean molasses. *J. Nat. Prod.* **1999**, *62*, 853−858.

(6) Hosny, M.; Rosazza, J. P. N. New isoflavone and triterpene glycosides from soybeans. *J. Nat. Prod.* **2002**, *65*, 805−813.

(7) Ali, Z.; Khan, S. I.; Khan, I. A. Soyasaponin Bh, a triterpene saponin containing a unique hemiacetal-functional five-membered ring from *Glycine max* (soybeans). *Planta Med.* **2009**, *75*, 371−374.

(8) Chang, S.; Han, M.; Han, S.; Kim, D. Metabolism of soyasaponin I by human intestinal microflora and its estrogenic and cytotoxic effects. *Biomol. Ther.* **2009**, *17*, 430−437.

(9) Chang, S.; Han, M. J.; Joh, E.; Kim, D. Liquid chromatography/mass spectrometry-based structural analysis of soyasaponin Ab metabolites by human fecal microflora. *J. Pharm. Biomed.* **2010**, *52*, 752−756.

(10) Hu, J.; Reddy, M. B.; Hendrich, S.; Murphy, P. A. Soyasaponin I and sapongenol B have limited absorption by Caco-2 intestinal cells and limited bioavailability in women. *J. Nutr.* **2004**, *134*, 1867−1873.

(11) Hu, J.; Zheng, Y. L.; Hyde, W.; Hendrich, S.; Murphy, P. A. Human fecal metabolism of soyasaponin I. *J. Agric. Food Chem.* **2004**, *52*, 2689−2696.

(12) Masungi, C.; Borremans, C.; Willems, B.; Mensch, J.; Dijck, A. V.; Augustijns, P.; Brewster, M. E.; Noppe, M. Usefulness of a novel Caco-2 cell perfusion system. I. In vitro prrediction of the absorption potential of passively diffused compounds. *J. Pharm. Sci.* **2004**, *98*, 2507−2521.

(13) Kang, J.; Sung, M.; Kawada, T.; Yoo, H.; Kim, Y.; Kim, J.; Yu, R. Soybean saponins suppress the release of proinflammatory mediators by LPS-stimulated peritoneal macrophages. *Cancer Lett.* **2005**, *230*, 219−227.

(14) Lee, I.; Park, Y.; Joh, E.; Kim, D. Soyasaponin Ab ameliorates colitis by inhibiting the binding of lipopolysaccharide (LPS) to Toll-like receptor (TLR) 4 on macrophages. *J. Agric. Food Chem.* **2011**, *59*, 13165−13172.

(15) Zha, L.; Mao, L.; Lu, X.; Deng, H.; Ye, J.; Chu, X.; Sun, S.; Luo, H. Anti-inflammatory effect of soyasaponins through suppressing nitric oxide production in LPS-stimulated RAW 264.7 cells by attenuation of NF-κB-mediated nitric oxide synthase expression. *Bioorg. Med. Chem. Lett.* **2011**, *21*, 2415−2418.

(16) Lee, I.; Park, Y.; Yeo, H.; Han, M. J.; Kim, D. Soyasaponin I attenuates TNBS-induced colitis in mice by inhibiting NF-κB pathway. *J. Agric. Food Chem.* **2010**, *58*, 10929−10934.

(17) Lee, S.; Bae, J.; Kim, S.; Jeong, S.; Choi, C.; Choi, S.; Kim, H.; Jung, W.; Imm, J.; Kim, S.; Chun, T. Saponins from soy bean and mung bean inhibit the antigen specific activation of helper T cells by blocking cell cycle progression. *Biotechnol. Lett.* **2013**, *35*, 165−173.

(18) Ahn, K.; Kim, J.; Oh, S.; Min, B.; Kinjo, J.; Lee, H. Effects of oleanane-type triterpenoids from fabaceous plants on the expression of ICAM-1. *Biol. Pham. Bull.* **2002**, *25*, 1105−1107.

(19) Oh, S.; Kinjo, J.; Shii, Y.; Ikeda, T.; Nohara, T.; Ahn, K.; Kim, J.; Lee, H. Effects of triterpenoids from *Pueraria lobata* on immunohemolysis: β-D-glucuronic acid plays an active role in anticomplementary activity in vitro. *Planta Med.* **2000**, *66*, 506−510.

(20) Jun, H.; Kim, S.; Sung, M. Protective effect of soybean saponins and major antioxidants against aflatoxin $B_1$-induced mutagenicity and DNA-adduct formation. *J. Med. Food* **2002**, *5*, 235−240.

(21) Berhow, M. A.; Wager, E. D.; Vaughn, S. F.; Plewa, M. J. Characterization and antimutagenic activity of soybean saponins. *Mutat. Res.* **2000**, *448*, 11−12.

(22) Tsai, C.; Chen, Y.; Chien, Y.; Huang, W.; Lin, S. Effect of soy saponin on the growth of human colon cancer cells. *World J. Gastroenterol.* **2010**, *16*, 3371−3376.

(23) Kang, J.; Han, I.; Sung, M.; Yoo, H.; Kim, Y.; Kim, J.; Kawada, T.; Yu, R. Soybean saponin inhibits tumor cell metastasis by modulating expressions of MMP-2, MMP-9 and TIMP- 2. *Cancer Lett.* **2008**, *261*, 84−92.

(24) Oh, Y.; Sung, M. Soybean saponins inhibit cell proliferation by suppressing PKC activation and induce differentiation of HT-29 human colon adenocarcinoma cells. *Nutr. Cancer* **2001**, *39*, 132−138.

(25) Kim, H.; Yu, R.; Kim, J.; Kim, Y.; Sung, M. Antiproliferative crude soy saponin extract modulates the expression of IκB-α, protein kinase C, and cyclooxygenase-2 in human colon cancer cells. *Cancer Lett.* **2004**, *210*, 1−6.

(26) Gurfinkel, D. M.; Rao, A. V. Soyasaponins: the relationship between chemical structure and colon anticarcinogenic activity. *Nutr. Cancer* **2003**, *47*, 24−33.

(27) Jorud, I. N. The effect of generational feeding of soy and genistein-supplemented diets on progression of precancerous lesions in colon of second generation male rats. Master's thesis, University of Illinois at Urbana−Champaign, USA, 2012.

(28) Ellington, A. A.; Berhow, M.; Singletary, K. W. Induction of macroautophagy in human colon cancer cells by soybean B-group triterpenoid saponins. *Carcinogenesis* **2005**, *26*, 159−167.
(29) Ellington, A. A.; Berhow, M.; Singletary, K. W. Inhibition of Akt signaling and enhanced ERK1/2 activity are involved in induction of macroautophagy by triterpenoid B-group soyasaponins in colon cancer cells. *Carcinogenesis* **2006**, *27*, 298−306.
(30) MacDonald, R. S.; Guo, J.; Copeland, J.; Browning, J. D.; Sleper, D.; Rottinghaus, G. E.; Berhow, M. A. Environmental influence on isoflavones and saponins in soybeans and their role in colon cancer. *J. Nutr.* **2005**, *135*, 1239−1242.
(31) Zhang, W.; Yeo, M.; Tang, F.; Popovich, D. G. Bioactive responses of Hep-G2 cells to soyasaponin extracts differs with respect to extraction conditions. *Food Chem. Toxicol.* **2009**, *47*, 2202−2208.
(32) Zhang, W.; Popovich, D. G. Group B oleanane triterpenoid extract containing soyasaponins I and III from soy flour induces apoptosis in Hep-G2 cells. *J. Agric. Food Chem.* **2010**, *58*, 5315−5319.
(33) Zhang, W.; Popovich, D. G. Effect of soyasapogenol A and soyasapogenol B concentrated extracts on Hep-G2 cell proliferation and apoptosis. *J. Agric. Food Chem.* **2008**, *56*, 2603−2608.
(34) Xiao, J.; Huang, G.; Zhu, C.; Ren, D.; Zhang, S. Morphological study on apoptosis HeLa cells induced by soyasaponins. *Toxicol. in Vitro* **2007**, *21*, 820−826.
(35) Xiao, J.; Huang, G.; Zhang, S. Soyasaponins inhibit the proliferation of HeLa cells by inducing apoptosis. *Exp. Toxicol. Pathol.* **2007**, *59*, 35−42.
(36) Yanamandra, N.; Berhow, M. A.; Konduri, S.; Dinh, D. H.; Olivero, W. C.; Nicolson, G. L.; Rao, J. S. Triterpenoids from *Glycine max* decrease invasiveness and induce caspase-mediated cell death in human SNB19 glioma cells. *Clin. Exp. Metastasis* **2003**, *20*, 375−383.
(37) Wu, C.; Hsu, C.; Chen, S.; Tsai, Y. Soyasaponin I, a potent and specific sialyltransferase inhibitor. *Biochem. Biophys. Res. Commun.* **2001**, *284*, 466−469.
(38) Hsu, C.; Lin, T.; Chang, W.; Wu, C.; Lo, W.; Wang, P.; Tsai, Y. Soyasaponin-I-modified invasive behavior of cancer by changing cell surface sialic acids. *Gynecol. Oncol.* **2005**, *96*, 415−422.
(39) Rowlands, J. C.; Berhow, M. A.; Badger, T. M. Estrogenic and antiproliferative properties of soy sapogenols in human breast cancer cells in vitro. *Food Chem. Toxicol.* **2002**, *40*, 1767−1774.
(40) Chang, W.; Yu, C.; Lin, T.; Wang, P.; Tsai, Y. Soyasaponin I decreases the expression of $\alpha$2,3-linked sialic acid on the cell surface and suppresses the metastatic potential of B16F10 melanoma cells. *Biochem. Biophys. Res. Commun.* **2006**, *341*, 614−619.
(41) Kinjo, J.; Ikeda, T.; Okawa, M.; Udayama, M.; Hirakawa, T.; Shii, Y.; Nohara, T. Hepatoprotective and heptotoxic activities of sophoradiol analogs on rat primary liver cell cultures. *Biol. Pharm. Bull.* **2000**, *23*, 1118−1121.
(42) Kinjo, J.; Hirakawa, T.; Tsuchihashi, R.; Nagao, T.; Okawa, M.; Nohara, T.; Okabe, H. Hepatoprotective constituents in plants 14. Effects of soyasapogenol B, sophoradiol, and their glucuronides on the cytotoxicity of *tert*-butyl hydroperoxide to HepG2 cells. *Biol. Pharm. Bull.* **2003**, *26*, 1357−1360.
(43) Kuzuhara, H.; Nishiyama, S.; Minowa, N.; Sasaki, K. Effects of triterpene compounds on cytotoxicity, apoptosis, and immune response in cultured cells. *J. Nat. Med.* **2006**, *60*, 113−120.
(44) Ishii, Y.; Tanizawa, H. Effects of soyasaponins on lipid peroxidation through the secretion of thyroid hormones. *Biol. Pharm. Bull.* **2006**, *29*, 1759−1763.
(45) Yang, X.; Dong, C.; Ren, G. Effect of soyasaponins-rich extract from soybean on acute alcohol-induced hepatotoxicity in mice. *J. Agric. Food Chem.* **2011**, *59*, 1138−1144.
(46) Kuzuhara, H.; Nishiyama, S.; Minowa, N.; Sasaki, K.; Omoto, S. Protective effects of soyasapogenol A on liver injury mediated by immune response in a concanavalin A-induced hepatitis model. *Eur. J. Pharmacol.* **2000**, *391*, 175−181.
(47) Sasaki, K.; Minowa, N.; Kuzuhara, H.; Nishiyama, S. Preventive effects of soyasapogenol B derivatives on liver injury in a concanavalin A-induced hepatitis model. *Bioorg. Med. Chem.* **2005**, *13*, 4900−4911.
(48) Quan, J.; Yin, X.; Jin, M.; Shen, M. Study on the inhibition of $\alpha$-glucosidase by soyasaponins. *Zhong Yao Cai* **2003**, *26*, 654−656.
(49) Takahashi, S.; Hori, K.; Shinbo, M.; Hiwatashi, K.; Gotoh, T.; Yamada, S. Isolation of human renin inhibitor from soybean: soyasaponin I is the novel human renin inhibitor in soybean. *Biosci., Biotechnol., Biochem.* **2008**, *72*, 3232−3236.
(50) Yuan, L.; Wu, J.; Aluko, R. E.; Ye, X. Kinetics of renin inhibition by sodium houttuyfonate analogs. *Biosci., Biotechnol., Biochem.* **2006**, *70*, 2275−2280.
(51) Takahashi, S.; Hori, K.; Hokari, M.; Gotoh, T.; Sugiyama, T. Inhibition of human renin activity by saponins. *Biomed. Res.* **2010**, *31*, 155−159.
(52) Lin, C.; Tsai, C.; Lin, S. Effects of soy components on blood and liver lipids in rats fed high-cholesterol diets. *World J. Gastroenterol.* **2005**, *11*, 5549−5552.
(53) Lee, S.; Simons, A.; Murphy, P. A.; Hendrich, S. Soyasaponins lowered plasma cholesterol and increased fecal bile acids in female golden Syrian hamsters. *Exp. Biol. Med.* **2005**, *230*, 472−478.
(54) Hiwatashi, K.; Shirakawa, H.; Hori, K.; Yoshiki, Y.; Suzuki, N.; Hokari, M.; Komai, M.; Takahashi, S. Reduction of blood pressure by soybean saponins, renin inhibitors from soybean, in spontaneously hypertensive rats. *Biosci., Biotechnol., Biochem.* **2010**, *74*, 2310−2312.
(55) El-Hawiet, A. M.; Toaima, S. M.; Asaad, A. M.; Radwan, M. M.; El-Sebakhy, N. A. Chemical constituents from *Astragalus annularis* Forssk. and *A. trimestriss* L., Fabaceae. *Braz. J. Pharmacogn.* **2010**, *20*, 860−865.
(56) Kinjo, J.; Yokomizo, K.; Hirakawa, T.; Shii, Y.; Nohara, T.; Uyeda, M. Anti-herps virus activity of fabaceous triterpenoidal saponins. *Biol. Pharm. Bull.* **2000**, *23*, 887−889.
(57) Ikeda, T.; Yokomizo, K.; Okawa, M.; Tsuchihashi, R.; Kinjo, J.; Nohara, T.; Uyeda, M. Anti-herps virus type 1 activity of oleanane-type triterpenoids. *Biol. Pharm. Bull.* **2005**, *28*, 1779−1781.
(58) Yoshiki, Y.; Kahara, T.; Okubo, K.; Sakabe, T.; Yamasaki, T. Superoxide- and 1,1-diphenyl-2-picrylhydrazyl radical-scavenging activities of soyasaponin $\beta$g related to gallic acid. *Biosci., Biotechnol., Biochem.* **2001**, *65*, 2162−2165.
(59) Xu, H.; Hao, Y.; Su, Y.; Li, Q.; Wu, J.; Fan, H.; Wang, M.; Yan, L.; An, H.; Zhang, Y. Effect of soyasaponin on expression of Fas/Fasl of Pneumonocyte in silicotic fibrosis rats. In *Inforamatics and Management Science*; Du, W., Ed.; Springer-Verlag: London, UK, 2013; pp 309−313, ISBN 978-1-4471-4802-9.
(60) Xu, H.; Su, Y.; Li, Q.; Wu, J.; Hao, Y.; Fan, H.; Wang, M.; Liu, N.; Zheng, G. Effect of soyasaponin on pulmonary tissue apoptosis of silicotic fibrosis rats. In *Inforamatics and Management Science*; Du, W., Ed.; Springer-Verlag: London, UK, 2013; pp 735−740, ISBN 978-1-4471-4802-9.
(61) Oda, K.; Matsuda, H.; Murakami, T.; Katayama, S.; Ohgitani, T.; Yoshikawa, M. Adjuvant and haemolytic activities of 47 saponins derived from medicinal and food plants. *Biol. Chem.* **2000**, *381*, 67−74.
(62) Oda, K.; Matsuda, H.; Murakami, T.; Katayama, S.; Ohgitani, T.; Yoshikawa, M. Relationship between adjuvant activity and amphipathic structure of soyasaponins. *Vaccine* **2003**, *21*, 2145−2151.
(63) Philbrick, D. J.; Bureau, D. P.; Collins, F. W.; Holub, B. J. Evidence that soyasaponin $B_b$ retards disease progression in a murine model of polycystic kidney disease. *Kidney Int.* **2003**, *63*, 1230−1239.

JOURNAL OF AGRICULTURAL AND FOOD CHEMISTRY

Article

pubs.acs.org/JAFC

# Simultaneous Degradation of Cypermethrin and Its Metabolite, 3-Phenoxybenzoic Acid, by the Cooperation of *Bacillus licheniformis* B-1 and *Sphingomonas* sp. SC-1

Fangfang Liu, Yuanlong Chi, Shuang Wu, Dongying Jia, and Kai Yao*

College of Light Industry and Food Engineering, Sichuan University, 610065 Chengdu, Sichuan, People's Republic of China

**ABSTRACT:** Cypermethrin (CY) and its metabolite, 3-phenoxybenzoic acid (3-PBA), generally coexist in agricultural soil and cause a toxic effect on the human body. In this study, CY and its metabolite 3-PBA were simultaneously degraded by the cooperation of *Bacillus licheniformis* B-1 and *Sphingomonas* sp. SC-1. The effects of the inoculation proportion and inoculation method of these two strains, cultivation time, and initial CY content on the degradation of CY and 3-PBA were investigated. Furthermore, the degradation of CY and 3-PBA in soil environment by using the cooperation of these two strains was also determined. When the inoculation proportion of the biomass of strain B-1/strain SC-1 was 3.3:6.7, strain B-1 was inoculated first, and strain SC-1 was inoculated after 24 h of cultivation, 75.60% CY (100 mg $L^{-1}$) was degraded at 72 h and the 3-PBA content was 10.31 mg $L^{-1}$. Compared with those by using only strain B-1, the half-life of CY by using these two strains was shortened from 71.90 to 35.71 h, and the yield coefficient of 3-PBA was decreased from 0.8938 to 0.2651. As in the soil environment, the CY content by using these two strains within a period of 25 days declined from 22.71 to 5.33 mg $kg^{-1}$ and the 3-PBA content was 1.84 mg $kg^{-1}$. Compared with those by using only strain B-1, the half-life of CY by using these two strains was shortened from 19.86 to 11.34 days and the yield coefficient of 3-PBA was decreased from 0.5302 to 0.2056. This work could develop a promising approach for the simultaneous degradation of CY and its metabolite 3-PBA in agricultural soil.

**KEYWORDS:** *cypermethrin, 3-phenoxybenzoic acid, simultaneous degradation, Bacillus licheniformis B-1, Sphingomonas sp. SC-1, cooperation*

## INTRODUCTION

Cypermethrin (CY), used as an important pyrethroid pesticide, has been extensively used for pest control in fruits and vegetables or as grain protectant against stored-product insect pests,[1−3] especially when the use of organophosphate and organochlorine is restricted due to their high toxicity.[2] However, CY often remains in agricultural soil and agricultural products owing to excess spraying,[4,5] and CY residues would be accumulated in human or mammal bodies through frequent contact or the food chain,[6] which might cause toxic effects on the reproductive system,[5] immune system,[7] and nervous system.[8] Therefore, to remediate CY-contaminated regions, biodegradation is generally considered as an effective method to remove CY residues, owing to its characteristics of high efficiency, easy application, and environmental friendliness.[9−11]

As reported, most CY-degrading organisms could not mineralize CY, but transformed it into 3-phenoxybenzoic acid (3-PBA).[12] 3-PBA could disrupt the normal secretion of reproductive hormones[13] and lead to sperm DNA fracture and sperm concentration decrease in the male body.[14] Moreover, 3-PBA is more likely to spread in the environment due to its stronger hydrophilicity compared with CY[15] and thus could cause some food safety problems.[16,17] Therefore, the biodegradation of 3-PBA has also attracted increasing attention.[15]

To the best of our knowledge, there are many research sutdies focused on the degradation of either CY[18,19] or 3-PBA[20,21] separately. Jilani et al. found that *Pseudomonas* IES-Ps-1 had a good degradation ability on CY and could degrade 51% of CY (80 mg $L^{-1}$) in 48 h.[22] Chen et al. reported that *Stenotrophomonas* sp. ZS-S-01 could degrade 82.9% of 3-PBA (250 mg $L^{-1}$) in 9 days.[23] However, no information about the simultaneous degradation of CY and 3-PBA is available. In fact, CY and 3-PBA generally coexisted in the CY degradation process. Therefore, the simultaneous degradation of these two compounds would be of important practical application value. Our previous studies proved that *Bacillus licheniformis* B-1 (strain B-1) and *Sphingomonas* sp. SC-1 (strain SC-1) had good degradation capacities on CY and 3-PBA, respectively.[21,24] In this study, these two strains were used for the cooperative degradation of CY and 3-PBA. The purpose is to enhance CY degradation and remove the metabolite 3-PBA simultaneously. Figure 1 shows the proposed degradation pathway of CY and 3-PBA by using strains B-1 and SC-1. CY is first degraded into 3-PBA through hydrolysis by strain B-1,[12] and then the 3-PBA is converted into muconic acid through benzene ring cleavage by strain SC-1.[21] The metabolite of muconic acid has been proved to be of no harm to the human body.[25]

## MATERIALS AND METHODS

**Materials.** Cypermethrin (CY, 99.7%) was purchased from the National Standard Substances Center (Beijing, China). 3-Phenoxybenzoic acid (3-PBA, 98%) was purchased from Sigma-Aldrich Chemical Co. (Shanghai, China). Chromatographic grade acetonitrile was purchased from Meridian Medical Technologies (Beijing, China). Acetonitrile, ethyl acetate, ethyl alcohol, $KH_2PO_4$, $K_2HPO_4$, $MgSO_4$,

Received: January 22, 2014
Accepted: July 28, 2014
Published: July 28, 2014

ACS Publications © 2014 American Chemical Society

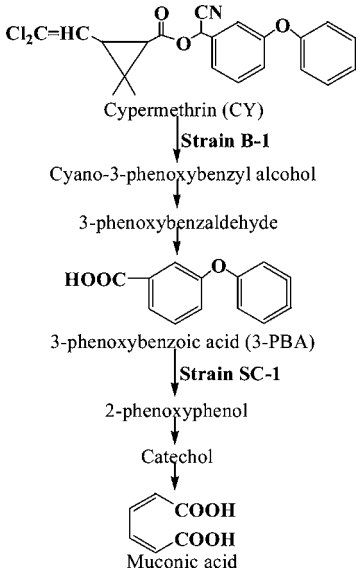


**Figure 1.** Proposed degradation pathway of CY and its metabolite 3-PBA by the cooperation of *Bacillus licheniformis* B-1 and *Sphingomonas* sp. SC-1.

NaCl, NaOH, $Na_2SO_4$, $(NH_4)_2SO_4$, and Tween 80 were of analytical grade and purchased from Kelong Chemical Co. (Chengdu, China).

**Microorganisms and Media.** The CY-degrading strain B-1 and the 3-PBA-degrading strain SC-1 were obtained from the soil in a tea garden (Ya'an, China) and from the sludge in a pesticide factory (Chengdu, China), respectively. Both were transferred to the laboratory by using sterile paper bags and domesticated by using enrichment culture technique. After several enrichment cultures, they were isolated by diluting the final cultures serially and spreading them on enrichment medium agar plates. On the basis of the analysis of morphological, physiological, and biochemical characteristics and 16S rDNA sequence (GenBank accession no.: strain B-1, HQ009796; strain SC-1, JN857975), strains B-1 and SC-1 were identified as *B. licheniformis*[24] and *Sphingomonas* sp.,[21] respectively. Both were stored in a 15% glycerol solution at −80 °C before experiments.

Several kinds of media were prepared. Luria−Bertani (LB) medium, containing 5.0 g $L^{-1}$ yeast extract, 10.0 g $L^{-1}$ peptone, and 10.0 g $L^{-1}$ NaCl, was used for CY degradation tests. Mineral salt (MS) medium, containing 0.2 g $L^{-1}$ $MgSO_4$, 0.5 g $L^{-1}$ $KH_2PO_4$, 0.5 g $L^{-1}$ NaCl, 1.5 g $L^{-1}$ $(NH_4)_2SO_4$, and 1.5 g $L^{-1}$ $K_2HPO_4$ was used for 3-PBA degradation tests. LB-MS medium, containing both LB and MS, was used for CY+3-PBA degradation tests. All media were adjusted to pH 7.0−7.5, and 0.2% Tween 80 (v/v) was added as an emulsifying agent before sterilization at 121 °C for 20 min.

**Inoculum Preparation.** Strain B-1 (or strain SC-1) was thawed and inoculated into a 100 mL Erlenmeyer flask, which contained 30 mL of LB-MS medium with 100 mg $L^{-1}$ CY (or 3-PBA). Then the flask was placed in a rotary shaker (Multitron-Pro, Infors, Switzerland) at 180 rpm and 30 °C, and the activated strain was obtained at 16 h of cultivation. After being centrifuged (ST40R, Thermo, German) at 10000 rpm and 4 °C for 10 min, the strain was collected and suspended in sterile *N*-saline (0.9% NaCl) to achieve a cell density of about $1.0 \times 10^8$ cells $mL^{-1}$. Then, the bacterial suspension was used as inoculum.

**Determination of the Content of CY and 3-PBA by HPLC.** *Pretreatment.* The broth culture was shaken by a vortex mixer for 30 s first, and 5 mL of broth culture was transferred to a 100 mL flask. Then, 5 mL of acetonitrile was added into the flask, and the flask was shaken by a vortex mixer for 30 s. The CY or 3-PBA in broth culture was extracted under ultrasonic (40 kHz and 300 W; B-3510E, Branson, America) for 30 min.[26] After centrifugation at 8000 rpm and 25 °C for 20 min, the supernatant was collected and filtered through a 0.22 μm membrane filter. Then, the collected filtrate was used for the determination of CY and/or 3-PBA contents.

*Determination of CY Content.* The content of CY was determined by an LC-20AT high-performance liquid chromatograph (HPLC, Shimadzu, Kyoto, Japan) equipped with an LC-20AT pump (Shimadzu), a CTO-20A column oven (Shimadzu), a Kromasil C18 column (250 mm × 4.60 mm, 5.0 μm; Sweden), and an SPD-M20A UV detector (Shimadzu). A series of CY acetonitrile solutions were prepared, and their contents ranged from 2.5 to 500 mg $L^{-1}$. After pretreatment as described under Pretreatment, 20 μL of the solution was injected manually, and elution was performed at 35 °C using 90% (v/v) aqueous acetonitrile solution with a flow rate of 1.0 mL $min^{-1}$. The detection wavelength was 210 nm.[26] Linear regression was taken between CY contents ($X$, mg $L^{-1}$) and their corresponding peak areas ($Y$), and then the calibration curve equation of CY was obtained as follows: $Y = 57585X + 99879$, $R^2 = 0.9996$, which was used for the calculation of CY content.

*Determination of 3-PBA Content.* The content of 3-PBA was determined by HPLC. A series of 3-PBA acetonitrile solutions with contents ranging from 1.0 to 200 mg $L^{-1}$ were prepared. HPLC detection was performed with a mobile phase of 60% (v/v) aqueous acetonitrile solution and a flow rate of 0.6 mL $min^{-1}$. Other chromatographic conditions were the same as those used for the determination of CY content. The calibration curve equation of 3-PBA was obtained as follows: $Y = 127025X + 84767$, $R^2 = 0.9998$, where $X$ and $Y$ represent the 3-PBA content (mg $L^{-1}$) and its corresponding peak area, respectively. It was used for the calculation of 3-PBA content.

**Degradation of CY by *B. licheniformis* B-1.** CY-degrading tests by using *B. licheniformis* B-1 were conducted in 250 mL Erlenmeyer flasks, which contained 30 mL of LB medium with 100 mg $L^{-1}$ CY. Strain B-1 inoculum was first shaken by a vortex mixer for 30 s, and then 1.5 mL of the inoculum was transferred into the medium (inoculated). The flask was shaken at 180 rpm and 30 °C. Uninoculated LB medium with 100 mg $L^{-1}$ CY served as control. Microbial biomass, CY degradation (%), and 3-PBA content (mg $L^{-1}$) in media were measured every 12 h. Microbial biomass was expressed by the optical density value measured at 600 nm ($OD_{600}$), and CY degradation was calculated according to eq 1, where $C$ is the content of CY in inoculated medium and $C_k$ is the content of CY in control.

$$\text{CY degradation (\%)} = (1 - C/C_k) \times 100 \quad (1)$$

**Degradation of 3-PBA by *Sphingomonas* sp. SC-1.** 3-PBA-degrading tests by using *Sphingomonas* sp. SC-1 were done in 250 mL Erlenmeyer flasks, which contained 30 mL of MS medium with 300 mg $L^{-1}$ 3-PBA. Strain SC-1 inoculum (1.5 mL) was inoculated to the medium, and the flask was shaken at 180 rpm and 30 °C. Uninoculated MS medium with 300 mg $L^{-1}$ 3-PBA was used as control. Microbial biomass and 3-PBA degradation (%) in media were measured every 2 h. 3-PBA degradation was calculated according to eq 2, where $C_1$ is the content of 3-PBA in inoculated medium and $C_{k1}$ is the content of 3-PBA in control.

$$\text{3-PBA degradation (\%)} = (1 - C_1/C_{k1}) \times 100 \quad (2)$$

**Degradation of CY and 3-PBA by Cooperation of Strains B-1 and SC-1.** *Effect of Inoculation Proportion of Strains B-1 and SC-1.* Mixed inocula of strains B-1 and SC-1 at different biomass ratios (10:0, 8:2, 7.5:2.5, 6.7:3.3, 5:5, 4:6, 3.3:6.7, 2.9:7.1, 2.5:7.5, 2:8, 0:10) were prepared, and the cell density of the mixed inocula were all $1.0 \times 10^8$ cells $mL^{-1}$. Each inoculum (1.5 mL) was separately inoculated to 30 mL of LB-MS media with 100 mg $L^{-1}$ CY. Uninoculated LB-MS medium with 100 mg $L^{-1}$ CY served as control. All of them were cultivated by shaker at 30 °C and 180 rpm for 72 h. Then, the CY degradation (%) and 3-PBA content (mg $L^{-1}$) in media were measured.

*Effect of Inoculation Method.* Strains B-1 and SC-1 at the biomass ratio of 3.3:6.7 were inoculated into 30 mL LB-MS medium with 100 mg $L^{-1}$ CY by using three different methods described below. Uninoculated LB-MS medium with 100 mg $L^{-1}$ CY served as control.

CY degradation (%) and 3-PBA content (mg $L^{-1}$) in media were measured after 72 h of cultivation.

Method 1: Strains B-1 and SC-1 were inoculated to the medium, simultaneously.

Method 2: Strain B-1 was first inoculated to the medium. At 24 h of cultivation, its biomass was determined as $N_0$. Strain SC-1 at the biomass of $6.7N_0/3.3$ was inoculated to the medium and cultivated for a further 48 h.

Method 3: Strain SC-1 was first inoculated to the medium. At 24 h of cultivation, its biomass was determined as $N_1$. Strain B-1 at the biomass of $3.3N_1/6.7$ was inoculated to the medium and cultivated for a further 48 h.

*Effect of Cultivation Time.* Degradation tests for a cultivation period of 96 h were done in 30 mL of LB-MS medium with 100 mg $L^{-1}$ CY. Strain B-1 was first inoculated to the medium. At 24 h of cultivation, its biomass was determined as $N$, and strain SC-1 at the biomass of $6.7N/3.3$ was inoculated and cultivated for a further 72 h. Uninoculated LB-MS medium containing 100 mg $L^{-1}$ CY served as control. Microbial biomass, CY degradation (%), and 3-PBA content (mg $L^{-1}$) in media were measured every 12 h.

*Effect of Initial CY Content.* Degradation tests at different initial CY contents (10, 25, 50, 100, 150 mg $L^{-1}$) in LB-MS media were conducted. Strain B-1 was first inoculated to the medium. At 24 h of cultivation, its biomass was determined as $N$, and strain SC-1 at the biomass of $6.7N/3.3$ was inoculated and cultivated for a further 48 h. Then the CY degradation (%) and 3-PBA content (mg $L^{-1}$) in media were measured. Uninoculated LB-MS medium containing a certain content of CY served as control.

**Degradation of CY and Its Metabolite 3-PBA in Soil Environment.** The soil was collected from the top 0−10 cm of a vegetable farmland in Sichuan University. The soil was sieved (mesh size = 2 mm) and air-dried overnight. The characteristics of the soil ($g^{-1}$, dry weight) were detected as follows: organic matter, 54.9 mg; total bacteria, $4.58 \times 10^8$ CFU; total actinomycetes, $1.33 \times 10^8$ CFU; total fungi, $1.67 \times 10^7$ CFU; and pH 7.86. A certain amount of CY was added to the soil to achieve a final content of 20 mg $kg^{-1}$, and then the soil was placed overnight.

Three soil samples with a weight of about 1000 g were used. One sample was inoculated with strain B-1 ($1.0 \times 10^8$ cells $g^{-1}$ soil, dry weight) and called B sample. Another sample was first inoculated with strain B-1 ($3.3 \times 10^7$ cells $g^{-1}$ soil, dry weight). At 24 h of cultivation, strain SC-1 ($6.7 \times 10^7$ cells $g^{-1}$ soil, dry weight) was inoculated and called BS sample. The third sample was uninoculated and used as control. The moisture contents of these three soil samples were kept at 40.0 ± 5.0% (w/w) by supplying water manually, and the average temperature was 22 °C. The contents (mg $L^{-1}$) of CY and 3-PBA in soil were measured every 2 days.

As for the extraction of CY and 3-PBA in the soil, the soil was dried to constant weight, and 5.0 g of soil was mixed with 10 mL of acetonitrile in a 100 mL flask under ultrasonic (40 kHz and 300 W) for 60 min. Ten milliliters of ethyl acetate was then added, and the supernatant was collected. The supernatant was purified by passing through an anhydrous $Na_2SO_4$ column.[26] After recovery of the organic solvent at 50 °C in a vacuum, the CY and 3-PBA solution was obtained by redissolving into 1 mL of acetonitrile. It was filtered through a 0.22 $\mu$m membrane filter and used for the determination of CY and 3-PBA contents.

## RESULTS AND DISCUSSION

**Degradation of CY by *B. licheniformis* B-1.** Microbial biomass ($OD_{600}$), CY degradation, and 3-PBA content in the CY degradation process by *B. licheniformis* B-1 are shown in Figure 2. In the initial cultivation phase (0−24 h), the $OD_{600}$ value and CY degradation all exhibited rapid increase trends, and the CY degradation reached 23.35% at 24 h, whereas only 0.72 mg $L^{-1}$ 3-PBA was detected. This might be due to the fact that CY was first degraded into cyano-3-phenoxybenzyl alcohol by esterase produced by strain B-1,[12] and only a very small

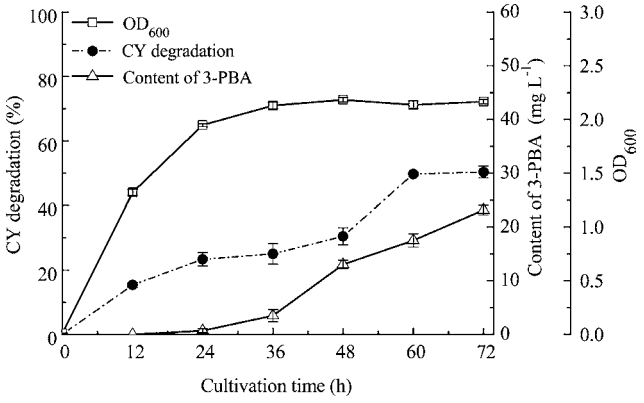


**Figure 2.** Microbial biomass ($OD_{600}$), CY degradation, and 3-PBA content in the CY degradation by *B. licheniformis* B-1. Results are expressed as the average and standard deviation of three parallel samples.

amount of cyano-3-phenoxybenzyl alcohol was transformed to 3-PBA. From 24 to 72 h, the CY degradation continued to increase, and the 3-PBA content began to increase quickly. These might be because cyano-3-phenoxybenzyl alcohol was gradually oxidized to 3-phenoxybenzaldehyde and then to 3-PBA.[12] At 72 h, CY degradation and 3-PBA content reached 50.36% and 23.16 mg $L^{-1}$, respectively. Compared with other CY-degrading organisms, such as *Pseudomonas* IES-Ps-1 isolated by Jilani and Khan that could degrade 51% CY (80 mg $L^{-1}$) in 48 h[22] and *Bacillus* sp. ISTDS2 reported by Sundaram and co-workers that could completely degrade CY (50 mg $L^{-1}$) in 180 h,[27] strain B-1 exhibited similar degradation ability on CY. However, the metabolite 3-PBA would be accumulated in the CY degradation process, and strain B-1 possessed poor degradation of 3-PBA.

**Degradation of 3-PBA by *Sphingomonas* sp. SC-1.** Microbial biomass ($OD_{600}$) and 3-PBA degradation in the 3-PBA degradation process by *Sphingomonas* sp. SC-1 were determined, and the results are shown in Figure 3. From 0 to 6

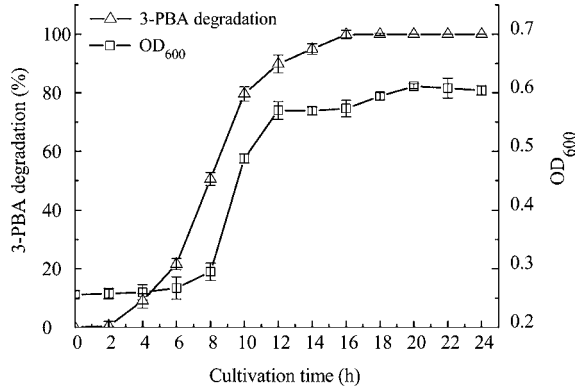


**Figure 3.** Microbial biomass ($OD_{600}$) and 3-PBA degradation in the 3-PBA degradation by *Sphingomonas* sp. SC-1. Results are expressed as the average and standard deviation of three parallel samples.

h, strain SC-1 could be in the lag growth phase, so its $OD_{600}$ value remained constant. Low 3-PBA degradation was found. From 6 to 16 h, 3-PBA was degraded rapidly and could be completely degraded at 16 h. The possible mechanism of 3-PBA degradation by strain SC-1 was described as follows. 3-PBA was first degraded to 2-phenoxyphenol under the effects of


dx.doi.org/10.1021/jf502835n | J. Agric. Food Chem. 2014, 62, 8256−8262

decarboxylase and hydroxylase produced from strain SC-1. Then 2-phenoxyphenol was converted into catechol owing to cleavage of the ether linkage and further degraded into muconic acid by the role of dioxygenase.[21] Chen et al. reported that *Stenotrophomonas* sp. ZS-S-01 could achieve 82.9% degradation of 3-PBA (250 mg $L^{-1}$) in 9 days,[23] and *Ochrobactrum lupine* DG-S-01 could completely degrade 100 mg $L^{-1}$ 3-PBA in 14 days.[28] Compared with these two strains, strain SC-1 exhibited a stronger degradation capacity on 3-PBA and could completely degrade 300 mg $L^{-1}$ 3-PBA in 16 h.

**Simultaneous Degradation of CY and Its Metabolite 3-PBA by Cooperation of Strains B-1 and SC-1.** *Effect of Inoculation Proportion of Strains B-1 and SC-1.* Strains B-1 and SC-1 have been proved to possess good degradation performance on CY and 3-PBA, respectively. Therefore, to improve the degradation of CY and decrease the metabolite 3-PBA content, simultaneously, the cooperation of these two strains was used in a CY degradation process.

The simultaneous degradation of CY and its metabolite 3-PBA was performed under different inoculation proportions of strains B-1 and SC-1, as the results show in Figure 4. When

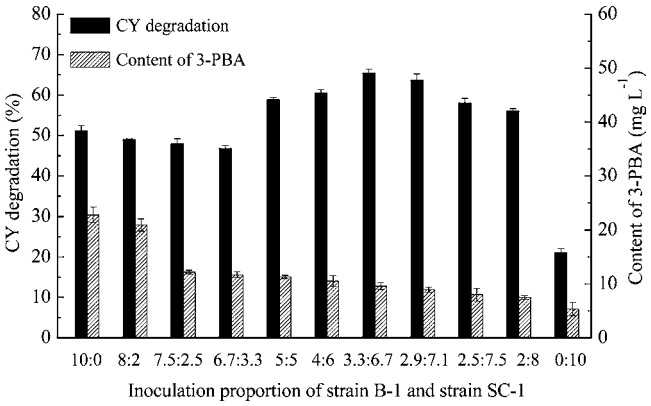


**Figure 4.** CY degradation and 3-PBA content by using different inoculation proportions of strains B-1 and SC-1. Results are expressed as the average and standard deviation of three parallel samples.

only strain B-1 was inoculated to the media (B-1/SC-1 = 10:0), 51.08% CY was degraded and 22.81 mg $L^{-1}$ 3-PBA was accumulated. As the inoculation proportion of strains B-1 and SC-1 ranged from 8:2 to 2:8, the 3-PBA content gradually decreased, which indicated that strain SC-1 can effectively degrade 3-PBA even in the coexistence of strain B-1 and CY. When the inoculation proportion was 3.3:6.7, the maximum CY degradation (65.36%) and only 9.6 mg $L^{-1}$ 3-PBA was observed. When only strain SC-1 was used (B-1/SC-1 = 0:10), only 21.08% CY could be degraded, indicating that strain SC-1 possessed poor degradation performance on CY. Therefore, strains B-1 and SC-1 used in a cooperative way can degrade CY and 3-PBA, simultaneously, and the proportion of 3.3:6.7 was appropriate and used in the following experiments.

*Effect of Inoculation Method.* The CY degradation and 3-PBA content by using three inoculation methods are shown in Figure 5. The CY degradations by using methods 1, 2, and 3 were 64.78, 75.60, and 53.89%, respectively. There was a statistically significant difference ($t$ test, $P < 0.05$) among the three methods. The 3-PBA contents by using these three methods were all about 10 mg $L^{-1}$. Therefore, method 2, in which strain B-1 was first inoculated and then strain SC-1 was

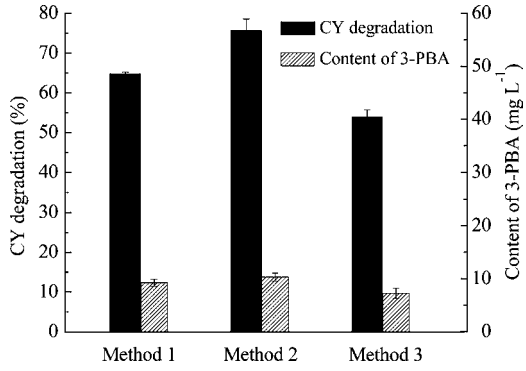


**Figure 5.** CY degradation and 3-PBA content by using three different inoculation methods. Results are expressed as the average and standard deviation of three parallel samples.

inoculated, was the most effective inoculation method for degrading CY and 3-PBA, simultaneously. It was presumably because (i) the antagonism and competition between strains B-1 and SC-1 might be minor[29] and (ii) CY was first degraded into 3-PBA by strain B-1 and then the 3-PBA was further degraded by strain SC-1, in accordance with the proposed degradation process of CY shown in Figure 1. Therefore, method 2 was used as the inoculation method in the following experiments.

*Effect of Cultivation Time.* Microbial biomass ($OD_{600}$), CY degradation, and 3-PBA content in the cultivation period of 96 h were investigated, and the results are shown in Figure 6. In

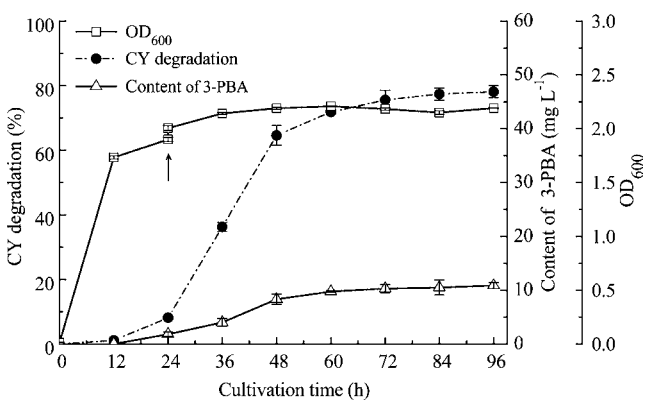


**Figure 6.** Microbial biomass ($OD_{600}$), CY degradation, and 3-PBA content in the cultivation period. ↑ represents addition of strain SC-1. Results are expressed as the average and standard deviation of three parallel samples.

the initial cultivation period (0–24 h, only strain B-1 was inoculated to the media), the $OD_{600}$ value increased quickly and reached 1.899 at 24 h, but only 8.13% CY was degraded. This was presumably because strain B-1 mainly utilized the nutrients in medium except CY to achieve fast growth in the initial phase. After the addition of strain SC-1 (24–96 h), CY degradation began to increase rapidly and reached 78.13% at 96 h, and only 10.87 mg $L^{-1}$ 3-PBA was detected. The possible mechanism of CY degradation by the cooperation of these two strains was as follows: CY was first degraded into 3-PBA by strain B-1, then 3-PBA was further degraded by strain SC-1. Meanwhile, the degradation of metabolite 3-PBA contributed to accelerate CY degradation. Compared with those by using only strain B-1 as described under Degradation of CY by *B. licheniformis* B-1, CY


dx.doi.org/10.1021/jf502835n | J. Agric. Food Chem. 2014, 62, 8256–8262

degradation by the cooperation of strains B-1 and SC-1 was improved from 50.36 to 75.60%, and the 3-PBA content declined from 23.16 to 10.31 mg $L^{-1}$ at 72 h of cultivation.

To further quantify the degradation efficiency of CY and 3-PBA by only strain B-1 or by the cooperation of strains B-1 and SC-1, the degradation rate constant ($k$) (eq 3) and half-life ($t_{1/2}$) (eq 4) of CY from a first-order degradation kinetic model and the yield coefficient ($Y$) of 3-PBA (eq 5) were calculated.[30]

$$C_t = C_0 \times e^{-kt} \quad (3)$$

$$t_{1/2} = \ln 2/k \quad (4)$$

$$Y = (P_t - P_0)/(S_0 - S_t) \quad (5)$$

$C_0$ is the initial content of CY, and $C_t$ is the content of CY at time $t$ (mg $L^{-1}$). $k$ and $t$ are the degradation rate constant ($h^{-1}$) and cultivation time (h), respectively. $P_0$ is the initial molar content of 3-PBA, and $P_t$ is the molar content of 3-PBA at time $t$ (mmol $L^{-1}$). $S_0$ is the initial molar content of CY, and $S_t$ is the molar content of CY at time $t$ (mmol $L^{-1}$). The molar masses of CY and 3-PBA are 416.32 and 214.2 g $mol^{-1}$, respectively.

The degradation rate constant and half-life of CY and the yield coefficient of 3-PBA at 72 h are shown in Table 1.

**Table 1. Degradation Rate Constant ($k$), Half-Life ($t_{1/2}$), and Correlation Coefficient ($R^2$) of CY and Yield Coefficient ($Y$) of 3-PBA after 72 h of Cultivation by Using Strain B-1 or a Cooperation of Strains B-1 and SC-1 in Media**

| treatment | regression eq | $k$ ($h^{-1}$) | $t_{1/2}$ (h) | $R^2$ | $Y$ |
|---|---|---|---|---|---|
| strain B-1 | $C_t = 99.3948\ e^{-0.0096t}$ | 0.0096 | 71.90 | 0.9143 | 0.8938 |
| strains B-1 and SC-1 | $C_t = 113.1823\ e^{-0.0194t}$ | 0.0194 | 35.71 | 0.9101 | 0.2651 |

Compared with those by using only strain B-1, the half-life ($t_{1/2}$) of CY by a cooperation of strains B-1 and SC-1 was shortened from 71.90 to 35.71 h, and the yield coefficient of 3-PBA was decreased from 0.8938 to 0.2651. Therefore, these results could further confirm that the cooperation of strains B-1 and SC-1 was an effective way to achieve the simultaneous degradation of CY and its metabolite 3-PBA.

*Effect of Initial CY Content.* The CY degradation and 3-PBA content by using different initial CY contents are shown in Figure 7. When the initial CY content was 10 mg $L^{-1}$, CY and its metabolite 3-PBA were completely degraded. When the initial CY content increased from 25 to 100 mg $L^{-1}$, the CY degradations were all >75% and the 3-PBA contents were ≤10 mg $L^{-1}$. When the initial CY content reached 150 mg $L^{-1}$, only 37.13% CY was degraded, and the 3-PBA content was still about 10 mg $L^{-1}$. This might be because when the CY reach a high content, it could produce a toxic effect on the voltage-sensitive $Na^+$ channels of strains B-1 and SC-1,[1] prolonging the lag growth phase of these two strains,[22] and so their degradation activity on CY or 3-PBA declined. These results indicated that the simultaneous degradation of CY and its metabolite 3-PBA by these two strains could be well achieved when the initial CY content was <100 mg $L^{-1}$. In fact, the CY content in the natural environment is at a very low level. For example, the content of CY in vegetables was from 0.02 to 0.19 mg $kg^{-1}$,[4] and the content of pyrethroid pesticide in soil is not more than 0.129 mg $kg^{-1}$.[31] Therefore, the cooperation of strains B-1 and SC-1 might be a promising method for the degradation of CY and its metabolite 3-PBA in agricultural soil, and this proposed method would be verified in the following.

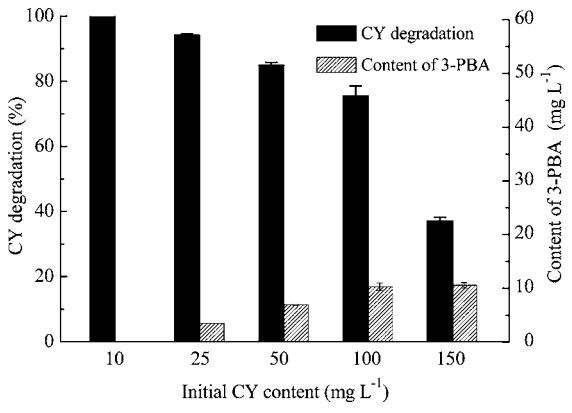


**Figure 7.** CY degradation and 3-PBA content by using different initial CY contents. Results are expressed as the average and standard deviation of three parallel samples.

**Degradation of CY and Its Metabolite 3-PBA in Soil Environment.** The contents of CY and its metabolite 3-PBA in the period of 25 days by using only strain B-1 or a cooperation of strains B-1 and SC-1 are shown in Figure 8. After incubation for 25 days, the CY content was 5.33 mg $L^{-1}$ in the soil inoculated with both strains B-1 and SC-1 (BS sample), whereas those in the soil inoculated with strain B-1 (B

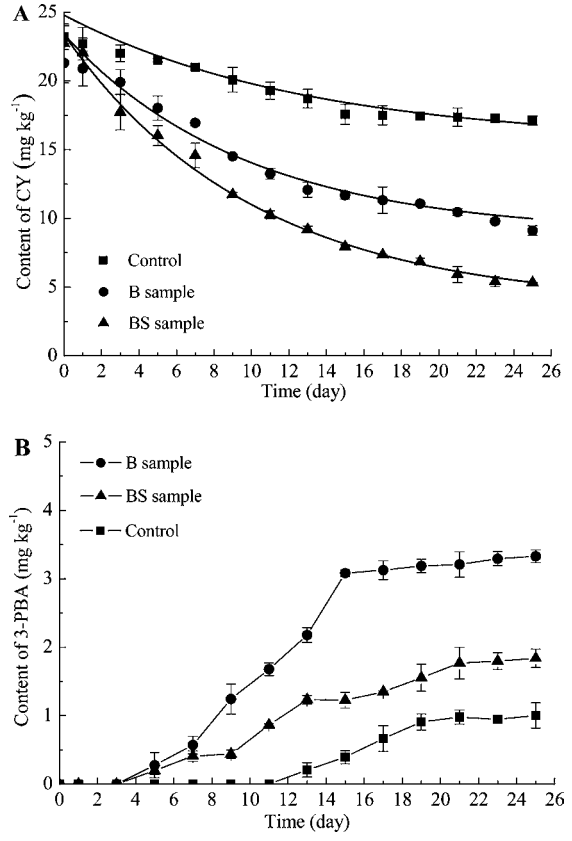


**Figure 8.** CY content (A) and 3-PBA content (B) in the soil by using only strain B-1 (B sample), in the soil by using the cooperation of strains B-1 and SC-1 (BS sample), and in the uninoculated soil (control). Results are expressed as the average and standard deviation of three parallel samples.


dx.doi.org/10.1021/jf502835n | J. Agric. Food Chem. 2014, 62, 8256−8262

sample) and the uninoculated soil (control) were 9.11 and 17.11 mg $L^{-1}$, respectively. As for the 3-PBA content, those in BS sample, B sample, and control were 1.84, 3.33, and 1.00 mg $L^{-1}$, respectively. These results indicated that the degradation of CY and its metabolite 3-PBA by a cooperation of strains B-1 and SC-1 was still much better than that by using only strain B-1 in the soil environment.

Furthermore, the degradation rate constant ($k$) and half-life ($t_{1/2}$) of CY from a first-order degradation kinetic model and the yield coefficient of 3-PBA ($Y$) at incubation on the 25th day were calculated and are summarized in Table 2. The half-lives

**Table 2. Degradation Rate Constant ($k$), Half-Life ($t_{1/2}$), and Correlation Coefficient ($R^2$) of CY and Yield Coefficient ($Y$) of 3-PBA after Incubation for 25 Days in the Uninoculated Soil (Control), in the Soil Inoculated with Strain B-1 (B Sample), or in the Soil Inoculated with both Strains B-1 and SC-1 (BS Sample)**

| treatment | regression eq | $k$ ($days^{-1}$) | $t_{1/2}$ (days) | $R^2$ | $Y$ |
|---|---|---|---|---|---|
| control | $C_t = 22.7303\, e^{-0.0133t}$ | 0.0133 | 52.12 | 0.9392 | 0.3200 |
| B sample | $C_t = 20.9596\, e^{-0.0349t}$ | 0.0349 | 19.86 | 0.9703 | 0.5302 |
| BS sample | $C_t = 21.5829\, e^{-0.0611t}$ | 0.0611 | 11.34 | 0.9853 | 0.2056 |

of CY in control, B sample, and BS sample were 52.12, 19.86, and 11.34 days, respectively. The B or BS sample has a longer half-life of CY than that in media, which might be because the soil environment has less nutrients and poor oxygen dissolving ability for the growth of strains B-1 and SC-1. The yield coefficients of 3-PBA in control, B sample, and BS sample were 0.3200, 0.5302, and 0.2056, respectively. A lower yield coefficient of 3-PBA in B or BS sample was observed as compared with that in media, which might be because part of the generated 3-PBA was degraded by the indigenous organisms in soil. From the above results, it could be further confirmed that the cooperation of strains B-1 and SC-1 could effectively remove the CY and its metabolite 3-PBA in agricultural soil.

## AUTHOR INFORMATION


### Corresponding Author

*(K.Y.) Phone/fax: +86 28 85404298. E-mail: yaokai555@126.com.



### Funding

This work was financially supported by the National Natural Science Foundation of China (31371775), the Specialized Research Fund for the Doctoral Program of Higher Education of China (20130181120094), the Open Fund for the Key Lab of Sichuan Province (13-R01), and the Applied Basic Research Program of High Education of Chengdu (11DXYB208NC-027).


### Notes

The authors declare no competing financial interest.

## REFERENCES


(1) Dorman, D. C.; Beasley, V. R. Neurotoxicology of pyrethrin and the pyrethroid insecticides. *Vet. Hum. Toxicol.* **1991**, *33*, 238−243.

(2) Katsuda, Y. Development of and future prospects for pyrethroid chemistry. *Pest Manag. Sci.* **1999**, *55*, 775−782.

(3) Athanassiou, C. G.; Kavallieratos, N. G.; Vayias, B. J.; Dimizas, C. B.; Papagregoriou, A. C.; Buchelos, C. Th. Residual toxicity of beta cyfluthrin, alpha cypermethrin and deltamethrin against *Tribolium confusum* Jacquelin du Val (Coleoptera: Tenebrionidae) on stored wheat. *Appl. Entomol. Zool.* **2004**, *39*, 195−202.

(4) Łozowicka, B.; Jankowska, M.; Kaczyński, P. Pesticide residues in *Brassica* vegetables and exposure assessment of consumers. *Food Control* **2012**, *25*, 561−575.

(5) McKinlay, R.; Plant, J. A.; Bell, J. N. B.; Voulvoulis, N. Endocrine disrupting pesticides: implications for risk assessment. *Environ. Int.* **2008**, *34*, 168−183.

(6) Schettgen, T.; Heudorf, U.; Drexler, H.; Angerer, J. Pyrethroid exposure of the general population-is this due to diet. *Toxicol. Lett.* **2002**, *134*, 141−145.

(7) Jin, Y.; Zheng, S.; Fu, Z. Embryonic exposure to cypermethrin induces apoptosis and immunotoxicity in zebrafish (*Danio rerio*). *Fish. Shellfish. Immunol.* **2011**, *30*, 1049−1054.

(8) Wolansky, M. J.; Harrill, J. A. Neurobehavioral toxicology of pyrethroids insecticides in adult animals: a critical review. *Neurotoxicol. Teratol.* **2008**, *30*, 55−78.

(9) Grant, R. J.; Betts, W. B. Biodegradation of the synthetic pyrethroid cypermethrin in used sheep dip. *Lett. Appl. Microbiol.* **2003**, *36*, 173−176.

(10) Fenlon, K. A.; Jones, K. C.; Semple, K. T. Development of microbial degradation of cypermethrin and diazinon in organically and conventionally managed soils. *J. Environ. Monit.* **2007**, *9*, 510−505.

(11) Liu, W.; Gan, J. J.; Lee, S.; Werner, I. Isomer selectivity in aquatic toxicity and biodegradation of cypermethrin. *J. Agric. Food Chem.* **2004**, *52*, 6233−6238.

(12) McCoy, M. R.; Yang, Z.; Fu, X.; Ahn, K. C.; Gee, S. J.; Bom, D. C.; Zhong, P.; Chang, D.; Hammock, B. D. Monitoring of total type II pyrethroid pesticides in citrus oils and water by converting to a common product 3-phenoxybenzoic acid. *J. Agric. Food Chem.* **2012**, *60*, 5065−5070.

(13) Han, Y.; Xia, Y.; Han, J.; Zhou, J.; Wang, S.; Zhu, P.; Zhao, R.; Jin, N.; Song, L.; Wang, X. The relationship of 3-PBA pyrethroids metabolite and male reproductive hormones among non-occupational exposure males. *Chemosphere* **2008**, *72*, 785−790.

(14) Ji, G.; Xia, Y.; Gu, A.; Shi, X.; Long, Y.; Song, L.; Wang, S.; Wang, X. Effects of non-occupational environmental exposure to pyrethroids on semen quality and sperm DNA integrity in Chinese men. *Reprod. Toxicol.* **2011**, *31*, 171−176.

(15) Halden, R. U.; Tepp, S. M.; Halden, B. G.; Dwyer, D. F. Degradation of 3-phenoxybenzoic acid in soil by *Pseudomonas pseudoalcaligenes* POB310 (pPOB) and two modified *Pseudomonas* strains. *Appl. Environ. Microbiol.* **1999**, *65*, 3354−3359.

(16) Ueyama, J.; Kimata, A.; Kamijima, M.; Hamajima, N.; Ito, Y.; Suzuki, K.; Inoue, T.; Yamamoto, K.; Takagi, K.; Saito, I.; Miyamoto, K.; Hasegawa, T.; Kondo, T. Urinary excretion of 3-phenoxybenzoic acid in middle-aged and elderly general population of Japan. *Environ. Res.* **2009**, *109*, 175−180.

(17) Riederer, A. M.; Bartell, S. M.; Barr, D. B.; Ryan, P. B. Diet and nondiet predictors of urinary 3-phenoxybenzoic acid in NHANES 1999−2002. *Environ. Health. Perspect.* **2008**, *116*, 1015−1022.

(18) Grant, R. J.; Daniell, T. J.; Betts, W. B. Isolation and identification of synthetic pyrethroid-degrading bacteria. *J. Appl. Microbiol.* **2002**, *92*, 534−540.

(19) Tallur, P. N.; Megadi, V. B.; Ninnekar, H. Z. Biodegradation of cypermethrin by *Micrococcus* sp. strain CPN 1. *Biodegradation* **2008**, *19*, 77−82.

(20) Topp, E.; Akhtar, M. H. Mineralization of 3-phenoxybenzoate by a two-membered bacterial co-culture. *Can. J. Microbiol.* **1990**, *36*, 495−499.

(21) Tang, J.; Yao, K.; Liu, S.; Jia, D.; Chi, Y.; Zeng, C.; Wu, S. Biodegradation of 3-phenoxybenzoic acid by a novel *Sphingomonas* sp. SC-1. *Fresenius' Environ. Bull.* **2013**, *22*, 1564−1572.

(22) Jilani, S.; Khan, M. A. Biodegradation of cypermethrin by *pseudomonas* in a batch activated sludge process. *Int. J. Environ. Sci. Technol.* **2006**, *3*, 371−380.

(23) Chen, S.; Yang, L.; Hu, M.; Liu, J. Biodegradation of fenvalerate and 3-phenoxybenzoic acid by a novel *Stenotrophomonas* sp. strain ZS-S-01 and its use in bioremediation of contaminated soils. *Appl. Microbiol. Biotechnol.* **2011**, *90*, 755−767.
(24) Lai, W.; Liu, S. L.; Zhao, N.; Yuan, H. Y. Isolation, identification and characterization of a cypermethrin-degrading strain. *Food Sci.* **2012**, *21*, 157−163.
(25) Wiwanitkit, V.; Soogarun, S.; Suwansaksri, J. A correlative study on red blood cell parameters and urine trans, trans-muconic acid in subjects with occupational benzene exposure. *Toxicol. Pathol.* **2007**, *35*, 268−269.
(26) Liu, S.; Yao, K.; Jia, D.; Zhao, N.; Lai, W.; Yuan, H. A pretreatment method for HPLC analysis of cypermethrin in microbial degradation systems. *J. Chromatogr. Sci.* **2012**, *50*, 469−476.
(27) Sundaram, S.; Das, M. T.; Thakur, I. S. Biodegradation of cypermethrin by *Bacillus* sp. in soil microcosm and in-vitro toxicity evaluation on human cell line. *Int. Biodeter. Biodegr.* **2013**, *77*, 39−44.
(28) Chen, S.; Hu, M.; Liu, J.; Zhong, G.; Yang, L.; Rizwan-ul-Haq, M.; Han, H. Biodegradation of beta-cypermethrin and 3-phenoxybenzoic acid by a novel *Ochrobactrum lupini* DG-S-01. *J. Hazard. Mater.* **2011**, *187*, 433−440.
(29) Christensen, B. B.; Haagensen, J. A.; Heydorn, A.; Molin, S. Metabolic commensalism and competition in a two-species microbial consortium. *Appl. Environ. Microbiol.* **2002**, *68*, 2495−2502.
(30) Cycon, M.; Wojcik, M.; Piotrowska-Seget, Z. Biodegradation of the organophosphorus insecticide diazinon by *Serratia* sp. and *Pseudomonas* sp. and their use in bioremediation of contaminated soil. *Chemosphere* **2009**, *76*, 494−501.
(31) Weston, D. P.; You, J.; Lydy, M. J. Distribution and toxicity of sediment-associated pesticides in agriculture-dominated water bodies of California's Central Valley. *Environ. Sci. Technol.* **2004**, *38*, 2752−2759.

JOURNAL OF AGRICULTURAL AND FOOD CHEMISTRY

Article

pubs.acs.org/JAFC

# Effect of Thermal Processing on Estimated Metabolizable Protein Supply to Dairy Cattle from Camelina Seeds: Relationship with Protein Molecular Structural Changes

Quanhui Peng,[†,‡] Nazir A. Khan,[†,⊥] Zhisheng Wang,[‡] Xuewei Zhang,[§] and Peiqiang Yu*[,†,§]

[†]Department of Animal and Poultry Science, University of Saskatchewan, Saskatoon, SK S7N 5A8, Canada

[‡]Animal Nutrition Institute, Sichuan Agriculture University, Sichuan 625014, China

[§]Tianjin Agricultural University, Tianjin 300384, China

Supporting Information

**ABSTRACT:** This study evaluated the effect of thermal processing on the estimated metabolizable protein (MP) supply to dairy cattle from camelina seeds (*Camelina sativa* L. Crantz) and determined the relationship between heat-induced changes in protein molecular structural characteristics and the MP supply. Seeds from two camelina varieties were sampled in two consecutive years and were either kept raw or were heated in an autoclave (moist heating) or in an air-draft oven (dry heating) at 120 °C for 1 h. The MP supply to dairy cattle was modeled by three commonly used protein evaluation systems. The protein molecular structures were analyzed by Fourier transform/infrared-attenuated total reflectance molecular spectroscopy. The results showed that both the dry and moist heating increased the contents of truly absorbable rumen-undegraded protein (ARUP) and total MP and decreased the degraded protein balance (DPB). However, the moist-heated camelina seeds had a significantly higher ($P < 0.05$) content of ARUP and total MP and a significantly lower ($P < 0.05$) content of DPB than did the dry-heated camelina seeds. The regression equations showed that intensities of the protein molecular structural bands can be used to estimate the contents of ARUP, MP, and DPB with high accuracy ($R^2 > 0.70$). These results show that protein molecular structural characteristics can be used to rapidly assess the MP supply to dairy cattle from raw and heat-treated camelina seeds.

**KEYWORDS:** *camelina seed, protein metabolic characteristics, protein molecular structure, protein evaluation system*

## INTRODUCTION

Camelina (*Camelina sativa* L. Crantz), commonly known as gold-of-pleasure or false flax, is an unexploited, short-seasoned oilseed crop in the family of Brassicaceae. Over the past few years, the demand for camelina seeds has increased because of its increased use in biodiesel and bio-oil production, and in animal feed.[1,2] Moreover, because of its early maturity and adaptability to diverse soil and environmental conditions, the crop grows well in the cold, semiarid, and marginal lands of North America. As a result, the cultivated area of camelina was estimated to reach 0.607 million hectares by 2013 in North America.[3] Camelina seeds contain over 35% oil,[3] with a remarkably high content (>37%) of C18:3n-3,[2,4] which makes it a valuable alternative source of omega-3 fatty acids in human and animal diets.[5] Moreover, it is well-known that camelina seeds are relatively rich in crude protein (CP, >25%) and essential amino acids,[3,6] indicating the potential of this oilseed as a high quality protein and oil supplement for dairy cattle, particularly during early lactation. The beneficial effects of feeding camelina-derived oil on animal health and the fatty acid profiles of meat and milk have been extensively evaluated;[7−13] however, to the author's knowledge, the metabolizable protein (MP) supply to dairy cattle from camelina seeds has not been evaluated.

Excessive degradation of oilseed-derived protein in the rumen decreases the efficiency of protein utilization and increases feed cost and N losses to the environment.[14,15] Thermal processing has been used widely to decrease the rumen degradation of protein; however, the establishment of optimal heating conditions is vital to optimize protein utilization in ruminants. Recent research has demonstrated that thermal processing alters protein digestive behavior by changing protein molecular structures.[16] Therefore, quantifying the heat-induced changes in protein molecular structures in relation to changes in protein digestive behavior in the rumen and intestines of dairy cattle can help to establish optimal heating conditions.[17,18] However, such studies are extremely rare, partly because of the lack of appropriate analytical techniques. Recent research has revealed that Fourier transform/infrared-attenuated total reflectance (FT/IR-ATR) molecular spectroscopy can be used as a fast, nondestructive, and noninvasive bioanalytical technique to detect protein molecular structural changes in feed tissues.[16,18,19]

Over the past few decades, various protein evaluation models such as the National Research Council (NRC)-2001 model,[20] the DVE/OEB system[21] (DVE, truly absorbed protein in the small intestine; OEB, degraded protein balance), and the PDI[22] (protein truly digestible in the small intestine) system have been developed, which estimate the MP supply to dairy cattle using in situ ruminal and intestinal protein digestibility data. So far, the MP content and feed milk value (FMV) of camelina seeds have not been investigated by employing and comparing different protein evaluation models. Therefore, the first objective

Received: March 18, 2014
Revised: July 21, 2014
Accepted: July 21, 2014
Published: July 21, 2014

 © 2014 American Chemical Society 

of the present study was to evaluate the metabolic characteristics of the protein in the rumen and intestines of dairy cattle and to estimate the MP supply to dairy cattle from raw and heat-treated camelina seeds. The second objective was to establish the relationship between the protein molecular structural characteristics and the MP supply to dairy cattle as predicted by three evaluation systems in order to provide a new tool for the rapid evaluation of protein nutritive value. We hypothesized that some specific protein structural characteristics can be used to estimate the MP content, degraded protein balance (DPB), and FMV of camelina seeds.

## MATERIALS AND METHODS

**Camelina Seeds, Heat Treatment and Processing.** Seeds of Blaine Creek and Celine varieties of camelina were sampled from three replicate plots in two different years (2010 and 2011) by the Feeds Innovation Institute (FII), University of Saskatchewan (Saskatoon, Canada). The seeds were used as a model for camelina-derived feed protein. The seeds (1 kg) of each camelina variety were spread (2 cm thin layer) in aluminum pans (23 cm × 33 cm × 5 cm high) and heated in an air-draft oven (dry heating) or an autoclave (Amsco Eagle SG-3031, Steris Corp., Mentor, OH) under 15 pounds per square inch pressure (moist heating) for 1 h at 120 °C. The heat processing was carried out in two replicate runs. After heat treatment, the seeds were immediately removed from the oven or autoclave, cooled at room temperature (22 ± 2 °C), and stored at 4 °C for further processing and analysis. The raw seeds were used as a control.

The seeds were ground through a 2 mm screen (Retsch ZM-1, Brinkmann Instruments Ltd., Mississauga, ON, Canada) for in situ incubation studies. For chemical analysis, the seeds were ground through a 1 mm screen, whereas for molecular spectral analyses, the seeds were finely ground through a 0.25 mm screen. For the fine grinding, the seeds were kept cool and were slowly fed into the grinder to avoid extrusion.

**Molecular Spectroscopy.** The protein molecular structural bands of the raw and heat-treated camelina seeds were analyzed using FT/IR-ATR microspectroscopy (Jasco-4200, Jasco Inc., Easton, MD) at the molecular spectroscopy laboratory of the Department of Animal and Poultry Science, University of Saskatchewan (Saskatoon, Canada). The FT/IR-ATR was equipped with a deuterated L-alanine-doped triglycine sulfate detector (JASCO Corp., Tokyo, Japan) and a ceramic infrared light source, and was outfitted with a MIRacle ATR accessory module and a ZnSe crystal and pressure clamp (Pike Technologies, Madison, WI, U.S.A.). For each sample, 128 scans were generated in the mid-infrared (ca. 4000−800 $cm^{-1}$) and fingerprint (ca. 1800−800 $cm^{-1}$) regions in a transmission mode at a spectral resolution of 4 $cm^{-1}$. Each sample was run five times. The spectra were collected with Jasco Spectra Manager II software, and the molecular structural features were quantified by Ominic 7.2 software (Spectra-Tech Inc., Madison, WI, U.S.A.). The specific spectral bands associated with protein functional groups, such as amide I and amide II, and protein secondary structures, such as $\alpha$-helix and $\beta$-sheet, were identified and quantified as reported by Peng et al.[3]

**In Situ Rumen Incubation.** Four nonlactating Holstein cows, fitted with flexible rumen cannula with an internal diameter of 10 cm (Bar Diamond Inc., Parma, ID, U.S.A.), were used for the in situ incubation. The cows were handled and cared for according to the guidelines of the Canadian Council on Animal Care.[23] The cows had free access to fresh drinking water and were individually fed twice each day with a balanced total mixed ration, containing 805 g barley silage and 195 g concentrate per kg DM, according to NRC maintenance requirements.[20] The detailed chemical composition of the concentrate and barley silage is reported earlier.[19] The rumen degradation kinetics of raw and heat-treated camelina seeds were determined according to the standard in situ method as described by Yan et al.[24]

**Rumen Degradation Characteristics.** The rumen degradation characteristics of protein were computed according to the first-order kinetics equation of Ørskov and McDonald[25] with a modification for lag time by Robinson et al:[26]

$$\mathrm{CP}\ (t) = U + (100 - S - U) \times \mathrm{e}^{-K_\mathrm{d}(t-T_0)}$$

where CP ($t$) is the CP (g/kg) present in the residues at time h incubation; $S$ is the soluble CP fraction (g/kg); $U$ is the rumen nondegradable CP fraction (g/kg); $K_\mathrm{d}$ is the degradation rate/h; and $T_0$ is the lag time (h). The results were analyzed using the PROC NLIN (nonlinear) procedure of Statistical Analysis System (SAS, 2009)[27] with an iterative least-squares regression (Gauss−Newton method). Rumen-degraded feed protein (RDP) and rumen-undegraded protein (RUP) were calculated according to the NRC-2001[20] model as

$$\mathrm{RDP\ (g/kg)} = S + D\left[\frac{K_\mathrm{d}}{(K_\mathrm{d} + K_\mathrm{p})}\right]$$

$$\mathrm{RUP\ (g/kg)} = U + D\left[\frac{K_\mathrm{p}}{(K_\mathrm{d} + K_\mathrm{p})}\right]$$

where $D$ is the potential degradable protein (g/kg) and was calculated as $D = 100 - S - U$, and $K_\mathrm{p}$ is the estimated outflow rate of digesta from rumen, which was assumed to be 6%/h for the three evaluation systems.

**Intestinal Protein Digestion Determination.** The intestinal digestibility of RUP was determined using the three-steps in vitro method of Calsamiglia and Stern[28] with slight modifications as described in our previous study by Peng et al.[3]

**Estimating Metabolizable Protein Supply to Dairy Cattle: NRC-2001 Model.** The detailed framework, concepts, and formulas of the NRC-2001 dairy model are provided by the NRC.[20] Briefly, the MP supply from raw and heat-treated camelina seeds to the small intestine of dairy cattle was calculated from (1) truly absorbable RUP ($\mathrm{ARUP_{NRC}}$), (2) truly absorbable ruminally synthesized microbial protein (microbial protein, MCP) ($\mathrm{AMCP_{NRC}}$), and (3) truly absorbable rumen endogenous protein ($\mathrm{AECP_{NRC}}$). The MP was calculated as follows:

$$\mathrm{MP\ (g/kg\,DM)} = \mathrm{ARUP_{NRC}\ (g/kg)} + \mathrm{AMCP_{NRC}\ (g/kg)} + \mathrm{AECP_{NRC}\ (g/kg)}$$

The $\mathrm{ARUP_{NRC}}$ content was estimated as follows:

$$\mathrm{ARUP_{NRC}\ (g/kg\,DM)} = \frac{\mathrm{dRUP\ (\%RUP)}}{100} \times \mathrm{RUP_{NRC}\ (g/kg\,DM)}$$

where, dRUP was the intestinal digestibility of RUP, determined according to the three-step in vitro procedure of Calsamiglia and Stern.[28] The RUP content was calculated as

$$\mathrm{RUP_{NRC}\ (g/kg\,DM)} = \mathrm{CP\ (g/kg\,DM)} \times \frac{\mathrm{RUP\ (\%CP)}}{100}$$

The $\mathrm{AMCP_{NRC}}$ was estimated from the predicted MCP synthesized in the rumen. The NRC (2001) assumes that the MCP contributed by bacteria and protozoa contains 80% true protein while the other 20% CP is contributed by nucleic acids, which are not available to dairy cattle. Moreover, it also assumes that the digestibility of true MCP is 80%. Thus,

$$\mathrm{AMCP_{NRC}} = \mathrm{MCP} \times 0.8 \times 0.8$$

According to the NRC-2001 model, the MCP was estimated from the total digestible nutrients (TDN). The model assumes that the yield of MCP from 1 kg TDN is 130 g. The $\mathrm{MCP_{TDN}}$ was calculated as follows:

$$\mathrm{MCP_{TDN}\ (g/kg\,DM)} = 0.130 \times \mathrm{TDN}$$

However, if RDP in the feed is less than $1.18 \times \mathrm{MCP_{TDN}}$, then MCP is calculated from RDP as follows:

$$\mathrm{MCP_{RDP}\ (g/kg\,DM)} = 0.85 \times \mathrm{RDP\ (g/kg\,DM)}$$


dx.doi.org/10.1021/jf5013049 | J. Agric. Food Chem. 2014, 62, 8263−8273

where the NRC (2001) assumes that 85% of the RDP is converted to MCP, and 1.18 results from 1.00/0.85.

The supply of endogenous crude protein (ECP) to the small intestine was calculated as

$$ECP_{NRC}\ (g/kg\,DM) = 6.25 \times 1.9 \times DM$$

The number 6.25 represents the protein−N conversion factor, and 1.9 indicates that 1.9 g of endogenous N was originated from 1 kg of DM. The NRC assumes that 50% of the $ECP_{NRC}$ passes to the duodenum, and 80% of the rumen ECP is true protein. The truly absorbed ECP in the small intestine ($AECP_{NRC}$) was estimated as

$$AECP_{NRC} = 0.50 \times 0.80 \times ECP_{NRC}$$

The $DPB_{NRC}$ was calculated as the difference between the potential $MCP_{RDP}$ and $MCP_{TDN}$, as follows:

$$DPB_{NRC}\ (g/kg\,DM) = MCP_{RDP}\ (g/kg\,DM) - 1.18 \times MCP_{TDN}\ (g/kg\,DM)$$

**Nutrient Supply Evaluated Using DVE/OEB System.** The calculation for estimating the MP supply using the DVE/OEB system[21] is summarized here. The MP (DVE) value of feed comprises truly absorbable RUP ($ARUP_{DVE}$), truly absorbable rumen-synthesized MCP ($AMCP_{DVE}$), and a correction for endogenous $ECP_{DVE}$ losses ($ENDP_{DVE}$). The $MP_{DVE}$ value was calculated as

$$MP_{DVE}\ (g/kg\,DM) = ARUP_{DVE} + AMCP_{DVE} - ENDP_{DVE}$$

The $ARUP_{DVE}$ was calculated on the basis of the content and digestibility of $RUP_{DVE}$. The $ARUP_{DVE}$ was calculated as

$$ARUP_{DVE}\ (g/kg\,DM) = \frac{dRUP\ (\%RUP)}{100} \times RUP_{DVE}\ (g/kg\,DM)$$

where dRUP was determined according to Calsamiglia and Stern.[28] The content of $RUP_{DVE}$ was calculated from the CP content of the feeds and RUP contents of the CP as follows:

$$RUP_{DVE}\ (g/kg\,DM) = 1.11 \times \left[CP\ (g/kg\,DM) \times \frac{RUP\ (\%CP)}{100}\right]$$

where 1.11 is the correction of the in situ data from the in vivo results.[21] The $AMCP_{DVE}$ was calculated as follows:

$$AMCP_{DVE}\ (g/kg\,DM) = 0.75 \times 0.85 \times MCP_{FOM}\ (g/kg\,DM)$$

where 0.75 is the assumed amount of true protein in the MCP, and 0.85 is the digestibility of $MCP_{FOM}$. The $MCP_{FOM}$ was calculated as

$$MCP_{FOM} = 0.15 \times FOM$$

where the factor 0.15 represents the assumption of the DVE system that for 1 kg of fermentable organic matter (FOM), 150 g of $MCP_{FOM}$ is synthesized in the rumen. The FOM was calculated as

$$FOM\ (g/kg\,DM) = DOM - Cfat - RUP - RUST - FP$$

where DOM is the digestible organic matter (OM); Cfat is the ether extract; RUST is the ruminally undegraded feed starch; and FP is fermentation products for conserved forages. For camelina seeds, FP and RUST were assumed to be zero.

The DVE/OEB system assumes that the ECP losses ($ENDP_{DVE}$) in the digestive tract are associated with the passage of the undigested DM (UDM). The $ECP_{DVE}$ was calculated as

$$ENDP_{DVE}\ (g/kg\,DM) = 0.075 \times UDM\ (g/kg\,DM)$$

where the DVE/OEB system assumed that 75 g of protein would be excreted per kilogram of UDM. The UDM was calculated as

$$UDM\ (g/kg\,DM) = (0.35 \times ash) + OM - \left[\frac{OM \times dOM}{100}\right]$$

where 0.35 is the constant utilized by CVB,[29] which indicates that 35% of the ash is not digested, and dOM is the degradability of OM after 120 h of rumen incubation.

The degraded protein balance ($DPB_{DVE}$) was calculated from the difference between the $MCP_{RDP}$ and the potential MCP based on the energy extracted during the anaerobic fermentation of FOM ($MCP_{FOM}$) in the rumen:

$$DPP_{DVE} = MCP_{RDP} - MCP_{FOM}$$

where $MCP_{RDP}$ was determined as follows:

$$MCP_{RDP} = CP\ (g/kg\,DM) \times \left[1 - \left(1.11 \times \frac{RUP\ (\%CP)}{100}\right)\right]$$

**Nutrient Supply Evaluated Using PDI System.** The principles and calculations of the PDI system[22,30] were used to calculate the supply of truly digestible protein (PDI) to the small intestine of dairy cattle from the raw and heat-treated camelina seeds. The PDI of feed comprises the truly absorbable RUP ($ARUP_{PDI}$) and the truly absorbable rumen-synthesized MCP ($AMCP_{PDI}$):

$$PDI\ (g/kg\,DM) = ARUP_{PDI} + AMCP_{PDI}$$

The $ARUP_{PDI}$ was calculated from the $RDP_{PDI}$ as

$$ARUP_{PDI}\ (g/kg\,DM) = CP\ (g/kg\,DM) \times (1.11 \times (1 - RDP)) \times TId$$

The PDI system assumes that 1.11 is a correction factor for the rumen bypass protein ($RUP_{PDI} = 1.11 \times (1 - RDP_{PDI})$ based on in vivo experiments. The RDP was calculated from the disappearance of protein from nylon bags during 48 h, assuming a rumen particle outflow rate of 6%/h. The TId is the true intestinal digestibility of RUP. TId was calculated as

$$TId\ (g/kg\,DM) = 88.3 + 0.371 \times CP - 0.0037 \times CP^2 - 1.07 \times ADL - 0.313 \times UDOM$$

where CP, acid detergent lignin (ADL), and undigested OM (UDOM) are expressed in (g/kg DM).

The $AMCP_{PDI}$ was calculated from (1) the MCP synthesized based on the available energy ($MCP_{ME}$), assuming that the degraded CP and other nutrients are not limiting, and (2) the MCP synthesized based on RDP ($MCP_{RDP}$), assuming that energy and other nutrients are not limiting. The $MCP_{ME}$ was estimated from the FOM and was calculated as follows:

$$MCP_{ME} = FOM \times 0.145 \times 0.8 \times 0.8$$

where 0.145 represents the yield of MCP that is assumed to be 145 g CP/kg FOM, and its true protein content and true digestibility in the small intestine are assumed to be 0.80 each. The FOM was calculated as follows:

$$FOM = DOM - EE - RUP_{PDI}$$

The DOM was calculated as

$$DOM = 87.75 - 0.314 \times CF\ (\%of\,DM) + \alpha$$

where $\alpha = 6.2$ for oilseeds. The $MCP_{RDP}$ was calculated as

$$MCP_{RDP} = 0.80 \times 0.80 \times RDP_{PDI}$$

as mentioned before, the true protein content of MCP and the true digestibility in the small intestine are 0.80 each. The $RDP_{PDI}$ was calculated as

$$RDP_{PDI}\ (g/kg\,DM) = 0.90 \times CP\ (g/kg\,DM) \times (1.11(1 - RDP))$$

where 0.90 is the efficiency of conversion of degraded N to rumen microbial N. The truly absorbable rumen-synthesized MCP in the small intestine ($AMCP_{PDI}$) was calculated as

$$AMCP_{PDI}\ (g/kgDM) = CP \times \frac{RDP_{PDI}}{DOM}$$

The degraded protein balance ($DPB_{PDI}$) was calculated as

$$DPB_{PDI}\ (g/kg\,DM) = (ARUP_{PDI} + MCP_{RDP}) - (ARUP_{PDI} + MCP_{ME})$$


dx.doi.org/10.1021/jf5013049 | J. Agric. Food Chem. 2014, 62, 8263−8273

**Feed Milk Value.** The FMVs of raw and heat-treated camelina seeds were calculated using the estimated MP supply as obtained with the NRC-2001, DVE/OEB, and PDI systems. The FMV was calculated as

$$FMV = MP \times 0.67 \times 0.033$$

Where, 0.67 is the efficiency of MP for milk production, and 0.033 is the protein content (g/g) of milk.

**Statistical Analysis.** The PROC MIXED procedure of the Statistical Analysis System (SAS)[27] was used to analyze the data on modeled protein supply, DPB, and FMV. The model used for analysis was

$$Y_{ij} = \mu + T_i + e_{ij}$$

where $Y_{ij}$ is an observation on the dependent variable $ij$; $\mu$ is the overall population mean; $T_i$ is the fixed effect of heat treatment (i = control, moist heating, and dry heating), and $e_{ij}$ is the random error associated with the observation $ij$. The plots were used as experimental replicates.

Comparisons among the three protein evaluation models were performed using the PROC MIXED procedure of SAS,[27] using the following model:

$$Y_{ij} = \mu + M_i + e_{ij}$$

where $Y_{ij}$ is an observation on the dependent variable $ij$; $\mu$ is the overall population mean; $M_i$ is the fixed effect of the protein evaluation model (i = NRC-2001, DVE/OEB, PDI); and $e_{ij}$ is the random error associated with the observation $ij$. The different treatments (control, dry heating, and moist heating) were used as replications. For variables with significant ($P < 0.05$) differences, posthoc analyses were carried out using the Tukey Test to compute pairwise differences in the means.

Stepwise, multiple-regression analyses were performed using the PROC REG procedure of SAS[27] to determine which of the protein molecular structural features can be used to estimate the modeled protein nutrient supply to dairy cattle from raw and heat-treated camelina seeds. The independent variables tested in the model were the $\alpha$-helix height, $\beta$-sheet height, amide-I area, amide-II area, ratio of the $\alpha$-helix to $\beta$-sheet height, and ratio of the amide I to amide II area. Only variables contributing significantly ($P < 0{\cdot}05$) to the estimation of the dependent variable were left in the final model. Collinearity among the independent variables was detected and avoided by the use of the variance inflation factor (VIF) option of SAS.[27]

## RESULTS

**Estimating Protein Supply to Dairy Cattle Using the NRC-2001 Model.** Heat processing increased the contents of $MCP_{TDN}$, $AMCP_{NRC}$, $ARUP_{NRC}$, and total MP, with the increase being significant ($P < 0.05$) for moist heating (Table 1). The FMV and $RUP_{NRC}$ contents increased ($P < 0.05$) with both dry and moist heating, and the highest ($P < 0.05$) values were estimated for moist heating. In contrast, the $MCP_{RDP}$ and $DPB_{NRC}$ contents decreased ($P = 0.01$) with heat processing, and the lowest value was computed for moist heating.

**Protein Supply to Dairy Cattle Using the DVE/OEB System.** Heat processing decreased the contents of $MCP_{FOM}$ and $DPB_{DVE}$, and the decrease was significant ($P < 0.05$) for moist heating (Table 2). Both the dry and moist heating significantly ($P < 0.05$) decreased the contents of $MCP_{RDP}$ and $AMCP_{DVE}$, and the lowest values were estimated for moist heating. In contrast, the contents of $RUP_{DVE}$, $ARUP_{DVE}$, $MP_{DVE}$, and $FMV_{DVE}$ increased ($P < 0.05$) with both dry and moist heating; however, the highest ($P < 0.05$) values were obtained with moist heating.

**Protein Supply to Dairy Cattle Using the PDI System.** Both dry and moist heating decreased ($P < 0.01$) the contents of $MCP_{ME}$, $MCP_{RDP}$, $AMCP_{PDI}$ and $DPB_{PDI}$, and the lowest values ($P < 0.05$) were obtained with moist heating (Table 3).

**Table 1. Dry and Moist Heat-Induced Changes in Protein Supply to Dairy Cattle from Camelina Seeds: Estimated by NRC-2001 Model[a]**

| | | heat treatments (HT)[b] | | | | contrast |
|---|---|---|---|---|---|---|
| item (g/kg DM) | control | HT-1 | HT-2 | SEM[c] | *P* value | control vs HT |
| Absorbable Microbial Protein Synthesized in the Rumen[d] | | | | | | |
| $MCP_{TDN}$ | 147.13b | 151.40a | 149.68ab | 0.540 | 0.025 | 0.014 |
| $MCP_{RDP}$ | 152.01a | 122.71b | 131.46ab | 2.304 | 0.010 | 0.005 |
| $AMCP_{NRC}$ | 94.16b | 96.90a | 95.80ab | 0.344 | 0.025 | 0.014 |
| Absorbable Endogenous True Protein in the Small Intestine[e] | | | | | | |
| $ECP_{NRC}$ | 11.09 | 10.98 | 11.59 | 0.042 | 0.052 | 0.242 |
| $AECP_{NRC}$ | 4.44 | 4.39 | 4.64 | 0.107 | 0.051 | 0.241 |
| Truly Absorbable Rumen-Undegraded Protein in Small Intestine[f] | | | | | | |
| $RUP_{NRC}$ | 68.29c | 111.93a | 88.39b | 1.514 | 0.002 | 0.001 |
| $ARUP_{NRC}$ | 33.41b | 78.64a | 46.52b | 3.021 | 0.002 | 0.003 |
| Total Metabolizable Protein[g] | | | | | | |
| $MP_{NRC}$ | 132.03b | 179.92a | 146.95b | 2.893 | 0.002 | 0.002 |
| Degraded Protein Balance[h] | | | | | | |
| $DPB_{NRC}$ | 36.88a | 3.31c | 15.23b | 2.133 | 0.001 | 0.001 |
| $FMV_{NRC}$ | 2.92c | 3.98a | 3.25b | 0.146 | 0.001 | 0.002 |

[a]Means within a row with different letters differ at the $P < 0.05$ level. [b]HT-1, moist-heated in an autoclave at 120 °C for 1 h; HT-2, dry-heated in an air-draft oven at 120 °C for 1 h. [c]SEM, standard error of mean. [d]$MCP_{TDN}$, MCP synthesized in the rumen based on available energy; $MCP_{RDP}$, MCP synthesized in the rumen based on available protein, calculated as 0.85 of rumen-degraded protein; $AMCP_{NRC}$, truly absorbable rumen-synthesized MCP in the small intestine. [e]ECP, rumen endogenous crude protein; AECP, truly absorbable endogenous protein in the small intestine. [f]$RUP_{NRC}$, ruminally undegraded crude protein; $ARUP_{NRC}$, truly absorbable rumen-undegraded feed protein in the small intestine. [g]MP, total metabolizable protein contributed by $ARUP_{NRC}$, $AMCP_{NRC}$, and AECP. [h]$DPB_{NRC}$, degraded protein balance, which reflects the difference between the potential MCP synthesis based on ruminally degraded feed protein and that based on energy (TDN) available for microbial fermentation in the rumen. $FMV_{NRC}$, feed milk value. The efficiency of use of the metabolizable protein for lactation is assumed to be 0.67,[19] and the protein content of milk is assumed to be 33 g/kg milk.

The contents of $RUP_{PDI}$ and FMV increased ($P < 0.05$) for both dry and moist heating; however, the highest ($P < 0.05$) values were obtained with moist heating. The contents of PDIE ($ARUP_{PDI}$ + $MCP_{ME}$) and PDIN ($ARUP_{PDI}$ + $MCP_{RDP}$) increased with heat processing with significant ($P < 0.05$) increase being observed with moist heating.

**Comparison of Estimated Protein Supply to Dairy Cattle by the NRC-2001 Model, DVE/OEB System, and PDI System.** Comparison of the estimated contents of protein nutrient supply and FMV of camelina seeds by the NRC-2001 model, DVE/OEB system, and PDI system are presented in Table 4. The estimated content (g/kg DM) of rumen-synthesized MCP on the basis of available energy was significantly higher ($P < 0.05$) in the NRC-2001 model (149.40) than that estimated by the DVE/OEB (59.51) and PDI (37.32) systems. Subsequently, the estimated content of truly absorbable rumen-synthesized MCP was substantially higher ($P < 0.05$) in the NRC-2001 model than those obtained with the DVE/OEB and PDI systems. In contrast, the rumen-synthesized MCP based on RDP was higher ($P < 0.05$) in the DVE/OEB and PDI systems than that in the NRC-2001 model. Moreover, the estimated content of truly absorbed rumen-synthesized MCP was higher ($P < 0.05$) in the DVE/OEB system than that in the PDI system.


dx.doi.org/10.1021/jf5013049 | J. Agric. Food Chem. 2014, 62, 8263−8273

**Table 2. Dry and Moist Heat-Induced Changes in Metabolizable Protein Supply to Dairy Cattle from Camelina Seeds: Estimated by DVE/OEB System[a]**

| | | heat treatments (HT)[b] | | | | contrast |
|---|---|---|---|---|---|---|
| item (g/kg DM) | control | HT-1 | HT-2 | SEM[c] | *P* value | control vs HT |
| Absorbable Microbial Protein Synthesis in the Rumen[d] | | | | | | |
| $MCP_{FOM}$ | 66.65a | 54.04b | 57.83ab | 2.120 | 0.035 | 0.046 |
| $MCP_{RDP}$ | 179.94a | 143.792c | 154.36b | 2.761 | 0.002 | 0.003 |
| $AMCP_{DVE}$ | 42.49a | 34.54b | 36.87b | 1.351 | 0.041 | 0.025 |
| Absorbable Endogenous True Protein in the Small Intestine[e] | | | | | | |
| $ECP_{DVE}$ | 11.43 | 12.63 | 13.09 | 1.14 | 0.623 | 0.384 |
| Truly Absorbable Rumen-Undegraded Protein in Small Intestine[f] | | | | | | |
| $RUP_{DVE}$ | 65.19c | 111.93a | 88.68b | 1.52 | 0.001 | 0.000 |
| $ARUP_{DVE}$ | 37.11c | 87.29a | 51.64b | 1.44 | 0.011 | 0.014 |
| Total Metabolizable Protein[g] | | | | | | |
| $MP_{DVE}$ | 68.17c | 109.48a | 75.42b | 4.663 | 0.008 | 0.015 |
| Degraded Protein Balance[h] | | | | | | |
| $DPB_{DVE}$ | 109.10a | 89.75b | 96.52ab | 6.388 | 0.035 | 0.028 |
| $FMV_{DVE}$ | 1.40c | 2.53a | 1.53b | 0.103 | 0.008 | 0.015 |

[a]Means within a row with different letters differ at the $P < 0.05$ level. [b]HT-1, moist-heated in an autoclave at 120 °C for 1 h; HT-2, dry-heated in an air-draft oven at 120 °C for 1 h. [c]SEM, standard error of mean. [d]$MCP_{FOM}$, MCP synthesized in the rumen based on available energy; $MCP_{DVE}$, MCP synthesized in the rumen based on rumen-degraded crude protein; $AMCP_{DVE}$, truly absorbable rumen-synthesized MCP in the small intestine. [e]$ECP_{DVE}$, endogenous protein losses in the digestive tract. [f]$RUP_{DVE}$, ruminally undegraded feed protein calculated according to the DVE/OEB model; $ARUP_{DVE}$, truly absorbable rumen-undegraded feed protein in the small intestine. [g]DVE, truly absorbable protein in the small intestine contributed by $RUP_{DVE}$, $MCP_{FOM}$, and a correction for ENDP. [h]$DPB_{DVE}$, reflects the difference between the potential MCP synthesis based on rumen-degraded feed crude protein and that based on energy (FOM) available for microbial fermentation in the rumen. $FMV^{NRC}$, feed milk value. The efficiency of use of the metabolizable protein for lactation is assumed to be 0.67,[19] and the protein content of milk is assumed to be 33 g/kg milk.

**Table 3. Dry and Moist Heat Induced Changes in Protein Supply to Dairy Cattle from Camelina Seeds: Estimated by PDI System[a]**

| | | heat treatments (HT)[b] | | | | contrast |
|---|---|---|---|---|---|---|
| item (g/kg DM) | Control | HT-1 | HT-2 | SEM[c] | *P* value | control vs HT |
| Absorbable Microbial Protein Synthesis in the Rumen[d] | | | | | | |
| $MCP_{ME}$ | 40.49a | 33.43c | 37.61b | 0.519 | 0.005 | 0.003 |
| $MCP_{RDP}$ | 117.26a | 92.04c | 100.55b | 1.432 | 0.002 | 0.001 |
| $AMCP_{PDI}$ | 35.41a | 27.44c | 32.14b | 0.480 | 0.003 | 0.002 |
| Truly Absorbable Rumen-Undegraded Protein in Small Intestine[e] | | | | | | |
| $RUP_{PDI}$ | 65.89c | 111.88a | 88.21b | 1.599 | 0.001 | 0.000 |
| $ARUP_{PDI}$ | 37.11b | 87.29a | 51.64ab | 3.352 | 0.002 | 0.003 |
| Degraded Protein Balance[f] | | | | | | |
| PDIN ($ARUP_{PDI}$ + $MCP_{RDP}$) | 138.46b | 170.11a | 140.55ab | 2.451 | 0.004 | 0.009 |
| PDIE ($ARUP_{PDI}$ + $MCP_{ME}$) | 77.45b | 121.63a | 88.49ab | 7.365 | 0.098 | 0.232 |
| $DPB_{PDI}$ (PDIN − PDIE) | 61.55a | 48.48c | 52.06b | 1.694 | 0.006 | 0.005 |
| $FMV_{PDI}$ | 2.26c | 3.03a | 2.66b | 0.060 | 0.001 | 0.001 |

[a]Means within a row with different letters differ at the $P < 0.05$ level. [b]HT-1, moist-heated in an autoclave at 120 °C for 1 h; HT-2, dry-heated in an air-draft oven at 120 °C for 1 h. [c]SEM, standard error of mean. [d]$MCP_{ME}$, amount of MCP that could be synthesized from the available energy in the rumen, when degraded nitrogen (N) is not limiting; $MCP_{RDP}$, amount of MCP that could be synthesized in the rumen from the degraded dietary N when energy is not limiting; $AMCP_{PDI}$, truly absorbable rumen-synthesized MCP in the small intestine. [e]$RUP_{PDI}$, ruminally undegraded feed protein; $ARUP_{PDI}$, truly absorbable ruminally undegraded feed protein. [f]PDIN, digestible proteins in the small intestine where N is the limiting factor for rumen microbial activity; PDIE, digestible proteins in the small intestine where energy is the limiting factor for rumen microbial activity; $DPB_{PDI}$, the difference between MCP synthesis based on rumen-degraded feed crude protein and that based on energy from anaerobic fermentation in the rumen. The efficiency of use of the metabolizable protein for lactation is assumed to be 0.67,[19] and the protein content of milk is assumed to be 33 g/kg milk.

The contents of ARUP did not differ significantly among the three evaluation systems. The MP content obtained with the NRC-2001 model was higher ($P < 0.05$; 152.97 vs 84.33) than that of the DVE/OEB system. The DPB was different ($P < 0.01$) among the three evaluation systems, and the highest ($P < 0.05$) value was obtained with the DVE/OEB system. The PDI system had a higher ($P < 0.05$) DPB value than did the NRC-2001 model. The FMV of camelina seeds differed among the three protein evaluation systems, and the highest ($P < 0.05$) value was recorded for the NRC-2001 model, followed by the PDI and DVE/OEB systems, respectively.

**Using Protein Molecular Structural Spectra to Predict the Estimated Protein Supply to Dairy Cattle.** The multiple-regression equations in Table 5 show that the protein secondary structure ($\alpha$-helix height) can be used to predict $ECP_{NRC}$ ($R^2$ = 0.73), $AECP_{NRC}$ ($R^2$ = 0.75), $ARUP_{NRC}$ ($R^2$ = 0.84),


dx.doi.org/10.1021/jf5013049 | J. Agric. Food Chem. 2014, 62, 8263−8273

**Table 4. Comparison of the NRC-2001 Model, DVE/OEB System, and PDI System in the Prediction of Metabolizable Protein Supply to Dairy Cattle from Camelina Seeds**

| item (g/kg DM) | mean[a] | | | SEM[b] | *P* value |
|---|---|---|---|---|---|
| | NRC-2001 | DVE/OEB | PDI | | |
| Microbial Protein Supply Based on Available Energy[c] | | | | | |
| $MCP_{TDN}$ vs $MCP_{FOM}$ vs $MCP_{ME}$ | 149.40a | 59.51b | 37.32c | 0.691 | <0.001 |
| Microbial Protein Supply Based on Ruminally Degraded Feed Protein[d] | | | | | |
| $MCP_{NRC}$ vs $MCP_{DVE}$ vs $MCP_{RDP}$ | 135.49b | 158.03a | 143.62ab | 4.880 | 0.004 |
| Truly Absorbable Rumen-Synthesized Microbial Protein[e] | | | | | |
| $AMCP_{NRC}$ vs $AMCP_{DVE}$ vs $AMCP_{PDI}$ | 95.62a | 37.94b | 31.63c | 0.680 | <0.001 |
| Truly Absorbable Rumen-Undegraded Protein[f] | | | | | |
| $ARUP_{NRC}$ vs $ARUP_{DVE}$ vs $ARUP_{PDI}$ | 52.86 | 56.68 | 58.68 | 6.453 | 0.833 |
| Endogenous Protein[g] | | | | | |
| $AECP_{NRC}$ vs $ECP_{DVE}$ | 4.47b | 12.38a | ND | 0.298 | 0.038 |
| Total Truly Metabolizable Protein[h] | | | | | |
| $MP_{NRC}$ vs $MP_{DVE}$ | 152.97a | 84.33b | ND | 5.635 | 0.016 |
| Compared Degraded Protein Balance[I] | | | | | |
| $DPB_{NRC}$ vs $DPB_{DVE}$ vs $DPB_{PDI}$ | 18.49c | 98.10a | 54.72b | 4.547 | 0.001 |
| Feed Milk Value[j] | | | | | |
| $FMV_{NRC}$ vs $FMV_{DEV}$ vs $FMV_{PDI}$ | 3.38a | 1.86c | 2.65b | 0.104 | 0.006 |

[a]Means within a row with different letters differ at the $P < 0.05$ level. ND, not defined. [b]SEM, standard error of mean. [c]$MCP_{TDN}$, MCP synthesized in the rumen based on available TDN (energy); $MCP_{FOM}$, MCP synthesized in the rumen based on available fermentable organic matter (energy); $MCP_{ME}$, MCP that could be synthesized from the fermentable organic matter (energy) when degraded nitrogen (N) is not limiting. [d]$MCP_{RDP}$, $MCP_{RDP}$, and $MCP_{RDP}$ are the contents of MCP that could be synthesized in the rumen from the degraded dietary protien. [e]$AMCP_{NRC}$, $AMCP_{DVE}$, and $AMCP_{PDI}$ are the truly absorbable rumen-synthesized MCPs in the small intestine. [f]$ARUP_{NRC}$, $ARUP_{DVE}$, and $ARUP_{PDI}$ are truly absorbable rumen-undegraded feed proteins in the small intestine [g]AECP, truly absorbable endogenous protein in the small intestine; $ECP_{DVE}$, endogenous protein losses in the digestive tract. [h]MP, truly metabolizable protein, contributed by $ARUP_{NRC}$, $AMCP_{NRC}$, and AECP; DVE, truly absorbable protein in the small intestine contributed by $RUP_{DVE}$, $MCP_{FOM}$, and a correction for $ECP_{DVE}$. [I]$DPB_{NRC}$ reflects the difference between the potential MCP synthesis based on ruminally degraded feed protein and that based on TDN-energy available for microbial fermentation in the rumen; $DPB_{DVE}$ and $DPB_{PDI}$ reflect the difference between the potential MCP synthesis based on rumen-degraded feed crude protein and that based on available energy from fermentable organic matter. [j]$FMV_{NRC}$, $FMV_{DEV}$, and $FMV_{PDI}$ represent feed milk value. The efficiency of use of the metabolizable protein for lactation is assumed to be 0.67,[19] and the protein content of milk is assumed to be 33 g/kg milk.

**Table 5. Regression Equations To Predict the NRC-2001 Model Estimated Protein Supply to Dairy Cattle from Protein Structural Characteristics Data[a]**

| predicted variable (*Y*, g/kg DM) | prediction equations | $R^2$ | RSD[b] | *P* value |
|---|---|---|---|---|
| Absorbable Microbial Protein Synthesis in the Rumen[c] | | | | |
| $MCP_{TDN}$ | No variables met the 0.05 significance level for entry into the model | | | |
| $MCP_{RDP}$ | $Y = -135.73 + 2018.59 \times \alpha$-helix + 63.87 × ratio of amide I to II area | 0.980 | 29.21 | 0.012 |
| $AMCP_{NRC}$ | No variables met the 0.05 significance level for entry into the model | | | |
| Absorbable Endogenous True Protein in the Small Intestine[d] | | | | |
| $ECP_{NRC}$ | $Y = 8.78 + 37.30 \times \alpha$-helix | 0.729 | 10.75 | 0.031 |
| $AECP_{NRC}$ | $Y = 3.51 + 15.01 \times \alpha$-helix | 0.747 | 11.79 | 0.027 |
| Truly Absorbable Rumen-Undegraded Protein in Small Intestine[e] | | | | |
| $RUP_{NRC}$ | No variables met the 0.05 significance level for entry into the model | | | |
| $ARUP_{NRC}$ | $Y = 183.22 - 2118.34 \times \alpha$-helix | 0.842 | 21.37 | 0.010 |
| Total Metabolizable Protein[f] | | | | |
| $MP_{NRC}$ | $Y = 286.05 - 2160.00 \times \alpha$-helix | 0.798 | 16.87 | 0.015 |
| Degraded Protein Balance[g] | | | | |
| $DPB_{NRC}$ | $Y = -308.72 + 2330.49 \times \alpha$-helix + 65.22 × ratio of amide I to II area | 0.989 | 38.71 | 0.008 |
| Feed Milk Value[h] | | | | |
| $FMV_{NRC}$ | $Y = 6.31 - 47.57 \times \alpha$-helix | 0.808 | 16.81 | 0.015 |

[a]Protein molecular structural characteristics measured with FT/IR-ATR molecular spectroscopy: amide I area and amide II area intensity with the baseline at about 1,715−1,485 $cm^{-1}$, $\alpha$-helix height centered at about 1,653 $cm^{-1}$, and $\beta$-sheet centered at about 1,630 $cm^{-1}$. [b]RSD, residual standard deviation. [c]$MCP_{TDN}$, MCP synthesized in the rumen based on available energy; $MCP_{RDP}$, MCP synthesized in the rumen based on available protein, calculated as 0.85 of rumen-degraded protein; $AMCP_{NRC}$, truly absorbable rumen-synthesized MCP in the small intestine. [d]$ECP_{NRC}$, rumen endogenous protein; $AECP_{NRC}$, truly absorbable endogenous protein in the small intestine. [e]$RUP_{NRC}$, ruminally undegraded protein calculated according to the NRC-2001 dairy model; $ARUP_{NRC}$, truly absorbable rumen-undegraded feed protein in the small intestine. [f]$MP_{NRC}$, truly metabolizable protein obtained from $ARUP_{NRC}$, $AMCP_{NRC}$, and AECP. [g]$DPB_{NRC}$ reflects the difference between the potential MCP synthesis based on ruminally degraded feed crude protein and that based on energy (TDN) available for microbial fermentation in the rumen. [h]$FMV_{NRC}$, feed milk value, the efficiency of use of the metabolizable protein for lactation is assumed to be 0.67,[19] and the protein content of milk is assumed to be 33 g/kg milk.

**Table 6. Regression Equations To Predict the DVE/OEB Model Estimated Protein Supply to Dairy Cattle from Protein Structural Characteristics Data[a]**

| predicted variable ($Y$) | prediction equations | $R^2$ | RSD[b] | $P$ value |
|---|---|---|---|---|
| Absorbable Microbial Protein Synthesis in the Rumen[c] | | | | |
| $MCP_{FOM}$ | $Y = 40.45 + 391.52 \times \alpha$-helix | 0.743 | 11.55 | 0.027 |
| $MCP_{RDP}$ | $Y = -190.09 + 2519.17 \times \alpha$-helix + 80.44 × ratio of amide I to II area | 0.983 | 35.58 | 0.009 |
| $AMCP_{DVE}$ | $Y = 25.80 + 249.38 \times \alpha$-helix | 0.742 | 11.47 | 0.028 |
| Absorbable Endogenous True Protein in the Small Intestine[d] | | | | |
| $ECP_{DVE}$ | $Y = -4.72 + 5.73 \times \alpha$-helix | 0.858 | 24.16 | 0.008 |
| Truly Absorbable Rumen-Undegraded Protein in Small Intestine[e] | | | | |
| $RUP_{DVE}$ | No variables met the 0.05 significance level for entry into the model | | | |
| $ARUP_{DVE}$ | $Y = 203.38 - 2351.50 \times \alpha$-helix | 0.842 | 21.37 | 0.010 |
| Total Metabolizable Protein[f] | | | | |
| $MP_{DVE}$ | $Y = 213.43 - 2003.93 \times \alpha$-helix | 0.830 | 19.58 | 0.012 |
| Degraded Protein Balance[g] | | | | |
| $DPB_{DVE}$ | $Y = 12.29 + 18.29 \times \alpha$-helix | 0.967 | 16.19 | 0.028 |
| Feed Milk Value[h] | | | | |
| $FMV_{DVE}$ | $Y = 4.74 - 44.65 \times \alpha$-helix | 0.808 | 19.57 | 0.012 |

[a]Protein molecular structural characteristics measured with FT/IR-ATR molecular spectroscopy: amide I area and amide II area intensity with the baseline at about 1,715−1,485 $cm^{-1}$, $\alpha$-helix height centered at about 1,653 $cm^{-1}$, and $\beta$-sheet centered at about 1,630 $cm^{-1}$. [b]RSD, residual standard deviation. [c]$MCP_{FOM}$, MCP synthesized in the rumen based on available energy; $MCP_{RDP}$, MCP synthesized in the rumen based on rumen-degraded protein; $AMCP_{DVE}$, truly absorbable rumen-synthesized MCP in the small intestine. [d]$ECP_{DVE}$, endogenous protein losses in the digestive tract. [e]$RUP_{DVE}$, ruminally undegraded feed protein calculated according to the DVE/OEB model; $ARUP_{DVE}$, truly absorbable rumen-undegraded feed protein in the small intestine. [f]$MP_{DVE}$, truly absorbable protein in the small intestine contributed by $RUP_{DVE}$, $MCP_{FOM}$, and a correction for ENDP. [g]$DPB_{DVE}$ reflects the difference between the potential MCP synthesis based on rumen-degraded feed crude protein and that based on energy (FOM) available for microbial fermentation in the rumen. [h]$FMV_{DVE}$, feed milk value, the efficiency of use of the metabolizable protein for lactation is assumed to be 0.67,[19] and the protein content of milk is assumed to be 33 g/kg milk.

$MP_{NRC}$ ($R^2$ = 0.80), and $FMV_{NRC}$ ($R^2$ = 0.81) with high accuracy. Similarly, the $\alpha$-helix height and the ratio of amide I to amide II area can be used to predict $MCP_{RDP}$ ($R^2$ = 0.98) and $DPB_{NRC}$ ($R^2$ = 0.99). However, no protein molecular peak intensities were left in the model to predict $MCP_{TDN}$, $AMCP_{NRC}$, and $RUP_{NRC}$.

The regression equations and their predictive power for the estimation of the protein nutrient supply and FMV obtained with the DVE/OEB system from protein molecular spectral characteristics are shown in Table 6. These equations demonstrated that the data on $\alpha$-helix height can be used to predict the supply of $MCP_{FOM}$ ($R^2$ = 0.74), $AMCP_{DVE}$ ($R^2$ = 0.74), $ECP_{DVE}$ ($R^2$ = 0.86), $ARUP_{DVE}$ ($R^2$ = 0.84), $MP_{DVE}$ ($R^2$ = 0.83), $DPB_{DVE}$ ($R^2$ = 0.97), and $FMV_{DVE}$ ($R^2$ = 0.81) with high accuracy. The $\alpha$-helix height and the ratio of amide I to amide II area provided a high prediction power for $MCP_{RDP}$ ($R^2$ = 0.98).

Equations in Table 7 show that the $\alpha$-helix height can be used to predict $ARUP_{PDI}$ ($R^2$ = 0.84), PDIA ($R^2$ = 0.70), and PDIE ($R^2$ = 0.87) with high accuracy. The amide I area can be used to predict $DPB_{PDI}$ ($R^2$ = 0.70), and the $\alpha$-helix height and the ratio of amide I to amide II area can be used to predict $MCP_{RDP}$ ($R^2$ = 0.98) and $AMCP_{PDI}$ ($R^2$ = 0.97). No protein spectral bands were left in the model to predict the supply of $MCP_{ME}$, $RUP^{PDI}$, or $FMV^{PDI}$.

## DISCUSSION

An accurate measurement of the feed protein degradation and MCP synthesis in the rumen and the intestinal digestibility of feed undegraded and MCP is required to optimize the efficiency of oilseed-derived protein utilization in dairy cattle, reduce feed costs, and reduce $NH_3$−N losses to the environment.[14,15] With the recent advances in the understating of protein metabolism in ruminants, various protein evaluation systems have been developed, which estimate the MP supply to dairy cattle from feeds. This study provides the first data set on the MP supply to dairy cattle from raw and heat-treated camelina seeds by employing and comparing three different protein evaluation systems. This study also provides information on the relationship between the protein molecular structural characteristics and the estimated MP supply to dairy cattle. This information will strengthen the current knowledge on the evaluation of feed protein nutritive value for dairy cattle and can also be used as an alternative tool for the rapid assessment of protein nutritive value.

**Heat-Induced Changes in the Metabolic Characteristics of Protein in Camelina Seeds.** The protein evaluation models estimated that both dry and moist heating (1 h at 120 °C) of camelina seeds increased the content of MP and improved the FMV. A similar increase in the supply of MP, estimated from the data obtained with in situ and mobile nylon techniques, from the toasting of whole-fat rapeseed[31] and lupine seeds[32] was reported earlier. The increase in MP supply with thermal processing was predominantly caused by the substantial increase in the supply of digestible RUP. This shift in protein degradation from the rumen to the small intestine of dairy cattle could be related to heat-induced changes in protein molecular structures and secondary chemical reactions, such as the Maillard reaction, between protein molecules and other compounds.[3,16] These structural and chemical changes decrease the protein degradation in the rumen by decreasing the protein solubility[3,17,18] and the access of microbes and proteolytic enzymes to protein molecules.[33−35] The improvement in MP supply was much higher with moist heating (>36%) than it was with dry heating (~11%). This could be related to a larger decrease in protein degradation in the rumen and an increase in the intestinal digestibility of the RUP with the moist heating of oilseeds compared to dry heating.[3,17] It is pertinent to mention that the validation of in situ-derived ruminal degradation data and the estimated MP content with in vivo results has been limited. However, several in vivo studies have shown a lower range in the RUP supply to the small intestine between raw and thermal processed protein feeds than in the large differences estimated by

**Table 7. Regression Equations To Predict the PDI Model Estimated Protein Supply to Dairy Cattle from Protein Structural Characteristics Data[a]**

| predicted variable ($Y$) | prediction equations | $R^2$ | RSD[b] | $P$ value |
|---|---|---|---|---|
| Absorbable Microbial Protein Synthesis in the Rumen[c] | | | | |
| $MCP_{ME}$ | No variables met the 0.05 significance level for entry into the model | | | |
| $MCP_{RDP}$ | $Y = -109.36 + 1450.18 \times \alpha$-helix + 46.30 × ratio of amide I to II area | 0.983 | 35.38 | 0.010 |
| $AMCP_{PDI}$ | $Y = -28.19 + 436.27 \times \alpha$-helix + 13.37 × ratio of amide I to II area | 0.967 | 16.19 | 0.028 |
| Truly Absorbable Rumen-Undegraded Protein in Small Intestine[d] | | | | |
| $RUP_{PDI}$ | No variables met the 0.05 significance level for entry into the model | | | |
| $ARUP_{PDI}$ | $Y = 203.37 - 2351.18 \times \alpha$-helix | 0.842 | 21.35 | 0.010 |
| Degraded Protein Balance[e] | | | | |
| PDIN ($ARUP_{PDI}$ + $MCP_{RDP}$) | $Y = 253.01 - 1595.17 \times \alpha$-helix | 0.696 | 9.17 | 0.039 |
| PDIE ($ARUP_{PDI}$ + $MCP_{ME}$) | $Y = 237.05 - 2259.33 \times \alpha$-helix | 0.865 | 25.59 | 0.007 |
| $DPB^{PDI}$ (PDIN−PDIE) | $Y = -2.05 + 12.00 \times$ amid I area | 0.704 | 9.52 | 0.037 |
| Feed Milk Value[f] | | | | |
| $FMV_{PDI}$ | No variables met the 0.05 significance level for entry into the model | | | |

[a]Protein molecular structural characteristics measured with FT/IR-ATR molecular spectroscopy: amide I area and amide II area intensity with the baseline at about 1,715−1,485 $cm^{-1}$, $\alpha$-helix height centered at about 1,653 $cm^{-1}$, and $\beta$-sheet centered at about 1,630 $cm^{-1}$. [b]RSD, residual standard deviation. [c]$MCP_{ME}$, amount of MCP that could be synthesized from the available energy in the rumen when degraded N is not limiting; $MCP_{RDP}$, the amount of MCP that could be synthesized in the rumen from the degraded dietary N when energy is not limiting; MPS, truly absorbed rumen-synthesized MCP in the small intestine. [d]$RUP_{PDI}$, ruminally undegraded feed crude protein; $ARUP_{PDI}$, truly absorbable ruminally undegraded feed protein. [e]PDIN, digestible proteins in the small intestine where N is the limiting factor for rumen microbial activity; PDIE, digestible proteins in the small intestine where energy is the limiting factor for rumen microbial activity; $DPB_{PDI}$, the balance between MCP synthesis based on rumen-degraded feed crude protein and that based on energy from anaerobic fermentation in the rumen. [f]$FMV_{PDI}$, feed milk value, the efficiency of use of the metabolizable protein for lactation is assumed to be 0.67,[19] and the protein content of milk is assumed to be 33 g/kg milk.

the in situ method, which could be related to the over estimation of RUP by the in situ method.[36]

The NRC-2001 model showed that heat processing caused a small increase (<3 g/kg DM), and the DVE/OEB and PDI systems showed that heat processing caused a small decrease (<8 g/kg DM) in the contents of truly absorbed MCP synthesis in the rumen. This discrepancy among the models is due to the energy inputs that these models use for the estimation of MCP synthesis. In the NRC-2001 model, the MCP synthesis is based on the energy extracted from the TDN, hence the increase in fat availability with heating[3] increased the TDN content and the estimated microbial biomass production from TDN. While in the DVE/OEB and PDI systems, the MCP syntheses are based on the FOM (FOM = DOM − fat − RUP), and the increase in fat and RUP contents[3] with heating would synergistically decrease the contents of FOM and the estimated MCP synthesis from FOM.

The DPB shows the difference between MCP syntheses that are potentially possible from the available RDP and those potentially possible from the energy extracted from anaerobic fermentation in the rumen. A positive DPB value indicates $NH_3$ (N) loss from the rumen, and a negative DPB value indicates a shortage of N in the rumen, which can impair MCP synthesis. The optimum DPB value for a dairy ration is, therefore, zero or slightly above.[21] The three protein evaluation models showed high positive values (>36 g/kg DM) of DBP for raw camelina seeds. In agreement with our findings, high DPB values have been reported for full fat oilseeds such as rapeseeds and lupine seeds.[31,32] The high DPB values and N loss in the rumen could be related to the high contents of rapidly degradable soluble protein (523.7 g/kg CP) and the extensive degradation of protein (754.5 g/kg CP) in the raw camelina seeds. The decrease in DPB values with heating, particularly with moist heating, improved feed protein utilization in the rumen, and the DPB values of the heated camelina seeds were still positive. The decrease in DPB values with heat processing could be related to the subsequent decrease in the soluble protein content and overall protein degradation in the rumen.

**Comparison of the Three Protein Evaluation Models in Predicting Protein Nutrient Supply to Dairy Cattle from Camelina Seeds.** The three models selected in the present study are prevalently used in the feed industry and in scientific research work in North America and Europe. The basic framework and principles of these protein evaluation systems are similar; however, some concepts and factors used to compute the MP contents of feedstuffs are different. Each evaluation system has its strengths and weaknesses for different types of feed ingredients.[33,34] For example, the three models adopted a similar concept of predicting MCP synthesis from the potentially available energy supply to the rumen; however, the three models differ in their sources of available energy, and they use different conversion factors in the calculations. The NRC-2001 model uses the available TDN as the energy source, whereas the DVE/OEB and PDI systems use the rumen FOM as the energy source. The FOM does not include fat as an energy source, while TDN does. For forages and other low fat containing feeds, the differences in the available energy and the MCP syntheses from FOM and TDN were not large.[35,37,38] However, our results showed that for high fat (381.7 g/kg DM) containing camelina seeds, the difference in energy inputs (TDN vs FOM) caused a substantial difference in the predicted energy supply to the rumen and MCP synthesis. In the present study, $MCP_{TDN}$ was markedly higher than were $MCP_{FOM}$ (>89 g/kg DM; 60%) and $MCP_{ME}$ (>112 g/kg DM; 75%). With the recent advances in fat metabolism in the rumen and on the basis of previous recommendations of other studies,[38] the concept of energy inputs adopted by the three models needs to be further standardized for different feed types. The RUP does not provide energy for MCP synthesis, which is taken into account by the DVE/OEB and PDI systems. However, the TDN used for MCP synthesis in the NRC-2001 model needs to be corrected for this RUP content. Fermented protein provides much less energy to rumen microbes than do

carbohydrates, but all of the protein evaluation systems ignore this concept.[39] The three systems assume a constant value for the efficiency of MCP synthesis and do not account for the decrease in digestibility with an increase in the feeding level, which may lead to an overestimation of MCP with increased feed intake. Secondly, the constants used by the three models are different. The NRC-2001 model assumes that 130 g of MCP is synthesized from 1 kg of energy substrate (TDN); the DVE/OEB system assumes that 150 g of MCP is synthesized from 1 kg of energy substrate (FOM); and the PDI system assumes that 145 g of MCP is synthesized from 1 kg of energy substrate (FOM). The three models use different conversion factors to compute the digestibility and amino acid N contents of the rumen-synthesized MCP. The DVE/OEB system assumes that the digestibility of MCP is 85% and that 75% of the MCP is presented in the form of amino acids. In the NRC-2001 and PDI models, the digestibility and amino acid N contents of MCP are assumed to be 80%, each. However, the combined value of these conversion factors (0.64; 0.85 × 0.75 vs 0.80 × 0.80) for the estimation of truly absorbable MCP is more or less similar.

The three models calculated the contents of truly absorbable RUP as the product of the RUP and the intestinal digestibility of RUP; however, the estimation of the RUP differs among the three models. The PDI and DVE/OEB systems use a coefficient of 1.11 to correct the in situ degradation data on in vivo results, whereas in the NRC-2001 model, no correction factor is used. On the basis of these differences, the content of truly absorbable RUP was 11% higher in the PDI and DVE/OEB systems than it was in the NRC-2001 model. However, these calculations only caused numerical differences among the contents of the truly absorbable RUP predicted by the three models. Our results are in agreement with literature values.[40]

In the three models, the protein degradation characteristics were determined by the in situ method, which contains several inherent limitations.[40] These limitations include the assumption that proteins in the soluble-fraction are completely degraded in the rumen; however, recent studies[41,42] have shown that dietary CP can escape from the rumen as nonammonia and nonmicrobial N. Moreover, small feed particles can escape the bags without being degraded. On the other hand, the physical restriction of feeds within the nylon bag and microbial contamination of the undigested residues can results in the under estimation of CP degradability. The model used for the estimation of the rumen degradation parameter assumes that the particles escaping the system are independent of factors such as particle size, specific gravity, and body size. In vivo studies, however, clearly showed a selective retention of forage particles in the rumen.[39] For concentrates, such as the camelina seed, with smaller particle sizes, the differences in retention time may not be very large.

The three systems differ in the concepts and calculations of the ECP. In the NRC-2001 model, the ECP (digestive enzymes, desquamated rumen epithelial cells, bile, and mucus) excretion in the gastrointestinal tract is considered as a contribution to the total MP, and its value is added to the requirements rather than subtracted from the supply. In contrast, in the DVE/OEB system, the ECPs are subtracted from the total truly MP. Although the ECP originates from the animal, the DVE/OEB system assumes that these losses are more related to the characteristics of the feed than to the animal. Moreover, the calculations of ECP also differ between the DVE/OEB and NRC-2001 models. The DVE/OEB system assumes that with the excretion of 1 kg of UDM, 75 g of truly absorbed $ECP_{DVE}$ is lost; therefore, the total truly absorbable MP is corrected ($ECP_{DVE}$ = 0.075 × UDM) for the endogenous losses, whereas the NRC-2001 model assumes that with the intake of 1 kg of DM, 4.75 g of truly absorbable ECP is added to the total truly MP supply. In our study, the $ECP_{DVE}$ content predicted by the DVE/OEB system was over two times higher than that obtained with the NRC-2001 model (12.38 g/kg DM vs 4.47 g/kg DM). Our results are in line with those of Yu et al.[40] Nevertheless, this was in contrast with the findings of Theodoridou and Yu[40] and Yu et al.[38] who reported higher values of $AECP_{NRC}$ than $ECP_{DVE}$. The discrepancy among these studies could be attributed to the intrinsic differences in the digestibility of the different feed types. Because no ECP excretion or losses are available for the PDI system, no comparison could be made with the NRC-2001 and DVE/OEB models. Consequently, no total truly MP was estimated for the PDI system.

The three models use different efficiencies for MCP synthesis based on the RDP. The NRC-2001 model assumes that the turnover efficiency of RDP into MCP is 85%.[19] The DVE/OEB system[21] assumes that 100% of the RDP could be potentially converted into MCP if enough energy is provided, whereas, the PDI system[22] assumes that 90% of the RDP is converted into MCP. The lower values of MCP synthesized from RDP in the NRC-2001 model than in the DVE/OEB and PDI systems are consistent with earlier studies[41,43,44] and could be related to lower turnover efficiency.

The DPB represents the difference between MCP synthesis potentially possible from the available RDP and the MCP synthesis potentially possible from the available energy. The DPB value of of the NRC-2001 model (18.49 g/kg DM) was much lower than the values estimated by the DVE/OEB (98.10 g/kg DM) and PDI (54.72 g/kg DM) systems. As discussed earlier, these large differences in DPB values among the three systems mainly originated from differences in the energy inputs (TDN vs FOM) between these systems. Similarly, the high MP and FMV values predicted by the NRC-2001 model compared to those by the DVE/OEB and PDI systems were predominantly associated with the higher predicted MCP synthesis based on a higher energy input (TDN vs FOM). Our results are consistent with those of Theodoridou and Yu.[35]

**Relationship between Protein Molecular Structural Characteristics and Predicted Metabolizable Protein Supply to Dairy Cattle.** Recent research has demonstrated that rumen degradation and the intestinal digestibility of feed protein is strongly related to protein intrinsic molecular structures.[3,17,44] Moreover, if feeds contain similar protein and amino acid contents, their nutritive values may be different if their protein molecular structures are different.[3] In addition, the heat-induced changes in the inherent molecular structure of proteins alter its degradation in the rumen[16] by changing the protein solubility[3,17,18] and the access of microbes and proteolytic enzymes to protein molecules in the gastrointestinal tract of dairy cattle.[33−35] This study provides information on the relationship between the protein molecular structures and MP supply to dairy cattle as predicted by three different protein evaluation systems and may provide an approach for the prediction of the protein value of feeds.

The large variation in the nutritive value of protein feeds highlights the need for a rapid and accurate assay to determine the quality of individual feedstuff in terms of their MP content. The traditional wet chemical analysis in combination with in situ protein degradation data and the intestinal digestibility

of RUP can be modeled to estimate the truly MP content of feed protein.[15] However, these procedures are time-consuming and expensive and could not be applied for routine analysis. Alternatively, FT/IR-ATR molecular spectroscopy is a noninvasive and nondestructive technique that can rapidly analyze a large number of feed samples. Our results demonstrate that the spectral bands intensities, such as the $\alpha$-helix height and the ratio of amide I to amide II area, can be used to quantitatively estimate the protein supply to the small intestine of dairy cattle with good accuracy.

Our results showed that dry and moist heating of camelina seeds increased the content of truly absorbable RUP, total MP, and FMV and decreased the DPB in dairy cattle. However, moist-heated camelina seeds had a significantly higher ($P < 0.05$) content of truly absorbable RUP, total MP, and FMV and a significantly lower ($P < 0.05$) content of DPB than did the dry-heated camelina seeds. Because of difference in energy inputs (TDN vs FOM), the NRC-2001 model predicted a significantly higher energy supply to the rumen microbes, which resulted in significantly higher contents of the predicted MCP, total truly MP, and FMV and lower contents of DPB than those predicted by the DVE/OEB and PDI systems. The regression equations showed that the protein molecular structural bands intensities, such as the $\alpha$-helix height and the ratio of amide I to amide II area, can be used to quantitatively estimate the contents of truly absorbable RUP, total MP, DPB, and FMV with good accuracy ($R^2 > 0.70$).

## ■ ASSOCIATED CONTENT

### Supporting Information

Dry and moist heat-induced changes in in situ ruminal CP degradation kinetics of camelina seeds. Dry and moist heat-induced changes in the protein molecular spectral characteristics of of camelina seeds as revealed by FT/IR-ATR molecular spectroscopy. This material is available free of charge via the Internet at http://pubs.acs.org.

## ■ AUTHOR INFORMATION


### Corresponding Author

*Phone: +1 306 966 4132. Fax: + 1 306 966 4151. E-mail: Peiqiang.yu@usask.ca.

### Present Address

⊥N.A.K.: Department of Animal Nutrition, the University of Agriculture Peshawar, Pakistan.



### Funding

The research projects of the (Professor Dr. Peiqiang Yu) chair group were supported by grants from the Natural Sciences and Engineering Research Council of Canada (NSERC), SaskCanola, Saskatchewan Agricultural Development Fund (ADF), Ministry of Agriculture Strategic Research Chair Program, and Thousand-Talent-People Program in Tianjin. Quanhui Peng (Ph.D. student scholarship) was financially supported by the China Scholarship Council.


### Notes

The authors declare no competing financial interest.

## ■ ACKNOWLEDGMENTS


The authors wish to thank Zhiyuan Niu, research assistant in the Department of Animal and Poultry Science, University of Saskatchewan, for providing assistance with the chemical analyses. We thank Colleen Christensen at Feed Innovation Institute for the collection of samples.


## ■ REFERENCES


(1) Putnam, D. H.; Budin, J. T.; Field, L. A.; Breene, W. M. Camelina: A promising low-input oilseed. In *New Crops*; Janick, J., Simon, J. E., Eds.; Wiley Publishing: New York, 1993; pp 314−322.

(2) Kirkhus, B.; Lundon, A. R.; Haugen, J. E.; Vogt, G.; Borge, G. I. A.; Henriksen, B. I. F. Effects of environmental factors on edible oil quality of organically grown *Camelina sativa*. *J. Agric. Food Chem.* **2013**, *61*, 3179−3185.

(3) Peng, Q.; Khan, N. A.; Wang, Z.; Yu, P. Moist and dry heating-induced changes in protein molecular structure, protein subfractions, and nutrient profiles in camelina seeds. *J. Dairy Sci.* **2014**, *97*, 446−457.

(4) Peiretti, P. G.; Mussa, P. P.; Prola, L.; Meineri, G. Use of different levels of false flax (*Camelina sativa* L.) seed in diets for fattening rabbits. *Livest. Sci.* **2007**, *107*, 192−198.

(5) Moloney, A. P.; Kennedy, C.; Noci, F.; Monahan, F. J.; Kerry, J. P. Lipid and colour stability of M. longissimus muscle from lambs fed camelina or linseed as oil or seeds. *Meat Sci.* **2012**, *92*, 1−7.

(6) Zubr, J. Qualitative variation of *Camelina sativa* seed from different locations. *Ind. Crops Prod.* **2003**, *17*, 161−169.

(7) Halmemies-Beauchet-Filleau, A.; Kokkonen, T.; Lampi, A. M.; Toivonen, V.; Shingfield, K. J.; Vanhatalo, A. Effect of plant oils and camelina expeller on milk fatty acid composition in lactating cattle fed diets based on red clover silage. *J. Dairy Sci.* **2011**, *94*, 4413−4430.

(8) Szumacher-Strabel, M.; Cieślak, A.; Zmora, P.; Pers-Kamczyc, E.; Bielińska, S.; Stanisz, M.; Wójtowski, J. *Camelina sativa* cake improved unsaturated fatty acids in ewe's milk. *J. Sci. Food Agric.* **2011**, *91*, 2031−2037.

(9) Cappellozza, B. I.; Cooke, R. F.; Bohnert, D. W.; Cherian, G.; Carroll, J. A. Effects of camelina meal supplementation on ruminal forage degradability, performance, and physiological responses of beef cattle. *J. Anim. Sci.* **2012**, *90*, 4042−4054.

(10) Ni Eidhin, D.; Burke, J.; Lynch, B.; O'Beirne, D. Effects of dietary supplementation with camelina oil on porcine blood lipids. *J. Food Sci.* **2003**, *68*, 671−679.

(11) Kakani, R.; Fowler, J.; Haq, A. U.; Murphy, E. J.; Rosenberger, T. A.; Berhow, M.; Bailey, C. A. Camelina meal increases egg n-3 fatty acid content without altering quality or production in laying hens. *Lipids* **2012**, *47*, 519−526.

(12) Morais, S.; Edvardsen, R. B.; Tocher, D. R.; Bell, J. G. Transcriptomic analyses of intestinal gene expression of juvenile Atlantic cod (*Gadus morhua*) fed diets with camelina oil as replacement for fish oil. *Comp. Biochem. Physiol., Part B: Biochem. Mol. Biol.* **2012**, *161*, 283−293.

(13) Salin, S.; Taponen, J.; Elo, K.; Simpura, I.; Vanhatalo, A.; Boston, R.; Kokkonen, T. Effects of abomasal infusion of tallow or camelina oil on responses to glucose and insulin in dairy cattle during late pregnancy. *J. Dairy Sci.* **2012**, *95*, 3812−3825.

(14) Habib, G.; Khan, N. A.; Ali, M.; Bezabih, M. In situ ruminal crude protein degradability of by-products from cereals, oilseeds, and animal origin. *Livest. Sci.* **2013**, *153*, 81−87.

(15) Van Duinkerken, G.; Blok, M. C.; Bannink, A.; Cone, J. W.; Dijkstra, J.; Van Vuuren, A. M.; Tamminga, S. Update of the Dutch protein evaluation system for ruminants: The DVE/$OEB_{2010}$ system. *J. Agric. Sci.* **2011**, *149*, 351−367.

(16) Yu, P. Protein molecular structures, protein subfractions, and protein availability affected by heat processing: A review. *Am. J. Biochem. Biotechnol.* **2007**, *3*, 70−90.

(17) Khan, N. A.; Peng, Q.; Xin, H.; Yu, P. Vibrational spectroscopic investigation of heat-induced changes in functional groups related to protein structural conformation in camelina seeds and their relationship to digestion in dairy cows. *Anim. Prod. Sci.* **2014**, DOI: 10.1071/an14400.

(18) Samadi; Yu, P. Dry and moist heating-induced changes in protein molecular structure, protein subfraction, and nutrient profiles in soybeans. *J. Dairy Sci.* **2011**, *94*, 6092−6102.

(19) Peng, Q.; Khan, N. A.; Wanga, Z.; Yu, P. Relationship of feeds protein structural makeup in common prairie feeds with protein

solubility, in situ ruminal degradation, and intestinal digestibility. *Anim. Feed Sci. Technol.* **2014**, *194*, 58−70.
(20) National Research Council. *Nutrient Requirements of Dairy Cattle*, 7th rev. ed.; National Academic Press: Washington, DC, 2001.
(21) Tamminga, S.; Van Straalen, W. M.; Subnel, A. P. J.; Meijer, R. G. M.; Steg, A.; Wever, C. J. G.; Blok, M. C. The Dutch protein evaluation system: The DVE/OEB system. *Livest. Prod. Sci.* **1994**, *40*, 139−155.
(22) Verite, R.; Geay, T. Evaluation and implementation of the PDI system in France. In *Feed Evaluation and Protein Requirement Systems for Ruminants*, Jarrige, R., Alderman, G., Eds.; ECSC-EEC-EAEC: Brussels, Belgium, 1987; pp 249−261.
(23) *Guide to the Care and Use of Experimental Animals*, Vol. *1*, 2nd ed.; Canadian Council on Animal Care: Ottawa, ON, Canada, 1993.
(24) Yan, X.; Khan, N. A.; Zhang, F.; Yang, L.; Yu, P. Microwave irradiation induced changes in protein molecular structures of barley grains: Relationship to changes in protein chemical profile, protein subfractions, and digestion in dairy cows. *J. Agric. Food Chem.* **2014**, *62*, 6546−6555.
(25) Øskov, E. R.; McDonald, I. The estimation of protein degradability in the rumen from incubation measurements weighted according to rate of passage. *J. Agric. Sci.* **1979**, *92*, 499−503.
(26) Robinson, P. H.; Fadel, J. G.; Tamminga, S. Evaluation of mathematical models to describe neutral detergent residue in terms of its susceptibility to degradation in the rumen. *Anim. Feed Sci. Technol.* **1986**, *15*, 249−271.
(27) SAS Institute. *Statistical Analysis System*, version 9.3; SAS Institute Inc.: Cary, NC, 2009.
(28) Calsamiglia, S.; Stern, M. D. A three-step in vitro procedure for estimating intestinal digestion of protein in ruminants. *J. Anim. Sci.* **1995**, *73*, 1459−1465.
(29) CVB. Table ruminants. In *Chemical Composition and Nutritional Values of Feedstuffs and Feeding Standards*; Central Bureau for Livestock Feeding (CVB): The Hague, The Netherlands, 1996.
(30) INRA. *Ruminant Nutrition: Recommended Allowances and Feed Tables*; Jarrige, R., Ed.; John Libbey: London, U.K., 1989; p 389.
(31) Azarfar, A.; Ferreira, C. S.; Goelema, J. O.; Van Der Poel, A. F. B. Effects of pressure toasting on in situ degradability and intestinal protein and protein-free organic matter digestibility of rapeseed. *J. Sci. Food Agric.* **2008**, *88*, 1380−1384.
(32) Yu, P. Modeling nutrient supply to dairy cattle from a feedstuff using NRC-2001 (a TDN-based model) with inputs based on in situ and mobile bag technique measurements. *Can. J. Anim. Sci.* **2005**, *85*, 513−519.
(33) McAllister, T. A.; Phillippe, R. C.; Rode, L. M.; Cheng, K. J. Effect of the protein matrix on the digestion of cereal grains by ruminal microorganisms. *J. Anim. Sci.* **1993**, *71*, 205−212.
(34) Yu, P.; Nuez-Ortín, W. G. Relationship of protein molecular structure to metabolisable proteins in different types of dried distillers grains with solubles: A novel approach. *Br. J. Nutr.* **2010**, *104*, 1429−1437.
(35) Theodoridou, K.; Yu, P. Application potential of ATR-FT/IR molecular spectroscopy in animal nutrition: Revelation of protein molecular structures of canola meal and presscake, as affected by heat-processing methods, in relationship with their protein digestive behavior and utilization for dairy cattle. *J. Agric. Food Chem.* **2013**, *61*, 5449−5458.
(36) Huhtanen, P.; Hetta, M.; Swensson, C. Evaluation of canola meal as a protein supplement for dairy cows: A review and a meta-analysis. *Can. J. Anim. Sci.* **2011**, *91*, 529−543.
(37) Nuez-Ortín, W. G.; Yu, P. Using the NRC chemical summary and biological approaches to predict energy values of new co-product from bio-ethanol production for dairy cattle. *Anim. Feed Sci. Technol.* **2011**, *170*, 165−170.
(38) Yu, P.; Christensen, D. A.; McKinnon, J. J. Comparison of the National Research Council-2001 model with the Dutch system (DVE/OEB) in the prediction of nutrient supply to dairy cattle from forages. *J. Dairy Sci.* **2003**, *86*, 2178−2192.
(39) Huhtanen, P. Critical aspects of feed protein evaluation systems for ruminants. *J. Anim. Feed Sci.* **2005**, *14* (Suppl. 1), 145−170.
(40) Theodoridou, K.; Yu, P. Metabolic characteristics of the proteins in yellow-seeded and brown-seeded canola meal and presscake in dairy cattle: Comparison of three systems (PDI, DVE, NRC) in nutrient supply and feed milk value (FMV). *J. Agric. Food Chem.* **2013**, *61*, 2820−2830.
(41) Choi, C. W.; Ahvenjärvi, S.; Vanhatalo, A.; Toivonen, V.; Huhtanen, P. Uantification of the flow of soluble non-ammonia nitrogen entering the omasal canal of dairy cows fed grass silage based diets. *Anim. Feed Sci. Technol.* **2002**, *96*, 203−220.
(42) Volden, H.; Mydland, L. T.; Olaisen, V. Apparent ruminal degradation and rumen escape of soluble nitrogen fractions in grass and grass silage administered intraruminally to lactating dairy cows. *J. Anim. Sci.* **2002**, *80*, 2704−2716.
(43) Yu, P.; Meier, J. A.; Christensen, D. A.; Rossnagel, B. G.; McKinnon, J. J. Using the NRC-2001 model and the DVE/OEB system to evaluate nutritive values of Harrington (malting-type) and Valier (feed-type) barley for ruminants. *Anim. Feed Sci. Technol.* **2003**, *107*, 45−60.
(44) Khan, N. A.; Booker, H.; Yu, P. Molecular structures and metabolic characteristics of protein in brown and yellow flaxseed with altered nutrient traits. *J. Agric. Food Chem.* **2014**, *62*, 6556−6564.

JOURNAL OF AGRICULTURAL AND FOOD CHEMISTRY

Article

pubs.acs.org/JAFC

# Understanding the Role of Saliva in Aroma Release from Wine by Using Static and Dynamic Headspace Conditions

Carolina Muñoz-González,[†] Gilles Feron,[§] Elisabeth Guichard,[§] J. José Rodríguez-Bencomo,[†] Pedro J. Martín-Álvarez,[†] M. Victoria Moreno-Arribas,[†] and M. Ángeles Pozo-Bayón*[,†]

[†]Instituto de Investigación en Ciencias de la Alimentación (CIAL) (CSIC-UAM), C/Nicolás Cabrera 9, 28049 Madrid, Spain

[§]Centre des Sciences du Goût et de l'Alimentation, UMR1324 INRA, UMR6265 CNRS, Université de Bourgogne, Agrosup Dijon, F-21000 Dijon, France

Supporting Information

**ABSTRACT:** The aim of this work was to determine the role of saliva in wine aroma release by using static and dynamic headspace conditions. In the latter conditions, two different sampling points ($t$ = 0 and $t$ = 10 min) corresponding with oral (25.5 °C) and postoral phases (36 °C) were monitored. Both methodologies were applied to reconstituted dearomatized white and red wines with different nonvolatile wine matrix compositions and a synthetic wine (without matrix effect). All of the wines had the same ethanol concentration and were spiked with a mixture of 45 aroma compounds covering a wide range of physicochemical characteristics at typical wine concentrations. Two types of saliva (human and artificial) or control samples (water) were added to the wines. The adequacy of the two headspace methodologies for the purposes of the study (repeatability, linear ranges, determination coefficients, etc.) was previously determined. After application of different chemometric analysis (ANOVA, LSD, PCA), results showed a significant effect of saliva on aroma release dependent on saliva type (differences between artificial and human) and on wine matrix using static headspace conditions. Red wines were more affected than white and synthetic wines by saliva, specifically human saliva, which provoked a reduction in aroma release for most of the assayed aroma compounds independent of their chemical structure. The application of dynamic headspace conditions using a saliva bioreactor at the two different sampling points ($t$ = 0 and $t$ = 10 min) showed a lesser but significant effect of saliva than matrix composition and a high influence of temperature (oral and postoral phases) on aroma release.

**KEYWORDS:** *saliva, wine, aroma release, static HS-SPME-GC/MS, dynamic HS-SPME-GC/MS*

## INTRODUCTION

Aroma is one of the most outstanding aspects related to food preferences and choices, especially in the case of wine, in which consumption is mainly triggered by a hedonic motivation. Therefore, aroma represents a relevant aspect in wine research, and many interesting works have focused on the characterization of aroma impact compounds of different wine types.[1−3] However, the retronasal aroma profile of a food during consumption might better represent the aroma fraction involved in the interaction with the olfactory receptors than the orthonasal aroma profile; therefore, it should be more closely related with aroma perception.[4]

In the case of the consumption of liquid foods, such as wine, retronasal aroma is produced by the breathing airflow after swallowing, sweeping the aroma molecules retained in the oral or throat cavities traveling via the nasopharynx from the mouth or throat to the nose.[5−7] It has been shown that orthonasal (odor sense when smelling a food) and retronasal aroma perceptions can be different.[8−10] Different factors involved in the intraoral release of aroma compounds during consumption (saliva, interaction with mucosa, temperature, breathing flows, in-mouth air cavity volumes, change, etc.) seem to be related to these differences[7,11−15,16]

Saliva is a complex dilute aqueous solution; its composition varies depending on the respective physiological status, type of food consumed, oral hygiene, etc.[17] Saliva contains numerous inorganic salts (sodium, calcium, potassium, chloride, phosphate, and bicarbonate)[18] and organic components such as enzymes (amylase, lipases, proteases, etc.)[17,19,20] and proteins (mucins, proline rich proteins, histidine rich proteins, etc.).[21,22] Previous studies have shown that saliva might exert an important role in aroma release through different physicochemical (dilution of aroma due to the aqueous phase of saliva, changes in the pH of the food, hydration of the food, which favors aroma release, interaction with salts causing a salting-out effect, interaction with proteins), chemical (degradation of odorants), biochemical (degradation of odorant or release from aroma precursors), or even physiological effects (impact on velum−tongue seal formation and swallowing performance), which form part of many previous works performed on this topic.[19,20,23−25]

Nonetheless, many of the studies performed on the saliva effect on aroma release in simple and real food systems seem to be contradictory. Some studies have shown that saliva reduces aroma release, for example, in pectin gels,[26] bell peppers,[25] or French beans,[24] whereas others have shown an increase in volatiles released from model gels[27] or primary and multilayer oil/water emulsions.[28]There are also other works showing the

Received: February 25, 2014
Accepted: July 30, 2014
Published: July 30, 2014

 © 2014 American Chemical Society 

**Table 1. Chromatographic and Physicochemical Characteristics of the Volatile Compounds Employed in This Study**

| no. | compound | RI exp.[a] | RI lit.[b] | ion Q[c] (*m*/*z*) | MW[d] (g/mol) | log *P*[e] | BP[f] (°C) | descriptor[g] | CAS Registry No. | concn[h] (mg/L) |
|---|---|---|---|---|---|---|---|---|---|---|
| 1 | ethyl propanoate | <1000 | 950 | 57 | 102 | 1.2 | 99.1 | fruit | 105-37-3 | 0.61 |
| 2 | isobutyl acetate | 1018 | 1018 | 56 | 116 | 1.8 | 116.5 | fruit, apple, banana | 110-19-0 | 0.33 |
| 3 | α-pinene | 1030 | 1035 | 93 | 136 | 4.8 | 156.0 | pine, turpentine | 80-56-8 | 0.20 |
| 4 | ethyl butanoate | 1043 | 1040 | 71 | 116 | 1.9 | 121.5 | apple | 105-54-4 | 0.54 |
| 5 | ethyl 2-methylbutanoate | 1060 | 1056 | 57 | 130 | 2.3 | 133.0 | apple | 7452-79-1 | 0.29 |
| 6 | butyl acetate | 1079 | 1079 | 43 | 116 | 1.8 | 126.1 | pear | 123-84 | 0.35 |
| 7 | isobutanol | 1100 | 1103 | 74 | 74 | 0.8 | 108.0 | wine, solvent, bitter | 78-83-1 | 1.38 |
| 8 | β-pinene | 1120 | 1118 | 93 | 136 | 4.4 | 164.0 | pine, resin, turpentine | 127-91-3 | 0.25 |
| 9 | isoamyl acetate | 1131 | 1117 | 70 | 130 | 2.3 | 142.5 | banana | 123-92-2 | 0.69 |
| 10 | 1-butanol | 1154 | 1145 | 56 | 74 | 0.8 | 117.0 | medicine, fruit | 71-36-3 | 0.93 |
| 11 | limonene | 1217 | 1208 | 68 | 136 | 4.8 | 176.0 | lemon, orange, citrus | 5989-27-5 | 0.23 |
| 12 | isoamylic alcohols | 1217 | 1208 | 55 | 86 | 1.3 | 128.0 | wine, onion | 123-51-3 | 30.01 |
| 13 | ethyl hexanoate | 1247 | 1231 | 88 | 136 | 2.8 | 167.0 | apple peel, fruit | 123-66-0 | 0.89 |
| 14 | hexyl acetate | 1286 | 1276 | 56 | 144 | 2.8 | 171.5 | fruit, herb | 142-92-7 | 0.92 |
| 15 | 1-hexanol | 1364 | 1362 | 56 | 102 | 2.0 | 156.0 | resin, flower, green | 111-27-4 | 0.91 |
| 16 | *trans*-3-hexen-1-ol | 1376 | 1386 | 67 | 100 | 1.6 | 156.5 | moss, fresh | 928-97-2 | 0.31 |
| 17 | *cis*-3-hexen-1-ol | 1399 | 1398 | 67 | 100 | 1.6 | 156.5 | grass | 928-96-1 | 0.33 |
| 18 | ethyl octanoate | 1453 | 1444 | 127 | 172 | 3.8 | 208.5 | fruit, fat | 106-32-1 | 0.79 |
| 19 | furfural | 1487 | 1466 | 95 | 96 | 0.4 | 161.7 | bread, almond, sweet | 98-01-1 | 0.85 |
| 20 | linalool | 1557 | 1544 | 93 | 154 | 3.0 | 198.0 | flower, lavender | 78-70-6 | 0.24 |
| 21 | 5-methylfurfural | 1603 | 1573 | 109 + 110 | 110 | 0.7 | 187.0 | almond, caramel, burnt | 620-02-0 | 0.54 |
| 22 | terpinen-4-ol | 1633 | 1606 | 93 | 154 | 3.3 | 209.0 | turpentine, nutmeg, must | 2438-10-0 | 0.30 |
| 23 | ethyl decanoate | 1658 | 1636 | 101 | 200 | 4.8 | 241.5 | grape | 110-38-3 | 0.38 |
| 24 | furfuryl alcohol | 1677 | 1672 | 98 | 98 | 0.3 | 171.0 | burnt | 98-00-0 | 0.55 |
| 25 | γ-butyrolactone | 1674 | 1647 | 42 | 86 | −0.6 | 204.0 | caramel, sweet | 96-48-0 | 1.97 |
| 26 | diethyl succinate | 1693 | 1647 | 101 | 174 | 1.2 | 217.7 | wine, fruit | 123-25-1 | 0.69 |
| 27 | α-terpineol | 1725 | 1688 | 59 | 154 | 3.0 | 217.5 | oil, anise, mint | 10482-56-1 | 0.20 |
| 28 | β-citronellol | 1780 | 1768 | 69 | 156 | 3.9 | 224.0 | rose | 106-22-9 | 0.28 |
| 29 | nerol | 1820 | 1792 | 69 | 154 | 3.6 | 225.0 | sweet | 106-25-2 | 0.23 |
| 30 | β-phenylethyl acetate | 1852 | 1829 | 104 | 164 | 2.3 | 232.6 | rose, honey, tobacco | 103-45-7 | 0.74 |
| 31 | ethyl dodecanoate | 1860 | 1842 | 88 | 228 | 5.7 | 281.2 | leaf | 106-33-2 | 0.43 |
| 32 | β-damascenone | 1860 | 1815 | 190 | 190 | 4.2 | 275.0 | apple, rose, honey | 23726-93-4 | 0.20 |
| 33 | α-ionone | 1894 | 1840 | 93 | 192 | 3.9 | 259.5 | wood, violet | 127-41-3 | 0.10 |
| 34 | hexanoic acid | 1900 | 1829 | 60 | 116 | 2.1 | 203.0 | sweat | 142-62-1 | 0.83 |
| 35 | benzyl alcohol | 1909 | 1897 | 79 | 108 | 1.1 | 205.3 | sweet, flower | 100-51-6 | 0.74 |
| 36 | *trans*-whiskey lactone | 1935 | 1977 | 99 | 156 | 2.0 | 260.6 | flower, lactone | 80041-01-6 | 0.69 |
| 37 | β-phenylethyl alcohol | 1948 | 1925 | 91 | 122 | 1.4 | 218.2 | honey, spice, rose, lilac | 60-12-8 | 3.28 |
| 38 | β-ionone | 1985 | 1912 | 177 | 192 | 3.8 | 262.9 | raspberry, violet, flower | 79-77-6 | 0.10 |
| 39 | *cis*-whiskey lactone | 2010 | 1985 | 99 | 156 | 2.0 | 260.6 | coconut | 80041-00-5 | 0.69 |
| 40 | 4-ethylguaicol | 2067 | 2031 | 137 | 152 | 2.4 | 248.39 | spice, clove | 2785-89-9 | 0.35 |
| 41 | γ-nonalactone | 2081 | 2042 | 85* | 156 | 2.1 | 243.0 | coconut, peach | 104-61-0 | 0.17 |
| 42 | octanoic acid | 2107 | 2083 | 60 | 144 | 3.1 | 239.0 | sweat, cheese | 124-07-2 | 1.96 |
| 43 | eugenol | 2205 | 2164 | 164* | 164 | 2.3 | 253.2 | clove, honey | 97-53-0 | 0.21 |
| 44 | 4-ethylphenol | 2205 | 2170 | 107* | 122 | 2.6 | 217.9 | must | 123-07-9 | 0.40 |
| 45 | decanoic acid | 2328 | 2361 | 60 | 172 | 4.1 | 278.6 | rancid, fat | 334-45 | 0.78 |

[a]Experimental retention index calculated with an alkane mixture (C5−C30) on a DB-WAX column. [b]Linear retention index from literature (NIST Chemistry Webbook). [c]Ion of quantification (*, compound determined in SIM mode). [d]Molecular weight. [e]Hydrophobic constant estimated using molecular modeling software EPI Suite (U.S. EPA 2000−2007). [f]Boiling point estimated using molecular modeling software EPI Suite (U.S. EPA 2000−2007). [g]From Flavornet database (http://www.flavornet.org; accessed October 2009), from NIST web chemistry book (2005) (http://www.webbook.nis.gov/chemistry). [h]Final concentration in the wine.

lack of effect of saliva on aroma release, for example, in model cheeses[29] and from starch and water liquid systems.[30]

Undoubtedly, the physicochemical characteristics of the volatile compounds are outstanding parameters in determining the degree of interaction with saliva components.[22] In addition, saliva might induce an array of processes with sometimes opposite effects on aroma release and perception. Therefore, the overall impact of saliva needs to be specifically studied for each food system and aroma composition. Moreover, in many of the above-mentioned works, different types of saliva had been used (human, artificial saliva with different compositions); therefore, a comparison of the effect of saliva performed in such different conditions is not straightforward.

As stated in a recent review on wine aroma analysis, studies regarding aroma release during wine consumption using in vitro or in vivo approaches are scarce,[31] and research on the role of different intraoral factors (such as saliva) that might be involved in aroma release during wine drinking is still incipient. The effect of saliva has been mainly studied because of its involvement in wine astringency.[32−37] However, there are very few studies focused on the role of saliva in wine aroma release.[38,39] Although the relatively short intraoral period of consumption of liquid foods could indicate a limited effect of saliva on aroma release, the formation of an intraoral (and pharyngeal) aroma reservoir[5] and the fact that natural swallowing of saliva is continuously performed make the idea that saliva might exert an important role in the perception of wine aroma during consumption perfectly viable and also affect the persistence of aroma perception during the postoral phase of wine consumption. Very recently, using in vivo conditions, it was shown that enzymatic degradation of palm wine odorants due to saliva was not noticeable among pyrazines, pyrrolines, and most alcohols but was quite pronounced among aldehydes, esters, and thiols.[40]

Likewise, in other food systems, the few studies concerning the effect of saliva on aroma release from wines are contradictory. In the work of Genovese and collaborators,[38] saliva induced, in general, a decrease on aroma release for most of the wine volatiles, and this effect seemed to be more important in white than in red wines. On the contrary, Mitropoulou and co-workers[39] observed an enhancement in the release of hydrophobic compounds from model wines and a decrease in the release of the most hydrophilic compounds in the presence of saliva, although this effect was dependent on the concentration of tannins and polysaccharides. Both works were, however, performed in very different conditions: by using dynamic conditions in the work by Genovese et al.[38] and by using a static headspace approach in the work of Mitropoulou et al.[39] The dynamic conditions are advisible to achieve conditions more realistic to those during food consumption; however, the static conditions have been shown to be better suited for the study of interacting effects that otherwise might be underestimated with the first approach.[23,41]

Therefore, the aim of this work was to determine the role of saliva in wine aroma release by using both static and dynamic headspace conditions. In an attempt to follow a systematic study, avoiding the influence of different factors other than those of interest in this work (saliva effect and wine type), both methodologies were applied to reconstituted wines (with different nonvolatile wine matrix compositions) and a synthetic wine (with no matrix effect), keeping the concentrations of ethanol and aroma compounds the same. In addition, two types of saliva (human and artificial) and control samples (with water) were used to better understand the different mechanisms that saliva might induce in the release of aroma compounds from wine.

## MATERIALS AND METHODS

**Wine Samples.** Two commercial Spanish wines representative of different wine matrix compositions were selected for this study: a young Verdejo white wine (W-wine) and a young Tempranillo red wine (R-wine).

**Reconstituted Wines.** *Deodorization Procedure.* Wines were deodorized with Amberlite XAD-2 (Supelco, Bellefonte, PA, USA). Two 25 cm length glass columns (Pobel, Madrid, Spain), one for each wine type, filled with 100 g of Amberlite XAD-2 were prepared by sequential conditioning with 250 mL of dichloromethane, then methanol, and finally 375 mL of a 12% (v/v) hydroethanolic solution. After this, wine samples were filtered through glass wool and loaded into the column by slowly passing 750 mL of each wine.

Deodorized wines (750 mL of each) were transferred to 250 mL vials and were completely dried in a lyophilizer (Labconco, Kansas City, MO, USA). Five samples per wine type were prepared using this procedure. To replace the oxygen from the samples, all of the dry samples were exposed to a nitrogen atmosphere and stored at 4 °C until sample preparation. This procedure practically ensured the complete elimination of the original aroma compounds in the wines as was confirmed by HS-SPME-GC/MS analysis.

*Wine Reconstitution.* Deodorized wines were reconstituted with a hydroalcoholic solution and spiked with a volatile mixture to a final ethanol concentration of 12%. This aroma mixture is composed of 45 aroma compounds (manufacturers: Aldrich, Fluka, Merck, Firmenich, Lancaster, and Scharlau) representative of a typical wine aroma profile to produce the final concentration of each aroma compound shown in Table 1. This table also shows some of the typical gas chromatography and physicochemical properties of these compounds.

As well as the two types of reconstituted wine matrix, a synthetic wine (S-wine) representing a sample with "no matrix effect" was prepared by mixing a hydroalcoholic solution with 4 g/L tartaric acid (Panreac, Barcelona, Spain) and adjusting the pH to 3.5 with NaOH (Panreac).

The influence of ethanol on the volatility of aroma compounds was not considered in this study, because it has been extensively demonstrated.[42−45] Therefore, ethanol was kept at the same concentration in all reconstituted and synthetic wines.

**Human Saliva.** Stimulated human saliva was collected from 20 volunteers as described before.[46] Participants could not consume food or water for 1 h before sampling. To stimulate production, volunteers chewed a little piece of Parafilm and spat out as much saliva in a bottle as they could. Sodium azide ($NaN_3$, Sigma-Aldrich, Saint Quentin Fallavier, France) was added at a final concentration of 0.02% to avoid bacterial and fungal contamination and development. To obtain the most representative salivary composition, the different saliva samples were pooled, mixed, and centrifuged at 15000*g* for 15 min. After that, the saliva pool was filtered through a 0.22 $\mu$m Sartorius device under vacuum at 4 °C to remove saliva bacteria. Finally, saliva was sampled into pots of 20 mL and stored at −80 °C until use.

**Artificial Saliva.** Artificial saliva was prepared as previously described[24] by dissolving in 1 L of water (purified by a Milli-Q system) 5.028 g of $NaHCO_3$, 1.369 g of $K_2HPO_4{\cdot}3H_2O$, 0.877 g of NaCl, 0.477 g of KCl, 0.441 g of $CaCl_2{\cdot}2H_2O$, and 2.16 g of mucin (type 1-S from bovine submaxillary glands) from Sigma (Milan, Italy). The artificial saliva was stored at 4 °C until use.

**Static Headspace-SPME Sampling Procedure.** In the human mouth, the average ratio of liquid food/saliva had previously been shown to be 5:1 w/v.[38] Therefore, blends containing the reconstituted white and red wines (W-wine, R-wine) or the synthetic wine (S-wine) were prepared by adding 10 mL of the wines spiked with the volatile mixture in a 20 mL vial (Agilent Technologies, Palo Alto, CA, USA). After that, 2 mL of water or human or artificial saliva was added. The headspace vials were immediately closed with a screw cap and polytetrafluoroethylene (PTFE)/silicone septum (Supelco, Bellefonte, PA, USA) and were placed in the incubator of an automatic headspace sampling device (GERSTEL MPS 2, Gerstel Inc., Mülheim an der Ruhr, Germany) at 11 °C. The wine/saliva mixture was previously preincubated for 12 min at 36 °C. In the control wine, the extraction was performed in the headspace of each vial at different incubation times (5, 15, 30, and 45 min) to follow the kinetic of aroma release and to determine the equilibrium time, using a DVB/CAR/PDMS (divinylbenzene/carboxen/polydimethylsiloxane 50/30 $\mu$m thickness, 2 cm length) coated SPME fiber (Supelco). After the incubation time, the fiber was exposed to the headspace above the sample for 2 min, and the vial was maintained at 36 °C. Desorption was performed in the injector of the GC system (Agilent 6890N) in splitless mode for 1.5 min at 270 °C. After each injection, the fiber was cleaned for 30 min to avoid any memory effect. Each analysis was performed in triplicate (one injection per sample vial). Linearity and reproducibility of the

procedure were previously determined by using a synthetic wine spiked with different amounts of the aroma solution (75, 150, and 300 μL) covering as closely as possible the wine aroma concentration expected in wines.[47]

The results of this study are shown in supplementary Table 1 in the Supporting Information. Herein, satisfactory values for the regression coefficients for most of the aroma compounds were obtained, which ranged from 0.910 to 1.000, and the regression RSDs were also acceptable, with values lower than 20% (except for γ-butyrolactone and ethyl dodecanoate). These results confirmed the lack of interactions between individual volatile aroma compounds in the mixture at the concentrations used,[48] confirming the adequacy of the technique to perform this study.

**Dynamic Headspace-SPME Sampling Procedure.** A saliva bioreactor cell was used for these assays.[49] This device was specifically designed to evaluate the particular role of saliva during liquid and semisolid food consumption. It was composed of a water-jacketed glass flask (100 mL), which allowed a temperature control of the sample set at 36 °C. This device has five orifices. The first permits clean air to enter the flask to purge the sample (100 mL/min), therefore reproducing the dynamic conditions of the breathing phenomena. A second orifice is the purge gas outlet, which is connected through a heated transfer line to a flowmeter. In the third orifice the SPME fiber is inserted, and the fourth opening is where the sample is introduced. Finally, to mix the sample as might occur in the mouth, a fifth orifice allowed the introduction of a stir bar with digital speed control. An agitation rate of 150 rpm was employed. This last orifice was firmly sealed around the stir bar shaft with a septum to avoid leaks from the flask. During the experiment setup, the sample was added to the apparatus using a glass funnel.

Following the above-mentioned 5:1 average ratio liquid food/saliva in the human mouth, 10 mL of water, human saliva, or artificial saliva was transferred into the sample flask (100 mL), which was kept at 36 °C, and then 50 mL of wine was then added. The headspace was continuously flushed with purified nitrogen gas (100 mL/min). Even if the experimental conditions were not directly comparable with conditions in the mouth, two sampling points were assayed to analyze the aroma release resulting from the incubation of control, red, and white wines in contact with water, human saliva, or artificial saliva (Figure 1). The first one, corresponding to an initial sampling time ($t$ = 0 min), in which the saliva/wine mixture temperature was raised from 25.5 to 32.3 °C that might correspond with the introduction of the sample in the mouth (oral phase). The second sampling point ($t$ = 10 min at 36 °C) was more related to the postoral phase in which aroma from the remaining wine sample could be released within the oral cavity at physiological temperature. In both cases, extraction was performed for 2 min. Two or three replicates for each sample type were analyzed depending on the experiment.

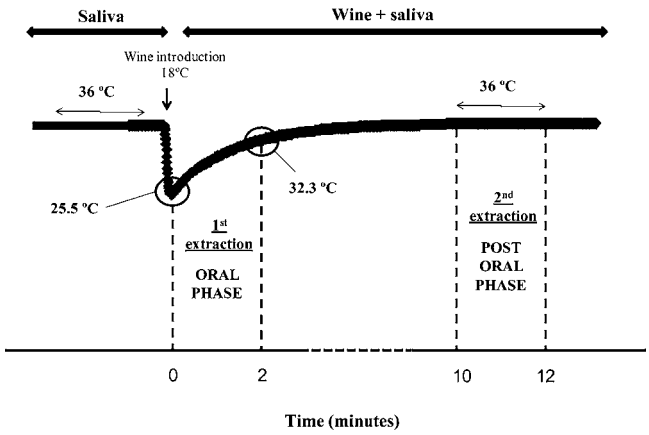


**Figure 1.** Representation of the sampling procedure employed during the dynamic HS-SPME-GC/MS analysis.

It has been shown that interfiber repeatability is lower than the intrafiber accuracy.[50−52] Therefore, a preliminary interfiber repeatability study was performed to select the most similar fibers to complete the study. For this study 9 SPME fibers were used to recover the 45 aroma compounds of the aroma mixture added to synthetic wines, and the 2 SPME fibers exhibiting the lowest variation (<10% RSDs for the extraction of the same aroma compound) were selected and used for the complete set of experiments.

In addition, because the dynamic HS-SPME sampling approach is based on a nonequilibrium situation, a linearity study was carried out to seek the relationship between the adsorbed amount of volatiles on the fiber and their initial concentration in the sample. To do so, a synthetic wine spiked with four different amounts of the aroma mixture was submitted to the dynamic HS extraction conditions as explained above. These results are shown in supplementary Table 1 in the Supporting Information. As can be seen, there is good linearity, high coefficients of determination ($R^2$) (>0.9 in the assayed concentration range, except for γ-butyrolactone), and adequate regression RSDs for most of the assayed compounds independent of the time at which sampling was performed (0 and 10 min). The lack of fit test also showed the adequacy of the proposed regression models ($p$ values > 0.01 for most of the aroma compounds) (data not shown). Therefore, the adsorbed amount of aroma compounds in the SPME was linearly proportional to their initial concentration in the sample matrix, highlighting the adequacy of the technique for quantification purposes, which is in agreement with other theoretical and experimental studies performed in simpler aroma systems.[53]

**GC/MS Analysis.** The identification of volatile compounds was carried out with an Agilent 6890N gas chromatograph coupled to an Agilent 5973 quadrupole mass detector. After desorption of the SPME fiber (270 °C, splitless), volatile compounds were separated on a DB-Wax polar capillary column (60 m × 0.25 mm i.d. × 0.50 μm film thickness) from Agilent (J&W Scientific, Folsom, CA, USA). Helium was the carrier gas at a flow rate of 1 mL/min. The oven temperature was initially held at 40 °C for 5 min, then increased at 4 °C/min to 240 °C, and held for 20 min.

For the MS system (Agilent 5973N), the temperatures of the transfer line, quadrupole, and ion source were 250, 150, and 230 °C, respectively. Electron impact mass spectra were recorded at 70 eV ionization voltages, and the ionization current was 10 μA. The acquisitions were performed in scan (from 35 to 350 amu) and SIM modes for some specific compounds as indicated in Table 1.

The identification of compounds was based on their retention indices (RIs) and comparison of retention times and mass spectra. RIs were calculated from the retention times of $n$-alkanes (C5−C30) on the same column. The mass spectra were compared with those from three databases: NIST 2.0, WILEY 138, and INRAMASS (internal database achieved using standard compounds).

To avoid possible wine matrix interaction phenomena,[47] instead of using an internal standard compound, release data were referred to absolute peak area, once the precision of the data was proven.

**Chemical Wine Matrix Composition.** Total acidity and pH, total polyphenols, neutral polysaccharides, residual sugar, and nitrogen compounds (total nitrogen, free amino acids, and peptides) were determined following previously described analytical procedures.[47]

**Saliva Biochemical Analysis.** *Protein Concentration.* The protein concentration was determined using the Bradford protein assay Quick Start (Bio-Rad, France) with γ-globulin as the standard for calibration.

*Enzymatic Activities.* Lipolysis, proteolysis, lysozyme, and amylase activities were measured as previously described.[17,46]

**Statistical Analysis.** Aroma release data (absolute peak area) were submitted to two-way ANOVA to determine significant effects of the studied factors (saliva type and wine type). In addition, for each aroma compound and wine type (red, white, and synthetic) differences between medium type (with human saliva, artificial saliva, and water) were subsequently examined by least significant difference (LSD) test. The significance level was $p$ = 0.05 throughout the study. Principal component analysis (PCA) was also applied to examine the relationship between aroma release data and wine samples. The

STATISTICA program for Windows version 7.1 was used for data processing (StatSoft, Inc., 2005; www.statsoft.com). Linear regression analysis to establish the calibration curves of each aroma compound and the lack of fit test to judge the adequacy of the models were performed by using the Statgraphics Centurion XV version 15.2 (Manugistics, Rockville, MD, USA).

## RESULTS AND DISCUSSION

To understand the effect of saliva composition on the release of aroma compounds, two types of wines, a white and a red wine, were previously deodorized, reconstituted to the same ethanol content, and aromatized at the same concentration with the aroma mixture (Table 1). With this procedure, it was guaranteed that ethanol did not affect the partition of volatile compounds into the headspace and that both wine matrices had the same concentration of aroma compounds. Therefore, the main differences between both wines were exclusively due to their matrix composition. Table 2 shows the chemical compositions of both reconstituted wines. The percentage of nonvolatile residue and the pH values were very similar. The nonvolatile residues were 2.17 and 2.99% (w/w) and the pH values were 3.23 and 3.79 for the white and red wines, respectively. Total acidity was slightly lower for the red wine (4.29 mg tartaric acid/L) compared to 5.66 mg tartaric acid/L in the case of white wine. The major differences were, however, in the total polyphenol content, neutral polysaccharides, residual sugars, and nitrogen-containing compounds (amino acids and peptides) that were significantly higher in the red wine. These differences in matrix composition have been previously shown to affect the release of aroma compounds in static conditions.[47] In addition to this, a synthetic wine with the same ethanol concentration and pH 3.5 that could be considered as a wine with "no matrix" effect was also prepared.

**Table 2. Chemical Composition of the Red and White Wines Employed in This Study**[a]

| | white wine | | red wine | |
|---|---|---|---|---|
| | mean | SD | mean | SD |
| nonvolatile residue (% w/w) | 2.17 | 0.11 | 2.99 | 0.08 |
| pH | 3.23 | 0.01 | 3.79 | 0.01 |
| total acidity (mg tartaric acid/L) | 5.66 | 0.1 | 4.29 | 0.2 |
| total polyphenols (mg gallic acid/L) | 269.95 | 17.2 | 1647.98 | 292.8 |
| neutral polysaccharides (g mannose/L) | 1.67 | 0.5 | 2.50 | 0.9 |
| residual sugars (g/L) | 1.12 | 0.2 | 3.68 | 0.5 |
| total nitrogen (mg/L) | 239.96 | 32.9 | 406.00 | 65.7 |
| amino acids + peptides (mg N/L) | 49.54 | 2.2 | 133.51 | 10.9 |
| amino acids (mg N/L) | 30.67 | 0.8 | 58.57 | 1.4 |
| peptides[b] (mg N/L) | 18.87 | | 79.94 | |

[a]Values are the average of two determinations except for pH (average of three determinations). [b]This value is indirectly determined as the difference between the analytical determination of amino acids plus peptides and free amino acids; therefore, standard deviation (SD) values are not included.

For the saliva experiments, two types of saliva were used: artificial saliva with mucin prepared in agreement with the recipe previously described and human saliva collected from different volunteers and mixed together to form a single pool. The composition, regarding total protein content and enzymes (amylase, lipase, lysozyme, and protease) was analyzed. The major enzymatic activity detected in the human saliva was lysozyme (698.06 U/mL) followed by proteolysis (16.77 U/mL) and amylase (8.01 U/mL) and, to a lesser extent, lipase (0.95 mU/mL). These values are in the same order of magnitude as those previously published[17,46,54] except for proteolysis activity, which was higher in our study. In addition to the two types of saliva, control experiments were also performed by adding the same amount of water instead of saliva. With this control, we also eliminated the dilution effect exerted by saliva on volatile release, which has also been described.[28,55] In addition, this type of experiment could provide us important information regarding whether saliva enzymes might have an impact on aroma release from wine as has been previously shown in simple aroma/saliva mixtures.[19,20,56]

**Effect of Saliva on Aroma Release Using Static Headspace Conditions.** Although static headspace conditions do not mimic the dynamic conditions during drinking or eating, this technique has been largely used to study aroma interactions with food matrix components to determine their effect on aroma release.[23,39,47,57] Even so, different authors have shown that this is a reliable approach to investigate partitioning in more controlled and simple conditions, which allows us to envisage this subtle phenomena with importance on aroma release that otherwise might be underestimated by using dynamic HS methods.[23,41]

In this work, the aroma release behavior of a mixture of 45 volatile compounds characteristic of the wine aroma profile and with very different physicochemical characteristics (Table 1) was evaluated in the presence and absence of human and artificial saliva by using a previously validated static HS-SPME approach (see Table 1 in Supporting Information). Preliminary experiments were performed to determine the equilibration time (5, 15, 30, 45 min) for most volatiles of the aroma mixture. From the analysis of the kinetic profiles it was found that 5 min of incubation was enough for the equilibration of most of the aroma compounds of the mixture. Only 10 of them (ethyl propanoate, isobutyl acetate, isobutanol, isoamyl acetate, 1-butanol, ethyl octanoate, furfuryl alcohol, $\alpha$-terpineol, benzyl alcohol, and decanoic acid) were not equilibrated after 5 min. Nonetheless, because the main objective of this work was to compare wine samples performed under identical experimental conditions, this should not be a constraint for the validity of the data, and 5 min was adopted as the sampling time to perform the experiment, which are conditions closer to real physiological situations.

Data corresponding to absolute peak areas of the aroma compounds determined by HS-SPME-GC/MS analysis in the three types of wines (white, red, and synthetic) incubated with the two types of saliva (artificial and human) and water were submitted to a two-factorial ANOVA to determine the magnitude of the effect of matrix composition and type of saliva on aroma release. Results of this analysis showed that both effects and the interactions (matrix composition × type of saliva) significantly affected the majority of aroma compounds. From a total of 45 aroma compounds, 37 were affected by the type of saliva and 33 by matrix composition (data not shown). This showed the similar importance of both factors in aroma release in static headspace conditions.

To gain insight into the impact of saliva on aroma release depending on wine matrix composition, a LSD test was also carried out for each type of wine and for each aroma compound. Table 3 shows these results taking into consideration the different aroma chemical families assayed. As can be seen, in general, the addition of saliva (artificial or

Table 3. Average Aroma Release Values and Results of LSD Test in the Wines Determined by Static HS-SPME-GC/MS[a]

| | synthetic wine | | | white wine | | | red wine | | |
|---|---|---|---|---|---|---|---|---|---|
| | water | artificial saliva | human saliva | water | artificial saliva | human saliva | water | artificial saliva | human saliva |
| **terpenes** | | | | | | | | | |
| *α*-pinene | 495.6 b | 398.4 a | 412.7 a | 466.3 b | 392.7 a | 381.6 a | 560.3 c | 442.8 a | 517.5 b |
| *β*-pinene | 584.8 b | 483.3 a | 488.4 a | 536.5 b | 461.1 a | 432.7 a | 648.0 c | 533.0 a | 574.1 b |
| limonene | 95.1 b | 76.5 a | 77.9 a | 89.0 b | 72.8 a | 72.1 a | 99.5 b | 82.9 a | 82.5 a |
| linalool | 2.3 a | 2.1 a | 2.2 a | 2.2 a | 2.1 a | 2.1 a | 2.4 b | 2.4 ab | 2.2 a |
| terpinen-4-ol | 1.8 a | 1.6 a | 1.6 a | 1.7 a | 1.6 a | 1.7 a | 1.8 b | 1.7 ab | 1.6 a |
| *α*-terpineol | 1.2 b | 1.0 a | 1.0 ab | 1.2 b | 1.1 a | 1.2 b | 1.2 b | 1.0 a | 1.0 a |
| *β*-citronellol | 2.3 b | 2.0 a | 2.0 a | 2.1 a | 2.0 a | 2.0 a | 2.3 b | 2.1 ab | 2.0 a |
| nerol (*cis*-geraniol) | 1.7 b | 1.5 a | 1.5 ab | 1.6 b | 1.5 a | 1.4 a | 1.7 b | 1.6 ab | 1.5 a |
| **esters** | | | | | | | | | |
| ethyl propanoate | 19.1 b | 17.9 a | 19.0 b | 17.9 a | 17.6 a | 17.2 a | 20.1 a | 18.9 a | 18.4 a |
| isobutyl acetate | 11.8 b | 11.0 a | 11.6 b | 10.8 a | 10.9 a | 10.5 a | 12.2 a | 11.4 a | 11.2 a |
| ethyl butanoate | 39.1 ab | 38.2 a | 41.4 b | 35.9 a | 36.1 a | 38.0 a | 41.9 b | 38.1 a | 36.9 a |
| ethyl 2-methylbutanoate | 29.4 c | 26.6 a | 27.7 b | 26.4 a | 25.5 a | 25.4 a | 30.4 b | 27.9 ab | 27.5 a |
| butyl acetate | 33.6 a | 31.7 a | 27.0 a | 31.6 a | 30.8 a | 31.0 a | 36.5 b | 34.1 a | 32.8 a |
| isoamyl acetate | 78.9 c | 71.3 a | 74.5 b | 72.9 a | 71.2 a | 70.1 a | 82.7 b | 74.5 a | 73.5 a |
| ethyl hexanoate | 194.5 b | 173.2 a | 179.0 a | 179.9 b | 169.7 a | 170.6 a | 201.4 b | 183.7 a | 176.6 a |
| hexyl acetate | 116.9 b | 104.7 a | 106.8 a | 107.7 b | 102.3 a | 102.7 a | 121.3 b | 111.1 a | 106.1 a |
| ethyl octanoate | 101.0 b | 83.8 a | 85.8 a | 88.5 b | 82.1 a | 82.3 a | 95.0 b | 87.5 a | 82.5 a |
| ethyl decanoate | 122.2 b | 96.5 a | 102.0 a | 104.1 b | 93.4 a | 93.0 a | 102.8 b | 106.5 b | 93.8 a |
| diethyl succinate | 1.6 a | 1.4 a | 1.5 a | 2.2 b | 2.0 a | 2.1 ab | 2.9 b | 3.4 c | 1.7 a |
| *β*-phenylethyl acetate | 13.4 b | 12.2 a | 12.5 ab | 12.8 a | 12.4 a | 12.6 a | 13.6 b | 12.7 ab | 12.1 a |
| ethyl dodecanoate | 294.3 b | 216.3 a | 212.4 a | 215.8 b | 187.4 a | 182.4 a | 218.5 b | 243.5 c | 163.3 a |
| **alcohols** | | | | | | | | | |
| isobutanol | 0.1 a | 0.1 a | 0.1 a | 0.1 a | 0.1 a | 0.1 a | 0.3 b | 0.3 b | 0.2 a |
| 1-butanol | 1.0 a | 1.0 a | 1.0 a | 1.0 a | 1.0 a | 1.0 a | 1.2 c | 1.1 b | 1.0 a |
| isoamylic alcohols | 53.4 a | 52.1 a | 56.1 a | 52.7 a | 52.1 a | 51.1 a | 59.8 b | 58.1 b | 54.0 a |
| 1-hexanol | 8.4 a | 8.1 a | 8.2 a | 8.1 a | 8.1 a | 8.0 a | 9.2 b | 8.6 a | 8.2 a |
| *trans*-3-hexen-1-ol | 1.0 a | 0.9 a | 1.0 a | 1.0 a | 0.9 a | 1.0 a | 1.1 b | 1.0 ab | 1.0 a |
| *cis*-3-hexen-1-ol | 1.1 a | 1.0 a | 1.0 a | 1.0 a | 1.0 a | 1.0 a | 1.1 b | 1.1 ab | 1.0 a |
| benzyl alcohol | 0.4 a | 0.3 a | 0.4 a | 0.4 a | 0.3 a | 0.4 a | 0.4 a | 0.4 a | 0.4 a |
| *β*-phenylethyl alcohol | 3.8 a | 3.1 a | 3.6 a | 3.4 a | 2.9 a | 3.0 a | 3.7 a | 4.0 a | 3.4 a |
| **lactones/furanic compounds** | | | | | | | | | |
| furfural | 3.0 b | 2.7 a | 2.9 b | 2.7 b | 2.6 a | 2.7 ab | 3.0 b | 2.8 b | 2.7 a |
| 5-methylfurfural | 1.3 b | 1.1 a | 1.2 ab | 1.2 a | 1.1 a | 1.2 a | 1.3 b | 1.2 b | 1.2 a |
| *γ*-butyrolactone | 0.2 a | 0.2 a | 0.2 a | 0.3 b | 0.2 a | 0.2 ab | 0.4 a | 0.5 a | 0.4 a |
| furfuryl alcohol | 0.2 a | 0.2 a | 0.2 a | 0.2 a | 0.2 a | 0.2 a | 0.2 a | 0.2 a | 0.2 a |
| *trans*-whiskey lactone | 0.9 a | 0.8 a | 0.8 a | 0.8 a | 0.8 a | 0.8 a | 0.9 a | 0.9 a | 0.8 a |
| *cis*-whiskey lactone | 0.7 a | 0.6 a | 0.6 a | 0.6 a | 0.6 a | 0.6 a | 0.7 b | 0.6 ab | 0.6 a |
| *γ*-nonalactone | 0.5 a | 0.4 a | 0.4 a | 0.4 a | 0.3 a | 0.4 a | 0.4 b | 0.4 b | 0.3 a |
| **volatile phenols** | | | | | | | | | |
| 2-methoxy-4-ethylphenol (4-ethylguaicol) | 1.7 b | 1.5 a | 1.5 ab | 1.6 a | 1.5 a | 1.6 a | 1.7 b | 1.6 b | 1.5 a |
| eugenol | 0.3 b | 0.3 a | 0.3 ab | 0.3 a | 0.3 a | 0.3 a | 0.3 b | 0.3 b | 0.3 a |
| 4-ethylphenol | 1.3 a | 1.1 a | 1.2 a | 1.2 a | 1.1 a | 1.1 a | 1.3 a | 1.3 a | 1.2 a |
| **C13-norisoprenoids** | | | | | | | | | |
| *β*-damascenone | 1.6 a | 1.5 a | 1.6 a | 1.6 a | 1.5 a | 1.5 a | 1.6 b | 1.5 ab | 1.4 a |
| *α*-ionone | 2.5 a | 2.3 a | 2.3 a | 2.4 b | 2.2 a | 2.3 a | 2.4 b | 2.3 b | 2.2 a |
| *β*-ionone | 4.4 b | 4.0 a | 3.9 a | 4.2 b | 3.9 a | 4.0 ab | 4.2 b | 4.0 ab | 3.7 a |
| **acids** | | | | | | | | | |
| hexanoic acid | 1.0 b | 0.8 a | 1.0 b | 0.9 a | 0.8 a | 0.9 a | 1.1 b | 0.8 a | 0.9 a |
| octanoic acid | 2.7 b | 2.2 a | 2.7 ab | 2.6 b | 2.4 a | 2.3 a | 2.8 b | 2.1 a | 2.3 a |
| decanoic acid | 2.5 b | 1.3 a | 1.4 a | 1.5 b | 1.3 ab | 1.2 a | 1.4 b | 1.1 a | 1.4 b |

[a]All values (area: arbitrary units) are divided by a factor of 10000. Different letters (a–c) for the same aroma compound in the same wine type (synthetic, white, red) denote statistical differences among saliva types after application of LSD test.

human) provoked a significant decrease (or higher retention) on the aroma release for most of the aroma compounds assayed. However, the extent of this effect was dependent on the type of wine and also on the type of aroma chemical class. In this sense, it is important to highlight that human saliva exerted a high impact on the aroma release from red wines, and


dx.doi.org/10.1021/jf503503b | J. Agric. Food Chem. 2014, 62, 8274–8288

practically all of the aroma compounds assayed were less released when human saliva was added to the wine. However, in the case of white wines this effect was more dependent on the type of aroma compound. For example, the addition of human or artificial saliva did not affect the release of any of the alcohols of the aroma mixture. As can be seen in the table, the effect of saliva seemed to be much lower in the case of synthetic wines.

To better understand the way in which both factors (type of saliva and wine matrix) affected the aroma release behavior, a PCA was also performed taking into consideration all of the aroma release data. Two principal components, PC1 and PC2, explaining 68.8% of data variations were obtained (Figure 2a). As can be seen in the graph, PC1 was mainly involved in the separation of the samples depending on the type of medium (with human saliva, artificial saliva, or water). In agreement with previous results, the clearest separation (or differences) among wine samples were obtained for red wines. As can be seen, red wines with human saliva showed positive values for PC1, whereas red wines with water showed high and negative values for this component. Red wines with artificial saliva showed an intermediate behavior and were placed between the other two types of wine samples (with human saliva and water). PC1 was negatively correlated with many volatile compounds (25 volatile compounds showed loadings lower than 0.8 and 15 of them, lower than 0.9). Among them, the variable projection (Figure 2b) showed that some aroma compounds such as limonene (11), hexyl acetate (14), *cis*-3-hexen-1-ol (17), linalool (20), or 5-methylfurfural (21), among others, were strongly correlated with PC1. On the contrary, PC2 separated wines as a function of wine type. Red wines exhibited negative values for this component, whereas white and synthetic wines appeared on the half top of the graph showing positive values for PC2.

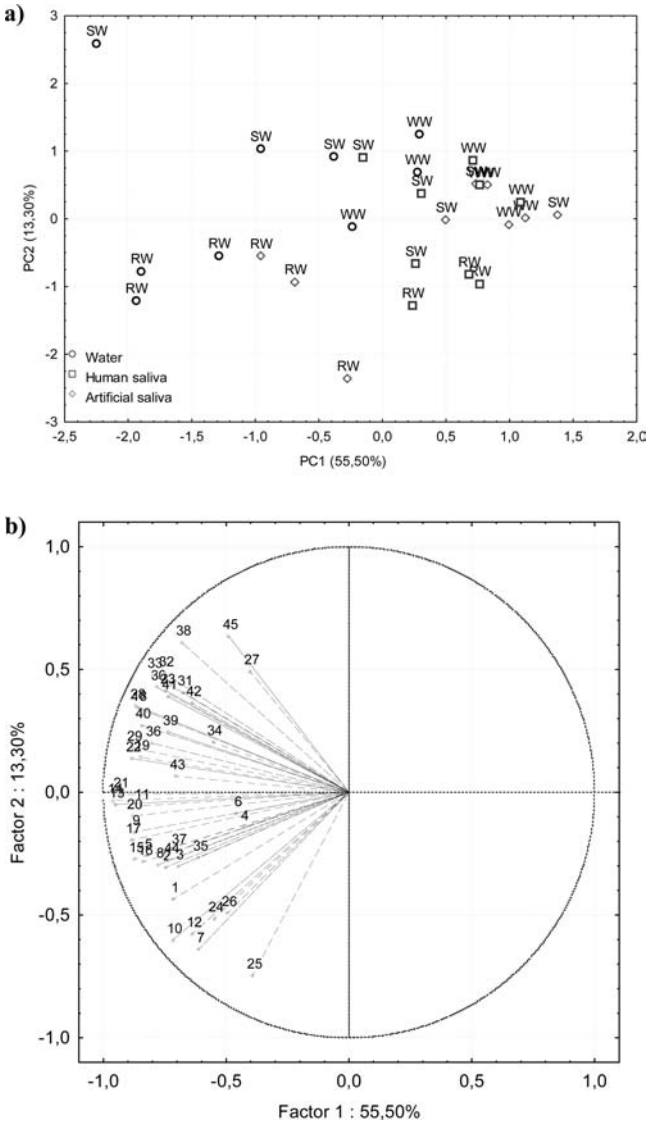


**Figure 2.** Graphic representation of the wine samples (a) and of the variables (b) obtained using PCA with the aroma release data from the static HS-SPME-GC/MS. Numbers of the variables in panel b correspond to the compounds listed in Table 1. RW, SW, and WW mean red, synthetic, and white wines, respectively.

These results emphasized an effect of saliva on aroma release dependent on wine matrix composition. Even more interestingly, red wines seemed to be more affected than white and synthetic wines. The most outstanding effect provoked by human saliva was a reduction in the aroma release of most of the aroma compounds independent of their chemical structure. This global effect could be the result of the combination of single effects that could be differently affecting the volatile compounds employed in this study.

For instance, it is already known that wine polyphenols, which are more abundant and structurally different in red than in white wines, might interact with aroma compounds through different mechanisms depending on polyphenol structure decreasing the amount of aroma release.[47,58−60] In addition to this effect, wine polyphenols (such as procyanidins) might form insoluble complexes with saliva proteins with colloidal structures[39] modifying the viscosity of the sample and, therefore, affecting aroma release. To check this hypothesis, the viscosity values of white and red wines with the two types of saliva and water were also determined. Table 4 shows that the viscosity values determined in all of the wines were very similar, ranging from 6.9 mPa·s for the white wine with water to 7.4 mPa·s for the white wine with artificial saliva. Therefore, there were no substantial differences between red and white wines. Although an increase in viscosity induced by saliva has been proposed to explain the lower aroma release observed in oil/water emulsions,[12,28] the low volume of saliva compared to the wine (1:5) employed in this study might not be enough to provoke a clear effect, at least in static headspace conditions as used here. Therefore, this factor did not seem a determinant parameter responsible for the higher retention of aroma compounds determined in red wines and specifically in those with human saliva.

The buffering capacity of saliva might be another important factor to explain aroma release, because this property might induce changes in the pH of the food matrix.[12,22] In fact, this factor has been pointed out, because it might influence the overall perception of aroma compounds during the in vivo consumption of palm wine.[61] To check this hypothesis, the pH values of the human and artificial saliva and the pH values of the wine/saliva mixtures were determined, and they are also shown in Table 4. The original pH value for the artificial saliva was a little bit higher (8.4) than the pH of the human saliva (8.2). As expected and for both white and red wines, the addition of water practically did not change the pH, whereas it increased with the addition of saliva. Artificial saliva seemed to induce higher changes in pH than human saliva, and this could

Table 4. Viscosity and pH Values Determined for the Saliva Samples and Wine/Saliva Mixtures ($n$ = 3)

| | viscosity (mPa·s) | | | pH | | |
|---|---|---|---|---|---|---|
| | water mean (SD) | human saliva mean (SD) | artificial saliva mean (SD) | water mean (SD) | human saliva mean (SD) | artificial saliva mean (SD) |
| salivas | | 7.0 (0.1) | 7.9 (0.2) | | 8.2 (0.1) | 8.4 (0.2) |
| red wine | 7.2 (0.1) | 7.3 (0.1) | 7.1 (0.1) | 3.8 (0) | 4.0 (0.1) | 4.2 (0.1) |
| white wine | 6.9 (0.0) | 7.3 (0.3) | 7.4 (0.5) | 3.1 (0) | 3.3 (0.1) | 3.7 (0.1) |

be due to its higher original pH compared to the human saliva. Therefore, differences induced by changes in pH did not seem relevant to explain the differences in the behavior of the aroma compounds in both wines whatever the matrix and type of medium.

To explain the retention effect induced by saliva, mainly in red wines, we have to propose an additional hypothesis. Previous works using static headspace conditions but with other food matrices have shown the ability of the saliva protein mucin to bind aroma compounds via hydrophobic interactions, leading to a reduction in aroma release into the headspace.[23] Moreover, this hypothesis has already been proposed to explain the lower release of a wide range of volatile compounds (e.g., esters, acetates, alcohols) from red and white wines.[38] However, in the present study, red wine with human saliva released lower amounts of aroma than the same wine with artificial saliva. The final amount of mucin in the wine/artificial saliva vial was 4.32 mg, whereas the amount of total protein (including mucin) in the wines samples with added human saliva was lower, 0.98 mg. Therefore, wines spiked with human saliva should have a minor interaction effect with mucin (and therefore higher aroma release) than wines spiked with artificial saliva, which does not explain our results. However, it is important to bear in mind that human saliva contains other proteins different from mucin, for instance, proline-rich proteins (PRPs), histidine-rich proteins (histatins or HRPs), lactoferrine, and enzymes ($\alpha$-amylase, lipase, etc.),[21] which could be also involved in specific interactions with aroma compounds explaining the lower aroma release of wines with human saliva. In particular, PRPs, which represent up to 70% of proteins originated from the parotid gland, are known to interact with tannins, leading to the formation of some aggregates.[62] Moreover, it has been shown that depending on the protein and tannin concentrations, dense aggregates might coexist with nonaggregated proteins, the latter also showing a significant number of bound tannin molecules.[62] We could hypothesize that the formation of this second type of aggregate might interact with aroma molecules without substantially changing the viscosity of the solution, as was observed in the present study in the case of red wines with added human saliva.

Moreover, besides tannins, other wine matrix components might be also involved in the formation of these types of aggregates. Mitropoulou et al.[39] have suggested, at least in reconstituted model wines, the possible formation of saliva protein−polyphenol−carbohydrate complexes able to encapsulate hydrophobic aroma molecules. In this sense, in addition to the higher concentration of polyphenols determined in the red wine employed in this study, the polysaccharide content was also higher (2502 mg mannose/L) compared to the white wines (1667 mg mannose/L) (see Table 2). The formation of these type of complexes involving saliva proteins and specific wine polyphenols (tannins) and polysaccharides, both at higher concentrations in red than in white wines, might explain why red wines, and specifically those with human saliva, retained more aroma molecules. Moreover, the fact that the very high hydrophobic aroma compounds (log $P$ > 2) of the aroma mixture showed higher retention (lower aroma release) in red wines with saliva than in the white wines might be in agreement with this hypothesis. The formation of these structures (protein−polyphenol−carbohydrate complexes) might, however, represent a reservoir of aroma molecules ready to be released by the exhalation breath during the in vivo red wine consumption, as has been recently proposed.[63]

Finally, the salivary metabolic activity might have also affected the release of certain aroma compounds. In this regard, a reduction of aldehydes to the corresponding alcohols and/or partial hydrolysis of certain aroma compounds such as esters might be expected.[19,20] In the case of the aldehydes employed in the aroma mixture (furfural and 5-methylfurfural), the release of these compounds was lower in red wines with human saliva, which could be in agreement with a possible transformation by an NADP-linked aldehyde reductase.[19] However, the increase of the corresponding alcohol (furfuryl alcohol in the case of furfural) was not significant in these samples. In addition, the involvement of aldehydes in the formation of condensation products such as Schiff bases (e.g., with salivary proteins) or other chemical reactions might be also possible.[19]

On the other hand, a reduction of esters in the HS of white but mainly red wines with saliva has been also shown in this work. However, this seems to be more related to the interaction of these compounds with the protein−polyphenol−carbohydrate complex than related to the esterase activity of saliva. Although the decrease in the release of some esters (ethyl butanoate, hexanoate, octanoate, etc.) in wines with human saliva compared to control wines (without saliva) has been attributed to the esterase activity,[38] the activity of these enzymes has been proven only in a very different environment (specifically, in an aqueous system at pH 5)[20] from that in wine (12% ethanolic system at pH 3.5). Therefore, it seems difficult to obtain straightforward relationships between the decrease in ester release and saliva esterase activity.

**Effect of Saliva on Aroma Release Using Dynamic Headspace Conditions.** In the present work, aroma release from different wine matrices in dynamic conditions was determined by using a bioreactor cell with controlled temperature and agitation conditions at two different sampling times (initial $t$ = 0 and final $t$ = 10 min) (Figure 1). The initial sampling time ($t$ = 0) might be related to the oral phase, in which the mixture of wine (generally cold) and saliva is at lower temperature (25.5 °C) than physiological temperature (36 °C). The final sampling time ($t$ = 10 min) could be more representative of the postoral phase, in which some volatiles could be released from the liquid sample remaining in the oral cavity after drinking[5] at oral temperature (36 °C).

Aroma release data collected from $t$ = 0 and $t$ = 10 min are shown in Tables 5 and 6, respectively. These data were submitted to two independent two-way ANOVA (one for each sampling time), considering the global effect of saliva type (artificial, human, water) and type of wine matrix (red, white,

Table 5. Average Aroma Release Values and Results of LSD Test in the Wines Determined by Dynamic HS-SPME-GC/MS at $t$ = 0 (Oral Phase)[a]

| | synthetic wine | | | white wine | | | red wine | | |
|---|---|---|---|---|---|---|---|---|---|
| | water | artificial saliva | human saliva | water | artificial saliva | human saliva | water | artificial saliva | human saliva |
| **terpenes** | | | | | | | | | |
| α-pinene | 49.1 b | 0.2 a | 19.0 a | 7.2 b | 2.0 a | 0.7 a | 10.9 c | 1.3 a | 3.7 b |
| β-pinene | 45.1 b | 0.0 a | 16.3 a | 9.9 b | 3.2 a | 1.1 a | 19.4 c | 3.3 a | 7.3 b |
| limonene | 14.8 b | 0.9 a | 7.1 a | 4.6 b | 3.4 b | 1.6 a | 3.9 c | 1.4 a | 2.3 b |
| linalool | 1.7 a | 1.6 a | 1.7 a | 1.9 a | 1.9 a | 1.9 a | 1.8 a | 1.6 a | 2.1 b |
| terpinen-4-ol | 1.2 a | 1.1 a | 1.1 a | 1.3 a | 1.3 a | 1.3 a | 1.3 ab | 1.1 a | 1.5 b |
| α-terpineol | 1.0 a | 1.1 a | 0.9 a | 0.7 a | 0.8 a | 0.8 a | 0.7 a | 0.6 a | 0.9 b |
| β-citronellol | 1.4 a | 1.1 a | 1.1 a | 1.3 a | 1.4 a | 1.3 a | 1.3 b | 1.1 a | 1.6 c |
| nerol (*cis*-geraniol) | 0.9 b | 0.7 a | 0.8 ab | 0.9 a | 0.9 a | 0.9 a | 0.9 ab | 0.8 a | 1.1 b |
| **esters** | | | | | | | | | |
| ethyl propanoate | 37.8 a | 36.1 a | 39.7 b | 39.1 a | 41.8 a | 41.2 a | 38.6 b | 37.1 a | 36.8 a |
| isobutyl acetate | 19.2 b | 16.8 a | 18.9 b | 19.0 a | 20.0 a | 19.2 a | 18.5 c | 17.2 a | 17.8 b |
| ethyl butanoate | 58.9 b | 52.0 a | 60.6 b | 58.5 a | 63.0 a | 58.2 a | 57.5 c | 53.5 a | 55.5 b |
| ethyl 2-methylbutanoate | 34.8 b | 28.7 a | 32.1 ab | 32.3 a | 34.4 a | 32.0 a | 31.3 c | 28.8 a | 30.2 b |
| butyl acetate | 48.0 a | 45.9 a | 48.4 a | 48.6 a | 51.6 a | 50.3 a | 47.8 a | 43.6 a | 47.6 a |
| isoamyl acetate | 100.1 b | 89.2 a | 96.6 ab | 94.7 a | 104.4 a | 88.8 a | 94.1 a | 82.9 a | 94.1 a |
| ethyl hexanoate | 184.0 b | 150.7 a | 164.7 ab | 169.9 a | 176.4 a | 164.3 a | 151.0 a | 136.4 a | 153.7 a |
| hexyl acetate | 112.4 b | 93.1 a | 101.1 ab | 104.7 a | 108.3 a | 101.7 a | 91.8 a | 82.6 a | 93.6 a |
| ethyl octanoate | 65.9 b | 46.6 a | 50.1 a | 56.5 a | 59.7 a | 53.3 a | 42.2 ab | 38.2 a | 43.5 b |
| ethyl decanoate | 35.4 b | 19.5 a | 19.3 a | 25.0 a | 26.4 a | 22.2 a | 17.8 a | 15.3 a | 17.8 a |
| diethyl succinate | 1.0 a | 0.9 a | 0.9 a | 1.1 a | 1.2 a | 1.1 a | 1.8 a | 1.9 a | 2.5 b |
| β-phenylethyl acetate | 11.5 a | 11.6 a | 11.0 a | 13.3 a | 13.9 a | 13.7 a | 12.7 ab | 11.8 a | 14.9 b |
| ethyl dodecanoate | 29.2 a | 14.0 a | 11.8 a | 13.0 a | 14.3 a | 11.2 a | 9.9 c | 6.1 a | 7.9 b |
| **alcohols** | | | | | | | | | |
| isobutanol | 0.2 a | 0.3 a | 0.4 a | 0.3 a | 0.3 a | 0.3 a | 0.5 a | 0.5 a | 0.5 a |
| 1-butanol | 1.6 a | 1.6 a | 2.0 a | 1.7 a | 1.7 a | 1.7 a | 1.8 a | 1.7 a | 1.9 a |
| isoamylic alcohols | 68.0 a | 77.3 b | 75.9 b | 78.7 a | 80.7 a | 79.6 a | 83.0 a | 78.4 a | 85.3 a |
| 1-hexanol | 9.2 a | 9.9 a | 9.9 a | 10.4 a | 10.6 a | 10.7 a | 10.7 a | 9.7 a | 11.3 a |
| *trans*-3-hexen-1-ol | 1.1 a | 1.1 a | 1.2 a | 1.1 a | 1.2 a | 1.2 a | 1.2 ab | 1.1 a | 1.3 b |
| *cis*-3-hexen-1-ol | 0.9 a | 0.9 a | 1.1 b | 1.0 a | 1.0 a | 0.9 a | 1.0 ab | 0.9 a | 1.2 b |
| benzyl alcohol | 0.2 a | 0.2 a | 0.3 a | 0.3 a | 0.3 a | 0.3 a | 0.3 a | 0.3 a | 0.4 b |
| β-phenylethyl alcohol | 1.9 a | 1.9 a | 1.9 a | 2.1 a | 2.6 a | 2.5 a | 2.1 a | 2.3 a | 3.2 b |
| **lactones/furanic compounds** | | | | | | | | | |
| furfural | 2.9 a | 2.7 a | 3.2 b | 2.1 a | 2.3 a | 2.1 a | 2.7 a | 2.6 a | 3.3 b |
| 5-methylfurfural | 1.2 a | 1.1 a | 1.2 b | 1.1 a | 1.2 a | 1.2 a | 1.1 a | 1.1 a | 1.4 b |
| γ-butyrolactone | 0.3 a | 0.3 a | 0.3 a | 0.3 a | 0.4 a | 0.4 a | 0.5 a | 0.4 a | 0.6 a |
| furfuryl alcohol | 0.1 a | 0.1 a | 0.1 b | 0.1 a | 0.2 a | 0.2 a | 0.1 a | 0.1 a | 0.2 a |
| *trans*-whiskey lactone | 0.6 a | 0.5 a | 0.5 a | 0.6 a | 0.7 a | 0.6 a | 0.6 a | 0.6 a | 0.8 b |
| *cis*-whiskey lactone | 0.4 a | 0.4 a | 0.3 a | 0.4 a | 0.5 a | 0.4 a | 0.4 a | 0.4 a | 0.6 b |
| γ-nonalactone | 0.2 a | 0.2 a | 0.2 a | 0.2 a | 0.3 b | 0.3 b | 0.3 a | 0.2 a | 0.3 b |
| **volatile phenols** | | | | | | | | | |
| 2-methoxy-4-ethylphenol (4-ethylguaicol) | 1.0 a | 1.0 a | 0.9 a | 1.1 a | 1.2 a | 1.2 a | 1.1 a | 1.1 a | 1.4 a |
| eugenol | 0.1 a | 0.2 a | 0.1 a | 0.2 a | 0.2 b | 0.2 b | 0.1 a | 0.2 ab | 0.2 b |
| 4-ethylphenol | 0.7 a | 0.7 a | 0.6 a | 0.8 a | 0.9 a | 0.9 a | 0.7 a | 0.8 a | 1.1 b |
| **C13-norisoprenoids** | | | | | | | | | |
| β-damascenone | 1.2 a | 1.2 a | 1.1 a | 1.4 a | 1.4 a | 1.4 | 1.3 ab | 1.1 a | 1.5 b |
| α-ionone | 1.9 a | 1.6 a | 1.5 a | 2.0 a | 2.0 a | 1.9 | 1.8 ab | 1.5 a | 2.1 b |
| β-ionone | 2.9 b | 2.5 ab | 2.2 a | 3.1 a | 3.1 a | 3.1 | 2.8 a | 2.5 a | 3.4 b |
| **acids** | | | | | | | | | |
| hexanoic acid | 0.6 b | 0.5 a | 0.7 b | 0.8 a | 0.8 a | 0.7 | 0.3 a | 0.5 a | 0.9 a |
| octanoic acid | 1.2 a | 1.1 a | 1.1 a | 1.6 a | 2.2 a | 1.5 | 1.8 a | 1.5 a | 2.0 a |
| decanoic acid | nd | nd | nd | nd | nd | nd | nd | nd | nd |

[a]All values (area: arbitrary units) are divided by a factor of 10000. Different letters (a–c) for the same aroma compound in the same wine type (synthetic, white, red) denote statistical differences among saliva types after application of LSD test.

synthetic). Results showed that in the oral phase ($t$ = 0) only 9 aroma compounds were affected by saliva type, whereas 30 of them were affected by wine matrix (data not shown). In addition, 11 compounds showed an effect of the interaction


dx.doi.org/10.1021/jf503503b | J. Agric. Food Chem. 2014, 62, 8274–8288

**Table 6. Average Aroma Release Values and LSD Test in the Wines Determined by Dynamic HS-SPME-GC/MS at $t$ = 10 min (Post Oral Phase)[a]**

| | synthetic wine | | | white wine | | | red wine | | |
|---|---|---|---|---|---|---|---|---|---|
| | water | artificial saliva | human saliva | water | artificial saliva | human saliva | water | artificial saliva | human saliva |
| **terpenes** | | | | | | | | | |
| α-pinene | 20.6 a | 0.2 a | 19.0 a | 6.8 b | 1.6 a | 0.7 a | 8.8 b | 1.2 a | 3.7 a |
| β-pinene | 21.6 a | 0.1 a | 18.4 a | 9.8 b | 2.8 a | 1.1 a | 17.5 b | 3.6 a | 7.5 a |
| limonene | 11.9 b | 1.3 a | 9.7 a | 5.5 c | 3.6 b | 2.2 a | 4.2 c | 1.7 a | 2.7 b |
| linalool | 4.4 a | 4.9 a | 4.6 a | 4.5 a | 4.5 a | 5.0 b | 4.3 a | 4.1 a | 4.3 a |
| terpinen-4-ol | 3.6 a | 3.8 a | 3.4 a | 3.5 a | 3.5 a | 3.6 a | 3.4 a | 3.2 a | 3.3 a |
| α-terpineol | 3.1 a | 3.5 a | 2.9 a | 2.0 a | 2.1 a | 2.3 a | 1.9 a | 1.8 a | 1.8 a |
| β-citronellol | 4.1 a | 4.0 a | 3.7 a | 3.8 ab | 3.5 a | 4.0 b | 3.6 a | 3.4 a | 3.5 a |
| nerol (*cis*-geraniol) | 2.3 a | 2.3 a | 2.4 a | 2.1 ab | 2.0 a | 2.4 b | 2.2 a | 2.1 a | 2.2 a |
| **esters** | | | | | | | | | |
| ethyl propanoate | 28.7 a | 32.5 b | 31.1 a | 32.1 a | 32.3 a | 32.3 a | 30.4 a | 28.9 a | 30.2 a |
| isobutyl acetate | 17.6 a | 19.1 a | 18.5 a | 18.5 a | 19.5 b | 18.6 a | 17.7 a | 17.0 a | 17.3 a |
| ethyl butanoate | 61.8 a | 65.2 a | 66.6 a | 64.2 a | 66.3 a | 62.7 a | 60.0 a | 56.2 a | 59.2 a |
| ethyl 2-methylbutanoate | 35.0 a | 37.9 a | 36.4 a | 35.4 ab | 36.9 b | 34.8 a | 33.5 b | 31.9 a | 32.2 ab |
| butyl acetate | 52.3 a | 59.7 b | 55.8 a | 55.4 a | 58.3 b | 56.3 a | 54.1 a | 52.8 a | 52.9 a |
| isoamyl acetate | 117.5 a | 124.9 a | 120.2 a | 118.1 a | 123.0 a | 117.9 a | 110.5 a | 110.6 a | 108.4 a |
| ethyl hexanoate | 256.6 a | 264.6 a | 257.3 a | 242.0 a | 248.2 a | 240.6 a | 216.9 a | 206.5 a | 210.6 a |
| hexyl acetate | 159.9 a | 163.8 a | 159.2 a | 150.4 a | 153.4 a | 149.5 a | 133.3 a | 126.1 a | 128.8 a |
| ethyl octanoate | 100.9 a | 94.7 a | 94.2 a | 84.6 a | 83.5 a | 83.2 a | 63.9 a | 59.5 a | 60.7 a |
| ethyl decanoate | 57.2 a | 45.8 a | 45.2 a | 45.0 a | 42.1 a | 42.6 a | 31.4 a | 28.2 a | 28.7 a |
| diethyl succinate | 2.2 a | 2.1 a | 2.1 a | 2.3 a | 2.2 a | 2.4 a | 4.2 a | 3.7 a | 4.0 a |
| β-phenylethyl acetate | 25.6 a | 29.5 a | 26.7 a | 28.3 a | 26.6 a | 28.8 a | 26.9 a | 25.5 a | 25.8 a |
| ethyl dodecanoate | 50.5 a | 31.7 a | 30.3 a | 25.6 b | 21.0 a | 20.3 a | 17.1 b | 10.7 a | 12.8 a |
| **alcohols** | | | | | | | | | |
| isobutanol | 0.2 a | 0.3 a | 0.3 a | 0.3 a | 0.3 a | 0.3 a | 0.5 a | 0.5 b | 0.5 a |
| 1-butanol | 1.9 a | 2.4 a | 2.4 a | 2.4 a | 2.5 a | 2.4 a | 2.3 a | 2.4 a | 2.3 a |
| isoamylic alcohols | 92.4 a | 116.7 b | 102.6 a | 113.3 a | 118.7 a | 117.6 a | 112.4 a | 117.0 b | 112.3 a |
| 1-hexanol | 17.5 a | 21.2 b | 19.0 a | 19.6 a | 20.3 a | 20.3 a | 19.5 a | 19.1 a | 19.2 a |
| *trans*-3-hexen-1-ol | 2.1 a | 2.5 a | 2.4 a | 2.3 a | 2.9 a | 2.5 a | 2.3 a | 2.2 a | 2.2 a |
| *cis*-3-hexen-1-ol | 1.7 a | 2.1 b | 2.1 b | 2.1 a | 2.1 a | 2.3 a | 2.0 a | 2.0 a | 2.2 b |
| benzyl alcohol | 0.4 a | 0.4 a | 0.4 a | 0.4 a | 0.4 a | 0.4 a | 0.4 a | 0.4 a | 0.4 a |
| β-phenylethyl alcohol | 3.8 a | 3.8 a | 3.7 a | 3.5 a | 3.4 a | 3.9 a | 3.9 a | 3.2 a | 3.7 a |
| **lactones/furanic compounds** | | | | | | | | | |
| furfural | 5.2 a | 6.1 b | 6.2 b | 4.8 b | 5.1 c | 4.5 a | 5.4 a | 5.6 a | 5.8 a |
| 5-methylfurfural | 2.2 a | 2.4 a | 2.5 a | 2.4 a | 2.3 a | 2.4 a | 2.4 a | 2.2 a | 2.5 a |
| γ-butyrolactone | 0.4 a | 0.5 a | 0.3 a | 0.4 a | 0.5 a | 0.5 a | 0.6 a | 0.5 a | 0.6 a |
| furfuryl alcohol | 0.2 a | 0.2 a | 0.2 a | 0.2 a | 0.2 a | 0.2 a | 0.2 a | 0.2 a | 0.2 a |
| *trans*-whiskey lactone | 1.4 a | 1.4 a | 1.3 a | 1.3 a | 1.3 a | 1.4 a | 1.4 a | 1.3 a | 1.3 a |
| *cis*-whiskey lactone | 0.9 a | 0.9 a | 0.8 a | 0.9 a | 0.9 a | 0.9 a | 1.0 a | 0.9 a | 0.9 a |
| γ-nonalactone | 0.5 a | 0.5 a | 0.5 a | 0.5 b | 0.5 a | 0.5 b | 0.5 a | 0.4 a | 0.5 a |
| **volatile phenols** | | | | | | | | | |
| 2-methoxy-4-ethylphenol (4-ethylguaicol) | 2.4 a | 2.4 a | 2.3 a | 2.4 a | 2.2 a | 2.5 a | 2.3 a | 2.2 a | 2.3 a |
| eugenol | 0.3 a | 0.3 a | 0.3 a | 0.3 ab | 0.3 a | 0.4 b | 0.3 a | 0.3 a | 0.3 a |
| 4-ethylphenol | 1.5 a | 1.6 a | 1.5 a | 1.5 a | 1.4 a | 1.7 a | 1.6 a | 1.4 a | 1.4 a |
| **C13-norisoprenoids** | | | | | | | | | |
| β-damascenone | 3.4 a | 3.8 a | 3.4 a | 3.6 a | 3.6 a | 3.8 a | 3.3 a | 3.1 a | 3.2 a |
| α-ionone | 5.4 a | 5.5 a | 4.9 a | 5.2 a | 5.2 a | 5.5 a | 4.7 a | 4.3 a | 4.5 a |
| β-ionone | 7.8 a | 8.1 a | 7.3 a | 8.3 a | 8.0 a | 8.7 a | 7.4 a | 6.7 a | 6.9 a |
| **acids** | | | | | | | | | |
| hexanoic acid | 1.0 a | 0.9 a | 1.1 a | 1.4 a | 1.4 a | 1.6 b | 1.3 b | 1.0 a | 1.1 a |
| octanoic acid | 2.5 a | 2.1 a | 2.6 a | 3.6 b | 3.1 a | 4.0 b | 3.0 a | 2.5 a | 2.4 a |
| decanoic acid | nd | nd | nd | nd | nd | nd | nd | nd | nd |

[a]All values (area: arbitrary units) are divided by a factor of 10000. Different letters (a–c) for the same aroma compound in the same wine type (synthetic, white, red) denote statistical differences among saliva types after application of LSD test.

factor. In the case of the postoral phase ($t$ = 10 min) the application of the same statistical treatment also showed a higher influence of wine matrix composition (22 compounds significantly affected) compared to the saliva effect (7


dx.doi.org/10.1021/jf503503b | J. Agric. Food Chem. 2014, 62, 8274–8288

compounds) and the interaction (5 compounds) (data not shown).

Compared to results from the previous static headspace analysis, the influence of saliva on aroma release seemed to be lower. The minor effect of saliva addition by using the dynamic approach compared to the static headspace analysis could have been due to a displacement of the equilibrium, which might reduce the retention effect produced by proteins[41] or by other nonvolatile wine matrix molecules, such as the above-mentioned protein−polyphenol−polysaccharide complexes. These findings are not surprising taking into consideration that several authors have already suggested that despite dynamic conditions might better simulate the consumption situation, static measurements are better suited for determining thermodynamic and kinetic parameters with good precision.[64]

In terms of amount of aroma release, it is interesting to note that higher releases for most of the aroma compounds were found during the postoral release step ($t$ = 10 min) (Table 6) compared to the oral phase (Table 5). This could be due to the higher extraction temperature in the postoral phase (36 °C) compared to the oral phase (25.5 °C). Previously, the effect of temperature (4, 23, 60 °C) on volatile release from oil/water emulsions using an artificial mouth system had been pointed out.[28] These authors showed a similar effect between 4 and 23 °C (release less pronounced), compared to 60 °C. In the present work, using more realistic temperatures closer to what was expected during wine consumption (25.5 and 36 °C), most of the volatile compounds showed higher release when the temperature was raised about 12 °C independent of the wine type. The increase in sampling temperature increases the partitioning of the volatiles into the gas phase following the van't Hoff law.[65] In addition, in ethanol solutions (as wine) and using dynamic headspace conditions, Tsachaki et al.[66] showed that the evaporation of ethanol at the solution vapor interface might create a surface tension gradient, making new ethanol molecules move from the bulk phase to replenish the depleted surface areas, carrying along an appreciable volume of underlying liquid with aroma compounds. This phenomenon, called the Marangoni effect,[67] might also explain the higher aroma release for most of the volatile compounds in the wines with a moderate increase in temperature.

To extract more conclusions on the role of saliva in aroma release using dynamic conditions, a LSD test for mean comparison was also performed for each type of wine (red, white, and artificial) in the oral and postoral phases. These results are also shown in Tables 5 and 6. Results show that during the oral phase ($t$ = 0), only three terpenes ($\alpha$- and $\beta$-pinenes, limonene) showed significantly lower release in the three types of wines with saliva (human and artificial) (Table 5). The same compounds were significantly less released in white and red wines with saliva during the postoral phase ($t$ = 10 min) (Table 6). These compounds are characterized by high log $P$ values, which seem to be in agreement with their involvement in the formation of hydrophobic interactions with wine polyphenols[58] or with their involvement in the formation of complexes with salivary proteins, polyphenols, and polysaccharides.

Surprisingly, and mainly during the oral phase, a relatively high number of aroma compounds were highly released in the wines with saliva, which seems to contradict results from the previous experiment performed in static conditions. This could be due to the higher sensitivity of the dynamic HS conditions over the static HS, which might have improved the detection of some aroma compounds.[41] For instance, some lactones (*cis*- and *trans*-whiskylactones, $\gamma$-nonalactone), furanic compounds (furfural, 5-methylfurfural), volatile phenols (eugenol, ethylphenol), C13 norisoprenoids ($\beta$-damascenone, $\alpha$-ionone, $\beta$-ionone), and terpene alcohols (linalool, terpinen-4-ol, $\alpha$-terpineol, $\beta$-citronellol, nerol) were more highly released in red wines with human saliva (Table 5). Some of these compounds, such as terpene alcohols, could have originated de novo from the corresponding grape glycosidic precursor that might have remained in the wine matrix after the desaromatization step. The existence of saliva glycoside activity has been recently shown.[68]

To better understand the impact of saliva on aroma release in the three types of wine matrices, aroma release data (peak area) taken at $t$ = 0 and $t$ = 10 min were independently submitted to PCA. Figure 3a shows the representation of the first two

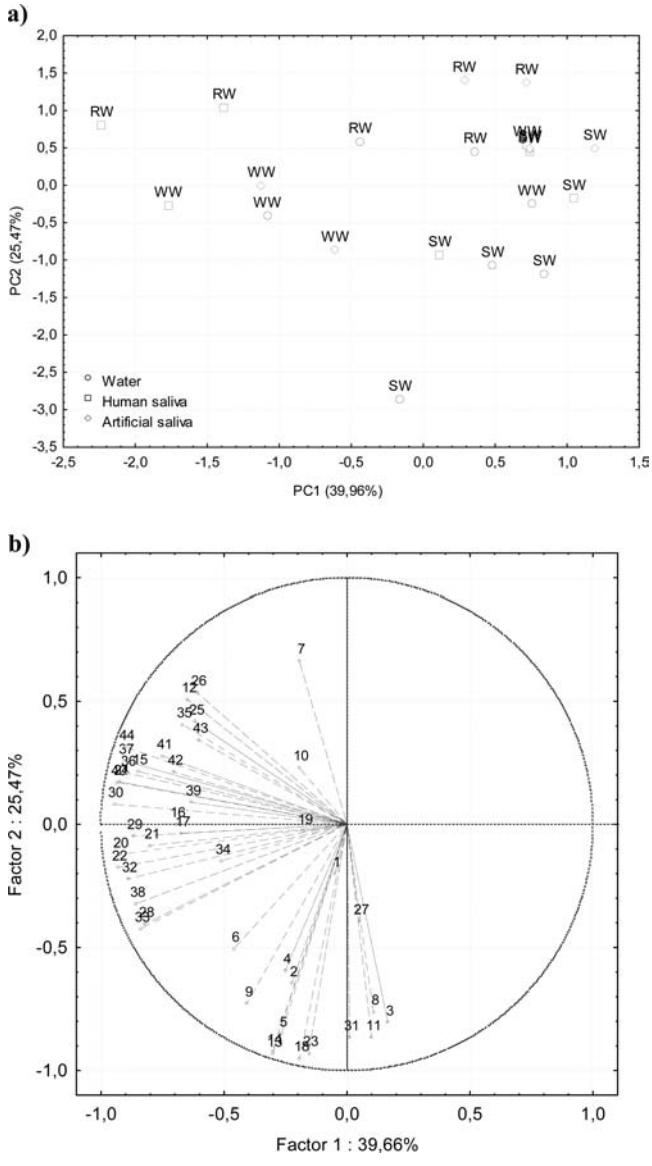


**Figure 3.** Graphic representation of the wine samples (a) and of the variables (b) obtained using PCA with the aroma release data from the dynamic HS-SPME-GC/MS analysis at $t$ = 0 (oral phase). Numbers of the variables in panel b correspond to the compounds listed in Table 1.


dx.doi.org/10.1021/jf503503b | J. Agric. Food Chem. 2014, 62, 8274−8288

principal components obtained after the application of this test to aroma release data collected from the wines at $t$ = 0. Both PCs explained >65% of data variation. As can be seen (Figure 3), similar to what happens in static conditions, the main differences among wine samples were found in the case of red wines. PC1 clearly separated red wines with water and artificial saliva from red wines with human saliva. The latter exhibited high and negative values for this component. The representation of the variables on the basis of the two first components (Figure 3b) shows how some variables such as *trans*- and *cis*-hexenol (16, 17), linalool (20), 5-methylfurfural (21), terpinen-4-ol (22), nerol (29), $\beta$-phenylethyl acetate (30), $\beta$-damascenone (32), and $\beta$-ionone (38), among others, were strongly and negatively correlated with PC1. Most of these compounds match those previously shown in the LSD test (Table 5) as significantly more released in red wines with saliva, which is the same conclusion obtained by PCA. In Figure 3a, PC2 also shows a separation of the samples depending on wine matrix composition. Red wines appeared on the top of the graph showing high values for this component, whereas white and mainly synthetic wines appeared in the low part of the graph with lower and even negative values for this component, especially in the water medium. As can be seen (Figure 3b), the most correlated (negatively) variables were, in general, ethyl esters such as ethyl octanoate (18), ethyl decanoate (23), and ethyl dodecanoate (31) and some nonalcoholic terpenes such $\alpha$-pinene (3), $\beta$-pinene (8), and limonene (11). It seems that these compounds (with high log $P$ values) might interact more with saliva protein and wine matrix than with synthetic wine. In the case of these three terpene compounds, this result was the same as previously shown in the LSD test.

Similar to the results found in the previous ANOVA and LSD tests, results from the PCA performed with release data collected during the postoral phase ($t$ = 10 min) did not show a clear grouping of wine samples depending on the medium composition (with human saliva, artificial saliva, or water) (Figure 4a). However, an influence on the wine matrix composition was indeed manifested. As can be seen, PC1 separates between red on the positive side of the graph and white and synthetic wines on the other side (Figure 4a), showing differences in their aroma release behaviors. Red wines exhibited higher values for this component than white wines. The projection of the variables on the plane defined by the first and second components (Figure 4b) shows that PC1 was highly correlated (negatively) with some aroma compounds such as terpinen-4-ol (22), $\beta$-citronellol (28), $\alpha$-ionone (33), $\beta$-phenylethyl alcohol (37), 4-ethylguaicol (40), and 4-ethylphenol (44), among others. In addition, PC2 also allowed a separation between synthetic wines with positive values for this component and white and red wines with negative values for it. In this case, PC2 was strongly and negatively correlated with some alcohols such as 1-butanol (10) or isoamylic alcohols (12) but positively with some nonalcoholic terpenes such as $\alpha$- and $\beta$-pinene (3, 8) and limonene (11).

In conclusion, the main finding of this work is that saliva has an important effect on aroma release from wine and this effect was different depending on wine matrix composition. In addition, we found differences depending on using human or artificial saliva, therefore proving that proteins other than mucins seem to have an important role in aroma release. Moreover, it has been shown that the effect of saliva on wine aroma release is more evident when using static than dynamic headspace conditions. In general, human saliva produces lower

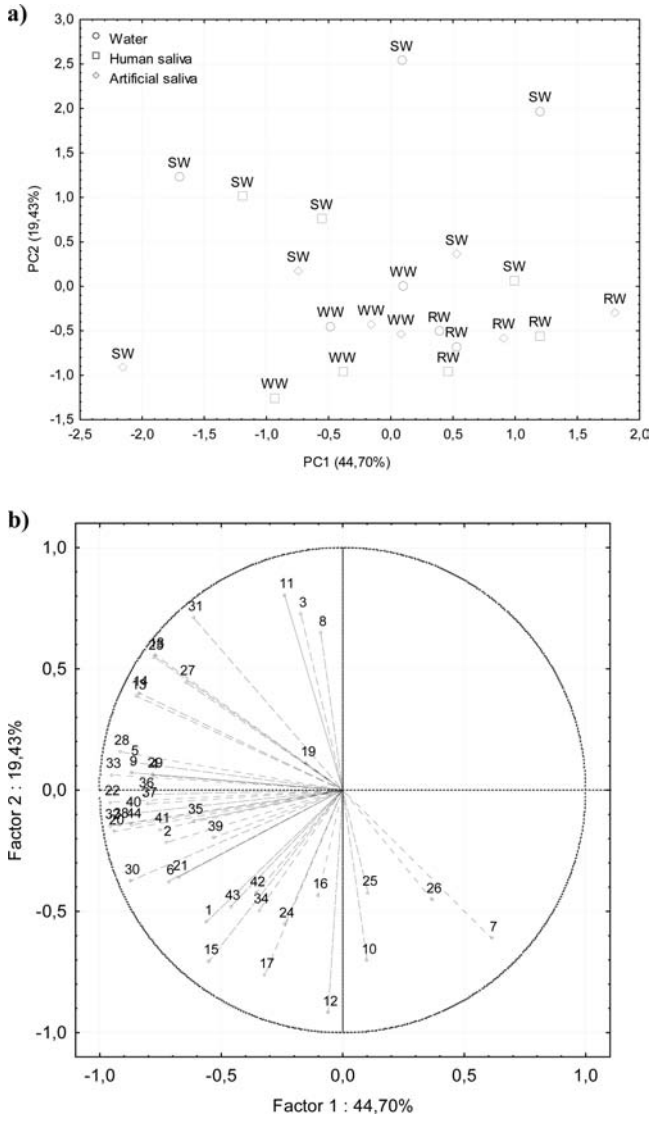


**Figure 4.** PCA of the graphic representation of the wine samples (a) and of the variables (b) obtained using PCA with the aroma release data from the dynamic HS-SPME-GC/MS analysis at $t$ = 10 min (post oral phase). Numbers of the variables in panel b correspond to the compounds listed in Table 1.

release for most of the wine volatile compounds, and this effect was more important in red than white wines. The interaction of aroma compounds with other proteins different from mucin or the formation of complexes involving saliva glycoproteins−wine polyphenols−wine polysaccharides and aroma compounds, preferentially for those aroma compounds with high log $P$ values (hydrophobic), seems to be responsible for the observed effect. In addition, large differences in the amount of aroma released depending on sampling temperature during the oral and postoral phases invite us to think about the importance of this second step of wine consumption as a mechanism in releasing aroma compounds from oral or throat wine reservoirs influencing long-lasting perception of aroma after swallowing. Finally, despite the minor impact of saliva observed in dynamic conditions, it is important to bear in mind that in vivo consumption conditions could represent a more dynamic process than that used in the present work, in which saliva is continuously produced and replenished (incorporating more proteins to interact with aroma compounds or enzymes) and


dx.doi.org/10.1021/jf503503b | J. Agric. Food Chem. 2014, 62, 8274−8288

also that "fresh" sample is continuously being provided. Therefore, the extent of its effect could be higher than that determined with the experimental in vitro dynamic headspace conditions used in this study. Overall, this work will contribute to insights into the role of oral physiology on wine aroma perception, which should be taken into consideration in the production of high-quality wines for targeted groups of consumers.

## ■ ASSOCIATED CONTENT

### Supporting Information

Table with the linear ranges and regression parameters calculated for the aroma compounds by using static and dynamic ($t$ = 0 and $t$ = 10 min) HS-SPME-GC/MS approaches. This material is available free of charge via the Internet at http://pubs.acs.org.

## ■ AUTHOR INFORMATION

### Corresponding Author

*(M.A.P.-B.) E-mail: m.delpozo@csic.es. Phone: +34 91 0017 961. Fax: +34 91 0017 905.

### Funding

This work was funded by the MINECO (AGL2012-04172-C02-01) and CONSOLIDER INGENIO 2010 (FUN-C-FOOD, CSD2007-063, Projects). C.M.-G. thanks CSIC for its research contract cofunded by the European Social Fund together with Regional Council for Burgundy and FEDER (European Union) for experiments realized in Dijon (France).

### Notes

The authors declare no competing financial interest.

## ■ ACKNOWLEDGMENTS

We give a special thank you to Karine Gourrat, Etienne Sémon, and Hélène Brignot for technical assistance, to the volunteers for providing us the saliva samples, and to ChemoSens Platform (CSGA, Dijon, France).

## ■ REFERENCES

(1) Ferreira, V.; Ortin, N.; Escudero, A.; Lopez, R.; Cacho, J. Chemical characterization of the aroma of Grenache rose wines: aroma extract dilution analysis, quantitative determination, and sensory reconstitution studies. *J. Agric. Food Chem.* **2002**, *50*, 4048−4054.

(2) Escudero, A.; Campo, E.; Farina, L.; Cacho, J.; Ferreira, V. Analytical characterization of the aroma of five premium red wines. Insights into the role of odor families and the concept of fruitiness of wines. *J. Agric. Food Chem.* **2007**, *55*, 4501−4510.

(3) Guth, H. Identification of character impact odorants of different white wine varieties. *J. Agric. Food Chem.* **1997**, *45*, 3022−3026.

(4) Pierce, J.; Halpern, B. P. Orthonasal and retronasal odorant identification based upon vapor phase input from common substances. *Chem. Senses* **1996**, *21*, 529−543.

(5) Buettner, A.; Beer, A.; Hannig, C.; Settles, M. Observation of the swallowing process by application of videofluoroscopy and real-time magnetic resonance imaging-consequences for retronasal aroma stimulation. *Chem. Senses* **2001**, *26*, 1211−1219.

(6) Buettner, A.; Beer, A.; Hannig, C.; Settles, M.; Schieberle, P. Physiological and analytical studies on flavor perception dynamics as induced by the eating and swallowing process. *Food Qual. Pref.* **2002**, *13*, 497−504.

(7) Taylor, A. J. Volatile flavor release from foods during eating. *Crit. Rev. Food Sci. Nutr.* **1996**, *36*, 765−784.

(8) Linforth, R.; Martin, F.; Carey, M.; Davidson, J.; Taylor, A. J. Retronasal transport of aroma compounds. *J. Agric. Food Chem.* **2002**, *50*, 1111−1117.

(9) Voirol, E.; Daget, N. Comparative-study of nasal and retronasal olfactory perception. *LWT−Food Sci. Technol.* **1986**, *19*, 316−319.

(10) Burdach, K. J.; Kroeze, J. H. A.; Koster, E. P. Nasal, retronasal, and gustatory perception − an experimental comparison. *Perception Psychophys.* **1984**, *36*, 205−208.

(11) Buettner, A.; Schieberle, P. Exhaled odorant measurement (EXOM) − a new approach to quantify the degree of in-mouth release of food aroma compounds. *LWT−Food Sci. Technol.* **2000**, *33*, 553−559.

(12) Buettner, A.; Beauchamp, J. Chemical input − sensory output: diverse modes of physiology-flavour interaction. *Food Qual. Pref.* **2010**, *21*, 915−924.

(13) Burdach, K. J.; Doty, R. L. The effects of tongue movements and swallowing on retronasal aroma perception. *Chem. Senses* **1987**, *12*, 181−181.

(14) Overbosch, P.; Afterof, W. G.; Haring, P. G. Flavor release in the mouth. *Food Rev. Int.* **1991**, *7*, 137−184.

(15) Harrison, M. Effect of breathing and saliva flow on flavor release from liquid foods. *J. Agric. Food Chem.* **1998**, *46*, 2727−2735.

(16) Mishellany-Dutour, A.; Woda, A.; Laboure, H.; Bourdiol, P.; Lachaze, P.; Guichard, E.; Feron, G. Retro-nasal aroma release is correlated with variations in the in-mouth air cavity volume after empty deglutition. *PLoS One* **2012**, *7*, 8.

(17) Neyraud, E.; Palicki, O.; Schwartz, C.; Nicklaus, S.; Feron, G. Variability of human saliva composition: possible relationships with fat perception and liking. *Arch. Oral Biol.* **2012**, *57*, 556−566.

(18) Drobitch, R. K.; Svensson, C. K. Therapeutic drug-monitoring in saliva − an update. *Clin. Pharmacokinetics* **1992**, *23*, 365−379.

(19) Buettner, A. Influence of human saliva on odorant concentrations. 2. Aldehydes, alcohols, 3-alkyl-2-methoxypyrazines, methoxyphenols, and 3-hydroxy-4,5-dimethyl-2(5*H*)-furanone. *J. Agric. Food Chem.* **2002**, *50*, 7105−7110.

(20) Buettner, A. Influence of human salivary enzymes on odorant concentration changes occurring in vivo. 1. Esters and thiols. *J. Agric. Food Chem.* **2002**, *50*, 3283−3289.

(21) McRae, J. M.; Kennedy, J. A. Wine and grape tannin interactions with salivary proteins and their impact on astringency: a review of current research. *Molecules* **2011**, *16*, 2348−2364.

(22) Salles, C.; Chagnon, M.-C.; Feron, G.; Guichard, E.; Laboure, H.; Morzel, M.; Semon, E.; Tarrega, A.; Yven, C. In-mouth mechanisms leading to flavor release and perception. *Crit. Rev. Food Sci. Nutr.* **2011**, *51*, 67−90.

(23) Friel, E. N.; Taylor, A. J. Effect of salivary components on volatile partitioning from solutions. *J. Agric. Food Chem.* **2001**, *49*, 3898−3905.

(24) vanRuth, S. M.; Roozen, J. P.; Nahon, D. F.; Cozijnsen, J. L.; Posthumus, M. A. Flavour release from rehydrated French beans (*Phaseolus vulgaris*) influenced by composition and volume of artificial saliva. *Z. Lebensm. Unters. Forsch.* **1996**, *203*, 1−6.

(25) van Ruth, S. M.; Buhr, K. Influence of saliva on temporal volatile flavour release from red bell peppers determined by proton transfer reaction-mass spectrometry. *Eur. Food Res. Technol.* **2003**, *216*, 220−223.

(26) Hansson, A.; Giannouli, P.; Van Ruth, S. The influence of gel strength on aroma release from pectin gels in a model mouth and in vivo, monitored with proton-transfer-reaction mass spectrometry. *J. Agric. Food Chem.* **2003**, *51*, 4732−4740.

(27) Boland, A. B.; Buhr, K.; Giannouli, P.; van Ruth, S. M. Influence of gelatin, starch, pectin and artificial saliva on the release of 11 flavour compounds from model gel systems. *Food Chem.* **2004**, *86*, 401−411.

(28) Benjamin, O.; Silcock, P.; Beauchamp, J.; Buettner, A.; Everett, D. W. Tongue pressure and oral conditions affect volatile release from liquid systems in a model mouth. *J. Agric. Food Chem.* **2012**, *60*, 9918−9927.

(29) Pionnier, E.; Nicklaus, S.; Chabanet, C.; Mioche, L.; Taylor, A. J.; Le Quere, J. L.; Salles, C. Flavor perception of a model cheese: relationships with oral and physico-chemical parameters. *Food Qual. Pref.* **2004**, *15*, 843−852.

(30) Rabe, S.; Linforth, R. S. T.; Krings, U.; Taylor, A. J.; Berger, R. G. Volatile release from liquids: a comparison of in vivo APCI-MS, in-mouth headspace trapping and in vitro mouth model data. *Chem. Senses* **2004**, *29*, 163−173.
(31) Muñoz-Gonzalez, C.; Rodriguez-Bencomo, J. J.; Moreno-Arribas, M. V.; Pozo-Bayon, M. A. Beyond the characterization of wine aroma compounds: looking for analytical approaches in trying to understand aroma perception during wine consumption. *Anal. Bioanal. Chem.* **2011**, *401*, 1497−1512.
(32) Cala, O.; Dufourc, E. J.; Fouquet, E.; Manigand, C.; Laguerre, M.; Pianet, I. The colloidal state of tannins impacts the nature of their interaction with proteins: the case of salivary proline-rich protein/procyanidins binding. *Langmuir* **2012**, *28*, 17410−17418.
(33) Rinaldi, A.; Gambuti, A.; Moio, L. Precipitation of salivary proteins after the interaction with wine: the effect of ethanol, pH, fructose, and mannoproteins. *J. Food Sci.* **2012**, *77*, 485−490.
(34) de Freitas, V.; Mateus, N. Protein/polyphenol interactions: past and present contributions. Mechanisms of astringency perception. *Curr. Org. Chem.* **2012**, *16*, 724−746.
(35) Mateus, N.; Pinto, R.; Ruao, P.; de Freitas, V. Influence of the addition of grape seed procyanidins to Port wines in the resulting reactivity with human salivary proteins. *Food Chem.* **2004**, *84*, 195−200.
(36) Simon, C.; Barathieu, K.; Laguerre, M.; Schmitter, J. M.; Fouquet, E.; Pianet, I.; Dufourc, E. J. Three-dimensional structure and dynamics of wine tannin-saliva protein complexes. A multitechnique approach. *Biochemistry* **2003**, *42*, 10385−10395.
(37) Kallithraka, S.; Bakker, J.; Clifford, M. N.; Vallis, L. Correlations between saliva protein composition and some T-I parameters of astringency. *Food Qual. Pref.* **2001**, *12*, 145−152.
(38) Genovese, A.; Piombino, P.; Gambuti, A.; Moio, L. Simulation of retronasal aroma of white and red wine in a model mouth system. Investigating the influence of saliva on volatile compound concentrations. *Food Chem.* **2009**, *114*, 100−107.
(39) Mitropoulou, A.; Hatzidimitriou, E.; Paraskevopoulou, A. Aroma release of a model wine solution as influenced by the presence of non-volatile components. Effect of commercial tannin extracts, polysaccharides and artificial saliva. *Food Res. Int.* **2011**, *44*, 1561−1570.
(40) Lasekan, O. A comparative analysis of the influence of human salivary enzymes on odorant concentration in three palm wines. *Molecules* **2013**, *18*, 11809−11823.
(41) Fabre, M.; Aubry, V.; Guichard, E. Comparison of different methods: Static and dynamic headspace and solid-phase microextraction for the measurement of interactions between milk proteins and flavor compounds with an application to emulsions. *J. Agric. Food Chem.* **2002**, *50*, 1497−1501.
(42) Escalona, H.; Piggott, J. R.; Conner, J. M.; Paterson, A. Effect of ethanol strength on the volatility of higher alcohols and aldehydes. *Ital. J. Food Sci.* **1999**, *11*, 241−248.
(43) Robinson, A. L.; Ebeler, S. E.; Heymann, H.; Boss, P. K.; Solomon, P. S.; Trengove, R. D. Interactions between wine volatile compounds and grape and wine matrix components influence aroma compound headspace partitioning. *J. Agric. Food Chem.* **2009**, *57*, 10313−10322.
(44) Rodriguez-Bencomo, J. J.; Conde, J. E.; Rodriguez-Delgado, M. A.; Garcia-Montelongo, F.; Perez-Trujillo, J. P. Determination of esters in dry and sweet white wines by headspace solid-phase microextraction and gas chromatography. *J. Chromatogr., A* **2002**, *963*, 213−223.
(45) Conner, J. M.; Birkmyre, L.; Paterson, A.; Piggott, J. R. Headspace concentrations of ethyl esters at different alcoholic strengths. *J. Sci. Food Agric.* **1998**, *77*, 121−126.
(46) Poette, J.; Mekoué, J.; Neyraud, E.; Berdeaux, O.; Renault, A.; Guichard, E.; Genot, C.; Feron, G. Fat sensitivity in humans: oleic acid detection threshold is linked to saliva composition and oral volume. *Flavour Fragrance J.* **2014**, *29*, 39−49.
(47) Rodriguez-Bencomo, J. J.; Muñoz-Gonzalez, C.; Andujar-Ortiz, I.; Martin-Alvarez, P. J.; Moreno-Arribas, M. V.; Pozo-Bayon, M. A. Assessment of the effect of the non-volatile wine matrix on the volatility of typical wine aroma compounds by headspace solid phase microextraction/gas chromatography analysis. *J. Sci. Food Agric.* **2011**, *91*, 2484−2494.
(48) Lubbers, S.; Decourcelle, N.; Vallet, N.; Guichard, E. Flavor release and rheology behavior of strawberry fatfree stirred yogurt during storage. *J. Agric. Food Chem.* **2004**, *52*, 3077−3082.
(49) Poette, J.; Lubbers, S.; Maison, B.; Andriot, I.; Pernin, K.; Guichard, E.; Cavellec, A.; Feron, G. The salivary reactor: an innovating tool for the categorization of food products through their aroma and taste compounds release profiles. In *Advances and Challenges in Flavor Chemistry and Biology*, Proceedings of the 9th Warburg Symposium; Hofmann, T., Meyerhof, W., Schieberle, P., Eds.; Deutsche Forschungsanstalt für Lebensmittelchemie: Freising, Germany, 2010; pp 386−389.
(50) Natera Marin, R.; Castro Mejias, R.; De Valme Garcia Moreno, M.; Garcia Rowe, F.; Garcia Barroso, C. Headspace solid-phase microextraction analysis of aroma compounds in vinegar. Validation study. *J. Cromatogr., A* **2002**, *967*, 261−267.
(51) Popp, P.; Paschke, A. Solid phase microextraction of volatile organic compounds using carboxen-polydimethylsiloxane fibers. *Chromatographia* **1997**, *46*, 419−424.
(52) Yang, S. S.; Huang, C. B.; Smetena, I. Optimization of headspace sampling using solid-phase microextraction for volatile components in tobacco. *J. Chromatogr., A* **2002**, *942*, 33−39.
(53) Ai, J. Solid phase microextraction for quantitative analysis in nonequilibrium situations. *Anal. Chem.* **1997**, *69*, 1230−1236.
(54) Mounayar, R.; Septier, C.; Chabanet, C.; Feron, G.; Neyraud, E. Oral fat sensitivity in humans: links to saliva composition before and after stimulation by oleic acid. *Chemosens. Percept.* **2013**, *6*, 118−126.
(55) van Ruth, S. M.; Grossmann, I.; Geary, M.; Delahunty, C. M. Interactions between artificial saliva and 20 aroma compounds in water and oil model systems. *J. Agric. Food Chem.* **2001**, *49*, 2409−2413.
(56) Hussein, M. M.; Kachikian, R.; Pidel, A. R. Analysis for flavor residuals in the mouth by gas-chromatography. *J. Food Sci.* **1983**, *48*, 1884−1885.
(57) Kopjar, M.; Andriot, I.; Saint-Eve, A.; Souchon, I.; Guichard, E. Retention of aroma compounds: an interlaboratory study on the effect of the composition of food matrices on thermodynamic parameters in comparison with water. *J. Sci. Food Agric.* **2010**, *90*, 1285−1292.
(58) Dufour, C.; Bayonove, C. Interactions between wine polyphenols and aroma substances. An insight at the molecular level. *J. Agric. Food Chem.* **1999**, *47*, 678−684.
(59) Jung, D. M.; de Ropp, J. S.; Ebeler, S. E. Study of interactions between food phenolics and aromatic flavors using one- and two-dimensional H-1 NMR spectroscopy. *J. Agric. Food Chem.* **2000**, *48*, 407−412.
(60) Aronson, J.; Ebeler, S. E. Effect of polyphenol compounds on the headspace volatility of flavors. *Am. J. Enol. Viticul.* **2004**, *55*, 13−21.
(61) Lasekan, O.; Buettner, A.; Christlbauer, M. Investigation of the retronasal perception of palm wine (*Elaeis guineensis*) aroma by application of sensory analysis and exhaled odorant measurement (EOM). *Afr. J. Food Agric. Nutr. Dev.* **2009**, *9*, 793−813.
(62) Canon, F.; Pate, F.; Cheynier, V.; Sarni-Manchado, P.; Giuliani, A.; Perez, J.; Durand, D.; Li, J.; Cabane, B. Aggregation of the salivary proline-rich protein IB5 in the presence of the tannin EgCG. *Langmuir* **2013**, *29*, 1926−1937.
(63) Muñoz-Gonzalez, C.; Martin-Alvarez, P. J.; Moreno-Arribas, M. V.; Pozo-Bayon, M. A. Impact of the nonvolatile wine matrix composition on the in vivo aroma release from wines. *J. Agric. Food Chem.* **2014**, *62*, 66−73.
(64) Juteau, A.; Cayot, N.; Chabanet, C.; Doublier, J. L.; Guichard, E. Flavour release from polysaccharide gels: different approaches for the determination of kinetic parameters. *Trends Food Sci. Technol.* **2004**, *15*, 394−402.
(65) Tromelin, A.; Andriot, I.; Kopjar, M.; Guichard, E. Thermodynamic and structure property study of liquid-vapor equilibrium for aroma compounds. *J. Agric. Food Chem.* **2010**, *58*, 4372−4387.
(66) Tsachaki, M.; Gady, A. L.; Kalopesas, M.; Linforth, R. S. T.; Athes, V.; Marin, M.; Taylor, A. J. Effect of ethanol, temperature, and

gas flow rate on volatile release from aqueous solutions under dynamic headspace dilution conditions. *J. Agric. Food Chem.* **2008**, *56*, 5308−5315.

(67) Spedding, P. L.; Grimshaw, J.; Ohare, K. D. Abnormal evaporation rate of ethanol from low concentration aqueous-solutions. *Langmuir* **1993**, *9*, 1408−1413.

(68) Mayr, C. M.; Parker, M.; Baldock, G. A.; Black, C. A.; Pardon, K. H.; Williamson, P. O.; Herderich, M. J.; Francis, I. L. Determination of the importance of in-mouth release of volatile phenol glycoconjugates to the flavor of smoke-tainted wines. *J. Agric. Food Chem.* **2014**, *62*, 2327−2336.

JOURNAL OF AGRICULTURAL AND FOOD CHEMISTRY

Article

pubs.acs.org/JAFC

# Dimethyl Sulfide as a Source of the Seaweed-like Aroma in Cooked Soybeans and Correlation with Its Precursor, *S*-Methylmethionine (Vitamin U)

Akira Morisaki,[†] Naohiro Yamada,[‡] Shiori Yamanaka,[†] and Kenji Matsui*[,†]

[†]Graduate School of Medicine (Agriculture) and Department of Biological Chemistry, Faculty of Agriculture, Yamaguchi University, Yamaguchi 753-8515, Japan

[‡]Nagano Vegetable and Ornamental Crops Experiment Station, Shiojiri, Nagano 399-6461, Japan

Supporting Information

**ABSTRACT:** Among the soybean germplasm in Japan, two varieties, Nishiyamahitashi 98-5 (NH) and Shinanokurakake (SKK), have an intense seaweed-like flavor after cooking. Gas−liquid chromatography with mass spectrometry (GC-MS) indicated that a significant amount (11.5 ± 3.46 $\mu$g g$^{-1}$ for NH and 6.66 ± 0.91 $\mu$g g$^{-1}$ for SKK) of dimethyl sulfide (DMS) was formed after heat treatment. DMS is formed from *S*-methylmethionine (SMM, vitamin U). SMM was detected in all soybean varieties examined here, but its concentration in NH and SKK seeds was >100-fold higher than in the other varieties and ranged from 75 to 290 $\mu$g g$^{-1}$. The SMM content and the ability to form DMS upon heat treatment correlated among them. The plumes and radicles contained SMM exclusively. This is the first report of soybean varieties containing SMM at a level equivalent to or higher than that in vegetables known to contain high levels of SMM, for example, turnip, cabbage, and celery.

**KEYWORDS:** *soybean, flavor, dimethyl sulfide, S-methylmethionine*

## INTRODUCTION

Soybean, *Glycine max* (L.) Merr., is the most important legume plant and the fifth most important crop in the world in terms of quantity of production after maize, rice, wheat, and potato (FAOSTAT, 2012, http://faostat3.fao.org/faostat-gateway/go/to/home/E). Soybean seeds contain large amounts of oils (18−20%) and proteins (40%−45%);[1] accordingly, they are widely used as a source of nutritious foods for humans and livestock. Recently, a variety of claims about health benefits of soy products increased the consumption of soybeans. Because of its importance, the soybean is regarded as a model legume crop, and in 2010, a whole-genome sequence of the representative variety Williams 82 was published.[2] At the same time, a wide diversity of agronomic and food-related chemical properties such as the level of proteins, lipids, isoflavones, and saponins as well as flavor properties have been reported for different varieties of soybean;[1,3,4] therefore, a lot of effort has been devoted to the establishment of germplasm collections worldwide. For example, approximately 11300 soybean-related accession numbers are available in the National Institute of Agrobiological Sciences Genebank, Japan (https://www.gene.affrc.go.jp/index_en.php). Each entry has a distinct color, shape, size, and other agronomic traits.[4] During our effort to identify new traits in the Japanese germplasm, we noticed a unique seaweed-like flavor in some of the traditional varieties locally cultivated and consumed in the central part of Japan (around Nagano prefecture). In these regions, soybean seeds with seed coat colors of green and black are widely consumed. The colored soybean seeds with the seaweed-like flavor are consumed after boiling of water-soaked seeds with a modicum of soy sauce and sugar. Colored soybeans such as black and green soybeans have high isoflavone and anthocyanin contents, respectively;[5] thus, their use as a functional food is to be expected.

Dimethyl sulfide (DMS) is a typical volatile organic sulfur compound with a characteristic seaweed-like and boiled cabbage-like odor. DMS is formed enzymatically in a lyase reaction involving dimethylsulfoniopropionate in a wide variety of seaweed species.[6] DMS is considered a key flavor constituent in cooked vegetables, such as tomato, cabbage, and asparagus.[7−9] DMS is one of the markers that differentiate black truffle (*Tuber melanosporum*) and Chinese truffle (*Tuber indicum*), with stronger aromatic contribution to the former.[10] Formation of DMS was also reported in soy milk prepared using heat treatment at 90 °C for 10 min.[11] DMS has a disagreeable odor at high concentrations but is beneficial to the aroma of lager types of beer at a concentration between 30 and 100 $\mu$g L$^{-1}$[12] and some types of red wine at a concentration of 100 $\mu$g L$^{-1}$.[13,14]

In vegetables and green malts, DMS is formed via thermal degradation of its precursor, *S*-methylmethionine (SMM).[9] The latter was originally called vitamin U because it has an antiulcerogenic activity, and it reduces gastric mucosal damage induced by ethanol in rats.[15] It is an active ingredient in an over-the-counter gastrointestinal drug widely used in Japan (Cabagin Kowa, Kowa Co., Ltd.). Furthermore, SMM has been shown to have a choline-sparing activity in poultry.[16] It is also reported that SMM inhibits adipocyte differentiation via down-regulation of adipogenic factors and up-regulation of AMP-

Received: April 4, 2014
Revised: August 3, 2014
Accepted: August 4, 2014
Published: August 4, 2014

ACS Publications © 2014 American Chemical Society



dx.doi.org/10.1021/jf501614j | J. Agric. Food Chem. 2014, 62, 8289−8294

activated protein kinase.[17] Such beneficial biological activities of SMM should make food products containing it attractive to consumers.

Until now, soybeans have not been recognized as food products containing high concentrations of SMM. The traditional soybean varieties that show an intense seaweed-like flavor especially after boiling are believed to contain a relatively high concentration of SMM, which would be degraded to DMS upon heating. We examined the SMM contents of several soybean varieties and compared them with those of other soybean varieties. Because of the unique flavor resulting from DMS and the possible pharmaceutical properties of SMM, identification of varieties that contain a substantial concentration of SMM should open up opportunities for novel uses of soybeans.

## MATERIALS AND METHODS

**Plant Materials.** Seeds of a leading Japanese cultivar, Fukuyutaka (FK), widely used for tofu in Japan,[18] were harvested at Saga City (E 130° 18′, N 33° 14′; annual mean temperature, 17 °C), Saga, Japan, in 2011 (provided by Dr. Toyoaki Anai, Saga University, Japan). The other varieties, Shinanomidori (SM), Shinanokuro (SK), Nakasennari (NS), Gankui (GK), Shinanokurakake (SKK), and Nishiyamahitashi 98-5 (NH; Figure 1), are traditional varieties in the Nagano prefecture

**Figure 1.** Seven varieties of soybean used in this study.

(central Japan) and were harvested in 2011 in an experimental field at the Nagano Vegetable and Ornamental Crops Experimental Station, Shiojiri City (E 137° 57′, N 36° 06′; annual mean temperature, 11 °C), Nagano, Japan. SKK and NH have a green color with a black patch and are known to produce a seaweed-like flavor. The seaweed-like flavor is enhanced after boiling. The seaweed-like flavor is hardly detected in the other varieties used here even after boiling. SM is a green soybean without a black patch, and SK and GK are black soybeans. NS is a yellow soybean and is used as a control similar to FK but grown in the same field with the other colored soybeans. The seeds were kept at 4 °C under dry conditions until use.

**Chemicals.** L-Methionine-*S*-methyl-$d_6$ sulfonium chloride ($d_6$-SMM) was purchased from Toronto Research Chemicals Inc. (Toronto, Ontario, Canada) via the distributor Funakoshi Co., Ltd. (Tokyo, Japan). DL-SMM sulfonium chloride was purchased from Tokyo Chemical Industry Co. (Tokyo, Japan). 1-Octen-3-ol was from Alfa Aesar (Lancashire, UK), and isobutanol, *n*-hexanal, *n*-hexan-1-ol, and dimethyl sulfide were purchased from Wako Pure Chemicals (Osaka, Japan).

**Analysis of Volatiles.** We collected volatiles at 25 °C to avoid any further changes that might happen at higher temperatures. The volatiles from intact soaked seeds, with and without heat treatment, were collected to analyze the way the colored seeds were consumed in the region where they were popular. The seeds (1 g, corresponding to 2−5 seeds depending on the seed size) were soaked in 8 mL of distilled water for 8 h at 4 °C in a glass vial (22 mL, PerkinElmer, Waltham, MA, USA). The vial was kept open during the soaking period. Thereafter, the vial was sealed tightly with a butyl rubber stopper and a crimp top seal (National Scientific, Rockwood, TN, USA). Heat treatment of soybean seeds was carried out at 80 °C for 30 min, keeping the vial sealed. This temperature was chosen because it is often used to prepare various types of soy milk.[19,20] Volatiles from the soaked seeds were collected without heat treatment. After chilling of the seeds to 25 °C, we collected the volatiles by using the solid-phase microextraction (SPME) fiber (50/30 μm DVB/Carboxen/PDMS, Supelco, Bellefonte, PA, USA; preconditioned immediately prior to use at 240 °C for 37 min) by exposing the fiber to the headspace for 30 min at 25 °C. The fiber was inserted into the insertion port of a gas chromatography−mass spectrometry (GC-MS) system (QP-5050, Shimadzu, Kyoto, Japan) equipped with a Stabilwax column (30 m × 0.25 mm i.d. × 0.25 μm film thickness, Restek, Bellefonte, PA, USA). The column temperature was programmed as follows: 40 °C for 5 min followed by an increase of 5 °C $min^{-1}$ to 200 °C. The carrier gas (He) was delivered at 86.1 kPa. The glass insert was an SPME sleeve (Supelco). Splitless injection with a sampling time of 1 min was used. The fiber was held in the injection port for 10 min to remove completely any compounds from the matrix. The temperature of the injector and interface was 240 °C. The mass detector was operated in the electron impact mode with ionization energy of 70 eV. Full-scan acquisition was used in the 40−350 atomic mass unit range of masses. To identify each compound, we used retention time and an MS profile of corresponding standard samples. The corresponding MS profiles in the NIST08 database (Shimadzu) were also used. For quantitation, an aqueous solution (10 mg $mL^{-1}$) of each compound was prepared in 10 mg $mL^{-1}$ Tween 20. The solutions were mixed at different ratios, and then water was added to 8 mL in a glass vial. Immediately after mixing of the solutions, the vial was tightly sealed, and the volatiles in the headspace were collected using the SPME fiber at 25 °C for 30 min. A calibration curve for each compound was constructed, and the area was calculated using integration software (GC-MS Solution, Shimadzu; Supporting Information Figure S1). The limit of detection for DMS, *n*-hexanal, *n*-hexan-1-ol, or 1-octen-3-ol was 30, 10, 20, or 20 ng $g^{-1}$, respectively. All measurements were performed in triplicate for each sample. The precision of the GC-MS method was determined by injecting a mixture of standards five times: dimethyl sulfide (5 μg), *n*-hexanal (0.1 μg), *n*-hexan-1-ol (0.1 μg), and 1-octen-3-ol (0.2 μg) suspended in 8 mL of $H_2O$. The relative standard errors (RSEs) for dimethyl sulfide, *n*-hexanal, *n*-hexan-1-ol, and 1-octen-3-ol were 3.08, 2.14, 1.03, and 2.46%, respectively. When the volatiles formed after treatment of NH seeds at 80 °C for 30 min were analyzed five times, RSEs for dimethyl sulfide, *n*-hexanal, *n*-hexan-1-ol, and 1-octen-3-ol were 5.15, 23.2, 10.2, and 14.4%, respectively.

**Quantitation of *S*-Methylmethionine.** This procedure was carried out essentially as per the procedure reported by Scherb et al.[9] The seeds were powdered using a force mill (Osaka Chemical Co., Ltd., Osaka, Japan). The powder (1 g) was suspended in 20 mL of 0.1 M sodium acetate buffer (pH 4.4). A portion (0.2 mL) of the suspension was mixed with 20 μL of 0.05 mg $mL^{-1}$ $d_6$-SMM in water as the internal standard and then mixed with 2 mL of MeOH/water (7:3, v/v). The mixture was shaken on a reciprocal shaker at 25 °C for 30 min. Thereafter, the mixture was centrifuged at 1500 rpm (Kubota 8100 centrifuge with RS 3000/6 rotor; Kubota Co., Tokyo, Japan) for 10 min at room temperature, and the resultant supernatant was collected. After removal of MeOH with $N_2$ gas flow, 1 mL of ethyl acetate was added, vigorously mixed, and centrifuged at 1500 rpm (same centrifuge) for 5 min. The lower aqueous phase was collected and cleared using Ekicrodisc 3 (0.45 μm, 3 mm, Wako Pure Chemicals). The cleared solution was mixed with acetonitrile/water (1:1, v/v) to the total volume of 2.5 mL.

Liquid chromatography with tandem mass spectrometry (LC-MS/MS) was performed on an AB Sciex (Framingham, MA, USA) 3200 Q-TRAP LS-MS/MS system equipped with a Prominence UFLC (Shimadzu). Chromatography was carried out on a Discovery HS F5 column (15 cm × 2.1 mm, 3 μm; Supelco) using 20% acetonitrile in water supplemented with 0.1% formic acid at a flow rate of 0.1 mL $min^{-1}$. The injection volume was 5 μL. The column temperature was set to 40 °C. The compound was detected using electrospray ionization (ESI) in the positive ion mode [ion spray voltage, 5500 V; nitrogen as the curtain gas (set to 35 arbitrary units)] with the multiple reaction monitoring (MRM) mode (Q1/Q3 mass, 164.113/102.000 for SMM and 170.113/102.000 for $d_6$-SMM; declustering potential, 16 V; energy potential, 5 V; collision energy potential, 10 V; collision

energy, 13 V). A calibration curve for SMM was constructed, and the area was calculated using integration software (Analyst, ABSciex; Supporting Information Figure S2). On the basis of the calibration curve, a response factor of 0.863 was calculated.

The precision of the LC-MS/MS method was determined by injecting a 1 $\mu$g mL$^{-1}$ solution of $d_6$-SMM four times. The RSE was found to be 0.84%. When SMM in NH seed powder was analyzed four times, the RSE for SMM was 2.22%. The recovery was validated by spiking the heat-treated NH seeds with a known amount of $d_6$-SMM. The results showed that 52.7% of the theoretical amount of $d_6$-SMM was recovered.

**Statistical Analysis.** All of the experiments were conducted at least in triplicate. The differences were evaluated using one-way analysis of variance (ANOVA) with Tukey's test in Excel Toukei (Social Survey Research Information Co., Ltd., Tokyo, Japan).

## RESULTS AND DISCUSSION

We collected six varieties of soybeans that are grown in the local area in the central part of Japan and one variety that is widely grown throughout Japan (Figure 1). Fukuyutaka (FK) is a strain widely grown in Japan as an ingredient of tofu and was used as a control in this study. Nakasennari (NS) is also a soybean variety that is widely grown (for tofu production) in the central part of Japan. Shinanokurakake (SKK) and Nishiyamahitashi 98-5 (NH) are the traditional varieties in the Nagano prefecture (central Japan). These soybean seeds are usually eaten after boiling with a modicum of soy sauce and sugar, and they are known to produce a seaweed-like flavor, especially after boiling. Their seed coat color is green with a black patch that resembles a saddle on horseback; therefore, they are sometimes called "saddle-bearing" soybeans (*Kurakakemame* in Japanese). Shinanomidori (SM) is also a traditional variety in Nagano prefecture and is consumed after boiling, but it does not smell like seaweed. It has a green seed coat without the black "saddle". Shinanokuro (SK) and Gankui (GK) are black soybeans. SM, SK, and GK were used as controls to evaluate the effect of the seed coat color on the flavor. To identify the compound responsible for the seaweed-like flavor after boiling, we examined volatiles formed before and after heat treatment in whole seeds.

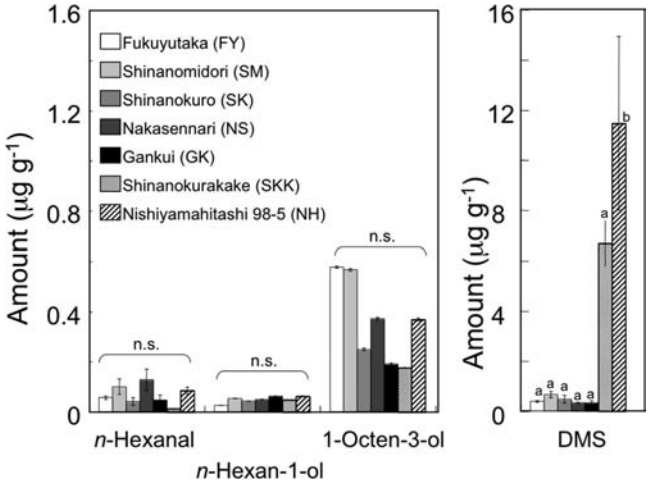


**Figure 2.** Concentration of volatile compounds formed in heat-treated soybean seeds. The concentrations of *n*-hexanal, *n*-hexan-1-ol, and 1-octen-3-ol (left panel) and dimethyl sulfide (DMS; right panel) detected in the headspace of heat-treated soybean seeds were determined using solid phase microextraction with gas–liquid chromatography and mass spectrometry. Means ± standard error (error bars) are shown ($n$ = 3). Different letters indicate significant differences, and n.s. means that there is no significant difference (analysis of variance, Tukey's test, $p < 0.05$).

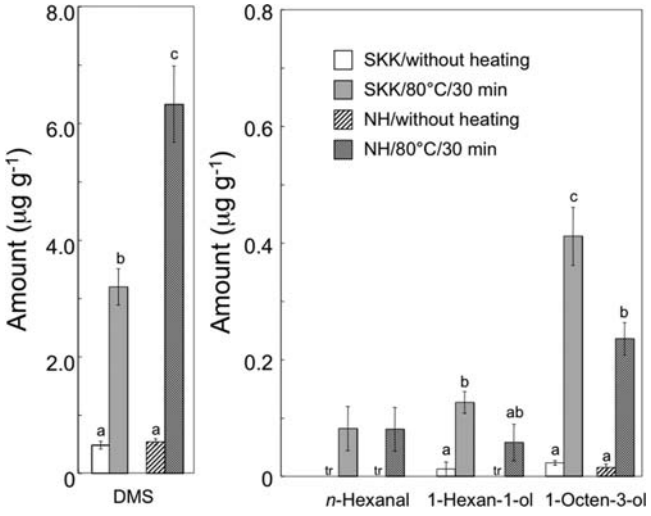


**Figure 3.** Effect of heat treatment on the concentration of dimethyl sulfide (DMS) in the headspace of Sinanokurakake (SKK) and Nishiyamahitashi (NH) soybean seeds. The seeds were soaked in 8 mL of water, and immediately, or after heating at 80 °C for 30 min, the concentration of DMS was determined. Means ± standard error (error bars) are shown ($n$ = 3). Different letters indicate significant differences (analysis of variance, Tukey's test, $p < 0.05$).

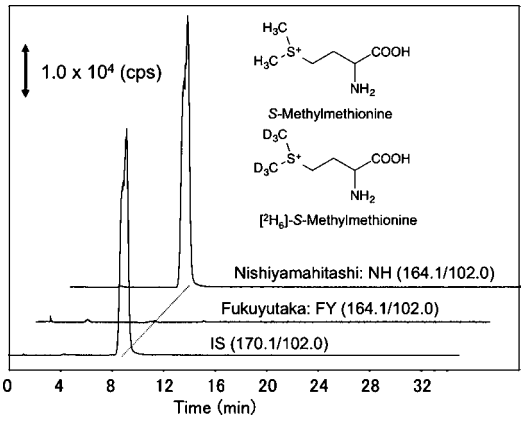


**Figure 4.** Detection of *S*-methylmethionine (SMM) in the multiple reaction monitoring (MRM) mode of liquid chromatography with tandem mass spectrometry (LC-MS/MS). We performed LC-MS/MS analyses of the extracts from Nishiyamahitashi (NH) and Fukuyutaka (FY) by following the signal of 164.113 (Q1)/102.000 (Q3) as well as the analysis of a standard sample of L-methionine-*S*-methyl-$d_6$ sulfonium chloride ($d_6$-SMM) by following the signal of 170.113 (Q1)/102.000 (Q3) (top, middle, and bottom chromatograms, respectively). The structures of SMM and $d_6$-SMM are shown.

After overnight soaking and heat treatment of the intact seeds, *n*-hexanal, *n*-hexan-1-ol, and 1-octen-3-ol were detected in all seven varieties (Figure 2; Supporting Information Figure S3). These were the typical volatile compounds most abundant in homogenized soybean seeds.[21,22] Even though the content of *n*-hexanal, *n*-hexan-1-ol, and 1-octen-3-ol somehow varied depending on the variety analyzed, the differences in their concentrations in the seven soybean varieties were insignificant (Figure 2). The concentrations of *n*-hexanal detected in heat-treated soybean seeds in this study (ranging from 0.01 to 0.13

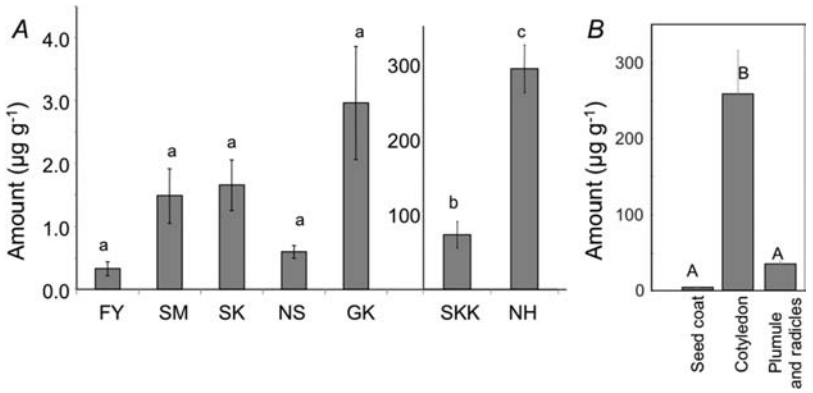


**Figure 5.** Concentration of SMM in whole seeds of each variety of soybean (A) and that in seed coats, cotyledons, and plumules with radicles in Nishiyamahitashi (NH) soybean seeds (B). Means ± standard error (error bars) are shown ($n$ = 3). Different letters indicate significant differences (analysis of variance, Tukey's test, $p < 0.05$).

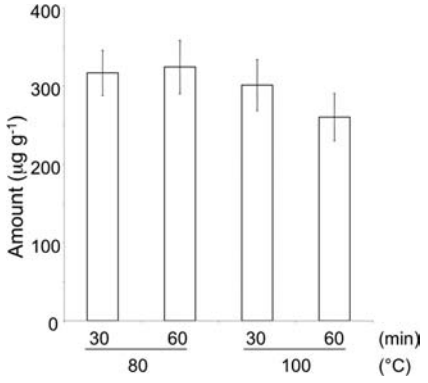


**Figure 6.** Effects of heating temperature and duration on the concentration of *S*-methylmethionine (SMM) remaining in the soaked soybean seeds (Nishiyamahitashi, NH). The seeds were soaked in 8 mL of water at 4 °C and were then heated at 80 or 100 °C for 30 or 60 min. After the seeds had chilled to room temperature, we quantified SMM using liquid chromatography with tandem mass spectrometry (LC-MS/MS). Means ± standard error (error bars) are shown ($n$ = 3). Statistical analysis by using analysis of variance and Tukey's test indicated no statistically significant differences among the treatments.

$\mu$g g$^{-1}$) were 7−500-fold lower than those in soy milk (ranging from 1 to 5.4 $\mu$g g$^{-1}$).[11,19−21] The difference might be attributable to the differences in processing procedures such as the method of heating and whether the seeds were homogenized. *n*-Hexan-1-ol was generally undetectable in soy milk prepared through homogenization of seeds with hot water (80 °C),[11,22] whereas a substantial level of *n*-hexan-1-ol was found here (ranging from 0.025 to 0.063 $\mu$g g$^{-1}$). Again, this effect might be explained by differences in the processing procedures, for example, rapid homogenization of seeds with hot water in the study by Lozano et al.[11] and a gradual temperature increase to 80 °C with intact seeds in the present study. The level of 1-octen-3-ol detected in the heat-treated soybean seeds used in this study was comparable to that reported for soy milk regardless of the differences in processing procedures. This is probably because the formation of 1-octen-3-ol is independent of disruption of soybean tissues.[21,23]

A low but substantial concentration of DMS was detected in FY, SM, SK, NS, and GK, whereas this concentration in SKK and NH was quite high and reached 6−11 $\mu$g g$^{-1}$ of seeds. The concentrations are roughly equivalent to the levels found in cooked vegetables: from 1.1 $\mu$g g$^{-1}$ (tomato) to 25 $\mu$g g$^{-1}$ (celery).[9] It was apparent that the ability to form DMS in soybean seeds was independent of the ability to form volatile oxylipins examined here.

The concentrations of *n*-hexanal, *n*-hexan-1-ol, 1-octen-3-ol, and DMS were low in SKK and NH seeds soaked for 8 h; however, these concentrations significantly increased after we heated the soaked seeds at 80 °C for 30 min (Figure 3). It was assumed that DMS was formed from an endogenous substrate. DMS is formed in large amounts by algae and bacteria, especially in marine environments through the action of a lyase enzyme on dimethylsulfoniopropionate.[6] On the contrary, it is known that DMS is formed as a result of thermal degradation of SMM in angiosperms including vegetables and green malt.[9]

SMM has been found in various vegetables such as cabbage, tomato, celery, and spinach.[9] Soybean has the ability to form SMM from methionine,[24] and SMM at 1.65 mg g$^{-1}$ was detected after acid hydrolysis (at 105 °C for 24 h in HCl) of dehulled-soybean meal.[16] We used a stable isotope dilution assay involving LC-MS/MS to measure the concentration of SMM, essentially as per the procedure developed by Scherb et al.[9] With the modified assay system, SMM was eluted at a retention time of 8.1 min and was detected with the limit of detection of 0.1 $\mu$g g$^{-1}$ with a signal/noise ratio >3 (Figure 4).

We quantified the concentration of SMM in soaked soybean seeds (Figure 5). The soybean varieties showing a low ability to form DMS, that is, FY, SM, SK, NS, and GK, contained SMM in the range between 0.5 and 3.0 $\mu$g g$^{-1}$ without any significant differences among these varieties. In contrast, the concentrations in SKK and NH were 75 and 290 $\mu$g g$^{-1}$: 30−600-fold higher than those in the other soybeans. The level found in SKK and NH was comparable to or even higher than that found in vegetables reported to contain a high concentration of SMM such as celery (176.0 $\mu$g g$^{-1}$), turnip cabbage (124.0 $\mu$g g$^{-1}$), leek (94.0 $\mu$g g$^{-1}$), beetroot (89.0 $\mu$g g$^{-1}$), and cabbage (81.0 $\mu$g g$^{-1}$).[9] Nonetheless, the concentration in SKK and NH was still much lower than that found in acid-hydrolyzed soybean meal (1.65 mg g$^{-1}$).[16] Because we estimated the concentration of SMM in its free form without acid hydrolysis, a large proportion of SMM might exist as its bound form as a component of a protein, as in the LaeA protein in *Aspergillus nidulans*.[25]

Most plant seeds have the biosynthetic pathway that produces SMM in seeds;[26] however, no studies have been reported to examine its distribution in seeds. When the seed of the NH soybean was dissected into the seed coat, cotyledon,

and plumules with radicles, the cotyledons accounted for ~87% of the total SMM found in the whole seeds, followed by the plumules and radicles, which comprised ~12% of the total SMM (Figure 6B). On the basis of the weight of each part, the plumules and radicles accounted for only 1.8% of the total weight of soaked soybean seeds, whereas the cotyledons accounted for 89%. Thus, the plumules and radicles contain the highest concentration of SMM (1071 ± 179 $\mu g\ g^{-1}$) followed by the cotyledons (159 ± 36.0 $\mu g\ g^{-1}$).

The concentration of SMM tended to decrease depending on the heating temperature and heating time, even though there was no statistically significant difference among the treatments (Figure 6). At low pH (pH 2−5), DMS is formed as a result of a nucleophilic substitution of the dimethyl sulfonium group by water, whereas at higher pH values (pH >7), an intramolecular nucleophilic substitution caused by the carboxyl group of SMM takes place.[27] Because the pH of the homogenate prepared from soybean seeds after soaking or after heat treatment was 5.7−6.0, both mechanisms might be possible. Under the experimental conditions used here, where soybean seeds (NH) are heated without disruption, ~90% of SMM found in intact seeds was retained even after heat treatment at 100 °C for 60 min. This yield was expected because the concentration of DMS (10−12 $\mu g\ g^{-1}$, see Figure 2) after heating of the NH seeds accounted for only 3−4% of the initial concentration of SMM found in intact seeds before heat treatment (Figure 5). The thermal stability of SMM is dependent on the pH value of the solution and on the matrix; therefore, its degradation in tomato or orange juice is higher than that in an aqueous buffer at the same pH.[9]

This seems to be the first study on soybean varieties that contain SMM at a level (75−290 $\mu g\ g^{-1}$) equivalent to or even higher than that in vegetables that are known to contain high concentrations of SMM such as cabbage and celery (80−180 $\mu g\ g^{-1}$).[9] It was reported that the biosynthetic pathway that produces SMM (SMM cycle) is widespread among angiosperms[28] and is active during seed development in alfalfa (*Medicago truncatula*)[29] and flax (*Linum usitatissimum*).[30] In fact, all of the soybean seeds examined here, except for the two that showed extraordinarily high SMM content, exhibited a low but substantial concentration of SMM. These findings suggest that a mutation in the metabolic pathway results in the high SMM concentration in the seeds of NH and SKK. The SMM cycle partly accounts for the methionine level, which is an important nutritional parameter of soybeans.[31] Therefore, deciphering the cause of the high SMM content of the two varieties at the molecular level would be worthwhile. Currently, we are trying to locate genetic loci responsible for the accumulation of SMM.

## ■ ASSOCIATED CONTENT

### Ⓢ Supporting Information

Calibration curves for DMS, *n*-hexanal, *n*-hexan-1-ol, 1-octen-3-ol, and SMM and typical total ion chromatograms of volatiles. This material is available free of charge via the Internet at http://pubs.acs.org.

## ■ AUTHOR INFORMATION

### Corresponding Author

*(K.M.) Phone: +81-83-933-5850. Fax: +81-83-933-5820. E-mail: matsui@yamaguchi-u.ac.jp.

### Funding

This work was supported in part by the Japan Society for the Promotion of Science (JSPS; KAKENHI, Grants 23580151 and 26660095) and by Yamaguchi University (Yobimizu Project; grant to M.K.).

### Notes

The authors declare no competing financial interest.

## ■ ABBREVIATIONS USED

DMS, dimethyl sulfide; SMM, *S*-methylmethionine; SPME, solid phase microextraction; GC, gas−liquid chromatography; LC, liquid chromatography; MS, mass spectrometry; ESI, electrospray ionization; MRM, multiple reaction monitoring

## ■ REFERENCES

(1) Hwang, E. Y.; Song, Q.; Jia, G.; Specht, J. E.; Hyten, D. L.; Costa, J.; Cregan, P. B. A genome-wide association study of seed protein and oil content in soybean. *BMC Genomics* **2014**, *15*, 1 DOI: 10.1186/1471-2164-15-1.

(2) Schmutz, J.; Cannon, S. B.; Schlueter, J.; Ma, J.; Mitros, T.; Nelson, W.; et al. Genome sequence of the palaeopolyploid soybean. *Nature* **2010**, *463*, 178−183.

(3) Kim, J. K.; Kim, E. H.; Park, I.; Yu, B. R.; Lim, J. D.; Lee, Y. S.; Lee, J. H.; Kim, S. H.; Chung, I. M. Isoflavones profiling of soybean [*Glycine max* (L.) Merrill] germplasms and their correlations with metabolic pathways. *Food Chem.* **2014**, *153*, 258−264.

(4) Kaga, A.; Shimizu, T.; Watanabe, S.; Tsubokura, Y.; Katayose, Y.; Harada, K.; Vaughan, D. A.; Tomooka, N. Evaluation of soybean germplasm conserved in NIAS genebank and development of mini core collections. *Breed. Sci.* **2012**, *61*, 566−592.

(5) Cho, K. M.; Ha, T. J.; Lee, Y. B.; Seo, W. D.; Kim, J. Y.; Ryu, H. W.; Jeong, S. H.; Kang, Y. M.; Lee, J. H. Soluble phenolics and antioxidant properties of soybean (*Glycine max* L.) cultivars with varying seed coat colours. *J. Funct. Foods* **2013**, *5*, 1065−1076.

(6) Bentley, R.; Chasteen, T. G. Environmental VOSCs-formation and degradation of dimethyl sulfide, methanethiol and related materials. *Chemosphere* **2004**, *55*, 291−317.

(7) Miers, J. C. Formation of volatile sulfur compounds in processed tomato products. *J. Agric. Food Chem.* **1966**, *14*, 419−423.

(8) Ney, K. J.; Freytag, W. Dimethyl sulfide as an essential component of asparagus flavor. Volatile components of boiled asparagus. *Z. Lebensm. Unters. Forsch.* **1972**, *149*, 154−155.

(9) Scherb, J.; Kreissl, J.; Haupt, S.; Schieberle, P. Quantitation of *S*-methylmethionine in raw vegetables and green malt by a stable isotope dilution assay using LC-MS/MS: comparison with dimethyl sulfide formation after heat treatment. *J. Agric. Food Chem.* **2009**, *57*, 9091−9096.

(10) Culleré, L.; Ferreira, V.; Venturini, M. E.; Marco, P.; Blanco, D. Potential aromatic compounds as markers to differentiate between *Tuber melanosporum* and *Tuber indicum* truffles. *Food Chem.* **2013**, *141*, 105−110.

(11) Lozano, P. R.; Drake, M.; Benitez, D.; Cadwallader, K. R. Instrumental and sensory characterization of heat-induced odorants in aseptically packaged soy milk. *J. Agric. Food Chem.* **2007**, *55*, 3018−3026.

(12) Anness, B. J.; Bamforth, C. W. Dimethyl sulphide − a review. *J. Inst. Brew.* **1982**, *88*, 244−252.

(13) Segurel, M. A.; Razungles, A. J.; Riou, C.; Salles, M.; Baumes, R. L. Contribution of dimethyl sulfide to the aroma of Syrah and Grenache Noir wines and estimation of its potential in grapes of these varieties. *J. Agric. Food Chem.* **2004**, *52*, 7084−7093.

(14) DeMora, S. J.; Knowles, S. J.; Eschenbruch, R.; Torrey, W. J. Dimethyl sulphide in some Australian red wines. *Vitis* **1987**, *26*, 79−84.

(15) Watanabe, T.; Ohara, S.; Miyazawa, S.; Saigenji, K.; Hotta, K. Augmentative effects of L-cysteine and methylmethionine sulfonium

chloride on mucin secretion in rabbit gastric mucous cells. *J. Gastroenterol. Hepatol.* **2000**, *15*, 45−52.
(16) Augspurger, N. R.; Scherer, C. S.; Garrow, T. A.; Baker, D. H. Dietary *S*-methylmethionine, a component of foods, has choline-sparing activity in chickens. *J. Nutr.* **2005**, *135*, 12−17.
(17) Lee, N. Y.; Park, K. Y.; Min, H. J.; Song, K. Y.; Lim, Y. Y.; Park, J.; Kim, B. J.; Kim, M. N. Inhibitory effect of vitamin U (*S*-methylmethionine sulfonium chloride) on differentiation in 3T3-L1 pre-adipocyte cell lines. *Ann. Dermatol.* **2012**, *24*, 39−44.
(18) Hwang, T. Y.; Sayama, T.; Takahashi, M.; et al. High-density integrated linkage map based on SSR markers in soybean. *DNA Res.* **2009**, *16*, 213−225.
(19) Zhang, Y.; Guo, S.; Liu, Z.; Chang, S. K. C. Off-flavor related volatiles in soymilk as affected by soybean variety, grinding, and heat-processing methods. *J. Agric. Food Chem.* **2012**, *60*, 7457−7462.
(20) Yuan, S.; Chang, S. K. C. Selected odor compounds in soymilk as affected by chemical composition and lipoxygenases in five soybean materials. *J. Agric. Food Chem.* **2007**, *55*, 426−431.
(21) Kobayashi, A.; Tsuda, Y.; Hirata, N.; Kubota, K.; Kitamura, K. Aroma constituents of soybean [*Glycine max* (L.) Merril] milk lacking lipoxygenase isozymes. *J. Agric. Food Chem.* **1995**, *43*, 2449−2452.
(22) Pulvera, Z. M.; Kitamura, K.; Hajika, M.; Shimada, K.; Matsui, K. Oxylipin metabolism in soybean seeds containing different sets of lipoxygenase isozymes after homogenization. *Biosci., Biotechnol., Biochem.* **2006**, *70*, 2598−2603.
(23) Matsui, K.; Takaki, S.; Shimada, K.; Hajika, M. Effects of anaerobic processing of soybean seeds on the properties of tofu. *Biosci., Biotechnol., Biochem.* **2011**, *75*, 1174−1176.
(24) Mudd, S. H.; Datko, A. H. The *S*-methylmethionine cycle in *Lemna paucicostata*. *Plant Physiol.* **1990**, *93*, 623−630.
(25) Patananan, A. N.; Palmer, J. M.; Garvey, G. S.; Keller, N. P.; Clarke, S. G. A novel automethylation reaction in the *Aspergillus nidulans* LaeA protein generates *S*-methylmethionine. *J. Biol. Chem.* **2013**, *288*, 14032−14045.
(26) Amir, R.; Han, T.; Ma, F. Bioengineering approaches to improve the nutritional values of seeds by increasing their methionine content. *Mol. Breed.* **2012**, *29*, 915−924.
(27) Cremer, D. R.; Eichner, K. Formation of volatile compounds during heating of spice paprika (*Capsicum annuum*) powder. *J. Agric. Food Chem.* **2000**, *48*, 2454−2460.
(28) Ranocha, P.; McNeil, S. D.; Ziemak, M. J.; Li, C.; Tarczynski, M. C.; Hanson, A. D. The *S*-methylmethionine cycle in angiosperms: ubiquity, antiquity and activity. *Plant J.* **2001**, *25*, 575−584.
(29) Gallardo, K.; Firnhaber, C.; Zuber, H.; Héricher, D.; Belghazi, M.; Henry, C.; Küster, H.; Thompson, R. A combined proteome and transcriptome analysis of developing *Medicago truncatula* seeds. *Mol. Cell. Proteomics* **2007**, *6*, 2165−2179.
(30) Barvkar, V. T.; Pardeshi, V. C.; Kale, S. M.; Kadoo, N. Y.; Giri, A. P.; Gupta, V. S. Proteome profiling of flax (*Linum usitatissimum*) seed: characterization of functional metabolic pathways operating during seed development. *J. Proteome Res.* **2012**, *11*, 6264−6276.
(31) Song, S.; Hou, W.; Godo, I.; Wu, C.; Yu, Y.; Matityahu, I.; Hacham, T.; Sun, S.; Ham, T.; Amir, R. Soybean seeds expressing feedback-insensitive cystathionine γ-synthase exhibit a higher content of methionine. *J. Exp. Bot.* **2013**, *64*, 1917−1926.

JOURNAL OF AGRICULTURAL AND FOOD CHEMISTRY

Article

pubs.acs.org/JAFC

# Comparison of the Volatiles Formed by Oxidation of Phosphatidylcholine to Triglyceride in Model Systems

Li Zhou,*[,†,‡] Minjie Zhao,[‡] Françoise Bindler,[‡] and Eric Marchioni[‡]

[†]College of Food Science and Technology, Nanjing Agricultural University, Nanjing, Jiangsu 210095, People's Republic of China

[‡]Equipe de Chimie Analytique des Molécules Bioactives (IPHC-LC4, UMR 7178), Université de Strasbourg, 74 route du Rhin, 67400 Illkirch, France

Supporting Information

**ABSTRACT:** The oxidative stability of oleoyl and linoleoyl residues esterified in the form of triglyceride (TAG) and phosphatidylcholine (PC) during thermal treatment was investigated. Headspace solid-phase microextraction (HS-SPME) followed by gas chromatography−mass spectrometry (GC−MS) analysis was used to determine the volatile compounds from oxidized PL and TAG molecular species. The results showed that aldehydes were the major volatile oxidized compounds (VOCs) of 1-stearoyl-2-oleoyl-*sn*-glycero-3-phosphocholine (SOPC), 1-stearoyl-2-linoleoyl-*sn*-glycero-3-phosphocholine (SLPC), and 1,3-distearoyl-2-linoleoyl-glycerol (SLS), while ketones, especially saturated methyl ketones, were the major VOCs of 1,3-distearoyl-2-oleoyl-glycerol (SOS). The monitoring of the oxidative degradation using liquid chromatography−electrospray ionization−mass spectrometry (LC−ESI−MS) showed that either monounsaturated or diunsaturated fatty acyl groups were less oxidized when in the form of PCs than when in the form of TAGs. This finding demonstrated that the choline group in the form of PCs could increase the stability of fatty acyl groups to oxidation in comparison to TAGs.

**KEYWORDS:** *phosphatidylcholine, triglycerides, oxidative stability, volatile oxidized compound, oleic acid, linoleic acid*

## INTRODUCTION

Polyunsaturated fatty acids (PUFAs) play very important roles in human health, in particular, in protecting the liver,[1,2] in improving memory and learning,[3,4] and in protecting the cardiovascular system.[5−7] Phospholipids (PLs) are rich in PUFAs and are an important source of PUFAs.[8] Supplementation of food products with PUFA-rich PLs has recently emerged as an interesting way of increasing the daily intake of PUFA and, thereby, received more and more attention. Another important source of PUFA is triglycerides (TAGs), which are the major carriers of fatty acids (FAs), with 50−100 g/day for an adult, followed by PLs, with 2−10 g/day.[9,10] However, according to the bioavailability of FAs, PLs are much more efficient than TAGs.[11−13] Moreover, cellular permeability to PUFA and their intracellular level were indeed much higher when linked to PL than to TAG,[10,14] which suggests that food supplementation with PUFA-rich PL could enhance essential FA assimilation.

The bioavailability of PUFA in the form of PL or TAG is an important factor that should be considered, but their stabilities in food sources are also as important. The information on the evaluation of relative stability of TAG and PL is limited. Most of the studies were contributed on the comparison of the stability of oil-enriched PLs to that of oils containing few or no PLs at all.[13,15,16]

Lipid oxidation is a major cause of quality deterioration of many natural and processed foods.[17,18] It leads to the development of undesirable off-flavors and potentially toxic compounds. Our previous studies have investigated the formation mechanism of non-volatiles of PLs.[19,20] As for volatile compounds, there are also major decomposition products of lipids.[21] We have identified the volatile compounds from oxidized phosphatidylcholine (PC) and figured out their origin.[22] However, to our knowledge, no studies have been carried out in detail on the comparison of volatiles by oxidation of PC to TAG.

Several methods are available to measure the progress of lipid oxidation. Conventional measurements for the assessment of lipid oxidation are usually determined by simple spectroscopic techniques, such as thiobarbituric acid reactive substances (TBARS), carbonyl group, and diene conjugate methods. However, these photometric assays could only roughly reflect the level of lipid oxidation, and their sensitivities are limited, while chromatographic techniques (gas chromatography and/or high-performance liquid chromatography together with different detectors, including mass spectroscopy) are useful for a more detailed description of the reaction products.

The aim of this study was to compare the oxidative stability of PC to TAG. As a model system, oleyol and linoleoyl residues in the form of PC and TAG were chosen, because they exist widely in food matrices, such as soybean, egg yolk, and ox liver, which were identified in our previous study.[4,19] The comparison of the oxidative stability of PC and TAG was made in terms of the kinetics of the formation of volatile oxidized compounds (VOCs), which was monitored by headspace solid-phase microextraction and gas chromatography−mass spectrometry (HS-SPME−GC−MS), and the kinetics of degradation of the starting material, which was

Received: April 26, 2014
Revised: July 27, 2014
Accepted: August 3, 2014
Published: August 3, 2014

ACS Publications © 2014 American Chemical Society

monitored using liquid chromatography−electrospray ionization−mass spectrometry (LC−ESI−MS).

## MATERIALS AND METHODS

**Materials.** The following standards (>95%) were used to identify the volatile compounds, including pentanal, hexanal, heptanal, octanal, nonanal, (*E*)-2-hexenal, (*E*)-2-heptenal, (*E*)-2-octenal, (*E*)-2-decenal, (*E*,*E*)-2,4-decadienal, 1-pentanol, 1-hexanol, 1-octen-3-ol, 1-heptanol, 1-octanol, 2-decanone, 2-undecanone, 1-octen-3-one, 2-pentyl-furan, (*E*)-2-undecenal, (*E*)-3-octen-2-one, 5-ethyldihydro-2(3*H*)-furanone, and dihydro-5-propyl-2(3*H*)-furanone. They were purchased from Sigma-Aldrich (St. Louis, MO).

1-Stearoyl-2-oleoyl-*sn*-glycero-3-phosphocholine (SOPC) (99.9%) and 1-stearoyl-2-linoleoyl-*sn*-glycero-3-phosphocholine (SLPC) (99.9%) were purchased from Avanti Polar Lipids (Alabaster, AL). 1,3-Distearoyl-2-oleoyl-glycerol (SOS) (99.9%) and 1,3-distearoyl-2-linoleoyl-glycerol (SLS) (99.9%) were obtained from Larodan (Malmö, Sweden). High-performance liquid chromatography (HPLC)-grade methanol and ammonium formate were purchased from VWR (Strasbourg, France). Chloroform of analytical grade was purchased from Riedel de Haën (Sigma-Aldrich, Seelze, Germany).

The SPME fiber tested in this study was 65 $\mu$m of polydimethylsiloxane/divinylbenzene (PDMS/DVB), purchased from Sigma-Aldrich (St. Louis, MO).

**Sample Preparation.** Stock solutions of 10 mg mL$^{-1}$ were prepared by weighing standards (SOPC, SLPC, SOS, and SLS) in a 5 mL amber vial and dissolving them in chloroform. A total of 100 $\mu$L of these solutions (1.0 mg of sample) were placed in a 20 mL dark glass injection vial previously desorbed, uncapped by a heating treatment at 200 °C during 2 h in an oven. After evaporation of chloroform at room temperature in the fume chamber, each injection vial was sealed with an aluminum crimp cap provided with a polytetrafluoroethylene/silicone septum (Agilent Technologies, Massy, France) and kept at −20 °C until oxidative treatment.

**Oxidative Treatments.** The samples were heated in an oven at a specified temperature comprised between 100 and 200 °C for a duration ranging from 0 to 180 min. After oxidation, samples were cooled quickly in ice for 5 min, then left at room temperature for 5 min, and finally injected in HS-SPME−GC−MS for analysis. A total of 1.0 mL of methanol was added in the vial; then a $^{1}/_{50}$ dilution was performed to obtain 0.02 mg/mL; and 10 $\mu$L was injected in the LC−ESI−MS system. All samples were analyzed in triplicate.

**HS-SPME.** Prior to analysis, the PDMS/DVB fiber was preconditioned (at 250 °C for 30 min) in the bakeout oven of the CombiPAL injector with the temperature and duration suggested by the manufacturers. The extraction was carried out for 25 min at 50 °C,[22] and each measurement was repeated 3 times.

**GC−MS Analysis of Volatiles.** GC−MS analysis was performed in a 450 Varian gas chromatograph fitted with a CombiPAL (CTC Analytics AG, Switzerland) automatic HS-SPME injector. Helium was used as the carrier gas at a constant flow rate of 1 mL min$^{-1}$. The injector operated in the splitless mode, and its temperature was set at 250 °C. The separation of VOCs was performed on a DB-wax column (60 m × 0.25 mm, 0.15 $\mu$m, Agilent, Santa Clara, CA). The oven temperature program started at 40 °C, was raised at a rate of 4 °C min$^{-1}$ to 220 °C (held for 5 min), and then was raised at a rate of 4 °C min$^{-1}$ to 240 °C (held for 17 min). The detection was performed by an Agilent 240 mass selective detector (ion trap) set in positive electron impact (+EI) mode with 70 eV of electron energy. The electron multiplier was set by the autotune procedure. MS data were collected with the daughter ion scan mode over the $m/z$ range from 50 to 315. Transfer line temperature, trap temperature, and ion source temperature were 110, 150, and 150 °C, respectively.

VOCs were tentatively identified by matching the experimental mass spectra with the reference mass spectra in the National Institute of Standards and Technology (NIST) mass spectral library. Most VOCs identified in this way were then confirmed by comparing their mass spectra and retention times to those obtained from authentic reference compound (STD) under the same analytical conditions. In addition, retention indices (RIs) were calculated on the basis of a series of *n*-alkanes with a chain length from $C_5$ to $C_{20}$. They were compared to literature values to support tentative identification.[23−25]

**LC−ESI−MS Analysis.** After oxidative treatment of the samples, the remaining PCs and TAGs were evaluated using a Varian Prostar HPLC system made of two 210 solvent delivery modules, a 410 autosampler, and a 1200 L triple quadrupole mass spectrometer with ESI operated in positive-ion mode (Agilent, Les Ulis, France). High-purity nitrogen (99.99%, Domnik Hunter) was used as the nebulizing gas, set at 317 kPa, and as the drying gas, set at 300 °C. Separation was performed on a Zorbax column C8 (250 × 4.6 mm, 5 $\mu$m, Agilent) using an isocratic elution of 100% $CH_3OH$ containing 5 mM ammonium formate at a flow rate of 1 mL min$^{-1}$. A total of 20 $\mu$L of each diluted oxidized sample was injected. A split system allowed for the HPLC effluent to enter the mass spectrometer at a flow rate of 0.2 mL min$^{-1}$. The injection volume was performed in positive mode in a mass range between $m/z$ 500 and 1000 and in selected ion monitoring (SIM) mode by extracting ion $[M + H]^+$ $m/z$ 788.6 for SOPC, $m/z$ 786.6 for SLPC, $m/z$ 889.8 for SOS, and $m/z$ 887.8 for SLS.

The percentage of the remaining precursors was determined as follows:

$$\% = \frac{(\text{area})_t}{(\text{area})_{t^\circ}} \times 100$$

where $(\text{area})_t$ is the area of the peak corresponding to the ion $m/z$ of the starting material (PC or TAG) after oxidation and $(\text{area})_{t^\circ}$ is the area of the same ion $m/z$ without oxidative treatment. All samples were analyzed in triplicate, and results are given as the mean ± standard deviation (SD).

## RESULTS

**Determination of Optimal Oxidation Temperatures.** To determine the optimal oxidation conditions of SOPC and SLPC, the total areas of VOCs generated at several temperatures was determined. The temperatures allowing for the highest yield of total VOCs were different for thermally oxidized SOPC and SLPC. According to our previous study,[22] the highest production of total VOCs was 175 and 125 °C for SOPC and SLPC, respectively, in the same oxidation time. This was in accordance with a previous report showing that free linoleic acid was more sensitive to oxidation than free oleic

**Scheme 1. Homolytic−Heterolytic Mechanism of the Decomposition of Hydroperoxides[28]**

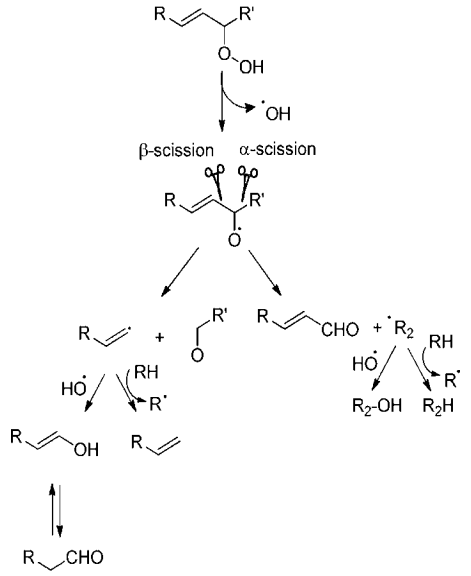

**Table 1. Volatile Compounds Identified from Oxidized SOPC and SOS[a]**

| VOCs | RI[b] | area (×10^6) SOPC[c] | area (×10^6) SOS[c] | origin[22] | identification[d] |
|---|---|---|---|---|---|
| | | Aldehyde | | | |
| hexanal | 1080 | 1.06 ± 0.03 | 6.57 ± 0.19 | O[e] | MS, STD, RI |
| heptanal | 1184 | 7.46 ± 0.06 | 19.9 ± 0.2 | O | MS, STD, RI |
| octanal | 1278 | 21.3 ± 0.0 | 28.4 ± 0.3 | O | MS, STD, RI |
| nonanal | 1380 | 27.7 ± 0.3 | 51.0 ± 0.1 | O | MS, STD, RI |
| 2-nonenal[f] | 1535 | 3.18 ± 0.10 | 8.95 ± 0.04 | O | MS, RI |
| (*E*)-2-decenal | 1645 | 29.4 ± 0.0 | 28.8 ± 0.1 | O | MS, STD, RI |
| (*E*)-2-undecenal | 1750 | 16.5 ± 0.2 | 11.6 ± 0.1 | O | MS, STD, RI |
| | | Alcohol | | | |
| 1-hexanol | 1357 | 1.36 ± 0.03 | 2.47 ± 0.03 | O | MS, STD, RI |
| 1-heptanol | 1460 | 6.56 ± 0.13 | 3.26 ± 0.08 | O | MS, STD, RI |
| 3-decen-1-ol[f] | 1507 | 3.06 ± 0.06 | 4.6 ± 0.2 | O | MS, RI |
| 1-octanol | 1562 | 11.8 ± 0.1 | 9.37 ± 0.10 | O | MS, STD, RI |
| | | Ketone | | | |
| 2-octanone[f] | 1262 | 5.86 ± 0.34 | 7.01 ± 0.15 | S[g] | MS, RI |
| 2-nonanone[f] | 1375 | 5.77 ± 0.12 | 15.2 ± 0.1 | S | MS, RI |
| 2-decanone | 1493 | 7.17 ± 0.03 | 37.2 ± 0.3 | S | MS, STD, RI |
| 2-undecanone | 1598 | 4.35 ± 0.06 | 40.1 ± 0.1 | S | MS, STD, RI |
| 2-dodecanone[f] | 1678 | 4.41 ± 0.13 | 45.9 ± 0.2 | S | MS, RI |
| dihydro-5-propyl-2(3*H*)-furanone | 1793 | 4.74 ± 0.03 | 42.4 ± 0.8 | O | MS, STD, RI |
| 5-butyldihydro-2(3*H*)-furanone[f] | 1853 | 3.62 ± 0.10 | 12.3 ± 0.1 | O | MS, RI |
| dihydro-5-pentyl-2(3*H*)-furanone[f] | 1898 | 1.4 ± 0.1 | 15.2 ± 0.1 | O | MS, RI |

[a]Results ($n$ = 3) were expressed as the mean ± SD. Extraction conditions: PDMS/DVB, 50 °C, and 25 min. Oxidation conditions: 175 °C and 120 min. [b]Retention indices (RIs) were determined on DB-wax using the homologous series of $n$-alkanes. [c]Data were expressed in terms of peak areas. [d]Identification: MS, by comparison of the reference mass spectra in the NIST mass spectral library; STD, by comparison of authentic reference compounds; and RI, by comparion of RIs to those from the literature. [e]O: VOCs formed from the oleic acid chain of SOPC or SOS. [f]Compound tentatively identified according to MS and by comparison of the RI to the literature. [g]S: VOCs formed from the stearic acid chain of SOPC or SOS.

**Table 2. Volatile Compounds Identified from SLPC and SLS[a]**

| VOCs | RI[b] | area (×10^6) SLPC[c] | area (×10^6) SLS[c] | origin[22] | identification[d] |
|---|---|---|---|---|---|
| | | Aldehyde | | | |
| pentanal | 984 | 3.57 ± 0.04 | 5.35 ± 0.21 | L[e] | MS, STD, RI |
| hexanal | 1080 | 30.1 ± 0.2 | 40.5 ± 3.0 | L | MS, STD, RI |
| (*E*)-2-hexenal | 1216 | 1.38 ± 0.07 | 0.22 ± 0.01 | L | MS, STD, RI |
| (*E*)-2-heptenal | 1320 | 31.6 ± 0.3 | 5.37 ± 0.09 | L | MS, STD, RI |
| (*E*)-2-octenal | 1425 | 36.2 ± 0.2 | 2.88 ± 0.14 | L | MS, STD, RI |
| 2-nonenal[f] | 1535 | 4.08 ± 0.11 | 0.15 ± 0.01 | L | MS, RI |
| 2,4-nonadienal[f] | 1667 | 6.89 ± 0.03 | 0.48 ± 0.03 | L | MS, RI |
| (*E*,*Z*)-2,4-decadienal[f] | 1788 | 3.53 ± 0.07 | 0.35 ± 0.06 | L | MS, RI |
| (*E*,*E*)-2,4-decadienal | 1810 | 3.35 ± 0.02 | 0.47 ± 0.06 | L | MS, STD, RI |
| 4-oxononanal[f] | 1832 | 4.53 ± 0.04 | 0.11 ± 0.04 | L | MS, RI |
| | | Alcohol | | | |
| 1-pentanol | 1250 | 6.25 ± 0.21 | 1.99 ± 0.02 | L | MS, STD, RI |
| 1-octen-3-ol | 1455 | 6.59 ± 0.01 | 2.18 ± 0.03 | L | MS, STD, RI |
| | | Ketone | | | |
| 2-heptanone[f] | 1180 | 5.1 ± 0.2 | 2.52 ± 0.06 | S[g] | MS, RI |
| 1-octen-3-one | 1280 | 7.16 ± 0.03 | 0.15 ± 0.03 | L | MS, STD, RI |
| (*E*)-3-octen-2-one | 1385 | 28.9 ± 0.3 | 2.0 ± 0.1 | L | MS, STD, RI |
| 3-nonen-2-one[f] | 1512 | 5.0 ± 0.0 | 2.03 ± 0.13 | L | MS, RI |
| 5-ethyldihydro-2(3*H*)-furanone | 1678 | 3.67 ± 0.04 | 7.28 ± 0.03 | L | MS, STD, RI |
| | | Furan | | | |
| 2-pentyl-furan | 1240 | 9.67 ± 0.02 | 5.56 ± 0.12 | L | MS, STD, RI |

[a]Results ($n$ = 3) were expressed as the mean ± SD. Extraction conditions: PDMS/DVB, 50 °C, and 25 min. Oxidation conditions: 125 °C and 90 min. [b]Retention indices (RIs) were determined on DB-wax using the homologous series of $n$-alkanes. [c]Data were expressed in terms of peak areas. [d]Identification: MS, by comparison of the reference mass spectra in the NIST mass spectral library; STD, by comparison of authentic reference compounds; and RI, by comparion of RIs to those from the literature. [e]L: VOCs formed from the linoleic acid chain of SLPC or SLS. [f]Compound tentatively identified according to MS and by comparison of the RI to the literature. [g]S: VOCs formed from the stearic acid chain of SLPC or SLS.

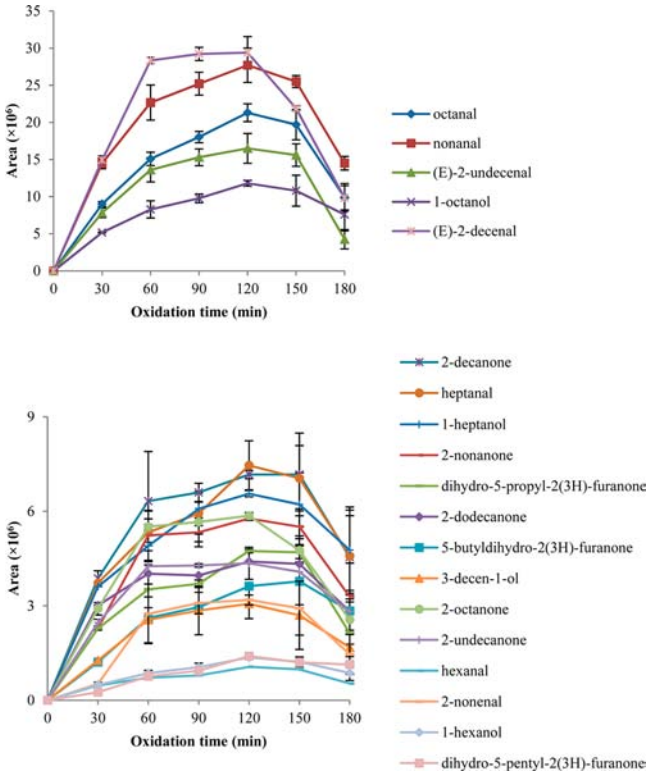


**Figure 1.** Kinetics of VOCs produced from oxidized SOPC during heat treatment at 175 °C monitored from 0 to 180 min.

acid.[9] To compare to the oxidative stability of TAG, 175 and 125 °C were chosen for SOS and SLS, respectively.

**Identification of VOCs.** A variety of volatile and nonvolatile secondary products are formed from hydroperoxides when lipid oxidation is carried out at elevated temperatures. The mechanism suggested for the formation of oxidized products involves the homolytic cleavage of the hydroperoxide group to yield an alkoxyl radical and a hydroxyl radical.[26] The further decomposition of an alkoxyl radical involving carbon−carbon bond scission is a major pathway for the formation of volatile products.[27] The $\alpha$-scission and $\beta$-scission of an alkoxyl radical lead to different decomposition products (Scheme 1).

Oxidation was performed in the solid state because chloroform was evaporated before oxidation. Because of the selectivity of the HS-SPME procedure, identified compounds were those that were present in the sample and were extracted by the PDMS/DVB fiber. Besides, there might be other VOCs that were present in the sample but not extracted by the fiber.

Table 1 gives the VOCs of SOPC and SOS at 175 °C with 120 min. A total of 19 VOCs were detected from oxidized SOPC. The major VOCs of SOPC were aldehydes, such as nonanal, (*E*)-2-decenal, octanal, and (*E*)-2-undecenal. However, ketones were the predominant group of VOCs formed from oxidized SOS. Among them, saturated methyl ketones, such as 2-octanone, 2-nonanone, 2-decanone, 2-undecanone, and 2-dodecanone, accounted for a large proportion of total VOCs. It was well-known from our previous study that these saturated methyl ketones were formed from the stearic acid chain of SOPC or SOS.[22] Three reactions, degradation, $\beta$-oxidation, and decarboxylation, occurring simultaneously were proposed to account for the homologous series of methyl ketones.[29] Furthermore, the results indicated that the total peak areas of saturated methyl ketones from oxidized SOS were

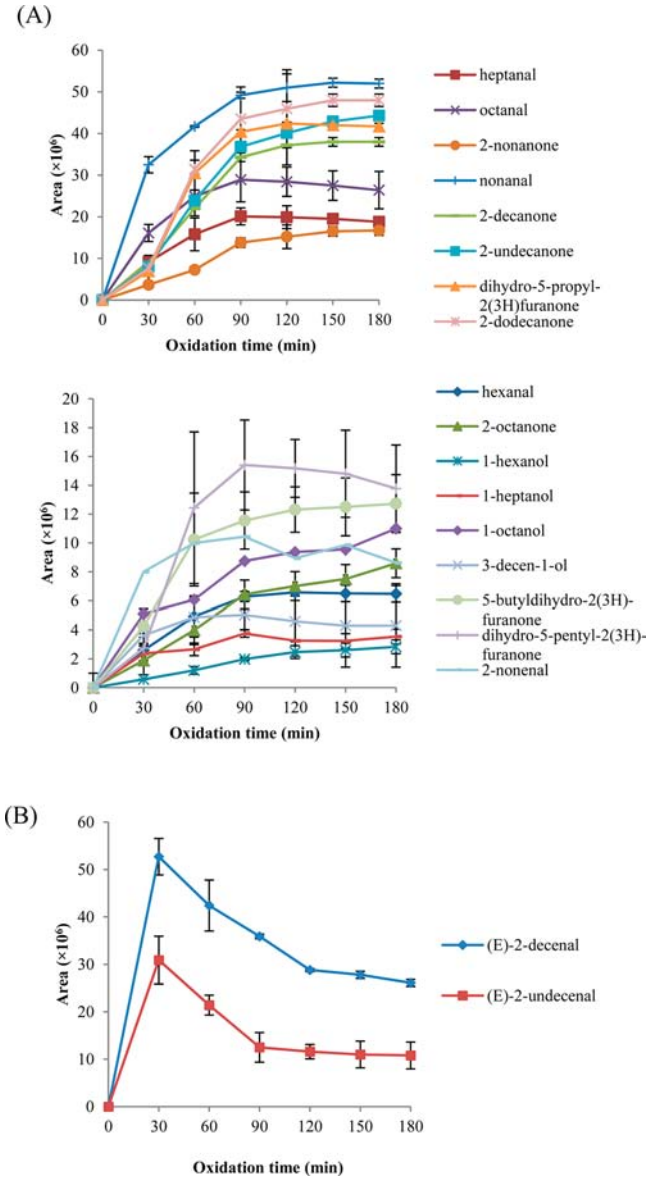


**Figure 2.** Kinetics of VOCs produced from oxidized SOS during heat treatment at 175 °C monitored from 0 to 180 min: (A) VOCs increased gradually until 90 min and then stabilized or increased slightly, and (B) VOCs increased in a sharp way before 30 min and decreased rapidly until 90 or 120 min.

obviously higher than that from oxidized SOPC. That was in agreement with the fact that SOS contained two stearic acid chains, while SOPC contained only one stearic acid chain.

A total of 18 VOCs were detected from oxidized SLPC and SLS (Table 2). Among them, aldehydes were also the major VOCs. In contrast to SOPC/SOS, oxidation of SLPC and SLS produced rather unsaturated ketones, such as (*E*)-3-octen-2-one, formed from linoleic acid chains, with saturated methyl ketones being only in trace amounts because only one (2-heptanone) was detected. Up to now, it is quite difficult to explain why SOPC/SOS and SLPC/SLS did not produce the same kind of ketones because they contain both the same C18:0 saturated FA. Perhaps the competitive oxidation equilibrium between *sn*-1 and *sn*-2 FA chains of PC/TAG may give information. The competition between stearoyl residues and oleoyl residues for VOC formation is relatively


dx.doi.org/10.1021/jf501934w | J. Agric. Food Chem. 2014, 62, 8295−8301

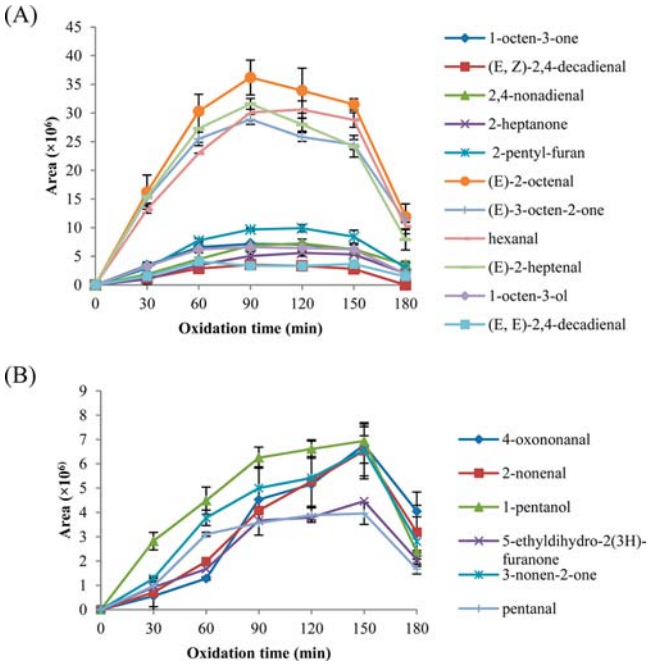


**Figure 3.** Kinetics of VOCs produced from oxidized SLPC during heat treatment at 125 °C monitored from 0 to 180 min: (A) VOCs increased until 90 min and then decreased, and (B) VOCs increased continuously until 150 °C and then decreased.

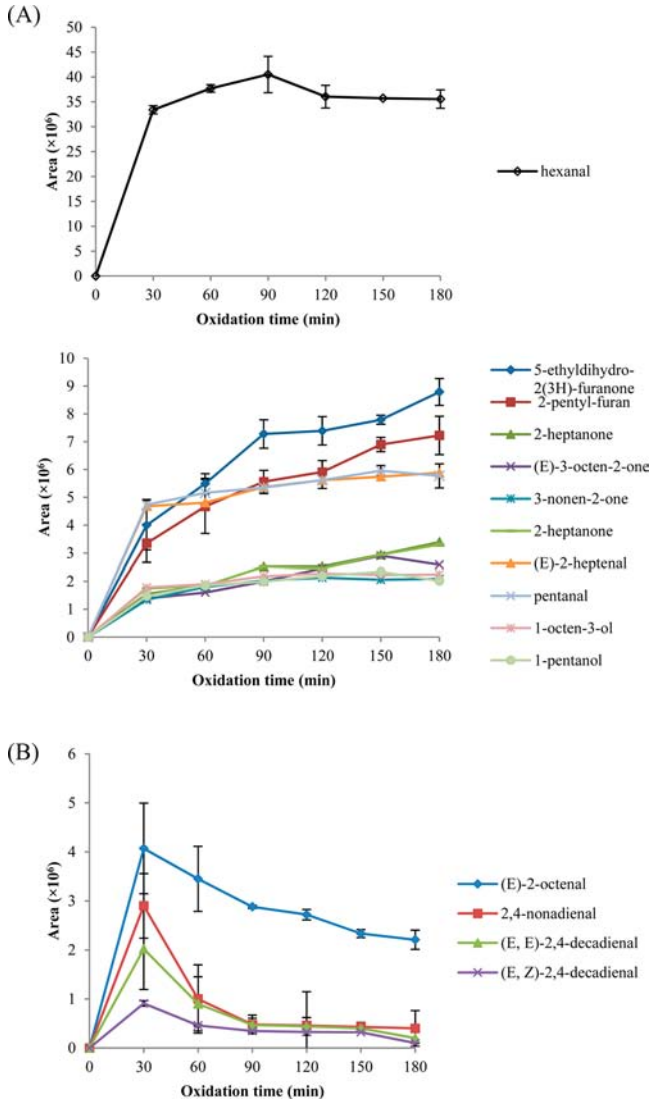


**Figure 4.** Kinetics of VOCs produced from oxidized SLS during heat treatment at 125 °C monitored from 0 to 180 min: (A) VOCs increased gradually with the increase of the oxidation time or increased to reach a maximum and then were kept stable, and (B) VOCs increased in a sharp way in the first 30 min and then decreased.

weak by comparison to stearoyl residues and linoleoyl residues. In other words, the *sn*-1 FA chains of SOPC/SOS and SLPC/SLS are stearic acids, but *sn*-2 FA chains of SOPC/SOS and SLPC/SLS are oleic and linoleic acids, respectively. Because linoleic acid is more sensitive to oxidation than oleic acid, it is easier to be oxidized. That is probably why more ketones tend to be formed from the linoleic acid chains of SLPC/SLS and less from the stearic acid chains. In comparison, more ketones, especially methyl ketones, were derived from the stearic acid chain of SOPC/SOS. It thereby showed that a higher amount of total saturated methyl ketones was formed from SOPC/SOS than that from SLPC/SLS.

**Oxidative Kinetics.** The oxidative kinetics of PLs and TAGs were investigated by analyzing HS-SPME−GC−MS peak areas of all VOCs produced as a function of the oxidation time. Some VOCs had relatively high occurrences in one chemical group. To let the low-content VOCs appear clearly, the curves of relatively high-content and low-content VOCs were divided into two separate figures.

The major VOCs of oxidized SOPC were (*E*)-2-decenal, nonanal, octanal, 2-undecenal, and 1-octanol (Figure 1). Almost all of the VOCs increased rapidly during 0−60 min and reached their maximum at 120 min, then were kept stable or decreased slowly until 150 min, but decreased rapidly after 150 min.

As for SOS (Figure 2), the VOCs can be separated into two groups: one group included the products that increased gradually until 90 min and then stabilized or increased slightly (Figure 2A), and the other group included (*E*)-2-decenal and (*E*)-2-undecenal, which increased in a sharp way before 30 min, decreased rapidly until 120 and 90 min, respectively, and then reached equilibrium or decreased slightly (Figure 2B).

Figure 3 shows kinetics of production of VOCs from oxidized SLPC. Two groups were obtained: one group (Figure 3A) reached their maximum rapidly at 90 min of oxidation, then were kept stable or decreased slowly until 150 min, and decreased sharply after 150 min, and the other group (Figure 3B) increased gradually until 150 min and then decreased rapidly.

As far as the VOCs of SLS were concerned, 18 VOCs were detected (Table 2). Hexanal was most abundant among the VOCs. It increased in a sharp way in the first 30 min, reached its maximum at 90 min, then decreased, and stabilized (Figure 4A). The amount of (*E*)-2-octenal, 2,4-nonadienal, (*E*,*Z*)-2,4-decadienal, and (*E*,*E*)-2,4-decadienal reached a maximum after 30 min of oxidation and then decreased (Figure 4B). Other VOCs increased gradually with the increase of the oxidation time (Figure 4A).

SOS is more sensitive to oxidation than SOPC. Two major VOCs of SOS identified, (*E*)-decenal and (*E*)-2-undecenal, reached their maximum after only 30 min of oxidative treatment and then decreased (Figure 2B), while most VOCs of SOPC reached their maximum after 120 min (Figure 1). Similarly, four VOCs, which were (*E*)-2-octenal, 2,4-non-


dx.doi.org/10.1021/jf501934w | J. Agric. Food Chem. 2014, 62, 8295−8301

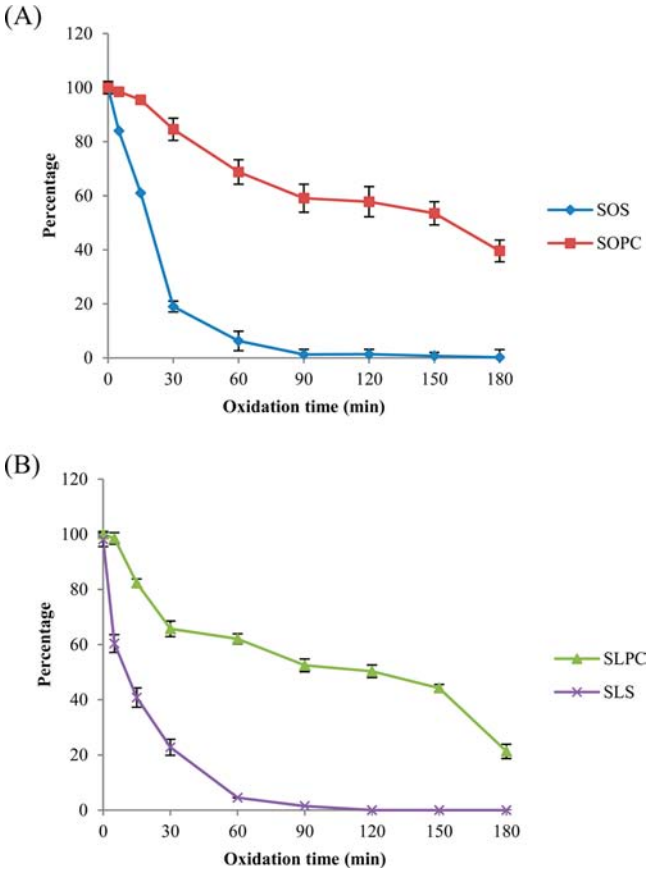


**Figure 5.** (A) Oxidative kinetics of SOPC and SOS was monitored over time of thermal treatment at 175 °C, and (B) oxidative kinetics of SLPC and SLS was monitored over time of thermal treatment at 125 °C.

adienal, (*E*,*E*)-2,4-decadienal, and (*E*,*Z*)-2,4-decadienal, reached a maximum at 30 min and then decreased (Figure 4B). While all of the VOCs of SLPC reached their maximum after 90 min, even some VOCs reached their maximum after 150 min (Figure 3B). That shows that SLS is also more sensitive to oxidation than SLPC.

**Degradation of Starting Material.** The quantities of the starting materials SOPC and SOS (SLPC and SLS), expressed as recovery percentages, were monitored by LC−ESI−MS as a function of the oxidation duration. An example of mass spectra of SOPC (A) and SLPC (B) were shown in Figure S1 of the Supporting Information. The percentage of SOPC decreased gradually over time of oxidation; SOPC was not completely decomposed at the end of 180 min; and the remaining percentage of SOPC was 39.6%. While in the case of SOS, the remaining percentage decreased rapidly (by 81%) during the first 30 min and then decreased slightly until an almost total loss of the precursor during 90 min of oxidation (Figure 5A).

Figure 5B shows the evolution of the relative amounts of SLPC and SLS over time at 125 °C. The trend of curves was similar to Figure 5A. The amounts of SLS decreased immediately and were significantly sharper than SLPC ($p < 0.05$). It also showed that SLS disappeared within 90 min of oxidation, while SLPC decreased gently down to 21.3% after 180 min of oxidation.

The kinetics of the loss of the precursors of SLS and SLPC followed the same trend as that of SOS and SOPC. PC species thereby appeared more resistant to thermal oxidation than TAG species. Our results were consistent with the results by Song et al.,[16] who demonstrated that docosahexaenoic acid (DHA) in the form of PLs was more resistant to oxidative degradation than DHA in the form of TAGs or ethyl esters. Results obtained by Lyberg et al.[30] followed the same trend that DHA was protected against hydroperoxide formation when it was incorporated at *sn*-1 and *sn*-2 positions of PC, while incorporation of DHA at any positions of a TAG was not an appropriate solution for protecting DHA. Therefore, the result suggests that the polar moiety of PC has a role to play in their stability to oxidation. This hypothesis was proposed by Yoshimoto et al.,[31] who supposed that PC can lead to the polarization of the oxygen−oxygen bond in the hydrogen peroxide, which allowed for a nucleophilic attack of an oxygen atom of another peroxide group. That can reduce the proparation phase of the oxidation process.

In this study, the results showed that PC species are more resistant to thermal oxidation than their corresponding TAG species, which supported a hypothesis that polar head groups affect oxidative kinetics of glycerol-based lipids. Therefore, concerning FA bioavailability and oxidative stability, supplementation with PUFA PLs was a more potential and interesting way than PUFA TAGs for food development.

## ■ ASSOCIATED CONTENT

### Ⓢ Supporting Information

Mass spectra of (A) SOPC *m*/*z* 788.6 and (B) SLPC *m*/*z* 786.6 (Figure S1). This material is available free of charge via the Internet at http://pubs.acs.org.

## ■ AUTHOR INFORMATION

### Corresponding Author

*Telephone/Fax: +86-25-84396791. E-mail: zhoul@njau.edu.cn.

### Funding

This work was supported by "Equipe de Chimie Analytique des Molécules Bioactives (IPHC-LC4, UMR 7178), Université de Strasbourg" and a grant from the Natural Science Foundation of Jiangsu Province (BK20140701).

### Notes

The authors declare no competing financial interest.

## ■ ABBREVIATIONS USED

GC−MS, gas chromatography−mass spectrometry; HS-SPME, headspace solid-phase microextraction; PC, phosphatidylcholine; PDMS/DVB, polydimethylsiloxane/divinylbenzene; PL, phospholipid; SLPC, 1-stearoyl-2-linoleoyl-*sn*-glycero-3-phosposphocholine; SOPC, 1-stearoyl-2-oleoyl-*sn*-glycero-3-phosphocholine; TAG, triglyceride; VOC, volatile oxidized compound; SOS, 1,3-distearoyl-2-oleoyl-glycerol; SLS, 1,3-distearoyl-2-linoleoyl-glycerol; PUFA, polyunsaturated fatty acid; FA, fatty acid

## ■ REFERENCES

(1) Shirouchi, B.; Nagao, K.; Inoue, N.; Furuya, K.; Koga, S.; Matsumoto, H.; Yanagita, T. Dietary phosphatidylinositol prevents the development of nonalcoholic fatty liver disease in Zucker (*fa*/*fa*) rats. *J. Agric. Food Chem.* **2008**, *56*, 2375−2379.

(2) Zhou, L.; Le Grandois, J.; Marchioni, E.; Zhao, M. J.; Ennahar, S.; Bindler, F. Improvement of total lipid and glycerophospholipid recoveries from various food matrices using pressurized liquid extraction. *J. Agric. Food Chem.* **2010**, *58*, 9912−9917.

(3) Bloklang, A.; Honig, W.; Browns, F.; Jolles, J. Cognition-enhancing properties of subchronic phosphatidylserine (PS) treatment in middle-aged rats: Comparison of bovine cortex PS with egg PS and soybean PS. *Nutrition* **1999**, *15*, 778−783.
(4) Zhou, L.; Zhao, M. J.; Ennahar, S.; Bindler, F.; Marchioni, E. Determination of phosphatidylethanolamine molecular species in a variety of food matrices by liquid chromatography−electrospray ionization−tandem mass spectrometry (LC−ESI−$MS^2$). *Anal. Bioanal. Chem.* **2012**, *403*, 291−300.
(5) Wat, E.; Tandy, S.; Kapera, E.; Kamili, A.; Chung, R. W. S.; Brown, A.; Rowney, M.; Cohn, J. S. Dietary phospholipid-rich dairy milk extract reduces hepatomegaly, hepatic steatosis and hyperlipidemia in mice fed a high-fat diet. *Atherosclerosis* **2009**, *205*, 144−150.
(6) Jian, B.; Llera-Moya, M.; Royer, L.; Rothblat, G.; Francone, O.; Swaney, J. B. Modification of the cholesterol efflux properties of human serum by enrichment with phospholipid. *J. Lipid Res.* **1997**, *38*, 734−744.
(7) Zhou, L.; Zhao, M. J.; Ennahar, S.; Bindler, F.; Marchioni, E. Liquid chromatography−tandem mass spectrometry for the determination of sphingomyelin species from calf brain, ox liver, egg yolk, and krill oil. *J. Agric. Food Chem.* **2012**, *60* (1), 293−298.
(8) Zhou, L.; Khalil, A.; Bindler, F.; Zhao, M. J.; Marcic, C.; Ennahar, S.; Marchioni, E. Effect of heat treatment on the content of individual phospholipids in coffee beans. *Food Chem.* **2013**, *141* (4), 3846−3850.
(9) Shahidi, F. *Nutraceutical and Specialty Lipid and Their Co-products*; CRC Press: Boca Raton, FL, 2006.
(10) Parmentier, M.; Sayed Mahmoud, C.; Linder, M.; Fanni, J. Polar lipids: n-3 PUFA carriers for membranes and brain: Nutritional interest and emgering processes. *Ol., Corps Gras, Lipides* **2007**, *14*, 224−229.
(11) Amate, L.; Gil, A.; Ramirez, M. Feeding infant piglets formula with long-chain polyunsaturated fatty acids as triacylglycerols or phospholipids influences the distribution of these fatty acids in plasma lipoprotein fractions. *J. Nutr.* **2001**, *131*, 1250−1255.
(12) Lemaitre-Delaunay, D.; Pachiaudi, C.; Laville, M.; Pousin, J.; Armstrong, M.; Lagarde, M. Blood compartmental metabolism of docosahexaenoic acid (DHA) in humans after ingestion of a single dose of [$^{13}$C] DHA in phosphatidylcholine. *J. Lipid Res.* **1999**, *40*, 1867−1874.
(13) Wijendran, V.; Huang, M. C.; Diau, G. Y.; Boehm, G.; Nathanielsz, P. W.; Brenna, J. T. Efficacy of dietary arachidonic acid provided as triglyceride or phospholipid as substrates for brain arachidonic acid accretion in baboon neonates. *Pediatr. Res.* **2002**, *51*, 265−272.
(14) Youdim, K. A.; Martin, A.; Joseph, J. A. Essential fatty acids and the brain: Possible health implications. *Int. J. Dev. Neurosci.* **2000**, *18*, 383−399.
(15) Moriya, H.; Kuniminato, T.; Hosokawa, M.; Fukunaga, K.; Nishiyama, T.; Myashita, K. Oxidative stability of salmon and herring roe lipids and their dietary effect on plasma cholesterol levels of rats. *Fish. Sci.* **2007**, *73*, 668−674.
(16) Song, J. H.; Inoue, Y.; Miyazawa, T. Oxidative stability of docosahexaenoic acid-containing oils in the form of phospholipids, triacylglycerols, and ethyl esters. *Biosci., Biotechnol., Biochem.* **1997**, *61*, 2085−2088.
(17) Velasco, J.; Berdeaux, O.; Márquez-Ruiz, G. Sensitive and accurate quantitation of monoepoxy fatty acids in thermoxidised oils by gas-liquid chromatography. *J. Chromatogr. A* **2002**, *982*, 145−152.
(18) Márquez-Ruiz, G.; Tasioula-Margari, M.; Dobarganes, M. C. Quantitation and distribution of altered fatty acids in frying fats. *J. Am. Oil Chem. Soc.* **1995**, *72*, 1171−1176.
(19) Le Grandois, J.; Marchioni, E.; Ennahar, S.; Giuffrida, F.; Bindler, F. Identification and kinetics of oxidized compounds from phosphatidylcholine molecular species. *Food Chem.* **2010**, *119*, 1233−1238.
(20) Le Grandois, J.; Marchioni, E.; Zhao, M. J.; Giuffrida, F.; Ennahar, S.; Bindler, F. Oxidative stability at high temperatures of oleoyl and linoleoyl residues in the forms of phosphatidylcholines and triacylglycerols. *J. Agric. Food Chem.* **2010**, *58*, 2973−2979.
(21) Asghar, A.; Gray, J. L.; Buckley, D. J.; Pearson, A. M.; Boeren, A. M. Perspectives of warmed-over flavour. *Food Technol.* **1988**, *42*, 102−108.
(22) Zhou, L.; Zhao, M. J.; Khalil, A.; Marcic, C.; Bindler, F.; Marchioni, E. Identification of volatiles from oxidised phosphatidylcholine molecular species using headspace solid-phase microextraction (HS-SPME) and gas chromatography−mass spectrometry (GC−MS). *Anal. Bioanal. Chem.* **2013**, *405*, 9125−9137.
(23) Garcia-Esteban, M.; Ansorena, D.; Astiasarán, I.; Ruiz, J. Study of the effect of different fiber coatings and extraction conditions on dry cured ham volatile compounds extracted by solid-phase microextraction (SPME). *Talanta* **2004**, *64*, 458−466.
(24) Plutowska, B.; Chmiel, T.; Dymerski, T.; Wardencki, W. A headspace solid-phase microextraction method development and its application in the determination of volatiles in honeys by gas chromatography. *Food Chem.* **2011**, *126*, 1288−1298.
(25) Vichi, S.; Isabel Castellote, A.; Pizzale, L.; Conte, L. S.; Buxaderas, S.; López-Tamames, E. Analysis of virgin olive oil volatile compounds by headspace solid-phase microextraction coupled to gas chromatography with mass spectrometric and flame ionization detection. *J. Chromatogr. A* **2003**, *983*, 19−33.
(26) Frankel, E. N.; Neff, W. E.; Selke, E. Analysis of autoxidized fats by gas chromatography−mass spectrometry: VII. Volatile thermal decomposition products of pure hydroperoxides from autoxidized and photosensitized oxidized methyl oleate, linoleate and linolenate. *Lipids* **1981**, *16*, 279−285.
(27) Frankel, E. N. *Lipid Oxidation*, 2nd ed.; The Oily Press: Bridgwater, U.K., 2005.
(28) Varlet, V.; Prost, C.; Serot, T. Volatile aldehydes in smorked fish: analysis methods, occurrence and mechanisms of formation. *Food Chem.* **2007**, *105*, 1536−1556.
(29) Selke, E.; Rohwedder, W. K.; Dutton, H. J. Volatile components from tristearin heated in air. *J. Am. Oil Chem. Soc.* **1975**, *52*, 232−235.
(30) Lyberg, A. M.; Fasoli, E.; Adlerrcreutz, P. Monitoring the oxidation of docosahexaenoic acid in lipids. *Lipids* **2005**, *40*, 969−979.
(31) Yoshimoto, M.; Miyazaki, Y.; Umemoto, A.; Walde, P.; Kuboi, R.; Nakao, K. Phosphoatidylcholine vesicle-mediated decomposition of hydrogen peroxide. *Langmuir* **2007**, *23*, 9416−9422.

JOURNAL OF AGRICULTURAL AND FOOD CHEMISTRY

Article

pubs.acs.org/JAFC

# Lichenysin, a Cyclooctapeptide Occurring in Chinese Liquor *Jiannanchun* Reduced the Headspace Concentration of Phenolic Off-Flavors via Hydrogen-Bond Interactions

Rong Zhang, Qun Wu, and Yan Xu*

State Key Laboratory of Food Science and Technology, Synergetic Innovation Center of Food Safety and Nutrition, Key Laboratory of Industrial Biotechnology of Ministry of Education, School of Biotechnology, Jiangnan University, 1800 Lihu Avenue, Wuxi, Jiangsu 214122, China

**ABSTRACT:** Nonvolatile compounds play important roles in the quality of alcoholic beverages. In our previous work, a type of cyclooctapeptide lichenysin was newly identified in Chinese strong-aroma type liquor. In this work, it was found that lichenysin could selectively affect aroma volatility in strong-aroma type (*Jiannanchun*) liquor. Interaction of lichenysin and volatile phenolic compounds (off-odors in strong-aroma type liquor) was characterized using headspace solid-phase microextraction coupled with gas chromatography−mass spectrometry (HS-SPME-GC-MS). HS-SPME results indicated that lichenysin very efficiently suppressed the volatility of phenolic compounds by 36−48% ($P < 0.05$). Thermodynamic analysis showed that the binding process was mainly mediated by hydrogen bonding. Furthermore, the mixture of lichenysin and 4-ethylguaiacol revealed intermolecular cross peaks between the *a*H (Val) of lichenysin and the 1H of 4-ethylguaiacol, by using nuclear Overhauser effect spectroscopy. This study will help to further understand the interaction mechanisms between flavor and nonvolatile matrix components in Chinese liquors.

**KEYWORDS:** *lichenysin, phenolic off-flavors, aroma volatility, hydrogen-bond interaction*

## INTRODUCTION

Chinese liquor is a traditionally indigenous and famous distilled beverage in China.[1] The various aroma profiles of Chinese liquors result from their complexity in manufacturing practices. During the production, Chinese liquor is typically distilled from fermented sorghum. The sorghum used for liquor fermentation is cooked and then mixed with a fermentation starter (Daqu powder). Daqu made from wheat is rich in various microorganisms including bacteria, yeast, and fungi. They are typically carried out at 28−32 °C under anaerobic conditions in the solid-state fermentation. After fermentation, the liquor is distilled out with steam from fermented sorghum by the means of traditional solid distillation. Then, it is aged in a china jar (sealed tightly) for more than 3 years at 15−25 °C.[1]

The quality of Chinese liquor depends on the volatile and nonvolatile compounds. In Chinese strong-aroma type liquors, a sum of 132 aroma compounds was detected using gas chromatography olfactometry (GC-O) coupled with mass spectrometry (MS).[2,3] Besides the volatile compounds, nonvolatile compounds also play important roles in the liquor quality. In past research, we isolated and identified a cyclooctapeptide lichenysin in many different Chinese liquors as a nonvolatile compound, using preparative high-performance liquid chromatography (HPLC) coupled with a quadrupole-time-of-flight (Q-TOF) mass spectrometer. Lichenysin is produced by *Bacillus licheniformis* in the fermented sorghum and is most likely to be distilled into the liquor with steam by means of traditional solid distillation. The concentration of this nonvolatile compound is the highest to reach 112 μg/L in the *Dongjiu* liquor (unpublished data). However, little information has been reported about the nonvolatile compounds affecting aroma perception in Chinese liquors, especially their interaction mechanism with aroma compounds.

The nature of interactions between odor and nonvolatile matrix components may depend on the physicochemical properties of the aroma compound and the binding mechanisms. The most frequent method to measure the interactions that occur between aroma compounds and other food or beverage constituents is headspace analysis, the headspace solid-phase microextraction (HS-SPME) method.[4−6] Aronson and Ebeler[7] have shown that gallic acid (in 1% ethanol solution) significantly decreased the volatility of 2-methylpyrazine by HS-SPME. To further explore the nature of the interactions between aroma compounds and nonvolatile wine compounds, NMR spectroscopy has been proven as one of the most powerful techniques. It was found that the interactions between the galloyl ring of gallic acid and the aromatic ring of methylpyrazine were stabilized by hydrogen bonds, using NMR techniques.[8] β-Cyclodextrin (β-CD) is usually used for the microencapsulation of aroma compounds in food processes. The binding nature of β-CD with benzyl alcohol and 2-methylbutyric acid was studied by using $^{1}H$ and $^{13}C$ NMR experiments.[9] Up to now, there is no report about the interaction mechanism between nonvolatile compounds and aroma compounds in Chinese liquor.

In this study, we characterized that the cyclooctapeptide lichenysin reduced the headspace concentration of phenolic off-

Received: April 30, 2014
Revised: July 13, 2014
Accepted: July 26, 2014
Published: July 26, 2014

ACS Publications © 2014 American Chemical Society

flavors in strong-aroma type liquor and the model solution, using HS-SPME-GC-MS and sensory evaluation. Furthermore, we used thermodynamic analysis and nuclear Overhauser effect spectroscopy (NOESY) to elucidate the nature of binding between lichenysin and phenolic compounds.

## MATERIALS AND METHODS

**Chemicals.** DMSO-$d_6$ and tetramethylsilane (TMS) were purchased from Sigma Technology (St. Louis, MO, USA). The chemical standards of all the aroma compounds and internal standards (hexyl formate and 2-octanol) were purchased from Acros Organics (Fair Lawn, NJ, USA). Formic acid was purchased from Acros Organics. Methanol and absolute alcohol were purchased from Tedia (Fairfield, OH, USA). The reference standards were prepared in an ethanol solvent. All standard solutions were flushed with nitrogen to avoid oxidation of the phenols and kept in the freezer at −20 °C in the dark. We got the $C_{15}$–lichenysin from the Chinese liquor sample *Dongjiu* liquor, from the Dongjiu distilleries. The compound was isolated from the fractions by means of preparative HPLC (autopurity system, Waters, Milford, MA, USA) material, by using an Xbridge Prep $C_{18}$ (250 mm × 19 mm, 10 μm) reversed-phase Xbridge steel column. The solvents were water containing 0.1% formic acid as solvent A and methanol as solvent B. The program was conducted by means of gradient elution, and the detection was selected at wavelength of 210 nm. The structure of $C_{15}$–lichenysin was confirmed by the Waters Synapt Q-TOF system. It is built from a heptapeptide and a β-hydroxy fatty acid with a chain of 15 carbon atoms. The purity of $C_{15}$–lichenysin that we got from the liquor can reach 99%. The Chinese liquor sample *Jiannanchun* liquor was purchased from the market. *Jiannanchun* is one of the most famous strong-aroma type liquors, which typically have strong fruity, pineapple-like, and banana-like aromas.[1] This liquor is the typical representatives of strong-aroma type.

**Sample Preparation for SPME Extraction and SPME Conditions.** An aliquot of $C_{15}$–lichenysin was dissolved in Chinese liquor (strong-aroma type liquor) and model solution. Phenol, 4-methylphenol (4-MP), 4-ethylphenol (4-EP), guaiacol, and 4-ethylguaiacol (4-EG) (Figure 1) were respectively dissolved in the model

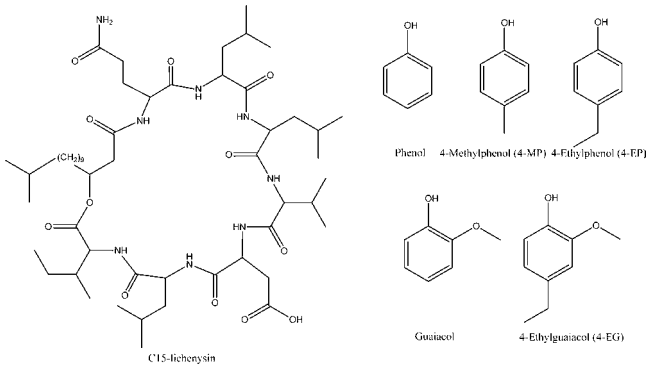


**Figure 1.** Chemical structures of $C_{15}$-Lichenysin and five phenolic compounds.

solution (46% ethanol/water solution, v/v). The phenol concentration was 1.28 mg/L, the 4-MP concentration was 3.20 mg/L, the 4-EP concentration was 0.38 mg/L, the guaiacol concentration was 0.38 mg/L, and the 4-EG concentration was 1.54 mg/L. The concentration of phenolic compound in the model solution reached close to the strong aroma type *Jiannanchun* liquor determined by HS-SPME-GC-MS.[10] The $C_{15}$–lichenysin is the highest to reach 75% of the total in Chinese liquor. Therefore, the effect of $C_{15}$–lichenysin on aroma compounds release was evaluated by HS-SPME-GC-MS.

For the SPME, an automatic headspace sampling system (Multi Purpose Sample MPS 2 with a SPME adapter, from GERSTEL Inc., Baltimore, MD, USA) with a 50/30 μm DVB/CAR/PDMS fiber (2 cm, Supelco Inc., Bellefonte, PA, USA) was used for analyte extraction. A total of 8 mL of sample was spiked with 10 μL of internal standard (hexyl formate for nonpolar compounds, 760 μg/L in ethanol, 2-octanol for polar compounds, 810 μg/L in ethanol). The sample was transferred to a screw-capped, straight-sided headspace vial with a 15 mL volume. The vial was tightly capped with a Teflon-faced silicone septum. The samples were equilibrated at 30 °C for 5 min and extracted for 45 min at the same temperature[6,7] under stirring (500 rpm, on for 20 s, off for 0 s). After extraction, the fiber was inserted into the injection port of the gas chromatograph (250 °C) for 5 min to desorb the analytes. All analyses were made in triplicate, using a modified HS-SPME method.[6,7]

**GC-MS Analysis and GC-MS Data Analysis.** For the GC-MS analysis, an Agilent 6890N gas chromatograph coupled to an Agilent 5975 mass selective detector (MSD) was used. The capillary column used was a DB-Wax column (30 m length × 0.25 mm i.d., 0.25 μm film thickness; Phenomenex, Torrance, CA, USA). The injector temperature was 250 °C, and the splitless mode was used. The conditions were as follows: starting temperature 50 °C (holding 2 min), then raised to 230 °C at the rate of 6 °C/min, and held at 230 °C for 30 min. The column carrier gas was helium with a purity of 99.9995% at a constant flow rate of 2 mL/min. The electron impact energy was 70 eV, and the ion source temperature was set at 230 °C. Full-scan acquisition was used in the ranges of masses (30−350 amu).

Identification of aroma compounds in Chinese liquor has been carried out on a DB-Wax column and a DB-5 column (30 m × 0.25 mm i.d., 0.25 μm film thickness, J&W Scientific, Folsom, CA, USA). It was based on the following criteria: comparing determined mass spectra and retention indices (RIs) with those of reference compounds. RIs were determined using a series of standard linear alkanes $C_5$–$C_{23}$ in accordance with a modified Kovats method.[11] Peak area integration of unique masses was conducted using MSD Chemstation (G1701-90057, Agilent, Santa Clara, CA, USA).

We compared the peak areas of aroma compounds in the control group (the liquor sample) with that of experiment group (the liquor sample added with lichenysin) by the means of HS-SPME-GC-MS. The net changes in peak areas were obtained by dividing the peak area of the control group subtracted from that of experiment group by the control. To eliminate the effect of other factors, we kept the control group and the experiment group at the same condition. From the net changes in peak areas, we studied about the effect of lichenysin on the volatility of different aroma compounds in the Chinese liquor. The use of peak area data to express aroma release was sufficient for the purpose of studying about aroma volatility in this work.

**Sensory Evaluation of Model Solutions.** The model solutions were presented to 10 panelists (China Distilled Spirit Appraisal Commissioner) at room temperature of 25 °C. According to Aronson's method,[7] the judges were trained in three test sessions and then carried up the experiment. They learned how to use the intensity scales by practicing with a number of samples. They familiarized themselves with the aroma and the low (zero) and high (the following concentrations) standards for each flavor compound. The model solution is 46% ethanol/water solution by volume, in which the phenol concentration is 1.28 mg/L, the 4-MP concentration is 3.20 mg/L, the 4-EP concentration is 0.38 mg/L, the guaiacol concentration is 0.38 mg/L, and the 4-EG concentration is 1.54 mg/L. Each flavor compound was evaluated respectively for two weeks. Samples of 30 mL were randomly presented in coded clear white wine glasses covered by tinfoil plates. The samples consisted of five controls and five phenolic/lichenysin solutions. The five phenolic compounds were respectively dissolved in the model solutions. Standards were used to anchor the ends of the scale for the judges.

The aroma intensity of the samples was marked on a 10 cm line scale in terms of deviation. The line scale was labeled "less than reference" and "more than reference" at the two ends. Judges were asked not to swirl the samples so as not to disturb the equilibrium. Lastly, they were allowed to resniff samples as long as they waited approximately 1 min before smelling the same sample a second time. All evaluations were conducted in a well-ventilated room. Each phenol and lichenysin combination was replicated during the triangle tests.


dx.doi.org/10.1021/jf502053g | J. Agric. Food Chem. 2014, 62, 8302−8307

Table 1. Effect of $C_{15}$−Lichenysin on Mean HS-SPME-GC-MS Peak Areas for Aroma Volatility in Chinese Liquor ($n$ = 3)

| compd | RI DB-Wax | RI DB-5 | odor descriptors[a] | identification[b] | control[c] | lichenysin, 160 μg/L | net change |
|---|---|---|---|---|---|---|---|
| ethyl acetate | 887 | 585 | pineapple | MS, RI | 2 085 585 ± 129 699a | 2 051 879 ± 61 274a | 1.62% |
| ethyl butanoate | 1031 | 800 | pineapple | MS, RI | 7 392 103 ± 376 057a | 7 222 882 ± 241 102a | 2.29% |
| ethyl pentanoate | 1144 | 900 | apple | MS, RI | 942 935 ± 29 573a | 951 414 ± 17 454a | 0.90% |
| ethyl hexanoate | 1233 | 1010 | fruity, floral | MS, RI | 3 581 850 ± 156 172a | 3 538 357 ± 156 168a | 1.21% |
| ethyl heptanoate | 1316 | 1095 | fruity | MS, RI | 2 360 905 ± 55 039a | 2 405 441 ± 61 676a | 1.89% |
| ethyl 2-hydroxypropanoate | 1348 | 815 | fruity | MS, RI | 164 962 234 ± 25 280 185a | 157 489 181 ± 27 761 731a | 4.53% |
| ethyl octanoate | 1410 | 1195 | fruity | MS, RI | 2 411 046 ± 115 910a | 2 478 513 ± 178 558a | 2.80% |
| ethyl decanoate | 1624 | 1390 | fruity, grape | MS, RI | 2 176 588 ± 42 168a | 2 249 724 ± 175 299a | 3.36% |
| 2-methylpropanol | 1112 | 610 | wine, solvent | MS, RI | 3 325 027 ± 143 751a | 3 438 090 ± 107 324a | 3.40% |
| 3-methylbutanol | 1210 | 783 | rancid, nail polish | MS, RI | 382 271 ± 133 554a | 384 928 ± 163 154a | 0.69% |
| acetic acid | 1473 | N.D. | acidic, vinegar | MS, RI | 2 391 796 ± 39 720a | 2 419 804 ± 35 247a | 1.17% |
| butanoic acid | 1641 | 795 | rancid, cheesy | MS, RI | 273 365 ± 10 054a | 291 606 ± 7584a | 6.67% |
| hexanoic acid | 1857 | N.D. | sweaty, cheesy | MS, RI | 368 519 ± 17 128a | 382 181 ± 24 427a | 3.71% |
| furfural | 1467 | 830 | sweet, almond | MS, RI | 153 321 ± 6164a | 175 827 ± 12 850a | 14.68% |
| benzaldehyde | 1501 | 960 | fruity, berry | MS, RI | 413 593 ± 1787a | 433 321 ± 22 105a | 4.77% |
| ethyl 2-phenylacetate | 1775 | 1247 | rosy, honey | MS, RI | 5 256 621 ± 346 629a | 4 656 515 ± 850 976a | 11.42% |
| ethyl 3-phenylpropanoate | 1878 | 1353 | fruity, floral | MS, RI | 148 759 ± 498a | 156 688 ± 6358a | 5.33% |
| phenol | 2007 | 970 | phenol, medicinal | MS, RI | 1785 ± 276a | 413 ± 272b | 76.86% |
| 4-methylphenol | 2090 | N.D. | animal, phenol | MS, RI | 1594 ± 261a | 656 ± 201b | 58.85% |
| 4-ethylphenol | 2185 | 1181 | smoky | MS, RI | 3457 ± 846a | 1798 ± 844b | 47.98% |
| guaiacol | 1862 | 1009 | spicy, animal | MS, RI | 62 831 ± 24 086a | 23 025 ± 6931b | 63.35% |
| 4-ethylguaiacol | 2031 | 1281 | clove, spicy | MS, RI | 4774 ± 541a | 2142 ± 664b | 55.14% |

[a]Odor descriptors of the aroma compounds were from refs 2 and 3. [b]Identification based on comparing determined MS and RI with that of reference compounds. [c]Different letters within a row denote significantly different means at $p \leq 0.05$.

Three samples include one control and two experiment groups. Judges periodically took some time to rest during the experiment to minimize fatigue. The responses for the test were decoded manually in centimeters and entered into an Excel spreadsheet.

**NMR Procedures.** NMR measurements were performed on a Bruker Avance 500 MHz spectrometer at 25 °C. Samples were prepared in DMSO-$d_6$; tetramethylsilane (TMS) were added to the DMSO-$d_6$ at a level of 0.05%. To investigate the concentration dependence of chemical shift changes, a 2.5 mM phenolic compound solution (0.5 mL) was mixed with various amounts of lichenysin covering molar ratios of 1:4, 1:2, 3:4, 1:1, 2:1, and 2.5:1 in DMSO-$d_6$ and observed by the single-pulse method. The chemical shift changes of protons were measured relative to the reference chemical shift. The experiments were carried out at 25, 45, and 60 °C, from which equilibrium association constants ($K_a$) and thermodynamic parameters ($\Delta H$ and $\Delta S$) were obtained using a nonlinear estimation program, ORIGIN (Microcal Software Co. Inc., Northampton, MA, USA). Then, a 2.5 mM lichenysin solution (0.5 mL) was mixed with various amounts of 4-EG to cover molar ratios of 1:0, 4:1, 4:2, 1:1, and 1:2 in DMSO-$d_6$. The NOESY spectrum was observed by the mean of NOESY measurement. The NOESY spectra were acquired with a spectral width of 7 kHz in 2K data points using 16 scans for each of the 512 $t_1$ increments. The spin lock power level and mixing time were set to 29 dB and 60 ms, respectively.

Data processing was performed by using Topspin NMR software (version 2.1; Bruker, Rheinstetten, Germany).

**Statistical Analysis Software.** Each sample was analyzed in triplicate for each analysis. Results presented in the tables were shown with standard deviations and the arithmetic means. All data were statistically assessed using SPSS version 19.0 for Windows statistical package (SPSS Inc.; Chicago, IL, USA). The significance of differences between mean values obtained was determined using a one-way ANOVA ($P < 0.05$).

## RESULTS AND DISCUSSION

**Interaction between $C_{15}$−Lichenysin and Aroma Compounds in Chinese Liquor by HS-SPME-GC-MS.** The study examined the effect of lichenysin on the volatility of aroma compounds in Chinese liquor (strong-aroma type liquor). In this study, a sum of 22 volatile compounds in Chinese liquor was identified and quantitated by using the HS-SPME method (Table 1). These following compounds were eight esters, two alcohols, three acids, two aldehydes, two aromatic compounds, and five phenolic compounds.

Addition of lichenysin (at concentration of 160 μg/L) to the liquor sample resulted in significant but variable suppressing effects on headspace concentration (HS-GC peak area) depending on the nature of flavor compound examined (Table 1). For esters, the headspace concentrations were influenced little by lichenysin, where the volatility of esters decreased by 1−5% in the liquor sample. For alcohols and aldehydes, the volatility of these compounds was affected the least by 1−15%. For volatile acids, the headspace concentrations were influenced by 1−7%. The most pronounced effects were interactions between lichenysin and phenolic compounds (phenol, 4-MP, 4-EP, guaiacol, and 4-EG). It might be because the phenolic hydroxyl group of these compounds formed hydrogen bonds with the carboxyl group of the lichenysin. The headspace concentration of phenol, 4-MP, 4-EP, guaiacol, and 4-EG significantly decreased by 77%, 59%, 48%, 63%, and 55%, respectively, in the liquor sample. The volatilities of esters, alcohols, aldehydes, and volatile acids were affected little. Thus, lichenysin selectively affected aroma volatility in Chinese liquor.

**Interaction between $C_{15}$−Lichenysin and Phenolic Compounds in Model Solutions by HS-SPME-GC-MS and Sensory Evaluation.** Volatile phenolic compounds in Chinese liquor are considered as off-odors,[10] in which 4-MP and 4-EG, respectively, give horsy and medical smells. We chose phenol, 4-MP, 4-EP, guaiacol, and 4-EG as aroma compounds. Interactions between lichenysin and phenolic


dx.doi.org/10.1021/jf502053g | J. Agric. Food Chem. 2014, 62, 8302−8307

compounds were studied in model solution by using the HS-SPME-GC-MS method. In Figure 2, lichenysin significantly

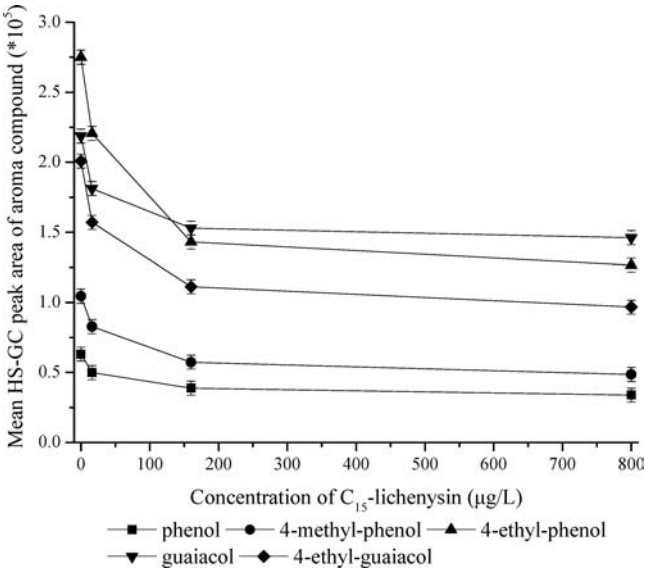


**Figure 2.** Effect of $C_{15}$–lichenysin concentration on mean HS-GC peak area for phenolic compounds in model solution (46%, ethanol/water solution, $n = 3$).

decreased the headspace concentration (HS-GC peak area) of the whole phenolic compounds relative to control group (without the addition of lichenysin), and the effect was the most pronounced when the concentration of lichenysin was 160 $\mu$g/L. The headspace concentrations of phenol, 4-MP, and 4-EP decreased by 39%, 45%, and 48%, respectively, ($p < 0.05$). The volatility of guaiacol and 4-EG in model solution decreased by 30% and 45% ($p < 0.05$). Later from that concentration, the effect of lichenysin on the volatility of phenolic compounds tended to reach an equilibrium state. When the concentration of lichenysin was 16 $\mu$g/L, the headspace concentrations of phenolic compounds decreased by 17−22%.

Ten trained sensory panelists were asked to test the aroma intensity scores of the model solution and also the one with lichenysin addition. Lichenysin (160 $\mu$g/L in model solution) significantly suppressed aroma perception of phenolic compounds ($p < 0.05$, Table 2). Thus, lichenysin could efficiently suppress the volatility of phenolic off-flavors in Chinese liquor.

**Thermodynamic Parameters and Acting Forces between Lichenysin and Phenolic Compounds.** To further study the nature of the phenolic/lichenysin interaction, the changes in the chemical shifts of protons in the phenolic compounds were evaluated by using $^1$H NMR, upon complexation with lichenysin in DMSO-$d_6$. Exchangeable protons such as those in carboxylic acids or alcohols do not give separate resonances in $D_2O$ or ethanol-$d_6$. Therefore, the solvent (DMSO-$d_6$) was chosen in which exchange is so slow that coupling between OH and adjacent protons can be observed. A titration process was then used to determine the concentration equilibrium constant, $K_a$, based on the chemical shift changes of phenolic protons. The 1H proton of each phenolic compound, which was most significantly affected by lichenysin complexation (Figure 3), was selected to obtain the association

**Table 2. Mean Perceived Aroma Intensity Scores[a] for Phenolic Compounds with Added Lichenysin**

| | control | 16 $\mu$g/L | 160 $\mu$g/L |
|---|---|---|---|
| phenol | 8.6 ± 0.6a | 6.8 ± 0.8a | 4.0 ± 0.4b |
| 4-methylphenol | 7.8 ± 0.4a | 6.6 ± 0.6a | 3.5 ± 0.8b |
| 4-ethylphenol | 8.0 ± 0.5a | 7.2 ± 0.8a | 3.0 ± 0.4b |
| guaiacol | 8.2 ± 0.7a | 7.6 ± 0.4a | 5.1 ± 0.5b |
| 4-ethylguaiacol | 7.9 ± 0.5a | 7.2 ± 0.4a | 4.2 ± 0.6b |

[a]Different letters within a row denote significantly different means at $p \leq 0.05$, $n = 10$.

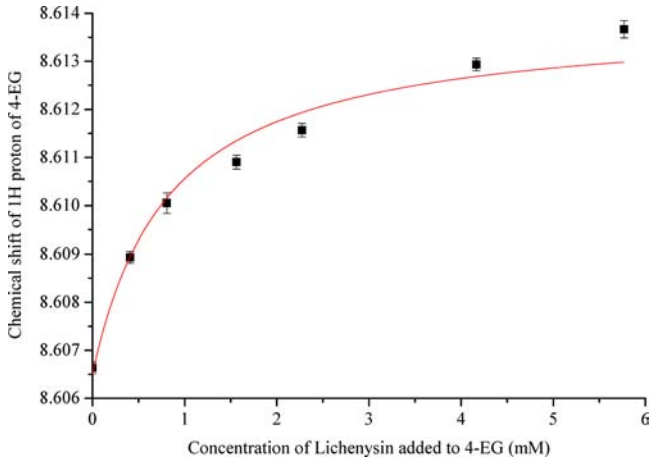


**Figure 3.** Nonlinear curve fitting of chemical shift data for mixtures of 4-EG (2.5 mM) and lichenysin in DMSO-$d_6$ at 25 °C.

constant, $K_a$, assuming a 1:1 stoichiometry between phenolic compound (2.5 mM) and lichenysin:

$$K_a = \frac{LP}{L \times P} \quad (1)$$

.In eq1, L, P, and LP represent the mole fractions of the free lichenysin, the free phenolic compound, and the bound form of the phenolic compounds, respectively. When fast exchange processes take place, the NMR spectrum for each proton shows a single signal, averaged in the proportions of the partial mole fractions of the complexed and free molecules. Therefore, the observed chemical shift ($\delta_{obs}$) of a signal is a weighted average of the chemical shifts in two possible environments—the chemical shift for the free flavor ($\delta_P$) and the chemical shift for the bound flavor ($\delta_{LP}$):

$$\delta_{obs} = \delta_P + (\delta_{LP} - \delta_P)\frac{LP}{P_0} \quad (2)$$

,where $P_0$ represents the total mole fraction of the phenolic compound. Values of $K_a$, $\delta_P$, and $\delta_{LP}$ leading to a best fit of the proton chemical shift changes were estimated by a nonlinear curve fitting program, and theoretical curves were derived from eq2. The curve fit of a 4-EG (2.5 mM) and lichenysin mixture is shown in Figure 3. Quantitative analysis of NMR spectra recorded at 25, 45, and 60 °C yielded association constants ($K_a$) for the interaction of the five phenolic compounds with lichenysin (Table 3).

The interaction forces between phenolic compounds and lichenysin mainly include four types: hydrogen bonding, hydrophobic interaction, electrostatic interaction, and van der Waals force. The thermodynamic parameters free energy change ($\Delta G$), enthalpy change ($\Delta H$), and entropy change


dx.doi.org/10.1021/jf502053g | J. Agric. Food Chem. 2014, 62, 8302−8307

**Table 3. Thermodynamic Parameters for Association between Lichenysin and Five Phenolic Compounds**

| | $K_{25°C}$ ($M^{-1}$) | $K_{45°C}$ ($M^{-1}$) | $K_{60°C}$ ($M^{-1}$) | $\Delta H$ (kJ/mol) | $\Delta S$ (J/(mol·K)) |
|---|---|---|---|---|---|
| phenol | 327.09 | 302.21 | 193.73 | −11.63 | 9.62 |
| 4-MP | 1243.47 | 927.66 | 888.49 | −8.20 | 31.51 |
| 4-EP | 1601.28 | 1081.24 | 559.39 | −24.07 | −19.55 |
| guaiacol | 2913.92 | 1344.43 | 438.00 | −43.57 | −79.09 |
| 4-EG | 1219.65 | 340.65 | 46.68 | −74.85 | −192.46 |

($\Delta S$) of the binding reaction can provide evidence for clarifying interaction modes. If $\Delta H$ does not change significantly over the temperature range studied, it can be regarded as a constant, and then, the values of $\Delta H$, $\Delta S$, and $\Delta G$ are estimated from the Van't Hoff equation:

$$\ln K_a = -\Delta H/RT + \Delta S/R \quad (3)$$

$$\Delta G = \Delta H - T \times \Delta S \quad (4)$$

where $K_a$ is the association constant at temperature $T$ and $R$ is the universal gas constant.

The signs and magnitudes of the thermodynamic parameters associated with various individual kinds of interaction that might take place in the protein association processes.[12] That is, for $\Delta H > 0$ and $\Delta S > 0$, the contributions to these changes mainly arise from hydrophobic interactions; for $\Delta H < 0$ and $\Delta S < 0$, van der Waals forces and hydrogen-bond formation play major roles; for $\Delta H \approx 0$ and $\Delta S > 0$, electrostatic forces are suggested as more important. The calculated $\Delta H$ and $\Delta S$ are summarized in Table 3. For 4-EP, guaiacol, and 4-EG, the values of both $\Delta H$ and $\Delta S$ were negative, which suggested the main acting force would be hydrogen bonding and/or van der Waals force. The carbonyl group of the amino acid residues of lichenysin is a neutral acceptor group for hydrogen bonding. For phenol and 4-MP, $\Delta S$ values were found to be positive, whereas $\Delta H$ values were negative. The positive $\Delta S$ values are supposed to provide evidence for hydrophobic interactions in the binding phenomenon between lichenysin and these two phenolic compounds. Meanwhile, the negative $\Delta H$ values may account for the involvement of hydrogen bonding in this interaction, as 1H atoms on the phenolic compounds can easily form hydrogen bonds with amino acid residues of lichenysin. Thus, the main acting force between lichenysin and phenolic compounds was hydrogen-bond interaction.

**$^1$H NMR and Two-Dimensional NOESY in the Complexes of Lichenysin and 4-EG.** To better evaluate the binding site of the interactions and determine the spatial proximity of interacting protons, we chose $^1$H NMR and two-dimensional (2D) NOESY for the complexes of lichenysin and 4-EG. When passing from the free to the complex state, the $^1$H NMR chemical shifts change for individual molecules in the complex. By using $^1$H NMR, the changes in the chemical shifts of protons in the lichenysin were evaluated, upon complexation with 4-EG in DMSO-$d_6$. For complexes of lichenysin and 4-EG, the special proton of both compounds underwent chemical shift changes compared to those of their free state. When the 4-EG molar concentration was onefold with respect to that of lichenysin, a gentle downfield shift (4.10 ppm) of *a*H (Val) of lichenysin is observed in Figure 4, as compared with that (4.07 ppm) of its free state. Lichenysin has a potential of hydrogen bonding to 4-EG, as it has some acyl groups.

The lichenysin/4-EG interactions were further evaluated using 2D NOESY. The cross peaks indicate spatial proximity among the peaks (<5 Å) in the NOESY spectra. As shown in Figure 5, the NOESY spectrum of a lichenysin and 4-EG mixture in DMSO-$d_6$ reveals intermolecular cross peaks between the *a*H (Val) of lichenysin and the 1H of 4-EG. The NOESY effect observed by means of 2D experiments suggests that, in the spatial geometry, the carbonyl oxygen of the acyl group (Val) of lichenysin can very easily form a hydrogen bond with the hydroxyl groups of 4-EG.

This study was the first one to characterize that the cyclooctapeptide lichenysin reduced the headspace concentration of phenolic off-flavors in the Chinese liquor

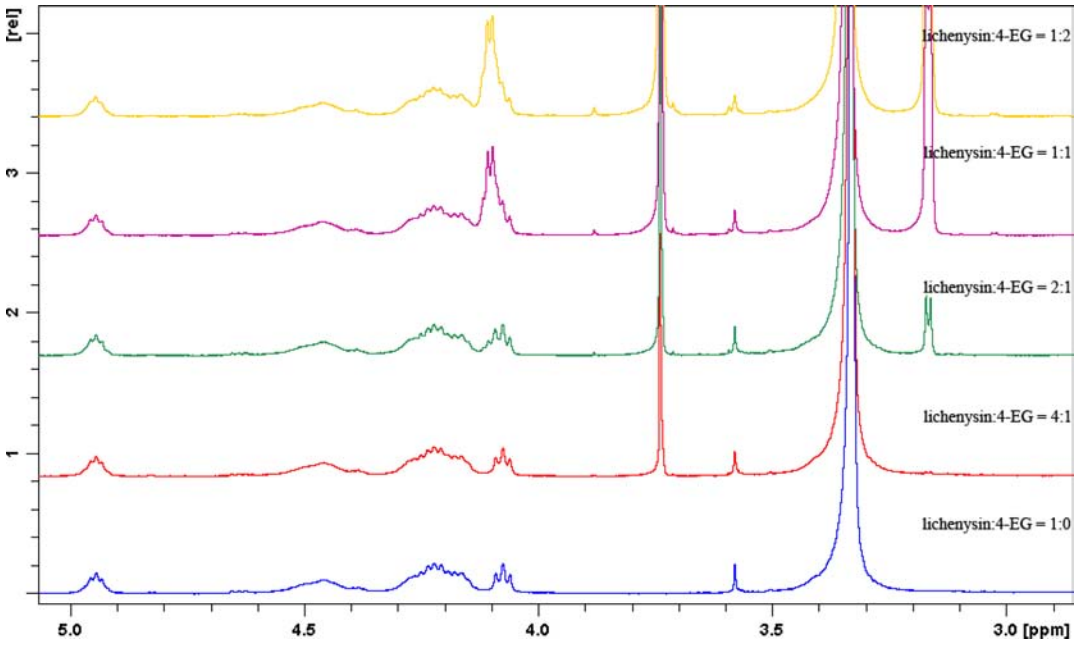


**Figure 4.** Change values of the chemical shift of lichenysin (2.5 mM) in DMSO-$d_6$ solution at 25 °C following the addition of 4-EG at the ratio of mole.


dx.doi.org/10.1021/jf502053g | J. Agric. Food Chem. 2014, 62, 8302−8307

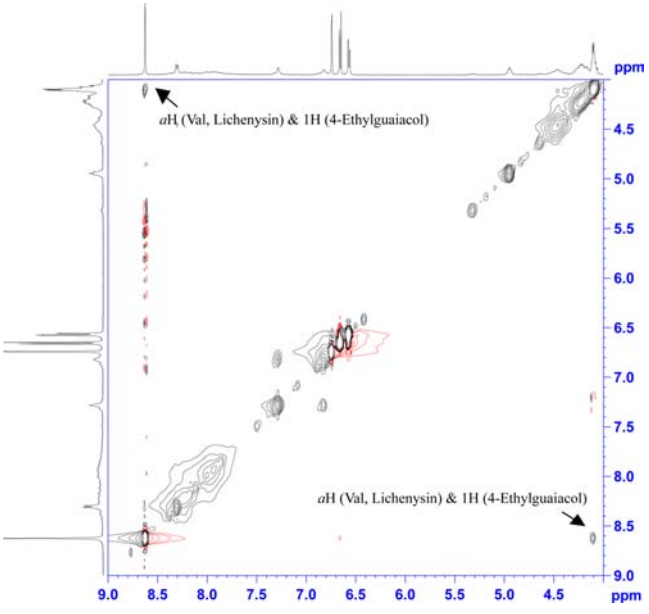


**Figure 5.** NOESY spectrum (4−9 ppm) of 2.5 mM lichenysin and 5.0 mM 4-EG in DMSO- $d_6$ at 25 °C.

*Jiannanchun*. Though limitations still existed, our investigation could contribute to a better understanding of Chinese liquor at the molecular level.

## AUTHOR INFORMATION

### Corresponding Author

*Phone: +86 510 85918197; fax: +86 510 85918201; e-mail: yxu@jiangnan.edu.cn.

### Funding

This work was supported by National High Technology Research and Development Program of China (2012AA021301, 2013AA102108), National Natural Science Foundation of China (31000806, 31371822, 31271921), Cooperation Project of Jiangsu Province among Industries, Universities and Institutes (BY2010116), 169 Plan of Chinese liquor, the Program of Introducing Talents of Discipline to Universities (111 Project) (111-2-06), and the Priority Academic Program Development of Jiangsu Higher Education Institution.

### Notes

The authors declare no competing financial interest.

## REFERENCES

(1) Mu, X. Q.; Xu, Y.; Fan, W. L.; Wang, H. Y.; Wu, Q.; Wang, D. Solid state fermented alcoholic beverages. In *Solid State Fermentation for Foods and Beverages*; Chen, J., Zhu, Y., Eds.; Taylor & Francis Group: Boca Raton, FL, 2014; pp 288−299.

(2) Fan, W.; Qian, M. C. Characterization of aroma compounds of Chinese "*Wuliangye*" and "*Jiannanchun*" liquors by aroma extract dilution analysis. *J. Agric. Food Chem.* **2006**, *54*, 2695−2704.

(3) Fan, W.; Qian, M. C. Headspace solid phase microextraction and gas chromatography−olfactometry dilution analysis of young and aged Chinese "*Yanghe Daqu*" liquors. *J. Agric. Food Chem.* **2005**, *53*, 7931−7938.

(4) Villamor, R. R.; Ross, C. F. Wine matrix compounds affect perception of wine aromas. *Annu. Rev. Food Sci. Technol.* **2013**, *4*, 1−20.

(5) Munoz-Gonzalez, C.; Rodriguez-Bencomo, J. J.; Moreno-Arribas, M. V.; Pozo-Bayon, M. A. Beyond the characterization of wine aroma compounds: Looking for analytical approaches in trying to understand aroma perception during wine consumption. *Anal. Bioanal. Chem.* **2011**, *401*, 1497−1512.

(6) Robinson, A. L.; Ebeler, S. E.; Heymann, H.; Boss, P. K.; Solomon, P. S.; Trengove, R. D. Interactions between wine volatile compounds and grape and wine matrix components influence aroma compound headspace partitioning. *J. Agric. Food Chem.* **2009**, *57*, 10313−10322.

(7) Aronson, J.; Ebeler, S. E. Effect of polyphenol compounds on the headspace volatility of flavors. *Am. J. Enol. Vitic.* **2004**, *55*, 13−21.

(8) Jung, D.-M.; Ropp, J. S. D.; Ebeler, S. E. Study of interactions between food phenolics and aromatic flavors using one- and two-dimensional $^1$H NMR spectroscopy. *J. Agric. Food Chem.* **2000**, *48*, 407−412.

(9) Goubet, I.; Dahout, C.; Sémon, E.; Guichard, E.; Le Quéré, J. L.; Voilley, A. Competitive binding of aroma compounds by $\beta$-cyclodextrin. *J. Agric. Food Chem.* **2001**, *49*, 5916−5922.

(10) Zhang, C.; Xu, Y.; Fan, W. Removal of off-odors from baijiu (Chinese liquor) with different adsorbents. *Sci. Technol. Food Ind.* **2012**, 60−65.

(11) Cates, V. E.; Meloan, C. E. Separation of sulfones by gas chromatography. *J. Chromatogr.* **1963**, *11*, 472−478.

(12) Zhang, J.; Zhuang, S.; Tong, C.; Liu, W. Probing the molecular interaction of triazole fungicides with human serum albumin by multispectroscopic techniques and molecular modeling. *J. Agric. Food Chem.* **2013**, *61*, 7203−7211.

JOURNAL OF AGRICULTURAL AND FOOD CHEMISTRY

Article

pubs.acs.org/JAFC

# Characterization of the Potent Odorants Contributing to the Characteristic Aroma of Chinese Green Tea Infusions by Aroma Extract Dilution Analysis

Ryoko Baba* and Kenji Kumazawa

Ogawa & Company, Ltd., 15-7 Chidori Urayasushi, Chiba 279-0032, Japan

Supporting Information

**ABSTRACT:** The volatile fractions of three famous Chinese green tea cultivar infusions (Longjing, Maofeng, and Biluochun) were prepared by a combination of the adsorptive column method and the SAFE techniques. The aroma extract dilution analysis (AEDA) applied to the volatile fractions revealed 58 odor-active peaks with flavor dilution (FD) factors between $4^1$ and $4^7$. Forty-six of the odorants, which included six odorants that have not been reported in the literature in Chinese green tea (2-isopropyl-3-methoxypyrazine, 2-ethenyl-3,5-dimethylpyrazine, *cis*-4,5-epoxy-(*E*)-2-decenal, 4-ethylguaiacol, (*E*)-isoeugenol, and 3-phenylpropionic acid), were identified or tentatively identified by GC-MS and GC-O. Among the perceived odorants, 4-hydroxy-2,5-dimethyl-3(2*H*)-furanone, 3-hydroxy-4,5-dimethyl-2(5*H*)-furanone, coumarin, vanillin, geraniol, (*E*)-isoeugenol, and 2-methoxyphenol showed high FD factors in all of the cultivars, irrespective of the cultivar or harvesting season, suggesting that these seven odorants are essential for the aroma of Chinese green tea. On the other hand, the contents of the odorants, FD factors of which were uneven between the cultivars, were suggested to influence the characteristic aroma of each cultivar. In addition, the formation mechanism of (*E*)-isoeugenol, one of the odorants which have not been reported in the literature with a high FD factor common to all the cultivars, was investigated, and it was suggested that the (*E*)-isoeugenol content of the tea products has a close correlation with the manufacturing process of the tea leaves.

**KEYWORDS:** *Chinese green tea, flavor, aroma, AEDA, isoeugenol, coniferyl alcohol*

## INTRODUCTION

Tea is one of the most widely consumed beverages in the world. Being differentiated by the degrees of fermentation by the endogenous enzymes in the leaves, three main types of teas are produced; i.e., fermented tea (black tea), semifermented tea (oolong tea), and unfermented tea (green tea). Each of them has its own characteristic aroma, despite being made from the same plant (*Camellia sinensis*). Among them, green tea, the leaves of which are immediately heated after being plucked to inactivate the endogenous enzymes, is the most popular tea in China, Japan, and other East Asian countries.

The manufacturing process of green tea is mainly divided into two types according to the heating process to inactivate the endogenous enzymes in the leaves, i.e., pan-firing and steaming, which are common in China and Japan, respectively. The difference in the heating process is said to be one of the factors which influences the aromas of the tea products; the steamed tea (Sen-cha), which is not affected by the enzymes because they are immediately inactivated, has a green, marine aroma. On the other hand, pan-fired tea, affected by the enzymatic reactions because the temperature of the leaves slowly rises and the enzymes are not immediately inactivated, has a sweet, floral aroma like fermented teas, besides the characteristic pan-fired aroma. Furthermore, in China, the leaves are generally withered before being pan-fired, during which the leaves are affected by the enzymes. In addition, there are numerous Chinese green tea cultivars classified by the subtle differences in the producing area, varieties of tea, and/or the manufacturing process (withering, heating, etc.), and each of them has its own characteristic aroma.

A number of volatile compounds in Chinese green tea have been identified by gas chromatography (GC) and GC/mass spectrometry (MS).[1−6] A number of potent odorants in green tea have also been identified (Japanese green tea,[4,7] Darjeeling green tea,[8] and Chinese green tea[4−6]). However, the investigations of Chinese green tea were only intended for some of the cultivars, despite there being many.[4−6] Therefore, they cannot fully explain the characteristic aroma of Chinese green tea in general.

In this investigation, in order to elucidate the potent odorants common to Chinese green tea in general, the three famous Chinese green tea cultivar infusions (Longjing, Maofeng, and Biluochun) were investigated by aroma extract dilution analysis (AEDA). Simultaneously, the characteristic odorants of each cultivar were also investigated. In addition, the formation mechanism of (*E*)-isoeugenol, which has not been reported in the literature in Chinese green tea, was studied.

## MATERIALS AND METHODS

**Materials.** Tea samples: Chinese green tea products, Longjing, Maofeng, and Biluochun (spring and summer crops), were produced in the Zhejiang, Anhui, and Jiangsu provinces (China) in 2012. Sen-cha was produced in the Shizuoka prefecture (Japan) in 2008 and

Received: May 15, 2014
Revised: July 28, 2014
Accepted: August 3, 2014
Published: August 3, 2014

ACS Publications © 2014 American Chemical Society

2012. The oolong tea products, Pouchong tea, Dongding oolong tea, Oriental Beauty tea, Tie Guan Yin tea, Golden Cassia, and Robe tea, were produced in Taiwan or China in 2001. The black tea products, Dimbura, Java tea, Kenyan tea, and Assam tea, produced in 2005, were purchased from Mitsui Norin Co., Ltd. (Tokyo, Japan). All of these products were of high grade based on the market price and stored at −80 °C until needed.

**Chemicals.** The following compounds were synthesized according to the literature procedures: 2-acetyl-1-pyrroline;[9] (*Z*)-1,5-octadien-3-one;[10] 4-mercapto-4-methyl-2-pentanone;[11] 2-ethenyl-3,5-dimethylpyrazine;[12] 3-methyl-2,4-nonanedione;[13] 2-acetyl-2-thiazoline;[14] and *cis*- and *trans*-4,5-epoxy-(*E*)-2-decenal.[15] Compounds (Table 2) **3**, **6**, **12**, **14**, **16**−**19**, **21**, **23**−**26**, **29**, **32**, **33**, **35**, **38**, **40**, **41**, **43**, **47**, **48**, **52**−**55**, **57**, and **58** were purchased from Tokyo Chemical Industry Co., Ltd. (Tokyo, Japan); compounds **4**, **15**, **30**, **45**, **46**, and **56** were purchased from Sigma-Aldrich Japan (Tokyo, Japan); **39**, **44**, and coniferyl alcohol were purchased from Wako Pure Chemical Industries (Osaka, Japan); **50** was purchased from the Zeon Corporation (Tokyo, Japan); cellulose and cinnamyl alcohol were purchased from Nacalai Tesque (Kyoto, Japan); and pectriase was purchased from the Shinnihon Chemicals Corporation (Chiba, Japan).

**Isolation of the Volatiles from Chinese Green Tea Infusion.** Distilled water (90 °C, 1500 g) was added to 75 g of Chinese green tea, and the leaves were filtered after standing for 5 min. The filtrate (1000 g) was immediately cooled in tap water and passed through a column packed with 20 mL of SP700 (Mitsubishi Chemical Corporation).[16] The adsorbed compounds were eluted with methylene chloride (100 mL). As the internal standard solution, 0.1% 2-octanol in methylene chloride (100 μL) was added to the eluate. The eluate was dried over anhydrous sodium sulfate and distilled under reduced pressure (<4.0 × $10^{-3}$ Pa, 40 °C) using the SAFE technique.[17] The solvent in the distillate was removed by rotary evaporation (35 °C, 550 mmHg) to about 5 mL in volume. Further concentration to approximately 100 μL was conducted using a nitrogen stream. The concentrate was used as the sample for the AEDA and the GC-MS analysis (*a*).

**Gas Chromatography−Olfactometry (GC-O).** An Agilent 6850 series gas chromatograph equipped with a thermal conductivity detector (TCD) (Agilent Technologies, Santa Clara, CA, USA) and fused silica column (30 m × 0.25 mm i.d., coated with a 0.25 μm film of DB-Wax; Agilent Technologies) was used in splitless injection mode from 40 to 210 °C at the rate of 5 °C/min for all runs. The injector and detector temperatures were both 250 °C. Helium was used as the carrier gas at a flow rate of 1 mL/min. A glass sniffing port was connected to the outlet of the TCD and heated by a ribbon heater along with moist air being pumped into the sniffing port at about 100 mL/min to quickly remove the odorant from the sniffing port that had been eluted from the TCD.

**Aroma Extract Dilution Analysis (AEDA).** The original odor concentrates of the Chinese green tea infusion were stepwise diluted with methylene chloride to $4^n$ ($n$ = 0−8), and aliquots (1 μL) of each sample were analyzed by capillary GC using a DB-Wax column. The odorants were then detected by GC eluate sniffing (GC-O). The flavor dilution (FD) factors of the odorants were determined by AEDA.[18] Prior to the FD factor measurement, two panelists repeatedly confirmed the retention time and the odor quality of the odorants using each diluted sample ($4^0$ and $4^1$), and then the FD factors of the odorants were defined as the dilution step that both panelists detected. For the purpose of selecting the potent odorants common to all of the cultivars or characteristics of each cultivar, the mean values and the relative standard deviations (RSD) of exponents of the FD factors ($\log_4$ (FD factor)) of all the samples were calculated; a compound with a high mean value and low RSD was considered to be a potent odorant common to all of the cultivars.

**Semi-Quantitative Analysis of Isoeugenol and Coniferyl Alcohol in the Various Teas.** Various tea infusions (three Japanese green teas, six Chinese green teas, six oolong teas, and four black teas) prepared by the same method as that described above (200 g) were passed through a column packed with 5 mL of SP700. The adsorbed compounds were eluted with a mixed solvent (diethyl ether: *n*-pentane (8:2), 50 mL). The internal standard solution, 0.1% 2-octanol in methylene chloride (20 μL), was added to the eluate. The eluate was dried over anhydrous sodium sulfate, and the solvent in the distillate was removed by rotary evaporation (35 °C, 550 mmHg) to about 1 mL in volume. Further concentration to approximately 100 μL was conducted using a nitrogen stream. The concentrates were used as the samples for the GC-MS analysis (*b*).

**Model Experiment for (*E*)-Isoeugenol Formation by Heating.** Coniferyl alcohol or cinnamyl alcohol mixed with cellulose in distilled water was lyophilized and placed in a 20 mL vial. After being sealed by a silicon septum, the vial was heated in the GC column oven (150 °C, 30 min) and analyzed by the GC-MS using the solid phase microextraction (SPME) method (*c*). As a control experiment, a nonheated sample was also analyzed.

**Model Experiment for Coniferyl Alcohol Formation by Enzymatic Reaction.** Japanese green tea infusion prepared by the same method as described above (200 g) was passed through a column packed with 5 mL of SP700. After the adsorbed compounds were eluted with the mixed solvent (diethyl ether/*n*-pentane (8:2), 50 mL), the nonvolatile compounds were eluted with methanol (50 mL). Methanol in the eluate was removed by rotary evaporation (35 °C, 120 mmHg), and then the nonvolatile fraction was lyophilized. The nonvolatile fraction (0.4 g) was put into a 10 mL glass vial and dissolved in the citrate phosphate buffer (pH 4.5, 7 mL). After pectriase (Shinnihon Chemicals, 2 mg) was added, the vial was capped and incubated in a water bath (40 °C, 3 h). The volatile compounds in the reaction liquid were extracted with 2 mL of a mixed solvent (diethyl ether/*n*-pentane (8:2)), then the extract was concentrated to approximately 100 μL by a nitrogen stream, and used as the sample for the GC-MS analysis (*d*).

**Gas Chromatography−Mass Spectrometry.** (*a*) An Agilent 7890A gas chromatograph coupled to an Agilent 5975C *inert* XL series mass spectrometer (Agilent Technologies) was used. The column was a 60 m × 0.25 mm i.d., fused silica capillary type, coated with a 0.25 μm film of DB-Wax (Agilent Technologies). The column temperature was programmed from 80 to 230 °C at the rate of 3 °C/min. The injector temperature was 250 °C, and the flow rate of the helium carrier gas was 1 mL/min. An injection volume of 1 μL was applied using the split mode (the split ratio was 1:30). The mass spectrometer was used with an ionization voltage of 70 eV (EI) and ion source temperature of 150 °C. (*b*) The conditions of the GC-MS were same as those in *a*. The semiquantitative contents of isoeugenol and coniferyl alcohol in the tea infusions were determined by the internal standard method from the total ion or the selected ion peak areas obtained by mass chromatography. The GC-MS was operated in the selected ion monitoring and scan (SIM-SCAN) mode, and the selected ions of 115 and 164 were monitored for 2-octanol (internal standard) and (*E*)-isoeugenol, respectively. The semiquantitative contents of these compounds in the tea infusions were calculated from the ratio of the total ion peak areas of the internal standard and those of the analytes. On the basis of the ratio of the selected ion versus the overall ions of the mass spectra for each authentic compound, the total ion peak area of each compound was converted from the selected ion peak area; total ion peak area = selected ion peak area × conversion factor. The conversion factors were 63.4 and 4.2 for 2-octanol and (*E*)-isoeugenol, respectively. The response factor of each odorant versus the internal standard was defined as 1. (*c*) The volatile compounds in the headspace were extracted by the SPME fiber, 50/30 μm StableFlex DVB/Carboxen/PDMS (Sigma-Aldrich), and analyzed by an Agilent 6850N gas chromatograph coupled to an Agilent 5973N series mass spectrometer (Agilent Technologies), equipped with the CycleComposer autosampler system (AMR Inc., Tokyo, Japan): CycleComposer with macro editor software, a sample tray, a temperature controlled agitator tray, and a fiber conditioning device system. All of the setup parameters of the autosampler are as follows: the agitator was 60 °C, 500 rpm (on for 5 s. and off for 2 s.), the pre-extraction equibration time was 10 min, the extraction time was 15 min, and the desorption time was 1 min. The column and its temperature, the injector temperature, and the flow rate of the helium

carrier gas were the same as those in *a*. (*d*) The conditions of the GC-MS were the same as those in *a*.

**Identification of the Components.** Each component was identified by comparing its Kovats GC retention index (RI), mass spectrum, and odor quality to those of the authentic compounds.

## RESULTS AND DISCUSSION

**Potent Odorants in Chinese Green Tea Infusions.** The three famous Chinese green tea cultivars, Longjing, Maofeng, and Biluochun, the spring crops and summer crops of each, were used. The shapes of the tea leaves differ with the cultivars, depending on the manufacturing process of pan-firing and drying. The leaves of Longjing had flat shapes because the leaves were pressed against the pans. Those of Maofeng, which were dried in baskets over charcoal fires, had big, twisted shapes. On the other hand, those of Biluochun had small, twisted shapes and white fluff on them because they were plucked early by their shoots and stirred in the pans. The characteristic aromas of the infusions evaluated by four panelists are shown in Table 1. The infusions of the spring crops had better and more characteristic aromas from each cultivar than those of the summer crops.

**Table 1. Characteristic Aromas of the Chinese Green Tea Infusions**

| cultivar | crop | characteristic aroma of infusion |
|---|---|---|
| Longjing | spring | roast, green sweet |
| Longjing | summer | roast, green |
| Maofeng | spring | roast, metallic |
| Maofeng | summer | soybean-like |
| Biluochun | spring | floral, japanese apricot-like |
| Biluochun | summer | roast |

The volatile concentrates of these Chinese green tea infusions were prepared by the combination of the adsorptive column method and the SAFE techniques, which makes it possible to efficiently and reproducibly extract the aroma components from a large volume of samples. The volatile concentrates obtained by this preparation without excessive heating well-reproduced the characteristic aroma of the infusions. Thus, it was regarded as the most preferable analytical sample for the screening of the potent odorants by GC-O. The AEDA applied to the volatile concentrates of the six Chinese green tea infusions revealed 58 odor-active peaks with FD factors between $4^1$ and $4^7$ (Table 2). Forty-six of the odorants, which included six odorants that have not been reported in the literature in Chinese green tea, were identified or tentatively identified by GC-MS and GC-O. Among the perceived odorants, 4-hydroxy-2,5-dimethyl-3(2*H*)-furanone (**40**: sweet, caramel-like), 3-hydroxy-4,5-dimethyl-2(5*H*)-furanone (**45**: seasoning-like, caramel-like), coumarin (**55**: sweet), vanillin (**57**: vanilla-like), geraniol (**32**: floral, green), (*E*)-isoeugenol (**52**: floral, spicy), and 2-methoxyphenol (**33**: burnt, rubber-like) showed high FD factors in all of the cultivars, irrespective of the cultivars or the harvesting seasons (the mean of $\log_4$ (FD factor) >4 and RSD <20%), suggesting that these odorants are essential for Chinese green tea aroma. Although most of the odorants in Table 2 are consistent with those reported in previous studies,[4−6] some compounds have not been reported. This is assumed to be due to the raw materials and/or analytical procedures; it is noteworthy that steam distillation was not applied in this investigation.

On the other hand, to elucidate the potent odorants responsible for the characteristic aroma of each cultivar, the FD factors of the compounds in the spring crops of the three cultivars were compared since the aromas of the spring crops were more characteristic than those of the summer crops. Among the odorants, except for the seven odorants mentioned above, the odorants, which had FD factors more than $4^3$ and higher by $4^2$ or more from the other cultivars, were selected. In Longjing and Maofeng, the FD factors of 2-isopropyl-3-methoxypyrazine (**12**: pea-like) and 3-methyl-2,4-nonanedione (**27**: green) were higher than those in Biluochun. Furthermore, in Maofeng, (*E*,*E*)-2,4-nonadienal (**26**: fatty) and *trans*-4,5-epoxy-(*E*)-2-decenal (**37**: sweet, juicy, metallic) also showed significantly high FD factors. These results did not contradict the characteristic aromas of each infusion, suggesting that the contents of these odorants are responsible for the characteristic aroma of each cultivar. It was assumed that various factors, such as the contents of the precursors in the tea leaves and the conditions during the manufacturing process, influence the contents of these odorants since most of the volatile compounds in tea are known to be generated during the enzymatic reaction or the heating reaction from various precursors, i.e., fatty acids, amino acids, sugar, and glycosides.[19]

On the basis of these results, it was suggested that sweet, floral, and burnt aromas are essential for the aroma of Chinese green tea, and some odorants influence the characteristic aroma of each cultivar. However, it is necessary to investigate more samples to confirm this hypothesis since there are an enormous number of Chinese green teas. Furthermore, since highly volatile compounds might be lost during the concentration by rotary evaporation or nitrogen stream, it is necessary to apply some other methods such as static headspace olfactometry to detect them.

**Proposed Formation Mechanism of (*E*)-Isoeugenol.** (*E*)-Isoeugenol (**52**: floral, spicy), which was newly identified in Chinese green tea and showed high FD factors in all of the cultivars, was suggested to play an important role in the characteristic flowery aroma of Chinese green tea. On the other hand, the **52** content of the tea leaves is reported to increase during the withering process.[20] Therefore, to elucidate the relationship between the **52** contents and the enzymatic reaction during the tea manufacturing process, the **52** contents of various tea infusions were semiquantified. As a result, the **52** contents of Chinese green tea (generally withered) infusions showed a tendency to be higher than those of the Sen-cha (not withered) infusions (Figure 1A). Furthermore, the **52** contents of six semifermented tea (Pouchong tea, Dongding oolong tea, Oriental Beauty tea, Tie Guan Yin tea, Golden Cassia, and Robe tea) and four black tea infusions (Dimbura, Java tea, Kenyan tea, and Assam tea) were extremely higher than those of the green tea infusions (Figure 1B). These results suggested that the enzymatic reaction during the tea manufacturing process has a close relationship with the formation of **52**.

There are some reports about the generation of **52** in plants. In the petunia flower, **52** is reported to be biosynthesized from coniferyl alcohol via coniferyl acetate by an enzymatic reaction.[21] On the other hand, in wood, **52** is reported to be generated from coniferyl alcohol by heat during delignification.[22] This information suggests that coniferyl alcohol is an important intermediate in the formation of **52** in plants. Thus, the coniferyl alcohol in the various tea infusions was analyzed by GC-MS. As a result, coniferyl alcohol was detected in all of the infusions (green tea, oolong tea, and black tea), and its

**Table 2. Potent Odorants Showing FD Factors (FD >1) in Chinese Green Tea**

| | | | | log$_4$ (FD factor) | | | | | |
|---|---|---|---|---|---|---|---|---|---|
| | | | | Longjing | | Maofeng | | Biluochun | |
| no. | R.I.[a] | compound[b] | odor quality[c] | spring | summer | spring | summer | spring | summer |
| 1 | 946 | unknown | stimulus | 2 | 1 | 2 | 1 | 2 | 1 |
| 2 | 1009 | unknown | fruity, green | | | | 1 | | |
| 3 | 1076 | hexanal | green, grassy | 1 | 1 | 1 | 1 | 1 | 1 |
| 4 | 1132 | (*Z*)-3-hexenal[c] | green | | | 2 | 2 | 1 | |
| 5 | 1189 | unknown | nutty | | | | | | 1 |
| 6 | 1294 | 1-octen-3-one | mushroom-like | | | 1 | | 1 | 1 |
| 7 | 1334 | 2-acetyl-1-pyrroline | roasty | 2 | 2 | 3 | 2 | | 1 |
| 8 | 1366 | (*Z*)- 1,5-octadien-3-one[c] | metallic | 1 | 1 | 3 | 1 | 2 | 1 |
| 9 | 1374 | 4-mercapto-4-methyl-2-pentanone[c] | green, meaty | 1 | | | | | |
| 10 | 1380 | unknown | green | | 1 | | 1 | | 1 |
| 11 | 1407 | unknown | nutty, green | | | 2 | | | 1 |
| 12 | 1422 | 2-isopropyl-3-methoxypyrazine[c,d] | pea-like | 3 | 2 | 3 | 2 | 1 | 3 |
| 13 | 1447 | unknown | nutty | | | | 1 | | |
| 14 | 1449 | methional | potato-like | 3 | 2 | 3 | 3 | 3 | 2 |
| 15 | 1459 | 2-ethyl-3,5-dimethylpyrazine | nutty | 3 | 2 | 3 | 2 | 2 | 2 |
| 16 | 1492 | 2,3-diethyl-5-methylpyrazine | nutty | 3 | 1 | 3 | 1 | 2 | 2 |
| 17 | 1521 | 2-isobutyl-3-methoxypyrazine[c] | earthy, musty | 2 | 2 | 3 | 2 | 1 | 2 |
| 18 | 1530 | (*E*)-2-nonenal | green, sweet | 2 | 2 | 1 | 2 | 1 | 2 |
| 19 | 1538 | linalool | floral | 2 | 1 | 3 | 1 | 4 | 1 |
| 20 | 1551 | 2-ethenyl-3,5-dimethylpyrazine[c,d] | nutty | 3 | | 2 | | 1 | 1 |
| 21 | 1581 | (*E*,*Z*)-2,6-nonadienal | green, cucumber-like | | 1 | | 2 | 2 | 2 |
| 22 | 1674 | unknown | roasty, sour, smoky | | | | 2 | | |
| 23 | 1625 | 2-acetylpyrazine | nutty | | | | | | 1 |
| 24 | 1633 | phenylacetaldehyde | sweet, honey-like | 2 | 1 | | 1 | | 1 |
| 25 | 1660 | isovaleric acid | sweaty, rancid | | | 2 | | | 1 |
| 26 | 1698 | (*E*,*E*)-2,4-nonadienal | fatty | 1 | 2 | 4 | 2 | | 2 |
| 27 | 1700 | 3-methyl-2,4-nonanedione | green | 4 | 4 | 4 | 3 | 2 | 3 |
| 28 | 1756 | 2-acetyl-2-thiazoline[c] | roasty | | 2 | 2 | 1 | | 1 |
| 29 | 1807 | (*E*,*E*)-2,4-decadienal | fatty | 1 | 1 | 1 | 1 | | 2 |
| 30 | 1817 | *β*-damascenone[c] | sweet, honey-like | 2 | 1 | 2 | 1 | | 1 |
| 31 | 1842 | unknown | sweaty, green | | | | | | 1 |
| 32 | 1842 | geraniol | floral, green | 4 | 5 | 4 | 4 | 5 | 5 |
| 33 | 1851 | 2-methoxyphenol | burnt, rubber-like | 6 | 5 | 7 | 5 | 5 | 4 |
| 34 | 1940 | unknown | green, sweaty | | | | | | 1 |
| 35 | 1961 | maltol | sweet | 1 | 2 | 2 | 2 | 2 | 2 |
| 36 | 1981 | *cis* -4,5-epoxy-(*E*)-2-decenal[d] | sweet, juicy | | | 1 | | | |
| 37 | 1996 | *trans* -4,5-epoxy-(*E*)-2-decenal | sweet, juicy, metallic | | | 3 | 2 | | |
| 38 | 2020 | 4-ethylguaiacol[d] | spicy | | | | | | 4 |
| 39 | 2023 | 4-nonanolide | sweet | | 1 | 3 | | 2 | |
| 40 | 2025 | 4-hydroxy-2,5-dineuhyl-3(2*H*)-furanone | sweet, caramel-like | 7 | 6 | 7 | 5 | 7 | 5 |
| 41 | 2075 | *p* -cresol | phenolic | | | | | | 2 |
| 42 | 2146 | unknown | sweet, green, floral | | | | 2 | | 2 |
| 43 | 2157 | eugenol | spicy | 4 | 3 | 5 | 4 | 3 | 4 |
| 44 | 2174 | 2-methoxy-4-vinylphenol | spicy | | | 2 | | | |
| 45 | 2190 | 3-hydroxy-4,5-dimethyl-2(5*H*)-furanone[c] | seasoning-like, caramel-like | 5 | 5 | 5 | 4 | 3 | 4 |
| 46 | 2196 | 5-decanolide[c] | lactone-like | | 2 | | 1 | | 2 |
| 47 | 2213 | *o* -aminoacetophenone | grape-like | 1 | | 3 | 2 | 2 | |
| 48 | 2236 | methyl anthranilate | grape-like | 1 | | 1 | 1 | 1 | 1 |
| 49 | 2253 | unknown | phenolic | | 1 | | | | 1 |
| 50 | 2259 | jasmin lactone | sweet, burnt | 2 | 1 | 2 | 2 | 2 | 3 |
| 51 | 2299 | unknown | green | | 2 | | 1 | | |
| 52 | 2338 | (*E*)-isoeugenol[d] | floral, spicy | 5 | 5 | 4 | 5 | 4 | 5 |
| 53 | 2389 | (*Z*)-methyl jasmonate | floral | 2 | 2 | 2 | 2 | 3 | 3 |
| 54 | 2432 | indole | animal-like | 1 | | 3 | 3 | 2 | 4 |
| 55 | 2446 | coumarin | sweet | 6 | 5 | 5 | 5 | 4 | 4 |
| 56 | 2540 | phenylacetic acid | sweet | 4 | 4 | 3 | 3 | 4 | 3 |
| 57 | 2551 | vanillin | vanilla-like | 5 | 4 | 5 | 5 | 5 | 5 |
| 58 | 2610 | 3-phenylpropionic acid[c,d] | animal-like | 3 | 2 | 3 | 2 | 3 | 2 |


dx.doi.org/10.1021/jf502308a | J. Agric. Food Chem. 2014, 62, 8308−8313

**Table 2. continued**

[a]Retention index on DB-Wax column (30 m × 0.25 mm i. d.; coated with a 0.25 μm film) observed for GC-O. [b]The compound was identified by comparison with the reference substance on the basis of the following criteria: retention index (R.I.) on stationary phase DB-Wax, mass spectra, and odor quality. [c]The MS signals were too weak for unequivocal interpretation. The compound was tentatively identified by comparison with the reference substance on the basis of the following criteria: retention index (R.I.) on stationary phase DB-Wax and odor quality. [d]The compound has not been reported in the literature in Chinese green tea. [e]Odor quality assigned during AEDA.

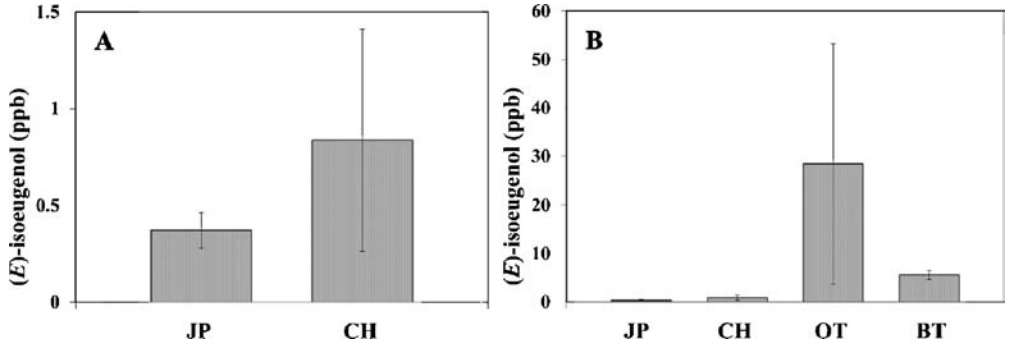


**Figure 1.** Semiquantified (*E*)-isoeugenol content of various tea (three Japanese green teas, six Chinese green teas, six oolong teas, and four black teas) infusions. Error bars show standard deviations. (JP, Japanese green tea (Sen-cha); CH, Chinese green tea; OT, oolong tea; BT, black tea.)

contents were correlated with those of **52**, suggesting that coniferyl alcohol might be an important intermediate in the formation of **52**, also in the tea leaves. The formation of **52** from coniferyl alcohol was assumed to be caused by heating during the manufacturing process, not by an enzymatic reaction, since coniferyl acetate was not detected in the tea infusions, and **52** was reported to be generated from coniferyl alcohol by heating. To confirm this assumption, coniferyl alcohol mixed with cellulose was heated under the same conditions as the pan-firing and drying process of the tea leaves (150 °C, 30 min), and then **52** and eugenol (**43**) were generated. It was assumed that **52** is formed from coniferyl alcohol during the reducing dehydration reaction. The mechanism presumed for this reaction includes the corresponding quinone methide intermediate since coniferyl alcohol has a hydroxyl group at the C-4 position on the benzene ring. To confirm this, the requirement of the hydroxyl group at the C-4 position on the benzene ring for this reaction was indirectly tested, i.e., cinnamyl alcohol, which has no hydroxyl group on the benzene ring like coniferyl alcohol, was heated (150 °C, 30 min). As a result, the corresponding product, 3-phenylpropene, was not generated, indicating that the hydroxyl group on the benzene ring is required for this dehydration reaction. Therefore, it was suggested that this reaction includes a quinone methide intermediate which is relatively stable, and thus this reaction would proceed under such moderate heating conditions (Figure 2).

On the other hand, coniferyl alcohol is known as a precursor of lignin, an essential substance of plants, and known to be accumulated as a glycoside called coniferin in plants because of its instability. In addition, coniferin is found in *Camellia taliensis*, a close relative of *Camellia sinensis*.[23] Considering that most of the alcohols in tea aroma are known to be generated from glycosides by enzymatic reactions during the manufacturing process,[19] a glycoside like coniferin is assumed to be involved in the formation of coniferyl alcohol. To confirm this assumption, a hydrolysis enzyme, pectriase, was added to the nonvolatile fraction of the Sen-cha infusion, in which glycosides were assumed to be included. As a result, coniferyl alcohol was generated.

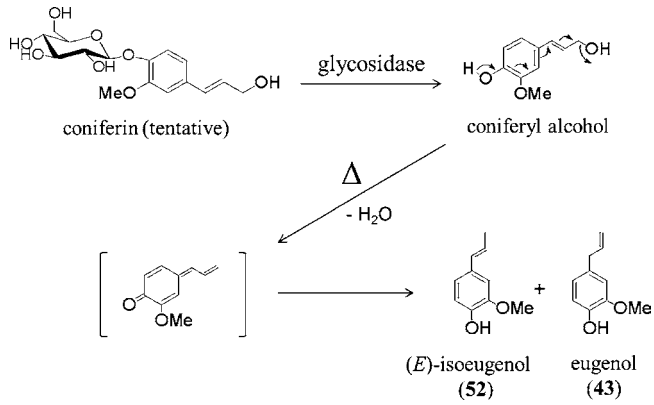


**Figure 2.** Proposed pathway for the formation of (*E*)-isoeugenol in tea leaves during the manufacturing process of Chinese green tea.

On the basis of these results, the formation mechanism of **52** in tea leaves during the manufacturing process was indirectly suggested as follows: first, coniferyl alcohol is generated from its glycoside like coniferin by an enzymatic reaction, and then **52** is formed from coniferyl alcohol by heating. In other words, it was suggested that coniferyl alcohol is generated from the precursor like coniferin by the endogenous enzymatic reaction during the withering and pan-firing processes and that then **52** is formed from coniferyl alcohol via the quinone methide intermediate by heating during the pan-firing and drying processes in tea leaves during the manufacturing process (Figure 2). These results indicated that the formation of **52**, which is assumed to be the important compound for the characteristic floral aroma of Chinese green tea, is closely correlated to the specific manufacturing process of Chinese green tea: withering the plucked leaves and slowly inactivating the endogenous enzymes in the leaves by pan-firing. However, the coniferyl alcohol content showed a tendency to be higher in the semifermented tea (oolong tea) than in the fermented tea (black tea), suggesting that the coniferyl alcohol content is not necessarily in proportion to the degree of fermentation. It seems possible that coniferyl alcohol once generated in the tea leaves by fermentation changes into other compounds as the

fermentation proceeds because coniferyl alcohol is an unstable compound. Therefore, further studies and elucidation of the precursor of coniferyl alcohol in tea leaves are necessary to clarify the relationship between the **52** contents of the tea leaves and the tea manufacturing process.

In this study, the essential volatile compounds and characteristics of the aroma of three famous cultivars of Chinese green tea were identified. It is assumed that the contents of these compounds are affected by the precursor contents of the tea leaves or their manufacturing process. However, the details about the formation mechanism of these compounds have not been clarified. Now that green tea has become increasingly popular around the world, it would be important to elucidate the potent odorants, their formation mechanism, and the effect of the manufacturing process on their contents to produce better-smelling and highly palatable green tea.

## ■ ASSOCIATED CONTENT

### Ⓢ Supporting Information

Correlation between the content of coniferyl alcohol and that of (*E*)-isoeugenol in various tea infusions; extracted-ion chromatogram of (*E*)-isoeugenol formed from coniferyl alcohol by heating; heating reaction of coniferyl alcohol and cinnamyl alcohol; and total ion chromatogram of coniferyl alcohol released from the crude glycosidic fraction of the Japanese green tea (Sen-cha) infusion. This material is available free of charge via the Internet at http://pubs.acs.org.

## ■ AUTHOR INFORMATION

### Corresponding Author

*Fax: +81-47-305-1423. E-mail: baba.ryoko@ogawa.net.

### Notes

The authors declare no competing financial interest.

## ■ REFERENCES

(1) Kosuge, M.; Aisaka, H.; Yamanishi, T. Aroma characteristics of Chinese green tea (in Japanese). *Eiyo to Shokuryo* **1980**, *33*, 101−104.

(2) Kosuge, M.; Aisaka, H.; Yamanishi, T. Flavor constituents of Chinese and Japanese pan-fired green teas (in Japanese). *Eiyo to Shokuryo* **1981**, *34*, 545−549.

(3) Kawakami, M.; Yamanishi, T. Flavor constituents of Longing tea. *Agric. Biol. Chem.* **1983**, *47*, 2077−2083.

(4) Kumazawa, K.; Masuda, H. Identification of potent odorants in different green tea varieties using flavor dilution technique. *J. Agric. Food. Chem.* **2002**, *50*, 5660−5663.

(5) Guth, H.; Grosh, W. Identification of potent odourants in static headspace samples of green and black tea powders on the basis of aroma extract dilution analysis (AEDA). *Flavour Fragrance J.* **1993**, *8*, 173−178.

(6) Cheng, Y.; Huynh-Ba, T.; Blank, I.; Robert, F. Temporal changes in aroma release of Longjing tea infusion: interaction of volatile and nonvolatile tea components and formation of 2-butyl-2-octenal upon aging. *J. Agric. Food. Chem.* **2008**, *56*, 2160−2169.

(7) Kumazawa, K.; Masuda, H. Identification of potent odorants in Japanese green tea (Sen-cha). *J. Agric. Food. Chem.* **1999**, *47*, 5169−5172.

(8) Schuh, C.; Schmid, K.; Schieberle, P. Aroma Active Compounds in a Green Tea Infusion (Darjeeling) − Comparison with Odorants of a Black Tea Beverage. In *Recent Highlights in Flavor Chemistry & Biology*; Hofmann, T., Meyerhof, W., Schieberle, P., Eds.; German Research Centre for Food Chemistry: Garching, Germany, **2007**; pp 117−122.

(9) Buttery, R. G.; Ling, L. C.; Juliano, B. O.; Turnbaugh, J. G. Cooked rice aroma and 2-acetylpyrroline. *J. Agric. Food. Chem.* **1983**, *31*, 823−826.

(10) Swoboda, P. A. T.; Peers, K. E. Metallic odour caused by vinyl ketones formed in the oxidation of butterfat. The identification of octa-1,*cis*-5-dien-3-one. *J. Sci. Food Agric.* **1977**, *28*, 1019−1024.

(11) Guth, H. Identification of character impact odorants of different white wine varieties. *J. Agric. Food. Chem.* **1997**, *45*, 3022−3026.

(12) Czerny, M.; Wagner, R.; Grosch, W. Detection of odor-active ethenylalkylpyrazines in roasted coffee. *J. Agric. Food. Chem.* **1996**, *44*, 3268−3272.

(13) Guth, H.; Grosch, W. 3-Methylnonane-2,4-dione − An intense odour compound formed during flavour reversion of soya-bean oil. *Fat Sci. Technol.* **1989**, *93*, 225−230.

(14) Cerny, C.; Grosch, W. Evaluation of potent odorants in roasted beef by aroma extract dilution analysis. *Z. Lebensm.-Unters. Forsch.* **1992**, *194*, 322−325.

(15) Kumazawa, K.; Wada, Y.; Masuda, H. Characterization of epoxydecenal isomers as potent odorants in black tea (Dimbula) infusion. *J. Agric. Food. Chem.* **2006**, *54*, 4795−4801.

(16) Kaneko, S.; Kumazawa, K.; Nishimura, O. Studies on the key aroma compounds in raw (unheated) and heated Japanese soy sauce. *J. Agric. Food. Chem.* **2013**, *61*, 3396−3402.

(17) Engel, W.; Bahr, W.; Schieberle, P. Solvent assisted flavour evaporation − a new and versatile technique for the careful and direct isolation of aroma compounds from complex food matrices. *Eur. Food Res. Technol.* **1999**, *209*, 237−241.

(18) Schieberle, P. New Developments in Methods for Analysis of Volatile Flavor Compounds and Their Precursors. In *Characterization of Food: Emerging Methods*; Goankar, A., Ed.; Elesevier: Amsterdam, The Netherlands, 1995; pp 403−431.

(19) Yang, Z.; Baldermann, S.; Watanabe, N. Recent studies of the volatile compounds in tea. *Food Res. Int.* **2013**, *53*, 585−599.

(20) Kobayashi, A.; Tachiyama, K.; Kawakami, M.; Yamanishi, T.; Juan, I.; Chiu, W. T. Effects of solar-withering and turn over treatment during indoor-withering on the formation of pouchong tea aroma. *Agric. Biol. Chem.* **1985**, *49*, 1655−1660.

(21) Koeduka, T.; Fridman, E.; Gang, D. R.; Vassao, D. G.; Jackson, B. L.; Kish, C. M.; Orlova, I.; Spassova, S. M.; Lewis, N. G.; Noel, J. P.; Baiga, T. J.; Dudareva, N.; Pichersky, E. Eugenol and isoeugenol, characteristic aromatic constituents of spices, are biosynthesized via reduction of a coniferyl alcohol ester. *Proc. Natl. Acad. Sci. U.S.A.* **2006**, *103*, 10128−10133.

(22) Sakai, K. Organosolv delignification. *Kami Parupu Gijutsu Kyokai shi* **1994**, *48*, 1003−1012.

(23) Gao, D.; Zhang, Y.; Yang, C.; Chen, K.; Jiang, H. Phenolic antioxidants from green tea produced from *Camellia taliensis*. *J. Agric. Food. Chem.* **2008**, *56*, 7517−7521.

JOURNAL OF AGRICULTURAL AND FOOD CHEMISTRY

Article

pubs.acs.org/JAFC

# Quantitation of *trans*-Aconitic Acid in Different Stages of the Sugar-Manufacturing Process

Guillermo Montoya,*[,†] July Londono,[†] Paola Cortes,[†] and Olga Izquierdo[§]

[†]Facultad de Ciencias Naturales, Grupo Natura, Universidad ICESI, Cali, Colombia

[§]Manuelita Sugarmill Km 7 vía Palmira-Cerrito, Palmira, Colombia

**ABSTRACT:** The sugar cane industry has seen how biomass production in sugar mills would be converted to a readily available source of molecules besides sugar. Properly managed, byproducts would be transformed into a sustainable source of renewable and environmentally friendly chemical products.[1] As a principal and more abundant organic acid in sugar cane juice, *trans*-aconitic acid (TAA) has been studied for use as a plasticizer in the polymer industry.[2] However, up to now no industrial-scale application has been reported. As a reasonable approach to recover TAA from a sugar mill, first, an analytical method to determine its presence in all stages of the sugar-manufacturing process is needed. A new modern method was developed to measure TAA in seven stages in a sugar mill located in Valle del Cauca, Colombia. The stages with higher content of TAA were syrup, with 3363.6 ± 589.3 mg/L, and honey (molasses), with 6110.05 ± 139.5 mg/L.

**KEYWORDS:** *sugar cane, trans-aconitic acid, solid phase extraction, UPLC-ESLD, byproducts, sugar mill*

## INTRODUCTION

Sugar from sugar cane is produced in around 120 countries worldwide, and Brazil is the biggest producer with an average annual production of 34 million tons per year.[3] Additional byproducts obtained in the Brazilian sugar cane industry are the bioelectricity commonly used by manufacturing plants and biopolymers (as raw materials for the production of packaging, bags, and bottles obtained from sugar, ethanol, and bagasse).[4,5] Whereas the use of byproducts in some countries is well established, others have not determined how to take advantage of these residuals. Exploratory work has been carried out to recover byproducts from the production process, and *trans*-aconitic acid is no exception; its industrial retrieval has been suggested by means of easy scaled-up techniques.[6] There is no consistent flowchart of a specific pathway to discover a recoverable molecule from industrial waste. However, the first step of a reasonable approach is an analytical evaluation of the target into the matrix where it is contained.

Colombia processes >20 million tons of sugar cane per year, obtaining around 2.4 million tons of sugar;[7] its residues are mainly employed for bioelectricity, in the paper industry, and to fertilize the sugar cane crops. Sugar cane is also one of the country's most widespread crops and therefore has an important impact in gross domestic product. Conversely, the economic progress of this agro-industrial business during the course of the lpast few decades has been stagnant; Colombia does not appear in the top 10 of the world's biggest producers. Another well-known issue in the sugar cane industry is the unpredictable volatile nature of the price of raw sugar,[8] which supports the idea that taking advantage of byproducts in sugar mills would be a rational alternative to increase the industry's economic value.

**Aconitic Acid and Special Considerations.** Aconitic acid is a tricarboxylic acid and the most abundant acid produced by sugar cane. The predominant form is the *trans*-aconitic acid isomer (TAA), which in Australian molasses averages 19.4 g/kg of the total dry solids[9] and in North American molasses averages 9−55 g/kg in dry solid bases. Several techniques have been used to try to recover TAA from molasses; two of the most popular are liquid−liquid extraction[10] and supported liquid membranes.[9] However, bioethanol plants operate with discarded molasses from sugar mills, and the scientific community is making enormous efforts to use bagasse as a source of second-generation alcohols.[11−13] Scientists are also trying to find the best matrix in the sugar-manufacturing stages to establish an industrial TAA extraction for the food, cosmetics, and chemical industries.

With regard to analytical methods, TAA is an organic acid with a low molar absorptivity coefficient and high hydrosolubility (Log $P = -1$); therefore, it is inadequately retained in hydrophobic chromatographic columns. The oldest methodologies described the use of octadecylsilane columns with an ion pair reagent; however, ion pair reagents make the column spoil quickly, so this practice is no longer used. Another option was to use amino columns under low-pH normal phase condition, which become weak anion exchangers capable of separating negatively charged molecules. Recently, polar embedded groups in reverse phase columns are gaining more attention for their rising hydrophilic interaction, capable of interacting with polar compounds such as carbohydrates and small organic acids.[14] Amide columns also offer a wider set of possibilities to separate very highly hydrophilic molecules.[15] This hydrophilic interaction chromatography is available in sub-2 $\mu$m particles, offering acceptable separation of molecules with physicochemical properties such as those described above, in short retention times and good peak shapes.

Received: February 24, 2014
Revised: August 1, 2014
Accepted: August 6, 2014
Published: August 6, 2014

ACS Publications © 2014 American Chemical Society



dx.doi.org/10.1021/jf5008874 | J. Agric. Food Chem. 2014, 62, 8314−8318

After good separation is achieved, properly detecting small organic aliphatic acids using chromatography is one of the biggest concerns. Generally, academics describe mass spectrometry as the perfect choice to couple with a separation technique; however, in most commercial industries, it is not always chosen because of its high cost. The lack of light absorption of organic acids and carbohydrates makes them unsuitable for UV detection (at least with high sensitivity and without derivatization), but other options are available to detect them, such as refractive index and conductivity. Recently, evaporative light-scattering detectors (ELSD) and charged aerosol detectors (CAD) have undergone some improvements that allow them to replace the refractive index in many applications. ELSD has the advantage of having a response independent of the solvent gradient, and despite the fact that the ELSD response is not necessarily linear, the selection of the appropriate concentration for calibration standards and the best fitted equation allow the analyst to quantify a wide range of analyte concentrations.

On the basis of these aspects, we decided to develop a method to measure the quantities of TAA in different stages of the sugar-manufacturing process. We suggest additional matrices from which TAA could be recovered. It is important to systematically identify the best stages in the sugar-manufacturing process where this byproduct is wasted and, consequently, promote its industrial recovery. The new methodology includes a sample treatment using ion exchange cartridges in solid phase extraction coupled with a faster LC analysis with an evaporative light-scattering detector (SPE-UPLC-ELSD).

## MATERIALS AND METHODS

**Materials.** The *trans*-aconitic and formic acids were purchased from Sigma-Aldrich. Methanol and acetonitrile of HPLC grade were obtained from Merck (Darmstadt, Germany). The sugar cane juices were obtained from the analytical laboratory of the Manuelita sugar cane mill (Km 7, Vía Palmira, Valle del Cauca, Colombia). Ultrapure water was obtained from a Sartorius ASTM ultrapure water system (total organic carbon < 5 ppb, conductivity at 0.05 $\mu$S/cm$^3$, and filtered using 0.22 $\mu$m pore size).

**Selection of Different Sugar-Manufacturing Process Stages.** In the pipelines of several sugar mills, the stage names would differ. Nevertheless, the sequence of steps remains the same. Briefly, the processing of sugar cane begins with crushing the stalk to obtain the juice (extraction); then the bagasse is re-extracted with water to contribute better sucrose extraction (dilution). Once extracted, the juice is transferred to an alkalization tank where the pH is controlled by adding lime (alkalization). After that, the juice is clarified, precipitating proteins, fats, and waxes to make a sludge (clarification). To make the process more efficient, the sludge is squeezed and filtered (filtration). The clarified juice is then transferred to multieffect evaporators, where almost 80% of the water content is eliminated to obtain the syrup; then the process is repeated twice to obtain honey. Thus, the stages of production are extraction, dilution, alkalization, clarification, and filtration, producing syrup and two final products: refined white sugar (ultrapure) and brown sugar. The juices were collected during the last week of October 2013 during four consecutive days in triplicate. A schematic flowchart of sugar cane manufacturing is shown in Figure 1.

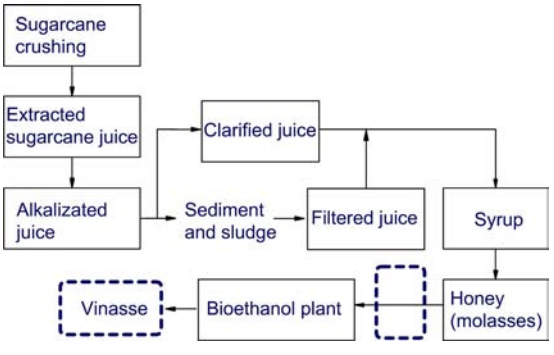


**Figure 1.** Flowchart of the sugar-manufacturing process. The arrows follow the workflow, and the solid line boxes show the stages sampled. Dashed boxes show the stages where TAA would be recovered.

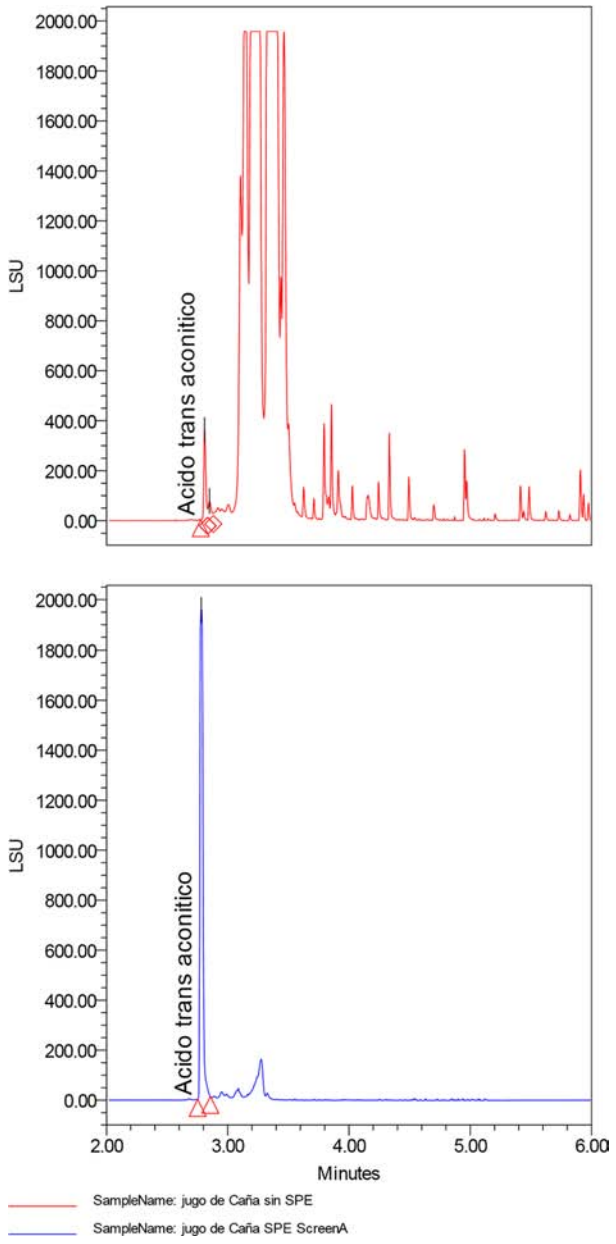


**Figure 2.** Comparison of chromatograms obtained with and without solid phase extraction: (top) sugar cane juice containing high levels of impurities; (bottom) well sample subjected to the SPE procedure. Both samples were diluted at equal volumes to manage the same concentration of solids, suggesting TAA was concentrated after SPE [by comparing light-scattering units (LSU)].

**Sample Treatment by Solid Phase Extraction.** Sugar cane liquors and standards were injected onto a Strata Screen-A cartridge (sorbent with C8 and anion exchange quaternary propylamine) conditioned with methanol and water. The loading of samples and


dx.doi.org/10.1021/jf5008874 | J. Agric. Food Chem. 2014, 62, 8314−8318

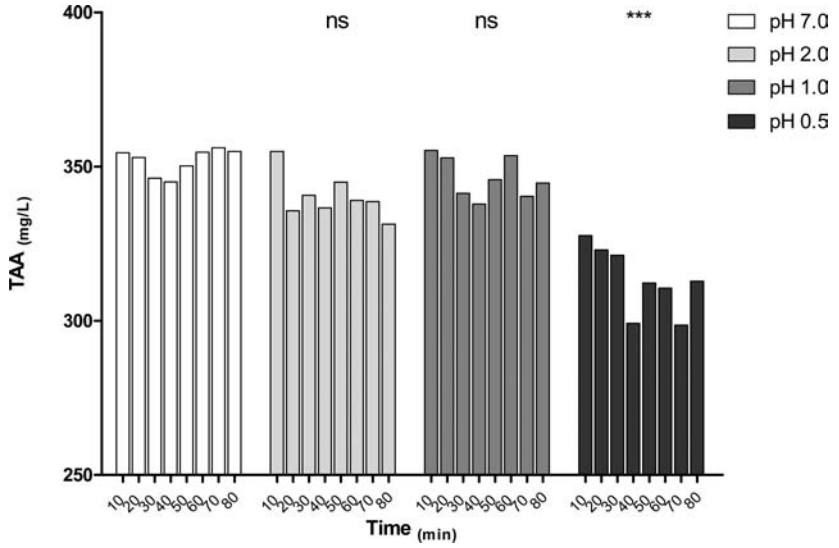


**Figure 3.** Stability test of TAA at 350 mg/L in different pH values over 80 min. Injections were made every 10 min. A Kruskal–Wallis test showed a significant difference ($p < 0.05$) between 8.0 and 0.5 pH values. No significant differences were found between 8.0 value and either the 2.0 or 1.0 pH value.

standards was performed on a solution at pH 7.0, and the washing stage was carried out with 90:10 methanol/water preserving the same pH value as the loading stage. The elution was performed with 20:80 methanol/water at pH 1.5 with diluted hydrochloric acid. All of the pH values as well as organic/water proportions were obtained by experimental design not shown. The stability of *trans*-aconitic acid at various pH values is discussed below.

**Equipment.** The UPLC system consisted of a Waters Acquity H-class equipped with a quaternary pump, degasser, and preheater modules. Detection was performed with an ELSD using gas pressure at 40 psi, gain set at 25, the nebulizer on cooling mode, and drift tube temperature set at 40 °C.

Chromatographic separation analysis was carried out on an amide BEH (2.1 mm × 100 mm, 1.7 $\mu$m particle size) column (Waters, USA). The mobile phase was a mixture of (A) deionized water/formic acid (FA) (99.9:0.1% v/v) and (B) acetonitrile/formic acid (FA) (99.9:0.1% v/v), and the flow rate was 0.5 mL/min in linear gradient without temperature control of the column.

**Statistical Analysis and Validation of the SPE-UPLC-ELSD Method.** All data processing was carried out with Empower 3.0. Calibration curves were analyzed by quadratic equation (second-order polynomial), and the coefficient correlations were always >0.9990 from a six-level curve ranging from 100 to 700 mg/L and relative standard deviation (RSD) <5% by quadruplicate. To validate the method, we used the logarithm of response (light-scattering units).[16] Limits of detection (LOD) and limits of quantitation (LOQ) were determined as 3 and 10 times the signal-to-noise ratio. LOD was 4 mg/L, and LOQ was 55 mg/L. The precision of intraday variation was determined by analyzing five standard solutions in triplicate within 1 day by two analysts. The recovery was determined in water and matrix (1 g of ultrapure sugar in 10 mL of pure water) at two concentrations, 200 and 500 mg/L. The results showed that the recovery of both water and matrix-spiked standard solutions ranged from 90 to 105% with RSDs <7%. Statistical analyses were performed by using GraphPad Prism 5.0 for Windows. A Kruskal–Wallis test was used to assess the significance of the differences of TAA concentration among pH values. All data were grouped by pH and compared against pH 7.0 (control group). $p < 0.05$ was considered statistically significant.

## RESULTS AND DISCUSSION

**Recovery of Aconitic Acid by Ion Exchange SPE.** We needed to develop analytical methods that were as simple as possible; sugar cane juice represents a complex matrix that contains fat, waxes, organic acids, polyphenols, and high concentrations of sugars. The average concentration of organic acids is estimated in the range of 0.5–2%. Taking this into consideration, we used a sample treatment method that would extend column lifetime. Figure 2 shows the differences between raw sugar cane juice and juice after SPE ion exchange preparation on separate UPLC runs. Despite the natural concentration of TAA being high enough to be quantified, we found that SPE not only concentrates the analytes but also prevents impurities such as waxes and long-chain alcohols from entering the column.

**Stability of TAA at pH Conditions.** As low pH is needed to elute the TAA from cartridges, we verified the stability of TAA at different pH values. Figure 3 shows a stability test of TAA at 350 mg/L under different pH values (from 0.5 to 7.0) over 80 min. TAA has three p$K_a$ values at 2.8, 4.6, and 6.3, and we selected pH 1.5 due to the observed stability in combination with the fact that it is >1 unit lower than the p$K_a$ value.

**Content of TAA in Different Sugar-Manufacturing Process Stages.** As shown in Figure 1, the main goal of a sugar mill is to whiten sugar cane juice and then crystallize sucrose. Most sugar mill engineers suggested that we evaluate primarily the sludge produced by alkalization tanks, because this stage eliminates most of the acidic metabolites from the juice, which precipitate under high pH value. These engineers were wrong, because we proved that TAA remains in all stages of the sugar-manufacturing process as shown in Figure 4. A large amount of TAA was found in syrup and honey, obeying the phenomenon of increasing concentration as water content evaporates and also because the sucrose is extracted. That is the same reason why honey TAA content is almost twice that of syrup, as shown in Figure 4. Ultrapure sugar lacks TAA, but brown sugar maintains around 158 mg/L TAA. The final molasses that does not crystallize into additional sugar is then used in bioethanol plants, making it off-limits for TAA recovery, unless an intermediate stage is proposed that depletes TAA from honey and preserves the sugar content needed in a biorefinery. One feasible matrix that contains TAA is vinasses (resulting after alcohol distillation of molasses); however, the matrix becomes more complex due to the high contents of tannins and colored compounds. TAA is most likely to be

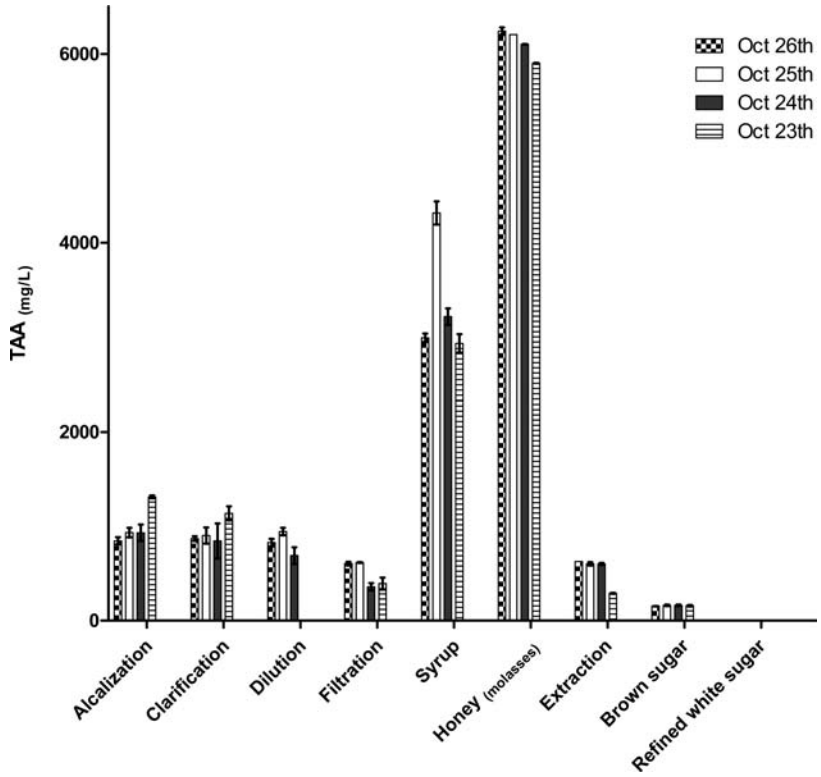


**Figure 4.** Quantification of *trans*-aconitic acid in seven stages of the sugar-manufacturing process. Samples were taken in triplicate over four consecutive days. Bars are plotted with a standard deviation bar between each day. The concentration of TAA decreased from alkalized to filtered. Brown sugar contains 158.45 ± 6.7 mg/L TAA, whereas refined white sugar (ultrapure sugar) does not have quantifiable amounts of TAA. Honey contains 6110.05 ± 139.5 mg/L TAA. The rest of the TAA contents were 1006.4 ± 193.5 mg/L alkalized, 938.5 ± 152.9 mg/L clarified, 820.8 ± 122.2 mg/L diluted, 492.6 ± 127.5 mg/L filtered, 3363.6 ± 589.3 mg/L syrup, and 547.5 ± 136.6 mg/L extract, respectively.

recovered in the dashed-line boxes in Figure 1. Decades ago, some scientists were dealing with the recovery of TAA from molasses,[9,17,18] but up to now, no commercial production has been carried out.

The chromatographic conditions prove that hydrophilic interaction by amide column represents a simple alternative to retain highly hydrophilic compounds instead of using a complex mix of solvents. Although light-scattering detectors have less sensitivity compared to ultraviolet ones, it is the best simple alternative for analytes with low absorptivity coefficients and simultaneously uses solvents with additives well adapted to the chemistry of the column. The honey (molasses) contains a high concentration of TAA, but a method that does not affect sugar and alcohol production is required to be feasible at a commercial level. Future research should explore the economic viability of these processes.

## AUTHOR INFORMATION

### Corresponding Author

*(G.M.) Phone: (057)-2-5552334, ext 8856. E-mail: glmontoya@icesi.edu.co.

### Funding

All authors acknowledge ICESI University for all financial support and laboratory facilities.

### Notes

The authors declare no competing financial interest.

## ACKNOWLEDGMENTS

We thank Manuelita Sugarmill (Km 7 vía Palmira-Cerrito, Colombia) for allowing us to sample and giving us access to a quality control chemical laboratory.

## REFERENCES

(1) Ekman, A.; Campos, M.; Lindahl, S.; Co, M.; Börjesson, P.; Karlsson, E. N.; Turner, C. Bioresource utilisation by sustainable technologies in new value-added biorefinery concepts − two case studies from food and forest industry. *J. Cleaner Prod.* **2013**, *57*, 46−58.

(2) Gil, N.; Saska, M.; Negulescu, I. Evaluation of the effects of biobased plasticizers on the thermal and mechanical properties of poly(vinyl chloride). *J. Appl. Polym. Sci.* **2006**, *102*, 1366−1373.

(3) Association, S. I. Sustainability Report 2011. In UNICA-Brazil, 2012.

(4) Harding, K. G.; Dennis, J. S.; von Blottnitz, H.; Harrison, S. T. L. Environmental analysis of plastic production processes: comparing petroleum-based polypropylene and polyethylene with biologically-based poly-*β*-hydroxybutyric acid using life cycle analysis. *J. Biotechnol.* **2007**, *130*, 57−66.

(5) Agroindustrial, P. Biocycle; http://www.biocycle.com.br/.

(6) Kanitkar, A.; Aita, G.; Madsen, L. The recovery of polymerization grade aconitic acid from sugarcane molasses. *J. Chem. Technol. Biotechnol.* **2013**, *88*, 4.

(7) CENICAÑ. Informe Anual 2012. In Centro de Investigación de la caña de azúcar en Colombia.

(8) Sugar prices fall to lowest since July '10 on Brazil crop. *Bloomberg* **2013** (May 14).

(9) McMurray, S. H.; Griffin, G. J. Extraction of aconitic acid from mixtures of organic acids and cane molasses solutions using supported liquid membranes. *J. Chem. Technol. Biotechnol.* **2002**, *77*, 1262−1268.

(10) Malmary, G. H.; Monteil, F.; Molinier, J. R.; Hanine, H.; Conte, T.; Mourgues, J. Recovery of aconitic acid from simulated aqueous effluents of the sugar-cane industry through liquid-liquid extraction. *Bioresour. Technol.* **1995**, *52*, 33−36.

(11) Li, H. G.; Luo, W.; Gu, Q. Y.; Wang, Q.; Hu, W. J.; Yu, X. B. Acetone, butanol, and ethanol production from cane molasses using

*Clostridium beijerinckii* mutant obtained by combined low-energy ion beam implantation and *N*-methyl-*N*-nitro-*N*-nitrosoguanidine induction. *Bioresour. Technol.* **2013**, *137*, 254−260.
(12) de Andrade, R. R.; Maugeri Filho, F.; Maciel Filho, R.; da Costa, A. C. Kinetics of ethanol production from sugarcane bagasse enzymatic hydrolysate concentrated with molasses under cell recycle. *Bioresour. Technol.* **2013**, *130*, 351−359.
(13) Rabelo, S. C.; Maciel Filho, R.; Costa, A. C. Lime pretreatment and fermentation of enzymatically hydrolyzed sugarcane bagasse. *Appl. Biochem. Biotechnol.* **2013**, *169*, 1696−1712.
(14) Gika, H. G.; Theodoridis, G. A.; Vrhovsek, U.; Mattivi, F. Quantitative profiling of polar primary metabolites using hydrophilic interaction ultrahigh performance liquid chromatography−tandem mass spectrometry. *J. Chromatogr., A* **2012**, *1259*, 121−127.
(15) Shen, G.; Zhang, F.; Yang, B.; Chu, C.; Liang, X. A novel amide stationary phase for hydrophilic interaction liquid chromatography and ion chromatography. *Talanta* **2013**, *115*, 129−132.
(16) Kong, W. J.; Xing, X. Y.; Xiao, X. H.; Wang, J. B.; Zhao, Y. L.; Yang, M. H. Multi-component analysis of bile acids in natural *Calculus bovis* and its substitutes by ultrasound-assisted solid-liquid extraction and UPLC-ELSD. *Analyst* **2012**, *137*, 5845−5853.
(17) Regna, E. A.; Bruins, P. F. Recovery of aconitic acid from molasses. *Ind. Eng. Chem.* **1956**, *48*, 1268−1277.
(18) Bloch, E.; Ritchie, R. J. Ion exchange − operation of commercial scale plant for demineralization of cane sirups and molasses. *Ind. Eng. Chem.* **1947**, *39*, 1581−1584.

JOURNAL OF AGRICULTURAL AND FOOD CHEMISTRY

Article

pubs.acs.org/JAFC

# A Simple Method for Simultaneous Quantification of Total Arabinoxylans and Fructans in Wheat Flour

Zhiqian Liu[†] and Simone Rochfort*[,†,‡]

[†]Department of Primary Industries, Biosciences Research Division, Bundoora, Victoria 3083, Australia

[‡]La Trobe University, Bundoora, Victoria 3086, Australia

Supporting Information

**ABSTRACT:** Current methods for measuring fructan and arabinoxylan concentrations in wheat flour are time-consuming, and each type of the polymers requires a separate method. Here, we report the development of a new method that allows simultaneous determination of arabinoxylan and fructan contents in wheat flour. The new method is based on a single hydrolysis procedure for both arabinoxylans and fructans and an optimized separation technique for all monomers released. Owing to the use of milder hydrolysis conditions that afforded higher recovery of pentoses, the level of arabinoxylans in wheat flour determined by this new method is slightly higher than that measured with the widely used hydrolysis protocol. On the basis of the finding that, for a given flour sample, the total fructose concentration after hydrolysis is highly correlated with its total fructan concentration, the fructan content of a wheat flour sample can thus be estimated directly by the total fructose content. By simplifying and combining the two separate methods used for arabonoxylan and fructan analysis, this new method enables the quantification of arabinoxylans and fructans in wheat flour using a single acid hydrolysis step and a single high-performance liquid chromatography run.

**KEYWORDS:** *arabinoxylans, fructans, quantification, HPLC, wheat flour*

## INTRODUCTION

Fructans are linear or branched polymers of fructose molecules, with or without a single internal or terminal glucose molecule. Fructans are present in approximately 15% of the angiosperm flora.[1] Arabinoxylans, consisting of a linear xylan backbone to which mostly single arabinose units are linked as side residues, are one of the major polysaccharides in all major cereal cell walls.[2] In white wheat flour, fructan content is below 3%,[3] whereas arabinoxylan content ranges from 1.5% to 2.5%.[4] Despite being a minor component of wheat flour, fructans and arabinoxylans are soluble dietary fiber and are claimed to have beneficial effects on human health by selectively promoting certain bacterial species of the gut flora (prebiotic effect).[5−7] For this reason, fructans are increasingly being used as functional additives to foods.[8] In addition to conferring health benefits when included in human diets,[9] arabinoxylans play an important role in the rheological properties of dough and bread-making quality of wheat flours.[10,11] Since wheat is a staple food crop, increasing its fructan and arabinoxylan levels could increase the intake of these nonstarch carbohydrates for a large number of people. As significant genotypic variation has been reported for fructan and arabinoxylan concentrations in wheat grain,[3,12] developing higher fructan and arabinoxylan wheat cultivars can be envisaged.[3,13] Therefore, a high-throughput yet reliable method for evaluating fructan and arabinoxylan concentrations in wheat flour samples has the potential to facilitate both genetic mapping of loci responsible for controlling fructan and arabinoxylan accumulation in grain and rapid and accurate screening for the identification of elite or improved germplasm.

Although various high-performance anion-exchange chromatography (HPAEC) based methods have been reported for quantification of fructans in plant tissues,[14−16] they may not be suitable for wheat flour samples that contain only a small amount of fructans.[3] Recently, specific methods for determination of fructan content in wheat flour have been developed.[17,18] These methods are accurate but complex and time-consuming because they involve two steps in sample treatment (extraction of fructans from flour samples using hot water followed by acid or enzymatic hydrolysis of fructans into hexoses), and two high-performance liquid chromatography (HPLC) runs are required to determine the level of total fructans.[17,18] Therefore, the current methods are low throughput and not suited for processing a large number of samples.

Different methods can also be found in the literature for determination of arabinoxylan content in wheat flour.[19−23] As colorimetric methods cannot provide information on pentose composition and gas chromatography based methods require an additional derivatization step following hydrolysis,[24,25] HPAEC is increasingly being used for arabinoxylan quantification. Similarly, the amount of arabinoxylans can be determined by quantifying the level of arabinose and xylose released after hydrolysis of the pentose polymers. A detailed method comprising optimization of the acid hydrolysis condition and HPAEC separation of released monomers was reported by Houben et al.,[22] and the hydrolysis protocol has been widely used since.[13,26] However, a recovery of about 85% for arabinose and about 75% for xylose was observed under these hydrolysis

Received: March 13, 2014
Revised: July 15, 2014
Accepted: July 22, 2014
Published: July 22, 2014

ACS Publications © 2014 American Chemical Society



dx.doi.org/10.1021/jf501198k | J. Agric. Food Chem. 2014, 62, 8319−8324

Table 1. Fructan Content of 12 Flour Samples Determined by the 2-Step Method

| sample | free sucrose[a] (%) | total glucose[b] (%) | total fructose[c] (%) | glucose and fructose ex sucrose[d] (%) | fructose ex fructan[e] (%) | glucose ex fructan[f] (%) | DP[g] | fructan[h] (%) |
|---|---|---|---|---|---|---|---|---|
| 1 | 0.32 | 0.52 | 1.75 | 0.17 | 1.58 | 0.36 | 5.5 | 1.78 |
| 2 | 0.33 | 0.53 | 1.63 | 0.17 | 1.46 | 0.36 | 5.1 | 1.67 |
| 3 | 0.41 | 0.47 | 1.20 | 0.22 | 0.98 | 0.25 | 4.9 | 1.14 |
| 4 | 0.40 | 0.57 | 1.63 | 0.21 | 1.42 | 0.36 | 4.9 | 1.64 |
| 5 | 0.29 | 0.46 | 1.33 | 0.15 | 1.18 | 0.30 | 4.9 | 1.36 |
| 6 | 0.44 | 0.65 | 2.28 | 0.23 | 2.05 | 0.42 | 5.9 | 2.27 |
| 7 | 0.32 | 0.46 | 1.25 | 0.17 | 1.08 | 0.29 | 4.8 | 1.26 |
| 8 | 0.42 | 0.55 | 1.45 | 0.22 | 1.23 | 0.33 | 4.7 | 1.44 |
| 9 | 0.36 | 0.34 | 0.80 | 0.19 | 0.61 | 0.15 | 5.0 | 0.70 |
| 10 | 0.37 | 0.38 | 0.96 | 0.19 | 0.77 | 0.18 | 5.2 | 0.88 |
| 11 | 0.33 | 0.35 | 1.04 | 0.17 | 0.87 | 0.18 | 5.8 | 0.96 |
| 12 | 0.31 | 0.37 | 0.98 | 0.16 | 0.82 | 0.20 | 5.0 | 0.94 |

[a]Obtained from analyzing the aqueous extract. [b]Obtained from analyzing the hydrolysate of the extract. [c]Obtained from analyzing the hydrolysate of the extract. [d]Calculated from $a(d = 0.526 \times a)$. [e]Calculated from $c$ and $d$ $(e = c - d)$. [f]Calculated from $b$ and $d$ $(f = b - d)$. [g]Calculated from $e$ and $f$ $(g = (e/f) + 1)$. [h]Calculated from $e$, $f$, and $g$ $(h = K(e + f)$, where $K = [180 + 162(g - 1)]/180g)$.

conditions (i.e., 90 min in 2 M HCl at 100 °C),[22] which could lead to underestimation of arabinoxylan content.

Although separate methods are available for the determination of fructans and arabinoxylans in wheat flour, to our knowledge, no attempt has been made to develop a comprehensive method that enables simultaneous quantification of both fructans and arabinoxylans in wheat flour. Here, we report on the development and validation of a new method for the quantitative analysis of fructans and arabinoxylans in wheat flour based on a direct acid hydrolysis of both types of polymers and a single HPLC run to quantify all monomers released.

## MATERIALS AND METHODS

**Wheat Flour.** Wet-milled white flour samples (150 in total) were prepared from different bread wheat cultivars and/or locations throughout Australia.

**Chemicals.** Standards of glucose, fructose, sucrose, arabinose, xylose, and raffinose were purchased from Sigma (USA). Sodium hydroxide (50% solution) and sodium acetate anhydrous used in the mobile phase were obtained from Fluka (Germany).

**Hydrolysis of Arabinoxylans.** Arabinoxylan content in wheat flour was determined by measuring the amount of arabinose and xylose released after hydrolysis of arabinoxylans. The method of direct acid hydrolysis of wheat flour was adopted in this work. Briefly, 10 mg of flour samples was accurately weighed out into 2 mL screw-cap tubes, and 1 mL of HCl of an appropriate concentration (as detailed below) was added to each tube. The hydrolysis was accomplished by incubating the tubes in heating blocks (90 °C) for 60 min. Following hydrolysis, the sample was neutralized by adding NaOH, and the amount of arabinose and xylose released was determined by HPAEC. The amount of arabinoxylans in a sample is calculated as the sum of arabinose and xylose, multiplied by 0.88 to correct for water uptake during hydrolysis.[22]

**Extraction and Hydrolysis of Fructans.** Fructan content in wheat flour was determined by measuring the amount of fructose and glucose released after hydrolysis of the fructose polymers. Two hydrolysis methods were used in this work: (1) extraction of fructans from wheat flour by hot water, followed by acid hydrolysis of the extracted fructans; (2) direct acid hydrolysis of fructans from wheat flour. The first method was adapted from that of Verspreet at al.[18] and is referred to as the 2-step method in this paper. Briefly, the extraction of fructans by hot water was performed in heating blocks (90 °C) for 60 min (step 1), followed by hydrolysis of an aliquot of the extract with 30 mM HCl in heating blocks (70 °C) for 90 min (step 2). The amount of free glucose, fructose, sucrose, and raffinose present in the aqueous extract before hydrolysis as well as that of total glucose and fructose after hydrolysis was determined by HPAEC. Fructan content was then calculated as described by Liu et al.[16] For the second method, the hydrolysis was performed by adding 1 mL of HCl of various concentrations into 2 mL screw-cap tubes containing 10 mg of a flour sample, followed by incubating the tubes in heating blocks (90 °C) for 30−120 min. The amount of fructose released from the flour sample was measured by HPAEC.

**HPAEC Analysis.** Carbohydrate analysis was performed using an ICS-5000 HPLC system (Dionex) equipped with a CarboPac PA100 column (4 × 250 mm) and an electrochemical detector working in pulsed amperometric mode using a gold working electrode and a combined pH−Ag/AgCl reference electrode. A standard quadruple-potential waveform for carbohydrates was used for all analyses (Supporting Information, Table S-1). Two elution programs were used in this work (Supporting Information, Tables S-2 and S-3): one for the quantification of arabinose, xylose, and fructose after hydrolysis, and the other for measuring free glucose, fructose, sucrose, and raffinose content before hydrolysis.

## RESULTS

**Correlation of the Total Fructose Content (after Hydrolysis) and the Fructan Content.** Rhamnose was used as an internal standard in our preliminary analysis, and comparable results were obtained with and without the internal standard. So, no internal standards were used in subsequent experiments. By using the 2-step method, the fructan content of a flour sample can be calculated based on the amount of glucose and fructose liberated from fructan molecules. To deduce the portion of fructose and glucose derived solely from fructans, two separate analyses are needed to quantify, respectively, total fructose and glucose after hydrolysis and free glucose, fructose, sucrose, and raffinose before hydrolysis, as both sucrose and raffinose also contain glucose and fructose units.

The analysis of the aqueous extract of 54 random flour samples indicates that free glucose, fructose, and raffinose are present in very small amount in wheat flour (Supporting Information, Table S-4). Consequently, only the amount of fructose and glucose derived from sucrose needs to be subtracted from the total fructose and glucose to calculate the fructan content. This implies that the concentration of fructan in a wheat flour sample can be calculated using only three values (total glucose and total fructose content after hydrolysis and free sucrose content before hydrolysis), as the amount of glucose and fructose released from sucrose hydrolysis can be directly calculated from sucrose content.

Table 1 shows the fructan content of 12 random flour samples as calculated using the three values determined by two separate HPLC analyses.

A close examination of the data in Table 1 reveals that the fructan content of the 12 samples is very close to their total fructose content after hydrolysis. The strong correlation between these two data series is clearly seen in Figure S-1 (Supporting Information). This suggests that the concentration of total fructose after hydrolysis can be potentially used to estimate the content of fructans in a flour sample. This will greatly simplify the fructan analysis procedure, as the total fructose content after hydrolysis can be determined by one single HPLC run.

**Simplification of the 2-Step Method in Fructan Analysis.** All the current methods for fructan analysis involve two steps: a hot water extraction step and a hydrolysis step.[16−18] Given the fact that, in the case of wheat flour, fructan content could be estimated directly by the total fructose content after hydrolysis, the 2-step method in fructan quantification can also be simplified into one single step, that is, direct hydrolysis of fructans from wheat flour under the same hydrolysis conditions. Indeed, the total fructose contents of 24 random flour samples determined after direct hydrolysis are very close to those measured using the 2-step method (Figure 1).

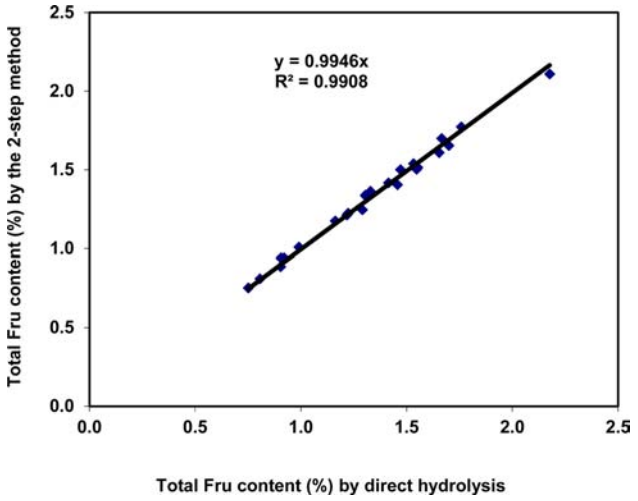


**Figure 1.** Correlation of the total fructose content of 24 wheat flour samples, as determined by the direct hydrolysis method and by the 2-step method. The direct hydrolysis was performed by incubating flour samples with 30 mM HCl at 70 °C for 90 min.

**Optimization of HPLC Separation for All Fructan and Arabinoxylan Monomers.** In order to develop a method allowing simultaneous quantification of fructans and arabinoxylans in wheat flour, chromatographic separation of all monomers (i.e., arabinose, xylose, glucose, and fructose) contained in these two types of carbohydrate polymers is required. A systematic evaluation of the performance of various columns and mobile phase concentrations allowed us to achieve baseline resolution of the four monomer in a standard mix as well as in a wheat flour hydrolysate, in which a large amount of glucose (derived from starch) is present (Figure 2). The optimum chromatographic conditions consist of a Carbopac PA100 ion-exchange column (Dionex) and a mobile phase containing 40 mM NaOH.

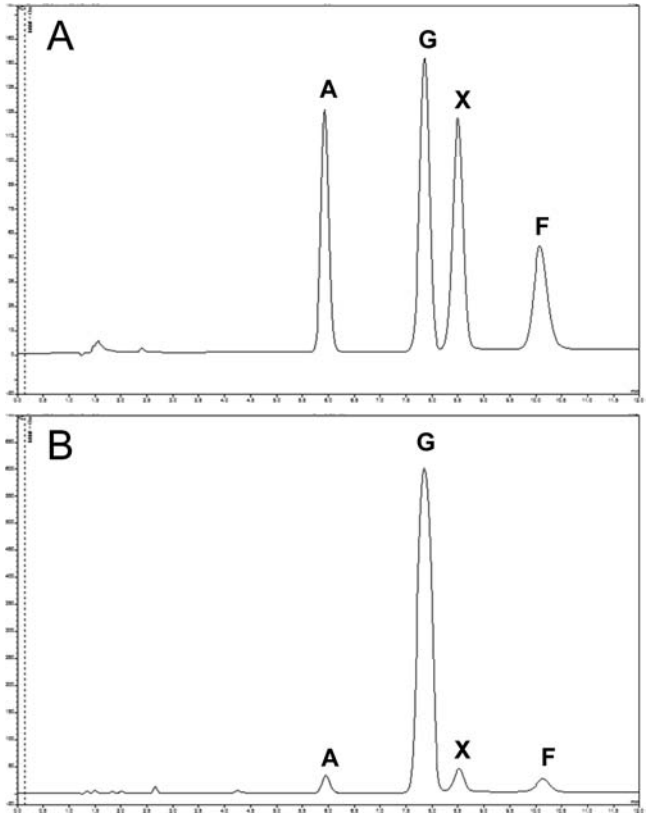


**Figure 2.** HPAEC separation of the four monomers (A) from a standard mix and (B) from the hydrolysate of a wheat flour sample. Peak annotations: A, arabinose; G, glucose; X, xylose; F, fructose. The hydrolysis of wheat flour was performed with 1 M HCl at 90 °C for 60 min.

**Optimization of Acid Hydrolysis for Arabinoxylans and Fructans.** Having demonstrated that fructan and arabinoxylan monomers can be quantified by a single HPLC analysis, a unified acid hydrolysis protocol for both types of polymers is needed in order to develop a higher throughput method. The yield of arabinose, xylose, and fructose was compared when one random flour sample was subjected to various hydrolysis conditions (by varying HCl concentrations, incubation time, and temperatures). Figure 3 shows the yield of arabinose, xylose, and fructose as a function of HCl concentration and incubation time at a fixed incubation temperature (90 °C). Clearly, the hydrolysis rate of arabinoxylans and fructans, as reflected by the yield of arabinose/xylose and fructose, respectively, is influenced by both the HCl concentration and the incubation time. It is also observed that the xylan backbone of arabinoxylans is more resistant to acid hydrolysis than the arabinose branches, whereas fructans can be depolymerised readily. Lowering the incubation temperature to 70 or 80 °C significantly prolongs the time required for complete hydrolysis of arabinoxylans (results not shown).

A combination of HCl concentration of 1 M, incubation time of 60 min, and incubation temperature of 90 °C appears to be the best compromise for the hydrolysis of both types of carbohydrate polymers in wheat flour. This unified hydrolysis protocol and the one-step HPAEC analysis of all monomers form our new method for simultaneous quantification of fructans and arabinoxylans in wheat flour.

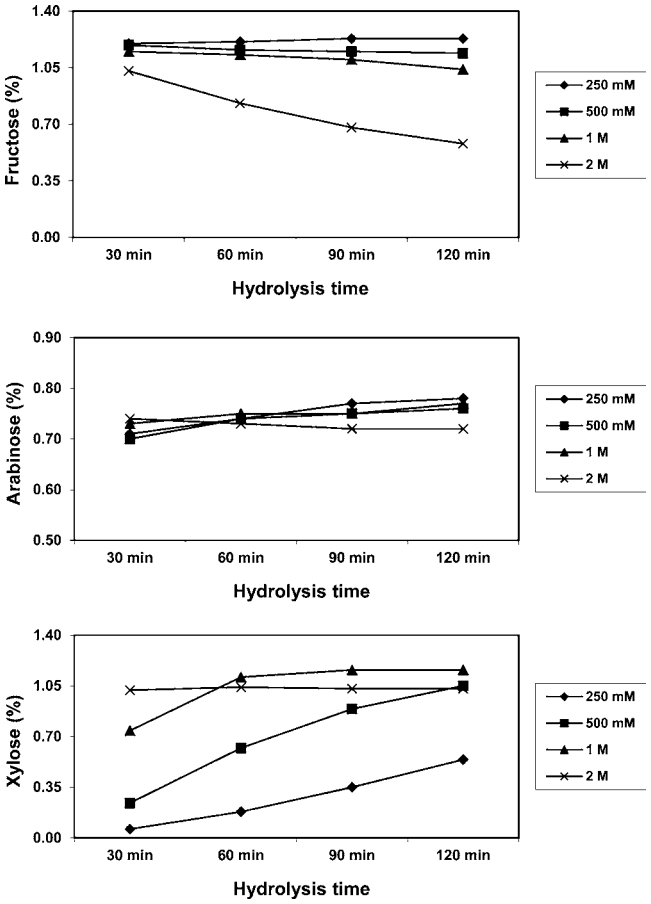


**Figure 3.** Yield of monomers as a function of HCl concentration and incubation time. All hydrolyses were performed at 90 °C, and all data points are the means of three replicates.

**Stability of Arabinose, Xylose, and Fructose under Acidic Conditions.** Having found the unified hydrolysis conditions for the two types of polymers, the stability of the monomers under these hydrolysis conditions needs to be assessed, as the content of the polymers is calculated based on the concentrations of the monomers. The stability of arabinose, xylose, and fructose was assessed by measuring the recovery of standard compounds (applied at 0.01%) after incubation in 1 M HCl at 90 °C for 30–90 min. Figure 4 shows that both arabinose and xylose are stable under the hydrolysis conditions, with a recovery rate close to 100% even after 90 min. By contrast, a slight degradation (or transformation) was observed for fructose (92% recovery after 60 min) (Figure 4).

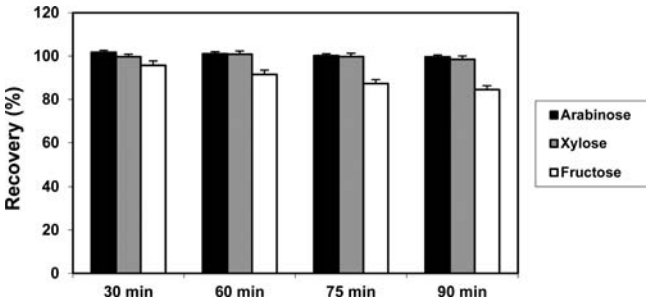


**Figure 4.** Recovery (%) of arabinose, xylose, and fructose after incubation in 1 M HCl at 90 °C. All values in this figure are the means of two replicates.

**Comparison between the New Method and the Standard Method for Arabinoxylan Quantification.** Ten randomly selected flour samples were used to compare our new method with the standard hydrolysis method in quantitative analysis of arabinoxylans. Overall, our new method produced similar results compared to the currently widely used direct hydrolysis method. However, owing to the improved recovery of arabinose and xylose, a slightly higher arabinxylan content was obtained with our new method for nearly all samples (Table 2).

**Table 2. Comparison of Arabinoxylan Content of 10 Flour Samples, as Determined by the New Method and by the Standard Method**

| | mean content[a] (%) ± SD | |
|---|---|---|
| sample | new method | standard method |
| A | 2.33 ± 0.06 | 2.24 ± 0.07 |
| B | 2.13 ± 0.04 | 1.99 ± 0.08 |
| C | 2.22 ± 0.04 | 2.15 ± 0.04 |
| D | 2.46 ± 0.02 | 2.40 ± 0.04 |
| E | 2.36 ± 0 | 2.20 ± 0.10 |
| F | 2.81 ± 0.02 | 2.68 ± 0.07 |
| G | 2.74 ± 0.01 | 2.59 ± 0.10 |
| H | 2.56 ± 0.03 | 2.42 ± 0.08 |
| I | 1.94 ± 0.02 | 1.77 ± 0.10 |
| J | 2.08 ± 0.05 | 1.96 ± 0.05 |

[a]Mean and SD values are calculated from two replicates.

**Comparison between the New Method and the 2-Step Method in Fructan Quantification.** To confirm the reliability of the new method in fructan quantification, a further set of 24 randomly selected samples was analyzed in parallel by the new method and the standard 2-step method. Fructan contents determined by the new method were highly correlated with those determined by the standard 2-step method (Figure 5). However, the overall fructan content measured by our new method is about 95% that determined by the 2-step method. As a result, a correction factor of 1.05 should be applied when using this new method for fructan quantification in wheat flour.

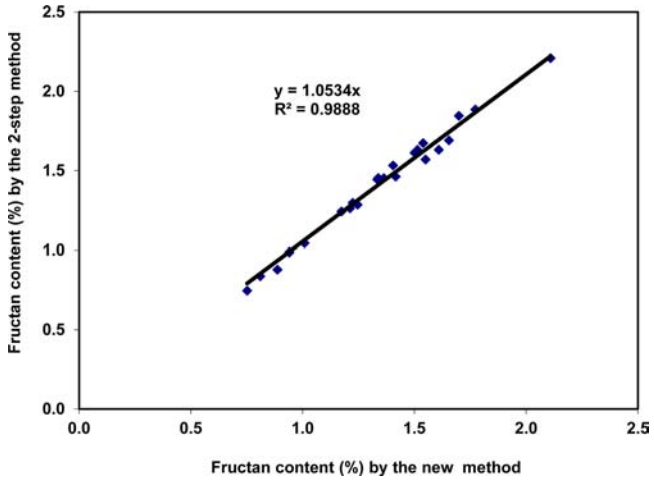


**Figure 5.** Correlation of fructan content of 24 random flour samples, as determined by the new method and by the standard 2-step method.


dx.doi.org/10.1021/jf501198k | J. Agric. Food Chem. 2014, 62, 8319–8324

Indeed, a recovery of about 94% and 99% before and after correction, respectively, was obtained with this new method when wheat flour was spiked with commercial fructan at two different concentrations (1% and 2% fructan of the flour wheat).

**Reproducibility of the New Method in Arabinoxylan and Fructan Quantification.** The reproducibility of the method in the quantification of fructans and arabinoxylans in wheat flour was assessed by the variation of measurement results between technical replicates taken from one single flour sample (Table 3). The content of both arabinoxylans and fructans shows very small variation between replicates, demonstrating the excellent repeatability of the method in fructan and arabinoxylan quantification.

**Table 3. Reproducibility of the Method in Arabinoxylan and Fructan Analysis[a]**

| carbohydrate | rep | content (%) | mean | SD | RSD (%) |
|---|---|---|---|---|---|
| arabinoxylans | 1 | 2.12 | 2.13 | 0.04 | 1.88 |
| | 2 | 2.16 | | | |
| | 3 | 2.16 | | | |
| | 4 | 2.07 | | | |
| fructans | 1 | 1.97 | 1.97 | 0.02 | 1.02 |
| | 2 | 1.98 | | | |
| | 3 | 1.94 | | | |
| | 4 | 1.97 | | | |

[a]Arabinoxylan content is calculated as the sum of arabinose and xylose multiplied by 0.88 to correct for water uptake. Fructan content is calculated using the total fructose content (after direct hydrolysis) multiplied by 1.05. SD, standard deviation. RSD, relative standard deviation.

## DISCUSSION

Quantitative analysis of arabinoxylans and fructans in grains is an important step in the understanding of the genetic control mechanisms for the accumulation of these carbohydrates and in research programs aiming to develop high arabinoxylan and/or fructan germplasm.

Currently, separate methods are available for the determination of total arabinoxylan and fructan contents in wheat flour. A systematic method development for arabinoxylan analysis was reported by Houben et al.,[22] in which a direct hydrolysis of the flour sample was adopted, resulting in significant simplification of the sample pretreatment procedure. However, an extra step was needed in this method to convert glucose into gluconic acid to prevent its interference in xylose quantification. Nguyen et al.[13] further simplified this method by a direct quantification of xylose and arabinose in the hydrolysate. We also found it unnecessary to convert or remove glucose (derived from starch) after hydrolysis, as the use of a CarboPac PA100 column together with an optimized mobile phase allowed complete separation of the four monomeric sugars. In addition, by fine-tuning the parameters used in hydrolysis (reducing the HCl concentration from 2 to 1 M and decreasing the incubation temperature from 100 to 90 °C), we have improved slightly the recovery of the pentoses while achieving complete breakdown of arabinoxylans.

In the case of fructan analysis in wheat flour, an excellent method was published by Verspreet et al.,[18] in which a mild acid hydrolysis (60 mM) was used to breakdown fructan polymers with no degradation of starch. By avoiding starch breakdown during acid hydrolysis, this method allowed accurate estimation of wheat flour fructans. However, this method involved two steps, that is, hot water extraction and acid hydrolysis, and is thus low throughput.

We have found that, in the case of wheat flour, the total fructose content after hydrolysis can be used directly to estimate the content of fructans. This is an important finding for simplifying the fructan analysis procedure. The possibility of using direct hydrolysis of flour to measure the total fructose content is a key step toward a unified hydrolysis protocol for both arabinoxylans and fructans. However, the easy breakdown of fructan molecules and the relative instability of fructose under acidic conditions imply that mild conditions would be preferred for fructan hydrolysis, whereas the backbone of arabinoxylans is much harder to break. Considerable effort was made to find a three-way combination (HCl concentration, incubation time, and temperature) of hydrolysis conditions that ensure complete conversion of arabinoxylans (into arabinose and xylose) and at the same time minimum degradation of fructose liberated from fructans. Under the optimized hydrolysis conditions, the content of arabinoxylans measured is slightly higher compared to the widely used hydrolysis protocol, and the content of fructan is about 95% that measured by the 2-step method. A correction factor of 1.05 is thus needed when using this method for fructan quantification in wheat flour. The reproducibility of the new method in the quantification of both arabinoxylans and fructans was finally confirmed by replicate analyses of the same sample.

In conclusion, a combined method for arabinoxylan and fructan quantification in wheat flour has been developed. This method, requiring one single sample preparation step and one single HPLC run, is simple and reliable and thus particularly suited for screening a large number of samples. Although it has been validated in wheat flour, this method should be applicable to other cereal species.

## ASSOCIATED CONTENT

### Supporting Information

Quadruple potential waveform used in HPAEC-PAD analysis of carbohydrates (Table S-1); gradient elution program used for the quantification of arabinose, xylose, and fructose after hydrolysis (Table S-2); gradient elution program used for the quantification of free glucose, fructose, sucrose, and raffinose before hydrolysis (Table S-3); content of free sugars in wheat flour (Table S-4); correlation between the total fructose content after hydrolysis and fructan content determined by the 2-step method (Figure S-1). This material is available free of charge via the Internet at http://pubs.acs.org.

## AUTHOR INFORMATION

### Corresponding Author

*E-mail: Simone.Rochfort@depi.vic.gov.au.

### Notes

The authors declare no competing financial interest.

## REFERENCES

(1) Pollock, C. J.; Cairns, A. J. Fructan metabolism in grasses and cereals. *Annu. Rev. Plant Physiol.* **1991**, *42*, 77−101.

(2) Skendi, A.; Biliaderis, C. G.; Izydorczyk, M. S.; Zervou, M.; Zoumpoulakis, P. Structural variation and rheological properties of water-extractable arabinoxylans from six Greek wheat cultivars. *Food Chem.* **2011**, *126*, 526−536.

(3) Huynh, B. L.; Wallwork, H.; Stangoulis, J. C. R.; Graham, R. D.; Willsmore, K. L.; Olson, S.; Mather, D. E. Quantitative trait loci for grain fructan concentration in wheat(*Triticum aestivum* L.). *Theor. Appl. Genet.* **2008b**, *117*, 701−709.
(4) Courtin, C. M.; Delcour, J. A. Arabinoxylans and endoxylanases in wheat flour bread-baking. *J. Cereal Sci.* **2002**, *35*, 225−243.
(5) Gibson, G. R.; Beatty, E. R.; Wang, X.; Cummings, J. H. Selective stimulation of bifidobacteria in the human colon by oligofructose and inulin. *Gastroenterology* **1995**, *108*, 975−982.
(6) Ferguson, L. R. Wheat bran and cancer: The role of dietary fibre. *Asia Pac. J. Clin. Nutr.* **1999**, *8*, 17−25.
(7) Ritsema, T.; Smeekens, S. Fructans: Beneficial for plants and humans. *Curr. Opin. Plant Biol.* **2003**, *6*, 223−230.
(8) Roberfroid, M. B.; Van Loo, J.; Gibson, G. R. The bifidogenic nature of chicory inulin and its hydrolysis products. *J. Nutr.* **1997**, *128*, 11−19.
(9) Lu, Z. X.; Walker, K. Z.; Muir, J. G.; O'Dea, K. Arabinoxylan fibre improves metabolic control in people with type II diabetes. *Eur. J. Clin. Nutr.* **2004**, *58*, 621−628.
(10) Biliaderis, C. G.; Izydorczyk, M. S.; Rattan, O. Effect of arabinoxylans on bread-making quality of wheat flours. *Food Chem.* **1995**, *53*, 165−171.
(11) Courtin, C. M.; Delcour, J. A. Arabinoxylans and endoxylanases in wheat flour bread-making. *J. Cereal Sci.* **2002**, *35*, 225−243.
(12) Li, S. B.; Morris, C. F.; Bettge, A. D. Genotype and environment variation for arabinoxylans in hard winter and spring wheats of the US Pacific Northwest. *Cereal Chem.* **2009**, *86*, 88−95.
(13) Nguyen, V. L.; Huynh, B. L.; Wallwork, H.; Stangoulis, J. Identification of quantitative trait loci for grain arabinoxylan concentration in bread wheat. *Crop Sci.* **2011**, *51*, 1143−1150.
(14) Clark, G. T.; Zuther, E.; Outred, H. A.; McManus, M. T.; Heyer, A. G. Tissue-specific changes in remobilisation of fructan in the xerophytic tussock species Festuca novae-zelandiae in response to a water deficit. *Funct. Plant Biol.* **2004**, *31*, 377−389.
(15) Monti, A.; Amaducci, M. T.; Pritoni, G.; Venturi, G. Growth, fructan yield, and quality of chicory (*Cichorium intybus* L.) as related to photosynthetic capacity, harvest time, and water regime. *J. Exp. Bot.* **2005**, *56*, 1389−1395.
(16) Liu, Z.; Mouradov, A.; Smith, K. F.; Spangenberg, G. An improved method for quantitative analysis of total fructans in plant tissues. *Anal. Biochem.* **2011**, *418*, 252−259.
(17) Huynh, B. L.; Palmer, L.; Mather, D. E.; Wallwork, H.; Graham, R. D.; Welch, R. M.; Stangoulis, J. C. R. Genotypic variation in wheat grain fructan content revealed by a simplified HPLC method. *J. Cereal Sci.* **2008a**, *48*, 69−378.
(18) Verspreet, J.; Pollet, A.; Cuyvers, S.; Vergauwen, R.; Van den Ende, W.; Delcour, J. A.; Courtin, C. M. A simple and accurate method for determining wheat grain fructan content and average degree of polymerization. *J. Agric. Food Chem.* **2012**, *60*, 2102−2107.
(19) Douglas, S. G. A rapid method for the determination of pentosans in wheat flour. *Food Chem.* **1981**, *7*, 139−145.
(20) Bell, B. M. A rapid method for dietary fibre estimation in wheat products. *J. Sci. Food Agric.* **1985**, *36*, 815−821.
(21) Hashimoto, S.; Shogren, M. D.; Pomeranz, Y. Cereal pentosan: Their estimation and significance. I. Pentosans in wheat and milled wheat products. *Cereal Chem.* **1987**, *64*, 30−34.
(22) Houben, R.; de Ruijter, C. F.; Brunt, K. Determination of the pentosan content of wheat products by hydrolysis, glucose oxidase treatment and analysis by HPAEC/PAD. *J. Cereal Sci.* **1997**, *26*, 37−46.
(23) Virkki, L.; Maina, N. H.; Johansson, L.; Tenkanen, M. New enzyme-based method for analysis of water-soluble wheat arabinoxylans. *Carbohydr. Res.* **2008**, *343*, 521−529.
(24) Courtin, C. M.; Van den Broeck, H.; Delcour, J. A. Determination of reducing end sugar residues in oligo- and polysaccharides by gas-liquid chromatography. *J. Chromatogr. A* **2000**, *866*, 97−104.
(25) Snelders, J.; Dornez, E.; Broekaert, W. F.; Delcour, J. A.; Courtin, C. M. Determination of the xylan backbone distribution of arabinoxylan-oligosaccharides. *Bioact. Carbohydr. Diet. Fibre* **2013**, *2*, 84−91.
(26) Krahl, M.; Müller, S.; Zarnkow, M.; Back, W.; Becker, T. Arabinoxylan and fructan in the malting and brewing process. *Qual. Assur. Saf. Crops Foods* **2009**, *1*, 246−255.

JOURNAL OF AGRICULTURAL AND FOOD CHEMISTRY

Article

pubs.acs.org/JAFC

# Highly Sensitive Detection of Zearalenone in Feed Samples Using Competitive Surface-Enhanced Raman Scattering Immunoassay

Jianzhi Liu, Yongjun Hu,* Guichi Zhu, Xiaoming Zhou, Li Jia, and Tao Zhang

Ministry of Education Key Laboratory of Laser Life Science & Institute of Laser Life Science, College of Biophotonics, South China Normal University, Guangzhou 510631, People's Republic of China

**ABSTRACT:** Accurate and quantitative analysis of mycotoxin (such as zearalenone) is particularly imperative in the field of food safety and animal husbandry. Here, we develop a sensitive and specific method for zearalenone detection using competitive surface-enhanced Raman scattering (SERS) immunoassay. In this assay, a functional gold nanoparticle was labeled with the Raman reporter and the zearalenone antibody, and a modified substrate was assembled with the zearalenone−bovine serum albumin. With the addition of free zearalenone, the competitive immune reaction between free zearalenone and zearalenone−bovine serum albumin was initiated for binding with zearalenone antibody labeled on gold nanoparticle, resulting in the change of SERS signal intensity. The proposed method exhibits high sensitivity with a detection limit of 1 pg/mL and a wide dynamic range from 1 to 1000 pg/mL. Furthermore, this method can be further applied to analyze the multiple natural feed samples contaminated with zearalenone, holding great potential for real sample detection.

**KEYWORDS:** *Zearalenone, mycotoxin, surface-enhanced Raman scattering, competitive, immunoassay, quantitative detection*

## INTRODUCTION

Contamination of agricultural commodities by mycotoxins is a serious problem worldwide due to their high toxicity and biological persistence. Zearalenone is one of the most important mycotoxins and results from the secondary metabolite of several Fusarium species.[1] Because of unusual weather conditions or improper storage, zearalenone contamination is frequent in agricultural commodities and cereal products such as flour, malt, soybeans, and beer.[2] Global trade also facilitates the occurrence of zearalenone contamination in food, feed, and feed raw materials.[3] Evidence suggests that the consumption of contaminated products might cause various toxic effects on humans and animals, including teratogenesis, carcinogenicity, neurotoxicity, abortion, and estrogenic effect.[4−9] Consequently, accurate and quantitative analysis of zearalenone in agricultural commodities is critical for food safety and animal husbandry.

Because of the adverse effects and the universal existence of zearalenone, a variety of methods such as chemical, physical, and biological processing approaches have been used to lower its level, and it is necessary to develop effective methods to detect and monitor the trace amount of residual zearalenone.[10,11] The traditional analytical methods used for zearalenone detection include high-performance liquid chromatography and ultra high performance liquid chromatography coupled with tandem mass spectrometry, but they usually require expensive instrumentation and complicated sample preparation processes, which might limit their applications in the routine monitoring of zearalenone.[12,13] To avoid this limitation, the immunoassay- and aptamer-based methods have been developed with the advantages of simplicity and low cost, but most of them are difficult to reach a satisfactory sensitivity.[14−20] Therefore, a simple and sensitive method is highly desirable for zearalenone detection in the real samples.

Surface-enhanced Raman scattering (SERS) is an emerging and powerful optical technology that can provide a nondestructive and ultrasensitive detection even down to a single molecular level.[21,22] With several characteristics of tremendous signal enhancement, narrow band widths, and alleviated photobleaching, SERS immunoassay has been widely applied for sensitive detection of nucleic acids, proteins, and microbes.[22−27] In SERS immunoassay, a novel labeling technique is employed. Herein, a SERS nanoprobe that relies on gold nanoparticle is labeled by dye molecules (Raman reporter, e.g., 4,4′-dipyridyl) and antibodies, respectively; thus, Raman signal of the reporter molecules can act as the tracer signal.[23] However, the conventional SERS immunoassay depends on the formation of a sandwich structure of "antibody−antigen−antibody", which demands the antigen with multiple recognition sites for binding antibody. For the detection of small molecules with small size and nonmultiple recognition sites, like zearalenone, this sandwich structure is unsuitable. To overcome this defect, the introduction of competitive concept into SERS immunoassay has gained attention.[23,28] Dufek et al.[29] first applied the competitive SERS immunoassay for the detection of 1,25-dihydroxy metabolite of vitamin $D_3$, but the antibody was chosen to attach to the substrate instead of antigen, which would increase the cost of the assay. Afterward, our group designed a low-cost competitive SERS immunoassay for the detection of adrenergic agonist of clenbuterol in pig urine;[30] nevertheless, the analysis of spiked clenbuterol samples could not confirm its presence in real samples.

**Received:** April 8, 2014
**Revised:** July 21, 2014
**Accepted:** July 23, 2014
**Published:** July 23, 2014

ACS Publications © 2014 American Chemical Society

Herein, we developed a new method based on a competitive SERS immunoassay, which was carried out between free zearalenone and zearalenone−bovine serum albumin fixed on the substrate, competitively binding with zearalenone antibody conjugated on the gold nanoparticles. In the present report, this method was used to detect the zearalenone in natural feed samples.

## MATERIALS AND METHODS

**Materials.** Zearalenone monoclonal antibody, zearalenone−bovine serum albumin, and zearalenone standard solution were purchased from Beijing Huaan Magnech Bio-Tech Co., Ltd. (Beijing, China). Aflatoxin $B_1$ standard solution and diethylstilbestrol standard solution were from Guangzhou Analysis Center Keli Technology Co., Ltd. (Guangzhou, China). 4,4′-Dipyridyl, bovine serum albumin, and trisodium citrate were purchased from Sigma Chemical (St. Louis). 3-Aminopropyl trimethoxysilane and glutaraldehyde were purchased from Aladdin China Ltd. (Shanghai, China). Chloroauric acid ($HAuCl_4$) was received from Sinopharm Chemical Reagent Co., Ltd. (Shanghai, China). The blank feed samples were obtained from Guangdong Medical Laboratory Animal Center (Guangdong, China). Sulfuric acid, nitric acid, 30% hydrogen peroxide, sodium chloride (NaCl), boric acid, borax, potassium dihydrogen phosphate, disodium hydrogen phosphate, and potassium chloride were from Guangzhou Chemical Regent Factory (Guangzhou, China).The following buffer solutions were used: borate buffer (pH 8.2) and phosphate-buffered saline (pH 7.4). The washing buffer was prepared by adding 0.05% Tween-20 to the phosphate-buffered saline. All these reagents were analytical grade or better and all aqueous solutions were prepared with ultrapure water processed by an ultrapure water system (ELGA, London).

**Equipment.** A microscopic Raman spectrometer (Nippon Optical System Co., Tokyo) was used to measure the Raman spectra. The excitation source was a He−Ne laser (Melles Griot, Carlsbad, CA) with a 632.8 nm excitation wavelength and a power of 1 mW was obtained. All spectra were calibrated referring to the 520 $cm^{-1}$ line of silicon. The typical accumulation time used in this study was 30 s. The Raman spectrum was collected by WinSpec/32 software and could be converted into digital data. Those data were processed with Origin 7.0 software. Thereafter, only a baseline calibration on the spectra was performed to remove the intense fluorescence, which came from the capture substrate. A UV/vis spectrometer (Perkin-Elmer, Waltham, MA) was used to determine the diameter of gold nanoparticles.

**Preparation of Gold Nanoparticles and SERS Nanoprobes.** The gold nanoparticles were prepared according to Frens' method,[31] with slight modification.[32] Generally, 100 mL of 1 mM $HAuCl_4$ aqueous solution was heated to boiling, and then 6.0 mL of freshly prepared 38.8 mM trisodium citrate solution was added rapidly. The solution turned deep red quickly and was boiled for another 20 min. Then the solution was allowed to cool down to room temperature with continuous stirring. The resulting red gold nanoparticles were obtained with a diameter of 30 nm and the diameter of the nanoparticles was determined by the UV/vis spectrometer.

The SERS nanoprobes were prepared by the procedure reported by Gu and co-workers with slight modification.[33,34] It was prepared in a typical two-step process: first, 4,4′-dipyridyl molecules were located on the gold nanoparticles through the spontaneous adsorption on gold nanoparticles surface. A total of 30 μL of 0.01 mM 4,4′-dipyridyl was added to 1.0 mL of uncoated gold nanoparticles and the resultant mixture was allowed to react for 10 min. The gold nanoparticles labeled with 4,4′-dipyridyl molecules were then separated from the solution by centrifugation at 12 000 rpm for 5 min and dispersed with 1.0 mL of borate buffer (pH 8.2). Second, zearalenone antibody was immobilized on the 4,4′-dipyridyl-labeled gold nanoparticles. Five microliters of 0.5 mg/mL zearalenone antibody was added to 1.0 mL of 4,4′-dipyridyl-labeled gold nanoparticles. The mixture was incubated at room temperature for 2 h. Then the SERS nanoprobes were purified by centrifugation for 10 min and resuspension with 1.0 mL of borate buffer (pH 8.2). Finally, 20 μL of 2.5% bovine serum albumin was added into the above SERS nanoprobes to block sites bare of 4,4′-dipyridyl and the mixture was incubated for 1 h at room temperature. After centrifugation and resuspension with 1.0 mL of phosphate-buffered saline (pH 7.4), the SERS nanoprobes were finally obtained and the nanoprobes are usually stable for 2−3 days when stored at 4 °C.

**Preparation of Capture Substrates.** The substrates that we used were concave glass slides and five steps were needed to modify them, which meant that the substrates were modified by piranha solution, 3-aminopropyl trimethoxysilane, glutaraldehyde,[35−38] zearalenone−bovine serum albumin, and bovine serum albumin. In the first step, the glass slides were immersed in piranha solution ($H_2SO_4$:$H_2O_2$, 7:3, v/v) for 30 min to yield hydroxyl on the surface. In the second step, after ultrasonic cleaning, the substrates were dipped in methanol solution containing 5% 3-aminopropyl trimethoxysilane for 12 h at room temperature. In the third step, 2.5% glutaraldehyde was added onto the 3-aminopropyl trimethoxysilane silanized substrates to form an 3-aminopropyl trimethoxysilane−glutaraldehyde surface. The slides were allowed to react for 4 h at room temperature, and the amino groups on the 3-aminopropyl trimethoxysilane silanized substrates reacted with the aldehyde groups of glutaraldehyde, thus yielding the 3-aminopropyl trimethoxysilane−glutaraldehyde surface. In the fourth step, 100 μL of 50 μg/mL zearalenone−bovine serum albumin were dropped onto the concave surface of the modified substrates. In the last step, the substrates were incubated in 2.5% bovine serum albumin for 1 h to block active sites on the modified substrates. After they were rinsed with ultrapure water and dried under a stream of nitrogen, the capture substrates were eventually obtained.

**Sample Preparation.** Zearalenone-free feed sample was spiked by adding zearalenone standard solution and the mixture was stored overnight at 4 °C. The concentrations of the spiked samples used in the experiment were 0, 1, 10, 100, and 1000 pg/mL for zearalenone.

A new extraction method, dispersive liquid−liquid extraction, for SERS immunoassay was investigated. Specifically, 5 g of the spiked ground sample was extracted with 30 mL of methanol and 20 mL of 50 g/L NaCl solution where methanol was used as extractant and NaCl was used to avoid emulsification. The mixture was first shaken for 10 min and then ultrasonically for 30 min. After filtering, the filtrate was placed in the separatory funnel and chloroform was used to extract zearalenone from the mixture. The zearalenone chloroform solution was evaporated to dryness before diluting 30-fold with phosphate-buffered saline (pH 7.4) containing 10% methanol (v/v) and 0.05% Tween 20 (v/v). Three natural feed samples contaminated with zearalenone were also handled according to the procedure above.

**Test Procedure.** The SERS procedure has been described previously,[30] with minor modification, as shown in Figure 1. In

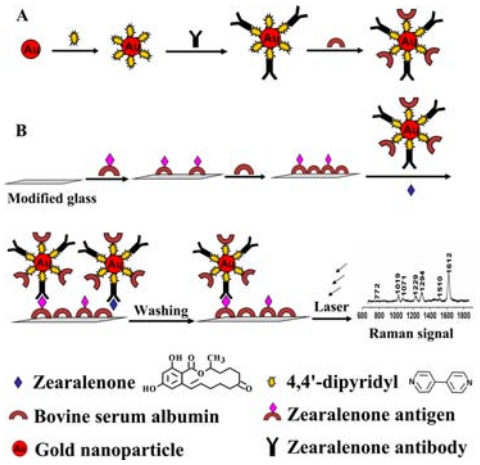


**Figure 1.** (A) Preparation of SERS nanoprobes. (B) Competitive SERS immunoassay for zearalenone.

the first step, the SERS nanoprobes were prepared as above. In the second step, the competitive SERS immunoassay was carried out. Zearalenone standard solution and SERS nanoprobes in the same volume were simultaneously dropped on the concave surface of the capture substrate, during which zearalenone–bovine serum albumin fixed on the capture substrate and zearalenone antigen suspending in the standard solution competitively conjugated with the zearalenone antibody labeled on the SERS nanoprobes. Finally, the 4,4′-dipyridyl Raman signal was obtained from the substrate with a microscopic Raman spectrometer if there are nanoprobes conjugating on the capture substrate. The control experiment was carried out to confirm the antibody and bovine serum albumin were actually labeled on the gold nanoprobes.

## RESULTS AND DISCUSSION

**Optimization of the SERS Nanoprobes.** 4,4′-Dipyridyl is a typical bifunctional Raman reporter, with two nitrogen atoms on both ends of the molecule (Figure 2). One can interact with the gold nanoparticles and the other conjugates with the

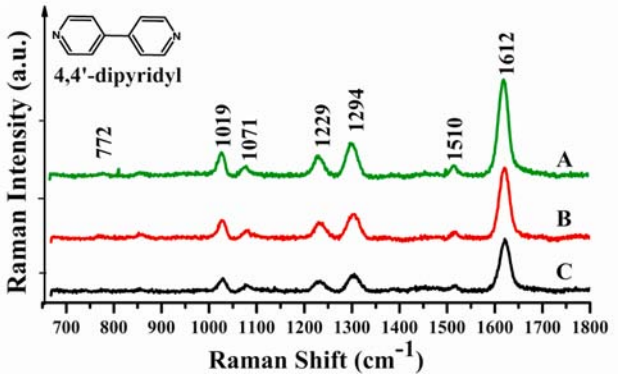


**Figure 2.** (A) SERS spectra of the 4,4′-dipyridyl labeled on gold nanoparticles. (B) SERS nanoprobes labeled with 4,4′-dipyridyl and antibody. (C) SERS nanoprobes labeled with 4,4′-dipyridyl and antibody, and then bovine serum albumin blocking the surplus 4,4′-dipyridyl on the gold nanoparticles surface.

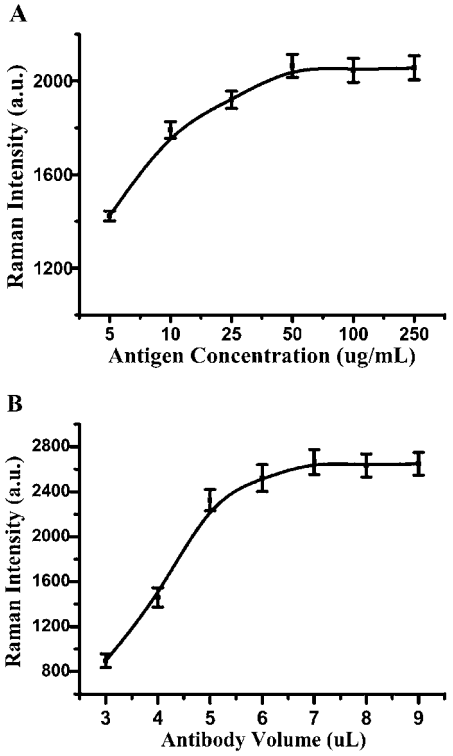


**Figure 3.** (A) SERS signal intensity with different concentrations of zearalenone–bovine serum albumin. (B) SERS signal intensity with different volumes of zearalenone antibody. The Raman intensities are those of the bands at 1612 $cm^{-1}$ of 4,4′-dipyridyl. Error bars indicate the standard deviations of three independent measurements.

zearalenone antibody or bovine serum albumin. A previous study showed bovine serum albumin could be used to block the surplus active sites of the 4,4′-dipyridyl.[33] 4,4′-Dipyridyl is able to be perpendicularly adsorbed on the surface of the gold nanoparticles, which makes the amount of the antibodies labeled on gold nanoparticles as large as possible.[39,40] Its fast-labeled and nontoxic properties make it an excellent Raman reporter. The characteristic peaks of 4,4′-dipyridyl are at 1612, 1510, 1984, 1229, 1071, 1019, and 772 $cm^{-1}$, respectively. The characteristic peak at 772 $cm^{-1}$ is assigned to ring breathing vibrational mode, $B_1$, and the characteristic peak at 1019 $cm^{-1}$ is related to ring breathing vibrational mode, $A_1$. The characteristic peak at 1071 $cm^{-1}$ is assigned to ring in-plane deformation vibrational mode and C–H bend vibrational mode, $A_1$. The band at 1229 $cm^{-1}$ is attributed to C–H in-plane bending vibrational mode, $A_1$. The band at 1294 $cm^{-1}$ is attributed to inter-ring stretching Ω, $B_1$. The band at 1510 $cm^{-1}$ is assigned to C–H in-plane bending vibrational mode and ring stretching, $A_1$. The band at 1612 $cm^{-1}$ is assigned to ring stretching vibrational mode, $A_1$.[39]

From Figure 2, we can see that the number and the locations of the 4,4′-dipyridyl peaks remain invariable, which means that the additions of zearalenone antibody and bovine serum albumin have no effect on 4,4′-dipyridyl adsorption and the 4,4′-dipyridyl is steadily adsorbed on the gold nanoparticles. Because of the long distance between the gold nanoparticles and the zearalenone antibody or bovine serum albumin, no SERS signal of zearalenone antibody or bovine serum albumin was observed. Hence, we chose 4,4′-dipyridyl as the Raman reporter for our experiment. To achieve the optimal Raman spectrum, we carried out a series of experiments to optimize the


dx.doi.org/10.1021/jf503191e | J. Agric. Food Chem. 2014, 62, 8325–8332

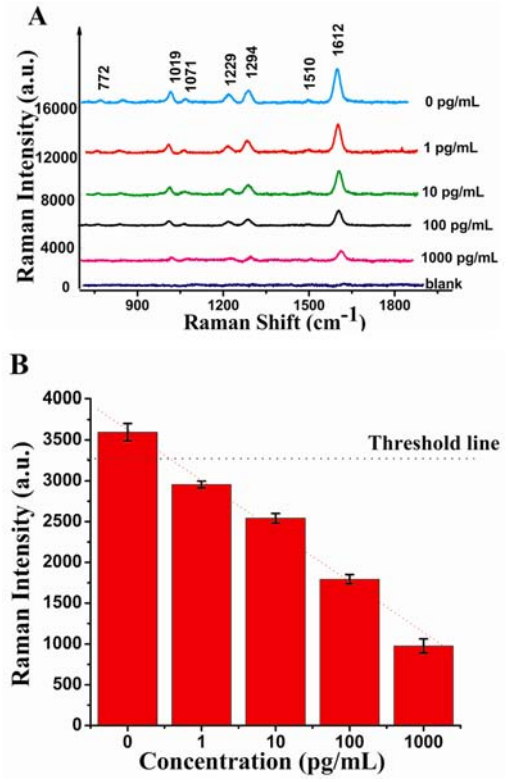


**Figure 4.** (A) SERS spectra acquired with different zearalenone antigen concentrations. (B) Concentration-dependent SERS intensity of the band at 1612 $cm^{-1}$ of 4,4′-dipyridyl using the competitive SERS immunoassay. Error bars indicate the standard deviations of three independent measurements.

4,4′-dipyridyl amount and the reaction time of 4,4′-dipyridyl and gold nanoparticles. The results indicate that the proper amount is ca. 30 μL of 0.01 mM 4,4′-dipyridyl and the proper incubation time is ca. 10 min, which corresponds with our previous work.[30]

**Optimization of the Concentrations of the Zearalenone−Bovine Serum Albumin and the Zearalenone Antibody.** For the sake of the optimal experimental results, determining the proper concentration of zearalenone−bovine serum albumin antigen is very important. As a high-cost reagent, we need to avoid unnecessary waste while making it detectable, so it is important to determine the proper concentration while meeting our experiment demands. To obtain the proper concentration, the same volume of zearalenone−bovine serum albumin antigens with the concentrations of 5, 10, 25, 50, 100, and 250 μg/mL were dropped respectively on the glass slides to incubate for 2 h and the antibody used in this test was sufficient. After 2 h incubation, the SERS calibration curves of different concentrations were obtained as shown in Figure 3A. It is found that the Raman intensity increases with the concentration when the concentrations are lower than 50 μg/mL. At 50 μg/mL, the Raman intensity reaches the maximum and when the concentration is over 50 μg/mL, the Raman intensity is unchanged. This indicates that the glass slide has not been completely occupied by the antigen when the concentrations are lower than 50 μg/mL, and when the concentration is beyond 50 μg/mL, zearalenone−bovine serum albumin antigens are excessive. Therefore, the optimal concentration of zearalenone−bovine serum albumin antigen used in our experiment is 50 μg/mL.

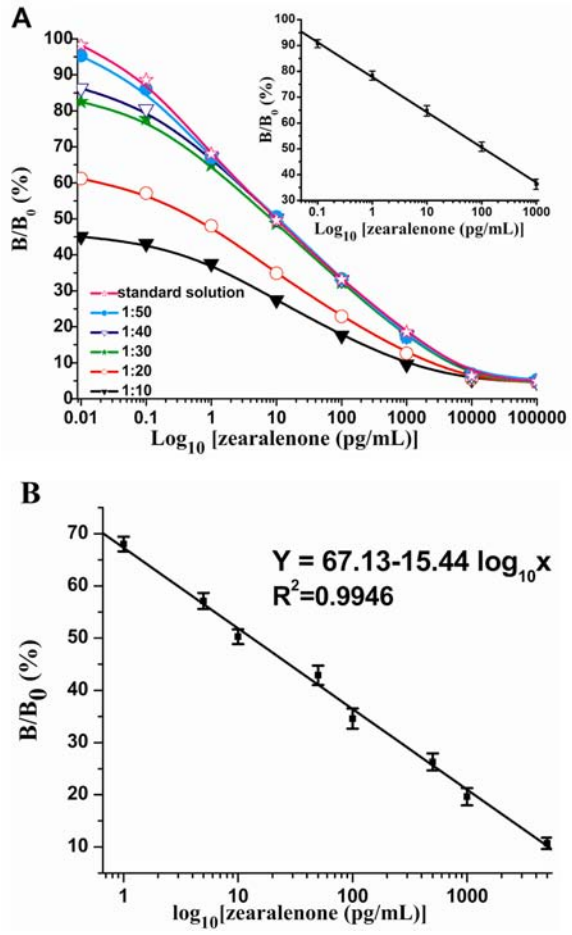


**Figure 5.** (A) Function of centrifugation on the matrix effect in different dilutions of the feed sample and standard curve of the standard solution. (B) Calibration curve for the competitive SERS immunoassay of zearalenone. $B/B_0$ represents the ratio of SERS intensities of different concentrations versus 0 pg/mL standard solution. Error bars indicate the standard deviations of three independent measurements.

**Table 1. Comparison of Zearalenone Detection by Competitive SERS and HPLC in Feed Samples ($n$ = 3)**

| | | sample 1 (ng/mL) | sample 2 (ng/mL) | sample 3 (ng/mL) |
|---|---|---|---|---|
| competitive SERS | $n$ = 1 | 36.8 | 108.4 | 781.1 |
| | $n$ = 2 | 34.1 | 102.6 | 1002.4 |
| | $n$ = 3 | 32.2 | 124.5 | 881.1 |
| | mean | 34.4 | 111.8 | 888.2 |
| | relative standard deviation (%) | 6.7 | 10.1 | 12.5 |
| HPLC[a] | test | 38.9 | 133.7 | 976.1 |

[a]Data are provided by Beijing Huaan Magnech Bio-Tech Co., Ltd.

The optimal concentration of zearalenone−bovine serum albumin antigen remains at the same level when the sample extract and zearalenone antibodies labeled on the SERS nanoprobes are added together on capture substrates.

Apart from zearalenone−bovine serum albumin antigen, zearalenone antibodies labeled on the SERS nanoprobes are vital and the amount of the antibodies also play an important role in this assay, which demands that the amount is neither too much nor too little. To ensure that the competitive


dx.doi.org/10.1021/jf503191e | J. Agric. Food Chem. 2014, 62, 8325−8332

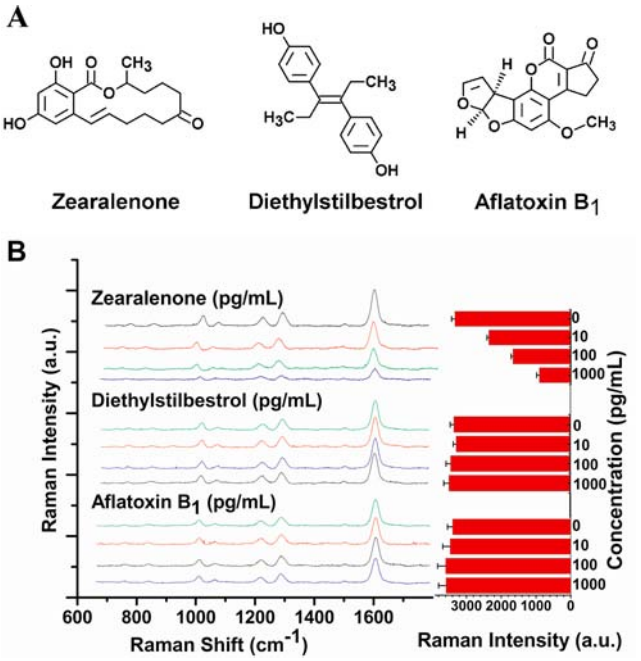


**Figure 6.** Specificity of zearalenone antibody–antigen. (A) The molecular structures of zearalenone, diethylstilbestrol, and aflatoxin $B_1$. (B) Raman spectra of the competitive SERS immunoassay and concentration-dependent SERS intensity of the band at 1612 $cm^{-1}$ of 4,4′-dipyridyl. Error bars indicate the standard deviations of three independent measurements.

immunoassay is established, the amount of antibodies used in the experiment should be comparable to that of zearalenone–bovine serum albumin. In this experiment, 10, 9, 8, 7, 6, 5, 4, and 3 $\mu$L of 0.5 mg/mL zearalenone antibodies were added on the SERS capture substrates with the identical volume 50 $\mu$L of 50 $\mu$g/mL zearalenone antigens, respectively. About 3 h later, we obtained the calibration curve of SERS spectra with different volumes of antibodies. Figure 3B indicates that the Raman intensity reaches the maximum when the volume is 6 $\mu$L. When it is more than 6 $\mu$L, the Raman intensities remain unchanged, which means that the antibodies are excessive. When it is lower than 6 $\mu$L, the Raman intensities increase sharply with the volumes of antibodies increasing. Thus, we determine 5 $\mu$L of 0.5 mg/mL antibodies as the optimal antibodies amount, which indicates that ca. 14 zearalenone antibody molecules are estimated to contact single gold nanoparticle. After we determined the optimal concentrations of the zearalenone–bovine serum albumin antigen and the zearalenone antibody, the free zearalenone concentration was the only variable factor; thus, we could investigate the corresponding relationship between the free zearalenone concentration and the SERS intensity.

**SERS Detection.** In this protocol, a series of zearalenone standard solutions with different concentrations were used to confirm the limit of detection, during which the concentrations of zearalenone standard solutions 1, 10, 100, and 1000 pg/mL, respectively, were used. A control experiment was simultaneously carried out with the solution containing only SERS nanoprobes and phosphate-buffered saline while no zearalenone antigen was added. A blank test was also performed to determine whether nonspecific adsorption existed or not. After SERS nanoprobes and zearalenone standard solutions have been simultaneously incubated on the capture substrate, about 3 h, which has been confirmed as the optimal incubation time, the Raman spectra of the SERS nanoprobes combining with the zearalenone–bovine serum albumin were obtained. In fact, antibody–antigen reaction is very rapid, and in 30 min, most of the reaction has finished.[41,42] We set 3 h as the incubation time to obtain the better sensitivity.

Figure 4A indicates that SERS signal intensities change with the concentrations of zearalenone standard solutions. It clearly shows that the higher the concentrations of zearalenone standard solutions, the weaker the SERS signal intensities. This is because when the concentrations of zearalenone standard solutions get higher, the amount of the SERS nanoprobes conjugated on the capture substrate lessens. This implies that the zearalenone–bovine serum albumin fastened on the capture substrate and the zearalenone antigens in the standard solutions have competitively bound with the zearalenone antibodies labeled on the SERS nanoparticles, which corresponds well with our experimental hypothesis about the detection scheme. To investigate the quantitative relation of SERS signal intensities and zearalenone concentrations in the standard solution, we drew a histogram with the band intensity at 1612 $cm^{-1}$ which is the most intense band. Figure 4B shows that the SERS signal intensity of the control experiment (0 pg/mL free zearalenone) is the highest, ca. 3595 ± 184 a.u., so we set 3227 a.u. (mean of the control intensity minus 2 times standard deviation) as the detection threshold value.[29] Moreover, it is also found that the SERS intensity of 1 pg/mL can be identified from the threshold value with ease and the intensities of any two adjacent concentrations from 1 to 1000 pg/mL can be easily separated. Therefore, ca.1 pg/mL estimated to be the limit of detection for zearalenone in standard solution is acceptable and reasonable. Furthermore, there is an underlying linear relationship between the SERS intensities and their corresponding zearalenone concentrations, implying that quantitative analysis of zearalenone may be feasible in this experiment.

**Feed Sample Analysis.** Whether this method is practical in the detection of zearalenone in feed sample is a question, so experiments were carried out to verify its feasibility. However, for the sake of fulfilling animal requirement of all kinds of nutrition, feed usually contains various ingredients including numerous additives, thus introducing difficulties in zearalenone detection, due to the matrix effect.[43,44] In the present experiment, the matrix is the feed samples diluted with phosphate-buffered saline. Under such circumstances, alleviating the matrix effect is an urgent problem to solve.[45] Only in this way can this method realize its practicability in feed detection. First, we directly detected spiked feed samples. Generally, calibration curves of the pure zearalenone standard solution and feed samples diluted with phosphate-buffered saline (with the final dilutions 1:10, 1:20, 1:30, 1:40, and 1:50) were plotted and the zearalenone concentration range was 0.1–$10^5$ pg/mL, during which $B/B_0$ ($B/B_0$ represents the SERS intensity ratios of different concentrations to 0 pg/mL standard solution) versus the zearalenone concentration is the coordinate axis. However, there is a perfect match only when the zearalenone concentration surpassed 10 pg/mL and the diluted multiples is more than 40. When the zearalenone concentration is lower than 10 pg/mL, none of the dilution curves correspond to the standard solution curve, which suggests that the matrix effect is more obvious in the lower concentration range.


dx.doi.org/10.1021/jf503191e | J. Agric. Food Chem. 2014, 62, 8325–8332

To further alleviate the matrix effect, centrifugal separation has been performed. After the feed sample has been diluted into different concentrations, the solutions were centrifuged for 10 min. Then the supernatant of the feed sample was separated and stored at 4 °C. We set 10 000 rpm as the optimal rotation speed to not only remove the components that are not analyzed but also keep zearalenone undestroyed. Figure 5A shows the function of centrifugation on alleviating the matrix effect and the standard curve of the standard solution which obeys the equation $Y = 77.73-13.59 \log_{10} X$, $R^2 = 0.9992$. After centrifugation, the calibration curves of the 1:30, 1:40, and 1:50 dilute feed samples were similar to that of zearalenone standard solution with the concentration range from 5 to 5000 pg/mL, which indicates that the matrix effect has been effectively diminished. Hence, all experiments were carried out when the feed samples have been diluted 30 times and centrifuged. Figure 5B shows a linear plot which obeys the equation $Y = 67.31-15.44 \log_{10} X$, $R^2 = 0.9969$. On the basis of the calibration curve above, recoveries of 99−105.2% ($n = 3$) and mean relative standard deviation of 8.1% are obtained, which further demonstrates the substantial elimination of the matrix effect compared with the former method. Therefore, this method is appropriate for the quantitative analysis of feed samples.

**Analysis of Zearalenone in Natural Feed Samples.** To validate its availability in natural feed samples, three natural feed samples were analyzed using this method. The feed samples were handled according to the procedure above. However, it was surprising that no SERS signal was obtained. Since matrix effect has been eliminated, the reason may exist in the gold colloid, the buffer pH, or the zearalenone content in the feed sample. The control variable method was used to determine the possible reasons and finally we focused on the zearalenone content, which means the zearalenone content is beyond our detection range. Dilution is a good method to reduce the zearalenone content, so we diluted the samples as 1:30, 1:50, 1:70, and 1:100. When the dilution ratio is 1:50, SERS signal appears, and we calculate the zearalenone content according to the calibration curve. The results are presented in Table 1, with the measured value 111.8 ng/mL ($n = 3$), and relative standard deviation 10.1%. Another two natural feed samples were also analyzed according to the procedure above. From the data in Table 1, we clearly see that the three feed samples are positive. To further confirm the results above, high-performance liquid chromatography (HPLC) was used and the results of the three feed samples have also been listed in Table 1, respectively. The competitive SERS method has a variation in determining zearalenone, which may be due to the difference of sample preparation, laser light intensity, and the instrument. Although HPLC has an excellent accuracy which is even better than ours,[46] the proposed method still has a good enough accuracy with the advantages of high sensitivity, high specificity, and low cost. Moreover, the whole spectrum collection by Raman spectrometry needs only ca. 30 s. It is shorter than that of HPLC, where at least several minutes are needed.[46] Therefore, our method has its characteristic advantages and is suitable to detect zearalenone residuue with very low concentration, especially for the trace detection.

**Investigation of Antibody−Antigen−Mycotoxin Specificity.** The experiments described in this section demonstrate the feasibility of combining SERS and competitive method to detect the presence of specific species in aqueous samples. Zearalenone−bovine serum albumin and free zearalenone competitively binding with antizearalenone monoclonal antibody are used for immunorecognition. Aflatoxin $B_1$, which is a commonly occurring mycotoxin, and diethylstilbestrol, which is another kind of estrogen, are selected to investigate the specificity of antibody−antigen−mycotoxin. Specifically, the competitive immunoassays are carried out as follows: the three reagents with the same concentration in the feed sample were dropped on the capture substrate respectively while SERS nanoprobes were simultaneously added on each capture substrate. After 3 h incubation under room temperature with certain humidity, SERS signals were obtained. Figure 6 shows the chemical structures of the three reagents and their SERS signals, and we also drew the histogram with the SERS band intensity at 1612 $cm^{-1}$ to compare the changes of SERS signal intensity with various concentrations. The SERS signal intensities of aflatoxin $B_1$ and diethylstilbestrol in different concentrations have little changes while that of zearalenone shows a dramatic decline and the histogram shows the changes of the signal intensities along with the concentrations, which indicates that there is a high specificity of zearalenone antibody in recognizing zearalenone antigen. The results of this experiment shown in Figure 6B further establish the viability of our assay concept in natural feed samples detection.

## AUTHOR INFORMATION

### Corresponding Author

*Telephone: (+86-20) 8521-1436, ext. 8107. Fax: (+86-20) 8521-6052. E-mail: yjhu@scnu.edu.cn.

### Funding

This research is supported by the NSFC (No. 11079020, 21273083, U1332132) and Guangdong-NSF (No. S2013010016551) grants, the scientific research foundation for the returned overseas Chinese scholars, State Education Ministry, the foundation for introduction of talents by the universities in Guangdong Province, and the project under scientific and technological planning by Guangzhou City.

### Notes

The authors declare no competing financial interest.

## ACKNOWLEDGMENTS

We would like to thank Beijing Huaan Magnech Bio-Tech Co., Ltd., for providing natural feed samples.

## REFERENCES

(1) Zinedine, A.; Soriano, J. M.; Molto, J. C.; Mañes, J. Review on the toxicity, occurrence, metabolism, detoxification, regulations and intake of zearalenone: an oestrogenic mycotoxin. *Food Chem. Toxicol.* **2007**, *45*, 1−18.

(2) Schatzmayr, G.; Streit, E. Global occurrence of mycotoxins in the food and feed chain: facts and figures. *World Mycotoxin J.* **2013**, *6*, 213−222.

(3) Streit, E.; Naehrer, K.; Rodrigues, I.; Schatzmayr, G. Mycotoxin occurrence in feed and feed raw materials worldwide: long-term analysis with special focus on Europe and Asia. *J. Sci. Food Agric.* **2013**, *93*, 2892−2899.

(4) Hussein, H. S.; Brasel, J. M. Toxicity, metabolism, and impact of mycotoxins on humans and animals. *Toxicology* **2001**, *167*, 101−134.

(5) Gazzah, A. C.; Camoin, L.; Abid, S.; Bouaziz, C.; Ladjimi, M.; Bacha, H. Identification of proteins related to early changes observed in human hepatocellular carcinoma cells after treatment with the mycotoxin zearalenone. *Exp. Toxicol. Pathol.* **2013**, *65*, 809−816.

(6) Schneider, E. P.; Dickert, K. J. Health costs and benefits of fungicide use in agriculture. *J. Agromedicine* **1994**, *1*, 19−37.

(7) Edgar, J. A. Toxins in temperate grasses—implications and solutions. *N. Z. J. Agric. Res.* **1994**, *37*, 341−347.
(8) Ryu, D.; Jackson, L.; Bullerman, L. Effects of processing on zearalenone. *Adv. Exp. Med. Biol.* **2002**, *504*, 205−216.
(9) Kuiper-Goodman, T.; Scott, P. M.; Watanabe, H. Risk assessment of the mycotoxin zearalenone. *Regul. Toxicol. Pharmacol.* **1987**, *7*, 253−306.
(10) Giménez, I.; Herrera, M.; Escobar, J.; Ferruz, E.; Lorán, S.; Herrera, A.; Ariño, A. Distribution of deoxynivalenol and zearalenone in milled germ during wheat milling and analysis of toxin levels in wheat germ and wheat germ oil. *Food Control* **2013**, *34*, 268−273.
(11) Shephard, G. S.; Burger, H. M.; Gambacorta, L.; Krska, R.; Powers, S. P.; Rheeder, J. P.; Solfrizzo, M.; Sulyok, M.; Visconti, A.; Warth, B.; van der Westhuizen, L. Mycological analysis and multimycotoxins in maize from rural subsistence farmers in the former Transkei, southern Africa. *J. Agric. Food Chem.* **2013**, *61*, 8232−8240.
(12) De Saeger, S.; Sibanda, L.; Van Peteghem, C. Analysis of zearalenone and α-zearalenol in animal feed using high-performance liquid chromatography. *Anal. Chim. Acta* **2003**, *487*, 137−143.
(13) Arroyo-Manzanares, N.; Huertas-Perez, J. F.; Gamiz-Gracia, L.; Garcia-Campana, A. M. A new approach in sample treatment combined with UHPLC-MS/MS for the determination of multiclass mycotoxins in edible nuts and seeds. *Talanta* **2013**, *115*, 61−67.
(14) Edupuganti, S. R.; Edupuganti, O. P.; O'Kennedy, R. Generation of anti-zearalenone scFv and its incorporation into surface plasmon resonance-based assay for the detection of zearalenone in sorghum. *Food Control* **2013**, *34*, 668−674.
(15) Tanaka, T.; Teshima, R.; Ikebuchi, H.; Sawada, J.; Ichinoe, M. Sensitive enzyme-linked immunosorbent assay for the mycotoxin zearalenone in barley and job's-tears. *J. Agric. Food Chem.* **1995**, *43*, 946−950.
(16) Li, X.; Li, P. W.; Zhang, Q.; Li, R.; Zhang, W.; Zhang, Z. W.; Ding, X. X.; Tang, X. Q. Multi-component immunochromatographic assay for simultaneous detection of aflatoxin $B_1$, ochratoxin A and zearalenone in agro-food. *Biosens. Bioelectron.* **2013**, *49*, 426−432.
(17) Shim, W. B.; Kim, K. Y.; Chung, D. H. Development and validation of a gold nanoparticle mmunochromatographic assay (ICG) for the detection of zearalenone. *J. Agric. Food Chem.* **2009**, *57*, 4035−4041.
(18) Liu, G.; Han, Z.; Nie, D. X.; Yang, J. H.; Zhao, Z. H.; Zhang, J. B.; Li, H. P.; Liao, Y. C.; Song, S. Q.; Saeger, D. S.; Wu, A. B. Rapid and sensitive quantitation of zearalenone in food and feed by lateral flow immunoassay. *Food Control* **2012**, *27*, 200−205.
(19) Wang, Y. K.; Yan, Y. X.; Ji, W. H.; Wang, H. A.; Li, S. Q.; Zou, Q.; Sun, J. H. Rapid simultaneous quantification of zearalenone and fumonisin $B_1$ in corn and wheat by lateral flow dual immunoassay. *J. Agric. Food Chem.* **2013**, *61*, 5031−5036.
(20) Chen, X. J.; Huang, Y. K.; Duan, N.; Wu, S. J.; Ma, X. Y.; Xia, Y.; Zhu, C. Q.; Jiang, Y.; Wang, Z. P. Selection and identification of ssDNA aptamers recognizing zearalenone. *Anal. Bioanal. Chem.* **2013**, *405*, 6573−6581.
(21) Hu, J. W.; Zhao, B.; Xu, W. Q.; Fan, Y. G.; Li, B. F.; Ozaki, Y. Simple method for preparing controllably aggregated silver particle films used as surface-enhanced Raman scattering active substrates. *Langmuir* **2002**, *18*, 6839−6844.
(22) Han, X. X.; Zhao, B.; Ozaki, Y. Surface-enhanced Raman scattering for protein detection. *Anal. Bioanal. Chem.* **2009**, *394*, 1719−1727.
(23) Huang, J. S.; Kim, K. H.; Choi, N.; Chon, H.; Lee, S.; Choo, J. Preparation of silica-encapsulated hollow gold nanosphere tags using layer-by-layer method for multiplex surface-enhanced Raman scattering detection. *Langmuir* **2011**, *27*, 10228−10233.
(24) Guven, B.; Basaran-Akgul, N.; Temur, E.; Tamer, U.; Boyac, İ. H. SERS-based sandwich immunoassay using antibody coated magnetic nanoparticles for Escherichia coli enumeration. *Analyst* **2011**, *136*, 740−748.
(25) Harper, M. M.; McKeating, K. S.; Faulds, K. Recent developments and future directions in SERS for bioanalysis. *Phys. Chem. Chem. Phys.* **2013**, *15*, 5312−5328.
(26) Liu, Z. M.; Hu, C. F.; Li, S. X.; Zhang, W.; Guo, Z. Y. Rapid intracellular growth of gold nanostructures assisted by functionalized graphene oxide and its application for surface-enhanced Raman spectroscopy. *Anal. Chem.* **2012**, *84*, 10338−10344.
(27) Chon, H.; Lee, S.; Son, S. W.; Oh, C. H.; Choo, J. Highly sensitive immunoassay of lung cancer marker carcinoembryonic antigen using surface-enhanced Raman scattering of hollow gold nanospheres. *Anal. Chem.* **2009**, *81*, 3029−3034.
(28) Brady, C. I.; Mack, N. H.; Brown, L. O.; Doorn, S. K. Self-assembly approach to multiplexed surface-enhanced Raman spectral-encoder beads. *Anal. Chem.* **2009**, *81*, 7181−7188.
(29) Dufek, E. J.; Ehlert, B.; Granger, M. C.; Sandrock, T. M.; Legge, S. L.; Herrmann, M. G.; Meikle, A. W.; Porter, M. D. Competitive surface-enhanced Raman scattering assay for the 1,25-dihydroxy metabolite of vitamin D3. *Analyst* **2010**, *135*, 2811−2817.
(30) Zhu, G. C.; Hu, Y. J.; Gao, J.; Zhong, L. Highly sensitive detection of clenbuterol using competitive surface-enhanced Raman scattering immunoassay. *Anal. Chim. Acta* **2011**, *697*, 61−66.
(31) Frens, G. Controlled nucleation for the regulation of the particle size in monodisperse gold suspensions. *Nat. Phys. Sci.* **1973**, *241*, 20−22.
(32) Xie, M.; Zhu, G. C.; Hu, Y. J.; Gu, H. M. Conformations of morpholine in liquid and adsorbed on gold nanoparticles explored by Raman spectroscopy and theoretical calculations. *J. Phys. Chem. C* **2011**, *115*, 20596−20602.
(33) Cui, Y.; Ren, B.; Yao, J. L.; Gu, R. A.; Tian, Z. Q. Multianalyte immunoassay based on surface-enhanced Raman spectroscopy. *J. Raman Spectrosc.* **2007**, *38*, 896−902.
(34) Jiang, Y.; Cui, Y.; Yao, J. L.; Gu, R. A. Surface enhanced Raman spectroscopic studies on immunoassay by 4,4′-bipyridyl as readout molecule. *Acta. Chim. Sin.* **2006**, *64*, 240−244.
(35) Nakanishi, K.; Muguruma, H.; Karube, I. A novel method of immobilizing antibodies on a quartz crystal microbalance using plasma-polymerized films for immunosensors. *Anal. Chem.* **1996**, *68*, 1695−1700.
(36) Cras, J. J.; Rowe-Taitt, C. A.; Nivens, D. A.; Ligler, F. S. Comparison of chemical cleaning methods of glass in preparation for silanization. *Biosens. Bioelectron.* **1999**, *14*, 683−688.
(37) Zhang, Z. J.; Hu, R. S.; Liu, Z. F. Formation of a porphyrin monolayer film by axial ligation of protoporphyrin IX zinc to an amino-terminated silanized glass surface. *Langmuir* **2000**, *16*, 1158−1162.
(38) Xu, S. P.; Ji, X. H.; Xu, W. Q.; Li, X. L.; Wang, L. Y.; Bai, Y. B.; Zhao, B.; Ozaki, Y. Immunoassay using probe-labelling immunogold nanoparticles with silver staining enhancement via surface-enhanced Raman scattering. *Analyst* **2004**, *129*, 63−68.
(39) Suzuki, M.; Niidome, Y.; Yamada, S. Adsorption characteristics of 4,4′-bipyridine molecules on gold nanosphere films studied by surface-enhanced Raman scattering. *Thin Solid Films* **2006**, *496*, 740−747.
(40) Joo, S. W. Surface-enhanced Raman scattering of 4,4′-bipyridine on gold nanoparticle surfaces. *Vibr. Spectrosc.* **2004**, *34*, 269−272.
(41) Myszka, D. G.; Morton, T. A.; Doyle, M. L.; Chaiken, I. M. Kinetic analysis of a protein antigen-antibody interaction limited by mass transport on an optical biosensor. *Biophys. Chem.* **1997**, *64*, 127−137.
(42) Malmborg, A. C.; Michaëlsson, A.; Ohlin, M.; Jansson, B.; Borrebaeck, C. A. K. Real time analysis of antibody-antigen reaction kinetics. *Scand. J. Immunol.* **1992**, *35*, 643−650.
(43) Matuszewski, B. K.; Constanzer, M. L.; Chavez-Eng, C. M. Strategies for the assessment of matrix effect in quantitative bioanalytical methods based on HPLC−MS/MS. *Anal. Chem.* **2003**, *75*, 3019−3030.
(44) Dams, R.; Huestis, M. A.; Lambert, W. E.; Murphy, C. M. Matrix effect in bio-analysis of illicit drugs with LC-MS/MS: Influence

of ionization type, sample preparation, and biofluid. *J. Am. Soc. Mass Spectrom.* **2003**, *14*, 1290−1294.
(45) Zhao, L.; Qin, H. Q.; Wu, R. A.; Zou, H. F. Recent advances of mesoporous materials in sample preparation. *J. Chromatogr. A* **2012**, *1228*, 193−204.
(46) Duca, R. C.; Bravin, F.; Delaforge, M.; Vladescu, L.; Badea, I. A.; Criste, R. D. Development of a new HPLC method used for determination of zearalenone and its metabolites in broiler samples. Influence of zearalenone on the nutritional properties of broiler meat. *J. Agric. Food Chem.* **2009**, *57*, 10497−10504.

JOURNAL OF AGRICULTURAL AND FOOD CHEMISTRY

Article

pubs.acs.org/JAFC

# A Control Method To Inspect the Compositional Authenticity of Minas Frescal Cheese by Gel Electrophoresis

Renata B. Magenis,[†,‡] Elane S. Prudêncio,[‡] Luciano Molognoni,[‡,§] and Heitor Daguer*[,§]

[†]Instituto Federal Catarinense, Campus Rio do Sul, Rio do Sul, Santa Catarina 89160-000, Brazil

[‡]Departamento de Ciência e Tecnologia de Alimentos, Universidade Federal de Santa Catarina, Florianópolis, Santa Catarina 88034-000, Brazil

[§]Laboratório Nacional Agropecuário, Ministério da Agricultura, Pecuária e Abastecimento, São José, Santa Catarina 88102-600, Brazil

**ABSTRACT:** This study introduces a qualitative method to inspect the compositional authenticity of white nonripened cheeses like Minas Frescal, a typical Brazilian cheese, especially when irregular replacement of milk by whey is suspected. A sodium dodecyl sulfate gel electrophoresis (SDS−PAGE) method, followed by image densitometry, was validated. Cheeses were freeze-dried to electrophoresis, and $\beta$-lactoglobulin ($\beta$-LG) was chosen as the adulteration marker. In gel trypsin digestion followed by matrix assisted laser desorption ionization time-of-flight (MALDI-TOF) mass spectrometry provided its identification. Cheeses with a minimum of 14 mg·g$^{-1}$ of $\beta$-LG are considered to be adulterated. The method shows satisfactory precision with a detection limit of 7 mg·g$^{-1}$. Forty-two commercial samples from inspected establishments were then assessed and subjected to cluster analysis. Compliant and noncompliant groups were set with 24 (57%) authentic samples and 18 (43%) adulterated samples, respectively, showing that proper analytical monitoring is required to inhibit this practice.

**KEYWORDS:** *SDS−PAGE, white cheeses, adulterations, dairy inspection, whey*

## INTRODUCTION

Minas Frescal is a widely consumed cheese in Brazil. It is a white fresh, ready to consume cheese, that usually presents a whitish internal color, a soft consistence, and a close texture with scarce irregular holes. It is a high moisture cheese, whose flavor ranges from mild to slightly acid.[1−3] A national regulation has been established by inspection authority for this product, which shall be obtained from whole or semiskimmed pasteurized milk by enzymatic clotting with rennet and/or other appropriate clotting enzymes, complemented or not by the action of specific lactic bacteria.[4]

In dairy products, modification of composition and adulteration with other dairy or nondairy ingredients may take place for economic reasons.[5,6] In a previous study, unexpected variations were observed in rheological and physicochemical properties of Minas Frescal cheese commercial samples acquired in Brazil. Moreover, based on the electrophoretic profile of those samples, it was suggested that whey was irregularly present in the composition of these products.[7] Considering the large excess and the low price of whey,[8] its fraudulent addition to Minas Frescal cheese production is easily accomplished for financial gain.

Although a reference method is available to detect cow milk in cheeses made from goat, buffalo, and ewe milk in European Union,[9] it seems that adulteration of white cheeses with whey has not been properly assessed, since no analytical method has been validated or is even available with this purpose. Recently, adulterated goat and ewe cheeses were detected in Croatia by isoelectric focusing.[10] Particularly, the addition of whey to several dairy products has been researched for a long time, and depending on the matrix susceptible to adulteration, a different protein marker has to be selected. Proteomic methods have been described with this purpose, such as the classic detection of caseinomacropeptide (CMP) in milk.[11] In Italy, a proteomic approach was performed to assess the adulteration of mozzarella "Fiordilatte" with stored curd and a fragment of the main proteolytic product obtained by rennet digestion of $\alpha_{S1}$-I casein has been patented as a marker protein.[12]

In Brazil, products of animal origin can be inspected by federal, state, or municipal governments. Since 2006, in an attempt to reduce trading restriction in inspected establishments and also to provide technical and sanitary equivalence among those three inspection levels, the Brazilian System of Inspection (SISBI) was created.[13] In that system, an authorized establishment, inspected by a state or municipal inspection service officially recognized as equivalent to the federal inspection service, is allowed to trade its products throughout the whole country. In this growing scenario, where the number of medium and small factories is increasing, the importance of having available analytical methods capable of detecting fraudulent trade practices is evident.

Analytical methodologies that allow the characterization of dairy products can be very useful to support regulative authorities as well as food manufacturers.[14] Polyacrylamide gel electrophoresis (PAGE) is a classic separation method which assisted by advanced scanner and image analysis can result in good separations and high resolutions, leading to accurate and reproducible results.[15] Dodecyl sulfate polyacrylamide gel electrophoresis (SDS−PAGE) has been widely used to identify proteins, and it fits well to dairy products, separating caseins and whey with good resolution.[16−21] This

Received: April 23, 2014
Revised: July 28, 2014
Accepted: July 30, 2014
Published: July 30, 2014

ACS Publications © 2014 American Chemical Society



dx.doi.org/10.1021/jf502864e | J. Agric. Food Chem. 2014, 62, 8333−8339

work aimed to validate an electrophoretic qualitative method to detect Minas Frescal cheese's adulteration by replacement of milk by whey, as a control tool to inspect its authenticity.

## MATERIALS AND METHODS

**Materials.** Whole pasteurized milk (from five different brands), food-grade lactic acid (Purac Sínteses, Campos dos Goytacazes, RJ, Brazil), calcium chloride (Vetec, Duque de Caxias, RJ, Brazil), and commercial rennet (Chr. Hansen A/S, Valinhos, SP, Brazil) were used to prepare cheese reference samples. Commercial Minas Frescal cheeses ($n$ = 42), processed by different state or federally inspected factories (from 7 different states), were purchased at various shops and market stalls in Brazil, within 2−3 weeks after manufacture. Defatted milk powder (Nestlé Brasil Ltda., Araraquara, SP, Brazil) and whole pasteurized milk were purchased at local market. Demineralized whey powder (12.5% net protein content) was obtained from Cooperativa Central Aurora Alimentos (Pinhalzinho, SC, Brazil). Trypsin from porcine pancreas and $\beta$-lactoglobulin (purity ≥90%) from bovine milk were purchased from Sigma-Aldrich (St. Louis, MO). All reagents employed to prepare buffers and solutions were electrophoresis grade and obtained from Bio-Rad Laboratories Inc. (Hercules, CA). All solvents and acids were of analytical grade for HPLC and were purchased from Merck KGaA (Darmstadt, Germany). Standard solution was prepared by diluting $\beta$-lactoglobulin to 1 mg·mL$^{-1}$ with sample buffer before analysis.

**Reference Samples.** Five cheeses were manufactured with commercial pasteurized milk as reference Minas Frescal samples at the laboratory. For the processing of each cheese, milk (4 L) was heated at 37 ± 1 °C, and lactic acid (0.25 mL·L$^{-1}$ of an 85% lactic acid solution), calcium chloride (0.4 mL·L$^{-1}$ of a 40% calcium chloride solution), and commercial rennet (0.9 mL·L$^{-1}$) were added, followed by incubation at 37 ± 1 °C for 40 min. Gel was gently cut into cubes, drained, placed in perforated circular containers (approximately 500 g capacity), and kept overnight under refrigeration for draining. Reference samples were then freeze-dried at a lyophilizer (Liobrás Comércio e Serviço de Liofilizadores, São Carlos, SP, Brazil) and kept at −18 °C.

**SDS−PAGE Analysis.** Freeze-dried cheeses were weighed into polypropylene centrifuge tubes and diluted to 4 mg·mL$^{-1}$ in sample buffer [0.1 M Tris−HCl, pH 6.8; 20% (v/v) glycerol, 2% (v/v) SDS, 5% (v/v) $\beta$-mercaptoethanol, and 0.01% bromophenol blue]. Tubes were moderately shaken on a "wrist action" shaker for 30 min and then heated in water (95 °C) for 5 min. SDS−PAGE was carried out as originally proposed by Laemmli (1970)[22] on a 15% (w/v) separating gel, and sample aliquots of 5 $\mu$L were loaded per well at a Mini Protean Tetra Cell cube (Bio-Rad Laboratories Inc., Hercules, CA). Gels were run at constant voltage (200 V) for 45 min. Molecular weight standards (MWS), consisting of a cocktail of proteins of known molecular weights (aprotinin, 6.5 kDa; lysozyme, 14.4 kDa; trypsin inhibitor, 21.5 kDa; carbonic anhydrase, 31 kDa; ovalbumin, 45 kDa; serum albumin, 66.2 kDa; phosphorylase b, 97.4 kDa; $\beta$-galactosidase, 116.25 kDa; myosin, 200 kDa) (Bio-Rad Laboratories Inc., Hercules, CA), were run together with cheese samples. MWS solution was prepared by diluting the standards 1:20 in sample buffer, followed by heating for 5 min at 95 °C. The solution was cooled, and an aliquot of 5 $\mu$L was loaded at the well. After electrophoresis, gels were stained for 16 h in Coomassie blue dye solution [0.3% (w/v) Coomassie blue R-250, 10% (v/v) acetic acid, and 40% (v/v) methanol] and then destained using 10% (v/v) acetic acid and 40% (v/v) methanol solution until the background color was completely removed. Gels were digitalized using a densitometer (Bio-Rad GS800) and the Quantity One 1-D Analysis software (Bio-Rad Laboratories Inc., Hercules, CA). Densitometry analyses were performed using lane-based background subtraction, followed by measurement of the spots by the area under the peaks. The values in optical density (OD) were then used for statistical analysis. Each sample was analyzed on duplicate gels. Proteins were identified by comparison of their relative mobilities with those of molecular weight standards and by comparison of electropherograms from previous reports.[16,17,20,23]

**Selection of a Marker Protein.** In order to identify a marker protein to evaluate the authenticity of Minas Frescal cheeses, the SDS−PAGE profiles of reference samples (processed as described above) were assessed. Milk powder and whey powder samples were also used as references. Milk powder and whey powder were weighed (10 mg), diluted in sample buffer (2.5 mL), and subjected to electrophoresis.

**Establishment of an Action Level.** Aiming to establish the level of the marker protein which can be accepted in authentic Minas Frescal cheeses, we assessed 42 commercial samples and five reference samples with SDS−PAGE. Optical density (OD) values were subjected to clustering using the $k$-means technique ($k$ = 2) and the R software.[24] The two groups formed were classified as compliant or noncompliant. From the compliant group's OD, an action level was then set as follows:

$$\text{action level} = X + 10s \quad (1)$$

where $X$ is the $\beta$-LG OD mean from compliant samples at cluster analysis and from reference samples and $s$ is standard deviation. Mean was obtained from duplicate determinations.

Aiming to obtain the concentration of the marker protein at the established action level, a reference sample was fortified with $\beta$-LG (six levels) and an analytical curve was built from concentrations (mg·g$^{-1}$ cheese) versus OD. Fortification was done by preparing a solution of freeze-dried cheese in sample buffer, to which the standard solution was added (at 0, 3.125, 6.25, 12.5, 25, and 50 mg·g$^{-1}$). The action level was then calculated in mg·g$^{-1}$ of cheese by linear regression from the theoretical concentrations of the fortified blank sample versus the respective OD.

**Performance Characteristics of Method.** Confirmation of identity of the marker protein, selectivity/specificity, limit of detection (LoD), and precision were assessed to evaluate the method's performance, as recommended by Eurachem (1998)[25] for qualitative methods.

**Confirmation of Identity of the Marker Protein and Selectivity/Specificity.** Protein spots corresponding to the selected marker were manually excised from stained gels obtained from whey and the reference sample. Spots were submitted to destaining in 400 $\mu$L of a 25 mM ammonium bicarbonate/acetonitrile solution (1:1, v/v). The solution was replaced by 200 $\mu$L of pure acetonitrile for 5 min and dried under vacuum for 15 min. The samples were incubated for 18 h at 37 °C in the presence of 10 $\mu$L of 0.01 $\mu$g·$\mu$L$^{-1}$ trypsin. The peptides were extracted by washing the gel pieces 3 times with 50% (v/v) acetonitrile and 5% (v/v) trifluoroacetic acid (TFA) solution, and then the supernatant containing digested peptides was transferred into clean tubes. The extract was dried under vacuum and solubilized in 0.1% TFA. Then 0.5 $\mu$L of sample was thoroughly mixed with 0.5 $\mu$L of a saturated matrix solution (10 mg of $\alpha$-cyano-4-hydroxycinnamic acid in 50% v/v acetonitrile, 1% v/v TFA, 49% water). This peptide matrix solution was spotted onto a target plate. The samples were then subjected to matrix assisted laser desorption ionization time-of-flight (MALDI-TOF) on an Autoflex III Smartbean mass spectrometer (Bruker Daltonics, Bremen, Germany) fitted with a 200 Hz Smartbeam pulsed nitrogen laser emitting at 337 nm and operated in reflectron mode. The extraction voltage was 19 kV. Spectral data were collected in the range of 700−3500 Da using positive ionization. Protein identification was performed by searching in the protein sequence database (Swiss-Prot) using the Mascot search engine (http://www.matrixscience.com). The following parameters were used for database search: taxonomy, mammalian; enzyme, trypsin; variable modifications, oxidized methionine; fragment mass tolerance, 0.5 Da; peptide charge, 1 H$^+$; precursor mass tolerance, 100 ppm. The search was initially performed on peptide mass fingerprinting method, and then the MS/MS Ion Search was used.

**Limit of Detection (LoD).** Limit of detection was established as follows:

$$\text{LoD} = X + 3s \quad (2)$$

where $X$ is the $\beta$-LG optical density mean from compliant commercial samples at cluster analysis and from reference samples and $s$ is


dx.doi.org/10.1021/jf502864e | J. Agric. Food Chem. 2014, 62, 8333−8339

standard deviation. LoD was then calculated in $mg \cdot g^{-1}$ of cheese by linear regression from the theoretical concentrations of fortified the blank sample versus the respective OD.

**Precision.** Both blank and fortified blank samples at concentrations below, at, and above the action level were randomly injected in electrophoresis gels. Blind analysis was carried out by two analysts, and then precision was assessed by calculating the rates of false positives/false negatives as follows:

$$\%\ \text{false positives} = \frac{\text{false positives} \times 100}{\text{total known negatives}} \quad (3)$$

$$\%\ \text{false negatives} = \frac{\text{false negatives} \times 100}{\text{total known positives}} \quad (4)$$

## RESULTS AND DISCUSSION

**SDS−PAGE Analysis.** The major proteins of the milk were individually resolved by SDS−PAGE and then visualized by Coomassie blue staining (Figure 1A). Our results show both typical milk and whey electrophoretic profiles and which major proteins could be identified, as caseins (molecular weight ranging from about 19 kDa to 25 kDa) and whey proteins such as $\beta$-LG (molecular weight of about 18.3 kDa) and $\alpha$-lactalbumin (molecular weight about 14 kDa), in accordance with those cited in the literature.[26,27] Moreover, some of milk's minor proteins, such as serum albumin, immunoglobulin G (IgG), and lactoferrin, were also resolved. As expected, the para-$\kappa$-casein peptide was present in all reference samples and in all authentic Minas Frescal cheese samples.

**Selection of a Marker Protein.** The broad objective in assessing food authentication is to identify markers to characterize the authenticity of food or their potential adulterants/contaminants and use them to resolve authenticity issues. The selected marker has to be specific, and its natural variation must be limited and well characterized.[28] Proteins have been widely used as adulteration markers in dairy products, allowing assessment of their animal species or even the irregular replacement of milk by whey.[11,12,29] In Minas Frescal, $\beta$-LG appeared with low optical density (Figure 1B). This behavior is expected, since milk clotting enzyme acts directly on casein, retaining it in the clot, while whey proteins are expelled with the aqueous phase.[30,31] Being the major protein in the composition of whey and in very low concentration in cheese, $\beta$-LG was chosen as the marker to assess the compositional authenticity of Minas Frescal with SDS−PAGE.

**Establishment of an Action Level.** A strong difference among the protein compositions of the samples was seen (Figure 2A). In 43% of samples ($n$ = 18), caseins appeared as moderately or slightly stained spots. This variable concentration is expected among noncompliant samples, suggesting that, when compositional adulteration occurs, milk is used in different combinations with whey. On the other hand, intense spots of $\beta$-LG can be seen. On the contrary, negligible amounts of $\beta$-LG can be seen in reference samples (Figure 2B). Since these commercial samples were declared by the producers as manufactured with milk, it can be assumed that, in white cheeses like Minas Frescal, a high concentration of $\beta$-LG suggests the use of whey as a raw material in its composition, which is inconsistent with the official regulation.[4]

Estimating a "basal value" is important when selecting an authenticity marker, since it can avoid natural errors in milk proteolysis, physiological responses related to feed and climate,

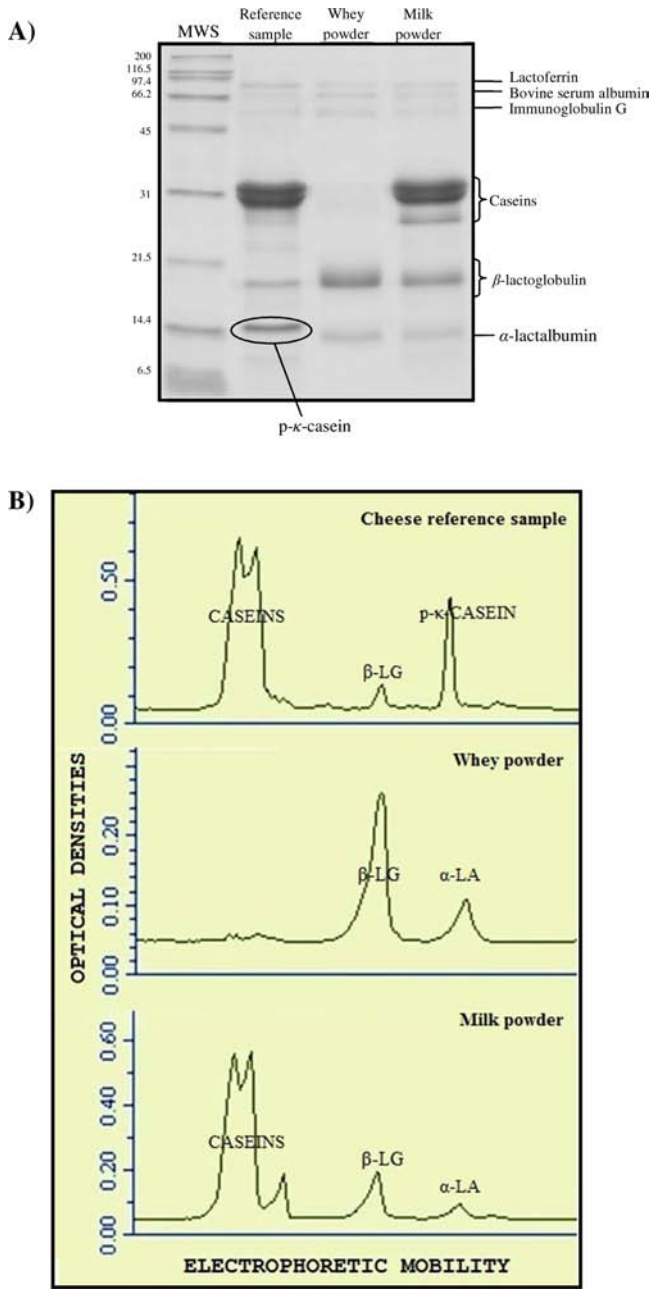


**Figure 1.** SDS−PAGE electrophoretic proteins profile of a Minas Frescal cheese reference sample, demineralized whey powder, and defatted milk powder (A) and respective densitograms (B). $\alpha$-LA: alfa-lactalbumin. $\beta$-LG: $\beta$-lactoglobulin. MWS: molecular weight standards (6.5 to 200 kDa).

and several other factors.[11] The presence/absence of an analyte is not considered to be an absolute measure related to a concentration level of zero but to a specific concentration level.[32] Below this limiting level, analyte concentration is considered insignificant and intrinsic of the sample's composition. In this study, the proposal of an action level aimed to set the maximum OD for the marker protein ($\beta$-LG) in a sample of cheese to be considered compliant (i.e., produced from coagulated milk enzyme). Previously, we tried to establish a casein/$\beta$-LG ratio from the densitometry analysis of cheeses, as a way to distinguish compliant from non-compliant Minas Frescal samples.[7] Although samples could be divided by cluster analysis into two significantly different


dx.doi.org/10.1021/jf502864e | J. Agric. Food Chem. 2014, 62, 8333−8339

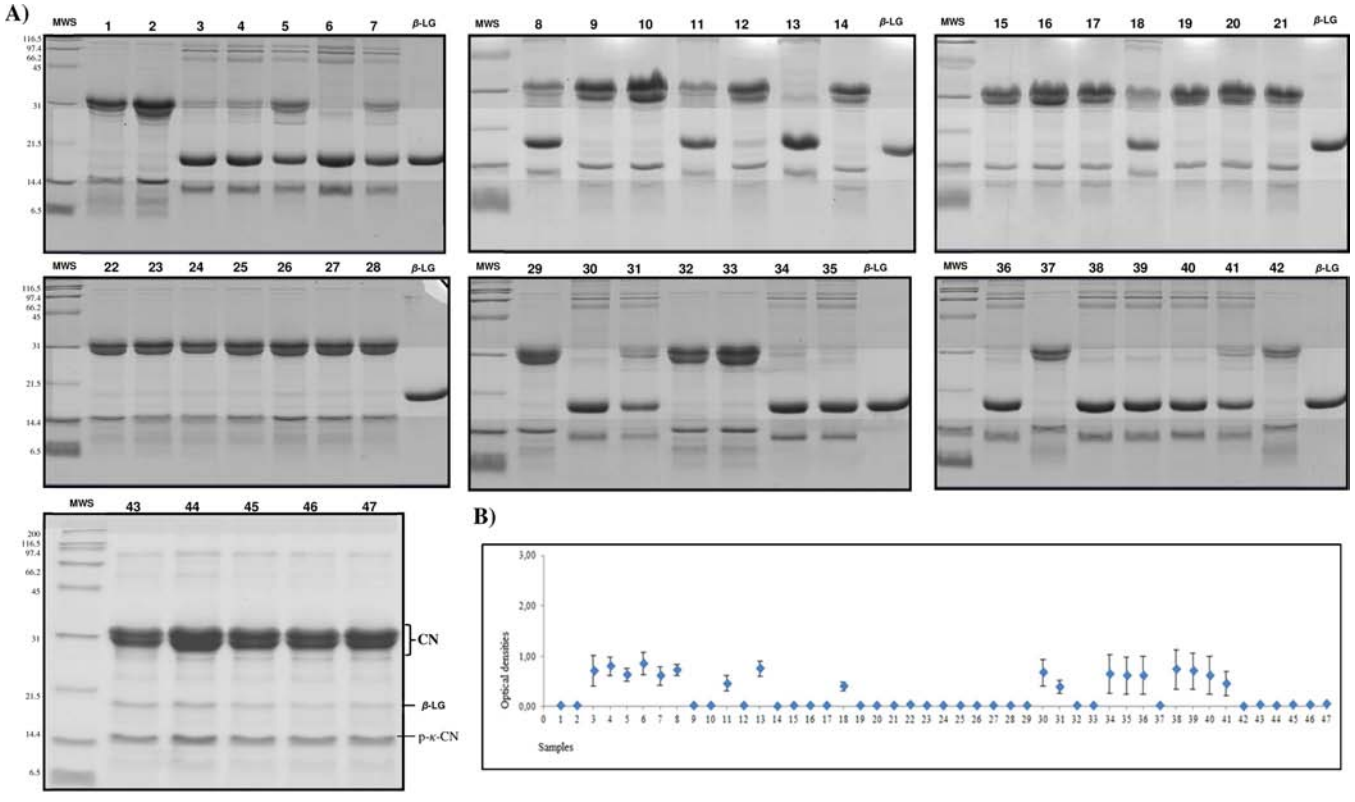


**Figure 2.** SDS−PAGE electrophoretic profiles (A) and mean values ($n$ = 2) of $\beta$-LG optical densities (B) from commercial samples (lanes 1−42) and from reference samples (lanes 43−47) of Minas Frescal cheese. MWS: molecular weight standards (6.5 to 200 kDa). $\beta$-LG: $\beta$-lactoglobulin. CN: caseins. p-$\kappa$-CN: para-kappa-casein.

groups, the wide variation led to set a single adulteration marker instead of calculating a cutoff value for this ratio.

Optical densities for the $\beta$-LG spots from both commercial and reference samples are shown in Figure 2B. Although a wide variation can be observed, cluster analysis revealed two distinct groups: compliant (group A) and noncompliant (group B). As expected, group A consisted of the reference samples and of most commercial cheeses (samples 1, 2, 9, 10, 12, 14−17, 19−29, 32, 33, 37, 42). This cluster showed low OD for the $\beta$-LG spot, ranging from 0.01 to 0.04. On the other hand, group B consisted of the reference samples and most of the commercial samples (samples 3−8, 11, 13, 18, 30, 31, 34−36, 38−41) which showed higher densities for that protein, ranging from 0.39 to 0.85. OD values ranging from 0.04 to 0.39 have not been observed for any sample. Since compliant Minas Frescal cheeses tended to present low OD for $\beta$-LG, an action level, based on the mean value (OD = 0.02) presented by this cluster plus the standard deviation multiplied by 10, could be set. Thus, compliant/noncompliant cheeses can be easily distinguished. Linear regression from the theoretical concentrations of fortified blank samples versus the respective OD resulted in the calculation of the concentration of $\beta$-LG at the action level (14 mg·g$^{-1}$). The results shown in Figure 3 indicated that the intensity of the $\beta$-LG spot was almost linearly related to the concentration of the analyte ($R^2$ = 0.992). A qualitative method must respond to either the presence or absence of the analyte detected either directly or indirectly in a certain amount of sample.[33] The final decision is made by comparing the response of a test sample to the response of a reference sample containing the analyte at the action level. Since the cutoff concentration (action level) has been set, a blank sample fortified with $\beta$-LG must be assessed at the same gel in which unknown samples are being analyzed. If an unknown sample has a higher OD than the fortified sample, it is considered to be positive (noncompliant), and whey must have been used in replacement of milk. On the other hand, if $\beta$-LG OD is lower than fortification, the sample is considered to be negative (compliant), and milk is presumed to have been properly processed.

**Performance Characteristics of Method.** Table 1 shows the results obtained during performance assessment for this qualitative method. By the position of the $\beta$-LG spots in terms of molecular weight and the peptide mass fingerprints obtained by MALDI-TOF mass spectrometry, identification was provided (Figure 4). The use of confirmatory techniques can be useful as a means of verifying the analyte's identity and so to assess the selectivity/specificity of a proposed method.[25] By matching the peptide masses generated following the trypsin digestion with those available in the database, the selected spots were successfully identified as homologous to *Bos taurus* $\beta$-LG, one of bovine milk's major proteins. Significant ($p$ < 0.05) protein scores were obtained (Mascot score = 146). To confirm the identification of $\beta$-LG, the MS/MS spectra of three greater intensity peptides ($m/z$ 837; 1635; 2313) were obtained. A total of 17 peptides matched with 80% of the $\beta$-LG sequence (Table 2). A number of unidentified peaks may represent contaminants from the gel, Coomassie staining, trypsin, or the matrix used. Mass spectrometry provides unequivocal molecular mass identification of peptides. The main advantages of MALDI are rapidity, simplicity, and sensitivity, especially if compared to electrophoretic and chromatographic techniques.[34] Recently, the combination of two-dimensional electro-

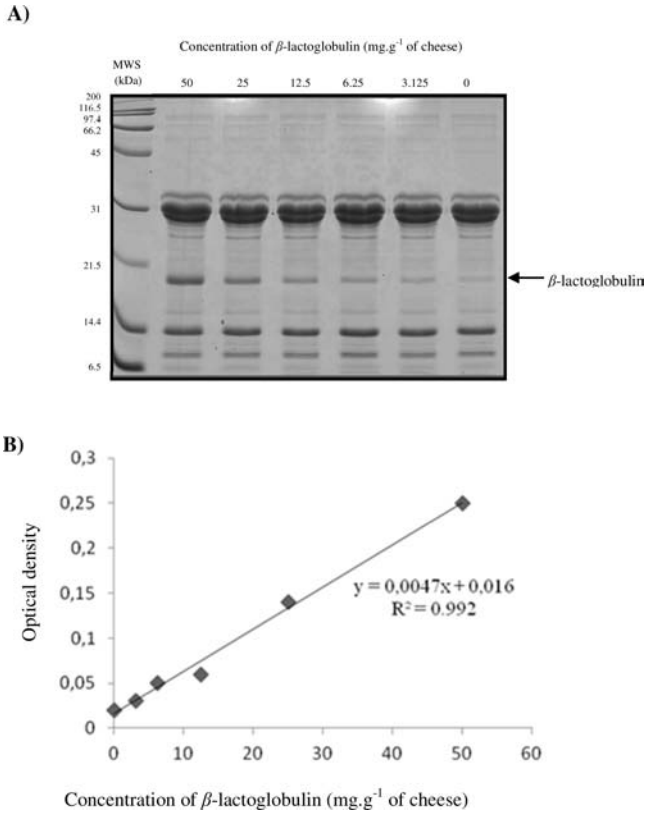


**Figure 3.** Electrophoretic profile (A) and linear regression (B) from a blank sample of Minas Frescal cheese fortified with $\beta$-lactoglobulin in different concentrations versus the respective optical density. MWS: molecular weight standards (6.5 to 200 kDa).

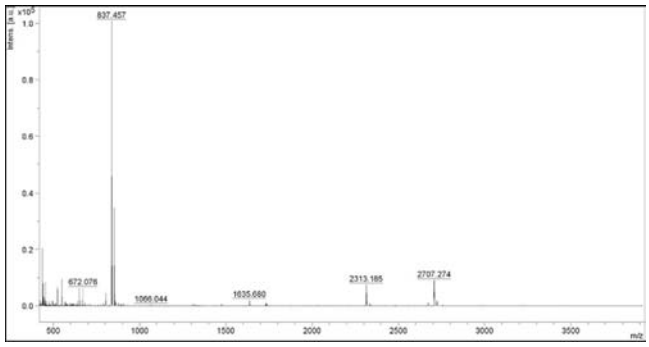

**Figure 4.** Matrix assisted laser desorption ionization time-of-flight (MALDI-TOF) mass spectrum of *Bos taurus* $\beta$-lactoglobulin after in gel digestion with trypsin.

**Table 2. Theoretical (Expected) and Experimental (Detected) $\beta$-Lactoglobulin Peptides ($m/z$) Obtained by Tryptic Digestions in Solution**

| | $M_r$ | |
|---|---|---|
| sequence | expected tryptic peptides[a] (calcd) | detected tryptic peptides (detected) |
| 3–24 | 2274.25 | 2275.28 |
| 25–30 | 672.38 | 673.43 |
| 31–56 | 2706.36 | 2707.27 |
| 57–76 | 2312.25 | 2313.18 |
| 86–91 | 700.44 | 701.47 |
| 87–93 | 801.49 | 802.96 |
| 92–99 | 902.55 | 903.52 |
| 94–99 | 673.41 | 674.47 |
| 94–107 | 1570.87 | 1571.96 |
| 100–107 | 915.46 | 916.56 |
| 108–116 | 1064.57 | 1066.04 |
| 108–117 | 1192.67 | 1193.59 |
| 141–151 | 1244.57 | 1245.44 |
| 141–154 | 1634.76 | 1635.68 |
| 155–164 | 1148.68 | 1149.73 |
| 158–164 | 836.46 | 837.45 |
| 165–178 | 1657.77 | 1657.67 |

[a]Theoretical digestion performed at Protein Prospector (http://prospector.ucsf.edu/prospector/mshome.htm).

phoresis and MALDI-TOF mass spectrometry was also applied to identify an adulteration marker in mozzarella.[12]

The LoD was set to 7 mg·g$^{-1}$, which corresponds to the lowest concentration of the analyte that can be confidently detected by this method. The method presented good precision, since neither false positives nor false negatives have been detected by any analyst below (7 mg·g$^{-1}$), at (14 mg·g$^{-1}$), and above (28 mg·g$^{-1}$) the action level. During the precision assessment, the chosen concentrations for $\beta$-LG fortification were considerably lower than the detected concentrations at the adulterated commercial samples, probably because whey is being deliberately used as a noncompliant raw material (Figure 2). Thus, it must be concluded that, when adulteration with whey is practiced during the manufacturing of Minas Frescal cheese, the concentration for $\beta$-LG is consistently higher than the action level set by the present method. Moreover,

**Table 1. Validation Data for the Qualitative Control Method To Inspect Compositional Authenticity of Minas Frescal Cheese by Gel Electrophoresis**

| validation parameter | methodology | results |
|---|---|---|
| precision | blind analysis of blank ($n$ = 3) and fortified blank samples ($n$ = 3/concentration) at concentrations below (7.0 mg·g$^{-1}$), at (14.0 mg·g$^{-1}$), and above (28.0 mg·g$^{-1}$) the action level by two analysts | FP = 0; FN = 0 (A1)[a] FP = 0; FN = 0 (A2)[a] |
| selectivity/ specificity | mass spectrometric characterization | confirmed identity for *Bos taurus* $\beta$-lactoglobulin (Mascot score = 146, sequence coverage = 80%, with 17 matching peptides) |
| limit of detection (LoD) | LoD = $X$ + 3$s$[b] | $s$ = 0.006, LoD = 7 mg·g$^{-1}$ |
| action level | action level = $X$ + 10$s$[b] | $s$ = 0.006, action level = 14 mg·g$^{-1}$ |

[a]FP = false positives; FN = false negatives; A1 = analyst 1; A2 = analyst 2. [b]$X$ = $\beta$-LG optical density mean from compliant commercial samples at cluster analysis and from reference samples; $s$ = standard deviation.


dx.doi.org/10.1021/jf502864e | J. Agric. Food Chem. 2014, 62, 8333–8339

adulteration with whey may be a common, underestimated feature in the processing of white nonripened cheeses. This situation may offer economic profit, since whey is cheaper than milk. As previously reported, when adulterated with whey, Minas Frescal cheeses assume some Ricotta-like properties, presenting a yellowish white color, lower moisture content, and less deformability and tending to be more viscous than elastic.[7] In fact, due to the impossibility of clotting the whey, it can be inferred that heating is employed during the fraud, in a very similar way to Ricotta processing. Adulterated products are then mislabeled, and milk is falsely declared as being used as raw material. Considering the difficulty of identifying this noncompliant practice during factory inspection, laboratory support and availability of a method to detect adulteration of Minas Frescal cheese compositional authenticity is quite convenient.

The proposed method in the present work has been successfully applied in our laboratory and constitutes a simple control tool to inspect Minas Frescal cheese compositional authenticity, being helpful to official dairy inspection. The main advantages of this method rely on the low cost and reasonable simplicity of SDS−PAGE, and the possibility of simultaneous analyzing of several samples. Noncompliant products (43%) were detected, enlightening the need for proper analytical monitoring in order to inhibit this practice.

## AUTHOR INFORMATION


### Corresponding Author

*Ministério da Agricultura, Pecuária e Abastecimento, Rua João Grumiché, 117, São José, SC 88102-600, Brazil. Phone: +55 48 3261 9918. E-mail: heitor.daguer@agricultura.gov.br.



### Funding

The present work was financially supported by CNPq (Conselho Nacional de Desenvolvimento Científico e Tecnológico), RENALI (Rede Nacional de Análise de Alimentos), and Ministério da Agricultura, Pecuária e Abastecimento.


### Notes

The authors declare no competing financial interest.

## ACKNOWLEDGMENTS


We dedicate and acknowledge Daniel Macedo Lorenzini (in memoriam) for this work, whose contribution and technical supervision was invaluable for its realization. MALDI-TOF mass spectrometry was carried out by Centro de Biologia Molecular e Estrutural (CEBIME) at Universidade Federal de Santa Catarina. We acknowledge Hernán Terenzi for this facility and Martina Blank for performing peptide identification.


## REFERENCES


(1) Planzer, S. B., Jr.; Da Cruz, A. G.; Sant'Ana, A. S.; Moura, M. R. L.; Carvalho, L. M. J. Food Safety Knowledge of Cheese Consumers. *J. Food Sci.* **2009**, *74*, 28−30.

(2) Naldini, M. C. M.; Viotto, W. H.; Kuaye, A. Y. Behaviour of Listeria monocytogenes inoculated into Minas Frescal cheese made by direct acidification or lactic culture during refrigerated storage. *Int. J. Dairy Technol.* **2009**, *62*, 361−365.

(3) Souza, C. H. B.; Saad, S. M. I. Viability of Lactobacillus acidophilus La-5 added solely or in co-culture with a yoghurt starter culture and implications on physico-chemical and related properties of Minas fresh cheese during storage. *LWT—Food Sci. Technol.* **2009**, *42*, 633−640.

(4) Brasil. Ministério da Agricultura, Pecuária e Abastecimento. *Instrução Normativa n° 4, de 01 de março de 2004. Altera o regulamento técnico de identidade e qualidade do queijo Minas Frescal*. Available at http://www.agricultura.gov.br (retrieved Dec 7, 2013).

(5) De La Fuente, M. A.; Juarez, M. Authenticity assessment of dairy products. *Crit. Rev. Food Sci. Nutr.* **2005**, *45*, 563−585.

(6) Hruzikova, J.; Milde, D.; Krajankova, P.; Ranc, V. Discrimination of cheese products for authenticity control by infrared spectroscopy. *J. Agric. Food Chem.* **2012**, *60*, 1845−1849.

(7) Magenis, R. B.; Prudêncio, E. S.; Fritzen-Freire, C. B.; Stephan, M. P.; Egito, A. S.; Daguer, H. Rheological, physicochemical and authenticity assessment of Minas Frescal cheese. *Food Control* **2014**, *45*, 22−28.

(8) Recio, I.; García-Risco, M. R.; López-Fandiño, R.; Olano, A.; Ramos, M. Detection of rennet whey solids in UHT milk by capillary electrophoresis. *Int. Dairy J.* **2000**, *10*, 333−338.

(9) European Commission. Commission Regulation (EC) No. 273/2008 of 5 march 2005 laying down detailed rules for the application of Council Regulation (EC) N° 1255/1999 as regards methods for the analysis and quality evaluation of milk and milk products. *Off. J. Eur. Union* **2008** L 81/53, 29.3.2008.

(10) Spoljaric, J.; Mikulec, N.; Plavljanic, D.; Radeljevic, B.; Havranek, J.; Antunac, N. Proving the adulteration of ewe and goat cheese. *Mljekarstvo* **2013**, *63*, 115−121.

(11) Motta, T. M. C.; Hoff, R. B.; Barreto, F.; Andrade, R. B. S.; Lorenzini, D. M.; Meneghini, L. Z.; Pizzolato, T. M. Detection and confirmation of milk adulteration with cheese whey using proteomic-like sample preparation and liquid chromatography-electrospray-tandem mass spectrometry analysis. *Talanta* **2014**, *120*, 498−505.

(12) Faccia, M.; Trani, A.; Loizzo, P.; Gagliardi, R.; La Gatta, B.; Di Luccia, A. Detection of $\alpha_{s1}$-I casein in mozzarella Fiordilatte: A possible tool to reveal the use of stored curd in cheesemaking. *Food Control* **2014**, *42*, 101−108.

(13) Brasil. Ministério da Agricultura, Pecuária e Abastecimento. *Decreto n° 5.741, de 30 de março de 2006. Regulamenta os artigos 27-A, 28-A e 29-A da Lei n 8.171, de 17 de janeiro de 1991, organiza o Sistema Unificado de Atenção à Sanidade Agropecuária, e dá outras providências.* Available at http://www.agricultura.gov.br (retrieved Jan 10, 2014).

(14) Miralles, B.; Bartolomé, B.; Ramos, M.; Amigo, L. Determination of whey protein to total protein ratio in UHT milk using fourth derivative spectroscopy. *Int. Dairy J.* **2000**, *10*, 191−197.

(15) Pesic, M.; Barac, M.; Vrvic, M.; et al. Qualitative and quantitative analysis of bovine milk adulteration in caprine and ovine milks using native-PAGE. *Food Chem.* **2011**, *125*, 1443−1449.

(16) Alomirah, H. F.; Alli, I. Separation and characterization of $\beta$-lactoglobulin and $\alpha$- lactalbumin from whey and whey protein preparations. *Int. Dairy J.* **2004**, *14*, 411−419.

(17) Patel, H. A.; Singh, H.; Anema, S. G.; Creamer, L. K. Effects of Heat and High Hydrostatic Pressure Treatments on Disulfide Bonding Interchanges among the Proteins in Skim Milk. *J. Agric. Food Chem.* **2006**, *54*, 3409−3420.

(18) Patel, H. A.; Anema, S. G.; Holroyd, S. E.; Singh, H.; Creamer, L. K. Methods to determine denaturation and aggregation of proteins in low-, medium- and high-heat skim milk powders. *Lait* **2007**, *87*, 251−268.

(19) Jovanovic, S.; Barac, M.; Macej, O.; Vucic, T.; Lacnjevac, C. SDS-PAGE analysis of soluble proteins in reconstituted milk exposed to different heat treatments. *Sensors* **2007**, *7*, 371−383.

(20) Outinen, M.; Heino, A.; Uusi-Rauva, J. Pre-treatment methods of Edam cheese milk. Effect on the whey composition. *LWT—Food Sci. Technol.* **2010**, *43*, 647−654.

(21) Puglisi, I.; Petrone, G.; Lo Piero, A. R. A kiwi juice aqueous solution as coagulant of bovine milk and its potential in Mozzarella cheese manufacture. *Food Bioprod. Process.* **2014**, *92*, 67−72.

(22) Laemmli, U. K. Cleavage of structural proteins during the assembly of the head of bacteriophage T4. *Nature* **1970**, *227*, 680−685.

(23) Basch, J. J.; Douglas, F. W., Jr.; Procino, L. G.; Holsinger, V. H.; Farrell, H. M., Jr. Quantitation of Caseins and Whey Proteins of

Processed Milks and Whey Protein Concentrates, Application of Gel Electrophoresis, and Comparison with Harland-Ashworth Procedure. *J. Dairy Sci.* **1985**, *68*, 23−31.
(24) R Core Team. R: A language and environment for statistical computing. R Foundation for Statistical Computing, Vienna, Austria, 2013. ISBN 3-900051-07-0, URL http://www.R-project.org/ (retrieved Nov 20, 2013).
(25) Eurachem. *The Fitness for Purpose of Analytical Methods. A Laboratory Guide to Method Validation and Related Topics*. Eurachem: 1998. Available at http://www.eurachem.org/images/stories/Guides/pdf/valid.pdf (retrieved Jun 2, 2013).
(26) Farrell, H. M., Jr.; Jimenez-Flores, R.; Bleck, G. T.; et al. Nomenclature of the proteins of cows' milk-sixth revision. *J. Dairy Sci.* **2004**, *87*, 1641−1674.
(27) Smolenski, G.; Haines, S.; Kwan, F.Y.-S.; Bond, J.; Farr, V.; Davis, S. R.; Stelwagen, K.; Wheeler, T. Characterisation of host defense proteins in milk using a proteomic approach. *J. Proteome Res.* **2007**, *6*, 207−215.
(28) Primrose, S.; Woolfe, M.; Rollinson, S. Food forensics: methods for determining the authenticity of foodstuffs. *Trends Food Sci. Technol.* **2010**, *21*, 582−590.
(29) Mafra, I.; Ferreira, I. M. P. L. V. O.; Oliveira, M. B. P. P. Food authentication by PCR-based methods. *Eur. Food Res. Technol.* **2008**, *227*, 649−665.
(30) Hinrichs, J. Incorporation of whey proteins in cheese. *Int. Dairy J.* **2001**, *11*, 495−503.
(31) De La Fuente, M. A.; Singh, H.; Hemar, Y. Recent advances in the characterization of heat-induced aggregates and intermediates of whey proteins. *Trends Food Sci. Technol.* **2002**, *13*, 262−274.
(32) Trullols, E.; Ruisánchez, I.; Rius, F. X. Validation of qualitative analytical methods. *TrAC, Trends Anal. Chem.* **2004**, *23*, 137−145.
(33) Feldsine, P.; Abeyta, C.; Andrews, W. H. AOAC International Methods Committee guidelines for validation of qualitative and quantitative food microbiology. *J. AOAC Int.* **2002**, *85*, 1187−1200.
(34) Calvano, C. D.; Monopoli, A.; Loizzo, P.; Faccia, M.; Zambonin, C. Proteomic approach based on MALDI-TOF MS to detect powdered milk in fresh cow's milk. *J. Agric. Food Chem.* **2012**, *61*, 1609−1617.

JOURNAL OF AGRICULTURAL AND FOOD CHEMISTRY

Article

pubs.acs.org/JAFC

# Simple and Fast Method for Iron Determination in White and Red Wines Using Dispersive Liquid–Liquid Microextraction and Ultraviolet–Visible Spectrophotometry

Juliana V. Maciel,[†] Bruno M. Soares,[†] Jaime S. Mandlate,[†] Rochele S. Picoloto,[‡] Cezar A. Bizzi,[‡] Erico M. M. Flores,[‡] and Fabio A. Duarte*,[‡]

[†]Escola de Química e Alimentos, Universidade Federal do Rio Grande, Rio Grande, Rio Grande do Sul 96203-900, Brazil

[‡]Departamento de Química, Universidade Federal de Santa Maria, Santa Maria, Rio Grande do Sul 97105-900, Brazil

**ABSTRACT:** This work reports the development of a method for Fe extraction in white and red wines using dispersive liquid–liquid microextraction (DLLME) and determination by ultraviolet–visible spectrophotometry. For optimization of the DLLME method, the following parameters were evaluated: type and volume of dispersive (1300 $\mu$L of acetonitrile) and extraction (80 $\mu$L of $C_2Cl_4$) solvents, pH (3.0), concentration of ammonium pyrrolidinedithiocarbamate (APDC, 500 $\mu$L of 1% m/v APDC solution), NaCl concentration (not added), and extraction time. The calibration curve was performed using the analyte addition method, and the limit of detection and relative standard deviation were 0.2 mg $L^{-1}$ and below 7%, respectively. The accuracy was evaluated by comparison of results obtained after Fe determination by graphite furnace atomic absorption spectrometry, with agreement ranging from 94 to 105%. The proposed method was applied for Fe determination in white and red wines with concentrations ranging from 1.3 to 4.7 mg $L^{-1}$.

**KEYWORDS:** *dispersive liquid–liquid microextraction, iron, wine, UV–vis spectrophotometry, food analysis, sample preparation, GFAAS*

## INTRODUCTION

Wine is defined as a beverage obtained exclusively by alcoholic fermentation of grapes.[1] With regard to its chemical composition, wine has a great concern considering nutritional and toxicological aspects, because it is a worldwide consumed beverage.[2] Among the main components present in wine, some of them can be cited as volatile organic compounds (ethanol), non-volatile organic compounds (superior alcohols, sugars, organic acids/salts, and others) and major and trace elements.[3] The presence of metals in wine can be originated from natural and/or anthropogenic sources.[2] The range and level of inorganic compounds in wine depends upon several factors, such as the type of grape, soil characteristics, environmental conditions, and contamination during the manufacturing process.[4]

Iron is an essential element, which plays an important role in biological systems, participating in the maintenance of cellular homeostasis and several metabolic and fermentation processes, such as enzymatic activator, stabilizer, or as a functional component of proteins. Iron deficiency leads manly to anemia, causing changes in muscle metabolism and dysfunctions in the immunological system.[5] Otherwise, excess of Fe cause hemochromatosis, characterized by pigmentation in the skin, pancreatic injury, such as diabetes, cirrhosis, and others.[6] The presence of iron (ferric salts) in wine may cause cloudiness and precipitation, which modify organoleptic characteristics.[7]

In general, detection techniques, such as flame atomic absorption spectrometry (FAAS),[7] graphite furnace atomic absorption spectrometry (GFAAS),[8] and inductively coupled plasma–optical emission spectrometry (ICP–OES),[9] have been applied for Fe determination in wine samples. Although there are a few works reporting ultraviolet–visible (UV–vis) spectrophotometry for the determination of Fe in wine, it is a useful technique and stands out mainly by its availability, simplicity, and relatively low cost when compared to other spectrometric techniques already cited.[10] However, the direct element determination at low concentrations by UV–vis is often difficult because of its insufficient sensitivity and selectivity. Besides, some wines (especially the red wines) show an intense color, which causes several interferences for UV–vis detection.[11] Therefore, a prior extraction and preconcentration step is convenient, especially for matrix removal. Thus, many sample preparation methods, such as solid-phase extraction (SPE),[7] cloud point extraction (CPE),[12,13] and liquid–liquid extraction (LLE),[14,15] have been evaluated for subsequent element determination in wine. However, some of these methods demand excessive solvent consumption, high waste generation, and long extraction times.

Recently, dispersive liquid–liquid microextraction (DLLME) was developed[16] as an alternative for conventional LLE. This method shows some advantages, such as simplicity, quickness, low waste generation, and good enrichment factors.[17] Initially, DLLME was employed for the extraction of organic analytes from aqueous samples.[16] However, it has recently been applied for element extraction[18] and selected chemical species.[19] It is important to mention that, when DLLME is applied for

Received: May 2, 2014
Revised: July 18, 2014
Accepted: July 29, 2014
Published: July 29, 2014

ACS Publications © 2014 American Chemical Society



dx.doi.org/10.1021/jf5019774 | J. Agric. Food Chem. 2014, 62, 8340–8345

extraction of elements (or their species), it is necessary to perform a chemical modification (addition of a complexant agent), which results in a complex with affinity by extraction solvent, which can be easily extracted.[20]

In this sense, the aim of this work was to develop a method for Fe extraction in white and red wine samples using DLLME to allow for the determination by UV−vis. Some parameters, such as type and volume of dispersive and extraction solvents, pH, complexant agent [ammonium pyrrolidinedithiocarbamate (APDC)] concentration, NaCl concentration, and extraction time, were exhaustively investigated. The optimized method was applied for Fe determination in commercial white and red wine samples. For accuracy evaluation, Fe was also determined by GFAAS in all samples after sample digestion.

## 2. EXPERIMENTAL SECTION

**2.1. Instrumentation.** Iron determination was performed in a Shimadzu UV−vis spectrophotometer (model UV-2550, Japan) with 1.0 cm quartz microcells. Iron was determined [as a complex of $Fe(APDC)_3$] at 587 nm using peak height.[18]

For results comparison, a graphite furnace atomic absorption spectrometer (model AAnalyst 800, PerkinElmer, Waltham, MA) equipped with a Zeeman-effect background correction system and an auto sampler (model AS 800, PerkinElmer) were used for the analysis of wine samples previously digested with nitric acid. Transversely heated pyrolytically coated graphite tubes using standard platforms were used throughout. A Fe hollow cathode lamp (Hamamatsu Photonics, Japan) was (248.3 nm). The spectral bandpass was set at 0.2 nm. The main conditions of the heating program were optimized, and the follow temperatures were chosen: drying 1, ramp of 15 °C $s^{-1}$ up to 90 °C and hold for 15 s; drying 2, ramp of 5 °C $s^{-1}$ up to 130 °C and hold for 10 s; pyrolysis, ramp of 15 °C $s^{-1}$ up to 1300 °C and hold for 20 s; atomization, ramp of 2000 °C $s^{-1}$ up to 2400 °C and hold for 6 s; and clean out, ramp of 500 °C $s^{-1}$ up to 2500 °C and hold for 3 s. Results were obtained using integrated absorbance (peak area), with 20 $\mu$L of reference solutions or sample extract and 5 $\mu$L of 1000 mg $L^{-1}$ Pd solution (Merck, Germany), which were injected into the graphite tube. Argon (99.999%, White Martins, Brazil) was used as the purge gas. Wine samples were digested in a heating block with open vessels. About 2 mL of sample were transferred to the vessels and submitted to a step for alcohol removal (80 °C for 2 h). After cooling, 4 mL of concentrated $HNO_3$ was added, followed by heating at 80 °C for 1 h and 120 °C for 1 h. After cooling, the digests were diluted with ultrapure water up to 50 mL for further Fe determination by GFAAS.

A centrifuge (model 80-2B, Centribio, Brazil) with 15 mL calibrated centrifuge tubes was used for separation of phases after the DLLME procedure. The pH was adjusted using HCl or NaOH solutions with a Hanna pH meter (model pH21, Brazil).

**2.2. Reagents.** All reagents used in this work were of analytical grade. Ultrapure water was purified by a Direct-Q UV3 purification system (resistivity of 18.2 MΩ cm, Millipore, Billerica, MA). Stock reference solutions of 100 mg $L^{-1}$ Fe were prepared by dissolving an appropriate amount of $FeNH_4(SO_4)_2{\cdot}12H_2O$ (Vetec, Brazil) in 1.0 mol $L^{-1}$ HCl (Merck). Other reference solutions were prepared daily by serial dilution of stock solution in ultrapure water. The complexant agent (APDC, purity of 99%, Sigma-Aldrich, St. Louis, MO) was prepared by dissolving an appropriate amount of this reagent in ultrapure water. Dichlorobenzene ($C_6H_4Cl_2$, $d$ = 1.30 g $mL^{-1}$), carbon tetrachloride ($CCl_4$, $d$ = 1.59 g $mL^{-1}$), monochlorobenzene ($C_6H_5Cl$, $d$ = 1.11 g $mL^{-1}$), and tetrachloroethylene ($C_2Cl_4$, $d$ = 1.62 g $mL^{-1}$) were evaluated as extraction solvents and purchased from Vetec. Acetone, acetonitrile, ethanol, methanol, and tetrahydrofuran (THF) were evaluated as dispersive solvents and obtained from J.T.Baker (Center Valley, PA). Solutions of 0.1 mol $L^{-1}$ HCl and 0.1 mol $L^{-1}$ NaOH (both Merck) were used to adjust the pH of wine samples. All materials used in this work were previously cleaned by immersion in 20% (v/v) $HNO_3$ (Merck) solution for 24 h and washed with ultrapure water.

**2.3. Samples.** Samples used in this work (two samples of white wine and five samples of red wine) were produced and purchased in Rio Grande do Sul State (Brazil). All samples were stored in glass bottles in the dark at room temperature and were named as WW1 and WW2 (white wine) and RW1, RW2, RW3, RW4, and RW5 (red wine). The alcohol content of samples ranged from 10 to 13.4%. Sample WW1 (1 mL of sample, pH adjustment and dilution up to 5 mL with water) was used for method optimization.

**2.4. DLLME Optimization.** Initially, experiments were performed to evaluate the wavelength with a maximum absorbance signal and less susceptible to interferences on Fe determination by UV−vis. The formation of the sedimented phase using all possible combinations between extraction and dispersive solvents was evaluated. Some parameters of DLLME, such as type of dispersive solvent (acetone, acetonitrile, ethanol, methanol, and THF), volume of dispersive solvent (100−1500 $\mu$L), type of extraction solvent ($C_6H_4Cl_2$, $CCl_4$, $C_6H_5Cl$, and $C_2Cl_4$), volume of extraction solvent (20−160 $\mu$L), pH (2−4), APDC concentration (0.1−3%, m/v), extraction time (0.5−5 min), and NaCl concentration (0−0.5 mol $L^{-1}$), were evaluated. For these experiments, samples were spiked with a Fe(III) solution up to a final Fe concentration of 2 mg $L^{-1}$, and results were shown as Fe recovery (%). Even considering the natural Fe concentration, samples were spiked to ensure the detectability of analyte and to allow for a suitable comparison of extraction conditions.

**2.5. DLLME Procedure.** Aliquots of 1 mL of wine and 500 $\mu$L of APDC solution were placed in a 15 mL glass tube with a conic bottom and diluted up to 5 mL with ultrapure water. The pH was adjusted with HCl or NaOH solutions. A mixture containing the dispersive and extraction solvent was quickly injected into the sample solution with aid of a 2.5 mL microsyringe. After injection, a cloudy solution was formed, which was centrifuged at 3000 rpm for 3 min, and small droplets of extraction solvent containing the complexed analyte [$Fe(APDC)_3$] were deposited at the bottom of the glass tube. To reduce some interference during the measurements, the sedimented phase (extract) was washed with ultrapure water (3 mL and centrifugation at 3000 rpm for 3 min). The aqueous phase was removed, and extract was further diluted up to 3 mL with acetonitrile for subsequent Fe determination by UV−vis.

All statistical calculations were performed using GraphPad InStat software (GraphPad InStat Software, Inc., version 3.06). A significance level of 95% was adopted for all comparisons.

## 3. RESULTS AND DISCUSSION

Initially, experiments were performed to find the spectral region with maximum absorbance for the $Fe(APDC)_3$ complex. In a previous study of our group,[18] APDC was used for complexation of Fe(II) and Fe(III) species. It was observed that Fe(III) is instantaneously complexed by APDC, while Fe(II) is complexed by APDC and quickly oxidized to Fe(III), making it difficult to perform Fe speciation analysis.[18] It was observed [using an aqueous solution containing Fe(III) and APDC] that $Fe(APDC)_3$ complex shows one absorption band in UV region (wavelength of maximum absorbance at 354.0 nm) and two absorption bands in visible region (wavelengths of maximum absorbance at 499.0 and 587.0 nm). Although the most intense absorption band was in the UV region (data not shown), it was highly influenced by the absorption band of APDC, making the use of this wavelength difficult for analytical purposes. Thus, to minimize possible interferences, the wavelength of 587.0 nm was selected for Fe determination by UV−vis.

**3.1. Effect of the Type of Extraction and Dispersive Solvents.** The choice of dispersive and extraction solvents is essential to obtain suitable analyte recoveries using DLLME. The extraction solvent should have the ability to extract the analytes and present low solubility in water.[21] Initially, several combinations between extraction and dispersive solvents were qualitatively evaluated (results not showed) for red and white

wines. The main parameters to choose the solvents that were used for subsequent experiments were taken into account, with the minimum amount of solids around the drop and the minimum undesirable effects (e.g., changes in baseline) during measurements by UV−vis. In this case, solvents with higher density than water, such as dichlorobenzene, carbon tetrachloride, monochlorobenzene, and tetrachloroethylene, were evaluated as the extraction solvent. These solvents were investigated using 50 $\mu$L of extraction solvent combined with 500 $\mu$L of acetonitrile as the dispersive solvent. As showed in Figure 1, the higher recovery (48%) was found using

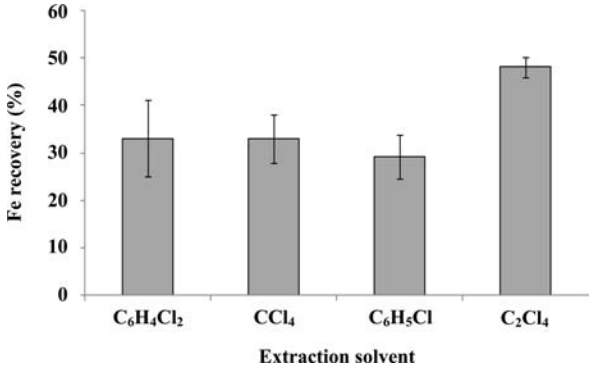


**Figure 1.** Effect of the type of extraction solvent on Fe recovery. Conditions: 5 mL of white wine sample (5 times diluted), addition of 240 $\mu$L of 25 mg $L^{-1}$ Fe(III) solution, 500 $\mu$L of 1% APDC, 50 $\mu$L of extraction solvent, 500 $\mu$L of dispersive solvent (acetonitrile), and pH 3.3. The error bars represent the standard deviation ($n$ = 5).

tetrachloroethylene, whereas the recoveries for other solvents were lower than 33%. Additionally, tetrachloroethylene presented the lowest relative standard deviation (RSD, about 3%), which was also considered for choosing this solvent for further experiments.

For the selection of the dispersive solvent, the key factor is the miscibility of dispersive solvent into the extraction solvent and aqueous sample.[22] The effect of dispersive solvent (acetone, acetonitrile, ethanol, methanol, and THF) on Fe extraction was evaluated using 500 $\mu$L of each solvent and 50 $\mu$L of tetrachloroethylene (as the extraction solvent). As can be seen in Figure 2, the highest recovery (about 48%) was obtained using acetonitrile, with RSD below 2%. Thus, acetonitrile was used as the dispersive solvent for subsequent experiments.

**3.2. Effect of Volumes of Dispersive and Extraction Solvents.** The volume of the dispersive solvent is an important parameter in DLLME because, at small volumes, the dispersion of the extraction solvent does not occur and the cloudy solution is not formed. On the other hand, the use of large volumes increases the solubility of the extraction solvent (and analyte) in the aqueous phase, decreasing the extraction efficiency.[23] After dispersive (acetonitrile) and extraction (tetrachloroethylene) solvents have been chosen, experiments were performed to evaluate the volume of these solvents. The volume of acetonitrile ranged from 200 to 1500 $\mu$L in combination with 50 $\mu$L of $C_2Cl_4$ and 500 $\mu$L of 1% (m/v) APDC at pH 3.3. As can be seen in Figure 3, Fe recovery increased according to the increase of acetonitrile volume up to 1300 $\mu$L. A significant difference (Tukey−Kramer test) between 1300 and 1500 $\mu$L of acetonitrile was not observed,

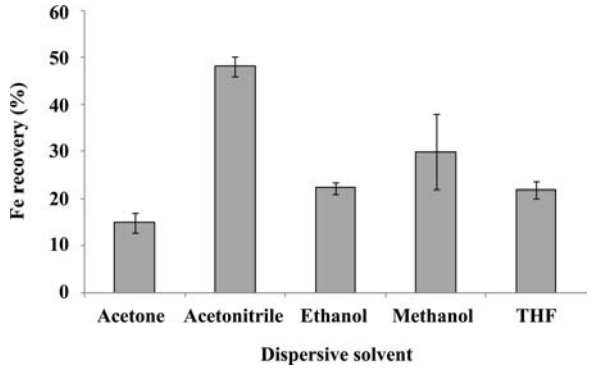


**Figure 2.** Effect of the type of dispersive solvent on Fe recovery. Conditions: 5 mL of white wine sample (5 times diluted), addition of 240 $\mu$L of 25 mg $L^{-1}$ Fe(III) solution, 500 $\mu$L of 1% APDC, 500 $\mu$L of dispersive solvent, 80 $\mu$L of extraction solvent ($C_2Cl_4$), and pH 3.3. The error bars represent the standard deviation ($n$ = 5).

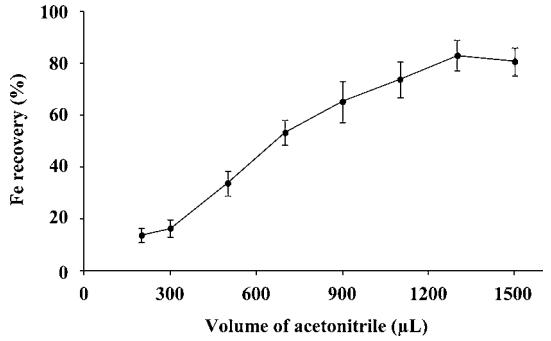


**Figure 3.** Effect of the dispersive solvent volume (acetonitrile) on Fe recovery. Conditions: 5 mL of white wine sample (5 times diluted), addition of 240 $\mu$L of 25 mg $L^{-1}$ Fe(III) solution, 500 $\mu$L of 1% APDC, 80 $\mu$L of extraction solvent ($C_2Cl_4$), and pH 3.3. The error bars represent the standard deviation ($n$ = 5).

and the condition using 1300 $\mu$L was selected for further experiments.

After optimization of the volume of acetonitrile (1300 $\mu$L), the volume of tetrachloroethylene was evaluated from 20 and 160 $\mu$L. Results are shown in Figure 4, and a significant difference (Tukey−Kramer test) was not observed among 40 and 160 $\mu$L of $CCl_4$. Considering the use of lower volumes of

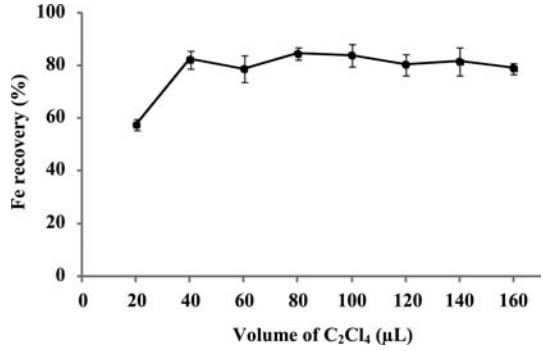


**Figure 4.** Effect of the extraction solvent volume ($C_2Cl_4$) on Fe recovery. Conditions: 5 mL of white wine sample (5 times diluted), addition of 240 $\mu$L of 25 mg $L^{-1}$ Fe(III) solution, 500 $\mu$L of 1% APDC, 1300 $\mu$L of dispersive solvent (acetonitrile), and pH 3.3. The error bars represent the standard deviation ($n$ = 5).


dx.doi.org/10.1021/jf5019774 | J. Agric. Food Chem. 2014, 62, 8340−8345

tetrachloroethylene (from 20 to 60 $\mu$L), it was difficult to handle the extract because of the low volume of solvent. Thus, 80 $\mu$L was chosen for the subsequent experiments, which presented the lowest RSD values (about 2%) and also assured a suitable amount of extraction solvent.

**3.3. Effect of pH.** The effect of pH for element extraction using DLLME has an important role on the formation of the complex and its subsequent extraction. The influence of pH in the Fe recovery was evaluated from 2 to 4. Results are shown in Figure 5. Using pH 3, Fe recovery of about 80% was obtained

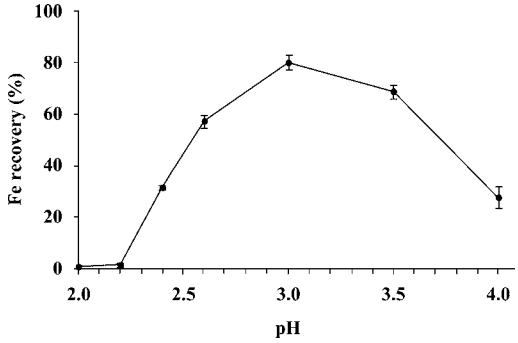


**Figure 5.** Effect of pH on Fe recovery. Conditions: 5 mL of white wine sample (5 times diluted), addition of 240 $\mu$L of 25 mg $L^{-1}$ Fe(III) solution, 500 $\mu$L of 1% APDC, 80 $\mu$L of extraction solvent ($C_2Cl_4$), and 1300 $\mu$L of dispersive solvent (acetonitrile). The error bars represent the standard deviation ($n$ = 5).

(RSD of 3%). For pH values below 3, low recovery values could be attributed to the protonation of APDC (complexant agent). Similarly, low recoveries were obtained at pH values higher than 3, which can be attributed to the formation of Fe–hydroxyl complexes. It can directly affect the transference of analyte to the extraction solvent because the formation of the Fe(APDC) complex is avoided.[24] Therefore, pH 3 was selected for further experiments. This pH (3) was in agreement with those found for Fe extraction using APDC as the complexant agent.[25]

**3.4. Effect of the APDC Concentration.** The effect of the APDC concentration was investigated using 500 $\mu$L of solution ranging from 0.1 to 3% (m/v). The maximum recoveries (about 80%) were found using 1% APDC solution, which remained constant up to 3%. Once significant differences ($p$ > 0.05) among the values ranging from 1 to 3% were not observed, 1% APDC solution was selected for further studies. For the APDC concentration below of 1%, the lower recoveries can be explained because of the low APDC concentration, which was not enough for complete complexation of the analyte, especially because of the presence of other ions that could compete with the analyte by complexation with APDC.

**3.5. Effect of the NaCl Addition.** Generally, the addition of salt in the DLLME procedure increases the extraction efficiency because of the salting out effect that promotes the transfer of analyte to the organic phase by decreasing its solubility in the aqueous phase.[26] To investigate the influence of ionic strength, experiments were performed by adding variable amounts of NaCl (from 0 to 25 g $L^{-1}$). Other experimental conditions were kept constant, but at this range of the NaCl concentration, no statistical difference (Tukey–Kramer test) on Fe recovery was observed. Thereby, for further studies, NaCl was not added.

**3.6. Effect of the Extraction Time.** In general, the extraction time for DLLME is defined as the time between the injection of the mixture of dispersive and extraction solvents before the centrifugation.[27] The extraction time was evaluated from 0.5 to 5 min, but results (not shown) did not presented significant influence (Tukey–Kramer test) on Fe recovery. Because of the large surface area between the extraction solvent and aqueous phase after the formation of a cloudy solution, the complex quickly diffuses into the extraction solvent.[28] Therefore, the DLLME procedure was considered time-independent, which is an important advantage of the proposed method.

**3.7. Analytical Performance.** The optimized DLLME method was evaluated considering some parameters, such as linearity, limit of detection (LOD), limit of quantification (LOQ), accuracy, and precision. A complementary study for evaluating the matrix effect on Fe determination by UV–vis was also performed comparing the slopes of calibration curves, through the DLLME method, in aqueous reference solution and wine samples. When these slopes were compared, suppression in the analytical curve of about 16 and 26% was found for white and red wines, respectively. This suppression was also observed during method optimization, once recoveries were not better than 84%. Thus, to minimize this effect, the instrument calibration was carried out using a calibration curve with analyte addition. It is important to point out that the behavior (slope) for the same type of wine (white or red) was similar for all samples. In this sense, for Fe determination in white wine, sample WW1 was used for instrument calibration. Similarly, for red wine, sample RW1 was used for instrument calibration for further Fe determination. The calibration range was linear from 0.75 to 2.5 mg $L^{-1}$ Fe(III) with coefficients of determination ($R^2$) of 0.9985 and 0.9988, for white and red wines, respectively. It is important to mention that the effect of coexisting ions was also investigated. As expected, it was observed that transition metals, such as $Cd^{2+}$, $Cr^{3+}$, $Mn^{2+}$, $Ni^{2+}$, $Pb^{2+}$, $Sn^{2+}$, and $Zn^{2+}$, with concentration below 1 mg $L^{-1}$, did not affect Fe extraction/determination by UV–vis spectrophotometry. For major elements, such as $Ca^{2+}$, $K^{+}$, $Mg^{2+}$, and $Na^{+}$, the concentration limit is about 5000 mg $L^{-1}$. It is important to mention that $Co^{2+}$ and $Cu^{2+}$ have a strong influence on Fe extraction/determination (concentration limit of about 0.4 mg $L^{-1}$).

The LOD and LOQ were estimated using a calibration curve with analyte addition, defined as 3 and 10 times the standard deviation of 10 measurements of blanks divided by the slope of the calibration curve.[29] The LOD and LOQ were 0.2 and 0.8 mg $L^{-1}$, which are significantly lower than the maximum Fe concentration established by Brazilian legislation. Considering that the proposed DLLME method is relatively fast and low cost, it can be an important alternative for Fe monitoring in a wine sample easily applied in routine analysis.

Because of the lack of a certified reference material presenting certified values for Fe in wine samples, accuracy was evaluated by comparison to Fe determination by GFAAS. It is important to mention that Fe determination by GFAAS was performed using samples decomposed in a heating block with open vessels. Results are summarized in Table 1. By comparison to results obtained by GFAAS, the proposed method showed an agreement ranging from 93 to 105% for all samples, with RSD lower than 7%. The proposed method was also applied for Fe determination in commercial white and red wine samples (Table 1), and the concentration ranged from 1.3 to 4.7 mg $L^{-1}$ and from 2.5 to 4.2 mg $L^{-1}$, respectively. It is

**Table 1. Iron Determination in White and Red Wines by UV−vis and GFAAS (Results in mg $L^{-1}$ ± Standard Deviation; $n$ = 5)**

| sample | UV−vis | GFAAS |
|---|---|---|
| white wine 1 | 1.3 ± 0.1 | 1.4 ± 0.1 |
| white wine 2 | 4.7 ± 0.1 | 5.0 ± 0.2 |
| red wine 1 | 4.2 ± 0.2 | 4.4 ± 0.2 |
| red wine 2 | 3.3 ± 0.1 | 3.2 ± 0.1 |
| red wine 3 | 3.9 ± 0.2 | 4.1 ± 0.3 |
| red wine 4 | 2.5 ± 0.1 | 2.5 ± 0.1 |
| red wine 5 | 3.0 ± 0.2 | 3.0 ± 0.2 |

worth highlighting that results are below the maximum limit of Fe in Brazilian legislation (maximum value of Fe in wine is 15 mg $L^{-1}$), making the proposed extraction procedure appropriate for Fe control in wines.

In summary, the proposed DLLME method combined with UV−vis spectrophotometry was successfully developed for total Fe determination in wine samples. This method was considered as environmentally friendly because it uses low volumes of organic solvents and showed the same suitable features, such as simplicity, quickness, and relatively low cost, when compared to AAS- or ICP-based techniques. In addition, the proposed method showed good results in terms of linearity, accuracy, and precision, providing evidence of the feasibility of UV−vis spectrophotometry as an alternative to routine quality control for Fe concentration in white and red wines.

## AUTHOR INFORMATION


### Corresponding Author

*Fax: +55-55-3220-9445. E-mail: fabioand@gmail.com.



### Funding

The authors are grateful to the Conselho Nacional de Desenvolvimento Científico e Tecnológico (CNPq), the Coordenação de Aperfeiçoamento de Pessoal de Nível Superior (CAPES), and the Fundação de Amparo à Pesquisa do Estado do Rio Grande do Sul (FAPERGS) for supporting this study.


### Notes

The authors declare no competing financial interest.

## REFERENCES


(1) Pohl, P. What do metals tell us about wine? *TrAC, Trends Anal. Chem.* **2007**, *26*, 941−949.

(2) Tariba, B. Metals in wine—Impact on wine quality and health outcomes. *Biol. Trace Elem. Res.* **2011**, *144*, 143−156.

(3) Grindlay, G.; Mora, J.; Gras, L.; de Loos-Vollebregt, M. T. C. Atomic spectrometry methods for wine analysis: A critical evaluation and discussion of recent applications. *Anal. Chim. Acta* **2011**, *691*, 18−32.

(4) Catarino, S.; Curvelo-Garcia, A. S.; Sousa, R. B. Measurements of contaminant elements of wines by inductively coupled plasma−mass spectrometry: A comparison of two calibration approaches. *Talanta* **2006**, *70*, 1073−1080.

(5) Bleackley, M. R.; MacGillivray, R. T. A. Transition metal homeostasis: From yeast to human disease. *BioMetals* **2011**, *24*, 785−809.

(6) World Health Organization (WHO). *Guidelines for Drinking-Water Quality*; WHO: Geneva, Switzerland, 1996.

(7) Pohl, P.; Prusisz, B. Application of tandem column solid phase extraction and flame atomic absorption spectrometry for the determination of inorganic and organically bound forms of iron in wine. *Talanta* **2009**, *77*, 1732−1738.

(8) Olalla, M.; González, M. C.; Cabrera, C.; López, M. C. Optimized determination of iron in grape juice, wines, and other alcoholic beverages by atomic absorption spectrometry. *J. AOAC Int.* **2000**, *83*, 189−195.

(9) Lara, R.; Cerutti, S.; Salonia, J. A.; Olsina, R. A.; Martinez, L. D. Trace element determination of Argentine wines using ETAAS and USN−ICP−OES. *Food Chem. Toxicol.* **2005**, *43*, 293−297.

(10) Abadi, M. D. M.; Ashraf, N.; Chamsaz, M.; Shemirani, F. An overview of liquid phase microextraction approaches combined with UV−vis spectrophotometry. *Talanta* **2012**, *99*, 1−12.

(11) Andruch, V.; Kocúrová, L.; Balogh, J. S.; Škrlíková, J. Recent advances in coupling single-drop and dispersive liquid−liquid microextraction with UV−vis spectrophotometry and related detection techniques. *Microchem. J.* **2012**, *102*, 1−10.

(12) Zheng, C.; Hongtao, Y.; Jia-Jian, H. Determination of trace iron in water and wine samples by spectrophotometry with cloud point extraction. *Acta Chim. Sin.* **2010**, *68*, 717−721.

(13) Paleologos, E. K.; Giokas, D. L.; Tzouwara-Karayanni, S. M.; Karayannis, M. I. Micelle mediated methodology for the determination of free and bound iron in wines by flame atomic absorption spectrometry. *Anal. Chim. Acta* **2002**, *458*, 241−248.

(14) Costa, R. C. C.; Araújo, A. N. Determination of Fe(III) and total Fe in wines by sequential injection analysis and flame atomic absorption spectrometry. *Anal. Chim. Acta* **2001**, *438*, 227−233.

(15) Tasev, K.; Karadjova, I.; Arpadjan, S.; Cvetković, J.; Stafilov, T. Liquid/liquid extraction and column solid phase extraction procedures for iron species determination in wines. *Food Control* **2006**, *17*, 484−488.

(16) Rezaee, M.; Assadi, Y.; Hosseini, M. R. M.; Aghaee, E.; Ahmadia, F.; Berijani, S. Determination of organic compounds in water using dispersive liquid−liquid microextraction. *J. Chromatogr. A* **2006**, *1116* (1−2), 1−9.

(17) Yan, H.; Wang, H. Recent development and applications of dispersive liquid−liquid microextraction. *J. Chromatogr. A* **2013**, *1295*, 1−15.

(18) Pereira, E. R.; Soares, B. M.; Maciel, J. V.; Caldas, S. S.; Andrade, C. F. F.; Primel, E. G.; Duarte, F. A. Development of a dispersive liquid−liquid microextraction method for iron extraction and preconcentration in water samples with different salinities. *Anal. Methods* **2013**, *5*, 2273−2280.

(19) Soares, B. M.; Pereira, E. R.; Maciel, J. V.; Vieira, A. A.; Duarte, F. A. Assessment of dispersive liquid−liquid microextraction for the simultaneous extraction, preconcentration, and derivatization of $Hg^{2+}$ and $CH_3Hg^+$ for further determination by GC−MS. *J. Sep. Sci.* **2013**, *36*, 3411−3418.

(20) Skrlíková, J.; Andruch, V.; Balogh, I. S.; Kocúrová, L.; Nagy, L.; Bazel, Y. A novel, environmentally friendly dispersive liquid−liquid microextraction procedure for the determination of copper. *Microchem. J.* **2011**, *99*, 40−45.

(21) Anthemidis, A. N.; Ioannou, K. G. Development of a sequential injection dispersive liquid−liquid microextraction system for electrothermal atomic absorption spectrometry by using a hydrophobic sorbent material: Determination of lead and cadmium in natural waters. *Anal. Chim. Acta* **2010**, *668*, 35−40.

(22) Anthemidis, A. N.; Ioannou, K. G. On-line sequential injection dispersive liquid−liquid microextraction system for flame atomic absorption spectrometric determination of copper and lead in water samples. *Talanta* **2009**, *79*, 86−91.

(23) Ma, J.; Lu, W.; Chen, L. Recent advances in dispersive liquid−-liquid microextraction for organic compounds analysis in environmental water: A review. *Curr. Anal. Chem.* **2012**, *8*, 78−90.

(24) Hulanick, A. Complexation reactions of dithiocarbamates. *Talanta* **1967**, *14*, 1371−1392.

(25) Sitko, R.; Kocot, K.; Zawisza, B.; Feist, B.; Pytlakowska, K. Liquid-phase microextraction as an attractive tool for multielement trace analysis in combination with X-ray fluorescence spectrometry: An example of simultaneous determination of Fe, Co, Zn, Ga, Se and Pb in water samples. *J. Anal. At. Spectrom.* **2011**, *26*, 1979−1985.

(26) Mirzaeia, M.; Behzadi, M.; Abadi, N. M.; Beizaei, A. Simultaneous separation/preconcentration of ultra-trace heavy metals in industrial wastewaters by dispersive liquid−liquid microextraction

based on solidification of floating organic drop prior to determination by graphite furnace atomic absorption spectrometry. *J. Hazard. Mater.* **2011**, *186*, 1739−1743.

(27) Wu, Q.; Wu, C.; Wang, C.; Lu, X.; Li, X.; Wang, Z. Sensitive determination of cadmium in water, beverage and cereal samples by a novel liquid-phase microextraction coupled with flame atomic absorption spectrometry. *Anal. Methods* **2011**, *3*, 210−216.

(28) Tabrizi, A. B. Development of a dispersive liquid−liquid microextraction method for iron speciation and determination in different water samples. *J. Hazard. Mater.* **2010**, *183*, 688−693.

(29) Ribani, M.; Bottoli, C. B. G.; Collins, C. H.; Jardim, I. C. S. F.; Melo, L. F. C. Validation for chromatographic and electrophoretic methods. *Quim. Nova* **2004**, *27*, 771−780.

JOURNAL OF AGRICULTURAL AND FOOD CHEMISTRY

Article

pubs.acs.org/JAFC

# Immunomodulatory Effect of a Wild Blueberry Anthocyanin-Rich Extract in Human Caco-2 Intestinal Cells

Valentina Taverniti,[†] Daniela Fracassetti,[‡] Cristian Del Bo',[‡] Claudia Lanti,[‡] Mario Minuzzo,[#] Dorothy Klimis-Zacas,[§] Patrizia Riso,*[,‡,∥] and Simone Guglielmetti[†,∥]

[†]Division of Food Microbiology and Bioprocessing and [‡]Division of Human Nutrition, Department of Food, Environmental and Nutritional Sciences (DeFENS), Università degli Studi di Milano, via Celoria 2, 20133 Milan, Italy

[#]Department of Biomolecular Sciences and Biotechnology, Università degli Studi di Milano, via Celoria 20, 20133 Milan, Italy

[§]Department of Food Science and Human Nutrition, University of Maine, Orono, Maine 04469, United States

**ABSTRACT:** Intestinal inflammation is a natural process crucial for the maintenance of gut functioning. However, abnormal or prolonged inflammatory responses may lead to the onset of chronic degenerative diseases, typically treated by means of pharmacological interventions. Dietary strategies for the prevention of inflammation are a safer alternative to pharmacotherapy. Anthocyanins and other polyphenols have been documented to display anti-inflammatory activity. In the present study, three bioactive fractions (anthocyanin, phenolic, and water-soluble fractions) were extracted from a wild blueberry powder. The Caco-2 intestinal model was used to test the immunomodulatory effect of the above fractions. Only the anthocyanin-rich fraction reduced the activation of NF-κB, induced by IL-1β in intestinal epithelial Caco-2 cells. Specifically, concentrations of 50 and 100 μg mL$^{-1}$ decreased NF-κB activation by 68.9 and 85.2%, respectively ($p \leq 0.05$). These preliminary results provide further support for the role of food bioactives as potential dietary anti-inflammatory agents.

**KEYWORDS:** *wild blueberry, anthocyanins, Caco-2 cells, NF-κB, luciferase reporter system*

## INTRODUCTION

Inflammation is a nonspecific immune response consisting of complex reactions as the body defends itself against injuries that are encountered daily by host cells such as the mucosal surface of the gastrointestinal tract. The orchestration of these responses guarantees both effective protection against harmful agents and maintenance of homeostasis. The nuclear factor κB (NF-κB) pathway is an immunological route through which inflammation processes are triggered and regulated. The NF-κB transcription factor exists in an inactive state in the cytosol of cells; upon its activation and translocation into the nucleus, the induction of genes involved in immune and pro-inflammatory responses is induced, leading to the expression of cytokines and chemokines, adhesion molecules, and inflammatory enzymes.[1]

In some individuals, or in particular conditions, the above system fails to suppress the inflammatory processes once activated, leading to exacerbated responses and to the onset of pathological consequences such as inflammatory bowel diseases (IBD). Usually, effective therapies are mainly based on pharmacological interventions, which are often connected with adverse side effects. Therefore, the potential of utilizing dietary strategies to prevent and/or reduce the inflammatory state may represent a safer and affordable tool.

Polyphenols are a class of phytochemicals that have been shown to modulate inflammatory processes.[2] In vitro and in vivo studies report that pure polyphenolic molecules, but also plant extracts, can interfere with immunological pathways and the production of inflammatory mediators.[3]

The anti-inflammatory abilities of polyphenols have been partially attributed to a direct action on the host immune system. It is reported that these bioactives could affect different intracellular pathways in the intestinal mucosa by triggering specific immune responses.[4] In fact, diverse phenolic compounds (e.g., kaempferol, quercitin, genistein, luteolin) have been documented to exert their effects through the attenuation of pro-inflammatory cytokines.[5,6] Consequently, it has been proposed that such compounds may decrease the risk of individuals to develop chronic inflammation.[4] Specifically, previous investigations (both in in vitro and in mouse models) documented that polyphenols can exert modulatory effects in the presence of different inflammatory stimuli.[2]

Anthocyanins (ACNs) are pigments of the polyphenol class that confer red to blue color to several common fruits and vegetables, which have been shown to exert different health-promoting properties as documented in both in vitro and in vivo studies.[7−12] Apart from their antioxidant activity,[13] ACNs play a key role in promoting host health through diverse mechanisms: from improvement of lipid profiles, vasomotor tone, and blood pressure to the modulation of detoxifying enzymes[7−10] and inflammation.[11,12,14]

ACNs are poorly absorbed,[15] even if new evidence suggests higher bioavailability than previously reported.[16] Consequently, most of them reach the colon, where their concentrations, as well as that of other polyphenols, can reach high concentrations, justifying a beneficial effect against IBD.[17]

Thus, the present study aims to investigate the effect of different bioactive fractions, obtained from an ACN-rich wild

Received: December 21, 2013
Revised: July 26, 2014
Accepted: July 30, 2014
Published: July 30, 2014

ACS Publications © 2014 American Chemical Society

blueberry (WB, *Vaccinium angustifolium*) powder, on immune responses in CaCo-2 cells following exposure to a pro-inflammatory stimulus.

## MATERIALS AND METHODS

**Chemicals and Materials.** Standards of cyanidin (Cy)-, delphinidin (Dp)-, petunidin (Pt)-, peonidin (Pe)-, and malvidin (Mv)-3-*O*-glucoside (glc), Cy- and Pt-3-*O*-arabinoside (ara), Cy-3-*O*-galactoside (gal), Dp, Cy, and Mv were purchased from Polyphenols Laboratory (Sandes, Norway). Eagle's minimum essential medium (EMEM), trypsin, fetal calf serum (FCS), D-luciferin, adenosine triphosphate (ATP), phosphate buffer saline (PBS), penicillin, streptomycin, nonessential amino acids, L-glutamine, HEPES, Tris-HCl buffer, interleukin 1$\beta$, and standards of chlorogenic, caffeic, ferulic, glucose, fructose, malic, and citric acid were obtained from Sigma-Aldrich. Hydrochloric acid, methanol, acetonitrile, triethylamine, phosphoric acid, trifluoroacetic acid (TFA), and ethyl acetate were from Merck (Darmstadt, Germany). Water was obtained from a Milli-Q apparatus (Millipore, Bedford, MA, USA). Zeocin and plasmid pNiFty2-Luc were purchased from Invivogen (Labogen, Rho, Italy). Freeze-dried WB powder, standardized at 1.5% total ACNs, was provided by Future-Ceuticals Co. (Momence, IL, USA).

**Separation and Chemical Characterization of WB Fractions.** *Extraction of Bioactives from the WB Powder.* The freeze-dried WB powder was used to extract three different fractions providing the main WB bioactives: the water-soluble fraction (containing mainly sugars and organic acids, WS fraction), the ethyl acetate-soluble fraction (containing mainly chlorogenic acid, Phe fraction), and the methanol-soluble fraction (containing mainly anthocyanins, ACN fraction).

Extraction was performed following the method described by Wrolstad[18] with a few modifications. Briefly, the WB powder was suspended in water, sonicated for 10 min, and centrifuged at 3000*g* for 10 min. Fraction separation from the supernatant was obtained through a solid-phase extraction (SPE) cartridge (Strata-X 300 mg/3 mL, Phenomenex, Torrence, CA, USA). Three milliliters of supernatant was loaded, and the elution of WS, Phe, and ACN fractions was carried out respectively with 0.01 N HCl (5 mL), ethyl acetate (10 mL), and methanol (5 mL) containing 0.1% HCl. The fractions were dried under vacuum with a rotavapor (RC Jouan 10, Jouan, Winchester, VA, USA) at 20 °C for ACN, at 40 °C for Phe, and at up to 60 °C for the WS fraction. The residues were dissolved in methanol acidified with HCl (0.05 mM) for the ACNs, methanol for the Phe, and water for the WS fractions. The solutions were analyzed for the content of ACNs, Phe, sugars, and organic acids and stored at −20 °C until use.

*Analysis of ACN and Phe-Rich Fractions.* Analysis was performed with a liquid chromatographic system, which consisted of an Alliance model 2695 (Water, Milford, MA, USA) equipped with a model 2998 photodiode array detector (Waters). The separation was carried out through a $C_{18}$ Kinetex column (150 × 4.6 mm, 2.6 $\mu$m, Phenomenex) at 45 °C with a 1.7 mL min$^{-1}$ flow rate. The eluents were (A) 1% $H_3PO_4$ and (B) acetonitrile/water (35:65, v/v). The elution gradient was linear as indicated: 0−15 min, 14% B; 15−25 min, from 14 to 20% B; 25−35 min, from 20 to 32% B; 35−45 min, from 32 to 50% B; 45−48 min, from 50 to 90% B; 90% for 3 min. Chromatographic data were acquired from 200 to 700 nm and integrated at 520 nm (ACNs) and 320 nm (Phe). Calibration curves ranging from 2 to 50 $\mu$g mL$^{-1}$ were obtained for Cy-, Dp-, Pt-, Pe-, and Mv-3-*O*-glc, Cy- and Pt-3-*O*-gal, and Pt-3-*O*-ara and chlorogenic acid. For the ACNs, the working solution was diluted from the stock solution with methanol acidified with 0.1% TFA. Each analysis was carried out in duplicate. The identification of single ACNs was confirmed by LC coupled to electrospray ionization−mass spectrometry (ESI-MS) as already described by Del Bo' et al.[9] Briefly, the mass spectrometer operated in positive full-scan mode in the range of 200−800 Da. The capillary voltage was set to 3.5 kV, the cone voltage to 20 V, the source temperature to 130 °C, and the desolvating temperature to 350 °C. Data were acquired by Masslinx 4.0 software (Micromass, Beverly, MA, USA).

*Analysis of Sugars.* Glucose and fructose were quantified in WB fractions by UPLC (Acquity, Waters) coupled with a triple-quadrupole mass spectrometer model Quattro micro (Micromass).

The separation was carried out on an ethylene-bridged hybrid (BEH) amide column (150 × 2.1 mm, 1.7 $\mu$m, Waters) at 35 °C. Solvents were (A) 0.2% triethylamine and (B) 0.2% triethylamine in acetonitrile. The flow rate was 0.40 mL min$^{-1}$. The calibration curve was obtained from 1 to 50 $\mu$g mL$^{-1}$ for both sugars. The mass spectrometer operated in ESI negative mode monitoring the ions with $m/z$ 179 (glucose, fructose). The capillary voltage was set to 3.0 kV, the cone voltage to 20 V, the source temperature to 120 °C, and the desolvating temperature to 250 °C.

*Analysis of Organic Acids.* Malic and citric acids were analyzed by UPLC (Acquity, Waters) coupled to a triple-quadrupole mass spectrometer model Quattro micro (Micromass). The separation was performed on a $C_{18}$ Atlantis T3 column (150 × 2.1 mm, 1.7 $\mu$m, Waters) at 45 °C, and the flow rate was 0.5 mL min$^{-1}$. The eluent was 0.05% formic acid. The calibration curves were obtained over the concentration range from 2 to 25 $\mu$g mL$^{-1}$ for both malic and citric acid. The capillary voltage was set to 3.5 kV, and the cone voltage and the collision energy were specific for each compound. The source temperature was 120 °C, the desolvating temperature was 300 °C, and argon was used at 1.3 × 10$^{-3}$ mbar to improve fragmentation in the collision cell. Masslinx 4.0 acquired data with Quan-Optimize option for fragmentation study. The fragmentation transitions for the multiple reaction monitoring (MRM) were $(m/z)^-$ 133 → 115 and 133 → 71 for malic and $(m/z)^-$ 191 → 111 and 191 → 87 for citric acid, with a dwell time of 0.2 s per transition.

**Immunomodulatory Activity of ACN-Rich Fraction Evaluated on Caco-2 Cell Line.** *In Vitro Cultivation.* Caco-2 cells (human epithelial colorectal adenocarcinoma cell line; ATCC HTB-37) are a well-established and validated model of the human intestinal barrier.[19] They were routinely grown in EMEM supplemented with 10% (v/v) heat-inactivated (30 min at 56 °C) FCS, 100 U mL$^{-1}$ penicillin, 100 $\mu$g mL$^{-1}$ streptomycin, 0.1 mM nonessential amino acids (NEAA), and 2 mM L-glutamine and were incubated at 37 °C in a water-jacketed incubator in an atmosphere of 95% air and 5% carbon dioxide.

*Study of NF-κB Activation.* Stable recombinant Caco-2 cell line was generated by transfecting cells with the plasmid pNiFty2-Luc as described by Guglielmetti et al.[20] This plasmid contains a promoter with five NF-κB-binding sites followed by the firefly luciferase reporter gene *luc*. Stimuli that activate NF-κB promote its binding to the vector promoter, resulting in the expression of the luciferase gene. Briefly, Caco-2 cells were transfected by means of the StoS transfection kit (GeneSpin, Milan, Italy), in accordance with the manufacturer's protocol. Afterward, cells were resuspended in fresh EMEM, seeded in 24-well plates, and incubated for 48 h to obtain the expression of the antibiotic resistance. Finally, stable recombinant clones were selected by adding into the culture medium 50 $\mu$g mL$^{-1}$ zeocin.

*Stimulation Protocol and NF-κB-Luciferase Assay.* After growth in the presence of 50 $\mu$g mL$^{-1}$ zeocin, differentiated cell monolayers (approximately 3 × 10$^5$ cells well$^{-1}$) were carefully washed with 0.1 M Tris-HCl buffer (pH 8.0). Subsequently, fresh EMEM containing 100 mM HEPES (pH 7.4) was added to Caco-2 cells. The WS-, Phe-, and ACN-rich fractions obtained by WB powder have been tested. Concentrations used were 25, 50, and 100 $\mu$g mL$^{-1}$ for the WS fraction (calculated considering the sugars and organic acid concentration) and 5, 25, 50, and 100 $\mu$g mL$^{-1}$ for the Phe-rich fraction (calculated considering the chlorogenic acid concentration) and the ACN-rich fraction (calculated considering the total ACN concentration). Only minor changes of pH were registered (pH 7.6 ± 0.1) when cells were supplemented with extract doses corresponding to the highest concentration. Recombinant Caco-2 cells were simultaneously stimulated with interleukin-1$\beta$ (IL-1$\beta$, 2 ng mL$^{-1}$), used as pro-inflammatory stimulus. After incubation at 37 °C for 4 h, 24-well plates were put on ice for 15 min; recombinant Caco-2 cells were detached mechanically from the bottom of a well, and samples were transferred into an eppendorf tube and subjected to sonication at maximum power for 5 s using a Bandelin SONOPLUS ultrasonic

homogenizer (Bandelin Electronic GmbH & Co., Berlin, Germany). Insoluble particles were removed by centrifugation, and the supernatants were transferred into a new tube. One hundred microliters of supernatants was aliquoted in duplicate into the wells of a 96-well white microtiter plate (PerkinElmer, Monza, Italy) by means of an epMotion Automated Pipetting System (Eppendorf, Milan, Italy). Then 12.5 $\mu$L of a 10 mM ATP solution (i.e., up to the final concentration of 1 mM) and 12.5 $\mu$L of 0.1 mM D-luciferin solution were added, and the emitted bioluminescence was immediately measured every 120 s with a VICTOR3 1420 multilabel counter (PerkinElmer). The maximum of light production curve was considered for comparison of results. All conditions were analyzed in duplicate in eight independent experiments.

*Cell Viability Assay.* The methosulfate (MTS) test is a spectrophotometric method used to evaluate the vitality and number of living cells.[21] The test was performed on cells treated with ACN-rich fraction (5, 25, 50, and 100 $\mu$g mL$^{-1}$), with media (control 1), and with media with added MetOH + 0.05 mM HCl (control 2). After incubation at 37 °C for 4 h, the medium was removed from Caco-2 cells, and the cells were carefully washed with 500 $\mu$L of PBS. Trypsin (0.25% trypsin, 2.5 g porcine trypsin + 0.2 g EDTA) was added to lyse cells. EMEM, containing 100 mM HEPES (pH 7.4), was added, and 100 $\mu$L of supernatant was aliquoted into a 96-well microtiter plate (PerkinElmer, Monza, Italy) by means of an epMotion automated pipetting system and then 10 $\mu$L of MTS was added. The plate was incubated at 37 °C for 90 min, and the absorbance of MTS at 490 nm was measured by a spectrophotometer (Biorad, UK).

**Statistical Analysis.** Statistical analysis was performed by means of STATISTICA software (Statsoft Inc., Tulsa, OK, USA). Analysis of variance (ANOVA), with type of treatment as the dependent factor, was used to evaluate the immunomodulatory activity of the different WB fractions on Caco-2 cells. The same analysis was performed to ensure cell viability following the ACN-rich fraction supplementation. Post hoc analysis of differences between treatments was assessed by the least significant difference (LSD) test with $p \leq 0.05$ as the level of statistical significance.

## RESULTS

**Characterization of WB Fractions.** The three fractions obtained from the WB powder were analyzed to evaluate the content of sugars and organic acids, phenols, and ACNs. The water-soluble fraction (WS) contained 4.12 $\mu$g mL$^{-1}$ sugars, corresponding to 2.28 ± 0.12 and 1.84 ± 0.13 $\mu$g mL$^{-1}$ of glucose and fructose, respectively. The contents of malic acid and citric acid were 19.9 ± 2.10 and 47.2 ± 4.23 $\mu$g mL$^{-1}$, respectively. Conversely, the contents of ACNs and phenols were negligible. Sugars and organic acids were detected only in the WS fraction.

In the Phe-rich fraction, throughout chlorogenic acid was the main phenolic compound (719.2 ± 21.4 $\mu$g mL$^{-1}$), with traces of caffeic and ferulic acids. No ACNs, sugars, or organic acids were detected.

The ACN-rich fraction composition is reported in Table 1. The total ACN content was 1563 ± 102 $\mu$g mL$^{-1}$. Fourteen different ACNs were detected in the fraction; the dominant compounds were Mv glycosides (about 540 $\mu$g mL$^{-1}$; 35% of the total ACN amount) and Dp glycosides (about 492 $\mu$g mL$^{-1}$; 31%) followed by Cy glycosides (about 293 $\mu$g mL$^{-1}$; 19%), whereas Pt and Pe glycosides represented about 11 and 4.2% of the total ACNs, respectively. The rank order for conjugated sugars was glucoside > galactoside > arabinoside from the most to the least representative (Table 1). No phenolic compounds, sugars, and organic acids were detected.

**Modulation of NF-κB Activation by WS, Phe, and ACN-Rich Fractions in Caco-2 Cells.** To identify the class of potential bioactive molecules provided by our WB powder, we tested the effects of the three different fractions isolated from WB (i.e., WS, Phe, ACN-rich) on NF-κB pathway activation. Experiments on Caco-2 cells were performed in the presence of the pro-inflammatory stimulus IL-1$\beta$. No significant differences in light emission levels were observed following Phe and WS exposure, and none of the Phe or the WS concentrations used (up to 100 $\mu$g mL$^{-1}$) resulted in a significant reduction in the NF-κB induction level compared to control. On the contrary, the ACN-rich fraction was able to reduce significantly NF-κB activation (Figure 1). In particular, the bioluminescence, and therefore NF-κB activation, was reduced by 68.9 and 85.2% at concentrations of 50 and 100 $\mu$g mL$^{-1}$, respectively ($p \leq 0.05$).

**Cell Viability.** No significant difference in cell viability was observed following Caco-2 cell supplementation. Thus, the reduction of NF-κB activation observed was not ascribable to a

**Table 1. Characterization of the ACN-Rich Fraction**

| | extracted | |
|---|---|---|
| compound | $\mu$g mL$^{-1}$[a] | % |
| malvidin 3-glc[b] | 251 ± 6.3 | 16.4 |
| malvidin 3-gal[c] | 224 ± 8.1 | 14.3 |
| malvidin 3-ara[d] | 65.1 ± 4.1 | 4.2 |
| delphinidin 3-glc | 224 ± 17.2 | 14.3 |
| delphinidin 3-gal | 166 ± 13.1 | 10.6 |
| delphinidin 3-ara | 102 ± 9.8 | 6.5 |
| cyanidin 3-glc | 99.1 ± 8.6 | 6.3 |
| cyanidin 3-gal | 69.1 ± 3.4 | 4.4 |
| cyanidin 3-ara | 124 ± 9.9 | 7.8 |
| petunidin 3-glc | 43.2 ± 2.3 | 2.8 |
| petunidin 3-gal | 107 ± 11.1 | 6.8 |
| petunidin 3-ara | 22.1 ± 3.7 | 1.4 |
| peonidin 3-glc | 28.2 ± 2.2 | 1.8 |
| peonidin 3-gal | 38.2 ± 2.1 | 2.4 |
| total | 1563 ± 102 | 100 |

[a]Data are reported as the mean ± standard deviation. [b]glc, glucoside. [c]gal, galactoside. [d]ara, arabinoside.

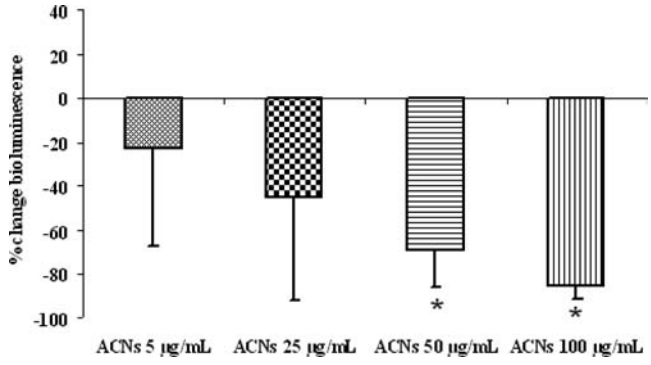


**Figure 1.** Modulation of light emission expressed by Caco-2 cells transfected with a NF-κB/luciferase reporter vector and incubated in the presence of interleukin-1$\beta$ with the ACN-rich fraction. Data are reported as percent variation of light emission, referred to the control. Control, Caco-2 cell layers incubated only with media supplemented with MetOH + 0.05 mM HCl. ACNs, anthocyanin-rich fraction. ACN concentrations (5, 25, 50, 100) are referred to $\mu$g mL$^{-1}$. The values are the means (± standard deviations) for eight independent experiments conducted in duplicate. Asterisks indicate statistically significant differences compared to results for the control (*, $p < 0.05$).

cytotoxic effect of high concentrations of the ACN-rich fraction (Table 2).

**Table 2. MTS Viability Test**[a]

| cell viability | % |
|---|---|
| control 1 | 100 |
| control 2 | 74.5 ± 18.3 |
| ACNs 5 $\mu$g mL$^{-1}$ | 77.4 ± 14.9 |
| ACNs 10 $\mu$g mL$^{-1}$ | 73.3 ± 18.9 |
| ACNs 50 $\mu$g mL$^{-1}$ | 65.7 ± 25.1 |
| ACNs 100 $\mu$g mL$^{-1}$ | 90.1 ± 10.2 |

[a]Data are reported as a measure of absorbance at 490 nm. Caco-2 cell layers incubated with ACN-rich fraction (5, 25, 50, 100 $\mu$g mL$^{-1}$) only with media (control 1) and media with MetOH + 0.05 mM HCl (control 2). ACNs, anthocyanin-rich fraction. Values are expressed as percentage mean (± standard deviations) for two independent experiments.

## DISCUSSION

Prolonged inflammation mediated by NF-κB activation may contribute to the pathogenesis of chronic diseases such as inflammatory bowel disease, diabetes, neurodegenerative diseases, cancer, and cardiovascular diseases.[3,22,23] In particular, the regulation of NF-κB activation at the epithelial interfaces, such as at gut level, is of particular importance for the maintenance of mucosal integrity, barrier function, and homeostasis. Excessive activation of NF-κB at the gut level has been associated with IBD.[24]

NF-κB is the main target in several anti-inflammatory therapies (e.g., nonsteroidal anti-inflammatory drugs)[25,26] that are not specific for NF-κB inhibition and are required in relatively high concentrations, leading to problems of adverse side effects and toxicity.[26]

The use of natural bioactive molecules, such as polyphenols, which possess the ability to attenuate NF-κB activation, might represent a safer and effective strategy in repressing inflammatory processes. Several studies suggest that blueberry polyphenols display anti-inflammatory effects that are not specifically related to their antioxidant properties.[27] ACNs, flavonols, and phenolic acids could be the phytochemicals mainly responsible for this activity. Thus, in our study, we extracted and characterized three fractions (WS, Phe, and ACN-rich fraction) from the freeze-dried WB powder to investigate the potential anti-inflammatory ability exerted by the different bioactive-rich fractions. The ACN profile of the WB used in the current research differs from that of previous studies in both qualitative and quantitative composition.[28,29] Generally, Mv-, Dp-, Cy-, Pt-, and Pe-glycosides are the most abundant ACNs found in wild blueberry.[9,30,31] In the ACN-rich fraction prepared for this study that originated from wild blueberry (*Vaccinium angustifolium*), the dominant compounds were Mv-glycosides (35% of the total ACN amount), Dp-glycosides (31%), and Cy-glycosides (19%). On the contrary, Yi et al.,[28] using three different blueberry cultivars (Briteblue, Tifblue, and Powderblue), reported higher levels of Pt- and Pe-glycosides in the ACN fraction, whereas Triebel et al.[29] detected higher levels of Dp-glycosides and Cy-glycosides from bilberry (*Vaccinium myrtillus* L.). These differences may be explained considering that the ACN profile of blueberry can vary between different cultivars and growing conditions;[32] finally, the extraction procedures may affect molecule recovery. However, it is noteworthy that the absorption of ACNs and their antiproliferative effects were demonstrated to be comparable in Caco-2 cell monolayers supplemented with different ACN fractions obtained from several blueberry cultivars.[31] Moreover, the authors reported that ACN absorption and average transport efficiency in the Caco-2 cell model were comparable to those evidenced in in vivo studies (i.e., about 3−4%).[33]

With regard to the Phe-rich fraction, chlorogenic acid was the main compound detected. Traces of hydroxycinnamic acids, such as caffeic and ferulic acids, were also found. These results disagree with findings by Yi et al.[28] in which gallic, caffeic, *p*-coumaric, and ferulic acids were identified in three different cultivars. The differences may be due to the blueberry cultivar investigated as well as to the freeze-drying process, which may contribute to the decrease in phenols.

Finally, the immunomodulatory effect of the WS fraction was investigated to ascertain the potential contribution of sugars (i.e., glucose and fructose) and organic acids (i.e., malic acid and citric acid), not included in the ACN- and Phe-rich fractions.

The WS fraction did not show any immunomodulatory potential, even though some studies suggest an induction of the NF-κB pathway following supplementation with sugars.[34] Similarly, no significant effect was observed following Phe-rich fraction exposure. These results are in contrast with other studies that documented an anti-inflammatory and inhibitory activity of phenolic compounds on NF-κB.[5,6,35] In particular, Rodriguez-Ramiro et al.[36] documented that a cocoa polyphenolic extract (10 $\mu$g mL$^{-1}$) decreased the nuclear levels of NF-κB and the expression of several cytokines in the colon of rats. Additionally, the authors confirmed in Caco-2 cells that the cocoa polyphenol-rich extract down-regulated the levels of inflammatory markers by inhibiting NF-κB activation. The capacity of polyphenols to down-regulate the NF-κB signaling pathway was also observed by Romier et al.[37] in a Caco-2 intestinal model upon supplementation with different polyphenols (50 $\mu$mol L$^{-1}$). Moreover, Kim et al.[38] reported that the flavonoid luteolin (50 $\mu$mol L$^{-1}$) prevented lipopolysaccharide (LPS)-induced NF-κB signaling and gene expression by blocking IκB kinase activity in intestinal epithelial cells. These conflicting results could be attributed to the different type and amount of polyphenols used and the specific role played by each phenolic compound.

In the present study, only the ACN-rich fraction tested revealed an immunomodulatory potential on transfected human intestinal epithelial Caco-2 cells. In particular, a significant decrease of NF-κB activation was observed at ACN-rich fraction concentrations of 50 and 100 $\mu$g mL$^{-1}$.

Our results are in agreement with others demonstrating the ability of ACNs in the modulation of NF-κB and downstream signaling in vitro in different cell models.[3,39−41] For example, supplementation with ACN-rich extract (100 $\mu$g mL$^{-1}$) isolated from bilberries and black currants modulated in vitro LPS-induced activation of NF-κB in monocytes.[3] Kim et al.[42] showed that the administration of a soybean seed coat extract (providing from 1 to 100 $\mu$g mL$^{-1}$ ACNs) significantly inhibited NF-κB activation in endothelial cells.

Beneficial effects were also observed in vivo with ACN-rich foods. For example, the use of a WB-enriched diet in Zucker rats was able to down-regulate the expression of NF-κB, both in the liver and in the abdominal adipose tissue, and to reduce several circulating inflammatory markers such as CRP, IL-6, and TNF-α.[14] Moreover, interestingly, in a parallel-design con-

trolled clinical trial, the supplementation of healthy subjects with ACNs from blueberry (Medox, 300 mg day$^{-1}$ for 3 weeks) reduced the levels of circulating NF-κB-dependent inflammatory mediators such as IL-8 and IFN-α.[3]

In the present in vitro study, the use of extracts instead of single ACNs is limited because it does not reveal the effect of single bioactive compounds on the NF-κB pathway. In this regard, the ACN-rich fraction was further characterized for the content of vitamins A and E,[43] ascorbic acid,[44] carotenoids,[43] fatty acids,[45] fiber,[46] and minerals eventually recovered during the extract preparation. None of the compounds were detectable apart from traces of fatty acids (palmitic, stearic, oleic, and linoleic acids). With regard to minerals, only traces of magnesium, phosphorus, and manganese were present, whereas calcium, sodium, and zinc were the main compounds found. However, Caco-2 cell supplementation with the ACN-rich fraction provided <1.1 μg mL$^{-1}$ of the above minerals. In addition, we cannot exclude that other bioactive compounds not identified in the ACN-rich fraction could have contributed to the anti-inflammatory effect observed. In fact, some of them might interact synergistically or additively with ACNs or other bioactives. In this regard, the contribution of ACN metabolites such as protocatechuic acid, the in vivo concentration of which is reported to be much higher than that of the parent compound,[47,48] cannot be ruled out. The extensive activity of the gut microbiota in the colon may also be another contributory factor.[49] Additionally, it is known from cell culture studies that under simulated physiological conditions (pH and temperature) a significant rate of degradation of ACNs occurs with formation of isoforms (e.g., chalcone, hemiketal) and phenolic acids that can contribute to the effects observed.[50,51] Finally, a possible limitation of cell culture studies in which food extracts are used is the omission of the step simulating gastrointestinal digestive processes as happens in vivo.

In conclusion, our preliminary results show that the ACN-rich fraction extracted from the WB powder displayed anti-inflammatory properties by decreasing the activation of NF-κB in the presence of the pro-inflammatory stimulus IL-1β. This ability might be particularly useful in the prevention/control of several inflammatory disorders, such as IBD, as already observed in a mouse model.[49]

Further investigations are necessary to identify the individual components and/or metabolites of the ACN-rich fraction responsible for this immunomodulatory ability. Future research should target the identification of potential functional components that could aid in the development of innovative strategies preventing chronic inflammatory diseases without the side effects of pharmacotherapy.

## AUTHOR INFORMATION


### Corresponding Author

*(P.R.) Phone: + 39 02 50316726. Fax: + 39 02 50316721. E-mail: patrizia.riso@unimi.it.

### Author Contributions

‖P.R. and S.G. contributed equally to this work.



### Funding

This work was supported by Grant 2010.2303 from Cariplo Foundation (Italy).


### Notes

The authors declare no competing financial interest.


## ACKNOWLEDGMENTS

We thank Antonella Brusamolino, Daniele Contino, and Giorgio Lucchini for their contribution in the characterization of the WB fractions. Moreover, we thank the Wild Blueberry Association of North America (WBANA) for providing the wild blueberries, and FutureCeuticals (Momence, IL, USA) for processing the wild blueberry powder.


## REFERENCES


(1) Wullaert, A.; Bonnet, M. C.; Pasparakis, M. NF-κB in the regulation of epithelial homeostasis and inflammation. *Cell Res.* **2011**, *21*, 146−158.

(2) Romier, B.; Schneider, Y. J.; Larondelle, Y.; During, A. Dietary polyphenols can modulate the intestinal inflammatory response. *Nutr. Rev.* **2009**, *67*, 363−378.

(3) Karlsen, A.; Retterstøl, L.; Laake, P.; Paur, I.; Bøhn, S. K.; Sandvik, L.; Blomhoff, R. Anthocyanins inhibit nuclear factor-kappaB activation in monocytes and reduce plasma concentrations of pro-inflammatory mediators in healthy adults. *J. Nutr.* **2007**, *137*, 1951−1954.

(4) Clarke, J. O.; Mullin, G. E. A review of complementary and alternative approaches to immunomodulation. *Nutr. Clin. Pract.* **2008**, *23*, 49−62.

(5) Paradkar, P. N.; Bluma, P. S.; Berhowb, M. A.; Baumannc, H.; Kuoa, S.-M. Dietary isoflavones suppress endotoxin-induced inflammatory reaction in liver and intestine. *Cancer Lett.* **2004**, *215*, 21−28.

(6) Porath, D.; Riegger, C.; Drewe, J.; Schwager, J. Epigallocatechin-3-gallate impairs chemokine production in human colon epithelial cell lines. *J. Pharmacol. Exp. Ther.* **2005**, *315*, 1172−1180.

(7) Mazza, G.; Kay, C. D.; Cottrell, T.; Holub, B. J. Absorption of anthocyanins from blueberries and serum antioxidant status in human subjects. *J. Agric. Food Chem.* **2002**, *50*, 7731−7737.

(8) Norton, C.; Kalea, A. Z.; Harris, P. D.; Klimis-Zacas, D. J. Wild blueberry-rich diets affect the contractile machinery of the vascular smooth muscle in the Sprague-Dawley rat. *J. Med. Food* **2005**, *8*, 8−13.

(9) Del Bo', C.; Ciappellano, S.; Klimi-Zacas, D.; Martini, D.; Gardana, C.; Riso, P.; Porrini, M. Anthocyanins adsorption, metabolism, and distribution from a wild-blueberry-enriched diet (*Vaccinium angustifolium*) is affected by diet duration in the Sprague-Dawley rat. *J. Agric. Food Chem.* **2010**, *58*, 2494−2497.

(10) Kristo, A. S.; Kalea, A. Z.; Schuschke, D. A.; Klimis-Zacas, D. Attenuation of alpha-adrenergic-induced vasoconstriction by dietary wild blueberries (*Vaccinium angustifolium*) is mediated by the NO-cGMP pathway in spontaneously hypertensive rats (SHRs). *Int. J. Food Sci. Nutr.* **2013**, *64*, 979−987.

(11) Bagchi, D.; Sen, C. K.; Bagchi, M.; Atalay, M. Anti-angiogenic, antioxidant, and anti-carcinogenic properties of a novel anthocyanin-rich berry extract formula. *Biochemistry (Moscow)* **2004**, *69*, 75−80.

(12) Vendrame, S.; Daugherty, A.; Kristo, A. S.; Klimis-Zacas, D. Wild blueberry (*Vaccinium angustifolium*)-enriched diet improves dyslipidaemia and modulates the expression of genes related to lipid metabolism in Zucker rats. *Br. J. Nutr.* **2014**, *111*, 194−200.

(13) Espín, J. C.; García-Conesa, M. T.; Tomás-Barberán, F. A. Nutraceuticals: facts and fiction. *Phytochemistry* **2007**, *68*, 2986−3008.

(14) Vendrame, S.; Daugherty, A.; Kristo, A. S.; Riso, P.; Klimis-Zacas, D. Wild blueberry (*Vaccinium angustifolium*) consumption improves inflammatory status in the obese Zucker rat model of the metabolic syndrome. *J. Nutr. Biochem.* **2013**, *24*, 1508−1512.

(15) Milbury, P. E.; Vita, J. A.; Blumberg, J. B. Anthocyanins are bioavailable in humans following an acute dose of cranberry juice. *J. Nutr.* **2010**, *140*, 1099−1104.

(16) Czank, C.; Cassidy, A.; Zhang, Q.; Morrison, D. J.; Preston, T.; Kroon, P. A.; Botting, N. P.; Kay, C. D. Human metabolism and elimination of the anthocyanin, cyanidin-3-glucoside: a $^{13}$C-tracer study. *Am. J. Clin. Nutr.* **2013**, *97*, 995−1003.

(17) Romier, B.; Schneider, Y. J.; Larondelle, Y.; During, A. Dietary polyphenols can modulate the intestinal inflammatory response. *Nutr. Rev.* **2009**, *67*, 363−378.

(18) Wrolstad, R. E.; Acree, T. E.; Decker, E. A.; Penner, M. H.; Reid, D. S.; Schwartz, S. J.; Shoemaker, S. F.; Smith, D. M.; Sporns, P. *Handbook of Analytical Chemistry: Pigments, Colorants, Flavor, Texture and Bioactive Food Components*; Wiley Interscience: Hoboken, NJ, USA, 2005; Vol. 2, pp 473−475.
(19) Sambuy, Y.; De Angelis, I.; Ranaldi, G.; Scarino, M. L.; Stammati, A.; Zucco, F. The Caco-2 cell line as a model of the intestinal barrier: influence of cell and culture-related factors on Caco-2 cell functional characteristics. *Cell Biol. Toxicol.* **2005**, *21*, 1−26.
(20) Guglielmetti, S.; Taverniti, V.; Minuzzo, M.; Arioli, S.; Stuknyte, M.; Karp, M.; Mora, D. Oral bacteria as potential probiotics for the pharyngeal mucosa. *Appl. Environ. Microbiol.* **2010**, *76*, 3948−3958.
(21) Malich, G.; Markovic, B.; Winder, C. The sensitivity and specificity of the MTS tetrazolium assay for detecting the in vitro cytotoxicity of 20 chemicals using human cell lines. *Toxicology* **1997**, *124*, 179−192.
(22) Nathan, C. Points of control in inflammation. *Nature* **2002**, *420*, 846−852.
(23) Blomhoff, R. Dietary antioxidants and cardiovascular disease. *Curr. Opin. Lipidol.* **2005**, *16*, 47−54.
(24) Schreiber, S.; Nikolaus, S.; Hampe, J. Activation of nuclear factor kappa B inflammatory bowel disease. *Gut* **1998**, *42*, 477−484.
(25) Yamamoto, Y.; Gaynor, R. B. Therapeutic potential of inhibition of the NF-kappaB pathway in the treatment of inflammation and cancer. *J. Clin. Invest.* **2001**, *107*, 135−142.
(26) Tas, S. W.; Vervoordeldonk, M. J.; Tak, P. P. Gene therapy targeting nuclearfactor-kappaB: towards clinical application in inflammatory diseases and cancer. *Curr. Gene Ther.* **2009**, *9*, 160−170.
(27) Lau, F. C.; Bielinski, D. F.; Joseph, J. A. Inhibitory effects of blueberry extract on the production of inflammatory mediators in lipopolysaccharide-activated BV2 microglia. *J. Neurosci. Res.* **2007**, *85*, 1010−1017.
(28) Yi, W.; Fischer, J.; Krewer, G.; Akoh, C. C. Phenolic compounds from blueberries can inhibit colon cancer cell proliferation and induce apoptosis. *J. Agric. Food Chem.* **2005**, *53*, 7320−7329.
(29) Triebel, S.; Trieu, H.-L.; Richling, E. Modulation of inflammatory gene expression by a bilberry (*Vaccinium myrtillus* L.) extract and single anthocyanins considering their limited stability under cell culture conditions. *J. Agric. Food Chem.* **2012**, *60*, 8902−8910.
(30) Nicoué, E. É.; Savard, S.; Belkacemi, K. Anthocyanins in wild blueberries of Quebec: extraction and identification. *J. Agric. Food Chem.* **2007**, *55*, 5626−5656.
(31) Zhao, Y. *Berry Fruit. Value-Added Products for Health Promotion*; CRC Press Taylor & Francis Group: Boca Raton, FL, USA, 2007.
(32) Connor, A. M.; Luby, J. J.; Tong, C. B. S. Genotypic and environmental variation in antioxidant activity, total phenolic content, and anthocyanin content among blueberry cultivars. *J. Am. Soc. Hortic. Sci.* **2002**, *127*, 89−97.
(33) Yi, W.; Akoh, C. C.; Fischer, J.; Krewer, G. Absorption of anthocyanins from blueberry extracts by Caco-2 human intestinal cell monolayers. *J. Agric. Food Chem.* **2006**, *54*, 5651−5658.
(34) Iwasaki, Y.; Kambayashi, M.; Asai, M.; Yoshida, M.; Nigiwara, T.; Hashimoto, K. High glucose alone, as well as in combination with proinflammatory cytokines, stimulates nucelar factor kappa-B-mediated transcription in hepatocytes in vitro. *J. Diabetes Complications* **2007**, *21*, 56−62.
(35) Sergent, T.; Piront, N.; Meurice, J.; Toussaint, O.; Scheneider, Y.-J. Anti-inflammatory effects of dietary phenolic compounds in an in vitro model of inflamed human intestinal epithelium. *Chem.−Biol. Interact.* **2010**, *188*, 659−667.
(36) Rodríguez-Ramiro, I.; Ramos, S.; López-Oliva, E.; Agis-Torres, A.; Bravo, L.; Goya, L.; Martín, M. A. Cocoa polyphenols prevent inflammation in the colon of azoximethane-treated rats in the TNF-$\alpha$-stimulated Caco-2 cells. *Br. J. Nutr.* **2013**, *110*, 206−215.
(37) Romier, B.; Van De Walle, J.; During, A.; Larondelle, Y.; Schneider, Y. J. Modulation of signalling nuclear factor-kappaB activation pathway by polyphenols in human intestinal Caco-2 cells. *Br. J. Nutr.* **2008**, *100*, 542−551.
(38) Kim, J. S.; Jobin, C. The flavonoid luteolin prevents lipopolysaccharide-induced NF-kappaB signalling and gene expression by blocking IkappaB kinase activity in intestinal epithelial cells and bone-marrow derived dendritic cells. *Immunology* **2005**, *115*, 375−387.
(39) Wang, J.; Mazza, G. Effects of anthocyanins and other phenolic compounds on the production of tumor necrosis factor $\alpha$ in LPS/IFN-$\gamma$-activated RAW 264.7 macrophages. *J. Agric. Food Chem.* **2002**, *50*, 4183−4189.
(40) Herath, H. M.; Takano-Ishikawa, Y.; Yamaki, K. Inhibitory effect of some flavonoids on tumor necrosis factor-alpha production in lipopolysaccharide-stimulated mouse macrophage cell line J774.1. *J. Med. Food* **2003**, *6*, 365−370.
(41) Cimino, F.; Ambra, R.; Canali, R.; Saija, A.; Virgili, F. Effect ofcyanidin-3-*O*-glucoside on UVB-induced response in human keratinocytes. *J. Agric. Food Chem.* **2006**, *54*, 4041−4047.
(42) Kim, H. J.; Tsoy, I.; Park, J. M.; Chung, J. I.; Shin, S. C.; Chang, K. C. Anthocyanins from soybean seed coat inhibit the expression of TNF-alpha-induced genes associated with ischemia/reperfusion in endothelial cells by NF-kappa-B dependent pathway and reduce rat myocardial damages incurred by ischemia and reperfusion in vivo. *FEBS Lett.* **2005**, *580*, 1391−1397.
(43) Riso, P.; Brusamolino, A.; Moro, M.; Porrini, M. Absorption of bioactive compounds from steamed broccoli and their effect on plasma glutathione S-transferase activity. *Int. J. Food Sci. Nutr.* **2009**, *60* (Suppl. 1), 56−71.
(44) Guarnieri, S.; Riso, P.; Porrini, M. Orange juice vs vitamin C: effect on hydrogen peroxide-induced DNA damage in mononuclear blood cells. *Br. J. Nutr.* **2007**, *97*, 639−643.
(45) Simonetti, P.; Ciappellano, S.; Gardana, C.; Bramati, L.; Pietta, P. Procyanidins from *Vitis vinifera* seeds: in vivo effects on oxidative stress. *J. Agric. Food Chem.* **2002**, *50*, 6217−6221.
(46) AOAC Method 991.43. Total, insoluble and soluble dietary fiber in food-enzymatic-gravimetric method, MES-TRIS bufferr. *Official Methods of Analysis*, 16th ed.; AOAC International: Gaithersburg, MD, USA, 1995.
(47) Vitaglione, P.; Donnarumma, G.; Napoletano, A.; Galvano, F.; Gallo, A.; Scalfi, L.; Fogliano, V. Protocatechuic acid is the major human metabolite of cyanidin-glucosides. *J. Nutr.* **2007**, *137*, 2043−2048.
(48) Bermúdez-Soto, M. J.; Tomás-Barberán, F. A.; García-Conesa, M. T. Stability of polyphenols in chokeberry (*Aronia melanocarpa*) subjected to in vitro gastric and pancreatic digestion. *Food Chem.* **2007**, *102*, 865−874.
(49) McGhie, T. K.; Walton, M. C. The bioavailability and absorption of anthocyanins: towards a better understanding. *Mol. Nutr. Food Res.* **2007**, *51*, 702−713.
(50) Woorward, G.; Kroon, P.; Cassidy, A.; Kay, C. Anthocyanin stability and recovery: implications for the analysis of clinical and experimental samples. *J. Agric. Food Chem.* **2009**, *57*, 5271−5278.
(51) Kay, C. D.; Kroon, P. A.; Cassidy, A. The bioactivity of dietary anthocyanins is likely to be mediated by their degradation products. *Mol. Nutr. Food Res.* **2009**, *53*, S92−S101.

JOURNAL OF AGRICULTURAL AND FOOD CHEMISTRY

Article

pubs.acs.org/JAFC

# Potential of a Renin Inhibitory Peptide from the Red Seaweed *Palmaria palmata* as a Functional Food Ingredient Following Confirmation and Characterization of a Hypotensive Effect in Spontaneously Hypertensive Rats

Ciaran Fitzgerald,*[,†] Rotimi E. Aluko,[‡] Mohammad Hossain,[†] Dilip K. Rai,[†] and Maria Hayes[†]

[†]Food Biosciences Department, Teagasc Food Research Centre, Ashtown, Dublin 15, Ireland

[‡]Department of Human Nutritional Sciences, University of Manitoba, Winnipeg R3T 2N2, Canada

**ABSTRACT:** This work examined the resistance of the renin inhibitory, tridecapeptide IRLIIVLMPILMA derived previously from a *Palmaria palmata* papain hydrolysate, during gastrointestinal (GI) transit. Following simulated GI digestion, breakdown products were identified using mass spectrometry analysis and the known renin and angiotensin I converting enzyme inhibitory dipeptide IR was identified. In vivo animal studies using spontaneously hypertensive rats (SHRs) were used to confirm the antihypertensive effects of both the tridecapeptide IRLIIVLMPILMA and the seaweed protein hydrolysate from which this peptide was isolated. After 24 h, the SHR group fed the *P. palmata* protein hydrolysate recorded a drop of 34 mm Hg in systolic blood pressure (SBP) from 187 (±0.25) to 153 (± 0.64) mm Hg SBP, while the group fed the tridecapeptide IRLIIVLMPLIMA presented a drop of 33 mm Hg in blood pressure from 187 (±0.95) to 154 (±0.94) mm Hg SBP compared to the SBP recorded at time zero. The results of this study indicate that the seaweed protein derived hydrolysate has potential for use as antihypertensive agents and that the tridecapeptide is cleaved and activated to the dipeptide IR when it travels through the GI tract. Both the hydrolysate and peptide reduced SHR blood pressure when administered orally over a 24 h period.

**KEYWORDS:** *in vitro simulated gastrointestinal digestion, spontaneously hypertensive rats, renin inhibitory peptides, red macroalga*

## INTRODUCTION

Therapeutic peptides of natural origin are used widely in the pharmaceutical industry.[1] Peptide therapies range from anticancer and antimicrobial applications to peptide use in the treatment of the symptoms of Alzheimer's disease.[1] Cardiovascular disease (CVD) is the biggest natural cause of death in Western society, and there is a focus by pharmaceutical and functional food manufacturers on the prevention of its onset.[2] High blood pressure or hypertension is the main contributory factor to CVD.[2] To fight hypertension, different components of the renin angiotensin aldosterone system (RAAS) can be positively affected. High blood pressure is ordinarily treated with the use of drugs such as captopril and enalopril that are proven and effective antihypertensive agents.[3] These drugs work by inhibiting angiotensin converting enzyme (ACE-I), the second rate-limiting enzyme of the renin angiotensin system (RAS) that forms part of the RAAS.[3] However, inhibition of this enzyme can lead to side effects such as development of a dry cough and angioneurotic edema due to the disruption of kinin metabolism.[4] The enzyme renin is the initial rate-limiting enzyme in the RAAS, and even though its importance within this system is known since 1898[5] and its substrate specificity described since 1957, commercialization of viable renin inhibitory drugs is a relatively recent occurrence.[6] Inhibition of renin has advantages over ACE-I inhibition as it is not associated with the negative side effects previously mentioned.[4] Peptides that inhibit ACE-I were discovered from a range of natural sources including soy,[7] cereal,[8] fish,[9] and macroalgae.[10] Similar to the trend observed with synthetic renin inhibitors, naturally occurring renin inhibitors have only recently been reported from sources such as peas[11] and hemp seed.[12]

Previous work carried out by this group isolated a renin inhibitory tridecapeptide with the amino acid sequence IRLIIVLMPILMA from a protein hydrolysate generated using the food-grade enzyme papain from the red seaweed *Palmaria palmata*.[13] This peptide, IRLIIVLMPILMA, had a renin inhibitory $IC_{50}$ value of 3.34 mM compared to the positive control used.

The aim of this work was to assess if the tridecapeptide IRLIIVLMPILMA could survive gastrointestinal (GI) digestion and therefore could be used as a viable functional food ingredient that positively affects hypertension. In silico cleavage analysis coupled with a simulated GI digestion method were used to assess the resistance of this peptide in vivo using spontaneously hypertensive rats (SHRs). The peptide hydrolysate from which the tridecapeptide IRLIIVLMPILMA was isolated along with the chemically synthesized peptide was administered separately via oral gavage to SHRs. The effect on the blood pressure of the animals was observed over 24 h.

## MATERIALS AND METHODS

**Chemicals.** The tridecapeptide IRLIIVLMPILMA was synthesized by GL Biochem Ltd. (Shanghai, China). All enzymes used for the simulated gastric digestion of the tridecapeptide including pepsin from

Received: February 25, 2014
Revised: July 23, 2014
Accepted: July 25, 2014
Published: July 25, 2014

ACS Publications © 2014 American Chemical Society



dx.doi.org/10.1021/jf500983n | J. Agric. Food Chem. 2014, 62, 8352−8356

porcine gastric mucosa, amylase, pancreatin, and porcine bile extract were obtained from Sigma–Aldrich (Dublin, Ireland). All reagents used in the formation of the gastric fluids including potassium chloride, monobasic potassium phosphate, sodium bicarbonate, sodium chloride, and magnesium chloride hexahydrate were also sourced from Sigma–Aldrich (Germany).

**In Silico Analysis of the Renin Inhibitory Peptide IRLIIVLMPILMA.** The program Expasy Peptide Cutter (http://web.expasy.org/peptide_cutter/) was used to predict where the main proteases of the GI tract could cleave the renin inhibitory peptide IRLIIVLMPILMA.

The online tool ToxinPred (http://crdd.osdd.net/raghava/toxinpred/index.html) was used to predict the toxicity of the peptide and its fragments after hydrolysis.[14]

**Simulated Gastric Digestion of the Peptide IRLIIVLMPILMA.** The simulated gastric digestion method was carried out according to the method described by the European Cooperation in Science and Technology (COST) funded group INFOGEST (http://www.cost-infogest.eu/). This method was devised under COST action FA1005 in an attempt to promote harmonization of currently used digestion models. Simulation of the gastric process was carried out in three phases as shown in Figure 1. Initially, an oral phase containing 1 g of

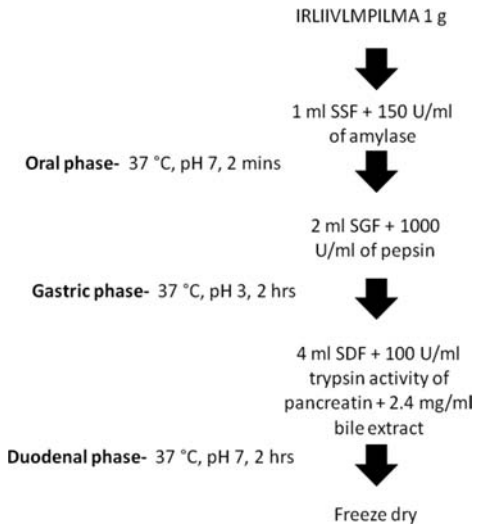


**Figure 1.** Schematic representation of the simulated, in vitro gastric digestion protocol used. The simulated digestion was carried out in three stages: (1) oral stage; (2) gastric stage; (3) duodenal stage.

the synthesized peptide was mixed with 1 mL of simulated salivary fluid (SSF) (Table 1) and 150 U/mL amylase. This mixture was left to stir in a water bath (Stuart shaking water bath, Staffordshire, UK) at 37 °C for 2 min. The second phase of the simulation was the gastric phase. The oral phase was mixed with 2 mL of the prepared simulated gastric fluid (SGF) (Table 1) along with pepsin at a concentration of 1000 U/mL SGF. The pH was adjusted to pH 3 using 1 M hydrochloric acid (HCl) and left to stir in a water bath (Stuart shaking water bath) at 37 °C for 2 h. The final stage of the digestion was the duodenal phase. For this phase, 4 mL of the simulated duodenal fluid (SDF) (Table 1) was added to the SGF along with pancreatin at a concentration of 100 U/mL trypsin activity. Porcine bile extract was also added at a concentration of 2.4 mg/mL of the total volume. The mixture was adjusted to pH 7 using 1 M NaOH and left to stir in a water bath at 37 °C for 2 h before being deactivated using heating at 90 °C for 20 min and subsequently freeze-dried.

**Removal of Polyethylene Glycols from *P. palmata* Protein Digested Samples Using a Titanium Dioxide Cleanup Procedure.** Digested samples were cleaned-up for further analysis using Pierce graphite spin columns available as part of the Pierce titanium dioxide phosphopeptide enrichment and cleanup kit (Thermo Fischer Scientific, Waltham, MA, USA). The graphite spin columns were used according to the manufacturer's instructions. Briefly, the column was prepared by placing it in a 1.5 mL Eppendorf tube followed by centrifugation at 2000*g* for 1 min to remove storage buffer. The column was then rinsed twice with 100 $\mu$L of $NH_4OH$ and subsequently centrifuged at 2000*g*. The graphite was activated by adding 100 $\mu$L of acetonitrile followed by centrifugation at 2000*g* for 1 min before adding 100 $\mu$L of 1% trifluoroacetic acid (TFA) in water (1:99 v/v) followed again by centrifugation of the column at 2000*g* for 1 min. After column preparation, 50 mg of the hydrolysate was added and allowed to bind to the column for 10 min with periodical vortexing. The column was then centrifuged at 1000*g* for 3 min, and the flow through was discarded. The column was subsequently placed in a new tube and washed with 200 $\mu$L of 1% TFA followed by centrifugation at 2000*g* for 1 min. The column was then placed in a new tube and spun at 2000*g* for 1 min following addition of 100 $\mu$L of 0.1% formic acid (FA) in a 50:50 acetonitrile/water v/v ratio. This step was repeated three times, and the resulting elution was freeze-dried.

**Tandem Mass Spectrometry Analysis of the Hydrolysate.** The enriched digested fraction was further analyzed using an electrospray ionization quadrupole time-of-flight (ESI-Q-TOF) mass spectrometer coupled to a nanoultra performance liquid chromatography (nano-UPLC) system (Waters Corporation, Milford, MA, USA) used in positive ionization mode. The sample was dissolved in water/acetonitrile (80:20, v/v). The redissolved hydrolysate was injected onto a nano-UPLC Acquity column BEH130 $C_{18}$ (100 $\mu$m × 100 mm, 1.7 $\mu$m particle size) preceded by a Symmetry $C_{18}$ (180 $\mu$m × 200 mm, 5 $\mu$m particle size) trapping column. Mobile phases consisted of solvent A, which contained 0.1% FA in water, and solvent B, which contained 0.1% FA in acetonitrile. Trapping of the peptide/peptide fragments was achieved using a loading time of 3 min at a flow rate of 5 $\mu$L/min with 98% solvent A and 2% solvent B and then elution onto the analytical column at 300 nL/min. Chromatographic conditions consisted of 95% solvent A and 5% solvent B isocratically for 2 min, followed by a linear gradient from 85% to 20% solvent A over 63 min.

Mass spectrometry (MS) data were acquired in $MS^e$ mode with collision energy for a full mass scan of 6 eV and a collision energy ramp of 15–35 eV for a mass range $m/z$ 155 to $m/z$ 1600. The Q-TOF was calibrated externally using MS/MS fragment ions of Glu-fibrinopeptide (Glu-fib).

**In Vivo Determination of the Antihypertensive Effect of the *P. palmata* Protein Hydrolysate and the Tridecapeptide IRLIIVLMPILMA in Spontaneously Hypertensive Rats.** All rat experiments were performed according to protocols approved by the University of Manitoba Animal Care Protocol and Management

**Table 1. Concentrations of Electrolytes Used to Create the Simulated Saliva Fluid, Simulated Gastric Fluid, and Simulated Duodenal Fluid**

| simulated saliva fluid | | simulated gastric fluid | | simulated duodenal fluid | |
|---|---|---|---|---|---|
| compd | conc (mM) | compd | conc (mM) | compd | conc (mM) |
| KCl | 12.50 | KCl | 35.08 | KCl | 6.91 |
| $KH_2PO_4$ | 14.02 | $KH_2PO_4$ | 0.63 | $KH_2PO_4$ | 0.56 |
| $NaHCO_3$ | 7.99 | $NaHCO_3$ | 25.98 | $NaHCO_3$ | 43.00 |
| NaCl | 4.10 | NaCl | 41.00 | NaCl | 32.85 |
| $MgCl_2(H_2O)_6$ | 0.29 | $MgCl_2(H_2O)_6$ | 0.59 | $MgCl_2(H_2O)_6$ | 0.32 |


dx.doi.org/10.1021/jf500983n | J. Agric. Food Chem. 2014, 62, 8352–8356

Review Committee in accordance to the Canadian Council on Animal Care regulations. Adult (20 week old) SHRs weighing between 360 and 400 g were kept under a 12 h day/night cycle at 21 °C and fed a standard chow diet and water ad libutum. The SHRs were split into four groups of four rats each and administered the following treatment: (a) *P. palmata* hydrolysate dissolved in phosphate buffer saline (PBS, pH 7.2) at 50 mg/kg body weight, (b) the synthesized tridecapeptide IRLIIVLMPILMA dissolved in PBS at 50 mg/kg body weight, (c) the positive control captopril dissolved in PBS at 10 mg/kg body weight, and (d) PBS only. Each group received a 1 mL dose of each treatment via oral gavage. Before blood pressure was determined, rats were first anesthetized in a chamber at 40 °C with 4% isofluorane for 4 min to avoid stress-related blood pressure effects. The systolic blood pressure (SBP) of the SHRs was measured at 0, 2, 4, 6, 8, and 24 h by the tail cuff method while the rats were in an unconscious state using the Mouse Rat Tail Cuff Blood Pressure System (IITC Life Sciences, Woodland Hills, CA, USA). The change in SBP mm Hg (ΔSBP) was determined by subtracting the SBP at time $n$ (where $n$ is equal to 2, 4, 6, 8, or 24 h) from the SBP at time 0.

**Statistical Analysis.** The student's $t$ test was performed using GraphPad Prism version 5.04 for Windows, GraphPad Software (La Jolla, CA, USA) and was considered significantly different if $P < 0.05$.

## RESULTS AND DISCUSSION

The feasibility of functional food or pharmaceutical application of bioactive peptides depends on overcoming several challenges including lack of oral bioavailability. In addition, bioactive peptide action is often hampered by proteolytic attack. In this work, the resistance of a renin inhibitory tridecapeptide with the amino acid sequence IRLIIVLMPILMA was assessed using a combination of in silico analysis followed by a simulated GI digestion procedure and in vivo administration to SHRs. Table 2 shows the resultant peptide fragments obtained from the tridecapeptide IRLIIVLMPILMA following in silico analysis using the online tool Expasy Peptide Cutter. It shows that the peptide is cleaved at position 3, 6, and 11 by pepsin at both pH 1.3 and pH > 2. More importantly, however, in terms of renin inhibitory activity, the enzyme trypsin cleaves the peptide at position 2 at the carboxy end of the amino acid arginine releasing the dipeptide, amino acid sequence IR. Previous work showed that this dipeptide inhibited renin, and ACE-I activities at concentrations of 1 mg/mL previously when isolated from a pea peptide hydrolysate.[11]

To confirm the results obtained using in silico analysis, the tridecapeptide was subjected to the in vitro simulated gastric digestion outlined in Figure 1. In addition, the sample was analyzed using UPLC-MS in order to identify the breakdown products and the dipeptide IR. Figures 2 and 3 show the UPLC chromatograms obtained following MS analysis of the tridecapeptide following in vitro simulated GI digestion according to the INFOGEST procedure and the corresponding nano-ESI-MS spectra data. The base peak intensity chromato-

**Table 2. Cleavage Points of the Peptide IRLIIVLMPILMA by the Main Enzymes of the Gastrointestinal Tract Using the Online Tool Expasy Peptide Cutter**

| name of enzyme | no. of cleavages | positions of cleavage sites |
|---|---|---|
| pepsin (pH 1.3) | 3 | 3, 6, 11 |
| pepsin (pH > 2) | 3 | 3, 6, 11 |
| trypsin | 1 | 2 |

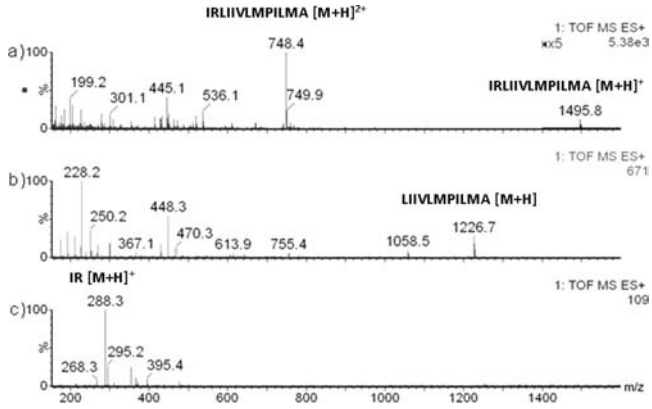


**Figure 3.** Nano-ESI-MS spectra data showing singly protonated molecular ions for (a) peptide IRLIIVLMPILMA at $m/z$ 1495 and doubly protonated at $m/z$ 748, (b) hydrolyzed peptide fragment LIIVLMPILMA at $m/z$ 1226, and (c) dipeptide IR at $m/z$ 288.

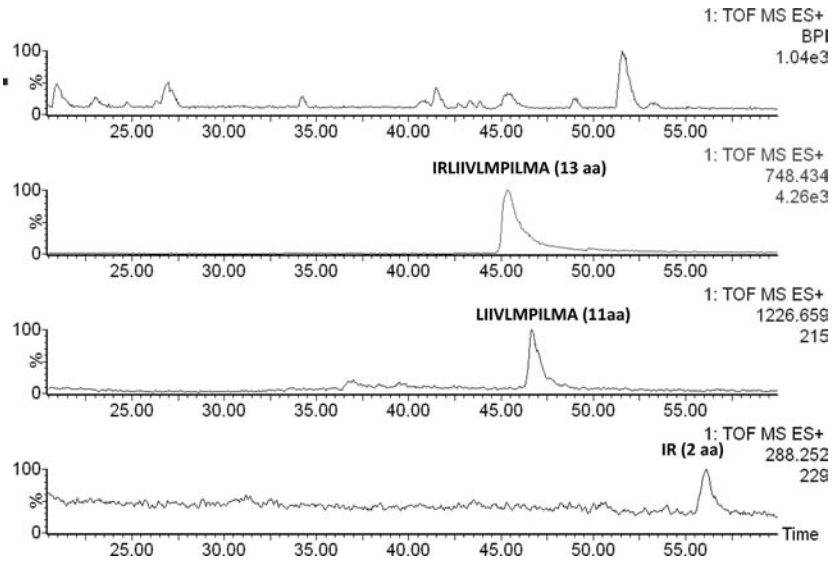


**Figure 2.** (a) Base peak intensity (BPI) chromatogram of the hydrolyzed analytes. (b) Extracted ion chromatograms (XIC) for $[M + 2H]^{2+}$ ions at $m/z$ 748.43. (c) $[M + H]^+$ ions at $m/z$ 1226. (d) $[M + H]^+$ ions at $m/z$ 288.


dx.doi.org/10.1021/jf500983n | J. Agric. Food Chem. 2014, 62, 8352−8356

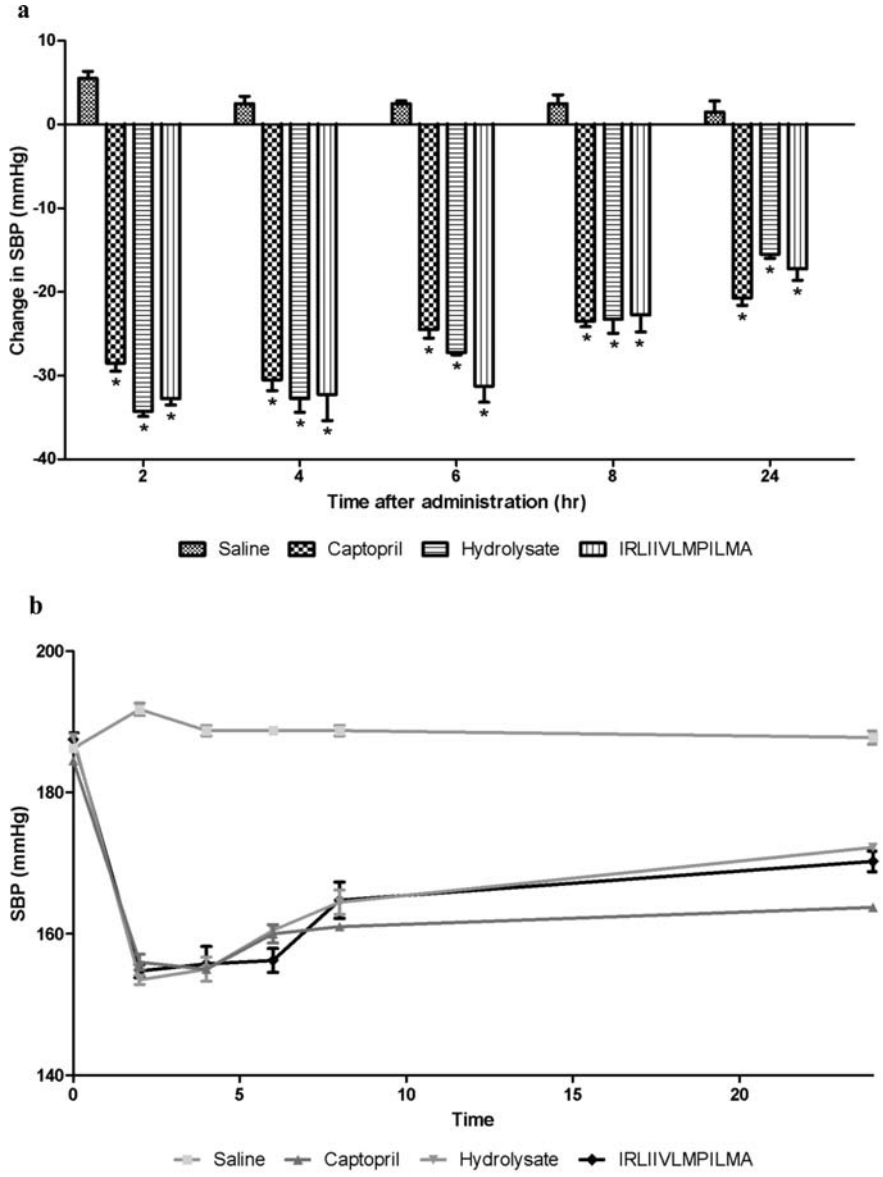


**Figure 4.** (a) Short-term (24 h) changes in systolic blood pressure (SBP) of spontaneously hypertensive rats (SHRs) after oral administration of saline, captopril, *P. palmata* protein hydrolysate, and the synthesized peptide IRLIIVLMPILMA. (b) SBP of SHR rats over 24 h after oral administration of saline, captopril, P. palmata protein hydrolysate, and the synthesized peptide IRLIIVLMPILMA. Values are mean ± SEM ($n$ = 3). *$P$ < 0.05 compared to the control (saline).

gram (Figure 2a) displays the peaks of all hydrolyzed analytes. The extracted chromatogram in Figure 2b displays doubly charged $[M + 2H]^{2+}$ ions at $m/z$ 748 representing the whole, uncleaved tridecapeptide IRLIIVLMPILMA (theoretical mass = 1494). The corresponding nano-ESI-MS spectra data in Figure 3a shows both the protonated molecular ions for IRLIIVLMP-ILMA at $m/z$ 1495 and the doubly protonated at $m/z$ 748. Figure 2c displays the extracted chromatogram highlighting the peaks corresponding to the $[M + H]^{+}$ ions at $m/z$ 1226 representing the cleaved fragment LIIVLMPILMA (theoretical mass = 1225). Figure 3b displays the resultant nano-ESI-MS spectra data hydrolyzed peptide fragment LIIVLMPILMA at $m/z$ 1226. Figure 2d shows the extracted ion chromatogram displaying $[M + H]^{+}$ ions at $m/z$ 288 the expected observed mass of the peptide IR (theoretical mass = 287) now cleaved from the parent peptide. The consequential nano-ESI-MS spectral data in Figure 3c shows the dipeptide IR at $m/z$ 288. The MS data obtained confirms the in silico cleavage analysis results that predicted that the renin inhibitory dipeptide IR remains intact during normal digestive processes. Previous studies examined the ACE-I inhibitory activity in pea and whey protein digests using in vitro digestion but chose to analyze the resulting hydrolysates with SDS-PAGE and HPLC.[15] In this study, ESI-Q-TOF mass spectrometry was used in tandem with UPLC due to the high sensitivity of peptide detection that ESI-Q-TOF offers along with the rapid and high degree of separation offered by UPLC.[16]

The results shown in Figure 4 present the short-term changes in SBP observed over a 24 h period of SHRs fed a diet of the seaweed protein papain hydrolysate, the synthesized tridecapeptide, a positive control (captopril), and a saline solution (negative control). Figure 4a displays changes in SBP over a 24 h period whereas Figure 4b shows the actual SBP over the same time period following administration of the

control (saline), the known blood pressure lowering drug captopril (3 mg/kg bw) as a positive control, the *P. palmata* protein hydrolysate (50 mg/kg bw), and the synthesized peptide IRLIIVLMPILMA (3 mg/kg bw). Interestingly, both the hydrolysate and the tridecapeptide IRLIIVLMPILMA displayed very similar trends in lowering the SBP of the rats over a 24 h period. After 2 h, the group that was fed with captopril recorded a 29 mm Hg drop in SBP from 184 (±0.28) mm Hg to 156 (±1.08) mm Hg . Likewise, the group fed the *P. palmata* protein hydrolysate recorded a drop of 34 mm Hg in SBP from 187 (±0.25) to 153 (±0.64) mm Hg SBP, while the group fed the tridecapeptide IRLIIVLMPLIMA presented a drop of 33 mm Hg in blood pressure from 187 (±0.95) to 155 (±0.94) mm Hg SBP. After 24 h, the effect of all blood pressure lowering agents was drops of 21, 16, and 17 mmHg SBP, respectively, compared to the SBP recorded at 0 h. Previous papers examined the blood pressure lowering effects of a pea peptide hydrolysate in SHRs.[17] Blood pressure was measured using the tail cuff plethysmography method to avoid stress-related blood pressure effects. However, the pea protein hydrolysates were administered at a concentration of 200 mg/kg, and this dose resulted in a 19 mm Hg drop in SBP of SHRs. Likewise, SHRs treated with an antihypertensive buckwheat hydrolysate recorded an initial decrease in SBP of 27 ± 7.6 mm Hg after 2 h but only when treated with 100 mg/kg body weight,[18] twice the concentration of the *P. palmata* protein hydrolysate and the tridecapeptide IRLIIVLMPLIMA used in this study. In silico analysis of the peptide using the online tool ToxinPred also showed that the peptide was nontoxic, which indicates that it is suitable for use in functional foods and pharmaceutical agents. In addition, an earlier study carried out by this group found that the *P. palmata* hydrolysate was nontoxic to zebrafish when administered at a concentration between 1 and 5 mg/mL.[19]

This study demonstrates that the tridecapeptide IRLIIVLMPLIMA is a renin inhibitory peptide with the ability to impart an antihypertensive effect in vivo confirmed by monitoring changes in SBP in SHRs over a 24 h period. Both the peptide and the *P. palmata* protein papain hydrolysate may have potential for use as functional ingredients in the growing nutraceutical market to prevent hypertension.

## AUTHOR INFORMATION

### Corresponding Author

*Phone: +353 (0) 1 8059500; fax: +353 (0)1 8059550; e-mail: ciaran.fitzgerald@teagasc.ie.

### Funding

This work was supported by the Irish Marine Functional Foods Research Initiative, NutraMara programme, which is funded by the Irish Department of Agriculture, Fisheries and Marine and the Marine Institute. It was also supported by the COST action INFOGEST, improving health properties of food by sharing knowledge on the digestive process FA1005. INFOGEST is supported by the EU Framework programme 2011-2015. C.F. is in receipt of the Teagasc Walsh Fellowship.

### Notes

The authors declare no competing financial interest.

## REFERENCES

(1) Lien, S.; Lowman, H. B. Therapeutic peptides. *Trends Biotechnol.* **2003**, *21*, 556−562.

(2) Callow, A. D. Cardiovascular disease 2005—The global picture. *Vasc. Pharmacol.* **2006**, *45*, 302−307.

(3) Gradman, A. H.; Kad, R. Renin inhibition in hypertension. *J. Am. Coll. Cardiol.* **2008**, *51*, 519−528.

(4) Gradman, A. H.; Schmieder, R. E.; Lins, R. L.; Nussberger, J.; Chiang, Y.; Bedigian, M. P. Aliskiren, a novel orally effective renin inhibitor, provides dose-dependent antihypertensive efficacy and placebo-like tolerability in hypertensive patients. *Circulation* **2005**, *111*, 1012−1018.

(5) Tigerstedt, R.; Bergman, P. Niere und Kreislauf. *Skand. Arch. Physiol.* **1898**, *8*, 223−271.

(6) Skeggs, L. T.; Kahn, J. R.; Lentz, K.; Shumway, N. P. The preparation, purification, and amino acid sequence of a polypeptide renin substrate. *J. Exp. Med.* **1957**, *106*, 439−453.

(7) Wu, J.; Ding, X. Characterization of inhibition and stability of soy-protein-derived angiotensin I-converting enzyme inhibitory peptides. *Food Res. Int.* **2002**, *35*, 367−375.

(8) Ma, M.-S.; Bae, I. Y.; Lee, H. G.; Yang, C.-B. Purification and identification of angiotensin I-converting enzyme inhibitory peptide from buckwheat (*Fagopyrum esculentum* Moench). *Food Chem.* **2006**, *96*, 36−42.

(9) Kim, S.-K.; Wijesekara, I. Development and biological activities of marine-derived bioactive peptides: A review. *J. Funct. Foods* **2010**, *2*, 1−9.

(10) Suetsuna, K.; Nakano, T. Identification of an antihypertensive peptide from peptic digest of wakame (*Undaria pinnatifida*). *J. Nutr. Biochem.* **2000**, *11*, 450−454.

(11) Li, H.; Aluko, R. E. Identification and inhibitory properties of multifunctional peptides from pea protein hydrolysate. *J. Agric. Food Chem.* **2010**, *58*, 11471−11476.

(12) Girgih, A. T.; Udenigwe, C. C.; Li, H.; Adebiyi, A. P.; Aluko, R. E. Kinetics of enzyme inhibition and antihypertensive effects of hemp seed (*Cannabis sativa L.*) protein hydrolysates. *J. Am. Oil Chem. Soc.* **2011**, *88*, 1767−1774.

(13) Fitzgerald, C.; Mora-Soler, L.; Gallagher, E.; O'Connor, P.; Prieto, J.; Soler-Vila, A.; Hayes, M. Isolation and characterization of bioactive pro-peptides with *in vitro* renin inhibitory activities from the macroalga *Palmaria palmata*. *J. Agric. Food Chem.* **2012**, *60*, 7421−7427.

(14) Gasteiger, E.; Hoogland, C.; Gattiker, A.; Wilkins, M. R.; Appel, R. D.; Bairoch, A. Protein identification and analysis tools on the ExPASy server. In *The Proteomics Protocols Handbook*; Springer: New York, 2005; pp 571−607.

(15) Vermeirssen, V.; van der Bent, A.; Van Camp, J.; van Amerongen, A.; Verstraete, W. A quantitative in silico analysis calculates the angiotensin I converting enzyme (ACE) inhibitory activity in pea and whey protein digests. *Biochimie* **2004**, *86*, 231−239.

(16) Yang, B.; Dong, W.; Zhang, A.; Sun, H.; Wu, F.; Wang, P.; Wang, X. Ultra performance liquid chromatography coupled with electrospray ionization/quadrupole-time of-flight mass spectrometry for rapid analysis of constituents of Suanzaoren decoction. *J. Sep. Sci.* **2011**, *34*, 3208−15.

(17) Li, H.; Prairie, N.; Udenigwe, C. C.; Adebiyi, A. P.; Tappia, P. S.; Aukema, H. M.; Jones, P. J.; Aluko, R. E. Blood pressure lowering effect of a pea protein hydrolysate in hypertensive rats and humans. *J. Agric. Food. Chem.* **2011**, *59*, 9854−60.

(18) Li, C. H.; Matsui, T.; Matsumoto, K.; Yamasaki, R.; Kawasaki, T. Latent production of angiotensin I-converting enzyme inhibitors from buckwheat protein. *J. Pept. Sci.* **2002**, *8*, 267−74.

(19) Fitzgerald, C.; Gallagher, E.; O'Connor, P.; Prieto, J.; Mora-Soler, L.; Grealy, M.; Hayes, M. Development of a seaweed derived platelet activating factor acetylhydrolase (PAF-AH) inhibitory hydrolysate, synthesis of inhibitory peptides and assessment of their toxicity using the Zebrafish larvae assay. *Peptides* **2013**, *50c*, 119−124.

JOURNAL OF AGRICULTURAL AND FOOD CHEMISTRY

Article

pubs.acs.org/JAFC

# Effect of Processing on Physicochemical Characteristics and Bioefficacy of β-Lactoglobulin−Epigallocatechin-3-gallate Complexes

Pauline Lestringant,[†,‡] Anilda Guri,*[,†] İbrahim Gülseren,[†,§] Perla Relkin,[‡] and Milena Corredig[†]

[†]Department of Food Science, University of Guelph, 50 Stone Road East, Guelph, Ontario N1G 2W1, Canada

[‡]UMR 1145, Food Process Engineering, AgroParisTech, 1 Avenue des Olympiades, F-91300 Massy, France

**ABSTRACT:** Varying amounts of epigallocatechin-3-gallate (EGCG) were encapsulated in β-lactoglobulin (β-Lg) nanoparticles, either native or processed, denoted as heated or desolvated protein. The stability, physical properties, and bioactivity of the β-Lg−EGCG complexes were tested. Native β-Lg−EGCG complexes showed comparable stability and binding efficacy (EGCG/β-Lg molar ratio of 1:1) to heated β-Lg nanoparticles (1% and 5% protein w/w). The sizes of heated and desolvated β-Lg nanoparticles were comparable, but the latter showed the highest binding affinity for EGCG. The presence of EGCG complexed with β-Lg did not affect the interfacial tension of the protein when tested at the soy oil−water interface but caused a decrease in dilational elasticity. All β-Lg complexes (native, heated, or desolvated) showed a decrease in cellular proliferation similar to that of free ECGC. In summary, protein−EGCG complexes did not alter the bioefficacy of EGCG and contributed to increased stability with storage, demonstrating the potential benefits of nanoencapsulation.

**KEYWORDS:** *β-lactoglobulin, EGCG, nanoencapsulation, fluorescence spectroscopy, interfacial tensiometry, bioefficacy, Caco-2 cells*

## 1. INTRODUCTION

Tea (*Camellia sinensis*) has been consumed for thousands of years and is the most common beverage after water.[1] Green tea extracts have shown antibacterial and antiviral activity[2] and also have been associated with a decreased risk of cancer or cardiovascular disease.[3] These activities are mainly attributed to the presence of polyphenolic compounds in tea leaves (i.e., flavonoids). Flavonoids contribute to color and taste of foods[3] and are widely found at high concentrations in plant-derived materials.[4]

In green tea, flavonoids are a large and heterogeneous group of molecules. Catechins account for 80% of total green tea flavonoids and include the majority of bioactive molecules in tea.[4] Epigallocatechin-3-gallate (EGCG) is the most prevalent (approximately 50%) and bioactive tea catechin[5] and is a highly water-soluble compound. As an anticarcinogen, EGCG inhibits the growth of cancer cells, such as human cervical cancer cells or colon cancer cells, and although its mechanisms of action are not fully understood, it has been shown to induce apoptosis and regulate gene expression in such cells.[6] However, recent in vivo studies on prostate cancer have led to the conclusion that green tea may not be considered yet as a chemopreventive agent.[7]

As an antioxidant, EGCG was demonstrated to act up to 10 times as effectively as L-ascorbate or β-carotene,[8] as assessed by the survival of *Escherichia coli* incubated with alkyl peroxyl radical (pH 7.3, 37 °C, 35 min). EGCG can be easily oxidized in aqueous environments, rendering it highly unstable in aqueous solutions, especially at neutral and basic pH.[9,10] The aqueous stability of EGCG can be improved by the addition of metal ion scavengers (such as ethylenediaminetetraacetic acid, EDTA) or other antioxidants (such as vitamin C) in the medium.[11] It is important to note that the bioavailability of EGCG depends not only on its stability but also on its complexed state in the food matrix, the extent of its intestinal absorption, and the extent of its bioconversion.[3]

In addition to their nutritional value, proteins are utilized for a variety of functional properties in foods, such as gelation, emulsification, or foam formation. They have the ability to bind with small hydrophilic and hydrophobic molecules, making them potential carriers of bioactive molecules in the human body[12] and in the creation of functional foods.[13−15] β-Lactoglobulin (β-Lg) is the major whey protein with an approximate concentration of 1 g·L$^{-1}$ in milk and a molecular mass of 18 400 Da.[16] Its ability to act as a nanocarrier system has been shown with model compounds such as bixin,[17] vanillin,[18] resveratrol,[19] and tea polyphenol extracts.[20]

The structure and functionality of β-Lg is highly dependent on environmental conditions such as pH and temperature. Previous studies showed that the EGCG-binding characteristics of β-Lg can be enhanced up to 3.5 times after thermal denaturation of the whey proteins.[9] The binding of polyphenols to proteins occurs mainly through hydrophobic interactions,[16] hydrogen bonding,[21] and, in some instances, electrostatic forces.[22] These interactions depend on the size and structure of the polyphenol molecules. EGCG has the highest binding affinity to whey proteins among tea catechins,[16] because of its esterification with gallic acid, which creates a galloyl functional group with multiple peptide binding sites, able to form hydrophobic interactions and hydrogen bonds with the proteins.[23]

The utilization of β-Lg as a delivery system for EGCG could potentially improve the stability of the polyphenol in a wider pH range, limit its gastric degradation, and enhance its

Received: February 25, 2014
Revised: July 29, 2014
Accepted: July 31, 2014
Published: July 31, 2014

ACS Publications © 2014 American Chemical Society

intestinal uptake. A well-designed β-Lg−EGCG system should not negatively affect the digestibility of the protein and the health-promoting properties of EGCG. The effect of tea polyphenols on digestive enzymes remains controversial, as shown by Shpigelman et al.[24] According to their results, complexation of β-Lg with EGCG did not significantly affect in vitro gastric digestion of the protein. Similar conclusions were drawn for casein−EGCG complexes: the presence of EGCG did not affect casein hydrolysis, in two different in vitro models.[25] In the literature, the role of β-Lg−EGCG interactions in the prevention of EGCG degradation in aqueous medium remains controversial regarding the extent to which EGCG is protected. It was demonstrated that the binding of EGCG to heat-denatured (85 °C, 20 min) β-Lg can effectively reduce the extent of oxidative degradation (up to 33 times) in 30 mM phosphate-buffered saline (PBS, pH 6.9), especially over the first 8 days.[24] However, it was also reported that degradation of EGCG over time is not significantly limited by binding with native or heated β-Lg.[4]

In vitro assays have been conducted to measure EGCG antioxidant activity as well as that of β-Lg−EGCG complexes.[26] To the best of our knowledge, the antioxidant activity of β-Lg−EGCG complexes has not been studied in cell culture experiments.

In this study, the interactions between β-Lg and EGCG as influenced by processing conditions were investigated. Thermal processing and desolvation were utilized in order to manufacture protein−EGCG complexes along with the unprocessed protein. The physicochemical characteristics of such complexes including encapsulation efficiency, particle size, and charge were studied by a variety of analytical techniques. It has been repeatedly shown in the literature that utilization of cell culture models in the testing of bioefficacy of medicinal drugs or bioactive compounds is a valuable approach prior to animal or human trials as an efficient and cost-effective strategy.[27,28] The bioefficacy of these complexes was studied in Caco-2 cells. This cell line was chosen as representative of epithelial tissues; it is one of the most commonly utilized cell culture models in current pharmacological studies. The effect of free EGCG, or EGCG associated with native protein, as well as protein nanoparticles, was tested by measuring their ability to inhibit cellular proliferation.

## 2. MATERIALS AND METHODS

**2.1. Sample Preparation.** Highly pure β-Lg (>99%) used in the experiments was purified from whey protein isolate (New Zealand Dairy Products, NZMP, Palmerston North, New Zealand) by preparative ion chromatography on Q-Sepharose (GE Healthcare) as previously reported.[29] β-Lg stock solution (2−5% w/w) was prepared in a buffer medium (see below) and kept refrigerated overnight (4 °C) to ensure complete hydration. The stock solution was then filtered through a 0.45 μm filter (Millipore, Millex HV, Billerica, MA). EGCG (min. 94%) was a gift of DSM Nutritional Products (Teavigo, Ayr, Ontario, Canada) and its stock solutions (0.1−5 mg·mL$^{-1}$) were freshly prepared and filtered as described for β-Lg solutions. Unless otherwise stated, all solutions were prepared in sodium phosphate buffer (20 mM, pH 7.0) that contained sodium azide as bacteriostat (0.02%). β-Lg stock solution was equilibrated at room temperature (30 min) before it was mixed with varying volumes of EGCG solutions to obtain different EGCG/β-Lg molar ratios (0−10). Each sample was immediately vortexed for 5 s.

**2.2. Fluorescence Spectroscopy.** β-Lg−EGCG complexes were prepared by mixing 10.9 μM β-Lg solution with equal volumes of diluted EGCG stock solutions ranging from 0 to 135.9 μM. Eleven different samples with EGCG/β-Lg molar concentration ratios of 0−10 were prepared, and 200 μL aliquots of each sample were transferred to a 96 well fluorescence plate (Fisher Scientific). The protein intrinsic fluorescence spectra (300−450 nm) were directly recorded with a Synergy H4Microplate Reader (Biotek, Winooski, VT) utilizing an excitation wavelength of 280 nm and slit width of 5 nm. The Stern−Volmer equation was used to determine the quenching mechanism that takes place due to EGCG binding to β-Lg molecules:

$$\frac{F_0}{F} = 1 + K_{SV}[\mathrm{EGCG}] \quad (1)$$

where $F_0$ is the initial fluorescence intensity of 0.02% (w/w) β-Lg solution, $F$ is the fluorescence intensity of the sample at the peak (325 nm emission), and $K_{SV}$ is the Stern−Volmer constant.[30] The binding constant and stoichiometry were calculated as follows:

$$\log\left(\frac{F_0 - F}{F}\right) = \log(K_s) + n\log[\mathrm{EGCG}] \quad (2)$$

where $K_s$ is the static binding constant and $n$ is the binding number.[20] All measurements were carried out at least in duplicate.

**2.3. Preparation of EGCG-Bearing β-Lactoglobulin Nanoparticles.** *2.3.1. Thermal Processing.* Thermal processing of β-Lg solutions was carried out at 85 °C (20 min, 400 rpm) with a thermomixer (Eppendorf 5436, Brinkmann Instruments, Mississauga, ON, Canada). The samples were immediately transferred to an ice bath and were mixed with EGCG solutions at room temperature at a molar ratio ranging from 0:1 to 3:1 (EGCG/β-Lg). The final β-lactoglobulin concentrations in the mixture were 1% or 5% (w/w) in all cases.

*2.3.2. Desolvation Procedure.* Whey protein nanoparticles were prepared by an established procedure.[14] To maximize electrostatic repulsion between protein molecules, pH of the native β-Lg solutions was adjusted to pH 9 with concentrated sodium hydroxide solution (2 M). Pure ethanol was then added to 2 mL of β-Lg solution at a rate of 1 mL·min$^{-1}$. The final volume of ethanol added was 5 times the volume of β-lactoglobulin solution (i.e., 10 mL). Immediately after desolvation, the mixture was diluted 20 times in 20 mM sodium citrate buffer (pH 3) to stabilize the desolvated particles. In this case, as heating was not applied, EGCG was dissolved in the dilution buffer prior to mixing (0−190.7 μM). Due to the high extent of dilution in the desolvation protocol (i.e., 120 times), all desolvation experiments were conducted at an initial protein concentration of 5% (w/w).

**2.4. Interfacial Tensiometry.** To further probe the formation of complexes and possible changes in the protein functionality, interfacial tensiometry was applied to determine changes in protein adsorption at the interface. This technique is based on analysis of the size and shape of a dispersed phase droplet (i.e., soy oil) suspended in a continuous phase (i.e., aqueous suspension of β-Lg−EGCG complexes). Interfacial tension was measured for at least 2 h to ensure that equilibrium was established. Immediately afterward, the oil droplet was sinusoidally oscillated around its initial volume (±10%) to measure the elastic modulus. A dilational amplitude range of 0−40% was within the linear viscoelastic range (data not shown).

The interfacial activity of EGCG-bearing β-Lg nanoparticles was determined by drop shape tensiometry at the aqueous dispersion−soybean oil interface (25 °C) (Tracker, IT Concept, Longessaigne, France). The oil phase was purified prior to the experiments by mixing it with Florisil (Sigma−Aldrich, catalog no. 46385, particle size 149−250 μm)[31] at a ratio of 10:1, shaking for 2 h (60 rpm) on a shaking plate, and then removal of Florisil by filtering (Whatman cellulose filter #52, 7 μm). The purification process was repeated three times prior to all measurements. A soy oil droplet (approximately 6 μL) was automatically formed at the tip of a syringe, which was immersed in a cuvette containing the aqueous dispersion of protein−EGCG complexes or protein only. The assembly of the cuvette and syringe was monitored by a charge-coupled device (CCD) camera for acquisition of high-quality images, and the shape of the oil droplet was automatically analyzed in order to calculate the time dependence of the interfacial tension up to a drop age of 10 000 s. Since the calculation of dynamic interfacial tension was based on the Young−

Laplace equation, the shape of the drop was periodically monitored to ensure a Laplacian shape and the absence of partial detachment of the drop throughout the run. All the measurements were carried out in duplicate. The focus, verticality of the syringe tip, and measured image volume were reset or recalibrated daily.[32]

Dilational elasticity gives an indication of the ability of the adsorbed moieties to stabilize the interface during droplet volume changes. The method utilized here is based on the automatically controlled, sinusoidal compression−expansion of the aqueous droplet at a defined oscillatory frequency and amplitude of dilation.[33] The interfacial modulus of dilational elasticity was calculated from the change in interfacial tension ($d\gamma$) relative to the change in droplet surface area ($dA$):

$$\varepsilon = \frac{d\gamma}{d \ln A} \quad (3)$$

Heated and desolvated $\beta$-Lg particles were prepared and EGCG was added to prepare complexes of these particles and along with native protein, as detailed above. The interfacial activity of the complexes was measured. A molar ratio range of 0:1 to 3:1 (EGCG/$\beta$-Lg) was utilized throughout the experiment. All measurements were carried out at least in duplicate.

**2.5. Determination of Apparent Particle Diameter and $\zeta$-Potential by Dynamic Light Scattering.** The particle size distribution and $\zeta$-potential of EGCG-bearing $\beta$-Lg nanoparticles was determined by dynamic light scattering (DLS) on a Zetasizer Nano (Malvern Instruments, Worcestershire, U.K.). No further dilution was carried out prior to DLS measurements due to the low extent of scattering of the protein dispersions. All particle size distributions reported here were determined on the basis of volume frequency, and the apparent mean diameter was measured.

**2.6. Separation of Uncomplexed Polyphenols.** To determine the amount of encapsulated EGCG, free EGCG was separated from bound EGCG on a desalting column (HiTrap desalting column, product no. 17-408-01, GE Healthcare, Uppsala, Sweden). The extent of EGCG encapsulation was then quantified on the basis of absorbance measurements (at a wavelength of 280 nm). The complexes were eluted with 20 mM sodium phosphate buffer (pH 7) that contained 50 mM NaCl. Free EGCG was removed from the column with 20% ethanol, and the absorbance measurements were carried out in ethanolic solution on a UV−visible spectrophotometer (RF-5301PC, Shimadzu, Japan). A range of EGCG controls (0−0.2 mg/mL) was also studied along with the samples.

**2.7. Cellular Proliferation Assays.** Caco-2 cells were provided form CRIFS culture collection (Canadian Research Institute for Food Safety) and were maintained in Dulbecco's modified Eagle medium (DMEM; Sigma−Aldrich Corp., Oakville, ON, Canada) supplemented with 10% (v/v) heat-inactivated fetal bovine serum (FBS) (Invitrogen Canada Inc., Burlington, ON, Canada), 2 mM L-glutamine, 1% (v/v) penicillin−streptomycin, and 1% (v/v) essential amino acids as well as 0.25% (v/v) *N*-(2-hydroxyethyl)piperazine-*N*′-ethanesulfonic acid (HEPES) buffer. Cells were passaged weekly (80−90% confluence) with 0.25% trypsin−EDTA (Invitrogen) and medium was changed every other day. Cells were kept daily at 37 °C in humidified atmosphere in 5% $CO_2$. Cells at passage 29−38 were used for the proliferation tests.

Freshly prepared EGCG−$\beta$-Lg and respective aged samples (24 h at 4 °C) were administered to the Caco-2 cell culture. Sulforhodamine B (SRB) assay was used to evaluate the influence of the samples on the proliferation rate of Caco-2 cancer cells.[34] Briefly, Caco-2 cells at a concentration of $6 \times 10^3$ cells/well were seeded on clear bottom 96 well plates (Fisher Scientific, Mississauga, ON, Canada) and allowed to adhere for 24 h. Afterward, fresh samples were added to the cells at a dilution rate of 1:5.6 in the medium (sample/medium v/v) and incubated for 24 h. Loading on the cells was calculated on the basis of the amount of EGCG originally present in the sample. The amount of protein $\beta$-Lg in final dilution in the well was 1.8 $\mu$g/mL for native and heated samples, while for desolvated samples it was 0.08 $\mu$g/mL. EGCG concentrations were 0.05 and 0.13 $\mu$g/mL for EGCG/$\beta$-Lg molar ratios of 1 and 3, respectively, when complexed with native or heated $\beta$-Lg. On the other hand, the EGCG concentration was 0.006 $\mu$g/mL when complexed with desolvated $\beta$-Lg to maintain a EGCG/$\beta$-Lg molar ratio of 3. Control samples (cells with medium only) along with blank samples (medium only) were also tested. The optical density of plates was measured on an automated 96-well plate reader (Synergy H4Microplate Reader, Biotek, Winooski, VT) at 570 nm. Results were expressed as percentage proliferation with respect to control wells grown with no sample treatments.

**2.8. Statistical Analyses.** Unless otherwise stated, all the experiments were carried out in triplicates and the results are expressed as means ± standard deviation (SD). Statistical differences were evaluated by analysis of variance (ANOVA) (XL Stats [7.5.2], Addinsoft, Paris, France). The differences were considered to be significant at $p < 0.05$.

## 3. RESULTS AND DISCUSSION

**3.1. Fluorescence Spectroscopy.** Figure 1 shows the changes in intrinsic fluorescence in native $\beta$-Lg solutions

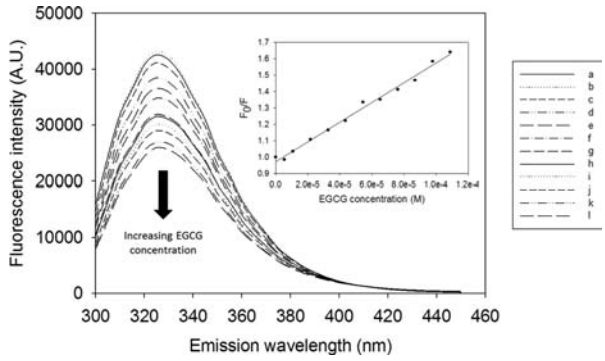


**Figure 1.** Fluorescence spectra of 0.02% (w/w) $\beta$-lactoglobulin and the influence of EGCG concentration (millimolar) on intrinsic fluorescence of the protein. The molar ratio range tested was 0−10. Curves a−l respectively correspond to EGCG/$\beta$-Lg molar ratios 0, 0.5, 1, 2, 3, 4, 5, 6, 7, 8, 9, and 10. Excitation was carried out at 280 nm. Representative runs are shown. (Inset) Stern−Volmer plot (eq 1) derived from fluorescence intensity data.

(0.02% w/w) as a function of EGCG concentration (0−0.05 mg·mL$^{-1}$, corresponding to EGCG/$\beta$-Lg molar ratios 0−10). For EGCG/$\beta$-Lg ratios that are lower than 4:1 (0.02 mg/mL EGCG), the absorbance values recorded for the mixture were lower than 0.1 (data not shown), thus rendering the measurements valid in this concentration range. In all cases, the intensity of the intrinsic fluorescence intensity of the protein decreased with EGCG addition. The linearity of the Stern−Volmer plot (Figure 1, inset) suggested that all fluorophores in the protein were equally accessible to the EGCG molecules.[30] The quenching was attributed to binding of EGCG to $\beta$-Lg.

Figure 2 illustrates the linearity of the double logarithmic plot (eq 2), employed to determine the binding constant ($K_s$) and number of EGCG binding sites per $\beta$-Lg molecule ($n$). These values were $4.3 \times 10^4$ M$^{-1}$ and 1.2, respectively. These figures were found to be comparable with those reported in previous studies where a similar fluorescence method was used: $1.25 \times 10^4$ M$^{-1}$ and 0.94[4] and $1.3 \times 10^4$ M$^{-1}$ and 1.3,[16] respectively, for binding constant and number of binding sites. On the basis of these findings, each native $\beta$-Lg molecule can be expected to bind approximately one EGCG molecule (i.e., 1:1 on a molar concentration basis).

Previous authors reported an increase in the EGCG binding capabilities of $\beta$-Lg with heating.[9] In the present work, the


dx.doi.org/10.1021/jf5029834 | J. Agric. Food Chem. 2014, 62, 8357−8364

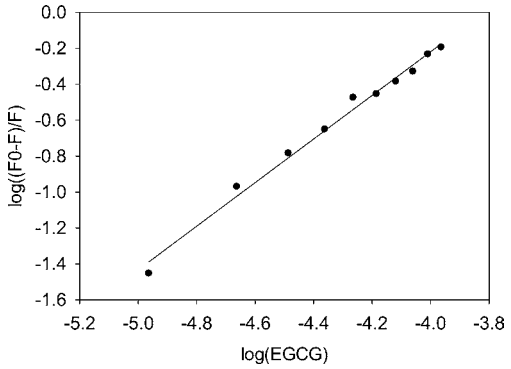


**Figure 2.** Double logarithmic plot of changes in fluorescence intensity as a function of EGCG concentration (10.9−108.8 $\mu$M). The binding constant and number of binding sites of $\beta$-Lg for EGCG binding can be inferred from the intercept and slope, respectively (eq 2).

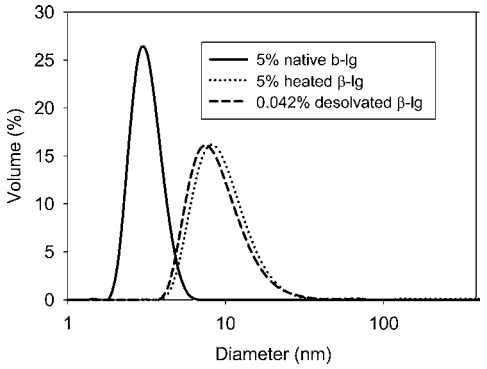


**Figure 3.** Particle size distribution of native (—), heated (85 °C, 20 min) (···), or desolvated (5× ethanol) (− − −) $\beta$-lactoglobulin solutions mixed with EGCG solutions at molar concentration ratio (EGCG/ $\beta$-Lg) of 3 as determined by dynamic light scattering (DLS). The protein concentration was 5% for native and heated protein, whereas it corresponded to 0.042% due to extensive dilution requirement for desolvated samples. Representative runs are shown.

association of EGCG with $\beta$-Lg was studied after preparation of protein nanoparticles by either thermal processing or desolvation techniques. We hypothesized that $\beta$-Lg−EGCG complexes could be obtained and that, in the complexed form, EGCG could maintain its bioefficacy in a cell culture model for intestinal cells (i.e., Caco-2 culture).

**3.2. Physicochemical Characteristics of EGCG-Bearing $\beta$-Lactoglobulin Particles.** The average apparent diameter for nanoparticles is summarized in Table 1, and Figure 3 shows the particle size distribution of EGCG-bearing $\beta$-Lg nanoparticles (heated or desolvated, 1:3 molar ratio of protein/EGCG) or native $\beta$-Lg, as measured by dynamic light scattering. Both heating and desolvation resulted in significantly larger protein complexes but <100 nm in average apparent diameter. The experiments were conducted at 10 and 50 $\mu$g·mL$^{-1}$ protein in the case of solutions heated at 85 °C for 20 min and at 50 $\mu$g·mL$^{-1}$ for desolvated nanoparticles (due to the high dilution in pH 3 buffer; see Materials and Methods). Native $\beta$-Lg solutions showed an average apparent diameter between 11 and 14 nm, and heating significantly increased the size to about 30 nm for 10 $\mu$g·mL$^{-1}$ and 40 nm for 50 $\mu$g·mL$^{-1}$ protein. The presence of EGCG did not affect the particle size significantly at the protein concentration levels studied (Table 1). This finding might be attributed to the molecular mass of EGCG (458 Da), which is considerably smaller compared to that of $\beta$-Lg (18.4 kDa) and the low extent of EGCG binding on a molar basis as shown by fluorescence measurements (i.e., $n$ = 1.2). Furthermore, EGCG interactions with the protein did not cause aggregation of the particles.

Desolvated $\beta$-Lg particles (with a starting solution of 50 $\mu$g·mL$^{-1}$) showed a significantly higher apparent diameter than both heated and native particles, with a larger standard deviation between experiments ($p$ < 0.05). This was due to a small fraction (1.2% of the volume) of larger particle (>1000 nm) in some of the replicate runs (data not shown). These results are in agreement with the observation of desolvated $\beta$-Lg samples by cryo-transmission electron microscopy (cryo-

**Table 1. Particle Size, $\zeta$ Potential, and Encapsulation Efficiency of EGCG-Bearing Native, Heated, or Desolvated Nanoparticles[a]**

| $\beta$-Lg concn (%) | EGCG/$\beta$-Lg molar ratio | diameter (nm) | $\zeta$ potential (mV) | encapsulation efficiency (% EGCG) | loading EGCG/$\beta$-Lg ($\mu$g·mg$^{-1}$) |
|---|---|---|---|---|---|
| | | | Native[b] | | |
| 1 | 0 | 14 ± 1 D | −17 ± 4 C | | |
| 1 | 1 | 11 ± 1 D | −21 ± 3 CD | 91 ± 13 A | 23 ± 3 |
| 1 | 3 | 12 ± 4 E | −27 ± 2 E | 69 ± 9 AB | 52 ± 7 |
| 5 | 0 | 12 E | −10 ± 2 B | | |
| 5 | 1 | 10 ± 0 E | −16 ± 3 C | 89 ± 12 A | 22 ± 3 |
| 5 | 3 | 11 ± 0 E | −21 ± 2 C | 22 ± 9 C | 16 ± 7 |
| | | | Heated[b] | | |
| 1 | 0 | 30 ± 0.5 CD | −17 ± 5 C | | |
| 1 | 1 | 30 ± 0.5 D | −21 ± 4 C | 94 ± 8 A | 21 ± 5 |
| 1 | 3 | 38 ± 8 BCD | −27 ± 3 E | 54 ± 13 BC | 44 ± 8 |
| 5 | 0 | 41 ± 1 BC | −27 ± 2 E | | |
| 5 | 1 | 42 ± 1 B | −26 ± 2 DE | 79 ± 2 AB | 20 ± 1 |
| 5 | 3 | 42 ± 3 B | −30 ± 3 E | 27 ± 3 C | 20 ± 2 |
| | | | Desolvated[c] | | |
| 0.042 | 0 | 71 ± 24 A | 28 ± 1 A | | |
| 0.042 | 3 | 101 ± 38 A | 26 ± 2 A | 91 ± 18 A | 68 ± 13 |

[a]Different letters in the same column indicate a statistically significant difference. [b]Native $\beta$-Lg or heated $\beta$-Lg nanoparticles at final protein concentrations of 1% and 5% (pH 7). [c]$\beta$-Lg nanoparticles prepared with desolvation at a final protein concentration of 0.042% (pH 3).


dx.doi.org/10.1021/jf5029834 | J. Agric. Food Chem. 2014, 62, 8357−8364

TEM) showing small spherical particles and some larger particles.[14]

The thermal denaturation point of β-Lg is ∼76 °C.[35] Previous studies[35,36] showed that the first steps of denaturation lead to formation of surface-exposed hydrophobic clusters that increase protein−protein interactions. At temperatures higher than 60 °C, β-Lg monomers are partially unfolded, exposing the thiol group.[37] The free sulfhydryl group of β-Lg becomes reactive and causes thiol/disulfide interchanges with the other β-Lg monomers.[37,38] Heating caused aggregation of β-Lg, and the size of the aggregates significantly increased with protein concentration from 10 to 50 $\mu g \cdot mL^{-1}$ ($p < 0.05$). This observation was previously attributed to an acceleration of the polymerization reaction with increasing protein concentration.[38] Although the tertiary structure of β-Lg is affected by heating, as shown by Fourier transform infrared (FTIR) measurements, a reversible change in secondary structure will take place once β-Lg is cooled down quickly after heating.[26] Furthermore, it was reported that binding of EGCG did not affect the secondary structure of the protein, which is composed primarily of β-strands (55%).[26] This was in contrast with the findings of Shpigelman et al.[24] who suggested, using attenuated total reflectance (ATR)-FTIR, that binding of EGCG on heated β-Lg changed the protein secondary structure toward a higher extent of random coils. In the case of desolvated nanoparticles, however, the addition of ethanol to a β-Lg solution triggers a change in solvent polarity that affects the protein secondary structure and its ability to bind with other molecules. It has been shown that, in the presence of ethanol, β-Lg increases its α-helix content, and the structural changes lead to aggregation of the monomers.[39]

The ζ-potential of native β-Lg and heated β-Lg nanoparticles was found to be negative at pH 7, for example, −17 mV for 1% native and heated protein alone. When measured at a higher protein concentration, the values for native β-Lg particles were significantly lower; this may indicate the presence of residual ions in the purified protein fractions, which increases the overall ionic strength in the medium with protein concentration. In all cases, the presence of EGCG significantly increased the magnitude of ζ-potential of native β-Lg, as well as for the heated β-Lg nanoparticles (Table 1). This is consistent with results reported by Thongkaew et al.[40] when adding catechins to whey protein isolate. At 50 $\mu g \cdot mL^{-1}$, the heated nanoparticles were significantly more negatively charged than the native proteins, and the ζ-potential was also found to significantly increase in magnitude with EGCG concentration (Table 1). These results were consistent with a previous study[24] showing that the stability of EGCG-bearing heated β-Lg complexes was greater than that of heated β-Lg alone, which demonstrated that EGCG tends to stabilize β-Lg particles. It can be explained by the fact that, at pH 7, EGCG phenolic groups are deprotonated, generating an oxygen center of negative charges that will prevent further aggregation of β-Lg−EGCG complexes.[37] A recent work also pointed out a change in the structure of the protein upon polyphenol addition, namely, an increase in α-helix and β-sheet secondary structures and a decrease in random coil.[16] This could also stabilize the β-Lg−EGCG complexes. However, at high polyphenol concentration (1% w/v), precipitation of whey protein isolate has been reported and attributed to the aggregation of soluble complexes forming insoluble flocs.[37] In the case of desolvated particles (Table 1), since pH 3 is below the isoelectric point of β-Lg, their ζ-potential was positive, as previously demonstrated.[14] The value did not significantly vary with the presence of EGGC. In all cases, the particles showed a charge of about +26 mV, which indicates stability of the particles.

**3.3. Encapsulation Efficiency of EGCG-Bearing β-Lg Nanoparticles.** The amount of EGCG associated with the protein was determined after separation of the protein fraction from the unbound EGCG by a gel-filtration method. The values of EGCG recovery and encapsulation efficiency are summarized in Table 1 for 10 and 50 $\mu g \cdot mL^{-1}$ protein. The amount of EGCG recovered with β-Lg in 10 $\mu g \cdot mL^{-1}$ solutions was not significantly different between native and heated β-Lg (Table 1). At a molar ratio of 1:1 (EGCG/β-Lg), most of the EGCG was found associated with the protein, which was consistent with the fluorescence data reported in Figures 1 and 2. Since the fluorescence measurements indicated a molar binding ratio of approximately 1.2, the two sets of measurements are coherent. However, at the same β-Lg concentration, upon further addition of EGCG to the system (EGCG/β-Lg molar ratio increasing from 1:1 to 3:1), the encapsulation efficiency (percent) significantly decreased to about 60%, which implied the saturation of complexes. On a weight basis, the extent of binding increased from about 20 to 50 $\mu g \cdot (\text{mg of protein})^{-1}$ when the EGCG/β-Lg molar ratio increased from 1:1 to 3:1.

Table 1 also summarizes the association behavior of EGCG at 50 $\mu g \cdot mL^{-1}$ β-Lg. At this concentration, again, as for the 10 $\mu g \cdot mL^{-1}$ samples, there was no significant difference between heated and unheated β-Lg particles, and in all cases, the percent encapsulated was about 80% for EGCG/β-Lg molar ratio 1:1. These results are in contrast with earlier reports showing that EGCG binding of β-Lg increases after thermal denaturation of the protein.[9] At the higher molar ratio, the amount of encapsulated EGCG significantly decreased to about 25%, and the amount of loading was consistent at approximately 20 μg of EGCG/mg of protein. When 1% native dispersion and heated β-Lg particles complexed with EGCG were compared, at a molar concentration ratio of 1, almost complete encapsulation of EGCG took place, whereas at higher EGCG/β-Lg ratios, part of the EGCG remained free in solution. These findings are in full agreement with the fluorescence data shown in Figures 1 and 2 (i.e., $n = 1.2$). The findings can be attributed to increased extent of protein−protein interactions upon thermal denaturation, which could limit protein−polyphenol interactions.

Desolvated β-Lg particles showed very different encapsulation behavior. Due to their high extent of dilution (to a final protein concentration of 0.42 $\mu g \cdot mL^{-1}$), the percentage encapsulated was tested only for a molar ratio of 3:1 (EGCG/β-Lg). The encapsulation efficiency for these samples was approximately 90%, which was significantly higher than the other methods. It has been previously demonstrated that desolvated whey protein particles show high encapsulation efficiency.[15] The data shown in Table 1 clearly demonstrate that most of the EGCG added was found associated with the desolvated protein particles. The amount of EGCG bound was 68 μg of EGCG/mg of β-Lg, which was significantly higher than the values obtained with heated β-Lg particles. Compared to native β-Lg, which can bind approximately 1 EGCG molecule/β-Lg protein molecule (as shown in Figures 1 and 2), desolvated particles can bind approximately 2.7 EGCG molecules/β-Lg protein molecule. The different pH value (pH 3) could clearly affect the structural attributes of the protein, including surface charge and secondary structure.[41] However, the high dilution ratio utilized here may limit the applicability in

food systems. Although the ethanolic desolvation procedure enhanced the molar encapsulation ratio and the encapsulation efficiency on a weight basis (mg/mg), the stabilization of desolvated proteins and the reduction in ethanol content require extensive dilution, which in turn limits the total amount of EGCG that can be encapsulated. However, this approach could extend the EGCG encapsulation characteristics of β-Lg to acidic pH values and relevant food products.[10]

**3.4. Interfacial Characteristics of EGCG-Bearing β-Lactoglobulin Nanoparticles.** β-Lactoglobulin is known for its interfacial properties, and it is commonly found as an ingredient in emulsion systems, due to its ability to adsorb at interfaces and stabilize oil droplets or air bubbles. The interfacial characteristics of β-Lg were studied to determine whether the interfacial characteristics of the protein could be modified by formation of a complex with EGCG. The interfacial characteristics of the samples (at EGCG/β-Lg molar ratios of 0:1 and 3:1) were studied at the soy oil−dispersion interface by drop shape tensiometry. It has been previously reported that EGCG in isolation does not demonstrate interfacial activity.[42]

In all experiments, β-Lg reduced the interfacial tension of the oil−water interface, initially measured at 30.7 $mN{\cdot}m^{-1}$,[32] regardless of presence or absence of EGCG (Table 2). The interfacial tension data show that there were no significant differences in equilibrium interfacial tension values between native, heated, or desolvated protein particles. In the absence of EGCG, interfacial tension values for the oil−water interface were approximately 16 $mN{\cdot}m^{-1}$. This was consistent with previous findings on desolvated whey protein particles.[14] The presence of EGCG did not significantly affect the equilibrium interfacial tension for any of the samples, which implied that EGCG binding does not limit the extent of protein adsorption at the oil−dispersion interface.

Dilational elasticity was also tested for native β-Lg dispersions, β-Lg nanoparticles, and their corresponding EGCG complexes, as shown in Table 2. The method of sample manufacture did not significantly alter the dilational elasticity characteristics of the interface. The presence of EGCG significantly decreased the dilational modulus in all cases. In the absence of EGCG, the elasticity modulus was approximately 33 $mN{\cdot}m^{-1}$, while at a molar ratio of 3:1 (EGCG/β-Lg), dilational elasticity decreased to 21, 23, and 29 $mN{\cdot}m^{-1}$ (Table 2), for native dispersion and heat-induced and desolvated particle systems, respectively. It was concluded that the association of EGCG with β-Lg may decrease the ability of the protein to interact with other protein molecules at the interface and therefore hinder the creation of a rigid interface. These results are in contrast with the study of Rossetti et al.,[42] who have shown that EGCG increases elasticity when complexed with other proteins (saliva proteins from whole human saliva). This may be due to the differences in proteins and environments. We can infer from the current findings that the presence of EGCG did not significantly affect interfacial tension but decreased the extent of protein−protein interactions at the interface. These results demonstrated that EGCG binding only slightly affected the functional, and possibly nutritional, properties of the protein.

**Table 2. Interfacial Tension and Dilational Elasticity Characteristics of EGCG-Bearing β-Lg Dispersions at the Soy Oil−Dispersion Interface as a Function of Composition and Processing Conditions[a]**

| EGCG/β-Lg molar ratio | interfacial tension ($mN{\cdot}m^{-1}$) | dilational elasticity ($mN{\cdot}m^{-1}$) |
|---|---|---|
| | Native | |
| 0 | 17.5 ± 2.1 | 32.8 ± 12.9 |
| 3 | 16.3 ± 2.4 | 21.2 ± 4.3 |
| | Heated | |
| 0 | 15.8 ± 1.2 | 33.3 ± 6.3 |
| 3 | 16.0 ± 1.6 | 23.7 ± 7.6 |
| | Desolvated | |
| 0 | 14.7 ± 0.5 | 34.8 ± 11.7 |
| 3 | 17.4 ± 0.0 | 29.3 ± 1.4 |

[a]Native and heated samples contained 1% protein, whereas due to extensive dilution, desolvated samples had a β-Lg concentration of 0.042%. Dilational elasticity was measured at a dilational frequency of 10 mHz, and the extent of dilation was 10% in all cases.

**3.5. Bioefficacy of β-Lactoglobulin−EGCG Complexes.** Proliferation tests were conducted on confluent Caco-2 cells after 24 h of growth. The viability (percent) of Caco-2 cells that were administered freshly prepared or aged samples (24 h, 4 °C) after incubation for 24 h is shown in Table 3. Since EGCG is known for its anticancer properties on the vast majority of cancer cell lines,[6,43,44] in this study, its antiproliferative capacity was investigated in isolation or complexed with native β-Lg or desolvated or heated β-Lg nanoparticles. In the case of

**Table 3. Caco-2 Cell Proliferation Measured for EGCG Complexed with Native β-Lg or Heated or Desolvated β-Lg Nanoparticles after 24 h of Incubation[a]**

| amt loaded ($\mu g{\cdot}mL^{-1}$) | | cell proliferation (%) | |
|---|---|---|---|
| protein | EGCG | fresh ($t$ = 0) | aged ($t$ = 24 h) |
| | | Native | |
| 1.8 | 0 | 106.3 ± 3.5 | 105.9 ± 1.6 |
| 1.8 | 0.05 | 18.4 ± 0.3 | 34.9 ± 2.1 |
| 1.8 | 0.13 | 17.1 ± 0.8 | 23.4 ± 1.9 |
| | | Heated | |
| 1.8 | 0 | 92.1 ± 11 | 106.2 ± 12 |
| 1.8 | 0.05 | 27.3 ± 0.6 | 42.8 ± 5.8 |
| 1.8 | 0.13 | 19.9 ± 0.8 | 34.7 ± 1.7 |
| | | Desolvated | |
| 0.08 | 0 | 104.7 ± 15 | 94.6 ± 5.5 |
| 0.08 | 0.006 | 34.8 ± 0.9 | 34.1 ± 15 |
| | | EGCG (pH 7) | |
| 0 | 0.05 | 20.5 ± 0.7 | 87.5 ± 16 |
| 0 | 0.13 | 34.1 ± 1.9 | 94.1 ± 19 |
| | | EGCG (pH 3) | |
| 0 | 0.05 | 31.3 ± 2.2 | 81.2 ± 7.5 |
| 0 | 0.13 | 29.4 ± 5.0 | 94.3 ± 18 |
| | | Phosphate Buffer | |
| 0 | 0 | 102.1 ± 4.5 | NA |
| | | Citrate Buffer | |
| 0 | 0 | 105.2 ± 4.9 | NA |
| | | Citrate Buffer + EtOH | |
| 0 | 0 | 100.1 ± 7.4 | NA |

[a]Final β-Lg and EGCG concentrations in the medium were calculated respectively on the basis of the amount loaded initially for 1 and 3 protein/EGCG molar ratios after final dilution in the medium (1:5.6 v/v). A high dilution ratio (120×) was applied on desolvated protein−EGCG complex. Controls of respective buffers and EGCG solution pH 3 and 7 were also tested.

unheated $\beta$-Lg and heated $\beta$-Lg nanoparticles, 1.8 $\mu g \cdot mL^{-1}$ solutions were tested at EGCG/$\beta$-Lg ratios of 1 and 3. On the other hand, for the desolvated nanoparticles, due to dilution effects, final dilutions brought the $\beta$-Lg concentration to 0.08 $\mu g \cdot mL^{-1}$, and a molar ratio of 3 was employed. In all cases, about 90% of the EGCG was encapsulated (see Table 1). Control samples containing buffer at pH 7 or citrate buffer at pH 3 (with or without traces of ethanol) were tested, and they did not affect Caco-2 viability. Free EGCG showed a significant decrease in cell proliferation in fresh samples ($p < 0.05$); however, in all cases, both at pH 7 and 3, the decrease in efficacy after storage of the EGCG solution at 4 °C was noticed. When EGCG was associated with native $\beta$-Lg, there was a clear decrease in cell proliferation. The values were comparable to those obtained with free EGCG. Similarly, heated $\beta$-Lg−EGCG complexes showed a statistically significant decrease in cell proliferation ($p < 0.05$). All the samples of EGCG complexed with proteins showed bioefficacy also after 24 h at the incubation temperature. In the desolvated $\beta$-Lg samples, due to the extensive dilution requirements in buffer at pH 3, a smaller amount of EGCG was added to the cell culture wells (see Table 3). The bioefficacy of EGGC in the desolvated $\beta$-Lg nanoparticles was fully maintained, with results not significantly different in fresh and aged samples. In both cases, the cell viability decreased up to 35%. Encapsulation of EGCG in nanostructures such as liposomes or casein micelles also has been shown to maintain its antiproliferative capacity on colon carcinoma cells.[45,46]

In this work we demonstrated that $\beta$-Lg, both native and after heat or desolvation treatment,can be an effective, protective carrier for EGCG. The bioactivity of $\beta$-Lg−EGCG complexes tested on Caco-2 cell monolayers did not alter its antiproliferative activity, and in all cases this activity was maintained. Furthermore, the results of this study confirm previous suggestions by Shpigelman et al.[9] that $\beta$-Lg−EGCG complexes provide considerable protection against oxidative degradation of EGCG. As shown in Table 3, such complexes were able to preserve the bioactivity of EGCG after 24 h storage of the solutions, compared to free EGCG solutions. Further studies should be conducted to investigate whether such processing conditions are able to protect EGCG activity after prolonged storage, if such complexes were to be considered in beverage formulations.

## AUTHOR INFORMATION


### Corresponding Author

*E-mail aguri@uoguelph.ca.

### Present Address

[§]Department of Food Engineering, İstanbul Sabahattin Zaim University, Istanbul, Turkey; e-mail: ibrahim.gulseren@izu.edu.tr.



### Funding

This work was partly funded by the Natural Science and Engineering Council of Canada (NSERC), under the Canada Research Chair program, as well as the Ontario Ministry of Agriculture and Food, under the Food and Health program.


### Notes

The authors declare no competing financial interest.

## ACKNOWLEDGMENTS

We thank DSM Nutritional products for donating the EGCG extract.

## ABBREVIATIONS

EGCG, epigallocatechin-3-gallate; $\beta$-Lg, $\beta$-lactoglobulin

## REFERENCES


(1) Graham, H. N. Green tea composition, consumption, and polyphenol chemistry. *Prev. Med.* **1992**, *21*, 334−350.

(2) Von Staszewski, M.; Pilosof, A.; Jagus, R. Antioxidant and antimicrobial performance of different Argentinean green tea varieties as affected by whey proteins. *Food Chem.* **2011**, *125*, 186−192.

(3) Papadopoulou, A.; Frazier, R. A. Characterization of Protein-Polyphenol Interactions. *Trends Food Sci. Technol.* **2005**, *15*, 186−190.

(4) Zorilla, R.; Liang, L.; Remondetto, G.; Subirade, M. Interaction of EGCG with $\beta$-lactoglobulin: Molecular characterization and biological implication. *Dairy Sci. Technol.* **2011**, *91*, 629−644.

(5) Maiti, T. K.; Ghosh, K. S.; Dasgupta, S. Interaction of EGCG with HSA: Fluorescence, FT-IR, CD and docking studies. *Proteins: Struct., Funct., Bioinf.* **2006**, *64*, 355−362.

(6) Ahn, W. S.; Huh, S. W.; Bae, S. M.; Lee, I. P.; Lee, J. M.; Namkoong, S. E.; Kim, C. K.; Sin, J. I. A major constituent of green tea, EGCG, inhibits the growth of a human cervical cancer cell line, CaSki cells, through apoptosis, G1 arrest, and regulation of gene expression. *DNA Cell Biol.* **2003**, *22*, 217−224.

(7) Jian, L.; Xie, L. P.; Lee, A. H.; Binns, C. W. Protective effect of green tea against prostate cancer: A case-control study in southeast China. *Int. J. Cancer* **2004**, *108*, 130−135.

(8) Nakao, M.; Takio, S.; Ono, K. Alkyl peroxyl radical-scavenging activity of catechins. *Phytochemistry* **1998**, *49* (8), 2379−2382.

(9) Shpigelman, A.; Israeli, Y.; Livney, Y. Thermally-induced protein-polyphenol co-assemblies: $\beta$-lg based nanocomplexes as protective nanovehicles for EGCG. *Food Hydrocolloids* **2010**, *24*, 735−743.

(10) Su, Y. L.; Leung, L. K.; Huang, Y.; Chen, Z. Y. Stability of tea theaflavins and catechins. *Food Chem.* **2003**, *83*, 189−195.

(11) Zhou, Q.; Chiang, H.; Portocarrero, C.; Zhu, Y.; Hill, S.; Heppert, K.; Jayaratna, H.; Davies, M.; Janle, E.; Kissinger, P. Investigating the stability of EGCG in aqueous media. *Curr. Sep.* **2003**, *20* (3), 83−86.

(12) Sahoo, B. K.; Ghosh, K. S.; Dasgputa, S. Investigating the binding of curcumin derivatives to bovine serum albumin. *Biophys. Chem.* **2008**, *132*, 81−88.

(13) Relkin, P.; Shukat, R. Food protein aggregates as vitamin-matrix carriers: Impact of processing conditions. *Food Chem.* **2012**, *134*, 2141−2148.

(14) Gülseren, İ.; Fang, Y.; Corredig, M. Whey protein nanoparticles prepared with desolvation with ethanol: Characterization, thermal stability and interfacial behavior. *Food Hydrocolloids.* **2012**, *29*, 258−264.

(15) Gülseren, İ.; Fang, Y.; Corredig, M. Zinc incorporation capacity of whey protein nanoparticles prepared with desolvation with ethanol. *Food Chem.* **2012**, *135*, 770−774.

(16) Kanakis, C. D.; Hasni, I.; Bourrassa, P.; Tarantilis, P. A.; Polissou, M. G.; Tajmir-Riahi, H. A. Milk $\beta$-lactoglobulin complexes with tea polyphenols. *Food Chem.* **2011**, *127*, 1046−1055.

(17) Zhang, Y.; Zhong, Q. Effects of thermal denaturation on binding between bixin and whey protein. *J. Agric. Food Chem.* **2012**, *60*, 7526−7531.

(18) Relkin, P.; Vermersh, J. Binding properties of vanillin to whey proteins: Effect on protein conformational stability and foaming properties. In *Food Colloids: Fundamentals of Formulation*; Dickinson, E., Muller, R., Eds.; The Royal Society of Chemistry: Cambridge, U.K., 2000; Sect. 4, pp 282−292.

(19) Hemar, Y.; Gerbeaud, M.; Oliver, C. M.; Augustin, M. A. Investigating into the interaction between resveratrol and whey proteins using fluorescence spectroscopy. *Int. J. Food Sci. Technol.* **2011**, *46*, 2137−2144.

(20) Stojadinovic, M.; Radosavljevic, J.; Ognjenovic, J.; Vesic, J.; Prodic, I.; Stanic-Vucinic, D.; Velickovic, T. Binding affinity between dietary polyphenols and $\beta$-lactoglobulin negatively correlates with the

protein susceptibility to digestion and total antioxidant activity of complexes formed. *Food Chem.* **2013**, *136*, 1263−1271.
(21) Rawel, H. M.; Kroll, J.; Hohl, U. C. Model studies on reactions of plant phenols with whey proteins. *Nahrung* **2001**, *45*, 72−81.
(22) Xu, C.; Chen, X. Molecular property−affinity relationship of the interaction between dietary polyphenols and bovine milk proteins. *Food Funct.* **2011**, *2*, 368−372.
(23) De Fretias, N.; Mateus, S. Structural features of procyanidin interactions with salivary proteins. *J. Agric. Food Chem.* **2001**, *49*, 940−945.
(24) Shpigelman, A.; Cohen, Y.; Livney, Y. Thermally-induced β-lactoglobulin-EGCG nanovehicles: Loading, stability, sensory and digestive-release study. *Food Hydrocolloids* **2012**, *29*, 57−67.
(25) Guri, A.; Haratifar, S.; Corredig, M. Bioefficacy of tea catechins associated with milk caseins tested using different in vitro digestion models. *Food Dig.* **2014**, 1−11.
(26) Li, B.; Du, W.; Jin, J.; Du, Q. Preservation of (−)-epigallocatechin-3-gallate antioxidant properties loaded in heat-treated β-lactoglobulin nanoparticles. *J. Agric. Food Chem.* **2012**, *60*, 3477−3484.
(27) Cilla, A.; Perales, S.; Lagarda, M. J.; Barbera, R.; Farre, R. Iron bioavailability in fortified fruit beverages using ferritin synthesis by Caco-2 cells. *J. Agric. Food Chem.* **2008**, *56*, 8699−8703.
(28) Bellion, P.; Hofmann, T.; Pool-Zobel, B. L.; Will, F.; Dietrich, H.; Knaup, B.; Richling, E.; Baum, M.; Eisenbrand, G.; Janzowski, C. Antioxidant effectiveness of phenolic apple juice extracts and their gut fermentation products in the human colon carcinoma cell line Caco-2. *J. Agric. Food Chem.* **2008**, *56*, 6310−6317.
(29) Andrew, A. T.; Taylor, M. D.; Owen, A. J. Rapid analysis of bovine milk proteins by fast protein liquid chromatography. *J. Chromatogr. A* **1985**, *348*, 177−185.
(30) Lakowicz, J. R. Quenching of fluorescence. In *Principles of Fluorescence Spectroscopy*, 3rd ed.; Springer:, New York, 2006; Chapt. 8, pp 278−327.
(31) Gaonkar, A. G. Interfacial tensions of vegetable oil/water systems: effect of oil purification. *J. Am. Oil Chem. Soc.* **1989**, *66*, 1090−1092.
(32) Gülseren, İ.; Corredig, M. Interactions at the interface between hydrophobic and hydrophilic emulsifiers: Polyglycerol polyricinoleate (PGPR) and milk proteins, studied by drop shape tensiometry. *Food Hydrocolloids* **2012**, *29*, 193−198.
(33) Lucassen-Reynders, E. H.; Cagna, A.; Lucassen, J. Gibbs elasticity, surface dilational modulus and diffusional relaxation in nonionic surfactant monolayers. *Colloids Surf., A* **2001**, *186*, 63−72.
(34) Vichai, V.; Kirtikara, K. Sulforhodamine B colorimetric assay for cytotoxicity screening. *Nat. Protoc.* **2006**, *1*, 1112−1116.
(35) Ju, Z. Y.; Hettiarachchy, N.; Kilara, A. Thermal properties of whey protein aggregates. *J. Dairy Sci.* **1999**, *82*, 1882−1889.
(36) Relkin, P. Reversibility of heat-induced conformational changes and surface exposed hydrophobic clusters of beta-lactoglobulin: Their role in heat-induced sol-gel state transition. *Int. J. Biol. Macromol.* **1998**, *22*, 59−66.
(37) Von Staszewski, M.; Jagus, R. J.; Pilosof, A. M. R. Influence of green tea polyphenols on the colloidal stability and gelation of WPC. *Food Hydrocolloids* **2011**, *25*, 1077−1084.
(38) Roefs, S.; De Kruif, K. A model for the denaturation and aggregation of β-lactoglobulin. *Eur. J. Biochem.* **1994**, *226*, 883−889.
(39) Dufour, E.; Haertlé, T. Temperature-induced folding changes of β- lactoglobulin in hydro-methanolic solutions. *Int. J. Biol. Macromol.* **1993**, *15*, 293−329.
(40) Thongkaew, C.; Gibis, M.; Hinrichs, J.; Weiss, J. Polyphenol interactions with whey protein isolate and whey protein isolate-pectin coacervates. *Food Hydrocolloids* **2014**, *41*, 103−112.
(41) Bhattacharjee, C.; Das, K. P. Thermal unfolding and refolding of β-lactoglobulin: An intrinsic and extrinsic fluorescence study. *Eur. J. Biochem.* **2000**, *267*, 3957−3964.
(42) Rossetti, D.; Ravera, F.; Liggieri, L. Effect of tea polyphenols on the dilational rheology of human whole saliva (HWS): Part 2, polyphenols−HWS interaction. *Colloids Surf., B* **2013**, *110*, 474−479.
(43) Yamamoto, T.; Hsu, S.; Lewis, J.; Wataha, J.; Dickinson, D.; Singh, B.; Bollag, W. B.; Lockwood, P.; Ueta, E.; Osaki, T.; Schuster, G. Green tea polyphenol causes differential oxidative environments in tumor versus normal epithelial cells. *J. Pharmacol. Exp. Ther.* **2003**, *307*, 230−236.
(44) Chen, D.; Wan, S. B.; Yang, H.; Yuan, J.; Chan, T. H.; Dou, Q. P. EGCG, green tea polyphenols and their synthetic analogs and prodrugs for human cancer prevention and treatment. *Adv. Clin. Chem.* **2011**, *53*, 53155−53177.
(45) Gülseren, İ.; Guri, A.; Corredig, M. Encapsulation of tea polyphenols in nanoliposomes prepared with milk phospholipids and their effect on the viability of HT-29 human carcinoma cells. *Food Dig.* **2012**, *3*, 36−45.
(46) Haratifar, S. *Nanoencapsulation of tea catechins in casein micelles: Effects on processing and biological functionalities*. Ph.D. Thesis, University of Guelph, Canada, 2012.

JOURNAL OF AGRICULTURAL AND FOOD CHEMISTRY

Article

pubs.acs.org/JAFC

# Steviol Glycoside Rebaudioside A Induces Glucagon-like Peptide-1 and Peptide YY Release in a Porcine ex Vivo Intestinal Model

Dina Ripken,*[,†,‡,§] Nikkie van der Wielen,[†,§] Heleen M. Wortelboer,[‡] Jocelijn Meijerink,[§] Renger F. Witkamp,[§] and Henk F. J. Hendriks[†,‡]

[†]Top Institute Food and Nutrition, Nieuwe Kanaal 9A, 6709 PA Wageningen, The Netherlands

[‡]Netherlands Organization for Applied Scientific Research (TNO), Utrechtseweg 48, 3704 HE Zeist, The Netherlands

[§]Division of Human Nutrition, Wageningen University, Bomenweg 2, 6703 HD Wageningen, The Netherlands

**ABSTRACT:** Glucagon-like peptide-1 (GLP-1) and peptide YY (PYY) are hormones important for satiation and are involved in the process called "ileal brake". The aim of this study was to investigate the GLP-1- and PYY-stimulating efficacy of rebaudioside A, casein, and sucrose. This was studied using tissue segments collected from various regions of the pig small intestine. GLP-1 release was strongest from the distal ileum. There, control release was 0.06 ± 0.01 (GLP-1) and 0.07 ± 0.01 (PYY) pmol/cm$^2$ of tissue. Rebaudioside A (2.5, 12.5, and 25 mM) stimulated GLP-1 release (0.14 ± 0.02, 0.16 ± 0.02, and 0.13 ± 0.02 pmol/cm$^2$ of tissue, $p < 0.001$) and PYY release (0.19 ± 0.02, 0.42 ± 0.06, and 0.27 ± 0.03 pmol/cm$^2$ of tissue, $p < 0.001$). Sucrose stimulated GLP-1 release (0.08 ± 0.01 pmol/cm$^2$ of tissue, $p < 0.05$) only at 10 mM. Casein (0.5%, 1%, and 2.5%, w/v) stimulated GLP-1 release (0.15 ± 0.03, 0.13 ± 0.02, and 0.14 ± 0.01 pmol/cm$^2$ of tissue, $p < 0.001$) and PYY release (0.13 ± 0.02, 0.20 ± 0.03, and 0.27 ± 0.03 pmol/cm$^2$ of tissue, $p < 0.01$). These findings may help in developing dietary approaches for weight management.

**KEYWORDS:** *rebaudioside A, GLP-1, PYY, ex vivo intestinal porcine model*

## INTRODUCTION

The presence of nutrients and other molecules in the small intestine stimulates the release of satiety hormones, such as cholecystokinin (CCK), glucagon-like peptide-1 (GLP-1), and peptide YY (PYY).[1,2] The release of these hormones results in decreased gastric emptying and activation of the so-called intestinal brake. This poorly explored mechanism refers to a physiological feedback mechanism that is triggered by nutrients at a specific location in the intestine, resulting in reduced appetite and food intake.[3,4] Lipids have been widely researched and are known to activate this ileal brake mechanism, resulting in the release of satiety hormones and reduced food intake.[5−8] However, whether other macronutrients such as carbohydrates and proteins could also activate the ileal brake mechanism is still unknown.[4] Knowledge of the satiety-hormone-inducing properties of macronutrients is relevant to better understanding the intestinal response to ingested food and may contribute to the development of products with satiating properties.

The efficacies of noncaloric sweeteners to induce the release of satiety hormones are also partly unknown. However, a study by Anton et al. showed that preloads containing the sweetener stevia reduced daily caloric intake by 301 kcal and reduced postprandial glucose and insulin levels compared to preloads containing sucrose.[9] Such a reduced caloric intake as well as glucose and insulin responses may be caused by reduced caloric content of the preload but may also be caused by other mechanisms such as GLP-1 release. The glycoside rebaudioside A is one of the most abundant sweet compounds extracted from the leaves of *Stevia rebaudiana* Bertoni. Rebaudioside A is reported to be the most potent sweetener among the steviol glycosides,[10] with a relative sweetness 200−400 times greater than that of sucrose.[11] Rebaudioside A is increasingly used in food products as a natural noncaloric sweetener. It has been approved in the United States since 2008[12] and by the European Union since 2010.[13]

It is unknown if ileal delivery of macronutrients other than lipids and sweeteners could also stimulate the release of satiety hormones and consequently activate the ileal brake. Stimulation of GLP-1 and PYY release from isolated ileal tissue has been demonstrated for lipids including unsaturated fatty acids. This was shown using a recently described ex vivo porcine intestinal model.[14] For other macronutrients such as sucrose and casein, such studies have not been performed yet, although their efficacy to induce gut hormone release has been shown in cell cultures.[15−17] The pig was chosen as a model because the gastrointestinal tract of the pig shows a high degree of macroscopic and microscopic resemblance to that of humans.[18−20] The present study primarily focused on the GLP-1- and PYY-inducing efficacy of casein, sucrose, and the noncaloric sweetener rebaudioside A at various locations of the small intestine. We hypothesize that rebaudioside A, the protein casein, and the carbohydrate sucrose are effective stimulators of GLP-1 and PYY release from various locations of the small intestine and thus may be effective activators of the ileal brake in vivo.

## MATERIALS AND METHODS

**Chemicals.** Casein protein (food grade, sodium caseinate purity >82%, batch number 158156) was obtained from Dutch Protein Services BV, Tiel, The Netherlands. Rebaudioside A (Figure 1, food

Received: March 5, 2014
Revised: July 23, 2014
Accepted: July 25, 2014
Published: July 25, 2014

 © 2014 American Chemical Society 

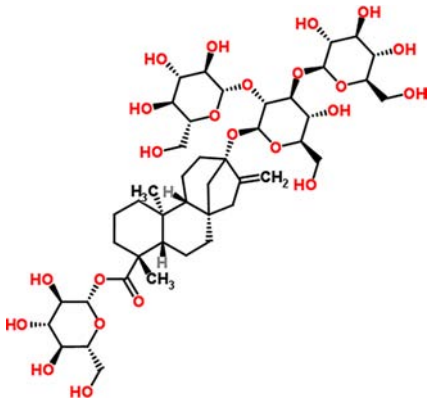

**Figure 1.** Chemical structure of rebaudioside A. Adapted from ChemSpider, ID 5294031.

grade, purity >97%, batch number 20110301, ChemSpider ID 5294031) was obtained from SteviJa Natuurlijk BV, Drachten, The Netherlands. Sucrose (food grade, purity >99.9%) was supplied by Suiker Unie, Oud Gastel, The Netherlands. Safflower oil (food grade, composed of 3−8% C16:0, 2−5% C18:0, 9−15% C18:1, and 75−85% C18:2) was provided by De Wit Specialty Oils, De Waal, The Netherlands. Xantham gum and guar gum were supplied by GF Supplies, Amsterdam, The Netherlands. Chemicals to make the Krebs−Ringer bicarbonate (KRB) buffer (D-glucose (1.8 g/L), magnesium chloride (0.0468 g/L), potassium chloride (0.34 g/L), sodium chloride (7.0 g/L), sodium phosphate dibasic (0.1 g/L), sodium phosphate monobasic (0.18 g/L), HEPES (5579 g/L)) were obtained from Sigma, Zwijndrecht, The Netherlands. The pH of the KRB buffer was adjusted to pH 7.4.

**Collection of Porcine Intestinal Tissues.** Intestinal tissues were obtained from 10 healthy male pigs (*Sus scrofa domesticus*). The pigs were considered healthy after evaluation by a veterinarian. The protocol for this study was approved by the Animal Ethics Committee Utrecht (Ethics Committee Permit Number 2012.I.09.096, Utrecht, The Netherlands). The pigs had a mean (±SEM) body mass of 141 ± 2 kg and mean (±SEM) age of 6 ± 0.1 months. They were housed in groups and were fed ad libitum with the standard pig diet (vitaal P 003103, de Heus, Ede, The Netherlands) and had free access to water. Within 10 min after the pigs were sacrificed, the intestines were excised, and segments of different anatomical regions were stored in ice-cold oxygenated (95% $O_2$, 5% $CO_2$) KRB buffer. Jejunum (4.5 m proximal to the ileocecal junction) and proximal, middle, and distal ileum (0.5 m of intestine sampled from 1.5, 1, and 0.5 m proximal to the ileocecal junction, respectively) were collected for the experiments. Tissues were transported to the laboratory and immediately used for ex vivo experiments. The time between excision and start of the experiments was approximately 30 min.

**Nutrient Exposure of Intestinal Tissue and Viability Tests.** Incubations with casein (0.5, 1, and 2.5%, w/v), rebaudioside A (2.5, 12.5, and 25 mM), sucrose (2.5, 5, and 10 mM), and safflower oil (3.35%, w/v) were performed with porcine intestinal tissue as described previously[14] with some minor adaptations. In brief, upon arrival at the laboratory, the intestine was rinsed with KRB buffer and cut open in a longitudinal direction. The outer muscle layers were carefully stripped off with the basolateral side upward. The mucosal tissue was placed on gauze (pores 250 μm, Sefar Nitex 03-250/50, Sefar, Heiden, Switzerland) with the apical side upward, and circles of tissue with a diameter of 11.8 mm (about 1.0 $cm^2$) were punched out using a biopsy punch. The intestinal segments were randomized, per region, in a beaker glass, transferred to a 24-well plate which was filled with 500 μL of ice-cold KRB buffer/well, and kept on ice until the start of the experiment. Thereafter, the tissues were brought to room temperature within 30 min, followed by a preincubation step at 37 °C for 1 h in a humidified incubator (5% (v/v) $CO_2$). To study the release of GLP-1 and PYY, incubations were initiated by replacing the KRB buffer solution with 500 μL of prewarmed (37 °C) KRB without D-glucose containing the test compounds. KRB buffer without D-glucose was used as a control since D-glucose might induce gastrointestinal hormone release. Then the tissue was put in a humidified incubator for 1 h at 37 °C and 5% (v/v) $CO_2$. After incubation, the solutions were collected, mixed with 100 μM phenylmethanesulfonyl floride (PMSF) (Sigma-Aldrich, Zwijndrecht, The Netherlands) to inactivate dipeptidyl peptidase IV, aliquoted, and stored at 4 °C for further analysis of lactate dehydrogenase (LDH) or stored at −80 °C for further analysis of GLP-1 and PYY.

Tissue viability was checked by measuring the leakage of intracellular LDH in supernatant. LDH, a stable cytosolic enzyme, was analyzed using an LDH kit (Sigma-Aldrich). LDH activity in the supernatant was expressed as a percentage of the total LDH activity present in control tissue collected before incubation. Total tissue levels of LDH were determined per region in 1.0 $cm^2$ tissue samples, which were homogenized in ice-cold KRB buffer with a Potter−Elvehjem-type Teflon pestle tissue grinder (Braun, Melsungen, Germany) for 5 min at 200 rounds/min. Samples were only included for further analysis when LDH leakage did not exceed 10% of the total LDH tissue content.[14,21] No samples had to be excluded applying this criterion.

**Analysis of Satiety Hormones GLP-1 and PYY.** GLP-1 active levels were analyzed using commercially available enzyme-linked immunosorbent assay (ELISA) kits obtained from Millipore (Billerica, MA) and used according to the manufacturer's instructions using a BioTek Synergy HT fluorescence microplate reader (BioTek Instru-

**Table 1. GLP-1 Concentrations Released from Jejunal and Proximal, Middle, and Distal Ileum Intestinal Tissue Segments after Exposure to Various Compounds[a]**

| | | GLP-1 concn released (pmol/$cm^2$ of tissue) | | | |
|---|---|---|---|---|---|
| solution | concn | jejunum | proximal ileum | middle ileum | distal ileum |
| control | | 0.04 ± 0.01 | 0.07 ± 0.02 | 0.07 ± 0.01 | 0.06 ± 0.01 |
| safflower oil | 3.35% | 0.07 ± 0.02 | 0.11 ± 0.03 a | 0.09 ± 0.02 | 0.13 ± 0.02 c |
| sucrose | 2.5 mM | 0.05 ± 0.01 | 0.10 ± 0.02 | 0.07 ± 0.01 | 0.06 ± 0.01 |
| | 5 mM | 0.05 ± 0.01 | 0.17 ± 0.05 | 0.08 ± 0.01 | 0.07 ± 0.01 |
| | 10 mM | 0.06 ± 0.01 | 0.07 ± 0.01 | 0.08 ± 0.01 | 0.08 ± 0.01 a |
| casein | 0.5% | 0.06 ± 0.01 | 0.12 ± 0.02 c | 0.09 ± 0.01 | 0.15 ± 0.03 c |
| | 1% | 0.09 ± 0.01 c | 0.09 ± 0.02 b | 0.08 ± 0.01 | 0.13 ± 0.02 c |
| | 2.5% | 0.08 ± 0.02 c | 0.13 ± 0.03 c | 0.08 ± 0.01 | 0.14 ± 0.01 c |
| rebaudioside A | 2.5 mM | 0.07 ± 0.01 | 0.14 ± 0.02 c | 0.13 ± 0.02 b | 0.14 ± 0.02 c |
| | 12.5 mM | 0.07 ± 0.01 b | 0.11 ± 0.02 c | 0.18 ± 0.04 c | 0.16 ± 0.02 c |
| | 25 mM | 0.07 ± 0.01 b | 0.14 ± 0.02 c | 0.13 ± 0.02 b | 0.13 ± 0.02 c |

[a]Key: a, $p < 0.05$; b, $p < 0.01$; c, $p < 0.001$. $p$ values are based on comparison to the control (ANOVA + Tukey correction). The incubations were performed in triplicate ($n = 6$ for jejunum and $n = 10$ for proximal, middle, and distal ileum).


dx.doi.org/10.1021/jf501105w | J. Agric. Food Chem. 2014, 62, 8365−8370

ments Inc., Winooski, VT). Since the GLP-1 hormone gene sequence is highly preserved, this kit could be applied for analyzing porcine GLP-1. The range of this assay is approximately 2−100 pM. The interassay coefficient of variation is 11%, and the intraassay variation is 6%. When necessary, samples were diluted in assay buffer from the kit to be in this range.

PYY release was measured from the distal ileum only, since PYY is known to be colocalized with GLP-1.[22] PYY concentrations were measured using a PYY ELISA kit for total PYY (Bachem, Penisula Laboratories, San Carlos, CA) according to the manufacturer's instructions using a BioTek Synergy HT microplate reader (BioTek Instruments Inc.). This kit measures porcine PYY, which is identical to human PYY.[23] The range of this assay is approximately 0.32−5 ng/mL (4.6−1150 pM). The interassay coefficient of variation for this assay is 6%, and the intraassay coefficient of variation is 3%. The lower detection limit of this kit was 20 pg/mL (4.6 pM). It was not necessary to dilute samples for this assay.

**Statistical Analysis.** Statistical analysis was performed using the SAS statistical software package (SAS version 9; SAS Institute, Cary, NC). Both variables GLP-1 and PYY were compared with a mixed analysis of variance (ANOVA) model. GLP-1 and PYY were both log transformed to meet the requirements for ANOVA. The ANOVA model included the fixed factors dose solution (control, sucrose (2.5, 5, and 10 mM), casein (0.5%, 1%, and 2.5%, w/v), rebaudioside A (2.5, 12, and 25 mM), and safflower oil (3.35%, w/v)), intestinal location (jejunum and proximal middle, and distal ileum), and number of incubations per condition (incubations were performed in triplicate). The factor pig, which specifies the individual pig, was added to the model as a random factor. The Tukey post hoc test was used to correct for multiple comparisons. Data are presented as the mean ± SEM and considered significant at $p < 0.05$.

## RESULTS

**Effects of Rebaudioside A and Other Compounds/Mixtures on GLP-1 Release.** Table 1 shows the GLP-1 concentrations in the medium following incubation with the test compounds or mixtures using tissues taken from different locations. In all parts of the small intestine investigated, rebaudioside A caused a significant release of GLP-1 already at the lowest concentration tested (2.5 mM) ($p < 0.01$), except for the jejunum where the release was significant at a concentration of 12.5 mM ($p < 0.05$). The highest relative increase of GLP-1 after incubation with rebaudioside A was seen in the distal ileum ($p < 0.001$). The release at 25 mM was not higher than that at 12.5 mM. As also shown in Table 1, safflower oil (3.35%, w/v) significantly increased GLP-1 release from the proximal ileum ($p < 0.05$) and even more from the distal ileum ($p < 0.001$). Safflower oil did not increase GLP-1 release from the middle ileum and only marginally increased it from the jejunum. At the concentrations tested sucrose did not stimulate GLP-1 release from jejunal and middle ileal tissue. The only significant stimulation was seen in tissues from the distal ileum at a sucrose concentration of 10 mM ($p < 0.05$).

Casein, at 1% and 2.5% (w/v), increased GLP-1 release ($p < 0.001$) from tissues collected from the jejunum, whereas 0.5% (w/v) casein did not. Both 0.5% and 2.5% (w/v) casein stimulated GLP-1 release from the proximal ileum ($p < 0.001$). A concentration of 1% (w/v) casein stimulated GLP-1 release from the proximal ileum ($p < 0.010$), but exposure to 0.5% and 2.5% (w/v) casein caused a higher GLP-1 release. None of the casein concentrations, 0.5%, 1%, and 2.5% (w/v), stimulated GLP-1 release from the middle ileum. All three casein concentrations stimulated GLP-1 release from the distal ileum ($p < 0.001$). Similar to that by rebaudioside A, the most pronounced stimulation of GLP-1 by casein was observed in the distal ileum.

**Regional Differences in GLP-1 Release.** Exposing intestinal tissue to the control did not result in regional differences in control GLP-1 release. However, after exposure to the nutrients, regional differences were observed. For GLP-1 both an overall incubation and location effect ($p < 0.001$) and an interaction effect between incubation and location ($p < 0.05$) were found. Overall GLP-1 release from all ileal locations (distal, middle, and proximal ileum) was higher than GLP-1 release from the jejunal locations ($p < 0.001$). Furthermore, GLP-1 release from the distal ileum was higher than GLP-1 release from the middle ileum ($p < 0.001$). Hormone release from the middle and proximal ileum did not differ, nor did release from the proximal and distal ileum ($p < 0.08$).

**Effects of Compounds and Mixtures on PYY Release.** The compounds and mixtures stimulating GLP-1 release were also tested for their PYY-releasing capacity from the distal ileum (Table 2). Safflower oil was found to stimulate PYY release, whereas sucrose at the concentrations tested did not. Casein stimulated PYY release from the distal ileum at all three concentrations tested. Release after exposure to 1% (w/v) casein was higher than that after exposure to 0.5% (w/v) casein ($p < 0.05$). Rebaudioside A stimulated PYY release from the distal ileum ($p < 0.001$). The effect at 12.5 mM rebaudioside A was higher than that at 2.5 mM ($p < 0.05$).

**Table 2. PYY Concentrations Released from Distal Ileum Intestinal Tissue Segments after Exposure to Various Compounds[a]**

| solution | concn | PYY concn released (pmol/cm$^2$ tissue) |
|---|---|---|
| control | | 0.07 ± 0.01 |
| safflower oil | 3.35% | 0.17 ± 0.01 c |
| sucrose | 2.5 mM | 0.14 ± 0.03 |
| | 5 mM | 0.12 ± 0.02 |
| | 10 mM | 0.08 ± 0.01 |
| casein (%) | 0.5% | 0.13 ± 0.02 b |
| | 1% | 0.20 ± 0.03 c |
| | 2.5% | 0.27 ± 0.03 c |
| rebaudioside A | 2.5 mM | 0.19 ± 0.02 c |
| | 12.5 mM | 0.42 ± 0.06 c |
| | 25 mM | 0.27 ± 0.03 c |

[a]Key: a, $p < 0.05$; b, $p < 0.01$; c, $p < 0.001$. $p$ values are based on comparison to the control (ANOVA + Tukey correction). The incubations were performed in triplicate ($n = 10$).

## DISCUSSION

Our study confirmed our hypothesis that rebaudioside A and casein induce GLP-1 and PYY release from porcine intestinal tissue segments. Remarkably, rebaudioside A was found to stimulate GLP-1 release from all ileal and jejunal regions investigated, whereas sucrose (10 mM) only caused GLP-1 release from the distal ileum. Rebaudioside was effective in stimulating hormone release from more locations of the small intestine than casein. Therefore, taking into account that the model and the tested concentrations make a direct comparison difficult, our results suggest that rebaudioside A and the protein casein are candidate substances that may activate the ileal brake in vivo via the release of GLP-1 and PYY.

Some sweeteners including sucralose were found not to affect satiety hormone release in vivo.[24,25] For stevia, Anton et al. demonstrated satiation-inducing properties which may be due to increased satiety hormone release. However, since satiety

hormones were not measured in that study, this association cannot be made from these findings. To our knowledge, no reports have shown the satiety-hormone-inducing capacity of the noncaloric sweetener rebaudioside A as was done in our study.

Nutrients such as casein and sucrose could stimulate satiety hormone release following interaction with G-protein-coupled receptors and some solute carrier transporters located on enteroendocrine cells in the intestinal epithelium.[26] A potential mechanism by which rebaudioside A could stimulate GLP-1 and PYY release is via the sweet taste receptor. Recently, it was found that rebaudioside A has affinity for the sweet taste receptor TAS1R2/TASR3.[10] This receptor is involved in glucose-dependent release of GLP-1 and PYY in vivo.[27] Furthermore, TAS1R2/TASR3 is present on brush cells and enteroendocrine cells.[28] However, mechanisms other than via the taste receptors by which rebaudioside A and casein could induce satiety hormone release cannot be excluded and should be further studied.

Already more than 100 compounds have been identified in *S. rebaudiana*. However, the steviol glycosides stevioside and rebaudioside A have been found to be the most abundant. Steviol glycosides are metabolized into steviol upon their arrival in the colon and are absorbed thereafter.[29] Incubation of the murine enteroendocrine STC-1 cells with stevia preparations resulted in higher GLP-1 and CCK release compared to incubation with sucrose,[17] which is in line with our findings. The same study also demonstrated GLP-1 and CCK release after incubation with sucralose. However, only relatively high concentrations of sucralose (150 and 300 mM) and sucrose (600 mM) were able to stimulate GLP-1 and CCK release from STC-1 cells. In our study 2.5 mM rebaudioside A resulted in higher GLP-1 release compared to 2.5 mM sucrose ($0.14 \pm 0.02$ vs $0.06 \pm 0.01$, $p < 0.001$, distal ileum). Concentrations of sucrose and rebaudioside A in this study were in the same range (0−25 mM). Further in vitro studies should explore the dose−effect relationships of these compounds.

Safflower oil was used as a positive control in our study. Safflower oil (3.35%) was found to activate the ileal brake in vivo and to increase satiety and gastrointestinal hormone concentrations.[5,7] As expected, safflower oil effectively stimulated GLP-1 release from the ileum mainly from the distal part whereas no such stimulation occurred from the middle ileum. This difference may relate to the enteroendocrine cell distribution. Enteroendocrine L-cells are most abundant in the distal part of the small intestine[30] corresponding to the intestinal tissue content of GLP-1.[14] The protein casein increases satiety in vivo,[31] and in vitro it stimulates GLP-1 release from enteroendocrine murine STC-1 and human NCI-H716 cells.[15,16,32] In our study casein induced GLP-1 and PYY release, which confirms these previous findings and suggests that casein is a candidate to induce the ileal brake in vivo.

Apart from the differences in efficacy of various nutrients to stimulate GLP-1 and PYY, some other questions remain. An important question is to what extent the effects on satiety hormone release found in our model can be reproduced in in vivo models and specifically in humans. Another relevant question is whether the capacity to induce satiety hormone release will lead to satiation in vivo. In one study by Veldhorst et al., it was shown that breakfast with a higher casein content (25% vs 10%) increased visual analogue scale (VAS) scores in fullness and satiety whereas subsequent energy intake was not reduced and GLP-1 plasma concentrations did not differ per condition.[33] Food intake is regulated by a whole cascade of responses which have to be taken into account if studying satiation in vivo. Therefore, knowledge of the satiety-hormone-releasing capacity of macronutrients and noncaloric sweeteners could be useful to understand this so-called "satiety cascade".[34]

The current in vivo data are based on lipid infusions mainly. Those data could be extended into infusion studies using rebaudioside A and casein since the results from this study suggest that the satiety-hormone-releasing effect of sweeteners and proteins might be at least as effective as that of fat. These human interventions will then further substantiate the relevance of this ex vivo intestinal model.

One could question whether the concentrations of the selected compounds are relevant in view of those reached in the gut after dietary intake. Nutrient concentrations in the small intestine depend on the rate of gastric emptying of a meal, the rate of absorption, and (or) digestion of the nutrients the meal contained.[35−37] Data on actual concentrations of the selected products are very scarce. There is only one animal study showing that luminal glucose concentrations after a meal vary between 0.2 and 48 mM depending on the postprandial time and the small intestinal region.[38] Although the data are limited, one could estimate intestinal concentrations on the following assumptions: 1 cup of coffee or tea (200 mL) with 0.3 g of rebaudioside A (based on an acceptable daily intake (ADI) of 0.4 mg/kg of body mass/day), or 1 cube of sugar (1 g), in a total volume of 300 mL (100 mL of gastric juice is added in the stomach).[17] These assumptions would yield an estimate of approximately 10 mM sucrose and 1 mM rebaudioside A for the small intestine. The estimate for casein is based on the assumption that one glass of milk is consumed (total volume including gastric juice 300 mL) with a casein concentration of 80% of the total milk protein content, which is approximately 35 g/L. This means that a concentration of approximately 3% may initially be reached in the small intestine. Although these values are estimates only, they suggest that the concentrations used in this study may be relevant from a dietary perspective.

The hormone-secreting capacity of nutrients and other compounds is often studied in vitro using enteroendocrine cell lines including murine STC-1,[15,39−41] GLUTag cells,[42] and the human NCI-H716 cell line.[43] The advantage of the current ex vivo model compared to cell lines is that this model consists of all different cell types present in the gut. Another model to study the GLP-1- and PYY-inducing capacity of nutrients is the Ussing chamber technology using animal or human biopsies.[44] It is, however, challenging to obtain human biopsies, especially from the ileum, which makes the ex vivo intestinal porcine segment system a valuable alternative. However, there are still some technical limitations such as tissue viability and intrasubject variation. In this study tissue viability was evaluated by LDH leakage as before,[14] and LDH leakage did not exceed 10%. Also, hormone release in the control condition was low. Both conditions indicate a good tissue viability. However, we cannot exclude that hormone release may be due to aspecific processes such as cell lysis. Also, a high number of replicates were needed because of a high intrasubject variation. This variation may be caused by the relatively low number of enteroendocrine cells (reported to account for only 1% of the epithelial cell population in the small intestine), and these cells may be unevenly distributed.[2,28]

In conclusion, the present study showed that rebaudioside A and casein, but not sucrose, induced satiety hormone release at various locations of the small intestine using an ex vivo model.

These findings may contribute to the development of dietary approaches improving weight management and glucose control. However, in vivo studies are necessary to confirm the potential satiety-inducing properties of rebaudioside A and casein in vivo.

## AUTHOR INFORMATION


### Corresponding Author

*Fax: +31 888 668767. Phone: +31 888 668701. E-mail: dina.ripken@tno.nl.


### Notes

The authors declare no competing financial interest.

## ACKNOWLEDGMENTS

We thank Ying Lu for her assistance with the conducted experiments. Furthermore, we thank Bas Swildens and Danielle Padilla de Beer from the Utrecht University for their help with the preparation of the study.

## ABBREVIATIONS USED

ANOVA, mixed analysis of variance; CCK, cholecystokinin; GLP-1, glucagon-like peptide-1; GI, gastrointestinal; GPR, G-protein-coupled receptor; KRB, Krebs−Ringer bicarbonate; LDH, lactate dehydrogenase; PYY, peptide YY; PMSF, phenylmethanesulfonyl fluoride; SEM, standard error of the mean; SD, standard deviation

## REFERENCES


(1) Gribble, F. M. The gut endocrine system as a coordinator of postprandial nutrient homoeostasis. *Proc. Nutr. Soc.* **2012**, *71*, 456−462.

(2) Tolhurst, G.; Reimann, F.; Gribble, F. M. Intestinal sensing of nutrients. *Handb. Exp. Pharmacol.* **2012**, *209*, 309−35.

(3) Maljaars, P. W.; Peters, H. P.; Mela, D. J.; Masclee, A. A. Ileal brake: A sensible food target for appetite control. A review. *Physiol. Behav.* **2008**, *95*, 271−281.

(4) Shin, H. S.; Ingram, J. R.; McGill, A. T.; Poppitt, S. D. Lipids, CHOs, proteins: Can all macronutrients put a 'brake' on eating? *Physiol. Behav.* **2013**, *120C*, 114−123.

(5) Maljaars, P. W.; Symersky, T.; Kee, B. C.; Haddeman, E.; Peters, H. P.; Masclee, A. A. Effect of ileal fat perfusion on satiety and hormone release in healthy volunteers. *Int. J. Obes.* **2008**, *32*, 1633−1639.

(6) Maljaars, J.; Romeyn, E. A.; Haddeman, E.; Peters, H. P.; Masclee, A. A. Effect of fat saturation on satiety, hormone release, and food intake. *Am. J. Clin. Nutr.* **2009**, *89*, 1019−1024.

(7) Maljaars, P. W.; Peters, H. P.; Kodde, A.; Geraedts, M.; Troost, F. J.; Haddeman, E.; Masclee, A. A. Length and site of the small intestine exposed to fat influences hunger and food intake. *Br. J. Nutr.* **2011**, *106*, 1609−1615.

(8) Maljaars, P. W.; van der Wal, R. J.; Wiersma, T.; Peters, H. P.; Haddeman, E.; Masclee, A. A. The effect of lipid droplet size on satiety and peptide secretion is intestinal site-specific. *Clin. Nutr.* **2012**, *31*, 535−542.

(9) Anton, S. D.; Martin, C. K.; Han, H.; Coulon, S.; Cefalu, W. T.; Geiselman, P.; Williamson, D. A. Effects of stevia, aspartame, and sucrose on food intake, satiety, and postprandial glucose and insulin levels. *Appetite* **2010**, *55*, 37−43.

(10) Hellfritsch, C.; Brockhoff, A.; Stahler, F.; Meyerhof, W.; Hofmann, T. Human psychometric and taste receptor responses to steviol glycosides. *J. Agric. Food Chem.* **2012**, *60*, 6782−6793.

(11) Fujimaru, T.; Park, J. H.; Lim, J. Sensory characteristics and relative sweetness of tagatose and other sweeteners. *J. Food Sci.* **2012**, *77*, S323−8.

(12) Joint FAO/WHO Expert Committee on Food Additives.. Safety evaluation of certain food additives. *WHO Food Addit. Ser.* **2009**, *60*, 183−220.

(13) EFSA Panel on Food Additives and Nutrient Sources (ANS).. Scientific opinion on safety of steviol glycosides for the proposed uses as a food additive. *EFSA J.* **2010**, *8* (4), 1537−1625.

(14) Voortman, T.; Hendriks, H. F.; Witkamp, R. F.; Wortelboer, H. M. Effects of long- and short-chain fatty acids on the release of gastrointestinal hormones using an ex vivo porcine intestinal tissue model. *J. Agric. Food Chem.* **2012**, *60*, 9035−9042.

(15) Geraedts, M. C.; Troost, F. J.; Fischer, M. A.; Edens, L.; Saris, W. H. Direct induction of CCK and GLP-1 release from murine endocrine cells by intact dietary proteins. *Mol. Nutr. Food Res.* **2011**, *55*, 476−484.

(16) Chen, Q.; Reimer, R. A. Dairy protein and leucine alter GLP-1 release and mRNA of genes involved in intestinal lipid metabolism in vitro. *Nutrition* **2009**, *25*, 340−349.

(17) Geraedts, M. C. P.; Troost, F. J.; Saris, W. H. M. Different tastants and low-caloric sweeteners induce differential effects on the release of satiety hormones. *Food Chem.* **2011**, *129*, 731−738.

(18) Clouard, C.; Meunier-Salaun, M. C.; Val-Laillet, D. Food preferences and aversions in human health and nutrition: how can pigs help the biomedical research? *Animal* **2012**, *6*, 118−136.

(19) Miller, E. R.; Ullrey, D. E. The pig as a model for human nutrition. *Annu. Rev. Nutr.* **1987**, *7*, 361−382.

(20) Patterson, J. K.; Lei, X. G.; Miller, D. D. The pig as an experimental model for elucidating the mechanisms governing dietary influence on mineral absorption. *Exp. Biol. Med. (Maywood, NJ, U.S.)* **2008**, *233*, 651−664.

(21) Verhoeckx, K. C.; Voortman, T.; Balvers, M. G.; Hendriks, H. F.; M Wortelboer, H.; Witkamp, R. F. Presence, formation and putative biological activities of N-acyl serotonins, a novel class of fatty-acid derived mediators, in the intestinal tract. *Biochim. Biophys. Acta, Mol. Cell Biol. Lipids* **2011**, *1811*, 578−586.

(22) Eissele, R.; Goke, R.; Willemer, S.; Harthus, H. P.; Vermeer, H.; Arnold, R.; Goke, B. Glucagon-like peptide-1 cells in the gastrointestinal tract and pancreas of rat, pig and man. *Eur. J. Clin. Invest.* **1992**, *22*, 283−291.

(23) Adrian, T. E.; Bacarese-Hamilton, A. J.; Smith, H. A.; Chohan, P.; Manolas, K. J.; Bloom, S. R. Distribution and postprandial release of porcine peptide YY. *J. Endocrinol.* **1987**, *113*, 11−14.

(24) Fujita, Y.; Wideman, R. D.; Speck, M.; Asadi, A.; King, D. S.; Webber, T. D.; Haneda, M.; Kieffer, T. J. Incretin release from gut is acutely enhanced by sugar but not by sweeteners in vivo. *Am. J. Physiol. Endocrinol. Metab.* **2009**, *296*, E473−9.

(25) Steinert, R. E.; Frey, F.; Topfer, A.; Drewe, J.; Beglinger, C. Effects of carbohydrate sugars and artificial sweeteners on appetite and the secretion of gastrointestinal satiety peptides. *Br. J. Nutr.* **2011**, *105*, 1320−1328.

(26) Depoortere, I. Taste receptors of the gut: Emerging roles in health and disease. *Gut* **2013**, *63*, 179−90.

(27) Gerspach, A. C.; Steinert, R. E.; Schonenberger, L.; Graber-Maier, A.; Beglinger, C. The role of the gut sweet taste receptor in regulating GLP-1, PYY, and CCK release in humans. *Am. J. Physiol. Endocrinol. Metab.* **2011**, *301*, E317−25.

(28) Janssen, S.; Depoortere, I. Nutrient sensing in the gut: New roads to therapeutics? *Trends Endocrinol. Metab.* **2013**, *24*, 92−100.

(29) Wolwer-Rieck, U. The leaves of *Stevia rebaudiana* (Bertoni), their constituents and the analyses thereof: A review. *J. Agric. Food Chem.* **2012**, *60*, 886−895.

(30) Moran-Ramos, S.; Tovar, A. R.; Torres, N. Diet: Friend or foe of enteroendocrine cells—How it interacts with enteroendocrine cells. *Adv. Nutr.* **2012**, *3*, 8−20.

(31) Hochstenbach-Waelen, A.; Veldhorst, M. A.; Nieuwenhuizen, A. G.; Westerterp-Plantenga, M. S.; Westerterp, K. R. Comparison of 2 diets with either 25% or 10% of energy as casein on energy expenditure, substrate balance, and appetite profile. *Am. J. Clin. Nutr.* **2009**, *89*, 831−838.

(32) Rafferty, E. P.; Wylie, A. R.; Elliott, C. T.; Chevallier, O. P.; Grieve, D. J.; Green, B. D. In vitro and in vivo effects of natural putative secretagogues of glucagon-like peptide-1 (GLP-1). *Sci. Pharm.* **2011**, *79*, 615−621.

(33) Veldhorst, M. A.; Nieuwenhuizen, A. G.; Hochstenbach-Waelen, A.; Westerterp, K. R.; Engelen, M. P.; Brummer, R. M.; Deutz, N. E.; Westerterp-Plantenga, M. S. Comparison of the effects of a high-and normal-casein breakfast on satiety, 'satiety' hormones, plasma amino acids and subsequent energy intake. *Br. J. Nutr.* **2009**, *101*, 295−303.
(34) Blundell, J.; De Graaf, C.; Hulshof, T.; Jebb, S.; Livingstone, B.; Lluch, A.; Mela, D.; Salah, S.; Schuring, E.; Van Der Knaap, H. Appetite control: Methodological aspects of the evaluation of foods. *Obes. Rev.* **2010**, *11*, 251−270.
(35) Meyer, J. H.; Hlinka, M.; Khatibi, A.; Raybould, H. E.; Tso, P. Role of small intestine in caloric compensations to oil premeals in rats. *Am. J. Physiol.* **1998**, *275*, R1320−33.
(36) Meyer, J. H.; Hlinka, M.; Tabrizi, Y.; DiMaso, N.; Raybould, H. E. Chemical specificities and intestinal distributions of nutrient-driven satiety. *Am. J. Physiol.* **1998**, *275*, R1293−307.
(37) Meyer, J. H.; Tabrizi, Y.; DiMaso, N.; Hlinka, M.; Raybould, H. E. Length of intestinal contact on nutrient-driven satiety. *Am. J. Physiol.* **1998**, *275*, R1308−19.
(38) Ferraris, R. P.; Yasharpour, S.; Lloyd, K. C.; Mirzayan, R.; Diamond, J. M. Luminal glucose concentrations in the gut under normal conditions. *Am. J. Physiol.* **1990**, *259*, G822−37.
(39) Abello, J.; Ye, F.; Bosshard, A.; Bernard, C.; Cuber, J. C.; Chayvialle, J. A. Stimulation of glucagon-like peptide-1 secretion by muscarinic agonist in a murine intestinal endocrine cell line. *Endocrinology* **1994**, *134*, 2011−2017.
(40) Geraedts, M. C.; Troost, F. J.; Saris, W. H. Peptide-YY is released by the intestinal cell line STC-1. *J. Food Sci.* **2009**, *74*, H79−82.
(41) McLaughlin, J. T.; Lomax, R. B.; Hall, L.; Dockray, G. J.; Thompson, D. G.; Warhurst, G. Fatty acids stimulate cholecystokinin secretion via an acyl chain length-specific, $Ca^{2+}$-dependent mechanism in the enteroendocrine cell line STC-1. *J. Physiol.* **1998**, *513* (Partt 1), 11−18.
(42) Reimer, R. A.; Darimont, C.; Gremlich, S.; Nicolas-Metral, V.; Ruegg, U. T.; Mace, K. A human cellular model for studying the regulation of glucagon-like peptide-1 secretion. *Endocrinology* **2001**, *142*, 4522−4528.
(43) Brubaker, P. L.; Schloos, J.; Drucker, D. J. Regulation of glucagon-like peptide-1 synthesis and secretion in the GLUTag enteroendocrine cell line. *Endocrinology* **1998**, *139*, 4108−4114.
(44) Geraedts, M. C.; Troost, F. J.; De Ridder, R. J.; Bodelier, A. G.; Masclee, A. A.; Saris, W. H. Validation of Ussing chamber technology to study satiety hormone release from human duodenal specimens. *Obesity* **2012**, *20*, 678−682.

JOURNAL OF AGRICULTURAL AND FOOD CHEMISTRY

Article

pubs.acs.org/JAFC

# Pterostilbene, a Dimethyl Ether Derivative of Resveratrol, Reduces Fat Accumulation in Rats Fed an Obesogenic Diet

Saioa Gómez-Zorita,[†,§] Alfredo Fernández-Quintela,[†,§] Arrate Lasa,[†,§] Leixuri Aguirre,[†,§] Agnes M. Rimando,[#] and María P. Portillo*[,†,§]

[†]Nutrition and Obesity Group, Department of Nutrition and Food Science, University of the Basque Country (UPV/EHU) and Lucio Lascaray Research Center, 01006 Vitoria, Spain

[§]CIBERobn Physiopathology of Obesity and Nutrition, Institute of Health Carlos III (ISCIII), Spain

[#]U.S. Department of Agriculture, Agricultural Research Service, Natural Products Utilization Research Unit, University, Mississippi, United States

**ABSTRACT:** The current study aimed to demonstrate the effects of pterostilbene in rats fed an obesogenic diet. For this purpose, pterostilbene was administered at doses of 15 mg/kg body weight/day (PT15 group) or 30 mg/kg body weight/day (PT30 group) for 6 weeks. Pterostilbene reduced adipose tissue mass −15.1% (PT15) and −22.9% (PT30). In this tissue, it decreased malic enzyme (−39.4 and −49.5% for PT15 and PT30 groups, respectively) and fatty acid synthase (−45 and −53.4% for PT15 and PT30) activities. Acetyl-CoA carboxylase activity was reduced and AMPK activity was increased only in the PT30 group. In the liver, pterostilbene (PT30) reduced malic enzyme (−29.5%) and glucose-6-P dehydrogenase (−43.2%) activities and increased carnitine palmitoyltransferase-1a (37.5%) and acyl-coenzyme A oxidase (42.5%) activities. This increased oxidative capacity was not associated with increased mitochondriogenesis. Among biochemical serum parameters, only insulin was modified by pterostilbene (−31.6%) in the PT15 group. The amounts of pterostilbene in serum and tissues from rats in the PT30 group were in not all cases 2-fold greater than those found in the PT15 group. In conclusion, pterostilbene shows antiobesity properties due, at least in part, to reduced lipogenesis in adipose tissue and increased fatty acid oxidation in liver.

**KEYWORDS:** *adipose tissue, bioavailability, fatty acid oxidation, lipogenesis, pterostilbene*

## INTRODUCTION

Obesity and overweight are major public health concerns that are spreading throughout the world, afflicting not only adults but also many children and adolescents. Moreover, obesity is associated with several chronic diseases, such as diabetes, strokes, and hypertension.[1] Considerable efforts are being made to identify naturally occurring molecules that are active and safe when administered orally and can be employed for obesity management, using a broad range of in vivo and in vitro methodologies.[2]

Phenolic compounds make up one of the groups of molecules that have been most frequently studied in recent years. In this context, resveratrol has been reported to decrease triacylglycerols in cultured adipocytes[3−5] and to reduce adipose tissue in various animal models, such as mice,[6] rats,[7] and primates.[8] However, resveratrol has a very low bioavailability as a consequence of its rapid metabolism in the gut and liver.[9] This poor bioavailability is highly dependent on its free hydroxyl groups, making it susceptible to glucuronidation and sulfation.[10] Due to this fact, the scientific community is looking for other resveratrol-related molecules showing higher bioavailability. In this context, pterostilbene, a dimethyl ether derivative of resveratrol that is less metabolized than resveratrol, is a good candidate.[11]

Pterostilbene is a phenolic compound biologically classified as a phytoalexin, which is part of a plant's defense system and is synthesized in response to pathogen infection, as well as to excessive ultraviolet exposure. Pterostilbene is known to have diverse benefits in the prevention and treatment of several diseases, including cancer,[12] dyslipidemia,[13] diabetes,[14] and cardiovascular and cognitive function degeneration.[15] However, the potential effects of pterostilbene on body fat accumulation have not been studied yet.

In this scenario, the aim of the present study was to determine the effect of pterostilbene on body fat in rats fed an obesogenic diet. The analysis of several mechanisms of action underlying this effect was also assessed.

## MATERIALS AND METHODS

**Chemicals.** 3T3-L1 preadipocytes were supplied by American Type Culture Collection (Manassas, VA, USA). Pterostilbene (purity > 98%) and resveratrol (purity > 98%) were obtained from Bertin Pharma (Montigny le Bretonneux, France). Dulbecco's modified Eagle medium (DMEM) was purchased from Life Technologies (Grand Island, NY, USA). Infinity Triglycerides reagent for triacylglyceride content and BCA reagent for protein determination were obtained from Thermo Scientific (Rockford, IL, USA). Antibodies for phosphorylated acetyl-CoA carboxylase (ACC1) (Ser 79), ACC1, phosphorylated-adenosine monophosphate-activated protein kinase (AMPK) (Thr 172), and AMPK were purchased form Cell Signaling Technology (Beverly, MA, USA). Trizol for RNA isolation was acquired from Invitrogen (Carlsbad, CA, USA). Primers for gene

Received: March 19, 2014
Revised: July 31, 2014
Accepted: August 1, 2014
Published: August 1, 2014

ACS Publications © 2014 American Chemical Society



dx.doi.org/10.1021/jf501318b | J. Agric. Food Chem. 2014, 62, 8371−8378

Table 1. Primer Sequences, Annealing Temperatures, and Primer Concentrations for PCR Amplification of Each Gene Studied

| gene[a] | sense primer | antisense primer | annealing (°C) | concn (nM) |
|---|---|---|---|---|
| FAS | 5′-AGCCCCTCAAGTGCACAGTG-3′ | 5′-TGCCAATGTGTTTTCCCTGA-3′ | 60.0 | 300 |
| ATGL | 5′-CACTTTAGCTCCAAGGATGA-3′ | 5′-TGGTTCAGTAGGCCATTCCT-3′ | 60.0 | 900 |
| HSL | 5′-CCCATAAGACCCCATTGCCTG-3′ | 5′-CTGCCTCAGACACACTCCTG-3′ | 60.0 | 300 |
| IL6 | 5′-TCCTACCCCAACTTCCAATGCTC-3′ | 5′-TTGGATGGTCTTGGTCCTTAGCC-3′ | 60.0 | 300 |
| CPT-1a | 5′-CGGTTCAAGAATGGCATCATC-3′ | 5′-TCACACCCACCACCACGAT-3′ | 60.0 | 300 |
| CD36 | 5′-GGTGTGCTCAACAGCCTTATC-3′ | 5′-TTATGGCAACCTTGCTTATG-3′ | 62.1 | 300 |
| TFAM | 5′-GCTTCCAGGGGGCTAAGGAT-3′ | 5′-CCCAATCCCAATGACAACTC-3′ | 60.0 | 300 |
| COX-II | 5′-AACAATTCTCCCAGCTGTCATTC-3′ | 5′-AGTCAAAGCATAGGTCTTCATAGTC-3′ | 60.0 | 300 |
| $\beta$-actin | 5′-TCTATGAGGGCTACGCTCTCC-3′ | 5′- CACGCTCGGTCAGGATCTTC-3′ | 60.0 | 300 |

[a]FAS, fatty acid synthase; ATGL, adipose triglyceride lipase; HSL, hormone sensitive lipase; IL6, interleukine 6; CPT, carnitine palmitoyltransferase; CD36, cluster of differentiation 36; TFAM, mitochondrial transcription factor; COX-II, cytochrome *c* oxidase subunit II.

expression were purchased from Integrated DNA Technologies, Inc. (Leuven, Belgium).

For pterostilbene analysis, $\beta$-glucuronidase (from *Escherichia coli*, Type IX-A) and sulfatase (from abalone entrails, Type VIII) were acquired from Sigma-Aldrich (St. Louis, MO, USA), and bis-[trimethylsilyl]-trifluoroacetamide/dimethylformamide (BSTFA/DMF, 1:1), the derivation reagent, was obtained from Pierce Biotechnology, Inc. (Rockford, IL, USA).

All other reagents and chemicals were of the highest purity grade available and from Sigma-Aldrich.

**Cell Culture.** 3T3-L1 preadipocytes were cultured in DMEM containing 10% fetal bovine serum (FBS). Two days after confluence (day 0), the cells were stimulated to differentiate with DMEM containing 10% FBS, 10 $\mu$g/mL insulin, 0.5 mM isobutylmethylxanthine (IBMX), and 1 $\mu$M dexamethasone for 2 days. On day 2, the differentiation medium was replaced by FBS/DMEM (10%) medium containing 10 $\mu$g/mL insulin and from day 4 onward by FBS/DMEM (10%) medium containing 0.2 $\mu$g/mL insulin. This medium was changed every 2 days until cells were harvested. All media contained 1% penicillin/streptomycin (10000 U/mL), and the media for differentiation and maturation contained 1% (v/v) biotin and panthothenic acid. Cells were maintained at 37 °C in a humidified 5% $CO_2$ atmosphere.

For the adipocyte treatment, cells grown in 6-well plates were incubated with pterostilbene or resveratrol at 1 $\mu$M (diluted in 95% ethanol) for 24 h on day 12 after differentiation. By that day, >90% of cells were mature adipocytes with visible lipid droplets. This cell treatment was carried out in triplicate.

**Adipocyte, Adipose Tissue, and Liver Triacylglycerol Content.** For triacylglycerol extraction, cells were washed extensively with phosphate-buffered saline (PBS) and incubated three times with 800 $\mu$L of hexane/isopropanol (2:1). The total volume was then evaporated under nitrogen, and the pellet was resuspended in 200 $\mu$L of Triton X-100 in 1% distilled water. Afterward, triacylglycerols were solubilized by a sonicator, and the content was measured using Infinity Triglycerides reagent. For protein determination, cells were lysed in 0.3 N NaOH and 0.1% SDS. Protein measurements were performed using the BCA reagent.

Adipose tissue and liver total lipids were extracted following the method described by Folch et al.[16] The lipid extract was dissolved in isopropanol and triacylglycerol content, was measured using a commercial kit (BioSystems, Barcelona, Spain).

**Cytotoxicity Assay.** Cell viability was assessed in cells treated for 24 h with 1 $\mu$M pterostilbene or resveratrol by the neutral red assay (TOX4 kit, Sigma-Aldrich, St. Louis, MO, USA).

**Animals, Diets, and Experimental Design.** The experiment was conducted with 27 male Wistar rats (6 weeks old) with an initial body weight of 180 ± 2 g purchased from Harlan Ibérica (Barcelona, Spain) and took place in accordance with the University of the Basque Country's guide for the care and use of laboratory animals (reference protocol approval CUEID CEBA/30/2010). The rats were individually housed in polycarbonate metabolic cages (Techniplast Gazzada, Guguggiate, Italy) and placed in an air-conditioned room (22 ± 2 °C) with a 12 h light−dark cycle. After a 6 day adaptation period, rats were randomly divided into three experimental groups of nine animals each and fed a commercial obesogenic diet, high in sucrose (20.0%) and fat (22.5%) (Harlan Ibérica, TD.06415). Pterostilbene (purity = 99.9%) was synthesized according to a published procedure.[15] This polyphenol was added to the diet in amounts that assured doses of 15 mg/kg body weight/day (PT15 group) or 30 mg/kg body weight/day (PT30 group). All animals had free access to food and water. Food intake and body weight were measured daily.

At the end of the experimental period (6 weeks), animals were sacrificed, after an overnight fasting, under anesthesia (chloral hydrate) by cardiac exsanguination. White adipose tissue from different anatomical locations (perirenal, epididymal, mesenteric, and subcutaneous) and liver were dissected and weighed. Serum was obtained from blood samples after centrifugation (1000*g* for 10 min at 4 °C). All samples were stored at −80 °C until analysis.

**Serum Parameters.** Serum insulin, triacylglycerols, and nonesterified fatty acids (NEFAs), as well as aspartate aminotransferase (AST/GOT) and alanine aminotransferase (ALT/GPT) activities, were measured using a commercial kits (BioSystems, Barcelona, Spain; EZRMI-13K, Linco, St. Charles, MO, USA; Roche Diagnostics GmbH, Mannheim, Germany; and Spinreact, Barcelona, Spain, respectively). An ELISA kit was used for interleukin 6 (IL6) determination (Quantikine ELISA, R&D Systems, Abingdon, UK).

**Enzyme Activities in White Adipose Tissue and Liver.** For lipogenic enzyme analysis, samples of subcutaneous adipose tissue (1 g) or liver (0.5 g) were homogenized in 5 mL of buffer (pH 7.6) containing 150 mM KCl, 1 mM $MgCl_2$, 10 mM *N*-acetylcysteine, and 0.5 mM dithiothreitol. After centrifugation at 100000*g* for 40 min at 4 °C, the supernatant fraction was used for quantitation of enzyme activities. Fatty acid synthase (FAS), glucose-6-phosphate dehydrogenase (G6PDH), malic enzyme (ME), and lipoprotein lipase (LPL) activities were measured as previously described.[17] Enzyme activities were expressed either as nanomoles of NADPH consumed (FAS) or as nanomoles of NADPH produced (G6PDH and ME) per minute per milligram of protein. Protein was assessed using the Bradford method.[18]

Carnitine palmitoyltransferase-1a (CPT-1a) and acyl-coenzyme A oxidase (ACO) activities in liver were assessed in the mitochondrial/peroxisomal fraction as previously described.[16] CPT-1a activity was expressed as nanomoles of CoA formed per minute per milligram of protein and ACO activity as nanomoles of NADH formed per minute per milligram of protein.

**Extraction and Analysis of RNA and Quantification by Reverse Transcription Polymerase Chain Reaction (Real-Time RT-PCR).** RNA samples were extracted from cells by using Trizol, according to the manufacturer's instructions. The integrity of the RNA extracted from all samples was verified and quantified using an RNA 6000 Nano Assay (Thermo Scientific, Wilmington, DE, USA). RNA samples were then treated with DNase I kit (Applied Biosystems, Foster City, CA, USA) to remove any contamination with genomic DNA.

One microgram of total RNA in a total reaction volume of 20 $\mu$L was reverse transcribed using the iScript cDNA Archive Kit (Applied

Table 2. Final Body Weight, Food Intake, Body Weight Gain, Adipose Tissue Weight, Liver Weight, and Liver Triacylglycerol Content of Rats Fed the Experimental Diets for 6 Weeks[a]

| | control | PT15 | PT30 | ANOVA |
|---|---|---|---|---|
| final body weight (g) | 382 ± 5 | 387 ± 9 | 376 ± 9 | NS |
| food intake (g/day) | 17.6 ± 0.3 | 17.7 ± 0.5 | 17.5 ± 0.3 | NS |
| body weight gain (g) | 202 ± 10 | 206 ± 9 | 200 ± 6 | NS |
| adipose tissue weights | | | | |
| epididymal (g) | 11.8 ± 0.9 | 10.5 ± 0.9 | 10.5 ± 1.1 | NS |
| perirenal (g) | 13.5 ± 0.8 a | 12.0 ± 1.1ab | 11.2 ± 1.0 b | $P < 0.05$ |
| mesenteric (g) | 6.02 ± 0.4 a | 5.19 ± 0.4 ab | 4.80 ± 0.5 b | $P < 0.05$ |
| subcutaneous (g) | 16.8 ± 1.1 a | 12.6 ± 1.2 b | 12.7 ± 1.6 b | $P < 0.05$ |
| PR + MS (g) | 18.8 ± 3.1 a | 17.2 ± 1.3 b | 14.7 ± 2.8 b | $P < 0.05$ |
| E + PR + MS (g) | 36.0 ± 3.1 a | 30.1 ± 2.5 b | 29.6 ± 2.8 b | $P = 0.08$ |
| total (g) | 47.5 ± 3.0a | 40.3 ± 3.0b | 36.6 ± 3.5b | $P < 0.05$ |
| liver | | | | |
| weight (g) | 9.40 ± 0.4 | 10.0 ± 0.3 | 10.1 ± 0.4 | NS |
| triacylglycerols (mg/g) | 33.1 ± 4.9 | 30.9 ± 3.0 | 35.5 ± 2.4 | NS |

[a]Values are means ± SEM ($n = 9$). Values in the same row with different letters are significantly different at $P < 0.05$ as determined by Newman–Keuls test. PT, pterostilbene; NS, not significant; PR, perirenal; MS, mesenteric; E, epididymal.

Biosystems Inc., Foster City, CA, USA) according to the manufacturer's protocols. Reactions were incubated initially at 25 °C for 10 min and subsequently at 37 °C for 120 min and at 85 °C for 5 min.

Relative mRNA levels were quantified using real-time PCR with an iCycler MyiQ Real Time PCR Detection System (Bio-Rad, Hercules, CA, USA). β-Actin mRNA levels were similarly measured and served as the reference gene. The PCR reagent mixture consisted of 1 μL of each cDNA (10 pmol/μL). Specific primers were synthesized commercially, and the sequences and PCR conditions are shown in Table 1.

**Western Blot Analysis.** For acetyl-CoA carboxylase (ACC) and adenosine monophosphate-activated protein kinase (AMPK) activity determinations, the amounts of total ACC and phosphorylated ACC or those of total AMPK and phosphorylated AMPK were measured.

Tissue extracts were obtained by homogenizing 100 mg of subcutaneous adipose tissue or liver in a PBS buffer (pH 7.4) and centrifuged (40*g*, 10 min, 4 °C). For ACC activity determination, 15 μg of tissue extracts in the case of subcutaneous adipose tissue or 60 μg in the case of liver was separated by electrophoresis in a SDS–polyacrylamide gel and transferred to PVDF membranes (Millipore, Bedford, MA, USA). For AMPK activity determination, 25 μg of subcutaneous adipose tissue extracts was used for eletrophoretic separation and transfer to PVDF membranes. Then, the membranes of the two assays were blocked with casein PBS–Tween buffer for 2 h.

The membranes were incubated overnight at 4 °C with ACC antibody (1:1000) or AMPK antibody (1:2000), respectively. Antibodies were visualized by using a chemiluminescent substrate (Thermo Scientific). The intensity of the bands was determined by densitometric analysis and quantified by a ChemiDoc MP imaging system (Bio-Rad). After antibody stripping, the membranes were blocked and then incubated with a phosphorylated ACC antibody (1:1000) or with a phosphorylated AMPK antibody (1:2000) and measured again.

**Analysis of Pterostilbene in Serum and Tissues.** Serum pterostilbene extraction was performed according to the procedure published by Kotani et al.,[19] with modifications. Serum from −80 °C storage was thawed on ice. Fifteen microliters of β-glucuronidase (from *E. coli*, Type IX-A; 250 U/15 mL sodium phosphate buffer, 0.1 M, pH 6.8) and 15 μL of sulfatase (from Abalone Entrails, Type VIII; 20 U/15 mL sodium phosphate buffer, 0.1 M, pH 6.8) were added to 50 μL of serum and then vortex-mixed. This mixture was incubated for 20 h at 37 °C while shaking at 750 rpm using an Eppendorf Thermomixer R (Eppendorf North America, Hauppauge, NY, USA), cooled to room temperature, and then partitioned with ethyl acetate (75 μL × 3). The ethyl acetate layers were combined and dried under nitrogen. The dried sample was derivatized with 40 μL of *N,O*-bis[trimethylsilyl]trifluoroacetamide/dimethylformamide (BSTFA/DMF, 1:1), heated at 70 °C for 40 min, and used for the analysis of pterostilbene by gas chromatography–mass spectrometry (GC-MS).

Pterostilbene in liver was extracted following a published procedure,[20] with minor modifications. One hundred milligrams of fresh tissues was homogenized in 1 mL of saline solution (0.9% NaCl in $H_2O$). Enzyme solution (300 μL; 793.67 U/mL sulfatase and 666.66 U/mL β-glucuronidase in sodium acetate buffer, pH 5), was added to the homogenates, vortex-mixed, and incubated at 37 °C for 16 h while shaking at 750 rpm. Then, 100 μL of 0.1 N HCl was added to this mixture and then partitioned with ethyl acetate (800 μL × 2). The ethyl acetate layers were combined and then dried under nitrogen. The dried sample was derivatized with BSTFA/DMF under the same conditions used for the analysis of pterostilbene in serum.

For the analysis of pterostilbene in adipose tissues, 100 mg of lyophilized tissue was homogenized in 300 μL of sodium acetate buffer and then sonicated for 30 min. Enzyme solution (300 μL; 793.67 U/mL sulfatase and 1333.33 U/mL β-glucuronidase in sodium acetate buffer, pH 5) was added to the homogenate, vortex-mixed, and incubated at 37 °C, with shaking at 750 rpm, for 16 h. After incubation, 500 μL of ice-cold acetonitrile were added, vortexed for 1 min, and then centrifuged (648.7*g*, Savant SpeedVac Concentrator; ThermoFisher Scientific, Waltham, MA, USA) for 20 min. The clear supernatant was collected and treated again with 500 μL of ice-cold acetonitrile, vortexed, and then centrifuged for 20 min. The supernatant was then dried under a stream of nitrogen and derivatized with BSTFA/DMF using the same conditions as in the analysis of pterostilbene in serum.

GC-MS analysis of pterostilbene in serum and tissues was performed using a J&W DB-5 capillary column (0.25 mm internal diameter, 0.25 μm film thickness, 30 m length; Agilent Technologies, Foster City, CA, USA) on a JEOL GCMate II Instrument (JEOL USA Inc., Peabody, MA, USA). For the serum samples, the GC temperature program was as follows: initial, 180 °C; held at this temperature for 1 min; increased to 264 °C at a 12 °C/min rate; held at this temperature for 4 min; increased to 300 °C at a rate of 30 °C/min; and held at this temperature for 0.5 min. The retention time of pterostilbene was 9.7 min. For the tissue samples, the GC temperature program was as follows: initial, 180 °C; held at this temperature for 1 min; increased to 263 °C at a 14 °C/min rate; held at this temperature for 5 min; increased to 300 °C at a rate of 35 °C/min; and held at this temperature for 0.5 min. The retention time of pterostilbene was 8.6 min. The carrier gas was ultrahigh-purity helium, at a 1 mL/min flow rate. The injection port, GC-MS interface, and ionization chamber were at 250, 230, and 230 °C, respectively. The volume of injection was 1 μL, splitless injection. The mass spectrum was acquired in positive, electron impact (70 eV), low-resolution, selected ion

Table 3. Serum Parameters of Rats Fed the Experimental Diets for 6 Weeks[a]

| | control | PT15 | PT30 | ANOVA |
|---|---|---|---|---|
| insulin ($\mu$U/mL) | 80.1 ± 10.9a | 54.8 ± 8.2b | 76.1 ± 6.1a | $P < 0.05$ |
| triacylglycerols (mg/dL) | 51.4 ± 7.4 | 45.1 ± 3.9 | 60.3 ± 9.1 | NS |
| NEFAs (mmol/L) | 0.26 ± 0.03 | 0.23 ± 0.02 | 0.23 ± 0.01 | NS |
| IL6 (pg/mL) | 26.5 ± 6.7 | 25.9 ± 8.1 | 26.5 ± 7.5 | NS |
| AST (U/L) | 81.9 ± 10.4 | 73.8 ± 8.8 | 76.2 ± 10.1 | NS |
| ALT (UL) | 25.3 ± 0.9 | 26.0 ± 2.2 | 26.6 ± 2.1 | NS |

[a]Values are means ± SEM ($n = 9$). Values in the same row with different letters are significantly different at $P < 0.05$ as determined by Newman−Keuls test. PT, pterostilbene; NS, not significant; NEFAs, nonesterified fatty acids;IL6, interleukin 6; AST/GO: aspartate aminotransferase; ALT/GPT, alanine aminotransferase.

Table 4. Adipose Tissue and Liver Lipogenic Enzyme Activities and Liver CPT-1a and ACO Activities of Rats Fed the Experimental Diets for 6 Weeks[a]

| | control | PT15 | PT30 | ANOVA |
|---|---|---|---|---|
| adipose tissue | | | | |
| G6PDH[b] | 63.5 ± 8.7 | 70.5 ± 9.6 | 50.2 ± 2.8 | NS |
| ME[b] | 94.2 ± 11.3a | 57.1 ± 6.1b | 47.6 ± 6.1b | $P < 0.01$ |
| FAS[c] | 43.6 ± 4.4a | 24.0 ± 3.8b | 20.3 ± 4.3b | $P < 0.01$ |
| HR-LPL[d] | 4.62 ± 0.9 | 4.79 ± 1.0 | 3.12 ± 0.6 | NS |
| liver | | | | |
| G6PDH[b] | 28.0 ± 4.2a | 19.7 ± 1.8ab | 15.9 ± 1b | $P < 0.05$ |
| ME[b] | 22.7 ± 2.3a | 16.8 ± 1.5ab | 16.0 ± 1.5b | $P < 0.05$ |
| FAS[c] | 5.42 ± 1.0 | 3.71 ± 0.6 | 3.33 ± 0.4 | NS |
| CPT-1a[e] | 6.48 ± 1.1a | 8.26 ± 1.1ab | 10.4 ± 0.4b | $P < 0.05$ |
| ACO[f] | 4.17 ± 0.7a | 4.54 ± 0.1a | 7.34 ± 0.5b | $P < 0.01$ |

[a]Values are means ± SEM. Values in the same row with different letterss are significantly different as determined by Newman−Keuls test. PT, pterostilbene; NS, not significant; G6PDH, glucose-6-phosphate dehydrogenase; ME, malic enzyme; FAS, fatty acid synthase; HR-LPL, heparin releasable lipoprotein lipase; CPT-1a, carnitine palmitoyltransferase 1a; ACO, acyl-CoA oxidase. [b]nmol NADPH formed/mg protein/min. [c]nmol NADPH consumed/mg protein/min. [d]nmol oleate released/min/g tissue. [e]nmol CoA formed/min/mg protein. [f]nmol NADH formed/min/mg protein.

monitoring mode using masses $m/z$ 328, 313, and 296. Quantitation was performed from a calibration curve of a standard sample of pterostilbene.

**Statistical Analysis.** Results are presented as means ± standard error of the means. Statistical analysis was performed using SPSS 17.0 (SPSS Inc., Chicago, IL, USA). All of the parameters are normally distributed according to the Shapiro--Wilks test. Thus, data from the in vivo experiment were analyzed by using one-way ANOVA followed by a Newman−Keuls post hoc test with the exception of pterostilbene amounts in serum and tissues, which were analyzed by using Student's $t$ test. Also in the in vitro experiment Student's $t$ test was used to compare treated cells with each dose of pterostilbene or resveratrol with control cells and also to compare both polyphenols at every dose. Statistical significance was set at the $P < 0.05$ level.

## RESULTS

**Final Body Weight, Food Intake, Body Weight Gain, White Adipose Tissue Weights, Fat Mass, Liver Weight, Liver Triacylglycerol Content, and Serum Parameters.** No statistical differences in food intake, body weight gain, and final body weight were found among experimental groups. Nevertheless, pterostilbene significantly reduced total adipose tissue mass (−15.1% in PT15 group and −22.9% in PT30 group) ($P < 0.05$). With regard to specific anatomical locations, whereas only the subcutaneous depot was significantly affected in the PT15 group, in the PT30 group perirenal, mesenteric, and subcutaneous locations were reduced ($P < 0.05$) (Table 2). This reduction was mirrored in fat mass data (expressed as percentage of body weight): 10.4 ± 1.6 in the control group, 7.80 ± 0.6 in the PT15 group, and 7.07 ± 0.4 in the PT30 group ($P < 0.05$).

As far as liver is concerned, no significant differences in organ weight or triacylglycerol content were observed among experimental groups (Table 2).

Serum parameters are shown in Table 3. Due to the fact that lipogenesis is controlled by insulin, we also measured serum concentrations of this hormone. No differences were found between the control rats and the rats treated with 30 mg/kg/day pterostilbene. By contrast, the rats treated with 15 mg/kg/day pterostilbene showed significantly reduced serum concentrations of this hormone ($P < 0.05$). No significant changes were observed in triacylglycerols and NEFAs.

AST and ALT activities were measured to assess potential liver damage induced by pterostilbene, and no significant changes were found among the experimental groups. Finally, serum concentrations of IL6, a marker of inflammation, remained unchanged (Table 3).

**Enzyme Activities in Adipose Tissue and Liver.** Table 4 shows that the activities of ME and FAS were significantly reduced in subcutaneous adipose tissue from rats of the PT15 and PT30 groups ($P < 0.01$). G6PDH and HR-LPL remained unchanged.

Phosphorylation of ACC leads to its inactivation. Thus, the phosphorylated-ACC/total ACC protein ratio is an index of ACC activity. This index was significantly increased by pterostilbene in rats from the PT30 group ($P < 0.05$), meaning that this enzyme was significantly inhibited (Figure 1A).

By contrast, the greater the phosphorylation rate of AMPK, the greater the activation of this enzyme. In the present study, only the higher dose of pterostilbene (30 mg/kg/day) increased the phosphorylatedAMPK/total AMPK protein

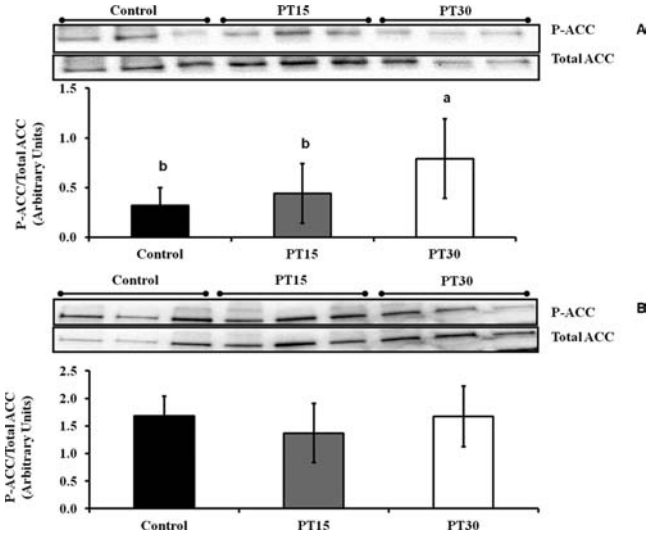


**Figure 1.** Phosphorylated-ACC/total ACC ratio in adipose tissue (A) or liver (B) of rats from the experimental groups. Values are means ± SEM for nine animals per group. Bars not sharing a common letter are significantly different ($P < 0.05$).

ratio ($P < 0.05$). This result means that AMPK was significantly activated in the PT30 group (Figure 2).

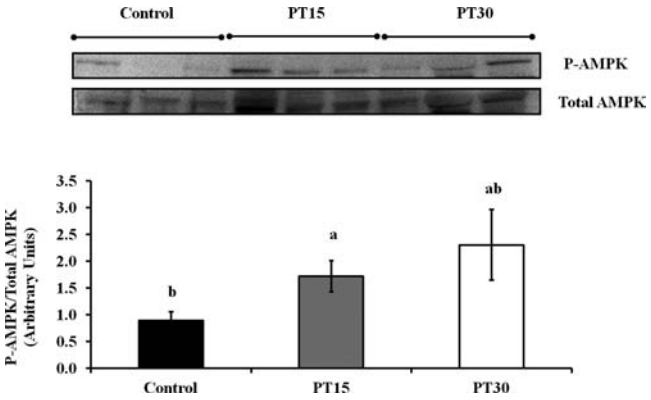


**Figure 2.** Phosphorylated AMPK/total AMPK ratio in adipose tissue of rats from the experimental groups. Values are means ± SEM for nine animals per group. Bars not sharing a common letter are significantly different ($P < 0.05$).

In liver, the activities of enzymes that provide NADPH for lipogenesis (ME and G6PDH) were decreased in rats from the PT30 group, but not in rats from the PT15 group ($P < 0.05$) (Table 4). By contrast, the activities of the rate-limiting lipogenic enzymes (FAS and ACC) were not modified (Table 4; Figure 1B).

As far as the activities of enzymes involved in fatty acid oxidation (CPT-1a and ACO) are concerned, both were significantly increased in the PT30 group ($P < 0.05$ and $P < 0.01$, respectively) (Table 4).

**Gene Expressions in Adipose Tissue and Liver.** In adipose tissue gene expressions of fatty acid synthase (FAS), adipose triglyceride lipase (ATGL), hormone sensitive lipase (HSL), and IL6 were measured. None of these genes showed significant changes after pterostilbene treatment (Table 5). Similarly, hepatic gene expressions of CPT-1a, cluster of differentiation 36 (CD36), mitochondrial transcription factor (TFAM), and cytochrome *c* oxidase subunit II (COX-II) remained unchanged (Table 5).

**Table 5. Gene Expression (Arbitrary Units) in Adipose Tissue and Liver of Rats Fed the Experimental Diets for 6 Weeks[a]**

| | control | PT15 | PT30 | ANOVA |
|---|---|---|---|---|
| adipose tissue | | | | |
| FAS | 1.00 ± 0.22 | 0.52 ± 0.22 | 1.30 ± 0.35 | NS |
| ATGL | 1.00 ± 0.13 | 1.34 ± 0.37 | 1.61 ± 0.42 | NS |
| HSL | 1.00 ± 0.28 | 1.03 ± 0.33 | 1.74 ± 0.41 | NS |
| IL6 | 1.00 ± 0.30 | 0.72 ± 0.20 | 0.82 ± 0.31 | NS |
| liver | | | | |
| CPT-1a | 1.00 ± 0.32 | 0.84 ± 0.17 | 1.12 ± 0.09 | NS |
| CD36 | 1.00 ± 0.46 | 1.49 ± 0.50 | 0.69 ± 0.58 | NS |
| TFAM | 1.00 ± 0.69 | 1.45 ± 0.37 | 0.88 ± 0.30 | NS |
| COX-II | 1.00 ± 0.68 | 1.22 ± 0.68 | 0.50 ± 0.23 | NS |

[a]FAS, fatty acid synthase; ATGL, adipose triglyceride lipase; HSL, hormone sensitive lipase; IL6, interleukin 6; CPT, carnitine palmitoyltransferase; CD36, cluster of differentiation 36; TFAM, mitochondrial transcription factor; COX-II, cytochrome *c* oxidase subunit II.

**Serum and Tissue Levels of Pterostilbene.** Pterostilbene was detected in the serum and in all of the tissues analyzed. The accumulation of this polyphenol was greater in the liver than in adipose tissue. Rats from the PT30 group received a dose of pterostilbene 2-fold higher than rats from the PT15 group, but the amounts of this molecule found in serum and tissues in rats from the PT30 group were not in all cases 2-fold greater than those found in rats from the PT15 group (Table 6).

**Table 6. Serum and Tissue Levels of Pterostilbene in Rats Fed Pterostilbene-Supplemented Diets for 6 Weeks[a]**

| | PT15 | PT30 |
|---|---|---|
| serum (ng/mL) | 384 ± 19.3 | 788 ± 100.6*** |
| liver (ng/100 mg FW) | 30.8 ± 4.8 | 70.6 ± 4.3*** |
| epididymal (ng/100 mg FW) | 1.09 ± 0.2 | 3.07 ± 0.4*** |
| subcutaneous (ng/100 mg FW) | 2.05 ± 0.5 | 3.54 ± 0.3* |

[a]Values are means ± SEM. Pterostilbene amounts in serum and tissues were analyzed by using Student's *t* test: *, $P < 0.05$; ***, $P < 0.001$. PT, pterostilbene; FW, fresh weight.

**Cell Viability and Triacylglycerol Content in Mature 3T3-L1 Adipocytes.** 3T3-L1 mature cells exposed to 1 μM pterostilbene and resveratrol for 24 h showed no loss of viability. Figure 3 shows the results obtained by the neutral red test after 24 h.

Pterostilbene, as well as resveratrol, showed a delipidating effect in 3T3-L1 mature adipocytes at 1 μM (Figure 4).

## DISCUSSION

As described in the Introduction, resveratrol, a polyphenol that has recently been reported to reduce body fat, shows a very low bioavailability. Consequently, interest in other resveratrol-related molecules that share the beneficial properties of resveratrol but show higher bioavailability is growing. In this context, the potential antiobesity properties of pterostilbene, a resveratrol dimethyl ether derivative, were analyzed in the present study.

It is known that the substitution of a hydroxy with a methoxy group in polyphenols increases their transport into cells, as well


dx.doi.org/10.1021/jf501318b | J. Agric. Food Chem. 2014, 62, 8371−8378

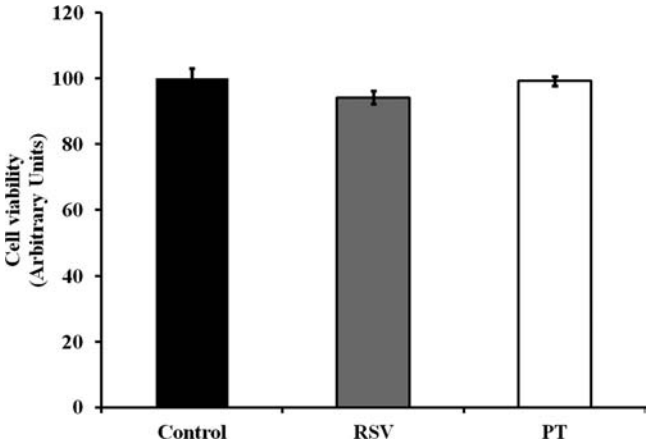


**Figure 3.** Cell viability in 3T3-L1 mature adipocytes treated for 24 h with resveratrol or pterostilbene at 1 $\mu$M. Values are means ± SEM. Comparisons between each treatment and the control were analyzed by Student's *t* test. RSV, resveratrol; PT, pterostilbene.

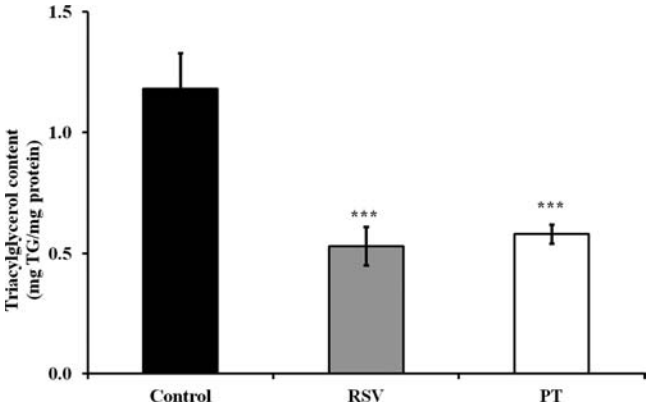


**Figure 4.** Triacylglycerol content in 3T3-L1 mature adipocytes treated for 24 h with resveratrol or pterostilbene at 1 $\mu$M. Values are means ± SEM. Comparisons between each treatment and the control were analyzed by Student's *t* test. Asterisks represent differences between pterostilbene- or resveratrol-treated cells and control cells: (***) $P < 0.001$. RSV, resveratrol; PT, pterostilbene.

as their bioavailability.[21] Pterostilbene is not as quickly glucuronidated and sulfated as resveratrol. The influence of the number and position of the hydroxy/methoxy groups in the stilbene-based molecular structure has not been extensively studied.[22,23] Thus, this issue needs further investigation. With regard to the antiobesity properties of pterostilbene, as far as we are aware few studies have been performed so far.[24]

In the present study, data concerning serum concentrations and tissue amounts of pterostilbene obtained in rats fed an obesogenic diet and treated with 15 or 30 mg pterostilbene/kg/day allowed us to confirm that this compound showed greater bioavailability than resveratrol. Resveratrol serum concentrations, after oral doses similar to those used in the present study, are in the nanomolar range (10−60 nM).[25−27] In good accordance with the literature,[10] we observed that pterostilbene serum concentrations were definitely higher. In the case of tissues, the greater bioavailability of pterostilbene as compared to that of resveratrol is even more evident. Whereas in the present study the amounts of pterostilbene found in liver and adipose tissue were in the range of nanomoles per gram after an overnight fasting, resveratrol, as the parent compound, was not found in a previous study from our laboratory carried out by using the same experimental conditions.[28]

To assess the antiobesity properties of pterostilbene, we analyzed its effect on body fat accumulation in the rats fed the obesogenic diet. This phenolic compound significantly reduced body fat accumulation. The antiobesity effect of the higher dose was greater than that of the lower dose (22.9 vs 15.1% decrease in total adipose tissue mass), but significant differences between these two groups were not found. As far as specific anatomical locations are concerned, whereas the lower dose mainly affected the subcutaneous depot, the higher dose reduced both subcutaneous and internal (mesenteric and perirenal) depots.

This reduction in fat accumulation was not due to a decrease in food intake. Thus, to find potential mechanisms underlying the body fat decrease, the effects of pterostilbene treatment on several metabolic pathways related to triacylglycerol metabolism were assessed. For this purpose, we chose subcutaneous adipose tissue because it showed the greatest reduction.

The activity of the enzymes involved in de novo lipogenesis was significantly reduced, meaning that the attenuation of this metabolic pathway was involved in the body fat lowering effect of pterostilbene. By contrast, the uptake of triacylglycerols from circulating lipoproteins, as well the lipolytic capacity, did not seem to be modified, because significant changes were not observed either in the activity of HR-LPL or in the gene expression of ATGL and HSL.

It has been reported that pterostilbene suppresses lipogenesis in human prostate cancer cells by activating AMPK.[29] To elucidate whether this mechanism also takes place in vivo in adipose tissue, AMPK activity was measured and seen to be increased by the higher dose of pterostilbene. This can justify the decreased ACC activity in the PT30 group, because it has been demonstrated that AMPK inhibits ACC activity by phosphorylation.[30] As far as FAS is concerned, we observed increased activity without changes in its gene expression, suggesting that this pterostilbene-mediated regulation took place at a post-transcriptional level.

It is well-known that insulin regulates the activity of lipogenic enzymes.[31] In the present study, the lack of a clear parallelism between changes in serum insulin concentrations and changes in lipogenic enzyme activities induced by pterostilbene suggests that the effects of pterostilbene do not seem to be mediated by this hormone.

The lack of change in serum insulin concentration in the PT30 group can be surprising. Nevertheless, this situation sometimes takes place with polyphenols. In a previous study performed by our group in obese Zucker rats treated with resveratrol at doses of 15 and 45 mg/kg/day, we observed that this polyphenol significantly increased hepatic CPT-1a activity and reduced serum transaminase concentrations when administered at 15 mg/kg body weight/day, but not at 45 mg/kg body weight/day.[32] Cho et al.[33] fed C57BL/J mice a diet supplemented with 0.02 or 0.005% resveratrol. They found that plasma total cholesterol was reduced by only the lower concentration. Moreover, the reductions induced in hepatic cholesterol and triacylglycerol contents by the lower concentration of resveratrol were significantly greater than those induced by the higher concentration. It seems that pterostilbene is showing the same pattern of response as its related compound, resveratrol.

Pterostilbene has been demonstrated to reduce several inflammatory markers, such as IL6 in 3T3-L1 adipocytes after induction of inflammation by TNF$\alpha$.[34] In the present study, no

changes either in adipose tissue gene expression or in serum concentrations of IL6 were observed. This lack of effect can be due to the fact that the increase in body fat induced by obesogenic feeding was not big enough to induce inflammation. In fact, serum concentration of this interleukin was no greater than that of lean rats fed a standard chow diet (data not shown).

The accumulation of fat in adipose tissue depends on lipid metabolism not only in this tissue but also in other tissues and organs such as the liver. Although pterostilbene, at a dose of 30 mg/kg/day, significantly reduced the activity of hepatic ME and G6PDH, two enzymes involved in the production of NADPH, the activity of hepatic FAS and ACC, two rate-limiting enzymes,[33] was not significantly modified. Therefore, the contribution to the antiobesity effects of pterostilbene of a reduced hepatic triacylglycerol synthesis, and thus of a reduced amount of triacylglycerols in plasma from the liver and available for adipose tissue uptake, may be disregarded.

To analyze the effects of pterostilbene on liver fatty acid oxidation, the activities of two rate-limiting oxidative enzymes, CPT-1a and ACO, were measured. Only the higher dose of pterostilbene significantly increased the activity of both enzymes. It is well-known that an increase in fatty acid oxidation is an underlying mechanism of action for the antiobesity effect of several molecules, such as resveratrol. Under these metabolic conditions fatty acids are channeled toward oxidative routes instead of toward storage routes.[35,36] The present results suggest that at 15 mg/kg/day the antiobesity effect of pterostilbene results from the direct action on adipose tissue and that an additional contribution of hepatic lipid metabolism takes place when pterostilbene doses increase. This could explain why the antiobesity effect of 30 mg/kg/day, although not significant, was greater than that of the lowest dose. The increased activity of CPT-1a seems not to be associated with increased mitochondria density because no changes were induced in the expression of TFAM, a mitochondriogenesis marker, and COX-II a mitochondrion-encoded protein embedded in the lipid bilayer of the inner mitochondrial membrane. When liver triacylglycerol content was measured, no differences were found among experimental groups. This suggests that apparently the increase in fatty acid oxidation was not sufficient to reduce liver fat accumulation. Although surprising, this fact has also been found in other studies.[37−39] To find a potential contribution of increased liver fatty acid uptake from serum to this situation, gene expression of CD36 was measured but no significant changes were observed.

If we compare the present results with those obtained in the study from our laboratory, carried out with resveratrol and previously mentioned,[35] we observe that pterostilbene was more efficient than resveratrol at a dose of 15 mg/kg/day. At 30 mg/kg/day both stilbenes showed similar responses. This can be justified, at least in part, by the higher bioavailability of pterostilbene. Nevertheless, a potential involvement of a higher activity of pterostilbene, due to its specific chemical structure (two additional methoxy groups as compared to resveratrol's structure) could not be discarded. The exclusive influence of a differential activity cannot be elucidated in an in vivo study, and as a consequence, an in vitro study was conducted.

The results obtained show that at a dose of 1 $\mu$M, pterostilbene and resveratrol showed similar delipidating effects, suggesting that the substitution of two hydroxyl groups by two methoxy groups did not modify the activity of pterostilbene. The reduction in triacylglycerol content induced by both phenolic compounds was not due to reduced cell viability.

In summary, pterostilbene shows antiobesity properties. Reduced lipogenesis in adipose tissue and increased fatty acid oxidation in liver contribute to this effect. In the range of the doses studied, a dose−response effect was not observed.

## AUTHOR INFORMATION


### Corresponding Author

*(M.P.P.) Mail: Dpt. Nutrition and Food Science, Faculty of Pharmacy, Paseo de la Universidad 7, 01006 Vitoria, Spain. Phone: +34-945-013067. Fax: +34-945-013014. E-mail: mariapuy.portillo@ehu.es.



### Funding

This study was supported by grants from the Ministerio de Ciencia e Innovación (AGL2008-01005-ALI) and Ministerio de Economía y Competitividad (AGL2011-27406-ALI), Instituto de Salud Carlos III (CIBERObn), the government of the Basque Country (IT-512-13), and the University of the Basque Country (UPV/EHU) (ELDUNANOTEK UFI11/32). S.G.-Z. is the recipient of a doctoral fellowship from the University of the Basque Country (UPV/EHU).


### Notes

The authors declare no competing financial interest.

## ACKNOWLEDGMENTS

We thank Gloria Hervey for her technical help.

## ABBREVIATIONS USED

ACO, acyl-coenzyme A oxidase; ALT/GPT, alanine aminotransferase; AMPK, AMP-activated protein kinase; AST/GOT, aspartate aminotransferase; ATGL, adipose triglyceride lipase; CD36, cluster of differentiation 36; COX-II, cytochrome *c* oxidase subunit II; CPT-1a, carnitine palmitoyltransferase-1a; DMEM, Dulbecco's modified Eagle medium; FAS, fatty acid synthase; FBS, fetal bovine serum; G6PDH, glucose-6-phosphate dehydrogenase; GC-MS, gas chromatography−mass spectrometry; HR-LPL, heparin releasable lipoprotein lipase; HSL, hormone sensitive lipase; IBMX, isobutylmethylxanthine; IL6, interleukin 6; LPL, lipoprotein lipase; ME, malic enzyme; NADH, reduced form of nicotinamide adenine dinucleotide; NADPH, reduced form of nicotinamide adenine dinucleotide phosphate; NEFA, nonesterified fatty acid; PBS, phosphate-buffered saline; PVDF, polyvinylidine fluoride; RSV, resveratrol; TFAM, mitochondrial transcription factor A; TNF$\alpha$, tumor necrosis factor alpha

## REFERENCES


(1) James, P.; Rigby, N.; Leach, R.; International Obesity Task Force. The obesity epidemic, metabolic syndrome and future prevention strategies. *Eur. J. Cardiovasc. Prev. Rehabil.* **2004**, *11*, 3−8.

(2) Wang, S.; Moustaid-Moussa, N.; Chen, L.; Mo, H.; Shastri, A.; Su, R.; Bapat, P.; Kwun, I.; Shen, C. L. Novel insights of dietary polyphenols and obesity. *J. Nutr. Biochem.* **2014**, *25*, 1−18.

(3) Bai, L.; Pang, W. J.; Yang, Y. J.; Yang, G. S. Modulation of Sirt1 by resveratrol and nicotinamide alters proliferation and differentiation of pig preadipocytes. *Mol. Cell. Biochem.* **2008**, *307*, 129−140.

(4) Picard, F.; Kurtev, M.; Chung, N.; Topark-Ngarm, A.; Senawong, T.; Machado De Oliveira, R.; Leid, M.; McBurney, M. W.; Guarente, L. Sirt1 promotes fat mobilization in white adipocytes by repressing PPAR-$\gamma$. *Nature* **2004**, *429*, 771−776.

(5) Rayalam, S.; Yang, J. Y.; Ambati, S.; Della-Fera, M. A.; Baile, C. A. Resveratrol induces apoptosis and inhibits adipogenesis in 3T3-L1 adipocytes. *Phytother. Res.* **2008**, *22*, 1367−1371.
(6) Lagouge, M.; Argmann, C.; Gerhart-Hines, Z.; Meziane, H.; Lerin, C.; Daussin, F.; Auwerx, J. Resveratrol improves mitochondrial function and protects against metabolic disease by activating SIRT1 and PGC-1α. *Cell* **2006**, *127*, 1109−1122.
(7) Alberdi, G.; Rodríguez, V. M.; Miranda, J.; Macarulla, M. T.; Arias, N.; Andrés-Lacueva, C.; Portillo, M. P. Changes in white adipose tissue metabolism induced by resveratrol in rats. *Nutr. Metab.* **2011**, *8*, 29−35.
(8) Dal-Pan, A.; Blanc, S.; Aujard, F. Resveratrol suppresses body mass gain in a seasonal non-human primate model of obesity. *BMC Physiol.* **2010**, *10*, 11.
(9) Wenzel, E.; Somoza, V. Metabolism and bioavailability of *trans*-resveratrol. *Mol. Nutr. Food Res.* **2005**, *49*, 472−481.
(10) Otake, Y.; Nolan, A. L.; Walle, U. K.; Walle, T. Quercetin and resveratrol potently reduce estrogen sulfotransferase activity in normal human mammary epithelial cells. *J. Steroid Biochem. Mol. Biol.* **2000**, *73*, 265−270.
(11) Kapetanovic, I. M.; Muzzio, M.; Huang, Z.; Thompson, T. H.; McCormick, D. L. Pharmacokinetics, oral bioavailability and metabolic profile of resveratrol and its dimethylether analog, pterostilbene, in rats. *Cancer Chemother. Pharmacol.* **2010**, *68*, 593−601.
(12) Rimando, A. M.; Suh, N. Biological/chemopreventive activity of stilbenes and their effect on colon cancer. *Planta Med.* **2008**, *74*, 1635−1643.
(13) Rimando, A. M.; Nagmani, R.; Feller, D. R.; Yokoyama, W. Pterostilbene, a new agonist for the peroxisome proliferator-activated receptor α-isoform, lowers plasma lipoproteins and cholesterol in hypercholesterolemic hamsters. *J. Agric. Food Chem.* **2005**, *53*, 3403−3407.
(14) Satheesh, M. A.; Pari, L. The antioxidant role of pterostilbene in streptozotocin-nicotinamide induced type 2 diabetes mellitus in Wistar rats. *J. Phar. Pharmacol.* **2006**, *58*, 1483−1490.
(15) Joseph, J. A.; Fisher, D. R.; Cheng, V.; Rimando, A. M.; Shukitt-Hale, B. Cellular and behavioral effects of stilbene resveratrol analogues: implications for reducing the deleterious effects of aging. *J. Agric. Food Chem.* **2008**, *56*, 10544−10551.
(16) Folch, J.; Lees, M.; Sloane Stanley, G. H. A simple method for the isolation and purification of total lipides from animal tissues. *J. Biol. Chem.* **1957**, *226*, 497−509.
(17) Miranda, J.; Fernández-Quintela, A.; Churruca, I.; Rodríguez, V. M.; Simón, E.; Portillo, M. P. Hepatomegaly induced by trans-10,cis-12 conjugated linoleic acid in adult hamsters fed an atherogenic diet is not associated with steatosis. *J. Am. Coll. Nutr.* **2009**, *28*, 43−49.
(18) Bradford, M. M. A rapid and sensitive method for the quantitation of microgram quantities of protein utilizing the principle of protein-dye binding. *Anal. Biochem.* **1976**, *72*, 248−254.
(19) Kotani, A.; Miyashita, N.; Kusu, F. Determination of catechins in human plasma after commercial canned green tea ingestion by high-performance liquid chromatography with electrochemical detection using a microbore column. *J. Chromatogr., B* **2003**, *788*, 269−275.
(20) Hou, Y. C.; Lin, S. P.; Tsai, S. Y.; Ko, M. H.; Chang, Y. C.; Lee, P. D. Flavonoid pharmacokinetics and tissue distribution after repeated dosing of the roots of *Scutellaria baicalensis* in rats. *Planta Med.* **2011**, *77*, 455−460.
(21) Wen, X.; Walle, T. Methylated flavonoids have greatly improved intestinal absorption and metabolic stability. *Drug Metab. Dispos.* **2006**, *34*, 1786−1792.
(22) Mikstacka, R.; Rimando, A. M.; Ignatowicz, E. Antioxidant effect of *trans*-resveratrol, pterostilbene, quercetin and their combinations in human erythrocytes in vitro. *Plant Foods Hum. Nutr.* **2010**, *65*, 57−63.
(23) Kondratyuk, T. P.; Park, E. J.; Marler, L. E.; Ahn, S.; Yuan, Y.; Choi, Y.; Yu, R.; van Breemen, R. B.; Sun, B.; Hoshino, J.; Cushman, M.; Jermihov, K. C.; Mesecar, A. D.; Grubbs, C. J.; Pezzuto, J. M. Resveratrol derivatives as promising chemopreventive agents with improved potency and selectivity. *Mol. Nutr. Food Res.* **2011**, *55*, 1249−1265.
(24) Hsu, C. L.; Lin, Y. J.; Ho, C. T.; Yen, G. C. Inhibitory effects of garcinol and pterostilbene on cell proliferation and adipogenesis in 3T3-L1 cells. *Food Funct.* **2012**, *3*, 49−57.
(25) Marier, J. F.; Vachon, P.; Gritsas, A.; Zhang, J.; Moreau, J. P.; Ducharme, M. P. Metabolism and disposition of resveratrol in rats: extent of absorption, glucuronidation and enterohepatic recirculation evidenced by a linked-rat model. *J. Pharmacol. Exp. Ther.* **2002**, *302*, 369−373.
(26) Azorín-Ortuño, M.; Yañez-Gascón, M. J.; Pallarés, F. J.; Vallejo, F.; Larrosa, M.; García-Conesa, M. T.; Tomás-Barberán, F.; Espín, J. C. Pharmacokinetic study of *trans*-resveratrol in adult pigs. *J. Agric. Food Chem.* **2010**, *58*, 11165−11171.
(27) Patel, K. R.; Scott, E.; Brown, V. A.; Gescher, J. A.; Steward, W. P.; Brown, K. Clinical trials of resveratrol. *Ann. N.Y. Acad. Sci.* **2011**, *1215*, 161−165.
(28) Andres-Lacueva, C.; Macarulla, M. T.; Rotches-Ribalta, M.; Boto-Ordóñez, M.; Urpi-Sarda, M.; Rodríguez, V. M.; Portillo, M. P. Distribution of resveratrol metabolites in liver, adipose tissue, and skeletal muscle in rats fed different doses of this polyphenol. *J. Agric. Food Chem.* **2012**, *60*, 4833−4840.
(29) Lin, V. C. H.; Tsai, Y. C.; Lin, J. N.; Fan, L. L.; Pan, M. H.; Ho, C. T.; Wu, J. Y.; Way, T. D. Activation of AMPK by pterostilbene suppresses lipogenesis and cell-cycle progression in p53 positive and negative human prostate cancer cells. *J. Agric. Food Chem.* **2012**, *60*, 6399−6407.
(30) Zhou, G.; Myers, R.; Li, Y.; Chen, Y.; Shen, X.; Fenyk-Melody, J.; Wu, M.; Ventre, J.; Doebber, T.; Fujii, N.; Musi, N.; Hirshman, M. F.; Goodyear, L. J.; Möller, D. E. Role of AMP-activated protein kinase in mechanism of metformin action. *J. Clin. Invest.* **2001**, *108*, 1167−1174.
(31) Wong, R. H.; Sul, H. S. Insulin signaling in fatty acid and fat synthesis: a transcriptional perspective. *Curr. Opin. Pharmacol.* **2010**, *10*, 684−691.
(32) Gómez-Zorita, S.; Fernández-Quintela, A.; Macarulla, M. T.; Aguirre, L.; Hijona, E.; Bujanda, L.; Milagro, F.; Martínez, J. A.; Portillo, M. P. Resveratrol attenuates steatosis in obese Zucker rats by decreasing fatty acid availability and reducing oxidative stress. *Br. J. Nutr.* **2012**, *107*, 202−210.
(33) Cho, S. J.; Jung, U. J.; Choi, M. S. Differential effects of low-dose resveratrol on adiposity and hepatic steatosis in diet-induced obese mice. *Br. J. Nutr.* **2012**, *108*, 2166−2175.
(34) Hsu, C. L.; Lin, Y. J.; Ho, C. T.; Yen, G. C. The inhibitory effect of pterostilbene on inflammatory responses during the interaction of 3T3-L1 adipocytes and RAW 264.7 macrophages. *J. Agric. Food Chem.* **2013**, *61*, 602−610.
(35) Alberdi, G.; Rodríguez, V. M.; Macarulla, M. T.; Miranda, J.; Churruca, I.; Portillo, M. P. Hepatic lipid metabolism pathways by resveratrol in rats fed an obesogenic diet. *Nutrition* **2013**, *29*, 562−567.
(36) Macarulla, M. T.; Alberdi, G.; Gómez, S.; Tueros, I.; Bald, C.; Rodriguez, V. M.; Portillo, M. P. Effects of different doses of resveratrol on body fat and serum parameters in rats fed a hypercaloric diet. *J. Physiol. Biochem.* **2009**, *65*, 369−376.
(37) Foxworthy, P. S.; Perry, D. N.; Hoover, D. M.; Eacho, P. I. Changes in hepatic lipid metabolism associated with lipid accumulation and its reversal in rats given the peroxisome proliferator LY171883. *Toxicol. Appl. Pharmacol.* **1990**, *106*, 375−383.
(38) Barazzoni, R.; Zanetti, M.; Bosutti, A.; Biolo, G.; Vitali-Serdoz, L.; Stebel, M.; Guarnieri, G. Moderate caloric restriction, but not physiological hyperleptinemia *per se*, enhances mitochondrial oxidative capacity in rat liver and skeletal muscle-tissue-specific impact on tissue triglyceride content and AKT activation. *Endocrinology* **2005**, *146*, 2098−2106.
(39) Lasa, A.; Simón, E.; Churruca, I.; Fernández-Quintela, A.; Macarulla, M. T.; Martínez, J. A.; Portillo, M. P. Effects of *trans*-10,*cis*-12 CLA on liver size and fatty acid oxidation under energy restriction conditions in hamsters. *Nutrition* **2011**, *27*, 116−121.

JOURNAL OF AGRICULTURAL AND FOOD CHEMISTRY

Article

pubs.acs.org/JAFC

# Preparation of Organogel with Tea Polyphenols Complex for Enhancing the Antioxidation Properties of Edible Oil

Rong Shi,[†,∥] Qiuyue Zhang,[†,∥] Frank Vriesekoop,[§] Qipeng Yuan,[†] and Hao Liang*[,†]

[†]State Key Laboratory of Chemical Resource Engineering, Beijing University of Chemical Technology, Beijing, People's Republic of China

[§]Department of Food Science, Harper Adams University, Newport, Shropshire TF10 8NB, England

**ABSTRACT:** Food-grade organogels are semisolid systems with immobilized liquid edible oil in a three-dimensional network of self-assembled gelators, and they are supposed to have a broad range of potential applications in food industries. In this work, an edible organogel with tea polyphenols was developed, which possesses a highly effective antioxidative function. To enhance the dispersibility of the tea polyphenols in the oil phase, a solid lipid−surfactant−tea polyphenols complex (organogel complex) was first prepared according to a novel method. Then, a food-grade organogel was prepared by mixing this organogel complex with fresh peanut oil. Compared with adding free tea polyphenols, the organogel complex could be more homogeneously distributed in the prepared organogel system, especially under heating condition. Furthermore, the organogel loading of tea polyphenols performed a 2.5-fold higher antioxidation compared with other chemically synthesized antioxidants (butylated hydroxytoluene and propyl gallate) by evaluating the peroxide value of the fresh peanut oil based organogel in accelerated oxidation conditions.

**KEYWORDS:** *organogel, tea polyphenols, antioxidation*

## INTRODUCTION

Oxidative deterioration of foods remains a very difficult and real problem while we attempt to maintain minimum quality standards. One of the principal causes of food quality deterioration is lipid peroxidation.[1,2] The oxidation of lipids is a free radical driven, chain reaction process, which can cause many deleterious changes including loss of nutritional values and formation of toxic compounds.[3,4] Most of these toxic compounds are known to damage DNA or cause cancers[5] and as a key phenomenon in chronic diseases.[6,7] At present, the principal method to minimize oxidative deterioration in lipid-containing foods and edible oils is the application of antioxidants. Antioxidants terminate the lipid peroxidation chain reactions by removing free radical intermediates and inhibit other oxidation reactions.[8] Synthetic antioxidants, such as butylated hydroxyanisole (BHA), butylated hydroxytoluene (BHT), and propyl gallate (PG), are widely used in the food and cosmetics industries[9,10] due to their high efficiency and relatively low costs. However, the safety of synthetic antioxidants with regard to human consumption has long been questioned.[11−14] In response, natural antioxidants are identified and used as safer and alternative sources of antioxidants in the prevention of oxidative deterioration of foods.[15,16]

Tea polyphenols, which include a wide range of chemical compounds, such as flavonoids, tannins, and catechins, possess outstanding antioxidative properties.[16,17] The main mechanisms for inhibition of oxidative reactions by tea polyphenols include scavenging reactive oxygen species, chelating redox-active transition metal ions, and inhibition of "pro-oxidant" enzymes.[18] However, tea polyphenols are severely restricted to direct use in foods with high lipid content, due to their low solubility in oil phase.

Organogel-based delivery systems for functional ingredients are relatively new in food science and drug delivery.[19−21] Organogels are semisolid systems containing liquid oil trapped within a three-dimensional networked structure, which is formed by the self-assembly of a relatively low concentration of organogelator molecules.[19,22] This structured network appears to be based on the orientational ordering of the hydrocarbon chains,[23] which can facilitate an improved dispersibility of aliphatic functional compounds in the oil phase.[24] Meanwhile, the structure also influences the oxidative stability of the oil entrapped in the system.[25] In recent years, these semisolid products have gained much importance in the food and nutraceutical industries due to applications including the restriction of oil mobility and their ability to control the rate of nutraceutical release.[19,26]

In this paper, we describe the development of an edible oil organogel laden with tea polyphenols, which has a thermal reversibility. To enhance the dispersibility of the tea polyphenols in the oil phase, a solid lipid−surfactant−tea polyphenols complex (organogel complex) was prepared using a novel method.

The resultant organogel displayed highly effective antioxidative properties. A novel method to produce the organogel complex formed of stearic acid, surfactant, and tea polyphenols was developed. The food-grade organogel was prepared by mixing this complex with fresh peanut oil. Microscopy, Fourier transform infrared (FTIR), and X-ray diffraction (XRD) were used to characterize the structure of the organogel complex. Furthermore, the antioxidative properties of the organogel

**Received:** April 1, 2014
**Revised:** July 26, 2014
**Accepted:** August 4, 2014
**Published:** August 4, 2014

ACS Publications © 2014 American Chemical Society



dx.doi.org/10.1021/jf501512y | J. Agric. Food Chem. 2014, 62, 8379−8384

containing tea polyphenols was also tested and analyzed and were compared with those of stearic acid based organogels with free tea polyphenols and chemically synthesized antioxidants.

## EXPERIMENTAL PROCEDURES

**Materials and Methods.** Tea polyphenols were obtained from Jiangsu Dehe Biotechnology Co., Ltd., China. The composition of these tea polyphenols was determined by using UPLC-MS (XEVO-G2QTOF, Waters, USA). The result is shown in Table 1. Stearic acid (98%, w/w) was purchased from Aladdin Co. (Shanghai, China). Sucrose erucate (ER290) was obtained from Mitsubishi-Kagaku Foods Corp. (Tokyo, Japan). HPLC-grade water was from Alfa Aesar (Lawrence, KS, USA). Glacial acetic acid, isooctane, potassium iodide, sodium thiosulfate, and starch were of analytical reagent grade.

**Table 1. Composition of the Tea Polyphenols (PLC-MS)**

| peak | retention time (min) | $[M - H]^-$ ($m/z$) | compound | area | % |
|---|---|---|---|---|---|
| 1 | 3.29 | 305 | gallocatechin (GC) | 2106 | 2.25 |
| 2 | 3.52 | 305 | epigallocatechin (EGC) | 7113 | 7.62 |
| 3 | 3.72 | 289 | catechin (C) | 4563 | 4.88 |
| 4 | 3.94 | 457 | epigallocatechin-3-gallate (EGCG) | 49175 | 52.65 |
| 5 | 3.99 | 457 | gallocatechin-3-gallate (GCG) | | |
| 6 | 4.22 | 471 | epigallocatechin-3-(3″-*O*-methyl)gallate (EGCmetG) | 3651 | 3.91 |
| 7 | 4.33 | 441 | epicatechin-3-gallate (ECG) | 26787 | 28.68 |

We chose peanut oil as the sample oil to prepare the organogel. Peanut oil possesses a well-balanced fatty acid profile and has been credited with cardioprotective and anti-inflammatory properties.[27] Fresh peanut oil was squeezed out using a small edible oil press (6YL-95A, SRS, China). During the process, the peanuts were mildly toasted to remove the internal water and then pressed to obtain fresh peanut oil.

**Procedure for Preparation of a Stearic Acid−Surfactant−Tea Polyphenols Complex (Organogel Complex).** One hundred milligrams of tea polyphenols dissolved in 2 mL of water was used as aqueous phase. Stearic acid (10 g) containing sucrose erucate ER290 (5%w/w) was placed in an 80 °C water bath and stirred at 500 rpm until a homogeneous clear solution was obtained. Then the aqueous phase and the oil phase were homogenized (HENC homogenizer, Shanghai, China) at 26000 rpm for 2 min to form a stable W/O emulsion. The aqueous and oil phases were homogenized at 80 °C to ensure that the oil phase remained in a liquid state during the homogenization process. The resulting emulsion was frozen rapidly in liquid nitrogen and subsequently lyophilized (FD-1C-50, Beijing, China). The control organogel complex was prepared in the same way only without tea polyphenols in aqueous phase.

**Determination of Critical Gelation Concentration (CGC) and Gel−Sol Transition Temperature.** Gelation was considered successful when the gels failed to flow under gravity on inversion of the vials.[28,29] The CGC is the lowest concentration of gelator (the organogel complex) that induces gelation of edible oil.[30] When determining the CGC, various amounts of the organogel complex were added to peanut oil, following which the mixture was carefully heated to 80 °C and stirred at 500 rpm and subsequently allowed to cool at room temperature under static conditions for 3 h before it was inverted. The lowest concentration of added organogel complex that induced gelation determined the CGC. Meanwhile, the homogeneity of tea polyphenols in the organogel could be visually inspected.

Gel (nonflow)−sol (flow) transition was determined using the inverting tube method. The inverting tube method used in our study was similar to the one used by Motulsky, Behare, and co-workers.[31,32] The organogels with tea polyphenols complex (5, 10, 20, or 30%) were heated in a temperature-controlled water bath as the temperature was varied from 20 to 80 °C at an increment of 2 °C. The samples were equilibrated for 5 min at the previous temperature for 5 min before the temperature increment was made. Sol−gel phase transition temperature ($T_{SG}$) and gel−sol phase transition temperature ($T_{GS}$) are defined as the midpoint of the temperature range above which gelation changes.[33] Sol−gel phase transition temperature was measured by cooling the sample stepwise to 20 °C, following the same procedure.

**Preparation of Different Organogel Samples.** Generally, the organogels with tea polyphenols complex (5, 10, 20, or 30%) were prepared to add organogel complex (1, 2, 4, or 6 g) in 20 g of peanut oil. Then, all of the samples were heated at 80 °C and stirred at 500 rpm to obtain the homogeneous solutions. The samples were cooled to room temperature and crystallized under static conditions. The control organogel was obtained in the same manner with the control organogel complex.

Organogel complex (0.04 g) and stearic acid (0.06 g) were added into 20 g of peanut oil and stirred at 500 rpm to obtain the homogeneous solution. The solution was cooled to room temperature and crystallized under static conditions. Then the organogel with tea polyphenols complex (2%) was prepared.

The organogels with free tea polyphenols, BHT, or PG (0.02%) were prepared by adding free tea polyphenols, BHT, or PG (0.004 g) into 20 g of peanut oil, respectively. The concentrations of BHT, PG, and free tea polyphenols were 0.02% (w/w) in peanut oil, which were the same as the content of tea polyphenols in the organogel containing 5% organogel complex. Then, all of the samples were heated at 80 °C and stirred at 500 rpm. The samples were cooled to room temperature and crystallized under static conditions.

**Characterizations of the Organogel Complex and Organogel Containing Tea Polyphenols.** *Microscopic Analysis.* A compound optical microscope (Olympus, Japan) was used for analyzing the microstructure of the organogels. Attempts were made to understand the mechanism of formation of the organogels through the variation of the proportions of organogel complex in the organogels.

*FTIR Spectra Analysis.* FTIR spectra were investigated to detect the functional groups of compounds through a TENSOR 27 FTIR spectrometer (Bruker, Germany). Stearic acid and representative complexes were prepared for scanning in the range from 4000 to 500 $cm^{-1}$ to examine the interactions among the components of the organogel complex.

*X-ray Diffractometry.* XRD analyses of the samples were carried out with an XRD-600 (Shimadzu, Japan). Samples were scanned in the range from 5° to 95°/2$\theta$, and the scanning rate was 2°/min. Measurements were operated at a voltage of 40 kV, 40 mA.

**Accelerated Oxidation Conditions and Determination of the Peroxide Value (PV).** A range of organogel samples with various antioxidant substances were placed in open transparent glass beakers. The range of organogel samples was prepared by the way of organogel preparation and contained different compositions (see details in Table 3). The range of samples contained various controls and was designed to investigate the effectiveness of tea polyphenols as an antioxidant in an organogel. To artificially induce an accelerated oxidation of the lipids, all samples were marked and stored in an oven at 90 °C for 84 h. During this process of oxidation, the PVs of samples were determined every 12 h.

The PV was evaluated following the NP-904 (1987) method. This method consists of a reaction carried out in darkness of a mixture of oil and isooctane/acetic acid 2:3 (v/v) with a saturated potassium iodide solution. Autoxidation causes the formation of peroxides, which in turn causes the release of iodine. The free iodine formed is then titrated with a sodium thiosulfate solution. The peroxide value was expressed as milliequivalents of active oxygen per kilogram of oil (mequiv/kg). The experiment was conducted in triplicate, and at least three determinations were performed for each sample.

## RESULTS AND DISCUSSION

**Preparation and Characterization of Organogel Complex.** In recent years, there has been a great deal of interest in studying gelling of edible oils with fatty acid derivatives.[34−36] However, saturated fatty alcohols showed lower efficiencies compared to saturated fatty acids of the same length in their ability to form oleogels with various oils.[34] Furthermore, the melting point of stearic acid is lower than that of (*R*)-12-hydroxystearic acid. The solubility of stearic acid in edible oil is higher than that of (*R*)-12-hydroxystearic acid. Thus, stearic acid was chosen as the organogelator to form an organogel complex in this work.

The addition of tea polyphenols to stearic acid resulted in a stable homogeneous emulsion when the tea polyphenols were added up to a concentration of 5% (w/w). At any concentration in excess of 5% (w/w) tea polyphenols, a precipitate would occur. Unless otherwise indicated, all experiments were carried out with a tea polyphenols loading of 1% (w/w).

To assess the molecular interactions due to the presence of tea polyphenols, we undertook FTIR spectroscopy, which included samples of pure stearic acid, control organogel complex (without tea polyphenols), and an organogel complex (with tea polyphenols). We observed that the spectra of the three samples were similar except the different intensity of the broad peaks in the range from 3700 to 3300 $cm^{-1}$ corresponding to O−H stretching (Figure 1). The intensity

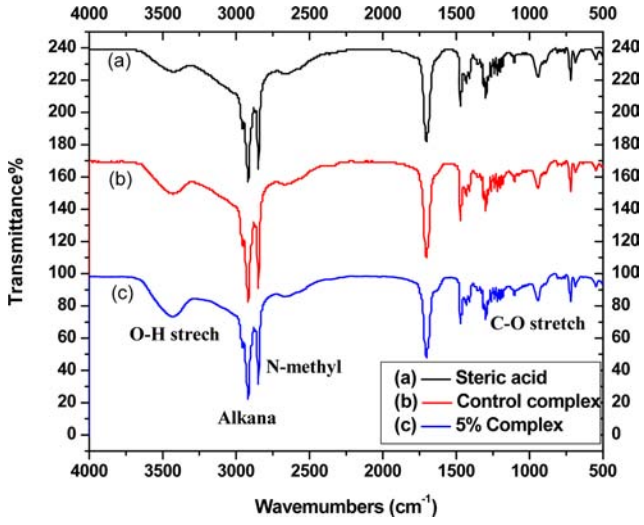


**Figure 1.** FTIR analyses of (a) pure stearic acid, (b) control organogel complex (no tea polyphenols), and (c) organogel complex with 1% (w/w) tea polyphenols.

of the peak corresponding to the O−H stretching vibration increased in the organogel complex containing 1% (w/w) tea polyphenols. This may have been due to the presence of a phenolic hydroxyl group in the tea polyphenol molecules. The characteristic functional groups stretches indicate the presence of alkane (3001 and 2934 $cm^{-1}$), *N*-methyl (2867 $cm^{-1}$), and C−O stretch (1156 $cm^{-1}$) in the samples.[37] There was no significant difference in the rest of the spectra, which indicates that the chemical functionality of the components within the organogel complex was conserved.

To further investigate the molecular arrangements of the structure forming those crystals within the organogel complex, XRD measurements were employed. A control organogel complex and organogel complexes containing 1 and 2% (w/w) tea polyphenols were taken as representative samples. The organogel complexes containing tea polyphenols displayed the same angle diffraction peaks compared to the control organogel complex (Figure 2). These peaks were the result of the

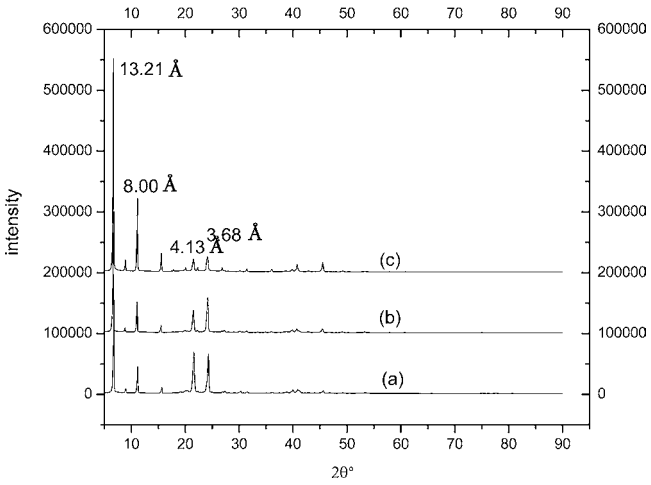


**Figure 2.** X-ray diffraction patterns of (a) control organogel complex, (b) organogel complex containing 1% (w/w) of tea polyphenols, and (c) organogel complex containing 2% (w/w) of tea polyphenols.

scattering associated with stearic acid and showed an elevated crystallinity with sharp peaks. A layer thickness of 13.21 Å can be observed in all of these samples. The results indicated that the crystals were well developed in this direction and cause clear diffraction intensity. All of these samples showed short spacings around 4.13 and 3.68 Å, which are characteristic for an orthorhombic packing, and were similar to the $\beta'$ packing of triacylglycerols.[38] As the concentration of tea polyphenols increased, a peak at 11° with higher intensity could be observed; on the contrary, the short spacings around 4.13 and 3.68 Å showed a weaker intensity (Figure 2), indicating that the corresponding crystals were much thinner in the direction of the unit cell. These results indicate that an increase in tea polyphenols affects the crystal structure and the texturing properties of the organogel complex.

**Preparation and Characterizations of Peanut Oil Based Organogels with Tea Polyphenols.** The dissolution of the organogel complex in peanut oil at 80 °C resulted in the formation of a homogeneous solution. When the temperature was reduced, a change in the solubility parameter of the organogel complex resulted in the crystallization of the stearic acid molecules in the oil continuous phase and formed self-assembled structures. Depending on the concentration of the organogel complex in peanut oil, the solution either remained cloudy and liquid or formed a semisolid-like structure. Through the inverse experiments, the CGC of the organogel was found to be 5% (w/w) (Figure 3); hence, further analyses of the organogels were performed using gels having complex concentration ≥5% (w/w).

The gel−sol and sol−gel transition temperatures were determined by using the inverting tube method. It is an important parameter for gel stability and shelf life.[39] $T_{GS}$ and $T_{SG}$ were very close, because of the same concentration of organogel complex (shown in Table 2). The temperature at which transition occurred increased with organogel complex


dx.doi.org/10.1021/jf501512y | J. Agric. Food Chem. 2014, 62, 8379−8384

**Figure 3.** CGC of organogel loading of tea polyphenols: S-1, organogel containing 4% (w/w) organogel complex; S-2, organogel containing 5% (w/w) organogel complex.

**Table 2. Results of Sol−Gel Phase and Gel−Sol Transition**

| organogel sample | $T_{SG}$[a] (°C) | $T_{GS}$[b] (°C) |
|---|---|---|
| organogel (5% complex)[c] | 48.0 | 51.0 |
| organogel (10% complex)[d] | 50.0 | 53.0 |
| organogel (20% complex)[e] | 54.0 | 57.0 |
| organogel (30% complex)[f] | 57.0 | 60.0 |

[a]Sol−gel phase transition temperature ($T_{SG}$). [b]Gel−sol phase transition temperature ($T_{GS}$). [c]Organogel contains 5% tea polyphenols organogel complex. [d]Organogel contains 10% tea polyphenols organogel complex. [e]Organogel contains 20% tea polyphenols organogel complex. [f]Organogel contains 30% tea polyphenols organogel complex.

concentration. Transitions were fully reversible, and the organogel had a thermal reversibility. The phenomenon of transition temperature was similar to reported results.[38,39]

Microstructure analysis showed the presence of needle-shaped crystals of stearic acid in peanut oil when 5% (w/w) organogel complex concentration was used (Figure 4A). As the concentration of organogel complex was increased, these clusters aggregated to form fiber-like structures (Figure 4B,C). The density of these fiber-like structures increased with the increase of the organogel complex concentration, and these fiber-like structures were found to form a networked skeleton, which helped in the immobilization of the peanut oil. To study the effect of incorporation of tea polyphenols on the crystallinity of the peanut oil based organogel, XRD measurements was also employed to test the representative samples (Figure 5). As the concentration of organogel complex increased from 20 to 30% (w/w), the organogels showed a higher crystallinity, which can be observed from the larger peaks in Figure 5. The larger peaks are indicative of a greater presence of stearic acid in the peanut oil, causing a more pronounced crystallinity in the organogels, and the broader peaks that can be evidenced in Figure 5 correspond to the peanut oil in the organogel.

**Determination of the Antioxidation of the Organogel Loading of Tea Polyphenols.** To test the effectiveness of the presence of tea polyphenols as antioxidants in the organogel, the generation of peroxides was monitored by a modified oven test at 90 °C for up to 84 h. Compared with the peanut oil (blank), the addition of stearic acid alone to peanut oil (control) did not reduce the kinetics of peroxide formation at the early stages of the oven test (Figure 6), but it did reduce the formation of peroxides by about 14% over 84 h, which seems to indicate that the structural characteristics of the organogel systems influence the oxidative reaction.[23] The addition of 5% organogel complex to fresh peanut oil (5% complex) caused a 60% reduction in the formation of peroxides (Figure 6). These

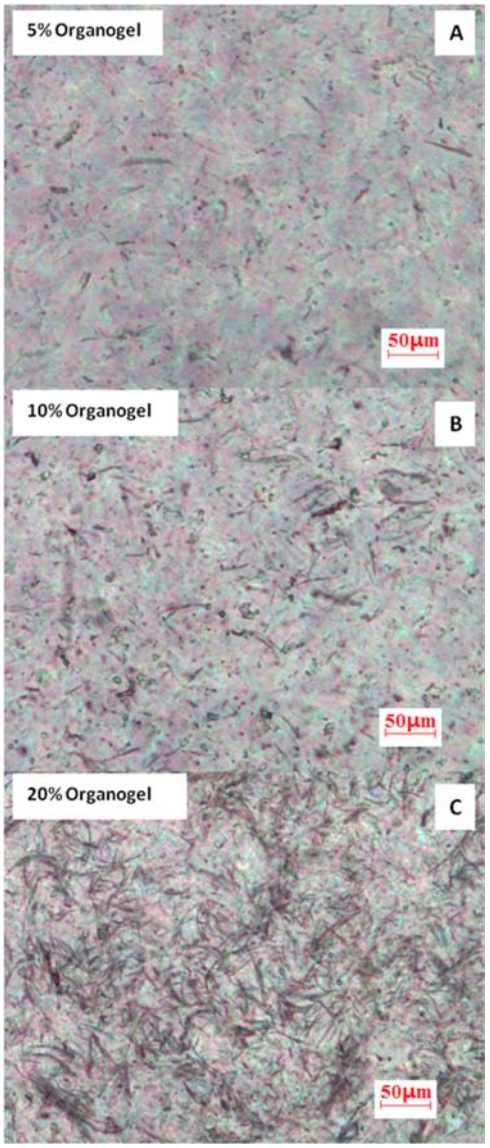


**Figure 4.** Micrographs of organogels. 5% organogel, organogel containing 5% (w/w) organogel complex; 10% organogel, organogel containing 10% (w/w) organogel complex; 20% organogel, organogel containing 20% (w/w) organogel complex.

results indicate that the organogel loading of tea polyphenols performs an obvious antioxidative effect.

To compare the function of different antioxidants, and according to the existing food additive regulations published by the U.S. Food and Drug Administration, BHA and PG can be used individually or in combination at a maximum accumulative level of 0.02%. Stearic acid based organogel samples containing 0.02% (w/w) of BHT, PG, and free tea polyphenols were also prepared (Table 3), and their ability to delay the onset of oxidative rancidity was determined (Figure 7). It is clear that the organogel (2% complex) has a much greater antioxidative effect than organogel with free tea polyphenols (0.02% free TPs), and both of them have the same weight of tea polyphenols, which indicates the organogel complex could improve the dispersibility of tea polyphenols in the oil phase. The addition of either BHT or PG at 0.02% in a stearic acid based organogel only slightly improves the antioxidative effect of organogel (Figures 6 and 7). The addition of 0.02% free tea

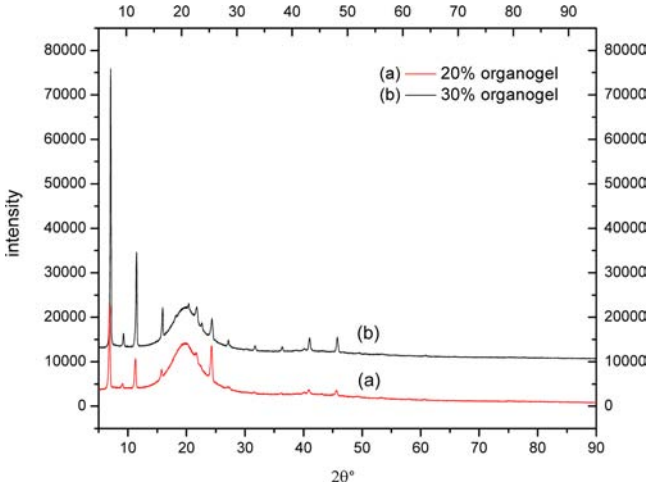


**Figure 5.** X-ray diffraction patterns of organogels. 20% organogel, organogel containing 20% (w/w) organogel complex; 30% organogel, organogel containing 30% (w/w) organogel complex.

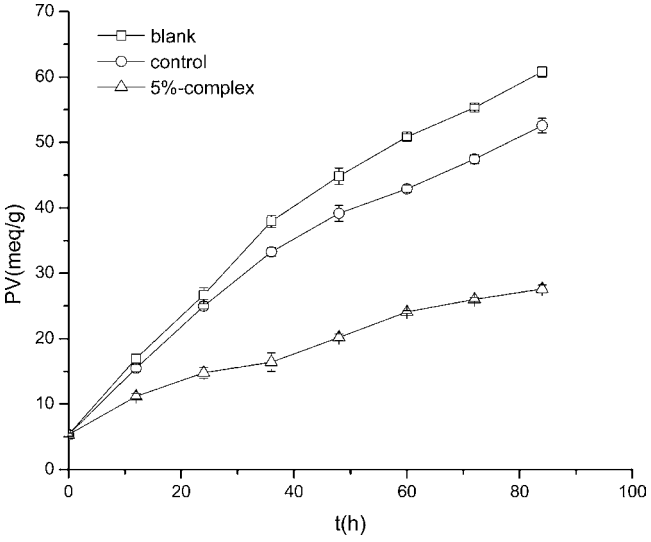


**Figure 6.** Influence of tea polyphenols on delaying the onset of rancidity as measured by changes in peroxide value of organogels as a function of storage time at 90 °C. The "blank" (□) contains pure peanut oil; the "control" (○) contains 5% stearic acid and no tea polyphenols in peanut oil; and "5% complex" organogel (△) contains no stearic acid and 5% organogel complex in peanut oil.

**Table 3. Composition of the Organogel Samples Used for Antioxidation Analysis**

| organogel sample code | fresh peanut oil (g) | stearic acid (%) | antioxidant |
|---|---|---|---|
| blank | 20 | 0 | |
| control | 20 | 0 | control organogel complex (1000 mg) |
| 5% complex | 20 | 0 | organogel complex[a] (1000 mg) |
| 2% complex | 20 | 3 | organogel complex[a] (400 mg) |
| 0.02% free TPs[b] | 20 | 5 | free tea polyphenols (4 mg) |
| 0.02% BHT | 20 | 5 | BHT (4 mg) |
| 0.02% PG | 20 | 5 | PG (4 mg) |

[a]Organogel complex contains 1% tea polyphenols. [b]Tea polyphenols.

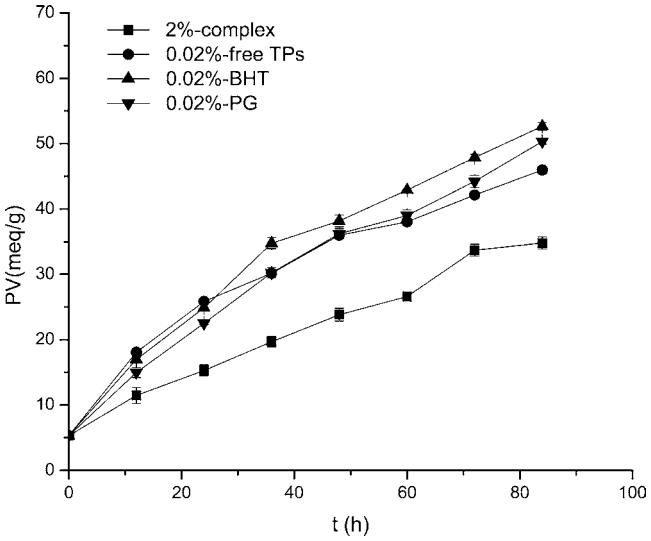


**Figure 7.** Influence of a range of antioxidants on delaying the onset of rancidity as measured by changes in peroxide value of organogels as a function of storage time at 90 °C. The "2% complex" organogel (■) contains 2% organogel complex plus 3% stearic acid in peanut oil; "0.02% free TPs" organogel (●) contains 5% stearic acid plus 0.02% tea polyphenols in peanut oil; "0.02% BHT" organogel (▲) contains 5% stearic acid plus 0.02% BHT in peanut oil; and "0.02% PG" organogel (▼) contains 5% stearic acid plus 0.02% PG in peanut oil.

polyphenols in a stearic acid based organogel yielded a slight improvement in antioxidative ability compared to either BHT or PG (Figure 7). In general, after the oven test for 84 h, the organogel 2% complex, which contained 0.02% tea polyphenols, reduced the formation of peroxides by about 45%, and the stearic acid based organogels, 0.02% TPs, 0.02% PG, and 0.02% BHT, separately caused 27, 18, and 15% reductions in the formation of peroxides. The organogel loading of tea polyphenols performed a 2.5-fold higher antioxidation compared with other chemically synthesized antioxidants (BHT, PG) by evaluating the peroxide value of the fresh peanut oil based organogel in the oven test.

In summary, a novel method was developed to prepare an organogel loaded with tea polyphenols, which significantly improved the dispersibility of tea polyphenols in the organogel system. Furthermore, the organogel loading of a stearic acid−tea polyphenols complex greatly enhanced the ability to delay the onset of oxidative rancidity. More importantly, the method developed here allows the addition of water-soluble, natural active ingredients into lipid-rich foods such as fried foods, cocoa butter, and cream products to improve the shelf life of the food.

## AUTHOR INFORMATION

### Corresponding Author

*(H.L.) Phone: +86 10 6443 1557. Fax: +86 10 6443 7610. E-mail: lianghao@mail.buct.edu.cn.

### Author Contributions

‖R.S. and Q.Z. contributed equally to this work.

### Funding

We acknowledge financial support from the Natural Science Foundation of China (20806005), the Beijing Higher Education Young Elite Teacher Project (YETP0520), and the National High Technology Research and Development Program of China (863 Program, Grants 2012AA021403 and 2014AA021705).

## Notes

The authors declare no competing financial interest.

## REFERENCES


(1) Frankel, E. N. Lipid oxidation. *Prog. Lipid Res.* **1980**, *19* (1−2), 1−22.

(2) Addis, P. B. Occurrence of lipid oxidation products in foods. *Food. Chem. Toxicol.* **1986**, *24* (10), 1021−1030.

(3) Ladikos, D.; Lougovois, V. Lipid oxidation in muscle foods: a review. *Food Chem.* **1990**, *35* (4), 295−314.

(4) Gray, J. I.; Monahan, F. J. Measurement of lipid oxidation in meat and meat products. *Trends Food Sci. Technol.* **1992**, *3*, 315−319.

(5) Esterbauer, H. Cytotoxicity and genotoxicity of lipid-oxidation products. *Am. J. Clin. Nutr.* **1993**, *57* (5), 779S−785S.

(6) Willcox, J. K.; Ash, S. L.; Catignani, G. L. Antioxidants and prevention of chronic disease. *Crit. Rev. Food Sci. Nutr.* **2004**, *44* (4), 275−295.

(7) Rahman, I.; van Schadewijk, A. A.; Crowther, A. J.; Hiemstra, P. S.; Stolk, J.; MacNee, W.; De Boer, W. I. 4-Hydroxy-2-nonenal, a specific lipid peroxidation product, is elevated in lungs of patients with chronic obstructive pulmonary disease. *Am. J. Resp. Crit. Care.* **2002**, *166* (4), 490−495.

(8) Halliwell, B.; Murcia, M. A.; Chirico, S.; Aruoma, O. I. Free radicals and antioxidants in food and in vivo: what they do and how they work. *Crit. Rev. Food Sci. Nutr.* **1995**, *35* (1−2), 7−20.

(9) Guan, Y.; Chu, Q.; Fu, L.; Ye, J. Determination of antioxidants in cosmetics by micellar electrokinetic capillary chromatography with electrochemical detection. *J. Chromatogr., A* **2005**, *1074* (1), 201−204.

(10) Guo, L.; Xie, M. Y.; Yan, A. P.; Wan, Y. Q.; Wu, Y. M. Simultaneous determination of five synthetic antioxidants in edible vegetable oil by GC−MS. *Anal. Bioanal. Chem.* **2006**, *386* (6), 1881−1887.

(11) Miková, K. The regulation of antioxidants in food. In *Antioxidants in Food*; Pokorny, J., Yanishlieva, N., Gordon, M., Eds.; CRC Press: Boca Raton, FL, USA, 2001; pp 287−284.

(12) Almeida, P. P.; Mezzomo, N.; Ferreira, S. R. Extraction of *Mentha spicata* L. volatile compounds: evaluation of process parameters and extract composition. *Food Bioprog. Technol.* **2012**, *5* (2), 548−559.

(13) Williams, G. M.; Iatropoulos, M. J.; Whysner, J. Safety assessment of butylated hydroxyanisole and butylated hydroxytoluene as antioxidant food additives. *Food Chem. Toxicol.* **1999**, *37* (9), 1027−1038.

(14) Botterweck, A. A. M.; Verhagen, H.; Goldbohm, R. A.; Kleinjans, J.; Van Den Brandt, P. A. Intake of butylated hydroxyanisole and butylated hydroxytoluene and stomach cancer risk: results from analyses in the Netherlands cohort study. *Food Chem. Toxicol.* **2000**, *38* (7), 599−605.

(15) Landete, J. M. Dietary intake of natural antioxidants: vitamins and polyphenols. *Crit. Rev. Food Sci. Nutr.* **2013**, *53* (7), 706−721.

(16) Akram, S.; Amir, R. M.; Nadeem, M.; Sattar, M. U.; Faiz, F. Antioxidant potential of black tea (*Camellia sinensis* L.) − review. *J. Food Sci.* **2012**, *22* (3), 128−132.

(17) El Gharras, H. Polyphenols: food sources, properties and applications − a review. *Int. J. Food Sci. Technol.* **2009**, *44* (12), 2512−2518.

(18) Perron, N. R.; Brumaghim, J. L. A review of the antioxidant mechanisms of polyphenol compounds related to iron binding. *Cell Biochem. Biophys.* **2009**, *53* (2), 75−100.

(19) Hughes, N. E.; Marangoni, A. G.; Wright, A. J.; Rogers, M. A.; Rush, J. W. Potential food applications of edible oil organogels. *Trends Food Sci. Technol.* **2009**, *20* (10), 470−480.

(20) Vintiloiu, A.; Leroux, J. C. Organogels and their use in drug delivery − a review. *J. Controlled Release* **2008**, *125* (3), 179−192.

(21) Ting, Y.; Jiang, Y.; Ho, C.-T.; Huang, Q. Common delivery systems for enhancing *in vivo* bioavailability and biological efficacy of nutraceuticals. *J. Funct. Foods* **2004**, *7*, 112−128.

(22) Rogers, M. A.; Wright, A. J.; Marangoni, A. G. Crystalline stability of self-assembled fibrillar networks of 12-hydroxystearic acid in edible oils. *Food Res. Int.* **2008**, *41* (10), 1026−1034.

(23) Pernetti, M.; van Malssen, K. F.; Flöter, E.; Bot, A. Structuring of edible oils by alternatives to crystalline fat. *Curr. Opin. Colloid Interface Sci.* **2007**, *12* (4), 221−231.

(24) Yu, H.; Shi, K.; Liu, D.; Huang, Q. Development of a food-grade organogel with high bioaccessibility and loading of curcuminoids. *Food Chem.* **2012**, *131* (1), 48−54.

(25) Da Pieve, S.; Calligaris, S.; Panozzo, A.; Arrighetti, G.; Nicoli, M. C. Effect of monoglyceride organogel structure on cod liver oil stability. *Food Res. Int.* **2011**, *44* (9), 2978−2983.

(26) Gunstone, F. D. Research highlights: lipid technology 11-12/2009. *Lipid Technol.* **2009**, *21*, 269−273.

(27) Akhtar, S.; Khalid, N.; Ahmed, I.; Shehzad, A.; Suleria, H. A. R. Physicochemical characteristics, functional properties and nutritional benefits of peanut oil: a review. *Crit. Rev. Food Sci. Nutr.* **2013**, *54*, 1562−1575.

(28) Maity, G. C. Low molecular mass gelators of organic liquids. *J. Phys. Sci.* **2007**, *11*, 156−171.

(29) Shaikh, I.; Jadhav, S. L.; Jadhav, K. R.; Kadam, V. J.; Pisal, S. S. Aceclofenac organogels: in vitro and in vivo characterization. *Curr. Drug Delivery* **2009**, *6* (1), 1−7.

(30) Schaink, H. M.; Van Malssen, K. F.; Morgado-Alves, S.; Kalnin, D.; Van der Linden, E. Crystal network for edible oil organogels: possibilities and limitations of the fatty acid and fatty alcohol systems. *Food Res. Int.* **2007**, *40* (9), 1185−1193.

(31) Motulsky, A.; Lafleur, M.; Couffin-Hoarau, A.-C.; Hoarau, D.; Boury, F.; Benoit, J.-P.; Leroux, J.-C. Characterization and biocompatibility of organogels based on L-alanine for parenteral drug delivery implants. *Biomaterials* **2005**, *26* (31), 6242−6253.

(32) Behera, B.; Patil, V.; Sagiri, S.; Pal, K.; Ray, S. Span-60-based organogels as probable matrices for transdermal/topical delivery systems. *J. Appl. Polym. Sci.* **2012**, *125* (2), 852−863.

(33) George, M.; Weiss, R. G. Low molecular-mass gelators with diyne functional groups and their unpolymerized and polymerized gel assemblies. *Chem. Mater.* **2003**, *15* (15), 2879−2888.

(34) Daniel, J.; Rajasekaran, R. Organogelation of plant oils and hydrocarbons by longchain saturated FA, fatty alcohols, wax esters, and dicarboxylic acids. *J. Am. Oil Chem. Soc.* **2003**, *80*, 417−421.

(35) Toro-Vazquez, J. F.; Morales-Rueda, J.; Torres-Martínez, A.; Charó-Alonso, M. A.; Mallia, V. A.; Weiss, R. G. Cooling rate effects on the microstructure, solid content, and rheological properties of organogels of amides derived from stearic and (*R*)-12-hydroxystearic acid in vegetable oil. *Langmuir* **2013**, *29* (25), 7642−7654.

(36) Mallia, V. A.; George, M.; Blair, D. L.; Weiss, R. G. Robust organogels from nitrogen-containing derivatives of (*R*)-12-hydroxystearic acid as gelators: comparisons with gels from stearic acid derivatives. *Langmuir* **2009**, *25* (15), 8615−8625.

(37) Coates, J. In *Encyclopedia of Analytical Chemistry*; Meyers, R. A., Ed.; Wiley: Chichester, UK, 2000; pp 10815−10837.

(38) Schaink, H. M.; Van Malssen, K. F.; Morgado-Alves, S.; Kalnin, D.; Van der Linden, E. Crystal network for edible oil organogels: possibilities and limitations of the fatty acid and fatty alcohol systems. *Food Res. Int.* **2007**, *40* (9), 1185−1193.

(39) Liu, J.; He, P.; Yan, J.; Fang, X.; Peng, J.; Liu, K.; Fang, Y. An organometallic supe-gelator with multiple-stimulus responsive properties. *Adv. Mater.* **2008**, *20* (13), 2508−2511.

JOURNAL OF AGRICULTURAL AND FOOD CHEMISTRY

Article

pubs.acs.org/JAFC

# *Camelina sativa* Defatted Seed Meal Contains Both Alkyl Sulfinyl Glucosinolates and Quercetin That Synergize Bioactivity

Nilanjan Das,[†] Mark A. Berhow,[‡] Donato Angelino,[†] and Elizabeth H. Jeffery*[,†]

[†]Department of Food Science and Human Nutrition, University of Illinois at Urbana−Champaign, 905 S. Goodwin Avenue, Urbana, Illinois 61801, United States

[‡]Agricultural Research Service, United States Department of Agriculture, Peoria, Illinois 61604, United States

**ABSTRACT:** *Camelina sativa* L. Crantz is under development as a novel oilseed crop, yet bioefficacy of camelina phytochemicals is unknown. Defatted camelina seed meal contains two major aliphatic glucosinolates (GSLs), glucoarabin (9-(methylsulfinyl)nonylglucosinolate; GSL 9) and glucocamelinin (10-(methylsulfinyl)decylglucosinolate; GSL 10), with traces of a third, 11(methylsulfinyl)undecylglucosinolate and several flavonoids, mostly quercetin glycosides. In Hepa1c1c7 cells, hydrolyzed GSLs (hGSLs) 9 and 10 upregulated the phase II detoxification enzyme quinone reductase (NQO1), with no effect on cytochrome P450 (CYP) 1A1 activity. Isobologram graphs revealed synergy of NQO1 induction for a combination of hGSL 9 and quercetin. These findings suggest that defatted camelina seed meal should be evaluated for anticancer activity, similar to broccoli and other Brassicaceae family members. Interestingly, synergy of NQO1 induction was also seen for physiologically relevant doses of sulforaphane (SF) and quercetin, two key bioactives present in broccoli. This suggests that SF within broccoli may be more potent than purified SF.

**KEYWORDS:** *camelina, glucosinolate, quercetin, NQO1, synergy, sulforaphane*

## INTRODUCTION

There is significant interest in developing novel oilseed crops in both the United States and Canada. *Camelina sativa* L. Crantz, a flowering plant belonging to the Brassicaceae family and commonly known as gold-of-pleasure or false flax, is native to Northern Europe and Central Asia, has been cultivated as an oilseed crop. Although, camelina was introduced more recently into North America, radiocarbon dating of archaeobotanical samples identifies its presence from 720 to 520 cal B.C.[1] Because of its high polyunsaturated C18-fatty acid content, less weather dependency, consistent yields, low requirements for tillage and weed control, and relatively cheap production cost, interest in camelina is growing rapidly for use as an oil crop, source of biodiesel production, and renewable feedstock.[2] Camelina oil consists of about 45% polyunsaturated fatty acids, 35% monounsaturated fatty acids, 10% saturated fatty acids, and up to 10% free fatty acids, tocopherols, sterols, other terpenes, and volatiles. High levels of omega-3 fatty acids and antioxidants such as tocopherols have been the focus of potential health benefits of camelina to date.[3,4] Defatted camelina seed consists of approximately 10% residual oils, 45% protein, up to 15% insoluble fiber, up to 10% soluble carbohydrates, 5% minerals, approximately 0.2% nucleic acids, and 14% or more of a mixture of phytochemical components consisting mostly of glucosinolates (GSLs) and flavonoids.[5] Camelina accumulates significant levels of two aliphatic GSL in its seeds: glucoarabin (9-(methylsulfinyl)nonylglucosinolate; GSL 9) and glucocamelinin (10-(methylsulfinyl)decyl-glucosinolate; GSL 10), with a trace amount of a third, 11(methylsulfinyl)undecylglucosinolate (GSL 11).[6] Moreover, mature camelina seed contains several flavonoids, the most plentiful of which is the flavonol quercetin.[7]

GSLs occur as secondary metabolites, mainly in the Brassicaceae. They act as natural pesticides, preventing herbivory.[8,9] Myrosinase, a thiohydrolase present in GSL-containing plants, can cleave glucose from GSL in the presence of water to form an unstable intermediate that rapidly rearranges to a thiocyanate, isothiocyanate, or nitrile; these serve to defend the plant.[10] Importantly, when ingested by mammals, isothiocyanates exhibit chemoprotective activity against the initiation of tumors, inducing detoxification enzymes, inhibiting enzyme activation, modifying steroid hormone metabolism, and generally improving the host-defense system.[11]

The bioactivity of the isothiocyanate sulforaphane (SF) from broccoli has been studied in detail.[12] Although SF and other hydrolysis products may have multiple sites of action, upregulation of the phase II detoxification enzyme NAD(P)-H:quinone oxidoreductase 1 (NQO1), is often used as a biomarker of beneficial bioactivity.[13] In addition to NQO1, aliphatic GSL hydrolysis products are typically associated with upregulation of antioxidant, anti-inflammatory, and anticancer effects. In contrast, aromatic and indolyl GSLs exert mixed effects, often including upregulation of cytochrome P450 (CYP) 1A1 as well as phase II enzymes, such as NQO1. Possibly associated with CYP1A1 induction, the aromatic and indolyl GSLs have been reported to promote some cancers, even though they protect against others.[14] In contrast, aliphatic GSL hydrolysis products have been found to act as inhibitors of CYP activation of carcinogens.[15]

**Received:** April 11, 2014
**Revised:** July 17, 2014
**Accepted:** July 22, 2014
**Published:** July 22, 2014

ACS Publications © 2014 American Chemical Society

Much research is ongoing to establish camelina as a biofuel crop, yet little is known about the potential bioefficacy of camelina GSLs and flavonoids. Preparative and countercurrent chromatography has been used to purify GSLs and flavonoids from camelina seed extract.[16] The GSLs in camelina are methyl sulfinyl aliphatics, similar to glucoraphanin the parent GSL to SF, suggesting that they may provide health benefits similar to those of SF. However, they are far larger molecules than the bioactive compounds found in common cruciferous vegetables: 9−11 carbons in length, rather than 3−5. For this reason, we decided to evaluate induction of phase I and phase II detoxification enzymes CYP1A1 and NQO1, as biomarkers of potential bioactivity. Because camelina seed extract also contains the bioactive flavonoid quercetin in several glycosidic forms including rutin, we chose to evaluate the impact of GSL 9, GSL 10, quercetin, and rutin individually, in combination, and as the defatted seed meal extract. We did not evaluate GSL 11, as it is present in negligible amounts (<2 mg/g of seed meal). We also evaluated interactive induction of NQO1 activity between major camelina GSLs and the flavonoid quercetin, comparing this to SF and quercetin, to determine if these were additive, synergistic, or antagonistic in their effect on NQO1 induction. A synergy of action has been reported previously for SF and quercetin in the inhibition of self-renewal of pancreatic cancer stem cells.[17] Our aim was to determine if defatted camelina seed meal might be a health promoting byproduct of biofuel production.

## MATERIALS AND METHODS

**Chemicals.** SF was purchased from LKT Laboratories (St. Paul, MN, USA). Glucose-6-phosphate dehydrogenase was obtained from Roche diagnostics (Indianapolis, IN, USA). Fetal bovine serum (FBS) was purchased from Atlanta Biologicals (Flowery Branch, GA, USA). All other chemicals including myrosinase from *Sinapis alba*, quercetin, and rutin were of the highest grade available and purchased from Sigma (St. Louis, MO, USA).

**Analytical Sample Preparation and Purification of Bioactive Compounds from Camelina Sseeds.** Camelina seeds were harvested according to the method described previously.[16] Camelina GSLs were purified from methanol extracts of defatted meal, using flash chromatography, followed by semipreparative reverse-phase HPLC,[16] or according to the modified counter-current chromatography method described by Toribio et al.[18] Purification of GSLs (GSL 9 > 95%; GSL 10 > 97%), confirmed by NMR addition analysis using acetone as a comparison standard, has been reported in detail elsewhere.[16]

**Cell Culture and Treatments.** Hepa1c1c7 mouse hepatoma cells ($10^4$ cells/mL) were purchased from the American Type Culture Collection (ATCC; Manassas, VA, USA). Cells were cultured in $\alpha$-MEM, enriched with 10% heated and charcoal-inactivated FBS, supplemented with 2.2 g/L $NaHCO_3$, penicillin (100 U/mL), and streptomycin (100 $\mu$g/mL), and maintained at 37 °C in 95% air and 5% $CO_2$. After 24 h incubation, SF (dissolved in DMSO at 0.1% final concentration), GSL 9 or GSL 10 (dissolved in cell culture medium), quercetin (dissolved in DMSO at 0.1% final concentration), and rutin (dissolved in water) were added to the culture medium alone or in combination according to the experimental design and incubated for 24 h. Myrosinase (20 mU/mL) was added to media containing camelina GSLs immediately before adding the media to cultured cells, since early studies showed that, without hydrolysis, GSLs were without effect. Medium treated with GSL 9 and GSL10 plus myrosinase formed the expected isothiocyanate hydrolysis products, confirmed by GC/MS.[16]

**MTT Cytotoxicity Assay.** Any adverse effects of SF or hydrolyzed GSLs (hGSLs) 9 or 10 on cell growth were determined using a standard MTT assay. Hepa1c1c7 cells were placed in 96-well culture plates ($10^4$ cells/well) in complete medium and incubated at 37 °C. After 24 h, the medium was replaced with treatment media containing camelina GSLs plus myrosinase (20 mU/mL) and incubated for another 24 h. Cytotoxicity of the hGSLs and SF was then evaluated using the MTT assay,[19] and results were quantified using a $\mu$Quant microplate reader (Bio-Tek Instruments, Winooski, VT, USA) at 595 nm. Data are reported as percent cell survival relative to respective controls.

**NQO1 Inductive Activity.** The NQO1 inducing activity of different samples was estimated as previously described.[20] Hepa1c1c7 cells, grown in $\alpha$-MEM and enriched with 10% FBS, were seeded in a 96-well plate at a density of $10^4$ cells/well and maintained at 37 °C in 95% ambient air and 5% $CO_2$. After 24 h, cells were exposed to fresh media containing SF, hGSL 9, hGSL 10, quercetin, or rutin for a further 24 h, alone or in combination. Concentrations used for the treatments with hGSL 9, hGSL 10, quercetin, and rutin were 1.25, 2.5, and 5 $\mu$M. In a second study, cells were treated with 2.5 mg seed extract/mL and with the individual components, at the concentration present in 2.5 mg seed extract/mL: 0.86 $\mu$M hGSL 9, 2.2 $\mu$M hGSL 10, together with 1.46 $\mu$M quercetin and 0.48 $\mu$M rutin. Treated cells were rinsed with phosphate buffer at pH 7.4, lysed with 50 $\mu$L 0.8% digitonin in 2 mM EDTA, incubated, and agitated for 10 min. A 200 $\mu$L aliquot of reaction mix was added to the lysed cells. Readings were made at five time points, 50 s apart, using a $\mu$Quant microplate reader at 610 nm. Immediately after completion of the readings, 50 $\mu$L of 0.3 mM dicumarol in 25 mM Tris−Cl buffer was added to each well, and the plate was read again (five time points, 50 s apart) to determine nonspecific MTT reduction. Total protein content was measured by the BioRad assay (Bio-Rad, Hercules, CA, USA) following manufacturer's instruction. Activity was expressed as NQO1 specific activity (nmol MTT reduced/min/mg protein). For each study, incubations were carried out in triplicate; studies were repeated three times.

**Measurement of CYP1A1 Catalytic Activity.** Hepa1c1c7 cells were seeded on 96-well plates at a density of $10^4$ cells/well in $\alpha$-MEM supplemented with 10% FBS and stabilized for 24 h. Cells were then treated for 24 h with 1.25, 2.5, and 5 $\mu$M GSLs 9 or 10 plus myrosinase (20 mU/mL) alone, in combination, and in the presence or absence of the CYP1A1 inducing agent $\beta$-naphthoflavone (5 $\mu$M). The catalytic activity of 7-ethoxyresorufin-*O*-deethylase (EROD) was measured as described elsewhere.[21] Briefly, monolayers were washed with PBS and then treated with 100 $\mu$L of serum free medium/well, containing 8 mM 7-ethoxyresorufin and 10 mM dicumarol (to inhibit cytosolic NQO1) followed by 150 $\mu$L Tris−MeOH (15% methanol in 50 mM Tris−Cl buffer). Fluorescence was measured at 530 nm excitation and 590 nm emission, using a FLx800 universal microplate reader. Specific activity was expressed as picomoles of resorufin formed per minute per milligram of protein, comparing the resorufin formed to the standard curve of known concentrations of resorufin.

**Synergy Study Using Major Camelina GSLs and Flavonoids.** To evaluate synergy between camelina bioactives, we developed an isobologram[22] using concentrations of GSL 9 and quercetin, individually or together, that doubled NQO1 activity in Hepa1c1c7 cells after 24 h incubation, compared to activity in untreated cells. We compared this to synergy between SF and quercetin, major bioactives present in broccoli, under similar conditions.

**Statistical Analysis.** One way analysis of variance (ANOVA) was used to identify differences among treatment groups. Between individual groups, statistical significance was assessed using Student's *t*-test with a *p* value of less than 0.05 indicating a significant difference between data sets.

## RESULTS

**Impact of Defatted Camelina Seed Extract and Its Individual Bioactive Components on Cellular Survival.** We tested the cytotoxicity of hGSL 9, hGSL 10, quercetin, and rutin for three doses 1.25, 2.5, and 5 $\mu$M as well as the existing concentration ratios in the seed extract (2.5 mg/mL) (Figure 1A). We also tested the cytotoxicity of the seed extract itself at three doses, 0.5, 1.25, and 2.5 mg/mL (Figure 1B). Neither the

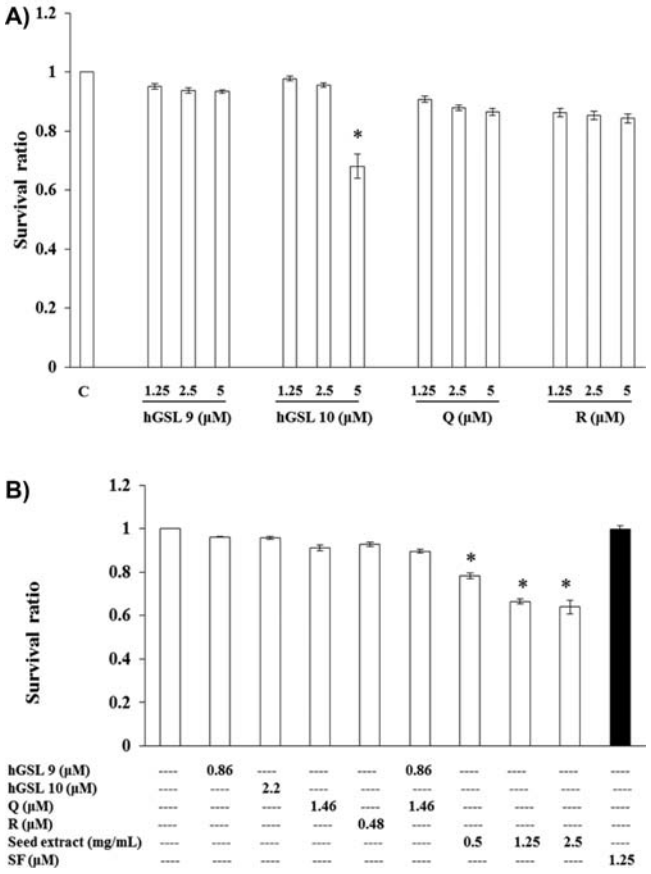


**Figure 1.** Cytotoxicity of camelina seed extract and of individual bioactives from camelina. (A) Individual cytotoxicity dose–response of hydrolyzed GSLs 9 (hGSL 9) and 10 (hGSL 10), quercetin (Q), and rutin (R). (B) Cytotoxicity of the camelina extract and of the components present in 2.5 mg extract/mL. Survival of treated cells was compared to the survival of the untreated control, which was set to 1. Values are mean ± SD; $n = 3$. *Different from control ($p < 0.05$, using Student's $t$ test).

hGSLs nor the flavonoids from the camelina seed extract exhibited cytotoxicity at the concentrations used to determine bioactivity. However, the highest concentration of hGSL 10 (5 $\mu$M) and all the doses of the seed extract showed some cytotoxicity.

**Induction of NQO1.** We found dose-dependent NQO1 induction with hGSL 9, hGSL 10, quercetin, and rutin, four major bioactives of defatted camelina seed meal (Figure 2). Treatment with 1.25, 2.5, and 5 $\mu$M hGSL 9 showed 2.6-, 3.2-, and 3.6-fold induction of NQO1 activity, respectively. Similar inducing activity was seen for hGSL 10, which showed 1.98-, 2.7-, and 3.3-fold induction, respectively. Quercetin also showed a similar range of activity, 1.7-, 2.7-, and 3-fold induction, respectively, as did rutin, with 1.4-, 2.25-, and 2.8-fold induction, respectively (Figure 2). Used as a positive control, SF (1.25 $\mu$M) showed 3.5-fold induction over control (Figure 2). In the study of NQO1 induction by the two GSL at the concentrations present in 2.5 mg/mL camelina seed meal extract (0.86 $\mu$M GSL 9 and 2.2 $\mu$M GSL 10), we found that induction was 1.42-fold and 2.1-fold by hGSLs 9 and 10, respectively. When used in combination at these low concentrations, these two GSLs caused 3.6-fold NQO1 induction, not different from the expected, theoretical value of 3.52 from addition of the individual values (Figure 3). All four major bioactives of camelina seed (GSL 9, GSL 10, quercetin, and rutin) caused NQO1 induction alone and in combination (Figure 4). The combination treatment of bioactives, reflecting that found in 2.5 mg defatted seed extract/mL medium (0.86 $\mu$M GSL 9 and 2.2 $\mu$M GSL 10, together with 1.46 $\mu$M quercetin and 0.48 $\mu$M rutin) caused 4.8-fold induction of NQO1, not significantly different from the 5.1-fold induction caused by the 2.5 mg extract/mL (Figure 4).

Interestingly, combination of only hGSL 9 and quercetin at these concentrations caused a far greater than additive, 4-fold induction of NQO1 (Figure 5). No other combination of camelina seed bioactives showed greater than the expected value from the theoretical addition of data from the individual treatments. Rather, combination of hGSL 10 and quercetin

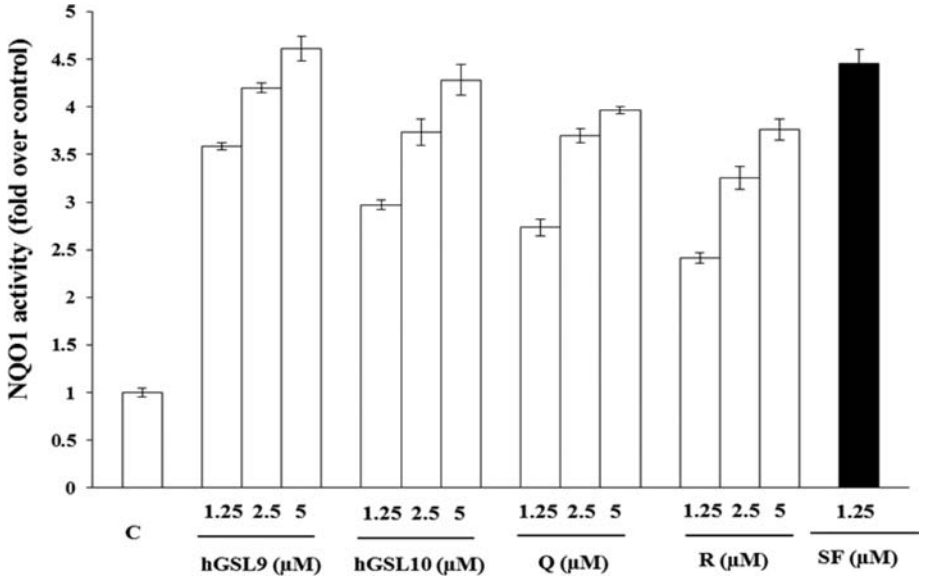


**Figure 2.** Induction of NQO1 activity by hydrolyzed GSLs 9 (hGSL 9) and 10 (hGSL 10), quercetin (Q), and rutin (R). Sulforaphane (SF) was used as a positive control. Myrosinase (20 mU/mL) was added to the medium for GSL hydrolysis. Relative NQO1 activity was calculated in relation to the untreated control, which was set to 1. Values are mean ± SD; $n = 3$ ($p < 0.05$).


dx.doi.org/10.1021/jf501742h | J. Agric. Food Chem. 2014, 62, 8385–8391

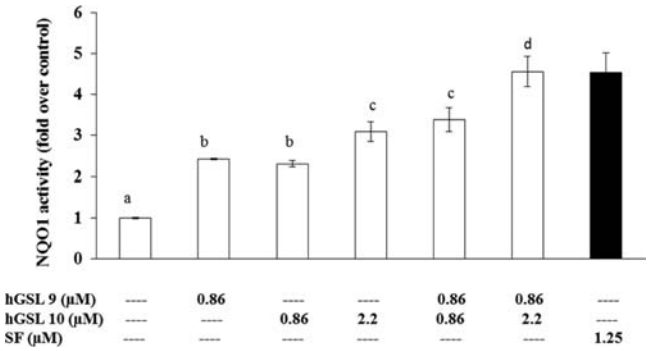


**Figure 3.** NQO1 activity of hydrolyzed GSLs 9 (hGSL 9) and 10 (hGSL 10) alone and in combination. Sulforaphane (SF) was used as a positive control. Relative NQO1 activity was calculated in relation to the untreated control, which was set to 1. Values are mean ± SD; $n$ = 3. Values with different superscripts are different ($p < 0.05$).

caused a small but nonsignificant loss of activity compared to theoretical addition of their individual activities.

**Synergistic Action of hGSL9 and Quercetin and Its Similarity to That of SF and Quercetin from Broccoli.** To evaluate in more detail the interactive activity between GSL 9 and quercetin, we developed an isobologram. First, a five-point concentration range was used to determine the dose needed to double NQO1 activity with GSL 9 or quercetin individually (data not shown). We found that individually, 0.48 μM hGSL 9 and 2.07 μM quercetin were necessary to double NQO1 activity in 24 h. By using different concentrations of hGSL9 ($^1/_{10}$, $^2/_{10}$, and $^3/_{10}$ of 0.48 μM hGSL 9, the concentration needed to double the NQO1 activity), a range of quercetin concentrations was evaluated at each of the GSL 9 doses, to determine the concentration of quercetin needed to enhance the GSL 9 effect sufficiently to double NQO1 activity. Synergy was apparent only at the $^3/_{10}$ and $^2/_{10}$ concentrations of GSL 9, whereas antagonism appeared at the $^1/_{10}$ concentration of hGSL 9 (Figure 6A). Because we had used SF as a positive control and because quercetin is present in broccoli, we evaluated synergy between SF and quercetin (Figure 6B), developing a similar isobologram. We found that 0.38 μM SF was required to double NQO1 activity. Then, we set the concentration combinations as we did for hGSL 9 and quercetin and found synergy with all three combinations evaluated, but again, we found the greatest synergy at lower quercetin concentrations.

**CYP1A1 Activity.** Although we evaluated CYP1A1 inducing activity of all four camelina bioactives under study, none of these compounds caused induction of CYP1A1 alone or in combination (Figure 7A). Further, we determined if any of these compounds were able to inhibit β-naphthoflavone-mediated induction of CYP1A1 activity, since β-naphthoflavone is a potent CYP1A1 inducer. However, we did not find any inhibitory action by camelina bioactives against β-naphthoflavone-mediated induction of CYP1A1 activity (Figure 7B).

## DISCUSSION

To our knowledge, this is the first article to evaluate the impact of camelina seed bioactives on detoxification enzymes, as a measure of bioactivity. We chose to evaluate defatted camelina seed meal as a potential bioactive food, not only because it is a byproduct of camelina fuel oil production but because it contains both GSLs and flavonoids, well-known for their health benefits. The content of GSLs can vary over a range of approximately 10−25 μmol/g defatted seed meal, due to variation in the growing environment, in the genotype, and in processing losses.[23] This is similar to the 20−75 μmol/g freeze-dried brassica vegetables and thus considerably greater than the GSL content of fresh brassica vegetables.[24] The dried methanol extract that we used for these studies contained ∼250 μmol GSL/g extract, about a 10-fold increase in concentration over the defatted seed meal. A dried ethanol extract, appropriate for human consumption, could be expected to be similar. The flavonoids in the extract are mainly quercetin glycosides, almost entirely in the form of rutin (quercetin rutinoside) or more complex glycosides of rutin.[23] Rutin is only partly absorbed whole, and no free quercetin was evident in the extract. However, we used the aglycone quercetin in these studies, since this is the form that is considered the active form within cells.

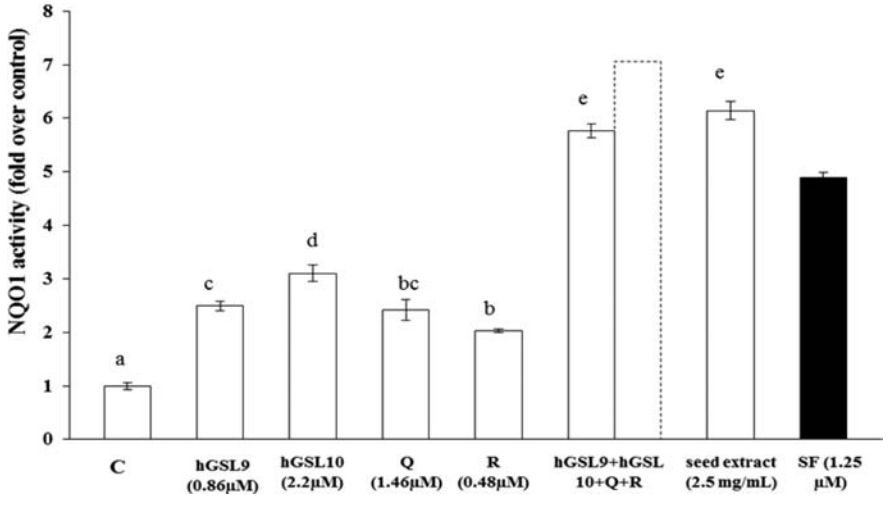


**Figure 4.** NQO1 activity of camelina seed extract and major components. Cells were treated with the four bioactives individually or combined, at the concentrations found in 2.5 mg extract/mL, and compared to the activity of whole extract, 2.5 mg/mL. Hydrolysed GSLs 9 (hGSL 9) and 10 (hGSL 10), quercetin (Q), rutin (R), and sulforaphane (SF). Relative NQO1 activity was calculated in relation to the control, which was set to 1. Values are mean ± SD; $n$ = 3. Values with different superscripts are different ($p < 0.05$). Dashed bars show the theoretical value, calculated by addition of values derived from individual agents.


dx.doi.org/10.1021/jf501742h | J. Agric. Food Chem. 2014, 62, 8385−8391

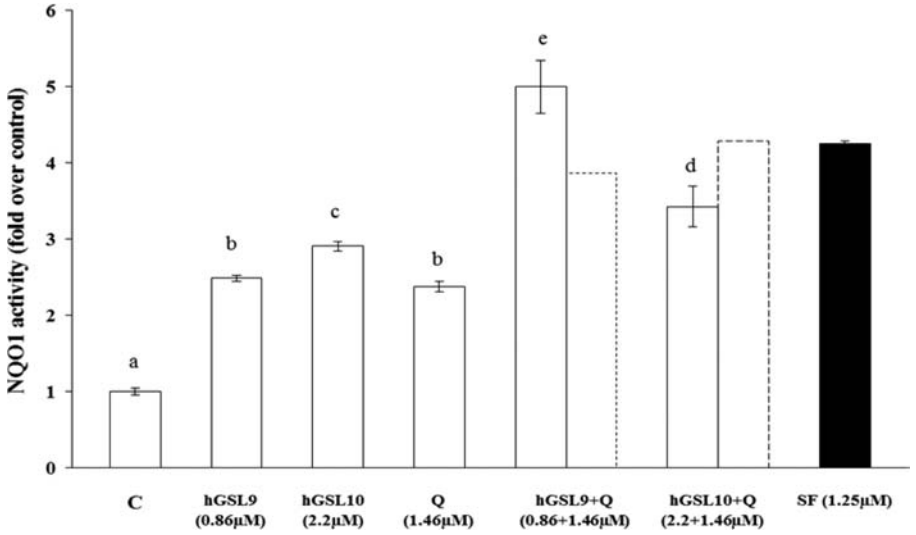


**Figure 5.** Interactive NQO1 activity between glucosinolates and quercetin. Relative NQO1 activity was calculated in relation to the untreated control, which was set to 1. Hydrolysed GSLs 9 (hGSL 9) and 10 (hGSL 10), quercetin (Q), and sulforaphane (SF).Values are mean ± SD of three experiments performed in triplicate. Values with different superscripts are different ($p < 0.05$). Dashed bars show the theoretical value, calculated by addition of values derived from individual agents.

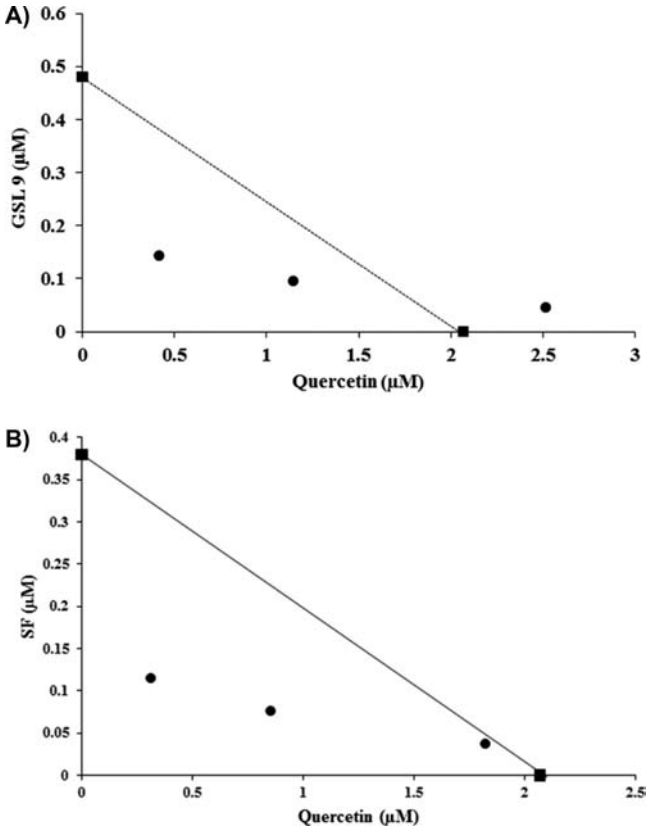


**Figure 6.** Isobolographic representation of interactive NQO1 inducing activity between different concentration combinations of (A) hGSL 9 and quercetin, (B) sulforaphane (SF) and quercetin. The squares are the concentrations of each individual bioactive necessary to double NQO1 activity in 24 h; the line joining them described the theoretical concentrations necessary to double NQO1 activity if activities are additive. The circles show concentrations found to double NQO1 activity when both compounds were present at the concentrations shown. For details on isobologram construction, see the Materials and Methods section.

Most quercetin glycosides are hydrolyzed in the gut, either by lactase phlorizin hydrolase, an enzyme of the brush border, or $\beta$-glucosidases present intracellularly.[25] The free quercetin is then conjugated within the cell, mainly to glucouronide or sulfate conjugates, and thought to be released at the surface of cells by a $\beta$-glucuronidase before it enters the cell in the free form to exert its activity.[26] We therefore chose to evaluate bioactivity of rutin and free quercetin, over a range representing that present in camelina seed meal.

Initially, we evaluated possible cytotoxicity of the four major bioactive components, GSL 9, GSL 10, quercetin, and rutin. At the concentrations tested, only hGSL 10 exhibited any toxicity, causing an approximately 30% loss of cell count at 24 h at the largest dose tested, 5 $\mu$M (Figure 1). The complete extract, at the dose containing this level of hGSL 10 (2.5 mg extract/mL culture medium) caused a similar loss in viability. However, lower doses also caused some losses, suggesting that, whereas hGSL 10 was a major cause of toxicity, it was not solely responsible for this loss of viability.

Following hydrolysis of the two GSLs, all four of the camelina bioactives under study caused a dose-dependent induction of NQO1, in the concentration range 1.25−5 $\mu$M, Figure 2. The two GSLs each induced NQO1 activity in a similar dose range to SF, and this was additive when they were both present, Figure 3.

When cells were treated with a mixture of all four bioactives, the effect on NQO1 induction was similar to that of the whole extract, Figure 4. In an effort to identify the major bioactives responsible for this combinatorial effect, we examined the interaction between hGSL 9 and free quercetin and found that together these gave a significantly greater than additive effect, although this was possibly countered by hGSL 10 and quercetin together causing less induction than expected, Figure 3. Focusing on the effect of hGSL 9 and quercetin, we decided to develop an isobologram, to determine if there was any synergy in the NQO1 inducing activity shown by their combination. The isobologram showed synergy, particularly strongly at the 20% and 30% of maximal GSL 9 doses. Although there are several ways to assess synergy, an advantage

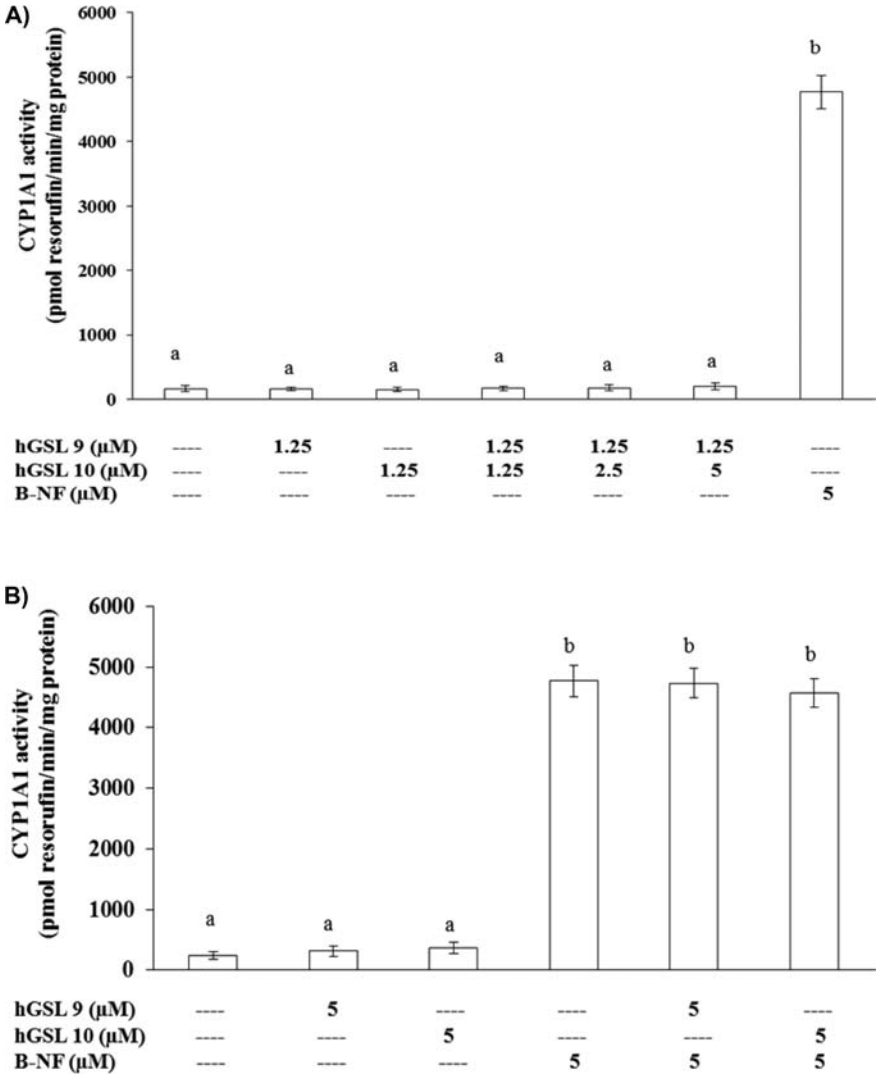


**Figure 7.** Influence of hGSL 9 and hGSL 10 on ethoxyresorufin-*O*-deethylase (CYP1A1) activity. (A) Cells were treated with GSLs or $\beta$-naphthoflavone ($\beta$-NF, 5 $\mu$M) as positive control. (B) Cells were treated with hGSLs and $\beta$-NF, to evaluate the potential of GSLs to inhibit $\beta$-NF-mediated CYP1A1 induction. Values are mean ± SD of three experiments performed in triplicate. Values with different superscripts are different ($p < 0.05$).

in using isobologram construction is that it is independent of the mode of action and thus applies under many conditions. An isobole is an "iso-effect" curve, in which a combination of constituents is represented on a graph, the axes of which are the dose axes of the individual agents.[22] A line is then drawn joining the individual concentrations that cause a chosen, specific effect; here, we chose doubling of NQO1 at 24h. If the two compounds do not cause an interactive effect (synergy or antagonism) when used in combination, then resulting dose combinations required to cause doubling will fall on the line joining the points. If there is a synergy, that is, the effect of the combination is greater than expected from their individual dose−response curves, the doses of the combination needed to produce the same effect will be less than for the sum of the individual components, and the curve will appear concave. The opposite applies for antagonism, in which the dose of the combination is greater than expected, and will produce a convex isobole. We found that, when hGSL 9 was provided at a very low dose (only 10% of that needed to provide doubling), the quercetin required was greater than that required individually to double induction, showing an antagonism or interference. Whereas we did not evaluate the mechanism further, one explanation would be that, when quercetin is at very high doses, it is competitive with hGSL 9.

In all our experiments, we used SF as a positive control for comparison, as it is known to have potent NQO1 inducing ability. We therefore did the same synergy evaluation for SF with quercetin, developing a second isobologram, Figure 6B. Just as we found that quercetin synergizes the upregulation of NQO1 by hGSL 9, we also saw synergy between quercetin and SF. This is particularly interesting, given that broccoli is a good source of quercetin as well as SF. We interpret this to mean that whole broccoli may exert a stronger potency than can be explained based on purified SF of the same concentration. The impact of quercetin on bioefficacy of broccoli is worthy of further study.

Because indolyl, but not aliphatic, GSLs have been reported to upregulate CYP1A1, we had hypothesized that camelina GSLs would not increase CYP1A1 activity. None of the camelina bioactives tested induced CYP1A1 or inhibited $\beta$-naphthoflavone-mediated induction of CYP1A1 activity. Compounds upregulating phase II detoxification enzymes

such as NQO1 but not the phase I CYP1A1 enzyme have been termed monfunctional. Monofunctional inducers are considered to have greater health promoting activity than bifunctional inducers that upregulate both phase I and phase II enzymes. This is based on the finding that some precarcinogens are activated by CYP1A1.[15] In this regard, camelina has even greater potential to be viewed as a food with positive health benefits. In summary, we found the *C. sativa* seed meal contains bioactivity stemming from two alkyl sulfinyl GSLs and quercetin. We also found that the major bioactive from broccoli, SF, exhibits a synergistic upregulation of NQO1 with quercetin, a flavonoid that is naturally present in broccoli.

## AUTHOR INFORMATION

### Corresponding Author

*Phone: (217) 333-3820; e-mail: ejeffery@illinois.edu.

### Funding

This work was funded by a grant to E.H.J. from the United States Department of Agriculture (USDA/NIFA 2010-65200-20398).

### Notes

Mention of trade names or commercial products in this publication is solely for the purpose of providing specific information and does not imply recommendation or endorsement by the U.S. Department of Agriculture. USDA is an equal opportunity provider and employer.

The authors declare no competing financial interest.

## REFERENCES

(1) Sostarić, R.; Alegro, A.; Hrsak, V.; Stancić, Z.; Küster, H. Plant remains from an Early Iron Age well at Hajndl, Slovenia. *Coll. Antropol.* **2009**, *33*, 1295−1301.

(2) Urbaniak, S. D.; Caldwell, C. D.; Zheljazkov, V. D.; Lada, R.; Luan, L. The effect of seeding rate, seeding date and seeder type on the performance of *Camelina sativa* L. in the Maritime provinces of Canada. *Can. J. Plant Sci.* **2008**, *88*, 501−508.

(3) Ruiz-Lopez, N.; Haslam, R. P.; Napier, J. A.; Sayanova, O. Successful high-level accumulation of fish oil omega-3 long-chain polyunsaturated fatty acids in a transgenic oilseed crop. *Plant J.* **2014**, *77*, 198−208.

(4) Aziza, A. E.; Quezada, N.; Cherian, G. Antioxidative effect of dietary Camelina meal in fresh, stored, or cooked broiler chicken meat. *Poult. Sci.* **2010**, *89*, 2711−2718.

(5) Zubr, J. Cabohydrates, vitamins, and minerals of Camelina sativa seed. *Nutr. Food Sci.* **2010**, *40*, 523−531.

(6) Vaughn, S. F.; Berhow, M. A. Glucosinolate hydrolysis products from various plant sources: pH effects, isolation, and purification. *Ind. Crops Prod.* **2005**, *21*, 193−204.

(7) Onyilagha, J.; Bala, A.; Hallett, R.; Gruber, M.; Soroka, J.; Westcott, N. Leaf flavonoids of the cruciferous species, *Camelina sativa*, *Crambe* spp., *Thlaspi arvense*, and several other genera of the family Brassicaceae. *Biochem. Syst. Ecol.* **2003**, *31*, 1309−1322.

(8) Fahey, J. W.; Wade, K. L.; Stephenson, K. K.; Chou, F. E. Separation and purification of glucosinolates from crude plant homogenates by high-speed counter-current chromatography. *J. Chromatogr.* **2003**, *A 996*, 85−93.

(9) Halkier, B. A.; Gershenzon, J. Biology and biochemistry of glucosinolates. *Annu. Rev. Plant Biol.* **2006**, *57*, 303−33.

(10) Spencer, G. F.; Daxenbichler, M. E. Gas chromatography-mass spectrometry of nitriles, isothiocyanates and oxazolidinethiones derived from cruciferous glucosinolates. *J. Sci. Food Agric.* **1980**, *31*, 359−367.

(11) Jeffery, E. H.; Araya, M. Physiological effects of broccoli consumption. *Phytochem. Rev.* **2009**, *8*, 283−298.

(12) Juge, N.; Mithen, R. F.; Traka, M. Molecular basis for chemoprevention by sulforaphane: A comprehensive review. *Cell. Mol. Life Sci.* **2007**, *64*, 1105−1127.

(13) Cuendet, M.; Oteham, C. P.; Moon, R. C.; Pezzuto, J. M. Quinone reductase induction as a biomarker for cancer chemoprevention. *J. Nat. Prod.* **2006**, *69*, 460−463.

(14) Androutsopoulos, V. P.; Tsatsakis, A. M.; Spandidos, D. A. Cytochrome P450 CYP1A1: Wider roles in cancer progression and prevention. *BMC Cancer* **2009**, *9*, 187.

(15) Skupinska, K.; Misiewicz-Krzeminska, I.; Stypulkowski, R.; Lubelska, K.; Kasprzycka-Guttman, T. Sulforaphane and its analogues inhibit CYP1A1 and CYP1A2 activity induced by benzo[a]pyrene. *J. Biochem. Mol. Toxicol.* **2009**, *23*, 18−28.

(16) Berhow, M. A.; Polat, U.; Glinski, J. A.; Glensk, M.; Vaughn, S. F.; Isbell, T.; Ayala-Diaz, I.; Marek, L.; Gardner, C. Optimized analysis and quantification of glucosinolates from *Camelina sativa* seeds by reverse-phase liquid chromatography. *Ind. Crops Prod.* **2013**, *43*, 119−125.

(17) Srivastava, R. K.; Tang, S. N.; Zhu, W.; Meeker, D.; Shankar, S. Sulforaphane synergizes with quercetin to inhibit self-renewal capacity of pancreatic cancer stem cells. *Front. Biosci.* **2011**, *3*, 515−528.

(18) Toribio, A.; Nuzillard, J. M.; Pinel, B.; Boudesocque, L.; Lafosse, M.; De La Poype, F.; Renault, J.-H. Pilot-scale ion-exchange centrifugal partition chromatography: Purification of sinalbin from white mustard seeds. *J. Sep. Sci.* **2009**, *32*, 1801−1807.

(19) van Meerloo, J.; Kaspers, G. J. L.; Cloos, J. Cell sensitivity assays: The MTT assay. In *Cancer Cell Culture: Methods and Protocols*, 2nd ed.; Cree, I. A., Ed.; Humana Press: New York, 2011; Vol. *731*, pp 237−245.

(20) Prochaska, H. J.; Santamaria, A. B. Direct measurement of NAD(P)H:quinone reductase from cells cultured in microtiter wells: A screening assay for anticarcinogenic enzyme inducers. *Anal. Biochem.* **1988**, *169*, 328−336.

(21) Vrzal, R.; Zdarilova, A.; Ulrichova, J.; Blaha, L.; Giesy, J. P.; Dvorak, Z. Activation of the aryl hydrocarbon receptor by berberine in HepG2 and H4IIE cells: Biphasic effect on CYP1A1. *Biochem. Pharmacol.* **2005**, *70*, 925−936.

(22) Williamson, E. M. Synergy and other interactions in phytomedicine. *Phytomedicine* **2001**, *8*, 401−409.

(23) Berhow, M. A.; Vaughn, S. F.; Moser, B. R.; Belenli, B.; Polat, U. Evaluating the phytochemical potential of camelina—An emerging new crop of old world origin. In *Phytochemicals—Biosynthesis, Function and Application, Recent Advances in Phytochemistry*; Springer: New York, 2014; Vol. *44*, pp 129−148.

(24) Falk, K. L.; Tokuhisa, J. G.; Gershenzon, J. The effect of sulfur nutrition on plant glucosinolate content: Physiology and molecular mechanisms. *Plant Biol.* **2007**, *9*, 573−581.

(25) Daya, A. J.; M. DuPonta, M. S.; Ridleyb, S.; Rhodes, M.; Rhodes, M. J. C.; Morgan, M. R. A.; Williamson, G. Deglycosylation of flavonoid and isoflavonoid glycosides by human small intestine and liver $\beta$-glucosidase activity. *FEBS Lett.* **1998**, *436*, 71−75.

(26) Perez-Vizcaino, F.; Duarte, J.; Santos-Buelga, C. The flavonoid paradox: Conjugation and deconjugation as key steps for the biological activity of flavonoids. *J. Sci. Food Agric.* **2012**, *92*, 1822−1825.

JOURNAL OF AGRICULTURAL AND FOOD CHEMISTRY

Article

pubs.acs.org/JAFC

# Identification of Bioactive Metabolites Dihydrocanadensolide, Kojic Acid, and Vanillic Acid in Soy Sauce Using GC-MS, NMR Spectroscopy, and Single-Crystal X-ray Diffraction

Ying Li,[†] Zi Teng,[†] Kirk L. Parkin,[#] Qin Wang,[†] Qingli Zhang,[⊥] Wei Luo,[○] Deyun Ma,[△] and Mouming Zhao*[,§]

[†]Department of Nutrition and Food Science, University of Maryland, College Park, Maryland 20742, United States

[§]College of Light Industry and Food Science, South China University of Technology, Guangzhou 510640, People's Republic of China

[#]Department of Food Science, University of Wisconsin—Madison, 1605 Linden Drive, Madison, Wisconsin 53705, United States

[⊥]Department of Animal and Food Sciences, Texas Tech University, Lubbock, Texas 79409, United States

[○]Analysis and Test Center of South China University of Technology, Guangzhou 510640, People's Republic of China

[△]School of Chemistry and Chemical Engineering, Zhaoqing University, Zhaoqing 526061, People's Republic of China

**ABSTRACT:** Microbial transformations of intrinsic substrates offer immense potential for generating new bioactive compounds in fermented food products. The aim of this work was to characterize the secondary metabolites in soy sauce, one of the oldest fermented condiments. Ethyl acetate extract (EAE) of soy sauce was separated using flash column chromatography, crystallized, and analyzed by nuclear magnetic resonance (NMR), single-crystal X-ray diffraction (SC-XRD), and mass spectroscopy. Dihydrocanadensolide (DHC), an antiulcer agent, was identified in a food for the first time. The natural stereostructure of DHC, which remained controversial for several decades, was determined as (3*S*,3a*S*,6*R*,6a*R*)-6-butyl-3-methyltetrahydrofuro[3,4-*b*]furan-2,4-dione using SC-XRD analysis. Kojic acid (KA) and vanillic acid (VA) were also identified from EAE as bioactive metabolic products of fungi and yeasts. Moreover, a new polymorphic form of KA was determined by SC-XRD.

**KEYWORDS:** *bioactive metabolites, soy sauce, dihydrocanadensolide (DHC), kojic acid, polymorphism, single-crystal X-ray diffraction (SC-XRD), NMR, GC-MS*

## INTRODUCTION

Fermented foods have fascinated humans since antiquity. Over the past few decades, extensive research has been done on the secondary metabolites in fermented foods and their potential health-promoting benefits. In fermented dairy foods, besides the notable B vitamins (over)produced by lactic acid bacteria (LAB), the essential biogenic peptides generated by LAB also drew attention because of their antihypertensive, antimicrobial, and immunomodulatory properties.[1−3] *Monascus* species-fermented "red mold rice" contains bioactive metabolites, such as monacolins, monascin, and monascopyridines; this red mold rice is a popular functional food regarded in East Asia as conferring antioxidant, cancer chemopreventive, hypolipidemic, hypotensive, and hypoglycemic benefits.[4,5] Kojic acid (KA), first isolated from cultures of *Aspergillus oryzae* in steamed rice, is widely used now as an antibrowning food additive and a skin-lightening agent in the cosmetics industry.[6] Discovery of the beneficial activities of secondary metabolites produced by microorganisms has resulted in renewed interest and exploration of fermentation processes.

Soy sauce, one of the world's oldest fermented soy products, is documented for being effective in suppressing inflammation and clearing toxins according to ancient Chinese literature.[7,8] Since the 1990s, there have been increasing studies on the chemopreventive, antioxidant, and antimicrobial activities of soy sauce.[9] Many aroma compounds in soy sauce, such as Furaneol, homofuraneol, norfuraneol, 4-ethylphenol, 4-ethylguaiacol, and 2-phenylethanol, exhibit antioxidant functions. These compounds were identified as byproducts of a salt-tolerant yeast *Zygosaccharomyces rouxii*.[10−13] The newly found phase II enzyme inducers in soy sauce, flazin and perlolyrin, are metabolic products of *Pediococcus halophilus*, and they are candidates for further evaluation as cancer preventive agents.[14,15] Owing to the complexity of the raw materials and the fact that mixed microbes collectively contribute to the whole fermentation process, soy sauce could be a rich reservoir of a diversity of food-derived microbial products that remain to be identified.[16]

In the present study, we report the isolation and identification of bioactive microbial metabolites in traditional fermented soy sauce based on solvent extraction, column chromatography, nuclear magnetic resonance (NMR), gas chromatography−mass spectrometry (GC-MS), and single-crystal X-ray diffraction (SC-XRD) analyses.

## MATERIALS AND METHODS

**Materials.** KA, vanillic acid (VA), formic acid, ethyl acetate, hexane, and acetone were purchased from Sigma-Aldrich Chemical Co. (St. Louis, MO, USA). Silica gel for column chromatography

Received: May 7, 2014
Revised: August 1, 2014
Accepted: August 4, 2014
Published: August 4, 2014

ACS Publications © 2014 American Chemical Society



dx.doi.org/10.1021/jf502159m | J. Agric. Food Chem. 2014, 62, 8392−8401

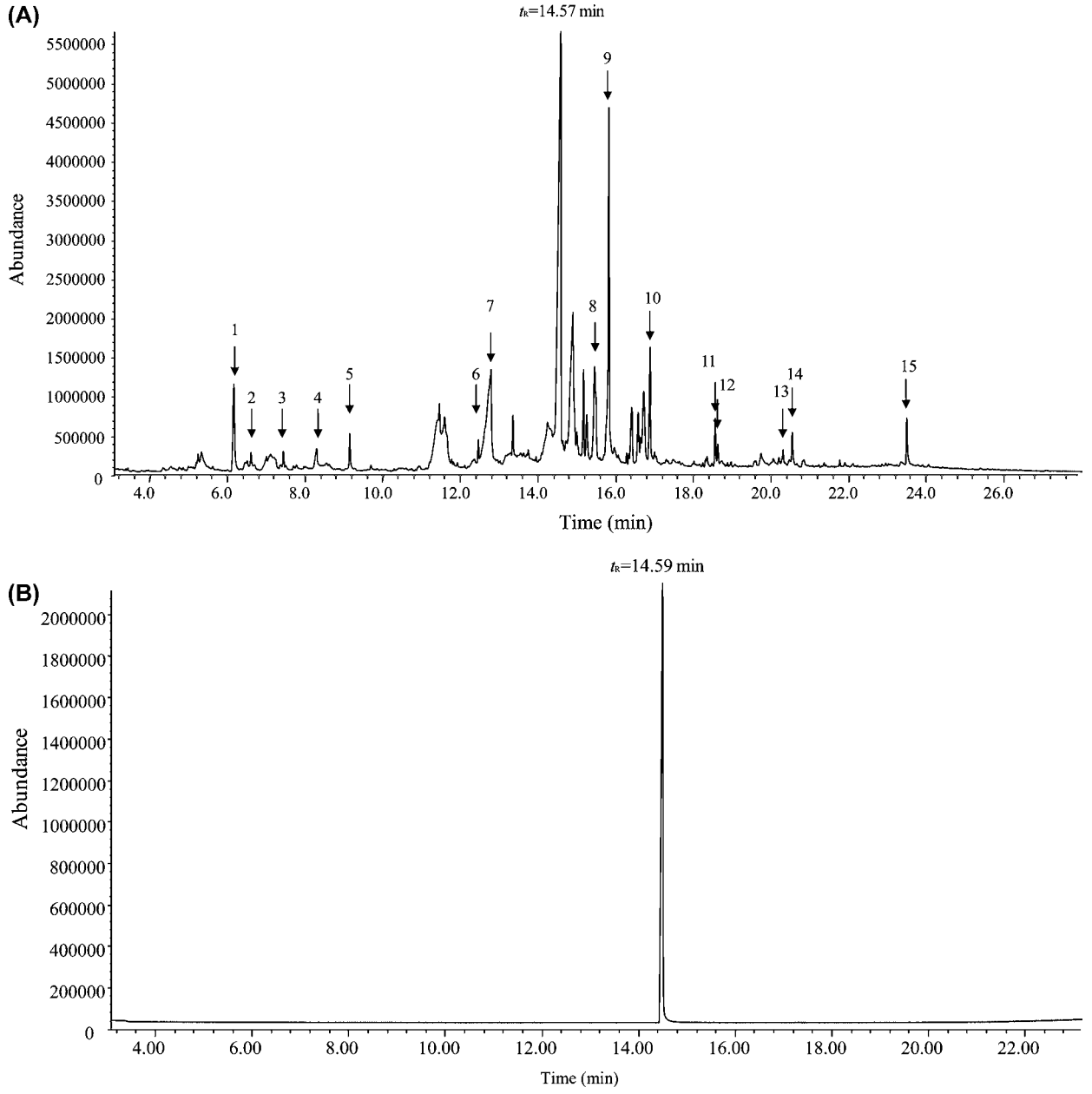


**Figure 1.** GC-MS total ion chromatograms of ethyl acetate extract of raw soy sauce (A) and dihydrocanadensolide (B). Peaks in (A): 1, maltol; 2, pyranone; 3, methylmaltol; 4, benzeneacetic acid; 5, 2-methoxy-4-vinylphenol; 6, 4-hydroxybenzoic acid; 7, vanillic acid; 8, syringic acid; 9, phthalic acid, isobutyl octyl ester; 10, palmitic acid; 11, oleic acid; 12, stearic acid; 13, oleylamide; 14, cyclo(phe-pro); 15, erucylamide.

(230−400 mesh, 60 Å) and thin-layer chromatography (TLC) glass plates (precoated with silica gel 60 $F_{254}$) were purchased from Merck (Darmstadt, Germany).

Soy sauce produced by the traditional high-salt dilute-state fermentation method was obtained from a local manufacturer (Guangdong, China). The fermentation process was conducted as follows: Raw whole soybeans were thoroughly cooked by steam at 125 °C for 15 min and mixed with wheat flour. Spore suspensions (*Aspergillus oryzae*) were inoculated (0.05%, w/w) into the mixtures of soybean and flour, and the medium was kept at 35−40 °C, relative humidity 70−90% for 2−3 days (*koji* process). After turning yellowish-green, the molded materials were mixed with NaCl solution (16−18%, w/v) to make wet mash (*moromi*). Finally, raw soy sauce was obtained by collecting liquid dripping from the wet mash after 3 months of fermentation. Raw soy sauce was batch-pasteurized at 80 °C for 30 min before analysis.

**Flash Column Chromatography.** One and a half liters of pasteurized soy sauce was extracted with ethyl acetate (1:1, v/v) three times by continuous shaking in a separatory funnel for 10 min each. The combined ethyl acetate phases were dried over anhydrous $Na_2SO_4$ and concentrated using a rotary evaporator under vacuum (Buchi rotavapor RII, Buchi Labortechnik AG, Flawil, Switzerland) to yield ∼3 g of solids from the ethyl acetate extract (EAE).

Two grams of EAE solids was redissolved in minimum volume of ethyl acetate and mixed with 10 g of silica gel. Then the mixture was dried in a vacuum desiccator at room temperature (∼25 °C) for 4 h. The extract-laden silica gel was then loaded onto a normal phase silica gel flash column (4.5 cm i.d. × 12.2 cm). The column was eluted successively with a gradient of hexane/acetone (9:1, 8:2, ..., 2:8, 1:9; 500 mL for each step). Portions (120 mL) of eluate collected were subject to solvent evaporation, and a small sample (∼10 μL) of each portion was applied to a 20 cm × 10 cm precoated TLC plate (silica gel 60 A $F_{254}$). Spots were detected by ultraviolet illumination (254


dx.doi.org/10.1021/jf502159m | J. Agric. Food Chem. 2014, 62, 8392−8401

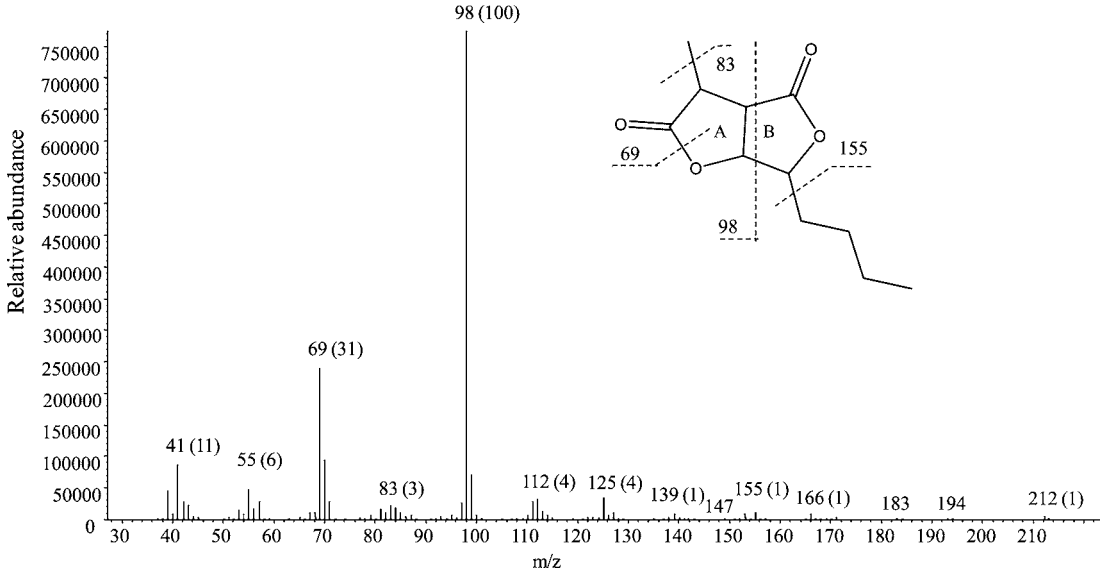


**Figure 2.** Mass spectra (EI/MS) fragmentation and cleavage sites of dihydrocanadensolide.

and 365 nm) and iodine vapors. The consecutive portions of eluate showing single spots with the same $R_f$ on TLC developed by the same developing solvents (mixtures of hexane and ethyl acetate) were combined into fractions and concentrated. Fraction 1 comprised material migrating to an $R_f$ of 0.26 on a TLC plate developed with hexane/ethyl acetate/formic acid (80:20:1, v/v/v). This fraction was concentrated under vacuum to ~2 mL and sealed in vials held at room temperature (~25 °C) to allow slow crystallization. The resulting colorless rectangular prismatic crystals (~40 mg) were washed carefully with methanol and recrystallized with ethyl acetate for further analysis. Fraction 2 was recovered as material migrating to an $R_f$ of 0.52 on TLC plates that were developed by hexane/ethyl acetate/formic acid (60:40:1, v/v/v). Upon evaporation of desorbing solvent, 15 mg of white powder was recovered. Fraction 3 was composed of material migrating to an $R_f$ of 0.37 on TLC plates developed by hexane/ethyl acetate/formic acid = 70:30:1 (v/v/v). The recovered material afforded colorless needle-shaped crystals (~18 mg) after slow solvent evaporation in sealed vials.

**Gas Chromatographic Analyses.** GC-MS analyses of EAE and dihydrocanadensolide (DHC) were performed on a 6890N gas chromatograph (Agilent Technologies, Palo Alto, CA, USA) with a mass spectrometer (MS 5975, Agilent Technologies). Helium was used as a carrier gas with a flow rate of 1 mL/min. Diluted EAE (0.2 $\mu$L) was injected into a splitless injector (270 °C). An HP-5MS (5% phenyl methyl siloxane) capillary GC column (30 m length, 0.25 mm i.d., 0.25 $\mu$m film thickness, Agilent Technologies) was used. The GC oven temperature was held at 80 °C for 3 min, then increased to 280 °C at 10 °C/min, and finally held for 5 min at 280 °C. The mass selective detector was operated in positive electron ionization (EI) mode (70 eV) with a mass scan range from $m/z$ 33 to 450. The database NIST.05 was used to determine compound structures. Quantitative GC analysis was carried out using an Agilent 5890 II instrument with a flame ionization detector (FID). The capillary column and temperature program were the same as those of the GC-MS analysis.

**Nuclear Magnetic Resonance (NMR) Analysis.** $^1$H NMR, $^{13}$C NMR, and gradient correlation spectroscopy (gCOSY) NMR spectra were recorded with a Bruker AVANCE spectrometer (Bruker DRX400, Bruker Biospin Co., Karlsruhe, Germany) using solvent signals as an internal standard. Chemical shifts ($\delta$) and coupling constants ($J$) are expressed in parts per million (ppm) and hertz (Hz), respectively. MestReNova V5.3 was used to visualize and process NMR data (Mestrelab, Escondido, CA, USA). Signal multiplicities were described as follows: s (singlet), d (doublet), dd (doublet of doublets), ddd (doublet of doublets of doublets), dt (doublet of triplets), dq (doublet of quartets), t (triplet), m (multiplet), and b (broad).

**Single-Crystal X-Ray Crystallography (SC-XRD) Analysis.** Well-shaped single crystals of fractions 1 and 3 were selected for the X-ray diffraction experiment. The crystals were mounted on glass fibers and positioned on the goniometer head. SC-XRD data of both fractions were collected on an R-axis Spider diffractometer (Rigaku, Japan) at 293(2) K using monochromatic Mo K$\alpha$ radiation ($\lambda$ = 0.71073 Å) at the Analytical and Testing Center of South China University of Technology. The programs SHELXS-97 and SHELXL-97 were used for structure determination and refinement. All H atoms were placed at calculated positions. Before the last cycle of refinement, all H atoms were fixed and were allowed to ride on their parent atoms.

## RESULTS AND DISCUSSION

**GC-MS Analysis of EAE.** Previous studies of GC-MS analysis of volatile compounds in soy sauce were usually conducted on polar GC capillary columns, such as DB-FFAP/HP-FFAP,[17,18] DB-WAX,[19] and HP-Innowax.[20] In this study, a nonpolar HP-5MS column was adopted, in the hope of searching for a different polarity category of metabolites in soy sauce. A total ion chromatogram of volatile compounds in EAE of soy sauce separated by the HP-5MS column was obtained (Figure 1A). Among the tentatively identified compounds, maltol, VA, and syringic acid were reported to possess antioxidant activities, nitric oxide scavenging effects, and cytoprotective ability in the prevention of diabetic neuropathy complications.[21−24] Other principal peaks included oleic acid, palmitic acid, and stearic acid, which were likely derived from soybean lipids.[25] However, no match was found for the mass spectrum of the major peak (retention time = 14.57 min) in the commercial mass spectra libraries or online mass spectra database. For structure identification, this unknown compound was isolated from EAE by silica gel column chromatography.

**Identification of DHC in Soy Sauce and Its Absolute Configuration.** Eluates of silica gel chromatography were pooled according to their TLC patterns. Fraction 1 formed colorless crystals after slow solvent evaporation. After washing and recrystallizing, the crystal emanated a strong characteristic odor of soy sauce. In GC-MS TIC spectra, the peak retention time and mass spectrum of this compound (Figure 1B) were consistent with those of the major peak in Figure1A. The


dx.doi.org/10.1021/jf502159m | J. Agric. Food Chem. 2014, 62, 8392−8401

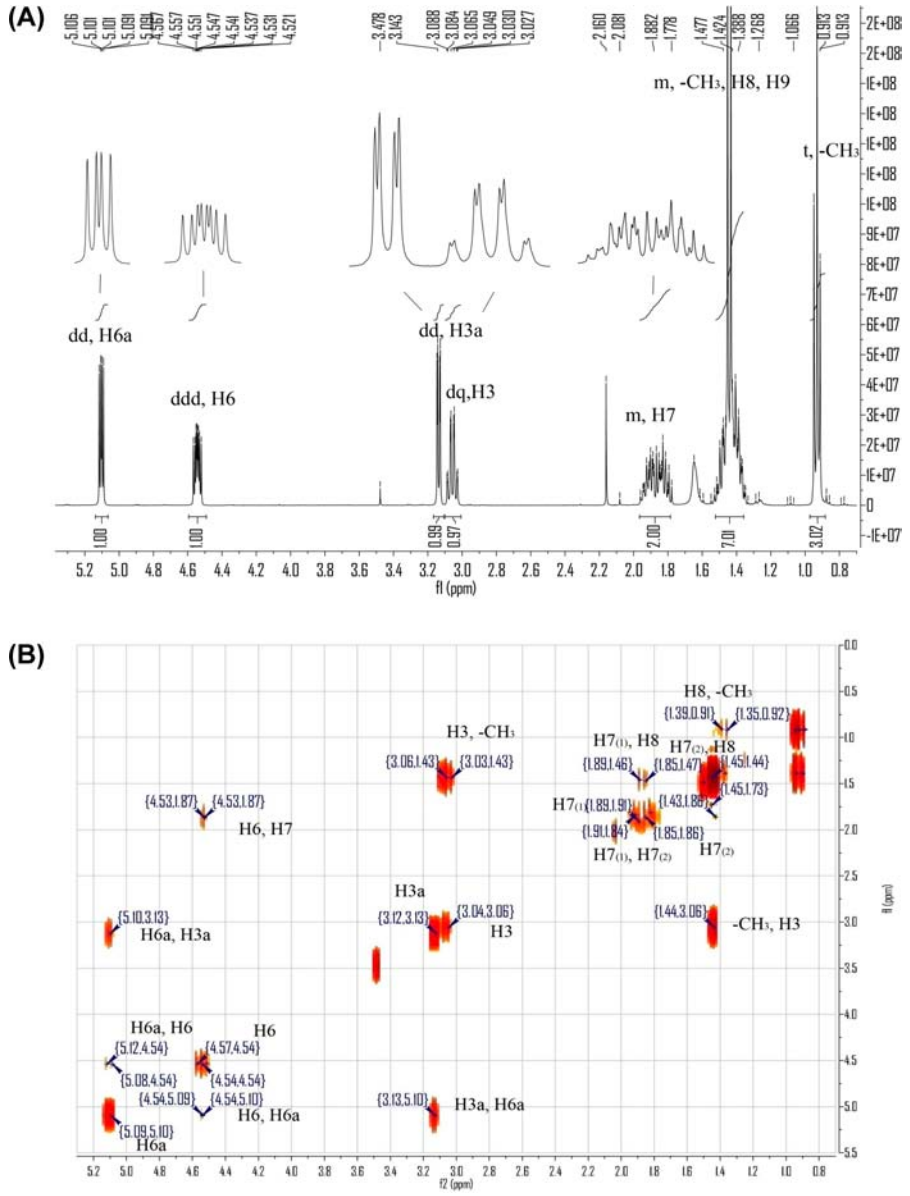


**Figure 3.** (A)$^{1}$H NMR spectrum of DHC in $CDCl_3$; (B) gCOSY spectrum of DHC in $CDCl_3$ For the convenience of interpretation, atomic numbers of C, H, and O were designated as shown in Figure 4.

molecular weight of the compound was $m/z$ 212 according to the EI mass spectrum (EI/MS) (Figure 2).

Confirmation of the structure and assignment of this compound were conducted from detailed analyses of the $^{13}$C NMR spectra, $^{1}$H NMR spectra (Figure 3A), gCOSY (Figure 3B), and EI/MS (Figure 2). First, the chemical shifts observed by $^{13}$C NMR analysis (in $CDCl_3$) were $\delta$ 13.98, 17.31, 22.59, 27.68, 28.72, 38.57, 49.22, 78.49, 82.61, 174.83, and 176.90. The chemical shifts in high field permitted the assignments of two R−COO−R′ groups. From the $^{1}$H NMR spectra, no signal was evident in the range of $\delta$ 6−14 ppm, indicating no carboxylic acid, benzene ring, or double bond present in the molecule. The integration of two peaks at $\delta$ 4.4−5.2 in $^{1}$H NMR were both 1, suggesting two $\alpha$ hydrogen within two −COO−CH− fragments. The $^{13}$C NMR signals at $\delta$ 78.49 and 82.61 imply two carbons are connected to oxygen atoms. Therefore, the two ester groups appeared to be confirmed. Second, the four chiral centers (C3, C3a, C6, and C6a in Figure 4A) in the *cis*-fused dilactonic ester structures could explain the characteristic splitting patterns in the $^{1}$H NMR spectra. The signals of protons on C3a and C6a were dd because they were affected not only by each other ($J$ = 6 Hz) but also by H3 and H6, respectively ($J$ = 1.4 and 4 Hz). For H3, the quartet intensity 1:3:3:1 ($J$ = 8 Hz) suggested that a methyl group was connected to C3, and the pattern of quartet peaks splitting to doublets occurred owing to the influence of H3a at the adjacent stereocenter ($J$ = 1.4 Hz). It is not surprising that H6 showed a similar pattern of ddd ($J$ = 8, 6, 4 Hz), which was also observed by Sharma.[26] Attention should be paid to the interpretation of the ddd effect of H6, evoked by vicinal coupling from H6a, and individual diastereotopic protons H7$_{(1)}$ and H7$_{(2)}$. This could be easily confused with a doublet of triplets, which was the case interpreted by Birch and led to stereostructure III in Table 1.[27] Third, an *n*-butyl residue on C6 could be deduced from the downfield $^{1}$H NMR spectra. The chiral center C6 may cause the restricted rotation of diastereotopic protons on C7, resulting in geminal coupling of these two protons. Similar geminal coupling effects were also recorded by Isaka in the


dx.doi.org/10.1021/jf502159m | J. Agric. Food Chem. 2014, 62, 8392−8401

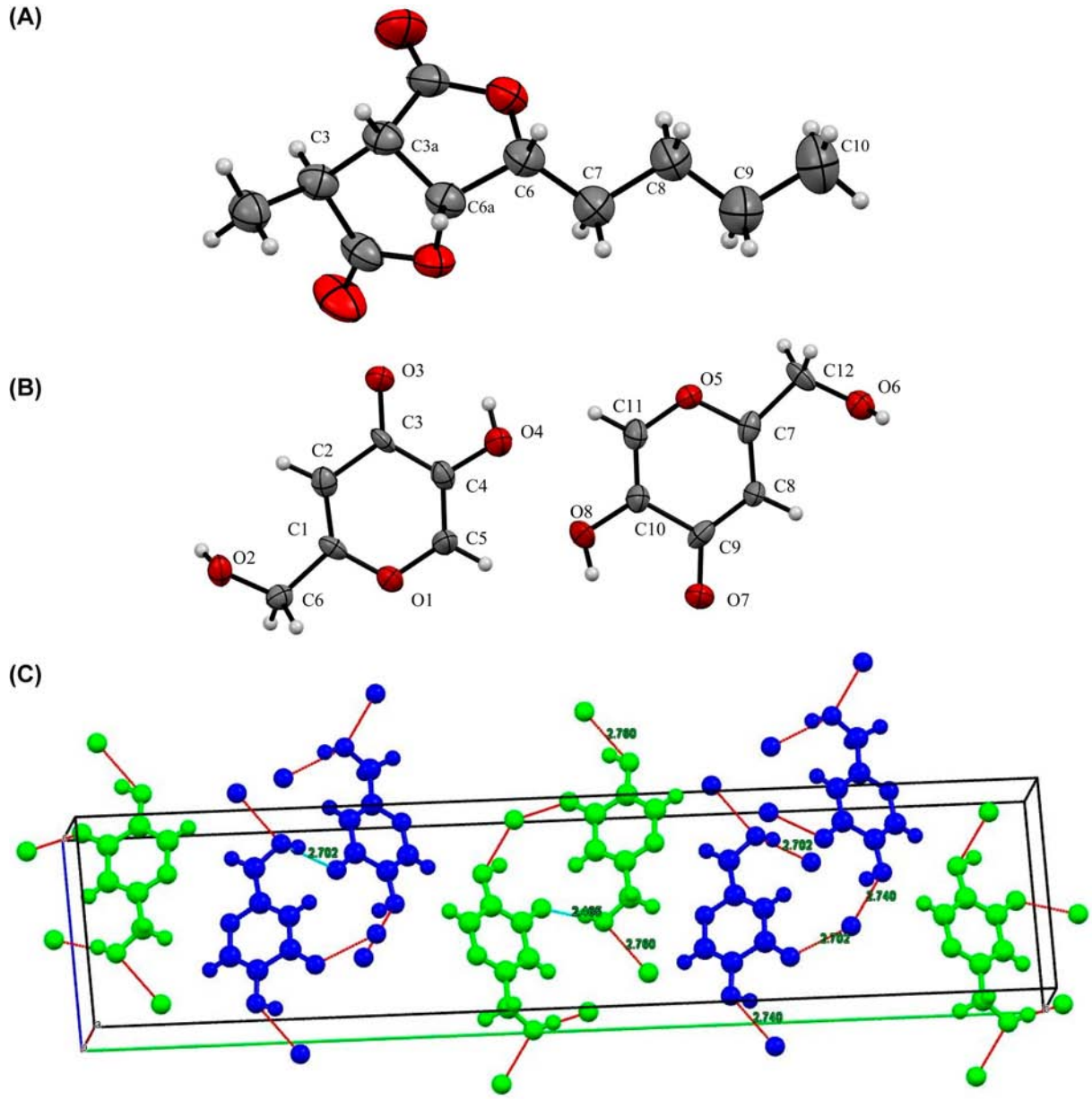


**Figure 4.** (A) Oak Ridge thermal ellipsoid plot (ORTEP) diagram for crystal structures of DHC; (B) ORTEP of KA; (C) packing diagram of KA. Molecules of equivalent symmetry are shown in the same color. Lengths of O−H···O hydrogen bond: 2.465, 2.702, 2.740, and 2.760 Å.

identification of a furofurandione.[28] Also considering the influence from H8, splitting patterns of H7 appeared to be more complex than a triplet of doublets (1.7−2.0 ppm in Figure 3A), consistent with locating the *n*-butyl group on C6 ($-CH_3$). These effects were confirmed by gCOSY spectra, which reflect the interactions between the coupling protons H3a−H6a, H6−H6a, H6−H7, H3−$CH_3$, $H7_{(1)}$−H8, $H7_{(2)}$−H8, and $H7_{(1)}$−$H7_{(2)}$ (Figure 3B). In addition, analysis of EI/MS spectra is consistent with the speculated structure of DHC (Figure 2). The parent peak indicated that *m*/*z* of the molecule was 212. The base peak at *m*/*z* 98 probably results from loss of the *n*-butyl connected B ring. The appearance of the second major molecular ion peak at *m*/*z* 69 can be ascribed to fragmentation by ring opening of ring A. The differences of 13, 15, 16, 18, and 29 among other minor ions were postulated to arise from the loss of the groups −CH, $-CH_3$, −O, $H_2O$ (or CO), and −CH−O, respectively (Figure 2). Although mass fragments of DHC were previously reported by Birch,[27] the detailed EI/MS spectra provided here have the advantage of indicating the relative abundance of fragments.

Because of the complexity brought about by the four chiral centers, there has been debate about the natural configuration of DHC since its discovery (Table 1). When McCorkindale first isolated DHC from synthetic medium of *Penicillum canadense*, the structure was suggested as **III**.[29] In the same year, Birch identified DHC, also as III, from *Aspergillus indicus*.[27] However, in their studies, the absence of NMR data of protons H7 precluded a discussion of the possibility of stereoconfiguration reflected by long-range couplings from H6a, if **III** was the correct assignment of structure. More recently, Yoshikoshi reported the protons on the B ring had been interpreted as *trans*-positioned by McCorkindale, and corrected the structure **III** to **II** by evidence obtained from stereoselective synthesis of (+)-canadensolide from hex-1-


dx.doi.org/10.1021/jf502159m | J. Agric. Food Chem. 2014, 62, 8392−8401

**Table 1. Dissension on Molecular Configuration of DHC**

| | Stereo-structures | Configuration of chiral centers | Studies |
|---|---|---|---|
| I | 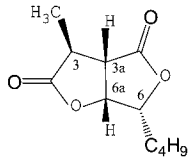 | 3*S*,3a*S*,6*R*,6a*R* | (*26*)<br>(*28*)<br>(*33*)<br>(*35*)<br>This study<br>CAS number: 20421-32-3 |
| II | 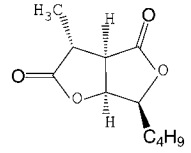 | 3*R*,3a*R*,6*S*,6a*S* | (*30*)<br>(*31*)<br>(*34*)<br>(*36*)<br>(*38*)<br>CAS number: 251950-91-1 |
| III | 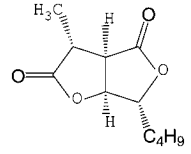 | 3*R*,3a*R*,6*R*,6a*S* | (*27*)<br>(*29*)<br>CAS number: 59796-36-0 |
| IV | 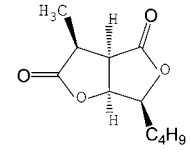 | 3*S*,3a*R*,6*S*,6a*S* | CAS number: 177187-30-3 |
| V | 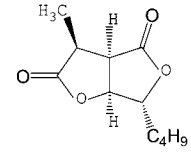 | 3*S*,3a*R*,6*R*,6a*S* | CAS number: 59796-19-9 |

yne.[30,31] However, this correction still mistakenly adopted the structure of a synthetic epimer as the natural configuration. After comparing samples from both McCorkindale and Yoshikoshi, Anderson and Fraser-Reid suggested a dehydro-**I** as the natural structure of canadensolide in 1978.[32] In 1975, Aldridge[32] patented a formula containing fermented DHC as a gastric and duodenal ulcer-healing agent and acknowledged **II** as the structure corrected by Yoshikoshi.[30,31] Over the past two decades, chemical synthesis of DHC in its natural configuration has been gaining increasing attention. Although extensive studies have been done by exploring the synthetic processes for **I**, **II**, and the epimers **III** and **IV**, the natural configuration of DHC has not been conclusively established.[26,30,33−37]

Molecular chirality is essential to activities of biologically/pharmacologically active compounds, as many drug components exhibit significant differences in their pharmacologic activities compared with their enantiomers.[39] Therefore, knowledge of the absolute configuration of chemicals that are potential therapeutic agents is extremely important. By far, the most powerful structural method for determination of the absolute configuration of molecules is single-crystal X-ray crystallography.[40] Because the anomalous dispersion effect of heavy atoms can be measured very accurately, the absolute stereostructure obtained by SC-XRD is clear and unambiguous.[41] The critical issue for SC-XRD is obtaining a single crystal with suitable size.[42] In this study, single crystals weighing up to 15 mg of DHC were obtained for SC-XRD analysis for the first time. Information on crystallographic data collection and structure refinement is summarized in Table 2. The

**Table 2. Crystal Data and Structure Refinements for DHC and KA**

| parameter | DHC | KA |
|---|---|---|
| diffraction radiation wavelength (Å) | 0.71073 | 0.71073 |
| diffraction radiation type | Mo K$\alpha$ | Mo K$\alpha$ |
| temperature (K) | 293(2) | 293(2) |
| crystal system | monoclinic | monoclinic |
| chemical formula | $C_{11}H_{16}O_4$ | $C_6H_6O_4$ |
| formula weight | 212.24 | 142.11 |
| unit cell dimensions | | |
| *a* (Å) | 10.008 (2) | 3.8334(7) |
| *b* (Å) | 8.6505(17) | 36.876(7) |
| *c* (Å) | 13.474(3) | 8.512(3) |
| $\alpha$ (deg) | 90 | 90 |
| $\beta$ (deg) | 103.03(3) | 96.66(3) |
| $\gamma$ (deg) | 90 | 90 |
| *V* (Å$^3$) | 1136.4(4) | 1195.1(5) |
| *Z* | 4 | 8 |
| *F* (000) | 520 | 592 |
| density (mg/cm$^3$) | 1.428 | 1.580 |
| absorption coefficient (mm$^{-1}$) | 0.117 | 0.136 |
| GOF (goodness of fit) | 1.036 | 1.085 |
| $\theta$ range for data collection (deg) | 3.10−25.19 | 3.27−25.19 |
| value of $R_{int}$ | 0.0202 | 0.0212 |
| residual factor *R* for all | 0.0447 | 0.0387 |

absolute configuration of DHC isolated from soy sauce was identified as (3*S*,3a*S*,6*R*,6a*R*)-6-butyl-3-methyltetrahydrofuro-[3,4-*b*]furan-2,4-dione (**I** in Table 1). A search of the Cambridge Structural Database and online databases showed no match with crystallographic data reported here for DHC. Detailed chemical bond lengths and bond angles of DHC can be found in the CIF format data deposited with the Cambridge Crystallographic Data Centre (CCDC) under reference no. 982491.

Previous studies on bioactivities of DHC were mostly focused on the antiulcer activities on gastric or duodenal ulcers. Animal experiments revealed that DHC produced by fermentation method showed better healing properties in gastric ulceration induced by betamethasone and fenclozic acid, compared to the commonly used drug carbenoxolone. In addition, DHC significantly reduced duodenal ulceration in rats induced by acetic acid, whereas carbenoxolone did not show this property.[38,43]

The reported fermentation method for producing DHC involved 10 days of agar fermentation and 33 days of submerged fermentation, which was similar to the *koji* (solid) and *moromi* (liquid) fermentation process of soy sauce, respectively.[38] DHC was discovered in the metabolites of *Penicillium canadense* and *Aspergillus indicus*.[29] *Penicillium* and *Aspergillus* species were also found in soy sauce. *A. oryzae* and *A. sojae* are two important starter fungi for soy sauce fermentation.[44,45] In our study, ∼40 mg of DHC crystals was obtained in 2 g of EAE (i.e., ∼40 mg/L soy sauce). Considering the loss during extraction, isolation, and crystallization processes, the concentration of DHC in soy sauce should be


dx.doi.org/10.1021/jf502159m | J. Agric. Food Chem. 2014, 62, 8392−8401

higher than this value. Quantification of DHC in the ether extract of raw soy sauce was performed by GC-FID under the same conditions as GC-MS described under Materials and Methods, using purified DHC (>99% judged by GC-MS) as an external standard. The results showed that the concentration of DHC in raw soy sauce was approximately 83 mg/L.

Although chemically diverse, all secondary metabolites are produced via a few common biosynthetic pathways.[46] Studies with [2-$^{14}$C]acetic acid suggested that DHC might arise from the condensation of two chains, octanoic acid and pyruvic acid (or oxaloacetic acid with subsequent decarboxylation).[27] Oxaloacetic acid is an intermediate in the citric acid cycle, a major metabolic pathway of primary metabolism found in living systems. On the basis of these facts, it is likely that DHC is derived from the citric acid cycle of fungi. Ma et al. reported that a nucleophile-promoted, biscyclization of keto acids could spontaneously happen, suggesting this mechanism might be involved in the biosynthesis of natural bicyclic lactones.[47] Similar biosynthetic routes have been defined for canadensolide, indicating that this compound was mainly formed by condensation of $\alpha$-methylene of a fatty acid and the carbonyl group of oxalacetic acid.[48] 1-$^{14}$C- and 2-$^{13}$C-labeling during the evolution of another bislactone, avenaciolide, gave more evidence for this biosynthetic pathway.[48]

**Identification of VA.** Identification of fraction 2 was conducted by GC-MS and $^1$H NMR. The EI/MS profile of fraction 2 matched that of VA in the NIST 0.05 database. Its retention time ($t_R$ of 12.78 min, Figure 1A) on an HP-5MS column, as well as $^1$H NMR profile [$\delta$ 7.59 (1H, dd, $J$ = 8.0 Hz, 2.0 Hz, H4), 7.56 (1H, d, $J$ = 2.0 Hz, H6), 6.92 (1H, d, $J$ = 8.0 Hz, H3), 3.90 (3H, s, $-OCH_3$), 400 MHz, acetone-$d_4$)] corresponded with that of the authentic compound. VA is a flavoring compound in soy sauce.[49] It might be derived directly from soybeans, which contain VA as a major phenolic acid.[50] Another phenolic compound, ferulic acid in soybeans, can be converted to VA through the metabolism of *Aspergillus niger*,[51] *Debaryomyces hansenii*,[52] and *Pseudomonas putida*.[53] Moreover, *Zygosaccharomyces rouxii*, a salt-tolerant yeast commonly found in soy sauce, is capable of producing VA as a metabolite.[54]

The concentration of VA in soy sauce recovered in this study was ~15 mg/L, which was within the range of 1.9−294 mg/L reported by others.[49,55,56] Considering the dry contents in soy sauce (25−58 g/100 mL),[57] the concentration of VA relative to total solids of soy sauce was comparable to that in the root of the medicinal plant *Angelica sinensis* (or Dang Gui), which contains the highest known amount of VA among all plants (6.1−94.4 mg/kg).[58,59] Hence, soy sauce may be a rich source for VA.

VA has been reported to exhibit potential antiulcer activity in ulcerative colitis.[60] It reduced the severity of the clinical signs of dextran sulfate sodium-induced colitis in mice, including weight loss and shortening of colon length, and the disease activity index. A hepatoprotective effect of VA was also reported.[61] VA significantly decreased the transaminase activity and suppressed the disorganization of the hepatic sinusoids in concanavalin A-treated mice. VA was capable of reducing plasma interleukin-6 in both ulcerative colitis-healing and hepatoprotective effects. Moreover, VA has been associated with antihypertensive and antioxidant activities demonstrated in rats.[62] VA restored systolic and diastolic blood pressure to normal levels, preserved the plasma nitric oxide metabolites concentration, and reduced plasma lipid peroxidation products and cellular defensing enzymes. The potential of inhibiting carcinogenesis[63] and preventing the secondary complications of diabetes[64] by VA have also gained increasing attention.

**Identification of KA.** Fraction 3 was separated by normal phase column chromatography and obtained as colorless needle-like crystals. $^1$H NMR spectra ($\delta$ 4.35 (2H, s, H6), 6.47 (1H, s, H2), 8.16 (1H, s, H5), 5.75 (1H, b, −O(2)H), 9.13 (1H, b, −O(4)H), 400 MHz, DMSO-$d_6$) and data obtained from an authentic compound confirmed this compound as 5-hydroxy-2-hydroxymethyl-4-pyrone (KA).[65] As the physical appearance of KA crystal obtained in this study was different from that described in the literature (0.1 × 0.15 × 0.15 mm, KA obtained from *Aspergillus tamaril* strain),[66] a further analysis oby SC-XRD was carried out to gain more insight into the crystal polymorphs, because SC-XRD was considered to outweigh other methodologies on providing detailed and undisputable crystal packing information.[67] A crystal of KA (1 × 0.8 × 3 mm) was mounted on a glass fiber and positioned on the goniometer head for SC-XRD analysis. Our results showed different unit cell dimensions from reports in the literature,[66] mainly in the observation that $Z$ = 8 molecules instead of 4 molecules (Table 1; Figure 4B,C). Another report showed that a crystal of KA (0.48 × 0.5 × 0.08 mm) obtained from the strain of *Aspergillus oryzae* WP-D-1 had the formula $(C_6H_6O_4)_2$.[68] The crystal packing of KA in our study was more complex than those previously reported. Whereas all KA molecules were connected by hydrogen bonding with three other molecules instead of two, they were aligned along the *b*-axis facing mainly two directions (Figure 4C). More specifically, the planes of KA were tilted ~23.4°, ~26.7°, ~153.3°, and ~156.6° off the *bc* plane and approximately normal to the *ab* plane. The difference in packing motif provides evidence for the polymorphism of KA, and our report added an additional polymorphic variety.

Because of its superior activities of antioxidant and inhibition of tyrosinase, KA has been used as an antibrowning food additive and a skin-lightening agent in the cosmetics industry.[6] Other health beneficial effects such as antimelasma and antineoplastic activities have also been reported.[69,70] Literature on the presence of kojic acid in soy sauce is the subject of debate. Nakadai claimed that KA was not detected in commercial soy sauce.[71] Shinshi studied 84 commercially used koji-mold strains for their capabilities of producing KA. Most of them generate <2 mg/mL KA under fermentation conditions for soy sauce, whereas some strains produced up to 24 mg/mL.[72] Decomposition of KA during soy sauce liquid fermentation was observed to be nearly 100% at the end of 140 days.[73] In our study, ~18 mg of KA was recovered from 2 g of EAE after extraction and isolation, so the concentration of KA was likely to be >18 mg/L in the original sample.

Kojic acid is produced by numerous *Aspergillus* species. Carbon sources for KA fermentation include reducing sugars, sugar acids, and sugar alcohols. The chain length of these compounds could be 2−7 carbons or 12 or 18 carbons. Polysaccharides can also serve as a carbon source for KA.[74] Although the studies on the biosynthesis of KA started six decades ago, the pathway remains speculative.[6] One important theory suggesting that KA can be synthesized from glucose via direct conversion was supported by isotope-traced D-glucose experiments.[75] Typically, oxidation of glucose to 3-ketoglucose by glucose 3-dehydrogenases was suggested as the initial step, followed by dehydration at the 4- and 5-positions of 3-ketoglucose to form KA. For carbon sources with fewer than six carbon atoms, it was difficult to determine the exact route,

because the presence of a $C_6$ precursor has not been definitely identified, and $^{14}C$ positions in the KA product were more extensively redistributed than direct conversion, by evidence obtained with [2-$^{14}$C]-dihydroxyacetone and [1-$^{14}$C]-D-ribose.[6,76]

Fermentation is the major production technology for soy sauce by far. Typically, the fermentation process consists of two stages, namely, *koji* (aerobic growth of the starter fungi on soy- and wheat-based materials for a few days) and *moromi* (anaerobic incubation of molded materials in salt solutions for months).[77] Depending on the temperature and the ratio of solid to brine solution, the producing methods are mainly categorized into high-salt dilute-state (HSDS) and low-salt solid-state (LSSS) fermentation. HSDS fermentation is widely adopted among Asian countries, although there are differences in raw materials (whole soybean, defatted soy flake, roast wheat, flour, and wheat bran), starter fungal species, and fermentation time for *moromi* (3−9 months). On the other hand, LSSS fermentation requires less time for both *koji* (1 day) and *moromi* (3 weeks) processes, a smaller volume of *moromi* brine solution (half that of HSDS), and a higher *moromi* temperature (40−45 °C).[78] It has been known that the amounts and compositions of amino acids and the aroma compounds in soy sauce can be regulated by controlling the fermentation conditions.[78,79] Similarly, it can be inferred that bioactive compounds can also be modulated. Considering the possible biosynthesis routes of KA, this compound may arise from heterocyclic compounds derived from the primary intermediates in the citric acid cycle of fungal metabolism during fermentation. The primary intermediates, particularly oxalacetic acid in the citric acid cycle, can be converted to secondary intermediates, which may be responsible for the formation of DHC in soy sauce. Secondary metabolites are usually not produced during the phase of rapid growth (trophophase); instead, they are synthesized during the subsequent production state (idiophase), especially when microbial growth is limited by the exhaustion of one key nutrient.[80] Therefore, the production of microbial secondary metabolites could be enhanced by (1) allowing sufficient microbial growth and exhaustive utilization of certain culturing ingredients in the *koji* process, followed by (2) proceeding to the *moromi* stage at which the brine solution could further inhibit the rapid growth of the microbes. This was supported by reports that solid fermentation followed by liquid fermentation resulted in a higher yield of KA, compared to adopting liquid fermentation alone.[6,81,82] The relatively short time (1 day) of *koji* and high temperature of *moromi* processes of the LSSS method are designed to achieve highest protease activities, which may compromise the adequate conditions for microbial trophophase growth and idiophase metabolite production, compared to HSDS fermentation. In addition, VA in soy sauce is generated from various sources, including the soy materials and enzymatic modification of ferulic acid by fungi, yeasts, or bacteria. Utilization of soy materials with high VA and/or ferulic acid contents may be beneficial for elevating the levels of VA in soy sauce. Until now, the key fermentation conditions that affect microbial survival status, metabolic pathways, and microbe-culturing material interaction are still largely unknown. Further studies need to be done on the effects of various fermentation factors on the contents of bioactive compounds in soy sauce.

The findings of the present study illustrate the isolation and structural determination of three bioactive microbial secondary metabolites, namely, DHC, VA, and KA. To our knowledge, this study is the first to offer SC-XRD data of DHC and identify DHC in a food. This is an advance over earlier attempts to resolve the long-lasting debate on natural configuration of DHC. In addition, polymorphism of KA was discovered by SC-XRD analysis. The polymorphic variety observed in this study had the crystal packing of eight molecules in a unit cell, and each molecule was connected with three other molecules via hydrogen bonding. These data, as well as the detailed information on EI fragmentation in EI/MS spectra of DHC, can extend our knowledge of the structural identification of similar microbial metabolites in a wide range of fungus-fermented foods. On the basis of the results from this study, future works can be done on the quantification of these bioactive compounds in various fermented foods, improvement of fermentation processes to enrich these metabolites, and development of new food products bearing potential ulcer protection activities.

## AUTHOR INFORMATION

### Corresponding Author

*(M.Z.) Phone/fax: 86-20-87113914. E-mail: femmzhao@scut.edu.cn.

### Funding

This work was supported by the National Science Technology Supporting Project for the 12th Five-Year Plan (Nos. 2012BAD34B03 and 2012BAK17B11) and the Key Technology R&D Program of Guangdong Province (No. 2012cxy004).

### Notes

The authors declare no competing financial interest.

## ABBREVIATIONS USED

GC, gas chromatography; GC-MS, gas chromatography−mass spectrometry; GC-FID, GC with flame ionization detector; NMR, nuclear magnetic resonance; SC-XRD, single-crystal X-ray diffraction; KA, kojic acid; VA, vanillic acid; TLC, thin-layer chromatography; EAE, ethyl acetate extract; DHC, dihydrocanadensolide; EI, electron ionization; MS, mass spectra; gCOSY, gradient correlation spectroscopy; ORTEP, Oak Ridge thermal ellipsoid plot

## REFERENCES

(1) Hayes, M.; Stanton, C.; Fitzgerald, G. F.; Ross, R. P. Putting microbes to work: dairy fermentation, cell factories and bioactive peptides. Part II: Bioactive peptide functions. *Biotechnol. J.* **2007**, *2*, 435−449.

(2) Stanton, C.; Ross, R. P.; Fitzgerald, G. F.; Sinderen, D. V. Fermented functional foods based on probiotics and their biogenic metabolites. *Curr. Opin. Biotechnol.* **2005**, *16*, 198−203.

(3) Hugenholtz, J.; Smid, E. J. Nutraceutical production with food-grade microorganisms. *Curr. Opin. Biotechnol.* **2002**, *13*, 497−507.

(4) Loret, M.-O.; Morel, S. Isolation and structural characterization of two new metabolites from *Monascus*. *J. Agric. Food Chem.* **2009**, *58*, 1800−1803.

(5) Wild, D.; Tóth, G.; Humpf, H.-U. New *Monascus* metabolite isolated from red yeast rice (angkak, red koji). *J. Agric. Food Chem.* **2002**, *50*, 3999−4002.

(6) Bentley, R. From miso, sake and shoyu to cosmetics: a century of science for kojic acid. *Nat. Prod. Rep.* **2006**, *23*, 1046−1062.

(7) Huang, G. Truth-seeking in materia medica (Ben Cao Qiu Zhen, 1769). In *Classical Ten Books of Materia Medica (Ben Cao Jing Dian Lun Zhu Shi Ren Shu)*; Academy Press (Xue Yuan): Beijing, China, 2011; Vol. 7, p 324.

(8) Tao, Z., Other records by famous doctors (Ming Yi Bie Lu, between 220−450 A.D). In *Compilation of Ancient Books of Traditional*

*Chinese Medicin Series (Zhong Yi Gu Ji Zheng Li Cong Shu)*; Shang, Z., Ed.; People's Medical Publishing House: Beijing, China, 1986; Vol. 3, p 314.
(9) Kataoka, S. Functional effects of Japanese style fermented soy sauce (shoyu) and its components. *J. Biosci. Bioeng.* **2005**, *100*, 227−234.
(10) Hecquet, L.; Sancelme, M.; Bolte, J.; Demuynck, C. Biosynthesis of 4-hydroxy-2,5-dimethyl-3(2*H*)-furanone by *Zygosaccharomyces rouxii*. *J. Agric. Food Chem.* **1996**, *44*, 1357−1360.
(11) Sasaki, M.; Nunomura, N.; Matsudo, T. Biosynthesis of 4-hydroxy-2(or 5)-ethyl-5(or 2)-methyl-3(2*H*)-furanone by yeasts. *J. Agric. Food Chem.* **1991**, *39*, 934−938.
(12) Suezawa, Y.; Suzuke, M. Bioconversion of ferulic acid to 4-vinylguaiacol and 4-ethylguaiacol and of 4-vinylguaiacol to 4-ethylguaiacol by halotolerant yeasts belonging to the genus *Candida*. *Biosci., Biotechnol., Biochem.* **2007**, *71*, 1058−1062.
(13) van der Sluis, C.; Tramper, J.; Wijffels, R. H. Enhancing and accelerating flavour formation by salt-tolerant yeasts in Japanese soy-sauce processes. *Trends Food Sci. Technol.* **2001**, *12*, 322−327.
(14) Li, Y.; Zhao, M.; Parkin, K. L. $\beta$-Carboline derivatives and diphenols from soy sauce are in vitro quinone reductase (QR) inducers. *J. Agric. Food Chem.* **2011**, *59*, 2332−2340.
(15) Kihara, K. Elucidation of shoyu pigment. 1. Formation of shoyu pigment from flazin and the end product. *Nippon Shoyu Kenkyusho Zasshi* **1995**, *21*, 187−196.
(16) O'Toole, D. K. The role of microorganisms in soy sauce production. In *Advances in Applied Microbiology*; Saul, L. N., Allen, I. L., Eds.; Academic Press: San Diego, CA, USA, 1997; Vol. 45, pp 87−152.
(17) Wanakhachornkrai, P.; Lertsiri, S. Comparison of determination method for volatile compounds in Thai soy sauce. *Food Chem.* **2003**, *83*, 619−629.
(18) Steinhaus, P.; Schieberle, P. Characterization of the key aroma compounds in soy sauce using approaches of molecular sensory science. *J. Agric. Food Chem.* **2007**, *55*, 6262−6269.
(19) Hayashida, Y.; Nishimura, K.; Slaughter, J. C. The influence of mash pre-aging on the development of the flavour-active compound, 4-hydroxy-2(or5)-ethyl-5(or2)-methyl-3(2*H*)-furanone (HEMF), during soy sauce fermentation. *Int. J. Food Sci. Technol.* **1997**, *32*, 11−14.
(20) Lee, S. M.; Seo, B. C.; Kim, Y.-S. Volatile compounds in fermented and acid-hydrolyzed soy sauces. *J. Food Sci.* **2006**, *71*, C146−C156.
(21) Kim, Y. B.; Oh, S. H.; Sok, D. E.; Kim, M. R. Neuroprotective effect of maltol against oxidative stress in brain of mice challenged with kainic acid. *Nutr. Neurosci.* **2004**, *7*, 33−39.
(22) Kang, K. S.; Yokozawa, T.; Kim, H. Y.; Park, J. H. Study on the nitric oxide scavenging effects of ginseng and its compounds. *J. Agric. Food Chem.* **2006**, *54*, 2558−2562.
(23) Zhao, H. F.; Chen, W. F.; Lu, J.; Zhao, M. M. Phenolic profiles and antioxidant activities of commercial beers. *Food Chem.* **2010**, *119*, 1150−1158.
(24) Huang, S.-M.; Chuang, H.-C.; Wu, C.-H.; Yen, G.-C. Cytoprotective effects of phenolic acids on methylglyoxal-induced apoptosis in Neuro-2A cells. *Mol. Nutr. Food Res.* **2008**, *52*, 940−949.
(25) Namgung, H. J.; Park, H. J.; Cho, I. H.; Choi, H. K.; Kwon, D. Y.; Shim, S. M.; Kim, Y. S. Metabolite profiling of doenjang, fermented soybean paste, during fermentation. *J. Sci. Food Agric.* **2010**, *90*, 1926−1935.
(26) Sharma, G. V. M; Gopinath, T. Radical-mediated stereoselective synthesis of (+)-dihydrocanadensolide and (−)-3-epi-dihydrocanadensolide from D-xylose. *Tetrahedron Lett.* **2001**, *42*, 6183−6186.
(27) Birch, A. J.; Qureshi, A. A.; Rickards, R. W. Metabolites of *Aspergillus indicus* − structure and some aspects of biosynthesis of dihydrocanadensolide. *Aust. J. Chem.* **1968**, *21*, 2775−2784.
(28) Isaka, M.; Chinthanom, P.; Boonruangprapa, T.; Rungjindamai, N.; Pinruan, U. Eremophilane-type sesquiterpenes from the fungus *Xylaria* sp BCC 21097. *J. Nat. Prod.* **2010**, *73*, 683−687.
(29) McCorkindale, N. J.; Wright, J. L. C.; Brian, P. W.; Clarke, S. M.; Hutchinson, S. A. Canadensolide − an antifungal metabolite of penicillium canadense. *Tetrahedron Lett.* **1968**, *9*, 727−730.
(30) Nubbemeyer, U. Diastereoselective zwitterionic aza-Claisen rearrangement: the synthesis of bicyclic tetrahydrofurans and a total synthesis of (+)-dihydrocanadensolide. *J. Org. Chem.* **1996**, *61*, 3677−3686.
(31) Kato, M.; Tanaka, R.; Yoshikoshi, A. Synthesis of (±)-canadensolide and its C-5 epimer. Revision of the stereochemistry. *J. Chem. Soc. D* **1971**, 1561−1562.
(32) Anderson, R. C.; Fraser-Reid, B. An asymmetric synthesis of naturally occurring canadensolide. *Tetrahedron Lett.* **1978**, *19*, 3233−3236.
(33) Sharma, G. V. M; Gopinath, T. Radical cyclisation approach for the synthesis of (+)dihydrocanadensolide, (+)dihydrosporothriolide and their C-3 epimers from d-xylose. *Tetrahedron* **2003**, *59*, 6521−6530.
(34) Aldridge, D. C.; Nicholson, S.; Taylor, P. J. Rates and mechanisms for the ring-opening, ring-closure and ring transformation reactions of the di-$\gamma$-lactone dihydrocanadensolide (DHC). *J. Chem. Soc., Perkin Trans. 2* **1995**, 1929−1938.
(35) Mulzer, J.; Kattner, L. Doubly stereodifferentiating hiyama addition with mismatched reactants; enantio- and diastereo-controlled synthesis of dihydrocanadensolide. *Angew. Chem., Int. Ed.* **1990**, *29*, 679−680.
(36) Chen, M.-J.; Narkunan, K.; Liu, R.-S. Total synthesis of natural bicyclic lactones (+)-dihydrocanadensolide, (±)-avenociolide, and (±)-isoavenociolide via tungsten-$\pi$-allyl complexes. *J. Org. Chem.* **1999**, *64*, 8311−8318.
(37) Adrio, J.; Carretero, J. C. Butenolide synthesis by molybdenum-mediated hetero-Pauson-Khand reaction of alkynyl aldehydes. *J. Am. Chem. Soc.* **2007**, *129*, 778−779.
(38) Aldridge, D. C.; Borrow, A.; Gerring, E. E. L. Pharmaceutical compositions. U.S. 3,930,014, 1975.
(39) Kasprzyk-Hordern, B. Pharmacologically active compounds in the environment and their chirality. *Chem. Soc. Rev.* **2010**, *39*, 4466−4503.
(40) Albright, A.; White, J. Determination of absolute configuration using single crystal X-ray diffraction. In *Metabolomics Tools for Natural Product Discovery*; Roessner, U., Dias, D. A., Eds.; Humana Press: Totowa, NJ, USA, 2013; Vol. 1055, pp 149−162.
(41) Fun, H.-K.; Boonnak, N.; Chantrapromma, S. Single crystal x-ray structural determination of natural products. *AIP Conf. Proc.* **2012**, *1455*, 19−28.
(42) Harada, N. Powerful chiral molecular tools for preparation of enantiopure alcohols and simultaneous determination of their absolute configurations by X-ray crystallography and/or $^1$H NMR anisotropy methods. In *Chirality in Drug Research*; Wiley-VCH Verlag: Weinheim, Germany, 2006; pp 283−321.
(43) Aldridge, D. C.; Crawley, G. C.; Strawson, C. J. Pharmaceutical compositions. U.S. 4,103,023 1978.
(44) Biesebeke, R. T.; Record, E. Scientific advances with *Aspergillus* species that are used for food and biotech applications. *Microbes Environ.* **2008**, *23*, 177−181.
(45) Pitt, J. I.; Hocking, A. D. *Fungi and Food Spoilage*, 2nd ed.; Blackie Academic and Professional: London, UK, 1997; p 593.
(46) Keller, N. P.; Turner, G.; Bennett, J. W. Fungal secondary metabolism − from biochemistry to genomics. *Nat. Rev. Microbiol.* **2005**, *3*, 937−947.
(47) Ma, G.; Nguyen, H.; Romo, D. Concise total synthesis of (±)-salinosporamide A, (±)-cinnabaramide A, and derivatives via a bis-cyclization process: implications for a biosynthetic pathway? *Org. Lett.* **2007**, *9*, 2143−2146.
(48) Hanson, J. R. *Fungal Metabolites Derived from the Citric Acid Cycle*; Royal Society of Chemistry: Cambridge, UK, 2008; pp 121−124.
(49) Kaneko, S.; Kumazawa, K.; Nishimura, O. Studies on the key aroma compounds in raw (unheated) and heated Japanese soy sauce. *J. Agric. Food Chem.* **2013**, *61*, 3396−3402.

(50) Chung, I.-M.; Seo, S.-H.; Ahn, J.-K.; Kim, S.-H. Effect of processing, fermentation, and aging treatment to content and profile of phenolic compounds in soybean seed, soy curd and soy paste. *Food Chem.* **2011**, *127*, 960−967.
(51) Lesage-Meessen, L.; Delattre, M.; Haon, M.; Thibault, J.-F.; Ceccaldi, B. C.; Brunerie, P.; Asther, M. A two-step bioconversion process for vanillin production from ferulic acid combining *Aspergillus niger* and *Pycnoporus cinnabarinus*. *J. Biotechnol.* **1996**, *50*, 107−113.
(52) Mathew, S.; Abraham, T. E.; Sudheesh, S. Rapid conversion of ferulic acid to 4-vinyl guaiacol and vanillin metabolites by *Debaryomyces hansenii*. *J. Mol. Catal. B: Enzym.* **2007**, *44*, 48−52.
(53) Muheim, A.; Lerch, K. Towards a high-yield bioconversion of ferulic acid to vanillin. *Appl. Microbiol. Biotechnol.* **1999**, *51*, 456−461.
(54) Naylin, N.; Suganuma, T.; Taing, O. Antioxidant activities of compounds isolated from fermented broth of *Zygosaccharomyces rouxii*. *Food Biotechnol.* **2006**, *20*, 131−141.
(55) Li, X.; Hiramoto, K.; Yoshida, M.; Kato, T.; Kikugawa, K. Identification of 2,5-dimethyl-4-hydroxy-3(2*H*)-furanone (DMHF) and 4-hydroxy-2(or 5)-ethyl-5(or 2)-methyl-3(2*H*)-furanone (HEMF) with DNA breaking activity in soy sauce. *Food Chem. Toxicol.* **1998**, *36*, 305−314.
(56) Kihara, K. Determination of benzoic acid and vanillic acid in shoyu by micro high-performance liquid chromatography. *Nippon Shoyu Kenkyusho Zasshi* **1981**, *7*, 112−115.
(57) Li, Y.; Zhao, H.; Zhao, M.; Cui, C. Relationships between antioxidant activity and quality indices of soy sauce: an application of multivariate analysis. *Int. J. Food Sci. Technol.* **2010**, *45*, 133−139.
(58) Świsłocka, R.; Piekut, J.; Lewandowski, W. The relationship between molecular structure and biological activity of alkali metal salts of vanillic acid: spectroscopic, theoretical and microbiological studies. *Spectrochim. Acta, Part A* **2013**, *100*, 31−40.
(59) Lü, J.-L.; Zhao, J.; Duan, J.-A.; Yan, H.; Tang, Y.-P.; Zhang, L.-B. Quality evaluation of *Angelica sinensis* by simultaneous determination of ten compounds using LC-PDA. *Chroma* **2009**, *70*, 455−465.
(60) Kim, S.-J.; Kim, M.-C.; Um, J.-Y.; Hong, S.-H. The beneficial effect of vanillic acid on ulcerative colitis. *Molecules* **2010**, *15*, 7208−7217.
(61) Itoh, A.; Isoda, K.; Kondoh, M.; Kawase, M.; Kobayashi, M.; Tamesada, M.; Yagi, K. Hepatoprotective effect of syringic acid and vanillic acid on concanavalin A-induced liver injury. *Biol. Pharm. Bull.* **2009**, *32*, 1215−1219.
(62) Kumar, S.; Prahalathan, P.; Raja, B. Antihypertensive and antioxidant potential of vanillic acid, a phenolic compound in L-NAME-induced hypertensive rats: a dose-dependence study. *Redox Rep.* **2011**, *16*, 208−215.
(63) Erdem, M. G.; Cinkilic, N.; Vatan, O.; Yilmaz, D.; Bagdas, D.; Bilaloglu, R. Genotoxic and anti-genotoxic effects of vanillic acid against mitomycin C-induced genomic damage in human lymphocytes in vitro. *Asian Pac. J. Cancer Prev.* **2012**, *13*, 4993−4998.
(64) Prabhakar, P. K.; Doble, M. Effect of natural products on commercial oral antidiabetic drugs in enhancing 2-deoxyglucose uptake by 3T3-L1 adipocytes. *Ther. Adv. Endocrinol. Metab.* **2011**, *2*, 103−114.
(65) Saruno, R. Kojic acid, a tyrosinase inhibitor from *Aspergillus albus*. *Agric. Biol. Chem.* **1979**, *43*, 1337−1338.
(66) Lokaj, J.; Kozisek, J.; Koren, B.; Uher, M.; Vrabel, V. Structure of kojic acid. *Acta Crystallogr. C* **1991**, *47*, 193−194.
(67) Gavezzotti, A.; Flack, H. *21. Crystal Packing*; University College Cardiff Press: Cardiff, Wales, 2001; pp 14−15.
(68) Zhang, L.-R.; Yan, X.-F.; Liu, S.-S.; Yu, M.; Chen, J.-J.; Shen, Y.-M. 5-Hydroxy-2-hydroxymethyl-4-pyrone, a major secondary metabolite isolated from the strain of *Aspergillus oryzae* WP-D-1. *J. Life Sci.* **2008**, *2*, 1−4.
(69) Novotný, L.; Rauko, P.; Abdel-Hamid, M.; Vachalkova, A. Kojic acid − a new leading molecule for a preparation of compounds with an anti-neoplastic potential. *Neoplasma* **1998**, *46*, 89−92.
(70) Lim, J. T. E. Treatment of melasma using kojic acid in a gel containing hydroquinone and glycolic acid. *Dermatol. Surg.* **1999**, *25*, 282−284.
(71) Nakadai, T. Kojic acid. *Nippon Shoyu Kenkyusho Zasshi* **2004**, *30*, 55−59.
(72) Eiichiro, S.; Masaru, M.; Tetshuhisha, G.; Yukiko, M.; Kenji, T.; Sinji, M. Studies on the fluorescent compounds in fermented foods. Part VII. The degradation of added kojic acid during soy sauce fermentation. *Nippon Shoyu Kenkyusho Zasshi* **1984**, *10*, 151−155.
(73) Tanaka, K.; Kushiro, M.; Manabe, M. A review of studies and measures to improve the mycotoxicological safety of traditional Japanese mold-fermented foods. *Mycotoxin Res.* **2006**, *22*, 153−158.
(74) Beélik, A. Kojic acid. In *Advances in Carbohydrate Chemistry*; Melville, L. W., Tipson, R. S., Eds.; Academic Press: New York, 1956; Vol. 11, pp 145−183.
(75) Arnstein, H. R. V.; Bentley, R. Kojic acid biosynthesis from 1-$C^{14}$-glucose. *Nature* **1950**, *166*, 948−949.
(76) Arnstein, H.; Bentley, R. The biosynthesis of kojic acid. 1. Production from [1-$^{14}$C] and [3:4-$^{14}C_2$] glucose and [2-$^{14}$C]-1:3-dihydroxyacetone. *Biochem. J.* **1953**, *54*, 493.
(77) Hui, Y. H. *Handbook of Food Science, Technology, And Engineering*; CRC Press: Boca Raton, FL, USA, 2006; Vol. 149.
(78) Laskin, A. I.; Bennett, J. W.; Gadd, G. M. *Advances in Applied Microbiology*; Academic Press: San Diego, CA, USA, 2003; Vol. 45, pp 104−132.
(79) Feng, Y.; Cui, C.; Zhao, H.; Gao, X.; Zhao, M.; Sun, W. Effect of koji fermentation on generation of volatile compounds in soy sauce production. *Int. J. Food Sci. Technol.* **2012**, *48*, 609−619.
(80) Pandey, A., Soccol, C. R., Larroche, C., Eds. *Current Developments in Solid-State Fermentation*; Asiatech Publishers: New Delhi, India, 2007; pp 304−305.
(81) Rosfarizan, M.; Ariff, A. B. Kinetics of kojic acid fermentation by *Aspergillus flavus* link S44-1 using sucrose as a carbon source under different pH conditions. *Biotechnol. Bioprocess. Eng.* **2006**, *11*, 72−79.
(82) Ogawa, A.; Wakisaka, Y.; Tanaka, T.; Sakiyama, T.; Nakanishi, K. Production of kojic acid by membrane-surface liquid culture of *Aspergillus oryzae* NRRL484. *J. Ferment. Bioeng.* **1995**, *80*, 41−45.

JOURNAL OF AGRICULTURAL AND FOOD CHEMISTRY

Article

pubs.acs.org/JAFC

# Comparison of Food Antioxidants and Iron Chelators in Two Cellular Free Radical Assays: Strong Protection by Luteolin

Tim Hofer,*[,†] Trond Ø. Jørgensen,[‡] and Ragnar L. Olsen[#]

[†]Department of Chemicals and Radiation, Division of Environmental Medicine, The Norwegian Institute of Public Health, N-0403 Oslo, Norway

[‡]MabCent-SFI and [#]Norwegian College of Fishery Science, University of Tromsø, N-9037 Tromsø, Norway

**ABSTRACT:** Liver (HepG2) cells were incubated with 21 edible flavonoids, carotenoids, polyunsaturated fatty acid (PUFA) chromones, and metal chelators for 1 h, washed in PBS, and challenged in the cellular antioxidant activity (CAA) and the cellular lipid peroxidation antioxidant activity (CLPAA) assays. These microplate format assays assess the compounds' ability to protect against cytosolic peroxyl radicals (CAA) and induced membrane lipid peroxidation (CLPAA), respectively. Incubation encompassing a broad compound concentration range determined half-maximal inhibitory concentrations ($IC_{50}$) by using sigmoidal curve fits. Overall, considering both assays, luteolin offered the greatest protection. The carotenoid astaxanthin offered only modest protection, whereas $\beta$-carotene was ineffective. Subtle structural differences between flavonoids were found to have amplified effects on protective abilities, and mechanisms of flavonoid antioxidant action are discussed. Membrane-permeable iron chelators (deferasirox and SIH) offered strong protective effects in CLPAA, but not in CAA, suggesting that CLPAA is dependent on membrane-associated free iron ions.

**KEYWORDS:** *catechin, curcumin, hydroxytyrosol, resveratrol, acetylsalicylic acid (ASA)*

## INTRODUCTION

Several human diseases and conditions involve free radicals and/or metal dyshomeostasis.[1−3] Iron levels rise in multiple tissues during disease states and aging,[1,4] increasing the likelihood of oxidative damages from reactive oxygen species (ROS; $O_2^{\bullet-}$, $H_2O_2$, ROOH, HOCl, etc.) during events such as inflammation and ischemia. ROS can induce lipid peroxidation,[5,6] a process generating other toxic reactive species, for example, aldehydes. Antioxidant mechanisms are commonly related to free radical scavenging and metal chelating. Low-molecular-weight antioxidants and metal chelators have received increased interest both as protectors from disease onset and as therapeutics.[7,8] A regular intake of fruits and vegetables containing antioxidants can counteract undesired health conditions, but it is not clear which dietary compounds are the most beneficial in terms of antioxidant effects. These effects are best evaluated in living cells and organisms. Antioxidants need to be constantly replenished because they are eventually oxidized (some are recycled, e.g., vitamin E and certain flavonoids)[9] or are metabolized and excreted.[10,11] Intake of flavonoid-rich foods (dark chocolate, red wine, green tea, etc.) have shown promising effects in humans, and flavonoids can scavenge radicals, chelate catalytic metal ions, and pass cellular membranes.[6,12,13] Clinically administered iron chelators treat iron overload conditions, but will cause iron deprivation and other toxicities in normal subjects.

Numerous papers describe the effects of antioxidants in chemical assays, but few demonstrate effects in living cells, which requires cell membrane passage and compound stability. Compound testing in cell cultures can provide valuable insights into which compounds are likely to have an impact in higher organisms. We recently established the cellular lipid peroxidation antioxidant activity (CLPAA) assay in the microplate format.[14,15] Another commonly used free radical assay is the cellular antioxidant activity (CAA) assay.[16−18] Both assays are described below. Loosely chelated iron from the labile iron pool (LIP) can redox cycle ($Fe^{3+} \leftrightarrow Fe^{2+}$) and mediate biomolecular oxidation reactions by ROS (Fenton chemistry) as well as accelerate lipid peroxidation reactions; however, the role of iron in the CLPAA and CAA assays has been less clear. The objective of this study was to test different classes of edible (low toxicity) hydrophilic and lipophilic antioxidants and investigate the role of LIP in the CAA and CLPAA assays using metabolically active human hepatocarcinoma cells (HepG2). The compounds studied are all much in focus as antioxidants and often studied using chemical antioxidant assays.

## MATERIALS AND METHODS

**Chemicals.** All chemicals used were of the highest quality, and purity is indicated when relevant. The compounds tested for bioactivities are shown in Figure 1. Acetylsalicylic acid (ASA; Sigma A7356; 99.8%), apigenin (Fluka 10798; 95.4%), L-ascorbic acid (Sigma A5960; 99.3%), astaxanthin (Sigma A9335; synthetic; 95.6%), $\beta$-carotene (Fluka 22040; 98.0%), cumene hydroperoxide (cumOOH; Aldrich 513296, 88% (*cautionary note: handle concentrated cumOOH inside a hood as vapors are toxic*)), deferoxamine mesylate (DFOM; Sigma D9533; 95.0%), 2′,7′-dichlorofluorescin diacetate (DCFH-DA; Fluka 35847), resveratrol (Sigma R5010; 99.0%), and quercetin (Sigma Q0125; >99.9%) were purchased from Sigma-Aldrich Corp., St. Louis, MO, USA. 2,2′-Azobis(2-amidinopropane (abbreviated ABAP or AAPH; 82235), (+)-catechin (70940; >99.9%), epigallocatechin gallate (EGCG, 70935; >99.9%), 3,4-dihydroxyphenylethanol (hydroxytyrosol; 70604; 98.0%), and luteolin (10004161; 99.0%) were purchased from Cayman Europe,

Received: May 16, 2014
Revised: July 28, 2014
Accepted: July 29, 2014
Published: July 29, 2014

ACS Publications © 2014 American Chemical Society

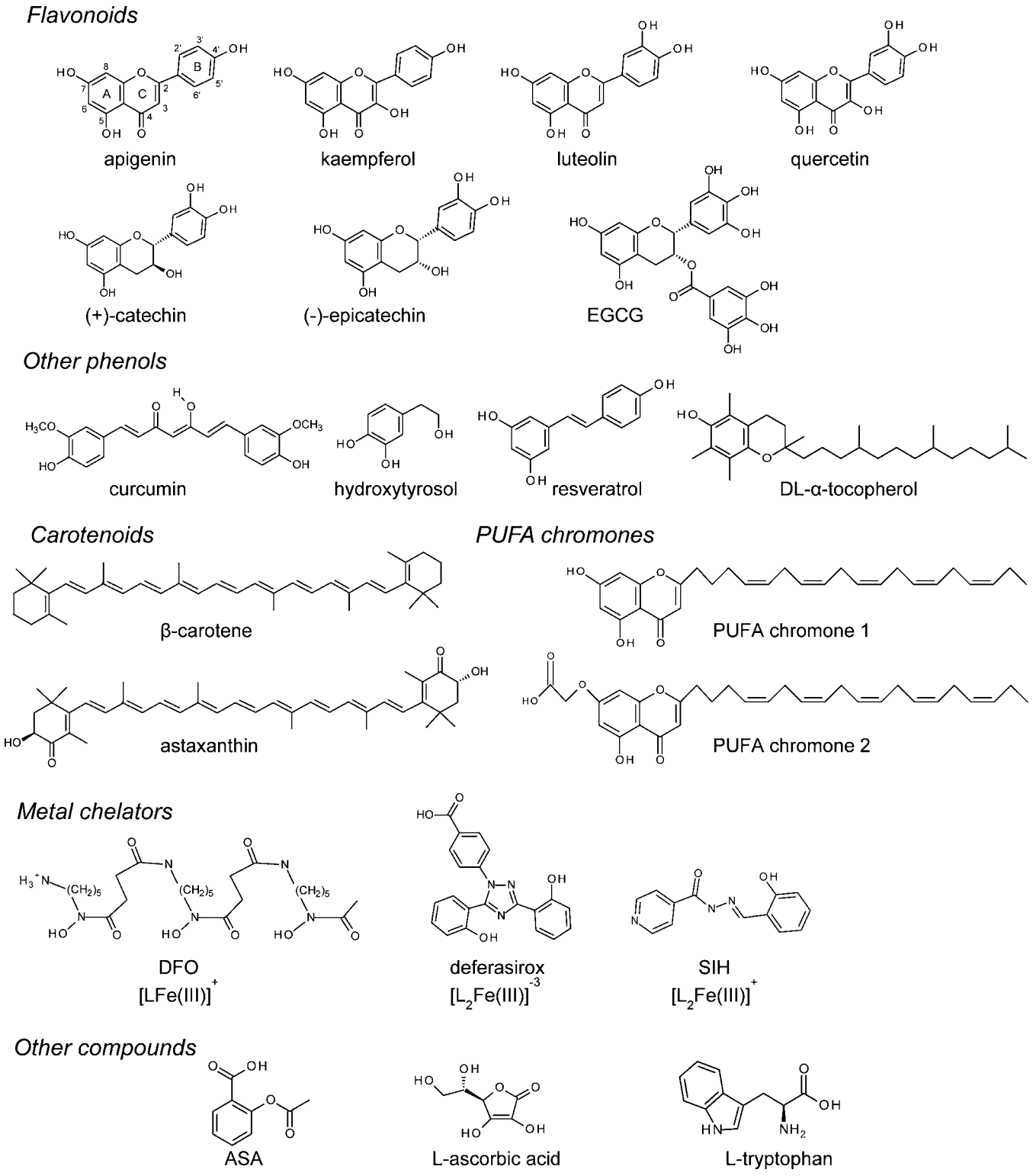


**Figure 1.** Categories and chemical structures of compounds tested. Numbering of the basic flavonoid structure is illustrated for apigenin. Apigenin and luteolin are flavones; kaempferol and quercetin are flavon-3-ols; and (+)-catechin, (−)-epicatechin, and EGCG are flavan-3-ols. Resveratrol is a stilbenoid, and DL-$\alpha$-tocopherol is a lipophilic methylated phenol (a member of the vitamin E family). For metal chelators the number of ligands in the resulting major Fe(III) complex and the net charge at pH 7.4 are indicated. DFOM dissolves as DFO (charge +1) at pH 7.4 and forms a ferrioxamine−$Fe^{3+}$ hexadentate ligand 1:1 complex with net charge +1. Deferasirox chelates $Fe^{3+}$ as a tridentate ligand 2:1 complex with net charge −3.[44] Also, SIH chelates $Fe^{3+}$ as a tridentate ligand 2:1 complex but with net charge +1.[43] Acetylsalicylic acid (ASA), the active ingredient in aspirin, is a small synthetic prodrug of salicylic acid, a phenol. L-Ascorbic acid (vitamin C) is a hydrophilic acidic sugar present as the ascorbate anion ($AscH^-$) at pH 7.4. L-Tryptophan is an amino acid containing an indole group.

Tallinn, Estonia. (−)-Epicatechin (A3894; >99.9%) and kaempferol (A3288; 98.9%) were from AppliChem GmbH, and L-tryptophan (108374; 99.5%) was from Merck Chemicals, both located in Darmstadt, Germany. DL-$\alpha$-Tocopherol (A17039; synthetic; 98.8%)


dx.doi.org/10.1021/jf5022779 | J. Agric. Food Chem. 2014, 62, 8402−8410

was from Alfa Aesar, Ward Hill, MA, USA. Curcumin was from Alexis Biochemicals (350-028; 99.0%) purchased through Enzo Life Sciences Inc., Farmingdale, NY, USA. 4,4-Difluoro-5-(4-phenyl-1,3-butadienyl)-4-bora-3a,4a-diaza-*s*-indacene-3-undecanoic acid ($C_{11}$-BODIPY, D3861) was from Invitrogen, Eugene, OR, USA. Deferasirox (ICL670; 99.9%) was kindly provided by Novartis Pharma AG, Basel, Switzerland, and salicylaldehyde isonicotinoyl hydrazone (SIH; 99.0%) by Dr. Katherine J. Franz, Duke University, Durham, NC, USA. PUFA chromone 1 (*all*-(*Z*)-5,7-dihydroxy-2-(4*Z*,7*Z*,10*Z*,13*Z*,16*Z*-nonadecapentaenyl) and PUFA chromone 2 (2-((5-hydroxy-2-((4*Z*,7*Z*,10*Z*,13*Z*,16*Z*)-nonadeca-4,7,10,13,16-pentaen-1-yl)-4-oxo-4*H*-chromen-7-yl)oxy)acetic acid) were synthesized as described[19] and donated by Dr. Trond V. Hansen, Oslo University, Norway. PUFA chromone 2 has a carboxylic acid group ether-linked to the chromone moiety, making it more hydrophilic than PUFA chromone 1 (see Figure 1). Screening a small synthetic library of natural compounds identified PUFA chromone 1 and PUFA chromone 2 as powerful antioxidants, particularly in CLPAA, but also in CAA.[19]

Compounds to be tested were weighed out in rubber-sealed cryo vials and dissolved in appropriate media using a vortex or, when necessary, an ultrasonicator combined with heating (60 °C) for the shortest possible time (minutes). Ascorbic acid, EGCG, (−)-epicatechin, DFOM, and L-tryptophan were dissolved in aqueous cell culture media (without fetal bovine serum, FBS). Quercetin was dissolved in 1 M NaOH. Catechin, hydroxytyrosol, kaempferol, luteolin, and resveratrol were dissolved in ethanol. Apigenin, astaxanthin, $\beta$-carotene, the chromones, curcumin, deferasirox, and SIH were dissolved in DMSO. Three stocks were prepared for each compound, which thereafter were stored at −80 °C. On assay days, two stocks containing different compounds were thawed and serially diluted 1:1 using cell culture media. Tested previously using HepG2 cells, short-term (1−2 h) incubations with up to 2% v/v dimethyl sulfoxide (DMSO) or ethanol did not significantly alter reaction rates or induce cell necrosis in any of the assays.[15] For compounds dissolved in ethanol, cells were maximally exposed to 2% v/v ethanol at the highest compound concentration investigated, and the ethanol concentration was negligible at lower compound concentrations. Lipophilic compounds dissolved in DMSO, however, were diluted in culture media maintaining a minimum 5% v/v DMSO so as not to stick to plastics and were eventually diluted 1:5 (20 + 80 $\mu$L) into each well, giving a final DMSO concentration of 1% v/v DMSO on cells also in control wells. DL-$\alpha$-Tocopherol, a highly sticky viscous liquid, was diluted in 100% DMSO but also incubated on cells at 1% v/v DMSO (final dilution 1 + 99 $\mu$L) along with controls. Aliquots of DCFH-DA (20 mM in ethanol), ABAP (200 mM in water), and $C_{11}$-BODIPY (6 mM in DMSO) were kept at −80 °C and thawed immediately prior to use.

**Cell Culture.** Human hepatocellular carcinoma (HepG2) cells were purchased from the American Type Culture Collection (Manassas, VA, USA) and routinely cultivated as monolayers in minimum essential medium Earle's (MEM Earle's; F0325 from Biochrom AG, Berlin, Germany) supplemented with gentamycin (10 $\mu$g/mL), L-alanyl-L-glutamine (2 mM), nonessential amino acids (1%), sodium pyruvate (1 mM), and 10% FBS in 175 $cm^2$ flasks in a humidified 5% $CO_2$ atmosphere at 37 °C. After washing cells with phosphate-buffered saline (PBS, $Mg^{2+}$- and $Ca^{2+}$-free), cells were detached using trypsinization and resuspended in cell culture medium. The cell concentration was determined by using Bürker chamber counting, and 80000 cells (in 100 $\mu$L) were seeded into wells (0.32 $cm^2$ cell growth surface area) of black microplates with transparent bottoms (product 3603) obtained from Corning Inc. Life Sciences, Tewksbury, MA, USA. Cells were allowed to settle at room temperature to minimize plate edge effects[20] before incubation at 37 °C. After 24 h, experiments were conducted when microplate wells had ∼50% monolayer cell confluence. Positive and negative controls were included on each microplate. $IC_{50}$ values are influenced by the cell density and other experimental conditions; hence, maintaining constant conditions is necessary for reproducible results. Background levels of antioxidants (vitamin E, selenium) in cultured cells are commonly low and dependent on culture media additives.

**CLPAA Assay.** To measure effects of antioxidants on cellular lipid membrane peroxidation, we recently established the cellular lipid peroxidation antioxidant activity (CLPAA) assay in microplate format,[14,15] where after cellular uptake of the lipophilic oxidation sensitive probe $C_{11}$-BODIPY (fluorescent red) and subsequent antioxidant uptake, lipid peroxidation is induced by adding cumene hydroperoxide (cumOOH; lipophilic), capable of generating oxidizing (and initiating lipid membrane peroxidation) hydroxyl radicals ($HO^{\bullet}$) in the presence of redox-cycling metals such as ferrous iron ($Fe^{2+}$).

$$\text{cumOOH} + Fe^{2+} \rightarrow \text{cumO}^{-} + HO^{\bullet} + Fe^{3+} \quad (1)$$

$$R - H + HO^{\bullet} \rightarrow R^{\bullet} + H_2O \quad (2)$$

$$R^{\bullet} + O_2 \rightarrow ROO^{\bullet} \quad (3)$$

$$ROO^{\bullet} + RH \rightarrow ROOH + R^{\bullet} \text{ and so on} \quad (4)$$

Free radical attack of $C_{11}$-BODIPY generates two similar fluorescent green products (both having lost a phenyl moiety), correlative to the degree of lipid peroxidation that has taken place.[21,22]

$$C_{11}\text{-BODIPY(red)} \ (+\text{oxidation}) \rightarrow C_{11}\text{-BODIPY oxidation products (green)} \quad (5)$$

Usage of the $C_{11}$-BODIPY probe provides an indirect measure of lipid peroxidation. The process generates reactive secondary oxidation products such as malondialdehyde (MDA) and 4-hydroxynonenal (4-HNE) that are more challenging to measure. HepG2 cells grown in serum-supplemented media sustain a non-ferritin-bound redox-active labile iron pool (LIP) (in isolated primary hepatocytes it is about 5−10 $\mu$M),[23,24] so the addition of extra $Fe^{3+}$ was found not to be necessary.[14]

After cells had been washed in PBS, 100 $\mu$L of cell culture medium (without FBS) containing 5 $\mu$M $C_{11}$-BODIPY was added (at 5 $\mu$M, $C_{11}$-BODIPY is not toxic to cells)[25] to the microplate and placed inside a 37 °C water-saturated 5% $CO_2$ chamber for 30 min. After medium withdrawal, 100 $\mu$L of cell culture medium (without FBS) containing diluted antioxidant was added before the microplate was placed back into the 5% $CO_2$ incubator at 37 °C. After 60 min, the cells were washed in PBS and 100 $\mu$L of clear Hanks' salt solution supplemented with 50 $\mu$M cumOOH was added. The microplate was immediately placed inside a Wallac VICTOR3 1420 multilabel counter (PerkinElmer, Waltham, MA, USA) preheated at 37 °C and set on bottom reading mode. The green (485/14 and 520/10 nm filters; CW-lamp setting: 20000)[14] fluorescence was monitored over 60 min. The rate (slope) of fluorescently green $C_{11}$-BODIPY oxidation product increase (obtained from linear regressions of slopes over 0−40 min using the inbuilt plate reader software Workout 2.0 from Dazdaq Solutions Ltd.) is related to the rate of cellular membrane lipid peroxidation.[14] As diluted peroxides are unstable, a 0.1 M cumOOH stock was prepared immediately prior to use on a daily basis.

**CAA Assay.** The CAA assay was used as described[16] with minor modifications.[15] CAA is based on simultaneous cellular uptake of antioxidants and the ROS-sensitive nonfluorescent probe 2′,7′-dichlorofluorescin diacetate (DCFH-DA), which is hydrolyzed into cytosolically trapped DCFH that upon oxidation by peroxyl radicals forms 2′,7′-dichlorofluorescein (DCF; fluorescent green), which is monitored.[15,16] The formation of peroxyl radicals from thermal decomposition of the azo compound ABAP is illustrated by the equations below:

$$-R—N{=}N—R-(+\text{heat}) \rightarrow 2\,-R^{\bullet} + N_2 \quad (6)$$

$$-R^{\bullet} + O_2 \rightarrow -ROO^{\bullet} \quad (7)$$

After cells had been washed in PBS, 100 $\mu$L of cell culture medium (without FBS) containing diluted antioxidants and DCFH-DA (25 $\mu$M) was added and the microplate placed inside a 37 °C water-saturated 5% $CO_2$ chamber. After 60 min of preincubation, the cells were washed in PBS, and 100 $\mu$L of clear Hanks' salt solution supplemented with glucose (L2035 from Biochrom) containing ABAP (600 $\mu$M) was added before starting ($t$ = 0 min) to monitor green fluorescence (485/14 nm excitation and 520/10 nm emission filters; CW lamp setting: 15000 stabilized

energy, 0.1 sec) inside a Wallac VICTOR3 1420 multilabel counter set at bottom reading mode. Control wells having no oxidant and a known potent antioxidant were included in all plates. The microplate was placed upon a specially designed alumina block in direct contact with all wells intended to provide uniform heating inside a water-saturated 5% $CO_2$ chamber held at 37 °C. Finally, the green fluorescence was monitored again ($t$ = 60 min). CAA data for each well were baseline corrected by subtracting the starting value from final value by using the inbuilt plate reader software Workout 2.0. This corrects for the antioxidant's own light absorption as well as probe background fluorescence and ensures evaluation of only experimentally generated DCF.

**Curve Fitting.** Log transformation of data and curve fitting was performed using Prism 5.0 (GraphPad Software, San Diego, CA, USA) by employing the four-parameter logistic equation (also called the Hill slope model) that yields half-maximal inhibitory concentrations ($IC_{50}$, a measure of the effectiveness of a compound) and Hill slopes (examples are shown in Figure 2). A strong concentration dependence was seen for potent antioxidants in the micromolar−millimolar range (−6 to −3 on a log scale, see Figure 2). In cases when full protection could not be achieved, approximate $IC_{50}$ values were obtained by extrapolating the curve to the lower plateau.

## RESULTS AND DISCUSSION

In this study, cells were preincubated with the compound of interest for 1 h prior to washing and thereafter exposed to a radical inducer. This preincubation should allow sufficient time for cell membrane passage of most compounds and antioxidant defense establishment prior to adding the inducer, which may otherwise pass cellular membranes more quickly than the antioxidant investigated. Preincubation also ensures that protective effects occur within cells, and are not due to antioxidants reacting with the radical inducer outside cells. Nevertheless, some compounds (e.g., DFO, being taken up by endocytosis)[26] may require longer incubations for effective cellular uptake, and rapidly membrane passing compounds could, to some extent, also leak from the cells and pass back into the medium. The HepG2 cell line was chosen due to its human origin, preservation of cellular functions,[27,28] metabolic activity,[28−30] ease of cultivation, and frequent use for similar tests.[16,31] However, HepG2 cells have been reported to express low basal levels of phase I cytochrome P450 metabolizing enzymes and may (for certain compounds) be less responsive than, for example, the HepaRG cell line[30,32] and human primary liver cells, in particular.[32,33] Human primary liver cells, however, can show profound interindividual differences[30] and are today unrealistically expensive for a study requiring large numbers of cells such as this one. Cellular uptake and eventual time-dependent compound metabolite formation may differ between cell types, and LIP levels may be influenced by the culturing conditions. These factors should be considered when results from different studies are compared. Testing two compounds simultaneously over broad concentration ranges for each microplate and then performing dose−response curve fitting by using the four-parameter logistic equation worked fine for both assays; see representative examples in Figure 2. The obtained $IC_{50}$ values (given in both mg/L and $\mu$M units) are shown in Table 1 (CLPAA) and Table 2 (CAA), respectively. These results can be useful for selecting candidate compounds for testing in higher organisms and also provide insight into how the CLPAA and CAA assays function similarly and differ from one another. No obvious correlations between size ($M_w$) or lipophilicity (XLogP3; a calculated octanol−water partition coefficient) with antioxidant effect ($IC_{50}$) among the tested compounds were found in either assay.

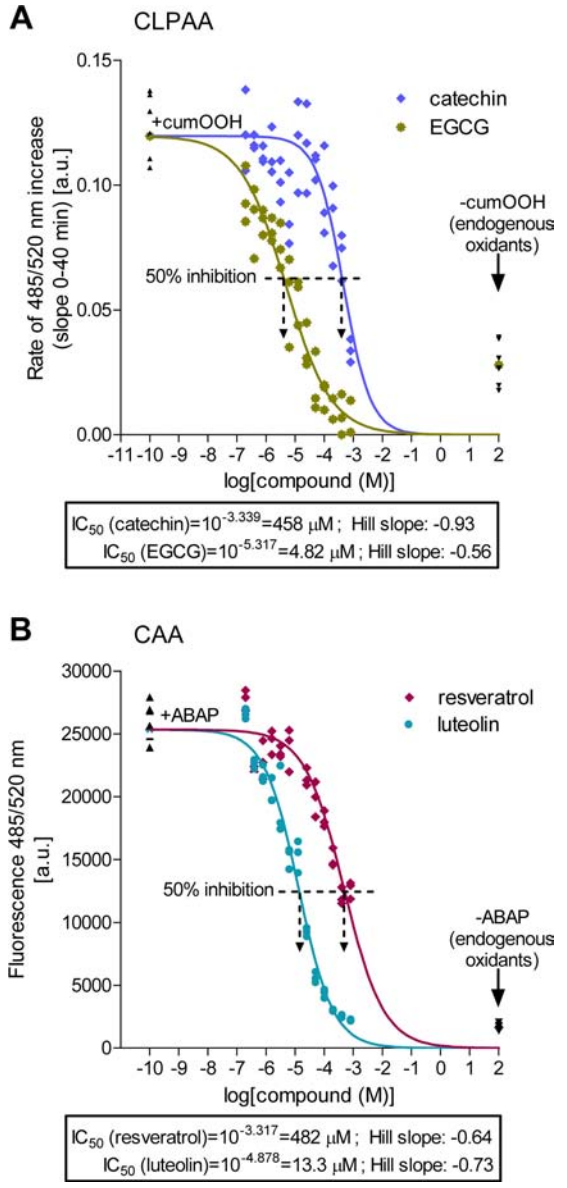


**Figure 2.** Dose−response testing compounds in the CLPAA and CAA assays. Representative examples are shown comparing two compounds in parallel over the range 0.2−800 $\mu$M using HepG2 cells. See Tables 1 and 2 for all obtained $IC_{50}$ values. (A) Parallel dose−response testing of catechin and EGCG in the CLPAA assay. For this particular run, catechin and EGCG produced $IC_{50}$ values of 458 and 4.82 $\mu$M, respectively. (B) Parallel dose−response testing of luteolin and resveratrol in the CAA assay. For this particular run, luteolin and resveratrol gave $IC_{50}$ values of 13.3 and 482 $\mu$M, respectively. Experiments were performed in a 96-well microplate, and each concentration was tested in triplicate ($N$ = 6 for each control (+added oxidant (▲); no added oxidant (▼)) selectively placed at concentrations distant from the tested range of antioxidants). For $IC_{50}$ value calculations a "theoretical zero level" is used as the lower plateau ($y$ value constrained to 0, reflecting a "perfect antioxidant") for extrapolation of dose−response curves. The top plateau is constrained to the mean of the +added oxidant (▲) value, a measure of both added and endogenous oxidants. a.u., arbitrary units.

**Flavonoids.** With the exception of apigenin, which displayed no activity in either assay and also not at realistically obtainable concentrations in vivo (protection was noticeable first at several mM), most flavonoids were effective antioxidants in both assays.


dx.doi.org/10.1021/jf5022779 | J. Agric. Food Chem. 2014, 62, 8402−8410

**Table 1. CLPAA Generated $IC_{50}$ Values Using HepG2 Cells[a]**

| compound | $M_w$ | XLogP3[b] | class | $IC_{50}$ (mg/L) | $IC_{50}$ ($\mu$M) | CV (%) | incubation in |
|---|---|---|---|---|---|---|---|
| SIH | 241.3 | 1.9 | $Fe^{3+}$ chelator, permeable | 0.201 ± 0.16 | 0.833 ± 0.65 | 77.7 | MEME + 1% DMSO |
| luteolin | 286.2 | 1.4 | flavone | 0.802 ± 0.39 | 2.80 ± 1.35 | 48.3 | MEME |
| deferasirox | 373.4 | 3.8 | $Fe^{3+}$ chelator, permeable | 1.05 ± 0.44 | 2.82 ± 1.18 | 41.6 | MEME + 1% DMSO |
| EGCG | 458.4 | 1.2 | flavan-3-ol | 2.38 ± 0.15 | 5.20 ± 0.33 | 6.38 | MEME |
| quercetin | 302.2 | 1.5 | flavonol | 2.90 ± 1.07 | 9.59 ± 3.53 | 36.8 | MEME |
| hydroxytyrosol[c] | 154.2 | −0.7 | phenolic | 5.27 ± 2.13 | 34.2 ± 13.8 | 40.5 | MEME |
| PUFA chromone 1[c] | 434.0 | 8.4[d] | PUFA chromone | 6.13 ± 3.94 | 14.13 ± 9.07 | 64.2 | MEME + 1% DMSO |
| curcumin | 368.4 | 3.2 | curcuminoid | 8.92 ± 0.67 | 24.2 ± 1.82 | 7.53 | MEME + 1% DMSO |
| DL-$\alpha$-tocopherol | 430.7 | 10.7 | methylated phenol (lipophilic) | 10.5 ± 4.98 | 24.5 ± 11.6 | 47.3 | MEME + 1% DMSO |
| PUFA chromone 2[c] | 492.0 | <8.4[d] | PUFA chromone | 14.2 ± 1.60 | 28.9 ± 3.26 | 11.3 | MEME + 1% DMSO |
| kaempferol | 286.2 | 1.9 | flavonol | 49.5 ± 53.4[e] | 173.05 ± 186.4 | 103 | MEME |
| resveratrol | 228.2 | 3.1 | stilbenoid | 75.8 ± 13.0 | 332.1 ± 56.9 | 17.1 | MEME |
| astaxanthin | 596.9 | 10.3 | carotenoid | 132.0 ± 12.0 | 221.1 ± 20.1 | 9.09 | MEME + 1% DMSO |
| (+)-catechin | 290.3 | 0.4 | flavan-3-ol | 132.9 ± 19.1 | 457.7 ± 66.0 | 14.4 | MEME |
| (−)-epicatechin | 290.3 | 0.4 | flavan-3-ol | 153.4 ± 47.7 | 528.5 ± 164.4 | 31.1 | MEME |
| apigenin | 270.2 | 1.7 | flavone | >550 | >4000 | | MEME +1% DMSO |
| DFOM | 656.8 | −0.614 | $Fe^{3+}$ chelator, impermeable | >550 | >4000 | | MEME |
| ASA | 180.2 | 1.2 | phenolic | >550 | >4000 | | MEME |
| $\beta$-carotene | 536.9 | 13.5 | carotenoid | >550 | >4000 | | MEME + 1% DMSO |
| L-tryptophan | 204.2 | −1.1 | amino acid (indole) | >550 | >4000 | | MEME |
| L-ascorbic acid | 176.1 | −1.6 | sugar acid | >550 | >4000 | | MEME |

[a]Data are shown as averages (mean ± SD) from three separate experiments where separate preparations were tested on separate days. The PUFA chromenone data have been published,[19] but are included for comparison. [b]Lipophilicity data were obtained from NCBI Pubchem. [c]For hydroxytyrosol and the PUFA chromones, only one preparation was available, which was tested on three different days. [d]Clog$P^a$ value from ref 19. [e]Kaempferol gave a biphasic effect curve with CLPAA, and only the protective range (up to 100 $\mu$M) was used for curve-fits. High kaempferol concentrations (≥200 $\mu$M) offered no protection and increased probe oxidation. MEME = minimum essential medium Earle's.

**Table 2. CAA Generated $IC_{50}$ Values Using HepG2 Cells[a]**

| compound | $M_w$ | XLogP3[b] | type | $IC_{50}$ (mg/L) | $IC_{50}$ as ($\mu$M) | CV (%) | incubation in |
|---|---|---|---|---|---|---|---|
| luteolin | 286.2 | 1.4 | flavone | 3.41 ± 0.40 | 11.90 ± 1.40 | 11.8 | MEME |
| kaempferol | 286.2 | 1.9 | flavonol | 3.80 ± 0.82 | 13.27 ± 2.86 | 21.5 | MEME |
| EGCG | 458.4 | 1.2 | flavan-3-ol | 8.51 ± 1.48 | 18.57 ± 3.23 | 17.4 | MEME |
| curcumin | 368.4 | 3.2 | curcuminoid | 14.5 ± 1.12 | 39.47 ± 3.04 | 7.7 | MEME + 1% DMSO |
| quercetin | 302.2 | 1.5 | flavonol | 21.5 ± 11.7 | 71.23 ± 38.6 | 54.1 | MEME |
| L-ascorbic acid | 176.1 | −1.6 | sugar acid | 64.7 ± 11.6 | 367.4 ± 66.1 | 18.0 | MEME |
| PUFA chromone 1[c] | 434.0 | 8.4[d] | PUFA chromone | 69.2 ± 10.7 | 159.5 ± 24.7 | 15.5 | MEME + 1% DMSO |
| resveratrol | 228.2 | 3.1 | stilbenoid | 118.5 ± 9.56 | 519.2 ± 41.9 | 8.1 | MEME |
| astaxanthin | 596.9 | 10.3 | carotenoid | 134.7 ± 14.8 | 225.7 ± 24.8 | 11.0 | MEME + 1% DMSO |
| hydroxytyrosol[c] | 154.2 | −0.7 | phenolic | 134.8 ± 37.3 | 874.0 ± 242 | 27.7 | MEME |
| PUFA chromone 2[c] | 492.0 | <8.4[d] | PUFA chromone | 168.0 ± 60.1 | 341.5 ± 122 | 35.8 | MEME + 1% DMSO |
| deferasirox | 373.4 | 3.8 | $Fe^{3+}$chelator, permeable | 242.1 ± 115.3 | 648.4 ± 308.9 | 47.6 | MEME + 1% DMSO |
| (+)-catechin | 290.3 | 0.4 | flavan-3-ol | 353.7 ± 172.5 | 1218.7 ± 594.1 | 48.8 | MEME |
| (−)-epicatechin | 290.3 | 0.4 | flavan-3-ol | 417.3 ± 66.0 | 1437.7 ± 227.4 | 15.8 | MEME |
| DFOM | 656.8 | −0.614 | $Fe^{3+}$ chelator, impermeable | >550 | 1676.3 ± 507.8 | 30.3 | MEME |
| $\beta$-carotene | 536.9 | 13.5 | carotenoid | >550 | >4000 | | MEME + 1% DMSO |
| L-tryptophan | 204.2 | −1.1 | amino acid (indole) | >550 | >4000 | | MEME |
| ASA | 180.2 | 1.2 | phenolic | >550 | >4000 | | MEME |
| DL-$\alpha$-tocopherol | 430.7 | 10.7 | methylated phenol, lipophilic | >550 | >4000 | | MEME + 1% DMSO |
| apigenin | 270.2 | 1.7 | flavone | >550 | >4000 | | MEME + 1% DMSO |
| SIH | 241.3 | 1.9 | $Fe^{3+}$ chelator, permeable | >550[e] | >4000 | | MEME + 1% DMSO |

[a]Data are shown as averages (mean ± SD) from three separate experiments where separate preparations were tested on separate days. The PUFA chromenone data have been published,[19] but are included for comparison. [b]Lipophilicity data were obtained from NCBI Pubchem. [c]For the PUFA chromones and hydroxytyrosol only one preparation was available, which was tested on three separate days. [d]Clog$P^a$ value from ref 19. [e]SIH provided no protection and even increased the fluorescence over that of the positive control at ≥200 $\mu$M.

Interestingly, luteolin, which displayed the highest antioxidant activity of all compounds tested considering both assays (see Tables 1 and 2), differs structurally from apigenin by just one extra hydroxyl group on the B-ring (Figure 1); both are flavones and have similar molecular weight and lipophilicity (Tables 1 and 2). Thus, luteolin's dual ortho-positioned 3′,4′-dihydroxy substituents (catechol-type) on its extruding aromatic B-ring appear to have provided the extra edge. Luteolin was found to have a half-peak oxidation potential (Ep/2) of +180 mV, whereas apigenin could not be oxidized up to the maximum tested 1 V.[12]

Still, both apigenin and luteolin display iron chelating abilities,[12] although not nearly as strong as the metal chelators tested in this study ($pFe^{3+}$ values of deferasirox, DFO, and SIH are 22.5, 26.6, and 50, respectively;[34] $pFe^{3+}$ values for most compounds investigated in this study could not be found but are considerably lower). Thus, it seems that a potent flavonoid lipid peroxidation inhibitory activity requires a combination of metal chelating ability and low oxidation potential. The large difference between apigenin and luteolin in redox potential likely explains how the two compounds differed in performances in the CAA assay as well. Luteolin exhibits a high degree of electrochemical reversibility that is substantially higher than that of quercetin, for example, which is an even better electron donor (Ep/2 = +30 mV)[12] that also can redox cycle its 3′,4′-dihydroxy substituents on its B-ring in a $2e^- -2H^+$ step,[9] implying that the C-ring structure affects the compound's electrochemical properties. Higher concentrations of luteolin stained the cells yellow. Both flavanols, kaempferol and quercetin, displayed protective effects in both assays. However, kaempferol produced a biphasic effect in CLPAA (an increased dose−response protection was observed up to around 200 μM, but at higher concentrations, the protective effect disappeared), so only the protective range (low concentration) was used for curve fits. The reason for the biphasic effect curve in CLPAA is unclear; however, concentrations >200 μM are not biologically realistic in any case. Kaempferol (Ep/2 = +120 mV)[12] has a single hydroxyl group on the B-ring as apigenin, but differs in that it is substituted with an oxidizable hydroxyl group at C-3 on its C-ring, which allows it to also oxidize as a conjugated system in a $2e^- -2H^+$ step (its B- and C-ring −OH substituents → =O).[35] The electrochemical reversibility of luteolin and kaempferol could potentially be a disadvantage[12] as redox cycling could produce ROS (as in the case of redox cycling quinones),[36] but only unrealistically high (≥200 μM) kaempferol (not luteolin) concentrations had a pro-oxidant effect in this study (in the CLPAA assay only). The large flavonoid EGCG offered protection in both assays. EGCG is relatively lipophilic and has two 3′,4′,5′-trihydroxy (pyrogallol-type) phenolic rings that are also easily oxidized.[9] (+)-Catechin and (−)-epicatechin (isomers) offered similar protection in both assays. The reason why (+)-catechin and (−)-epicatechin offered much less protection in comparison to luteolin (all three have ortho-positioned 3′,4′-dihydroxy substituents on the B-ring, and catechin's Ep/2 of +160 mV[12] is nearly the same as that of luteolin) and EGCG is unclear but may be due to the catechins' different C-ring structure, which likely influences the compound's reversibility or their lower lipophilicity. Possibly their metal chelatability or a cellular metabolic effect (HepG2 cells are metabolically active) may have affected the outcome. Several flavonoids were found to reach and protect the nuclei in HepG2 cells with maximum incorporation after 30 min, and quercetin and luteolin were found to be effective in suppressing ABAP-induced 8-oxodG formation in DNA.[31]

**Other Phenols.** It has been suggested that in particular the *o*-diphenolic substitution gives high antioxidant ability, as opposed to *m*-diphenolic or single hydroxyl substitution.[8] This observation in addition to the obtained results for the flavonoids is further supported by the performance of hydroxytyrosol. Hydroxytyrosol is a small but major olive oil *o*-diphenolic derived from hydrolysis of oleuropein,[8] which offered protection in both assays. DL-α-Tocopherol displayed antioxidant activity in cellular membranes (CLPAA), but not in the aqueous cytosol (CAA). It was previously observed that the oxidation of $C_{11}$-BODIPY in rat-1 fibroblast was prevented by preincubation of the cells with a mixture of α- and γ-tocopherol.[21] Curcumin and resveratrol offered protection in both assays, and at higher curcumin concentrations (≥100 μM) necrotic (cell detachment, etc.) effects were visually observed, reflecting cytotoxicity on the HepG2 cells; however, toxicity in cancer cells (i.e., HepG2) may be considered beneficial.

**Carotenoids.** Carotenoids are highly lipophilic and partition into cellular membranes. Carotenoids contain multiple carbon−carbon double bonds that absorb UV light[2] and can react with singlet oxygen ($^1O_2$) produced from UV light-induced photosensitization reactions;[37] however, $^1O_2$ is of relatively low physiological importance. Carotenoids may also react with peroxyl radicals[38] and are oxidized during lipid peroxidation reactions but seem incapable of stalling this process, becoming degraded themselves.[39] In humans, carotenoids are well absorbed, contrary to many experimental animals, but it has been suggested that their antioxidant role in humans is not very strong.[40] In this study, astaxanthin and β-carotene stained the cells intensely red and orange, respectively, reflecting high cellular uptake. However, astaxanthin's low and β-carotene's absent effects in CLPAA suggest poor stalling of lipid peroxidation. The suggestion that astaxanthin would be a "super vitamin E"[41] could not be supported. It should, however, be noted that oxidative damage indicative probes such as $C_{11}$-BODIPY and DCFH could potentially oxidize more easily than biomolecules such as proteins or certain lipid constituents, and cellular membranes consist of a whole range of different lipids. For example, in a cell-free system measuring oxidation of 1-stearoyl-2-arachidonyl-*sn*-glycero-3-phosphocholine (SAPC), $C_{11}$-BODIPY was more sensitive to oxidative damage than the SAPC lipid.[42]

**PUFA Chromones.** The PUFA chromones tested are novel unexplored compounds that may offer promising activities in vivo. However, further toxicokinetic and toxicity testing is required. The more lipophilic PUFA chromone 1 resulted in a somewhat stronger response than PUFA chromone 2 (the PUFA chromone results were recently published[19] but are included for comparison as the testing conditions were identical).

**Metal Chelators.** The protective effects offered by the lipophilic cell membrane permeable $Fe^{3+}$ chelators SIH[43] and deferasirox[44] in CLPAA (Table 1) suggest that this assay involves membrane-associated Fe ions that catalyze membrane peroxidation reactions upon cumOOH addition and eventually cause $C_{11}$-BODIPY oxidation with the formation of measurable green fluorescent $C_{11}$-BODIPY products. Thus, the CLPAA assay should be suitable for screening new Fe chelators. The low, or lacking, protective effect by deferasirox and SIH in CAA (Table 2), however, demonstrates that ABAP-induced oxidation of intracellular DCFH is largely independent of labile Fe ions. In CAA, SIH was the only compound that at higher (≥200 μM) concentrations increased the fluorescence compared to the positive control in a dose−response manner. Noticeably, deferasirox offered a relatively limited protection in CAA compared to its strong protection in CLPAA. The hydrophilic membrane impermeable $Fe^{3+}$ chelator DFO offered no protection at reasonable concentrations in either assay (noticeable effects appeared first at mM concentrations; $IC_{50}$ was 1.7 mM in CAA and even higher in CLPAA). DFO is mainly taken up intracellularly into lysosomes by endocytosis (a slow process)[26] and requires subcutaneous infusion for optimal effect in patients. Whereas deferasirox and DFO are clinically used, SIH is not, presumably due to lower stability in vivo.

**Other Compounds.** ASA has anti-inflammatory and antiplatelet (inactivates cyclooxygenase enzymes COX-1 and -2) physiological effects but is also a free radical scavenger,


dx.doi.org/10.1021/jf5022779 | J. Agric. Food Chem. 2014, 62, 8402−8410

particularly against free hydroxyl radicals ($^{\bullet}OH$).[3,45] Here, however, ASA offered no protection in either assay, indicating that free $^{\bullet}OH$ has no major role in the CLPAA and CAA assays. Thus, the initiating CLPAA assay reactions 1 and 2 above appear to be "caged" events (no freely diffusing $^{\bullet}OH$).[46] L-Ascorbic acid (vitamin C) offered protection in the CAA assay, but not in the CLPAA assay. Passive plasma membrane passage of ascorbate ($AscH^-$) is expected to be very low due to low lipophilicity and charge, but active ascorbate import is mediated in most cell types (also hepatocytes) by sodium vitamin C transporters SVCT1 and SVTC2.[47] The amino acid L-tryptophan (contains an indole group) offered no protection in either assay and was merely included as a negative control.

**Comparisons between CLPAA and CAA and Mechanistic Assay Insights.** The two biologically relevant assays measure different parameters. CLPAA measures lipid peroxidation inhibition, and CAA measures intracellular peroxyl radical scavenging; hence, these are very complementing assays.[14−16] For CLPAA, we previously concluded that the rate of green fluorescence appearance ($C_{11}$-BODIPY decomposition products) was more sensitive than the disappearance of red fluorescence ($C_{11}$-BODIPY)[14] and that the background fluorescence from the plastic microplate interfered in the red light range.[14] As CLPAA is based on analyzing the slope of green BODIPY product formation, it is not affected by individual absorption from tested compounds. With CAA, however, light-absorbing effects by the compound can be an issue for particularly strong light (excitation and/or emitted light) absorbing compounds such as carotenoids by producing a false effect (increased effect at increased compound concentration). This can be checked and possibly normalized for by using a blank control with only the addition of test compound to cell-free medium containing a known concentration of the fluorescent probe. Moreover, the CAA assay is also more sensitive toward plate heating effects than CLPAA, and the variation among positive control values in CAA also increases (more than for CLPAA) with incubation time. Random placement of samples in the microplate can circumvent edge and corner effects (outer wells generally warm up more rapidly).

Overall, our results together with those by others[48,49] suggest that peroxides (cumOOH, $H_2O_2$, etc.) depend upon catalytic transition metal ions to oxidize organic compounds, whereas both production of azo compound (e.g., ABAP) oxidizing peroxyl radicals ($ROO^{\bullet}$ as in the CAA assay) and their oxidation of organic compounds can take place independent of transition metals. Thus, the choice of oxidant in an assay relates to which antioxidant characteristics are being assessed.

**Implications.** This study encourages further in vivo studies with administration of the better performing compounds (Tables 1 and 2), and an increased intake of foods rich in these compounds could be beneficial for our health. Luteolin, the most promising compound in this study, is present in multiple plants to various degrees; for example, high luteolin contents are present in peanut shells (here extractable luteolin exists in the studied aglycone form)[50] and in certain edible herbs such as peppermint and sage,[51] where luteolin mainly exists chemically attached to sugars (i.e., rutinose or glucose), bonds that hydrolyze during gastrointestinal passage.[10,52] Interestingly, chrysanthemum flower tea extract is rich in luteolin constituents and has been used in folk medicine for centuries.[52]

## AUTHOR INFORMATION


### Corresponding Author

*(T.H.) E-mail: tim.hofer@fhi.no. Phone: +47-21076671. Fax: +47-21076686.



### Funding

We are grateful to the Norwegian Research Council (Project 208463) for financial support.


### Notes

The authors declare no competing financial interest.


## ACKNOWLEDGMENTS

We thank Novartis Pharma AG, Dr. Katherine J. Franz, and Dr. Trond V. Hansen for kindly supplying deferasirox, SIH, and the PUFA chromones, respectively.


## ABBREVIATIONS USED

ABAP (or AAPH), 2,2′-azobis(2-amidinopropane); ASA, acetylsalicylic acid; CAA, cellular antioxidant activity; $C_{11}$-BODIPY, 4,4-difluoro-5-(4-phenyl-1,3-butadienyl)-4-bora-3a,4a-diaza-*s*-indacene-3-undecanoic acid; CLPAA, cellular lipid peroxidation antioxidant activity; cumOOH, cumene hydroperoxide; DCF, 2′,7′-dichlorofluorescein; DCFH, 2′,7′-dichlorofluorescin; DCFH-DA, 2′,7′-dichlorofluorescin diacetate; DFOM, deferoxamine mesylate; DMSO, dimethyl sulfoxide; EGCG, epigallocatechin gallate; FBS, fetal bovine serum; FRAP, ferric reducing antioxidant power; HepG2, human hepatocellular liver carcinoma cell line; $IC_{50}$, half-maximal inhibitory concentration; PUFA chromone 1, *all*-(*Z*)-5,7-dihydroxy-2-(4*Z*,7*Z*,10*Z*,13*Z*,16*Z*)-nonadecapentaenyl; PUFA chromone 2, 2-((5-hydroxy-2-((4*Z*,7*Z*,10*Z*,13*Z*,16*Z*)-nonadeca-4,7,10,13,16-pentaen-1-yl)-4-oxo-4*H*-chromen-7-yl)oxy)acetic acid; SIH, salicylaldehyde isonicotinoyl hydrazone

## REFERENCES


(1) Myhre, O.; Utkilen, H.; Duale, N.; Brunborg, G.; Hofer, T. Metal dyshomeostasis and inflammation in Alzheimer's and Parkinson's diseases: possible impact of environmental exposures. *Oxid. Med. Cell. Longev.* **2013**, *2013*, 1−19.

(2) Snodderly, D. M. Evidence for protection against age-related macular degeneration by carotenoids and antioxidant vitamins. *Am. J. Clin. Nutr.* **1995**, *62*, 1448S−1461S.

(3) Thome, J.; Zhang, J. J.; Davids, E.; Foley, P.; Weijers, H. G.; Wiesbeck, G. A.; Boning, J.; Riederer, P.; Gerlach, M. Evidence for increased oxidative stress in alcohol-dependent patients provided by quantification of in vivo salicylate hydroxylation products. *Alcohol.: Clin. Exp. Res.* **1997**, *21*, 82−85.

(4) Hofer, T.; Marzetti, E.; Xu, J. Z.; Seo, A. Y.; Gulec, S.; Knutson, M. D.; Leeuwenburgh, C.; Dupont-Versteegden, E. E. Increased iron content and RNA oxidative damage in skeletal muscle with aging and disuse atrophy. *Exp. Gerontol.* **2008**, *43*, 563−570.

(5) Zhang, R.; Brennan, M. L.; Shen, Z.; MacPherson, J. C.; Schmitt, D.; Molenda, C. E.; Hazen, S. L. Myeloperoxidase functions as a major enzymatic catalyst for initiation of lipid peroxidation at sites of inflammation. *J. Biol. Chem.* **2002**, *277*, 46116−46122.

(6) Laguerre, M.; Lecomte, J.; Villeneuve, P. Evaluation of the ability of antioxidants to counteract lipid oxidation: existing methods, new trends and challenges. *Prog. Lipid Res.* **2007**, *46*, 244−282.

(7) Rossi, L.; Mazzitelli, S.; Arciello, M.; Capo, C. R.; Rotilio, G. Benefits from dietary polyphenols for brain aging and Alzheimer's disease. *Neurochem. Res.* **2008**, *33*, 2390−2400.

(8) Tripoli, E.; Giammanco, M.; Tabacchi, G.; Di Majo, D.; Giammanco, S.; La Guardia, M. The phenolic compounds of olive oil: structure, biological activity and beneficial effects on human health. *Nutr. Res. Rev.* **2005**, *18*, 98−112.

(9) Hendrickson, H. P.; Kaufman, A. D.; Lunte, C. E. Electrochemistry of catechol-containing flavonoids. *J. Pharm. Biomed.* **1994**, *12*, 325−334.
(10) Manach, C.; Donovan, J. L. Pharmacokinetics and metabolism of dietary flavonoids in humans. *Free Radical Res.* **2004**, *38*, 771−785.
(11) Crozier, A.; Jaganath, I. B.; Clifford, M. N. Dietary phenolics: chemistry, bioavailability and effects on health. *Nat. Prod. Rep.* **2009**, *26*, 1001−1043.
(12) van Acker, S. A.; van den Berg, D. J.; Tromp, M. N.; Griffioen, D. H.; van Bennekom, W. P.; van der Vijgh, W. J.; Bast, A. Structural aspects of antioxidant activity of flavonoids. *Free Radical Biol. Med.* **1996**, *20*, 331−342.
(13) Melidou, M.; Riganakos, K.; Galaris, D. Protection against nuclear DNA damage offered by flavonoids in cells exposed to hydrogen peroxide: the role of iron chelation. *Free Radical Biol. Med.* **2005**, *39*, 1591−1600.
(14) Hofer, T.; Olsen, R. L. Cellebasert metode for måling av lipid peroksidasjon og antioksidantaktivitet. *Bioingeniøren* (Norwegian; archived at www.bioingenioren.no) **2010**, *10*, 6−12.
(15) Hofer, T.; Eriksen, T. E.; Hansen, E.; Varmedal, I.; Jensen, I. J.; Andersen, J. H.; Olsen, R. L. Cellular and chemical assays for discovery of novel antioxidants in marine organisms. In *Studies on Experimental Models*; Basu, S., Wiklund, L., Eds.; Springer Science, Humana Press: New York, 2011; p 680.
(16) Wolfe, K. L.; Liu, R. H. Cellular antioxidant activity (CAA) assay for assessing antioxidants, foods, and dietary supplements. *J. Agric. Food Chem.* **2007**, *55*, 8896−8907.
(17) Song, W.; Derito, C. M.; Liu, M. K.; He, X. J.; Dong, M.; Liu, R. H. Cellular antioxidant activity of common vegetables. *J. Agric. Food Chem.* **2010**, *58*, 6621−6629.
(18) Wolfe, K. L.; Kang, X. M.; He, X. J.; Dong, M.; Zhang, Q. Y.; Liu, R. H. Cellular antioxidant activity of common fruits. *J. Agric. Food Chem.* **2008**, *56*, 8418−8426.
(19) Mohamed, Y. M. A.; Vik, A.; Hofer, T.; Andersen, J. H.; Hansen, T. V. Polyunsaturated fatty acid-derived chromones exhibiting potent antioxidant activity. *Chem. Phys. Lipids* **2013**, *170*−*171*, 41−45.
(20) Lundholt, B. K.; Scudder, K. M.; Pagliaro, L. A simple technique for reducing edge effect in cell-based assays. *J. Biomol. Screen.* **2003**, *8*, 566−570.
(21) Pap, E. H.; Drummen, G. P.; Winter, V. J.; Kooij, T. W.; Rijken, P.; Wirtz, K. W.; Op den Kamp, J. A.; Hage, W. J.; Post, J. A. Ratio-fluorescence microscopy of lipid oxidation in living cells using C11-BODIPY(581/591). *FEBS Lett.* **1999**, *453*, 278−282.
(22) Drummen, G. P.; Gadella, B. M.; Post, J. A.; Brouwers, J. F. Mass spectrometric characterization of the oxidation of the fluorescent lipid peroxidation reporter molecule C11-BODIPY(581/591). *Free Radical Biol. Med.* **2004**, *36*, 1635−1644.
(23) Ma, Y.; de Groot, H.; Liu, Z.; Hider, R. C.; Petrat, F. Chelation and determination of labile iron in primary hepatocytes by pyridinone fluorescent probes. *Biochem. J.* **2006**, *395*, 49−55.
(24) Petrat, F.; Rauen, U.; de Groot, H. Determination of the chelatable iron pool of isolated rat hepatocytes by digital fluorescence microscopy using the fluorescent probe, phen green SK. *Hepatology* **1999**, *29*, 1171−1179.
(25) Drummen, G. P.; van Liebergen, L. C.; Op den Kamp, J. A.; Post, J. A. C11-BODIPY(581/591), an oxidation-sensitive fluorescent lipid peroxidation probe: (micro)spectroscopic characterization and validation of methodology. *Free Radical Biol. Med.* **2002**, *33*, 473−490.
(26) Persson, H. L.; Yu, Z. Q.; Tirosh, O.; Eaton, J. W.; Brunk, U. T. Prevention of oxidant-induced cell death by lysosomotropic iron chelators. *Free Radical Biol. Med.* **2003**, *34*, 1295−1305.
(27) Javitt, N. B. Hep-G2 cells as a resource for metabolic studies − lipoprotein, cholesterol, and bile-acids. *FASEB J.* **1990**, *4*, 161−168.
(28) Roe, A. L.; Snawder, J. E.; Benson, R. W.; Roberts, D. W.; Casciano, D. A. HepG2 cells − an in vitro model for P450-dependent metabolism of acetaminophen. *Biochem. Biophys. Res. Commun.* **1993**, *190*, 15−19.
(29) Huang, M.; Zhang, L.; Mesaros, C.; Zhang, S. H.; Blaha, M. A.; Blair, I. A.; Penning, T. M. Metabolism of a representative oxygenated polycyclic aromatic hydrocarbon (PAH) phenanthrene-9,10-quinone in human hepatoma (HepG2) cells. *Chem. Res. Toxicol.* **2014**, *27*, 852−863.
(30) Jetten, M. J. A.; Kleinjans, J. C. S.; Claessen, S. M.; Chesne, C.; van Delft, J. H. M. Baseline and genotoxic compound induced gene expression profiles in HepG2 and HepaRG compared to primary human hepatocytes. *Toxicol. in Vitro* **2013**, *27*, 2031−2040.
(31) Kanazawa, K.; Uehara, M.; Yanagitani, H.; Hashimoto, T. Bioavailable flavonoids to suppress the formation of 8-OHdG in HepG2 cells. *Arch. Biochem. Biophys.* **2006**, *455*, 197−203.
(32) Gerets, H. H. J.; Tilmant, K.; Gerin, B.; Chanteux, H.; Depelchin, B. O.; Dhalluin, S.; Atienzar, F. A. Characterization of primary human hepatocytes, HepG2 cells, and HepaRG cells at the mRNA level and CYP activity in response to inducers and their predictivity for the detection of human hepatotoxins. *Cell Biol. Toxicol.* **2012**, *28*, 69−87.
(33) Wilkening, S.; Stahl, F.; Bader, A. Comparison of primary human hepatocytes and hepatoma cell line HEPG2 with regard to their biotransformation properties. *Drug. Metab. Dispos.* **2003**, *31*, 1035−1042.
(34) Fakih, S.; Podinovskaia, M.; Kong, X.; Collins, H. L.; Schaible, U. E.; Hider, R. C. Targeting the lysosome: fluorescent iron(III) chelators to selectively monitor endosomal/lysosomal labile iron pools. *J. Med. Chem.* **2008**, *51*, 4539−4552.
(35) Brown, J. E.; Khodr, H.; Hider, R. C.; Rice-Evans, C. A. Structural dependence of flavonoid interactions with $Cu^{2+}$ ions: implications for their antioxidant properties. *Biochem. J.* **1998**, *330*, 1173−1178.
(36) Taguchi, K.; Shimada, M.; Fujii, S.; Sumi, D.; Pan, X.; Yamano, S.; Nishiyama, T.; Hiratsuka, A.; Yamamoto, M.; Cho, A. K.; Froines, J. R.; Kumagai, Y. Redox cycling of 9,10-phenanthraquinone to cause oxidative stress is terminated through its monoglucuronide conjugation in human pulmonary epithelial A549 cells. *Free Radical Biol. Med.* **2008**, *44*, 1645−1655.
(37) Di Mascio, P.; Devasagayam, T. P.; Kaiser, S.; Sies, H. Carotenoids, tocopherols and thiols as biological singlet molecular oxygen quenchers. *Biochem. Soc. Trans.* **1990**, *18*, 1054−1056.
(38) El-Agamey, A.; Lowe, G. M.; McGarvey, D. J.; Mortensen, A.; Phillip, D. M.; Truscott, T. G.; Young, A. J. Carotenoid radical chemistry and antioxidant/pro-oxidant properties. *Arch. Biochem. Biophys.* **2004**, *430*, 37−48.
(39) Chen, G.; Djuric, Z. Carotenoids are degraded by free radicals but do not affect lipid peroxidation in unilamellar liposomes under different oxygen tensions. *FEBS Lett.* **2001**, *505*, 151−154.
(40) Krinsky, N. I. Carotenoids as antioxidants. *Nutrition* **2001**, *17*, 815−817.
(41) Miki, W. Biological functions and activities of animal carotenoids. *Pure Appl. Chem.* **1991**, *63*, 141−146.
(42) MacDonald, M. L.; Murray, I. V. J.; Axelsen, P. H. Mass spectrometric analysis demonstrates that BODIPY 581/591 C11 overestimates and inhibits oxidative lipid damage. *Free Radical Biol. Med.* **2007**, *42*, 1392−1397.
(43) Charkoudian, L. K.; Pham, D. M.; Franz, K. J. A pro-chelator triggered by hydrogen peroxide inhibits iron-promoted hydroxyl radical formation. *J. Am. Chem. Soc.* **2006**, *128*, 12424−12425.
(44) Bruin, G. J. M.; Faller, T.; Wiegand, H.; Schweitzer, A.; Nick, H.; Schneider, J.; Boernsen, K. O.; Waldmeier, F. Pharmacokinetics, distribution, metabolism, and excretion of deferasirox and its iron complex in rats. *Drug. Metab. Dispos.* **2008**, *36*, 2523−2538.
(45) Shi, X. L.; Ding, M.; Dong, Z. G.; Chen, F.; Ye, J. P.; Wang, S. W.; Leonard, S. S.; Castranova, V.; Vallyathan, V. Antioxidant properties of aspirin: Characterization of the ability of aspirin to inhibit silica-induced lipid peroxidation, DNA damage, NF-$\kappa$B activation, and TNF-$\alpha$ production. *Mol. Cell. Biochem.* **1999**, *199*, 93−102.
(46) Hofer, T. Oxidation of 2′-deoxyguanosine by $H_2O_2$-ascorbate: evidence against free OH• and thermodynamic support for two-electron reduction of $H_2O_2$. *J. Chem. Soc., Perkin Trans. 2* **2001**, 210−213.
(47) Liang, W. J.; Johnson, D.; Jarvis, S. M. Vitamin C transport systems of mammalian cells. *Mol. Membr. Biol.* **2001**, *18*, 87−95.

(48) Balcerczyk, A.; Kruszewski, M.; Bartosz, G. Does the cellular labile iron pool participate in the oxidation of 2′,7′-dichlorodihydrofluorescein? *Free Radical Res.* **2007**, *41*, 563−570.
(49) Lebel, C. P.; Ischiropoulos, H.; Bondy, S. C. Evaluation of the probe 2′,7′-dichlorofluorescin as an indicator of reactive oxygen species formation and oxidative stress. *Chem. Res. Toxicol.* **1992**, *5*, 227−231.
(50) Zhou, P.; Li, L. P.; Luo, S. Q.; Jiang, H. D.; Zeng, S. Intestinal absorption of luteolin from peanut hull extract is more efficient than that from individual pure luteolin. *J. Agric. Food Chem.* **2008**, *56*, 296−300.
(51) Fecka, I.; Turek, S. Determination of water-soluble polyphenolic compounds in commercial herbal teas from *Lamiaceae*: peppermint, melissa, and sage. *J. Agric. Food Chem.* **2007**, *55*, 10908−10917.
(52) Lu, X. Y.; Sun, D. L.; Chen, Z. J.; Chen, T.; Li, L. P.; Xu, Z. H.; Jiang, H. D.; Zeng, S. Relative contribution of small and large intestine to deglycosylation and absorption of flavonoids from *Chrysanthemun morifolium* extract. *J. Agric. Food Chem.* **2010**, *58*, 10661−10667.

JOURNAL OF AGRICULTURAL AND FOOD CHEMISTRY

Article

pubs.acs.org/JAFC

# α-Amylase Inhibitory Triterpene from *Abrus precatorius* Leaves

Ryuta Yonemoto, Miyuki Shimada, Maria D. P. T. Gunawan-Puteri, Eisuke Kato, and Jun Kawabata*

Division of Applied Bioscience, Graduate School of Agriculture, Hokkaido University, Sapporo, Hokkaido 060-8589, Japan

**ABSTRACT:** In the screening experiments for porcine pancreatic α-amylase inhibitors in 18 plants obtained from Indonesia, a potent inhibitory activity was detected in the extract of leaves of *Abrus precatorius*. The enzyme assay-guided fractionation of the extract led to the isolation of a triterpene ketone, lupenone (**1**), as a potent α-amylase inhibitor, together with 24-methylenecycloartenone (**2**) and luteolin (**3**). The mode of inhibition of compound **1** against porcine pancreatic α-amylase was a mixed inhibition. This is the first report that describes the potent α-amylase inhibitory activity of the low-polar triterpene ketone similar to compound **1**. A comparison of the activities of the isolate and related compounds indicated the importance of C-3 ketone and the lupane skeleton in the α-amylase inhibitory activity.

**KEYWORDS:** *Abrus precatorius, α-amylase inhibitor, triterpene ketone*

## INTRODUCTION

Diabetes mellitus is a typical chronic disease related to both obesity and aging and has thus become a serious global health problem.[1] One of the therapeutic approaches for preventing diabetes is the suppression of intestinal digestion and absorption of dietary carbohydrates through the inhibition of carbohydrate-hydrolyzing enzymes, α-amylase and α-glucosidase, in the digestive organs.[2] In this context, several research efforts have screened for effective α-amylase and α-glucosidase inhibitors from natural sources to develop a physiological functional food or lead compounds for the use of antidiabetic medicines.[3,4]

In the course of our continuing search for rat intestinal α-glucosidase inhibitory principles from plants, we have isolated and identified several active compounds from a variety of plants.[5−9] However, the search for α-amylase inhibitors from natural sources have led to relatively scarce results.[10−12] It is well-known that α-amylase recognizes a consecutive glucose chain as a substrate using its subsite.[13] In fact, acarbose, a typical α-amylase inhibitor, has a strong affinity for the enzyme because of its pseudo-tetrasaccharide structure.[14] This is partly the reason for the limited number of cases involved with the identification of small-molecule α-amylase inhibitors from natural sources. Most of these are polyphenols with low enzyme specificity.[15−19] Recently, a triterpene glycoside has been isolated as a specific inhibitor by high-throughput screening,[20] and more surprisingly, a simple low-polar ketone, chalcone, has been found to possess considerable α-amylase inhibitory activity.[21] The molecular docking study revealed that the low-polar small molecule could interact with hydrophobic amino acid residues near the active site of the enzyme. From these results, we have thus focused on searching for non-polyphenolic low-polar α-amylase inhibitors from plant origin.

In this paper, we present the results of a study on α-amylase inhibition and identification of active principles from the plant extract of indigenous plants obtained from Indonesia that show a potent inhibitory activity. In the screening experiments for porcine pancreatic α-amylase (PPA) inhibitors in 18 plants obtained from Indonesia, the potent α-amylase inhibitory activity was found in a tannin-free low-polar extract of the leaves of *Abrus precatorius*. *A. precatorius* (Fabaceae) is a perennial climber found in tropical and subtropical regions. It is famous for its beans, which contain a proteinaceous toxin.[22,23] In addition, several other biological activities have been reported,[24−26] although there have been no reports on α-amylase and α-glucosidase inhibitory activities of this plant.

## MATERIALS AND METHODS

**Materials.** A total of 18 Indonesian plants, including *A. precatorius* leaves, were purchased from Merapi Farma Traditional Herbs Distributor, Yogyakarta, Indonesia, in January 2007. PPA (A3176) was obtained from Sigma-Aldrich Co. (Tokyo, Japan). All chemicals used in the present study were of reagent grade and were purchased from Wako Pure Chem. Co. (Osaka, Japan), unless otherwise stated.

**General Procedure.** Nuclear magnetic resonance (NMR) spectra were recorded on Bruker AMX500 ($^1$H, 500 MHz; $^{13}$C, 125 MHz) and Jeol EX-270 ($^1$H, 270 MHz) instruments. Chemical shifts were determined relative to a reference signal of tetramethylsilane in chloroform-*d* ($\delta_H$, 0.00 ppm; $\delta_C$, 0.0 ppm) or a residual solvent signal of methanol-$d_4$ ($\delta_H$, 3.30 ppm). Field desorption mass spectra (FD-MS) were determined by a Jeol T100GCV instrument.

**PPA Inhibitory Activity Determination.** The PPA inhibitory activity was determined using the method described by Ali et al.,[27] with a slight modification. PPA was dissolved in sodium phosphate buffer (20 mM, pH 6.9) containing 6.7 mM NaCl to give a concentration of 0.5 unit/mL solution. Potato starch (0.01 g/mL) in the same buffer was used as a substrate solution. A coloring reagent [3,5-dinitrosalicylic acid (DNS)] was prepared by mixing a 4.8 M 3,5-dinitrosalicylic acid solution (20 mL) and a solution of (+)-sodium potassium tartrate tetrahydrate (12 g) in 0.4 M NaOH (40 mL). A sample solution (100 μL) in 50% dimethyl sulfoxide (DMSO) and the PPA solution (150 μL) were mixed in a microtube (1.5 mL). The tube was stoppered and preincubated at 37 °C for 15 min. The starch solution (250 μL) was then added, and the mixture was incubated at 37 °C for 15 min. To terminate the reaction, the tube was dipped in boiling water for 1 min. After cooling, the contents of the microtube were directly passed through a small ODS (Cosmosil 75$C_{18}$-OPN, Nacalai Tesque Co., Kyoto, Japan) column (3 mL) to remove any

Received: June 9, 2014
Revised: August 1, 2014
Accepted: August 4, 2014
Published: August 4, 2014

ACS Publications © 2014 American Chemical Society

sample constituents that may interfere with the following color reaction. The reaction mixture (100 μL) was then mixed with DNS reagent (50 μL) in a microtube, stoppered, and heated in boiling water for 15 min. The ice-cooled mixture was diluted with water (450 μL); the solution (200 μL) was transferred to a 96-well microplate; and the optical density was determined at a wavelength of 540 nm. The control experiment was performed using 50% DMSO in place of the sample solution. Blank experiments for the sample and control were performed using the sodium phosphate buffer in place of the enzyme solution, and each blank value was subtracted from the sample and the control values, respectively. The inhibitory activity (%) was calculated as $[1 - OD_{540}\ (\text{sample})/OD_{540}\ (\text{control})] \times 100$.

**Screening Experiment.** The screening experiments for PPA inhibition were performed with extracts of 18 plant species. Each dried plant was extracted with 50% aqueous methanol. The extracts were evaporated and partitioned with chloroform/methanol/water (4:1:5). The organic phase was washed with 1% saline to give a tannin-free extract,[28] which was then evaporated, redissolved in 50% aqueous DMSO, and subjected as the test sample to the assay for PPA inhibitory activity at the final concentration of the extractable constituents obtained from 0.3 g of plant material in 1 mL of solution.

**Isolation of Lupenone (1), 24-Methylenecycloartenone (2), and Luteolin (3) from *A. precatorius* Leaves.** Dried leaves (40 g) of *A. precatorius* were extracted with 50% aqueous MeOH. The extract was concentrated and partitioned with chloroform/methanol/water (4:1:5). The organic phase was washed with 1% saline and evaporated to give a tannin-free chloroform-soluble part (1.5 g). This fraction was charged onto a silica gel column and eluted successively with hexane/ethyl acetate (9:1, F1), hexane/ethyl acetate (3:1, F2), hexane/ethyl acetate (1:1) containing 0.1% formic acid (F3), ethyl acetate containing 0.1% formic acid (F4), and methanol containing 0.1% formic acid (F5). The PPA inhibitory activity was observed in F1, F4, and F5.

The less polar F1 (114 mg) was further fractionated by silica gel column chromatography with a hexane/ethyl acetate gradient. The PPA inhibitory activity was eluted mainly in a hexane/ethyl acetate (30:1) eluate (F1-2, 78 mg). F1-2 was further purified by silica gel preparative thin-layer chromatography (TLC) (11:1 hexane/ethyl acetate) to give an active band (F1-2-2, $R_f$ = 0.50, 11 mg). F1-2-2 was finally purified by preparative high-performance liquid chromatography (HPLC) [column, Inertsil ODS-3, 4.6 × 250 mm, GL-Science Co., Tokyo, Japan; mobile phase, MeOH; flow rate, 1.0 mL/min; and detection, ultraviolet (UV) at 210 nm]. Two major peaks were collected and identified as lupenone (**1**, $t_R$ = 21.0 min, 0.7 mg) and 24-methylenecycloartenone (**2**, $t_R$ = 16.0 min, 0.3 mg).

The more polar active fraction (F4, 200 mg) of the first silica gel column was rechromatographed by a silica gel column (hexane/ethyl acetate/methanol). The most polar fraction (F4-4, 110 mg) eluted by hexane/ethyl acetate (1:5) and methanol showed PPA inhibitory activity. The final polar fraction (F5, 480 mg) of the first column was expected to contain the similar active constituents to F4-4, and thus, F4-4 and F5 were merged (F45) and subjected to further fractionation. F45 was chromatographed on a silica gel column with a chloroform/methanol gradient. The PPA inhibitory activity was eluted in a chloroform/methanol (10:1 and 7:1) eluate (F45-5, 75 mg). F45-5 gave a single peak ($t_R$ = 41.3 min) by HPLC analysis [column, Inertsil ODS-3, 4.6 × 250 mm; mobile phase, 10−100% MeOH in water containing 0.1% formic acid (0−60 min); flow rate, 1.0 mL/min; and detection, UV at 254 nm] and was identified as luteolin by comparison to an authentic sample.

*Lupenone (**1**).* FD-MS *m/z*: 424 ([M]$^+$). $^1$H NMR (500 MHz, chloroform-*d*) δ: 0.80 (3H, s), 0.93 (3H, s), 0.96 (3H, s), 1.00−1.16 (3H, m), 1.02 (3H, s), 1.07 (3H, s), 1.07 (3H, s), 1.17−1.52 (15H, m), 1.66−1.72 (2H, m), 1.68 (3H, s), 1.86−1.98 (2H, m), 2.33−2.54 (2H, m), 2.41 (1H, m), 4.57 (1H, m), 4.69 (1H, m). $^{13}$C NMR (125 MHz, chloroform-*d*) δ: 14.5, 15.8, 16.0, 18.0, 19.3, 19.7, 21.0, 21.5, 25.2, 26.7, 27.4, 29.8, 33.6, 34.2, 35.5, 36.9, 38.2, 39.6, 40.0, 40.8, 42.9, 42.9, 47.3, 48.0, 48.3, 49.8, 55.0, 109.4, 150.9, 218.2.

*24-Methylenecycloartenone (**2**).* FD-MS *m/z*: 438 ([M]$^+$). $^1$H NMR (500 MHz, chloroform-*d*) δ: 0.58 (1H, d, *J* = 4.4 Hz), 0.79 (1H, d, *J* = 4.4 Hz), 0.90 (3H, d, *J* = 5.6 Hz), 0.91 (3H, s), 1.00 (3H, s), 1.03 (3H, d, *J* = 6.8 Hz), 1.04 (3H, d, *J* = 6.8 Hz), 1.05 (3H, s), 1.10 (1H, m), 1.10 (3H, s), 1.13 (2H, m), 1.14 (1H, m), 1.31 (1H, m), 1.32 (2H, m), 1.40 (1H, m), 1.41 (1H, m), 1.54 (1H, m), 1.55 (2H, m), 1.59 (1H, m), 1.64 (1H, m), 1.67 (2H, m), 1.71 (1H, dd, *J* = 12.0 and 4.4 Hz), 1.86 [1H, dt, *J* = 14.0 (t) and 5.6 (d) Hz], 1.89 (1H, m), 1.92 (1H, m), 2.05 (1H, m), 2.13 (1H, m), 2.24 (1H, m), 2.30 (1H, m), 2.71 [1H, dt, *J* = 14.0 (t) and 5.6 (d) Hz], 4.67 (1H, brs), 4.72 (1H, brs). $^{13}$C NMR (125 MHz, chloroform-*d*) δ: 18.1, 18.3, 19.3, 20.8, 21.1, 21.5, 21.9, 22.0, 22.2, 25.9, 26.0, 26.8, 28.2, 29.6, 31.3, 32.8, 33.4, 33.8, 35.0, 36.1, 37.5, 45.4, 47.9, 48.5, 48.8, 50.2, 52.3, 106.0, 156.9, 216.6.

*Luteolin (**3**).* FD-MS *m/z*: 286 ([M]$^+$). $^1$H NMR (270 MHz, methanol-$d_4$) δ: 6.20 (1H, d, *J* = 2.1 Hz), 6.43 (1H, d, *J* = 2.1 Hz), 6.54 (1H, s), 6.90 (1H, d, *J* = 8.7 Hz), 7.38 (2H, m).

## RESULTS AND DISCUSSION

In the screening experiment, tannin-free extracts from 2 of 18 Indonesian plants, namely, *A. precatorius* leaves (73%) and *Baeckea frutescens* bark (58%), showed >50% PPA inhibitory activity (Table 1). On the basis of this result, we chose extracts of *A. precatorius* for identifying active principles.

**Table 1. PPA Inhibitory Activity of Tannin-Free Extracts of Indonesian Plants**

| plant | part | inhibitory activity (%)[a] |
|---|---|---|
| *Abrus precatorius* | leaf | 73 |
| *Carica papaya* | leaf | 33 |
| *Gynura procumbens* | aerial part | 6 |
| *Menta arvensis* | leaf | 15 |
| *Ruella napifera* | leaf | 15 |
| *Sida rhombifolia* | aerial part | 12 |
| *Tribulus terrestris* | aerial part | 0 |
| *Caesalpinia sappan* | bark | 0 |
| *Ruellia tuberosa* | fruit | 23 |
| *Helicteres isora* | leaf | 4 |
| *Sonchus arvensis* | fruit | 5 |
| *Cryptocarya massoy* | bark | 0 |
| *Piper nigrum* | seed | 18 |
| *Bruceal javanica* | seed | 2 |
| *Alyxia stellata* | bark | 39 |
| *Baeckea frutescens* | bark | 58 |
| *Murraya paniculata* | aerial part | 22 |
| *Borreria hispida* | leaf | 21 |

[a]The concentration was adjusted to the extractable constituents obtained from 0.3 g of plant material in 1 mL of solution.

The tannin-free organic phase of *A. precatorius* leaves was chromatographed on a silica gel column, and PPA inhibitory activity was observed in two discrete fractions. The less polar active fraction was further chromatographed on a silica gel column followed by silica gel preparative TLC and reverse-phase HPLC to afford two major peaks in the final active fraction. These two constituents were identified as lupenone (**1**)[29] and 24-methylenecycloartenone (**2**)[30] by comparison of their analytical data to those reported in the references and an authentic specimen of lupenone. The more polar active fraction of the first column was also chromatographed on silica gel, and the resultant active eluate showed a single peak in the reverse-phase HPLC analysis. The active constituent of the final fraction was identified as luteolin (**3**) by comparison to an authentic specimen (Figure 1).

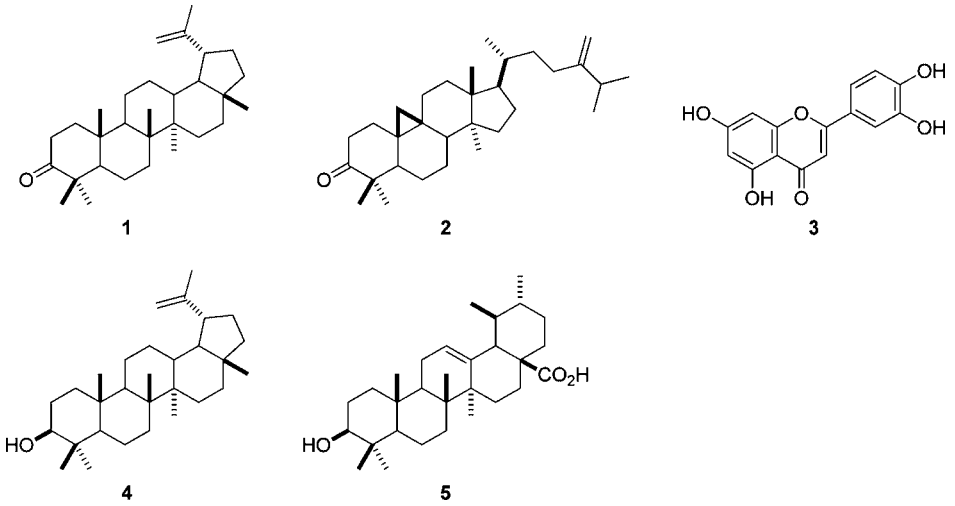


**Figure 1.** Structures of compounds **1**–**5**.

The PPA inhibitory assay of the isolates showed a potent activity of compound **1** ($IC_{50}$ = 31 $\mu$M) and a weaker activity of compound **3** ($IC_{50}$ = 3.1 mM) (Table 2). The activity was not observed in compound **2** (0%) at 0.6 mM, although a further experiment using a higher concentration could not be performed because of the limited sample amount. The potent inhibitory activity of compound **1** against PPA has not ever been reported, whereas compound **3** has been known as a moderate PPA inhibitor.[15,19] The inhibition mode of compound **1** was determined to be mixed-inhibition-type by the double-reciprocal plot experiment (Figure 2).

**Table 2. PPA Inhibitory Activity of Isolated and Related Compounds**

| | inhibitory activity (%) | |
|---|---|---|
| | 50 $\mu$M | 100 $\mu$M |
| **1** | 84 | 87 |
| **2** | *a* | 0[b] |
| **3** | *a* | *a* and *c* |
| **4** | 8 | 16 |
| **5** | 32 | 45 |

[a]Not tested. [b]0% at 0.6 mM. [c]$IC_{50}$ = 3.1 mM.

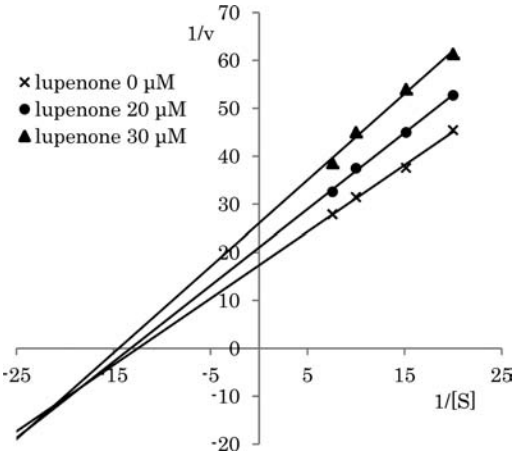


**Figure 2.** Double-reciprocal plot (Lineweaver–Burk) for the $\alpha$-amylase inhibition by lupenone (**1**).

It is interesting that a low-polar triterpene, such as compound **1**, showed significant PPA inhibition, because only few studies have investigated the PPA inhibitory activity of triterpenes. Ali et al. reported triterpenic inhibitors, ursolic acid, oreanolic acid, and lupeol, from a Malaysian plant, *Phyllanthus amarus*, and ursolic acid showed the highest activity among the isolates.[27] The structural similarity of those triterpenes and compound **1** prompted us to perform brief activity comparison experiments. The PPA inhibitory assay of commercially available lupenone (**1**), lupeol (**4**), and ursolic acid (**5**) (Figure 1) at a concentration of 50 $\mu$M showed the strongest activity of compound **1** (84%), followed by compound **5** (32%), and the lowest activity of compound **4** (8%) (Table 2). These results together with the low inhibitory activity of compound **2** show that both the lupane skeleton and a ketone at C-3 would be essential for exerting a potent PPA inhibition. To the best of our knowledge, this is the first finding of the potent PPA inhibitory activity of lupenone, although some other biological activities,[29,31] including $\alpha$-glucosidase inhibition,[32] have been reported for compound **1**. There are a few examples of non-polyphenolic low-polar small-molecular inhibition against PPA. It should be interesting to determine how efficiently a low-polar molecule, such as compound **1**, could associate with the PPA enzyme.

In conclusion, the enzyme assay-guided fractionation of the extract from the dried leaves of *A. precatorius* led to the isolation of a triterpene ketone, lupenone (**1**), as a potent PPA inhibitor, together with lower active luteolin (**3**). The relatively higher activity of compound **1** and the larger amount of compound **3** present in *A. precatorius* leaves suggest that both compounds contribute to the inhibitory activity of this plant. *A. precatorius* may have a potential for the treatment of diabetes, although *in vivo* experiments are warranted.

## AUTHOR INFORMATION

### Corresponding Author

*Telephone/Fax: +81-11-706-2496. E-mail: junk@chem.agr.hokudai.ac.jp.

### Notes

The authors declare no competing financial interest.

## ■ ACKNOWLEDGMENTS

The authors thank Yusuke Takata and Dr. Eri Fukushi of the GC−MS and NMR Laboratory, Faculty of Agriculture, Hokkaido University, for their skillful measurements of mass spectra.

## ■ REFERENCES

(1) King, H.; Aubert, R. E.; Herman, W. H. Global burden of diabetes, 1995−2025; prevalence, numerical estimates, and projections. *Diabetes Care* **1998**, *21*, 1414−1431.

(2) Puls, W.; Keup, U.; Krause, H. P.; Thomas, G.; Hofmeister, F. Glucosidase inhibition: A new approach to the treatment of diabetes, obesity, and hyperlipoproteinaemia. *Naturwissenschaften* **1977**, *64*, 536−537.

(3) Matsui, T.; Ogunwande, I. A.; Abesundara, K. J. M.; Matsumoto, K. Anti-hyperglycemic potential of natural products. *Mini-Rev. Med. Chem.* **2006**, *6*, 109−120.

(4) Kumar, S.; Narwal, S.; Kumar, V.; Prakash, O. α-Glucosidase inhibitors from plants: A natural approach to treat diabetes. *Pharmacogn. Rev.* **2011**, *5*, 19−29.

(5) Jong-Anurakkun, N.; Bhandari, M. R.; Kawabata, J. α-Glucosidase inhibitors from devil tree (*Alstonia scholaris*). *Food Chem.* **2007**, *103*, 1319−1323.

(6) Gao, H.; Huang, Y.-N.; Gao, B.; Xu, P.-Y.; Inagaki, C.; Kawabata, J. α-Glucosidase inhibitory effect by the flower buds of *Tussilago farfara* L. *Food Chem.* **2008**, *106*, 1195−1201.

(7) Yoshida, K.; Hishida, A.; Iida, O.; Hosokawa, K.; Kawabata, J. Flavonol caffeoylglycosides as α-glucosidase inhibitors from *Spiraea cantoniensis* flower. *J. Agric. Food Chem.* **2008**, *56*, 4367−4371.

(8) Takahashi, K.; Yoshioka, Y.; Kato, E.; Katsuki, S.; Iida, O.; Hosokawa, K.; Kawabata, J. Methyl caffeate as an α-glucosidase inhibitor from *Solanum torvum* fruits and the activity of its related compounds. *Biosci., Biotechnol., Biochem.* **2010**, *74*, 741−745.

(9) Gunawan-Puteri, M. D. P. T.; Kawabata, J. Novel α-glucosidase inhibitors from *Macaranga tanarius* leaves. *Food Chem.* **2010**, *123*, 384−389.

(10) Hansawasdi, C.; Kawabata, J.; Kasai, T. α-Amylase inhibitors from roselle (*Hibiscus sabdariffa* Linn.) tea. *Biosci., Biotechnol., Biochem.* **2000**, *64*, 1041−1043.

(11) Bhandari, M. R.; Jong-Anurakkun, N.; Gao, H.; Kawabata, J. α-Glucosidase and α-amylase inhibitory activities of Nepalese medicinal herb Pakhanbhed (*Bergenia ciliata* Haw.). *Food Chem.* **2008**, *106*, 247−252.

(12) Gunawan-Puteri, M. D. P. T.; Kato, E.; Kawabata, J. α-Amylase inhibitors from an Indonesian medicinal herb, *Phyllanthus urinaria*. *J. Sci. Food Agric.* **2012**, *92*, 606−609.

(13) Brayer, G. D.; Sidhu, G.; Maurus, R.; Rydberg, E. H.; Braun, C.; Wang, Y.; Nguyen, N. T.; Overall, C. M.; Withers, S. G. Subsite mapping of the human pancreatic α-amylase active site through structural, kinetic, and mutagenesis techniques. *Biochemistry* **2000**, *39*, 4778−4791.

(14) Li, C.; Begum, A.; Numao, S.; Park, K. H.; Withers, S. G.; Brayer, G. D. Acarbose rearrangement mechanism implied by the kinetic and structural analysis of human pancreatic α-amylase in complex with analogues and their elongated counterparts. *Biochemistry* **2005**, *44*, 3347−3357.

(15) Kim, J.-S.; Kwon, C.-S.; Son, K. H. Inhibition of α-glucosidase and amylase by luteolin, a flavonoid. *Biosci., Biotechnol., Biochem.* **2000**, *64*, 2458−2461.

(16) McDougall, G. J.; Shpiro, F.; Dobson, P.; Smith, P.; Blake, A.; Stewart, D. Different polyphenolic components of soft fruits inhibit α-amylase and α-glucosidase. *J. Agric. Food Chem.* **2005**, *53*, 2760−2766.

(17) He, Q.; Lv, Y.; Yao, K. Effects of tea polyphenols on the activities of α-amylase, pepsin, trypsin and lipase. *Food Chem.* **2006**, *101*, 1178−1182.

(18) Li, H.; Tanaka, T.; Zhang, Y.-J.; Yang, C.-R.; Kouno, I.; Rubusuaviins, A.-F. Monomeric and oligomeric ellagitannins from Chinese sweet tea and their α-amylase inhibitory activity. *Chem. Pharm. Bull.* **2007**, *55*, 1325−1331.

(19) Piparo, E. L.; Scheib, H.; Frei, N.; Williamson, G.; Grigorov, M.; Chou, C. J. Flavonoids for controlling starch digestion: Structural requirements for inhibiting human α-amylase. *J. Med. Chem.* **2008**, *51*, 3555−3561.

(20) Tarling, C. A.; Woods, K.; Zhang, R.; Brastianos, H. C.; Brayer, G. D.; Andersen, R. J.; Withers, S. G. The search for novel human pancreatic α-amylase inhibitors: High-throughput screening of terrestrial and marine natural product extracts. *ChemBioChem* **2008**, *9*, 433−438.

(21) Najafian, M.; Ebrahim-Habibi, A.; Hezareh, N.; Yaghmaei, P.; Parivar, K.; Larijani, B. *trans*-Chalcone: A novel small molecule inhibitor of mammalian α-amylase. *Mol. Biol. Rep.* **2011**, *38*, 1617−1620.

(22) D'Silva, I.; Vaidyanathan, C. S.; Podder, S. K. Ribosome-inactivating proteins and agglutinins from callus and suspension cultures of *Ricinus communis* L. and *Abrus precatorius* L. *Plant Sci.* **1993**, *94*, 161−172.

(23) Olsnes, S. The history of ricin, abrin and related toxins. *Toxicon* **2004**, *44*, 361−370.

(24) Attal, A. R.; Otari, K. V.; Shete, R. V.; Upasani, C. D.; Nandgude, T. D. *Abrus precatorius* Linnaeus: A phytopharmacological review. *J. Pharm. Res.* **2010**, *3*, 2585−2587.

(25) De Britto, A. J.; Kumar, P. B. J. R.; Gracelin, D. H. S. *Abrus precatorius* L.: A medicinal plant with potential as antibacterial agent. *J. Pharm. Res.* **2012**, *5*, 1207−1209.

(26) Shenoy, A.; Varghese, B. P.; Rajan, M. S.; Koshy, S.; Joshi, M.; Shabaraya, A. R. Anticonvulsant activity of ethanolic extract of *Abrus precatorius* leaves. *Adv. Res. Pharm. Biol.* **2012**, *2*, 53−61.

(27) Ali, H.; Houghton, P. J.; Soumyanath, A. α-Amylase inhibitory activity of some Malaysian plants used treat diabetes; with particular reference to *Phyllanthus amarus*. *J. Ethnopharmacol.* **2006**, *107*, 449−455.

(28) Wall, M. E.; Wan, M. C.; Brown, D. M.; Fullas, F.; Olwald, J. B.; Josephson, F. F.; Thornton, N. M.; Pezzuto, J. M.; Beecher, C. W. W.; Farnsworth, N. R.; Cordell, G. A.; Kinghorn, A. D. Effect of tannins on screening of plant extracts for enzyme inhibitory activity and techniques for their removal. *Phytomedicine* **1996**, *3*, 281−285.

(29) Na, M.; Kim, B. Y.; Osada, H.; Ahn, J. S. Inhibition of protein tyrosine phosphatase 1B by lupeol and lupenone isolated from *Sorbus commixta*. *J. Enzyme Inhib. Med. Chem.* **2009**, *24*, 1056−1059.

(30) Jayasinghe, U. L. B.; Vithana, H. S. K.; Wannigama, G. P.; Fujimoto, Y. 24-Methylenecycloartenone from *Bhesa nitidissima*. *Fitoterapia* **2001**, *72*, 594−595.

(31) Ahn, E.-K.; Oh, J. S. Lupenone isolated from *Adenophora triphylla* var. *japonica* extract inhibits adipogenic differentiation through the downregulation of PPARγ in 3T3-L1 cells. *Phytother. Res.* **2013**, *27*, 761−766.

(32) Mohamed, I. E.; El Nur, E. B. E.; Choudhary, M. I.; Khan, S. N. Bioactive natural products from two Sudanese medicinal plants *Diospyros mespiliformis* and *Croton zambesicus*. *Rec. Nat. Prod.* **2009**, *3*, 198−203.

JOURNAL OF AGRICULTURAL AND FOOD CHEMISTRY

Article

pubs.acs.org/JAFC

# Capsaicinoids but Not Their Analogue Capsinoids Lower Plasma Cholesterol and Possess Beneficial Vascular Activity

Weihuan Huang,[†,§] Wai San Cheang,[‡] Xiaobo Wang,[†] Lin Lei,[†] Yuwei Liu,[†] Ka Ying Ma,[†] Fangrui Zheng,[#] Yu Huang,[‡] and Zhen-Yu Chen*[,†]

[†]Food and Nutritional Sciences Program, School of Life Sciences, [‡]School of Biomedical Sciences, and [#]Department of Chemistry, The Chinese University of Hong Kong, Shatin, NT, Hong Kong, China

[§]Institute of Traditional Chinese Medicine and Natural Products, Jinan University, Guangzhou, China

Supporting Information

**ABSTRACT:** Capsaicinoids exist in chili peppers, whereas capsinoids are present in some sweet peppers. The present study investigated the effects of capsaicinoids and capsinoids on plasma lipids, relaxation of the aorta, atherosclerotic plaque development, and fecal sterol excretion in hamsters fed a high-cholesterol diet. Five groups of male hamsters were given the control diet or one of the four experimental diets containing 1.3 mmol of capsaicinoids (NL), 2.6 mmol of capsaicinoids (NH), 1.3 mmol of capsinoids (OL), or 2.6 mmol of capsinoids (OH), respectively. Results showed capsaicinoids but not capsinoids could decrease plasma total cholesterol (TC), reduce the formation of atherosclerotic plaque, and relax the aortic artery. This was accompanied by a 28−175% increase in fecal excretion of acidic sterols in hamsters fed the diets containing capsaicinoids. Similarly, capsaicinoids but not capsinoids could decrease the pad weights of epididymal and prerenal adipose tissues. It was concluded that capsaicinoids but not capsinoids could favorably modulate plasma lipids and possess beneficial vascular activity.

**KEYWORDS:** *aorta, capsaicinoids, capsinoids, cholesterol, atherosclerosis, pepper*

## INTRODUCTION

Capsaicinoids refer to a group of well-known pungent compounds found in the fruits of chili pepper plant *Capsicum*, whereas capsinoids are the nonpungent analogues of capsaicinoids isolated in the fruits of sweet pepper *Capsicum* CH-19.[1,2] Capsaicinoids consists of mainly two isomers, namely, capsaicin and dihydrocapsaicin, whereas capsinoids also have two major isomers, capsiate and dihydrocapsiate (Figure 1). The structural difference is that capsaicinoids are fatty acid amides linked with vanillylamine, whereas capsinoids are fatty acid esters linked with vanillyl alcohol.

Health benefits associated with the consumption of capsaicinoids have been well reported. It has been shown that capsaicinoids can promote weight reduction by enhancing fat oxidation and increasing adrenergic activity and energy expenditure.[3] Research has also demonstrated that capsaicinoids have some beneficial effect on the human cardiovascular system, possess some antitumor activity, and also decrease plasma lipids.[4−8] Like capsaicinoids, capsinoids are also able to reduce body fat by increasing thermogenesis[9] and possess some antitumor activity.[4]

Capsaicinoids are beneficial for people who love spicy foods, whereas capsinoids may be an alternative for people who cannot tolerate spicy foods. In view of the structural similarity between capsaicinoids and capsinoids, the present study was the first to examine if capsaicinoids and capsinoids were both able to reduce plasma cholesterol concentration and formation of atherosclerosis plaque. We also sought to ascertain whether capsaicinoids and capsinoids could improve endothelial function and possess beneficial vascular activity. The major findings were that only capsaicinoids but not capsinoids could reduce the plasma cholesterol concentration and possessed vasorelaxation activity.

## MATERIALS AND METHODS

**Capsinoid Synthesis.** Capsinoids are not commercially available in large quantities. We therefore had to use capsaicinoids as starting materials to synthesize their corresponding capsinoids. Capsaicinoids containing 51.3% capsaicin and 46.2% dihydrocapsaicin were purchased from Henan Bis-Biotech Co. Ltd. (Henan, China). Vanillyl alcohol was purchased from Sigma-Aldrich Chemical Co. (St. Louis, MO, USA). Lipase enzyme (Lipozyme 435) was purchased from Guangzhou Minagyao Trading Co. Ltd. (Guangzhou, China). To obtain a capsinoid mixture of 51.3% capsiate and 46.2% dihydrocapsiate, the mixture of acyl donors was prepared with capsaicinoids according to the method described by Kobata et al.[10] and Dong et al.[11] In brief, 3 g of capsaicinoids was dissolved in 1 L of 4 N HCl in 67% methanol and was refluxed for 48 h. Then *n*-hexane was added to the solution to extract the acyl donors (Figure 1). Capsinoids were synthesized by adding 10 g of Lipozyme 435 into a solution of acetone (1 L) containing vanillyl alcohol (7.7 g) and acyl donors (14.2 g). After being incubated in a shaker at 25 °C for 48 h, the reaction mixture was filtered to remove the enzymes, and the solvent was evaporated in a rotary evaporator. The crude capsinoids were loaded onto a silica column and eluted using a solvent mixture of hexane and ethyl acetate (6:1, v/v), producing 4 g of capsinoids. Structures of synthesized capsinoids were confirmed using NMR (Supporting Information Supplementary Figures 1 and 2). HPLC analysis found that capsinoids consisted of 52.4% capsiate and 44.9% dihydrocapsiate

Received: June 18, 2014
Revised: July 31, 2014
Accepted: July 31, 2014
Published: July 31, 2014

 © 2014 American Chemical Society 

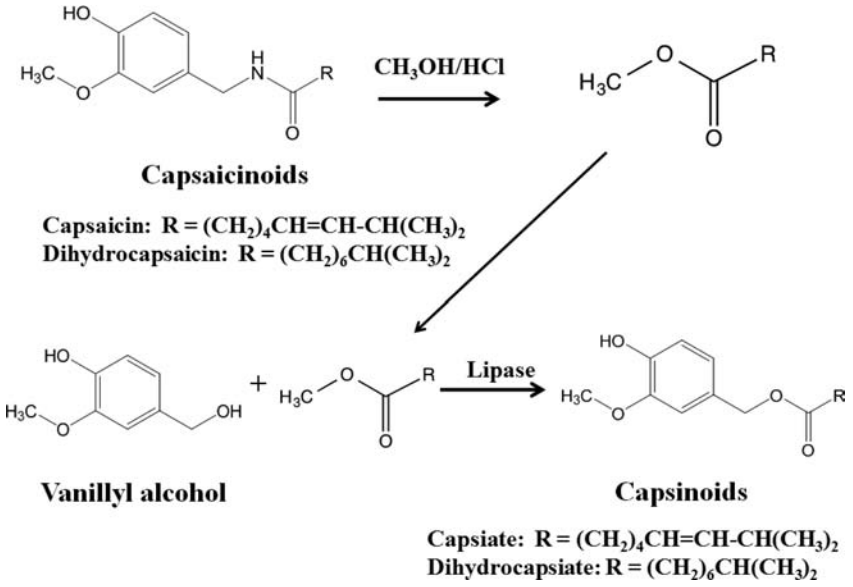


**Figure 1.** Synthesis of capsinoids (capsiate and dihydrocapsiate) from capsaicinoids (capsaicin and dihydrocapsaicin). Modified from reference 11.

with such a ratio being similar to that in sweet pepper (Supporting Information Supplementary Figure 3).

**Diet.** Five diets were prepared by modifying the formulation as we previously described.[12] The control diet was prepared by mixing all powdered ingredients (g/kg): corn starch, 507; casein, 241; lard, 50; sucrose, 119; mineral mix, 40, vitamin mix, 20; geltatin, 20; DL-methionine, 1; cholesterol, 2 (Table 1). The four experimental diets were similarly prepared by mixing the control diet with 1.3 mmol of capsaicinoids (NL), 2.6 mmol of capsaicinoids (NH), 1.3 mmol of capsinoids (OL), or 2.6 mmol of capsinoids (OH), respectively. Such amounts of capsaicinoids and capsinoids added into diets were equivalent to a daily dose of 7−14 mg/kg body weight, which could be achieved by humans who love chili hot foods.[13] All five diets contained 0.2% cholesterol by weight and had 68.2, 26.4, and 5.4% energy from carbohydrate, protein, and fat, respectively.

**Table 1. Composition of the Control Diet and Four Experimental Diets Containing 1.3 mmol of Capsaicinoids (NL), 2.6 mmol of Capsaicinoids (NH), 1.3 mmol of Capsinoids (OL), or 2.6 mmol of Capsinoids (OH), Respectively**

| ingredient (per kg diet) | control | NL | NH | OL | OH |
|---|---|---|---|---|---|
| corn starch (g) | 507 | 507 | 507 | 507 | 507 |
| casein (g) | 241 | 241 | 241 | 241 | 241 |
| sucrose (g) | 119 | 119 | 119 | 119 | 119 |
| lard (g) | 50 | 50 | 50 | 50 | 50 |
| mineral mixture AIN-76 (g) | 40 | 40 | 40 | 40 | 40 |
| vitamin mixture AIN-76A (g) | 20 | 20 | 20 | 20 | 20 |
| gelatin (g) | 20 | 20 | 20 | 20 | 20 |
| DL-methionine (g) | 1 | 1 | 1 | 1 | 1 |
| cholesterol (g) | 2 | 2 | 2 | 2 | 2 |
| capsaicinoids (mmol) | 0 | 1.3 | 2.6 | 0 | 0 |
| capsinoids (mmol) | 0 | 0 | 0 | 1.3 | 2.6 |

**Hamsters.** We chose hamsters as model because cholesterol metabolism in hamsters is close to that in humans.[14] The experiments were approved and conducted in accordance with the guidelines set by the Animal Experimental Ethics Committee, The Chinese University of Hong Kong. Golden hamsters ($n$ = 50, body weight = 116 ± 6 g) were divided into five groups and fed the control or one of the four experimental diets as described above for 6 weeks. All hamsters were given fresh diet daily and housed in an animal room at 23 °C with a 12/12 h light/dark cycle. The hamsters were allowed free access to food and water. Blood sample was taken from the retro-orbital sinus under light anesthesia using a mixture of ketamine, xylazine, and saline (4:1:5; v/v/v) after overnight fasting at weeks 0, 3, and 6. At the end of experiment, all hamsters were killed under carbon dioxide anesthesia; the abdomen was opened with blood being sampled from the aorta into a syringe. The fecal output from each hamster was collected and pooled at weeks 1 and 6, then freeze-dried, ground, and saved for neutral and acidic sterol analyses.

**Plasma Lipids.** Plasma total cholesterol (TC), high-density lipoprotein cholesterol (HDL-C), and triacylglycerols (TG) were measured using their respective commercial enzymatic kits from Infinity (Waltham, MA, USA) and Stanbio Laboratories (Boerne, TX, USA), respectively. Non-HDL cholesterol (non-HDL-C) was calculated by deducting HDL-C from the TC.

**Atherosclerotic Plaque.** The aorta was used to assess atherosclerosis as we previously described.[12] In brief, the thoracic aorta was cut open vertically followed by staining in a 10 mL ethanol solution containing 0.5 g of Sudan III for 3 h. Afterward, Sudan III was washed with distilled water three times and scanned with a table scanner. The area of atherosclerotic plaque was measured with the aid of a computer image analysis program (Sigma Scan Pro 5.0, SPSS, Inc., Chicago, IL, USA).[12]

**Hepatic Cholesterol.** Total cholesterol in the liver was quantified as previously described.[15] Total liver cholesterol was extracted using a mixture of chloroform/methanol (2:1, v/v). 5$\alpha$-Cholestane as an internal standard was added during the extraction. Other lipids were saponified and removed. The nonsaponified fraction containing cholesterol was saved, and free cholesterol was converted to its TMS-ether derivative by a commercial TMS reagent (Sigma, Hong Kong). Analysis of the cholesterol TMS-ether derivative was performed in an SAC-5 column in a Shimadzu GC-14B GLC equipped with a flame ionization detector. Hepatic cholesterol was calculated according to the amount of internal standard 5$\alpha$-cholestane added.

**Fecal Neutral and Acidic Sterols.** The total fecal output was collected and saved for the measurement of total fecal neutral and acidic sterols as previously described.[15] In brief, total fecal sterols were extracted with 5$\alpha$-cholestane being added as an internal standard for quantification of fecal neutral sterols, whereas hyodeoxycholic acid was added as an internal standard for the quantification of total acidic sterols. First, the fecal samples were saponified, the total neutral sterols were extracted into cyclohexane, and the neutral sterols were converted into their TMS derivatives. Second, total fecal acidic sterols in the aqueous phase after cyclohexane extraction were also extracted

**Table 2. Change in Food Consumption, Body Weight, and Relative Organ Weights in Hamsters Fed the Control and the Four Experimental Diets Diets Containing 1.3 mmol of Capsaicinoids (NL), 2.6 mmol of Capsaicinoids (NH), 1.3 mmol of Capsinoids (OL), or 2.6 mmol of Capsinoids (OH), Respectively, at Week 6[a]**

| | control | NL | NH | OL | OH |
|---|---|---|---|---|---|
| food intake (g/day) | 8.5 ± 0.3 | 7.9 ± 0.4 | 7.8 ± 0.3 | 8.5 ± 0.4 | 7.8 ± 0.3 |
| body weight (g) | | | | | |
| initial | 116.7 ± 4.3 | 115.1 ± 6.6 | 118.9 ± 5.2 | 116.4 ± 6.9 | 116.5 ± 7.8 |
| final | 125.8 ± 4.7 | 121.9 ± 5.0 | 124.4 ± 1.0 | 124.1 ± 8.6 | 121.7 ± 8.5 |
| relative weight (% body weight) | | | | | |
| liver | 5.0 ± 0.3 | 4.9 ± 0.3 | 5.2 ± 0.5 | 5.2 ± 0.2 | 5.1 ± 0.3 |
| heart | 0.33 ± 0.02 | 0.32 ± 0.01 | 0.32 ± 0.01 | 0.32 ± 0.02 | 0.33 ± 0.02 |
| kidney | 0.9 ± 0.1 | 0.9 ± 0.1 | 1.0 ± 0.1 | 0.9 ± 0.1 | 0.9 ± 0.1 |
| testis | 2.7 ± 0.3 | 2.6 ± 0.4 | 2.3 ± 0.8 | 2.2 ± 0.5 | 2.5 ± 0.5 |
| epididymal fat pad | 1.9 ± 0.3a | 1.6 ± 0.3b | 1.5 ± 0.2b | 1.8 ± 0.3ab | 1.7 ± 0.2ab |
| perirenal fat pad | 1.2 ± 0.3a | 1.0 ± 0.2ab | 0.8 ± 0.2b | 1.1 ± 0.2ab | 1.1 ± 0.1ab |

[a]Data are expressed as the mean ± SD; $n = 10$. Means in the same row with different letters differ significantly at $P < 0.05$.

**Table 3. Changes in Plasma Total Cholesterol (TC), Triacylglycerols (TG), HDL-Cholesterol (HDL-C), Non-HDL-Cholesterol (Non-HDL-C), Non-HDL-C/HDL-C, HDL/TC, Liver Total Cholesterol, and Aortic Atherosclerotic Plaque in Hamsters Fed the Control or One of the Four Experimental Diets Containing 1.3 mmol of Capsaicinoids (NL), 2.6 mmol of Capsaicinoids (NH), 1.3 mmol of Capsinoids (OL), or 2.6 mmol of Capsinoids (OH), Respectively[a]**

| | control | NL | NH | OL | OH |
|---|---|---|---|---|---|
| week 0 | | | | | |
| TC (mg/dL) | 127.9 ± 9.7 | 127.9 ± 9.5 | 125.1 ± 10.2 | 127.3 ± 13.3 | 127.8 ± 12.0 |
| HDL-C (mg/dL) | 65.3 ± 13.8 | 64.0 ± 14.3 | 65.1 ± 20.7 | 65.2 ± 23.6 | 67.7 ± 17.7 |
| TG (mg/dL) | 79.0 ± 24.4 | 80.7 ± 38.4 | 77.8 ± 30.1 | 80.4 ± 36.9 | 79.1 ± 23.6 |
| non-HDL-C (mg/dL) | 62.6 ± 14.1 | 63.9 ± 14.4 | 60.0 ± 26.6 | 62.1 ± 19.9 | 60.0 ± 17.0 |
| non-HDL-C/HDL-C | 1.0 ± 0.4 | 1.0 ± 0.4 | 1.1 ± 0.6 | 1.2 ± 0.8 | 1.0 ± 0.6 |
| HDL/TC | 0.5 ± 0.1 | 0.5 ± 0.1 | 0.5 ± 0.2 | 0.5 ± 0.2 | 0.5 ± 0.1 |
| week 3 | | | | | |
| TC (mg/dL) | 240.6 ± 27.6a | 217.1 ± 29.7ab | 202.8 ± 36.3b | 237.8 ± 25.2a | 239.5 ± 29.7a |
| HDL-C (mg/dL) | 117.6 ± 13.6a | 102.2 ± 12.2b | 100.5 ± 19.2b | 120.8 ± 11.8a | 120.8 ± 10.0a |
| TG (mg/dL) | 150.8 ± 63.4ab | 138.3 ± 31.5b | 121.0 ± 33.9b | 181.7 ± 43.5a | 163.1 ± 41.7ab |
| non-HDL-C | 123.1 ± 20.9a | 114.9 ± 18.6ab | 102.4 ± 20.4b | 117.2 ± 18.8ab | 118.6 ± 15.6ab |
| non-HDL-C/HDL-C | 1.05 ± 0.19ab | 1.12 ± 0.08a | 1.04 ± 0.18ab | 0.98 ± 0.16b | 0.98 ± 0.11b |
| HDL/TC | 0.48 ± 0.05ab | 0.47 ± 0.05b | 0.49 ± 0.05ab | 0.51 ± 0.04a | 0.51 ± 0.04ab |
| week 6 | | | | | |
| TC (mg/dL) | 216.2 ± 35.3a | 203.9 ± 30.1ab | 179.3 ± 56.7b | 220.9 ± 30.5a | 219.2 ± 33.0a |
| HDL-C (mg/dL) | 114.7 ± 13.5a | 108.8 ± 21.5a | 90.4 ± 28.4b | 103.8 ± 15.9ab | 109.0 ± 16.9a |
| TG (mg/dL) | 171.2 ± 13.2 | 168.8 ± 42.3 | 169.4 ± 56.2 | 173.5 ± 43.5 | 151.5 ± 39.2 |
| non-HDL-C (mg/dL) | 101.2 ± 25.6abc | 95.2 ± 15.8bc | 88.9 ± 27.2c | 117.0 ± 20.4a | 110.2 ± 22.1ab |
| non-HDL-C/HDL-C | 0.88 ± 0.18b | 0.86 ± 0.19b | 0.98 ± 0.29ab | 1.18 ± 0.22a | 1.01 ± 0.19a |
| HDL-C/TC | 0.53 ± 0.05b | 0.53 ± 0.05b | 0.50 ± 0.15ab | 0.47 ± 0.05a | 0.5 ± 0.05a |
| liver cholesterol (mg/g) | 53.5 ± 16.6a | 43.2 ± 12.0b | 37.9 ± 9.7b | 50.6 ± 11.2ab | 56.6 ± 10.4a |
| aortic atherosclerotic plaque (% area) | 25.7 ± 4.6a | 18.1 ± 6.3b | 17.8 ± 6.7b | 26.8 ± 5.5a | 24.1 ± 3.0a |

[a]Data are expressed as the mean ± SD; $n = 10$. Means in the same row with different letters differ significantly at $P < 0.05$.

and similarly converted into their TMS derivatives. Individual neutral and acidic sterol TMS derivatives were then subjected to GC analysis on an SAC-5 column in a Shimadzu GC-14B GLC equipped with a flame ionization detector.

**Endothelium-Dependent Relaxation in Rat Mesenteric Artery.** To assess the effect of capsaicinoids and capsinoids on the functionality of the artery, endothelium-dependent relaxation was measured in rat mesenteric artery as previously described.[16] In brief, rats were sacrificed by $CO_2$ suffocation. Superior mesenteric arteries were dissected out and placed in ice-cold Krebs solution (mmol/L): 119 NaCl, 4.7 KCl, 2.5 $CaCl_2$, 1 $MgCl_2$, 25 $NaHCO_3$, 1.2 $KH_2PO_4$, and 11 D-glucose. Arteries were cleaned of adhering tissue and cut into ring segments of 2 mm in length. Rings were suspended in a myograph (Danish Myo Technology, Aarhus, Denmark) for recording of changes in isometric tension. After a 60 min equilibration period, each ring was first contracted by 60 mmol/L KCl and then washed in Krebs solution three times. Phenylephrine at 1 μmol/L was used to induce steady contraction of the ring and the effect of capsaicinoids or capsinoids was then determined.

**Culture of Human Umbilical Cord Vein Endothelial Cells (HUVECs).** HUVECs (CC-3317, Clonetics, Lonza, Walkersville, MD, USA) were grown in endothelial cell growth medium (Clonetics) supplemented with bovine brain extract and 1% penicillin and streptomycin. Cells were grown in 75 $cm^2$ flasks and maintained at 37 °C in a 95% humidified air/5% $CO_2$ atmosphere. Medium was changed every 2 days. Confluent cells were passaged by trypsinization (0.25% trypsin with 2.5 mmol/L EDTA in PBS). Experiments were performed on cells at passage 4−8 when 80−90% confluency was achieved.

**Measurement of Intracellular $Ca^{2+}$ Concentration by Fluorescence Microscopy.** HUVECs were treated at 37 °C for 60 min with 10 μmol/L calcium indicator fluo-4 AM (Molecular Probes,

Table 4. Cholesterol Intake and Changes in Fecal Sterol Profile in Hamsters Fed the Control or One of the Four Experimental Diets Containing 1.3 mmol of Capsaicinoids (NL), 2.6 mmol of Capsaicinoids (NH), 1.3 mmol of Capsinoids (OL), or 2.6 mmol of Capsinoids (OH), Respectively, at Week 6[a]

| | control | NL | NH | OL | OH |
|---|---|---|---|---|---|
| cholesterol intake (mg/hamster/day) | 16.98 ± 0.54 | 15.78 ± 0.72 | 15.58 ± 0.68 | 16.98 ± 0.85 | 15.98 ± 0.69 |
| fecal neutral sterols (mg/hamster/day) | | | | | |
| coprostanol | 0.32 ± 0.10 | 0.49 ± 0.31 | 0.64 ± 0.10 | 0.47 ± 0.07 | 0.38 ± 0.04 |
| coprostanone | 0.31 ± 0.15 | 0.26 ± 0.26 | 0.10 ± 0.06 | 0.09 ± 0.04 | 0.09 ± 0.03 |
| cholesterol | 0.82 ± 0.58 | 0.71 ± 0.37 | 1.01 ± 0.22 | 0.58 ± 0.23 | 0.56 ± 0.09 |
| dihydrocholesterol | 0.17 ± 0.10 | 0.12 ± 0.04 | 0.17 ± 0.02 | 0.17 ± 0.03 | 0.13 ± 0.02 |
| total sterols | 1.62 ± 0.57 | 1.58 ± 0.59 | 1.91 ± 0.28 | 1.32 ± 0.30 | 1.15 ± 0.11 |
| fecal acidic sterols (mg/hamster/day) | | | | | |
| lithocholic acid | 1.39 ± 0.46b | 1.66 ± 0.62b | 4.00 ± 0.78a | 1.45 ± 0.53b | 1.30 ± 0.63b |
| deoxycholic acid | 0.37 ± 0.16 | 0.44 ± 0.15 | 0.58 ± 0.07 | 0.41 ± 0.32 | 0.28 ± 0.17 |
| chenodeoxycholic acid | 0.47 ± 0.21b | 0.74 ± 0.46b | 1.55 ± 0.26a | 0.61 ± 0.27b | 0.48 ± 0.20b |
| total acid sterols | 2.23 ± 0.71b | 2.85 ± 1.23b | 6.13 ± 0.7a | 2.48 ± 0.58b | 2.08 ± 0.54b |

[a]Data are expressed as the mean ± SD; $n$ = 10 each group. Means in the same row with different letters differ significantly at $P < 0.05$.

Eugene, OR, USA) in normal physiological saline solution containing (mmol/L) 140 NaCl, 5 KCl, 1 $CaCl_2$, 1 $MgCl_2$, 10 glucose, and 5 HEPES (pH ~7.4). Fluorescent images were obtained under a fluorescence microscope (Olympus, Tokyo, Japan) (excitation, 495 nm; emission filter, 505−525 nm) every 5 s continuously. Changes in intracellular $Ca^{2+}$ concentration triggered by the addition of capsaicinoids or capsinoids was expressed as $F_1/F_0$ ratio, where $F_1$ is the fluorescence intensity at a specific time point and $F_0$ is the signal measured at the starting point of image recording.

**Statistical Analysis.** Data are expressed as the mean ± SD ($n$ = 10 for the experiment on hamsters and $n$ = 4 for the experiment on aortic relaxation). One-way analysis of variance followed by using Fisher's LSD method was used to statistically evaluate differences in plasma lipids, aortic functions, and atherosclerotic plaque among the five groups.

## RESULTS

**Food Intake and Body and Organ Weights.** No differences in food intake, body weight, and relative weights of heart, kidney, and testis were seen among the five groups (Table 2). However, the relative weights of epididymal and perirenal fat pats were smaller in NL and NH groups fed the diets containing capsaicinoids compared with those in the control hamsters ($P < 0.05$). However, no significant difference was seen among the control, OL, and OH hamsters.

**Plasma TC, HDL-C, Non-HDL-C, and TG.** The five groups of hamsters had similar concentrations of plasma TC, HDL-C, non-HDL-C, and TG at week 0 (Table 3). When the experiment reached the end of weeks 3 and 6, NH groups had plasma TC, non-HDL-C, and TG concentrations significantly lower than the control hamsters. It was clear that capsaicinoids decreased plasma cholesterol in a dose-dependent manner ($P < 0.05$). However, two capsinoids groups, OL and OL, had no effect on plasma TC, non-HDL-C, and HDL (Table 3).

**Liver Cholesterol and Atherosclerotic Plaque.** Two capsaicinoids groups, NL and NH, significantly decreased hepatic cholesterol concentrations in a dose-dependent manner compared with the control hamsters, whereas two capsinoids groups, OL and OH, had no effect on hepatic cholesterol concentration (Table 3). A similar trend in atherosclerotic plaque was seen. Hamsters fed NL and NH diets had less atherosclerotic plaque, whereas those fed OL and OH groups had levels of atherosclerotic plaque similar to those of the control hamsters (Table 3).

**Fecal Neutral and Acidic Sterols.** In the colon, cholesterol is subjected to microbial bioconversion, producing series of cholesterol microbial metabolites with coprostanol and dihydrocholesterol being the major products. To simplify the presentation, only data on fecal samples collected from week 6 are reported. As shown in Table 4, capsaicinoids had a trend of increasing the excretion of fecal cholesterol and coprostanol; however, the effect was statistically insignificant. Capsinoids had no effect on total excretion of fecal neutral sterols. With regard to fecal acidic sterol excretion, it was evident that capsaicinoids but not capsinoids increased their excretion.

**Endothelium-Dependent Relaxation.** In phenylephrine-contracted superior mesenteric arteries, capsaicinoids beneficially induced relaxation in a dose-dependent manner. By contrast, capsinoids were without any beneficial effect (Figure 2A).

**$Ca^{2+}$ Influx.** Acute exposure to capsaicinoids stimulated an increase of intracellular $Ca^{2+}$ level in HUVECs in a concentration-dependent manner (Figure 2B), whereas capsinoids led to little rise of intracellular $Ca^{2+}$ (Figure 2C).

## DISCUSSION

Capsaicinoids are present in large quantity in most chili peppers and can induce strong pungent sensations, whereas capsinoids are not pungent and are present in only a small amount in sweet pepper CH-19.[1] It has been estimated that the consumption of chili pepper by humans who like hot spicy foods could reach 2.5−20 g/person/day, equivalent to 0.5−4 mg capsaicinoids/kg body weight/day provided that capsaicinoids in chili pepper are 1% by weight.[17] In contrast, no data are available for us to assess the intake of capsinoids in humans. Structurally, capsaicinoids and capsinoids are similar except that the former are the amides of vanillylamine with fatty acids, whereas the latter are the esters of vanillyl alcohol with fatty acids (Figure 1). For individuals who like spicy foods, capsaicinoids provide a pleasurable sensation upon ingestion. In addition to the use for releasing pain, capsaicinoids also act as an antioxidant and increase the oxidation of body fat, thus being used as a target for obesity management.[18,19] However, the burning and pungent sensation may prevent their wide application, particularly for people who dislike or cannot tolerate spicy foods. In this regard, capsinoids could be an alternative if they had bioactivity similar to that of capsaicinoids because they are nonpungent. In fact, capsinoids have been

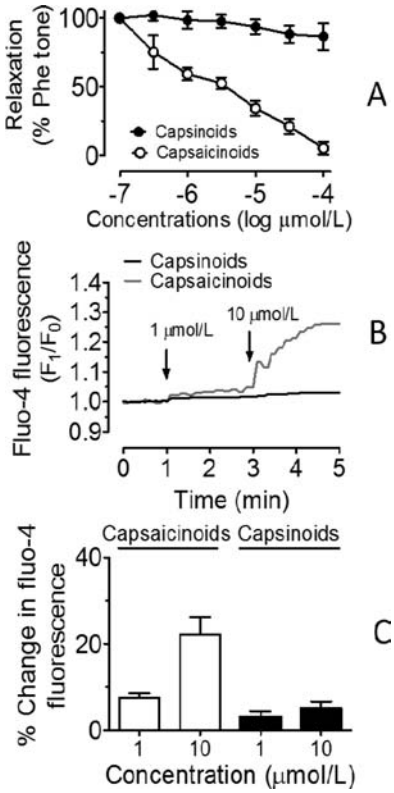


**Figure 2.** Effect of capsaicinoids and capsinoids on the relaxation of rat mesenteri artery and intracellular $Ca^{2+}$ concentration in human umbilical cord endothelial cells (HUVECs). (A) Capsaicinoids but not capsinoids caused vasodilatation on phenylephrine (1 $\mu$mol/L)-contracted mesenteric arteries. (B) Representative tracing and (C) summarized data show that capsaicinoids stimulated $Ca^{2+}$ entry in HUVECs in a concentration-dependent manner, whereas capsinoids had little effect. Data are expressed as the mean ± SEM; $n$ = 4.

similarly proposed to be a dietary supplement in weight management, as they are equally effective in increasing the energy expenditure by increasing fatty acid oxidation in vivo.[20] The present results demonstrated that capsaicinoids could reduce the size of both epididymal and prerenal fat pads, which were the two visible adipose tissues in rodents (Table 2). However, the effects of dietary capsinoids on two fat pads were found to be insignificant. This discrepancy with previous studies was probably because the duration of the present study was only 6 weeks, which might be not long enough for capsinoids to exert any antiobesity effect in hamsters.

The present study was the first time to compare the effect of capsaisinoids on plasma TC with that of capsinoids. Results clearly demonstrated that capsaicinoids but not capsinoids were able to decrease plasma TC in hamsters fed a 0.2% cholesterol diet (Table 3). Reduction in plasma TC caused by dietary capsaicinoids was accompanied by a decrease in both liver cholesterol and atherosclerotic plaque. The result regarding the effect of capsaicinoids on plasma TC was in agreement with that of Liang et al.[13] In another study, it was found that 0.015% capsaicinoids in the diet could reduce serum TC by 23% in Sprague–Dawley rats fed a 30% fat diet.[7] In the present hamster model fed a diet containing 5% lard and 0.2% cholesterol, we found that reduction in plasma TC could reach 16%.

To explain why capsaicinoids but not capsinoids could decrease plasma TC, we quantified the excretion of fecal total sterols. It was clear that both capsaicinoids and capsinoids had no significant effect on the excretion of fecal neutral sterols. However, only capsaicinoids but not capsinoids could increase the excretion of fecal bile acids (Table 4). To be specific, it was found that dietary capsaicinoids at 1.3 and 2.6 mmol in the diet could increase the excretion of fecal bile acids by 28 and 175%, respectively. The present result was in agreement with that of Zhang et al., who found that the gavage of capsaicinoids at 10 mg/kg body weight could increase the excretion of fecal bile acids by 13% in rats given a 2% cholesterol diet.[21] In contrast, no significant effect of capsinoids on the excretion of fecal bile acids was seen. Because excess cholesterol in mammals is usually disposed of via bile fluid duct or by conversion to bile acids, the increase in bile acid excretion is likely the primary mechanism underlying the plasma TC-reducing activity of capsaicinoids.

Capsaicinoids have been shown to decrease atherosclerotic plaque and possess some beneficial effect on aortic function.[13,21] To ascertain if capsinoids also had similar activity, we studied the vasodilatory effect of both capsaicinoids and capsinoids in the mesenteric arteries from rats. It was clear that only capsaicinoids but not capsinoids beneficially induced the relaxation of mesenteric arteries. Moreover, acute treatment of capsaicinoids triggered a favorable increase of intracellular $Ca^{2+}$ concentration in endothelial cells, which in turn promotes nitric oxide formation and causes endothelium-dependent relaxation. It has been shown that the favorable effect of capsaicinoids on the aorta is at least in part mediated by their inhibition on either activity or expression of cylco-oxygenase 2 (COX-2).[13] Up-regulation of COX-2 is associated with endothelial dysfunction, atherosclerotic plaque, and inflammation.[22]

In summary, capsaicinoids and capsinoids are naturally present in chili or sweet peppers; however, their biological properties differ in many ways. Under the present physiological conditions, capsaicinoids were able to favorably modulate plasma lipoprotein profile and possess beneficial vascular activity, whereas analogue capsinoids had no such properties. It was therefore concluded that nonpungent capsinoids could not be used as an alternative of pungent capsaicinoids in relation to their favorable modification of plasma lipids and cardiovascular benefit.

## ■ ASSOCIATED CONTENT

### Ⓢ Supporting Information

Supplementary Figures 1–3. This material is available free of charge via the Internet at http://pubs.acs.org.

## ■ AUTHOR INFORMATION

### Corresponding Author

*(Z.-Y.C.) Fax: (852) 2603-7246. E-mail: zhenyuchen@cuhk.edu.hk.

### Funding

This project was supported by a grant from the Hong Kong Research Grant Council (CUHK 462813).

### Notes

The authors declare no competing financial interest.

## ■ REFERENCES

(1) Yazawa, S.; Suetome, N.; Okamoto, K.; Namiki, T. Content of capsaicinoids and capsaicinoid-like substances in fruit of pepper (*Capsicum annuum* L.) hybrids made with 'CH-19 sweet' as a parent. *J. Jpn. Soc. Hortic. Sci.* **1989**, *58*, 601–607.

(2) Barbero, G. F.; Ruiz, A. G.; Liazid, A.; Palma, M.; Vera, J. C.; Barroso, C. G. Evolution of total and individual capsaicinoids in peppers during ripening of the cayenne pepper plant (*Capsicum annuum* L.). *Food Chem.* **2014**, *153*, 200−206.
(3) Josse, A. R.; Sherriffs, S. S.; Holwerda, A. M.; Andrews, R.; Staples, A. W.; Phillips, S. M. Effects of capsinoid ingestion on energy expenditure and lipid oxidation at rest and during exercise. *Nutr. Metab.* **2010**, *7*, 65.
(4) Luo, X. J.; Peng, J.; Li, Y. J. Recent advances in the study on capsaicinoids and capsinoids. *Eur. J. Pharmacol.* **2011**, *650*, 1−7.
(5) Peng, J.; Li, Y. J. The vanilloid receptor TRPV1: role in cardiovascular and gastrointestinal protection. *Eur. J. Pharmacol.* **2010**, *627*, 1−7.
(6) Rajput, S.; Mandal, M. Antitumor promoting potential of selected phytochemicals derived from spices: a review. *Eur. J. Cancer Prev.* **2012**, *21*, 205−215.
(7) Manjunatha, H.; Srinivasan, K. Hypolipidemic and antioxidant effects of curcumin and capsaicin in high-fat-fed rats. *Can. J. Physiol. Pharmacol.* **2007**, *85*, 588−596.
(8) Seo, S.; Kim, J.; Noh, S. Effect of enteral capsaicin on the lymphatic absorption and fats in rat. *Han'guk Sikp'um Yongyang Kwahak Hoechi* **2009**, *38*, 1712−1717.
(9) Saito, M.; Yoneshiro, T. Capsinoids and related food ingredients activating brown fat thermogenesis and reducing body fat in humans. *Curr. Opin. Lipidol.* **2013**, *24*, 71−77.
(10) Kobata, K.; Kawaguchi, M.; Watanabe, T. Enzymatic synthesis of a capsinoid by the acylation of vanillyl alcohol with fatty acid derivatives catalyzed by lipases. *Biosci., Biotechnol., Biochem.* **2002**, *66*, 319−327.
(11) Dong, X. R.; Liu, Z. H.; Li, Y. H.; Xie, D. P. Lipase-catalyzed synthesis and bioactivity of capsinoids. *Nat. Prod. Res. Dev.* **2009**, *21*, 570−573.
(12) Ng, C. H.; Qiang Yao, X.; Huang, Y.; Chen, Z. Y. Oxidised cholesterol is more hypercholesterolaemic and atherogenic than non-oxidised cholesterol in hamsters. *Br. J. Nutr.* **2008**, *99*, 749−755.
(13) Liang, Y. T.; Tian, X. Y.; Chen, J. N.; Peng, C.; Ma, K. Y.; Zuo, Y.; Jiao, R.; Lu, Y.; Huang, Y.; Chen, Z. Y. Capsaicinoids lower plasma cholesterol and improve endothelial function in hamsters. *Eur. J. Nutr.* **2013**, *52*, 379−388.
(14) Zhang, Z. S.; Wang, H.; Jiao, R.; Peng, C.; Wong, Y. M.; Yeung, V. S. Y.; Huang, Y.; Chen, Z. Y. Choosing hamsters but not rats as a model for studying plasma cholesterol-lowering activity of functional foods. *Mol. Nutr. Food Res.* **2009**, *53*, 921−930.
(15) Jiao, R.; Zhang, Z.; Yu, H.; Huang, Y.; Chen, Z. Y. Hypocholesterolemic activity of grape seed proanthocyanidin is mediated by enhancement of bile acid excretion and up-regulation of CYP7A1. *J. Nutr. Biochem.* **2010**, *21*, 1134−1139.
(16) Chen, Z. Y.; Su, Y. L.; Lau, C. W.; Law, W. I.; Huang, Y. Endothelium-dependent contraction and direct relaxation induced by baicalein in rat mesenteric artery. *Eur. J. Pharmacol.* **1999**, *374*, 41−47.
(17) Opinion of the Scientific Committee on Food on Capsaicin, European Commission Health and Consumer Protection Directorate − General: SCF/CS/FLAV/FLAVOUR/8 ADD1 Final, Feb 28,2002.
(18) Materska, M.; Perucka, I. Antioxidant activity of the main phenolic compounds isolated from hot pepper fruit (*Capsicum annuum* L.). *J. Agric. Food Chem.* **2005**, *53*, 1750−1756.
(19) Janssens, P. L.; Hursel, R.; Martens, E. A.; Westerterp-Plantenga, M. S. Acute effects of capsaicin on energy expenditure and fat oxidation in negative energy balance. *PLoS One* **2013**, *8*, No. e67786.
(20) Ludy, M. J.; Moore, G. E.; Mattes, R. D. The effects of capsaicin and capsiate on energy balance: critical review and meta-analyses of studies in humans. *Chem. Senses* **2012**, *37*, 103−121.
(21) Zhang, L.; Fang, G.; Zheng, L.; Chen, Z.; Liu, X. Hypocholesterolemic effect of capsaicinoids in rats fed diets with or without cholesterol. *J. Agric. Food Chem.* **2013**, *61*, 4287−4293.
(22) Wong, W. T.; Tian, X. Y.; Chen, Y.; Leung, F. P.; Liu, L.; Lee, H. K.; Ng, C. F.; Xu, A.; Yao, X.; Vanhoutte, P. M.; Tipoe, G. L.; Huang, Y. Bone morphogenic protein-4 impairs endothelial function through oxidative stress−dependent cyclooxygenase-2 upregulation implications on hypertension. *Circ. Res.* **2010**, *107*, 984−991.

JOURNAL OF AGRICULTURAL AND FOOD CHEMISTRY

Article

pubs.acs.org/JAFC

# Chemical and Thermal Characterization of Potato Peel Waste and Its Fermentation Residue as Potential Resources for Biofuel and Bioproducts Production

Shaobo Liang[†] and Armando G. McDonald*[,†,‡]

[†]Environmental Science Program, University of Idaho, Moscow, Idaho 83844-3006, United States

[‡]Department of Forest, Rangeland and Fire Science, University of Idaho, Moscow, Idaho 83844-1132, United States

**ABSTRACT:** The growing demand for renewable fuels has driven the interest in the utilization of alternative waste materials such as potato peel waste (PPW) which contains fermentable carbohydrate. Fermentation of PPW using a mixed microbial consortium yielded about 60% unreacted PPW fermentation residue (PPW-FR). The PPW and PPW-FR were characterized by a combination of Fourier transform infrared (FTIR) and nuclear magnetic resonance (NMR) spectroscopies, gas chromatography−mass spectrometry (GC-MS), and thermogravimetric analysis (TGA) to quantify changes after fermentation. Fermentation of PPW resulted in fermentation of starch and concentrating lignin plus suberin and lipids in PPW-FR. TGA analysis showed that decomposition peaks differed for PPW (423 °C) and PPW-FR (457 °C). Pyrolysis-GC/MS showed an increase in phenolic and long chain fatty acid compounds with a concomitant decrease in carbohydrate derived compounds in the PPW after fermentation. Both the PPW and PPW-FR have shown potential based on properties to be converted into crude biofuel via thermochemical processes.

**KEYWORDS:** *potato peel waste, fermentation residue, chemical analysis, thermo gravimetric analysis*

## INTRODUCTION

Potatoes are the world's fourth largest crop behind corn, rice, and wheat and have experienced a steady growth over the last two decades as a stable food crop and a major source of starch.[1] According to data from the National Potato Council,[2] United States (U.S.) ranks fifth of potato producing countries with a production over 21.7 billion kg in 2011. A typical potato processing plant can generate 6−10% potato peel waste (PPW) from the peeling process,[3] and other defect removal, trimming, and cutting processes can generate an additional 15% waste. This combined waste stream can pose a significant waste management effort, and therefore, knowing this waste's composition will facilitate its utilization into bioproducts.

The composition of steam PPW was determined by Camire et al.[4] and shown to contain starch (25%), nonstarch polysaccharide (30%), acid insoluble and acid soluble lignin (20%), protein (18%), lipids (1%), and ash (6%). The lipid fraction was shown to comprise long chain fatty acids, triglycerides, alcohols, sterols, sterol esters, and phenolics.[5] Suberin, a rubbery polyester material composed of polyaromatic and polyaliphatic domains, has been found in the cell walls of potatoes.[6] Lignin, a three-dimensional polymer made up of phenylpropane units, has also been detected in the plant cell wall.[7]

PPW has been utilized in a variety of applications and traditionally has been used for local animal feed.[4,8−12] Suberin and lignin fractions have been pressure extracted from PPW to obtain value added antioxidants and bioactive chemicals.[8,9] While fermentation of PPW starch has been employed to generate alcohols and organic acids. Arapoglou et al.[10] converted PPW by sequential enzymatic hydrolysis and fermentation using *Saccharomyces cereviciae* to yield ethanol. Lactic acid has also been produced from PPW using pure cultures of *Lactobacillus* var. or *Rhizupus* var.[11,12] Recently, PPW has been directly converted to primarily lactic acid, a useful chemical building block for the production of polylactic acid, using undefined mixed microbial culture fermentation.[13,14] The advantage of using a mixed microbial system is that the fermenters do not require expensive pure cultures or sterilized conditions to operate, and the microbial community self-regulated to predominately lactic acid producing bacteria.[13] However, a significant amount of unreacted solid PPW fermentation residue (PPW-FR) was obtained in the process.[10,13,14] This PPW-FR waste will also need to be managed and forms the basis of this characterization study to maximize its utilization. Another popular option for waste management of PPW is by anaerobic digestion (AD) to produce $CH_4$ and electricity.[15] However, AD systems require large digesters based on the slow methanogenic bacterial conversion of biomass to $CH_4$ and unpleasant odor (namely, $H_2S$) generation.[15] Work by Kang and Min[16] has used PPW as a novel substrate for making biobased flexible films for packaging applications with good barrier properties.

Currently, food crops such as corn and soybean are the two predominant biomass resources widely used for liquid bioethanol and biodiesel production worldwide.[17] However, the controversy between food and fuel also promoted the utilization of other noneligible biomass materials, such as agricultural and forestry residues,[18] animal manure,[15] algae,[19]

Received: February 19, 2014
Revised: August 4, 2014
Accepted: August 5, 2014
Published: August 5, 2014

ACS Publications © 2014 American Chemical Society



dx.doi.org/10.1021/jf5019406 | J. Agric. Food Chem. 2014, 62, 8421−8429

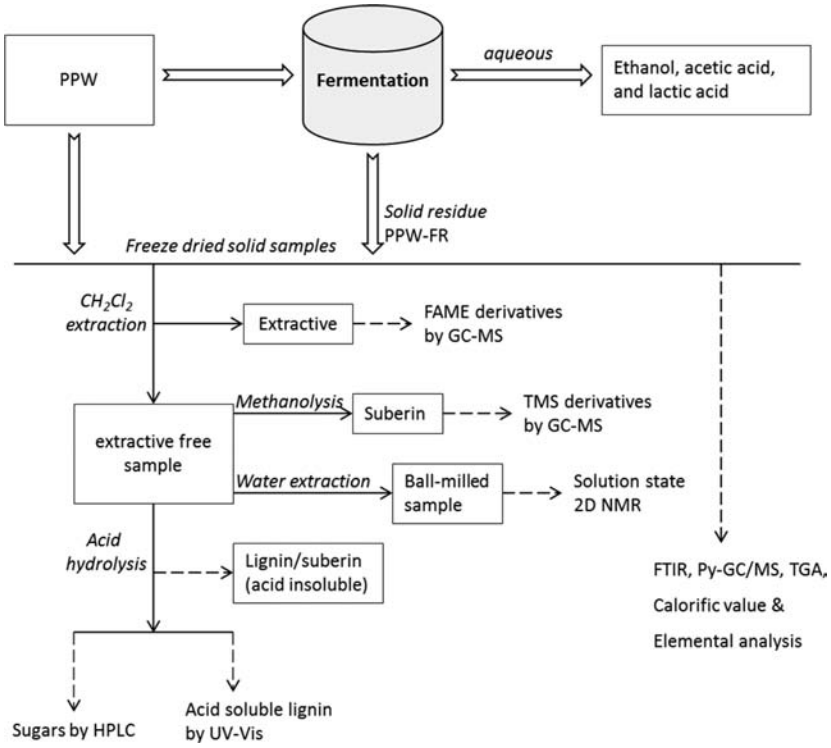


**Figure 1.** Schematic diagram of PPW and PPW-FR sample generation and analytical procedures.

and food processing wastes.[20] PPW and more recently PPW-FR are promising carbon rich waste resources for producing value added biofuels and bioproducts. Onal et al.[21] used steam pyrolysis of PPW (at 500 °C) to generate >25% bio-oil and contained significant amounts of aliphatics that could be used in transportation fuels. Biochar from pyrolyzed PPW, another coproduct, was shown to remove heavy metals from aqueous solutions.[22] These approaches to utilize PPW will minimize waste streams, reduce the carbon footprint, mitigate greenhouse gases, and generate a range of bioproducts.

The aim of this study is to characterize the chemical and thermal properties of PPW and PPW-FR, an uncharacterized bioresource, in order to target possible thermochemical processes, such as pyrolysis, for conversions of these wastes into biofuel and bioproducts. A combination of characterization techniques was employed, and the results of this study can be used in future work to evaluate the pyrolysis based biofuel and bioproduct production from PPW and PPW-FR.

## MATERIALS AND METHODS

**Sample Preparation.** The PPW (*Russet Burbank*) sample was collected from a potato processing plant (J.R. Simplot Company, Nampa, ID) over a 2 h period in May 2012, and the sample was mixed thoroughly and stored frozen for fermentation studies using a consistent feed stock and a portion freeze-dried for subsequent analysis. Hybrid poplar (*Populus deltoides* × *Populus tremuloides*) sample was obtained from Greenwood Resources (Portland, OR) and Wiley milled to <0.5 mm particle size.

The fermentation process primarily produced lactic acid and to a lesser extent ethanol, and acetic acid from PPW was described by Liang.[13,14] A 1 L glass bottle with an air-lock was used as a reactor, operated in sequencing batch mode with moderate mixing speed and at 35 °C. The fermenter was inoculated with 5% mixed microbial cultures (sewage sludge from Moscow Wastewater Treatment Plant, Idaho) only at the first day running. Gelatinized PPW (boiled for 30 min and cooled down) was fed daily with the same amount of mixed slurry that was drawn off and using a retention time of 2 days and solid loading of 40 g $L^{-1}$ was kept constant. Sampling was conducted after 4 weeks running to obtain a steady state, and the PPW-FR was collected over a 3−4 week period, then recovered by centrifugation, and freeze-dried for subsequent analyses. A detailed characterization flow process is shown in Figure 1. All of the results in this study were calculated on a dry weight basis biomass and measured in triplicate.

**Compositional and Calorific Analyses.** Freeze-dried samples (4−5 g) were Soxhlet extracted with $CH_2Cl_2$ (150 mL) for 16 h according to ASTM D 1108-96[23] and the extractives (lipids) were determined gravimetrically. The lignin and suberin complex was divided into acid insoluble and acid soluble fractions, and the analyses were performed on extractive free samples according to ASTM D 1106-96[24] and Schoening and Johansson,[25] respectively. Carbohydrate analysis was performed on the 2-stage acid-hydrolyzates according to ASTM E 1758-01.[26] More specifically, the dried sample (200 mg) was incubated in 72% $H_2SO_4$ (2 mL) for 1 h at 30 °C, then diluted into 4% $H_2SO_4$, and subjected to secondary hydrolysis in an autoclave (117 KPa and 121 °C) for 30 min. The hydrolyzate was filtered to obtain acid insoluble (Klason lignin + suberin) residue content gravimetrically. The hydrolysis filtrate was made up to 250 mL and an aliquot portion taken to determine acid soluble lignin (+ suberin complex) fraction content at 205 nm using an absorption coefficient of 110 L $g^{-1}$ $cm^{-1}$ (Beckman DU640 spectrometer). An aliquot portion of the hydrolyzate (5 mL) was transferred to a centrifuge tube to which internal standard (inositol, 1 mL, 0.5 mg $mL^{-1}$) and $PbCO_3$ (0.16 g) were added, mixed well, centrifuged, and the supernatant (4 mL) deionized (column of Amberlite IR-120 $H^+$ (0.5 mL) and Amberlite IRA35 $OH^-$ (0.5 mL) resins) and filtered (0.45 $\mu$m) into HPLC vials. Monosaccharides were the quantified by HPLC using two RPM columns in series (7.8 mm × 30 cm, Phenomenex) at 85 °C equipped with a differential refractive index detector (Waters Associates model 2414) on elution with 0.5 mL $min^{-1}$ water. Starch content was estimated by an enzymatic hydrolysis assay according to AACC method 76-11[27] using glucoamylase (Sigma-Aldrich) and the sugars analyzed by HPLC. More specifically, the sample (0.50 g) was dissolved in water (25 mL) and heated to 135 °C for 1 h, cooled, acetate buffer (pH 4.8, 2.5 mL) and glucoamylase (5 mL, 150 IU)


dx.doi.org/10.1021/jf5019406 | J. Agric. Food Chem. 2014, 62, 8421−8429

added to the solution, incubated at 55 °C for 2 h, and analyzed by HPLC.

The ash content was determined by furnacing samples at 600 °C according to ASTM D 1102-84.[28] The C, H, and N content was determined using a CE-440 elemental analyzer (EAI Exeter Analytical), and O content was calculated by the difference. The calorific values for pressed dried pellet samples (5.5 mm × 6.3 mm Ø) were determined by bomb calorimetry (Model 1261, Parr Instruments) according to ASTM D 5865-04.[29]

**GC-MS Analysis of $CH_2Cl_2$ Extractives and Suberin.** The $CH_2Cl_2$ extract (5.0 mg) was weighed into a 5 mL reacti-vial to which 2 mL of $CH_3OH/H_2SO_4/CHCl_3$ (1.7:0.3:2.0 v/v/v) was added, and the mixture was heated for 90 min at 90 °C to form fatty acid methyl ester (FAME) derivatives.[30] $CHCl_3$ contained 1-napthalaneacetic acid as an internal standard (50 $\mu$g mL$^{-1}$). To the cooled mixture, water (1 mL) was added, vigorously shaken, centrifuged, the $CHCl_3$ layer removed, dried through anhydrous sodium sulfate, and transferred to a GC vial. The prepared FAME derivatives were analyzed by GC-$MS_{EI}$ (FOCUS-ISQ, ThermoScientific); temperature profile, 40 °C (1 min) to 320 °C at 5 °C min$^{-1}$ with injector temperature of 320 °C, mass transfer line temperature of 325 °C, and ion source temperature of 240 °C; GC capillary column, RTx-5MS (30 m, 0.25 mm Ø, 0.25 $\mu$m film thickness, Restek). The eluted compounds were identified with authentic standards (C12, C14, C16, and C18) and by spectral matching with the National Institute of Standards and Technology (NIST) 2008 mass spectral library. The abundance of each compound was referenced against the area of internal standard.

Suberin analysis was performed on samples by $NaOCH_3$-catalyzed methanolysis and subsequent GC-MS analysis.[6] The $CH_2Cl_2$ extractive free sample (500 mg) was refluxed in freshly prepared 12 mmol L$^{-1}$ $NaOCH_3$ in dry $CH_3OH$ (50 mL) for 3 h. The reaction mixture was filtered (glass fiber paper) and the residue washed with $CH_3OH$ (25 mL) and $CHCl_3$ (25 mL). The filtrate (1 mL) in a GC vial was concentrated to dryness to which $CH_2Cl_2$ (containing anthracene as internal standard (50 $\mu$g mL$^{-1}$, 1 mL)), *N,O*-bis (trimethylsilyl)-trifluoro-acetamide containing 1% trimethylchlorosilane (50 $\mu$L), and pyridine (50 $\mu$L) were added and then heated to 70 °C for 30 min. Suberin derived trimethylsilyl (TMS) derivatives were analyzed by GC-$MS_{EI}$ (Focus-ISQ, ThermoScientific)); temperature profile, 40 °C (1 min) to 300 °C (20 min) at 5 °C min$^{-1}$ with an injector temperature of 320 °C, mass transfer line temperature of 300 °C, and ion source temperature of 240 °C; GC capillary column, RTx-5MS (30 m, 0.25 mm Ø, 0.25 $\mu$m film thickness, Restek). The eluted compounds were identified with authentic standards, literature, and by spectral matching with the NIST 2008 mass spectral library, and the abundance of each compound was referenced against the area of internal standard.

**Spectroscopy.** FTIR spectroscopic analysis was performed using an Avatar 370 spectrophotometer (Thermo Nicolet) with an attenuated total reflection (ATR) probe (ZnSe crystal). The spectra were ATR and baseline corrected using Omnic v7.0 software.

$^{13}C-^{1}H$ HSQC NMR spectroscopy was performed on a 500 MHz Bruker AVANCE 500 spectrometer. $CH_2Cl_2$ extractive free samples (10 g) were extracted with water overnight and the solid residue freeze-dried and ball-milled in a porcelain jar (0.5 L) for 14 d. The ball-milled samples (40 mg) were dissolved in dimethyl sulfoxide (DMSO)-$d_6$ (1 mL) with the aid of sonication and analyzed according to Kim et al.[31]

**Thermogravimetric Analysis.** TGA was performed on samples (4−6 mg) using a TGA-7 (PerkinElmer) instrument using a temperature program of 30 to 900 °C at a heating rate of 5, 10, 20, 30, 40 K min$^{-1}$ under $N_2$ (30 mL min$^{-1}$). TGA and differential thermogravimetry (DTG) data were analyzed using Pyris v8 software. Activation energy ($E$) and pre-exponential factor ($A$) were calculated according to ASTM E 1641-07.[32] The decomposition kinetics was assumed to be first-order to determine $E$ and $A$ by the following equations:

$$E = -\left(\frac{R}{b}\right) \times \frac{\Delta(\log \beta)}{\Delta(1/T)} \quad (1)$$

$$A = -\left(\frac{\beta'}{E_r}\right) \times R \times \ln(1-\alpha) \times 10^a \quad (2)$$

where, $R$ is the gas constant, 8.314 J mol$^{-1}$ K$^{-1}$, $b$ is the approximate derivative given by ASTM E 1641 numerical integration constants, $\beta$ is the heating rate at K min$^{-1}$, $\beta'$ is the heating rate nearest the midpoint of the experimental heating rates at K min$^{-1}$, $T$ is the temperature (K) at constant conversion, $E_r$ is the refined value of Arrhenius $E$, $\alpha$ is the conversion value of decomposition, and $a$ is the approximation integral taken from ASTM E 1641 of numerical integration constants.

**Py-GC/MS Analysis.** Samples (<0.1 mg) were injected into a quartz capillary tube and pyrolyzed at 500 °C in an inert atmosphere (He, 0.125 MPa) using a Pyrojector II unit (SGE Analytical Science) coupled to a GC-$MS_{EI}$ (FOCUS-ISQ, ThermoScientific) instrument. The compounds were separated on a RTx-5ms (30 m × 0.25 mm Ø, 0.25 $\mu$m film thickness, Restek) capillary column with a temperature program of 50 to 250 °C (10 min) at 5 °C min$^{-1}$ with an injector temperature of 255 °C, a mass transfer line temperature of 255 °C, and an ion source temperature of 240 °C. The eluted compounds were identified with the NIST 2008 library matching and by their mass spectra, and the relative abundance of each derived compound was calculated using $CO_2$ as internal standard.[30,33]

**Statistical Analysis.** Statistical analyses of obtained data were conducted by SAS 9.3 (SAS Inc., Cary, NC, USA) under analysis of variance (ANOVA) at an $\alpha$ level of 0.05 to determine significant differences between the measured properties.

## RESULTS AND DISCUSSION

**Chemical, Elemental, and Calorific Value Analyses.** Chemical, elemental, and calorific value analyses were performed to obtain base chemical properties of the PPW and PPW-FR materials and establish what classes of components have been removed by fermentation. PPW and PPW-FR compositions, elemental contents, and calorific values are given in Table 1, which were significantly different. The PPW contained approximately 17% starch and 22% nonstarch polysaccharides. It was observed that most of the starch was consumed and converted to ethanol, acetic acid, and lactic acid during fermentation leaving 2% residual starch and 20% nonstarch polysaccharides in the PPW-FR.[13,14] Lignin and

**Table 1. Compositional, Elemental, and Calorific Value Analyses of PPW and PPW-FR**

| component | PPW (% dry basis) | PPW-FR (% dry basis) |
|---|---|---|
| carbohydrate | | |
| starch | 16.83 ± 0.52 | 2.07 ± 0.13 |
| nonstarch glucan[a] | 7.75 ± 0.68 | 7.79 ± 0.31 |
| galactan | 6.91 ± 0.10 | 5.31 ± 0.14 |
| mannan | 0.75 ± 0.07 | 1.35 ± 0.07 |
| xylan | 3.52 ± 0.21 | 1.47 ± 0.10 |
| arabinan | 3.53 ± 0.06 | 4.44 ± 0.08 |
| nonstarch polysaccharide | 22.46 ± 0.79 | 20.36 ± 0.08 |
| lignin and suberin | | |
| acid insoluble | 15.94 ± 0.04 | 30.31 ± 0.20 |
| acid soluble | 5.70 ± 0.20 | 6.68 ± 0.00 |
| $CH_2Cl_2$ extractive | 1.98 ± 0.15 | 7.68 ± 0.00 |
| ash | 11.05 ± 0.07 | 7.47 ± 0.00 |
| C | 43.78 ± 0.15 | 47.81 ± 0.01 |
| H | 5.96 ± 0.12 | 6.41 ± 0.04 |
| N | 4.06 ± 0.01 | 4.02 ± 0.08 |
| O | 46.21 ± 0.28 | 41.78 ± 0.05 |
| calorific value (MJ kg$^{-1}$) | 17.37 ± 0.38 | 19.19 ± 0.03 |

[a]The nonstarch glucan, galactan, mannan, xylan, and arabinan are listed as anhydro-sugar units present in nonstarch polysaccharides.


dx.doi.org/10.1021/jf5019406 | J. Agric. Food Chem. 2014, 62, 8421−8429

suberin complex content increased during fermentation from 22% to 37% with a concomitant removal of carbohydrate. The extractives (lipids and secondary metabolites) comprise fats, waxes, long-chain fatty acids, and alcohols, accounting for 2 and 8%, respectively, in PPW and PPW-FR. After fermentation, extractives accumulated in PPW-FR, which is in accordance with the distiller dried grains from ethanol fermentation.[34]

A decrease of ash content from 11% to 7% was observed and could be attributable to solubilization. Elemental composition analysis showed a significant difference between the PPW-FR and PPW. The C and H content increased, while the O content decreased after fermentation due to the removal of carbohydrates. The C (48%) and H (6.4%) contents in the PPW-FR were similar to hardwood biomass (48−52% C; 4.5−6.5% H) but higher than herbaceous biomass (wheat straw (43% C; 5.0% H) and corn stover (44% C; 5.6% H)).[35] A 10% increase in calorific value was observed after biomass fermentation (19.2 MJ $kg^{-1}$), and this is consistent with the higher C/H ratio obtained by other researchers on fermentation residues (19−21 MJ $kg^{-1}$)[36] and comparable to that of some hardwoods (13.5−19.4 MJ $kg^{1-}$).[35] These findings suggest that the PPW-FR could be a promising biomass resource for biofuel production.

**Compositional Analysis of Extractives and Suberin.** Lipids are an important class of compounds because they are used in biodiesel production and therefore were characterized to determine composition. The $CH_2Cl_2$ extracts were converted to their FAME derivatives and semiquantitatively analyzed by GC/MS, in which total 17 compounds ranging from C12 (lauric acid) to C30 (melissic acid) were identified (Table 2 and Figure 2). The total biomass lipid content increased from 7.5 to 14.3 mg $g^{-1}$ after fermentation. Linoleic (C18:2, 39%), palmitic (C16:0, 18%), and linolenic (C18:3, 16%) acids were the main components in PPW and were in agreement with the results from Dobson et al.[5] The levels of linoleic, palmitic, and linolenic acids increased, respectively, by 29.7%, 70.8, and 84.3% upon fermentation. Other minor (<10%) fatty acids were also found: lauric (C12:0), myristic (C14:0), pentadecanoic (C15:0), heptadecenoic (C17:0), stearic (C18:0), eicosanoic (C20:0), heneicosanoic (C21:0), docosanoic (C22:0), tricosanoic (C23:0), tetracosanoic (C24:0), hexacosanoic (C26:0) acids, montanic acid (C28:0), nonacosylic acid (C29:0), and melissic acid (C30:0). Dobson et al.[5] quantified lipids, as FAMEs, in two potato species from C14 to C24 and also detected odd numbered (C15:0, C17:0, C21:0, and C23:0) fatty acids. The total 17 fatty acids increased by 90% after fermentation, and the increasing lipids could be produced by microorganisms during fermentation.[37]

We determined the abundances of the lignin and suberin complex in the previous section at 22 and 37%, respectively, for PPW and PPW-FR. Suberin is regarded as a major constituent of potato cell walls,[6] and a further semiquantitative analysis to obtain a better content value and composition was necessary. Figure 3 shows the composition of suberin, which mainly comprised glycerol, alkanoic acids, $\alpha,\omega$-diacids, and $\omega$-hydroxyacids, as well as minor amounts of alkan-1-ols, hydroxycinnamic acids, and amino acids. Similar suberin constituents were also identified by other researchers.[38,39] Glycerol was the most abundant component in suberin at 48%, a cross-linker of the aliphatic and aromatic domains, and content is consistent with the literature.[40] Estimated suberin content was shown to increase in PPW after fermentation from 58 to 166 mg $g^{-1}$ as starch levels decreased.

**Table 2. FAME Derivatives of PPW and PPW-FR Extracts**

| no. | compound | retention time (min) | $M^+$ ($m/z$) | PPW (mg/g) | PPW-FR (mg/g) |
|---|---|---|---|---|---|
| 1 | lauric acid (C12:0) | 22.59 | 214 | 0.00 | 0.01 |
| 2 | myristic acid (C14:0) | 27.07 | 242 | 0.02 | 0.03 |
| 3 | pentadecanoic acid (C15:0) | 29.15 | 256 | 0.02 | 0.02 |
| 4 | palmitic acid (C16:0) | 31.13 | 270 | 1.37 | 2.34 |
| 5 | heptadecenoic acid (C17:0) | 33.04 | 284 | 0.01 | 0.02 |
| 6 | linoleic acid (C18:2) | 34.31 | 294 | 2.93 | 3.80 |
| 7 | linolenic acid (C18:3) | 34.43 | 296 | 1.21 | 2.23 |
| 8 | stearic acid (C18:0) | 34.86 | 298 | 0.25 | 0.38 |
| 9 | eicosanoic acid (C20:0) | 38.27 | 326 | 0.06 | 0.10 |
| 10 | heneicosanoic acid (C21:0) | 39.89 | 340 | 0.02 | 0.03 |
| 11 | docosanoic acid (C22:0) | 41.42 | 354 | 0.09 | 0.14 |
| 12 | tricosanoic acid (C23:0) | 42.91 | 368 | 0.01 | 0.02 |
| 13 | tetracosanoic acid (C24:0) | 44.34 | 282 | 0.20 | 0.28 |
| 14 | hexacosanoic acid (C26:0) | 47.07 | 410 | 0.28 | 0.58 |
| 15 | montanic acid (C28:0) | 49.61 | 438 | 0.67 | 2.61 |
| 16 | nonacosylic acid (C29:0) | 50.82 | 452 | 0.14 | 0.60 |
| 17 | melissic acid (C30:0) | 51.99 | 466 | 0.26 | 1.15 |
| | total | | | 7.54 | 14.33 |

**Spectroscopic Analysis.** FTIR spectroscopy was further used to analyze chemical functional group changes of PPW and PPW-FR, and their spectra are shown in Figure 4. The main characteristics were attributed to the presence of cellulose/starch, hemicellulose, lignin−suberin complex, and protein. A strong hydrogen bonded O−H stretching band[18] at 3329 $cm^{-1}$ and C−H ($CH_3$, $CH_2$) stretching vibration bands at 2974, 2915, and 2849 $cm^{-1}$ were observed for PPW, whereas similar characteristic bands appeared at 3339, 2917, and 2850 $cm^{-1}$, respectively, for PPW-FR. Absorption ester bands for fatty acid, hydroxy fatty acid, and diacids in lipids and suberin polymers[38] were detected at 1735 $cm^{-1}$ (C═O) and 1238 $cm^{-1}$ (−C-O-C) in PPW-FR. However, these bands were detected, at low intensity, in PPW at 1733 and 1255 $cm^{-1}$ and were reflective of lower lipid and suberin contents. These results are in agreement with the compositional analysis mentioned above. A distinct amide I C═O stretching band,[41] for protein, was detected at 1609 $cm^{-1}$ in PPW, whereas the band was shifted to 1628 $cm^{-1}$ in PPW-FR. Other functional groups associated with proteins were observed and overlapped with carbohydrate and lignin bands at 3640−3040 $cm^{-1}$ for N−H stretching and 1600−1500 $cm^{-1}$ for amide II C−N stretching and N−H bonding absorptions.[42]

In general, the absorption bands from 1600 to 1400 $cm^{-1}$ derived from C═C vibration of the aromatic ring were assigned to lignin.[43] Three distinct bands at 1515, 1452, and 1418 $cm^{-1}$ were detected in PPW-FR, while only two bands at 1514 and 1408 $cm^{-1}$ and a shoulder around 1450 $cm^{-1}$were detected in PPW. A clear absorption band at 1370 $cm^{-1}$


dx.doi.org/10.1021/jf5019406 | J. Agric. Food Chem. 2014, 62, 8421−8429

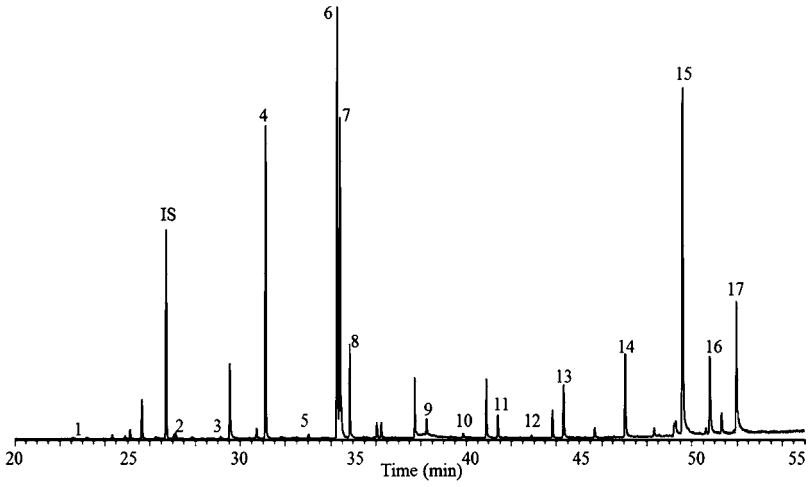


**Figure 2.** Total ion chromatogram of FAME derivatives of the $CH_2Cl_2$ extract of PPW-FR (IS, 1-naptheneacetic acid; peak numbers and identified compounds are given in Table 2).

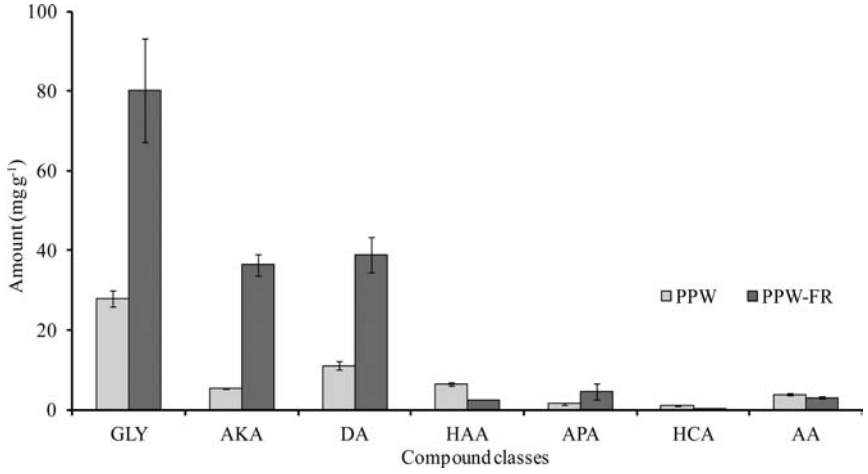


**Figure 3.** Levels of suberin derived compound classes present in PPW and PPW-FR by methanolysis (GLY, glycerol; AKA, alkanoic acids; DA, diacids; HAA, hydroxyalkanoic acids; APA, aliphatic alcohols; HCA, hydrocinnamic acids; AA, amino acids; triplicate tests were performed).

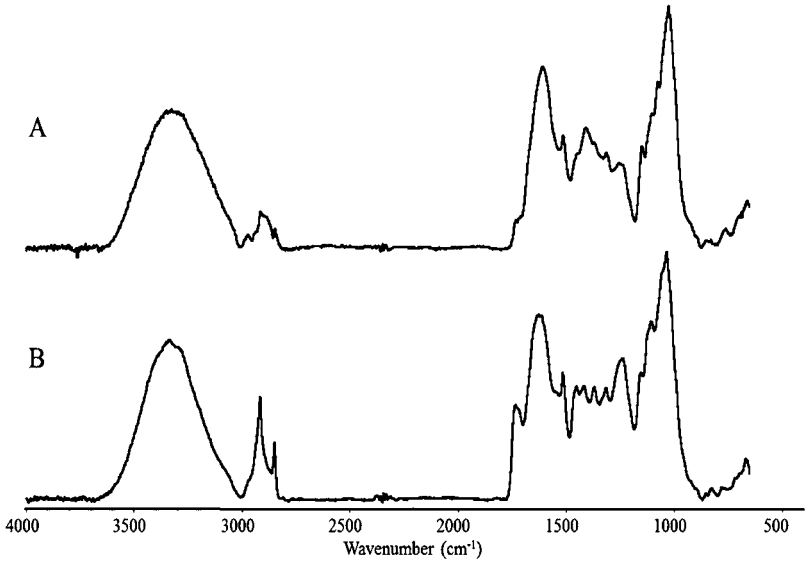


**Figure 4.** FTIR spectra of PPW (A) and PPW-FR (B).

denoted as aliphatic C−H stretching[44] in $CH_3$, or phenolic OH was observed only in PPW-FR. The band at 1314 $cm^{-1}$ was assigned to C−H vibration. Finally, a strong band ranging from 1200 to 900 $cm^{-1}$ was assigned to −C-O-C− vibration of


dx.doi.org/10.1021/jf5019406 | J. Agric. Food Chem. 2014, 62, 8421−8429

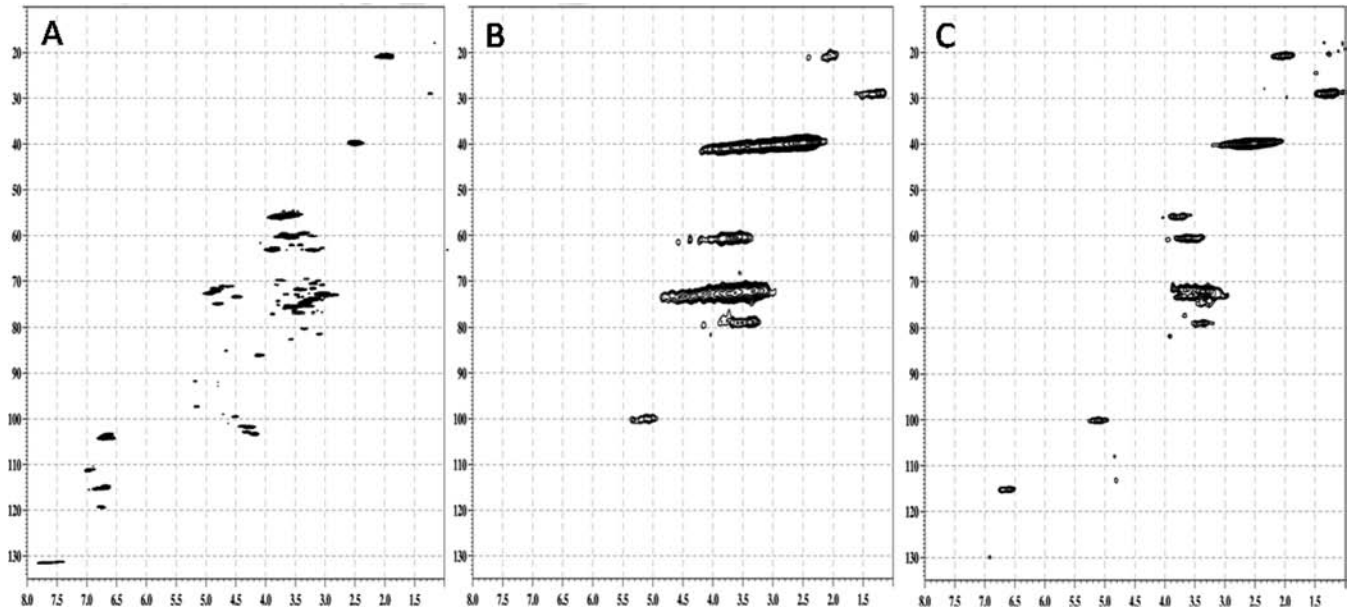


**Figure 5.** HSQC $^{1}H-^{13}C$ NMR spectra of (A) hybrid poplar, (B) PPW, and (C) PPW-FR in DMSO-$d_6$.

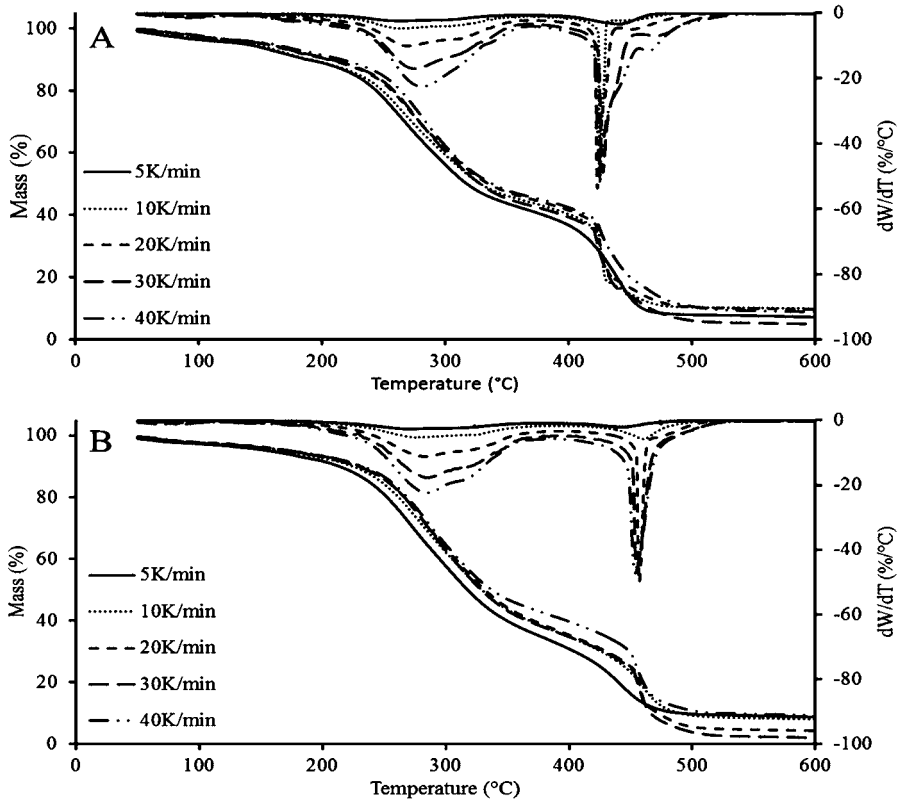


**Figure 6.** TGA and DTG thermograms of PPW (A) and PPW-FR (B) at different heating rates (5 to 40 K $min^{-1}$).

pyranose sugar rings (carbohydrates) in both PPW and PPW-FR samples.

2D-NMR spectroscopy was employed to nondestructively analyze PPW and PPW-FR by fully solubilizing the samples in DMSO following the approach by Kim et al.[31] and Lu and Ralph,[45] which were developed for woody biomass. This approach was out to trial to assess its suitability to characterize PPW. Figure 5 shows the 2D HSQC $^{13}C-^{1}H$ correlation spectra of ball-milled hybrid poplar, PPW, and PPW-FR samples. Most of the $^{1}H-^{13}C$ correlations in the $\delta_C/\delta_H$ 50–120/2.5–5.5 ppm region belong to polysaccharides, and the $\delta_C/\delta_H$ 100–150/6–8 ppm region is contributed by aromatic components. Hybrid poplar as a model lignocellulosic substrate exhibited significant cellulose, hemicellulose, and lignin signals, where the anomeric C/H correlation of cellulose and xylan appear at $\delta_C/\delta_H$ 103/4.4 ppm for (1 → 4)-$\beta$-D-Glc*p*, 104/4.2 ppm for (1 → 6)-$\beta$-D-Glc*p*, and 102/4.3 ppm for (1 → 4)-$\beta$-D-Xyl*p*. Correlations of lignin appear at $\delta_C/\delta_H$ 104/6.7 ppm for $C_2-H_2$ and $C_6-H_6$ in syringyl units, 111/7.0, 115/6.7, and 119/6.8 ppm for $C_2-H_2$, $C_5-H_5$, and $C_6-H_6$ in the guaiacyl


dx.doi.org/10.1021/jf5019406 | J. Agric. Food Chem. 2014, 62, 8421–8429

**Table 3. Compounds Released by Py-GC/MS of PPW and PPW-FR**

| no. | compound | retention time (min) | $M^+$ ($m/z$) | formula | relative abundance (%) | |
|---|---|---|---|---|---|---|
| | | | | | PPW | PPW-FR |
| 1 | acetaldehyde | 1.36 | 44 | $C_2H_4O$ | 2.89 | 2.17 |
| 2 | acetic acid | 1.66 | 60 | $C_2H_4O_2$ | 14.00 | 7.02 |
| 3 | acetic anhydride | 2.05 | 102 | $C_4H_6O_3$ | 7.92 | 5.13 |
| 4 | pyrrole | 2.98 | 67 | $C_4H_5N$ | 2.37 | 2.12 |
| 5 | toluene | 3.12 | 92 | $C_7H_8$ | 2.80 | 2.53 |
| 6 | acetamide | 3.27 | 59 | $C_2H_5NO$ | 0.45 | 1.39 |
| 7 | 2,3-butanediol | 3.47 | 90 | $C_4H_{10}O_2$ | 2.09 | 0.00 |
| 8 | 2-oxo-3-cyclopentene-1-acetaldehyde | 4.27 | 124 | $C_7H_8O_2$ | 1.72 | 1.70 |
| 9 | 3-methylpyrrole | 4.38 | 81 | $C_5H_7N$ | 1.20 | 0.60 |
| 10 | 3-furylmethnol | 4.71 | 98 | $C_5H_6O_2$ | 1.01 | 0.76 |
| 11 | 6-hydroxy-hexan-2-one | 5.01 | 116 | $C_6H_{12}O_2$ | 0.92 | 1.54 |
| 12 | 1,2,3-cyclopentanetriol | 5.72 | 118 | $C_5H_{10}O_3$ | 0.24 | 0.20 |
| 13 | 2-methyl-2-cyclopentenone | 5.85 | 96 | $C_6H_8O$ | 0.72 | 0.48 |
| 14 | 2(5*H*)-furanone | 6.06 | 84 | $C_4H_4O_2$ | 2.03 | 1.38 |
| 15 | 1,2-cyclopentanedione | 6.30 | 98 | $C_5H_6O_2$ | 1.76 | 2.11 |
| 16 | 1-methyl-1-cyclopenten-3-one | 7.33 | 96 | $C_6H_8O$ | 1.39 | 0.64 |
| 17 | 4-methyl-2(5*H*)-furanone | 7.74 | 98 | $C_5H_6O_2$ | 0.57 | 0.71 |
| 18 | phenol | 7.83 | 94 | $C_6H_6O$ | 5.28 | 5.74 |
| 19 | 3-methyl-1,2-cyclopentanedione | 9.04 | 112 | $C_6H_8O_2$ | 3.19 | 2.83 |
| 20 | 2-methyl-phenol | 9.83 | 108 | $C_7H_8O$ | 2.10 | 1.61 |
| 21 | 3-methyl-phenol | 10.44 | 108 | $C_7H_8O$ | 3.32 | 3.87 |
| 22 | guaiacol | 10.76 | 124 | $C_7H_8O_2$ | 3.21 | 5.34 |
| 23 | 3-ethyl-2-hydroxy-2-cyclopenten-1-one | 11.62 | 126 | $C_7H_{10}O_2$ | 1.57 | 1.09 |
| 24 | 2,3-dimethyl-phenol | 13.01 | 122 | $C_8H_{10}O$ | 2.54 | 2.39 |
| 25 | 3-ethyl-phenol | 13.09 | 122 | $C_8H_{10}O$ | 2.24 | 2.23 |
| 26 | 4-methyl-guaiacol | 13.68 | 138 | $C_8H_{10}O_2$ | 0.82 | 1.45 |
| 27 | 1,4:3,6-dianhydro-hexopyranose | 14.17 | 144 | $C_6H_8O_4$ | 0.50 | 0.87 |
| 28 | coumaran | 14.49 | 120 | $C_8H_8O$ | 1.45 | 2.83 |
| 29 | 2-ethyl-methyl-phenol | 14.96 | 136 | $C_9H_{12}O_2$ | 0.91 | 0.90 |
| 30 | 4-ethyl-guaiacol | 16.03 | 152 | $C_9H_{12}O_2$ | 0.76 | 1.42 |
| 31 | 1,4-benzenediol | 16.23 | 110 | $C_6H_6O_2$ | 0.29 | 0.61 |
| 32 | indolizine | 16.47 | 117 | $C_8H_7N$ | 1.99 | 1.79 |
| 33 | 4-vinyl-guaiacol | 16.98 | 150 | $C_9H_{10}O_2$ | 2.73 | 4.97 |
| 34 | syringol | 17.97 | 154 | $C_8H_{10}O_3$ | 0.27 | 0.52 |
| 35 | propioguaiacone | 20.44 | 180 | $C_{10}H_{12}O_3$ | 0.72 | 1.26 |
| 36 | $\alpha$-hydroxydodecanoic acid | 21.34 | 216 | $C_{12}H_{24}O_3$ | 0.57 | 0.53 |
| 37 | tetradecanoic acid | 27.54 | 228 | $C_{14}H_{28}O_2$ | 0.95 | 1.28 |
| 38 | pentadecanoic acid | 29.54 | 242 | $C_{15}H_{30}O_2$ | 0.90 | 0.83 |
| 39 | hexadecenoic acid | 31.11 | 254 | $C_{16}H_{30}O_2$ | 0.95 | 0.88 |
| 40 | hexadecanoic acid | 31.47 | 256 | $C_{16}H_{32}O_2$ | 5.53 | 5.51 |
| 41 | 2,6,10-trimethyltetradecane | 33.91 | 240 | $C_{17}H_{36}$ | 1.03 | 1.25 |
| 42 | octadecyonic acid | 34.61 | 280 | $C_{18}H_{32}O_2$ | 1.40 | 1.69 |
| 43 | oxacycloheptadec-8-en-2-one | 34.91 | 252 | $C_{16}H_{28}O_2$ | 1.80 | 3.83 |
| 44 | eicosane | 37.35 | 282 | $C_{20}H_{42}$ | 1.67 | 2.40 |
| 45 | vaccenic acid | 38.88 | 282 | $C_{18}H_{34}O_2$ | 2.05 | 2.81 |
| 46 | heneicosene | 40.43 | 295 | $C_{21}H_{42}$ | 1.05 | 1.17 |
| 47 | 2-methyleicosane | 40.51 | 296 | $C_{21}H_{44}$ | 1.34 | 2.19 |
| 48 | eicosenoic aicd | 41.95 | 310 | $C_{20}H_{38}O_2$ | 0.84 | 0.98 |
| 49 | 2-methyl-eicosane | 43.64 | 296 | $C_{21}H_{44}$ | 1.00 | 1.80 |
| 50 | erucic acid | 45.55 | 338 | $C_{22}H_{42}O_2$ | 0.92 | 0.67 |

unit, respectively. Other clusters of C/H correlations for polysaccharides and lignin were also observed, and the results are in accordance with Lu and Ralph.[45] In this research, nonderivatized solution state 2D NMR was first introduced to analyze potato peel samples (Figure 5), and the NMR spectra of PPW and PPW-FR samples were quite different from those of hybrid poplar. The clusters of $^1H-^{13}C$ correlations were associated with polysaccharides, suberin, and lignin. The methyl signal appears at $\delta_C/\delta_H$ 21/2.1 ppm for the acetyl group in polysaccharides,[31] aliphatic methylenic groups ($-CH_2-$) appear at $\delta_C/\delta_H$ 29/1.4 ppm for suberin components,[39] C6 appears at $\delta_C/\delta_H$ 61/3.8 ppm for $C_6-H_6$ in cellulose and $C_\gamma$-$H_\gamma$ in $\beta$-O-4 substructures, C5 and C4 appear at $\delta_C/\delta_H$ 73−74/3.6−3.8 ppm for $C_5-H_5$ and $C_4-H_4$ correlations in cellulose, and anomeric C1 appears at $\delta_C/\delta_H$ 100/4.9−5.3 ppm for anomeric C/H of (1 → 4)-$\alpha$-D-Glc*p* and (1 → 6)-$\alpha$-D-Glc*p* in


dx.doi.org/10.1021/jf5019406 | J. Agric. Food Chem. 2014, 62, 8421−8429

starch[31,45,46] and were present in both PPW and PPW-FR. Signals attributable to lignin at $\delta_C/\delta_H$ 56/3.6−3.9 ppm (methoxyl group) and $\delta_C/\delta_H$ 115/6.5−6.8 ppm ($C_5$−$H_5$ correlation for guaiacyl) were observed only in the PPW-FR, which are in agreement with FTIR and Py-GC/MS data. Unfortunately, due to the poor spectral dispersion in the NMR spectra of PPW and PPW-FR limited chemical information was obtained. This may be due to the complex nature of PPW samples (containing protein, suberin, and lipids) as compared to that of hybrid poplar. Therefore, this approach to analyze PPW directly by NMR was not successful and may require further optimization.

**TGA/DTG Analysis.** TGA analysis was performed to examine the thermal degradation behavior of PPW and PPW-FR, which will provide useful information on the pyrolysis of these materials, such as pyrolysis temperature and decomposition kinetics. Figure 6 shows the TGA and DTG thermograms for PPW and PPW-FR samples. Thermal degradation of biomass can be classified into four regions: (i) dewatering at 50−130 °C; (ii) evaporation of volatile compounds due to degradation 130−220 °C; (iii) thermolysis/pyrolysis of polymers (depolymerization) at 220−460 °C; and (iv) char formation at >460 °C.[47,48] Thermal decomposition of the following main constituents occurs at 280−350 °C for starch; 315−400 °C for cellulose; and 220−315 °C for hemicelluloses; and starts at 250 °C for lignin and 290 °C for suberin. Two distinct peaks were observed from the DTG thermograms at 279 and 423 °C for PPW and 285 and 457 °C for PPW-FR, respectively. In addition, less char/ash was seen in the PPW-FR than PPW, which is in accordance with ash content determination. The $E$ before 70% $\alpha$ of samples at 5% conversion intervals were calculated based on ASTM methods. Generally, the $E$ values for PPW and PPW-FR were similar, where decreased trends were observed in both samples after 45% conversion. However, slightly lower values were found in PPW-FR than PPW after $\alpha$ reached 45%. The average $E$ and $A$ values were, respectively, 214 kJ mol$^{-1}$ and $9.18 \times 10^{24}$ for PPW and 209 kJ mol$^{-1}$ and $1.65 \times 10^{22}$ for PPW-FR. Similar values of $E$ and $A$ for the wheat straw sample were observed at 260 kJ mol$^{-1}$ and $2.00 \times 10^{22}$.[47] The lower $E$ in PPW-FR indicates that less energy is required for thermal decomposition and suitable for pyrolysis.[49]

**Py-GC/MS Analysis.** Py-GC/MS was used as a tool to rapidly analyze biomass samples and assess potential pyrolysis bio-oil chemical products. Py-GC/MS products of PPW and PPW-FR at 500 °C are listed in Table 3. A total of 51 pyrolysis products were identified with the main product being $CO_2$ followed by acetic acid (14% for PPW and 7.0% for PPW-FR), acetic anhydride (7.9% and 5.1%), hexadecenoic acid (5.5% and 5.5%), and phenol (5.3% and 5.7%). A range of phenolic compounds, including guaiacyl and syringyl derivatives, were observed totaling at 26.7% in PPW and 35% in PPW-FR. Long chain fatty acids and alkane were derived from lipid and suberin decomposition,[30,50] and the relative percentage increased from 22% into 28% after fermentation. The carbohydrate derived compounds decreased from 45% into 31% from PPW during fermentation. Nitrogen containing compounds (such as pyrrole, methylpyrrole, acetamide, and indolizine) derived from protein were also identified with similar relative percentages in both PPW and PPW-FR samples, which is in agreement with the C, H, and N analyses.

In this study, we have performed a comprehensive chemical and thermal characterization of PPW and PPW-FR to obtain information to improve the utilization of this resource for the production of bioproducts, via thermochemical conversion. A significant increase of lignin/suberin, C/H contents, and calorific value was observed in PPW-FR as a result of fermentation, which will provide higher levels of phenolics and long chain hydrocarbon products after thermochemical conversion. Thermal characterization by TGA and Py-GC/MS analyses indicated that PPW-FR required less energy and lower temperature for thermal conversion processes, such as pyrolysis, and more high value chemical compounds (phenolics and long chain fatty acids, alcohols, and hydrocarbons) can be recovered and upgraded catalytically to transportation fuels. The composition (high in lipids, suberin, and lignin) and thermal properties of PPW-FR, and to a lesser extent PPW, make it a promising renewable biomass for biofuel and bioproducts production. Future work will explore the thermochemical conversion of PPW and PPW-FR in an Auger reactor to produce a crude bio-oil, fractionation of the bio-oil into aqueous and nonaqueous fractions, and their characterization as biofuels.

## AUTHOR INFORMATION


### Corresponding Author

*Tel: +1 208 885 9454. Fax: +1 208 885 6226. E-mail: armandm@uidaho.edu.



### Funding

Funding for this research was provided by the J. R. Simplot Company.


### Notes

The authors declare no competing financial interest.

## ACKNOWLEDGMENTS


We acknowledge Dr. Jean'ne M. Shreeve for providing elemental analysis, Dr. Alexander Blumenfeld for technical assistance in obtaining NMR spectra, Steve Vernon from the J. R. Simplot Company for providing potato peels, and a Waters Technologies Corporation equipment grant for the refractive index detector.


## REFERENCES


(1) FAO. FAOSTAT Agricultural Data. Food and Agricultural Commodities Production. Available at http://faostat.fao.org/site/339/default.aspx (accessed Jun 12, 2014).

(2) NPC. National Potato Council 2012 Potato Statistical Yearbook. Available at http://www.nationalpotatocouncil.org/files/1613/3926/5517/FINAL_2012Statbook_smallerfilesizeforweb.pdf (accessed Jun 12, 2014).

(3) Mader, J.; Rawel, H.; Kroh, L. Composition of phenolic compounds and glycoalkaloids $\alpha$-solanine and $\alpha$-chaconine during commercial potato processing. *J. Agric. Food Chem.* **2009**, *57*, 6292−6297.

(4) Camire, M. E.; Violette, D.; Dougherty, M. P.; McLaughlin, M. A. Potato peel dietary fiber composition: effects of peeling and extrusion cooking processes. *J. Agric. Food Chem.* **1997**, *45*, 1404−1408.

(5) Dobson, G.; Griffiths, D. W.; Davies, H. V.; McNicol, J. W. Comparison of fatty acid and polar lipid contents of tubers from two potato species, *Solanum tuberosum* and *Solanum phureja*. *J. Agric. Food Chem.* **2004**, *52*, 6306−6314.

(6) Graca, J.; Pereira, H. Suberin structure in potato periderm: glycerol, long-chain monomers, and glyceryl and feruloyl dimmers. *J. Agric. Food Chem.* **2000**, *48*, 5476−5483.

(7) Bunzel, M.; Schubler, A.; Saha, G. T. Chemical characterization of Klason lignin preparations from plant-based foods. *J. Agric. Food Chem.* **2011**, *59*, 12506−12513.

(8) Wijngaard, H. H.; Ballay, M.; Brunton, N. The optimization of extraction of antioxidants from potato peel by pressurized liquids. *Food Chem.* **2012**, *133*, 1123−1130.
(9) Piletska, E. V.; Burns, R.; Terry, L. A.; Piletsky, S. A. Application of molecularly imprinted polymer for the extraction of kukoamine A from potato peels. *J. Agric. Food Chem.* **2012**, *60*, 95−99.
(10) Arapoglou, A.; Varzakas, T.; Vlyssides, A.; Israilides, C. Ethanol production from potato peel waste. *Waste Manage* **2010**, *30*, 1898−1920.
(11) Afifi, M. M. Enhancement of lactic acid production by utilizing liquid potato wastes. *Int. J. Biol. Sci. Chem.* **2011**, *5*, 91−102.
(12) Liu, Y.; Wen, Z.; Liao, W.; Liu, C.; Chen, S. Optimization of the process for the production of L(+)-lactic acid from cull potato by *Rhizopus oryzae*. *Eng. Life Sci.* **2005**, *5*, 343−349.
(13) Liang S. Value Added Bioproducts from Potato Peel Waste. Ph.D. Dissertation, University of Idaho, 2014.
(14) Liang, S.; McDonald, A. G.; Coats, E. R. Lactic acid production with undefined mixed culture fermentation of potato peel waste. *Waste Management* **2014**, DOI: 10.1016/j.wasman.2014.07.009.
(15) Coats, E. R.; Searcy, E.; Feris, K.; Shrestha, D.; McDonald, A. G.; Briones, A.; Magnuson, T.; Prior, M. An integrated two-stage anaerobic digestion and biofuel production process to reduce life cycle GHG emissions from U.S. dairies. *Biofuels, Bioprod. Biorefin.* **2013**, *7*, 459−473.
(16) Kang, H. J.; Min, S. C. Potato peel-based biopolymer film development using high-pressure homogenization, irradiation, and ultrasound. *LWT Food Sci. Technol.* **2010**, *43*, 903−909.
(17) Manuel, J. Battle of the biofuels. *Environ. Health Perspect.* **2007**, *115*, 92−95.
(18) Soria, J. A.; McDonald, A. G. Chapter 13: Liquefaction of Softwoods and Hardwoods in Supercritical Methanol: A Novel Approach to Bio-Oil Production. *Biomass Conversion: The Interface of Biotechnology, Chemistry and Materials Science*; Baskar, C., Baskar, S., Dhillon, R. S.; Springer: Berlin, Germany, 2012; pp 421−433.
(19) Chakraborty, M.; Miao, C.; McDonald, A. G.; Chen, S. Concomitant extraction of bio-oil and value added polysaccharides from *Chlorella sorokiniana* using a unique sequential hydrothermal extraction technology. *Fuel* **2012**, *95*, 63−70.
(20) Wang, L. J. Production of bioenergy and bioproducts from food processing wastes: a review. *Trans. ASAE* **2013**, *56*, 217−230.
(21) Onal, E. P.; Uzun, B. B.; Putun, A. E. Steam pyrolysis of an industrial waste for bio-oil production. *Fuel Process. Technol.* **2011**, *92*, 879−885.
(22) Moreno-Pirajan, J. C.; Giraldo, L. Immersion calorimetry applied to the study of the adsorption of phenolic derivatives onto activated carbon obtained by pyrolysis of potato peel. *Mater. Express* **2012**, *2*, 121−129.
(23) *Standard Test Method for Dichloromethane Solubles in Wood*; ASTM Standard D 1108-96; ASTM International: West Conshohocken, PA, 2001.
(24) *Standard Test Method for Acid-Insoluble Lignin in Wood*; ASTM Standard D 1106-96; ASTM International: West Conshohocken, PA, 2001.
(25) Schoening, A. G.; Johansson, G. Absorptiometric determination of acid-soluble lignin in semichemical bisulfite pulps and in some woods and plants. *Svensk Papperstid.* **1965**, *68*, 607−613.
(26) *Standard Test Method for Determination of Carbohydrates in Biomass by High Performance Liquid Chromatography*; ASTM Standard E 1758-01; ASTM International: West Conshohocken, PA, 2007.
(27) *Starch-Glucoamylase Method with Subsequent Measurement of Glucose with Glucose Oxidase*; AACC Method 76-11; AACC International: St. Paul, MN, 1999.
(28) *Standard Test Method for Ash in Wood*; ASTM Standard D 1102-84; ASTM International: West Conshohocken, PA, 2001.
(29) *Standard Test Method for Gross Calorific Value of Coal and Coke*; ASTM Standard D 5856-04; ASTM International: West Conshohocken, PA, 2001.
(30) Osman, N. B.; McDonald, A. G.; Laborie, M. P. G. Analysis of DCM extractable components from hot-pressed hybrid poplar. *Holzforschung* **2012**, *66*, 927−934.
(31) Kim, H.; Ralph, J.; Akiyama, T. Solution-state 2D NMR of ball-milled plant cell wall gels in DMSO-d6. *Bioenerg. Res.* **2008**, *1*, 56−66.
(32) *Standard Test Method for Decomposition Kinetics by Thermogravimetry*; ASTM Standard E 1641-07; ASTM International: West Conshohocken, PA, 2007.
(33) Pillai, K. V.; McDonald, A. G.; Wagner, F. G. Developing a model system in vitro to understand tracheary element development in Douglas-fir (*Pseudostuga mensziesii*) *Maderas. Cienc. Tecnol.* **2011**, *13*, 3−18.
(34) Belyea, R. L.; Rausch, K. D.; Tumbleson, M. E. Composition of corn and distillers dried grains with solubles from dry grind ethanol processing. *Bioresour. Technol.* **2004**, *94*, 293−298.
(35) Sannigrahi, P.; Ragauskas, A. J.; Tuskan, G. A. Poplar as a feedstock for biofuels: a review of compositional characteristics. *Biofuels, Bioprod. Biorefin.* **2010**, *4*, 209−226.
(36) Sannigrahi, P.; Ragauskas, A. J. Characterization of fermentation residues from the production of bio-ethanol from lignocellulosic feedstocks. *J. Biobased Mater. Bioenergy* **2011**, *5*, 514−519.
(37) Liu, W.; Wang, Y.; Yu, Z.; Bao, J. Simultaneous saccharification and microbial lipid fermentation of corn stover by oleaginous yeast *Trichosporon cutaneum*. *Bioresour. Technol.* **2012**, *118*, 13−18.
(38) Mattinen, M. L.; Filpponen, I.; Rvinen, R. J.; Li, B.; Kallio, H.; Lehtinen, P.; Argyropoulos, D. Structure of the polyphenolic component of suberin isolated from potato (*Solanum tuberosum var. Nikola*). *J. Agric. Food Chem.* **2009**, *57*, 9747−9753.
(39) Wang, W.; Tian, S.; Stark, R. E. Isolation and identification of triglycerides and ester oligomers from partial degradation of potato suberin. *J. Agric. Food Chem.* **2010**, *58*, 1040−1045.
(40) Moire, L.; Schmutz, A.; Buchala, A.; Yan, B.; Stark, R. E.; Ryser, U. Glycerol is a suberin monomer: new experimental evidence for an old hypothesis. *Plant Physiol.* **1999**, *119*, 1137−1146.
(41) Schilling, C. H.; Tomasik, P.; Karpovich, D. S.; Hart, B.; Shepardson, S.; Garcha, J.; Boettcher, P. T. Preliminary studies on converting agricultural waste into biodegradable plastics, part I: Corn distillers' dry grain. *J. Polym. Environ.* **2004**, *12*, 257−264.
(42) Zarrinbakhsh, N.; Mohanty, A. K.; Misra, M. Fundamental studies on water-washing of the corn ethanol coproduct (DDGS) and its characterization for biocomposite applications. *Biomass Bioenerg.* **2013**, *55*, 251−259.
(43) Mattinen, M. L.; Suortti, T.; Gosselink, R.; Argyropoulos, D. S.; Evtuguin, D.; Suurnakki, A.; de Jong, E.; Tamminen, T. Polymerization of different lignins by laccase. *Bioresource* **2008**, *3*, 549−565.
(44) Singh, R.; Singh, S.; Pandare, T. K. V.; Bastawade, K. B.; Gokhale, D. V.; Varma, A. J. Lignin-carbohydrate complexes from sugarcane bagasse: preparation, purification, and characterization. *Carbohydr. Polym.* **2005**, *62*, 57−66.
(45) Lu, F.; Ralph, J. Solution-state NMR of lignocellulosic biomass. *J. Biobased Mater. Bioenergy* **2011**, *5*, 169−180.
(46) Cheng, H. N.; Neiss, T. G. Solution NMR spectroscopy of food polysaccharides. *Polym. Rev.* **2012**, *52*, 81−114.
(47) Gao, A. H.; Bule, M. V.; Laskar, D. D.; Chen, S. Structural and thermal characterization of wheat straw pretreated with aqueous ammonia soaking. *J. Agric. Food Chem.* **2012**, *60*, 8632−8639.
(48) Wei, L.; McDonlad, A. G.; Freitag, C.; Morrell, J. J. Effects of wood fiber esterification on properties, weatherability and biodurability of wood plastic composites. *Polym. Degrad. Stab.* **2013**, *98*, 1348−1361.
(49) Meszaros, E.; Varhegyi, G.; Jakab, E.; Marosvolgyi, B. Thermogravimetric and reaction kinetic analysis of biomass samples from an energy plantation. *Energy Fuels* **2004**, *18*, 497−507.
(50) Turner, J. W.; Hartman, B. E.; Hatcher, P. G. Structural characterization of suberin isolated from river birch (*Betula nigra*) bark. *Org. Geochem.* **2013**, *57*, 41−53.

JOURNAL OF AGRICULTURAL AND FOOD CHEMISTRY

Article

pubs.acs.org/JAFC

# Improving Rheology and Enzymatic Hydrolysis of High-Solid Corncob Slurries by Adding Lignosulfonate and Long-Chain Fatty Alcohols

Hongming Lou,[†,‡] Shun Wu,[†] Xiuli Li,[†] Tianqing Lan,[§] Dongjie Yang,[†] Yuxia Pang,[†] Xueqing Qiu,*[,†,‡] Xuehui Li,[†] and Jinhao Huang[†]

[†]School of Chemistry and Chemical Engineering and [‡]State Key Laboratory of Pulp and Paper Engineering, South China University of Technology, Guangzhou, China

[§]Faculty of Chemical Engineering, Kunming University of Science and Technology, Kunming, China

**ABSTRACT:** The effects of lignosulfonate (SXSL) and long-chain fatty alcohols (LFAs) on the rheology and enzymatic hydrolysis of high-solid corncob slurries were investigated. The application of 2.5% (w/w) SXSL increased the substrate enzymatic digestibility (SED) of high-solid corncob slurries at 72 h from 31.7 to 54.0%, but meanwhile it increased the slurry's yield stress and complex viscosity to make the slurry difficult to stir and pump. The smallest molecular weight (MW) SXSL fraction had the strongest enhancement on SED. The SXSL fraction with large MW had a negative effect on rheology. *n*-Octanol (C8) and *n*-decanol (C10) improved the rheological properties of high-solid slurry and are strong enough to counteract the negative effect of SXSL. Furthermore, C8 and C10 clearly enhanced the enzymatic hydrolysis of high-solid corncob slurries with and without SXSL. A mechanism was proposed to explain the observed negative effect of SXSL and the positive effect of LFAs on the rheological properties.

**KEYWORDS:** *lignosulfonate, long-chain fatty alcohols, high-solid enzymatic hydrolysis, rheology, corncob slurry*

## INTRODUCTION

Enzymatic hydrolysis of lignocellulosic biomass has been recognized as a main method to depolymerize the lignocellulose into fermentable sugars for conversion to biofuels and other chemicals.[1,2] However, it still needs technological improvements to make the products of lignocellulose economically competitive.[3] The consumption of lignocellulose feedstock and enzymes and the energy inputs for pretreatment and distillation are the important factors that cause the high cost of lignocellulosic ethanol.[3,4] Economic analyses suggested that the ethanol concentration in fermentation broth should be above 4% (w/w) to make the subsequent distillation economical.[4] Therefore, enzymatic hydrolysis should be conducted at high-solid loadings to increase the concentration of sugar and ethanol and decrease the cost of distillation processes.[5,6]

However, high-solid slurries have difficulties in mixing and pumping for lack of water.[7,8] Improving the rheological properties of high-solid lignocellulosic slurry can result in economic benefits because of (1) decreased utility costs associated with pumping and mixing of slurries, (2) decreased capital costs associated with increased pump and reactor lifetimes, and (3) decreased capital costs associated with smaller reaction vessels.[9] Therefore, several chemical additives were studied for their ability to modify the rheology of lignocellulosic biomass, including polymers, proteins, and nonionic, anionic, and cationic surfactants.[10] Although anionic surfactants, such as sodium dodecyl benzenesulfonate and sodium dodecyl sulfonate, were very effective at reducing the yield stress, their presence was very detrimental to the enzymatic hydrolysis of high-solid cellulosic slurries.[10]

Meanwhile, the enzymatic hydrolysis efficiency of lignocellulosic substrate at high-solid loading is always lower than that at low-solid loading.[11] Increasing the enzymatic hydrolysis efficiency of lignocellulose at high-solid loading can reduce the consumption of substrate and enzymes to decrease the production cost. Therefore, a low-cost additive with strong improvement on the rheology properties and enzymatic hydrolysis efficiency of high-solid lignocellulosic slurry is urgently required to lower the cost of lignocellulosic ethanol.

In previous studies, we have reported that lignosulfonate (SXSL), as an anionic polymeric surfactant from pulping waste liquor of the papermaking industry, has the potential to increase the enzymatic hydrolysis efficiency of low-solid lignocellulose through reducing the nonproductive binding of cellulose and improving the cellulase adsorption on cellulose.[12−14] However, the effect of SXSL on enzymatic hydrolysis efficiency of high-solid lignocellulose has not been discovered. Especially, the adsorption of SXSL on lignin could increase the hydrophilicity and negative charge of lignocellulose substrate.[12] The former would increase the slurry viscosity; the latter would decrease it. Therefore, the effect of SXSL on the rheology properties of high-solid lignocellulose slurry should be explored for its application.

On the other hand, long-chain fatty alcohols (LFAs) could improve the physicochemical properties of calcium lignosulfonate solution, such as dynamic and equilibrium surface tension

Received: May 27, 2014
Revised: August 5, 2014
Accepted: August 6, 2014
Published: August 6, 2014

ACS Publications © 2014 American Chemical Society



dx.doi.org/10.1021/jf502534s | J. Agric. Food Chem. 2014, 62, 8430−8436

and apparent viscosity.[15,16] It has been found that LFAs could improve the enzymatic hydrolysis of lignocellulose and the rheology properties.[14] Synergistic effects between SXSL and LFAs on the improvement of enzymatic hydrolysis and the rheology properties of high-solid lignocellulosic slurries could be expected.

In China, >20 million tons of corncobs are generated annually.[17] Corncob is an important feedstock for xylose and xylitol production due to its high xylan content. The xylan fraction of corncob can easily be hydrolyzed into xylose by diluted acids.[18] The cellulose and lignin fractions remain in the solid residue. Currently, approximately half a million tons of corncob residues are produced annually,[17] which are usually burned to get heat energy. Because the upstream diluted acid hydrolysis has greatly removed its hemicellulose fraction and destroyed its lignocellulose cell wall structure and its cellulose content is >60%,[17,19] it is a cheap raw material for ethanol and biorefinery and needs no pretreatment.

This study is focused on the effects of SXSL and LFAs on the enzymatic hydrolysis and rheology of high-solid corncob residue slurry. The objectives are (1) to investigate the synergistic effects between SXSL and LFAs on enzymatic hydrolysis and rheology and (2) to discover the effect of SXSL molecular weight on enzymatic hydrolysis and rheology.

## MATERIALS AND METHODS

**Substrates.** Brown corncob residue particles were provided by Shengquan Corp. Ltd. (Jinan, Shandong province, China). Prior to enzymatic hydrolysis, the corncob residues were treated at 121 °C for 1 h by autoclave and then washed by deionized water. The washed corncob residues were directly used for enzymatic liquefaction and hydrolysis without sieving. The chemical composition of the washed corncob residues was analyzed and is given in Table 1.

**Table 1. Chemical Composition of Washed Lignocellulosic Substrates**

| | main carbohydrates (%) | | lignin (%) | | |
|---|---|---|---|---|---|
| substrate | glucan | xylan | acid-soluble lignin | acid-insoluble lignin | ash (%) |
| washed corncob residue | 74.40 | 0.08 | 0.72 | 18.84 | 1.18 |

**Additives.** Lignosulfonate was produced from sulfite pulping of poplar wood by Shixian Papermaking Corp. Ltd. (Yanbian, Jilin province, China). SXSL was separated into four fractions by an ultrafiltration apparatus (Wuxi Membrane Science and Technology Corp., China). The fractions with molecular weight (MW) ranges of >50000 (SL1), 10000−50000 (SL2), 2500−10000 (SL3), and <2500 (SL4) were used. Table 2 shows the properties of all MW fractions used in this study. Long-chain fatty alcohols (*n*-octanol and *n*-decanol, AR) were purchased from Tianjin Kemiou Chemical Reagent Co., Ltd.

**Enzymes.** Commercial cellulase enzyme Cellic CTec2 (abbreviated CTec2) derived from the fungus *Trichoderma reesei* (*Hypocrea jecorina*) was generously provided by Novozymes North America (Franklinton, NC, USA). The cellulase activity was 150 filter paper units (FPU)/mL as determined according to a literature method,[20] and its protein concentration was 73.6 mg/mL by using the Bradford method.[21]

**High-Solid Enzymatic Hydrolysis.** Enzymatic hydrolysis of corncob residues was conducted at 13% (w/w) solid loading with acetate buffer (50 mM) in a shaker (DDHZ-300, Jiangsu Taicang equipment factory, China) at 50 °C and 200 rpm. The dosage of SXSL and LAFs by weight was on an oven-dry substrate basis. The pH of the slurries was adjusted to 4.8. The CTec2 loading was 3 FPU/g glucan. Aliquots of 1 mL were taken at 72 h for glucose analysis after centrifugation at 10000 rpm for 10 min. Glucose in enzymatic hydrolysates was measured with a commercial SBA-40E biosensor by a $H_2O_2$ electrode sensor (Institute of Biology of the Shandong Academy of Sciences, China). Control experiments without substrates were also carried out for comparison. Substrate enzymatic digestibility (SED), defined as the percentage of substrate glucan enzymatically hydrolyzed to glucose, was used to represent the enzymatic hydrolysis efficiency. Each data point is the average of two analyses. The experimental error in enzymatic hydrolysis was <2.5% based on replicate runs. Error bars are shown in the figures.

**Rheometry.** High-solid lignocellulosic slurries were prepared with sieved corncob (40 mesh) and acetate buffer (50 mM, pH 4.8) without cellulase, and their rheological properties were investigated at 25 °C by a Haake Mars-III rotational rheometer (Thermo Scientific, Germany) with vane-in-cup geometry. The average particle diameter was 118.4 ± 6.4 μm measured by using an MS2000 laser diffraction particle size analyzer (Malvern Instruments, Malvern, UK). The cup diameter was 26 mm, and the vane diameter was 22 mm, resulting in a gap width of 1 mm.

## RESULTS AND DISCUSSION

**Effect of Lignosulfonate on Enzymatic Hydrolysis Efficiency and Rheology of High-Solid Corncob Slurries.** Lignocellulosic residues from corncob by acidolysis to convert xylan into furfural were enzymatically hydrolyzed with SXSL dosage on dry substrate ranging from 0.25 to 5.0% at a high-solid dry content of 13% (Figure 1). The enzymatic hydrolysis was conducted at a CTec2 loading of 3 FPU/g glucan and 50 °C in acetate buffer of pH 4.8. The addition of 2.5 and 5.0% SXSL increased the SED of corncob residues at 72 h from 31.7 to 54.0 and 67.7%. This result was consistent with the enhancement of lignosulfonate on the enzymatic hydrolysis of softwood and hardwood substrates in our previous studies at a low-solid dry content of 2%.[12,13] This indicated that lignosulfonate could be used to improve the enzymatic hydrolysis efficiency of high-solid lignocellulosic slurries. The enhancement on enzymatic hydrolysis of high-solid lignocellulosic substrate increases with the dosage of SXSL.

Lignosulfonate is an amphiphilic polymer with hydrophobic phenylpropanoid backbone linked to the hydrophilic sulfonate group. It was proved that lignosulfonate would bind to solid

**Table 2. Properties of the Four Lignosulfonate Fractions Used**

| sample label | MW (Da) | weight percentage | sulfonic acid group (mmol/g) | lignosulfonate content (%) | glucose content (%) | conductivity[a] (ms/cm) |
|---|---|---|---|---|---|---|
| SXSL | 9900 | 100 | 2.11 ± 0.04 | 49.60 | 3.63 | 1.66 |
| SL1 | 19900 | 42 | 1.67 ± 0.01 | 100 | 0 | 0.13 |
| SL2 | 6000 | 22 | 1.98 ± 0.02 | 86.03 | 0 | 0.47 |
| SL3 | 4300 | 18 | 2.44 ± 0.07 | 63.11 | 0.32 | 1.23 |
| SL4 | 2360 | 18 | 2.96 ± 0.05 | 16.23 | 9.85 | 6.77 |

[a]Conductivity was measured in lignosulfonate aqueous solution for which the concentration was the same with the high-solid corncob slurries.


dx.doi.org/10.1021/jf502534s | J. Agric. Food Chem. 2014, 62, 8430−8436

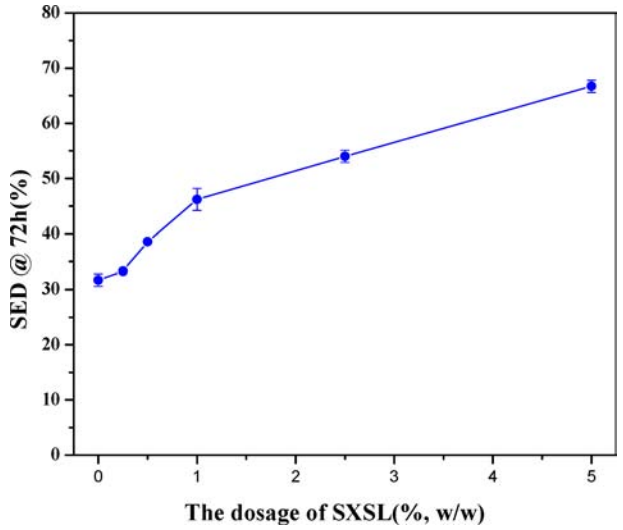


**Figure 1.** Effects of dosage of lignosulfonate on SED of high-solid corncob slurries at 72 h.

lignin in substrate by hydrophobic interaction to reduced nonproductive cellulase binding to lignin to improve the enzymatic hydrolysis in previous studies.[13,18,22] Lignosulfonate is more hydrophilic than lignin in substrate because of its higher sulfonic acid group content. The application of lignosulfonate may increase the hydrophilicity of substrate by covering the surface of lignin in substrate and modifying the viscosity and rheology of corncob slurries.

Transient flow rheometer experiment is a reliable measurement of the yield stress for high-solid lignocellulosic slurries.[10] The stress−strain measurements of Figure 2a were taken at a shear rate of 0.01 $s^{-1}$, as low as that in other studies.[10] Considering the inhomogeneity of high-solid slurries, these experiments were carried out in duplicate to ensure the repeatability. As shown in Figure 2a, the shear stress initially increases linearly with the vane displacement as the slurries are elastically deformed. The shear stress reaches a peak when plastic deformation dominates and then declines as the slurries are plastically deformed. The peak shear stress in these measurements is an indication of the characteristic yield stress of the slurry. The yield stress of the control slurries ranged from 72.3 to 82.7 Pa, averaging 77.5 Pa. The application of 2.5% SXSL nearly doubled the yield stress, increasing to about 140 Pa. Results of the oscillatory frequency sweeps are shown in Figure 2b. The complex viscosity is an essential parameter to characterize the rheological properties of a viscoelastic slurry, which does not vary with oscillatory stresses in the linear viscoelastic region. Slurries with a low value of complex viscosity are relatively "soft" and more easily deformed, whereas slurries with a high value of complex viscosity tend to be considered "hard" and deformation is more difficult.[10] As shown in Figure 2b, the addition of SXSL generally provided a small increase in the complex viscosity of the high-solid corncob slurries.

Although SXSL improved the enzymatic hydrolysis of high-solid corncob slurry, it increased the slurry's viscosity, which would produce a higher mixing and pumping power to increase the cost. Therefore, it needs to develop a way to decrease the viscosity of high-solid corncob slurries with application of SXSL.

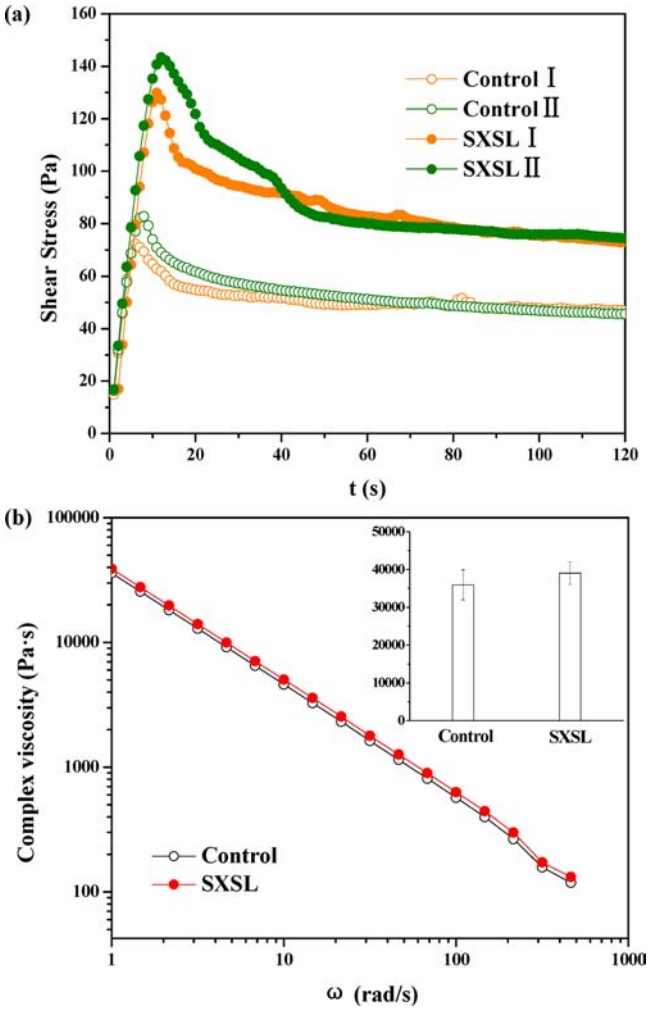


**Figure 2.** Effects of SXSL on the rheology of high-solid corncob slurries: (a) typical transient flow curves of control slurries and those with added 2.5% (w/w) SXSL (multiple flow curves are shown for each condition to show the reproducibility of the method); (b) typical oscillatory frequency sweep recorded from control suspensions and those with added 2.5% (w/w) SXSL using 10 Pa stress; (inset) complex viscosity on a linear scale with $\omega$ at 1 rad/s.

**Effect of LFAs on the Rheological Properties with SXSL.** LFAs derived from plant oils or fats by hydrolysis and catalytic hydrogenation[23] have been observed to enhance the enzymatic hydrolysis of crystalline cellulose and improve the rheological properties of high-solid lignocellulosic slurry in our previous studies.[14] LFAs were applied to improve the rheological properties of high-solid corncob slurries with the addition of SXSL. The effect of LFAs on the yield stresses and complex viscosity of the corncob slurries at dry content of 13% are shown in Figures 3 and 4. The application of 2.5% (w/w) C8 and C10 clearly reduced the shear stress at a shear rate of 0.01 $s^{-1}$ (Figure 3a), and the yield stress decreased from 136.7 to 86.7 and 58.7 Pa, as shown in Figure 3b. Meanwhile, C8 and C10 reduced the complex viscosity at the rotating speed range from 1 to 100 rad/s (Figure 4a). The complex viscosity at 1 rad/s decreased from 39060 to 21850 and 14770 Pa·s (Figure 4b), and the yield stress and complex viscosity of the high-solid corncob slurry with 2.5% SXSL and 2.5% C10 was lower than those without SXSL and C10. The results indicated that LFAs could improve the rheological properties of high-solid corncob


dx.doi.org/10.1021/jf502534s | J. Agric. Food Chem. 2014, 62, 8430−8436

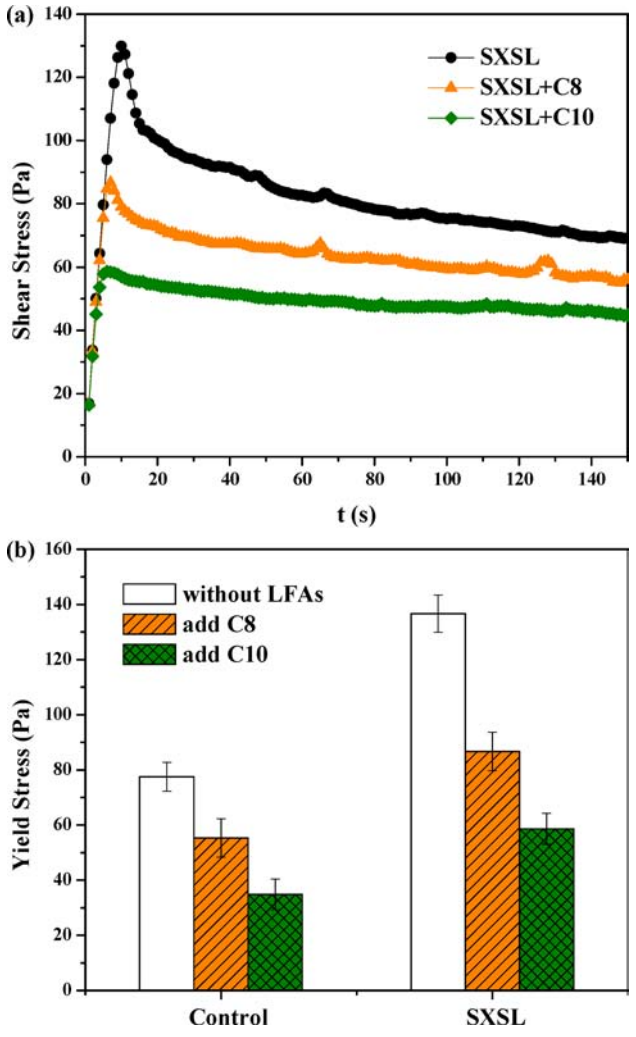


**Figure 3.** Effects of LFAs on the yield stress of high-solid corncob slurries at additives' concentration of 2.5% (w/w): (a) typical transient flow curves; (b) yield stresses of high-solid corncob slurries.

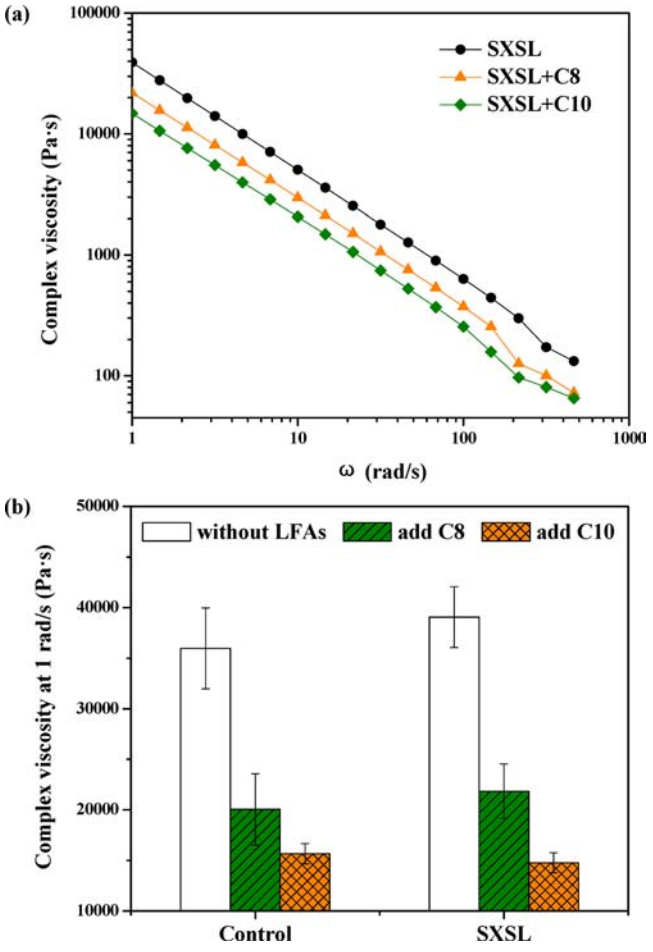


**Figure 4.** Effects of LFAs on the complex viscosity of high-solid corncob slurries at additives' concentration of 2.5% (w/w): (a) oscillatory frequency sweep; (b) complex viscosity of high-solid slurries on a linear scale with $\omega$ at 1 rad/s.

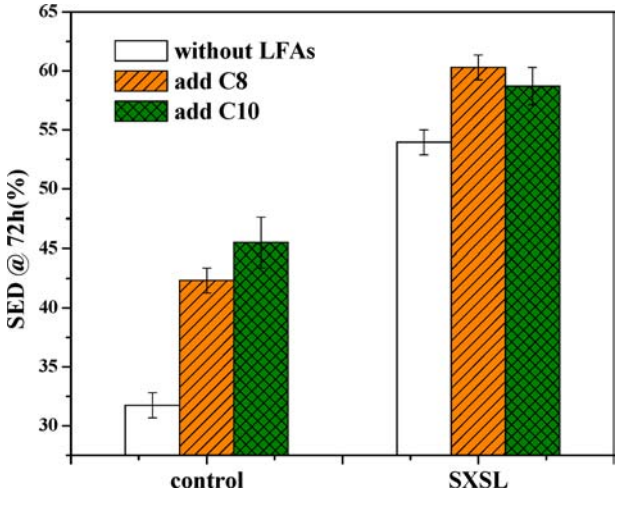


**Figure 5.** Effects of C8 and C10 on SED of high-solid corncob slurries at 72 h.

slurry with and without the application of lignosulfonate. The improvement of LFAs increases with the carbon chain length, and 2.5% C10 is enough to counteract the negative effect of 2.5% lignosulfonate on high-solid corncob slurry.

**Effect of LFAs on the SED of High-Solid Corncob Residues with SXSL.** The effects of C8 and C10 on the SED of high-solid corncob slurries at 72 h are shown in Figure 5. In the absence of SXSL, 2.5% C8 and C10 increased the SED at 72 h from 31.7 to 42.3 and 45.5%, respectively. This observed enhancement agrees with our previous study.[14] In the presence of 2.5% SXSL, 2.5% C8 and C10 increased the SED at 72 h from 54.0 to 60.3 and 58.7%, respectively. These results indicated that LFAs could improve the enzymatic hydrolysis of high-solid corncob slurry with and without lignosulfonate.

**Lignosulfonate MW Effects on the Enzymatic Hydrolysis and Rheology of High-Solid Corncob Slurries.** Four SXSL fractions prepared by ultrafiltration were applied to compare the enzymatic hydrolysis efficiency and rheological properties of high-solid corncob slurry at the same loading of 2.5% with and without LFAs. The SXSL fraction concentrations were corrected by UV measurement. As shown in Figure 6, in the absence of LFAs, all SXSL fractions enhanced the enzymatic hydrolysis of high-solid corncob, in agreement with the observed enhancement of woody substrate at dry content of 2% in our previous study.[13] The order of enhancement at 72 h is SL4 > SL3 ≈ SL2 > SL1. The small MW fraction SL4 doubled the SED of corncob slurries at 13% from 31.7 to 63.5%. In the presence of SXSL fractions, the application of C8


dx.doi.org/10.1021/jf502534s | J. Agric. Food Chem. 2014, 62, 8430−8436

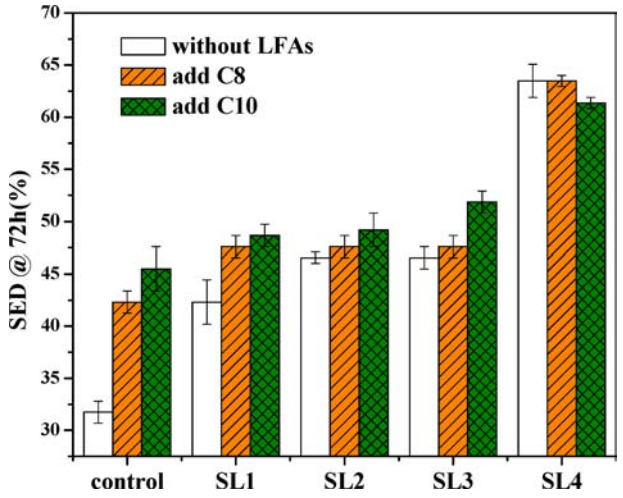


**Figure 6.** Effects of MW of lignosulfonate on SED of high-solid corncob slurries at 72 h.

and C10 improved the enzymatic hydrolysis of corncob slurries with large MW fractions of SL1, SL2, and SL3 and had negligible effect on that with small MW fraction SL4 containing much sugars and inorganic salts. The mechanism of lignosulfonate enhancement on enzymatic hydrolysis mainly includes the effect on cellulase nonproductive adsorption on lignin[12,24] and the effect on enzymatic hydrolysis of pure cellulose.[25] It has been found that lignosulfonate could efficiently reduce the cellulase nonproductive adsorption on lignin in lignocellulosic substrate by increasing the lignin surface hydrophilicity and by electrostatic repulsion between lignosulfonate adsorbed on lignin and cellulase.[12,26] SXSL fraction with higher MW had a stronger blocking effect on cellulase nonproductive adsorption on lignin due to its larger adsorption on lignin. On the other hand, the concept of "lignosulfonate-cellulase aggregate stabilized and enhanced cellulase binding to cellulose" has been proposed to explain the lignosulfonate enhancement on enzymatic hydrolysis of pure cellulose in our previous study.[25] SXSL fraction with lower MW had stronger enhancement on pure cellulose by increasing the cellulase adsorption at a buffer pH of 4.8 and with a relatively low dosage. In the high-solid corncob slurry, the SXSL fraction effect on the cellulase adsorption on cellulose may be the dominant factor of enhancement on enzymatic hydrolysis. Therefore, SXSL fraction with lower MW had stronger enhancement on the enzymatic hydrolysis of corncob. LFAs have been found to improve the lignosulfonate adsorption on $TiO_2$ particles.[15] LFAs could improve the enzymatic hydrolysis of high-solid corncob slurry with SXSL by increasing the SXSL fraction adsorption on cellulase to stabilize cellulase binding on cellulose. SL4, the smallest MW fraction, is highly sulfonated with high negative charges. The highly negatively charged SL4–cellulase aggregates would produce sufficiently strong electrostatic repulsion between the aggregates on cellulose to limit the cellulase adsorption on cellulose, even if LFAs could improve the formation of SL4–cellulase aggregates. Therefore, LFAs have negligible enhancement on the enzymatic hydrolysis of high-solid corncob with 2.5% SL4.

In addition, four SXSL fractions were applied to investigate the effect of lignosulfonate MW on the rheological properties of high-solid corncob slurry at the same loading of 2.5%. As shown in Figure 7, the largest MW faction SL1 increased the yield stress and complex viscosity of high-solid corncob slurry. SL2

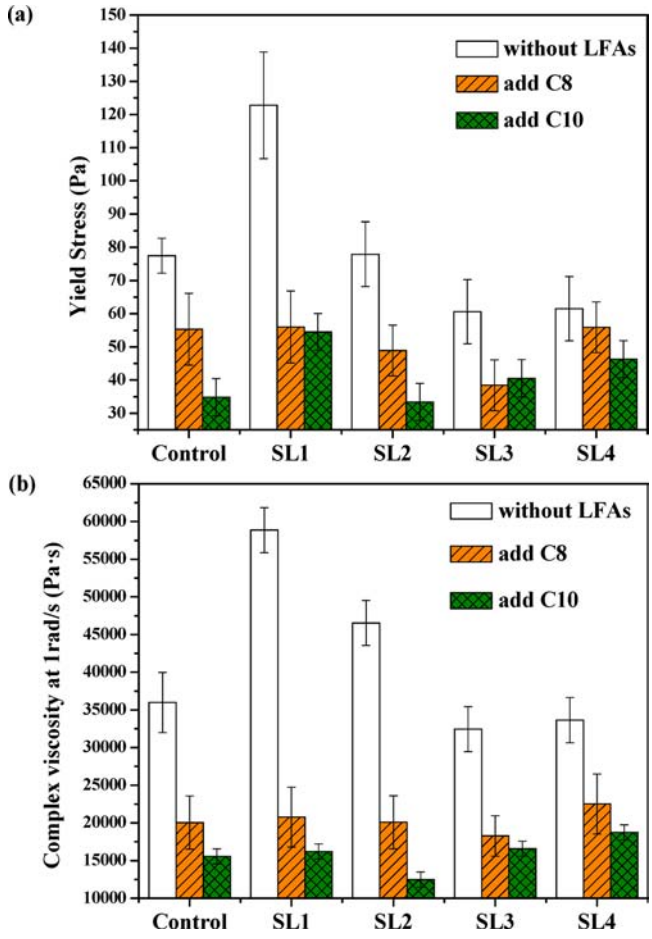


**Figure 7.** Effects of MW of lignosulfonate on rheology of high-solid corncob slurries: (a) changes in yield stresses measured via transient flow experiments; (b) changes in complex viscosity measured by typical frequency sweep on a linear scale with $\omega$ at 1 rad/s.

had negligible effect on the yield stress, but increased the complex viscosity. The small MW fractions of SL3 and SL4 slightly reduced the shear stress and yield stress. After the addition of LFAs, the yield stress and complex viscosity at 1 rad/s of the corncob slurry with SXSL fractions clearly decreased and was lower than that without the application of lignosulfonate and LFAs (control run). LFAs strongly improved the rheology of high-solid slurry with SL1 loaded and made it similar to other fractions. Furthermore, C10 has a stronger reduction in the yield stress and complex viscosity than C8.

**Mechanism Understanding of Lignosulfonate and LFAs on Rheology of Lignocellulosic Substrate.** The negative effect of SXSL on the rheological properties of corncob slurries could be explained using a cartoon shown in Figure 8. In the absence of lignosulfonate, lignocellulose would absorb water through hydrogen bonding between hydroxyl groups in cellulose or hemicellulose and water molecules. A hydration layer would form on the surface of cellulose and hemicellulose parts in lignocellulosic substrate. Because lignin is more hydrophobic than cellulose and hemicellulose, it is difficult to form a hydration layer on the lignin surface in lignocellulose. After adding lignosulfonate, lignosulfonate can be adsorbed on the surface of lignin by $\pi-\pi$ interactions between aromatic rings in lignin and lignosulfonate[27] and hydrophobic interactions.[12] The hydrophilic part (e.g., sulfonic


dx.doi.org/10.1021/jf502534s | J. Agric. Food Chem. 2014, 62, 8430–8436

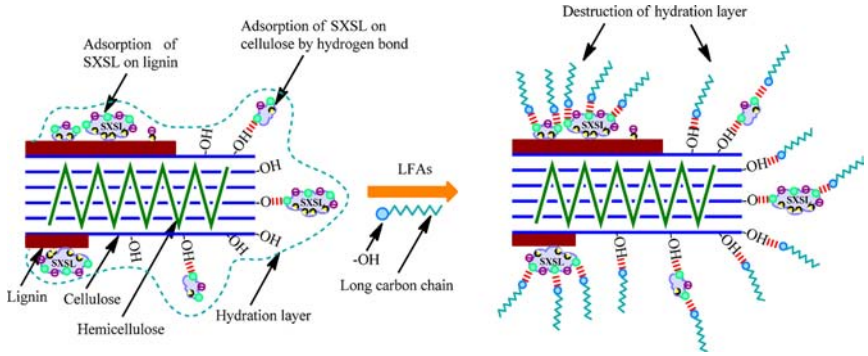


**Figure 8.** Schematic diagram of the effect of lignosulfonate and LFAs on the rheological properties of high-solid lignocellulosic slurries.

acid group, hydroxyl group, carboxyl group) of lignosulfonate would face toward water and make the lignin surface hydrophilic. Thus, the lignosulfonate on lignin surface would adsorb water in the slurry and form a hydration layer. As a result of the reduction of free water in the slurry, the rheological properties would become poor, such as the observed increment of yield stress and complex viscosity. On the other hand, lignosulfonate can be adsorbed on the cellulose surface to disrupt the network of high-solid lignocellulose slurry formed among the lignocellulose particles by hydrogen bonds, which made lignocellulose particles negatively charged and dispersive to improve the rheology. However, the yield stress measured at a very low shear rate of 0.01 $s^{-1}$, which is too slow to disrupt the lignocellulose network in slurry, increased significantly due to the reduction of free water with the application of lignosulfonate. Because the adsorption amount of lignosulfonate fraction on lignin increases with its MW,[12] more SL1 and free water would be adsorbed on lignin to result in a more negative effect on the rheological properties. Complex viscosity measured at a high rotating speed of 1 rad/s, equivalent to 1100 times that in yield stress measurement, was affected not only by the reduction of free water but also by the dispersion improvement. As a balanced result, there is a small increase in the complex viscosity after the addition of lignosulfonate.

LFAs are composed of a long alkyl chain and a hydroxyl group. LFAs would bind to the hydroxyl group on cellulose, hemicellulose, lignin, and lignosulfonate on lignin through hydrogen bonding. The alkyl chain in LFAs would make the lignocellulose surface more hydrophobic and destroy the hydration layers around cellulose and lignosulfonate, freeing water molecules and improving the rheological properties of high-solid lignocellulosic slurry.

Lignosulfonate enhanced the enzymatic hydrolysis of high-solid corncob slurry, and the enhancement increased with the decrease of the MW. Lignosulfonate with high MW and low sulfonation degree increased the slurry's yield stress and complex viscosity to make it difficult to stir and pump. LFAs including C8 and C10 could clearly decrease the yield stress and complex viscosity with and without lignosulfonate and be strong enough to counteract the negative effect of lignosulfonate. Both the negative effect of lignosulfonate and the positive effect of LFAs on rheology may be attributed to the hydrophobicity change of lignocellulose particles. Furthermore, LFAs would improve the enzymatic hydrolysis of high-solid corncob slurry with and without lignosulfonate, but further investigation is needed to better understand the synergistic effect mechanism between LFAs and lignosulfonate on the enhanced enzymatic hydrolysis of lignocellulose.

## AUTHOR INFORMATION

### Corresponding Author

*(X.Q.) Phone: 86-20-87114968. Fax: 86-20-87114721. E-mail: xueqingqiu66@163.com.

### Funding

This research was financially supported by the National Natural Science Foundation of China (21376100, 21336002), International S&T Cooperation Program of China (2013DFA41670), the National Basic Research Program of China 973 (2012CB215302), and the Fundamental Research Funds for the Central Universities.

### Notes

The authors declare no competing financial interest.

## ACKNOWLEDGMENTS

We acknowledge Liu Hao (State Key Laboratory of Pulp and Paper Engineering, SCUT) for giving the CTec2 sample.

## ABBREVIATIONS USED

SXSL, lignosulfonate; LFAs, long-chain fatty alcohols; SED, substrate enzymatic digestibility; C8, *n*-octanol; C10, *n*-decanol; MW, molecular weight

## REFERENCES

(1) Himmel, M. E.; Ding, S. Y.; Johnson, D. K.; Adney, W. S.; Nimlos, M. R.; Brady, J. W.; Foust, T. D. Biomass recalcitrance: engineering plants and enzymes for biofuels production. *Science* **2007**, *315* (5813), 804−807.

(2) Lan, T. Q.; Gleisner, R.; Zhu, J. Y.; Dien, B. S.; Hector, R. E. High titer ethanol production from SPORL-pretreated lodgepole pine by simultaneous enzymatic saccharification and combined fermentation. *Bioresour. Technol.* **2013**, *127*, 291−297.

(3) Zhu, J. Y.; Zhuang, X. S. Conceptual net energy output for biofuel production from lignocellulosic biomass through biorefining. *Prog. Energy Combust. Sci.* **2012**, *38*, 583−598.

(4) Wingren, A.; Galbe, M.; Zacchi, G. Techno-economic evaluation of producing ethanol from softwood: comparaison of SSF and SHF and identification of bottlenecks. *Biotechnol. Prog.* **2003**, *19*, 1109−1117.

(5) Hsieh, C. W. C.; Cannella, D.; Jørgensen, H.; Felby, C.; Thygesen, L. G. Cellulase inhibition by high concentrations of monosaccharides. *J. Agric. Food Chem.* **2014**, *62* (17), 3800−3805.

(6) Huang, R.; Cao, M.; Guo, H.; Qi, W.; Su, R.; He, Z. Enhanced ethanol production from pomelo peel waste by integrated hydrothermal treatment, multi-enzymes formulation and fed-batch operation. *J. Agric. Food Chem.* **2014**, *62* (20), 4643−4651.

(7) Modenbach, A. A.; Nokes, S. E. Enzymatic hydrolysis of biomass at high-solids loadings − a review. *Biomass Bioenergy* **2013**, *56*, 526−544.
(8) Jørgensen, H.; Vibe-Pedersen, J.; Larsen, J.; Felby, C. Liquefaction of lignocellulose at high-solids concentrations. *Biotechnol. Bioeng.* **2007**, *96* (5), 862−870.
(9) Knutsen, J. S.; Liberatore, M. W. Rheology modification and enzyme kinetics of high-solids cellulosic slurries: an economic analysis. *Energy Fuels* **2010**, *24* (12), 6506−6512.
(10) Knutsen, J. S.; Liberatore, M. W. Rheology modification and enzyme kinetics of high solids cellulosic slurries. *Energy Fuels* **2010**, *24* (5), 3267−3274.
(11) Ramachandriya, K. D.; Wilkins, M.; Atiyeh, H. K.; Dunford, N. T.; Hizifoglu, S. Effect of high dry solids loading on enzymatic hydrolysis of acid bisulfite pretreated Eastern red cedar. *Bioresour. Technol.* **2013**, *147*, 168−176.
(12) Lou, H.; Wang, M.; Lai, H.; Lin, X.; Zhou, M.; Yang, D.; Qiu, X. Reducing non-productive adsorption of cellulase and enhancing enzymatic hydrolysis of lignocelluloses by noncovalent modification of lignin with lignosulfonate. *Bioresour. Technol.* **2013**, *146*, 478−484.
(13) Zhou, H.; Lou, H.; Yang, D.; Zhu, J.; Qiu, X. Lignosulfonate to enhance enzymatic saccharification of lignocelluloses: role of molecular weight and substrate lignin. *Ind. Eng. Chem. Res.* **2013**, *52* (25), 8464−8470.
(14) Lou, H.; Lai, H.; Wu, S.; Li, X.; Yang, D.; Qiu, X.; Huang, J.; Yi, C. Enhancing enzymatic hydrolysis of crystalline cellulose and lignocellulose by adding long-chain fatty alcohols. *Cellulose* **2014**, DOI: 10.1007/s10570-014-0331-2.
(15) Qiu, X.; Yan, M.; Yang, D.; Pang, Y.; Deng, Y. Effect of straight-chain alcohols on the physicochemical properties of calcium lignosulfonate. *J. Colloid Interface Sci.* **2009**, *338* (1), 151−155.
(16) Li, R. The dynamic adsorption behavior and regulation of lignosulfonate at the interfaces. Ph.D. dissertation, South China University of Technology, Guangzhou, China, 2012.
(17) Gu, H.; Zhang, J.; Bao, J. Inhibitor analysis and adaptive evolution of *Saccharomyces cerevisiae* for simultaneous saccharification and ethanol fermentation from industrial waste corncob residues. *Bioresour. Technol.* **2014**, *157*, 6−13.
(18) Chen, M.; Xia, L.; Xue, P. Enzymatic hydrolysis of corncob and ethanol production from cellulosic hydrolysate. *Int. Biodeterior. Biodegrad.* **2007**, *59* (2), 85−89.
(19) Liu, K.; Lin, X.; Yue, J.; Li, X.; Fang, X.; Zhu, M.; Lin, J.; Qu, Y.; Xiao, L. High concentration ethanol production from corncob residues by fed-batch strategy. *Bioresour. Technol.* **2010**, *101*, 4952−4958.
(20) Wood, T. M.; Bhat, K. M. Methods for measuring cellulase activities. *Methods Enzymol.* **1988**, *160*, 87−112.
(21) Bradford, M. M. A rapid and sensitive method for the quantitation of microgram quantities of protein utilizing the principle of protein-dye binding. *Anal. Biochem.* **1976**, *72*, 248−254.
(22) Del Rio, L. F.; Chandra, R. P.; Saddler, J. N. The effects of increasing swelling and anionic charges on the enzymatic hydrolysis of organosolv-pretreated softwoods at low enzyme loadings. *Biotechnol. Bioeng.* **2011**, *108* (7), 1549−1558.
(23) Fernández-Arche, A.; Marquez-Martín, A.; Vazquez, R. D. L. P.; Perona, J. S.; Terencio, C.; Perez-Camino, C.; Ruiz-Gutierrez, V. Long-chain fatty alcohols from pomace olive oil modulate the release of proinflammatory mediators. *J. Nutr. Biochem.* **2009**, *20* (3), 155−162.
(24) Kumar, L.; Arantes, V.; Chandra, R.; Saddler, J. The lignin present in steam pretreated softwood binds enzymes and limits cellulose accessibility. *Bioresour. Technol.* **2012**, *103* (1), 201−208.
(25) Lou, H.; Zhou, H.; Li, X.; Wang, M.; Zhu, J. Y.; Qiu, X. Understanding the effects of lignosulfonate on enzymatic saccharification of pure cellulose. *Cellulose* **2014**, *21* (3), 1351−1359.
(26) Lou, H.; Zhu, J. Y.; Lan, T. Q.; Lai, H.; Qiu, X. pH-Induced lignin surface modification to reduce nonspecific cellulase binding and enhance enzymatic saccharification of lignocelluloses. *ChemSusChem* **2013**, *6* (5), 919−927.
(27) Deng, Y.; Feng, X.; Yang, D.; Yi, C.; Qiu, X. $\pi$-$\pi$ stacking of the aromatic groups in lignosulfonates. *BioResources* **2012**, *7* (1), 1145−1156.

JOURNAL OF AGRICULTURAL AND FOOD CHEMISTRY

Article

pubs.acs.org/JAFC

# Impact of Several Pre-treatments on the Extraction of Phenolic Compounds in Winegrape Varieties with Different Anthocyanin Profiles and Skin Mechanical Properties

Susana Río Segade,[†,§] Fabrizio Torchio,[†,§] Simone Giacosa,[†] Davide Ricauda Aimonino,[†] Paolo Gay,[†] Milena Lambri,[‡] Roberta Dordoni,[‡] Vincenzo Gerbi,[†] and Luca Rolle*[,†]

[†]Dipartimento di Scienze Agrarie, Forestali e Alimentari, Università degli Studi di Torino, Via Leonardo da Vinci 44, 10095 Grugliasco, Torino, Italy

[‡]Istituto di Enologia e Ingegneria Agro-Alimentare, Università Cattolica del Sacro Cuore, Via Emilia Parmense 84, 29122 Piacenza, Piacenza, Italy

**ABSTRACT:** This study was performed to evaluate and compare the effects of different pre-treatments of whole grape berries (freezing with dry ice or in a cold room, steam blanching with different exposure times, and microwave heating with different exposure times and microwave power density) on total content of some phenolic compounds and the composition of individual anthocyanins released into the pulp during the treatment and those extracted during the maceration step. Two red winegrape varieties with different proportions of di- and trisubstituted anthocyanins were used (Nebbiolo and Barbera, respectively). Pulp-extracted anthocyanins were more significantly influenced by the pre-treatment. The results highlighted that freezing with dry ice, followed by freezing in a cold room and steam blanching for 5 min, have a great potential from an industrial point of view. They facilitated the extraction of anthocyanins in the must prior to maceration, when compared with the control samples, increasing their total content (+37.8−83.6%), and modifying the anthocyanin profile through the enrichment in the most stable compounds (+2.8−6.6% malvidin derivatives) to the detriment of others more prone to oxidation (−0.8−11.0% cyanidin derivatives). In Nebbiolo winegrapes, an improved extraction of low- and high-molecular weight flavanols into the pulp was also observed (+60.4−73.4%). Significant relationships between the phenolic composition of treated berries and the corresponding skin mechanical properties were also studied, but they were variety dependent. Discriminant analysis permitted a correct classification of the samples according to the variety and pre-treatment.

**KEYWORDS:** *grape pre-treatments, anthocyanins, flavanols, extraction, skin mechanical properties, dry ice, microwave*

## INTRODUCTION

The biosynthesis of grape anthocyanins depends on several factors, including maturity, climate, seasonal variations, soil, variety and viticultural practices.[1−3] Nevertheless, the grapevine genome determines the characteristic anthocyanin profile of each variety. In fact, the anthocyanin fingerprinting enables the chemotaxonomic differentiation of red winegrape varieties.[4−7]

The degradation of the cell-wall polysaccharide structures during grape ripening is a fundamental step to increase the release of anthocyanins from grape skins during winemaking, and the chemical composition of berry skin cell walls at harvest is important for the anthocyanin extractability.[8−10] On the other hand, the mechanical properties of berry skin also influence the anthocyanin extraction from the grape skin into the must/wine. Therefore, the anthocyanin extraction can be successfully predicted by instrumental texture analysis. In particular, the berry skin break force can be considered the best mechanical parameter to estimate anthocyanin extraction kinetics with adequate reliability.[11]

However, these colored compounds are only partially extracted during fermentation/maceration. In the initial phase of maceration, 3′-hydroxylated anthocyanins are preferentially extracted from winegrape varieties with hard skins and may be easily oxidized by the enzymes present in the juice.[12] Once released, anthocyanin compounds suffer chemical reactions (oxidation, hydrolysis, cycloaddition, condensation, and polymerization), may be adsorbed by the yeasts, and also fixed again onto the solid parts of the grapes. This affects the color stability and taste of the must/wine. Particularly, the formation of flavanol−anthocyanin complexes promotes the color stability and contributes favorably to the sensory characteristics by decreasing the astringency perception.[13,14] Therefore, the extraction of flavanols is also of great relevance for the color of the final product.

Alternative techniques to traditional maceration have been used to promote the diffusion of phenolic compounds from the berry skin and their solubilization in the must. The rate and extent of the extraction of anthocyanins and proanthocyanidins are influenced by the enological technique applied.[15] In particular, the use of pectolytic enzymes, maceration temperature and time, and ethanol content affect the cell and membrane permeability in grape berries.[16−21]

Grape freezing and heat treatment prior to crushing do not constitute maceration techniques themselves but are possible pre-treatments aiming at the preparation of the grapes to

Received: January 29, 2014
Revised: July 29, 2014
Accepted: July 31, 2014
Published: July 31, 2014

ACS Publications © 2014 American Chemical Society

encourage release of phenolic compounds from the skins. Grape freezing causes the berry cells to burst, breaking the cell membranes and thus releasing preferentially water-soluble compounds into the must.[22] Consequently, the anthocyanin extraction from the skins is enhanced.[18,23−25] The thermal treatment of grape berries also damages the hypodermal cell membranes, favoring preferential anthocyanin release into the must.[22] Nevertheless, some authors reported that the heat can cause partial thermal degradation of anthocyanins[26] and adverse effects on the sensory attributes of the final product.[27]

The use of microwave heating as an alternative to conventional grape blanching and drying has been recently reported in the literature.[27−29] Moreover, the advantages of microwave-assisted extraction of anthocyanins in alcoholic and/or acidic medium from grape skins have been investigated.[30,31] Microwave energy has a high penetration power, which allows rapid heating throughout the sample while reducing both the exposure time and the impact of temperature on thermolabile compounds and sensory characteristics.[32] Lin and Brewer[33] also demonstrated that microwaves enable an efficient heat transfer with little or without water, which reduces nutrient losses compared with the traditional method. In fact, microwave hydrodiffusion permits the rapid juice extraction by internal heating of the water present inside the grape until its boiling point because of the expansion of the cells and consequent cell-wall rupture.[34] The same principle could be applied to the release of the cell constituents into the surrounding juice enhancing the extraction efficiency. In this sense, many attempts were carried out to produce a grape juice enriched in polyphenols.[35]

The new enological trends aim at implementing the production of high-quality red wines and colored juices from the exploitation of the intrinsic chromatic characteristics of the grapes and their preservation in the final product. Therefore, the aim of this work was to evaluate and compare the impact of different treatments on winegrapes prior to crushing, such as grape freezing, steam blanching, and microwave heating, on the skin mechanical properties and the extraction of anthocyanins from red winegrapes. Many experimental conditions influencing the anthocyanin release from berry skins were investigated. In particular, the study was carried out on *Vitis vinifera* L. cv. Nebbiolo and Barbera to assess the effect in grape berries with a high proportion of di- and tri-substituted anthocyanins, respectively, because of the different trends of these compounds to be lost during winemaking. Given the relevance for color, the extraction of low- and high-molecular weight flavanols from the skin was also evaluated. These are important and well-known Italian varieties, giving grapes used for the production of renowned red wines that are commercialized worldwide.

## MATERIALS AND METHODS

**Grape Samples.** Twenty whole bunches of red grape cultivars *Vitis vinifera* L. cv. Nebbiolo and Barbera were harvested at technological maturity (24.0°Brix, 8.41 g/L tartaric acid and 24.3°Brix, 6.66 g/L tartaric acid, respectively) from as many vines in commercial vineyards located in the same growing zone (Piedmont, Cuneo province, northwest Italy) in 2012. Once in the laboratory, for each variety, a subsample of approximately 1.5 kg of grapes (1000−1200 berries) was randomly selected by picking berries with attached pedicels, cut in the proximity of the receptacle, from different positions in the cluster (shoulders, middle and bottom). The presence of the pedicel prevents grape must losses. For each subsample, the berries were sorted according to their density by flotation using different saline solutions (from 100 to 190 g/L sodium chloride corresponding to densities comprising between 1069 and 1125 kg/m$^3$) and following the protocol described by Rolle et al.[2] This densimetric sorting allows obtaining more homogeneous samples and minimizing the possible ripening effect among berries. The comparative study was carried out on the berries belonging to the most representative class with a density of 1107 kg/m$^3$ and a relative weight of 60% w/w. The sorted berries were washed with water and visually inspected; those with damaged skins were discarded. For each variety studied, seven sets of 30 sorted berries (three replicates of 10 berries)[36] were randomly selected to apply the different pre-treatments, and another one of 30 sorted berries was used as control sample (untreated grapes, CS).

**Grape Pre-treatments.** Three grape pre-treatments were studied at different experimental conditions: steam blanching, freezing, and microwave heating. Each replicate of sorted berries was weighed by means of a technical balance (Gibertini E1700, Modena, Italy). Therefore, three replicates of each experiment were performed for a total of seven experiments. The grape berries were treated using the following methods.

*Steam Blanching.* The berries were treated with the vapor released during water heating at 100 °C for 1 min (HS1) or 5 min (HS5). Subsequently, the grapes were quickly cooled at 4 °C in a refrigerator down to ambient temperature (20 ± 1 °C).

*Freezing.* The berries were frozen using two different cooling methods: direct freezing in a freezer at −18 °C for 2 days (DF), or by adding 3 mm thick dry ice pellets in the same amount as the berries weight (DI) as proposed by Busse-Valverde et al.[15] for crushed grapes. Then, the grapes were defrosted at ambient temperature.

*Microwave Heating.* Microwave treatments were conducted by using a 2450 MHz microwave oven with maximum delivered power of 1000 W (Panasonic NE 1037). The berries were arranged in a single layer on the rotating glass plate and placed in the center of the oven. The treatments were performed at two different microwave power densities and exposure times using 1 W/g for 30 s (MW1D30), 1 W/g for 60 s (MW1D60), or 2 W/g for 60 s (MW2D60), thereby preventing grape must losses during the treatment.[34] The grapes were quickly cooled at 4 °C in a refrigerator down to ambient temperature.

Pulp and surface temperatures of grape berries were measured immediately after heating pre-treatments (HS1, HS5, MW1D30, MW1D60, MW2D60) employing two different techniques. Pulp temperature was measured inserting a T-type thermocouple (0.6 mm diameter and 10 mm long junction) in the center of two berries. A DeltaOHM HD32.8.16 thermocouple datalogger recoded data. Surface temperature was evaluated adopting the infrared (IR) thermography technique. IR images were acquired by an Avio TVS-500 camera and analyzed with the Goramtec Thermography Studio (GTS 4.8) software. Emissivity parameter was assessed heating a sample of ten grape berries at 30, 40, 50, and 60 °C in a thermostatic chamber and acquiring, for each condition, an IR image once the thermal equilibrium was achieved. The cooling time of the berries was evaluated considering the pulp temperature for each heating pre-treatment. In particular, the temperature was monitored during the entire cooling process, and the cooling time was assumed as the time required to the three thermocouples to achieve the temperature of 20 ± 0.5 °C. The same technique was followed to assess the thawing time for DF and DI pre-treatments and the freezing time for DI pre-treatment. In this last case, the pulp temperature of grape berries was measured until they achieved the same temperature of dry ice.

**Instrumental Texture Analysis.** A Universal Testing Machine (UTM) TA.XTplus texture analyzer (Stable Micro Systems, Godalming, Surrey, UK), equipped with an HDP/90 platform and a 5 kg load cell, was used for grape texture analysis. The berry skin hardness was assessed by a puncture test using an SMS P/2N needle probe (Stable Micro Systems), a test speed of 1 mm/s and a penetration depth of 3 mm.[37] Each berry (untreated or treated) was individually punctured in the lateral face, and two parameters were measured: skin break force (N, as $F_{sk}$) and skin break energy (mJ, as $W_{sk}$). The first variable corresponds to the skin resistance to the needle probe penetration, and the second variable is represented by the area under the force−time curve, which is limited between 0 and $F_{sk}$.[37] The use of

a needle probe allows separate estimation of this skin mechanical characteristic, minimizing the possible interferences caused by the pulp firmness on the results. All data acquisitions were made at 500 points per second, and the skin mechanical properties were calculated from force−distance curves using the Texture Exponent software package (Stable Micro Systems).

**Chemical Analysis.** Solvents of HPLC-gradient grade and all other chemicals of analytical-reagent grade were purchased from Sigma (Milan, Italy). The solutions were prepared in deionized water produced by a Purelab Classic system (Elga Labwater, Marlow, UK). Anthocyanin standards (delphinidin-3-*O*-glucoside chloride, malvidin-3-*O*-glucoside chloride, petunidin chloride, peonidin-3-*O*-glucoside chloride, and cyanidin-3-*O*-glucoside chloride), (+)-catechin, and cyanidin chloride were supplied from Extrasynthèse (Genay, France).

*Technological Ripeness Parameters.* Soluble solids concentration (°Brix) was measured using an Atago 0−32 Brix temperature compensating refractometer (Atago Corporation, Tokyo, Japan), and titratable acidity (g/L tartaric acid) was estimated using the OIV method.[38]

*Extraction and Determination of Phenolic Compounds.* Once the berries have been punctured, the berry skins were manually removed from the pulp using a laboratory spatula. The pulp was introduced into a tube containing 100 mg sodium metabisulfite, weighed, and subsequently diluted (9:1, m/m) with 5 mol/L sulfuric acid.[39] Afterward, the pulp was homogenized at 9500 rpm for 30 s with an Ultraturrax T10 high-speed homogenizer (IKA Labortechnik, Staufen, Germany) and centrifuged in a PK 131 centrifuge (ALC International, MI, Italy) for 15 min at 3000*g* at 20 °C. In the resulting solution, pulp phenolic compounds were determined in untreated berries and compared to those extracted during the grape pre-treatment. The skins were weighed and quickly immersed into 25 mL of a hydroalcoholic buffer at pH 3.2 containing 5 g/L tartaric acid, 100 mg/L sodium metabisulfite and 12% v/v ethanol. After remaining 48 h at 25 °C, the solution was used for determining extracted skin phenolic compounds during the maceration step.[40] In these conditions, an extraction time of 48 h was sufficient to achieve a plateau for all compounds investigated.[11,40] The residual berry skins were quickly immersed into 25 mL of a new hydroalcoholic buffer containing 600 mg/L sodium metabisulfite. Afterward, the skins were homogenized at 8000 rpm for 1 min with an Ultraturrax T25 high-speed homogenizer (IKA Labortechnik, Staufen, Germany) and centrifuged for 15 min at 3000*g* at 20 °C. The supernatant was then used for determining non-extracted skin phenolic compounds.[40] Total contents of anthocyanins (expressed as mg malvidin-3-*O*-glucoside chloride/kg grape, as TA), proanthocyanidins (expressed as mg cyanidin chloride/kg grape, as PRO) and flavanols reactive to vanillin (expressed as mg (+)-catechin/kg grape, as FRV) were determined by spectrophotometric methods[39,41] using an UV-1800 spectrophotometer (Shimazdu Corporation, Kyoto, Japan).

The determination of the anthocyanin profile was performed after the berry skin or pulp extract had been submitted to reversed-phase solid-phase extraction using a 1 g SEP-PAK $C_{18}$ cartridge (Waters Corporation, Milford, MA, USA) with methanol as the eluent.[42] The HPLC-DAD system and chromatographic conditions were those used in a previous work.[42] A LiChroCART analytical column (25 cm × 0.4 cm i.d.) purchased from Merck (Darmstadt, Germany), which was packed with LiChrospher 100 RP-18 (5 $\mu$m) particles supplied by Alltech (Deerfield, IL, U.S.A.), and a Spectra Focus diode array detector (DAD, Spectra Physics Analytical, Inc.) operating at 520 nm were used. The mobile phases were: A = formic acid/water (10:90, v/v); B = formic acid/methanol/water (10:50:40, v/v), working at a flow-rate of 1 mL/min. The identification of the free forms of anthocyanins was achieved by comparing their retention times with those of pure standards. The acylated forms of anthocyanins were identified by matching the DAD spectrum and retention time of each chromatographic peak, and by comparing these data with those available in the literature.[7] Individual anthocyanins were expressed in percentages. All of the analyses were performed in duplicate and then averaged.

**Statistical Analysis.** Statistical analyses were carried out using the SPSS Statistics software package version 19.0 (IBM Corporation, Armonk, NY, U.S.A.).

## RESULTS AND DISCUSSION

As a consequence of minimizing the ripening effect by densimetric sorting of berries, all the berries belonging to the same density class of 1107 kg/m$^3$ have similar soluble solids concentration of 24.2 ± 0.2 and 24.2 ± 0.1°Brix for Barbera and Nebbiolo winegrapes, respectively, and titratable acidity value of 8.74 ± 0.11 and 6.81 ± 0.03 g/L tartaric acid, respectively.

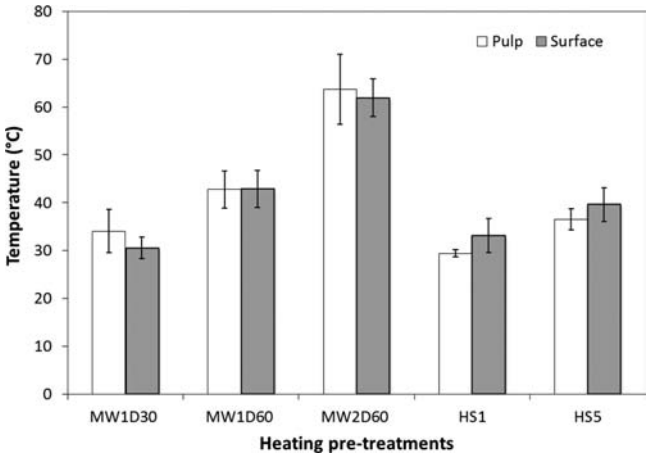


**Figure 1.** Pulp and surface temperatures of grape berries measured immediately after heating pre-treatments. MW1D30 = microwave heating at 1 W/g for 30 s, MW1D60 = microwave heating at 1 W/g for 60 s, MW2D60 = microwave heating at 2 W/g for 60 s, HS1 = steam blanching at 100 °C for 1 min, HS5 = steam blanching at 100 °C for 5 min.

**Grape Pre-treatments.** Figure 1 shows pulp and surface temperatures of grape berries measured immediately after heating pre-treatments by steam and microwave energy (HS1, HS5, MW1D30, MW1D60, and MW2D60). The temperatures achieved increased with longer heating times and/or higher microwave power density. The cooling time of the berries to achieve the temperature of 20 ± 0.5 °C was 8, 16, 21, 26, and 30 min, respectively. The freezing time for the DI pre-treatment (−77 °C) was 38 min, whereas the thawing time for the DF and DI pre-treatments was 85 and 220 min, respectively.

**Total Anthocyanins and Flavanols.** Total content of phenolic compounds released from the skin to the pulp during the grape pre-treatment, extracted skin phenolic compounds during the maceration step and non-extracted skin phenolic compounds for the two red winegrape varieties studied is shown in Table 1. As regards total skin anthocyanins (sum of pulp, extracted skin, and non-extracted skin anthocyanins) of Barbera grapes, the concentration obtained (753 ± 52 mg/kg) was lower than that reported for berries with higher contents of reducing sugars.[41] This agreed with the significant increase (16−31%) in the concentration of total anthocyanins (TA) in Barbera grapes with increasing the sugars content between 235 and 269 g/L for most of the production zones evaluated.[41] The concentration of total skin anthocyanins in Nebbiolo grapes (440 ± 29 mg/kg), although low, was usual for this variety as shown in other works performed on berries containing a similar content of reducing sugars or belonging to the same density


dx.doi.org/10.1021/jf502656d | J. Agric. Food Chem. 2014, 62, 8437−8451

**Table 1. Total Content of Phenolic Compounds in Barbera and Nebbiolo Winegrapes Before and After Different Pre-Treatments**

| parameter[a] | grape pre-treatment[b] | | | | | | | | |
|---|---|---|---|---|---|---|---|---|---|
| | HS1 | HS5 | DF | DI | MW1D30 | MW1D60 | MW2D60 | CS | sign[c] |
| | | | | | Barbera | | | | |
| pulp TA (mg/kg) | 10.8 ± 2.0a | 28.6 ± 8.2ab | 44.0 ± 14.3b | 67.7 ± 8.3c | 15.8 ± 3.0a | 20.5 ± 2.4a | 23.5 ± 6.9a | 17.8 ± 0.4a | *** |
| extracted skin TA (mg/kg) | 481.6 ± 29.8 | 451.1 ± 19.6 | 474.2 ± 12.5 | 470.1 ± 16.8 | 451.6 ± 6.2 | 474.3 ± 18.5 | 450.6 ± 15.4 | 449.6 ± 18.6 | ns |
| non-extracted skin TA (%) | 34.6 ± 3.7bc | 36.3 ± 1.8bc | 31.2 ± 0.3ab | 28.6 ± 3.1a | 37.9 ± 1.2c | 34.3 ± 2.2bc | 37.0 ± 1.4bc | 37.9 ± 2.5c | *** |
| pulp PRO (mg/kg) | 25.2 ± 3.2 | 37.9 ± 16.4 | 56.1 ± 14.2 | 60.3 ± 16.1 | 34.0 ± 9.5 | 30.3 ± 1.6 | 32.0 ± 9.7 | 43.6 ± 11.0 | ns |
| extracted skin PRO (mg/kg) | 350.9 ± 3.8 | 315.6 ± 7.5 | 378.5 ± 39.8 | 362.5 ± 26.5 | 295.8 ± 80.0 | 350.2 ± 14.5 | 332.7 ± 7.3 | 230.8 ± 82.5 | ns |
| non-extracted skin PRO (%) | 37.5 ± 1.2ab | 41.3 ± 4.0ab | 27.8 ± 4.2a | 29.8 ± 1.7a | 45.2 ± 11.7ab | 36.8 ± 2.2ab | 39.4 ± 0.4ab | 54.4 ± 11.9b | * |
| pulp FRV (mg/kg) | 3.4 ± 0.9 | 7.7 ± 5.9 | 10.4 ± 1.6 | 8.0 ± 1.2 | 4.7 ± 0.4 | 6.4 ± 0.8 | 4.8 ± 0.9 | 3.9 ± 1.1 | ns |
| extracted skin FRV (mg/kg) | 164.5 ± 0.8 | 160.7 ± 9.6 | 167.7 ± 8.4 | 160.0 ± 5.6 | 163.3 ± 2.2 | 167.3 ± 4.7 | 165.6 ± 1.1 | 154.7 ± 2.1 | ns |
| non-extracted skin FRV (%) | 16.2 ± 0.0ab | 15.9 ± 1.9ab | 11.1 ± 3.4a | 16.1 ± 3.4ab | 16.1 ± 0.9ab | 13.3 ± 2.0ab | 14.9 ± 0.1ab | 20.8 ± 0.5b | * |
| | | | | | Nebbiolo | | | | |
| pulp TA (mg/kg) | 14.8 ± 1.5a | 74.8 ± 17.1c | 44.2 ± 11.1b | 60.9 ± 9.0bc | 19.6 ± 4.2a | 22.8 ± 3.1a | 21.0 ± 2.1a | 12.3 ± 0.3a | *** |
| extracted skin TA (mg/kg) | 339.2 ± 14.6 | 314.2 ± 14.0 | 333.8 ± 10.5 | 314.5 ± 16.8 | 345.9 ± 10.4 | 331.8 ± 13.6 | 340.3 ± 1.2 | 342.3 ± 6.7 | ns |
| non-extracted skin TA (%) | 19.6 ± 3.0c | 11.7 ± 1.1a | 14.2 ± 0.1ab | 14.8 ± 1.8ab | 17.0 ± 1.5bc | 19.5 ± 2.4c | 18.0 ± 0.7bc | 19.5 ± 1.5c | *** |
| pulp PRO (mg/kg) | 292.3 ± 95.7a | 639.3 ± 69.9b | 655.7 ± 50.5b | 629.5 ± 1.7b | 317.2 ± 179.8a | 333.3 ± 53.2a | 380.5 ± 15.0ab | 249.4 ± 8.6a | ** |
| extracted skin PRO (mg/kg) | 1886.3 ± 70.7 | 1670.3 ± 110.1 | 1626.4 ± 0.6 | 1585.5 ± 2.0 | 1801.9 ± 158.0 | 1797.1 ± 0.9 | 1774.6 ± 63.0 | 1776.4 ± 31.7 | ns |
| non-extracted skin PRO (%) | 19.3 ± 0.9abc | 14.5 ± 1.5a | 15.5 ± 1.9ab | 18.0 ± 0.1abc | 21.5 ± 0.8cd | 21.1 ± 2.0cd | 20.2 ± 1.8bcd | 25.0 ± 1.5d | ** |
| pulp FRV (mg/kg) | 89.4 ± 44.0a | 252.9 ± 45.4b | 193.1 ± 34.0ab | 246.5 ± 11.1b | 106.7 ± 64.1a | 103.3 ± 24.3a | 118.3 ± 12.3a | 67.2 ± 2.2a | ** |
| extracted skin FRV (mg/kg) | 854.7 ± 30.2b | 716.7 ± 53.6a | 761.1 ± 43.9ab | 704.7 ± 13.2a | 785.7 ± 45.3ab | 780.3 ± 9.7ab | 794.7 ± 4.6ab | 804.3 ± 15.1ab | * |
| non-extracted skin FRV (%) | 14.5 ± 1.2ab | 12.2 ± 0.7a | 13.6 ± 0.9ab | 13.9 ± 0.2ab | 19.2 ± 1.7c | 20.0 ± 1.3c | 17.3 ± 1.5bc | 21.1 ± 1.6c | *** |

[a]TA = total anthocyanins, PRO = proanthocyanidins, FRV = flavanols reactive to vanillin. [b]HS1 = steam blanching at 100 °C for 1 min, HS5 = steam blanching at 100 °C for 5 min, DF = direct freezing in a freezer at −18 °C for 2 days, DI = freezing by adding dry ice, MW1D30 = microwave heating at 1 W/g for 30 s, MW1D60 = microwave heating at 1 W/g for 60 s, MW2D60 = microwave heating at 2 W/g for 60 s, CS = control. All data are expressed as average value ± standard deviation ($n = 3$). Different Latin letters within the same row indicate significant differences ([c]) among pre-treatments according to Tukey-b test ($p < 0.05$). [c]Sign: *, **, *** and ns indicate significance at $p < 0.05$, 0.01, 0.001 and not significant, respectively.



dx.doi.org/10.1021/jf502656d | J. Agric. Food Chem. 2014, 62, 8437−8451

**Table 2. Anthocyanin Profile of Barbera Winegrapes Before and After Different Pre-treatments**

| | grape pre-treatment[a] | | | | | | | | |
|---|---|---|---|---|---|---|---|---|---|
| cmpd | HS1 | HS5 | DF | DI | MW1D30 | MW1D60 | MW2D60 | CS | sign[b] |
| | | | | | Pulp Anthocyanins (%) | | | | |
| ∑ delphinidin derivatives | 6.58 ± 0.39d | 3.54 ± 0.68a | 4.85 ± 0.56abc | 4.53 ± 0.33ab | 6.18 ± 0.65cd | 5.74 ± 0.2bcd9 | 5.79 ± 0.80bcd | 6.34 ± 0.72cd | *** |
| ∑ cyanidin derivatives | 9.53 ± 0.70cd | 8.87 ± 0.83bcd | 7.74 ± 0.98abc | 7.11 ± 0.72ab | 8.70 ± 1.02bcd | 10.65 ± 0.26d | 6.64 ± 0.46a | 9.62 ± 0.88cd | *** |
| ∑ petunidin derivatives | 10.50 ± 0.57d | 8.04 ± 0.70a | 8.89 ± 0.48abc | 8.46 ± 0.44ab | 10.28 ± 0.52cd | 9.62 ± 0.27bcd | 10.21 ± 0.6cd | 9.93 ± 0.49cd | *** |
| ∑ peonidin derivatives | 10.09 ± 1.22ab | 12.08 ± 0.58b | 12.54 ± 1.37b | 10.30 ± 0.72ab | 10.44 ± 1.25ab | 12.70 ± 0.14b | 9.23 ± 0.52a | 10.97 ± 1.22ab | ** |
| ∑ malvidin derivatives | 63.30 ± 1.21ab | 67.47 ± 1.85bc | 65.98 ± 2.51abc | 69.59 ± 1.64c | 64.40 ± 3.00abc | 61.29 ± 0.45a | 68.13 ± 2.38bc | 63.15 ± 2.38ab | ** |
| ∑ simple glucosides | 91.53 ± 0.32bc | 92.12 ± 0.37c | 90.45 ± 0.25ab | 89.92 ± 0.71a | 90.65 ± 0.28ab | 90.23 ± 0.33ab | 90.87 ± 0.96abc | 92.04 ± 0.41c | *** |
| ∑ acetyl glucosides | 1.22 ± 0.08abc | 1.13 ± 0.06ab | 2.68 ± 0.12d | 3.17 ± 0.40e | 1.36 ± 0.11bc | 1.66 ± 0.12c | 1.47 ± 0.25bc | 0.88 ± 0.03a | *** |
| ∑ cinnamoyl glucosides | 7.24 ± 0.25abc | 6.75 ± 0.36a | 6.87 ± 0.14ab | 6.91 ± 0.35ab | 7.99 ± 0.37bc | 8.12 ± 0.21c | 7.67 ± 0.82abc | 7.08 ± 0.41abc | ** |
| | | | | | Extracted Skin Anthocyanins (%) | | | | |
| ∑ delphinidin derivatives | 9.55 ± 0.60 | 9.48 ± 0.46 | 9.55 ± 0.55 | 10.04 ± 0.43 | 9.30 ± 0.59 | 9.55 ± 0.27 | 9.54 ± 0.31 | 9.54 ± 0.13 | ns |
| ∑ cyanidin derivatives | 3.58 ± 0.26ab | 4.61 ± 0.47b | 3.32 ± 0.54a | 4.18 ± 0.15ab | 3.93 ± 0.50ab | 3.47 ± 0.47a | 3.64 ± 0.26ab | 3.80 ± 0.34ab | * |
| ∑ petunidin derivatives | 13.21 ± 0.37a | 13.75 ± 0.40a | 13.97 ± 0.21a | 15.42 ± 0.20b | 13.33 ± 0.64a | 13.42 ± 0.04a | 13.45 ± 0.31a | 13.37 ± 0.09a | *** |
| ∑ peonidin derivatives | 5.08 ± 0.31ab | 6.09 ± 0.46b | 4.67 ± 0.77a | 5.63 ± 0.40ab | 5.66 ± 0.50ab | 4.97 ± 0.51ab | 5.07 ± 0.34ab | 5.39 ± 0.57ab | * |
| ∑ malvidin derivatives | 68.57 ± 1.29 | 66.06 ± 1.56 | 68.50 ± 1.66 | 64.73 ± 0.61 | 67.78 ± 2.16 | 68.59 ± 1.26 | 68.30 ± 1.17 | 67.90 ± 0.82 | ns |
| ∑ simple glucosides | 75.22 ± 3.21 | 75.24 ± 0.99 | 72.73 ± 0.56 | 75.74 ± 0.44 | 74.51 ± 2.09 | 75.60 ± 3.91 | 76.48 ± 1.59 | 74.59 ± 0.50 | ns |
| ∑ acetyl glucosides | 15.83 ± 3.30 | 16.45 ± 0.90 | 17.80 ± 0.29 | 15.28 ± 0.58 | 16.40 ± 1.75 | 15.28 ± 3.67 | 14.93 ± 1.69 | 16.72 ± 0.43 | ns |
| ∑ cinnamoyl glucosides | 8.95 ± 0.35ab | 8.31 ± 0.20a | 9.47 ± 0.48b | 8.98 ± 0.15ab | 9.09 ± 0.43ab | 9.12 ± 0.24ab | 8.59 ± 0.10ab | 8.69 ± 0.41ab | * |
| | | | | | Non-extracted Skin Anthocyanins (%) | | | | |
| ∑ delphinidin derivatives | 15.30 ± 1.49 | 14.21 ± 0.83 | 13.69 ± 0.97 | 13.30 ± 0.54 | 14.82 ± 1.12 | 14.53 ± 0.86 | 15.35 ± 0.73 | 15.53 ± 0.23 | ns |
| ∑ cyanidin derivatives | 3.91 ± 0.30ab | 5.07 ± 0.55b | 3.62 ± 0.68a | 4.72 ± 0.08ab | 4.24 ± 0.53ab | 3.77 ± 0.71ab | 3.84 ± 0.26ab | 4.10 ± 0.42ab | * |
| ∑ petunidin derivatives | 19.35 ± 0.83 | 19.54 ± 0.44 | 19.20 ± 0.24 | 19.50 ± 0.43 | 19.36 ± 0.69 | 19.38 ± 0.27 | 19.84 ± 0.49 | 19.56 ± 0.26 | ns |
| ∑ peonidin derivatives | 4.70 ± 0.24 | 5.65 ± 0.32 | 4.55 ± 0.71 | 5.45 ± 0.39 | 5.10 ± 0.44 | 4.64 ± 0.49 | 4.52 ± 0.24 | 5.03 ± 0.59 | ns |
| ∑ malvidin derivatives | 56.75 ± 2.81 | 55.53 ± 2.02 | 58.94 ± 2.28 | 57.03 ± 0.59 | 56.49 ± 2.39 | 57.67 ± 2.20 | 56.47 ± 1.50 | 55.78 ± 0.87 | ns |
| ∑ simple glucosides | 74.52 ± 2.63 | 73.30 ± 1.28 | 71.68 ± 1.29 | 74.88 ± 2.69 | 72.78 ± 1.48 | 70.81 ± 1.57 | 74.02 ± 1.10 | 75.33 ± 3.67 | ns |
| ∑ acetyl glucosides | 11.33 ± 1.55 | 12.79 ± 1.01 | 12.67 ± 0.26 | 10.66 ± 1.52 | 13.05 ± 0.71 | 14.49 ± 0.60 | 12.62 ± 1.16 | 12.25 ± 2.96 | ns |
| ∑ cinnamoyl glucosides | 14.15 ± 1.73 | 13.91 ± 0.62 | 15.65 ± 1.36 | 14.47 ± 1.66 | 14.17 ± 0.82 | 14.69 ± 0.98 | 13.36 ± 0.21 | 12.42 ± 0.72 | ns |

[a]HS1 = steam blanching at 100 °C for 1 min, HS5 = steam blanching at 100 °C for 5 min, DF = direct freezing in a freezer at −18 °C for 2 days, DI = freezing by adding dry ice, MW1D30 = microwave heating at 1 W/g for 30 s, MW1D60 = microwave heating at 1 W/g for 60 s, MW2D60 = microwave heating at 2 W/g for 60 s, CS = control. All data are expressed as average value ± standard deviation ($n$ = 3). Different Latin letters within the same row indicate significant differences ([b]) among pre-treatments according to Tukey-b test ($p < 0.05$). [b]Sign: *,**,*** and ns indicate significance at $p < 0.05$, 0.01, 0.001 and not significant, respectively.



dx.doi.org/10.1021/jf502656d | J. Agric. Food Chem. 2014, 62, 8437−8451

**Table 3. Anthocyanin Profile of Nebbiolo Winegrapes Before and After Different Pre-Treatments**

| | grape pre-treatment[a] | | | | | | | | |
|---|---|---|---|---|---|---|---|---|---|
| cmpd | HS1 | HS5 | DF | DI | MW1D30 | MW1D60 | MW2D60 | CS | sign[b] |
| | | | | | Pulp Anthocyanins (%) | | | | |
| ∑ delphinidin derivatives | 3.89 ± 0.39a | 5.84 ± 0.33b | 4.38 ± 0.60a | 4.83 ± 0.36ab | 4.06 ± 0.37a | 4.10 ± 0.48a | 4.47 ± 0.63a | 4.63 ± 0.50a | ** |
| ∑ cyanidin derivatives | 36.58 ± 3.07b | 24.05 ± 0.84a | 24.31 ± 1.30a | 23.91 ± 2.11a | 32.45 ± 2.73b | 32.68 ± 1.83b | 32.74 ± 1.19b | 34.86 ± 1.72b | *** |
| ∑ petunidin derivatives | 3.43 ± 0.15a | 4.47 ± 0.15b | 3.68 ± 0.42a | 4.01 ± 0.30ab | 3.67 ± 0.19a | 3.54 ± 0.31a | 3.86 ± 0.24ab | 3.69 ± 0.12a | ** |
| ∑ peonidin derivatives | 45.44 ± 1.00ab | 48.53 ± 0.78cd | 50.10 ± 1.69d | 47.70 ± 1.89bcd | 46.66 ± 0.59abc | 46.80 ± 0.61abc | 45.48 ± 1.02ab | 43.85 ± 0.49a | *** |
| ∑ malvidin derivatives | 10.66 ± 1.64a | 17.11 ± 1.02bc | 17.53 ± 1.74bc | 19.55 ± 3.37c | 13.17 ± 2.64ab | 12.89 ± 1.50ab | 13.45 ± 1.77ab | 12.97 ± 1.63ab | *** |
| ∑ simple glucosides | 97.13 ± 0.10cd | 95.96 ± 0.22a | 97.17 ± 0.30d | 96.22 ± 0.15ab | 96.53 ± 0.36abc | 96.56 ± 0.22abcd | 96.75 ± 0.28bcd | 96.88 ± 0.12cd | *** |
| ∑ acetyl glucosides | 0.36 ± 0.06a | 0.73 ± 0.02b | 0.72 ± 0.11b | 0.93 ± 0.06c | 0.45 ± 0.06a | 0.38 ± 0.05a | 0.38 ± 0.06a | 0.35 ± 0.03a | *** |
| ∑ cinnamoyl glucosides | 2.50 ± 0.04ab | 3.31 ± 0.20c | 2.11 ± 0.20a | 2.86 ± 0.17bc | 3.02 ± 0.34bc | 3.06 ± 0.17c | 2.87 ± 0.26bc | 2.77 ± 0.11bc | *** |
| | | | | | Extracted Skin Anthocyanins (%) | | | | |
| ∑ delphinidin derivatives | 6.12 ± 0.54 | 6.89 ± 0.21 | 6.73 ± 0.24 | 6.60 ± 0.72 | 6.05 ± 0.57 | 6.20 ± 0.16 | 6.42 ± 0.57 | 6.76 ± 0.19 | ns |
| ∑ cyanidin derivatives | 20.75 ± 2.69 | 20.40 ± 1.49 | 17.19 ± 1.21 | 18.72 ± 1.26 | 17.45 ± 2.39 | 17.14 ± 1.52 | 18.99 ± 2.82 | 18.15 ± 0.14 | ns |
| ∑ petunidin derivatives | 5.01 ± 0.53 | 5.12 ± 0.17 | 5.49 ± 0.08 | 5.44 ± 0.55 | 5.03 ± 0.40 | 5.19 ± 0.18 | 5.18 ± 0.16 | 5.42 ± 0.06 | ns |
| ∑ peonidin derivatives | 48.11 ± 2.49 | 47.47 ± 0.52 | 47.33 ± 1.16 | 48.08 ± 3.31 | 47.49 ± 2.93 | 48.02 ± 1.10 | 45.99 ± 0.83 | 46.26 ± 0.63 | ns |
| ∑ malvidin derivatives | 20.02 ± 4.19 | 20.11 ± 1.46 | 23.26 ± 2.16 | 21.15 ± 3.28 | 23.98 ± 4.28 | 23.44 ± 1.77 | 23.42 ± 2.89 | 23.40 ± 0.52 | ns |
| ∑ simple glucosides | 89.60 ± 0.85b | 86.46 ± 0.24a | 88.19 ± 0.64b | 88.15 ± 0.55b | 88.85 ± 0.72b | 88.65 ± 0.21b | 88.30 ± 0.78b | 88.12 ± 0.08b | *** |
| ∑ acetyl glucosides | 4.29 ± 0.43 | 4.88 ± 0.32 | 4.62 ± 0.32 | 4.45 ± 0.34 | 4.39 ± 0.34 | 4.79 ± 0.06 | 4.63 ± 0.14 | 4.88 ± 0.07 | ns |
| ∑ cinnamoyl glucosides | 6.10 ± 0.47a | 8.66 ± 0.10c | 7.18 ± 0.36b | 7.40 ± 0.23b | 6.76 ± 0.38ab | 6.56 ± 0.27ab | 7.07 ± 0.65ab | 7.00 ± 0.02ab | *** |
| | | | | | Non-extracted Skin Anthocyanins (%) | | | | |
| ∑ delphinidin derivatives | 6.99 ± 0.74ab | 6.51 ± 0.10a | 6.83 ± 0.20ab | 6.27 ± 0.58a | 6.69 ± 0.35ab | 7.05 ± 0.29ab | 7.02 ± 0.62ab | 7.75 ± 0.18b | * |
| ∑ cyanidin derivatives | 20.86 ± 2.10 | 20.43 ± 1.78 | 17.45 ± 1.34 | 18.81 ± 0.98 | 17.64 ± 2.73 | 17.67 ± 1.32 | 19.62 ± 2.92 | 18.72 ± 0.46 | ns |
| ∑ petunidin derivatives | 5.36 ± 0.59 | 5.05 ± 0.21 | 5.60 ± 0.04 | 5.34 ± 0.49 | 5.35 ± 0.33 | 5.63 ± 0.28 | 5.48 ± 0.17 | 5.96 ± 0.11 | ns |
| ∑ peonidin derivatives | 47.53 ± 2.66 | 48.22 ± 0.53 | 47.57 ± 1.21 | 48.75 ± 3.26 | 47.11 ± 2.84 | 47.86 ± 1.59 | 45.58 ± 0.73 | 45.03 ± 1.21 | ns |
| ∑ malvidin derivatives | 19.26 ± 3.38 | 19.80 ± 1.99 | 22.55 ± 2.35 | 20.83 ± 3.15 | 23.21 ± 5.07 | 21.79 ± 1.82 | 22.29 ± 3.00 | 22.54 ± 0.80 | ns |
| ∑ simple glucosides | 86.31 ± 1.09c | 82.31 ± 0.42a | 82.78 ± 1.58ab | 82.10 ± 0.76a | 85.07 ± 1.37bc | 84.84 ± 0.60bc | 85.20 ± 0.80bc | 84.54 ± 0.41abc | *** |
| ∑ acetyl glucosides | 3.57 ± 0.45 | 3.77 ± 0.33 | 3.59 ± 0.53 | 3.78 ± 0.52 | 3.88 ± 0.51 | 4.13 ± 0.12 | 3.59 ± 0.12 | 4.12 ± 0.18 | ns |
| ∑ cinnamoyl glucosides | 10.13 ± 0.66a | 13.92 ± 0.10b | 13.63 ± 1.06b | 14.12 ± 0.27b | 11.06 ± 0.86a | 11.03 ± 0.50a | 11.20 ± 0.70a | 11.34 ± 0.32a | *** |

[a]HS1 = steam blanching at 100 °C for 1 min, HS5 = steam blanching at 100 °C for 5 min, DF = direct freezing in a freezer at −18 °C for 2 days, DI = freezing by adding dry ice, MW1D30 = microwave heating at 1 W/g for 30 s, MW1D60 = microwave heating at 1 W/g for 60 s, MW2D60 = microwave heating at 2 W/g for 60 s, CS = control. All data are expressed as average value ± standard deviation ($n$ = 3). Different Latin letters within the same row indicate significant differences ([b]) among pre-treatments according to Tukey-b test ($p < 0.05$). [b]Sign: *,**,*** and ns indicate significance at $p < 0.05$, 0.01, 0.001 and not significant, respectively.



dx.doi.org/10.1021/jf502656d | J. Agric. Food Chem. 2014, 62, 8437−8451

Table 4. Skin Mechanical Properties of Barbera and Nebbiolo Winegrapes Before and After Different Pre-Treatments

| parameter | grape pre-treatment[a] | | | | | | | | |
|---|---|---|---|---|---|---|---|---|---|
| | HS1 | HS5 | DF | DI | MW1D30 | MW1D60 | MW2D60 | CS | sign[b] |
| | | | | | Barbera | | | | |
| $F_{sk}$ (N)[c] | 0.837 ± 0.118 | 0.874 ± 0.146 | 0.767 ± 0.134 | 0.831 ± 0.150 | 0.777 ± 0.150 | 0.797 ± 0.142 | 0.840 ± 0.126 | 0.852 ± 0.123 | ns |
| $W_{sk}$ (mJ)[d] | 0.859 ± 0.189bc | 0.921 ± 0.214c | 0.781 ± 0.270bc | 0.574 ± 0.231a | 0.726 ± 0.205b | 0.779 ± 0.208bc | 0.925 ± 0.188c | 0.803 ± 0.229bc | *** |
| | | | | | Nebbiolo | | | | |
| $F_{sk}$ (N)[c] | 0.635 ± 0.110b | 0.785 ± 0.129c | 0.510 ± 0.106a | 0.603 ± 0.121b | 0.570 ± 0.084ab | 0.580 ± 0.144ab | 0.628 ± 0.123b | 0.575 ± 0.077ab | *** |
| $W_{sk}$ (mJ)[d] | 0.468 ± 0.140abc | 0.657 ± 0.171d | 0.504 ± 0.208bc | 0.528 ± 0.176c | 0.386 ± 0.100a | 0.387 ± 0.135a | 0.461 ± 0.128abc | 0.410 ± 0.093ab | *** |

[a]HS1 = steam blanching at 100 °C for 1 min, HS5 = steam blanching at 100 °C for 5 min, DF = direct freezing in a freezer at −18 °C for 2 days, DI = freezing by adding dry ice, MW1D30 = microwave heating at 1 W/g for 30 s, MW1D60 = microwave heating at 1 W/g for 60 s, MW2D60 = microwave heating at 2 W/g for 60 s, CS = control. All data are expressed as average value ± standard deviation ($n$ = 30). Different Latin letters within the same row indicate significant differences ([b]) among pre-treatments according to Tukey-b test ($p < 0.05$). [b]Sign: *** and ns indicate significance at $p < 0.001$ and not significant, respectively. [c]$F_{sk}$ = skin break force, [d]$W_{sk}$ = skin break energy.

class.[2,42] In addition to the ripening effect, the influence of the growing location on the content of TA has been observed for both Barbera and Nebbiolo varieties in several studies.[41,42]

For Nebbiolo untreated berries, the average anthocyanin extraction yield was 80.5% (100-non-extracted skin anthocyanins, expressed as percentage), this value being lower than that published (91.1−94.2%) for different harvest dates and berry densities.[2] However, the average percentage obtained of non-extracted skin anthocyanins (19.5%, Table 1) agreed with that reported (19.9%) for Nebbiolo berries with hard skins.[11] For Barbera grapes, no study has been previously carried out on the extraction yield of anthocyanins from the skin into the pulp or a wine-like solution, and only the cellular maturity index (EA%) was determined in some works.[41]

The sum of pulp, extracted skin, and non-extracted skin contents of proanthocyanidins (PRO) and flavanols reactive to vanillin (FRV) (602 ± 116 and 200 ± 39 mg/kg for Barbera grapes, and 2700 ± 288 and 1104 ± 98 mg/kg for Nebbiolo grapes, respectively) was in the range published for total contents in the skin of the same varieties,[2,41] with the exception of FRV in Barbera grapes for which the values obtained in the present work were higher. The influence of the growing location on the content of FRV in the skin was very evident.[41] For Nebbiolo untreated berries, the average extraction yields of PRO and FRV were 75.0 and 78.9% (100-non-extracted skin compounds, expressed as percentage), respectively; these values agreed with those reported for different harvest dates and berry densities.[2]

TA contents in the pulp lower than 18 and 13 mg/kg for Barbera and Nebbiolo untreated berries, respectively, could be due in part to the inevitable manipulation of the sample during the step of removing the skin from the pulp. Only direct freezing of berries in a freezer (DF) and by adding dry ice (DI) facilitated the releasing of skin anthocyanins to the pulp for both Barbera and Nebbiolo winegrapes, as well as the pre-treatment of the berries by steam blanching for 5 min (HS5) for Nebbiolo. For the Barbera variety, the highest content of pulp TA was obtained when the pre-treatment with dry ice was used (67.7 mg/kg). For the Nebbiolo variety, the highest contents were associated with the pre-treatment by steam blanching for 5 min (74.8 mg/kg), but they were not significantly different from the ones corresponding to the pre-treatment with dry ice (60.9 mg/kg). For each variety, there were no significant differences in the content of extracted skin TA among treated and untreated berries. Therefore, in Barbera winegrapes, the percentage of non-extracted anthocyanins was significantly lower for the DI pre-treatment than for untreated berries (CS) or those treated with heat (HS or MW). On the other hand, non-extracted TA were significantly lower for the HS5 pre-treatment in Nebbiolo winegrapes although they did not differ from TA remaining in the skin after freezing (DF and DI).

As occurred for TA in Nebbiolo winegrapes, the DF, DI, and HS5 pre-treatments facilitated the releasing of PRO and FRV from the skin to the pulp. The lowest percentages of non-extracted skin PRO and FRV corresponded to the HS5 pre-treatment, although they did not differ significantly from PRO and FRV remaining in the skin after freezing (DF and DI) or shorter steam blanching (HS1). In Barbera winegrapes, significant differences were only found in the percentages of non-extracted skin PRO and FRV. In this case, the percentage of non-extracted skin PRO was significantly lower for freezing pre-treatments (DF and DI), as well as that of FRV for the DF

**Table 5. Pearson's Correlation Coefficients Between Skin Mechanical Properties and Phenolic Composition of Treated Barbera and Nebbiolo Winegrapes**

| cmpd[a] | Barbera | | Nebbiolo | |
|---|---|---|---|---|
| | $F_{sk}$ (N)[b,c] | $W_{sk}$ (mJ)[b,d] | $F_{sk}$ (N)[b,c] | $W_{sk}$ (mJ)[b,d] |
| **Pulp Phenolic Compounds** | | | | |
| TA (mg/kg) | ns | −0.553** | 0.433* | 0.736*** |
| PRO (mg/kg) | ns | −0.576** | ns | 0.640** |
| FRV (mg/kg) | ns | ns | ns | 0.681*** |
| ∑ delphinidin derivatives (%) | ns | ns | 0.731*** | 0.775*** |
| ∑ cyanidin derivatives (%) | ns | ns | ns | −0.692*** |
| ∑ petunidin derivatives (%) | ns | ns | 0.717*** | 0.724*** |
| ∑ peonidin derivatives (%) | ns | ns | ns | ns |
| ∑ malvidin derivatives (%) | ns | ns | ns | 0.597** |
| ∑ simple glucosides (%) | 0.468* | 0.608** | −0.519* | ns |
| ∑ acetyl glucosides (%) | ns | −0.665** | ns | 0.605** |
| ∑ cinnamoyl glucosides (%) | ns | ns | 0.514* | ns |
| **Extracted Skin Phenolic Compounds** | | | | |
| TA (mg/kg) | −0.456* | ns | ns | −0.455* |
| PRO (mg/kg) | ns | ns | ns | −0.456* |
| FRV (mg/kg) | ns | ns | ns | −0.454* |
| ∑ delphinidin derivatives (%) | ns | ns | ns | 0.595** |
| ∑ cyanidin derivatives (%) | ns | ns | ns | ns |
| ∑ petunidin derivatives (%) | ns | −0.648** | ns | ns |
| ∑ peonidin derivatives (%) | ns | ns | ns | ns |
| ∑ malvidin derivatives (%) | ns | ns | ns | ns |
| ∑ simple glucosides (%) | ns | ns | −0.546* | −0.678*** |
| ∑ acetyl glucosides (%) | ns | ns | ns | ns |
| ∑ cinnamoyl glucosides (%) | −0.614** | −0.453* | 0.553** | 0.721*** |
| **Non-extracted Skin Phenolic Compounds** | | | | |
| TA (%) | ns | 0.615** | ns | −0.721*** |
| PRO (%) | ns | ns | ns | −0.751*** |
| FRV (%) | ns | ns | ns | −0.755*** |
| ∑ delphinidin derivatives (%) | ns | 0.451* | ns | ns |
| ∑ cyanidin derivatives (%) | ns | ns | ns | ns |
| ∑ petunidin derivatives (%) | 0.500* | ns | ns | ns |
| ∑ peonidin derivatives (%) | ns | ns | ns | ns |
| ∑ malvidin derivatives (%) | −0.461* | ns | ns | ns |
| ∑ simple glucosides (%) | ns | ns | ns | −0.549** |
| ∑ acetyl glucosides (%) | ns | ns | ns | ns |
| ∑ cinnamoyl glucosides (%) | ns | ns | ns | 0.622** |

[a]TA = total anthocyanins, PRO = proanthocyanidins, FRV = flavanols reactive to vanillin. [b]Sign: *,**,*** and ns indicate significance at $p <$ 0.05, 0.01, 0.001 and not significant, respectively ($n$ = 21). [c]$F_{sk}$ = skin break force, [d]$W_{sk}$ = skin break energy.

pre-treatment, than for CS berries. Therefore, the improved extraction of anthocyanins and flavanols from the skin could favor the long-term color stability through the formation of pigmented polymers.[13,14] Furthermore, an increase in the proportion of PRO (high-molecular weight flavanols) released from the skin usually leads to a softening effect on the mouthfeel because of the lower astringency perception.[15]

Other studies revealed that the wines obtained using different low-temperature pre-fermentative treatments (grape freezing in a freezer, must freezing with dry ice, and cold maceration) show higher concentrations of TA at the end of fermentative maceration than the control wine.[15,18,19,43] Particularly, freezing may provide better results in winegrape varieties characterized by skins having a more rigid structure.[18] The use of dry ice also facilitated the extraction of high-molecular weight PRO from skins by degrading the structures.[15] Freezing with dry ice facilitates the extraction of phenolic compounds probably due to a quick thermal shock that induces the formation of ice crystals within the berry skin. The increased volume of the intracellular liquids causes the breakage of the cell walls and membranes. An additional advantage of dry ice is the protective effect against oxidation of extracted anthocyanins before fermentation, as it sublimates to gaseous carbon dioxide displacing completely the oxygen present in the medium and inhibits the activity of polyphenoloxidase enzymes.[15,22,25] The carbon dioxide saturation maintains the inhibitory effect even when temperature reaches normal fermentation values.[18] However, other works reported that the effectiveness of these treatments depends on the grape ripeness, the berry size, and the composition of the skin cell walls.[20,23,44]

In the scientific literature, dry ice is usually added to the must after grapes crushing, whereas the uncrushed grapes are directly frozen in a freezer. The comparative studies carried out on the use of these two pre-fermentative cold treatments provide contradictory results. Gil-Muñoz et al.[18] pointed out that must freezing with dry ice leads to higher contents of TA at the end of alcoholic fermentation. However, Heredia et al.[25] justified lower anthocyanin contents on the basis of a local effect on the skin just in the mass being directly in contact with dry ice. When pre-fermentative cold maceration of the must with the solid parts (crushed grapes) was carried out, higher extraction of TA was achieved with the addition of dry ice instead of keeping the sample in the freezer.[20] In the present study, the two pre-treatments (DF and DI) were applied to uncrushed berries, and the release and solubilization of anthocyanins into the pulp for Barbera and Nebbiolo winegrapes were also more favored using the DI pre-treatment as compared with the DF pre-treatment.

According to the results obtained for steam blanching of whole berries, TA, PRO, and FRV released into the pulp during the pre-treatment seem to increase with increasing heating time for the Nebbiolo variety. In some works, higher concentrations of anthocyanins in wines were obtained by heating partially dejuiced grapes at 90−95 °C for 1 min,[45] by mash thermal


dx.doi.org/10.1021/jf502656d | J. Agric. Food Chem. 2014, 62, 8437−8451

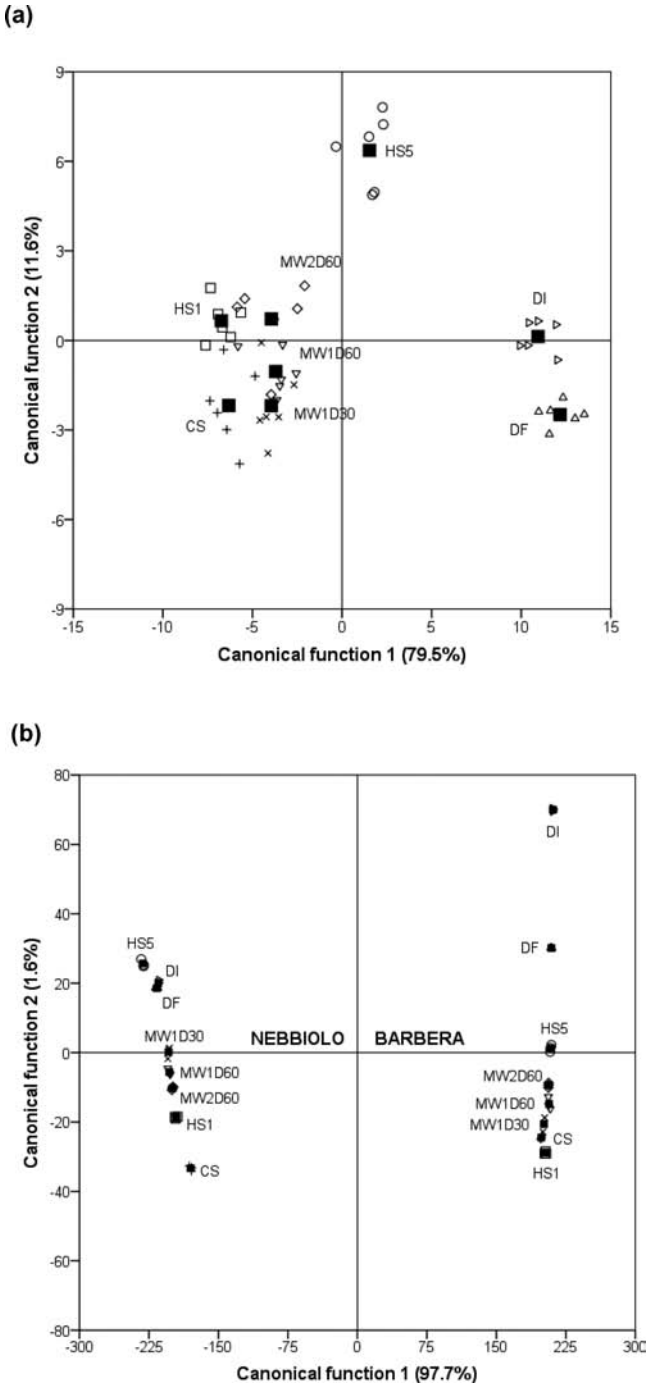


**Figure 2.** Projection of winegrape berries untreated and submitted to the different pre-treatments studied in the plane defined by the two first canonical functions considering Barbera and Nebbiolo varieties simultaneously (a) and separately (b). HS1 = steam blanching at 100 °C for 1 min, HS5 = steam blanching at 100 °C for 5 min, DF = direct freezing in a freezer at −18 °C for 2 days, DI = freezing by adding dry ice, MW1D30 = microwave heating at 1 W/g for 30 s, MW1D60 = microwave heating at 1 W/g for 60 s, MW2D60 = microwave heating at 2 W/g for 60 s, CS = control.

treatment at 50 °C for 15 min[46] or by mash pre-fermentative heating up to 65 °C and cooling down for 24 h (30 °C)[47] than using the untreated grapes. On the contrary, other researchers reported lower content of TA but higher one of total flavanols in the wine obtained by mash pre-fermentative heating at 65 °C for 8 h than in the control wine.[16] Therefore, temperature and time of heating seem to be important factors. Although the degradation of monomeric anthocyanins occurs more rapidly with increasing temperature, shorter treatment time at higher temperatures might be ideal for enhancing the extraction of thermally labile compounds.[26] Mild blanching of the berries can inactivate polyphenoloxidase enzymes, protecting anthocyanins against enzymatic degradation.[48] On the other hand, the water content is the most common absorbing phase for microwave energy and, therefore, plays a key role during the microwave treatment of grapes. In the present work, significant differences were not found in the content of pulp TA for microwave-treated berries (MW) in relation to untreated berries (CS). According to the results obtained, the anthocyanin degradation was not observed using the thermal pre-treatments of whole berries with steam or microwave energy, probably due to the short treatment times and/or low microwave power densities.[49]

**Anthocyanin Profile.** The qualitative composition of skin anthocyanins released into the pulp before and after the grape pre-treatment, extracted skin anthocyanins during the maceration step, and non-extracted skin anthocyanins for Barbera and Nebbiolo winegrapes are shown in Tables 2 and 3, respectively. For Barbera untreated grapes, malvidin derivatives were the predominant anthocyanin compounds (about 62%), and the richness in trisubstituted anthocyanin forms ranged from 77% to 92% (Table 2). However, the anthocyanin profile was slightly different as a function of the extraction easiness of anthocyanins (Table 2). In particular, peonidin derivatives were the second most abundant pulp anthocyanins (11%), whereas petunidin derivatives were for extracted and non-extracted skin anthocyanins (13% and 20%, respectively). Furthermore, simple glucoside (free or unacylated) forms accounted for around 75% of extracted and non-extracted skin anthocyanins, but they achieved 92% of pulp anthocyanins mainly at the expense of acetylated forms. Although the general profile of extracted and non-extracted skin anthocyanins in Barbera untreated winegrapes was similar, non-extracted skin anthocyanins showed slightly lower percentages of malvidin derivatives, which resulted in higher abundance of the other trisubstituted anthocyanins. Despite some small differences attributable to the growing zone and seasonal variability,[6] the anthocyanin profile of Barbera untreated grapes was similar to the extractable anthocyanin profile previously reported in other works,[5,36,41] particularly for extracted and non-extracted skin anthocyanins. The works published to date did not consider pulp anthocyanins during the manipulation step of the berry skin.

Regarding the Nebbiolo variety, Table 3 shows that untreated winegrapes were rich in disubstituted anthocyanin forms with percentages ranging from 63% to 81%. The major anthocyanin compounds were peonidin derivatives (about 45%). Malvidin derivatives were also abundant extracted and non-extracted skin anthocyanins (about 23%), although lower than peonidin forms. However, cyanidin derivatives (35%) predominated over malvidin derivatives (13%) in pulp anthocyanins. This constitutes an important enological aspect because of the high percentage of disubstituted anthocyanin forms easily extracted in the pulp (77−81%). As occurred in Barbera untreated grapes, simple glucoside forms accounted for 97% of pulp anthocyanins, whereas they only reached percentages comprising between 84% and 88% of extracted and non-extracted skin anthocyanins. The qualitative composition of extracted and non-extracted skin anthocyanins for Nebbiolo untreated grapes was quite similar and agreed, with


dx.doi.org/10.1021/jf502656d | J. Agric. Food Chem. 2014, 62, 8437−8451

**Table 6. Standardized Coefficients of Canonical Discriminant Functions for Barbera and Nebbiolo Winegrapes Considered Simultaneously**

| | function | | | | | | |
|---|---|---|---|---|---|---|---|
| parameter[a] | 1 | 2 | 3 | 4 | 5 | 6 | 7 |
| | | | | Pulp Phenolic Compounds | | | |
| TA (mg/kg) | 0.144 | 1.841 | 0.696 | 0.106 | 1.148 | 2.075 | 0.248 |
| FRV (mg/kg) | 2.052 | 1.100 | 2.965 | 1.768 | −0.791 | 4.980 | −1.199 |
| ∑ delphinidin derivatives (%) | −0.639 | −3.546 | −1.361 | −2.309 | 0.798 | 2.250 | −0.036 |
| ∑ cyanidin derivatives (%) | −8.930 | −0.999 | 1.870 | −2.664 | 3.169 | 6.336 | −4.794 |
| ∑ petunidin derivatives (%) | −4.343 | 8.550 | 2.744 | 9.475 | −2.922 | −7.608 | 0.547 |
| ∑ peonidin derivatives (%) | 7.191 | −2.894 | 3.927 | 5.085 | 11.810 | −1.986 | 5.815 |
| ∑ simple glucosides (%) | 10.389 | −0.065 | −5.460 | −0.748 | 0.259 | 1.666 | 0.221 |
| ∑ acetyl glucosides (%) | 7.349 | −3.378 | −2.210 | 0.404 | −1.146 | 0.200 | −0.538 |
| | | | | Extracted Skin Phenolic Compounds | | | |
| TA (mg/kg) | 1.244 | 6.135 | 1.896 | 4.564 | 3.356 | 13.140 | 5.936 |
| PRO (mg/kg) | −5.531 | 10.516 | 6.538 | 12.672 | 0.186 | 9.027 | −1.470 |
| ∑ delphinidin derivatives (%) | −0.188 | 2.548 | 0.811 | −0.883 | −0.410 | 1.666 | −1.107 |
| ∑ cyanidin derivatives (%) | 1.264 | −6.596 | −8.635 | −2.407 | −1.189 | 1.009 | 12.490 |
| ∑ peonidin derivatives (%) | −1.543 | 9.009 | 2.455 | −3.817 | −9.353 | 5.289 | 6.042 |
| ∑ simple glucosides (%) | −1.931 | 0.365 | 1.216 | 0.218 | −1.324 | 2.868 | −2.595 |
| | | | | Non-extracted Skin Phenolic Compounds | | | |
| TA (%) | 2.655 | 1.518 | 2.454 | 3.909 | 2.437 | 12.145 | 3.501 |
| ∑ cyanidin derivatives (%) | 1.483 | 7.712 | 1.873 | 5.326 | 0.059 | −9.420 | −7.925 |
| ∑ acetyl glucosides (%) | 1.285 | 1.628 | 2.631 | −0.585 | 1.132 | −1.225 | −0.616 |
| | | | | Skin Mechanical Properties | | | |
| $F_{sk}$ (N) | −3.058 | 2.912 | 1.433 | −0.709 | −1.105 | −0.002 | 1.101 |
| $W_{sk}$ (mJ) | 0.501 | 0.548 | −2.584 | 0.658 | 1.450 | 0.861 | −1.867 |

[a]TA = total anthocyanins, PRO = proanthocyanidins, FRV = flavanols reactive to vanillin, $F_{sk}$ = skin break force, $W_{sk}$ = skin break energy.

some small differences, with the extractable anthocyanin profile previously reported in the scientific literature.[2,5,42,50]

When the profile of extracted skin anthocyanins was compared with that of pulp anthocyanins in untreated and treated berries, greater percentages of delphinidin, petunidin and malvidin derivatives were usually observed in the former for both Barbera and Nebbiolo varieties, whereas the percentages of cyanidin and peonidin forms were lower. The diffusion of disubstituted anthocyanins is faster than the one corresponding to trisubstituted anthocyanins,[12] which justifies the higher relative abundance of the first compounds in the pulp, but the percentage of trisubstituted anthocyanins increases during the first days of maceration.[12] On the other hand, the proportion of unacylated forms in extracted skin anthocyanins was lower in favor of higher proportions of acetylated and cinnamoylated glucosides. Acylated anthocyanins are very important because they participate in intramolecular copigmentation processes, protecting the flavylium cation.[18] In the present work, some exceptions were found to this general behavior, particularly in malvidin and peonidin derivatives for Barbera and Nebbiolo winegrapes, respectively. Therefore, for a given variety the different pre-treatments studied on whole berries may influence the anthocyanin profile of the final product, favoring preferential releasing of a certain anthocyanin form from the skin into the must. This fact is of great importance because the reactivity of the different anthocyanins depends on their structure. Particularly, 3′-hydroxylated molecules (delphinidin, cyanidin, and petunidin) are more prone to oxidation and thermolabile,[51,52] and therefore the juices/wines with higher proportions of these molecules are more sensitive to color degradation. In fact, anthocyanins without ortho-hydroxylated groups can interact with flavanols and ethanal, leading to a stable red pigmentation. In varieties characterized by an important presence of disubstituted anthocyanins, such as Nebbiolo, a remarkable loss of these anthocyanin compounds has been also noticed during winemaking.[53] The next step was to evaluate the effect of each grape pre-treatment studied on the profile of pulp, extracted skin and non-extracted skin anthocyanin compounds for Barbera and Nebbiolo berries.

The different pre-treatments of the berries caused changes of different magnitude in the anthocyanin profile of Barbera grapes if compared with untreated berries (Table 2). Most of significant differences were found in pulp anthocyanins. Freezing with dry ice (DI) was the grape pre-treatment that affected more significantly the profile of pulp anthocyanins. Although the proportions of trisubstituted anthocyanins like delphinidin and petunidin forms experienced a significant decrease, total trisubstituted anthocyanins were more abundant in the berries treated with dry ice because of a significant decrease in the percentage of cyanidin derivatives and the largest increase in the percentage of malvidin derivatives (+6.4%). This effect of the DI pre-treatment on the profile of pulp anthocyanins agreed with the observed in wines made from winegrapes rich in trisubstituted anthocyanins.[54] The DI pre-treatment also induced the greatest decrease in the relative abundance of simple glucoside anthocyanins in favor of the more significant increase in acetylated glucosides (+2.3%). The influence of freezing of the berries in a freezer (DF) on the profile of pulp anthocyanins was similar to the one corresponding to the DI pre-treatment but to a much lesser extent. Microwave heating at 2 W/g for 60 s (MW2D60) also promoted a marked increase in the percentage of total trisubstituted anthocyanins as a consequence of the lowest percentages of cyanidin and peonidin derivatives released from the skin into the pulp during the berries pre-treatment

**Table 7. Standardized Coefficients of Canonical Discriminant Functions for Barbera and Nebbiolo Winegrapes Considered Separately**

| | function | | | | | | |
|---|---|---|---|---|---|---|---|
| parameter[a] | 1 | 2 | 3 | 4 | 5 | 6 | 7 |
| | | | | Pulp Phenolic Compounds | | | |
| TA (mg/kg) | 4.339 | 1.427 | 1.845 | −0.624 | −2.529 | 2.809 | 0.976 |
| PRO (mg/kg) | −6.219 | 2.861 | 2.189 | −1.654 | 1.589 | 0.624 | 1.060 |
| ∑ delphinidin derivatives (%) | −0.126 | −5.192 | 0.701 | 2.026 | −1.453 | −1.412 | 1.073 |
| ∑ cyanidin derivatives (%) | 0.327 | −5.585 | −1.274 | 0.880 | −0.450 | 0.239 | 0.559 |
| ∑ petunidin derivatives (%) | −0.048 | 1.579 | 0.326 | −2.553 | 1.452 | 0.652 | −1.087 |
| ∑ peonidin derivatives (%) | −0.350 | 2.124 | 0.285 | −0.685 | 1.087 | −0.859 | 0.551 |
| ∑ simple glucosides (%) | −0.023 | 2.365 | −0.715 | −0.212 | −1.257 | −0.091 | 0.073 |
| ∑ acetyl glucosides (%) | −0.174 | 3.846 | −1.845 | −0.205 | −0.524 | −0.824 | 0.410 |
| | | | | Extracted Skin Phenolic Compounds | | | |
| TA (mg/kg) | 8.200 | 2.807 | 3.240 | −2.432 | −3.096 | 3.579 | 3.202 |
| PRO (mg/kg) | −9.838 | 5.677 | 1.446 | −3.020 | 6.352 | −0.589 | 0.951 |
| FRV (mg/kg) | 2.770 | −2.576 | −1.479 | 0.086 | −4.358 | 1.136 | −1.035 |
| ∑ delphinidin derivatives (%) | 4.905 | −5.230 | 6.835 | 7.082 | −3.178 | 4.945 | 2.428 |
| ∑ cyanidin derivatives (%) | 3.529 | 6.584 | 0.671 | −5.988 | −0.220 | −0.360 | −1.900 |
| ∑ petunidin derivatives (%) | −2.162 | 0.155 | −2.718 | −1.396 | 2.317 | −0.995 | −2.589 |
| ∑ peonidin derivatives (%) | 4.024 | −1.767 | 7.144 | 4.539 | −1.269 | 4.788 | 0.694 |
| ∑ simple glucosides (%) | 2.058 | −13.482 | 5.693 | 20.092 | −3.961 | 4.514 | −0.145 |
| ∑ acetyl glucosides (%) | 1.397 | −13.246 | 4.681 | 19.334 | −4.221 | 3.719 | −0.406 |
| | | | | Non-extracted Skin Phenolic Compounds | | | |
| TA (%) | 7.929 | −1.548 | 4.026 | 0.620 | −3.171 | 3.369 | 2.191 |
| PRO (%) | −4.980 | 0.746 | 0.599 | −1.046 | 2.605 | −0.254 | 0.654 |
| FRV (%) | 0.034 | 1.890 | −0.671 | −0.162 | 0.269 | 0.743 | 0.766 |
| ∑ delphinidin derivatives (%) | −5.084 | −2.537 | −3.024 | −3.006 | −4.992 | −1.518 | −1.264 |
| ∑ cyanidin derivatives (%) | −2.781 | −0.490 | −3.842 | 1.553 | 1.513 | −1.195 | 0.432 |
| ∑ petunidin derivatives (%) | 2.824 | 6.289 | 1.493 | −0.717 | 4.005 | −0.572 | 1.317 |
| ∑ peonidin derivatives (%) | −5.049 | 1.806 | −4.467 | −2.711 | 1.798 | −3.436 | −0.817 |
| ∑ simple glucosides (%) | 0.350 | 12.254 | −5.398 | −9.922 | 8.486 | −2.902 | −0.654 |
| ∑ acetyl glucosides (%) | 0.136 | 9.404 | −4.406 | −6.819 | 7.056 | −2.074 | −1.314 |
| | | | | Skin Mechanical Properties | | | |
| $F_{sk}$ (N) | 0.012 | 0.530 | −0.034 | −1.271 | −2.063 | 1.675 | 1.077 |
| $W_{sk}$ (mJ) | 0.075 | −2.081 | 0.989 | 0.083 | 1.633 | −0.278 | −1.104 |

[a]TA = total anthocyanins, PRO = proanthocyanidins, FRV = flavanols reactive to vanillin, $F_{sk}$ = skin break force, $W_{sk}$ = skin break energy.

(decreasing −3.0% and −1.7%, respectively). The MW2D60 pre-treatment and steam blanching for 5 min (HS5) caused an important increase in the percentage of malvidin derivatives. In the case of the HS5 pre-treatment, the lowest percentages of other trisubstituted anthocyanins like delphinidin and petunidin derivatives were obtained (decreasing −2.8% and −1.9%, respectively). Microwave heating at 1 W/g for 60 s (MW1D60) was the grape pre-treatment giving the highest proportion of disubstituted anthocyanins and the greatest decrease in the percentage of malvidin derivatives in the pulp (−1.9%). Microwave heating using any experimental condition investigated permitted a significant increase in the proportion of acetylated glucoside anthocyanins at the expense of simple glucoside forms.

The effect of the different pre-treatments applied to the berries on the anthocyanin profile of Nebbiolo winegrapes is shown in Table 3. As already mentioned for the Barbera variety, most of significant differences among untreated and treated berries were found in pulp anthocyanins. The most influential grape pre-treatments were DI, DF and HS5. The DI pre-treatment caused the largest increase in the percentage of malvidin compounds (+6.6%) and the greatest decrease in the proportion of cyanidin derivative pulp anthocyanins (−11.0%). Although this last treatment also favored the significant increase in the percentage of peonidin derivatives, total trisubstituted anthocyanins were more abundant in the berries treated with dry ice. Furthermore, the more significant increase in the proportion of acetylated glucoside pulp anthocyanins at the expense of free glucosides corresponded to the DI pre-treatment. On the other hand, the greatest increase in the percentage of peonidin derivatives (+6.3%) was associated with the DF pre-treatment, but it was balanced with a significant reduction in the proportion of cyanidin derivatives and an important increase in the percentage of malvidin forms of pulp anthocyanins. This fact implied that the relative abundance of total trisubstituted anthocyanins was not significantly different among freezing pre-treatments (DF and DI). The percentage of these compounds also agreed with that obtained in the pulp after the HS5 pre-treatment of the berries, as a consequence of the highest increase found in the proportions of delphinidin and petunidin derivatives (+1.2% and +0.8%, respectively) together with a significant reduction in the percentage of cyanidin derivatives and an important increase in malvidin forms in relation to untreated berries. However, the percentage of peonidin derivatives increased significantly. Furthermore, the lowest proportion of free glucoside pulp anthocyanins (decreasing −0.9%), in favor of acetylated glucosides, corresponded to the HS5 pre-treatment. The anthocyanin


dx.doi.org/10.1021/jf502656d | J. Agric. Food Chem. 2014, 62, 8437−8451

profile of the berries steam blanched for 1 min (HS1) or microwave heated (MW) was not significantly different from the one corresponding to untreated berries.

For each variety, only a few significant differences were found in the profile of extracted and non-extracted skin anthocyanins among untreated and treated berries. Because the grape pre-treatment can cause changes in the skin tissues that facilitate the extraction of anthocyanins during the maceration step, the profile of extracted skin anthocyanins for Barbera winegrapes showed some significant changes affecting mainly petunidin derivatives (+2.1%) when the DI pre-treatment was applied (Table 2). For the Nebbiolo variety (Table 3), the only significant difference was the lowest percentage of simple glucosides (−1.7%) when the berries were submitted to the HS5 pre-treatment in favor of cinnamoylated glucosides. Regarding the qualitative composition of anthocyanins that remain in the skin after maceration, the most important changes were observed for Nebbiolo berries where the greatest decrease in the percentages of delphinidin derivatives and simple glucosides (about −1.4% and −2.3%, respectively), in favor of cinnamoylated glucosides, was obtained after the DI and HS5 pre-treatment.

Regarding general trends, some aspects are particularly relevant. Freezing of whole berries (DF and DI) improved the extraction of malvidin derivatives from the skin into the pulp for both Barbera and Nebbiolo winegrapes, which agreed with the increased extraction of malvidin-3-glucoside into the wine using different pre-fermentative cold maceration treatments of crushed berries.[23,54] Since malvidin derivatives are the most stable forms of anthocyanins (particularly acylated forms), their higher diffusion into the pulp may contribute favorably to the color stability of the resulting juice/wine. When acylation was considered, higher percentages of acylated glucosides were observed in pulp anthocyanins after the DI pre-treatment of Barbera and Nebbiolo winegrapes than after the DF pre-treatment. Heredia et al.[25] have also found lower abundance of monoglucosides during cryomaceration with dry ice when compared with refrigeration of the berries in a freezer.

According to the results obtained, the effect of heating time and/or microwave power density depended on the variety. Microwave power density affected mainly the anthocyanin profile of Barbera winegrapes, whereas the effect of treatment time was particularly important for the Nebbiolo variety using steam as heating source. Other work showed that, after alcoholic fermentation, the wine obtained by pre-fermentative mash heating at 65 °C for 8 h contains less malvidin-3-glucoside and more delphinidin-3-glucoside and petunidin-3-glucoside than the control wine, even though malvidin-3-glucoside is the most abundant monomeric anthocyanin in Okuzgozu grapes.[16] These results disagreed with those obtained in the present work. The variety and the experimental conditions of heating may be very influential factors on the anthocyanin profile of the resulting juices/wines and, therefore, on their color stability.

**Instrumental Texture Analysis.** The skin mechanical properties of Barbera and Nebbiolo winegrapes before and after the different pre-treatments studied are shown in Table 4. The values obtained in untreated berries are comprised in the usual range for these varieties, particularly from Piedmont growing zone.[41,42,50] The magnitude of the effect of the different freezing and heating pre-treatments on the instrumental texture parameters defining the skin hardness ($F_{sk}$ and $W_{sk}$) depended on the variety. For Barbera winegrapes, freezing with dry ice (DI) reduced significantly the skin break energy ($W_{sk}$), achieving the lowest values in relation to berries untreated and treated with any other methodology studied. No significant difference was found in the skin break force ($F_{sk}$) among untreated and treated berries for the Barbera variety. For Nebbiolo winegrapes, the hardest skins were found after the thermal pre-treatment of the berries by steam blanching for 5 min (HS5), with values of $F_{sk}$ and $W_{sk}$ being significantly higher than those corresponding to untreated and differently treated berries. A possible explanation could be the caramelization of sugars closer to the skin, which occurs at high temperatures. The DI pre-treatment also promoted a significant increase in the values of $W_{sk}$ in relation to untreated berries.

Instrumental texture parameters of the skin have been proposed as anthocyanin extractability markers.[11] However, the relationships between the skin mechanical properties and the anthocyanin extraction yield are variety dependent. The chemical composition of grape skin cell walls may determine the mechanical resistance of the berry skin to the anthocyanin release.[8] In Nebbiolo grapes, higher values of $F_{sk}$ facilitated more complete anthocyanin release from the skin.[11] In the present work, significant correlations (correlation factor $R > 0.5$, $p < 0.05$) were found for each variety between the value of $W_{sk}$ in treated whole berries and the corresponding content of TA ($n = 21$, 7 treatments × 3 replicates of 10 berries). Thus, the amount of pulp TA and the percentage of non-extracted skin TA were better correlated with the value of $W_{sk}$ for Nebbiolo ($R = 0.736$, $p < 0.001$ and $R = -0.721$, $p < 0.001$, respectively) than for Barbera winegrapes ($R = -0.553$, $p < 0.01$ and $R = 0.615$, $p < 0.01$, respectively), as shown in Table 5. Furthermore, the relationships were inverse for the two varieties. The results obtained agreed with those reported by Rolle et al.[11] for the Nebbiolo variety, the higher the skin hardness the higher the extracted anthocyanins. Because higher skin hardness probably involves greater cell wall fragility, the higher the $W_{sk}$ values the higher the amounts of pulp flavanols (PRO and FRV) ($R = 0.640$, $p < 0.01$ and $R = 0.681$, $p < 0.001$, respectively) for Nebbiolo winegrapes, and therefore the lower the percentages of non-extracted skin flavanols ( $R = -0.751$, $p < 0.001$ and $-0.755$, $p < 0.001$, respectively). As occurred for TA in Barbera winegrapes, the content of PRO (high-molecular weight flavanols) released into the pulp was negatively correlated with the value of $W_{sk}$ ($R = -0.576$, $p < 0.01$), whereas no significant correlation was found for FRV (low-molecular weight flavanols).

The berry skin hardness also affected the individual anthocyanin composition of the hydroalcoholic extracts for Nebbiolo skins.[11] Only in the early phases of the anthocyanin diffusion, harder skins (more fragile) exhibited significantly higher percentages of extracted petunidin-3-glucoside (+0.8%), cyanidin-3-glucoside (+3.6%), and peonidin-3-glucoside (+6.0%) derivatives at the expense of malvidin-3-glucosides (−9.6%). After macerating for 10 min, no significant differences were found in the extracted anthocyanin profile of skins with different hardness. Since the values obtained of $F_{sk}$ in the present work for Nebbiolo winegrapes correspond to hard skins, higher proportions of peonidin derivatives in pulp anthocyanins (+1.6−6.3%) are justified for treated berries if compared with untreated berries. On the other hand, a higher number of significant relationships between the berry skin mechanical properties and the anthocyanin profile were associated with pulp anthocyanins (Table 5), probably due to the fact that they were more quickly released from the skin.

Considering only the most significant correlations (Table 5, $R > 0.675$, $p < 0.001$), in Nebbiolo treated winegrapes, the percentages of delphinidin and petunidin glucosides increased with increasing values of $F_{sk}$ and $W_{sk}$, whereas those of cyanidin decreased with increasing $W_{sk}$, for pulp anthocyanins. However, the most important variation in pulp anthocyanins with $W_{sk}$ corresponded to the percentages of cyanidin and malvidin glucosides. Harder skins of Nebbiolo treated berries provided lower relative abundance of cyanidin glucosides (sensitive to oxidation reactions) and higher percentage of malvidin glucosides (highly stable). Furthermore, the proportion of unacylated glucosides decreased significantly, and the relative amount of cinnamoylated forms increased with rising values of $W_{sk}$ for extracted skin anthocyanins in Nebbiolo treated berries. In Barbera treated winegrapes, the significant correlations were less numerous and weaker than in Nebbiolo ones (Table 5, $R < 0.670$, $p > 0.001$) with general inverse trends for the two varieties.

**Multivariate Analysis.** Discriminant analysis based on the contents of TA, PRO and FRV, and the composition of individual anthocyanins released into the pulp, extracted during maceration and remaining in the skin (as defined in the Materials and Methods section), and the skin mechanical properties for treated and untreated Barbera and Nebbiolo winegrapes (Tables 1−4) showed a very clear classification of the berries according to the pre-treatment (Figure 2a). A perfect clustering of scores of the samples for each pre-treatment was observed. The two first canonical functions accounted for 91.0% of total variance in the original data. Function 1 explained 79.5% of the variability and was mainly related to the percentages of cyanidin and peonidin derivatives of pulp anthocyanins, particularly unacylated forms. The highest positive values of function 1 corresponded to the berries frozen (DF and DI pre-treatments). Function 2 accounted for 11.6% of the cumulative variance and was mainly associated with the relative abundance of pulp petunidin derivatives, extracted skin cyanidin and peonidin derivatives, and non-extracted skin cyanidin derivatives, as well as the content of extracted skin TA and PRO, the thermal pre-treatment HS5 corresponding to the highest positive values. The standardized coefficients of canonical functions are shown in Table 6. Although the differentiation of berries untreated and treated by other thermal pre-treatments was not so clear, 95.8% of the samples were correctly classified. When discriminant analysis was carried out separately on Barbera and Nebbiolo winegrapes (Figure 2b), a perfect clustering of scores of the samples for each variety and pre-treatment was observed. The two first canonical functions accounted for 99.2% of total variance in the original data. Function 1 explained 97.7% of the variability and was mainly related to the content of pulp PRO, extracted skin TA and PRO and non-extracted skin TA. The highest positive and negative values of function 1 were associated with Barbera and Nebbiolo winegrapes, respectively. Therefore, function 1 permitted a good differentiation of the samples according to the variety. Function 2 accounted for 1.6% of the cumulative variance and was mainly associated with the percentage of cyanidin derivatives of extracted skin anthocyanins and the relative abundance of petunidin derivatives of non-extracted skin anthocyanins, particularly unacylated and acetylated forms. The highest positive values of function 2 corresponded to freezing pre-treatments (DF and DI) and the thermal pre-treatment HS5, whereas the highest negative values were associated with untreated berries (CS) and the thermal pre-treatment HS1. The standardized coefficients of the seven first canonical functions are shown in Table 7. In this case, 100% of the samples were correctly classified. Therefore, function 2 facilitated the differentiation of untreated berries and those submitted to the different pre-treatments studied.

In conclusion, different pre-treatments of whole berries (freezing with dry ice, freezing in a freezer and steam blanching for 5 min) enhanced mainly the releasing of anthocyanins from the skin into the pulp. Nevertheless, the magnitude of the effect depended on the grape pre-treatment, experimental conditions used, anthocyanin compound and variety. The varietal effect may be related to the changes occurring in the skin tissue during the pre-treatment, which affected the facility to break the cell-walls and to release anthocyanins. In fact, the significance and strength of the correlations between the berry skin mechanical properties and the phenolic composition of treated berries depended strongly on the variety studied. Freezing with dry ice can be considered a promising treatment for industrial processing of uncrushed grape berries, not only because of increased total content of pulp extracted anthocyanins but also the modified anthocyanin profile in favor of more stable compounds. It is particularly important for winegrape varieties with a high proportion of disubstituted anthocyanins, such as Nebbiolo. For this variety, the use of dry ice also facilitated the release of low and high molecular weight flavanols from the skin into the pulp, which may lead to more colored juices/wines with lower astringency perception. In future works, the practical application of the most advantageous pre-treatments will be thoroughly evaluated by means of chemical, chromatic and sensory quality of the juices and/or wines obtained. Particularly, the production of grape juices rich in anthocyanins could be of great interest for offering a product with higher nutritional value, better chromatic characteristics and improved acceptance by consumers.

## AUTHOR INFORMATION

### Corresponding Author

*E-mail: luca.rolle@unito.it. Tel.: +39 011 6708558. Fax: +39 011 6708549.

### Author Contributions

§These authors contributed equally to the study.

### Notes

The authors declare no competing financial interest.

## REFERENCES

(1) Gil-Muñoz, R.; Fernández-Fernández, J. I.; Vila-López, R.; Martinez-Cutillas, A. Anthocyanin profile in Monastrell grapes in six different areas from Denomination of Origen Jumilla during ripening stage. *Int. J. Food Sci. Technol.* **2010**, *45*, 1870−1877.

(2) Rolle, L.; Río Segade, S.; Torchio, F.; Giacosa, S.; Cagnasso, E.; Marengo, F.; Gerbi, V. Influence of grape density and harvest date on changes in phenolic composition, phenol extractability indices, and instrumental texture properties during ripening. *J. Agric. Food Chem.* **2011**, *59*, 8796−8805.

(3) Tarara, J. M.; Lee, J.; Spayd, S. E.; Scagel, C. F. Berry temperature and solar radiation alter acylation, proportion, and concentration of anthocyanin in Merlot grapes. *Am. J. Enol. Vitic.* **2008**, *59*, 235−247.

(4) Dimitrovska, M.; Bocevska, M.; Dimitrovski, D.; Murkovic, M. Anthocyanin composition of Vranec, Cabernet Sauvignon, Merlot and Pinot Noir grapes as indicator of their varietal differentiation. *Eur. Food Res. Technol.* **2011**, *232*, 591−600.

(5) Ferrandino, A.; Carra, A.; Rolle, L.; Schneider, A.; Schubert, A. Profiling of hydroxycinnamoyl tartrates and acylated anthocyanins in

the skin of 34 *Vitis vinifera* genotypes. *J. Agric. Food Chem.* **2012**, *60*, 4931−4945.
(6) Ortega-Regules, A.; Romero-Cascales, I.; López-Roca, J. M.; Ros-García, J. M.; Gómez-Plaza, E. Anthocyanin fingerprint of grapes: environmental and genetic variations. *J. Sci. Food Agric.* **2006**, *86*, 1460−1467.
(7) Pomar, F.; Novo, M.; Masa, A. Varietal differences among the anthocyanin profiles of 50 red table grape cultivars studied by high performance liquid chromatography. *J. Chromatogr. A* **2005**, *1094*, 34−41.
(8) Hernández-Hierro, J. M.; Quijada-Morín, N.; Martínez-Lapuente, L.; Guadalupe, Z.; Ayestarán, B.; Rivas-Gonzalo, J. C.; Escribano-Bailón, M. T. Relationship between skin cell wall composition and anthocyanin extractability of *Vitis vinifera* L. cv. Tempranillo at different grape ripeness degree. *Food Chem.* **2014**, *146*, 41−47.
(9) Ortega-Regules, A.; Romero-Cascales, I.; Ros-García, J. M.; López-Roca, J. M.; Gómez-Plaza, E. A first approach towards the relationship between grape skin cell-wall composition and anthocyanin extractability. *Anal. Chim. Acta* **2006**, *563*, 26−32.
(10) Romero-Cascales, I.; Ortega-Regules, A.; López-Roca, J. M.; Fernández-Fernández, J. I.; Gómez-Plaza, E. Differences in anthocyanin extractability from grapes to wines according to variety. *Am. J. Enol. Vitic.* **2005**, *56*, 212−219.
(11) Rolle, L.; Torchio, F.; Ferrandino, A.; Guidoni, S. Influence of wine-grape skin hardness on the kinetics of anthocyanin extraction. *Int. J. Food Prop.* **2012**, *15*, 249−261.
(12) González-Neves, G.; Gil, G.; Barreiro, L. Influence of grape variety on the extraction of anthocyanins during the fermentation on skins. *Eur. Food Res. Technol.* **2008**, *226*, 1349−1355.
(13) Cheynier, V.; Dueñas-Paton, M.; Salas, E.; Maury, C.; Souquet, J.-M.; Sarni-Manchado, P.; Fulcrand, H. Structure and properties of wine pigments and tannins. *Am. J. Enol. Vitic.* **2006**, *57*, 298−305.
(14) Fulcrand, H.; Dueñas, M.; Salas, E.; Cheynier, V. Phenolic reactions during winemaking and aging. *Am. J. Enol. Vitic.* **2006**, *57*, 289−297.
(15) Busse-Valverde, N.; Gómez-Plaza, E.; López-Roca, J. M.; Gil-Muñoz, R.; Bautista-Ortín, A. B. The extraction of anthocyanins and proanthocyanidins from grapes to wine during fermentative maceration is affected by the enological technique. *J. Agric. Food Chem.* **2011**, *59*, 5450−5455.
(16) Borazan, A. A.; Bozan, B. The influence of pectolytic enzyme addition and prefermentative mash heating during the winemaking process on the phenolic composition of Okuzgozu red wine. *Food Chem.* **2013**, *138*, 389−395.
(17) Canals, R.; Llaudy, M. C.; Valls, J.; Canals, J. M.; Zamora, F. Influence of ethanol concentration on the extraction of color and phenolic compounds from the skin and seeds of Tempranillo grapes at different stages of ripening. *J. Agric. Food Chem.* **2005**, *53*, 4019−4025.
(18) Gil-Muñoz, R.; Moreno-Pérez, A.; Vila-López, R.; Fernández-Fernández, J. I.; Martínez-Cutillas, A.; Gómez-Plaza, E. Influence of low temperature prefermentative techniques on chromatic and phenolic characteristics of Syrah and Cabernet Sauvignon wines. *Eur. Food Res. Technol.* **2009**, *228*, 777−788.
(19) Koyama, K.; Goto-Yamamoto, N.; Hashizume, K. Influence of maceration temperature in red wine vinification on extraction of phenolics from berry skins and seeds of grape (*Vitis vinifera*). *Biosci. Biotechnol. Biochem.* **2007**, *71*, 958−965.
(20) Ortega-Heras, M.; Pérez-Magariño, S.; González-Sanjosé, M. L. Comparative study of the use of maceration enzymes and cold pre-fermentative maceration on phenolic and anthocyanic composition and colour of a Mencía red wine. *LWT - Food Sci. Technol.* **2012**, *48*, 1−8.
(21) Parenti, A.; Spugnoli, P.; Calamai, L.; Ferrari, S.; Gori, C. Effects of cold maceration on red wine quality from Tuscan Sangiovese grape. *Eur. Food Res. Technol.* **2004**, *218*, 360−366.
(22) Sacchi, K. L.; Bisson, L. F.; Adams, D. O. A review of the effect of winemaking techniques on phenolic extraction in red wines. *Am. J. Enol. Vitic.* **2005**, *56*, 197−206.
(23) Álvarez, I.; Aleixandre, J. L.; García, M. J.; Lizama, V. Impact of prefermentative maceration on the phenolic and volatile compounds in Monastrell red wines. *Anal. Chim. Acta* **2006**, *563*, 109−115.
(24) Coletta, A.; Trani, A.; Faccia, M.; Punzi, R.; Dipalmo, T.; Crupi, P.; Antonacci, D.; Gambacorta, G. Influence of viticultural practices and winemaking technologies on phenolic composition and sensory characteristics of Negroamaro red wines. *Int. J. Food Sci. Technol.* **2013**, *11*, 2215−2227.
(25) Heredia, F. J.; Escudero-Gilete, M. L.; Hernanz, D.; Gordillo, B.; Meléndez-Martínez, A. J.; Vicario, I. M.; González-Miret, M. L. Influence of the refrigeration technique on the colour and phenolic composition of Syrah red wines obtained by pre-fermentative cold maceration. *Food Chem.* **2010**, *118*, 377−383.
(26) Monrad, J. K.; Srinivas, K.; Howard, L. R.; King, J. W. Design and optimization of a semicontinuous hot−cold extraction of polyphenols from grape pomace. *J. Agric. Food Chem.* **2012**, *60*, 5571−5582.
(27) Carranza-Concha, J.; Camacho, M. M.; Martínez-Navarrete, N. Effects of blanching on grapes (*Vitis vinifera*) and changes during storage in syrup. *J. Food Process. Preserv.* **2012**, *36*, 11−20.
(28) Carranza-Concha, J.; Benlloch, M.; Camacho, M. M.; Martínez-Navarrete, N. Effects of drying and pretreatment on the nutritional and functional quality of raisins. *Food Bioprod. Process.* **2012**, *90*, 243−248.
(29) Dev, S. R. S.; Padmini, T.; Adedeji, A.; Gariépy, Y.; Raghavan, G. S. V. A comparative study on the effect of chemical, microwave, and pulsed electric pretreatments on convective drying and quality of raisins. *Dry. Technol.* **2008**, *26*, 1238−1243.
(30) Liazid, A.; Guerrero, R. F.; Cantos, E.; Palma, M.; Barroso, C. G. Microwave assisted extraction of anthocyanins from grape skins. *Food Chem.* **2011**, *124*, 1238−1243.
(31) Li, Y.; Han, L.; Ma, R.; Xu, X.; Zhao, C.; Wang, Z.; Chen, F.; Hu, X. Effect of energy density and citric acid concentration on anthocyanins yield and solution temperature of grape peel in microwave-assisted extraction process. *J. Food Eng.* **2012**, *109*, 274−280.
(32) Heddleson, R. A.; Doores, S. Factors affecting microwave-heating of foods and microwave-induced destruction of foodborne pathogens − A review. *J. Food Prot.* **1994**, *57*, 1025−1037.
(33) Lin, S.; Brewer, M. S. Effects of blanching method on the quality characteristics of frozen peas. *J. Food Qual.* **2005**, *28*, 350−360.
(34) Cendres, A.; Chemat, F.; Maingonnat, J.-F.; Renard, C. M. G. C. An innovative process for extraction of fruit juice using microwave heating. *LWT - Food Sci. Technol.* **2011**, *44*, 1035−1041.
(35) Al Bittar, S.; Périno-Issartier, S.; Dangles, O.; Chemat, F. An innovative grape juice enriched in polyphenols by microwave-assisted extraction. *Food Chem.* **2013**, *141*, 3268−3272.
(36) Ferrandino, A.; Guidoni, S. Anthocyanins, flavonols and hydroxycinnamates: An attempt to use them to discriminate *Vitis vinifera* L. cv 'Barbera' clones. *Eur. Food Res. Technol.* **2010**, *230*, 417−427.
(37) Letaief, H.; Rolle, L.; Zeppa, G.; Gerbi, V. Assessment of grape skin hardness by a puncture test. *J. Sci. Food Agric.* **2008**, *88*, 1567−1575.
(38) OIV. *Recueil international des méthodes d'analyse des vins et des moûts [International Compendium of methods for the analysis of wines and musts]*. Organisation Internationale de la Vigne et du Vin: Paris, France, 2008.
(39) Di Stefano, R.; Cravero, M. C. Metodi per lo studio dei polifenoli dell'uva [Methods for the study of grape polyphenols]. *Riv. Vitic. Enol.* **1991**, *44*, 37−45.
(40) Río Segade, S.; Giacosa, S.; Gerbi, V.; Rolle, L. Berry skin thickness as main texture parameter to predict anthocyanin extractability in winegrapes. *LWT-Food Sci. Technol.* **2011**, *44*, 392−398.
(41) Torchio, F.; Cagnasso, E.; Gerbi, V.; Rolle, L. Mechanical properties, phenolic composition and extractability indices of Barbera grapes of different soluble solids contents from several growing areas. *Anal. Chim. Acta* **2010**, *660*, 183−189.

(42) Rolle, L.; Torchio, F.; Giacosa, S.; Río Segade, S.; Cagnasso, E.; Gerbi, V. Assessment of physicochemical differences in Nebbiolo grape berries from different production areas and sorted by flotation. *Am. J. Enol. Vitic.* **2012**, *63*, 195−204.
(43) Gordillo, B.; López-Infante, M. I.; Ramírez-Pérez, P.; González-Miret, M. L.; Heredia, F. J. Influence of prefermentative cold maceration on the color and anthocyanic copigmentation of organic Tempranillo wines elaborated in a warm climate. *J. Agric. Food Chem.* **2010**, *58*, 6797−6803.
(44) González-Neves, G.; Gil, G.; Favre, G.; Ferrer, M. Influence of grape composition and winemaking on the anthocyanin composition of red wines of Tannat. *Int. J. Food Sci. Technol.* **2012**, *47*, 900−909.
(45) Gao, L.; Girard, B.; Mazza, G.; Reynolds, A. G. Changes in anthocyanins and color characteristics of Pinot Noir wines during different vinification processes. *J. Agric. Food Chem.* **1997**, *45*, 2003−2008.
(46) El Darra, N.; Grimi, N.; Maroun, R. G.; Louka, N.; Vorobiev, E. Pulsed electric field, ultrasound, and thermal pretreatments for better phenolic extraction during red fermentation. *Eur. Food Res. Technol.* **2013**, *236*, 47−56.
(47) Netzel, M.; Strass, G.; Bitsch, I.; Könitz, R.; Christmann, M.; Bitsch, R. Effect of grape processing on selected antioxidant phenolics in red wine. *J. Food Eng.* **2003**, *56*, 223−228.
(48) Patras, A.; Brunton, N. P.; O'Donnell, C.; Tiwari, B. K. Effect of thermal processing on anthocyanin stability in foods; mechanisms and kinetics of degradation. *Trends Food Sci. Technol.* **2010**, *21*, 3−11.
(49) Zhao, M.; Li, Y.; Xu, X.; Wu, J.; Liao, X.; Chen, F. Degradation kinetics of malvidin-3-glucoside and malvidin-3,5-diglucoside exposed to microwave treatment. *J. Agric. Food Chem.* **2013**, *61*, 373−378.
(50) Santini, D.; Rolle, L.; Cascio, P.; Mannini, F. Modifications in chemical, physical and mechanical properties of Nebbiolo (*Vitis vinifera* L.) grape berries induced by mixed virus infection. *S. Afr. J. Enol. Vitic.* **2011**, *32*, 183−189.
(51) Cheynier, V.; Souquet, J. M.; Kontek, A.; Moutounet, M. Anthocyanin degradation in oxidising grape musts. *J. Sci. Food Agric.* **1994**, *66*, 283−288.
(52) Song, B. J.; Sapper, T. N.; Burtch, C. E.; Brimmer, K.; Goldschmidt, M.; Ferruzzi, M. G. Photo- and thermodegradation of anthocyanins from grape and purple sweet potato in model beverage systems. *J. Agric. Food Chem.* **2013**, *61*, 1364−1372.
(53) Cagnasso, E.; Rolle, L.; Caudana, A.; Gerbi, V. Relationship between grape phenolic maturity and red wine phenolic composition. *Ital. J. Food Sci.* **2008**, *20*, 365−380.
(54) Soto Vázquez, E.; Río Segade, S.; Orriols Fernández, I. Effect of the winemaking technique on phenolic composition and chromatic characteristics in young red wines. *Eur. Food Res. Technol.* **2010**, *231*, 789−802.

JOURNAL OF AGRICULTURAL AND FOOD CHEMISTRY

Article

pubs.acs.org/JAFC

# Isoflavones of the Soybean Components and the Effect of Germination Time in the Cotyledons and Embryonic Axis

Alécio Quinhone Júnior[†] and Elza Iouko Ida*[,†]

[†]Departamento de Ciência e Tecnologia de Alimentos, Programa de Pós Graduação em Ciência de Alimentos, Universidade Estadual de Londrina, Londrina, Paraná 86057-970, Brazil

**ABSTRACT:** The aim of this study was to evaluate the content of different forms of isoflavones of BRS 284 soybean components and the effect of germination time in the cotyledons, radicle, and hypocotyl. Seeds were germinated until 168 h at 35 °C and collected each 24 h. The isoflavone content was determined by ultraperformance liquid chromatography, and the data were subjected to regression analysis. In cotyledons, germination time had a quadratic effect on daidzin and genistin contents and a linear effect on malonyldaidzin and malonylgenistin contents. In radicles, germination time had a quadratic effect on daidzin, glycitin, malonylgenistin, and malonylglycitin contents in addition to a linear effect on malonyldaidzin content. In hypocotyls, germination time showed a cubic effect on daidzin and genistin contents, a quadratic effect on malonyldaidzin, malonylgenistin, and malonylglycitin contents, and a linear effect on genistein content; glycitin, daidzein and glycitein were detected in a few germination times.

**KEYWORDS:** *soybean sprouts, hypocotyl, aglycone, radicle, seedling*

## INTRODUCTION

Soybean (*Glycine max* (L.) Merrill) and its derivatives have received more attention in recent years due to their potential beneficial effects on human health, such as protective effects against bone loss in postmenopausal women,[1] prevention of cardiovascular diseases,[2] relief of menopausal symptoms,[3] and protective effects against breast cancer[4] and prostate cancer.[5]

The main soy isoflavones are divided into aglycones (daidzein, genistein, and glycitein), $\beta$-glucosides (daidzin, genistin, and glycitin), malonylglucosides (6″-*O*-malonyldaidzin, 6″-*O*-malonylgenistin, and 6″-*O*-malonylglycitin), and acetylglucosides (6″-*O*-acetyldaidzin, 6″-*O*-acetylgenistin, and 6″-*O*-acetylglycitin).[6] During seed development of soybean, aglycones are synthesized by the phenylpropanoid metabolic pathway and stored in vacuoles as $\beta$-glucosides and malonylglucosides.[7,8] However, aglycones and acetylglucosides are absent or in low concentrations.[9,10]

Isoflavone contents in soybean seeds display a broad range of variation because their synthesis and accumulation are affected by multiple environmental and genetic factors.[11,12] Isoflavones may vary between soybean components. Total isoflavone content in the embryonic axis can be 5.0−25.0-fold higher than that in the cotyledons, whereas the seed coat is substantially free of isoflavones.[8,13,14]

During the course of soybean domestication, China gradually transformed soybean seeds in various forms of foods that are versatile, tasty, and digestible, such as tofu, sauce, paste, extract, and soybean sprouts.[15] Soybean sprouts, which are produced after 6−7 days of germination, are an important vegetable source, are rich in nutrients, are available all year, and have been consumed for thousands of years in countries, such as Korea, China, and Japan.[16] However, interest in healthy and functional foods has increased the demand for soybean sprouts in the West.[17]

Soybean germination can be used as a processing method to improve the sensorial quality[6] and nutritional value[10,18] of soybean seeds because it reduces the amount of undesirable substances, such as phytic acid,[19,20] oligosaccharides,[17,21] and trypsin inhibitors, in addition to lipoxygenase activity.[10] Germination can also promote a significant increase of vitamins,[22] phytosterols, tocopherols,[23] isoflavones,[24,25] and isoflavone aglycones.[10,14,17,23] In addition, the germination process is simple and inexpensive, and soybean sprouts have been investigated for several decades due to the high content and quality of protein and essential amino acids.[6]

The germination time may exert distinct effects depending on the soybean sprout components or isoflavone forms. In soybean cotyledons germinated for 72 h, the content of $\beta$-glucosides does not vary significantly, but the malonylglucoside content increases throughout the germination time. In radicles, however, a decrease in malonylglucoside and $\beta$-glucosides content occurs.[13] In contrast, in cotyledons and hypocotyls germinated for 120 h, a decrease in malonylglucoside and $\beta$-glucoside contents in addition to an increase in aglycone content have been reported.[14] However, the biotransformation of the various forms of isoflavones in soy components as a function of germination time has not been fully explored, and a few existing studies did not follow the entire process of germination considering the different forms of isoflavones in the various components of the germinated soybeans.

The objective of this study was to evaluate the content of different forms of isoflavones of BRS 284 soybean components and the effect of germination time up to 168 h on the content of these isoflavones in cotyledons and the embryonic axis.

**Received:** March 7, 2014
**Revised:** July 28, 2014
**Accepted:** July 29, 2014
**Published:** July 29, 2014

ACS Publications © 2014 American Chemical Society



dx.doi.org/10.1021/jf502927m | *J. Agric. Food Chem.* 2014, 62, 8452−8459

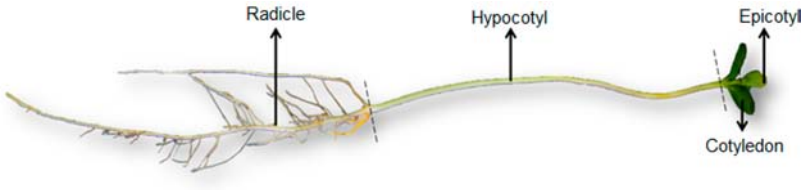


**Figure 1.** Components of soybean seeds germinated by 168 h.

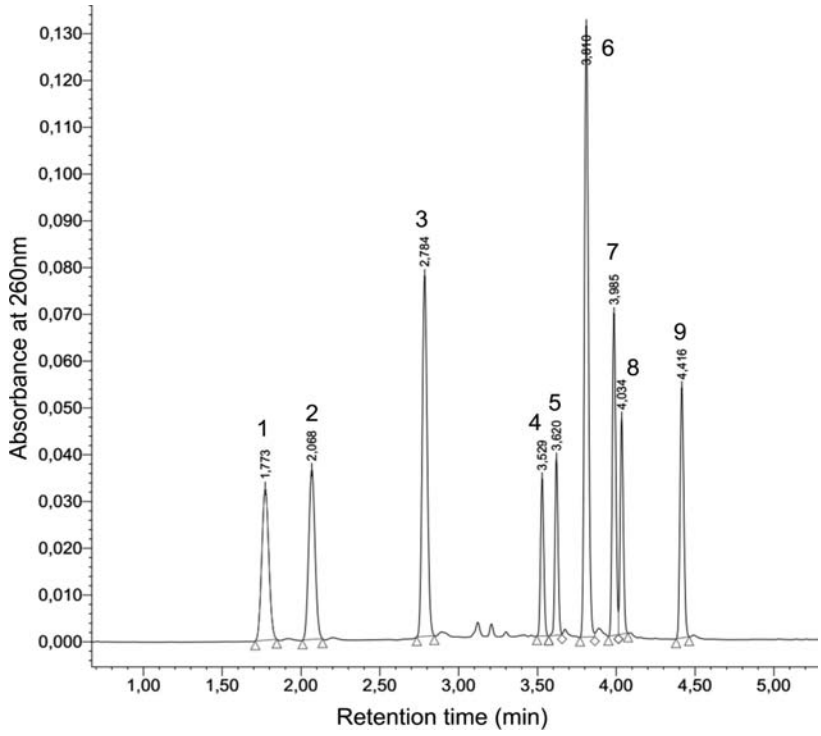


**Figure 2.** Typical UPLC chromatogram of isoflavones in a standard solution.

## MATERIALS AND METHODS

**Materials and Reagents.** Soybean seeds of the BRS 284 cultivar, a conventional cultivar, grown during the 2011/2012 season were provided by a specialist company in the region and were used for this study. According to the Empresa Brasileira de Pesquisa Agropecuária,[26] this cultivar is used for industrial processing, and it has an average size of 14.6 g per 100 seeds and contains 38.7% protein and 20.4% lipids; because of these characteristics, BRS 284 was used for this study. All reagents used were of analytical grade and from different sources. Acetylglucosides and malonylglucosides were obtained from Wako Pure Chemical Industries, Ltd. (Osaka, Japan), and the $\beta$-glucosides and aglycones were obtained from Sigma–Aldrich Co. (St. Louis, MO, USA) and were used as isoflavone standards. All standard solutions were filtered through a 0.22 $\mu$m syringe filter (Millex-GV, Millipore, Billerica, MA, USA) prior to injection into the ultraperformance liquid chromatography (UPLC) instrument.

**Experimental Design of the Germination Process.** Soybean seeds were previously selected to eliminate damaged seeds, stained seeds, or any foreign material. Fifty soybean seeds were placed on two pieces of germination paper (37.5 cm × 28.2 cm; Germitest) previously wetted with distilled water and supported by a perforated plate. The seeds were then covered with another piece of paper of which the bottom edge was folded, and the papers were curled longitudinally to form rolls.

To evaluate the effect of soybean germination time on the different forms of isoflavones in cotyledons and the embryonic axis, a randomized complete block design with three replications was used. For each block and germination time, 15 paper rolls were used. Germination was performed in a germination chamber (model Mangelsdorf, J. Prolab - São José dos Pinhais, PR, BR) with natural light at 35 °C (±1 °C) and relative humidity of 100% for 24, 48, 72, 96, 120, 144, and 168 h, as described by Yoshiara et al.[27] The effect of germination time on the isoflavone content in radicles and hypocotyls was considered only after 48 h of germination when it was possible to observe these components and separate them manually. Germinated seeds were collected at each germination time, and the cotyledons, hypocotyls, and radicles (Figure 1) were separated manually and in sufficient quantity for analysis. Epicotyls and seed coats of germinated seeds were discarded. Thereafter, the components were identified, freeze-dried, ground (model A-11, Ika), placed in polyethylene bags, and stored at −22 °C for analysis. The components of ungerminated seeds were used for comparison.

**Analytical Procedures.** Moisture content of the lyophilized samples was determined in a drying oven at 105 °C. The percentage of each structural part of the soybean seed was determined in triplicate using 100 g of seeds. Cotyledons, the embryonic axis, and seed coats were manually separated and weighed. The content of the different forms of isoflavones was also analyzed in these components.

Prior to quantification of isoflavones, the lyophilized and milled samples were defatted with hexane at 1:10 (w/v) for 1 h at room temperature by continuous and rotary agitation followed by vacuum filtration. The isoflavone extraction was performed in triplicate with 0.1 g of defatted sample with 2 mL of extraction solution containing ultrapure water, acetone, and ethanol (1:1:1, v/v/v) as described by Yoshiara et al.[28] The quantification of all isoflavones forms was performed simultaneously, in triplicate, using a UPLC system as described by Handa et al.[29] The different forms of isoflavones and the sum of all forms of isoflavones were expressed as micromoles of the form

Table 1. Isoflavone Content ($\mu$mol g$^{-1}$) in Seeds, Cotyledons, and the Embryonic Axis of BRS 284 Soybeans[a]

| isoflavone | seed | cotyledon | embryonic axis |
|---|---|---|---|
| glucoside | 2.273 ± 0.249a | 2.056 ± 0.067a | 15.819 ± 1.284b |
| daidzin | 0.618 ± 0.030a | 0.464 ± 0.019a | 5.059 ± 0.340b |
| genistin | 1.376 ± 0.192a | 1.592 ± 0.048a | 2.459 ± 0.288b |
| glycitin | 0.279 ± 0.031a | nd | 8.301 ± 0.656b |
| malonylglucoside | 6.381 ± 0.315a | 5.401 ± 0.185a | 37.701 ± 2.550b |
| malonyldaidzin | 1.530 ± 0.124a | 1.134 ± 0.034a | 12.715 ± 0.961b |
| malnoylgenistin | 4.132 ± 0.088a | 4.267 ± 0.152a | 6.405 ± 0.372b |
| malonylglycitin | 0.718 ± 0.109a | nd | 18.581 ± 1.217b |
| aglycone | 0.104 ± 0.004a | 0.109 ± 0.002a | 0.324 ± 0.029b |
| daidzein | nd | nd | 0.223 ± 0.022 |
| genistein | 0.104 ± 0.004a | 0.109 ± 0.002a | 0.101 ± 0.008a |
| glycitein | nd | nd | nd |
| total isoflavone | 8.757 ± 0.566a | 7.565 ± 0.254a | 53.844 ± 3.863b |

[a]Mean ± standard deviation; nd: not detected; value with different letter in the same row is significantly different at 5% level according to Tukey's test.

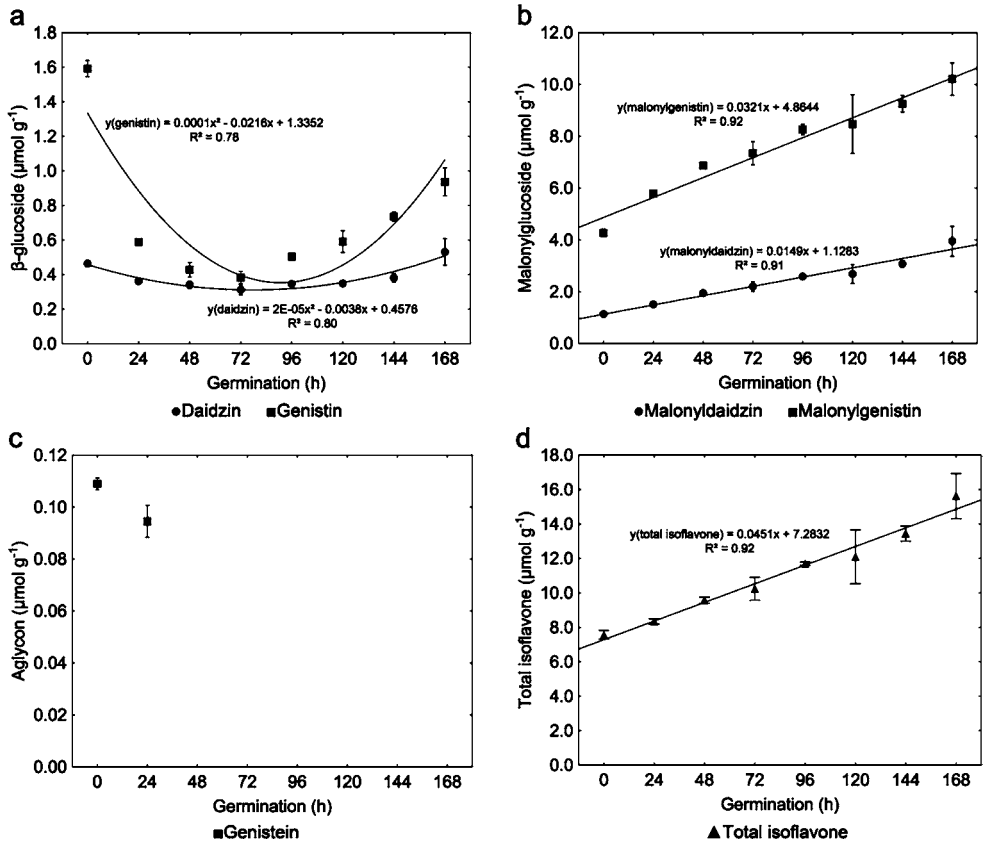


Figure 3. (a) $\beta$-glucoside, (b) malonylglucoside, (c) aglycone, and (d) total isoflavone contents in cotyledons of germinated BRS 284 soybeans.

of isoflavone per gram of sample on a dry and defatted basis. A typical UPLC chromatogram of isoflavones in the standard is show in Figure 2.

**Experimental Design and Statistical Analysis.** The results of the content of different forms of isoflavones in soybean seeds and their components were subjected to analysis of variance (ANOVA), and the means were compared by Tukey's test ($p < 0.05$). Regression analyses between germination time and content of different forms of isoflavones were also performed using all the experimental data with Statistica 10.0 software (StatSoft Inc., Tulsa, OK, USA).

## RESULTS AND DISCUSSION

**Content of Different Forms of Isoflavones in Soybean Seed Components.** The BRS 284 soybean seeds were composed of 89.9% cotyledons, 2.4% embryonic axis, and 7.7% seed coat. These results were similar to those reported by Yuan et al.[14] However, Ribeiro et al.[13] reported that BRS 213 soybeans have 86.8% cotyledons, 3.2% embryonic axis, and 10.0% seed coat. According to Phommalth et al.,[25] the proportion of soybean components depends on its size, so smaller seed sizes result in a greater percentage being the embryonic axis.

BRS 284 soybeans (Table 1) had 8.757 ± 0.566 $\mu$mol of total isoflavones per gram of soybean on a dry basis. The isoflavone content of soybean seeds can vary according to biotic and abiotic factors, such as cultivar, harvest year,[30,31] sowing date, growing location,[9] pathogen load in soybean growing season,[32] and elicitors.[33]

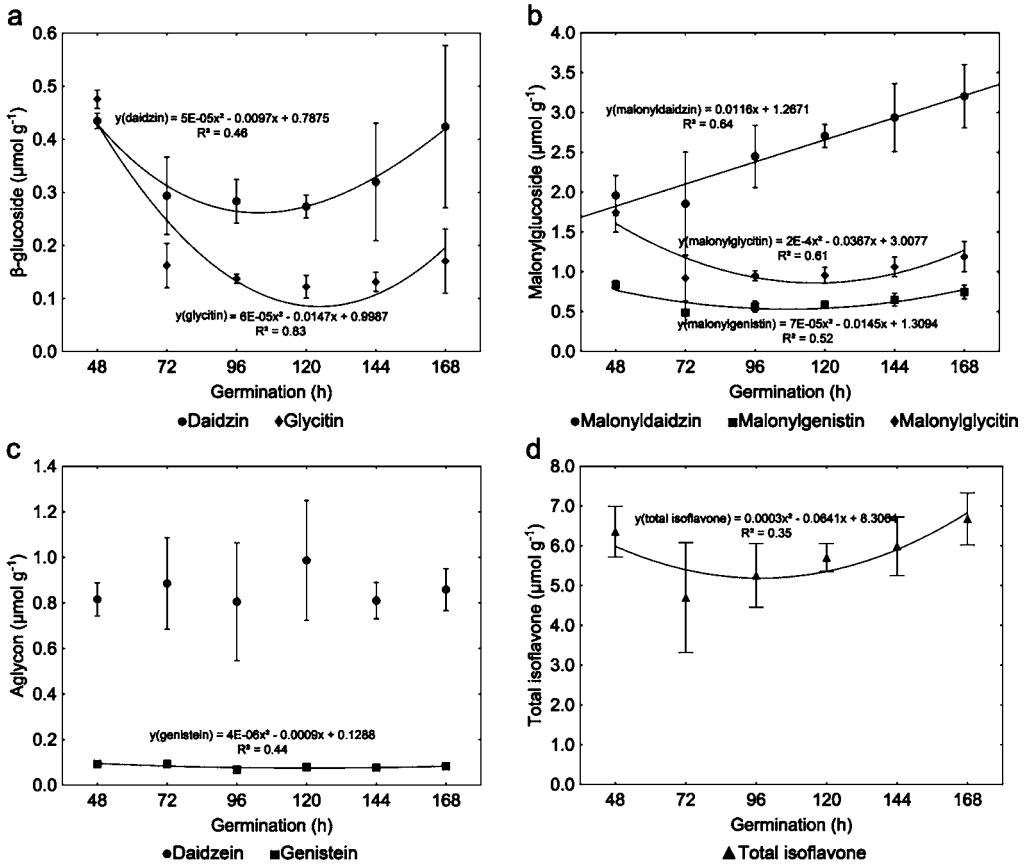


**Figure 4.** (a) $\beta$-glucoside, (b) malonylglucoside, (c) aglycone, and (d) total isoflavone contents in radicles of germinated BRS 284 soybeans.

The concentration of the various forms of isoflavones in BRS 284 soybean (Table 1) varied according to its components ($p < 0.05$). The total isoflavone content in the embryonic axis was 7.1-fold higher than that in cotyledons. These results were similar to those described by Yuan et al.[14] However, Silva et al.[34] reported that the total isoflavone content in the embryonic axis is 6.5–15.5-fold higher than in cotyledons. In addition, Berger et al.[31] observed that the total isoflavone content in cotyledons is dependent on environmental conditions and that the embryonic axis genotype has greater influence.

Isoflavone forms have not been found in seed coats of BRS 284 soybeans as observed.[8,34] Thus, considering the percentage of each component in the soybean, 84.2% and 15.8% of the total isoflavones are present in cotyledons and the embryonic axis, respectively. Similar results have been observed by Tsukamoto et al.[9] However, 51.8% and 48.2% of total isoflavone content is located in cotyledons and the embryonic axis, respectively, in BRS 213 soybeans.[13] These differences in the concentration and distribution of isoflavones among soybean components may be attributed to differences in cultivars, growing conditions,[30,31] seed size,[35] and other factors.

In BRS 284 soybeans, cotyledons and the embryonic axis showed similar proportions of $\beta$-glucosides, malonylglucosides, and aglycones isoflavones (Table 1). In relation to total isoflavones, the seeds, cotyledons, and embryonic axis showed 26.0%, 27.2%, and 29.4% $\beta$-glucosides, 72.9%, 71.4%, and 70.0% malonylglucosides, and 1.2%, 1.4%, and 0.6% aglycones, respectively. In soybean, the daidzein, genistein, and glycitein isoflavones are synthesized via the phenylpropanoid pathway and are stored in the vacuole as malonylglucosides and $\beta$-glucosides.[7,8]

**Effect of Soybean Germination Time on Different Forms of Isoflavones in Cotyledons.** Regression analysis of the effect of germination time on daidzin ($R^2 = 0.80$, $p < 0.01$) and genistin ($R^2 = 0.78$, $p < 0.01$) contents in germinated soybean cotyledons indicated that the quadratic model showed a good fit to the experimental data (Figure 3a). However, glycitin was not detected in germinated cotyledons.

In cotyledons germinated up to 72 h, the daidzin and genistin contents decreased by 1.5- and 4.2-fold followed by an increase of 1.7- and 2.5-fold between 72 and 168 h, respectively. This initial decrease in daidzin and genistin contents may be associated with the translocation of these isoflavones from cotyledons to radicles.[7] The daidzin content in cotyledons germinated for 168 h was similar to ungerminated cotyledons, but the concentration of genistin was reduced by 1.7-fold (Figure 3a). In soybean cotyledons, the amount of $\beta$-glucosides decreases until 120 h of germination.[14] However, Ribeiro et al.[13] described that the germination time of 72 h of BRS 213 soybean cotyledons does not influence the profile of the genistin and daidzin isoflavones. The nondetection of glycitin in soybean cotyledons throughout the germination process has also been observed by Kudou et al.[8] in ungerminated soybean cotyledons and by Ribeiro et al.[13] in ungerminated soybean cotyledons and soybean cotyledons germinated for 72 h.

Regression analysis of the effect of germination time on malonyldaidzin ($R^2 = 0.91$, $p < 0.01$) and malonylgenistin ($R^2 = 0.92$, $p < 0.01$) contents in germinated soybean cotyledons indicated that the linear model showed a good fit to the experimental data (Figure 3b). However, malonylglycitin was not detected in germinated cotyledons. Between 0 and 168 h of germination, the malonyldaidzin and malonylgenistin contents


dx.doi.org/10.1021/jf502927m | J. Agric. Food Chem. 2014, 62, 8452–8459

increased by 3.5- and 2.4-fold, respectively. According to Ribeiro et al.,[13] the malonyldaidzin and malonylgenistin contents in BRS 213 soybean cotyledons germinated for 72 h are 3.3- and 2.6-fold higher than those in ungerminated cotyledons, respectively. It is noteworthy that the soybean cotyledons germinated for 168 h had 25.3% malonyldaidzin and 65.3% malonylgenistin in relation to the total isoflavone content. The malonylglycitin isoflavone was not detected in ungerminated soybean cotyledons and soybean cotyledons germinated up to 168 h. Similar results of malonyl isoflavones have been reported by Ribeiro et al.[13]

It was not possible to perform regression analysis on the aglycone content for germinated soybean cotyledons, since genistein was only detected in ungerminated cotyledons and cotyledons germinated for 24 h without differing in 0 and 24 h of germination ($p > 0.05$) presenting an average of 0.102 ± 0.010 $\mu$mol g$^{-1}$ of cotyledons (Figure 3c). Additionally, daidzein and glycitein were not detected in the cotyledons during the entire germination process. According to Ribeiro et al.,[13] genistein is the only isoflavone aglycone present in BRS 213 soybean cotyledons that are either ungerminated or germinated for 6 h. However, in cotyledons of 17 soybeans germinated for 120 h with and without light, three types of aglycones are detected with daidzein showing higher concentrations than genistein and glycitein.[24] According to Wang and Murphy,[30] these differences may be associated with the cultivar, crop year, and location of soybean cultivation.

Regression analysis of the effect of germination time on total isoflavone content ($R^2 = 0.92$, $p < 0.01$) in germinated soybean cotyledons indicated that the linear model showed a good fit to the experimental data (Figure 3b) with an increase of 1.4- and 2.1-fold in total isoflavone content after 72 and 168 h of germination, respectively. Similar results have been reported by Phommalth et al.,[25] who described that total isoflavone contents in cotyledons of Aga3 and Pungsannamulkong soybeans germinated for 168 h at 20 °C are 1.5- and 1.7-fold higher than in ungerminated cotyledons, respectively. However, Ribeiro et al.[13] observed an increase of 2.4-fold in total isoflavone content from BRS 213 soybean cotyledons germinated for 72 h. During germination, the increase in the concentration of total isoflavones can be attributed to activity and/or synthesis of novel enzymes[36] that are responsible for the isoflavone biosynthesis and metabolism as well as the degradation of proteins, lipids, or carbohydrates that can promote a reduction in seed dry matter[17,37] and contribute to an increase in the relative concentration of total isoflavones.

**Effect of Soybean Germination Time on Different Forms of Isoflavones in Radicles.** The effect of germination time on the isoflavone content in radicles was considered only after 48 h of germination when it was possible to observe the radicles and manually separate them from the other components of the embryonic axis.

Regression analysis of the effect of germination time on daidzin ($R^2 = 0.46$, $p = 0.01$) and glycitin ($R^2 = 0.83$, $p < 0.01$) contents in germinated soybean radicles indicated that the quadratic model fitted to the experimental data (Figure 4a). However, genistin was not detected in germinated radicles. The concentration of daidzin from germinated soybean radicles showed a decrease of 1.6-fold until 120 h with a new increase of 1.5-fold up to 168 h of germination, but the glycitin content showed a marked reduction of 2.9-fold between 48 and 72 h of germination and then remained constant averaging 0.145 ± 0.021 $\mu$mol g$^{-1}$ between 72 and 168 h. When compared to the embryonic axis of ungerminated seeds, it was observed that the daidzin and glycitin contents decreased by 17.2- and 51.2-fold after 72 h of germination, respectively. However, Ribeiro et al.[13] reported that the concentration of the daidzin and glycitin isoflavones in BRS 213 soybean radicles germinated for 72 h decrease by 6.7- and 10.9-fold, respectively. The decrease in daidzin and genistin in the early stages of germination may be associated with an intense metabolic activity of seeds and conversion of these isoflavones into aglycones and subsequent exudation by the root system.[7]

Genistin was not detected in radicles of germinated seeds, which has also been observed by Ribeiro et al.[13] in radicles of BRS 213 soybeans germinated up to 72 h. However, Kim et al.[38] reported that the genistin content ranges from 0.074 to 0.437 $\mu$mol g$^{-1}$ radicles in three soybean cultivars germinated for 168 h. However, the genistin content in radicles of 17 soybean cultivars germinated for 120 h in the presence of light ranges from 0.377 to 5.480 $\mu$mol g$^{-1}$ radicle.[24]

Regression analysis of the effect of germination time on malonyldaidzin ($R^2 = 0.64$, $p < 0.01$) content in germinated soybean radicles indicated that the linear model fit to the experimental data and that the quadratic model fit to the experimental data of malonylgenistin ($R^2 = 0.52$, $p < 0.01$) and malonylglycitin ($R^2 = 0.61$, $p < 0.01$) contents (Figure 4b). The malonyldaidzin content increased by 1.6-fold between 48 and 168 h of germination. However, the malonylgenistin and malonylglycitin contents decreased between 48 and 72 h with a less pronounced increase after 72 h of germination (Figure 4b). When compared to the embryonic axis of ungerminated seeds, the malonyldaidzin, malonylgenistin, and malonylglycitin contents in radicles germinated for 72 h decreased by 6.9-, 13.1-, and 20.2-fold, respectively. Ribeiro et al.[13] also observed a reduction in malonylglucoside content in BRS 213 soybean radicles germinated for 72 h with light. According to Graham,[7] the conjugates of daidzein and genistein in addition to several unidentified aromatic metabolites are selectively excreted into root and seed exudates, and the analysis of seed exudates suggests that this is a continuous but saturable event.

Regression analysis of the effect of germination time on daidzein content in soybean radicles germinated indicated that the linear, quadratic, or cubic models did not fit the experimental data ($p > 0.05$). However, the quadratic model showed a low fit to the experimental data for the genistein concentration ($R^2 = 0.44$, $p = 0.01$). These results indicated that there was little influence of germination time on the concentration of these two aglycones between 48 and 168 h. Thus, it was verified that the mean concentration of genistein and daidzein between 48 and 168 h of germination was 0.860 ± 0.069 and 0.082 ± 0.010 $\mu$mol g$^{-1}$ radicle, respectively. Glycitein was not detected in radicles throughout the entire germination time. However, radicles of 17 soybean varieties germinated for 120 h with and without light have 2.9% glycitein relative to total isoflavone content.[24] In relation to total isoflavone content, the percentage of aglycone in germinated soybean radicles was 14.1%. The highest percentage of isoflavone aglycones in radicles compared to cotyledons and hypocotyls can be attributed to the highest activity of the $\beta$-glucosidase enzyme in radicles[39] with subsequent hydrolysis and release of aglycones that participate in interactions between plants and symbiotic microorganisms as well as act as a defense agent against infection by pathogens.[40] The daidzein and genistein isoflavones are the major components in soybean root extracts responsible for inducing *nod* genes in *Bradyrhizobium japonicum*, which are responsible for the formation of nitrogen-fixing root nodules.[41]

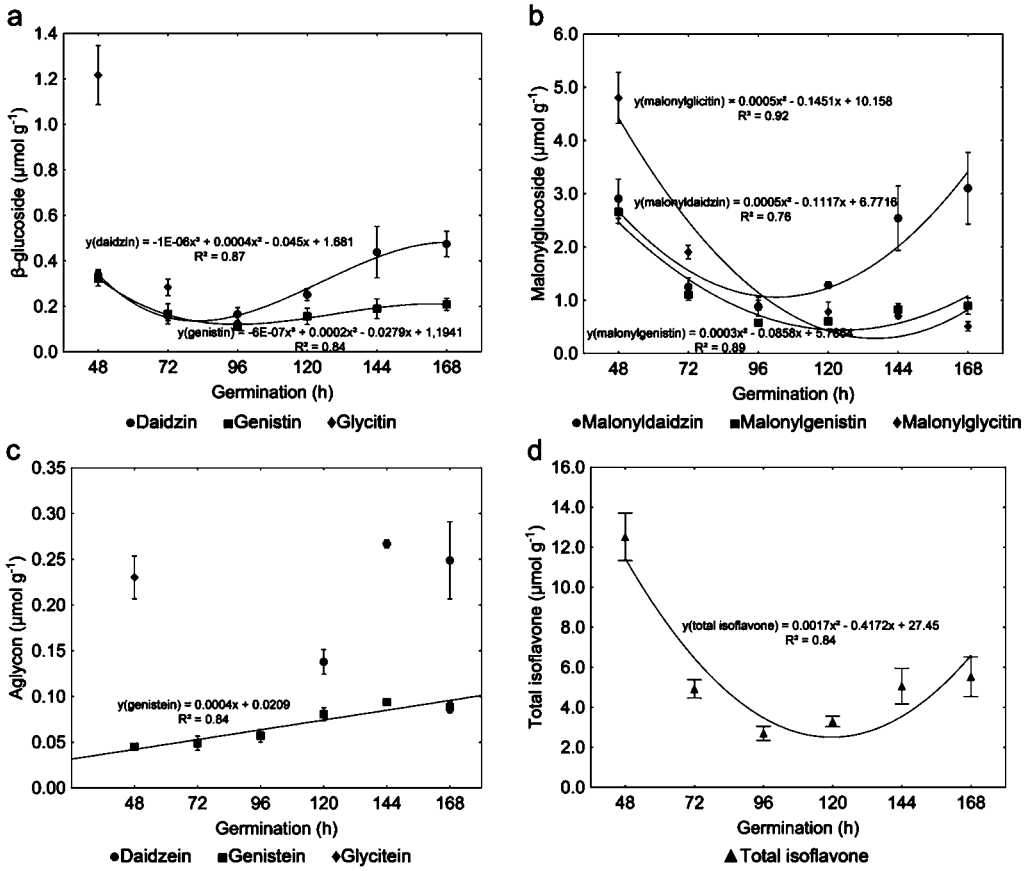


**Figure 5.** (a) $\beta$-glucoside, (b) malonylglucoside, (c) aglycone, and (d) total isoflavone contents in hypocotyls of germinated BRS 284 soybeans.

Regression analysis of the effect of germination time on total isoflavone content ($R^2 = 0.35$, $p = 0.04$) in germinated soybean radicles indicated that the quadratic model showed a low fit to the experimental data (Figure 4d), thereby indicating that the germination time between 48 and 168 h had a low effect on the total isoflavone content. Thus, in this interval of germination, the average total isoflavone content was 5.778 ± 0.125 $\mu$mol g$^{-1}$ radicle. The low change observed for isoflavone content in radicles may be due to high variability in the experimental data, which is intrinsic to the experiment because germination is a biological phenomenon in which several factors in addition to time can influence the isoflavone content.

In the embryonic axis of ungerminated soybean seeds, the total isoflavone content was 53.844 ± 3.863 $\mu$mol g$^{-1}$ sample. Thus, after 168 h of germination, the total isoflavone content decreased by 9.3-fold. A decrease of 6.3-fold was observed by Ribeiro et al.[13] in BRS 213 soybean radicles germinated for 72 h. This decline may be associated with exudation of isoflavones to the external environment or metabolism of isoflavones in other constituents.[7]

**Effect of Soybean Germination Time on Different Forms of Isoflavone in Hypocotyls.** The effect of germination time on the isoflavone content in hypocotyls was considered only after 48 h of germination when it was possible to observe the hypocotyls and to manually separate them from the other components of the embryonic axis.

Regression analysis of the effect of germination time on daidzin ($R^2 = 0.87$, $p < 0.01$) and genistin ($R^2 = 0.84$, $p < 0.01$) contents in germinated soybean hypocotyls indicated that the cubic model fit to the experimental data (Figure 5a). Thus, the daidzin and genistin contents in soybean hypocotyls decreased by 2.1- and 2.9-fold between 72 and 96 h of germination, respectively, followed by an increase of 2.8- and 1.7-fold, respectively, up to 144 h with a little tendency to change between 144 and 168 h. The glycitin isoflavone was detected at 48 h with a reduction of 4.3-fold at 72 h. After this germination time, glycitin was not detected, thus excluding regression analysis for glycitin. However, the glycitin content ranges from 0.100 to 0.776 $\mu$mol g$^{-1}$ hypocotyl in 17 soybean cultivars germinated for 120 h with light.[24] When compared to the embryonic axis of ungerminated seeds, the daidzin, genistin, and glycitin contents decreased by 15.0-, 7.6-, and 6.8-fold, respectively, after 48 h of germination. Graham[7] reported a higher concentration of daidzein and genistein conjugates in hypocotyl hooks and reported that the contents of these isoflavones undergo a programmed and dramatic decrease between 48 and 96 h of germination. Additionally, Graham found an inverse correlation between the concentration of isoflavone conjugates and expansion of the hypocotyl hook.

Regression analysis of the effect of germination time on malonyldaidzin ($R^2 = 0.76$, $p < 0.01$), malonylgenistin ($R^2 = 0.89$, $p < 0.01$), and malonylglycitin ($R^2 = 0.92$, $p < 0.01$) contents in germinated soybean hypocotyls indicated that the quadratic model showed a good fit to the experimental data (Figure 5b). The malonyldaidzin content decreased by 3.3-fold up to 96 h of germination and returned to the initial concentration after 168 h of germination. However, the malonylgenistin and malonylglycitin contents decreased by 4.6- and 5.3-fold, respectively, up to 96 h of germination with little change between 96 and 168 h. When compared to the embryonic axis of ungerminated seeds, the malonyldaidzin content decreased by 22.0- and 4.1-fold at 96 and 168 h, respectively, and the malonylgenistin and malonylglycitin contents were decreased by 7.2- and 36.7-fold


dx.doi.org/10.1021/jf502927m | J. Agric. Food Chem. 2014, 62, 8452−8459

after 168 h of germination. These results showed similar tendencies to those observed by Yuan et al.,[14] who found a reduction of 9.0-, 25.6-, and 125.0-fold for the malonyldaidzin, malonylgenistin, and malonylglycitin contents in soybean hypocotyls germinated for 120 h in the presence of light.

Regression analysis of the effect of germination time on genistein ($R^2$ = 0.84, $p < 0.01$) content in germinated soybean hypocotyls indicated that the linear model showed a good fit to the experimental data (Figure 5c). The genistein content increased by 2.0-fold between 48 and 168 h of germination. Similar trends were observed by Yuan et al.,[14] who reported an increase of 9.7-fold for the genistein content in soybean hypocotyls germinated for 72 h followed by a decrease of 1.4-fold between 72 and 120 h of germination. In hypocotyls, daidzein was detected only after 120 h, and glycitein was detected only after 48 h of germination. Therefore, no regression analysis was performed for these components. In hypocotyls, the daidzein content doubled between 120 and 144 h and remained constant up to 168 h with an average of 0.258 ± 0.013 $\mu$mol g$^{-1}$ hypocotyl. In hypocotyls of 17 soybean cultivars germinated for 120 h, the daidzein content ranges between 0.231 and 1.019 $\mu$mol g$^{-1}$ hypocotyl.[24] The daidzein content in soybean hypocotyls germinated for 120 h increases by 5.1-fold compared to nongerminated hypocotyls.[14] The glycitein content after 48 h of germination was 0.230 ± 0.023 $\mu$mol g$^{-1}$ hypocotyl. However, in hypocotyls of 17 soybean cultivars germinated for 120 h with and without light, the glycitein concentrations range from 0.067 to 0.814 $\mu$mol g$^{-1}$.[24]

Regression analysis of the effect of germination time on total isoflavone content ($R^2$ = 0.84, $p < 0.01$) in germinated soybean hypocotyls indicated that the quadratic model showed a low fit to the experimental data (Figure 5d). The total isoflavone content decreased by 4.6-fold between 48 and 96 h of germination followed by a 2.0-fold increase between 96 and 168 h. Comparing the embryonic axis of ungerminated soybeans with soybean hypocotyls germinated for 168 h, the total isoflavone content decreased by 9.8-fold (Table 1). Similar results have been observed in the Aga3 and Pungsannamulkong cultivars germinated for 168 h.[25]

In conclusion, soybean BRS 284 showed 89.9% cotyledons, 2.4% embryonic axis, and 7.7% seed coat, and 84.2% and 15.8% of total isoflavones are present in cotyledons and the embryonic axis, respectively; however, the total isoflavone content in the embryonic axis was 7.1-fold higher than that in cotyledons. The germination time exerted different effects depending on the components of germinated soybeans and the different forms of isoflavones. In cotyledons germinated up to 168 h, the total isoflavone content increased 2.1-fold in relation to ungerminated cotyledons, and aglycones were not detected. In radicles, germination time exerted low influence on the daidzein and genistein content, while the malonyldaidzin increased 1.6-fold between 48 and 168 h, and in hypocotyl, the genistein content increased by 2.0-fold between 48 and 168 h of germination. Therefore, in this study, it was concluded that, in the germination process by 168 h, the total isoflavones showed higher concentration in the cotyledons and aglycones were detected only in the hypocotyl and radicle.

In the present study, the effects of germination time were modeled, and it was possible to monitor the whole process of germination in relation to the content of different forms of isoflavones and different components of soybeans germinated. Our results imply that, to obtain soybean sprouts for human consumption with higher levels of total isoflavones, it is necessary to carry germination until 168 h and not eliminate the cotyledons. In addition, if the main purpose is the intake of aglycones isoflavones, the consumption of radicle and hypocotyls may be sufficient as cotyledons germinated for 168 h does not contain these forms of isoflavones.

## AUTHOR INFORMATION


### Corresponding Author

*Phone: +55 43 3371 5971; fax: +55 43 3371 4080; e-mail: elida@uel.br.



### Funding

This work was partially funded by Fundação Araucária de Desenvolvimento Científico e Tecnológico do Paraná/Conselho Nacional de Desenvolvimento Científico e Tecnológico-CNPq (PRONEX Program). A.Q.Jr. would like to thank CNPq for a graduate scholarship, and E.I.I. is a CNPq Research Fellow.


### Notes

The authors declare no competing financial interest.

## REFERENCES


(1) Atteritano, M.; Mazzaferro, S.; Frisina, A.; Cannata, M. L.; Bitto, A.; D'anna, R.; Squadrito, F.; Macrì, I.; Frisina, N.; Buemi, M. Genistein effects on quantitative ultrasound parameters and bone mineral density in osteopenic postmenopausal women. *Osteoporosis Int.* **2009**, *20* (11), 1947−1954.

(2) Chan, Y.-H.; Lau, K.-K.; Yiu, K.-H.; Li, S.-W.; Chan, H.-T.; Tam, S.; Shu, X.-O.; Lau, C.-P.; Tse, H.-F. Isoflavone intake in persons at high risk of cardiovascular events: Implications for vascular endothelial function and the carotid atherosclerotic burden. *Am. J. Clin. Nutr.* **2007**, *86*, 938−945.

(3) Williamson-Hughes, P. S.; Flickinger, B. D.; Messina, M. J.; Empie, M. W. Isoflavone supplements containing predominantly genistein reduce hot flash symptoms: A critical review of published studies. *Menopause* **2006**, *13*, 831−839.

(4) Wada, K.; Nakamura, K.; Tamai, Y.; Tsuji, M.; Kawachi, T.; Hori, A.; Takeyama, N.; Tanabashi, S.; Matsushita, S.; Tokimitsu, N.; Nagata, C. Soy isoflavone intake and breast cancer risk in Japan: From the Takayama study. *Int. J. Cancer.* **2013**, *133*, 952−960.

(5) Dong, X.; Xu, W.; Sikes, R. A.; Wu, C. Combination of low dose of genistein and daidzein has synergistic preventive effects on isogenic human prostate cancer cells when compared with individual soy isoflavone. *Food Chem.* **2013**, *141*, 1923−1933.

(6) Liu, K. *Soybeans as Functional Foods and Ingredients*; AOCS Press: Champaign, IL, 2004; p 331.

(7) Graham, T. L. Flavonoid and isoflavonoid distribution in developing soybean seedling tissues and in seed and root exudates. *Plant Physiol.* **1991**, *95*, 594−560.

(8) Kudou, S.; Fleury, Y.; Welti, D.; Magnolato, D.; Uchida, T.; Kitamura, K.; Okubo, K. Malonyl isoflavone glycosides in soybean seeds (*Glycine max* Merrill). *Agric. Biol. Chem.* **1991**, *55*, 2227−2233.

(9) Tsukamoto, C.; Shimada, S.; Igita, K.; Kudou, S.; Kokubun, M.; Okubo, K.; Kitamura, K. Factors affecting isoflavone content in soybean seeds: Changes in isoflavones, saponins, and composition of fatty acids at different temperatures during seed development. *J. Agric. Food Chem.* **1995**, *43*, 1184−1192.

(10) Paucar-Menacho, L. M.; Berhow, M. A.; Mandarino, J. M. G.; Chang, Y. K.; Mejia, E. G. D. Effect of time and temperature on bioactive compounds in germinated Brazilian soybean cultivar BRS 258. *Food Res. Int.* **2010**, *43*, 1856−1865.

(11) Hoeck, J. A.; Fehr, W. R.; Murphy, P. A.; Welke, G. A. Influence of genotype and environment on isoflavone contents of soybean. *Crop Sci.* **2000**, *40* (1), 48−51.

(12) Mebrahtu, T.; Mohamed, A.; Wang, C. Y.; Andebrhan, T. Analysis of isoflavone contents in vegetable soybeans. *Plant Foods Hum. Nutr.* **2004**, *59*, 55−61.

(13) Ribeiro, M. L. L.; Mandarino, J. M. G.; Carrão-Panizzi, M. C.; Oliveira, M. C. N.; Campo, C. B. H.; Nepomuceno, A. L.; Ida, E. I. *β*-Glucosidase activity and isoflavone content in germinated soy bean radicles and cotyledons. *J. Food Biochem.* **2006**, *30*, 453−465.
(14) Yuan, J.-P.; Liu, Y.-B.; Peng, J.; Wang, J.-H.; Liu, X. Changes of isoflavone profile in the hypocotyls and cotyledons of soybeans during dry heating and germination. *J. Agric. Food Chem.* **2009**, *57*, 9002−9010.
(15) Liu, K. Food use of whole soybeans. In *Soybeans Chemistry, Production, Processing, and Utilization*; Lawrence, A. J., White, P. J., Galloway, R., Eds.; AOCS Press: Urbana, IL, 2008; pp 441−482.
(16) Lee, J. D.; Hwang, Y. H.; Cho, H. Y.; Kim, D. U.; Chung, M. G. Comparison of characteristics related with soybean sprouts between Glycine max and G. soja. *Korean J. Crop Sci.* **2002**, *47*, 189−198.
(17) Kim, W.-J.; Lee, H.-Y.; Won, M. H.; Yoo, S.-H. Germination effect of soybean on its contents of isoflavones and oligosaccharides. *Food Sci. Biotechnol.* **2005**, *14*, 498−502.
(18) Kim, S.-L.; Lee, J.-E.; Kwon, Y.-U.; Kim, W.-H.; Jung, G.-H.; Kim, D.-W.; Lee, C.-K.; Lee, Y.-Y.; Kim, M.-J.; Kim, Y.-H.; Hwang, T.-Y.; Chung, I.-M. Introduction and nutritional evaluation of germinated soy germ. *Food Chem.* **2013**, *136*, 491−500.
(19) Ribeiro, M. L. L.; Ida, E. I.; Oliveira, M. C. N. Efeito da germinação de soja cv. BR-13 e Paraná sobre ácido fítico, fósforo total e inibidores de tripsina. *Pesqui. Agropecu. Bras.* **1999**, *34*, 31−36.
(20) Ramadan, E. A. Effect of processing and cooking methods on the chemical composition, sugars and phytic acid of soybeans. *Food Public Health* **2012**, *2*, 11−15.
(21) Martín-Cabrejas, M. A.; Díaz, M. F.; Aguilera, Y.; Benítez, V.; Mollá, E.; Esteban, R. M. Influence of germination on the soluble carbohydrates and dietary fibre fractions in non-conventional legumes. *Food Chem.* **2008**, *107*, 1045−1052.
(22) Ahmad, S.; Pathak, D. K. Nutritional changes in soybean during germination. *J. Food Sci. Technol.* **2000**, *37*, 665−666.
(23) Shi, H.; Nam, P.; Ma, A. Comprehensive profiling of isoflavones, phytosterols, tocopherols, minerals, crude protein, lipid, and sugar during soybean (*Glycine max*) germination. *J. Agric. Food Chem.* **2010**, *58*, 4970−4976.
(24) Lee, S. J.; Ahn, J. K.; Khanh, T. D.; Chun, S. C.; Kim, S. L.; Ro, H. M.; Song, H. K.; Chung, I. M. Comparison of isoflavone concentrations in soybean (*Glycine max* (L.) Merrill) sprouts grown under two different light conditions. *J. Agric. Food Chem.* **2007**, *55*, 9415−9421.
(25) Phommalth, S.; Jeong, Y.-S.; Kim, Y.-H.; Hwang, Y.-H. Isoflavone composition within each structural part of soybean seeds and sprouts. *J. Crop Sci. Biotechnol.* **2008**, *11*, 57−62.
(26) Embrapa. *Cultivares de Soja: Regiões sul e Central do Brasil 2010/2011*, 1ª ed.; Embrapa Soja: Londrina, Puerto Rico, 2010; p 62.
(27) Yoshiara, L. Y.; Madeira, T. B.; Ribeiro, M. L. L.; Mandarino, J. M. G.; Carrão-Panizzi, M. C.; Ida, E. I. *β*-Glucosidase activity of soybean (Glycine max) embryonic axis germinated in the presence or absence of light. *J. Food Biochem.* **2012**, *36*, 699−705.
(28) Yoshiara, L. Y.; Madeira, T. B.; Delaroza, F.; Silva, J. B.; Ida, E. I. Optimization of soy isoflavone extraction with different solvents using the simplex-centroid mixture design. *Int. J. Food Sci. Nutr.* **2012**, *63*, 978−986.
(29) Handa, C. L.; Couto, U. R.; Vicensoti, A. H.; Georgetti, S. R.; Ida, E. I. Optimisation of soy flour fermentation parameters to produce *β*-glucosidase for bioconversion into aglycones. *Food Chem.* **2014**, *152*, 56−65.
(30) Wang, H.; Murphy, P. A. Isoflavone composition of American and Japanese soybeans in Iowa: Effects of variety, crop year, and location. *J. Agric. Food Chem.* **1994**, *42*, 1674−1677.
(31) Berger, M.; Rasolohery, C. A.; Cazalis, R.; Daydé, J. Isoflavone accumulation kinetics in soybean seed cotyledons and hypocotyls: Distinct pathways and genetic controls. *Crop Sci.* **2008**, *48*, 700−708.
(32) Wegulo, S. N.; Yang, X.-B.; Martinson, C. A.; Murphy, P. A. Effects of wounding and inoculation with *Sclerotinia sclerotiorumon* isoflavone concentrations in soybean. *Can. J. Plant Sci.* **2005**, *85*, 749−760.
(33) Zhang, B.; Hettiarachchy, N.; Chen, P.; Horax, R.; Cornelious, B.; Zhu, D. Influence of the application of three different elicitors on soybean plants on the concentrations of several isoflavones in soybean seeds. *J. Agric. Food Chem.* **2006**, *54*, 5548−5554.
(34) Silva, C. E.; Carrão-Panizzi, M. C.; Mandarino, J. M. G.; Leite, R. S.; Mônaco, A. P. A. Teores de isoflavonas em grãos inteiros e nos componentes dos grãos de diferentes cultivares de soja (Glycine max (L.) Merrill). *Braz. J. Food Technol.* **2012**, *15*, 150−156.
(35) Lee, S. J.; Kim, J. J.; Moon, H. I.; Ahn, J. K.; Chun, S. C.; Jung, W. S.; Lee, O. K.; Chung, I. M. Analysis of isoflavones and phenolic compounds in Korean soybean [*Glycine max* (L.) Merrill] seeds of different seed weights. *J. Agric. Food Chem.* **2008**, *56*, 2751−2758.
(36) Bewley, J. D.; Black, A. M. *Seeds-Physiology of Development and Germination*, 2ª ed.; Plenum Press: New York, 1994; p 445.
(37) Bordingnon, J. R.; Ida, E. I.; Oliveira, M. C.; Mandarino, J. M. Effect of germination on the protein content and on the level of specific activity of lipoxygenase-1 in seedlings of three soybean cultivars. *Arch. Latinoam. Nutr.* **1995**, *45*, 222−226.
(38) Kim, E. M.; Lee, K. J.; Chee, K.-M. Comparison in isoflavone contents between soybean and soybean sprouts of various soybean cultivar. *Korean J. Nutr.* **2004**, *37*, 45−51.
(39) Hsieh, M. C.; Graham, T. L. Partial purification and characterization of a soybean *β*-glucosidase with high specific activity towards isoflavone conjugates. *Phytochemistry (Elsevier)* **2001**, *58*, 995−1005.
(40) Suzuki, H.; Takahashi, S.; Watanabe, R.; Fukushima, Y.; Fujita, N.; Noguchi, A.; Yokoyama, R.; Nishitani, K.; Nishino, T.; Nakayama, T. An isoflavone conjugate-hydrolyzing-glucosidase from the roots of soybean (*Glycine max*) seedlings: Purification, gene cloning, phylogenetics, and cellular localization. *J. Biol. Chem.* **2006**, *281*, 30251−30259.
(41) Kosslak, R. M.; Bookland, R.; Barkei, J.; Paaren, H. E.; Appelbaum, E. R. Induction of *Bradyrhizobium japonicum* common *nod* genes by isoflavones isolated from *Glycine max*. *Proc. Natl. Acad. Sci. U.S.A.* **1987**, *84*, 7428−7432.

JOURNAL OF AGRICULTURAL AND FOOD CHEMISTRY

Article

pubs.acs.org/JAFC

# Cloning and Characterization of a Cold-Adapted Endo-1,5-α-L-arabinanase from *Paenibacillus polymyxa* and Rational Design for Acidic Applicability

Shaohua Wang,[†,∥] Ying Yang,[†,∥] Rujian Yang,[†] Jian Zhang,[†] Min Chen,[†] Shingo Matsukawa,[§] Jingli Xie,*[,†] and Dongzhi Wei[†]

[†]State Key Laboratory of Bioreactor Engineering, Department of Food Science and Technology, School of Biotechnology, East China University of Science and Technology, Shanghai 200237, People's Republic of China

[§]Department of Food Science and Technology, Tokyo University of Marine Science and Technology, Tokyo 108-8477, Japan

**ABSTRACT:** AbnZ1, with optimal pH of 6.0 and optimal temperature of 40 °C, is a cold-adapted endo-1,5-α-L-arabinanase encoded by the gene *abnZ1* from *Paenibacillus polymyxa* Z6. The specific activity of AbnZ1 remained 54.1% of maximum at 5 °C. To apply AbnZ1 in acidic conditions, three basic hsitidine (His) residues, $His^{48}$, $His^{218}$, and $His^{297}$, around the catalytic domain were selected as mutation sites, which were replaced with Asp, Glu, Arg, and Lys, respectively, to yield 12 mutants, H48D/E/R/K, H218D/E/R/K, and H297D/E/R/K. The optimum pH of mutant H218D shifted toward the acidic direction by 0.5 unit, and the relative activity was enhanced from 20.4 to 55.7% at pH 5.0. Furthermore, the specific activity of H218D in optimal conditions was 82.6 U/mg versus that of wild type, 73.4 U/mg, and the $K_m$ decreased from 11.9 to 7.1 mg/mL. This work provided an arabinanase candidate for juice clarification and pectin extraction.

**KEYWORDS:** *arabinanase, cold-adapted, site-directed mutagenesis, molecular modeling, pH stability*

## INTRODUCTION

Arabinans, mainly composed of α-L-arabinofuranosyl residues, are generally arranged in α-1,5-linked chains with various numbers of residues substituted with other α-L-arabinofuranosides at the O2 and/or O3 position.[1] In the plant primary cell wall, arabinans are concentrated on rhamnogalacturonan I regions of pectin and act as a vital neutral sugar side chain of pectin, which connects pectin to cellulose.[1,2]

Enzymes that can release arabinoses are found in various bacteria and fungi. These enzymes involved in degradation of arabinan can be mainly divided into three types by their action mode and substrate specificity:[3] (1) Endo-1,5-α-L-arabinanases (endo-ABNs, EC 3.2.1.99) cleave internal linkages of arabinan backbone, producing arabino-oligosaccharides. (2) Exo-α-L-arabinanases cleave arabinan backbone from terminal arabinose, yielding arabinoses. (3) The last is α-L-arabinofuranosidases (AFs, EC 3.2.1.55), exotype enzyme, which hydrolyze terminal nonreducing residues from arabinose-containing polysaccharides and are active on 4-nitrophenyl-α-L-arabinofuranoside.[4] AFs remove arabinan side chain, allowing ABNs to cleave the glycosidic bonds of the arabinan backbone.

The arabinan is soluble in water, whereas debranched arabinan produced by AFs is insoluble in cold water. Therefore, in fruit and vegetable juice processing, if AFs in the enzyme preparations cause haze formation due to the precipitation of polymeric debranched arabinans, endoarabinanases can be applied to prevent haze formation by degrading polymeric debranched arabinan.[5,6] In addition, as arabinan was one of the major components in plant cell wall, endoarabinanase could be used with AFs together in the juice industry for improving the yield of juice because they can promote the degradation of the pectin in fruits and vegetables. Endoarabinanases from several microorganisms have been characterized, but most of them were mesophilic and thermophilic. Their optimal temperatures are 50 °C for *Aspergillus niger*,[7] 60 °C for *Bacillus subtilis* and *Penicillium chrysogenum*,[8,9] 70 °C for *Bacillus thermodentrificans*, and 73 °C for *Thermotoga petrophila*.[10,11] Compared with the mesophilic and thermophilic endoarabinanases, cold-active endoarabinanases should be more attractive in the juice industry as colder conditions hamper spoilage and avoid changes in nutritional properties.[12] However, only a few cold-active endoarabinanases have been reported, such as Abnc from *Penicillium chrysogenum* 31B, which was mostly active at 30−40 °C and remained 55% of maximal activity at 10 °C.[6]

Besides, endoarabinanases have potential application in the enzymatic extraction of pectin. As a vital member of protopectinases, endoarabinanases can promote the solubilization of protopectin through cleaving the link between protopectin and cellulose.[13,14] However, the raw material used for industrial pectin extraction, such as pomace from fruit juice processing, is usually at lower pH than the optimal pH for most natural endoarabinanases. Large-scale pH adjustments will significantly increase costs for pH modifier and treatment of wastewater with high ionic strength, and the same problem happened in the application of endoarabinanases in juice clarification because of the acidity of juices. Such issues can be resolved by modification of the enzyme molecule through site-directed mutagenesis based on rational design to

Received: March 17, 2014
Revised: July 25, 2014
Accepted: July 31, 2014
Published: July 31, 2014

ACS Publications © 2014 American Chemical Society

**Table 1. Primers Used in This Work**[a]

| primer | oligonucleotide sequence | $T_m$ (°C) |
|---|---|---|
| abn-f11 | 5′-TGTGGATCCTTGAAAGCATGGAAAAAA-3′ | 59.22 |
| abn-r11 | 5′-GGTCTCGAGGTACGTAGGCCAACC-3′ | 63.10 |
| H48D | 5′-TGGCAGTAGAT**GAT**CCGTCCATCACCAAGGAAGGC-3′ | 73.22 |
| | 5′-GACGG**ATC**ATCTACTGCCACATCGCCTGTTAACGCC-3′ | 73.35 |
| H48E | 5′-GGCGATGTGGCAGTA**GAG**GATCCGTCCATCACC-3′ | 71.27 |
| | 5′-GGTGATGGACGGATC**CTC**TACTGCCACATCGCC-3′ | 71.27 |
| H218D | 5′-GCACCG**GAT**GTTACATACCGCAATGGCTATTATTATC-3′ | 68.52 |
| | 5′-TGTAAC**ATC**CGGTGCTTCCAAACCACCAGCCGTACG-3′ | 73.79 |
| H218E | 5′-GTGGTTTGGAAGCACCG**GAG**GTTACATACCGCAATG-3′ | 71.93 |
| | 5′-CCATTGCGGTATGTAAC**CTC**CGGTGCTTCCAAACCA-3′ | 71.93 |
| H297D | 5′-TTGCGCGT**GAT**GCCTATGATGCCACTGATGGCGGA-3′ | 74.33 |
| | 5′-AGGC**ATC**ACGCGCAATCACACTGTTGTTATAGACAG-3′ | 70.25 |
| H297E | 5′-CAACAGTGTGATTGCGCGT**GAG**GCCTATGATGCCAC-3′ | 72.45 |
| | 5′-GTGGCATCATAGGC**CTC**ACGCGCAATCACACTGTTG-3′ | 72.45 |

[a]Nucleotides printed in bold and underlined were the positions chosen for mutation. *Bam*HI and *Xho*I restriction sites are underlined. The mutations of H48R/K, and H218R/K and H297R/K were not shown.

improve the protein stability and catalytic efficiency under acidic conditions.

In this study, we cloned and characterized a novel endoarabinanase from *Paenibacillus polymyxa* Z6 with excellent cold-adapted properties such as remaining at 54.1% of maximum activity at 5 °C. Following site-directed mutagenesis based on rational design, 12 mutants were generated, among which the replacement of His with Asp in the position 218 produced an apparent positive mutant with a shift of pH optima from pH 6.0 to pH 5.5 and higher pH stability in lower pH.

## MATERIALS AND METHODS

**Chemicals and Reagents.** Sugar beet linear $\alpha$-1,5-L-arabinan, sugar beet red debranched arabinan, sugar beet arabinan, wheat flour arabinoxylan (medium viscosity), larch arabinogalactan, arabinose, arabinobiose, arabinotriose, and arabinotetraose were obtained from Megazyme International Ireland Co., Ltd. (Wicklow, Ireland). Xylan from beechwood and 4-nitrophenyl-$\alpha$-L-arabinofuranoside were purchased from Sigma-Aldrich Co., Ltd. (St. Louis, MO, USA). Gum arabic and soluble starch were obtained from Shanghai Hushi Co., Ltd. (Shanghai, China). Genomic DNA extraction kits, plasmid extraction kits, gel extraction kits, and Ni-Sepharose resin were purchased from Tiangen Biotech Co., Ltd. (Beijing, China). Kod plus mutagenesis kit was from Toyobo Biotech Co., Ltd. (Shanghai, China). All other molecular cloning reagents were from Takara Biotechnology Co., Ltd. (Dalian, China).

**Strain, Media, and Plasmids.** The *P. polymyxa* Z6 used in this study was screened from a planting soil sample collected from an apple orchard in Xi'an, Shanxi province, China. The *P. polymyxa* Z6 was deposited in the China Center for Type Culture Collection (CCTCC AB 2014036). *Escherichia coli* DH5$\alpha$, *E. coli* BL21 (DE3), and the plasmid pET21a (+) were used for cloning and expression of the gene *abnZ1*. Transformants were grown in LB medium (1% peptone, 1% NaCl, and 0.5% yeast extract) with 100 $\mu$g/mL ampicillin.

**Cloning, Expression, and Purification of AbnZ1.** The coding sequence of *abn*Z1 was amplified by PCR with the forward primer abn-f11 and the reverse primer abn-r11 by using genomic DNA of *P. polymyxa* Z6 as the template (Table 1). The products of PCR reaction were cloned in the plasmid pET21a (+) containing a C-terminal His-tag for purification of AbnZ1.

The recombinant plasmid was transformed into *E. coli* BL21 (DE3) and grown on solid LB medium containing 100 $\mu$g/mL ampicillin. Then the positive recombinant *E. coli* was cultivated in 50 mL of liquid LB medium at 37 °C with 100 $\mu$g/mL ampicillin until the $OD_{600}$ reached 0.6. After that, 0.2 mM IPTG was added to the medium to induce enzyme expression, and the culture continued to grow at 20 °C for 20 h.

The target protein was purified by using Ni-Sepharose through elution with imidazole in a linear gradient from 10 to 250 mM. Phosphate buffer (pH 7.0, 100 mM) was used in the Ni-Sepharose column. The concentrated active fractions were stored in 100 mM phosphate buffer (pH 7.0) containing 10% glycerol at −20 °C.

**Site-Directed Mutagenesis.** The mutants were obtained by using the KOD-plus-Mutagenesis Kit (Toyobo, Shanghai, China) to amplify the recombinant plasmid pET21a (+)-*abnZ1*. The primers used for the site-directed mutagenesis are listed in Table 1. The mutants of the recombinant plasmid was transformed into *E. coli* BL21 (DE3) and grown on solid LB medium containing 100 $\mu$g/mL ampicillin. The clones grown on the ampicillin-resisted plates were transferred to liquid LB medium containing 100 $\mu$g/mL ampicillin and selected for DNA sequencing. Then, the positive clones were stored in 15% glycerol at −20 °C and used for further research.

**Determination of Protein Content, Molecular Mass, and Association Form.** The protein content was determined using the Bradford reagent with bovine albumin as standard. A 5800 MALDI-TOF/TOF (AB SCIEX, USA) was used to detect the association form and the molecular weight of AbnZ1. A solution of CCA was prepared by dissolving 10 mg of matrix in 1 mL of water solvent containing 0.1% TFA and 50% ACN. The protein solution (1.0 g/L) was placed on a MALDI plate and evaporated at room temperature. Following this, 1 $\mu$L of different matrix solutions was used to overlay the protein sample spots, and the resulting droplets were left for crystallization by air-drying. Mass spectrometric measurements were performed using a 5800 MALDI-TOF-TOF instrument. An accelerating voltage of 20 kV was used. Mass spectra were recorded in the linear mode.

**Enzyme Activity Assay.** The arabinanase activity was determined by measuring the amount of reducing sugar released in a reaction mixture containing 200 $\mu$L of 0.25% arabinan in 100 mM buffer and 50


dx.doi.org/10.1021/jf501328n | J. Agric. Food Chem. 2014, 62, 8460−8469

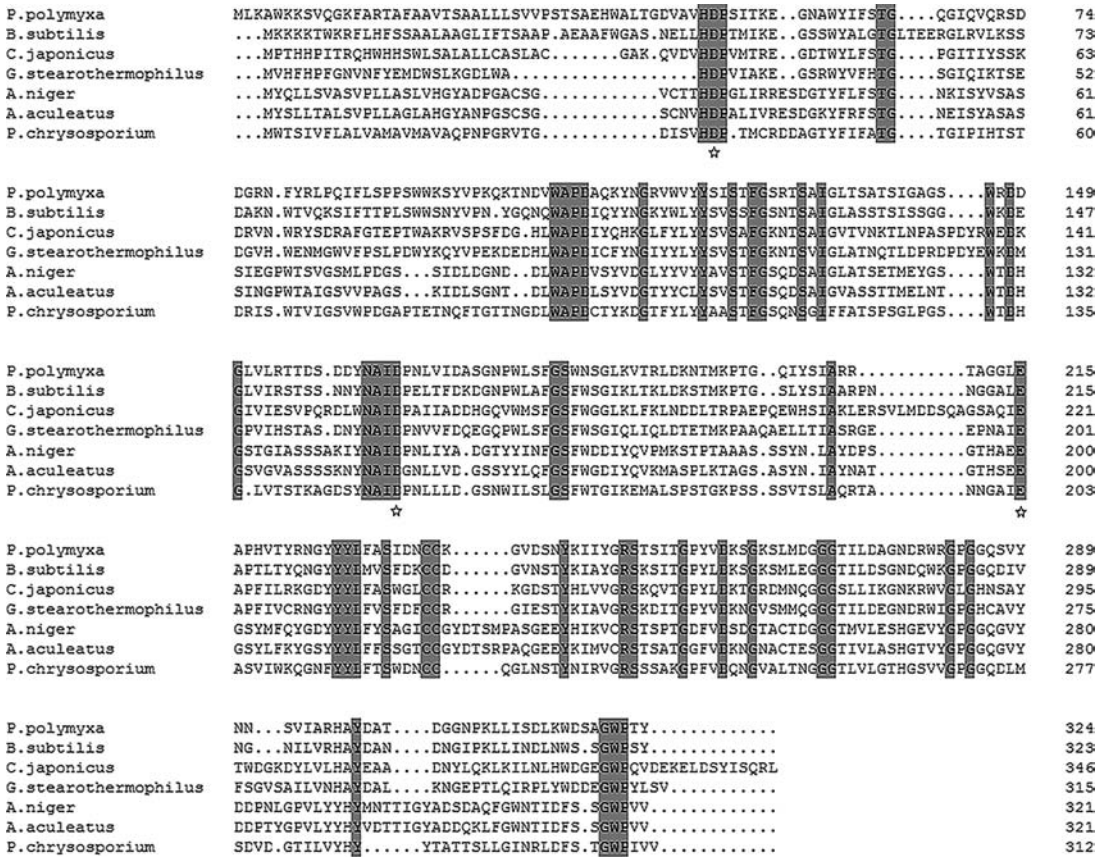


**Figure 1.** Multiple sequence alignment of AbnZ1 with some GH43 endoarabinanases. AbnZ1 was compared with endo-1,5-$\alpha$-L-arabinanase from *B. subtilis* 168T+ (AAV87172), *C. japonicus* (CAA71485), *G. stearothermophilus* (B3EYM8), *A. niger* (P42256), *A. aculeatus* (Q9HFS9), and *P. chrysosporium* (AFN42888). The catalytic residues are marked with asterisks. Residues that are identical in all sequences are shaded in gray.

$\mu$L of enzyme samples. Reducing sugars were measured by using the 3,5-dinitrosalicylic acid (DNS) method.[5] One unit of enzyme activity was defined as 1 $\mu$mol of reducing sugar as arabinose produced per minute.

**Determination of pH and Temperature Optima and Stability.** The optimal pH was measured at 37 °C for 30 min from pH 4.0 to 9.0 by using sodium acetate buffer (pH 4.0−6.0), sodium phosphate buffer (pH 6.0−8.0), and Tris-HCl buffer (pH 8.0−9.0). The optimal temperature was measured at temperatures ranging from 5 to 70 °C in 100 mM sodium acetate buffer (pH 6.0) for 30 min. For pH stability, the enzyme was incubated in buffers ranging from pH 5.0 to 7.0 at 20 °C for various periods. For temperature stability, the enzyme was incubated in 100 mM sodium acetate buffer (pH 6.0) at temperatures ranging from 20 to 50 °C for various phases. Then, the residual enzyme activity was measured at an optimal pH and temperature for 30 min. Substrate was 0.25% (w/v) debranched arabinan.

**Substrate Specificity and Degradation Pattern of AbnZ1.** The substrate specificity was determined by measuring the enzyme activity with sugar beet linear 1,5-$\alpha$-L-arabinan, sugar beet red debranched arabinan, sugar beet arabinan, 4-nitrophenyl-$\alpha$-L-arabinofuranoside, xylan from beechwood, wheat flour arabinoxylan, larch arabinogalactan, gum arabic, and starch soluble at the optimal pH and temperature for 5 min.

For the degradation pattern, high-performance anion exchange chromatography (HPAEC) was used to determine hydrolysis products. The hydrolysis products of 1% sugar beet linear 1,5-$\alpha$-arabinan were analyzed with HPAEC using an Agilent 1100 series system (Agilent, Santa Clara, CA, USA) with a 300 × 6.5 mm Sugarpak1 column (Waters, Milford, MA, USA) maintained at 80 °C using double-distilled deionized and degassed water as mobile phase at a flow rate of 0.5 mL/min. The effluent was monitored with a differential refractive index detector.

**Determination of Kinetic Parameters.** The kinetic parameters were determined through the Lineweaver−Burk plot method at the optimal pH and temperature by using the linear 1,5-$\alpha$-L-arabinan at concentrations ranging from 0.1 to 1% (w/v) for 5 min.[15]

**Sequence Analysis.** Multiple nucleotide sequence alignment of gene *abnZ1* was calculated and presented by using the DNAMAN program. The signal peptide was predicted by the SignalP program. The molecular weight and p*I* were predicted by using the Compute pI/Mw tool on the ExPASy Bioformatics Resources Portal (http://web.expasy.org/compute_pi/).

**3-D Structure Model Analysis of Wild-Type and Mutants.** A theoretical structure of AbnZ1 with residues 47−324 was built by automated protein structure homology modeling from the Swiss Model server (http://swissmodel.expasy.org/) with the crystal structure of endo-1,5-$\alpha$-L-arabinanase (1UV4) from *B. subtilis* 168+ as template. The estimated absolute model quality (QMEAN *Z*-score) of modeling structure was 0.22,[16] and the sequence identity between template and target was 60.2%.[17−19] The 3-D model and structure alignment between AbnZ1 and BsArb43B (2x8f) from *B. subtilis* were conducted and shown by the software PyMOL. Amino acid mutations were inserted into the structure using the mutation tool Swiss-Viewer followed by energy minimization.

**Nucleotide Sequence Accession Number.** The nucleotide sequence data of the wild-type gene *abnZ1* reported in this study were submitted to Genbank under accession no. KF481913.

## RESULTS

**Sequence Analysis of *P. polymyxa* AbnZ1.** The gene *abn*Z1 had an open reading frame of 972 bp encoding 324 amino acids. The molecular weight and p*I* of AbnZ1 were

predicted as 35 477 Da and 9.18, respectively. AbnZ1 was classified as a member of the glycoside hydrolase family 43 (GH43) according to its primary protein sequence and displayed 99% identity to the product of the *abnA* gene from *P. polymyxa* M1. Moreover, the amino acid sequence of AbnZ1 displayed 55, 39, 51, 33, 33, and 37% identity with the sequences of endo-1,5-α-L-arabinanase from *B. subtilis* 168T+, *Cellvibrio japonicus*, *Geobacillus stearothermophilus*, *A. niger*, *A. aculeatus*, and *Phanerochaete chrysosporium* (Figure 1).

The active sites of endoarabinanases consisted of three key amino acids, Asp, Asp, and Glu, which were conserved in glycoside hydrolase (GH) family 43.[20] Such amino acid residues are $Asp^{49}$, $Asp^{165}$, and $Glu^{215}$, conserved in the mature AbnZ1 according to the result of multiple sequence alignment (Figure 1).

**Expression in *E. coli* and Purification of Recombinant AbnZ1.** We cloned and expressed the gene *abn*Z1 in pET21a (+) with a $His_6$-tag at the C-terminus. Parts of the recombinant AbnZ1 overexpressed in *E. coli* BL21 (DE3) were soluble and active (Figure 2a). The enzyme was purified by using a Ni-

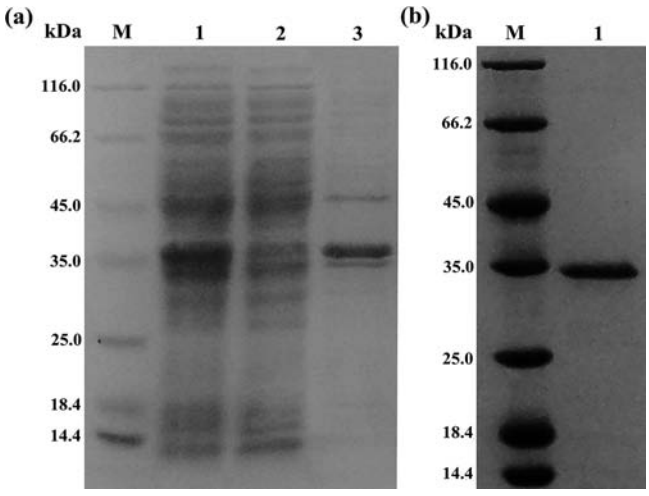


**Figure 2.** Expression and purification of AbnZ1: (a) analysis of the protein expression (lanes: 1, crude cell lysate after cold osmotic shock; 2, soluble fraction of the crude cell lysate after cold osmotic shock; 3, insoluble fraction of the crude cell lysate after cold osmotic shock); (b) recombinant AbnZ1 purified by Ni-Sepharose column. The proteins were separated by 12.5% SDS-PAGE gels.

Sepharose column. The specific activity measured under pH 6.0 and 40 °C was 73.4 U/mg. The purified AbnZ1 is shown in Figure 2b, which indicated that the molecular weight of the recombinant protein after purification was about 35 kDa, in good accordance with the predicted molecular weight (Figure 2b). The result of further MALDI-TOF/TOF testing (Figure 3) showed that the monomeric molecular weight of AbnZ1 was about 32.6 kDa, whereas that of the dimer was 65.2 kDa, and there was no distinct peak of its trimer formation to be determined, which indicated that the association form of AbnZ1 is dimer.

**Biochemical Properties of Purified AbnZ1.** The optimal reaction temperature of purified AbnZ1 ranged from 30 to 40 °C (Figure 4a). The specific activity of AbnZ1 was kept about 54.1% of maximal activity at 5 °C (Figure 4a), which was rare in reported arabinanases. AbnZ1 could maintain most of the initial activity after incubation at 20 °C for 4 h while losing most activity when incubated at 50 °C for 30 min (Figure 4b).

AbnZ1 reached the highest activity at pH 6.0 and 40 °C in 100 mM sodium acetate buffer and achieved about 20.4 and 83.6% of the maximal activity at pH 5.0 and 7.0, respectively (Figure 4c). AbnZ1 was stable at pH 7.0 compared with 55.5 and 5.78% of maximal activity remaining after 30 min of incubation at pH 6.0 and 5.0 respectively (Figure 4d).

The substrate specificity of recombinant AbnZ1 was measured on linear α-1,5-L-arabinan, red debranched arabinan, sugar beet arabinan, 4-nitrophenyl-α-L-arabinofuranoside, xylan from beechwood, wheat flour arabinoxylan, larch arabinogalactan, gum arabic, and soluble starch. AbnZ1 was found to be active toward only linear arabinan, red debranched arabinan, and sugar beet arabinan with specific activities of 73.4, 44.0, and 9.3 U/mg, respectively, but showed no activity toward the rest of the substrates.

Linear α-1,5-L-arabinan was selected as substrate for product analysis.[21] HPAEC mutagenesis, forming six mutan analysis (Figure 5) showed arabinobiose and arabinotriose were the major final products of the hydrolysis by the recombinant AbnZ1, which supported that AbnZ1 is an endoarabinanase.

Kinetic parameters toward the optimal substrate linear α-1,5-L-arabinan were measured at 40 °C and pH 6.0 for 5 min by the Lineweaver−Burk plot method. The $K_m$ and $V_{max}$ toward linear arabinan were 11.6 mg/mL and 117.7 μmol $min^{-1}$ $mg^{-1}$, respectively. Kinetic parameters of AbnZ1 toward linear arabinan are listed in Table 2.

**Theoretical Three-Dimensional Model and Site-Directed Mutagenesis of AbnZ1.** A 3-D model was constructed by the Swiss model with the structure of endoarabinanase Ara43a (1UV4) as template to determine the mutation site of AbnZ1 for improving acidic-adapted ability of AbnZ1. As shown in Figure 6a, AbnZ1 displayed a characteristic β-propeller fold structure, containing five β-sheets called blades arranged around a pseudo axis. An α-helix was located after blade I, which exists commonly in endoarabinanases.[22] The catalytic domain of AbnZ1 comprised three key active sites $Asp^{49}$, $Asp^{165}$, and $Glu^{215}$, which were conserved in all members of GH families 32, 43, 62, and 68.[20]

The function of three key active sites from the arabinanase BsArb43B has been identified.[22] On the basis of the results of multiple sequence alignment (Figure 1) and structure alignment between AbnZ1 and BsArb43B (Figure 6b), $Asp^{49}$ in AbnZ1 was deduced to serve as a general base catalyst, deprotonating the nucleophilic water molecule that attacks the bond, whereas $Glu^{215}$ served as a general acid catalyst protonating the glycosidic oxygen.[23] Putative roles of $Asp^{165}$ include acting as a $pK_a$ modulator and maintaining the correct alignment of the general acid residue relative to the substrate.[24]

Given the similar catalytic mechanism among the glycoside hydrolases and the importance of the electrostatic interactions around the active sites, three basic histidine (His) residues around the catalytic domain of AbnZ1 were selected as mutation sites (Figure 6a) according to the 3-D model of AbnZ1, which were $His^{48}$, $His^{218}$, and $His^{297}$. They were further replaced respectively with acidic amino acid residues, aspartate and glutamate, and alkaline amino acid residues, arginine and lysine, via site-directed mutagenesis, forming 12 mutants H48D/E/R/K, H218D/E/R/K, and H297D/E/R/K.

The mutants H48D/E/R/K, H297D/E/R/K, and H218R/K lost their activity (data not shown). Mutant H218E was active, but it did not change the enzymatic property obviously under acidic condition compared with the wild type. Fortunately, the optimal pH of H218D shifted toward the acidic direction.


dx.doi.org/10.1021/jf501328n | J. Agric. Food Chem. 2014, 62, 8460−8469

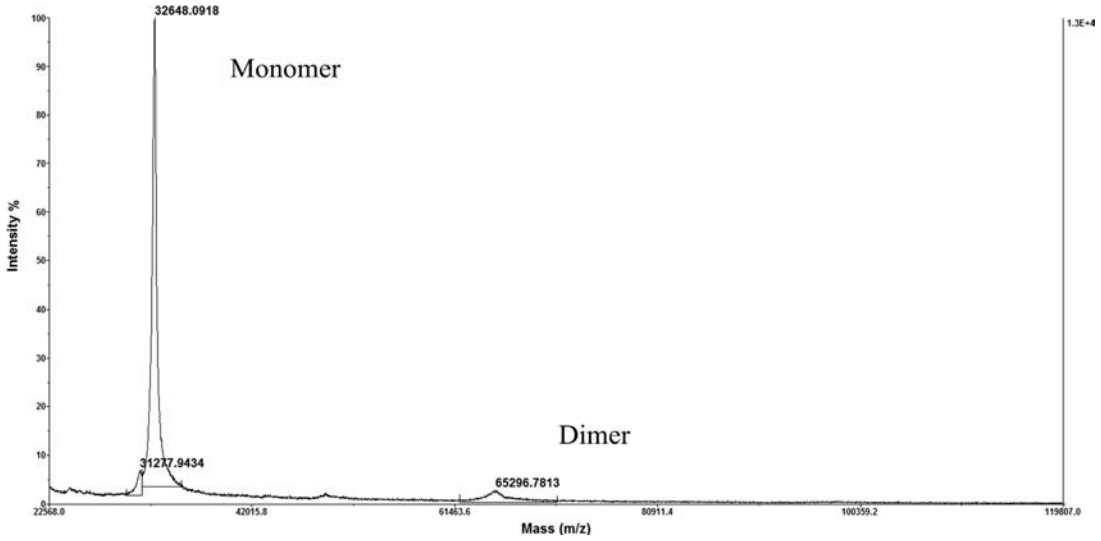


**Figure 3.** MALDI-TOF/TOF showing the association form and molecular weight of AbnZ1.

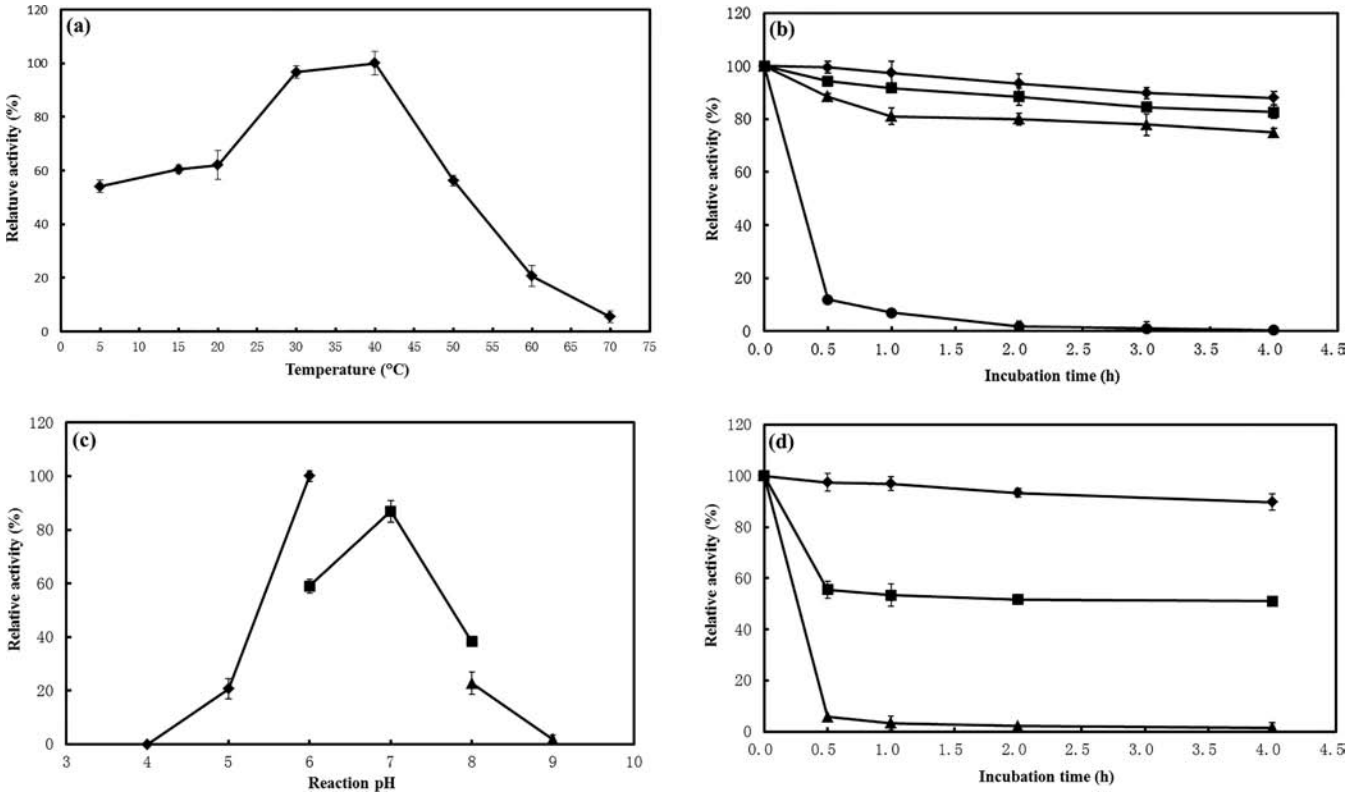


**Figure 4.** (a) Effect of temperature on enzyme activity. Reactions were conducted for 30 min in 100 mM, pH 6.0, sodium acetate buffer. (b) Effect of temperature on enzyme stability. The enzyme was incubated at temperatures ranging from 20 to 50 °C in 100 mM, pH 6.0, sodium acetate buffer for a period of time, and residual activity was assayed at optimal temperature and pH by using the DNS method. Solid rhombuses, squares, triangles, and circles represent AbnZ1 at 20, 30, 40, and 50 °C, respectively. (c) Effect of pH on enzyme activity. Activity was measured at 40 °C for 30 min at the indicated pH values in 100 mM of each buffer: sodium acetate (pH 4.0−6.0, solid rhombuses), sodium phosphate (pH 6.0−8.0, solid squares), and Tris-HCl (pH 8.0−9.0, solid triangles). (d) Effect of pH on enzyme stability. The enzyme was incubated at 20 °C in pH 5.0−7.0 100 mM buffers for a period of time. After that, residual activity was assayed at optimal temperature and pH by using the DNS method. Solid rhombuses, squares, and triangles represent AbnZ1 at pH 7.0 sodium phosphate, pH 6.0 sodium acetate, and pH 5.0 sodium acetate. In all panels, the highest activity was taken as 100%. Reaction substrate was 0.25% red debranched arabinan.

**Biochemical Characterization of Mutant Enzyme H218D.** There were no obvious differences in recombinant protein concentration between the wild-type AbnZ1 and the mutant H218D according to the graph of SDS-PAGE (Figure 7a), which implied the substitution of His residue did not affect the expression of recombinant protein. A single band in Figure 7b indicated H218D was successfully purified. The specific activity of H218D was 82.6 U/mg under pH 6.0 and 40 °C. The optimal pH of H218D is 5.5, and the specific activity of H218D in pH 5.0 was 55.7% of the highest activity compared


dx.doi.org/10.1021/jf501328n | J. Agric. Food Chem. 2014, 62, 8460−8469

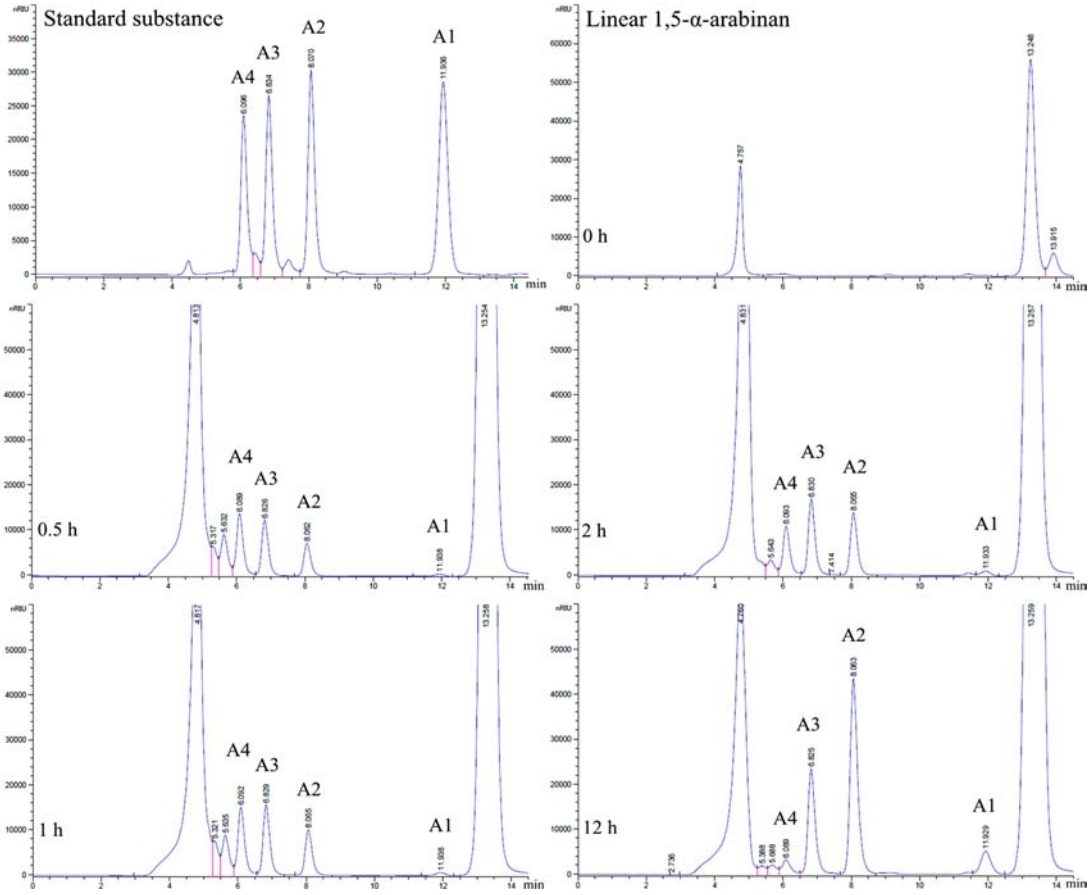


**Figure 5.** HPAEC chromatogram showing enzymatic products of linear arabinan with AbnZ1. A1, arabinose; A2, arabinobiose; A3, arabinotriose; A4, arabinotetraose.

**Table 2. Enzymatic Properties and Kinetic Parameters of AbnZ1, H218D, and Some Reported ABNs[a]**

| enzyme | optimal temperature (°C) | optimal pH | specific activity (U/mg) | $k_{cat}$ ($s^{-1}$) | $K_m$ (mg/mL) | $k_{cat}/K_m$ |
|---|---|---|---|---|---|---|
| wild-type AbnZ1 | 40.0 | 6.0 | 73.4 | 68.7 ± 8.3 | 11.6 ± 1.6 | 5.9 |
| mutant H218D | 40.0 | 5.5 | 82.6 | 99.7 ± 6.0 | 7.1 ± 1.9 | 14.0 |
| Abn2[3] | 37.0 | 7.0 | 72.8 | | 2.0 | |
| Abnc[6] | 40.0 | 6.5 | 6.5 | | | |
| AbnA[11] | 73.0 | 6.0 | 152.1 | | 19.9 | |
| ABN[25] (*B. licheniformis*) | 35.0 | 6.0 | 27.0 | 160 | 19 | 8.47 |
| ABN[26] (*C. saccharolyticus*) | 75.0 | 6.5 | 12.0 | 50 | 18 | 2.8 |

[a]Specific activity was measured by purified recombinant AbnZ1 with linear arabinan at 40 °C, pH 6.0. The data of AbnZ1 shown are the averages and standard deviations of three independent experiments.

with that of the wild AbnZ1, 20.4% (Figure 8a). Meanwhile, the stability of H218D at pH 6.0 was slightly higher than that of the wild AbnZ1 (Figure 8b). Sixty percent of the initial activity was retained after H218D had been incubated in pH 6.0 at 20 °C for 4 h, whereas that for wild-type was 50%. Besides, the mutation did not bring about change in the reaction temperature between the H218D and the wild AbnZ1 (Figure 8c).

The $V_{max}$ and $K_m$ of H218D were changed to 171.3 μmol $min^{-1}$ $mg^{-1}$ and 7.1 mg/mL, and $K_{cat}$ was improved about 45% versus that of the wild AbnZ1. Kinetic parameters of H218D and the wild AbnZ1 toward linear arabinan are listed in Table 2, which showed that H218D was given higher catalytic efficiency.

## DISCUSSION

Unlike AFs have been grouped into GH families 3, 10, 43, 51, 54, and 62 on the basis of their amino acid sequences; all known endoarabinanases are in GH family 43.[9] Among the reported arabinanases, cold-adapted arabinanases were scarce but valuable in the food industry. We cloned and characterized a novel cold-adapted endo-1,5-α-L-arabinanase gene *abnZ1* from *P. polymyxa* Z6 in this study.

Most reported endoarabinanases were mesophilic and thermophilic. Compared with most reported endoarabinanases, the optimal reaction temperature of purified AbnZ1 ranged from 30 to 40 °C and was lower. Furthermore, the specific activity of AbnZ1 was about 54.1% of maximal activity at 5 °C, which was rare in reported arabinanases. Only a few cold-active endoarabinanases have been reported, such as Abnc from *Penicillium chrysogenum* 31B, which was mostly active at 30−40


dx.doi.org/10.1021/jf501328n | J. Agric. Food Chem. 2014, 62, 8460−8469

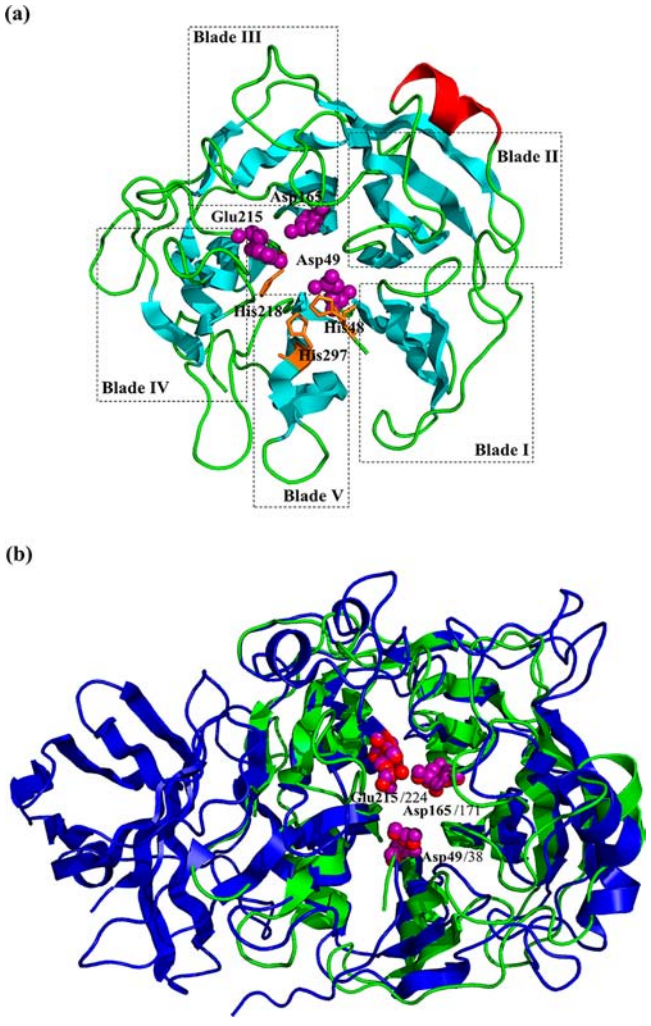


**Figure 6.** (a) 3-D model structure of wild-type AbnZ1 created by Swiss model and processed by PyMol. AbnZ1 contains a five-blade $\beta$-propeller, which is a characteristic structure in GH43. Blade I to blade V is marked with a dotted box. The $\alpha$-helices and $\beta$-sheets are shown in red and cyan, respectively. Loops and other secondary structure are shown in green. The catalytic residues Asp[49], Asp[165], and Glu[215] are shown in purple balls. The positions of the point mutation are shown in orange sticks. (b) Structure alignment with endoarabinanase BsAra43B from *B. subtilis* (2x8f). The 3-D model structure was created by PyMol. AbnZ1 is shown in green and BsArb43B in blue. The catalytic residues of AbnZ1 are shown in purple balls and printed in bold. The catalytic residues of BsArb43B are shown in red balls.

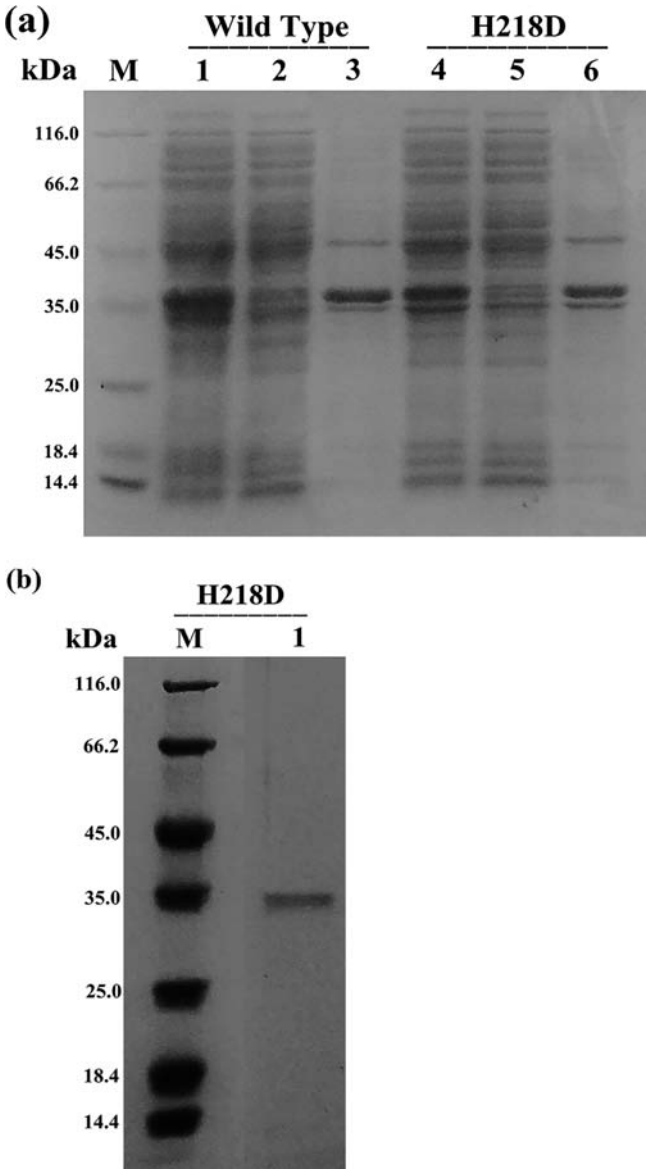


**Figure 7.** Expression of purification of the mutant H218D: (a) analysis of protein expression (lanes: 1 and 4, crude cell lysate after cold osmotic shock; 2 and 5, soluble fraction of the crude cell lysate after cold osmotic shock; 3 and 6, insoluble fraction of the crude cell lysate after cold osmotic shock); (b) recombinant H218D purified by Ni-Sepharose column. The proteins were separated by 12.5% SDS-PAGE gels.

°C and retained 55% of maximal activity at 10 °C,[6] indicating AbnZ1 performed better than Abnc under the low temperature. In addition, AbnZ1 had a higher specific activity, 73.4 U/mg, when compared with Abnc, the specific activity of which was 6.5 U/mg.[6] Thus, AbnZ1 was an excellent cold-adapted enzyme and would have potential application in some food processing under lower temperature.

The HPAEC result supported that AbnZ1 was an endoarabinanase. Generally, in the case of exoacting enzymes, only monomers or dimers accumulate throughout the enzyme reaction, whereas in the case of endoacting enzymes, bigger oligomers, such as arabinotriose and arabinotetraose, formed even in the initial stage of hydrolysis (Figure 5). Besides, the ability of hydrolyzing red debranched arabinan also indicated that AbnZ1 acts in an endo manner, because dye molecules attached to nonreducing terminal arabinose of arabinan prevent the exoarabinanases from releasing arabinose from the nonreducing end.[3]

The optimal pH of reported endoarabinanases is mostly at ≥6.0, such as 6.0−7.0 for AbnS1 from *P. chrysogenum*,[9] 6.0 for an endoarabinanase from *Bacillus licheniformis*,[25] 6.5 for that from *Caldicellulorsiruptor saccharolyticus*, 7.0 for Abn2 from *B. subtilis*,[3,26] and 6.0 for the present AbnZ1. AbnZ1 also showed rapidly decreased specific activity under acidic environment, which would limit its application for either enzymatic extraction of pectin or juice clarification, the pH of the raw material usually being about 4.0−4.5. Considering the situation of pectin extraction from fruit pomace, as the pH modifier (alkali) was used, the advantages of enzymatic extraction of pectin would be lost compared with the present industrial acidolysis method.


dx.doi.org/10.1021/jf501328n | J. Agric. Food Chem. 2014, 62, 8460−8469

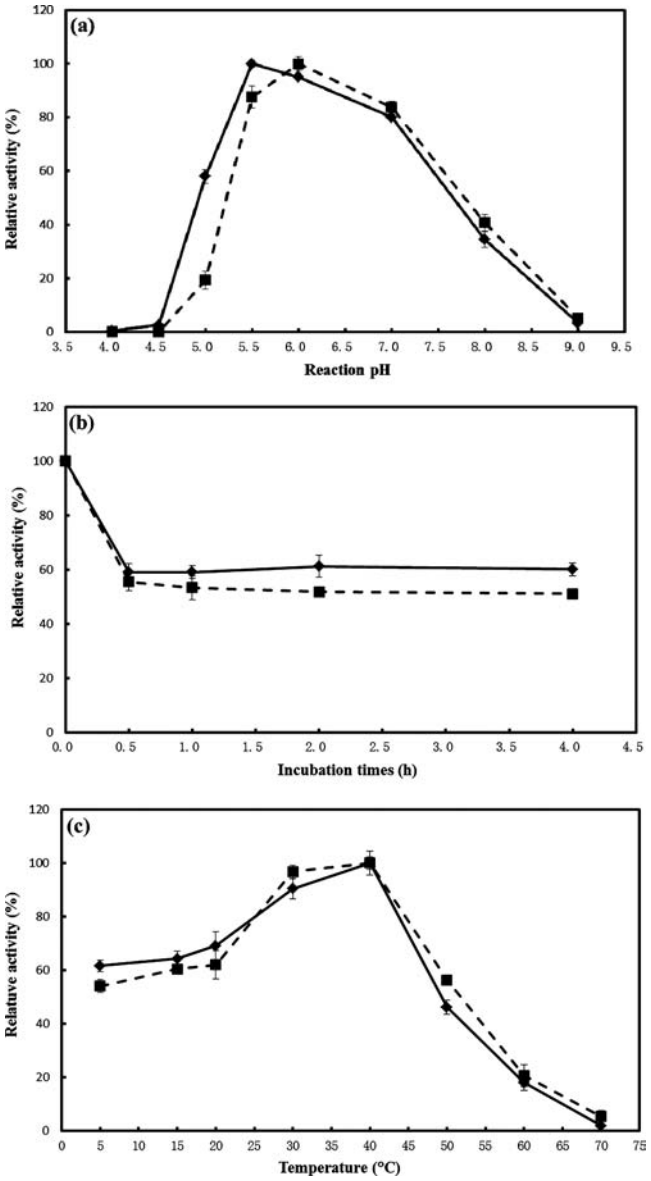


**Figure 8.** (a) Effects of mutation on the reaction pH. Activity was measured at 40 °C for 30 min at the indicated pH values in 100 mM of each buffer: sodium acetate (pH 4.0–6.0). (b) Effects of mutation on the pH stability at pH 6.0. The enzyme was incubated at 20 °C in pH 6.0, 100 mM, buffer for a period of time. After that, residual activity was assayed at optimal temperature and pH by using the DNS method. (c) Effects of mutation on the reaction temperature. Reactions were conducted for 30 min in 100 mM, pH 6.0, sodium acetate buffer. In all panels, full lines and dotted lines represented mutant H218D and wild-type AbnZ1, respectively. The highest activity was taken as 100%. The 0.25% red debranched arabinan was used as reaction substrate.

Therefore, modification of the AbnZ1 molecule aimed at acidic reaction condition is necessary. A directed evolution method (also called irrational design, such as error PCR and DNA shuffling) is a common way to change the property of an enzyme. However, directed evolution needs a lot of experimental work, which costs a lot of time and labor. More recently, rational design based on the catalytic mechanism and protein structure is booming. Some research has succeeded in improving protein efficiency under acidic conditions of some glycoside hydrolases though rational design, such as amylase.[27] However, there are no analogous reports about arabinanases so far.

Glycoside hydrolases hydrolyze the glycosidic bonds requiring two critical residues, a proton donor and a nucleophilic catalytic base, via general acid catalysis. Two major mechanisms, retaining mechanism and inverting mechanism, were involved in glycosidic bond hydrolysis.[23] Within GH family 43, the enzymes work in an inversion manner, in which protonation of the glycosidic oxygen and aglycone departure are accompanied by a concomitant attack of a water molecule that is activated by the base residue. Accordingly, $Asp^{49}$ worked as a nucleophilic catalytic base and $Glu^{215}$ worked as a proton donor on the basis of the 3-D structure of AbnZ1 (Figure 6b).

The specific activity of mutant enzyme was influenced by the distance between the mutant group and the catalytic site. The distance between $His^{48}$ and $Asp^{49}$ was 5.41 Å, and the distance between $His^{297}$ and $Asp^{49}$ was only 3.74 Å, which indicated that these two mutation sites were adjacent to $Asp^{49}$, one of the active sites (Figure 9a). When $His^{48}$ and $His^{297}$ were replaced by Asp/Glu or Arg/Lys, the active site $Asp^{49}$ might be not correctly deprotonated and then the general base catalyst $Asp^{49}$ could not deprotonate the nucleophilic water molecule, which caused the complete activity loss of H48D/E/R/K and H297D/E/R/K.

The decreased $K_m$ and improved $K_{cat}$ of H218D toward linear arabinan indicated the affinity between the enzyme and substrate as well as the catalytic efficiency was enhanced. The changed kinetic parameters of AbnZ1 after substitution of $His^{218}$ by Asp displayed that position 218 was important for the catalytic efficiency of arabinanase at an acidic reaction condition. On the one hand, it was previously reported that $Asp^{49}$ must be deprotonated in the first step of hydrolysis reaction of glycosidic bonds, whereas the general acid $Glu^{215}$ must be protonated at the same time according to the proposed GH catalytic mechanism.[27,28] After mutation, the acidic amino acid $Asp^{218}$ near the hydrogen donor $Glu^{215}$ (Figure 9a) could bear a negative charge and would stabilize the protonated form of $Glu^{215}$ according to Liu et al.[29] This change in structure caused the increment of catalytic efficiency under acidic condition and the shift of pH optima. On the other hand, the residue $His^{218}$ locating around the catalytic domain had a bigger side chain than Asp; thus, the steric hindrance might be reduced after the substitution of His by Asp, which resulted in the reduced steric hindrance and easier substrate attack of the catalytic domain and, subsequently, the decreased $K_m$. These two factors might cause the change of kinetic parameters and improve the catalytic efficiency of endoarabinanase.

As for the stability of enzyme, the hydrogen bonding network around the catalytic domain played critical roles. After the substitution of His with Asp at position 218, four new hydrogen bonds formed and one hydrogen bond disappeared, and the number of hydrogen bonds around the mutation site was increased from 8 to 11 (Figure 9b,c). Thus, the stability of endoarabinanase at pH 6.0 after the mutation might be enhanced by the three newly formed hydrogen bonds according to Yang et al.[27]

In this study, we found a novel cold-adapted endo-$\alpha$-1,5-L-arabinanase, AbnZ1, which would be especially attractive in both juice clarification under low processing temperature, to hamper spoilage and avoid changes in nutritional properties, and enzymatic extraction of pectin. The substitution of the basic residue by an acidic residue around the catalytic domain

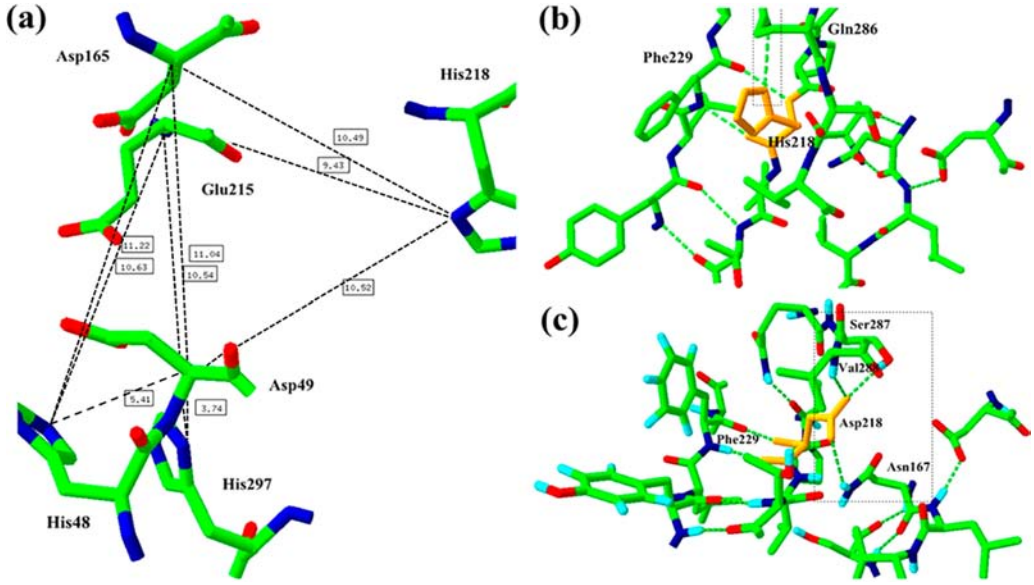


**Figure 9.** (a) Distances from the respective catalytic residues to $His^{48}$, $His^{218}$, and $His^{297}$ in AbnZ1, respectively. (b, c) Local hydrogen bonding network (amino acids within 6 Å around the mutation site; b, wild-type AbnZ1; c, mutant H218D). The oxygen atoms, nitrogen atoms, and hydrogen atoms are shown in red, blue, and cyan, respectively. Change in the number of hydrogen bonds is marked with a dotted box. The positions of the point mutation are shown in orange.

was performed for modification of the enzyme molecule to overcome the unsteady enzyme activity under the acidic condition. On the basis of this study, our next work will focus on two aspects to enhance the catalytic efficiency of endoarabinanases under acidic condition, including more basic amino acids around the catalytic domain chosen as mutation sites, such as arginine (Arg) and lysine (Lys). The distance between mutation sites and key active sites will also be considered as an important factor for the choice of mutation sites. After that, we hope that AbnZ1 will have greater prospects for application in the food industry.

## AUTHOR INFORMATION


### Corresponding Author

*(J.X.) Mail: P.O. Box 283, East China University of Science and Technology, 130 Meilong Road, Shanghai 200237, China. Fax: +86-21-64252563. E-mail: jlxie@ecust.edu.cn.

### Author Contributions

‖S.W. and Y.Y., the same contribution as the first coauthor.



### Funding

This work supported by the National Special Fund for State Key Laboratory of Bioreactor Engineering (2060204), partially supported by the National Natural Science Foundation of China (No. 31201296) and the Fundamental Research Funds for the Central Universities, People's Republic of China.


### Notes

The authors declare no competing financial interest.

## REFERENCES


(1) Zykwinska, A.; Thibault, J. F.; Ralet, M. C. Organization of pectic arabinan andgalactan side chains in association with cellulose microfibrils in primary cellwalls and related models envisaged. *J. Exp. Bot.* **2007**, *58* (7), 1795−1802.

(2) Willats, W. G.; Knox, P.; Mikkelsen, J. D. Pectin: new insights into an old polymer are startin to gel. *Trends Food Sci. Technol.* **2006**, *17* (3), 97−104.

(3) Inácio, J. M.; de Sá-Nogueira, I. Characterization of *abn2*(*yxiA*), encoding a *Bacillus subtilis* GH43 arabinanase, Abn2, and its role in arabino-polysaccharide degradation. *J. Bacteriol.* **2008**, *190* (12), 4272−4280.

(4) Saha, B. C. α-L-Arabinofuranosidases: biochemistry, molecular biology and application in biotechnology. *Biotechnol. Adv.* **2000**, *18* (5), 403−423.

(5) Wong, D. W. S.; Chan, V. J.; McCormack, A. A. Functional cloning and expression of a novel endo-α-1,5-L-arabinanase from a metagenomic library. *Protein Pept. Lett.* **2009**, *16* (12), 1435−1441.

(6) Sakamoto, T.; Ihara, H.; Kozaki, S.; Kawasaki, H. A cold-adapted endo-arabinanase from *Penicillium chrysogenum*. *Biochim. Biophys. Acta (Gen. Subj.)* **2003**, *1624* (3), 70−75.

(7) Rombouts, F. M.; Voragen, A. G. J.; Searle-van Leeuwen, M. F.; Geraeds, C. C. J. M.; Schols, H. A.; Pilnik, W. The arabinanases of *Aspergillus niger*-purification and characterisation of two α-L-arabinofuranosidases and an endo-1,5-α-L-arabinanase. *Carbohydr. Polym.* **1988**, *9* (1), 25−47.

(8) Leal, T. F.; de Sá-Nogueira, I. Purification, characterization and functional analysis of an endo-arabinanase (AbnA) from *Bacillus subtilis*. *FEMS Microbiol. Lett.* **2004**, *241* (1), 41−48.

(9) Sakamoto, T.; Inui, M.; Yasui, K.; Tokuda, S.; Akiyoshi, M.; Kobori, Y.; Nakaniwa, T.; Tada, T. Biochemical characterization and gene expression of two endo-arabinanases from *Penicillium chrysogenum* 31B. *Appl. Microbiol. Biotechnol.* **2012**, *93* (3), 1087−1096.

(10) Takao, M.; Yamaguchi, A.; Yoshikawa, K.; Terashita, T.; Sakai, T. Molecular cloning of the gene encoding thermostable endo-1,5-α-L-arabinase of *Bacillus thermodenitrifcans* TS-3 and its expression in *Bacillus subtilis*. *Biosci., Biotechnol., Biochem.* **2002**, *66* (2), 430−433.

(11) Squina, F. M.; Santos, C. R.; Ribeiro, D. A.; Cota, J.; de Oliveira, R. R.; Ruller, R.; Mort, A.; Murakami, M. T.; Prade, R. A. Substrate cleavage pattern, biophysical characterization and low-resolution structure of a novel hyperthermostable arabinanase from *Thermotoga petrophila*. *Biochem. Biophys. Res. Commun.* **2010**, *399* (4), 505−511.

(12) Padma, P. N.; Anuradha, K.; Reddy, G. Pectinolytic yeast isolates for cold-active polygalacturonase production. *Innovative Food Sci. Emerging Technol.* **2011**, *12* (2), 178−181.

(13) Bonnin, E.; Dolo, E.; Le Goff, A.; Thibault, J. F. Characterisation of pectin subunits released by an optimized combination of enzymes. *Carbohydr. Res.* **2002**, *337* (18), 1687−1696.

(14) Chen, J.; Yang, R.; Chen, M.; Wang, S.; Li, P.; Xia, Y.; Zhou, L.; Xie, J.; Wei, D. Production optimization and expression of pectin

releasing enzyme from *Aspergillus oryzae* PO. *Carbohydr. Polym.* **2014**, *101*, 89−95.
(15) Lineweaver, H.; Burk, D. The determination of enzyme dissociation constants. *J. Am. Chem. Soc.* **1934**, *56* (3), 658−666.
(16) Benkert, P.; Biasini, M.; Schwede, T. Toward the estimation of the absolute quality of individual protein structure models. *Bioinformatics* **2011**, *27* (3), 343−350.
(17) Arnold, K.; Bordoli, L.; Kopp, J.; Schwede, T. The SWISS-MODEL workspace: a web-based environment for protein structure homology modelling. *Bioinformatics* **2006**, *22* (2), 195−201.
(18) Schwede, T.; Kopp, J.; Guex, N.; Peitsch, M. C. SWISS-MODEL: an automated protein homology-modeling server. *Nucleic Acids. Res.* **2003**, *31* (13), 3381−3385.
(19) Guex, N.; Peitsch, M. C. SWISS-MODEL and the Swiss-PdbViewer: an environment for comparative protein modeling. *Electrophoresis* **1997**, *18* (15), 2714−2723.
(20) Pons, T.; Naumoff, D. G.; Martínez-Fleites, C.; Hernández, L. Three acidic residues are at the active site of a $\beta$-propeller architecture in glycoside hydrolase families 32, 43, 62, and 68. *Proteins* **2004**, *54* (3), 424−432.
(21) Wong, D. W. S.; Chan, V. J.; Batt, S. B. Cloning and characterization of a novel exo-$\alpha$-1,5-L-arabinanase gene and the enzyme. *Appl. Microbiol. Biotechnol.* **2008**, *79* (6), 941−949.
(22) de Sanctis, D.; Inácio, J. M.; Lindley, P. F.; de Sá-Nogueira, I.; Bento, I. New evidence for the role of calcium in the glycosidase reaction of GH43 arabinanases. *FEBS J.* **2010**, *277* (21), 4562−4574.
(23) Davies, G.; Henrissat, B. Structures and mechanisms of glycosyl hydrolases. *Structure* **1995**, *3* (9), 853−859.
(24) Brüx, C.; Ben-David, A.; Shallom-Shezifi, D.; Leon, M.; Niefind, K.; Shoham, G.; Shoham, Y.; Schomburg, D. The structure of an inverting GH43 $\beta$-xylosidase from *Geobacillus stearothermophilus* with its substrate reveals the role of the three catalytic residues. *J. Mol. Biol.* **2006**, *359* (1), 97−109.
(25) Seo, E. S.; Lim, Y. R.; Kim, Y. S.; Park, C. S.; Oh, D. K. Characterization of a recombinant endo-1,5-$\alpha$-L-arabinanase from the isolated bacterium *Bacillus licheniformis*. *Biotechnol. Bioprocess Eng.* **2010**, *15* (4), 590−594.
(26) Hong, M. R.; Park, C. S.; Oh, D. K. Characterization of a thermostable endo-1,5-$\alpha$-L-arabinanase from *Caldicellulorsiruptor saccharolyticus*. *Biotechnol. Lett.* **2009**, *31* (9), 1439−1443.
(27) Yang, H.; Liu, L.; Shin, H.; Chen, R. R.; Du, G.; Chen, J. Structure-based engineering of histidine residues in the catalytic domain of $\alpha$-amylase from *Bacillus subtilis* for improved protein stability and catalytic efficiency under acidic conditions. *J. Biotechnol.* **2013**, *164* (1), 59−66.
(28) Wind, R. D.; Uitdehaag, J. C. M.; Buitelaar, R. M.; Dijkstra, B. W.; Dijkhuizen, L. Engineering of cyclodextrin product specificity and pH optima of the thermostable cyclodextrin glycosyltransferase from *Thermoanaerobacterium thermosulfurigenes* EM1. *J. Biol. Chem.* **1998**, *273* (10), 5771−5779.
(29) Liu, Y.; Lu, F.; Li, Y.; Wang, J.; Gao, C. Acid stabilization of *Bacillus licheniformis* $\alpha$-amylase through introduction of mutations. *Appl. Microbiol. Biotechnol.* **2008**, *80* (5), 795−803.

JOURNAL OF AGRICULTURAL AND FOOD CHEMISTRY

Article

pubs.acs.org/JAFC

# Identification of Bitter Modulating Maillard-Catechin Reaction Products

Liyun Zhang,[†] Youlin Xia,[‡] and Devin G. Peterson*[,†]

[†]Department of Food Science and Nutrition, University of Minnesota, 1334 Eckles Avenue, St. Paul, Minnesota 55108, United States
[‡]MNMR Center, University of Minnesota, St. Paul, Minnesota 55455, United States

**ABSTRACT:** The influence of thermally induced reaction products of a known dietary bitter compound, catechin, on bitterness perception was investigated. Catechin was reacted in low-moisture simple Maillard models (200 °C for 15 min) consisting of glycine and a reducing sugar (D-glucose, D-xylose, or D-galactose). Based on liquid chromatrography−mass spectrometry (LC-MS) isotopic labeling techniques, eight reaction products were identified and subsequently structurally elucidated by tandem LC-MS/MS and two-dimensional NMR analysis; six were report to be flavan-3-ol−spiro-C-glycosides reaction products. One of the spiro products was reported to significantly suppress the perceived bitterness intensity of a caffeine solution. Additionally, this specific spiro product was further identified in cocoa and reported to increase in concentration during bean roasting.

**KEYWORDS:** *Maillard reaction, bitter modulation, catechin, roasting*

## INTRODUCTION

Bitter taste is one of the basic gustatory taste sensations that can cause consumer dislike in foods and beverages.[1] Common approaches for decreasing the bitterness of commercial foods often involve the addition of sugar or salt.[2] However, with the increasing demand for healthier but tasty foods, the discovery of novel ingredients that are able to modulate bitterness is desirable. Consequently, the discovery of compounds with bitter modulator activity is of commercial interest to improve the palatability of food with bitter attributes, particular for reduced sugar and salt formulations.

Screening and identifying bitter modulating compounds is an analytically challenging task.[3] Recently, a series of flavan-3-ol−*C*-glycosides isolated from cocoa were suggested to suppress the bitter intensity of cocoa beverages.[4] Additionally, $\beta$-D-glucopyranosides were reported to activate one of the human bitter receptors (T2Rs) with high specificity and stereoselectivity, based on the conformation at the C1 position of the pyranose moiety.[5] Therefore, slight changes of the compound structure (e.g., the pyranose moiety attached to a flavonoid) have been reported to influence the taste profile or even modulate the bitter perception.[3]

Natural product taste compounds are known to be chemically modified by food reactions during food manufacture; however, how common food reactions could modulate these taste attributes is not well understood. Previously our group has reported that dietary bitter compounds, the flavan-3-ols, were chemically modified by reactive carbonyl species (i.e., dicarbonyls) generated by food reactions, such as Maillard pathways.[6,7] The main goal of the current study was thus to investigate if the modification of known dietary bitter compounds, such as the flavanols, generated new chemical species that modulated the perception of bitterness intensity. These results were further extrapolated to cocoa beans to investigate if related phenolic-Maillard adducts existed.

## MATERIALS AND METHODS

**Chemicals.** D-Glucose, D-xylose, D-galactose, glycine, (+)-catechin hydrate (≥98%), high-purity quartz sand, formic acid, and methanol-$d_4$ (99.8% enrichment) were obtained from Sigma-Aldrich Co. (St. Louis, MO, USA). High-performance liquid chromatography (HPLC) grade acetonitrile and methanol were obtained from Fisher Scientific (Fair Lawn, NJ, USA). Distilled deionized water was further purified through a Barnstead Nanopure Diamond water purification system (Thermo Scientific, Dubuque, IA, USA). $^{13}C_6$-Glucose, $^{13}C_6$-galactose, and $^{13}C_1$-xylose were obtained from Cambridge Isotope Laboratories, Inc. (Andover, MA, USA).

**Low-Moisture Maillard Reaction Model with Catechin.** Reactions were conducted according to those of Jiang et al.[8] Briefly, the reaction apparatus consisted of a round-bottom flask (500 mL) attached with a Vigreux column and a glass stirrer fitted with a Teflon blade (Ace Glass, Vineland, NJ, USA). The reaction vessel was heated by oil bath and connected to a rheostat (PowerStat, The Superior Electric Co., Bristol, CT, USA) for temperature control. The reactants (reported in Table 1) were mixed with 15 g of quartz sand (previously cleaned and dried) and 1.5 g of water. The reactant mixture was mixed at 40−60 rpm in the round-bottom flask for 2−3 min. The apparatus was then placed in an oil bath maintained at 200 °C, and the reaction was conducted for 15 min, then immediately removed from the oil bath, and prepared for further analysis.

**Sample Preparation for Model Reactions.** Extraction was performed with methanol (3 × 30 mL), the isolate was filtered, and the filtrate was separated by means of ultrafiltration equipped with 1 kDa MW cutoff membrane (8200 Series stirred cell, EMD Millipore, Billerca, MA, USA). The permeate fraction was concentrated until precipitate appeared under vacuum (Buchi Rotavapor, model R110, New Castle, DE, USA; 0.1 atm; water bath was maintained at 30 °C) and subsequently filtered through a 0.2 $\mu$m Nylon tip filter (Sigma-Aldrich Co.) and analyzed by liquid chromatography−mass spectrometry (LC-MS).

Received: April 29, 2014
Revised: July 29, 2014
Accepted: July 31, 2014
Published: July 31, 2014

ACS Publications © 2014 American Chemical Society



dx.doi.org/10.1021/jf502040e | J. Agric. Food Chem. 2014, 62, 8470−8477

**Table 1. Maillard-Catechin Model Reaction under Low-Moisture Condition[a]**

| | reactant (mmol) | | | | | | | |
|---|---|---|---|---|---|---|---|---|
| | hexose | | | | pentose | | | |
| | glucose | | galactose | | xylose | | amino acid | phenolic |
| model system | unlabeled | labeled | unlabeled | labeled | unlabeled | labeled | glycine | (+)-catechin |
| A | 5 | | | | | | 5 | 5 |
| B | | | | | 5 | | 5 | 5 |
| C | | | 5 | | | | 5 | 5 |
| D | 2.5 | 2.5 | | | | | 5 | 5 |
| E | | | | | 2.5 | 2.5 | 5 | 5 |
| F | | | 2.5 | 2.5 | | | 5 | 5 |
| G | 5 | | | | | | | 5 |
| H | 5 | | | | | | 5 | |
| I | | | | | | | | 5 |

[a]Conditions: 10% moisture; 200 °C for 15 min.

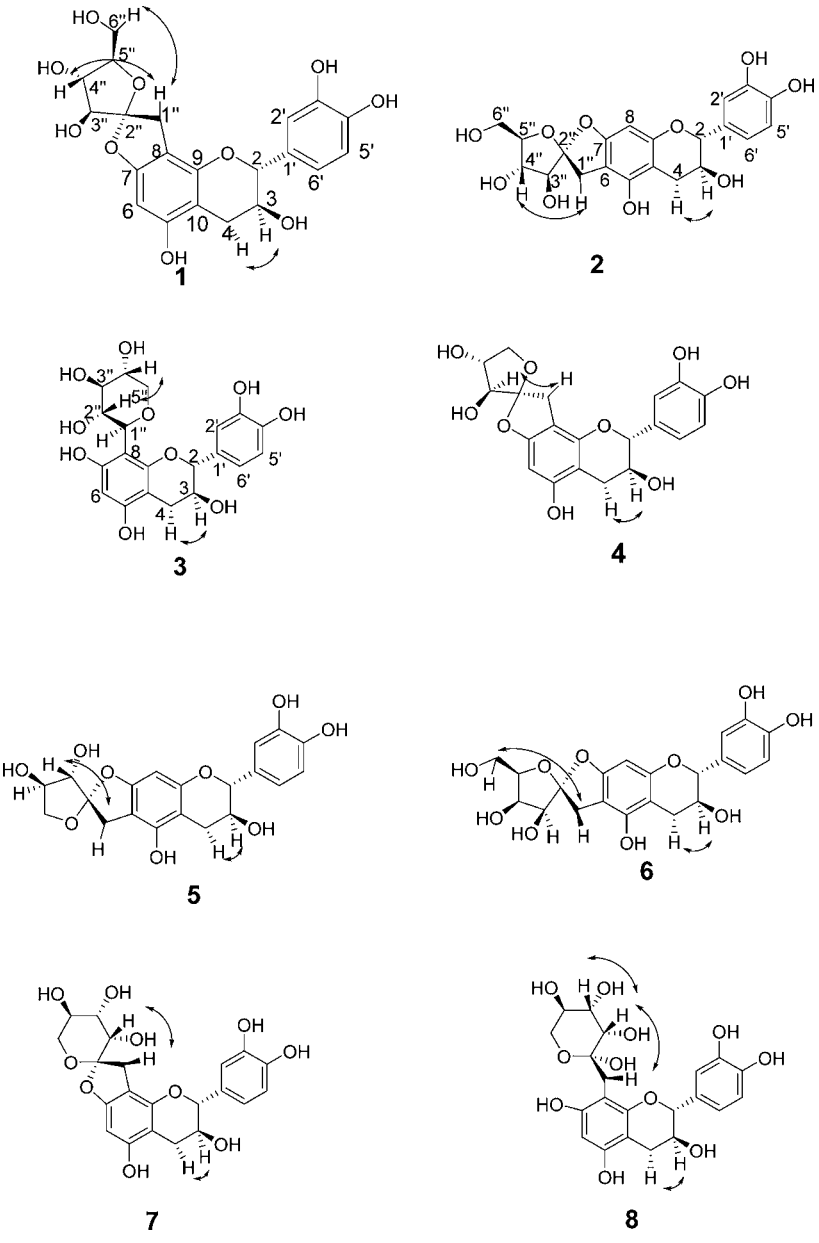


**Figure 1.** Structure and key NOESY correlations of the successfully isolated Maillard-catechin products.


dx.doi.org/10.1021/jf502040e | J. Agric. Food Chem. 2014, 62, 8470−8477

*LC-MS-TOF Isotopomeric and Accurate Mass Analysis.* Maillard-phenolic reaction products were characterized by identifying isotopomers as previously reported (Table 1,[6]). Analysis was conducted with a Waters 2D UPLC Acquity iClass coupled with a Xevo G2 QTof system (Waters, Milford, MA, USA). Accurate mass acquisition of the ion of interest was performed by chromatography injection using dual electroscpray ion source. Reserpine (100 mg/L) was used as the lockspray injecting at 10 μL/min. Injections of 2 μL each of the extracts were injected on ACQUITY UPLC BEH C18 1.7 μm column (2.1 mm × 50 mm; Waters) maintained at a temperature of 25 °C. The mobile phase was maintained at a flow rate of 0.3 mL/min using a binary solvent system of 0.1% formic acid in water (A) and methanol (B). The elution gradient started at 10% B, linearly increased to 90% B (1−6.35 min), held at 100% B (6.35−8.35 min), and then held at 10% B (8.35−10 min). Mass spectrometric ionization conditions were as follows: desolvation temperature of 400 °C; source temperature of 110 °C; capillary voltage of 1.1 kV. For samples analyzed in both positive and negative sensitivity scan mode, the scan range was 50−1000 Da.

**Prep-LC.** Target analytes were purified using a LC system that consisted of a binary pumping system (LC-10 ADvp), a degasser (DGU-14A), an autosampler (SIL-10vp), a variable-wavelength UV−vis detector at 254 and 280 nm (Shimadzu, SPD-10A), a fraction collector (Shimadzu, FRC-10A), and a RP-C18 column (150 mm × 21.2 mm, Pursuit 5, Varian, USA). The HPLC condition was as follows: the injection volume was 1.5 mL, the column temperature was 25 °C, binary mobile system A was 0.1% formic acid aqueous solution, pH 3.0 and B was 100% acetonitrile, column and flow rate was 10 mL/min. The gradient was started with 5% B (0−10 min), then increased to 50% B (10−40 min), then held at 100% B (40−50 min), and then decreased to 5% B (50−70 min). The total run time was 70 min. The effluent was collected with a fraction collector. Compounds **1** and **2**, generated from model A, were collected at 19.5 and 20.5 min, respectively; compounds **3**, **4**, and **5** obtained from model B were collected at 20.3, 21.0, 22.0 min, respectively; compounds **6**, **7**, and **8** were collected at 20.4, 21.4, and 21.9 min, respectively (refer to Figure 1 for compound structures). Second dimension off-line liquid chromatography was conducted for further purification until at least 95% purity was achieved based on $^1$H NMR. The binary mobile phase for the second dimension was as follows: mobile phase A was water with pH = 7; mobile phase B was methanol. The second dimension gradient was started with 5% B (0−5 min), then increased to 20% B (5−10 min), then slowly increased to 30% B (10−40 min), then further increased to 100% B (41−50 min), and then decreased to 5% B (50−60 min). About 0.5−1 mg of the Maillard-catechin adducts was collected as dry mass for each model reaction (models A−C, Table 1).

**Circular Dichroism Spectrum.** For circular dichroism (CD) spectrum, methanolic solutions of the samples were analyzed by means of a Jasco Model CD-1595 circular dichroism chiral detector (Easton, MD, USA; 0.190 ± 0.30° for D- and L-camphorsulfonic acid as references).

**Nuclear Magnetic Resonance Spectrum.** $^1$H, correlation spectroscopy (COSY), heteronuclear multiple quantum coherence (HMQC), heteronuclear multiple bond correlation (HMBC), $^{13}$C, and nuclear Overhauser enhancement spectroscopy (NOESY) nuclear magnetic resonance (NMR) measurements were performed on a Bruker 700 MHz spectrometer with TXI cryoprobe and a Bruker 850 MHz spectrometer with TCI cryoprobe. Data were processed and analyzed with Topspin 3.1 and MestRenova 8.1. Methanol-$d_4$ was used as the NMR solvent. The solvent residual peak of methanol-$d_4$ at $\delta$ 4.78 was set as the internal reference. NOESY correlations were verified within reasonable range (<4 Å) using ChemBio 3D software.

**Sensory Analysis.** *Subjects and Training.* A panel of eight judges (ages 23−45, 3 males and 5 females) from the Department of Food Science and Nutrition, St. Paul, MN, evaluated the bitterness of the test solutions. Prior to analysis, all panelists participated in 12 training sessions of approximately 1 h in duration over a period of 4 weeks. Panelists were initially trained on a 10-point scale with four references provided (0.03, 0.04, 0.08, and 0.15% (w/w) of caffeine in water), corresponding to bitterness intensity ratings of 2, 3.5, 5, and 10, respectively. Inconsistencies in the ratings were addressed with panelists as part of the training.

*Evaluation.* The test samples (Figure 1) were evaluated for bitterness modulation activity. Two separate sample evaluations were conducted. In the first session, all eight test compounds were evaluated followed by a second session consisting of two select compounds (numbers **2** and **7**, Figure 1). For all evaluation sessions, the samples were evaluated in duplicate. Three reference levels were provided (0.03, 0.04, and 0.08% (w/w) of caffeine in water), corresponding to bitterness intensity ratings of 2, 3.5, and 5, respectively. All samples were prepared the morning of the evaluation. During the first session, each test compound (1.9 mg) was added to 32 mL of 0.04% caffeine solution. The ratio of test compound to caffeine was 1:7 (w/w), which was based on the quantification of these two analytes in roasted cocoa (Figure 3).

For the second evaluation session the concentrations of compounds **2** and **7** were doubled to 3.8 mg of each test compound in the 32 mL of 0.04% caffeine solution (ratio of 2:7 (w/w)). Solutions were stirred for 10 min, and then 2 mL of each solution was dispensed in sample cups labeled with three-digit codes. Panelists used a PTFE dropper to dispense 2 mL of solution on the center of their tongue. Water and unsalted crackers were used as palate cleansers.

*Data Analysis.* Ratings were averaged and the differences among treatments were evaluated by analysis of variance (ANOVA) followed by Tukey's HSD pairwise comparison. All analyses were performed with Statistix Software (version 9). Significance was established at $p < 0.05$.

**Sample Preparation of Cocoa Samples.** Samples of 15 g amounts of unroasted or roasted beans (135 °C for 15 min) were ground for 2 min then extracted with a mixture (2:1, v/v; 3 × 100 mL) of ethanol and water for 2 h at room temperature with stirring. The ethanol/water extract was added with methylparaben (100 ppm) as internal standard. Then it was concentrated until precipitate appeared under vacuum (Buchi rotavapor, model R110, New Castle, DE, USA; 0.1 atm; water bath was maintained at 30 °C) and then filtered through a 0.2 μm Nylon tip filter (Sigma-Aldrich Co.) and analyzed by LC-MS.

**LC-MS Identification of Compounds 2 and 7 in Cocoa.** Cocoa isolates were analyzed on a Waters ACQUITY UPLC system interfaced with a Quattro Premier XE mass spectrometer (Waters). Two microliters were injected on to an ACQUITY UPLC BEH C18 1.7 μm column (2.1 mm × 50 mm; Waters) at 25 °C. The mobile phase was maintained at a flow rate of 0.3 mL/min using a binary solvent system of 0.1% formic acid in water (A) and methanol (B). The elution gradient started at 10% B, linearly increased to 90% B (1−6.35 min), held at 100% B (6.35−8.35 min), and then held at 10% B (8.35−10 min). The Quattro Premier XE mass spectrometer was equipped with an electrospray ionization probe, and the operational parameters were positive ion mode, with a source temperature of 110 °C, desolvation temperature of 350 °C, and capillary voltage of 3.0 kV. Data were collected in multiple-reaction monitoring (MRM) mode. The ion transitions for the compounds were optimized according to the ion intensity of the product ion through full scan MS/MS. The MRM method was optimized by direct infusion of authentic compounds. The MS acquisition was collected as follows: compound **2**, $m/z$ 435 → 283 and 435 → 417, cone 35 V, collision 15 V; compound **7**, $m/z$ 435 → 247 and 435 → 123, cone 30 V, collision 20 V.

**LC-MS Quantification of Compound 2 and Caffeine in Cocoa.** Analysis was conducted by LC-MS in MRM mode. The ion transitions for the compounds were as follows: compound **2**, $m/z$ 435 → 283 and 435 → 417, cone 30 V, collision 15 V; caffeine, $m/z$ 195 → 138 and 195 → 110, cone 30 V, collision 20 V. The dwell time was 0.5 s for the analytes; the interscan delay was 0.1 s, and interchannel delay was 0.005 s. All samples were analyzed in duplicate. Quantification was conducted by internal standard (methylparaben, 0.3 M) and external five-point calibration curve of compound **2** and caffeine at $10^{-2}$−$10^2$ mM that showed good linearity with regression coefficient ranging from 0.97 to 0.99.

**Spectral Data of Compounds 1−8 (Figure 1).** *Compound **1**, (2R,2′R,3S,3′S,4S,5R)-2′-(3,4-Dihydroxyphenyl)-5-(hydroxymethyl)-2′,3′,4,4′,5,9′-hexahydro-3H-spiro[furan-2,8′-furo[2,3-h]chromene]-3,3′,4,5′-tetraol.* CD (MeOH): 280 (−0.12). MS-TOF: *m/z* 433.1123 ([M − H]$^-$, 3 ppm). $^1$H NMR (700 MHz, $CD_3OD$): $\delta$ 2.46 [dd, 1H, *J* = 16.1, 7 Hz, H−C(4b)], 2.69 [dd, 1H, *J* = 16.1, 4.9 Hz, H−C(4a)], 2.82 [d, 1H, *J* = 16.8 Hz, H−C(1″b)], 3.30 [d, 1H, *J* = 16.8 Hz, H−C(1″a)], 3.55 [dd, 1H, *J* = 11.9, 3.5 Hz, H−C(6″b)], 3.65 [dd, 1H, *J* = 11.9, 3.5 Hz, H−C(6″a)], 3.87 [dd, 1H, *J* = 5.6, 3.5 Hz, H−C(4″)], 3.94 [m, 1H, H−C(3)], 3.95 [m, 1H, H−C(5″)], 4.02 [d, 1H, *J* = 3.5 Hz, H−C(3″)], 4.61 [d, 1H, *J* = 7 Hz, H−C(2)], 5.87 [s, 1H, H−C(6)], 6.65 [dd, 1H, *J* = 7.7, 2.1 Hz, H−C(6′)], 6.70 [d, 1H, *J* = 7.7 Hz, H−C(5′)], 6.73 [d, 1H, *J* = 2.1 Hz, H−C(2′)]. $^{13}$C NMR (175 MHz, $CD_3OD$): $\delta$ 28.1 [C-4], 33.6 [C-1″], 62.9 [C-6″], 68.6 [C-3], 78.9 [C-4″], 82.5 [C-3″], 82.6 [C-2], 85.6 [C-5″], 91.2 [C-6], 101.6 [C-10], 103.3 [C-8], 114.9 [C-2′], 116.2 [C-5′], 119.7 [C-6′], 121.1 [C-2″], 132.2 [C-1′], 146.2 [C-3′, C-4′], 152.1[C-9], 156.9 [C-5], 158.8 [C-7].

*Compound **2**, (2R,3S,4S,5R,6′S,7′R)-7′-(3,4-Dihydroxyphenyl)-5-(hydroxymethyl)-4,5,6′,7′-tetrahydro-3H,3H′,5′H-spiro[furan-2,2′-furo[3,2-g]chromene]-3,4,4′,6′-tetraol.* CD (MeOH): 280(−0.22). MS-TOF: *m/z* 433.1123 ([M − H]$^-$, 3 ppm). $^1$H NMR (700 MHz, $CD_3OD$): $\delta$ 2.50 [dd, 1H, *J* = 16.1, 7.7 Hz, H−C(4b)], 2.80 [dd, 1H, *J* = 16.1, 5.6 Hz, H−C(4a)], 2.89 [d, 1H, *J* = 16.8 Hz, H−C(1″b)], 3.42 [d, 1H, *J* = 16.8 Hz, H−C(1″a)], 3.63 [dd, 1H, *J* = 11.9, 3.5 Hz, H−C(6″b)], 3.74 [dd, 1H, *J* = 11.9, 3.5 Hz, H−C(6″a)], 3.93 [m, 1H, H−C(4″)], 3.95 [m, 1H, H−C(3)], 4.00 [m, 1H, H−C(5″)], 4.18 [d, 1H, *J* = 3.5 Hz, H−C(3″)], 4.56 [d, 1H, *J* = 7 Hz, H−C(2)], 5.88 [s, 1H, H−C(8)], 6.68 [dd, 1H, *J* = 8.4, 2.1 Hz, H−C(6′)], 6.72 [d, 1H, *J* = 8.4 Hz, H−C(5′)], 6.80 [d, 1H, *J* = 1.4 Hz, H−C(2′)]. $^{13}$C NMR (175 MHz, $CD_3OD$): $\delta$ 28.9 [C-4], 33.8 [C-1″], 62.9 [C-6″], 68.7 [C-3], 78.9 [C-4″], 82.6 [C-3″], 82.8 [C-2], 85.5 [C-5″], 91.2 [C-8], 102.3[C-10], 104.6 [C-6], 115.2 [C-2′], 116.2 [C-5′], 120.0[C-6′], 120.8 [C-2″], 132.2 [C-1′], 146.3 [C-3′, C-4′], 152.5 [C-5], 156.2 [C-9], 159.0 [C-7].

*Compound **3**, (2R,3S)-2-(3,4-dihydroxyphenyl)-8-((2S,3R,4S,5R)-3,4,5-trihydroxytetrahydro-2H-pyran-2-yl)chromane-3,5,7-triol.* MS-TOF: *m/z* 421.1148 ([M − H]$^-$, 1 ppm). $^1$H NMR (700 MHz, $CD_3OD$): $\delta$ 2.45 [dd, 1H, *J* = 16.1, 7.7 Hz, H−C(4b)], 2.67 [dd, 1H, *J* = 16.1, 4.9 Hz, H−C(4a)], 3.22 [dd, 1H, *J* = 11.2, 10.5 Hz, H−C(5″b)], 3.31 [dd, 1H, *J* = 9.1, 8.4, H−C(3″)], 3.54 [ddd, 1H, *J* = 10.5, 9.1, 5.6 Hz, H−C(4″)], 3.58 [dd, 1H, *J* = 9.4, 8.4, H−C(2″)], 3.90 [ddd, 1H, *J* = 7, 7, 4.9 Hz, H−C(3)], 3.95 [dd, 1H, *J* = 11.2, 5.6 Hz, H−C(5″a)], 4.53 [d, 1H, *J* = 7 Hz, H−C(2)], 4.65 [d, 1H, *J* = 9.4 Hz, H−C(1″)], 5.86 [s, 1H, H−C(6)], 6.59 [dd, 1H, *J* = 8.4, 2.1 Hz, H−C(5′)], 6.64 [d, 1H, *J* = 8.4 Hz, H−C(6′)], 6.70 [d, 1H, *J* = 2.1 Hz, H−C(2′)]. $^{13}$C NMR (175 MHz, $CD_3OD$): $\delta$ 27.7 [C-4], 68.2 [C-3], 70.9 [C-4″], 71.7 [C-5″], 74.3 [C-2″], 78.0 [C-1″], 79.5 [C-3″], 82.1 [C-2], 96.1 [C-6]. 101.9 [C-10], 103.1 [C-8], 110.5 [C-2′], 115.7 [C-6′], 119.3 [C-5′], 132.1 [C-1′], 146.3 [C-3′, C-4′], 156.0 [C-5], 156.1 [C-9], 156.2 [C-7].

*Compound **4**, (2S,2′R,3S,3′S,4R)-2′-(3,4-dihydroxyphenyl)-3′,4,4′,5-tetrahydro-2′H,3H,9′H-spiro[furan-2,8′-furo[2,3-h]chromene]-3,3′,4,5′-tetraol.* MS-TOF: *m/z* 403.1015 ([M − H]$^-$, 4 ppm). $^1$H NMR (700 MHz, $CD_3OD$): $\delta$ 2.43 [dd, 1H, *J* = 16.1, 7 Hz, H−C(4b)], 2.72 [dd, 1H, *J* = 16.1, 5.6 Hz, H−C(4a)], 2.78 [d, 1H, *J* = 16.1 Hz, H−C(1″a)], 3.28 [d, 1H, *J* = 16.1 Hz, H−C(1″b)], 3.73 [dd, 1H, *J* = 8.4, 3.5 Hz, H−C(5″b)], 3.91 [ddd, 1H, *J* = 7, 7, 5.6 Hz, H−C(3)], 3.98 [d, 1H, *J* = 1.4 Hz, H−C(3″)], 4.13 [m, 1H, H−C(4″)], 4.16 [dd, 1H, *J* = 8.4, 7.7 Hz, H−C(5″a)], 4.45 [d, 1H, *J* = 7 Hz, H−C(2)], 5.85 [s, 1H, H−C(6)], 6.62 [dd, 1H, *J* = 8.4, 2.1 Hz, H−C(6′)], 6.66 [d, 1H, *J* = 8.4 Hz, H−C(5′)], 6.73 [d, 1H, *J* = 2.1 Hz, H−C(2′)]. $^{13}$C NMR (175 MHz, $CD_3OD$): $\delta$ 28.2 [C-4], 33.4 [C-1″], 68.7 [C-3], 74.4 [C-5″], 78.1 [C-4″], 82.2 [C-3″], 82.7 [C-2], 96.2 [C-6], 101.5 [C-10], 103.3 [C-8], 114.9 [C-2′], 116.1 [C-5′], 119.7 [C-6′], 121.5 [C-2″], 132.2 [C-1′], 146.3 [C-3′, C-4′], 152.1 [C-9], 156.8 [C-5], 158.8 [C-7].

*Compound **5**, (2S,3S,4R,6′S,7′R)-7′-(3,4-Dihydroxyphenyl)-4,5,6′,7′-tetrahydro-3H,3′H,5′H-spiro[furan-2,2′-furo[3,2-g]chromene]-3,4,4′,6′-tetraol.* MS-TOF: *m/z* 403.1015 ([M − H]$^-$, 4 ppm). $^1$H NMR (700 MHz, $CD_3OD$): $\delta$ 2.44 [dd, 1H, *J* = 16.1, 7.7 Hz, H−C(4b)], 2.72 [dd, 1H, *J* = 16.1, 3.5 Hz, H−C(4a)], 2.89 [d, 1H, *J* = 16.1 Hz, H−C(1″b)], 3.12 [d, 1H, *J* = 16.1, H−C(1″a)], 3.53 [dd, 1H, *J* = 9.1, 5.6 Hz, H−C(5″b)], 3.84 [d, 1H, *J* = 7.7 Hz, H−C(3″)], 3.90 [m, 1H, H−C(3)], 4.12 [m, 1H, H−C(5″a)], 4.29 [m, 1H, H−C(4″)], 4.57 [d, 1H, *J* = 7 Hz, H−C(2)], 5.87 [s, 1H, H−C(8)], 6.60 [dd, 1H, *J* = 8.4 1.4 Hz, H−C(6′)], 6.65 [d, 1H, *J* = 8.4 Hz, H−C(5′)], 6.71 [d, 1H, *J* = 1.4 Hz, H−C(2′)]. $^{13}$C NMR (175 MHz, $CD_3OD$): $\delta$ 30.0 [C-4], 35.5 [C-1″], 69.0 [C-3], 72.5 [C-5″], 75.7 [C-4″], 83.2 [C-3″], 83.3 [C-2], 91.7 [C-8], 102.1 [C-10], 103.6 [C-6], 115.4 [C-2′], 116.5 [C-5′], 118.1 [C-2″], 120.2 [C-6′], 132.6 [C-1′], 146.7 [C-3′, C-4′], 152.5 [C-9], 157.6 [C-5], 159.6 [C-7].

*Compound **6**, (2R,3S,4R,5R,6′S,7′R)-7′-(3,4-Dihydroxyphenyl)-5-(hydroxymethyl)-4,5,6′,7′-tetrahydro-3H,3′H,5′H-spiro[furan-2,2′-furo[3,2-g]chromene]-3,4,4′,6′-tetraol.* MS-TOF: *m/z* 433.1123 ([M − H]$^-$, 3 ppm). $^1$H NMR (700 MHz, $CD_3OD$): $\delta$ 2.47 [dd, 1H, *J* = 16.1, 8.4 Hz, H−C(4b)], 2.80 [dd, 1H, *J* = 16.1, 5.6 Hz, H−C(4a)], 2.88 [d, 1H, *J* = 16.1 Hz, H−C(1″b)], 3.42 [d, 1H, *J* = 16.1 Hz, H−C(1″a)], 3.66 [dd, 1H, *J* = 19.6, 4.2, H−C(6″b)], 3.67 [dd, 1H, *J* = 19.6, 4.2 Hz, H−C(6″a)], 3.90 [m, 1H, H−C(3)], 3.97 [d, 1H, *J* = 5.6 Hz, H−C(3″)], 4.17 [m, 1H, H−C(5″)], 4.48 [d, 1H, *J* = 7.7 Hz, H−C(2)], 4.53 [m, 1H, H−C(4″)], 5.78 [s, 1H, H−C(8)], 6.63 [dd, 1H, *J* = 7.7, 1.4 Hz, H−C(6′)], 6.68 [d, 1H, *J* = 7.7 Hz, H−C(5′)], 6.75 [d, 1H, *J* = 1.4 Hz, H−C(2′)]. $^{13}$C NMR (175 MHz, $CD_3OD$): $\delta$ 29.0 [C-4], 33.9 [C-1″], 61.6 [C-6″], 68.9 [C-3], 72.7 [C-4″], 76.5 [C-3″], 81.8 [C-5″], 83.0 [C-2], 91.1 [C-8], 102.4 [C-10], 104.7 [C-6], 115.4 [C-2′], 116.2 [C-5′], 120.1 [C-6′], 120.2 [C-2″], 132.3 [C-1′], 146.4 [C-3′, C-4′], 152.6 [C-5], 156.4 [C-9], 159.0 [C-7].

*Compound **7**, (2R,3S,3′S,4′S,5′R,8S)-2-(3,4-Dihydroxyphenyl)-3,3′,4,4′,5′,6′-hexahydro-2H,9H-spiro[furo[2,3-h]chromene-8,2′-pyran]-3,3′,4′,5,5′-pentaol.* CD (MeOH): 280 (−0.06). MS-TOF: *m/z* 433.1223 ([M − H]$^-$, 3 ppm). $^1$H NMR (700 MHz, $CD_3OD$): $\delta$ 2.47 [dd, 1H, *J* = 17.2, 5.1 Hz, H−C(4b)], 2.72 [dd, 1H, *J* = 17.2, 6.9 Hz, H−C(4a)], 2.84 [d, 1H, *J* = 17.2 Hz, H−C(1″b)], 3.13 [d, 1H, *J* = 17.2 Hz, H−C(1″a)], 3.55 [dd, 1H, *J* = 11.1, 11.1 Hz, H−C(6″b)], 3.61 [dd, 1H, *J* = 11.1, 5.6 Hz, H−C(6″a)], 3.73 [dd, 1H, *J* = 11.1, 3.4 Hz, H−C(4″)], 3.75 [d, 1H, *J* = 3.4 Hz, H−C(3″)], 3.81 [ddd, 1H, *J* = 11.1, 11.1, 5.6 Hz, H−C(5″)], 3.93 [ddd, 1H, *J* = 7.7, 6.9, 5.1 Hz, H−C(3)], 4.60 [d, 1H, *J* = 7.7 Hz, H−C(2)], 5.87 [s, 1H, H−C(6)], 6.62 [dd, 1H, *J* = 8.5, 1.7 Hz, H−C(6′)], 6.67 [d, 1H, *J* = 8.5 Hz, H−C(5′)], 6.74 [d, 1H, *J* = 1.7 Hz, H−C(2′)]. $^{13}$C NMR (175 MHz, $CD_3OD$, HSQC and HMBC): $\delta$ 26.1 [C-4], 36.3 [C-1″], 63.2 [C-6″], 65.1 [C-5″], 67.0 [C-3], 70.6 [C-4″], 70.8 [C-3″], 79.8 [C-2], 88.4 [C-6], 100.3 [C-10], 101.2 [C-8], 101.0 [C-2′], 112.2 [C-2″], 116.5 [C-5′], 118.4 [C-6′], 130.4 [C-1′], 143.2 [C-3′, C-4′], 150.6 [C-9], 155.2 [C-5], 158.3 [C-7].

*Compound **8**, (2R,3S,4S,5R)-2-(((2R,3S)-2-(3,4-dihydroxyphenyl)-3,5,7-trihydroxychroman-8-yl)methyl)tetrahydro-2H-pyran-2,3,4,5-tetraol.* CD (MeOH): 280 (−0.10). MS-TOF: *m/z* 451.1235 ([M − H]$^-$, 2 ppm). $^1$H NMR (700 MHz, $CD_3OD$): $\delta$ 2.45 [dd, 1H, *J* = 16.1, 8.4 Hz, H−C (4b)], 2.77 [d, 1H, *J* = 14.7 Hz, H−C (1″b)], 2.80 [dd, 1H, *J* = 16.1, 5.6 Hz, H−C(4a)], 2.98 [d, 1H, *J* = 14.7 Hz, H−C(1″a)], 3.45 [d, 1H, *J* = 3.5 Hz, H−C(3″)], 3.48 [dd, 1H, *J* = 9.8, 9.8 Hz, H−C(6″b)], 3.49 [dd, 1H, *J* = 9.8, 6.3 Hz, H−C(6″a)], 3.60 [dd, 1H, *J* = 9.8, 3.5 Hz, H−C(4″)], 3.68 [ddd, 1H, *J* = 9.8, 9.8, 6.3 Hz, H−C(5″)], 3.95 [ddd, 1H, *J* = 7.7, 7.7, 5.6 Hz, H−C(3)], 4.58 [d, 1H, *J* = 7.7 Hz, H−C(2)], 5.99 [s, 1H, H−C(6)], 6.64 [dd, 1H, *J* = 8.4, 1.4 Hz, H−C(6′)], 6.68 [d, 1H, *J* = 8.4 Hz, H−C(5′)], 6.74 [d, 1H, *J* = 1.4 Hz, H−C(2′)]. $^{13}$C NMR (175 MHz, $CD_3OD$, HSQC and HMBC): $\delta$ 28.0 [C-4], 31.2 [C-1″], 63.0 [C-6″], 67.1 [C-5″], 67.5 [C-3], 71.2 [C-4″], 73.4 [C-3″], 83.6 [C-2], 96.9 [C-6], 100.2 [C-10], 101.1 [C-8], 114.5 [C-2′], 115.3 [C-5′], 119.2 [C-6′], 132.0 [C-1′], 145.3 [C-3′, C-4′], 154.1 [C-9], 155.5 [C-7], 156.2 [C-5].

## RESULTS AND DISCUSSION

In order to investigate the influence of thermal reactions on the modulation of bitterness in food, catechin, a known dietary bitter compound, was reacted in simple Maillard reaction model systems consisting of a simple sugar (glucose, galactose, or xylose) and glycine (Table 1, Models A−C). It was expected

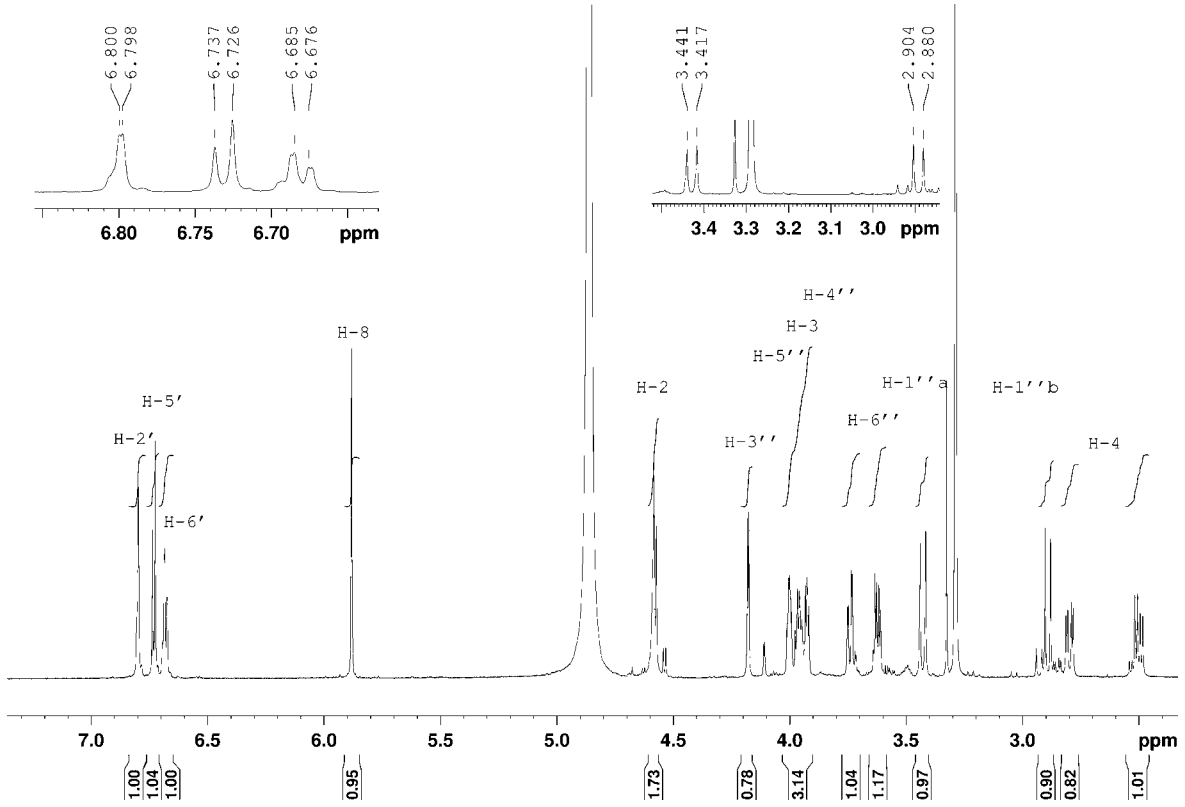


**Figure 2.** $^{1}$H spectrum of compound **2**.

**Table 2. Assignment of $^{1}$H and $^{13}$C of Compound 2 Generated from Glucose−Glycine−Catechin Model Reaction**[a,b]

| assignment | | $\delta_H$ | $\delta_C$ | COSY | HMBC |
|---|---|---|---|---|---|
| glucose | 1″a | 3.42 (d, $J$ = 16.8 Hz) | 33.8 | | C5, C6, C7, C2″, C3″ |
| | 1″b | 2.89 (d, $J$ = 16.8 Hz) | | | |
| | 2″ | / | 120.8 | | H1″a, H1″b, H3″ |
| | 3″ | 4.18 (d, $J$ = 3.5 Hz) | 82.6 | | C2″, C4″ |
| | 4″ | 3.93 (m) | 78.9 | | C3″ |
| | 5″ | 4.00 (m) | 85.5 | H6″ | C4″ |
| | 6″a | 3.74 (dd, $J$ = 11.9, 3.5 Hz) | 62.9 | H5″ | C4″, C5″ |
| | 6″b | 3.63 (dd, $J$ = 11.9, 3.5 Hz) | | | |
| catechin | 2 | 4.56 (d, $J$ = 7 Hz) | 82.8 | H3 | C4, C3, C1′, C2′, C6′, C9 |
| | 3 | 3.95 (m) | 68.7 | H2, H4a, H4b | C2, C4, C10, C1′ |
| | 4a | 2.80 (dd, $J$ = 16.1, 5.6 Hz) | 28.9 | H3 | C3, C2, C10, C5, C9 |
| | 4b | 2.50 (dd, $J$ = 16.1, 7.7 Hz) | | | |
| | 5 | / | 152.5 | | H4a, H4b, H1″a, H1″b |
| | 6 | / | 104.6 | | H1″a, H1″b |
| | 7 | / | 159.0 | | H8, H1″a, H1″b |
| | 8 | 5.88 (s) | 91.2 | | C7, C9 |
| | 9 | / | 156.2 | | H8, H4a, H4b |
| | 10 | / | 102.3 | | H3, H4a, H4b |
| | 1′ | / | 132.2 | | H2, H3, H2′, H5′, H6′ |
| | 2′ | 6.80 (d, $J$ = 1.4 Hz) | 115.2 | | C1′, C3′, C4′, C6′ |
| | 3′ | / | 146.3 | | H2′, H5′ |
| | 4′ | / | 146.3 | | H2′, H5′, H6′ |
| | 5′ | 6.72 (d, $J$ = 8.4 Hz) | 116.2 | H6′ | C4′, C6′, C1′, C3′ |
| | 6′ | 6.68 (dd, $J$ = 8.4, 2.1 Hz) | 120.0 | H5′ | C1′, C5′, C2′, C4′ |

[a] $^{1}$H NMR experiment was conducted on a 700 MHz cryoprobe. Samples were dissolved in $CD_3OD$. [b] The identified structure is matched with ref 10.

the unique stereocenters of the two hexose sugars would be transferred to catechin-Maillard reaction products, providing the ability to investigate structure−activity relationships on bitter perception. Additionally, the pentose sugar (xylose) was selected similarly to provide additional reaction products. Utilization of simple Maillard model systems provided the


dx.doi.org/10.1021/jf502040e | J. Agric. Food Chem. 2014, 62, 8470−8477

**Scheme 1. Proposed Mechanism for Generating the spiro-*C*-Glycosides**

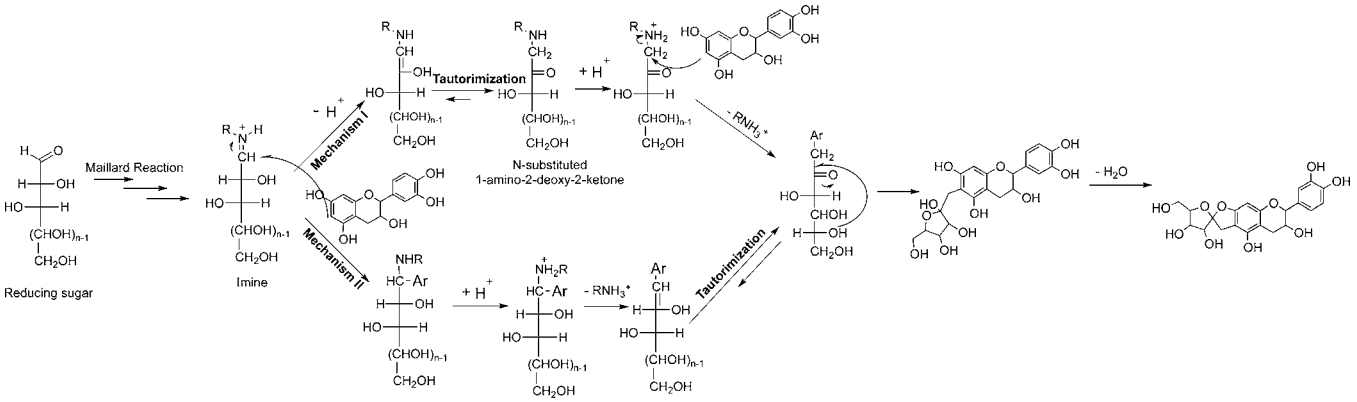


ability to enrich one of the reactants (in this example the simple sugar) with $^{13}$C-labeling for the identification of phenolic-Maillard reaction products (Table 1, Models D−F) as we as we have previously reported.[6]

**Identification of Catechin−*C*-spiro-Glycoside Adducts.** Adducts were identified by LC-MS isotopomeric analysis of Models D−F, with the same unlabeled parent ion reported in Models A−C, respectively, at the same retention time. Isotopomeric analysis of models D−F indicated an intact sugar moiety was incorporated in the selected products. No reaction products were also detected in models H (glucose and glycine) and I (catechin only). Similarly reaction products were not identified in model G (glucose and catechin), indicating the importance of the amino acid for product generation. Overall, eight main reaction products were identified and isolated for structural determination.

Two reaction products (compound **1** and compound **2**, Figure 1) were isolated from model A (catechin, glucose, and glycine). The carbons from the sugar moiety are noted as 1″ to 6″ while the carbons from catechin are marked as 2 to 9 and 1′ to 6′. For compound **1**, the majority of the $^{1}$H spectra of (+)-catechin (data not shown) were easily deduced. A pair of doublets at 3.30 and 2.82 with *J*-coupling of 16.8 Hz indicated a pair of geminal hydrogens is incorporated and connected directly to the A ring of catechin, which is unique compared with other flavan-3-ol−*C*-glycosides that have been reported.[4] According to NMR HMBC spectrum, the sugar moiety was connected through C-8. In considering the distinctive carbon chemical shifts, the 7-hydroxyl loses one molecule of water with the C-2″ acetal group forming a spiro [4,4] structure. The structure of the sugar moiety is supported by ref 9. NOESY spectrum shows spatial correlation between H-1″ and H-6″ and correlation between H-1″ and H-4″. In consideration of the stereochemistry of the starting material as well, the stereochemistry of compound **1** is indicated in Figure 1.

Compound **2**, based on the $^{1}$H spectrum (Figure 2), again shows a pair of geminal hydrogens connecting between catechin and the sugar moiety; compound **2** is distinctive in its HMBC correlations compared with the assignment of compound **1**. The presence of $^{3}J_{\text{H1″-C7}}$ and $^{3}J_{\text{H1″-C5}}$ indicate that the sugar moiety is connected to the C-6 of catechin as shown in Table 2. Spatial correlation is shown in Figure 1 according to NOESY correlations.[10] It is found that the volume ratio of H3″−H4″ cross-peak and H1″a−H1″b (1.8 Å) cross-peak is 0.0053, which shows H3″ and H4″ have a very weak NOESY correlation; thus H3″ and H4″ are not planar.

For model B (catechin, xylose, and glycine, Table 1) compounds **3**, **4**, and **5** (Figure 1) were isolated. According to the molecular mass (MW = 422), compound **3** is different from other analytes isolated in model B (MW = 404), which indicates one less dehydration step occurred. Moreover, no methylene moiety is found in connection with the A ring of catechin which renders compound **3** structurally different from others. The $^{13}$C chemical shift (82−68 ppm) indicates no acetal group was incorporated. Additionally, a pyran ring formed for the distinctive chemical shift of C-3″ and C-4″(<78 ppm). The *J*-coupling constants of H1″−H2″, H2″−H3″, H3″−H4″, and H4″−H5″b are 9−10 Hz while H4″−H5″a is 5 Hz, indicating all of the hydrogens of the sugar moiety are axial hydrogens except H5″a is equatorial.[11] The structure of xyloside moiety is further supported by ref 12.

For compounds **4** and **5**, HMBC spectrum shows xyloside is connected to catechin C-8 for compound **4** while the xyloside of compound **5** is attached to the C-6 of catechin. A typical furan carbohydrate carbon chemical shift is observed for compound **4** and compound **5**. H-1″ has NOESY correlation with H-3″ in compound **4** and compound **5** supported by refs 13−15.

For model C (catechin, galactose, and glycine) compounds **6**, **7**, and **8** (Figure 1) were isolated. For compound **6**, COSY and HMBC spectra followed the same trend as that of compound **2**. However, the chemical shifts of the sugar moiety at the 3″, 4″, and 5″ and the coupling constants are unique compared with compound **2**; hence, the stereochemistry of the sugar moiety of compound **6** is different from compound **2**. NOESY shows H1″−H6″ and H3″−H4″ correlations of similar strengths, indicating that the stereochemistry of compound **6** at the 4″ position is different from that at compound **2**. For compound **6**, H-3″ is much closer to H-4″ compared with that in compound **2** since the volume ratio of NOESY correlations H3″−H4″ and H1″a−H1″b is 0.88, much higher than that for compound *2*. Therefore, compound *6* was reported as a diastereomer of compound *2*.

The HMBC spectrum of compound **7** shows H-1″ has correlations with C-7 and C-9; thus the reaction happens on the C-7 and the C-8 of catechin. Moreover, HMBC correlations confirm that there are correlations between H6″−C2″ corresponding to a pyran ring spiro-fused with a furan ring. Additionally, the carbon chemical shifts of the sugar moiety belong to a [4,5] ring instead of a [4,4] ring structure. H1″−H3″ NOESY correlation indicates the stereochemistry as shown in Figure 2.[16,17]


dx.doi.org/10.1021/jf502040e | J. Agric. Food Chem. 2014, 62, 8470−8477

For compound **8**, it is a C-8 substituted *C*-glycoside adduct. The 6″ hydroxyl group loses one molecule of water to form the acetal with C-1″ as confirmed by HMBC correlation (C1″−H6″). As illustrated above, the stereochemistry of compound **8** is discussed by both NOESY and *J*-coupling constants.[18,19]

**Plausible Mechanisms for the Spirocyclic Catechin-Maillard Products Generation.** To gain insights into how the catechin−*C*-spiro-glycosides were generated in these simple model Maillard reaction systems, two mechanisms are proposed. In mechanism I (see Scheme 1), the Maillard-derived imine rearranges to the keto form of the N-substituted 1-amino-2-deoxy-2-ketone, which is then protonated and trapped by catechin at the $\alpha$ to the carbonyl group.[20,21] The 5-hydroxyl group of the sugar moiety then attacks the carbonyl to form an acetal. According to LC-MS, one molecule of water is lost; hence, the spirocyclic glycoside catechin is formed. For mechanism II, catechin traps the cation of the imine, then undergoes elimination followed with tautomerization to afford the same catechin-Maillard intermediate, and then dehydrated and ring-closed to generate the spiro-*C*-glycosides product.

**Taste-Modifying Activity of Maillard-Catechin Products.** The eight isolated Maillard-catechin compounds (Figure 1) were screened for bitter modulation activity in a caffeine solution (see Table 3). Caffeine was selected because it is a highly ubiquitous dietary bitter compound and has been previously used to screen for bitter masking compounds.[22] Additionally, caffeine is also a major bitter compound found in cocoa.[23] To provide perhaps a more food-relevant dosage, both compounds **2** and **7** were screened in cocoa beans. Only compound **2** was identified in cocoa and was subsequently quantified in addition to caffeine. The concentration of compound **2** is reported in Figure 3, for both unroasted and roasted cocoa. The concentration of compound **2** in roasted cocoa is approximately three times higher in comparison to unroasted cocoa, suggesting it was not only a natural product of microbial provenance in cocoa beans but also generated through roasting (thermal treatment) as well. Similar compound structures (*C*-spiro-glycoside flavonoids) such as compound **2** have been previously reported as fungal products with anti-inflammation activities.[24,25] Comparing the concentration of compound **2** (0.15 mg/g) to the concentration of caffeine (1.03 mg/g) in roasted cocoa, a concentration ratio of 7:1 (caffeine:test compound) was determined. At the same concentration level (caffeine:test compound = 7:1, w/w) trends in the bitterness enhancement or suppression were observed among the different compound structures, albeit there were no significant differences in bitter ratings between caffeine base and caffeine with test compounds added. Unfortunately, dose−response analysis was beyond the scope of this project due to the limited quantities of the reaction products available. However, based on the noted suppression of the average bitterness rating for both compounds **2** (generated from glucose, glycine, and catechin) and **7** (generated from galactose, glycine, and catechin), these compounds were further selected for evaluation at a higher dosage level. Subsequently, compound **2** was added at a double dosage level (caffeine:test compound = 7:2, w/w) to further investigate potential modulation activity (see Table 4); compound **7** was also included for comparison. In the cocoa sample, an isomer of compound **2** consisting of epicatechin (as apposed to catechin) was also predicted by MS/MS fragmentation analysis and reported to be at a similar concentration (data not shown). This suggested epicatechin reaction product was not isolated from cocoa, nor was the taste activity tested. Given that compound **2** was a natural (fungal) product in the raw beans and also generated by thermal processing as well as other similar reaction products could be generated, the assessment of compound **2** at 2-fold the concentration reported in the beans used in the current study (Figure 3) was predicted to be within normal natural product variation. At this higher dosage level compound **2** was reported to significantly decrease the bitterness perception of the caffeine solution or compound **2**

**Table 3. Mean Bitterness Intensity Ratings of 0.04% Caffeine Solution with and without Maillard-Catechin (MC) Compounds at a 7:1 Mass Ratio**

| samples (7:1, w/w)[a] | bitterness ratings[b] | SD |
|---|---|---|
| caffeine: MC 5 | 3.95a | 0.95 |
| caffeine: MC 6 | 3.77a | 0.73 |
| caffeine: MC 1 | 3.60a | 0.99 |
| caffeine: MC 3 | 3.51a | 0.68 |
| caffeine: MC 4 | 3.45a | 0.82 |
| caffeine: MC 8 | 3.40a | 1.46 |
| caffeine | 3.31a | 0.71 |
| caffeine: MC 7 | 3.06a | 0.79 |
| caffeine: MC 2 | 3.05a | 1.08 |

[a]Derived from quantitation of MC 2 and caffeine in roasted cocoa (Figure 3). [b]Bitterness ratings are based on 10-point rating scale; a rating of 2, 3.5, and 5 corresponded to 0.03%, 0.04%, and 0.08% caffeine solution, respectively. Mean ratings with letters in common do not differ significantly (5% significance level).

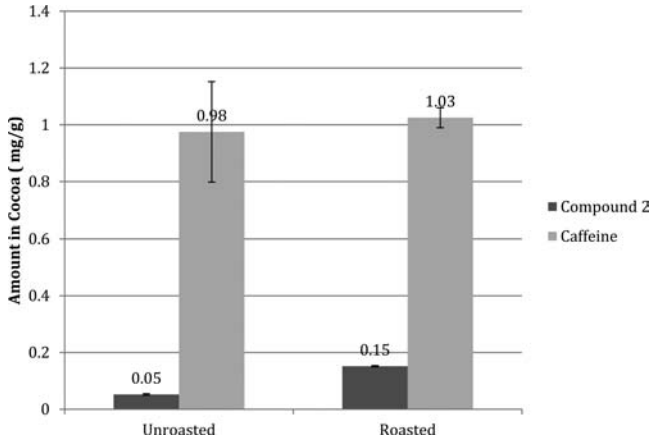


**Figure 3.** Mean concentrations of compound **2** and caffeine in roasted and unroasted cocoa. (Error bars represent standard deviation from duplicate extraction.)

**Table 4. Mean Bitterness Intensity Ratings of 0.04% Caffeine Solutions with and without Maillard-Catechin (MC) Compounds 2 and 7 at a Scaled-up 7:2 Mass Ratio**

| test samples (7:2, w/w) | bitterness rating[a] | SD |
|---|---|---|
| caffeine | 3.50a | 0.46 |
| caffeine: MC 7 | 3.19ab | 0.85 |
| caffeine: MC 2 | 2.75b | 0.66 |

[a]Bitterness ratings are based on 10-point rating scale; a rating of 2, 3.5, and 5 corresponded to 0.03%, 0.04%, and 0.08% caffeine solution, respectively. Mean ratings with letters in common do not differ significantly (5% significance level).

functioned as a bitter blocker (Table 4). This finding suggested the bitterness attributes of cocoa beans and related products could be influenced not just by bitter compounds but also by compounds that modulate this taste attribute.

In summary, the chemical modification of a dietary bitter compound by common thermally induced food reactions was reported to modulate this taste attribute. The role of reaction products of taste compounds on the flavor properties of foodstuffs is not well understood and provides a novel basis to develop food processing strategies for flavor optimization by suppressing or enhancing specific taste attributes of interest.

## AUTHOR INFORMATION

### Corresponding Author

*E-mail: dgp@umn.edu. Phone: (612)624-3201. Fax: (612) 625-5272.

### Notes

The authors declare no competing financial interest.

## ACKNOWLEDGMENTS

We acknowledge the Minnesota NMR center for the use of the NMR instrumentation as well as Wei You (Indiana University, Bloomington) for assistance on data interpretation.

## REFERENCES

(1) Hofmann, T.; Ho, C.; Pickenhagen, W. Challenges in taste research: Present knowledge and future implications. *Challenges Taste Chem. Biol.* **2004**, *867*, 1−24.

(2) Gaudette, N. J.; Pickering, G. J. The efficacy of bitter blockers on health-relevant bitterants. *J. Funct. Foods* **2012**, *4*, 177−184.

(3) Ley, J. P. Masking bitter taste by molecules. *Chemosens. Percept.* **2008**, *1*, 58−77.

(4) Stark, T.; Hofmann, T. Application of a molecular sensory science approach to alkalized cocoa (*Theobroma cacao*): Structure determination and sensory activity of nonenzymatically C-glycosylated flavan-3-ols. *J. Agric. Food Chem.* **2006**, *54*, 9510−9521.

(5) Behrens, M.; Meyerhof, W. Bitter taste receptors and human bitter taste perception. *Cell. Mol. Life Sci.* **2006**, *63*, 1501−1509.

(6) Totlani, V. M.; Peterson, D. G. Influence of epicatechin reactions on the mechanisms of Maillard product formation in low moisture model systems. *J. Agric. Food Chem.* **2007**, *55*, 414−420.

(7) Totlani, V. M.; Peterson, D. G. Reactivity of epicatechin in aqueous glycine and glucose Maillard reaction models: quenching of C2, C3, and C4 sugar fragments. *J. Agric. Food Chem.* **2005**, *53*, 4130−4135.

(8) Jiang, D.; Chiaro, C.; Maddali, P.; Prabhu, K. S.; Peterson, D. G. Identification of hydroxycinnamic acid—Maillard reaction products in low-moisture baking model systems. *J. Agric. Food Chem.* **2009**, *57*, 9932−9943.

(9) Qi, J.; Lu, J.; Liu, J.; Yu, B. Flavonoid and a rare benzophenone glycoside from the leaves of Aquilaria sinensis. *Chem. Pharm. Bull.* **2009**, *57*, 134−137.

(10) Bläs, B.; Zapp, J.; Becker, H. *ent*-Clerodane diterpenes and other constituents from the liverwort *Adelanthus lindenbergianus* (Lehm.) Mitt. *Phytochemistry* **2004**, *65*, 127−137.

(11) Pretsch, E.; Bühlmann, P.; Affolter, C. *Structure determination of organic compounds*; Springer: Berlin, 2000.

(12) Shie, J.; Chen, C.; Lin, C.; Ku, A. F.; Cheng, T. R.; Fang, J.; Wong, C. Regioselective synthesis of di-C-glycosylflavones possessing anti-inflammation activities. *Org. Biomol. Chem.* **2010**, *8*, 4451−4462.

(13) Aghmiz, M. L.; Díaz, Y.; Jana, G. H.; Matheu, M. I.; Echarri, R.; Castillón, S.; Jimeno, M. L. The reaction of pyranoside 2-uloses with DAST revised. Synthesis of 1-fluoro-ketofuranosyl fluorides and their reactivity with alcohols. *Tetrahedron* **2001**, *57*, 6733−6743.

(14) Zhang, P.; Xu, S. Flavonoid ketohexosefuranosides from the leaves of *Crataegus pinnatifida* Bge. var. *major* N.E.Br. *Phytochemistry* **2001**, *57*, 1249−1253.

(15) Zhang, P.; Zhou, Y.; Xu, S. Two Novel Flavonoid Glycosides from *Crataegus Pinnatifida*. *J. Asian Nat. Prod. Res.* **2001**, *3*, 77−82.

(16) Kumazawa, T.; Asahi, N.; Matsuba, S.; Sato, S.; Furuhata, K.; Onodera, J. Conversion of *β*-D- *C*-glucopyranosyl phloroacetophenone to a spiroketal compound. *Carbohydr. Res.* **1998**, *308*, 213−216.

(17) Sato, S.; Miura, M.; Sekito, T.; Kumazawa, T. Effective Conversion of three diacetyl-C-(*β*-D-glycopyranosyl) phloroglucinols to spiroketal derivatives by refluxing in water. *J. Carbohydr. Chem.* **2008**, *27*, 86−102.

(18) Preobrazhenskaya, M.; Rozhkov, I.; Lazhko, E.; Yudina, L.; Korolev, A. Reaction of vanilmandelic acid and 4-hydroxybenzyl alcohol derivatives with *L*-ascorbic acid. *Tetrahedron* **1997**, *53*, 6971−6976.

(19) Kizu, H.; Kaneko, E.; Tomimori, T. Studies on Nepalese crude drugs. XXVI. Chemical constituents of panch aunle, the roots of *Dactylorhiza hatagirea* D. don. *Chem. Pharm. Bull.* **1999**, *47*, 1618−1625.

(20) Conant, J.; Kirner, W. The relation between the structure of organic halides and the speed of their reaction with inorganic iodides. I. The problem of alternating polarity in chain compounds. *J. Am. Chem. Soc.* **1924**, *46*, 232−252.

(21) Bach, R. D.; Coddens, B. A.; Wolber, G. J. Origin of the reactivity of allyl chloride and .alpha.-chloroacetaldehyde in SN2 nucleophilic substitution reactions: a theoretical comparison. *J. Org. Chem.* **1986**, *51*, 1030−1033.

(22) Ley, J. P.; Blings, M.; Paetz, S.; Krammer, G.; Bertram, H. J. New bitter-masking compounds: Hydroxylated benzoic acid amides of aromatic amines as structural analogues of homoeriodictyol. *J. Agric. Food Chem.* **2006**, *54*, 8574−8579.

(23) Graham, D. M. Caffeine—Its Identity, dietary sources, intake and biological effects. *Nutr. Rev.* **2009**, *36*, 97−102.

(24) Perron, F.; Albizati, K. F. Chemistry of spiroketals. *Chem. Rev.* **1989**, *89*, 1617−1661.

(25) Awasaguchi, K.; Miyazawa, M.; Uoya, I.; Inoue, K.; Nakamura, K.; Yokoyama, H.; Kakuda, H.; Hirai, Y. Synthesis of spiro *C*-arylglycoriboside via Pd (II)-catalyzed spirocyclization. *Synlett* **2010**, *16*, 2392−2396.

JOURNAL OF AGRICULTURAL AND FOOD CHEMISTRY

Article

pubs.acs.org/JAFC

Open Access on 07/31/2015

# Relationship between Medium-Chain Fatty Acid Contents and Organoleptic Properties of Japanese Sake

Kei Takahashi,*[,†] Fumihiko Tsuchiya,[‡,∥] and Atsuko Isogai[†,§]

[†]National Research Institute of Brewing, 3-7-1 Kagamiyama, Higashi-hiroshima, Hiroshima, 739-0046, Japan

[‡]LECO Japan Corporation, 2-13-4 Shiba, Minato-ku, Tokyo, 105-0014, Japan

[§]Department of Molecular Biotechnology, Graduate School of Advanced Sciences of Matter, Hiroshima University, 1-3-2 Kagamiyama, Higashi-hiroshima, Hiroshima, 739-8511, Japan

Supporting Information

**ABSTRACT:** Medium-chain fatty acids (MCFAs) and ethyl esters are considered to contribute to some organoleptic properties, such as fatty odor and bitterness in Japanese sake. However, the relationships between these compounds and the organoleptic properties of sake remain unclear. Here, we quantified MCFAs and ethyl hexanoate in *ginjo* sake using gas chromatography with a flame ionization detector (GC-FID). The hexanoic acid concentration strongly correlated with fatty odor ($p < 0.0001$). The octanoic acid/hexanoic acid ratio correlated with butanoic acid concentration, which is likely correlated with inharmonious bitter taste. Multiple comparison analysis revealed that the ethyl hexanoate level was negatively correlated with bitterness. We then identified other chemical compounds correlating with fatty odor and bitterness using comprehensive two-dimensional GC coupled with time-of-flight mass spectrometry. By performing correlation analysis between certain compounds and sensory values following statistical selection for chemical compounds, we identified several candidate compounds correlating with fatty odor and bitterness in sake.

**KEYWORDS:** *medium-chain fatty acid (MCFA), ethyl hexanoate, Japanese sake, alcoholic beverage, gas chromatography with a flame ionization detector (GC-FID), comprehensive two-dimensional gas chromatography coupled with time-of-flight mass spectrometry (GC × GC−TOFMS)*

## INTRODUCTION

Medium-chain fatty acid (MCFA) ethyl esters in premium Japanese sake (*ginjo* sake) provide a pleasant, fruity apple-like flavor. This flavor is an essential trait for *ginjo* sake, and MCFA ethyl esters are considered to play an important role in flavor quality. On the other hand, MCFAs such as hexanoic acid and octanoic acid, precursors to ethyl esters, are recognized as a rancid or unpleasant fatty odor in reconstituted sake.[1] In sake fermentation, although the mechanism of MCFA ethyl ester formation during sake fermentation is poorly understood, it is considered that they are chemically generated (without enzymes) or by biosynthesis through enzymes in sake yeast, *Saccharomyces cerevisiae*.[2] Cerulenin-resistant sake yeast is generally used in modern *ginjo* sake brewing. This yeast harbors a point mutation at base 3748 of the fatty acid synthase 2 gene, encoding the alpha subunit of the fatty acid synthesis enzyme complex.[3,4] In this type of sake yeast, MCFAs, which are intermediates in the biosynthesis of long-chain fatty acids, accumulate to high concentrations. In turn, MCFAs combine during fermentation to form ethyl alcohol and generate MCFA ethyl esters.[3,5,6] Therefore, it is increasingly important to quantify MCFA concentrations during the brewing process and to develop techniques that control the production of these compounds during *ginjo* sake fermentation.

In our previous work, we developed a simple method for simultaneously quantifying MCFAs and ethyl hexanoate in sake using gas chromatography with a flame ionization detector (GC-FID). Based on these quantification data, we proposed a concept regarding the efficiency of ethyl ester production in sake.[7] In addition, this low-cost method is less labor intensive than other data analysis methods, and it is therefore suitable for processing large sample numbers. In contrast, this method is not suitable for analyzing target chemicals that are present in less than sub-ppm concentrations or for nontarget analyses.

In recent developments of analytical instruments and data processing techniques, the comprehensive two-dimensional gas chromatography (GC × GC) coupled with high-speed data acquisition using time-of-flight mass spectrometry (GC × GC−TOFMS) has emerged as a powerful analytical method that can be used to reveal large numbers of metabolites in complex samples. In combination with a statistical approach that combines multidimensional data, including first and second retention times, mass spectra, and variance of replicates, the compositional differences between samples can be effectively determined.[8,9] Many studies of relationships between brewing conditions, organoleptic properties, and metabolites have been published in the context of winemaking[10−15] and beer brewing.[16,17] However, whereas comprehensive metabolomics studies on sake were performed by Sakamoto et al.[18] using GC−MS, and by Sugimoto et al.[19,20] using capillary electro-

Received: May 2, 2014
Revised: July 31, 2014
Accepted: July 31, 2014
Published: July 31, 2014

ACS Publications © 2014 American Chemical Society

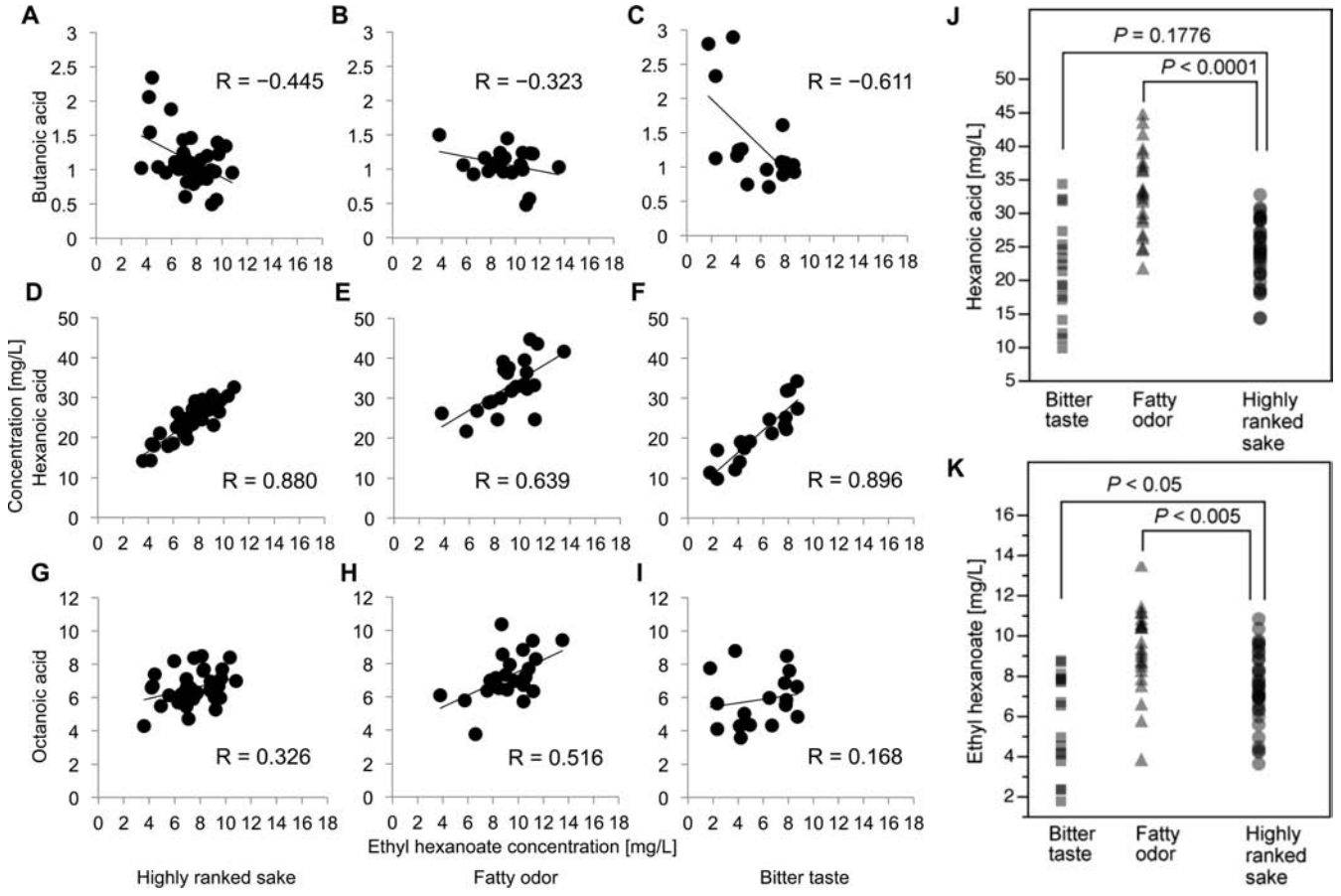


**Figure 1.** Correlation between ethyl hexanoate and MCFAs in Japanese sake. Indicated chemical compounds (ethyl hexanoate, butanoic acid, hexanoic acid, and octanoic acid) in sake were quantified using GC-FID. Graphs (A), (D), and (G) show results from the highly ranked sake (control). Graphs (B), (E), and (H) show results from fatty odor sake, and graphs (C), (F), and (I) show results from inharmonious bitter taste sake. Panels (J) and (K) show the statistically significant differences in hexanoic acid and ethyl hexanoate concentrations between highly ranked sake and fatty odor sake. Statistically significant differences were identified using the Dunnett's post hoc test. Typical data from three independent analytical procedures are shown.

phoresis TOFMS (CE−TOFMS), no metabolomics studies of sake report data from GC × GC−TOFMS analyses.

In this study, we determined MCFA and ethyl hexanoate concentrations in *ginjo* sake using GC-FID, and investigated correlations between MCFA and ethyl hexanoate with fatty odor and inharmonious bitter taste. Subsequent analysis of MCFAs and ethyl hexanoate in the sake mash *moromi* demonstrated that MCFA composition appeared to associate with ethyl hexanoate generation. We finally used GC × GC−TOFMS to analyze and identify other chemical compounds that correlate with fatty odor and inharmonious bitter taste in sake.

## MATERIALS AND METHODS

**Materials.** Premium Japanese sake samples were selected from entries in the National New Sake Awards competition held by the National Research Institute of Brewing (NRIB) in Japan during 2009, 2010, and 2011. Other samples were obtained by brewing at the NRIB using 40 kg of polished rice (Japanese cultivar: *Yamadanishiki*) and a cerulenin-resistant sake yeast strain (Kyokai No. 1801). Sake mash (*moromi*) was sampled in the morning dairy on days 2−39. *Moromi* samples were paper-filtered, and liquid fractions were used for chemical analysis. Samples were dispensed and preserved at −30 °C until use.

All chemicals were purchased from Wako Pure Chemical Industries Ltd. (Osaka, Japan). HP-FFAP capillary columns were purchased from Agilent Technologies (Palo, Alto, CA, USA), and DB-1 and BPX-50 capillary columns were purchased from Agilent Technologies and SGE Analytical Science Japan Inc. (Yokohama, Japan), respectively.

**Sensory Evaluation.** Sensory evaluations were performed by 15 well-trained panelists, as described in Japanese governmental reports.[21−23] To semiquantify sensory properties, the presence or absence of fatty odor and inharmonious bitter taste was determined on the basis of "check-all-that-apply (CATA)" assessments.[24,25] Sake samples in which fatty odor or inharmonious bitter taste were identified by more than four panelists were defined as fatty odor or inharmonious bitter taste sake, respectively.

**Sample Pretreatment for GC-FID Analysis.** Analysis of chemical components using GC-FID was performed according to a previously described Method[7] with some modifications. Briefly, 400-$\mu$L aliquots of sake samples were mixed with 2-propanol (1.2 mL). After centrifugation (17,000*g* for 5 min at room temperature), the supernatant was separated from the precipitate. An equal volume of 100% (v/v) 2-propanol was then added to the supernatant, diluting the sample. To estimate injection and detection efficiencies, an internal standard comprising 500 mg/L 1-pentanol (for ethyl hexanoate) and 200 mg/L heptanoic acid (for butanoic acid, hexanoic acid, and octanoic acid) in 17.0% ethanol was added to the diluted samples at a ratio of 9:1 (sample:internal standard).

**Quantification of MCFAs and Ethyl Hexanoate Using GC-FID.** A GC-FID (GC-17A-FID version 1; Shimadzu, Kyoto, Japan) coupled with an AOC-20i autosampler (Shimadzu, Kyoto, Japan) was used as previously described.[7] Splitless injections were performed for all samples with injection volumes of 1.2 $\mu$L. Two HP-FFAP columns

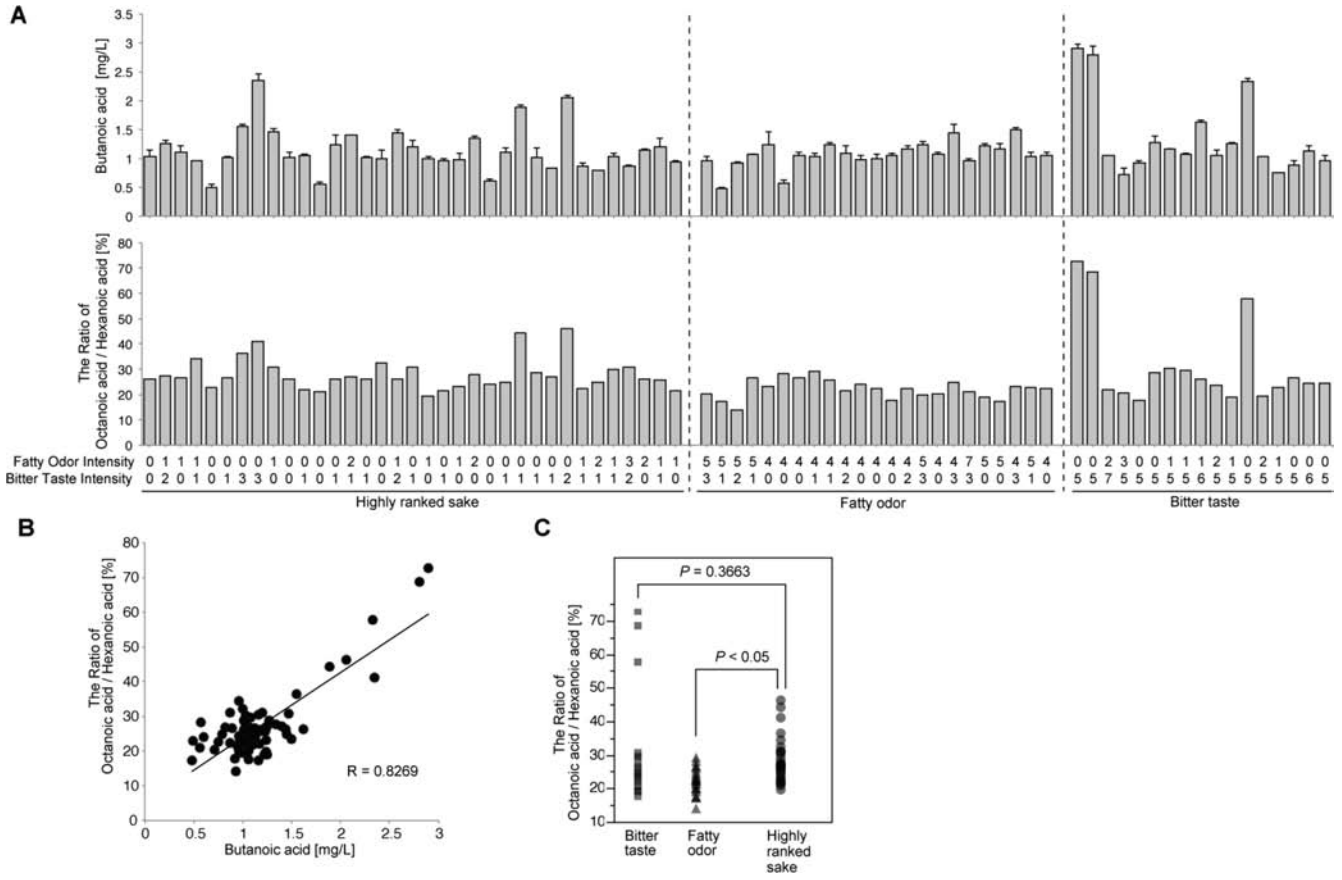


**Figure 2.** Positive correlation of butanoic acid concentrations and the octanoic acid/hexanoic acid (OA/HA) ratios in Japanese sake. Indicated chemical compounds (butanoic acid, hexanoic acid, and octanoic acid) were quantified using GC-FID. (A) *Upper panel*, The butanoic acid concentrations in sake are grouped according to the characteristics (highly ranked sake, fatty odor, and inharmonious bitter taste sake). Groupings are based on the numbers of sensory evaluation panelists who identified fatty odor or inharmonious bitter taste (shown below the graph). *Lower panel*, corresponding OA/HA ratios in sake. (B) Correlation between the OA/HA ratio and butanoic acid concentrations in all sake. (C) No statistically significant differences in OA/HA ratios between highly ranked and inharmonious bitter taste sake were identified using the Dunnett's post hoc test. Error bars indicate the variance between two technical replicates. Typical data from three independent analytical processes are shown.

(30 m × 0.32 mm i.d., 0.25-$\mu$m film thickness) were connected in tandem using a universal press-tight column connector (Restek, Bellefonte, PA, USA). The oven was initially set at 50 °C (for 3 min), and the temperature was increased from 50 to 235 °C at 7 °C/min, and was then maintained at 235 °C for 15 min. The temperature was subsequently increased from 235 to 240 °C at 30 °C/min and was maintained at 240 °C for 5 min. Peak areas on the chromatograms were quantified using GC-solution software version 2 (Shimadzu).

**Analysis of General Components of *moromi* and Sake.** The general components of the *moromi* during fermentation and those of sake were analyzed by the standard method established by the National Tax Administration Agency of Japan. In this analysis, ethanol content was determined using GC with an Rtx-624 column (Restek).

**Analysis of Choline-Containing Phospholipids.** The amount of choline-containing phospholipids in sake samples was determined using a colorimetric enzyme assay for detecting serum lipids with minor modification (Phospholipid C kit 433-36201, Wako Pure Chemicals, Osaka, Japan). Briefly, 10 $\mu$L of sake, filtered sake mash (*moromi*), or standards were mixed with 1.5 mL of assay reagent, incubated for 5 min at 37 °C, and the absorbance was measured at 600 nm.

**Sample Pretreatment for GC × GC−TOFMS Analysis.** The following manipulations were performed below 15 °C. Eleven sake samples (15 mL each), which were entries into the 2011 NRIB National New Sake Awards competition, were diluted with equal volumes of water and were passed through a 1-cc Oasis HLB cartridge containing 30 mg of sorbent (Waters, Milford, MA, USA) under slightly negative pressure (approximately from −0.002 to −0.005 MPa) using a GL-SPE vacuum manifold system (GL Science, Tokyo, Japan). After washing with 200 $\mu$L of water, the chemical components were eluted with 400 $\mu$L of organic solvent (2-propanol:methanol = 4:1), and 37.5-fold condensed elutes were tightly packed in glass vials and stored at 4 °C until further analysis.

**GC × GC−TOFMS Analysis.** The GC × GC system comprised an Agilent 7890N instrument equipped with an auto sampler 7683B series injector (Agilent). The nonpolar DB-1 (30 m × 0.25 mm i.d., 0.25-$\mu$m film thickness) was used as a primary separation column, and the BPX-50 (1.5 m × 0.1 mm i.d., 0.1-$\mu$m film thickness), which enables medium polarity separation, was used as a secondary column. A LECO Pegasus 4D TOFMS (LECO, St. Joseph, MI, USA) was connected in series with the GC × GC separation system. During modulation, cold pulses were generated using dry nitrogen gas cooled by liquid nitrogen, and heated dry air was used for hot pulses. Injector, transfer line, and ion source temperatures were set at 250 °C. The oven temperature program for the primary column began at 40 °C (for 5 min) and increased to 310 °C at 7 °C/min, and then the temperature was maintained at 310 °C for 1 min. The oven temperature program for the secondary column began at 55 °C (for 5 min) and increased to 325 °C at 7 °C/min, and then the temperature was maintained at 325 °C for 2 min. The modulator offset was +10 °C relative to the primary oven, and the modulation period was 5 s. Ultra-high-purity helium (>99.9999%) was used as a carrier gas with a constant flow rate of 1.5 mL/min. The injection volume was 1.0 $\mu$L.

Mass spectrometry parameters included electron ionization at 70 eV with a detector voltage of −1750 V, a mass range between 29 and 500


dx.doi.org/10.1021/jf502071d | J. Agric. Food Chem. 2014, 62, 8478−8485

Da, and an acquisition rate of 200 spectra/s. Data are presented as nominal mass.

Analyses were performed 4 times per sample, and the first data set obtained for each sample was discarded to avoid contamination by carryover compounds from the previous analysis. Data from the subsequent three analyses were then processed.

**Data Processing and Semiquantification.** Deconvolution of GC × GC−TOFMS spectra was conducted using ChromaTOF software ver. 4.50, which was optimized for the LECO Pegasus 4D TOFMS instrument. Chromatograms were processed with a baseline offset of 0.5, automatic peak smoothing, peak find with a minimum signal-to-noise ratio (S/N) of 30, a first dimension peak width of 15 s, and a second dimension peak width of 0.1 s. Compound mass spectral data were compared against the Wiley09 database library to calculate "similarity" and "reverse" parameters. Analytical conditions and parameters are summarized in Supporting Information Table 1.

**Statistical Analyses.** Descriptive statistical, multiple variance, and principal component analyses were conducted using JMP software version 10.0.2 (SAS Institute Inc., Cary, NC, USA).

## RESULTS AND DISCUSSION

**Quantification of MCFAs and Ethyl Hexanoate in Sake Using GC-FID.** Premium Japanese sake "*ginjo* sake" is known for its fruity flavor. However, little is known of the flavor-generating mechanisms in sake. In particular, sensory evaluations of sake sometimes identify problematic fatty odor and inharmonious bitter taste, although the relevant chemical compounds remain uncharacterized. To address this issue, we initially selected three types of sake, which were entries into the NRIB National New Sake Awards Competition from 2009 to 2011, for use as samples. Highly ranked sake samples were used as controls, and sake samples with fatty odor or inharmonious bitter taste were examined. The numbers of highly ranked sake were 9 (2009), 13 (2010), and 13 (2011). The numbers of sake with fatty odor were 5 (2009), 12 (2010), and 6 (2011), and the numbers of sake with inharmonious bitter taste were 4 (2009), 8 (2010), and 5 (2011).

After selection of sake samples, we quantified the concentrations of butanoic acid, hexanoic acid, octanoic acid, and ethyl hexanoate in sake using GC-FID. Figure 1 shows correlations between ethyl hexanoate and MCFAs. As expected, higher ethyl hexanoate and MCFAs concentrations were found in sake samples (Figure 1) than in commercial sake products that were previously determined.[7] Using multiple comparison analysis, we found that ethyl hexanoate and hexanoic acid were present in significantly higher quantities in fatty odor sake than in the highly ranked sake (Figure 1J and K). The average hexanoic acid concentration in highly ranked sake was 24.2 mg/L, whereas that in fatty odor sake was 9.9 mg/L higher (34.1 mg/L). In contrast, the average octanoic acid concentration differed by only 0.7 mg/L. Yamane et al. previously showed that the addition of 8 mg/L hexanoic acid to sake resulted in increased perceptions of unpleasant fatty-related odors,[1] which is consistent with our results. Furthermore, we performed verification tests by adding 20 mg/L hexanoic acid to three sake samples containing 14.2−19.6 mg/L hexanoic acid, resulting in increased perception of fatty odor ($p < 0.01$ by $\chi^2$ test). As shown in Figure 1D−F, ethyl hexanoate was positively correlated with hexanoic acid, as previously described.[26] A stronger positive correlation between ethyl hexanoate and hexanoic acid ($R = 0.88$) was observed in highly ranked sake (Figure 1D). As expected, the addition of 6 mg/L ethyl hexanoate to sake did not increase any perception of fatty odor, but unexpectedly rather decreased perception of fatty odor ($p < 0.01$ by $\chi^2$ test). These results suggested that increased hexanoic acid but not ethyl hexanoate concentration is a primary contributor to fatty odor in sake.

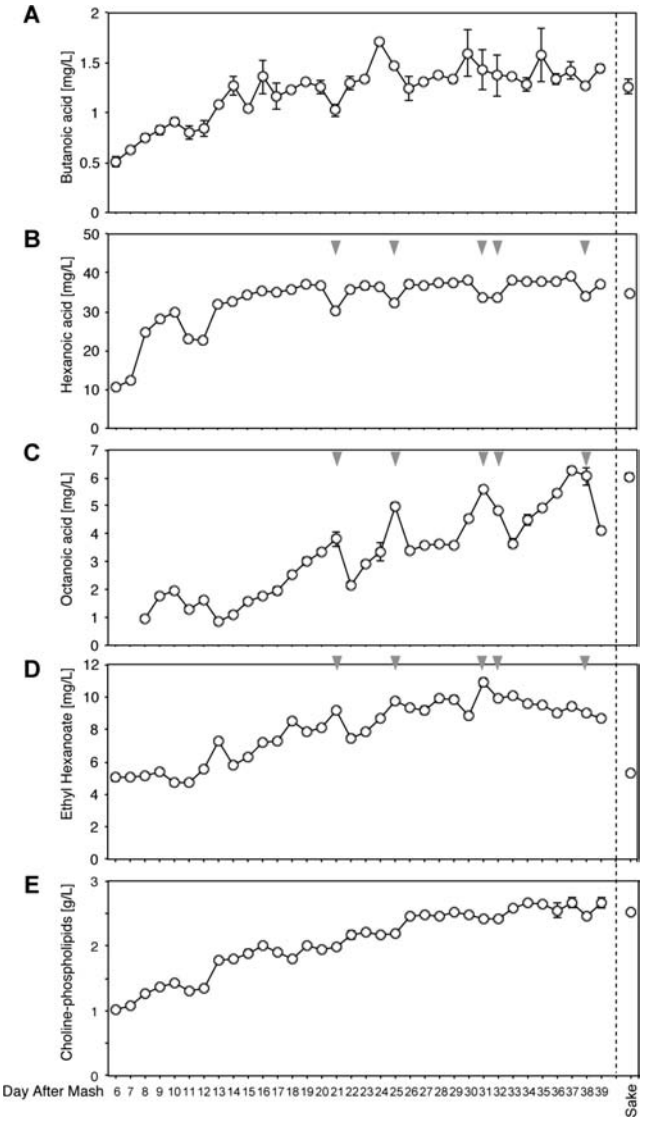


**Figure 3.** Variable patterns of MCFA and ethyl hexanoate concentrations in sake mash. Japanese sake was brewed on a semi-industrial scale, and chemical compounds concentrations were determined in samples taken during the fermentation period, and in samples of the final product (separated by dotted lines). (A) Butanoic acid, (B) hexanoic acid, (C) octanoic acid, (D) ethyl hexanoate, (E) choline-phospholipids concentrations in *moromi* samples and in final product; the *x*-axis shows the number of days after starting the mash. Gray arrowheads indicate days on which uncharacteristic patterns of hexanoic acid, octanoic acid, and ethyl hexanoate concentrations were observed. Errors bar indicate the variance between two technical replicates. Typical data from three independent analytical processes are shown.

No significant differences in hexanoic acid levels were found between highly ranked and inharmonious bitter taste sake. However, ethyl hexanoate levels were relatively lower in inharmonious bitter taste sake (Figure 1J and K), suggesting that ethyl hexanoate negatively correlated with inharmonious bitter taste.

Unexpectedly, ethyl hexanoate levels were found to negatively correlate with butanoic acid (Figure 1A−C). Butanoic acid concentration varied considerably even brewed


dx.doi.org/10.1021/jf502071d | J. Agric. Food Chem. 2014, 62, 8478−8485

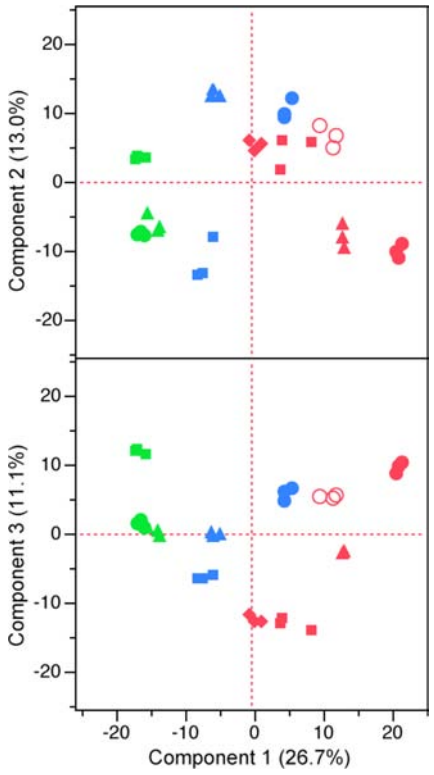


**Figure 4.** Principal component analysis (PCA) of Japanese sake. After selecting compounds using Fisher ratio criteria, PCA was performed for 11 sake samples in triplicate. Highly ranked sake ($n$ = 5) is shown in red, fatty odor sake ($n$ = 3) is shown in green, and inharmonious bitter taste sake ($n$ = 3) is shown in blue.

using the same fermentation materials and under the same conditions, including rice species, yeast strain, and *shubo* (seed mash) type. However, butanoic acid concentration tended to be slightly higher in sake samples, brewed using rice species, *Omachi*.

**Positive Correlation between Butanoic Acid and the Octanoic Acid/Hexanoic Acid Ratio.** Because we were interested in our findings showing that MCFAs did not uniformly vary between sample groups (Figure 1), the molecular ratios of chemical compounds were analyzed. Figure 2A shows the butanoic acid concentrations and the octanoic acid/hexanoic acid (OA/HA) ratios. Some sake samples with high butanoic acid concentrations also had high OA/HA ratios (Figure 2A), which were likely to be correlated with inharmonious bitter taste. As shown in Figure 2B, butanoic acid concentration correlated with the OA/HA ratios. Although inharmonious bitter taste was not significantly correlated with butanoic acid or the OA/HA ratios (Figure 2C), some inharmonious bitter taste sake samples contained higher butanoic acid concentrations, or higher OA/HA ratios (Figure 2A and B).

**Variable Patterns of MCFA and Ethyl Hexanoate Concentrations in Sake Mash.** To determine when MCFAs and ethyl hexanoate were generated during the sake brewing process, we brewed *ginjo* sake. In the sake brewing process, *moromi* stirring was minimized to promote the discharge of $CO_2$ gas during fermentation. The final ethanol concentration in the sake product was 16.2%. Parts A–C of Figure 3 show changes in butanoic acid, hexanoic acid, and octanoic acid concentrations, respectively, over time in *moromi*. Hexanoic acid concentrations reached a maximum level during the early-to-middle stage of the fermentation period (Figure

**Table 1. Positive Correlation of Chemical Compounds with Fatty Odor Sake[a]**

| no. | 1st RT | 2nd RT | unique mass | name | corr coeff | similarity | reverse | type |
|---|---|---|---|---|---|---|---|---|
| 1 | 815 | 1.405 | 74 | octanoic acid, methyl ester (CAS) | 0.792 | 884 | 888 | MCFA |
| 2 | 590 | 1.335 | 96 | 2-furancarboxaldehyde (CAS) | 0.790 | 666 | 903 | furfural |
| 3 | 2225 | 1.535 | 57 | eicosane, 2-methyl- (CAS) | 0.788 | 770 | 834 | long-chain alkane |
| 4 | 560 | 1.325 | 74 | hexanoic acid, methyl ester (CAS) | 0.781 | 868 | 955 | ethyl hexanoate |
| 5 | 1570 | 1.825 | 104 | butanoic acid, 3-methyl-, 2-phenylethyl ester (CAS) | 0.773 | 844 | 852 | ester |
| 6 | 2300 | 1.735 | 71 | nonadecane, 2-methyl- (CAS) | 0.773 | 882 | 884 | long-chain alkane |
| 7 | 1540 | 3.19 | 135 | adenine | 0.768 | 871 | 879 | adenine |
| 8 | 2040 | 2.98 | 143 | pentanamide, *N*-[2-(indol-3-yl)]ethyl- | 0.761 | 776 | 778 | ester |
| 9 | 1735 | 1.855 | 104 | butanoic acid, 3-methyl-, 2-phenylethyl ester (CAS) | 0.758 | 751 | 815 | ester |
| 10 | 2245 | 1.645 | 71 | nonadecane, 2-methyl- (CAS) | 0.737 | 908 | 911 | long-chain alkane |
| 11 | 750 | 2.46 | 42 | 2H-pyran-2-one, tetrahydro-6-methyl- (CAS) | 0.730 | 928 | 938 | cyclohexanoate |
| 12 | 830 | 1.245 | 54 | 1,2-nonadiene (CAS) | 0.717 | 768 | 850 | alkene |
| 13 | 1280 | 1.66 | 159 | 1S,*cis*-calamenene | 0.711 | 812 | 875 | wood-like |
| 14 | 2190 | 1.585 | 71 | nonadecane, 2-methyl- (CAS) | 0.693 | 848 | 882 | long-chain alkane |
| 15 | 1110 | 1.535 | 60 | decanoic acid | 0.693 | 909 | 909 | MCFA |
| 16 | 1060 | 1.425 | 74 | decanoic acid, methyl ester (CAS) | 0.690 | 819 | 868 | MCFA |
| 17 | 2215 | 1.58 | 71 | eicosane, 2-methyl- (CAS) | 0.685 | 770 | 834 | long-chain alkane |
| 18 | 2065 | 1.505 | 71 | eicosane (CAS) | 0.678 | 860 | 888 | long-chain alkane |
| 19 | 285 | 1.395 | 85 | 1-methoxy-3-pentene | 0.669 | 694 | 884 | alkene ether |
| 20 | 1805 | 2.28 | 120 | tyrosol acetate | 0.669 | 686 | 793 | ester |
| 21 | 1900 | 2.875 | 143 | pentanamide, *N*-[2-(indol-3-yl)]ethyl- | 0.664 | 768 | 782 | indole-related |
| 22 | 1530 | 3.525 | 144 | 1H-indole-3-carboxaldehyde (CAS) | 0.660 | 889 | 904 | indole-related |
| 23 | 1120 | 2.37 | 130 | 1H-indole, 3-methyl- (CAS) | 0.656 | 931 | 931 | indole-related |
| 24 | 1300 | 2.65 | 143 | quinoline, 3-methyl- (CAS) | 0.645 | 857 | 880 | quinoline |
| 25 | 2130 | 1.54 | 71 | nonadecane, 2-methyl- (CAS) | 0.625 | 903 | 905 | long-chain alkane |

[a]Retention time is provided as seconds.


dx.doi.org/10.1021/jf502071d | J. Agric. Food Chem. 2014, 62, 8478–8485

Table 2. Positive Correlation of Chemical Compounds with Inharmonious Bitter Taste Sake[a]

| no. | 1st RT | 2nd RT | unique mass | name | corr coeff | similarity | reverse | type |
|---|---|---|---|---|---|---|---|---|
| 1 | 1430 | 1.725 | 81 | 2-octylfuran | 0.69 | 694 | 741 | furan |
| 2 | 315 | 1.15 | 86 | 2-pentanone (CAS) | 0.636 | 907 | 912 | ketone |
| 3 | 975 | 1.7 | 95 | ethanone, 1-(2-furanyl)- (CAS) | 0.622 | 659 | 752 | furan |
| 4 | 955 | 1.725 | 135 | (+)-(1*R*,5*R*)-2(10)-PINEN-4-ONE | 0.605 | 834 | 843 | ketone |
| 5 | 990 | 1.93 | 82 | 2-cyclohexen-1-one, 3,5-dimethyl- | 0.579 | 682 | 762 | ketone |
| 6 | 620 | 1.26 | 101 | ethyl 4-hydroxypent-2-enoate | 0.555 | 698 | 856 | ester |

[a]Retention time is provided as seconds.

3B). In contrast, octanoic acid concentrations increased with ethyl alcohol production (data not shown) and reached a maximum at a later stage of the fermentation period (Figure 3C). These differences may reflect differences in hydrophobicity. Figure 3D shows the ethyl hexanoate concentration in *moromi*, which reached a maximum during the middle stage, and was markedly decreased in the final product. This phenomenon has long been observed in the sake industry and was expected because ethyl hexanoate is thought to exist in the yeast cells, although details of its localization are unknown. Interestingly and unexpectedly, we observed several points: the lower hexanoic acid concentrations, but higher concentrations of octanoic acid and ethyl hexanoate (Figure 3B−D). These changes in concentrations were probably attributable to the minimal *moromi* stirring before sampling. In previous reports, yeast ethyl ester biosynthesis 1 (Eeb1) and ethanol hexanoyl transferase 1 (Eht1) catalyzed the esterification of hexanoic acid (hexanoyl-coenzyme A) and ethanol, producing ethyl hexanoate.[2] Saerens et al. also showed that the *EEB1* gene was particularly considered to be robustly upregulated in the presence of octanoic acid.[27] Thus, the variable concentration of hexanoic acid, octanoic acid, and ethyl hexanoate in *moromi* may reflect the expression of genes such as *EEB1 and EHT1*. The butanoic acid concentrations in *moromi* did not change significantly over time (Figure 3A) and were not associated with the OA/HA ratio, indicating that butanoic acid concentration does not always correlate with OA/HA ratio.

Choline-containing phospholipids in *moromi* were positively correlated with hexanoic acid (Figure 3E). Although we did not identify predominating choline-containing phospholipid species and fatty acids in cerulenin-resistant yeast, the concentration of choline-containing phospholipids in *moromi* was positively correlated with hexanoic acid, but not with octanoic acid.

In conclusion, MCFA and ethyl hexanoate concentrations did not uniformly increase in *moromi*. This pattern has not been previously observed in the sake fermentation process. In yeast cells, MCFAs are primarily generated in the cytosol by the traditional fatty acid synthase complex. However, MCFAs such as octanoic acid, which is involved in the formation of $\alpha$-lipoic acid, are also generated in the mitochondria.[28,29] Hence, cytosolic MCFA composition may differ from that generated in the mitochondria. In the present study, sake fermentation was performed under completely anaerobic conditions, indicating that sake yeast does not require the tricarboxylic acid cycle to produce energy in mitochondria. However, the mechanisms behind MCFA generation and accumulation in sake yeast during the brewing process remain unknown, and further targeted cell biology studies are required.

**Comprehensive Analysis of Compounds Using GC × GC−TOFMS.** We showed that fatty odor and inharmonious bitter taste in sake correlate with MCFA contents, indicating that yeast metabolism may change during sake brewing. Thus, the present comparisons of sake metabolites other than MCFA in these three types of Japanese sake (highly ranked sake, fatty odor sake, and inharmonious bitter taste sake) are critical for understanding the factors that contribute to certain organoleptic properties. Hence, a comprehensive analysis of volatile compounds in these three types of sake was performed using a GC × GC−TOFMS system.

In these experiments, 11 sake samples, including 5 highly ranked sake samples, 3 fatty odor sake samples, and 3 inharmonious bitter taste sake samples, were selected from entries into the NRIB National New Sake Awards competition held in 2011. Sake samples were analyzed in triplicate using GC × GC−TOFMS equipped with a LECO Pegasus 4D system, giving a total of 33 sets of two-dimensional total ion chromatogram (TIC) data. Analytical conditions are summarized in Supporting Information Table 1. Typical TIC data for each type of sake are shown in Supporting Information Figure 1A−C, and corresponding intensity data are shown in Supporting Information Figure 1D−F. Supporting Information Figure 1 shows similar patterns of most peaks from the three different types of sake, although some differences are indicated. Subsequently, after performing peak deconvolution using ChromaTOF software, an automatic data mining program was applied, and detected peaks were aligned using the statistical-compare function of ChromaTOF software.

**Correlations of Chemical Compounds with Fatty Odor and Inharmonious Bitter Tastes.** GC × GC−TOFMS analyses showed >3,000 peaks. For convenience, peaks with poor reproducibility were denoted as "unknown", and peaks with good reproducibility (with similarities of >600) were denoted as "analytes". Specific compound names were assigned to peaks with similarities >650. A total of 1,182 analytes were thus identified, and specific chemical compounds were inferred for 1,110 of these. Using the area values of these compounds, we performed a Fisher ratio calculation using ANOVA to identify significant differences between samples. Consequently, 568 peaks remained after Fisher ratio selection with $F$ values of >5.0. Principal component analysis (PCA) was performed using semiquantification data from the 568 peaks as parameters. The results of PCA show clear separation of fatty odor sake from highly ranked sake and inharmonious bitter taste sake (Figure 4). Highly ranked sake may not have been clearly separated from inharmonious bitter taste sake because nonvolatile compounds contributed more to the bitter taste than volatile compounds. Although the replicates were repeatable, the five highly ranked sake samples were not tightly clustered (Figure 4). Nonetheless, fatty odor sake was clearly distinguished by component 1, indicating that numerous chemical compounds in sake contribute to its characteristics. Hence, loading plot analysis after PCA was not used to estimate correlations of chemical compounds with class separation. Instead, we correlated certain compounds with semiquantitative sensory

data (numbers of notations for fatty odor and inharmonious bitter taste) using a relational analysis method.

Compounds that correlated with fatty odor and inharmonious bitter taste are listed in Tables 1 and 2, respectively. Several compounds, such as long-chain alkanes, some MCFA-related compounds, and some indole-related compounds, were positively correlated with fatty odor (Table 1). Alkanes in yeast can be generated intracellularly by the decarboxylation of fatty acids.[30] MCFAs and fatty acids with longer carbon chains may be converted to more volatile alkanes in decarboxylation reactions and may enhance fatty odor. MCFAs are toxic to microorganisms.[31−33] Hence, for protection against exposure to MCFAs, yeast may express proteins that esterify or export MCFAs.[34,35] Fungi similarly express enzymes that decarboxylate MCFAs such as *E,E*-2,4-dihexenoic acid (common name, sorbic acid).[36] Thus, the presence of alkanes in sake may reflect microbe-assisted decarboxylation reactions. Accordingly, MCFA-related compounds were correlated with fatty odor (Table 1), and this finding corresponded with the results shown in Figure 1. Although hexanoic acid was not identified in fatty odor sake, the derivative lactone (2H-pyran-2-one, tetrahydro-6-methyl-) was present (Table 1), despite the strong correlation between hexanoic acid concentrations and fatty odor. Some failures in peak picking were caused by peak saturation of some high concentration compounds such as hexanoic acid, and they may have lowered the Fisher ratio value to <5.0 in this experiment. Semiquantitative analysis of decanoic acid using GC-FID showed that decanoic acid positively correlated with both octanoic acid and hexanoic acid with correlation coefficients of $R = 0.59$ and $R = 0.33$, respectively (data not shown). For further information on MCFA-related compounds and alkanes, targeted analysis for these compounds is required.

Furan and ketone compounds were positively correlated with inharmonious bitter taste (Table 2). Furan is a well-known thermally generated compound that imparts food a bitter taste. Moreover, among ketones, 2-en ketone was particularly correlated with inharmonious bitter taste. However, neither direct nor indirect mechanisms have been described for the relationship between inharmonious bitter taste and these compounds.

Because GC analysis detects only volatile compounds, nonvolatile compounds were not identified. Thus, the GC analysis of derivatized compounds, and analysis using alternative instruments such as liquid chromatography and CE, may be required to investigate the roles of nonvolatile compounds in sensory qualities.

In conclusions, we quantified MCFAs and ethyl hexanoate in premium Japanese *ginjo* sake using GC-FID. These experiments showed a strong correlation between hexanoic acid and fatty odor, and a possible correlation between butanoic acid and the OA/HA ratio, and inharmonious bitter taste. The variable MCFA content in *moromi* apparently correlates with ethyl hexanoate concentrations, and can be linked to the expression of yeast genes. Furthermore, the chemical compounds found in fatty odor and inharmonious bitter taste sake were investigated using comprehensive GC × GC−TOFMS analysis. These experiments revealed direct correlations of MCFA derivatives and long-chain alkanes, and fatty odor. Taken together, MCFAs, MCFA derivatives, and long-chain alkanes could contribute to unpleasant fatty odor in sake. The present data indicate relationships between volatile compounds and the organoleptic properties of sake and provide fundamental knowledge for future research into the production of alcoholic beverages.

## APPENDIX

Names for sake brewing procedures are written in *italics* in this manuscript, in accordance with the English edition of the sake handbook, published by the NRIB of Japan (http://www.nrib.go.jp/English/sake/pdf/sl_e.pdf; http://www.nrib.go.jp/English/sake/pdf/guidesse01.pdf; http://www.nrib.go.jp/English/sake/pdf/SakeNo01_en.pdf: most recent access date, 20 July 2014).

## ASSOCIATED CONTENT

### Supporting Information

Table S1, Analytical conditions of comprehensive two-dimensional gas chromatography coupled with time-of-flight mass spectrometry (GC × GC−TOFMS); Figure S1, Representative contour plots of Japanese sake of total ion chromatographs from comprehensive two-dimensional gas chromatography coupled with TOFMS. This material is available free of charge via the Internet at http://pubs.acs.org.

## AUTHOR INFORMATION

### Corresponding Author

*Tel.: +81-82-420-0812; Fax: +81-82-420-0850 E-mail address: k.takahashi@nrib.go.jp.

### Present Address

[‖](F.T.) ThermoFisher Scientific, 3-9 Moriya-cho, Kanagawa-ku, Yokohama city, Kanagawa, 221-0022, Japan.

### Notes

The authors declare no competing financial interest.

## ACKNOWLEDGMENTS

This work involved the study of *ginjo* sake samples, which were supplied by entrants into the NRIB National New Sake Awards competition. We greatly appreciate all the participating breweries, particularly those that entered in the competition in 2011. We wish to thank Ms. Fumie Kabashima (LECO Corporation Japan) and Ms. Hiromi Kohno for scientific help.

## REFERENCES

(1) Yamane, Y.; Takemiya, S.; Kawase, N.; Saiki, H. Sensory Properties of Some Fatty Acids in Sake. *J. Brew. Soc. Jpn.* **1997**, *92* (3), 224−227.

(2) Saerens, S. M.; Verstrepen, K. J.; Van Laere, S. D.; Voet, A. R.; Van Dijck, P.; Delvaux, F. R.; Thevelein, J. M. The Saccharomyces cerevisiae EHT1 and EEB1 genes encode novel enzymes with medium-chain fatty acid ethyl ester synthesis and hydrolysis capacity. *J. Biol. Chem.* **2006**, *281* (7), 4446−56.

(3) Aritomi, K.; Hirosawa, I.; Hoshida, H.; Shiigi, M.; Nishizawa, Y.; Kashiwagi, S.; Akada, R. Self-cloning yeast strains containing novel FAS2 mutations produce a higher amount of ethyl caproate in Japanese sake. *Biosci. Biotechnol. Biochem.* **2004**, *68* (1), 206−14.

(4) Inokoshi, J.; Tomoda, H.; Hashimoto, H.; Watanabe, A.; Takeshima, H.; Omura, S. Cerulenin-resistant mutants of Saccharomyces cerevisiae with an altered fatty acid synthase gene. *Mol. Gen. Genet.* **1994**, *244* (1), 90−6.

(5) Ichikawa, E.; Hosokawa, N.; Hata, Y.; Abe, Y.; Suginami, K.; Imayasu, S. Breeding of a Sake Yeast with Improved Ethyl Caproate Productivity. *Agric. Biol. Chem.* **1991**, *55* (8), 2153−2154.

(6) Verstrepen, K. J.; Derdelinckx, G.; Dufour, J. P.; Winderickx, J.; Thevelein, J. M.; Pretorius, I. S.; Delvaux, F. R. Flavor-active esters: adding fruitiness to beer. *J. Biosci. Bioeng.* **2003**, *96* (2), 110−8.

(7) Takahashi, K.; Goto-Yamamoto, N. Simple method for the simultaneous quantification of medium-chain fatty acids and ethyl hexanoate in alcoholic beverages by gas chromatography-flame ionization detector: Development of a direct injection method. *J. Chromatogr., A* **2011**, *1218* (43), 7850−6.
(8) Groger, T.; Schaffer, M.; Putz, M.; Ahrens, B.; Drew, K.; Eschner, M.; Zimmermann, R. Application of two-dimensional gas chromatography combined with pixel-based chemometric processing for the chemical profiling of illicit drug samples. *J. Chromatogr., A* **2008**, *1200* (1), 8−16.
(9) Pierce, K. M.; Hoggard, J. C.; Hope, J. L.; Rainey, P. M.; Hoofnagle, A. N.; Jack, R. M.; Wright, B. W.; Synovec, R. E. Fisher ratio method applied to third-order separation data to identify significant chemical components of metabolite extracts. *Anal. Chem.* **2006**, *78* (14), 5068−75.
(10) Perestrelo, R.; Barros, A. S.; Camara, J. S.; Rocha, S. M. In-depth search focused on furans, lactones, volatile phenols, and acetals as potential age markers of Madeira wines by comprehensive two-dimensional gas chromatography with time-of-flight mass spectrometry combined with solid phase microextraction. *J. Agric. Food Chem.* **2011**, *59* (7), 3186−204.
(11) Robinson, A. L.; Boss, P. K.; Heymann, H.; Solomon, P. S.; Trengove, R. D. Development of a sensitive non-targeted method for characterizing the wine volatile profile using headspace solid-phase microextraction comprehensive two-dimensional gas chromatography time-of-flight mass spectrometry. *J. Chromatogr., A* **2011**, *1218* (3), 504−17.
(12) Robinson, A. L.; Boss, P. K.; Heymann, H.; Solomon, P. S.; Trengove, R. D. Influence of yeast strain, canopy management, and site on the volatile composition and sensory attributes of cabernet sauvignon wines from Western Australia. *J. Agric. Food Chem.* **2011**, *59* (7), 3273−84.
(13) Welke, J. E.; Manfroi, V.; Zanus, M.; Lazarotto, M.; Alcaraz Zini, C. Characterization of the volatile profile of Brazilian Merlot wines through comprehensive two dimensional gas chromatography time-of-flight mass spectrometric detection. *J. Chromatogr., A* **2012**, *1226*, 124−39.
(14) Welke, J. E.; Manfroi, V.; Zanus, M.; Lazarotto, M.; Alcaraz Zini, C. Differentiation of wines according to grape variety using multivariate analysis of comprehensive two-dimensional gas chromatography with time-of-flight mass spectrometric detection data. *Food Chem.* **2013**, *141* (4), 3897−3905.
(15) Bordiga, M.; Rinaldi, M.; Locatelli, M.; Piana, G.; Travaglia, F.; Coisson, J. D.; Arlorio, M. Characterization of Muscat wines aroma evolution using comprehensive gas chromatography followed by a post-analytic approach to 2D contour plots comparison. *Food Chem.* **2013**, *140* (1−2), 57−67.
(16) Charry-Parra, G.; Dejesus-Echevarria, M.; Perez, F. J. Beer volatile analysis: optimization of HS/SPME coupled to GC/MS/FID. *J. Food Sci.* **2011**, *76* (2), C205−11.
(17) Van Opstaele, F.; De Causmaecker, B.; Aerts, G.; De Cooman, L. Characterization of novel varietal floral hop aromas by headspace solid phase microextraction and gas chromatography-mass spectrometry/olfactometry. *J. Agric. Food Chem.* **2012**, *60* (50), 12270−81.
(18) Sakamoto, K.; Mitsuya Shimoda; Osajima, Y. Concentration in Porapak Q Column of Volatile Compounds in Sake for Analysis. *Nippon Nogeikagaku Kaishi* **1993**, *67* (4).
(19) Sugimoto, M.; Koseki, T.; Hirayama, A.; Abe, S.; Sano, T.; Tomita, M.; Soga, T. Correlation between sensory evaluation scores of Japanese sake and metabolome profiles. *J. Agric. Food Chem.* **2010**, *58* (1), 374−83.
(20) Sugimoto, M.; Kaneko, M.; Onuma, H.; Sakaguchi, Y.; Mori, M.; Abe, S.; Soga, T.; Tomita, M. Changes in the charged metabolite and sugar profiles of pasteurized and unpasteurized Japanese sake with storage. *J. Agric. Food Chem.* **2012**, *60* (10), 2586−93.
(21) Sudo, S.; Isogai, A.; Fujita, A.; Iwata, H.; Hiramatsu, J. *Analysis of Sake Components Presented to the Sake Contest in 2009*; NATIONAL RESEARCH INSTITUTE OF BREWING: Higashi-hiroshima city, Hiroshima, Japan, 2010; pp 1−15.
(22) Sudo, S.; Isogai, A.; Fujita, A.; Hiramatsu, J. *Analysis of Sake Components Presented to the Sake Contest in 2010*; NATIONAL RESEARCH INSTITUTE OF BREWING: Higashi-hiroshima city, Hiroshima, Japan, 2011; pp 1−15.
(23) Matsumaru, K.; Isogai, A.; Fujita, A.; Sudo, S.; Kizaki, Y. *Analysis of Sake Component Presented to Sake Contests in 2011*; NATIONAL RESEARCH INSTITUTE OF BREWING: Higashi-hiroshima city, Hiroshima, Japan, 2012; pp 1−15.
(24) Dooley, L.; Lee, Y.-s.; Meullenet, J.-F. The application of check-all-that-apply (CATA) consumer profiling to preference mapping of vanilla ice cream and its comparison to classical external preference mapping. *Food Qual. Prefer.* **2010**, *21* (4), 394−401.
(25) Reinbach, H. C.; Giacalone, D.; Ribeiro, L. M.; Bredie, W. L. P.; Frøst, M. B. Comparison of three sensory profiling methods based on consumer perception: CATA, CATA with intensity and Napping. *Food Qual. Prefer.* **2014**, *32* (Part B), 160−166.
(26) Utsunomiya, H.; Yamada, O.; Hashiguchi, T. Analysis of Free Fatty Acids, Higher Alcohols and Esters in Ginjyo-shu Produced in the Northern Part of Kyushu. *J. Brew. Soc. Jpn.* **2000**, *95* (3), 214−218.
(27) Saerens, S. M.; Delvaux, F.; Verstrepen, K. J.; Van Dijck, P.; Thevelein, J. M.; Delvaux, F. R. Parameters affecting ethyl ester production by Saccharomyces cerevisiae during fermentation. *Appl. Environ. Microbiol.* **2008**, *74* (2), 454−61.
(28) Hiltunen, J. K.; Schonauer, M. S.; Autio, K. J.; Mittelmeier, T. M.; Kastaniotis, A. J.; Dieckmann, C. L. Mitochondrial fatty acid synthesis type II: more than just fatty acids. *J. Biol. Chem.* **2009**, *284* (14), 9011−5.
(29) Tehlivets, O.; Scheuringer, K.; Kohlwein, S. D. Fatty acid synthesis and elongation in yeast. *Biochim. Biophys. Acta* **2007**, *1771* (3), 255−70.
(30) Radakovits, R.; Jinkerson, R. E.; Darzins, A.; Posewitz, M. C. Genetic engineering of algae for enhanced biofuel production. *Eukaryot. Cell* **2010**, *9* (4), 486−501.
(31) Liu, P.; Chernyshov, A.; Najdi, T.; Fu, Y.; Dickerson, J.; Sandmeyer, S.; Jarboe, L. Membrane stress caused by octanoic acid in Saccharomyces cerevisiae. *Appl. Microbiol. Biotechnol.* **2013**, *97* (7), 3239−51.
(32) Viegas, C. A.; Rosa, M. F.; Sa-Correia, I.; Novais, J. M. Inhibition of Yeast Growth by Octanoic and Decanoic Acids Produced during Ethanolic Fermentation. *Appl. Environ. Microbiol.* **1989**, *55* (1), 21−8.
(33) Ullah, A.; Orij, R.; Brul, S.; Smits, G. J. Quantitative analysis of the modes of growth inhibition by weak organic acids in Saccharomyces cerevisiae. *Appl. Environ. Microbiol.* **2012**, *78* (23), 8377−87.
(34) Legras, J. L.; Erny, C.; Le Jeune, C.; Lollier, M.; Adolphe, Y.; Demuyter, C.; Delobel, P.; Blondin, B.; Karst, F. Activation of two different resistance mechanisms in Saccharomyces cerevisiae upon exposure to octanoic and decanoic acids. *Appl. Environ. Microbiol.* **2010**, *76* (22), 7526−35.
(35) Piper, P.; Mahe, Y.; Thompson, S.; Pandjaitan, R.; Holyoak, C.; Egner, R.; Muhlbauer, M.; Coote, P.; Kuchler, K. The pdr12 ABC transporter is required for the development of weak organic acid resistance in yeast. *EMBO J.* **1998**, *17* (15), 4257−65.
(36) Stratford, M.; Plumridge, A.; Pleasants, M. W.; Novodvorska, M.; Baker-Glenn, C. A.; Pattenden, G.; Archer, D. B. Mapping the structural requirements of inducers and substrates for decarboxylation of weak acid preservatives by the food spoilage mould Aspergillus niger. *Int. J. Food Microbiol.* **2012**, *157* (3), 375−83.

JOURNAL OF AGRICULTURAL AND FOOD CHEMISTRY

Article

pubs.acs.org/JAFC

# Evaluation of Emerging Factors Blocking Filtration of High-Adjunct-Ratio Wort

Ting Ma,[†,‡,§] Linjiang Zhu,[†,‡,§] Feiyun Zheng,[†,‡] Yongxian Li,[†,‡] and Qi Li*[,†,‡]

[†]Synergetic Innovation Center of Food Safety and Nutrition, School of Biotechnology, and [‡]The Key Laboratory of Industrial Biotechnology, Ministry of Education, School of Biotechnology, Jiangnan University, Wuxi 214122, China

**ABSTRACT:** Corn starch has become a common adjunct for beer brewing in Chinese breweries. However, with increasing ratio of corn starch, problems like poor wort filtration performance arise, which will decrease production capacity of breweries. To solve this problem, factors affecting wort filtration were evaluated, such as the size of corn starch particle, special yellow floats formed during liquefaction of corn starch, and residual substance after liquefaction. The effects of different enzyme preparations including $\beta$-amylase and $\beta$-glucanase on filtration rate were also evaluated. The results indicate that the emerging yellow floats do not severely block filtration, while the fine and uniform-shape corn starch particle and its incompletely hydrolyzed residue after liquefaction are responsible for filtration blocking. Application of $\beta$-amylase preparation increased the filtration rate of liquefied corn starch. This study is useful for our insight into the filtration blocking problem arising in the process of high-adjunct-ratio beer brewing and also provides a feasible solution using enzyme preparations.

**KEYWORDS:** *beer brewing, corn starch, high-adjunct-ratio brewing, filtration blocking, wort filtration*

## INTRODUCTION

As an important industrial raw material, corn starch is applied widely in various bioprocesses, such as production of syrup, lactic acid,[1−3] itaconic acid,[4] and ethanol.[5−7] It is also often used as adjunct in the brewing industry.[8−10] Corn starch has been used as an adjunct for beer brewing since 1970s and is proved to have no negative influence on wort quality and beer flavor except slightly thin flavor.[11]

In the beer brewing industry, starch-rich materials are often used as adjuncts, for example, corn starch, rice, wheat, and barley.[10,12] Corn starch and rice are the most widely used due to their low-cost and abundant resources in China. The beer made from corn starch as adjunct is characterized by light color, white foam, light flavor, and pure taste,[12] which exactly meet the tastes of Chinese consumers. Besides, corn starch has a higher degree of fermentability than other adjuncts. With the application of high-gravity brewing technology,[13] high-adjunct-ratio beer brewing technology is adopted widely in some Chinese breweries.

However, severe problems like sluggish wort filtration using frame filter often occur when corn starch is used with a high proportion such as 50%, which significantly decreases production capacity of brewery. In contrast, this filtration problem does not occur when rice flour is used as adjunct. There are multiple factors that may cause slower lautering including incompletely degraded cell wall fragments (e.g., hemicelluloses and pentosans) causing high wort viscosity and incompletely hydrolyzed small starch granules resulting in longer lautering time.[14] Particle size distribution of fines in mash is also the predominant factor affecting wort filtration performance.[15,16]

These factors causing slower lautering all originate from malt and have been studied widely. Some combinational enzyme preparations such as $\beta$-glucanase, xylanase, and glucoamylase have been developed to solve these problems of filtration blocking. However, few investigations have been done with respect to the adjunct in the process of high-adjunct-ratio brewing. As practical experience, the high proportion of corn starch caused severe extension of lautering time, while combinational application of corn starch and rice flour does not. To evaluate factors causing slower lautering and origin from pure adjunct of corn starch, we focused on comparative analysis of corn starch, rice flour, and their liquefied mash using scanning electron microscopy and particle size distribution in this study. The components in incompletely hydrolyzed residue of liquefied corn starch were also analyzed, and the effects of some amylolytic enzymes on filtration rate were evaluated.

## MATERIALS AND METHODS

**Brewing Materials and Enzyme Preparations.** Corn starch was purchased from COCFO Biochemical Energy Co., Ltd. (Jilin Province, China). Rice was milled in a Buhler Miag disk mill (DLEUW 22050, Buhler Miag) using a fine grind and sieved through 80 mesh to obtain rice flour. The Canada Harrington barley was malted in Dalian malting (Liaoning Province, China). Malt was milled with a disk mill set at 0.2 mm disk distance.

Thermostable $\alpha$-amylase preparation and $\beta$-glucanase preparation were provided by Novozymes. Liquid $\beta$-amylase preparation was purchased from a local enzyme plant, Boli Biological Products Co., Ltd. (Jiangsu Province, China). The usage amount of enzyme preparation was according to the manufacturer's instructions. The specifications of all enzyme preparations used in this study are shown in Table 1.

**Assay of the Content of Total Starch, Total Nitrogen, and Fat.** Total starch content was analyzed by the dinitrosalicylic acid (DNS) method.[17] Samples (0.1 g) were hydrolyzed in 10 mL of 6 mol/L HCl at 100 °C for 30 min, and the concentration of glucose in the hydrolysate was determined by the DNS method. The obtained hydrolysate was adjusted with 6 mol/L NaOH to neutral pH using phenolphthalein as an indicator and then was filtered with a filter paper. The filtrate was diluted

Received: May 19, 2014
Revised: August 3, 2014
Accepted: August 3, 2014
Published: August 4, 2014

ACS Publications © 2014 American Chemical Society



dx.doi.org/10.1021/jf5023109 | J. Agric. Food Chem. 2014, 62, 8486−8490

**Table 1. Commercial Enzyme Preparations Used in the Study**

| | description | optimum pH | optimum temp (°C) | activity | product |
|---|---|---|---|---|---|
| Termamyl SC | $\alpha$-amylase | 5.0−7.0 | 85−95 | 120 KNU-S/g | liquid |
| Ultraflo Max | $\beta$-glucanase xylanase | 4.0−6.0 | 63−68 | $\beta$-glucanase 700 EGU/g xylanase 250 FXU/g | liquid |
| $\beta$-amylase | $\beta$-amylase | 5.0−5.5 | 55−65 | 6000 U/mL | liquid |

by 10-fold with deionized water for further analysis. One milliliter of the diluted hydrolysate was added to 1 mL of DNS solution (6.3‰ w/v) and 1 mL of water. The mixture was boiled for 5 min and then cooled in water for 2 min. 22 mL of deionized water was added, and the mixture was used to measure the absorbance at 540 nm. The absorbance was used to calculate the concentration of reducing sugar according to a standard curve of glucose solution (0−0.6 mg/mL). The total starch content was calculated as the concentration of reducing sugar × 0.9.

Total nitrogen content was determined using a Kjeldahl 8400 Analyzer Unit (Foss).[18] Protein content was estimated as 6.25 times total nitrogen content.

Fat content was analyzed by Soxhlet extraction method using diethyl ether. Samples (3.0 g) were weighed in an extraction thimble and placed in the extraction tube, which was connected to a condenser above and a flask below. Diethyl ether was added to 1/2 to 3/5 of the volume of the flask. Extraction was carried out by diethyl ether reflux at 55 °C for 6−8 h. After extraction, diethyl ether was subjected to evaporation at the rotary evaporator and the flask was dried at 105 °C for 90 min until constant weight (weight difference was within 0.0002 g). The fat content was calculated according to the increased weight of the flask.

**The Procedures of Gelatinization, Liquefaction, and Mashing in the High-Adjunct-Ratio Brewing Process.** In the high-adjunct-ratio brewing process used in this study, a high ratio of material to water (1:2.5) was used during gelatinization and liquefaction of the adjunct. 50 g of the adjunct was mixed with 125 mL of preheated water (55 °C) in the mashing cup of Agreement Saccharification Instrument (BGT-8A, Bioer) and stirred immediately. The mixture was heated to 75 °C and incubated for 10 min and then heated to 95 °C and incubated for 30 min. The thermostable $\alpha$-amylase preparation (0.6 mg/g corn starch) was added at the beginning of gelatinization at 55 °C. The evaporated water was readded into the cup according to its weight.

The mashing procedure was as follows: 30 min at 48 °C, 40 min at 63 °C, 20 min at 72 °C and before mashing off at 78 °C. The heating rate for temperature ramp up was 1 °C per min. 50 g of malt barley was milled and mashed with a water-to-malt ratio of 3.5:1 in the mashing bath (BGT-8A, Bioer). After the step of 30 min at 48 °C, the mash was mixed with the above liquefied adjunct and was heated to 63 °C.

**Analysis of Scanning Electron Microscopy (SEM).** The samples for SEM analysis were prepared as follows: corn starch and milled rice were directly used as the samples; yellow floats and the incompletely degraded residue in liquefied corn starch were collected on a filter paper as the samples. All of the collected samples were fixed with glutaraldehyde, then washed with 35% (v/v) alcohol solution before dehydration, and dried at the critical temperature. Samples were then mounted on a SEM stub with silver plate and spatter-coated with platinum by ion coater, and they were observed under a constant accelerating voltage of 5.0 kV using a scanning electron microscope (FEI Quanta 200, Holland).

**Particle Size Analysis.** Particle size was measured in a Microtrac SDC laser-diffraction analyzer (Microtrac Inc., USA) using the flow-through, 300 mL reservoir. Starch granules and starch slurries were added into the reservoir until the concentration value reach between 12% and 17%. Settings were optimized for the refractive index of starch in water, and particle size was recorded as volume average diameter automatically by transferring light scattering signals to electrical signals.

**Evaluation of Filtration Rate.** The liquefied solution of adjunct and the mash were filtered through a filter paper and the filtrate was collected by a graduated cylinder. The volume of filtrate was recorded every 10 min in the first 60 min and then every 20 min for another 60 min. The filtration rate was evaluated by the collected total volume of filtrate. Another evaluation method of filtration rate is dependent upon the filtration time. This method was carried out as follows: the first 100 mL of filtrate was collected and refiltrated, and the time for 150 mL of filtrate was recorded and used to evaluate the filtration rate. Each experiment of filtration was carried out in triplicates.

## RESULTS

**The Differences in Component and Dimension between Corn Starch and Rice Flour.** Both corn starch and rice flour are commonly used as adjunct in the brewing process. However, corn starch often causes a serious extension of lautering time, while rice flour does not. The differences in component and dimension were compared. Protein content in rice flour was more than that in corn starch (Table 2). Corn starch granules were polygonal granules with several edges and a uniform shape (Figure 1A). The size of the granule in diameter was from about 5 to 25 $\mu$m with an average volume diameter of 14 $\mu$m (Figure 1C). In contrast, the dimension of rice flour granules was irregular (Figure 1B), from about several microns to hundreds of microns in diameter, and its average volume diameter was 173 $\mu$m (Figure 1C).

**Table 2. Components of Corn Starch and Rice Flour (w/w)[a]**

| content (%) | corn starch | rice flour |
|---|---|---|
| starch | 94.6 ± 2.1 | 86.7 ± 1.8 |
| protein | 0.34 ± 0.1 | 8.3 ± 0.1 |
| fat | 0.57 ± 0.2 | 0.7 ± 0.1 |

[a]Date are means ± standard deviation of three replicates.

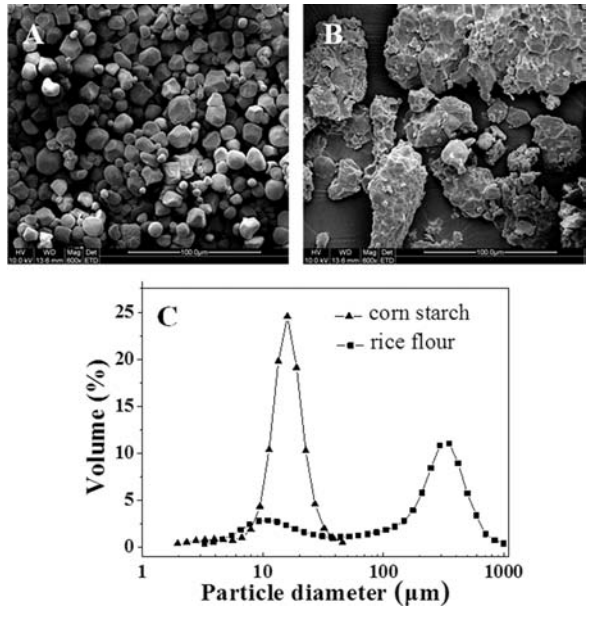


**Figure 1.** Comparative analysis between corn starch and rice flour using SEM imaging (600×) and particle size analysis. (A) SEM image of corn starch particle. (B) SEM imaging of rice flour particle. (C) Particle size distributions of corn starch particle and rice flour particle.


dx.doi.org/10.1021/jf5023109 | J. Agric. Food Chem. 2014, 62, 8486−8490

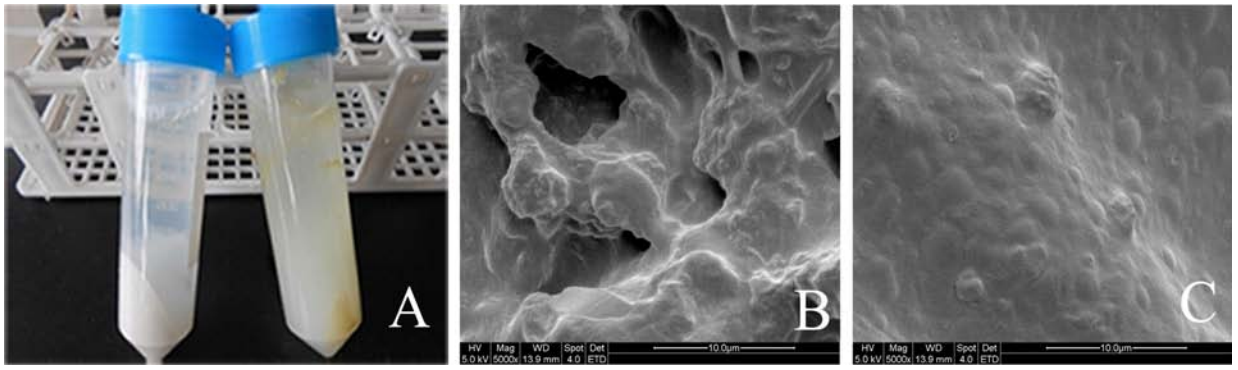


**Figure 2.** Special yellow floats formed during liquefaction of corn starch. (A) The comparison of liquefied solution between rice flour (right) and corn starch (left). (B) SEM image (5000×) of the yellow floats from liquefied corn starch. (C) SEM image (5000×) of the bottom precipitate from liquefied corn starch.

**Analysis of Yellow Floats in Liquefied Corn Starch.** The differences in liquefied adjuncts between corn starch and rice flour mainly included yellow floats and residual insoluble particle. After liquefaction using the thermostable $\alpha$-amylase, liquefied corn starch was a uniform, highly viscous, and colloidal solution, while liquefied rice flour was not viscous and contained many visible granules. Especially, during liquefaction of corn starch, some yellow substances floated on the surface of thick mash, which were intuitively thought as a main potential factor of filtration blocking.

After centrifugation at 8,000 rpm for 10 min, there was a distinct difference between liquefied corn starch and liquefied rice flour (Figure 2A). The upper layer of liquefied rice flour was clean and did not contain any floats, so the upper liquid layer was clean and transparent and the bottom layer was sedimentation. Unlike rice flour, some yellow floats appeared in the upper layer of liquefied corn starch, moreover, the boundary between the middle liquid layer and the bottom sedimentation layer was obscure due to many suspended particles, which may contain very small and incompletely degraded corn starch particles.

The factors that affected the formation of yellow floats during liquefaction of corn starch were also evaluated. The results indicated that the high ratio of corn starch to water, liquefaction time, boiling process, and boiling time significantly promoted formation of yellow floats (data not shown). The more the ratio of corn starch to water increased and the longer the liquefaction time and boiling time, the more corn floats formed. Especially, the boiling process produced quite a lot of yellow floats arising on the surface of liquefied corn starch.

To analyze the dimensions and components of yellow floats, these floats were collected, dried, and then analyzed by SEM analysis and chemical analysis methods. As SEM photographs showed (Figure 2B,C), yellow floats had a relatively loose structure compared with the bottom sedimentation in liquefied corn starch. Overall compositions of corn floats formed under different conditions were similar, which contained polysaccharides (70 ± 5%), ether-soluble substances (13 ± 1%), proteins (5 ± 1%), and other unknown components (12%). The density of yellow floats was lower than that of liquefied corn starch since it floats on the surface, which can also be explained by its loose structure and relatively high fat content over the raw material of corn starch. However, its density was still larger than that of water. Yield of yellow floats was around 0.8 g (dry weight)/100 g of corn starch, and yield of the sedimentation was 1.52 g (dry weight)/100 g of corn starch. Components in sedimentation consisted of polysaccharides (61.4 ± 0.6%), proteins (0.5 ± 0.04%), and fat (2 ± 0.2%). Therefore, the main components in both yellow floats and sedimentation were incompletely degraded corn starch, which might be the main reason for filtration blocking.

**Evaluation of Factors of Filtration Blocking in Liquefied Corn Starch.** Since corn starch can block filtration while rice flour does not, the retention substances on a filter paper from the two-type liquefied adjuncts were compared by SEM imaging. As shown in Figure 3A, the filtration rate of liquefied corn starch was significantly slower than that of rice flour. The SEM photos showed that filter medium formed from liquefied rice flour was porous and loose (Figure 3D), which did not cause the problem of filtration blocking. In contrast, filter medium formed from liquefied corn starch was very dense (Figure 3C), which could seriously block filtration. The dense filter medium of corn starch should result from the mixture of yellow floats and sedimentation, therefore, its main component should be the incompletely degraded starch particle.

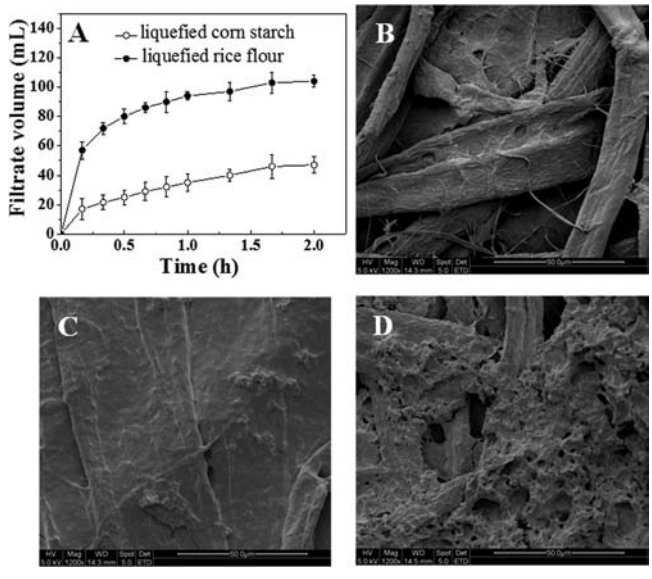


**Figure 3.** Comparison of filtration rate of liquefied adjunct and SEM analysis of the filter medium (1200×). (A) The filtration rate of liquefied corn starch and liquefied rice flour within 2 h. (B) SEM image of filter paper (blank). (C) SEM image of filter medium formed from liquefied corn starch. (D) SEM image of filter medium formed from liquefied rice flour.


dx.doi.org/10.1021/jf5023109 | J. Agric. Food Chem. 2014, 62, 8486−8490

In consideration of increased fat content in yellow floats that may influence filtration, the effects of yellow floats on filtration rate were compared with those of liquid corn oil. As shown in Figure 4, when 5% (w/w) of corn oil was added into liquefied

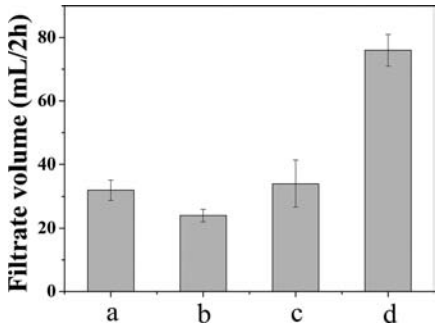


**Figure 4.** Effects of corn floats, corn oil and $\beta$-amylase on filtration rate of liquefied corn starch. (a) Liquefied corn starch. (b) Liquefied corn starch with addition of 5% (w/w) corn oil. (c) Liquefied corn starch with removal of yellow floats. (d) Liquefied corn starch with addition of 100 U/g of $\beta$-amylase.

corn starch, the filtration rate did not change significantly, which indicated that the corn oil should not be the main reason for filtration blocking. When the yellow float was removed from the surface of liquefied corn starch, the filtration rate also did not change significantly (Figure 4). When 100 U/g of $\beta$-amylase was added to further degrade the liquefied corn starch for 1 h, the filtration rate was increased by 2-fold (Figure 4). These results indicated that the main reason for filtration blocking of corn starch was the incompletely degraded starch particle.

**Evaluation of Factors of Filtration Blocking in Mash.** As for the mash that mixed liquefied adjunct with malt, the problem of filtration blocking was similar to that of pure adjunct (Figure 5A). The filtration rate of mash mixed with rice flour was rapid and almost a constant, while that of mash mixed with corn starch was slower and gradually reduced. The filter medium formed after mash filtration was different. The medium mixed with rice flour was more loose and stable, which maintained filtration rate as a constant. In contrast, filter media mixed with corn starch are viscous and layered, where fine particles gradually accumulated in the upper layer of filter media. The layer of fine particles was very thin but greatly weakened filter layer permeability and thus significantly reduced filtration rate.

As permeability of filter medium was greatly dependent on decomposition of cell-wall components from malt such as $\beta$-glucan and xylan and the corn starch particles, effects of $\beta$-amylase and Ultraflo Max (combinational enzyme preparation of $\beta$-glucanase and xylanase) were added into mash respectively, to further degrade the corn starch particles and cell-wall components of malt. The result showed that the filtration rate of mash was increased significantly when the amount of enzyme preparations was increased (Figure 5B,C). Therefore, amylolytic enzyme preparations and cell wall degrading enzymes should be a potential solution for improving high corn starch ratio wort filtration performance.

## DISCUSSION

A rapid mash filtration rate is necessary for high productivity of brewery, so some enzyme preparations have been widely applied to degrade the component causing filtration blocking in the brewing industry like $\beta$-glucanase and xylanase. However, when new material and brewing technology were used in recent years in China like high corn starch ratio beer brewing, new factors blocking mash filtration arose. The emerging problem of filtration blocking cannot be solved very well only by the available brewing enzyme preparations. This study was carried out to evaluate these emerging factors in the process of high corn starch ratio beer brewing and provide new solutions of enzyme preparation for brewery. The results indicate that the emerging factors of filtration blocking should be the incompletely degraded and fine corn starch particles. These residual corn starch particles could not be degraded well by the thermostable $\alpha$-amylase under the condition of high ratio of corn starch to water (1:2.5) even if its dosage was increased by 10 times (data not shown), but could be further degraded by some mesophilic amylolytic enzymes like $\beta$-amylase. However, its industrial application should be further optimized in consideration of the cost of enzyme preparations. Since malts contain intrinsic mesophilic $\beta$-amylase and $\alpha$-amylase, their activity might be not enough for degradation of corn starch during the mashing process when a high adjunct ratio (up to 50%) was used.

Unlike rice flour, corn starch causes obvious extension of lautering time. Besides, the mixture of corn starch and rice flour can reduce the lautering time significantly. According to comparative analysis of the two adjuncts, the distinct filtration performance caused by corn starch and rice flour should mainly result from their different particle character. Corn starch granules were small and uniform in shape, which formed dense and

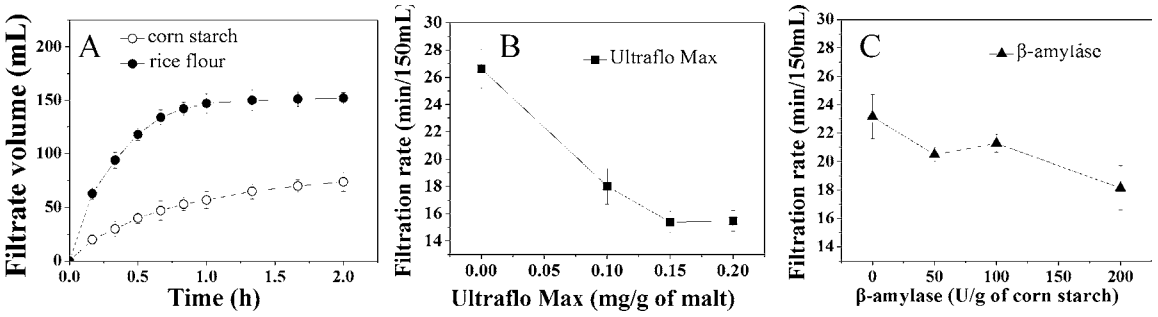


**Figure 5.** Evaluation of enzyme preparations on filtration rate of the mash mixed with high-ratio adjunct (corn starch and rice flour). (A) The filtration rates of mash mixed with different adjuncts (malt:adjunt = 1:1 (w/w)). The filtration rate was evaluated by the total volume of filtrate. (B, C) The effect of different amount of enzyme preparations on filtration rate of mash mixed 50% corn starch (B, Ultraflo Max; C, $\beta$-amylase). Mash mixed corn starch was filtered through a filter paper. The first 100 mL of filtrate was collected and refiltrated, and the filtration time for 150 mL of filtrate was used to evaluate the filtration rate.


dx.doi.org/10.1021/jf5023109 | J. Agric. Food Chem. 2014, 62, 8486−8490

viscous filter media, while rice flour granules were large and irregular, which formed loose and stable filter media. Besides, corn starch particles were easily suspended in wort and could not uniformly deposit with malt husk and formed a thin and dense layer of filter medium on the upper part of the filter medium, which greatly reduced the filtration rate of mash. Therefore, as an adjunct, rice flour can help to form a stable skeleton structure in filter media to maintain a constant filtration rate, while corn starch blocks the filtration pore and forms a dense layer on the surface of filter media to gradually reduce the filtration rate.

The other feature of corn starch that distinguished it from rice flour was the formation of yellow floats. At the later stage of liquefaction of corn starch with high ratio of material to water (1:2.5), some yellow substances floated on the surface and were called yellow floats. They were intuitively thought of as main factors blocking filtration by most breweries' technicians. According to the component analysis, the yellow floats contained a large proportion of polysaccharides and little fat and proteins. Compared with components in the material of corn starch, both the fat content and protein content in corn floats slightly increased, but their amount was still very small. The formation of corn floats was promoted by a high ratio of material to water and elongation of liquefaction time and boiling time. According to these results, we speculate the formation mechanism of yellow floats as follows: high ratio of material to water causes high density of solution; extension of liquefaction time and boiling time caused more water evaporation, resulting in an increased liquid density; some fine corn starch particles interact with pigment, protein, and a small amount of fat to form an aggregation with a low density and loose structure, which floats on the surface. Therefore, the main component in yellow floats is corn starch particles; although they float on the surface, yellow floats are not the factors blocking filtration.

In conclusion, for the filtration process of high corn starch ratio wort, the major factor blocking filtration is the incompletely degraded and fine corn starch particles. Filtration rate mainly depends on the degradation of these small particles. Additional $\beta$-amylase preparation could effectively increase filtration rate. Ultraflo Max that can degrade the known blocking factors like $\beta$-glucan and xylan also performed well. Therefore, the results in this study are useful for our insight into solving the filtration problem causing by high-ratio corn starch, and a combined enzyme preparation including mesophilic amylolytic enzyme and glucanase is proposed.

## AUTHOR INFORMATION


### Corresponding Author

*Jiangnan University, No. 1800 Lihu Avenue, Wuxi, Jiangsu, 214122, China. E-mail: liqi@jiangnan.edu.cn. Phone: +86-510-85918176.

### Author Contributions

§These authors contributed equally to this work.



### Funding

This work was supported by the Fundamental Research Funds for the Central Universities (JUDCF13008 and JUSRP51402A), the Priority Academic Program Development of Jiangsu Higher Education Institutions, and Program of Introducing Talents of Discipline to Universities (No. 111-2-06).


### Notes

The authors declare no competing financial interest.

## ACKNOWLEDGMENTS

We thank Novozymes for kindly providing the enzyme preparations.

## REFERENCES


(1) Cheng, P.; Mueller, R.; Jaeger, S.; Bajpai, R.; Iannotti, E. Lactic acid production from enzyme-thinned corn starch usingLactobacillus amylovorus. *J. Ind. Microbiol.* **1991**, *7*, 27−34.

(2) Xiaodong, W.; Xuan, G.; Rakshit, S. Direct fermentative production of lactic acid on cassava and other starch substrates. *Biotechnol. Lett.* **1997**, *19*, 841−843.

(3) Yin, P.; Nishina, N.; Kosakai, Y.; Yahiro, K.; Pakr, Y.; Okabe, M. Enhanced production of L(+)-lactic acid from corn starch in a culture of *Rhizopus oryzae* using an air-lift bioreactor. *J. Ferment. Bioeng.* **1997**, *84*, 249−253.

(4) Yahiro, K.; Shibata, S.; Jia, S.-R.; Park, Y.; Okabe, M. Efficient itaconic acid production from raw corn starch. *J. Ferment. Bioeng.* **1997**, *84*, 375−377.

(5) Krishnan, M.; Taylor, F.; Davison, B.; Nghiem, N. Economic analysis of fuel ethanol production from corn starch using fluidized-bed bioreactors. *Bioresour. Technol.* **2000**, *75*, 99−105.

(6) Krishnan, M. S.; Nghiem, N. P.; Davison, B. H. Ethanol production from corn starch in a fluidized-bed bioreactor. *Appl. Biochem. Biotechnol.* **1999**, *78*, 359−372.

(7) Shigechi, H.; Koh, J.; Fujita, Y.; Matsumoto, T.; Bito, Y.; Ueda, M.; Satoh, E.; Fukuda, H.; Kondo, A. Direct production of ethanol from raw corn starch via fermentation by use of a novel surface-engineered yeast strain codisplaying glucoamylase and $\alpha$-amylase. *Appl. Environ. Microbiol.* **2004**, *70*, 5037−5040.

(8) Poreda, A.; Czarnik, A.; Zdaniewicz, M.; Jakubowski, M.; Antkiewicz, P. Corn grist adjunct—application and influence on the brewing process and beer quality. *J. Inst. Brew.* **2014**, *120*, 77−81.

(9) Delcour, J. A.; Hennebert, M. M.; Vancraenenbroeck, R.; Moerman, E. Unmalted cereal products for beer brewing. Part I. The use of high percentages of extruded or regular corn starch and sorghum. *J. Inst. Brew.* **1989**, *95*, 271−276.

(10) Lloyd, W. Adjuncts. *J. Inst. Brew.* **1986**, *92*, 336−345.

(11) Russell, I.; Stewart, G. G. Brewing. In *Biotechnology Set*, 2nd ed.; Rehm, H.-J., Reed, G., Eds.; Wiley-VCH Verlag GmbH: Weinheim, Germany, 1995; pp 419−462, 10.1002/9783527620999.ch11j.

(12) Goldammer, T. Adjuncts. In *The brewers' handbook*; KVP Publishers: Clifton, VA, 1999; pp 121−134.

(13) Puligundla, P.; Smogrovicova, D.; Obulam, V. S. R.; Ko, S. Very high gravity (VHG) ethanolic brewing and fermentation: a research update. *J. Ind. Microbiol. Biotechnol.* **2011**, *38*, 1133−1144.

(14) Webster, R. Prediction of the lautering performance of malt. *J. Inst. Brew.* **1981**, *87*, 52−56.

(15) Barrett, J.; Clapperton, J.; Divers, D.; Rennie, H. Factors affecting wort separation. *J. Inst. Brew.* **1973**, *79*, 407−413.

(16) Bühler, T.; McKechnie, M.; Wakeman, R. Temperature induced particle aggregation in mashing and its effect on filtration performance. *Food Bioprod. Process.* **1996**, *74*, 207−211.

(17) Kim, B. S.; Chang, H. N. Production of poly (3-hydroxybutyrate) from starch by Azotobacter chroococcum. *Biotechnol. Lett.* **1998**, *20*, 109−112.

(18) Garcia, A. M.; Walter, W. M., Jr. Physicochemical Characterization of Starch From Peruvian Sweetpotato Selections. *Starch/Staerke* **1998**, *50*, 331−337.

JOURNAL OF AGRICULTURAL AND FOOD CHEMISTRY

Article

pubs.acs.org/JAFC

# Betalain Profile, Phenolic Content, and Color Characterization of Different Parts and Varieties of *Opuntia ficus-indica*

María Jesús Cejudo-Bastante,[†] Makhlouf Chaalal,[§] Hayette Louaileche,[§] Juan Parrado,[#] and Francisco J. Heredia*,[†]

[†]Food Color and Quality Laboraty, Departament of Nutrition and Food Science, Faculty of Pharmacy, University of Sevilla, 41012 Sevilla, Spain

[§]Laboratoire de Biochimie Appliquée, Faculté des Sciences de la Nature et de la Vie, Université de Bejaia, 06000 Bejaia, Algeria

[#]Department of Biochemistry and Molecular Biology, School of Pharmacy, University of Seville, 41012 Seville, Spain

**ABSTRACT:** Three different varieties of *Opuntia ficus-indica* (R, red; Y, yellow; RY, red-yellow) have been considered in this study. Attention was focused on differential tristimulus colorimetry and on the analysis of individual betalains (HPLC-DAD-ESI-ToF-MS) and phenolic content, scarcely previously reported in these kinds of samples. The importance of this research stems from the elucidation of the parts and varieties of cactus pear more optimal for use as natural colorants and sources of phenolics and betalains. Thus, the RY pulp was appropriate to obtain colorants with high color intensity ($C^*_{ab}$ = 66.5), whereas the whole Y fruit and R pulp reached powerful and stable yellow and red colors, respectively ($C^*_{ab}/h_{ab}$, 57.1/84.7 and 61.1°/81.8°). This choice was also based on the visually appreciable differences ($\Delta E^*_{ab} > 5$) among samples, mainly quantitative ($\%\Delta^2L$, $\%\Delta^2C$). In addition, seeds of all *Opuntia* varieties showed significantly ($p < 0.05$) similar phenolic content (around 23.3 mg/g) and color characteristics.

**KEYWORDS:** *Opuntia ficus-indica, differential tristimulus colorimetry, betalains, phenolics, HPLC-DAD-ESI-ToF-MS*

## INTRODUCTION

In the past few years, consumers have become more conscious of the importance of healthy and natural food both in the manufacture or in consumption. One part of this reality is the use of natural products as colorants. In this way, there is a large extent of natural colorants, extracted from different natural raw materials, rich in compounds such as anthocyanins, carotenoids, and chlorophylls. Apart from those, there is a group of chemical compounds that it is still poorly investigated, betalains.

Betalains are water-soluble compounds present in a restricted number of families of the plant order Caryophyllales and of the genus *Amanita* of the Basidiomycetes.[1] Numerous advantageous on consuming betalain-rich food have been reported, such as antioxidant activity, antiviral, anti-inflammatory, and anticarcinogenic effects.[2,3] Betalains are structured in two chemical families (betacyanins and betaxanthin). The common moiety of both chemical families corresponds to betalamic acid, and the nature of the additional residue determines the pigment classification as betacyanin (hydroxycinnamic acid derivatives or sugars) or betaxanthin (amines or amino acids),[4] with maximum absorptions around 540 and 480 nm, respectively.[2,5]

There are manifold species and varieties used as natural food colorants. In that way, although the most studied and widely distributed source of betalains is the red beet (*Beta vulgaris* L.),[6−8] betalains have been also studied in other raw materials. Some examples are the Swiss chard vegetable,[9] flowers (*Gomphrena globosa* L. and *Bougainvillea* sp.),[10] and fruits such as pitaya[11] and cactus pear (*Opuntia* sp.).[12−16]

*Opuntia ficus-indica* is a type of cactus that provides edible prickly pears. This kind of cactus is widely cultivated in the world due to its adaptability to difficult growing conditions (arid and semiarid zones).[17] Recently, the study of cactus pear has become more and more prominent because of its high content of betalains and other phenolic compounds. In fact, those compounds have been previously studied on this matter in different edible and nonedible parts of prickly pears such as pulps,[14] skins,[16] and seeds.[18,19] These research studies have been focused on the general chemical characterization,[12,20] the total content of both phenolic and betalains,[21−23] and the antioxidant activity determination.[24] However, only a few studies have been developed about individual betalains in that raw material.[13,14,25] Moreover, although this fruit has a potential enterprise projection as natural colorant, hitherto, scarce advanced colorimetric studies have been developed.[12,21,26] Therefore, there are still many aspects to be elucidated about the repercussion on the color of *O. ficus-indica* when it is added as safe colorant.

Therefore, the aim of this research was to carry out an extensive chemical and colorimetric characterization of *O. ficus-indica* [L.] Mill cultivated in Algeria. Different parts of three cactus pear varieties were taken into account, which have not been previously considered in conjunction. Our interest was focused on the study of the phenolic content and individual betalain profile and also on colorimetric characteristics by applying differential tristimulus colorimetry, scarcely reported in the literature. Therefore, the objective is not only the chemical characterization of different parts of prickly pears but

Received: May 23, 2014
Revised: July 23, 2014
Accepted: July 30, 2014
Published: July 30, 2014

ACS Publications © 2014 American Chemical Society

**Table 1. Mean CIELAB Parameters and Mean Values of Total Polyphenols (TP) Concentration Corrected for Ascorbic Acid (and Standard Deviations) of Different Parts of the Fruit of the Three Varieties: Influence of the Tested Factors As Assessed by Univariate Statistical Analysis[a]**

| | | | | | statistical main effects | | | | | | | | | | |
|---|---|---|---|---|---|---|---|---|---|---|---|---|---|---|---|
| | | | | | by part of fruit | | | | | | by variety | | | | |
| | $L^*$ | $C^*_{ab}$ | $h_{ab}$ | TP | | | $L^*$ | $C^*_{ab}$ | $h_{ab}$ | TP | | | $L^*$ | $C^*_{ab}$ | $h_{ab}$ | TP |
| YS | 97.7 ± 0.7 | 4.4 ± 0.6 | 92.5 ± 1.8 | 3.8 ± 0.5 | | S/W | * | * | * | * | | Y/R | | | | |
| YW | 88.7 ± 0.9 | 57.1 ± 3.2 | 84.7 ± 0.1 | 13.3 ± 1.1 | Y | S/P | * | * | * | * | S | Y/RY | | | | |
| YP | 84.8 ± 7.8 | 54.5 ± 0.4 | 85.2 ± 1.1 | 8.1 ± 0.5 | | W/P | | | | * | | R/RY | | | | |
| RS | 95.7 ± 2.8 | 6.2 ± 2.1 | 90.9 ± 4.1 | 4.1 ± 0.4 | | S/W | * | * | * | * | | Y/R | | | * | * |
| RW | 88.7 ± 1.4 | 54.9 ± 2.1 | 83.4 ± 0.1 | 6.6 ± 1.5 | *R* | S/P | * | * | * | * | W | Y/RY | | | * | * |
| RP | 80.8 ± 1.7 | 61.1 ± 0.8 | 81.8 ± 0.3 | 11.8 ± 1.3 | | W/P | * | * | * | * | | R/RY | | * | | |
| RYS | 94.9 ± 3.5 | 7.7 ± 2.9 | 88.7 ± 2.6 | 4.0 ± 0.1 | | S/W | | * | * | * | | Y/R | | * | * | * |
| RYW | 89.3 ± 0.2 | 62.5 ± 3.7 | 83.7 ± 0.1 | 8.4 ± 1.0 | *RY* | S/P | * | * | * | * | P | Y/RY | | * | * | * |
| RYP | 88.9 ± 0.9 | 66.5 ± 0.1 | 83.1 ± 0.4 | 12.9 ± 1.4 | | W/P | | | | * | | R/RY | * | * | * | |

[a]Asterisks denote significant differences by pairs according to Tukey test ($p < 0.05$). S, seeds; P, pulp; W, whole fruit; R, red variety; Y, yellow variety; RY, red-yellow variety.

its practical application as a natural colorant by deepening the study of differential colorimetry and betalain profile.

## MATERIALS AND METHODS

**Chemicals and Solvents.** Methanol of analytical or HPLC grade was purchased from J. T. Baker (Baker Mallinckrodt, Mexico), and formic acid and Folin−Ciocalteu reagent were supplied by Sigma-Aldrich (St. Louis, MO, USA). HPLC grade water was obtained by a Milli-Q plus water purification system (Millipore Corp., Bedford, MA, USA). Sodium ascorbate and L-ascorbic acid were from Panreac (Barcelona, Spain). Betanin was supplied by Cymit Quimica S.L. (Barcelona, Spain).

**Samples.** Three different cultivars of prickly pear fruits (*O. ficus-indica* [L.] Mill.) with diverse physical qualities have been selected for this study. Those cactus pear varieties were typically cultivated in the area of Bousselam (Setif, Algeria). Fully ripe cactus pears were collected in August from different points of the plant and in various parts of the parcel. Samples were selected on the basis of their color (both pulp and skin) and the shape and presence of cladode spines (R, red, ovoid and cladode spineless; Y, yellow, elongate with cladode spines; RY, red-yellow, ovoid with cladode spines). Fruits were harvested at a desirable maturity and in good sanitary conditions (R, Y, and RY: pH, 6.14, 5.86 and 5.95; titratable acidity, 0.10, 0.11, and 0.09; °Brix, 12.83, 11.55, and 14.22, respectively).

Fruits were carefully washed and manually peeled. The seeds were removed from the pulp and washed with distilled water. Three different parts of each variety was studied, corresponding to the edible part of the fruit: seeds, pulp, and whole fruit (seeds + pulp). They were separately lyophilized (Christ, Alpha 1-4 LD plus, Germany), ground with a crusher (IKA A 11B, Germany), and passed through a 500 μm sieve.

**Preparation of Extracts.** Lyophilized samples (1 g) were added to 3 mL of methanol/water (50:50) containing 50 mM sodium ascorbate (for avoiding possible oxidations). Subsequently, samples were stirred at 225 rpm for 10 min in darkness. Afterward, samples were centrifuged at 12000*g* at 10 °C for 5 min, separating supernatants from the plant tissue. To achieve the complete discoloration of the plant material, the residues was rinsed once more with the extraction solution and finally with 100% methanol. The extracts were then concentrated in a vacuum (30 °C) until around 3 mL to remove methanol, adding purified water until a total of 4 mL. The mean pH values of the resulting extracts were similar among varieties, as follows: seeds, 5.83; pulp, 6.20; and whole fruit, 6.04. All experiments were carried out in triplicate.

**Colorimetric Measurements.** A Hewlett-Packard UV−vis HP8452 spectrophotometer (Palo Alto, CA, USA) was used to carry out color measurements. The whole visible spectrum (380−770 nm) was recorded at constant intervals ($\Delta\lambda$ = 2 nm) using 2 mm path length glass cells and distilled water as reference. The CIELAB parameters ($L^*$, $a^*$, $b^*$, $C^*_{ab}$, and $h_{ab}$) were determined by using the original software CromaLab[27] following the Commission Internationale de L'Eclariage's recommendations,[28] the CIE 1976 10° Standard Observer and the Standard Illuminant D65. Euclidean distances between two points in the three-dimensional space define by $L^*$, $a^*$, and $b^*$ were used for calculating color differences ($\Delta E^*_{ab}$ of CIELAB): $\Delta E^*_{ab} = [(\Delta L^*)^2 + (\Delta a^*)^2 + (\Delta b^*)^2]^{1/2}$. Moreover, the relative contribution of the three color attributes with respect to $\Delta^2 E^*_{ab}$ that constitutes the total CIELAB color difference was also calculated, expressed as percentage of the quadratic increases of lightness, chroma, and hue.[29]

**Total Phenolic (TP) Content.** TP content was determined using a modification of the Folin−Ciocalteu method.[30] Absorbance was measured at 765 nm, and the results were expressed as milligrams of gallic acid per liter (mg GAE/L). Subsequently, total phenolic content was expressed as milligrams per gram of dry weight (DW). To eliminate the contribution of ascorbic acid to the measurement of absorbance in the Folin−Ciocalteu assay, a correction factor was calculated,[31] quantifying also the ascorbic acid present in each sample.[32] Subsequently, the impact of ascorbic acid in terms of milligrams of GAE per liter was deduced from the spectrophotometrically determined total polyphenol values.

**HPLC-DAD-ESI-ToF-MS Analysis of Betalains.** HPLC separation, identification, and semiquantification of betalains were performed in an Agilent 1200 chromatographic system equipped with a quaternary pump, an UV−vis diode array detector, an automatic injector, and ChemStation software (Palo Alto, CA, USA). Prior to direct injection, the samples were filtered through a 0.45 μm nylon filter (E0034, Análisis Vínicos, Spain). All analyses were made in triplicate.

The betalains' identification was carried out following the method proposed by Castellanos-Santiago and Yahia,[14] using 1% formic acid in water (v/v, eluent A) and methanol (eluent B). Betalains were separated in a Zorbax C18 column (250 × 4.6 mm, 5 μm particle size) maintained at 25 °C, at a flow rate of 1 mL/min. The injection of the volume for all extracts was 20 μL. Betalain compounds were separated starting with 100% A, followed by a linear gradient from 0 to 10% B in 20 min, then a linear gradient from 10 to 30% B in 10 min, and from 30 to 100% B in 5 min. To re-establish the initial conditions, a linear gradient from 100% B to 100% A was used during 5 min. UV−vis spectra were recorded from 200 to 800 nm with a bandwidth of 1.0 nm. Betacyanins and betaxanthins were monitored at 535 and 482 nm, respectively. The identification of each chromatographic peak was tentatively assigned by their visible spectral characteristics in comparison with standard and retention times according to the method proposed by Castellanos-Santiago and Yahia.[14] Semi-

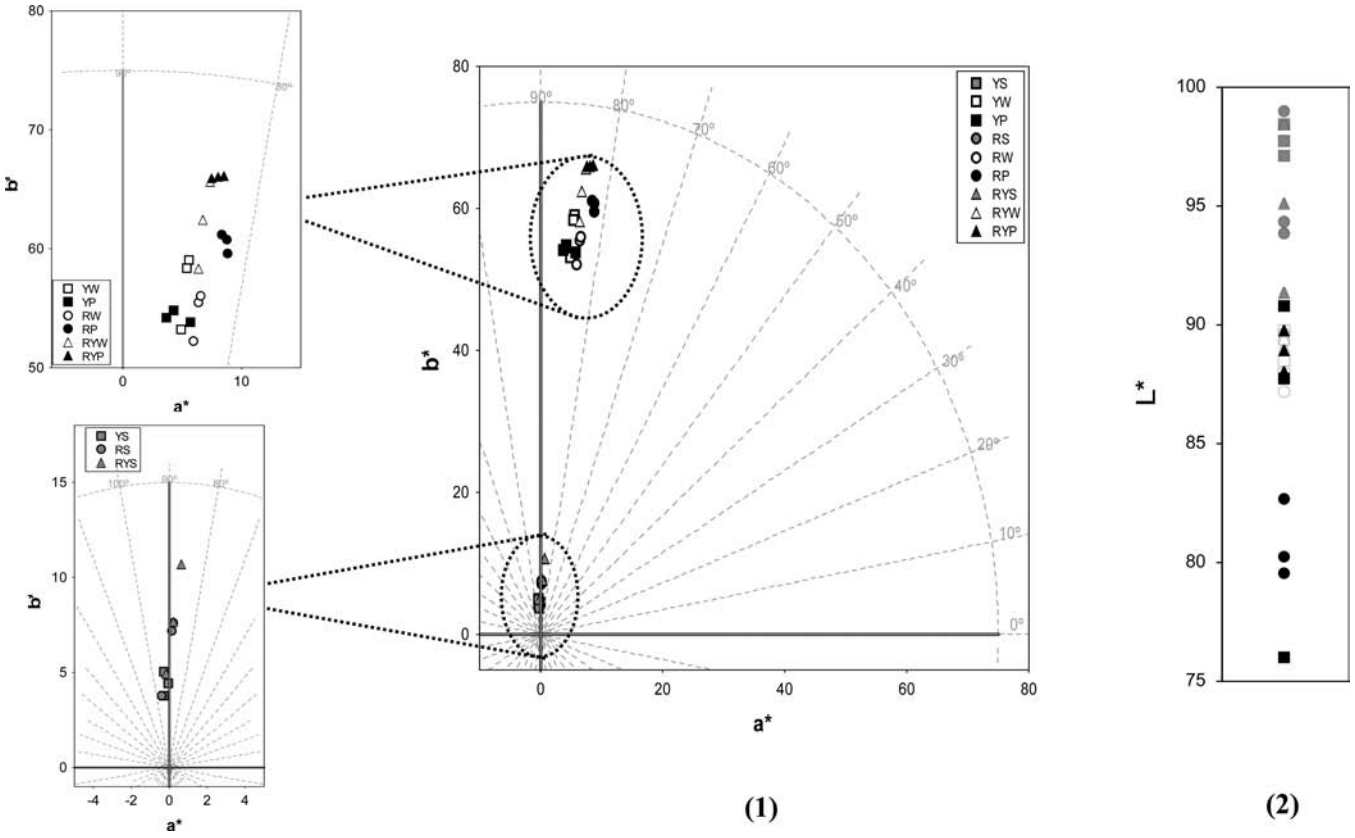


**Figure 1.** Representation of *Opuntia ficus-indica* extracts obtained from different parts of the fruit of three varieties in the ($a^*b^*$) plane (1) and representation of their $L^*$ (lightness) values (2). S, seeds; P, pulp; W, whole fruit; R, red variety; Y, yellow variety; RY, red-yellow variety.

quantification was done on the basis of the mean areas of individual betalains.

The identity of individual betalains was confirmed by mass spectrometry. The separation was performed in a Dionex Ultimate 3000RS U-HPLC (Thermo Fisher Scientific, Waltham, MA, USA), using the column and mobile phase above indicated but with a postcolumn split of 0.4 mL/min. The mass spectra was obtained using a microToF-QII high-resolution time-of-flight mass spectrometer (UHR-ToF) with Q-ToF geometry (Bruker Daltonics, Bremen, Germany) equipped with an electrospray ionization (ESI) source. The instrument was operated in positive ion mode using a scan range from $m/z$ 50 to 1200. Nitrogen was used as the dry gas at a flow rate of 8 mL/min with nebulizing (1.2 bar), and the nebulized temperature was set at 200 °C. Mass spectra were acquired in MS full scan mode, and data were used to perform multiple target screening using Target Analysis 1.2 software (Bruker Daltonics). Instrument control was performed using Bruker Daltonics HyStar 3.2. The accurate mass data of the molecular ions were processed through the software Data Analysis (Bruker Daltonics). The accepted accuracy threshold for confirmation of elemental compositions has been established at 5 ppm.

**Statistical Analysis.** Statistical analysis was carried out by using Statistica version 8.0 software.[33] Univariate analyses of variance (Tukey test and ANOVA) and correlation analysis were applied to discriminate among the means of chemical data by "variety" and by "part of the fruit" factors.

## RESULTS AND DISCUSSION

**Colorimetric Characteristics.** The color was objectively calculated by tristimulus colorimetry, and the values of $L^*$, $C^*_{ab}$, and $h_{ab}$ of each sample are shown in Table 1. The color points represented in the ($a^*b^*$) color diagram as well as the lightness of the sample extracts appear in Figure 1.

The different locations of the diverse parts of *Opuntia* varieties could permit the objective establishment of the chromatic characteristics of the fruits. As can be seen, two different groups are formed: seeds (S), on the one hand, and pulp (P) and whole fruit (W), on the other hand. Regardless of the "variety", P and W were located in the first quadrant (positive values of $a^*$ and $b^*$) of the ($a^*$–$b^*$) plane, whereas S was situated between the first and second quadrants (positive values of $b^*$). It can be noted that, although seed extracts showed intense yellowish tonalities (values of hue close to 90°), their chromatic intensity was very low (values of $C^*_{ab}$ between 4 and 8) (Table 1). However, P and W had a very intense orange-yellow color (values of $C^*_{ab}$ and $h_{ab}$ around 60° and 82°, respectively) (Table 1). Pulp extracts of the different varieties were clearly separated in the space according to both $b^*$ and $a^*$ parameters, whereas the whole fruits were discriminated only on the basis of $b^*$ (Figure 1). Moreover, a separation "by variety" of these samples was observed (Figure 1). Thus, the red-yellow (RY) variety showed the highest values of $b^*$, whereas $a^*$ is the predominant parameter in the red (R) variety. With regard to the lightness, seeds and pulp (especially RP) were noted to occupy opposite positions, keeping the whole fruit extracts in an intermediate stage.

Among "variety" and "part of the fruit" factors, it was largely the latter the most influenced color (Table 1). When ANOVA was applied to the set of data to draw attention to the possible significant differences according to "variety" and "part of the fruit" ($n$ = 27 and $n$ = 9, respectively; data not shown), only the latter factor showed significance. For a better understanding, a comparison by pairs using the Tukey test was applied (Table 1). Thus, when the "part of the fruit" factor was considered, the

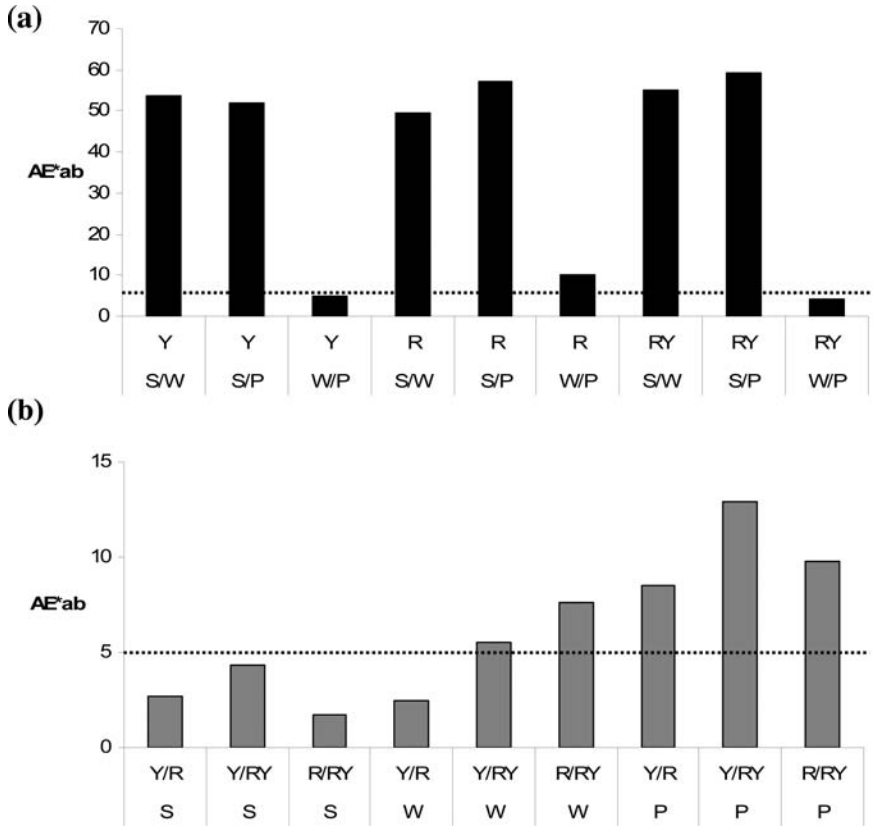


**Figure 2.** Color variation ($\Delta E^*_{ab}$) by pairs in relation to the part of the fruit (a) and variety (b) factors. S, seeds; P, pulp; W, whole fruit; R, red variety; Y, yellow variety; RY, red-yellow variety. Dotted line represents the value of $\Delta E^*_{ab}$ appreciable to the human eye.

major significant variations on CIELAB parameters were assigned to the R variety. Clearly, as could be expected, S significantly differed from P and W for all *Opuntia* varieties in all colorimetric parameters. Moreover, due to the absence of significance ($p > 0.05$) in $C^*_{ab}$ and $h_{ab}$ between P and W extracts in Y and RY varieties, both pulp and whole fruit for both varieties could lend the same color to foods and they could be used indistinctly as natural yellow colorants. However, the values of chroma in P extracts of R variety were significantly higher when compared with W, with a considerably strong red tonality. Seeds could contribute to those differences between W and P because of their low values of chroma, producing an attenuation of the color intensity of W (Table 1). Therefore, it is more suitable to use the pulp of R variety to confer a more powerful red color.

With regard to the "variety" factor, P was considered the most influential part of the fruit to discriminate among varieties, above all regarding chroma and hue. Thus, if pulp extract was considered to be used as natural colorant, the Y variety would confer the significantly highest yellow tonalities.[34] On the contrary, if the whole fruit extract was taken into account, the RY variety should be employed, due to its noticeably higher chromatic intensity. It was also remarkable that the colorimetric characteristics were not significantly affected by "variety" when S extracts were taken into account.

From an industrial point of view, it is easier and economically advantageous to avoid the time-consuming manipulation that some technological procedures require, such as the separation of the seeds from the pulp. Therefore, the whole Y fruit and the pulp of R varieties are optimal for use as yellow and red colorants, respectively, whereas the whole RY fruit could be useful as an additive to confer vivid colors.

**Differential Colorimetry.** In an attempt to evaluate the colorimetric differences among "varieties" and "parts of the fruit", the mean color difference ($\Delta E^*_{ab}$) among samples was calculated (Figure 2). Taking into account that $\Delta E^*_{ab}$ of up to 5 CIELAB units indicates "big color differences" appreciable to the human eye,[35,36] it was confirmed that visually perceptible color differences were observed among the different parts of the fruit of each variety (Figure 2a). On the one hand, the significant variations among S/P and S/W for all varieties previously commented were also appreciable to human eyes. This fact is predictable because they greatly differ from the phenolic profile and, consequently, from the color.[34] When the role of each color attribute with respect to $\Delta^2 E^*_{ab}$ was calculated ($\%\Delta^2 L$, $\%\Delta^2 C$, $\%\Delta^2 H$), results evidenced that these differences were mainly quantitative, with major values of quadratic variations of chroma ($\%\Delta^2 C > 90$) and practically negligible values of lightness and hue. In addition, also noticeable and quantitative color differences were seen for W and P in R variety, lightness being mainly responsible ($\%\Delta^2 L > 65$). The negligible quadratic percentages of hue demonstrated that this parameter did not contribute to the establishment of significant differences of color.

On the other hand, when a comparison among varieties was carried out (Figure 2b), it was observed that several significant differences in the pulps were mainly due to chroma ($\%\Delta^2 C \sim 65$ and 87 when Y/R and Y/RY, respectively, were compared). However, it was lightness that was mainly responsible for the discrepancy between R/RY varieties ($\%\Delta^2 L = 68$). In the case of the whole fruit, only quantitative variations contributed to


dx.doi.org/10.1021/jf502465g | J. Agric. Food Chem. 2014, 62, 8491−8499

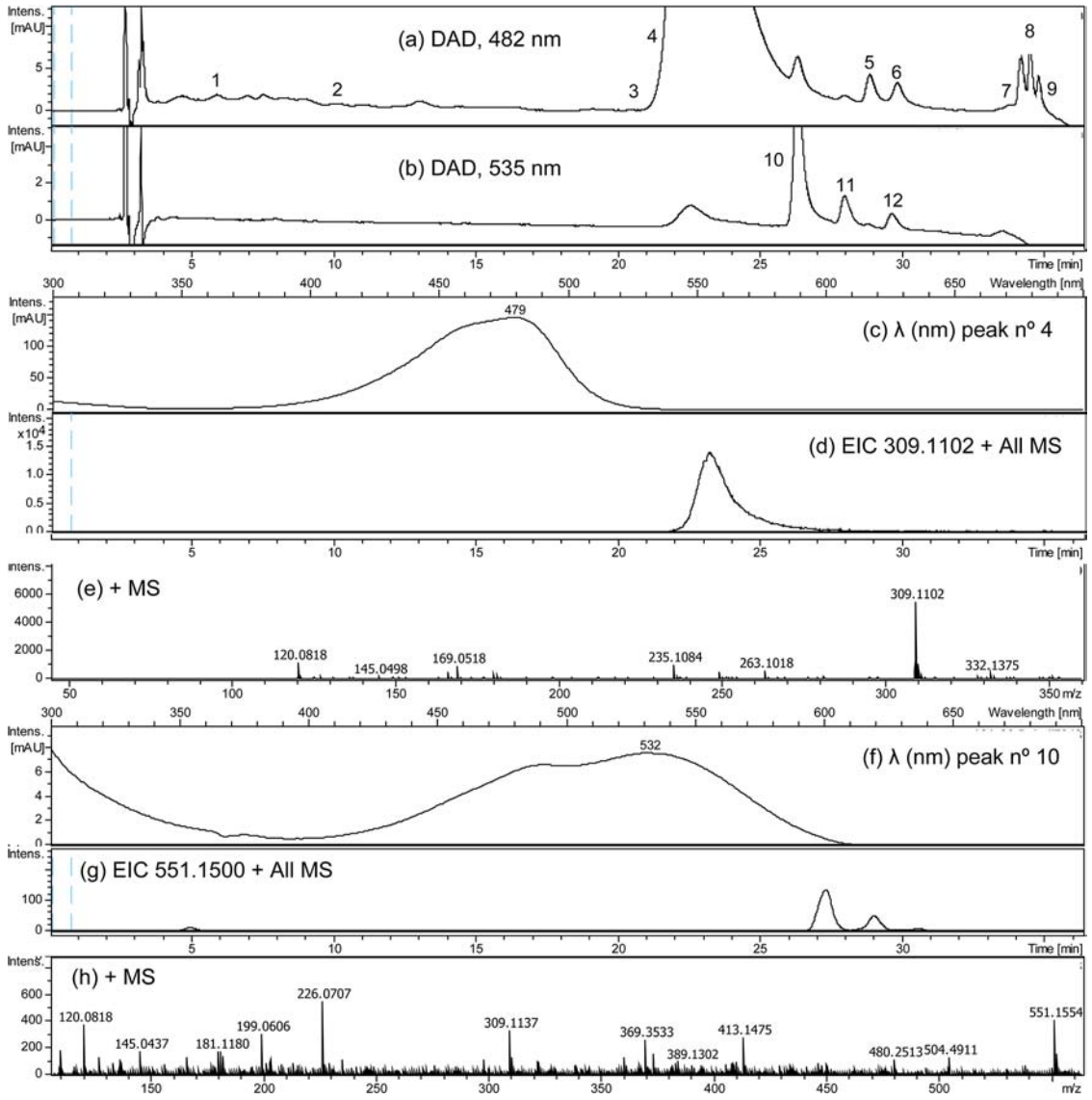


**Figure 3.** HPLC chromatogram corresponding to the fraction of betaxanthins and betacyanins of the whole fruit of the red-yellow *Opuntia ficus-indica* variety as representative sample: DAD chromatogram at (a) 482 nm and (b) 535 nm and visible spectrum (c, f), EIC chromatogram in positive mode (d, g), and MS positive mode (e, h) of the major compounds of each kind of betalains, indicaxanthin and betanin, respectively.

**Table 2. Molecular Formula, Retention Times, UV−Vis Data, and Mass Spectral Data of Betalains Identified in *Opuntia ficus-indica* by HPLC-DAD-ESI-ToF-MS**

| peak | compound | molecular formula | $t_r$ (min) | UV−vis maxima (nm) | $m/z$ $[M + H]^+$ | MS ion |
|---|---|---|---|---|---|---|
| | betaxanthins | | | | | |
| 1 | histidine-betaxanthin (muscaarin) | $C_{15}H_{16}N_4O_6$ | 5.9 | 476 | | |
| 2 | glutamine-betaxanthin (vulgaxanthin I) | $C_{14}H_{17}N_3O_7$ | 10.1 | 472 | | |
| 3 | aminobutyric acid-betaxanthin | $C_{13}H_{16}N_2O_6$ | 19.2 | 462 | 297.1106 | 253.1227 |
| 4 | proline-betaxanthin (indicaxanthin) | $C_{14}H_{16}N_2O_6$ | 22.7 | 479 | 309.1102 | 263.1018 |
| 5 | valine-betaxanthin | $C_{14}H_{18}N_2O_6$ | 29.0 | 472 | 311.1275 | 137.0628 |
| 6 | valine-betaxanthin isomer | $C_{14}H_{18}N_2O_6$ | 30.0 | 471 | 311.1295 | 137.0654 |
| 7 | isoleucine-betaxanthin | $C_{15}H_{20}N_2O_6$ | 34.4 | 472 | 325.1408 | 219.1094 |
| 8 | leucine-betaxanthin (vulgaxanthin IV) | $C_{15}H_{20}N_2O_6$ | 34.7 | 471 | 325.1369 | 209.0844 |
| 9 | phenylalanine-betaxanthin | $C_{18}H_{18}N_2O_6$ | 35.0 | 468 | | |
| | betacyanins | | | | | |
| 10 | betanin | $C_{24}H_{26}N_2O_{13}$ | 26.5 | 534 | 551.1554 | 389.1302 |
| 11 | isobetanin | $C_{24}H_{26}N_2O_{13}$ | 28.1 | 534 | 551.1485 | 389.1243 |
| 12 | gomphrenin | $C_{24}H_{26}N_2O_{13}$ | 29.8 | 535 | 551.1987 | 389.1223 |


dx.doi.org/10.1021/jf502465g | J. Agric. Food Chem. 2014, 62, 8491−8499

Table 3. Mean Areas and Standard Deviations of Betalain Compounds Belonging to Different Chemical Families (Betacyanins and Betaxanthins)[a]

| | YW | RW | RYW | YP | RP | RYP |
|---|---|---|---|---|---|---|
| betanin | 155.9 ± 24.7 | 182.4 ± 13.2 | 226.3 ± 11.5 | 25.3 ± 1.1 | 169.1 ± 6.3 | 216.2 ± 39.8 |
| isobetanin | 46.1 ± 15.2 | 38.4 ± 5.7 | 55.4 ± 10.6 | 10.8 ± 2.4 | 82.5 ± 12.6 | 45.3 ± 3.1 |
| gomphrenin I | 6.5 ± 1.1 | 8.8 ± 0.6 | 11.0 ± 0.7 | 5.4 ± 1.2 | 8.8 ± 0.7 | 11.8 ± 1.3 |
| sum of betacyanins | 208.5 ± 38.9 | 229.6 ± 13.5 | 292.6 ± 21.6 | 37.9 ± 1.8 | 260.4 ± 17.9 | 273.3 ± 39.2 |
| histidine-betaxanthin (muscaarin) | 152.0 ± 44.8 | 90.0 ± 15.8 | 155.6 ± 42.4 | 55.0 ± 1.4 | 50.6 ± 7.1 | 21.3 ± 1.5 |
| glutamine-betaxanthin (vulgaxanthin) | 76.6 ± 5.1 | 30.5 ± 2.7 | 48.7 ± 3.1 | 38.3 ± 9.8 | 25.4 ± 10.6 | 11.5 ± 0.8 |
| aminobutyric acid-betaxanthin | 86.2 ± 4.8 | 51.3 ± 1.2 | 100.2 ± 3.8 | 61.3 ± 10.1 | 84.9 ± 12.4 | 68.6 ± 12.8 |
| proline-betaxanthin (indicaxanthin) | 6550.6 ± 336.4 | 7224.0 ± 617.1 | 7656.1 ± 277.3 | 6180.3 ± 279.0 | 8525.3 ± 297.9 | 8987.1 ± 502.5 |
| valine-betaxanthin | 34.1 ± 3.7 | 15.4 ± 0.2 | 43.9 ± 3.3 | 16.5 ± 0.5 | 25.9 ± 2.7 | 22.0 ± 3.8 |
| valine-betaxanthin isomer | 30.7 ± 0.5 | 12.4 ± 1.0 | 33.0 ± 9.6 | 14.4 ± 4.0 | 21.3 ± 3.4 | 24.8 ± 1.0 |
| isoleucine-betaxanthin | 58.5 ± 3.8 | 36.5 ± 2.1 | 72.9 ± 1.0 | 53.3 ± 6.0 | 54.5 ± 5.0 | 65.7 ± 8.1 |
| leucine-betaxanthin (vulgaxanthin) | 64.8 ± 4.4 | 44.2 ± 2.4 | 69.7 ± 2.1 | 44.9 ± 9.2 | 46.6 ± 5.6 | 56.5 ± 8.7 |
| phenylalanine-betaxanthin | 32.6 ± 3.0 | 26.3 ± 0.2 | 51.1 ± 9.5 | 13.5 ± 1.3 | 26.9 ± 4.0 | 38.4 ± 7.6 |
| sum of betaxanthins | 7086.2 ± 397.4 | 7530.5 ± 614.6 | 8231.3 ± 259.7 | 6477.3 ± 279.4 | 8861.3 ± 336.6 | 9295.9 ± 524.5 |
| total betalains | 7294.7 ± 427.6 | 7760.1 ± 619.5 | 8523.9 ± 248.8 | 6515.2 ± 280.2 | 9121.7 ± 319.3 | 9569.2 ± 528.8 |

[a]S, seeds; P, pulp; W, whole fruit; R, red variety; Y, yellow variety; RY, red-yellow variety.

the color differences among RY/Y and R/RY (%$\Delta^2C$ > 95). The contribution of quadratic variations of lightness was negligible. No appreciable color differences among varieties were found in seeds.

**Polyphenolic Content.** The values of phenolic compounds of the different parts of cactus pears are shown in Table 1. The ANOVA test applied to the whole set of data revealed that no significant differences were assigned either by "part of the fruit" or by "variety" (data not shown). However, as was performed with CIELAB parameters, the Tukey test was applied to elucidate possible significant variations by pairs. It is highlighted that the "part of the fruit" factor showed significance for all three varieties (Table 1). In the case of the Y variety, as expected, the phenolic content of W was the most predominant, followed by P and S. Khatabi et al.[34] also reported an abundant amount of polyphenols in the whole fruit and pulp of Moroccan prickly pears. Furthermore, according to the "variety" factor, Y variety (both P and S) had the significantly lowest phenolic content in comparison with the rest of the varieties. Similar results were also obtained by Khatabi et al.[34] when comparing pulps of yellow and red varieties of prickly pears. Furthermore, seeds were attributed minor values of total polyphenols, but, even so, prickly pear seeds could be considered as an important natural source of polyphenols with direct application in the food or health industry.[18,19] No variance in the polyphenolic content among varieties was found, contrarily to that observed by Morales et al.[22] in seeds of diverse species of *Opuntia*.

**Betalain Identification.** In this research, several types of betalains have been identified by HPLC coupled with electrospray mass spectrometry. The identities of betalains were achieved on the basis of the retention times, spectra, and $m/z$ values. Figure 3 shows the chromatographic pattern and peak assignment of the two families of betalains (betacyanins and betaxanthin), monitored at 535 and 482 nm, respectively. As well, the EIC chromatogram and MS positive mode of the major compounds belonged to each kind of betalains (betanin and indicaxanthin, respectively) were included. These compounds are summarized in Table 2, which shows the retention times, UV−vis data, and mass spectra of each betalain identified of *O. ficus-indica* by HPLC-DAD-ESI-ToF-MS. Concretely, the whole fruit of the red-yellow variety has been selected as representative because of its higher values of areas. Individual betalains were identified in both pulp and whole fruit. However, seeds lacked betalains.

A great number of betaxanthins have been identified in this study. Among them, the presence of indicaxanthin, well-described in cactus pears, has been confirmed (peak 4, molecular ion at 309.1102 $m/z$ units, and a daughter ion at $m/z$ 263.1018) (Table 2; Figure 3). Moreover, the identification of several additional betaxanthins is highlighted, the structures of which involved amino acids such as aminobutyric acid (peak 3, $m/z$ 297.1106 and 253.1227), valine (peak 5, $m/z$ 311.1275 and 137.0628), isovaline (peak 6, $m/z$ 311.1195 and 137.0654), isoleucine (peak 7, $m/z$ 325.1408 and 219.1094), and leucine (peak 8, $m/z$ 325.1369 and 209.0844) (Table 2). Other betalains have been tentatively identified on the basis of UV−vis spectra and the retention times of the chromatographic method used:[14] muscaarin (peak 1, 476 nm), vulgaxanthin (peak 2, 472 nm), and phenylalanine (peak 9, 468 nm). In addition, three betacyanin compounds have been correctly assigned: the well-known betanin (peak 10, $m/z$ 551.1554), its isomer isobetanin (peak 11, $m/z$ 551.1485), and a minor one, poorly described, called gomphrenin (peak 12, $m/z$ 551.1987). The different attachment of the glucose moiety (C-6 and C-5) caused the different elution times between gomphrenin and betanin, respectively.[14] All betacyanins produced a fragment near $m/z$ 389.1243 units corresponding to the protonate aglycones ($[\text{betanidin} + H]^+$ or $[\text{isobetanidin} + H]^+$) (loss of a fragment of $m/z$ 162 units corresponding to the glucose molecule).

**Semiquantification of Betalain.** Two different wavelengths have been monitored to carry out the semiquantification of betalains, 535 nm for betacyanins and 482 nm for betaxanthins. It is noteworthy that, although both betacyanins and betaxanthins were present in all cactus pear varieties, the mean areas of betaxanthins were, by far, considerably higher in comparison with that of betacyanins (Table 3). Among them, indicaxanthin was the major betaxanthin compound in *O. ficus-indica*, with an average

**Table 4. Influence of the Tested Factors (Part of the Fruit and Variety) on Betalain Compounds As Assessed by Univariate Statistical Analysis[a]**

| | by part of fruit | | | by variety | | | | | |
|---|---|---|---|---|---|---|---|---|---|
| | Y | R | RY | W | | | P | | |
| | W/P | W/P | W/P | Y/R | Y/RY | R/RY | Y/R | Y/RY | R/RY |
| betanin | * | | | | * | * | * | * | |
| isobetanin | * | * | | | | | * | * | * |
| gomphrenin I | | | | * | * | * | * | * | * |
| sum of betacyanins | * | | | | * | * | * | * | |
| histidine-betaxanthin (muscaarin) | * | * | * | | | | | * | * |
| hlutamine-betaxanthin (vulgaxanthin) | * | | * | * | * | * | | * | |
| aminobutyric acid-betaxanthin | * | * | * | * | * | * | | | |
| proline-betaxanthin (indicaxanthin) | | * | * | | * | | * | * | |
| valine-betaxanthin | * | * | * | * | * | * | * | | |
| valine-betaxanthin isomer | * | * | | * | | * | | * | |
| isoleucine-betaxanthin | | * | | * | * | * | | | |
| leucine-betaxanthin (vulgaxanthin) | * | | | * | | * | | | |
| phenylalanine-betaxanthin | * | | | * | * | * | * | * | |
| sum of betaxanthins | * | * | * | | * | | * | * | |
| total betalains | * | * | * | | * | | * | * | |

[a]Asterisks denote significant differences by pairs according to Tukey test ($p < 0.05$). S, seeds; P, pulp; W, whole fruit; R, red variety; Y, yellow variety; RY, red-yellow variety.

percentage of area around 90%. Similar results were reported in the pulps of different Mexican and Moroccan prickly pear cultivars.[14,34] Muscaarin took second place, with 2% of the total mean area of betalains, followed by the aminobutyric acid moiety betaxanthin (around 1%). With regard to betacyanins, betanin was the dominate compound in *O. ficus-indica*, but represents only 2% of the total area of betalains.[12] The rest of the identified betaxanthins and betacyanins were found in an area percentage below 1%.

When ANOVA was applied to the set of data, and similarly to that described for the color of extracts, the "part of the fruit" was largely the most influential factor of significant variance in virtually all betalain compounds (data not shown). In fact, all individual betalains were highly ($p < 0.05$) correlated with chromatic characteristics (positive for $L^*$ and $h_{ab}$, and negative for $C^*_{ab}$). Concretely, $C^*_{ab}$ and $h_{ab}$ were the chromatic parameters more correlated with betalains (Pearson correlation coefficients: $C^*_{ab}$, 0.8500; $h_{ab}$, −0.7000; $L^*$, −0.5500), so the chromatic intensity and the tonality of the samples were directly related with the content of betalains. The "variety" factor, however, practically did not affect this kind of compound. To test the diversity among pairs of samples, statistical main differences (Tukey test) on the main areas of betalain compounds were scrutinized (Table 4). As can be seen, the major considerable differences on betacyanins among W and P were ascribed to the Y variety, with remarkable areas in the whole fruit. With regard to betaxanthins, pulps of R and RY varieties had main areas in plenty in comparison with that observed in the whole fruit. These results were in concordance with the phenolic content previously commented. In fact, individual betalains and phenolic content were positively and highly correlated ($p < 0.05$), with Pearson correlation coefficients >0.7000 in the majority of individual betalains. Moreover, although Y was the variety with most differences on individual betaxanthins ($p < 0.05$), muscaarin, aminobutyric acid, and valine moiety compounds were the betalains with significance in all three prickly pears.

With regard to the "variety" factor, when the whole fruit was considered, RY significantly held the first position of total area of individual betacyanins and betaxanthins, whereas Y and R were at the tail end ($p < 0.05$) (Table 3). However, different behaviors followed the pulp extracts, with significantly lower values of Y variety and without variance among R and RY varieties. That pattern was in concordance with the aforementioned content of total polyphenols. In short, the Y variety showed the significantly lowest areas of betalains, the pulp of the RY variety being the one that adopted the greater values.

In summary, it might be concluded that *O. ficus-indica* could be an important choice for use as a natural colorant and source of phenolic and betalain compounds. The choice of the best part of cactus pears with that objective has been directed not only toward the highest values of polyphenols and betalains but also to the best color properties. Thus, the whole grain of yellow cactus pear could be more suitable as yellow colorant, whereas it could be more appropriate to use the pulp of the red variety to obtain a more reddish colorant. Finally, also the pulp of red-yellow prickly pear is optimal as a complement due to its high colorant intensity. Moreover, regardless of the variety, *Opuntia* seeds could be used as an important source of polyphenols. In addition, the possibility of the presence of essential amino acids in the structure of betaxanthins makes possible the use of *O. ficus-indica* as an important essential dietary colorant or as a diet fortification with essential amino acids. This study could be a great step forward in the food, cosmetics, and drug industries, among others.

## AUTHOR INFORMATION

### Corresponding Author

*(F.J.H.) Phone: +34 954556495. Fax: +34 954556110. E-mail: heredia@us.es.

### Funding

We are indebted to Consejería de Economía, Innovación y Ciencia, Junta de Andalucía, Spain (Projects P11-AGR-7843 and P11-RNM-7887), and Ministerio de Ciencia y Tecnología, Spain (Projects Plan Nacional I+D CTM2011-29930) for financial support. We are also grateful to the Algerian Ministry of Higher Education and Scientific Research for the award of a grant.

### Notes

The authors declare no competing financial interest.

## ■ ACKNOWLEDGMENTS

We thank the technical staff of Biology Service (SGI, Universidad de Sevilla) and Instituto de Biomedicina de Sevilla (IBiS, Universidad de Sevilla) for technical assistance. We also thank María Gil Vicente for her support in the analytical assays.

## ■ REFERENCES

(1) Waterman, P. G. Alkaloid chemosystematics. In *The Alkaloids, Chemistry and Pharmacology*; Academic: San Diego, CA, USA, 1998; Vol. 50.

(2) Strack, D.; Vogt, T.; Schliemann, W. Recent advances in betalain research. *Phytochemistry* **2003**, *62*, 247−269.

(3) Reddy, M. K.; Alexander-Lindo, R. L.; Nair, M. G. Relative inhibition of lipid peroxidation, cyclooxygenase enzymes, and human tumor cell proliferation by natural food colors. *J. Agric. Food Chem.* **2005**, *53*, 9268−9273.

(4) Herbach, K. M.; Stintzing, F. C.; Carle, R. Betalain stability and degradation − structural and chromatic aspects. *J. Food Sci.* **2006**, *71*, R41−R50.

(5) Azeredo, H. M. C. Betalains: properties, sources, applications, and stability − a review. *Int. J. Food Sci. Technol.* **2009**, *44*, 2365−2376.

(6) De Azeredo, H. M. C.; Pereira, A. C.; De Souza, A. C. R.; Gouveia, S. T.; Mendes, K. C. B. Study on efficiency of betacyanin extraction from red beetroots. *Int. J. Food Sci. Technol.* **2009**, *44*, 2464−2469.

(7) Nemzer, B.; Pietrzkowski, Z.; Spórna, A.; Stalica, P.; Thresher, W.; Michałowski, T.; Wybraniec, S. Betalainic and nutritional profiles of pigment-enriched red beet root (*Beta vulgaris* L.) dried extracts. *Food Chem.* **2011**, *127*, 42−53.

(8) Pavokovi, D.; Krsnik-Rasol, M. Complex biochemistry and biotechnological production of betalains. *Food Technol. Biotechnol.* **2011**, *49*, 145−155.

(9) Kugler, F.; Stintzing, F. C.; Carle, R. Identification of betalains from petioles of differently colored Swiss chard (*Beta vulgaris* L. ssp. *cicla* [L.] Alef. cv. Bright Lights) by high-performance liquid chromatography-electrospray ionization mass spectrometry. *J. Agric. Food Chem.* **2004**, *52*, 2975−2981.

(10) Kugler, F.; Stintzing, F. C.; Carle, R. Characterisation of betalain patterns of differently coloured inflorescences from *Gomphrena globosa* L. and *Bougainvillea* sp. by HPLC-DAD-ESI-MSn. *Anal. Bioanal. Chem.* **2007**, *387*, 637−648.

(11) Stintzing, F. C.; Schieber, A.; Carle, R. Betacyanins in fruits from red-purple pitaya, *Hylocereus polyrhizus* (Weber) Britton & Rose. *Food Chem.* **2002**, *77*, 101−106.

(12) Stintzing, F. C.; Schieber, A.; Carle, R. Evaluation of colour properties and chemical quality parameters of cactus juices. *Eur. Food Res. Technol.* **2003**, *216*, 303−311.

(13) Stintzing, F. C.; Schieber, A.; Carle, R. Identification of betalains from yellow beet (*Beta vulgaris* L.) and cactus pear [*Opuntia ficus-indica* (L.) Mill.] by high-performance liquid chromatography-electrospray ionization mass spectrometry. *J. Agric. Food Chem.* **2002**, *50*, 2302−2307.

(14) Castellanos-Santiago, E.; Yahia, E. M. Identification and quantification of betalains from the fruits of 10 Mexican prickly pear cultivars by high-performance liquid chromatography and electrospray ionization mass spectrometry. *J. Agric. Food Chem.* **2008**, *56*, 5758−5764.

(15) Yahia, E. M.; Castellanos, E.; Mondragon-Jacobo, C. Identification and quantification of pigments in prickly pear fruit. *Acta Hortic.* **2010**, *877*, 1129−1136.

(16) Moussa-Ayoub, T. E.; El-Samahy, S. K.; Rohn, S.; Kroh, L. W. Flavonols, betacyanins content and antioxidant activity of cactus *Opuntia macrorhiza* fruits. *Food Res. Int.* **2011**, *44*, 2169−2174.

(17) Stintzing, F. C.; Carle, R. Cactus stems (*Opuntia* spp.): a review on their chemistry, technology, and uses. *Mol. Nutr. Food Res.* **2005**, *49*, 175−194.

(18) Chaalal, M.; Touati, N.; Louaileche, H. Extraction of phenolic compounds and in vitro antioxidant capacity of prickly pear seeds. *Acta Bot. Gallica* **2012**, *159*, 467−475.

(19) Chaalal, M.; Louaileche, H.; Touati, N.; Bachir Bey, M. Phytochemicals, in vitro antioxidant capacity and antiradical potential of whole and ground seeds of three prickly pear varieties: a comparative study. *Ind. Crops Prod.* **2013**, *49*, 386−391.

(20) Medina, E. M. D.; Rodríguez, E. M. R.; Romero, C. D. Chemical characterization of *Opuntia dillenii* and *Opuntia ficus indica* fruits. *Food Chem.* **2007**, *103*, 38−45.

(21) Felker, P.; Stintzing, F. C.; Müssig, E.; Leitenberger, M.; Carle, R.; Vogt, T.; Bunch, R. Colour inheritance in cactus pear (*Opuntia ficus-indica*) fruits. *Ann. Appl. Biol.* **2008**, *152*, 307−318.

(22) Morales, P.; Ramírez-Moreno, E.; Sanchez-Mata, M. D. C.; Carvalho, A. M.; Ferreira, I. C. F. R. Nutritional and antioxidant properties of pulp and seeds of two xoconostle cultivars (*Opuntia joconostle* F.A.C. Weber ex Diguet and *Opuntia matudae* Scheinvar) of high consumption in Mexico. *Food Res. Int.* **2012**, *46*, 279−285.

(23) Yahia, E. M.; Mondragon-Jacobo, C. Nutritional components and anti-oxidant capacity of ten cultivars and lines of cactus pear fruit (*Opuntia* spp.). *Food Res. Int.* **2011**, *44*, 2311−2318.

(24) Jorge, A. J.; De La Garza, T. H.; Alejandro, Z. C.; Ruth, B. C.; Noé, A. C. The optimization of phenolic compounds extraction from cactus pear (*Opuntia ficus-indica*) skin in a reflux system using response surface methodology. *Asian Pac. J. Trop. Biomed.* **2013**, *3*, 436−442.

(25) Stintzing, F. C.; Herbach, K. M.; Mosshammer, M. R.; Carle, R.; Yi, W.; Sellappan, S.; Akoh, C. C.; Bunch, R.; Felker, P. Color, betalain pattern, and antioxidant properties of cactus pear (*Opuntia* spp.) clones. *J. Agric. Food Chem.* **2005**, *53*, 442−451.

(26) Guzmán-Maldonado, S. H.; Herrera-Hernández, G.; Hernández-López, D.; Reynoso-Camacho, R.; Guzmán-Tovar, A.; Vaillant, F.; Brat, P. Physicochemical, nutritional and functional characteristics of two underutilised fruit cactus species (Myrtillocactus) produced in central Mexico. *Food Chem.* **2010**, *121*, 381−386.

(27) Heredia, F. J.; Álvarez, C.; González-Miret, M. L.; Ramírez, A. CromaLab, Análisis de color. Registro General de la Propiedad Intelectual, 2004.

(28) CIE. *Technical Report Colorimetry*; Commission Internationale de l'Eclairage Central Bureau: Vienna, Austria, 2004.

(29) Gordillo, B.; Rodríguez-Pulido, F. J.; Escudero-Gilete, M. L.; González-Miret, M. L.; Heredia, F. J. Comprehensive colorimetric study of anthocyanic copigmentation in model solutions. Effects of pH and molar ratio. *J. Agric. Food Chem.* **2012**, *60*, 2896−2905.

(30) Singleton, V. L.; Rossi, J. A. Colorimetry of total phenolics with phosphomolybdic-phosphotungstic acid reagents. *Am. J. Enol. Vitic.* **1965**, *16*, 144−158.

(31) Asami, D. K.; Hong, Y. J.; Barrett, D. M.; Mitchell, A. E. Comparison of the total phenolic and ascorbic acid content of freeze-dried and air-dried marionberry, strawberry, and corn grown using conventional, organic, and sustainable agricultural practices. *J. Agric. Food Chem.* **2003**, *51*, 1237−1241.

(32) Mau, J. L.; Tsai, S. Y.; Tseng, Y. H.; Huang, S. J. Antioxidant properties of methanolic extracts from Ganoderma tsugae. *Food Chem.* **2005**, *93*, 641−649.

(33) StatSoft Inc. *STATISTICA (Data Analysis Software System)*, v. 8; StatSoft Inc.: Tulsa, OK, USA, 2007.

(34) Khatabi, O.; Hanine, H.; Elothmani, D.; Hasib, A. Extraction and determination of polyphenols and betalain pigments in the Moroccan prickly pear fruits (*Opuntia ficus indica*). *Arab. J. Chem.* **2013**, DOI: 10.1016/j.arabjc.2011.04.001.
(35) Martínez, J. A.; Melgosa, M.; Pérez, M. M.; Hita, E.; Negueruela, A. I. Note. Visual and instrumental color evaluation in red wines. *Food Sci. Technol. Int.* **2001**, *7*, 439−444.
(36) Melgosa, M.; Hita, E.; Poza, A. J.; Alman, D. H.; Berns, R. S. Suprathreshold color-difference ellipsoids for surface colors. *Color Res. Appl.* **1997**, *22*, 148−155.

JOURNAL OF AGRICULTURAL AND FOOD CHEMISTRY

Article

pubs.acs.org/JAFC

# Studies on the Reaction of *trans*-2-Heptenal with Peanut Proteins

Martin Globisch, Marco Schindler, Jana Kreßler, and Thomas Henle*

Institute of Food Chemistry, Technische Universität Dresden, D-01062 Dresden, Germany

**ABSTRACT:** Hexanal, 2-heptenal, and nonanal were identified as relevant reaction products formed in the course of the lipid peroxidation of heated peanut oil. For the identification of potential amino acid side chain adducts, kinetic studies between $N^{\alpha}$-benzoylglycyl-L-lysine as a model for protein-bound lysine and *trans*-2-heptenal were performed, showing a strong decrease of the lysine-derivative whereupon the loss of *trans*-2-heptenal was moderate. Following acid hydrolysis of the incubation mixture of $N^{\alpha}$-acetyl-L-lysine and *trans*-2-heptenal, two UV-active major lipation products were observed, isolated and identified as isomeric pyridinium-derivatives, namely (*Z*)- and (*E*)-1-(5-amino-5-carboxypentyl)-4-butyl-3-(pent-1-en-1-yl)pyridin-1-ium (*cis*- and *trans*-BPP-lysine). After heating of a native peanut protein extract with *trans*-2-heptenal, both derivatives were quantitated by LC-ESI-MS/MS after acid hydrolysis and the modification of lysine was measured by amino acid analysis. At low, "food-relevant", concentrations of *trans*-2-heptenal, up to 80% of the lysine modification could be explained by the formation of *cis*- and *trans*-BPP-lysine, showing that these two lipation derivatives represent good markers for a protein modification by the lipid peroxidation product *trans*-2-heptenal.

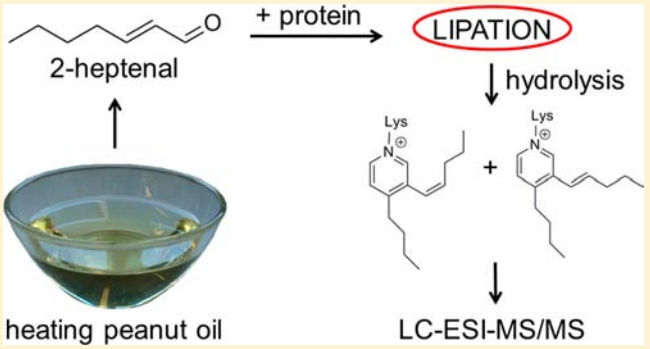


**KEYWORDS:** *peanuts, lipid peroxidation, 2-heptenal, lipation, pyridinium derivatives, BPP-lysine, carbonyl-protein-reaction*

## INTRODUCTION

Peanuts are a common food and serve as ingredients for many foods, being a rich source of protein (25%) and fat (48%).[1] In the U.S. and Europe, peanuts are commonly consumed roasted, whereas in Asian countries peanuts are mostly consumed boiled or fried.[2,3] Heat-induced protein modifications occurring during food processing can influence the allergenic potential of peanuts. Findings concerning a relationship between heating of peanuts and their allergenic potential are currently contradictory. On the one hand, no difference in the immunoreactivity between proteins isolated from raw and commercially roasted peanuts was observed[4] and even a reduction of the allergenic potential of Ara h 1 was measured following boiling of the isolated protein.[5] On the other hand, extracts from roasted peanuts exhibited at 90-fold higher binding to serum IgE of allergic patients when compared to the raw extracts.[6] Additionally, Ara h 1 and Ara h 3 modified with advanced glycation endproducts (AGEs) were found to interact with the receptor for AGEs (RAGE), and thus may be involved in allergic sensitization.[7] After heating of Ara h 1 at low moisture in the presence or absence of glucose, the degranulation capacity of basophils was increased, whereas for Ara h 2 the degranulation capacity was decreased.[8] These results show that heating in the presence or absence of reactive carbonyls can have different effects, depending on the protein structure. Among the reactions that can occur during the roasting process, besides glycation, the lipid peroxidation is of particular importance. Recently, it could be shown that up to 30−40% of lysine was modified as a result of peanut roasting.[9] However, only about one tenth of the totally observed lysine modification could be explained by the formation of the Maillard reaction products $N^{\epsilon}$-fructosyllysine, pyrraline and $N^{\epsilon}$-carboxymethyllysine. Taking into account the relatively high content of fat in peanuts and the fact that about 85% of the fatty acids are unsaturated,[10] it is highly likely that lipid peroxidation occurs in the course of the peanut roasting process. Actually, a large variety of secondary lipid peroxidation products have been detected by analyzing peanut oils obtained from raw and roasted peanuts,[11] ranging for monocarbonyl compounds from 8 to 26 μmol per 100 g oil, respectively.[12] Well known secondary products are α,β-unsaturated aldehydes like 4-hydroxyalkenals and 2-alkenals.[13,14] Due to their high reactivity, these electrophiles readily form covalent adducts, for example with nucleophilic amino acid side chains of proteins.[15] Having two electrophilic centers, 2-alkenals initially can form Michael- and Schiff base-adducts which can undergo further reactions. In model mixtures consisting of *trans*-2-hexenal and $N^{\alpha}$-acetylglycyllysine methyl ester, several pyridinium derivatives resulting from the reaction of alkenals with one amino group and arising cross-links were detected, but no information about formation of corresponding compounds at proteins under conditions relevant for food processing were given.[16] Under physiological conditions, *trans*-2-nonenal was found to

**Received:** May 26, 2014
**Revised:** July 14, 2014
**Accepted:** July 26, 2014
**Published:** July 26, 2014

ACS Publications © 2014 American Chemical Society

modify human and bovine serum albumin, resulting mainly in a modification of lysine residues and the formation of two *cis*–*trans*-isomeric pyridinium derivatives.[17] After acid hydrolysis, both derivatives could be quantitated in model proteins as well as in oxidatively modified LDL (*ox*LDL) and mice kidneys after exposure of the animals to ferric nitrilotriacetate.[17]

Regarding reactions in food, very little information is available concerning modification of proteins by lipid peroxidation products. Using ELISA, protein adducts in beef and rice seeds were detected, which resulted from reactions with 4-hydroxynonenal-, malondialdehyde- and alkenals with 6 to 9 C atoms.[18] In 22 fresh food products ε-*N*-pyrrolylnorleucine, representing a reaction product of 4,5-epoxy-2-alkenals and the ε-amino group of lysine,[19] was quantified by capillary electrophoresis after alkaline hydrolysis.[20] The concentration ranged from 0.24 to 6.36 μmol/g of food and the amount in peanuts was 2.89 μmol/g. The authors concluded that ε-*N*-pyrrolylnorleucine is a normal component of fresh food products.

The aim of this study, therefore, was to identify newly formed lipation products in food proteins and to develop an LC-ESI-MS/MS method for direct quantification. To identify potential precursors for amino acid side chain modifications arising during the peanut roasting process, peanut oil was heated under roasting conditions and volatile secondary products were semiquantitated by GC-MS. In kinetic studies, the reaction behavior of *trans*-2-heptenal and the lysine derivative $N^{\alpha}$-benzoylglycyl-L-lysine was studied by HPLC. For identification of relevant reaction products with the ε-amino group of lysine, $N^{\alpha}$-acetyl-L-lysine was incubated with *trans*-2-heptenal and reaction products were identified by LC-ESI-MS/MS. After isolation of two isomeric pyridinium derivatives arising from *trans*-2-heptenal and the ε-amino group of lysine, both derivatives were quantitated for the first time in peanut proteins by LC-ESI-MS/MS. Additionally, modification of lysine was measured by amino acid analysis.

## MATERIALS AND METHODS

**Materials.** Heptanal, pepsin (EC 3.4.23.1), Pronase E (EC 3.4.24.4), and hydrochloric acid (37%) were obtained from Merck (Darmstadt, Germany). Leucine aminopeptidase (EC 3.4.11.1), prolidase (EC 3.4.13.9), dialysis tubing cellulose membrane (MWCO 14 kDa), *trans*-2-heptenal (≥95%), hexanal, 2-hexenal, octanal, *p*-xylene, 1,3-diethylbenzene, tetradeuteromethanol, and petroleum ether (boiling point 40–60 °C) were obtained from Sigma-Aldrich (Taufkirchen, Germany). $N^{\alpha}$-acetyl-L-lysine, $N^{\alpha}$-benzoylglycyl-L-lysine, and *N*-benzoylglycyl-L-phenylalanine were obtained from Bachem (Bubendorf, Switzerland). Nonanal, methanol, dichloromethane, heptafluorobutyric acid, and cyclohexanol were obtained from VWR (Darmstadt, Germany). Acetonitrile was obtained from Fischer Scientific (Schwerte, Germany). Sodium bicarbonate, monosodium phosphate, and disodium phosphate were obtained from Grüssing (Filsum, Germany). Tris(hydroxymethyl)aminomethan was obtained from Serva (Heidelberg, Germany). Thymol was obtained from Carl Roth (Karlsruhe, Germany). All chemicals were of highest purity unless otherwise indicated. For all experiments, ultrapure water was used prepared by an ELGA LabWater Purelab Plus water system (Celle, Germany). For LC-ESI-MS/MS-measurements, double-distilled water, prepared in the presence of potassium permanganate, was used. Refined peanut oil was obtained from a local market.

**GC-MS (EI) Analysis of Volatile Compounds Formed during Heating of Peanut Oil.** After adding 75 μL of an internal standard solution containing *p*-xylene and 1,3-diethylbenzene in dichloromethane (6 mM each) to 50 g of peanut oil, the sample was heated in a three-neck flask while stirring for 20 min at 170 °C using a gentle airstream to transfer the volatile compounds in the head space into a gas washing bottle filled with 100 mL dichloromethane. After evaporation of the dichloromethane to a volume of 5 mL using a rotary evaporator at atmospheric pressure at 46 °C, an aliquot was used for GC-MS (EI) analysis. This was performed using an Agilent 7890A System, consisting of an 7683 Series injector with a sample tray, a 5975C MS detector working in EI mode, a HP-5MS capillary column (30.0 m × 0.25 mm ID, 0.25 μm film thickness), all from Agilent (Böblingen, Germany), and a Zebron Z-guard column (deactivated, 5.0 m × 0.25 mm ID, Phenomenex, Germany). Helium was used as carrier gas with a constant flow of 1 mL/min. The injector temperature was set to 250 °C and 1 μL sample was injected by using the pulsed splitless mode. The auxiliary temperature was set to 250 °C, ion source and quadrupole to 230 and 150 °C, respectively. The initial oven temperature was set to 40 °C and held for 9 min, then raised at 3 °C/min to 61 °C and held for 3 min, then raised at 3 °C/min to 76 °C, at 6 °C/min to 90 °C, at 20 °C/min to 110 °C and held for 1 min and finally raised at 30 °C/min to 300 °C. The post run time was set to 3 min at 300 °C. The mass spectrometer was working in electron impact mode at 70 eV in the SCAN mode (mass range: $m/z$ 30.0–300.0). Identification of the analytes was performed by comparing retention times and mass spectra to corresponding standard samples. Semiquantitation of the volatile compounds was performed by evaluating the peak areas of the analytes related to the peak areas of the internal standards. Depending on their boiling points, hexanal, 2-hexenal, and heptanal were evaluated related to *p*-xylene whereas 2-heptenal, octanal, and nonanal were evaluated related to 1,3-diethylbenzene. Identification of compounds was obtained by reference compounds.

**Kinetic Studies on the Incubation of *trans*-2-Heptenal with $N^{\alpha}$-Benzoylglycyl-L-lysine.** $N^{\alpha}$-benzoylglycyl-L-lysine and *trans*-2-heptenal, 4 mM each in methanol, were incubated for 24 h at 37 °C under nitrogen atmosphere. Every 2 h an aliquot of 400 μL was taken and mixed with 1200 μL of water to stop further reactions. Samples were filtered (0.45 μm) and *trans*-2-heptenal and $N^{\alpha}$-benzoylglycyl-L-lysine quantitated using a Knauer HPLC system (Berlin, Germany), which consisted of a degasser, a solvent organizer K-1500, a WellChrom pump K-1001, a dynamic mixing chamber K-5001, an automatic injector Basic Marathon, a column oven and a diode array detector WellChrom K-2700. Samples of 20 μL were separated using an Eurospher 100–5 C18 column (250 × 4.6 mm$^2$) from Knauer (Berlin, Germany) at 30 °C at a flow rate of 0.9 mL/min and a detection wavelength of 227 nm. A gradient was used with solvent A (water) and B (acetonitrile), each containing 13 mM heptafluorobutyric acid. Gradient was as follows: Increased from 10% B to 70% B within 30 min, to 90% B within 5 min, held at 90% B for 10 min, decreased within 2 min to 10% B and held at 10% B for 10 min. For external calibration, *trans*-2-heptenal and $N^{\alpha}$-benzoylglycyl-L-lysine were used.

**Nuclear Magnetic Resonance spectroscopy (NMR).** $^{1}$H NMR was recorded on a Bruker Avance 600 instrument (Rheinstetten, Germany) at 600,16 MHz. $^{13}$C NMR was recorded on a Bruker DRX 500 instrument at 150,9 MHz. Tetradeuteromethanol (MeOH-d4) was used as solvent. All chemical shifts are given in parts per million (ppm) relative to the solvent signal serving as internal standard. The following 2D-NMR experiments were performed additionally: COSY (correlation spectroscopy), NOESY (nuclear overhauser enhancement spectroscopy), HSQC (heteronuclear single quantum coherence), and HMBC (heteronuclear multiple bond correlation).

**Elemental Analysis.** Elemental analysis was performed using an EuroEA3000 (Eurovector, Milan, Italy) to quantitate the product content in the purified standards. *Cis*- and *trans*-BPP-lysine were isolated as salts of heptafluorobutyric acid, so the molecular ratio of cationic pyridinium derivative and heptafluorobutyric acid in the isolated products was not known. Therefore, the analyzed percentage of nitrogen was compared to the calculated nitrogen percentage. The pure amount of cationic pyridinium derivative in the product without counterion is expressed in percent by weight.

**Acid and Enzymatic Hydrolysis.** For acid hydrolysis of proteins, a ratio of 3 mg protein per 1.0 mL 6 M hydrochloric acid was used. Samples were hydrolyzed under nitrogen for 23 h at 110 °C. For enzymatic hydrolysis,[21] 3.0 mg of protein were dissolved in 1.0 mL of

0.02 M hydrochloric acid (HCl) containing a crystal of thymol and incubated with 1 FIP-U of pepsin for 24 h at 37 °C. After adding 0.25 mL of 2 M TRIS-HCl buffer (pH 8.2) and 400 PU of Pronase E, samples were incubated for 24 h at 37 °C. Following addition of 0.3 U of leucine aminopeptidase and 2 U of prolidase, samples were incubated for another 24 h at 37 °C and finally lyophilized.

**Amino Acid Analysis.** Amino acid analyses were performed using a SYKAM S4300 amino acid analyzer (Fürstenfeldbruck, Germany) after acid hydrolysis for the acid-stable amino acids valine, histidine, lysine, and arginine and enzymatic hydrolysis for the acid-labile amino acid cysteine. Amino acids were separated by cationic ion exchange chromatography, derivatized by ninhydrin, and detected using a wavelength of 570 nm.[22] Valine was taken as internal standard and amino acids were expressed as valine equivalents.

**Incubation of *trans*-2-Heptenal with $N^{\alpha}$-Acetyl-L-lysine.** For identification of major amino acid side chain reaction products between *trans*-2-heptenal and $N^{\alpha}$-acetyl-L-lysine, 10 mM *trans*-2-heptenal and 10 mM $N^{\alpha}$-acetyl-L-lysine were heated for 4 h at 75 °C in 5 mL methanol in a 10 mL round-bottom flask under reflux. 1.0 mL was taken for direct HPLC-DAD-ESI-MS/MS analysis and 3.0 mL were evaporated under a gentle stream of nitrogen. After hydrolysis with 3 mL of 6 M hydrochloric acid for 23 h at 110 °C under nitrogen, 1.0 mL of the sample was dried at 37 °C in vacuo by using a SpeedVac vacuum concentrator (Thermo Fisher Scientific, Waltham, U.S.A.), redissolved in 2.0 mL methanol and analyzed by LC-DAD-ESI-MS/MS.

**Preparation of Modified Peanut Proteins.** Previously shelled and skinned raw peanuts were crushed and defatted by Soxhleth extraction using petroleum ether for 6 h at 78 °C. For protein extraction, 21 mL 0.1 M sodium bicarbonate (pH 10.4) were added to 3.0 g defatted peanut meal.[23] Samples were homogenized using an ultraturrax at 11.200 rpm for 2 min and proteins extracted for 1 h at 6 °C while stirring constantly. After centrifugation at 8643*g* for 15 min at 4 °C, the supernatant was collected and the residue was extracted analogously. Following dialysis (14 kDa MWCO) against deionized water for 48 h at 6 °C, the samples were lyophilized. Protein content was analyzed by the Kjeldahl method using the factor 5.3 for oilseeds.[24] Amino acid composition was analyzed by amino acid analysis. Amino acid contents of cysteine, histidine, lysine, and arginine were 3.83 ± 0.79, 19.27 ± 0.06, 32.58 ± 1.39, and 70.58 ± 3.22 mmol/100 g protein, respectively. Approximately 100 mg of peanut proteins were dissolved in 0.1 M phosphate buffer (pH 7.4) and *trans*-2-heptenal was added in 1.0 mL methanol in following molar ratios related to the sum of relevant reactive amino acids histidine, lysine, and arginine: 0.1:1, 0.2:1, 0.5:1, 1:1, 5:1, and 10:1. Finally, the samples were made up to 25 mL with phosphate buffer (pH 7.4). Additionally, a blank sample consisting of peanut proteins without *trans*-2-heptenal was prepared. The incubation was carried out under a nitrogen atmosphere for 24 h at 37 °C while stirring. After dialysis (14 kDa MWCO) against deionized water for 24 h at 6 °C, the samples were lyophilized and protein contents were analyzed by the Kjeldahl method. For analysis of the amino acid modification rate (lysine, histidine, and arginine), the samples were hydrolyzed by hydrochloric acid and subjected to amino acid analysis. For cysteine analysis, samples were hydrolyzed enzymatically. For analysis of BPP-lysine, 12 mg of samples were hydrolyzed by 4 mL 6 M hydrochloric acid for 23 h at 110 °C. 1.0 mL of samples were dried in vacuo using a SpeedVac vacuum concentrator (Thermo Fisher Scientific, Waltham, U.S.A.) at 37 °C, redissolved in 0.25 mL deionized water, 0.2 mL methanol and 0.05 mL of internal standard *N*-benzoylglycyl-L-phenylalanine in methanol:water (50:50, v/v) with a final concentration of 1 μg/mL. After filtration (0.45 μm), samples were subjected to HPLC-ESI-MS/MS analysis.

**Isolation of (*Z*)-1-(5-Amino-5-carboxypentyl)-4-butyl-3-(pent-1-en-1-yl)pyridin-1-ium (*cis*-BPP-lysine) and (*E*)-1-(5-Amino-5-carboxypentyl)-4-butyl-3-(pent-1-en-1-yl)pyridin-1-ium (*trans*-BPP-lysine).** In a 500 mL round-bottom flask 376.5 mg (2.0 mmol) $N^{\alpha}$-acetyl-L-lysine and 827.0 μL (6.0 mmol) *trans*-2-heptenal were heated for 4 h at 75 °C in 200 mL methanol under reflux. After evaporation of methanol in vacuo at 40 °C, 150 mL 6 M hydrochloric acid were added and heated for 23 h at 110 °C. Afterward, the hydrochloric acid was removed using a water-jet vacuum pump at 40 °C. *cis*- and *trans*-BPP-lysine were purified using a semipreparative HPLC system. The system consisted of a Smartline solvent manager 5000, a Smartline pump 1000, and a Smartline UV-detector 2500 (all from Knauer, Berlin, Germany). Two mg of the unpurified reaction mixture were dissolved in 1.0 mL of methanol and separated after filtration (0.45 μm) using an Eurospher 100−10 C18 column (250 × 16 $mm^2$; Knauer, Berlin, Germany) at 23 °C room temperature, a flow rate of 3 mL/min and a detection wavelength of 227 nm. A gradient was used with solvent A (water) and B (acetonitrile), each containing 13 mM heptafluorobutyric acid. The gradient program started with 25% solvent B for 5 min, increased to 50% B within 20 min, followed by isocratic elution with 50% B for 31 min, a flow reduction to 0.7 mL/min from 35 to 55 min, increased to 95% B within 2 min at a flow rate of 3 mL/min, isocratic elution with 95% B for 5 min, decreased to 25% B within 2 min, isocratic elution with 25% B for 15 min. *cis*- and *trans*-BPP-lysine eluted between 37 and 41 min and 41 and 51 min, respectively. Multiple separations were performed, relevant fractions containing the two compounds combined and finally the solvent was evaporated in vacuo at 40 °C. To increase purity, both compounds were purified for a second time prior to HPLC-ESI-MS/MS and one- and two-dimensional NMR analysis. For *cis*-BPP-lysine, results were as follows: ESI-MS (positive mode), $[M]^+$ $m/z$ 333.3; $^1$H NMR (600 MHz, MeOH-d4): $\delta$ 0.98 (t, 3H, $J$ = 7.5 Hz, H-16), 1.04 (t, 3H, $J$ = 7.5 Hz, H-20), 1.51 (m, 2H, H-19), 1.57 (m, 2H, H-15), 1.72 (m, 2H, H-18), 1.60−1.69 (m, 2H, H-8A,B), 2.03−2.10 (m, 2H, H-9A,B), 2.13 (m, 2H, H-7), 2.19 (q, 2H, $J$ = 7.5 Hz, H-14), 2.96 (t, 2H, $J$ = 7.9 Hz, H-17), 4.05 (t, 1H, $J$ = 6.4 Hz, H-10), 4.67 (t, 2H, $J$ = 7.5 Hz, H-6), 6.24 (dt, 1H, $J$ = 7.5 Hz, $J$ = 11.3 Hz, H-13), 6.60 (d, 1H, $J$ = 11.3 Hz, H-12), 8.02 (d, 1H, $J$ = 6.4 Hz, H-5), 8.75 (s, 1H, H-3), 8.81 (d, 1H, $J$ = 6.4 Hz, H-4). Purity of cation based on elemental analysis: 42.9%. For *trans*-BPP-lysine, results were as follows: ESI-MS (positive mode), $[M]^+$ $m/z$ 333.3; $^1$H NMR (600 MHz, MeOH-d4): $\delta$ 1.06 (t, 3H, $J$ = 7.5 Hz, H-20), 1.08 (t, 3H, $J$ = 7.5 Hz, H-16), 1.53 (m, 2H, H-19), 1.60−1.71 (m, 2H, H-8A,B) 1.66 (m, 2H, H-15), 1.72 (m, 2H, H-18), 2.04−2.09 (m, 2H, H-9A,B), 2.15 (m, 2H, H-7), 2.41 (q, 2H, $J$ = 7.2 Hz, H-14), 3.02 (t, 2H, $J$ = 7.9 Hz, H-17), 4.07 (t, 1H, $J$ = 6.4 Hz, H-10), 4.65 (t, 2H, $J$ = 7.5 Hz, H-6), 6.62 (dt, 1H, $J$ = 6.8 Hz, $J$ = 15.8 Hz, H-13), 6.76 (d, 1H, $J$ = 15.8 Hz, H-12), 7.93 (d, 1H, $J$ = 6.4 Hz, H-5), 8.71 (d, 1H, $J$ = 6.4 H, H-4), 9.04 (s, 1H, H-3). Purity of cation based on elemental analysis: 35.7%.

**HPLC-DAD-ESI-MS/MS Analysis.** For identification of major reaction products between *trans*-2-heptenal and $N^{\alpha}$-acetyl-L-lysine, for characterization of isolated BPP-standards and for quantitation of *cis*- and *trans*-BPP-lysine in modified peanut proteins, HPLC-DAD-ESI-MS/MS analysis were performed. The HPLC system consisted of a degasser, a pump, an autosampler and a diode array detector, all from Agilent Technologies 1200 Series (Böblingen, Germany). For MS/MS-measurements, a Triple Quad LC/MS 6410 from Agilent Technologies was used. For identification of major reaction products between *trans*-2-heptenal and $N^{\alpha}$-acetyl-L-lysine, 5 μL of samples were separated using an Eurospher 100−5 C18 column (250 × 3.0 $mm^2$; Knauer, Berlin, Germany) at 30 °C, a flow rate of 0.38 mL/min and a detection wavelength of 227 nm. A gradient was used with solvent A (water) and B (acetonitrile), each containing 2 mM heptafluorobutyric acid and 11 mM acetic acid. The gradient increased from 5% B to 70% B within 50 min, to 90% B within 15 min, held at 90% B for 20 min, followed by a decrease within 3 min to 5% B and isocratic elution at 5% B for 10 min. At first full scan analyses and then product ion scans were performed. Full scan analyses were performed from 5.1 to 78.0 min in positive mode, scan ranges were from $m/z$ 70 to 1000, scan time 500 ms, fragmentor voltage was set to 135 V, gas temperature to 300 °C, gas flow to 11 mL/min and nebulizer pressure to 15 psi. Product ion scans were performed for the hydrolyzed sample from 25 to 45 min with precursor ion $m/z$ 333.3, using the same conditions as described above. Product ion scan ranges were from $m/z$ 60 to 500 with a scan time of 200 ms, a fragmentor voltage of 135 V and a collision voltage of 25 V for *cis*- and 20 V for *trans*-BPP-lysine,

respectively. For quantitation of BPP-lysine in modified peanut proteins 1 to 10 μL of samples were separated using a Zorbax SB-C18 column (50 × 2.1 mm) from Agilent Technologies (Böblingen, Germany) at 30 °C and a flow rate of 0.25 mL/min. A gradient was used with solvent A (water) and B (acetonitrile), each containing 2 mM heptafluorobutyric acid and 11 mM acetic acid. Gradient was as follows: 2% B was held for 5 min, increased to 51% B within 17 min, to 90% B within 2 min, held at 90% B for 6 min, decreased to 2% B within 1 min and held at 2% B for 6 min. Measurements were performed using the multi reaction monitoring (MRM) mode in positive mode, gas temperature was set to 300 °C, gas flow to 11 mL/min and nebulizer pressure to 15 psi. Internal standard *N*-benzoylglycyl-L-phenylalanine was analyzed from 18 to 20.1 min with a mass transition from *m*/*z* 327.1 to 166.1 for quantitation using fragmentor and collision voltages of 80 and 4 V, respectively and a dwell time of 300 ms. Mass transition from *m*/*z* 327.1 to 105.1 was used for qualification using fragmentor and collision voltages of 80 and 32 V, respectively and a dwell time of 300 ms. *cis*-BPP-lysine was analyzed from 20.1 to 21.0 min with a mass transition from *m*/*z* 333.3 to 204.2 for quantitation using fragmentor and collision voltages of 133 and 21 V, respectively, and a dwell time of 100 ms. Mass transition from *m*/*z* 333.3 to 84.2 was used for qualification using fragmentor and collision voltages of 133 and 33 V, respectively, and a dwell time of 100 ms. *trans*-BPP-lysine was analyzed from 21.0 to 23.5 min with a mass transition from *m*/*z* 333.3 to 204.2 for quantitation using fragmentor and collision voltages of 134 and 21 V, respectively, and a dwell time of 100 ms. Mass transition from *m*/*z* 333.3 to 84.2 was used for qualification using fragmentor and collision voltages of 134 and 30 V, respectively and a dwell time of 100 ms. Quantification was realized using authentic *cis*-and *trans*-BPP-lysine in a native peanut protein hydrolyzate matrix calibration after addition of internal standard *N*-benzoylglycyl-L-phenylalanine with a final concentration of 1 μg/mL.

**Statistical Treatment.** Results are expressed as mean values ± standard deviations of two separate measurements.

## RESULTS AND DISCUSSION

**Identification of Volatile Secondary Lipid Peroxidation Products of Heated Peanut Oil.** To identify potential precursors for amino acid side chain modifications formed in the course of lipid peroxidation during roasting of peanuts, refined peanut oil was heated under roasting conditions for 20 min at 170 °C. Figure 1 shows selected volatile carbonyl compounds in the headspace analyzed by GC-MS (EI). Identification was achieved by comparing retention times and mass spectra to corresponding reference material. Compounds were semiquantitated by evaluating the peak areas of the analytes related to the peak areas of the internal standards *p*-xylene and 1,3-diethylbenzene. Hexanal, 2-heptenal, and nonanal are the most important secondary products of lipid peroxidation. Hexanal and 2-heptenal are mainly formed by the autoxidation of linoleic acid and nonanal is mainly formed from oleic acid.[14] Being a rich source of unsaturated fatty acids, peanut oil consists of about 55% oleic acid and 22% linolenic acid.[1] Considering the high reactivity of the 2-alkenals,[15−17] it is likely that in the presence of peanut proteins, these compounds can easily react with nucleophilic amino acid side chains for example the ε-amino group of lysine.

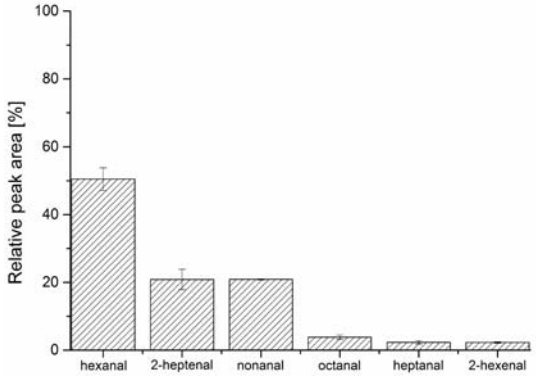


**Figure 1.** Semiquantitated amounts of selected volatile lipid peroxidation products of peanut oil heated under roasting conditions for 20 min at 170 °C.

**Kinetic Studies on the Reaction of *trans*-2-Heptenal and $N^{\alpha}$-Benzoylglycyl-L-lysine.** Focusing on 2-heptenal, kinetic studies were performed to get an insight into the reaction behavior with the ε-amino-group of lysine using $N^{\alpha}$-benzoylglycyl-L-lysine as a model for protein bound lysine. *trans*-2-Heptenal and $N^{\alpha}$-benzoylglycyl-L-lysine were incubated in equimolar amounts under mild reaction conditions at 37 °C for 24 h in methanol. Analogously, blank samples consisting only of *trans*-2-heptenal or $N^{\alpha}$-benzoylglycyl-L-lysine, respectively, were incubated. Figure 2 shows that the amounts of

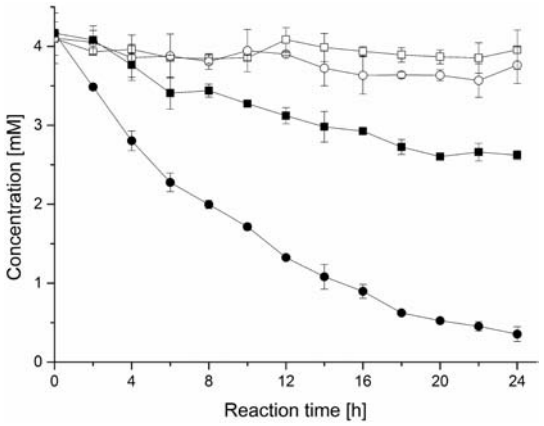


**Figure 2.** Kinetic studies on the reaction of equimolar amounts of *trans*-2-heptenal and $N^{\alpha}$-benzoylglycyl-L-lysine at 37 °C for 24 h in methanol. Open squares, blank samples of $N^{\alpha}$-benzoylglycyl-L-lysine; open circles, blank samples of *trans*-2-heptenal; filled squares, $N^{\alpha}$-benzoylglycyl-L-lysine in equimolar reaction mixture; filled circles, *trans*-2-heptenal in equimolar reaction mixture.

*trans*-2-heptenal and $N^{\alpha}$-benzoylglycyl-L-lysine in the blank samples were stable over the reaction time, whereas both the amounts of *trans*-2-heptenal and $N^{\alpha}$-benzoylglycyl-L-lysine in the equimolar reaction mixture were decreasing. The observation that *trans*-2-heptenal decreased more than 2-fold faster than $N^{\alpha}$-benzoylglycyl-L-lysine may indicate *trans*-2-heptenal was decomposed or polymerized in the presence of the ε-amino-group of lysine. A proposed reaction pathway for polymerization initially starts with the formation of Schiff base adducts which polymerize by aldol condensation resulting in polymers from which the amino compound even may cleave.[25,26] Another possibility is that he majority of the newly formed adducts arised by the reaction of two or more molecules of *trans*-2-heptenal and one molecule $N^{\alpha}$-benzoylglycyl-L-lysine. Possible reaction products are pyridinium derivatives as previously described for other 2-alkenales and the ε-amino-group of lysine (see the Introduction).[16,17,27]

**Identification of Major Reaction Products of *trans*-2-Heptenal and $N^{\alpha}$-Acetyl-L-lysine.** For the identification of major reaction products of *trans*-2-heptenal and the ε-amino-group of lysine, *trans*-2-heptenal and $N^{\alpha}$-acetyl-L-lysine were

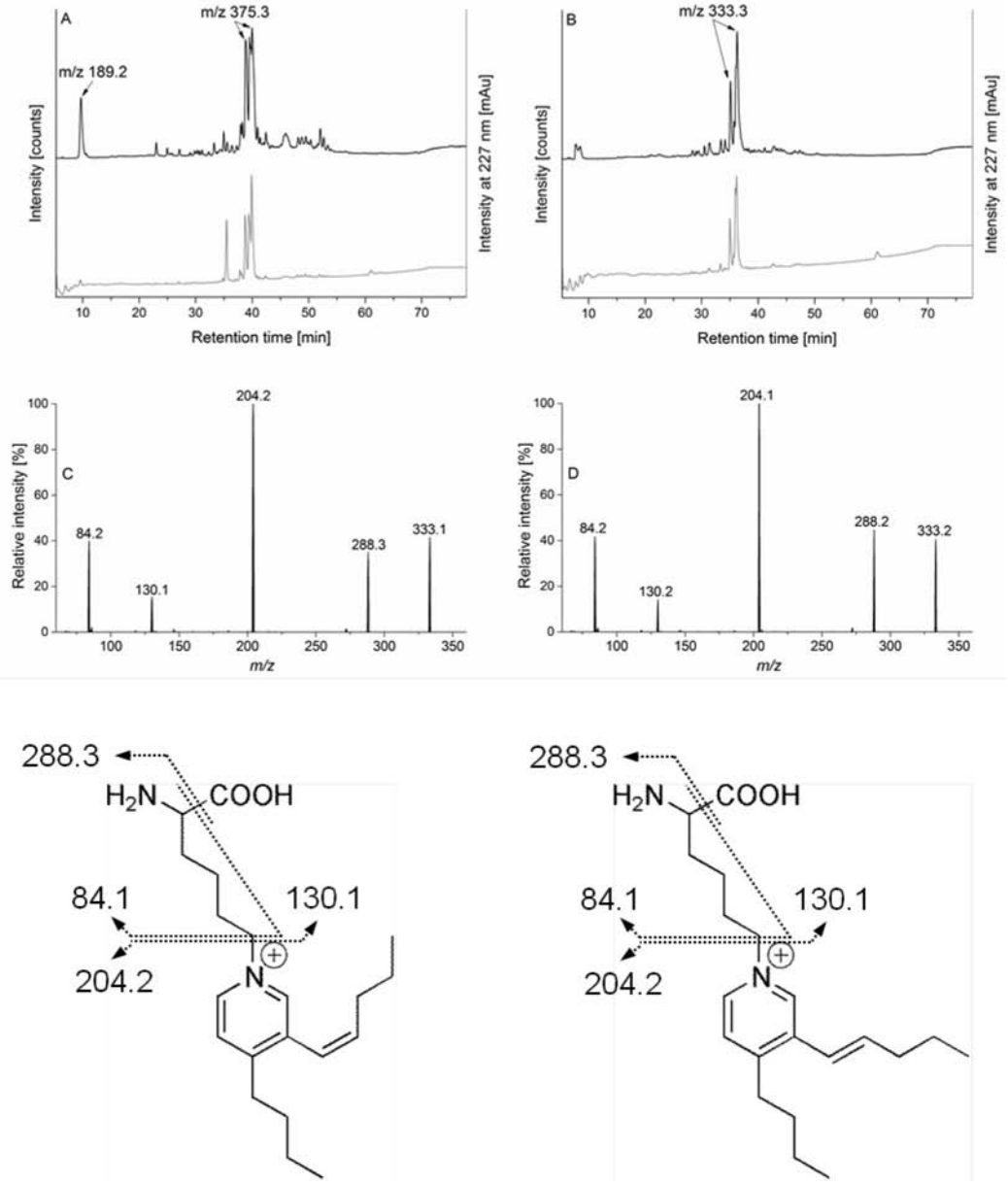


**Figure 3.** Identification of *cis*- and *trans*-BPP-lysine by HPLC-DAD-ESI-MS/MS after incubation of $N^{\alpha}$-acetyl-L-lysine with *trans*-2-heptenal in equimolar amounts in methanol for 4 h at 75 °C. (A, B) HPLC-ESI-MS-scan-chromatograms and HPLC-UV-chromatograms (gray) at 227 nm before and after acid hydrolysis, respectively. Arrows indicate peaks resulting from $N^{\alpha}$-acetyl-L-lysine ($m/z$ 189.2) and the two pyridinium derivatives ($m/z$ 375.3 and $m/z$ 333.3). (C, D) product ion patterns after fragmentation of the hydrolyzed pyridinium derivatives with $m/z$ 333.3 (first and second peak) and individual ions resulting from *cis*- and *trans*-pyridinium derivatives with $m/z$ 333.3, respectively.

incubated in equimolar amounts in methanol for 4 h at 75 °C. Newly formed products were analyzed before and after acid hydrolysis by HPLC-DAD-ESI-MS/MS. Figure 3A shows that under these conditions, two UV-active main products with monoisotopic masses of $m/z$ 375.3 were detectable. These masses are indicative for pyridinium derivatives resulting from one molecule $N^{\alpha}$-acetyl-L-lysine, two molecules of *trans*-2-heptenal, the loss of two water molecules and an oxidation step. As previously described, *cis*- and *trans*-derivatives may be formed, being the cis-derivative of the compound eluting earlier in the chromatogram.[16,17] Even when the reaction partners were incubated in equimolar ratio, some amounts of $N^{\alpha}$-acetyl-L-lysine ($M+H^+$ peak at $m/z$ 189.2) were remaining. This fits with the previous results of the kinetic studies, underlining that the formed adducts consist of more than one molecule of *trans*-2-heptenal. After acid hydrolysis, two UV-active main adducts with $m/z$ 333.3 were detectable, showing that the deacetylation (mass difference, −42) was successful (Figure 3B). The stability of pyridinium derivatives against acid hydrolysis was analogously described for lysine-2-nonenal-pyridinium derivatives.[17] To ensure these findings, product ion scans of the two hydrolyzed adducts were performed. Figure 3C,D indicates that both substances lead to the same product ions. The fragmentation patterns show typical lysine fragments with $m/z$ 84.2 and $m/z$ 130.1 as well as a decarboxylation step with $m/z$ 288.3. The ions with $m/z$ 204.2 result from a fragmentation between the $\delta$-carbon of lysine and the $\epsilon$-nitrogen being incorporated in the pyridinium structure and therefore are strong hints for the existence of pyridinium derivatives. Due to the fact that both structures gave the same fragmentation


dx.doi.org/10.1021/jf502501f | J. Agric. Food Chem. 2014, 62, 8500−8507

patterns, the presence of the *cis*- and *trans*-pyridinium derivatives can be assumed. The formation of the cis-derivative with *trans*-2-heptenal as reactant may be due to an isomerization of the *trans*-2-heptenal in the presence of the ε-amino-group of lysine.[17] On the basis of the UV-chromatograms before and after acid hydrolysis, it can be seen that the trans-derivative is the major product. This may be due to its thermodynamically preferred structure or due to the fact that the isomerization only leads to lower amounts of the cis-derivative. This is confirmed by a recent literature report, in which *cis*- and *trans*-nonenal-pyridinium derivatives were quantitated in mice kidneys in comparable amounts after exposing the animals to ferric nitrilotriacetate.[14] It is, therefore, likely that in real food samples, the *cis*- and *trans*-2-heptenal derivatives of lysine will also appear in equimolar amounts.

For the isolation and unequivocal structure elucidation of the formed reaction products, $N^{\alpha}$-acetyl-L-lysine was incubated with a 3-fold excess of *trans*-2-heptenal to induce the formation of the pyridinium derivatives. After acid hydrolysis, the products were separated and isolated by semipreparative HPLC with UV-detection, using an RP-18 column. Identification was realized by LC-ESI-MS/MS measurements and one and two-dimensional NMR spectroscopy. Following collision-induced fragmentation, both substances showed the same identical fragmentation patterns as previously described. Figure 4 shows

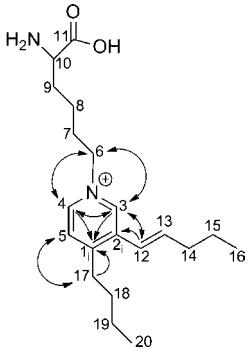

**Figure 4.** Structure of *trans*-BPP-lysine showing the observed relevant heteronuclear multiple bond correlations (HMBC).

exemplarily the structure of (*E*)-1-(5-amino-5-carboxypentyl)-4-butyl-3-(pent-1-en-1-yl)pyridin-1-ium (*trans*-BPP-lysine) and relevant heteronuclear multiple bond correlations (HMBC). The couplings in the HMBC spectrum of (Z)-1-(5-amino-5-carboxypentyl)-4-butyl-3-(pent-1-en-1-yl)pyridin-1-ium (*cis*-BPP-lysine) were analogous. Differentiation of *cis*- and *trans*-BPP-lysine was possible on the basis of the $^1$H vinyl proton (H-12 and H-13) coupling constants $J$ = 11.3 Hz for the cis-derivative and $J$ = 15.8 Hz for the trans-derivative and by means of 2D $^1$H/$^1$H NOESY experiments. Strong NOEs were observed between proton 3 and protons 14, 15, and 16 (weak) being indicative for the *cis*-product. Additionally, no NOE was observed between protons 3 and 13 and only a weak NOE was observed between protons 12 and 14. In contrast, no NOEs were observed between proton 3 and protons 14, 15, 16 by analyzing the trans-product, whereas strong NOEs between protons 3 and 13 and protons 12 and 14 were observed. To the best of our knowledge, this is the first profound structural characterization of these two lysine derivatives. Analogously to the reaction of the ε-amino-group of lysine with *trans*-2-hexenal,[16] an exemplarily proposed reaction mechanism for the formation of *trans*-BPP-lysine following the reaction of *trans*-2-heptenal with the ε-amino-group of lysine is given in Figure 5. In the first step, *trans*-2-heptenal probably reacts with the ε-amino-group of lysine, resulting in a Schiff's base adduct, followed by a Michael addition of a second molecule of *trans*-2-heptenal, cyclization, and oxidation reaction to the final pyridinium derivative.

**Quantitation of BPP-Lysine Derivatives in Modified Peanut Proteins.** To investigate whether the pyridinium derivatives can be formed in food proteins as well, extracted proteins of native peanuts were incubated with *trans*-2-heptenal under mild physiological conditions at 37 °C for 24 h in phosphate buffer (pH 7.4) as previously described for other 2-alkenals.[17,28,29]

Incubations were performed in different molar ratios between *trans*-2-heptenal and the sum of relevant reactive amino acids histidine, lysine and arginine. The amounts of these amino acids in the native peanut protein extract were 19.27 ± 0.06, 32.58 ± 1.39 and 70.58 ± 3.22 mmol/100 g protein, respectively. Cysteine was not regarded as a relevant amino acid because of its low amount in peanut proteins (3.83 ± 0.79 mmol/100 g protein) and its ability to form disulfide bonds. After acid hydrolysis, both BPP-lysine derivatives were quantitated by LC-ESI-MS/MS (MRM mode). Figure 6 shows a representative LC-ESI-MS/MS-chromatogram ($m/z$ 333.3 > 204.2) of the hydrolyzed peanut proteins modified in the 0.1:1 ratio. It can be seen that the separation of the cis- and trans-derivatives can be achieved using an RP-18 column and addition of heptafluorobutyric acid to the regular ion pair reagent acetic acid. The quantitated amounts of both derivatives are shown in Figure 7. These results show clearly that a modification of peanut proteins by *trans*-2-heptenal is possible and that the amounts of formed BPP-lysine derivatives depend on the amount of *trans*-2-heptenal within the incubation samples. In the blank sample, consisting of peanut proteins treated in the same way but without *trans*-2-heptenal,

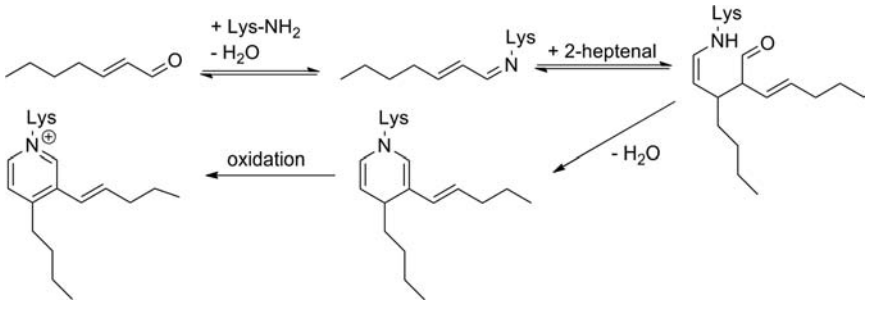


**Figure 5.** Proposed formation pathway for the formation of *trans*-BPP-lysine.


dx.doi.org/10.1021/jf502501f | J. Agric. Food Chem. 2014, 62, 8500−8507

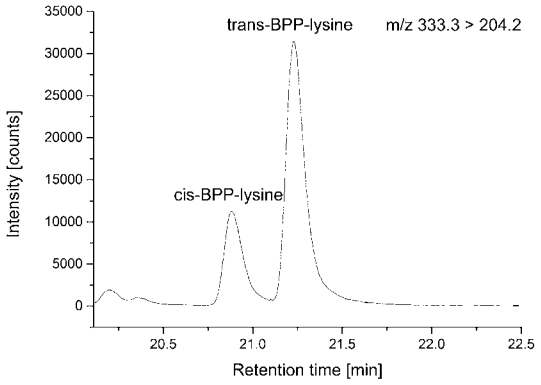


**Figure 6.** Representative LC-ESI-MS/MS-chromatogram (MRM mode, transition $m/z$ 333.3 > 204.2) of the acid hydrolyzate of the peanut protein extract modified by *trans*-2-heptenal in the ratio 0.1 to 1 related to the sum of the potentially reactive amino acids histidine, lysine and arginine.

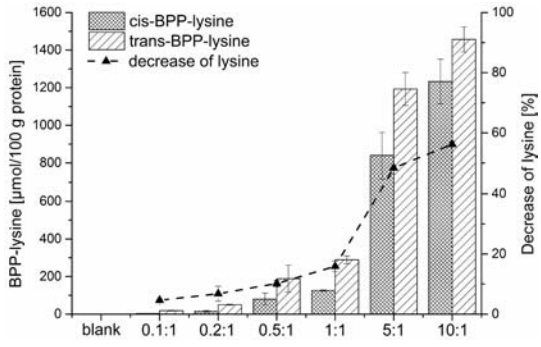


**Figure 7.** Quantitated amounts of *cis*- and *trans*-BPP-lysine in modified peanut protein extracts by LC-ESI-MS/MS and decrease of lysine analyzed by amino acid analysis.

no derivatives could be measured. As previously discussed, the *trans*-derivative is the major product formed. Additionally, a direct relationship between the formation of the BPP-lysine derivatives and the decrease in lysine can be seen (Figure 8). In the slightly modified samples, up to 80% of the decrease in lysine can be explained by the formed BPP-lysine derivatives. At higher levels of *trans*-2-heptenal further reactions will become relevant. Having two electrophilic centers, possible reactions might be the formation of Michael- and Schiff's base-adducts. These can lead for example to lysine cross-links by involving

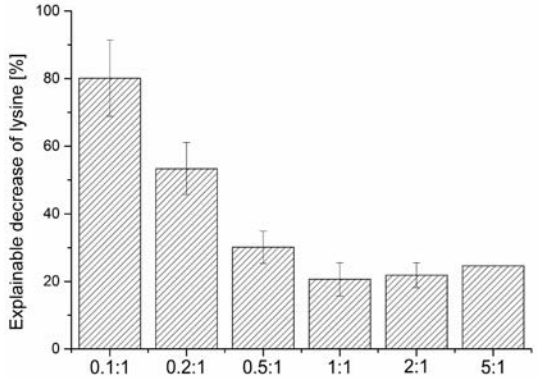


**Figure 8.** Explainable decreases of lysine due to the formation of *cis*- and *trans*-BPP-lysine.

only one molecule of *trans*-2-heptenal. Further cross-linking may occur due to a Michael addition of a pyridinium derivative to a Schiff base-adduct.[16] Taking into account that the amounts of 2-heptenal formed in the course of lipid peroxidation as a result of peanut roasting will be probably lower than the amounts of *trans*-2-heptenal added to the peanut protein extract samples, it can be shown that especially in the presence of small amounts of *trans*-2-heptenal, nearly the whole lysine modification can be explained by the formation of the BPP-lysine derivatives. So it is possible to cover most of the adducts formed by the reaction of the $\varepsilon$-amino group of lysine and 2-heptenal by measuring the two BPP-lysine derivatives.

In conclusion, we were able to show that *trans*-2-heptenal, a well-known secondary product formed in the course of the autoxidation of linoleic acid,[14] is one of the most important volatile carbonyl compounds formed during heating peanut oil under roasting conditions and is able to modify the $\varepsilon$-amino group of lysine, leading to the formation of two isomeric pyridinium derivatives. Considering the whole peanut, it is likely that the volatile compounds formed in the course of the lipid peroxidation during the roasting process are able to react with the amino acid side chains of peanut proteins. Hence, these two derivatives represent good markers for a protein modification by 2-heptenal. Taking into account that other 2-alkenals, like 2-hexenal, 2-octenal, or 2-nonenal, are able to form analogous adducts[16,17,27] and that "mixed" derivatives consisting for example of one molecule each of lysine, 2-hexenal, and 2-heptenal, respectively, are possible, a large variety of adducts can be expected. Furthermore, other secondary products of the lipid peroxidation like alkanals, 2,4-alkadienals or 4-hydroxyalkenals are also able to form adducts with amino acid side chains.[13,30,31] Due to the broad spectrum of possible precursors, we conclude that in food, especially as a result of roasting lipid-rich peanuts, a complex spectrum of adducts between amino acid side chains and secondary products of lipid peroxidation can be formed accounting for the large modification rate of lysine. Analogous to glycation reactions between reducing carbohydrates and amino compounds (also referred to a Maillard reaction or nonenzymatic glycosylation), the complex reactions involving carbonyl compounds from lipid peroxidation and amino acids could be called "lipation". Due to the formation of these post-translationally formed lipation products, the binding ability of immunoglobulines E against peanut proteins may be altered. This could have an influence on the allergenic potential of roasted peanuts. Further studies are needed to investigate whether lipation products are formed in roasted peanuts as well and whether these modifications have an influence on the allergenic potential of roasted peanuts.

## AUTHOR INFORMATION

### Corresponding Author

* Phone: +49-351-463-34647; fax: +49-351-463-34138; e-mail: Thomas.Henle@chemie.tu-dresden.de.

### Notes

Parts of this study were presented as poster contributions on the "11th International Symposium on the Maillard Reaction", September 16−20, 2012, Nancy, France, and at the conference "Chemical Reactions in Foods VII", November 14−16, 2012, Prague, Czech Republic.

The authors declare no competing financial interest.

## ■ ACKNOWLEDGMENTS

We thank Karla Schlosser, Institute of Food Chemistry, for performing the amino acid analysis, Anke Peritz, Institute of Organic Chemistry, for performing the elemental analysis and Dr. Margit Gruner, Institute of Organic Chemistry, for performing the NMR analysis.

## ■ ABBREVIATIONS USED:

AGE, advanced glycation endproduct; IgE, immunoglobulin E; *cis*-BPP-lysine, (*Z*)-1-(5-amino-5-carboxypentyl)-4-butyl-3-(pent-1-en-1-yl)pyridin-1-ium; *trans*-BPP-lysine, (*E*)-1-(5-amino-5-carboxypentyl)-4-butyl-3-(pent-1-en-1-yl)pyridin-1-ium; CML, $N^{\epsilon}$-carboxymethyllysine; MWCO, molecular weight cut off; GC-MS (EI), gas chromatography with mass spectrometry after electron-impact ionization; LC-DAD-ESI-MS/MS, liquid chromatography-diode array detector-electrospray ionization-tandem mass spectrometry

## ■ REFERENCES

(1) Souci, S. W.; Fachmann, W.; Kraut, H. *Food Composition and Nutrition Tables*, 7th ed.; MedPharm Scientific Publishers: Stuttgart, Germany, 2008; p 397.

(2) Beyer, K.; Morrow, E.; Li, X. M.; Bardina, L.; Bannon, G. A.; Burks, A. W.; Sampson, H. A. Effects of cooking methods on peanut allergenicity. *J. Allergy Clin. Immunol.* **2001**, *107*, 1077−1081.

(3) Cong, Y.-J.; Lou, F.; Li, L.-F.; Xue, W.-T.; Wang, J.; Zhang, H.; Fan, J.-F. Identification and quantification of major peanut allergens (in China) with IgE-binding property. *J. Food Biochem.* **2008**, *32*, 353−367.

(4) Mondoulet, L.; Drumare, M.-F.; Ah-Leung, S.; Paty, E.; Scheinmann, P.; Wal, J.-M.; Bernard, H. Influence of thermal processing on the IgE binding capacity of peanut allergens. *Rev. Fr. Allergol.* **2003**, *43*, 486−491.

(5) Blanc, F.; Vissers, Y. M.; Adel-Patient, K.; Rigby, N. M.; Mackie, A. R.; Gunning, A. P.; Wellner, N. K.; Skov, P. S.; Przybylski-Nicaise, L.; Ballmer-Weber, B.; Zuidmeer-Jongejan, L.; Szépfalusi, Z.; Ruinemans-Koerts, J.; Jansen, A. P. H.; Bernard, H.; Wal, J.-M.; Savelkoul, H. F. J.; Wichers, H. J.; Mills, E. N. C. Boiling peanut Ara h 1 results in the formation of aggregates with reduced allergenicity. *Mol. Nutr. Food Res.* **2011**, *55*, 1887−1894.

(6) Maleki, S. J.; Chung, S.-Y.; Champagne, E. T.; Raufman, J.-P. The effects of roasting on the allergenic properties of peanut proteins. *J. Allergy Clin. Immunol.* **2000**, *106*, 763−768.

(7) Mueller, G. A.; Maleki, S. J.; Johnson, K.; Hurlburt, B. K.; Cheng, H.; Ruan, S.; Nesbit, J. B.; Pomés, A.; Edwards, L. L.; Schorzman, A.; Deterding, L. J.; Park, H.; Tomer, K. B.; London, R. E.; Williams, J. G. Identification of Maillard reaction products on peanut allergens that influence binding to the receptor for advanced glycation end products. *Allergy* **2013**, *68*, 1546−1554.

(8) Vissers, Y. M.; Iwan, M.; Adel-Patient, K.; Skov, P. S.; Rigby, N. M.; Johnson, P. E.; Müller, P. M.; Przybylski-Nicaise, L.; Schaap, M.; Ruinemans-Koerts, J.; Jansen, A. P. H.; Mills, E. N. C.; Savelkoul, H. F. J.; Wichers, H. J. Effect of roasting on the allergenicity of major peanut allergens Ara h 1 and Ara h 2/6: the necessity of degranulation assays. *Clin. Exp. Allergy* **2011**, *41*, 1631−1642.

(9) Wellner, A.; Nußpickel, L.; Henle, T. Glycation compounds in peanuts. *Eur. Food Res. Technol.* **2012**, *234*, 423−429.

(10) Maguire, L. S.; O'Sullivan, S. M.; Galvin, K.; O'Connor, T. P.; O'Brien, N. M. Fatty acid profile, tocopherol, squalene and phytosterol content of walnuts, almonds, peanuts, hazelnuts and the macadamia nut. *Int. J. Food Sci. Nutr.* **2004**, *55*, 171−178.

(11) Liu, X.; Jin, Q.; Liu, Y.; Huang, J.; Wang, X.; Mao, W.; Wang, S. Changes in volatile compounds of peanut oil during the roasting process for production of aromatic roasted peanut oil. *J. Food Sci.* **2011**, *76*, 404−412.

(12) Brown, D. F.; Senn, V. J.; Stanley, J. B.; Dollear, F. G. Comparison of carbonyl compounds in raw and roasted runner peanuts. I. Major qualitative and some quantitative differences. *J. Agr. Food Chem.* **1972**, *20*, 700−706.

(13) Esterbauer, H.; Schaur, R. J.; Zollner, H. Chemistry and biochemistry of 4-hydroxynonenal, malondialdehyde and related aldehydes. *Free Radic. Biol. Med.* **1991**, *11*, 81−128.

(14) Esterbauer, H.; Zollner, H.; Schaur, R. J. Aldehydes Formed by Lipid Peroxidation: Mechanisms of Formation, Occurence, And Determination. In *Membrane Lipid Oxidation*; Vigo-Pelfrey, C., Ed.; CRC Press: Boca Raton, FL, 1990; Vol. *1*, pp 239−283.

(15) Uchida, K. Role of reactive aldehyde in cardiovascular diseases. *Free Radic. Biol. Med.* **2000**, *28*, 1685−1696.

(16) Baker, A.; Zidek, L.; Wiesler, D.; Chmelik, J.; Pagel, M.; Novotny, M. V. Reaction of *N*-acetylglycyllysine methyl ester with 2-alkenals: An alternative model for covalent modification of proteins. *Chem. Res. Toxicol.* **1998**, *11*, 730−740.

(17) Ishino, K.; Wakita, C.; Shibata, T.; Toyokuni, S.; Machida, S.; Matsuda, S.; Matsuda, T.; Uchida, K. Lipid peroxidation generates body odor component *trans*-2-nonenal covalently bound to protein in vivo. *J. Biol. Chem.* **2010**, *285*, 15302−15313.

(18) Lynch, M. P.; Faustman, C.; Silbart, L. K.; Rood, D.; Furr, H. C. Detection of lipid-derived aldehydes and aldehyde:protein adducts in vitro and in beef. *J. Food Sci.* **2001**, *66*, 1093−1099.

(19) Zamora, R.; Hidalgo, F. J. Modification of lysine amino groups by the lipid-peroxidation product 4,5(*E*)-epoxy-2(*E*)-heptenal. *Lipids* **1994**, *29*, 243−249.

(20) Zamora, R.; Alaiz, M.; Hidalgo, F. J. Determination of $\epsilon$-*N*-pyrrolylnorleucine in fresh food products. *J. Agric. Food Chem.* **1999**, *47*, 1942−1947.

(21) Henle, T.; Walter, H.; Klostermeyer, H. Evaluation of the extent of the early Maillard-reaction in milk-products by direct measurement of the Amadori-product lactuloselysine. *Z. Lebensm. Unters. Forsch.* **1991**, *193*, 119−122.

(22) Henle, T.; Walter, H.; Krause, I.; Klostermeyer, H. Efficient determination of individual Maillard compounds in heat-treated milk products by amino acid analysis. *Int. Dairy J.* **1991**, *1*, 125−135.

(23) Chung, S. Y.; Champagne, E. T. Allergenicity of Maillard reaction products from peanut proteins. *J. Agric. Food Chem.* **1999**, *47*, 5227−5231.

(24) Matissek, R.; Steiner, G.; Fischer, M. *Lebensmittelanalytik*, 4th ed.; Springer-Verlag: Berlin Heidelberg, 2010.

(25) Hidalgo, F. J.; Zamora, R. The role of lipids in nonenzymatic browning. *Grasas y Aceites* **2000**, *51*, 35−49.

(26) Gardner, H. W. Lipid hydroperoxide reactivity with proteins and amino-acids: a review. *J. Agric. Food Chem.* **1979**, *27*, 220−229.

(27) Alaiz, M.; Barragán, S. Reaction of a lysyl residue analogue with *E*-2-octenal. *Chem. Phys. Lipids* **1995**, *75*, 43−49.

(28) Furuhata, A.; Ishii, T.; Kumazawa, S.; Yamada, T.; Nakayama, T.; Uchida, K. *N*-epsilon-(3-methylpyridinium)lysine, a major antigenic adduct generated in acrolein-modified protein. *J. Biol. Chem.* **2003**, *278*, 48658−48665.

(29) Ichihashi, K.; Osawa, T.; Toyokuni, S.; Uchida, K. Endogenous formation of protein adducts with carcinogenic aldehydes—Implications for oxidative stress. *J. Biol. Chem.* **2001**, *276*, 23903−23913.

(30) Fenaille, F.; Tabet, J.-C.; Guy, P. A. Study of peptides containing modified lysine residues by tandem mass spectrometry: precursor ion scanning of hexanal-modified peptides. *Rapid Commun. Mass Spectrom.* **2004**, *18*, 67−76.

(31) Kato, H.; Kaneko, S.; Okitani, A.; Ito, M.; Hayase, F. Modification of lysine residues to alkyl-substituted pyridiniums on exposure of proteins to vaporized hexanal. *Agric. Biol. Chem.* **1986**, *50*, 1223−1228.

JOURNAL OF AGRICULTURAL AND FOOD CHEMISTRY

Article

pubs.acs.org/JAFC

# Octopus Lipid and Vitamin E Composition: Interspecies, Interorigin, and Nutritional Variability

Álvaro Torrinha,[†] Rebeca Cruz,[‡] Filipa Gomes,[†] Eulália Mendes,[‡] Susana Casal,*[,‡] and Simone Morais*[,†]

[†]REQUIMTE, Instituto Superior de Engenharia do Porto, Instituto Politécnico do Porto, Rua Dr. António Bernardino de Almeida, 431, 4200-072 Porto, Portugal

[‡]REQUIMTE, Laboratório de Bromatologia e Hidrologia, Faculdade de Farmácia, Universidade do Porto, Rua de Jorge Viterbo Ferreira, 228, 4050-313 Porto, Portugal

Supporting Information

**ABSTRACT:** *Octopus vulgaris*, *Octopus maya*, and *Eledone cirrhosa* from distinct marine environments [Northeast Atlantic (NEA), Northwest Atlantic (NWA), Eastern Central Atlantic, Western Central Atlantic (WCA), Pacific Ocean, and Mediterranean Sea] were characterized regarding their lipid and vitamin E composition. These species are those commercially more relevant worldwide. Significant interspecies and interorigin differences were observed. Unsaturated fatty acids account for more than 65% of total fatty acids, mostly $\omega$-3 PUFA due to docosahexaenoic (18.4−29.3%) and eicosapentanoic acid (11.4−23.9%) contributions. The highest $\omega$-3 PUFA amounts and $\omega$-3/$\omega$-6 ratios were quantified in the heaviest specimens, *O. vulgaris* from NWA, with high market price, and simultaneously in the lowest graded samples, *E. cirrhosa* from NEA, of reduced dimensions. Although having the highest cholesterol contents, *E. cirrhosa* from NEA and *O. maya* from WCA have also higher protective fatty acid indexes. Chemometric discrimination allowed clustering the selected species and several origins based on lipid and vitamin E profiles.

**KEYWORDS:** *octopus, fatty acids, cholesterol, vitamin E, nutritional assessment, chemometric discrimination*

## INTRODUCTION

Cephalopods are part of the traditional diet of Japan, Korea, Argentina, Taiwan, and China, and of coastal communities of southern Europe, such as Spain, Portugal, Morocco, Mauritania, Greece, and Italy. Unfortunately, octopus catches have been declining through time mainly due to stock overexploitation in some areas.[1] Still, cephalopods comprise, in general, a major food resource for human consumption with catches of 3.77 million tonnes in 2010 and representing always high values in terms of auction transaction of the wholesale market registered for marine species.[1,2] In terms of world trade and landing, *Octopus vulgaris* (common octopus), *Eledone cirrhosa* (curled octopus), and *Octopus maya* (Mexican four-eyed octopus) represent the most important octopus species available to consumers being those selected for this study. The two former species are the most abundant species from their taxonomical genus.[3] Based on FAO information, the world geographical distribution of the three species is presented in Figure 1. As it can be seen, *O. vulgaris* have a wide distribution, being found in the Atlantic, Indian, and Pacific Oceans (PO) as well as in the Mediterranean Sea (MS). The endemic species *O. maya* is specifically found in the Yucatan peninsula, in the Gulf of Mexico. On the other hand, *E. cirrhosa* is distributed in the Northeast Atlantic Ocean (NEA) and in the MS.[3]

Seafood is known to be very important in human nutrition regarding the prevention of health disorders due to the presence of polyunsaturated fatty acids in their lipid composition [including the essential linoleic (C18:2) and alpha-linolenic (C18:3) acids, as well as docosahexaenoic (DHA; C22:6$\omega$-3) and eicosapentanoic acids (EPA; C20:5$\omega$-3)][4] and octopus species are no exception. Thus, some nutritional parameters such as total fat, fatty acids, cholesterol, and fat soluble vitamins are nowadays taken into account in order to maintain a good nutritional balance, since they are positively or negatively associated with health problems. To the best of our knowledge, *O. vulgaris* from MS[5−9] and NEA[10−13] have been analyzed for their fatty acids, but there is a lack of information on this subject concerning other geographical provenance, as well as regarding the other most relevant species, *E. cirrhosa*[14] and *O. maya*.[15] Also, data are very limited regarding the levels of cholesterol and vitamin E in these species and their different origins, being inexistent for *O. maya*. Furthermore, several studies[16−18] reported that cephalopods are highly sensitive to the environmental changes during all stages of the cephalopod's life, being able to respond to these changes actively (for example, migrating to areas with more propitious environmental conditions for feeding or spawning) or passively (using optimum environmental conditions to reach certain life stages at different growth rates between different generations).[17]

Thus, the aim of the present work was to characterize the total fat, fatty acids, cholesterol, and vitamin E concentrations in the arms of the three aforementioned species of octopus from distinct marine environments [NEA, Northwest Atlantic Ocean (NWA), Eastern Central Atlantic Ocean (ECA), Western Central Atlantic Ocean (WCA), PO, and MS]. The selected species are representative of the current octopus

Received: May 28, 2014
Revised: July 30, 2014
Accepted: August 3, 2014
Published: August 4, 2014

 © 2014 American Chemical Society 

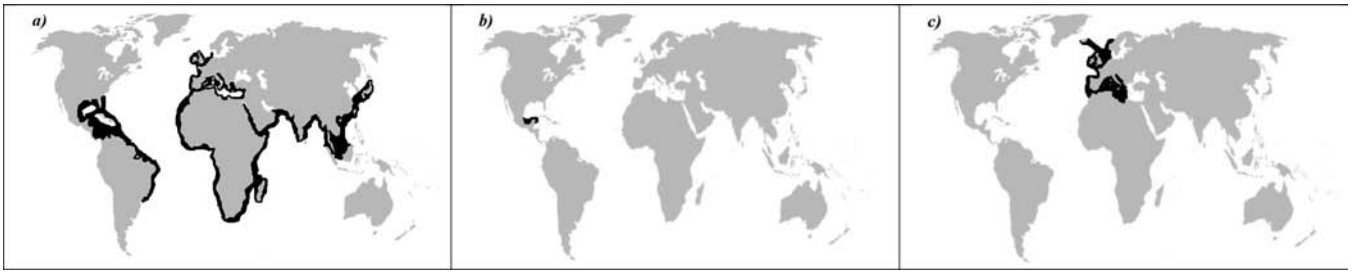


**Figure 1.** Geographical distribution of (a) *O. vulgaris*, (b) *O. maya*, and (c) *E. cirrhosa* according to FAO (1984).

generally consumed worldwide, being those commercially available in Portugal. The interspecies and interorigin composition variability and the associated benefit−risk balance of consumption of these species were evaluated. Also, the suitability of using fatty acids, cholesterol, and vitamin E concentrations as chemical descriptors to differentiate the octopus species and oceanic provenance was assessed.

## MATERIAL AND METHODS

**Reagents.** For cholesterol, vitamin E, fatty acids, and total fat analysis, propan-2-ol, cyclohexane, and HPLC grade *n*-hexane were purchased from Merck (Darmstadt, Germany), while 1,4-dioxane was from Sigma-Aldrich (Steinheim, Germany). Methanol and potassium hydroxide were acquired from Panreac (Spain). Boron trifluoride in methanol (14%), butylated hydroxytoluene (BHT), and ascorbic acid were obtained from Sigma-Aldrich. The internal standard for fatty acids quantification, triundecanoin, was also from Sigma-Aldrich (Steinheim, Germany), while the internal standard for vitamin E quantification, tocol, was obtained from Matreya (USA). Alfa-tocopherol and cholesterol standards were from Sigma-Aldrich (Steinheim, Germany), and the fatty acids methyl esters (FAMEs) standard was from Supelco (Bellefonte, PA). All other chemicals were of analytical grade from diverse suppliers.

**Sample Collection.** Octopus ($n$ = 69) from the different geographical origins available to Portuguese consumers was purchased frozen randomly from the markets in the NW region of Portugal during spring 2012. The species collected were *O. vulgaris* from NWA ($n$ = 8), NEA ($n$ = 8), ECA ($n$ = 8), WCA ($n$ = 8), PO ($n$ = 8), and MS ($n$ = 5); *O. maya* from ECA ($n$ = 8) and WCA ($n$ = 8); and *E. cirrhosa* from NEA ($n$ = 8). The origin was established based on the label information, as well as the date of capture (from 11 October to 9 December 2011). Sample collection, biometric characterization, and preparation were performed in accordance with the EPA Guide No. 823-B-00-07, DL No. 187/2005,[19] and CE Regulation No. 333/2007.[20] Specimens were carefully identified and manually eviscerated. Only the edible tissues were preserved. Homogenization was performed mechanically with a blender until a smooth paste was obtained. For each sample, three independent subsamples were defined. Samples were preserved at −18 °C, and subportions were freeze-dried (Telstar Cryodos-80, Terrassa, Barcelona) for fatty acid, cholesterol, and vitamin E quantification.

Moisture was evaluated using 10 g of sample according to the Portuguese Standard NP 2282-1991 and the official AOAC method.[21]

**Fatty Acids, Cholesterol, and Vitamin E Analysis.** For total fat content, approximately 1 g (accurately weighed) of the homogenized sample was extracted with 30.0 mL of acetone:ether petroleum (1:2, v/v) by microwave-assisted extraction, according to Ramalhosa et al.[22]

Extraction and analysis of fatty acids, cholesterol, and vitamin E were performed according to a validated study, conducted by Cruz and co-workers.[23] Briefly, an accurate freeze-dried sample portion (300 mg) was extracted with a ternary mixture of propan-2-ol, cyclohexane, and 0.9% (m/v) KCl, in the presence of the internal standards (tocol and triundecanoate), plus antioxidants (ascorbic acid and BHT). One-third of the organic extract was directly used for vitamin E analysis by HPLC, after being taken to dryness under a gentle nitrogen stream and reconstituted in *n*-hexane. The remaining extract was hydrolyzed with KOH (0.5 mol/L in methanol) at 100 °C (10 min) and further methylated with $BF_3$ (30 min at 100 °C) to convert the acyl-*sn*-glycerols and free fatty acids in the samples to volatile methyl esters (FAMEs). The lipids were extracted with *n*-hexane, and the solution was used initially for cholesterol quantification by HPLC, and thereafter for fatty acids analysis by GC-FID.

**HPLC Conditions for Vitamin E and Cholesterol Analysis.** The liquid chromatograph consisted of a Jasco integrated system (Japan) equipped with an LC-NetII/ADC data unit, a refrigerated autosampler (AS-2057 Plus), a PU-980 Intelligent Pump, and a multiwavelength DAD (MD-910, recorded at 210 nm), connected in series to a FD (FP-2020 Plus; $\lambda_{exc}$ = 290 nm and $\lambda_{em}$ = 330 nm; gain 10). The chromatographic separation was achieved on a Supelcosil LC-SI column (75 × 3.0 mm, 3 μm; Supelco, Bellefonte, PA) operating at constant room temperature (23 °C). A mixture of *n*-hexane and 1,4-dioxane (97.5:2.5, v/v) was used as eluent at a flow rate of 0.8 mL/min. Data were analyzed with the ChromNAV Control Center—JASCO Chromatography Data Station (Japan). The compounds were identified by chromatographic comparisons with authentic standards, by coelution, and by their UV spectra. Vitamin E was evaluated by the internal standard method based on the fluorescence data. Cholesterol was quantified at 210 nm, with calibration based on external standard solutions.

**Gas Chromatographic Conditions for Fatty Acids Analysis.** Gas chromatography was performed on a Chrompack CP 9001 chromatograph (Chrompack, Middelburg, The Netherlands) equipped with a split−splitless injector, a flame-ionization detector, and a Chrompack CP-9050 autosampler. The temperatures of the injector and detector were 250 and 270 °C, respectively. Separation was achieved on a 50 m × 0.25 mm i.d. CP-Sil 88 column (0.19 μm film; Chrompack-Varian), using a temperature program from 140 to 220 °C. Helium was used as the carrier gas at an internal pressure of 120 kPa. Fatty acid identification (from C14:0 to C22:6ω-3) was accomplished by comparing the relative retention times of FAMEs of commercially available fatty acids methyl esters (Supelco 37-FAME mix, Supelco, USA). Total fatty acids content was estimated on the basis of the total fatty acid methyl ester area counts in comparison with the undecanoic methyl ester by converting the FAMEs to their respective fatty acid equivalents using the appropriate conversion factors. Individual fatty acids were initially quantified on a g/100 g fatty acids basis and then converted to mg/100 g wet weight (ww) using the fatty acid internal standard (C11:0) and moisture content. Saturated fatty acids (SFA) include 12:0, 14:0, 15:0, 16:0, 17:0, 18:0, 20:0, and 22:0; monounsatured fatty acids (MUFA) include 16:1 isomers (ω-7 plus ω-9), 18:1 (ω-7 and ω-9), 20:1ω-9, 22:1ω-9, and 24:1ω-9; while polyunsaturated fatty acids (PUFA) include several omega-6 (18:2ω-6, 20:2ω-6, 20:3ω-6, 20:4ω-6, and 22:4ω-6) and omega-3 (18:3ω-3, 20:5ω-3, 22:2ω-6, 22:5ω-3, and 22:6ω-3) fatty acids.

**Nutritional Assessment.** The most relevant nutritional lipid quality indexes such as total ω-3/ω-6 ratio, PUFA/SFA, DHA + EPA sum, atherogenicity index (AI), thrombogenicity index (TI), and hypocholesterolemic:hypercholesterolemic ratio (HH) were estimated.[24] AI, TI, and HH indexes were calculated using eqs 1, 2, and 3, respectively:


dx.doi.org/10.1021/jf502502b | J. Agric. Food Chem. 2014, 62, 8508−8517

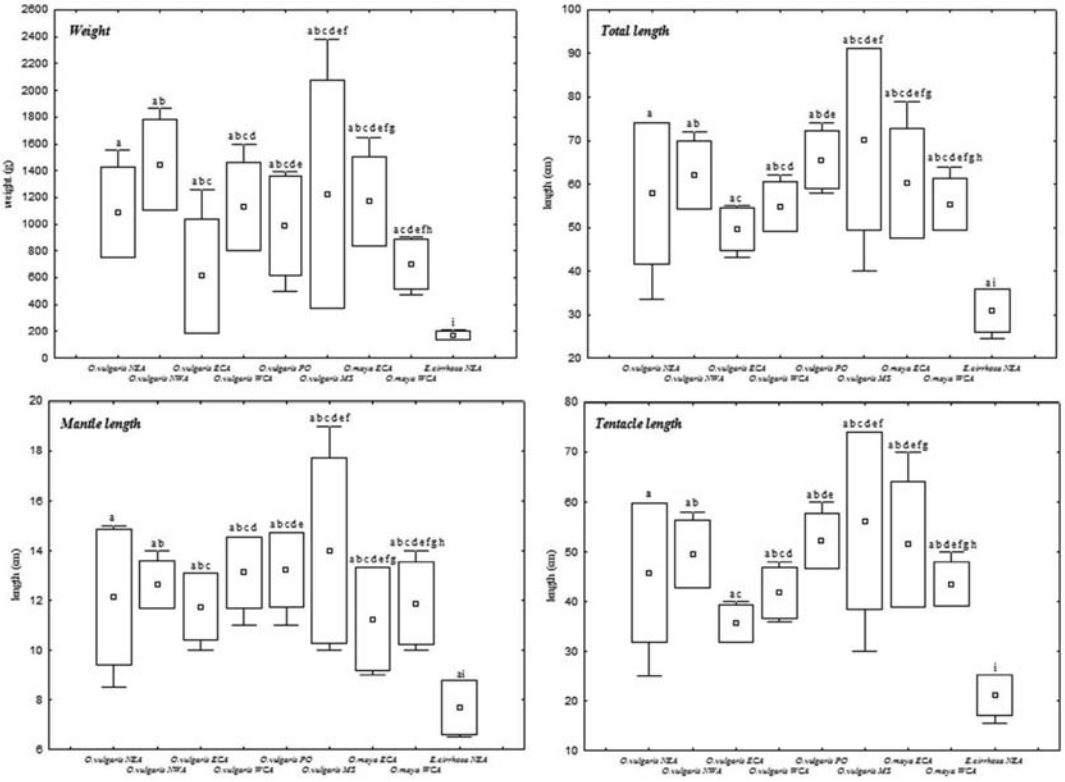


**Figure 2.** Biometric parameters (□, mean; rectangles, mean ± standard deviation; bars above and below rectangles, range) of the characterized octopus species ($n$ = 69). Each letter (a–i) corresponds to a species and inherent origin (a, *O. vulgaris* from Northeast Atlantic Ocean (NEA); b, *O. vulgaris* from Northwest Atlantic Ocean (NWA); c, *O. vulgaris* from Eastern Central Atlantic Ocean (ECA); d, *O. vulgaris* from Western Central Atlantic Ocean (WCA); e, *O. vulgaris* from Pacific Ocean (PO); f, *O. vulgaris* from Mediterranean Sea (MS); g, *O. maya* from ECA; h, *O. maya* from WCA; i, *E. cirrhosa* from NEA). The same letters in a box plot indicate that the given means are not statistically different ($p > 0.05$).

$$\mathrm{AI} = \frac{\mathrm{C12{:}0} + 4 \times \mathrm{C14{:}0} + \mathrm{C16{:}0}}{\sum \mathrm{MUFA} + \sum \omega\text{-}3 + \sum \omega\text{-}6} \quad (1)$$

$$\mathrm{TI} = \frac{\mathrm{C14{:}0} + \mathrm{C16{:}0} + \mathrm{C18{:}0}}{0.5\sum \mathrm{MUFA} + 0.5\sum \omega\text{-}6 + 3\sum \omega\text{-}3} \quad (2)$$

$$\mathrm{HH} = (\mathrm{C18{:}1}\omega\text{-}9 + \mathrm{C18{:}2}\omega\text{-}6 + \mathrm{C20{:}4}\omega\text{-}6 + \mathrm{C18{:}3}\omega\text{-}3 + \mathrm{C20{:}5}\omega\text{-}3 + \mathrm{C22{:}5}\omega\text{-}3 + \mathrm{C22{:}6}\omega\text{-}3)/(\mathrm{C14{:}0} + \mathrm{C16{:}0}) \quad (3)$$

**Statistical Analysis.** Statistical analysis was performed using the SPSS (IBM SPSS Statistics 20) and Statistica software (v. 7, StatSoft Inc., USA). Data were expressed as mean ± standard deviation and range and were grouped according to species and origins. Mean values were compared through the nonparametric Mann–Whitney $U$ test, since normal distribution was not observed by Shapiro–Wilk's test. Statistical significance was defined as $p \leq 0.05$. Principal components analysis (PCA) was applied, after variable standardization to mean zero and unit variance to assess which variables may be used as chemical descriptors among the three species or origins.

## RESULTS AND DISCUSSION

**Biometric Data.** The collected biometric data is presented in Figure 2. Generally, *E. cirrhosa* may be clearly distinguished from the other species due to its statistically significantly reduced dimensions, which explain its lower market price. On average, the heavier specimens were from *O. vulgaris* from NWA (1443 ± 336 g) while the biggest (14.0 ± 3.7 cm for mantle, 56.3 ± 17.9 cm for tentacle, and 70.3 ± 21.0 cm for total length) were from MS *O. vulgaris* species. Generally, the commercialized individuals of each species and origin were highly heterogeneous in length and weight, particularly *O. vulgaris* from the MS, which hindered the identification of biometric differences between the several tested species and geographical origins. Still, this high variability is in accordance with other documented results and may be related to biological factors.[7,10,12,13,25,26]

**Fatty Acids Composition.** In opposition to the biometric data, the fatty acids composition (as relative percentage of total fatty acids) was highly homogeneous in terms of fatty acids classes among the samples analyzed. PUFA is the more abundant class, followed by SFA and MUFA. Total PUFA ranged from 51.9% (*O. maya* from ECA) to 59.0% (*O. vulgaris* from NWA), followed by SFA from 25.6% (*E. cirrhosa* from NEA) to 31.1% (*O. maya* from ECA) and MUFA from 11.6% (*O. vulgaris* from WCA and MS) to 14.1% (*O. vulgaris* from NEA). Unsaturated fatty acids (PUFA + MUFA) account for more than 65% of total fatty acids.

The majority of the published studies in octopus composition concern *O. vulgaris* caught in MS. The attained results for this species are in accordance with Estefanell et al.,[5,6] Ozogul et al.,[7] and Passi et al.[8] while much higher SFA contents were reported by Karakoltsidis et al.[9] (41%). In particular, some authors have determined the fatty acid profiles of *O. vulgaris* captured in NEA. The reported values are similar to ours with only slight variations: SFA 31.9–34.6%, MUFA 9.2–11.6%, PUFA 55.7%;[10] SFA 27.3–33.2%, MUFA 9.6–10.4%, PUFA 54.8–59.2%;[12] SFA 34.2–40.8%, MUFA 4.5–7.9%, PUFA 47.6–56.4%;[11] SFA 25.9%, MUFA 15.5%, PUFA 58.6%.[13] The results reached for *O. vulgaris* from PO and *E. cirrhosa* are also


dx.doi.org/10.1021/jf502502b | J. Agric. Food Chem. 2014, 62, 8508–8517

in agreement with those scarce previously published (Turner et al.[27] for *O. vulgaris* from PO; Rosa et al.[14] for *E. cirrhosa*).

To the best of our knowledge, no information exists in the literature about fatty acids composition of *O. vulgaris* from NWA, ECA, and WCA, as well as wild *O. maya*. Studies concerning reared octopus were not used for comparison purposes since marine specimens created in captivity show differences from the wild ones because feeding habits are different.[28] In recent years, chemical and nutritional compositions of cephalopods have been extensively studied for aquaculture and industrial production purposes. Benthic species like *O. vulgaris* and *O. maya* are examples with high potential for aquaculture due to the worldwide high consumption demand and to their physiological, behavioral, and environmental characteristics.[28]

Regarding the fatty acids composition on an edible basis (mg/100 g ww) only the ones with more quantitative/nutritional importance are detailed in Table 1. There were wide variation and significant differences ($p < 0.05$) among the fatty acid profiles of the different species and origins in terms of total and individual compounds. Overall, *E. cirrhosa* stands out for its statistically significantly greater concentrations of the three main classes of fatty acids (SFA, MUFA, and PUFA) followed by *O. maya* from WCA. The MUFA and PUFA levels of *O. maya* from WCA were only similar to those from *O. vulgaris* from NWA. Within the different oceanic regions of *O. vulgaris*, the maximum total fatty acids mean (including the higher average value per fatty acid class) was observed in specimens from NWA. In contrast, the poorest species in fatty acids content was the most expensive and consumed worldwide species, *O. vulgaris* from MS. Still, its PUFA and SFA levels were similar to those from the same species from NEA and ECA, as well as to those of *O. maya* from ECA.

Concerning total PUFA averages, more than 56% (*O. maya* from WCA) up to 89% (*O. vulgaris* from NWA) are $\omega$-3 fatty acids, ranging respectively from 83 ± 27 to 341 ± 60 mg/100 g on a fresh basis. Marine organisms living in cold waters have usually a higher percentage of $\omega$-3 fatty acids composition,[29] which is consistent with this benthic species. The compounds that contributed most for total PUFA proportions in the fatty acids were, by descending order, docosahexaenoic acid (DHA; C22:6$\omega$-3) with 18.4% for *O. maya* from ECA (47 ± 18 mg/100 g ww) to 29.3% for *E. cirrhosa* from NEA (195 ± 31 mg/100 g ww), followed by eicosapentanoic acid (EPA; C20:5$\omega$-3) ranging 11.4% for *O. maya* WCA (31 ± 11 mg/100 g ww) to 23.9% (94 ± 11 mg/100 g ww) for *O. vulgaris* NWA, and arachidonic acid (ARA; C20:4$\omega$-6) with 4.6% for *O. vulgaris* NWA (19 ± 2 mg/100 g ww) to 19.4% for *O. maya* WCA (86 ± 10 mg/100 g ww). This pattern of variation is slightly different for *O. vulgaris* from WCA and PO, as well as for *O. maya* from ECA due to the higher contribution of ARA than EPA. In absolute amounts, as consumed, the lowest DHA (27 mg/100 g ww) and EPA (15 mg/100 g ww) contents were detected in *O. maya* from ECA while the highest were determined in *E. cirrhosa* from NEA, with 252 and 171 mg/100 g ww, respectively. Interestingly, the same *O. maya* but from WCA was the third group with higher DHA amounts (82 ± 11 mg/100 g), just after *O.vulgaris* from NWA. DHA and EPA are important in marine species since they are components in membrane cells where they maintain structural functions and their extremely low freezing temperatures are consistent with the demands of a life in cold seas. Taking a deeper look into the $\omega$-6 PUFA concentrations, it can be also observed that *O. maya* from WCA exhibits the highest levels (1.6−3.9 times higher) of $\omega$-6 PUFA mainly due to the contributions of ARA and C22:4$\omega$-6 and supported by the higher lipids content.

MUFA content ranged from 23.0 mg/100 g ww (*O. vulgaris* from MS and *O. maya* from ECA) to 126 mg/100 g ww (for *E. cirrhosa* from NEA). Oleic acid (C18:1; here reported as the sum of $\omega$-7 and $\omega$-9 isomers) was the most abundant within the monounsaturated class representing 31% (*O. vulgaris* from PO) to 46% (*O. vulgaris* from NWA) of the total MUFA mean amounts. Considering all species and origins, the strongest significant differences in C18:1 concentrations were detected between *E. cirrhosa* and the others ($p < 0.01$), as well as among *O. vulgaris* NWA and all the species apart from *O. maya* from WCA. Within the studied *O. vulgaris* sources, individuals from the NWA location presented the major statistical differences.

SFA values varied from 51 mg/100 g ww (*O. maya* from ECA) to 219 mg/100 g ww (*E. cirrhosa* from NEA). Statistical differences were found between *E. cirrhosa* and the other species ($p < 0.01$), as well as among *O. maya* WCA and all the remaining ones ($p < 0.01$). Palmitic acid (C16:0) followed by stearic acid (C18:0) were the compounds that contributed most for the total SFA mean. C16:0 corresponded to 13.9% (*O. maya* WCA) to 17.7% (*O. vulgaris* NWA) while C18:0 represented 5.4% (*E. cirrhosa* NEA) to 10.4% (*O. maya* ECA). The same statistical differences as those for the SFA class were found between species for C16:0 and C18:0.

Among all the factors influencing cephalopod fatty acid composition, diet is the most important and what affects most.[30] Several reports about cultured octopus have shown that fatty acid profile is significantly affected by the prey composition.[28,31−33] The availability of certain preys and the feeding habits of the species are connected, to some extent, with the geographical region. Octopus lipid composition is also largely influenced by water temperature (which depends on location and season), such that in colder water they store more fat.[15,34] Other influencing factors are oogenesis, spermatogenesis, and starvation of females during brooding.[7,9,11,12]

**Vitamin E.** The high prevalence of unsaturated fatty acids requires effective measures to protect them from oxidation. In nature, vitamin E levels are usually allied with high concentrations of unsaturated fatty acids.[35,36] The oxidation of a methyl group in PUFA gives formation to a free radical by a hydrogen atom removal becoming reactive and goes under chain reaction. Vitamin E that is incorporated in biological membranes acts as chain-breaking antioxidant. The phenol group of vitamin E compounds donates a hydrogen atom to the peroxyl radical, forming a tocopherol radical and a lipid hydroperoxide. The tocopherol radical can then link to another peroxyl radical forming inactive molecular products.[35]

Vitamin E embraces several lipophilic tocochromanols with antioxidant properties, but in the octopus samples analyzed only $\alpha$-tocopherol was detected and quantified. As expected, higher amounts of vitamin E were quantified in the samples with higher PUFA amounts (Figure 3 and Table 1). Detectable concentrations of vitamin E varied from 0.29 (for *O. vulgaris* from WCA) to 2.5 mg/100 g ww (for *O. vulgaris* from NWA). The results varied about a factor of 10 showing high intervariability between species and origins. The mean vitamin E content of *O. vulgaris* from NWA (1.60 ± 0.5 mg/100 g ww), *E. cirrhosa* from NEA (1.25 ± 0.46 mg/100 g ww), and *O. vulgaris* from PO (1.00 ± 0.45 mg/100 g ww) may be clearly distinguished from the other species by their highest contents. No statistical differences were verified between the mean of *E.*

**Table 1. Moisture (%) and Total and Fatty Acids Composition (Mean ± Standard Deviation and Range; mg/100 g wet weight) in the Arms of Octopus from Different Origins[a]**

| | *O. vulgaris* | | | | | | *O. maya* | | *E. cirrhosa* |
|---|---|---|---|---|---|---|---|---|---|
| | NEA ($n$ = 8) | NWA ($n$ = 8) | ECA ($n$ = 8) | WCA ($n$ = 8) | PO ($n$ = 8) | MS ($n$ = 5) | ECA ($n$ = 8) | WCA ($n$ = 8) | NEA ($n$ = 8) |
| moisture | 88.7 ± 3.6 a (84.5−92.4) | 81.5 ± 1.0 b (80.7−82.8) | 91.7 ± 4.1 ac (88.4−97.4) | 85.9 ± 0.6 ad (85.6−86.7) | 89.2 ± 0.6 ace (88.5−89.9) | 91.0 ± 2.8 acef (88.5−94.3) | 92.2 ± 2.0 acfg (90.5−94.9) | 86.1 ± 1.7 adh (84.0−88.0) | 84.1 ± 1.6 abdhi (82.0−85.9) |
| total fatty acids | 271 ± 73 a (194−389) | 394 ± 40 b (346−457) | 257 ± 50 ac (196−311) | 337 ± 24 ad (289−364) | 319 ± 42 ade (254−375) | 241 ± 32 acf (190−277) | 263 ± 102 acfg (181−448) | 450 ± 53 h (386−531) | 686 ± 119 i (518−901) |
| C14:0 | 3.1 ± 1.3 a (1.3−4.7) | 3.9 ± 1.5 ab (2.0−6.3) | 3.1 ± 1.2 abc (2.0−5.0) | 3.5 ± 0.3 abcd (3.1−4.0) | 3.4 ± 0.5 abcde (2.9−4.2) | 2.8 ± 0.5 abcf (2.3−3.6) | 2.1 ± 0.6 ag (1.4−3.0) | 3.3 ± 0.8 abcdefh (2.4−5.2) | 4.7 ± 0.7 bi (3.8−5.7) |
| C16:0 | 44 ± 15 a (28−65) | 69 ± 8 b (60−79) | 42 ± 9 ac (32−53) | 48 ± 5 acd (38−57) | 46 ± 11 acde (29−58) | 39 ± 5 acef (32−46) | 40 ± 18 acefg (23−71) | 62 ± 8 h (51−74) | 108 ± 15 i (87−130) |
| C18:0 | 20 ± 4 a (14−24) | 28 ± 2 b (24−32) | 18 ± 3 ac (14−22) | 33 ± 2 d (28−36) | 28 ± 9 bde (16−39) | 17 ± 2 acf (14−22) | 26 ± 12 aeg (17−49) | 44 ± 4 h (38−52) | 36 ± 5 di (28−46) |
| C20:0 | 0.4 ± 0.3 a (0.1−1.1) | 0.3 ± 0.1 ab (0.1−0.4) | 0.3 ± 0.2 bc (0.1−0.7) | 0.4 ± 0.2 abcd (0.2−0.9) | 0.8 ± 1.1 ade (0.2−4.1) | 0.9 ± 0.5 ef (0.2−1.7) | 1.2 ± 1.3 abcdefg (0.2−4.1) | 0.1 ± 0.1 h (n.d. - 0.3) | 2.9 ± 3.5 fgi (0.2−12.5) |
| SFA[b] | 79 ± 19 a (56−109) | 109 ± 10 b (96−122) | 73 ± 13 ac (58−87) | 103 ± 9 bd (85−114) | 90 ± 21 ade (59−117) | 69 ± 6 acf (57−76) | 82 ± 36 acefg (51−147) | 129 ± 15 h (110−148) | 176 ± 25 i (138−219) |
| C16:1 | 6.0 ± 1.0 a (4.4−7.5) | 6.2 ± 1.0 ab (5.1−8.2) | 8.3 ± 1.2 c (5.8−10.3) | 8.6 ± 1.6 cd (6.2−11.7) | 8.1 ± 1.7 cde (5.9−11.6) | 7.0 ± 1.2 abef (5.1−9.2) | 4.4 ± 1.6 g (2.5−7.1) | 9.9 ± 2.5 cdeh (6.1−13.3) | 10.0 ± 1.4 hi (7.8−12.8) |
| C18:1 | 15 ± 4 a (10−21) | 23 ± 4 b (17−30) | 11 ± 3 c (7−15) | 17 ± 4 ad (13−24) | 14 ± 3 ade (11−17) | 11 ± 1 cf (9−13) | 14 ± 5 acefg (9−24) | 25 ± 4 bh (20−31) | 34 ± 9 i (25−49) |
| C20:1$\omega$-9 | 6.6 ± 3.2 a (3.0−11.4) | 10.1 ± 1.3 b (8.4−11.6) | 6.3 ± 2.1 ac (3.9−9.4) | 6.7 ± 0.9 acd (6.0−9.4) | 8.1 ± 4.5 abcde (3.9−15.0) | 5.6 ± 1.4 acdef (4.1−7.2) | 4.5 ± 1.0 aeg (3.3−5.8) | 9.1 ± 1.5 abeh (6.3−11.5) | 18.0 ± 2.6 i (14.8−22.9) |
| MUFA[c] | 38 ± 8 a (30−53) | 50 ± 8 b (38−60) | 34 ± 6 ac (26−43) | 39 ± 5 acd (33−48) | 45 ± 5 abe (32−52) | 28 ± 3 f (23−31) | 35 ± 10 acdg (23−54) | 55 ± 8 bh (43−73) | 89 ± 20 i (68−126) |
| C18:2$\omega$-6 | 2.2 ± 0.8 a (1.2−3.4) | 3.5 ± 1.5 b (1.3−6.0) | 1.4 ± 0.5 c (0.7−2.1) | 1.9 ± 0.5 acd (1.4−2.8) | 1.9 ± 0.9 acde (0.8−3.0) | 1.8 ± 0.6 acdef (0.9−2.5) | 2.1 ± 1.4 acdefg (0.9−4.6) | 2.8 ± 0.4 abh (2.2−3.7) | 3.6 ± 1.2 bi (2.4−5.8) |
| C20:2$\omega$-6 | 1.3 ± 0.5 a (0.7−2.1) | 0.5 ± 0.8 b (0.1−2.9) | 1.1 ± 0.4 ac (0.8−1.8) | 1.8 ± 0.2 d (1.4−2.2) | 2.5 ± 1.0 de (1.2−3.9) | 1.2 ± 0.2 acf (0.9−1.5) | 2.0 ± 2.1 acg (0.6−5.7) | 2.6 ± 0.4 eh (2.0−3.1) | 2.2 ± 0.9 dei (1.3−4.0) |
| C20:4$\omega$-6 | 21 ± 8 a (13−34) | 19 ± 2 ab (16−23) | 17 ± 4 abc (10−22) | 56 ± 11 d (41−72) | 45 ± 16 e (28−69) | 21 ± 6 abcf (16−33) | 39 ± 24 eg (18−81) | 86 ± 10 h (75−108) | 40 ± 10 egi (28−56) |
| C22:2$\omega$-6 | 0.9 ± 0.2 a (0.7−1.4) | 0.5 ± 0.3 b (0.2−1.2) | 0.6 ± 0.2 bc (0.2−0.9) | 0.9 ± 0.2 ad (0.7−1.2) | 1.0 ± 0.5 ade (0.2−1.7) | 0.9 ± 0.2 adef (0.7−1.2) | 0.9 ± 0.6 acdefg (0.4−2.0) | 1.0 ± 0.2 adefgh (0.7−1.5) | 3.8 ± 1.0 i (2.5−5.6) |
| C22:4$\omega$-6 | 2.2 ± 1.3 a (1.1−4.5) | 1.4 ± 0.3 b (1.0−2.0) | 1.8 ± 0.4 ac (1.2−2.4) | 7.3 ± 2.5 d (4.7−11.6) | 5.7 ± 2.1 de (3.0−8.7) | 2.3 ± 0.8 acf (1.7−3.6) | 4.9 ± 4.0 efg (1.6−11.7) | 12.9 ± 2.1 h (9.9−17.2) | 4.3 ± 1.2 egi (2.7−6.8) |
| $\omega$-6 PUFA | 28 ± 10 a (18−45) | 23 ± 3 ab (20−30) | 23 ± 5 abc (14−29) | 69 ± 15 d (50−92) | 59 ± 21 de (34−90) | 27 ± 7 abf (22−41) | 51 ± 35 eg (23−111) | 110 ± 12 h (98−138) | 59 ± 14 egi (39−83) |
| C18:3$\omega$-3 | 0.7 ± 0.2 a (0.5−1.3) | 0.6 ± 0.1 ab (0.5−0.8) | 0.6−0.2 abc (0.4−1.0) | 1.7 ± 0.7 d (1.0−3.6) | 0.9 ± 0.4 ace (0.2−1.4) | 0.6 ± 0.3 abcf (0.1−1.0) | 1.0 ± 0.5 aeg (0.5−1.9) | 1.7 ± 0.6 dh (1.1−2.7) | 1.5 ± 0.5 dhi (0.9−2.2) |
| C20:3$\omega$-3 | 1.3 ± 1.0 a (0.3−2.8) | 3.0 ± 0.5 b (2.5−4.1) | 1.0 ± 0.4 ac (0.5−1.6) | 0.6 ± 0.2 ad (0.4−1.0) | 0.6 ± 0.1 ade (0.4−0.7) | 1.4 ± 0.8 acdf (0.3−2.3) | 0.4 ± 0.2 deg (0.2−0.7) | 0.8 ± 0.2 acfh (0.6−1.2) | 4.6 ± 1.4 i (2.6−6.5) |
| C20:5$\omega$-3 (EPA) | 46 ± 25 a (18−82) | 94 ± 11 b (80−112) | 49 ± 14 ac (30−65) | 41 ± 8 acd (28−51) | 39 ± 11 ade (26−57) | 44 ± 12 acdef (31−60) | 31 ± 11 adeg (15−46) | 50 ± 14 acfh (27−65) | 127 ± 24 i (94−171) |
| C22:5$\omega$-3 | 4.5 ± 1.4 a (3.2−6.9) | 6.5 ± 1.1 b (4.6−8.1) | 5.2 ± 1.1 c (4.2−7.1) | 5.8 ± 0.6 bd (5.0−6.7) | 7.0 ± 3.1 bcde (4.4−12.3) | 3.9 ± 0.6 af (3.2−4.9) | 4.3 ± 2.4 afg (2.2−8.6) | 9.9 ± 3.0 h (6.9−15.0) | 12.7 ± 4.0 i (9.3−20.4) |
| C22:6$\omega$-3 (DHA) | 63 ± 23 a (38−99) | 102 ± 12 b (87−125) | 62 ± 14 ac (44−78) | 64 ± 8 acd (55−79) | 65 ± 8 acde (42−74) | 59 ± 13 acdef (43−77) | 47 ± 18 aefg (27−76) | 82 ± 11 ah (64−96) | 195 ± 31 i (150−252) |
| $\omega$-3 PUFA | 115 ± 50 a (60−190) | 206 ± 24 b (181−249) | 119 ± 28 ac (87−148) | 113 ± 14 acd (96−137) | 113 ± 13 acde (100−134) | 109 ± 26 acdef (80−140) | 83 ± 27 afg (45−117) | 144 ± 27 ah (100−175) | 341 ± 60 i (257−448) |
| PUFA[d] | 145 ± 44 a (101−217) | 232 ± 25 b (206−276) | 143 ± 32 ac (104−178) | 184 ± 12 d (161−202) | 174 ± 19 acde (142−202) | 138 ± 23 acf (105−166) | 137 ± 55 acfg (92−233) | 257 ± 35 bh (204−316) | 403 ± 74 i (298−536) |
| $\omega$-3/$\omega$-6 | 4.9 ± 2.8 a (1.4−8.4) | 9.2 ± 1.2 b (7.1−10.8) | 5.3 ± 1.1 ac (3.8−6.7) | 1.7 ± 0.5 d (1.1−2.3) | 2.2 ± 0.9 de (1.2−3.6) | 4.3 ± 1.6 af (2.2−5.9) | 2.2 ± 1.3 deg (1.0−3.8) | 1.3 ± 0.2 gh (1.0−1.5) | 5.9 ± 0.7 ai (4.6−6.7) |



dx.doi.org/10.1021/jf502502b | J. Agric. Food Chem. 2014, 62, 8508−8517

Table 1. continued

| | *O. vulgaris* | | | | | *O. maya* | | *E. cirrhosa* |
|---|---|---|---|---|---|---|---|---|
| | NEA ($n$ = 8) | NWA ($n$ = 8) | ECA ($n$ = 8) | WCA ($n$ = 8) | PO ($n$ = 8) | MS ($n$ = 5) | ECA ($n$ = 8) | WCA ($n$ = 8) | NEA ($n$ = 8) |
| DHA/EPA | 1.6 ± 0.4 a (1.2–2.2) | 1.1 ± 0.1 b (1.0–1.2) | 1.3 ± 0.2 ac (1.1–1.7) | 1.6 ± 0.3 ad (1.4–2.1) | 1.8 ± 0.6 ade (1.2–2.7) | 1.4 ± 0.1 acdef (1.2–1.6) | 1.6 ± 0.6 acdefg (1.0–2.4) | 1.7 ± 0.4 adegh (1.5–2.4) | 1.6 ± 0.1 adeghi (1.5–1.6) |
| AI[e] | 0.30 ± 0.03 a (0.24–0.35) | 0.30 ± 0.03 ab (0.26–0.37) | 0.31 ± 0.03 abc (0.27–0.35) | 0.28 ± 0.02 d (0.25–0.30) | 0.27 ± 0.05 abde (0.20–0.37) | 0.30 ± 0.02 abcf (0.27–0.33) | 0.28 ± 0.02 deg (0.24–0.29) | 0.24 ± 0.03 eh (0.20–0.28) | 0.26 ± 0.03 degi (0.23–0.29) |
| TI[f] | 0.18 ± 0.03 a (0.15–0.25) | 0.15 ± 0.01 b (0.14–0.18) | 0.16 ± 0.01 ac (0.15–0.17) | 0.22 ± 0.02 d (0.19–0.24) | 0.20 ± 0.05 ade (0.12–0.27) | 0.17 ± 0.03 abcef (0.14–0.20) | 0.23 ± 0.06 deg (0.17–0.29) | 0.22 ± 0.03 degh (0.19–0.28) | 0.14 ± 0.01 i (0.12–0.15) |
| HH[g] | 3.3 ± 0.2 a (3.1–3.7) | 3.4 ± 0.2 ab (2.9–3.7) | 3.3 ± 0.2 abc (3.1–3.7) | 3.7 ± 0.2 d (3.4–4.0) | 3.7 ± 0.8 abcde (2.4–5.1) | 3.4 ± 0.3 abcef (3.1–3.8) | 3.4 ± 0.4 abcefg (3.1–4.0) | 4.0 ± 0.6 deh (3.1–4.8) | 3.7 ± 0.4 bdefghi (3.2–4.2) |

[a]Each letter (a–i) corresponds to a species and inherent origin (a, *O. vulgaris* from Northeast Atlantic Ocean (NEA); b, *O. vulgaris* from Northwest Atlantic Ocean (NWA); c, *O. vulgaris* from Eastern Central Atlantic Ocean (ECA); d, *O. vulgaris* from Western Central Atlantic Ocean (WCA); e, *O. vulgaris* from Pacific Ocean (PO); f, *O. vulgaris* from Mediterranean Sea (MS); g, *O. maya* from ECA; h, *O. maya* from WCA; i, *E. cirrhosa* from NEA). The same letters in a row indicate that the given means are not statistically different ($p > 0.05$). [b]SFA = saturated fatty acids. [c]MUFA = monounsaturated fatty acids. [d]PUFA = polyunsaturated fatty acids. [e]AI = atherogenic índex. [f]TI = thrombogenic index. [g]HH = hypocholesterolaemic/hypercholesterolaemic ratio.

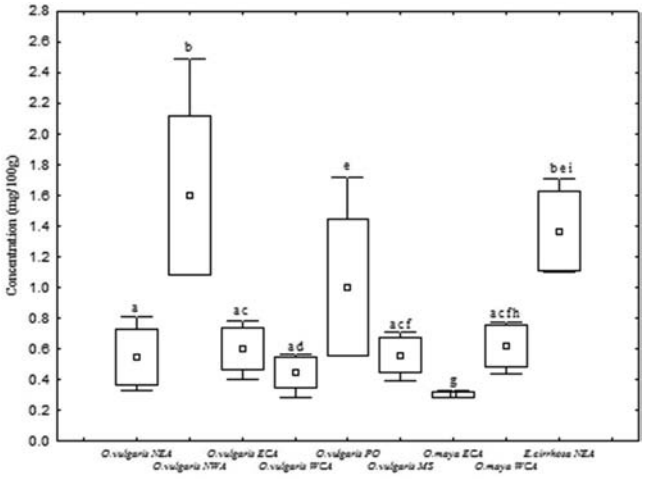


**Figure 3.** Vitamin E concentrations (□, mean; rectangles, mean ± standard deviation; bars above and below rectangles, range; mg/100 g wet weight) in the edible tissues of the characterized octopus species. Each letter (a–i) corresponds to a species and inherent origin (a, *O. vulgaris* from Northeast Atlantic Ocean (NEA); b, *O. vulgaris* from Northwest Atlantic Ocean (NWA); c, *O. vulgaris* from Eastern Central Atlantic Ocean (ECA); d, *O. vulgaris* from Western Central Atlantic Ocean (WCA); e, *O. vulgaris* from Pacific Ocean (PO); f, *O. vulgaris* from Mediterranean Sea (MS); g, *O. maya* from ECA; h, *O. maya* from WCA; i, *E. cirrhosa* from NEA). The same letters in a box plot indicate that the given means are not statistically different ($p > 0.05$).

*cirrhosa* and those of *O. vulgaris* from NWA and from PO. In contrast, *O. maya* ECA was the octopus with the lowest vitamin E content, being simultaneously among the ones with lower PUFA content. Statistical differences were found between *O. maya* ECA and all the other species ($p = 0.01$).

Data concerning vitamin E levels in octopus species are quite scarce and were not found for *O. vulgaris* from NWA, ECA, WCA, and PO, as well as for *O. maya* and *E. cirrhosa*. The attained concentrations for *O. vulgaris* from MS and NEA are in agreement with those previously reported by Passi et al.[8] (0.74 mg/100 g ww for *O. vulgaris* from MS), Nunes et al.[37] (0.73 mg/100 g ww for *O. vulgaris* from NEA), and Dias et al.[38] (0.78 mg/100 g ww for *O. vulgaris* consumed in Portugal with no indication of the geographical provenance). Villanueva and co-workers[36] characterized the vitamin E contents in the early life stages of *O. vulgaris* laboratory hatchlings and wild juveniles (9.2–14.2 g ww) from MS. They reported a much higher value (9.1 mg/100 g ww) possibly because vitamin E content seems to be higher in the early stages of cephalopods compared to adult stages and due to the fact that vitamin E was analyzed in whole octopus instead of in edible parts. It is known that digestive gland and gonads have higher contents of lipids than muscle parts.[10,14]

**Cholesterol.** Cephalopod consumption is usually associated with elevated cholesterol ingestion. Cholesterol plays an important role in cephalopods, with structural functions in cell membranes, and acts as a precursor of steroid hormones.[14] In opposition, and humans having the inherent ability to synthesize cholesterol, dietary cholesterol has been positively associated with low density lipoprotein (LDL) cholesterol and deleterious health outcomes. Therefore, in order to support adequately the data obtained from the nutritional point of view, the intra- and interspecific variability of the cholesterol concentrations in octopus edible tissues was also analyzed (Figure 4). Cholesterol mean content ranged from 85 ± 14

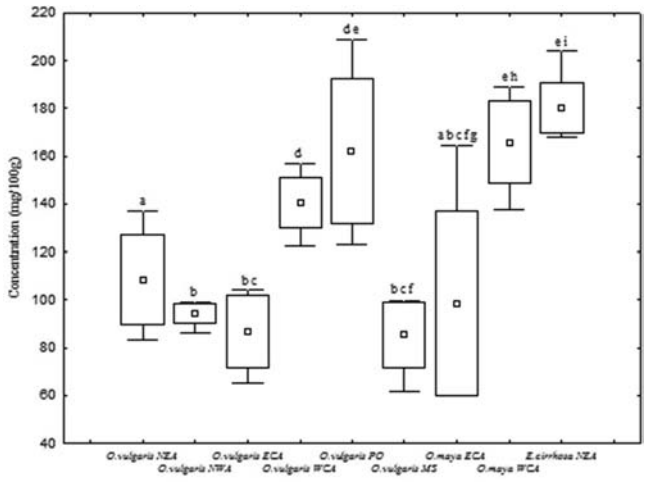


**Figure 4.** Cholesterol concentrations (□, mean; rectangles, mean ± standard deviation; bars above and below rectangles, range; mg/100 g wet weight) in the edible tissues of the characterized octopus species. Each letter (a−i) corresponds to a species and inherent origin (a, *O. vulgaris* from Northeast Atlantic Ocean (NEA); b, *O. vulgaris* from Northwest Atlantic Ocean (NWA); c, *O. vulgaris* from Eastern Central Atlantic Ocean (ECA); d, *O. vulgaris* from Western Central Atlantic Ocean (WCA); e, *O. vulgaris* from Pacific Ocean (PO); f, *O. vulgaris* from Mediterranean Sea (MS); g, *O. maya* from ECA; h, *O. maya* from WCA; i, *E. cirrhosa* from NEA). The same letters in a box plot indicate that the given means are not statistically different ($p > 0.05$).

mg/100 g ww for *O. vulgaris* from MS to 180 ± 11 mg/100 g ww for *E. cirrhosa* (Figure 4). This variability is highly interesting from the nutritional point of view indicating that one cannot classify all species and origins on the same basis regarding this parameter. Edible tissues of *O. vulgaris* from WCA (141 ± 11 mg/100 g ww) and from PO (162 ± 30 mg/100 g ww), *O. maya* from WCA (166 ± 17 mg/100 g ww), and *E. cirrhosa* from NEA exhibited significantly higher mean levels of cholesterol than the other species. Although some authors have concluded that cholesterol is not correlated with fat content (Oehlenschläger, 2006),[38] as confirmed in the present study, these species have all superior SFA and ω-6 PUFA amounts. In humans, some studies indicate that SFA as C16:0 and myristic acid (C14:0) raise blood cholesterol by decreasing LDL receptors that are responsible for cholesterol regulation.[4] *O. maya* from WCA and *E. cirrhosa* from NEA only exhibited similarity with *O. vulgaris* from PO ($p = 0.76$ and $p = 0.16$, respectively). The highest intravariability was observed for *O. maya* from ECA (65−164 mg/100 g ww), but the mean content (99 ± 39 mg/100 g ww) was not statistically different from those of *O. vulgaris* from NEA (109 ± 19 mg/100 g ww), from NWA (94 ± 4 mg/100 g ww), from ECA (87 ± 15 mg/100 g ww), and from MS (85 ± 14 mg/100 g ww).

There is limited information about cholesterol levels in octopus species. Data was found for only *E. cirrhosa*[14,25] and *O. vulgaris* from NEA[37,39] and from MS,[9,26,40,41] ranging from 64 mg/100 g ww[37] to 158 mg/100 g ww;[40]. Morillo-Velarde et al.[41] reported lower values in the muscle of *O. vulgaris* caught in the MS (31.6−62.2 mg/100 g ww) which may be explained by the fact that the individuals were analyzed after artificial feeding or absence of it (induced starvation of 4 days). Octopus natural preys are bivalves and crustaceans like shrimp, crab, and lobster,[3] all containing elevated cholesterol amounts. However, the food habits of octopuses are not completely known especially in the paralarva stage. According to Rosa et al.,[10] other factors, besides dietary, such as the demand during oogenesis and spermatogenesis, may affect the cholesterol content in cephalopods.

**Nutritional Assessment.** Although no specific data concerning octopus per capita consumption were found, cephalopod species are highly appreciated, particularly in Mediterranean and Asian countries. According to FAO,[1] in 2010 the average cephalopod intake varied widely worldwide, being 3.4 kg per capita per year in Portugal and reaching 6.5 kg per capita per year in Korea, of which octopuses represent an important part. Nowadays, there is clear evidence that the type of fat is more important in diminishing metabolic and cardiovascular disease risk than the total quantity of fat in the diet.[4] In addition, marine lipids are generally regarded as healthy, due to their high amounts of long chain PUFA, particularly EPA and DHA. Thus, to assess the potential health outcomes from the consumption of the characterized octopus species, the most important nutritional quality indexes were analyzed. Regarding the fatty acid composition, all the selected species had a favorable ω-3/ω-6 ratio, from 1.7 ± 0.5 to 9.2 ± 1.2 for *O. vulgaris* from WCA and NWA, respectively, 1.3 ± 0.2 to 2.2 ± 1.3 for *O. maya* from WCA and ECA, respectively; and 5.9 ± 0.7 for *E. cirrhosa* from NEA, confirming the importance of these species for ingestion of ω-3 PUFAs. The geographical provenance of *O. vulgaris* showed a marked influence on this ratio. A portion of 78 g (*E. cirrhosa* from NEA) to 321 g (*O. maya* from ECA) provides 250 mg of DHA + EPA, the daily recommended intake.[42] DHA and EPA are described as hypotriacylglycerolemic, antiarrhythmic, antiatherogenic, antithrombotic, and anti-inflammatory, being considered as protective agents against coronary heart diseases.[43] Also, the attained PUFA/SFA ratios are significantly higher (1.7 for *O. maya* from ECA to 2.2 for *E. cirrhosa* from NEA) than the recommended minimum of 0.45.[44]

The atherogenic and thrombogenic indexes, AI and TI, estimated on the basis of the fatty acid composition, are indicative of potential cardiovascular disease risk factors and therefore must be kept low. The fatty acid influence on cholesterol synthesis is also frequently estimated by the hypocholesterolemic/hypercholesterolemic (HH) index (Table 1). The AI attained mean (0.24 ± 0.03 (*O. maya* from WCA) to 0.31 ± 0.03 (*O. vulgaris* from ECA)) and TI from 0.14 ± 0.01 (*E. cirrhosa* from NEA) to 0.23 ± 0.06 (*O. maya* from ECA) can be considered favorable for the consumption of all species due to the cardioprotective effect of their MUFA and PUFA concentrations. Concerning the obtained HH index (3.3 ± 0.2 for *O. vulgaris* from ECA and NEA to 4.0 ± 0.6 for *O. maya* from WCA) high values are desired from a nutritional standpoint[24] since it estimates effects of specific fatty acids on cholesterol metabolism. *E. cirrhosa* from NEA and *O. maya* from WCA presented simultaneously the highest cholesterol amounts and the more protective HH indexes. Therefore, despite the elevated cholesterol amount in some species and origins, the octopus HH is protective from the nutritional point of view, balancing the potential health effects derived from cholesterol ingestion. These results constitute an added value for food consumption choices since these species are marketed at lower prices when compared with *O. vulgaris*.

Still, to exceed the guideline target of less than 300 mg/day established by the American Heart Association,[45] a portion of 20 to 25% of the whole collected specimens should be consumed corresponding to the entire individual for *E. cirrhosa*.


dx.doi.org/10.1021/jf502502b | J. Agric. Food Chem. 2014, 62, 8508−8517

The potential negative effects of dietary cholesterol are relatively small compared to those of SFA.[4] The SFA levels in octopus species are considerably lower than those of meat products (about 40%). Both SFA and cholesterol are unavoidable in omnivorous diets, and attempts to reduce intake completely would require significant changes to dietary patterns and introduce undesirable effects, such as inadequate intakes of micronutrients and protein.[4]

The reached AI, TI, and HH compare favorably in terms of nutritional evaluation with those determined for other cephalopods, such as squids[46] and common cuttlefish,[47] as well as for other worldwide consumed marine species (hake, silver and black scabbardfish, ray, angler, blackbelly rosefish, and megrim).[48,49]

Although existing at low concentrations in the studied species, vitamin E protects unsaturated fatty acids from peroxidation, preventing the formation of free radicals and subsequent health disorders.[35,50] The ingestion of a portion of 100 g of octopus will contribute to 2.0 (*O. maya* from ECA) to 10.7% (*O. vulgaris* from NWA) of the recommended dietary allowance (RDA) established for adult males and females (15 mg/day) by the Food and Nutrition Board of Institute of Medicine.[51]

**Principal Components Analysis.** PCA was applied as a pattern recognition technique to identify chemical descriptors for the selected species (Figure 5) or origins (Figure 1S, Supporting Information). PCA allowed explaining 93.8% of total data variance by using two principal components based on seven individual fatty acids (C18:1, C16:0, C22:6$\omega$-3, C22:5$\omega$-3, C20:5$\omega$-3, C22:4$\omega$-6, and C20:4$\omega$-6).

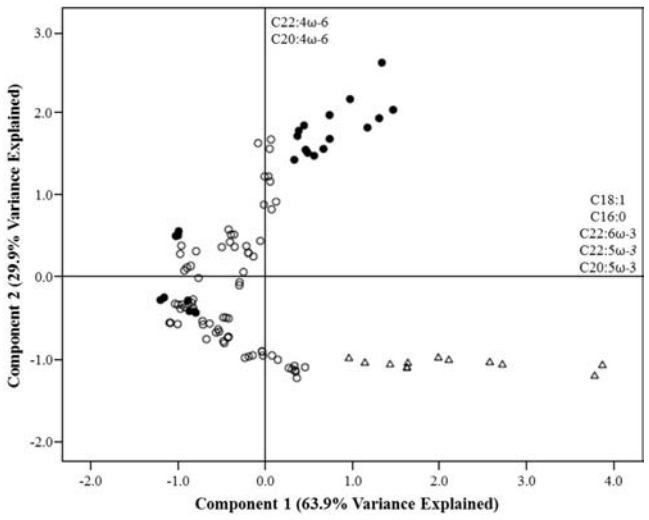


**Figure 5.** Principal components analysis of the characterized octopus species (○, *O. vulgaris*; ●, *O. maya*; and △, *E. cirrhosa*) based on concentrations of selected individual fatty acids (C18:1, C16:0, C22:6$\omega$-3, C22:5$\omega$-3, C20:5$\omega$-3, C22:4$\omega$-6, and C20:4$\omega$-6).

In Figure 5, three distinct octopus groups are represented corresponding to *O. vulgaris*, *O. maya*, and *E. cirrhosa* clusters. The first principal component factor (PC1), which comprises 63.9% of the total variance, is able to separate the three groups, being *O. maya* and *E. cirrhosa*, in general, located in the positive region, while *O. vulgaris* is positioned in the negative region. Still, some *O. maya* samples revealed greater similarities to those of *O. vulgaris*. All these may be justified by the fact that *O. maya* and *E. cirrhosa* samples, in general, reported higher figures for C18:1 (PC1 loading = 0.956), C16:0 (PC1 loading = 0.953), C22:6$\omega$-3 (PC1 loading = 0.933), C22:5$\omega$-3 (PC1 loading = 0.895), and C20:5$\omega$-3 (PC1 loading = 0.843) than *O. vulgaris* samples. The second component factor (PC2), which justifies 29.9% of the total variance observed, was able to separate at least *O. maya* from *E. cirrhosa*, which may be explain by the higher C22:4$\omega$-6 (PC2 loading = 0.937) and C20:4$\omega$-6 (PC2 loading = 0.910) content of the former. PCA was also tested to infer the oceanic origin of octopus species. Four main clusters corresponding to NEA, WCA, NWA, and PO/ECA/MS can be distinguished based on both components. NEA samples are characterized by lower C22:4$\omega$-6 and C20:4$\omega$-6 amounts than WCA samples. On the other hand, both of these oceans showed higher C18:1, C16:0, C22:6$\omega$-3, C22:5$\omega$-3, and C20:5$\omega$-3 contents than all the remaining ones. The observed results match the statistical differences observed in the fatty acids composition. Despite the difficulty of defining a biochemical profile representative of a specific species and oceanic area based on a limited number of individuals, the attained differentiation may be useful for authenticity control. It can be particularly relevant for mislabeling detection since *O. vulgaris* is usually highly rated on the market when compared with *O. maya* and *E. cirrhosa*. Prato and Biandolino[52] and Torrinha et al.[46] also applied successfully chemometric discrimination to cluster several marine organisms based on the most important fatty acids.

## ■ ASSOCIATED CONTENT

### Supporting Information

Figure depicting principal components analysis of the octopus oceanic origins. This material is available free of charge via the Internet at http://pubs.acs.org.

## ■ AUTHOR INFORMATION

### Corresponding Authors

*E-mail: sucasal@ff.up.pt. Phone: +351-2220428638. Fax: +351-226093390.

*E-mail: sbm@isep.ipp.pt. Phone: +351-228340500. Fax: +351-228321159.

### Funding

This work received financial support from the European Union (FEDER funds through COMPETE) and National Funds (FCT, Fundação para a Ciência e Tecnologia) through Projects PTDC/AGR-AAM/102316/2008 and Pest-C/EQB/LA0006/2013. The work also received financial support from the European Union (FEDER funds) under the framework of QREN through Project NORTE-07-0124-FEDER-000069.

### Notes

The authors declare no competing financial interest.

## ■ ACKNOWLEDGMENTS

To all financing sources the authors are greatly indebted.

## ■ ABBREVIATIONS USED

AI, atherogenic index; ARA, arachidonic acid; CDA, canonical discriminant analysis; DHA, docosahexaenoic acid; ECA, East Center Atlantic; EPA, eicosapentanoic acid; HH, hypocholesterolemic/hypercholesterolemic; MCS, mean canonical score; MS, Mediterranean sea; MUFA, monounsaturated fatty acids; NEA, Northeast Atlantic; NWA, Northwest Atlantic; PO, Pacific Ocean; PUFA, polyunsaturated fatty acids; RDA,

recommended dietary allowance; SFA, saturated fatty acids; TI, thrombogenic index; WCA, West Center Atlantic

## REFERENCES


(1) FAO. *1961−2010 Fish and fishery products: world apparent consumption statistics based on food balance sheets*; FAO Yearbook, Fishery and Aquaculture Statistics; Food and Agriculture Organization of the United Nations: Rome, 2013.

(2) Lourenço, D.; Silva, L. J. G.; Lino, C. M.; Morais, S.; Pena, A. SPE-LC-FD Determination of polycyclic aromatic hydrocarbon monohydroxy derivatives in cephalopods. *J. Agric. Food Chem.* **2014**, *62*, 2685−2691.

(3) FAO. *FAO Species Catalogue—Vol. 3 Cephalopods of the World*; FAO Fisheries Synopsis N. 125, Volume 3, 1984.

(4) US Department of Agriculture and US Department of Health and Human Services. *Report of the Dietary Guidelines Advisory Committee (DGAC) on the dietary guidelines for Americans, Part D. Section 3: Fatty Acids and cholesterol*; Washington, DC, 2010; pp 210−258. Available at: http://www.cnpp.usda.gov/DGAs2010-DGACReport.htm. Accessed on September 20th 2013.

(5) Estefanell, J.; Socorro, J.; Tuya, F.; Izquierdo, M.; Roo, J. Growth, protein retention and biochemical composition in *Octopus vulgaris* fed on different diets based on crustaceans and aquaculture by-products. *Aquaculture* **2011**, *322−323*, 91−98.

(6) Estefanell, J.; Roo, J.; Guirao, R.; Afonso, J.; Fernández-Palacios, H.; Izquierdo, M.; Socorro, J. Efficient utilization of dietary lipids in Octopus vulgaris (Cuvier 1797) fed fresh and agglutinated moist diets based on aquaculture by-products and low price trash species. *Aquacult. Res.* **2013**, *44*, 93−105.

(7) Ozogul, Y.; Duysak, O.; Ozogul, F.; Özkütük, A.; Türeli, C. Seasonal effects in the nutritional quality of the body structural tissue of cephalopods. *Food Chem.* **2008**, *108*, 847−852.

(8) Passi, S.; Ctaudell, S.; Di Marco, P.; De Simone, F.; Rastrelli, L. Fatty Acid Composition and Antioxidant Levels in Muscle Tissue of Different Mediterranean Marine Species of Fish and Shellfish. *J. Agric. Food Chem.* **2002**, *50*, 7314−7322.

(9) Karakoltsidis, P.; Zotos, A.; Constantinides, S. Composition of the commercially important Mediterranean finfish, Crustaceans and molluscs. *J. Food Compos. Anal.* **1995**, *8*, 258−273.

(10) Rosa, R.; Costa, P.; Nunes, M. Effect of sexual maturation on the tissue biochemical composition of *Octopus vulgaris* and *O. defilippi* (Mollusca: Cephalopoda). *Mar. Biol.* **2004**, *145*, 563−574.

(11) Rosa, R.; Nunes, L.; Reis, C. Seasonal changes in the biochemical composition of *Octopus vulgaris* Cuvier, 1797, from three areas of the Portuguese coast. *Bull. Mar. Sci.* **2002**, *71*, 739−751.

(12) Sieiro, M.; Aubourg, S.; Rocha, F. Seasonal study of the lipid composition in different tissues of the common octopus (*Octopus vulgaris*). *Eur. J. Lipid Sci. Technol.* **2006**, *108*, 479−487.

(13) Vaz-Pires, P.; Barbosa, A. Sensory, microbiological, physical and nutritional properties of iced whole common octopus (*Octopus vulgaris*). *Lebensm.-Wiss. Technol.* **2004**, *37*, 105−114.

(14) Rosa, R.; Costa, P.; Pereira, J.; Nunes, M. Biochemical dynamics of spermatogenesis and oogenesis in *Eledone cirrhosa* and *Eledone moschata* (Cephalopoda: Octopoda). *Comp. Biochem. Physiol., Part B* **2004**, *139*, 299−310.

(15) Noyola, J.; Mascaró, M.; Caamal-Monsreal, C.; Noreña-Barroso, E.; Díaz, F.; Re, D.; Sánchez, A.; Rosas, C. Effect of temperature on energetic balance and fatty acid composition of early juveniles of *Octopus maya*. *J. Exp. Mar. Biol. Ecol.* **2013**, *445*, 156−165.

(16) Morais, S.; Gomes, F.; Ramalhosa, M. J.; Delerue-Matos, C.; Oliveira, M. B. P. P. Occurrence of Polycyclic Aromatic Hydrocarbons in Cephalopods. In *Handbook of Polycyclic Aromatic Hydrocarbons: Chemistry, Occurrence and Health Issues*; Bandeira, G. C., Meneses, H. E., Eds.; Nova Science Publishers, Inc.: New York, 2013; pp 197−216.

(17) Pierce, G. J.; Valavanis, V. D.; Guerra, A.; Jereb, P.; Orsi-Relini, L.; Bellido, J. M.; Katara, I.; Piatkowski, U.; Pereira, J.; Balguerias, E.; Sobrino, I.; Lefkaditou, E.; Wang, J.; Santurtun, M.; Boyle, P. R.; Hastie, L. C.; Macleod, C. D.; Smith, J. M.; Viana, M.; González, A. F.; Zuur, A. F. A review of cephalopod−environment interactions in European Seas. *Hydrobiologia* **2008**, *612*, 49−70.

(18) Pecl, G. T.; Jackson, G. D. The potential impacts of climate change on inshore squid: biology, ecology and fisheries. *Rev. Fish Biol. Fish.* **2008**, *18*, 373−385.

(19) United States Environmental Protection Agency (USEPA). *Guidance for Assessing Chemical Contaminant Data for Use in Fish Advisories, Vol. 1, Fish Sampling and Analysis; EPA 823-B-00-007*, 3rd ed.; Office of Science and Technology: Washington, DC, 2000.

(20) European Commission. Regulation (EC) No 333/2007 of 28 March 2007 laying down the methods of sampling and analysis for the official control of the levels of lead, cadmium, mercury, inorganic tin, 3-MCPD and benzo(a)pyrene in foodstuffs. *Off. J. Eur. Union* **2007**, L 88/29.

(21) AOAC. *Official Methods of Analysis of AOAC International*, 18th ed.; AOAC International: Arlington, VA, 2007.

(22) Ramalhosa, M. J.; Paíga, P.; Morais, S.; Alves, M. R.; Delerue-Matos, C.; Oliveira, M. B. P. P. Lipid content of frozen fish: comparison of different extraction methods and variability during freezing storage. *Food Chem.* **2012**, *131*, 328−336.

(23) Cruz, R.; Casal, S.; Mendes, E.; Costa, A.; Santos, C.; Morais, S. Validation of a single-extraction procedure for sequential analysis of vitamin E, cholesterol, fatty acids, and total fat in seafood. *Food Anal. Methods* **2013**, *6*, 1196−1204.

(24) Guimarães, R. C. A.; Macedo, M. L. R.; Munhoz, C. L.; Filiu, W.; Viana, L. H.; Nozaki, V. T.; Hiane, P. A. Sesame and flaxseed oil: nutritional quality and effects on serum lipids and glucose in rats. *Food Sci. Technol. (Campinas)* **2013**, *33*, 209−217.

(25) Rosa, R.; Pereira, J.; Nunes, M. L. Biochemical composition of cephalopods with different life strategies with special reference to a giant squid *Architeuthis sp*. *Mar. Biol.* **2005**, *146*, 739−751.

(26) Valverde, J.; Hernández, M.; García-Garrido, S.; Rodríguez, C.; Estefanell, J.; Gairín, J.; Rodríguez, C.; Tomás, A.; García, B. Lipid classes from marine species and meals intended for cephalopod feeding. *Aquacult. Int.* **2012**, *20*, 71−89.

(27) Turner, N.; Hulbert, A.; Else, P. Sodium pump molecular activity and membrane lipid composition in two disparate ectotherms, and comparison with endotherms. *J. Comp. Physiol., B* **2005**, *175*, 77−85.

(28) Prato, E.; Portacci, G.; Biandolino, F. Effect of diet on growth performance, feed efficiency and nutritional composition of *Octopus vulgaris*. *Aquaculture* **2010**, *309*, 203−211.

(29) Çelik, M.; Diler, A.; Küçükgülmez, A. 2005. A comparison of the proximate compositions and fatty acid profiles of zander (*Sander lucioperca*) from two different regions and climatic conditions. *Food Chem.* **2005**, *92*, 637−641.

(30) Kaya, Y.; Erdem, M. E. Seasonal comparison of wild and farmed brown trout (*Salmo trutta forma fario* L., 1758): crude lipid, gonadosomatic index and fatty acids. *Int. J. Food Sci. Nutr.* **2009**, *60*, 413−423.

(31) Biandolino, F.; Portacci, G.; Prato, E. Influence of natural diet on growth and biochemical composition of Octopus vulgaris Cuvier, 1797. *Aquacult. Int.* **2010**, *18*, 1163−1175.

(32) Miliou, H.; Fintikaki, M.; Tzitzinakis, M.; Kountouris, T.; Verriopoulos, G. Fatty acid composition of the common octopus, *Octopus vulgaris*, in relation to rearing temperature and body weight. *Aquaculture* **2006**, *256*, 311−322.

(33) Navarro, J.; Villanueva, R. Lipid and fatty acid composition of early stages of cephalopods: an approach to their lipid requirements. *Aquaculture* **2000**, *183*, 161−177.

(34) Harris, K.; Fleming, J.; Kris-Etherton, P. Challenges in estimating omega-3 fatty acid content of seafood from US nutrient databases: A salmon case study. *J. Food Compos. Anal.* **2011**, *24*, 1168−1173.

(35) Kulawik, P.; Özogul, F.; Glew, R.; Özogul, Y. Significance of antioxidants for seafood safety and human health. *J. Agric. Food Chem.* **2013**, *61*, 475−491.

(36) Villanueva, R.; Escudero, J.; Deulofeu, R.; Bozzano, A.; Casoliva, C. Vitamin A and E content in early stages of cephalopods and their

dietary effects in Octopus vulgaris paralarvae. *Aquaculture* **2009**, *286*, 277−282.
(37) Nunes, M.; Bandarra, N.; Oliveira, L.; Batista, I.; Calhau, M. Composition and nutritional value of fishery products consumed in Portugal. In *Seafood research from fish to dish: quality, safety and processing of wild and farmed fish*; Luten, J. B., Jacobsen, C., Bekaert, K., Saebo, A., Oehlenschläger, J., Eds.; Wageningen Academic Publishers: Netherlands, 2006; pp 477−487.
(38) Dias, G.; Sánchez, V.; Bártolo, H.; Oliveira, L. Vitamin content of fish and fish products consumed in Portugal. *Electron. J. Environ., Agric. Food Chem.* **2003**, *2*, 510−513.
(39) Oehlenschläger, J. Cholesterol content in food, data from the last decade: a review. In *Seafood research from fish to dish: quality, safety and processing of wild and farmed fish*; Luten, J. B., Jacobsen, C., Bekaert, K., Saebo, A., Oehlenschläger, J., Eds.; Wageningen Academic Publishers: The Netherlands, 2006; pp 41−57.
(40) García-Garrido, S.; Hachero-Cruzado, I.; Garrido, D.; Rosas, C.; Domingues, P. Lipid composition of the mantle and digestive gland of *Octopus vulgaris* juveniles (Cuvier, 1797) exposed to prolonged starvation. *Aquacult. Int.* **2010**, *18*, 1223−1241.
(41) Morillo-Velarde, P. S.; Valverde, J. C.; Llinares, R. M. S.; García, B. G. Changes in lipid composition of different tissues of common octopus (*Octopus vulgaris*) during short-term starvation. *Aquacult. Res.* **2013**, *44*, 1177−1189.
(42) EFSA. EFSA panel on dietetic products, nutrition, and allergies (NDA); Scientific opinion on dietary reference values for fats, including saturated fatty acids, polyunsaturated fatty acids, monounsaturated fatty acids, trans fatty acids, and cholesterol. *EFSA J.* **2010**, *8*, 1461.
(43) Wijendran, V.; Hayes, K. C. Dietary n-6 and n-3 fatty acid balance and cardiovascular health. *Annu. Rev. Nutr.* **2004**, *24*, 597−615.
(44) Department of Health. *Nutritional aspects of cardiovascular disease: report on Health and social subjects*; HMSO: London, 1994.
(45) Lichtenstein, A. H.; Appel, L. J.; Brands, M.; Carnethon, M.; Daniels, S.; Franch, H. A.; Franklin, B.; Kris-Etherton, P. M.; Harris, W. S.; Howard, B.; Karanja, N.; Lefevre, M.; Rudel, L.; Sacks, F.; Horn, L. V.; Winston, M.; Wylie-Rosett, J. Diet and lifestyle recommendations revision 2006. A scientific statement from the American Heart Association nutrition committee. *Circulation* **2006**, *114*, 82−96.
(46) Torrinha, A.; Gomes, F.; Oliveira, M.; Cruz, R.; Mendes, E.; Delerue-Matos, C.; Casal, S.; Morais, S. Commercial squids: Characterization, assessment of potential health benefits/risks and discrimination based on mineral, lipid and vitamin E concentrations. *Food Chem. Toxicol.* **2014**, *67*, 44−56.
(47) Ayas, D.; Ozogul, Y.; Ozogul, I.; Uçar, Y. The effects of season and sex on fat, fatty acids and protein contents of Sepia officinalis in the northeastern Mediterranean Sea. *Int. J. Food Sci. Nutr.* **2012**, *63*, 440−445.
(48) Afonso, C.; Lourenço, H. M.; Cardoso, C.; Bandarra, N. M.; Carvalho, M. L.; Castro, M.; Nunes, M. L. From fish chemical characterization to the benefit-risk assessement − Part A. *Food Chem.* **2013**, *137*, 99−107.
(49) Afonso, C.; Cardoso, C.; Lourenço, H. M.; Anacleto, P.; Bandarra, N. M.; Carvalho, M. L.; Castro, M.; Nunes, M. L. Evaluation of hazards and benefits associated with the consumption of six fish species from the Portuguese coast. *J. Food Compos. Anal.* **2013**, *32*, 59−67.
(50) Maestre, R.; Pazos, M.; Medina, I. Role of the raw composition of pelagic fish muscle on the development of lipid oxidation and rancidity during storage. *J. Agric. Food Chem.* **2011**, *59*, 6284−6291.
(51) FNIC. *Dietary Reference Intakes (DRIs): Recommended Dietary Allowances and Adequate Intakes, Vitamins; Food and Nutrition Board*; Institute of Medicine, National Academy of Sciences: Washington, DC, 2010.
(52) Prato, E.; Biandolino, F. Total lipid content and fatty acid composition of commercially important fish species from the Mediterranean, Mar Grande Sea. *Food Chem.* **2012**, *131*, 1233−1239.

JOURNAL OF AGRICULTURAL AND FOOD CHEMISTRY

Article

pubs.acs.org/JAFC

# Thermally Induced Oxidative Decarboxylation of Copper Complexes of Amino Acids and Formation of Strecker Aldehyde

Ossanna Nashalian and Varoujan A. Yaylayan*

Department of Food Science and Agricultural Chemistry, McGill University, 21111 Lakeshore, Sainte Anne de Bellevue, Quebec H9X 3V9, Canada

**ABSTRACT:** In the Maillard reaction, independent degradations of amino acids play an important role in the generation of amino-acid-specific products, such as Strecker aldehydes or their Schiff bases. Such oxidative decarboxylation reactions are expected to be enhanced in the presence of metals. Preliminary studies performed through heating of alanine and various metal salts (Cu, Fe, Zn, and Ca) under pyrolytic conditions indicated that copper(II) and iron(III) because of their high oxidation potentials were the only metals able to induce oxidative decarboxylation of amino acids and formation of Strecker aldehyde or its derivatives as detected by gas chromatography/mass spectrometry. Furthermore, studies performed with synthetic alanine and glycine copper complexes indicated that they constituted the critical intermediates undergoing free-radical oxidative degradation, followed by the loss of carbon dioxide and the generation of Strecker aldehydes, which were detected either as stable Schiff base adducts or incorporated in moieties, such as pyrazine or pyridine derivatives.

**KEYWORDS:** *Strecker aldehydes, metal salts, amino acid metal complexes, oxidative decarboxylation of amino acids*

## INTRODUCTION

Metal salts, such as copper sulfate, are commonly found or added to foods for a variety of reasons. The corresponding metal complexes formed during processing with amino acids and sugars (Figure 1) or other Maillard reaction products[1] may alter their chemical reactivity during thermal treatment, generating or enhancing specific reaction products, such as those of oxidation or decomposition. Understanding how these independent complexes thermally degrade provides important insight into their fundamental behavior in the context of the Maillard reaction. Over the past few decades, the role of metal salts and their potential to affect the Maillard reaction has been studied by several researchers.[1−4] Considerable efforts have been expended to study the catalytic role of metal salts in promoting oxidation pathways and affecting the rates of the reaction in aqueous systems. Moreover, recently, it has been demonstrated that metal ions can accelerate the formation of specific Maillard reaction products, such as advanced glycosylation end product (AGE)-modified peptides.[5] On the other hand, the use of cations and their salts were explored in mitigation strategies in lowering or preventing the formation of certain Maillard reaction products, such as acrylamide, in both model systems involving asparagine and sugars and food models.[6,7] Although the exact mechanism of how metal ions can affect the Maillard reaction is still not clear, it has been proposed that metals increase the rate of the reaction because of their ability to oxidize Amadori compounds, accelerating the formation of melanoidins.[3] High-molecular-weight reductones have also been reported to form complexes with metal ions through polynuclear ligands.[1,3] Their ability to complex with amino acids, change the structural configurations of proteins, catalyze redox reactions, and act as Lewis acid catalysts by forming metal coordination complexes with sugars has also been reported.[8] Amino acids could be considered as prime targets for metal complex formation, and although the role of such complexes in the Maillard reaction has not been studied, enhancements in the Strecker aldehyde formation were reported in the presence of copper ions by Hofmann and Schieberle.[9] Furthermore, copper was found to catalyze the oxidative decarboxylation of a synthetic amino dioic acid in aqueous solution, converting it into an amino monocarboxylic acid.[10] Recently, Yablokov et al.[11] reported the kinetics of thermal degradation of copper complexes of several amino acids at 230 °C, indicating an oxidative degradation mechanism of the complex initiated with the formation of carboxylamine free radical, followed by the loss of carbon dioxide and the generation of alkylamine radicals and its recombination products. Furthermore, the rate constants for the thermal degradation reactions of various amino acid copper complexes were highly dependent upon the nature and bulkiness of their side chains, and rates of degradation of such amino acid complexes decreased in the following order: Ser > Phe > Leu > Ile > Val > Gly > Ala.

The objective of this study was to explore the thermal degradation of synthetic copper complexes of various amino acids, particularly alanine and glycine, and their degradations in the presence of various metal salts {iron(II) or iron(III) chlorides, zinc chloride, calcium chloride [two generally recognized as safe (GRAS) metal chloride salts], and copper(I) and (II) chlorides}. The chloride salts of metals were selected because of their ability to form more volatile chlorinated reaction products.[12] In this study, we explore the role of metal salts and amino acid metal complexes in the decomposition reactions of amino acids.

**Received:** June 9, 2014
**Revised:** July 30, 2014
**Accepted:** July 31, 2014
**Published:** July 31, 2014

ACS Publications © 2014 American Chemical Society



dx.doi.org/10.1021/jf502751n | J. Agric. Food Chem. 2014, 62, 8518−8523

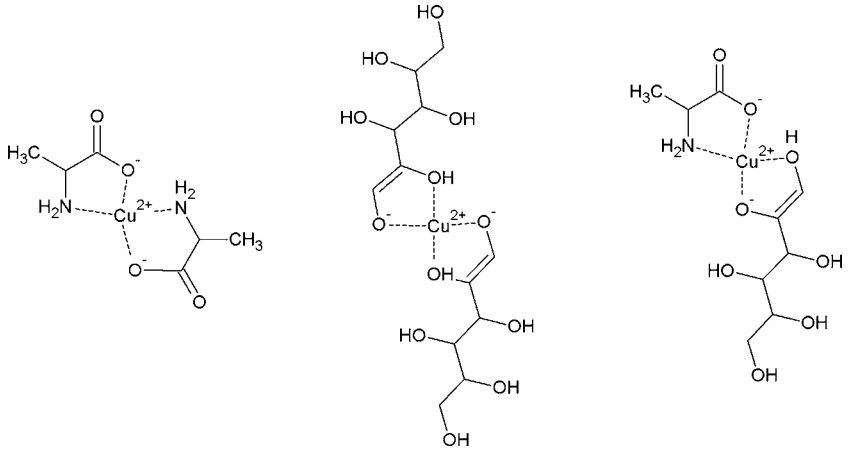

**Figure 1.** Possible complexes of copper with glucose and alanine.

## MATERIALS AND METHODS

**Materials and Reagents.** L-Alanine (99%), L-methionine (99%), L-leucine (99%), L-glycine (98%), copper(II) chloride ($CuCl_2$) (99.9%), copper(I) chloride (CuCl) (97%), calcium chloride ($CaCl_2$), zinc chloride ($ZnCl_2$) (98%), chloral hydrate (98%), 2-methylpyridine (98%), potassium hydroxide, D-glucose, and acetaldehyde (99.5%) were purchased from Sigma-Aldrich Chemical Co. (Oakville, Ontario, Canada). [$^{13}$C-1]Alanine (98%), [$^{13}$C-2]alanine (98%), [$^{13}$C-3]alanine (98%), [$^{15}$N]alanine, and [$^{13}$C-1, $^{13}$C-2]glycine (98%) were purchased from Cambridge Isotope Laboratories (Andover, MI).

**Preparation of Model Systems.** Model systems comprising of amino acids alone, amino acids with metal salts (in a 2:1 relative molar ratio), or synthetic amino acid metal complexes (see Table 1) were homogenized and mixed using a microscale porcelain mortar and pestle. After thorough homogenization, approximately 0.5 mg of the individual reactants or their mixtures were weighed into a quartz tube (0.3 mm thickness), plugged at both ends with glass wool (Supelco, Bellefonte, PA), inserted inside the coil probe, and pyrolyzed at 250 °C for 20 s under a helium atmosphere, as described below. All samples were analyzed in duplicate.

**Table 1. Composition of the Reactants in the Model Systems**

| amino acid[a] | metal salt | synthetic metal complex |
|---|---|---|
| alanine | $CuCl_2$/CuCl | $(Gly)_2Cu$ |
| glycine | $FeCl_2$/$FeCl_3$ | $(Ala)_2Cu$ |
| leucine | $ZnCl_2$ | (Gly)Cu(Ala) |
| methionine | $CaCl_2$ | |

[a]All of the listed amino acids were studied in the presence and absence of metal ions. The amino acids alanine and glycine were studied with all of the metal salts listed in the table and as synthetic metal complexes. Leucine and methionine were studied only with $CuCl_2$.

**Synthesis of Amino Acid–Metal Adducts.** Alanine–copper and glycine–copper complexes or mixed complexes were prepared by dissolving alanine (0.89 g), glycine (0.75 g), [$^{13}$C-1, $^{13}$C-2]glycine, or an equimolar mixture of alanine and glycine at room temperature in methanol (10 mL) in the presence of KOH (0.05 g) and stirred until all completely dissolved, followed by the addition of 0.5 mol of $CuCl_2$. The dark blue (with $CuCl_2$) precipitates were filtered, washed with methanol, and dried.

**Pyrolysis–Gas Chromatography/Mass Spectrometry (Py–GC/MS).** A Varian CP-3800 gas chromatograph coupled to a Saturn 2000 ion-trap detector interfaced to a CDS Pyroprobe 2000 unit through a valved interface (CDS 1500) was used for Py–GC/MS analysis of model systems shown in Table 1. The samples were packed in the quartz tube inserted inside the coil probe and pyrolyzed at 250 °C for 20 s under a helium atmosphere.

The separation was performed using a fused silica DB-5MS column (50 m length × 0.2 mm inner diameter × 33 μm film thickness). The GC method used for the analysis of the volatiles was as follows: The GC column flow rate was regulated by an electronic flow controller (EFC) and set at a pressure pulse of 55 psi for the first 3 min, then decreased to 32 psi at the rate of 300 psi/min, and finally, increased to 70 psi at a rate of 1.23 psi/min for the rest of the run. The GC oven temperature was set at −5 °C for first 5 min using $CO_2$ as the cryogenic cooling source and then increased to 50 °C at a rate of 50 °C/min. Then, the oven temperature was again increased to 270 °C at a rate of 8 °C/min and kept at 270 °C for 5 min. The samples were detected using an ion-trap mass spectrometer. The MS transfer-line temperature was set at 250 °C; the manifold temperature was set at 50 °C; and the ion-trap temperature was set at 175 °C. The ionization voltage of 70 eV was used, and electron multiplier voltage (EMV) was set at 2000 V. The generated data was analyzed using the AMDIS_32, version 2.69, computer software, and peak identification will be performed using the National Institute of Standards and Technology (NIST), version 2.0, mass spectral research program.

**Liquid Chromatography–Mass Spectrometry (LC–MS) Analysis of the Amino Acid–Copper Synthetic Adducts.** The dry samples were dissolved in deionized water (Millipore, Billerica, MA) to a concentration of 1 mL/mg. The sample was then diluted 10-fold in 10% methanol prior to analysis by LC–MS. The LC–electrospray ionization (ESI)–MS analysis comprised of a Dionex Ultimate 3000 RS liquid chromatograph (Dionex, Germering, Germany) coupled to a Bruker Maxis Impact quadruple-time-of-flight mass spectrometer (Bruker Daltonics, Bremen, Germany) in positive mode. A total of 1 μL of the sample was injected directly into LC–MS. The electrospray interphase settings were the following: nebulizer pressure, 0.6 bar; drying gas, 8 L/min; temperature, 180 °C; and capillary voltage, 4500 V. The scan range was from $m/z$ 100 to 1000. The data were analyzed using Bruker Compass DataAnalysis software, version 4.1.

**Structural Identification.** Specific reaction products (listed in Table 2) were identified by comparison of their retention times and mass spectra to commercial or *in-situ*-generated standards in addition to NIST library matches and stable isotope labeling data (Table 2). Elemental composition of selected metal complexes was based on their accurate mass determination by ESI–QqTOF analysis [alanine–copper complex at $m/z$ 261.9985 [M + Na] (calculated for $C_6H_{12}CuN_2NaO_4$ with an error of −1.4 ppm and glycine copper complex at $m/z$ 233.9665 [M + Na] (calculated for $C_4H_8N_2O_4CuNa$ with an error of 5.443 ppm].

## RESULTS AND DISCUSSION

Under the Maillard reaction conditions, independent degradation reactions of amino acids play an important role in the generation of amino-acid-specific products that result from thermal decarboxylation or oxidative decarboxylation (Figure


dx.doi.org/10.1021/jf502751n | J. Agric. Food Chem. 2014, 62, 8518–8523

**Table 2. Decomposition Products Observed in the Alanine−Copper Complex and Alanine $CuCl_2$ Mixtures**

| model system | structure | retention time[a] (min) | isotope incorporation |
|---|---|---|---|
| Alanine-$CuCl_2$ | 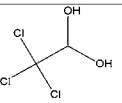 chloral hydrate | 10.2 (10.2) | 1 x C-2<br>1 x C-3<br>0 x N |
| Alanine-$CuCl_2$<br>Alanine-CuCl | 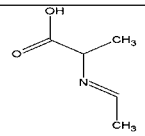 2-ethylideneamino propanoic acid[b] | 13.2 (13.2) | 1 x C-1<br>2 x C-2<br>2 x C-3<br>1 x N |
| Alanine-$CuCl_2$ | 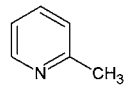 2-methylpyridine | 12.2 (12.2) | 3 x C-2<br>3 x C-3<br>1 x N |
| Alanine-$CuCl_2$ | 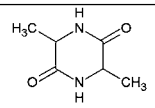 3,6-dimethyl piperazine-2,5-dione | 25.9 (25.9) | 2 x C-2<br>2 x C-3<br>2 x N |

[a]Values in parentheses represent those of the commercial or synthesized standards. [b]The *in situ* preparation of 2-ethylideneamino propanoic acid comprised 0.5 mg of alanine and 1 $\mu$L of acetaldehyde mixed and pyrolyzed under standard pyrolytic conditions.

2), leading to the formation of amines[13] and Strecker aldehydes captured as imines by the amino acid or its corresponding

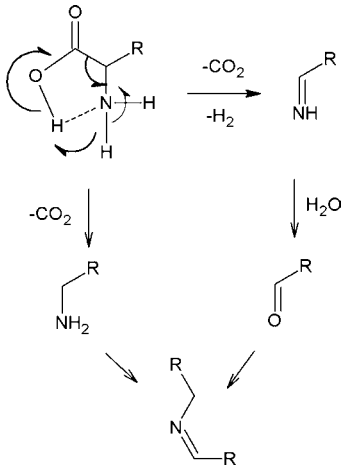


**Figure 2.** Proposed mechanism of thermally induced oxidative autodecarboxylation of amino acids.

amine.[14,15] Such oxidative decarboxylation reactions are expected to be enhanced in the presence of oxidizing species, such as copper,[10] and contribute to the pool of aroma-active aldehydes. On the other hand, oxidative decomposition of sugars leads to the formation of $\alpha$-dicarbonyl compounds, such as glucosone and deoxyglucosone, that can trigger the Strecker reaction of amino acids, producing even more Strecker aldehydes along with 2-aminocarbonyl compounds, the precursors of pyrazines. Currently, the relative contribution of the two pathways of generating Strecker aldehydes is not known in food products. Because of the importance of these aldehydes, enhancement of the pathways generating them could be a critical factor in flavor production and control. Because of the oxidative capacity of some metal salts, such as copper salts, it was predicted that, in their presence, the oxidative decarboxylation reactions could be encouraged. To understand metal−amino acid interactions and their influence on the production of specific reaction products, such as Strecker aldehydes, model systems containing amino acids were studied in the presence and absence of metal ions as both their free salts or synthesized amino acid−copper complexes (see Table 1). The purpose of the latter was to eliminate the effect of counterions, such as chlorides, and assess its importance as an intermediate.

Unlike other amino acids with longer side chains, such as leucine and methionine,[15] alanine when pyrolyzed in the absence of metal salts did not generate any significant amount of degradation products that could be observed under the experimental conditions. However, when the synthetic copper salt ($Ala_2Cu$) of alanine was pyrolyzed, a single major peak was observed that was characterized, resulting from the Schiff base formation between the intact alanine and its Strecker aldehyde (see Table 2). The same peak was also observed in the various copper and iron(III) salt/alanine mixtures along with other products. On the other hand, leucine and methionine in the absence of metal salts generated under pyrolytic conditions Schiff bases of Strecker aldehydes with their corresponding decarboxylated amino acids[15] (see Figure 2). Similarly, the formation of these Schiff bases was increased in the presence of copper salts. These observations clearly indicated that, although some amino acids can undergo thermally induced oxidative decarboxylation on their own and generate Strecker aldehydes, however, in the presence of copper or iron(III) salts, this ability is greatly facilitated or even accelerated by the formation of copper complexes.


dx.doi.org/10.1021/jf502751n | J. Agric. Food Chem. 2014, 62, 8518−8523

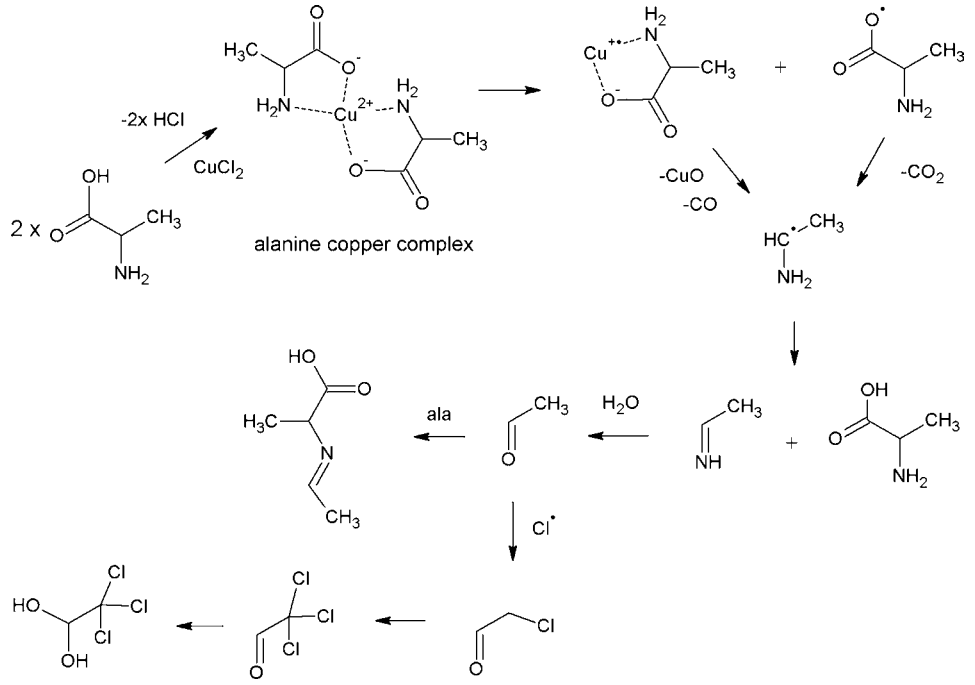


**Figure 3.** Proposed mechanism of copper-assisted thermal decarboxylation of alanine and acetaldehyde formation.

To confirm the generality of this observation, another amino acid glycine was chosen that behaves similar to alanine and does not undergo oxidative decarboxylation on its own. However, when glycine was pyrolyzed in the presence of copper salts or as its copper complex, it generated various Strecker aldehyde derivatives, such as pyrazines,[16] that were verified through NIST library searches and isotope-labeling studies using synthetic [$^{13}$C-1, $^{13}$C-2]glycine−copper complex, which generated pyrazine and two of its derivatives methyl- and 2,6-dimethyl pyrazines, incorporating four, five, and six glycine atoms, respectively. This label incorporation pattern was consistent with those reported by Guerra and Yaylayan.[16] Pyrazine and alkyl-substituted pyrazines can be formed through dimerization of azomethine ylides, which, in turn, can be formed from the Schiff base adducts of glycine and formaldehyde, the Strecker aldehyde of glycine. The same complex also generated 4-hydroxybutanal, the aldol product of two acetaldehyde molecules. Guerra and Yaylayan[16] also demonstrated that acetaldehyde can be generated from glycine and formaldehyde through a chain elongation reaction.

Although other metals, such as calcium and zinc, can also complex with amino acids, however, when copper or iron(III) chloride was replaced with calcium or zinc chlorides in the reaction mixtures, they did not promote Strecker aldehyde formation. This observation underlines the significance of the nature and reactivity of the metal ions in these complexes, considering that copper in its oxidation sate +2 and iron in its oxidation state +3 are known to have higher redox potentials compared to the other metals studied. The high redox potential enhances the electron affinity of copper, which, in turn, affects its reactivity and how easily it can accept and donate electrons.[17] In addition, the Lewis acid character of the metal ions also influences the stability of the complexes by forming metal−amino acid bonds with differing bond strengths depending upon the metal type, which, in turn, would affect their thermal dissociation capacity. On the other hand, when alanine was replaced with other amino acids, such as leucine and methionine, in the $CuCl_2$ reaction mixtures, similar enhancements in their corresponding Strecker aldehyde concentrations were observed relative to the model systems lacking $CuCl_2$ salts. Interestingly, when the mixed glycine/alanine copper complex (AlaCuGly) was analyzed, a significant enhancement in the formation of pyrroles, pyridines, and pyrazines relative to single amino acid complexes was observed. Furthermore, ethylamine and acetic acid were observed in iron(III) chloride/alanine model systems, in addition to the Schiff base adducts of Strecker aldehyde, indicating the ability of the iron to oxidize acetaldehyde and generate nitrogen-centered free radicals.

**Proposed Mechanism of Copper-Assisted Oxidative Decarboxylation of Alanine and Acetaldehyde Formation.** The analysis of the metal salt−alanine reaction products indicated that the influence of the metal ions on the thermal degradation profile of alanine was highly dependent upon the type of metal ion. Among the metal chloride salts investigated, CuCl, $CuCl_2$, and $FeCl_3$ were found to be the only salts that induced significant changes to the thermal degradation profile of alanine that could be observed under the experimental conditions, causing the generation of new products (see Table 2). The results pointed to the role of copper to be stoichiometric rather than catalytic, as supported by the generated products and their formation mechanism (see Figure 3). $CuCl_2$ can form stable complexes with 2 mol of alanine with the release of HCl, as shown in Figure 3, and the resulting complex can undergo thermal decomposition through an intramolecular redox reaction to generate a copper-centered radical cation and a carboxylamine radical.[11,18] Both products can be converted into the ethylamine radical, the former through the loss of CuO and CO and the latter through the thermal decarboxylation mechanism. A subsequent disproportionation reaction between the carboxylamine radical and ethylamine radical generates free alanine and ethanimine molecules. The hydrolysis of imine can lead to the formation of the Strecker aldehyde, which can immediately form a Schiff


dx.doi.org/10.1021/jf502751n | J. Agric. Food Chem. 2014, 62, 8518−8523

base adduct with the released free alanine, as shown in Figure 3. This identified adduct, which confirms the formation of both acetaldehyde and alanine, as predicted in the proposed mechanism, was the main product observed when the synthetic copper complex of alanine was pyrolyzed. The identity of this adduct was verified through comparison of its retention time to that of pyrolytically generated standard from alanine and acetaldehyde and through isotope-labeling experiments with [$^{13}$C-1]alanine, [$^{13}$C-2]alanine, [$^{13}$C-3]alanine, and [$^{15}$N]-alanine (see Table 2), in addition to its mass spectral fragmentation pattern, which was consistent with the proposed structure (see Figure 4). Further evidence for the release of free

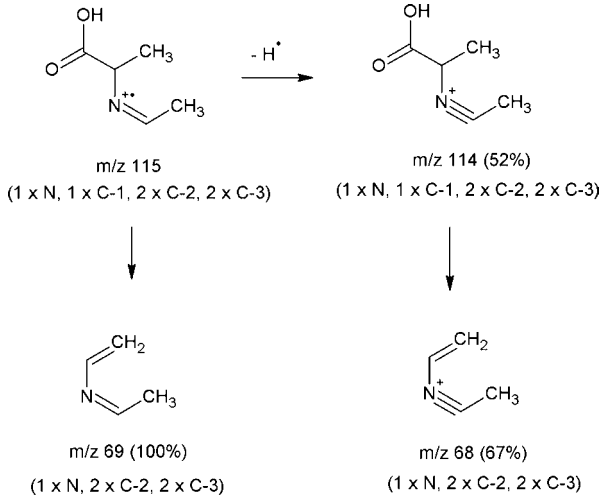


**Figure 4.** Mass spectral fragmentation patterns of 2-ethylidineamino propionic acid (values in parentheses represent the observed alanine atom incorporations).

alanine was the detection of 3,6-dimethyl piperazine-2,5-dione, as shown in Table 2. The same diketopiperazine was also observed in the alanine copper complexes analyzed at 270 °C by Yablokov et al.[11] On the other hand, the model systems containing chloride salts, such as $CuCl_2$, that can release HCl provided additional evidence for the formation of acetaldehyde because of the ability of HCl to chlorinate acetaldehyde and form chloral hydrate (Figure 3). The structure of chloral hydrate was confirmed by comparison of its mass spectrum and retention time to a commercially available standard (Table 2). Additionally, the labeling studies confirmed that chloral hydrate contains $^{13}$C-2 and $^{13}$C-3 atoms of alanine, while the number of chlorine atom incorporation was confirmed through its natural isotope abundance pattern. In addition to chloral hydrate, several chlorinated and non-chlorinated methylpyridines were also detected in $CuCl_2$–alanine model systems. Isotope-labeling studies have indicated that 2-methylpyridine incorporated three $^{13}$C-2, three $^{13}$C-3 atoms, and one nitrogen atom from alanine, implying an aldol-type condensation involving acetaldehyde and ethanimine, followed by cyclization (Figure 5). The mass spectra and retention time of 2-methylpyridine were further confirmed using a commercially available standard.

Copper(II) and iron(III) were found to be the most reactive metals that are able to complex with amino acids, promote their oxidative decarboxylation in a thermally induced free-radical pathway, and enhance the formation of important Strecker aldehydes. This ability was demonstrated when the amino acid was replaced with the alanine copper complex in a Maillard model system consisting of glucose and alanine. In this reaction system, the total intensity of ethyl-substituted pyrazines that incorporated $^{13}$C-2 atoms of alanine was increased by 10-fold compared to the total intensity of corresponding ethyl-substituted pyrazines in the glucose alanine model system, indicating enhanced production of the Strecker aldehyde acetaldehyde and its subsequent reaction with dihydropyrazines to generate various ethyl-substituted derivatives. With the absence of any toxicological evidence to prohibit their use as flavor-potentiating additives, these amino acid–metal complexes might provide a cost-effective way to enhance the flavor of heated foods. This pathway of generating Strecker aldehydes through thermal degradation of easily available metal–amino acid complexes in the absence of sugar-derived $\alpha$-dicarbonyl compounds can be considered a convenient strategy to introduce such aroma-active volatiles in foods lacking carbohydrates or a sugar source.

## AUTHOR INFORMATION

### Corresponding Author

*Telephone: 514-398-7918. Fax: 514-398-7977. E-mail: varoujan.yaylayan@mcgill.ca.

### Funding

The authors acknowledge funding for this research from the Natural Sciences and Engineering Research Council of Canada (NSERC).

### Notes

The authors declare no competing financial interest.

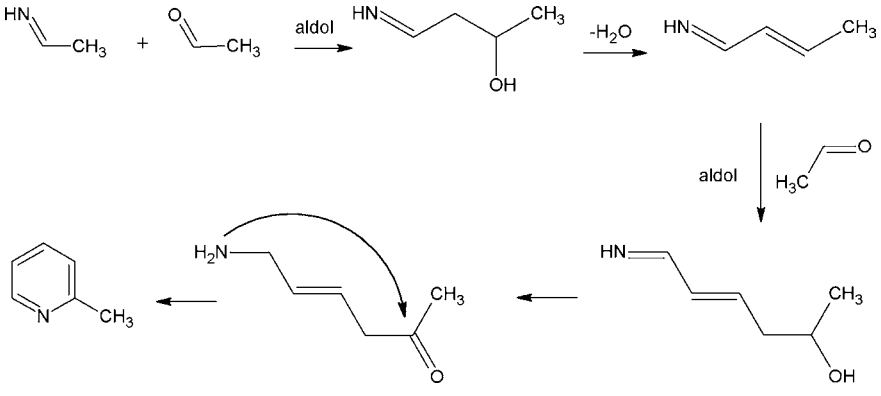


**Figure 5.** Proposed mechanism of 2-methylpyridine formation from acetaldehyde.

## REFERENCES


(1) O'Brien, J.; Morrissey, P. A. Metal ion complexation by products of the Maillard reaction. *Food Chem.* **1997**, *58*, 17−27.

(2) Kwak, E. J.; Lim, S. I. The effect of sugar, amino acid, metal ion, and NaCl on model Maillard reaction under pH control. *Amino Acids* **2004**, *27*, 85−90.

(3) Ramonaitytė, D. T.; Keršienė, M.; Adams, A.; Tehrani, K. A.; Kimpe, N. D. The interaction of metal ions with Maillard reaction products in a lactose−glycine model system. *Food Res. Int.* **2009**, *42*, 331−336.

(4) Rendleman, J. A., Jr.; Inglett, G. E. The influence of $Cu^{2+}$ in the Maillard reaction. *Carbohydr. Res.* **1990**, *201*, 311−326.

(5) Frolov, A.; Schmidt, R.; Spiller, S.; Greifenhagen, U.; Hoffmann, R. Arginine-derived advanced glycation end products generated in peptide−glucose mixtures during boiling. *J. Agric. Food Chem.* **2014**, *62*, 3626−3635.

(6) Gökmen, V.; Şenyuva, H. Z. Acrylamide formation is prevented by divalent cations during the Maillard reaction. *Food Chem.* **2007**, *103*, 196−203.

(7) Sadd, P. A.; Hamlet, C. G.; Liang, L. Effectiveness of methods for reducing acrylamide in bakery products. *J. Agric. Food Chem.* **2008**, *56*, 6154−6161.

(8) Choudhary, V.; Mushrif, S. H.; Ho, C.; Anderko, A.; Nikolakis, V.; Marinkovic, N. S.; Frenkel, A. I.; Sandler, S. I.; Vlachos, D. G. Insights into the interplay of Lewis and Brønsted acid catalysts in glucose and fructose conversion to 5-(hydroxymethyl)furfural and levulinic acid in aqueous media. *J. Am. Chem. Soc.* **2013**, *135*, 3997−4006.

(9) Hofmann, T.; Schieberle, P. Formation of aroma-active Strecker-aldehydes by a direct oxidative degradation of Amadori compounds. *J. Agric. Food Chem.* **2000**, *48*, 4301−4305.

(10) Fitzpatrick, J. H.; Hopgood, D. Metal ion catalyzed decarboxylation. Kinetics and mechanism of the oxidative decarboxylation of copper (II) complexes of aminomalonic acid in aqueous solution. *Inorg. Chem.* **1974**, *13*, 568−574.

(11) Yablokov, V. A.; Smeltsova, I. L.; Faerman, V. I. Kinetics of heat-induced transformation of copper complexes with amino acids. *Russ. J. Gen. Chem.* **2014**, *84*, 568−570.

(12) Troise, A. D.; Fogliano, V. Reactants encapsulation and Maillard reaction. *Trends Food Sci. Technol.* **2013**, *33*, 63−74.

(13) Moldoveanu, S. C. Pyrolysis of organic molecules with applications to health and environmental issues. In *Techniques and Instrumentation in Analytical Chemistry*; Serban, C. M., Ed.; Elsevier: Amstersdam, Netherlands, 2010; Vol. *28*, pp 527−578.

(14) Yaylayan, V. A. Recent advances in the chemistry of Strecker degradation and Amadori rearrangement: Implications to aroma and color formation. *Food Sci. Technol. Res.* **2003**, *9*, 1−6.

(15) Yaylayan, V. A.; Keyhani, A. Carbohydrate and amino acid degradation pathways in L-methionine/D-[$^{13}$C] glucose model systems. *J. Agric. Food Chem.* **2001**, *49*, 800−803.

(16) Guerra, P. V.; Yaylayan, V. A. Dimerization of azomethine ylides: An alternate route to pyrazine formation in the Maillard reaction. *J. Agric. Food Chem.* **2010**, *58*, 12523−12529.

(17) Bishop, K. C. Transition metal catalyzed rearrangements of small ring organic molecules. *Chem. Rev.* **1976**, *76*, 461−486.

(18) Shelkovnikov, V. V.; Yeroshkin, V. I. Two-stagedness of thermal decomposition of copper glycinate. *Izv. Sib. Otd. Akad. Nauk SSSR, Ser. Khim. Nauk* **1985**, *11*, 86−93.

JOURNAL OF AGRICULTURAL AND FOOD CHEMISTRY

Article

pubs.acs.org/JAFC

# Isotope-Labeling Studies on the Formation Pathway of Acrolein during Heat Processing of Oils

Alice Ewert,[†] Michael Granvogl,[‡] and Peter Schieberle*[,†,‡]

[†]Deutsche Forschungsanstalt für Lebensmittelchemie and

[‡]Lehrstuhl für Lebensmittelchemie, Technische Universität München, Lise-Meitner-Straße 34, D-85354 Freising, Germany

**ABSTRACT:** Acrolein (2-propenal) is classified as a foodborne toxicant and was shown to be present in significant amounts in heated edible oils. Up to now, its formation was mainly suggested to be from the glycerol part of triacylglycerides, although a clear influence of the unsaturation of the fatty acid moiety was also obvious in previous studies. To unequivocally clarify the role of the glycerol and the fatty acid parts in acrolein formation, two series of labeled triacylglycerides were synthesized: [$^{13}C_3$]-triacylglycerides of stearic, oleic, linoleic, and linolenic acid and [$^{13}C_{54}$]-triacylglycerides with labeled stearic, oleic, and linoleic acid, but with unlabeled glycerol. Heating of each of the seven intermediates singly in silicon oil and measurement of the formed amounts of labeled and unlabeled acrolein clearly proved the fatty acid backbone as the key precursor structure. Enzymatically synthesized pure linoleic acid and linolenic acid hydroperoxides were shown to be the key intermediates in acrolein formation, thus allowing the discussion of a radical-induced reaction pathway leading to the formation of the aldehyde. Surprisingly, although several oils contained high amounts of acrolein after heating, deep-fried foods themselves, such as donuts or French fries, were low in the aldehyde.

**KEYWORDS:** *Acrolein, foodborne toxicant, frying, fatty acid hydroperoxides, labeling studies*

## INTRODUCTION

Acrolein (2-propenal) is a highly reactive aldehyde commonly formed by incomplete combustion of organic material. Thus, the aldehyde has been found in cigarette smoke, fireplaces, incense, candles, and fuels.[1−4] Furthermore, acrolein has been detected in the exhaust of kitchens and thermally processed cooking oils[5−10] as well as in biological samples.[11,12]

Acrolein has been classified by the U.S. Environmental Protection Agency (EPA) as a pulmonary toxicant and is among the air toxicants posing the greatest health risk.[13−18] Its toxicity is related to a reaction with, for example, the sulfhydryl group of cysteine in proteins and glutathione, leading to interferences in the intermediary cell metabolism and to modified proteins by introducing inter- and intramolecular cross-links.[8,19,20] Furthermore, administration of acrolein to rats decreased lung and liver levels of glutathione, ascorbic acid, and $\alpha$-tocopherol.[21] In addition, acrolein has been reported to induce the generation of oxygen radicals[22,23] and has been associated with several illnesses, such as atherosclerosis,[24] Alzheimer's disease,[25] and cancer.[26,27]

Despite extensive toxicological studies, data on the formation pathway of acrolein from food constituents are scarcely available in the literature. Presently, two published major hypotheses can be found: acrolein may be generated by either partial hydrolysis of triacylglycerides, followed by dehydration of liberated glycerol to acrolein,[28,29] or, in particular, a degradation of the unsaturated fatty acid backbone.[7,30] Fujisaki et al.[26] showed that the amount of acrolein in processed oil was well correlated with the experimental oxygen concentration (2−20%) in the air, and Bastos and Pereira[31] observed a clear increase of acrolein during oil processing in the presence of metal ions, suggesting that hydroperoxide formation is involved.

Umano and Shibamoto[7] assumed the necessity of free fatty acids for acrolein formation, and acrolein generation was suggested from linolenic acid via its 13-hydroperoxide as key intermediate.[10] Esterbauer et al.[32] proposed that acrolein originates from the center of the fatty acid chain involving $\beta$-cleavage of the 9-hydroperoxide. However, this formation mechanism needs $\omega$-3 or $\omega$-6 fatty acids, respectively, as precursors, but it remains unclear how acrolein can also be generated from, for example, oleic acid. The ability of free fatty acids as well as their esters to generate acrolein was also observed by Tamura et al.[33] as well as by Pan et al.[34]

Recently, it was shown by our group that the amount of acrolein generated during heat processing of different edible fats and oils was well correlated with the content of unsaturated fatty acids in the oil sample.[6] However, the reaction pathway leading to acrolein from triacylglycerides is still unclear. Thus, the objectives of this study were, first, to identify the most efficient precursor structures using several $^{13}C$-labeled triacylglycerides as well as unlabeled fatty acid hydroperoxides in a model system with silicon oil, and, second, to quantitate acrolein in different types of fried foods and to correlate the amounts with the concentrations present in the frying oil.

## MATERIALS AND METHODS

*CAUTION:* Acrolein, as well as [$^{13}C_3$]-acrolein, is classified as toxic and may cause cancer. Be careful when handling these chemicals.

**Food Samples.** Vegetable oils, potato chips, precooked French fries, and donuts were purchased in local supermarkets.

Received: March 31, 2014
Revised: July 2, 2014
Accepted: July 4, 2014
Published: July 4, 2014

ACS Publications © 2014 American Chemical Society

**Chemicals.** [$^{13}C_3$]-Acrolein was obtained from Isotec Stable Isotopes (St. Louis, MO), and acrolein and dicyclohexyl carbodiimide were from Fluka (Steinheim, Germany). Glycerol, stearic acid, oleic acid, $\alpha$-linoleic acid, $\alpha$-linolenic acid, [$^{13}C_3$]-glycerol, [$^{13}C_{18}$]-stearic acid, [$^{13}C_{18}$]-oleic acid, [$^{13}C_{18}$]-linoleic acid, 4-(dimethylamino)-pyridine, soybean lipoxygenase type I, and xylenol orange were obtained from Sigma-Aldrich (Taufkirchen, Germany). L-Ascorbic acid, D,L-*all-rac*-$\alpha$-tocopherol, silicon oil, sulfuric acid (96%), and ferrous ammonium sulfate hexahydrate were from VWR International (Darmstadt, Germany). Silica gel (230−400 mesh, grade 60) and LiChroprep Diol (40−63 $\mu$m) were from Merck (Darmstadt). Argon, oxygen, and liquid nitrogen were obtained from Linde (Munich, Germany). All other reagents were of analytical grade.

**Synthesis of $^{13}$C-Labeled Triacylglycerides.** The glycerides were prepared according to a general procedure published previously.[35] Either unlabeled glycerol (0.15 mmol) was reacted with each of the carbon-13 labeled fatty acids (0.5 mmol), or [$^{13}C_3$]-glycerol was reacted with each of the unlabeled fatty acids dissolved in dichloromethane (2.5 mL) under an argon atmosphere. The solution was stirred and cooled to 0 °C while dicyclohexyl carbodiimide (0.75 mmol) and 4-(dimethylamino)pyridine (0.05 mmol) were added within 5 min. The reaction mixture was stirred for 3 h at room temperature, and the dicyclohexyl urea formed was removed by filtration. After extraction with hydrochloric acid (0.5 mol/L; total volume = 40 mL) and an aqueous saturated sodium bicarbonate solution (total volume = 40 mL), the organic phase was dried over anhydrous sodium sulfate and concentrated to a final volume of ∼1 mL using a rotary evaporator. The crude product obtained was purified by column chromatography (220 mm × 22 mm i.d.) on silica gel (230−400 mesh, grade 60). Elution was performed with dichloromethane/*n*-pentane (8:2; v/v). Structures of the seven target compounds were confirmed by LC-MS in positive atmospheric pressure chemical ionization (APCI$^+$) mode as well as by $^1$H and $^{13}$C NMR spectroscopy ([$^{13}C_3$]-labeled compounds). Yields of synthesized $^{13}$C-labeled triacylglycerides were determined by LC-MS (APCI$^+$) and calculated from external five-point calibration curves using defined triacylglyceride solutions. Reference solutions were prepared in dichloromethane from a stock solution (5 mg/mL) in the concentration range between 10 and 200 $\mu$g/mL.

**Analytical Data of the Synthesized Triacylglycerides.** *[$^{13}C_3$]-Glyceryl tristearate:* MS-APCI$^+$, *m/z* (%) 611.3 (100), 551.3 (30), 648.9 (15), 895.4 ([M + H]$^+$; 10).

$^1$H NMR (400 MHz; $CDCl_3$; 298 K): $\delta$ 0.90 (t, 7.0 Hz, H-C18′/H-C18″), 1.21−1.39 (m, H-C4′−H-C17′/H-C4″−H-C17″), 1.55−1.70 (m, H-C3′/H-C3″), 2.33 (t, 7.6 Hz, H-C2′), 2.34 (t, 7.5 Hz, H-C2″), 4.17 (dm, 145.6 Hz, $H_a$-C1), 4.23 (dm, 148.3 Hz, $H_b$-C1), 5.29 (dm, 149.2 Hz, H-C2). Numbering of carbon atoms refers to Figure 1.

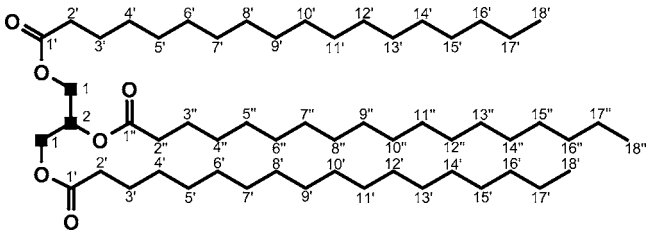

**Figure 1.** Structure of [$^{13}C_3$]-labeled glyceryl tristearate. (■) $^{13}$C-labeling.

$^{13}$C NMR (100 MHz; $CDCl_3$; 298 K): $\delta$ 14.1 (C18′/C18″), 22.7 (C17′/C17″), 24.88 (C3′), 24.92 (C-3″), 29.0-29.9 (C4′-C15′/C4″-C15″), 31.9 (C16′/C16″), 34.1 (C2′), 34.2 (C2″), 62.1 (d, 43.6 Hz, C1), 68.9 (t, 43.3 Hz, C2), 172.9 (C1″), 173.3 (C1′).

*[$^{13}C_{54}$]-Glyceryl tristearate:* MS-APCI$^+$, *m/z* (%) 643.3 (100), 579.3 (30), 880.3 (15), 946.3 ([M + H]$^+$; 10).

*[$^{13}C_3$]-Glyceryl trioleate:* MS-APCI$^+$, *m/z* (%) 888.9 ([M + H]$^+$; 100), 606.8 (30), 270.0 (30), 551.2 (30), 458.0 (25), 523.2 (20), 663.3 (20), 796.3 (10).

*[$^{13}C_{54}$]-Glyceryl trioleate:* MS-APCI$^+$, *m/z* (%) 940.6 ([M + H]$^+$; 100), 639.5 (35), 663.2 (30), 439.2 (25), 383.2 (15), 523.3 (10).

*[$^{13}C_3$]-Glyceryl trilinoleate:* MS-APCI$^+$, *m/z* (%) 883.4 ([M + H]$^+$; 100), 620.2 (25), 602.0 (20), 390.9 (15), 278.9 (10).

*[$^{13}C_{54}$]-Glyceryl trilinoleate.* MS-APCI$^+$, *m/z* (%) 934.6 ([M + H]$^+$; 100), 635.5 (35), 600.3 (10).

*[$^{13}C_3$]-Glyceryl trilinolenate:* MS-APCI$^+$, *m/z* (%) 877.3 ([M + H]$^+$; 100), 739.3 (50), 598.3 (20), 321.4 (10), 472.5 (10).

**Preparation of Hydroperoxides.** Fatty acid hydroperoxides were prepared as previously described.[36] Either linoleic acid or linolenic acid (200 mg each) was treated with soybean lipoxygenase type I (4 mg) for 60 min under an atmosphere of pure oxygen at room temperature. Separation of the hydroperoxides from the residual fatty acids was performed by means of preparative flash-column chromatography using a LiChroprep Diol stationary phase and *n*-hexane/2-propanol/methanol/water (900:50:2:1; v/v/v/v) as the mobile phase. Due to the high regio- and stereospecifity of LOX I (94−97% of 13-hydroperoxy-(*Z*,*E*)-9,11-octadienoic acid), no further separation of the isomers was needed.[37] The 13-hydroperoxides were identified by LC-MS (APCI$^+$). Quantitation of the fatty acid hydroperoxides was performed photometrically.[38]

*13-Hydroperoxy-(Z,E)-9,11-octadecadienoic acid:* MS-APCI$^+$, *m/z* (%) 279.9 (100), 294.9 (50), 207.0 (40), 313.0 ([M + H]$^+$; 35), 608.2 (30), 625.3 (25), 592.2 (20), 349.1 (20).

*13-Hydroperoxy-(Z,E,Z)-9,11,15-octadecatrienoic acid:* MS-APCI$^+$, *m/z* (%) 311.1 ([M + H]$^+$; 100), 277.8 (60), 293.1 (60), 603.5 (40), 587.6 (20), 621.4 (10).

**Heating of Oils.** Rapeseed oil (100 g) or a commercial frying fat (100 g) was mixed either with D,L-*all-rac*-$\alpha$-tocopherol (100 mg) or with L-ascorbic acid (100 mg; finely powdered, forming a suspension), respectively, before heat treatment. For comparison, rapeseed oil or the frying fat was analyzed without antioxidants. All samples were heated at 180 °C for 4 h.

**Degradation of Labeled Triacylglycerides or Monohydroperoxides.** Silicon oil (5 mL) was mixed singly either with each of the isotopically labeled triacylglycerides or with the hydroperoxides as well as with the respective free fatty acids (20 mg each). A control experiment was performed by heating silicon oil without any additives to prove the absence of signals and background interferences within the mass traces of acrolein (*m/z* 57 in chemical ionization (CI) mode) or [$^{13}C_3$]-acrolein (*m/z* 60), respectively. Samples were heated at 140 °C for 4 h under continuous stirring in closed glass vessels in a thermocontrolled metal block.

**Preparation of Food and Frying.** *Donuts.* Yeast (42 g) was suspended in warm water, and wheat flour (500 g), whole milk (150 mL), sugar (50 g), eggs (100 g), and water (25 mL) were added to obtain a homogeneous dough, which was divided into pieces of about 50 g and stored at 30 °C for 2 h before frying.

*Different foods (potato chips, precooked French fries, and donuts)* were fried at 180 °C either in rapeseed oil, in safflower oil, or in a commercial frying fat: potato chips (peeled, 1.5 mm of cross section) for 2 min, French fries for 3.5 min, and donuts for 6 min. To provide similar reaction conditions, the first five batches of the respective fried foods were discarded, and only the sixth batch was used for analysis. The frying process (100 g of each food) was carried out in a DF320 Kenwood deep-fryer (Heusenstamm, Germany) containing 2.3 L of oil, which was preheated for 10 min prior to frying.

**Quantitation of Acrolein.** *Model System with Antioxidants, Free Fatty Acids, and Hydroperoxides.* Immediately after cooling to room temperature, the internal standard [$^{13}C_3$]-acrolein (dissolved in dichloromethane; 1−214 $\mu$g, depending on the amounts determined in preliminary experiments) was added to an aliquot of each sample (5 g). The sample was vortexed (1 min) and ultrasonified (5 min), and aliquots (1 g) were weighed into gastight headspace vials (20 mL), which were immediately capped and stirred for 20 min at room temperature prior to headspace GC-MS measurement (CI mode) as recently described.[6]

*Model System with Labeled Triacylglycerides.* Quantitation was performed by preparing acrolein standards in dichloromethane from a stock solution (1.372 mg/mL) in the concentration range from 1 to

500 μg acrolein/mL containing a fixed amount of internal standard (10 μg/mL). Calibration curves were newly prepared prior to each measurement and showed good-quality fit ($r^2 > 0.993$).

For acrolein quantitation in foods, the material was frozen in liquid nitrogen and ground with a laboratory mill. Aliquots (5 g) were weighed into gastight headspace vials (100 mL) containing silicon oil (30 mL). After addition of [$^{13}C_3$]-acrolein (100 ng), the vials were immediately capped, and the suspensions were stirred for 20 min at 30 °C prior to headspace GC-MS measurement (CI mode) as recently described.[6]

**High-Performance Liquid Chromatography–Mass Spectrometry (HPLC-MS).** Mass spectrometry was performed by means of an LCQ ion trap mass spectrometer connected to an SCM 1000 high-performance liquid chromatography system (both Finnigan MAT, Bremen, Germany) equipped with a 150 mm × 2.0 mm i.d., 4 μm Synergi Polar RP 80 Å column kept at 30 °C and connected to a 4 mm × 2.0 mm i.d. polar RP precolumn (both Phenomenex, Aschaffenburg, Germany). Elution was done isocratically using a mixture of *n*-hexane/2-propanol/methanol/water (900:50:2:1; v/v/v/v). Flow rate was set at 0.8 mL/min, and injection volume was 50 μL. Analytes were detected in full scan using APCI$^+$ mode. The sheath and auxiliary gas nitrogen nebulized the effluent with flows of 80 and 20 arb, respectively. Further parameters were the following: discharge current, 5 μA; vaporizer temperature, 400 °C; heated capillary temperature, 200 °C; capillary voltage, 4 V; and tube lens offset, 30 V. The ion trap operated at a helium pressure of $1.3 \times 10^{-4}$ kPa.

**Nuclear Magnetic Resonance (NMR) Spectroscopy.** $^1$H and $^{13}$C NMR spectra were recorded using a 400 MHz DRX spectrometer (Bruker, Rheinstetten, Germany). Sample was dissolved in deuterated chloroform ($CDCl_3$; 0.7 mL), and chemical shifts ($^1$H NMR) were determined using either tetramethylsilane (0.03%) as the internal standard or the carbon signal of $CDCl_3$ at 77.0 ppm ($^{13}$C NMR), respectively.

## RESULTS AND DISCUSSION

**Model Studies.** *Effect of Antioxidants on Acrolein Formation.* To check if a radical mechanism is involved in acrolein generation, in a first series of experiments, the antioxidant α-tocopherol or L-ascorbic acid was singly added to rapeseed oil as well as to a commercial frying fat before heating. The oils were selected on the basis of their different fatty acid compositions: the frying fat consisted of >50% of saturated fatty acids, whereas rapeseed oil mainly consisted of unsaturated fatty acids. Compared to the samples heated without antioxidant addition (expt 3) (Table 1), in the presence of both antioxidants, acrolein formation was strongly reduced during heating, although to a lesser extent in the frying fat (expts 1 and 2) (Table 1). In the presence of α-tocopherol, which was the more effective antioxidant, acrolein concentration in rapeseed oil was reduced to ∼15% compared to the oil heated without the antioxidant. The results supported data on wok-cooking[19] indicating that acrolein emissions were reduced when the antioxidant BHA was added to the cooking oil. The more effective reduction of acrolein found for α-tocopherol in comparison to L-ascorbic acid might be explained by the better solubility of α-tocopherol in the fatty matrix. On the basis of these results, it can be assumed that acrolein generation in oils involves a radical-induced degradation of the triacylglycerides.

**Table 1. Amounts of Acrolein Formed by Heating of Rapeseed Oil and a Common Frying Fat at 180 °C for 4 h in the Presence or Absence of Antioxidants**

| | | concn (mg/kg)[a] in | |
|---|---|---|---|
| expt | additive | rapeseed oil | frying fat |
| 1 | α-tocopherol[b] | 9.8 (7.6–12.1) | 19.6 (17.8–21.4) |
| 2 | ascorbic acid[b] | 16.9 (15.8–17.1) | 35.4 (33.4–37.6) |
| 3 | without[c] | 67.5 (63.2–69.7) | 51.8 (48.9–53.1) |

[a]Mean values of three independent experiments. Concentration ranges in parentheses. [b]100 mg per 100 g of oil and fat. [c]Control experiment without antioxidant addition.

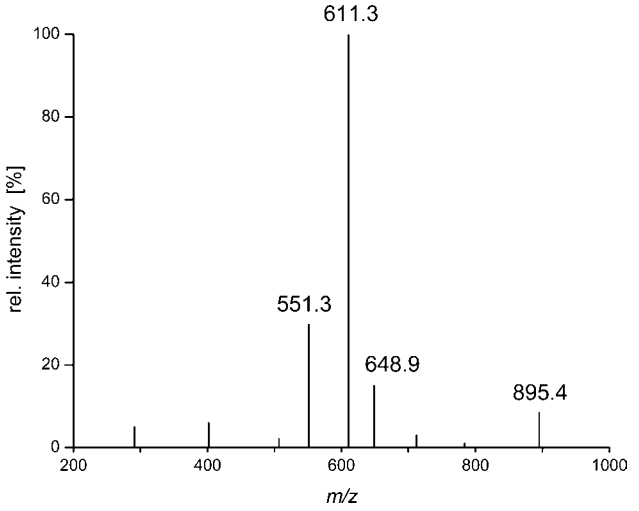


**Figure 2.** Mass spectrum (APCI$^+$) of [$^{13}C_3$]-glyceryl tristearate.

*Stable Isotope Labeling Studies with Triacylglycerides.* To get further insight into the formation pathway of acrolein from triacylglycerides, experiments using isotopically labeled precursors were undertaken. Recently, it was shown that acrolein formation from oils containing linoleic or linolenic acid is significantly higher than from oils mainly consisting of saturated or monounsaturated fatty acids.[6] However, up to now, no systematic investigations on the formation pathway of acrolein were reported in the literature.

Thus, two kinds of labeled triacylglycerides were synthesized: in one group of four triacylglycerides only the glycerol backbone was carbon-13 labeled, and in the other group of three labeled triacylglycerides the entire fatty acid moiety of either stearic, oleic, and linoleic acid was labeled, whereas glycerol was left unlabeled. All compounds were characterized by LC-MS analysis in APCI$^+$ mode and by NMR spectroscopy ([$^{13}C_3$]-labeled compounds). As an example, the mass spectrum of [$^{13}C_3$]-tristearate (Figure 2) and the respective $^{13}$C NMR spectrum (Figure 3) are shown.

In the next step, the four triacylglycerides labeled in the glycerol backbone were individually heated at 140 °C for 4 h in silicon oil, and the formation of acrolein was measured. In a control experiment, the oil did not show any mass traces at *m/z* 57 (acrolein) or *m/z* 60 ([$^{13}C_3$]-acrolein) when heated for 4 h.

When [$^{13}C_3$]-trioleate was heated (expt 2) (Table 2), the amount of unlabeled acrolein was higher by a factor of >8 compared to the carbon-13 labeled acrolein, clearly indicating the fatty acid moiety as the main precursor structure. The labeled acrolein formed from [$^{13}C_3$]-trilinoleate and [$^{13}C_3$]-trilinolenate (expts 3 and 4) (Table 2) was also as low as found for [$^{13}C_3$]-trioleate, but the amounts of unlabeled acrolein increased with the number of double bonds in the fatty acid moiety, amounting to 6240 μmol/mol from the linolenic acid residues. By contrast, from the saturated [$^{13}C_3$]-tristearate no acrolein was formed (expt. 1) (Table 2). Altogether, these results proved that the acrolein originates from the fatty acid

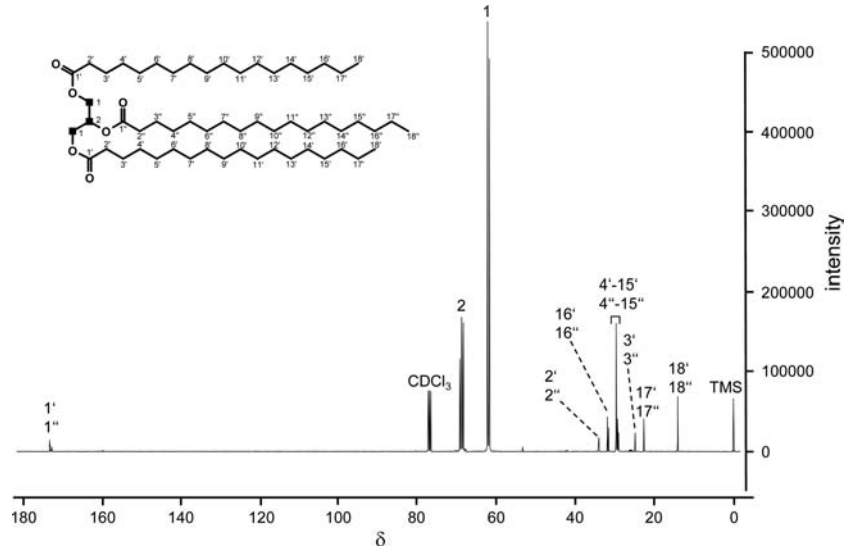


**Figure 3.** $^{13}C$ NMR spectrum of [$^{13}C_3$]-glyceryl tristearate. (■) $^{13}C$-labeling.

**Table 2. Amounts of Unlabeled Acrolein and [$^{13}C$]-Acrolein Formed by Heating of Triacylglycerides Labeled either in the Glycerol Backbone ([$^{13}C_3$]-Compounds) or in the Fatty Acid Moieties ([$^{13}C_{54}$]-Compounds) at 140 °C for 4 h**

| | | concn[a] (μmol/mol precursor) | |
|---|---|---|---|
| expt | precursor | [$^{13}C_3$]-acrolein | acrolein |
| 1 | [$^{13}C_3$]-tristearate | nd[b] | nd |
| 2 | [$^{13}C_3$]-trioleate | 30 (10−40) | 260 (240−280) |
| 3 | [$^{13}C_3$]-trilinoleate | 30 (20−40) | 710 (680−740) |
| 4 | [$^{13}C_3$]-trilinolenate | 40 (30−60) | 6240 (5980−6310) |
| 5 | [$^{13}C_{54}$]-tristearate | nd | nd |
| 6 | [$^{13}C_{54}$]-trioleate | 240 (220−260) | 20 (10−40) |
| 7 | [$^{13}C_{54}$]-trilinoleate | 780 (760−810) | 20 (10−30) |

[a]Mean values of three independent heat processings. Concentration ranges in parentheses. [b]Not detected (limit of detection = 0.25 μmol).

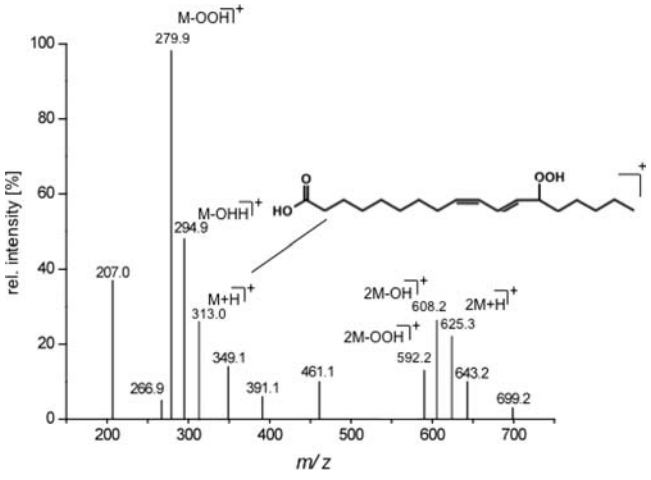


**Figure 4.** Mass spectrum (APCI$^+$) of 13-hydroperoxy-(*E*,*Z*)-9,11-octadecadienoic acid.

moiety of triacylglycerides containing at least one double bond. Further experiments with the triglycerides containing the labeled fatty acid moieties corroborated this finding. From these precursor triacylglycerides, higher amounts of [$^{13}C_3$]-acrolein were formed as compared to unlabeled acrolein, with trilinoleate being more effective than trioleate (expts 6 and 7) (Table 2). Again, the labeled tristearate did not form acrolein, which leads to the suggestion that at least one double bond in the fatty acid moiety is needed to initiate the formation of acrolein from the fatty acid moiety or the glycerol backbone. Thus, these results are additional proof that the fatty acid moiety plays the major role in acrolein formation. For the first time, the high precursor potential of unsaturated fatty acid moieties compared to the glycerol backbone, which was considered as a main acrolein precursor until now,[28] was proven. Hence, this model system is well in line with former findings that linseed oil containing high amounts of linolenic acid showed the highest precursor potential.[6]

**Table 3. Amounts of Acrolein Formed either from Free Linoleic Acid and Free Linolenic Acid or from 13-Hydroperoxy-(*Z*,*E*)-9,11-octadecadienoic Acid (13-HPOD) and 13-Hydroperoxy-(*Z*,*E*,*Z*)-9,11,15-octadecatrienoic Acid (13-HPOT) during Heating at 140 °C for 4 h**

| expt | precursor | concn[a] (μmol/mol precursor) |
|---|---|---|
| 1 | linoleic acid | 350 (260−390) |
| 2 | linolenic acid | 2210 (2050−2390) |
| 3 | 13-HPOD | 560 (210−840) |
| 4 | 13-HPOT | 3100 (2930−3310) |

[a]Mean values of triplicates. Concentration ranges in parentheses.

*Stable Isotope Labeling Studies with Fatty Acid Hydroperoxides.* To get more information about the transient reaction steps of acrolein formation from fatty acids, the precursor potential of fatty acid hydroperoxides was studied. The high regio- and stereospecifity of soybean lipoxygenase type I was used to synthesize the 13-hydroperoxides of linoleic as well as of linolenic acid. The mass spectrum of the 13-hydroperoxide from linolenic acid showed high fragmentation (APCI$^+$) (Figure 4), which was advantageous for the identification of the target molecule.

Single-model experiments with defined amounts of either free linoleic acid or linolenic acid as well as the respective 13-hydroperoxides were performed in silicon oil at 140 °C for 4 h. Also, the free linoleic acid and the free linolenic acid generated acrolein, with linolenic acid being the better precursor (expts 1

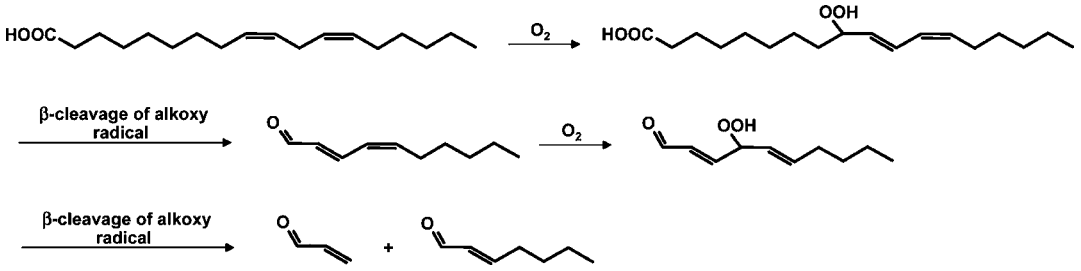


**Figure 5.** Reaction pathway leading to acrolein via 9-hydroperoxy-(*E*,*Z*)-10,12-octadecadienoic acid (following the idea of ref 32).

**Table 4. Influence of the Type of Fat Used in the Frying Process of Several Foods on Acrolein Formation**

| | acrolein concn[a] (μg/kg) in food after frying using | | | |
|---|---|---|---|---|
| sample | safflower oil | rapeseed oil | frying fat | commercial samples[b] |
| potato chips | 17.0 (15.3−17.9) | 23.3 (22.0−24.9) | 16.3 (15.1−17.1) | 18.3 (16.9−19.7) |
| French fries | 18.1 (15.5−19.8) | 14.8 (12.6−17.1) | 19.9 (17.4−22.5) | 18.5 (16.4−19.8) |
| donuts | 14.4 (11.3−15.5) | 15.0 (14.1−15.9) | 14.1 (11.7−16.3) | 16.9 (15.3−18.0) |

[a]Mean values from three independent frying processes. Concentration ranges in parentheses. LoD = 3 μg/kg, LoQ = 9 μg/kg according to ref 39. [b]For comparison.

and 2) (Table 3). Heating of the respective hydroperoxides led to higher amounts of acrolein with the 13-linolenic acid hydroperoxide generating higher amounts (expts 3 and 4) (Table 3). Thus, these results suggest that the formation of hydroperoxides is an important step in acrolein formation, leading to the introduction of the oxygen moiety.

In the literature, it was proposed that acrolein may originate from the unsaturated part of the aliphatic chain, that is, by *β*-cleavage of 9-hydroperoxides resulting in the respective aldehyde and an alkyl fragment. By Hock fragmentation, the released carbonyls lead to two aldehyde fragments (Figure 5). Contrary to the suggested mechanism via linolenic acid 13-hydroperoxide,[10] this pathway may also explain acrolein generation from the monounsaturated oleic acid. To the best of our knowledge, these results are the first proof for acrolein generation from fatty acid hydroperoxides.

**Identification and Quantitation of Acrolein in Fried Foods.** In the next experiments, it was clarified whether a high concentration of acrolein in the frying oil must consequently result in high amounts in the fried food. Thus, French fries, donuts, and potato chips were fried either in oils high in unsaturated fatty acids, such as safflower oil and rapeseed oil, or in a commercial frying fat. As previously shown,[6] rapeseed oil in particular generated the highest amounts of acrolein simply by heating without foods. Acrolein quantitation in the self-prepared as well as in the commercial samples revealed comparable amounts of acrolein, nearly independently from the type of frying oil used (Table 4). Acrolein concentrations in fried potato chips ranged from 16.3 μg/kg prepared with a common frying fat to 23.3 μg/kg using rapeseed oil, and the analysis of commercial potato chips revealed an acrolein concentration of 18.3 μg/kg. The average acrolein content in French fries ranged from 14.8 μg/kg prepared in rapeseed oil to 19.9 μg/kg in frying fat. Analysis of fried donuts showed slightly lower acrolein concentrations compared to the other food samples with 14.1 μg/kg in donuts fried in frying fat, 15.0 μg/kg in donuts prepared in rapeseed oil, and 16.9 μg/kg in donuts from a local bakery (Table 4).

Compared to the acrolein amounts measured in heated fats and oils from previous studies (46.8 mg/kg of safflower oil, 55.8 mg/kg of frying fat, 157 mg/kg of rapeseed oil; heating conditions, 180 °C/24 h),[6] the fried food itself does not seem to be a significant source of free acrolein in the human diet.

In conclusion, the formation pathways of the toxicologically relevant acrolein were proven on the basis of labeling experiments. A formation pathway from the carbon backbone of unsaturated fatty acids, in particular, linolenic acid via the 13-hydroperoxide, seems very likely, whereas the glycerol backbone does not play a key role. Surprisingly, however, acrolein was low in different types of foods, although the investigated oils and fat were high in acrolein. This result suggests that acrolein might be bound to, for example, macromolecular structures in foods, thus no longer existing in the free state. Experiments to study this assumption are currently underway due to the fact that Watzek et al.[40] were able to show that the amounts of acrolein-related mercapturic acids excreted in urine after potato crisp intake were much higher than calculated from the previously analyzed amounts of free acrolein in the crisps.

## AUTHOR INFORMATION

### Corresponding Author

*(P.S.) Phone: +49 8161 71 2932. Fax: +49 8161 71 2970. E-mail: Peter.Schieberle@ch.tum.de.

### Notes

The authors declare no competing financial interest.

## ACKNOWLEDGMENTS

The authors thank Dr. Johanna Kreißl and Dr. Johannes Polster for measurement and interpretation of the NMR spectra.

## REFERENCES

(1) Ho, S. S. H.; Yu, J. Z. Feasibility of collection and analysis of airborne carbonyls by on-sorbent derivatization and thermal desorption. *Anal. Chem.* **2002**, *74*, 1232−1240.

(2) Kataoka, H.; Kondo, T.; Sumida, A. Gas chromatographic determination of aldehydes in combustion smoke samples. *Anal. Chim. Acta* **1998**, *358*, 269−275.

(3) Singer, B. C.; Hodgson, A. T. Gas-phase organics in environmental tobacco smoke. 1. Effects of smoking rate, ventilation, and furnishing level on emission factors. *Environ. Sci. Technol.* **2002**, *5*, 846−853.

(4) Gilbert, N. L.; Guay, M.; Miller, J. D.; Judek, S.; Chan, C. C.; Dales, R. E. Levels and determinants of formaldehyde, acetaldehyde,

and acrolein in residential indoor air in Prince Edward Island, Canada. *Environ. Res.* **2005**, *99*, 11−17.
(5) Seaman, V. Y.; Bennett, D. H.; Cahill, T. M. Indoor acrolein emission and decay rates resulting from domestic cooking events. *Atmos. Environ.* **2009**, *43*, 6199−6204.
(6) Ewert, A.; Granvogl, M.; Schieberle, P. Development of two stable isotope dilution assays for the quantitation of acrolein in heat-processed fats. *J. Agric. Food Chem.* **2011**, *59*, 3582−3589.
(7) Umano, K.; Shibamoto, T. Analysis of acrolein from heated cooking oils and beef fat. *J. Agric. Food Chem.* **1987**, *35*, 14−18.
(8) Casella, I. G.; Contursi, M. Quantitative analysis of acrolein in heated vegetable oils by liquid chromatography with pulsed electrochemical detection. *J. Agric. Food Chem.* **2004**, *52*, 5816−5821.
(9) Fullana, A.; Carbonell-Barrachina, A. A.; Sidhu, S. Comparison of volatile aldehydes present in the cooking fumes of extra virgin olive, olive, and canola oils. *J. Agric. Food Chem.* **2004**, *52*, 5207−5214.
(10) Da Silva, T. O.; de Paula Pereira, P. A. Influence of time, surface-to-volume ratio, and heating process (continuous or intermittent) on the emission rates of selected carbonyl compounds during thermal oxidation of palm and soybean oils. *J. Agric. Food Chem.* **2008**, *56*, 3129−3135.
(11) Takamoto, S.; Sakura, N.; Namera, A.; Yashiki, M. Monitoring of urinary acrolein concentration in patients receiving cyclophosphamide and ifosphamide. *J. Chromatogr., B* **2004**, *806*, 59−63.
(12) Paci, A.; Rieutord, A.; Guillaume, D.; Traoré, F.; Ropenga, J.; Husson, H.-P.; Brion, F. Quantitative high-performance liquid chromatographic determination of acrolein in plasma after derivatization with Luminarin® 3. *J. Chromatogr., B* **2000**, *739*, 239−246.
(13) International Agency for Research on Cancer. Acrolein. *IARC Monogr. Eval. Carcinog. Risks Hum.* **1995**, *63*, 337−372.
(14) Yoshida, M.; Tomitori, H.; Machi, Y.; Hagihara, M.; Higashi, K.; Goda, H.; Ohya, T.; Niitsu, M.; Kashiwagi, K.; Igarashi, K. Acrolein toxicity: comparison with reactive oxygen species. *Biochem. Biophys. Res. Commun.* **2009**, *378*, 313−318.
(15) LoPachin, R. M.; Gavin, T.; Petersen, D. R.; Barber, D. S. Molecular mechanism of 4-hydroxy-2-nonenal and acrolein toxicity: nucleophilic targets and adduct formation. *Chem. Res. Toxicol.* **2009**, *22*, 1499−1508.
(16) Horton, N. D.; Mamiya, B. M.; Kehrer, J. P. Relationships between cell density, glutathione and proliferation of A549 human lung adenocarcinoma cells treated with acrolein. *Toxicology* **1997**, *122*, 111−122.
(17) Rudra, P. K.; Krokan, H. E. Acrolein cytotoxicity and glutathione depletion in n-3 fatty acid-sensitive and -resistant human tumor cells. *Anticancer Res.* **1999**, *19*, 461−469.
(18) U.S. Environmental Protection Agency.. Control of hazardous air pollutants from mobile sources: final rule. 40 CFR Parts 59, 80, 85, and 86. *Fed. Regist.* **2007**, *72*, 8428−8570.
(19) Shields, P. G.; Xu, G. X.; Blot, W. J.; Fraumeni, J. F., Jr.; Trivers, G. E.; Pellizzari, E. D.; Qu, Y. H.; Gao, Y. T.; Harris, C. C. Mutagens from heated Chinese and U.S. cooking oils. *J. Natl. Cancer Inst.* **1995**, *87*, 836−841.
(20) Beauchamp, R. O., Jr.; Andjelkovich, D. A.; Kligerman, A. D.; Morgan, K. T.; Heck, H. D. A critical review of the literature on acrolein toxicity. *Crit. Rev. Toxicol.* **1985**, *14*, 309−380.
(21) Arumugam, N.; Sivakumar, V.; Thanislass, J.; Sadasivan Pillai, K.; Niranjali Devaraj, S.; Devaraj, H. Acute pulmonary toxicity of acrolein in rats − underlying mechanism. *Toxicol. Lett.* **1999**, *104*, 189−194.
(22) Adams, J. D., Jr.; Klaidman, L. K. Acrolein-induces oxygen radical formation. *Free Radical Biol. Med.* **1993**, *15*, 187−193.
(23) Patel, J. M. Stimulation of cyclophosphamide-induced pulmonary microsomal lipid peroxidation by oxygen. *Toxicology* **1987**, *45*, 79−91.
(24) Srivastava, S.; Sithu, S. D.; Vladykovskaya, E.; Haberzettl, P.; Hoetker, D. J.; Siddiqui, M. A.; Conklin, D. J.; D'Souza, S. E.; Bhatnagar, A. Oral exposure to acrolein exacerbates atherosclerosis in apoE-null mice. *Atherosclerosis* **2011**, *215*, 301−308.
(25) Calingasan, N. Y.; Uchida, K.; Gibson, G. E. Protein-bound acrolein: a novel marker of oxidative stress in Alzheimer's disease. *J. Neurochem.* **1999**, *72*, 751−756.
(26) Fujisaki, M.; Endo, Y.; Fujimoto, K. Retardation of volatile aldehyde formation in the exhaust of frying oil by heating under low oxygen atmospheres. *J. Am. Oil Chem. Soc.* **2002**, *79*, 909−914.
(27) Crook, T. R.; Souhami, R. L.; McLean, A. E. Cytotoxicity, DNA cross-linking, and single strand breaks induced by activated cyclophosphamide and acrolein in human leukemia cells. *Cancer Res.* **1986**, *46*, 5029−5034.
(28) Nawar, W. Thermal and radiolytic decomposition of lipids. In *Chemical Changes in Food during Processing*; Richardson, T., Finley, J., Eds.; AVI: Westport, CT, 1985; pp 79−105.
(29) Zhu, X.; Wang, K.; Zhu, J.; Koga, M. Analysis of cooking oil fumes by ultraviolet spectrometry and gas chromatography-mass spectrometry. *J. Agric. Food Chem.* **2001**, *49*, 4790−4794.
(30) Schauer, J. J.; Kleeman, M. J.; Cass, G. R.; Simoneit, B. R. Measurement of emissions from air pollution sources. 4. $C_1$-$C_{27}$ organic compounds from cooking with seed oils. *Environ. Sci. Technol.* **2002**, *36*, 567−575.
(31) Bastos, L. C. S.; de Paula Pereira, P. A. Influence of heating time and metal ions on the amount of free fatty acids and formation rates of selected carbonyl compounds during the thermal oxidation of canola oil. *J. Agric. Food Chem.* **2010**, *58*, 12777−12783.
(32) Esterbauer, H.; Schaur, R. J.; Zollner, H. Chemistry and biochemistry of 4-hydroxynonenal, malonaldehyde and related aldehydes. *Free Radical Biol. Med.* **1991**, *11*, 81−128.
(33) Tamura, H.; Kitta, K.; Shibamoto, T. Formation of reactive aldehydes from fatty acids in a $Fe^{2+}/H_2O_2$ oxidation system. *J. Agric. Food Chem.* **1991**, *39*, 439−442.
(34) Pan, X.; Kaneko, H.; Ushio, H.; Ohshima, T. Oxidation of all-*cis*-7,10,13,16,19-docosapentaenoic acid ethyl ester. Hydroperoxide distribution and volatile characterization. *Eur. J. Lipid Sci. Technol.* **2005**, *107*, 228−238.
(35) Neises, B.; Steglich, W. Simple method for the esterification of carboxylic acids. *Angew. Chem., Int. Ed. Engl.* **1978**, *17*, 522−524.
(36) Schieberle, P.; Grosch, W.; Kexel, H.; Schmidt, H.-L. A study of oxygen isotope scrambling in the enzymic and non-enzymic oxidation of linoleic acid. *Biochim. Biophys. Acta* **1981**, *666*, 322−326.
(37) Browne, R. W.; Armstrong, D. HPLC analysis of lipid-derived polyunsaturated fatty acid peroxidation products in oxidatively modified human plasma. *Clin. Chem.* **2000**, *46*, 829−836.
(38) Jiang, Z.-Y.; Woollard, A. C. S.; Wolff, S. P. Lipid hydroperoxide measurement by oxidation of $Fe^{2+}$ in the presence of xylenol orange. Comparison with the TBA assay and an iodometric method. *Lipids* **1991**, *26*, 853−856.
(39) Granvogl, M. Development of three stable isotope dilution assays for the quantitation of (*E*)-2-butenal (crotonaldehyde) in heat-processed edible fats and oils as well as in food. *J. Agric. Food Chem.* **2014**, *62*, 1272−1282.
(40) Watzek, N.; Scherbl, D.; Feld, J.; Berger, F.; Doroshyenko, O.; Fuhr, U.; Tomalik-Scharte, D.; Baum, M.; Eisenbrand, G.; Richling, E. Profiling of mercapturic acids of acrolein and acrylamide in human urine after consumption of potato crisps. *Mol. Nutr. Food Res.* **2012**, *56*, 1825−1837.

JOURNAL OF AGRICULTURAL AND FOOD CHEMISTRY

Article

pubs.acs.org/JAFC

# $^1$H NMR Profiling as an Approach To Differentiate Conventionally and Organically Grown Tomatoes

Monika Hohmann,*[†,§] Norbert Christoph,[†] Helmut Wachter,[†] and Ulrike Holzgrabe[§]

[†]Bavarian Health and Food Safety Authority, Luitpoldstraße 1, 97082 Würzburg, Germany

[§]Institute of Pharmacy and Food Chemistry, University of Würzburg, Am Hubland, 97074 Würzburg, Germany

**ABSTRACT:** This study describes the approach of $^1$H NMR profiling for the authentication of organically produced tomatoes (*Solanum lycopersicum*). Overall, 361 tomato samples of two different cultivars and four different producers were regularly analyzed during a 7 month period. The results of principal component analysis showed a significant trend for the separation between organically and conventionally produced tomatoes ($p < 0.001$ using the $t$ test). Linear discriminant analysis demonstrated good discrimination between the growing regimens, and external validation showed 100% correctly classified tomato samples. Further validation studies, however, also disclosed unexpected differences between individual producers, which interfere with the aim of predicting the cultivation method, yet the results indicate significant differences between $^1$H NMR spectra of organically and conventionally grown tomatoes.

**KEYWORDS:** *$^1$H NMR, multivariate data analysis, tomato, Solanum lycopersicum, organic, conventional*

## INTRODUCTION

The demand for organically produced food has been increasing considerably; it almost tripled between 2002 and 2011, when its market share reached a worth of U.S. $62.8 billion.[1] Because consumers are prepared to purchase organic food at higher prices, the risk for conventional produce fraudulently labeled as "organic" has also been increasing. To prevent and detect counterfeit, there is a strong need for analytical methods that allow the verification of organic cultivation. This study examines the differentiation between organically and conventionally grown tomatoes (*Solanum lycopersicum*), which are widely consumed in Europe,[2] by means of multivariate data analysis of $^1$H NMR spectra.

Within the European Union, the requirements for organic farming are stated in Council Regulation (EC) 834/2007 and Commission Regulation (EC) 889/2008. With respect to the ban of the use of synthetic pesticides and synthetic mineral fertilizer for organic farming, there are a variety of starting points for analytical differentiation.

Organically produced food is often associated with statements about a better nutritional value due to allegedly increased contents of bioactive compounds and lower levels of pesticides and contaminants. Higher contents of polyphenolic compounds and higher antioxidant capacity were analyzed for tomatoes,[3] tomato ketchup,[4] and tomato juice.[5] However, the amounts of bioactive compounds are influenced by variations due to crop year, origin,[6,7] amount of fertilizer and soil nitrate,[8] stage of maturity,[9,10] and ripening type.[11] Thus, differences in organic and conventional tomatoes were occasionally inconsistent within different varieties or crop years,[12,13] and individual results are hardly comparable due to different conditions in cultivation.[14] Pesticide screening of organic food is meaningful to detect the illegitimate usage of synthetic pesticides, yet residue findings can also be the result of contaminations from nearby conventional farms or anthropogenic inherited waste. Furthermore, conventional farming is not necessarily combined with the use of pesticides for plant protection, which, especially in greenhouse cultivation, can also be performed by means of beneficial insects.

Other studies show that nitrogen fertilization affects the composition of amino acids in vegetables,[15] whereas these results are likewise affected by variety[16] and degree of ripeness.[17,18] Furthermore, variations in the pattern of mineral concentrations in organically and conventionally grown tomatoes have been described,[19] which may be attributed to the metabolism of arbuscular mycorrhizal fungi in organic soils.[20]

Up to now, the most reliable analytical method for authentication is presented by the composition of the nitrogen isotope: the nitrogen isotope composition of the fertilizer predefines the nitrogen isotope composition of the grown crop.[21−23] As the nitrogen of synthetic mineral fertilizer originates from atmospheric nitrogen with a $\delta^{15}$N value around 0‰ ($\delta^{15}$N is expressed as the relative difference from atmospheric nitrogen as standard), improper usage of conventional fertilizers can be identified by lower $\delta^{15}$N values than common values for organic farming.[21] However, there exists an overlap between the $\delta^{15}$N values of organically and conventionally grown crops[24] that suggests the development of further analytical methods for the verification of the growing regime.

As recently described by Esslinger et al.,[25] the application of spectroscopic data combined with multivariate data analysis to verify food authenticity is becoming increasingly important. Using these profiling techniques is especially reasonable in the area of food products, where attributes of authenticity represent unique quality parameters and legitimate higher prices, as is the case for organic food. Previous examples of use cover authenticity control in terms of analyzing botanical[26] or geographical origin[27,28] and adulteration[29] of honey, geographical origin[30−33]

Received: May 7, 2014
Revised: July 27, 2014
Accepted: July 28, 2014
Published: July 28, 2014

ACS Publications © 2014 American Chemical Society

and adulteration[34] of olive oil, botanical[35] or geographical origin[36−40] and quality[41] of wine and authenticity control of fruit juice.[42] Both the multitude of recent applications and their output of results show the importance of $^1$H NMR profiling in terms of authenticity analysis.

Previous NMR measurements of tomatoes and tomato products focused on carotenoid composition,[43] degree of ripeness,[44,45] quantitative NMR,[4] magnetic resonance imaging (MRI) measurements,[46] or diverse 2D NMR experiments.[47] Here, the suitability of $^1$H NMR profiling for the purpose of differentiation between organic and conventional tomatoes is discussed. Our key aim is the development of a sufficient method for an authentication of organic tomatoes against the background of food surveillance and consumer protection, independent from nutritional perspectives.

Because no set definition for organic or conventional farming exists, there is ample scope for a variety of cultivation methods. For example, numerous fertilizers may be used and fruits can be grown in greenhouses as well as on open land. It is accordingly unfeasible to create an experimental design that fulfills the possible growing conditions in all facets. In this study, attention was turned on greenhouse cultivation, and authentic tomatoes were grown conventionally with mineral substrate and mineral fertilizers as well as organically with soil and organic fertilizers. An essential difference of these cultivation methods may be represented by different nitrogen availabilities. This cultivation experiment certainly does not reflect the wide range of actually existing ways of farming, but rather demonstrates a proper starting point to verify the basic suitability of $^1$H NMR profiling for a differentiation between organically and conventionally grown tomatoes.

## MATERIALS AND METHODS

**Sample Collection.** *Cultivation Experiment (CE).* The tomato cultivars Mecano and Tastery were grown in two different greenhouses at the Bavarian State Research Institute of Viticulture and Horticulture, both organically and conventionally (LWG, Bamberg, Germany; tomato samples are referred to as "CE organic" and "CE conv" in the following text). Thereby, conventional growing conditions were carried out as hydroponic culture using perlite substrate and mineral fertilizer, whereas organic growing conditions were carried out using soil and clover-grass silage, vinasse, Patentkali, sheep's wool, and winter rye (previous culture for green manure) as organic fertilizer. Except for conventionally grown tomatoes of the cultivar Mecano (planted in both January and March), all plants were grown in March. For each cultivar and farming method at least three parcels of tomato plants (each consisting of 10 plants) were grown: for organic cultivation of Mecano, 4 parcels, and for Tastery, 4 parcels; for conventional cultivation of Mecano, 7 parcels (thereof 3 parcels with tomatoes planted in January and 4 parcels planted in March), and for Tastery, 5 parcels. Harvesting was performed at regular intervals of 2 weeks between weeks 21 and 45 (13 harvest times), and sampling was done by picking tomatoes systematically from different plants in the greenhouse. Tomatoes from each parcel were analyzed individually and, in addition, tomatoes from equal parcel of the same cultivation method and cultivar were pooled to one mixed sample for analysis. At this, altogether 325 CE samples were analyzed, with 52 samples from tomatoes planted in January and 273 samples from tomatoes planted in March.

*Trading Firms (TF).* Additionally, three trading firms (referred to as "TF organic", "TF conv 1", and "TF conv 2" in the following text) cultivated the same cultivars (Mecano and Tastery). Conventional growing conditions were again carried out as hydroponic culture using perlite substrate and mineral fertilizer, and organic growing conditions were carried out using soil and hair meal and compost as organic fertilizer. Fruits were harvested from May to October once a month, so that in total 36 tomato samples were analyzed (3 producers × 2 cultivars × 6 months).

*Validation Data Set Comprising CE and TF Tomato Samples.* To test the suitability of statistical models, an external validation data set was created by systematically excluding both CE and TF tomato samples from calibration (validation of LDA1): overall, 81 tomato samples, organically grown at CE (harvested at weeks 23, 31 and 39), conventionally grown at CE (harvested at weeks 27, 35, and 43; excluding tomatoes planted in January), and organically grown at TF (harvested at weeks 21, 29, and 37) as well as conventionally grown at TF (harvested at weeks 24, 32 and 40), were used for validation purposes.

*Additional Tomato Samples for Validation.* In addition, several other fruits were analyzed and used for validation (validation of LDA2):

The cultivar Tica was grown under the same conditions as organically grown CE tomatoes. Fruits from six different parcels were harvested individually and as a pooled sample of these parcels at week 30 and another pooled sample of these parcels at week 35, resulting in overall eight tomato samples.

Furthermore, cultivars Mecano and Tastery, grown at the CE (planted in March), were harvested as ripening (red-turning) tomatoes at week 35. Overall, 4 tomato samples were measured, one for each cultivar and type of farming.

From another producer (school for horticulture in Fürth, Germany), the cultivar Mecano was grown conventionally in a greenhouse using mineral fertilizer and different substrates: cocos-plate, wood-perlite mixture, and perlite. Fruits were harvested at weeks 30 and 31, with one tomato sample for each substrate, yielding six tomato samples.

**Chemicals.** For 1 M NaOH and 1 M HCl, NaOH pellets were purchased from VWR (Leuven, Belgium) and HCl (37%) from Sigma-Aldrich (St. Louis, MO, USA). $TSPd_4$ (3-(trimethylsilyl)propionic acid-$d_4$ sodium salt, 98 atom % D), $D_2O$ (99.9 atom % D), EDTA (ethylenediaminetetraacetic acid), and $NaN_3$ were purchased from Merck (Darmstadt, Germany).

**Sample Preparation.** At least 250 g of tomato was pureed and subsequently stored at −18 °C. After thawing, the samples were centrifuged for 5 min at 3528*g*, and the residual liquid tomato phase was used for subsequent $^1$H NMR measurement. For this purpose, 900 $\mu$L of liquid tomato phase was mixed with 100 $\mu$L of TSPd4 solution (containing 7 mM TSPd4, 10 mM EDTA, and 2 mM $NaN_3$ in $D_2O$), and the pH value of all samples was adjusted to pH 4.00 ± 0.03 using 1 M NaOH or 1 M HCl. Finally, 600 $\mu$L of the pH-adjusted solutions was filled into 5 mm NMR tubes (PP-507, purchased from Rototec-Spintec, Griesheim, Germany) for NMR measurement.

**$^1$H NMR Measurement.** Hardware and software equipment used for NMR measurement was completely purchased from Bruker (Bruker BioSpin, Rheinstetten, Germany) comprising a Bruker Avance 400 spectrometer with a 5 mm SEI probe with *Z*-gradient coils, an automatic sample changer (B-ACS-60), a BCU 05 temperature unit, and TopSpin 3.0 software.

All tomato samples were measured at 301.8 ± 0.1 K, without rotation and using 4 dummy scans prior to 128 scans. Acquisition parameters have been set as follows: size of fid = 64K, spectral width = 20.5524 ppm, receiver gain = 16, acquisition time = 3.98 s, relaxation delay = 10 s, FID resolution = 0.25 Hz. Data acquisition was achieved using an experiment with a NOESY presaturation pulse sequence (Bruker 1D noesygppr1d) with water suppression via irradiation of the water frequency during the recycle and mixing time delays. The spectra were automatically phased, baseline-corrected, and calibrated to the TSP signal at 0.0 ppm.

**Multivariate Statistical Analysis.** Data reduction was achieved by transforming NMR spectra into buckets (bundling spectral regions to one rectangular bucket, whereas the value of a bucket represents the signal intensity of the respective spectral region). Two different types of buckets (given in Table 1) were generated with Amix 3.9.12 software (Bruker Biospin GmbH).

Subsequent multivariate data analysis was done on the assumption of normally distributed data. Principal component analysis (PCA) was performed with Unscrambler X version 10.0.1 (Camo Software AS, Oslo, Norway) with buckets of $^1$H NMR spectra scaled to unit variance. Linear discriminant analysis (LDA) of buckets was carried out with SPSS statistics 21 (IBM Corp., Armonk, NY, USA) using equal a priori probabilities for all groups and stepwise selection procedure

**Table 1. Description of the Bucketing Process and the Application of Buckets for Multivariate Data Analysis**

| | bucketing 1 | bucketing 2 |
|---|---|---|
| spectral region | 0.00−10.00 ppm | 2.86−8.67 ppm |
| exclusions | 4.85−4.67 ppm | 7.91−6.67 ppm |
| | 3.70−3.60 ppm | 6.12−5.39 ppm |
| | 1.22−1.14 ppm | 5.02−4.49 ppm |
| | | 3.15−2.98 ppm |
| reason for exclusions | elimination of residual water and ethanol signals (NMR tubes were reused and washed with ethanol) | elimination of irrelevant signals for a differentiation between organic and conventional tomato samples |
| bucket width | 0.200 ppm | 0.007 ppm |
| application | PCA, LDA1 | LDA2 |

(chosen method, minimization of Wilks' lambda; selection criterion, $F$ probabilities of 0.050 for inclusion and 0.100 for exclusion for LDA1 and 0.005 for inclusion and 0.010 for exclusion for LDA2). $t$ tests were performed using OriginPro 9G software (OriginLab Corp., Northampton, MA, USA).

## RESULTS AND DISCUSSION

**$^1$H NMR Measurement and Optimization of Sample Preparation.** On average, tomatoes contain 94% water and the remaining 6% of dry matter consists of 55% sugar (mainly glucose and fructose), 20% alcohol-soluble constituents (proteins, cellulose, pectin, and polysaccharides), 12% organic acids (mainly citric acid), 8% inorganic substances (minerals), and 5% of other substances, such as amino acids.[48] Hence, $^1$H NMR spectra of tomatoes are dominated by signals of sugar and citric acid, whereas an enlarged view also reveals diverse amino acids and other minor components (Figure 1 and Table 2). Thereby, the signals obtained are in good agreement with those reported previously.[49]

As several citrate species exist in fast exchange with each other (protonated or ionic, complexed with $Ca^{2+}$ and $Mg^{2+}$), the observed citrate signal represents an average of the signals from those species.[50] Additionally, broadened lines can arise from paramagnetic substances that lead to enlarged values of line width by shortening T2 relaxation times.[51,52] To achieve high resolution and optimized line widths, small amounts of EDTA were added to each sample, because EDTA enables signal sharpening via serving as chelating agent. With regard to the $^1$H NMR spectra of tomato samples, especially the line width of citric acid was clearly reduced by the addition of EDTA, whereas no major effects on chemical shifts could be detected.

For the best possible conditions for multivariate data analysis, highest reproducibility has to be achieved. Therefore, all samples were pH adjusted (pH 4.00 ± 0.03) to minimize variation in chemical shifts due to protonation or deprotonation processes. As the chemical shift of citric acid is highly influenced by deviations from the requested pH value, it was used as a quality marker for adequate pH adjustment to define control limits for tolerable chemical shift deviations (deviations up to ±3.5 Hz from the left signal top of the citric acid duplet at 2.881 ppm were accepted).

**Principal Component Analysis.** To get an overview of the given data, PCA was performed with $^1$H NMR spectra of tomatoes from both cultivars and types of farming (309 tomato samples are included in the evaluation, 273 from CE, excluding fruits planted in January, and 36 from TF).

The scatter plot of PC1 versus PC4 (Figure 2) shows the separation of the two cultivars Mecano (circles) and Tastery (triangles) along PC1. With the aim of recognizing the effect of different cultivars, two very dissimilar cultivars were analyzed (Tastery is small fruited with an average weight of 20 g/fruit, and Mecano is normally fruited with an average weight of 100 g/fruit) and, thus, differentiation according to their cultivar is quite

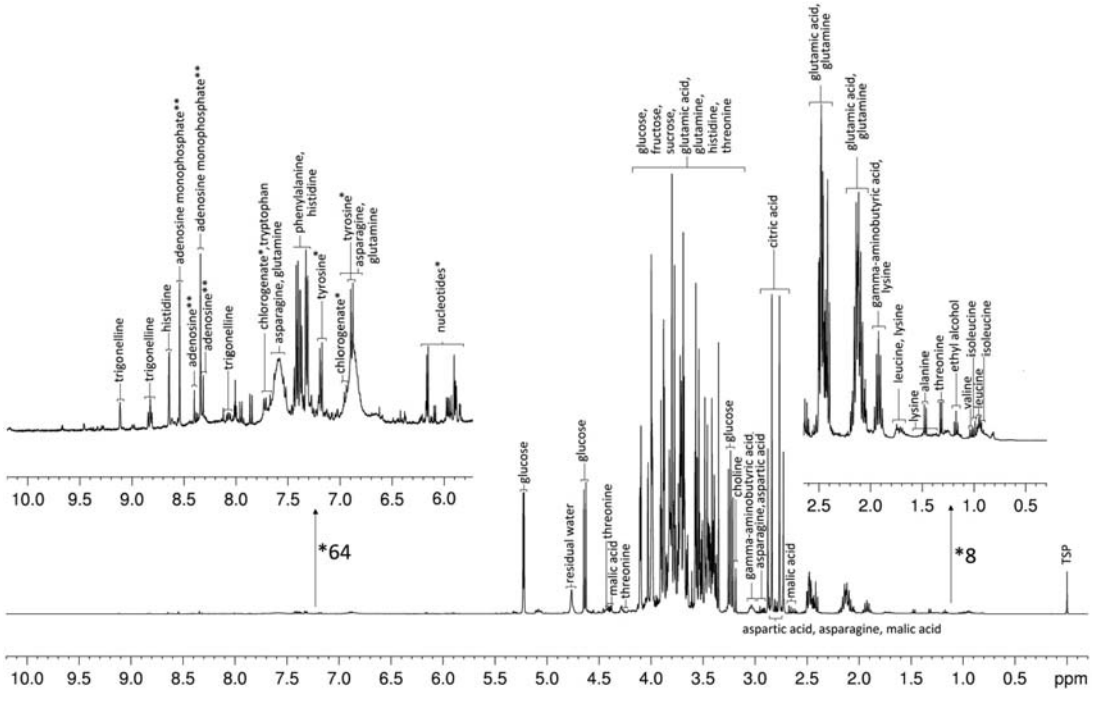


**Figure 1.** $^1$H NMR spectrum of the aqueous phase of a tomato sample with an enlarged view on the spectral range from 0.5 to 2.6 ppm (*8) and from 5.8 to 10.0 ppm (*64), measured with a 400 MHz spectrometer. Signal assignments are based on reference spectra and the literature (*Mounet et al.;[45] and **Le Gall et al.[53]).


dx.doi.org/10.1021/jf502113r | J. Agric. Food Chem. 2014, 62, 8530−8540

**Table 2. Resonance Assignments of Signals in $^1$H NMR Spectra of the Aqueous Phase of Tomatoes with Chemical Shift and Spin−Spin Coupling,[49] Using a 400 MHz NMR Spectrometer**

| molecule | chemical shift | multiplicity | molecule | chemical shift | multiplicity |
|---|---|---|---|---|---|
| isoleucine | 0.93 | t | β-D-fructofuranose | 3.67 | dd |
| leucine | 0.95 | m | isoleucine | 3.67 | |
| valine | 0.98 | d | α-D-fructofuranose | 3.68 | |
| isoleucine | 1.00 | d | β-D-fructopyranose | 3.70 | dd |
| valine | 1.03 | d | α-D-glucose | 3.70 | td |
| ethyl alcohol | 1.17 | t | β-D-fructopyranose | 3.70 | d |
| isoleucine | 1.26 | m | β-D-glucose | 3.71 | dd |
| threonine | 1.32 | d | α-D-glucose | 3.75 | dd |
| lysine | 1.47 | m | glutamine | 3.77 | t |
| alanine | 1.47 | d | glutamic acid | 3.77 | m |
| isoleucine | 1.47 | m | alanine | 3.78 | |
| leucine | 1.70 | m | alanine | 3.78 | |
| lysine | 1.71 | m | β-D-fructopyranose | 3.79 | dd |
| lysine | 1.89 | m | β-D-fructofuranose | 3.79 | dd |
| γ-aminobutyric acid | 1.93 | m | α-D-fructofuranose | 3.80 | |
| isoleucine | 1.97 | m | α-D-glucose | 3.81 | m |
| glutamic acid | 2.09 | m | α-D-glucose | 3.82 | m |
| glutamine | 2.13 | m | β-D-fructofuranose | 3.83 | m |
| glutamic acid | 2.15 | m | β-D-fructopyranose | 3.89 | dd |
| valine | 2.26 | m | β-D-glucose | 3.89 | dd |
| γ-aminobutyric acid | 2.42 | t | aspartic acid | 3.94 | dd |
| glutamine | 2.45 | m | β-Dfructopyranose | 3.99 | ddd |
| glutamic acid | 2.48 | m | phenylalanine | 3.99 | dd |
| malic acid | 2.65 | dd | α-D-fructofuranose | 3.99 | |
| citric acid | 2.75 | d | asparagine | 4.00 | dd |
| aspartic acid | 2.76 | dd | β-D-fructopyranose | 4.01 | dd |
| malic acid | 2.83 | dd | histidine | 4.02 | dd |
| asparagine | 2.84 | dd | α-D-fructofuranose | 4.05 | |
| citric acid | 2.86 | d | α-D-fructofuranose | 4.10 | d |
| aspartate | 2.88 | dd | threonine | 4.26 | |
| asparagine | 2.95 | dd | malic acid | 4.40 | dd |
| lysine | 3.02 | m | β-D-glucose | 4.63 | d |
| γ-aminobutyric acid | 3.03 | m | α-D-glucose | 5.22 | d |
| phenylalanine | 3.11 | dd | glutamine | 6.85 | |
| choline | 3.19 | s | asparagine | 6.89 | |
| β-D-glucose | 3.23 | dd | tryptophan | 7.19 | t |
| histidine | 3.28 | m | tryptophan | 7.28 | t |
| phenylalanine | 3.28 | dd | phenylalanine | 7.32 | dd |
| histidine | 3.34 | m | phenylalanine | 7.37 | t |
| β-D-glucose | 3.39 | dd | histidine | 7.38 | s |
| α-D-glucose | 3.40 | dd | phenylalanine | 7.42 | td |
| β-D-glucose | 3.45 | ddd | tryptophan | 7.53 | d |
| β-D-glucose | 3.48 | t | glutamine | 7.57 | |
| α-D-glucose | 3.52 | dd | asparagine | 7.62 | |
| β-D-fructofuranose | 3.54 | d | tryptophan | 7.73 | d |
| β-D-fructopyranose | 3.56 | d | trigonelline | 8.06 | dd |
| threonine | 3.59 | m | histidine | 8.64 | s |
| β-D-fructofuranose | 3.59 | d | trigonelline | 8.80 | m |
| valine | 3.61 | m | trigonelline | 8.82 | m |
| α-D-fructofuranose | 3.65 | | trigonelline | 9.10 | s |
| ethyl alcohol | 3.65 | m | | | |

understandable. In addition, a separation of the organically and conventionally grown groups is apparent for each cultivar, notably along PC4: both Mecano and Tastery show higher values of PC4 for the conventional than for the organic group. Given the existing overlap of organic and conventional tomato samples, values of PC4 are not capable of a reliable classification of organic fruits. Nevertheless, the findings confirm the approach that $^1$H NMR spectra show significant differences between the cultivation methods ($p < 0.001$ using $t$ test of PC4 values).

Comparability of all other impact parameters has to be ensured to reason that differences between organic and conventional tomato samples can be attributed to the kind of growing regimen. As immoderate heating of greenhouses is contradictory to the concepts of environmental acceptability for organic cultivation,


dx.doi.org/10.1021/jf502113r | J. Agric. Food Chem. 2014, 62, 8530−8540

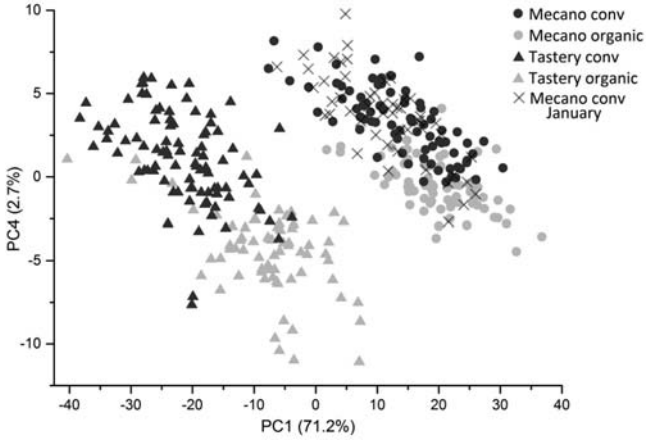


**Figure 2.** Scatter plot of PC1 versus PC4: triangles, Tastery; circles, Mecano; dark gray data points, conventional tomatoes; light gray data points, organic tomatoes. The group of Mecano conventionally planted in January is projected into the PCA plot and marked by crosses.

the planting is commonly performed later than in case of conventional farming using intensively heated greenhouses. To determine whether potential differences in organic and conventional tomatoes are irrespective of the planting date, Mecano cultivar was planted conventionally in both January and March, and $^1$H NMR spectra were subsequently checked for differences. When the group of Mecano cultivar planted in January was projected into the previously mentioned PCA model, no data separation from the group of conventionally grown Mecano cultivar planted in March is recognizable (Figure 2). Hence, the planting date evidently did not affect the composition of tomato ingredients.

Next, PCA was performed with each cultivar individually with overall 148 NMR spectra for Mecano cultivar (130 for CE planted in March and 18 for TF) and 161 NMR spectra for Tastery cultivar (143 for CE and 18 for TF). PCA scatter plots show a significant separation ($p < 0.001$ using $t$ test) between the groups of organically and conventionally grown tomatoes for both cultivars, observed along PC3 for Mecano and along PC1 for Tastery (Figure 3). Because PC3 explains only 4.6% of the data variance for the PCA of Mecano in comparison to PC1 with 55.8% explained variance for the PCA of Tastery, variations of $^1$H NMR spectra according to the type of farming seem to have a higher impact on the total variance in $^1$H NMR spectra for Tastery than for Mecano.

**Linear Discriminant Analysis.** Just as PCA, LDA forms linear combinations of variables to best explain the given data. The main difference between PCA and LDA is the fact that LDA is a supervised method. At first, each sample is assigned to a group subject to the sample's properties. Second, discriminant variables are examined by weighing the sample's variables, so that the differentiation between the predefined groups is maximized and differences of samples within one group are minimized. Once a discriminant analysis has been carried out, the resulting model can serve for an assignment of unknown samples to one of the predefined groups.

At first, LDA was performed with the two groups of organically or conventionally produced tomatoes (LDA1; altogether 309 NMR spectra were used for examination, 273 for CE, with tomatoes planted in March, and 36 for TF). As can be seen in Figure 4, the groups are successfully separated without any region of overlap. Moreover, the unwanted differentiation of the cultivars Mecano and Tastery does not occur because variables for cultivar separation are consciously weighted low in the computation of LDA.

The major disadvantage of supervised multivariate data analysis techniques such as LDA is the risk for building overfitted models. A possibly biased focus on model samples can hamper the application of group prediction for other samples. Hence, representative model samples are a key prerequisite for capable LDA models. In this context, validation of LDA1 was performed to evaluate the suitability for a prediction of the group membership.

The data set was separated into a calibration data set and a validation data set in two different ways. First, the calibration data set was created by systematically excluding both tomato samples

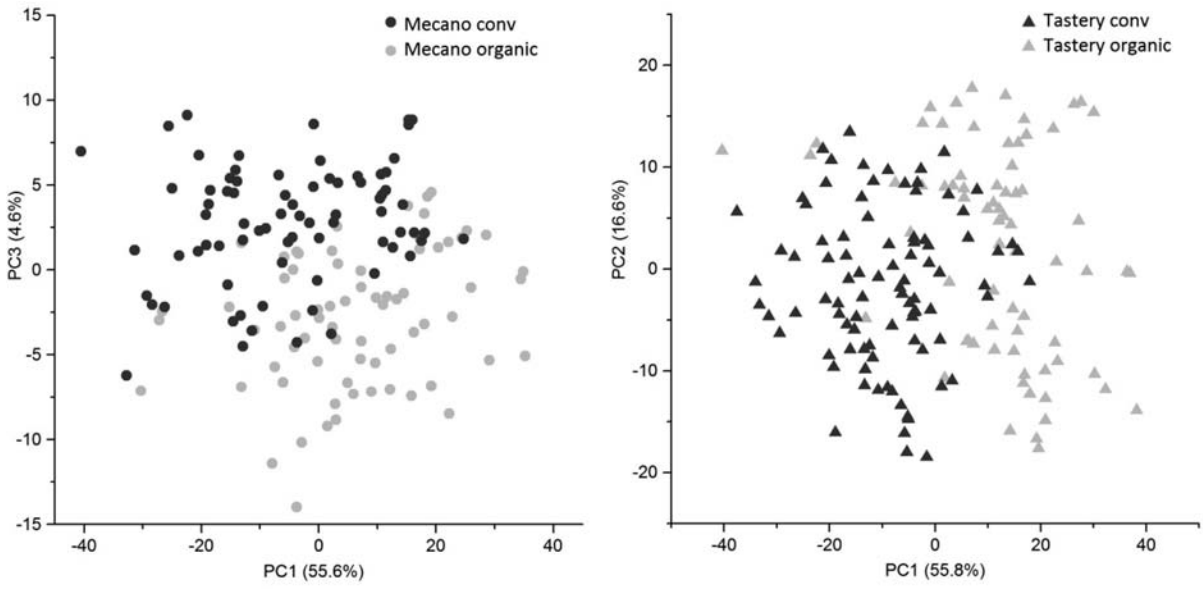


**Figure 3.** Scatter plots of PC1 versus PC3 of PCA for Mecano samples (circles; left side) and PC1 versus PC2 for Tastery samples (triangles; right side): dark gray data points, conventional tomatoes; light gray data points, organic tomatoes.


dx.doi.org/10.1021/jf502113r | J. Agric. Food Chem. 2014, 62, 8530−8540

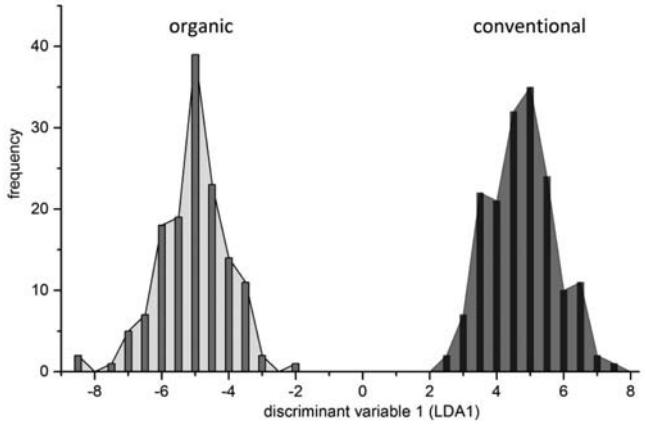


**Figure 4.** Frequency histogram of the values of discriminant variable 1 obtained by LDA1: dark gray, conventional tomato samples; light gray, organic tomato samples.

from CE and TF for validation. Overall, 81 tomato samples formed the validation data set, which is 26.21% of all 309 tomato samples (see Materials and Methods). In this case, validation showed excellent results with 100% correctly predicted group identities. Second, fruits from CE were used as calibration data set and fruits from TF as validation data set. Thus, merely 72.2% of group identities were predicted correctly.

When the calibration model is based only on fruits grown at CE, it is rather differentiating between the two specific CE greenhouses than between organic and conventional tomatoes in general, which makes it inapplicable for a group prediction of tomatoes from TF. In this context, the promising validation results (when both CE and TF tomato samples are included in the calibration data set) need to be questioned critically in terms of a basic suitability for an authentication of organic tomatoes from other producers. However, this validation illustrates the potential for differentiation if representative cultivation conditions are taken into consideration for LDA.

At this point the question arises whether it is possible to build a sufficient database of $^{1}$H NMR spectra from authentic tomatoes that fulfills the requirement to reflect the actually given variety of variable organically and conventionally grown tomatoes. Given the limitation of the present data set, this question cannot be answered yet, but the results so far suggest an extension of the experimental design with additional tomato varieties, producers, and farming conditions.

Moreover, it is reasonable to further examine the unwanted differences between greenhouses of the same growing regimen. For this, another LDA (LDA2) was performed with CE and TF tomato samples from each greenhouse classified with a single group, resulting in overall five groups (CE organic, CE conv, TF conv 1, TF conv 2, TF organic). Best separation results were achieved when a selection of spectral regions was used instead of the whole range from 0 to 10 ppm (Table 1). The selection was based on spectral regions with apparent differences between NMR spectra of organically and conventionally grown tomatoes, defined by a visual comparison when overlaying spectra with different colors according to organic and conventional cultivation. This rather represents a preselection, because another stepwise selection (using critical $F$ values) is performed when buckets are undergoing LDA.

The results of LDA2 can be seen at Figure 5. As the two groups of conventional TF tomato samples are hardly separated, it can be assumed that no relevant differences exist between them, yet all other groups are separated well. The unwanted differentiation between CE groups (circles) and TF groups (triangles and squares) appears along discriminant variable 2, showing higher values for CE groups than for TF groups. Besides, the key information on LDA2 is the separation achieved by discriminant variable 1: the conventional groups show higher values of discriminant variable 1 than the organic groups (Figure 5). Thus, the type of farming obviously represents a latent factor herein, and it was tested if LDA2 enables a prediction of the growing regimen based on the value of discriminant variable 1.

For this purpose, first validation steps with additional tomato samples were performed. Basically, two cases of wrong

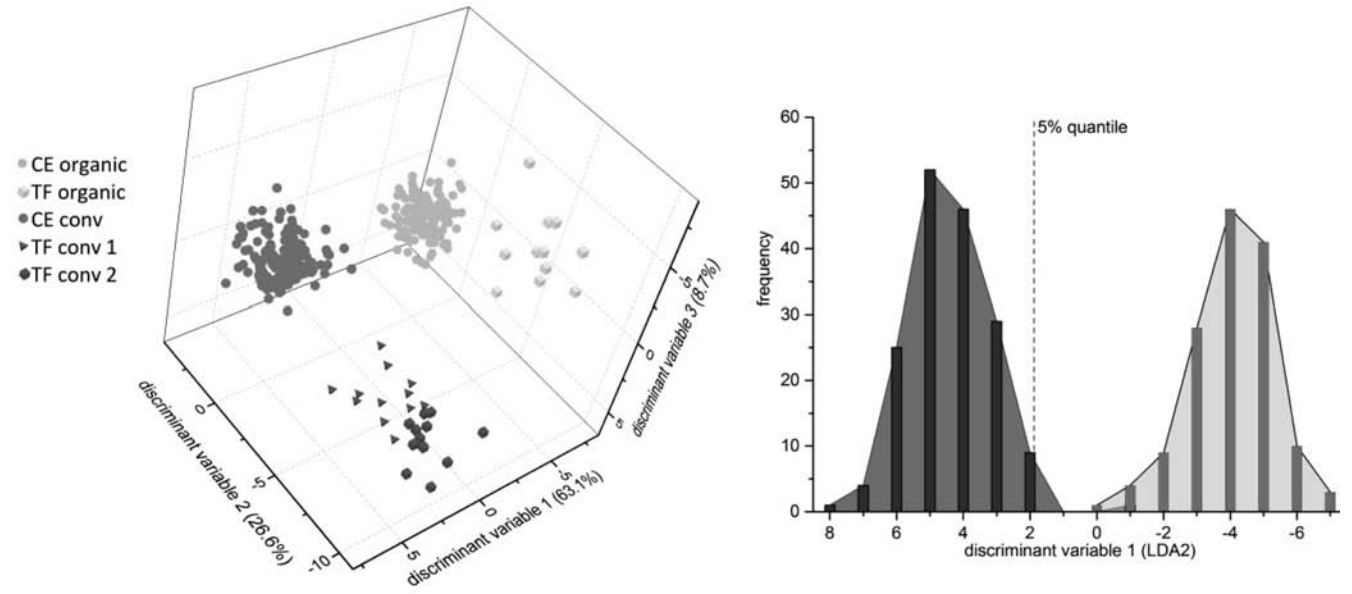


**Figure 5.** 3D scatter plot of discriminant variables 1, 2, and 3, with sphere symbols for CE samples, tetrahedral symbols for TF organic and TF conv 1, and cube symbols for TF conv 2: dark gray data points, conventional tomaotes; light gray data points, organic tomatoes (left side). Frequency histogram of the values of discriminant variable 1 obtained by LDA2: dark gray, conventional samples; light gray, organic samples (the auxiliary line shows the 5% quantile of the values of discriminant variable 1 for conventional tomato samples; right side).


dx.doi.org/10.1021/jf502113r | J. Agric. Food Chem. 2014, 62, 8530−8540

**Table 3. Results for the Prediction of the Growing Regimen Based on the Value of Discriminant Variable 1 (Obtained by LDA2) for Several Additional Tomato Samples (See Materials and Methods)**

| sample type and no. of samples ($n$) | | dv1 (LDA2) | growing regimen | prediction |
|---|---|---|---|---|
| (i) tomatoes of cultivar Tica organically grown at CE ($n$ = 8) | Tica | −1.56 | organic | organic |
| | Tica | −3.85 | organic | organic |
| | Tica | −2.73 | organic | organic |
| | Tica | −5.19 | organic | organic |
| | Tica | −1.79 | organic | organic |
| | Tica | −5.84 | organic | organic |
| | Tica | −5.10 | organic | organic |
| | Tica | −3.76 | organic | organic |
| (ii) tomatoes (cultivar Mecano) of another producer (Fürth, Germany) organically grown using different substrates, ($n$ = 6) | wood-perlite | 1.51 | conventional | organic |
| | wood-perlite | 4.19 | conventional | conventional |
| | cocos | 2.93 | conventional | conventional |
| | cocos | 5.38 | conventional | conventional |
| | perlite | 2.87 | conventional | conventional |
| | perlite | 3.68 | conventional | conventional |
| (iii) unripe (red-turning) tomatoes (cultivars Mecano and Tastery) organically/conventionally grown at CE ($n$ = 4) | Mecano | −3.20 | organic | organic |
| | Tastery | −4.04 | organic | organic |
| | Mecano | 2.41 | conventional | conventional |
| | Tastery | 4.83 | conventional | conventional |

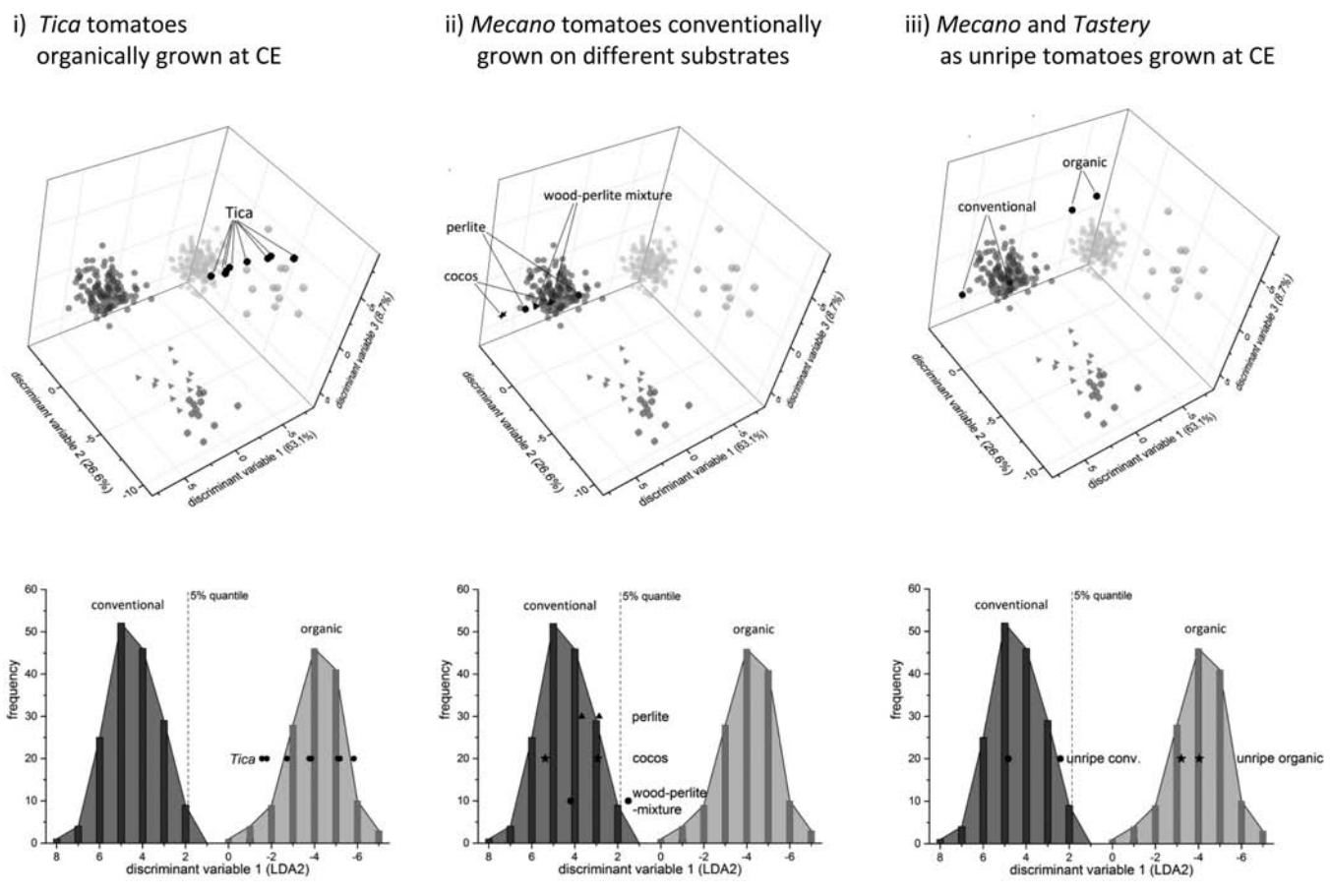


**Figure 6.** Projection of the prediction results for (i) Tica samples (left), (ii) Mecano samples conventionally grown on different substrates (middle), and (iii) unripe CE samples of Mecano and Tastery (right) into the 3D scatter plot of LDA2 (top; see Figure 5) and into the frequency histogram of the values of discriminant variable 1 obtained by LDA2 (bottom; see Figure 5).

predictions can occur: an organic fruit is falsely determined as conventional or a conventional fruit is falsely determined as organic. With the aim of preventing unjust allegations against reliable organic producers, the risk for conventionally grown tomatoes being falsely assigned as organic is rather accepted than the risk for organically grown tomatoes being falsely identified as


dx.doi.org/10.1021/jf502113r | J. Agric. Food Chem. 2014, 62, 8530−8540

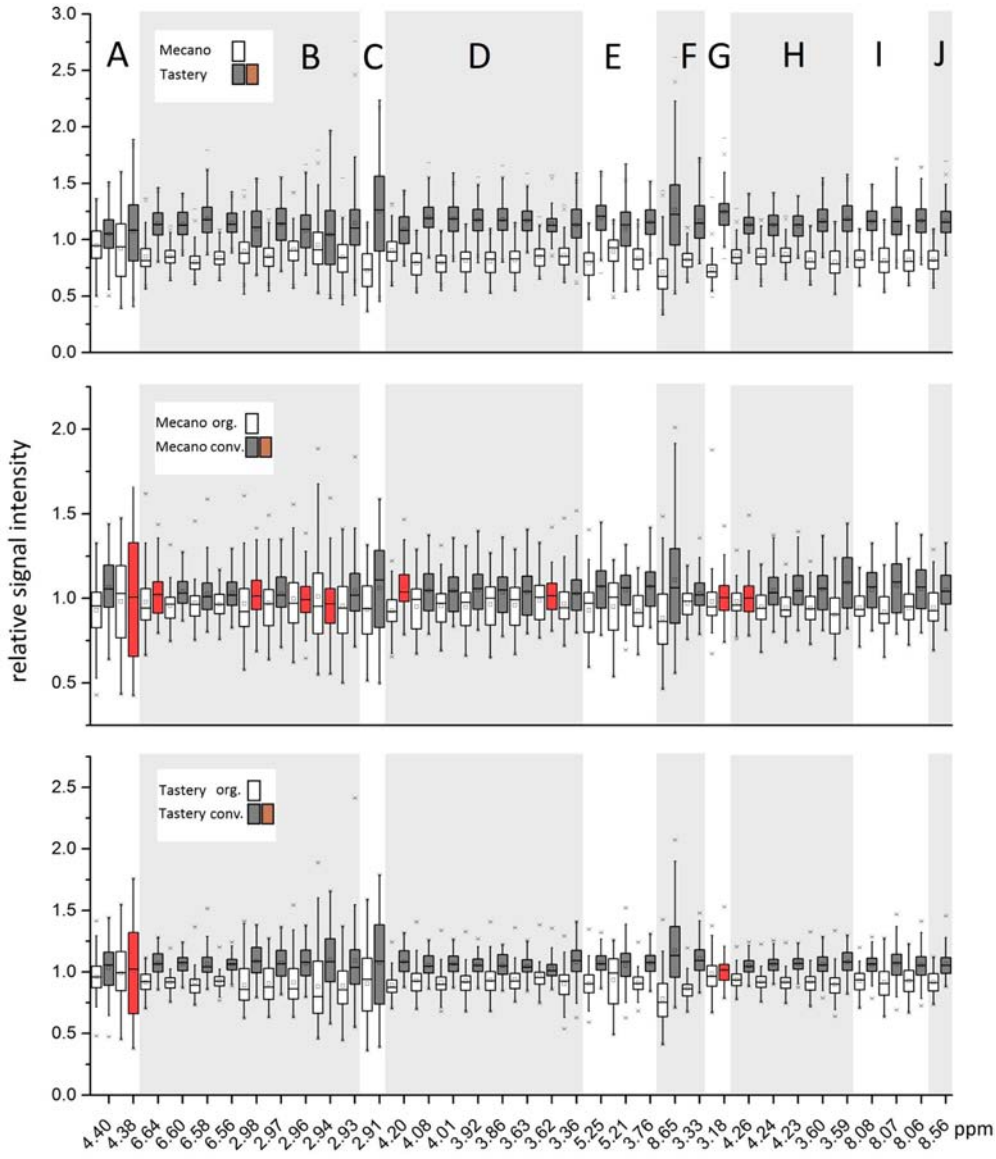


**Figure 7.** Box plot of relative bucket intensities for the cultivars Mecano and Tastery (top) and organically and conventionally grown tomatoes for Mecano (middle) and Tastery (bottom). Each box is determined by the 25th and 75th percentiles and each whisker by the 5th and 95th percentiles. Values higher than 75th percentile +1.5*interquartile range and lower than 25th percentile −1.5*interquartile range are marked by a cross as outliers. Significantly different bucket intensities are colored white/gray, and nonsignificantly different bucket intensities are colored white/red.

conventional. Hence, the decision rule for an assignment was built on the consideration that no more than 5% of conventional tomato samples are accepted to be falsely predicted as organically grown fruits. The value of discriminant variable 1 within LDA2 served as predictive indicator for the validation data set: values lower than the 5% quantile for discriminant variable 1 of conventional tomato samples (discriminant variable < 1.88) were assigned to organic farming and higher values to conventional farming (Figure 5).

In this way prediction was applied for several additional fruits that vary in cultivar, type of substrate for conventional farming, and degree of ripeness (see Materials and Methods). Results are displayed in Table 3 and Figure 6.

The results for the cultivar Tica are very promising, especially when considering that this cultivar was not taken into account within the LDA2 model. Because the cultivar Tica is close to Mecano, it can be assumed that once a cultivar type is part of the model, adequate prediction for similar cultivars can be performed. The results for additional tomato samples grown on different substrates are also satisfying: although no further tomato samples of this specific producer are part of the LDA2 model, correct predictions were achieved for five of six tomato samples, and the falsely predicted one has a value very close to the decision limit of the 5% quantile. Hence, the sort of substrate did not interfere with a prediction of conventional farming. The prediction for unripe fruits of Mecano and Tastery cultivar was right for all samples and, consequently, the degree of ripeness did not hamper an assignment of the cultivation method.

**Designation of Substances That Are Relevant for Differentiation.** In view of the differentiation between organically and conventionally grown tomatoes based on $^{1}$H NMR spectra, it is especially interesting to detect spectral regions and the corresponding substances that are responsible for data separation.

Given the promising validation results for an assignment of the growing regimen based on discriminant value 1 of LDA2, the


dx.doi.org/10.1021/jf502113r | J. Agric. Food Chem. 2014, 62, 8530−8540

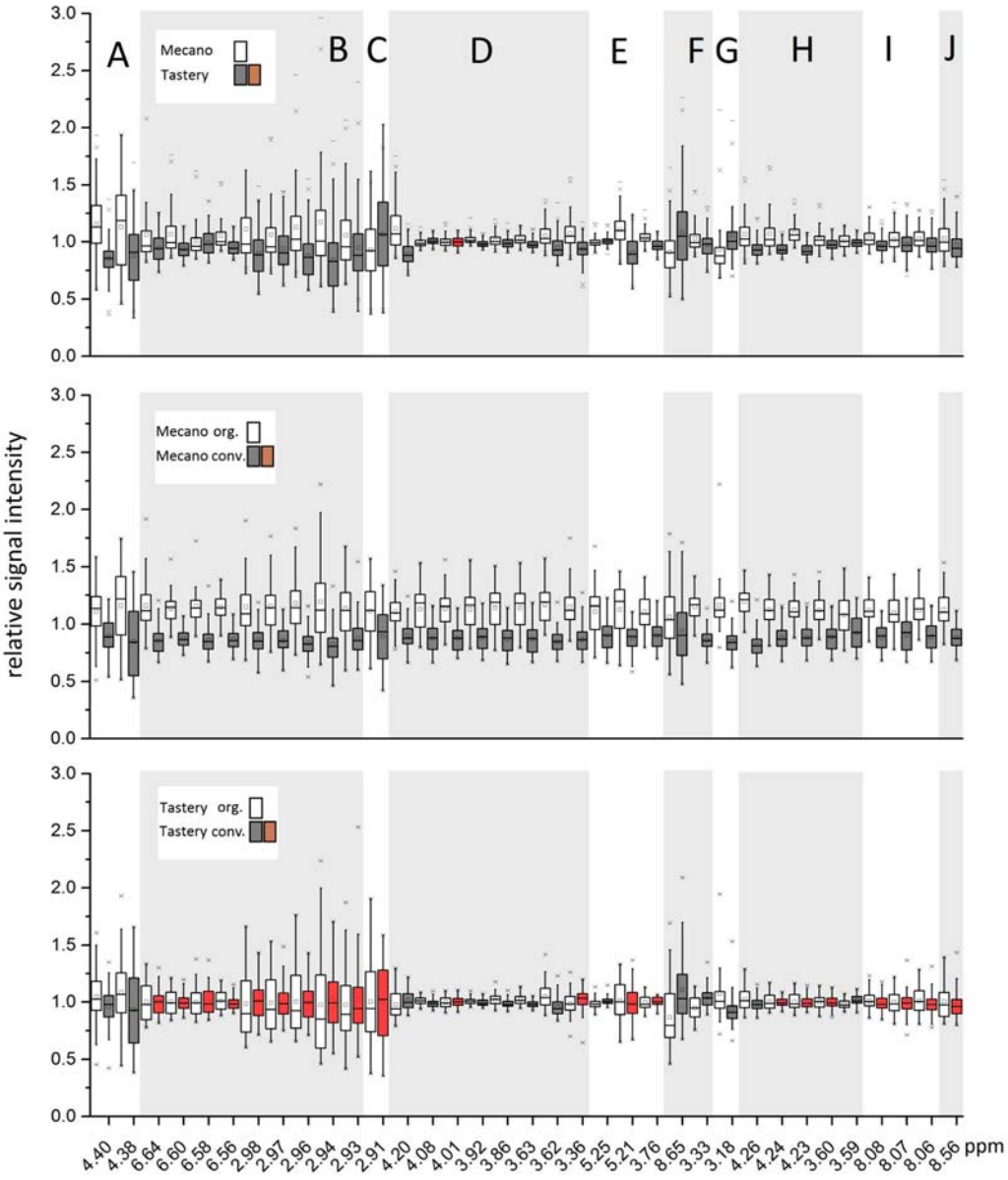


**Figure 8.** Box plot of relative bucket intensities, scaled to total signal intensities of the respective NMR spectra, for the cultivars Mecano and Tastery (top) and organically and conventionally grown tomatoes for Mecano (middle) and Tastery (bottom). Each box is determined by the 25th and 75th percentiles, and each whisker by the 5th and 95th percentiles. Values higher than 75th percentile +1.5*interquartile range and lower than 25th percentile −1.5*interquartile range are marked by a cross as outliers. Significantly different bucket intensities are colored white/gray, and nonsignificantly different bucket intensities are colored white/red.

overall 66 buckets used for its calculation were analyzed in more detail. Thirty-five buckets could be assigned to the reference signals of malic acid (A), asparagine (B), aspartic acid (C), fructose (D), glucose (E), histidine (F), choline (G), threonine (H), trigonelline (I), and adenosine monophosphate (J; assignment according to the literature[53]). These buckets were checked for significant differences between the cultivars Mecano and Tastery as well as for differences between organically and conventionally grown tomatoes between each cultivar.

Figures 7 and 8 show a comparison of the relative bucket intensities within cultivars and growing regimens in a box-plot diagram, whereby nonsignificantly different bucket intensities are highlighted white/red ($t$ test: $p > 0.05$) and significantly different bucket intensities are colored white/gray ($t$ test: $p < 0.05$). Figure 7 illustrates that the bucket intensities are mainly influenced by the tomato cultivar and consistently higher for the group of Tastery than for the group of Mecano. Additionally, within both cultivars, the signal intensities show on average higher values for conventionally grown than for organically grown tomatoes. In this connection, the differences are more distinct for Tastery than for Mecano.

Because the bucket intensities are continuously increased for the respective conventional group, this may be attributed to increased dry matter levels in conventionally grown fruits[2] instead of compositional differences. To reduce the influence of dry matter, the bucket intensities were referred to the total signal intensity of the spectra and again compared within cultivars and cultivation methods (Figure 8; the total intensity was defined as signal intensity from 0 to 10 ppm minus the regions of water and ethanol signals from 4.85−4.67, 3.70−3.60 and 1.22−1.14 ppm).

This scaling procedure massively changes the image of bucket intensities: the separation of Mecano and Tastery as well as the separation of the organic and conventional group for Tastery deteriorated, whereas the separation of organic and conventional Mecano tomato samples improved. Moreover, higher signal intensities are averaged for the organic group compared to the conventional group, opposed to previous results for unscaled buckets.

However, individual buckets show irregular distributions, although they are actually assigned to the same substance. For example, the bucket at 4.40 ppm shows significant differences between organically and conventionally grown tomatoes for Mecano cultivar, whereas the bucket at 4.38 ppm is non-significantly different for these growing regimens (Figure 7), despite both buckets being attributed to malic acid (A). This is presumably due to an overlap with signals from other ingredients that are not assigned yet. Thus, the present results are first estimations, and at this point classical quantitative methods are needed to confirm these results.

## AUTHOR INFORMATION


### Corresponding Author

*(M.H.) Phone: +49 9131 68087159. Fax: +49 9131 68087210. E-mail: monika.hohmann@lgl.bayern.de.



### Funding

This research was funded by the Bavarian State Ministry of the Environment and Consumer Protection within Research Project 11-33.

### Notes

The authors declare no competing financial interest.


## ACKNOWLEDGMENTS


Special thanks are due to colleagues from the Bavarian State Research Institute of Viticulture and Horticulture (LWG, Bamberg, Germany) for the helpful introduction into agricultural implementations and the realization of the cultivation experiment. Furthermore, particular thanks are given to all producers for providing authentic tomato samples.


## REFERENCES


(1) Sahota, A. The world of organic agriculture, statistics and emerging trends 2013, the global market for organic food and drink; https://www.fibl.org/fileadmin/documents/shop/1606-organic-world-2013.pdf (accessed April 28, 2014).

(2) Caris-Veyrat, C.; Amiot, M. J.; Tyssandier, V.; Grasselly, D.; Buret, M.; Mikolajczak, M.; Guilland, J. C.; Bouteloup-Demange, C.; Borel, P. Influence of organic versus conventional agricultural practice on the antioxidant microconstituent content of tomatoes and derived purees; consequences on antioxidant plasma status in humans. *J. Agric. Food Chem.* **2004**, *52*, 6503−6509.

(3) Mitchell, A. E.; Hong, Y. J.; Koh, E.; Barrett, D. M.; Bryant, D. E.; Denison, R. F.; Kaffka, S. Ten-year comparison of the influence of organic and conventional crop management practices on the content of flavonoids in tomatoes. *J. Agric. Food Chem.* **2007**, *55*, 6154−6159.

(4) Vallverdú-Queralt, A.; Medina-Remón, A.; Casals-Ribes, I.; Amat, M.; Lamuela-Raventós, R. M. A metabolomic approach differentiates between conventional and organic ketchups. *J. Agric. Food Chem.* **2011**, *59*, 11703−11710.

(5) Vallverdú-Queralt, A.; Medina-Remón, A.; Casals-Ribes, I.; Amat, M.; Lamuela-Raventós, R. M. Is there any difference between the phenolic content of organic and conventional tomato juice? *Food Chem.* **2012**, *130*, 222−227.

(6) Hallmann, E.; Lipowski, J.; Marszalek, K.; Rembialkowska, E. The seasonal variation in bioactive compounds content in juice from organic and non-organic tomatoes. *Plant Foods Hum. Nutr.* **2013**, *68*, 171−176.

(7) Aherne, S. A.; Jiwan, M. A.; Daly, T.; O'Brien, N. M. Geographical location has greater impact on carotenoid content and bioaccessibility from tomatoes than variety. *Plant Foods Hum. Nutr.* **2009**, *64*, 250−256.

(8) Gravel, V.; Blok, W.; Hallmann, E.; Carmona-Torres, C.; Wang, H. Y.; Van de Peppel, A.; Còndor Golec, A. F.; Dorais, M.; Van Meeterens, U.; Heuvelink, E.; Rembialkowska, E.; Van Bruggen, A. H. C. Differences in N uptake and fruit quality between organically and conventionally grown greenhouse tomatoes. *Agron. Sustain. Dev.* **2010**, *30*, 797−806.

(9) Rodríguez-Munoz, E.; Herrera-Ruiz, G.; Pedraza-Aboytes, G.; Loarca-Pina, G. Antioxidant capacity and antimutagenic activity of natural oleoresin from greenhouse grown tomatoes (*Lycopersicon esculentum*). *Plant Foods Hum. Nutr.* **2009**, *64*, 46−51.

(10) Dalal, K. B.; Salunkhe, D. K.; Boe, A. A.; Olson, L. E. Certain physiological and biochemical changes in developing tomato fruit (*Lycopersicon esculentum* Mill). *J. Food Sci.* **1965**, *30*, 504−508.

(11) Giovanelli, G.; Lavelli, V.; Peri, C.; Nobili, S. Variation in antioxidant components of tomato during vine and post-harvest ripening. *J. Sci. Food Agric.* **1999**, *79*, 1583−1588.

(12) Migliori, C.; Di Cesare, L. F.; Lo Scalzo, R.; Campanelli, G.; Ferrari, V. Effects of organic farming and genotype on alimentary and nutraceutical parameters in tomato fruits. *J. Sci. Food Agric.* **2012**, *92*, 2833−2839.

(13) Hallmann, E. The influence of organic and conventional cultivation systems on the nutritional value and content of bioactive compounds in selected tomato types. *J. Sci. Food Agric.* **2012**, *92*, 2840−2848.

(14) Nelson, L.; Giles, J.; Macilwain, C.; Gewin, V. Organic FAQs. *Nature* **2004**, *428*, 796−798.

(15) Eppendorfer, W. H.; Bille, S. W. Free and total amino acid composition of edible parts of beans, kale, spinach, cauliflower and potatoes as influenced by nitrogen fertilisation and phosphorus and potassium deficiency. *J. Sci. Food Agric.* **1996**, *71*, 449−458.

(16) Muttucumaru, N.; Powers, S. J.; Elmore, J. S.; Mottram, D. S.; Halford, N. G. Effects of nitrogen and sulfur fertilization on free amino acids, sugars, and acrylamide-forming potential in potato. *J. Agric. Food Chem.* **2013**, *61*, 6734−6742.

(17) Boggio, S. B.; Palatnik, J. F.; Heldt, H. W.; Valle, E. M. Changes in amino acid composition and nitrogen metabolizing enzymes in ripening fruits of *Lycopersicon esculentum* Mill. *Plant Sci.* **2000**, *159*, 125−133.

(18) Valle, E. M.; Boggio, S. B.; Heldt, H. W. Free amino acid composition of phloem sap and growing fruit of *Lycopersicon esculentum*. *Plant Cell Physiol.* **1998**, *39*, 458−461.

(19) Kelly, S. D.; Bateman, A. S. Comparison of mineral concentrations in commercially grown organic and conventional crops − tomatoes (*Lycopersicum esculentum*) and lettuces (*Lactuca sativa*). *Food Chem.* **2010**, *119*, 738−745.

(20) Gosling, P.; Hodge, A.; Goodlass, G.; Bending, G. D. Arbuscular mycorrhizal fungi and organic farming. *Agric. Ecosyst. Environ.* **2006**, *113*, 17−35.

(21) Bateman, A. S.; Kelly, S. D.; Jickells, T. D. Nitrogen isotope relationships between crops and fertilizer: implications for using nitrogen isotope analysis as an indicator of agricultural regime. *J. Agric. Food Chem.* **2005**, *53*, 5760−5765.

(22) Yoneyama, T.; Kouno, K.; Yazaki, J. Variation of natural $^{15}N$ abundance of crops and soils in Japan with special reference to the effect of soil conditions and fertilizer applications. *Soil Sci. Plant Nutr.* **1990**, *36*, 667−675.

(23) Nakano, A.; Uehara, Y.; Yamauchi, A. Effect of organic and inorganic fertigation on yields, $\delta^{15}N$ values and $\delta^{13}C$ values of tomato (*Lycopersicon esculentum* Mill. cv. Saturn). *Plant Soil* **2003**, *255*, 343−349.

(24) Bateman, A. S.; Kelly, S. D.; Woolfe, M. Nitrogen isotope composition of organically and conventionally grown crops. *J. Agric. Food Chem.* **2007**, *55*, 2664−2670.

(25) Esslinger, S.; Riedl, J.; Fauhl-Hassek, C. Potential and limitations of non-targeted fingerprinting for authentication of food in official control. *Food Res. Int.* **2014**, *60*, 189−204.
(26) Boffo, E. F.; Tavares, L. A.; Tobias, A. C. T.; Ferreira, M. M. C.; Ferreira, A. G. Identification of components of Brazilian honey by $^1$H NMR and classification of its botanical origin by chemometric methods. *Food Sci. Technol.−LEB* **2012**, *49*, 55−63.
(27) Consonni, R.; Cagliani, L. R. Geographical characterization of polyfloral and acacia honeys by nuclear magnetic resonance and chemometrics. *J. Agric. Food Chem.* **2008**, *56*, 6873−6880.
(28) Donarski, J. A.; Jones, S. A.; Charlton, A. J. Application of cryoprobe $^1$H nuclear magnetic resonance spectroscopy and multivariate analysis for the verification of Corsican honey. *J. Agric. Food Chem.* **2008**, *56*, 5451−5456.
(29) Bertelli, D.; Lolli, M.; Papotti, G.; Bortolotti, L.; Serra, G.; Plessi, M. Detection of honey adulteration by sugar syrups using one-dimensional and two-dimensional high-resolution nuclear magnetic resonance. *J. Agric. Food Chem.* **2010**, *58*, 8495−8501.
(30) Longobardi, F.; Ventrella, A.; Napoli, C.; Humpfer, E.; Schütz, B.; Schäfer, H.; Kontominas, M. G.; Sacco, A. Classification of olive oils according to geographical origin by using $^1$H NMR fingerprinting combined with multivariate analysis. *Food Chem.* **2012**, *130*, 177−183.
(31) Alonso-Salces, R. M.; Héberger, K.; Holland, M. V.; Morena-Rojas, J. M.; Mariani, C.; Bellan, G.; Reniero, F.; Guillou, C. Multivariate analysis of NMR fingerprint of the unsaponifiable fraction of virgin olive oils for authentication purposes. *Food Chem.* **2010**, *118*, 956−965.
(32) Alonso-Salces, R. M.; Moreno-Rojas, J. M.; Holland, M. V.; Reniero, F.; Guillou, C.; Heberger, K. Virgin olive oil authentication by multivariate analyses of $^1$H NMR fingerprints and $\delta^{13}$C and $\delta^2$H data. *J. Agric. Food Chem.* **2010**, *58*, 5586−5596.
(33) Mannina, L.; Marini, F.; Gobbino, M.; Sobolev, A. P.; Capitani, D. NMR and chemometrics in tracing European olive oils: the case study of Ligurian samples. *Talanta* **2010**, *80*, 2141−2148.
(34) Mannina, L.; D'Imperio, M.; Capitani, D.; Rezzi, S.; Guillou, C.; Mavromoustakos, T.; Molero Vilchez, M. D.; Herrera Fernández, A.; Thomas, F.; Aparicio, R. $^1$H NMR-based protocol for the detection of adulterations of refined olive oil with refined hazelnut oil. *J. Agric. Food Chem.* **2009**, *57*, 11550−11556.
(35) Son, H. S.; Hwang, G. S.; Ahn, H. J.; Park, W. M.; Lee, C. H.; Hong, Y. S. Characterization of wines from grape varieties through multivariate statistical analysis of $^1$H NMR spectroscopic data. *Food Res. Int.* **2009**, *42*, 1483−1491.
(36) Lopez-Rituerto, E.; Savorani, F.; Avenoza, A.; Busto, J. H.; Peregrina, J. M.; Engelsen, S. B. Investigations of La Rioja terroir for wine production using $^1$H NMR metabolomics. *J. Agric. Food Chem.* **2012**, *60*, 3452−3461.
(37) Anastasiadi, M.; Zira, A.; Magiatis, P.; Haroutounian, S. A.; Skaltsounis, A. L.; Mikros, E. $^1$H NMR-based metabonomics for the classification of Greek wines according to variety, region, and vintage. Comparison with HPLC data. *J. Agric. Food Chem.* **2009**, *57*, 11067−11074.
(38) Godelmann, R.; Fang, F.; Humpfer, E.; Schütz, B.; Bansbach, M.; Schäfer, H.; Spraul, M. Targeted and nontargeted wine analysis by $^1$H NMR spectroscopy combined with multivariate statistical analysis. Differentiation of important parameters: grape variety, geographical origin, year of vintage. *J. Agric. Food Chem.* **2013**, *61*, 5610−5619.
(39) Papotti, G.; Bertelli, D.; Graziosi, R.; Silvestri, M.; Bertacchini, L.; Durante, C.; Plessi, M. Application of one- and two-dimensional NMR spectroscopy for the characterization of protected designation of origin Lambrusco wines of Modena. *J. Agric. Food Chem.* **2013**, *61*, 1741−1746.
(40) Son, H. S.; Hwang, G. S.; Kim, K. M.; Ahn, H. J.; Park, W. M.; Van Den Berg, F.; Hong, Y. S.; Lee, C. H. Metabolomic studies on geographical grapes and their wines using $^1$H NMR analysis coupled with multivariate statistics. *J. Agric. Food Chem.* **2009**, *57*, 1481−1490.
(41) Ali, K.; Maltese, F.; Toepfer, R.; Choi, Y. H.; Verpoorte, R. Metabolic characterization of Palatinate German white wines according to sensory attributes, varieties, and vintages using NMR spectroscopy and multivariate data analyses. *J. Biomol. NMR* **2011**, *49*, 255−266.
(42) Spraul, M.; Schütz, B.; Rinke, P.; Koswig, S.; Humpfer, E.; Schäfer, H.; Mörtter, M.; Fang, F.; Marx, U. C.; Minoja, A. NMR-based multi parametric quality control of fruit juices: SGF profiling. *Nutrients* **2009**, *1*, 148−155.
(43) Tiziani, S.; Schwartz, S. J.; Vodovotz, Y. Profiling of carotenoids in tomato juice by one- and two-dimensional NMR. *J. Agric. Food Chem.* **2006**, *54*, 6094−6100.
(44) Sánchez Perez, E. M.; Iglesias, M. J.; López Ortiz, F.; Sánchez Perez, I.; Mártinez Galera, M. Study of the suitability of HRMAS NMR for metabolic profiling of tomatoes: application to tissue differentiation and fruit ripening. *Food Chem.* **2010**, *122*, 877−887.
(45) Mounet, F.; Lemaire-Chamley, M.; Maucourt, M.; Carbasson, C.; Giraudel, J. L.; Deborde, C.; Lessire, R.; Gallusci, P.; Betrand, W.; Gaudillére, M.; Rothan, C.; Rolin, D.; Moing, A. Quantitative metabolic profiles of tomato flesh and seeds during fruit development: contemporary analysis with ANN and PCA. *Metabolomics* **2007**, *3*, 273−288.
(46) Musse, M.; Quellec, S.; Devaux, M. F.; Cambert, M.; Lahaye, M.; Mariette, F. An investigation of the structural aspects of the tomato fruit by means of quantitative nuclear magnetic resonance imaging. *Magn. Reson. Imaging* **2009**, *27*, 709−719.
(47) Moing, A.; Maucourt, M.; Renaud, C.; Gaudillere, M.; Brouquisse, R.; Lebouteiller, B.; Gousset-Dupont, A.; Vidal, J.; Granot, D.; Denoyes-Rothan, B.; Lerceteau-Kohler, E.; Rolin, D. Quantitative metabolic profiling by 1-dimensional $^1$H-NMR analyses: application to plant genetics and functional genomics. *Funct. Plant Biol.* **2004**, *31*, 889−902.
(48) Herrmann, K. Übersicht über die Inhaltsstoffe der Tomaten. *Z. Lebensm. Unters. Forsch.* **1979**, *169*, 179−200.
(49) Sobolev, A. P.; Segre, A.; Lamanna, R. Proton high-field NMR study of tomato juice. *Magn. Reson. Chem.* **2003**, *41*, 237−245.
(50) Barton, R. H.; Waterman, D.; Bonner, F. W.; Holmes, E.; Clarke, R.; Procardis, C.; Nicholson, J. K.; Lindon, J. C. The influence of EDTA and citrate anticoagulant addition to human plasma on information recovery from NMR-based metabolic profiling studies. *Mol. Biosyst.* **2010**, *6*, 215−224.
(51) Friebolin, H. Relaxation. In *Ein- und zweidimensionale NMR-Spektroskopie, eine Einführung*, 2nd ed.; Wiley VCH, Weinheim, Germany, 1992; pp 176−177.
(52) Holzgrabe, U. Quantitative NMR spectroscopy in pharmaceutical applications. *Prog. Nucl. Magn. Reson. Spectrosc.* **2010**, *57*, 229−240.
(53) Le Gall, G.; Colquhoun, I. J.; Davis, A. L.; Collins, G. J.; Verhoeyen, M. E. Metabolite profiling of tomato (*Lycopersicon esculentum*) using $^1$H NMR spectroscopy as a tool to detect potential unintended effects following a genetic modification. *J. Agric. Food Chem.* **2003**, *51*, 2447−2456.

JOURNAL OF AGRICULTURAL AND FOOD CHEMISTRY

Addition/Correction

pubs.acs.org/JAFC

# Correction to Overview of Plant Chitinases Identified as Food Allergens

Mariateresa Volpicella, Claudia Leoni, Immacolata Fanizza, Antonio Placido, Elide A. Pastorello, and Luigi R. Ceci*

*J. Agric. Food Chem.* **2014**, *62* (25), 5734−5742. DOI: 10.1021/jf5007962

The correct version of Figure 1 appears below. Correction is required because in the original submission the Roman numerals in the pink boxes were wrong.

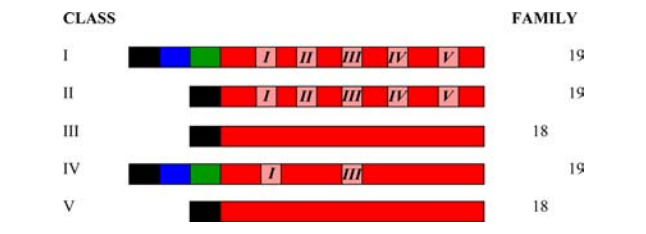


**Figure 1.** Schematic representation of different classes of chitinases of the 18 and 19 GH families. Color code: black = PM, blue = CtBM, green = LM, red = CM, and pink = surface loops. In order to adhere to previous literature, classes and surface loops have been both indicated with Roman figures, but italic font has been introduced for loops. Lengths of structural modules and positions of surface loops are only indicative. Adapted with permission from ref 24. Copyright 2009 Springer.

**Published:** August 8, 2014

ACS Publications © 2014 American Chemical Society

JOURNAL OF AGRICULTURAL AND FOOD CHEMISTRY

Addition/Correction

pubs.acs.org/JAFC

# Correction to Zingiberenol, (1*R*,4*R*,1′*S*)-4-(1′,5′-Dimethylhex-4′-enyl)-1-methylcyclohex-2-en-1-ol, Identified as the Sex Pheromone Produced by Males of the Rice Stink Bug *Oebalus poecilus* (Heteroptera: Pentatomidae)

Márcio Wandré Morais de Oliveira, Miguel Borges, Carlos Kleber Zago Andrade, Raul Alberto Laumann, José Alexandre Freitas Barrigossi, and Maria Carolina Blassioli-Moraes*

*J. Agric. Food Chem.* **2013**, *61* (32), 7777−7785. DOI: 10.1021/jf402765b

The configuration is now correctly shown in the title above.

**Published:** August 11, 2014

ACS Publications © 2014 American Chemical Society

JOURNAL OF AGRICULTURAL AND FOOD CHEMISTRY

Article

pubs.acs.org/JAFC

# Impact of Cationic Surfactant on the Self-Assembly of Sodium Caseinate

Marko Vinceković,*[,†] Marija Ćurlin,[‡] and Darija Jurašin*[,§]

[†]Department of Chemistry, Faculty of Agriculture, and [‡]Department of Histology and Embryology, School of Medicine, University of Zagreb, Zagreb, Croatia

[§]Division of Physical Chemistry, Ruđer Bošković Institute, Zagreb, Croatia

**ABSTRACT:** The impact of a cationic surfactant, dodecylammonium chloride (DDACl), on the self-assembly of sodium caseinate (SC) has been investigated by light scattering, zeta potential, and rheological measurements as well as by microscopy (transmission electron and confocal laser scanning microscopy). In SC dilute solutions concentration-dependent self-assembly proceeds through the formation of spherical associates and their aggregation into elongated structures composed of connected spheres. DDACl interacts with SC via its hydrophilic and hydrophobic groups, inducing changes in SC self-assembled structures. These changes strongly depend on the surfactant aggregation states (monomeric or micellar) as well as concentration ratio of both components, leading to the formation of soluble and insoluble complexes of nano- to microdimensions. DDACl monomers interact with SC self-assembled entities in a different way compared to their micelles. Surfactant monomers form soluble complexes (similar to surfactant mixed micelles) at lower SC concentration but insoluble gelatinous complexes at higher SC concentration. At surfactant micellar concentration soluble complexes with casein chains wrapped around surfactant micelles are formed. This study suggests that the use of proper cationic surfactant concentration will allow modification and control of structural changes of SC self-assembled entities.

**KEYWORDS:** *casein, cationic surfactant, self-assembling, complexation*

## INTRODUCTION

Biopolymers and surfactants are often used simultaneously in the food, pharmaceutical, and cosmetics industries, production of agrochemicals, etc. Understanding their interactions at the molecular level is therefore of great importance in tailoring the final properties of manufactured products. Intensive research on intermolecular interactions between biopolymers (proteins or polysaccharides) and low molecular weight surfactants has provided many new insights into the processes and mechanisms of interactions; however, there is no universal theory describing their complex interactions.[1−3] Understanding the behavior of mixtures containing amphiphilic molecules, such as proteins and low molecular weight surfactants, is not straightforward because these species self-assemble in bulk solution and at interfaces by different mechanisms, leading to competitive association and adsorption processes.[2] Although much is known about the interactions between surfactants and proteins, knowledge of their molecular structure/reactivity relationship in relationship to their functionality in complex systems is still rather limited, and empirical approaches continue to be required in tackling the problem of improvement and optimization of processing conditions.

Depending on aqueous conditions (pH, ionic strength, temperature) and features of the molecular structures of both proteins and surfactants as well as on their concentration and molar ratio, the overall character of their interactions may be significantly different. Addition of small-molecule surfactants to protein solutions modifies the protein functional properties both at the interfaces and in bulk. It was found that hydrophobic and electrostatic interactions as well as hydrogen bonding are the main factors governing protein and surfactant complexation, resulting in specific surface properties of complexes and conformational changes of proteins.[3] This is of special concern in controlled release application, such as plant protection. There are increasing concerns about the level of plant protection active agents found in soil and plant materials causing environmental and health problems. In line with global efforts toward sustainable agriculture, encapsulation with biopolymer matrices has been recognized as an effective method for controlled release of an active agent used for plant protection.[4] The development of systems for controlled release strongly depends on adequate physicochemical properties of biopolymers and on economically sustainable production. Milk proteins are widely available, inexpensive, and generally recognized as safe raw materials with many structural properties and functionalities that make them highly suitable natural vehicles for bioactives.[5] The presence of anionic phosphoserine and other anionic amino acid residues makes caseins available for cation binding, which is important for the delivery of bioactive cations (copper, iron, etc.) to plants in acceptable form. The main objective of the present work was to explore the possibility of guiding the self-assembly of sodium caseinate (SC) with the model cationic surfactant dodecylammonium chloride (DDACl) and consequently to enhance the suitability of SC self-assembled structures for loading bioactive cations.

Most of the studies dealing with the impact of surfactants on the supramolecular organization of the main milk proteins,

Received: April 8, 2014
Revised: June 18, 2014
Accepted: July 31, 2014
Published: July 31, 2014

ACS Publications © 2014 American Chemical Society



dx.doi.org/10.1021/jf5016472 | J. Agric. Food Chem. 2014, 62, 8543−8554

caseins, have been conducted with anionic or nonionic surfactants.[3,6] Data on the interaction with cationic surfactants are relatively scarce.[7−10] One of the interesting features of the mixture of oppositely charged amphiphilic molecules is that the self-assembled structures and the charge of their electrical double layer can be manipulated by simple variation of concentrations and molar ratio of components.

Sodium caseinate is the sodium salt of the main milk proteins, caseins. Caseins are relatively small, amphiphilic, randomly or flexibly structured molecules composed of four main proteins: $\alpha_{s1}$-, $\alpha_{s2}$-, $\beta$-, and $\kappa$-caseins. They are proteins characterized by an open structure and a high degree of hydration. In none of their native states do they adopt random coil conformation, but they contain significant amounts of defined secondary structure with few tertiary folds, but do not, for various reasons, fold into compact globular proteins.[11] Casein monomers as complex amphiphilic copolymers exhibit differences in self-association due to the different hydrophobic and hydrophilic regions along the protein chain; $\beta$- and $\kappa$-caseins self-assemble as surfactants, whereas $\alpha_s$-caseins associate in a series of consecutive steps to form open aggregates, which can be rigid worm-like structures.[12] Besides expressed self-association, casein molecules also interact with each other, forming associated structures with the $\kappa$-casein mainly located on the surface and other caseins mainly located in the interior of self-assembled entities.[13−16] The microenvironment, such as pH, ionic strength, concentration, temperature, and surfactant, can significantly alter the self-assembled structures of casein molecules.[12,17,18]

All literature data dealing with casein and oppositely charged surfactant interactions rely on the experiments performed at various surfactant concentrations and constant casein concentration. On the contrary, our data rely on experiments performed at a constant concentration of cationic surfactant and various SC concentrations to show how surfactant aggregation state (monomer or micellar) affects SC self-assembly. The major novelty of our research is the comprehensive focus on the overall changes in the mechanism of SC self-assembly induced by the addition of constant concentration, both monomer and micellar, of model cationic surfactant. We hope that the results obtained will provide better insight into the nature of interactions between caseins and an oppositely charged surfactant, providing an opportunity to control the formation of SC self-assembled structures.

## EXPERIMENTAL PROCEDURES

**Materials and Sample Preparation.** Commercial food-grade SC containing protein with sodium ≤3% and calcium ∼0.1% (Sigma-Aldrich, USA) was used throughout without purification and was dried in a vacuum before weighing. Preparation and purification of DDACl were described earlier.[19] Stock solutions were prepared by dissolving dried SC or DDACl in deionized water, treated in an ultrasonic bath, filtered through a 0.45 $\mu$m filter (Millipore Corp.), and left to stand overnight.

Numerous literature data relating to casein self-assembly have generally been obtained at adjusted pH and ionic strength. On the contrary, we prepared samples with various SC concentrations in the presence or absence of constant DDACl concentrations (monomer (0.001 mol dm$^{-3}$) or micellar (0.03 mol dm$^{-3}$)) with no pH adjustment or salt added. Samples were left to equilibrate for 24 h in a water bath at 298 K. All samples contained 0.01 wt % $NaN_3$ as a bacteriostatic agent.

**Methods.** *Electrical Conductivity and Surface Tension Measurements.* Electrical conductivity ($\kappa$) measurements were performed in a temperature-controlled double-walled glass container with a circulation of water using a conductivity meter (Metrohm, Herisau, Switzerland). The $\kappa$ was measured to within 0.01 $\mu$S. The surface tension ($\gamma$) was determined using the Du Noüy ring method (interfacial tensiometer K100, Krűss, Hamburg, Germany). The $\gamma$ was measured to within 0.001 mN m$^{-1}$. These values then were corrected by using the tables of Huh and Mason. The surface tension of water was measured regularly to provide values for the pure solvent and to check that the technique was being properly carried out. All measurements were performed at 298 K.

*Light Scattering and Zeta Potential Measurements.* Light scattering and electrophoretic measurements were performed using Zetasizer Nano ZS (Malvern Instruments, Malvern, UK). The size of particles ($d$) was determined by means of a dynamic light scattering (DLS) technique using a photon correlator spectrophotometer equipped with a 532 nm "green" laser. DLS measurements were performed at a backscatter angle of 173° to reduce the extent of multiple scattering as well as the effects of dust. Numerous static and DLS studies in SC solutions have shown that variation in their chemical composition resulting from the preparation procedure and methods of sample preparation (centrifugation, filtration, etc.) as well as the experimental conditions led to differences in the reported light scattering data.[20−24] Casein self-assembled entities are polydisperse in size, including in some cases the coexistence of several populations as well as a residual lipid material that could not be completely removed upon sample purification. In a polydisperse sample, the scattering intensity of large particles dominates that of smaller ones and the meaning of the average hydrodynamic size is not straightforward; that is, the intensity-weighted size distribution given by DLS overestimates larger aggregates. To distinguish the contribution of SC from that of large particles, DLS data have been analyzed by relying on the volume and number size distributions. The data processing was done by the Zetasizer software 6.32 (Malvern Instruments). The mean diameters derived from volume and number size distributions were always based on six or more measurements with a relative standard deviation of ±20%.

The zeta potential ($\zeta$) of particles was calculated from the measured electrophoretic mobility by means of the Henry equation using the Smoluchowski approximation ($f$(Ka) = 1.5). Results are reported as an average value of five measurements with a relative standard deviation of ±10%. Samples were prepared by dilution of stock solutions in triple-distilled water, which was previously filtered through a 0.45 $\mu$m Millipore filter.

All measurements were performed at 298 K.

*Rheological Measurements.* Rheological measurements were employed to obtained the flow behavior and viscosity data. Measurements were performed with a stress-controlled rheometer with a double-gap Couette cell (MC1, Paar Physica, Graz, Austria). Flow curves were determined by recording the steady shear rate ($\gamma$) for a series of imposed shear stress ($\sigma$). All flow curves revealed that SC solutions behaved as Newtonian fluids. The plots of shear stress versus shear rate gave straight lines, from which viscosity ($\eta$) was derived with the linear regression coefficient close to unity for all plots. All measurements were run in triplicate and performed at 298 K.

*Microscopic Observations.* Microscopic phases were identified by transmission electron microscopy (TEM 902A, Zeiss, Thornwood, NY, USA) and confocal laser scanning microscopy (CLSM; TCP SP2, Wetzlar, Germany). The transmission electron microscope (TEM) was operated in bright field mode at an acceleration voltage of 80 kV. Images were recorded with a Canon Power Shot S50 camera attached to the microscope. Samples for TEM were were negatively stained with uranyl acetate (2 wt %). A drop of the sample solution was placed on a carbon-coated mesh copper grid. The sample was allowed to dry for 5 min, and then any excess solution was removed by filter paper; dried sample was stained and allowed to dry. All sample preparations for microscopic observation were performed at room temperature.

Samples for CLSM were stained with Rhodamine B (RhB). RhB (0.05 wt %) was dispersed in the SC solution prior to its mixing with DDACl.

*pH Measurements.* pH measurements were performed using a combined electrode connected to an ion meter (Metrohm).

## RESULTS AND DISCUSSION

**Self-Assembly in SC Dilute Solutions.** Sodium caseinate is a heterogeneous mixture of phosphorus-containing proteins containing many ionizable groups on the side chains of their amino acids as well as their amino and carboxyl termini. Depending on solution conditions, functional groups of the side chains belonging to amino acids combined into the protein polypeptide chain can be either protonated or deprotonated.[25−27] The polar regions of the caseins are dominated by phosphoseryl residues and thus carry a net negative charge above the pH called the isoelectric point (p*I*). The average p*I* of caseins is around 4.6 at 293 K;[28] at p*I* casein is electrically neutral due to the presence of an equal amount of oppositely charged ionizable groups. The increase of the net negative charge beyond the p*I* arises from the deprotonation of carboxyl groups, loss of positive charge on the histidines and lysines, and increased negative charge on the phosphoseryl residues.[29]

Figure 1a shows variation of pH with SC concentration. It is evident that at very low concentrations SC aqueous solutions are basic, showing rapid pH decrease with increasing concentration up to the critical concentration, denoted *c**. The pH decrease with increasing SC concentration indicates a release of hydrogen ions into solution. As the SC concentration increased beyond the *c**, the pH continued to decrease to a smaller extent, approaching the pH of milk. The self-buffering power of proteins is diminished in dilute solutions,[30] and it seems that small amount of ions commonly present in a commercial sample overcome the SC self-buffering capacity. This effect is compensated at higher SC concentration.

Like other amphiphilic molecules, caseins self-assemble in aqueous solutions, thus inducing changes in the behavior of physicochemical properties (such as conductivity, surface tension, light scattering, etc.). Figure 1b shows the plots of specific conductivity and surface tension against SC concentration. The intersection point between two linear parts of the $\kappa$-*c*(SC) curve (denoted *c**) indicates a change in the conductivity behavior of the species present, that is, a change in the SC self-assembled structures.

The considerable exposure of hydrophobic amino acid residues caused by the open structure of casein molecules underlies the ability of SC to adsorb readily at the air/water interface, thus decreasing the surface tension. It can be seen in the inset that the decrease in surface tension starts immediately at a very low SC concentration. The break point between the steeply descending and fairly constant branch of the $\gamma$-*c*(SC) curve indicates the monolayer formation at the air/water interface and corresponds to the *c** obtained by pH and specific conductivity measurements. Constant surface tension beyond the *c** indicated that the air/liquid interface is occupied with surface active casein molecules. Compared to a conventional surfactant, SC lowers the surface tension of water to a smaller extent. Our results are in good agreement with literature data; maximum lowering of surface tension is consistent with the equilibrium surface tension obtained for sodium caseinate dissolved in water with 0.1 mol dm$^{-3}$ NaCl.[31]

The origin of an abrupt change in measured physicochemical properties of SC solutions was systematically examined by light scattering, zeta potential, and rheological measurements. Literature data based on light scattering measurements revealed polydispersity as a characteristic property of SC solutions. Commonly, a bimodal size distribution with the variable relationship between peak areas (PA) depending on the origin

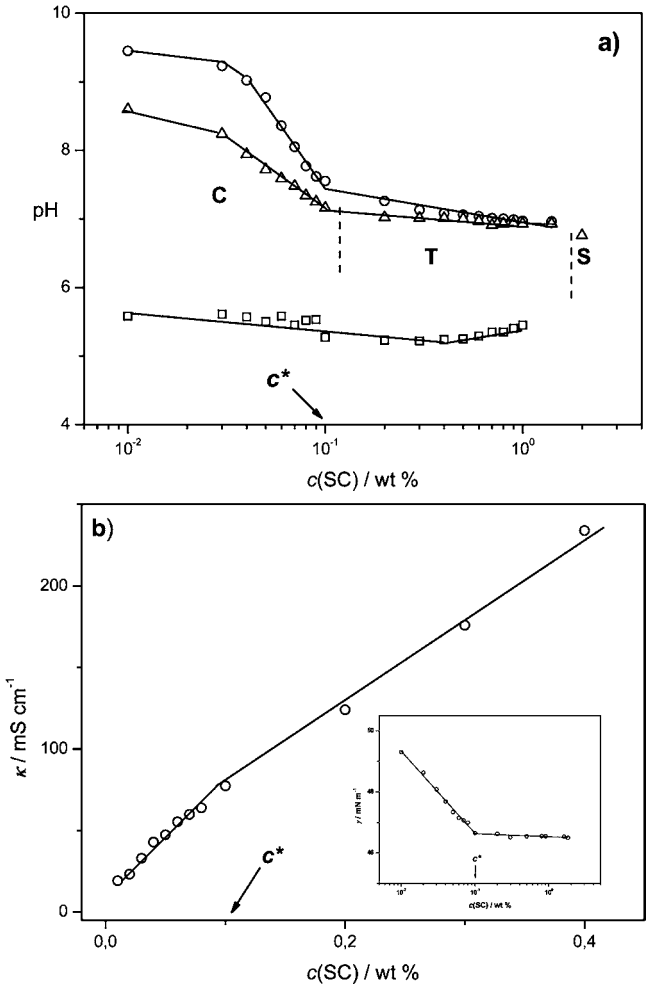


**Figure 1.** (a) Variation of pH with SC concentration (*c*(SC)) for samples without (○) and with constant DDACl concentration (*c*(DDACl) = 0.001 mol dm$^{-3}$ (△) and 0.03 mol dm$^{-3}$ (□)). (b) Variation of specific conductivity ($\kappa$) and surface tension ($\gamma$) (inset) with SC concentration (*c*(SC)). All SC samples were dispersed in water without addition of salt or pH adjustment. Critical SC concentration (*c**) is denoted by an arrow. Capital letters denote the appearance of samples in various concentration regions at constant monomeric DDACl concentration: C, clear region; T, turbid region; S, sedimentation region. Temperature is 298 K.

of SC sample and the experimental conditions was obtained.[15,23,32,33] To avoid overestimation arising from the scattering intensity of large particles (especially of a small weight fraction of complexes containing fat that cannot be removed completely by sample purification),[15] we have analyzed DLS data relying on the comparison between volume and number size distributions. Volume and number size distributions were used to estimate the relative amounts of multiple size peaks and are not considered absolute.

A typical example of volume size distributions for SC samples below the *c** presented in Figure 2a shows the existence of two particle populations. A population of smaller particles with the *d* value of 25 nm at the peak maximum (PA = 57%; *d* varies in the range from 16 to 50 nm) along with a population of larger particles with the *d* value of 191 nm at the peak maximum (PA = 43%; *d* varies in the range from 70 to 712 nm) were observed. The number size distribution (Figure 2b) revealed the presence of 99.7% of smaller particles and a negligible


dx.doi.org/10.1021/jf5016472 | J. Agric. Food Chem. 2014, 62, 8543−8554

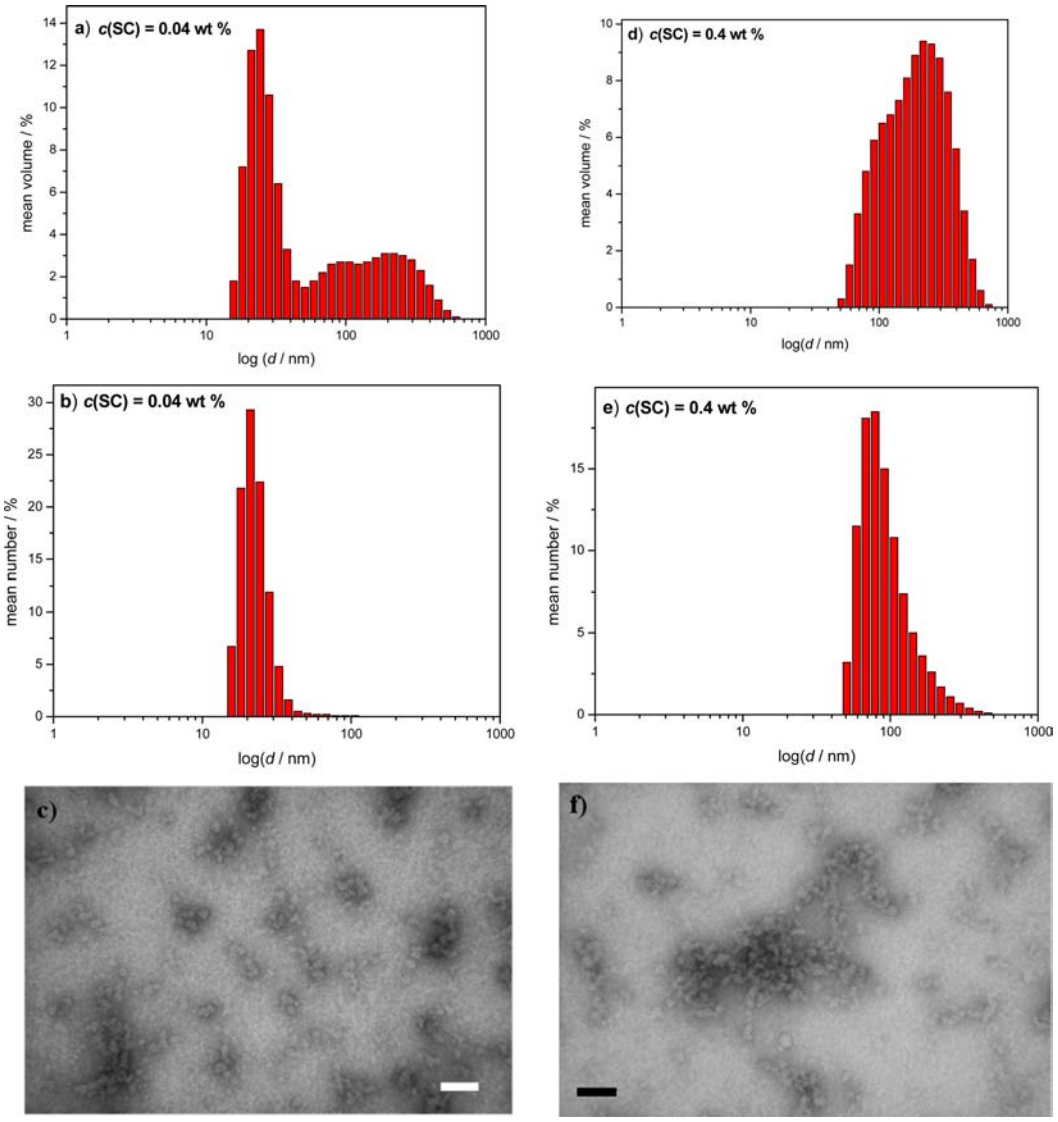


**Figure 2.** Size distribution by volume (a, d) and number (b, e) of casein associates (left) and aggregates (right). SC samples (concentrations as denoted) were dispersed in water with no salt and no pH adjustment. Corresponding images taken with transmission electron microscope (c, f); bars = 100 nm.

amount of larger particles. Complementary information obtained by TEM observation (Figure 2c) confirmed the coexistence of prevailing small spherical particles and their aggregates with the size consistent with those obtained by DLS measurements.

On the contrary, volume size distributions of samples beyond the $c^*$ generally indicated the existence of one population of particles with a broad size distribution. A typical example presented in Figure 2d shows volume size distribution ($d$ varies in the range from 69 to 710 nm) with the value of 216 nm at the peak maximum. The number size distribution (Figure 2e) revealed that particles having smaller size are dominant. It is not possible to discern the structure of formed particles from DLS data; however, evidence from electron microscopy revealed the presence of more or less elongated and flexible aggregates composed of small spheres with a diameter close to that of the individual spherical particles below the $c^*$ (Figure 2f).

To distinguish the contribution of prevailing SC self-assembled entities, DLS data are presented in Figure 3a as the change of the peak maximum volume sizes of dominant particles with $c$(SC). Two separate concentration regions can be recognized, below and above the $c^*$. The first region is dominated by the presence of spherical associates with the size very close to the formerly reported size of SC in the presence of electrolyte[23,32,33] as well as to the value reported for the size of native casein micelle building blocks, called submicelles.[34]

Like other proteins, casein molecules carry charges according to their amino acid sequence and the aqueous pH in which they are dissolved. Generally, when pH >4.6, caseins have a net negative charge and when pH <4.6, caseins have a net positive charge. It can be clearly seen in Figure 3b that spherical associates are negatively charged. Owing to the relatively high negative $\zeta$-potential value, they are relatively stable, showing only a slight change in size up to $c^*$. An abrupt increase in the peak maximum volume size and the absolute value of the average zeta potential decrease at the $c^*$ indicated the onset of aggregation, that is, formation of elongated aggregates (Figure 2f). The size of elongated aggregates is consistent with the size of the dominant population detected in sodium caseinate aqueous solutions under similar experimental conditions[33] as


dx.doi.org/10.1021/jf5016472 | J. Agric. Food Chem. 2014, 62, 8543−8554

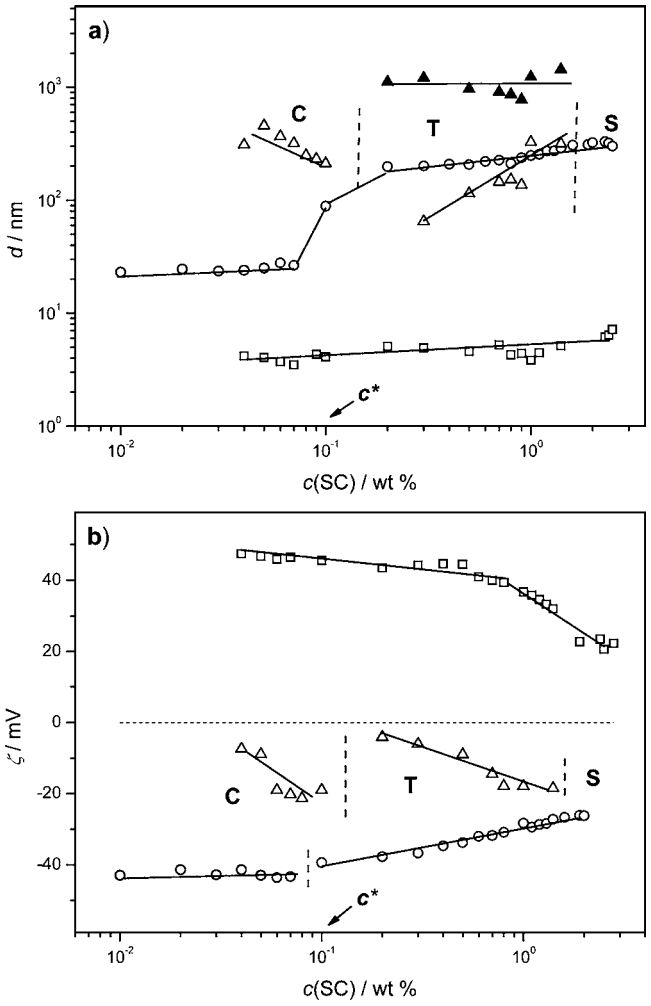


**Figure 3.** (a) Variation of the peak maximum volume size ($d$) and (b) the average zeta potential ($\zeta$) with SC concentration ($c$(SC)) for samples without (○) and with constant DDACl concentration; $c$(DDACl) = 0.001 mol dm$^{-3}$ (△ and ▲ denote the peak volume size of population with smaller and larger particles (a), and △ denotes the average zeta potential ($\zeta$) (b)), and $c$(DDACl) = 0.03 mol dm$^{-3}$ (□). All SC samples were dispersed in water without addition of salt or pH adjustment. Critical SC concentration ($c$*) is denoted by an arrow. Capital letters denote the appearance of samples in various concentration regions at constant monomeric DDACl concentration: C, clear region; T, turbid region; S, sedimentation region. Temperature is 298 K.

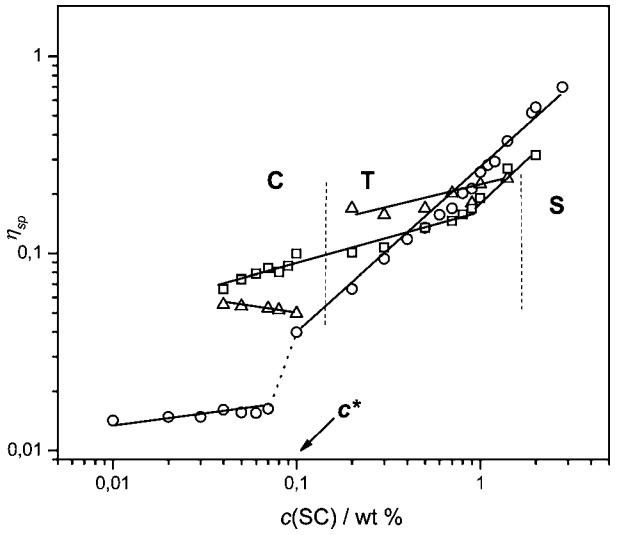


**Figure 4.** Variation of specific viscosity ($\eta_{sp}$) with SC concentration ($c$(SC)) for samples without (○) and with constant DDACl concentration ($c$(DDACl) = 0.001 mol dm$^{-3}$ (△) and 0.03 mol dm$^{-3}$ (□)). All SC samples were dispersed in water without addition of salt or pH adjustment. Critical SC concentration ($c$*) is denoted by an arrow. Capital letters denote the appearance of samples in various concentration regions at constant monomeric DDACl concentration: C, clear region; T, turbid region; S, sedimentation region. Temperature is 298 K.

well as with the size of native casein micelles containing calcium phosphate.[27,35−37] With the increase in SC concentration, the size of elongated aggregates as well as the absolute value of the average zeta potential increased due to the partial charge neutralization caused by the interactions between oppositely charged functional groups of casein molecules.

The change in SC self-assembly behavior around $c$* was also confirmed by rheological measurement. Over the range of concentrations investigated, viscosity did not depend on the shear rate, that is, at least up to $\dot{\gamma} = 10^3$ s$^{-1}$. This finding is in reasonable agreement with literature data for SC suspension at concentrations below $c$ < 7 wt %.[38] Figure 4 shows the concentration dependence on the specific viscosity. The specific viscosity slightly increased up to $c$* due to an insignificant change in size and charge of the spherical associates. An abrupt increase in the specific viscosity beyond the $c$* can be attributed to the onset of aggregation. Results are consistent with literature data (continuous shear rheology and TEM micrographs),[14] which also attributed the viscosity enhancement to aggregation into weakly branched rod-like aggregates.

Viewing individual casein molecules as amphiphilic block copolymers, the formation of small spherical associates can be explained via a balance of attractive hydrophobic interactions and electrostatic repulsion.[12,14] The high proline content in caseins causes a particular bending of the protein chain and inhibits the formation of ordered structures; that is, they have a relatively random, open structure. Without an ordered structure there is considerable exposure of hydrophobic residues, which promotes self-association in water and adsorption at interfaces at very low concentrations. Increase in SC concentration followed by a pH decrease and $\zeta$-potential decrease promotes aggregation beyond the $c$*. Aggregation of SC spherical associates into elongated structures may be ascribed to decreased electrostatic repulsions forcing them to interact more frequently with each other. Like other proteins, casein contains a large number of ionizable groups (acidic and basic residues) to which protons can be attached. Depending on solution conditions they can be either protonated or depronated, giving to the molecule a complex electric charge distribution.[30,39] In dilute solutions and low ionic strength this fluctuating charge may significantly contribute to the intermolecular interactions, thus causing aggregation.

Comparison of supramolecular organization between native casein and SC self-assembled entities revealed differences, sponge-like micelles of the former and soft fragile aggregates of the latter.[15,32,40] The difference in their structures arises from the fact that native casein micelles are, besides hydrophobic and steric interactions, additionally stabilized by specific interactions of colloidal calcium phosphate with casein chains.[41,42] Native casein micelles are similar to surfactant micelles only in the sense that a hydrophilic part resides at the surface and that they


dx.doi.org/10.1021/jf5016472 | J. Agric. Food Chem. 2014, 62, 8543−8554

are spherical. In comparison with surfactant micelles having a homogeneous hydrophobic core, the interior of casein micelles containing submicelles is heterogeneous, porous, and hydrated.[16] The minor amount of calcium arising from the commercial SC sample could not play an important role in aggregation at $c^*$; the hydrophobic interaction and hydrogen bond and electrostatic actions are the main factors governing their formation.[18]

**Self-Assembling of SC in DDACl Solutions.** Interactions between proteins and surfactants have many similarities to interactions between surfactants and polyelectrolytes.[1] Proteins may be considered as amphoteric polyelectrolytes with some hydrophobic groups or as amphiphilic polymers with variable charge density. Interactions between a polyelectrolyte and an oppositely charged surfactant are characterized by the fact that the complexation takes place in a highly cooperative manner. Strong complexation between oppositely charged species is primarily of electrostatic origin, although hydrophobic interactions also enhance the binding of surfactants to polyelectrolyte chains. Surfactants could interact with protein self-assembled entities via their hydrophilic and hydrophobic groups, inducing changes in their organization. These changes strongly depend both on the surfactant and protein structure and on their concentrations.[6]

Earlier, we denoted the self-assembled entities in SC dilute aqueous solutions as small spherical associates below and elongated aggregates beyond the $c^*$. On the other hand, DDACl, as a conventional cationic surfactant, self-assembles in aqueous solutions beyond the cmc (0.015 mol dm$^{-3}$); in dilute aqueous solutions DDACl is present in the form of monomers and beyond the cmc as micelles and monomers. DDACl is a salt of the weak base dodecylamine (DDA) and hydrolyzes in aqueous solutions. In acidic and neutral pH range, DDACl solutions contain only dodecylammonium ions ($C_{12}-NH_3^+$). As the pH increased beyond pH 8, the concentration of $C_{12}-NH_3^+$ drastically decreased as a result of hydrolysis into dodecylamine ($C_{12}-NH_2$), and around pH 9 phase separation of DDA occurred.[43] The increasing concentration of DDA drastically changes important surfactant parameters such as solubility, Krafft point, and cmc.[44]

Having in mind the self-assembly of both SC and DDACl, we have studied the influence of DDACl monomers and micelles on the SC spherical associates and elongated aggregates. Addition of DDACl to SC solutions resulted in pH decrease due to the release of protons from the carboxylic groups of casein molecules (Figure 1a) as was similarly observed upon complexation with positively charged lactoferrin.[45] To avoid hydrolysis of DDACl, all experiments were performed only with samples at pH <8.

*Cross Section with DDACl Monomers.* Samples at the cross section with the constant DDACl monomer and increasing SC concentration range from clear (C) to turbid (T) and to the sedimentation region (S), showing a clear difference in comparison with single SC samples, which were clear and appeared slightly turbid only when approaching 2 wt % of SC. The most turbid milky samples were observed around 0.2 wt % of SC (Figure 5). The difference in the sample appearance with and without DDACl may be primarily attributed to the interactions of surfactant monomers with spherical associates at lower and elongated aggregates at higher SC concentrations.

Interactions between SC spherical associates and DDACl monomers resulted in their complexation. Complexes are significantly larger in size (Figure 3a) and less net negatively charged (Figure 3b) than SC spherical associates. Volume size distributions of samples below the $c^*$ generally indicated the existence of one population of particles. A typical example in Figure 6a shows a broad volume size distribution with the value of 310 nm at the peak maximum ($d$ varies in the range from 100 to 700 nm). Complementary information obtained by TEM observation (Figure 6b) revealed the coexistence of individual spherical particles with size around 4−5 times higher than that of SC spherical associates. With the increase in SC concentration, the size of complexes continuously decreased and the absolute value of zeta potential increased. Zeta potential measurement is a way of evaluating the electrostatic interactions between SC and DDACl. At a constant monomer concentration level and increasing $c$(SC), the continuous increase in the absolute zeta potential value can be explained by the increasing SC/DDACl molar ratio in complexes. Continuous increase in zeta potential indicates an increase in net negative charge, thus enhancing electrostatic repulsion and diminishing the size of complexes.

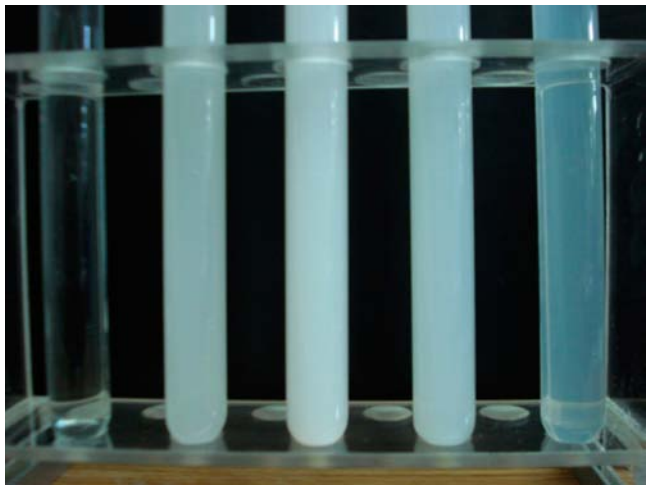

**Figure 5.** Photographs of samples from the turbid region containing, from left to right, increasing concentrationd of SC and constant $c$(DDACl) = 0.001 mol dm$^{-3}$. From left to right, SC concentrations are 0.10, 0.15, 0.20, 0.50, and 0.70 wt %. Note maximum turbidity of the central sample.

Beyond the $c^*$, DDACl monomers interact with SC elongated aggregates. Immediately beyond the $c^*$, DLS measurements (Figure 6c) detected the appearance of one population with large micrometer-sized complexes, which are slightly negatively charged (Figure 3b), indicating almost matching charges. The abrupt decrease in the absolute value of the average zeta potential can be explained by charge neutralization upon complexation and the appearance of larger complexes, which is an additional factor determining the electrophoretic mobility from which zeta potential is derived.[46] Microphotographs from the milky region show that the largest complexes are visible under CSLM as red spots (Figure 6d). It can be seen that fluorescence was regularly distributed in the photograph, indicating the complexes were spread all over the sample. Further increase in $c$(SC) was followed by the appearance of additional particle population. A typical example of volume size distribution is presented in Figure 6e. The population of smaller particles with the value of 145 nm at the peak maximum (PA = 7%; $d$ varies in the range from 79 to 255 nm) coexists along with population of larger particles with the value of 728 nm at the peak maximum (PA = 93%; $d$ varies in

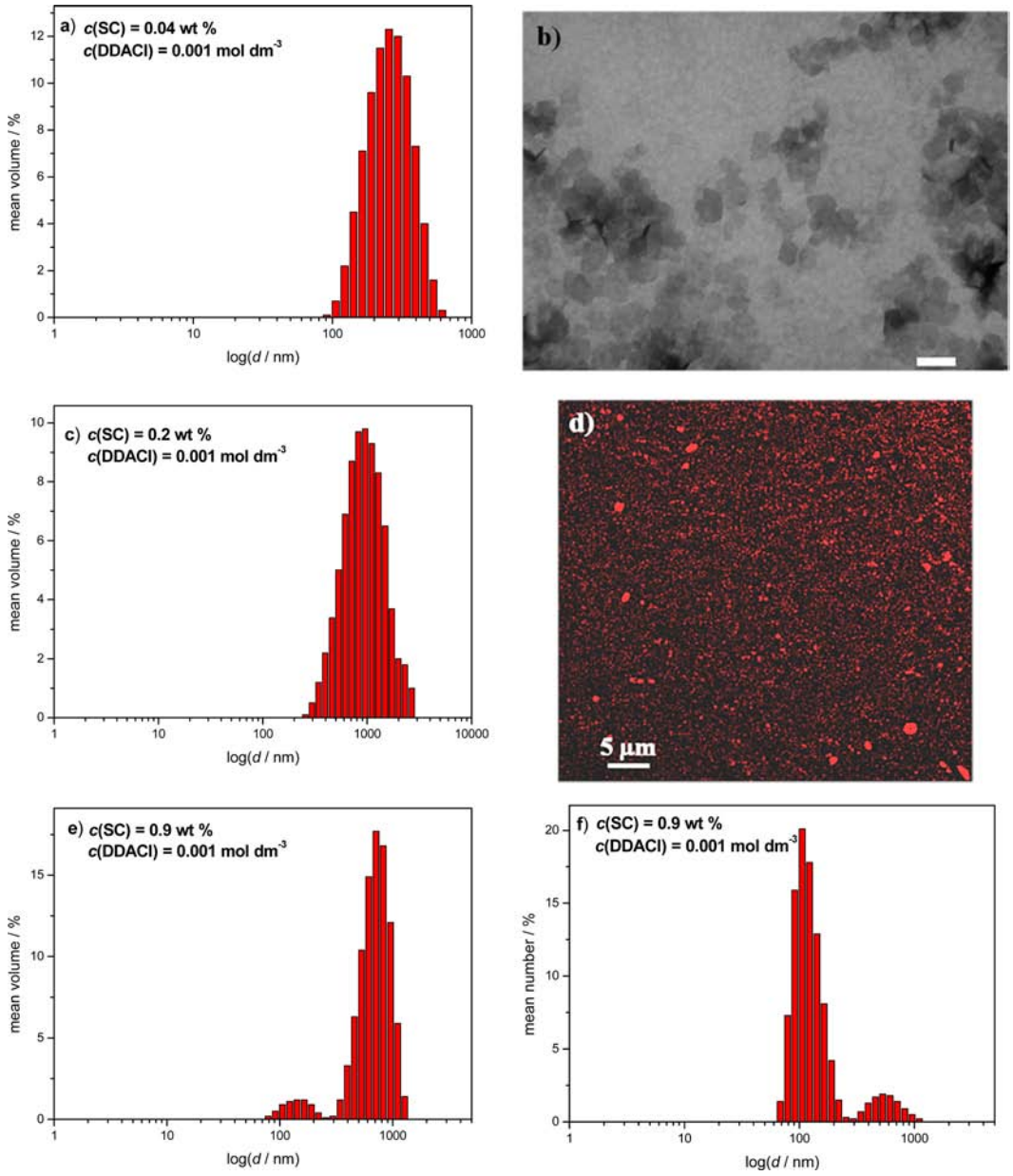


**Figure 6.** Size distribution by volume (a, c, e) and number (f) of DDACl/SC complexes prepared at denoted SC concentration ($c$(SC)) and constant DDACl concentration ($c$(DDACl) = 0.001 mol dm$^{-3}$). All SC samples were dispersed in water without addition of salt or pH adjustment. Corresponding images taken with transmission electron microscope ((b), bar = 100 nm) and confocal laser scanning microscope (CLSM) (d) are displayed at right. Sample for visualization with CLSM was stained with Rhodamine B.

the range from 295 to 1300 nm). Corresponding number size distribution (Figure 6f) revealed the presence of a small amount of larger particles. The absolute value of the average zeta potential continuously increased with increasing $c$(SC). It seems that only close to the $c^*$ is there enough DDACl for complete complexation with SC elongated aggregates. Number size analysis indicated that the fraction of larger particles continuously decreased from 1 at $c$(SC) = 0.2 wt % to 0.1 at $c$(SC) = 1 wt % concomitantly with the increasing fraction of smaller particles. Somewhat lower average size of smaller particles than the size of SC elongated aggregates without DDACl indicates their fragile structure. The observed decrease in size could be also attributed to the change of particle shape from spherical to elongated structures.

Plots of shear stress versus shear rate of samples with DDACl monomers suggested Newtonian behavior of all investigated samples. Higher specific viscosity (Figure 4) than that of single SC solutions is a consequence of complex formation, as observed in mixtures of polyelectrolytes and monomers of oppositely charged surfactants.[47,48] DDACl interacts with SC through electrostatic and hydrophobic interactions, leading to a strengthened association between casein chains and thus to increased specific viscosity in comparison with a single SC solution. Decrease of the specific viscosity up to the $c^*$ is consistent with the decreasing size and increasing charge of complexes (Figure 3). An abrupt increase in the specific viscosity beyond the $c^*$ is related to the appearance of micrometer-sized complexes. Further increase in $c$(SC) drastically decreases the fraction of larger complexes from ~1


dx.doi.org/10.1021/jf5016472 | J. Agric. Food Chem. 2014, 62, 8543−8554

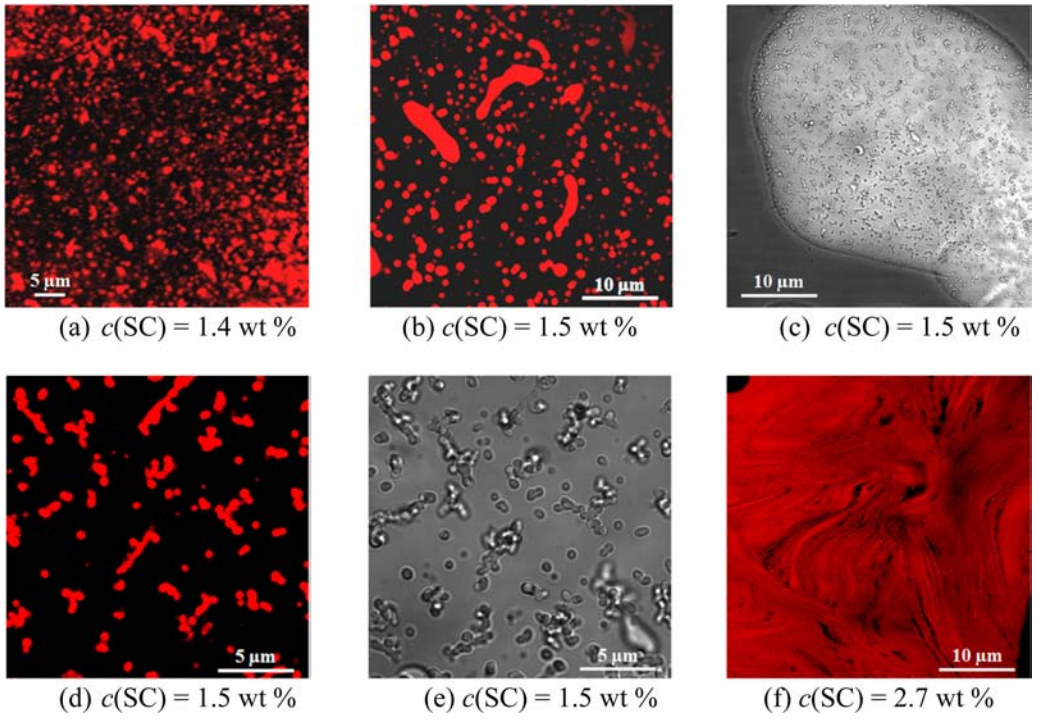


**Figure 7.** Images taken with confocal laser scanning microscope (CLSM) of samples in fluorescence (a, b, d, f) and reflection (c, e) modes, taken at denoted SC ($c$(SC)) and constant monomer DDACl concentration ($c$(DDACl) = 0.001 mol dm$^{-3}$). Samples for visualization with CLSM were stained with Rhodamine B. Bars are indicated.

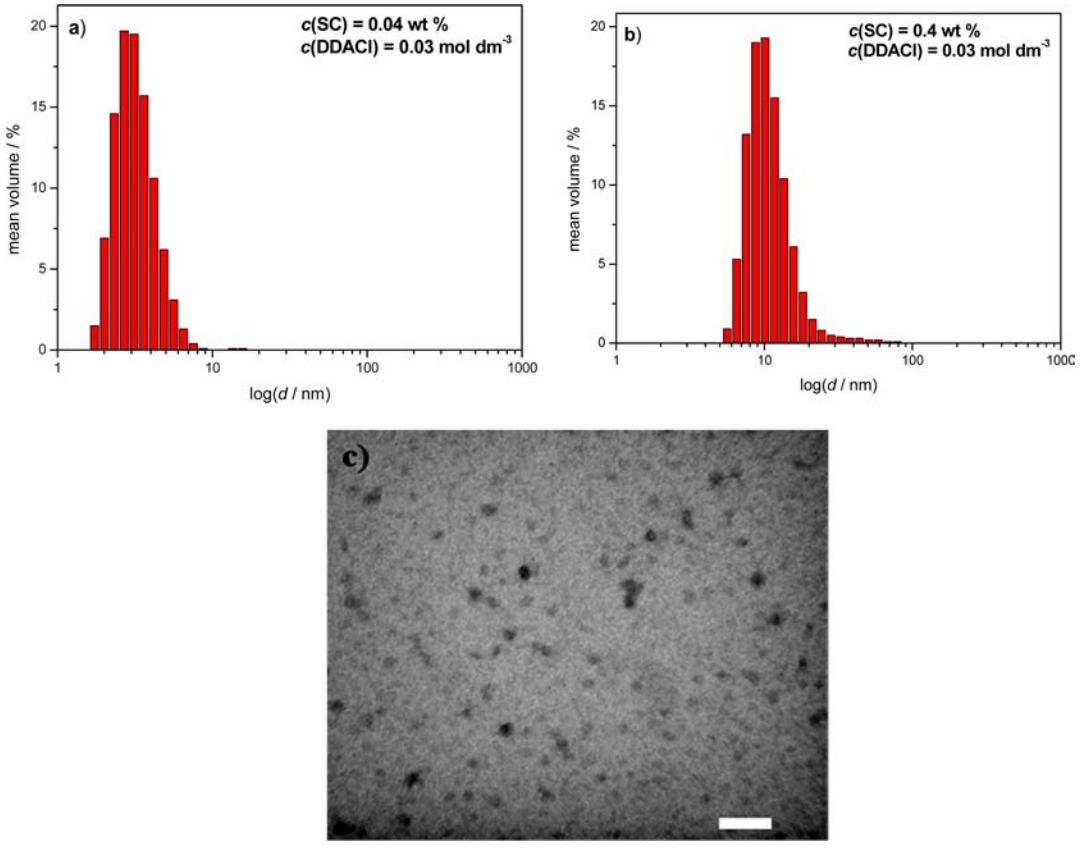


**Figure 8.** Size distribution by volume (a, b) of DDACl/SC complexes prepared at denoted SC concentration ($c$(SC)) and constant DDACl concentration ($c$(DDACl) = 0.03 mol dm$^{-3}$). (c) Transmission electron microscope image of the sample which corresponding volume distribution is shown on the right ($c$(SC) = 0.4 wt %); bar = 100 nm.


dx.doi.org/10.1021/jf5016472 | J. Agric. Food Chem. 2014, 62, 8543−8554

to 0.1 and, consequently, approaching the gelatinous sediment region, specific viscosity increases more slowly than the specific viscosity of single SC solutions.

Light scattering, electrophoretic, and rheological measurements were not performed beyond 1.4 wt % $c$(SC) because due to the presence of a gelatinous phase they could not provide correct information. Labeling with RhB allowed us to see the structure of larger SC/DDACl complexes, which appear red in the micrographs. At the beginning of the sedimentation region, sample microphotographs show a large number of aggregates (Figure 7a), which at slightly higher SC concentration coexist with the fragments of gelatinous phase (Figure 7b). Gel-like fragments formed at this relatively low SC concentration undergo sedimentation under their own weight without forming a continuous gel phase through the medium. Figure 7c clearly shows the coexistence of gelatinous sediment and embedded bulk phase containing spherical complexes; most of them joined into worm-like structures. The sedimented gel-like phase appeared homogeneously red. The enlarged part of Figure 7c shows some spherical complexes are joined into beaded chains (Figure 7d,e). An unstable and very viscous gelatinous phase evolved into a more compact structure at higher SC concentration. The CLSM microphotograph of an insoluble complex (Figure 7f) exhibited the appearance of flexible layers; however, preliminary X-ray analysis has not indicated any ordering. It seems that the SC complex with DDACl retained the tendency of casein micelles to self-aggregate into elongated structures.[8,14] Sedimentation of caseins with net negative charge on binding of a cationic surfactant is a common phenomenon, the behavior analogous to that of mixtures of polyelectrolytes and oppositely charged surfactants.[19,48]

*Cross Section with DDACl Micelles.* At the cross section with micellar DDACl the pH is shifted to the slightly acidic region, showing a slight decrease up to the $c^*$ and a small increase when approaching higher SC concentration (Figure 1). All samples were clear, indicating the formation of soluble complexes. Volume size distributions revealed the presence of particles with the size close to or slightly higher than DDACl micelles ($d_{DDACl} \sim 3.2$ nm[17]). Typical examples of volume size distribution for samples below and beyond the $c^*$ are presented in panels a and b, respectively, of Figure 8. Figure 8a presents the population of small particles with the value of 4.1 nm at the peak maximum ($d$ varies in the range from 1.8 to 7.4 nm). A negligible amount of larger particles (PA = 0.3%) with $d$ varied in the range from 12 to 18 nm was not detected in the number size analysis. From low to the highest SC concentrations the value of the peak maximum volume size distribution was shifted to ∼10 nm (Figure 3a) concomitant with broadening of volume size distribution and increasing fraction of larger particles. Figure 8b presents typical volume size distribution beyond the $c^*$; $d$ varies in the range from 5.9 to 79 nm. Complementary information obtained by TEM observation (Figure 8c) revealed the presence of individual globular particles with the size in accordance with DLS data.

All complexes are positively charged (Figure 3b), indicating strong electrostatic interactions between SC and DDACl. The absolute zeta potential value continuously decreases from 50 mV at 0.04 wt % to 23 mV at 2.8 wt % of SC. This high net charge decrease is followed by a relatively small variation in size. Obtained results suggested that the DDACl micellar concentration induces disintegration of both spherical associates and elongated aggregates. Decrease in the zeta potential value and a slight increase in complex size indicate that casein chains with negatively charged sites bind to the positively charged surfactant head groups located at the micelle/solution interface and wrap around DDACl micelles. It seems that due to very high excess of DDACl compared to SC, only a part of DDACl micelles may be wrapped by casein chains.

Plots of shear stress versus shear rate of samples with DDACl micellar concentration suggested Newtonian behavior of all investigated samples. It can be seen in Figure 4 that at lower SC concentration specific viscosity is higher than that of single SC solutions, although lower than that of DDACl micellar solution (0.463)[49] due to mixed complex formation. Differences in the specific viscosity between samples with and without DDACl disappear around 0.5 wt % SC, and after that, become slightly lower than the viscosity of single SC solutions.

In summary, the presented results give evidence of the concentration-dependent SC self-assembly in dilute aqueous solutions and of changes induced by a cationic surfactant addition. Self-assembly in single SC solutions proceeds in several steps, leading to the formation of spherical associates below and elongated aggregates beyond the $c^*$, showing strong structural difference in comparison with native casein, which, due to the presence of colloidal calcium phosphate, self-assemble into casein micelles.

Surfactants can interact with protein self-assembled entities via their hydrophilic and hydrophobic groups, leading to complexation. The three most commonly encountered models for protein and ionic surfactant complexes are (i) the pearl necklace model,[50] (ii) the rod-like prolate ellipsoidal model,[51] and (iii) the flexible capped helical model.[52] Some literature data concerning the influence of cationic surfactants on casein self-assembly suggested the pearl necklace model to describe the structure of cationic surfactant−casein complexes.[7−9] Both the results obtained with constant casein concentration at levels, at which caseins are present as random coil chains[7] or as micelles,[8,9] and those obtained with increasing concentration of cationic surfactants were described by a mechanism adopted for a polyelectrolyte chain and oppositely charged surfactant; electrostatic binding of cationic head groups to the negatively charged amino acid sites on casein chains at lower concentration; aggregation of micelle-like aggregates at casein chains at critical concentration; insoluble complex precipitation due to negative casein charge neutralization; redissolution of insoluble complexes in the excess of cationic surfactant; and formation of positively charged casein/surfactant complexes and cationic surfactant free micelles.

In this work, we have investigated the impact of constant DDACl concentration on SC self-assembled structures that evolved with increasing concentration from spherical associates to elongated aggregates. Both SC spherical associates and elongated aggregates have hydrophobic domains in their interior, where the hydrophobic part of DDACl monomers can be solubilized and accordingly the formation of complexes with varying stoichiometry may be regarded similar to a mixed micelle of two oppositely charged surfactants.[1] Bearing a net negative charge, SC associates will interact with the positively charged surfactant head groups predominantly via electrostatic attraction. Electrostatic attractions between the positively charged surfactant headgroup and negatively charged SC associates promote hydrophobic interactions.

Hydrophobic segments of casein molecules have some hydrophilic and polar amino acid residues in the sequence. These residues modify the packing behavior in the interior of

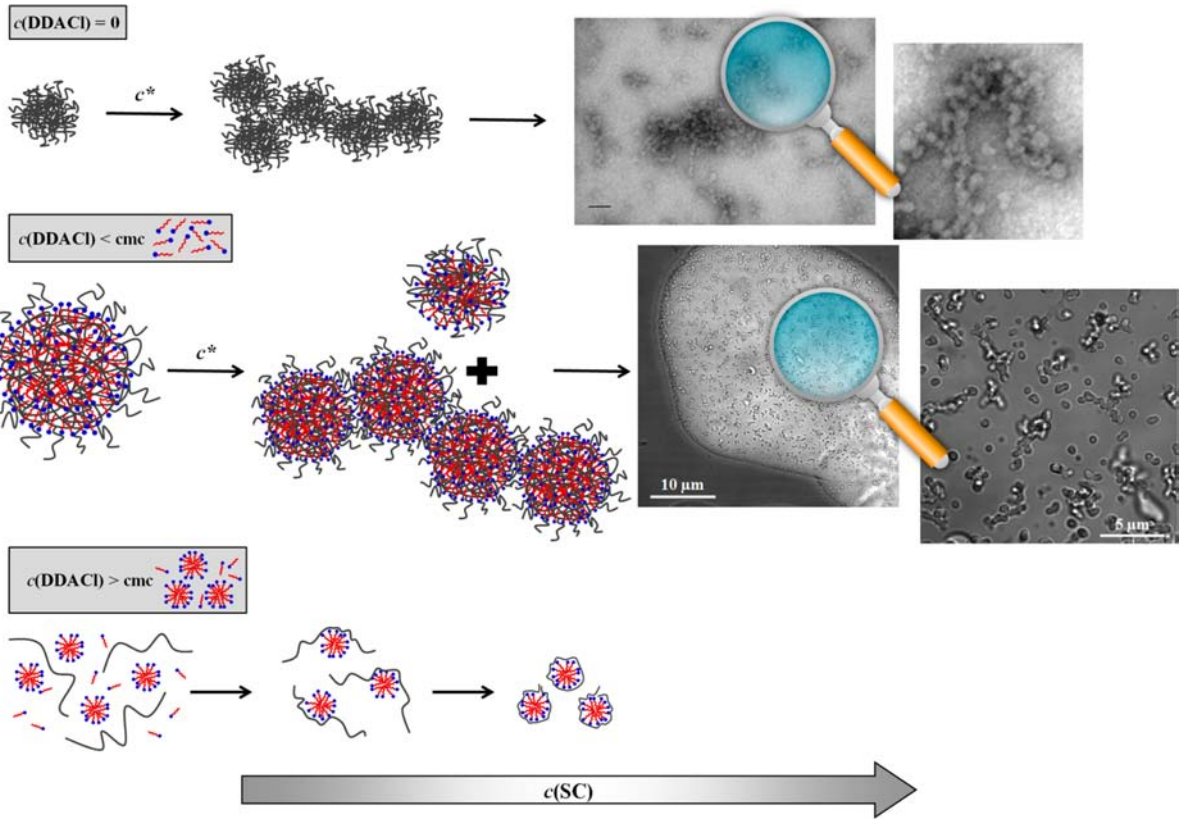


**Figure 9.** Schematic presentation describing interactions of DDACl monomers ($c$(DDACl) < cmc) and monomers and micelles ($c$(DDACl) > cmc) with SC spherical associates and elongated aggregates. Black color represents casein chains, red color represents DDACl hydrophobic tails, and blue color represents surfactant head groups. CLSM image taken from the sedimentation region clearly shows the coexistence of spherical and wormlike aggregates and gelatinous sediment (bars are denoted). TEM image, bar = 100 nm.

casein associates and make it less compact compared to a surfactant micelle.[15,21,40] The relatively open structure of SC associates allows a relatively easy transfer of DDACl hydrocarbon chains into the interior. It seems that despite the decreasing fraction of larger complexes, the increasing number of smaller particles at higher SC concentration forced them to interact more frequently with each other, leading to sedimentation of the gelatinous phase. At the beginning of the sedimentation region, CLSM microphotographs show spherical complexes connected like pearls, indicating that complexes retained the tendency of SC spherical associates to aggregate into elongated structures.[8]

The observed impact of DDACl micellar concentration may be attributed to the influence of the high ionic strength; thus, SC chains may reach only their limited size comparable with the size of DDACl micelles. Another possible scenario of DDACl effects at micellar concentration might involve the influence of both DDACl monomers and micelles. In the micellar region, surfactant micelles and monomers are in equilibrium, and it is generally accepted that the surfactant monomer concentration is equal to the critical micelle concentration, remaining constant at higher concentrations. Owing to the very high monomer concentration (~0.015 mol $dm^{-3}$),[19] one may suppose two steps of interactions, the first step comprising disintegration of SC self-assembled entities into single casein chains due to the incorporation of a large amount of DDACl monomers, and the second step comprising the binding of casein negatively charged sites to the positively charged surfactant head groups located at the micelle/solution interface; casein chains are wrapped around DDACl micelles. It seems that fast disintegration of casein associates into single chains was immediately followed by electrostatic interactions with surfactant micelles. Acting as a multivalent electrolyte, casein chains induce very strong electrostatic binding concomitant with the release of counterions from both the surfactant and casein chains.[53] This scenario is similar to the effect of surfactants on the denaturation of globular proteins. It was shown that depending on surfactant concentration, the unfolding pathway during globular protein denaturation involves several steps and formation of intermediates/complexes; the initial monomer concentration shows a propensity to stimulate protein aggregation, whereas micellar surfactant concentration exhibits strong dispersive abilities.[54]

We did not detect particles with a size corresponding to the size of SC small associates. The small size of complexes may be ascribed to increased ionic strength as well as to the high excess of surfactant micelles wrapped by casein chains without cross-linking.

DDACl monomer antinomian effects leading to the formation of mixed complexes at lower or DDACl micelles wrapped with SC chain at higher concentration may be explained by the influence of the SC/DDACl molar ratio. Owing to their flexible and dynamic nature, casein molecules associate into a loose hierarchical structure of substructures having a hydrophobic interior and a hydrophilic surface with some hydrophobic patches.[12] Addition of a lower monomer concentration results in monomer incorporation and formation of mixed complexes similar to mixed micelles. Both possible


dx.doi.org/10.1021/jf5016472 | J. Agric. Food Chem. 2014, 62, 8543−8554

scenarios, the effect of the high ionic strength or incorporation of a high excess of monomers inside loose SC structures, in the micellar region result in SC chains wrapped around DDACl micelles.

Considering all of the results described, two mechanisms are supposed to describe the complexation of caseins at a constant level of DDACl concentration, one with surfactant monomers and the other with monomers and micelles (Figure 9). In the absence of DDACl, SC exists in several aggregation states, spherical associates below and elongated aggregates beyond the $c^*$. For simplicity, casein associates are shown as spherical aggregates with a hairy layer.

A better understanding of the mechanisms of interactions between SC and oppositely charged surfactants may provide an opportunity to modify and control structural changes of their complexes useful for the production of new materials and may also find a potential in encapsulation and controlled release of bioactive compounds (plant protection agents, drugs, nutraceuticals, etc.).

## AUTHOR INFORMATION


### Corresponding Authors

*Marko Vinceković, Ph.D. E-mail: mvincekovic@agr.hr; Tel: + 385 1 239 3953.

*Darija Jurašin, Ph.D. E-mail: djurasin@irb.hr; Tel: + 385 1 456 0941.



### Funding

Financial support from the Ministry of Science, Education and Sports of the Republic of Croatia (Grants 178-1780469-3591 and 098-0982915-2949) is gratefully acknowledged.


### Notes

The authors declare no competing financial interest.

## ACKNOWLEDGMENTS

We are indebted to Zoran Štefanić for preliminary X-ray analysis and Nada Filipović-Vinceković for helpful discussions and manuscript reading.

## REFERENCES


(1) Holmberg, K.; Jönsson, B.; Kronberg, B.; Lindman, B. *Surfactant and Polymers in Aqueous Solutions*, 2nd ed.; Wiley: Chichester, UK, 2002.

(2) Otzen, D. Protein-surfactant interactions: a tale of many states. *Biochim. Biophys. Acta (BBA)—Proteins Proteomics* **2011**, *1814*, 562—591.

(3) Antipova, A. S.; Semenova, M. G.; Belyakova, L. E.; Il'in, M. M. On relationships between molecular structure, interaction and surface behaviour in mixture: small—molecule surfactant + protein. *Colloids Surf. B: Biointerfaces* **2001**, *21*, 217—230.

(4) Thies, C. Microencapsulation. In *Kirk-Othmer Encyclopedia of Chemical Technology*, 5th ed.; Seidel, A., Ed.; Wiley: Hoboken, NJ, USA, 2006; pp 438—463.

(5) Livney, Y. D. Milk proteins as vehicles for bioactives. *Curr. Opin. Colloid Interface Sci.* **2010**, *15*, 73—83.

(6) Semenova, M. G. Thermodynamic analysis of the impact of molecular interactions on the functionality of food biopolymers in solution and in colloidal systems. *Food Hydrocolloids* **2007**, *21*, 23—45.

(7) Liu, Y.; Guo, R. Interaction between casein and the oppositely charged surfactant. *Biomacromolecules* **2007**, *8*, 2902—2908.

(8) Chakraborty, A.; Basak, S. Effect of surfactants on casein structure: a spectroscopic study. *Colloids Surf. B: Biointerfaces* **2008**, *63*, 83—90.

(9) Liu, Y.; Yang, L.; Guo, R. Interaction between $\beta$-casein micelles and imidazolium based ionic liquid surfactant. *Soft Matter* **2013**, *9*, 3671—3680.

(10) Sun, L.-H.; Sun, Y.-L.; Yang, L. Y.; Zhang, J.; Chen, Z.-X. Controllable self-assembly of sodium caseinate with a zwitterionic vitamin-derived bolaamphiphile. *J. Agric. Food Chem.* **2013**, *61*, 10582—10589.

(11) Farrell, M.; Brown, E. M.; Malin, E. L. Higher order structures of the caseins: a paradox? In *Advanced Dairy Chemistry. Vol. 1A: Proteins: Basic Aspects*, 4th ed.; McSweeney, P. L. H., Fox, P. F., Eds.; Springer: New York, 2013; Chapter 5, pp 161—185.

(12) Horne, D. S. Casein interactions: casting light on the *black boxes*, the structure in dairy products. *Int. Dairy J.* **1998**, *8*, 171—177.

(13) de Kruif, C. G.; Huppertz, T.; Urban, V. S.; Petukhov, A. V. Casein micelles and their internal structure. *Adv. Colloid Interface Sci.* **2012**, *171—172*, 36—52.

(14) Farrer, D.; Lips, A. On the self-assembly of sodium caseinate. *Int. Dairy J.* **1999**, *9*, 281—286.

(15) HadjSadok, A.; Pitkowski, A.; Nicolai, T.; Benyahia, L.; Moulai-Mostefa, N. Characterisation of sodium caseinate as a function of ionic strength, pH and temperature using static and dynamic light scattering. *Food Hydrocolloids* **2008**, *22*, 1460—1466.

(16) Fox, P. F.; Brodkorb, A. The casein micelle: historical aspects, current concepts and significance. *Int. Dairy J.* **2008**, *18*, 677—688.

(17) Horne, D. S. Casein micelles as hard spheres: limitations of the model in acidified gel formation. *Colloids Surf. A: Physicochem. Eng. Aspects* **2003**, *213*, 255—263.

(18) Liu, Y.; Guo, R. pH-dependent structures and properties of casein micelles. *Biophys. Chem.* **2008**, *136*, 67—73.

(19) Vinceković, M.; Bujan, M.; Šmit, I.; Filipović-Vinceković, N. Phase behavior in mixtures of cationic surfactant and anionic polyelectrolytes. *Colloids Surf. A: Physicochem. Eng. Aspects* **2005**, *255*, 181—191.

(20) Semenova, M. G.; Belyakova, L. E.; Polikarpov, Y. N.; Stankovic, I.; Antipova, A. S.; Anokhina, M. S. Analysis of light scattering data on the sodium caseinate assembly as a response to the interactions with likely charged anionic surfactant. *Food Hydrocolloids* **2007**, *21*, 704—715.

(21) Lucey, J. A.; Srinivsan, M.; Singh, H.; Munro, P. A. Characterization of commercial and experimental sodium caseinates by multiangle laser light scattering and size-exclusion chromatography. *J. Agric. Food Chem.* **2000**, *48*, 1610—1616.

(22) Panouillé, M.; Nicolai, T.; Durand, D. Heat induced aggregation and gelation of casein submicelles. *Int. Dairy J.* **2004**, *14*, 297—303.

(23) Chu, B.; Zhou, Z.; Wu, G.; Farrell, H. M. J. Laser light scattering of model casein solutions. *J. Colloid Interface Sci.* **1995**, *170*, 102—112.

(24) Nash, W.; Pinder, W.; Hemar, Y.; Singh, H. Dynamic light scattering investigation of sodium caseinate and xanthan mixtures. *Int. J. Biol. Macromol.* **2002**, *30*, 269—271.

(25) Fox, P. F. Milk proteins: general and historical aspects. In *Advanced Dairy Chemistry, Vol. 1: Proteins*; Fox, P. F., McSweeney, P. L. H., Eds.; Kluwer Academic/Plenum Publishers: New York, 2003; pp 1—41.

(26) Swaisgood, H. E. Chemistry of the caseins. In *Advanced Dairy Chemistry, Vol. 1: Proteins*; Fox, P. F., McSweeney, P. L. H., Eds.; Kluwer Academic/Plenum Publishers: New York, 2003; pp 139—187.

(27) Walstra, P. Casein sub-micelles do they exist? *Int. Dairy J.* **1999**, *9*, 189—192.

(28) Hu, M.; McClements, D. J.; Decker, E. A. Lipid oxidation in corn-oil-in-water emulsions stabilized by casein, whey protein isolate and soy protein isolate. *J. Agric. Food Chem.* **2003**, *51*, 1696—1700.

(29) Post, A. E.; Arnold, B.; Weiss, J.; Hinrichs, J. Effect of temperature and pH on the solubility of caseins: environmental influences on the dissociation of $\alpha_S$- and $\beta$-casein. *J. Dairy Sci.* **2012**, *95*, 1603—1616.

(30) Timasheff, S. N.; Dintizs, H. M.; Kirkwood, J. G.; Coleman, B. D. Light scattering investigation of charge fluctuations in isoionic serum albumin. *J. Am. Chem. Soc.* **1957**, *79*, 782—791.

(31) Rouimi, S.; Schorsch, C.; Valentini, C.; Vaslin, S. Foam stability and interfacial properties of milk protein−surfactant systems. *Food Hydrocolloids* **2005**, *19*, 467−478.
(32) Pitkowski, A.; Durand, D.; Nicolai, T. Structure and dynamical mechanical properties of suspensions of sodium caseinate. *J. Colloid Interface Sci.* **2008**, *326*, 96−102.
(33) Semenova, M. G.; Belyakova, L. E.; Polikarpov, Y. N.; Antipova, A. S.; Dickinson, E. Light scattering study of sodium caseinate + dextran sulfate in aqueous solution: relationship to emulsion stability. *Food Hydrocolloids* **2009**, *23*, 629−639.
(34) Rollema, H. S. Chemistry of milk proteins. In *Developments in Dairy Chemistry−1. Proteins*; Fox, P. F., Ed.; Applied Sciences: London, UK, 1992; pp 111−140.
(35) Horne, H. D. Casein micelle structure: models and muddles. *Curr. Opin. Colloid Interface Sci.* **2006**, *11*, 148−153.
(36) Nair, P. K.; Dalgleish, D. G.; Corredig, M. Colloidal properties of concentrated heated milk. *Soft Matter* **2013**, *9*, 3815−3824.
(37) Dalgleish, D. G. On the structural models of bovine casein micelles − review and possible improvements. *Soft Matter* **2011**, *7*, 2265−2272.
(38) Konstance, R. P.; Strange, E. D. Solubility and viscous behaviour of caseins and caseinates. *J. Food Sci.* **1991**, *56*, 556−559.
(39) Lund, M.; Jönsson, B. Charge regulation in biomolecular solution. *Q. Rev. Biophys.* **2013**, *46*, 265−281.
(40) Bouchoux, A.; Schorr, D.; Daffé, A.; Cambert, M.; Gésan-Guiziou, G.; Mariette, F. Molecular mobility in dense protein systems: an investigation through $^{1}$H NMR relaxometry and diffusometry. *J. Phys. Chem. B* **2012**, *116*, 11744−11753.
(41) McMahon, D. J.; Oommen, B. S. Casein micelle structure, functions, and interactions. In *Advanced Dairy Chemistry. Vol. 1A: Proteins: Basic Aspects*, 4th ed.; McSweeney, P. L. H., Fox, P. F., Eds.; Springer: New York, 2013; Chapter 6, pp 185−209.
(42) Phadungath, C. Casein micelle structure: a concise review. *Songklanakarin J. Sci. Technol.* **2005**, *27*, 201−212.
(43) Matulis, D.; Bloomfield, V. A. Thermodynamics of the hydrophobic effect. I. Coupling of aggregation and pK shifts in solutions of aliphatic amines. *Biophys. Chem.* **2001**, *93*, 37−51.
(44) Dai, Q.; Laskowaki, J. S. The Krafft point of dodecylammonium chloride: pH effect. *Langmuir* **1991**, *7*, 1361−1364.
(45) Anema, S. G.; de Kruif, C. G. Co-acervates of lactoferrin and caseins. *Soft Matter* **2012**, *8*, 4471−4478.
(46) Moriyama, Y.; Takeda, K.; Murakami, K. Electrophoretic behaviour of complexes between sodium dextran sulphate and cationic surfactant. *Langmuir* **2000**, *6*, 7629−7633.
(47) Vinceković, M.; Bujan, M.; Sikirić, D. Nano- and micro-complexes of biopolymer carrageenans and dodecylammonium chloride. *J. Polym. Eng.* **2011**, *31*, 115−123.
(48) Kötz, J.; Kosmella, S.; Beitz, T. Self-assembled poleylectrolyte systems. *Prog. Polym. Sci.* **2001**, *26*, 1199−1232.
(49) Vinceković, M.; Katona, J.; Bujan, M.; Sovilj, V. Nano- and microcomplexes of biopolymer carrageenans and dodecylammonium chloride. *Colloids Surf. A: Physicochem. Eng. Aspects* **2011**, *383*, 739−748.
(50) Turro, N. J.; Lei, X.; Ananthapadmanabhan, K. P.; Aronson, M. Spectroscopic probe analysis of protein−surfactant interactions: the BSA/SDS system. *Langmuir* **1995**, *11*, 2525−2533.
(51) Reynolds, J. A.; Tanford, C. The gross conformation of protein−sodium dodecyl sulfate complexes. *J. Biol. Chem.* **1970**, *245*, 5161−5165.
(52) Lundahl, P.; Greijer, E.; Sandberg, M.; Cardell, S.; Eriksson, K. O. A model for ionic and hydrophobic interactions and hydrogen-bonding in sodium dodecyl sulfate−protein complexes. *Biochim. Biophys. Acta* **1986**, *873*, 20−26.
(53) Allen, R. J.; Warren, P. B. Complexation and phase behavior of oppositely charged polyelectrolyte/macroion systems. *Langmuir* **2004**, *20*, 1997−2009.
(54) Andersen, K. K.; Oliveira, C. L. P.; Larsen, K. L.; Poulsen, F. M.; Callisen, T. H.; Westh, P.; Pedersen, J. S.; Otzen, D. E. The role of decorated SDS micelles in sub-cmc protein denaturation and association. *J. Mol. Biol.* **2009**, *391*, 207−226.

JOURNAL OF AGRICULTURAL AND FOOD CHEMISTRY

Article

pubs.acs.org/JAFC

# Allelochemicals in the Rhizosphere Soil of *Euphorbia himalayensis*

Quan Liu,[†,‡] Dengxue Lu,[§] Hui Jin,[†] Zhiqiang Yan,[†] Xiuzhuang Li,[†] Xiaoyan Yang,[†] Hongru Guo,[†] and Bo Qin*[,†]

[†]Key Laboratory of Chemistry of Northwestern Plant Resources of the Chinese Academy of Sciences (CAS) and Key Laboratory for Natural Medicine of Gansu Province, Lanzhou Institute of Chemical Physics, Chinese Academy of Sciences, Lanzhou, Gansu 730000, People's Republic of China

[‡]State Key Laboratory of Grassland Agro-ecosystems, College of Pastoral Agriculture Science and Technology, Lanzhou University, Lanzhou, Gansu 730020, People's Republic of China

[§]Institute of Biology, Gansu Academy of Sciences, Lanzhou, Gansu 730000, People's Republic of China

**ABSTRACT:** Weed infestation has been known to cause considerable reductions in crop yields, thereby hindering sustainable agriculture. Many plants in genus *Euphorbia* affect neighboring plants and other organisms by releasing chemicals into the environment. In view of the serious threat of weeds to agriculture, the allelochemicals of *Euphorbia himalayensis* and their allelopathic effects were investigated. The extract of root exudates from rhizosphere soil exhibited allelopathic activities against crops (wheat, rape, and lettuce) and grasses (*Poa annua*, *Festuca rubra*, and red clover). Bioassay-guided fractionation and isolation from the root extract of *E. himalayensis* led to the characterization of two ellagic acid derivatives and a jatrophane diterpene, which observably showed phytotoxic activities against lettuce, *Festuca arundinacea*, and *F. rubra*. They were further confirmed by ultra-performance liquid chromatography−tandem mass spectrometry to have concentrations of 3.6, 3.8, and 8.99 nmol/g in the rhizospere soil, respectively. Bioassay indicated that the combination of the allelochemicals could be selective plant growth regulator in agriculture.

**KEYWORDS:** *Euphorbia himalayensis, root exudates, ellagic acid derivatives, esulone A, allelopathy*

## INTRODUCTION

Weeds pose an important biological constraint to crop productivity. Many weeds release allelochemicals to interfere with the germination and growth of crops growing around them.[1] It has long been suspected that an allelopathic mechanism should play an important role in the interference of weed with the crop plants.

The genus *Euphorbia* is one of the largest and most widely distributed in the spurge family (Euphorbiaceae), in which most species are found in temperate regions. The plants of the genus are herbs, shrubs, and cactus-like, growing in nearly all climate types, and are often characterized by the presence of a milky latex.[2] Many plants in the genus, such as leafy spurge, are reported to affect adjacent plants through allelochemicals released into the environment.[3,4] A yield reduction of 4−85% has been reported in field crops with different *Euphorbia* species and distinct occurrence densities. The plants in this genus decrease herbage production by 10−100% in pasture and rangelands.[5] *Euphorbia* species have herbicidal and insecticidal properties, but there is a need to establish their commercial utility potential as environmentally friendly plant protection measures.

*Euphorbia himalayensis* Boiss. commonly grows in non-irrigated farmlands and infests cultivated fields in the Tibetan Plateau. The plant is also toxic to livestock and poses a serious threat to crop and livestock production. In light of the ecological benefits of *E. himalayensis* in farmland, the investigation of chemical constituents with phytotoxic activities was processed. Using a bioassay-directed approach, three active compounds were isolated and elucidated, which were responsible for obvious phytotoxic activities. Furthermore, these allelochemicals were identified from the rhizosphere soil by high-performance liquid chromatography (HPLC) and ultraperformance liquid chromatography−mass spectrometry (UPLC−MS). To the best of our knowledge, this is the first report of this plant on the phytochemical investigation and allelopathic activities. These results would be useful to explore how *E. himalayensis* becomes a successful competitor against other plants in nature. In this study, a rapid and highly sensitive method was developed with the use of ultraperformance liquid chromatography−tandem mass spectrometry (UPLC−MS/MS) to determine the levels of allelochemicals in the rhizospere soil.

## MATERIALS AND METHODS

**General Experimental Instruments and Procedures.** Electron ionization−mass spectrometry (EI−MS) was recorded on a VG ZABHS instrument (VG, East Sussex, U.K.), and electrospray ionization (ESI) ion-trap data were recorded on an Esquire 6000 instrument (Bruker Daltonics, Billerica, MA). $^{1}H$ and $^{13}C$ nuclear magnetic resonance (NMR) spectra with tetramethylsilane (TMS) as the internal standard were measured on a Varian Mercury-400BB instrument (Bruker, Karlsruhe, Germany) operating at 400 and 100 MHz, respectively. Silica gel (200−300 mesh) (Qingdao Haiyang Chemical Co., Ltd., Qingdao, China), Sephadex LH-20 (25−100 mm) (Pharmacia Fine Chemical Co., Ltd., Berlin, Germany), and silica gel 60 RP18 (230−400 mesh) (Merck, Whitehouse Station, NJ) were used in column chromatography (CC). Thin-layer chromatography (TLC) was performed on precoated silica

Received: April 28, 2014
Revised: July 27, 2014
Accepted: August 2, 2014
Published: August 2, 2014

ACS Publications © 2014 American Chemical Society



dx.doi.org/10.1021/jf502020v | J. Agric. Food Chem. 2014, 62, 8555−8561

gel 60 $F_{254}$ plates (Qingdao Haiyang Chemical Co., Ltd., Qingdao, China), and spots on the plates were observed under ultraviolet (UV) light of 254 nm and visualized by spraying with 5% $H_2SO_4$ in EtOH (v/v), followed by heating.

The HPLC analysis was performed on a HP1200 system (Agilent, Santa Clara, CA) with a diode array (G1315D) and the GraceSmart RP18 C18 column (2.5 cm × 4.6 mm, 5 μm) (Grace Corporation, Columbia, MD). Liquid chromatography (LC)-grade methanol and acetonitrile were purchased from Tedia Company, Inc. (Anhui Fulltime Co., Ltd., Hefei, China) and filtered through a 0.45 μm membrane filter before HPLC analysis. Ultrapure water was purified by a water purification system (Shanghai Laikie Instrument Co., Ltd., Shanghai, China) and filtered through a 0.45 μm membrane filter before use.

**Plant Material.** Roots of *E. himalayensis* were collected among the mountains (91° 51′ E, 29° 46′ N) in Maizhokunggar county, Tibet province, China, in August of 2012 and identified by Prof. Huanyang Qi from Lanzhou Institute of Chemical Physics, Chinese Academy of Sciences (CAS). The plant mainly grew in the side of farmland as the dominant species. The *Euphorbia* specimens collected in the study were healthy and in the fruit period. The voucher specimen (Eh001) was deposited in Lanzhou Institute of Chemical Physics, CAS. The seeds of wheat, rape, red clover, lettuce, *Poa annua*, *Festuca arundinacea*, and *Festuca rubra* were bought from the seed market in Lanzhou. Wheat and rape were the main crops in Tibet, and the other plants were associated plants of *E. himalayensis*.

**Sample Preparation Procedures of Root Exudates.** The plants of *E. himalayensis* were carefully uprooted. The roots with soil were taken in tubes and fiercely shaken off rhizosphere soil. The rhizosphere soil of *E. himalayensis* (8.58 kg, $1.80 \times 10^{-2}$ $m^3$) was extracted ultrasonically with methanol 3 times (30 min each). The filtrate was concentrated in vacuum to near dryness on a rotary evaporator, yielding the root exudates (2.66 g). Then, 70 mg of the extract was dissolved in 8.75 mL of 80% methanol to prepare a solution that was filtered through a Millipore filter (0.45 μm) prior to HPLC analysis and bioassay.

**Biology Assays.** Inhibitory activities on the growth of crops and other plants were evaluated using the plate-culture method.[6] The seeds of the tested plants were soaked in 0.1% mercuric chloride (w/v) for 7 min, washed by distilled sterile water 5 times, and germinated on filter paper with a photoperiod condition of 16/8 h day/night at 22 °C. After 3 days, the lettuce seedlings were transferred to 12-well plates (VWR Scientific, Inc., Shanghai, China) supplemented with $^1/_2$ MS liquid medium, and then the extracts, root exudates, and chemicals isolated were diluted with dimethyl sulfoxide (DMSO) and added to each of the treated pores. The extracts and root exudates were prepared in the final concentrations of 200 and 100 μg/mL, and compounds **1**−**3** were prepared for 200, 100, and 50 μg/mL. Four replicates were performed per treatment. Then, the plants were incubated in a constant temperature humidity chamber at 22 °C for 3 days, under 16 h light/8 h dark photoperiod conditions. The fresh weights and root length were measured at the end of the experiment. Inhibitory ratios (%) of root lengths were determined by the formula: [(control root length − plant length treated)/control root length] × 100. The inhibitory ratios (%) of fresh weights were also calculated by reference to the control. Control bioassays only contained the same amount of DMSO. Significant differences were evaluated by analysis of variation (ANOVA) ($p < 0.05$). Similar procedures were taken to evaluate the phytotoxic activities against other plants. The 2-day-old seedlings of wheat were monitored for 2 days. The 3-day-old seedlings of red clover and rape were monitored for 3 days. The 14-day-old seedlings of *P. annua*, *F. arundinacea*, and *F. rubra* were monitored for 7 days.

**Bioactivity-Driven Isolation of Phytotoxins.** Air-dried roots of *E. himalayensis* (472 g) were smashed and extracted with EtOH at room temperature, and then the solution was concentrated under reduced pressure to obtain the root extract (28 g). The root extract was submitted to silica gel CC (18 × 145 cm) with petroleum ether/$Me_2CO$ [1:0 (3 L), 50:1 (3 L), 20:1 (4 L), 10:1 (5 L), 5:1 (8 L), 2:1 (5 L), and 0:1 (2.3 L)], to give fractions A−G by means of TLC analysis. The fractions E and F showed significant inhibitory activities in the bioassays against lettuce seedlings. Fraction E was separated by CC on silica gel CC (2 × 75 cm), eluted with a gradient of petroleum ether/$Me_2CO$ [10:1 (1.5 L), 5:1 (0.8 L), 2:1 (0.6 L), and 0:1 (0.32 L)], and then repeated silica gel CC to produce compound **3** (9 mg). Fraction F was chromatographed on silica gel CC (2 × 75 cm), eluting with a $CHCl_3/CH_3OH$ gradient [20:1 (0.5 L), 5:1 (1 L), 2:1 (1.6 L), and 0:1 (0.4 L)], then was passed through a Sephadex LH-20 column (1.1 × 60 cm, 30 g) (1:1 $CHCl_3/CH_3OH$), and repeated silica gel CC to produce compound **1** (16 mg) and compound **2** (6 mg).

*Compound* ***1***. White amorphous powder. ESI−MS *m/z*: 461.13 $[M - H]^-$. $^1$H NMR (400 MHz, DMSO) *δ*: 7.73 (s, 1H, H-5), 7.48 (s, 1H, H-5′), 4.09 (s, 3H, 3-OMe), 4.05 (s, 3H, 3′-OMe), 5.16 (d, 1H, *J* = 7.6 Hz, H-1″), 3.21−3.87 (m, 5H, H-2″, H-3″, H-4″, H-5″). $^{13}$C NMR (100 MHz, DMSO) *δ*: 114.0 (C-1), 141.4 (C-2), 141.7 (C-3), 151.1 (C-4), 111.7 (C-5), 112.6 (C-6), 158.3 (C-7), 110.9 (C-1′), 140.8 (C-2′), 140.0 (C-3′), 152.7 (C-4′), 111.7 (C-5′), 112.6 (C-6′), 158.2 (C-7′), 61.5 (3-OMe), 60.9 (3′-OMe), 101.7 (C-1″), 72.9 (C-2″), 76.0 (C-3″), 69.1 (C-4″), 65.7 (C-5″).

*Compound* ***2***. White amorphous powder. ESI−MS *m/z*: 329.10 $[M - H]^-$. $^1$H NMR (400 MHz, DMSO) *δ*: 7.48 (s, 2H, H-5, H-5′), 4.03 (s, 6H, 2× OMe). $^{13}$C NMR (100 MHz, DMSO) *δ*: 111.5 (C-1, C-1′), 141.1 (C-2, C-2′), 140.1 (C-3, C-3′), 152.1 (C-4, C-4′), 111.3 (C-5, C-5′), 112.0 (C-6, C-6′), 158.3 (C-7, C-7′), 60.8 (2× OMe).

*Compound* ***3***. White amorphous powder. ESI−MS *m/z*: 689.25 $[M - H]^-$. $^1$H NMR (400 MHz, DMSO) *δ*: 2.47 (m, 1H, H-1a), 2.93 (m, 1H, H-1b), 5.43 (dd, 1H, *J* = 4.2 and 1.0 Hz, H-3), 3.75 (dd, 1H, *J* = 4.2 and 9.0 Hz, H-4), 6.03 (d, 1H, *J* = 9.0 Hz, H-5), 6.08 (s, 1H, H-7), 4.81 (d, 1H, *J* = 9.2 Hz, H-8), 6.12 (d, 1H, *J* = 16.0 Hz, H-11), 5.88 (dd, 1H, *J* = 16.0 and 9.0 Hz, H-12), 4.34 (m, 1H, H-13), 1.31 (s, 3H, H-16), 5.75 (brs, 1H, H-17a), 6.12 (brs, 1H, H-17b), 1.34 (s, 3H, H-18), 1.26 (s, 3H, H-19), 1.41 (d, 3H, *J* = 6.0 Hz, H-20), 2.03 (s, 3H, 3-OAc), 2.08 (s, 3H, 15-OAc), 7.03−7.35 (m, 6H, 2× OBz), 7.52−7.81 (m, 4H, 2× OBz), 2.34 (s, 1H, 2-OH), 3.30 (d, 1H, *J* = 9.2 Hz, 8-OH). $^{13}$C NMR (100 MHz, DMSO) *δ*: 50.6 (C-1), 79.0 (C-2), 80.6 (C-3), 46.6 (C-4), 65.6 (C-5), 136.8 (C-6), 72.6 (C-7), 72.8 (C-8), 211.5 (C-9), 48.4 (C-10), 134.3 (C-11), 134.8 (C-12), 42.0 (C-13), 205.1 (C-14), 90.8 (C-15), 25.1 (C-16), 124.0 (C-17), 23.0 (C-18), 20.0 (C-19), 23.5 (C-20), 169.7 [3-OAc(CO)], 20.5 [3-OAc(Me)], 169.8 [15-OAc(CO)], 21.9 [15-OAc(Me)], 165.0 [5-OBz(CO)], 128.5 (1′,5-OBz), 129.6 (2′,6′,5-OBz), 127.9 (3′,5′,5-OBz), 133.1 (4′,5-OBz), 166.0 [7-OBz(CO)], 128.8 (1″,7-OBz), 129.7 (2″,6″,7-OBz), 128.0 (3″,5″,7-OBz), 133.1 (4″,7-OBz).

**HPLC Analysis.** HPLC analysis was measured on an Agilent apparatus equipped with a diode array detector (DAD) and a reverse-phase C18 column with 5 μm particle sizes. UV spectra were recorded at 200−400 nm, and the compounds were monitored at 254 and 275 nm. The mobile phase was composed of (A) 0.1% aqueous acetic acid and (B) methanol/acetonitrile (1:2, v/v) for analysis of compounds **1** and **2** and programmed as follows: 0−5 min, 15% B; 5−10 min, from 15 to 40% B; 10−20 min, from 40 to 55% B; 20−35 min, from 55 to 70% B; and 35−42 min, 70% B. The flow rate was 0.6 mL/min with an injection volume of 20 μL at the temperature of 30 °C. To analyze compound **3** in the root exudates, the other mobile phase was composed of (A) 0.1% aqueous acetic acid and (B) methanol. The gradient schedule was as follows: 0−5 min, 40% B; 5−10 min, from 40 to 55% B; 10−20 min, from 55 to 60% B; 20−25 min, 60% B; 25−40 min, from 60 to 70% B; 40−45 min, from 70 to 90% B; and 45−50 min, from 90 to 100% B. The method for analysis of compounds **1**−**3** in the extract of roots at the concentration of 0.1 mg/mL was the same as that with the compounds **1** and **2**.

The analytical HPLC methods described above were validated by compounds **1** and **3**. Mean recovery rates (accuracy) were >98% with a relative standard deviation of <5% and were decided by adding a certain amount of standards into the extract of soil samples. Precision of the intraday assay was determined using six continuous injections during the same day, while that of the interday assay was measured in 3 consecutive days. All relative standard deviation (RSD) values of peak area were found to be <5%.

**Identification and Quantitation of Allelochemicals in the Rhizosphere Soil.** Identifications of the phenolic compounds in the

rhizosphere soil of *E. himalayensis* were completed by comparing the retention times and UV spectra to the standards of compounds **1**−**3**. The standard curves were performed using the linear regression method, and peak areas at 275 nm were plotted versus concentrations. The regression equations of compounds **1**−**3** were $y = 17619x + 59.108$ ($r^2 = 0.9999$), $y = 16519x + 39.108$ ($r^2 = 0.9979$), and $y = 869.86x - 1925.8$ ($r^2 = 0.9964$) in the concentration range of 0.001−0.2 mg/mL, respectively. Limit of detection (LOD) was defined as the concentration for which the signal-to-noise ratio was 3, and limit of quantitation (LOQ) was defined as the concentration for which the signal-to-noise ratio was 10. The LOD was calculated to be 0.03 μg/mL, and the LOQ was 0.1 μg/mL for compounds **1**−**3**. Compounds **1**−**3** were also verified to exist in the soils by the internal standard method.[6] The same soil sample used in the HPLC analysis was further analyzed by UPLC−MS/MS.

**UPLC−MS/MS Equipment and Conditions.** UPLC was measured on a Waters Acquity Ultra Performance LC system (Waters Corp., Milford, MA), which was equipped with a binary solvent delivery pump, a column oven, a photodiode array detector, and an auto-sampler and coupled to a TQD mass spectrometer (Waters Corp., Milford, MA) with an ESI source. The analytes were separated on a BEH C18 column with 1.7 μm particle sizes (50 mm length and 2.1 mm inner diameter) (Waters Corp., Milford, MA) at the temperature of 30 °C. Chromatographic separation was performed through a 6 min gradient delivery of a mixture of (A) methanol and (B) 0.1% aqueous acetic acid, at a flow rate of 0.3 mL/min. The gradient schedule was as follows: 0−1 min, 30% A; 1−2 min, 30−45% A; 2−4 min, 45−50% A; 4−5 min, 50−80% A; and 5−6 min, 80% A. The system was re-equilibrated with 30% A for 2 min before the next sample run. The absorption spectra of the compounds were recorded in the range of 190−400 nm. The injection volume was 2 μL.

MS/MS detection was performed on a Waters Micromass Quattro Premier triple quadrupole mass spectrometer with an ESI source at the negative mode. The cone gas flow was set at 50 L/h; desolvation gas flow was 600 L/h; and capillary voltage was operated at 3.0 kV. The source and desolvation temperatures were 110 and 350 °C, respectively. The argon gas collision energy was set with the cone voltage at 35 V.

## RESULTS AND DISCUSSION

**Allelopathic Effects of the Root Exudates of *E. himalayensis* on Crops and Grasses.** Wheat and rape are common crops in the Tibetan Plateau. The bioassay showed that the extract of the root exudates from rhizosphere soil of *E. himalayensis* had significant allelopathic effects on crops (wheat, rape, and lettuce) and grasses (*F. rubra*, *P. annua*, and red clover) (Figures 1 and 2), indicating that the plant exudes sufficient quantities of allelochemicals to influence other neighboring plants. Interestingly, it was found that the extract of the root exudates showed an inhibitory effect at a concentration of 100 μg/mL but promoted the growth and development of wheat seedlings when the tested concentration was increased to 200 μg/mL (Figure 1), indicating that the allelochemicals and their combination could be explored as a selective plant growth regulator for weed control and a friendly promoter for the growth of wheat in the agricultural ecosystem.

**Allelopathic Metabolites Isolated from Roots of *E. himalayensis*.** The isolations of allelopathic compounds from roots of *E. himalayensis* were achieved by a bioactivity-guided fractionation approach. Three compounds including 4-*O*-[*β*-D-xylopyranosyl]-3,3′-di-*O*-methylellagic acid (**1**),[7] 3,3′-di-*O*-methylellagic acid (**2**),[7] and esulone A (**3**)[8] were isolated from the active fractions of the root extracts and characterized by spectroscopic methods (Figure 3).

Compound **1** was obtained as a white amorphous powder. The $^1$H and $^{13}$C NMR with [distortionless enhancement by

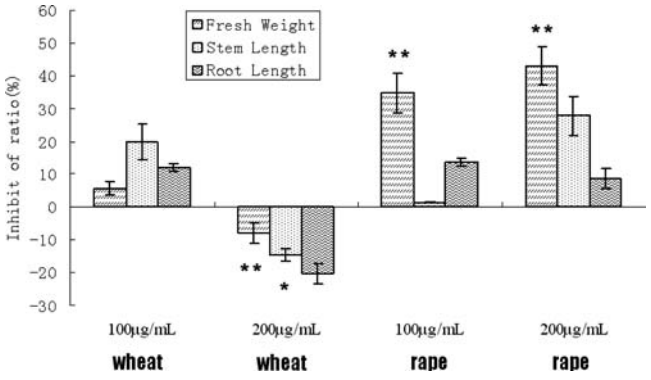


**Figure 1.** Phytotoxic effects of root exudates of *E. himalayensis* against wheat and rape at the concentrations of 100 and 200 μg/mL, respectively. Values are presented as a percentage of the mean compared to the control. Means significantly lower than the DMSO controls are indicated with one asterisk (∗) (Dunnett's one-sided *t* test; $p < 0.05$) or two asterisks (∗∗) ($p < 0.01$). Error bars are one standard error of the mean. $N = 4$.

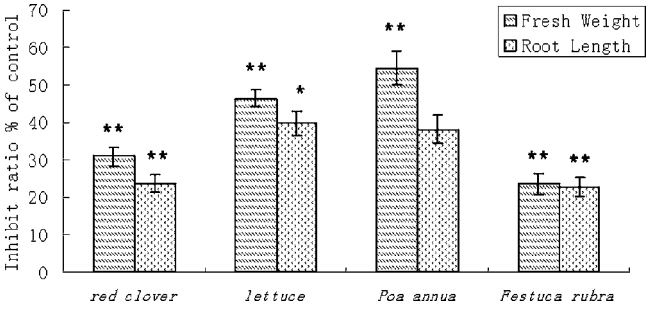


**Figure 2.** Phytotoxic effects of root exudates of *E. himalayensis* at the concentration of 200 μg/mL. Values are presented as a percentage of the mean compared to the control. Means significantly lower than the DMSO controls are indicated with one asterisk (∗) (Dunnett's one-sided *t* test; $p < 0.05$) or two asterisks (∗∗) ($p < 0.01$). Error bars are one standard error of the mean. $N = 4$.

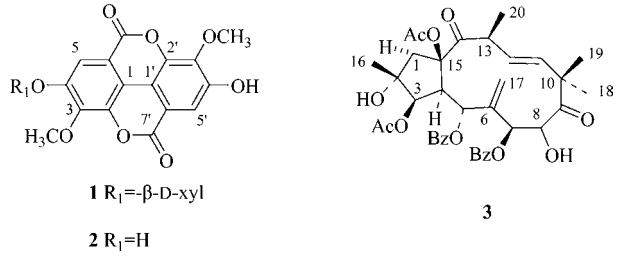


**Figure 3.** Structures of allelopathic compounds isolated from the roots of *E. himalayensis*.

polarization transfer (DEPT)] spectra of compound **1** displayed signals of 2 methoxyls, 1 methylenes, 6 methines, and 12 quaternary carbon atoms (including 2 carbonyl and 10 aromatic carbon atoms). In particular, six proton signals at $\delta_H$ 5.16 (d, 1H, $J = 7.6$ Hz) and 3.21−3.87 (m, 5H) in the $^1$H NMR together with five carbon atoms at $\delta_C$ 101.7, 72.9, 76.0, 69.1, and 65.7 in the $^{13}$C NMR enabled us to establish the skeleton of ellagic acid as well as xylopyranosyl group connection. The structure of compound **1** was finally established as 4-*O*-[*β*-D-xylopyranosyl]-3,3′-di-*O*-methylellagic acid by comparison to the reported data.[7]

The $^1$H and $^{13}$C NMR spectra of compound **2** were similar to those of compound **1**, except lacking the signals of the xylopyranosyl group. By comparison to the literature values,[7]


dx.doi.org/10.1021/jf502020v | J. Agric. Food Chem. 2014, 62, 8555−8561

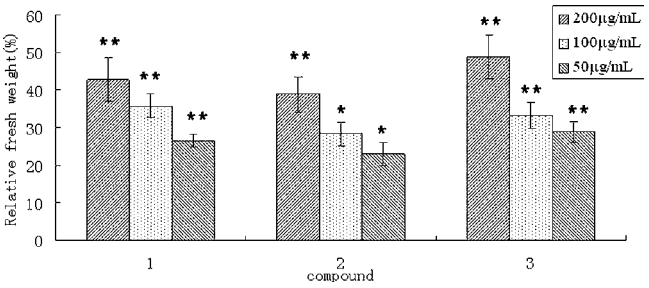


**Figure 4.** Effects of compounds **1**–**3** isolated from the roots of *E. himalayensis* on fresh weights of lettuce seedlings. Values are presented as a percentage of the mean compared to the control. Means significantly lower than the DMSO controls are indicated with one asterisk (∗) (Dunnett's one-sided *t* test; $p < 0.05$) or two asterisks (∗∗) ($p < 0.01$). Error bars are one standard error of the mean. $N = 4$.

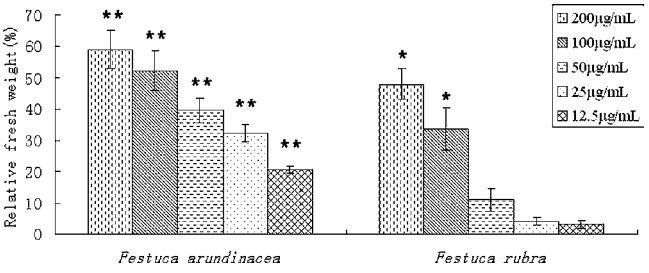


**Figure 5.** Effects of compound **3** on fresh weights of *F. arundinacea* and *F. rubra* seedlings. Values are presented as a percentage of the mean compared to the control. Means significantly lower than the DMSO controls are indicated with one asterisk (∗) (Dunnett's one-sided *t* test; $p < 0.05$) or two asterisks (∗∗) ($p < 0.01$). Error bars are one standard error of the mean. $N = 4$.

the structure of compound **2** was identified as 3,3′-di-*O*-methylellagic acid.

Compound **3** was found to possess a molecular formula of $C_{38}H_{42}O_{12}$ requiring 18 degrees of unsaturation, which was evidenced by ESI–MS at $m/z$ 689.25 $[M - H]^-$ and $^{13}C$ NMR. Four characteristic methyl groups at $\delta_H$ 1.31 (s, 3H, H-16), 1.34 (s, 3H, H-18), 1.26 (s, 3H, H-19), and 1.41 (d, 3H, $J$ = 6.0 Hz, H-20) and $\delta_C$ 25.1 (C-16), 23.0 (C-18), 20.0 (C-19), and 23.5 (C-20) and one exocyclic double bond at $\delta_H$ 5.75 (brs, 1H, H-17a) and 6.12 (brs, 1H, H-17b) and $\delta_C$ 136.8 (C-6) and 124.0 (C-17) suggested that compound **3** was a jatrophane diterpene. The structure of compound **3** was determined to be esulone A, which had been reported in literature isolated from the plant belonging to the same genus *Euphorbia*.[8]

**Allelopathic Activities of the Purified Metabolites.** Compounds **1**–**3** isolated and purified from the roots of *E. himalayensis* were evaluated by the bioassays of the allelopathic activities against seedlings of lettuce, *F. arundinacea*, and *F. rubra*. Results indicated that the growth of the tested lettuce seedlings were inhibited by all three compounds to different degrees, with compounds **1**–**3** showing obvious inhibitory effects (Figure 4). The allelopathic effects of three compounds showed dose-dependent alterations. Compound **3** had an inhibitory activity against weeds *F. arundinacea* and *F. rubra* (Figure 5), while the other compounds only exhibited very slight activities. In addition, the inhibitory activity of compound **3** against *F. arundinacea* was stronger than that against *F. rubra*, especially at low concentrations. It was found that compound **3** did not kill the other plants but mainly inhibited the growth of their roots. These results may be induced by the compound through mediating the polar auxin transport or inhibiting the synthesis of auxin, which should be

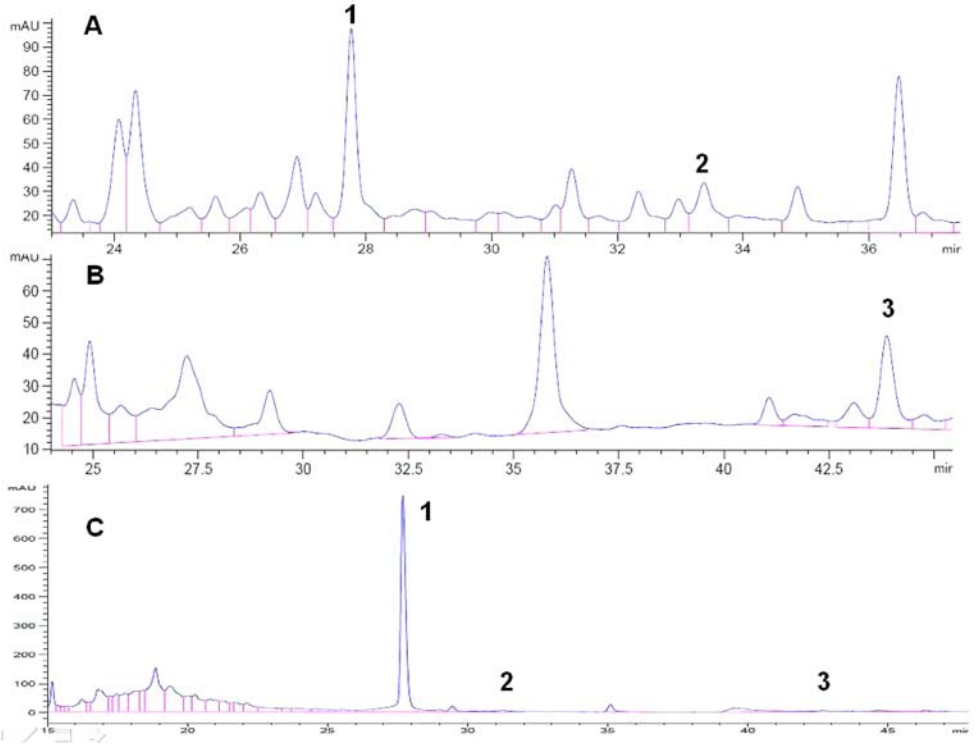


**Figure 6.** HPLC analysis of the rhizosphere soil and root of *E. himalayensis*. (A and B) Compounds **1**, **2**, and **3** were shown in the HPLC chromatogram of the rhizosphere soil at 275 nm and had the following LC retention times of 27.77, 33.38, and 43.87 min, respectively. (C) Compounds **1**, **2**, and **3** were shown in the HPLC chromatogram of the root at 275 nm and had the following LC retention times of 27.77, 33.38, and 41.13 min, respectively.


dx.doi.org/10.1021/jf502020v | J. Agric. Food Chem. 2014, 62, 8555–8561

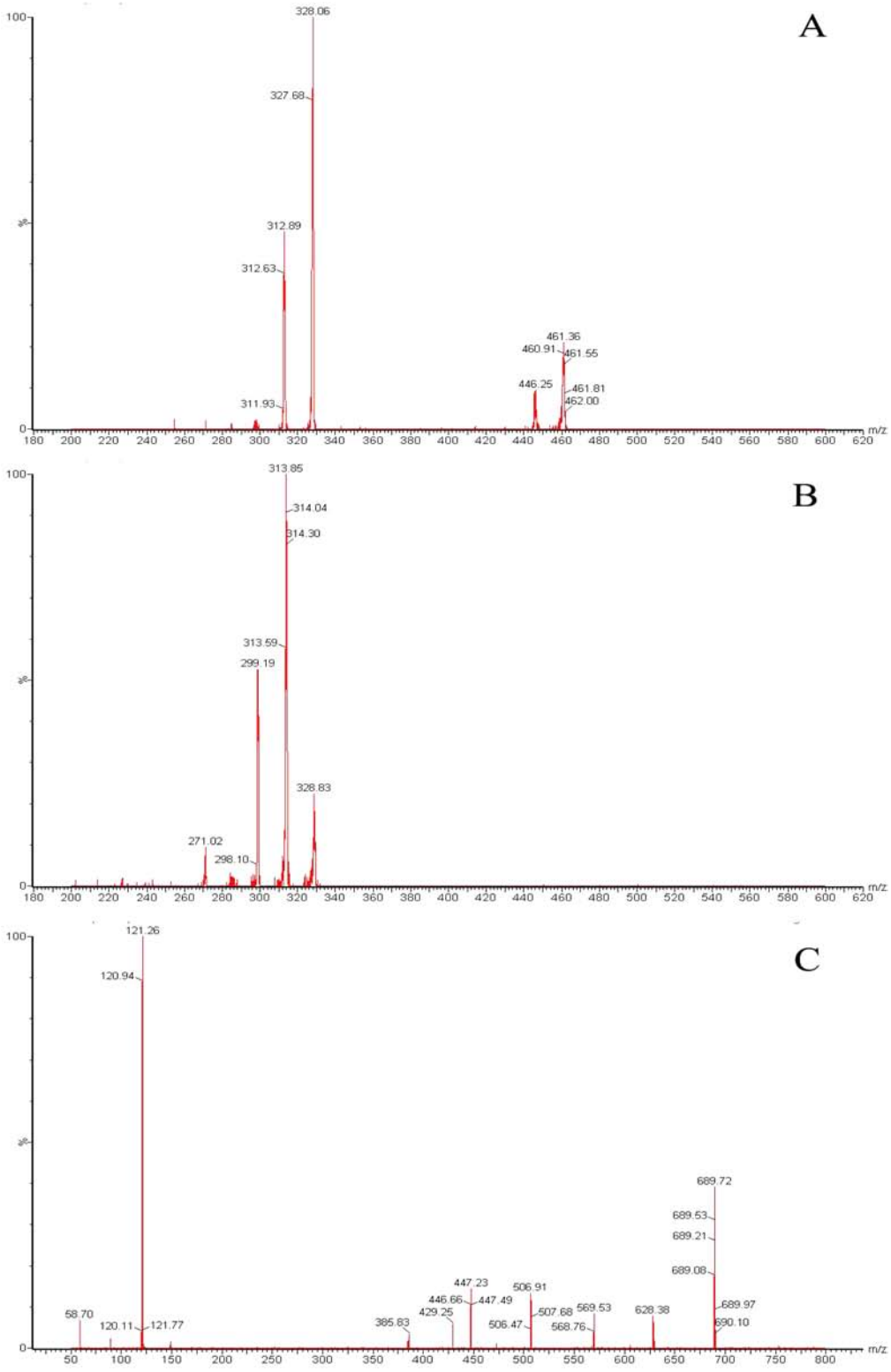


**Figure 7.** (A–C) Tandem mass spectra of compounds **1**–**3**, respectively.

demonstrated by further studies. Thus, the identification of these compounds could lead to the discovery of new, natural herbicides, which can be more environmentally friendly and potentially have new modes of action when compared to the currently used synthetic herbicides.

**Identification and Quantitation of Allelochemicals in the Rhizosphere Soil.** To achieve identification of the allelochemicals released from the plant into soil during its growth, HPLC was used to confirm the existence of the allelochemicals in the rhizosphere soil (Figure 6). The chromatogram was measured at 275 nm, at which most of the compounds had absorbance. Compounds **1**–**3** were identified as allelochemicals in the rhizosphere soil and confirmed by the internal standard method.[6] In comparison to the chromatogram of the soil, the


dx.doi.org/10.1021/jf502020v | J. Agric. Food Chem. 2014, 62, 8555–8561

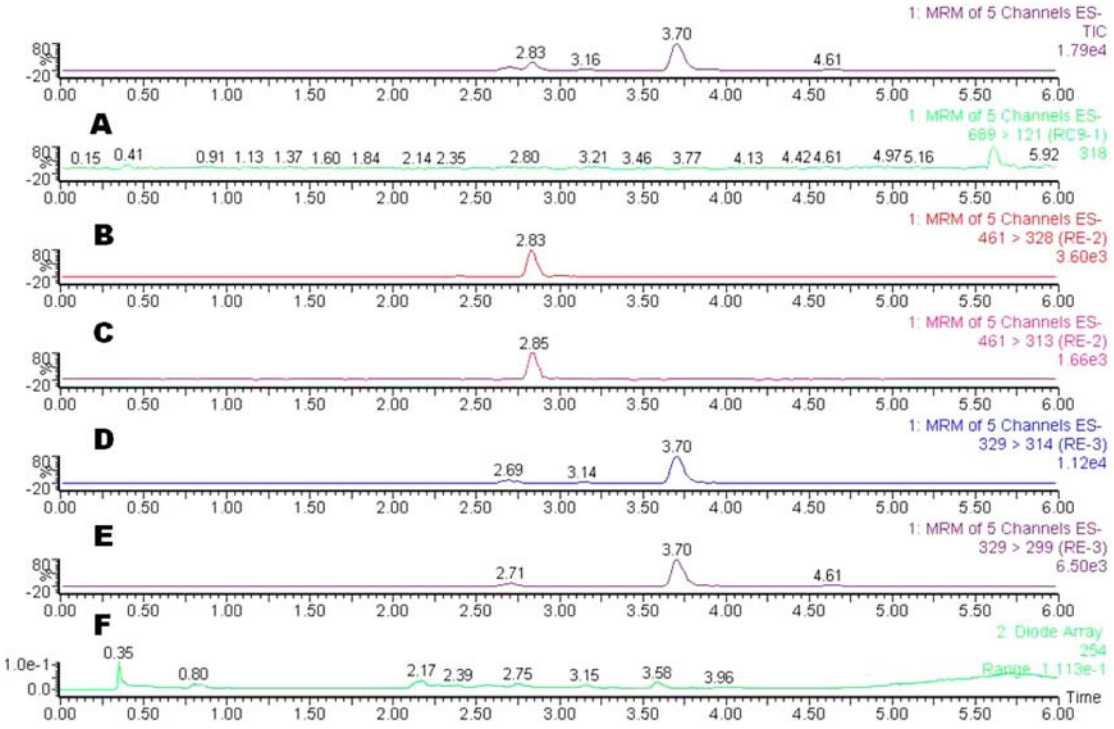


**Figure 8.** UPLC analysis of the root exudates of *E. himalayensis*. Compounds **1**, **2**, and **3** are shown in the UPLC chromatogram and had the following LC retention times of 2.85, 3.70, and 5.62 min, respectively: (A) compound **3** (689 > 121), (B) compound **1** (461 > 328), (C) compound **1** (461 > 313), (D) compound **2** (329 > 314), (E) compound **2** (329 > 299), and (F) UPLC chromatogram with a photodiode array detector at 254 nm.

peaks of compounds **1**−**3** were enhanced obviously after the injection of the standards into soil samples and no new peaks appeared.

The allelochemicals in the soil matrix were further identified by means of mass spectra, because they were the key to research of allelopathic effects. UPLC−MS/MS and HPLC−DAD were successfully used in this study to determine the existence of the allelochemicals in the rhizosphere soil of *E. himalayensis*. Accurate MS and MS/MS data confirmed the composition of each of the daughter ions. Fragmentation of the protonated molecular ion of compound **1** ($[M - H]^-$ $m/z$ 461) in negative-ion ESI mode produces a number of daughter ions, notably $m/z$ 446 (loss of $CH_3$), $m/z$ 328 (loss of $C_4H_6O_5$), and $m/z$ 313 (loss of xylopyranosyl) (Figure 7). Although compounds **1** and **2** have the same nucleus, the protonated molecular ion $[M - H]^-$ $m/z$ 329 of compound **2** produces corresponding daughter ions of $m/z$ 314 (loss of $CH_3$) and $m/z$ 299 (loss of two $CH_3$). The most dominant daughter ion observed at $m/z$ 121 was chosen as the transition ($m/z$ 689 → 121) for verification of compound **3** using a multiple reaction monitoring (MRM) program on UPLC−MS/MS. The detection of three compounds in the UPLC−MS/MS chromatogram of the rhizosphere soil is shown in Figure 8.

The standard curves were obtained by use of the linear regression method, and peak areas at 275 nm were plotted to calculate concentrations; thus, the concentrations of compounds **1**, **2**, and **3** in the soil were determined as 3.6, 3.8, and 8.99 nmol/g of soil, respectively.

It is well-known that plants usually synthesize secondary metabolites used to adapt to the environment and enable their survival and well-being. The compounds of ellagic acid type, which belonged to compounds **1** and **2**, were reported to exhibited varied activities, such as inhibitors of auxin transport.[9] Allelochemicals **1** and **2** possessed the same skeleton and maybe mutual reverse in nature. The replacement of the xylose group at the C-4 position would improve the water solubility and enlarge the application range of compound **2**, although the activity of compound **2** was slightly weaker than that of compound **1**. Compound **3** belongs to jatrophane diterpenes usually isolated from Euphorbiaceae plants and exhibits cytotoxic, antitumor, insect deterrent, and antimicrobial activities *in vitro*.[10] The phytotoxic compounds isolated from roots were also present in the root exudates, suggesting that they were allelochemicals of *E. himalayensis*. These two types of compounds might be leached into the soil and accumulated in the rhizosphere, resulting in a competitive superiority for *E. himalayensis* with its neighboring plants in the natural plant ecosystem.

It is also interesting to note that compounds **1**−**3** have been reported to present in roots of leafy spurge, an invasive species in the same genus.[7,11] Of particular interest is the observation that compounds **1** and **2** were also found in the root exudates of leafy spurge. It is known that the skeletal structures of secondary metabolites from the same genera are usually the same or similar.[12]

*E. himalayensis*, a toxic weed to livestock and humans in the Tibetan Plateau, exhibits allelopathic effects on crops, but the phytotoxic activities of the purified metabolites have not been reported thus far. In this study, compounds **1**−**3** isolated from the root extract of *E. himalayensis* showed observably phytotoxic activities. These compounds were also determined as allelochemicals of the plant released into the soil environment. The bioassay showed that the extract of the root exudates from the rhizosphere soil of *E. himalayensis* had significant allelopathic effects on crops and grasses. Our findings suggest that *E. himalayensis* is able to exert an effect on other plants through the release of allelochemicals. Production of these


dx.doi.org/10.1021/jf502020v | J. Agric. Food Chem. 2014, 62, 8555−8561

chemicals can increase the fitness of *E. himalayensis* and provide the plant a superiority to become a successful competitor in the natural plant ecosystem. The bioassay results showed that the extract of the root exudates had an inhibitory effect at a lower concentration but promoted the growth of wheat seedlings once the test concentration was increased to 200 μg/mL, suggesting that the combination of the allelochemicals could be explored as a plant growth inhibitor for weed control and promoter for the growth and development of Gramineae crops, such as wheat in agriculture.

## AUTHOR INFORMATION

### Corresponding Author

*Telephone: +86-931-4968372. Fax: +86-931-8277088. E-mail: bqin@licp.cas.cn.

### Funding

This work was funded by the National Natural Science Foundation of China (21102154 and 31070386), the Associate Scholar Program for Talents Cultivation Plan of "Western Light" of CAS, and the Basic Research Program of Lanzhou Institute of Chemical Physics, CAS (080423SYR1).

### Notes

The authors declare no competing financial interest.

## REFERENCES

(1) Zhou, B.; Kong, C. H.; Li, Y. H.; Wang, P.; Xu, X. H. Crabgrass (*Digitaria sanguinalis*) allelochemicals that interfere with crop growth and the soil microbial community. *J. Agric. Food Chem.* **2013**, *61*, 5310−5317.

(2) Escrig, P. V.; Iglesias, D. J.; Corma, A.; Primo, J.; Primo-Millo, E.; Cabedo, N. *Euphorbia characias* as bioenergy crop: A study of variations in energy value components according to phenology and water status. *J. Agric. Food Chem.* **2013**, *61*, 10096−10109.

(3) Steenhagen, D. A.; Zimdahl, R. L. Allelopathy of leafy spurge (*Euphorbia esula*). *Weed Sci.* **1979**, *27*, 1−3.

(4) Ghodake, S. D.; Jagtap, M. D.; Kanade, M. B. Allelopathic effect of three *Euphorbia* species on seed germination and seedling growth of wheat. *Ann. Biol. Res.* **2012**, *3*, 4801−4803.

(5) Tanveer, A.; Khaliq, A.; Javaid, M. M.; Chaudhry, M. N.; Awan, I. Implications of weeds of genus *Euphorbia* for crop production: A review. *Planta Daninha* **2013**, *31*, 723−731.

(6) Liu, Q.; Xu, R.; Yan, Z. Q.; Jin, H.; Cui, H. Y.; Lu, L. Q.; Zhang, D. H.; Qin, B. Phytotoxic allelochemicals from roots and root exudates of *Trifolium pratense*. *J. Agric. Food Chem.* **2013**, *61*, 6321−6327.

(7) Khac, D. D.; Tran-Van, S.; Campos, A. M.; Lallemand, J.; Fetizon, M. Ellagic compounds from *Diplopanax stachyanthus*. *Phytochemistry* **1990**, *29*, 251−256.

(8) Manners, G. D.; Wong, R. Y. The absolute stereochemical characterization of two new jatrophane diterpenes from *Euphorbia esula*. *J. Chem. Soc., Perkin Trans. 1* **1985**, 2075−2081.

(9) Vieitez, F. J.; Ballester, A. Presence of root inhibitors in chestnut cuttings. *Bol. Acad. Galega Cienc.* **1986**, *5*, 125−132.

(10) Devappa, R. K.; Makkar, H. P. S.; Becker, K. *Jatropha* diterpenes: A review. *J. Am. Oil Chem. Soc.* **2011**, *88*, 301−322.

(11) Qin, B.; Perry, L. G.; Broeckling, C. D.; Du, J.; Stermitz, F. R.; Paschke, M. W.; Vivanco, J. M. Phytotoxic allelochemicals from roots and root exudates of leafy spurge (*Euphorbia esula* L.). *Plant Signaling Behav.* **2006**, *1*, 1−5.

(12) Griffin, W. J.; Lin, G. D. Chemotaxonomy and geographical distribution of tropane alkaloids. *Phytochemistry* **2000**, *53*, 623−637.

JOURNAL OF AGRICULTURAL AND FOOD CHEMISTRY

Article

pubs.acs.org/JAFC

# Effect of pH and Recombinant Barley (*Hordeum vulgare* L.) Endoprotease B2 on Degradation of Proteins in Soaked Barley

Jesper Bjerg Christensen,[†] Giuseppe Dionisio,[‡] Hanne Damgaard Poulsen,[†] and Henrik Brinch-Pedersen*[,‡]

[†]Aarhus University, Research Center Foulum, Department of Animal Science, DK-8830 Tjele, Denmark

[‡]Aarhus University, Research Center Flakkebjerg, Department of Molecular Biology and Genetics, DK-4200 Slagelse, Denmark

Supporting Information

**ABSTRACT:** Nonfermented soaking of barley feedstuff has been established as an in vitro procedure prior to the feeding of pigs as it can increase protein digestibility. In the current study, two feed cultivars of barley (Finlissa and Zephyr) were soaked in vitro either nonbuffered or buffered at pH 3.6 and 4.3. Solubilized and degraded proteins evaluated by biuret, SDS-PAGE, and differential proteomics revealed that pH 4.3 had the greatest impact on both solubilization and degradation. In order to boost proteolysis, the recombinant barley endoprotease B2 (rec-HvEP-B2) was included after 8 h using the pH 4.3 regime. Proteolysis evaluated by SDS-PAGE and differential proteomics confirmed a powerful effect of adding rec-HvEP-B2 to the soaked barley, regardless of the genotype. Our study addresses the use of rec-HvEP-B2 as an effective feed enzyme protease. HvEP-B2 has the potential to increase the digestibility of protein in the pig, either supplied as recombinant additive or as possible new selection criterion in barley breeding.

**KEYWORDS:** *pH, barley, Hordeum vulgare L., soaking, protein, cysteine endoprotease B2, rec-HvEP-B2*

## INTRODUCTION

Inefficient nitrogen utilization in intensive animal production results in environmental pollution problems. When barley (*Hordeum vulgare* L.) is used as dry porcine feedstuff, the apparent total tract digestibility of protein is ∼73%.[1] This may be the result of relative low retention times in the stomach and ileum (5 h in total[2]) and limited accessibility of the digestive proteases to the nutrients. When cereals are soaked or fermented prior to feeding of the pig, an increased apparent ileal digestibility of protein is reported,[3] indicating a "predigestion" of the cereal protein. In vitro methods, estimating the ileal digestibility of feed protein, assume that soluble and proteolyzed peptides with molecular sizes smaller than 5 kDa is digested and absorbed in vivo.[4−6] However, soaking of barley in liquid feed preparations may activate barley proteases to degrade water-insoluble hordeins to a degree that fulfills the digestibility criteria. During germination of the barley grain, cysteine endoproteases degrade and solubilize storage proteins,[7,8] which are further proteolyzed into amino acids[9,10] and transported to the growing embryo.[11,12] The cysteine endoproteases have acidic pH optima and are active during the first 7 days of the germination when the pH becomes acidic in the storage vacuole.[13,14] Acidification also takes place when ground cereals are soaked or fermented for liquid feed, creating optimal conditions for endoprotease activity. Unfortunately, acidification under these conditions can take up to 24 h.[15−17] This period of time is not realistic in the case of nonfermented liquid feed, which is preferred for fast feed preparation. Acidifying and buffering pH in the range of the pH optima of endogenous proteases may speed up the proteolysis and thereby shorten the time of degradation and soaking. Moreover, the addition of additional protease activity may improve the protein digestibility and shorten the soaking time even further. A promising protease is the *H. vulgare* cysteine endoprotase B2 (HvEP-B2), which has been produced recombinantly and proved to be effective for hydrolyzing barley hordein storage proteins in vitro.[18,19] Recombinant HvEP-B2 (rec-HvEP-B2) degrades hordeins at pH 4.5 and may be a new candidate for improving protein digestibility in soaked barley.[18]

The present study was conducted to investigate if it is possible to increase the proteolytic degradation of the barley storage proteins during soaking. This was attempted by the means of pH buffering and addition of rec-HvEP-B2.

## MATERIALS AND METHODS

**Materials.** Two winter barley feed cultivars, Finlissa and Zephyr were used in this study. Two cultivars were selected to increase the statistical strength of the study. Finlissa and Zephyr were provided by Sejet Plant Breeding and were selected from multiplication fields in 2010.[20] Grains (100 g) of each cultivar were grinded using a hammer mill with a 0.5 mm sieve. The total amount of nitrogen in the grain was determined using a modified Kjeldahl method.[21] The protein content was calculated by use of a protein-to-nitrogen conversion factor of 5.45, which is specific for barley.[22]

**Soaking of Barley and Buffering pH.** Samples of Finlissa and Zephyr were weighed out in repetitions of three for six time points: 0, 4, 8, 12, 24, and 48 h. Samples of 1.5 g ground barley were weighed out in 10 mL screw cap tubes and mixed with water or buffer in a 1:2.75 (w/w) ratio.[23] Three conditions were tested: (1) nonbuffered, where the dry samples were mixed with water in the ratio mentioned

Received: May 8, 2014
Revised: August 1, 2014
Accepted: August 12, 2014
Published: August 12, 2014

 © 2014 American Chemical Society 

above; (2) pH 4.3, where 100 mM acetic acid pH 4.3 was used; and (3) pH 3.6, obtained by soaking the sample with 100 mM lactic acid pH 3.6 buffer. The pH increased 0.2 units during the initial mixing of buffer and barley flour, resulting in samples with pH 4.5 and 3.8, respectively, for conditions 2 and 3. The samples were soaked at 20 °C under shaking conditions (250 rpm) and subsequently at the chosen time points, centrifuged at 4200*g*, 4 °C for 20 min after incubation. The amount of water-soluble proteins in the supernatant was measured using a modified biuret method[24] and were correlated with the total amount of protein in the cultivars. The proteins in the soluble fraction and the pellet were analyzed by SDS-PAGE (NuPAGE 4−12%, Life Technologies, U.S.A.) and stained by Coomassie (Brilliant Blue R-250) for monitoring the level of proteolysis.

**Addition of Rec-HvEP-B2.** Before the addition of rec-HvEP-B2 (produced recombinantly in *Pichia pastoris*[18]), it was activated by adding 4 mM cysteine (final concentration in the soaking) to reduce the nucleophilic cysteine in the active site. It was tested if the addition of 4 mM cysteine itself in the soaking mixture would affect the proteolysis. SDS-PAGE analysis on the pellet fraction revealed no changes after addition of 4 mM cysteine (not shown). The soluble fraction was analyzed by label-free differential LC-MS analysis, but in this case, no significant changes were observed (Table 4 in Supporting Information). Next, the addition of 4 mM cysteine along with rec-HvEP-B2 was tested. The amount of rec-HvEP-B2 protease to add was determined by initial titration experiments where increasing amounts of soaked barley ground seeds were added to a fixed amount of rec-HvEP-B2. In detail, 500 mg of 0.5 mm ground Finlissa and Zephyr were soaked at 20 °C in 5 mL of 100 mM acetic acid pH 4.3 containing 4 mM cysteine for 1 h and thereafter centrifuged at 4000*g* for 10 min. Different volumes of extracts were mixed with 0.04 U of activated rec-HvEP-B2, and the activity was measured with an 0.1 mM of endoprotease specific chromogenic substrate, (*Z*)-Phe-Arg-*p*NA-HCl (Z-F-R-pNA, Bachem) as described by Rosenkilde et. al 2013.[18] In this study, one rec-HvEP-B2 unit equals 1 μmol per min of *p*-nitroaniline liberated at 42 °C. Increasing amounts of barley extracts caused a decreasing rec-HvEP-B2 activity, compared to the positive control (0.04 U activated rec-HvEP-B2 without barley extracts). This indicated a clear inhibitory effect of rec-HvEP-B2 by barley.

The amount of rec-HvEP-B2 exceeding the inhibitory effect was calculated to be 6 and 6.7 U of rec-HvEP-B2 for 1 g of Finlissa and Zephyr, respectively. Hence, 9 U per g barley was chosen as the amount of rec-HvEP-B2 calculated in excess for breaking the endogenous inhibitory activity of barley extracts. Prior to the addition, the cultivars were soaked at 20 °C in 2.5 mL of 100 mM acetic acid, pH 4.5, for 8 h, which allowed the endogenous proteases to hydrolyze endogenous substrates.

After 8 h of soaking, 2.25 U of rec-HvEP-B2 was added to 250 mg of fine ground barley cultivars (Finlissa and Zephyr). The samples were then incubated for additional 4 h. After centrifugation at 4200*g* for 20 min, the soluble fraction and the pellet sample were mixed 1:3 with 3× SDS sample buffer, boiled for 10 min, and analyzed by SDS-PAGE for monitoring the level of proteolysis, compared to untreated controls. The proteins in the pellet were extracted with 1:2.75 (w/w) ratio 8 M urea, shaken for 30 min at RT, and centrifuged for 3 min at 20.000*g*. The supernatant of the 8 M extracted pellet was mixed 1:3 with the 3× SDS sample buffer and directly loaded for SDS-PAGE.

**Electro-Elution of Proteins.** Soluble fractions after 12 h soaking for each condition (water, pH 4.3, and pH 3.6) were separated using a Gelfree 8100 apparatus (Expedeon, U.S.A.). Electro-elution was performed after 60, 75, and 90 min of a total of 3 h run of a 12% polyacrylamide cartridge, using settings described by the manufacturer.[25] At the different time points, withdrawals were sampled for proteomic analysis and for SDS-PAGE for visualizing the size of the proteins/peptides obtained (Figure 3A,B).

**Statistical Analysis.** For each treatment, three replicates were measured. Soluble proteins determined by biuret were statistically evaluated by the MIXED procedure of SAS version 9.3 (SAS Institute Inc., 2011). Comparison of the inhibition curves (Figure 4) was performed using the Student's *t*-test. The differential proteomics were evaluated by one-way ANOVA obtained from Progenesis LC-MS software. Effects were considered significant when $P \leq 0.05$. The results presented are least-mean square means (LS means). Standard error of mean is given as a measure for variance.

**Sample Preparation for Proteomic Analysis.** Soluble proteins (200 μL) were denatured, and disulfide bonds were reduced with 200 μL of 8 M urea, 10 μL of 1 M DTT, 50 μL of 1 M ABC (ammonium bicarbonate buffer pH 8.0) buffer at 37 °C for 30 min. Pellet proteins were solubilized as described above, and 200 μL of the 8 M urea solubilized proteins were treated with 5 μL of 1 M DTT, 25 μL of 1 M ABC buffer at 37 °C for 30 min. Cysteine alkylation was performed adding 30 μL and 15 μL of 0.5 M iodoacetamide in 100 mM $NH_4HCO_3$, respectively, for the soluble and pellet proteins. This mixture was incubated for 45 min at RT in the dark. After that, the alkylated proteins were desalted by $C_4$ silica spin chromatography (VYDAC 214TP) by lowering the pH with 20 μL of 100% formic acid (FA) and loading the samples onto a spin column containing 20 mg of the $C_4$ resin. The spin column was centrifuged at 2000*g* for 1 min and the pass through was discarded. Bound proteins were washed three times by 0.1% FA solution and spun at 2000*g* for 1 min. The alkylated proteins were eluted in two batches with 50 μL each of 80% acetonitrile (ACN) containing 0.1% FA.

The alkylated proteins were lyophylized using a speedyvac (Concentrator 5201, Eppendorf). The protein pellet was resuspended in 50 μL 0.1 M ABC buffer containing 0.1% Rapigest surfactant (Waters, Milford, U.S.A.), and either 1 μg of proteomics grade trypsin or chymotrypsin (Pierce, Thermoscientific, U.S.A.). The digestion was performed at 37 °C for 2 h and then stopped by adding 5 μL of 5% FA. Peptide desalting was performed by Supel-Tips C18 Micropipette Tips (Sigma-Aldrich, Supelco) according to the manufacturer specifications. The desalted peptides were lyophilized and dissolved in 0.1% FA containing 3% ACN. The amount of peptides per sample was evaluated by 280 nm Abs using a Nanodrop 1000 (Thermoscientific, U.S.A.).

Per sample, 500 ng of desalted peptides were analyzed in triplicate onto an Xbridge BEH130 C18 5 μm desalting/trap column with a BEH300 C18 1.7 μm nanoUPLC analytical capillary column (100 μm x 100 mm) on an Acquity nanoUPLC-LC system interfaced with a nano source to a Q-TOF Premiere MS (Waters, Milford, MA, U.S.A.). The entire length of the LC run was 90 min, starting with a gradient of ACN/0.1 FA (0 to 40%) from 0 to 70 min followed by 90% ACN wash. Data acquisition was performed in V positive mode. MS and MS/MS data was recorded in DDA mode (MS scan every 1 s, MS/MS every 1 s with selection of 4−8 ions and real time mass exclusion) and MSe mode by the software Masslynx version 4.1 (Waters). $MS^E$ runs were analyzed by the Protein Lynx Global Server 2.5 software and ExpressionE using a lock mass standard of 556.2771 $m/z$ for leucine-enkephaline (Leu-Enk), 60 ppm error tolerance for MS data and 30 ppm error for MSe data. Search parameters included HvEP-B2 main cleavage specificity "/Q-\P", where/indicate the cleavage site and −the amino group of the P1 site; also "\P" indicate no cutting if Q was followed by a proline. Furthermore, a semi trypsin or chymotrypsin, cleavage was selected, with one missed cleavage and no specificity from one end of the peptide as other cleavage options. The fixed modification was the carbamidomethyl cysteine (ΔMass +57.02), and many other variable modifications: deamination NQ (+.98), oxidation MHW (15.99), carbamilation N-term (+43.01), Dehydration DSTY, C-term (−18.01), Hydroxylation DKNPRY (+15.99), Pyrrolidinone P (−30.01), Pyroglutamic P (13.98), Pyro-glu from Q (−17.03) and Pyro-glu from E (−18.01).

**Differential Proteomics.** A differential approach involving the shot gun proteomics of the soluble and insoluble (pellet) fraction was performed with both the ExpressionE software ver. 2.5 (Waters) and the Progenesis LC-MS ver. 4.1 (Nonlinear Dynamics, U.K.). The different samples were compared according to their exact mass versus retention time ratio after normalization with 50 fmol of enolase 1 (swissprot P00924, ENO1, *Saccharomyces cerevisiae*) standard tryptic digest (MASSprep Enolase, Waters). Peptides were identified using the mass search engines PLGS 2.5 and PEAKS 6.0.

**Differential Proteomic Analysis of the pH Effect.** Up or down regulation of proteolysis of soluble proteins is indicated by the fold

**Table 1. Top 20 up and down Proteolyzed Proteins Identified by ExpressionE Analysis for Finlissa Samples after 12 h Soaked at Different pH versus the Non-Buffered Condition (Water)**

| max fold change | ANOVA (*P*) | highest mean | lowest mean | description | UniProt accession |
|---|---|---|---|---|---|
| 20.23 | $3.37 \times 10^{-8}$ | $H_2O$ | pH 4.3 | endochitinase | F2EK36 |
| 11.74 | $5.61 \times 10^{-5}$ | pH 4.3 | $H_2O$ | metallothionein-like protein type 4 | Q84L51 |
| 10.00 | $3.70 \times 10^{-8}$ | pH 3.6 | pH 4.3 | alpha amylase/trypsin inhibitor CMc fragment | E7BB45; E7BB46 |
| 8.63 | $1.99 \times 10^{-7}$ | pH 4.3 | pH 3.6 | pathogenesis-related protein 4 (PR4) | P93180 |
| 7.21 | $4.77 \times 10^{-7}$ | $H_2O$ | pH 4.3 | beta glucosidase fragments OS | Q9S9H4 |
| 7.17 | $4.45 \times 10^{-6}$ | $H_2O$ | pH 4.3 | translationally controlled tumor protein | F2DWT1 |
| 6.90 | $2.06 \times 10^{-5}$ | pH 4.3 | $H_2O$ | beta amylase | Q9FUK7; F2EFV1; Q9SB23 |
| 6.24 | $2.86 \times 10^{-6}$ | $H_2O$ | pH 4.3 | alpha amylase/trypsin inhibitor CMd3 protein | O24000; O23982 |
| 5.53 | $5.39 \times 10^{-6}$ | $H_2O$ | pH 3.6 | aldo-keto NADPH-dependent reductase | F2DXQ5 |
| 5.45 | $3.04 \times 10^{-5}$ | $H_2O$ | pH 4.3 | endochitinase | F2ELX8; F2CSS7 |
| 5.08 | $2.88 \times 10^{-8}$ | $H_2O$ | pH 4.3 | thaumatin/thaumatin-like protein TLP8 | F2DNP3; Q946Y8 |
| 4.50 | $6.09 \times 10^{-5}$ | $H_2O$ | pH 3.6 | glucose and ribitol dehydrogenase-like protein | F2CSK4 |
| 4.20 | $1.84 \times 10^{-5}$ | $H_2O$ | pH 4.3 | thaumatin | F2CTV7; F2CVM0; O22462; O23997; Q5MBN2; Q946Y9; Q946Z0 |
| 3.90 | 0.0001 | pH 4.3 | $H_2O$ | beta amylase | E0W6Z7 |
| 3.78 | $3.43 \times 10^{-5}$ | $H_2O$ | pH 4.3 | barwin-like_endoglucanase | F2DXR4 |
| 2.43 | 0.0233 | $H_2O$ | pH 3.6 | non-specific lipid transfer protein | Q42848 |
| 1.92 | 0.00161 | pH 3.6 | pH 4.3 | alpha amylase/trypsin inhibitor BTI CMe2 1 | O49861; O49862 |
| 1.91 | $3.23 \times 10^{-5}$ | $H_2O$ | pH 4.3 | Baker's asthma allergen BDP | Q9S8H1 |
| 1.71 | 0.00073 | $H_2O$ | pH 3.6 | beta amylase | Q84T20; Q9AVJ8; Q9FSI3; Q9FUK6 |
| 1.70 | 0.00062 | $H_2O$ | pH 4.3 | beta amylase | A8CFR3; D6BU16; Q6SNP7; Q84T19; Q9SBH7 |

**Table 2. Top 20 up and down Proteolyzed Proteins Identified by ExpressionE Analysis for Zephyr Samples after 12 h Soaked at Different pH versus the Non-Buffered Condition (Water)**

| max fold change | ANOVA (*P*) | highest mean | lowest mean | description | UniProt accession |
|---|---|---|---|---|---|
| 109 | 0.00142 | pH 3.6 | pH 4.3 | trypsin inhibitor CMc | E7BB46; E7BB45 |
| 55.3 | 0.00481 | $H_2O$ | pH 4.3 | endochitinase | F2ELX8; F2EK36 |
| 41.3 | $1.11 \times 10^{-7}$ | $H_2O$ | pH 4.3 | beta amylase fragment OS *Hordeum vulgare* PE 2 SV 1 | Q9FUK7; A8CFR3; C1IIM6; D6BU16; E0W6Z7; F2EFV1; Q6SNP7; Q84T19; Q84T20; Q9AVJ8; Q9FSI3; Q9FUK6; Q9SB23; Q9SBH7 |
| 34.5 | $2.42 \times 10^{-8}$ | $H_2O$ | pH 4.3 | alpha amylase/trypsin inhibitor BTI CMe4 protein | O49863; E7BB44; O49867; Q84VT9 |
| 32.6 | $2.09 \times 10^{-8}$ | pH 3.6 | pH 4.3 | putative bZIP transcription factor superfamily protein | F2ECK6 |
| 13.1 | $1.04 \times 10^{-5}$ | $H_2O$ | pH 4.3 | chloroplast Cu Zn SOD1 | K4KCI3; F8R513 |
| 11.0 | $1.49 \times 10^{-6}$ | $H_2O$ | pH 4.3 | alpha amylase/trypsin inhibitor BTI CMe2 1 protein | O49861 |
| 8.06 | 0.00600 | $H_2O$ | pH 3.6 | predicted protein OS *Hordeum vulgare* var. distichum PE 2 SV 1 | F2CSK4 |
| 6.89 | $3.41 \times 10^{-5}$ | pH 3.6 | $H_2O$ | gamma thionin | Q39999 |
| 6.79 | $8.84 \times 10^{-8}$ | $H_2O$ | pH 4.3 | thaumatin-like protein TLP6 OS *Hordeum vulgare* PE 2 SV 1 | Q946Z0 |
| 6.47 | 0.000761 | pH 3.6 | pH 4.3 | CMd subunit of tetrameric alpha amylase inhibitor | O23982; O24000 |
| 5.67 | $6.52 \times 10^{-5}$ | $H_2O$ | pH 4.3 | protein disulfide isomerase (PDI) | F2D284 |
| 5.57 | $1.36 \times 10^{-5}$ | $H_2O$ | pH 4.3 | thionin | F2EE63 |
| 4.83 | 0.000141 | $H_2O$ | pH 4.3 | thaumatin | F2CTV7; O22462; Q946Y9 |
| 4.56 | 0.00660 | $H_2O$ | pH 4.3 | glucose and ribitol dehydrogenase-like protein | Q42848 |
| 4.46 | 0.00189 | $H_2O$ | pH 4.3 | Baker's asthma allergen BDP | Q9S8H1 |
| 3.76 | $5.92 \times 10^{-5}$ | pH 4.3 | pH 3.6 | alpha amylase/trypsin inhibitor BTI CMe2 2 protein | O49862 |
| 2.46 | $2.49 \times 10^{-9}$ | $H_2O$ | pH 4.3 | putative cell wall protein-like | F2EKA5 |
| 2.45 | 0.000389 | $H_2O$ | pH 4.3 | beta glucosidase fragments OS *Hordeum vulgare* PE 1 SV 1 | Q9S9H4 |
| 1.80 | 0.00256 | $H_2O$ | pH 4.3 | Barwin-like_endoglucanase | F2DXR4 |

changes (log of the expression ratio value). Proteins remaining in the soluble fractions of the three conditions were treated with trypsin, and the $MS^E$ search was carried out only for trypsin cleavages. Hence, the fold changes reported here represent the effective amount of intact proteins in the different conditions not proteolyzed by barley endogenous proteases (Tables 1 and 2). The highest mean for the presence of a detected protein at a given condition represents the effective solubilization or proteolysis.

## RESULTS

**Effect of pH, Time, and Cultivar.** The amount of soluble protein increased during the soaking, depending on time, genotype, and acidic buffering (Figure 1). For Finlissa, comparable increases in soluble protein for the three soaking conditions were observed until 8 h (Figure 1). After 12 h, the pH 4.3 condition diverged from the two others by solubilizing

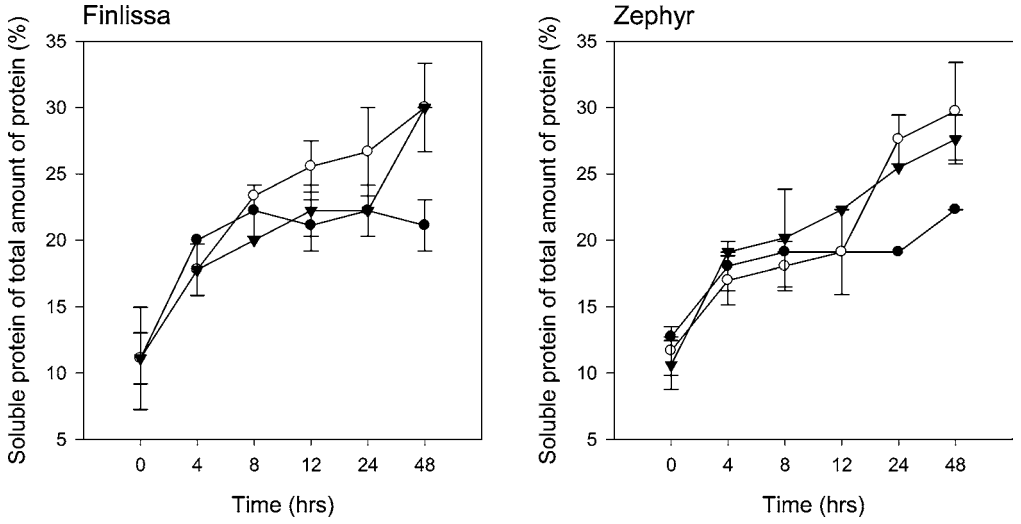


**Figure 1.** Effect of pH on the solubilization of barley protein during 48h of soaking. (●) Nonbuffered soaking. (▼) 100 mM acetic acid pH 3.6. (○) 100 mM lactic acid pH 4.3. Number of replicates was three. Standard deviations are shown as error bars for each data point.

significantly more of the total grain protein (26% vs ∼22%). For the buffered conditions, the difference was equalized after 48 h of soaking where in both cases ∼30% of the total protein was solubilized. This is ∼9% units more than for the nonbuffered condition ($P < 0.0001$).

For Zephyr, no difference was observed between the three conditions up to 8 h (Figure 1). Significant differences were first apparent after 24 h. Both buffered conditions diverged from the nonbuffered condition by solubilizing 25−28% of the total grain protein. This is 6−9% more than for the nonbuffered condition ($P < 0.0001$). After 48 h of soaking, the amount of soluble proteins at pH 3.6 and 4.3 increased to 28 and 30%, respectively.

**Protein Degradation Monitored by SDS-PAGE.** SDS-PAGE on soluble proteins at the different time points revealed that hydrolysis reached a maximal level after 12 h of soaking (data not shown). Compared to the nonbuffered sample, a significant higher degradation was seen in the buffered samples. Predominant bands (i.e., at ∼60 kDa) almost disappeared at condition pH 4.3 (Figure 2). The degradation was also affected at pH 3.6 for both cultivars (lane 3 and 6). Hence, for both cultivars, the highest degree of proteolysis was found at the pH 4.3 condition. SDS-PAGE analysis on the pellet proteins revealed no visible degradation (not shown).

**Differential Proteomic Analysis of the pH Effect.** In order to further elucidate the extent of proteolysis after 12 h of soaking, a label-free LC-MS-based differential proteomics analysis was performed. The point of interest was the small molecular weight (proteolyzed) peptides, which are highly relevant from a feed perspective. For both genotypes, the lowest proteolysis values of the identified peptides were found in the nonbuffered conditions (highest mean in $H_2O$) compared to the buffered conditions (Table 1 and 2). This indicated a pH-dependent proteolysis by endogenous proteases. The largest max fold change occurred between the nonbuffered (water soaking) and the pH 4.3 buffered condition (Table 1 and 2). A Progenesis LC-MS analysis performed on the same samples, covering both genotypes, showed a more profound proteolysis for Finlissa at pH 4.3 than for Zephyr (Table 1 in Supporting Information). This revealed a possible interaction between pH and genotype. However, the LC separation of the peptides using a total shotgun proteomic

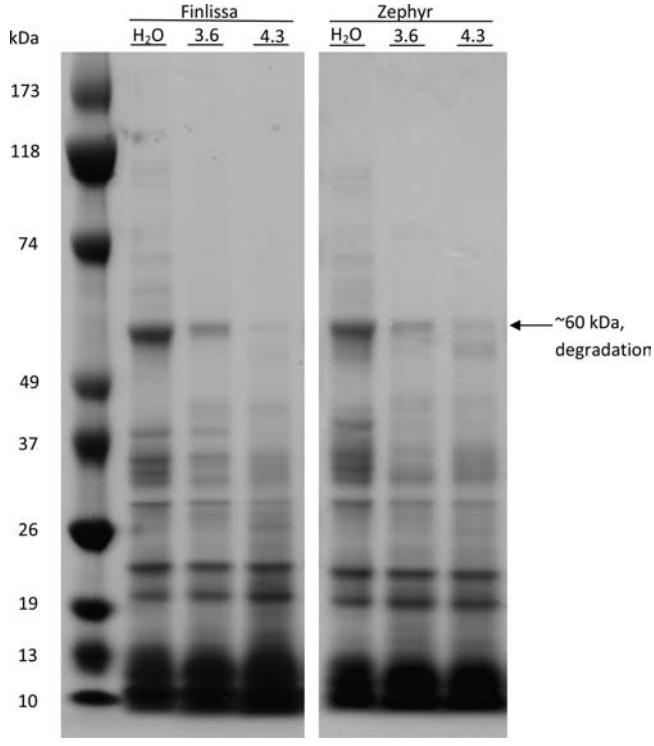


**Figure 2.** Effect of pH on the degradation of soluble proteins after 12 h of soaking. Coomassie staining of water-extractable proteins/peptides visualized in a 4−12% SDS-PAGE gel.

analysis can lead to a so-called ion-suppression effect, resulting in underestimating the quantity and quality of the peptides. This is in particular relevant for small proteolyzed peptides and can in theory cause a biasing of the results. To alleviate a potential ion suppression effect, low molecular weight peptides were isolated prior to proteomic analysis, using a Gelfree 8100 electro-elution after 60, 75, and 90 min run (Figure 3A,B). After 60 min, electro-elution only gave a limited number of hits in the subsequent Progenesis LC-MS analysis, and these samples were therefore excluded from further analysis. After 75 and 90 min, low molecular weight peptides were efficiently eluted, accompanied for 90 min by a significant amount of


dx.doi.org/10.1021/jf502170v | J. Agric. Food Chem. 2014, 62, 8562−8570

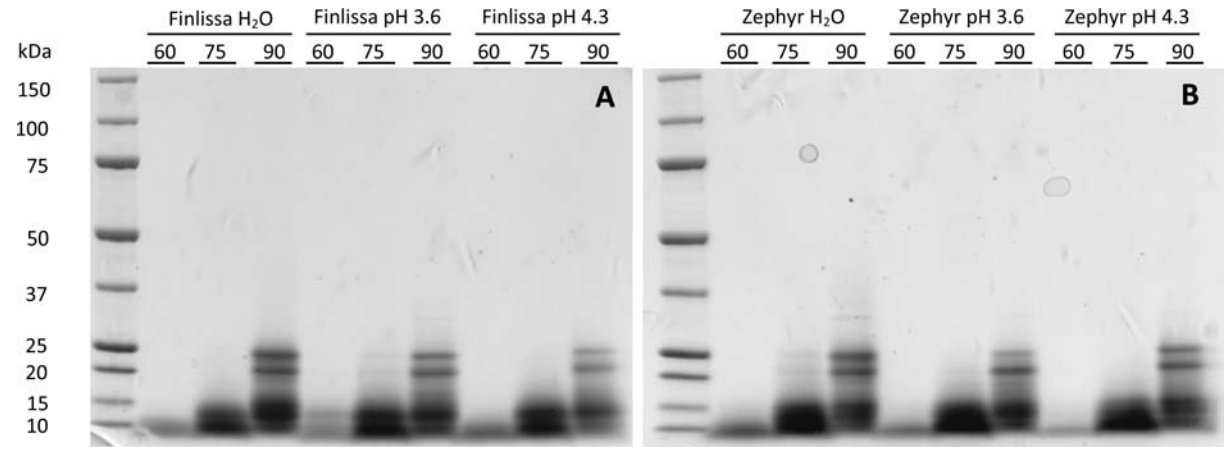


**Figure 3.** SDS-PAGE of Gelfree 8100 electro-eluted proteins after 30, 75, and 90 min of gel electrophoresis. (A) Finlissa; (B) Zephyr. Soaked for 12 h.

larger peptides. A pair-wise comparison at the different conditions as well as phenotypes revealed no obvious differences between the three conditions and the genotypes. Based on Progenesis LC-MS analysis, soaking at pH 4.3 showed a higher degree of proteolysis than soaking at pH 3.6, which again showed greater proteolysis than the nonbuffered soaking (water) condition (Tables 2 and 3 in Supporting Information). However, analysis of the pellet fraction proteins by SDS-PAGE showed no proteolysis of the hordein storage proteins as a result of the soaking (data not shown). It was therefore decided to add rec-HvEP-B2 to the soaking process.

**Addition of Rec-HvEP-B2.** Initial studies using SDS-PAGE with fixed amounts of rec-HvEP- B2 in soaked ground barley (1−2 U/g barley) showed very little or no effect on the proteolysis of soluble and insoluble proteins (data not shown). Moreover, no protease activity was seen when rec-HvEP-B2 was mixed with barley extracts and the chromogenic substrate Z-F-R-pNA. This indicated a potential inhibition by endogenous barley protease inhibitors. By mixing different volumes of barley extracts with a fixed amount of rec-HvEP-B2 endoprotease (0.04 U) and chromogenic substrate (Z-F-R-pNA), protease inhibition curves could be plotted ($P$ = 0.006) (Figure 4). For the chromogenic substrate, the effect of barley endogenous inhibitors was competitive. A barley extract corresponding to 12 $\mu$g material caused 50% of inhibition ($K_i$) on the amount of rec-HvEP-B2 activity used (0.04 U, Figure 4). From these ratios, it can be calculated that 6 and 6.7 U of enzyme per g Zephyr and Finlissa, respectively, is needed to get a 100% noncompetitive activity of rec-HvEP-B2.

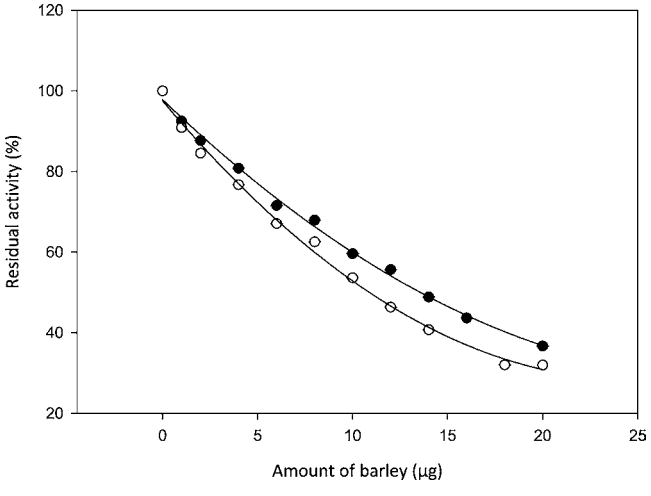


**Figure 4.** Titration of the activity of 0.04 U rec-HvEP-B2 with different volumes of barley extracts. (●) Finlissa and (○) Zephyr.

In order to further study the proteolysis by rec-HvEP-B2 in the soaking process, an experiment was carried out where the amounts of Finlissa and Zephyr were scaled down. The protease was introduced after 8 h of soaking at pH 4.3, allowing the preformed endogenous proteases to initiate the hydrolysis of endogenous substrates. Rec-HvEP-B2 was then allowed to hydrolyze the proteins for an additional 4 h. After the 12 h of total soaking, a substantial proteolysis of the water-insoluble proteins (pellets) was observed in samples incubated including rec-HvEP-B2 (Figure 5). Moreover, the addition of rec-HvEP-B2 caused a substantial hydrolytic effect on the proteins in the soluble fraction (Lanes 4 and 5 in Figure 6). Because the 4−12% polyacrylamide gels used in the initial studies does not effectively retain proteins with a molecular size smaller than 5 kDa, label-free LC-MS was used to quantify and assess qualitatively the extent of the proteolysis.

**Differential Proteomics after Addition of Rec-HvEP-B2.** As evaluated by SDS-PAGE, clear effects of the added protease (visible as decreasing band size, intensities, and smearing) were seen for both water-soluble and insoluble proteins (Figures 5 and 6). Differential proteomics was performed in order to further elucidate the proteolytic effect and to reveal potential genotypic effects. Proteolytic fragments of the typical water-insoluble hordeins D, B2, and B3 were found among the water-soluble proteins after addition of rec-HvEP-B2 (Table 3). The substrate specificity of HvEP-B2 produced in *E. coli* has previously been studied,[34] and according to this, short time incubation (10−30 min) gives mainly hydrolytic cleavages after glutamine residues. Longer and extended incubation time results in increased nonspecific cleavage leading to end products of di or tri peptides. In the present proteomic analysis, the soluble and insoluble proteins/peptides were further treated with trypsin which cleaves immediately after arginine or lysine residues. In the current study, the ratio of tryptic cleaved peptide versus both tryptic from one side and HvEP-B2 from the other was used as evaluation parameter in the Progenesis LC-MS software. The hordeins were detected with the "lowest mean", indicating that


dx.doi.org/10.1021/jf502170v | J. Agric. Food Chem. 2014, 62, 8562−8570

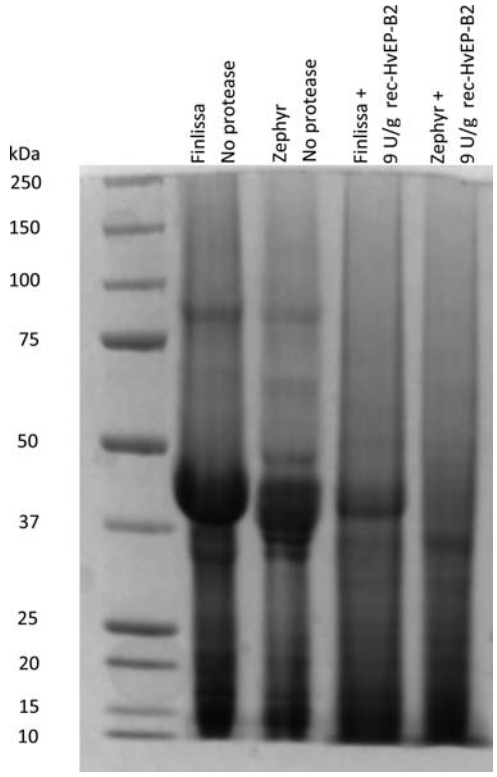


**Figure 5.** Proteolysis of insoluble proteins in Finlissa and Zephyr, with and without rec-Hv-EP-B2. Analyzed by SDS-PAGE.

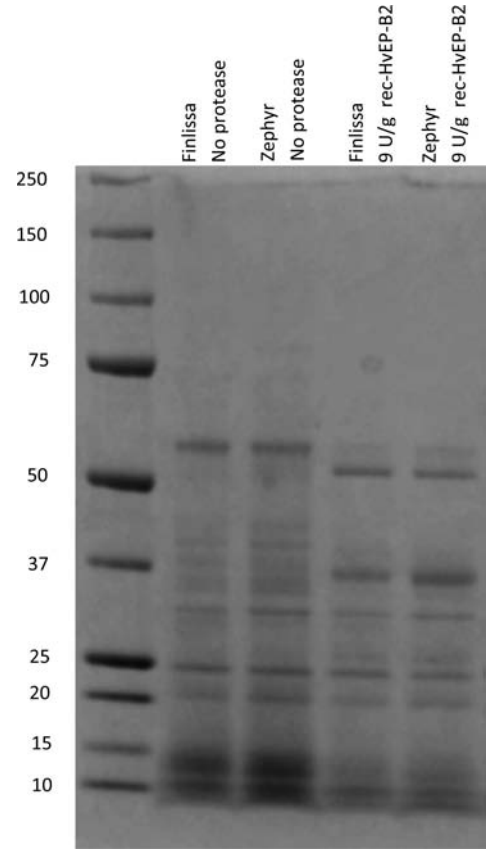


**Figure 6.** Proteolysis of water-soluble proteins analyzed by SDS-PAGE.

these proteins were effectively proteolyzed by rec-HvEP-B2 (Table 3). Proteins not affected by the rec-HvEP-B2 are included as highest mean conditions, meaning that most of the peptides detected were full tryptic peptides (Table 3). Examples on solubilized proteins that stayed intact after addition of rec-HvEP-B2 are heat shock protein 70 (HSP70), the protease inhibitor I4 (serpin), and the endochitinase. Effective rec-HvEP-B2 proteolysis is observed when D and B3 hordein fragments are found in the water-soluble phase. Rec-HvEP-B2 was more effective in hydrolyzing D hordein when rec-HvEP-B2 was added to Finlissa than to Zephyr. In contrast, better proteolysis of B3 hordein was observed when rec-HvEP-B2 added to Zephyr than to Finlissa. Among the insoluble proteins, the following substrates were good substrates: B1, B3, D, Gamma-1,-2, −3 hordeins, hordoindoline b, alpha glucosidase, alpha amylase inhibitor, peroxidase, PDI and thaumatin (Table 4). A genotypic effect was also observed here. Finlissa was better than Zephyr in the hydrolysis of all the hordein isoforms except for the B3 hordein (Table 4 and Figure 5, lane 4, band between 37 and 50 kDa, identified as B3-hordein by LC-MS). Zephyr was also effective in the hydrolysis of the hordeins except for the gamma-2 hordein (Table 4 and Figure 5, band slightly smaller than 37 kDa).

## DISCUSSION

The present study has investigated the possibility of increasing the proteolytic solubilization and degradation of proteins in soaked barley. This can potentially increase the digestibility of proteins in pig feed and speed up the preparation of nonfermented liquid feed. To increase the hydrolytic activity in the barley, pH was buffered in the range of the optima of plant endogenous acidic protease (pH 3.5 to 4.5).[14] Moreover, to further increase proteolysis, a recombinant barley cysteine endoprotease B2 was added under pH 4.3 buffered conditions. Preformed proteases in barley seeds are thought to act primarily on reserve proteins during early germination. This is not directly comparable with the soaking process for cereal-based feed. However, potentially, preformed enzymes could get activated during soaking and initiate the degradation of abundant grain proteins such as hordeins, 7S and 11S globulins. However, hydrolysis by preformed protease such as phytepsin and carboxypeptidase II[26] constitutes only a limited contribution to the concerted hydrolysis of storage proteins. The activities by preformed proteases is accompagnied by a substantial de novo synthesis of proteases during germination. A main de novo synthesized specific proteolytic activity in germination barley derives from the cysteine endoproteases. Moreover, in addition to regulation of proteolytic potential by temporal and spatial synthesis patterns, endogenous protease activity is also regulated via endogenous polypeptide inhibitors.[27,28] For the cysteine endoproteases, the protein is synthesized as an inactive pro-enzyme, including a pro-domain, which is cleaved and thereby activated upon exposure to low pH and reducing agents.[26] Thus, besides optimizing the proteolysis by lowering the pH, low pH may also have a mediating effect by activating preformed proteases.

**Effect of Buffering pH.** Lowering the pH in the soaking had a clear effect on protein solubilization in soaked barley (Figures 1 and 2). This may be due to optimized conditions for endogenous acidic barley endoproteases.[7] Endoproteases from barley are most active between pH 3.5 and pH 4.5,[29] a similar pH range that occurs after ∼24 h of soaking.[15−17] The significant interaction between time and pH shows that most of


dx.doi.org/10.1021/jf502170v | J. Agric. Food Chem. 2014, 62, 8562−8570

**Table 3. Top Highly Proteolyzed Soluble Proteins after the Adding of the Rec-HvEP-B2 to Soaked Barley[a]**

| max fold change | ANOVA (*P*) | samples | genotype | highest mean | lowest mean | description | UniProt accession |
|---|---|---|---|---|---|---|---|
| 149.95 | 0.000185 | 2 | 1 | no adding | plus HvEP-B2 | late embryogenesis abundant (LEA) protein | F2EKY2 |
| 38.19 | 0.00175 | 2 | 1 | no adding | plus HvEP-B2 | D hordein | I6TRS8 |
| 27.59 | $1.48 \times 10^{-06}$ | 1;2 | 2 | plus HvEP-B2 | no adding | cysteine endopeptidase EP-A | O04675 |
| 26.08 | $9.60 \times 10^{-05}$ | 1;2 | 2 | no adding | plus HvEP-B2 | hordoindoline b-2 | G1UH43 |
| 26.00 | 0.00159 | 1;2 | 2 | plus HvEP-B2 | no adding | heat shock protein 70 (HSP70) | Q40058 |
| 6.90 | 0.000591 | 1;2 | 2 | plus HvEP-B2 | no adding | protease inhibitor I4, serpin | F2DHX6 |
| 5.45 | 0.000259 | 1;2 | 2 | no adding | plus HvEP-B2 | B3 hordein | I6TMW4 |
| 4.31 | 0.00133 | 2 | 1 | plus HvEP-B2 | no adding | B1-hordein (fragment) 39K seed protein (fragments), serpin superfamily inhibits | Q40022 |
| 3.95 | $8.20 \times 10^{-05}$ | 1;2 | 2 | no adding | plus HvEP-B2 | alpha-chymotrypsin | Q7M273 |
| 3.84 | 0.0126 | 1;2 | 2 | no adding | plus HvEP-B2 | beta-amylase | A9E4H2 |
| 3.40 | 0.00153 | 1;2 | 2 | plus HvEP-B2 | no adding | endochitinase | F2D743 |
| 3.34 | $8.54 \times 10^{-05}$ | 1;2 | 2 | no adding | plus HvEP-B2 | triosephosphate isomerase | F2EHF8 |
| 3.04 | 0.00394 | 1 | 1 | no adding | plus HvEP-B2 | barley trypsin inhibitor CMc | E7BB45 |
| 2.52 | 0.00397 | 2 | 1 | no adding | plus HvEP-B2 | thaumatin-like protein TLP5 | Q5MBN2 |
| 1.71 | 0.000680 | 1 | 1 | no adding | plus HvEP-B2 | B2 hordein | C7FB16 |
| 1.67 | 0.464 | 1 | 1 | no adding | plus HvEP-B2 | gamma-thionin | Q39999 |
| 1.62 | 0.00111 | 1;2 | 2 | no adding | plus HvEP-B2 | CMd subunit of tetrameric alpha-amylase inhibitor | O23982 |
| 1.31 | 0.209 | 1 | 1 | no adding | plus HvEP-B2 | thaumatin | F2CVM0 |
| 1.23 | 0.465 | 2 | 1 | no adding | plus HvEP-B2 | pectinesterase inhibitor | F2EEQ1 |

[a]These results are related to Finlissa (1) and Zephyr (2) peptides obtained after 4 h of proteolysis with rec-HvEP-B2 and hence further cleaved by trypsin and analyzed by Progenesis LC-MS. Trypsin plus unspecific cut was searched for the related peptides.

**Table 4. Top Highly Proteolyzed Insoluble Proteins after the Adding of the RecHvEP-B2 to Soaked Barley[a]**

| max fold change | ANOVA (*P*) | samples | genotypes | highest mean | lowest mean | description | UniProt accession |
|---|---|---|---|---|---|---|---|
| 7.43 | 0.00130 | 1 | 1 | no adding | plus HvEP-B2 | B1 hordein fragment | Q40020 |
| 6.54 | 0.00200 | 1 | 1 | plus HvEP-B2 | no adding | eukaryotic initiation factor 4A-1 | F2DPE3 |
| 4.48 | 0.000251 | 1 | 1 | no adding | plus HvEP-B2 | gamma 3 hordein | I6TEV2 |
| 4.03 | $2.77 \times 10^{-05}$ | 1;2 | 2 | plus HvEP-B2 | no adding | 11S seed storage globulin (cupin) | F2E9N0 |
| 3.15 | $1.55 \times 10^{-05}$ | 1;2 | 2 | no adding | plus HvEP-B2 | D hordein | I6SW34 |
| 3.13 | 0.00778 | 1;2 | 2 | plus HvEP-B2 | no adding | endochitinase | F2DYI6 |
| 2.83 | 0.000610 | 2 | 1 | plus HvEP-B2 | no adding | papain-like cysteine proteinase | B4ESF2 |
| 2.69 | 0.00114 | 1 | 1 | plus HvEP-B2 | no adding | sucrose synthase | C6H0M2 |
| 2.69 | $2.14 \times 10^{-05}$ | 1;2 | 2 | no adding | plus HvEP-B2 | hordoindoline b2 | Q5IUF4 |
| 2.42 | 0.00510 | 1 | 1 | no adding | plus HvEP-B2 | alpha-glucosidase | F2DV72 |
| 2.19 | 0.00127 | 1;2 | 2 | plus HvEP-B2 | no adding | beta-amylase | F2DY58 |
| 2.10 | 0.00183 | 2 | 1 | plus HvEP-B2 | no adding | soluble starch synthase IIIa | G1FUQ4 |
| 2.08 | $1.27 \times 10^{-05}$ | 1;2 | 2 | no adding | plus HvEP-B2 | B3 hordein | I6SJ26 |
| 1.98 | 0.000125 | 1 | 1 | no adding | plus HvEP-B2 | gamma 2 hordein (fragment) | Q70IB4 |
| 1.65 | 0.00185 | 1;2 | 2 | no adding | plus HvEP-B2 | barley dimeric alpha-amylase inhibitor (Bdai-1) | Q546U1 |
| 1.58 | 0.357 | 1 | 1 | no adding | plus HvEP-B2 | peroxidase BP 2A | Q42853 |
| 1.54 | 0.00474 | 1 | 1 | no adding | plus HvEP-B2 | B hordein | C7FB13 |
| 1.50 | 0.000925 | 1;2 | 2 | no adding | plus HvEP-B2 | protein disulfide isomerase (PDI) | F2D284 |
| 1.37 | 0.0334 | 1 | 1 | no adding | plus HvEP-B2 | Barperm1 (thaumatin) | O22462 |
| 1.36 | 0.000723 | 1;2 | 2 | no adding | plus HvEP-B2 | gamma 1 hordein | I6TMV6 |

[a]These results are related to Finlissa (1) and Zephyr (2) peptides obtained after 4 h of proteolysis with rec-HvEP-B2 and hence further cleaved by Trypsin and analyzed by Progenesis LC-MS. Trypsin plus unspecific cut was searched for the related peptides.

the proteins and peptides are solubilized after 24 to 48 h of soaking when pH is lowered. This is consistent with previous characterization of the barley proteolytic activity[8,30] and in agreement with a general cultivar and time-dependent solubilization (Christensen, unpublished). Cultivar variations regarding enzymatic activity or target proteins have so far not been reported but may nevertheless be at least part of the reason for the observed genotypic variations. Differential proteomics including the electro-elution of the small molecular mass peptides confirmed that proteolysis at pH 4.3 was more effective than at pH 3.6 and in water, respectively (Tables 1 and 2, and Tables 1, 2, and 3 in Supporting Information). However, no degradation of the hordeins, which accounts for more than 50% of total grain proteins, was observed. The missing hordein degradation could be due to lack of activation of preformed cysteine endoproteases, low abundance, a tight regulation by pH, an unsuitable redox potential,[31,32] or by endogenous inhibitory polypeptides (i.e., cystatins). In order to uncover a potential redox effect, soaking was carried out at pH 4.3, plus or minus the addition of cysteine. However, no visible effects of

cysteine addition alone were observed in the insoluble and soluble proteins (data not shown). This indicates that the cysteine proteases are not main contributors to the degradation seen during the pH-induced degradations.

**Effect of Barley Inhibitors and Addition of Rec-HvEP-B2.** The hypothesis of this section was that cysteine endoproteases constitutes a limiting factor for protein degradation during soaking. However, initial studies including 0.04−1.0 U of rec-HvEP-B2 to 1.5 g of soaked barley (pH 4.3) showed no activity toward Z-F-R-pNA included in the sample. The lack of activity was hypothesized to be mediated by endogenous protease inhibitors.[33] In order to estimate the level of protease inhibition in the grain flour, a fixed amount of rec-HvEP-B2 and increasing amounts of extracts from the two cultivars were added. By these means, it was possible to unravel the amount of enzyme needed to exceed the inhibitory effect. Moreover, it showed that the inhibition curves for the two cultivars were not identical, indicating cultivar-dependent differences in the content of inhibitors.

In order to reveal an effect of the recombinant protease, a high level of rec-HvEP-B2 (9 U/g barley flour) was added. Following the addition, a comprehensive proteolysis of the hordeins in the pellets of the two genotypes could be observed. This is supported by previous studies reporting an efficient hydrolysis of the hordeins by HvEP-B2.[18]

Based on criteria for estimating ileal digestibility of protein, it seems likely that buffering at low pH during soaking plus addition of rec-HvEP-B2, in amounts exceeding the endogenous inhibitor, increases the digestibility of barley proteins. Internal inhibitor levels of the cultivars needs to be taken into account when strategies for improving digestibility are designed. Here, optimized conditions including rec-HvEP-B2 above inhibitor level (here 9 U/g barley), pH 4.3 and 4 mM cysteine, led to a substantial increased hydrolysis including mobilization of peptides from the insoluble pellet fraction to the soluble fraction. D and B3 hordein were highly proteolyzed after the addition of rec-HvEP-B2. A genotype effect was visible in the proteolysis of the hordeins in the insoluble pellet fraction. Thus, Finlissa was better than Zephyr for hydrolyzing all hordein isoforms except for hordein B3.

In conclusion, by using the best pH condition, pH 4.3, and after 4 h of partial proteolysis with a titrated amount of rec-HvEP-B2, for two barley feed genotypes, quantitative and qualitative differential proteolytic action revealed that rec-HvEP-B2 caused highly improved hydrolysis of soluble and insoluble barley storage proteins. For analysis purposes, it was necessary to stop the reaction after 4 h. Otherwise, the hydrolysis could have led to di- or tripeptides that are difficult to assign to the protein of origin by proteomic analysis. Therefore, the hydrolysis pattern of the current study cannot be considered as complete. However, on the basis of the current data, we propose that rec-HvEP-B2 constitutes a promising feed additive for mobilizing the insoluble proteins in liquid feed. In addition to this, it may also represent a new selection criterion in plant breeding as well as a candidate enzyme for genetic modifications of barley cultivars.

## ■ ASSOCIATED CONTENT

### Supporting Information

Progenesis and label-free LC-MS analysis of the soluble fraction as noted in the text. This material is available free of charge via the Internet at http://pubs.acs.org.

## ■ AUTHOR INFORMATION


### Corresponding Author

* E-mail: Henrik.BrinchPedersen@agrsci.dk.



### Funding

The authors greatly acknowledge the financial support by the Ministry of Food, Agriculture and Fisheries of Denmark, The Danish AgriFish Agency, and Aarhus University.


### Notes

The authors declare no competing financial interest.

## ■ ACKNOWLEDGMENTS


Sejet Plant Breeding I/S, Denmark is thanked for providing the barley and triticale cultivars used in the study. All members of the project team are acknowledged for fruitful discussions.


## ■ ABBREVIATIONS USED

rec-HvEP-B2,recombinant *Hordeum vulgare* endoprotease B2; FA,formic acid; ACN,acetonitrile; ABC,ammonium bicarbonate buffer

## ■ REFERENCES


(1) Just, A.; Jørgenssen, H.; Fernández, J. A.; Bech-Andersen, S.Forskellige foderstoffers kemiske sammensætning, fordøjelighed, energi- og proteinværdi til svin. *556. Beretning fra Statens Husdyrbrugsforsøg*. København: Landhusholdningsselskabets Forl., 1983

(2) Wilfart, A.; Montagne, L.; Simmins, H.; Noblet, J.; van Milgen, J. Digesta transit in different segments of the gastrointestinal tract of pigs as affected by insoluble fibre supplied by wheat bran. *Br. J. Nutr.* **2007**, *98*, 54−62.

(3) Lyberg, K.; Lundh, T.; Pedersen, C.; Lindberg, J. E. Influence of soaking, fermentation and phytase supplementation on nutrient digestibility in pigs offered a grower diet based on wheat and barley. *Anim. Sci.* **2006**, *82*, 853−858.

(4) Boisen, S.; Fernandez, J. A. Prediction of the Apparent Ileal Digestibility of Protein and Amino-Acids in Feedstuffs and Feed Mixtures for Pigs by In-Vitro Analyses. *Anim. Feed Sci. and Technol.* **1995**, *51*, 29−43.

(5) Boisen, S.; Moughan, P. J. Different expressions of dietary protein and amino acid digestibility in pig feeds and their application in protein evaluation: A theoretical approach. *Acta Agric. Scand., Sect. A* **1996**, *46*, 165−172.

(6) Qiao, Y.; Lin, X.; Odle, A.; Whittaker, A.; van Kempen, T. A. T. G. Refining in vitro digestibility assays: Fractionation of digestible and indisgestible peptides. *J. Anim. Sci.* **2004**, *82*, 1669−1677.

(7) Sopanen, T.; Takkinen, P.; Mikola, J.; Enari, T. M. Rate-Limiting Enzymes in the Liberation of Amino-Acids in Mashing. *J. Inst. Brew.* **1980**, *86*, 211−215.

(8) Rastogi, V.; Oaks, A. Hydrolysis of Storage Proteins in Barley Endosperms - Analysis of Soluble Products. *Plant Physiol.* **1986**, *81*, 901−906.

(9) Simpson, D. J. Proteolytic degradation of cereal prolamins - the problem with proline. *Plant Sci.* **2001**, *161*, 825−838.

(10) Enari, T. M.; Sopanen, T. Mobilization of Endospermal Reserves During the Germination of Barley. *J. Inst. Brew.* **1986**, *92*, 25−31.

(11) Higgins, C. F.; Payne, J. W. The Peptide Pools of Germinating Barley Grains - Relation to Hydrolysis and Transport of Storage Proteins. *Plant Physiol.* **1981**, *67*, 785−792.

(12) West, C. E.; Waterworth, W. M.; Stephens, S. M.; Smith, C. P.; Bray, C. M. Cloning and functional characterisation of a peptide transporter expressed in the scutellum of barley grain during the early stages of germination. *Plant J.* **1998**, *15*, 221−229.

(13) Mikola, L.; Mikola, J. Mobilization of Proline in the Starchy Endosperm of Germinating Barley-Grain. *Planta* **1980**, *149*, 149−154.

(14) Jones, B. L. Endoproteases of barley and malt. *J. Cereal Sci.* **2005**, *42*, 139−156.
(15) Canibe, N.; Jensen, B. B. Fermented liquid feed-Microbial and nutritional aspects and impact on enteric diseases in pigs. *Anim. Feed Sci. Technol.* **2012**, *173*, 17−40.
(16) Canibe, N.; Jensen, B. B. Fermented liquid feed and fermented grain to piglets- effect on gastrointestinal ecology and growth performance. *Livest. Sci.* **2007**, *108*, 198−201.
(17) Lyberg, K.; Olstorpe, M.; Passoth, V.; Schnurer, J.; Lindberg, J. E. Biochemical and microbiological properties of a cereal mix fermented with whey, wet wheat distillers' grain or water at different temperatures. *Anim. Feed Sci. Technol.* **2008**, *144*, 137−148.
(18) Rosenkilde, A. L.; Dionisio, G.; Holm, P. B.; Brinch-Pedersen, H. Production of barley endoprotease B2 in *Pichia pastoris* and its proteolytic acticity against native and recombinant hordeins. *Phytochemistry* **2014**, *97*, 11−19.
(19) Davy, A.; Sørensen, M. B.; Svendsen, I.; Cameron-Mills, V.; Simpson, D. J. Prediction of Protein Cleavage Sites by the Barley Cysteine Endoproteases EP-A and EP-B Based on the Kinetics of Synthetic Peptide Hydrolysis. *Plant Physiol.* **2000**, *122*, 137−146.
(20) Knowlegde Centre for Agriculture. Sortinfo, www.sortinfo.dk. 2012 (accessed January, 11, 2010).
(21) AOAC. *Official Methods of Analysis of AOAC International No. 984.13*, 17th ed.; Association of Official Analytical Chemists International: Gaithersburg, MD., 2000.
(22) Mariotti, F.; Tome, D.; Mirand, P. P. Converting nitrogen into protein—Beyond 6.25 and Jones' factors. *Critical Rev. Food Sci. Nutr.* **2008**, *48*, 177−184.
(23) Blaabjerg, K.; Carlsson, N. G.; Hansen-M?ller, J.; Poulsen, H. D. Effect of heat-treatment, phytase, xylanase and soaking time on inositol phosphate degradation in vitro in wheat, soybean meal and rapeseed cake. *Anim. Feed Sci. Technol.* **2010**, *162*, 123−134.
(24) American Association of Cereal Chemists (AACC). *Approved Methods of American Association of Cereal Chemists*, 11th ed.; Method 46-15.01. Biuret. American Association of Cereal Chemists: St. Paul, MN, 2013.
(25) GELFREE 8100 Fractionation System Molecular weight fractionation with liquid phase recovery. Expedeon 2013. http://www.expedeon.com/Portals/0/product%20manuals/G8100_Manual_v1-4.pdf (accessed October 17, 2013.
(26) Sreenivasulu, N.; Usadel, B.; Winter, A.; Radchuk, V.; Scholz, U.; Stein, N.; Weschke, W.; Strickert, M.; Close, T. J.; Stitt, M.; Graner, A.; Wobus, U. Barley Grain Maturation and Germination: Metabolic Pathway and Regulatory Network Commonalities and Differences Highlighted by New MapMan/PageMan Profiling Tools. *Plant Physiol.* **2008**, *146*, 1738−1758.
(27) Lampl, N.; Alkan, N.; Davydov, O.; Fluhr, R. Set-point control of RD21 protease activity by AtSerpin1 controls cell death in Arabidopsis. *Plant J.* **2013**, *74*, 498−510.
(28) Martinez, M.; Cambra, I.; Carrillo, L.; Diaz-Mendoza, M.; Diaz, I. Characterization of the Entire Cystatin Gene Family in Barley and Their Target Cathepsin L-Like Cysteine-Proteases, Partners in the Hordein Mobilization during Seed Germination. *Plant Physiol.* **2009**, *151*, 1531−1545.
(29) Zhang, N. Y.; Jones, B. L. Characterization of Germinated Barley Endoproteolytic Enzymes by 2-Dimensional Gel-Electrophoresis. *J. Cereal Sci.* **1995**, *21*, 145−153.
(30) Koehler, S. M.; Ho, T. H. D. Hormonal-Regulation, Processing, and Secretion of Cysteine Proteinases in Barley Aleurone Layers. *Plant Cell* **1990**, *2*, 769−783.
(31) Jones, B. L.; Budde, A. D. Effect of Reducing and Oxidizing Agents and pH on Malt Endoproteolytic Activities and Brewing Mashes. *J. Agric. Food Chem.* **2003**, *51*, 7504−7512.
(32) Stephen, A. G.; Powls, R.; Beynon, R. J. Activation of Oxidized Cysteine Proteinases by Thioredoxin-Mediated Reduction Invitro. *Biochem. J.* **1993**, *291*, 345−347.
(33) Jones, B. L. Interactions of malt and barley (*Hordeum vulgare* L.) endoproteinases with their endogenous inhibitors. *J. Agric. Food Chem.* **2001**, *49*, 5975−5981.
(34) Davy, A.; Svendsen, I.; Sørensen, S. O.; Blom Sørensen, M.; Rouster, J.; Meldal, M.; Simpson, D. J.; Cameron-Mills, V. Substrate specificity of barley cysteine endoproteases EP-A and EP-B. *Plant Physiol.* **1998**, *117*, 255−261.

JOURNAL OF AGRICULTURAL AND FOOD CHEMISTRY

Article

pubs.acs.org/JAFC

# Synthesis and Fungistatic Activity of Bicyclic Lactones and Lactams against *Botrytis cinerea*, *Penicillium citrinum*, and *Aspergillus glaucus*

Paulina Walczak, Jakub Pannek, Filip Boratyński, Agata Janik-Polanowicz, and Teresa Olejniczak*

Department of Chemistry, Wrocław University of Environmental and Life Sciences, Norwida 25, 50-375 Wrocław, Poland

Supporting Information

**ABSTRACT:** Six analogues of natural *trans*-4-butyl-*cis*-3-oxabicyclo[4.3.0]nonan-2-one (**3**) and three derivatives, **11**, **12**, and **13**, of Vince lactam (**10**) were synthesized and tested as fungistatic agents against *Botrytis cinerea* AM235, *Penicillium citrinum* AM354, and six strains of *Aspergillus*. Moreover, bioresolution carried out by means of whole cell microorganisms and commercially available enzymes afforded opposite enantiomerically enriched (−) and (+) isomers of Vince lactam (**10**), respectively. The effect of compound structures and stereogenic centers on biological activity has been discussed. The highest fungistatic activity was observed for four lactones: **3**, **4**, **7**, and **8** ($IC_{50}$ = 104.6−115.2 μg/mL) toward *B. cinerea* AM235. *cis*-5,6-Epoxy-2-aza[2.2.1]heptan-3-one (**13**) indicated significant fungistatic activity ($IC_{50}$ = 107.1 μg/mL) against *Aspergillus glaucus* AM211. *trans*-4-Butyl-*cis*-3-oxabicyclo[4.3.0]nonan-2-one (**3**) and *trans*-4-butyl-*cis*-3-oxabicyclo[4.3.0]non-7-en-2-one (**7**) exhibited high fungistatic activity ($IC_{50}$ = 143.2 and 110.2 μg/mL, respectively) against *P. citrinum* AM354 as well.

**KEYWORDS:** *lactones, Vince lactam, $IC_{50}$, Botrytis cinerea, Penicillium thomi*

## INTRODUCTION

It has been assessed that pathogenic fungi, mainly filamentous ones, are the cause of at least 20% of losses in the food industry and crop production,[1] and also they are responsible for mycotoxin contamination of foods.[2,3] Filamentous fungi pose a serious health hazard for people with low immunoresistance, causing dermatomycosis and pulmonary mycosis during hospital treatment. Additionally, they are often the cause of allergies.[4−6]

Nowadays, there is growing interest in new compounds that inhibit growth of filamentous fungi.[7−9] The most attractive are the ones of low toxicity and high biodegradability or the ones of high selectivity of action, not affecting the growth of saprophytic fungi.

Such compounds may include natural lactones biosynthesized by plants. Plants have evolved many secondary metabolites involved in their defense against phytopathogens.[10−13] Compounds with a lactone moiety display a wide spectrum of biological activities, such as fungistatic, bacteriostatic, and cytostatic ones.[14−16] They are often found among insect pheromones.[17] Additionally, several lactones are present in vegetables, fruits, and food products, being responsible for their aromas (mainly fruity ones) and taste (sweet, coconut, or spicy).[18]

In this regard we have developed interest in bicyclic lactones produced by plants of the family Apiaceae Lindl. (*Ligusticum officinale* (loveroot, old English lovage), *Ligusticum chuanxiong*, *L. wallichii* (Chinese lovage), *Angelica sinensis* (Chinese angelica), *Apium graveolens* (celeriac), and *Petroselinum crispum* (parsley)). Some of them are described in the literature.[19−23] There is a need to perform a systematic study on the relationship between structure and biological activity of these compounds. For this purpose we have synthesized natural lactone, its derivatives, and lactam analogues.

In this paper we have obtained bicyclic lactones, compounds of selective growth inhibition activities toward filamentous fungi of the genera *Aspergillus*,[24,25] *Penicillium*,[26,27] and *Botrytis*,[28−30] and we analyzed them with respect to the structure−activity relationship, including the effect of a stereogenic center. The fact that (+)- and (−)-enantiomers may have different biological activities is the background of the modern approach to understanding the mechanisms of action of biologically active compounds.[31]

The biocatalytic potential of microorganisms and their enzymes is used in the production of many valuable chemical compounds.[32] Microbial systems are very profitable due to the short time in which they can double their biomass. Additionally, the methods of genetic manipulations of microorganisms are well-known and established.[33] Therefore, biotransformations using microorganisms and isolated enzymes have enormous potential in the production of pharmaceuticals and compounds useful in agriculture.

## MATERIALS AND METHODS

**Analytical Methods.** Composition of extraction mixtures after biotransformations, syntheses, and purity of products were determined on the basis of complementary information received from gas chromatography (GC) and thin layer chromatography (TLC). TLC analyses were carried out on glass plates covered with silica gel (silica gel 60 $F_{254}$ (Merck)) and developed in eluting systems containing hexane/acetone or methylene chloride/methanol. The same eluents were applied for separation of the products by column chromatography (silica gel 60, 230−400 mesh).

GC analyses were performed with an Agilent 6890N GC instrument, equipped with a flame ionization detector (FID) and

Received: May 9, 2014
Revised: August 5, 2014
Accepted: August 11, 2014
Published: August 11, 2014

ACS Publications © 2014 American Chemical Society



dx.doi.org/10.1021/jf502148h | J. Agric. Food Chem. 2014, 62, 8571−8578

capillary columns Carbowax (30 m, 0.53 mm, film = 0.88 μm) and HP-1 (25 m, 0.32 mm, film = 0.25 μm), using $H_2$ as carrier gas at 2 mL/min of flow. Enantiomeric excesses of the products were determined on chiral columns: Cyclosil-B (30 m × 0.25 mm × 0.25 μm). Specific optical rotations were measured with an Autopol IV automatic polarimeter (Rudolph), equipped with a thermostatic system.

The structures of compounds were determined by means of spectral analysis: $^1$H NMR, $^{13}$C NMR, IR. and GC-MS. NMR spectra were recorded with a Bruker Avance DRX-500 spectrometer in $CDCl_3$ solutions. IR spectra were measured with a Mattson FTIR-300 Thermo Nicolet spectrometer. Molecular weights of products were established on the basis of GC-MS spectra (ionization energy = 70 eV), recorded with a Varian Chrompack GC/MS CP-3800 Saturn 2000 instrument.

**Chemicals.** The chemicals used for the syntheses were purchased from Sigma-Aldrich and Fluka. Potato dextrose agar (PDA) for fungistatic tests was purchased from BTL in Poland. Didecyldimethylammonium chloride (DDAC; 50% solution in propan-2-ol/water 2:3) was purchased from Merck. The substrate for biotransformation and fungistatic tests, racemic 2-azabicyclo[2.2.1]hept-5-en-3-one (**10**), was purchased from Sigma-Aldrich.

**Enzymes.** The following hydrolases were used for bioresolution of racemic lactam **10**: isolated esterase immobilized on Eupergit C from hog liver and esterase from *Rhizomucor miehei* recombinant from *Aspergillus oryzae* were purchased from Fluka, and lipases from *Aspergillus niger* (Amano), *Burkholderia cepacia*, *Candida antarctica* (lipase B immobilized on Innobead 150, recombinant from *Aspergillus oryzae*), *Mucor javanicus*, *Mucor miehei*, *Penicillium camemberti*, *Rhizopus oryzae*, and Lipozymer from *Mucor miehei* were purchased from Sigma-Aldrich.

**Microorganisms.** In our study, in both biotransformation processes and fungistatic activity tests, the microorganisms from the collection of the Institute of Botany of Medical University of Wrocław were used.

The following microorganisms were used: *Aspergillus candidus* AM386, *Aspergillus glaucus* AM211, *Aspergillus nidulans* AM243 *Aspergillus ochraceus* AM456, *Aspergillus* sp. AM31, *Aspergillus wenthi* AM 413, *Botrytis cinerea* AM235, *Candida viswanathi* AM120, *Fusarium culmorum* AM282, *Fusarium oxysporum* AM13, *Inonotus radiatus* AM70, *Laetiporus sulphurens* AM514, *Penicillium camemberti* AM83, *Penicillium citrinum* AM354, *Penicillium notatum* AM904, *Penicillium thomi* AM91, *Pezicula cinnamomea* AM53, *Poria placenta* AM38, *Prosthemium* sp. AM52, *Rhodotorula marina* AM77, *Rhodotorula rubra* AM4, *Sclerophoma pythiophila* AM55, *Sparassis crispa* AM535, *Stemphylium botryosum* AM279, *Yarrowia lipolytica* AM77.

**Synthesis of Lactones 2−4 and 6−8.** *cis-3-Oxabicyclo[4.3.0]-nonan-2-one* (**2**) *and cis-3-Oxabicyclo[4.3.0]non-7-en-2-one* (**6**) were prepared in good yields according to the literature procedures[34] and confirmed by GC-EIMS: 141 (M + 1) for lactone **2**; 139 (M + 1) for lactone **6**.

*trans-4-Butyl-cis-3-oxabicyclo[4.3.0]nonan-2-one* (**3**) was obtained in a three-step synthesis: To 0.48 g (0.02 mol) of magnesium activated with iodine was added anhydrous diethyl ether (50 mL), and the mixture was stirred, followed by the slow addition of freshly distillated *n*-butyl bromide (2.88 g; 0.021 mol). The reaction was continued until all magnesium reacted, and then the reaction mixture was heated under reflux for 1 h. After the mixture had cooled to room temperature, anhydrous cadmium chloride (1.65 g; 0.009 mol) was added, and the reaction mixture was heated under reflux for 1 h. After the mixture had cooled to room temperature, a diethyl ether solution of *cis*-1,2,3,6-tetrahydrophthalic anhydride (**1**) (1.39 g; 0.009 mol) was added dropwise at room temperature and heated under reflux for 6 h. The reaction mixture was poured into 10% HCl and extracted with diethyl ether (5 × 50 mL). The extract was dried over $MgSO_4$, and then solvent was evaporated off.

*Reduction.* Crude product was diluted with 50 mL of methanol and reduced by $NaBH_4$ (0.342 g; 0.009 mol) with 200 μL of 0.1 M NaOH. The reaction mixture was stirred overnight at room temperature, and then methanol was evaporated off.

*Lactonization.* Crude product of reduction was diluted with a solution of 50 mL of THF/$H_2O$ (2:1 v/v), and then 70% $HClO_4$ was dropped until the pH of the reaction mixture was acidic. The reaction mixture was heated under reflux for 3 h. THF was evaporated, and the product was extracted with diethyl ether (5 × 50 mL). The extract was dried over $MgSO_4$, then solvent was evaporated off, and finally crude product was purified by column chromatography using hexane/acetone (3:1) as eluent to give lactone 0.76 g (43% yield after three-step synthesis and purification).

The physical and spectral data of lactone **3** are a follows: mp 104 °C; $^1$H NMR (500 MHz, $CDCl_3$) $\delta$ 0.90 (t, 3, $J$ = 7.1 Hz, $CH_3$-13), 1.07−1.10 (m, 2, $CH_2$-12), 1.29−1.36 (m, 2, $CH_2$-9), 1.37−1.65 (m, 8, $CH_2$-6, $CH_2$-7, $CH_2$-8, $CH_2$-11), 1.70−1.72 (m, 1, one of $CH_2$-10), 2.15−2.18 (m, 1, one of $CH_2$-10), 2.29−2.31 (m, 1, CH-5), 2.69−2.72 (m, 1, CH-1), 4.20−4.24 (m, 1, CH-4); $^{13}$C NMR (151 MHz) $\delta$ 13.91 ($CH_3$-13), 22.48 ($CH_2$-12, $CH_2$-11), 22.55 ($CH_2$-7), 22.88 ($CH_2$-10), 23.58 ($CH_2$-8, $CH_2$-6), 27.96 ($CH_2$-9), 38.95 (CH-5), 42.08 (CH-1), 82.03 (C-4), 178.10 (C-2); IR (NaCl, $cm^{-1}$) 3019 (s), 2400 (m), 2253 (m), 1765 (s); GC-EIMS 197 (M + 1).

*trans-4-Butyl-cis-3-oxabicyclo[4.3.0]non-7-en-2-one* (**7**) was obtained by using the same procedure as for *trans*-4-butyl-*cis*-3-oxabicyclo[4.3.0]-nonan-2-one (**3**) from *cis*-4-cyclohexene-1,2-dicarboxylic anhydride (**5**) (1.37 g; 0.009 mol). Lactone **7** was obtained with 45% (0.79 g) yield. The physical and spectral data of lactone 7 are as follows: oil; $^1$H NMR (500 MHz, $CDCl_3$) $\delta$ 0.85 (t, 3, $J$ = 7.1 Hz, $CH_3$-13), 1.28−1.39 (m, 3, one of $CH_2$-11, $CH_2$-12), 1.45−1.50 (m, 1, one of $CH_2$-11), 1.50−1.54 (m, 2, one of $CH_2$-11, one of $CH_2$-10), 1.68−1.74 (m, 1, one of $CH_2$-10), 1.77−1.82 (m, 1, one of $CH_2$-6), 1.94−1.97 (m, 1, one of $CH_2$-6), 2.30−2.32 (m, 1, one of $CH_2$-9), 2.38−2.41 (m, 1, one of $CH_2$-9), 2.49−2.51 (m, 1, CH-5), 2.78−2.81 (m, 1, CH-1), 4.29−4.32 (m, 1, CH-4), 5.63−5.65 (m, 2, CH-7, CH-8); $^{13}$C NMR (151 MHz) $\delta$ 13.92 ($CH_3$-13), 19.63 ($CH_2$-12), 21.98 ($CH_2$-6), 22.56 ($CH_2$-9), 28.00 (CH-1), 28.91 ($CH_2$-11), 35.32 ($CH_2$-10), 39.95 (CH-5), 82.61 (CH-4), 124.35 (CH-7), 125.22 (CH-8), 178.65 (C-2); IR (NaCl, $cm^{-1}$) 3019 (s), 2400 (m), 1767 (s), 1521 (m); GC-EIMS 195 (M + 1).

*4,4-Dibutyl-cis-3-oxabicyclo[4.3.0]nonan-2-one* (**4**). To a stirred solution of 1.24 g (0.05 mol) of magnesium (activated with iodine) in anhydrous diethyl ether (80 mL) was slowly added *n*-butyl bromide (6.85 g; 0.05 mol). The reaction was continued until all of the magnesium was reacted, and then *cis*-1,2,3,6-tetrahydrophthalic anhydride (**1**) (2.62 g; 0.017 mol) was added dropwise at room temperature. After 12 h, the reaction mixture was poured into 10% HCl and extracted with diethyl ether (5 × 60 mL). The extract was dried over $MgSO_4$, the solvent was evaporated off, and the crude product was purified by column chromatography using hexane/acetone (3:1) as eluent to give 3.31 g of lactone **4** (yield = 77%). The physical and spectral data of lactone **4** are as follows: mp 43−45 °C; $^1$H NMR (500 MHz, $CDCl_3$) $\delta$ 0.87−0.91 (m, 6, $CH_3$-13, $CH_3$-13′), 1.02−1.14 (m, 4, $CH_2$-12, $CH_2$-12′), 1.19−1.34 (m, 8, $CH_2$-7, $CH_2$-8, $CH_2$-11, $CH_2$-11′), 1.49−1.51 (m, 4, $CH_2$-6, $CH_2$-9), 1.70−1.75 (m, 3, $CH_2$-10′, one of $CH_2$-10), 2.11−2.18 (m, 2, CH-5, one of $CH_2$-10), 2.94−2.97 (m, 1, CH-1); $^{13}$C NMR (151 MHz) $\delta$ 14.01 ($CH_3$-13, $CH_3$-13′), 22.79 ($CH_2$-12), 22.95 ($CH_2$-12′), 23.14 ($CH_2$-11′), 23.17 ($CH_2$-11), 31.04 ($CH_2$-7), 24.65 ($CH_2$-10′), 25.85 ($CH_2$-10), 26.16 ($CH_2$-8), 31.41 ($CH_2$-6), 34.04 ($CH_2$-9), 39.79 (CH-5), 41.74 (CH-1), 88.79 (C-4), 177.90 (C-2); IR (NaCl, $cm^{-1}$) 3019 (s), 2400 (m), 1765 (s); GC-EIMS 253 (M + 1).

*4,4-Dibutyl-cis-3-oxabicyclo[4.3.0]non-7-en-2-one* (**8**) was obtained by using the same procedure as for 4,4-dibutyl-*cis*-3-oxabicyclo[4.3.0]-nonan-2-one (**4**) from *cis*-4-cyclohexene-1,2-dicarboxylic anhydride (**5**) (2.59 g; 0.017 mol). Lactone **8** was obtained with 75% (3.19 g) yield. The physical and spectral data of lactone **8** are as follows: oil; $^1$H NMR (500 MHz, $CDCl_3$) $\delta$ 0.87−0.91 (m, 6, $CH_3$-13, $CH_3$-13′), 1.22−1.34 (m, 8, $CH_2$-11, $CH_2$-12, $CH_2$-11′, $CH_2$-12′), 1.52−1.59 (m, 2, one of $CH_2$-10, one of $CH_2$-10′), 1.68−1.74 (m, 2, one of $CH_2$-10, one of $CH_2$-10′), 1.71−1.73 (m, 1, one of $CH_2$-6), 2.03−2.08 (m, 1, one of $CH_2$-6), 2.26−2.28 (m, 1, one of $CH_2$-9), 2.33−2.39 (m, 1, one of $CH_2$-9), 2.42−2.46 (m, 1, CH-5), 3.00−3.04 (m, 1, CH-1), 5.73−5.76 (m, 2, CH-7, CH-8); $^{13}$C NMR (151 MHz) $\delta$ 13.95 ($CH_3$-13′),

13.97 ($CH_3$-13), 21.83 ($CH_2$-12), 23.68 ($CH_2$-12′), 23.16 ($CH_2$-11), 23.17 ($CH_2$-11′), 25.86 ($CH_2$-9), 26.07 (CH-6), 32.42 ($CH_2$-10), 35.67 (CH-10′), 38.22 (CH-1), 39.67 (CH-5), 89.72 (C-4), 125.70 (CH-7), 126.01 (CH-8), 178.97 (C-2); IR (NaCl, $cm^{-1}$) 3019 (s), 2400 (m), 1757 (s), 1522 (m), 1425 (m); GC-EIMS 251 (M + 1).

**Synthesis of Lactams 9 and 11−13.** *cis-3-Azabicyclo[4.3.0]non-7-en-2-one (**9**).* Synthesis of lactam **9** was performed using a high-pressure autoclave Berghof HR equipped with a Teflon liner. To the solution of *cis*-3-oxabicyclo[4.3.0]nonan-2-one (**6**) (1.518 g, 0.011 mol) in 2.0 mL of DMF placed in the Teflon liner was added 60 mL of 25% ammonia. The Teflon liner was put in a tightly closed autoclave. The reaction mixture was stirred with heating at 160 °C for 15 h (pressure increases to 21 bar). Product was extracted with diethyl ether (5 × 50 mL). The extract was dried over $MgSO_4$, and the solvent was evaporated off. Crude product was purified by column chromatography methylene chloride/methanol (97:3). Lactam **9** was obtained with 65% (0.98 g) yield. The physical and spectral data of lactone **9** are as follows: mp 63−66 °C; $^1$H NMR (500 MHz, $CDCl_3$) $\delta$ 1.80−1.85 (m, 1, one of $CH_2$-6), 2.11−2.17 (m, 1, one of $CH_2$-9), 2.23−2.26 (m, 1, one of $CH_2$-6), 2.38−2.41 (m, 1, CH-1), 2.48−2.50 (m, 2, one of $CH_2$-9, CH-5), 2.94−2.95 (m, 1, one of $CH_2$-4), 3.41−3.44 (m, 1, one of $CH_2$-4), 5.66−5.72 (m, 2, CH-7, CH-8), 6.14 (s, 1, NH); $^{13}$C NMR (151 MHz) $\delta$ 21.82 ($CH_2$-6), 25.91 ($CH_2$-9), 31.71 (CH-5), 38.71 (CH-1), 47.65 ($CH_2$-4), 125.46 (CH-7), 126.07 (CH-8), 180.13 (C-2); IR (NaCl, $cm^{-1}$) 3154 (s), 2253 (s), 1695 (s); GC-EIMS 138 (M + 1).

*2-Butyric-2-azabicyclo[2.2.1]hept-5-en-3-one (**11**).* To 2-azabicyclo[2.2.1]hept-5-en-3-one (**10**) (0.3 g, 2.47 × $10^{-3}$ mol) was added anhydrous THF (5 mL), followed by the addition of NaH (8.3 × $10^{-3}$ mol). Then, butyric acid chloride at room temperature was added dropwise (5.64 × $10^{-3}$ mol). The reaction was continued until all of the substrate was reacted (checked by TLC, 48 h). The reaction mixture was filtered and purified by column chromatography using methylene chloride/methanol (98:2.5) as eluent to give 0.24 g of pure product **11** and 0.07 g of contaminated product **11** (yield = 63%, $R_f$ = 0.27). The physical and spectral data of lactone **11** are as follows: oil; $^1$H NMR (500 MHz, $CDCl_3$) $\delta$ 0.92 (t, 3, $J$ = 7.4 Hz, $CH_3$-11), 1.56−1.69 (m, 2, $CH_2$-10), 2.17 (dt, 1, $J$ = 8.6, 1.7 Hz, one of $CH_2$-7), 2.27 (dt, 1, $J$ = 8.6, 1.7 Hz, one of $CH_2$-7), 2.67−2.74 (m, 2, $CH_2$-9), 3.40−3.41 (m, 1, CH-4), 5.26−5.27 (m, 1, CH-1), 6.62−6.64 (m, 1, CH-5), 6.87−6.88 (m, 1, CH-6); $^{13}$C NMR (151 MHz) $\delta$ 13.69 ($CH_3$-11), 17.81 ($CH_2$-10), 37.80 ($CH_2$-9), 54.69 ($CH_2$-7), 54.77 (CH-1), 60.24 (CH-4), 138.10 (CH-5), 140.50 (CH-6), 173.02 (C-8), 177.53 (C-3); IR (NaCl, $cm^{-1}$) 3019 (s), 2400 (m), 1700 (m), 1521 (m); GC-EIMS 180 (M + 1).

*2-Butyl-2-azabicyclo[2.2.1]hept-5-en-3-one (**12**).* To 2-azabicyclo[2.2.1]-hept-5-en-3-one (**10**) (0.3 g, 2.47 × $10^{-3}$ mol) was added anhydrous THF (5 mL), followed by the addition of NaH (8.3 × $10^{-3}$ mol). Then, butyl bromide at room temperature was added dropwise (4.96 × $10^{-3}$ mol). The reaction was continued until all of the substrate was reacted (checked by TLC, 48 h). The reaction mixture was filtered and purified by column chromatography using methylene chloride/methanol (98:2.5) as eluent to give 0.15 g of pure product **12** and 0.097 g of contaminated product **12** (yield = 54.4%; $R_f$ = 0.33). The physical and spectral data of lactone **12** are as follows: oil; $^1$H NMR (500 MHz, $CDCl_3$) $\delta$ 0.90 (t, 3, $J$ = 7.4 Hz, $CH_3$-11), 1.22−1.27 (m, 4, $CH_2$-9, $CH_2$-10), 2.11 (dt, 1, $J$ = 7.5, 1.7 Hz, one of $CH_2$-7), 2.28 (dt, 1, $J$ = 5.8, 1.7 Hz, one of $CH_2$-7), 2.84−2.88 (m, 1, one of $CH_2$-8), 3.09−3.14 (m, 1, one of $CH_2$-8), 3.30−3.31 (m, 1, CH-4), 4.14−4.15 (m, 1, CH-1), 6.62 (dt, 1, $J$ = 7.3, 5.6 Hz, CH-5), 6.69 (dt, 1, $J$ = 7.3, 4.8 Hz, CH-6); $^{13}$C NMR (151 MHz) $\delta$ 13.81 ($CH_3$-11), 20.09 ($CH_2$-10), 29.92 ($CH_2$-9), 43.43 ($CH_2$-8), 54.00 ($CH_2$-7), 59.10 (CH-4), 63.14 (CH-1), 138.16 (CH-5), 139.66 (CH-6), 180.52 (C-3); IR (NaCl, $cm^{-1}$) 3019 (s), 2400 (m), 1695 (m), 1518 (m); GC-EIMS 165 (M + 1).

*cis-5,6-Epoxy-2-azabicyclo[2.2.1]heptan-3-one (**13**).* To 2-azabicyclo[2.2.1]hept-5-en-3-one **10** (0.3 g, 2.47 × $10^{-3}$ mol) was added methylene chloride (15 mL), followed by the addition of *m*-CPBA (4.14 × $10^{-3}$ mol). The reaction was continued until all of the substrate was reacted (checked by TLC, 24 h). The reaction mixture was purified by column chromatography using methylene chloride/methanol (98:2.5) as eluent to give 0.265 g (yield = 77.3%; $R_f$ = 0.29). The physical and spectral data of lactone **13** are as follows: mp 95−100 °C; $^1$H NMR (500 MHz, $CDCl_3$) $\delta$ 1.62−1.64 (m, 1, one of $CH_2$-7), 1.80−1.82 (m, 1, one of $CH_2$-7), 2.84−2.90 (m, 1, CH-4), 3.56−3.58 (m, 1, CH-5), 3.64−3.69 (m, 1, CH-6), 3.87−3.90 (m, 1, CH-1), 6.24−6.26 (s, 1, NH); $^{13}$C NMR (151 MHz) $\delta$ 31.12 ($CH_2$-7), 46.88 (CH-4), 51.46 (CH-1), 55.61 (CH-5), 55.63 (CH-6), 180.43 (C-3); IR (NaCl, $cm^{-1}$) 3019 (s), 2400 (m), 1720 (s), 1518 (m), 1422 (m); GC-EIMS 126 (M + 1).

**Bioresolution of (±)-2-Azabicyclo[2.2.1]hept-5-en-3-one ((±)-10).** *Microbial Transformations of (±)-2-Azabicyclo[2.2.1]hept-5-en-3-one ((±)-**10**).* (a) Screening Scale Biotransformation. Microorganisms were cultivated in Erlenmeyer flasks (300 mL) containing 75 mL of the cultivation medium S (a solution of peptone 1% and glucose 3%) or C (an aqueous solution of $NaNO_3$ 0.3%, $KH_2PO_4$ 0.1%, KCl 0.05%, $MgSO_4·7H_2O$ 0.005%, $FeSO_4·7H_2O$ 0.001 g, and saccharose 3%). After 3−5 days of growth, 0.02 g of substrate (±)-**10** in 0.5 mL of acetone was added to the shaken cultivation mixture. The transformation was continued for 24, 72, 120, and 144 h. The products were extracted with diethyl ether or chloroform and analyzed using TLC and GC techniques. Enantiomeric excesses were determined by GC using chiral column Cyclosil-B (30 m × 0.25 mm × 0.25 $\mu$m with temperature program 80 °C (1 min), 130 °C (1 °C/min), and 250 °C (40 °C/min). For selected microorganisms optimization of biotransformation conditions was performed with regard to increased enantioselectivity and efficiency of a biocatalyst.

(b) Preparative Scale Biotransformation in Bench-Bioreactor. Bench-scale batch runs were carried out in 7 L vessels of the bioreactor (Brunswick, USA) in the selected conditions established on the basis of screening experiments. Growth of *P. thomi* AM91 was performed with the following parameters under control: medium volume (3 L), aeration rate (1 v/m), stirring speed (200−300 rpm), temperature (26 °C), pH. After 4 days of growth on mineral medium ($NaNO_3$ 0.3%, $KH_2PO_4$ 0.1%, KCl 0.05%, $MgSO_4·7H_2O$ 0.005%, $FeSO_4·7H_2O$ 0.001 g, and saccharose 3%) (pH 4.2), 30 g of peptone was added (pH 8.3). After 4 h, 1.0 g of (±)-**10** in 2 mL of acetone was added. The biotransformation was followed by GC with chiral column, once the substrate (±)-**10** was not detectable; the reaction mixture was overnight extracted in the same manner as in the screening procedure. The crude product was purified by column chromatography (methylene chloride/methanol, 97:3). The yield of the biotransformation calculated only for lactam **10** was 70% and the enantiomeric excess, 93% (GC, chiral column); $[\alpha]_{589}^{20}$ = −565° (*c* 2.0, $CHCl_3$) ($[\alpha]_{589}^{20}$ = −525.9° (*c* 1.0, $CH_3OH$)).[35] The physical and spectral data of lactone **10** are as follows: mp 55 °C; $^1$H NMR (500 MHz, $CDCl_3$) $\delta$ 2.19−2.20 (m, 1, one of $CH_2$-7), 2.37 (dt, 1, $J$ = 6.0, 1.7 Hz, one of $CH_2$-7), 3.19−3.23 (m, 1, CH-4), 4.31−4.35 (m, 1, CH-1), 5.85 (s, 1, NH), 6.64 (dt, 1, $J$ = 7.4, 5.0 Hz, CH-5), 6.76 (dd, 1, $J$ = 7.4, 5.0 Hz, CH-6); $^{13}$C NMR (151 MHz) $\delta$ 53.21 ($CH_2$-7), 59.32 (CH-1), 60.29 (CH-4), 138.18 (CH-5), 141.12 (CH-6), 185.34 (C-3); IR (NaCl, $cm^{-1}$) 3019 (s), 2400 (m), 1709 (s), 1521 (m); GC-EIMS 110 (M + 1).

*Biotransformations of (±)-2-Azabicyclo[2.2.1]hept-5-en-3-one ((±)-**10**) with the Use of Isolated Enzymes.* (a) Screening Scale Biotransformation. Substrate (±)-**10** (5 mg) was added to enzyme (the amount equal to 20 enzyme units of activity), dissolved in 0.5 mL of the phosphate buffer of pH 7.2. The reaction was stirred at room temperature. At the end of the process the reaction mixture was filtered through Celite, and the biotransformation products were extracted with diethyl ether. The enantiomeric excess of substrate **10** was determined by means of GC with application of chiral columns.

(b) Preparative Scale Biotransformation. Substrate (±)-**10** (0.2 g) was added to enzyme (the amount equal to 800 enzyme units of activity of Lipase B from *Candida antarctica* immobilized on Innobead 150, recombinant from *Aspergillus oryzea*), dissolved in 40 mL of the phosphate buffer of pH 7.2. The reaction was stirred at room temperature. At the end of the process the reaction mixture was filtered through Celite, and the biotransformation products were extracted with diethyl ether. The enantiomeric excess of substrate **10**

was determined by means of GC with application of chiral columns. The crude product was purified by column chromatography (methylene chloride/methanol, 97:3). The yield of the biotransformation was calculated only for lactam **10** and reached 74% with enantiomeric excess of (+)-**10**, ee = 99% (GC, chiral column); $[\alpha]_{589}^{20}$ = +565° (*c* 2.0, $CHCl_3$) ($[\alpha]_{589}^{20}$ = +555.9° (*c* 0.5, $CH_3OH$)).[35]

**Antifungal Assays.** All compounds dissolved in DMSO were mixed with sterilized PDA (0.01 mL of DMSO for 1 mL of agar) to achieve concentrations of 50, 100, 150, 200, 250, or 300 μg/mL, and the solution was poured into 6 cm Petri dishes. After inoculation by mycelium of a fungus, the tested dishes were incubated at 27 °C and 60−80% of relative humidity. The growth of mycelium was continued until the diameter of the growth zone in control sample dishes (nutrient with DMSO, without compound added) reached 4.5−5.0 cm. Then, the growth zone in experimental dishes was measured. All of the compounds were tested tripled at a concentration of 200 μg/mL as well as at three more concentrations, which were chosen individually. Fungistatic activity, expressed in $IC_{50}$ (the half-maximal inhibitory concentration) values for each tested compound, was determined on the basis of four measured values, as a percent of growth inhibition. $IC_{50}$ values were calculated according to the formula: $(1 - D_a/D_b) \times 100\%$, where $D_a$ is the diameter of the growth zone in the experimental dish (cm) and $D_b$ is the diameter of the growth zone in the control dish (cm). DDAC was used as reference compound. Statistical analysis was done using ANOVA ($p = 0.05$), and the means were compared by calculating the least significant difference (LSD, Tukey).

## RESULTS AND DISCUSSION

On the one hand, the aim of our research was the synthesis of *trans*-4-butyl-*cis*-3-oxabicyclo[4.3.0]nonan-2-one (**3**), one of the possible diastereoisomers of naturally occurring lactones. On the other hand, we planned to obtain a number of its derivatives from two groups of compounds: bicyclic lactones and bicyclic lactams. Our goal was to compare the fungistatic activities of natural lactone **3** and both groups of synthesized derivatives with those of lactone and lactam moiety. Moreover, we conducted enantioselective hydrolysis of lactam (±)-**10** by applying whole cells of fungi and isolated enzymes as well. The resulting compounds, including enantiomerically enriched isomers of lactam **10**, were tested for fungicidal activity against selected strains of filamentous fungi of the *Botrytis*, *Penicillium*, and *Aspergillus* genera.

**Synthesis of Bicyclic Lactones 2−4 and 6−8.** Taking into consideration the structure of natural lactone **3** (Figure 1), the effects of substituents at carbon atom C-4 and the C7−C8 double bond on fungistatic activity were investigated. Therefore, starting from two commercially available anhydrides, *cis*-1,2,3,6-tetrahydrophthalic anhydride (**1**) and *cis*-4-cyclohexene-1,2-dicarboxylic anhydride (**5**), the corresponding lactones without substituents ((±)-**2**, (±)-**6**), with *n*-butyl substituent ((±)-**3**, (±)-**7**), with two *n*-butyl substituents ((±)-**4**, (±)-**8**) at carbon atom C-4 were synthesized (Scheme 1). The influence of the double bond on the biological activity was also examined by comparing the results obtained from lactones (±)-**6**, (±)-**7**, and (±)-**8** possessing a C7−C8 double bond with their saturated derivatives (±)-**2**, (±)-**3**, and (±)-**4**.

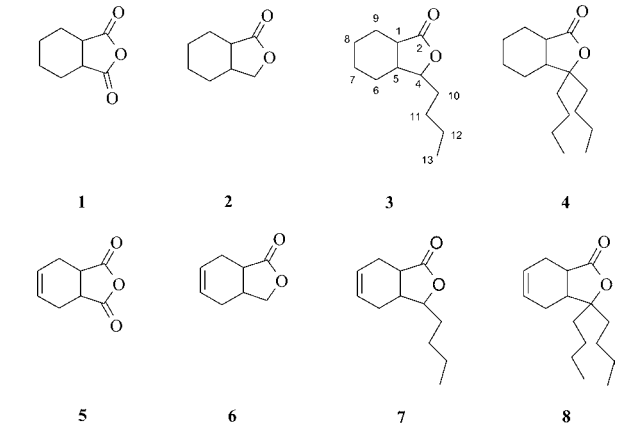


**Figure 1.** Structures of anhydrides (**1**, **5**) and bicyclic lactones (**2**−**4**, **6**−**8**) examined for fungistatic tests.

**Scheme 1**[a]

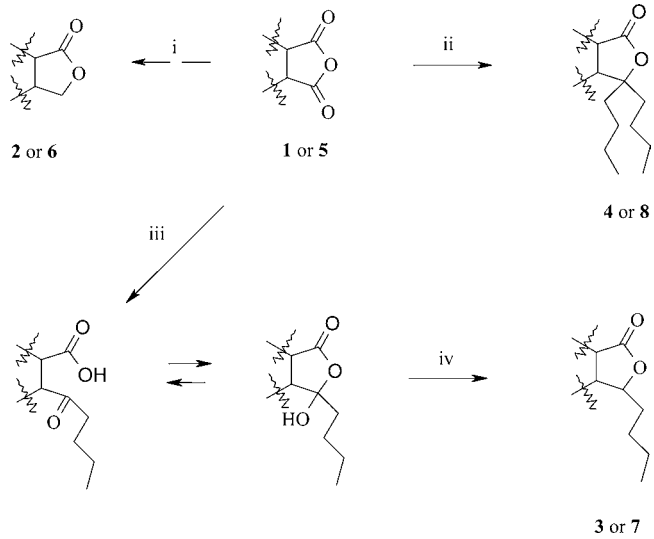


[a]i, $LiAlH_4$ $Et_2O$; ii, *n*-$C_4H_9MgBr$ (3 equiv), $Et_2O$ or THF; iii, (1) $Cd(n\text{-}C_4H_9)_2$, $Et_2O$ or THF, (2) HCl; iv, (1) $NaBH_4$, MeOH, (2) $THF/H_2O/HClO_4$, reflux.

Lactones (±)-3-oxabicyclo[4.3.0]nonan-2-one ((±)-**2**) and (±)-3-oxabicyclo[4.3.0]non-7-en-2-one ((±)-**6**) were obtained with high yield in reduction of the respective anhydrides **1** and **5** with lithium aluminum hydride in anhydrous diethyl ether. Signals in the $^1H$ NMR spectrum from two protons at carbon atom C-4 from lactone **2** were observed at 3.92 ppm (d, 1, $J$ = 8.8 Hz, one of $CH_2$-4) and 4.16 ppm (dd, 1, $J$ = 8.8, 5.0 Hz, one of $CH_2$-4); and from lactone **6** at 4.00 ppm (dd, 1, $J$ = 8.8, 2.0 Hz, one of $CH_2$-4) and 4.30 ppm (dd, 1, $J$ = 8.8, 5.1 Hz, 1H, one of $CH_2$-4).

(±)-*trans*-4-Butyl-*cis*-3-oxabicyclo[4.3.0]nonan-2-one ((±)-**3**), of the structure of the natural lactone,[19−23] was obtained in a three-step synthesis carried out without purification of intermediate products. In the first step the anhydride **1** reacted with a cadmium−organic compound[36,37] obtained from the reaction of *n*-butylmagnesium bromide with cadmium chloride. The reaction product isolated from acidic condition was a mixture of ketoacid and its cyclic form. The purification process of mixtures of ketoacid and the product of its cyclization was inefficient. Therefore, after evaporation of solvents, reduction with $NaBH_4$ in methanol and subsequent product cyclization in a mixture of $THF/H_2O/HClO_4$ was performed. Finally, the purification of reaction mixture on column chromatography afforded only one diastereoisomer, (±)-*trans*-**3**. The structure of the expected lactone (±)-*trans*-**3** was confirmed by the presence of a multiplet at 4.20−4.24 ppm from one proton at C-4 in the $^1H$ NMR spectrum. Lactone (±)-*trans*-4-butyl-*cis*-3-oxabicyclo[4.3.0]non-7-en-2-one


dx.doi.org/10.1021/jf502148h | J. Agric. Food Chem. 2014, 62, 8571−8578

((±)-**7**) was prepared from the respective anhydride **5** in the same procedure. The signal from proton at carbon atom C-4 was observed as a multiplet at 4.29−4.32 ppm.

The other two lactones, (±)-4,4-dibutyl-*cis*-3-oxabicyclo-[4.3.0]nonan-2-one ((±)-**4**) and (±)-4,4-dibutyl-*cis*-3-oxabicyclo[4.3.0]non-7-en-2-one ((±)-**8**), were obtained with good yields in Grignard reactions of 3 equiv of *n*-butylmagnesium bromide with 1 equiv of the corresponding anhydrides **1** and **5** (Scheme 1).

**Synthesis of Bicyclic Lactams 9−13.** Our studies concerned also bicyclic lactams, the second group of lactone **3** derivatives. We were interested in how the substitution of oxygen to nitrogen will influence the biological activity in the pair of lactone (±)-*cis*-3-oxabicyclo[4.3.0]non-7-en-2-one (**6**) and lactam (±)-*cis*-3-azabicyclo[4.3.0]non-7-en-2-one (**9**). The spectrum range of lactams applied in our research was increased by Vince lactam (2-azabicyclo[2.2.1]hept-5-en-3-one (**10**),[29−41] which we added to our studies (Figure 2). Both bicyclic lactams **9** and **10** have a double bond and γ-lactam moiety as well; however, they differ in the ring structure.

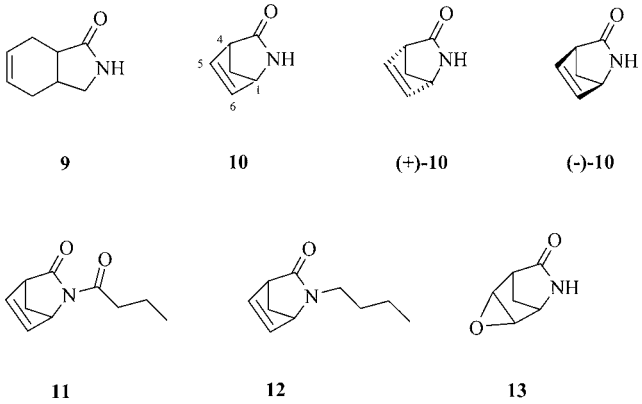


**Figure 2.** Structures of bicyclic lactams examined for fungistatic tests.

The obtained lactone (±)-**6** was used as the substrate for synthesis of lactam (±)-**9** conducted in a high-pressure autoclave (Berghof) using aqueous ammonia at high temperature and pressure as well (Scheme 2).

**Scheme 2**[a]

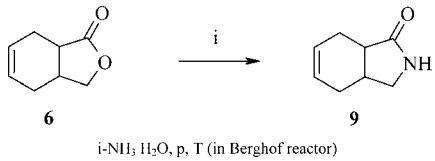


[a] i, $NH_3$ $H_2O$, p, T (in Berghof reactor).

Lactam (±)-**10**, with a structure similar to that of lactone **3** counterpart, was achieved by acylation of the nitrogen atom with butyric acid chloride, affording (±)-2-butyric-2-azabicyclo[2.2.1]hept-5-en-3-one ((±)-**11**) (Scheme 3). On the other hand, alkylation of lactam (±)-**10** with butyl bromide gave (±)-2-butyl-2-azabicyclo[2.2.1]hept-5-en-3-one ((±)-**12**) (Scheme 3). It was also worth checking the influence of the epoxy group on biological activity. Therefore, lactone (±)-**10** was oxidized to (±)-*cis*-5,6-epoxy-2-azabicyclo[2.2.1]heptan-3-one ((±)-**13**).

**Scheme 3**[a]

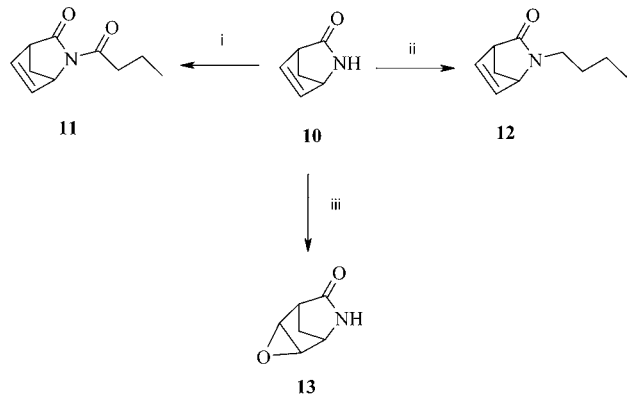


[a] i, NaH, THF, butyrate chloride; ii, NaH, THF butyl bromide; iii, *m*-CPBA, $CH_2Cl_2$.

**Bioresolution of (±)-2-Azabicyclo[2.2.1]hept-5-en-3-one ((±)-10).** Resolution of the racemic mixture of lactam (±)-**10** involved screening of nine commercially available enzymes (Scheme 4; Table 1). All enzymes (entries 1−9, Table 1)

**Scheme 4**

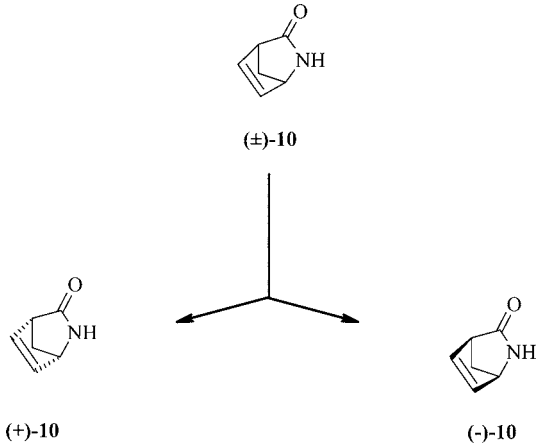


hydrolyzed more quickly enantiomer (−)-(1*R*,4*S*)-**10**, leaving in a reaction mixture unreacted optically active (+)-(1*S*,4*R*)-2-azabicyclo[2.2.1]hept-5-en-3-one ((+)-**10**) isomer. All enzymatic transformations were carried out in phosphate buffer solution. The best result was obtained after 7 days of biotranformation with *Candida antarctica* lipase B (recombinant in *Aspergillus oryzea*). The (−)-enantiomer of **10** was hydrolyzed preferentially, whereas the opposite isomer, (+)-**10** (ee = 99%), was extracted from the reaction mixture. The scale-up methodology (up to 200 mg of the substrate) was easily increased.

In parallel to enzymatic reactions, the lactam (±)-**10** was subjected to a microbial transformations with the following 18 strains: *Aspergillus ochraceus* AM456, *Candida viswanathi* AM120, *Fusarium culmorum* AM282, *Fusarium oxysporum* AM13, *Inonotus radiatus* AM70, *Laetiporus sulphurens* AM514, *Penicillium camemberti* AM83, *Penicillium notatum* AM904, *Penicillium thomi* AM91, *Pezicula cinnamomea* AM53, *Poria placenta* AM38, *Prosthemium* sp. AM52, *Rhodotorula marina* AM77, *Rhodotorula rubra* AM4, *Sclerophoma pythiophila* AM55,


dx.doi.org/10.1021/jf502148h | J. Agric. Food Chem. 2014, 62, 8571−8578

**Table 1. Enantiomeric Excess of 2-Azabicyclo[2.2.1]hept-5-en-3-one 10 after 7 Days of Biotransformations**

| entry | bioreagent | enantiomer | ee (%) |
|---|---|---|---|
| 1 | esterase immobilized on Eupergit C from hog liver | (+)-1*S*,4*R* | 42 |
| 2 | esterase from *Rhizomucor miehei* recombined from *Aspergillus oryzae* | (+)-1*S*,4*R* | 14 |
| 3 | lipase A (Amano) from *Aspergillus niger* | (+)-1*S*,4*R* | 40 |
| 4 | lipase from *Burkholderia cepacia* | (+)-1*S*,4*R* | 70 |
| 5 | lipase B *Candida antarctica* recombined from *Aspergillus oryzae* | (+)-1*S*,4*R* | 99 |
| 6 | lipase from *Mucor javanicus* | (+)-1*S*,4*R* | 75 |
| 7 | lipase from *Mucor miehei* | (+)-1*S*,4*R* | 30 |
| 8 | lipase from *Penicillium camemberti* | (+)-1*S*,4*R* | 93 |
| 9 | Lipozymer, immobilized from *Mucor miehei* | (+)-1*S*,4*R* | 6 |
| 10 | *Candida viswanathi* AM120 | (−)-1*R*,4*S* | 57 |
| 11 | *Penicillium camemberti* AM83 | (−)-1*R*,4*S* | 91 |
| 12 | *Penicillium notatum* AM904 | (−)-1*R*,4*S* | 66 |
| 13 | *Penicillium thomi* AM91 | (−)-1*R*,4*S* | 96 |
| 14 | *Sclerophoma pythiophila* AM55 | (−)-1*R*,4*S* | 77 |

*Sparassis crispa* AM535, *Stemphylium botryosum* AM279, and *Yarrowia lipolytica* AM77.

Only strains of the *Penicillium* genus and *C. viswanathi* AM120 possess enzymes capable of the enantioselective hydrolysis of the γ-lactam ring. It needs to be emphasize that selected strains were not previously described as biocatalysts useful in racemic resolution of (±)-**10**. In our opinion the aforementioned strains are a valuable source of lactam hydrolases, and in this regard they can be considered for further investigation.

It should be noted that lipase isolated from *P. camemberti* catalyzed hydrolysis of the opposite enantiomer of (±)-**10** than whole cell culture of *P. camemberti* AM83. We assume that other enzymes from a broad range of lipases were involved in biotransformation.

In preparative biotransformation of (±)-**10** *P. thomi* AM91 was applied. This strain enantioselectively hydrolyzed (+)-**10** isomer, leaving enantiomerically enriched (−)-**10** isomer (ee = 93%) (structures given in Figure 2). During condition optimization of the biotransformation, it was noted that the enzymes involved in amide bond hydrolization were biosynthesized in the presence of peptone growth medium or in a similar source of nitrogen. In contrast, in the mineral medium supplemented with $NaNO_3$, hydrolysis did not occur. Therefore, in the preparative biotransformation, *P. thomi* AM91 initially grew on a mineral medium until peptone induction. After 4 days, 1% of peptone was added, and the pH of the medium increased to 8.3. After another 4 h, 1 g of (±)-**10** was added. Finally, (−)-**10** isomer with an enantiomeric excess of 93% was formed after 2 days of biotransformation.

**Fungistatic Activity.** The fungistatic activity of racemic mixtures of lactones **2**−**4** and **6**−**8** (Figure 1), lactams **9**−**13**, and enantiomerically enriched (+)-**10** and (−)-**10** isomers (Figure 2) against three phytopathogenic strains (*P. citrinum* AM354, *B. cinerea* AM235, *A. glaucus* AM211) was estimated. Screening tests were conducted at a concentration of 200 μg/mL. Then, $IC_{50}$ in the range from 0 to 350 for each connection was determined. Compounds of $IC_{50}$ above 350 were considered as not active, and the $IC_{50}$ value was not specified.

Among the studied compounds, six of them ((±)-**3**, (±)-**4**, (±)-**7**, (±)-**8**, (±)-**9**, (±)-**10**) indicated high activity with $IC_{50}$ from 104.6 to 130.0 μg/mL (entries 2, 3, and 5−8, Table 2) against *B. cinerea* AM235, the pathogen of grapes. Promising high fungistatic activity of lactones **3** ($IC_{50}$ = 143.2 μg/mL) and **7** ($IC_{50}$ = 110.2 μg/mL) against *P. citrinum* AM354, in contrast to low fungistatic activity against *A. glaucus* AM211 (epoxylactam **13** $IC_{50}$ = 107.2 μg/mL), was observed. Our interests focused on combating fungi of the *Aspergillus* genus; therefore, we examined the activity of racemic lactones **2**−**4** and **6**−**8** and lactams **9** and **10** against the other five strains belonging to species of *Aspergillus*. Figure 3 shows the percentage of mycelium growth inhibition at a concentration of 200 μg/mL.

**Table 2. Half-Maximal Inhibitory Concentration ($IC_{50}$) for Compounds 2−4 and 6−13 against *Aspergillus glaucus* AM211, *Botrytis cinerea* AM235, and *Penicillium citrinum* AM354[a]**

| entry | compound no. | *A. glaucus* AM211 (μg/mL) | *B. cinerea* AM235 (μg/mL) | *P. citrinum* AM354 (μg/mL) |
|---|---|---|---|---|
| 1 | **2** | 142.9 | >350 | >350 |
| 2 | **3** | 246.3 | 104.6 | 143.2 |
| 3 | **4** | 238.6 | 115.2 | >350 |
| 4 | **6** | >350 | >350 | >350 |
| 5 | **7** | >350 | 107.7 | 110.2 |
| 6 | **8** | >350 | 103.3 | >350 |
| 7 | **9** | 250.0 | 127.4 | 220.0 |
| 8 | **10** | 262.6 | 130.4 | 219.0 |
| 9 | (+)-**10** | 245.0 | 125.3 | 220.6 |
| 10 | (−)-**10** | 282.4 | 147.5 | 256.2 |
| 11 | **11** | 203.8 | >350 | >350 |
| 12 | **12** | 226.9 | >350 | >350 |
| 13 | **13** | 107.1 | >350 | 289.0 |
| 14 | DDAC | 57.1 | 30.4 | 41.3 |

[a]Statistical analysis was done using ANOVA ($p$ = 0.05), and the means were compared by calculating the least significant difference (LSD, Tukey). $IC_{50}$ was calculated on the basis of standard curve with standard deviation ±1.745−2.050.

**Fungistatic Acticity of Bicyclic Lactones 2−4 and 6−8.** The tests were performed with six racemic bicyclic lactones **2**−**4** and **6**−**8** (Scheme 1) of the structure allowing determination of the effect of substituents on carbon atom C-4 and the influence of the C7−C8 double bond on fungistatic activity

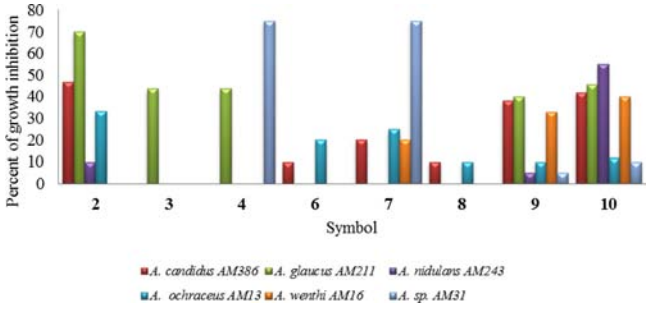


**Figure 3.** Percentage of growth inhibition of *Aspergillus* genus mycelium at a concentration of 200 μg/mL for lactones **2**−**4** and **6**−**8** and lactams **9** and **10**. Statistical analysis was done using ANOVA ($p$ = 0.05), and the means were compared by calculating the least significant difference (LSD, Tukey). $IC_{50}$ was calculated on the basis of standard curve with standard deviation ±1.745−2.050.


dx.doi.org/10.1021/jf502148h | J. Agric. Food Chem. 2014, 62, 8571−8578

against *A. glaucus* AM211, *B. cinerea* AM235, and *P. citrinum* AM354.

**Effect of Substituents on Carbon Atom C-4 on Fungistatic Activity.** Lactones (±)-**2** and (±)-**6**, without a substituent at carbon atom C-4, exhibited low fungistatic activity against tested strains (Table 2). Introducing one or two butyl groups caused a significant increase in fungistatic activity against *B. cinerea* AM 235 for (±)-**3** ($IC_{50}$ = 104.6 μg/mL (entry 2, Table 2)), (±)-7 ($IC_{50}$ = 107.7 μg/mL (entry 5, Table 2)), (±)-**4** ($IC_{50}$ = 115.2 μg/mL (entry 3, Table 2)), and (±)-**8** ($IC_{50}$ = 103.3 μg/mL (entry 6, Table 2)), respectively.

Otherwise, the aforementioned lactones affected the growth of *P. citrinum* AM354. Lactones with only one butyl group at C-4 were active: lactone (±)-**3** with the structure of natural lactone ($IC_{50}$ = 143.2 μg/mL (entry 2, Table 2)) and its analogue (±)-7 with the double bond at position C-7 ($IC_{50}$ = 110.2 μg/mL (entry 5, Table 2)).

**Effect of the C7−C8 Double Bond on Fungistatic Activity.** The presence of the C7−C8 double bond in the racemic lactones **6**−**8** indicated negligible or no effect on fungistatic activity against *P. citrinum* AM354 and *B. cinerea* AM235. In contrast, significant differences exist while for the inhibition of the growth of mycelium of *A. glaucus* AM211. Saturated racemic lactones **2**−**4** ($IC_{50}$ between 142.2 and 246.3 μg/mL, entries 1−3, Table 2) were more active than their analogues **6**−**8** ($IC_{50}$ > 350 μg/mL, entries 4−6, Table 2) with a double bond.

**Fungistatic Activity of Bicyclic Lactams 9−13.** *Effect of Heteroatom in the Five-Membered Ring on Fungistatic Activity.* By comparing the fungistatic activities against *B. cinerea* AM235 of lactone (±)-**6** and its analogue, lactam (±)-**9** (entries 4 and 7, Table 2), a significant increase in activity (from $IC_{50}$ > 350 μg/mL for lactone **6** to $IC_{50}$ = 127.4 μg/mL for lactam **9**) was observed.

*Effect of Ring Structure on Fungistatic Activity.* Both bicyclic lactams (±)-**9** and (±)-**10** possessed a γ-lactam ring and a double bond; however, they differed in the space structure (Scheme 3). These compounds inhibited the growth of all tested fungi to a comparable extent (entries 7 and 8, Table 2); therefore, we assumed that the γ-lactam ring and the nitrogen proton N−H significantly affect the biological activity.

*Effect of Substituents on the Nitrogen Atom of γ-Lactams on Fungistatic Activity.* The fungistatic activity of substituted lactams (±)-**11** and (±)-**12**, especially against *B. cinerea* AM235 and *P. citrinum* AM354, considerably decreased in comparison to that of unsubstituted lactam (±)-**10** from $IC_{50}$ = 130.0 μg/mL and 219.0 μg/mL (entry 8, Table 2) to $IC_{50}$ > 350 μg/mL (entries 11 and 12, Table 2).

*Effect of Double-Bond Oxidation on Fungistatic Activity.* Lactam (±)-**13**, the epoxy derivative of lactam (±)-**10**, was active ($IC_{50}$ = 107.1 μg/mL) against *A. glaucus* AM211 (entry 13, Table 2), but did not inhibit the growth of the other two strains tested.

*Effect of the Stereogenic Center on Fungistatic Activity.* Isomer (+)-(1*S*,4*R*)-**10** (ee = 91%) (entry 9, Table 2) inhibited more strongly the mycelium growth of all three strains (*A. glaucus* AM211, *B. cinerea* AM235, *P. citrinum* AM354), with an average of 15−20%, than its mirror image, (−)-(1*R*,4*S*)-**10** (ee = 93%) (entry 10, Table 2). Moreover, the (+)-**10** isomer was more active than the racemic mixture of 2-azabicyclo[2.2.1]hept-5-en-3-one ((±)-**10**).

**Fungistatic Activity against the *Aspergillus* Genus.** In general, synthesized lactones **2**−**4** and **6**−**8** and lactams **9** and **10** indicated low activity against *A. candidus* AM386, *A. nidulans* AM243, and *A. ochraceus* AM456 (Figure 3). Only compounds without an *n*-butyl substituent, (±)-3-oxabicyclo[4.3.0]nonan-2-one ((±)-**2**), (±)-3-azabicyclo[4.3.0]non-7-en-2-one ((±)-**9**), and (±)-2-aza-bicyclo[2.2.1]hept-5-en-3-one ((±)-**10**), inhibited more strongly the growth of mycelium of tested *Aspergillus* genus. Moreover, the growth of *A. glaucus* AM211 was inhibited by lactone (±)-**2**. Lactone (±)-4,4-dibutyl-3-oxabicyclo[4.3.0]nonan-2-one ((±)-**4**) and its analogue with a double bond ((±)-7) inhibited more strongly the growth of *Aspergillus* sp. AM31.

Analogues of natural *trans*-4-butyl-*cis*-3-oxabicyclo[4.3.0]-nonan-2-one (**3**) with a double bond at C-7 (**7**) or an additional butyl group at C-4 (lactones **4** and **8**) indicated the highest fungistatic activity ($IC_{50}$ = 104.6−115.2 μg/mL) toward *B. cinerea* AM235. However, only *trans*-4-butyl-*cis*-3-oxabicyclo-[4.3.0]nonan-2-one (**3**) and *trans*-4-butyl-*cis*-3-oxabicyclo-[4.3.0]non-7-en-2-one (**7**) exhibited high fungistatic activity ($IC_{50}$ = 143.2 and 110.2 μg/mL, respectively) against *P. citrinum* AM354, whereas lactones **3**, **4**, and **6**−**8** slightly inhibited the growth of mycelium of *A. glaucus* AM211.

The effect of a heteroatom in the five-membered ring on fungistatic activity was checked by comparing *cis*-3-oxabicyclo-[4.3.0]non-7-en-2-one (**6**) and its analogue, lactam *cis*-3-azabicyclo[4.3.0]non-7-en-2-one ((±)-**9**). A significant increase in activity (from $IC_{50}$ > 350 μg/mL for lactone **6** to $IC_{50}$ = 127.4 μg/mL for lactam **9**) against *B. cinerea* AM235 was observed. Also, (+)- and (−)-enantiomers of Vince lactam (**10**) and its three derivatives **11**−**13** were tested as fungistatic agents against *B. cinerea* AM235, *P. citrinum* AM354, and *A. gluacus* AM211. Isomer (+)-(1*S*,4*R*)-**10** with an average of 15−20% strongly inhibited mycelium growth of all tested strains.

The fungistatic activity of substituted nitrogen atom γ-lactams (±)-**11** and (±)-**12** considerably decreased in comparison to that of unsubstituted lactam (±)-**10** against *B. cinerea* AM235 and *P. citrinum* AM354. In contrast, oxidation of the double bond of lactam (±)-**10** increased the activity of epoxy derivative (**13**) ($IC_{50}$ = 107.1 μg/mL) against *A. glaucus*. As we indicated low activity of tested compounds against *A. glaucus* AM211, we have checked other *Aspergillus* genus species. Only compounds without an *n*-butyl substituent ((±)-3-oxabicyclo[4.3.0]nonan-2-one ((±)-**2**), (±)-3-azabicyclo[4.3.0]non-7-en-2-one ((±)-**9**), and (±)-2-aza-bicyclo[2.2.1]hept-5-en-3-one ((±)-**10**)) strongly inhibited growth of mycelium of tested *Aspergillus* genus species. Lactone (±)-4,4-dibutyl-3-oxabicyclo[4.3.0]nonan-2-one ((±)-**4**) and its analogue with a double bond ((±)-**8**) strongly inhibited growth of *Aspergillus* sp. AM31.

## ■ ASSOCIATED CONTENT

### Supporting Information

$^{1}H$ NMR and $^{13}C$ NMR spectra of lactones 3, 4, 7, 8 and lactams 9−13. This material is available free of charge via the Internet at http://pubs.acs.org.

## ■ AUTHOR INFORMATION

### Corresponding Author

*(T.O.) Phone: 048 71 320 52 67. Fax: 048 71 328 35 76. E-mail: teresa.olejniczak@up.wroc.pl.

### Funding

This work was financed by the National Science Centre, Grant 2011/03/B/NZ9/05005.

## Notes

The authors declare no competing financial interest.

## REFERENCES


(1) Chattapadhyay, T. K.; Dureja, P. Antifungal activity of 4-methyl-6-alkyl-2*H*-pyran-2-ones. *J. Agric. Food Chem.* **2006**, *54*, 2129−2133.

(2) Prieto-Simon, B.; Noguer, T.; Campas, M. Emerging biotools for assessment of mycotoxins in the past decade. *Trends Anal. Chem.* **2007**, *7*, 698−702.

(3) Dors, G. C.; Caldas, S. S.; dos Santos Hackbart, H. C.; Primel, E. G.; Fagundes, C. A. A.; Badiale-Furlong, E. Fungicides and the effects of mycotoxins on milling fractions of irrigated rice. *J. Agric. Food Chem.* **2013**, *61*, 1985−1990.

(4) Tomee, J. F. Ch.; Van der Werf, T. S. Pulmonary *aspergillosis*. *Neth. J. Med.* **2001**, *59*, 244−258.

(5) Malo, J. L. Antifungal therapy for allergic bronchopulmonary *aspergillosis*. *J. Allergy Clin. Immun.* **2003**, *111*, 934−935.

(6) Appendino, G.; Taglialatela-Scafati, O.; Romano, A.; Pollastro, F.; Avonto, C.; Rubiolo, P. Genepolide, a sesterpene γ-lactone with a novel carbon skeleton from Mountain Wormwood (*Artemisia umbellifomis*). *J. Nat. Prod.* **2009**, *72*, 340−344.

(7) Amorati, R.; Foti, M. C.; Valgimigli, L. Antioxidant activity of essential oils. *J. Agric. Food Chem.* **2013**, *61*, 10835−10847.

(8) Li, W.; Li, Q.; Liu, D.; Ding, M. Synthesis, fungicidal activity, and aterol 14α-demethylase binding interaction of 2-azolyl-3,4 dihydroquinazolines on *Penicillium digitatum*. *J. Agric. Food Chem.* **2013**, *61*, 1419−1426.

(9) Grabarczyk, M.; Mączka, W.; Wińska, K.; Żarowska, B.; Anioł, A. The new halolactones and hydroxylactone with trimethylcyclohexene ring obtained through combined chemical and microbial. *J. Mol. Catal. Enzym.: B* **2014**, *102*, 195−203.

(10) Jing, L.; Lei, Z.; Li, L.; Xie, R.; Xi, W.; Guan, Y.; Sumner, L. W.; Zhou, Z. Antifungal activity of citrus essential oils: a review. *J. Agric. Food Chem.* **2014**, *62*, 3011−3033.

(11) Liu, Q.; Shao, C.; Gu, Y.; Blum, M.; Gan, L.; Wang, K.; Chen, M.; Wang, C. Antifouling and fungicidal resorcylic acid lactones from the sea anemone-derived fungus *Cochliobolus lunatus*. *J. Agric. Food Chem.* **2014**, *62*, 3183−3191.

(12) Peretto, G.; Du, W.; Avena-Bustillos, R. J.; Berrios, J.; Sambo, P.; McHugh, T. H. Optimization of antimicrobial and physical properties of alginate coatings containing carvacrol and methyl cinnamate for strawberry application. *J. Agric. Food Chem.* **2014**, *62*, 984−990.

(13) Song, H.; Liu, Y.; Liu, Y.; Wang, L.; Wang, Q. Synthesis and antiviral and fungicidal activity evaluation of β-carboline, dihydro-β-carboline, tetrahydro-β-carboline alkaloids, and their derivatives. *J. Agric. Food Chem.* **2014**, *62*, 1010−1018.

(14) Queiroz, S. C. N.; Cantrell, C. L.; Duke, S. O.; Wedge, D. E.; Nandula, V. K.; Moraes, R. M.; Cerdeira, A. L. Bioassay-directed isolation and identification of phytotoxic and fungitoxic acetylenes from *Conyza canadensis*. *J. Agric. Food Chem.* **2012**, *60*, 5893−5898.

(15) Truchado, P.; Gil-Izquierdo, A.; Tomás-Barberán, F.; Allende, A. Inhibition by chestnut honey of *N*-acyl-L-homoserine lactones and biofilm formation in *Erwinia carotovora*, *Yersinia enterocolitica*, and *Aeromonas hydrophila*. *J. Agric. Food Chem.* **2009**, *57*, 11186−11193.

(16) Peters, A. M.; Haagsma, N.; Gensch, K.; van Amerongen, A. Production and characterization of polyclonal antibodies against the bitter sesquiterpene lactones of chicory (*Cichorium intybus* L.). *J. Agric. Food Chem.* **1996**, *44*, 3611−3615.

(17) Gravier-Pelletier, Ch.; Saniere, M.; Charvet, I.; Le Merrer, Y.; Depezay, J.-C. Synthesis of (−)-muricatacin and (−)-(5*R*,6*S*)-6-acetoxy-5-hexadecanolide, the mosquito oviposition attractant pheromone, from D-isoascorbic acid. *Tetrahedron Lett.* **1994**, *35*, 115−118.

(18) Boratyński, F.; Smuga, M.; Wawrzeńczyk, C. Lactones 42. Stereoselective enzymatic/microbial synthesis of optically active isomers of whisky lactone. *Food Chem.* **2013**, *141*, 419−427.

(19) Beck, J. J.; Chou, S. The structural diversity of phthalides from the *Apiaceae*. *J. Nat. Prod.* **2007**, *70*, 891−900.

(20) Bartschat, D.; Beck, T.; Mosandl, A. Stereoisomeric flavor compounds. 79. Simultaneous enantioselectivea of 3-butylphthalide and 3-butylhexahydrophthalide stereoisomers in celery, celeriac, and fennel. *J. Agric. Food Chem.* **1997**, *45*, 4554−4557.

(21) Momin, R. A.; Nair, M. G. Mosquitocidal, nematicidal, and antifungal compounds from *Apium graveolens* L. seeds. *J. Agric. Food Chem.* **2001**, *49*, 142−145.

(22) Bjeldanes, L. F.; Kim, I.-S. Phthalide components of celery essential oil. *J. Org. Chem.* **1977**, *42*, 2333−2335.

(23) Jiao, X.-Z.; Xie, P.; Zu, L.-S.; Liang, X.-T. Study of stereoselective synthesis of (±)-neocnidilide. *J. Asian Nat. Prod. Res.* **2003**, *5*, 165−169.

(24) Cheli, F.; Battaglia, D.; Pinotti, L.; Baldi, A. State of the art in feedstuff analysis: a technique-oriented perspective. *J. Agric. Food Chem.* **2012**, *60*, 9529−9542.

(25) Tao, Y.; Xu, X.; Ma, S.; Liang, G.; Wu, X.; Long, M.; Chen, Q. Cellulase hydrolysis of rice straw and inactivation of endoglucanase in urea solution. *J. Agric. Food Chem.* **2011**, *59*, 10971−10975.

(26) Mornar, A.; Sertic, M.; Nigović, B. Development of a rapid LC/DAD/FLD/MS*n* method for the simultaneous determination of *Monacolins* and *Citrinin* in red fermented rice products. *J. Agric. Food Chem.* **2013**, *61*, 1072−1080.

(27) Singh, P. K. Synthesis and fungicidal activity of novel 3-(substituted/unsubstituted phenylselenonyl)-1-ribosyl/deoxyribosyl-1*H*-1,2,4-triazole. *J. Agric. Food Chem.* **2012**, *60*, 5813−5818.

(28) Peretto, G.; Du, W.; Avena-Bustillos, R. J.; Berrios, J.; Sambo, P.; McHugh, T. H. Optimization of antimicrobial and physical properties of alginate coatings containing carvacrol and methyl cinnamate for strawberry application. *J. Agric. Food Chem.* **2014**, *62*, 984−990.

(29) Zheng, Y.; Hong, H.; Chen, L.; Li, J.; Shen, L. LEMAPK1, LEMAPK2, and LEMAPK3 are associated with nitric oxide-induced defense response against *Botrytis cinerea* in the *Lycopersicon esculentum* fruit. *J. Agric. Food Chem.* **2014**, *62*, 1390−1396.

(30) Yang, Z.; Zheng, Y.; Zhenfeng, S.; Cao, S. Effect of high oxygen atmosphere storage on quality, antioxidant enzymes, and DPPH-radical scavenging activity of chinese bayberry fruit. *J. Agric. Food Chem.* **2009**, *57*, 176−181.

(31) Canonne, P.; Akssira, M. Syntheses stereoselectives des γ-lactones bicycliques condenses. *Tetrahedron* **1985**, *41*, 3695−3704.

(32) Ward, O. P.; Singh, A. Enzymatic asymmetric synthesis by decarboxylases. *Curr. Opin. Biotechnol.* **2000**, *11*, 520−526.

(33) Singh, A. Engineering enzyme properties. *Ind. J. Microbiol.* **1999**, *39*, 65−77.

(34) Olejniczak, T.; Boratyński, F.; Białońska, A. Fungistatic activity of bicyclo[4.3.0]-γ-lactones. *J. Agric. Food Chem.* **2011**, *59*, 6071−6081.

(35) Taylor, S. J. C.; McCague, R.; Wisdom, R.; Lee, C.; Dickson, K.; Ruecroft, G.; O'Brien, F.; Littlechild, J.; Bevan, J.; Roberts, S. M.; Evans, C. T. Development of the biocatalytic resolution of 2-azabicyclo[2.2.1]hept-5-en-3-one as an entry to single-enantiomer carbocyclic nucleosides. *Tetrahedron Asymmetry* **1993**, *4*, 1117−1128.

(36) Kitayama, T. Microbial asymmetric syntheses of 3-alkylphthalide derivatives. *Tetrahedron Asymmetry* **1997**, *8*, 3765−3774.

(37) Yang, H.; Hu, G.; Chen, J.; Wang, Y.; Wang, Z. Synthesis, resolution, and antiplatelet activity of 3-substituted 1(3*H*)-isobenzofuranone. *Bioorg. Med. Chem. Lett.* **2007**, *17*, 5210−5213.

(38) Singh, R.; Vince, R. 2-Azabicyclo[2.2.1]hept-5-en-3-one: chemical profile of a versatile synthetic building block and its impact on the development of therapeutics. *Chem. Rev.* **2012**, *112*, 4642−4686.

(39) Szczepankiewicz, B. G.; Dai, H.; Koppetsch; Qian, D.; Jiang, F.; Mao, C.; Perni, R. B. Synthesis of carba-NAD and the structures of its ternary complexes with SIRT3 and SIRT5. *J. Org. Chem.* **2012**, *77*, 7319−7329.

(40) Torres, L. L.; Schließmann, M.; Silva-Martin, N.; Hermoso, J. A.; Berenguer, J.; Bornscheuer, U. T.; Hidalgo, A. Promiscuous enantioselective (−)-γ-lactamase activity in the *Pseudomonas fluorescens* esterase I. *Org. Biomol. Chem.* **2012**, *10*, 3388−3392.

(41) Li, F.; Zhao, D.; Chen, G.; Zhang, H.; Yue, H.; Wang, L.; Wang, Z. Enantioselective transesterification of *N*-hydroxymethyl Vince lactam catalyzed by lipase under ultrasound irradiation. *Biocatal. Biotransform.* **2013**, *31* (6), 299−304.

JOURNAL OF AGRICULTURAL AND FOOD CHEMISTRY

Article

pubs.acs.org/JAFC

# Pharmacokinetics and Toxicity Predictors of New *s*-Triazines, Herbicide Candidates, in Correlation with Chromatogrpahic Retention Constants

Nataša Milošević,*[,†] Nataša Janjić,[‡] Nataša Milić,[†] Maja Milanović,[†] Jovan Popović,[§] and Dušan Antonović[∥]

[†]Department of Pharmacy, [‡]Department of Orthopaedic Surgery and Traumatology, and [§]Department of Pharmacology and Toxicology, Faculty of Medicine, University of Novi Sad, Hajduk Veljkova 3, 21000 Novi Sad, Serbia

[∥]Department of Organic Chemistry, Faculty of Technology and Metallurgy, University of Belgrade, Karnegijeva 4, 11000 Belgrade, Serbia

**ABSTRACT:** Herbicides, which are ubiquitously present in soil and food, have been proven to cause human health hazard effects, hence development of new herbicide-active compounds is recommended. In this paper, nine 2,4-bis(cycloalkyl)-6-chloro-*s*-triazines were considered as herbicide candidates and their pharmacokinetics and toxicity were reviewed on the basis of in silico descriptors. Both, pharmacokinetic and toxicity predictors were presented as functions of their lipophilicity, quantified with retention constants that were obtained by liquid chromatography. None of the candidates investigated has functional groups for genotoxicity hazards and endocrine disruptions; they have acceptable toxicity and favorable pharmacokinetic properties based on computer-aided analyses. Two candidates have been selected as lead compounds for further research.

**KEYWORDS:** *herbicide candidates, triazines, in silico, pharmacokinetics, toxicity*

## INTRODUCTION

*s*-Triazines are compounds with pharmaceutical, chemosterilant and industrial importance. They are widely used as herbicides in agriculture and industry, and some of the compounds also have fungicidal properties.[1] Several of the most widely used herbicides (the class of 2-chloro-*s*-triazines) have been proven to induce the human aromatase enzyme (which converts androgens to estrogens) in vitro at relatively low concentrations. During critical developmental periods, aromatase induction may contribute to estrogen-mediated toxicities and inappropriate sexual differentiation.[2,3]

Hence, development of new *s*-triazine derivatives that have herbicide activity but fewer side effects is justified. It can be very informative to apply the main postulates of a drug designing process in an herbicide candidate screening process and to determine both compounds that have preferable pharmacokinetic and biological properties and to alert for those compounds with highly undesirable behavior in the human body in order to avoid late-stage attrition.[4] The implementation of appropriate management strategies requires that adequate information be developed regarding the types, physical and chemical properties, and toxicity of these compounds. The biological activity of a compound depends, among other factors, on its ability to reach the intended site of action.[5−7]

The physicochemical properties of a drug or pesticide have an important impact on its pharmacokinetic and metabolic fate in the body. Measurement and prediction of physicochemical characteristics are crucial in the development process of in silico models that allow early estimation on absorption, distribution, metabolism, and excretion (ADME) and toxicity data (together called ADMET data). Today, simple multiple linear regression and modern multivariate analysis techniques are now being applied to the analysis of ADME data and present the most applied quantitative structure−activity (or property) relationship [QSA(P)R] strategies.[8]

One of the most commonly referred descriptors in QSA(P)R analyzes is lipophilicity of a substance. It is usually quantified as the logarithm of the water−octanol partition coefficient for partitioning of the agent between the two immiscible solvent phases and expressed as log *P*. Partition coefficient, *P*, quantified as log *P*, can be precisely computed by using atomic or fragment-addition approaches or experimentally determined by a traditional shake-flask method or by application of chromatographic methods. In addition, the presence of more than one species (ionizable and molecular) in solutions with different pH values results in an apparent partition coefficient or distribution coefficient *D*, expressed as log *D*.[9]

The chromatographic methods are a useful alternative for lipophilicity quantification of drug or pesticide candidates. Net of bonds and interactions of the molecule with nonpolar stationary and polar mobile phase are very similar to the partitioning between the phospholipids bilayer and body fluids, which influences pharmacokinetic properties.[10,11] Thin-layer chromatography (TLC) allows the possibility of simultaneous analysis of several analytes, it is simple and economical, and it equalizes the differences that arise from the application of various organic solvent−water mixtures because extrapolated values to 0% of the organic solvents are applied; so it has still been an attractive method for lipophilicity quantification.[12] In

Received: May 21, 2014
Revised: August 2, 2014
Accepted: August 5, 2014
Published: August 5, 2014

ACS Publications © 2014 American Chemical Society



dx.doi.org/10.1021/jf502405k | J. Agric. Food Chem. 2014, 62, 8579−8585

this paper some *s*-triazines are overviewed as herbicides candidates, their pharmacokinetic and toxicity descriptors are discussed and presented as a function of lipophilicity described as retention constants.

## MATERIALS AND METHODS

A new series of nine *s*-triazine derivatives (Table 1) has been studied for their retention behavior on reversed-phase thin layer chromatography (RP-TLC), and the obtained retention constants $R_M^0$, which reflect their lipophilicity, have been correlated to pharmacokinetic and toxicological descriptors obtained with acd/i-lab-2.0 software package. RP-TLC was performed on silica gel C18 (Macherey-Nagel) with five different volume fractions ($\varphi$) of acetone in water−acetone mobile phase. Solutions for chromatographic investigations were prepared by dissolving in chloroform and were spotted on the plates with micropipette. Approximately 0.2 $\mu$L of each freshly prepared solution was spotted on the plates. Ascending technique has been used for chromatographic development. Dried plates after development were examined at 254 nm. $R_f$ values were calculated as an average out of three measurements.

**Table 1. Structures of Analyzed *s*-Triazines**

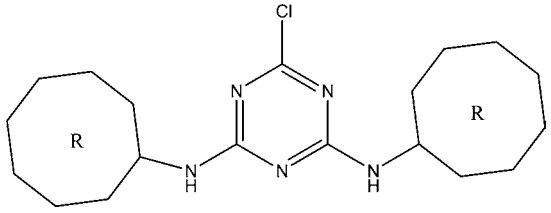


| compd | name | no. of C atoms in rings |
|---|---|---|
| **1** | 2,4-bis(cyclopropylamino)-6-chloro-*s*-triazine | 3 |
| **2** | 2,4-bis(cyclobutylamino)-6-chloro-*s*-triazine | 4 |
| **3** | 2,4-bis(cyclopentylamino)-6-chloro-*s*-triazine | 5 |
| **4** | 2,4-bis(cyclohexylamino)-6-chloro-*s*-triazine | 6 |
| **5** | 2,4-bis(cycloheptylamino)-6-chloro-*s*-triazine | 7 |
| **6** | 2,4-bis(cyclooctylamino)-6-chloro-*s*-triazine | 8 |
| **7** | 2,4-bis(cyclodecylamino)-6-chloro-*s*-triazine | 10 |
| **8** | 2,4-bis(cycloundecylamino)-6-chloro-*s*-triazine | 11 |
| **9** | 2,4-bis(cyclododecylamino)-6-chloro-*s*-triazine | 12 |

## RESULTS AND DISCUSSION

The retention behavior of *s*-triazines was investigated by changing the amount of organic modifier in the mobile phase and has been already previously reported.[13−16] The $R_M$ value for each compound was calculated as

$$R_M = \log\left(\frac{1}{R_f} - 1\right) \quad (1)$$

Relationships between retention values, $R_M$, of the compound and the volume fraction, $\varphi$, of organic modifier in the mobile phase were, as expected, linear and are expressed by the well-known equation:

$$R_M = R_M^0 + b\varphi \quad (2)$$

where $R_M^0$ (intercepts) are the extrapolated values corresponding to $\varphi$ = 0% and $b$ are the slopes of the linear plot. Regression equations derived for individual compounds are characterized by different slopes, which means that changes in mobile-phase composition have different effects on the $R_M$ values and that the slopes, $b$, correlate with the eluent strength of organic modifier. Linear relationships between the intercept, $R_M^0$, and the volume fraction of the organic modifier were characterized by high correlation coefficients (Table 2).

**Table 2. Intercepts and Slopes of the Linear TLC Equation Calculated for Each Analyzed Compound[a]**

| | $R_M = R_M^0 + b\varphi$ | | |
|---|---|---|---|
| compd | intercept ($R_M^0$) | slope ($b$) | adj $r^2$ |
| **1** | 1.695 | −2.885 | 0.998 |
| **2** | 2.023 | −3.667 | 0.986 |
| **3** | 2.553 | −3.745 | 0.985 |
| **4** | 3.055 | −3.875 | 0.986 |
| **5** | 3.678 | −4.599 | 0.989 |
| **6** | 4.121 | −4.610 | 0.992 |
| **7** | 5.242 | −6.117 | 0.989 |
| **8** | 5.325 | −5.652 | 0.990 |
| **9** | 5.860 | −6.640 | 0.996 |

[a] $p < 0.0001$.

In partition chromatography there is usually a linear correlation between $R_M^0$ and slope $b$. If linearity is observed, the compounds form a congeneric class.[17] Linear relationship between intercept $R_M^0$ and slope $b$ is given as

$$R_M^0 = -1.754 - 1.181b$$

where adj $r^2$ = 0.949, $F$ = 148.628, and $p < 0.0001$.

Sum effect of intermolecular interactions between analyte, stationary phase, and mobile phase define the chromatographic behavior of a molecule. Hydrophobic interactions dominantly guide the retention process of agents in reversed-phase liquid chromatography, hence good correlations (linear or parabolic) between the retention factor, $R_M^0$ and the standard lipophilicity parameter, log $P$, can be expected.[18]

Linear correlation was obtained between retention constants determined in RP TLC and log $P$ (ClogP and ACDlogP calculated by different software packages; Table 3) and more importantly with log $D$ (Table 3), which is consistent with literature data[19] in which a linear relationship between the retention constant log $k_w$ determined in HPLC and different log $P$ values has been described. Since the relationship between slopes $b$ and intercepts $R_M^0$ of the RP TLC equations has excellent statistical quality, the slopes can be considered alternative to intercepts for lipophilicity parameters. The slopes $b$ of RP TLC equations were correlated with log $P$ and log $D$ from calculation chemistry. It is evident that the slopes $b$ of TLC equation (eq 2) may be applied for lipophilicity expression (Table 4) of the compounds investigated with similar reliability like the intercepts, which well agrees with a report by Valko.[20]

Both retention constants $R_M^0$ and $b$ also vary with the size of the molecules quantified as molecular weight (MW)—that is, the number of C atoms (nC) in the substituent rings—since other physicochemical properties of the analytes do not alter with the change of their structure. Namely, the polarity of the molecules, described as total polar surface area (TPSA), number of hydrogen-bond donors (NHBD) and acceptors (NHBA), and elasticity of the molecules, quantified as number


dx.doi.org/10.1021/jf502405k | J. Agric. Food Chem. 2014, 62, 8579−8585

Table 3. Main Physicochemical Properties of the Analytes[a]

| nC | NHBD | NHBA | NRB | TPSA | MW | ClogP | ACDlogP | log $S$ (pH = 7.4) | log $D$ (pH = 7.4) |
|---|---|---|---|---|---|---|---|---|---|
| 3 | 2 | 5 | 4 | 62.73 | 225.68 | 2.5 | 1.96 | −4.18 | 2.62 |
| 4 | 2 | 5 | 4 | 62.73 | 253.73 | 3.16 | 3.08 | −4.68 | 3.04 |
| 5 | 2 | 5 | 4 | 62.73 | 281.78 | 4.28 | 4.21 | −5.17 | 4.16 |
| 6 | 2 | 5 | 4 | 62.73 | 309.84 | 5.4 | 5.34 | −5.63 | 4.80 |
| 7 | 2 | 5 | 4 | 62.73 | 337.89 | 6.52 | 6.47 | −6.06 | 6.27 |
| 8 | 2 | 5 | 4 | 62.73 | 365.94 | 7.63 | 7.6 | −6.47 | 7.34 |
| 10 | 2 | 5 | 4 | 62.73 | 422.05 | 9.87 | 9.85 | −7.23 | 8.53 |
| 11 | 2 | 5 | 4 | 62.73 | 450.1 | 10.99 | 10.98 | −7.57 | 9.23 |
| 12 | 2 | 5 | 4 | 62.73 | 478.15 | 12.11 | 12.11 | −7.89 | 9.89 |

[a]nC, number of C atoms in substituent rings; NHBD, number of hydrogen-bond donors; NHBA, number of hydrogen-bond acceptors; NRB, number of rotatable bonds; TPSA, total polar surface area; MW, molecular weight.

Table 4. Retention Constants $R_M^0$ and $b$, Presented as Functions of Computer-Calculated ClogP, ACDlogP, and log $D$ (pH = 7.4)

| equation | adj $r^2$ | $p$-value |
|---|---|---|
| $R_M^0 = 0.697 + 0.437\text{ClogP}$ | 0.991 | $1.074 \times 10^{-8}$ |
| $b = -2.196 - 0.353\text{ClogP}$ | 0.936 | $1.220 \times 10^{-5}$ |
| $R_M^0 = 0.827 + 0.424\text{ACDlogP}$ | 0.992 | $7.951 \times 10^{-9}$ |
| $b = -2.298 - 0.343\text{ACDlogP}$ | 0.940 | $9.855 \times 10^{-6}$ |
| $R_M^0 = 0.256 + 0.559 \log D$ | 0.991 | $1.242 \times 10^{-8}$ |
| $b = -1.870 - 0.447 \log D$ | 0.913 | $3.681 \times 10^{-5}$ |

of rotatable bonds (NRB), are constant for the analytes observed in this paper (Table 3), so the factors that influence the retention behavior of molecules are their lipophilicity and molecular size (Figure 1).

Pharmacokinetic predictors, calculated by use of computation program i-lab 2.0, are presented in Table 5.

High oral bioavailability is an important factor for the development of bioactive molecules as therapeutic agents but is undesirable for any xenobiotic that can be ingested. The rate and extent of intestinal absorption are mainly dependent on (i) dissolution rate of the drug (xenobiotics) in gastrointestinal fluids and (ii) rate of transport across the intestinal membrane. In light of present knowledge, it is probable that the predominant process of absorption for most conventional drugs (and xenobiotics) is passive diffusion. Varying types of approaches are used to predict the rate of passive intestinal absorption of drug candidates (or xenobiotics).[21]

Models applied in the early discovery phase typically allow rapid screens of a large number of compounds. The highest throughput can be obtained with computational quantitative structure−property relationship (QSPR) models.[22] Models developed to predict passive intestinal absorption can be evaluated by employing them to predict the intestinal absorption of a set of passively absorbed compounds with known values of the percentage of dose absorbed (abs%) in humans or constant of absorption $k_a$, defined as the ratio of natural logarithm of 2 and the half-time of compound absorption ($t_{a1/2}$): $k_a = \ln 2/(t_{a1/2})$. Compared with predicted abs%, predicted $k_a$ is more informative in the drug discovery process because the rate of absorption among completely absorbed drugs can vary.[9]

Properties of molecules such as bioavailability or membrane permeability have often been connected to simple molecular descriptors such as log $P$, MW, or counts of hydrogen-bond acceptors and donors in a molecule.[23−25] Lipinski et al.[26] have used these molecular properties to formulate the "rule of five". The rule states that most molecules with good membrane permeability have ClogP ≤ 5, molecular weight ≤ 500, number of hydrogen-bond acceptors ≤ 10, and number of hydrogen-bond donors ≤ 5. Investigated *s*-triazines have molecular weight under 500, two hydrogen-bond donors, five hydrogen-bond acceptors, and four rotatable bonds (Table 3). However, only three compounds have ClogP under 5, for which good oral absorption can be assumed. Compounds with more than 6 C atoms in substituent rings have ClogP over 5 and violate one rule; hence, for these compounds low membrane permeability can be expected, due to very low solubility (Table 3), and consequently very poor absorption. Nevertheless, absorption constants for compounds investigated are predicted to be low (0.048−0.06 $\text{min}^{-1}$, Table 5); that is, they have short half-times of absorption (11−15 min), which practically guarantee unomitted permeation through enterocytes. However, very low solubility for over 6C-in-rings-compounds should not be neglected for herbicide candidates.

The absorption constant defines the rate of transport through membrane and it is completely associated with lipophilicity quantifiers $R_M^0$ and $b$:

$$k_a = 0.066 - 0.004R_M^0$$

where adj $r^2 = 0.983$, $F = 466.892$, and $p < 0.0001$, and

$$k_a = 0.072 + 0.004b$$

where adj $r^2 = 0.902$, $F = 74.658$, and $p < 0.0001$, although only compounds with 3, 4, 5, and eventually 6 carbons in the rings should be considered for further pharmacokinetic profiling on the basis of violation of Lipinski's rule for the rest of the compounds. This good and fast absorption for compounds can be expected for these four molecules, so their further action in the human body will be the key in the selection process of herbicide candidates with the least side effects. The change of pharmacokinetic behavior of all considered compounds, however, is very informative, and all compounds will be considered.

The concentration of drug (or xenobiotic) in the plasma or tissues depends on the amount of xenobiotic systemically absorbed and the volume in which the xenobiotic is distributed. The apparent volume of distribution in the body, $V_d$, is the most important pharmacokinetic parameter that determines the extent of drug or any other xenobiotic distribution. It is simply a proportionality constant that relates the amount of xenobiotic in the body and/or compartments of the body (peripheral compartments) to its plasma (central compartment) concen-


dx.doi.org/10.1021/jf502405k | J. Agric. Food Chem. 2014, 62, 8579−8585

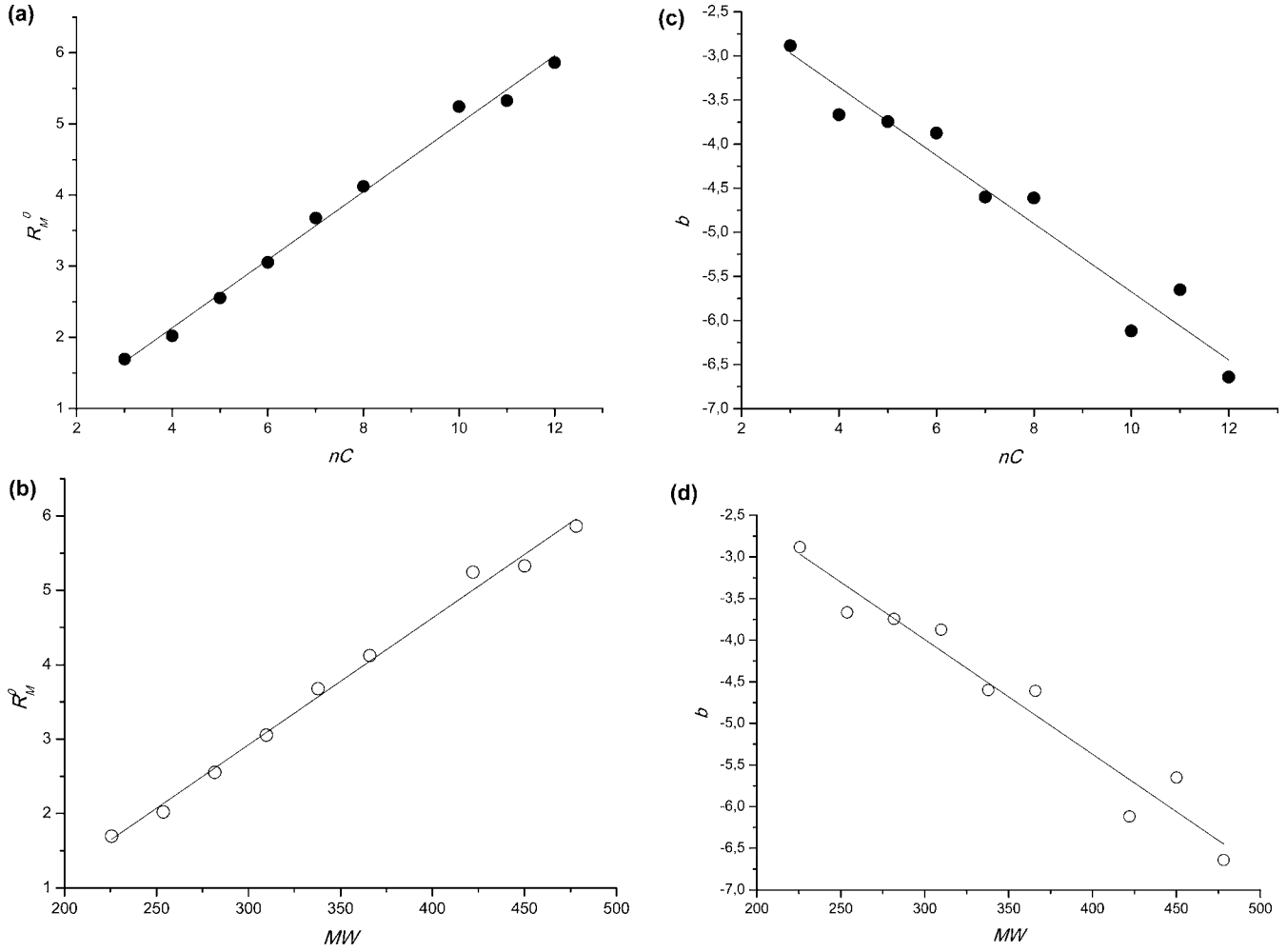


**Figure 1.** Linear dependence of retention constants $R_M{}^0$ from (a) number of C atoms in substituent rings, given as $R_M{}^0 = 0.222 + 0.478$nC [adj $r^2 = 0.992$, $F = 1004.25$, $p = 8.053 \times 10^{-9}$] or from (b) molecular weight, described as $R_M{}^0 = -2.191 + 0.017$MW [adj $r^2 = 0.992$, $F = 1004.56$, $p = 8.044 \times 10^{-9}$]. Linear dependence of slope $b$ from (c) number of C atoms in substituent rings, characterized as $b = -1.808 - 0.387$nC [adj $r^2 = 0.940$, $F = 126.75$, $p = 9.744 \times 10^{-6}$] or from (d) molecular weight, estimated as $b = 0.143 - 0.014$MW [adj $r^2 = 0.940$, $F = 126.75$, $p = 9.744 \times 10^{-6}$].

**Table 5. In Silico-Determined Pharmacokinetic Parameters**[a]

| compd | $k_a$ ($min^{-1}$) | $V_d$ (L/kg) | PPB (%) | log BBB |
|---|---|---|---|---|
| **1** | 0.061 | 1.80 | 91.77 | −0.17 |
| **2** | 0.059 | 2.16 | 92.23 | 0.06 |
| **3** | 0.057 | 2.48 | 95.97 | 0.37 |
| **4** | 0.054 | 2.85 | 96.99 | 0.53 |
| **5** | 0.053 | 3.93 | 96.89 | 0.77 |
| **6** | 0.051 | 4.26 | 98.16 | 0.60 |
| **7** | 0.048 | 5.63 | 99.49 | 0.3 |
| **8** | 0.047 | 6.48 | 99.62 | 0 |
| **9** | 0.046 | 7.10 | 99.69 | 0 |

[a] $k_a$, constant of absorption; $V_d$, volume of distribution; PPB, plasma protein binding affinity; log BBB, logarithm of blood−brain barrier permeation.

tration. $V_d$ is assumed to be constant for a xenobiotic that follows a one-compartment pharmacokinetic model and is calculated as the dose taken divided by the plasma concentration of the compound at time zero ($C_0$):[27,28] $V_d$ = dose/$C_0$.

Since accumulation of xenobiotic in fat tissue causes major problems and for many xenobiotics is the main health concern, $V_d$ of newly synthesized compounds that may have frequent use in everyday life is an important subject. These homologous series of investigated compounds have moderate predicted $V_d$ values (range 1.8−7.1 L/kg) (Table 5), indicating that no serious accumulation of compound in fat tissue occurs. $V_d$ can be larger for very hydrophobic compounds, which accumulate in the fat tissue. Lipophilicity of analytes has a leading role in the distribution process (as in absorption process) of investigated triazines. Figure 2 shows the change of $V_d$ with lipophilicity of the triazines investigated. The most important observation is that compounds which should have good oral absorption (**1**−**4**) are the least lipophilic compounds and are presumed to have the smallest $V_d$, which is highly preferable.

In the drug development process, it is desirable to recognize those drug candidates which are potential high binders for plasma proteins in early virtual screening procedures. Drug bound to plasma proteins is not active i.e. —that is, it is not able to cross membranes, pass the central compartment, and diffuse into the interstitial space—hence it cannot permeate to the site of action nor bind to receptors.[29] Although drugs require low binding values for xenobiotics, it is preferable to have a small free compound concentration in plasma in order to prevent possible side effects and remain nonpharmacologically active in the human body. From Table 5 it can be observed that compounds investigated are expected to have


dx.doi.org/10.1021/jf502405k | J. Agric. Food Chem. 2014, 62, 8579−8585

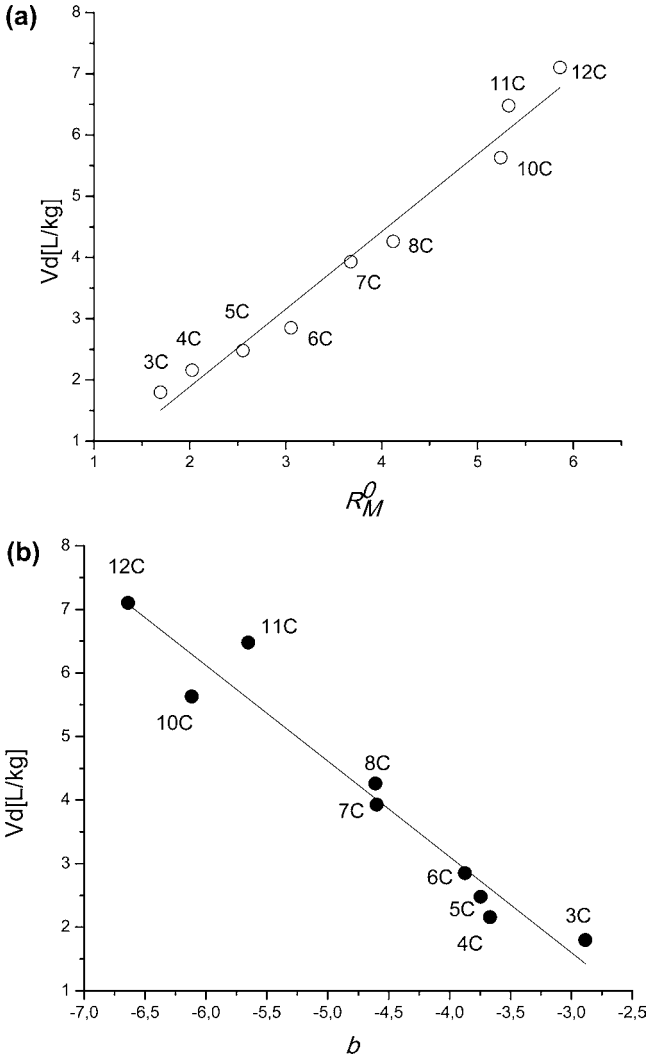


**Figure 2.** In silico estimated volume of distribution, $V_d$, presented as linear function of (a) lipophilicity of the analytes, quantified as $R_M{}^0$ and given as $V_d = -0.642 + 1.266R_M{}^0$ [adj $r^2 = 0.970$, $F = 262.309$, $p = 8.324 \times 10^{-7}$], and (b) slopes $b$, presented as $V_d = -2.914 - 1.506b$ [adj $r^2 = 0.936$, $F = 118.626$, $p = 1.215 \times 10^{-5}$].

very low free concentration (only 8% or less) in plasma, which guarantees small or no pharmacological effectiveness in the human body. It is widely accepted that protein binding and especially binding of drugs and other xenobiotics to serum albumin is generally nonspecific and strongly influenced by hydrophobic interactions within small congeneric series of compounds. However, lipophilicity seems not to be the dominant chemical property for albumin binding affinity when structurally different drugs or xenobiotics are compared.[30]

Since we are dealing with structurally similar compounds, the examination of dependence between PPB and lipophilicity is strongly recommended. Statistically high square function was determined between lipophilicity and PPB. As the number of C atoms in the ring increases, both lipophilicity and affinity for albumins elevate until the highest level (over 99% bound for human plasma albumins) is achieved for compounds that have 10 or more C atoms in rings:

$$\text{PPB} = 83.572 + 5.727R_M{}^0 - 0.512(R_M{}^0)^2$$

where adj $r^2 = 0.941$, $F = 64.256$, and $p < 0.0001$, and

$$\text{PPB} = 72.027 - 8.719b - 0.686b^2$$

where adj $r^2 = 0.807$, $F = 17.718$, and $p < 0.005$. It should be emphasized that high affinity for plasma proteins and very small free plasma concentration is characteristic for these sets of compounds, including those that are expected to absorb easily and in great percentage.

The blood–brain barrier is the formidable obstacle that restricts the brain entry of most hydrophilic compounds. Permeation of drugs through the blood–brain barrier is usually described as a logarithmic value. For many neurological drugs, a positive value for log BBB that tends to reach 1 is preferable, while for most xenobiotics, a negative value for log BBB or values close to zero indicate that those compounds are unable to gain access to the brain or lack sufficient concentration for an appropriate time; hence neurotoxicity should be diminished.[31,32]

The novel set of compounds observed in this paper, as demonstrated in Table 5, have log BBB values that vary from −0.17 up to 0.77. It can be assumed that compounds with only 3 and 4 C atoms or those with more than 10 C atoms in the rings are expected to have very low log BBB. Nevertheless, compounds with 5–8 C atoms in rings have moderate log BBB, and for them poor penetration in the brain can be predicted. These assumptions agree with Clark's[33] rule of thumb, on which basis all compounds violate at least one of the following rules:

- Rule 1: The sum of nitrogen and oxygen (N + O) atoms in a molecule should be five or fewer to facilitate brain permeation.
- Rule 2: ClogP − (N + O) > 0 is recommended.
- Rule 3: Polar surface area (PSA) of the compound should be below 90 Å$^2$ (60–70 Å$^2$).
- Rule 4: If molecular weight (MW) is below 450, then the molecule has a high chance of entering the brain.
- Rule 5: If log $D$ value is in the range 1–3, then log BBB is likely to be positive.

These compounds do have polar surface area around 60 Å$^2$ and molecular weight around 450 and less, as well as a sum of nitrogen and oxygen atoms 5 or fewer. However, all compounds violate rule 1 or rule 5. Compounds with 5 or fewer C atoms in the substituent rings do not obey the rule ClogP − (N + O) > 0, while rule 5, log $D$ = 1–3, is broken by compounds with 5 or more C atoms in rings. For potential herbicides that can be absorbed in the human body, low permeation in the brain is desirable as it is predicted. The most important is the small brain permeability by compounds with 3C, 4C and 5C atoms in the substituent rings, which have the best features for herbicide candidates.

The generally accepted physicochemical models of BBB permeability have recognized as their primary determinants for passive transport the analyte's lipophilicity and polarity.[34] Having in mind the constant polarity of the compounds (Table 3), log BBB should be associated only with the lipophilicity of the analytes. For this set of compounds, parabolic correlation with high statistical quality has been established between log BBB and lipophilicity of the solutes:

$$\log \text{BBB} - 1.981 + 1.384R_M{}^0 - 0.182(R_M{}^0)^2$$

where adj $r^2 = 0.864$, $F = 26.350$, and $p < 0.005$, and

$$\log \text{BBB} = -4.634 - 2.157b - 0.220b^2$$


dx.doi.org/10.1021/jf502405k | J. Agric. Food Chem. 2014, 62, 8579–8585

where adj $r^2$ = 0.802, $F$ = 15.151, $p < 0.01$, and compound **8** is excluded.

The increment of C atom number in the rings leads to elevation of the molecular weight and lipophilicty of the molecules which at first facilitates permeability into the brain. Further elevation of lipophilicity diminishes their permeation, probably due to low solubility and dissociation in water body fluids.

The critical point in drug development programs, which is recognized by the pharmaceutical industry and safety assessment regulatory authorities, is the early identification of serious toxicological issues in order to prevent significant investment of time and resources for new drugs in late stages of clinical development.[35] For new herbicide candidates, low animal and human toxicity is one of the most important issues. On the basis of in silico calculations, predicted acute toxicity of the compounds investigated (Table 6) compared to data for

**Table 6. Predicted $LD_{50}$ Values for Compounds Investigated**[a]

| | $LD_{50}$ (mg/kg) | | | | | |
|---|---|---|---|---|---|---|
| | mouse | | | | rat | |
| compd | ip | po | iv | sc | ip | po |
| **1** | 240 | 540 | 81 | 28 | 38 | 400 |
| **2** | 240 | 920 | 43 | 61 | 530 | 3200 |
| **3** | 260 | 1900 | 61 | 35 | 98 | 850 |
| **4** | 240 | 1900 | 49 | 33 | 49 | 960 |
| **5** | 150 | 1300 | 31 | 33 | 98 | 3300 |
| **6** | 180 | 550 | 20 | 16 | 110 | 1700 |
| **7** | 140 | 1400 | 16 | 98 | 50 | 3300 |
| **8** | 130 | 1200 | 12 | 76 | 48 | 3900 |
| **9** | 120 | 1100 | 10 | 80 | 46 | 4500 |

[a]ip, intraperitoneal; po, per os; iv, intravenous; sc, subcutaneous.

toxicity of atrazine,[36,37] simazine,[38−42] propazine,[43−47] and terbuthylazine[48,49] indicates slight to moderate toxicity to humans and other animals for the compounds investigated; that is, they have acceptable toxic properties.

In addition, not only do predicted oral absorption and distribution of compounds investigated depend on their lipophilicity, but values of toxicity predictors are also changed in accordance with lipophilicity alternation. There is a linear increment of both intravenous and intraperitoneal toxicity in mouse (i.e., decrement of $LD_{50}$ dosages predicted on the basis of structure) with the elevation of lipophilicity of the analytes experimentally quantified as retention constants $R_M{}^0$ and $b$:

$$LD_{50}\ (\text{ip mouse}) = 315.490 - 33.959R_M{}^0$$

where adj $r^2$ = 0.825, $F$ = 38.646, and $p < 0.0005$;

$$LD_{50}\ (\text{iv mouse}) = 90.866 - 14.747R_M{}^0$$

where adj $r^2$ = 0.811, $F$ = 35.259, and $p < 0.001$;

$$LD_{50}\ (\text{ip mouse}) = 376.480 + 40.400b$$

where adj $r^2$ = 0.796, $F$ = 32.123, and $p < 0.001$; and

$$LD_{50}\ (\text{iv mouse}) = 118.021 + 17.688b$$

where adj $r^2$ = 0.797, $F$ = 32.441, and $p < 0.001$.

Finally, investigated compounds were tested in silico as possible causes of human endocrine system disorders and genotoxic hazards. Namely, several members of the class of 2-chloro-*s*-triazine herbicides (atrazine, simazine, and propazine) induce the human aromatase enzyme (which converts androgens to estrogens) in vitro at relatively low concentrations. A logical concern would be that exposure of wildlife and humans to triazine herbicides, which are produced and used in large quantities and are ubiquitous environmental contaminants, may similarly contribute to estrogen-mediated toxicities and inappropriate sexual differentiation.[50,51] Investigated derivatives of *s*-triazine, according to in silico analyses, do not have functional groups for genotoxicity hazards and endocrine disruptions.

On the basis of the obtained results, it can be concluded that for further herbicide candidates, compounds **1** and **2** with 3C and 4C atoms in the substituent rings can be reviewed.

## AUTHOR INFORMATION


### Corresponding Author

*Telephone/fax +381(0)21-422-760; e-mail milosevic_natasa@ymail.com or natasabm@uns.ac.rs.



### Funding

This study was performed with the support of the Ministry of Education, Science and Technological Development of the Republic of Serbia, Project OI 172013.


### Notes

The authors declare no competing financial interest.

## REFERENCES


(1) Martin, H., Worthing, C. R., Eds. *Pesticide Manual*, 4th ed.; British Crop Protection Council: Worcestershire, England, 1974.

(2) Benachour, N.; Moslemi, S.; Sipahutar, H.; Seralini, G. E. Cytotoxic effects and aromatase inhibition by xenobiotic endocrine disrupters alone and in combination. *Toxicol. Appl. Pharmacol.* **2007**, *222*, 129−140.

(3) Vandenberg, L. N.; Colborn, T.; Hayes, T. B.; Heindel, J. J.; Jacobs, D. R., Jr.; Lee, D. H.; Shioda, T.; Soto, A. M.; vom Saal, F. S.; Welshons, W. V.; Zoeller, R. T.; Myers, J. P. Hormones and endocrine-disrupting chemicals: Low-dose effects and nonmonotonic dose responses. *Endocr. Rev.* **2012**, *33* (3), 378−455.

(4) Cimmino, A.; Zonno, M. C.; Andolfi, A.; Troise, C.; Motta, A.; Vurro, M.; Evidente, A. Agropyrenol, a phytotoxic fungal metabolite, and its derivatives: A structure−activity relationship study. *J. Agric. Food Chem.* **2013**, *61* (8), 1779−1783.

(5) Henchoz, Y.; Bard, B.; Guillarme, D.; Carrupt, P. A.; Veuthey, J. L.; Martel, S. Analytical tools for the physicochemical profiling of drug candidates to predict absorption/distribution. *Anal. Bioanal. Chem.* **2009**, *394*, 707−729.

(6) Kerns, E. H.; Di, L. Pharmaceutical profiling in drug discovery. *Drug Discovery Today* **2003**, *8* (7), 316−323.

(7) Li, A. P. Screening for human ADME/Tox drug properties in drug discovery. *Drug Discovery Today* **2001**, *6* (7), 357−366.

(8) van de Waterbeemd, H.; Gifford, E. ADMET in silico modelling: towards prediction paradise? *Nat. Rev. Drug Discovery* **2003**, *2* (3), 192−204.

(9) Hou, T.; Wang, J.; Zhang, W.; Wang, W.; Xu, X. Recent advances in computational prediction of drug absorption and permeability in drug discovery. *Curr. Med. Chem.* **2006**, *13* (22), 2653−2667.

(10) Lambert, W. J. Modeling oil-water partitioning and membrane permeation using reversed-phase chromatography. *J. Chromatogr. A* **1993**, *656*, 469−484.

(11) Gocan, S.; Cimpan, G.; Comer, J. Lipophilicity measurements by liquid chromatography. *Adv. Chromatogr.* **2006**, *44*, 79−176.

(12) Komsta, L.; Skibinski, R.; Berecka, A.; Gumieniczek, A.; Radkiewicz, B.; Radon, M. Revisiting thin-layer chromatography as a lipophilicity determination tool: A comparative study on several techniques with a model solute set. *J. Pharm. Biomed. Anal.* **2010**, *53* (4), 911−918.

(13) Djakovic-Sekulic, T. L.; Perisic-Janjic, N. U. Comparative study of the retention of s-triazines on octadecylsilica, cyano, and amino HPTLC plates by use of a QSPR model. *J. Planar. Chromatogr. − Mod. TLC* **2007**, *20* (5), 365−371.
(14) Perisic-Janjic, N. U.; Jovanovic, B. Z.; Janjic, N. J.; Rajkovic, O. S.; Antonovic, D. G. Study of the retention behavior of newly synthesized s-triazine derivatives in RP TLC systems, and the lipophilicity of the compounds. *J. Planar Chromatogr.—Mod. TLC* **2003**, *16* (6), 452−432.
(15) Djakovic-Sekulic, T. L.; Smolinski, A.; Perisic-Janjic, N. U.; Janicka, M. Chemometric characterization of (chromatographic) lipophilicity parameters of newly synthesized s-triazine derivatives. *J. Planar Chromatogr.—Mod. TLC* **2008**, *22* (3−4), 195−202.
(16) Perisic-Janjic, N. U.; Jovanovic, B. Z. Reversed-phase thin-layer chromatographic behaviour of some s-triazine derivatives. *J. Planar Chromatogr.—Mod. TLC* **2003**, *16* (1), 71−75.
(17) Cserhati, T. Lipophilicity determination of some monoamine oxidase inhibitors: The effect of methanol and ammonium chloride. *J. Liq. Chromatogr.* **1993**, *16*, 1805−1817.
(18) Guillot, A.; Henchoz, Y.; Moccand, C.; Guillarme, D.; Veuthey, J. L.; Carrupt, P. A.; Martel, S. Lipophilicity determination of highly lipophilic compounds by liquid chromatography. *Chem. Biodiversity* **2009**, *6*, 1828−1836.
(19) Janicka, M.; Kwietniewski, L.; Perisic-Janjic, N. U. Determination of retention factors of s-triazines homologous series in water using a numerical method basing on Oscik's equation. *Chromatographia* **2006**, *63*, 587−593.
(20) Valko, K. Measurements of physical properties for drug design in industry. In *Separation Methods in Drug Synthesis and Purification*; Valko, K., Ed.; Elsevier: Amsterdam, 2000; pp 535−583.
(21) Obata, K.; Sugano, K.; Saitoh, R.; Higashida, A.; Nabuchi, Y.; Machida, M.; Aso, Y. Prediction of oral drug absorption in humans by theoretical passive absorption model. *Int. J. Pharm.* **2005**, *293* (1−2), 183−192.
(22) Kaliszan, R. QSRR Quantitative structure−(chromatographic) retention relationships. *Chem. Rev.* **2007**, *107*, 3212−3246.
(23) Remko, M.; Swart, M.; Bickelhaupt, F. M. Theoretical study of structure, p$K_a$, lipophilicity, solubility, absorption, and polar surface area of some centrally acting antihypertensives. *Bioorg. Med. Chem.* **2006**, *14*, 1715−1728.
(24) Remko, M. Molecular structure, lipophilicity, solubility, absorption, and polar surface area of novel anticoagulant agents. *J. Mol. Struct.: THEOCHEM* **2009**, *916*, 76−85.
(25) Remko, M. Molecular structure, pKa, lipophilicity, solubility and absorption of biologically active aromatic and heterocyclic sulfonamides. *J. Mol. Struct.: THEOCHEM* **2010**, *944*, 34−42.
(26) Lipinski, C. A.; Lombardo, F.; Dominy, B. W.; Feeney, P. J. Experimental and computational approaches to estimate solubility and permeability in drug discovery and development settings. *Adv. Drug Delivery Rev.* **2001**, *46*, 3−26.
(27) Ghafourian, T.; Barzegar-Jalali, M.; Dastmalchi, S.; Khavari-Khorasani, T.; Hakimiha, N.; Nokhodchi, A. QSPR models for the prediction of apparent volume of distribution. *Int. J. Pharm.* **2006**, *319*, 82−97.
(28) Stepensky, D. Use of unbound volumes of drug distribution in pharmacokinetic calculations. *Eur. J. Pharm. Sci.* **2011**, *42*, 91−98.
(29) Kratochwil, N. A.; Huber, W.; Müller, F.; Kansy, M.; Gerber, P. R. Predicting plasma protein binding of drugs: a new approach. *Biochem. Pharmacol.* **2002**, *64* (9), 1355−1374.
(30) Láznícek, M.; Láznícková, A. The effect of lipophilicity on the protein binding and blood cell uptake of some acidic drugs. *J. Pharm. Biomed. Anal.* **1995**, *13*, 823−828.
(31) Pardridge, W. M. Blood-brain barrier biology and methodology. *J. Neurovirol.* **1999**, *5* (6), 556−569.
(32) Lundquist, S.; Renftel, M.; Brillault, J.; Fenart, L.; Cecchelli, R.; Dehouck, M. P. Prediction of drug transport through the blood-brain barrier *in vivo:* A comparison between two *in vitro* cell models. *Pharm. Res.* **2002**, *19* (7), 976−981.
(33) Clark, D. E. In silico prediction of blood−brain barrier permeation. *Drug Discovery Today* **2003**, *8*, 927−933.
(34) Goodwin, J. T.; Clark, D. E. In silico predictions of blood-brain barrier penetration: Considerations to "keep in mind". *J. Pharmacol. Exp. Ther.* **2005**, *315* (2), 477−483.
(35) Valerio, L. G., Jr. Review of in silico toxicology for the pharmaceutical sciences. *Toxicol. Appl. Pharmacol.* **2009**, *241* (3), 356−370.
(36) *Herbicide Handbook of the Weed Science Society of America*, 7th ed.; Weed Science Society of America: Champaign, IL, 1994.
(37) U.S. National Library of Medicine. *Hazardous Substances Databank*. Bethesda, MD, 1995.
(38) Hayes, W. J., Laws, E. R., Eds. *Handbook of Pesticide Toxicology, Vol. 3: Classes of Pesticides*; Academic Press: New York, 1990.
(39) Meister, R. T., Ed. *Farm Chemicals Handbook '92*. Meister Publishing Company: Willoughby, OH, 1992.
(40) Ciba-Geigy Corp. *Toxicological Overview for Simazine Technical*; Agricultural Division, Ciba-Geigy Corp: Greensboro, NC, 1990.
(41) *Herbicide Handbook of the Weed Science Society of America*, 6th ed.; Weed Science Society of America: Champaign, IL, 1989.
(42) *MSDS for Simazine*; Occupational Health Services, Inc.: Secaucus, NJ, 1991.
(43) Berg, G. L., Ed. *Farm Chemicals Handbook '87*; Meister Publishing Company: Willoughby, OH, 1987.
(44) *Registry of Toxic Effects of Chemical Substances*. National Institute for Occupational Safety and Health: Cincinnati, OH, 1986.
(45) Worthing, C. R., Ed. *The Pesticide Manual: A World Compendium*; The British Crop Protection Council: Croydon, England, 1983.
(46) U.S. Environmental Protection Agency. *Propazine: health advisory*. Office of Drinking Water, US EPA: Washington, DC, 1998.
(47) *SCS/ARS/CES Pesticide Properties Database: version 2.0 (summary)*; USDA Soil Conservation Service: Syracuse, NY, 1990.
(48) Mercier, O. Terbuthylazine: test to evaluate the acute toxicity following a single oral administration (LD 50) in the rat. Lab project number 012333:904139; Unpublished study prepared by Hazleton-France, 1991; p 45.
(49) Mercier, O. Terbuthylazine: test to evaluate the acute toxicity following a single cutaneous application (limit test) in the rat. Lab project number 012319:904151; Unpublished study prepared by Hazleton-France, 1991; p 30.
(50) Sanderson, J. T.; Seinen, W.; Giesy, J. P.; van den Berg, M. 2-Chloro-*s*-triazine herbicides induce aromatase (CYP19) activity in H295R human adrenocortical carcinoma cells: a novel mechanism for estrogenicity? *Toxicol. Sci.* **2000**, *54* (1), 121−127.
(51) Sanderson, J. T.; Letcher, R. J.; Heneweer, M.; Giesy, J. P.; van den Berg, M. Effects of chloro-s-triazine herbicides and metabolites on aromatase activity in various human cell lines and on vitellogenin production in male carp hepatocytes. *Environ. Health. Perspect.* **2001**, *109*, 1027−1031.

JOURNAL OF AGRICULTURAL AND FOOD CHEMISTRY

Article

pubs.acs.org/JAFC

# Analytical Method for the Determination of Trace Toxic Elements in Milk Based on Combining $Fe_3O_4$ Nanoparticles Accelerated UV Fenton-like Digestion and Solid Phase Extraction

Xi Ai,[†] Li Wu,[‡] Mengni Zhang,[†] Xiandeng Hou,[†,‡] Lu Yang,[§] and Chengbin Zheng*[,†]

[†]Key Laboratory of Green Chemistry & Technology of MOE, College of Chemistry, Sichuan University, Chengdu, Sichuan 610064, People's Republic of China

[‡]Analytical & Testing Center, Sichuan University, Chengdu, Sichuan 610064, People's Republic of China

[§]Chemical Metrology, Measurement Science and Standards, National Research Council Canada, Ottawa, Ontario K1A 0R6, Canada

Supporting Information

**ABSTRACT:** A UV Fenton-like digestion method was developed first time for a complete digestion of milk samples by using 1.6 g $L^{-1}$ $Fe_3O_4$ magnetic nanoparticles, 0.2% (v/v) nitric acid, and 6% (w/w) $H_2O_2$. During the digestion, the liberated As-, Sb-, and Bi-containing species were preconcentrated onto the surface of $Fe_3O_4$ magnetic nanoparticles, which were conveniently separated with a hand-held magnet and subsequently dissolved in hydrochloric acid prior to hydride generation atomic fluorescence spectrometric detection. Owing to the integration of UV Fenton-like digestion, solid phase extraction, and magnetic separation into a single step, the developed method significantly simplifies sample preparation steps and reduces chemical consumption and hazardous waste. Limits of detection of 0.0015, 0.0022, and 0.0025 $\mu$g $L^{-1}$ were obtained for As, Sb, and Bi, respectively, using a 50 mL milk sample. The method was applied to the determination of these elements in a Certified Reference Material and milk samples.

**KEYWORDS:** *$Fe_3O_4$ MNPs, Fenton reaction, sample pretreatment, hydride generation, solid phase extraction*

## INTRODUCTION

Generally, the accurate and precise determination of toxic or essential elements in food samples involves a sample pretreatment step (e.g., digestion, separation, and concentration) and a signal acquisition step. The performance of the latter has been significantly improved in recent years; however, the sample pretreatment techniques have changed little. Unfortunately, sample pretreatment not only seriously affects the accuracy and reproducibility of final results but also generates wastes which are toxic and have adverse effects on the environment. Consequently, there is a growing interest in developing green sample pretreatment procedures that produce less hazardous wastes to the environment.[1−4] For the determination of trace metals in solid or organic matrix food samples by atomic spectrometry, samples need to be digested into homogeneous aqueous solutions prior to their analyses. Typically, digestion is carried out by either open-vessel or closed-vessel techniques with relative large amounts of concentrated acids (e.g., HCl, $HNO_3$, $H_2SO_4$) at high temperature conditions.[5−10] Major drawbacks of open-vessel digestion techniques include the potential analyte loss and generation of toxic acid mist through volatilization. Closed-vessel digestion techniques, especially microwave assisted-digestion, can reduce digestion time, minimize analyte loss, and alleviate toxic wastes. However, the concentrated mineral acids in the digested solutions are not favorable to the subsequent measurements, thus, a tedious and time-consuming procedure of separation and concentration is needed, such as extraction and evaporation.

UV photo-oxidation is considered as a green alternative for the digestion of organic matrix sample.[11] Compared to the conventional acid digestion, only small amounts of reagents are required. Thus, the potential pollution is significantly minimized, which benefits the operator and the environment. In general, a few hours are needed for a complete digestion of samples in typical UV digestion (UVD).[11] As a result, microwave assistance[12−14] was frequently applied in this system to improve the digestion efficiency. The Fenton reaction may be considered as one of the most efficient and advanced oxidation techniques because of its long historical association with degradation of organic compounds and other pollutants.[15−17] Similar to UVD, the active species (for example, $^{\bullet}OH$) are produced by the reduction of $H_2O_2$ with Fe(II) or other transition metal ions at a suitable pH range. As a result, Fenton reaction has been frequently combined with UVD to significantly improve the degradation efficiencies of pollutants and reduce the degradation time.[18,19] Although homogeneous Fenton reaction using Fe(II) or other transition metal ions is of high efficiency, it remains several disadvantages including narrow working pH range (2.5−3.5) and the accumulation of large excess of unrecyclable transition metals containing sludge to environment.[20] To overcome these drawbacks, the development of heterogeneous Fenton reaction such as using solid iron oxides is gaining popularity as an alternative to homogeneous Fenton reaction.[21,22] Unfortunately, additional energies are required due to their weak catalytic activity of bulk materials.[23]

Received: April 8, 2014
Revised: July 24, 2014
Accepted: July 29, 2014
Published: July 29, 2014

ACS Publications © 2014 American Chemical Society



dx.doi.org/10.1021/jf501638k | J. Agric. Food Chem. 2014, 62, 8586−8593

Despite its 120-year history, Fenton reaction technique has been continuously improved over the last of a few decades. Recently, an intriguing oxidase-mimic property of $Fe_3O_4$ magnetic nanoparticles (MNPs) which can convert $H_2O_2$ into $^{\bullet}OH$ radicals to efficiently break down organic substances, was discovered by Yan et al.[24] Other nanomaterials have also attracted attention on their use for the degradation of various organic compounds.[25−29] Despite an increased interest in the Fenton reaction over the past 50 years, applications in sample pretreatment have remained limited. Recently, Shelor et al.[30] reported an interesting study on the use of homogeneous Fenton reaction for the digestion of milk prior to the determination of iodine by isotope dilution inductively coupled plasma mass spectrometry (ID ICP-MS), but the whole digestion had to be held in an oven overnight at 60 °C. On the basis of previous studies,[24−30] it is suggested that the performance of UV Fenton digestion (FD) may be significantly improved by the oxidase activity of $Fe_3O_4$ MNPs. However, no such attempt has emerged.

In general, the accurate determination of trace elements in many environmental and biological samples is a challenge even when complete digestion of sample can be realized, because of their very low contents. Thus, numerous preconcentration protocols have been developed to improve the detection limits.[31−33] Among those, solid phase extraction (SPE) using $Fe_3O_4$ MNPs has been proven to be a simple, organic solvent free and environmentally benign technique for the preconcentration of analytes, wherein analytes can be conveniently separated from matrix by using a permanent hand-held magnet.[34−36] In this study, a novel UV Fenton-like digestion (FLD) method using $Fe_3O_4$ MNPs and UV-FD under simple and mild conditions was developed for the determination of trace metals in food samples. The determination of As, Sb, and Bi in milk was selected to evaluate the proposed methodology since these elements are very toxic to humans and animals.[35,36] To the best of our knowledge, this is the first study utilizing $Fe_3O_4$ MNPs as an effective catalyst and adsorbent to accomplish complete digestion of milk, and to integrate UV-FLD, SPE and magnetic separation into a single step. The separated $Fe_3O_4$ MNPs were dissolved in hydrochloric acid prior to hydride generation (HG) AFS detection. The proposed method not only significantly alleviates the disadvantages of conventional acid digestion but also provides unique advantages of excellent digestion efficiency, high sample throughput, green analytical chemistry, and the elimination of tedious separation steps during SPE.

## MATERIALS AND METHODS

**Chemicals.** All reagents used were analytical grade or better. 18.2 MΩ-cm deionized water (DIW) produced by a water purification system (Chengdu Ultrapure Technology Co., LTD, China) was used to prepare solutions throughout the study. Standard solutions were prepared daily by diluting stock solutions (1000 mg $L^{-1}$) of As(III), Sb(III), and Bi(III) that were purchased from National Research Center of China (NRCC, Beijing, China). Thiourea was purchased from Kelong Chemical Reagents Co. (Chengdu, China) and used for prereduction of high oxidation state of As, Sb, and Bi prior to hydride generation. $H_2O_2$ (30%, w/w), HCl, $HNO_3$, KOH, $KBH_4$, $FeCl_2$, $FeCl_3$, $FeSO_4$, and $NH_3{\cdot}H_2O$ were also purchased from Kelong Chemical Reagents Co. $KBH_4$ solution was prepared daily by dissolving a proper amount of solid reagent in 0.5% (w/v) KOH. High-purity argon (Ar) and nitrogen ($N_2$) were obtained from Qiaoyuan Gas Co. (Chengdu, China).

A commercial milk sample (HX) spiked at 20 μg $L^{-1}$ of Sb(III) and 10 μg $L^{-1}$ of As(III) and Bi(III) was used to investigate the optimum experimental conditions. A Certified Reference Material (CRM, milk powder, GBW10017-GSB-8) from Beijing Century Oak Biotechnology Co., Ltd. and four commercial milk products (HX, YL, GM, and MN) bought at the local market were analyzed to evaluate the accuracy of the proposed method.

**Instrumentation.** A homemade UV digestion device consisting of a 15 W low pressure UV mercury lamp (Philips Co., Holland), a cylindrical glass container, a black rubber stopper, and six quartz digestion tubes (11 cm length × 8 mm i.d. × 10 mm o.d.; about 7 mL internal volume) or four bigger quartz digestion tubes (11 cm length × 28 mm × 30 mm o.d.; about 60 mL internal volume) was used to digest milk samples. The lamp and the quartz tubes were tightly bound together and further fastened through the holes made on the stopper, and then jam-packed and housed in the container over which a flow of Ar was passed to eliminate oxygen to avoid ozone generation. The container was wrapped with aluminum foil to reflect UV radiation from the lamp, enhancing digestion efficiency, and protecting the operator.

A commercial double-channel HG nondispersive atomic fluorescence spectrometer (AFS, Model AFS-2202, Beijing Haiguang Instrument Co., Beijing, China) was used for all measurements. This instrument as described in details in previous works[37,38] was equipped with coded high intensity hollow cathode lamps (HCL) of As, Sb, and Bi, a quartz argon−hydrogen flame atomizer and a hydride generator consisting of a four-channel peristaltic pump and a quartz gas liquid separator (GLS). An Agilent 7700x inductively coupled plasma mass spectrometer (ICP-MS) (Aglient Technologies, U.S.A.) was also used to evaluate the proposed method. An inductively coupled plasma optical emission spectrometer (ICP-OES) (ARCOS FHS12, SPECTRO Analytical Instruments GmbH, Germany) was used to determine the concentration of $Fe^{2+}/Fe^{3+}$ leached from $Fe_3O_4$ MNPs. Typical operating conditions for AFS and ICP-MS are summarized in Table S1 (see Section 1 of the Supporting Information, SI).

The size and surface morphology of $Fe_3O_4$ MNPs were characterized by scanning electron microscopy (SEM, JSM-7500F, JEOL, Japan). Wide-angle (10−70°, 40 kV/35 mA) powder X-ray diffraction (XRD) measurements were carried out using a X'Pert Pro X-ray diffractometer (Philips, Holland) with Cu K$\alpha$ radiation ($K$ = 1.5406 Å).

**Preparation and Characterization of $Fe_3O_4$ MNPs.** $Fe_3O_4$ MNPs were prepared following a previous coprecipitation method[39] (See section 2 of the SI). The representative SEM images of the prepared $Fe_3O_4$ MNPs were reported in our previous study,[39] and showed that these MNPs are spherical and homogeneous. The crystalline structure and the purity of the prepared MNPs were further characterized by powder X-ray diffraction. The positions and relative intensities of diffraction peaks agree well with the standard pattern of $Fe_3O_4$ indexed from the JCPDS 75-1609 card.

**$Fe_3O_4$ MNPs Accelerated UV Fenton-like Digestion.** Digestion of milk samples using the proposed method was performed for five samples and one blank simultaneously. One milliliter of each tested milk sample was transferred to individual quartz digestion tube, and then 8.0 mg of $Fe_3O_4$ MNPs with diameter of 30 nm, 1.0 mL of 30% (w/w) $H_2O_2$ and 2.0 mL of DIW were added. The contents in each tube were mixed on a vortex mixer (XH-B, Jiangsu Kangjian Medical Apparatus Co., Ltd., China). The mixture was acidified with 10 μL of $HNO_3$ and subsequently diluted to 5 mL with DIW. The digestion tubes were capped loosely and inserted into the UVD device, and allowed to expose to UV irradiation for 60 min. After the UV irradiation, $Fe_3O_4$ MNPs were deposited onto the bottom of the digestion tube with the aid of a permanent hand-held magnet. The supernatant was discarded, and the residual MNPs were directly dissolved in 0.3 mL of HCl and diluted to 5 mL solution with thiourea solution prior to analysis by HG-AFS.

In order to demonstrate the feasibility of both digestion and solid phase extraction, 10 mL of milk and proportional amounts of MNPs, $H_2O_2$ and $HNO_3$ were added into a 60 mL quartz digestion tube and operated using the above-described procedure except that the residual

MNPs were dissolved and diluted to 2.5 mL solution with thiourea prior to analysis.

**Microwave Assisted Digestion.** In order to evaluate the accuracy of the proposed method, a microwave assisted digestion method was employed to digest milk samples prior to their determination by ICP-MS. Briefly, each 5 mL of the tested milk samples, 10 mL of concentrate nitric acid and 5 mL of 30% (m/v) hydrogen peroxide were added into precleaned Teflon vessels. Sample blanks were processed along with the samples. The vessels were closed, fastened, and then placed in a microwave oven (Master 40, Shanghai Sineo Microwave Chemistry Technology Co., China) for microwave-assisted digestion. The digestion program was performed as follows: 5 min at 130 °C and 2200 W; 10 min at 150 °C and 2200 W; and 15 min at 180 °C and 2200 W. After cooling, the caps were removed and the digests were transferred to precleaned 50 mL volume Teflon tubes. The digests were then diluted to 50 mL with DIW prior to analysis by ICP-MS.

**Analytical Procedure and Data Analysis.** Quantification of As, Sb, and Bi was accomplished by flow injection HG-AFS, which is similar to our previous works.[37,38] Briefly, 2 mL of tested solution was initially directed to the sample loop through a six-port valve by a peristaltic pump. The valve was activated to pass the carrier solution (3% (v/v) HCl solution) to flush the digested solution to mix with 2% (m/v) $KBH_4$ solution containing 0.5% (m/v) KOH for the generation of As, Sb, and Bi hydrides. Finally, the sample was flushed into a GLS by the carrier solution and Ar carrier gas, wherein the resultant hydrides were separated from liquid phase and then introduced into the AFS for detection. Peak area signal of the atomic fluorescence intensity was recorded.

For comparison purpose, samples were also digested using a conventional microwave oven and analyzed by ICP-MS. Statistical analysis of *t* test was applied to the results obtained using the proposed method in the Certified Reference Material in order to validate the method.

## RESULTS AND DISCUSSION

**Experiment Design and Possible Reaction Mechanism.** An initial attempt was made to integrate conventional UVD and FD for the digestion of milk sample aiming to achieve high sample throughput, minimize chemical consumption, and analyte loss, and alleviate interference on the subsequent hydride generation. Unfortunately, complete digestion of a milk sample was not possible under conditions of 5 mL mixture containing 1 mL of milk, 100 $\mu$L of 0.1 M $Fe^{2+}$, 1 mL of 30% (w/w) $H_2O_2$, and 20 $\mu$L of $HNO_3$ even with a long digestion time of 6 h. Since $Fe_3O_4$ MNPs can catalytically generate $^{\bullet}OH$ radicals from $H_2O_2$ for a rapid degradation of complex organic substances, 20 mg of $Fe_3O_4$ MNP with diameter of 80 nm was thus added into 5 mL mixture containing 1 mL of milk, 1 mL of 30% (w/w) $H_2O_2$ and 20 $\mu$L of $HNO_3$. This mixture was subsequently exposed to UV irradiation. The milk solution turned clear and transparent within 90 min.

To investigate the possible mechanism of the above reaction, free iron ion concentration in the leaching solution was determined by ICP-AES. $Fe_3O_4$ MNPs with diameter of 30 nm were incubated under typical experimental conditions of 0.2% (v/v) $HNO_3$ and 6% (w/w) $H_2O_2$ for 60 min, and then removed by a hand-held magnet. The iron content of the leaching solution was found to be 0.45 mM, which agrees well with the amount required in the conventional Fenton reaction.[15,16,33] A comparison study to evaluate the digestion efficiencies induced by the leaching solution of $Fe_3O_4$ MNPs, 0.45 mM $FeSO_4$, or 10 mg of $Fe_3O_4$ with diameter of 30 nm, was performed by using each 5 mL mixture containing 1 mL milk sample, 6% (w/w) $H_2O_2$ and 0.2% (v/v) $HNO_3$. As shown in Figure 1, the milk sample was still opaque in the case of using either the leaching solution (Figure 1A) or 0.45 mM $FeSO_4$ (Figure 1B) even with the digestion time longer than 120 min, whereas it became clear and transparent within 60 min with use of $Fe_3O_4$ MNPs (Figure 1C). This observation indicates that the digestion activity provided by the MNPs is not only generated from the iron ions leaching into solution, but also attributed to the MNPs. The role of UV irradiation in the digestion was investigated by comparing the digestion efficiencies that carried out with and without UV irradiation, respectively. In the absence of UV, the tested milk samples could not be completely digested within 8 h with use of 30 nm of $Fe_3O_4$ MNPs as catalyst, confirming that the generation efficiency of hydroxyl radical was improved in the presence of UV irradiation.

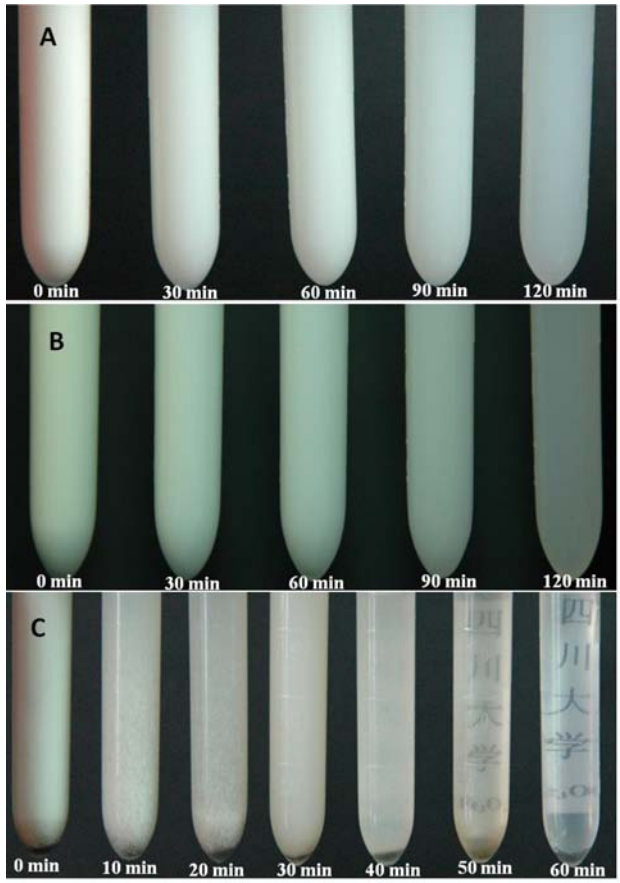


**Figure 1.** UV digestion of 5 mL mixture containing 1 mL milk sample, 6% $H_2O_2$ and 0.2% (v/v) $HNO_3$ using different catalyst. (A) the leaching solution of $Fe_3O_4$ MNPs; (B) 0.45 mM $FeSO_4$ solution; and (C) 10 mg of $Fe_3O_4$ with diameter of 30 nm.

According to the previous studies by Yan,[24] Xu,[25] Luo,[26] and Ai,[39] and their colleagues, this rapid digestion may be mainly attributed to the iron species of $\equiv Fe^{2+}$/ $\equiv Fe^{3+}$, rather than just the free $Fe^{2+}$ ions leached from the MNPs as previously presumed in the conventional Fenton reaction, where $\equiv Fe^{2+}$ and $\equiv Fe^{3+}$ represent Fe(II) and Fe(III) sites on the MNPs surface, respectively. On the basis of the observations from previous studies[24−26,39] and the above study, the reaction mechanism may consist of a dominant digestion and a subsidiary digestion, which have occurred on the surface of MNPs and in the leaching solution, respectively. Figure 1A,B shows that the mixture can be digested to some extent in the


dx.doi.org/10.1021/jf501638k | J. Agric. Food Chem. 2014, 62, 8586−8593

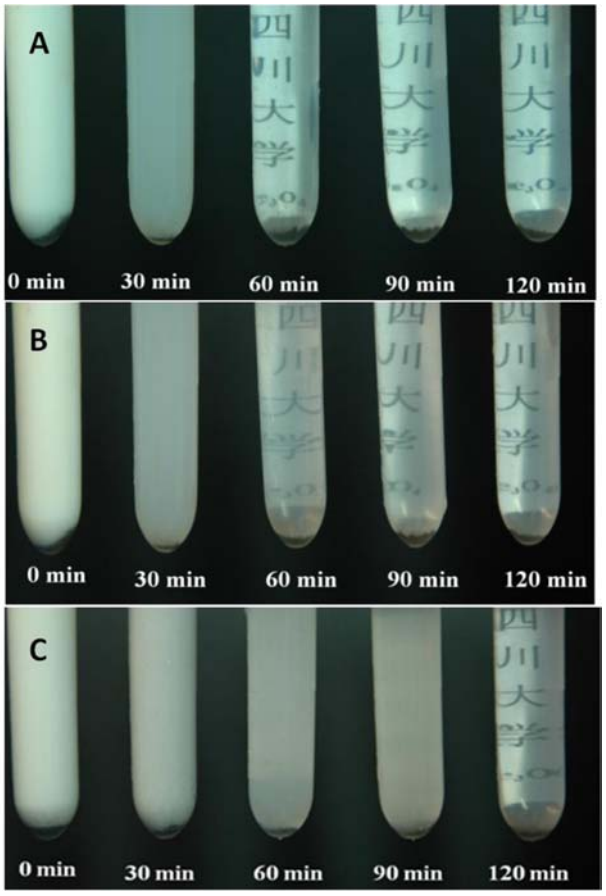


**Figure 2.** Effect of the diameter of $Fe_3O_4$ MNPs on the UV Fenton-like digestion: (A) 30 nm; (B) 80 nm, and (C) 120 nm. Experimental condition: 5 mL of mixture containing 1 mL of spiked milk, 10 mg $Fe_3O_4$ MNPs, 9% (w/w) $H_2O_2$, and 0.3% (v/v) $HNO_3$.

cases using leaching solution or 0.45 mM $FeSO_4$ solution. This supports the generally accepted mechanism of conventional FD[18,19,30] that part of organic compounds (OC) in milk were degraded by free hydroxyl radicals ($^{\bullet}OH_{free}$ and $^{\bullet}OOH_{free}$) produced from free Fe ions. The dominant digestion of the sample has occurred on the surface of MNPs because the milk sample can only be completely digested in the presence of $Fe_3O_4$ MNPs (Figure 1C). $\equiv Fe^{2+}$ react with $H_2O_2$ to generate surface-bound hydroxyl radicals ($^{\bullet}OH_{ads}$) and $\equiv Fe^{3+}$. Then the original $\equiv Fe^{3+}$ together with the generated $\equiv Fe^{3+}$ interact with $H_2O_2$ or $^{\bullet}OOH$ to produce more $\equiv Fe^{2+}$, which further improve the generation of $^{\bullet}OH_{ads}$. Moreover, the $^{\bullet}OH_{ads}$ can react with $H_2O_2$ to produce $^{\bullet}OOH_{ads}$. Finally, the OC of milk were adsorbed onto the surface of MNPs and then efficiently decomposed to $CO_2$ and $H_2O$ by $^{\bullet}OH_{ads}/^{\bullet}OOH_{ads}$ on the surface of MNPs.

**Experimental Conditions for MNP Based Digestion.** In order to investigate the effect of diameter of MNPs on the milk digestion and to gain further insight into the role played by the MNPs in the proposed method. $Fe_3O_4$ MNPs with diameter of 30, 80, and 120 nm were tested to digest the milk mixture under the same experimental conditions, as shown in Figure 2. Interestingly, catalytic activity of $Fe_3O_4$ MNPs was clearly decreased with increasing of its particle diameter, and the milk solution can be completely digested within 60 min using MNPs with 30 nm diameters, while a much longer time was required in the case of MNPs with 80 or 120 nm diameters. This much more efficient digestion may be attributed to the fact that smaller MNPs provide higher adsorption capability and more $\equiv Fe^{2+}/\equiv Fe^{3+}$ because of its greater surface-to-volume ratio. $Fe_3O_4$ MNPs with a diameter of 30 nm were thus chosen in all subsequent experiments.

As previously reported, the catalytic activity of $Fe_3O_4$ MNPs is also strongly dependent on the concentrations of $Fe_3O_4$ MNPs and $H_2O_2$ as well as acidity and reaction temperature. Thus, further investigations of these parameters are necessary. The effect of the concentration of MNPs on response is summarized in Figure 3A. The results show that the responses of As, Sb, and Bi increased in a range from 0.4 to 1.6 g $L^{-1}$ $Fe_3O_4$ MNPs, and followed by a plateau at higher concentrations. This is probably due to inefficient digestion at lower concentrations of $Fe_3O_4$ MNPs. A concentration of 1.6 g $L^{-1}$ $Fe_3O_4$ MNPs was chosen for the subsequent experiments. The effects of concentrations of $H_2O_2$ and $HNO_3$ on the digestion efficiencies of milk samples are presented in Figure 3B,C, respectively. The AFS responses increased as $H_2O_2$ concentration increased from 0 to 3% (w/w) and reached a plateau at higher concentrations. Consequently, the concentration of 6% (w/w) $H_2O_2$ was selected for all subsequent experiments in a consideration of achieving efficient digestion and the minimization of $H_2O_2$ consumption. The responses for As(III), Sb(III), and Bi(III) increased as $HNO_3$ concentration increased from 0 to 0.2% (v/v), remained relatively stable in the range of 0.2−0.5% (v/v), and then decreased at higher concentrations. Low acidity results in low catalytic activity of the $Fe_3O_4$ MNPs and insufficient digestion of milk, while high acidity leads to dissolution of MNPs and thus decreases its catalytic activity. Consequently, a concentration of 0.2% (v/v) of $HNO_3$ was chosen for further studies, which is much lower than that needed in the conventional acid digestion and benefits the reduction of chemical consumption and subsequent hydride generation.

The digestion time is usually reduced by increasing the digestion temperature during UVD.[12] To gain insight into the effect of temperature on digestion, a mercury thermometer was inserted into the quartz digestion tube to measure the temperature. The temperature was found to increase to about 65 °C after 20 min of UV irradiation and remained relatively stable at longer irradiation times. Therefore, the effect of temperature on the digestion time was investigated by putting the UVD device in a water bath to conveniently control the digestion temperature at 30, 40, 60, 70, and 90 °C, respectively. The results show that the digestion time was reduced with increased temperature from 30 to 70 °C. However, dark brown floccules were formed and the mixture could not be completely digested at 90 °C. This phenomenon may be resulted from the fact that the proteins in milk solution were denaturized and deposited onto the bottom of digestion tube at this temperature. Fortunately, on the basis of the above results, the optimal digestion temperature can be achieved with use of UV lamp only, and thus no additional heating source is required, which significantly simplified the operational process and experimental setup.

The effect of digestion time on response was investigated under the previously optimized conditions of 6% (w/w) $H_2O_2$, 0.2% (v/v) of $HNO_3$, and 1.6 g $L^{-1}$ of 30 nm $Fe_3O_4$ MNPs. The effect of digestion time on response is summarized in Figure 3D. It is evident that maximum responses can be achieved with a 40 min digestion or longer. Sixty min of


dx.doi.org/10.1021/jf501638k | J. Agric. Food Chem. 2014, 62, 8586−8593

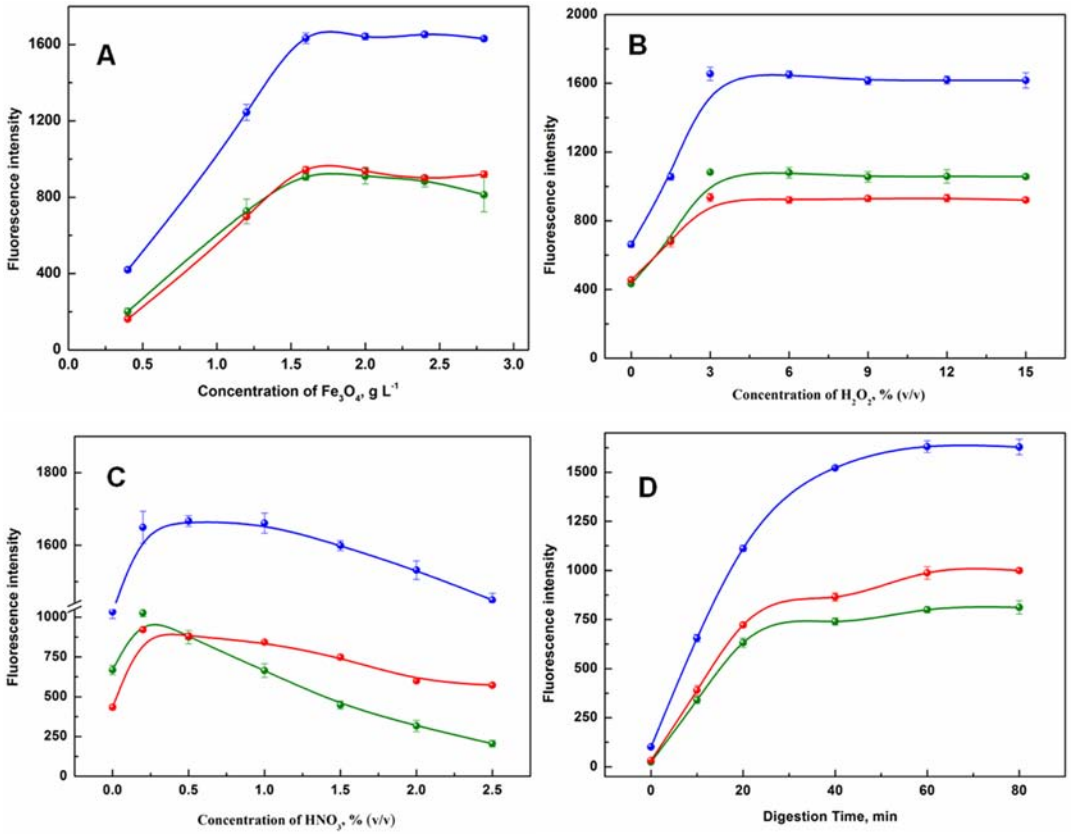


**Figure 3.** Effects of experimental conditions on the $Fe_3O_4$ MNPs accelerated, and UV-induced Fenton-like digestion (blue, As; red, Sb; green, Bi). (A) effect of the concentration of $Fe_3O_4$; (B) effect of the concentration of $H_2O_2$; (C) effect of the concentration of $HNO_3$; and (D) effect of the digestion time. Error bars indicate standard error of the mean ($n$ = 5).

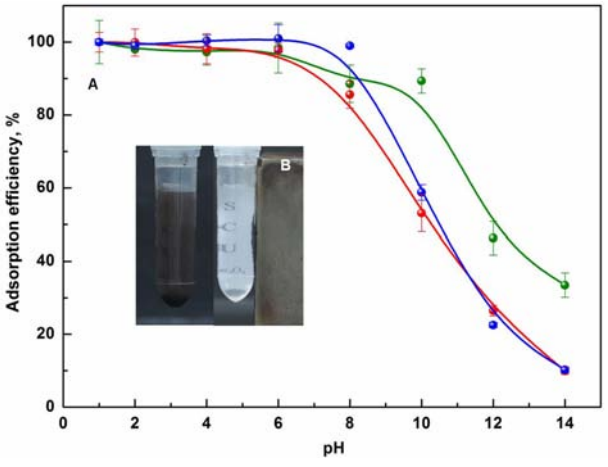


**Figure 4.** (A) Effect of pH of sample solution on the adsorption efficiencies of As(III), Sb(III), and Bi (III) (blue, As; red, Sb; green, Bi; $n$ = 5, error bars indicate standard error of the mean); and (B) visual demonstration of the feasibility of magnetic separation of the prepared $Fe_3O_4$ MNPs.

digestion time was thus chosen for all subsequent experiments to ensure a complete digestion.

**Experimental Conditions for $Fe_3O_4$ MNPs Based Solid Phase Extraction.** In order to improve limits of detection of the proposed method, $Fe_3O_4$ MNPs were used not only as a catalyst to improve digestion, but also as an adsorbent to preconcentrate analytes. SPE efficiency for metals is normally dependent on the pH of the sample solution and the adsorption time. Therefore, 50 mL mixture containing 10 mL spiked milk was used to investigate effects of these parameters on the adsorption efficiencies of As(III), Sb(III), and Bi(III). The adsorption efficiency was estimated from a comparison of the relative concentrations of analytes in the tested solution and in its supernatant after SPE. In order to avoid the dissolution of MNPs, the effect of pH on the adsorption efficiencies of analyte ions was studied in a range of pH 1.0−14.0. The adsorption efficiency was estimated from a comparison of the relative concentrations of analytes in the tested standard solution and in its supernatant after the adsorption by $Fe_3O_4$ MNPs. As shown in Figure 4A, all these tested analytes can be efficiently adsorbed in the pH range of 1.0−6.0, which agree well with those reported earlier.[40,41] This optimum pH range is particularly beneficial, since tedious pH adjustment is eliminated prior to analysis because the pH value of the digested sample solution is about 2, within this optimum pH range.

**Table 1. Figures of Merit**

| | without preconcentration | preconcentration |
|---|---|---|
| As/LOD, $\mu$g $L^{-1}$ | 0.027 | 0.0015 |
| Sb/LOD, $\mu$g $L^{-1}$ | 0.038 | 0.0022 |
| Bi/LOD, $\mu$g $L^{-1}$ | 0.040 | 0.0025 |
| As[a]/precision ($n$ = 9), % RSD | 2.4 | 5.2 |
| Sb[a]: precision ($n$ = 9), % RSD | 3.6 | 4.4 |
| Bi[a] precision ($n$ = 9), % RSD | 4.0 | 5.1 |

[a]5 $\mu$g $L^{-1}$ (without preconcentration); 0.5 $\mu$g $L^{-1}$ (preconcentration)


dx.doi.org/10.1021/jf501638k | J. Agric. Food Chem. 2014, 62, 8586−8593

**Table 2. Analytical Results of As, Sb, and Bi in Milk Samples**

| sample | added, $\mu$g L$^{-1}$ | | | detected[a,b] $\mu$g L$^{-1}$ | | | recovery, % | | |
|---|---|---|---|---|---|---|---|---|---|
| | As | Sb | Bi | As | Sb | Bi | As | Sb | Bi |
| HX | 10 | 20 | 10 | 10.5 ± 0.2 (10.0 ± 0.1) | 17.7 ± 0.8 (18.8 ± 0.6) | 8.9 ± 0.5 (10.2 ± 0.3) | 105 | 88 | 89 |
| YL | 10 | 20 | 10 | 10.6 ± 0.1 (9.8 ± 0.3) | 18.0 ± 0.6 (19.5 ± 0.4) | 9.2 ± 0.5 (10.1 ± 0.2) | 106 | 90 | 92 |
| GM | 10 | 20 | 10 | 10.6 ± 0.4 (9.6 ± 0.3) | 18.2 ± 0.5 (20.2 ± 0.5) | 8.7 ± 0.2 (9.7 ± 0.2) | 106 | 91 | 87 |
| MN | 10 | 20 | 10 | 10.3 ± 0.2 (10.5 ± 0.4) | 18.0 ± 0.8 (19.5 ± 0.3) | 9.3 ± 0.4 (10.3 ± 0.1) | 103 | 90 | 93 |
| GBW10017-GSB-8[c] | 0.031 ± 0.007[d] | | | 0.030 ± 0.002 | | | | | |

[a]Mean and standard deviation ($n$ = 3). [b]Detected by ICP-MS after microwave assisted digestion. [c]mg kg$^{-1}$. [d]Certified value.

The adsorption time counted after the digestion procedure, and its effect on adsorption efficiencies of As(III), Sb(III), and Bi(III) was investigated. The results show that adsorption equilibriums were obtained within a short time of less than 1 min. This remarkably fast adsorption actually can be attributed to the fact that the adsorption must be synchronized with the digestion. Therefore, no additional adsorption time was needed for subsequent experiments, and the sample throughput is increased.

The adsorption capacities of the prepared $Fe_3O_4$ MNPs for As(III), Sb(III), and Bi(III) were also evaluated via spiking various amounts of these analytes into 5 mL milk sample solutions and with each 8 mg $Fe_3O_4$ MNPs added. Saturation of the adsorption capacities of $Fe_3O_4$ was found to be 10, 5, and 8 mg g$^{-1}$ for As(III), Sb(III), and Bi(III), respectively, which can meet the requirement of routine analysis. Magnetic separation is simpler, faster, and more convenient than centrifuge separation. In order to visually demonstrate the feasibility of magnetic separation of the prepared $Fe_3O_4$ MNPs, the magnetic separation of 8 mg of $Fe_3O_4$ after complete digestion and adsorption of analytes ions in 5 mL sample solution is shown in Figure 4B. This fast magnetic separation arising from the strong magnetic response of the prepared $Fe_3O_4$ MNPs significantly simplified the separation procedure, eliminated organic solvent and reduced overall analysis time.

**Optimization of the HG-AFS Determination.** As a sample introduction technique, HG provides unmatched sensitivity and analyte−matrix separation, elemental specificity, and high sample introduction efficiency for atomic spectrometry, and is enjoying increasing interest for inorganic trace analysis. Previous study[42] found that HG efficiencies of As, Sb, and Bi were affected by many factors, especially $KBH_4$ concentration, concentration of prereducing reagent and the reaction medium. Therefore, these factors were carefully investigated, as shown in Figure S1 (see section 3 of the SI). Six percent (v/v) HCl, 2% (m/v) $KBH_4$, 1.0% (m/v) thiourea, and 10 min of prereduction time were finally chosen for better responses.

Since Fe MNPs were dissolved together with analytes and then directly reacted with $KBH_4$ for the generation of their hydrides, the effects of $Fe^{2+}/Fe^{3+}$ concentration on the HG efficiencies of 10 $\mu$g L$^{-1}$of As, Sb and Bi were thus investigated. No significant interferences was observed using the proposed method, even at a concentration of $Fe^{2+}/Fe^{3+}$ as high as 2 g L$^{-1}$.

**Analytical Performance.** A series of 5 mL mixture containing 1 mL milk and various concentrations of As(III), Sb(III), and Bi(III) were analyzed to establish the calibration curves under optimal experimental conditions, as shown in Figure S2A (see Section 4 of the SI). The linear coefficient for each curve is higher than 0.999. The limits of detection (LODs) defined as the analyte concentration equivalent to three times of the standard deviation of 11 measurements of a blank solution, were 0.027, 0.038, and 0.040 $\mu$g L$^{-1}$ for As, Sb, and Bi, respectively. Precisions of replicate measurements, expressed as relative standard deviations (RSDs, $n$ = 9), are better than 6% at 5 $\mu$g L$^{-1}$ analytes concentrations. In order to evaluate the improvement of sensitivity and LODs by $Fe_3O_4$ based SPE, a series of 50 mL of mixture containing 10 mL milk and various concentrations of As(III), Sb(III), and Bi(III) were used. After digestion, the MNPs were dissolved and diluted to a final 2.5 mL prior to analysis. The obtained calibration curves were described in Figure S2B (see section 4 of the SI). LODs of 0.0015, 0.0022, and 0.0025 $\mu$g L$^{-1}$ were obtained for As, Sb, and Bi, respectively, providing 18-, 17-, and 16-fold improvements over those obtained from this method without preconcentration. The analytical figures of merit achieved are summarized in Table 1.

**Preliminary Analytical Application.** Four milk samples obtained from a local market were analyzed to check the accuracy of the proposed method. Analytical results are summarized in Table 2 using external standard calibration. It was necessary to spike all the original milk samples with 10 $\mu$g L$^{-1}$ As, 20 $\mu$g L$^{-1}$ Sb and 10 $\mu$g L$^{-1}$ Bi because their endogenous concentrations were not detectable by the proposed method. Good spike recoveries of arsenic (103−106%) for these samples were achieved, and the analytical results are in good agreement with those obtained by use of microwave assisted digestion and ICP-MS detection, confirming the accuracy of the proposed methodology for routine elemental analysis of milk. Slightly lower recoveries for Sb and Bi maybe due to sample matrix effects, and their recoveries could be increased to 92−101% when a longer digestion time (80 min) was used. The accuracy of the proposed technique was further demonstrated by the determination of As in a Certified Reference Material (milk powder, GBW10017-GSB-8), as shown in Table 2. The $t$ test showed that the analytical results obtained by the proposed method were not significantly different from the certified value for As at the confidence level of 95%.

In summary, a unique and green method combining heterogeneous UV Fenton-like digestion, solid phase extraction, and magnetic separation was developed for the determination of trace toxic elements in milk. This method not only overcomes disadvantages associated with conventional acid digestion and UV digestion, but also provides several unique advantages including: simpler operation, greener analytical chemistry, higher sample throughput, cost-effectiveness, and reduction of chemical consumption. In addition, a tedious and time-consuming separation procedure was simplified in the proposed method because of the simple and convenient magnetic separation.

## ■ ASSOCIATED CONTENT

### Supporting Information

Instrumental parameters, preparation of $Fe_3O_4$, microwave assisted digestion of milk samples, optimization of the HG-AFS determination, and calibration curves. This material is available free of charge via the Internet at http://pubs.acs.org.

## ■ AUTHOR INFORMATION


### Corresponding Author

*Tel: +862885415810; fax: +862885412907; e-mail: abinscu@scu.edu.cn.


### Author Contributions

The manuscript was written through contributions of all authors. All authors have given approval to the final version of the manuscript.


### Funding

The authors gratefully acknowledge the National Nature Science Foundation of China (No. 21128006) for financial support. C.B.Z. is grateful for the financial support by Ministry of Education of China through Grant NCET-11-0361.


### Notes

The authors declare no competing financial interest.

## ■ ACKNOWLEDGMENTS


We also thank Dr. Xi Wu of Analytical & Testing Center for technical support.


## ■ REFERENCES


(1) Flores, É. M. M.; Barin, J. S.; Paniz, J. N. G.; Medeiros, J. A.; Knapp, G. Microwave-assisted sample combustion: A technique for sample preparation in trace element determination. *Anal. Chem.* **2004**, *76*, 3525−3529.

(2) Keith, L. H.; Gron, L. U.; Young, J. L. Green analytical methodologies. *Chem. Rev.* **2007**, *107*, 2695−2708.

(3) Mar, J. L. G; Reyes, L. H.; Rahman, G. M. M.; Kingston, H. M. S. Simultaneous extraction of arsenic and selenium species from rice products by microwave-assisted enzymatic extraction and analysis by ion chromatography-inductively coupled plasma-mass spectrometry. *J. Agric. Food Chem.* **2009**, *57*, 3005−3013.

(4) Zheng, C. B.; Yang, L.; Sturgeon, R. E.; Hou, X. D. UV Photochemical vapor generation sample introduction for determination of Ni, Fe, and Se in biological tissue by isotope dilution ICPMS. *Anal. Chem.* **2010**, *82*, 3899−3904.

(5) Mesko, M. F.; Pereira, J. S. F.; Moraes, D. P.; Barin, J. S.; Mello, P. A.; Paniz, J. N. G.; Nóbrega, J. A.; Korn, M. G. A.; Flores, E. M. M. Focused Microwave-induced combustion: A new technique for sample digestion. *Anal. Chem.* **2010**, *82*, 2155−2160.

(6) López-García, I.; Vicente-Martínez, Y.; Hernández-Córdoba, M. Nonchromatographic speciation of selenium in edible oils using dispersive liquid−liquid microextraction and electrothermal atomic absorption spectrometry. *J. Agric. Food Chem.* **2013**, *61*, 9356−9361.

(7) Araújo, G. C. L.; Nogueira, A. R. A.; Nóbrega, J. A. Single vessel procedure for acid-vapour partial digestion in a focused microwave: Fe and Co determination in biological samples by ETAAS. *Analyst* **2000**, *125*, 1861−1864.

(8) Chen, L. G.; Song, D. Q.; Tian, Y.; Ding, L.; Yu, A. M.; Zhang, H. Q. Application of on-line microwave sample-preparation techniques. *TrAC, Trends Anal. Chem.* **2008**, *27*, 151−159.

(9) Silvestre, D. M.; Nomura, C. S. Direct determination of potentially toxic elements in rice by SS-GF AAS: Development of methods and applications. *J. Agric. Food Chem.* **2013**, *61*, 6299−6303.

(10) Peixoto, R. R. A.; Oliveira, A.; Cadore, S. Multielemental determinations in chocolate drink powder using multivariate optimization and ICP OES. *J. Agric. Food Chem.* **2012**, *60*, 8117−8122.

(11) Capelo-Martínez, J. L.; Ximénez-Embún, P.; Madrid, Y.; Cámara, C. Advanced oxidation processes for sample treatment in atomic spectrometry. *TrAC, Trends Anal. Chem.* **2004**, *23*, 331−340.

(12) Florian, S.; Knapp, G. High-temperature, microwave-assisted UV digestion: A promising sample preparation technique for trace element analysis. *Anal. Chem.* **2001**, *73*, 1515−1520.

(13) Pereira, S. F.; Picoloto, R. S.; Pereira, L. S. F.; Guimarães, R. C. L.; Guarnieri, R. A.; Flores, E. M. M. High-efficiency microwave-assisted digestion combined to in situ ultraviolet radiation for the determination of rare earth elements by ultrasonic nebulization ICPMS in crude oils. *Anal. Chem.* **2013**, *85*, 11034−11040.

(14) Angeli, V.; Ferrari, C.; Longo, I.; Onor, M.; D'Ulivo, A.; Bramanti, E. Microwave-assisted photochemical reactor for the online oxidative decomposition and determination of *p*-hydroxymercurybenzoate and its thiolic complexes by cold vapor generation atomic fluorescence detection. *Anal. Chem.* **2011**, *83*, 338−343.

(15) Rivas, F. J.; Beltrán, F. J.; Gimeno, O.; Frades, J. Treatment of olive oil mill wastewater by Fenton's reagent. *J. Agric. Food Chem.* **2001**, *49*, 1873−1880.

(16) Pignatello, J. J.; Liu, D.; Huston, P. Evidence for an additional oxidant in the photo-assisted Fenton reaction. *Environ. Sci. Technol.* **1999**, *33*, 1832−1839.

(17) Morelli, R.; Russo-Volpe, S.; Bruno, N.; Lo Scalzo, R. Fenton-dependent damage to carbohydrates: Free radical scavenging activity of some simple sugars. *J. Agric. Food Chem.* **2003**, *51*, 7418−7425.

(18) Vermilyea, A. W.; Voelker, B. M. Photo-Fenton reaction at near neutral pH. *Environ. Sci. Technol.* **2009**, *43*, 6927−6933.

(19) Dong, M. M.; Rosario-Ortiz, F. L. Photochemical formation of hydroxyl radical from effluent organic matter. *Environ. Sci. Technol.* **2012**, *46*, 3788−3794.

(20) Cheng, M. M.; Ma, W. H.; Li, J.; Huang, Y. P.; Zhao, J. C. Visible-light-assisted degradation of dye pollutants over Fe(III)-loaded resin in the presence of $H_2O_2$ at neutral pH values. *Environ. Sci. Technol.* **2004**, *38*, 1569−1575.

(21) Deng, J. H.; Jiang, J. Y.; Zhang, Y. Y.; Lin, X. P.; Du, C. M.; Xiong, Y. $FeVO_4$ as a highly active heterogeneous Fenton-like catalyst towards the degradation of Orange II. *Appl. Catal. B: Environ.* **2008**, *84*, 468−473.

(22) Costa, R. C. C.; Moura, F. C. C.; Ardisson, J. D.; Fabris, J. D.; Lago, R. M. Highly active heterogeneous Fenton-like systems based on $Fe^0/Fe_3O_4$ composites prepared by controlled reduction of iron oxides. *Appl. Catal. B: Environ.* **2008**, *83*, 131−139.

(23) Zhang, G. K.; Gao, Y. Y.; Zhang, Y. L.; Guo, Y. D. $Fe_2O_3$-pillared rectorite as an efficient and stable fenton-like heterogeneous catalyst for photodegradation of organic contaminants. *Environ. Sci. Technol.* **2010**, *44*, 6384−6389.

(24) Gao, L. Z.; Zhuang, J.; Nie, L.; Zhang, J. B.; Zhang, Y.; Gu, N. W.; Feng, J.; Yang, D. L.; Perrett, S.; Yan, X. Y. Intrinsic peroxidase-like activity of ferromagnetic nanoparticles. *Nat. Nanotechnol.* **2007**, *9*, 577−583.

(25) Luo, W.; Zhu, L. H.; Wang, N.; Tang, H. Q.; Cao, M. J.; She, Y. B. Efficient removal of organic pollutants with magnetic nanoscaled $BiFeO_3$ as a reusable heterogeneous Fenton-like catalyst. *Environ. Sci. Technol.* **2010**, *44*, 1786−1791.

(26) Xu, L. J.; Wang, J. L. Magnetic nanoscaled $Fe_3O_4/CeO_2$ composite as an efficient Fenton-like heterogeneous catalyst for degradation of 4-chlorophenol. *Environ. Sci. Technol.* **2012**, *46*, 10145−10153.

(27) Yang, X. J.; Xu, X. M.; Xu, J.; Han, Y. F. Iron oxychloride (FeOCl): An efficient Fenton-like catalyst for producing hydroxyl radicals in degradation of organic contaminants. *J. Am. Chem. Soc.* **2013**, *135*, 16058−16061.

(28) Navalon, S.; de Miguel, M.; Martin, R.; Alvaro, M.; Garcia, H. Enhancement of the catalytic activity of supported gold nanoparticles for the Fenton reaction by light. *J. Am. Chem. Soc.* **2011**, *133*, 2218−2226.

(29) Navalon, S.; Martin, R.; Alvaro, M.; Garcia, H. Gold on diamond nanoparticles as a highly efficient Fenton catalyst. *Angew. Chem., Int. Ed.* **2010**, *49*, 8403−8407.

(30) Shelor, C. P.; Campbell, C. A.; Kroll, M.; Dasgupta, P. K.; Smith, T. L.; Abdalla, A.; Hamilton, M.; Muhammad, T. W. Fenton digestion of milk for iodinalysis. *Anal. Chem.* **2011**, *83*, 8300−8307.
(31) Date, Y.; Aota, A.; Terakado, S.; Sasaki, K.; Matsumoto, N.; Watanabe, Y.; Matsue, T.; Ohmura, N. Trace-level mercury ion ($Hg^{2+}$) analysis in aqueous sample based on solid-phase extraction followed by microfluidic immunoassay. *Anal. Chem.* **2013**, *85*, 434−440.
(32) Deng, D. Y.; Zhou, J. R.; Ai, X.; Yang, L.; Hou, X. D.; Zheng, C. B. Ultrasensitive determination of selenium by atomic fluorescence spectrometry using nano-$TiO_2$ pre-concentration and in situ hydride generation. *J. Anal. At. Spectrom.* **2012**, *27*, 270−275.
(33) Liu, J. F.; Chao, J. B.; Liu, R.; Tan, Z. Q.; Yin, Y. G.; Wu, Y.; Jiang, G. B. Cloud point extraction as an advantageous preconcentration approach for analysis of trace silver nanoparticles in environmental waters. *Anal. Chem.* **2009**, *81*, 6496−6502.
(34) Chen, L. G.; Wang, T.; Tong, J. Application of derivatized magnetic materials to the separation and the preconcentration of pollutants in water samples. *TrAC, Trends Anal. Chem.* **2011**, *30*, 1095−1108.
(35) Prucek, R.; Tuček, J.; Kolařík, J.; Filip, J.; Marušák, Z.; Sharma, V. K.; Zbořil, R. Ferrate(VI)-induced arsenite and arsenate removal by in situ structural incorporation into magnetic iron(III) oxide nanoparticles. *Environ. Sci. Technol.* **2013**, *47*, 3283−3292.
(36) VanDorn, D.; Ravalli, M. T.; Small, M. M.; Hillery, B.; Andreescu, S. Adsorption of arsenic by iron oxide nanoparticles: a versatile, inquiry-based laboratory for a high school or college science course. *J. Chem. Educ.* **2011**, *88*, 1119−1122.
(37) Zheng, C. B.; Li, Y.; He, Y. H.; Ma, Q.; Hou, X. D. Photo-induced chemical vapor generation with formic acid for ultrasensitive atomic fluorescence spectrometric determination of mercury: Potential application to mercury speciation in water. *J. Anal. At. Spectrom.* **2005**, *20*, 746−750.
(38) Zheng, C. B.; Wu, L.; Ma, Q.; Lv, Y.; Hou, X. D. Temperature and nano-$TiO_2$ controlled photochemical vapor generation for inorganic selenium speciation analysis by AFS or ICP-MS without chromatographic separation. *J. Anal. At. Spectrom.* **2008**, *23*, 514−520.
(39) Ai, X.; Wang, Y.; Hou, X. D.; Yang, L.; Zheng, C. B.; Wu, L. Advanced oxidation using $Fe_3O_4$ magnetic nanoparticles and its application in mercury speciation analysis by high performance liquid chromatography-cold vapor generation atomic fluorescence spectrometry. *Analyst* **2013**, *138*, 3494−3501.
(40) Mishra, M.; Farrell, J. Evaluation of mixed valent iron oxides as reactive adsorbents for arsenic removal. *Environ. Sci. Technol.* **2005**, *39*, 9689−9694.
(41) Jang, M.; Chen, W. F.; Cannon, F. S. Preloading hydrous ferric oxide into granular activated carbon for arsenic removal. *Environ. Sci. Technol.* **2008**, *42*, 3369−3374.
(42) Long, Z.; Chen, C.; Hou, X. D.; Zheng, C. B. Recent advance of hydride generation−analytical atomic spectrometry: Part II—Analysis of real samples. *Appl. Spectrosc. Rev.* **2012**, *47*, 495−517.

JOURNAL OF AGRICULTURAL AND FOOD CHEMISTRY

Article

pubs.acs.org/JAFC

# Water Distribution in Tofu and Application of $T_2$ Relaxation Measurements in Determination of Tofu's Water-Holding Capacity

Teng Li, Xin Rui, Wei Li, Xiaohong Chen, Mei Jiang, and Mingsheng Dong*

College of Food Science and Technology, Nanjing Agricultural University, Nanjing, Jiangsu 210095, People's Republic of China

**ABSTRACT:** Low-field nuclear magnetic resonance (LF-NMR) was introduced for the elucidation of tofu in the present study. After multiexponential analysis of relaxation decays, three water fractions centered at about 1.5−2.6, 24−114, and 132−305 ms were detected and identified as $T_{2b}$, $T_{21}$, and $T_{22}$, respectively. Principal component analysis (PCA) of the data revealed that sample aggregation was dependent on solubility of coagulants and contained anions. Stepwise centrifugation and microwave drying were employed as dehydration methods. Significant correlations were observed between $T_{21}$ and $T_{22}$ relaxation times and water-holding capacity (WHC) in both dehydration processes, which implied LF-NMR measurements could be an efficient method for determination and prediction of tofu's water-holding capacity. Ten linear equations that could be applied in prediction of WHC for tofu were reported. LF-NMR was suggested to be a powerful tool for the study of tofu.

**KEYWORDS:** *tofu, low-field nuclear magnetic resonance, water-holding capacity*

## INTRODUCTION

Tofu or soybean curd is a gel-like food made by adding different coagulants to soymilk.[1] In order to optimize production technologies and expand understanding of the coagulant's effects on tofu formation, various physical and chemical properties of tofu have been studied.[2−4] The ability of tofu to retain water in its matrix, also known as the water-holding capacity (WHC), is of paramount importance as it relates to tofu's yield and sensory attributes. However, due to limited analytical techniques, WHC of tofu has generally been studied in isolation.

In recent years, many instruments have been applied to the study of tofu. Electrical impedance spectroscopy was introduced for the study of tofu's coagulation process by Li et al.[5] Hsieh et al.[6] studied proteomic profiling of the coagulation of soymilk proteins induced by magnesium chloride using two-dimensional polyacrylamide gel electrophoresis. Other technologies, such as scanning electronic microscopy (SEM) and sodium dodecyl sulfate−polyacrylamide gel electrophoresis (SDS−PAGE) have been utilized in the characterization of tofu-making.[7−9] However, the measurement of tofu's WHC is still limited to centrifugation, which is a sample-consuming and destructive method.

Low-field nuclear magnetic resonance (LF-NMR) technologies have been widely applied in food study. Due to the contribution of Bertram et al.,[10,11] LF-NMR measurements have been widely applied in the evaluation of WHC of pork. Besides, the applications of LF-NMR have been successfully expanded to the effects of cooking and different freezing storage conditions on the quality of various meats.[12−15] The relaxation behaviors of different water fractions in water−casein system and milk have been studied in depth by Mariette and co-workers.[16−19] It has been demonstrated that LF-NMR measurement is a highly sensitive method to study changes of water mobility and corresponding water populations during the cooking process of potatoes.[20,21] Bosman and co-workers[22−24] reported that LF-NMR could be used as a powerful tool to evaluate various properties of different types of bread. Although the self-diffusion coefficient of water in $CaCl_2$-induced tofu was reported by Young et al.,[25] the number of water fractions and their spatial locations in different types of tofu are still unknown. Besides, due to the intimate connection between water distribution and microstructure, LF-NMR is assumed to build a bridge between water-related properties to structure-related properties of tofu. Therefore, in the present study, LF-NMR was introduced into the study of water distribution in different types of tofu. Centrifugation and microwave drying were performed to achieve a series of different WHC gradients for each type of tofu. The potential use of LF-NMR for determination and prediction of tofu's WHC were exploited.

## 2. MATERIALS AND METHODS

**Materials.** The coagulants of calcium sulfate (CS), magnesium sulfate (MS), calcium chloride (CC), magnesium chloride (MC), and glucono-$\delta$-lactone (GDL) were obtained from a local food ingredient supplier. All the chemicals were analytical-grade. Commercial soybeans from northeast China were kindly provided by Key Laboratory of Biology and Genetic Improvement of Soybean, Ministry of Agriculture, P. R. China (Nanjing, P. R. China).

**Preparation of Soymilk.** Soybeans were rinsed and soaked in deionized water in a ratio of 1:3 (w/w) for 12 h at 20 °C. Once hydrated, soybeans were rinsed once more and placed into a household soymilk maker BL-747 (Deer Co., Ltd., Guangdong, China) and ground with deionized water in ratios of 1:10 and 1:5 (w/w), respectively, for salt-induced tofu and GDL tofu. After the soymilk maker cycle was completed, okara (soymilk insoluble fiber) was removed by filtering the soymilk through a strainer and passing twice through double layers of cheesecloth. The soymilk was then stored at 4 °C until further use.

Received: April 25, 2014
Revised: August 4, 2014
Accepted: August 5, 2014
Published: August 5, 2014

ACS Publications © 2014 American Chemical Society



dx.doi.org/10.1021/jf503427m | J. Agric. Food Chem. 2014, 62, 8594−8601

**Preparation of Salt-Induced Tofu.** Soymilk was heated to the boiling point, maintained for 3 min with stirring, and cooled to 90 °C. Dispersions of four divalent salt coagulants were prepared at concentration of 3% (w/w) in hot deionized water (90 °C). The prepared coagulant dispersions were added into the soymilk immediately to achieve a final coagulant concentration of 15 mM. As coagulants were added into soymilk, the mixtures were continuously stirred with a stainless steel spoon for 10 s. Then the soymilk was decanted into a water bath for heat preservation at 90 °C for 20 min for better coagulation of soybean proteins. After that, the mixtures were transferred to a wooden mold and pressed in order to obtain tofu curd and exclude the whey. In order to avoid the influences of different pressing pressures on water distribution of salt-induced tofu, all salt-induced tofu was pressed at 0.01 kg/cm$^2$ for 30 min. After pressing, tofu was stored in airtight containers at 4 °C before analysis.

**Preparation of Glucono-$\delta$-lactone Tofu.** For GDL tofu, soymilk was heated to the boiling point, maintained for 3 min with stirring, and cooled to 80 °C, and then 2% (w/w) GDL solution was added to achieve a final concentration of 0.4% (w/w). The mixtures were incubated in a water bath at 80 °C for 30 min. The coagulation of GDL tofu could form automatically without external pressures. The final tofu curd was stored in airtight containers at 4 °C before analysis.

**Vacuum Freeze-Drying Pretreatment of Tofu Samples.** Vacuum freeze-drying (VFD) was employed to pretreat the tofu samples used for evaluation of influence of fat on $T_2$ measurements. The samples were prefrozen at −18 °C for 24 h and then decanted to a Labconco freezone 12 L console freeze-dry system (Labconco Co., Ltd., Kansas City, MO) with temperature of −50 °C for 30 h.

**Centrifugation Treatments of Tofu Curds.** Thirty grams of cylindrical samples were obtained from the central portion of three tofu curds (CS, MC, and GDL) with a stainless cylindrical cutter and placed into a CT15RT centrifugal filter system (Techcomp Co., Ltd., Shanghai, China). Stepwise centrifugation was performed at 420*g*, 650*g*, 1660*g*, 2600*g*, 3740*g*, 5000*g*, 6640*g*, 8400*g*, 10380*g*, 12560*g*, and 14940*g* for 15 min at 20 °C (for GDL and CS tofu). The centrifugation of MC tofu only reached 8400*g* since no significant change of WHC was observed at higher centrifugation force. The weight of released water was subsequently measured. Water-holding capacity was expressed as the ratio of sample weight after centrifugation to initial weight:

$$\text{WHC}\ (\%) = \frac{(A - B)}{A} \times 100 \tag{1}$$

where $B$ is the weight (grams) of water lost from the tofu sample during centrifugation and $A$ is the initial weight (grams) of the sample. Each measurement was performed in triplicate.

**Microwave Treatments of Tofu Curds.** Microwave treatments were employed to provide another way to generate a series of different WHC gradients of tofu. Samples of CS and MC tofu were cut into cuboids of 1.5 cm thick, 15 cm long, and 1.5 cm wide and placed in an EM-309Eb1 microwave oven (Sanyo Co., Ltd., Osaka, Japan). Samples were heated for 30, 45, 60, 75, 90, 105, 120, 135, 150, or 165 s at 600 W. Three replicate tests were carried out for each heating time. WHC was calculated according to eq 1.

**Low-Field Nuclear Magnetic Resonance Measurements.** Low-field nuclear magnetic resonance measurements (LF-NMR) were performed on a 22.4 MHz NMR Analyzer PQ001 (Niumag Co., Ltd., Shanghai, China). After storage at 4 °C for 1 h, the tofu samples were thermostated to 32 °C in a water bath for 20 min. Approximately 2 g of different tofu samples were taken from the middle of tofu curd and placed into 15 mm NMR glass tubes. Then the tubes were inserted in the NMR probe. $T_2$ relaxation times were measured by use of a Carr−Purcell−Meiboom−Gill sequence. The $T_2$ measurements were performed with a $\tau$-value of 150 $\mu$s (time between 90° and 180° pulse). Data from 3000 echoes were acquired as 16 scan repetitions. The repetition time between two successive scans was 3 s. The relaxation measurements were performed at 32 °C.

MultiExp Inv Analysis software (Niumag Co., Ltd., Shanghai, China) was employed for data analysis. This software performs distributed exponential curve fitting. In the time domain, spin−spin relaxation data is presumed to be a sum of exponentials:

$$R_{\text{mag}}(t) = \sum_{j=1}^{n} p_{2j} \exp\left(\frac{-t}{T_{2j}}\right) + e(t) \tag{2}$$

where $R_{\text{mag}}$ is the residual magnetization as a function of acquisition time $t$; $P_{2j}$ and $T_{2j}$ are the transverse relaxation amplitude and time, respectively, of the $j$th component; and $e$ is residual error. MultiExp Inv Analysis software performed multiexponential fitting analysis on the relaxation data according to a modified inversion method of Xiao et al.[26] Plots of relaxation amplitude versus relaxation time were obtained. The relaxation time $T_{2i}$ and its corresponding water population (signal area ratio) $M_{2i}$ were recorded.

**Statistical Analysis.** Principal component analysis (PCA) was performed with the software Simca-P+ (Umetrics AB). PCA was achieved on $T_2$ relaxation data to identify cluster patterns. Statistical analyses were performed with SPSS version 18.0. Linear regression analysis was performed with Origin 8.1. Adjust determination coefficients (adj-$R^2$) were used to evaluate the fitting degree and are defined as

$$\text{adj-}R^2 = 1 - \frac{(n - 1)(1 - R^2)}{n - m} \tag{3}$$

where $R^2$ is the original determination coefficient and $n$ and $m$ are the number of samples and variables, respectively. The significance levels are defined as (*) $p < 0.05$ and (**) $p < 0.01$.

## RESULTS AND DISCUSSION

**LF-NMR Analysis of Different Tofu Curds.** Since oil can be detected by LF-NMR,[25,27] the influence of oil on tofu's $T_2$ measurements should be evaluated before further studies are performed. Although soybean is rich in oil, the final oil content in tofu curd is very limited. Previous data showed that the oil content of final tofu matrix ranged from 1.4% to 2.2% when similar proportion of soybean and water was used.[7] In order to evaluate the influence of constant oil content on tofu's $T_2$ measurements, tofu samples were pretreated by vacuum freeze-drying (VFD) and then measured by LF-NMR. Figure 1 shows the multiexponential fitting relaxation curves of three types of tofu before and after VFD treatments. After pretreatment by VFD, samples presented two weak peaks. The component centered at about 86−100 ms was likely to be the signal of oil in tofu, which accounted for less than 1% compared to that of samples without VFD treatment. Therefore, the influence of oil in tofu on its $T_2$ relaxation measurements is negligible.

A representative LF-NMR $T_2$ measurement distribution of five types of tofu curds (without dehydration treatment) after multiexponential fitting is presented in Figure 2. All five types of tofu samples showed three peaks, and these peaks were identified as $T_{2b}$, $T_{21}$, and $T_{22}$ according to previous assignments.[10,11] The number of fractions was similar to the number detected in meat but lower than that of potato and other plant tissues.[10,11,20,27] $T_{2b}$ was a minor fraction with a relaxation time between 1.5 and 2.6 ms and accounted for only 1−2.5% of total signal. The mean value of $T_{2b}$ relaxation time was about 2 ms regardless of the type of tofu (data not shown). $T_{21}$ was regarded as the major fraction (about 90% of total signal) with a relaxation time of 24−114 ms, while $T_{22}$ was the slowest fraction with a relaxation time of 114−305 ms.

LF-NMR results after multiexponential fitting are shown in Table 1. $T_{21}$ values descended in the following order: GDL > CS > MS > MC > CC. Pronounced differences in $T_{21}$ relaxation times were observed between GDL tofu and salt-induced tofu, which might be explained by their different coagulation


dx.doi.org/10.1021/jf503427m | J. Agric. Food Chem. 2014, 62, 8594−8601

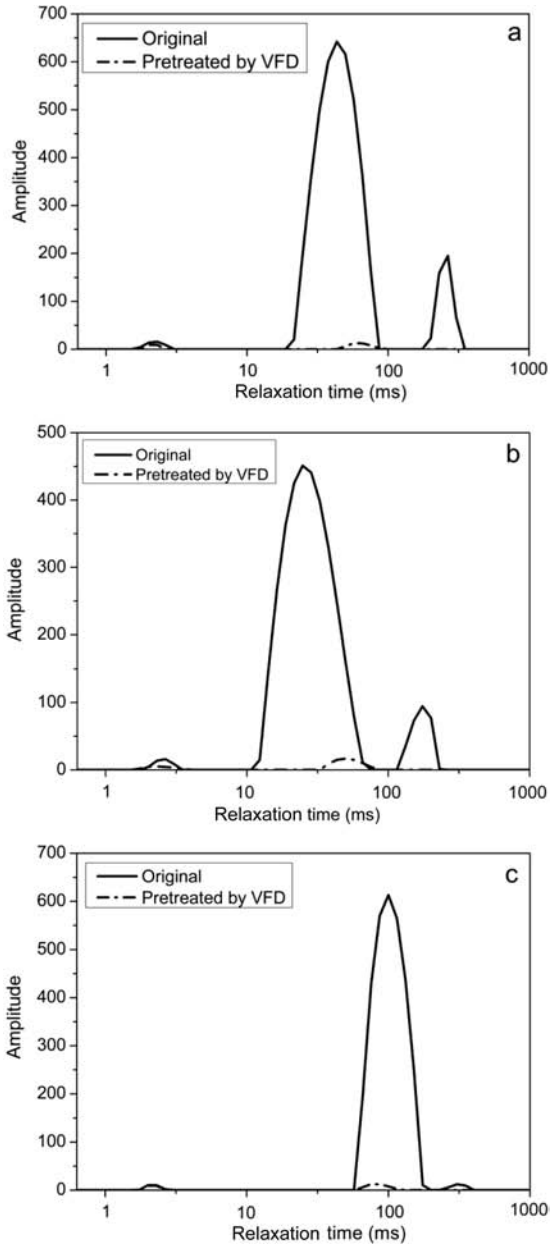


**Figure 1.** LF-NMR $T_2$ relaxation curves of three types of tofu samples before and after VFD treatment: (a) CS, (b) MC, and (c) GDL tofu.

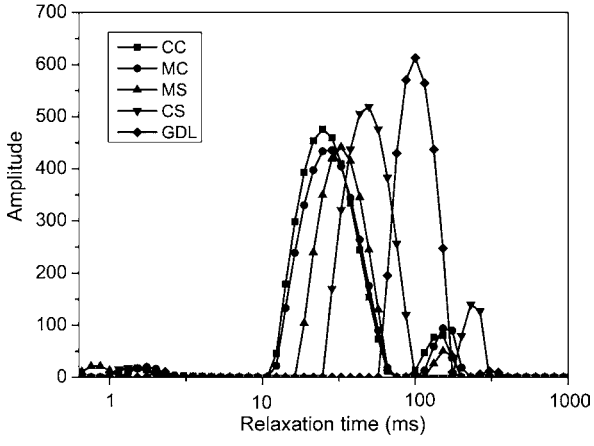


**Figure 2.** LF-NMR $T_2$ relaxation curves of five types of tofu samples.

mechanisms and final microstructures. The formation of salt-induced tofu is usually considered to be driven by salt-bridge effects between soybean proteins and coagulants.[28] Due to the pH reducing effect, mechanism of GDL tofu's formation is generally regarded as a special form of acid-induced coagulation.[29] Noh et al.[7] reported a globular stacked (or honeycomb) microstructure of salt-induced tofu which proteins were integrated into clumps. Bin et al.[30] found a well-connected network microstructure of GDL tofu. $T_{21}$ water fraction of GDL tofu, which accounted for 98% of total signal, was higher than the other samples, while salt-induced tofu samples shared similar $T_{21}$ water populations of approximately 90%; nevertheless, $T_{21}$ water fraction was the dominant population in all types of tofu. $T_{22}$ relaxation times of different tofu samples presented the same tendency as $T_{21}$ relaxation times but with inverse population order among different samples. GDL tofu showed the lowest value of $T_{22}$ water population of 1.73%, while salt-induced tofu shared similar values of about 7%.

Interpretation of $T_2$ transverse relaxation of heterogeneous systems has been extensively discussed. On the basis of the diffusive and chemical exchange model of heterogeneous system established by Hills et al.,[31−33] different water fractions in many biological tissues have been identified. Three water fractions detected in meat are generally regarded as $T_{2b}$ (water bound to proteins), $T_{21}$ (water trapped within the myofibrils), and $T_{22}$ (water outside the cell).[10,11] In the case of plant tissues, the component with the slowest relaxation time (550−650 ms) is ascribed to vacuolar water, while the second (200−250 ms) and third components (50−60 ms) are assigned to cytoplasmic and extracellular water, respectively. The component with the shortest relaxation time, about 5−10 ms, is considered to be water associated with the cell wall.[27] As suggested by Hills et al.,[31] proton relaxation measurements reflect the state of biopolymers and morphology rather than the state of water. Due to the existence of membrane systems, the microstructures of food matrixes mentioned above are different from that of tofu. Tofu is formed by aggregation of soybean protein and lacks a membrane system. However, cheese, a membrane-free milk protein matrix induced by rennet, is much more similar to tofu compared to biological tissues. Therefore, the studies of different water fractions in cheese may be pertinent to the present study. Water distribution in milk protein mixtures has been widely studied.[34,35] In general, transverse water proton relaxation in heterogeneous systems like cheese and tofu is influenced by the network structure of food matrix because water is influenced by its surroundings. The distance between water and the surrounding protein network is the key factor giving rise to the different relaxation times of three water fractions in tofu. Gianferri et al.[34] reported four fractions in mozzarella cheese. Except for the fraction derived from fat droplets, the other three fractions were considered to be water fractions located in different spatial areas of cheese's microstructure. The slowest fraction with a relaxation time of 488 ms was ascribed to water free of the influence of protein surface. The intermediate fraction was considered to be water molecules entrapped in meshes of gel. The fastest fraction, with a relaxation time centered at about 7.2 ms, was attributed to water molecules trapped within casein junction zones.[34] Although the microstructures of salt-induced tofu and GDL tofu are different, they still show some similarities. Thus, both salt-induced tofu and GDL tofu are characterized by the presence of big pores and small meshes in the microstructure.[2,7,30] Based on the identification of different water


dx.doi.org/10.1021/jf503427m | J. Agric. Food Chem. 2014, 62, 8594−8601

Table 1. $T_2$ Relaxation Times ($T_{21}$, $T_{22}$) and Populations ($M_{21}$, $M_{22}$) of Five Types of Tofu[a]

| coagulant ($n$ = 15) | $T_{21}$ (ms) | $M_{21}$ (%) | $T_{22}$ (ms) | $M_{22}$ (%) |
|---|---|---|---|---|
| GDL | 109.98 ± 7.31 a | 98.16 ± 1.12 a | 301.46 ± 6.38 a | 1.73 ± 0.11 a |
| CS | 45.61 ± 3.16 b | 90.75 ± 1.81 b | 251.77 ± 7.45 b | 7.44 ± 0.70 bc |
| CC | 24.54 ± 0.86 c | 90.05 ± 0.67 b | 133.61 ± 5.29 c | 7.57 ± 0.21 b |
| MS | 32.18 ± 1.50 d | 91.66 ± 0.23 c | 226.99 ± 10.58 d | 7.07 ± 0.21 d |
| MC | 27.02 ± 2.26 e | 90.22 ± 0.55 b | 174.75 ± 6.58 e | 7.16 ± 0.32 cd |

[a]Results are presented as the mean ± standard deviation. Lowercase letters (a–e) in the same column indicate significant differences ($p$ < 0.05).

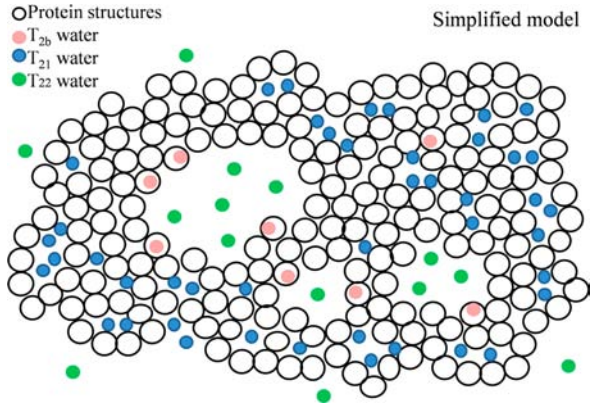


**Figure 3.** Simplified model of tofu's microstructure. Pores and meshes with different sizes exist in tofu's three-dimensional network. Color-coded circles represent water molecules of different fractions.

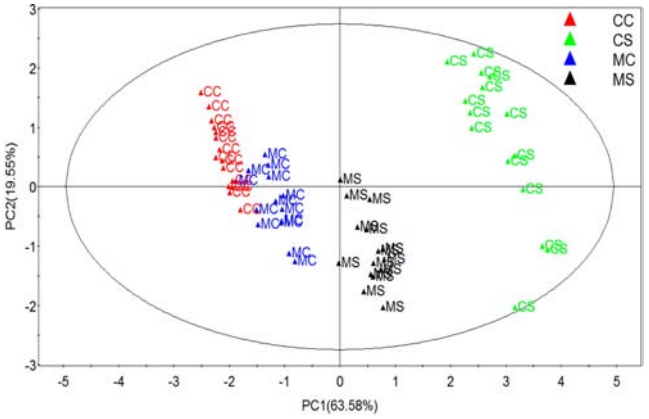


**Figure 4.** PCA plot ($n$ = 60) obtained on distributed NMR $T_2$ relaxation data of four types of salt-induced tofu samples. CC, MC, CA, and MA represent the samples containing these coagulants.

fractions in cheese and the microstructure of tofu, the following assignments to the three fractions in tofu's microstructure are proposed. The slowest fraction $T_{22}$ is ascribed to water molecules remote from the protein network whose motion can be little affected by the protein network. In conjunction with the microstructure of tofu, the big pores and gaps in tofu's three-dimensional network may provide space for $T_{22}$ water fraction. The intermediate component $T_{21}$ can be ascribed to water molecules near to the surface of protein network and is influenced by the interaction between protein network and water molecules. Due to the Brownian movement of water molecules, $T_{21}$ water fraction diffuses from the bulk to protein interface and its $T_2$ value is controlled by diffusive exchange. Small meshes in tofu's microstructure and gaps in the space of protein's tertiary and quaternary structures may provide space for the $T_{21}$ water fraction. The fastest fraction $T_{2b}$, with a relaxation time about 2 ms, can be assigned to the water molecules tightly associated with protein and can be regarded as an integral part of the protein structure. Its transverse relaxation time is essentially dominated by a fast chemical exchange with exchangeable protons of hydrophilic groups, such as hydroxyl, carboxyl, and sulfydryl, resulting in a short $T_2$ relaxation time. According to previous research,[10] the influence of $T_{2b}$ fraction on physical characteristics and WHC is minor, and it will therefore not be further discussed in this paper. On the basis of assignments of different water fractions in tofu matrix, we established a simplified model of tofu's microstructure (Figure 3). Pores and meshes with different sizes exist in tofu's three-dimensional network, leading to a heterogeneous microenvironment and multiple-exponential relaxation behavior of water in it.

The effects of divalent salts on the coagulation process of soymilk have been intensively studied, but no convincing conclusion has been obtained yet.[28,36] Both cation and anion seem to affect the coagulation process as well as the physical properties of final matrix.[37] Parameters such as viscosity[38] and turbidity[39] have been introduced for coagulation studies of tofu. Although differences were observed between GDL tofu and salt-induced tofu, the differences among four types of salt-induced tofu were not intuitively revealed. In order to obtain an overview of variation in the multivariate LF-NMR relaxation data of salt-induced tofu, PCA analysis was performed. As shown in Figure 4, PC1 explained 63.58% of the variation in the data and discriminated clearly according to the different divalent salts of tofu. PC2, explaining 19.55% of the variation in the data, was considered to be largely due to the variation between replicates. A clear separation of CS tofu from other samples in PC1 was observed and might be explained by low water solubility of CS. The amount of cations and anions available for reactions in CS–soymilk mixtures were lower than the other three salt–soymilk mixtures due to the low water solubility of CS, which might lead to different coagulation speeds, microstructures, and final water distribution. It is noteworthy that the separation of MS tofu and chloride salt-induced tofu in PC1 seemed to be determined by type of anion. Previous studies have demonstrated that anions affect the coagulation speed and textural properties of tofu,[38,39] which is in accordance with our results.

**Relationship between WHC and LF-NMR.** Water-holding capacity defines the capacity of tofu to retain water in its microstructure and is an important parameter. Centrifugation is a process that removes water through physical pressure without any chemical reaction between water and macromolecules. Due to a similar principle, stepwise centrifugation can simulate different pressures under which salt-induced tofu is made. CS, MC, and GDL tofu was stepwise centrifuged (Table 2). Both $T_{21}$ and $T_{22}$ relaxation times of all three tofu samples decreased with increases in centrifugation force. Similar findings were observed in a study of centrifugation


dx.doi.org/10.1021/jf503427m | J. Agric. Food Chem. 2014, 62, 8594–8601

Table 2. $T_{21}$, $T_{22}$, and WHC of Three Tofu Samples at Different Centrifugation Forces[a]

| | GDL ($n$ = 3) | | | $CaSO_4$ ($n$ = 3) | | | $MgCl_2$ ($n$ = 3) | | |
|---|---|---|---|---|---|---|---|---|---|
| centrifugation (g) | $T_{21}$ (ms) | $T_{22}$ (ms) | WHC (%) | $T_{21}$ (ms) | $T_{22}$ (ms) | WHC (%) | $T_{21}$ (ms) | $T_{22}$ (ms) | WHC (%) |
| 420 | 100.00 ± 0.00 a | 297.56 ± 6.89 a | 86.86 ± 1.84 a | 41.41 ± 3.26 a | 242.54 ± 11.53 a | 86.15 ± 1.24 a | 26.01 ± 0.14 a | 174.75 ± 0.00 a | 91.56 ± 1.21 a |
| 650 | 95.66 ± 7.52 b | 292.13 ± 12.96 ab | 73.91 ± 0.96 b | 39.53 ± 1.01 a | 192.20 ± 8.72 b | 83.32 ± 1.04 b | 24.77 ± 0.00 bc | 167.17 ± 7.58 a | 88.74 ± 0.68 b |
| 1660 | 91.31 ± 7.86 bc | 278.87 ± 7.25 bc | 72.53 ± 3.02 b | 34.38 ± 2.83 b | 183.48 ± 5.11 bc | 80.27 ± 1.74 c | 22.62 ± 1.86 cd | 145.39 ± 11.42 b | 87.75 ± 0.08 b |
| 2600 | 86.97 ± 0.00 cd | 265.61 ± 8.72 c | 65.44 ± 0.76 c | 32.75 ± 0.00 b | 174.75 ± 5.74 bcd | 75.24 ± 0.28 d | 20.61 ± 1.62 de | 138.79 ± 6.59 bc | 84.56 ± 0.36 c |
| 3740 | 79.42 ± 6.54 de | 254.08 ± 9.97 c | 62.67 ± 0.57 d | 31.26 ± 2.64 bc | 167.17 ± 7.58 d | 73.45 ± 1.48 e | 18.05 ± 3.03 ef | 131.29 ± 5.73 cde | 77.83 ± 0.45 d |
| 5000 | 72.36 ± 5.69 e | 242.54 ± 11.53 cd | 58.86 ± 1.16 e | 28.48 ± 0.00 cd | 159.58 ± 13.14 ef | 69.50 ± 1.93 ef | 15.59 ± 1.22 fg | 126.45 ± 9.94 def | 74.05 ± 1.02 e |
| 6640 | 60.08 ± 4.94 f | 220.98 ± 10.03 de | 56.30 ± 0.58 f | 26.01 ± 2.14 de | 145.39 ± 11.42 efg | 64.97 ± 1.60 fg | 14.88 ± 1.06 g | 120.71 ± 6.42 ef | 73.07 ± 0.81 e |
| 8400 | 59.57 ± 5.45 f | 210.95 ± 11.37 de | 53.63 ± 0.16 g | 24.77 ± 0.00 ef | 138.79 ± 6.59 fgh | 64.58 ± 0.29 g | 14.17 ± 0.00 g | 115.91 ± 4.99 f | 71.28 ± 1.28 f |
| 10380 | 52.22 ± 0.76 gf | 202.23 ± 8.15 ef | 48.15 ± 1.31 h | 23.69 ± 1.86 fg | 132.19 ± 11.76 fgh | 62.84 ± 0.96 h | | | |
| 12560 | 49.77 ± 0.00 f | 192.20 ± 9.11 f | 45.39 ± 0.86 i | 21.54 ± 0.00 gh | 126.45 ± 9.94 gh | 60.73 ± 0.53 i | | | |
| 14940 | 45.45 ± 3.74 f | 174.75 ± 0.00 g | 42.13 ± 0.49 j | 19.63 ± 1.62 h | 120.71 ± 9.97 h | 58.17 ± 0.55 g | | | |

[a]Results are presented as the mean ± standard deviation. Lowercase letters (a–j) in the same column mean significant differences ($P < 0.05$).

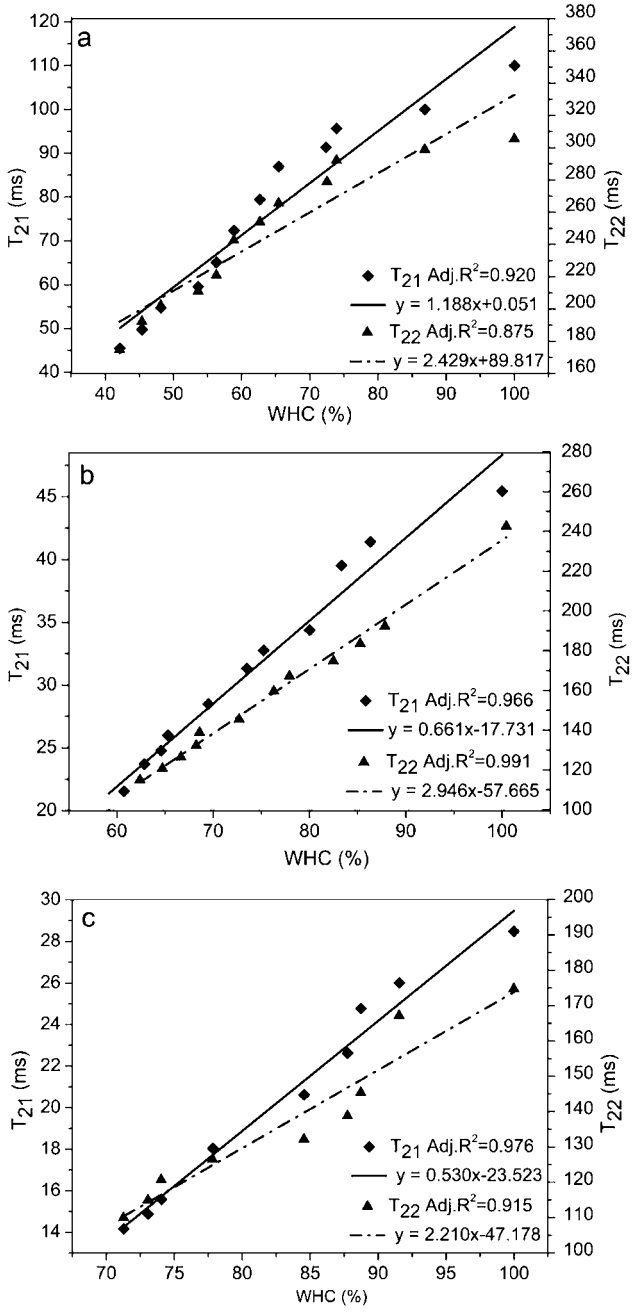


**Figure 5.** Linear regression equations to explain the linear relationships between WHC and $T_{2i}$ relaxation times during the process of centrifugation. (a) GDL tofu ($n$ = 12); (b) CS tofu ($n$ = 12); (c) MC tofu ($n$ = 9).

of pork.[10,11] As the centrifugation force increased, tofu formed a more compact microstructure, which shortened the distance of water molecule diffusion from the bulk to protein network interface, resulting in less mobility of water and lower values of $T_{21}$ and $T_{22}$ relaxation times.

Due to potential correlations between $T_{21}$ and $T_{22}$ relaxation times and WHC of tofu, Pearson correlation analysis was carried out, and the results are shown in Table 3. In the case of centrifugation, $T_{21}$ relaxation times presented significant correlations with WHC. This was in agreement with the results derived from continuous distribution analysis of pork reported by Bertram et al.[10] However, in the present study, the correlations between $T_{22}$ relaxation times and WHC were

Table 3. Pearson Correlation Analysis and Levels of Significance for Correlations between WHC and $T_{21}$, $T_{22}$, $M_{21}$, and $M_{22}$[a]

| parameter | centrifugation | microwave | parameter | centrifugation | microwave |
|---|---|---|---|---|---|
| | | GDL Tofu | | | |
| $T_{21}$ | 0.963** | | $M_{21}$ | 0.659* | |
| $T_{22}$ | 0.942** | | $M_{22}$ | −0.455 | |
| | | CS Tofu | | | |
| $T_{21}$ | 0.984** | 0.996** | $M_{21}$ | 0.374 | 0.806** |
| $T_{22}$ | 0.996** | 0.995** | $M_{22}$ | 0.539 | −0.712* |
| | | MC Tofu | | | |
| $T_{21}$ | 0.990** | 0.994** | $M_{21}$ | 0.642* | 0.920** |
| $T_{22}$ | 0.962** | 0.978** | $M_{22}$ | 0.425 | −0.591 |

[a]Levels of significance are defined as (*) $p < 0.05$ and (**) $p < 0.01$.

Table 4. $T_{21}$, $T_{22}$, and WHC of CS and MC Tofu at Different Microwave Drying Times[a]

| | $CaSO_4$ ($n$ = 3) | | | $MgCl_2$ ($n$ = 3) | | |
|---|---|---|---|---|---|---|
| drying time (s) | $T_{21}$ (ms) | $T_{22}$ (ms) | WHC (%) | $T_{21}$ (ms) | $T_{22}$ (ms) | WHC (%) |
| 30 | 41.41 ± 1.88 a | 254.61 ± 9.23 a | 94.53 ± 1.45 a | 23.69 ± 1.86 a | 171.85 ± 9.72 a | 93.83 ± 0.56 a |
| 45 | 39.53 ± 3.25 a | 242.07 ± 8.97 ab | 85.82 ± 0.44 b | 20.61 ± 1.62 b | 165.32 ± 12.53 bc | 86.16 ± 0.25 b |
| 60 | 34.38 ± 1.63 b | 220.55 ± 7.29 bc | 79.74 ± 1.25 c | 19.67 ± 0.93 b | 158.98 ± 7.37 bc | 80.24 ± 0.30 c |
| 75 | 28.67 ± 2.30 c | 210.51 ± 6.37 cd | 72.23 ± 0.70 d | 16.40 ± 2.28 c | 151.65 ± 6.24 cd | 71.32 ± 0.76 d |
| 90 | 26.01 ± 1.23 c | 192.98 ± 7.37 d | 66.95 ± 1.47 e | 14.27 ± 1.98 cd | 137.22 ± 5.12 de | 67.10 ± 0.88 e |
| 105 | 20.61 ± 1.62 d | 167.58 ± 4.14 e | 60.85 ± 0.13 f | 11.79 ± 0.92 de | 131.48 ± 4.12 e | 61.94 ± 0.55 f |
| 120 | 17.92 ± 1.41 de | 159.36 ± 6.43 ef | 55.20 ± 0.38 g | 10.39 ± 1.22 ef | 129.17 ± 7.13 ef | 53.61 ± 0.65 g |
| 135 | 14.97 ± 1.32 ef | 145.79 ± 8.03 efg | 49.62 ± 0.48 h | 8.92 ± 0.70 fg | 125.89 ± 3.48 fg | 50.41 ± 1.47 h |
| 150 | 13.25 ± 0.92 fi | 138.39 ± 3.78 fg | 46.43 ± 0.17 i | 6.44 ± 0.53 gh | 124.75 ± 0.00 fg | 45.43 ± 0.41 i |
| 165 | 9.33 ± 0.53 i | 132.59 ± 2.42 g | 41.38 ± 1.26 j | 5.87 ± 0.46 h | 116.98 ± 2.29 h | 44.69 ± 0.29 i |

[a]Results are presented as the mean ± standard deviation. Lowercase letters (a−j) in the same column indicate significant differences ($p < 0.05$).

also significant. Besides, Bertram et al.[10] revealed that $T_{2i}$ populations presented closer relationships with WHC compared with $T_{2i}$ relaxation times in the determination of WHC in pork, while $T_{2i}$ populations of three types of tofu were almost unchanged during the centrifugation process (data not shown) and the correlations were insignificant. We deduce that the dissimilar changes of $T_2$ parameters between tofu and pork meat during centrifugation processes can be ascribed to their different microstructures. $T_{21}$ and $T_{22}$ water fractions of meat exist in different compartments of muscular tissues. Cell membranes are considered to act as physical barriers for the different water fractions, giving rise to their different contribution to centrifugation water loss and significant correlations between $T_{2i}$ populations and WHC. Compared with meat, the water transfer in tofu during centrifugation can be faster and unhindered because, unlike a membrane system, water in tofu is present in a system regardless of obstacles. Water transfer in tofu during centrifugation is most likely a dynamic process. Due to shrinkage of tofu matrix, both $T_{21}$ and $T_{22}$ water fractions could be expelled outside without the obstacles of cellular tissues during centrifugation.

According to previous studies, linear relationships existed between $T_{2i}$ relaxation times and WHC of different food matrixes.[11,15] In order to analyze the quantitative relationships between $T_{2i}$ relaxation times and WHC, mean values of $T_{21}$ and $T_{22}$ relaxation times and WHC were used to establish simple linear equations. Six equations were obtained from linear regression (Figure 5). High adj-$R^2$ values (0.875−0.991) indicated high fitting degrees of prediction equations. Accordingly, LF-NMR could be an effective method to monitor and predict the WHC of tofu during centrifugation.

Microwave drying was introduced as another method of dehydration. Unlike centrifugation, microwave drying achieved dehydration by heating the tofu matrix integrally. Moreover, microwave induced a high temperature condition which might cause some chemical and physical changes of soybean proteins. GDL tofu was not included because severe destruction of texture occurred during microwave drying. Table 4 shows the LF-NMR results of microwave drying of tofu made with CS and MC. $T_{21}$ and $T_{22}$ relaxation times decreased along with the microwaving, which was similar to the centrifugation results. With increasing drying time, $T_{21}$ populations decreased while $T_{22}$ populations increased, which might indicate the density of water in tofu's matrix changed due to potential changes of tofu microstructure during microwave drying. It is noteworthy that the relaxation time of the major water fraction decreased to below 10 ms, which was generally regarded as the boundary relaxation time between $T_{2b}$ and $T_{21}$. In centrifugation, limits of $T_{21}$ relaxation time (above 10 ms) and WHC seem to exist when centrifugation force reached a threshold. Like MC tofu, when centrifugation reached 8400$g$, no significant changes of WHC and $T_{2i}$ relaxation times were observed at centrifugation forces exceeding this level. However, even though the water loss was much more than that of centrifugation, the $T_{21}$ relaxation time and WHC had not reached their limits during microwave drying. In microwave drying, both the microstructure and chemical properties of protein network might extensively alter due to the high temperature induced by microwave. Thus, different mechanisms of these two dehydration methods are considered to be the reason for the dissimilar changes of $T_2$ parameters and WHC. Although the relaxation time of the major water component was below 10 ms, this portion was still likely to be responsible for further water loss from 46% to 41% (CS tofu) and from 53% to 44% (MC tofu). As mentioned before, $T_{2b}$ water could hardly contribute to water loss of food matrix. Besides, the $T_2$

relaxation time of the major component was still significantly slower than tofu's $T_{2b}$ (0.80−2.6 ms). So it seems to be reasonable that the major portion of water was assigned as $T_{21}$ water fraction.

It is noteworthy that when drying time exceeded 60 s (165 s for CS tofu), a new fraction, of which the relaxation time was 72−37 ms, was observed and identified as $T_{21n}$ (Figure 6). The population of $T_{21n}$ increased from 1% to 14% (for MC tofu) along with prolonged drying time. A previous study demonstrated that microwave treatment could transform soybean protein dispersions to a gel-like curd.[40] Consequently the formation of this new fraction may be explained by further changes of tofu's microstructure driven by microwave drying. During the microwave drying process, some proteins experienced thermal denaturation and formed special microstructures, which could retain the water molecules expelled from inner spaces. This portion of water might become the source of $T_{21n}$ water.

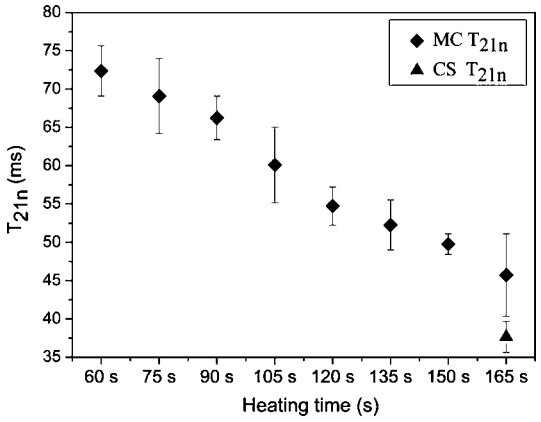


**Figure 6.** Relaxation time of new water component $T_{21n}$ in MC and CS tofu samples.

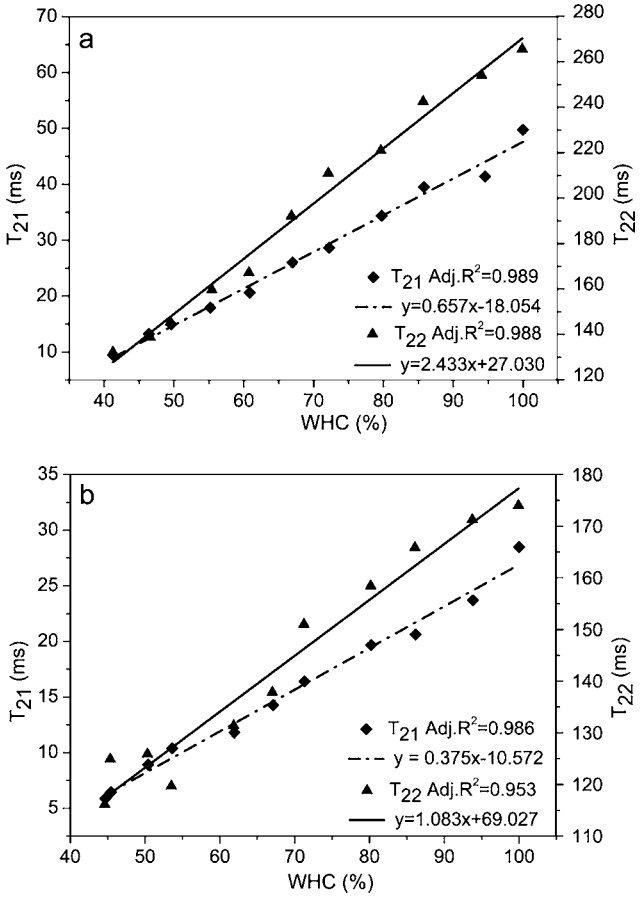


**Figure 7.** Linear regression equations to explain the linear relationships between WHC and $T_{2i}$ relaxation times during the process of microwave drying. (a) CS ($n$ = 11); (b) MC tofu ($n$ = 11).

Pearson's correlations between $T_2$ data and WHC are shown in Table 3. Significant correlations between $T_{2i}$ relaxation times and WHC were observed in the case of centrifugation. Although the mechanism of decrease of $T_{2i}$ relaxation times may be complex due to overlying effects in microwave drying, it still seems to be feasible to make a prediction of tofu's WHC by its $T_{2i}$ relaxation times because of the significant correlations between them. Therefore, linear regression analysis was performed on mean values of $T_{2i}$ relaxation times and WHC (Figure 7). Four equations with adj-$R^2$ ranging from 0.953 to 0.989 were obtained to explain the correlations between $T_{2i}$ relaxation times and WHC.

In conclusion, we consider that the $T_{21}$ and $T_{22}$ relaxation times can be good parameters in monitoring tofu's WHC during microwave dehydration.

## AUTHOR INFORMATION

### Corresponding Author

*Telephone +86 25 84396989; fax +86 25 84399090; e-mail dongms@njau.edu.cn.

### Funding

This work was cofinanced by High-Tech Research and Development Program of China (2011AA100903 and 2013BAD18B01-4) and National Natural Science Foundation of China (31201422 and 31371807) and was also supported by the Project Funded by the Priority Academic Program Development of Jiangsu Higher Education Institutions (PAPD).

### Notes

The authors declare no competing financial interest.

## ACKNOWLEDGMENTS

We thank the technical support staff from Key Laboratory of Meat Processing and Quality Control, Ministry of Education (Nanjing, P. R. China). We also thank Gao Yangwen and Yang Peiqiang for their illuminating discussions on this topic.

## ABBREVIATIONS USED

Low field nuclear magnetic resonance (LF-NMR); water holding capacity (WHC); calcium sulfate (CS); magnesium chloride (MC); Glucono-delta-lactone (GDL); vacuum freeze-drying (VFD); and adjust determination coefficient (*Adj.*$R^2$)

## REFERENCES

(1) Obatolu, V. A. Effect of different coagulants on yield and quality of tofu from soymilk. *Eur. Food Res. Technol.* **2008**, *226*, 467−472.

(2) Liu, Z. S.; Chang, S. K. C.; Li, L. T.; Tatsumi, E. Effect of selective thermal denaturation of soybean proteins on soymilk viscosity and tofu's physical properties. *Food Res. Int.* **2004**, *37*, 815−822.

(3) Miyahara, M.; Saito, Y. Effects of the processing steps in tofu production on pesticide residues. *J. Agric. Food Chem.* **1994**, *42*, 369−373.

(4) Liu, Z. S.; Chang, S. K. C.; Li, L. T.; Tatsumi, E. Development of a rapid titration method for predicting optimal coagulant concentration for filled tofu. *J. Agric. Food Chem.* **2003**, *51*, 815−822.

(5) Li, X. S.; Toyoda, K.; Ihara, I. Coagulation process of soymilk characterized by electrical impedance spectroscopy. *J. Food Eng.* **2011**, *105*, 563−568.
(6) Hsieh, J. F.; Yu, C. J.; Tsai, T. Y. Proteomic profiling of the coagulation of soymilk proteins induced by magnesium chloride. *Food Hydrocolloids* **2012**, *29*, 219−225.
(7) Noh, E. J.; Park, S. Y.; Park, J. I.; Hong, S. T.; Yun, S. E. Coagulation of soymilk and quality of tofu as affected by freeze treatment of soybeans. *Food Chem.* **2005**, *91*, 715−721.
(8) Kao, F. J.; Su, N. W.; Lee, M. H. Effect of calcium sulfate concentration in soymilk on the microstructure of firm tofu and the protein constitutions in tofu whey. *J. Agric. Food Chem.* **2003**, *51*, 6211−6216.
(9) Cai, T. D.; Chang, K. C. Characteristics of production-scale tofu as affected by soymilk coagulation method: propeller blade size, mixing time and coagulant concentration. *Food Res. Int.* **1998**, *31*, 289−295.
(10) Bertram, H. C.; Dønstrup, S.; Karlsson, A. H.; Andersen, H. J. Continuous distribution analysis of $T_2$ relaxation in meat: An approach in the determination of water-holding capacity. *Meat Sci.* **2002**, *60*, 279−285.
(11) Bertram, H. C.; Andersen, H. J.; Karlsson, A. H. Comparative study of low-field NMR relaxation measurements and two traditional methods in the determination of water holding capacity of pork. *Meat Sci.* **2001**, *57*, 125−132.
(12) Bertram, H. C.; Kohler, A.; Böcker, U.; Ofstad, R.; Andersen, H. J. Heat-induced changes in myofibrillar protein structures and myowater of two pork qualities. A combined FT-IR spectroscopy and low-field NMR relaxometry study. *J. Agric. Food Chem.* **2006**, *54*, 1740−1746.
(13) Bertram, H. C.; Aaslyng, M. D.; Andersen, H. J. Elucidation of the relationship between cooking temperature, water distribution and sensory attributes of pork: A combined NMR and sensory study. *Meat Sci.* **2005**, *70*, 75−81.
(14) Bertram, H. C.; Andersen, R. H.; Andersen, H. J. Development in myofibrillar water distribution of two pork qualities during 10-month freezer storage. *Meat Sci.* **2007**, *75*, 128−133.
(15) Sánchez-Alonso, I.; Martínez, I.; Sánchez-Valencia, J.; Careche, M. Estimation of freezing storage time and quality changes in hake (*Merluccius merluccius* L.) by low field NMR. *Food Chem.* **2012**, *135*, 1626−1634.
(16) Mariette, F.; Topgaard, D.; Jonsson, B.; Soderman, O. $^1$H NMR diffusometry study of water in casein dispersions and gels. *J. Agric. Food Chem.* **2002**, *50*, 4295−4302.
(17) Dean, A. L.; Mariette, F.; Marin, M. $^1$H nuclear magnetic resonance relaxometry study of water state in milk protein mixtures. *J. Agric. Food Chem.* **2004**, *52*, 5449−5455.
(18) Salami, S.; Maoura-Rondeau, C.; Van Duynhoven, J.; Mariette, F. PFG-NMR self-diffusion in casein dispersions: Effects of probe size and protein aggregate size. *Food Hydrocolloids* **2013**, *31*, 248−255.
(19) Mariette, F.; Tellier, C.; Brule, G.; Marchal, P. Multinuclear NMR study of the pH dependent water state in skim milk and caseinate solutions. *J. Dairy Res.* **1993**, *60*, 175−188.
(20) Margit, M.; Anettek, K. T.; Bertram, H. C.; Andersen, H. J.; Engelsen, S. B. Cooking effects on water distribution in potatoes using nuclear magnetic resonance relaxation. *J. Agric. Food Chem.* **2005**, *53*, 5976−5981.
(21) Hansen, C. L.; Thybo, A. K.; Bertram, H. C.; Viereck, N.; Van Denberg, F.; Engelsen, S. B. Determination of dry matter content in potato tubers by low-field nuclear magnetic resonance (LF-NMR). *J. Agric. Food Chem.* **2010**, *58*, 10300−10304.
(22) Hager, A.-S.; Bosman, G. M.; Delcour, J. A. Physical and molecular changes during the storage of gluten-free rice and oat bread. *J. Agric. Food Chem.* **2014**, *62*, 5682−5689.
(23) Bosman, G. M.; Lagrain, B.; Fierens, E.; Delcour, J. A. Impact of amylases on biopolymer dynamics during storage of straight-dough wheat bread. *J. Agric. Food Chem.* **2013**, *61*, 6525−6532.
(24) Bosman, G. M.; Lagrain, B.; Ooms, N.; Fierens, E.; Delcour, J. A. Biopolymer interactions, water dynamics, and bread crumb firming. *J. Agric. Food Chem.* **2013**, *61*, 4646−4654.
(25) Young, S. H.; Cherl, H. L. Self-diffusion coefficient of water in tofu determined by pulsed field gradient nuclear magnetic resonance. *J. Agric. Food Chem.* **2006**, *54*, 219−223.
(26) Xiao, Z.; Wang, Z.; Liu, T. Application of multi-exponential inversion method to NMR measurements. *Petro Sci.* **2004**, *1*, 19−22.
(27) Shao, X.; Li, Y. Application of low-field NMR to analyze water characteristics and predict unfrozen water in blanched sweet corn. *Food Bioprocess Technol.* **2013**, *6*, 1593−1599.
(28) Rha, C.; Lee, C. H. Microstructure of soybean protein aggregates and its relation to the physical and textural properties of the curd. *J. Food Sci.* **1978**, *43*, 79−84.
(29) Kohyama, K.; Yoshida, M.; Nishinara, K. Rheological study on gelation of soybean 11S protein by glucono-$\delta$-lactone. *J. Agric. Food Chem.* **1992**, *40*, 740−744.
(30) Bin, M. D.; Yasir, S.; Sutton, K. H.; Newberry, M. P.; Andrews, N. R.; Gerrard, J. A. The impact of Maillard cross-linking on soy proteins and tofu texture. *Food Chem.* **2007**, *104*, 1502−1508.
(31) Hills, B. P.; Takacs, S. F.; Belton, P. S. A new interpretation of proton NMR relaxation time measurements of water in food. *Food Chem.* **1990**, *37*, 95−111.
(32) Belton, P. S.; Hills, B. P. The effects of diffusive exchange in heterogeneous system on NMR line shapes and relaxation processes. *Mol. Phys.* **1987**, *61*, 999−1018.
(33) Belton, P. S.; Hills, B. P.; Raimbaud, E. R. The effects of morphology and exchange on proton NMR relaxation in agarose gels. *Mol. Phys.* **1988**, *63*, 825−842.
(34) Gianferri, R.; Maioli, M.; Delfini, M.; Brosio, E. A low resolution and high-resolution NMR integrated approach to investigate the physical structure and metabolic profile of Mozzarella di Bufala Campana cheese. *Int. Dairy J.* **2007**, *17*, 167−176.
(35) Metais, M.; Cambert, M.; Riaublanc, A.; Mariette, F. Influence of fat globule membrane composition on water holding capacity and water mobility in casein rennet gel: A nuclear magnetic resonance self-diffusion and relaxation study. *Int. Dairy J.* **2006**, *16*, 344−353.
(36) Lu, J. Y.; Carter, E.; Chung, R. A. Use of calcium salts for soybean curd preparation. *J. Food Sci.* **1980**, *45*, 32−34.
(37) Tay, S. L.; Tan, H. Y.; Perera, C. The coagulating effects of cations and anions on soy protein. *Int. J. Food Prop.* **2006**, *9*, 317−323.
(38) Zhang, Q.; Li, W.; Feng, M.; Dong, M. Effects of different coagulants on coagulation behavior of acid-induced soymilk. *Food Hydrocolloids* **2013**, *33*, 106−110.
(39) Molina, M. I.; Wagner, J. R. The effects of divalent cations in the presence of phosphate, citrate and chloride on the aggregation of soy protein isolate. *Food Res. Int.* **1999**, *32*, 135−143.
(40) Bhattacharya, S.; Jena, R. Gelling behavior of defatted soybean flour dispersions due to microwave treatment: Textural, oscillatory, microstructural and sensory properties. *J. Food Eng.* **2007**, *78*, 1305−1314.

JOURNAL OF AGRICULTURAL AND FOOD CHEMISTRY

Article

pubs.acs.org/JAFC

# Differential Production of Phytotoxins from *Phomopsis* sp. from Grapevine Plants Showing Esca Symptoms

Mary-Lorène Goddard,[†,‡] Nicolas Mottier,[†,⊥] Julie Jeanneret-Gris,[†] Danilo Christen,[§,#] Raphaël Tabacchi,[†] and Eliane Abou-Mansour*[,†,∥]

[†]Institute of Chemistry, University of Neuchâtel, Rue Emile Argand 11, CH-2009 Neuchâtel, Switzerland

[‡]Laboratoire de Chimie Organique et Bioorganique, Université de Haute-Alsace-ENSCMu, 3 bis rue A. Werner, 68093 Mulhouse cedex, France

[§]Phytopathology Group, Institute of Integrative Biology, Swiss Federal Institute of Technology, CH-8092 Zürich, Switzerland

[∥]Plant Biology, Department of Biology, University of Fribourg, Chemin du Musée 10, 1700 Fribourg, Switzerland

Supporting Information

**ABSTRACT:** Nine strains of the fungus *Phomopsis* spp. were isolated from a vineyard showing decline from the disease esca. Strains were screened for their ability to produce secondary metabolites showing chemical diversity. The culture extracts of each strain were analyzed by liquid chromatography−ultraviolet−diode array detection−mass spectrometry. Three strains were selected for the isolation and characterization of eight of the major metabolites. Structures were elucidated by spectroscopic analyses including two-dimensional NMR and mass spectrometry and by comparison to literature data. Among the isolated metabolites were the known phomopsolide B (**1**), sydowinin A (**6**), sydowinol (**7**), cytosporone B (**8**), and four new furanones named phomopsolidones A−D (**2**−**5**). The fungal strains were identified as *Phomopsis* sp., *Phomopsis viticola* Sacc and, *Phomopsis viticola* complex. Biological assays on *Vitis vinifera* leaves and callus tissue, antibacterial, and insecticidal activities were evaluated. The results revealed variability regarding secondary metabolites with species of *Phomopsis* sp. associated with grapevine, raising the question of cultivar-driven strain selection and phytotoxins biosynthesis in grapevine plants.

**KEYWORDS:** *Phomopsis sp., Phomopsis viticola, phytotoxins, grapevine, esca*

## INTRODUCTION

Esca, one of the grapevines trunk disease, causes decline and premature dieback of vineyards and has become a growing threat to grapevines worldwide.[1] The disease is most damaging when wet weather occurs early in the season. The disease does not spread rapidly but builds up progressively in a vineyard over a number of years, leading to a general decline in vigor and yield of the vines.[2] The foliar symptoms are characterized by interveinal chlorosis that later develops into large necrotic areas in summer.[2] More than a 158 fungal species have been reported from the necrotic wood of adult plants showing esca symptoms,[3−5] mainly *Phaeomoniella chlamydospora*, *Phaeoacremonium aleophilum*, *Fomitiporia mediterranea*, *Eutypa lata*, *Cadophora* sp., *Botryosphaeria* sp., and *Phomopsis* sp. fungal species have been reported to have medium to high incidence. *Phomopsis viticola* is a fungus responsible for the phomopsis cane blight and leaf spot disease[6] of grapevine and is more often reported together with the Botryosphaeriacea from esca symptomatic plants.[5] In grapevine trunk disease, pathogens are isolated from both symptomatic and asymptomatic plants, and it remains unclear whether fungi act successively and/or in combination and whether wood-inhabiting microflora influences the decay process.[5] The endophytic genus *Phomopsis* sp. comprises plant pathogens often associated with disease of agricultural crops and is known to be a rich source of bioactive secondary metabolites with diverse structures,[7] but to our knowledge, there have been no reports of secondary metabolites isolated from the grapevine pathogen *P. viticola* Sacc. Since the fungus cannot be detected in leaves of infected grapevine trunk diseased plants, it was hypothesized that foliar symptoms are caused by toxic compounds produced by the fungi in wood tissue that are either translocated to the leaves or induce chain reactions leading to the symptoms on the leaves. A comprehensive review highlighting the metabolites biosynthesized by some of the fungi inhabiting the wood of grapevine has been published.[8]

In an ongoing effort to identify phytotoxic metabolites from pathogenic fungi of grapevine trunk disease,[9−11] we investigated several strains of *Phomopsis* isolated from *V. vinifera* Merlot, Cabernet sauvignon, and Cabernet franc showing or not esca symptoms. We report here the isolation and structural elucidation of eight metabolites isolated from three different strains of *Phomopsis* sp. Their phytotoxicity was assessed on grapevine leaves and callus tissue as well as their antimicrobial and larvicidal activities. Finally, a correlation between cultivars susceptibility, strain species, and their capacity to biosynthesize secondary metabolites was attempted.

## MATERIALS AND METHODS

**General Experimental Procedures.** $^{1}H$ and $^{13}C$ NMR spectra were recorded on a Bruker AMX 400 spectrometer (400 MHz)

Received: March 8, 2014
Revised: July 8, 2014
Accepted: July 29, 2014
Published: July 29, 2014

ACS Publications © 2014 American Chemical Society



dx.doi.org/10.1021/jf501141g | J. Agric. Food Chem. 2014, 62, 8602−8607

Table 1. $^{1}H$ and $^{13}C$ NMR (400 and 100 MHz) Spectral Data of Compounds 2−5 ($CDCl_3$, $\delta$ in ppm, $J$ in hertz)

| | compd 2 | | | compd 3 | | |
|---|---|---|---|---|---|---|
| | $\delta$ C | $\delta$ H | HMBC ($^{1}H-^{13}C$) | $\delta$ C | $\delta$ H | HMBC ($^{1}H-^{13}C$) |
| 2 | 172.4 | | | 176.9 | | |
| 3 | 123.3 | 6.21 (dd, 2.0, 5.8) | C2−C5 | 28.1 | 2.56 (m) | C5 |
| 4 | 152.6 | 7.45 (dd, 1.6, 5.8) | C2−C5 | 23.7 | 2.34 (dddd, 7.7, 7.7, 9.2, 13.2) | C6 |
| | | | | | 2.08 (dddd, 5.5, 7.7, 9.2, 13.2) | C5 |
| 5 | 83.3 | 5.21 (ddd, 1.6, 2.0, 4.1) | C4−C6−C1′ | 80.1 | 4.69 (ddd, 4.4, 5.5, 7.7) | C3−C4−C6 |
| 6 | 71.7 | 5.64 (dd, 4.1, 6.0) | C4−C5−C1′−C2′ | 74.6 | 5.47 (dd, 4.4, 5.5) | C5−C2′−C1″ |
| 1′ | 125.7 | 5.85 (dd, 6.0, 15.6) | C6−C3′ | 126.2 | 5.88 (ddd, 1.0, 6.0, 15.5) | C6−C1′−C2′−C3′ |
| 2′ | 135.5 | 5.92 (dd, 5.4, 15.6) | C6−C1′ | 135.2 | 5.88 (ddd, 1.0, 6.0, 15.5) | C1′ |
| 3′ | 76.2 | 3.93 (dd, 5.4, 6.3) | C1′−C2′−C4′−C5′ | 76.3 | 3.93 (dd, 4.6, 6.3) | C1′−C2′−C4′−C5′ |
| 4′ | 70.5 | 3.68 (qt, 6.3) | C2′−C3′−C5′ | 70.4 | 3.68 (qt, 6.3) | C2′−C3′−C5′ |
| 5′ | 18.8 | 1.20 (d, 6.3) | C3′ | 18.9 | 1.20 (d, 6.3) | |
| 1″ | 166.5 | | | 166.8 | | |
| 2″ | 127.7 | | | 128.0 | | |
| 2″−Me | 14.5 | 1.83 (d, 1.7) | C1″−C2″−C4″ | 14.6 | 1.86 (d, 1.2) | C3″ |
| 3″ | 139.2 | 6.90 (qq, 1.7, 7.3) | C1″−C4″ | 139.1 | 6.92 (qq, 1.2, 7.0) | C1″ |
| 4″ | 11.9 | 1.82 (d, 7.3) | C3″−C2″−C2″−Me | 12.1 | 1.83 (d, 7.0) | C3″ |
| 3′−OH | | 1.91 (br s) | | | 1.28 (br s) | |
| 4′−OH | | 1.91 (br s) | | | 1.28 (br s) | |

(Fällenden, Switzerland). Chemical shifts were referenced to TMS. Optical rotations were determined on a PerkinElmer 241 digital polarimeter (Waltham, MA, USA) with a 1 dm cell. IR spectra were obtained on a PerkinElmer 1720 X spectrometer. UV spectra were recorded on a Shimadzu UV-190. High-performance liquid chromatography (HPLC) analysis and purification was carried out on an Agilent 1100 (Palo Alto, CA, USA) coupled to a diode array detector (DAD). Mass spectra were measured on an Agilent 1100 LCMSD Trap using the electrospray ionization (ESI) source in negative or positive ionization mode. High-resolution electrospray ionization mass spectrometry (HRESI MS) was performed on a Bruker FTMS 4.7T BioAPEX II or an Agilent 3100 QTof.

**Plant Materials and Fungal Strain Isolation.** Ten plants of 15 years old of *V. vinifera* cv. Merlot, Cabernet sauvignon, and Cabernet franc were rooted in 2003 for further analysis from a vineyard in Riva San Vitale (Ticino, Switzerland). Half of the plants already exhibited esca foliar symptoms in 2000 and/or 2001. Plants were ripped out and cut in disks as reported.[12]

**Strain Growth and Extraction Method for Strain Screening.** Nine strains of *Phomopsis* sp. (DC110, DC275, DC283, DC180, DC239, DC279, DC281, DC282, and DC301,) were isolated and maintained on potato dextrose agar (PDA) (Difco, Sparks, MD, USA) (Table 2) for chemical analysis. For each strain, 10 replicates were grown from 7 day old native cultures and incubated at 25 °C in the dark. The fungal cultures were extracted separately with ethyl acetate (EtOAc) (3 × 600 mL) and evaporated under reduced pressure to dryness. An aliquot (10 mg/mL) was dissolved in MeOH for LC-DAD-MS analysis, and 20 $\mu$L was examined by reverse-phase chromatography (Nucleosil 100-7, C-18, 250 $\mu$m × 4.6 $\mu$m, 7 $\mu$m, Machery−Nagel, Duren, Germany) on a gradient of methanol and water starting at 40% of methanol for 5 min, increasing to 90% at 30 min and to 100% at 40 min at the flow rate of 1 mL/min.

**Growth Conditions and Extraction Methods.** Four strains were selected for their chemical diversity and identified by the Belgium Coordinated Collections of Microorganisms (BCCM) as *Phomopsis* sp. DC275 isolated from asymptomatic cv. Merlot, *P. viticola* complex DC239 isolated from asymptomatic cv. Cabernet sauvignon and DC281 isolated from symptomatic Cabernet franc, and finally, *P. viticola* (Sacc.) Sacc. DC180 isolated from asymptomatic cv. Cabernet Sauvignon. Three strains (DC275, DC239, and DC180) were selected for high scale culture. Each strain was grown on 40 PDA Petri plates for 21 days at 25 °C in the dark. Cultures were extracted with EtOAc (3 × 3 L) to yield dry residues of 1.68 g for DC275, 1.8 g for DC239, and 1.0 g for DC180. Crude extract of each strain was dissolved in water and extracted with *n*-hexane for defatting.

The remaining defatted material from *Phomopsis* sp. DC275 was further extracted with dichloromethane ($CH_2Cl_2$). This extract showed the highest phytotoxic activity against grape leaves and was further purified by a successive column chromatography (CC) on Si gel 60°A eluted with a gradient solvent of *n*-hexane/$CH_2Cl_2$ (1:1, v/v) to $CH_2Cl_2$/MeOH (1:1, v/v). A final purification by the solvent mixture $CHCl_3$/*i*PrOH (9:1, v/v) afforded three pure compounds **1** (75 mg), **2** (3.2 mg), and **3** (3.6 mg) and a mixture of **4** and **5** (10 mg).

Ethyl acetate extracts from *P. viticola* complex DC239 and *P. viticola* Sacc. DC180 were subjected to Sephadex LH-20 (70 cm × 1.2 cm) CC (GE Healthcare, Piscataway, NJ, USA). The eluent was a mixture of chloroform/methanol (1:1, v/v) for the first extract and methanol for the second one. The final pure compounds from the strain DC239 were obtained by purification with semipreparative HPLC using a gradient of MeOH/$H_2O$ (starting with 70% MeOH and reaching 80% MeOH after 15 min, at the flow rate of 3.5 mL/min on a Nucleosil 100-7 C-18 column, (250 mm × 8 mm i.d., Macherey−Nagel, Düren, Germany). *P. viticola* complex afforded three compounds **6** (7 mg), **7** (1.3 mg), and **8** (2 mg). Finally, using the same HPLC conditions as above, the strain (DC181) afforded **8** (8 mg).

*Phomopsolide B (**1**).* Colorless needles (75 mg); $[\alpha]_D^{25}$ +183.1° (MeOH; *c* 0.47); HRESI MS (+) *m*/*z* 319.1153 $[M + Na]^+$ (calcd for $C_{15}H_{20}O_6Na$ 319.1152); IR (KBr disc) $\nu_{max}$ $cm^{-1}$: 3562, 3394, 2915, 1710, 1649, 1456, 1380, 1259, 1135, 1065, 976, 826, 733; UV (MeOH) $\lambda_{max}$ nm (log $\varepsilon$): 227 (4.36); $^{1}H$ NMR ($CDCl_3$) $\delta_H$ 1.15 ($CH_3$, d, 6.3 Hz), 1.79 ($CH_3$, d, 7.3 Hz), 1.81 (CH, d, 1.8 Hz), 2.83 (OH, br s), 2.83 (OH, br s), 3.60 (CHOH, qt, 6.3 Hz), 3.91 (CHOH, t, 6.0 Hz), 5.11 (CH, dd, 3.0, 5.9 Hz), 5.37 (CH, dd, 3.0, 5.5 Hz), 5.88 (CH, ddd, 1.0, 5.9, 15.7 Hz), 6.00 (CH, ddd, 1.0, 6.0, 15.7 Hz), 6.22 (CH, d, 9.7 Hz), 7.01 (CH, dd, 5.5, 9.7 Hz); $^{13}C$ NMR $\delta_C$ 11.9 ($CH_3$), 14.4 ($CH_3$), 18.6 ($CH_3$), 63.3 (CH), 70.4 (CH), 76.0 (CH), 78.6 (CH), 124.4 (CH), 124.7 (CH), 124.4 (CH), 127.4 (C), 135.0 (C), 139.8 (CH), 141.0 (CH), 162.5 (CO), 166.7 (CO).

*Phomopsolidone A (**2**).* Colorless oil (3.2 mg); $[\alpha]$ $^{25}_D$ −19.7° (MeOH; *c* 0.32); HRESI MS (+) *m*/*z* 319.1153 $[M + Na]^+$ (calcd for $C_{15}H_{20}O_6Na$ 319.1152); IR (film) $\nu_{max}$ $cm^{-1}$: 3435, 2917, 1749, 1648, 1455, 1385, 1261, 1130, 1077, 980, 822, 734; UV (MeOH) $\lambda_{max}$ nm (log $\varepsilon$): 233 (4.41); for $^{1}H$ and $^{13}C$ NMR data see Table 1.

*Phomopsolidone B (**3**).* Colorless oil (2.6 mg); $[\alpha]$ $^{25}_D$ −15.1° (MeOH; *c* 0.26); HRESI MS (1) *m*/*z* 321.1309 $[M + Na]^+$ (calcd for $C_{15}H_{22}O_6Na$ 321.1308); IR (film) $\nu_{max}$ $cm^{-1}$: 3419, 2926, 1767, 1707,


dx.doi.org/10.1021/jf501141g | J. Agric. Food Chem. 2014, 62, 8602−8607

1649, 1564, 1440, 1382, 1264, 1138, 1078, 979, 735; UV (MeOH) $\lambda_{max}$ nm (log $\varepsilon$): 237 (4.38); for $^1$H and $^{13}$C NMR data see Table 1.

*Phomopsolidone C (**4**) and D (**5**).* Colorless oil (10 mg); HRESI MS (+) *m/z* 219.0637 $[M + Na]^+$ (calcd for $C_{10}H_{12}O_4Na$, 219.0627); UV (MeOH) $\lambda_{max}$ nm (log $\varepsilon$): 227 (3.72). *Phomopsolidone C* (**4**) $^1$H NMR ($CDCl_3$) $\delta_H$ 1.22 ($CH_3$, d, 6.6 Hz), 3.71(CH, qt, 6.6 Hz), 4.03 (CH, tapp, 6.6 Hz), 5.86 (CH, d, 11.2 Hz), 6.05 (CH, dd, 6.6, 15.5 Hz), 6.21 (CH, d, 5.4), 6.86 (CH, ddd, 1.2, 11.2, 15.5 Hz), 7.41 (CH, d, 5.4 Hz); $^{13}$C NMR ($CDCl_3$) 19.1 ($CH_3$), 70.6 (CH), 77.2 (CH), 113.2 (CH), 119.5 (CH), 125.0 (CH), 139.1 (CH), 143.3 (CH), 149.1 (C), 169.5 (CO). *Phomopsolidone D* (**5**) $^1$H NMR ($CDCl_3$) $\delta_H$ 1.22 ($CH_3$, d, 6.6 Hz), 3.71(CH, qt, 6.6 Hz), 4.03 (CH, tapp, 6.6 Hz), 5.86 (CH, d, 11.2 Hz), 6.05 (CH, dd, 6.6, 15.5 Hz), 6.21 (CH, d, 5.4), 6.86 (CH, ddd, 1.2, 11.2, 15.5 Hz), 7.41 (CH, d, 5.4 Hz); $^{13}$C NMR ($CDCl_3$) 19.2 ($CH_3$), 70.8 (CH), 77.3 (CH), 114.5 (CH), 120.2 (CH), 124.1 (CH), 139.3 (CH), 143.2 (CH), 150.9 (C), 169.4 (CO).

*Sydowinin A (**6**).* Yellowish powder (7 mg). ESI MS (+) *m/z* 323.1 $[M + Na]^+$ calcd for $C_{16}O_6H_{12}Na$; IR (film) $\nu_{max}$ cm$^{-1}$: 3430, 1735, 1720, 1649, 1620, 1600; UV (MeOH) $\lambda_{max}$ nm (log $\varepsilon$): 233 (3.81), 257 (3.78), 291 (2.7), 362 (1.9). $^1$H NMR ($CDCl_3$) $\delta_H$ 4.0 ($CH_3$, s), 4.75 ($CH_2$, s), 6.70 (CH, d, 1.3 Hz), 6.95 (CH, d, 1.3 Hz), 7.33 (CH, dd, 6.9; 2.6 Hz), 7.56 (CH, dd, 6.9; 2.9 Hz), 7.78 (CH, dd, 6.9 Hz), 12.1(OH, s); $^{13}$C NMR ($CDCl_3$) $\delta_C$ 133.8 (C), 122.9 (CH), 135.4 (CH), 119.9 (CH), 156.4 (C), 156.3 (C), 104.5 (CH), 152.5 (C), 108.5 (CH), 162.0 (C), 108.2 (C), 117.8 (C), 180.9 (C), 170.0 (C), 53.6 ($CH_3$), 64.7 ($CH_2$).

*Sydowinol (**7**).* Yellow powder (1.3 mg), HRESI MS (−) *m/z* 315.0532 $[M - H]^-$ (calcd for $C_{16}O_7H_{12}$, 315.0510); IR (film) $\nu_{max}$ cm$^{-1}$: 3430, 1728, 1720, 1656, 1585, 1550; UV (MeOH) $\lambda_{max}$ nm (log $\varepsilon$): 233 (4.30), 257 (4.18), 291 (2.1), 362 (1.9); $^1$H NMR (MeOH-$d_4$) $\delta_H$ 3.96 ($CH_3$, s), 4.67 ($CH_2$, s), 6.73 (CH, d, *J* = 1.1 Hz), 6.97 (d, *J* = 1.1 Hz), 7.37 (d, *J* = 9.1 Hz), 7.51 (d, *J* = 9.1 Hz); $^{13}$C NMR (MeOH-$d_4$), $\delta_C$ 52.23 ($CH_3$), 63.36 ($CH_2$), 104.25 (CH), 107.49 (C), 120.30 (C), 118.06 (C), 125.05 (CH), 130.39 (C), 150.02 (C), 151.37 (C), 153.3 (C), 156.5 (C), 161.65 (C), 169.2 (C), 181.12 (C).

*Cytosporone B (**8**).* Colorless powder (9 mg); HRESI MS (+) $[M + Na]^+$ *m/z* 345.1674 (calcd for $C_{18}H_{27}O_5Na$, 345.1672) . ESI $MS^2$ (−) of *m/z* 321.3 $[M - H]^-$ gave the fragment 275 $[M-C_2H_5OH-H]^-$; IR (film) $\nu_{max}$ cm$^{-1}$: 3234, 1732, 1622, 1456, 1368, 1174 cm$^{-1}$; UV ($CH_3CN$) $\lambda_{max}$ nm (log $\varepsilon$): 219 (4.33), 268 (3.33); $^1$H NMR ($CDCl_3$) $\delta_H$ 6.30 (CH, d, 2.4 Hz), 6.28 (CH, d, 2.4 Hz), 4.22 (2H, t, 7 Hz), 3.85 (2H, s), 2.84 (2H, t, 7), 1.26−1.27−1.28−1.29−1.32 (8H, bm) 1.30 (3H, t, 7 Hz), 0.88 (3H, t, 7 Hz); $^{13}$C NMR ($CDCl_3$) $\delta_C$ 171.9 (C), 42.2 ($CH_2$), 137.0 (C), 103.7 (CH), 160.8 (C), 113.1 (CH), 160.8 (C), 207.1 (C), 117.0 (C), 43.8 ($CH_2$), 25.4 ($CH_2$), 29.5 ($CH_2$), 29.6 ($CH_2$), 32.1 ($CH_2$), 23.0 ($CH_3$), 14.5 ($CH_3$), 62.1 ($CH_2$), 14.6 ($CH_3$).

**Biological Assays.** *Grapevine Leaf Disc Assays.* The compounds were dissolved in 2% aqueous ethanol at concentrations of 500, 250, and 100 μg/mL. Grapevine leaves *V. vinifera* cv. Chasselas were cut into discs of 5 mm of diameter with a cork borer and immersed in 1 mL of the solutions. The phytotoxicity of the crude extracts and the pure compounds was evaluated by measuring the area of necrotic tissues related to the total leaf disc area. Eutypine was used as a positive control and 2% ethanol as a negative control.

*Grapevine Callus Assay.* Phomopsolide B (**1**) was also tested on grapevine callus tissue from *Vitis vinifera* cv. Gamay (kindly supplied by Prof. Roustan, INRA, Toulouse, France). Callus cultures were cultivated on a growth medium according to a method previously described[11] with 12 h daylight for 28 days at 28 °C. Calli were weighed before and after incubation, and percent growth was calculated.

*Antibacterial Assays.* The antibacterial activity was measured by the bioautography method on thin-layer chromatography plates. Different concentrations of test compounds were prepared by the 2-fold serial dilution method described previously.[13]

*Larvicidal Efficiency.* Phomopsolide B (**1**) and phomopsolidones A (**2**) and B (**3**) were screened for larvicidal activities. The assay was performed at the Research Station Agroscope Changins-Wädenswil (Nyon, Switzerland) according to a method previously described.[14] In short, *Lobesia botrana* larvae were reared on an artificial diet of "Manduca - Heliothis Premix" (Stonefly Industries, Bryan, TX, USA) containing the dissolved product. By using a spatula, 1−2 g of the contaminated diet (1 and 10 ppm) was placed into each of 60 small plastic boxes. One newborn larva from rearing was then placed into each box. The larvae were reared under laboratory conditions at 25 °C. After 14 days, a first count of the surviving larvae was made. Rearing was then continued to the adult stage. The development time of the larvae was also assessed.

## RESULTS AND DISCUSSION

We investigated nine strains of *Phomopsis* isolated from grapevine plants showing esca symptoms in Ticino, Switzerland. Ten PDA Petri dishes of each strain were extracted with ethyl acetate and screened for secondary metabolites by HPLC-DAD-MS analyses and for phytotoxic activity on grapevine leaf disc assays. Three strains DC275, DC239, and DC180 were selected for further study according to the chemical differences in the secondary metabolites produced.

The first strain *Phomopsis* sp. DC275, isolated from a Merlot cultivar, afforded five pure compounds, phomopsolide B (**1**) as the major compound and four new furanones (**2**−**5**) given the trivial names phomopsolidones A−D (Figure 1). The HRESI

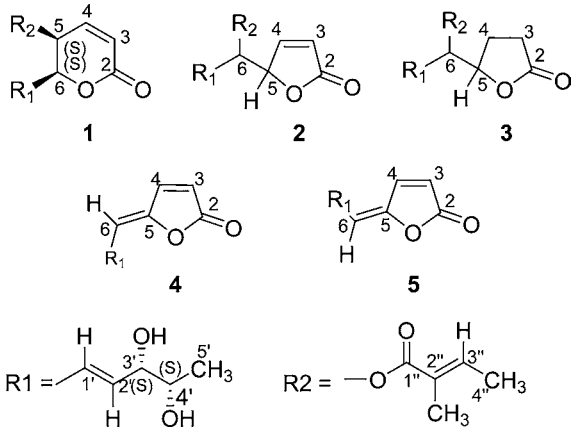


**Figure 1.** Compounds isolated from *Phomopsis* sp. DC275: phomopsolide B (**1**) and phomopsolidones A−D (**2**−**5**).

MS (+) spectrum *m/z* 319.1153 $[M + Na]^+$ of **1** indicated a molecular formula of $C_{15}H_{20}O_6Na$ supported by detailed IR, UV, $^1$H, $^{13}$C, one-dimensional (1D) and two-dimensional (2D) NMR, and MS data. The carbonyl group was also deduced from IR spectra and a signal at $\delta$ 162.5 in the $^{13}$C NMR spectrum. On the basis of COSY and HMBC and optical rotation spectra, compound **1** was identified as phomopsolide B (**1**) previously reported from cultures of *Phomopsis* species.[15−17]

Compound **2** showed the same molecular mass and HRESI MS (+) mass spectrum as **1** *m/z* 319.1153 $[M + Na]^+$ with the same molecular formula $C_{15}H_{20}O_6Na$. The downfield shift of the carbonyl atom signal of C-2, C-4, C-5, and C-6 at $\delta$ 172.4, $\delta$ 152.6, $\delta$ 83.3, and $\delta$ 71.7, respectively, in the $^{13}$C NMR spectrum indicated that the main differences occurred on the unsaturated $\gamma$-lactone moiety. Furthermore, the downfield chemical shift of H-3 ($\delta$ 6.21) and H-4 ($\delta$ 7.45) and the coupling constant (*J* = 1.6, 2.0, and 4.1) between H-3, H-4, and H-5 were characteristic of a 2-furanone ring indicating that group 2-methyl-but-2-enoic acid substituted at C-5 of **1** migrated to C-6 of **2** inducing a shielding of the H-6 chemical shift ($\delta$ 5.64). Thus, compound **2** was isolated for the first time and named phomopsolidone A.


dx.doi.org/10.1021/jf501141g | J. Agric. Food Chem. 2014, 62, 8602−8607

Compound **3** named phomopsolidone B had a molecular mass of 298, HRESI MS (1) *m/z* 321.1309 $[M + Na]^+$ indicating a molecular formula of $C_{15}H_{22}O_6Na$. The $^1H$ and $^{13}C$ NMR spectra of **3**, compared to those of **2**, indicated a hydrogenation of the furanone ring at positions C-3 and C-4 leading to a dihydrofuranone. However, the absolute configurations of **2** and **3** were not elucidated in this study, although the optical rotation spectra were similar to the results reported for the furanones from *Nigrospora sacchari*.[18]

Compounds **4** and **5**, named phomopsolidones C and D, were obtained as a mixture of two isomers. Because of the low amount of compounds available and the lack of activity, no further purification was performed. Nevertheless, HRESI MS and $^1H$ and $^{13}C$ NMR spectra, compared to those of **2**, indicated the presence of the furanone ring with the elimination of the group $R_2$. The presence of two new carbon atoms at $\delta$ 149.1 and $\delta$ 113.5 for compound **4** and $\delta$ 150.9 and $\delta$ 114.5 for compound **5** indicated the formation of an ethylenic bond between C-5 and C-6 with the configuration *Z* and *E*. A long-range coupling constant between H-3 and H-4 and H-6 in compound **5**, characteristic of a W system, indicated an *E* configuration of the double bond between C-5 and C-6. HRESI MS (+) *m/z* 219.0637 $[M + Na]^+$ confirmed the molecular formula $C_{10}H_{12}O_4Na$.

The second strain DC239 afforded three compounds (Figure 2). Compound **6**, a yellow amorphous solid, had a UV

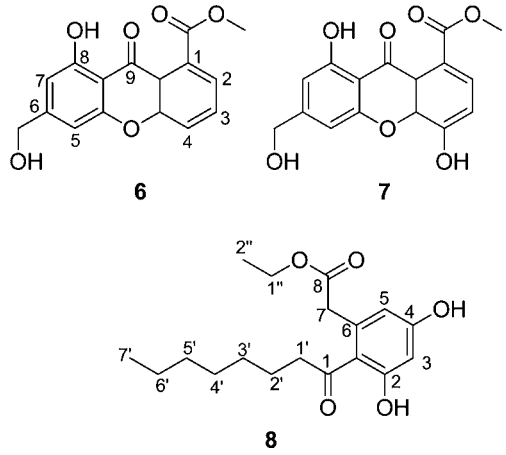


**Figure 2.** Compounds isolated from *P. viticola* complex and Sacc. DC239 and DC180: sydowinin A (**6**), sydowinol (**7**), and cytosporone B (**8**).

spectrum specific for a xanthone, with $\lambda_{max}$ at 233, 257, 291, 301, 362 nm. The molecular formula was deduced from $^1H$ NMR, $^{13}C$ NMR, DEPT, COSY, HMBC, and HMQC data as $C_{16}O_6H_{12}$ according to ESI MS (+) *m/z* 300.09 $[M + H]^+$ and $MS^2$ *m/z* 269.2 corresponded to the loss of a methoxyl group. Thus, compound **6** was identified as sydowinin A previously described from *Aspergillus sydowii*.[19]

The molecular formula $C_{16}O_7H_{12}$ for **7** was deduced from $^1H$ NMR, $^{13}C$ NMR, and DEPT data combined with MS data. The HRESI MS (−) *m/z* 315.0532 $[M - H]^-$ and $MS^2$ *m/z* 285.2 corresponded to the loss of the group methoxyl. 2D NMR data allowed the identification of compound **7** as sydowinol.[19] However, the identification of compounds **6** and **7** was reported only by $^1H$ NMR data; we report, in the Materials and Methods section, the complete spectral characterization by $^{13}C$ NMR.

The third compound **8** isolated from the second strain DC239, also isolated from the third strain *P. viticola* (Sacc.) Sacc. DC180, had a molecular formula of $C_{18}H_{26}O_5$, as deduced from $^1H$, $^{13}C$, and DEPT NMR spectroscopic data and HRESI MS (+) 345.1674 $[M + Na]^+$. The 1D and 2D NMR spectra in comparison with the literature led to the identification of compound **8** as cytosporone B, previously isolated from *Cytospora* sp. and *Diaporthe* sp.[20]

Biological activities for phomopsolide B (**1**) were previously reported for its antiboring/antifeeding activity against the elm bark beetle *Scolytus* sp.[16] and its good antibacterial activity against *Staphylococcus. aureus*.[21] Cytosporone B (**8**) was reported to have broad antifungal activities against *Aspergillus niger*, *Trichoderma* sp., *Fusarium* sp., and *Candida albicans*[22] and antibacterial activity against the methicillin-resistant *S. aureus* (MRSA ) bacterial strain;[23] however, there were no biological activities reported for sydowinin A and sydowinol.

Phytotoxic activity on grapevine leaves of cv. Chasselas was examined for all isolated compounds at the concentrations of 100, 250, and 500 $\mu$g/mL. Eutypine, the major phytotoxin isolated from *E. lata*,[24] was used as positive control at 500 $\mu$g/mL. Leaf necrosis was assessed 24 h after inoculation, and the values obtained are the mean of three replicates. Necrosis started to appears after 6 h at 500 $\mu$g/mL for cytosporone B (**8**) and eutypine. After 12 hours, eutypine, cytosporone B (**8**), and phomopsolide B (**1**) induced full necrosis on the leaf discs, whereas sydowinin A (**6**) and sydowinol (**7**) showed necrosis only on the leaf edges and phomopsolidones A−D did not induce leaf necrosis. The necrosis induced by phomopsolide B (**1**) was a bleaching type in opposition to the brownish ones usually observed, whereas cytosporone B induced a brown necrosis and the green part of the leaf became darker. Phytotoxicity against grapevine callus tissue was performed only with the major compound phomopsolide B (**1**) that induced 100% inhibition of callus growth at 60 $\mu$g/mL.

The antibacterial activity of compounds **1**−**3** was measured by the bioautography method on thin-layer chromatography against *Bacillus subtilis* and *Escherichia coli*. All three compounds showed minimal inhibitory concentration (MIC) at 0.1 ng against *B. subtilis* but did not show activity at 200 ng on *E. coli*.

Compounds **1**−**3**) were subjected to a larvicidal assay on larvae of the grapevine moth *L. botrana*. The trial was carried out at 1 and 10 ppm (mg/kg). The larvicidal activity of the product was calculated in relation to the corresponding control experiment for both the larval surviving rate at 14 days and also for the whole duration of the trial up to moth emergence. For the larvae reared with the contaminated diet, no significant difference in the survival rate was observed. The larval survival rates with 10 ppm at adult emergence reached 91.7% in the control, 65.0% with phomopsolide B (**1**), 90.0% with phomopsolidone A (**2**), and 68.3% with phomopsolidone B (**3**). The development delay at 10 ppm was more significant. The mean development time for the larvae for the control was 28 days, for phomopsolide B (**1**) was 31.41 days, for phomopsolidone A (**2**) was 30.48 days, and for phomopsolidone B (**3**) was 34.41 days.

Phomopsolidones A and B (**2** and **3**) with the furanone moiety displayed weaker phytotoxic and antibacterial activities than phomopsolide B (**1**) with the pyranone moiety; these results are in accordance with the herbicidal activity reported for phomalactone A (pyranone) and its furanone cometabolites isolated from *N. sacchari*.[24]


dx.doi.org/10.1021/jf501141g | J. Agric. Food Chem. 2014, 62, 8602−8607

Table 2. Strain Number, Species, Metabolites, and Cultivar Relationships: A Qualitative Analysis of Ethyl Acetate Extracts in HPLC-DAD-ESI MS as Reported in the Material and Methods Section[a]

| strain | species | isolated from | 1 | 2 | 6 | 7 | 8 |
|---|---|---|---|---|---|---|---|
| DC275[b] | *Phomopsis* sp. | Merlot As | X | X | nd | nd | nd |
| DC110 | *Phomopsi* sp. | Merlot As | X | X | nd | nd | nd |
| DC283 | *Phomopsis* sp. | Merlot As | X | X | nd | nd | nd |
| DC279 | *Phomopsis* sp. | Cabernet franc S | X | X | nd | nd | X |
| DC282 | *Phomopsis* sp. | Cabernet franc S | X | X | nd | nd | X |
| DC281[b] | *P. viticola* v. complex | Cabernet franc S | nd | nd | nd | X | X |
| DC239[b] | *P. viticola* v. complex | Cabernet sauvignon As | nd | nd | X | X | X |
| DC180[b] | *P. viticola* Sacc. | Cabernet sauvignon As | nd | nd | nd | nd | X |
| DC301 | *Phomopsis*sp. | Cabernet sauvignon S | X | X | nd | nd | X |

[a]As: asymptomatic plants; S: plants showing esca symptoms. [b]Strains identified by the Belgium Coordinated Collections of Microorganisms.

Four out of the nine strains studied were identified by the Belgian Coordinated Collections of Microorganisms (BCCM) of the Catholic University of Louvain-la-Neuve. Strain DC180 was identified as the typical type of strain found on *Vitis*, *P. viticola* (Sacc.) Sacc. Strains DC239 and DC281) were described as being very similar, with the dimensions of $\alpha$-conidia slightly bigger than those described for the typical *viticola* strain. The molecular biological analysis and sequencing of the ITS and 28S zones made it possible to note that the two samples have a succession of bases similar to that described by Mostert et al.[1] called *Phomopsis* sp. 2 and taken up in the "*P. viticola* complex". Strain DC275 showed smaller $\alpha$-conidia and shorter $\beta$-conidia than those described for the *viticola* species, but a molecular biological study did not give results allowing further identification of the strain. Thus, the strain could only be identified as being a species belonging to the *Phomopsis* sp.

In order to examine the compounds produced as a function of strain species, the original LC-DAD-MS data of the nine strains were reinvestigated in the light of the identified metabolites (Table 2). The strains could be divided into three groups. The first group included the strain producing phomopsolide, phomopsolidones, and cytosporone B (strains DC110, DC275, DC283, DC279, DC282, and DC301) and correlate with *Phomopsis* sp. The second group included a strain producing cytosporone B (**8**) alone corresponding to *P. viticola* (Sacc.) Sacc (DC180), and finally, the third group producing cytosporone B (**8**) together with sydowinin A (**6**) and sydowinol (**7**) corresponded to *P. viticola* v. complex (strains DC239 and DC281). Three out of the six strains producing the phytotoxic phomopsolide B (**1**) were isolated from asymptomatic cv. Merlot (a less susceptible cultivar). From plants showing esca symptoms,[12] two strains were isolated from Cabernet franc and one from Cabernet sauvignon (both sensitive cultivars); these strains produce compounds **1** and **2** together with cytosporone B (**8**). Strains producing cytosporone B (**8**) and xanthones **6** and **7** were isolated from symptomatic Cabernet franc and asymptomatic cv. Cabernet sauvignon. These results indicate that *Phomopsis* sp. of sensitive cultivars in plants showing esca symptoms produce the phytotoxic compounds phomopsolide B (**1**) and cytosporone B (**8**) raising the question of cultivar-driven strain selection and the stimulation of phytotoxins biosynthesis in grapevine plants. Phomopsolide B (**1**) has been reported from several species of *Phomopsis* from several host plants such as elm willow, quercus, platanus, heliconia, myrica, and liriodendron,[7] indicating that the biosynthesis of this secondary metabolite does not seem to be correlated with the host plant from which the *Phomopsis* isolate was obtained. It is likewise for cytosporone B (**8**) reported from *Phomopsis* sp. isolated from different host plants such as cacao, coffee, and mango.[25,26]

This study revealed that the *Phomopsis* isolates, associated with grapevine showing esca decline, show high variability with regard to secondary metabolites production. The role played by the fungi is not clear, but they may be weak pathogens, saprophytes, or endophytes.[5] The complexity of signaling between microorganisms and plants and between microorganisms themselves in grapevine trunk disease is still poorly understood. Characterization of metabolites biosynthesized by several fungi infecting grapevine wood is crucial not only for the phytotoxic properties but also is essential to better understand the conditions under which the fungi start producing the toxins and modify their lifestyle from endophytic to saprotrophic.

## ■ ASSOCIATED CONTENT

### Supporting Information

HRESI MS spectra of compounds **1**−**5**, **7** and **8**; ESI MS spectrum of **6**; IR, $^{1}$H NMR, $^{13}$C NMR, COSY, HSQC, and HMBC spectra of compounds **2** and **3**. This material is available free of charge via the Internet at http://pubs.acs.org.

## ■ AUTHOR INFORMATION


### Corresponding Author

*Phone: +41 26 300 88 05; e-mail: eliane.abou-mansour@unifr.ch.

### Present Addresses

⊥Nicolas Mottier: Philip Morris Products SA, Quai Jeanrenaud 5, 2000 Neuchâtel, Switzerland.

#Danilo Christen: Agroscope, Centre de recherche Conthey, Route des vergers 18, CH-1964 Conthey, Switzerland.



### Funding

We thank Swiss National Science Foundation for their financial support (project no. 20-67972-02) and the National Centre of Competence in Research (NCCR) Plant Survival.


### Notes

The authors declare no competing financial interest.

## ■ ACKNOWLEDGMENTS

We thank S. Unternaehrer for the biological tests on callus tissue. We thank Dr. P. Larignon (Institut Français de la Vigne et du Vin) for leaves and trunk necrosis photographs of the graphic, and Dr. Antony Buchala for English revision.

## ■ REFERENCES

(1) Mostert, L.; Crous, P. W.; Kang, J.-C. Species of *Phomopsis* and a *Libertella* sp. occurring on grapevines with specific reference to South

Africa: Morphological, cultural, molecular and pathological characterization. *Mycologia* **2001**, *93*, 146−167.
(2) Pearson, R. C.; Goheen, R. C. *Compendium of Grape Diseases*; American Phytpathological Society Press: St. Paul, MN, 1994; pp 17−18.
(3) Fisher, M.; Kassemeyer, H.-H. Fungi associated with Esca disease of grapevine in Germany. *Vitis* **2003**, *42*, 109−116.
(4) Urbez-Torres, J. R.; Leavitt, G. M.; Voegel, T. M.; Gubler, W. D. Identification and distribution of *Botryosphaeria* spp. associated with grapevine cankers in California. *Plant Dis.* **2006**, *90*, 1490−1503.
(5) Hofstetter, V.; Buyck, B.; Croll, D.; Viret, O.; Couloux, A.; Gindro, K. What if esca disease of grapevine were not a fungal disease? *Fungal Diversity* **2012**, *54*, 51−67.
(6) Phillips, A. J. L. The relationship between *Diaporthe perjuncta* and *Phomopsis viticola* on grapevines. *Mycologia* **1999**, *91*, 1001−1007.
(7) Udayanga, D.; Liu, X.; McKenzie, E. H. C.; Chukeatirote, E.; Bahkali, A. H. A.; Hyde, K. D. The genus *Phomopsis*: Biology, applications, species concepts and names of common phytopathogens. *Fungal Diversity* **2011**, *50*, 189−225.
(8) Andolfi, A.; Mugnai, L.; Luque, J.; Surico, G.; Cimmino, A.; Evidente, E. Phytotoxins produced by fungi associated with grapevine trunk diseases. *Toxins* **2011**, *3*, 1569−1605.
(9) Tabacchi, R.; Fkyerat, A.; Poliart, C.; Dubin, G.-M. Phytotoxins from fungi of esca of grapevine. *Phytopathol. Mediterr.* **2000**, *39*, 156−161.
(10) Djoukeng, J. D.; Polli, S.; Larignon, P.; Abou-Mansour, E. Identification of phytotoxins from *Botryosphaeria obtusa*, a pathogen of black dead arm disease of grapevine. *Eur. J. Plant Pathol.* **2009**, *124*, 303−308.
(11) Abou-Mansour, E.; Couché, E.; Tabacchi, R. Do fungal naphthalenones have a role in the development of esca symptoms? *Phytopathol. Mediterr.* **2004**, *43*, 75−82.
(12) Christen, D.; Schönmanna, S.; Jermini, M.; Strasser, R. J.; Défago, G. Characterization and early detection of grapevine (*Vitis vinifera*) stress responses to esca disease by in situ chlorophyll fluorescence and comparison with drought stress. *Environ. Exp. Bot.* **2007**, *60*, 504−514.
(13) Hadacek, F.; Greger, H. Testing of antifungal natural products: Methodologies, comparability of results and assay choice. *Phytochem. Anal.* **2000**, *11*, 137−147.
(14) Charmillot, P. J.; Pasquier, D.; Verneau, S. Efficacité larvicide de différents insecticides incorporés au milieu artificiel d'élevage sur les vers de la grappe 1. Tests sur eudémis *Lobesia botrana*. *Rev. Suisse Vitic., Arboric., Hortic.* **2004**, *36*, 141−145.
(15) Grove, J. F. Metabolic products of *Phomopsis oblonga*. Part 2.sup.1. Phomopsolide A and B, tiglic esters of two 6-substituted 5, 6-dihydro-5-hydroxypyran-2-ones. *J. Chem. Soc., Perkin Trans I* **1985**, *4*, 865−869.
(16) Claydon, N.; Grove, J. F.; Pople, M. Elm bark beetle boring and feeding deterrents from *Phomopsis oblonga*. *Phytochemistry* **1985**, *24*, 937−943.
(17) Horn, W. S.; Simmonds, M. S. J.; Schwartz, R. E.; Blaney, W. M. Variation in the production of phomodiol and phomopsolide B by *Phomopsis. spp*. *Mycologia* **1996**, *88*, 588−595.
(18) Fukushima, T.; Tanaka, M.; Gohbara, M.; Fujimori, T. Phytotoxicity of three lactones from *Nigrospora sacchari*. *Phytochemistry* **1998**, *48*, 625−630.
(19) Hamasaki, T.; Sato, Y.; Hatsuda, Y. Structure of sydowinin A, sydowinin B, and sydowinol, metabolites from *Aspergillus sydowi*. *Agric. Biol. Chem.* **1975**, *39*, 2341−5.
(20) Brady, S. F.; Wagenaar, M. M.; Singh, M. P.; Janso, J. E.; Clardy, J. The cytosporones, new octaketide antibiotics isolated from an endophytic fungus. *Org. Lett.* **2000**, *2*, 4043−4046.
(21) Stierle, D. B.; Stierle, A. A.; Ganser, B. New phomopsolides from a *Penicillium* sp. *J. Nat. Prod.* **1997**, *60*, 1207−1209.
(22) Huang, Z.; Cai, X.; Shao, C.; She, Z.; Xia, X.; Chen, Y.; Yang, J.; Zhou, S.; Lin, Y. Chemistry and weak antimicrobial activities of phomopsins produced by mangrove endophytic fungus *Phomopsis* sp. ZSU-H76. *Phytochemistry* **2008**, *69*, 1604−1608.
(23) Beau, J.; Mahid, N.; Burda, W.; Harrington, L.; Shaw, L.; Mutka, T.; Kyle, D. E.; Barisic, B.; Van Olphen, A.; Baker, B. Epigenetic tailoring for the production of anti-infective cytosporones from the marine fungus *Leucostoma persoonii*. *Mar. Drugs* **2012**, *10*, 762−774.
(24) Renaud, J.-M.; Tsoupras, G.; Tabacchi, R. Biologically active natural acetylenic compounds from *Eutypa lata* (Pers.:Fr.)Tul. *Helv. Chim. Acta* **1989**, *72*, 929−932.
(25) Toshiro, F.; Masayasu, T.; Masatoshi, G.; Takane, F. Phytotoxicity of three lactones from *Nigrospora sacchari*. *Phytochemistry* **1998**, *48*, 625−630.
(26) Abreu, L. M.; Costa, S. S.; Penning, L. H.; Takahashi, J. A.; Larsen, T. O.; Andersen, B. Chemical and molecular characterization of *Phomopsis* and *Cytospora*-like endophytes from different host plants in Brazil. *Fungal Biol.* **2012**, *116*, 249−260.

JOURNAL OF AGRICULTURAL AND FOOD CHEMISTRY

Article

pubs.acs.org/JAFC

# Functional Analyses on Antioxidant, Anti-inflammatory, and Antiproliferative Effects of Extracts and Compounds from *Ilex latifolia* Thunb., a Chinese Bitter Tea

Ting Hu, Xiao-Wei He, and Jian-Guo Jiang*

College of Food and Bioengineering, South China University of Technology, Guangzhou 510640, China

**ABSTRACT:** *Ilex latifolia* Thunb., widely distributed in China, has been used as a functional food and drunk for a long time. This study was aimed to identify the bioactive constituents with antioxidant, antitumor, and anti-inflammatory properties. *I. latifolia* was extracted with 95% ethanol and then partitioned into four fractions: petroleum ether fraction, ethyl acetate fraction, *n*-butanol fraction, and water fraction. Results showed that the ethyl acetate fraction was found to have significant ferric reducing antioxidant power activity, DPPH radical scavenging activity, and oxygen radical absorbance capacity, cytotoxicity against human cervix carcinoma HeLa cells, and inhibitory effect on NO production in macrophage RAW 264.7 cells. Five compounds were isolated from the ethyl acetate fraction, and they were identified as ethyl caffeate (**1**), ursolic acid (**2**), chlorogenic acid (**3**), 3,4-di-*O*-caffeoylquinic acid methyl ester (**4**), and 3,5-di-*O*-caffeoylquinic acid methyl ester (**5**), the last two of which were isolated for the first time from *I. latifolia*. Compounds **4** and **5** exhibited cytotoxicity actions against tumor cell line. Compound **3** showed the strongest anti-inflammatory activity of all the compounds. The results obtained in this work might contribute to the understanding of biological activities of *I. latifolia* and further investigation on its potential application values for food and drug.

**KEYWORDS:** *I. latifolia, antioxidant, antitumor, anti-inflammatory, ursolic acid, chlorogenic acid, 3,4-di-O-caffeoylquinic acid methyl ester, 3,5-di-O-caffeoylquinic acid methyl ester*

## INTRODUCTION

*Ilex latifolia* Thunb. is a bitter tea of Chinese origin. It has been consumed traditionally as a kind of tea in China and southeastern Asia for a long time. The taste of *I. latifolia* is much more bitter than that of tea made from the leaves of *Camellia sinensis*.[1] The main species are *I. latifolia* and *Ilex cornuta*, which belong to the same genus as Mate (*Ilex paraguariensis*).[2−4] *I. latifolia* has gained attention as a functional tea in the past decade because of its potential health and economic significance. Many beneficial functions of *I. latifolia* such as cardiovascular, antioxidant, antiobesity, antidiabetic, anti-inflammatory, hepatoprotective, and neuroprotective effects have been reported.[5,6]

There is a growing interest in *I. latifolia* about its chemical composition and functions due to its applications in cancer chemotherapy and other various pharmacological effects, particularly antitumor and anti-inflammatory activities.[7,8] *I. latifolia* remains an underutilized natural resource. To develop its health-promoting compounds into new food ingredients or nutraceutical applications, more research is urgently needed for the isolation and identification of the compounds with efficient procedures from *I. latifolia* extracts.

The main purpose of the present study was to isolate the bioactive constituents with antioxidant, antitumor, and anti-inflammatory properties. The crude extract and four fractions (petroleum ether fraction, ethyl acetate fraction, *n*-butanol fraction, and water fraction), which partitioned from a 95% ethanol extract of *I. latifolia*, were measured to compare their activities by the use of ferric reducing antioxidant power assay (FRAP), 2,2-diphenyl-1-picrylhydrazyl (DPPH) radical scavenging assay, oxygen radical absorbance assay (ORAC), cell proliferation assay against human cervix carcinoma HeLa cells, and inhibitory effect on NO production in LPS-induced RAW 264.7 macrophages. The activities of five compounds isolated from the ethyl acetate fraction were also determined.

## MATERIALS AND METHODS

**Plant Material.** *I. latifolia*, derived from Wuzhishan city (Hainan province, China), was purchased from Forest Drugstore Chain Co., Ltd., of Guangzhou, China. Samples were air-dried under shade for 1 week and pulverized to powder. The dried materials were stored in a well-closed container for further use.

**Reagents.** Methanol, HPLC grade water, Folin−Ciocalteu phenol reagent, and sodium carbonate were purchased from chemical reagent factory (Tianjing, China). DPPH, lipopolysaccharide (LPS), 3-(4,5-dimethylthiazol-2-yl)-2,5-diphenyltetrazolium bromide (MTT), *N*-1-naphthylethylenediamine dihydrochloride, sulfanilamide, 5-fluorouracil, gallic acid, and Trolox were purchased from Sigma Chemical Co. (USA). Human cervix carcinoma HeLa cell line and mouse macrophage RAW 264.7 cell line were obtained from the cell bank of the Chinese Academy of Sciences (CAS, Shanghai, China). Cell culture medium and all other materials required for cell culture were purchased from Life Technologies Corp. (Grand Island, NY, USA). All the other chemicals were of analytical grade.

**Extraction, Isolation, and Purification.** The process of *I. latifolia* extraction and isolation is shown in Figure 1. The dried powder (3 kg) of *I. latifolia* was extracted with 95% ethanol (3 × 10 L) for 3 h at 80 °C. The crude extract was evaporated to dryness under reduced pressure. The extract was suspended in water (1.5 L) first and then partitioned with petroleum ether, ethyl acetate, and *n*-butanol in sequence with the same volume (shaken sharply to mixt, then allowed to stand for 4 h at room temperature and atmosphere pressure every

Received: April 9, 2014
Revised: August 13, 2014
Accepted: August 13, 2014
Published: August 13, 2014

 © 2014 American Chemical Society  dx.doi.org/10.1021/jf501670v | J. Agric. Food Chem. 2014, 62, 8608−8615

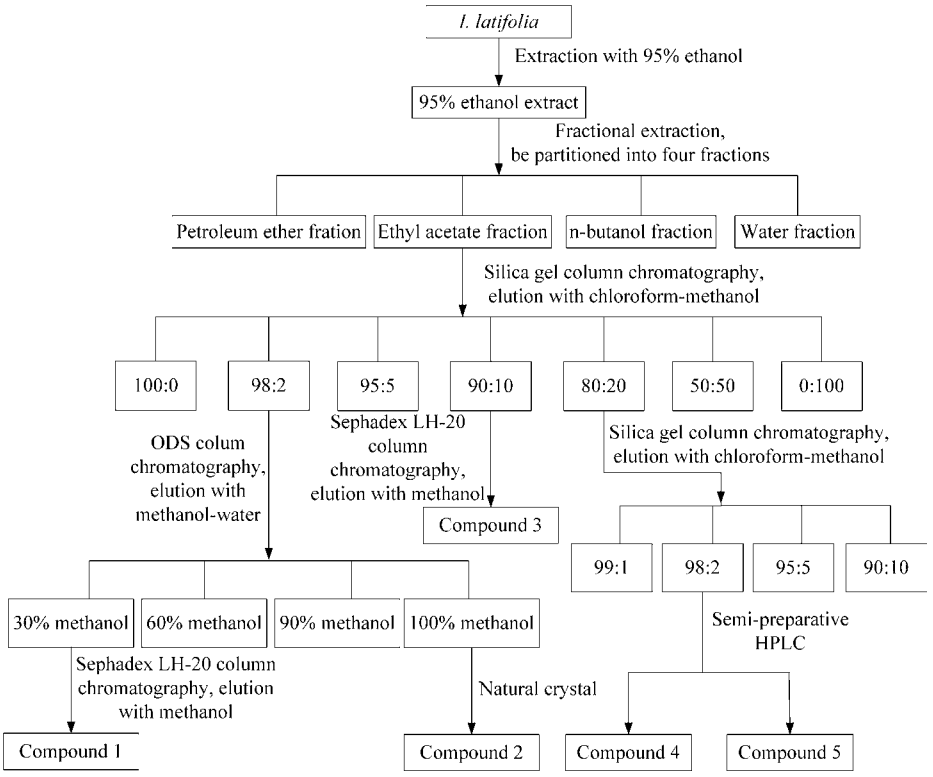


**Figure 1.** Extraction and isolation procedure of compounds from the 95% ethanol extract of *I. latifolia*.

**Table 1. Total Phenolic Contents (TPC) and Ferric Reducing Antioxidant Power (FRAP), Scavenging of the Free Radical DPPH, Oxygen Radical Absorbance Capacity (ORAC), and Percent (w/w) Extraction Yield of *I. latifolia* Ethanol Extract and Its Four Fractions on the Basis of Freeze-Dried Starting Material[a]**

| sample | TPC (mg GAE/g DW) | FRAP ($\mu$mol TE/g DW) | DPPH ($IC_{50}$, $\mu$g/mL) | ORAC ($\mu$mol TE/g DW) | extraction yield (w/w, %) |
|---|---|---|---|---|---|
| 95% ethanol extract | 84.4 ± 1.3 c | 148.65 ± 0.04 c | 28.7 ± 2.1 b | 1198 ± 89 c | 30.4 |
| petroleum ether fraction | 32.5 ± 0.6 d | 112.38 ± 0.04 d | not found | 139 ± 5 e | 3.7 |
| ethyl acetate fraction | 125.7 ± 7.8 a | 265.05 ± 1.5 a | 16.3 ± 3.3 c | 2367 ± 108 a | 15.2 |
| *n*-butanol fraction | 93.2 ± 6.2 b | 175.65 ± 0.09 b | 29.5 ± 1.5 b | 1921 ± 23 b | 5.1 |
| water fraction | 87.9 ± 4.1 c | 139.22 ± 0.04 c | 47.7 ± 2.6 a | 652 ± 36 d | 5.9 |

[a]Data are expressed as means ± standard deviation. Averages followed by different lower case letters in different columns differ significantly by one-way analysis of variance−Duncan's multiple-range test ($p \leq 0.05$). GAE, gallic acid equivalent; TE, Trolox equivalent; DW, dry weight.

time), which yielded a petroleum ether fraction (111.3 g), an ethyl acetate fraction (456.2 g), an *n*-butanol fraction (153.5 g), and a water fraction (177.4 g), respectively (for extraction yields see Table 1). The ethyl acetate fraction was chosen for further isolation becausse of its better activity among the four fractions in the biological activity screening tests.

It was dissolved in chloroform, applied to a silica gel (200−300 mesh) column (7.5 cm × 1.2 m), and eluted with a gradient of chloroform and methanol (100:0, 98:2, 95:5, 90:10, 80:20, 50:50, 0:100, v/v, each 10 L). The eluates were pooled into 28 fractions (100:0, fractions 1−2; 98:2, fractions 3−7; 95:5, fractions 8−12; 90:10, fractions 13−17; 80:20, fractions 18−22; 50:50, fractions 23−27; 0:100, fraction 28) on the basis of thin-layer chromatography (TLC) and high-performance liquid chromatography (HPLC). Fraction 6 (from the 98:2 fraction) was loaded on an ODS column and eluted with a mixture of methanol and water (30, 60, 90, and 100%, v/v, each 2.5 L) to obtain four fractions. The 30% methanol fraction was further purified by Sephadex LH-20 column chromatography, and compound **1** was obtained (300 mg). The 100% fraction appears as a crystal, and compound **2** was obtained (13 g). Fraction 17 was purified by Sephadex LH-20 column chromatography eluted with methanol, and compound **3** was obtained (5 g). Fraction 20 (from 90:10 fraction) was dissolved in chloroform and applied on a second silica gel column (5 cm × 80 cm). The column was eluted with a stepwise mixture of chloroform and methanol (99:1, 98:2, 95:5, 90:10, v/v, each 5 L), and the 98:2 fraction continued to separate followed by semipreparative HPLC using a 48% methanol solution as the mobile phase, to yield compounds **4** (1.2 g) and **5** (900 mg). The yields of extraction of five compounds (based on the initial 3 kg of dried *I. latifolia*) are 0.01, 0.43, 0.17, 0.04, and 0.03%, respectively.

The isolated compounds and 95% EtOH extract were dissolved in methanol (approximately 2 mg/mL) filtered through a 0.45 $\mu$m micropore membrane before use, and 20 $\mu$L was injected into the HPLC instrument for analysis. The relative contents in percentage of each compound in the initial extract were determined and calculated with the area normalization method, which are 0.22, 2.09, 1.07, 0.35, and 0.28%, respectively. The purity of the five compounds was detected by HPLC, and all were >95%.

**Determination of Total Phenolic Content (TPC).** A precisely weighed amount of samples was used for TPC, which were dissolved in methanol solution. The TPC was determined by using Folin−Ciocalteu's reagent method.[9] Briefly, the appropriate sample solution was oxidized with the Folin−Ciocalteu reagent, and sodium carbonate was used to neutralize the reaction. After a 30 min incubation period, absorbance was measured at 765 nm. The concentration was calculated using gallic acid as standard, and the results were expressed as


dx.doi.org/10.1021/jf501670v | J. Agric. Food Chem. 2014, 62, 8608−8615

milligrams of gallic acid equivalents (GAE) per gram of dry weight (DW) and are shown in Table 1.

**Assays for FRAP.** Assays for FRAP were measured by using the method of Benzie and Strain,[10] in which the absorbance at 593 nm was measured. Results were expressed as Trolox equivalents per gram of dry weight (TE/g DW).

**Assays for DPPH Radical Scavenging.** Assays for DPPH radical scavenging were determined by the method of Villaño et al.[11] with some modifications. Briefly, a total of 0.1 mL of sample in ethanol was added to 3.0 mL of DPPH ethanolic solution. Absorbance was measured at 517 nm after 30 min at room temperature in the dark. All measurements were performed in triplicate. The percent DPPH scavenging ability was calculated as DPPH scavenging ability = $(A_{control} - A_{sample}/A_{control}) \times 100$. $IC_{50}$ values calculated denote the concentration of a sample required to decrease the absorbance at 517 nm by 50%. The lower the $IC_{50}$ value, the more powerful the antioxidant capacity.

**Assays for ORAC.** Assays for PRAC were determined according to the method of Dávalos et al.[12] with some modifications. In brief, samples were diluted with $NaH_2PO_4$–$Na_2HPO_4$ solution (75 mM, pH 7.4) and then placed on microplates along with fluorescein solution (39.9 $\mu$M) and AAPH solution (38.25 mM). The plates were incubated in an automated microplate reader at 37 °C and read every minute for 70 min using a fluorescence detector with an excitation wavelength of 485 nm and an emission wavelength at 520 nm. A calibration curve was prepared using Trolox, and the results were expressed as Trolox equivalents per gram of dry weight (TE/g DW).

**Cell Culture.** The cell lines used in this study were human cervix carcinoma HeLa and mouse macrophage RAW 264.7. Cells were maintained and cultured in tissue culture flasks (25 $cm^2$, Corning) containing DMEM (Gibco BRL) supplemented with 10% fetal bovine serum (FBS), 1% penicillin (100 IU/mL), and streptomycin (100 $\mu$g/mL) at 37 °C in a humidified incubator with 5% $CO_2$. The medium was changed every 24–48 h.[13]

Dried samples were first dissolved in DMSO and then were diluted with the culture medium into different concentrations. The final concentration of DMSO in the culture medium was maintained at <0.5% (v/v) to avoid solvent toxicity.

**Antitumor Activity.** The effect of samples on the proliferation of HeLa cell was tested by MTT assay. MTT is captured by cells and reduced intracellularly in a mitochondrion-dependent reaction to yield formazan product. The ability of cells to reduce MTT provides an indication of their intactness and mitochondrial activity that serves as a measure of viability.[14,15] Exponential growth phase HeLa cells were plated into 96-well culture plates ($5 \times 10^4$ cells/mL, 100 $\mu$L/well) and incubated overnight. When the cells were attached to the plates, an equal volume of fresh medium containing different concentrations of samples was added. After 24 h, the supernatant was discarded and cells were washed with PBS two times. Two hundred microliters of fresh medium containing 20 $\mu$L of MTT (0.5 mg/mL) solution was added to each well followed by incubation for 4 h at 37 °C. After this period, the supernatant was removed and 150 $\mu$L of DMSO was added to dissolve formazan crystals. The absorbance was measured at 490 nm after the plates had been shaken for 8 min. 5-Fluorouracil is a kind of natural antitumor drug, and it shows a strong effect in antitumor assays. It was very popularly used as a positive control in antitumor activities. Therefore, 5-fluorouracil was used as a positive control in this work. The percentage of cell proliferation inhibition was calculated using the following formula (eq 1):[16]

$$\text{cell proliferation inhibition (\%)} = \left(1 - \frac{OD_{sample}}{OD_{control}}\right) \times 100\% \quad (1)$$

**Anti-inflammatory Assays.** The anti-inflammatory activities of total crude extraction fraction, ethyl acetate fraction, petroleum ether fraction, water fraction, *n*-butyl alcohol fraction, and isolated compounds were tested with RAW 264.7 macrophages in vitro. First, a cytotoxicity test should be performed by MTT assay to choose the samples for further investigation, which were nontoxic to normal cells. Thereafter, the samples with no toxicity could be done using the anti-inflammatory activity below.

Exponential growth phase RAW 264.7 cells were seeded into 96-well culture plates ($1 \times 10^5$ cells/mL, 100 $\mu$L/well) and incubated overnight. When the cells were attached to the plates, an equal volume of fresh medium containing different concentrations of samples was added. Then cells were stimulated with LPS (final concentration was 1 $\mu$g/mL). After 24 h, the supernatants were collected to measure NO content using the Griess reaction[17] with minor modifications. In brief, 100 $\mu$L of cell supernatants was added with 50 $\mu$L of 0.1% *N*-1-naphthylethylenediamine dihydrochloride in distilled water and 50 $\mu$L of 1% sulfanilamide in 5% $H_3PO_4$. The absorbance was measured at 540 nm after the plates were allowed to stand for 8 min at room temperature. A sodium nitrite standard curve was obtained and used to calculate the nitrite level in samples. NO inhibition rate was calculated using the following formula (eq 2):[18]

$$\text{NO inhibition (\%)} = \frac{OD_{LPS} - OD_{LPS+sample}}{OD_{LPS} - OD_{blank}} \times 100\% \quad (2)$$

**Statistical Analysis.** All of the experiments were carried out in three replications. The data were expressed as the mean ± standard deviation (SD). SPSS statistical analysis software was used to perform analysis of variance (ANOVA). Each group treated was compared with the corresponding controls by means of Student's *F* test and correlation test. Significant difference was checked by Duncan's multiple-range test, and the level was set at $p < 0.05$.

## RESULTS AND DISCUSSION

**Total Phenolic Content and Antioxidant Activity of Extract and Fractions from *I. latifolia*.** The crude extract (95% EtOH) made from *I. latifolia* with 95% ethanol was fractionated through solvent–solvent partitioning to obtain four fractions: petroleum ether fraction (PE), ethyl acetate fraction (EA), *n*-butanol fraction (*n*-BuOH), and water fraction (W). The extraction yields of 95% EtOH, PE, EA, *n*-BuOH, and W on the basis of freeze-dried starting material (3 kg) were 30.4, 3.7, 15.2, 5.1, and 5.9%, respectively (Table 1). The total recovery of the four fractions was 29.9%, and the remaining 0.5% may be lost during the solvent–solvent partition, concentration, and lyophilization.

The Folin–Ciocalteu reagent is used to obtain a crude estimate of the amount of phenolic compounds present in an extract. In the present study, a TPC of 95% EtOH and the four fractions was determined using the Folin–Ciocalteu method. As a result, TPC of the crude extract and four fractions decreased in the following order: EA > *n*-BuOH > 95% EtOH > W > PE, which is shown in Table 1. The TPC of the ethyl acetate fraction was much higher than those of the 95% EtOH and other fractions. It seems that ethyl acetate was the most suitable solvent to concentrate phenolic substances. Moreover, a lower TPC was found in the petroleum ether fraction.

Dietary antioxidants have been shown to prevent the oxidation of biomolecules, which can be regarded as effective scavengers of detrimental free radicals.[24,25] Tea is a good source of dietary antioxidants, such as caffeoylquinic acids and tea polyphenols. The antioxidant properties of tea are primarily owed to the phenolic content, and several epidemiological research studies have shown the chemoprotective properties of polyphenols.[26] In this work, the antioxidant activities of extract and fractions from *I. latifolia* have been evaluated in vitro. The crude extract (95% EtOH) and its four fractions, PE, EA, *n*-BuOH, and W, were evaluated for antioxidant activities using FRAP, DPPH radical scavenging activity, and ORAC, and the results were compared (Table 1). The activities decreased in the order EA > *n*-BuOH > 95% EtOH > W > PE, according to the FRAP and ORAC assays, with the exception of the rank order of *n*-BuOH and 95% EtOH in the DPPH assay.

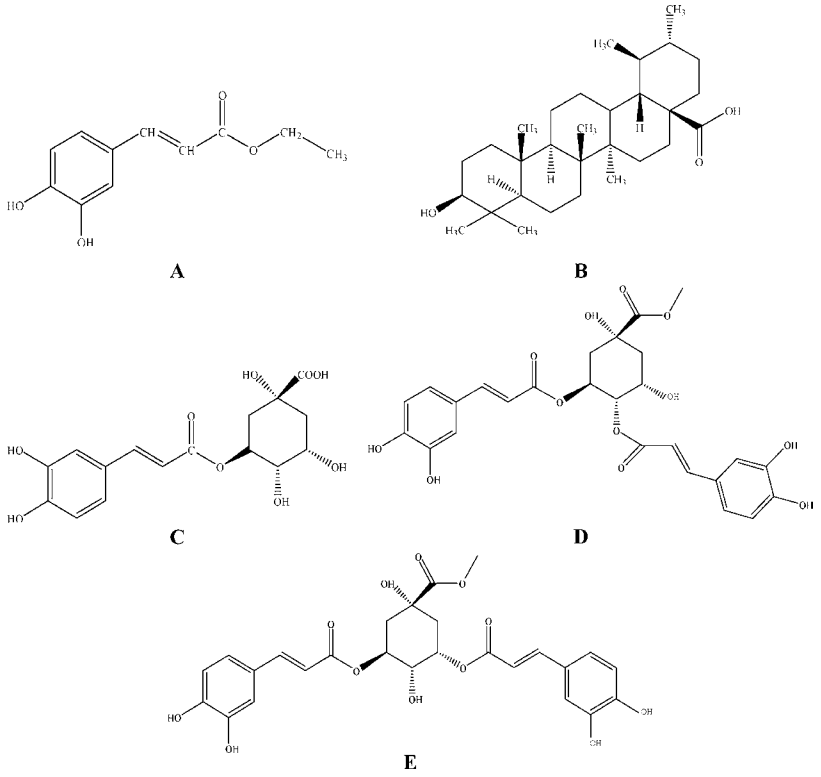


**Figure 2.** Compounds and their chemical structures isolated from *I. latifolia*: (A) ethyl caffeate; (B) ursolic acid; (C) chlorogenic acid; (D) 3,4-di-*O*-caffeoylquinic acid methyl ester; (E) 3,5-di-*O*-caffeoylquinic acid methyl ester.

This trend was similar to that observed for the TPC. The ethyl acetate fraction of *I. latifolia* exhibited a remarkable FRAP value (265.05 ± 1.5 μmol TE/g DW), free radical scavenging activity against DPPH ($IC_{50}$ = 16.3 ± 3.3 μg/mL), and ORAC value (2367 ± 88 μmol TE/g DW). By comparing 95% EtOH and its four fractions, the antioxidant power of 95% EtOH was less than those of EA and *n*-BuOH in the FRAP and ORAC assays, which may result from the active components through condensation effects during the solvent−solvent partitioning progress. The extract of *I. latifolia* was certified to contain a large number of caffeoylquinic acids, which contributed to the antioxidant activity.[27] It is observed that *I. latifolia* is a beneficial herbal drink due to its antioxidant activity.

**Identification of Isolated Compounds.** The structure identification of isolated compounds was performed with MS, $^1$H NMR, and $^{13}$C NMR analyses and comparison with the previously reported spectral data; the chemical structures of five compounds were identified and are shown in Figure 2. Spectroscopic data are described below.

*Compound **1** was obtained as a brown acicular crystal.* The negative ESI-MS showed a quasi-molecular ion at *m*/*z* 206.8 $[M - H]^-$. $^1$H NMR ($CD_3OD$-$d_4$, 400 MHz) δ 7.52 (1H, d, *J* = 15.9 Hz), 6.23 (1H, d, *J* = 15.9 Hz), 7.03 (1H, d, *J* = 1.9 Hz), 6.77 (1H, d, *J* = 8.4 Hz), 6.92 (1H, dd, *J* = 1.9, 8.4 Hz), 4.18 (2H, q, *J* = 6.6 Hz), 1.30 (3H, t, *J* = 6.6 Hz); $^{13}$C NMR ($CD_3OD$-$d_4$, 101 MHz) δ 167.4 (C-1), 114.8 (C-2), 145.5 (C-3), 127.4 (C-4), 115.5 (C-5), 146.2 (C-6), 148.7 (C-7), 116.2 (C-8), 122.3 (C-9), 60.4 (C-1′), 14.5 (C-2′). Compared with the NMR and MS data given in ref 19, compound **1** was identified as ethyl caffeate.

*Compound **2** was obtained as a white prismatic crystal.* The negative ESI-MS showed a quasi-molecular ion at *m*/*z* 455.2 $[M - H]^-$. $^1$H NMR ($CD_3Cl$-$d_4$, 400 MHz) δ 2.10 (1H, d, H-18), 3.13 (1H, t, H-3), 5.26 (1H, t, H-12), 0.80 (3H, d, *J* = 7.6 Hz, H-29), 0.70 (3H, d, *J* = 7.6 Hz, H-30), 1.26, 1.10, 0.89, 0.86, 0.78 (5 × 3H, s); $^{13}$C NMR ($CD_3Cl$-$d_4$, 101 MHz) δ 38.7 (C-1), 27.3 (C-2), 79.1 (C-3), 38.8 (C-4), 55.3 (C-5), 18.4 (C-6), 33.0 (C-7), 39.6 (C-8), 47.7 (C-9), 37.1 (C-10), 23.4 (C-11), 125.9 (C-12), 138.0 (C-13), 42.1 (C-14), 28.2 (C-15), 24.3 (C-16), 47.9 (C-17), 52.8 (C-18), 39.1 (C-19), 38.8 (C-20), 30.7 (C-21), 36.8 (C-22), 28.1 (C-23), 15.6 (C-24), 15.5 (C-25), 17.0 (C-26), 23.6 (C-27), 181.2 (C-28), 17.5 (C-29), 21.4 (C-30). These ESI-MS, $^1$H NMR, and $^{13}$C NMR data were similar to those in a previous paper;[20] therefore, compoud **2** was identified as ursolic acid. It was found to be the major constituent isolated from *I. latifolia*.

*Compound **3** was obtained as a white powder.* The negative ESI-MS showed a quasi-molecular ion at *m*/*z* 352.7 $[M - H]^-$. $^1$H NMR ($CD_3OD$-$d_4$, 400 MHz) δ 2.21 (dd, *J* = 13.6, 3.1 Hz), 2.07 (dd, *J* = 13.6, 4.4 Hz), 4.20 (ddd, *J* = 3.1, 4.4, 3.1 Hz), 3.76 (dd, *J* = 8.5, 3.1 Hz), 5.37 (ddd, *J* = 9.3, 4.8, 8.5 Hz), 2.11 (dd, *J* = 13.6, 9.3 Hz), 2.26 (dd, *J* = 13.6, 4.8 Hz), 7.08 (d, *J* = 2.0 Hz), 6.81 (d, *J* = 8.2 Hz), 6.98 (dd, *J* = 8.2, 2.0 Hz), 7.59 (d, *J* = 15.9 Hz), 6.29 (d, *J* = 15.9 Hz); $^{13}$C NMR ($CD_3OD$-$d_4$, 101 MHz) δ 126.6 (C-1), 114.1 (C-2), 144.2 (C-3), 147.0 (C-4), 116.0 (C-5), 122.6 (C-6), 145.9 (C-7), 115.2 (C-8), 168.9 (C-9), 76.6 (C-10), 38.8 (C-11), 70.6 (C-12), 72.8 (C-13), 71.0 (C-14), 37.3 (C-15), 180.1 (C-16). These data were in good agreement with the reported compound, chlorogenic acid.[21]

*Compound **4** was obtained as a yellow powder.* The negative ESI-MS showed a quasi-molecular ion at *m*/*z* 529 $[M - H]^-$. $^1$H NMR (DMSO-$d_6$, 400 MHz) δ 6.82 (2H, br d, *J* = 8.1 Hz, H-5′,5″), 7.03 (2H, dd, *J* = 8.1, 2.1 Hz, H-6′,6″), 7.07 (2H, d, *J* = 2.1 Hz, H-2′,2″), 7.56 (1H, d, *J* = 15.9 Hz, H-7′), 7.47 (1H, d, *J* = 15.9 Hz, H-7″), 6.32 (1H, d, *J* = 15.9 Hz, H-8′), 6.19 (1H, d, *J* = 15.9 Hz, H-8″), 5.32 (1H, m, H-3), 5.02


dx.doi.org/10.1021/jf501670v | J. Agric. Food Chem. 2014, 62, 8608−8615

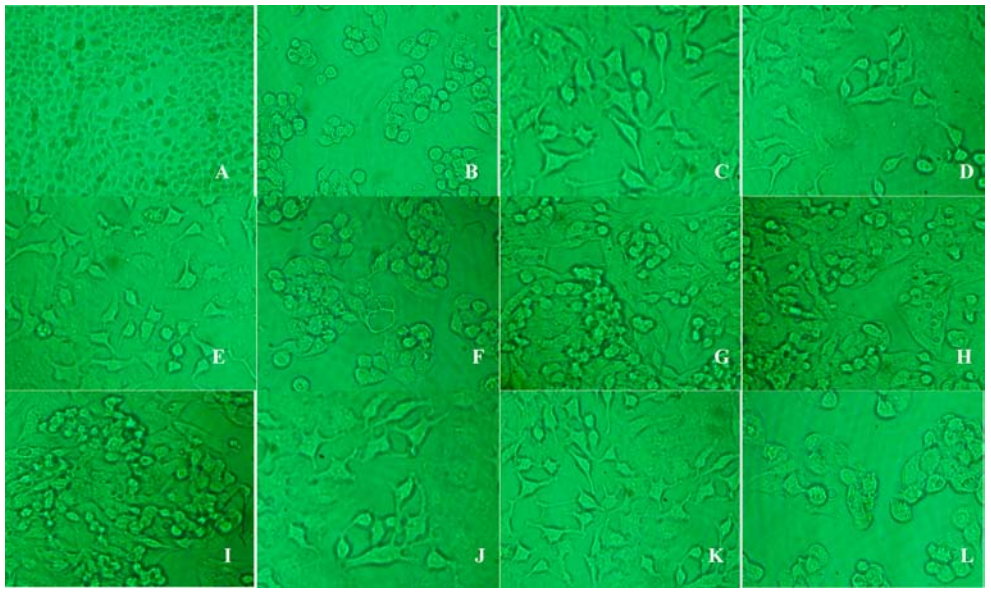


**Figure 3.** Morphological changes in the growth and survival of HeLa cells as examined by phase-contrast microscopy (magnification, 200×): (A) control group or blank group; (B) 95% EtOH (50 $\mu$g/mL); (C) petroleum ether fraction (50 $\mu$g/mL); (D) ethyl acetate fraction (50 $\mu$g/mL); (E) *n*-butanol fraction (50 $\mu$g/mL); (F) water fraction (50 $\mu$g/mL); (G) ethyl caffeate (10 $\mu$M); (H) ursolic acid (10 $\mu$M); (I) chlorogenic acid (10 $\mu$M); (J) 4-CAME (10 $\mu$M); (K) 5-CAME (10 $\mu$M); (L) 5-fluorouracil (10 $\mu$M).

(1H, m, H-4), 4.20 (1H, m, H-5), 3.65 (3H, s, $OCH_3$), 2.27 (2H, m, H-2, 6), 2.00 (2H, m, H-1,7); $^{13}$C NMR (DMSO-$d_6$, 101 MHz) $\delta$ 73.2 (C-1), 37.8 (C-2), 67.9 (C-3), 72.4 (C-4), 65.5 (C-5), 36.8 (C-6), 173.5 (C-7), 125.6 (C-1′), 125.3 (C-1″), 114.5 (C-2′,2″), 145.7 (C-3′), 145.5 (C-3″), 148.7 (C-4′), 148.6 (C-4″), 115.9 (C-5′), 114.9 (C-5″), 121.5 (C-6′), 121.0 (C-6″), 147.6 (C-7′), 147.1 (C-7″), 113.9 (C-8′), 113.4 (C-8″), 166.6 (C-9′), 165.3 (C-9″), 52.1 ($OCH_3$). By comparison of the above data with the literature,[22] compound **4** was identified as 3,4-di-*O*-caffeoylquinic acid methyl ester (4-CAME).

*Compound **5** was obtained as a yellow powder.* The negative ESI-MS showed a quasi-molecular ion at *m*/*z* 529 $[M - H]^-$. $^1$H NMR (DMSO-$d_6$, 400 MHz) $\delta$ 2.09−2.33 (4H, m, H-2,6), 3.71 (3H, s, $OCH_3$), 4.34 (1H, m, H-5), 5.10 (1H, dd, *J* = 8.0, 3.2 Hz, H-4), 5.50 (1H, m, H-3), 6.16 (1H, d, *J* = 16.0 Hz, H-8′), 6.28 (1H, d, *J* = 16.0 Hz, H-8″), 6.74 (2H, d, *J* = 8.0 Hz, H-5′,5″), 6.90 (1H, m, H-6′,6″), 7.00 (1H, d, *J* = 2.0 Hz, H-2′), 7.02 (1H, d, *J* =2.0 Hz, H-2″), 7.49 (1H, d, *J* = 16.0 Hz, H-7′), 7.59 (1H, d, *J* = 16.0 Hz, H-7″); $^{13}$C NMR (DMSO-$d_6$, 101 MHz) $\delta$ 177.5 (C-7), 168.4 (C-9″), 167.9 (C-9′), 149.7 (C-4′,4″), 147.7 (C-7″), 147.6 (C-7′), 146.7 (C-3′,3″), 127.7 (C-1″), 127.5 (C-1′), 123.1 (C-6′,6″), 116.5 (C-5″), 116.4 (C-5′), 115.1 (C-2′,2″), 114.7 (C-8′,8″), 75.8 (C-1), 74.9 (C-4), 69.0 (C-5), 68.6 (C-3), 53.0 ($OCH_3$), 38.5 (C-2), 38.3 (C-6). Compound **5** was identified as 3,5-di-*O*-caffeoylquinic acid methyl ester (5-CAME) according to the literature.[23]

Compounds **4** and **5** were isolated and identified from *I. latifolia* for the first time.

**Evaluation of Cytotoxicity against HeLa Cells.** In this investigation, the 95% EtOH extract, fractions, and isolated compounds **1**−**5** from *I. latifolia* were evaluated for their antiproliferative activities against HeLa human cervix carcinoma cell line using the MTT bioassay. Figure 3 indicates the morphological changes on the growth and survival of HeLa cells as examined by phase-contrast microscopy. The cell proliferation inhibition rates of samples are shown in Figure 4. Among the crude extract and four fractions, 95% EtOH and EA both exhibited the strongest cytotoxicity (Figure 4A). Although the inhibition rate of extract and four fractions was lower than that of 5-fluorouracil, the inhibition rate of 95% EtOH and EA fraction reached nearly 50 and 55%, respectively, at the concentration of 50 $\mu$g/mL. This result showed that the active ingredients on antitumor were concentrated in the EA fraction after 95% EtOH was partitioned into four fractions.

The isolated compounds show significant cytotoxicity against HeLa cell line except chlorogenic acid (Figure 4B). When the concentration was below 4 $\mu$M, all compounds showed very lower inhibition rates as compared to positive control. However, the inhibition rates of 4-CAME and 5-CAME increased significantly at concentrations of 6−10 $\mu$M. The inhibition rate of ursolic acid rose with the increase of concentration and reached about 28% at the maximum concentration. The further increase of concentration resulted in the inhibition rate of chlorogenic acid changing slightly. Ethyl caffeate also exhibited a poor effect at concentrations from 1 to 10 $\mu$M.

4-CAME and 5-CAME are derivatives of caffeoylquinic acid found in several plants. There is little study of the antitumor activity on these two compounds, but the physicochemical property of caffeoylquinic acid was widely reported in the literature. Hu et al.[28] reported that methyl 3,5-dicaffeoylquinate inhibited proliferation in a dose-dependent manner as detected by MTT, trypan blue exclusion, and flow cytometric assays using HT-29 cells. 5-Caffeoylquinic acid was used in preparing antitumor medicine in the form of tablets, capsules, or slow-release tablets or used for inhibiting growth and transfer of tumors. In our study, the two derivatives (4-CAME and 5-CAME) showed significant cytotoxicity against HeLa cell line, which can be potential antitumor drugs in the future.

**Effect of the Extract, Fractions, and Compounds on NO Production in RAW 264.7 Macrophages.** MTT colorimetric assays were carried out to evaluate the toxic effect of compounds on RAW 264.7 macrophage cell line, and the results were shown as relative cell viability referred to control

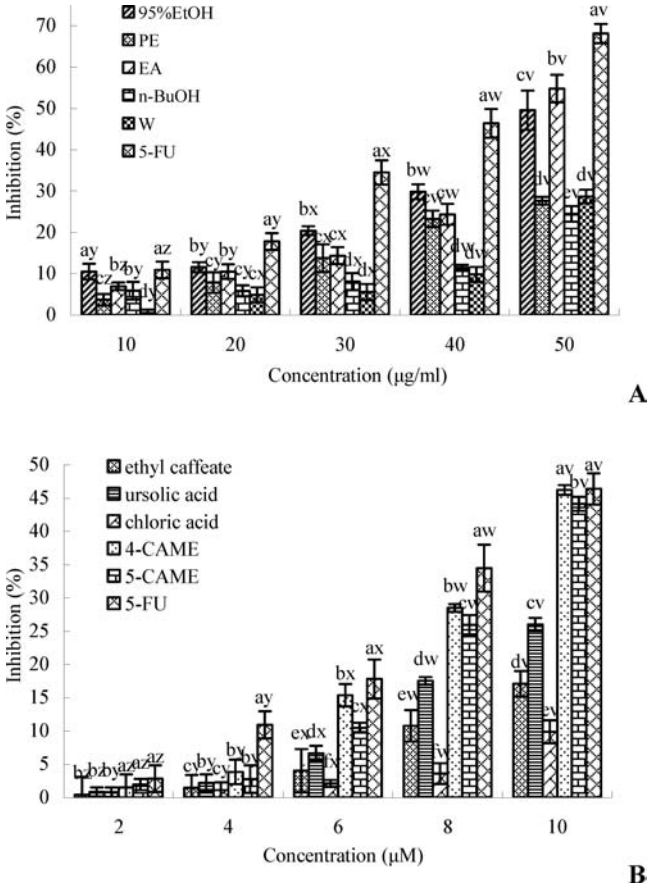


**Figure 4.** Cell proliferation inhibition rates of samples: (A) 95% ethanol extract (95% EtOH), petroleum ether fraction (PE), ethyl acetate fraction (EA), *n*-butanol fraction (*n*-BuOH), and water fraction (W), 5-FU (5-fluorouracil); (B) isolated compounds ethyl caffeate, ursolic acid, chlorogenic acid, 3,4-di-*O*-caffeoylquinic acid methyl ester (4-CAME), 3,5-di-*O*-caffeoylquinic acid methyl ester (5-CAME), 5-FU (5-fluorouracil). Letters a−e refer to significant differences within a fraction and v−z to comparisons across fractions by one-way analysis of variance−Duncan's multiple-range test ($p \leq 0.05$). Results are means ± standard deviation, which were calculated on the basis of data from three trials with three replicates per trial.

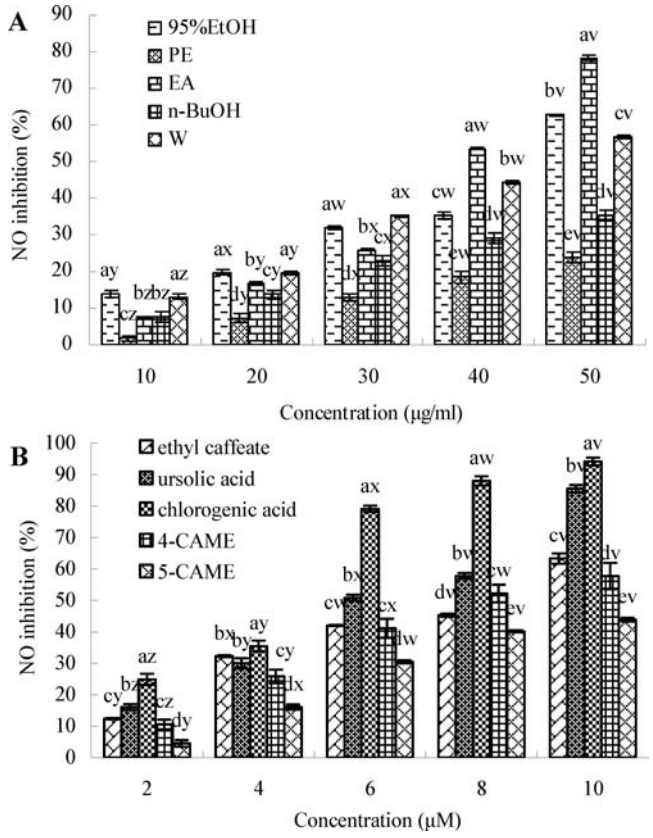


**Figure 5.** Inhibitory effect on NO production of total extract, four fractions, and isolated compounds from *I. latifolia* in LPS-induced RAW 264.7 macrophages: (A) 95% ethanol extract (95% EtOH), petroleum ether fraction (PE), ethyl acetate fraction (EA), *n*-butanol fraction (*n*-BuOH), water fraction (W); (B) isolated compounds ethyl caffeate, ursolic acid, chlorogenic acid, 3,4-di-*O*-caffeoylquinic acid methyl ester (4-CAME), 3,5-di-*O*-caffeoylquinic acid methyl ester (5-CAME). Letters a−e refer to significant differences within a fraction and v−z to comparisons across fractions by one-way analysis of variance−Duncan's multiple-range test ($p \leq 0.05$). Results are means ± standard deviation, which were calculated on the basis of data from three trials with three replicates per trial.

(equal to 100%). Cell viabilities all reached >92% (data not shown). Generally speaking, it could be considered as non-toxicity that the survival rate was >90% when treated with samples.

Current research has demonstrated the participation of reactive oxygen species in systems of inflammation.[29] *I. latifolia* was studied as a potential inhibitor of NO production in inflammatory reactions. Stimulation of LPS-induced RAW 264.7 cell leads to overproduction of NO, and it could be detected and quantified. Figure 5A displays that crude extract and four fractions significantly inhibited NO release and decreased in the order EA (78.16%), 95% EtOH (62.78%), W (56.63%), *n*-BuOH (35.11%), and PE (23.87%) at the concentration of 50 μg/mL. It was clear that EA showed the most active anti-inflammatory effect among the crude extract and all fractions. Many previous literature papers have shown that methanol/ethanol extracts or fractions had good anti-inflammatory activity. Yang et al.[30] reported that the ethyl acetate fraction of the seeds of *Brucea javanica* showed a significant decrease on NO production in LPS-induced RAW 264.7 macrophages. In addition, Pinheiro et al.[31] reported that ethanol extract and hexane and ethyl acetate fractions from *Couroupita guianensis* Aublet leaves exhibited anti-inflammatory activity. In this study, the ethyl acetate fraction showed a better anti-inflammatory ability than that of the 95% ethanol extract.

Inhibitory rates of compounds **1**−**5** on NO production decreased in a turn of chlorogenic acid ($EC_{50}$ = 4.15 μM), ursolic acid ($EC_{50}$ = 6.49 μM), ethyl caffeate ($EC_{50}$ = 7.72 μM), 4-CAME ($EC_{50}$ = 7.81 μM), and 5-CAME ($EC_{50}$ > 10 μM). Among the five isolated compounds, ursolic acid and chlorogenic acid showed strong anti-inflammatory ability on NO production in RAW 264.7 macrophages (Figure 5B). Chlorogenic acid was reported to efficiently inhibit LPS-induced pro-inflammatory responses in hepatic stellate cells, and the anti-inflammatory effect may be due to inhibition of the LPS/ROS/NF-κB signaling pathway.[32]

According to the above results, ursolic acid showed the best radical quenching capacity and a similar ferric reducing capacity as chlorogenic acid, whereas the latter showed the best anti-inflammatory activity and the worst antiproliferative effect. Thus, it can be seen that different compounds often have different biological activities. They may exert a strong effect in a certain activity, but a very weak effect in others. Chlorogenic


dx.doi.org/10.1021/jf501670v | J. Agric. Food Chem. 2014, 62, 8608−8615

acid showed a better antioxidant capacity and anti-inflammatory activity, which may be related to its structure with a lot of hydroxyl groups. However, the mechanism of antioxidant and anti-inflammatory activity in ursolic acid and chlorogenic acid should be further investigated in a future study.

In conclusion, an efficient method for bioassay-guided preparative isolation was used for identifying the antioxidant, antitumor, and anti-inflammatory constituents in *I. latifolia*. Five compounds were isolated and identified. Antioxidant, antitumor, and anti-inflammatory effects of extract, four fractions, and five isolated compounds were evaluated. The ethyl acetate fraction was found to exhibit effective antioxidant, antitumor, and anti-inflammatory activities. In the evaluation of cytotoxicity against tumor cell line, compounds 4-CAME and 5-CAME showed fine activities at high concentrations in comparison to 5-fluorouracil. In addition, chlorogenic acid showed stronger anti-inflammatory activity than the others. These results indicated that after the fractional extraction of 95% EtOH into four fractions, the active ingredients were concentrated into the ethyl acetate fraction. Compounds 4-CAME and 5-CAME are the bioactive chemical compositions isolated from *I. latifolia*, and they were isolated and identified from *I. latifolia* for the first time. The results obtained in this work might contribute to understanding the biological activity and further investigation of *I. latifolia* Thunb. for food and drug application.

## AUTHOR INFORMATION


### Corresponding Author

*(J.-G.J.) E-mail: jgjiang@scut.edu.cn. Phone: +86-20-87113849. Fax: +86-20-87113843.


### Notes

The authors declare no competing financial interest.

## ABBREVIATIONS USED

| | |
|---|---|
| *I. latifolia* | *Ilex latifolia* Thunb. |
| DPPH | 2,2-diphenyl-1-picrylhydrazyl |
| LPS | lipopolysaccharide |
| MTT | 3-(4,5-dimethylthiazol-2-yl)-2,5-diphenyltetrazolium bromide |
| GAE | gallic acid equivalent |
| TLC | thin-layer chromatography |
| HPLC | high-performance liquid chromatography |
| DMSO | dimethyl sulfoxide |
| OD | optical density |
| 4-CAME | 3,4-di-*O*-caffeoylquinic acid methyl ester |
| 5-CAME | 3,5-di-*O*-caffeoylquinic acid methyl ester |
| 95% EtOH | 95% ethanol extract |
| PE | petroleum ether fraction |
| EA | ethyl acetate fraction |
| *n*-BuOH | *n*-butanol fraction |
| W | water fraction |
| 5-FU | 5-fluorouracil |
| TPC | total phenolic content |
| TE | Trolox equivalent |

## REFERENCES


(1) Liu, L. X.; Sun, Y.; Laura, T.; Liang, X. F.; Ye, H.; Zeng, X. X. Determination of polyphenolic content and antioxidant activity of kudingcha made from *Ilex kudingcha* C.J. Tseng. *Food Chem.* **2009**, *112*, 35−41.

(2) Filip, R.; Lopez, P.; Giberti, G.; Coussio, J.; Ferraro, G. Phenolic compounds in seven South American *Ilex* species. *Fitoterapia* **2001**, *72*, 774−778.

(3) Bravo, L.; Goya, L.; Lecumberri, E. LC/MS characterization of phenolic constituents of mate (*Ilex paraguariensis*, St. Hil.) and its antioxidant activity compared to commonly consumed beverages. *Food Res. Int.* **2007**, *40*, 393−405.

(4) Heck, C. I.; De Mejia, E. G. Yerba Mate tea (*Ilex paraguariensis*): a comprehensive review on chemistry, health implications, and technological considerations. *J. Food Sci.* **2007**, *72*, R138−R151.

(5) Chen, Y.; Li, K. S.; Xie, T. G. Hypotensive action of the extract of kudingchadongqingye (*Ilex kudingcha*). *Chinese Tradit. Herb Drugs* **1995**, *26*, 250−252.

(6) Nishimura, K.; Fukuda, T.; Miyase, T.; Noguchi, H.; Chen, X. M. Activity-guided isolation of triterpenoid acyl CoA cholesteryl acyl transferase (ACAT) inhibitors from *Ilex kudincha*. *J. Nat. Prod.* **1999**, *62*, 1061−1064.

(7) Hirano, T.; Gotoh, M.; Oka, K. Natural flavonoids and lignans are potent cytostatic agents against human leukemic HL-60 cells. *Life Sci.* **1994**, *55*, 1061−1069.

(8) Su, B. N.; Jones, W. P.; Cuendet, M.; Kardono, L. B. S.; Ismail, R.; Riswan, S.; Fong, H. H. S.; Farnsworth, N. R.; Pezzuto, J. M.; Kinghorn, A. D. Constituents of the stems of *Macrococculus pomiferus* and their inhibitory activities against cyclooxygenases-1 and -2. *Phytochemistry* **2004**, *65*, 2861−2866.

(9) Yildirim, A.; Mavi, A.; Kara, A. Determination of antioxidant and antimicrobial activities of *Rumex crispus* L. extracts. *J. Agric. Food Chem.* **2001**, *49*, 4083−4089.

(10) Benzie, I. F. F.; Strain, J. J. The ferric reducing ability of plasma (FRAP) as a measure of "antioxidant power": the FRAP assay. *Anal. Biochem.* **1996**, *239*, 70−76.

(11) Villaño, D.; Fernández-Pachón, M. S.; Moyá, M. L.; Troncoso, A. M.; García-Parrilla, M. C. Radical scavenging ability of polyphenolic compounds towards DPPH free radical. *Talanta* **2007**, *71*, 230−235.

(12) Dávalos, A.; Gómez-Cordovés, C.; Batolomé, B. Extending applicability of the oxygen radical absorbance capacity (ORAC-fluorescein) assay. *J. Agric. Food Chem.* **2004**, *52*, 48−54.

(13) Huang, N.; Rizshsky, L.; Hauck, C.; Nikolau, B. J.; Murphy, P. A.; Birt, D. F. Identification of anti-inflammatory constituents in *Hypericum perforatum* and *Hypericum gentianoides* extracts using RAW 264.7 mouse macrophages. *Phytochemistry* **2011**, *72*, 2015−2023.

(14) Yang, L.; Wu, D. F.; Luo, K. W.; Wu, S. H.; Wu, P. Andrographolide enhances 5-fluorouracil-induced apoptosis via caspase-8-dependent mitochondrial pathway involving p53 participation in hepatocellular carcinoma (SMMC-7721) cells. *Cancer Lett.* **2009**, *276*, 180−188.

(15) Mosmann, T. Rapid colorimetric assay for cellular growth and survival: application to proliferation and cytotoxicity assays. *J. Immunol. Methods* **1983**, *65*, 55−63.

(16) Franchi, G. C.; Moraes, C. S.; Toreti, V. C.; Daugsch, A.; Nowill, A. E.; Park, Y. K. Comparison of effects of the ethanolic extracts of Brazilian propolis on human heukemic cells as assessed with the MTT assay. *Evidence-Based Complement. Altern. Med.* **2012**, *2012*, 918956−918962.

(17) Green, S. J.; Meltzer, M. S.; Hibbs, J. B., Jr.; Nacy, C. A. Activated macrophages destroy intracellular *Leishmania major* amastigotes by an L-arginine-dependent killing mechanism. *J. Immunol.* **1990**, *144*, 278−283.

(18) Ma, L. S.; Chen, H. X.; Dong, P.; Lu, X. M. Anti-inflammatory and anticancer activities of extracts and compounds from the mushroom *Inonotus obliquus*. *Food Chem.* **2013**, *139*, 503−508.

(19) Shi, S. Y.; Zhao, Y.; Zhou, H. G.; Zhang, Y. P.; Jiang, X. Y.; Huang, K. L. Identification of antioxidants from *Taraxacum mongolicum* by high-performance liquid chromatography-diode array detection-radical-scavenging detection-electrospray ionization mass spectrometry and nuclear magnetic resonance experiments. *J. Chromatogr. A* **2008**, *1209*, 145−152.

(20) Gordo, J.; Maximo, P.; Cabrita, E.; Lourenco, A.; Oliva, A.; Almeida, J.; Filipe, M.; Cruz, P.; Barcia, R.; Santos, M.; Cruz, H. *Thymus mastichina*: chemical constituents and their anti-cancer activity. *Nat. Prod. Commun.* **2012**, *7*, 1491−1494.

(21) Dai, X. P.; Huang, Q.; Zhou, B. T.; Gong, Z. C.; Liu, Z. Q.; Shi, S. Y. Preparative isolation and purification of seven main antioxidants from *Eucommia ulmoides* Oliv. (Du-zhong) leaves using HSCCC guided by DPPH-HPLC experiment. *Food Chem.* **2013**, *139*, 563−570.
(22) Jiang, H. L.; Xu, L. Z.; Yang, X. D.; Zhang, D.; Yang, S. L.; Zou, Z. M. Quinic acid esters from herba of *Siphonostegia chinensis*. *China J. Chinese Mater. Med.* **2002**, *27*, 923−926.
(23) Mao, Q.; Cao, D.; Jia, X. S. Studies on the chemical constituents of *Lonicera magranthoides* Hand. -Msaa. *Acta Pharm. Sinica* **1993**, *28*, 271−281.
(24) Halliwell, B.; Aeschbach, R.; Loliger, J.; Aruoma, O. I. The characterization of antioxidants. *Food Chem. Toxicol.* **1995**, *33*, 601−617.
(25) Pietta, P. G. Flavonoids as antioxidants. *J. Nat. Prod.* **2000**, *63*, 1035−1042.
(26) Riboli, E.; Norat, T. Epidemiological evidence of the protective effects of fruits and vegetables on cancer risk. *Am. J. Clin. Nutr.* **2003**, *78*, 559−569.
(27) Li, L.; Xu, L. J.; Ma, G. Z.; Dong, Y. M.; Peng, Y.; Xiao, P. G. The large-leaved Kudingcha (*Ilex latifolia* Thunb and *Ilex kudingcha* C.J. Tseng): a traditional Chinese tea with plentiful secondary metabolites and potential biological activities. *J. Nat. Med.* **2013**, *67*, 425−437.
(28) Hu, W.; Shen, T.; Wang, M. H. Cell cycle arrest and apoptosis induced by methyl 3,5-dicaffeoyl quinate in human colon cancer cells: involvement of the PI3K/Akt and MAP kinase pathways. *Chem. Biol. Interact.* **2011**, *194*, 48−57.
(29) Chu, Y. F.; Wise, M. L.; Gulvady, A. A.; Chang, T.; Kendra, D. F.; van Klinken, B. J. W.; Shi, Y. H.; O'Shea, M. *In vitro* antioxidant capacity and anti-inflammatory activity of seven common oats. *Food Chem.* **2013**, *139*, 426−431.
(30) Yang, J. H.; Li, S. C.; Xie, C. F.; Ye, H. Y.; Tang, H.; Chen, L. J.; Peng, A. H. Anti-inflammatory activity of ethyl acetate fraction of the seeds of *Brucea javanica*. *J. Ethnopharmacol.* **2013**, *147*, 442−446.
(31) Pinheiro, M. M. G.; Fernandes, S. B. O.; Fingolo, C. E.; Boylan, F.; Fernandes, P. D. Anti-inflammatory activity of ethanol extract and fractions from *Couroupita guianensis* Aublet leaves. *J. Ethnopharmacol.* **2013**, *146*, 324−330.
(32) Shi, H. T.; Dong, L.; Dang, X. Y.; Liu, Y. P.; Jiang, J.; Wang, Y.; Lu, X. L.; Guo, X. Y. Effect of chlorogenic acid on LPS-induced proinflammatory signaling in hepatic stellate cells. *Inflamm. Res.* **2013**, *62*, 581−587.

JOURNAL OF AGRICULTURAL AND FOOD CHEMISTRY

Article

pubs.acs.org/JAFC

# Possible Antioxidant Mechanism of Melanoidins Extract from Shanxi Aged Vinegar in Mitophagy-Dependent and Mitophagy-Independent Pathways

Lei Yang,[†,§] Xuping Wang,[†] and Xiaolan Yang*[,†]

[†]College of Life Science, Shanxi University, Taiyuan 030006, China

[§]College of Life Sciences, Nankai University, Tianjin 300073, China

**ABSTRACT:** Melanoidins are widely reported to have antioxidant activity; however, their mechanism has not been frequently studied. In this study, we found that melanoidins from Shanxi aged vinegar induced mitopahgy, the specific autophagic elimination of mitochondria, as assessed by up-regulation of the autophagy markers LC3-II and Beclin1 as well as degradation of the autophagy substrate p62 and mitochondrial proteins. Melanoidins reduced reactive oxygen species (ROS) in normal human liver cells and mouse livers through a mitophagy-dependent pathway, by the observation that the reducing ROS effect of melanoidins was partially lost when mitophagy was inhibited by chloroquine. Impaired Akt signaling was found in cells treated with melanoidins, which might explain the activation of autophagy induced by melanoidins. These results suggest that in addition to direct free radical scavenging activity, melanoidins decreased ROS levels through mitophagy in which damaged mitochondria, the source of ROS, were degraded.

**KEYWORDS:** *antioxidant, melanoidins, autophagy, mitophagy, oxidative stress, reactive oxygen species, vinegar, mouse livers*

## INTRODUCTION

Interest in the potential health effects of dietary vinegar is increasing worldwide. In China, vinegar has been traditionally produced from cereals for more than 3000 years.[1] Studies have reported antioxidative health effects of fruit vinegar,[2−4] but little is known about cereal vinegar. Shanxi aged vinegar (SAV) is a traditional Chinese cereal vinegar. Its unique fermentation and roasting processing (6 days at 85 °C) lead to the formation of high amounts of melanoidins,[5] which are high molecular weight nitrogenous, brown compounds[6] that contribute to the flavor and color of SAV. The potential health impacts of melanoidins include antioxidant, antimicrobial, anticariogenic, anti-inflammatory, antihypertensive, and antiglycative activities.[7] The in vitro antioxidant activity of melanoidins that has been evaluated includes 1,1-diphenyl-2-picrylhydrazyl (DPPH) radical-scavenging activity, reducing power, and inhibitory effects on hydroxyl radicals.[8] Protection of cells against oxidative damage by melanoidin has been reported for coffee,[9] biscuits,[10] and prunes.[11] However, because of the complexity of cells, the underlying molecular mechanisms of cellular antioxidant activity remain unclear, and a deeper exploration is needed.

Mitochondria are responsible for 90% of cellular energy. In ATP synthesis through mitochondrial oxidative phosphorylation, reactive oxygen species (ROS) are produced by electrons prematurely reacting with $O_2$, especially at respiratory chain complexes I and III.[12] Accumulating evidence demonstrates that ROS are involved in liver injuries including alcohol abuse, hepatitis C virus infection, iron overload, and chronic cholestasis.[13,14] Antioxidants have been proposed as therapies in experimental models and patients with chronic liver injury.[15,16] However, clinical studies have been controversial, with limited or no benefit reported from chronic administration of antioxidants such as vitamin A, vitamin E, or $\beta$-carotene.[17] These antioxidants not effective enough to attenuate oxidative stress-induced disorders or diseases, possibly because of an inability to target mitochondria, the primary source of ROS.[18]

Pharmacological inducers of autophagy have been described as ROS scavengers. For example, resveratrol, a natural polyphenol known to have antioxidative effects since the 1990s,[19] was believed to explain the "French paradox," in which a relatively low incidence of coronary heart disease is seen in a population with a high dietary intake of cholesterol and saturated fats.[20] However, the concentrations of resveratrol in red wine are low and cannot entirely account for this phenomenon.[21] The possible underlying mechanisms might relate to the autophagic activity of resveratrol. Duan et al. found that in addition to ROS clearance, autophagy is involved in resveratrol prevention of oxidative stress in restrained mice,[22] which might explain the antioxidant effect of resveratrol.

In this study, we found that melanoidins from SAV induced mitopahgy, the specific autophagic elimination of mitochondria, which reduced ROS in normal human liver cells and mice livers. The ability of melanoidins to reduce ROS and protect cells was lost when mitophagy was inhibited by chloroquine (CQ). Impaired Akt signaling was found in cells treated with melanoidins, which might explain the activation of autophagy induced by melanoidins. Thus, melanoidins and SAV acted as pro-autophagic compounds and could be beneficial in oxidative damage-related disease.

**Received:** April 9, 2014
**Revised:** July 31, 2014
**Accepted:** August 7, 2014
**Published:** August 7, 2014

ACS Publications © 2014 American Chemical Society



dx.doi.org/10.1021/jf501690e | J. Agric. Food Chem. 2014, 62, 8616−8622

## MATERIALS AND METHODS

**Chemicals, Cell Lines, and Culture Conditions.** SAV was from local supermarkets. Blue dextran-2000, L-tyrosine, bovine serum albumin, chicken egg albumin, curd protease A, cytochrome *c*, 3-(4,5-dimethylthiazol-2-yl)-2,5-diphenyltetrazolium bromide (MTT), dimethyl sulfoxide (DMSO), hydrogen peroxide ($H_2O_2$) CQ, 2′,7′-dichlorofluorescein diacetate (DCFH-DA), and bromobenzene (BB) were from Sigma-Aldrich (St. Louis, MO, USA). Immortalized human liver LO2 cells and HepG2 cells were cultured according to the method of Zhang et al.[23] Cells were seeded in 6- or 96-well plates and adapted to the culture substrate for 12−24 h before experiments.

**Melanoidins Isolation and Purification.** Components of SAV were prepared as in Figure 1. Briefly, 2 L of SAV was diluted with 2 L of distilled water. The resulting dispersion was filtered through Whatman filter paper 4 to remove insoluble matter. The filtrate was concentrated under vacuum using an RE-52 rotary evaporator (Yarong Experimental Instrument Co., Ltd., Shanghai, China) and freeze-dried to obtain Shanxi aged vinegar extract (SAVE), which was 21.3% of the SAV. To obtain high molecular weight material (HMW), 100 g of SAVE was dissolved in 2 L of distilled water and fractionated through ultrafiltration membranes (AMFOR, 10 kDa cutoff) with two washings with 2 L of distilled water to reduce contamination in the retentate from low molecular weight material (LMW). The resulting filtrate (MW <10 kDa, LMW, 73.6% of SAVE) and retentate (MW >10 kDa, HMW, 26.4% of SAVE) were frozen and freeze-dried.

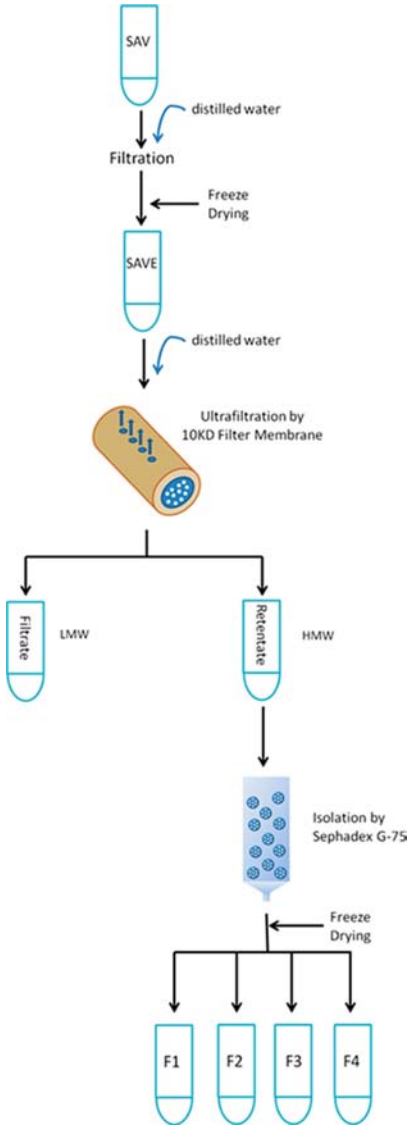


**Figure 1.** Scheme for melanoidin isolation and purification from Shanxi aged vinegar (SAV).

HMW was subjected to a second purification by size exclusion chromatography with a Sephadex G-75 column (60 × 1.6 cm). Freeze-dried HMW was dissolved to 10 mg/mL in distilled water and filtered with 0.45 μm microporous membranes to 2 mL of filtrate for chromatographic separation. The eluent was distilled water at a flow rate of 0.5 mL/min, continuously monitored by absorbance at 280 nm. Collection was 3 mL, and total sugars were determined by using the phenol−sulfuric acid method at 490 nm.[24] A color index was determined by absorbance at 420 nm. Column exclusion ($V_0$) was determined with blue dextran-2000 (20000 kDa) and total volume ($V_t$) was determined with L-tyrosine (181 Da). Fractions 1−4 (F1−F4) (F1, 6.8% of HMW; F2, 82.4% of HMW; F3, 7.2% of HMW; and F4, 3.6% of HMW) were collected, and the molecular weight was calculated by log MW − $V_e$ protein standard curves: lg MW = $-0.0288V_e + 5.9402$, $3r = 0.996$, which was calculated by four protein markers: bovine serum albumin (67 kDa), chicken egg albumin (43 kDa), curd protease A (25 kDa), and cytochrome *c* (12.4 kDa).

**DPPH Radical-Scavenging Activity Assays.** DPPH radical-scavenging activity was determined according to the method of Slusarczyk et al.[25] with slight changes. Test samples were mixed with DPPH radical solution in ethanol (1:2 v/v) and incubated at room temperature in the dark for 30 min, and absorbance was measured at 517 nm. Each test was repeated three times. DPPH radical-scavenging activity was calculated as DPPH radical scavenging (%) = $[A_0 - (A_1 - A_2)]/A_0 \times 100$, where $A_0$ is the absorbance of the DPPH solution, $A_1$ is the absorbance of the mixture of sample and DPPH solution after incubation, and $A_2$ is the absorbance of the sample.

**Total Reducing Power Assays.** Total reducing power was determined as in Zhu et al.[26] with slight changes. A test sample of 0.5 mL was mixed with 2.5 mL of phosphate buffer (0.2 mol/L, pH 6.6) and 2.5 mL of potassium ferricyanide (1%), incubated at 50 °C for 20 min, mixed with 2.5 mL of trichloroacetic acid (10%), blended, and centrifuged at 3000 rpm for 10 min. A 2.5 mL supernatant sample was mixed with 2.5 mL of distilled water and 1 mL of $FeCl_3$ (0.1%) and reacted for 10 min, and absorbance was measured at 700 nm.

**Determination of Cell Viability.** Cell viability was determined by using the MTT assay as previously described.[27] Cells were cultured in 96-well microtiter plates and exposed to $H_2O_2$ or F2 for 24 h. After treatment, 5 mg/mL MTT solution was added and incubated for 4 h at 37 °C. After a washing with PBS, purple-blue formazan was dissolved in 1 mL of DMSO, and absorbance was determined at 550 nm.

**Determination of Cellular ROS Level.** Samples were incubated with 20 μM DCFH-DA for 30 min. Intracellular ROS-mediated oxidation of DCFH-DA to the fluorescent compound DCF was measured.[28] Cells were harvested, and pellets were suspended in 1 mL of PBS and analyzed by flow cytometer (Becton Dickinson, Franklin Lakes, NJ, USA) with excitation of 488 nm and emission of 535.

**Western Blotting.** Cells were washed with ice-cold PBS, harvested, and lysed for 1 h in ice-cold lysis buffer (1% NP40, 0.5% sodium deoxycholate, 0.1% SDS, 1 mM EDTA, 1 mM EGTA, 1 mM $Na_3VO_4$, 20 mM NaF, 0.5 mM DTT, 1 mM PMSF, protease inhibitor cocktail in PBS, pH 7.4). After centrifugation at 4 °C (12000*g*, 10 min), supernatants were collected and solubilized in 6× loading buffer (0.5 M Tris-HCl, pH 6.8, 30% glycerol, 10% SDS, 5% β-mercaptoethanol, 0.012% bromophenol blue). Lysates were separated by 10 or 15% SDS-PAGE and transferred to PVDF membranes (Millipore, Billerica, MA, USA). Proteins were detected with antibodies and HRP-conjugated secondary antibodies. ECL Western Blotting Substrate (Thermo Fisher Scientific) was the HRP substrate. Antibodies were against β-actin (Sigma), beclin1, p62, LC3, tom20, tim23, cytochrome *c* (BD), phosphor-Akt ($Ser^{47}$), pan-Akt, and the C subunit of protein phosphatase 2A (PP2A-C) (Cell Signaling Technology).

**Animals and Treatment.** Hepatotoxicity assays were performed with 48 male Kunming mice from Shanxi Medical University Animal Research Center. Mice were housed in a temperature- and humidity-


dx.doi.org/10.1021/jf501690e | J. Agric. Food Chem. 2014, 62, 8616−8622

controlled room with a 12 h light−dark cycle and free access to a standard pellet diet and water. All animal protocols were approved by the Animal Care Committee of Shanxi University. After 1 week of adaptation, mice were randomly divided into six groups of eight mice per group: control, BB, low-dose SAVE (ig 500 mg/kg SAVE + BB), medium-dose SAVE (ig 1000 mg/kg SAVE + BB), high-dose SAVE (ig 2000 mg/kg SAVE + BB), and CQ+SAVE (ip 60 mg/kg CQ + ig 1000 mg/kg SAVE + BB). Mice were administered compounds or distilled water for 30 days and challenged ig with BB dispersed in 0.2 mL of plant oil at 0.47 mg $kg^{-1}$ body weight, followed by an 18−22 h recovery stage before determination of liver biochemical parameters. All biochemical parameters, thiobarbituric acid reactive substances (TBARS), superoxide dismutase (SOD), and glutathione peroxidase (GSH-Px) were measured as previously reported.[29]

**Statistical Analysis.** All data were expressed as the mean ± standard deviation (SD) and analyzed using SPSS statistical software (SPSS Inc., Chicago, IL, USA). One-way ANOVA with Duncan's test was used for intergroup comparison. $P$ values of <0.05 were considered statistically significant.

## RESULTS

**SAV Contains Melanoidin Complexes.** HMW separated from aqueous extracts of food by ultrafiltration as melanoidins have been explored for biological activity without purification to remove non-melanoidin material.[30,31] In our study, we obtained purified melanoidins and screened for highly antioxidative substances by obtaining HMW (26.4% of SAVE) by ultrafiltration and subjecting HMW to a second purification by size exclusion chromatography. Most HMW was under 80 kDa, and a small part was eluted at the $V_0$ of the column (Figure 2A). The four fractions had molecular weights of F1, >80 kDa; F2, 80−10 kDa; F3, 10−3 kDa; and F4, <3 kDa. F3 and F4 were probably LMW contaminants in the HMW that should not pass though a 10 kDa ultrafiltration membrane. Another possibility is that the LMW material present in the HMW isolated by ultrafiltration can be loosely linked to the HMW by hydrogen bonds or other noncovalent interactions that are released during the size exclusion chromatography method. Melanoidins are defined as brown HMW that are a final product of a Maillard reaction between reducing sugars and compounds with a free amino group.[6] Therefore, an index of total sugar (measured at 490 nm), protein (measured at 280 nm), and brown color (measured at 420 nm) was determined. Results showed that total sugar and protein elution profiles almost perfectly matched the brown color elution profile of F1, F2, and F3, which fit the compositional characteristics of melanoidins. These results demonstrated that we obtained purified melanoidins. F4 appeared to contain free proteins that did not participate in the Maillard reaction.

**In Vitro Antioxidative Activity of SAVE.** We evaluated the in vitro antioxidant activity of SAVE by DPPH radical-scavenging activity assays and total reducing power assays. At 0.05−2.5 mg/mL, SAVE had dose-dependent DPPH radical-scavenging activity with an $IC_{50}$ of 0.49 mg/mL (Figure 2B). SAVE had a dose-dependent total reducing power at 0.5−4.5 mg/mL with an $EC_{50}$ of 4.29 mg/mL (Figure 2C).

**SAVE F2 Is Responsible for Its in Vitro Antioxidative Activity.** To determine if the main antioxidative component in SAVE was melanoidins, we further separated HMW from SAVE. HMW had higher DPPH radical-scavenging activity and total reducing power than LMW and SAVE at the same concentration (Figure 2D,E). To avoid interference from non-melanoidins in the soluble HWM, such as unreacted proteins and carbohydrates, HMW was purified by size exclusion chromatography. Four fractions were collected (F1−F4), and in

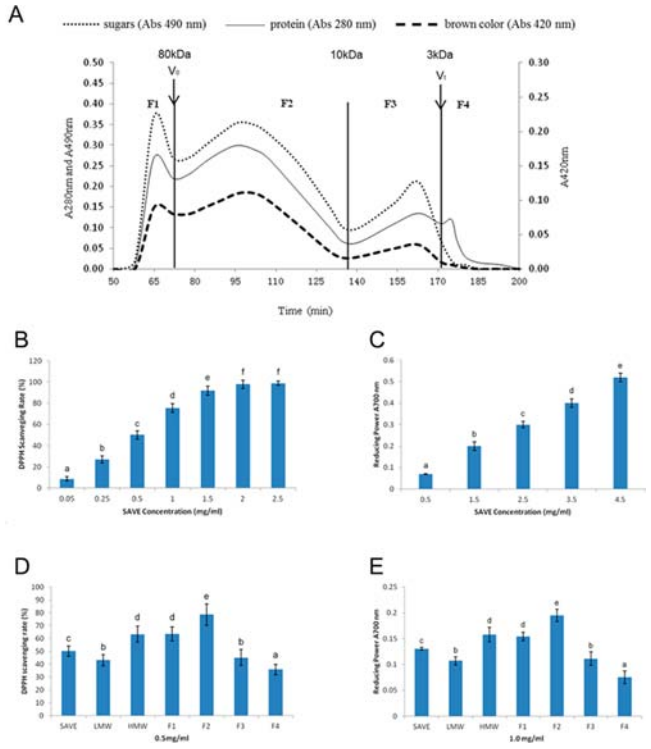


**Figure 2.** Fraction 2 (F2) in Shanxi aged vinegar extracts (SAVE) is responsible for in vitro antioxidative activity. (A) High molecular weight material (HMW) was subjected to a second purification by size exclusion chromatography. Panels B and C show DPPH radical-scavenging activity and total reducing power of SAVE. Panels D and E show DPPH radical-scavenging activity and total reducing power of different SAVE molecular weight fractions. Values are means ± SD, $n$ = 3. Different letters above columns indicate significant differences ($P$ < 0.05).

vitro antioxidative activity showed that F2 had the highest DPPH radical-scavenging activity and total reducing power (Figure 2D,E). The greatest amount of all fractions obtained by size exclusion chromatography was F2 (Figure 2A). These results indicated that F2 had further purified melanoidins responsible for the antioxidative activity of SAVE in vitro. We used F2 to evaluate antioxidative effects in cells.

**F2 Had No Toxicity to Human LO2 Normal Liver Cells.** For food safety and potential clinical use, F2 needed to be tested for toxic effects. Cell survival and redox status were determined for cells treated for 24 h with different concentrations of F2. At 50−1000 μg/mL, F2 did not influence LO2 growth (Figure 3A). Consistent with the MTT results, flow cytometer assays that analyzed the fluorescence intensity of intracellular ROS labeled by DCFH-DA showed that F2 did not influence intracellular basal ROS levels (Figure 3B,C). These results indicated that F2 had no toxicity at the selected concentrations and could safely be studied for potential protective effects.

**F2 Inhibited Cellular ROS Production Induced by $H_2O_2$.** We first established the concentration of $H_2O_2$ needed to increase ROS generation in LO2 cells. Cell survival was tested by an MTT method following treatment with 50−450 μM $H_2O_2$ for 24 h. $H_2O_2$ significantly decreased cell survival to about 60% at 50 μM (Figure 3D), suggesting abundant ROS generation. Cells treated with 250 μg/mL F2 were rescued from 50 and 150 μM $H_2O_2$-induced damage, indicating that F2 attenuated the state of oxidative stress in cells. To quantify the


dx.doi.org/10.1021/jf501690e | J. Agric. Food Chem. 2014, 62, 8616−8622

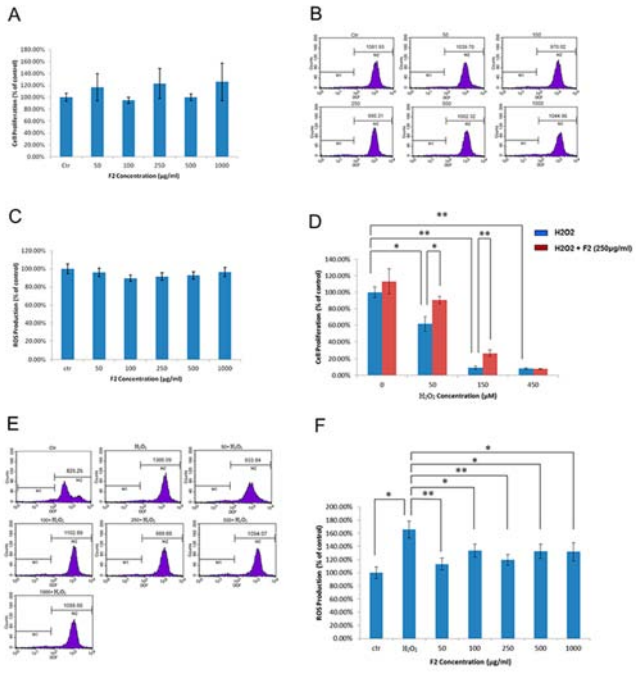

**Figure 3.** F2 attenuated reactive oxygen species (ROS) production in LO2 cells. (A) F2 did not affect cell proliferation measured by MTT test. (B, C) F2 did not affect intracellular basal redox status measured by flow cytometry for fluorescence intensity of intracellular ROS labeled with DCFH-DA. LO2 cells were treated with F2 at 50−1000 $\mu$g/mL for 24 h. (D) Cells treated with 250 $\mu$g/mL F2 rescued 50 and 150 $\mu$M $H_2O_2$ damage. (E, F) F2 non-dose-dependently inhibited cellular ROS production by $H_2O_2$. Values are means ± SD of three experiments. (*) $P < 0.05$; (**) $P < 0.01$.

protective effect of F2, 50 $\mu$M $H_2O_2$ for 24 h was chosen. Compared to the control group, increased ROS generation in the $H_2O_2$-treated group was mitigated by the addition of F2 at different concentrations (Figure 3E,F). The ROS-reducing effect of F2 was not dose-dependent, indicating that in addition to direct free radical-scavenging ability, F2 used another mechanism to attenuate ROS production.

**F2 Triggered Mitophagy in LO2 Cells.** Mitochondria are a major source of ROS, so mitophagy might be a mechanism to eliminate ROS. We hypothesized that the ROS-reducing effect of F2 in cells depended on mitophagy. To estimate the promotion of mitophagy by F2 in LO2 cells, expression of autophagy-related and mitochondrial proteins was determined by Western blots (Figure 4A). F2 at 250 $\mu$g/mL induced autophagy by increasing an endogenous, membrane-associated, phosphatidylethanolamine-conjugated form of LC3 (LC3-II). Beclin1, a mammalian protein that mediates autophagy,[32] was also up-regulated. The autophagy substrate p62, a polyubiquitin-binding protein that is degraded by autophagy and functions as an adaptor protein for selective types of macroautophagy such as mitophagy,[33] was degraded by F2 treatment. To monitor the last step of mitochondrial degradation, three mitochondrial proteins were analyzed to represent mitochondrial mass. The proteins were tom20 (an outer mitochondrial membrane protein), tim23 (an inner mitochondrial membrane protein), and cytochrome *c* (a mitochondrial intermembrane space protein). All three mitochondrial proteins were degraded. Taken together, the results showed that F2 could induce mitophagy.

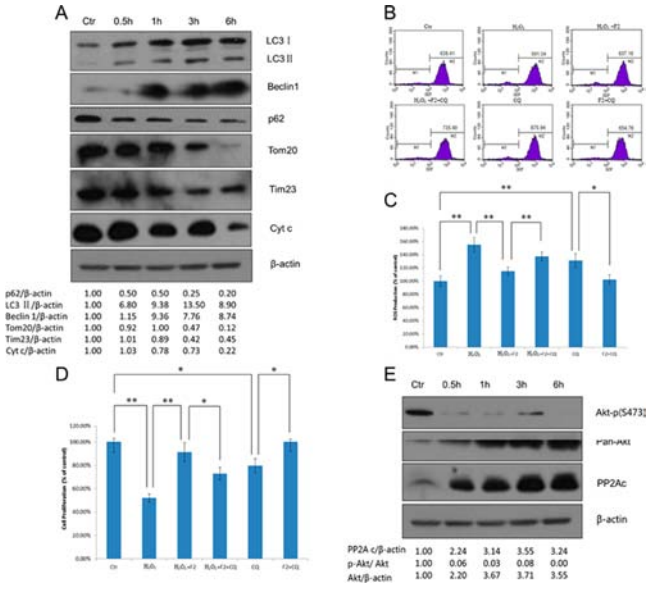

**Figure 4.** Mechanism of F2 antioxidant effect in mitophagy-dependent and mitophagy-independent pathways. (A) At 250 $\mu$g/mL, F2 triggered mitophagy in LO2 cells. (B, C) ROS-reducing effect of F2 was partly prevented by the autophagy inhibitor chloroquine (CQ). (D) MTT results were consistent with flow cytometry: protection by F2 against $H_2O_2$ was inhibited by CQ. (E) F2 activated autophagy through PP2A/Akt signaling. $\beta$-Actin was the loading control. Values are means ± SD of three experiments. (*) $P < 0.05$; (**)$P < 0.01$.

**F2 Used a Different Pathway to Lower ROS Production in Cells.** To determine if mitophagy might be partly involved in the effect of F2 on reducing oxidative stress, we inhibited autophagy by co-incubating cells with the lysosomal inhibitor CQ. Flow cytometry showed that the ROS-reducing effects of F2 were partly prevented by CQ (Figure 4B,C) and cell survival decreased (Figure 4D). We also found that the ROS promotion effect of CQ was blocked by F2, which supported F2 having an ROS-reducing effect that contributed to mitophagy and direct free radical-scavenging activity. These results indicated that F2 had two ways to lower ROS production in cells: (1) mitophagy to degrade damaged mitochondria that are the source of ROS and (2) direct free radical scavenging.

**F2 Activated the PP2A-AKT Signaling Pathway To Induce Autophagy.** Melanoidins impair the Akt signaling pathway,[34] which positively regulates autophagy, suggesting Akt might be the target in an upstream signaling pathway induced by F2. Therefore, we explored changes in the phosphorylation of Akt kinase in LO2 cells. Western blots showed that F2 at 250 $\mu$g/mL markedly reduced Akt phosphorylation at $Ser^{473}$ (Figure 4E), indicating that Akt kinase activity decreased. We also investigated the Akt negative regulator PP2A. After treatment with F2, expression of PP2A-C increased, suggesting that PP2A activity was increased by F2.

**Protective Effect of SAVE on BB-Induced Hepatotoxicity.** To determine if the in vitro biological activities attributed to melanoidins in SAVE were observed in vivo, we tested the antioxidative activity of SAVE in a BB-induced mouse hepatotoxicity model. No differences in body weight or food intake were observed among the six experimental groups (data not shown). Compared with the control group, the BB group showed significantly increased liver TBARS levels and significantly decreased SOD and GSH-Px activities (Table 1),


dx.doi.org/10.1021/jf501690e | J. Agric. Food Chem. 2014, 62, 8616−8622

**Table 1. Protective Effect of SAVE on BB-Induced Hepatotoxicity in Mice[a]**

| group | Ctr | BB | low SAVE | medium SAVE | high SAVE | medium SAVE + CQ |
|---|---|---|---|---|---|---|
| TBARS (nmol/mg protein) | 5.78 ± 0.55 | 9.11 ± 0.98** | 8.51 ± 0.86 | 6.71 ± 0.63## | 5.33 ± 0.59## | 8.09 ± 0.88△ |
| SOD (U/mg protein) | 634.70 ± 47.50 | 427.50 ± 47.30** | 462.60 ± 69.50 | 593.10 ± 66.90## | 680.80 ± 76.20## | 495.85 ± 75.10△ |
| GSH-Px (U/mg protein) | 425.10 ± 33.30 | 328.80 ± 34.20** | 353.30 ± 43.70 | 467.30 ± 35.20## | 488.60 ± 54.70## | 387.53 ± 48.20△ |

[a]Values are means ± SD ($n$ = 8): (**) $P < 0.01$ vs Ctr group; (##) $P < 0.01$ vs BB group; (△) $P < 0.05$ vs medium SAVE group. Ctr, control; BB, bromobenzene; SAVE, Shanxi aged vinegar extracts; CQ, chloroquine; TBARS, thiobarbituric acid reactive substances; SOD, superoxide dismutase; GSH-Px, glutathione peroxidase.

indicating that the construction of a BB-damaged mouse model was successful. Compared with the BB group, groups receiving medium or high doses of SAVE showed significantly decreased liver TBARS levels and significantly increased liver SOD and GSH-Px activities. The medium dose of SAVE was chosen to test whether the antioxidative activity of SAVE was dependent on mitophagy. The hepatic protective effect of SAVE was partially inhibited by CQ, consistent with results obtained with LO2 cells.

## DISCUSSION

In this study, we evaluated the in vitro antioxidative activity of SAVE and SAVE fractions with melanoidins of different molecular weights. DPPH radical-scavenging activity assays and total reducing power assays showed that SAVE had antioxidant activity in vitro and that the HMW fraction had higher antioxidant activity than the LMW fraction. This result was consistent with other studies. Borrelli et al. found that low molecular mass melanoidin fractions from bread and biscuits showed low antioxidant activity.[30] Morales et al. found that high molecular mass fractions (>10 kDa) were more effective as antioxidants than other fractions because of the direct scavenging activity against radicals and a stronger metal-chelating capability.[31] However, larger molecular weight melanoidins do not necessarily have stronger antioxidative ability. Our purification to produce HMW showed that F2 (10−80 kDa) had higher DPPH radical-scavenging activity and total reducing power than F1 (>80 kDa). Although the mechanism remains unclear, this result might be related to differences in the composition of melanoidins in fractions with different molecular weights, with different melanoidin populations exhibiting antioxidative capacities through different mechanisms.[7] We observed that the antioxidative ability of melanoidins of different molecular weights correlated with their polyphenol content (data not shown). Further study of melanoidin structures will improve the understanding of their antioxidant properties.

To evaluate the ROS-reducing effect of F2 in cells, we used $H_2O_2$ to activate mitochondrial oxidative stress. $H_2O_2$, a specific ROS, was sufficient and essential for inducing oxidative stress. $H_2O_2$ interacts with metal ions such as $Fe^{2+}$, forming metal-centered oxygen radicals and hydroxyl radicals ($OH^{\bullet}$) that are highly reactive and oxidatively damage mitochondria.[35] Mitochondria are the major site of ROS production and the major target of their detrimental effects.[36] We found a significantly increased ROS level in $H_2O_2$-treated groups, indicating that mitochondria were damaged and produced excessive ROS. Consistent with these studies, we observed a decrease in cell survival rates in $H_2O_2$-treated groups. Treatment with F2 reduced ROS levels and improved cell survival, indicating that F2 had protective effects on LO2 cells.

Autophagy can be nonselective or selective. Nonselective autophagy is an evolutionarily conserved mechanism in which intracellular proteins or organelles are degraded in lysosomes during nutrient deprivation, providing cells with recycled cellular components and energy from degraded components. Conversely, even under nutrient-rich conditions selective autophagy occurs, which specifically removes protein aggregates and damaged organelles, for example, in mitophagy, which targets permeabilized mitochondria.[37] Autophagy is vital for organisms. Autophagic ability decreases in older organisms,[38] which might lead to age-related diseases such as neurodegeneration and cancer. In this study, we hypothesized that the ROS-reducing effect of F2 depended on autophagic stimulation to remove oxidized mitochondria. We tested this hypothesis using Western blots to check if F2 selectively removed mitochondria. Removal of damaged mitochondria through autophagy requires two steps: (1) activation of general autophagy and (2) priming of mitochondria for selective autophagic recognition. First, we determined if F2 altered the expression autophagy markers in LO2 cells. The conversion of atg8/LC3 (LC3) from the soluble form (LC3-I) to the autophagosome-associated form (LC3-II) implies an increase of autophagosomes within cells.[39] F2 significantly up-regulated LC3-II expression. Beclin 1 (Vps30/Atg6), a mammalian protein that mediates autophagy,[32] was also up-regulated. We also determined the expression of p62/SQSTM1, an adaptor that, through direct interaction with LC3, recruits autophagosomal membranes to the mitochondria.[40] P62 was degraded, indicating that F2 induced mitophagy. Analysis of mitochondrial mass showed degradation of the outer mitochondrial membrane protein tom20. Recent studies suggest that most outer mitochondrial membrane proteins are preferentially degraded by the ubiquitin proteasome system, whereas matrix proteins are degraded through autophagy, although the exact mechanisms and reasons for the different degraded mechanisms are not clear.[41] Hence, we also analyzed proteins from all mitochondrial compartment proteins: outer mitochondrial protein tom20, inner mitochondrial protein tim23, and intermembrane-space protein cytochrome *c*. All three mitochondrial proteins were significantly degraded, demonstrating that F2 induced mitophagy.

Enhancement of mitophagy or autophagy might be a way for cells to reduce oxidative stress. In normal conditions, mitochondria and the cytoplasm have detoxifying enzymes and nonenzymatic antioxidant systems that prevent oxidative damage.[42] However, under stress or pathological conditions, damaged mitochondria produce excess ROS that overcome cellular defenses and oxidatively modify cellular components. Therefore, enhancement of autophagic ability with an autophagy inducer might maintain mitochondrial quality by eliminating damaged mitochondria and preventing oxidative damage. Dutta et al. showed that activation of autophagy by rapamycin protects cardiomyocytes from oxidative stress-induced toxicity.[43] Kurihara et al. demonstrated that mitophagy contributes to mitochondrial quantity and quality control in

yeast by eliminating mitochondria to a basal level and preventing excess ROS production.[44] Han et al. reported that curcumin protects human endothelial cells from oxidative damage via autophagy.[45] Our results also support these findings. We observed that activation of autophagy by F2 protected cells from oxidative stress and decreased cell survival and that CQ treatment blocked this protective effect.

Akt kinase (protein kinase B) is a serine/threonine protein kinase that negatively regulates autophagy.[46] Because melanoidins impair the Akt signaling pathway[34] and down-regulation of phospho-Akt (P-Akt) activates autophagy, we hypothesized that autophagic activity by F2 might be because of Akt kinase inhibition. F2 decreased the Akt protein kinase activity by impaired Akt phosphorylation at serine 473. Akt phosphorylation is determined by a balance between kinases and phosphatases.[47] Therefore, we investigated F2 effects on PP2A and P-Akt. PP2A is in a family of serine/threonine phosphatases that down-regulate Akt phosphorylation. Increasing evidence shows that PP2A is important in autophagy promotion.[48] PP2A contains a highly active core dimer of a catalytic C subunit (PP2A-C) and a structural A subunit (PP2A-A) that recruits one of several regulatory B subunits (PP2A-B) to form a PP2A heterotrimeric complex.[49,50] F2 treatment notably up-regulated PP2A-C expression, indicating that F2 increased PP2A activity. These results indicated that F2 might have activated autophagy through the PP2A/Akt signaling pathway.

Autophagy is protective against liver injury.[51−53] We did not obtain enough F2 for animal tests, so we used SAVE. We imitated pathological hepatic conditions using a BB-induced liver injury model to evaluate the antioxidative activities of SAVE. We previously demonstrated that BB is a strong oxidant that causes hepatic lipid peroxidation.[29] Liver oxidative damage was evaluated by lipid peroxidation production of TBARS and two antioxidant enzymes, SOD and GSH-px. The hepatic protective effect of SAVE was partially inhibited by CQ (Table 1). Similar to our results in LO2 cells, which showed that F2 had mitophagy-dependent pathways to lower ROS production (Figure 4B−D), the in vivo experiment also showed that SAVE had mitophagy-dependent pathways to lower liver oxidative damage, which suggested that F2 might contribute to the protective effect of SAVE in vivo, through mitophagy-dependent pathways. Taken together, these results suggested that F2-mediated autophagy might be important for preventing liver injury in vivo.

We demonstrated that mitophagy was involved in the ability of melanoidins extracted from SAV to protect the liver from oxidative stress in vitro and in vivo. Melanoidins might activate autophagy through the PP2A/Akt signaling pathway. This study provides novel insights into the cellular mechanisms of the antioxidative effect of melanoidins and potential future therapeutic strategies.

## AUTHOR INFORMATION

### Corresponding Author

*(X.Y.) Phone: +86-351-7011590. Fax: +86-351-7011590. E-mail: 13934214833@163.com.

### Funding

This work was supported by the National Natural Science Foundation of China (Grant 31171748).

### Notes

The authors declare no competing financial interest.

## ACKNOWLEDGMENTS

We are grateful to International Science Editing for providing language editing assistance.

## ABBREVIATIONS USED

SAV, Shanxi aged vinegar; SAVE, Shanxi aged vinegar extracts; HMW, high molecular weight material; LMW, low molecular weight material; F1−F4, fractions 1−4; ROS, reactive oxygen species; CQ, chloroquine; BB, bromobenzene

## REFERENCES

(1) Shi, G. Talk about Chinese vinegar. *China Brew.* **1999**, *6*, 39−40.
(2) Verzelloni, E.; Tagliazucchi, D.; Conte, A. From balsamic to healthy: Traditional balsamic vinegar melanoidins inhibit lipid peroxidation during simulated gastric digestion of meat. *Food Chem. Toxicol.* **2010**, *48*, 2097−2102.
(3) Falcone, P. M.; Giudici, P. Molecular size and molecular size distribution affecting traditional balsamic vinegar aging. *J. Agric. Food Chem.* **2008**, *56*, 7057−7066.
(4) Tagliazucchi, D.; Verzelloni, E.; Conte, A. Contribution of melanoidins to the antioxidant activity of traditional balsamic vinegar during aging. *J. Food Biochem.* **2010**, *34*, 1061−1078.
(5) Wang, A. L.; Zhang, J.; Li, Z. G. Correlation of volatile and nonvolatile components with the total antioxidant capacity of tartary buckwheat vinegar: influence of the thermal processing. *Food Res. Int.* **2012**, *49*, 65−71.
(6) Hodge, J. E. Chemistry of browning reactions in model systems. *J. Agric. Food Chem.* **1953**, *1*, 928−943.
(7) Moreira, A. S.; Nunes, F. M.; Domingues, M. R.; Coimbra, M. A. Coffee melanoidins: structures, mechanisms of formation and potential health impacts. *Food Funct.* **2012**, *3*, 903−915.
(8) Xu, Q. P.; Tao, W. Y.; Ao, Z. H. Antioxidant activity of vinegar melanoidins. *Food Chem.* **2007**, *102*, 841−849.
(9) Perrone, D.; Farah, A.; Donangelo, C. M. Influence of coffee roasting on the incorporation of phenolic compounds into melanoidins and their relationship with antioxidant activity of the brew. *J. Agric. Food Chem.* **2012**, *60*, 4265−4275.
(10) Martin, M. A.; Ramos, S.; Mateos, R.; Rufian-Henares, J. A.; Morales, F. J.; Bravo, L.; Goya, L. Biscuit melanoidins of different molecular masses protect human HepG2 cells against oxidative stress. *J. Agric. Food Chem.* **2009**, *57*, 7250−7258.
(11) Posadino, A. M.; Cossu, A.; Piga, A.; Madrau, M. A.; Del Caro, A.; Colombino, M.; Paglietti, B.; Rubino, S.; Iaccarino, C.; Crosio, C.; Sanna, B.; Pintus, G. Prune melanoidins protect against oxidative stress and endothelial cell death. *Front. Biosci. (Elite Ed.)* **2011**, *3*, 1034−1041.
(12) Zhang, H.; Bosch-Marce, M.; Shimoda, L. A.; Tan, Y. S.; Baek, J. H.; Wesley, J. B.; Gonzalez, F. J.; Semenza, G. L. Mitochondrial autophagy is an HIF-1-dependent adaptive metabolic response to hypoxia. *J. Biol. Chem.* **2008**, *283*, 10892−10903.
(13) Poli, G.; Parola, M. Oxidative damage and fibrogenesis. *Free Radical Biol. Med.* **1997**, *22*, 287−305.
(14) Parola, M.; Robino, G. Oxidative stress-related molecules and liver fibrosis. *J. Hepatol.* **2001**, *35*, 297−306.
(15) Boigk, G.; Stroedter, L.; Herbst, H.; Waldschmidt, J.; Riecken, E. O.; Schuppan, D. Silymarin retards collagen accumulation in early and advanced biliary fibrosis secondary to complete bile duct obliteration in rats. *Hepatology* **1997**, *26*, 643−649.
(16) Houglum, K.; Venkataramani, A.; Lyche, K.; Chojkier, M. A pilot study of the effects of D-α-tocopherol on hepatic stellate cell activation in chronic hepatitis C. *Gastroenterology* **1997**, *113*, 1069−1073.
(17) Bjelakovic, G.; Nikolova, D.; Gluud, L. L.; Simonetti, R. G.; Gluud, C. Mortality in randomized trials of antioxidant supplements for primary and secondary prevention: systematic review and meta-analysis. *JAMA, J. Am. Med. Assoc.* **2007**, *297*, 842−857.

(18) Rocha, M.; Hernandez-Mijares, A.; Garcia-Malpartida, K.; Banuls, C.; Bellod, L.; Victor, V. M. Mitochondria-targeted antioxidant peptides. *Curr. Pharm. Des.* **2010**, *16*, 3124−3131.
(19) Frankel, E. N.; Waterhouse, A. L.; Kinsella, J. E. Inhibition of human LDL oxidation by resveratrol. *Lancet* **1993**, *341*, 1103−1104.
(20) Lagouge, M.; Argmann, C.; Gerhart-Hines, Z.; Meziane, H.; Lerin, C.; Daussin, F.; Messadeq, N.; Milne, J.; Lambert, P.; Elliott, P.; Geny, B.; Laakso, M.; Puigserver, P.; Auwerx, J. Resveratrol improves mitochondrial function and protects against metabolic disease by activating SIRT1 and PGC-1$\alpha$. *Cell* **2006**, *127*, 1109−1122.
(21) Baur, J. A.; Pearson, K. J.; Price, N. L.; Jamieson, H. A.; Lerin, C.; Kalra, A.; Prabhu, V. V.; Allard, J. S.; Lopez-Lluch, G.; Lewis, K.; Pistell, P. J.; Poosala, S.; Becker, K. G.; Boss, O.; Gwinn, D.; Wang, M.; Ramaswamy, S.; Fishbein, K. W.; Spencer, R. G.; Lakatta, E. G.; Le Couteur, D.; Shaw, R. J.; Navas, P.; Puigserver, P.; Ingram, D. K.; de Cabo, R.; Sinclair, D. A. Resveratrol improves health and survival of mice on a high-calorie diet. *Nature* **2006**, *444*, 337−342.
(22) Duan, W. J.; Liu, F. L.; He, R. R.; Yuan, W. L.; Li, Y. F.; Tsoi, B.; Su, W. W.; Yao, X. S.; Kurihara, H. Autophagy is involved in the effects of resveratrol on prevention of splenocyte apoptosis caused by oxidative stress in restrained mice. *Mol. Nutr. Food Res.* **2013**, *57*, 1145−1157.
(23) Zhang, S.; Shan, C.; Kong, G.; Du, Y.; Ye, L.; Zhang, X. MicroRNA-520e suppresses growth of hepatoma cells by targeting the NF-$\kappa$B-inducing kinase (NIK). *Oncogene* **2011**, *31*, 3607−3620.
(24) Dubois, N.; Gilles, K. A.; Hamilton, J. K.; Rebers, P. A.; Smith, F. Colorimetric method for determination of sugars and related substances. *Anal. Chem.* **1956**, *28*, 350−356.
(25) Slusarczyk, S.; Hajnos, M.; Skalicka-Wozniak, K.; Matkowski, A. Antioxidant activity of polyphenols from *Lycopus lucidus* Turcz. *Food Chem.* **2009**, *113*, 134−138.
(26) Zhu, Q. Y.; Hackman, R. M.; Ensunsa, J. L.; Holt, R. R.; Keen, C. L. Antioxidative activities of oolong tea. *J. Agric. Food Chem.* **2002**, *50*, 6929−6934.
(27) Chen, G.; Bower, K. A.; Ma, C.; Fang, S.; Thiele, C. J.; Luo, J. Glycogen synthase kinase 3beta (GSK3$\beta$) mediates 6-hydroxydopamine-induced neuronal death. *FASEB J.* **2004**, *18*, 1162−1164.
(28) Wolfe, K. L.; Liu, R. H. Cellular antioxidant activity (CAA) assay for assessing antioxidants, foods, and dietary supplements. *J. Agric. Food Chem.* **2007**, *55*, 8896−8907.
(29) Wang, X.; Yang, L.; Yang, X.; Tian, Y. In vitro and in vivo antioxidant and antimutagenic activities of polyphenols extracted from hops (*Humulus lupulus* L.). *J. Sci. Food Agric.* **2013**, DOI: 10.1002/jsfa.6534.
(30) Borrelli, R. C.; Mennella, C.; Barba, F.; Russo, M.; Russo, G. L.; Krome, K.; Erbersdobler, H. F.; Faist, V.; Fogliano, V. Characterization of coloured compounds obtained by enzymatic extraction of bakery products. *Food Chem. Toxicol.* **2003**, *41*, 1367−1374.
(31) Morales, F. J.; Fernandez-Fraguas, C.; Jimenez-Perez, S. Iron-binding ability of melanoidins from food and model systems. *Food Chem.* **2005**, *90*, 821−827.
(32) Scherz-Shouval, R.; Shvets, E.; Fass, E.; Shorer, H.; Gil, L.; Elazar, Z. Reactive oxygen species are essential for autophagy and specifically regulate the activity of Atg4. *EMBO J.* **2007**, *26*, 1749−1760.
(33) Geisler, S.; Holmstrom, K. M.; Skujat, D.; Fiesel, F. C.; Rothfuss, O. C.; Kahle, P. J.; Springer, W. PINK1/Parkin-mediated mitophagy is dependent on VDAC1 and p62/SQSTM1. *Nat. Cell Biol.* **2010**, *12*, 119−131.
(34) Langner, E.; Nunes, F. M.; Pozarowski, P.; Kandefer-Szerszen, M.; Pierzynowski, S. G.; Rzeski, W. Antiproliferative activity of melanoidins isolated from heated potato fiber (potex) in glioma cell culture model. *J. Agric. Food Chem.* **2011**, *59*, 2708−2716.
(35) Wen, Y. D.; Wang, H.; Kho, S. H.; Rinkiko, S.; Sheng, X.; Shen, H. M.; Zhu, Y. Z. Hydrogen sulfide protects HUVECs against hydrogen peroxide induced mitochondrial dysfunction and oxidative stress. *PLoS One* **2013**, *8*, No. e53147.
(36) Marchi, S.; Giorgi, C.; Suski, J. M.; Agnoletto, C.; Bononi, A.; Bonora, M.; De Marchi, E.; Missiroli, S.; Patergnani, S.; Poletti, F.; Rimessi, A.; Duszynski, J.; Wieckowski, M. R.; Pinton, P. Mitochondria-ros crosstalk in the control of cell death and aging. *J. Signal Transduct.* **2012**, *2012*, No. 329635.
(37) Kanki, T.; Klionsky, D. J. Mitophagy in yeast occurs through a selective mechanism. *J. Biol. Chem.* **2008**, *283*, 32386−32393.
(38) Del Roso, A.; Vittorini, S.; Cavallini, G.; Donati, A.; Gori, Z.; Masini, M.; Pollera, M.; Bergamini, E. Ageing-related changes in the in vivo function of rat liver macroautophagy and proteolysis. *Exp. Gerontol.* **2003**, *38*, 519−527.
(39) Kimura, S.; Fujita, N.; Noda, T.; Yoshimori, T. Monitoring autophagy in mammalian cultured cells through the dynamics of Lc3. *Methods Enzymol.: Autophagy Mammalian Syst.* **2009**, *452* (Part B), 1−12.
(40) Ding, W. X.; Yin, X. M. Mitophagy: mechanisms, pathophysiological roles, and analysis. *Biol. Chem.* **2012**, *393*, 547−564.
(41) Yoshii, S. R.; Kishi, C.; Ishihara, N.; Mizushima, N. Parkin mediates proteasome-dependent protein degradation and rupture of the outer mitochondrial membrane. *J. Biol. Chem.* **2011**, *286*, 19630−19640.
(42) Andreyev, A. I.; Kushnareva, Y. E.; Starkov, A. A. Mitochondrial metabolism of reactive oxygen species. *Biochemistry (Moscow)* **2005**, *70*, 200−214.
(43) Dutta, D.; Xu, J. Z.; Kim, J. S.; Dunn, W. A.; Leeuwenburgh, C. Upregulated autophagy protects cardiomyocytes from oxidative stress-induced toxicity. *Autophagy* **2013**, *9*, 328−344.
(44) Kurihara, Y.; Kanki, T.; Aoki, Y.; Hirota, Y.; Saigusa, T.; Uchiumi, T.; Kang, D. Mitophagy plays an essential role in reducing mitochondrial production of reactive oxygen species and mutation of mitochondrial DNA by maintaining mitochondrial quantity and quality in yeast. *J. Biol. Chem.* **2012**, *287*, 3265−3272.
(45) Han, J.; Pan, X. Y.; Xu, Y.; Xiao, Y.; An, Y.; Tie, L.; Pan, Y.; Li, X. J. Curcumin induces autophagy to protect vascular endothelial cell survival from oxidative stress damage. *Autophagy* **2012**, *8*, 812−825.
(46) Jung, C. H.; Ro, S. H.; Cao, J.; Otto, N. M.; Kim, D. H. mTOR regulation of autophagy. *FEBS Lett.* **2010**, *584*, 1287−1295.
(47) Hennessy, B. T.; Smith, D. L.; Ram, P. T.; Lu, Y. L.; Mills, G. B. Exploiting the PI3K/AKT pathway for cancer drug discovery. *Nat. Rev. Drug Discovery* **2005**, *4*, 988−1004.
(48) Banreti, A.; Lukacsovich, T.; Csikos, G.; Erdelyi, M.; Sass, M. PP2A regulates autophagy in two alternative ways in *Drosophila*. *Autophagy* **2012**, *8*, 623−636.
(49) Shi, Y. G. Serine/threonine phosphatases: mechanism through structure. *Cell* **2009**, *139*, 468−484.
(50) Janssens, V.; Longin, S.; Goris, J. PP2A holoenzyme assembly: in cauda venenum (the sting is in the tail). *Trends Biochem. Sci.* **2008**, *33*, 113−121.
(51) Yang, L.; Rozenfeld, R.; Wu, D.; Devi, L. A.; Zhang, Z.; Cederbaum, A. Cannabidiol protects liver from binge alcohol-induced steatosis by mechanisms including inhibition of oxidative stress and increase in autophagy. *Free Radical Biol. Med.* **2014**, *68*, 260−267.
(52) Ding, W. X.; Li, M.; Chen, X.; Ni, H. M.; Lin, C. W.; Gao, W.; Lu, B.; Stolz, D. B.; Clemens, D. L.; Yin, X. M. Autophagy reduces acute ethanol-induced hepatotoxicity and steatosis in mice. *Gastroenterology* **2010**, *139*, 1740−1752.
(53) Ding, W. X.; Li, M.; Yin, X. M. Selective taste of ethanol-induced autophagy for mitochondria and lipid droplets. *Autophagy* **2011**, *7*, 248−249.

JOURNAL OF AGRICULTURAL AND FOOD CHEMISTRY

Article

pubs.acs.org/JAFC

# Determination of Antioxidant Capacities, α-Dicarbonyls, and Phenolic Phytochemicals in Florida Varietal Honeys Using HPLC-DAD-ESI-MS$^n$

Sara M. Marshall, Keith R. Schneider, Katherine V. Cisneros, and Liwei Gu*

Food Science and Human Nutrition Department, Institute of Food and Agricultural Sciences, University of Florida, Gainesville, Florida 32611, United States

**ABSTRACT:** Honeys contain phenolic compounds and α-dicarbonyls with antioxidant and antimicrobial capacities, respectively. The type and concentration of these compounds vary depending on the floral source and geographical location where the honey is produced. Seventeen varietal honeys, including 12 monofloral and 5 multifloral honeys, were sampled from different regions of Florida. The monofloral honeys included those from citrus, tupelo, palmetto, and gallberry. These honeys were evaluated for their antioxidant capacity, total phenolic content, and free radical scavenging capacity and compared with three New Zealand Manuka honeys. Phenolic phytochemicals and α-dicarbonyls were identified and quantified using HPLC-DAD-MS$^n$. Several honey varieties from gallberry, Manuka, and multifloral displayed a total phenolic content >1000 μg GAE/g. A citrus honey had the lowest total phenolic content of 286 μg GAE/g. The oxygen radical absorbance capacity of the honeys ranged from 1.48 to 18.2 μmol TE/g. All honeys contained 3-deoxyglucosone at a higher concentration than methylglyoxal or glyoxal. Manuka honeys had higher concentrations of methylglyoxal than other varieties. Plant hormones 2-*cis*,4-*trans*-abscisic acid and 2-*trans*,4-*trans*-abscisic acid were the most abundant phytochemicals in all honeys. Coumaric acid, rutin, chrysin, pinocembrin, quercetin, luteolin, and kaempferol were also found in samples but at lower concentrations.

**KEYWORDS:** *honey, Manuka, carbonyls, methylglyoxal, phytochemicals*

## INTRODUCTION

Honey is a natural product produced by bees from the nectar of various plants. The composition of honey is known to vary depending on the season, geographical location, and floral source. Honey is mostly composed of fructose and glucose, but it has also been shown to contain phenolic phytochemicals. These compounds are mostly phenolic acid derivatives and flavonoid aglycones, although some flavonoid glycosides have also been identified.[1,2] Flavonoids are ubiquitous in plants, and they possess antioxidant, radical scavenging, antimuntagenic, anti-inflammatory, and anticarcinogenic functions.[3] Phenolic compounds, specifically flavonoids, are known to contribute to the sensory characteristics of honey, such as color, flavor, and taste as well as potential health-promoting properties. The composition of these compounds was proposed as a quicker and easier way than pollen analysis to determine the floral source of honeys.[1,4−8]

Honeys have also been shown to contain α-dicarbonyls including glyoxal, methylglyoxal, and 3-deoxyglucosone. These compounds react with proteins to produce advanced glycation end products (AGEs) through the Maillard reaction.[9,10] Manuka honey from New Zealand and Australia have well-documented antimicrobial properties.[11−13] The high concentration of methylglyoxal in Manuka honeys is considered the major factor contributing to their high antimicrobial capacity.[11,12,14] Manuka honeys are classified and sold according to their methylglyoxal concentration or "Unique Manuka Factor"; the larger the Unique Manuka Factor value, the higher the antimicrobial capacity. In addition to α-dicarbonyls, some phenolic compounds such as kaempferol, quercetin, and myricetin also possess antimicrobial properties.[13,15]

There are several studies on the phenolic composition of honey from Europe, New Zealand, and Asia, but little exists on the phenolic and α-dicarbonyl composition of North American honey.[16−18] The present work aims to identify and quantify the phenolic compounds from various Florida honeys while determining their antioxidant capacities. Furthermore, the identification and quantification of the main α-dicarbonyls in honey were also performed.

## MATERIALS AND METHODS

**Chemicals.** 2,2′-Azobis(2-amidinopropane) (AAPH) was a product of Wako Chemicals Inc. (Bellwood, RI, USA). Trolox (6-hydroxy-2,5,7,8-tetramethylchroman-2-carboxylic acid), 2,2-diphenyl-1-picrylhydrazyl (DPPH), glyoxal (40% aqueous solution), pinocembrin, ellagic acid, luteolin, apigenin, morin, and galangin were purchased from Sigma-Aldrich (St. Louis, MO, USA). The 3-deoxyglucosone standard was a product of Toronto Research Chemicals Inc. (Toronto, Canada). Folin−Ciocalteu reagent, HPLC grade methanol, formic acid, acetic acid, 2-*cis*,4-*trans*-abscisic acid, coumaric acid, chlorogenic acid, syringic acid, naringenin, hesperetin, rutin, quercetin, chrysin, and kaempferol were purchased from Fisher Scientific (Pittsburgh, PA, USA). The $C_{18}$ (3 mL) solid phase extraction cartridges were from Dionex (Sunnyvale, CA, USA). Methylgloxal (40% aqueous solution) was purchased from MP Biomedicals, LLC (Solon, OH, USA).

Received: April 17, 2014
Revised: July 9, 2014
Accepted: August 7, 2014
Published: August 7, 2014

ACS Publications © 2014 American Chemical Society

**Samples.** A total of 20 honey samples, 15 monofloral and 5 multifloral honeys, were collected from Florida apiarists. The monofloral honeys included those from citrus, tupelo, palmetto, gallberry, and Manuka honeys. Their harvesting regions are listed in Table 1. Three Manuka honeys with certified antimicrobial capacity indices of 12+, 15+, and 16+ were purchased from New Zealand. A lower index number corresponds to a lower capacity, whereas a higher number corresponds to stronger antimicrobial capacity based on the Unique Manuka Factor index. The honeys were stored in darkness at 4 °C prior to analysis. On the day of analysis honeys were removed from refrigeration, and samples were run under warmed water to help create a homogeneous liquid sample.

**Table 1. Floral Sources and Harvesting Region of Honeys[a]**

| sample | floral type | region of Florida (FL, USA) and season |
|---|---|---|
| 1a | citrus | central, West Bradenton, FL, spring 2011 |
| 1b | citrus | north, Lake City, FL, spring 2011 |
| 1c | citrus | south/central, Zolfo Springs, FL, spring 2011 |
| 2a | gallberry | central, Land O' Lakes, FL, spring 2011 |
| 2b | gallberry | north, Wacissa, FL, spring 2011 |
| 2c | gallberry | central, Winter Park, FL, spring 2011 |
| 3a | Manuka 16+ | New Zealand |
| 3b | Manuka 15+ | New Zealand |
| 3c | Manuka 12+ | New Zealand |
| 4a | palmetto | north, Gulf Breeze, FL, spring 2010 |
| 4b | palmetto | central, Geneva, FL, summer 2010 |
| 4c | palmetto | south/central, Zolfo Springs, FL, spring/summer 2011 |
| 5a | tupelo | central, Land O' Lakes, FL, spring 2011 |
| 5b | tupelo | north, Bristol, FL, spring 2011 |
| 5c | tupelo | north, Chipley, FL, spring 2011 |
| 6 | multifloral | north, Fleming Island, FL, early summer 2010 |
| 7 | multifloral | south, Fort Myers, FL, fall 2010 |
| 8 | multifloral | central, Geneva, FL, late summer 2010 |
| 9 | multifloral | south, Fort Myers, FL, fall 2010 |
| 10 | multifloral | north, Lake City, FL, spring 2011 |

[a]Due to the year-round blooming of *Leptospermum scoparium*, the harvesting time for commercial Manuka honey was unknown. North region is defined above 29.28° N, the central region from 29.21° to 27.08° N, and the south region below 26.95° N.

**Total Phenolic and Antioxidant Capacity Assay.** Total phenolic content was determined using the Folin−Ciocalteu assay.[19,20] Contents were expressed as microgram gallic acid equivalents per gram of honey (μg GAE/g). The DPPH scavenging activities of honeys were measured according to a published method.[21] DPPH scavenging activities were expressed as micromole Trolox equivalents per gram of honey (μmol TE/g). Oxygen radical absorbance capacity (ORAC) values for each honey were determined using a modified method from Huang et al.[22] Samples (1 g) were diluted with 10 mL of the phosphate buffer solution and then brought to a final dilution of 1:300. No acetone/water extraction solution was used. Antioxidant capacities were expressed as micromole Trolox equivalents per gram of honey (μmol TE/g).

**Color Assay.** The color of honeys was determined using a published method on a SPECTRAmax 190 microplate reader (Molecular Devices, Sunnyvale, CA, USA).[23] Honey was diluted 50% (w/v) with warm water. The solutions were sonicated for 5 min and filtered through 0.45 μm filter units to remove large particles. The absorbance was measured at 450 nm using 720 nm as a reference wavelength to determine the color of honeys. Color was expressed as absorbance units (AU) at the 450 nm wavelength.

**Derivatization and HPLC Analysis of α-Dicarbonyls.** α-Dicarbonyls were analyzed as their corresponding quinoxalines after derivatization with *o*-phenylenediamine following the method from Mavric et al.[12] One milliliter of 15% (w/v) honeys in phosphate buffer (0.5 M, 6.5 pH) was mixed with 0.6 mL of 1% (w/v) *o*-phenylenediamine in phosphate buffer. The honey solutions were kept in darkness at room temperature for at least 12 h for the reaction to complete. After derivatiztion, solutions were filtered through a membrane (0.45 μm), and 20 μL was injected for HPLC analysis.

An Agilent 1200 HPLC system consisting of an autosampler, a binary pump, and a diode array detector (Agilent Technologies, Palo Alto, CA, USA) were interfaced to a HCT ion trap mass spectrometer (Bruker Daltonics, Billerica, MA, USA). A Zorbax SB-C18 column (250 mm × 4.6 mm, 5 μm particle size, Agilent Technologies) was used for the separation. Column temperature was set at 30 °C. The binary mobile phase consisted of (A) methanol/acetic acid (99.85:0.15 v/v) and (B) methanol/acetic acid (99.97:0.03 v/v). The 49 min gradient is described as follows: 0−2 min, 20% B isocratic; 2−22 min, 20−40% B linear; 22−37 min, 40−100% B linear; 37−42 min, 100% B isocratic; 42−49 min, 100−20% B linear, at a flow rate of 0.8 mL/min followed, by 5 min of re-equilibration of the column before the next sample run.[12] The detection wavelength was 312 nm. The estimated limits of detection for glyoxal, methylglyoxal, and deoxyglucosone were 0.083, 0.063, and 0.130 μg/mL, respectively. Electrospray ionization in positive mode was performed using nebulizer, 50 psi; drying gas, 10 L/min; drying temperature, 290 °C; and capillary, 4000 V. The full scan mass spectra of the quinoxalines were recorded in a range of $m/z$ 100−3000. Auto $MS^2$ was conducted with 80% compound stability and 80% trap drive level. Pure compounds of methylglyoxal, glyoxal, and 3-deoxyglucosone were used as external standards to quantify the quinoxalines formed after derivatization. The concentration ranges of external standard for 3-deoxglucosone, glyoxal, and methylglyoxal were 3−520, 0.1−60, and 0.1−250 mg/L, respectively. The α-dicarbonyls were identified on the basis of full scan and product ion mass spectra and UV−vis spectra on a diode array detector and compared to authentic standards.[10,12,24]

**HPLC Analyses of Phenolic Phytochemicals.** The procedure for the extraction of phenolic phytochemicals from honeys was adapted from that of Hadjmohammadi et al.[25] Honey (10 g) was mixed with 40 mL of deionized water. The solution was filtered to remove any solid residue. The SPE C18 cartridges (0.5 g packing) were preconditioned with 6 mL of methanol followed by 3 mL of deionized water. The honey solutions were loaded on the individual cartridges and rinsed with 15 mL of water followed by 3 mL of 10% (v/v) methanol to remove potential sugars. The phenolic fractions were recovered by eluting the cartridge with 6 mL of methanol. The eluent was dried in a SpeedVac concentrator (Thermo scientific ISS110, Waltham, MA, USA) overnight at room temperature. The dried extracts were then dissolved in 500 μL of methanol, sonicated for 10 min, and centrifuged at 17000*g* for 5 min. Twenty microliters of the supernatant was injected for analysis on HPLC.

A Zorbax SB-C18 column (250 mm × 4.6 mm, 5 μm particle size, Agilent Technologies) was used for the separation. The binary mobile phase consisted of (A) water/formic acid (99.5:0.5, v/v) and (B) methanol at a constant flow rate of 0.8 mL. A 60 min gradient was adapted from a published paper.[7,26] The gradient is described as follows: 0−5 min, 5% B isocratic; 5−20 min, 5−30% B linear; 20−32 min, 30−35% B linear; 32−45 min, 35−50% B linear; 45−50 min, 50−80% B linear; 50−60 min, 80−5% B linear, followed by 5 min of re-equilibration of the column before the next injection. The detection wavelengths were set at 290 and 340 nm, because a majority of the phenolics' UV absorption maxima are at these wavelengths.[5,27−29] Electrospray ionization in negative mode was performed using nebulizer, 50 psi; drying gas, 11 L/min; drying temperature, 350 °C; and capillary, 4000 V. The full scan mass spectra of the phytochemicals were recorded from $m/z$ 100 to 1000. Auto $MS^2$ was conducted with 80% compound stability and 50% trap drive level. Galangin, pinocembrin, quercetin, 2-*cis*,4-*trans*-abscisic acid, luteolin, rutin, coumaric acid, chrysin, and kaempferol were used as external standards to quantify flavonoids and phenolic acids that were identified from mass analysis. Phenolic phytochemicals were identified using a combination of full scan and product ion mass spectra, UV−vis spectra on diode array detector with comparison to authentic standards, and comparison with published papers.[3]

Table 2. Total Phenolic Content, Free Radical Scavenging, Antioxidant Capacities, and Color Analysis of Honeys[a]

| honey | total phenolics (μg/g) | DPPH (μmol TE/g honey) | ORAC (μmol TE/g honey) | $ABS_{450}$ (AU, 50% w/v) |
|---|---|---|---|---|
| 1a, citrus | 829 ± 17.8 b | 1.40 ± 0.00500 a | 6.16 ± 3.35 c | 0.348 ± 0.0180 a |
| 1b, citrus | 593 ± 28.4 d | 0.282 ± 0.115 d | 1.48 ± 1.36 d | 0.0770 ± 0.00500 d |
| 1c, citrus | 286 ± 3.30 d | 0.384 ± 0.251 d | 4.87 ± 2.08 d | 0.0840 ± 0.00300 d |
| 2a, gallberry | 1004 ± 13.7 a | 0.826 ± 0.326 d | 16.5 ± 1.78 a | 0.272 ± 0.0100 b |
| 2b, gallberry | 694 ± 47.6 c | 0.970 ± 0.0770 c | 3.18 ± 0.575 d | 0.115 ± 0.000 d |
| 2c, gallberry | 736 ± 11.9 c | 0.870 ± 0.128 d | 11.6 ± 2.91 b | 0.172 ± 0.115 c |
| 3a, Manuka 16+ | 1080 ± 14.2 a | 1.37 ± 0.665 b | 15.4 ± 9.31 a | 0.298 ± 0.0180 b |
| 3b, Manuka 15+ | 774 ± 27.0 b | 1.35 ± 0.218 b | 6.92 ± 0.233 c | 0.310 ± 0.0140 a |
| 3c, Manuka 12+ | 1030 ± 46.1 a | 1.38 ± 0.244 a | 11.3 ± 3.22 b | 0.224 ± 0.0100 c |
| 4a, palmetto | 767 ± 27.1 c | 0.679 ± 0.231 d | 5.09 ± 0.420 c | 0.163 ± 0.00800 d |
| 4b, palmetto | 851 ± 12.3 b | 1.22 ± 0.250 c | 12.8 ± 0.961 a | 0.248 ± 0.0650 b |
| 4c, palmetto | 530 ± 7.76 d | 1.22 ± 0.130 c | 4.77 ± 0.632 d | 0.284 ± 0.0650 b |
| 5a, tupelo | 820 ± 23.0 b | 1.36 ± 0.324 b | 7.69 ± 0.639 b | 0.241 ± 0.0170 c |
| 5b, tupelo | 773 ± 15.7 c | 1.13 ± 0.182 c | 6.86 ± 1.14 c | 0.145 ± 0.00300 d |
| 5c, tupelo | 691 ± 15.8 c | 1.78 ± 0.0990 a | 12.7 ± 4.56 b | 0.192 ± 0.0100 c |
| 6, multifloral | 936 ± 3.84 b | 1.08 ± 0.0140 c | 18.2 ± 5.10 a | 0.220 ± 0.0170 c |
| 7, multifloral | 1040 ± 12.6 a | 1.49 ± 0.233 a | 15.9 ± 1.68 a | 0.341 ± 0.0190 a |
| 8, multifloral | 981 ± 6.82 a | 1.28 ± 0.132 b | 4.67 ± 3.16 d | 0.480 ± 0.0350 a |
| 9, multifloral | 662 ± 12.1 d | 2.07 ± 0.124 a | 6.70 ± 0.0400 c | 0.380 ± 0.0560 a |
| 10, multifloral | 478 ± 10.2 d | 1.27 ± 0.113 b | 9.34 ± 6.24 b | 0.299 ± 0.0350 b |
| range | 286−1080 | 0.282−2.07 | 1.48−18.2 | 0.077−0.508 |
| average | 778 | 1.17 | 9.11 | 0.245 |

[a]Results are the mean ± SD of three determinations on a fresh weight basis. ORAC values are the mean of two determinations. Values in each column are grouped into four quartiles (a > 75th, b = 50th−75th, c = 25th−50th, and d < 25th percentile).

**Statistical Analysis.** Data was expressed as the mean ± standard deviation of three independent observations per each honey sample unless otherwise stated. Total phenolic content, antioxidant capacities, and color of honeys were grouped into four quartiles. The lowest and highest values were in quartiles 1st−25th and 75th−100th, respectively. Pearson correlation for the different comparable assays was determined using SigmaPlot software (version 12, Systat software Inc., Chicago, IL, USA).

## RESULTS AND DISCUSSION

**Total Phenolic Content, Antioxidant Capacity, and Color Analysis of Honeys.** Table 2 shows the total phenolic content, antioxidant capacity, and color analysis results of the 20 honeys analyzed, including the 3 New Zealand Manuka honeys. The total phenolic content in the monofloral and multifloral honeys ranged from 286 to 1080 μg GAE/g on a fresh weight basis. This range of values was in agreement with previously published values of honeys from other regions of the world.[3,17,23,30,31] Manuka honeys had the highest total phenolic content (averaging 961 μg GAE/g) among all of the honeys. This value is similar to those reported in honeydew honeys (1150 μg GAE/g) from Burkina Faso.[31] The highest total phenolic content in the multifloral honeys was 1040 μg GAE/g in sample 6b. This honey was collected from southern Florida during the fall season. There was no apparent correlation between total phenolic content and harvesting time or location for the multifloral honeys. This may be due to the fact that Florida's subtropical climate allows for the same plants to be grown in multiple seasons and multiple areas of the state. A previous study from Cuba and Portugal showed that the highest total phenolic content for honeys produced in these countries was 700 μg GAE/g.[32,33] These contents were comparable to Florida monofloral honeys of tupelo and palmetto, which had average total phenolic contents of 761 and 716 μg GAE/g, respectively. The multifloral varieties had a higher average total phenolic content of 819 μg GAE/g than most of the monofloral varieties examined.

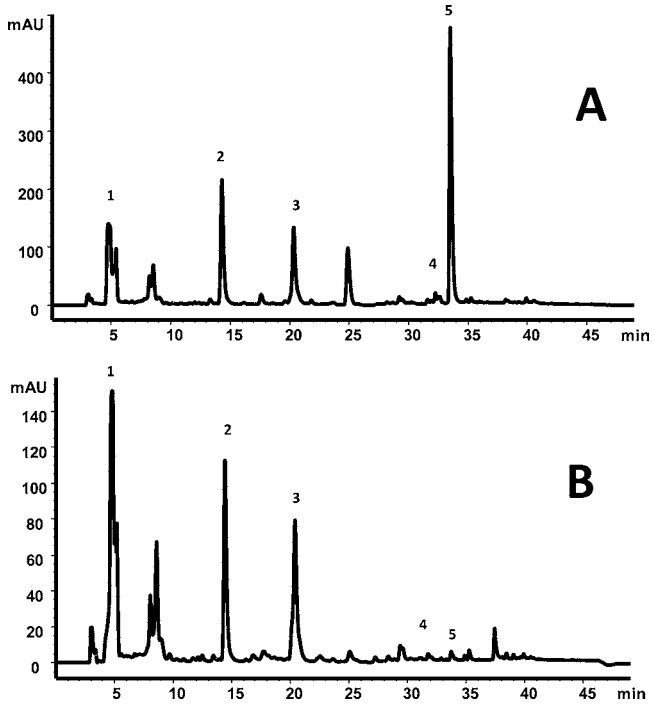


Figure 1. HPLC chromatogram of α-dicarbonyls in Manuka honey 3b (A) and multifloral honey 6 (B) after derivatization. Peaks 1, 2, 3, 4, and 5 are *o*-phenylenediamine, glucosone, 3-deoxyglucosone, glyoxal, and methylglyoxal, respectively.

It has been shown that color can also be an indicator of total phenolic content and honey's antioxidant capacity. Darker honeys often have a higher phenolic content and antioxidant capacity.[17,23] The color of honeys ranged from 77 mAU in a


dx.doi.org/10.1021/jf501329y | J. Agric. Food Chem. 2014, 62, 8623−8631

**Table 3. α-Dicarbonyl Content of Honeys[a]**

| sample | 3-deoxyglucosone (μg/g) | glyoxal (μg/g) | methylglyoxal (μg/g) | total carbonyl (μg/g) |
|---|---|---|---|---|
| 1a, citrus | 684 ± 34.5 b | 4.53 ± 1.01 a | 6.09 ± 1.27 b | 695 ± 33.2 b |
| 1b, citrus | 288 ± 11.9 d | 5.70 ± 0.462 a | 6.19 ± 1.46 b | 300 ± 12.7 d |
| 1c, citrus | 206 ± 21.4 d | 2.19 ± 0.345 d | 3.68 ± 1.49 d | 212 ± 21.6 d |
| 2a, gallberry | 517 ± 3.15 c | 3.75 ± 1.39 b | 7.09 ± 2.52 b | 528 ± 6.55 c |
| 2b, gallberry | 466 ± 24.9 d | 2.76 ± 0.694 c | 4.88 ± 1.05 d | 474 ± 26.6 d |
| 2c, gallberry | 701 ± 39.9 b | 7.35 ± 0.935 a | 13.0 ± 4.30 a | 722 ± 35.3 b |
| 3a, Manuka 16+ | 636 ± 48.8 b | 4.39 ± 0.660 b | 86.9 ± 0.967 a | 727 ± 49.8 b |
| 3b, Manuka 15+ | 558 ± 13.2 c | 5.13 ± 0.0740 a | 483 ± 10.7 a | 1047 ± 23.6 a |
| 3c, Manuka 12+ | 646 ± 40.2 b | 3.09 ± 0.182 c | 92.1 ± 0.343 a | 741 ± 39.8 b |
| 4a, palmetto | 474 ± 35.1 c | 2.95 ± 0.222 c | 5.80 ± 0.255 c | 483 ± 34.8 c |
| 4b, palmetto | 831 ± 3.46 a | 6.10 ± 0.315 a | 10.8 ± 1.77 a | 848 ± 23.2 a |
| 4c, palmetto | 730 ± 28.7 a | 2.23 ± 0.109 d | 4.53 ± 1.01 d | 737 ± 29.1 b |
| 5a, tupelo | 614 ± 23.4 c | 2.90 ± 1.19 c | 4.85 ± 0.619 d | 622 ± 24.8 c |
| 5b, tupelo | 502 ± 23.5 c | 3.93 ± 1.22 b | 5.90 ± 1.35 c | 512 ± 24.5 c |
| 5c, tupelo | 259 ± 12.7 d | 2.68 ± 0.257 d | 4.97 ± 0.582 c | 266 ± 13.3 d |
| 6, multifloral | 372 ± 17.2 d | 2.44 ± 0.778 d | 5.23 ± 1.15 c | 380 ± 19.0 d |
| 7, multifloral | 754 ± 17.6 a | 4.11 ± 1.56 b | 6.80 ± 1.98 b | 765 ± 18.0 a |
| 8, multifloral | 678 ± 109 b | 3.96 ± 0.915 b | 5.31 ± 0.948 c | 687 ± 111 c |
| 9, multifloral | 884 ± 21.8 a | 2.49 ± 0.321 d | 3.63 ± 0.284 d | 890 ± 22.3 a |
| 10, multifloral | 727 ± 8.95 a | 3.27 ± 0.245 c | 6.38 ± 0.187 b | 753 ± 37.7 a |
| range | 206–884 | 2.19–7.35 | 3.63–483 | 212–890 |
| average | 576 | 3.80 | 38.4 | 619 |

[a]Results are the mean ± standard deviation of three determinations on a fresh weight basis. Values in each column are grouped into four quartiles (a > 75th, b = 50th–75th, c = 25th–50th, and d < 25th percentile).

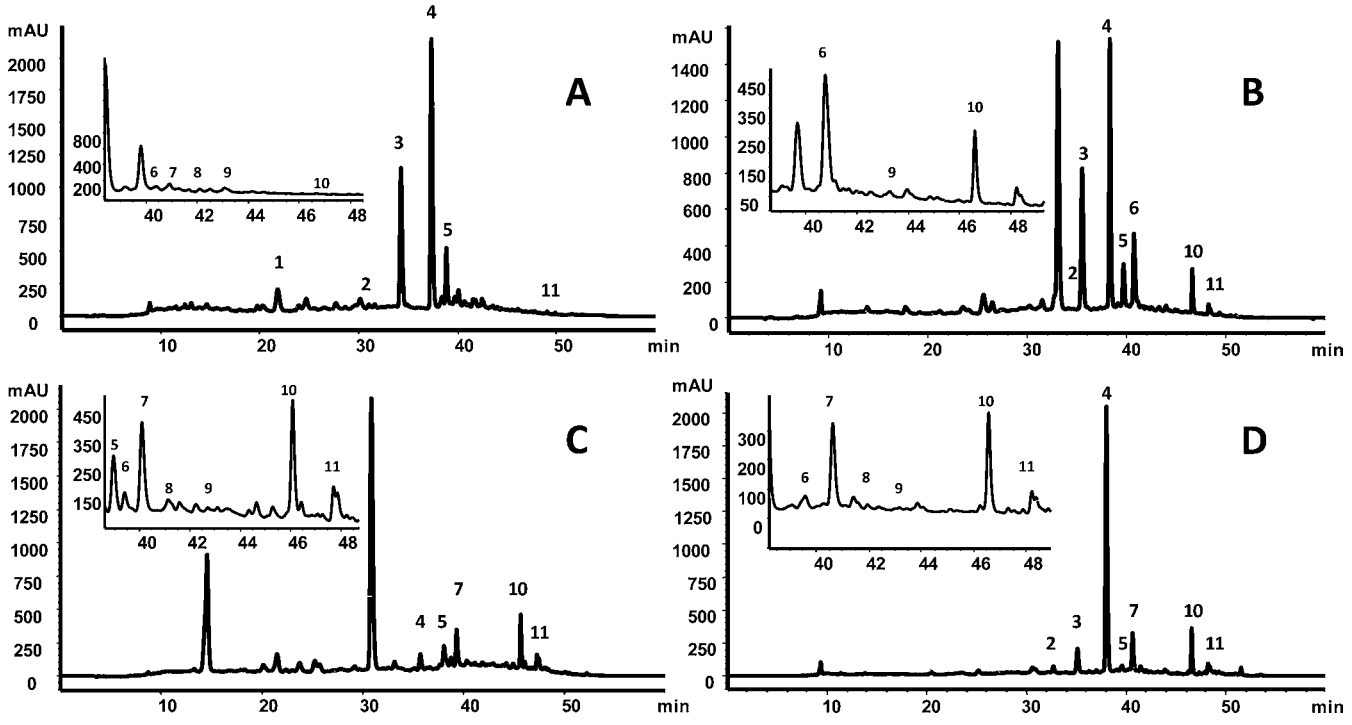


**Figure 2.** HPLC chromatogram of phenolic phytochemicals in palmetto honey 4a (A), palmetto honey 4b (B), Manuka honey 3b (C), and citrus honey 1a (D). Peak number and identification are listed in Table 4.

light colored citrus honey to 480 mAU in a multifloral honey. The range of absorbance is consistent with previously reported values.[23,34] Citrus honeys 1b and 1c had the lowest absorbance and were visually fairer than the other varieties. Two multifloral honeys, 6c and 6d, had the highest absorbances at 480 and 380 mAU, respectively, among all of the honeys analyzed. Citrus honey 1c showed lower values for color, total phenolic content, and antioxidant capacity (Table 2). This observation helps to support the conclusion that color and total phenolic content in honey are directly correlated. The multifloral variety had an average absorbance of 344 mAU, which was higher than the average absorbance of monofloral honeys (212 mAU). The correlation coefficient ($r$) between total phenolic concentration and color was 0.47. This $r$ value is lower than those reported


dx.doi.org/10.1021/jf501329y | J. Agric. Food Chem. 2014, 62, 8623–8631

**Table 4. Identification of Phytochemicals in Honeys by HPLC-DAD-ESI-MS$^{n}$[a]**

| peak | compound | mol wt | retention time (min) | $[M-H]^-$ ($m/z$) | $MS^2$ ($m/z$) |
|---|---|---|---|---|---|
| 1 | coumaric acid | 164 | 23.3 | 163 | 119 |
| 2 | rutin | 610 | 32.6 | 609 | 301 |
| 3 | 2-*trans*,4-*trans*-abscisic acid[b] | 264 | 35.1 | 263 | 219, 204, 201 |
| 4 | 2-*cis*,4-*trans*-abscisic acid | 264 | 38.4 | 263 | 219, 153 |
| 5 | unidentified | 286 | 39.5 | 285 | 267, 252, 239 |
| 6 | quercetin | 302 | 40.2 | 301 | 179, 151 |
| 7 | unidentified | 272 | 41.0 | 271 | 253, 215, 151 |
| 8 | luteolin | 286 | 42.0 | 285 | 243, 223, 199, 151 |
| 9 | kaempferol | 286 | 43.3 | 285 | 267, 257, 151 |
| 10 | pinocembrin | 256 | 46.7 | 255 | 213, 151 |
| 11[c] | chrysin | 254 | 48.0 | 253 | 209 |
| 11[c] | galangin | 270 | 48.0 | 269 | 227, 213, 197, 153 |

[a]Nine compounds were identified by comparison with authentic standards. Peaks 5 and 7 were unidentified. [b]2-*trans*,4-*trans*-Abscisic acid was tentatively identified using tandem mass spectra. [c]Chrysin and galangin coeluted in peak 11.

between total phenolics and color in other foods.[23,31] However, the correlation was significant at $p < 0.05$. The color of honeys can be attributed to flavonoids and Maillard reaction products, which can differ according to floral source and age of honey. Researchers have shown that proline content correlates with honey color.[35] Also, vitamins such as ascorbic acid may have an influence on honey's unique color. Carotenoids, minerals, and pollen are other pigment compounds that can be read at 450 nm and may be contributing to the low correlation between total phenolics and color.[36]

The DPPH scavenging activity of honeys ranged from 0.282 to 2.07 μmol TE/g honey. Multifloral honey 6d had the highest free radical scavenging capability among all honeys. The orange blossom honeys 1b and 1c had the lowest free radical scavenging values at 0.282 and 0.384 μmol TE/g honey, respectively. Honeys with paler colors, such as the citrus honeys, had lower absorbance and scavenging capacities compared to other varieties. It has been suggested that darker honeys generally have higher radical scavenging potential.[23] The correlation between total phenolic concentration and DPPH concentration was close to significant with a $p$ value of 0.058. Whereas correlation between total phenolic content and DPPH assay was shown for honeys, lack of correlation was also observed.[37] The DPPH assay measures the presence of compounds able to donate an electron to scavenge the DPPH radical. Phenolic compounds are not the only compounds capable of donating an electron. Islam et al. showed that amino acids and other nonphenolic compounds were also able to scavenge DDPH.[38] Honeys are complex matrices of compounds with different scavenging capabilities; therefore, it is possible that total phenolics and DPPH scavenging do not significantly correlate.

The antioxidant capacity of honeys, expressed as ORAC values, ranged from 1.48 to 18.2 μmol TE/g honey, which are comparable with those reported previously.[23] The ORAC value of multifloral honey 6a was higher than those of all other honeys tested. The multifloral varieties had an average ORAC value of 11 μmol TE/g, which is comparable to that of the gallberry honeys (10 μmol TE/g). The correlation coefficient ($r$) between total phenolic concentration of the honeys and ORAC values was 0.60 with $p < 0.05$. The ORAC assay does not measure antioxidant capacity due to phenolics alone; amino acids and other nucleophiles may also quench the free radicals in this method. The $r$ value between the ORAC and DPPH assays was 0.29. This low $r$ value was likely caused by the differences in the chemistry of these two methods. The ORAC assay is based on a hydrogen atom transfer reaction, whereas the DPPH assay uses an electron transfer mechanism.[39]

**Identification and Quantification of α-Dicarbonyls in Honey.** Carbonyl compounds were detected using UV−vis detection at 312 nm after a derivatization step with *o*-phenylenediamine to form quinoxalines (Figure 1). Peak 1 was excessive *o*-phenylenediamine. Peak 2 was tentatively identified as glucosone according to $[M + H]^+$ 251 and a published study.[24,40,41] Peak 3 produced $m/z$ 235 $[M + H]^+$, which fragmented into $m/z$ 217 and 199. These spectra were consistent with 3-deoxyglucosone.[24,41] Peak 4 was identified as glyoxal by comparing UV−vis and retention time with standard. Peak 5 yielded $m/z$ 145 $[M + H]^+$ and was identified as the quinoxaline formed after the reaction between *o*-phenylenediamine and methylglyoxal.[12,24] The α-dicarbonyl profiles in honeys differed according to floral sources and harvesting locations. For example, Manuka honey (Figure 1A) showed a predominant peak for methylglyoxal, whereas the methylglyoxal concentration in all of the other varieties was much lower (Figure 1B).

Table 3 provides the concentrations of glyoxal, methylglyoxal, and 3-deoxyglucosone in monofloral and multifloral honeys. Glucosone was not quantified in this experiment due to its artificial formation in select buffers and sample matrices. The contents of methylglyoxal in Manuka honeys 3a, 3b, and 3c were 86.9, 483, and 92.1 μg/g, respectively. Methylglyoxal concentration in other honeys ranged from 3.63 to 13.0 μg/g. Methylglyoxal in Manuka was 7−37 times more concentrated than the next highest (gallberry honey, 2c). Other studies have shown methylglyoxal concentrations ranging from undetectable to >1500 μg/g.[11,12,14,18,42] Stephen et al. showed that the longer a Manuka honey was aged, the higher the methylglyoxal concentration became.[18] The high levels of methylglyoxal in the Manuka honeys were not seen in any other foods.[12] A number of researchers suggested that the high levels of methylglyoxal in Manuka honeys are the major contributing factor to high antimicrobial capacity.[12] Glyoxal concentrations ranged from 2.19 to 7.35 μg/g, which is similar to the concentrations reported in honeys collected from other regions of the world.[11,12,15,34] Among three α-dicarbonyls, 3-deoxyglucosone had the highest concentration in all honeys. The higher concentration of 3-deoxyglucosone relative to methylglyoxal and glyoxal in honeys is expected because 3-deoxyglucosone is the initial product of glucose degradation and honey has a high sugar content.[10] Retro-aldolization of 3-deoxyglucosone produces methylglyoxal.[10] Thus, when 3-deoxyglucosone decreases, methylglyoxal should increase. This was not confirmed as a processing study was not performed on honeys to examine this reaction.

**Identification and Quantification of Phenolic Phytochemicals.** Figure 2 depicts the HPLC chromatograms of phenolic phytochemicals in different honeys after samples were purified using solid phase extraction. Chromatograms were recorded at 290, 340, and 520 nm, although only the chromatograms at 290 nm are shown. This is because most phenolic compounds can be detected at this wavelength.[20]

**Table 5. Content of Phenolic Compounds in Honeys ($\mu$g/g)[a]**

| sample | coumaric acid | rutin | 2-*trans*,4-*trans*-abscisic acid | 2-*cis*,4-*trans*-abscisic acid | quercetin | luteolin | kaempferol | pinocembrin | chrysin + galangin | total |
|---|---|---|---|---|---|---|---|---|---|---|
| 1a, citrus | ND | 0.232 ± 0.070 | 6.36 ± 1.2 | 35.8 ± 4.0 | 0.353 ± 0.12 | 0.401 ± 0.13 | 0.497 ± 0.16 | 1.65 ± 0.27 | 2.24 ± 0.14 | 47.6 ± 11 |
| 1b, citrus | 0.437 ± 0.26 | 0.555 ± 0.020 | 5.80 ± 0.080 | 15.1 ± 0.11 | 0.650 ± 0.040 | ND | 1.55 ± 0.11 | 1.07 ± 0.010 | 1.16 ± 0.050 | 26.4 ± 4.7 |
| 1c, citrus | ND | 0.597 ± 0.010 | 2.03 ± 0.11 | 5.12 ± 0.27 | 1.15 ± 0.060 | ND | 3.12 ± 0.16 | 0.146 ± 0.010 | ND | 12.2 ± 1.7 |
| 2a, gallberry | 0.185 ± 0.050 | ND | 7.53 ± 0.49 | 24.0 ± 1.8 | 0.317 ± 0.24 | ND | 0.392 ± 0.030 | 0.357 ± 0.040 | 0.348 ± 0.010 | 33.1 ± 7.7 |
| 2b, gallberry | 0.295 ± 0.14 | ND | 26.1 ± 11 | 27.6 ± 12 | 0.341 ± 0.16 | ND | 0.322 ± 0.17 | 0.084 ± 0.020 | 0.164 ± 0.040 | 55.0 ± 12 |
| 2c, gallberry | 0.508 ± 0.16 | 0.218 ± 0.030 | 13.1 ± 1.0 | 24.3 ± 2.6 | 0.344 ± 0.070 | ND | 0.425 ± 0.040 | 1.04 ± 0.16 | 1.03 ± 0.10 | 41.0 ± 8.2 |
| 3a, Manuka 16+ | ND | ND | 0.710 ± 0.11 | 1.55 ± 0.19 | 0.552 ± 0.060 | 1.05 ± 0.11 | 0.693 ± 0.090 | 0.742 ± 0.090 | 2.04 ± 0.19 | 7.34 ± 0.65 |
| 3b, Manuka 15+ | ND | ND | ND | 0.525 ± 0.22 | 0.495 ± 0.24 | 0.907 ± 0.16 | 0.260 ± 0.11 | 2.75 ± 0.69 | 4.56 ± 0.65 | 9.49 ± 1.5 |
| 3c, Manuka 12+ | ND | ND | 3.08 ± 0.78 | 5.54 ± 1.4 | 0.792 ± 0.21 | 1.26 ± 0.30 | 0.804 ± 0.34 | 1.03 ± 0.30 | 1.04 ± 0.080 | 13.5 ± 1.8 |
| 4a, palmetto | 0.745 ± 0.030 | 0.337 ± 0.050 | 14.4 ± 0.40 | 25.5 ± 1.0 | 0.689 ± 0.24 | 0.277 ± 0.060 | 1.49 ± 0.13 | 0.064 ± 0.020 | 0.140 ± 0.020 | 43.7 ± 8.7 |
| 4b, palmetto | ND | 0.534 ± 0.12 | 12.7 ± 1.9 | 21.1 ± 2.5 | ND | ND | 0.583 ± 0.14 | 1.17 ± 0.19 | 1.40 ± 0.090 | 37.5 ± 7.3 |
| 4c, palmetto | 1.21 ± 0.49 | 0.360 ± 0.14 | 2.08 ± 0.73 | 8.00 ± 2.7 | 0.711 ± 0.25 | 0.386 ± 0.16 | 1.52 ± 0.52 | 2.25 ± 0.76 | 2.94 ± 1.0 | 19.5 ± 2.4 |
| 5a, tupelo | 0.604 ± 0.29 | ND | 19.1 ± 5.1 | 27.0 ± 1.9 | 1.22 ± 0.070 | ND | 2.11 ± 0.050 | 2.65 ± 0.080 | 3.17 ± 0.12 | 55.8 ± 9.6 |
| 5b, tupelo | 0.219 ± 0.040 | ND | 7.50 ± 0.36 | 9.70 ± 0.38 | 0.436 ± 0.040 | ND | 0.610 ± 0.32 | 0.152 ± 0.050 | 0.393 ± 0.050 | 19.0 ± 3.6 |
| 5c, tupelo | 0.355 ± 0.18 | ND | 4.53 ± 1.3 | 5.95 ± 0.78 | ND | ND | 1.18 ± 0.30 | 1.63 ± 0.14 | 1.46 ± 0.19 | 15.1 ± 2.1 |
| 6, multifloral | 0.278 ± 0.10 | 0.175 ± 0.020 | 25.3 ± 4.3 | 72.9 ± 5.1 | 0.614 ± 0.19 | 0.525 ± 0.17 | 0.625 ± 0.30 | 1.24 ± 0.17 | 0.686 ± 0.12 | 102 ± 24.0 |
| 7, multifloral | 0.166 ± 0.010 | ND | 6.46 ± 0.13 | 18.8 ± 0.27 | 0.473 ± 0.010 | 0.797 ± 0.070 | 1.08 ± 0.31 | 0.107 ± 0.00 | 0.144 ± 0.020 | 28.0 ± 6.0 |
| 8, multifloral | 2.39 ± 0.33 | ND | 2.29 ± 0.060 | 8.95 ± 0.21 | 0.617 ± 0.020 | 0.135 ± 0.00 | ND | 1.50 ± 0.00 | 2.42 ± 0.14 | 18.3 ± 2.7 |
| 9, multifloral | 0.616 ± 0.10 | 0.441 ± 0.020 | 0.723 ± 0.23 | 2.41 ± 0.49 | 0.578 ± 0.12 | 0.196 ± 0.020 | 0.636 ± 0.12 | 0.258 ± 0.050 | 0.408 ± 0.050 | 6.27 ± 0.66 |
| 10, multifloral | 0.272 ± 0.21 c | 0.301 ± 0.080 | 9.35 ± 1.1 | 17.5 ± 1.3 | 0.557 ± 0.16 | 0.226 ± 0.080 | 1.75 ± 0.50 | 1.57 ± 0.19 | 1.73 ± 0.39 | 33.3 ± 5.7 |

[a]Results are the mean ± standard deviation of three determinations on a fresh weight basis. ND, not detected. 2-*trans*,4-*trans*-abscisic acid was quantified using the 2-*cis*,4-*trans*-abscisic acid as a standard.



dx.doi.org/10.1021/jf501329y | J. Agric. Food Chem. 2014, 62, 8623−8631

Mass spectrometry was operated in the negative mode due to its higher sensitivity toward flavonoids than positive ionization mode.[43] Phenolic compounds in honeys were identified on the basis of mass spectra, UV−vis spectra from diode array detector, and comparison with standards. The retention time, $[M - H]^-$, and production ions of identified phenolic acids and flavonoids are listed in Table 4. Nine compounds were identified in honeys by comparison with authentic standards and using $MS^n$. 2-*trans*,4-*trans*-Abscisic acid was tentatively identified using $MS^n$. Identification of two peaks was inconclusive. Identified compounds included flavones, flavonols, flavanones, isomers of the terpenoid abscisic acid, phenolic acids, and phenolic derivatives. These compounds had all been previously reported in other honey varieties or propolis.[4,5,7,27,44−50]

*Phenolic Acids.* Peak 1 was confirmed to be coumaric acid by comparing retention time and mass spectra with authentic standards.

*Terpenoids.* Peak 4 was identified as 2-*cis*,4-*trans*-abscisic acid by comparison with authentic standard. It produced a $[M - H]^-$ at $m/z$ 263 that further dissociated to form $m/z$ 219 and 153 after loss of $CO_2$ and the side chain, respectively. Peak 3 also produced $m/z$ 263 $[M - H]^-$. This peak had two main fragments, $m/z$ 204 after the loss of both $CO_2$ and $CH_3$, and $m/z$ 219 after the loss of $CO_2$. The peak was tentatively identified as 2-*trans*,4-*trans*-abscisic acid. Both isomers of abscisic acid had been identified in other honey varieties.[5,32,47,49]

*Flavanones.* Peak 10 was identified as pinocembrin by comparison of the retention time and mass spectra with its standard. Peak 10 gave an ion at $m/z$ 255 $[M - H]^-$, which further dissociated into $m/z$ 213 from the loss of $C_2H_2O$ (42 Da) and $m/z$ 151 from the RDA reaction.[46]

*Flavonols.* Multiple flavonols were identified in the honeys. Peak 2 was rutin. It produced $m/z$ 609 $[M - H]^-$, which further dissociated into $m/z$ 301 after the loss of the rutinose group corresponding to the deprotonated quercetin aglycone.[43,51] Peak 6 was confirmed to be quercetin. The maximum absorbance was seen at 340 nm. Its retention time and mass spectrum matched those of an authentic standard. Peak 9 was identified as kaempferol by comparison of the retention time and mass spectra with those of authentic standards. Kaempferol produced an ion at $m/z$ 285 $[M - H]^-$ and two product ions at $m/z$ 267 $[M - H - H_2O]^-$ and $m/z$ 151 from RDA reaction. Peak 11 contained two flavonoids, galangin and chrysin. Galangin produced an ion with $m/z$ 269 $[M - H]^-$, which further dissociated into $m/z$ 197, which was formed from the loss of both a $CO_2$ and a CO (62 Da) group and $m/z$ 227.

*Flavones.* Luteolin (peak 8) and chrysin (peak 11) were identified in honey by comparison of retention times and mass spectra with standards. Chrysin has been previously identified in many different varieties of honeys, and thus its presence would not be beneficial in authenticating a particular variety of honey.[8,52,53] We did not detect flavonoid glycosides in honey samples. There are two possible explanations for the predominance of aglycone in honey. First, flavonoids in the nectar are different from those in the plant. Second, bees have glucosidase enzymes that can hydrolyze flavonoid glycosides.[54]

*Unidentified Peaks.* Peak 5 produced $m/z$ 285 $[M - H]^-$, which further dissociated into $m/z$ 267 and 252. Peak 7 produced $m/z$ 271 $[M - H]^-$, which further dissociated into $m/z$ 253, corresponding to the loss of water. Identification of these two peaks was inconclusive.

The concentrations of the 10 phenolic compounds quantified in the honeys are listed in Table 5. Figure 2 shows the phenolic phytochemical profiles were similar in honeys of the same variety. These profiles in palmetto honey show the phenolic "fingerprints" of honeys and may help to identify the floral source of unknown honeys. It was speculated that the multifloral honeys could be classified according to composition of phenolic phytochemicals. The Manuka honey (sample 3a) in Figure 2C had two large peaks that were unidentifiable from mass data. Honey is a complex mixture that may include other compounds such as pesticides, antibiotics, peptides, amino acids, dicarboxylic acids, and other residues that may not be easily identifiable with the current method.[35,36,55,56]

The concentrations and profiles of phenolics in the multifloral honeys varied according to seasons, locations, and apiarists. There was a higher concentration of abscisic acids in multifloral honey 6 than in all other honeys.

A majority of the phenolic compounds identified and quantified were in small amounts of <1 $\mu$g/g. The plant hormone, abscisic acid, was seen in almost all honeys in two isomeric forms, 2-*cis*,4-*trans*-abscisic acid and 2-*trans*,4-*trans*-abscisic acid. 2-*cis*,4-*trans*-Abscisic acid (peak 4) was the most abundant phytochemical found in most of the honeys. The presence of abscisic acid was not surprising as it is commonly seen in all plants. Abscisic acid has also been documented in other honey varieties.[5,32,47,49]

Honey samples in this study were collected by experienced beekeepers. The floral sources of honey were reported by beekeepers but were not verified by pollen counting. It is often difficult to determine the floral sources of a honey because bees can forage over 32000 acres. We speculated that some of the monofloral honeys may contain honeys from other floral sources. This remains a limitation of this study.

In conclusion, Florida honeys contain antioxidant phenolic phytochemicals and antimicrobial $\alpha$-dicarbonyls. The concentrations and compositions of these compounds varied according to floral source, harvesting season, and location. Floral source appears to be the most significant influence on honey characteristics. Several Florida varietal honeys, such as gallberry and multifloral honeys, had higher antioxidant capacities and concentrations of flavonoids, phenolic acids, and $\alpha$-dicarbonyls. These honeys may have better health-promoting properties and other medicinal benefits.

## AUTHOR INFORMATION


### Corresponding Author

*(L.G.) Phone: (352) 392-1991, ext. 210. Fax: (352) 392-9467. E-mail: Lgu@ufl.edu.



### Funding

Funding for this research was provided in part by Specialty Crop Block Fund from the Florida Department of Agriculture and Consumer Service and the Florida State Beekeepers Association.

### Notes

The authors declare no competing financial interest.

## ACKNOWLEDGMENTS

We give special thanks to Jerry Hayes of the Apiary Inspection Services and James Ellis of the UF Bee College and the Entomology and Nematology Department for their help in assisting with the collection of honeys for this research.

## REFERENCES


(1) Alvarez-Suarez, J. M.; Gonzalez-Paramas, A. M.; Santos-Buelga, C.; Battino, M. Antioxidant characterization of native monofloral Cuban honeys. *J. Agric. Food Chem.* **2010**, *58*, 9817−9824.

(2) Ferreres, F.; Tomas-Barberan, F. A.; Soler, C.; Garcia-Viguera, C.; Ortiz, A.; Tomas-Lorente, F. A simple extractive technique for honey flavonoid HPLC analysis. *Apidologie* **1994**, *25*, 21−30.

(3) Gheldof, N.; Wang, X. H.; Engeseth, N. J. Identification and quantification of antioxidant components of honeys from various floral sources. *J. Agric. Food Chem.* **2002**, *50*, 5870−5877.

(4) Yaoa, L.; Jiang, Y. M.; Singanusong, R.; Datta, N.; Raymont, K. Phenolic acids in Australian *Melaleuca*, *Guioa*, *Lophostemon*, *Banksia* and *Helianthus* honeys and their potential for floral authentication. *Food Res. Int.* **2005**, *38*, 651−658.

(5) Yao, L. H.; Datta, N.; Tomas-Barberan, F. A.; Ferreres, F.; Martos, I.; Singanusong, R. Flavonoids, phenolic acids and abscisic acid in Australian and New Zealand *Leptospermum* honeys. *Food Chem.* **2003**, *81*, 159−168.

(6) Truchado, P.; Ferreres, F.; Tomas-Barberan, F. A. Liquid chromatography-tandem mass spectrometry reveals the widespread occurrence of flavonoid glycosides in honey, and their potential as floral origin markers. *J. Chromatogr., A* **2009**, *1216*, 7241−7248.

(7) Andrade, P.; Ferreres, F.; Amaral, M. T. Analysis of honey phenolic acids by HPLC, its application to honey botanical characterization. *J. Liq. Chromatogr. Relat. Technol.* **1997**, *20*, 2281−2288.

(8) Ferreres, F.; Garcia-Viguera, C.; Tomas-Lorente, F.; Tomas-Barberan, F. A. Hesperetin − a marker of the floral origin of citrus honey. *J. Sci. Food Agric.* **1993**, *61*, 121−123.

(9) Liu, H.; Liu, H.; Wang, W.; Khoo, C.; Taylor, J.; Gu, L. Cranberry phytochemicals inhibit glycation of human hemoglobin and serum albumin by scavenging reactive carbonyls. *Food Funct.* **2011**, *2*, 475−482.

(10) Weigel, K. U.; Opitz, T.; Henle, T. Studies on the occurrence and formation of 1,2-dicarbonyls in honey. *Eur. Food Res. Technol.* **2004**, *218*, 147−151.

(11) Atrott, J.; Henle, T. Methylglyoxal in Manuka honey − correlation with antibacterial properties. *Czech J. Food Sci.* **2009**, *27*, S163−S165.

(12) Mavric, E.; Wittmann, S.; Barth, G.; Henle, T. Identification and quantification of methylglyoxal as the dominant antibacterial constituent of Manuka (*Leptospermum scoparium*) honeys from New Zealand. *Mol. Nutr. Food Res.* **2008**, *52*, 483−489.

(13) Weston, R. J.; Mitchell, K. R.; Allen, K. L. Antibacterial phenolic components of New Zealand manuka honey. *Food Chem.* **1999**, *64*, 295−301.

(14) Adams, C. J.; Manley-Harris, M.; Molan, P. C. The origin of methylglyoxal in New Zealand manuka (*Leptospermum scoparium*) honey. *Carbohydr. Res.* **2009**, *344*, 1050−1053.

(15) Adams, C. J.; Boult, C. H.; Deadman, B. J.; Farr, J. M.; Grainger, M. N. C.; Manley-Harris, M.; Snow, M. J. Isolation by HPLC and characterization of the bioactive fraction of New Zealand manuka (*Leptospermum scoparium*) honey (2008, Vol. 343, p 651). *Carbohydr. Res.* **2009**, *344*, 2609−2609.

(16) Aljadi, A. M.; Kamaruddin, M. Y. Evaluation of the phenolic contents and antioxidant capacities of two Malaysian floral honeys. *Food Chem.* **2004**, *85*, 513−518.

(17) Bertoncelj, J.; Dobersek, U.; Jamnik, M.; Golob, T. Evaluation of the phenolic content, antioxidant activity and colour of Slovenian honey. *Food Chem.* **2007**, *105*, 822−828.

(18) Stephens, J. M.; Schlothauer, R. C.; Morris, B. D.; Yang, D.; Fearnley, L.; Greenwood, D. R.; Loomes, K. M. Phenolic compounds and methylglyoxal in some New Zealand manuka and kanuka honeys. *Food Chem.* **2010**, *120*, 78−86.

(19) Singleton, V. L.; Rossi, J. A. Colorimetry of total phenolics in grapes and wine with phosphomolybdic-phosphotungstic acid reagents. *Am. J. Enol. Vitic.* **1965**, *16*, 144−158.

(20) Sandhu, A. K.; Gu, L. Antioxidant capacity, phenolic content, and profiling of phenolic compounds in the seeds, skin, and pulp of *Vitis rotundifolia* (Muscadine grapes) as determined by HPLC-DAD-ESI-MS*n*. *J. Agric. Food Chem.* **2010**, *58*, 4681−4692.

(21) Brand-Williams, W.; Cuvelier, M. E.; Berset, C. Use of a free radical method to evaluate antioxidant activity. *Lebensm.-Wiss. Technol.* **1995**, *28*, 25−30.

(22) Huang, D. J.; Ou, B. X.; Hampsch-Woodill, M.; Flanagan, J. A.; Prior, R. L. High-throughput assay of oxygen radical absorbance capacity (ORAC) using a multichannel liquid handling system coupled with a microplate fluorescence reader in 96-well format. *J. Agric. Food Chem.* **2002**, *50*, 4437−4444.

(23) Beretta, G.; Granata, P.; Ferrero, M.; Orioli, M.; Facino, R. M. Standardization of antioxidant properties of honey by a combination of spectrophotometric/fluorimetric assays and chemometrics. *Anal. Chim. Acta* **2005**, *533*, 185−191.

(24) Marceau, E.; Yaylayan, V. A. Profiling of $\alpha$-dicarbonyl content of commercial honeys from different botanical origins: identification of 3,4-dideoxyglucoson-3-ene (3,4-DGE) and related compounds. *J. Agric. Food Chem.* **2009**, *57*, 10837−10844.

(25) Hadjmohammadi, M. R.; Nazari, S.; Kamel, K. Determination of flavonoid markers in honey with SPE and LC using experimental design. *Chromatographia* **2009**, *69*, 1291−1297.

(26) Petrus, K.; Schwartz, H.; Sontag, G. Analysis of flavonoids in honey by HPLC coupled with coulometric electrode array detection and electrospray ionization mass spectrometry. *Anal. Bioanal. Chem.* **2011**, *400*, 2555−2563.

(27) Martos, I.; Cossentini, M.; Ferreres, F.; Tomas-Barberan, F. A. Flavonoid composition of Tunisian honeys and propolis. *J. Agric. Food Chem.* **1997**, *45*, 2824−2829.

(28) Martos, I.; Ferreres, F.; Tomas-Barberan, F. A. Identification of flavonoid markers for the botanical origin of *Eucalyptus* honey. *J. Agric. Food Chem.* **2000**, *48*, 1498−1502.

(29) Martos, I.; Ferreres, F.; Yao, L. H.; D'Arcy, B.; Caffin, N.; Tomas-Barberan, F. A. Flavonoids in monospecific *Eucalyptus* honeys from Australia. *J. Agric. Food Chem.* **2000**, *48*, 4744−4748.

(30) Al-Mamary, M.; Al-Meeri, A.; Al-Habori, M. Antioxidant activities and total phenolics of different types of honey. *Nutr. Res. (N.Y.)* **2002**, *22*, 1041−1047.

(31) Meda, A.; Lamien, C. E.; Romito, M.; Millogo, J.; Nacoulma, O. G. Determination of the total phenolic, flavonoid and proline contents in Burkina Fasan honey, as well as their radical scavenging activity. *Food Chem.* **2005**, *91*, 571−577.

(32) Jasicka-Misiak, I.; Poliwoda, A.; Deren, M.; Kafarski, P. Phenolic compounds and abscisic acid as potential markers for the floral origin of two Polish unifloral honeys. *Food Chem.* **2012**, *131*, 1149−1156.

(33) Estevinho, L.; Pereira, A. P.; Moreira, L.; Dias, L. G.; Pereira, E. Antioxidant and antimicrobial effects of phenolic compounds extracts of northeast Portugal honey. *Food Chem. Toxicol.* **2008**, *46*, 3774−3779.

(34) Brudzynski, K.; Miotto, D. The relationship between the content of Maillard reaction-like products and bioactivity of Canadian honeys. *Food Chem.* **2011**, *124*, 869−874.

(35) Barganska, Z.; Slebioda, M.; Namiesnik, J. Pesticide residues levels in honey from apiaries located of northern Poland. *Food Control* **2013**, *31*, 196−201.

(36) Daniele, G.; Maitre, D.; Casabianca, H. Identification, quantification and carbon stable isotopes determinations of organic acids in monofloral honeys. A powerful tool for botanical and authenticity control. *Rapid Commun. Mass Spectrom.* **2012**, *26*, 1993−1998.

(37) Norshazila, S.; Syed Zahir, I.; Mustapha Suleiman, K.; Aisyah, M. R.; Kamarul Rahim, K. Antioxidant levels and activities of selected seeds of malaysian tropical fruits. *Malays. J. Nutr* **2010**, *16*, 149−159.

(38) Islam, A.; Khalil, I.; Islam, N.; Moniruzzaman, M.; Mottalib, A.; Sulaiman, S. A.; Gan, S. H. Physicochemical and antioxidant properties of Bangladeshi honeys stored for more than one year. *BMC Complement. Altern. Med.* **2012**, *12*, 177.

(39) Huang, D.; Ou, B.; Prior, R. L. The chemistry behind antioxidant capacity assays. *J. Agric. Food Chem.* **2005**, *53*, 1841−1856.

(40) Mittelmaier, S.; Fuenfrocken, M.; Fenn, D.; Fichert, T.; Pischetsrieder, M. Identification and quantification of the glucose degradation product glucosone in peritoneal dialysis fluids by HPLC/DAD/MSMS. *J. Chromatogr., B—Anal. Technol. Biomed. Life Sci.* **2010**, *878*, 877—882.
(41) Gensberger, S.; Mittelmaier, S.; Glomb, M. A.; Pischetsrieder, M. Identification and quantification of six major α-dicarbonyl process contaminants in high-fructose corn syrup. *Anal. Bioanal. Chem.* **2012**, *403*, 2923—2931.
(42) Oelschlaegel, S.; Gruner, M.; Wang, P.-N.; Boettcher, A.; Koelling-Speer, I.; Speer, K. Classification and characterization of manuka honeys based on phenolic compounds and methylglyoxal. *J. Agric. Food Chem.* **2012**, *60*, 7229—7237.
(43) Biesaga, M.; Pyrzynska, K. Liquid chromatography/tandem mass spectrometry studies of the phenolic compounds in honey. *J. Chromatogr., A* **2009**, *1216*, 6620—6626.
(44) Falcao, S. I.; Vilas-Boas, M.; Estevinho, L. M.; Barros, C.; Domingues, M. R. M.; Cardoso, S. M. Phenolic characterization of northeast Portuguese propolis: usual and unusual compounds. *Anal. Bioanal. Chem.* **2010**, *396*, 887—897.
(45) Gardana, C.; Scaglianti, M.; Pietta, P.; Simonetti, P. Analysis of the polyphenolic fraction of propolis from different sources by liquid chromatography-tandem mass spectrometry. *J. Pharm. Biomed. Anal.* **2007**, *45*, 390—399.
(46) Medana, C.; Carbone, F.; Aigotti, R.; Appendino, G.; Baiocchi, C. Selective analysis of phenolic compounds in propolis by HPLC-MS/MS. *Phytochem. Anal.* **2008**, *19*, 32—39.
(47) Bertoncelj, J.; Polak, T.; Kropf, U.; Korosec, M.; Golob, T. LC-DAD-ESI/MS analysis of flavonoids and abscisic acid with chemometric approach for the classification of Slovenian honey. *Food Chem.* **2011**, *127*, 296—302.
(48) Truchado, P.; Vit, P.; Ferreres, F.; Tomas-Barberan, F. Liquid chromatography tandem mass spectrometry analysis allows the simultaneous characterization of *C*-glycosyl and *O*-glycosyl flavonoids in stingless bee honeys. *J. Chromatogr., A* **2011**, *1218*, 7601—7607.
(49) Ferreres, F.; Andrade, P.; Tomas-Barberan, F. A. Natural occurrence of abscisic acid in heather honey and floral nectar. *J. Agric. Food Chem.* **1996**, *44*, 2053—2056.
(50) Tomas-Barberan, F. A.; Martos, I.; Ferreres, F.; Radovic, B. S.; Anklam, E. HPLC flavonoid profiles as markers for the botanical origin of European unifloral honeys. *J. Sci. Food Agric.* **2001**, *81*, 485—496.
(51) Sun, J.; Liang, F.; Bin, Y.; Li, P.; Duan, C. Screening non-colored phenolics in red wines using liquid chromatography/ultraviolet and mass spectrometry/mass spectrometry libraries. *Molecules* **2007**, *12*, 679—693.
(52) Gil, M. I.; Ferreres, F.; Ortiz, A.; Subra, E.; Tomas-Barberan, F. A. Plant phenolic metabolites and floral origin of rosemary honey. *J. Agric. Food Chem.* **1995**, *43*, 2833—2838.
(53) Fabre, N.; Rustan, I.; de Hoffmann, E.; Quetin-Leclercq, J. Determination of flavone, flavonol, and flavanone aglycones by negative ion liquid chromatography electrospray ion trap mass spectrometry. *J. Am. Soc. Mass Spectrom.* **2001**, *12*, 707—715.
(54) Pontoh, J.; Low, N. H. Purification and characterization of beta-glucosidase from honey bees (*Apis mellifera*). *Insect Biochem. Mol. Biol.* **2002**, *32*, 679—690.
(55) Hammel, Y.-A.; Mohamed, R.; Gremaud, E.; LeBreton, M.-H.; Guy, P. A. Multi-screening approach to monitor and quantify 42 antibiotic residues in honey by liquid chromatography-tandem mass spectrometry. *J. Chromatogr., A* **2008**, *1177*, 58—76.
(56) Hermosin, I.; Chicon, R. M.; Cabezudo, M. D. Free amino acid composition and botanical origin of honey. *Food Chem.* **2003**, *83*, 263—268.

JOURNAL OF AGRICULTURAL AND FOOD CHEMISTRY

Article

pubs.acs.org/JAFC

# Enhancement of Non-heme Iron Absorption by Anchovy (*Engraulis japonicus*) Muscle Protein Hydrolysate Involves a Nanoparticle-Mediated Mechanism

Haohao Wu,[†] Suqin Zhu,[†] Mingyong Zeng,*[,†] Zunying Liu,[†] Shiyuan Dong,[†] Yuanhui Zhao,[†] Hai Huang,[§] and Y. Martin Lo[#]

[†]College of Food Science and Engineering, Ocean University of China, 5 Yushan Road, Qingdao, Shandong Province 266003, China

[§]School of Aquatic Products, Rizhao Polytechnic, No. 16 North of Yantai Road, Rizhao, Shandong Province 276826, China

[#]Department of Nutrition and Food Science, University of Maryland, College Park, Maryland 20742, United States

**ABSTRACT:** The mechanisms by which meat enhances human absorption of non-heme iron remain unknown. Recently, anchovy (*Engraulis japonicus*) muscle protein hydrolysate (AMPH) was found to mediate the formation of nanosized ferric hydrolysis products in vitro. The current paper evaluates the effects of AMPH on the bioavailability and the intestinal speciation of non-heme iron in rats, followed by an investigation of cellular uptake pathways of in vitro-formed AMPH-stabilized nanosized ferric hydrolysis products (ANPs) by polarized human intestinal epithelial (Caco-2) cells. The hemoglobin regeneration efficiencies in anemic rats followed the order ferric citrate (9.79 ± 2.02%) < commercial bare $\alpha$-$Fe_2O_3$ nanoparticles (16.37 ± 6.65%) < mixture of ferric citrate and AMPH (40.33 ± 6.36%) ≈ ferrous sulfate (40.88 ± 7.67%) < ANPs (56.25 ± 11.35%). Percentage contents of intestinal low-molecular-weight iron in the groups of FC+AMPH, $FeSO_4$, and ANPs were significantly lower than the corresponding hemoglobin regeneration efficiencies ($P < 0.05$), providing strong evidence for the involvement of nanosized iron in intestinal iron absorption from FC+AMPH, $FeSO_4$, and ANPs. Calcein-fluorescence measurements of the labile iron pool of polarized Caco-2 cells revealed the involvement of both divalent transporter 1 and endocytosis in apical uptake of ANPs, with endocytosis dominating at acidic extracellular pH. Overall, AMPH enhancement of non-heme iron absorption involves a nanoparticle-mediated mechanism.

**KEYWORDS:** *iron bioavailability, muscle protein, anchovy, rats, Caco-2 cell, nanoparticle*

## INTRODUCTION

After birth, humans have to acquire iron from the diet to support growth and compensate for iron loss; over 2 billion people worldwide suffer from iron deficiency. Although dietary iron can be found in the form of heme or non-heme iron, interventions to reduce iron deficiency usually focus on increasing non-heme iron absorption, which is greatly influenced by various dietary components. Inhibitors of non-heme iron absorption in humans include phytates, oxalates, polyphenols, fibers, calcium, copper, and zinc; ascorbic acid and muscle foods (i.e., meat, poultry, and fish) enhance non-heme iron absorption.[1] The enhancing effect of muscle foods on non-heme iron absorption is usually attributed to certain "meat factors" (e.g., peptides, acidic polysaccharides, and L-$\alpha$-glycerophosphocholine), which may react with non-heme iron in the intestinal lumen, thereby increasing iron solubilization and absorption.[2−4] However, the chemical nature of such soluble non-heme iron has still not been fully elucidated.

One economical meat source that could be used to combat iron deficiency in developing countries is the anchovy, a small marine pelagic fish harvested in huge quantity worldwide, mainly for nonfood uses.[5] Recently, we demonstrated that anchovy (*Engraulis japonicus*) muscle protein hydrolysate (AMPH) could mediate the formation of nanosized ferric hydrolysis products within a pH range similar to that of human digestive lumen;[6] thus, AMPH might enhance non-heme iron absorption in humans via a nanoparticle-mediated mechanism. The current research examined the effects of AMPH on the bioavailability and the intestinal speciation of non-heme iron in rats, followed by an investigation of cellular uptake pathways of in vitro-formed AMPH-stabilized nanosized ferric hydrolysis products (ANPs) in polarized human intestinal epithelial (Caco-2) cells.

## MATERIALS AND METHODS

**Materials.** Japanese anchovies, *E. japonicus* (5−8 cm total length), caught in the Yellow Sea by Allen Ship Service Co. Ltd. (Shandong, China) were frozen immediately at −35 °C on board and transported in a Styrofoam-insulated box to the laboratory refrigerator (−20 °C) within 4 h. Trypsin from bovine pancreas with a declared activity of 250 U/mg was purchased from Sinopharm Chemical Co. Ltd. (Shanghai, China). Nano-$\alpha$-$Fe_2O_3$ powder with declared diameters of 20−30 nm was purchased from Beijing Nachen Co. Ltd. (Beijing, China). Bathophenanthrolinedisulfonic acid (BPDS), deferoxamine mesylate (DFB), ethylenediaminetetraacetic acid (EDTA), nitrilotriacetic acid (NTA), phytic acid sodium salt, diethylenetriaminepentaacetic acid (DTPA), *trans*-1,2-cyclohexanediaminetetraacetic acid (CDTA), sodium selenite, hydrocortisone, and triiodothyronine were obtained from Sigma-Aldrich Co. (St. Louis, MO, USA). Calcein

Received: April 18, 2014
Revised: July 27, 2014
Accepted: July 29, 2014
Published: July 29, 2014

 © 2014 American Chemical Society 

acetoxymethylester, cell culture mediums, insulin, and epidermal growth factor were purchased from Gibco (Grand Island, NY, USA). All other reagents used in this study were commercially available and of analytical grade.

**Preparation of AMPH and ANPs.** AMPH was obtained as described previously.[7] Briefly, 25% (w/v) homogenates of anchovy meat were hydrolyzed by trypsin with a 25:1 substrate to enzyme ratio (w/w) at 37 °C and pH 8 for 4 h with continuous magnetic stirring, followed by heat inactivation of the enzyme in a boiling water bath for 10 min, and the reaction mixture was then centrifuged at 10000*g* for 20 min. The supernatant was stored at 4 °C for no more than 48 h and filtered through 0.22 μm cellulose acetate filters before use. Total protein concentration in the supernatant was determined according to Lowry's method using bovine serum albumin as the standard protein.[8]

ANPs were prepared according to the procedure described by Wu et al.[6] with slight modification. Briefly, 1 volume of freshly prepared ferric chloride (20 mM) was added dropwise into 10 volumes of magnetically stirred AMPH solution (20 g peptide/L) with the solution pH maintained at 7.0 ± 0.2 using 1 M sodium hydroxide. The obtained sample solution was stored at 4 °C for no more than 24 h and filtered through 0.22 μm cellulose acetate filters before use. For the structural characterization of ANPs, sample solutions were dropped onto carbon-coated copper grids, allowed to air-dry, and then examined in a JEM 1200 EX (JEOL, Tokyo, Japan) electron microscope. Iron content in the sample solution was determined by flame atomic absorption spectroscopy using a Shimadzu AA-6800 spectrometer (Kyoto, Japan).

**Animal Experiments.** All animal handling was conducted according to the principles and guidelines outlined in the National Institutes of Health (NIH) *Guide for the Care and Use of Laboratory Animals* and approved by the Ethical Committee of Animal Care and Use at Ocean University of China (Permit 20001013). Sprague−Dawley rats were obtained from Shandong Lukang Pharmaceutical Group Co., Ltd. (Shandong, China). Pelletized purified AIN-93G-based diets were prepared by TROPHIC Animal Feed High-tech Co., Ltd. (Nantong, China). The Fe-deficient diet contained ∼10 mg/kg iron derived from raw materials. The Fe-sufficient diet contained ∼25 mg/kg iron in the form of ferric citrate (FC) and ∼10 mg/kg iron derived from raw materials. The Fe-repletion diets contained ∼10 mg/kg iron derived from raw materials and ∼20 mg/kg iron in the forms of ferrous sulfate ($FeSO_4$), ANPs, FC, mixture of FC and AMPH (FC +AMPH), and commercial bare $\alpha$-$Fe_2O_3$ nanoparticles (Nano-$\alpha$-$Fe_2O_3$). The iron compounds were incorporated into the diets during preparation of the wet ingredient mixtures. $FeSO_4$, FC, or Nano-$\alpha$-$Fe_2O_3$ equivalent to 20 mg iron was mixed with 1 kg of the other dry ingredients and 200 mL of Milli-Q water to obtain the wet ingredient mixture. To incorporate the solution form of AMPH (18 g peptide/L) and ANPs (1.8 mM iron and 18 g peptide/L), 200 mL of either of them was mixed with 1 kg of the other dry ingredients to make the wet ingredient mixture. After being pelletized, the wet ingredient mixture was dried overnight at 40 °C in a drying oven. Iron contents in the dried pelletized diets were determined by flame atomic absorption spectroscopy using a Shimadzu AA-6800 spectrometer. Rats received Milli-Q water ad libitum throughout the experiments. Body weight was recorded at the beginning and end of each experimental period.

The iron bioavailability was measured in anemic rats using a hemoglobin regeneration bioassay.[9,10] Female Sprague−Dawley rats ($n$ = 12) breastfeeding male pups (16 days old; $n$ = 52) were housed in individual stainless steel cages with four to five pups each and fed a Fe-deficient diet ad libitum for a week. On the weaning day, 52 male rats (23 days old) were transferred into individual stainless steel cages under controlled conditions at temperatures of 22 ± 2 °C and relative humidities of 55 ± 10% with a light/dark cycle of 12/12 h. The just-weaned rats were stratified according to body weight and within each stratum were randomly allocated to two groups: the Fe-depleted group ($n$ = 48) fed a Fe-deficient diet ad libitum and a control group ($n$ = 4) fed a Fe-sufficient diet ad libitum. After a Fe-depletion period of 27 days, 20 μL of fresh rat blood sampled by tail vein incision was diluted with EDTA and subsequently analyzed using a Cell-Dyn 1600 hematology analyzer (Abbott Laboratories, Abbott Park, IL, USA). The mean hemoglobin concentrations of the Fe-depleted group and the control group were 71.1 ± 13.8 and 153.8 ± 13.9 g/L, respectively. Rats in the Fe-depleted group were stratified by the hemoglobin concentrations and randomized into six groups (eight rats each). The rats in each group consumed one of the five Fe-repletion diets containing $FeSO_4$, ANPs, FC, FC+AMPH, or Nano-$\alpha$-$Fe_2O_3$ or the Fe-deficient diet for 13 days (the repletion period) ad libitum. Rats in the control group remained on the Fe-sufficient diet during the repletion period.

Periodically, the daily food intake of each rat was manually recorded. A known and adequate amount of a diet was given to a rat in the feeding container between 9:00 and 10:00 a.m. After 24 h, the diet remaining in the feeding container and at the bottom of the cage was reweighed; calculating the differences showed the rat's daily food intake.

At the end of the repletion period, blood samples were once again taken by tail vein incision. The rats were anesthetized with ether before their livers were taken, rinsed with saline, and stored at −20 °C. Iron concentration in the liver was measured by flame atomic absorption spectroscopy using a Shimadzu AA-6800 spectrometer.

Hemoglobin (Hb) iron pool (mg), assuming a total rat blood volume of 6.7% body weight and an iron content in hemoglobin of 0.335%, was calculated as follows:[10]

$$\text{Hb iron pool (mg)} = \text{body wt (kg)} \times 0.067 \times \text{Hb concn (g/L)} \times 3.35$$

The hemoglobin regeneration efficiency was calculated by using the following equation:

$$\text{Hb regeneration efficiency (\%)} = [\text{final Hb iron pool (mg)} - \text{initial Hb iron pool (mg)}] / \text{total iron consumed (mg)} \times 100$$

The relative biological value was calculated on the basis of the hemoglobin regeneration efficiencies:

$$\text{relative biological value (\%)} = \text{Hb regeneration efficiency of each animal} / \text{av Hb regeneration efficiency of the } FeSO_4 \text{ group} \times 100$$

Iron speciation analysis of rat intestinal contents was carried out as previously described by Kapsokefalou and Miller[11] and Simpson et al.[12] with some modifications. Male Sprague−Dawley rats (53 days old; $n$ = 40) weighing 290−310 g were stratified according to body weight and within each stratum were randomly distributed into five groups (eight rats each). The rats were fed the Fe-deficient diet for a week before they were daytime fasted for 9 h. The fasted rats in each group then consumed one of the five Fe-repletion diets for 30 min ad libitum and were anesthetized with ether 90 min after consumption of the meal. The rats were killed by cervical dislocation before an abdominal midline incision was performed. After the small intestine was removed from the carcass, the content in the proximal one-third segment was flushed with saline into a centrifuge tube and further fractionated into two fractions using Millipore filters (Göttingen, Germany): the 0.22 μm filtrate and the 3 kDa (≈1 nm) filtrate. Iron concentrations in the intestinal content, 0.22 μm filtrate, and 3 kDa filtrate were determined by flame atomic absorption spectroscopy using a Shimadzu AA-6800 spectrometer.

**Cellular Uptake Experiment.** Caco-2 cells were obtained from the Cell Bank of the Chinese Academy of Sciences (Shanghai, China) and seeded at a density of $5 \times 10^4$ cells/cm$^2$ in collagen-treated 24-well plates (BD Biosciences, San Jose, CA, USA). The cells were routinely maintained in high-glucose (4.5 g/L) Dulbecco's modified Eagle medium supplemented with 10% heat-inactivated fetal bovine serum, 25 mM HEPES, 4 mM glutamine, and 1 mM sodium pyruvate at 37 °C in an incubator with a 95% air/5% $CO_2$ atmosphere at constant humidity, and the medium was renewed every 2 days. After reaching confluence (2−3 days postseeding), the cells were maintained in


dx.doi.org/10.1021/jf5018719 | J. Agric. Food Chem. 2014, 62, 8632−8639

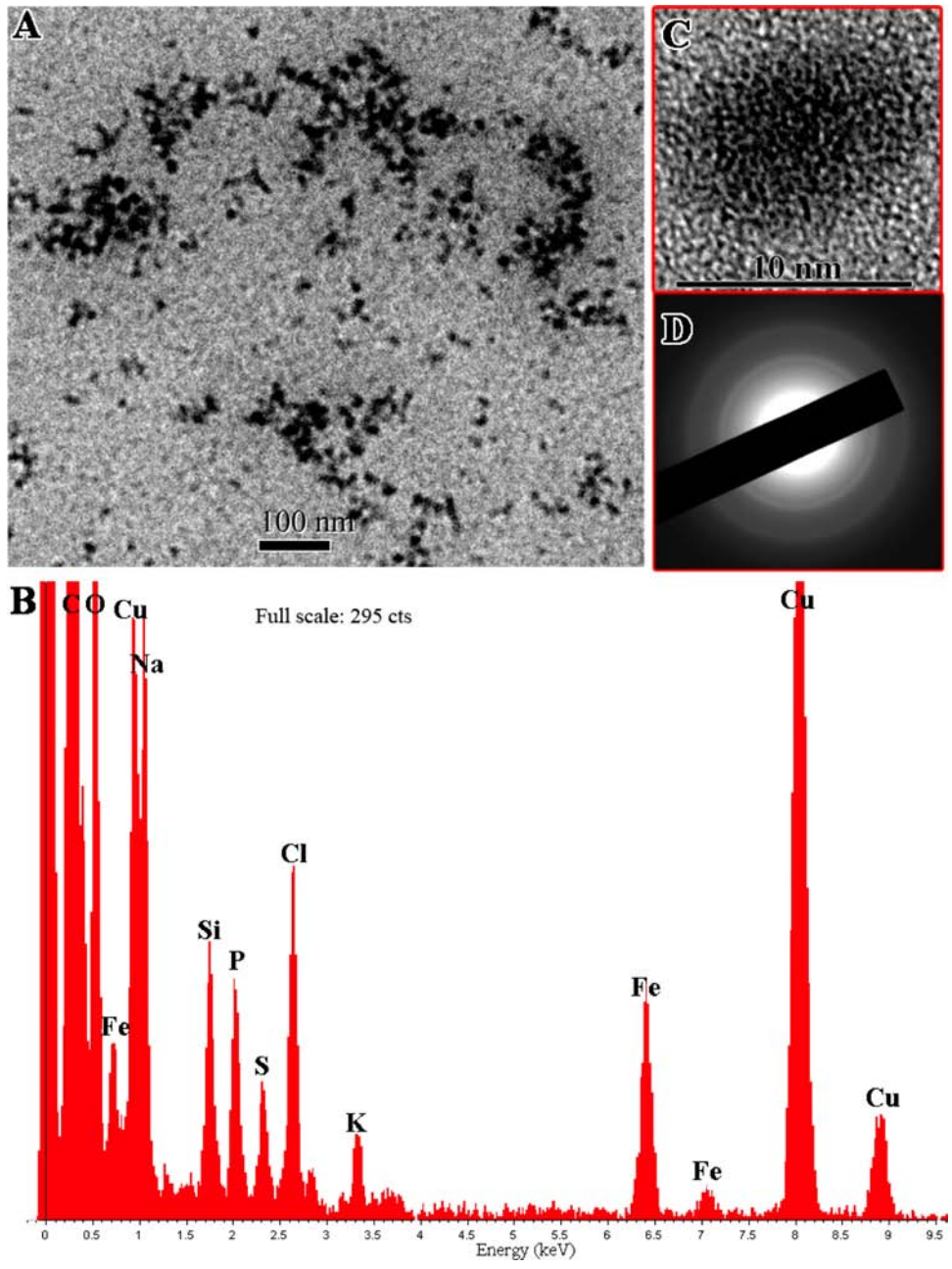


**Figure 1.** Structural characterization of in vitro-formed nanosized ferric hydrolysis products stabilized by anchovy muscle protein hydrolysate (ANPs): (A) transmission electron microscopy images collected from a drop of ANPs; (B) whole area energy dispersive X-ray analysis of one of the particles in panel A showing elemental compositions (peaks for sodium (Na), copper (Cu), potassium (K), silicon (Si), phosphorus (P), sulfur (S), chlorine (Cl), carbon (C), and oxygen (O) are identified); (C) high-resolution transmission electron microscopy; (D) selected area electron diffraction.

complete Dulbecco's modified Eagle medium for another 12 days to differentiate completely and further incubated for 24 h in serum-free minimum essential medium supplemented with 4 mg/L hydrocortisone, 5 mg/L insulin, 5 $\mu$g/L selenium, 34 $\mu$g/L triiodothyronine, and 20 $\mu$g/L epidermal growth factor. Following this, the medium was aspirated, and the cells were stained with 1 $\mu$M calcein acetoxymethylester in Hanks' balanced salt solution (HBSS) for 30 min at 37 °C before being washed three times with HBSS. The cells were then incubated in Tyrode solution (137 mM NaCl, 2.7 mM KCl, 1 mM $MgCl_2$, 1.8 mM $CaCl_2$, 5.5 mM D-glucose) buffered with 20 mM MES (pH 5.5) or MOPS (pH 7.0) containing $FeSO_4$, ANPs, or any of 1:1 ferric chelates of NTA, phytate, EDTA, DTPA, CDTA, and DFB at the concentration equivalent to 20 $\mu$M iron in a Synergy H4 hybrid microplate reader (Bio-Tek, Winooski, VT, USA) at 37 °C for 2.5 h, and calcein fluorescence (485 nm excitation, 530 nm emission) was monitored every 5 min. To trap and detect ferrous iron, 100 $\mu$M BPDS was used, and the absorbance of the ferrous tris(BPDS) complex was measured at 536 nm (molar extinction coefficient, $\varepsilon$ = $1.927 \times 10^4$ L $mol^{-1}$ $cm^{-1}$). Stock solution of $FeSO_4$ (1 mM) was freshly prepared before use. Stock solution of ferric chelates (1:1 molar ratio) of NTA, phytate, EDTA, DTPA, CDTA, and DFB was prepared by mixing equal volumes of chelators (2 mM) and freshly prepared $FeCl_3$ (2 mM).

**Statistical Analysis.** Data are expressed as the mean ± standard deviation (SD). Differences between groups were tested for significance by the least significant difference (LSD) mean comparison using the SPSS software program (SPSS Inc., Chicago, IL, USA). The relationship between variables was determined by the Pearson


dx.doi.org/10.1021/jf5018719 | J. Agric. Food Chem. 2014, 62, 8632−8639

**Table 1. Details and Results of the Hemoglobin Regeneration Bioassay**

| | group[a] | | | | | | |
|---|---|---|---|---|---|---|---|
| | Fe-deficient | $FeSO_4$ | ANPs | FC | FC+AMPH | Nano-$\alpha$-$Fe_2O_3$ | Fe-sufficient |
| *N* | 8 | 8 | 8 | 8 | 8 | 8 | 4 |
| diet iron (mg/kg) | 10.5 ± 1.5 | 32.4 ± 2.3 | 30.5 ± 0.7 | 29.8 ± 2.0 | 28.8 ± 0.2 | 31.8 ± 2.4 | 36.8 ± 2.5 |
| diet intake (g) | 265 ± 30.5a | 419.5 ± 70.3c | 332.1 ± 32.7ab | 268.2 ± 43.7a | 380.6 ± 70.0bc | 267.2 ± 16.9a | 383.9 ± 37.9b |
| baseline BW (g) | 222.7 ± 21.5 | 221.0 ± 20.1 | 221.4 ± 39.2 | 222.4 ± 38.8 | 215.0 ± 17.2 | 219.9 ± 11.8 | 297.5 ± 33.9 |
| BW gain[b] (g) | 62.4 ± 27.8a | 101.7 ± 32.9bc | 109.7 ± 37.2c | 79.7 ± 25.9ab | 88.7 ± 28.9ab | 75.6 ± 26.7ab | 85.0 ± 3.6ab |
| baseline Hb (g/L) | 71.1 ± 11.9 | 71.4 ± 16.8 | 73.7 ± 10.5 | 70.5 ± 15.3 | 71.9 ± 12.7 | 71.1 ± 19.0 | 153.8 ± 13.9 |
| Hb change[c] (g/L) | −14.4 ± 11.1a | 50 ± 19.8b | 52.8 ± 19.8b | −6.9 ± 21.7a | 42.8 ± 21.0b | 0.125 ± 17.2a | −25.3 ± 23.8 |

[a]Abbreviations: $FeSO_4$, ferrous sulfate; ANPs, in vitro-formed AMPH-stabilized nanosized ferric hydrolysis products; FC, ferric citrate; FC+AMPH, mixture of ferric citrate and anchovy muscle protein hydrolysate; Nano-$\alpha$-$Fe_2O_3$, commercial bare $\alpha$-$Fe_2O_3$ nanoparticles. Values are means ± SD. Means in a column without a common letter (a−c) are statistically different, $P < 0.05$. [b]BW, body weight. [c]Hb, hemoglobin.

correlation test. The probability level <0.05 was considered statistically significant.

## RESULTS AND DISCUSSION

To evaluate the structural properties of ANPs, that is, the products of ferric hydrolysis in the presence of AMPH in vitro at room temperature, we used transmission electron microscopy (TEM), high-resolution transmission electron microscopy (HRTEM), electron diffraction, and energy dispersive X-ray spectroscopy (EDX). TEM imaging (Figure 1A) showed that the average particle size ranged from 10 to 20 nm, and this size was greater than that of pure two-line ferrihydrite (2−4 nm).[13] Whole area EDX analysis (Figure 1B) of one of the particles in Figure 1A revealed three peaks (0.7, 6.4, and 7.1 keV) that corresponded to the L$\alpha$, K$\alpha$, and K$\beta$ lines of iron, respectively, so the particles in the TEM image were iron-containing. In addition, the EDX spectra also showed prominent peaks for copper, sodium, potassium, chloride, sulfur, carbon, oxygen, phosphorus, and silicon. The copper obviously represented the supporting copper grid, and the silicon peak was presumably due to contamination. Spurious silicon peaks have been recognized as a problem in EDX analysis of biological specimens due to silicon contamination from oils or greases during the course of specimen preparation or from the vacuum system of the electron microscope.[14] Any remaining peaks would presumably represent true compositions of AMPH or the specimen support film. The HRTEM image (Figure 1C) revealed no recognizable lattice fringe, suggesting the amorphous property of ANPs. The selected area electron diffraction (Figure 1D) showed a two-ring pattern similar to that of two-line ferrihydrite with the obtained *d*-spacing values (2.90 and 1.97 Å), a little higher than typical corresponding values of the latter (~2.5 and 1.5 Å). ANPs are likely to be a poorly crystalline ferric oxyhydroxide similar to two-line ferrihydrite. It is known that poorly crystalline iron oxides are prone to electron beam damage,[15] so the actual structure of ANPs might vary somewhat in size and crystalline phase from that observed under TEM, HRTEM, and electron diffraction.

Details and results of the hemoglobin regeneration bioassay are shown in Table 1. It is known that body iron is distributed in hemoglobin (65%), iron stores (ferritin and hemosiderin, 30%), myoglobin (3.5%), and other heme proteins (1.5%).[16] Liver iron stores did not show a significant increase in all Fe-repletion groups during the repletion period (Figure 2), so most of the iron absorbed should be used to generate new hemoglobin molecules, amounts of which could be calculated from changes of blood volumes and hemoglobin concentrations. The negative changes of the hemoglobin concentrations in Fe-deficient, FC, and Fe-sufficient groups were the result of a marked increase in blood volume, which is proportional to body weight, during fast growth of the anemic rat. As shown in Table 1, body weights and hemoglobin concentrations varied independently among the groups, so to measure iron bioavailability by hemoglobin regeneration in anemic rats, it is necessary to calculate the hemoglobin regeneration efficiencies from body weight gain, diet intake, diet iron content, and hemoglobin concentration.

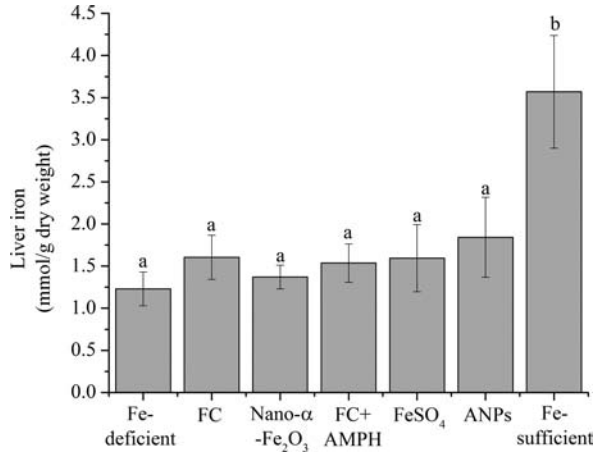


**Figure 2.** Liver iron concentrations at the end of the iron repletion period. Abbreviations: FC, ferric citrate; FC+AMPH, mixture of ferric citrate and anchovy muscle protein hydrolysate; $FeSO_4$, ferrous sulfate; ANPs, in vitro-formed nanosized ferric hydrolysis products stabilized by anchovy muscle protein hydrolysate; Nano-$\alpha$-$Fe_2O_3$, commercial bare $\alpha$-$Fe_2O_3$ nanoparticles. Values are means ± standard deviations of a representative experiment ($n = 4$ for the Fe-sufficient group; $n = 8$ for the other groups). Groups not sharing a common letter are significantly different ($P < 0.05$).

As shown in Table 2, the hemoglobin regeneration efficiency of FC+AMPH was as high as that of $FeSO_4$, a gold standard in iron bioavailability studies, and significantly higher than that of FC alone ($P < 0.05$). Apparently, AMPH effectively enhanced iron absorption from FC. ANPs displayed an even higher hemoglobin regeneration efficiency than FC+AMPH and $FeSO_4$, although not statistically significant ($P = 0.06$ and 0.12, respectively). Because crystallized bare iron oxide nanoparticles feature simple production process and low cost, we examined the bioavailability of iron from Nano-$\alpha$-$Fe_2O_3$, a commercial product with declared size similar to that of ANPs. The hemoglobin regeneration efficiency of Nano-$\alpha$-$Fe_2O_3$ was found to be significantly lower than that of ANPs ($P < 0.05$). Interestingly, the relative biological value of Nano-$\alpha$-$Fe_2O_3$


dx.doi.org/10.1021/jf5018719 | J. Agric. Food Chem. 2014, 62, 8632−8639

**Table 2. Hemoglobin Regeneration Efficiencies and Percentage Contents of Intestinal Iron species in different groups**

| group[b] | hemoglobin regeneration efficiency (%) | percentage contents of intestinal iron species[a] | | |
|---|---|---|---|---|
| | | total soluble iron[c] | low-molecular-weight iron[d] | nanosized iron[e] |
| FC | 9.79 ± 2.01a | 43.18 ± 4.49ef | 12.44 ± 3.47ab | 30.74 ± 6.49d |
| Nano-$\alpha$-$Fe_2O_3$ | 16.37 ± 6.65abc | 56.57 ± 11.69fg | 24.35 ± 4.67cd | 32.22 ± 12.24de |
| FC+AMPH | 40.33 ± 6.36ef | 60.74 ± 6.84g | 18.31 ± 4.16bc | 42.43 ± 3.40ef |
| $FeSO_4$ | 40.88 ± 7.67ef | 59.01 ± 9.02g | 19.21 ± 5.26bc | 39.80 ± 8.87def |
| ANPs | 56.25 ± 11.35fg | 61.24 ± 11.01g | 14.47 ± 2.63ab | 46.77 ± 8.89f |

[a]Values are means ± SD of a representative experiment ($n$ = 8). Means in a column without a common letter (a−g) are statistically different, $P$ < 0.05. [b]Abbreviations: FC, ferric citrate; Nano-$\alpha$-$Fe_2O_3$, commercial bare $\alpha$-$Fe_2O_3$ nanoparticles; $FeSO_4$, ferrous sulfate; ANPs, in vitro-formed nanosized ferric hydrolysis products stabilized by anchovy muscle protein hydrolysate; FC+AMPH, mixture of ferric citrate and anchovy muscle protein hydrolysate. [c]Iron in the 0.22 $\mu$m filtrate. [d]Iron in the 3 kDa filtrate. [e]Calculated by subtraction of low-molecular-weight iron from total soluble iron. Abbreviations:

(39.0 ± 15.8%) was also found to be significantly lower than those of previously reported ZnO-, MgO-, CaO-, or $FePO_4$-doped iron oxide nanopowders, namely, $Fe_2O_3$/ZnO/MgO (81.8−100.1%), $Fe_2O_3$/ZnO/CaO (72.4−92.6%), $Fe_2O_3$/ZnO (68.0−87.5%), and $Fe_2O_3$/$FePO_4$ (69.0−87.4%),[9] which might be explained by the higher iron dissolution rates of these latter iron oxide nanostructures in gastric acid due to doping with compounds more soluble in dilute acid than iron oxide.[17]

To elucidate whether nanosized iron involved iron absorption in vivo, we analyzed iron speciation in the luminal content of the proximal one-third segment of the small intestine, where dietary iron is mainly absorbed.[18] Iron in the 3 kDa filtrates was regarded as the truly dissolved iron species or low-molecular-weight (LMW) iron, whereas that in the 0.22 $\mu$m filtrate was supposed as total soluble iron including both LMW iron and nanosized colloidal iron. As shown in Table 2, percentage contents of intestinal LMW iron in the groups of FC+AMPH, $FeSO_4$, and ANPs were significantly lower than the corresponding hemoglobin regeneration efficiencies ($P$ < 0.05), so LMW iron alone was unlikely to account for total iron absorption in these groups. This provided strong evidence for the involvement of nanosized iron in intestinal iron absorption from FC+AMPH, $FeSO_4$, and ANPs.

LMW iron in the intestinal tract might be ferrous iron or ferric chelates. Except for $FeSO_4$, the other four iron compounds in the present study are all in the form of ferric iron. The reducing power of *tert*-butylhydroquinone, the fat-soluble antioxidant added in the AIN-93G diet, might not contribute to the formation of intestinal LMW iron due to its very low solubility in the aqueous phase. Although meat digestion products are capable of reducing non-heme ferric iron to the ferrous form in vitro,[19] AMPH and ANPs did not increase the percentage content of LMW iron (Table 2), which might be explained by the oxidation of protein sulfhydryl groups during the preparation and storage of AMPH and pelletized diets.[20] There are usually considerable amounts of residual phytates in the commercial starch that comprises an important part of the AIN-93G diet,[21] so iron phytate chelates might account for part of the intestinal LMW iron in the present study. It is also possible that some vitamins added in the AIN-93G diet could form LMW ferric complexes in the intestinal lumen.[22]

Ferric hydrolytic polymers could be stabilized at the nanoscale by biomacromolecules (e.g., polysaccharides and peptides) derived from some common food components (e.g., starch, carrageenan, pectin, alginate, casein, whey, and muscle protein) or gastrointestinal secretions (e.g., mucins).[6,23−27] The percentage contents of nanosized iron in the rat proximal small intestinal tracts were calculated by subtraction of LMW iron from total soluble iron (Table 2) and were found to be >30% in all five groups, suggesting that the AIN-93G diet could induce a high basal level of intestinal nanosized iron. This might be attributed to the digestion products of maltodextrin, starch, and casein in the basal formulation of AIN-93G diet or gastrointestinal secretions. Interestingly, the percentage of nanosized iron for the $FeSO_4$ group was also significantly higher than that of its LMW counterpart ($P$ < 0.05), which might be explained by the formation of nanosized iron via rapid in situ oxidation and hydrolysis of ferrous iron bound to soluble macromolecules in the presence of swallowed oxygen in the intestinal tract. Due to their tendency to aggregate and sediment in aqueous solutions, bare iron oxide nanoparticles are difficult to disperse into stable suspensions within the nanoscale range unless very efficient dispersing techniques (e.g., probe ultrasonication) are employed,[28] so it is unsurprising that Nano-$\alpha$-$Fe_2O_3$ induced a significantly lower level of intestinal nanosized iron than ANPs ($P$ < 0.05).

The involvement of intestinal nanosized iron in iron absorption from FC+AMPH, $FeSO_4$, and ANPs raises questions about how gut epithelial cells absorb intraluminal nanosized iron. Usually, exogenous iron enters the cellular labile iron pool before it is stored in ferritin, exported from the cell, or used to synthesize iron proteins.[29] Calcein, a fluorescence probe for the labile iron pool, has been frequently used to monitor cellular iron uptake in real time.[30,31] We thus used calcein-loaded polarized Caco-2 cell monolayers as a gut epithelial model to investigate the intestinal iron absorption from ANPs, a mimetic for intraluminal nanosized iron. As shown in Figure 3, iron uptake from $FeSO_4$ and ANPs at concentrations equivalent to 20 $\mu$M iron was monitored by the quenching of calcein fluorescence, that is, the incorporation of exogenous iron into the cellular labile iron pool, under two pH conditions (5.5 and 7.0) simulating those in the proximal and distal small intestine.[32] BPDS, a strong ferrous chelator, was used to block iron absorption via the divalent metal transporter 1 (DMT1). As expected, cellular iron uptake from $FeSO_4$ was completely blocked by BPDS at pH 5.5 and 7.0 (data for the latter pH are not shown), whereas iron uptake from ANPs was only partially blocked at both pH values, suggesting that both DMT1-dependent and DMT1-independent mechanisms are involved in iron absorption from ANPs.

The two best known DMT1-independent iron uptake mechanisms are by means of heme carrier protein 1 and endocytosis. Heme carrier protein 1 is specific to heme iron uptake,[33] so endocytosis, a very common mechanism for cellular entry of nanoparticles, attracted much attention in

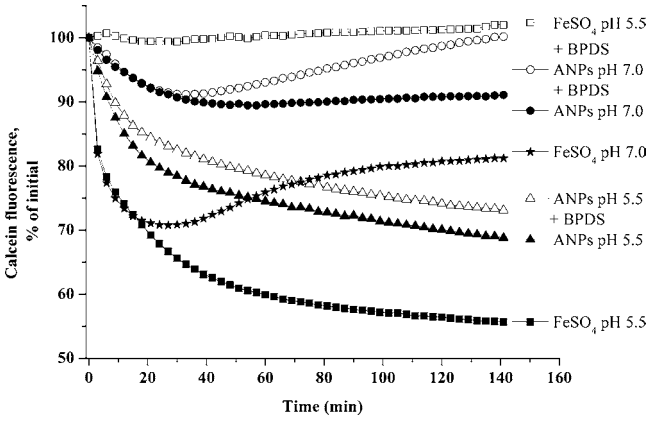


**Figure 3.** Iron uptake by polarized Caco-2 cell monolayers in the presence of 20 $\mu$M iron at extracellular pH values of 5.5 and 7.0. Abbreviations: $FeSO_4$, ferrous sulfate; ANPs, in vitro-formed AMPH-stabilized nanosized ferric hydrolysis products; BPDS, bathophenanthrolinedisulfonic acid. Cellular uptake of exogenous iron into the labile iron pool was measured as the quenching of calcein fluorescence. BPDS is a strong ferrous chelator to block the divalent metal transportor-1 pathway. Data are means of three independent experiments with standard deviations of <1.6.

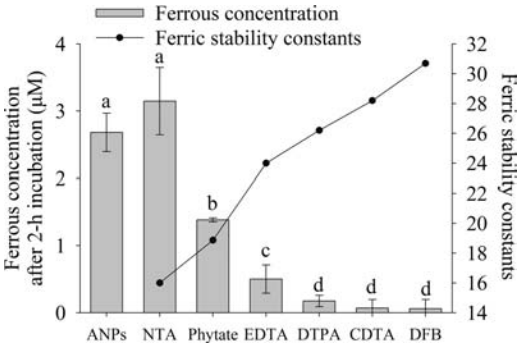


**Figure 4.** Ferrous concentrations after 2 h of incubation of 20 $\mu$M different forms of ferric iron with polarized Caco-2 cell monolayers at an extracellular pH of 5.5. Abbreviations: ANPs, in vitro-formed nanosized ferric hydrolysis products stabilized by anchovy muscle protein hydrolysate; CDTA, *trans*-1,2-cyclohexanediaminetetraacetic acid; DFB, deferoxamine mesylate; DTPA, diethylene triamine pentaacetic acid; EDTA, ethylenediaminetetraacetic acid; NTA, nitrilotriacetic acid. Ferric stability constants were obtained from the literature.[40] Data are presented as means ± standard deviations of three independent experiments. Groups not sharing a common letter are significantly different ($P < 0.05$).

recent studies on intestinal absorption of nanosized iron. Work by Theil and colleagues demonstrated that iron absorption from ferritin (i.e., ferrihydrite-like nanostructures encapsulated by a protein cage) is independent of heme iron and ferrous salts in both female human and rat intestinal segments,[34] and a paper published later by Antileo et al. revealed an endocytic pathway of ferritin in Caco-2 cells using TEM and fluorescence confocal microscopy.[35] The elegant studies of Pereira et al. and Powell et al.,[36,37] utilizing Caco-2 cells and mice, proved that intestinal uptake of luminally hydrolyzed nanosized iron invokes a nanoparticulate endocytic pathway. Thus, endocytosis could be the mechanism for DMT1-independent apical uptake of ANPs.

The calcein fluorescence changes in Figure 3 also showed a more noticeable uptake of iron from ANPs at pH 5.5 in the presence of BPDS than those observed at pH 7.0, suggesting a lower intraluminal pH in the proximal small intestine favors the endocytic uptake of ANPs. Acidic extracellular pH enhancement of endocytosis due to the proton-induced change of cellular membrane properties has been well-documented,[38] so it is not surprising that in the present study an extracellular pH of 5.5 was more favorable for the endocytic uptake of ANPs compared to pH 7.0. The marginal inhibition of iron absorption from ANPs by BPDS at pH 5.5 indicated the dominant role of the endocytic pathway at acidic extracellular pH. Iron uptake from $FeSO_4$ at pH 7.0 without the presence of BPDS was less evident than that at pH 5.5 after about 20 min of incubation, which could be explained by the relatively fast oxidation rate of ferrous iron at pH 7.0.[39]

Ferric iron must be reduced to the ferrous form by duodenal cytochrome *b* in the apical membrane of enterocytes before being absorbed by the DMT1 pathway, so the part played by the DMT1-dependent pathway in apical uptake of ANPs depends on the reducibility of ANPs. As shown in Figure 4, the reducibility of ferric chelates of NTA, phytate, EDTA, DTPA, CDTA, and DFB to polarized Caco-2 cells followed the reversed order of ferric stability constants of the chelators,[40] and ANPs were as reducible as ferric NTA, which is the most reducible of these ferric chelates.

Some previous studies have revealed that reduction rates of ferric chelates by plant roots (*Arachis hypogeae* L.) and yeast (*Saccharomyces cerevisiae*) were inversely related to the ferric stability constants,[41,42] and our data confirmed the previous observations in human intestinal cells. The reducibility of iron oxides is greatly dependent on their crystalline phases (e.g., ferrihydrite, lepidocrocite, maghemite, goethite, and hematite) and surrounding organic substances. Ferrihydrite is the most reducible phase of iron oxides. The phase of intestinal nanosized iron in the present study should be similar to ANPs, a poorly crystalline ferric oxyhydroxide-like two-line ferrihydrite. Iron-binding organic substances such as AMPH in the present study might enhance reduction dissolution of iron oxides via solubilizing ferric iron from the oxide surface or complexation of ferrous iron.[43] The high reducibility of ANPs to polarized Caco-2 cell monolayers could thus be easily understood.

In summary, our data suggest that intestinal nanosized iron involves AMPH enhancement of non-heme iron absorption in rats. Although both DMT1 and endocytosis play parts in the intestinal absorption of luminal nanosized iron, endocytosis dominates at acidic extracellular pH levels.

## AUTHOR INFORMATION

### Corresponding Author

*(M.Z.) Fax: +86 0532 82032400. E-mail: mingyz@ouc.edu.cn.

### Funding

Financially supported by the National Natural Science Foundation of China (No. 31371758), National Key Technology Research and Development Program of China (No. 2012BAD28B05), and China Scholarship Council (No. 201306330015).

### Notes

The authors declare no competing financial interest.

## ABBREVIATIONS USED

AMPH, anchovy muscle protein hydrolysate; ANPs, in vitro-formed nanosized ferric hydrolysis products stabilized by anchovy muscle protein hydrolysate; BPDS, bathophenanthro-

linedisulfonic acid; CDTA, *trans*-1,2-cyclohexanediaminetetraacetic acid; DFB, deferoxamine mesylate; DMT1, divalent metal transporter-1; DTPA, diethylenetriaminepentaacetic acid; EDTA, ethylenediaminetetraacetic acid; EDX, energy dispersive X-ray spectroscopy; FC, ferric citrate; FC+AMPH, mixture of ferric citrate and anchovy muscle protein hydrolysate; $FeSO_4$, ferrous sulfate; HRTEM, high-resolution transmission electron microscopy; LMW, low-molecular-weight; Nano-$\alpha$-$Fe_2O_3$, commercial bare $\alpha$-$Fe_2O_3$ nanoparticles; NTA, nitrilotriacetic acid; TEM, transmission electron microscopy

## REFERENCES


(1) WHO/UNICEF/UNU. *Iron Deficiency Anemia Assessment, Prevention, and Control*; World Health Organization: Geneva, Switzerland, 2001.

(2) Storcksdieck genannt Bonsmann, S.; Hurrell, R. F. Iron-binding properties, amino acid composition, and structure of muscle tissue peptides from *in vitro* digestion of different meat sources. *J. Food Sci.* **2007**, *72*, S019−029.

(3) Laparra, J. M.; Tako, E.; Glahn, R. P.; Miller, D. D. Isolated glycosaminoglycans from cooked haddock enhance non-heme iron uptake by Caco-2 cells. *J. Agric. Food Chem.* **2008**, *56*, 10346−10351.

(4) Armah, C. N.; Sharp, P.; Mellon, F. A.; Pariagh, S.; Lund, E. K.; Dainty, J. R.; Teucher, B.; Fairweather-Tait, S. J. L-$\alpha$-Glycerophosphocholine contributes to meat's enhancement of non-heme iron absorption. *J. Nutr.* **2008**, *138*, 873−877.

(5) Food and Agriculture Organization of the United Nations. Global Capture Production 1950−2010; http://www.fao.org.proxy-um.researchport.umd.edu/fishery/statistics/global-capture-production/query/en (accessed March 2014).

(6) Wu, H.; Liu, Z.; Dong, S.; Zhao, Y.; Huang, H.; Zeng, M. Formation of ferric oxyhydroxide nanoparticles mediated by peptides in anchovy (*Engraulis japonicus*) muscle protein hydrolysate. *J. Agric. Food Chem.* **2013**, *61*, 219−224.

(7) Wu, H.; Liu, Z.; Zhao, Y.; Zeng, M. Enzymatic preparation and characterization of iron-chelating peptides from anchovy (*Engraulis japonicus*) muscle protein. *Food Res. Int.* **2012**, *48*, 435−441.

(8) Lowry, O. H.; Rosebrough, N. J.; Farr, A. L.; Randall, R. J. Protein measurement with the Folin phenol reagent. *J. Biol. Chem.* **1951**, *193*, 265−275.

(9) Hilty, F. M.; Arnold, M.; Hilbe, M.; Teleki, A.; Knijnenburg, J. T.; Ehrensperger, F.; Hurrell, R. F.; Pratsinis, S. E.; Langhans, W.; Zimmermann, M. B. Iron from nanocompounds containing iron and zinc is highly bioavailable in rats without tissue accumulation. *Nat. Nanotechnol.* **2010**, *5*, 374−380.

(10) Mahoney, A. W.; Van Orden, C. C.; Hendricks, D. G. Efficiency of converting food iron into hemoglobin by the anemic rat. *Nutr. Metab.* **1974**, *17*, 223−230.

(11) Kapsokefalou, M.; Miller, D. D. Iron speciation in intestinal contents of rats fed meals composed of meat and nonmeat sources of protein and fat. *Food Chem.* **1995**, *52*, 47−56.

(12) Simpson, R. J.; Sidhar, S.; Peters, T. J. Application of selective extraction to the study of iron species present in diet and rat gastrointestinal tract contents. *Br. J. Nutr.* **1992**, *67*, 437−444.

(13) Janney, D. E.; Cowley, J. M.; Buseck, P. R. Transmission electron microscopy of synthetic 2- and 6-line ferrihydrite. *Clays Clay Miner.* **2000**, *48*, 111−119.

(14) Smith, N. K. A review of sources of spurious silicon peaks in electron microprobe X-ray spectra of biological specimens. *Anal. Biochem.* **1979**, *94*, 100−104.

(15) Pan, Y. H.; Vaughan, G.; Brydson, R.; Bleloch, A.; Gass, M.; Sader, K.; Brown, A. Electron-beam-induced reduction of $Fe^{(3+)}$ in iron phosphate dihydrate, ferrihydrite, haemosiderin and ferritin as revealed by electron energy-loss spectroscopy. *Ultramicroscopy* **2010**, *110*, 1020−1032.

(16) Hoffbrand, V.; Moss, P. *Essential Haematology*, 6th ed.; Wiley: West Sussex, UK, 2011; pp 34−36.

(17) Hilty, F. M.; Knijnenburg, J. T. N.; Teleki, A.; Krumeich, F.; Hurrell, R. F.; Pratsinis, S. E.; Zimmermann, M. B. Incorporation of Mg and Ca into nanostructured $Fe_2O_3$ improves Fe solubility in dilute acid and sensory characteristics in foods. *J. Food Sci.* **2011**, *76*, N2−N10.

(18) McKie, A.; Simpson, R. Intestinal iron absorption. In *Iron Physiology and Pathophysiology in Humans*; Anderson, G., McLaren, G. D., Eds.; Humana Press: Totowa, NJ, USA, 2012; pp 101−116.

(19) Kapsokefalou, M.; Miller, D. D. Effects of meat and selected food components on the valence of non-heme iron during in vitro digestion. *J. Food Sci.* **1991**, *56*, 352−355.

(20) Karava, N. B.; Mahoney, R. R. Lyophilization decreases the formation of dialyzable iron by extraction and digestion of chicken breast muscle. *Int. J. Food Sci. Nutr.* **2011**, *62*, 397−403.

(21) Ma, G.; Jin, Y.; Piao, J.; Kok, F.; Guusje, B.; Jacobsen, E. Phytate, calcium, iron, and zinc contents and their molar ratios in foods commonly consumed in China. *J. Agric. Food. Chem.* **2005**, *53*, 10285−10290.

(22) Layrisse, M.; García-Casal, M. N.; Solano, L.; Barón, M. A.; Arguello, F.; Llovera, D.; Ramírez, J.; Leets, I.; Tropper, E. New property of vitamin A and $\beta$-carotene on human iron absorption: effect on phytate and polyphenols as inhibitors of iron absorption. *Arch. Latinoam. Nutr.* **2000**, *50*, 243−248.

(23) Somsook, E.; Hinsin, D.; Buakhrong, P.; Teanchai, R.; Mophan, N.; Pohmakotr, M.; Shiowatana, J. Interactions between iron(III) and sucrose, dextran, or starch in complexes. *Carbohydr. Polym.* **2005**, *61*, 281−287.

(24) Chaud, M. V.; Izumi, C.; Nahaal, Z.; Shuhama, T.; Bianchi Mde, L.; de Freitas, O. Iron derivatives from casein hydrolysates as a potential source in the treatment of iron deficiency. *J. Agric. Food Chem.* **2002**, *50*, 871−877.

(25) Jones, F.; Cölfen, H.; Antoneitti, M. Iron oxyhydroxide colloids stabilized with polysaccharides. *Colloid Polym. Sci.* **2000**, *278*, 491−501.

(26) Hurrell, R. F.; Lynch, S. R.; Trinidad, T. P.; Dassenko, S. A.; Cook, J. D. Iron absorption in humans as influenced by bovine milk proteins. *Am. J. Clin. Nutr.* **1989**, *49*, 546−552.

(27) Conrad, M. E.; Umbreit, J. N. A concise review: iron absorption—the mucin-mobilferrin-integrin pathway. A competitive pathway for metal absorption. *Am. J. Hematol.* **1993**, *42*, 67−73.

(28) Dickson, D.; Liu, G.; Li, C.; Tachiev, G.; Cai, Y. Dispersion and stability of bare hematite nanoparticles: effect of dispersion tools, nanoparticle concentration, humic acid and ionic strength. *Sci. Total Environ.* **2012**, *419*, 170−177.

(29) Kakhlon, O.; Cabantchik, Z. I. The labile iron pool: characterization, measurement, and participation in cellular processes. *Free Radical Biol. Med.* **2002**, *33*, 1037−1046.

(30) San Martin, C. D.; Garri, C.; Pizarro, F.; Walter, T.; Theil, E. C.; Núñez, M. T. Caco-2 intestinal epithelial cells absorb soybean ferritin by $\mu_2$ (AP2)-dependent endocytosis. *J. Nutr.* **2008**, *138*, 659−666.

(31) Ma, Y.; Yeh, M.; Yeh, K. Y.; Glass, J. Iron Imports. V. Transport of iron through the intestinal epithelium. *Am. J. Physiol. Gastrointest. Liver Physiol.* **2006**, *290*, G417−G422.

(32) Dressman, J. B.; Berardi, R. R.; Dermentzoglou, L. C.; Russell, T. L.; Schmaltz, S. P.; Barnett, J. L.; Jarvenpaa, K. M. Upper gastrointestinal (GI) pH in young, healthy men and women. *Pharm. Res.* **1990**, *7*, 756−761.

(33) Latunde-Dada, G. O.; Takeuchi, K.; Simpson, R. J.; McKie, A. T. Haem carrier protein 1 (HCP1): expression and functional studies in cultured cells. *FEBS Lett.* **2006**, *580*, 6865−6870.

(34) Theil, E. C.; Chen, H.; Miranda, C.; Janser, H.; Elsenhans, B.; Núñez, M. T.; Pizarro, F.; Schümann, K. Absorption of iron from ferritin is independent of heme iron and ferrous salts in women and rat intestinal segments. *J. Nutr.* **2012**, *142*, 478−483.

(35) Antileo, E.; Garri, C.; Tapia, V.; Muñoz, J. P.; Chiong, M.; Nualart, F.; Lavandero, S.; Fernández, J.; Núñez, M. T. Endocytic pathway of exogenous iron-loaded ferritin in intestinal epithelial (Caco-2) cells. *Am. J. Physiol. Gastrointest. Liver. Physiol.* **2013**, *304*, G655−G661.

(36) Pereira, D. I. A.; Mergler, B. I.; Faria, N.; Bruggraber, S. F. A.; Aslam, M. F.; Poots, L. K.; Prassmayer, L.; Lönnerdal, B.; Brown, A. P.; Powell, J. J. Caco-2 cell acquisition of dietary iron(III) invokes a nanoparticulate endocytic pathway. *PLoS One* **2013**, *8*, No. e81250.
(37) Powell, J. J.; Bruggraber, S. F.; Faria, N.; Poots, L. K.; Hondow, N.; Pennycook, T. J.; Latunde-Dada, G. O.; Simpson, R. J.; Brown, A. P.; Pereira, D. I. A nano-disperse ferritin-core mimetic that efficiently corrects anemia without luminal iron redox activity. *Nanomedicine* **2014**, DOI: 10.1016/j.nano.2013.12.011.
(38) Ben-Dov, N.; Korenstein, R. Proton-induced endocytosis is dependent on cell membrane fluidity, lipid-phase order and the membrane resting potential. *Biochim. Biophys. Acta* **2013**, *1828*, 2672−2681.
(39) Morgan, B.; Lahav, O. The effect of pH on the kinetics of spontaneous Fe(II) oxidation by $O_2$ in aqueous solution–basic principles and a simple heuristic description. *Chemosphere* **2007**, *68*, 2080−2084.
(40) Martell, A. E., Smith, R. M., Eds. *NIST Standard Reference Database 46: NIST Critically Selected Stability Constants of Metal Complexes*, version 8; National Istitute of Standards and Technology, Gaithersburg, MD, USA, 2004.
(41) Römheld, V.; Marschner, H. Mechanism of iron uptake by peanut plants. I. Fe(III) reduction, chelate splitting, and release of phenolics. *Plant Physiol.* **1983**, *71*, 949−954.
(42) Lesuisse, E.; Raguzzi, F.; Crichton, R. R. Iron uptake by the yeast *Saccharomyces cerevisiae*: involvement of a reduction step. *J. Gen. Microbiol.* **1987**, *133*, 3229−3236.
(43) Wu, H.; Yin, J. J.; Wamer, W. G.; Zeng, M.; Lo, Y. M. Reactive oxygen species-related activities of nano-iron metal and nano-iron oxides. *J. Food Drug. Anal.* **2014**, *22*, 86−94.

JOURNAL OF AGRICULTURAL AND FOOD CHEMISTRY

Article

pubs.acs.org/JAFC

# Utility of Hesperidinase for Food Function Research: Enzymatic Digestion of Botanical Extracts Alters Cellular Antioxidant Capacities and Anti-inflammatory Properties

Lu Yu,[†] Haiqiu Huang,[†] Liangli (Lucy) Yu,*[,†] and Thomas T. Y. Wang*[,§]

[†]Department of Nutrition and Food Science, University of Maryland, College Park, Maryland 20742, United States

[§]Diet, Genomics and Immunology Laboratory, Beltsville Human Nutrition Research Center, ARS, U.S. Department of Agriculture, Beltsville, Maryland 20705, United States

**ABSTRACT:** Food-derived phytochemicals, many known for their health beneficial effects, often exist in conjugated forms containing sugar moieties such as glucose or rhamnose in foods. The uptake of these compounds requires colonic bacterial cleavage of sugar moieties. However, most studies involved in screening extracts for biological activities do not take this process into account. This study seeks to determine the utility of commercially available hesperidinase to mimic colonic digestion and to test the effects of this treatment on the biological properties of extracts. Using hesperidinase resulted in efficient hydrolysis of *Engelhardia roxburghiana* Wall. extract containing rhamnose conjugates. Enzymatic digestion enhanced the extract's cellular antioxidant ability by 2-fold in HepG2/C3A and the anti-inflammatory effect on lipopolysaccharide-induced interleukin (IL)-1$\beta$ and IL-6 expression in mouse macrophage J774A.1 and human monocyte THP-1 cells. Enzymatic digestion also efficiently processed extracts with mixed rhamnose and glucose conjugates and altered their biological activities. Results of the present study supported the importance of considering enzymatic digestion during the biological activity studies of botanicals.

**KEYWORDS:** *hesperidinase, enzymatic digestion, antioxidant, anti-inflammation, xenobiotic metabolism*

## INTRODUCTION

Research has led to a wealth of evidence supporting the consumption of plant-based foods rich in phytonutrients as being closely linked to lowered risks of various chronic noncommunicable diseases including inflammation, cardiovascular disease, and cancers as well as aging.[1−3] A variety of naturally occurring phenolic compounds have been reported to possess antioxidant and anti-inflammatory properties along with an ability to induce xenobiotic metabolizing enzymes involved in drug and carcinogen removal.[4−6] The most common and largest class of polyphenols is the flavonoids, which are known to be responsible for the color, flavor, and potential beneficial effects of plants.[7] Also, flavonoids are often considered as safe diet-derived health-promoting substances. The C6−C3−C6 backbone is the basic structure of all flavonoids.[8] In nature, flavonoids often exist as conjugated forms[9] that are attached to various sugar moieties, such as rhamnose and glucose.[10] The phenolic ring, the hydroxyl groups, and the double bonds of a flavonoid structure are thought to contribute to its antioxidant capacity, such as free radical neutralization and ROS inhibition, by donating hydrogen atoms.[11] Moreover, oxidative stress, which is caused by the imbalance of oxidants and antioxidants, plays a crucial role in the damage of proteins, lipids, carbohydrates, and DNA.[12] Oxidative stress has been demonstrated as a mediator of chronic inflammation by activating the expression of over 500 genes including growth factors, chemokines, and inflammatory cytokines.[13] Both enzymatic and nonenzymatic antioxidants are involved in the reduction of ROS formation, and they help to prevent, intercept, and repair damage from oxidative stress.[14] Hence, the modulation of oxidative stress and inflammation, as well as the induction of xenobiotic metabolizing enzymes, may be the mechanisms by which phytochemicals, such as flavonoids, can benefit human health.

Flavonoid glycosides are digested, absorbed, and excreted as they traverse through the gastrointestinal (GI) tract in humans.[15] More than 95% of polyphenols are not absorbed in the small bowel or stomach but transit into the colon,[16] where they are degraded by gut microbiota.[17] The degradation process in the colon includes the removal of glycosides from the conjugated phytochemicals. This naturally occurring process in our body causes changes to the chemical structures of flavonoids, thereby increasing their absorption.[18] Approximately 5000 naturally occurring flavonoids have been identified;[7] however, the majority of them possess one or more sugar groups (e.g., glucose, rhamnose, rutinose) while occasionally existing as aglycones.[11] In our previous study with *Engelhardia roxburghiana* Wall. (ER), we isolated and characterized astilbin and engeletin, which are the major constituents in the ER leaf extracts.[19] Our study has demonstrated that *Gynostemma pentaphyllum* (Thunb.) Makino (GP), another purported health-promoting plant, showed complex conjugated flavonoid composition.[20] It appears that the removal of glycosides might be necessary to release the active forms of flavonoids, and the differences in the structures of aglycones and glycosides might lead to significant differences in their polarities, bioavailabilities, biological activities, and

Received: April 25, 2014
Revised: July 13, 2014
Accepted: August 5, 2014
Published: August 5, 2014

ACS Publications © 2014 American Chemical Society

effects on human health.[18] A recent study by a Korean research group has demonstrated that most of the flavonoid glycosides could be efficiently degraded by gastrointestinal enzymes to their aglycone forms.[21]

Microbial enzymes involved in the processing of glycosides have been studied.[22,23] α-L-Rhamnosidase (EC 3.2.1.40) is an enzyme that cleaves the terminal α-L-rhamnose from natural glycosides.[22] This enzyme has been reported to occur in animal tissues, fungi, and bacteria.[22] Flavonoid glycosides, such as quercetin-3-*O*-rhamnoside, could be efficiently catalyzed and hydrolyzed to quercetin by gut microflora, for example, α-rhamnosidase-containing *Bacteroides distasonis*.[22] Other microorganism-derived enzymes, such as hesperidinase, are enzymes with both α-L-rhamnosidase (EC 3.2.1.40) and β-D-glucosidase (3.2.1.21) activities that can remove both rhamnose and glucose. Recently, approximately $10^{12}$ microorganisms/$cm^3$ have been reported to exist in the colon.[23] Thus, these microbial-derived enzymes may account for a significant aspect of flavonoid processing in the colon. Interestingly, in most studies of biological activities of naturally derived extracts, such as antioxidant and anti-inflammatory capacities, colonic processing of glycosides is often not considered.[24−26]

The purpose of this study is to explore the utility of commercially available hesperidinase from *Penicillium* sp. in mimicking colonic digestion of flavonoid glycosides and to test if (1) the treatment with hesperidinase catalyzes the processing of conjugated extracts and (2) the treatment with hesperidinase alters the biological activities of the extracts. In this study, a simplified assay system for the enzymatic digestion was developed using a water extraction from ER. Also, we validated the effects of enzymatic digestion on bioactivities, including antioxidant property, anti-inflammatory effect, and xenobiotic metabolizing capacity. The utility of enzymatic digestion was further evaluated on five complex extracts from leaf and whole-plant samples of diploid and tetraploid GP.[20] Our results indicated that the alteration of biological activities by enzyme treatment and the incorporation of hesperidinase digestion might provide a more realistic assessment of biological functions during in vitro screening of health-promoting properties of plant extracts.

## MATERIALS AND METHODS

**Materials and Reagents.** Human hepatocarcinoma cell HepG2/C3A, mouse macrophage J774A.1, and human leukemic cell THP-1 were purchased from American Type Culture Collection. Hesperidinase from *Penicillium* sp., HPLC grade water, acetic acid, sodium acetate, HEPES, hydrocortisone, penicillin, streptomycin, gentamicin, insulin, and dimethyl sulfoxide were purchased from Sigma-Aldrich (St. Louis, MO, USA). 2′,7′-Dichlorofluorescin diacetate, Williams' medium E without phenol red, RPMI medium with phenol red, and Hanks' balanced salt solution were purchased from Gibco Life Technologies (Grand Island, NY, USA). An ATPlite Luminescence Assay System Kit was from PerkinElmer Life and Analytical Sciences (Boston, MA. USA). DMEM, antibiotic−antimycotic, fetal bovine serum, and TRIzol reagent were purchased from Invitrogen (Carlsbad, CA, USA). 2,2-Azobis(2-amidinopropane) dihydrochloride (ABAP) was obtained from Wako Chemicals USA, Inc. (Richmond, VA, USA). All other chemicals were of analytical reagent grade and used without any further purification.

**Plant Extract Preparations.** Leaves of ER were collected and prepared as described in previous work.[19] All of the dried botanical materials were stored at room temperature in the dark before being used. GP samples including two diploid leaf samples (GP1 and GP2), two tetraploid leaf samples (GP3 and GP4), and one tetraploid whole-plant sample (GP5) were obtained and prepared following the published protocol.[20] To obtain the extracts, 2 g of ground ER leaves was weighed, added to 200 mL of water, and set in an 80 °C water bath for 15 min to simulate the tea-making procedure. Next, samples were filtered and freeze-dried. Five grams of pulverized GP dried leaves was weighed and extracted in pure methanol for 6 h using a Soxhlet apparatus. The sample solutions were filtered through a 0.45 μm membrane filter, and methanol was vaporized using gas nitrogen as described.[20]

**Enzyme Digestion Procedure.** Digestion reaction was performed in a 10 mL total volume containing 400 μg/mL of ER or GP samples and 400 μg/mL hesperidinase in either acetic acid−sodium acetate buffer (10 mM, pH 5.0) or HPLC grade water at 37 °C for 2 h. The enzyme was then inactivated at 80 °C in a water bath for 3 min. Digested samples were filtered by a 0.2 μm membrane filter, freeze-dried, and redissolved in 500 μL of DMSO for subsequent HPLC analysis or cell-based studies.

**Analysis of Astilbin, Engeletin, and Their Enzymatic Metabolites Taxifolin and Dihydrokaempferol in ER by HPLC.** Astilbin and engeletin, as well as their metabolites taxifolin and dihydrokaempferol, were identified using an HPLC-DAD method. ER extract before or after hydrolysis dissolved in DMSO was analyzed using a Shimadzu LC-20AD with an autosampler plus a C18, 250 × 4.6 mm, 5 μm column at 35 °C. The flow rate was kept at 1 mL/min. A binary gradient system was used with mobile phase A consisting of acetonitrile and mobile phase B consisting of 0.1% acetic acid in water. At 0−2 min, the constitution of mobile phase A was increased from 16 to 20% (linearly), then at 2−12 min increased from 20 to 40%, at 12−16 min increased from 40 to 90%, and at 16−19.5 min decreased from 90 to 16%. The wavelength for UV−vis detection was set at 290 nm. All of the flavonoids in ER were identified via comparison to the standards for retention time and UV spectrum, and the amount of flavonoids was compared via the area under the peaks.

Conversion rate was calculated by using the following formula:

$$\text{conversion rate} = \frac{\text{area under the peak of digested}}{\text{area under the peak of undigested}} \times 100\%$$

**Cytotoxicity Test of ER before and after Digestion in HepG2/C3A Cell Line.** Cell viability test was conducted using ATPlite assay[27] according to the manufacturer's protocol (PerkinElmer Life and Analytical Sciences). Briefly, $6 \times 10^4$ cells per well of HepG2 human hepatoma cells were plated into 96-well plates in Williams' medium E at 37 °C with 5% $CO_2$. After 24 h, culture medium was aspirated and 100 μL of control medium and medium containing 62.5, 125, or 250 μM ER before and after hesperidinase digestion was added to different wells. After 24 h of treatment, 100 μL of reconstituted ATPlite solution was added to each well, and luminescence was read using a Victor[3] multiwell plate reader (PerkinElmer) immediately. Experiments were conducted in triplicate.

**Cell-Based Antioxidant Activities.** Cell-based antioxidant assays were performed according to Wolfe's protocol.[28] Briefly, HepG2/C3A, $6 \times 10^4$ cells per well, was seeded in 96-well plates and kept in a 37 °C incubator with 5% $CO_2$. After 24 h, culture medium was removed and replaced with medium containing test extracts/compounds. After 24 h of pretreatment, the medium was removed and the cells were washed with prewarmed HBSS. HepG2/C3A cells were then treated with the extracts and 25 μM DCFHDA for 1 h. Next, 100 μL of 37 °C 600 μM ABAP was added to the cells. Fluorescence was read in 5 min intervals for 1 h with emission at 538 nm and excitation at 485 nm at 37 °C. Cell-based antioxidant activities of samples were expressed as micromoles of quercetin per gram of dried ER leaves.

**Effects of Enzymatic Digestion on Anti-inflammatory Properties of ER in Mouse J774A.1 Macrophages, Human THP-1 Monocytes, Human THP-1 Macrophages, and Xenobiotic Metabolism Activities of ER in Human THP-1 Monocytes.** The effects of enzymatic digestion on inflammatory response were first evaluated in mouse macrophage J774A.1, a cell line widely used for inflammation studies and anti-inflammation investigation.[29] A 2 mL cell suspension of J774A.1 ($7.5 \times 10^4$/mL) was seeded in a 6-well plate overnight in DMEM with 10% FBS and 1% antibiotic−antimycotic and reached 80% confluence at 37 °C with 5% $CO_2$.

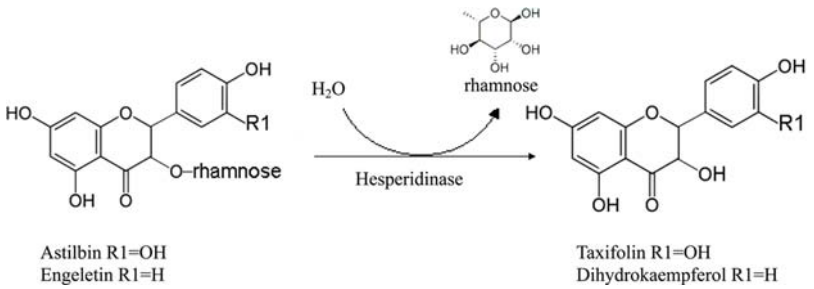


**Figure 1.** Transformation of major components in ER using hesperidinase.

For human THP-1 monocytes, 2 mL of cells ($2.5 \times 10^5$ cells/mL) was plated in 6-well plates in RPMI medium with 10% FBS and 1% antibiotic–antimycotic at 37 °C with 5% $CO_2$.

To prepare differentiated human THP-1 macrophages, 2 mL of human THP-1 monocytes ($5 \times 10^5$ cells/mL) with the differentiating agent PMA (25 ng/mL)[30] was plated in 6-well plates in RPMI medium with 10% FBS and 1% antibiotic–antimycotic at 37 °C with 5% $CO_2$ for 48 h until cells were all localized and attached to the plate. Treatments were initiated after this incubation.

Concentrations of 0, 10, and 25 $\mu$M (calibrated by the average molecular weight of two main components) of ER samples before and after digestion dissolved in DMSO solution were used for anti-inflammatory studies. Treatment was started 24 h after cell plating, and the treatment medium was replaced every 24 h by fresh medium containing the extract. After 48 h of treatment, lipopolysaccharide (LPS) was added at the concentration of 10 ng/mL for 4 h. mRNA isolation, cDNA synthesis, and real-time PCR were conducted according to our previously published protocol.[29,31] TATA-binding protein (Tbp) mRNA was used as housekeeping gene for normalization. TaqMan Assay-On-Demand gene expression assays were obtained from Applied Biosystems: Tbp (Mm00446973_m1; Hs00427620_m1), IL-1$\beta$ (Mm01336189_m1; Hs01555410_m1), IL-6 (Mm00446190_m1; Hs00985639_ml), and CYP1B1 (Hs02382916_s1). The amplification parameters were set as follows for PCR: 50 °C for 2 min, 95 °C for 10 min, and 46 cycles of amplification at 95 °C for 15 s and 60 °C for 1 min.

**Statistical Analysis.** Tests were conducted in triplicate, and data are reported as means ± standard deviation. The significance level of differences in means was analyzed using one-way ANOVA and Tukey's test. Statistics software SPSS for Windows (version rel. 10.0.1, 1999, SPSS Inc., Somers, NY, USA) was used. Statistical significance was defined at $P \leq 0.05$.

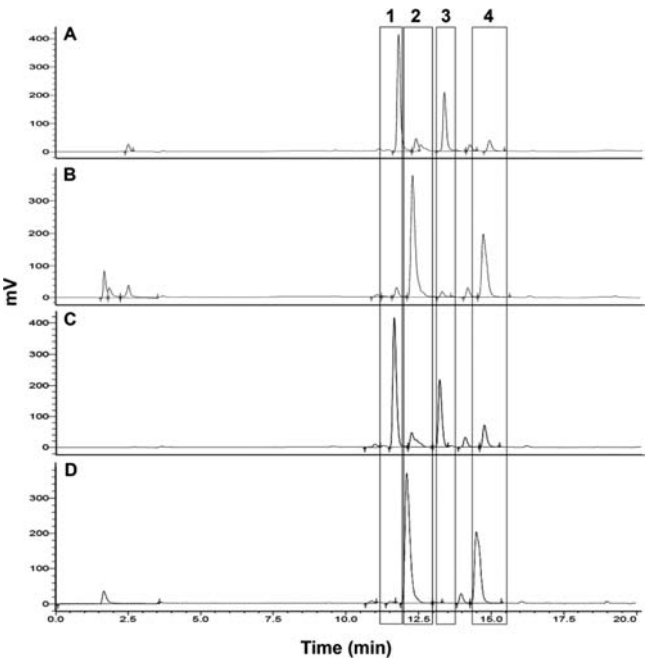


**Figure 2.** HPLC analysis of components of ER water extracts before and after 2 h of enzymatic digestion by hesperidinase from *Penicillium* sp.: (A) ER before digestion in buffer system; (B) ER after digestion in buffer system; (C) ER before enzymatic digestion in water system; (D) ER after enzymatic digestion in water system. Components in ER: (1) astilbin; (2) taxifolin; (3) engeletin; (4) dihydrokaempferol.

## RESULTS

**Effects of Hesperidinase Digestion on ER Extract.** As previously reported, ER extract contains a relatively simple array of two major compounds, astilbin and engeletin (Figure 1).[19] Therefore, we used ER extract to test the utility of hesperidinase treatments. The enzyme activity of hesperidinase was tested in two systems, a sodium acetate (NaAc) buffer system and a water system. The NaAc system was selected to mimic the colonic pH of ~5.0. The water system was chosen for its simplicity, as no additional components in the solvent after removal will affect subsequent bioactivity assays. On the basis of the preliminary optimization trials (data not shown), 400 $\mu$g/mL of ER extract and 400 $\mu$g/mL of hesperidinase were selected for the efficiency of glycosides hydrolysis. Compositions of ER extract in buffer system before and after enzymatic digestion were compared in the HPLC analysis. As illustrated in Figure 2, four major peaks were detected exclusively before and after digestion. Peaks designated 1–4 represent astilbin, taxifolin, engeletin, and dihydrokaempferol (retention times of 11.55, 12.12, 13.08, and 14.51 min), respectively. In NaAc-buffered condition (Figure 2A,B), rhamnosides astilbin and engeletin were efficiently degraded after digestion. Their aglycones, taxifolin and dihydrokaempferol, were the major components observed after hydrolysis (Figure 2B). The results of the water system as shown in Figure 2C,D were identical to those of the buffered system. The 400 $\mu$g/mL extracts with 400 $\mu$g/mL hesperidinase were selected for subsequent experiments.

Both the NaAc-buffered system and water system were further characterized to compare their effects on the efficiency of hesperidinase to catalyze the hydrolysis of naturally occurring flavonoids. For the buffered system, 10 mM sodium acetate was used and the pH was adjusted to 5.0. In the water system, the pH remained at 7.0 during the 2 h of enzymatic digestion. As illustrated in Figure 3, the hydrolysis rates of astilbin and engeletin for buffered and water systems were 92 and 97%, respectively. In the water system, the conversion was comparable to or even slightly higher than that in the buffered system. These results indicated that the $\alpha$-L-rhamnosidase processing ability was not affected by the pH ranging from 5.0 to 7.0 at 37 °C after 2 h of incubation. These results also indicated that the water system might be a simple, convenient

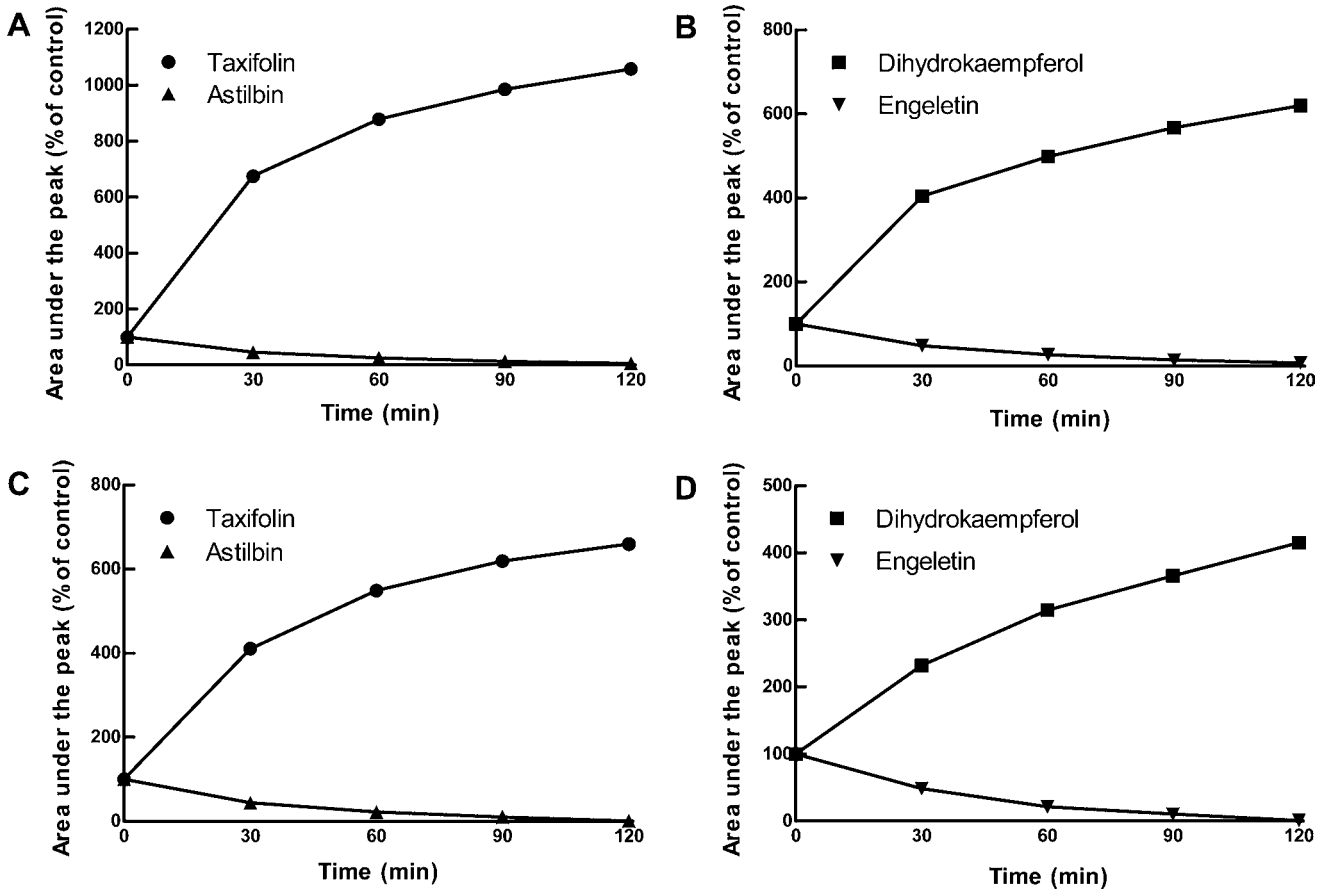


**Figure 3.** Comparison of the conversion rates of astilbin and engeletin to their hydrolyates taxifolin and dihydrokaempferol by hesperidinase treatment of ER extract during 2 h. Conversion rates of glycosides and aglycones were expressed as percent of the control: (A) astilbin and taxifolin in buffer; (B) engeletin and dihydrokaempferol in buffer; (C) astilbin and taxifolin in water; (D) engeletin and dihydrokaempferol in water.

condition for hesperidinase processing of extract in vitro. Therefore, the water assay system was used for the subsequent experiments.

**Analysis of Cytotoxicity and Cellular Antioxidant Activity of ER Water Extracts before and after Enzymatic Digestion in HepG2/C3A Cell Line.** We first examined the effect of ER extracts on cytotoxicity as a global end point. As shown in Figure 4A, concentrations up to 250 $\mu$M were nontoxic to HepG2 cells. Furthermore, digestion did not affect the cytotoxicity of ER extract as no changes in the proliferation index were observed. The effect of digestion on antioxidant properties of extracts using the cellular antioxidant activity assay (CAA) was examined, as flavanoids are known to possess antioxidant properties. A 250 $\mu$M ER water extract was used for CAA on the basis of cytotoxicity data. As illustrated in Figure 4B, after the digestion, the antioxidant activity of the ER extract increased from 14.23 to 24.99 $\mu$mol quercetin equivalents/g dried ER leaves. The enzymatic digestion of ER significantly enhanced its antioxidant capacity by ~2-fold.

**Anti-inflammatory Effects of ER before and after Digestion.** Exposure of monocyte/macrophage to LPS mimics the response of inflammation in vitro by the induction of inflammation-related cytokines such as interleukin-1$\beta$ (IL-1$\beta$), IL-6, and tumor necrosis factor-$\alpha$ (TNF-$\alpha$). Hence, we examined the response of monocyte/macrophage to LPS to assess the effects of enzymatic digestion on inflammation. As shown in Figure 5, the mRNA level of both IL-1$\beta$ and IL-6 in mouse J774A.1 cell line was increased by LPS stimulation.

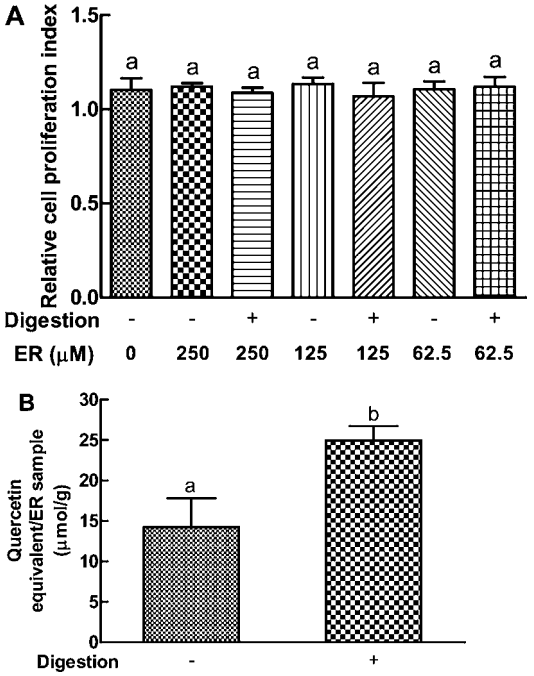


**Figure 4.** (A) Cytotoxicity and (B) cellular antioxidant capacity of ER water extracts before and after digestion in HepG2/C3A cell line. Each column represents the mean ± SD ($n$ = 3). Columns marked by different letters are significantly different from each other ($P \leq 0.05$).


dx.doi.org/10.1021/jf501963a | J. Agric. Food Chem. 2014, 62, 8640−8647

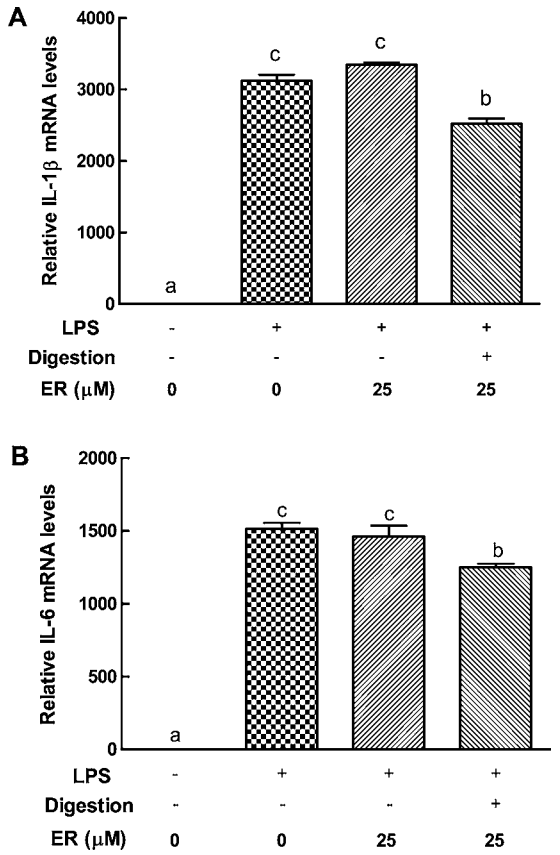


**Figure 5.** Anti-inflammation study of ER before and after digestion in mouse macrophage J774A.1 cell line: (A) IL-1$\beta$ expression; (B) IL-6 expression. Each column represents the mean ± SD ($n$ = 3). Columns marked by different letters are significantly different from each other ($P \leq 0.05$).

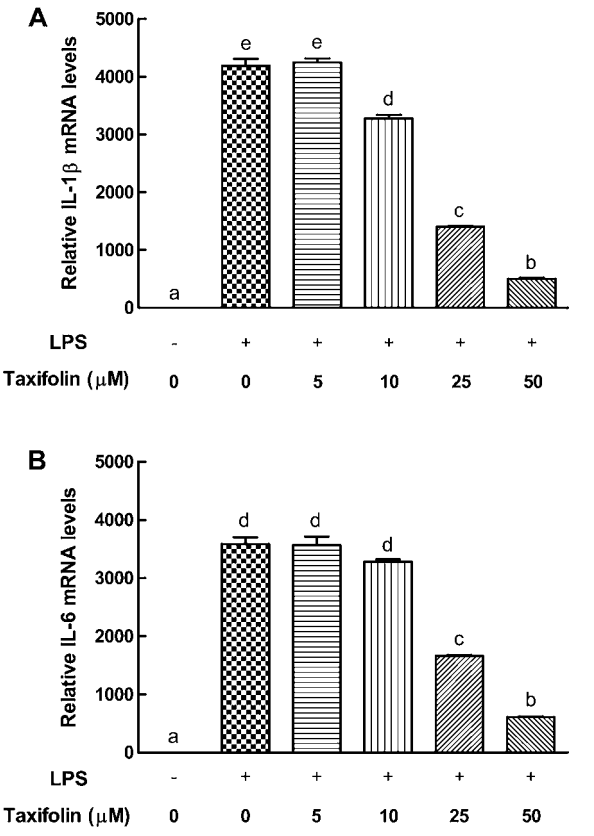


**Figure 6.** Anti-inflammation study of taxifolin in mouse macrophage J774A.1 cell line: (A) IL-1$\beta$ expression; (B) IL-6 expression. Each column represents the mean ± SD ($n$ = 3). Columns marked by different letters are significantly different from each other ($P \leq 0.05$).

Enzymatically digested extract (25 $\mu$M) exhibited significantly higher inhibitory effects on LPS induction of IL-1$\beta$ and IL-6 mRNA than that before digestion. The inhibitions of IL-1$\beta$ and IL-6 mRNA expression by 25 $\mu$M digested ER extract were 24.67 and 14.38%, respectively. As illustrated in Figure 6, elevated taxifolin concentrations resulted in greater IL-1$\beta$ and IL-6 mRNA down-regulation.

The anti-inflammatory effects of ER before and after hesperidinase digestion in human THP-1 monocytes and PMA differentiated THP-1 macrophage were also examined. Phorbol 12-myristate 13-acetate (PMA) was added to THP-1 cells to induce differentiation into adherent macrophage-like cells.[30] Consistent with the results found in mouse macrophage, 25 $\mu$M ER after digestion exhibited significantly higher capacity to inhibit the mRNA level of IL-1$\beta$ and IL-6 (Figure 7). Additionally, significant inhibition of IL-1$\beta$ was also observed in differentiated THP-1 macrophages (Figure 8).

**Enzymatic Digestion Effects on Xenobiotic Activities by ER before and after Digestion in Human THP-1 Monocytes.** Cytochrome P450 1B1 (CYP1B1) is a member of the CYP 1 gene family that metabolizes xenobiotics and carcinogens.[32] As illustrated in Figure 9, digestion led to an induction of CYP1B1 in human THP-1 monocytes. Furthermore, stimulation of THP-1 cells by LPS inhibited CYP1B1 mRNA expression, and treatment with digested ER extract reversed the effects of LPS and increased the mRNA of CYP1B1 to the control level.

**Cellular Antioxidant Activity of Five GP Species before and after Enzymatic Digestion in HepG2/C3A Cell Line.** We further tested our water digestion system in a more complex extract system to see if enzyme digestion may affect biological activities of the extracts. Five extracts from diploid and tetraploid GP leaves and whole plant were used to undergo the same digestion process by hesperidinase. The cellular antioxidant activities were determined. As illustrated in Figure 10, the digestion process altered the biological efficacies of the samples. Digestion increased the antioxidant capacity of GP1 by >2-fold. The antioxidant ability of GP2 was decreased after enzymatic treatment. GP3 and GP4 did not show significant changes of cellular antioxidant properties before and after digestion, whereas GP5 increased the oxidative level after digestion.

## DISCUSSION

Microbial-derived enzymes contribute significantly to flavonoid processing in the colon. This process occurs naturally in the human body, which might cause changes to the bioactivities of flavonoids. Our study focused on mimicking the colonic enzymatic digestion of flavonoid-rich botanicals to reveal their physiological bioactivities using commercially available hesperidinase. The use of enzyme hesperidinase sufficiently cleaved the rhamnose groups from astilbin and engeletin in both buffer and water systems at 37 °C, with hydrolysis rates of 92 and 97%, respectively (Figure 3). High efficiency in the water system is especially attractive because it allows for minimal manipulation and once removed, as in our case by


dx.doi.org/10.1021/jf501963a | J. Agric. Food Chem. 2014, 62, 8640−8647

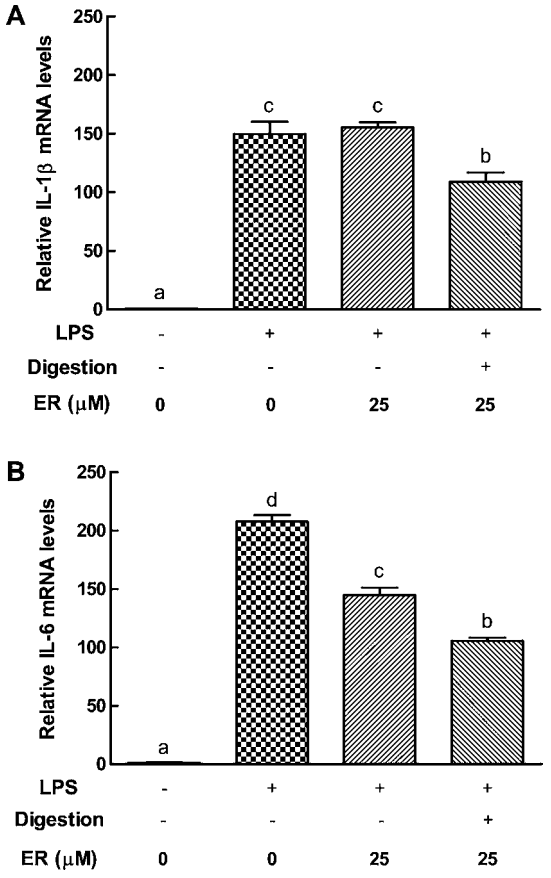


**Figure 7.** Anti-inflammation study of ER before and after digestion in human monocyte THP-1 cell line: (A) IL-1$\beta$ expression; (B) IL-6 expression. Each column represents the mean ± SD ($n$ = 3). Columns marked by different letters are significantly different from each other ($P \leq 0.05$).

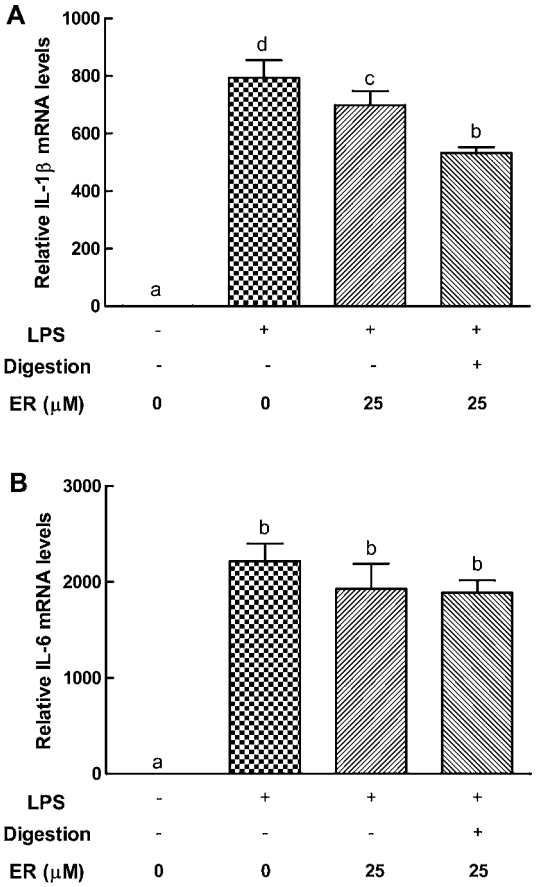


**Figure 8.** Anti-inflammation study of ER before and after digestion in human differentiated THP-1 cell line: (A) IL-1$\beta$ expression; (B) IL-6 expression. Each column represents the mean ± SD ($n$ = 3). Columns marked by different letters are significantly different from each other ($P \leq 0.05$).

lyophilization, should not affect subsequent biological activity. The efficiency of hesperidinase on the digestion of ER (Figure 2) supported the selectivity of the enzyme on removal of $\alpha$-L-rhamnose sugar groups in flavonoids and the use of commercially available hesperidinase from *Penicillium* sp. to simulate the enzymatic digestion of flavonoids in the gut. The composition of ER is comparably simple as it contains only two major components, astilbin and engeletin. However, most of the botanicals might consist of far more complex compositions, and how they could be digested and affect human health will need further investigation. For example, the GP extracts we studied contain 40 different compounds that vary with ploidies and parts of the plant.[19] Some of the identified components are known as quercetin-di(rhamno)hexoside, kaempferol 3-*O*-di-*p*-coumaroylhexoside, kaempferol 3-*O*-di-*p*-coumaroylhexoside, quercetin-rhamnohexoside, rutin, kaempferol-rhamnohexoside, kaempferol-3-*O*-rutinoside, quercetin, and kaempferol.[19] As listed, most phytochemicals in GP are glycosides. Our assay of hesperidinase digestion efficiently processed this complex mixture (Figure 10), suggesting that the hesperidinase was able to remove rhamnose and glucose from glycosides, although further authentication is necessary.

As hypothesized, enzymatic processing altered the biological activity of an extract. The cellular antioxidant activity of the ER water extract was nearly doubled after the digestion process when compared to the undigested extract (Figure 4). The smaller and less polar chemical structures of taxifolin and dihydrokaempferol were likely to result in stronger ROS inhibition after digestion, because it would be easier for these compounds to migrate through cell membranes. Inflammation has been reported to be a critical component associated with the development of chronic diseases including cancer, obesity, heart disease, and others.[33−35] Inhibitory effects on pro-inflammatory cytokines IL-1$\beta$ and IL-6 were elevated in both mouse macrophage J774A.1 cells and human THP-1 monocytes when ER extracts went through digestion (Figures 5, 7, and 8). Additionally, ER extract after digestion also up-regulated the mRNA level of the xenobiotic enzyme CYP1B1 in human THP-1 monocytes, whereas undigested extract did not affect CYP1B1 expression, indicating that digested extract might be more efficient in getting into the cells. The enzymatic digestion process therefore might increase the metabolizing capacity of toxic or carcinogenic compounds. Moreover, the expression of CYP1B1 was found inversely correlated with inflammatory activity. Our results indicated that the removal of rhamnose might be important for the biological efficacies of ER extract. The digestion also accounted for significant changes in the biological efficacies of the GP extracts. The effects varied among the extracts (Figure 10). In some cases, digestion of GP extracts (for example, diploid GP1 and tetraploid GP5; Figure 10) led to significant alteration in antioxidant activity. These results further supported the value of our hesperidinase treatment procedures as the physiologically relevant properties


dx.doi.org/10.1021/jf501963a | J. Agric. Food Chem. 2014, 62, 8640−8647

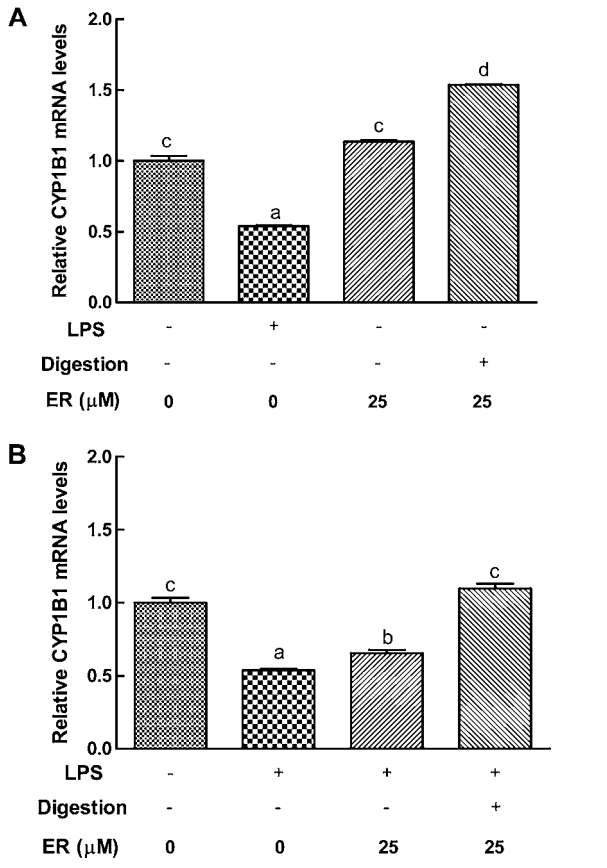


**Figure 9.** CYP1B1 activity of human THP-1 monocytes by ER before and after digestion: (A) CYP1B1 level in uninduced THP-1 monocytes; (B) CYP1B1 in THP-1 monocytes induced with LPS. Each column represents the mean ± SD ($n$ = 3). Columns marked by different letters are significantly different from each other ($P \leq 0.05$).

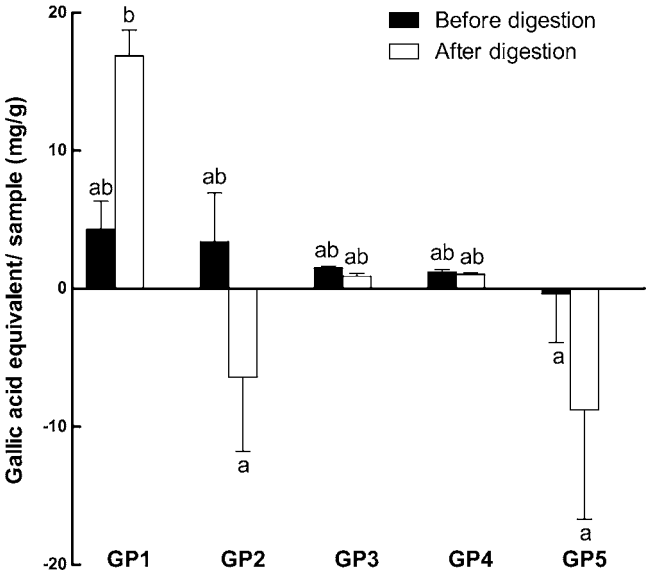


**Figure 10.** Cellular antioxidant activities of five types of GP before and after 2 h of enzymatic digestion. Each column represents the mean ± SD ($n$ = 3). Columns marked by different letters are significantly different from each other ($P \leq 0.05$).

of an extract may depend on the release of aglycones. It is also indicated that how food is processed in the colon might affect its biological activity. Hence, the consideration of enzyme processing during the screening of extracts is important.

In summary, the current study demonstrated the utility of commercially available hesperidinase from *Penicillium* sp. in simulating colonic processing of phytochemicals in vitro. We determined that a simple water system can be used for enzymatic digestion on the basis of the conversion rate of flavonoid glycosides to their aglycones. More importantly, we showed that digestion can result in the alteration of biological properties of an extract such as anti-inflammation property, antioxidant ability, and xenobiotic metabolizing potential. These results suggest that colonic enzymatic processing during food digestion alters the structure of food components and changes of their biofunctions, which may ultimately lead to different health-promoting effects in human. We recommend incorporating this simple enzymatic digestion step into functional food research studies of the biological efficacies in health promotion and disease prevention of foods.

## AUTHOR INFORMATION

### Corresponding Authors

*(T. T. Y. Wang) Mail: Diet, Genomics and Immunology Laboratory, Beltsville Human Nutrition Research Center, ARS, USDA, BARC-EAST, Building 307C, Room 132, Beltsville, MD 20705, USA. Phone: (301) 504-8459. E-mail: Tom.Wang@ars.usda.gov.

*(Liangli Yu) Mail: Department of Nutrition and Food Science, 0112 Skinner Building, University of Maryland, College Park, MD 20742, USA. Phone: (301) 405-0761. Fax: (301) 314-3313. E-mail: lyu5@umd.edu

### Funding

This research was supported by USDA appropriate fund Project 1235-51530-053-00D (T.T.Y.W.).

### Notes

The authors declare no competing financial interest.

## ACKNOWLEDGMENTS

We thank Dr. Norberta W. Schoene for her editorial assistance.

## ABBREVIATIONS USED

ER, *Engelhardtia roxburghiana* Wall.; GP, *Gynostemma pentaphyllum* (Thunb.) Makino; ROS, reactive oxygen species; LPS, lipopolysaccharide; TBP, TATA-binding protein; IL-1$\beta$, interleukin-1$\beta$; IL-6, interleukin-6; CYP1B1, cytochrome P450 1B1

## REFERENCES

(1) Mastaloudis, A.; Wood, S. M. Age-related changes in cellular protection, purification, and inflammation-related gene expression: role of dietary phytonutrients. *Ann. N.Y. Acad. Sci.* **2012**, *1259*, 112−120.

(2) Riccioni, G.; Speranza, L.; Pesce, M.; Cusenza, S.; D'Orazio, N.; Glade, M. J. Novel phytonutrient contributors to antioxidant protection against cardiovascular disease. *Nutrition* **2012**, *28*, 605−610.

(3) D'Ambrosio, S. M. Phytonutrients: a more natural approach toward cancer prevention. *Semin. Cancer Biol.* **2007**, *17*, 345−346.

(4) Haminiuk, C. W. I.; Maciel, G. M.; Plata-Oviedo, M. S. V.; Peralta, R. M. Phenolic compounds in fruits − an overview. *Int. J. Food Sci. Technol.* **2012**, *47*, 2023−2044.

(5) Zenkov, N. K.; Menshchikova, E. B.; Kandalintseva, N. V.; Oleynik, A. S.; Prosenko, A. E.; Gusachenko, O. N.; Shklyaeva, O. A.; Vavilin, V. A.; Lyakhovich, V. V. Antioxidant and antiinflammatory

activity of new water-soluble sulfur-containing phenolic compounds. *Biochemistry* **2007**, *72*, 644−651.
(6) Kale, A.; Gawande, S.; Gawande, S.; Kotwal, S. Cancer phytotherapeutics: role for flavonoids at the cellular level. *Phytother. Res.* **2008**, *22*, 567−577.
(7) Ross, J. A.; Kasum, C. M. Dietary flavonoids: bioavailability, metabolic effects, and safety. *Annu. Rev. Nutr.* **2002**, *22*, 19−34.
(8) Yao, L. H.; Jiang, Y. M.; Shi, J.; Tomás-Barberán, F. A.; Datta, N.; Singanusong, R.; Chen, S. S. Flavonoids in food and their health benefits. *Plant Food Hum. Nutr.* **2004**, *59*, 113−122.
(9) Kinoshita, T.; Lepp, Z.; Kawai, Y.; Terao, J.; Chuman, H. An integrated database of flavonoids. *BioFactors* **2006**, *26*, 179−188.
(10) Yokozawa, T.; Chen, C. P.; Dong, E.; Tanaka, T.; Nonaka, G. I.; Nishioka, I. Study on the inhibitory effect of tannins and flavonoids against the 1,1-diphenyl-2-picrylhydrazyl radical. *Biochem. Pharmacol.* **1998**, *56*, 213−222.
(11) Tsao, R. Chemistry and biochemistry of dietary polyphenols. *Nutrients* **2010**, *2*, 1231−1246.
(12) Chu, Y. F.; Wise, M. L.; Gulvady, A. A.; Chang, T.; Kendra, D. F.; Van Klinkena, B. J.W.; Shi, Y. H.; O'Shea, M. *In vitro* antioxidant capacity and anti-inflammatory activity of seven common oats. *Food Chem.* **2013**, *139*, 426−431.
(13) Reuter, S.; Gupta, S. C.; Chaturvedi, M. M.; Aggarwal, B. B. Oxidative stress, inflammation, and cancer: how are they linked? *Free Radical Biol. Med.* **2010**, *49*, 1603−1616.
(14) Sies, H. Oxidative stress: oxidants and antioxidants. *Exp. Physiol.* **1997**, *82*, 291−295.
(15) Cook, N. C.; Samman, S. Flavonoids − chemistry, metabolism, cardioprotective effects, and dietary sources. *J. Nutr. Biochem.* **1996**, *7*, 66−76.
(16) Miene, C.; Weise, A.; Glei, M. Impact of polyphenol metabolites produced by colonic microbiota on expression of COX-2 and GSTT2 in human colon cells (LT97). *Nutr. Cancer* **2011**, *63*, 653−662.
(17) Aherne, S. A.; O'Brien, N. M. Dietary flavonols: chemistry, food content and metabolism. *Nutrition* **2002**, *18*, 75−81.
(18) Manach, C.; Scalbert, A.; Morand, C.; Rémésy, C.; Jiménez, L. Polyphenols: food sources and bioavailability. *Am. J. Clin. Nutr.* **2004**, *79*, 727−747.
(19) Huang, H. Q.; Cheng, Z. H.; Shi, H. M.; Xin, W. B.; Wang, T. T. Y.; Yu, L. L. Isolation and characterization of two flavonoids, engeletin and astilbin, from the leaves of *Engelhardtia roxburghiana* and their potential anti-inflammatory properties. *J. Agric. Food Chem.* **2011**, *59*, 4562−4569.
(20) Xie, Z. H.; Zhao, Y.; Chen, P.; Jing, P.; Yue, J.; Yu, L. L. Chromatographic fingerprint analysis and rutin and quercetin compositions in the leaf and whole-plant samples of di- and tetraploid *Gynostemma pentaphyllum*. *J. Agric. Food Chem.* **2011**, *59*, 3042−3049.
(21) Kim, D. H.; Jung, E. A.; Sohng, I. S.; Han, J. A.; Kim, T. H.; Han, M. J. Intestinal bacterial metabolism of flavonoids and its relation to some biological activities. *Arch. Pharm. Res.* **1998**, *21*, 17−23.
(22) Yadav, V.; Yadav, P. K.; Yadav, S.; Yadav, K. D. S. α-L-Rhamnosidase: a review. *Process Biochem.* **2010**, *45*, 1226−1235.
(23) Scalbert, A.; Williamson, G. Dietary intake and bioavailability of polyphenols. *J. Nutr.* **2000**, *130*, 2073S−2085S.
(24) Djeridane, A.; Yousfi, M.; Nadjemi, B.; Boutassouna, D.; Stocker, P.; Vidal, N. Antioxidant activity of some algerian medicinal plants extracts containing phenolic compounds. *Food Chem.* **2006**, *97*, 654−660.
(25) Trouillas, P.; Calliste, C. A.; Allais, D. P.; Simon, A.; Marfak, A.; Delage, C.; Duroux, J. L. Antioxidant, anti-inflammatory and antiproliferative properties of sixteen water plant extracts used in the Limousin countryside as herbal teas. *Food Chem.* **2003**, *80*, 399−407.
(26) Park, H. S.; Lim, J. H.; Kim, H. J.; Choi, H. J.; Lee, I. S. Antioxidant flavone glycosides from the leaves of *sasa borealis*. *Arch. Pharm. Res.* **2007**, *30*, 161−166.
(27) Slavin, M.; Kenworthy, W.; Yu, L. L. Antioxidant properties, phytochemical composition, and antiproliferative activity of Maryland-grown soybeans with colored seed coats. *J. Agric. Food Chem.* **2009**, *57*, 11174−11185.
(28) Wolfe, K. L.; Liu, R. H. Cellular antioxidant activity (CAA) assay for assessing antioxidants, foods, and dietary supplements. *J. Agric. Food Chem.* **2007**, *55*, 8896−8907.
(29) Huang, H. Q.; Fletcher, A.; Niu, Y. G.; Wang, T. T. Y.; Yu, L. L. Characterization of lipopolysaccharide-stimulated cytokine expression in macrophages and monocytes. *Inflamm. Res.* **2012**, *61*, 1329−1338.
(30) Takashiba, S.; Van Dyke, T. E.; Amar, S.; Murayama, Y.; Soskolne, A. W.; Shapira, L. Differentiation of monocytes to macrophages primes cells for lipopolysaccharide stimulation via accumulation of cytoplasmic nuclear factor κB. *Infect. Immun.* **1999**, *67*, 5573−5578.
(31) Trasino, S. E.; Kim, Y. S.; Wang, T. T. Y. Ligand, receptor, and cell type-dependent regulation of ABCA1 and ABCG1 mRNA in prostate cancer epithelial cells. *Mol. Cancer Ther.* **2009**, *8*, 1934−1945.
(32) Rochat, B.; Morsman, J. M.; Murray, G. I.; Figg, W. D.; Mcleod, H. L. Human CYP1B1 and anticancer agent metabolism: mechanism for tumor-specific drug inactivation? *J. Pharmacol. Exp. Ther.* **2001**, *296*, 537−541.
(33) Zhou, H. P.; Lutterodt, H.; Cheng, Z. H.; Yu, L. L. Anti-inflammatory and antiproliferative activities of trifolirhizin, a flavonoid from *Sophora flavescens* roots. *J. Agric. Food Chem.* **2009**, *57*, 4580−4585.
(34) Coussens, L. M. Inflammation and cancer. *Toxicol. Pathol.* **2004**, *32*, 732.
(35) Yudkin, J. S.; Kumari, M.; Humphries, S. E.; Mohamed-Ali, V. Inflammation, obesity, stress and coronary heart disease: is interleukin-6 the link? *Atherosclerosis* **2000**, *148*, 209−214.

JOURNAL OF AGRICULTURAL AND FOOD CHEMISTRY

Article

pubs.acs.org/JAFC

# Intracellular Antioxidant Detoxifying Effects of Diosmetin on 2,2-Azobis(2-amidinopropane) Dihydrochloride (AAPH)-Induced Oxidative Stress through Inhibition of Reactive Oxygen Species Generation

Wenzhen Liao, Zhengxiang Ning, Luying Chen, Qingyi Wei, Erdong Yuan, Jiguo Yang,* and Jiaoyan Ren*

College of Light Industry and Food Sciences, South China University of Technology, Guangzhou 510640, China

**ABSTRACT:** The intracellular antioxidant activities of diosmetin were evaluated by cellular antioxidant activity (CAA) assay, 2,2-azobis(2-amidinopropane) dihydrochloride (AAPH)-induced erythrocyte hemolysis assay and cupric chloride ($CuCl_2$)-induced plasma oxidation assay. The results showed that diosmetin exhibits strong cellular antioxidant activity ($EC_{50}$ = 7.98 $\mu$mol, CAA value = 58 $\mu$mol QE/100 $\mu$mol). It was also found that diosmetin treatment could effectively attenuate AAPH-induced erythrocyte hemolysis (91.0% inhibition at 100 $\mu$g/mL) and $CuCl_2$-induced plasma oxidation through inhibition of intracellular reactive oxygen species (ROS) generation. Diosmetin could significantly restore AAPH-induced increase of intracelluar antioxidant enzyme (SOD, GPx, and CAT) activities to normal levels, as well as inhibit intracellular malondialdehyde (MDA) formation. Thus, the intracellular antioxidant detoxifying mechanism of diosmetin is associated with both nonenzymatic and enzymatic defense systems.

**KEYWORDS:** *diosmetin, cellular antioxidant activity, oxidative hemolysis, plasma oxidation*

## INTRODUCTION

Diosmetin (3′,5,7-trihydroxy-4′-methoxyflavone) is bioflavonoid found in citrus fruits, spearmint, and legume leaves[1] that has antibacterial activity against *Helicobacter pylori*(1),[2] *Staphylococcus aureus*,[3] and *Bacillus subtilis*.[4] In addition, diosmetin also exhibits antimutagenic, antioxidant, and anti-inflammatory activities.[5,6] Recent evidence had revealed that diosmetin possessed immunoregulating activity; for example, it could modulate macrophage colony-stimulating factor (M-CSF) induced proliferation and reduced the production of transforming growth factor beta 1 (TGF-$\beta$1), interleukin-10 (IL-10), and tumor necrosis factor alpha (TNF-$\alpha$) in mouse macrophages.[7] Other studies in cancer cell lines and animal models indicated that diosmetin had strong cancer chemopreventive and antiproliferative abilities.[8−12] The latest study also demonstrated that diosmetin could significantly enhance adenosine triphosphate (ATP) levels in liver and kidney cells.[13]

One factor underlying the pathology of many diseases, including cancer, diabetes, and coronary artery disease, is an increase in oxidative stress;[14−16] this suggests that the numerous beneficial properties of diosmetin may be related to its antioxidant activity. However, although the extracellular antioxidant activity of diosmetin has been extensively studied, there is little information on its antioxidant properties within cells. This is significant because extracellular assays mostly rely on chemical methods that do not take the metabolism and bioavailability of antioxidants into account. Therefore, tests of diosmetin's intracellular antioxidant activity, which address issues of uptake, distribution, and metabolism, are urgently needed.

The cellular antioxidant activity (CAA) assay is a newly developed approach that quantifies the antioxidant capacity of bioactive compounds in cell cultures.[17] The CAA assay represents a marked improvement over traditional chemical antioxidant activity assays because it simulates cellular biochemical processes, including cellular uptake and metabolism. Therefore, the CAA assay should allow a better understanding of how antioxidants behave under physiological conditions. To date, little information about the evaluation of the antioxidant activity of diosmetin by CAA has been done.

One of the main causes of intracellular oxidation is the presence of reactive oxygen species (ROS); for example, ROS can react with unsaturated fatty acids in phospholipids to form lipid peroxides, leading to damage of the cell membrane. The production and destruction of ROS is normally maintained in a steady-state balance by inherent cellular defense systems, including enzymatic and nonenzymatic antioxidants.[18,19] However, oxidative stress will occur either when there is an excess of ROS or when the intrinsic defenses are damaged. In cell models, oxidative stress can be induced by many reagents, for example, 2,2-azobis(2-amidinopropane) dihydrochloride (AAPH).[20,21] Thus, an AAPH-induced erythrocyte hemolysis assay can visually reveal biologically relevant radical-scavenging ability by measuring ROS and malondialdehyde (MDA) levels, as well as activities of intracellular antioxidant enzyme activities (superoxide dismutase, SOD; glutathione peroxidase, GPx; and catalase, CAT). Up to now, little information about the protective effects of diosmetin on AAPH-induced erythrocyte hemolysis is available.

A variety of studies suggested that cupric chloride ($CuCl_2$) was a pro-oxidant agent, which could cause lipid oxidation.

Received: May 20, 2014
Revised: July 22, 2014
Accepted: July 30, 2014
Published: July 30, 2014

ACS Publications © 2014 American Chemical Society

Although copper (Cu) is an essential component of many enzymes and participates in various physiological processes, Cu releases from proteins can facilitate the formation of hydroxyl radicals and lead to lipid peroxidation.[22] Thus, the $CuCl_2$-induced plasma oxidation assay can be used as a biologically relevant method for evaluating the antioxidant capacity of bioactive compounds. In this research, the $CuCl_2$-induced plasma oxidation assay was first applied to investigate the intracellular antioxidant capacity of diosmetin.

In the present study, the intracellular antioxidant properties of diosmetin were investigated using the CAA, AAPH-induced erythrocyte hemolysis, and copper-induced plasma oxidation assays. The results showed that diosmetin exhibited potent antioxidant activity via both nonenzymatic and enzymatic mechanisms.

## MATERIALS AND METHODS

**Materials.** Diosmetin, AAPH, and 4-(2-hydroxyethyl)-1-piperazineethanesulfonic acid (HEPES) were purchased from Sigma Co. (St. Louis, MO, USA). An MDA kit was purchased from Nanjing Jiancheng Institute of Biotechnology (Jiangsu, China). Kits for the determination of SOD, cellular GPx, CAT, ROS, and bicinchoninic acid (BCA) were purchased from Beyotime Institute of Biotechnology (Shanghai, China). Dulbecco's modified Eagle's medium (DMEM), Hank's balanced salt solution (HBSS), and phosphate-buffered saline (PBS, pH 7.4) were obtained from Gibco Life Technologies (Grand Island, NY, USA). Human hepatocellular carcinoma (HepG2) cells were obtained from the Medical College of Sun Yat-Sen University (Guangzhou, China). Heat-inactivated fetal bovine serum (FBS) was purchased from Sijiqing Co. Ltd. (Hangzhou, China). Ultrapure water was obtained from a Milli-Q water purification system (Millipore, Bedford, MA, USA).

**CAA Assay.** *CAA of Diosmetin.* The intracellular antioxidant capacity of diosmetin was assessed using the CAA assay as described[16] with some modifications. Briefly, HepG2 cells were grown in DMEM with 10% FBS, 100 $\mu$g/mL streptomycin, and 100 units/mL penicillin.[23] During the logarithmic growth phase, cells ($6 \times 10^5$/mL) were seeded into a 96-well microplate (100 $\mu$L/well) and incubated for 24 h in a fully humidified atmosphere in a 5% $CO_2$, 37 °C incubator. The culture medium was then removed, and the cells were washed with 200 $\mu$L of PBS and incubated for an additional 2.5 h with medium that contained diosmetin and 2′,7′-dichlorofluorescein diacetate (DCFH-DA) (final concentration = 25 $\mu$M). The culture medium was then removed, and the cells were washed with 200 $\mu$L of PBS, after which 100 $\mu$L of new medium (HBSS plus 10 mM HEPES) containing 600 $\mu$M AAPH was added to each well. The 96-well microplate was placed in a Fluoroskan Ascent microplate fluorometer (Thermo Electron Corp., Vantaa, Finland), and the fluorescence was monitored every 5 min for 1 h (ex/em, 488/525 nm). Each plate included triplicate blank wells, which contained cells treated without oxidant.

*Quantification of CAA.* The blank and initial fluorescence values were subtracted, and the CAA value of each diosmetin concentration was calculated as the integration of the area below the curve of fluorescence versus time, according to the following equation:[24] CAA (units) = $1 - (\int SA/\int CA)$, where $\int SA$ is the integration of the area under the sample fluorescence versus time curve and $\int CA$ refers to the integration of the area under the control curve. The 50% effective concentration ($EC_{50}$) for diosmetin was determined from the median effect plot of $\log(f_a/f_u)$ versus log(dose), where $f_a$ is the effective fraction of the treatment (CAA units) and $f_u$ is the ineffective fraction (1 − CAA units) of the treatment. The $EC_{50}$ was presented as the mean ± SD and calculated for triplicate data sets. $EC_{50}$ values were expressed as micromoles of quercetin equivalents (QE) per 100 $\mu$mol of diosmetin; the $EC_{50}$ value for quercetin was obtained from four separate experiments.

**Assay for Erythrocyte Hemolysis Mediated by Peroxyl Free Radicals.** The intracellular antioxidant activity of diosmetin was evaluated as the inhibition of erythrocyte hemolysis based on the method described by Cheung et al.[25] with some modifications. Blood samples were collected from normal male adult volunteers under 30 years of age. Erythrocytes were separated from plasma by centrifugation at 1200*g* for 10 min at 4 °C and washed three times with PBS (pH 7.4). An aliquot of 0.2 mL of a 20% erythrocyte suspension in PBS was mixed with 0.2 mL of PBS (absorbance A) or diosmetin (absorbance B) at different concentrations. The mixture was incubated at 37 °C for 20 min with gentle shaking, after which 0.4 mL of 200 mM AAPH was added, and the incubation continued at the same temperature for another 2 h. Finally, the reaction solution was diluted with 8 mL of PBS and centrifuged at 1200*g* for 10 min at 4 °C. The absorbance of the supernatant was measured at 540 nm. To achieve complete hemolysis, 8 mL of ultrapure water was added to the mixture, which was then centrifuged at 1200*g* for 10 min at 4 °C, and the absorbance of the supernatant was determined at 540 nm. The percentage of hemolysis inhibition was calculated as

$$\%\ \text{hemolysis inhibition} = (1 - A/B) \times 100\%$$

where *A* refers to the absorbance A and *B* refers to absorbance B as metioned above.

**Plasma Oxidation Assay.** Plasma samples were obtained from blood by centrifugation at 1200*g* for 10 min at 4 °C and then diluted 40-fold with PBS and stored at 4 °C until use. Then 0.2 mL of plasma was mixed with 0.2 mL of PBS or diosmetin at different concentrations and incubated at 37 °C for 20 min with gentle shaking. Subequently, 0.4 mL of 200 $\mu$M $CuCl_2$ was added as oxidant and the incubation continued for another 2 h. Levels of conjugated dienes were determined every 10 min by measuring absorption at 245 nm.

**Scanning Electron Microscopy (SEM).** Erythrocyte imaging was carried out using a scanning electron microscope (Hitachi TM3000, Hitachi Ltd., Tokyo, Japan). A film consisting of a single layer of red blood cells was made by spreading the treated blood samples onto newly split mica and settled with 2.5% glutaraldehyde, after which the film was placed on the specimen holder and images of blood samples were acquired.

**Determination of Intracellular ROS Level.** A ROS assay kit with DCFH-DA as a fluorescent probe was used to determine the relative levels of intracellular ROS. Treated red blood cells were collected by centrifuging at 1200*g* for 10 min at 4 °C, washed three times with PBS, and then incubated at 37 °C for 20 min in the presence of 10 $\mu$M DCFH-DA. DCFH-DA is transformed to the fluorescent compound 2′,7′-dichlorofluorescin (DCF) within cells. The fluorescence intensity of cells was measured using a Fluoroskan Ascent microplate fluorometer (ex/em, 488/525 nm).

**MDA, GPx, SOD, and CAT Assays.** Red blood cells were collected and washed as described above. Cells were then resuspended in 600 $\mu$L of cold ultrapure water and stored at −80 °C before determination. A BCA protein assay kit and microscale MDA kit were used to monitor the protein and MDA contents, respectively. The Cellular Glutathione Peroxidase Kit, Total Superoxide Dismutase Assay Kit, and Catalase Assay Kit were used to measure the activities of GPx, SOD, and CAT according to the manufacturer's instructions.

**Statistics.** Experiments were carried out in triplicate, and all data are reported as the mean ± standard deviation (SD). The significant differences between the means of parameters were calculated by Duncan's multiple-range test ($p < 0.05$) using SPSS 17.0 software (SPSS, Inc., Chicago, IL, USA).

## RESULTS AND DISCUSSION

**Cellular Antioxidant Activity of Diosmetin.** The intracellular antioxidant activity of diosmetin was evaluated using the CAA assay, which was regarded as a more biologically relevant assay than commonly used chemical antioxidant activity assays.[26] For the CAA assay, the membrane-permeable intracellular probe DCFH-DA was deacetylated to DCFH by cellular esterases in HepG2 cells. DCFH was then trapped within the cells and oxidated by peroxyl radicals generated from

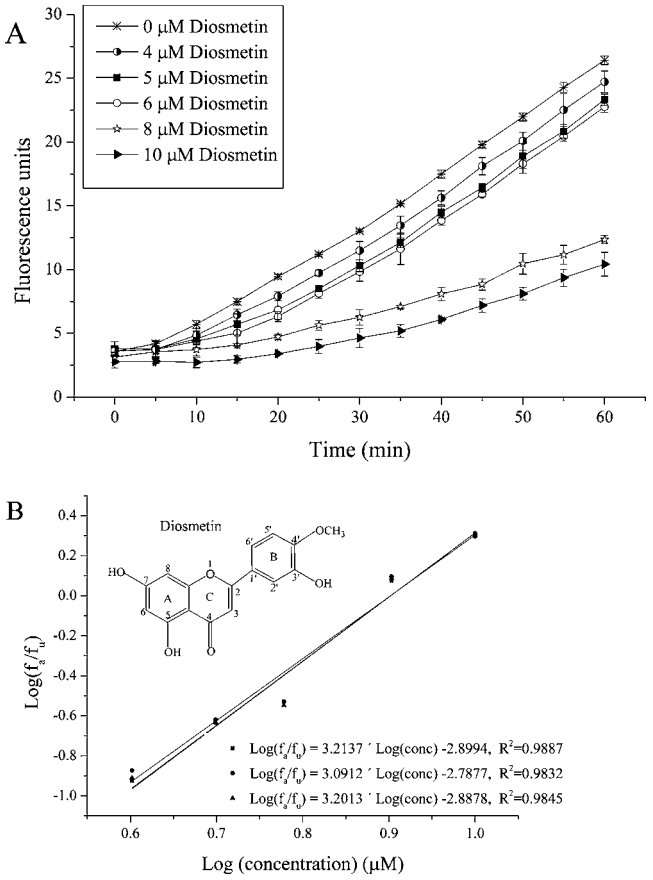


**Figure 1.** Inhibitory effects of diosmetin on peroxyl radical-induced oxidation of DCFH in HepG2 cells (A) and $EC_{50}$ plots for inhibition of peroxyl radical-induced DCFH oxidation by diosmetin (B).

**Table 1. $EC_{50}$ Value and CAA Value of the Inhibitory Effect of Diosmetin on AAPH-Induced DCFH Oxidation at Different Concentrations (2−10 μmol)**

| compound | $EC_{50}$ (μmol) | CAA (μmol QE[b]/100 μmol diosmetin) |
|---|---|---|
| quercetin | 4.626 ± 0.272 | |
| diosmetin | 7.98 ± 0.003 | 58.0 ± 0.019 |
| EGCG | 15.8 ± 0.4 | 33.1 ± 1.0[17] |
| myricetin | 15.4 ± 0.5 | 36.8 ± 3.8[17] |
| luteolin | 23.1 ± 1.0 | 32.3 ± 0.9[17] |
| kaempferol | 6.31 ± 0.21 | 81.1 ± 2.7[17] |

[b]QE, quercetin equivalents.

AAPH to form a fluorescent substance, DCF. The level of fluorescence was proportional to the degree of oxidation. The reduction of cellular fluorescence compared to the control group indicates the antioxidant activity of the tested samples.[27−29]

The kinetics of DCFH oxidation induced by AAPH are shown in Figure 1A. It was found that diosmetin significantly inhibited this oxidation process in a dose-dependent manner as indicated by the obvious decrease of the fluorescence level. The $EC_{50}$ for the inhibitory action of diosmetin on DCFH oxidation was calculated from the median effect curve plotted for each concentration (Figure 1B). On the basis of the fitting curves, the CAA value of diosmetin was determined (Table 1). Quercetin was used as a standard, as it has already been shown previously to have high CAA capacity compared to other

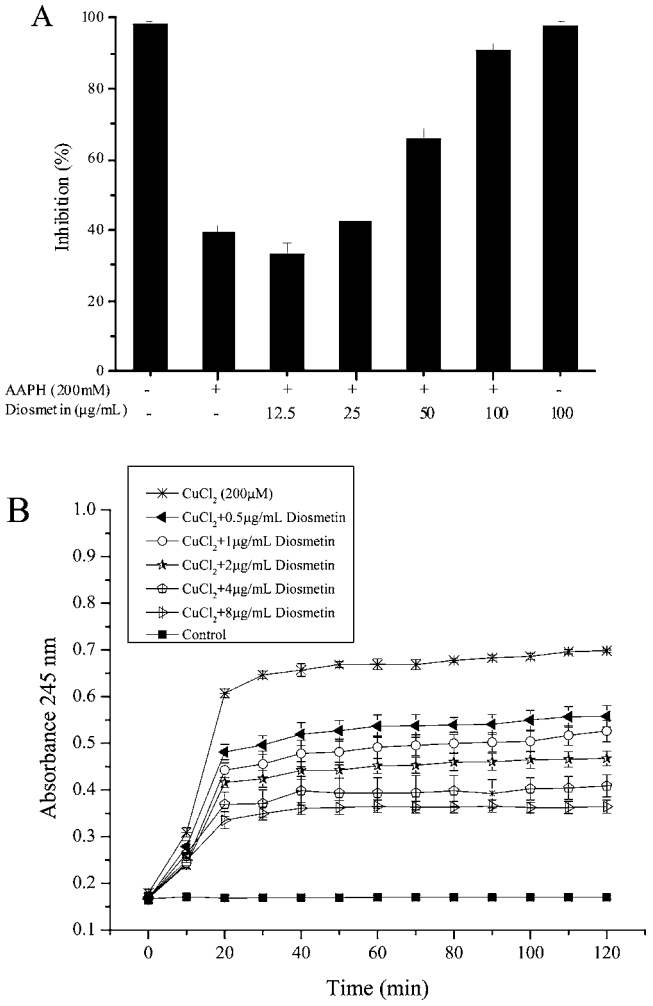


**Figure 2.** Protective effects of diosmetin on AAPH-induced erythrocyte hemolysis assay (A) and $CuCl_2$-induced accumulation of conjugated dienes in plasma (B). Erythrocytes were pretreated with different concentrations (12.5−100 μg/mL) of diosmetin for 25 min prior to AAPH (200 mM) treatment for 2 h; the positive group was treated with 200 mM AAPH only. Plasma was pretreated with different concentrations (0.5−8 μg/mL) of diosmetin for 10 min prior to $CuCl_2$ (200 μM) treatment for 2 h. The positive group was treated with 200 μM $CuCl_2$ only.

known phytochemicals such as kaempferol, myricetin, epigallocatechin gallate (EGCG) and luteolin.[16]

The $EC_{50}$ value of diosmetin was 7.98 ± 0.20 μmol, and the CAA value of diosmetin was 58.0 ± 0.02 μmol QE/100 μmol diosmetin, which is higher than those of EGCG (33.1 ± 1.0 μmol of QE/100 μmol), myricetin (36.8 ± 3.8 μmol of QE/100 μmol), and luteolin (32.3 ± 0.9 μmol of QE/100 μmol), and lower than that of only kaempferol (81.1 ± 2.7 μmol of QE/100 μmol), as reported by Wolfe et al.,[17] indicating that diosmetin had strong cellular antioxidant activity. This high activity probably results from the chemical structure of the diosmetin molecule (Figure 1B). It has three hydroxyl groups, one each attached to C3′, C5, and C7. Of these, the hydroxyl group attached to C3′ has the most positive effect on the free radical scavenging activity of diosmetin.[30] The 2,3-double bond conjugated with a 4-oxo group in the C ring of diosmetin also contributes significant activity against oxidation by $H_2O_2$.[29]

**Attenuation of Erythrocyte Hemolysis and Plasma Oxidation by Diosmetin.** The antioxidant ability of


dx.doi.org/10.1021/jf502359x | J. Agric. Food Chem. 2014, 62, 8648−8654

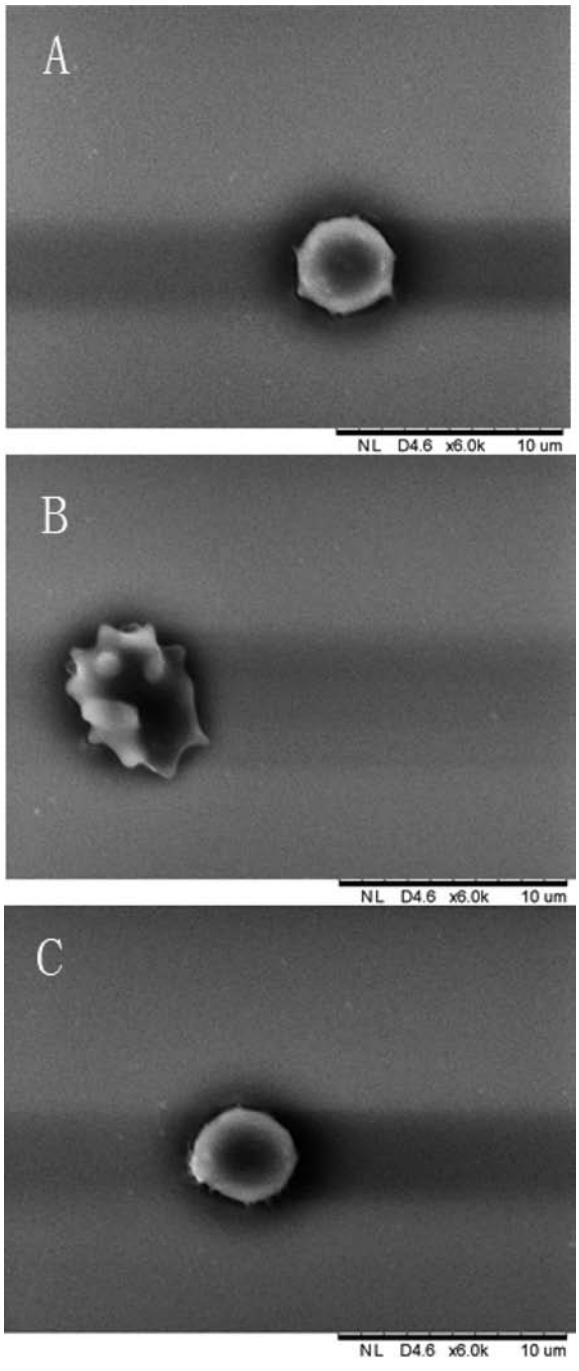


**Figure 3.** SEM micrographs of erythrocyte samples: (A) normal erythrocyte; (B) AAPH-treated erythrocyte; (C) erythrocyte pre-incubated with diosmetin prior to AAPH treatment.

diosmetin was further examined using erythrocyte hemolysis and plasma oxidation assays. In the erythrocyte hemolysis assay, AAPH, which can decompose at 37 °C to generate an alkyl radical, is used as an initiator. In the presence of oxygen, these alkyl radicals will be converted to peroxyl radicals that can cause lipid peroxidation and loss of erythrocyte membrane integrity, which could ultimately lead to hemolysis. Therefore, the rate of inhibition of hemolysis is an indirect way to measure the antioxidant activity of diosmetin. As shown in Figure 2A, erythrocyte hemolysis induced by AAPH was effectively attenuated by diosmetin in a dose-dependent manner: the inhibition rate was enhanced as diosmetin concentration

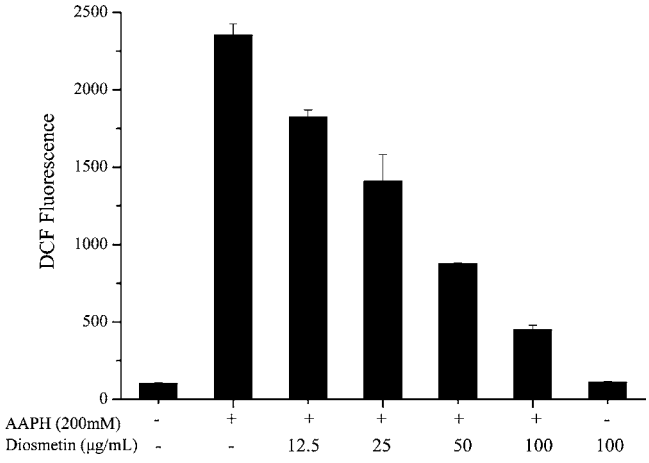


**Figure 4.** Inhibitory activity of diosmetin on AAPH-induced ROS overexpression in human erythrocytes. Erythrocytes were pretreated with different concentrations (12.5−100 μg/mL) of diosmetin for 30 min prior to AAPH (200 mM) treatment for 2 h; the positive group was treated with 200 mM AAPH only.

increased from 0 to 100 μg/mL. At a dose of 100 μg/mL, the inhibition rate of diosmetin on erythrocyte hemolysis was 91.0%, which was comparable to that of vitamin C, a well-known antioxidant with an inhibition rate of 96.9% at 1 mg/mL (data not shown).

Using SEM, we examined the morphological effect of oxidation on the red cell membranes with or without the addition of diosmetin. The normal biconcave discoid shape of erythrocytes can be clearly seen in Figure 3A. After treatment with AAPH, the erythrocyte lost its normal profile and showed a spiny configuration on its surface due to the severe damage of the cell membrane (Figure 3B). However, this damage was dramatically reduced in cells pretreated with 100 μg/mL diosmetin before the addition of AAPH (Figure 3C). This result confirmed the protective effect of diosmetin on AAPH-induced morphological changes in the red cell.

Lipoprotein oxidation in plasma has great pathological significance on atherosclerosis and hyperlipemia. Oxidation of low-density lipoprotein (LDL) is thought to be a great contributing factor to the development of atherosclerosis, whereas oxidation of high-density lipoprotein (HDL) may lead to hypercholesterolemia.[31] In a further test of the antioxidant activity of diosmetin, we used the plasma oxidation assay, where plasma is treated with $CuCl_2$, which can induce the formation of conjugated dienes. As shown in Figure 2B, the concentration of conjugated dienes increases over time. Diene accumulation, a hallmark of lipid peroxidation, was induced when plasma was treated with 200 μM copper(II) ions, as indicated by the high absorbance value at 245 nm. Diosmetin at different concentrations (0.5, 1.0, 2.0, 4.0, and 8.0 μg/mL) could significantly decrease copper-induced diene accumulation, which showed indirect protection of plasma from oxidative damage. Again, dose dependence could be demonstrated.

**Diosmetin Inhibits AAPH-Induced ROS Generation in Erythrocytes.** The antioxidant protection of erythrocytes by diosmetin is considered to be due to its effect on intracellular ROS generation.[32] To further test this, intracellular ROS generation was quantified using DCFH-DA, a fluorescein-labeled dye that can cross the plasma membrane into the cytoplasm, where it is hydrolyzed by nonspecific esterases to nonfluorescent DCFH. In the presence of ROS, DCFH is

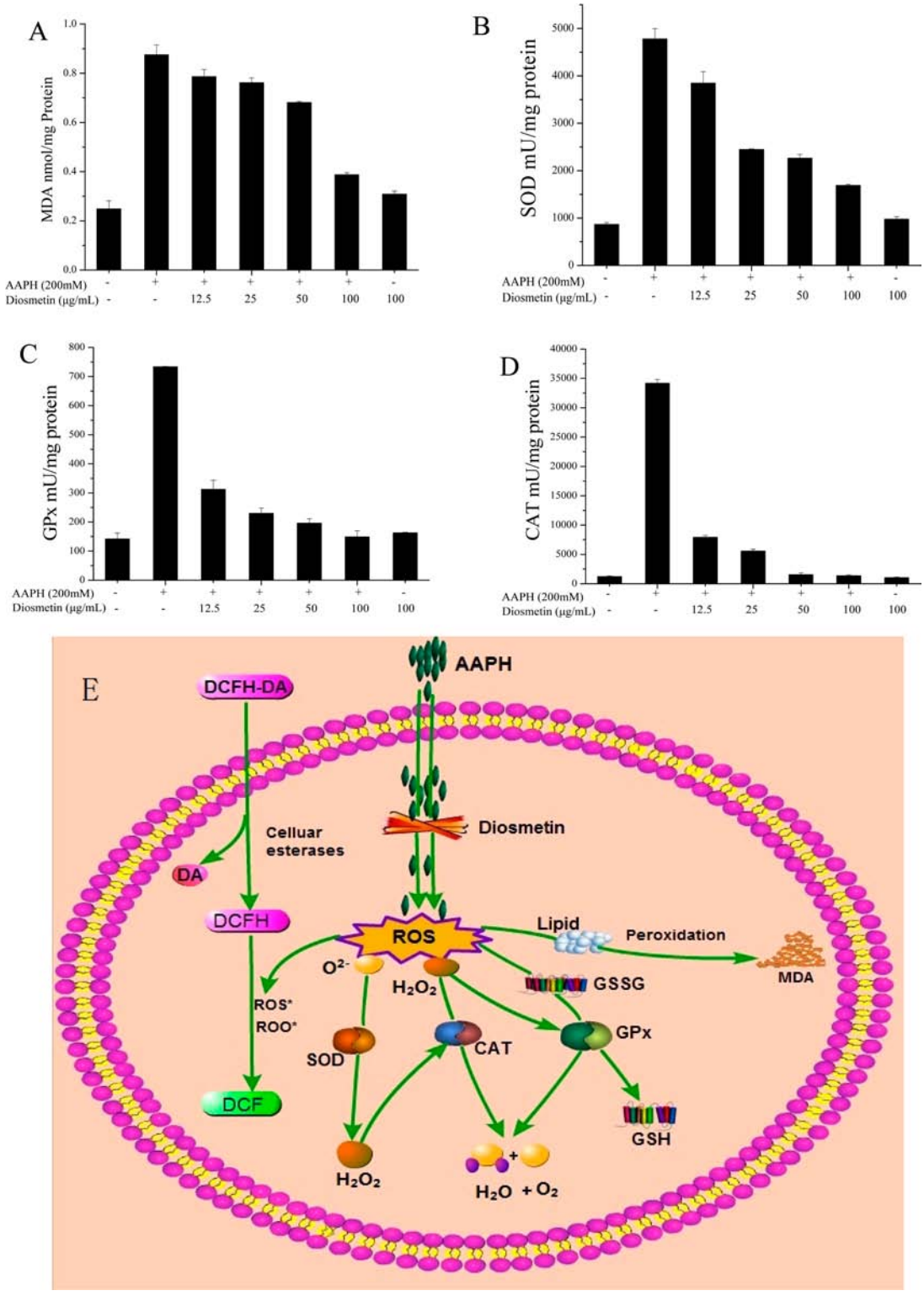


**Figure 5.** Changes in MDA content (A) and enzyme activities of SOD (B), GPx (C), and CAT (D) in erythrocytes. Erythrocytes were pretreated with different concentrations (12.5−100 μg/mL) of diosmetin for 30 min prior to AAPH (200 mM) treatment for 2 h; the positive group was treated with 200 mM AAPH only. (E) Possible intracellular antioxidant detoxifying mechanisms of diosmetin that attenuate AAPH-induced oxidative stress through inhibition of ROS generation.

oxidized to DCF, a highly fluorescent compound. Therefore, inhibition by diosmetin of AAPH-induced ROS generation can be measured by the ability of the diosmetin to prevent the oxidation of DCFH and, as a result, the formation of DCF. As shown in Figure 4, the DCF fluorescence intensity of erythrocytes exposed to AAPH (200 mM) was much higher than that of the control, demonstrating that AAPH treatment produced a large amount of ROS. However, cells pretreated with diosmetin (12.5, 25, 50, and 100 μg/mL) exhibited apparently lower DCF fluorescence intensity in a dose-


dx.doi.org/10.1021/jf502359x | J. Agric. Food Chem. 2014, 62, 8648−8654

dependent manner, indicating that diosmetin inhibited ROS generation. As a control, cells treated with diosmetin without AAPH addition did not show significantly different DCF fluorescence, implying that diosmetin itself did not cause ROS generation in normal erythrocytes. Taken together, these results confirm that diosmetin can reduce intracellular oxidative stress.

**Diosmetin Prevents AAPH-Induced MDA Accumulation and Modulates Intracellular Antioxidant Enzyme (GPx, SOD, and CAT) Activities.** AAPH-induced ROS generation can cause lipid peroxidation and result in the release of MDA. MDA is involved in tumor promotion, cellular metabolism disruption, and cell membrane dysfunction due to its high reactivity. Excess MDA can ultimately lead to disruption of cellular metabolism.[32] As seen in Figure 5A, the MDA level in erythrocytes was significantly increased from 0.25 to 0.87 nmol/mg protein after treatment with 200 mM AAPH for 2 h, indicating the occurrence of lipid peroxidation caused by AAPH-induced oxidative stress. For the cells incubated with different concentrations of diosmetin (12.5, 25, 50, and 100 $\mu$g/mL), the level of MDA in erythrocytes was decreased, especially at the high diosmetin concentration (100 $\mu$g/mL), where the MDA concentration declined almost to that of the control. For cells incubated with diosmetin without AAPH supplementation, the MDA level was comparable to that of the control, showing that diosmetin itself does not induce MDA formation. Thus, lipid peroxidation caused by ROS generation was efficiently inhibited by diosmetin.

Major radical scavenging antioxidant enzymes in the human body include SOD, GPx, and CAT. These enzymes constitute an intracellular defense system, which can coordinate the elimination of free radicals through a series of chain reactions. Changes in the activities of these antioxidant enzymes may be related to the cell's antioxidant response. The intracellular level of these antioxidants is crucial for maintaining a steady state of superoxide radicals and hydrogen peroxide.[33,34] SOD can catalyze the dismutation of the highly reactive superoxide anion $O_2^{\bullet-}$ into $O_2$ and hydrogen peroxide ($H_2O_2$), which is less reactive. CAT converts the $H_2O_2$ generated within cells to $H_2O$ and $O_2$ and prevents the conversion of $H_2O_2$ into more active species, such as hydroxyl radicals ($^{\bullet}OH$), which can ultimately lead to cell death. As for GPx, it catalyzes the reaction of hydroperoxides with glutathione (GSH), thereby protecting cells from oxidative damage. As shown in panels B, C, and D of Figure 5, the activities of SOD, GPx, and CAT in erythrocytes were significantly increased after 200 mM AAPH treatment for 2 h, showing that AAPH treatment activated the enzymatic antioxidant defense systems in erythrocytes.

The cellular antioxidant system depends on quenching of $O_2^{\bullet-}$ by SOD and further protection by CAT to convert $H_2O_2$ to $H_2O$ (Figure 5E). Pretreatment with diosmetin provided effective control of red cell antioxidant defense systems as indicated by the lower GPx (Figure 5B), SOD (Figure 5C), and CAT (Figure 5D) levels. This was particularly the case for high (100 $\mu$g/mL) diosmetin treatment, which maintained enzyme activities at normal levels. Thus, diosmetin can effectively attenuate AAPH-induced oxidative stress in erythrocytes, mainly through the inhibition of ROS generation, as illustrated in Figure 5E.

In conclusion, in a cell-based CAA assay, diosmetin efficiently attenuated AAPH-induced oxidative stress in human erythrocytes. Diosmetin prevented the generation of intracellular ROS, inhibited the formation of MDA, and regulated intracellular antioxidant enzyme (GPx, SOD, and CAT) activities. The particular chemical structure of diosmetin, for example, the hydroxyl group attached to C3′ and the 2,3-double bond conjugated with a 4-oxo group in the C ring, contributes significantly to its antioxidant activity. Diosmetin effectively attenuated AAPH-induced oxidative stress in erythrocytes and plasma by inhibition of intracellular ROS generation. It also significantly decreased copper-induced diene accumulation and protected plasma from oxidative damage. Because oxidative stress is involved in the pathogenesis of a number of chronic diseases including heart disease, cancer, type 2 diabetes, and inflammatory diseases,[35] our results demonstrated that diosmetin could be good candidate for the treatment of diseases in which ROS overproduction is the etiological factor. It can be developed either as functional foods or as complementary medicines.

## AUTHOR INFORMATION


### Corresponding Authors

*(J.Y.) Phone: (+86) 20-87112594. E-mail: yangjg@scut.edu.cn,.

*(J.R.) Phone: (+86) 20-87112594. E-mail: jyren@scut.edu.cn.



### Funding

This study was supported by the National Key Technology R&D Program of China in the 12th five-year period (No. 2012BAD33B11), the Fundamental Research Funds for the Central Universities (No. 2014ZZ0063 and 2013ZZ0061), and Guangdong Natural Science Funds for Distinguished Young Scholars (No.S2013050013954).

### Notes

The authors declare no competing financial interest.


## ACKNOWLEDGMENTS


We express thanks to Professor Alan Tunnacliffe, Department of Chemical Engineering and Biotechnology, University of Cambridge, for improvement of writing.


## REFERENCES


(1) Patel, K.; Gadewar, M.; Tahilyani, V.; Patel, D. K. A review on pharmacological and analytical aspects of diosmetin: a concise report. *Chin. J. Integr. Med.* **2013**, *19*, 792−800.

(2) Bae, E.; Kim, D. H. In vitro anti-*Helicobacter pylori* activity of some flavonoids and their metabolites. *Planta Med.* **1999**, *65*, 442−443.

(3) Chan, B. C.; Ip, M.; Gong, H.; Lui, S. L.; See, R. H.; Jolivalt, C.; Fung, K. P.; Leung, P. C.; Reiner, N. E.; Lau, C. Synergistic effects of diosmetin with erythromycin against ABC transporter over-expressed methicillin-resistant *Staphylococcus aureus* (MRSA) RN4220/pUL5054 and inhibition of MRSA pyruvate kinase. *Phytomedicine* **2013**, *20*, 611−614.

(4) Meng, J. C.; Zhu, Q. X.; Tan, R. X. New antimicrobial mono- and sesquiterpenes from *Soroseris hookeriana* subsp. *erysimoides*. *Planta Med.* **2000**, *66*, 541−544.

(5) Seelinger, G.; Merfort, I.; Schempp, C. M. Anti-oxidant, anti-inflammatory and anti-allergic activities of luteolin. *Planta Med.* **2008**, *74*, 1667−1677.

(6) Lyseng-Williamson, K. A.; Perry, C. M. Micronised purified flavonoid fraction. *Drugs* **2003**, *63*, 71−100.

(7) Comalada, M.; Ballester, I.; Bailón, E.; Sierra, S.; Xaus, J.; Gálvez, J.; Medina, F. S. D.; Zarzuelo, A. Inhibition of pro-inflammatory markers in primary bone marrow-derived mouse macrophages by naturally occurring flavonoids: analysis of the structure−activity relationship. *Biochem. Pharmacol.* **2006**, *72*, 1010−1021.

(8) Yang, M.; Tanaka, T.; Hirose, Y.; Deguchi, T.; Mori, H.; Kawada, Y. Chemopreventive effects of diosmein and hesperidin on *N*-butyl-*N*-(4-hydroxybutyl)nitrosamine-induced urinary-bladder carcinogenesis in male ICR mice. *Int. J. Cancer* **1997**, *73*, 719−724.
(9) Kuntz, S.; Wenzel, U.; Daniel, H. Comparative analysis of the effects of flavonoids on proliferation, cytotoxicity, and apoptosis in human colon cancer cell lines. *Eur. J. Nutr.* **1999**, *38*, 133−142.
(10) Tanaka, T.; Makita, H.; Kawabata, K.; Mori, H.; Kakumoto, M.; Satoh, K.; Hara, A.; Sumida, T.; Fukutani, K.; Ogawa, H. Modulation of *N*-methyl-*N*-amylnitrosamine-induced rat oesophageal tumourigenesis by dietary feeding of diosmin and hesperidin, both alone and in combination. *Carcinogenesis* **1997**, *18*, 761−769.
(11) Tanaka, T.; Makita, H.; Ohnishi, M.; Mori, H.; Satoh, K.; Hara, A.; Sumida, T.; Fukutani, K.; Tanaka, T.; Ogawa, H. Chemoprevention of 4-nitroquinoline 1-oxide-induced oral carcinogenesis in rats by flavonoids diosmin and hesperidin, each alone and in combination. *Cancer Res.* **1997**, *57*, 246−252.
(12) Tanaka, T.; Makita, H.; Kawabata, K.; Mori, H.; Kakumoto, M.; Satoh, K.; Hara, A.; Sumida, T.; Ogawa, H. Chemoprevention of azoxymethane-induced rat colon carcinogenesis by the naturally occurring flavonoids, diosmin and hesperidin. *Carcinogenesis* **1997**, *18*, 957−965.
(13) Poór, M.; Veres, B.; Jakus, P. B.; Antus, C.; Montskó, G.; Zrínyi, Z.; Vladimir-Knežević, S.; Petrik, J.; Kőszegi, T. Flavonoid diosmetin increases ATP levels in kidney cells and relieves ATP depleting effect of ochratoxin A. *J. Photochem. Photobiol. B* **2014**, *20*, 1011−1344.
(14) Moon, Y. J.; Wang, X.; Morris, M. E. Dietary flavonoids: effects on xenobiotic and carcinogen metabolism. *Toxicol. in Vitro* **2006**, *20*, 187−210.
(15) Williams, R. J.; Spencer, J. P.; Rice-Evans, C. Flavonoids: antioxidants or signalling molecules? *Free Radical Biol. Med.* **2004**, *36*, 838−849.
(16) Hodek, P.; Trefil, P.; Stiborová, M. Flavonoids-potent and versatile biologically active compounds interacting with cytochromes P450. *Chem.−Biol. Interact.* **2002**, *139*, 1−21.
(17) Wolfe, K. L.; Liu, R. H. Cellular antioxidant activity (CAA) assay for assessing antioxidants, foods, and dietary supplements. *J. Agric. Food Chem.* **2007**, *55*, 8896−8907.
(18) Manna, C.; Galletti, P.; Cucciolla, V.; Montedoro, G.; Zappia, V. Olive oil hydroxytyrosol protects human erythrocytes against oxidative damages. *J. Nutr. Biochem.* **1999**, *10*, 159−165.
(19) Takenaka, Y.; Miki, M.; Yasuda, H.; Mino, M. The effect of α-tocopherol as an antioxidant on the oxidation of membrane protein thiols induced by free radicals generated in different sites. *Arch. Biochem. Biophys.* **1991**, *285*, 344−350.
(20) Joshi, G.; Perluigi, M.; Sultana, R.; Agrippino, R.; Calabrese, V.; Butterfield, D. A. In vivo protection of synaptosomes by ferulic acid ethyl ester (FAEE) from oxidative stress mediated by 2,2-azobis(2-amidinopropane) dihydrochloride (AAPH) or $Fe^{2+}/H_2O_2$: insight into mechanisms of neuroprotection and relevance to oxidative stress-related neurodegenerative disorders. *Neurochem. Int.* **2006**, *48*, 318−327.
(21) Brand, M. D.; Affourtit, C.; Esteves, T. C.; Green, K.; Lambert, A. J.; Miwa, S.; Pakay, J. L.; Parker, N. Mitochondrial superoxide: production, biological effects, and activation of uncoupling proteins. *Free Radical Biol. Med.* **2004**, *37*, 755−767.
(22) Maria, V. L.; Bebianno, M. J. Antioxidant and lipid peroxidation responses in *Mytilus galloprovincialis* exposed to mixtures of benzo-(a)pyrene and copper. *Comp. Biochem. Physiol. C* **2011**, *154*, 56−63.
(23) Wu, S.; Pang, F.; Wen, Y.; Zhang, H.; Zhao, Z.; Hu, J. Antiproliferative and apoptotic activities of linear furocoumarins from *Notopterygium incisum* on cancer cell lines. *Planta Med.* **2010**, *76*, 82−85.
(24) Wang, L.; Chen, J.; Xie, H.; Ju, X.; Liu, R. H. Phytochemical profiles and antioxidant activity of adlay varieties. *J. Agric. Food Chem.* **2013**, *61*, 5103−5113.
(25) Cheung, L. M.; Cheung, P. C.; Ooi, V. E. Antioxidant activity and total phenolics of edible mushroom extracts. *Food Chem.* **2003**, *81*, 249−255.
(26) Song, W.; Derito, C. M.; Liu, M. K.; He, X.; Dong, M.; Liu, R. H. Cellular antioxidant activity of common vegetables. *J. Agric. Food Chem.* **2010**, *58*, 6621−6629.
(27) Wolfe, K. L.; Liu, R. H. Cellular antioxidant activity (CAA) assay for assessing antioxidants, foods, and dietary supplements. *J. Agric. Food Chem.* **2007**, *55*, 8896−8907.
(28) Wolfe, K. L.; Kang, X.; He, X.; Dong, M.; Zhang, Q.; Liu, R. H. Cellular antioxidant activity of common fruits. *J. Agric. Food Chem.* **2008**, *56*, 8418−8426.
(29) Wolfe, K. L.; Liu, R. H. Structure−activity relationships of flavonoids in the cellular antioxidant activity assay. *J. Agric. Food Chem.* **2008**, *56*, 8404−8411.
(30) Magnani, L.; Gaydou, E. M.; Hubaud, J. C. Spectrophotometric measurement of antioxidant properties of flavones and flavonols against superoxide anion. *Anal. Chim. Acta* **2000**, *411*, 209−216.
(31) Rifici, V. A.; Khachadurian, A. K. Effects of dietary vitamin C and E supplementation on the copper mediated oxidation of HDL and on HDL mediated cholesterol efflux. *Atherosclerosis* **1996**, *127*, 19−26.
(32) Roche, M.; Tarnus, E.; Rondeau, P.; Bourdon, E. Effects of nutritional antioxidants on AAPH-or AGEs-induced oxidative stress in human SW872 liposarcoma cells. *Cell Biol. Toxicol.* **2009**, *25*, 635−644.
(33) Ohta, Y.; Ohashi, K.; Matsura, T.; Tokunaga, K.; Kitagawa, A.; Yamada, K. Octacosanol attenuates disrupted hepatic reactive oxygen species metabolism associated with acute liver injury progression in rats intoxicated with carbon tetrachloride. *J. Clin. Biochem. Nutr.* **2008**, *42*, 118−125.
(34) Mittler, R. Oxidative stress, antioxidants and stress tolerance. *Trends Plant Sci.* **2002**, *7*, 405−410.
(35) Valko, M.; Leibfritz, D.; Moncol, J.; Cronin, M. T. D.; Mazur, M.; Telser, J. Free radicals and antioxidants in normal physiological functions and human disease. *Int. J. Biochem. Cell B* **2007**, *39*, 44−84.

JOURNAL OF AGRICULTURAL AND FOOD CHEMISTRY

Article

pubs.acs.org/JAFC

# Preparation of Novel Cross-Linked and Octylated Caseinates Using a Biphasic Enzymatic Procedure and Their Functional Properties

Yaqiong Zhang,[†] Yuge Niu,*[,†] Fangyi Yao,[†] Bona Dai,[‡] Qin Wang,[§] and Liangli (Lucy) Yu*[,†,§]

[†]Institute of Food and Nutraceutical Science, School of Agriculture and Biology and [‡]Instrumental Analysis Center, Shanghai Jiao Tong University, Shanghai 200240, China

[§]Department of Nutrition and Food Science, University of Maryland, 0112 Skinner Building, College Park, Maryland 20742, United States

Supporting Information

**ABSTRACT:** A novel microbial transglutaminase-catalyzed aqueous−organic biphasic reaction system was successfully developed to prepare caseinate derivatives by cross-linking and incorporating nonpolar octyl tails for the first time. SDS-PAGE and $^1$H NMR analysis confirmed that cross-linking and octyl conjugation occurred simultaneously. The octyl substitution degree (SD) was measured by $^1$H NMR and used as an index to determine a suitable reaction condition. It was found that at the condition of 0.125% (w/v) protein concentration and 6 h of reaction time, the modified caseinate had the highest SD of 28.96%. The modified caseinate also had an increased surface hydrophobicity, better emulsifying activity, and improved thermal and salt stabilities. However, its emulsion stability or in vitro enzymatic digestibility was slightly lower than that of the native caseinate.

**KEYWORDS:** *sodium caseinate, octylamine, microbial transglutaminase, biphasic system, functional properties*

## INTRODUCTION

Milk proteins are widely used in the food industry. As a major protein fraction in the milk, casein provides many important functions for processed foods, including film-forming,[1] emulsifying,[2] foaming,[3] and microencapsulating capacities.[4] The further improvement in functional properties through physical, chemical, or enzymatic modification might increase and extend the applicability of casein in different food systems. Among various modifications applied to casein, the interaction between casein and reducing sugars through Maillard reaction has been widely studied and shown to produce marked changes in the functional properties, such as solubility,[5] antioxidant,[6] foam and emulsion stability,[7] and heat stability,[8] as well as micro- and nanoencapsulating properties.[9,10] However, the Maillard reaction of food proteins might generate mutagenic compounds and undesired color, consequently affecting the sensory attributes of the final product or causing safety issues.[11,12] Therefore, the enzymatic approach, which requires milder reaction conditions, allows for easier control of the extent of the reaction, and yields minimal formation of byproduct, is much more preferable.[13]

Transglutaminase (TGase, EC 2.3.2.13) catalyzes an acyl-transferring reaction in which $\varepsilon$-($\gamma$-glutamyl) lysine bonds are formed using the $\gamma$-carboxyamide groups of peptide-bound glutamine residues and the amino groups of lysine side chains.[14,15] Transglutaminase is mainly classified into the microbial transglutaminase (MTGase) derived from *Streptomyces mobaraensis*, and the tissue transglutaminase (TGase), such as guinea pig liver transglutaminase. MTGase has several essential advantages in comparison to TGase, such as lower molecular weight, calcium-independent, and broader suitable pH and temperature ranges.[16] The effect of TGase-induced cross-linking through the formation of $\varepsilon$-($\gamma$-glutamyl) lysine intra- and intermolecular cross-links on the functional properties of various food proteins has been investigated. Treatment of millet protein by TGase was found to improve the heat stability and emulsifying capacity of the protein.[17] The cross-linked soy protein prepared using TGase as the catalyst was able to act as an effective wall-forming agent and increase the storage stability and emulsion-controlled release behavior.[18] Besides cross-linking of natural proteins, many attempts were made to incorporate lysine alternatives into protein, such as lysine analogue $\omega$-amino acids,[16] glucosamine,[19] and oligosaccharide using alkylamine as an alkyl donor.[20] Moreover, Ohtsuka et al. investigated the substrate specificity of TGase for aliphatic primary amines and suggested that four carbon atoms or more are required for an aliphatic primary amine without side chains to be a substrate for TGase.[21] The ability to arbitrarily incorporate various functional groups into the glutamine residues of proteins using TGase would allow for the introduction of nonpolar tails into a protein molecule or cross-links within and between protein molecules. However, the propensity of TGase to interact with a protein substrate is also dependent upon its molecular structure and conformation through altering the accessibility of its glutamine and lysine residues.[22] It has been noted that casein, a flexible random coil protein, is an excellent target protein for TGase.[23]

In fact, the incorporation of nonpolar groups into protein macromolecules may improve their surface activity dramatically.[24] Casein is a block copolymer comprising blocks containing hydrophobic and hydrophilic amino acid residues. Therefore, casein exhibits a strong tendency to self-assemble into casein micelles. Through the chemical reaction of casein

Received: May 25, 2014
Revised: July 31, 2014
Accepted: August 4, 2014
Published: August 4, 2014

ACS Publications © 2014 American Chemical Society

with fatty acids, casein derivatives exhibited better surface tension, wetting ability, and foaming properties than native casein.[25] Nevertheless, there is little information in the literature on modifying casein with nonpolar groups by using a TGase-induced enzymatic method. This may be because TGase generally catalyzes a reaction in aqueous systems, whereas nonpolar groups have little solubility in water, thus greatly impairing the reaction efficiency. On the other hand, the biphasic reaction system is widely used in peptide synthesis and enzymatic hydrolysis to overcome insolubility of substrates, unfavorable thermodynamic equilibrium, difficult product recovery, and enzyme inhibition by reagents and/or products.[26,27]

Therefore, the present work tried for the first time to use a commercial microbial transglutaminase (MTGase) as a biocatalytic agent, sodium caseinate as the acyl donor, and octylamine as the acyl acceptor in an aqueous−organic biphasic system to modify caseinate and obtain cross-linked and octyl-conjugated caseinate derivatives. The effects of reaction conditions on the substitution degree of octyl groups in the modified caseinates were also investigated using a $^1$H NMR-based analysis. The physicochemical and functional properties of the modified caseinate, including surface hydrophobicity, emulsifying activity and stability, thermal and salt stabilities, and in vitro digestibility, were evaluated and compared to those of the native caseinate.

## MATERIALS AND METHODS

**Chemicals.** Sodium caseinate, octylamine (>99% purity), 8-anilino-1-naphthalenesulfonic acid (ANS, 97% purity), pepsin (≥250 units/mg solid), trypsin (≥10000 BAEE units/mg protein), and trichloroacetic acid (TCA, >99% purity) were purchased from Sigma-Aldrich Chemical Co., Ltd. (St. Louis, MO, USA). Microbial transglutaminase (MTGase) was kindly donated by Jiangsu Yiming Fine Chemical Industry Co., Ltd. (Qinxing, Jiangsu, China) with a declared activity of 100 units/g. The Bradford reagent and standard protein markers used in SDS-PAGE analysis were purchased from Bio-Rad Co. (Richmond, CA, USA). Dialysis membranes (molecular weight cutoff (MWCO) 3500 Da) were purchased from Spectrum Laboratories, Inc. (Rancho Dominguez, CA, USA). All other reagents were of analytical grade and used without further purification. Water purified with a Milli-Q system was used for all experiments.

**Developing a MTGase-Catalyzed Aqueous−Organic Biphasic Reaction Procedure for Structural Modification of Sodium Caseinate.** The modification of sodium caseinate was carried out with sodium caseinate and octylamine as the substrates and MTGase as the catalyst. The reaction mixture containing sodium caseinate in 0.1 M Tris·HCl buffer (pH 7.5) with different concentrations (0.0625, 0.125, 0.25, and 0.5% w/v) and octylamine (feed mass ratio to sodium caseinate of 1:5) in cyclohexane were added into a 250 mL conical flask with a ground-in glass stopper, and the reaction was started by adding MTGase (10 units/g sodium caseinate) to the aqueous phase and carried out in a thermostatic oscillator (SWB25, Thermo Fisher Scientific Inc., Waltham, MA, USA) at 37 °C with continuous vibration at 60 rpm. At different reaction time points (2, 4, 6, 8, and 10 h), the organic phase was removed from the reaction system, and MTGase in the aqueous phase was inactivated immediately by heat treatment at 85 °C for 10 min. The heat-treated aqueous phase was cooled rapidly to ambient temperature and dialyzed against distilled water for 48 h. The prepared samples were then lyophilized and stored at −20 °C for further study. To serve as a control, a cross-linked caseinate was also prepared under the selected conditions in the absence of octylamine. Suitable reaction conditions, including protein concentration and reaction time, were selected on the basis of the maximum substitution degree (SD) value of octyl groups introduced into the modified product and applied to prepare a modified product for further study.

**Determination of Substitution Degree.** SD values were determined by $^1$H NMR using a Bruker AVANCE III 400 MHz NMR spectrometer at 298 K. Octylamine was dissolved in $d_6$-DMSO, and protein samples were dissolved in $D_2O$ at the concentration of 0.5% (w/v), using TMS as an internal reference (0 ppm). $D_2O$ signal was suppressed by the presaturation method.[28] For the $^1$H NMR spectrum of octylamine, the parameters for observation were as follows: number of data points, 64 K; spectral width, 8223.68 Hz; acquisition time, 4.00 s; relaxation delay time, 1.0 s; number of scans, 16. The parameters for the $^1$H NMR spectra of protein samples were as follows: number of data points, 32 K; spectral width, 8012.82 Hz; acquisition time, 2.04 s; relaxation delay time, 5.0 s; number of scans, 256. An exponential line broadening (0.30 Hz), automatic phase correction, and baseline correction (degree of polynomial equal to 5) were applied to each spectrum.

**SDS-PAGE Analysis.** Protein samples were analyzed by SDS-PAGE according to a procedure reported by Jiang et al.,[19] using a 12% separating gel and a 5% stacking gel. The sample solution (0.08% w/v) was prepared in a buffer containing 2% (w/v) sodium dodecyl sulfate (SDS), 5% (v/v) $\beta$-mercaptoethanol, 10% (v/v) glycerol, 0.02% (w/v) bromophenol blue, and 70 mM Tris·HCl (pH 6.8) and heated at 95 °C for 5 min. The samples and a protein ladder were loaded into separated wells (6 μL/well). Following electrophoresis, the gels were stained with Coomassie Brilliant Blue R250 and digitized using an Epson perfection 1270 image scanner (Epson America Inc., Long Beach, CA, USA).

**Determination of Surface Hydrophobicity.** ANS fluorescence assay[29] was carried out to determine the surface hydrophobicity of native caseinate and the modified products. Protein samples (10 mg) were dissolved in 1 mL of 0.1 M phosphate buffer (pH 7.0) and stirred overnight. The sample dispersions were then centrifuged at 20000*g* for 20 min to sediment insoluble proteins. The resultant supernatants were subjected to protein content determination using the Bradford method.[30] Then, the protein solutions were diluted 10, 20, 50, 80, and 100 times to make a series of diluted protein solutions. The ANS (100 μg/mL) was prepared in the same buffer and filtered through a 0.22 μm Acrodisc syringe filter membrance (Pall Co., Newquay, UK). The diluted protein solutions were mixed with the same volume of ANS solution. After 1 h of incubation at 25 °C (HERATHERM Incubator, Thermo Fisher Scientific Inc.), the mixture was observed for its fluorescence intensity (FI) on a TECAN Infinite M200 PRO multilabel plate reader (Tecan Group Ltd., Mannedorf, Switzerland). The excitation and emission wavelengths were 355 and 460 nm, respectively. For each protein sample, a linear regression equation was established for FI versus protein concentration ($R^2$ > 0.99), and the slope ($S_0$) was used as an index for surface hydrophobicity.

**Thermogravimetry/Derivative Thermogravimetry (TG/DTG) Determination.** TG/DTG analysis of protein samples was performed in a Pyris 1 TGA device by PerkinElmer (Santa Clara, CA, USA) in the temperature range from 30 to 600 °C, using platinum crucibles with ∼5 mg of samples, under a dynamic nitrogen atmosphere (20 mL/min) and heating rate of 10 °C/min.

**Determination of Emulsifying Capacity.** The emulsifying capacity of the protein samples was evaluated by assessing the emulsifying activity index (EAI) and emulsion stability index (ESI) using a classic turbidimetric method.[31] To prepare emulsions, 1.0 mL of soybean oil and 3.0 mL of a protein solution (0.2% w/v) in 0.1 M phosphate buffer (pH 7.0) were homogenized with a high-speed homogenizer (VWR VDI 12, Radnor, PA, USA) at 12000 rpm for 1 min. The freshly prepared emulsion (50 μL) was taken from the bottom of the beaker and dispersed into 5 mL of 0.1% (w/v) SDS solution. The absorbance of the solution was measured at 500 nm against a 0.1% (w/v) SDS blank. The prepared emulsion was kept undisturbed for 10 min. Then, 50 μL aliquots were taken from the bottom of the beaker and dispersed into 5 mL of 0.1% (w/v) SDS solution. The absorbance of the sample was measured at 500 nm against 0.1% (w/v) SDS as described above. EAI and ESI of the protein samples were calculated by using eqs 1 and 2, respectively:

**Scheme 1. Proposed MTGase-Catalyzed Acyl-Transferring Reactions**

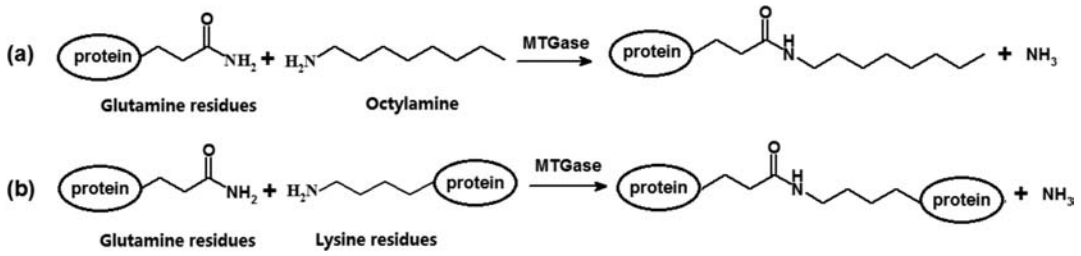


$$\mathrm{EAI}\left(\frac{\mathrm{m}^2}{\mathrm{g}}\right) = \frac{2 \times 2.303 \times A_{500} \times \text{dilution}}{C \times (1 - \Phi) \times 10^4} \quad (1)$$

$$\mathrm{ESI}\ (\%) = \frac{A_{10}}{A_0} \times 100 \quad (2)$$

In these equations, $A_{500}$ is the absorbance of the sample at 500 nm, $C$ is protein concentration (g/mL) before emulsion, $\Phi$ is the oil volume fraction (v/v) of the emulsion, dilution = 100, and $A_{10}$ and $A_0$ are the absorbance at 500 nm after 10 min and at time zero, respectively.

**Determination of Salt Stability.** The protein samples (50 mg) were dispersed in 10 mL of NaCl solutions with different concentrations (1−5 M) and stirred overnight. The sample dispersions were centrifuged at 20000*g* for 20 min to sediment insoluble proteins. The supernatant was diluted 20 times and assayed for protein content using the Bradford method.[30] Salt stability of protein samples was indirectly assessed using the protein solubility in the salt solution, whereas protein solubility was expressed as the percentage of protein content in the supernatant with respect to the protein content in the dispersion. All assays were performed in triplicates.

**Determination of in Vitro Digestibility.** The in vitro digestibility of the protein samples were examined using one-step and two-step hydrolysis as reported by Zhang et al.[32] with slight modifications. For one-step hydrolysis, 10 mL of protein dispersion of 1% (w/v) at pH 2.0 (by addition of 1 M HCl) was prepared, followed by the addition of 2 mg of pepsin. The hydrolysis was carried out at 37 °C for 2 h and stopped by adding an equal volume of 20% (w/v) TCA. For two-step hydrolysis, the starting dispersion was prepared and treated as above. After incubation at 37 °C for 1 h, the hydrolysis was stopped by heating at 90 °C for 5 min and cooling to 4 °C. Then the dispersion was lyophilized and reconstituted in 10 mL of 0.2 M phosphate buffer (pH 8.0), followed by the addition of 6 mg of trypsin. The incubation was carried out at 37 °C for 1 h, and then the hydrolysis was stopped by adding an equal volume of 20% (w/v) TCA. The suspensions were centrifuged at 10000*g* for 20 min to collect the supernatant. The TCA-soluble nitrogen released into the supernatant was diluted with a 6-fold volume of distilled water and monitored for absorbance at 280 nm. The value obtained was used to reflect in vitro digestibility of the protein sample.

**Statistical Analysis.** Data were reported as the mean ± SD for triplicate determinations. One-way ANOVA and Tukey's test were employed to identify differences in means. Statistics were analyzed using SPSS for Windows (version rel. 10.0.5, 1999, SPSS Inc., Chicago, IL, USA). Statistical significance was declared at $P < 0.05$.

## RESULTS AND DISCUSSION

**Developing a MTGase-Catalyzed Aqueous−Organic Biphasic Reaction Procedure for Structural Modification of Sodium Caseinate.** MTGase has been recognized for its ability to catalyze the cross-linking between the γ-carboxyamide groups and the ε-amino group of lysine residues to form an ε-(γ-glutamyl) lysine isopeptide bond in caseinate molecules.[14] The reactive lysine may be substituted by certain different compounds containing appropriate primary amino groups, giving different derivatives.[21] However, little previous study has tested the possibility of performing the MTGase-catalyzed reaction in a nonaqueous solvent system, which has limited the substrates to polar chemicals with adequate water solubility. In this study, a MTGase-catalyzed aqueous−organic biphasic reaction procedure was developed to modify sodium caseinate with nonpolar octylamine. It was hypothesized that octylamine might compete with the ε-amino group of lysine residues to incorporate into caseinate molecules at the interphase, and the cross-linking and octyl conjugation may occur simultaneously in the modified product (Scheme 1). To test the hypothesis, a reaction was performed with sodium caseinate and octylamine as the substrate and MTGase as the catalyst in a solvent system consisting of Tris·HCl buffer and cyclohexane. SDS-PAGE (Figure 1) and $^1$H NMR analyses (Figure 2) confirmed that the

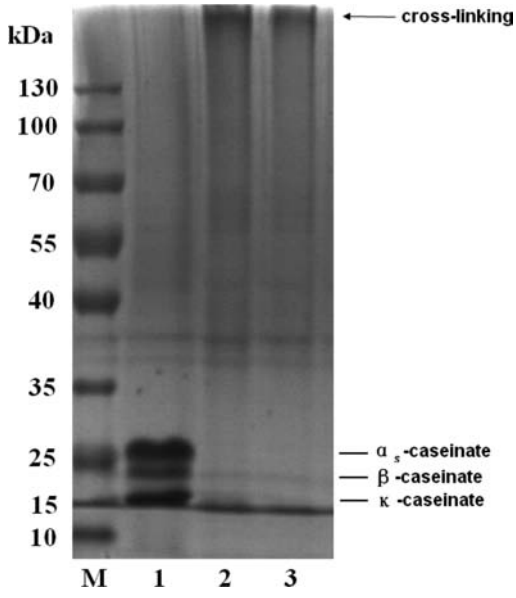


**Figure 1.** SDS-PAGE profiles of protein samples. Lanes: M, standard protein markers; 1, native caseinate; 2, cross-linked caseinate; 3, octyl-conjugated caseinate.

MTGase was able to successfully cross-link and introduce octyl conjugation in the caseinate molecule under the experimental condition. In Figure 1, lane 1 shows major protein components (subunits) of $\alpha_s$-, β-, and κ-caseinates in the native caseinate. In contrast, these bands for most of the subunits in the cross-linked and octyl-conjugated caseinates became less dense. Meanwhile, some new bands at higher molecular weights (>130 kDa) appeared on the top of the separating gel in lanes 2 and 3, evidencing the cross-linking between caseinate molecules, as octyl conjugation might not increase the molecular weight of caseinate to this extent. The $^1$H NMR spectra of octylamine and those for the native, cross-linked, and octyl-conjugated


dx.doi.org/10.1021/jf5024998 | J. Agric. Food Chem. 2014, 62, 8655−8662

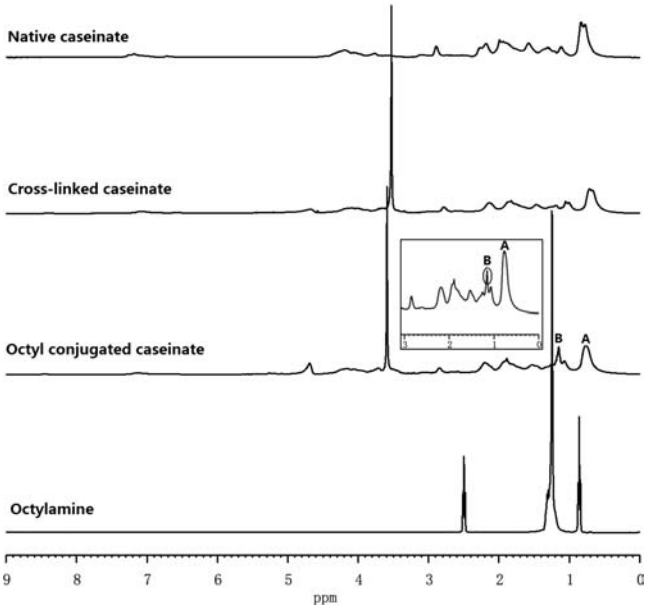


**Figure 2.** $^1$H NMR spectra of 0.5% (w/v) octylamine dissolved in $d_6$-DMSO and protein samples dissolved in $D_2O$. The substitution degree of octyl group in the octyl conjugated caseinate is 28.96%. The sharp peak at 3.7 ppm in the cross-linked and octyl-conjugated caseinate is due to residual Tris buffer.[34]

caseinate are shown in Figure 2. Octylamine showed multiple signals at 0.86, 1.28, and 2.50 ppm, which could be attributed to the protons of its methyl, methylene, and amino groups. Because of the high molecular weights of protein samples, the signals were considerably broader and less well-resolved than that for the smaller molecule octylamine. In the characteristic aliphatic hydrogen resonance region (0−3 ppm), a new peak B at 1.15 ppm (as a circle indicated in the inset) was detected only in the spectrum of the octyl-conjugated caseinate, but not in that of the native or cross-linked caseinate. This new peak originated very probably from the methylene protons of octyl groups covalently linked to the glutamine residues in caseinate, although chemical shifts of methylene protons in small molecules of octylamine (1.28 ppm) and octyl groups of the modified caseinate (1.15 ppm) showed a slight difference. This slight difference might be due to the different chemical environments of methylene protons in the octylamine and the modified protein.

To achieve the desired degree of octyl conjugation, the reaction conditions were examined for their influence on the degree of octyl conjugation, including feed protein concentration (0.0625, 0.125, 0.25, and 0.5% w/v) and reaction time (2, 4, 6, 8, and 10 h). At the protein concentration of 0.0625% (w/v), the obtained octyl-conjugated caseinate showed very poor solubility in water, regardless of the reaction time. This made the measurement of SD value of conjugated octyl groups and further application of the modified products in the food industry less possible. For the protein concentration of 0.125−0.5% (w/v), the modified products showed a good solubility in water.

**Determination of Substitution Degree.** A novel approach was developed in the present study to determine the SD value of conjugated octyl groups in the modified proteins according to the relative intensity between broad peak A (0.04−0.93 ppm) and peak B (1.15 ppm). The broad peak A between 0.04 and 0.93 ppm corresponded to the methyl protons of isoleucine, leucine, and valine residues[33] and octyl groups conjugated to the caseinate, whereas a new peak B at 1.15 ppm was attributed to the methylene protons of octyl groups (Figure 2). The SD of octyl groups conjugated into caseinate could be defined as the moles of conjugated octyl groups in the modified caseinate per mole glutamine units in the caseinate before modification and could be calculated by eqs 3−5:

$$I_{\text{peak A}} = (M_{\text{isoleucine}} \times N_{\text{isoleucine}} + M_{\text{leucine}} \times N_{\text{leucine}} + M_{\text{valine}} \times N_{\text{valine}} + yN_{\text{octylamine-CH}_3}) \times x \quad (3)$$

$$I_{\text{peak B}} = yN_{\text{octylamine-CH}_2} \quad (4)$$

$$\text{SD}\ (\%) = \frac{y}{N_{\text{glutamine}} \times x} \times 100 \quad (5)$$

In these equations, $I_{\text{peak A}}$ and $I_{\text{peak B}}$ are average integral areas of peaks A and B, $x$ is the mole number of the tested octyl conjugated caseinate, $y$ is the mole number of octyl groups in the tested octyl conjugated caseinate, $N_{\text{isoleucine}}$, $N_{\text{leucine}}$, $N_{\text{valine}}$, and $N_{\text{octylamine-CH}_3}$ are the number of protons of methyl signal in isoleucine (6H), leucine (6H), valine (6H), and octylamine (3H), $N_{\text{octylamine-CH}_2}$ is the number of protons of methylene signal in octylamine (14H), and $M_{\text{isoleucine}}$, $M_{\text{leucine}}$, $M_{\text{valine}}$, and $M_{\text{glutamine}}$ are the mole numbers of isoleucine (11.73), leucine (18.39), valine (14.61), and glutamine (18.54) residues per mol caseinate before modification, respectively. These data may be calculated from the amino acid compositions of each subunit of caseinate, which is available in the Supporting Information.

A group of octyl-conjugated caseinates with different SD values were prepared (Table 1). Table 1 shows that the SD of octyl groups increased with the reaction time increasing from 2 to 6 h and then decreased upon further increasing reaction time. At the same reaction time of 6 h, the maximal octyl conjugation was achieved for 0.125% (w/v) of protein concentration. Under this reaction condition, about 28.96% of glutamine units in caseinate were conjugated with octyl groups.

**Table 1. Effect of Protein Concentration and Reaction Time on the Substitution Degree of the Octyl Group in the Octyl-Conjugated Caseinates**

| | substitution degree (%) | | | | |
|---|---|---|---|---|---|
| protein sample | 2 h | 4 h | 6 h | 8 h | 10 h |
| octyl-conjugated caseinate, 0.125% (w/v) | 10.30 | 13.00 | 28.96 | 6.11 | 5.22 |
| octyl-conjugated caseinate, 0.25% (w/v) | 12.44 | 13.66 | 19.49 | 11.75 | 8.28 |
| octyl-conjugated caseinate, 0.50% (w/v) | 6.30 | 11.68 | 16.40 | 11.71 | 9.70 |

**Surface Hydrophobicity.** The surface hydrophobicity index, measured using ANS as a fluorescence probe, is an important parameter indicative of the hydrophobic region in a protein. The surface hydrophobicity index of the native, cross-linked, and octyl-conjugated protein samples is shown in Figure 3. The cross-linking and octyl conjugation increased the surface hydrophobicity index significantly ($P < 0.05$), from 23.92 (native caseinate) to 27.07 (cross-linked caseinate) and 32.66 (octyl-conjugated caseinate). This observation was in good agreement with a previous report that transglutaminase

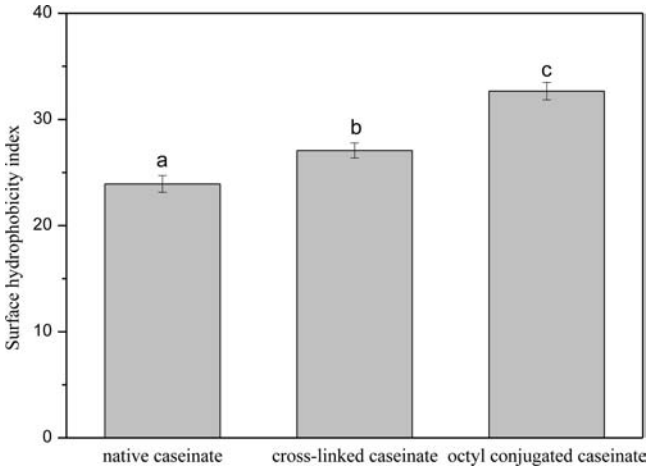


**Figure 3.** Surface hydrophobicity index of native caseinate, cross-linked caseinate, and octyl-conjugated caseinate. Different letters (a–c) above the columns indicate that the data are significantly different ($P < 0.05$). Values are expressed as means ± standard derivatives of triplicate measurements.

treatment increased surface hydrophobicity of sodium caseinate, whey protein isolate, and total milk protein by Hiller and Lorenzen.[35] They suggested that the increase in protein hydrophobicity corresponded to an unfolding of protein structure upon enzymatic treatment and thus an exposure of hydrophobic amino acid residues buried within the tertiary structure of original protein molecules. The conjugation of the octyl group, which is neutral and hydrophobic, could further increase the surface hydrophobicity of the modified caseinate.

**Thermal Stability.** Figure 4 and Table 2 present TGA/DTG curves and characteristic parameters of native, cross-linked, and octyl-conjugated caseinate under a flow of $N_2$ at a heating rate of 10 °C/min. The onset temperatures (temperature at 5% mass loss, $T_{5\%}$) proceeded at a relatively low temperature range (230.83–258.29 °C), at which chemical bonds could not be broken, and it could be attributable to the elimination of water physically retained by caseinate.[36] Comparable with those of native caseinate, the $T_{50\%}$ and $T_{max}$ of the cross-linked caseinate increased 10.99 and 16.84 °C, whereas these indices of the octyl-conjugated caseinate increased 9.05 and 20.23 °C, respectively. These data demonstrated that the thermal stabilities of cross-linked and octyl-conjugated protein samples were better than that of the native caseinate. Similar results were reported for millet protein and whey protein isolate polymerized by transglutaminase.[17,37] According to Flanagan,[38] this is probably due to the formation of intra- and intermolecular association between protein polymers, which delayed a heat-induced unfolding and denaturation of MTGase-treated proteins.

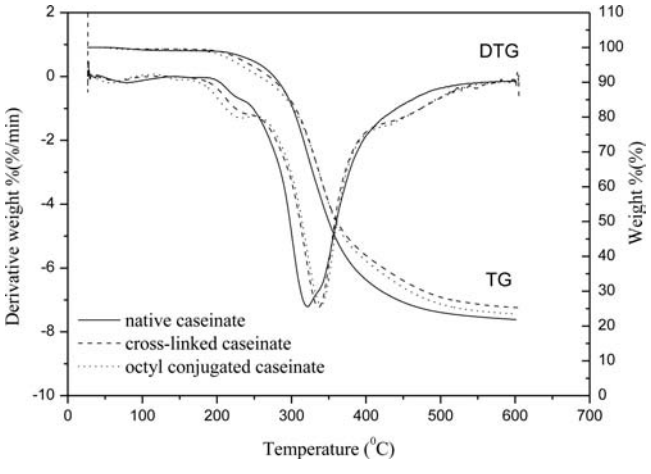


**Figure 4.** TGA/DTG curves of native caseinate, cross-linked caseinate, and octyl-conjugated caseinate under nitrogen atmosphere at a heating rate of 10 °C/min.

**Table 2. Characteristic Parameters for the Native, Cross-Linked, and Octyl-Conjugated Caseinates by TGA/DTG**

| protein sample | $T_{5\%}$ (°C) | $T_{50\%}$ (°C) | $T_{max}$ (°C) | residue weight (wt %) |
|---|---|---|---|---|
| native caseinate | 258.29 | 350.06 | 319.34 | 21.85 |
| cross-linked caseinate | 244.84 | 361.05 | 336.18 | 25.31 |
| octyl-conjugated caseinate | 230.83 | 359.11 | 339.57 | 23.47 |

**Emulsifying Property.** The emulsifying activity and emulsion stability index of the three protein samples were measured and expressed as EAI and ESI (Figure 5). The EAIs were 20.52, 33.50, and 37.38 $m^2/g$ and the ESIs were 7.42, 6.82, and 4.45% for the native, cross-linked, and octyl-conjugated caseinates, respectively. Compared with those of native caseinate, cross-linked and octyl-conjugated caseinate had significantly increased EAIs by 63.25 and 82.16%, and decreased ESIs by 8.08 and 40.02%, respectively. Surface hydrophobicity is positively associated with the ability of protein to act as an emulsifer.[39] In an earlier study, Sen et al.[40] have shown that highly alkylated casein derivatives had a better emulsion activity than the unmodified protein. For most proteins, higher surface hydrophobicity indicates a better emulsifying property as a large portion of hydrophobic residues may anchor to the surface of oil droplets and form a strong film.[41] However, it should be pointed out that increasing protein hydrophobicity may have in many instances adverse effects on emulsifying activity,[31,42] which implies the involvement of other factors in determining emulsion activity of proteins, such as protein solubility and distribution of hydrophobic and hydrophilic residues in the polypeptide

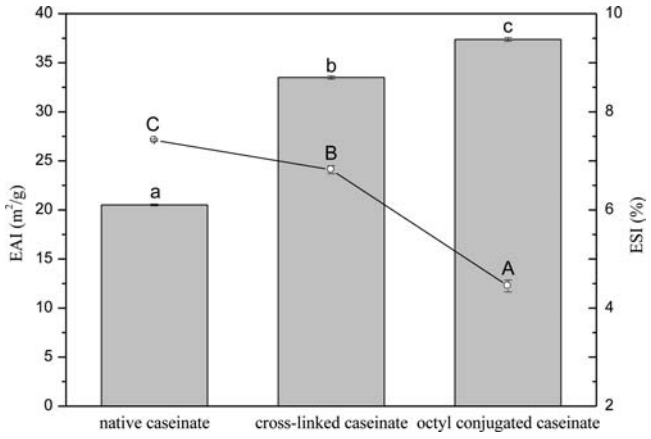


**Figure 5.** Emulsifying activity index (EAI, column) and emulsion stability index (ESI, curve) of native caseinate, cross-linked caseinate, and octyl-conjugated caseinate. Different letters (a–c or A–C) above the columns or curve indicate significant differences ($P < 0.05$), respectively. Values are expressed as means ± standard derivatives of triplicate measurements.


dx.doi.org/10.1021/jf5024998 | J. Agric. Food Chem. 2014, 62, 8655–8662

Table 3. Solubility Measurements of Different Protein Samples at Selected NaCl Concentrations

| protein sample | protein solubility[a] (%) | | | | |
|---|---|---|---|---|---|
| | 1 M | 2 M | 3 M | 4 M | 5 M |
| native caseinate | 97.73 b ± 0.46 | 94.67 a ± 2.61 | 92.80 c ± 1.11 | 22.40 a ± 0.72 | ~0 a[b] |
| cross-linked caseinate | 92.27 a ± 1.40 | 90.20 a ± 1.71 | 89.40 b ± 1.64 | 88.53 c ± 1.01 | 4.47 c ± 0.07 |
| octyl-conjugated caseinate | 93.07 a ± 2.27 | 92.80 a ± 1.05 | 86.00 a ± 0.5 | 77.13 b ± 1.21 | 4.32 b ± 0.04 |

[a]Values are expressed as means ± standard derivatives of triplicate measurements. Different lower case letters in the same column indicate significant differences ($P < 0.05$). [b]The absorbance was below the lowest detection limit of the calibration curve, which was established on the basis of the Bradford method.

chains.[43] Moreover, the impaired effect of cross-linking and octyl conjugation on ESIs may be explained by the fact that the huge, extended protein oligomers/polymers facilitate aggregation and coalescence by simultaneously participating in the interface areas of different oil droplets.

**Salt Stability.** Salt stability of protein samples was indirectly assessed using the protein solubility in the NaCl solution. The solubilities of native, cross-linked, and octyl-conjugated caseinates in different concentrations (1−5 M) of NaCl solutions were evaluated by measuring protein solubilities in supernatants after protein dispersions had been centrifuged (Table 3). The native caseinate exhibited high solubilities in 1 M (97.73%), 2 M (94.67%), and 3 M (92.80%) NaCl solutions. Upon cross-linking and octyl conjugation, <8% changes in solubilities were observed for cross-linked and octyl-conjugated caseinate at the above-mentioned NaCl concentration range. However, native caseinate exhibited a sharply reduced solubility (22.40%) in 4 M NaCl concentration, which was significantly lower than those of cross-linked (88.53%) and octyl-conjugated caseinates (77.13%) at the same NaCl concentration. The salt solubility of native caseinate supported the earlier argument that salts at low concentrations normally stabilize proteins and may prevent proteins from initial binding and subsequent conformation changes and aggregation. At a high ionic strength, excessive charge shielding may cause protein aggregation.[44] The improved salt stability of the cross-linked and octyl-conjugated caseinate might be explained by Melander and Horvath's extended cavity theory,[45] which was originally developed by Sinanoglu and Abdulnur.[46] At higher salt concentrations, protein molecules require the surface free energy to greatly exclude salts and create a cavity for themselves. A higher concentraion of salts renders a larger surface tension increment of water; that is, a greater surface free energy is required for proteins, although such surface free energy to create a cavity is reduced, upon protein−protein interactions, which reduces the total surface area. Therefore, the cross-linked and octyl-conjugated caseinates could tolerate higher salt concentration (4 M), due to the formation of intra- and intermolecular protein polymers. When the NaCl concentration increased to 5 M, nearly all of the protein samples aggregated (Table 3).

**In Vitro Digestibility.** Figure 6 shows the absorbance at 280 nm for the supernatants collected during in vitro pepsin or pepsin−trypsin hydrolysis of native, cross-linked, and octyl-conjugated caseinate, reflecting the TCA-soluble peptides released. Under these two hydrolysis conditions, an impaired in vitro digestibility of the cross-linked and octyl-conjugated caseinates were observed as the released amount of the peptides with significantly reduced molecular mass, compared to that of the native caseinate. The results implied that the cross-linking and octyl-conjugated caseinates might sterically shield the peptide bonds against proteolysis, thus decreasing enzymatic digestibility in vitro. The observation agreed with the previous report by Tang et al.[47] that TGase-induced cross-linking of soy protein isolates led to a decrease of its pepsin−trypsin digestibility.

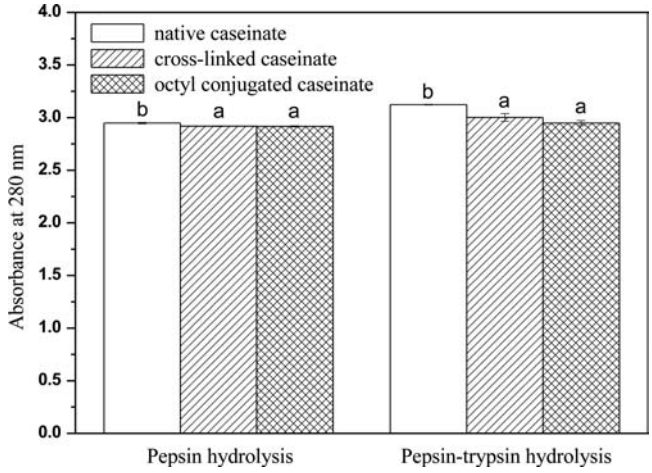


**Figure 6.** In vitro digestibility of protein samples evaluated by pepsin (one-step) or pepsin−trypsin (two-step) hydrolysis, respectively. Different letters (a, b) above the columns indicate significant differences ($P < 0.05$), respectively. Values are expressed as means ± standard derivatives of triplicate measurements.

In conclusion, a novel MTGase-catalyzed procedure was successfully developed to modify sodium caseinate by cross-linking and octylation in an aqueous−organic biphasic solvent system. The substitution degree of conjugated octyl groups was determined using a $^1$H NMR-based analysis for the first time, and this new analysis method could also be applied to other alkylation substitutions. Compared with the native caseinate, the octyl-conjugated caseinate has improved functional properties, such as better emulsifying activity and higher heat and salt stabilities. The reaction may also be applied to modify other food and nonfood proteins.

## ■ ASSOCIATED CONTENT

### Supporting Information

Amino acid compositions of $\alpha_{s1}$-, $\alpha_{s2}$-, $\beta$-, and $\kappa$-caseinates and mole numbers of isoleucine, leucine, valine, and glutamine residues. This material is available free of charge via the Internet at http://pubs.acs.org.

## ■ AUTHOR INFORMATION

### Corresponding Authors

*(L.Y.) Phone: +86 021 34205828. Fax: +86 021 34204107. E-mail: liangli.yu@sjtu.edu.cn.
*(Y.N.) Phone: +86 021 34204538. Fax: +86 021 34204107. E-mail: yugeniu@sjtu.edu.cn.

## Funding

This work was supported by the National High Technology Research and Development Program of China (Grants 2013AA102202 and 2013AA102207); a special fund for Agro-scientific Research in the Public Interest (Grant 201203069); and the SJTU startup fund for young talent (Grant 13X100040047) and SJTU 985-III disciplines platform and talent fund (Grants TS0414115001 and TS0320215001).

## Notes

The authors declare no competing financial interest.

## REFERENCES

(1) Cardoso, J. C.; Albuquerque, R. L. C., Jr.; Padilha, F. F.; Bittencourt, F. O.; De Freitas, O.; Nunes, P. S.; Pereira, N. L.; Fonseca, M. J. V.; Araújo, A. A. S. Effect of the Maillard reaction on properties of casein and casein films. *J. Therm. Anal. Calorim.* **2011**, *104*, 249−254.

(2) Roman, J. A.; Sgarbieri, V. C. The hydrophilic, foaming and emulsifying properties of casein concentrates produced by various methods. *Int. J. Food Sci. Technol.* **2006**, *41*, 609−617.

(3) Maldonado-Valderrama, J.; Langevin, D. On the difference between foams stabilized by surfactants and whole casein or $\beta$-casein. Comparison of foams, foam films, and liquid surfaces studies. *J. Phys. Chem. B* **2008**, *112*, 3989−3996.

(4) Pan, K.; Chen, H.; Davidson, P. M.; Zhong, Q. Thymol nanoencapsulated by sodium caseinate: physical and antilisterial properties. *J. Agric. Food Chem.* **2014**, *62*, 1649−1657.

(5) Grigorovich, N. V.; Moiseenko, D. V.; Antipova, A. S.; Anokhina, M. S.; Belyakova, L. E.; Polikarpov, Y. N.; Korica, N.; Semenova, M. G.; Baranov, B. A. Structural and thermodynamic features of covalent conjugates of sodium caseinate with maltodextrins underlying their functionality. *Food Funct.* **2012**, *3*, 283−289.

(6) Gu, F. L.; Kim, J. M.; Abbas, S.; Zhang, X. M.; Xia, S. Q.; Chen, Z. X. Structure and antioxidant activity of high molecular weight Maillard reaction products from casein-glucose. *Food Chem.* **2010**, *120*, 505−511.

(7) Oliver, C. M.; Augustin, M. A.; Sanguansri, L. Maillard-based casein-carbohydrate microcapsules for the delivery of fish oil: emulsion stability during in vitro digestion. *Aust. J. Dairy Technol.* **2009**, *64*, 80−83.

(8) Aminlari, M.; Ramezani, R.; Jadidi, F. Effect of Maillard-based conjugation with dextran on the functional properties of lysozyme and casein. *J. Sci. Food Agric.* **2005**, *85*, 2617−2624.

(9) Markman, G.; Livney, Y. D. Maillard-conjugate based core-shell co-assemblies for nanoencapsulation of hydrophobic nutraceuticals in clear beverages. *Food Funct.* **2012**, *3*, 262−270.

(10) Dong, S.; Wei, B.; Chen, B.; McClements, D. J.; Decker, E. A. Chemical and antioxidant properties of casein peptide and its glucose Maillard reaction products in fish oil-in-water emulsions. *J. Agric. Food Chem.* **2011**, *59*, 13311−13317.

(11) Brands, C. M.; Alink, G. M.; van Boekel, M. A.; Jongen, W. M. Mutagenicity of heated sugar-casein systems: effect of the Maillard reaction. *J. Agric. Food Chem.* **2000**, *48*, 2271−2275.

(12) Guerra-Hernandez, E.; Gomez, C. L.; Garcia-Villanova, B.; Sanchez, N. C.; Gomez, J. M. R. Effect of storage on non-enzymatic browning of liquid infant milk formulae. *J. Sci. Food Agric.* **2002**, *82*, 587−592.

(13) Sheng, W. W.; Zhao, X. H. Functional properties of limited hydrolysed cross-linked casein-gelatin composites. *Int. J. Food Sci. Technol.* **2013**, *48*, 260−266.

(14) Yokoyama, K.; Nio, N.; Kikuchi, Y. Properties and applications of microbial transglutaminase. *Appl. Microbiol. Biotechnol.* **2004**, *64*, 447−454.

(15) Lorand, L.; Lockridge, O. M.; Campbell, L. K.; Myhrman, R.; Bruner-Lorand, J. Transamidating enzymes. II. A continuous fluorescent method suited for automating measurements of factor XIII in plasma. *Anal. Biochem.* **1971**, *44*, 221−231.

(16) Kulik, C.; Heine, E.; Weichold, O.; Möller, M. Synthetic substrates as amine donors and acceptors in microbial transglutaminase-catalysed reactions. *J. Mol. Catal. B−Enzym.* **2009**, *57*, 237−241.

(17) Hassan, A. B.; Osman, G. A.; Babiker, E. E. Effect of chymotrypsin digestion followed by polysaccharide conjugation or transglutaminase treatment on functional properties of millet proteins. *Food Chem.* **2007**, *102*, 257−262.

(18) Cho, Y. H.; Shim, H. K.; Park, J. Encapsulation of fish oil by an enzymatic gelation process using transglutaminase cross-linked proteins. *J. Food Sci.* **2003**, *68*, 2717−2723.

(19) Jiang, S. J.; Zhao, X. H. Transglutaminase-induced cross-linking and glucosamine conjugation of casein and some functional properties of the modified product. *Int. Dairy J.* **2011**, *21*, 198−205.

(20) Yan, S. C. B. Colvent attachment of oligosaccharide-asparagine derivatives: incorporation into glutamine residues with the enzyme transglutaminase. *Methods Enzymol.* **1987**, *138*, 413−418.

(21) Ohtsuka, T.; Sawa, A.; Kawabata, R.; Nio, N.; Motoki, M. Substrate specificities of microbial transglutaminase for primary amines. *J. Agric. Food Chem.* **2000**, *48*, 6230−6233.

(22) Kellerby, S. S.; Gu, Y. S.; McClements, D. J.; Decker, E. A. Lipid oxidation in a menhaden oil-in-water emulsion stabilized by sodium caseinate cross-linked with transglutaminase. *J. Agric. Food Chem.* **2006**, *54*, 10222−10227.

(23) Yin, W. W.; Su, R. X.; Qi, W. A casein-polysaccharide hybrid hydrogel cross-linked by transglutaminase for drug delivery. *J. Mater. Sci.* **2012**, *47*, 2045−2055.

(24) Nesterenko, A.; Alric, I.; Silvestre, F.; Durrieu, V. Comparative study of encapsulation of vitamins with nativeand modified soy protein. *Food Hydrocolloids* **2014**, *38*, 172−179.

(25) Lin, L. H.; Wang, C. C.; Chen, K. M.; Lin, P. C. Synthesis and physicochemical properties of casein-derived surfactants. *Colloid Surf. A−Physicochem. Eng. Asp.* **2009**, *346*, 47−51.

(26) Barberis, S. B.; Quiroga, E.; Arribere, M. C. Peptide synthesis in aqueous-organic biphasic systems catalyzed by a protease brachystephana isolated from *Morrenia* (Asclepiadaceae). *J. Mol. Catal. B−Enzym.* **2002**, *17*, 39−47.

(27) Kurita, T.; Izu, H.; Sano, M.; Ito, M.; Kato, I. Enhancement of hydrolytic activity of sphingolipid ceramide *N*-deacylase in the aqueous-organic biphasic system. *J. Lipid Res.* **2000**, *41*, 846−851.

(28) Berger, S.; Braun, S. *200 and More NMR Experiments: A Practical Course*; Wiley-VCH: New York, 2004; pp 213−215.

(29) Teng, Z.; Li, Y.; Luo, Y.; Zhang, B.; Wang, Q. Cationic $\beta$-lactoglobulin nanoparticles as a bioavailability enhancer: protein characterization and particle formation. *Biomacromolecules* **2013**, *14*, 2848−2856.

(30) Bradford, M. M. A rapid and sensitive method for the quantitation of microgram quantities of protein utilizing the principle of protein-dye binding. *Anal. Biochem.* **1976**, *72*, 248−254.

(31) Song, C. L.; Zhao, X. H. Rheological, gelling and emulsifying properties of a glycosylated and cross-linked caseinate generated by transglutaminase. *Int. J. Food Sci. Technol.* **2013**, *48*, 2595−2602.

(32) Zhang, Y. N.; Zhao, X. H. Study on the functional properties of soybean protein isolate cross-linked with gelatin by microbial transglutaminase. *Int. J. Food Prop.* **2013**, *16*, 1257−1270.

(33) Rollema, H. S.; Brinkhuis, J. A. A $^1$H-NMR study of bovine casein micelles; influence of pH, temperature and calcium ions on micellar structure. *J. Dairy Res.* **1989**, *56*, 417−425.

(34) de Kruif, C. G.; Tuinier, R.; Holt, C.; Timmins, P. A.; Rollema, H. S. Physicochemical study of $\kappa$- and $\beta$-casein dispersions and the effect of cross-linking by transglutaminase. *Langmuir* **2002**, *18*, 4885−4891.

(35) Hiller, B.; Lorenzen, P. C. Functional properties of milk proteins as affected by enzymatic oligomerisation. *Food Res. Int.* **2009**, *42*, 899−908.

(36) Mocanu, A. M.; Moldoveanu, C.; Odochian, L.; Paius, C. M.; Apostolescu, N.; Neculau, R. Study on the thermal behavior of casein under nitrogen and air atmosphere by means of the TG-FTIR technique. *Thermochim. Acta* **2012**, *546*, 120−126.

(37) Damodaran, S.; Agyare, K. K. Effect of microbial transglutaminase treatment on thermal stability and pH-solubility of heat-shocked whey protein isolate. *Food Hydrocolloids* **2013**, *30*, 12−18.
(38) Flanagan, J.; Gunning, Y.; FitzGerald, R. J. Effect of cross-linking with transglutaminase on the heat stability and some functional characteristics of sodium caseinate. *Food Res. Int.* **2003**, *36*, 267−274.
(39) Banach, J. C.; Lin, Z.; Lamsal, B. P. Enzymatic modification of milk protein concentrate and characterization of resulting functional properties. *LWT−Food Sci. Technol.* **2013**, *54*, 397−403.
(40) Sen, L. C.; Lee, H. S.; Feeney, R. E.; Whitaker, J. R. In vitro digestibility and functional properties of chemically modified casein. *J. Agric. Food Chem.* **1981**, *29*, 348−354.
(41) Damodaran, S. Protein-stabilized foams and emulsions. In *Food Proteins and Their Applications*; Dekker: New York, 1997; pp 57−110.
(42) Seo, S.; Karboune, S.; L'Hocine, L.; Yaylayan, V. Characterization of glycated lysozyme with galactose, galactooligosaccharides and galactan: effect of glycation on structural and functional properties of conjugates. *LWT−Food Sci. Technol.* **2013**, *53*, 44−53.
(43) Chobert, J.-M.; Bertrand-Harb, C.; Nicolas, M.-G.; Gaertner, H. F.; Puigserver, A. J. Solubility and emulsifying properties of caseins chemically modified by covalent attachment of L-methionine and L-valine. *J. Agric. Food Chem.* **1987**, *35*, 638−644.
(44) Tsumoto, K.; Ejima, D.; Senczuk, A. M.; Kita, Y.; Arakawa, T. Effects of salts on protein-surface interactions: applications for column chromatography. *J. Pharm. Sci.* **2007**, *96*, 1677−1690.
(45) Melander, W.; Horvath, C. Salt effect on hydrophobic interactions in precipitation and chromatography of proteins: an interpretation of the lyotropic series. *Arch. Biochem. Biophys.* **1977**, *183*, 200−215.
(46) Sinanoglu, O.; Abdulnur, S. Effect of water and other solvents on the structure of biopolymers. *Fed. Proc.* **1965**, *24*, S12−S23.
(47) Tang, C. H.; Li, L.; Yang, X. Q. Influence of transglutaminase-induced cross-linking on in vitro digestibility of soy protein isolates. *J. Food Biochem.* **2006**, *30*, 718−731.

JOURNAL OF AGRICULTURAL AND FOOD CHEMISTRY

Article

pubs.acs.org/JAFC

# Biofunctional Constituent Isolated from *Citrullus colocynthis* Fruits and Structure−Activity Relationships of Its Analogues Show Acaricidal and Insecticidal Efficacy

Ju-Hyun Jeon and Hoi-Seon Lee*

Department of Bioenvironmental Chemistry and Institute of Agricultural Science and Technology, College of Agriculture and Life Sciences, Chonbuk National University, Jeonju 561-756, Republic of Korea

**ABSTRACT:** The acaricidal and insecticidal potential of the active constituent isolated from *Citrullus colocynthis* fruits and its structurally related analogues was evaluated by performing leaf disk, contact toxicity, and fumigant toxicity bioassays against *Tetranychus urticae*, *Sitophilus oryzae*, and *Sitophilus zeamais* adults. The active constituent of *C. colocynthis* fruits was isolated by chromatographic techniques and was identified as 4-methylquinoline on the basis of spectroscopic analyses. To investigate the structure−activity relationships, 4-methylquinoline and its structural analogues were tested against mites and two insect pests. On the basis of the $LC_{50}$ values, 7,8-benzoquinoline was the most effective against *T. urticae*. Quinoline, 8-hydroxyquinoline, 2-methylquinoline, 4-methylquinoline, 6-methylquinoline, 8-methylquinoline, and 7,8-benzoquinoline showed high insecticidal activities against *S. oryzae* and *S. zeamais* regardless of the application method. These results indicate that introduction of a functional group into the quinoline skeleton and changing the position of the group have an important influence on the acaricidal and insecticidal activities. Furthermore, 4-methylquinoline isolated from *C. colocynthis* fruits, along with its structural analogues, could be effective natural pesticides for managing spider mites and stored grain weevils.

**KEYWORDS:** *Citrullus colocynthis, Sitophilus oryzae, Sitophilus zeamais, structure−activity relationship, Tetranychus urticae*

## INTRODUCTION

Both spider mites and weevils are pests of various plants, vegetables, and postharvest grains in a wide range of agricultural environments.[1−3] Populations of these insect pests cause serious economic losses and a decline in the grain quality of agricultural products worldwide.[1,4] The management of these insect pests has principally been carried out using synthetic chemical applications such as contact, fumigant, or spraying treatments with organophosphate and insect-growth regulators.[3,5] Although these substances are useful for controlling insect pests, their repeated use could pose a meaningful risk to human health and cause environmental pollution, as well as unwanted toxicity on nontarget organisms.[3,4,6] For these reasons, various studies have investigated the effects of phytochemicals as useful alternatives to insect pest management agents.

Botanical pesticides have long been used as an alternative source to synthetic chemicals for pest management because plant secondary metabolites show a broad range of insecticidal effects against agricultural, hygienic, and stored product insect pests, such as aphids, mites, mosquitoes, and weevils.[1,3,7,8] Moreover, because plant-derived materials have multiple novel target points of action, the chance of developing a resistant individual is very low.[9] *Citrullus colocynthis*, a member of the Cucurbitaceae family, is a medicinal plant distributed throughout Asia, which has been used in material for traditional medicines for arthritis, diabetes, inflammatory disorders, and stomachache.[10−13] However, the acaricidal and insecticidal activities of the active constituent isolated from *C. colocynthis* fruits and its structurally related analogues against *Tetranychus urticae*, *Sitophilus oryzae*, and *Sitophilus zeamais* adults have not yet been reported. Therefore, the aim of the current study was to investigate the acaricidal and insecticidal properties of *C. colocynthis* fruits against the mites and two insect pests and to determine their structure−activity relationships.

## MATERIALS AND METHODS

**Chemicals and Plant Material.** Quinoline (98%), 2-hydroxyquinoline (98%), 4-hydroxyquinoline (98%), 6-hydroxyquinoline (95%), 8-hydroxyquinoline (99%), 2-methylquinoline (98%), 6-methylquinoline (98%), 8-methylquinoline (97%), and 7,8-benzoquinoline (97%) were purchased from Sigma-Aldrich Chemical Co. (St. Louis, MO, USA) (Figure 1). Abamectin and dichlorvos, which were used as positive control, were obtained from Fluka Chemical Co. (Buchs, Switzerland). All other chemical materials used in the study were of reagent grade and are commercially available. The fruits of *C. colocynthis* were supplied from the International Biological Material Research Center in Daejeon, South Korea. A voucher specimen was authenticated by Prof. Jeongmoon Kim and deposited in the herbarium at the Department of Landscape Architecture, Chonbuk National University.

**Plant Preparation.** *C. colocynthis* fruits were air-dried and ground to a powder. The dried *C. colocynthis* fruits (100 g) were extracted twice with methanol (10 L) in a shaking incubator at 25 ± 2 °C for 36 h and filtered (filter paper No. 2, Toyo Roshi, Tokyo, Japan) under vacuum. The methanol extracts were concentrated and combined under a vacuum at 45 °C to yield a crude extract (12.7%, based on the dry weight of the fruits). The methanol extract (10 g) was sequentially partitioned into hexane (1.93 g), chloroform (2.88 g), ethyl acetate (1.52 g), butanol (1.81 g), and water-soluble (1.56 g) fractions for

Received: May 28, 2014
Revised: August 6, 2014
Accepted: August 11, 2014
Published: August 11, 2014

ACS Publications © 2014 American Chemical Society

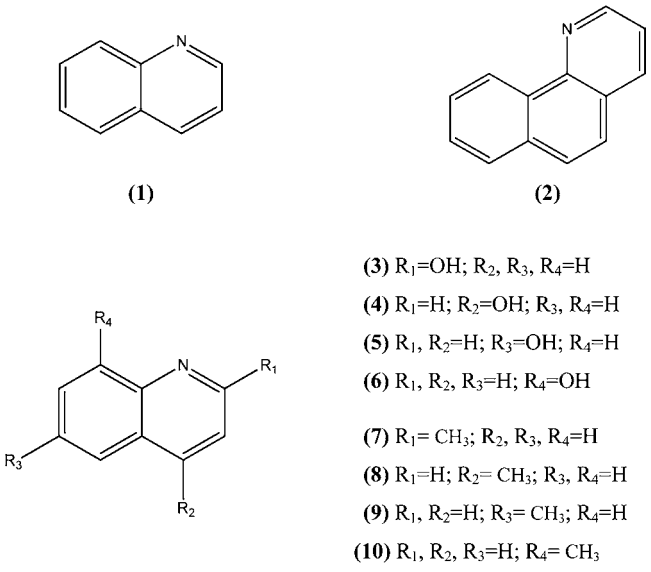


**Figure 1.** Quinoline structural analogues: (**1**) quinoline; (**2**) 7,8-benzoquinoline; (**3**) 2-hydroxyquinoline; (**4**) 4-hydroxyquinoline; (**5**) 6-hydroxyquinoline; (**6**) 8-hydroxyquinoline; (**7**) 2-methylquinoline; (**8**) 4-methylquinoline; (**9**) 6-methylquinoline; (**10**) 8-methylquinoline.

subsequent bioassays. The fractions were concentrated using rotary vacuum evaporation and were refrigerated prior to use at 4 °C.

**Isolation and Identification.** To isolate the active compound of the chloroform fraction derived from the methanol extract of *C. colocynthis* fruits, the chloroform fraction was chromatographed on a silica gel column (Merck 70−230 mesh, 12 × 15 cm; Rahway, NJ, USA) and eluted with a gradient of chloroform/ethyl acetate (from 10:0 to 0:10, v/v). The separated fractions were collected and analyzed by thin-layer chromatography (TLC; chloroform/ethyl acetate = 8:1, v/v), and similar fractions based on their TLC pattern were combined to yield subfractions designated CF1−CF5. The active CF4 fraction was chromatographed on a silica gel column and was eluted with chloroform/ethyl acetate (9:1, 8:2, 7:3, and 5:5, v/v). The active CF43 fraction was also chromatographed on a silica gel column and eluted with chloroform/ethyl acetate (7:3, v/v), and the fractions obtained were bioassayed against the target insects. To determine the insecticidal constituent in fraction CF432, further isolation was performed using preparative HPLC (recycling preparative HPLC; Japan Analytical Industry Co., Ltd.). A JAI gel W series column (W 253 500 mm + W 252 500 mm) was used with chloroform (100%) as the mobile phase at a flow rate of 3.5 mL/min. During this step, three subfractions (CF4321−CF4323) were obtained and were then bioassayed. The active CF4322 fraction was subjected to further chromatography using a JAI gel GS series column (GS 310 500 mm + GS 310 300 mm) with chloroform (100%) at a flow rate of 3.0 mL/min. Finally, the potent active principle (CF43221) was isolated to a single peak. The structure of CF43221 was determined by spectroscopic analyses. Electron ionization (EI) mass spectra were obtained on a GSX 400 mass spectrometer (JEOL Ltd., Tokyo, Japan). $^1$H and $^{13}$C NMR spectra were analyzed in $CD_3OD$, using a JNM-ECA600 spectrometer, at 600 and 150 MHz (with tetramethylsilane as an internal standard), respectively, with the chemical shifts expressed in $\delta$ (ppm).

**Mite and Insect Rearing Conditions.** Respective cultures of *T. urticae*, *S. oryzae*, and *S. zeamais* used for the bioassay were obtained from the National Academy of Agricultural Science, Rural Development Administration (Suwon, Korea). *T. urticae* were reared in the laboratory on kidney bean (*Phaseolus vulgaris* L.) seedlings, and *S. oryzae* and *S. zeamais* were reared on rice grains in plastic containers (30 × 30 × 30 cm). They were maintained in the laboratory at 25 ± 1 °C, 65 ± 5% relative humidity (RH), and a 16 h light/8 h dark photoperiod. No mites and insects were exposed to any known acaricides or insecticides during maintenance.

**Bioassay.** The acaricidal and insecticidal activities against the three insect species were evaluated by leaf disk, contact, and fumigant bioassays using *C. colocynthis* extract, the active constituent, and its structural analogues, using the bioassays presented by Akhtar et al.[1] and Jeon et al.[3] The initial concentrations were chosen in a previous screening. Adults of mixed sex were used for each bioassay.

To evaluate the residual toxicity against *T. urticae*, leaf disks (2.5 cm diameter) cut from kidney bean were dipped in solutions (2.0, 1.0, 0.5, 0.1, 0.05, 0.025, 0.010, and 0.005 $\mu$g/mL) of the test materials for 15 s, and the disks were then evaporated for 20 min in a hood. Acetone was utilized as a carrier solvent. Twenty *T. urticae* adults were introduced onto the leaf disk supported by a cotton pad in a Petri dish (60 × 15 mm), which was then covered with a lid.

To evaluate the contact toxicity of the test materials against *S. oryzae* and *S. zeamais* adults, various amounts (2.10, 1.05, 0.52, 0.26, 0.13, 0.06, 0.03, 0.01, 0.005, 0.001, and 0.0005 mg/cm$^2$) of each material were liquefied in ethanol and applied to filter paper (5 cm

**Table 1. Acaricidal and Insecticidal Activities of Methanol Extract and Solvent Fractions Derived from *Citrullus colocynthis* Fruits**

| | | | mortality (%, mean ± SE)[a] | | | |
|---|---|---|---|---|---|---|
| species | method | dose | methanol extract | hexane fraction | chloroform fraction | control (solvent only) |
| *T. urticae* | leaf disk | 5.0 mg/mL | 5.3 ± 0.4 b | 0 b | 7.1 ± 1.2 b | 0 a |
| *S. oryzae* | contact | 2.1 mg/cm$^2$ | 100.0 ± 0.0 a | 18.3 ± 1.7 a | 100.0 ± 0.0 a | 0 a |
| | | 1.0 mg/cm$^2$ | 62.1 ± 1.5 bc | 0 b | 100.0 ± 0.0 a | –[b] |
| | | 0.5 mg/cm$^2$ | 13.8 ± 0.7 d | – | 73.5 ± 2.1 b | – |
| | fumigant | 1.4 mg/cm$^3$ | 100.0 ± 0.0 a | 14.1 ± 2.2 a | 100.0 ± 0.0 a | 0 a |
| | | 0.7 mg/cm$^3$ | 41.8 ± 1.2 c | 0 b | 91.3 ± 1.4 a | – |
| | | 0.3 mg/cm$^3$ | 11.4 ± 0.6 d | – | 47.6 ± 2.3 c | – |
| *S. zeamais* | contact | 2.1 mg/cm$^2$ | 100.0 ± 0.0 a | 16.8 ± 1.8 a | 100.0 ± 0.0 a | 0 a |
| | | 1.0 mg/cm$^2$ | 79.2 ± 1.7 ab | 0 b | 100.0 ± 0.0 a | – |
| | | 0.5 mg/cm$^2$ | 18.9 ± 2.2 d | – | 61.8 ± 1.9 bc | – |
| | fumigant | 1.4 mg/cm$^3$ | 100.0 ± 0.0 a | 17.5 ± 0.9 a | 100.0 ± 0.0 a | 0 a |
| | | 0.7 mg/cm$^3$ | 43.5 ± 1.8 c | 0 b | 94.6 ± 0.7 a | – |
| | | 0.3 mg/cm$^3$ | 15.3 ± 0.9 d | – | 41.1 ± 2.2 c | – |

[a]Means within a column followed by the same letter are not significantly different ($P$ = 0.05; Scheffe's test). [b]–, not tested.


dx.doi.org/10.1021/jf502536e | J. Agric. Food Chem. 2014, 62, 8663−8667

diameter) (Whatman Co., Maidstone, UK), with an ethanol-only negative control. Each filter paper was placed in the bottom of a Petri dish (5.5 cm diameter × 1.5 cm) after being dried in a fume hood for 10 min. Groups of 20 insects were separately placed in the Petri dish, and the lid was replaced. To evaluate the fumigant toxicity against *S. oryzae* and *S. zeamais*, filter papers were impregnated with ethanol solutions (100 μL) of different concentrations (1.40, 0.70, 0.35, 0.18, 0.09, 0.05, 0.01, 0.005, 0.001, and 0.0005 mg/cm$^3$) of each test material. Filter paper treated with ethanol (100 μL) was used as a negative control. After drying in a hood for 10 min, each filter paper was placed in the lid of a Petri dish (5.5 cm diameter × 1.5 cm). Twenty adult weevils were then placed in the Petri dish, which was covered with a 60 mesh cloth to avoid direct contact with the samples tested, and the lid was replaced to assess the fumigant action. *T. urticae*, *S. oryzae*, and *S. zeamais* adults placed in treated Petri dishes were kept under the same conditions as for rearing. All treatments were replicated three times, and mortalities were recorded after 48 h of treatment.

**Statistical Analysis.** $LC_{50}$ values were determined and transformed to arcsine square root values for analysis of variance (ANOVA).[14] The effects of each treatment were determined to be significantly different at $P < 0.05$.

## RESULTS AND DISCUSSION

The acaricidal and insecticidal toxicities of the methanol extract and the five fractions (hexane, chloroform, ethyl acetate, butanol, and water-soluble) obtained from *C. colocynthis* fruits are shown in Table 1, from evaluations using the leaf disk, contact toxicity, and fumigant toxicity applications against *T. urticae*, *S. oryzae*, and *S. zeamais*. Significant differences were observed in the acaricidal and insecticidal toxicities against the different insects. Upon examination of the methanol extract of the *C. colocynthis* fruits, a clear dose−response relationship was observed against *S. oryzae* and *S. zeamais*. Moreover, the chloroform and hexane fractions produced strong and weak insecticidal toxicities against *Sitophilus* spp., respectively. However, no activity was observed from the ethyl acetate, butanol, and water-soluble fractions (data not shown). When tested against *T. urticae*, the methanol extract of *C. colocynthis* fruits and its fractions showed a dramatic decrease in the acaricidal toxicity during the leaf disk bioassay. No mortality was observed for the negative controls (solvent only). These results indicate that the acaricidal and insecticidal toxicities of plant-derived materials can have different potencies depending on the species of insect investigated.

Due to the strong insecticidal toxicities observed from the chloroform fraction of the methanol extract of *C. colocynthis* fruits, the active constituent was isolated from this fraction by silica gel column chromatography and preparative HPLC. Structural determination of the isolated constituent was performed by spectroscopic analyses, including EI/MS, $^1$H NMR, $^{13}$C NMR, COSY, DEPT, and HMQC NMR and then by direct comparison with an authentic reference compound. The active compound was characterized as 4-methylquinoline. It was identified on the basis of the following evidence: 4-methylquinoline ($C_{10}H_9N$); EI/MS (70 eV) $m/z$ M$^+$ 143 (100, base peak), 135 (40), 105 (39), 107 (40), 79 (46), 51 (13); $^1$H NMR ($CD_3OD$, 600 MHz) $\delta$ 2.61 (s), 7.26−7.27 (d, $J$ = 6.7 Hz), 7.42−7.43 (t, $J$ = 6.9 Hz), 7.63−7.75 (t, $J$ = 83.1 Hz), 8.00−8.05 (d, $J$ = 35.7 Hz), 8.09−8.11 (d, $J$ = 7.3 Hz), 8.42−8.43 (d, $J$ = 1.6 Hz); $^{13}$C NMR ($CD_3OD$, 150 MHz) $\delta$ 150.6, 148.2, 135.5, 130.0, 128.5, 128.1, 126.5, 124.4, 122.9, 19.6. The spectroscopic data of authentic 4-methylquinoline were found to be similar to those of the previous data.[10,15]

The acaricidal and insecticidal activities of 4-methylquinoline isolated from *C. colocynthis* fruits and structurally related analogues against three insect pests were evaluated using the leaf disk, contact toxicity, and fumigant toxicity bioassays. Acaricidal activities of 4-methylquinoline and its structural analogues against *T. urticae* were examined by the leaf disk method (Figure 2). On the basis of the 48 h mortality rates, the

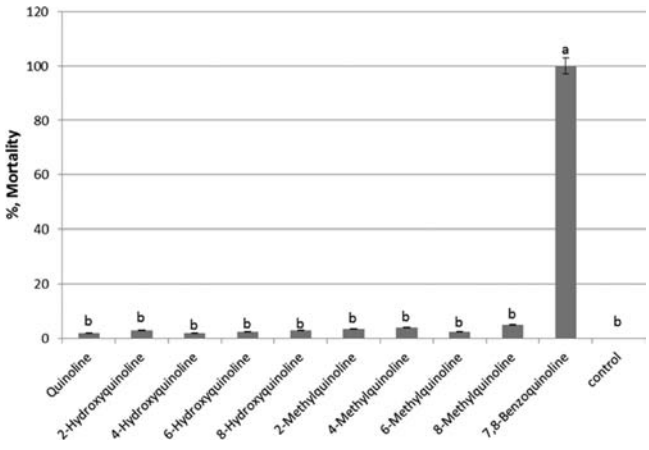


**Figure 2.** Responses of *T. urticae* adults to 4-methylquinoline and its structural analogues, determined by a leaf disk assay at 1.0 mg/mL, at 48 h. Twenty adults per replicate; 3 replicates per treatment; $n$ = 60. Mean values corresponding to each treatment with the same letters are not significantly different ($P$ = 0.05; Scheffe's test).

analogue 7,8-benzoquinoline demonstrated the highest mortality (100% at 1.0 mg/mL). However, other compounds (quinolone, 2-hydroxyquinoline, 4-hydroxyquinoline, 6-hydroxyquinoline, 8-hydroxyquinoline, 2-methylquinoline, 4-methylquinoline, 6-methylquinoline, and 8-methylquinoline) were found to have no acaricidal activity against *T. urticae*. The excellent acaricidal activity of 7,8-benzoquinoline against *T. urticae* was compared with that of a synthetic acaricide (abamectin) (Table 2). On the basis of the $LC_{50}$ values to *T. urticae* calculated from the leaf disk method, 7,8-benzoquinoline (0.017 μg/mL) was determined to be 31.06 times more toxic than abamectin (0.528 μg/mL). These results indicate that 7,8-benzoquinoline was the most effective for control of *T. urticae*, due to the low concentration required to produce strong activity.

The insecticidal activities of 4-methylquinoline and its structural analogues against *S. oryzae* and *S. zeamais* were tested on the basis of their active radicals ($R_1$, $R_2$, $R_3$, and $R_4$) by comparing the $LC_{50}$ values using contact toxicity and a fumigant toxicity bioassay (Tables 3 and 4). From the 48 h $LC_{50}$ values obtained with the contact toxicity bioassay, the most toxic compound against *S. ozryae* was 8-methylquinoline (0.001 mg/cm$^2$), followed by quinoline (0.071 mg/cm$^2$), 7,8-benzoquinoline (0.077 mg/cm$^2$), 2-methylquinoline (0.094 mg/cm$^2$), 4-methylquinoline (0.132 mg/cm$^2$), 8-hydroxyquinoline (0.163 mg/cm$^2$), and 6-methylquinoline (0.166 mg/cm$^2$). 8-Methylquinoline (0.001 mg/cm$^3$) was also the most toxic compound identified from the fumigant toxicity bioassay against *S. oryzae*, followed by 2-methylquinoline (0.034 mg/cm$^3$), 7,8-benzoquinoline (0.045 mg/cm$^3$), quinoline (0.064 mg/cm$^3$), 6-methylquinoline (0.081 mg/cm$^3$), 4-methylquinoline (0.096 mg/cm$^3$), and 8-hydroxyquinoline (0.109 mg/cm$^3$). Among the 4-methylquinoline analogues, 8-methylquinoline (which has a methyl group at the $R_4$ position in the quinoline


dx.doi.org/10.1021/jf502536e | J. Agric. Food Chem. 2014, 62, 8663−8667

**Table 2. Comparison of Acaricidal Activity of 7,8-Benzoquinoline and Synthetic Acaricide against *T. urticae***

| sample | concn ($\mu$g/mL) | % mortality (mean ± SE) | $LC_{50}$ ($\mu$g/mL) | 95% confidence limit | RT[a] |
|---|---|---|---|---|---|
| 7,8-benzoquinoline | 0.050 | 100.0 ± 0.0 | 0.017 | 0.014−0.019 | 31.06 |
| | 0.025 | 69.4 ± 1.9 | | | |
| | 0.010 | 27.2 ± 1.6 | | | |
| | 0.005 | 11.8 ± 1.1 | | | |
| abamectin | 1.500 | 85.4 ± 1.4 | 0.528 | 0.511−0.543 | 1.00 |
| | 1.000 | 70.3 ± 1.8 | | | |
| | 0.500 | 49.5 ± 0.7 | | | |
| | 0.250 | 39.6 ± 1.3 | | | |
| control (solvent only) | | 0 | | | |

[a]Relative toxicity = $LC_{50}$ value of abamectin/$LC_{50}$ value of 7,8-benzoquinoline.

**Table 3. Contact Toxicity of 4-Methylquinoline and Its Structural Analogues against *Sitophilus* spp. Adults, 48 h**

| | *Sitophilus oryzae* | | | *Sitophilus zeamais* | | |
|---|---|---|---|---|---|---|
| compound | $LC_{50}$ (mg/cm$^2$) | slope ± SE | 95% confidence limit | $LC_{50}$ (mg/cm$^2$) | slope ± SE | 95% confidence limit |
| quinoline | 0.071 | 2.1 ± 0.61 | 0.0515−0.0771 | 0.057 | 2.8 ± 0.74 | 0.0465−0.0701 |
| 2-hydroxyquinoline | >0.210 | | | >0.210 | | |
| 4-hydroxyquinoline | >0.210 | | | >0.210 | | |
| 6-hydroxyquinoline | >0.210 | | | >0.210 | | |
| 8-hydroxyquinoline | 0.163 | 2.3 ± 0.47 | 0.1552−0.1807 | 0.159 | 2.4 ± 0.89 | 0.1438−0.1702 |
| 2-methylquinoline | 0.094 | 3.1 ± 1.05 | 0.0811−0.1095 | 0.078 | 2.5 ± 0.56 | 0.0771−0.0893 |
| 4-methylquinoline | 0.132 | 2.1 ± 0.55 | 0.1255−0.1508 | 0.135 | 2.9 ± 0.67 | 0.1214−0.1431 |
| 6-methylquinoline | 0.166 | 4.7 ± 1.14 | 0.1538−0.1793 | 0.150 | 3.7 ± 1.14 | 0.1414−0.1715 |
| 8-methylquinoline | 0.001 | 1.4 ± 0.74 | 0.0008−0.0017 | 0.001 | 1.9 ± 0.83 | 0.0009−0.0016 |
| 7,8-benzoquinoline | 0.077 | 2.9 ± 0.84 | 0.0624−0.0855 | 0.076 | 2.7 ± 0.96 | 0.0599−0.0820 |
| dichlorvos (positive control) | 0.00043 | 3.5 ± 1.24 | 0.0003−0.0005 | 0.00039 | 2.8 ± 1.08 | 0.0003−0.0004 |
| control (solvent only) | | | | | | |

**Table 4. Fumigant Toxicity of 4-Methylquinoline and Its Structural Analogues against *Sitophilus* spp. Adults, 48 h**

| | *Sitophilus oryzae* | | | *Sitophilus zeamais* | | |
|---|---|---|---|---|---|---|
| compound | $LC_{50}$ (mg/cm$^3$) | slope ± SE | 95% confidence limit | $LC_{50}$ (mg/cm$^3$) | slope ± SE | 95% confidence limit |
| quinoline | 0.064 | 2.1 ± 1.05 | 0.0448−0.0652 | 0.042 | 2.8 ± 0.74 | 0.0381−0.0533 |
| 2-hydroxyquinoline | >0.140 | | | >0.140 | | |
| 4-hydroxyquinoline | >0.140 | | | >0.140 | | |
| 6-hydroxyquinoline | >0.140 | | | >0.140 | | |
| 8-hydroxyquinoline | 0.109 | 3.3 ± 1.08 | 0.0899−0.1204 | 0.094 | 2.8 ± 1.01 | 0.0825−0.1053 |
| 2-methylquinoline | 0.034 | 2.5 ± 0.98 | 0.0244−0.0428 | 0.039 | 3.1 ± 1.21 | 0.0223−0.0551 |
| 4-methylquinoline | 0.096 | 3.1 ± 1.09 | 0.0835−0.1087 | 0.084 | 3.3 ± 1.08 | 0.0638−0.0980 |
| 6-methylquinoline | 0.081 | 4.5 ± 1.47 | 0.0734−0.0907 | 0.063 | 4.1 ± 1.36 | 0.0511−0.0808 |
| 8-methylquinoline | 0.001 | 2.5 ± 0.88 | 0.0009−0.0016 | 0.001 | 2.3 ± 0.53 | 0.0009−0.0016 |
| 7,8-benzoquinoline | 0.045 | 3.3 ± 0.97 | 0.0368−0.0554 | 0.038 | 2.8 ± 1.36 | 0.0255−0.0497 |
| dichlorvos (positive control) | 0.00032 | 3.8 ± 0.74 | 0.0002−0.0004 | 0.00027 | 3.3 ± 0.96 | 0.0002−0.0004 |
| control (solvent only) | | | | | | |

skeleton) showed the most toxicity against *Sitophilus* spp. and was approximately 57.0−71.0 times more effective than quinoline (the parent structure). However, whereas the introduction of a hydroxyl group in the $R_1$, $R_2$, and $R_3$ positions of quinoline showed no activities, introduction at the $R_4$ position caused an increase in insecticidal activities. The insecticidal activities of 4-methylquinoline analogues against *S. zeamais* were similar to those against *S. oryzae*. These results demonstrate that introducing various functional groups (hydroxyl, methyl, and arene) into the quinoline structure can change the insecticdal activity of the compound. In addition, the placement of hydroxyl or methyl groups in the $R_4$ position seems to be very important for increasing insecticidal toxicities against *Sitophilus* spp. Furthermore, 7,8-benzoquinoline (which has an arene group in the quinoline's benzene ring) showed higher potential toxicity than the other quinoline analogues against *T. ureticae*. In our earlier study, we reported that the biological activity depends on the presence of various functional groups in the parent structure (benzene, naphthoquinone, anthraquinone, or quinoline).[16−19] Taken together, introducing or changing the position of the functional groups in the quinoline skeleton had potent acaricidal and insecticidal activities against the three insect species. Our study is the first report on the acaricidal and insecticidal activity of the constituent isolated from *C. colocynthis* fruits against *T. urticae*, *S. oryzae*, and *S. zeamais*.

Recent studies have sought to develop newer and safer control agents to replace older pesticides due to toxicity, pest resistance, and environmental damage.[20] Diwan et al.[21] reported that the acute lethal doses of the methanol extract and water-soluble fraction derived from *C. colocynthis* were 200 and 2000 mg/kg, respectively. According to the safety database,[22] the oral $LD_{50}$ values in mammals of 8-hydroxyquinoline (1200 mg/kg), 2-methylquinoline (1230 mg/kg), and 6-methylquinoline (800 mg/kg) indicate low and moderate acute toxicities. Sakthivadivel and Daniel[23] reported larvicidal activity of the petroleum ether extract of *C. colocynthis* against *Culex quinquefasciatus*, *Anopheles stephensi*, and *Aedes aegypti*. Moreover, quinoline analogues have been widely used as components in the food industry and in traditional medicines for many years.[19,24,25] On the basis of our results, 4-methylquinoline isolated from natural sources and its structurally relative analogues would be good replacements for synthetic pesticides. For this reason, further studies should be conducted to evaluate the effects of the 4-methylquinoline analogues on a wide range of insect pests, as well as to develop formulations to increase the potency and stability.

## AUTHOR INFORMATION


### Corresponding Author

*(H.-S.L.) Phone: +82-63-270-2544. Fax: +82-63-270-2550. E-mail: hoiseon@jbnu.ac.kr.



### Funding

This research was carried out with the support of the Cooperative Research Program for Agriculture Science and Technology Development (Project PJ01004502, Development of integrated pest management techniques using natural products in the grain storage), Rural Development Administration, Republic of Korea.

### Notes

The authors declare no competing financial interest.


## REFERENCES


(1) Akhtar, Y.; Isman, M. B.; Lee, C. H.; Lee, S. G.; Lee, H. S. Toxicity of quinones against two-spotted spider mite and three species of aphids in laboratory and greenhouse conditions. *Ind. Crops Prod.* **2012**, *37*, 536−541.

(2) Johnson, W. T.; Lyon, H. H. *Insects That Feed on Trees and Shrubs*; Cornell University Press: Ithaca, NY, USA, 1991; pp 468−470.

(3) Jeon, J. H.; Kim, M. G.; Lee, H. S. Insecticidal activities of *Ruta chalepensis* leaves-isolated constituent and structure-relationships of its analogues against *Sitophilus oryzae*. *J. Korean Soc. Appl. Biol. Chem.* **2013**, *56*, 591−596.

(4) Kim, S. I.; Yoon, J. S.; Jung, J. W.; Hong, K. B.; Ahn, Y. J.; Kwon, H. W. Toxicity and repellency of origanum essential oil and its components against *Tribolium castaneum* (Coleoptera: Tenebrionidae) adults. *J. Asia−Pac. Entomol.* **2010**, *13*, 369−373.

(5) Jeon, J. H.; Lee, H. S. Acaricidal activity of *Tabebuia impetiginosa* bark-derived constituent against domestic and spider mites (Arachnida: Acari). *J. Korean Soc. Appl. Biol. Chem.* **2011**, *54*, 551−557.

(6) Jeong, E. Y.; Kim, M. G.; Lee, H. S. Acaricidal activity of triketone analogues derived from *Leptospermum scoparium* oil against house-dust and stored-food mites. *Pest Manage. Sci.* **2009**, *65*, 327−331.

(7) Akhtar, Y.; Isman, M. B.; Niehaus, L. A.; Lee, C. H.; Lee, H. S. Antifeedant and toxic effects of naturally occurring and synthetic quinones to the cabbage looper *Trichoplusia ni*. *Crop Prot.* **2012**, *31*, 8−14.

(8) Kim, M. G.; Jeon, J. H.; Lee, H. S. Larvicidal activity of the active constituent isolated from *Tabebuia avellanedae* bark and structurally related derivatives against three mosquito species. *J. Agric. Food Chem.* **2013**, *61*, 10741−10745.

(9) Nguyen, D. M. C.; Seo, D. J.; Park, R. D.; Jung, W. J. Antifungal, nematicidal and antioxidant activity of the methanol extracts obtained from medicinal plants. *J. Appl. Biol. Chem.* **2013**, *56*, 199−204.

(10) Kim, M. G.; Lee, S. E.; Yang, J. Y.; Lee, H. S. Antimicrobial potentials of active component isolated from *Citrullus colocynthis* fruits and structure-activity relationships of its analogues against foodborne bacteria. *J. Sci. Food Agric.* **2014**, *94*, 2529−2533.

(11) Huseini, F. H.; Darvishzadeh, G.; Heshmat, R.; Jafariazar, Z.; Raza, M.; Larijai, B. The clinical investigation of *Citrullus colocynthis* (L.) Schrad fruit in treatment of type 2 diabetic patients: a randomized, double blind, placebo-controlled clinical trial. *Phytother. Res.* **2009**, *23*, 1186−1189.

(12) Marzouk, B.; Marzouk, Z.; Haloui, E.; Fenina, N.; Bouraoui, A.; Aouni, M. Screening of analgesic and anti-inflammatory activities of *Citrullus colocynthis* from southern Tunisia. *J. Ethnopharmacol.* **2010**, *128*, 15−19.

(13) Najafi, S.; Sanadgol, N.; Nejad, B. S.; Beiragi, M. A.; Snadgol, E. Phytochemical screening and antibacterial activity of *Citrullus colocynthis* (Linn.) Schrad against *Staphylococcus aureus*. *J. Med. Plant Res.* **2010**, *4*, 2321−2325.

(14) *SAS/STAT User's Guide*, version 9; SAS Institute: Cary, NC, USA, 2004.

(15) Shmidt, E. Y.; Senotrusova, E. Y.; Ushakov, I. A.; Protsuk, N. I.; Mikhaleva, A. I.; Trofimov, B. A. Eletrophilic addition of alcohols to 1-vinyl-2-phenylazopyrroles and unexpected formation of 2-methylquinoline. *Russ. J. Organ. Chem.* **2007**, *43*, 1502−1508.

(16) Yang, Y. C.; Lim, M. Y.; Lee, H. S. Emodin isolated from *Cassia obtusifolia* (Leguminosae) seed shows larvicidal activity against three mosquito species. *J. Agric. Food Chem.* **2003**, *51*, 7629−7631.

(17) Yang, J. Y.; Cho, K. S.; Chung, N. H.; Kim, C. H.; Suh, J. W.; Lee, H. S. Constituents of volatile compounds derived from *Melaleuca alternifolia* leaf oil and acaricidal toxicities against house dust mites. *J. Korean Soc. Appl. Biol. Chem.* **2013**, *56*, 91−94.

(18) Lee, H. S. Acaricidal activity of constituents identified in *Foeniculum vulgare* fruit oil against *Dermatophagoides* spp. (Acari: Pyroglyphidae). *J. Agric. Food Chem.* **2004**, *52*, 2887−2889.

(19) Lee, C. H.; Jeon, J. H.; Lee, S. G.; Lee, H. S. Insecticidal properties of Euphorbiaceae: *Sebastiania corniculata*-derived 8-hydroxyquinoline and its derivatives against three planthopper species (Hemiptera: Delphacidae). *J. Korean Soc. Appl. Biol. Chem.* **2010**, *53*, 464−469.

(20) Kim, M. G.; Yang, J. Y.; Lee, H. S. Acaricidal potentials of active properties isolated from *Cynanchum paniculatum* and acaricidal changes by introducing functional radicals. *J. Agric. Food Chem.* **2013**, *61*, 7568−7573.

(21) Diwan, F. H.; Abdel-Hassan, I. A.; Mohammed, S. T. Effect of saponin on mortality and histopathological changes in mice. *East Mediterr. Health J.* **2000**, *6*, 345−351.

(22) Sigma-Aldrich. *Material Safety Data Sheet (MSDS): Toxicological Information, Section 11*; Sigma-Aldrich: St. Louis, MO, USA, 2010.

(23) Sakthivadivel, M.; Daniel, T. Evaluation of certain insecticidal plants for the control of vector mosquitoes viz. *Culex quinquefasciatus*, *Anopheles stephensi* and *Aedes aegypti*. *Appl. Entomol. Zool.* **2008**, *43*, 57−63.

(24) Jeon, J. H.; Lee, C. H.; Lee, H. S. Antimicrobial activities of 2-methyl-8-hydroxyquinoline and its derivatives against human intestinal bacteria. *J. Korean Soc. Appl. Biol. Chem.* **2009**, *52*, 202−205.

(25) Lee, C. H.; Lee, H. S. Growth inhibiting activity of quinaldic acid isolated from *Ephedra pachyclada* against intestinal bacteria. *J. Korean Soc. Appl. Biol. Chem.* **2009**, *52*, 331−335.

JOURNAL OF AGRICULTURAL AND FOOD CHEMISTRY

Article

pubs.acs.org/JAFC

# Antioxidant Defense and Hepatoprotection by Procyanidins from Almond (*Prunus amygdalus*) Skins

Van-Long Truong,[†] Min-Ji Bak,[†] Mira Jun,[‡] Ah-Ng Tony Kong,[§] Chi-Tang Ho,[∥] and Woo-Sik Jeong*[,†]

[†]Department of Smart Foods and Drugs, Department of Food and Life Sciences, College of Biomedical Science and Engineering, Inje University, Gimhae 621-749, Korea

[‡]Department of Food Science and Nutrition, Dong-A University, Busan 604-714, Korea

[§]Department of Pharmaceutics, Ernest Mario School of Pharmacy, , Rutgers, The State University of New Jersey, Piscataway, New Jersey 08854, United States

[∥]Department of Food Science, Rutgers, The State University of New Jersey, New Brunswick, New Jersey 08903, United States

Supporting Information

**ABSTRACT:** Procyanidins, polymeric flavan-3-ols, are known to possess antioxidant, antiatherogenic, and anticarcinogenic properties. In the present study, we investigated the role of almond (*Prunus amygdalus*) skin procyanidins (ASP) in regulating the protein expression of phase II detoxifying and antioxidant enzymes in HepG2 cells and acetaminophen (APAP)-treated hepatotoxic mice. Treatments of ASP significantly induced the expression of phase II enzymes including NAD(P)H:quinone-oxidoreductase 1, catalase, glutathione peroxidase, and superoxide dismutase in the cells and mice. ASP also potently enhanced the expression of nuclear factor-E2-related factor 2 (Nrf2) and antioxidant response element (ARE)-reporter gene activity in vitro. APAP-induced hepatotoxic markers including AST and ALT in mice were inhibited by ASP administration. However, regulation of upstream kinases by ASP was different between in vitro and in vivo models. Collectively, ASP could induce the activation of Nrf2/ARE-mediated phase II detoxifying/antioxidant enzymes but with differential regulation on upstream kinases between in vitro and in vivo.

**KEYWORDS:** *Prunus amygdalus, almond skin, procyanidins, Nrf2, ARE, antioxidant enzymes, MAPKs, cytoprotection, acetaminophen, hepatotoxicity*

## INTRODUCTION

One of the important strategies of chemopreventive phytochemicals against cancer is the activation of cellular defensive mechanisms to block or prevent cells/tissues from exposure to carcinogens including chemical carcinogens and reactive oxygen species (ROS).[1,2] This could be achieved from the induction of the phase II detoxifying and/or antioxidant enzymes such as heme oxygenase-1 (HO-1), NAD(P)H:quinoneoxidoreductase 1 (NQO1), catalase (CAT), superoxide dismutase (SOD), glutathione peroxidase (GPx), and glutathione *S*-transferase (GST). Most of these enzymes are known to contain a specific nucleotide sequence called antioxidant response element (ARE) in their 5′-upstream promoter region and regulated by the nuclear factor-E2-related factor 2 (Nrf2), a member of CNC family of bZIP transcription factor.[3,4] Activation of Nrf2 by stimuli leads to the liberation of Nrf2 from Keap1 (a cytosolic repressor, Kelch-like ECH-associated protein 1) and facilitates Nrf2 translocation to the nucleus, where it heterodimerizes with small Maf proteins and transcriptionally activates ARE-mediated phase II detoxifying and antioxidant genes.[5] Many studies have indicated that the mechanism of signal transduction for the activation of Nrf2 and Nrf2/ARE-driven detoxifying and antioxidant enzymes is related to the activation of the upstream protein kinases including mitogen-activated protein kinases (MAPKs), protein C kinase (PCK), and phosphatidylinositol-3-kinase (PI3K) via phosphorylation.[6,7]

Acetaminophen (APAP) is a well-known and widely used analgesic and antipyretic drug that is regarded safe at therapeutic doses.[8] However, an overdose of APAP can lead to severe liver damage resulting from the formation of the highly reactive intermediate *N*-acetyl-*p*-benzoquinone imine (NAPQI) due to saturation and incompletion of detoxifying metabolism of APAP by glucuronidation and sulfation.[9] The covalent binding of NAPQI to cellular macromolecules can lead to series of molecular events, including protein alkylation, membrane lipid peroxidation, and formation of ROS and reactive nitrogen species (RNS), which are responsible for acute liver failure.[10] These events lead to a decline of intracellular defense system consisting of various antioxidant enzymes, which results in cell death caused by oxidative stress.[11]

Procyanidins are phenolic polymers mainly composed of the monomeric flavan-3-ol units such as (+)-catechin and (−)-epicatechin, and they are found in various fruits, vegetables, nuts, seeds, and grains.[12] Biological activities of procyanidins may depend on their isomerization, monomer bonding type, and degree of polymerization. Recent reports support that the consumption of dietary procyanidins is an

Received: June 7, 2014
Revised: July 26, 2014
Accepted: July 31, 2014
Published: July 31, 2014

ACS Publications © 2014 American Chemical Society



dx.doi.org/10.1021/jf5027247 | J. Agric. Food Chem. 2014, 62, 8668−8678

important strategy to promote health due to their beneficially biological properties, such as prevention of cardiovascular diseases and cancer.[13,14] Procyanidins have also been well-known as a strong anti-inflammatory agent both in vitro and in vivo by modulating nuclear factor κB (NF-κB) and MAPKs pathways.[15,16] Almond skin has been reported to contain abundant phenolic compounds including catechins and the polymer procyanidins with different degrees of polymerization. Existence of catechins, B-type procyanidin dimers, procyanidin trimers, tetramers and A- and B-type oligomers has been determined in almond skins.[17,18] A roasted almond skin has recently been reported to contain a series of procyanidin polymers with up to 11-mer.[19] Although the composition of almond skin procyanidins has been relatively well-characterized, the biological roles of almond skin procyanidins have not been extensively studied. Previous findings on biological properties of almond skin procyanidins have been limited to radical scavenging antioxidant activity, α-amylase inhibition, and metabolic profiles in human.[17−20] However, chemopreventive and cytoprotective roles of almond skin procyanidins (ASP) have been poorly characterized.

In this study, we isolated ASP and evaluated their cytoprotective properties and the underlying mechanism in regulation of Nrf2/ARE pathway in the human hepatoma-HepG2 cell line as well as in the APAP-induced hepatotoxic mouse model.

## MATERIALS AND METHODS

**Reagents.** The skins of almond (*Prunus amygdalus*) resulting from the blanching of almonds were a courtesy gift of Almond Board of California (Modesto, CA). Phloroglucinol and Toyopearl HW-40F were supplied by Sigma Chemical Co (St. Louis, MO). Solvents for column chromatography and HPLC analysis were of HPLC grade and purchased from Fisher Scientific (Springfield, NJ). MTT [3-(4,5-dimethylthiazol-2-yl)-2,5-diphenyltetrazolium bromide], sulforaphane (SFN), DMSO, acetaminophen, and silymarin were purchased from Sigma-Aldrich (St. Louis, MO). The colorimetric aspartate transaminase (AST) and alanine transaminase (ALT) assay kits were supplied by Young-Dong Co. (Seoul, Korea). Anti-Nrf2, anti-NQO1, anti-SOD2, anti-GPx, and horseradish-peroxidase-conjugated antigoat immunoglobulin IgG antibodies were purchased from Santa Cruz Biotechnology Inc. (Santa Cruz, CA). Anti-p-ERK, anti-p-JNK, anti-p-p38, anti-p-Akt, anti-CAT, and horseradish-peroxidase-conjugated antirabbit immunoglobulin IgG were purchased from Cell Signaling Technology (Beverly, MA). U0126 (MEK1/2 inhibitor), SP600125 (JNK inhibitor), SB202190 (p38 inhibitor), and LY294002 (PI3K inhibitor) were purchased from Cell Signaling Technology. All other reagents used in this study were of the highest grade commercially available.

**Preparation of ASP.** ASP was purified from aqueous extracts of almond skins. Briefly, almond skins (100 g) were milled to fine particles and extracted in 70% aqueous acetone for 48 h at room temperature. After the extraction, the solution was filtered twice through Whatman No.1 filter paper, and the acetone was evaporated using a rotary evaporator with vacuum at 35 °C. After removing the lipids by hexane, the aqueous residue was lypophilized to yield a dry powder. The powder sample was dissolved in 50% methanol and loaded onto a size exclusion chromatographic column packed with Toyopearl TSK HW-40-F (Sigma), which was preconditioned by eluting with 50% methanol (three times of column volume). After preconditioning, the loaded sample was washed with 50% methanol to remove monomeric phenolic compounds, and then eluted with 66% acetone to obtain procyanidins isolate. The eluted ASP isolate was further analyzed.

**BuOH-HCl Hydrolysis and Vanillin Assay in Glacial Acetic Acid.** To determine the presence of interflavan units of ASP isolate, a butanol-acid hydrolysis was carried out according to the methods of Guyot et al.[21] and Porter et al.[22] Two and half milliliters of acidic reagent [5% (v/v) concd HCl in BuOH] and 100 μL of iron reagent [2% (w/v) solution of $NH_4Fe(SO_4)_2 12H_2O$ in 2 M HCl] were added to about 5 mg of the procyanidin isolate in a glass screw-capped test tube. The tube was sealed with a screw cap, agitated vigorously, and heated for 40 min at 95 °C. To determine the presence of procyanidin and the degree of polymerization of ASP isolate, the vanillin assay in glacial acetic acid was performed by the method of Butler et al.[23] The isolate was dissolved in a minimum volume of methanol and filled up to 1 mL with glacial acetic acid. The isolate solution was reacted with 5 mL of vanillin reagent consisting of 0.5% vanillin and 4% concd HCl in glacial acetic acid (1:1, v/v) at room temperature for 20 min. The absorbance of the reaction mixture was measured at 510 nm. Catechin was used as a standard.

**Depolymerization of Procyanidins with Phloroglucinol.** Depolymerization of ASP was performed according to the method of Kennedy and Jones[24] with slight modification. ASP (10 mg), phloroglucinol (20 mg), and ascorbic acid (5 mg) were dissolved in 1 mL of 0.1 N HCl in methanol. The mixture was shaken vigorously and reacted at 50 °C for 20 min. After reaction, the solvent was evaporated by a stream of nitrogen gas and dissolved in 500 μL of distilled water. The solution was extracted 5 times with 1 mL of ethyl acetate. The ethyl acetate extracts were combined, and the solvent was removed by nitrogen gas. The residue was dissolved in 500 μL of methanol and analyzed by HPLC-MS.

**HPLC-Mass Spectrometry (MS) Analyses.** HPLC-MS was carried out using a VG Platform II mass spectrometer (Micromass, Beverly, MA) equipped with atmospheric pressure chemical ionization (APCI) probe in the positive ion mode. The HPLC system consisted of a Varian 9012 HPLC equipped with Varian 9050 UV detector and a Supelcosil LC-18 column (250 × 4.6 mm, particle size 5 μm). Detection wavelength was set at 280 nm, and injection volume was 20 μL. The mobile phase included 1% acetic acid (A) and methanol (B) as follows; isocratic: 0% B, 5 min; gradient: 0−15% B, 5−30 min; 15−60% B, 30−65 min; 60−90% B, 65−90 min. The mass was scanned between 50 and 2000 amu. The source temperature was set at 150 °C, and the probe temperature was 450 °C. The cone voltage and the corona discharge were 15 V and 3 kV, respectively. The scan rate and interscan delay were 2 and 0.3 s, respectively.

**Cell Culture and Treatment.** The human hepatoma cell line, HepG2, purchased from American Type Culture Collection (Rockville, MD), was maintained at 37 °C, humidified atmosphere of 5% $CO_2$ in Dulbecco's modified Eagle's medium (DMEM) supplemented with 10% fetal bovine serum (FBS), streptomycin (100 μg/mL), penicillin (100 units/mL), 1% essential amino acids, and 1% glutamax. The culture medium was renewed once after 2 days. HepG2 cells were allowed to grow about 80−90% confluency and then starved overnight with serum-free DMEM medium prior to treatment with either vehicle (DMSO, 0.1%) or various concentrations of ASP for the indicated periods.

**Cell Viability Assay.** The viability of HepG2 cells in medium containing ASP was determined by MTT assay, which is based on the metabolism of mitochondrial succinate dehydrogenase in viable cells. The cells were seeded onto 24-well plates at a density of $5 \times 10^5$ cells/well and incubated at 37 °C, 5% $CO_2$ for 24 h in a complete medium. After starvation, the cells were treated with a series of ASP concentrations for 24 h and followed by incubation with 50 μL of MTT solution (5 mg/mL) at 37 °C for 4 h in dark. A product from MTT metabolism, formazan crystal, was dissolved in DMSO (500 μL/well). The absorbance was read at 570 nm with a microplate reader (BioTek, Winooski, VT). The levels of cell survival were expressed as a percentage of that in 0.1% DMSO-treated control.

**Preparation of Cytosolic and Nuclear Extract.** The cytosolic and nuclear proteins were prepared by using a Nuclear and Cytoplasmic Extraction Reagents kit (Pierce Biotechnology Inc., Rockford, IL) according to the manufacturer's instructions. Protein concentrations were measured by BCA protein assay (Pierce Biotechnology).

**Assay of Reporter Gene Activity.** The HepG2-C8 cell line containing pARE-T1-luciferase reporter gene was previously de-

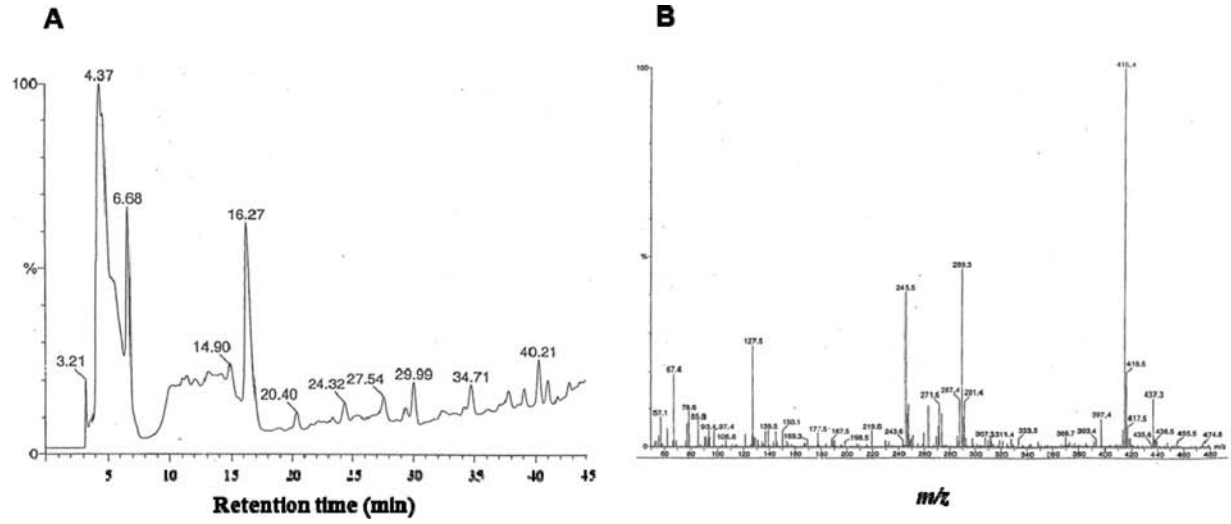


**Figure 1.** HPLC chromatogram of depolymerization products from ASP (A) and APCI-MS spectrum of major peak (peak at 16.27 min) (B).

scribed.[25] ARE-luciferase activity was measured by using luciferase kit (Promega, Madison, WI) following the manufacturer's instruction. Briefly, after treatment with ASP for 12 h, the cells were collected in 1× cell lysis buffer containing 25 mM Tris (pH 7.8 with $H_3PO_4$), 2 mM EDTA, 2 mM DTT, 10% glycerol, 1% triton X-100. After centrifugation, a 10 $\mu$L aliquot of supernatant was assayed for luciferase activity by using GloMax 20/20 luminometer (Promega). Luciferase activity was normalized against total protein concentration, determined by BCA protein assay, and expressed as a fold of induction over that in vehicle-treated control.

**Assay for Antioxidant Enzymes Activity.** For samples from cells, after exposure to ASP for 12 h, the cells were homogenized in ice-cold 50 mM phosphate buffer (pH 7.4) by sonication, followed by centrifugation at 10 000*g* for 20 min to separately obtain supernatant and pellet for further experiments. For samples from mice, liver tissues were collected and homogenized in phosphate buffer (pH 7.0). The protein content was determined using the BCA protein assay (Pierce). CAT activity was determined by the method of Abei[26] following the decrease in absorbance of $H_2O_2$ at 240 nm. One unit of CAT was defined as the amount of enzymes that decomposes 1.0 $\mu$M of $H_2O_2$ in a minute. GPx activity was performed according to the method of Bongdanska et al.[27] A unit of GPx was defined as an amount of enzyme that oxidized 1 nM of NADPH per minute. SOD activity was determined by the method of Oyanagui.[28] The amount of protein required for 50% inhibition in the absorbance at 550 nm was defined as one unit of SOD activity.

**Animals and Experimental Design.** Male Balb/c mice (6 weeks old, 20−25 g) used in the study were obtained from Hyochang Science (Daegu, Korea). The mice were housed in an environmentally controlled room at 25 ± 2 °C, 55−60% humidity, 12 h light/dark cycle and allowed free access to standard laboratory diet and distilled water ad libitum for at least 1 week prior to the experiments. The mice were assigned to six groups ($n$ = 5) and treated as follows: Group1 (control group), animals received only 50% polyglycol as vehicle. Group 2 (ASP group), animals were orally gavaged with 10 mg/kg ASP for three times per week. Group 3 (APAP group), mice were received 50% polyglycol for three times per week and then injected intraperitoneally (ip) with a single dose of APAP (300 mg/kg) in 10 mL/kg saline. Groups 4 and 5 (APAP + ASP group), animals were orally administered with 1 or 10 mg/kg of ASP, per os three times per week and then were exposed to APAP (300 mg/kg, ip) 2 h after the last dose of ASP. Group 6 (APAP + silymarin group), silymarin (50 mg/kg) was administered for three times per week and followed by single dose of APAP (300 mg/kg) once only. Silymarin has been well-known as a natural hepatoprotective agent in treatment of toxic liver diseases and is therefore considered as a positive control in this experiment.[29] Eight hours after APAP administration, the mice were sacrificed to obtain their blood and livers for further biochemical analysis.

**Measurement of Serum ALT and AST Levels in APAP-Treated Mice.** The level of liver damage was determined by detecting the enzymatic activities of plasma ALT and AST. Blood samples from mice were centrifuged at 3000*g* at 4 °C for 10 min, and the ALT and AST activities in serum supernatant were measured using commercially available kits (Youngdong Tech Co., Ltd).

**Western Blot Analysis.** For samples from cells, HepG2 cells were washed with ice-cold PBS (pH 7.4) after treatments, and cells were lysed in 200 $\mu$L of cold cell lysis buffer (20 mM Tris-HCl (pH 7.4), 150 mM NaCl, 1 mM $Na_2EDTA$, 1 mM EGTA, 1% triton, 2.5 mM sodium pyrophosphate, 1 mM $\beta$-glycerophosphate, 1 mM $Na_3VO_4$, 1 $\mu$g/mL leupeptin, 1 mM phenylmethanesulfonyl fluoride) on ice, for 1 h. To analyze protein expression, the proteins (40 $\mu$g) of each sample, normalized by BCA protein assay kit (Pierce), were resolved on SDS-PAGE gels and then transferred onto polyvinylidene fluoride membranes using semidry transfer system (Bio-Rad, Hercules, CA). The membranes were then blocked in PBST (0.1% Tween 20 in phosphate-buffered saline) containing 5% nonfat dried milk for 2 h at 4 °C and followed by incubation with specific primary antibodies overnight at 4 °C. After hybridization with primary antibodies, the membranes were washed with PBST four times, incubated with horseradish-peroxidase-conjugated antirabbit or antigoat immunoglobulin IgG secondary antibodies for 3 h at 4 °C, and washed with PBST four times. Finally, blots were visualized using enhanced chemiluminescence Western blotting reagents (Santa Cruz Biotechnology). For samples from mice, liver tissues were collected and homogenized in cell lysis buffer. Liver tissue homogenates were then centrifuged at 13 000 rpm for 10 min, 4 °C to obtain supernatants. The analytical procedure was the same as that mentioned above.

**Statistical Analysis.** Data were expressed as means ± SD. Statistical comparisons were evaluated using analysis of variance (ANOVA) followed by Tukey's test. $P < 0.05$ was considered as significant.

## RESULTS

**Isolation and Detection of Procyanidins.** Isolation and purification of ASP was carried out by conventional isolation methods as described in the Materials and Methods section. The presence of procyanidins in ASP isolate was determined by hydrolytic reactions such as BuOH-HCl and vanillin assays. The BuOH-HCl hydrolysis reaction of the ASP isolate in the presence of iron(III) salts and heat (95 °C) produced a deep red color (data not shown). Accordingly, these results indicate the presence of interflavan bonds procyanidins in ASP.[21,22] The

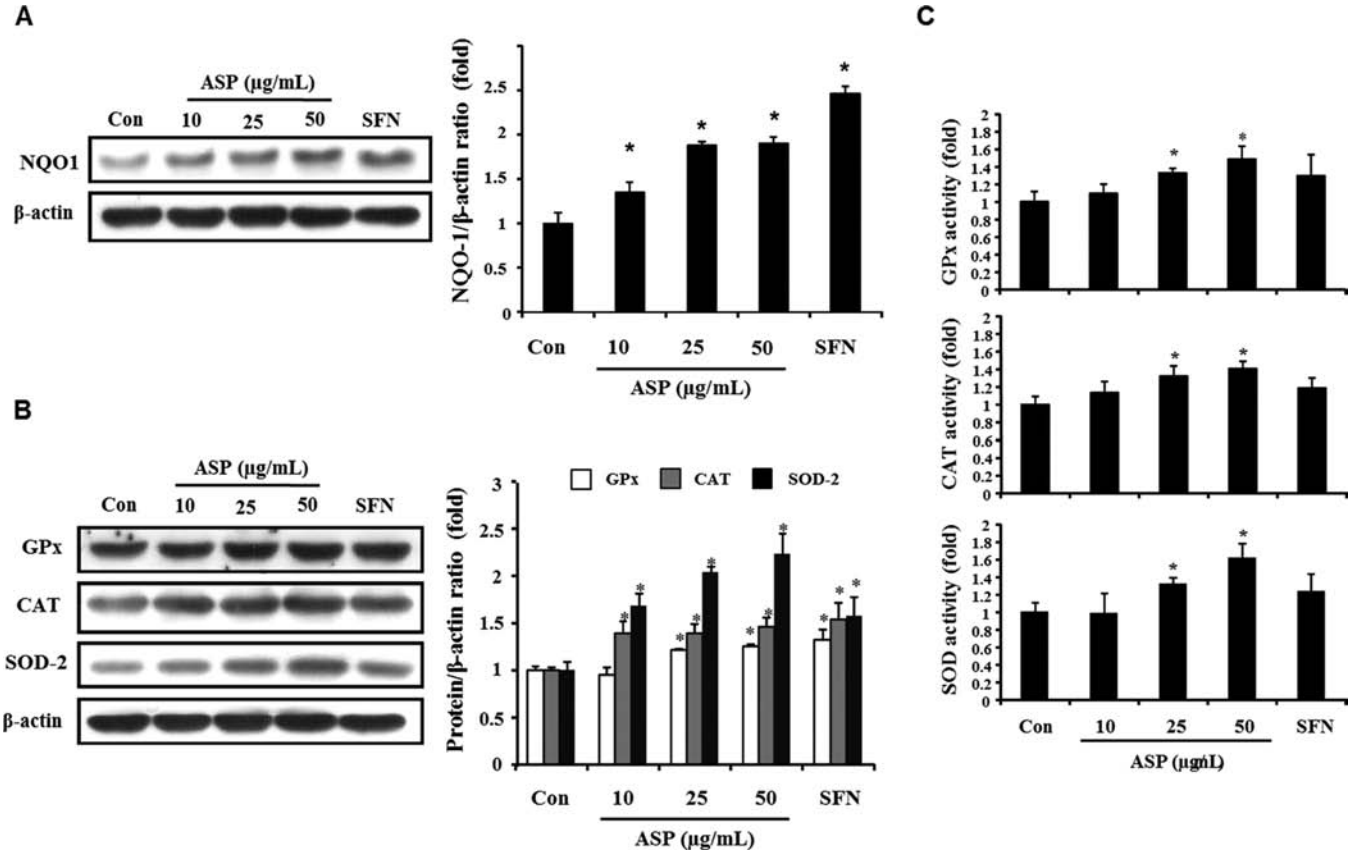


**Figure 2.** Induction of phase II detoxifying and antioxidant enzymes by ASP in HepG2 cells. (A) Protein expression of NQO1. (B) Protein expression of GPx, CAT, and SOD-2. The cells were treated with either vehicle (DMSO 0.1%) or indicated concentrations of ASP for 12 h. Equal amounts of total protein were subjected to Western blotting to analyze the expression of each protein. The results were quantitated by densitometry, and the levels of proteins were normalized with $\beta$-actin. (C) Enzyme activity of GPx, CAT, and Mn-SOD. After treatment with indicated concentration of ASP, the activity of CAT, GPx, and Mn-SOD enzymes was determined, as described in Materials and Method section. Sulforaphane (SFN, 25 $\mu$M) was used as a positive control. Data represent the average ± SD of three independent experiments with the similar results. (*) $p < 0.05$ compared to the vehicle-treated control.

approximate polyphenol content of the ASP isolate by vanillin assay in glacial acetic acid was also carried out. As a result, the ASP isolate showed about 24.1% polyphenol content when catechin, one of major monomeric flavan-3-ol units of procyanidins, was used to standardize this assay. The vanillin assay is a sensitive and simple method to determine flavan-3-ols, dihydrochalcones, and procyanidins. Although the ASP isolate might contain other compounds, the values could be underestimated because the assay has the limitation that only the terminal units of procyanidins react with vanillin in glacial acetic acid. However, this characteristic of the vanillin assay makes it possible to estimate the degree of polymerization. The degree of polymerization can be estimated as the ratio of absorbance of monomer to polymer when measured as the same amount.[23] As a result, the polymerization degree of ASP was found to be 4.2.

**HPLC-MS Analysis of ASP.** The ASP was directly analyzed by HPLC with C18 column, and a broad hump peak at 280 nm was observed (see the Supporting Information Figure S1), which strongly demonstrated the presence of polymeric procyanidins as major constituents in the isolate. Moreover, depolymerization reaction of the ASP isolate with phloroglucinol permitted the evaluation of ASP composition. The interflavan bonds of procyanidins can be cleaved under acidic condition, releasing extension and terminal subunits. The releasing extension subunit intermediates (electrophiles) can be trapped by phloroglucinols (nucleophiles) to produce detectable adducts.[24] The HPLC-MS analysis permitted the determination of cleavage products from the polymeric almond skin procyanidins. The depolymerization of procyanidins yielded several peaks (Figure 1A). However, except for the peaks before 7 min attributed to solvent, ascorbic acid and phloroglucinol, only one major peak at 16.27 min was observed from the HPLC chromatogram. The mass spectrum of the major peak showed $m/z$ = 415 $[M + H]^+$ as base peak, $m/z$ = 437 $[M = Na]^+$, $m/z$ = 289 $[M - H]^+$, $m/z$ = 245 $[289 - CO_2]$, and $m/z$ = 127 [phloroglucinol + $H]^+$ (Figure 1B). Therefore, the major peak was assigned as phloroglucinol adduct resulting from the reaction between phloroglucinol and flavanol extension unit of polymeric procyanidins. These findings suggest that there is only one predominant flavanol as extension subunits in the polymer, which is either (+)-catechin or (−)-epicatechin. A polymeric procyanidin fraction from unripe almond fruit flesh has been shown to contain only procyanidins presenting (−)-epicatechin in their extension units but with both catechin and epicatechin as terminal units (ratio of 3:2).[30] (+)-Catechin (peak at 20.4 min) and (−)-epicatechin (peak at 24.32 min) as terminal subunits were found in the depolymerization reaction mixture by the HPLC-MS analysis. These compounds were identified by the interpretation of their mass spectrum as well as by comparison of their retention time with standard materials and with the


dx.doi.org/10.1021/jf5027247 | J. Agric. Food Chem. 2014, 62, 8668−8678

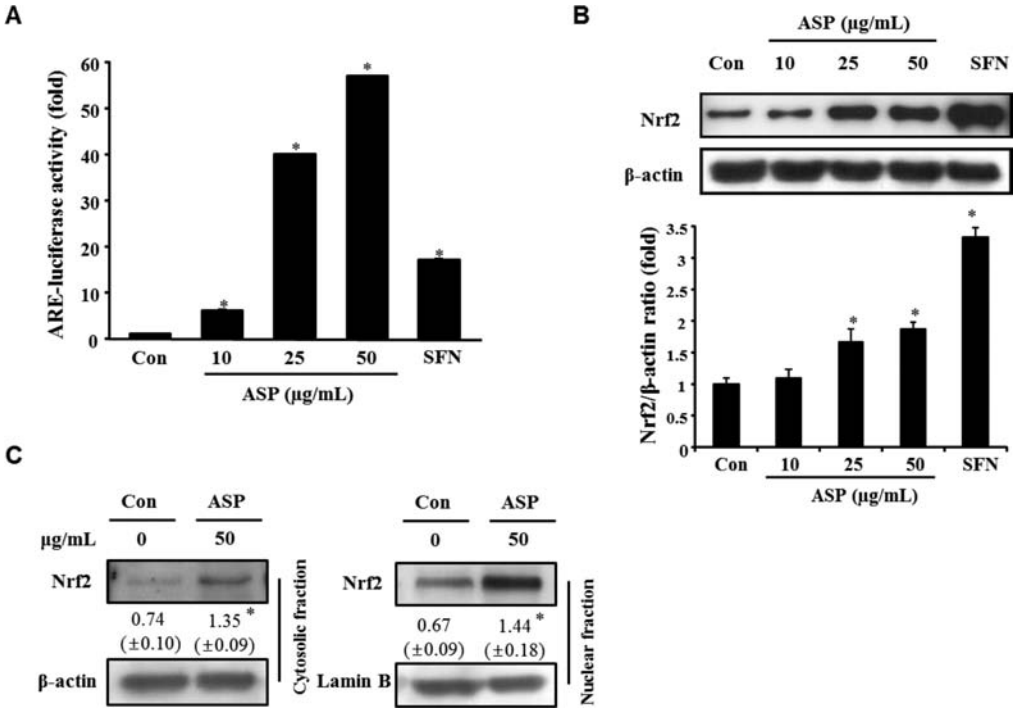


**Figure 3.** Induction of ARE-reporter gene activity and Nrf2 expression by ASP in HepG2-C8/HepG2 cells. (A) ARE-luciferase acidity. HepG2-C8 cells stably transfected with pARE-luciferase reporter gene were treated with either vehicle (DMSO 0.1%) or ASP (10, 25, and 50 $\mu$g/mL) for 12 h. Luciferase activity was normalized with total protein content and expresses as fold induction of vehicle-treated control. (B) Nrf2 expression. HepG2 cells were exposed to either vehicle or indicated concentrations of ASP for 2 h. Equal amounts of total protein were subjected to Western blot analysis using specific antibodies for Nrf2 and $\beta$-actin. (C) Nuclear localization of Nrf2. Cytosolic and nuclear fractions were prepared and analyzed by Western blotting. The results were quantitated by densitometry, and Nrf2 protein levels were normalized with $\beta$-actin (cytosolic fraction) or Lamin B (nuclear fraction). Sulforaphane (SFN, 25 $\mu$M) was used as a positive control. All data represent means ± SD of three independent experiments. (*) $p < 0.05$ compared to the vehicle-treated control.

literature.[24,31] The amount of these terminal subunits was quite small compared to the extension subunits, suggesting that the almond skin polymeric procyanidins might have a very high degree of polymerization. The HPLC-MS analysis also showed compounds with MW 576, $m/z$ = 577 $[M + H]^+$ (peak at 29.99 min). The molecular ion at 577 is two units lower than the (epi)catechin dimer with C−C interflavan bond, indicating that the presence of A-type double interflavan linkage.[30] A- and B-type procyanidins have been found in almond skin with polymerization degrees from dimer to 11-mer.[18,19,30]

**Expression and Activity of Phase II/Antioxidant Enzymes by ASP in HepG2 Cells.** To determine the appropriate concentrations of ASP in HepG2 cells, cell viability was determined after treatments with various concentrations of ASP (0−200 $\mu$g/mL) using the MTT assay. Over 90% of the cells survived after treatments with up to 100 $\mu$g/mL ASP for 24 h and 80% at the dose range 100−200 $\mu$g/mL (see the Supporting Information Figure S2). Based on the cell viability data, doses below 50 $\mu$g/mL of ASP were used for further experiments.

Expression of NQO1, a phase II detoxifying enzyme, in HepG2 cells was examined by Western blotting after exposure of cells to 10, 25, and 50 $\mu$g/mL of ASP for 12 h. As illustrated in Figure 2A, ASP treatment significantly increased the NQO1 protein expression in a dose-dependent manner. The maximal induction of NQO1 (1.8 fold) was obtained at 50 $\mu$g/mL ASP, whereas sulforaphane displayed more potent induction of the protein expression (2.3-fold).

To determine the effects of ASP on the expression of antioxidant enzymes, the protein levels of SOD-2, CAT, and GPx were measured after incubating HepG2 cells with ASP. The expressions of all three antioxidant enzymes were significantly and concentration-dependently upregulated by ASP treatment in the cells (Figure 2B). Especially, the protein expression levels of SOD-2 induced by ASP at the indicated dose range were greater than that induced by SFN (25 $\mu$M). These inductions of antioxidant enzymes by ASP have been found to be correlated with the activity of these enzymes. Correlation coefficients ($R^2$) between protein expressions and enzyme activities of CAT, GPx, and Mn-SOD are 0.66, 0.83, and 0.82, respectively. As displayed in Figure 2C, ASP treatments resulted in the enhancement of the enzymes' activity, although Mn-SOD activity was most potently induced by ASP at 50 $\mu$g/mL.

**Induction of ARE-Reporter Gene Activity and Nuclear Translocation of Nrf2 by ASP in Cells.** To elucidate whether the induction of phase II detoxifying and antioxidant enzymes by ASP was mediated by activation of Nrf2/ARE pathway, the HepG2-C8 cells stably transfected with a pARE-TI-luciferase reporter gene were treated with ASP for 12 h. As illustrated in Figure 3A, the luciferase activity dramatically increased in response to ASP treatments at the indicated doses. The cells exposed to 10, 25, and 50 $\mu$g/mL of ASP displayed the ARE-luciferase activity to 6-, 40-, 55-fold compared to untreated control, respectively. The induction of ARE-luciferase activity by ASP at above 25 $\mu$g/mL was much greater than that induced by SFN (18-fold). Transcription factor Nrf2 is known to play a crucial role in the expression of ARE-mediated phase II detoxifying/antioxidant enzymes such as NQO1, SOD, CAT, and GPx.[32,33] Therefore, we further evaluated whether the

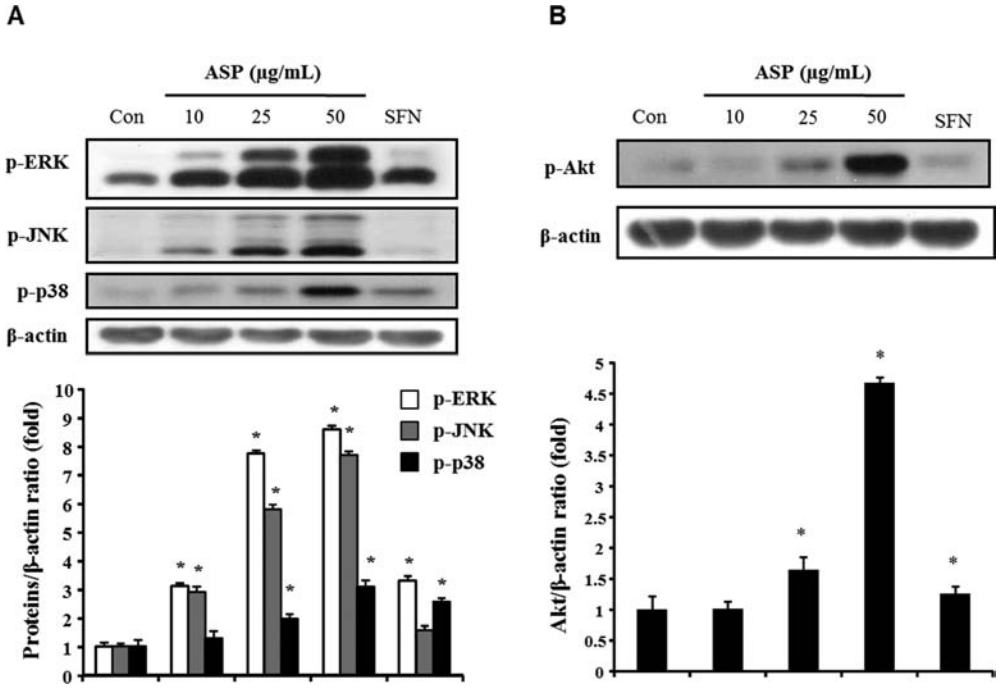


**Figure 4.** Effects of ASP on phosphorylations of MAPKs (A) and Akt (B) in HepG2 cells. The cells incubated in the absence or presence of ASP (10, 25, and 50 $\mu$g/mL) for 1 h were subjected to Western blot analysis using specific antibodies for p-ERK, p-JNK, p-p38, p-Akt, and $\beta$-actin. The intensity of indicated proteins was detected by densitometry and expressed as fold of vehicle-treated control. Sulforaphane (SFN, 25 $\mu$M) was used as a positive control. Each data represents the means ± SD of three independent experiments. (*) $p < 0.05$ compared to the vehicle-treated control.

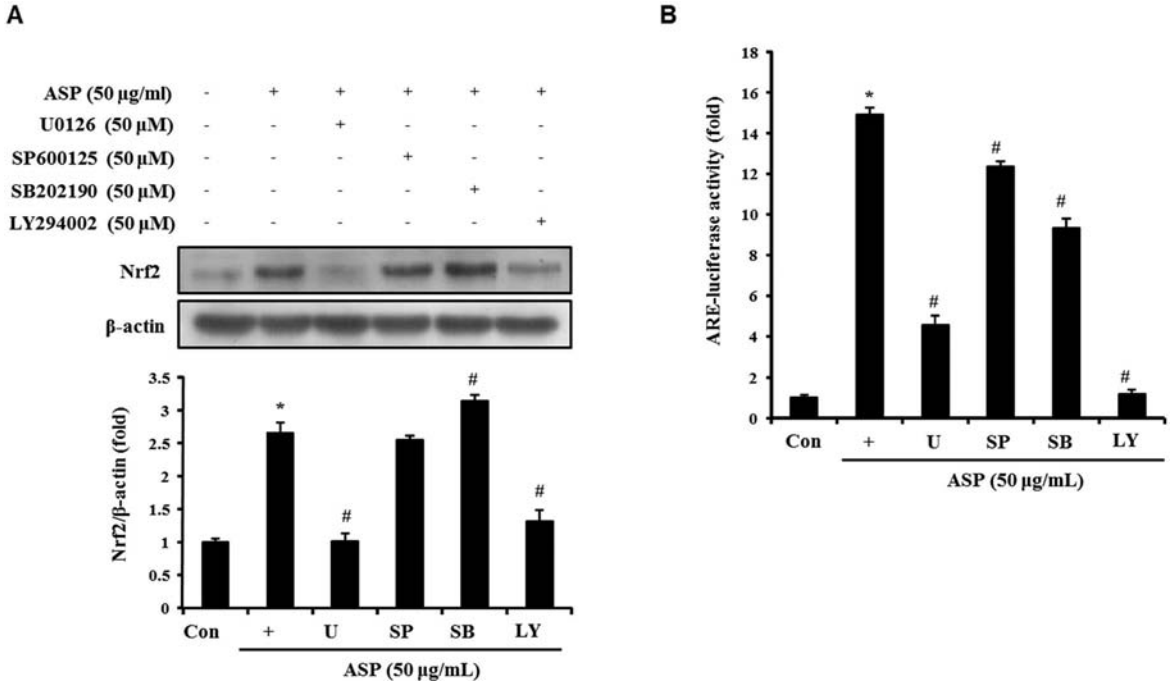


**Figure 5.** Effect of MAPK inhibitors on ASP-induced Nrf2 expression (A) and ARE-luciferase activity (B) in HepG2/HepG2-C8 cells. Cells were pretreated with or without U0126 (MEK1/2 inhibitor), SP600125 (JNK inhibitor), SB202190 (p38 inhibitor), and LY294002 (PI3K inhibitor) for 1 h and then incubated in the absence or presence of ASP (50 $\mu$g/mL) for another 1 h (A) or 12 h (B). The Nrf2 expression was determined by Western blotting, and ARE-luciferase activity was evaluated as described in the Materials and Methods section. The intensity of indicated proteins was detected by densitometry and expressed as fold of vehicle-treated control. Each data represents the means ± SD of three independent experiments. (*) $p < 0.05$ compared to the vehicle-treated control. (#)$p < 0.05$ indicates difference from the ASP alone group.

enhanced expressions of ARE-mediated phase II enzymes by ASP were associated with the induction of Nrf2. As expected, the ASP-treated HepG2 cells exhibited an increased expression of Nrf2 protein in a dose-dependent manner (Figure 3B). Moreover, ASP treatment resulted in the translocation of Nrf2 protein from cytosol to the nucleus (Figure 3C). These data strongly suggest that the induction of phase II detoxifying/antioxidant enzymes by ASP may be mediated by the enhanced

expression and nuclear translocation of Nrf2 in cooperation with ARE.

**Phosphorylations of Upstream Protein Kinases by ASP in Cells.** In order to elucidate whether ASP participates in the Nrf2/ARE-related upstream signaling pathways, we examined the phosphorylations of three MAPK subfamilies including ERK, JNK, and p38 as well as PI3K/Akt. As shown in Figure 4, ASP dramatically and dose-dependently stimulated the phosphorylation levels of all three MAPKs as well as Akt. The phosphorylation levels of ERK, JNK, p38, and Akt by ASP at the highest concentration of 50 $\mu$g/mL reached approximately 8.6-, 7.6-, 3.1-, and 4.6-fold, respectively, compared to that by vehicle-treated control. We further analyzed which upstream kinases were more responsible for the ASP-mediated Nrf2/ARE activation, using specific inhibitors for each kinase: U0126 (MEK1/2 inhibitor), SP600125 (JNK inhibitor), SB202190 (p38 inhibitor) and LY294002 (PI3K inhibitor). Pretreatment with U0126 or LY294002 prior to ASP treatment completely blocked the ASP-induced Nrf2 expression to near basal level, whereas SP600125 and SB202190 were not as effective as U0126 or LY294002 in the blockade of the ASP-induced Nrf2 expression (Figure 5A). Similarly, the ASP-induced ARE-luciferase activity was more effectively suppressed by the inhibitors of ERK and Akt (Figure 5B). Taken together, these results indicate that the ASP-induced activation of Nrf2/ARE-pathway might be at least in part through the activation of ERK and PI3K/Akt pathways in HepG2 cells.

**Effects of ASP on Serum ALT and AST Levels in APAP-Treated Mice.** In the present study, APAP treatment (300 mg/kg) resulted in a dramatic increase in activity of serum ALT and AST, biomarkers of hepatotoxicity,[34] compared to vehicle treatment (Figure 6). Plasma ALT and AST levels increased 9- and 7-fold after an 8 h APAP challenge, respectively, suggesting a significant damage in the hepatocytes by APAP. Preadministrations with ASP at 1 mg/kg and 10 mg/kg, however, significantly attenuated the levels of the ALT and AST activity. Silymarin (50 mg/kg), reported to possess protective capacity against APAP-mediated liver necrosis, similarly inhibited the APAP-elevated activity of ALT and AST. The administration of ASP alone did not affect the basal activity of these transaminases.

**Induction of Nrf2 and Phase II Enzyme Expression by ASP in the Liver of APAP-Treated Mice.** The activation of Nrf2 and phase II enzyme NQO1 in the cell line was further evaluated in APAP-treated animal model. The injection of APAP dramatically lowered the expression of Nrf2 as well as that of NQO1; however, administrations of ASP at both 1 mg/kg and 10 mg/kg restored the reduced expression levels of Nrf2 by APAP to near basal level, whereas administration of ASP alone did not change the basal protein levels (Figure 7). Moreover, the level of NQO1 expression induced by ASP was higher than that induced by the positive control silymarin. Our study is the first in vivo report demonstrating that procyanidins from almond skins have hepatoprotective activity through activation of Nrf2 and Nrf2/ARE-mediated antioxidant defense mechanism.

**Effects of ASP on the Expression and Activity of Antioxidant Enzymes in the Liver of APAP-Treated Mice.** The expression and activity of antioxidant enzymes including SOD-2, GPx, and CAT by ASP were also determined in the APAP-treated mice. Similar to the data observed in Figure 7, the injection of APAP to mice resulted in significant reduction in the expressions of all three antioxidant enzymes. However,

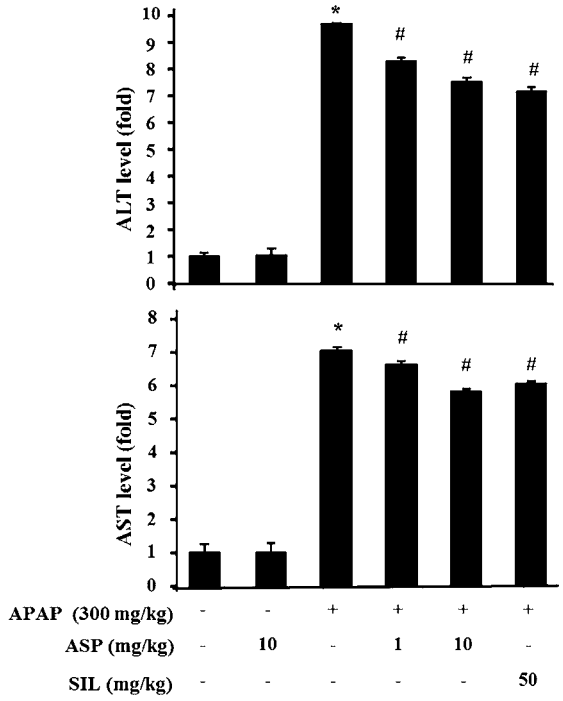


**Figure 6.** Effects of ASP administration on serum ALT and AST levels in APAP-treated mice. Vehicle or ASP (1 or 10 mg/kg) or silymarin (SIL, 50 mg/kg) was orally administered three times per week before intraperitoneal injection of APAP (300 mg/kg) injection. Activities of plasma ALT and AST were measured 8 h after the APAP injection, as described in the Materials and Methods. The data are expressed by means ± SD for five mice. (*) $p < 0.05$, significantly different from the vehicle control group. (#) $p < 0.05$, significantly different from the APAP-treated group.

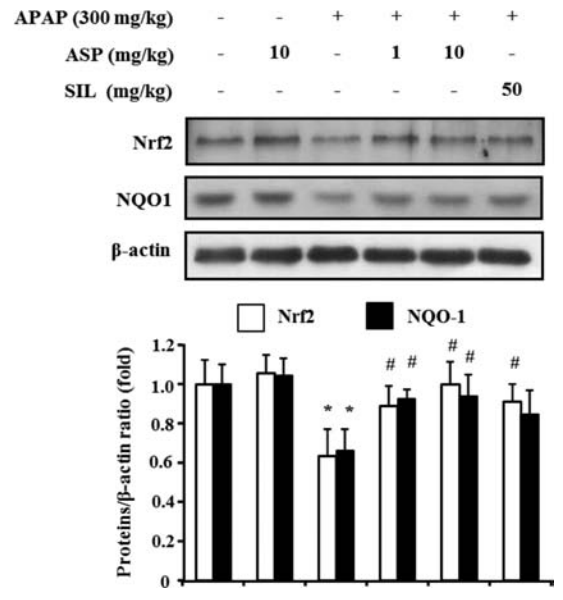


**Figure 7.** Effects of ASP administration on Nrf2 and NQO1 expression in APAP-treated mice liver. Liver tissues were collected at 8 h following APAP challenge to analyze Nrf2 and NQO1. Silymarin (SIL, 50 mg/kg) was used as a positive control. The data are expressed by means ± SD for five mice. (*) $p < 0.05$, significantly different from the vehicle control group. (#) $p < 0.05$, significantly different from the APAP-treated group.


dx.doi.org/10.1021/jf5027247 | J. Agric. Food Chem. 2014, 62, 8668−8678

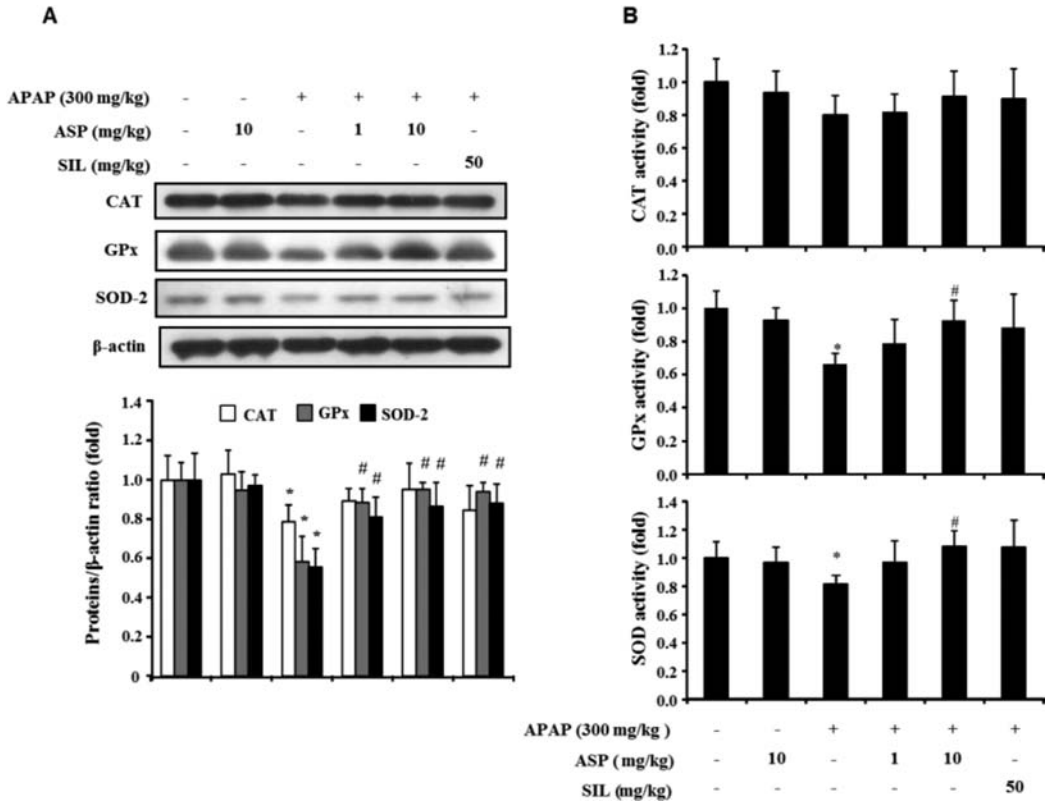


**Figure 8.** Effects of ASP administration on the expression (A) and activity (B) of antioxidant enzymes in APAP-treated mice liver. Liver tissues were collected at 8 h following APAP challenge to analyze antioxidant enzymes. Silymarin (SIL, 50 mg/kg) was used as a positive control. The data are expressed by means ± SD for five mice. (*) $p < 0.05$, significantly different from the vehicle control group. (#) $p < 0.05$, significantly different from the APAP-treated group.

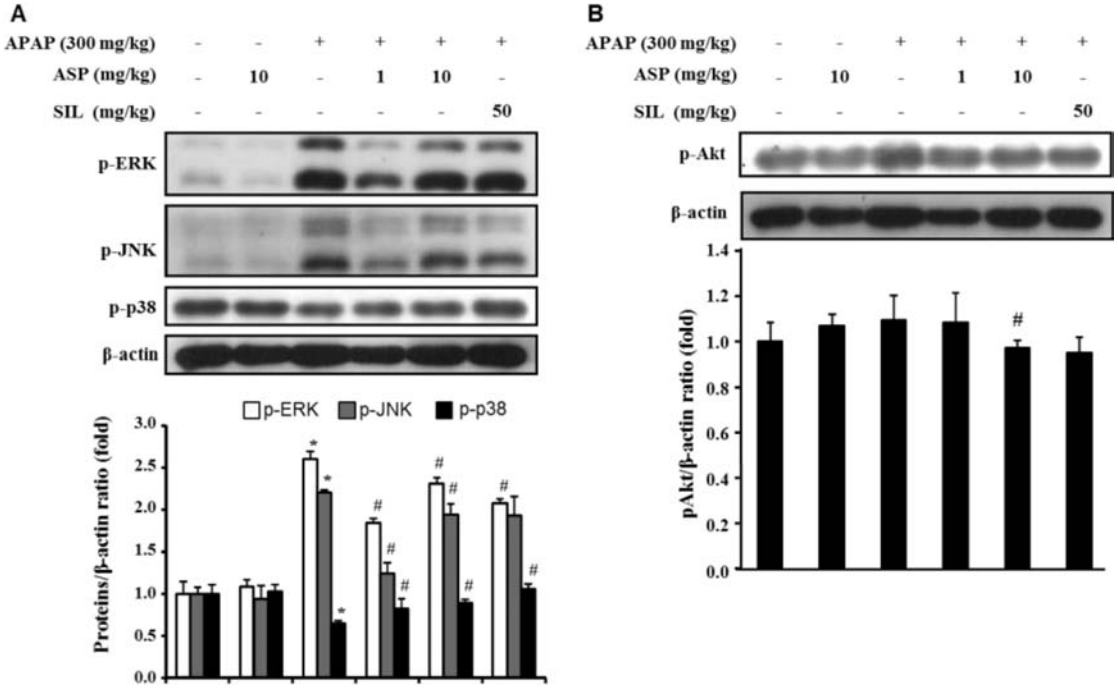


**Figure 9.** Effects of ASP administration on upstream kinases in APAP-treated mice liver. Liver tissues were collected at 8 h following APAP challenge to analyze phosphorylations of ERK, JNK, p38 (A) and Akt (B). Silymarin (SIL, 50 mg/kg) was used as a positive control. The data are expressed by means ± SD for five mice. (*) $p < 0.05$, significantly different from the vehicle control group. (#) $p < 0.05$, significantly different from the APAP-treated group.


dx.doi.org/10.1021/jf5027247 | J. Agric. Food Chem. 2014, 62, 8668−8678

ASP preadministration significantly restored the APAP-reduced protein levels of GPx and SOD-2 at doses of both 1 and 10 mg/kg, although the restoration of CAT expression by ASP was not statistically significant ($p < 0.05$) (Figure 8A). The activity of these antioxidant enzymes was also measured in the differentially treated mouse groups. Similar to the data of protein levels, APAP challenge caused reductions in the enzymes activities; however, only decreases in GPx and Mn-SOD activity were significant but not in CAT activity (Figure 8B). Restoration of GPx and Mn-SOD activity was observed only in ASP 10 mg/kg group. The positive control silymarin was not significantly effective in the restoration of antioxidant enzyme activity decreased by APAP treatment in this mouse model system. These data demonstrated that the enhancement of both expression and activity of hepatic antioxidant enzymes by ASP might contribute to attenuate the acute hepatotoxic effect caused by APAP in mice.

**Effects of ASP on Upstream Kinases in APAP-Treated Mice.** Based on the regulatory roles of ASP on MAPKS observed in cells, we further examined the modulation of MAPKs by ASP in APAP-treated mice. In the present study, exposure of mice to 300 mg/kg of APAP resulted in strong increases in the phosphorylation levels of ERK and JNK (2.3−2.7-fold) (Figure 9A). However, APAP treatment significantly downregulated the phosphorylation level of p38 in the mice. Preadministration of ASP (1 or 10 mg/kg) or silymarin (50 mg/kg) inhibited the APAP-induced phosphorylations of the hepatic ERK and JNK. However, the decreased p38 phosphorylations by APAP were significantly restored by ASP or silymarin preadministrations. The phosphorylation level of Akt was not significantly changed by APAP but significantly lowered in ASP treatment at 10 mg/kg (Figure 9B). Overdose of APAP-caused liver damage in rodents has been related to an early oxidative stress and the involvement of JNK activation.[11] The inhibitory effect on the JNK phosphorylation plays vital role in protection of cell/tissue against APAP toxicity. Saito et al. suggested that the JNK inhibitor SP600125 protects mice against APAP-induced liver injury mainly by preventing the mitochondrial oxidant stress and peroxynitrite formation.[35] A recent study also has demonstrated sustained activation of JNK and ERK by APAP in mice and possible protection by ROS scavenging antioxidant.[36] Additionally, PI3K/Akt pathway has been demonstrated to be involved in hepatotoxicity caused by toxicants such as carbon tetrachloride.[37] However, effects of APAP toxicity on the phosphorylation of Akt have not been fully understood yet.

## DISCUSSION

In the present study, various analytical tools confirmed the existence of procyanidins in almond skins with the average polymerization degree about 4.2. Although the exact structures of ASP still remain unclear due to the structural complexity as well as the variety differences. In spite of the efforts for the structural analyses on almond skin procyanidins, their biological roles and the underlying molecular mechanisms have been largely unknown. Our present study shows the cytoprotective activity of ASP in cells as well as in APAP-induced mice.

Protection of cells/tissues from endogenous and/or exogenous carcinogens has been regarded as a key defense mechanism of cancer chemoprevention by natural products. This can be mainly achieved by the induction of phase II detoxifying/antioxidant enzymes such as NQO1, GST, CAT, GPx, and SOD, which are capable of scavenging ROS, metabolizing and eliminating chemicals and their metabolites.[1,33] In this study, our results indicate that ASP possesses an ability to stimulate these phase II detoxifying and antioxidant enzymes in vitro and in vivo. The phase II detoxifying enzyme NQO1 catalyzes the two-electron reductive metabolism and detoxification of quinones and their derivatives resulting in protection of cells against chemical-oxidative stress and cancer.[38] Moffit et al. have shown enhanced levels of hepatic NQO1 may reduce the reactive NAPQI availability by converting it to the parent APAP compound.[39] Role of cellular defensive phytochemicals against oxidative stress can be roughly classified into two categories; direct scavenger of ROS/free radicals or indirect stimulator of cellular antioxidant defense systems including antioxidant enzymes. The major ROS in the mechanism of APAP-induced hepatotoxicity in mice has been superoxide anion radical ($O_2^-$), which dismutates to molecular oxygen and hydrogen peroxide or reacts with nitric oxide (NO) to form peroxynitrite ($ONOO^-$), a potent oxidant and nitrating species.[10] Our results clearly show that ASP significantly induces the expression and activity of SOD in cell and APAP-treated mice, indicating cytoprotection of liver cells/tissues from APAP damage by ASP-mediated SOD activation. Our findings suggest that ASP potentiates the cellular defense system through activation of phase II and antioxidant enzymes both in vitro and in vivo.

Induction of phase II/antioxidant enzymes has been positively associated with transcription factor Nrf2 expression and its nuclear translocation.[33] Therefore, we assume that the induction of the phase II/antioxidant enzymes and cytoprotection by ASP may be due to the activation of Nrf2/ARE pathway. Our previous study has also proclaimed that procyanidins from wild grape (*Vitis amuresis*) seed is a potential chemopreventive agent that activates the phase II enzymes through the regulation of Nrf2/ARE pathway.[40]

Stress-response kinases have been involved in the regulation of cellular signaling pathways in response to a variety of stresses from both external and internal environments.[1] Previous studies have shown that activation of PI3K/Akt and MAPKs including ERK, JNK and p38 MAPK has been shown to participate in the activation of Nrf2 and induction of ARE-mediated gene expressions in various in vitro and in *vivo* models.[41] Yu et al. have indicated that the induction of phase II detoxifying enzymes by SFN and *tert*-butyl hydroquinone is mediated by activation of ERK pathway.[25] Also, it has been shown that JNK implicates in the induction of phase II enzymes by phenethyl isothiocyanate, whereas p38 MAPK activates Nrf2 in response to quercetin in HepG2 cells.[42,43] Although we have found similar effects of ASP in the activation of Nrf2 and phase II/antioxidant genes both in vitro and in vivo models, however, the modulation of upstream kinases by ASP seems to be different between cell line and mouse model. In the HepG2 cell model, ASP potently upregulated the phosphorylations of all three upstream MAPKs and Akt. Moreover, blockade of ERK and Akt using the corresponding specific inhibitor resulted in the inhibition of ASP-induced Nrf2-ARE activation, indicating involvement of these kinases in ASP-mediated stimulation of cytoprotective mechanisms. However, data on upstream kinases from mice were quite different from those observed in cells. ASP administration did not alter the basal phosphorylation levels of these kinases in the liver of mice while overdose of APAP significantly changed the phosphorylation levels. In addition, APAP seemed to differentially regulate each MAPK in mice; it induced phosphorylation of ERK and JNK but

inhibited that of p38 and did not affect Akt phosphorylation. In any case, however, the pretreatment of ASP significantly changed the phosphorylation levels of these kinases toward basal levels. For example, ASP administration reduced the phosphorylations of ERK and JNK stimulated by overdose of APAP while it induced the phosphorylation of p38 reduced by APAP. The reason for this discrepancy in the regulation of the upstream kinases by ASP between cell line and mouse model is not clear at this moment. However, it might come from difference in bioavailability and/or pharmacokinetics between models in vitro and in vivo or the presence/absence of stimuli (APAP in this case).

Despite of abundant data on biological activities of procyanidins, the in vivo bioavailability and efficacy of procyanidins have been continuously questioned. Procyanidins up to tetramers but not higher degrees of polymer have been shown to be absorbed and present in blood circulation.[44−46] Therefore, ASP with average polymerization degree of 4.2 in our study might be able to be, at least in part, absorbed and exert its cytoprotective activity in the current mouse model. However, further studies on the exact molecular mechanisms and pharmacokinetics of ASP should be followed.

## ■ ASSOCIATED CONTENT

### Supporting Information

Figure S1 shows HPLC chromatogram of almond skin procayanidins. Figure S2 shows the effect of almond skin procyanidins on viability of HepG2 cells. This material is available free of charge via the Internet at http://pubs.acs.org.

## ■ AUTHOR INFORMATION

### Corresponding Author

*E-mail: jeongws@inje.ac.kr. Fax: +82-55-320-0691. Tel.: +82-55-320-3238.

### Funding

This research was supported by Basic Science Research Program through the National Research Foundation of Korea (NRF) funded by the Ministry of Education, Science and Technology (Grant No. 2013R1A1A2012599).

### Notes

The authors declare no competing financial interest.

## ■ ACKNOWLEDGMENTS

We are grateful to the Almond Board of California for providing us the skins of almonds. We also thank to Dr. Paul A. Lachance for his guidance to initiate this research.

## ■ ABBREVIATIONS USED

ASP,almond skin procyanidins; ARE,antioxidant response element; ROS,reactive oxygen species; Nrf2,nuclear factor-E2-related factor 2; CAT,catalase; GPx,glutathione peroxidase; SOD,superoxide dismutase; NQO1,NAD(P)-H:quinoneoxidoreductase 1; MAPK,mitogen-activated protein kinase; ERK,extracellular regulated kinase; JNK,c-Jun N-terminal kinase; PI3K,phosphoinositide 3-kinase; HPLC-MS,high-performance liquid chromatography− mass spectrometry

## ■ REFERENCES

(1) Kong, A.-N. T.; Yu, R.; Hebbar, V.; Chen, C.; Owuor, E.; Hu, R.; Ee, R.; Mandlekar, S. Signal transduction events elicited by cancer prevention compounds. *Mutat. Res.* **2001**, *480−481*, 231−241.

(2) Surh, Y.-J. Cancer chemoprevention with dietary phytochemicals. *Nat. Rev. Cancer* **2003**, *3*, 768−780.

(3) Nguyen, T.; Nioi, P.; Pickett, C. B. The Nrf2-Antioxidant Response Element Signaling Pathway and Its Activation by Oxidative Stress. *J. Biol. Chem.* **2009**, *284*, 13291−13295.

(4) Dhakshinamoorthy, D.; Jaiswal, A. K. Functional characterization and role of INrf2 in antioxidant response element-mediated expression and antioxidant induction of NAD(P)H:quinone oxidoreductase1 gene. *Oncogene* **2001**, *20*, 3906−3917.

(5) Taguchi, K.; Motohashi, H.; Yamamoto, M. Molecular mechanisms of the Keap1−Nrf2 pathway in stress response and cancer evolution. *Genes Cells* **2011**, *16*, 123−140.

(6) Yang, C.-M.; Huang, S.-M.; Liu, C.-L.; Hu, M.-L. Apo-8′-lycopenal Induces Expression of HO-1 and NQO-1 via the ERK/p38-Nrf2-ARE Pathway in Human HepG2 Cells. *J. Agric. Food Chem.* **2012**, *60*, 1576−1585.

(7) Yeh, C.-T.; Yen, G.-C. Involvement of p38 MAPK and Nrf2 in phenolic acid-induced P-form phenol sulfotransferase expression in human hepatoma HepG2 cells. *Carcinogenesis* **2006**, *27*, 1008−1017.

(8) Rumack, B. H. Acetaminophen misconceptions. *Hepatology* **2004**, *40*, 10−15.

(9) Ishibe, T.; Kimura, A.; Ishida, Y.; Takayasu, T.; Hayashi, T.; Tsuneyama, K.; Matsushima, K.; Sakata, I.; Mukaida, N.; Kondo, T. Reduced acetaminophen-induced liver injury in mice by genetic disruption of IL-1 receptor antagonist. *Lab. Invest.* **2009**, *89*, 68−79.

(10) Jaeschke, H.; Knight, T. R.; Bajt, M. L. The role of oxidant stress and reactive nitrogen species in acetaminophen hepatotoxicity. *Toxicol. Lett.* **2003**, *144*, 279−288.

(11) McGill, M. R.; Williams, C. D.; Xie, Y.; Ramachandran, A.; Jaeschke, H. Acetaminophen-induced liver injury in rats and mice: comparison of protein adducts, mitochondrial dysfunction, and oxidative stress in the mechanism of toxicity. *Toxicol. Appl. Pharmacol.* **2012**, *264*, 387−394.

(12) Jeong, W.-S.; Kong, A.-N. T. Biological Properties of Monomeric and Polymeric Catechins: Green Tea Catechins and Procyanidins. *Pharm. Biol.* **2004**, *42*, 84−93.

(13) Corder, R.; Mullen, W.; Khan, N. Q.; Marks, S. C.; Wood, E. G.; Carrier, M. J.; Crozier, A. Oenology: Red wine procyanidins and vascular health. *Nature* **2006**, *444*, 566.

(14) Gossé, F.; Guyot, S.; Roussi, S.; Lobstein, A.; Fischer, B.; Seiler, N.; Raul, F. Chemopreventive properties of apple procyanidins on human colon cancer-derived metastatic SW620 cells and in a rat model of colon carcinogenesis. *Carcinogenesis* **2005**, *26*, 1291−1295.

(15) Bak, M. J.; Truong, V. L.; Kang, H. S.; Jun, M.; Jeong, W. S. Anti-inflammatory effect of procyanidins from wild grape (*Vitis amurensis*) seeds in LPS-induced RAW 264.7 cells. *Oxid. Med. Cell. Longev.* **2013**, *2013* (Article ID 409321), 1−11.

(16) Martinez-Micaelo, N.; González-Abuín, N.; Ardèvol, A.; Pinent, M.; Blay, M. T. Procyanidins and inflammation: Molecular targets and health implications. *BioFactors* **2012**, *38*, 257−265.

(17) Sang, S.; Lapsley, K.; Jeong, W.-S.; Lachance, P. A.; Ho, C.-T.; Rosen, R. T. Antioxidative Phenolic Compounds Isolated from Almond Skins (*Prunus amygdalus* Batsch). *J. Agric. Food Chem.* **2002**, *50*, 2459−2463.

(18) Monagas, M.; Garrido, I.; Lebrón-Aguilar, R.; Bartolome, B.; Gómez-Cordovés, C. Almond (*Prunus dulcis* (Mill.) D.A. Webb) Skins as a Potential Source of Bioactive Polyphenols. *J. Agric. Food Chem.* **2007**, *55*, 8498−8507.

(19) Tsujita, T.; Shintani, T.; Sato, H. α-Amylase inhibitory activity from nut seed skin polyphenols. 1. Purification and characterization of almond seed skin polyphenols. *J. Agric. Food Chem.* **2013**, *61*, 4570−4576.

(20) Bartolome, B.; Monagas, M.; Garrido, I.; Gomez-Cordoves, C.; Martin-Alvarez, P. J.; Lebron-Aguilar, R.; Urpi-Sarda, M.; Llorach, R.; Andres-Lacueva, C. Almond (*Prunus dulcis* (Mill.) D.A. Webb) polyphenols: from chemical characterization to targeted analysis of phenolic metabolites in humans. *Arch. Biochem. Biophys.* **2010**, *501*, 124−33.

(21) Guyota, S.; Doco, T.; Souquet, J.-M.; Moutounet, M.; Drilleau, J.-F. Characterization of highly polymerized procyanidins in cider apple (*Malus sylvestris var. kermerrien*) skin and pulp. *Phytochemistry* **1997**, *44*, 351−357.
(22) Porter, L. J.; Hrstich, L. N.; Chan, B. G. The conversion of procyanidins and prodelphinidins to cyanidin and delphinidin. Phytochemistry. *Phytochemistry* **1986**, *25*, 223−230.
(23) Butler, L. C.; Price, M. L.; Brotherton, J. E. Vanillin assay for proanthocyanidins (condensed tannins): Modification of the solvent for estimation of the degree of polymerization. *J. Agric. Food Chem.* **1982**, *30*, 1087−1089.
(24) Kennedy, J. A.; Jones, G. P. Analysis of Proanthocyanidin Cleavage Products Following Acid-Catalysis in the Presence of Excess Phloroglucinol. *J. Agric. Food Chem.* **2001**, *49*, 1740−1746.
(25) Yu, R.; Lei, W.; Mandlekar, S.; Weber, M. J.; Der, C. J.; Wu, J.; Kong, A.-N. T. Role of a Mitogen-activated Protein Kinase Pathway in the Induction of Phase II Detoxifying Enzymes by Chemicals. *J. Biol. Chem.* **1999**, *274*, 27545−27552.
(26) Aebi, H. Catalase *in vitro*. *Methods Enzymol.* **1984**, *105*, 121−126.
(27) Bogdanska, J. J.; Korneti, P.; Todorova, B. Erythrocyte superoxide dismutase, glutathione peroxidase and catalase activities in healthy male subjects in Republic of Macedonia. *Bratisl. Lek. Listy* **2013**, *104*, 108−114.
(28) Oyanagui, Y. Reevaluation of assay methods and establishment of kit for superoxide dismutase activity. *Anal. Biochem.* **1984**, *142*, 290−296.
(29) Lee, N.-H.; Seo, C.-S.; Lee, H.-y.; Jung, D.-Y.; Lee, J.-K.; Lee, J.-A.; Song, K. Y.; Shin, H.-k.; Lee, M.-Y.; Seo, Y. B.; Kim, H.; Ha, H. Hepatoprotective and Antioxidative Activities of *Cornus officinalis* against Acetaminophen-Induced Hepatotoxicity in Mice. *J. Evidence-Based Complementary Altern. Med.* **2012**, *2012*, 8.
(30) de Pascual-Teresa, S.; Gutiérrez-Fernández, Y.; Rivas-Gonzalo, J. C.; Santos-Buelga, C. Characterization of monomeric and oligomeric flavan-3-ols from unripe almond fruits. *Phytochem. Anal.* **1998**, *9*, 21−27.
(31) Koupai-Abyazani, M. R.; McCallum, J.; Bohm, B. A. Identification of the constituent flavanoid units in sainfoin proanthocyanidins by reversed-phase high-performance liquid chromatography. *J. Chromatogr. A* **1992**, *594*, 117−123.
(32) Cho, H. Y.; Reddy, S. P.; Debiase, A.; Yamamoto, M.; Kleeberger, S. R. Gene expression profiling of NRF2-mediated protection against oxidative injury. *Free Radical Biol. Med.* **2005**, *38*, 325−343.
(33) Dreger, H.; Westphal, K.; Weller, A.; Baumann, G.; Stangl, V.; Meiners, S.; Stangl, K. Nrf2-dependent upregulation of antioxidative enzymes: a novel pathway for proteasome inhibitor-mediated cardioprotection. *Cardiovasc. Res.* **2009**, *83*, 354−361.
(34) Ozer, J.; Ratner, M.; Shaw, M.; Bailey, W.; Schomaker, S. The current state of serum biomarkers of hepatotoxicity. *Toxicology* **2008**, *245*, 194−205.
(35) Saito, C.; Lemasters, J. J.; Jaeschke, H. c-Jun N-terminal kinase modulates oxidant stress and peroxynitrite formation independent of inducible nitric oxide synthase in acetaminophen hepatotoxicity. *Toxicol. Appl. Pharmacol.* **2010**, *246*, 8−17.
(36) Noh, J. R.; Kim, Y. H.; Hwang, J. H.; Gang, G. T.; Kim, K. S.; Lee, I. K.; Yun, B. S.; Lee, C. H. Davallialactone protects against acetaminophen overdose-induced liver injuries in mice. *Food Chem. Toxicol.* **2013**, *58*, 14−21.
(37) Guo, C.; Xu, L.; He, Q.; Liang, T.; Duan, X.; Li, R. Anti-fibrotic effects of puerarin on CCl4-induced hepatic fibrosis in rats possibly through the regulation of PPAR-$\gamma$ expression and inhibition of PI3K/Akt pathway. *Food Chem. Toxicol.* **2013**, *56*, 436−442.
(38) Zhang, M.; An, C.; Gao, Y.; Leak, R. K.; Chen, J.; Zhang, F. Emerging roles of Nrf2 and phase II antioxidant enzymes in neuroprotection. *Prog. Neurobiol.* **2013**, *100*, 30−47.
(39) Moffit, J. S.; Aleksunes, L. M.; Kardas, M. J.; Slitt, A. L.; Klaassen, C. D.; Manautou, J. E. Role of NAD(P)H:quinone oxidoreductase 1 in clofibrate-mediated hepatoprotection from acetaminophen. *Toxicology* **2007**, *230*, 197−206.
(40) Bak, M. J.; Jun, M.; Jeong, W. S. Procyanidins from Wild Grape (*Vitis amurensis*) Seeds Regulate ARE-Mediated Enzyme Expression via Nrf2 Coupled with p38 and PI3K/Akt Pathway in HepG2 Cells. *Int. J. Mol. Sci.* **2012**, *13*, 801−818.
(41) Li, W.; Kong, A.-N. Molecular mechanisms of Nrf2-mediated antioxidant response. *Mol. Carcinog.* **2009**, *48*, 91−104.
(42) Keum, Y.-S.; Owuor, E.; Kim, B.-R.; Hu, R.; Kong, A. N. T. Involvement of Nrf2 and JNK1 in the Activation of Antioxidant Responsive Element (ARE) by Chemopreventive Agent Phenethyl Isothiocyanate (PEITC). *Pharm. Res.* **2003**, *20*, 1351−1356.
(43) Granado-Serrano, A. B.; Martín, M. A.; Bravo, L.; Goya, L.; Ramos, S. Quercetin modulates Nrf2 and glutathione-related defenses in HepG2 cells: Involvement of p38. *Chem. Biol. Interact.* **2012**, *195*, 154−164.
(44) Liu, H.; Zou, T.; Gao, J. M.; Gu, L. Depolymerization of cranberry procyanidins using (+)-catechin, (−)-epicatechin, and (−)-epigallocatechin gallate as chain breakers. *Food Chem.* **2013**, *141*, 488−494.
(45) Shoji, T.; Masumoto, S.; Moriichi, N.; Akiyama, H.; Kanda, T.; Ohtake, Y.; Goda, Y. Apple procyanidin oligomers absorption in rats after oral administration: analysis of procyanidins in plasma using the porter method and high-performance liquid chromatography/tandem mass spectrometry. *J. Agric. Food. Chem.* **2006**, *54*, 884−892.
(46) Tsang, C.; Auger, C.; Mullen, W.; Bornet, A.; Rouanet, J. M.; Crozier, A.; Teissedre, P. L. The absorption, metabolism and excretion of flavan-3-ols and procyanidins following the ingestion of a grape seed extract by rats. *Br. J. Nutr.* **2005**, *94*, 170−181.

JOURNAL OF AGRICULTURAL AND FOOD CHEMISTRY

Article

pubs.acs.org/JAFC

# Membrane Lipid Variability in *Saccharomyces cerevisiae* Wine Strains Rehydrated in the Presence of Metabolic Activators

Patricia Díaz-Hellín,[†] Sergio Gómez-Alonso,[†] Anna Borrull,[§] Nicolas Rozès,[§] Ricardo Cordero-Otero,[§] and Juan Úbeda*[,†]

[†]Tecnología de Alimentos, IRICA, Universidad de Castilla-La Mancha, Edificio Marie Curie, Avenida Camilo José Cela 10, 13071 Ciudad Real, Spain

[§]Departament de Bioquímica i Biotecnologia, Universitat Rovira i Virgili, Marcel·lí Domingo s/n, 43007 Tarragona, Spain

**ABSTRACT:** Slight variations in lipid composition of wine yeast membranes can alter some essential functions including selective nutrient transport and ion permeability. The absence of oxygen during alcoholic fermentation inhibits fatty acid desaturation and sterol biosynthesis, thereby reducing the stress resistance of yeast cells. In this work, membrane lipids in two commercial active dry yeast strains rehydrated in the presence of three activators (ergosterol, tetrahydrofolic acid, and manganese) were studied. Each was assayed at three different concentrations. The effect of these activators on the phospholipid, neutral lipid, and fatty acid contents in cell membranes was assessed. Also, cell viability and fermentation kinetics were determined. Ergosterol was found to shorten the lag phase and improve cell viability and membrane lipid composition; tetrahydrofolic acid raised neutral lipid levels; and manganese(II) increased cell viability and modified phospholipid composition and linoleic acid concentration. All activators interacted with yeasts in a strain-dependent way.

**KEYWORDS:** *Saccharomyces cerevisiae, membrane lipids, fatty acids, active dry yeasts, metabolic activators*

## INTRODUCTION

Wine yeasts suffer osmotic, thermal, nutritional, anaerobic, and toxic stress during alcoholic fermentation. Nutritional and osmotic stresses typically occur in high-sugar musts with poorly available nitrogen, whereas anaerobic−toxic stresses take place in the presence of ethanol and short- and medium-chain fatty acids. Those stressing conditions can lead to stuck or sluggish fermentations.

Inoculation with active dry yeasts (ADYs) is a common winemaking practice. On rehydration, ADYs recover their ability to ferment sugars in the must. The dehydration−rehydration process is cell-damaging; thus, cells lose nucleotides, ions, and most soluble cellular components.[1] However, most rehydrated cells keep their reproductive ability if they are grown under optimum conditions after rehydration.[2] ADY manufacturers address this problem by marketing "fermentation activators", including growth factors, which affect cell replication, and survival factors, molecules that yeasts are unable to produce under anaerobic conditions.[3]

The plasma membrane of *Saccharomyces cerevisiae* is about 7.5 nm thick and exhibits cytoplasmic invagination in some regions. The lipid composition of this membrane strongly influences its tolerance to various types and/or levels of stress, as well as its resistance to toxic compounds such as ethanol, acetic acid, acetaldehyde, and medium-chain fatty acids.[4] In addition, lipid composition of the plasma membrane plays a prominent role in the adaptive response of cells.[5] Small changes in it can alter some essential functions such as ion permeability or transport.[6,7]

Some environmental factors (e.g., temperature, oxygen availability), growth rate, and the presence of sterols can modify the lipid bilayer and/or unsaturated fatty acid composition of yeast cell membranes during alcoholic fermentation. The effect of these modifications includes reducing membrane fluidity and altering some essential functions (particularly selective transport of sugars and amino acids).[8]

Sterols take part in the construction and maintenance of eukaryotic membranes by regulating their permeability and fluidity in addition to their ethanol resistance and plasma $H^+$-ATPase activity.[9] It should be pointed out that ergosterol plays a different role depending on its concentration in the medium.[10] Thus, trace contents of this sterol help trigger cell replication, whereas high levels enable active growth and membrane synthesis. The remarkable enrichment of the plasma membrane in ergosterol parallels the preferential location of cholesterol in the plasma membrane of animal cells.[11] Secretory vesicles are second highest in ergosterol concentration, suggesting that these vesicles contribute to the flow of ergosterol from the endoplasmic reticulum to the plasma membrane.[12] On the other hand, Soubeyrand et al.[13] found the in situ addition of sterols during rehydration enhances the fermentation capacity of yeasts.

Several lipids, which have an important rol in membrane fluidity, exhibit dramatic differences in membrane concentration in a temperature-dependent manner.[14]

Phospholipids (particularly phosphatidylcholine, phosphatidylethanolamine, and, to a lesser extent, phosphatidylserine and phosphatidylglycerol) improve membrane fluidity.[15]

The unsaturation degree of fatty acids largely influences the physical properties of the cell membrane.[14,16] Oleic (C18:1), palmitoleic (C16:1), palmitic (C16:0), and stearic (C18:0) are

Received: February 20, 2014
Revised: July 4, 2014
Accepted: July 9, 2014
Published: July 9, 2014

ACS Publications © 2014 American Chemical Society



dx.doi.org/10.1021/jf500895y | J. Agric. Food Chem. 2014, 62, 8679−8685

the main fatty acids in cell membranes.[17] Besides, fluidity is also governed by the packing degree of these fatty acids. Thus, the less unsaturated and long-chained a fatty acid is, the tighter it packs and the less disordered and fluid is the resulting structure. By contrast, the more unsaturated the fatty acid is, the greater is the fluidity of the membrane and the more easily it can adapt to adverse conditions such as a high ethanol concentration or low temperature during fermentation.[18] Consequently, the correlation of unsaturated fatty acid content with ethanol tolerance is potentially due to increased membrane fluidity. *S. cerevisiae* yields saturated and monounsaturated fatty acids of 16 and 18 carbon atoms, but it is unable to produce polyunsaturated acids (PUFAs).[19]

Nonpolar lipids such as triacylglycerides (TAGs) provide an energy pool for the synthesis of membrane lipids[20] and also serve as precursor pool for phospholipids.

The absence of oxygen during alcoholic fermentation suppresses fatty acid desaturation and sterol biosynthesis, thereby reducing the ability of cells to adapt to the dramatic environmental changes involved in the process.[21]

Díaz-Hellín et al.[22] found rehydration of some commercially available yeast strains with different metabolic activators, such as ergosterol or ascorbic acid, to increase their fermentation capacity and sugar consumption. Ergosterol is a cell membrane component that enhances membrane plasticity under hyperosmotic conditions and thus favors nutrient transport;[23] tetrahydrofolic acid plays a role in energy-generating reactions through the biochemical oxidation of carbohydrates, fats, and proteins; and finally manganese(II) is a component of certain ATP-dependent coenzymes and reactions.

The main purpose of this work was to study the membrane lipid composition of two commercial active dry wine yeast strains following rehydration in the presence of three metabolic activators: ergosterol, tetrahydrofolic acid ($FH_4$), and Mn. The last one was selected instead of other oxidation states because it is involved in specific metabolic cycles. To this end, phospholipid (PL), neutral lipid (NL), and fatty acid (FA) compositions of yeasts cell membranes were determined. Yeast viability and fermentation kinetics were also measured.

## MATERIALS AND METHODS

**Yeast Strains and Metabolic Activators.** Two different commercially available active *S. cerevisiae* ADYs designated L2 and L4 and three activators were selected because they improved the behavior of the studied yeasts.[22] Half a gram of each yeast strain was rehydrated in 4.5 mL of physiological solution (0.9% w/v) at 35 °C for 30 min in the presence of $4.5 \times 10^{-2}$ g/L ergosterol plus $3.0 \times 10^{-2}$ g/L Tween 80 (used as emulsifier), 0.56 g/L tetrahydrofolic acid ($FH_4$), or 1.51 g/L manganese(II) sulfate 1 Hidrate (Sigma). The activators were used at normal dose (N) in addition to half-dose (0.5N) and double dose (2N) for kinetics studies and viability. For lipid membrane assays, normal dose (N) and half-dose (0.5N) were used.

Rehydrated cells in the presence of Tween 80 or 0.9% (w/v) physiological solution were used as controls for each treatment.

**Flow Cytometry Analysis.** Following rehydration, viable cell counts were carried out in duplicate using flow cytometry on CyFlow SPACE equipment (Partec GmbH, Münster, Germany) fitted with a 22 mW ion laser for excitation (488 nm) while monitoring with a single emission channel (575 nm band-pass filter). FloMax software (Quantum Analysis GmbH, Münster, Germany) was used for instrument control, data acquisition, and data analysis. As control of full viabililty (99% by propidium iodide stain), an overnight YPD culture of each reference strain was used.

**Growth Kinetics.** Growth kinetics was examined using a sterile synthetic must (125 g/L glucose, 125 g/L fructose, 4.15 g/L YNB with amino acids, 3 g/L malic acid, 2 g/L tartaric acid, and 0.5 g/L citric acid, at pH 3.7). The initial concentration of viable cells was $5 \times 10^6$ cells/mL. A calibration curve was obtained for cell counts using a Thoma chamber versus optical density (OD) (absorbance at 600 nm) using a spectrophotometer (V-530, JASCO, Tokyo, Japan). Tests were performed in microtitration plates and involved reading the OD at 600 nm at 20 min intervals until stationary growth was reached. Plates were read with a Polar Star Omega ELISA instrument (BMG Labtech GmbH, Ortenberg, Germany). Each determination was performed in octuplicate.

**Lipid Extraction from Rehydrated Yeast Cells.** Prior to lipid extraction, a solution of 100 $\mu$L of methanol and 20 $\mu$L of 0.1 mM EDTA was added to the pellet of rehydrated yeast cells with 1 g of 0.5 mm glass beads (Biospec Products, Bartlesville, OK, USA) in Eppendorf tubes and then mixed for 5 min in a Mini-Beadbeater-8 (Qiagen, Hilden, Germany).[24] Lipid extraction was performed in four steps: The first one involved extracting the organic layer with 200 $\mu$L of methanol and 600 $\mu$L of chloroform under stirring on an Orbit M60 vortexer for 1 h, followed by centrifugation at 5000 rpm for 1 min. This procedure was repeated three times with different extractant combinations: 300 $\mu$L of methanol plus 600 $\mu$L of chloroform, 450 $\mu$L of methanol plus 450 $\mu$L of chloroform, and 600 $\mu$L of methanol plus 300 $\mu$L of chloroform. The volume of organic layer extracted in each run was placed in a glass tube that was cleaned with one-fourth of the total extract volume of an 0.88% (w/v) KCl solution. This was followed by vortexing, cooling at 4 °C for 10 min, and centrifugation at 3000 rpm for 5 min. The organic phase was collected and finally concentrated to dryness under a nitrogen stream in a Supelco solid-phase evaporator. The resulting residue was dissolved in a 2:1 (v/v) chloroform/methanol mixture and stored in an amber-colored vial with a glass insert.

**Separation and Quantification of Phospholipids (PLs) in Cell Membrane by High-Performance Thin Layer Chromatography (HPTLC).** Phospholipids (phosphatidic acid (PA), phosphatidylethanolamine (PE), phosphatidylcholine (PC), and phosphatidylinositol plus phosphatidylserine (PI + PS)) were separated by one-dimensional HPTLC on silica gel plates (10 × 20 cm, 200 $\mu$m) (Merck, Darmstadt, Germany) with chloroform, acetone, methanol, glacial acetic acid, and water (50:15:10:10:5, v/v/v/v/v). Samples were loaded by using a Linomat semiautomatic applicator, and the mobile phase was held in a Camag semiautomatic cell. After the plate had been charred with 10% $CuSO_4$ in 8% $H_3PO_4$ and heated at 180 °C for 4 min,[25] PLs were identified using known standards: phosphatidic acid, phosphatidylethanolamine, phosphatidylcholine, phosphatidylinositol, and phosphatidylserine (Sigma). Calibration curves using standards of every phospholipid at a concentration of 0.5, 1, 2, or 4 $\mu$g/ $\mu$L were constructed. An image of the plate was acquired with an image scanner from Amersham Biosciences (Piscataway, NJ, USA). Each spot of the image was quantified with the software ImageJ (National Institutes of Health, Bethesda, MD, USA). All phospholipids were determined in triplicate.

**Separation and Quantification of Neutral Lipids (NLs) in Cell Membrane by Thin Layer Chromatography (TLC).** NLs (squalene, sterol esters, lanosterol, ergosterol, and free fatty acids) were separated by one-dimensional TLC on silica gel plates (10 × 20 cm, 250 $\mu$m) from Merck. Each plate was developed in three steps with (1) 50:50 (v/v) methyl *tert*-butyl ether (MTBE)/glacial acetic acid, (2) 80:20:1 (v/v/v) hexane/MTBE/glacial acetic acid, and (3) pure hexane. Plates were processed as described in under Separation and Quantification of Phospholipids (PLs) in Cell Membrane by High-Performance Thin Layer Chromatography (HPTLC), and Sigma standards (squalene, cholesteryl oleate, diolein, triolein, lanosterol, ergosterol, and ethyl oleate) were used to quantify NLs: calibration curves were constructed from the application of standards to every plate at a concentration of 0.5, 1, 2, or 4 $\mu$g/ $\mu$L.

**Quantification of Fatty Acids (FAs) in Cell Membrane by Gas Chromatography (GC).** Following rehydration, saturated fatty acids (SFAs; C10:0, C12:0, C14:0, C16:0, and C18:0) and unsaturated fatty acids (UFAs; C14:1, C16:1, C18:1, C18:2. and C18:3) were measured. Also, mean fatty acid chain length (ChL) was determined to ease the interpretation of the results. ChL was calculated according to the

following equation: ChL = Σ $(C_i n_{C,i})/\Sigma C_i$, where $C_i$ corresponds to the "$i$" fatty acid concentration and $n_{C,i}$ is the number of carbon atoms in the mentioned acid.

Sedimented cells ($10^8$ cells/mL) in sealed tubes with a Teflon-lined screw cap were saponified using 1 mL of 5% NaOH in 50% methanol/water[26] and placed in a dry bath (100 °C) for 30 min. After that, the saponified material was cooled at room temperature, and 2 mL of 6 M HCl and 1 mL of $BCl_3$ were added to obtain methylated free fatty acids. Then, samples were heated at 80 °C in the water bath for 10 min. At that point, fatty acid methyl esters were extracted with 1 mL of hexane; samples were vortexed for 30 s, and the organic phase was collected after centrifugation (3000 rpm, 3 min). The extraction step was repeated again, and then the combined organic phase extract was washed with 5 mL of Milli-Q water to remove excess HCl. Finally, the organic extract was dried with anhydrous sodium sulfate ($Na_2SO_4$).

Fatty acid methyl esters were separated on a gas chromatograph model 6890 equipped with a 7863 autosampler (Agilent, Santa Clara, CA, USA), a split/splitless injector, and a flame ionization detector (FID). The capillary column used (50 m long × 0.25 mm i.d.) was coated with a 0.25 μm thick film of SGL-1000 (acidified polyethylene glycol) stationary phase, (Sugelabor, Madrid, Spain). The carrier gas was helium at 1 mL/min, the injection volume 3 μL, and the split ratio 8:1. The injector and detector temperatures were both 250 °C. The temperature program was as follows: 100 °C (held for 3 min), 15 °C/min ramp to 210 °C, and a hold for 20 min. Heptanoic acid (20 mg/mL) and heptadecanoic acid (40 mg/mL) were used as internal standards. The amounts of fatty acids found were related to cell dry weights and expressed as percentages of total fatty acids. The determinations were performed in triplicate.

**Statistical Analysis.** Changes in membrane lipid composition upon rehydration of the ADYs in the presence of the metabolic activators were checked by one-way analysis of variance (ANOVA) at the 95% significance level ($p \leq 0.05$), using Duncan's test (SPSS v. 17.0). Data were processed in triads (i.e., each sample was compared with its corresponding control).

## RESULTS AND DISCUSSION

**Cell Viability.** In a previous work, Díaz-Hellín et al.[22] found that rehydration of L2 in the presence of glutathione and glycerol increased cell viability in this yeast strain after 15 days of fermentation. Likewise, L4 exhibited an increase of viability after rehydration in the presence of tetrahydrofolic acid ($FH_4$) and ascorbic acid.

Some extrinsic variables in relation with the transport and conservation of the dry yeasts could influence this parameter. Dehydrated yeast can lose up to 30% of soluble cell compounds when rehydrated, which proves the nonfunctionality of the cell membrane.[1] A faster reduction in nucleotides and trehalose leakage are therefore beneficial for the vitality of rehydrated yeast cells.[2] As can be seen in Figure 1, L2 exhibited higher viability than L4 in all studied cases. This could be a consequence of a specific strain factor because viability percentages hardly vary compared with controls in both strains.

By exception, ergosterol and manganese increased L2 viability in a statistically significant manner, whereas L4 exhibited significantly increased viability when rehydrated in the presence of manganese irrespective of its dose, contrary to what happened with ergosterol, which produced a significant decrease.

**Growth Kinetics.** Besides the lag period and the asymptotic value, another valuable parameter of the growth curve is the maximum specific growth rate ($\mu_{max}$). Because the logarithm of the absorbance is used, $\mu_{max}$ is given by the slope of the line when the organisms grow exponentially.[27] In this work, the growth kinetics of the two yeast strains in terms of initial population ($N_0$), maximum population ($N_{max}$), specific growth rate ($\mu_{max}$), lag time (T-Lag), and duplication time (T-d) were examined.

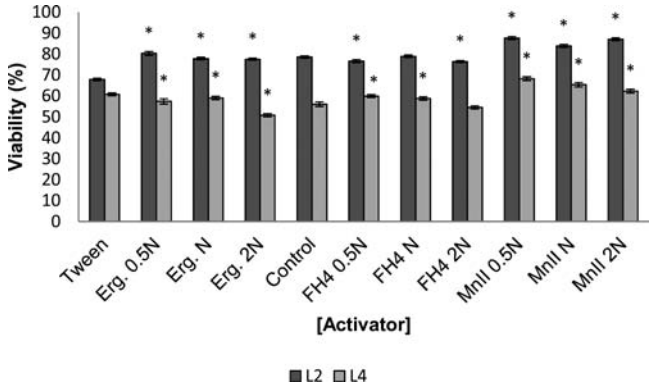


**Figure 1.** Percentage of viability of L2 (black bars) and L4 (gray bars) strains after rehydration with ergosterol (Erg.) + Tween 80, $FH_4$, and Mn(II) at half (0.5N), normal (N), and double (2N) doses. Controls: Tween 80 (rehydration with Tween 80) and control (rehydration with physiological solution). Values are means of $n = 2 \pm$ standard deviations. (*) Significantly different from each control ($p \leq 0.05$, $n = 2$).

L2 reached the stationary growth phase after 38 h of incubation and L4, after 83 h (data not shown). As viability, the lag time (T-Lag) was strain-dependent. Thus, L2 rehydrated in 0.5N ergosterol exhibited a shorter lag phase than both the control and the samples rehydrated with ergosterol at the other two doses (Table 1). It also affected the duplication rate, which was higher than the control and the other evaluated samples. Similar differences were observed in L4 rehydrated with a 0.5N or N dose of ergosterol. As can be seen from Table 1, $\mu_{max}$ and $N_{max}$ for L4 (0.44 $h^{-1}$ and 0.12, respectively) doubled the values for L2 (0.22 $h^{-1}$ and 0.06, respectively), and none of the activators succeeded in increasing them in either strain.

Rehydration in the presence of the tested activators had an effect on either $\mu_{max}$ or $N_{max}$; thus, the strain that started cell division later (L4) grew faster. This could be a result of the fact that the slower the yeast adaptation to the medium, the LAG phase, the better the fermentation kinetic in the LOG phase.

It is noticeable that double doses (2N) did not give remarkable results compared to the other dosages, so it was decided to reject them for further assays.

**Phospholipids and Neutral Lipids.** Overall, PL contents were higher in L2 than in L4 irrespective of the particular rehydration treatment (Figure 2). On the other hand, the NL content was invariably higher in L4 (Figure 3).

The ergosterol treatment significantly increased the content in phosphatidylcholine and phosphatidylinositol−phosphatidylserine in the L2 membrane (Figure 2A), as well as those in all neutral lipids except lanosterol (Figure 3A). Worthy of special note is the accumulation of ergosterol in L2 treated with this activator and also the increase in sterol esters resulting from esterification of sterols. On the contrary, ergosterol had no influence on either the composition or the concentration of the L4 strain phospholipids, except for PA at 0.5N dose, for which concentration diminished significantly (Figure 2B).

$FH_4$ increased the contents in phospholipids and some neutral lipids (squalene, sterol esters, and lanosterol) of L2. By contrast, it caused a slight decrease in the PL concentration of L4 at half-dose (0.5N) and increased it at the normal dose (N), but never overcoming significantly the value of the control.

Manganese(II) affected significantly neutral lipid content in L2 and FA, lanosterol, and squalene for L4. On the other hand, it decreased the contents in all PLs of L4 and only PA in L2 (Figures 2 and 3).


dx.doi.org/10.1021/jf500895y | J. Agric. Food Chem. 2014, 62, 8679−8685

**Table 1. Growth Kinetics of L2 and L4 Strains Rehydrated with Ergosterol + Tween 80, $FH_4$, or Mn(II) at Half (0.5N), Normal (N), and Double (2N) Doses Measured by Means of Optical Density at 600 nm[a]**

| | | | $N_0$[b] | $N_{max}$[b] | $\mu_{max}$ | T-Lag | T-d |
|---|---|---|---|---|---|---|---|
| L2 | Tween 80 | | −0.64 ± 0.03 | 0.06 ± 0.01 | 0.21 ± 0.05 | 6.59 ± 0.70 | 3.23 ± 0.16 |
| | ergosterol | 0.5N | −0.70 ± 0.03 | 0.04 ± 0.01 | 0.16 ± 0.04 | 1.82 ± 0.48 | 4.42 ± 0.20 |
| | | N | −0.70 ± 0.03 | 0.07 ± 0.01 | 0.20 ± 0.04 | 4.90 ± 0.95 | 3.43 ± 0.15 |
| | | 2N | −0.74 ± 0.03 | 0.04 ± 0.01 | 0.23 ± 0.04 | 5.61 ± 0.51 | 3.07 ± 0.14 |
| | control | | −0.68 ± 0.03 | 0.05 ± 0.01 | 0.22 ± 0.05 | 6.03 ± 0.60 | 3.09 ± 0.15 |
| | $FH_4$ | 0.5N | −0.67 ± 0.03 | 0.06 ± 0.01 | 0.20 ± 0.04 | 6.39 ± 0.78 | 3.44 ± 0.15 |
| | | N | −0.73 ± 0.03 | 0.06 ± 0.01 | 0.22 ± 0.04 | 5.52 ± 0.63 | 3.14 ± 0.14 |
| | | 2N | −0.69 ± 0.03 | 0.08 ± 0.01 | 0.19 ± 0.04 | 5.22 ± 0.15 | 3.67 ± 0.16 |
| | Mn(II) | 0.5N | −0.67 ± 0.03 | 0.06 ± 0.01 | 0.20 ± 0.04 | 6.39 ± 0.78 | 3.44 ± 0.15 |
| | | N | −0.73 ± 0.03 | 0.07 ± 0.01 | 0.22 ± 0.04 | 6.03 ± 0.45 | 3.16 ± 0.12 |
| | | 2N | −0.74 ± 0.03 | 0.08 ± 0.01 | 0.23 ± 0.04 | 6.13 ± 0.28 | 2.99 ± 0.11 |
| L4 | Tween 80 | | −1.01 ± 0.01 | 0.12 ± 0.01 | 0.44 ± 0.03 | 10.8 ± 0.3 | 1.57 ± 0.04 |
| | ergosterol | 0.5N | −1.00 ± | 0.12 ± | 0.35 ± | 7.95 ± | 1.99 ± |
| | | N | −0.10 ± 0.02 | 0.09 ± 0.01 | 0.32 ± 0.03 | 6.86 ± 0.58 | 2.17 ± 0.06 |
| | | 2N | −0.99 ± 0.01 | 0.09 ± 0.01 | 0.44 ± 0.03 | 10.1 ± 0.3 | 1.57 ± 0.04 |
| | control | | −1.06 ± 0.01 | 0.10 ± 0.01 | 0.39 ± 0.02 | 9.24 ± 0.29 | 1.79 ± 0.04 |
| | $FH_4$ | 0.5N | −1.04 ± 0.01 | 0.10 ± 0.01 | 0.41 ± 0.02 | 9.67 ± 0.26 | 1.69 ± 0.04 |
| | | N | −1.06 ± 0.01 | 0.11 ± 0.01 | 0.44 ± 0.02 | 10.3 ± 0.2 | 1.57 ± 0.04 |
| | | 2N | −1.00 ± 0.01 | 0.09 ± 0.01 | 0.45 ± 0.03 | 11.8 ± 0.2 | 1.55 ± 0.04 |
| | Mn(II) | 0.5N | −0.95 ± 0.01 | 0.10 ± 0.01 | 0.39 ± 0.02 | 8.56 ± 0.32 | 1.78 ± 0.04 |
| | | N | −1.00 ± 0.02 | 0.10 ± 0.01 | 0.40 ± 0.02 | 10.6 ± 0.4 | 2.00 ± 0.04 |
| | | 2N | −0.98 ± 0.02 | 0.10 ± 0.01 | 0.37 ± 0.02 | 7.59 ± 0.36 | 1.89 ± 0.04 |

[a]Controls: Tween 80 (rehydration with Tween 80) and control (rehydration with phisiological solution). $N_0$, initial population, $N_{max}$, maximum population, $\mu_{max}$, maximum specific growth rate ($h^{-1}$), T-Lag, lag time (h); T-d, duplication time (h). Values are means of $n = 8 \pm$ standard deviation. [b]Logarithmic scale.

**Table 2. Percentage Composition of Fatty Acids (C14:1, C16:0, C16:1, C18:0, C18:1, C18:2, and C18:3) in L2 and L4 Strains Rehydrated with Ergosterol + Tween 80 (A1), $FH_4$ (A2), and Mn(II) (A3) at Half (0.5N) and Normal (N) Doses[a]**

| | | | C14:1 | C16:0 | C16:1 | C18:0 | C18:1 | C18:2 | C18:3 |
|---|---|---|---|---|---|---|---|---|---|
| L2 | Tween 80 | | 0.11 ± 0.04 | 16.0 ± 1.1 | 39.7 ± 0.9 | 6.77 ± 0.22 | 30.6 ± 1.1 | 5.56 ± 0.17 | 0.49 ± 0.01 |
| | ergosterol | 0.5N | 0.15 ± 0.05 | 16.6 ± 0.4 | 37.1 ± 1.1 | 7.43 ± 0.87 | 31.7 ± 0.5 | 5.71 ± 0.49 | 0.35 ± 0.06[b] |
| | | N | 0.08 ± 0.01 | 16.5 ± 0.3 | 41.8 ± 2.0 | 5.82 ± 0.56 | 29.1 ± 1.3 | 5.53 ± 0.21 | 0.43 ± 0.02 |
| | control | | 0.06 ± 0.01 | 16.8 ± 0.6 | 38.4 ± 3.7 | 8.31 ± 1.52 | 29.2 ± 1.7 | 6.00 ± 0.17 | 0.39 ± 0.10 |
| | $FH_4$ | 0.5N | 0.07 ± 0.00 | 16.4 ± 0.6 | 39.9 ± 1.5 | 7.46 ± 0.64 | 28.6 ± 0.9 | 6.26 ± 0.48 | 0.41 ± 0.07 |
| | | N | 0.11 ± 0.01[b] | 17.0 ± 0.5 | 39.5 ± 0.8 | 6.79 ± 0.59 | 29.2 ± 0.5 | 5.99 ± 0.31 | 0.48 ± 0.03 |
| | control | | 0.06 ± 0.01 | 16.8 ± 0.6 | 38.4 ± 3.7 | 8.31 ± 1.52 | 29.2 ± 1.7 | 6.00 ± 0.17 | 0.39 ± 0.10 |
| | Mn(II) | 0.5N | 0.07 ± 0.01 | 17.1 ± 0.9 | 37.3 ± 0.6 | 8.00 ± 0.77 | 30.4 ± 0.4 | 6.01 ± 0.23 | 0.50 ± 0.00 |
| | | N | 0.08 ± 0.01 | 17.0 ± 0.1 | 37.7 ± 1.7 | 7.65 ± 0.85 | 30.5 ± 1.0 | 6.01 ± 0.20 | 0.27 ± 0.02 |
| L4 | Tween 80 | | 0.00 ± 0.00 | 21.2 ± 2.5 | 55.5 ± 8.7 | 6.61 ± 0.56 | 21.7 ± 0.5 | 0.32 ± 0.05 | 0.26 ± 0.11 |
| | ergosterol | 0.5N | 0.28 ± 0.01 | 20.5 ± 1.0 | 49.2 ± 2.8 | 5.30 ± 0.33[b] | 23.3 ± 1.8 | 0.38 ± 0.11 | 0.10 ± 0.02 |
| | | N | 0.25 ± 0.15 | 19.8 ± 1.2 | 48.0 ± 2,4 | 6.89 ± 0.89 | 23.1 ± 1.6 | 0.41 ± 0.28 | 0.12 ± 0.02 |
| | control | | 0.13 ± 0.06 | 19.2 ± 1.4 | 48.5 ± 3.6 | 6.08 ± 0.36 | 22.5 ± 0.2 | 0.03 ± 0.05 | 0.23 ± 0.11 |
| L4 | $FH_4$ | 0.5N | 0.16 ± 0.01 | 19.4 ± 2.2 | 51.3 ± 4.9 | 5.84 ± 0.45 | 22.9 ± 3.2 | 0.24 ± 0.03[b] | 0.46 ± 0.13 |
| | | N | 0.19 ± 0.05 | 18.4 ± 1.1 | 55.6 ± 0.7 | 5.20 ± 1.13 | 21.0 ± 0.2 | 0.31 ± 0.05[b] | 0.54 ± 0.04 |
| | control | | 0.13 ± 0.06 | 19.2 ± 1.4 | 48.5 ± 3.6 | 6.08 ± 0.36 | 22.5 ± 0.2 | 0.03 ± 0.05 | 0.23 ± 0.11 |
| | Mn(II) | 0.5N | 0.06 ± 0.02 | 20.4 ± 1.0 | 50.2 ± 4.5 | 5.82 ± 1.24 | 23.3 ± 2.3 | 0.00 ± 0.00 | 0.13 ± 0.02 |
| | | N | 0.08 ± 0.01 | 20.7 ± 0.2 | 49.8 ± 0.3 | 5.66 ± 0.28 | 23.5 ± 0.2 | 0.17 ± 0.02[b] | 0.13 ± 0.02 |

[a]Controls: Tween (rehydration with Tween 80) and control (rehydration with physiological solution). Values are means of $n = 3 \pm$ standard deviation. [b]Statistically significant differences of the treated sample with respect to its control (one-way ANOVA; $p \leq 0.05$; $n = 3$).

On the basis of the kinetic study results, T-Lag (Table 1), ergosterol (0.5N) was the most efficient activator. Therefore, its presence can have a beneficial effect on both yeasts. Ergosterol has been found to accumulate in cells during the initial fermentation stage;[28] also, it is added together with some amino acids and vitamins to some yeast preparations to accelerate fermentation.[29] As stated above, this compound was the most efficient activator for both yeast strains.

Tween 80 had an unexpected effect: whereas L2 was unaffected by its presence, L4 exhibited increased amounts of all neutral lipids (Figure 3).

**Fatty Acid Composition.** The composition of plasma membrane is especially relevant to the production of industrial

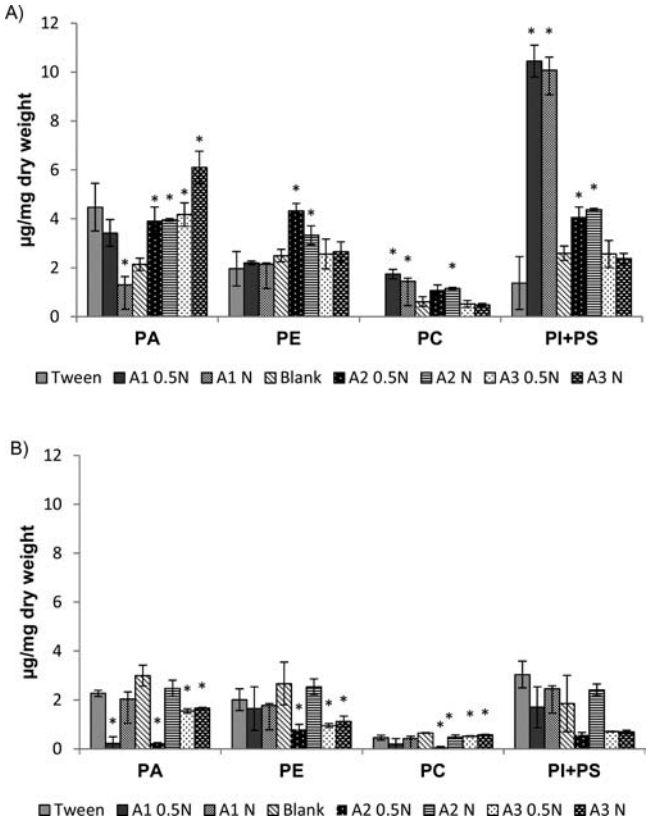


**Figure 2.** Concentrations ($\mu$g/mg dry weight) of phosphatidic acid (PA), phosphatidylethanolamine (PE), phosphatidylcholine (PC), and phosphatidylinositol + phosphatidylserine (PI + PS) determined by TLC in L2 (A) and L4 (B) strains. Treatments are defined in the legend. Controls: (black bars) Tween 80 (rehydration with Tween 80); (slashed bars) control (rehydration with physiological solution). Values are means of $n = 3 \pm$ standard deviations. (*) Significantly different from each control ($p \leq 0.05$, $n = 3$).

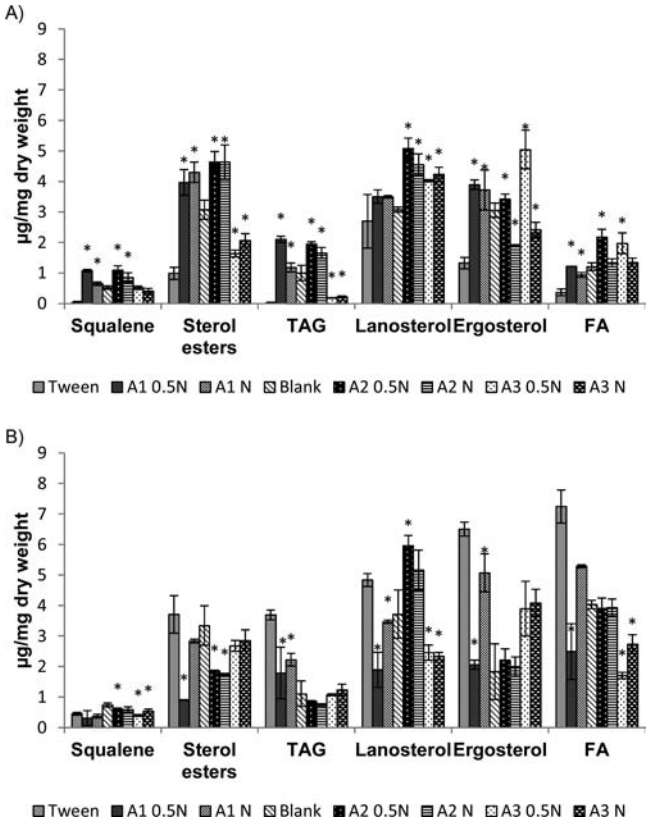


**Figure 3.** Concentration ($\mu$g/mg dry weight) of squalene, sterol esters, triacylglycerides (TAG), lanosterol, ergosterol, and fatty acids (FA) determined by TLC in L2 (A) and L4 (B) strains. Treatments are defined in the legend. Controls: (gray bars) Tween 80 (rehydration with Tween 80); (slashed bars) control (rehydration with physiological solution). Values are means of $n = 3 \pm$ standard deviations. (*) Significantly different from each control ($p \leq 0.05$, $n = 3$).

yeast strains in submerged stirred cultures; thus, enriching cell membranes with linoleic acid (C18:2) and ergosterol has been found to improve their ethanol tolerance.[30] Table 2 lists the proportions of membrane fatty acids in the yeasts after rehydration with the different activators. Overall, the activators had little impact on such proportions; nevertheless, L2 membranes had higher contents in C18 fatty acids (stearic, oleic, linoleic, and linolenic) than L4 membranes irrespective of the particular treatment; therefore, this variable is strain-dependent because already it is known. By contrast, L4 contained greater amounts of C16:0 and C16:1. Rehydrating with manganese(II) (N) or $FH_4$ at any dose significantly increased the content in C18:2 of L4. In the same manner, the N dose of $FH_4$ increased C14:1 of L2. By contrast, the presence of ergosterol decreased the content in C18:3 of L4.

As can be seen in Table 3, the contents in SFAs and UFAs were similar (i.e., treatment-independent) in all samples, with no significant differences among activators or doses. Nevertheless, L2 showed a lesser SFA and a higher UFA content than L4. Moreover, mean chain lengths (ChL) were similar in both strains. Besides, only ergosterol (N dose) caused a statistically significant change (a decrease) in ChL and exclusively in L2. In summary, metabolic activator treatment modified (increased or decreased) the production of fatty acids in both yeasts, but failed to alter their proportions.

Both strains showed different viabilities. L2 exhibited the highest viability in all cases. This could be a consequence of a specific strain factor. Numerous extrinsic variables in relation with the transport and conservation of the dry yeasts could influence this parameter, too.

In general, rehydration in the presence of the tested molecules caused no substantial change in cell viability, which suggests that maybe yeasts require a longer exposure time. Nevertheless, ergosterol was proved to be the most efficient of the three activators assayed. On the basis of the kinetic results, 0.5N dose reduced the lag time of both yeast strains. It also improved cell viability and membrane lipid composition; tetrahydrofolic acid raised neutral lipid levels, and manganese-(II) increased cell viability and modified phospholipid composition and linoleic acid concentration. All activators interacted with yeasts in a strain-dependent way.

As is already known, the content of membrane fatty acids is strain-dependent; the activators had little impact on such proportions. L2 cell membranes had higher contents in C18 fatty acids (stearic, oleic, linoleic, and linolenic) than L4 cell membranes.

Ergosterol treatment resulted in cellular accumulation of this lipid but only in L2. A quantitative lipid analysis revealed the presence of not only free but also esterified ergosterol (as sterol esters). This would make yeasts more robust and efficient in industrial processes under osmotic and hydric stress conditions than they are in alcoholic fermentation.[13]

It should be noted that the target parameters were assessed on freshly rehydrated yeasts. Taking into account that the

**Table 3. Percentage (Micrograms per Milligram Dry Weight) of Saturated (SFA; C16:0 and C18:0) and Unsaturated (UFA; C14:1, C16:1, C18:1, C18:2, and C18:3) Fatty Acids and Chain Length [ChL = $\Sigma(C_i n_{C,i})/\Sigma C_i$] of L2 and L4 Strains after Rehydration with Ergosterol + Tween 80, $FH_4$, and Mn(II) at Half (0.5N) and Normal (N) Doses[a]**

| | | | SFA | UFA | ChL |
|---|---|---|---|---|---|
| L2 | Tween 80 | | 23.5 ± 1.1 | 76.5 ± 1.1 | 16.8 ± 0.0 |
| | ergosterol | 0.5N | 25.0 ± 0.9 | 75.0 ± 0.9 | 16.9 ± 0.0 |
| | | N | 23.2 ± 0.9 | 76.8 ± 0.9 | 16.8 ± 0.0[b] |
| | control | | 25.9 ± 2.1 | 74.1 ± 2.1 | 16.9 ± 0.1 |
| | FH4 | 0.5N | 24.6 ± 0.9 | 75.4 ± 0.9 | 16.8 ± 0.0 |
| | | N | 24.7 ± 1.2 | 75.3 ± 1.2 | 16.8 ± 0.0 |
| | control | | 25.9 ± 2.1 | 74.1 ± 2.1 | 16.9 ± 0.1 |
| | Mn(II) | 0.5N | 25.9 ± 0.1 | 74.1 ± 0.1 | 16.9 ± 0.0 |
| | | N | 25.5 ± 0.9 | 74.6 ± 0.9 | 16.9 ± 0.0 |
| L4 | Tween 80 | | 28.5 ± 3.2 | 71.5 ± 3.2 | 16.4 ± 0.2 |
| | ergosterol | 0.5N | 26.8 ± 1.1 | 73.2 ± 1.1 | 16.5 ± 0.0 |
| | | N | 28.1 ± 1.0 | 71.9 ± 1.0 | 16.5 ± 0.1 |
| | control | | 25.4 ± 1.1 | 74.6 ± 1.1 | 16.6 ± 0.1 |
| | FH4 | 0.5N | 25.3 ± 2.0 | 74.7 ± 2.1 | 16.6 ± 0.1 |
| | | N | 23.6 ± 2.0 | 76.4 ± 2.0 | 16.5 ± 0.0 |
| | control | | 25.4 ± 1.1 | 74.6 ± 1.1 | 16.6 ± 0.1 |
| | Mn(II) | 0.5N | 26.3 ± 2.3 | 73.7 ± 2.3 | 16.6 ± 0.1 |
| | | N | 26.4 ± 0.2 | 73.6 ± 0.2 | 16.6 ± 0.0 |

[a]Controls: Tween 80 (rehydration with Tween 80) and control (rehydration with physiological solution). Values are means of $n = 3 \pm$ standard deviation. [b]Statistically significant differences of the treated sample with respect to its control (one-way ANOVA; $p \leq 0.05$; $n = 3$).

above-described changes occur within the first 24 h of cell growth, it would therefore be interesting to perform another subsequent sampling during lag phase to ensure the effect of the different treatments tested.

## AUTHOR INFORMATION

### Corresponding Author

*(J.Ú.) Phone: +34 926 295300, ext. 4324. Fax: +34 926 295318. E-mail: juan.ubeda@uclm.es.

### Notes

The authors declare no competing financial interest.

## REFERENCES

(1) Rapoport, A. I.; Khrustaleva, G. M.; Chamanis, G. Y.; Beker, M. E. Yeast anhydrobiosis − permeability of the plasma-membrane. *Microbiology* **1995**, *64* (2), 229−232.

(2) Rodríguez-Porrata, B.; Novo, M.; Guillamón, J.; Rozès, N.; Mas, A.; Cordero Otero, R. Vitality enhancement of the rehydrated active dry wine yeast. *Int. J. Food Microbiol.* **2008**, *126*, 116−122.

(3) Rodríguez-Porrata, B.; Lopez-Martinez, G.; Redon, M.; Sancho, M.; Mas, A.; Rozès, N.; Cordero-Otero, R. Enhancing yeast cell viability after dehydration by modification of the lipid profile. *World J. Microbiol. Biotechnol.* **2010**, *27* (1), 75−83.

(4) Bisson, L. Stuck and sluggish fermentations. *Am. J. Enol. Vitic.* **1999**, *50*, 107−119.

(5) Sajbidor, J. Effect of some environmental factors on the content and composition of microbial membrane lipids. *Crit. Rev. Biotechnol.* **1997**, *17*, 87−103.

(6) Keenan, M. H. J.; Rose, A. H.; Silverman, B. W. Effect of plasma-membrane phospholipid unsaturation on solute transport into *Saccharomyces cerevisiae* NCYC 366. *J. Gen. Microbiol.* **1982**, *128*, 2547−2556.

(7) Hazel, J. R.; Williams, E. E. The role of alterations in membrane lipid composition in enabling physiological adaptation of organisms to their physical environment. *Prog. Lipid Res.* **1990**, *29*, 167−227.

(8) Henschke, P. A.; Rose, A. H. *Plasma Membranes in the Yeasts*, 2nd ed.; Academic Press: London, UK, 1991; pp 297−435.

(9) Deytieux, C.; Mussard, L.; Biron, M. J.; Salmon, J. M. Fine measurement of ergosterol requirements for growth of *Saccharomyces cerevisiae* during alcoholic fermentation. *Appl. Environ. Microbiol.* **2005**, *68*, 266−271.

(10) Rodríguez, R. J.; Low, C.; Bottema, C.; Parks, L. W. Multiple functions for sterols in *Saccharomyces cerevisiae*. *Biochim. Biophys. Acta* **1985**, *837*, 336−343.

(11) Lange, Y.; Swaisgood, M. H.; Ramos, B. V.; Steck, T. L. Plasma membranes contain half the phospholipid and 90% of the cholesterol and sphingomyelin in cultured human fibroblasts. *J. Biol. Chem.* **1989**, *264*, 3786−3793.

(12) Zinser, E.; Sperka-Gottlieb, C. D.; Fasch, E. V.; Kohlwein, S. D.; Paltauf, F.; Daum, G. Phospholipid synthesis and lipid composition of subcellular membranes in the unicellular eukaryote *Saccharomyces cerevisiae*. *J. Bacteriol.* **1991**, *173* (6), 2026−2034.

(13) Soubeyrand, V.; Luparia, V.; Pascale, W.; Doco, T.; Vernhet, A.; Ortiz-Julien, A.; Salmon, J. M. Formation of micelle containing solubilized sterols during rehydration of active dry yeasts improves their fermenting capacity. *J. Agric. Food Chem.* **2005**, *53*, 8025−8032.

(14) Henderson, C. M.; Zeno, W. F.; Lerno, L. A.; Longo, M. L.; Block, D. E. Fermentation temperature modulates phosphatidylethanolamine and phosphatidylinositol levels in the cell membrane of *Saccharomyces cerevisiae*. *Appl. Environ. Microbiol.* **2103**, *79*, 5345−5356.

(15) Walker, G. M. *Yeast Physiology and Biotechnology*; Wiley: West Sussex, UK, 1998; pp 19−21.

(16) Avery, S. V.; Howlett, N. G.; Radice, S. Copper toxicity towards *Saccharomyces cerevisiae*: dependence on plasma membrane fatty acid composition. *Appl. Environ. Microbiol.* **1996**, *62*, 3960−3966.

(17) Daum, G.; Lees, N. D.; Bard, M.; Dickson, R. Biochemistry cell biology and molecular biology of lipids of *Saccharomyces cerevisiae*. *Yeast* **1998**, *14*, 1471−1510.

(18) Guilloux-Benatier, M.; Fur, Y. L.; Feuillat, M. Influence of fatty acids on the growth of wine microorganisms *Saccharomyces cerevisiae* and *Oenococcus oeni*. *J. Ind. Microbiol. Biotechnol.* **1998**, *20*, 144−149.

(19) Yazawa, H.; Iwahashi, H.; Kamisaka, Y.; Kimura, K.; Uemura, H. Production of polyunsaturated fatty acids in yeast *Saccharomyces cerevisiae* and its relation to alkaline pH tolerance. *Yeast* **2009**, *26*, 167−184.

(20) Grillitsch, K.; Connerth, M.; Köfeler, H.; Arrey, T. N.; Rietschel, B.; Wagner, B.; Karas, M.; Daum, G. Lipid particles/ droplets of the yeast *Saccharomyces cerevisiae* revisited: lipidome meets proteome. *Biochim. Biophys. Acta* **2011**, *1811*, 1165−1176.

(21) Rodríguez- Vargas, S.; Sánchez- García, A.; Martínez- Rivas, J. M.; Prieto, J. A.; Randez- Gil, F. Fluidization of membrane lipids enhances the tolerance of *Saccharomyces cerevisiae* to freezing and salt stress. *Appl. Environ. Microbiol.* **2006**, *73*, 110−116.

(22) Díaz-Hellín, P.; Úbeda, J.; Briones, A. Improving alcoholic fermentation by activation of *Saccharomyces* sp. during rehydration stage. *LWT−Food Sci. Technol.* **2013**, *50*, 126−131.

(23) Dupont, S.; Beney, L.; Ferreira, T.; Gervais, P. Nature of sterols affects plasma membrane behavior and yeast survival during dehydration. *Biochim. Biophys. Acta−Biomembranes* **2011**, *1808*, 1520−1528.

(24) Tronchoni, J.; Rozès, N.; Querol, A.; Guillamón, J. M. Lipid composition of wine strains of *Saccharomyces kudriavzevii* and *Saccharomyces cerevisiae* grown at low temperature. *Int. J. Food Microbiol.* **2012**, *155* (3), 191−198, DOI: 10.1016/j.ijfoodmicro.2012.02.004.

(25) Redón, M.; Guillamón, J. M.; Mas, A.; Rozès, N. Effect of active dry wine yeast storage upon viability and lipid composition. *World J. Microbiol. Biotechnol.* **2008**, *24*, 2555−2563.

(26) Rozès, N.; García-Jares, C.; Larue, F.; Lonvaud-Funel, A. Differentiation between fermenting and spoilage yeasts in wine by total free fatty acid analysis. *J. Sci. Food Agric.* **1992**, *59*, 351−357.
(27) Zwietering, M. H.; Jongenburger, I.; Rombouts, F. M.; Van't Riet, K. Modeling of the bacterial growth curve. *Appl. Environ. Microbiol.* **1990**, *56* (6), 1875−1881.
(28) Higgins, V. J.; Beckhouse, A. G.; Oliver, A. D.; Rogers, P. J.; Dawes, I. W. Yeast genome-wide expression analysis identifies a strong ergosterol and oxidative stress response during the initial stages of an industrial lager fermentation. *Appl. Environ. Microbiol.* **2003**, *69* (8), 4777−4787.
(29) Pozo-Bayón, M. A.; Andújar-Ortiz, I.; Moreno-Arribas, M. V. Scientific evidences beyond the application of inactive dry yeast preparations in winemaking. *Food Res. Int.* **2009**, *42*, 754−761.
(30) Rose, A. H. Composition of the envelope layers of *Saccharomyces cerevisiae* in relation to flocculation and ethanol tolerance. *J. Appl. Bacteriol. Symp. Suppl.* **1993**, *74*, 110S−118S.

JOURNAL OF AGRICULTURAL AND FOOD CHEMISTRY

Article

pubs.acs.org/JAFC

# Genetic Variability in Anthocyanin Composition and Nutritional Properties of Blue, Purple, and Red Bread (*Triticum aestivum* L.) and Durum (*Triticum turgidum* L. ssp. *turgidum* convar. *durum*) Wheats

Donatella B. M. Ficco,[†] Vanessa De Simone,[†] Salvatore A. Colecchia,[†] Ivano Pecorella,[†] Cristiano Platani,[†] Franca Nigro,[†] Franca Finocchiaro,[§] Roberto Papa,[†] and Pasquale De Vita*[,†]

[†]Consiglio per la Ricerca e la sperimentazione in Agricoltura − Centro di Ricerca per la Cerealicoltura (CRA-CER), S.S. 673, Km 25,200, 71122 Foggia, Italy

[§]Consiglio per la Ricerca e la sperimentazione in Agricoltura − Centro di Ricerca per la Genomica (CRA-GPG), Via S. Protaso, 29017 Fiorenzuola d'Arda (PC), Italy

Supporting Information

**ABSTRACT:** Renewed interest in breeding for high anthocyanins in wheat (*Triticum* ssp.) is due to their antioxidant potential. A collection of different pigmented wheats was used to investigate the stability of anthocyanins over three crop years. The data show higher anthocyanins in blue-aleurone bread wheat (*Triticum aestivum* L.), followed by purple- and red-pericarp durum wheat (*Triticum turgidum* L. ssp. *turgidum* convar. *durum*), using cyanidin 3-*O*-glucoside as standard. HPLC of the anthocyanin components shows five to eight major anthocyanins for blue wheat extracts, compared to three anthocyanins for purple and red wheats. Delphinidin 3-*O*-rutinoside, delphinidin 3-*O*-glucoside, and malvidin 3-*O*-glucoside are predominant in blue wheat, with cyanidin 3-*O*-glucoside, peonidin 3-*O*-galactoside, and malvidin 3-*O*-glucoside in purple wheat. Of the total anthocyanins, 40−70% remain to be structurally identified. The findings confirm the high heritability for anthocyanins, with small genotype × year effects, which will be useful for breeding purposes, to improve the antioxidant potential of cereal-based foods.

**KEYWORDS:** *pigmented durum and bread wheats, total anthocyanin content, qualitative parameters, anthocyanin composition, genotype by environment interaction, minerals, total polyphenol, trolox equivalent antioxidant capacity*

## INTRODUCTION

Wheat (*Triticum* ssp.) is one of the most common human foods in the world, and recently the focus has been on the possibility of increasing the content of bioactive compounds to improve health and prevent disease.[1] Some bioactive compounds can be specific to certain cereals, for example, γ-oryzanol in rice, avenanthramides and saponins in oat, β-glucans in oat and barley, alkylresorcinols in rye, and anthocyanins and carotenoids in pigmented cereal grains.[1−3] In particular, there is extensive literature on anthocyanins in colored rice, corn, and to a lesser extent, in barley, buckwheat, sorghum, millet, bread (*Triticum aestivum* L.) and durum wheat (*Triticum turgidum* L. ssp. *turgidum* convar. *durum*).[2,4−9]

Anthocyanins are recognized as having the ability to scavenge free radicals that can cause oxidative stress in human cells.[10] For a long time, the accumulation of anthocyanins in wheat grain was not considered in breeding programs, except as a genetic marker for specific purposes (feed) to enable their distinction from that used for human consumption or in genetic studies, for example, when carrying out an indirect selection program.[11] Indeed, anthocyanin accumulation is an extremely rare trait, which is seen in some forms of tetraploid wheats, with its high frequency in Ethiopian wheat germplasm.[11] More recently, a series of blue wheats have been developed through intraspecies crosses from *Triticum boeticum*, *Triticum monococcum*, and related wheat species (*Agropyron* ssp.) with bread wheat.[11−13] Early studies confirmed that the purple pigment is localized to the grain pericarp (outer layer), whereas the blue pigment is localized to the grain aleurone layer.[11]

The anthocyanins were identified and quantified in various blue, purple, and red bread wheats by Abdel-Aal et al.[4] The total anthocyanin contents varied from 7.1 to 211.9 μg/g. These pigments normally exist as glycosides (bonded to a sugar moiety), as the anthocyanidin (or aglycon) component alone is extremely unstable. The most common anthocyanin in purple wheat is cyanidin 3-*O*-glucoside (Cy-3-Glc), followed by peonidin 3-*O*-glucoside (Pn-3-Glc), whereas delphinidin 3-*O*-glucoside (Dp-3-Glc) is the most abundant anthocyanin in blue wheat.[2,14]

Carotenoids are the most important natural pigments, and these compounds have a wide distribution, different structures, and numerous biological functions. In humans, the nutritional importance of carotenoids arises mainly from the pro-vitamin A activity of β-carotene. In addition to their role as precursors of vitamin A, carotenoids have been associated with reduced risk of cancer, decreased cardiovascular disease, protection of the macula region of the retina, prevention of cataracts, and increased iron absorption. The concentration of carotenoids is higher in durum wheat (1.50−4.00 μg/g) than in bread wheat (0.50−2.00 μg/g)[15,16] as a result of selection in durum wheat

Received: January 22, 2014
Revised: July 24, 2014
Accepted: July 29, 2014
Published: July 29, 2014

ACS Publications © 2014 American Chemical Society

breeding programs for high yellow pigment concentrations.[17] Inheritance of grain or semolina pigment concentrations is complex, although the overall heritability of pigment concentrations is relatively high, ranging from 0.78 to 0.96.[18]

Recent studies have shown genetic variability for both anthocyanin[4,8,19,20] and carotenoid[3,17] contents in wheat. For breeding programs, the availability of genetic variability is a key factor to consider, as well as the interaction of genotype × environment (G×E). Few studies have been conducted to evaluate the effects of the environment, defined as a combination of location (L), year (Y), and agronomic management of the crop (M), on the total content of anthocyanins in wheat[14] whereas up to now, no studies have been conducted to evaluate the technological performance of these genetic materials.

The objectives of the present study were to (i) explore the genetic variability of the total anthocyanin content (TAC) and other qualitative parameters [yellow pigment (YP), thousand-kernel weight (TKW), protein content (PC), sodium dodecyl sulfate (SDS) sedimentation volume, and ash content (ASH)] and nutritional parameters [minerals, total polyphenol (TPC), Trolox equivalent antioxidant capacity (TEAC)] in wheat grain; (ii) identify the main anthocyanin compounds in a collection of wheats that includes accessions of tetraploid and hexaploid wheats; and (iii) estimate the effects of G×Y over three growing seasons for all of the traits evaluated. This will thus provide information on the existing variability and genetic resources available to breeders to improve the nutritional value of pasta, bread, and other wheat-based end-products.

## MATERIALS AND METHODS

**Genotypes and Field Experiments.** In all, 76 pigmented wheat genotypes were analyzed in the present study. These included 70 (27 purple, 43 red) that were durum wheat (*T. turgidum* L. ssp. *turgidum* convar. *durum* Desf; $2n = 4x = 28$; tetraploid AABB genome) and three that were blue bread wheat (*T. aestivum* L.; $2n = 6x = 42$; hexaploid AABBDD genome) (Supporting Information Table S1). The collection also included two Italian durum wheat genotypes (Preco, PR22D89) and one Italian bread wheat genotype (Spada), which were used as commercial yellow controls, that is, nonpigmented. The 76 genotypes were grown in field trials during three consecutive growing seasons (2008−2009, 2009−2010, 2010−2011) at the CRA-CER in Foggia, Italy. The experimental design was a randomized complete block with three replications. Each experimental unit consisted of a 1 $m^2$ plot (two rows of 1 m length, with 0.5 m between rows).

During the growing season, standard cultivation practices were used. Table S2 (Supporting Information) reports the monthly precipitation and temperature ranges throughout the entire growth cycle of the durum wheat, from November to June.

Whole plots were harvested mechanically on June 13, 2009, June 15, 2010, and June 20, 2011, and the grains were kept at 4 °C until analysis. Approximately 100 g of grain was sampled from each plot shortly before analysis and used for the preparation of whole meal, using an experimental mill (Tecator Cyclotec 1093) with a 0.05 mm sieve.

**Chemicals and Reagents.** Sulfuric acid, hydrogen peroxide, SDS, lactic acid, potassium chloride, sodium acetate ($CH_3CO_2Na{\cdot}3H_2O$), formic acid, 6-hydroxy-2,5,7,8-tetramethylchroman-3-carboxylic acid (Trolox), sodium hydroxide, 2,2′-azinobis(3-ethylbenzothiazoline-6-sulfonic acid) diammonium salt (ABTS), potassium ferricyanide ($K_3Fe(CN)_6$), iron(III) chloride, the gum arabic and catechin standards were purchased from Sigma-Aldrich (Milan, Italy). Methanol, *n*-butanol, hydrogen chloride, acetonitrile, acetone, and acetic acid were purchased from Carlo Erba (Milan, Italy). All chemicals and solvents used in the present study were of high-pressure liquid chromatography (HPLC) grade. Eleven anthocyanin standards were purchased: Cy-3-Glc, cyanidin 3-*O*-galactoside (Cy-3-Gal), malvidin 3-*O*-glucoside (Mv-3-Glc), pelargonidin 3-*O*-glucoside (Pg-3-Glc), and Pn-3-Glc from Extrasynthese (Genay, France); and cyanidin 3-*O*-rutinoside (Cy-3-Rut), Dp-3-Glc, delphinidin 3-*O*-rutinoside (Dp-3-Rut), peonidin 3-*O*-arabinoside (Pn-3-Ara), peonidin 3-*O*-galactoside (Pn-3-Gal), and Pt-3-Glc from Polyphenols Laboratory (Sandnes, Norway).

**Quality Traits Assessment.** Thousand-kernel weight was calculated from the mean weight of three sets of 100 grains per plot. PC was assayed using the micro-Kjeldahl method, according to the AACC International,[21] which was then multiplied by 5.7. The SDS sedimentation volume was measured on 0.6 g of whole meal flour, according to the UNI 10277 method (*Ente Nazionale Italiano di Unificazione*[22]), expressed as a specific SDS sedimentation volume of whole meal flour (in mL/g). The ash content was determined according to the UNI 2171 method[23] for the determination of ash yield by complete combustion. These data are expressed as percentages. Yellow pigments were analyzed according to method 14-50 of AACC International,[24] as modified by in ref 25 for microsamples. The data were expressed as micrograms per gram on dry matter.

**Total Anthocyanin Content Using the pH Differential Method.** The extraction and purification of TAC was performed according to the mehtod of Hosseinian,[9] with slight modifications. A mixture of methanol acidified with 1 N HCl (85:15; v/v) (8 mL) was added to the whole meal samples (0.5 g) in 50 mL centrifuge tubes and sonicated for 18 min at room temperature in an ultrasonic bath (DT 510 Sonorex, DIGITEC). After centrifugation at 9000*g* for 15 min at room temperature, the supernatants were recovered into 15 mL centrifuge tubes. The pellets were extracted with a further 4 mL of the acidified methanol, and following the same centrifugation, the second supernatants were added to the first. These total supernatants were incubated at −20 °C in the dark for 48 h to facilitate macromolecule precipitation. After this incubation, the samples were centrifuged at 9000*g* for 15 min, and the supernatants were filtered using 0.45 μm regenerated cellulose syringe filters (Phenomenex, Torrance, CA, USA).

Total anthocyanin content was evaluated using a colorimetric method with different pH solutions. Two aliquots of the supernatants extracted (750 μL) were put into different tubes and diluted (1:2, v/v) with either potassium chloride buffer (0.03 M KCl), for pH 1.00, or sodium acetate buffer (0.4 M $CH_3CO_2Na{\cdot}3H_2O$), for pH 4.50. The resulting samples were incubated for 30 min at room temperature in the dark and then filtered with 0.45 μm regenerated cellulose syringe filters. The absorbances of the samples at 520 nm were measured against distilled water as the blank. Total anthocyanin content was corrected for the dry matter and is expressed as Cy-3-Glc equivalents as micrograms per gram dry matter.

**Anthocyanin Composition Using HPLC Analysis.** The anthocyanins were extracted according to the method described by Abdel-Aal and Hucl,[14] with slight modifications. Briefly, 500 mg of material was extracted twice by mixing 8 mL of acidified methanol with 1.0 N HCl (85:15; v/v), which was then left in an ultrasonic bath for 30 min, with nitrogen gas introduced into the tubes. The crude extracts were centrifugated at 3000*g* for 15 min at 10 °C and then stored at −80 °C to precipitate the large molecules. The extracts were recentrifuged at 3000*g* for 15 min at 10 °C and concentrated in centrifugal evaporators (JOUAN RC 1022, Thermo Electron Corp.). The concentrated extracts (5 mL) were filtered through 0.45 μm regenerated cellulose syringe filters (Phenomenex) before analysis by HPLC. The anthocyanins were separated and quantified with a 1200 series chromatography system (Agilent Technologies, Waldbron, Germany) equipped with a G1379B degasser, G1312B binary pump, G1367D temperature-controlled injector, G1330B temperature-controlled column thermostat, G1316B photodiode array detector, and Chemstation Rev. B03.02. A 100 mm × 4.6 mm, 2.6 μm, C18 Kinetex column (Phenomenex) was used for the anthocyanin separation. The column temperature was 40 °C, and the mobile phase consisted of (A) 5% formic acid and (B) methanol 22.5%,

Table 1. Combined Analysis of Variance (ANOVA), Genetic ($\sigma^2_G$) and Genotype × Year Interaction ($\sigma^2_{GY}$) Variances (±SE) and Narrow-Sense Heritability Estimates on a Genotype-Mean Basis for Qualitative Traits Evaluated of 76 Pigmented Wheat Genotypes over Three Growing Seasons at Foggia, Italy[a]

| | DF | TAC | YP | TKW | PC | SDS | ASH |
|---|---|---|---|---|---|---|---|
| year | 2 | $4.450 \times 10^{2}$§[b] | 63.72§ | 8479.515§ | $9.267 \times 10^{2}$§ | 11.52§ | 10.28§ |
| genotype | 75 | $2.553 \times 10^{5}$§ | 408.19§ | 8823.235§ | $7.824 \times 10^{2}$§ | 4.55§ | 79.79§ |
| G×Y | 150 | $1.276 \times 10^{4}$§ | 98.98§ | 5135.975§ | $6.473 \times 10^{2}$§ | 5.69§ | 66.62§ |
| residual | 228 | $2.618 \times 10^{1}$ | 7.79 | 269.954 | $8.368 \times 10^{-1}$ | 0.31 | 3.18 |
| total | 455 | $2.685 \times 10^{5}$ | 578.69 | 22708.678 | $2.357 \times 10^{3}$ | 22.08 | 159.86 |
| $\sigma^2_G$ | | 553.12 ± 92.6 | 0.79 ± 0.15 | 13.90 ± 3.3 | 1.02 ± 0.3 | 0.10 ± 0.03 | 0.0037 ± 0.002 |
| ($\sigma^2_{GY}$) | | 42.49 ± 4.9 | 0.31 ± 0.04 | 16.52 ± 2.0 | 2.15 ± 0.2 | 0.21 ± 0.02 | 0.0183 ± 0.002 |
| heritability ($H^2_B$, %) | | 92.8 | 69.7 | 43.9 | 32.1 | 31.1 | 16.1 |

[a]TAC, total anthocyanin content (μg/g); YP, yellow pigment (μg/g); TKW, thousand-kernel weight (g); PC, protein content (%); SDS, sodium dodecyl sulfate sedimentation volume (mL/g); ASH, ash content (%). [b]§, significant at $p \leq 0.001$.

acetonitrile 22.5%, and ultrapure water, at a flow rate of 0.5 mL/min. The gradient was programmed as follows: 0 → 12 min, 9% B; 12 → 25 min, 35% B; 25 → 30 min, 50% B; 30 → 35 min, 9% B. The anthocyanins were detected at 520 nm and identified according to their retention times, using UV−vis spectra authenticated standards. The stock standard solutions were prepared by weighing 1 mg of each standard and dissolving each in 1 mL of acidified methanol. The working standard solutions were prepared by diluting the stock solution, and then they were injected. The range of injected standard was from 0 to 40 ng. All of the coefficients ($R^2$) ranged from 0.99981 to 0.99998. Data are expressed as micrograms per gram dry matter.

**Mineral Element Analysis.** The mineral element concentrations (Fe, Mn, Cu, Zn) of the whole meal were determined using a Varian Vista-MPX simultaneous inductively coupled plasma optical emission spectrometer, with CCD detection, as described in detail by Ficco et al.[26]

All of the mineral determinations were compared to certified reference materials (NIST SRM 8436: durum wheat flour on dry weight). The moisture content was determined by oven-drying samples of each material at 60 °C for 24 h and then allowing the samples to cool in a desiccator for 4 h prior to reweighing. The data are expressed as milligrams per kilogram.

**Total Polyphenol Content.** Total polyphenol content was quantified using the Prussian blue assay,[27] as modified and described in detail by Finocchiaro et al.[5] The absorbance was measured at 700 nm using a DU-64 spectrophotometer (Beckman Instruments, Brea, CA, USA). Increasing concentrations of catechin standard (from 0.3 to 1.0 mmol/L, initial concentrations) were used to construct the calibration curve. To verify the linearity of the curve in the range in these samples, the assay was standardized against 0.001 M catechin, and the polyphenols were expressed as catechin equivalents as grams per kilogram dry matter.

**Trolox Equivalent Antioxidant Capacity.** Total antioxidant capacity was evaluated according to the Trolox equivalent antioxidant capacity method,[28] as described in detail by Finocchiaro et al.[5] The TEAC method is based on decoloration of the ABTS radical cation at 734 nm in the presence of antioxidants. The data are expressed in millimoles of Trolox (used as the antioxidant reference) per kilogram dry matter.

**Statistical Analysis.** The results of TAC, YP, TKW, PC, SDS, and ASH were subjected to a combined analysis of variance (ANOVA) using Statistica software (StatSoft version 7.1 StatSoft, Inc., Tulsa, OK, USA) (1), whereas the analysis of minerals, TPC, and TEAC were subject to one-way ANOVA (2), according to the following equations:

$$y_{ijk} = \mu + \alpha_i + \beta_j + (\alpha\beta)_{ij} + e_{ijk} \quad (1)$$

$$y_{ijk} = \mu + \alpha_i + e_{ik} \quad (2)$$

$\mu$ represents the overall mean of all plots in all years, $\alpha_i$ represents the effect of the $i$th genotype, $\beta_j$ represents the effect of $j$th year, and $\alpha\beta_{ij}$ represents the effect of interaction of genotype $i$ with year $j$, whereas $e$ represents the residual effect.

Means were identified as being significantly different on the basis of Fischer's protected least significant differences (LSD) at a probability level of 5%. The variance components were calculated from a mixed model (genotype and genotype by year random effects; year and block within year fixed effects), as analyzed using the restricted maximum likelihood procedure.

Narrow-sense heritability ($H^2_B$) was estimated from the resulting variance components on a genotype-mean basis. Pearson correlation coefficients ($r$) were used to study the relationship among the qualitative traits evaluated.

## RESULTS

**ANOVA and Year Effect.** The results of combined analysis of variance (ANOVA) made on data obtained from three growing seasons are given in Table 1. Highly significant year (Y), genotype (G), and G×Y effects were detected for each of the investigated traits. Component of variance ($\sigma^2_G$ and $\sigma^2_{GY}$) and narrow-sense heritability estimates on a genotype-mean basis were also evaluated (Table 1). Total anthocyanin content showed the highest $H^2_B$ (92.8%) value followed by YP (69.7%). The narrow-sense heritability estimates were small for all other traits, ranging from 16.1% (ASH) to 43.9% (TKW).

The three experimental years showed similar annual temperature ranges, whereas the variations in the total rainfall levels were more significant (Supporting Information Table S2). In particular, the growing seasons of 2009−2010 and 2010−2011 had analogous rainfall, as 435.8 mm and 470.2 mm, respectively. This rainfall was more concentrated in the winter months with respect to the 2008−2009 growing season, during which it was distributed over the entire cycle of the plants, with about 2-fold the rainfall considered as the seasonal average over the past 52 years. These data significantly influenced all of the parameters analyzed, and in particular the PC, SDS sedimentation volume, and ASH, for which the highest values were recorded in the third year (16.90%, 3.03 mL/g, and 2.39%, respectively; Table 2). The behavior observed for TAC, however, was completely the opposite. In this case, the values were higher for those recorded in the first two growing seasons (19.0 and 18.8 μg/g, in 2008−2009 and 2009−2010, respectively), whereas the lowest TAC (17.1 μg/g) was recorded in the third study year (2010−2011). The levels of YP did not follow any clear trend, with an increased accumulation of carotenoids observed in the second growing season (2009−2010), when the minimum value of TKW was also recorded (35.1 g).

**Table 2. Mean Values of TAC and Qualitative Traits of 76 Pigmented Wheat Genotypes Evaluated over Three Growing Seasons at Foggia, Italy[a]**

| year | TAC | YP | TKW | PC | SDS | ASH |
|---|---|---|---|---|---|---|
| 2008−2009 | 18.98 | 5.90 | 45.48 | 13.93 | 2.69 | 2.21 |
| 2009−2010 | 18.82 | 6.75 | 35.08 | 13.83 | 2.99 | 2.03 |
| 2010−2011 | 17.14 | 6.02 | 41.88 | 16.90 | 3.03 | 2.39 |
| $LSD_{(0.05)}$ | 0.07 | 0.04 | 0.24 | 0.01 | 0.03 | 0.01 |

[a]TAC, total anthocyanin content (μg/g); YP, yellow pigment (μg/g); TKW, thousand-kernel weight (g); PC, protein content (%); SDS, sodium dodecyl sulfate sedimentation volume (mL/g); ASH, ash content (%).

**Qualitative Parameters among and within the Blue, Purple, and Red Wheat Groups.** The data reported in Table 3 subdivide the genotypes according to the color of the pericarp and their ploidy level, and these show higher values of TAC in the pigmented wheat than in the commercial varieties, with values close to zero. In particular, the blue wheat had a higher mean TAC (118.37 μg/g) than the purple (22.60 μg/g) and red (9.91 μg/g). This means that TAC in the blue wheat genotypes was 5-fold greater than for the purple and 12-fold greater than for the red tetraploid wheat.

The blue wheat was also characterized by the highest mean SDS sedimentation volume (4.40 mL/g). Compared to the bread and durum commercial varieties, the pigmented wheat also showed greater accumulation of ash in the grain than the commercial varieties (2.38, 2.21, and 2.22%, for blue, purple, and red wheats, respectively). Different behavior was seen for YP of the grain. In this case, the commercial varieties of durum wheat, which were genetically improved for this YP trait,[17,29] showed the highest YP (9.84 μg/g) compared to both the commercial control bread wheat variety Spada (4.49 μg/g) and the pigmented durum wheat (about 6 μg/g). A good level of variability was also seen for PC, for which the means were included in the range from 11.90 to 13.72% in the commercial wheat; among the pigmented wheats, the red had the highest PC (15.10%), followed by the purple (14.89%) and blue (13.54%). Contrary to what was observed for PC, the qualitative responses of the genetic materials in terms of SDS sedimentation volume were higher for the blue wheat (4.40 mL/g) with respect to the wheat with purple and red pericarp grain (2.80 mL/g each).

Thousand-kernel weight was significantly affected by the level of ploidy and the genetic improvements carried out with these two wheat species over the past decades.[30,31] Indeed, the tetraploid wheat, with particular reference to the durum wheat varieties used as references in the present study, showed higher mean TKW (49.18 g) as compared to pigmented blue wheat (35.46 g).

Considering the genotypic variability within each group (Supporting Information Table S1), among the blue wheat group, Sebesta Blue2 was the genotype with the highest TAC (174.27 μg/g), YP (7.01 μg/g), SDS sedimentation volume (4.90 mL/g), and ash (2.45%) but also the lowest TKW (32.05 g). Compared to the commercial bread wheat (Spada), the blue wheat showed good qualitative traits, in terms of both pigment content (anthocyanins and carotenoids) and technological traits (PC and SDS sedimentation volume).

The purple durum wheats were characterized by a wide range of values for all of the traits evaluated. Wide variations were seen for TAC, which ranged from 8.12 μg/g (Mog) to 50.22 μg/g (378b), for PC, which ranged from 12.47% (MP3) to 17.88% (ELS 6304-56), and for TKW, which ranged from 34.53 g (286b) to 49.70 g (ELS 6404-130-3). The 378b genotype showed the best performance in terms of TAC, PC, and SDS sedimentation volume.

The group of red durum wheats followed the same trend as the purple wheat, with the major differences being for TAC, which ranged from 1.20 μg/g (ELS 6404-139-3) to 24.57 μg/g (ELS 6304-71), for TKW, which ranged from 27.91 g (ELS 6404-114-2) to 49.75 g (ELS 6404-139-3), and for PC, which ranged from 13.02% (ELS 6404-116-3) to 18.38% (ELS 6404-159-2). Interestingly, the lower ash values ranged from 1.98% (337) to 2.06% (ELS 6404-85-2). Both of the durum pigmented groups are characterized by relatively variable YP and SDS sedimentation volume (from 5.26 to 7.34 μg/g and from 2.2 to 3.9 mL/g, respectively).

**Anthocyanin Composition of Pigmented Wheats.** The anthocyanin composition according to the HPLC analysis for the three different pigmented groups collected in the year 2010−2011 are reported in Table 4 and the Supporting Information (Table S3). These show different profiles for each of the groups in terms of the 11 standard compounds used as references for their identification (see Materials and Methods; Figure 1A). No anthocyanins were detected in the commercial wheats used as references (Figure 1C,F).

In the bread wheat, the blue aleurone was most represented by Dp-3-Rut (33.44 μg/g), Dp-3-Glc (13.68 μg/g), and Mv-3-Glc (12.04 μg/g), followed, with lower levels, by Cy-3-Rut (8.42 μg/g), Cy-3-Glu (3.07 μg/g), Pn-3-Ara (2.22 μg/g), Pn-3-Gal (1.94 μg/g), and Pn-3-Glc (0.88 μg/g) (Figure 1B). Among the genotypes belonging to this group, Sebesta Blue2

**Table 3. Descriptive Statistics of TAC and Qualitative Traits Evaluated in a Collection of 76 Pigmented Wheat Groups over Three Growing Seasons (2009−2011) at Foggia, Italy[a]**

| | *Triticum aestivum* | | | *Triticum durum* | | | | | |
|---|---|---|---|---|---|---|---|---|---|
| | blue ($n$ = 3) | | control ($n$ = 1) | purple ($n$ = 27) | | red ($n$ = 43) | | control ($n$ = 2) | |
| | mean | range | mean | mean | range | mean | range | mean | $LSD_{(0.05)}$ |
| TAC | 118.37 | 82.75−174.27 | 0.75 | 22.60 | 8.12−50.22 | 9.91 | 1.20−24.57 | 0.00 | 0.37 |
| YP | 6.13 | 5.01−7.01 | 4.49 | 6.20 | 5.26−7.10 | 6.12 | 5.28−7.34 | 9.84 | 0.21 |
| TKW | 35.46 | 32.05−38.59 | 43.28 | 40.45 | 34.53−49.70 | 40.97 | 27.91−49.75 | 49.18 | 1.23 |
| PC | 13.54 | 12.75−14.64 | 11.90 | 14.89 | 12.47−17.88 | 15.10 | 13.02−18.38 | 13.72 | 0.07 |
| SDS | 4.40 | 4.10−4.90 | 3.10 | 2.80 | 2.20−3.40 | 2.80 | 2.20−3.90 | 3.20 | 0.13 |
| ASH | 2.38 | 2.28−2.45 | 1.91 | 2.21 | 2.05−2.31 | 2.22 | 1.98−2.39 | 1.99 | 0.04 |

[a]TAC, total anthocyanin content (μg/g); YP, yellow pigment (μg/g); TKW, thousand-kernel weight (g); PC, protein content (%); SDS, sodium dodecyl sulfate sedimentation volume (mL/g); ASH, ash content (%).


dx.doi.org/10.1021/jf5003683 | J. Agric. Food Chem. 2014, 62, 8686−8695

**Table 4. Anthocyanin Components (μg/g) of 76 Pigmented Wheat Groups Evaluated over the 2010−2011 Growing Season at Foggia, Italy[a]**

| | *Triticum aestivum* | | *Triticum durum* | | | |
|---|---|---|---|---|---|---|
| | blue ($n$ = 3) | | purple ($n$ = 27) | | red ($n$ = 43) | |
| anthocyanin component | mean | range | mean | range | mean | range |
| Cy-3-Glc | 3.07 | 1.17−5.57 | 10.34 | 0.63−29.00 | 4.02 | 0.59−10.23 |
| Cy-3-Rut | 8.42 | 7.12−10.97 | − | | − | |
| Dp-3-Glc | 13.68 | 9.88−18.81 | − | | − | |
| Dp-3-Rut | 33.44 | 31.77−35.86 | − | | − | |
| Pn-3-Glc | 0.88 | 0.76−0.99 | − | | − | |
| Pn-3-Gal | 1.94 | 1.94 | 0.58 | 0.06−3.11 | 0.33 | 0.06−3.87 |
| Pn-3-Ara | 2.22 | 0.95−3.49 | − | | − | |
| Mv-3-Glc | 12.04 | 10.26−13.81 | 0.48 | 0.17−2.35 | 0.22 | 0.06−0.43 |

[a]Cy-3-Glc, cyanidin 3-*O*-glucoside; Mv-3-Glc, malvidin 3-*O*-glucoside; Pg-3-Glc, pelargonidin 3-*O*-glucoside; Cy-3-Gal, cyanidin 3-*O*-galactoside; Pn-3-Glc, peonidin 3-*O*-glucoside; Cy-3-Rut, cyanidin 3-*O*-rutinoside; Dp-3-Glc, delphinidin 3-*O*-glucoside; Dp-3-Rut, delphinidin 3-*O*-rutinoside; Pn-3-Gal, peonidin 3-*O*-galactoside; Pn-3-Ara, peonidin 3-*O*-arabinoside; Pt-3-Glc, petunidin 3-*O*-glucoside; −, not detectable.

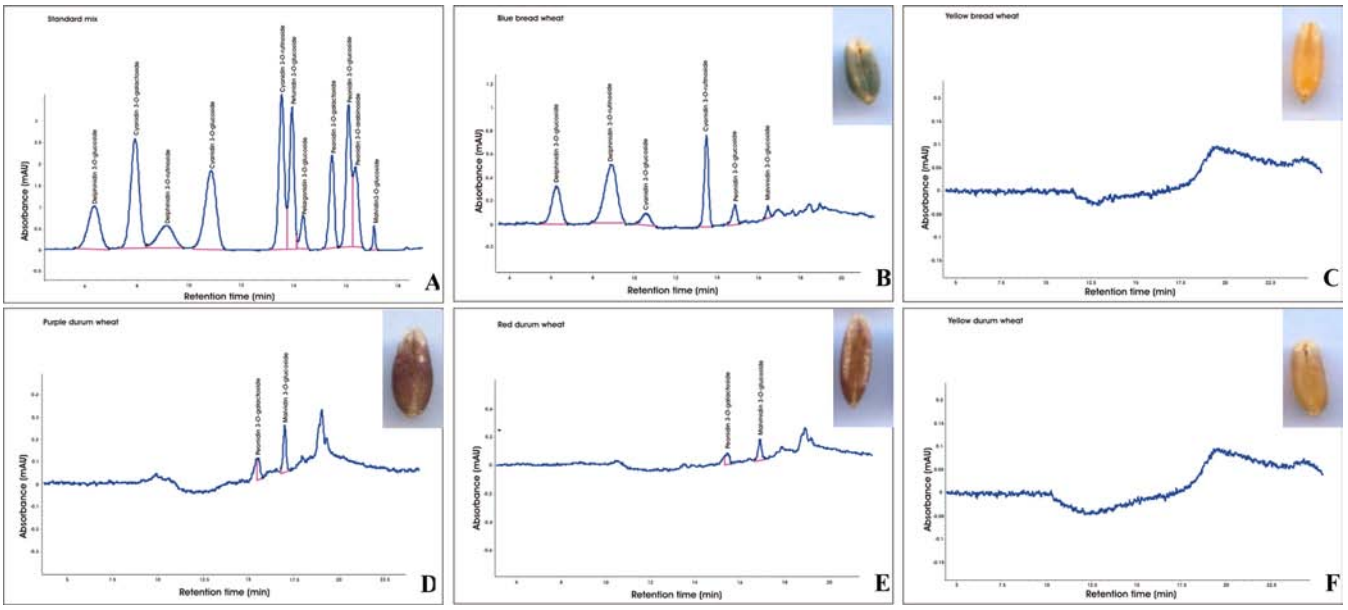


**Figure 1.** Typical HPLC chromatogram for standard mixture (A), blue bread wheat (B) versus yellow commercial bread (C), purple durum wheat (D), and red durum wheat (E) versus commercial durum wheat (F).

also showed the highest levels of anthocyanin compounds (85.36 μg/g) by HPLC, as compared to the spectrophotometric analysis.

The anthocyanin profile of the durum wheat genotypes with purple pericarp was simpler than that for the blue wheat. For the purple, HPLC analysis showed a total anthocyanin compound of 11.81 μg/g, with the most representative compound being Cy-3-Glc (10.34 μg/g), followed by Pn-3-Gal (0.58 μg/g) and Mv-3-Glc (0.48 μg/g) (Figure 1D). Within this group, the behavior of the individual genotypes was relatively diverse, especially for the content of Cy-3-Glc, which oscillated between 0.63 μg/g (ELS 6304-69) and 29.00 μg/g (T-1303). T-1303 is the genotype that also showed the highest Mv-3-Glc (2.35 μg/g). For all of the other compounds, extremely small quantities were detected.

A profile similar to that of the previous group was also seen for the red wheat (Figure 1E). In this case, the data confirm the presence of the same anthocyanin compounds, although in smaller quantities. Cy-3-Glc was also confirmed as the most representative compound for this group of wheat (4.02 μg/g), followed by Pn-3-Gal (0.33 μg/g) and Mv-3-Glc (0.22 μg/g). ELS 6404-117-4 was the genotype with the highest levels of anthocyanin compounds (11.39 μg/g), in agreement with its TAC (20.78 μg/g) detected with the spectrophotometric system. For 10 of the 43 wheat genotypes with red pericarp, these anthocyanins were not detected, probably because the amount is below the threshold of detectability of the instrument used.

To quantitatively analyze and confirm the relationships among anthocyanin components, TAC, YP, TKW, PC, SDS, and ASH, the Pearson correlation analysis was applied to the obtained data (Table 5). Higher TAC, but not TKW, was significantly associated with an increase in the concentration of almost all individual anthocyanin components, a finding suggesting that among the tested genotypes there was not a direct influence of the seed weight on the anthocyanin concentration. Positive associations were also recorded between SDS and the anthocyanin content in the grain. In contrast, YP and PC were correlated negatively with each other, but in relation to other characters, they did not show any association.


dx.doi.org/10.1021/jf5003683 | J. Agric. Food Chem. 2014, 62, 8686−8695

**Table 5. Pearson Correlation Coefficients among Anthocyanin Components, TAC, YP, TKW, PC, SDS, and ASH of 76 Pigmented Wheat Genotypes Evaluated over Three Growing Seasons at Foggia, Italy[a]**

| | Dp-3-Glc | Dp-3-Rut | Cy-3-Glc | Cy-3-Rut | Pn-3-Gal | Pn-3-Glc | Pn-3-Ara | Mv-3-Glc | TAC | YP | TKW | PC | SDS | ASH |
|---|---|---|---|---|---|---|---|---|---|---|---|---|---|---|
| Dp-3-Glc | 1.000 | | | | | | | | | | | | | |
| Dp-3-Rut | **0.974** | 1.000 | | | | | | | | | | | | |
| Cy-3-Glc | **0.866** | **0.783** | 1.000 | | | | | | | | | | | |
| Cy-3-Rut | **0.996** | **0.987** | **0.844** | 1.000 | | | | | | | | | | |
| Pn-3-Gal | 0.183 | 0.127 | **0.395** | 0.171 | 1.000 | | | | | | | | | |
| Pn-3-Glc | **0.911** | **0.819** | **0.864** | **0.873** | 0.207 | 1.000 | | | | | | | | |
| Pn-3-Ara | **0.578** | **0.698** | **0.350** | **0.644** | 0.025 | 0.189 | 1.000 | | | | | | | |
| Mv-3-Glc | 0.075 | 0.060 | **0.467** | 0.066 | **0.359** | 0.116 | −0.051 | 1.000 | | | | | | |
| TAC | **0.915** | **0.872** | **0.895** | **0.908** | **0.271** | **0.846** | **0.504** | **0.284** | 1.000 | | | | | |
| YP | 0.005 | −0.013 | 0.048 | 0.007 | −0.043 | −0.015 | 0.042 | 0.021 | 0.025 | 1.000 | | | | |
| TKW | **−0.270** | **−0.251** | **−0.252** | **−0.264** | −0.099 | **−0.265** | −0.117 | −0.043 | **−0.327** | −0.035 | 1.000 | | | |
| PC | −0.201 | −0.211 | −0.206 | −0.211 | 0.040 | −0.130 | −0.220 | −0.128 | −0.176 | **−0.328** | 0.134 | 1.000 | | |
| SDS | **0.722** | **0.711** | **0.562** | **0.724** | 0.032 | **0.636** | **0.460** | −0.065 | **0.637** | −0.030 | −0.099 | 0.000 | 1.000 | |
| ASH | **0.240** | 0.194 | **0.245** | 0.224 | 0.042 | **0.286** | 0.004 | 0.037 | **0.282** | 0.093 | **−0.233** | **0.231** | 0.158 | 1.000 |

[a]Cy-3-Glc, cyanidin 3-*O*-glucoside; Mv-3-Glc, malvidin 3-*O*-glucoside; Pg-3-Glc, pelargonidin 3-*O*-glucoside; Cy-3-Gal, cyanidin 3-*O*-galactoside; Pn-3-Glc, peonidin 3-*O*-glucoside; Cy-3-Rut, cyanidin 3-*O*-rutinoside; Dp-3-Glc, delphinidin 3-*O*-glucoside; Dp-3-Rut, delphinidin 3-*O*-rutinoside; Pn-3-Gal, peonidin 3-*O*-galactoside; Pn-3-Ara, peonidin 3-*O*-arabinoside; Pt-3-Glc, petunidin 3-*O*-glucoside; TAC, total anthocyanin content; YP, yellow pigment; TKW, thousand-kernel weight; PC, protein content; SDS, sodium dodecyl sulfate sedimentation volume; ASH, ash content. The coefficients in bold are significant at $p < 0.05$.



dx.doi.org/10.1021/jf5003683 | J. Agric. Food Chem. 2014, 62, 8686−8695

Table 6. Grain Minerals Concentration for Pigmented Wheat Groups Evaluated during the 2010−2011 Growing Season at Foggia, Italy

| | *Triticum aestivum* | | | | | *Triticum durum* | | | |
|---|---|---|---|---|---|---|---|---|---|
| | blue ($n$ = 3) | | control ($n$ = 1) | purple ($n$ = 27) | | red ($n$ = 43) | | control ($n$ = 2) | |
| mineral | mean | range | mean | mean | range | mean | range | mean | $LSD_{(0.05)}$ |
| Fe (mg/kg) | 46.13 | 43.90−47.30 | 30.30 | 36.71 | 30.10−42.00 | 36.71 | 30.80−46.80 | 32.85 | 5.61 |
| Mn (mg/kg) | 40.90 | 37.80−46.50 | 37.20 | 41.07 | 17.60−51.50 | 41.25 | 30.80−51.70 | 38.05 | 7.75 |
| Cu (mg/kg) | 6.00 | 4.80−7.70 | 5.70 | 6.87 | 4.30−9.60 | 6.71 | 3.80−9.20 | 7.40 | 1.64 |
| Zn (mg/kg) | 33.13 | 31.30−36.30 | 21.60 | 31.28 | 24.10−40.40 | 31.54 | 22.90−40.60 | 25.55 | 4.87 |

**Other Qualitative Parameters and Nutritional Properties of Pigmented Wheat.** To complete the characterization of the pigmented wheat, the 76 genotypes collected in the crop year 2010−2011 were also explored for the mineral content of their grain (Table 6 and Supporting Information Table S4). The highest levels of Fe were in blue wheat (46.13 mg/kg), whereas for the other pigmented groups, the means for Fe were lower. A similar trend was seen for Zn in the grain. The blue wheat showed the highest Zn (33.13 mg/kg), followed by the red and purple wheats (31.54 and 31.28 mg/kg, respectively). The other two elements analyzed, Mn and Cu, do not show a definite trend, and the commercial variety PR22D89 showed the highest concentrations of Mn (42.40 mg/kg) and Cu (9.50 mg/kg). Considering the genotypic variability within each group, the blue bread wheat did not show as wide a range as for the purple wheat. Indeed, the data show variations for Fe, from 30.10 mg/kg (286b) to 42.00 mg/kg (ELS 6304-56), for Mn, from 17.60 mg/kg (226) to 51.50 mg/kg (ELS 6304-56), for Cu, from 4.30 (286b) to 9.60 mg/kg (ELS 6404-75-3, ELS 6304-56), and for Zn, from 24.10 mg/kg (9503) to 40.40 mg/kg (ELS 6404-75-3).

Within the red group, for Fe, the range was from 30.80 mg/kg (377b) to 46.80 mg/kg (ELS 6404-159-4), for Mn, from 30.80 mg/kg (377b) to 51.70 mg/kg (ELS 6404-92-4), for Cu, from 3.80 mg/kg (ELS 6404-139-3) to 9.20 mg/kg (1842), and for Zn, from 22.90 mg/kg (377b) to 40.60 mg/kg (ELS 6404-92-4).

Table 7 shows the means for TPC and TEAC in relation to a selected number of genotypes, as representative of each group considered in the present study. These data show a significant correlation between the means of TPC and TEAC (0.97; $p \leq 0.001$). In particular, there was greater accumulation of TPC in the blue-pigmented wheat, as > purple, > red, which is reflected in the performance of the TEAC.

The commercial variety Preco appeared to show abnormal behavior, where a high TPC was seen (4.79 g/kg), and its TEAC was comparable to that for purple durum wheat (19.44 vs 20.08 mmol Trolox/kg).

Table 7. Mean Values of TPC and TEAC for a Subset of Pigmented Wheat Genotypes Collected during the 2010−2011 Growing Season at Foggia, Italy[a]

| species | color | genotype | TPC | TEAC |
|---|---|---|---|---|
| *Triticum aestivum* | blue | Sebesta Blue1 | 6.82 | 24.11 |
| *Triticum durum* | purple | World Seeds3 | 6.26 | 24.61 |
| | | MP3 | 5.67 | 20.53 |
| | | ELS 6404-115-5 | 3.16 | 15.11 |
| | red | ELS 6404-140-2 | 3.34 | 14.23 |
| | | ELS 6404-116-1 | 3.23 | 15.57 |
| | control | Preco | 4.79 | 19.44 |
| $LSD_{(0.05)}$ | | | 0.96 | 0.74 |

[a]TPC, total polyphenol content (g/kg); TEAC, Trolox equivalent antioxidant capacity in wheat grain (mmol Trolox/kg).

## DISCUSSION

Increasing attention has been paid to anthocyanins, due to their frequent presence in plants, particularly berry fruits, vegetables, grapes, and more recently in pigmented (black/blue/purple) cereal grains, for their health benefits as dietary antioxidants.[4,19] Most of the studies in the literature have been related to pigmented bread wheat and field trials conducted in a single growing season, and only rarely these investigations were carried out on tetraploid wheat genotypes. In the present study, the results are reported for a large collection of wheat genotypes. These are primarily represented by durum wheat genotypes, but also by bread wheat, with the aim being not only to evaluate the anthocyanin levels and composition in the grain but also to characterize other qualitative traits, which have not been investigated to date. The agronomic evaluation conducted for 3 years has also allowed estimation of the effect of growing season (Y) on the qualitative performance of these genetic materials.

**Total Anthocyanin Content, Qualitative Traits, and Nutritional Properties of Pigmented Wheats.** Our results confirm that blue wheat has, among wheat genetic resources, the highest TAC in the grain.[32−34] Recently, Syed Jaafar et al.[35] analyzed the TAC levels in a series of genotypes of wheat, including the same three Sebesta Blue genotypes analyzed in the present study. Although their mean TACs were relatively higher (159.8, 251.8, and 130.2 μg/g, for Sebesta Blue1, Sebesta Blue2, and Sebesta Blue3, respectively), the authors also confirm the graded list in the present study in which the Sebesta Blue2 genotype shows the highest TAC.

In particular, the TAC range observed in the present study, for the three Sebesta Blue genotypes throughout the entire study period (82.7−174.3 μg/g), was quite similar to that found in blue wheat by Abdel-Aal and Hucl[32] and Zofajova et al.[33] (157 and 193.3 μg/g, respectively).

However, sligthly lower were the values reported by Eticha et al.[34] and Knievel et al.,[19] between 39.9 and 106 μg/g. By contrast, higher values ranging from 76 to 286 μg/g were reported in refs 4, 7, and 19, although these other studies investigated different genotypes with respect to those considered in the present study.

Comparison with the literature of TAC in purple and red durum wheats is difficult, as most of the studies reported were conducted using hexaploid wheat varieties. The means recorded in the present study for purple durum wheat are comparable to


dx.doi.org/10.1021/jf5003683 | J. Agric. Food Chem. 2014, 62, 8686−8695

those reported in numerous other studies.[2,35] In these cases, TACs ranged from 27.0 μg/g[34] for the variety BVAL 258034 to 476.9 and 522.7 μg/g, recorded by Knievel et al.[19] for the breeding of a purple wheat line and by Hossenian et al.[9] in a stressed field trial, respectively. In the case of red wheat, the mean TACs in the present study were lower than for purple wheat, and in agreement with the means of 5, 5.2, and 5.76−7.97 μg/g observed by Escribano-Bailòn et al., Abdel-Aal et al., and Syed Jaafar et al.,[2,32,35] respectively.

The carotenoid pigments were lower than the anthocyanin pigments, which is in agreement with Abdel-Aal et al.,[32] who reported lower YP than TAC. Moreover, Eticha et al.[34] reported a range of YP from 2.6 to 7.6 μg/g for 13 blue and purple wheat genotypes. Here, no significant differences were observed among the three pigmented wheat groups, which suggests that for this character, there has been no selection, in contrast to the commercial varieties of durum wheat. For these latter, the present study indeed shows very high YP, which confirms the strong selective pressure that has been exerted by breeders to increase the content of the carotenoid pigments in the durum wheat grain.[17] The highest PC recorded in the present study is also comparable to the studies of Abdel-Aal et al.[32] and Eticha et al.[34] for both bread and durum wheats and the blue and purple wheats, whereas the red durum wheat shows values similar to those of the two commercial varieties used as controls.

Total polyphenol and TAC are also good indicators of antioxidant capacity, and some studies have reported high correlation between antioxidant capacity and TPC.[36,37] On a selected number of the genotypes chosen within each of the groups of the pigmented wheat in the present study, TPC and TEAC were determined. The positive association (0.64; $p < 0.001$) between TPC and the ability of these compounds to capture reactive oxygen species confirms previous studies on wheat[38−40] and on other crop species.[41] Our data confirm in part also the results obtained by Eticha et al.[34] relating to the antioxidant effects produced by TAC. Indeed, although it is less than that for TPC, the positive association between TAC and TEAC is significant (data not shown). However, the mean TEAC for durum wheat varieties (e.g., Preco) that are characterized by the absence of TAC and a high content of YP suggests that TEAC for some genotypes might be due to one or more other groups of pigments. This confirms the significant, but not exclusive, role that the anthocyanins appear to have in the control and capture of reactive oxygen species.[42]

For the mineral concentrations across the entire collection, the data in the present study are within the ranges defined previously by Ficco et al., Liu et al., and Ozkan et al.[26,43,44] on nonpigmented tetraploid wheat. With the exception of Cu, the concentrations of Mn, Zn, and Fe in purple wheat were higher than those of the commercial varieties (3.0, 5.8, and 3.9%, respectively). Interestingly, the mineral contents in the blue wheat analyzed in the present study are characterized by the highest Fe content (46.13 mg/kg), with a limited range of variation, whereas the red wheat is characterized by the highest Zn content, which is more variable. These data indicate that these variations can be exploited for breeding activities to improve the mineral availability in the final products.

**Effects of Year on Total Anthocyanin Content and Qualitative Parameters of Pigmented Wheats.** In our work we did not observe a strong effect of the growing season and of the G×Y effect on the TAC. Indeed, our results are similar to those obtained by Bustos et al.,[45] who analyzed the effect of crop management on TAC. Different from when a wider range of environmental conditions were explored, a larger effect associated with a significant G×E was observed. Moreover, the results of the G×E response on the accumulation of anthocyanins in wheat grain and their results appear to conflict. For instance, whereas water stress, as argued by Eticha et al.,[34] results in lower accumulation of TAC, Hossenian et al.[9] reported that this stress promotes accumulation of anthocyanin pigments in grain. Moreover, Abdel-Aal et al.[7] argued that in blue and purple wheats, the anthocyanin concentration is significantly influenced by growing conditions and that the environmental effect is much stronger in purple wheat, due to the pigment location in the outer pericarp. Probably, the intensity and duration of the stress may also produce substantialy different outcomes associated with the differences in environmental conditions not different from what is also occurring for complex traits such as grain yield.[29] Considering our results, the behavior of anthocyanin pigments appears similar to that of carotenoid pigments, for which there is a wide literature available that supports for this trait a strong genotypic component and a high heritability.[18,46,47] For the other traits evaluated (TKW, PC, ASH, and SDS), the data reveal that these are more influenced by genotype and G×Y, confirming a greater difficulty in obtaining a genetic progress as reported in refs 29 and 48.

**Anthocyanin Composition of Pigmented Wheat.** Compared to other cereals, such as maize and rice, the anthocyanin composition of pigmented wheat is not well characterized.[2,8] Moreover, the studies reported in the literature have almost always referred to a few selected genotypes of durum wheat. For these reasons, the present study appears to be the first that has examined a large number of purple/red tetraploid wheats. Our analysis was conducted using 11 standard compounds of the anthocyanins, with reference to bread wheat. Our data confirm delphinidin (Dp-3-Rut and Dp-3-Glc) as the main aglycone in blue wheat, as it represents 68.9% of the total anthocyanins,[4,7,8,19,49] followed by cyanidin, in the form of Cy-3-Glu and Cy-3-Rut. However, compared to previous studies, in all three Sebesta genotypes evaluated, relatively large levels of Mv-3-Glc were also found, whereas the peonidin aglycone is always present, and it is glycosylated with various sugars (glucoside, arabinoside, and galactoside) for each of the three genotypes.

To date, more than 15 types of anthocyanins have been identified in purple wheat,[35] which suggests greater complexity in the genetic control of purple durum wheat compared to blue bread wheat.[20] However, with the exception of the study of Hossenian et al.,[9] in which they identified and quantified 13 anthocyanin compounds using HPLC analysis, in all of the other studies, the number of compounds identified was limited to cyanidin in the form of Cy-3-Glc and Cy-3-Rut.[4,35] Although the chromatographic profiles of purple wheat appear more simple than those generated by blue wheat, the retention times overlapped only in part. In the purple and red tetraploid wheats in the present study, Cy-3-Glc was confirmed as the predominant anthocyanin, at 87.5 and 91.4% of TAC in purple and red wheats, respectively, followed by Pn-3-Gal (4.91−7.50%) and Mv-3-Glc (4.06−5.00%), which is consistent with previous results.[9,50] It must be emphasized, however, that with respect to blue wheat, purple and red wheats express lower levels of TAC, and although the chromatograms of wheat with purple and red pericarp appear simpler, this does not mean that other compounds are not present. It could be that the

extraction, identification, and quantification methods used have not allowed for the identification of all of the compounds examined. When the relationship between TAC determined by colorimetry and the sum of the individual anthocyanins determined by HPLC was examined, a significant positive correlation was obtained, with a correlation coefficient of 0.90 ($p < 0.05$). The difference might be due to the contribution of other pigments present in the grain that have an absorbance at 520 nm, and to be sure of this, there is the need to know more through more sensitive detection systems.

In conclusion, pigmented wheat genotypes exhibited large variations in quality and composition of anthocyanins as well as antioxidant activity. Cyanidin and delphinidin are the main anthocyanidins identified in the present collection of pigmented wheat and, although there is a need for more reliable and sensitive methods for their identification and quantification, the knowledge gained from the present study represents a very important aspect toward our better understanding of the genetic mechanisms that regulate the pathways of synthesis of anthocyanins in wheat.

For wheat, these genetic materials represent a source of genes/traits that will be very interesting for the improvement and development of new genotypes with enhanced nutritional properties. The high heritability values recorded for TAC and YP in wheat grain suggest that both traits can be combined, through specific crossing programs, in commercial wheat varieties with high technological grain quality to improve their nutritional value.

The characterization of these materials was also extended to the minerals content and, the higher contents of Fe and Zn make it even more attractive for the production of functional foods and also as added ingredients. In this way, the antioxidant activity of the wheat-derived products can be improved significantly.

However, to ensure a real effect of wheat grain pigments and minerals on human health, it is necessary to undertake further studies to evaluate the stability of these compounds during the manufacture of the final products (bread, pasta, and bakery products), milling, bread- and pasta-making, and cooking and to estimate the effects on human health through the evaluation of biomarkers of target functions and biological response.

## ■ ASSOCIATED CONTENT

### Supporting Information

Tables S1 and S2. This material is available free of charge via the Internet at http://pubs.acs.org.

## ■ AUTHOR INFORMATION

### Corresponding Author

*(P.D.V.) Phone: +39-0881-742972. Fax +39-0881-713150. E-mail: pasquale.devita@entecra.it.

### Funding

This study was supported by the Italian Ministry of Agriculture (MiPAAF), with the special grant RGV/Trattato FAO (*Risorse Genetiche Vegetali*), and by the Italian Ministry of Economic Development, with the special grant PAQ (Pasta e Nuovi Prodotti Alimentari ad Alta Qualità da Cereali Italiani).

### Notes

The authors declare no competing financial interest.

## ■ ACKNOWLEDGMENTS

Original seeds of pigmented wheats were kindly provided by Dr. Harold Bockelaman, (USDA-ARS, National Small Grain Collection, Aberdeen, ID, USA). We thank Cecilia di Paola for technical assistance and Dr. Antonio Troccoli for meteorological data support. We are grateful to Dr. Christopher Berrie for scientific English language editorial assistance.

## ■ ABBREVIATIONS USED

Cy-3-Gal, cyanidin 3-*O*-galactoside; Cy-3-Glc, cyanidin 3-*O*-glucoside; Cy-3-Rut, cyanidin 3-*O*-rutinoside; Dp-3-Glc, delphinidin 3-*O*-glucoside; Dp-3-Rut, delphinidin 3-*O*-rutinoside; G×E, genotype × environment; G×Y, genotype × year; HPLC, high-performance liquid chromatography; Mv-3-Glc, malvidin 3-*O*-glucoside; PC, protein content; Pg-3-Glc, pelargonidin 3-*O*-glucoside; Pn-3-Ara, peonidin 3-*O*-arabinoside; Pn-3-Gal, peonidin 3-*O*-galactoside; Pn-3-Glc, peonidin 3-*O*-glucoside; Pt-3-Glc, petunidin 3-*O*-glucoside; SDS, sodium dodecyl sulfate; TAC, total anthocyanin content; TEAC, Trolox equivalent antioxidant capacity; TKW, thousand-kernel weight; TPC, total polyphenol; YP, yellow pigment

## ■ REFERENCES

(1) Gani, A.; Wani, S. M.; Masoodi, F. A.; Gousia, H. Whole-grain cereal bioactive compounds and their health benefits: a review. *J. Food Process Technol.* **2012**, *3*, 146−155.

(2) Escribano-Bailón, M. T.; Santos-Buelga, C.; Rivas-Gonzalo, J. C. Anthocyanins in cereals. *J. Chromatogr. A* **2004**, *1054*, 129−141.

(3) Ficco, D. B. M.; Mastrangelo, A. M.; Trono, D.; Borrelli, G. M.; De Vita, P.; Fares, C.; Beleggia, R.; Platani, C.; Papa, R. The colours of durum wheat: a review. *Crop Pasture Sci.* **2014**, *65*, 1−15.

(4) Abdel-Aal, E. S. M.; Young, J. C.; Rabalski, I. Anthocyanin composition in black, blue, pink, purple, and red cereal grains. *J. Agric. Food Chem.* **2006**, *54*, 4696−4704.

(5) Finocchiaro, F.; Ferrari, B.; Gianinetti, A. A study of biodiversity of flavonoid content in the rice caryopsis evidencing simultaneous accumulation of anthocyanins and proanthocyanidins in a black-grained genotype. *J. Cereal Sci.* **2010**, *51*, 28−34.

(6) Eticha, F.; Grausgrever, H.; Berghoffer, E. Multivariate analysis of agronomic and quality traits of hull-less spring barley (*Hordeum vulgare* L.). *J. Plant Breed. Crop Sci.* **2010**, *2*, 81−95.

(7) Abdel-Aal, E. S. M.; Abou-Arab, A. A.; Gamel, T. H.; Hucl, P.; Young, J. C.; Rabalski, I. Fractionation of blue wheat anthocyanin compounds and their contribution to antioxidant properties. *J. Agric. Food Chem.* **2008**, *56*, 11171−11177.

(8) Hu, C.; Cai, Y. Z.; Li, W.; Corke, H.; Kitts, D. Anthocyanin characterization and bioactivity assessment of a dark blue grained wheat (*Triticum aestivum* L. cv. Hedong Wumai) extract. *Food Chem.* **2007**, *104*, 955−961.

(9) Hosseinian, F. S.; Li, W.; Beta, T. Measurement of anthocyanins and other phytochemicals in purple wheat. *Food Chem.* **2008**, *109*, 916−924.

(10) Shipp, J.; Abdel-Aal, El-S. M. Food applications and physiological effects of anthocyanins as functional food ingredients. *Open Food Sci. J.* **2010**, *4*, 7−22.

(11) Zeven, A. C. Wheats with purple and blue grains: a review. *Euphytica* **1991**, *56*, 243−258.

(12) Zeller, F. J.; Cermeno, M. C.; Miller, T. E. Cytogenetical analysis on the distribution and origin of the alien chromosome pair conferring blue aleurone colour in several European common wheat (*Triticum aestivum* L.) strains. *Theor. Appl. Genet.* **1991**, *81*, 551−558.

(13) Morrison, L. A.; Metzger, R. J.; Lukaszewski, A. J. Origin of the blue-aleurone gene in Sebesta Blue wheat genetic stocks and a protocol for its use in apomixes screening. *Crop Sci.* **2004**, *44*, 2063−2067.

(14) Abdel-Aal, E. S. M.; Hucl, P. Composition and stability of anthocyanins in blue-grained wheat. *J. Agric. Food Chem.* **2003**, *51*, 2174−2180.
(15) Hentschel, V.; Kranl, K.; Hollmann, J.; Lindhauer, M. G.; Bohmand, V.; Bitsch, R. Spectrophotometric determination of yellow pigment content and evaluation of carotenoids by high-performance liquid chromatography in durum wheat grain. *J. Agric. Food Chem.* **2002**, *50*, 6663−6668.
(16) Hidalgo, A.; Brandolini, A.; Pompei, C. Carotenoids evolution during pasta, bread and water biscuit preparation from wheat flours. *Food Chem.* **2010**, *121*, 746−751.
(17) Digesù, A. M.; Platani, C.; Cattivelli, L.; Mangini, G.; Blanco, A. Genetic variability in yellow pigment components in cultivated and wild tetraploid wheats. *J. Cereal Sci.* **2009**, *50*, 210−218.
(18) Blanco, A.; Colasuonno, P.; Gadaleta, A.; Mangini, G.; Schiavulli, A.; Simeone, R.; Digesù, A. M.; De Vita, P.; Mastrangelo, A. M.; Cattivelli, L. Quantitative trait loci for yellow pigment concentration and individual carotenoid compounds in durum wheat. *J. Cereal Sci.* **2011**, *54*, 255−264.
(19) Knievel, D. C.; Abdel-Aal, E. S. M.; Rabalski, I.; Nakamura, T.; Hucl, P. J. Grain colour development and the inheritance of high anthocyanin blue aleurone and purple pericarp in spring wheat (*Triticum aestivum* L.). *J. Cereal Sci.* **2009**, *50*, 113−120.
(20) Khlestkina, E. K.; Röder, M. S.; Börner, A. Mapping genes controlling anthocyanin pigmentation on the glume and pericarp in tetraploid wheat (*Triticum durum* L.). *Euphytica* **2010**, *171*, 65−69.
(21) AACC International (formerly the American Association of Cereal Chemists). *Approved Methods of the AACC*, 11th ed.; St. Paul, MN, USA, 2001; Method 46-13.01.
(22) UNI 10277 (Ente Nazionale Italiano di Unificazione). Durum wheat. Determination of sedimentation index. The sodium dodecyl sulfate method [in Italian], 1993.
(23) UNI ISO 2171 (Ente Nazionale Italiano di Unificazione). Determination of ash in cereals intended for food use [in Italian], 2010.
(24) AACC International (formerly the American Association of Cereal Chemists). *Approved Methods of the AACC*, 11th ed.; St. Paul, MN, USA, 2013; Method 14-50.01.
(25) Beleggia, R.; Platani, C.; Nigro, F.; Cattivelli, L. A micro-method for the determination of yellow pigment content in durum wheat. *J. Cereal Sci.* **2010**, *52*, 106−110.
(26) Ficco, D. B. M.; Riefolo, C.; Nicastro, G.; De Simone, V.; Di Gesù, A. M.; Beleggia, R.; Platani, C.; Cattivelli, L.; De Vita, P. Phytate and mineral elements concentration in a collection of Italian durum wheat cultivars. *Field Crop Res.* **2009**, *111*, 235−242.
(27) Graham, H. D. Stabilization of the Prussian blue color in the determination of polyphenols. *J. Agric. Food Chem.* **1992**, *40*, 801−805.
(28) Pellegrini, N.; Re, R.; Yang, M.; Rice-Evans, C. A. Screening of dietary carotenoids and carotenoid-rich fruit extracts for antioxidant activities applying the 2,2′-azinobis(3-ethylbenzothiazoline-6-sulfonic acid) radical cation decoloration assay. *Methods Enzymol.* **1999**, *299*, 379−389.
(29) De Vita, P.; Li Destri Nicosia, O.; Nigro, F.; Platani, C.; Riefolo, C.; Di Fonzo, N.; Cattivelli, L. Breeding progress in morpho-physiological, agronomical and qualitative traits of durum wheat cultivars released in Italy during the 20th century. *Eur. J. Agron.* **2007**, *26*, 39−53.
(30) Gegas, V. C.; Nazari, A.; Griffiths, S.; Simmonds, J.; Fish, L.; Orford, S.; Sayers, L.; Doonan, J. H.; Snapea, J. W. A genetic framework for grain size and shape variation in wheat. *Plant Cell* **2010**, *22*, 1046−1056.
(31) Wang, L.; Ge, H.; Hao, C.; Dong, Y.; Zhang, X. Identifying loci influencing 1,000-kernel weight in wheat by microsatellite screening for evidence of selection during breeding. *PLoS One* **2012**, *7*, e29432.
(32) Abdel-Aal, E. S. M.; Hucl, P. A rapid method for quantifying total anthocyanins in blue aleurone and purple pericarp wheats. *Cereal Chem.* **1999**, *76*, 350−354.
(33) Zofajova, A.; Psenova, I.; Havrlentova, M. M.; Piliarova, M. Accumulation of total anthocyanins in wheat grain. *Agriculture* **2012**, *58*, 50−56.
(34) Eticha, F.; Grausgruber, H.; Siebenhand-Ehn, S.; Berghofer, E. Some agronomic and chemical traits of blue aleurone and purple pericarp wheat (*Triticum* L.). *J. Agric. Sci. Technol. B* **2011**, *1*, 48−58.
(35) Syed Jaafar, S. N.; Baron, J.; Siebenhandl-Ehn, S.; Rosenau, T.; Böhmdorfer, S.; Grausgruber, H. Increased anthocyanin content in purple pericarp × blue aleurone wheat crosses. *Plant Breed.* **2013**, *132*, 48−58.
(36) Pellegrini, N.; Simonetti, P.; Gardana, C.; Brenna, O.; Brighenti, F.; Pietta, P. Polyphenol content and total antioxidant activity of vini novelli (young red wines). *J. Agric. Food Chem.* **2000**, *48*, 732−735.
(37) Simonetti, P.; Piergiorgio, P.; Testolin, G. Polyphenol content and total antioxidant potential of selected Italian wines. *J. Agric. Food Chem.* **1997**, *45*, 1152−1155.
(38) Yu, L.; Haley, S.; Perret, J.; Harris, M.; Wilson, J.; Qian, M. Free radical scavenging properties of wheat extracts. *J. Agric. Food Chem.* **2002**, *50*, 1619−1624.
(39) Liu, Q.; Qui, Y.; Beta, T. Comparison of antioxidant activities of different coloured wheat grains and analysis of phenolic compounds. *J. Agric. Food Chem.* **2010**, *58*, 9235−9241.
(40) Siebenhandl, S.; Grausgruber, H.; Pellegrini, N.; Del Rio, D.; Fogliano, V.; Pernice, R.; Berghofer, E. Phytochemical profile of main antioxidants in different fractions of purple and blue wheat and black barley. *J. Agric. Food Chem.* **2007**, *55*, 8541−8547.
(41) Lako, J.; Trenerry, C. V.; Wahlqvist, M.; Wattanapenpaiboon, N.; Sotheeswaran, S.; Premier, R. Phytochemical flavonols, carotenoids and the antioxidant properties of a wide selection of Fijian fruit, vegetables and other readily available foods. *Food Chem.* **2007**, *101*, 1727−1741.
(42) Zhou, K.; Laux, J. J.; Yu, L. L. Comparison of swiss red wheat grain and fractions for their antioxidant properties. *J. Agric. Food Chem.* **2004**, *52*, 1118−1123.
(43) Liu, Z. H.; Wang, H. Y.; Wang, X. E.; Zhang, G. P.; Chen, P. D.; Liu, D. J. Genotypic and spike positional difference in grain phytase activity, phytate, inorganic phosphorus, iron, and zinc contents in wheat (*Triticum aestivum* L.). *J. Cereal Sci.* **2006**, *44*, 212−219.
(44) Ozkan, H.; Brandolini, A.; Torun, A.; AltInta, S.; Eker, S.; Kilian, B.; Braun, H. J.; Salamini, F.; Cakmak, I. Natural variation and identification of micro-elements content in seeds of Einkorn wheat (*Triticum monococcum*). In *Wheat Production in Stressed Environments*; Buck, H. T., Nisi, J. E., Salomón, N., Eds.; Springer: Dordrecht, The Netherlands, 2007; Vol. 12, pp 455−462.
(45) Bustos, D. V.; Riegel, R.; Calderini, D. F. Anthocyanin content of grains in purple wheat is affected by grain position, assimilate availability and agronomic management. *J. Cereal Sci.* **2012**, *55*, 257−264.
(46) Zhang, W.; Dubcovsky, J. Association between allelic variation at the phytoene synthase 1 gene and yellow pigment content in the wheat grain. *Theor. Appl. Genet.* **2008**, *116*, 635−645.
(47) Elouafi, I.; Nachit, M. M.; Martin, L. M. Identification of a microsatellite on chromosome 7B showing a strong linkage with yellow pigment in durum wheat (*Triticum turgidum* L. var.*durum*). *Hereditas* **2001**, *135*, 255−261.
(48) Blanco, A.; Pasqualone, A.; Troccoli, A.; Di Fonzo, N.; Simeone, R. Detection of grain protein content QTL across environments in tetraploid wheats. *Plant Mol. Biol.* **2002**, *48*, 615−623.
(49) Tyl, C. E.; Bunzel, M. Antioxidant activity-guided fractionation of blue wheat (UC66049 *Triticum aestivum* L.). *J. Agric. Food Chem.* **2012**, *60*, 731−739.
(50) Chen, W.; Muller, D.; Richling, E.; Wink, M. Anthocyanin-rich purple wheat prolongs the life span of *Caenorhabditis elegans* probably by activating the DAF-16/FOXO transcription factor. *J. Agric. Food Chem.* **2013**, *61*, 3047−3053.

JOURNAL OF AGRICULTURAL AND FOOD CHEMISTRY

Article

pubs.acs.org/JAFC

# Identification of the Environmental Neurotoxins Annonaceous Acetogenins in an *Annona cherimolia* Mill. Alcoholic Beverage Using HPLC-ESI-LTQ-Orbitrap

Jessica Le Ven,[†] Isabelle Schmitz-Afonso,*[,‡] Guy Lewin,[†] Alain Brunelle,[‡] David Touboul,[‡] and Pierre Champy[†]

[†]Laboratoire de Pharmacognosie, CNRS UMR 8076 BioCIS, Faculté de Pharmacie, Université Paris-Sud, 5 rue J.-B. Clément, 92296 Châtenay-Malabry, France

[‡]Centre de Recherche de Gif, Institut de Chimie des Substances Naturelles, CNRS, avenue de la terrasse, 91198 Gif-sur-Yvette Cedex, France

Supporting Information

**ABSTRACT:** Epidemiological and toxicological studies have suggested Annonaceaeous acetogenins to be environmental neurotoxins responsible for sporadic atypical parkinsonism/dementia in tropical areas. These compounds are present in the tropical genus *Annona* (Annonaceae), known for its fruit-yielding cultivated species such as *Annona cherimolia*. This species is widely cultivated in South America, Spain, and Portugal and yields acetogenins in its seeds, stems, and roots. The presence of these compounds in the pulp of its fruit and in derived food products is unclear. An innovative and sensitive methodology by HPLC-ESI-LTQ-Orbitrap with postcolumn infusion of lithium iodide was used to identify the presence of low levels of acetogenins in an *A. cherimolia* Mill. fruit-based commercial alcoholic beverage. More than 80 representatives were detected, and the 31 most intense acetogenins were identified. All together these findings indicate that this species should be considered as a risk factor within the framework of a worldwide problem of food toxicity.

**KEYWORDS:** *acetogenins, Annona cherimolia Mill., Annonaceae, annonacin, dereplication, environmental neurotoxins, mass spectrometry, HPLC-MS/MS*

## INTRODUCTION

The tropical family Annonaceae has economic importance in the food-processing industry and fresh fruit local markets, mainly with members of the genus *Annona*. Species such as *Annona cherimolia* Mill. (annona, chirimoya), *Annona muricata* L. (soursop), and *Annona squamosa* L. (custard apple) are appreciated for their edible fruits and derived food products.[1] These plants are also widely used in traditional medicine.[2] Case-control studies[3−5] have suggested consumption of the fruits of Annonaceae and herbal infusions derived from these plants as the cause of the high prevalence of sporadic atypical Parkinsonism/dementia clusters reported in Guadeloupe (French West Indies)[6,7] and New Caledonia.[8] They might also be involved in atypical Parkinsonism observed in some communities in London[9] and on the island of Guam.[10] Phytochemical and toxicological studies have identified Annonaceous acetogenins (AAGs), a class of polyketides specific to the Annonaceae,[11,12] as candidate neurotoxins. The French food safety agency expressed its concern about this issue.[13]

AAGs constitute a chemically homogeneous class of polyketides with a common skeleton consisting of an $\alpha,\beta$-saturated or unsaturated $\gamma$-methyl-$\gamma$-lactone, optionally hydroxylated, substituted in position 2 by a long alkyl chain of 32 or 34 carbons. The aliphatic chain most often bears one or two tetrahydrofuranic cycles (THF) flanked by adjacent hydroxyls, free hydroxyls (possibly acetylated), ketones, epoxides, or double bonds. These compounds are potent inhibitors of mitochondrial complex I, with structure−activity relationships based on the above-mentioned structural features and global lipophilicity.[12,14] In agreement with clinical and anatomopathological observations, toxicological studies showed that these compounds induce hyperphosphorylation and redistribution of Tau and cell death in striatal and cortical neuronal primary cultures.[14−17] Annonacin, the major AAG of *A. muricata*, induces neurodegeneration after subchronic systemic intoxication in rats and Tau hyperphosphorylation in neurons of mice transfected with the human mutated Tau gene.[18−20] Chemical homogeneity among members of the Annonaceae family suggests that all edible species might be sources of AAGs. Indeed, phytochemical studies of *A. muricata*, *A. squamosa*, and *Asimina triloba* Dunnal. (paw paw) revealed significant quantities of AAGs in their fruits.[17,21−24] In addition, soursop processed nectars from different origins were also shown to contain AAGs.[21−23,25]

The fruit of *A. cherimolia* is cultivated and eaten in South America and Asia and also in southern Europe, with Spain as the main producer and an annual volume of 300 tons for the Portuguese island of Madeira only.[26] However, it is unclear whether the species is a dietary source of AAGs. Indeed, the chemical composition of this fruit is poorly known apart from essential oil and kaurane diterpenes.[27−29] According to the literature, 27 AAGs have been isolated from the seed, stem, and

Received: March 9, 2014
Revised: August 3, 2014
Accepted: August 3, 2014
Published: August 4, 2014

ACS Publications © 2014 American Chemical Society

root of this species, including 3 artifactual compounds.[12,30] Our previous study showed the absence of AAGs in fruits originating from Spain.[29] We recently developed an innovative approach for the detection of AAGs, using reversed-phase high-performance liquid chromatography coupled to a hybrid linear trap/Orbitrap mass spectrometer (LTQ-Orbitrap) with post-column infusion of lithium.[25] Under these conditions, intense lithium adducts of AAGs are preferably formed, with enhanced detection compared to other metabolites, providing useful fragment ions for structural studies. This technique was here used to investigate an industrial alcoholic beverage prepared with *A. cherimolia* originating from Madeira (Portugal). In the total ethyl acetate (EtOAc) extract, numerous AAGs could be detected, and those yielding the most intense $[M + Li]^+$ ions could be identified or structurally characterized.

## MATERIALS AND METHODS

**Chemical Reagents.** Ethyl acetate (EtOAc), methanol (MeOH, LC-MS grade), acetonitrile (HPLC grade), and $H_2SO_4$ were purchased from VWR-Prolabo (Fontenay-sous-Bois, France). Lithium iodide (LiI) and sodium sulfate ($Na_2SO_4$) were purchased from Sigma-Aldrich (Saint Quentin-Fallavier, France). Milli-Q water was prepared in house.

**Standards.** Diepomuricanin-B (**1**) ($C_{35}H_{62}O_4$; monoisotopic mass = 546.4648 Da), corossolin (**3**) ($C_{35}H_{64}O_6$; monoisotopic mass = 580.4703 Da), annonacin (**6**) and *cis*-annonacin (**7**) ($C_{35}H_{64}O_7$; monoisotopic mass = 596.4652 Da), *trans*-corossolone (**13**) and *cis*-corossolone (**14**) ($C_{35}H_{62}O_6$; monoisotopic mass = 585.4701 Da) were obtained as previously described.[12,31] Stock solutions were prepared in methanol at a concentration of 1 $\mu$M.

**Extracted Material.** *A. cherimolia* Mill. alcoholic beverage (brand Licor de Annona, J. Faria and Filhos, LDA; no batch number), packaged in a glass bottle (total volume = 0.7 L), was purchased in Madeira (Portugal). Its composition was "water, 20° alcohol, sugar and annona".

**Extraction.** The beverage (0.5 L) was acidified with $H_2SO_4$ (0.5 N) to pH 3 and then extracted (L/L) three times with EtOAc (3 × 300 mL) followed by centrifugation for 15 min at 4000 rpm to remove the emulsion produced by sugars. The organic phases were combined, dried over anhydric $Na_2SO_4$, and evaporated to dryness under reduced pressure to obtain a sample of 141 mg (yield = 4.7 × $10^{-2}$% w/v). The extract was kept at 4 °C. Aliquots were extemporaneously dissolved in MeOH (1 mg/mL) and filtered using an Acrodisc CR 4 mm syringe filter (0.45 $\mu$m PTFE membrane) before injection in the chromatographic system.

**High-Performance Liquid Chromatography with Tandem Mass Spectrometry (HPLC-MS/MS).** HPLC was performed on an HPLC Ultimate 3000 system (Dionex, Voisins-le-Bretonneux, France) consisting of a degasser, a quaternary pump, an autosampler, a column oven, and a photodiode array detector. Separation was achieved on an octadecyl column (Sunfire, 100 × 2.1 mm, 3.5 $\mu$m particle size; Waters, Guyancourt, France), equipped with a guard column. Column oven temperature was set at 30 °C. Elution was conducted with a mobile phase consisting of water (A) and acetonitrile (B), following the gradient 40 to 100% B in 25 min, then maintaining 100% B for 7 min at a flow rate of 0.3 mL/min. Injection volume was 10 $\mu$L (full loop) for standards and extract solutions. After LC separation, UV detection was operated at 210 nm. The HPLC system was interfaced to a hybrid linear trap/Orbitrap mass spectrometer (LTQ-XL Orbitrap, Thermo Scientific, Les Ulis, France) equipped with an electrospray (ESI) ionization source. Accessible ranges were $m/z$ 250−1200 for full-scan MS experiment and $m/z$ 160−700 for $MS^2$ experiments. Mass resolutions (fwhm) were fixed at 60000 and 30000 for MS and $MS^2$ experiments, respectively. The source parameters in the positive ion mode were as follows: spray voltage set at 5 kV, capillary temperature at 300 °C, capillary voltage at 45 V, and tube lens voltage at 165 V. The optimal collision energy was 50 au, and activation time was 33 ms. Postcolumn infusion of lithium iodide (2 mM in MeOH) was performed at a flow rate of 5 $\mu$L/min. Mass measurements were obtained with a mass precision below 3 ppm using an external calibration. The LOD (UV, MS) of purified annonacin (**6**) was evaluated in the same conditions, based on triplicate injection (10 $\mu$L) of the targeted concentration, with a signal-to-noise ratio above 3.

**AAGs Classification.** After structural identification, the AAGs contained in the extract were ranked using the classification established by Cavé et al.[11] The first rank classification type is based on the layout of the aliphatic chain: A-type (mono-THF), B-type (adjacent bis-THF), or C-type (nonadjacent bis-THF). These THF cycles are always flanked by two adjacent hydroxyl groups, except for a few representatives with one hydroxyl only, placed on the methyl-terminal end. E-type AAGs contain no THF, but epoxides and/or double bonds. The second rank classification is the subtype depending on the nature of the lactone ring. The most frequently referenced are subtype 1a ($\alpha,\beta$-unsaturated $\gamma$-methyl-$\gamma$-lactone) and subtype 1b ($\alpha,\beta$-unsaturated $\gamma$-methyl-$\gamma$-lactone with a hydroxyl on the C-4 position).

**Data Analyses.** The search for AAGs formulas corresponding to lithiated adducts was carefully achieved following the method described below. $[M + H]^+$, $[M + Na]^+$, and $[M + K]^+$ ions were excluded on the basis of the raw formulas assigned for each of these ions (precision better than 3 ppm). The characteristic structural fragments of lithiated adducts were sought according to the method established in our previous publication.[31] To validate that these compounds are AAGs, characteristic fragments of AAGs were first sought in the $MS^2$ spectra of C35 and C37 compounds corresponding to the AAGs: loss of CO (−27.9949 amu), $CO_2$ (−43.9898 amu), and cleavage on $\beta$ of the lactone.

Second, other characteristic structural fragments were searched, according to the classification established by Laprévote et al.: terminal $CH_3$-containing X-fragments, produced by an $\alpha$-cleavage of hydroxyl group; lactone-containing B-fragments for cleavage of a THF group; terminal $CH_3$-containing Y-fragments by breaking of bis-THF (B-type AAGs) and nonadjacent-THF groups (C-type AAGs); and finally lactone-containing c-fragments for the cleavage of an epoxide cycle.[25,31] Numeral subscripts used with these letters distinguish the different ions belonging to the same series (e.g., $X_1$ is the fragment produced by $\alpha$-cleavage to the first hydroxyl group, starting from the methyl end) (Figure 1). Fragments corresponding to successive water losses are not specific to the number of hydroxyls and therefore were not used. The relative intensity of the fragment corresponding to the $\beta$-cleavage of the lactone can differentiate subtype 1a (<100%) from subtype 1b (100%). However, no fragment allowed full characterization of the part between THF and terminal $CH_3$, the second epoxide, ketones, and double bonds.

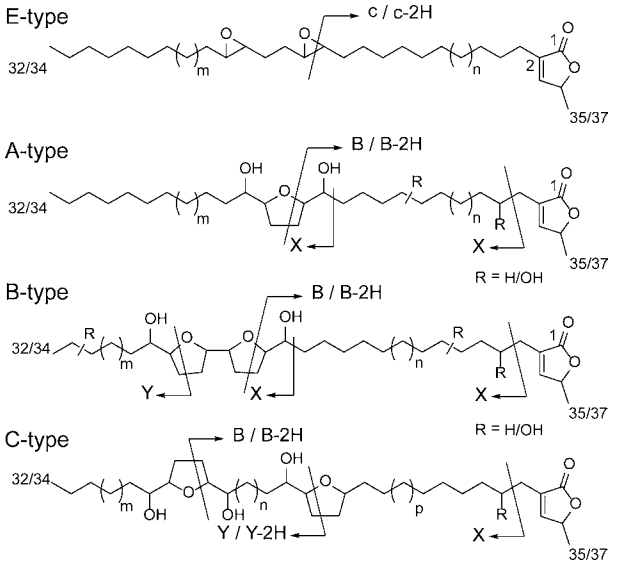


**Figure 1.** Fragmentation patterns for the $[M + Li]^+$ adduct ions of AAGs identified in the *Annona cherimolia* alcoholic beverage.


dx.doi.org/10.1021/jf501174j | J. Agric. Food Chem. 2014, 62, 8696−8704

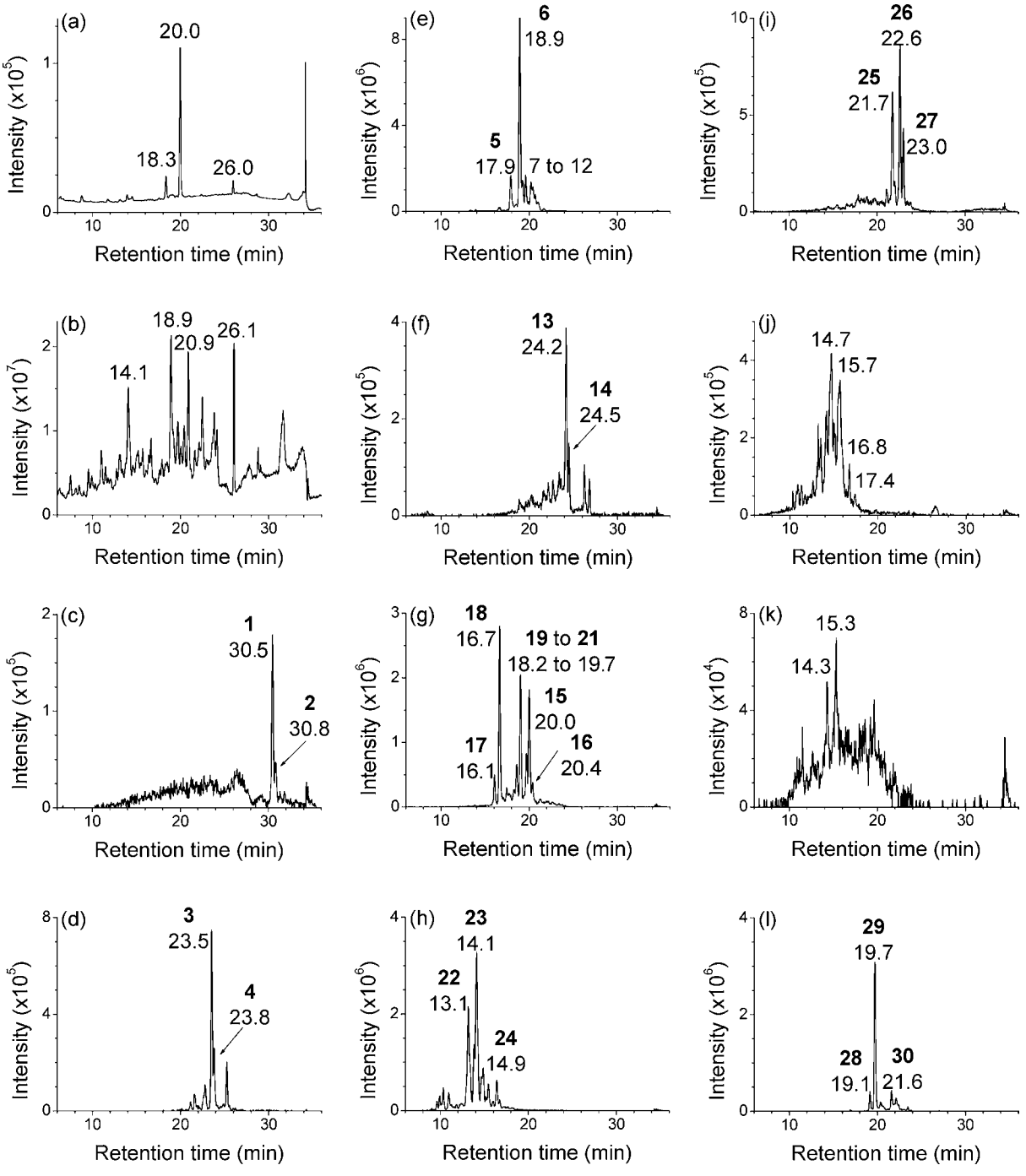


**Figure 2.** Chromatograms obtained for the ethyl acetate extract of *Annona cherimolia* alcoholic beverage using HPLC-UV-ESI-LTQ-Orbitrap: (a) UV 210 nm; (b) TIC ($m/z$ 250.00−1200.00) with postcolumn infusion of LiI; (c) EIC $m/z$ range 553.47−553.49, i.e., $[C_{35}H_{62}O_4Li]^+$; (d) EIC $m/z$ range 587.47−587.49, i.e., $[C_{35}H_{64}O_6Li]^+$; (e) EIC $m/z$ range 603.47−603.49, i.e., $[C_{35}H_{64}O_7Li]^+$; (f) EIC $m/z$ range 585.45−585.47, i.e., $[C_{35}H_{62}O_6Li]^+$; (g) EIC $m/z$ range 601.46−601.47, i.e., $[C_{35}H_{62}O_7Li]^+$; (h) EIC $m/z$ range 617.45−617.46, i.e., $[C_{35}H_{62}O_8Li]^+$; (i) EIC $m/z$ range 599.44−599.46, i.e. $[C_{35}H_{60}O_7Li]^+$; (j) EIC $m/z$ range 619.465−619.48, i.e., $[C_{35}H_{64}O_8Li]^+$; (k) EIC $m/z$ range 615.44−615.45, i.e., $[C_{35}H_{60}O_8Li]^+$; (l) EIC $m/z$ range 629.49−629.50, i.e., $[C_{37}H_{66}O_7Li]^+$.

## RESULTS AND DISCUSSION

**Detection of AAGs.** Analysis of the EtOAc extract of the *A. cherimolia* fruit alcoholic beverage was performed by HPLC-UV-LTQ-Orbitrap with postcolumn infusion of lithium under previously described conditions.[25] Three major molecules at retention times Rt = 18.3, 20.0, and 26.0 min, respectively, are distinguishable by UV detection (Figure 2a). These compounds with respective formulas $C_{25}H_{38}O_5$, $C_{26}H_{40}O_5$, and $C_{24}H_{38}O_4$ do not match with AAGs structural definition (C35 or C37). $MS^2$ studies did not show the characteristic fragments of AAGs described in our previous publication (loss of CO, $CO_2$, and lactone). In the total ion current chromatogram (TIC) different peaks corresponding to mass-to-charge ratio of AAGs are however detected (Figure 2b). The low TIC intensity and the absence of detection of AAGs by UV, despite the high amount of extract injected (10 $\mu$g), show the little quantity of these compounds in our extract in comparison to *A. muricata* pulp


dx.doi.org/10.1021/jf501174j | J. Agric. Food Chem. 2014, 62, 8696−8704

extract.[25] Indeed, the LOD of annonacin (**6**) was $5.10^{-7}$ M in UV ($\lambda$ = 210 nm) and $2.10^{-10}$ M in MS with postcolumn lithium infusion.

**AAGs Profile.** More than 80 AAGs are detected as lithiated adducts, including 20 different formulas. These results offer new insight on the chemical composition of the species, in which 27 AAGs corresponding to 7 different raw formulas had been identified so far. Most of the chromatographic peaks corresponding to AAGs are observed between 10 and 22 min, with about 12 main representatives (Figure 2b). Thirty-one AAGs could be precisely and unambiguously characterized and classified into types and subtypes, among which 18 were identified.

**C35 AAGs.** Thirteen different nominal $m/z$ values were attributed to the $[M + Li]^+$ ions of AAGs bearing 35 carbon atoms. Eight of them correspond to AAGs already isolated from the Annonaceae family, whereas only four were known in the case of *A. cherimolia* ($C_{35}H_{60}O_7$; $C_{35}H_{62}O_7$; $C_{35}H_{64}O_7$; $C_{35}H_{66}O_7$).[12] The formula $C_{35}H_{60}O_8$ had never been described within the AAGs group. Over 55 different C35 AAGs were detected, that is, 66% of the total number of AAGs. Preferential biosynthesis of AAGs of such length was indeed suggested by previous isolation works and is observed in most *Annona* species studied so far.[11,12]

**E-Type: Aliphatic AAGs.** No E-type AAG has been described in *A. cherimolia* so far. Two species with the same formula $C_{35}H_{62}O_4$ are detected at very low intensity ($4 \times 10^4$) and closely eluted at retention times Rt = 30.5 (**1**) and 30.8 min (**2**) (Figure 2c). Their $MS^2$ spectra exhibit major fragment ions corresponding to the loss of water, CO, and $CO_2$, whereas cleavage in $\beta$ of the lactone ring is not noticeable, indicating that they belong to subtype 1a (i.e., no hydroxyl in C-4). However, the c and c-2H fragments are detected (Table 1), indicating the presence of an epoxide between C-17 and C-18 carbons (Figure 1). Finally, coelution with a standard of the bis-epoxydic diepomuricanin-B confirmed the identity of **1**. Structural knowledge of E-type AAGs designates **2** as its diastereoisomer (Figure 3), the second epoxide being located in the $\gamma$-position of the first.[11] E-type AAGs are considered as biosynthetic precursors of THF-bearing, biologically active AAGs and are minor compounds in Annonaceae.[12,32] Their low amount in the extract could thus be expected. However, only compounds **19**–**24** are possible biosynthetic derivatives of **1** and **2**, which cannot be proposed as precursors of any of the A-type AAG identified in the extract (see below).

**A-Type A: Mono-THF.** Three main compounds are attributed to the formula $C_{35}H_{64}O_6$, along with about five minor peaks. Two of them were partially separated, at retention times Rt = 23.5 min (**3**) and 23.8 min (**4**), respectively. Both showed low intensity ($1 \times 10^5$) (Figure 2d). The fragment resulting from the cleavage in $\beta$ of the lactone shows that they belong to subtype 1a ($[M - C_6H_8O_2 + Li]^+$, relative intensity $\leq$ 10%). In addition, for the first compound, in the $MS^2$ spectrum of $m/z$ 587.48–587.49 ion, a B-fragment is detected, allowing placement of a THF ring between C-16 and C-19 carbons ($B_1 - 2H$ fragment), flanked by hydroxyl groups (postulated for C-20) (Figure 1). According to coelution with a standard, these two molecules are unambiguously assigned to corossolin (**3**) and a stereoisomer (**4**) (Figures 2d and 3). Neither has ever been described in this species. The third compound (retention time Rt = 25.3 min) is an AAG of subtype 1b (i.e., hydroxylated in C-4), but no other fragment was detected.

The most intense peaks ($7.8 \times 10^6$) correspond to AAGs with the formula $C_{35}H_{64}O_7$ (Figure 2e). Along with four minor peaks, eight main molecules are detected in the chromatogram, all of them bearing a hydroxyl in position C-4 on the aliphatic chain (subtype 1b, $X_4$ fragment, relative intensity = 100%). The four most polar compounds have an $\alpha,\alpha'$-dihydroxylated THF system placed between the C-15 and C-20 carbons ($B_1$, $B_1 - 2H$, $B_1 - 2H - H_2O$, and $X_2$ fragments). Three of them (retention times Rt = 17.9, 18.9, and 19.2 min) have their last hydroxyl located at C-10 ($X_3$ fragment). Compared with standards, these molecules are identified as annonacin (i.e., *trans*-annonacin) at retention time Rt = 18.9 min (**6**), *cis*-annonacin at Rt = 19.2 min (**7**), and a diastereoisomer such as annonacin-A, which was previously described in the species (**5**, Rt = 17.9 min).[12] The last compound (**8**, Rt = 19.6 min), with the same THF pattern and position, bears a hydroxyl at C-8 ($X_3$ fragment) and corresponds to xylopianin (*Xylopia aromatica*) or one of its stereoisomers (Figures 1 and 2). The four slightly polar AAGs show an $\alpha,\alpha'$-dihydroxy-mono-THF system between carbons C-13 and C-18 (**9**, Rt = 20.2 min; **10**, Rt = 20.4 min; **11**, Rt = 20.7 min; **12**, Rt = 21.0 min), because the $MS^2$ spectra of compounds **9** and **10** exhibit a $B_1 - H_2O$ fragment at $m/z$ 315.2140, whereas the THF position could be established by comparison with the LC-MS profile previously published for *A. muricata* for compounds **11** and **12**.[25] The free hydroxyl position was confirmed at C-10 for compound **11** ($X_3$ fragment). These compounds could correspond to goniothalamicin (**11**), previously isolated from *A. muricata*,[12] and to different diastereoisomers (**9**–**12**; Figure 3).

Ten compounds with formula $C_{35}H_{62}O_6$ are detected in the extracted ion chromatogram at $m/z$ 585.47–585.49 (Figure 2f), with two major peaks (**13**, Rt = 24.2; and **14**, Rt = 24.5 min). The respective $MS^2$ spectra show that these major peaks correspond to subtype 1a AAGs (fragment similar to $X_3$, relative intensity $\leq$ 10%). The detection of typical fragments for the AAG **13** confirms that this compound corresponds to an A-type AAG, with a THF positioned between C-16 and C-19 carbons and flanked by adjacent hydroxyls ($B_1$; $B_1 - 2H$, and $X_2$ fragments). These $B_1$ and $B_1 - 2H$ fragments have a mass difference of 2 amu when compared to compounds **5**–**7** ($C_{35}H_{64}O_6$). A ketone replacing the hydroxyl between the THF and the lactone is a frequent feature among AAGs. Indeed, **13** and **14** respectively match the retention times and the fragments of the standards *trans*- and *cis*-corossolones, isolated from *A. muricata* (Figure 3).[12] Noteworthy, at least eight minor peaks with the same molecular mass are detected with retention times ranging between 19 and 28 min. The low intensity of the $MS^2$ fragment ion peaks did not allow their identification.

The $C_{35}H_{62}O_7$ formula represents one of the major AAGs groups on the chromatogram (intensity $3 \times 10^6$) (Figure 2g). In the extracted ion chromatogram, more than 10 partially coeluted AAGs are detected, corresponding to AAGs of heterogeneous structures (i.e., different types and subtypes), all regrouped by retention time. According to the $MS^2$ spectra, two compounds (**15**, Rt = 20.0; and **16**, Rt = 20.4 min) belong to A-type, with THF between their C-16 and C-19 carbons ($B_1$, $B_1 - 2H$, and $X_2$ fragments) and to subtype 1b ($X_3$ fragment, relative intensity = 100%). The mass difference of 2 amu with the formula $C_{35}H_{64}O_7$ can be attributed to a carbonyl group placed between the THF and the lactone instead of a hydroxyl. These compounds could therefore be annocherin, which is an AAG previously isolated from *A. cherimolia* and bearing a carbonyl at C-10, a favored decoration site as evidenced above and exemplified in the literature, or position isomers (Figure 3).[12]

**Table 1. $[M + Li]^+$ and Characteristic Fragment Ions of the AAGs Identified in the *Annona cherimolia* Alcoholic Beverage**

| | Rt (min) | $m/z$ $[M + Li]^+$ | Δ (ppm) | formula | $MS^2$ characteristic fragment ions[a] | structural type[b] |
|---|---|---|---|---|---|---|
| **1** | 30.5 | 553.4789 | −1.5 | $C_{35}H_{62}O_4$ | c: $C_{20}H_{34}O_3Li$, $m/z$ 329.2660, $\Delta_{m/z}$ = −1.5 ppm; c − 2H: $C_{20}H_{32}O_3Li$, $m/z$ 327.2508, $\Delta_{m/z}$ = 0.2 ppm | E1a (bis-epoxide) |
| **2** | 30.8 | 553.4784 | −1.9 | $C_{35}H_{62}O_4$ | c: $C_{20}H_{34}O_3Li$, $m/z$ 329.2660, $\Delta_{m/z}$ = 3.2 ppm; | E1a (bis-epoxide) |
| **3** | 23.5 | 587.4851 | −1.1 | $C_{35}H_{64}O_6$ | $[M - C_6H_8O_2 + Li]^+$: $C_{29}H_{56}O_4Li$, $m/z$ 475.4334, $\Delta_{m/z}$ = 0.2 ppm; $B_1$ − 2H: $C_{20}H_{32}O_4Li$, $m/z$ 343.2449, $\Delta_{m/z}$ = −1.7 ppm | A1a, 3 hydroxyls |
| **4** | 23.8 | 587.4852 | −1.0 | $C_{35}H_{64}O_6$ | $[M - C_6H_8O_2 + Li]^+$: $C_{29}H_{56}O_4Li$, $m/z$ 475.4327, $\Delta_{m/z}$ = −1.4 ppm | A1a, 3 hydroxyls |
| **5** | 17.9 | 603.4794 | −2.1 | $C_{35}H_{64}O_7$ | $X_4$: $C_{29}H_{56}O_5Li$, $m/z$ 491.4275, $\Delta_{m/z}$ = −1.6 ppm; $X_3$: $C_{23}H_{44}O_4Li$, $m/z$ 391.3597, $\Delta_{m/z}$ = −1.3 ppm; $B_1$ − 2H: $C_{20}H_{32}O_5Li$, $m/z$ 359.2400, $\Delta_{m/z}$ = −1.3 ppm; $B_1$ − 2H − $H_2O$: $C_{20}H_{30}O_4Li$, $m/z$ 341.2296, $\Delta_{m/z}$ = −0.7 ppm; $X_2$: $C_{18}H_{34}O_3Li$, $m/z$ 305.2655, $\Delta_{m/z}$ = −2.5 ppm | A1b, 4 hydroxyls |
| **6** | 18.9 | 603.4794 | −2.1 | $C_{35}H_{64}O_7$ | $X_4$: $C_{29}H_{56}O_5Li$, $m/z$ 491.4271, $\Delta_{m/z}$ = −2.3 ppm; $X_3$: $C_{23}H_{44}O_4Li$, $m/z$ 391.3388, $\Delta_{m/z}$ = −1.6 ppm; $B_1$: $C_{20}H_{34}O_5Li$, $m/z$ 361.2556, $\Delta_{m/z}$ = −1.2 ppm; $B_1$ − 2H: $C_{20}H_{32}O_5Li$, $m/z$ 359.2400, $\Delta_{m/z}$ = −1.0 ppm; $B_1$ − 2H − $H_2O$: $C_{20}H_{30}O_4Li$, $m/z$ 341.2297, $\Delta_{m/z}$ = −0.6 ppm; $X_2$: $C_{18}H_{34}O_3Li$, $m/z$ 305.2663, $\Delta_{m/z}$ = 0.2 ppm | A1b, 4 hydroxyls |
| **7** | 19.2 | 603.4794 | −2.1 | $C_{35}H_{64}O_7$ | $X_4$: $C_{29}H_{56}O_5Li$, $m/z$ 491.4273, $\Delta_{m/z}$ = −1.8 ppm; $X_3$: $C_{23}H_{44}O_4Li$, $m/z$ 391.3385, $\Delta_{m/z}$ = −2.2 ppm; $B_1$− 2H − $H_2O$: $C_{20}H_{30}O_4Li$, $m/z$ 341.2298, $\Delta_{m/z}$ = −0.2 ppm; $X_2$: $C_{18}H_{34}O_3Li$, $m/z$ 305.2660, $\Delta_{m/z}$ = −0.7 ppm | A1b, 4 hydroxyls |
| **8** | 19.6 | 603.4797 | −1.6 | $C_{35}H_{64}O_7$ | $X_4$: $C_{29}H_{56}O_5Li$, $m/z$ 491.4273, $\Delta_{m/z}$ = −1.8 ppm; $X_3$: $C_{25}H_{48}O_4Li$, $m/z$ 419.3704, $\Delta_{m/z}$ = −0.8 ppm; $B_1$: $C_{20}H_{34}O_5Li$, $m/z$ 361.2551, $\Delta_{m/z}$ = −2.7 ppm; $B_1$ − 2H: $C_{20}H_{32}O_5Li$, $m/z$ 359.2402, $\Delta_{m/z}$ = −0.8 ppm; $B_1$ − 2H − $H_2O$: $C_{20}H_{30}O_4Li$, $m/z$ 341.2297, $\Delta_{m/z}$ = −0.5 ppm | A1b, 4 hydroxyls |
| **9** | 20.2 | 603.4795 | −1.9 | $C_{35}H_{64}O_7$ | $X_4$: $C_{29}H_{56}O_5Li$, $m/z$ 491.4272, $\Delta_{m/z}$ = −2.1 ppm; $B_1$−$H_2O$: $C_{18}H_{28}O_4Li$, $m/z$ 315.2140, $\Delta_{m/z}$ = −0.8 ppm | A1b, 4 hydroxyls |
| **10** | 20.4 | 603.4794 | −2.1 | $C_{35}H_{64}O_7$ | $X_4$: $C_{29}H_{56}O_5Li$, $m/z$ 491.4273, $\Delta_{m/z}$ = −2.0 ppm; $B_1$ − $H_2O$: $C_{18}H_{28}O_4Li$, $m/z$ 315.2141, $\Delta_{m/z}$ = −0.5 ppm | A1b, 4 hydroxyls |
| **11** | 20.7 | 603.4796 | −1.8 | $C_{35}H_{64}O_7$ | $X_4$: $C_{29}H_{56}O_5Li$, $m/z$ 491.4274, $\Delta_{m/z}$ = −1.7 ppm; $X_3$: $C_{23}H_{44}O_4Li$, $m/z$ 391.3391, $\Delta_{m/z}$ = −0.8 ppm | A1b, 4 hydroxyls |
| **12** | 21.0 | 603.4796 | −1.8 | $C_{35}H_{64}O_7$ | $X_4$: $C_{29}H_{56}O_5Li$, $m/z$ 491.4274, $\Delta_{m/z}$ = −1.7 ppm | A1b, 4 hydroxyls |
| **13** | 24.2 | 585.4693 | −1.3 | $C_{35}H_{62}O_6$ | $X_3$: $C_{29}H_{54}O_4Li$, $m/z$ 473.4171, $\Delta_{m/z}$ = −1.1 ppm; $B_1$: $C_{20}H_{32}O_4Li$, $m/z$ 343.2456, $\Delta_{m/z}$ = 0.4 ppm; $B_1$ − 2H: $C_{20}H_{30}O_4Li$, $m/z$ 341.2296, $\Delta_{m/z}$ = −0.7 ppm; $X_2$: $C_{18}H_{34}O_3Li$, $m/z$ 305.2663, $\Delta_{m/z}$ = 0.1 ppm | A1a, 2 hydroxyls, 1 ketone |
| **14** | 24.5 | 585.4694 | −1.2 | $C_{35}H_{62}O_6$ | $X_3$: $C_{29}H_{54}O_4Li$, $m/z$ 473.4173, $\Delta_{m/z}$ = −0.7 ppm | A1a, 2 hydroxyls, 1 ketone |
| **15** | 20.0 | 601.4639 | −1.9 | $C_{35}H_{62}O_7$ | $X_3$: $C_{29}H_{54}O_5Li$, $m/z$ 489.4116, $\Delta_{m/z}$ = −2.0 ppm; $B_1$: $C_{20}H_{32}O_5Li$, $m/z$ 359.2402, $\Delta_{m/z}$ = −0.7 ppm; $B_1$ − 2H: $C_{20}H_{30}O_5Li$, $m/z$ 357.2245, $\Delta_{m/z}$ = −0.8 ppm; $X_2$: $C_{18}H_{34}O_3Li$, $m/z$ 305.2660, $\Delta_{m/z}$ = −0.7 ppm | A1b, 3 hydroxyls, 1 ketone |
| **16** | 20.4 | 601.4638 | −1.9 | $C_{35}H_{62}O_7$ | $X_3$: $C_{29}H_{54}O_5Li$, $m/z$ 489.4117, $\Delta_{m/z}$ = −1.9 ppm; $B_1$ − 2H: $C_{20}H_{30}O_5Li$, $m/z$ 357.2251, $\Delta_{m/z}$ = 0.8 ppm; $X_2$: $C_{18}H_{34}O_3Li$, $m/z$ 305.2671, $\Delta_{m/z}$ = 2.7 ppm | A1b, 3 hydroxyls, 1 ketone |
| **17** | 16.1 | 601.4639 | −1.9 | $C_{35}H_{62}O_7$ | $[M - C_6H_8O_2 + Li]^+$: $m/z$ 489.4118, $\Delta_{m/z}$ = −1.5 ppm; $B_1$ − 2H: $C_{18}H_{28}O_3Li$, $m/z$ 299.2189, $\Delta_{m/z}$ = −1.5 ppm; $B_2$: $C_{22}H_{36}O_4Li$, $m/z$ 371.2774, $\Delta_{m/z}$ = 1.7 ppm | B1a, 3 hydroxyls |
| **18** | 16.7 | 601.4639 | −1.9 | $C_{35}H_{62}O_7$ | $[M - C_6H_8O_2 + Li]^+$: $m/z$ 489.4120, $\Delta_{m/z}$ = −1.2 ppm; $B_1$: $C_{18}H_{30}O_3Li$, $m/z$ 301.2349, $\Delta_{m/z}$ = −0.1 ppm; $B_1$ − 2H: $C_{18}H_{28}O_3Li$, $m/z$ 299.2191, $\Delta_{m/z}$ = −0.5 ppm; $B_2$: $C_{22}H_{36}O_4Li$, $m/z$ 371.2766, $\Delta_{m/z}$ = −0.6 ppm | B1a, 3 hydroxyls |
| **19** | 18.2 | 601.4637 | −2.2 | $C_{35}H_{62}O_7$ | $[M - C_6H_8O_2 + Li]^+$: $m/z$ 489.4119, $\Delta_{m/z}$ = −1.3 ppm; $B_1$ − 2H: $C_{18}H_{28}O_4Li$, $m/z$ 315.2142, $\Delta_{m/z}$ = −0.2 ppm; $B_2$: $C_{22}H_{36}O_5Li$, $m/z$ 387.2707, $\Delta_{m/z}$ = −2.6 ppm | B1a, 3 hydroxyls |
| **20** | 19.0 | 601.4639 | −1.8 | $C_{35}H_{62}O_7$ | $X_3$: $C_{29}H_{54}O_5Li$, $m/z$ 489.4117, $\Delta_{m/z}$ = −1.9 ppm; $B_1$ − 2H: $C_{18}H_{28}O_4Li$, $m/z$ 315.2141, $\Delta_{m/z}$ = −0.5 ppm; $B_2$: $C_{22}H_{36}O_5Li$, $m/z$ 387.2714, $\Delta_{m/z}$ = −0.7 ppm | B1b, 3 hydroxyls |
| **21** | 19.7 | 601.4638 | −2.0 | $C_{35}H_{62}O_7$ | $X_3$: $C_{29}H_{54}O_5Li$, $m/z$ 489.4118, $\Delta_{m/z}$ = 0.0 ppm; $B_1$ − 2H: $C_{18}H_{28}O_4Li$, $m/z$ 315.2144, $\Delta_{m/z}$ = 0.5 ppm; $B_2$: $C_{22}H_{36}O_5Li$, $m/z$ 387.2715, $\Delta_{m/z}$ = −0.6 ppm | B1b, 3 hydroxyls |
| **22** | 13.1 | 617.4591 | −1.4 | $C_{35}H_{62}O_8$ | $X_4$: $C_{29}H_{54}O_6Li$, $m/z$ 505.4069, $\Delta_{m/z}$ = −1.2 ppm; $X_3$: $C_{25}H_{46}O_5Li$, $m/z$ 433.3497, $\Delta_{m/z}$ = −0.6 ppm; $B_1$: $C_{18}H_{28}O_5Li$, $m/z$ 331.2093, $\Delta_{m/z}$ = 0.5 ppm; $B_1$ − $H_2O$: $C_{18}H_{26}O_4Li$, $m/z$ 313.1987, $\Delta_{m/z}$ = 0.5 ppm; $B_2$: $C_{22}H_{36}O_6Li$, $m/z$ 403.2666, $\Delta_{m/z}$ = −0.1 ppm; $Y_2$ − 2H: $C_{17}H_{32}O_2Li$, $m/z$ 275.2561, $\Delta_{m/z}$ = 1.4 ppm | B1b, 4 hydroxyls |
| **23** | 14.1 | 617.4589 | −1.7 | $C_{35}H_{62}O_8$ | $X_4$: $C_{29}H_{54}O_6Li$, $m/z$ 505.4067, $\Delta_{m/z}$ = −1.6 ppm; $X_3$: $C_{25}H_{46}O_5Li$, $m/z$ 433.3496, $\Delta_{m/z}$ = −0.8 ppm; $B_1$: $C_{18}H_{28}O_5Li$, $m/z$ 331.2093, $\Delta_{m/z}$ = 0.6 ppm; $B_1$ − $H_2O$: $C_{18}H_{26}O_4Li$, $m/z$ 313.1984, $\Delta_{m/z}$ = −0.4 ppm; $B_2$: $C_{22}H_{36}O_6Li$, $m/z$ 403.2666, $\Delta_{m/z}$ = −0.2 ppm; $Y_2$ − 2H: $C_{17}H_{32}O_2Li$, $m/z$ 275.2558, $\Delta_{m/z}$ = 0.2 ppm | B1b, 4 hydroxyls |
| **24** | 14.9 | 617.4588 | −1.9 | $C_{35}H_{62}O_8$ | $X_4$: $C_{29}H_{54}O_6Li$, $m/z$ 505.4065, $\Delta_{m/z}$ = −2.0 ppm; $B_1$: $C_{18}H_{28}O_5Li$, $m/z$ 331.2095, $\Delta_{m/z}$ = 1.2 ppm; $B_1$ − $H_2O$: $C_{18}H_{26}O_4Li$, $m/z$ 313.1982, $\Delta_{m/z}$ = −1.1 ppm; $B_2$: $C_{22}H_{36}O_6Li$, $m/z$ 403.2658, $\Delta_{m/z}$ = −1.9 ppm | B1b, 4 hydroxyls |
| **25** | 21.7 | 599.4481 | −2.1 | $C_{35}H_{60}O_7$ | $C_{29}H_{52}O_5Li$, $m/z$ 487.3961, $\Delta_{m/z}$ = −1.8 ppm; $C_{26}H_{48}O_4Li$, $m/z$ 431.3702, $\Delta_{m/z}$ = −1.2 ppm; $B_1$: $C_{20}H_{30}O_5Li$, $m/z$ 357.2241, $\Delta_{m/z}$ = −2.0 ppm; $B_1$ − 2H: $C_{20}H_{28}O_5Li$, $m/z$ 355.2088, $\Delta_{m/z}$ = −1.0 ppm; $B_1$ − 2H − $C_6H_8O_2$: $C_{14}H_{20}O_3Li$, $m/z$ 243.1562, $\Delta_{m/z}$ = −2.2 ppm | A1, THP (C-4−C-8) |
| **26** | 22.6 | 599.4483 | −1.8 | $C_{35}H_{60}O_7$ | $C_{29}H_{52}O_5Li$, $m/z$ 487.3961, $\Delta_{m/z}$ = −1.7 ppm; $C_{26}H_{48}O_4Li$, $m/z$ 431.3703, $\Delta_{m/z}$ = −0.9 ppm; $B_1$: $C_{20}H_{30}O_5Li$, $m/z$ 357.2244, $\Delta_{m/z}$ = −1.0 ppm; $B_1$ − 2H: $C_{20}H_{28}O_5Li$, $m/z$ 355.2090, $\Delta_{m/z}$ = −0.4 ppm | A1, THP (C-4−C-8) |
| **27** | 23.0 | 599.4486 | −1.4 | $C_{35}H_{60}O_7$ | $C_{29}H_{52}O_5Li$, $m/z$ 487.3960, $\Delta_{m/z}$ = −1.9 ppm; $C_{26}H_{48}O_4Li$, $m/z$ 431.3702, $\Delta_{m/z}$ = −1.3 ppm; $B_1$: $C_{20}H_{30}O_5Li$, $m/z$ 357.2252, $\Delta_{m/z}$ = 1.1 ppm; $B_1$ − 2H: $C_{20}H_{28}O_5Li$, $m/z$ 355.2088, $\Delta_{m/z}$ = −1.0 ppm | A1, THP (C-4−C-8) |
| **28** | 19.1 | 629.4950 | −2.0 | $C_{37}H_{66}O_7$ | $X_4$: $C_{31}H_{58}O_5Li$, $m/z$ 517.4430, $\Delta_{m/z}$ = −1.8 ppm; $B_1$ − 2H: $C_{20}H_{32}O_3Li$, $m/z$ 327.2500, $\Delta_{m/z}$ = −1.9 ppm; $B_2$: $C_{24}H_{40}O_4Li$, $m/z$ 399.3076, $\Delta_{m/z}$ = −1.2 ppm | B1a, 3 hydroxyls |
| **29** | 19.7 | 629.4951 | −2.0 | $C_{37}H_{66}O_7$ | $X_4$: $C_{31}H_{58}O_5Li$, $m/z$ 517.4433, $\Delta_{m/z}$ = −1.1 ppm; $B_1$ − 2H: $C_{20}H_{32}O_3Li$, $m/z$ 327.2505, $\Delta_{m/z}$ = −0.4 ppm; $B_2$: $C_{24}H_{40}O_4Li$, $m/z$ 399.3077, $\Delta_{m/z}$ = −1.1 ppm; $B_2$ − 2H: $C_{24}H_{38}O_4Li$, $m/z$ 397.2920, $\Delta_{m/z}$ = −1.2 ppm | B1a, 3 hydroxyls |



dx.doi.org/10.1021/jf501174j | J. Agric. Food Chem. 2014, 62, 8696−8704

Table 1. continued

| | Rt (min) | $m/z$ $[M + Li]^+$ | Δ (ppm) | formula | $MS^2$ characteristic fragment ions[a] | structural type[b] |
|---|---|---|---|---|---|---|
| **30** | 21.6 | 629.4951 | −1.9 | $C_{37}H_{66}O_7$ | $X_4$; $C_{31}H_{58}O_4Li$, $m/z$ 517.4430, $\Delta_{m/z}$ = −1.6 ppm; $B_1$ − 2H: $C_{20}H_{32}O_4Li$, $m/z$ 343.2448, $\Delta_{m/z}$ = −2.1 ppm; $B_2$: $C_{24}H_{40}O_3Li$, $m/z$ 415.3024, $\Delta_{m/z}$ = −1.5 ppm | B1b, 3 hydroxyls |
| **31** | 16.4 | 645.4900 | −1.9 | $C_{37}H_{66}O_8$ | $X_4$; $C_{31}H_{58}O_5Li$, $m/z$ 533.4379, $\Delta_{m/z}$ = −1.6 ppm; $B_2$: $C_{24}H_{40}O_4Li$, $m/z$ 431.2968, $\Delta_{m/z}$ = −2.6 ppm; $B_2$ − 2H: $C_{24}H_{38}O_4Li$, $m/z$ 429.2818, $\Delta_{m/z}$ = −1.2 ppm; $Y_2$ − 2H: $C_{21}H_{38}O_4Li$, $m/z$ 361.2921, $\Delta_{m/z}$ = −1.1 ppm | C1b, 4hydroxyls |

[a]All AAGs displayed loss of CO (−27.9949 amu) and $CO_2$ (−43.9898 amu). [b]Types: A (mono-THF), B (adjacent bis-THF), C (nonadjacent bis-THF); THP, tetrahydropyranic ring. Subtypes: 1a (unsaturated lactone without OH at C-4), 1b (unsaturated lactone with OH at C-4). Structures of **1**–**31** are depicted in Figure 3.

**B-Type: Adjacent Bis-THF.** Five other AAGs with the same molecular formula are also clearly distinguished in the extracted ion chromatogram of $m/z$ 601.46−601.47 ($C_{35}H_{62}O_7$) (Figure 2g). The $MS^2$ spectra show that three of them are of B-type and subtype 1a (fragment similar to $X_3$, relative intensity < 100%). The $MS^2$ spectra of the two most polar molecules (**17**, Rt = 16.1 min; and **18**, Rt = 16.7 min) showed the characteristic fragments of an adjacent bis-THF moiety between C-14 and C-21 carbons ($B_1$, $B_1$ − 2H, and $B_2$ fragments), with flanking hydroxyl groups (postulated for C-22) (Figure 1) and an additional hydroxyl between the THF and the $CH_3$ terminal part. For example, squamocin-B (*A. squamosa*)[12] corresponds to the structural features of these two compounds. The third AAG is detected at a retention time of 18.2 min (**19**). Its α,α′-dihydroxy-bis-THF system lies between C-13 and C-22 carbons ($B_1$ − 2H and $B_2$ fragments) Its third hydroxyl group is positioned between the lactone and the THF. Compound **19** could therefore be bullacin-B (*A. squamosa*)[12] or a position isomer (Figure 3). Finally, two other AAGs (**20**, Rt = 19.0 min; **21**, Rt = 19.7 min; Figure 2g) are of subtype 1b ($X_3$ fragment, relative intensity = 100%) and of B-type. According to the $MS^2$ spectra, their bis-THF is placed between the C-14 and C-21 carbons ($B_1$ − 2H and $B_2$ fragments). Therefore, they could correspond to molvizarin-1, already obtained from *A. cherimolia*,[12] and/or diastereoisomers (Figure 3). Interestingly, relationships between structures of AAGs and their retention times can be proposed: for the same molecular formula, AAGs of B-type are more polar than that of A-type bearing a ketone. Moreover, the presence of a hydroxyl between the THF and the lactone ring increases the retention times in comparison with a substitution on the methyl-terminal end.

Thirteen $C_{35}H_{62}O_8$ AAGs are detected in the extract (Figure 2h). The three most intense ones are evidenced as being of subtype 1b ($X_4$ fragment, relative intensity = 100%) and of B-type (THF between carbons C-14 and C-21: $B_1$, $B_1$ − $H_2O$, and $B_2$ fragments) (Figures 2h and 3). Two of them (**22**, Rt = 13.1 min; and **23**, Rt = 14.1 min) generate an $X_3$ fragment showing the presence of a fourth hydroxyl group at position C-8. This structure corresponds to that of annonisin, isolated from the species *A. atemoya* (a hybrid of *A. cherimolia* and *A. squamosa*)[12] and/or diastereoisomers (Figure 3). For the third major AAG of this group (**24**, Rt = 14.9 min), the lack of a fragment similar to $X_3$ suggests its free hydroxyl group lies in the methyl-terminal end. To our knowledge, such an AAG was never identified so far, despite a classical substitution pattern.

**C-Type: Nonadjacent Bis-THF.** No C-type AAG in C35 was observed in this study, which is consistent with literature data.

**Atypical C35 AAGs.** The $MS^2$ spectra of the three main peaks at $m/z$ 599.4494 ($C_{35}H_{60}O_7$; **25**, Rt = 21.7 min; **26**, Rt = 22.6 min; **27**, Rt = 23.0 min) were surprisingly different from the other spectra obtained during this study (Figure 2i). Similar compounds were identified in our previous study by LC-LTQ-Orbitrap performed with an *A. muricata* nectar[25] and were attributed, according to their fragmentation pattern, to AAGs bearing a THP ring between the C-4 and C-8 carbons (fragments at $m/z$ 487.3961 and $m/z$ 431.3703, see Table 1 and Supporting Information Figure S1) in addition to an α,α′-dihydroxylated mono-THF in C-15/C-20 ($B_1$ and $B_1$ − 2H fragments) and a ketone between C-6 and C-14 (Figure 3). Compounds **25**−**27**, displaying close retention times and identical $MS^2$ spectra, are proposed to be assigned to montanacin-D

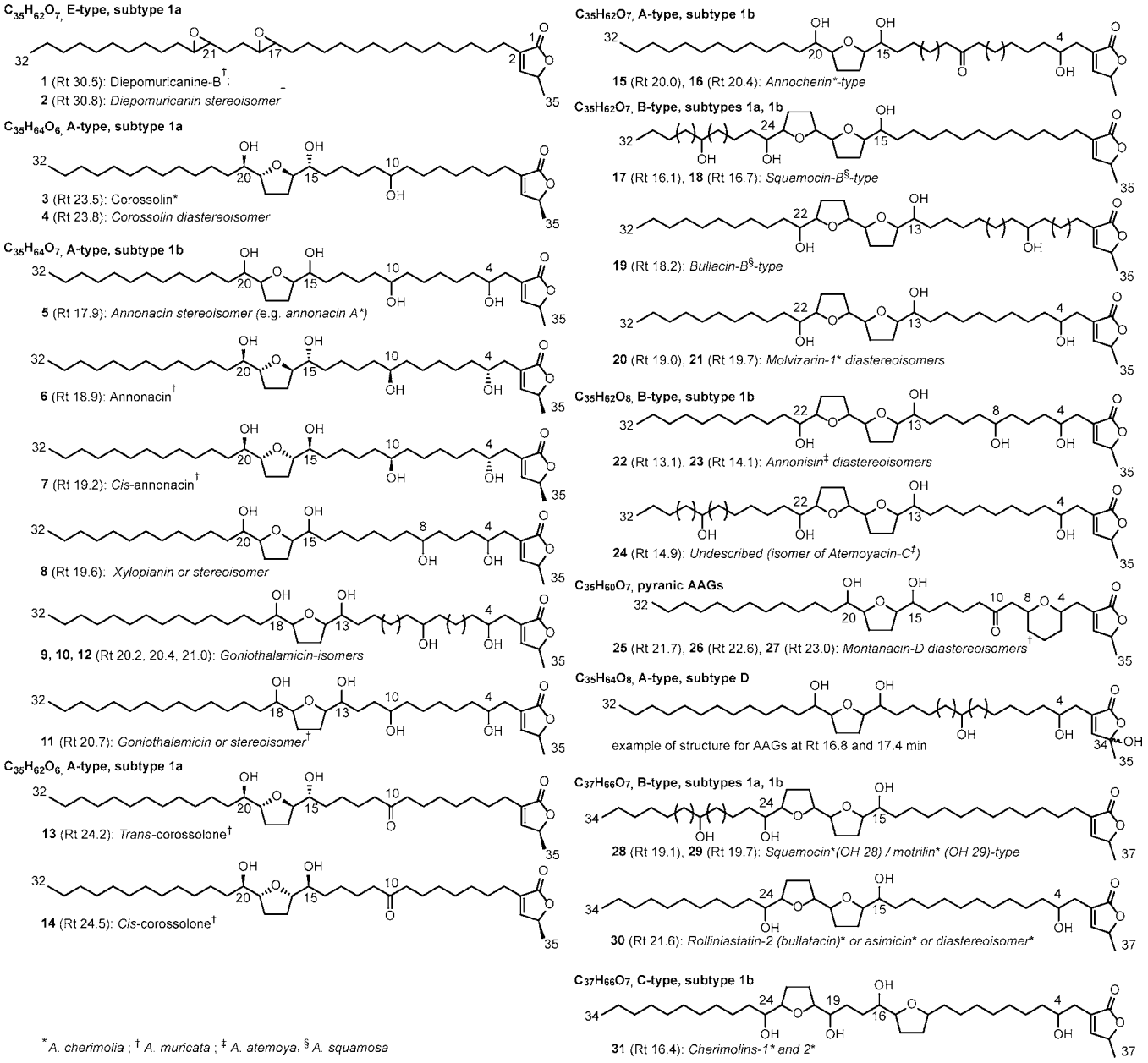


**Figure 3.** Structures of AAGs identified in the *Annona cherimolia* alcoholic beverage. Compounds were previously isolated from (*) *A. cherimolia*, (†) *A. muricata*, (‡) *A. atemoya* (*A. cherimolia* × *A. squamosa*), and (§) *A. squamosa*).

and/or diastereoisomers or position isomers for the carbonyl group (Figures 2i and 3). Interestingly, aromin-A ($C_{35}H_{60}O_7$), an AAG of close structural features except for a THF at C4−C-7, bearing a carbonyl group in C-9, was previously isolated from *A. cherimolia*.[12] The $MS^2$ spectra of minor peaks (Rt < 21 min) did not allow identification of typical fragments of this molecule.

AAGs with the formula $C_{35}H_{64}O_8Li$ are frequently encountered in *Annona* spp. At least eight peaks are detected in the extracted chromatogram of ion $m/z$ 619.44−619.45 (Figure 2j), all showing low intensity. Two original compounds are detected at Rt = 16.8 and 17.4 min. In the $MS^2$ spectra of $m/z$ 619, the cleavage in $\beta$ of the lactone shows a difference of 16 amu from the expected fragment ($C_{29}H_{56}O_5Li$, $m/z$ 491.4271, $\Delta_{m/z}$ = −2.3 ppm), corresponding to a hydroxylated unsaturated lactone, possibly in position C-34 (lactonic type L-D in the classification of Bermejo et al.;[12] Figure 3). Such AAGs are only scarcely distributed, but two ketonic analogues were already described in *A. cherimolia* (annomolons-A and -B, $C_{35}H_{62}O_7$ and $C_{35}H_{62}O_8$, respectively).[12]

Finally, no AAG of formula $C_{35}H_{60}O_8$ was identified so far, whereas at least five matching peaks are detected, as minor compounds (lowest signal intensity, $9.3 \times 10^4$) (Figure 2k). The two main peaks can be distinguished at Rt = 14.3 and 15.3 min in the extracted ion chromatogram. The $MS^2$ spectra show that these AAGs are of subtype 1b, but no other characteristic fragment is observed.

**C37 AAGs.** Extracted ion chromatogram analysis also shows the presence of C37 AAGs in the extract. Their intensities are lower than C35 AAGs (between $10^4$ and $10^6$), and the chromatographic profiles show that they are outnumbered by C35 AAGs. At least 27 C37 AAGs with 7 different formulas were detected here, whereas 13 were isolated from *A. cherimolia* so far. Most of their formulas were retrieved in our analysis


dx.doi.org/10.1021/jf501174j | J. Agric. Food Chem. 2014, 62, 8696−8704

($C_{37}H_{66}O_7$, Rt = 16−24 min; $C_{37}H_{66}O_8$, Rt = 11−20 min; $C_{37}H_{68}O_8$, Rt = 17−19 min). However, AAGs with the formula $C_{37}H_{68}O_8$ were not detected, although several representatives were identified in the species (asimicin, itrabin).[12] The other formulas identified in our analysis were $C_{37}H_{64}O_7$ (Rt = 13−25 min), $C_{37}H_{64}O_8$ (Rt = 13−22 min), $C_{37}H_{66}O_9$ (Rt = 7−14 min), and $C_{37}H_{68}O_9$ (Rt = 8−11 min). Due to numerous coeluting compounds and low ionic intensities, only AAGs with the formulas $C_{37}H_{66}O_7$ and $C_{37}H_{66}O_8$ could be structurally characterized. However, C37 AAGs belonging to E-, A-, and C-types were detected in the other most prominent groups.

**B-Type: Adjacent Bis-THF.** As for C35 AAGs, the C37 AAGs bearing seven oxygen atoms (here with three degrees of unsaturation; $C_{37}H_{66}O_7$) are those with the peaks of the highest intensity ($3.8 \times 10^6$). The extracted ion chromatogram shows at least seven peaks, with the major one at Rt = 19.7 min (**29**) (Figure 2l). The $MS^2$ spectrum of this compound is identical to that of the AAG at Rt = 19.1 min (**28**). Both compounds correspond to AAGs of subtype 1a ($X_4$ fragment, relative intensity <10%) and B-type with a THF located between the C-16 and C-23 carbons ($B_1 - 2H$, $B_2$ and $B_2 - 2H$ fragments). These two molecules are thus similar to motrilin and squamocin, both previously isolated from *A. cherimolia*.[11,12] A third AAG (**30**), detected at Rt = 21.6 min, is also of B-type but belongs to subtype 1b. Its $\alpha,\alpha'$-dihydroxy-bis-THF is located between C-15 and C-24 ($X_4$ fragment, relative intensity = 100%, $B_1 - 2H$, $B_2$). This AAG could possibly correspond to asimicin or rolliniastatin-2, both already isolated from *A. cherimolia*.[11]

**C-Type: Nonadjacent Bis-THF.** In the extracted ion chromatogram of *m/z* 645.45−645.55 ($C_{37}H_{66}O_8$; not shown), a prominent peak at Rt = 16.4 min displays an unusual $MS^2$ spectrum, evidencing an AAG (**31**) of subtype 1b ($X_4$ fragment, relative intensity = 100%), bearing two nonadjacent THF cycles (C-type). The first one is evidenced by a typical $Y_2 - 2H$ fragment indicating its location between C-12 and C-15, with a single hydroxyl flanking group, according to the typical structural features of this group of AAGs. The second one is visible between C-20 and C-23, with adjacent hydroxyl groups ($B_2$ and $B_2 - 2H$ fragments; Figure 1). Compound **31** therefore corresponds to cherimolin-1 or cherimolin-2 (both previously isolated from the species)[12] or to a stereoisomer (Figure 3). However, the presence of minor diastereoisomers of **31** in the extract cannot be excluded.

**Comparison with Literature, Human Exposure to AAGs.** Among the 80 AAGs detected here, the majority are constituted by C35 species. According to the $MS^2$ spectra of resolved or coeluted peaks, approximately 17 AAGs (21%) are of A-type, 17 (21%) of B-type, and 7 (9%) belong to other types. The structure of the THF moiety remains undetermined for 39 (50%) species. With regard to the lactone, 29 AAGs (36%) belong to subtype 1a and 48 (60%) to subtype 1b. Atypical hydroxylation of the lactone, which distinguishes *A. cherimolia* from other *Annona* spp.,[12] was observed. These structural features are in agreement with the compounds isolated from the plant.[11,12,30] The tandem mass spectrometry analyses of the ions corresponding to the major peaks allowed identification of 31 AAGs, of which 8 could be confirmed by comparison with isolated standards. The main AAGs belong to A-type and subtype 1b and have a 13 C alkyl spacer between the lactone and the THF moiety. Bearing these characteristics, annonacin (**6**), the main AAG in the species *A. muricata*, exhibited the most prominent AAG peak in this *A. cherimolia* sample, although it had surprisingly never been firmly identified in the species so far.[30] Given the LOD of our detection method, the amount of annonacin (**6**) per liter of beverage would be >35 ng. This is less than the concentrations measured in samples of *A. muricata* leaf herbal teas.[21] Moreover, this amount is negligible in comparison to the fruit pulps of *A. muricata* and *Asimina triloba*.[17,23,24]

This is the first evidence of the presence of AAGs in a dietary product derived from *A. cherimolia*. These results are not in agreement with our previous study made by MALDI-TOF MS (LOD ~ $1.5 \times 10^{-7}$ M for annonacin), which showed an absence of AAGs in the pulp of the fruit.[21,22,29] This might be due to the lower sensitivity of the method used here. However, this discrepancy could also be attributed to genetic or external factors. Indeed, 5-fold seasonal variations in AAGs content have been measured for the twigs of *Asimina triloba*.[33] Varieties and cultural conditions also are likely to influence secondary metabolites contents. Our previous study on *A. cherimolia* was performed with fruits harvested in southern Spain (Mediterranean climate, 38° N latitude), whereas the fruits used for preparation of the beverage studied here originated from Madeira (tropical climate, 32° N latitude). Nevertheless, a contamination of the beverage with seed fragments cannot be excluded. *A. cherimolia* thus appears as a minor source of exposure to environmental neurotoxins. Its consumption and that of derived products should, however, be considered as a risk factor in surveys about sporadic atypical Parkinsonism and dementia.

## ■ ASSOCIATED CONTENT

### Supporting Information

Figure S1: MS/MS spectrum of *m/z* 599.45, compound **26**. This material is available free of charge via the Internet at http://pubs.acs.org.

## ■ AUTHOR INFORMATION


### Corresponding Author

*(I.S.-A.) Phone: +33 1 69 82 30 16. E-mail: isabelle.schmitz-afonso@cnrs.fr.



### Funding

J.L.V. is the recipient of a doctoral fellowship from the French Ministry of Research.


### Notes

The authors declare no competing financial interest.

## ■ ACKNOWLEDGMENTS

We thank Dr. J. Quintin for providing plant material as well as K. Leblanc and B. Séon-Méniel for technical assistance.

## ■ ABBREVIATIONS USED

AAG, Annonaceous acetogenin; HPLC, high-performance liquid chromatography; LOD, limit of detection; MS, mass spectrometry; THF, tetrahydrofuran; TIC, total ion current; THP, tetrahydropyran

## ■ REFERENCES


(1) Morton, J. *Fruits of Warm Climates*; Creative Resource Systems: Miami, FL, USA, 1987; 505 pp.

(2) Longuefosse, J.-L.; Nossin, E. Medical ethnobotany survey in Martinique. *J. Ethnopharmacol.* **1996**, *53*, 117−142.

(3) Caparros-Lefèbvre, D.; Elbaz, A. Possible relation of atypical parkinsonism in the French West Indies with consumption of tropical plants: a case-control study. *Lancet* **1999**, *354*, 281−286.

(4) Caparros-Lefèbvre, D.; Sergeant, N.; Lees, A.; Camuzat, A.; Daniel, S.; Lannuzel, A.; Brice, A.; Tolosa, E.; Delacourte, A.; Duyckaerts, C. Guadeloupean parkinsonism: a cluster of progressive supranuclear palsy-like tauopathy. *Brain* **2002**, *125*, 801−811.
(5) Lannuzel, A.; Höglinger, G. U.; Verhaeghe, S.; Gire, L.; Belson, S.; Escobar-Khondiker, M.; Poullain, P.; Oertel, W. H.; Hirsch, E. C.; Dubois, B.; Ruberg, M. Atypical parkinsonism in Guadeloupe: a common risk factor two closely related phenotypes? *Brain* **2007**, *130*, 816−827.
(6) Camuzat, A.; Romana, M.; Dürr, A.; Feingold, J.; Brice, A.; Ruberg, M.; Lannuzel, A. The PSP-associated MAPT H1 subhaplotype in Guadeloupean atypical Parkinsonism. *Movement Disord.* **2008**, *23*, 2384−2391.
(7) Apartis, E.; Gaymard, B.; Verhaeghe, S.; Roze, E.; Vidailhet, M.; Lannuzel, A. Predominant cortical dysfunction in Guadeloupean parkinsonism. *Brain* **2008**, *131*, 2701−2709.
(8) Angibaud, G.; Gaultier, C.; Roscol, O. Atypical parkinsonism and Annonaceae consumption in New Caledonia. *Movement Disord.* **2004**, *19*, 603−605.
(9) Chaudhuri, K. R.; Hu, M. T.; Brooks, D. J. Atypical Parkinsonism in Afro-caribean and Indian origin immigrants to the UK. *Movement Disord.* **2000**, *15*, 18−23.
(10) Steele, J. C.; Caparros-Lefèbvre, D.; Lees, A.; Sacks, O. Progressive supranuclear palsy and its relation to pacific foci of the parkinsonism-dementia complex and Guadeloupean Parkinsonism. *Parkinsonism Relat. Dis.* **2002**, *9*, 39−54.
(11) Cavé, A.; Figadère, B.; Laurens, A.; Cortes, D. Acetogenins from Annonaceae. In *Progress in the Chemistry of Organic Natural Products*; Herz, W., Kirby, G. W., Moore, R. E., Steglich, W., Tamm, C., Eds.; Springer: Vienna, Austria, 1997; pp 81−288.
(12) Bermejo, A.; Figadère, B.; Zafra-Polo, M.-C.; Barrachina, I.; Estornell, E.; Cortes, D. Acetogenins from Annonaceae: recent progress in isolation, synthesis and mechanisms of action. *Nat. Prod. Rep.* **2005**, *22*, 269−303.
(13) Agence Française de Sécurité Sanitaire des Aliments. Avis de l'Agence française de sécurité sanitaire des aliments relatif aux risques liés à la consommation de corossol et de ses préparations (saisine 2008-SA-0171, 2010/04/28); 2010; 7 pp.
(14) Höllerhage, M.; Matusch, A.; Champy, P.; Lombès, A.; Ruberg, M.; Oertel, W. H.; Höglinger, G. U. Natural lipophilic inhibitors of mitochondrial complex I are candidate toxins for sporadic neurodegenerative tau pathologies. *Exp. Neurol.* **2009**, *220*, 133−142.
(15) Lannuzel, A.; Michel, P. P.; Höglinger, G. U.; Champy, P.; Jousset, A.; Medja, F.; Lombès, A.; Darios, F.; Gleye, C.; Laurens, A.; Hocquemiller, R.; Hirsch, E. C.; Ruberg, M. The mitochondrial complex I inhibitor annonacin is toxic to mesencephalic dopaminergic neurons by impairement of energy metabolism. *Neurosciences* **2003**, *121*, 287−296.
(16) Escobar-Khondiker, M.; Höllerhage, M.; Muriel, M. P.; Champy, P.; Bach, A.; Depienne, C.; Respondek, G.; Yamada, E. S.; Lannuzel, A.; Yagi, T.; Hirsch, E. C.; Oertel, W. H.; Jacob, R.; Michel, P. P.; Ruberg, M.; Höglinger, G. U. Annonacin, a natural mitochondrial complex I inhibitor, causes tau pathology in cultured neurons. *J. Neurosci.* **2007**, *27* (29), 7827−7837.
(17) Potts, L. F.; Luzzio, F. A.; Hetman, M.; Champy, P.; Litvan, I. Annonacin in *Asimina triloba* fruit: implication for neurotoxicity. *Neurotoxicology* **2012**, *33*, 53−58.
(18) Champy, P.; Höglinger, G. U.; Féger, J.; Gleye, C.; Hocquemiller, R.; Laurens, A.; Guérineau, V.; Laprévote, O.; Medja, F.; Lombès, A.; Michel, P. P.; Lannuzel, A.; Hirsch, E. C.; Ruberg, M. Annonacin, a lipophilic inhibitor of mitochondrial complex I, induces nigral and striatal neurodegeneration in rats: possible relevance for atypical parkinsonism in Guadeloupe. *J. Neurochem.* **2004**, *88*, 63−69.
(19) Rottscholl, R.; Lunow, M.; Jainsch, B.; de Andrade, A.; Respondek, G.; Höllerhage, M.; Champy, P.; Oertel, W. H.; Yamada, E.; Höglinger, G. Gene−environment interaction in a mouse tauopathy-model. *Basal Ganglia* **2011**, *1*, 29.
(20) Yamada, E. S.; Respondek, G.; Müssner, S.; de Andrade, A. C. F.; Höllerhage, M.; Depienne, C.; Rastetter, A.; Tarze, A.; Friguet, B.; Salama, M.; Champy, P.; Oertel, W. H.; Höglinger, G. U. Annonacin, a natural lipophilic mitochondrial complex I inhibitor, increases phophorylation of tau in the brain of FTDP-17 transgenic mice. *Exp. Neurol.* **2014**, DOI: 10.1016/j.expneurol.2013.12.017.
(21) Champy, P.; Melot, A.; Guérineau, V.; Gleye, C.; Fall, D.; Höglinger, G. U.; Ruberg, M.; Lannuzel, A.; Laprévote, O.; Laurens, A.; Hocquemiller, R. Quantification of acetogenins in *Annona muricata* linked to atypical parkinsonism in Guadeloupe. *Movement Disord.* **2005**, *20*, 1629−1633.
(22) Champy, P.; Guérineau, V.; Laprévote, O. MALDI-TOF MS profiling of Annonaceous acetogenins in *Annona muricata* products of human consumption. *Molecules* **2009**, *14*, 5235−5246.
(23) Bonneau, N.; Le Ven, J.; Schmitz-Afonso, I.; Guérineau, V.; Bajin ba Ndob, I.; Baloul, L.; Lewin, G.; Laprévote, O.; Brunelle, A.; Touboul, D.; Champy, P. Annonaceous acetogenins as environmental neurotoxins: human exposure from edible *Annona* fruits. *Planta Med.* **2012**, *78*, PH25.
(24) Pomper, K. W.; Lowe, J. D.; Crabtree, S. B.; Keller, W. Identification of Annonaceous acetogenins in the ripe fruit of the North American pawpaw (*Asimina triloba*). *J. Agric. Food Chem.* **2009**, *57*, 8339−8343.
(25) Le Ven, J.; Schmitz-Afonso, I.; Lewin, G.; Laprévote, O.; Brunelle, A.; Touboul, D.; Champy, P. Comprehensive characterization of Annonaceous acetogenins within a complex extract by HPLC-ESI-LTQ-Orbitrap® using post-column lithium infusion. *J. Mass Spectrom.* **2012**, *47*, 1500−1509.
(26) http://madereacores.blogspot.fr/2012/11/anone-de-madere-annona-cherimola-mill.html (last consulted Feb 1, 2014).
(27) Ferreira, L.; Perestrelo, R.; Câmara, J. S. Comparative analysis of the volatile fraction from *Annona cherimola* Mill. cultivars by solid-phase microextraction and gas chromatography-quadrupole mass spectrometry detection. *Talanta* **2009**, *77*, 1087−1096.
(28) Miyashita, H.; Nishida, M.; Okawa, M.; Nohara, T.; Yoshimitsu, H. Four new *ent*-kaurane diterpenoids from the fruits of *Annona cherimola*. *Chem. Pharm. Bull.* **2010**, *58*, 765−768.
(29) Guillopé, R.; Escobar-Khondiker, M.; Guérineau, V.; Laprévote, O.; Höglinger, G. U.; Champy, P. Kaurenoic acid from pulp of *Annona cherimolia* in regard to Annonaceae-induced Parkinsonism. *Phytother. Res.* **2011**, *20*, 1861−1864.
(30) García-Aguirre, K. K.; Zepeda-Vallejo, L. G.; Ramón-Gallegos, E.; Alvárez-González, I.; Madrigal-Bujaidar, E. Genotoxic and cytotoxic effects produced by acetogenins obtained from *Annona cherimolia* Mill. *Biol. Pharm. Bull.* **2008**, *31*, 2346−2349.
(31) Allegrand, J.; Touboul, D.; Schmitz-Afonso, I.; Guérineau, V.; Giuliani, A.; Le Ven, J.; Champy, P.; Laprévote, O. Structural study of acetogenins by tandem mass spectrometry under high and low collision energy. *Rapid Commun. Mass Spectrom.* **2010**, *24*, 3602−3608.
(32) Sahpaz, S.; Hocquemiller, R.; Cavé, A. Diepoxyrollin and diepomuricanin B: two new diepoxyacetogenins from *Rollinia membranacea* seeds. *J. Nat. Prod.* **1997**, *60*, 199−201.
(33) Gu, Z.-M.; Zhou, D.-W.; Lewis, J. L.; Wu, J.; Johnson, H. A.; McLaughlin, J.-L.; Gordon, J. Quantitative evaluation of Annonaceous acetogenins in monthly samples of paw paw (*Asimina triloba*) twigs by liquid chromatography/electrospray ionization/tandem mass spectrometry. *Phytochem. Anal.* **1999**, *10*, 32−38.

JOURNAL OF AGRICULTURAL AND FOOD CHEMISTRY

Article

pubs.acs.org/JAFC

# Characterization of *Musa* sp. Fruits and Plantain Banana Ripening Stages According to Their Physicochemical Attributes

Claudine Valérie Passo Tsamo,[†,‡] Christelle M. Andre,[*,§] Christian Ritter,[∥] Kodjo Tomekpe,[⊥] Gérard Ngoh Newilah,[▽] Hervé Rogez,[○] and Yvan Larondelle[†]

[†]Institut des Sciences de la Vie, Université Catholique de Louvain, B-1348 Louvain-la-Neuve, Belgium

[‡]Centre for Food and Nutrition Research, Institute of Medical Research and Medicinal Plant Studies (IMPM), P.O. Box 6163, Yaounde, Cameroon

[§]Environment and Agro-biotechnologies Department, Public Research Centre, Gabriel Lippmann L-4422 Belvaux, Luxembourg

[∥]Statistical Methodology and Computing Service, Université Catholique de Louvain, B-1348 Louvain-la-Neuve, Belgium

[⊥]Agricultural Research Centre for International Development, CIRAD, Avenue Agropolis, 34398, Montpellier, Cedex 5, France

[▽]African Research Centre on Banana and Plantain (CARBAP), Njombe, P.O. Box 832 Douala, Cameroon

[○]Centre for Agro-food Valorisation of Amazonian Bioactive Compounds (CVACBA), Universidade Federal do Pará, 66.095-780 Belém-PA, Brazil

**ABSTRACT:** This study aimed at understanding the contribution of the fruit physicochemical parameters to *Musa* sp. diversity and plantain ripening stages. A discriminant analysis was first performed on a collection of 35 *Musa* sp. cultivars, organized in six groups based on the consumption mode (dessert or cooking banana) and the genomic constitution. A principal component analysis reinforced by a logistic regression on plantain cultivars was proposed as an analytical approach to describe the plantain ripening stages. The results of the discriminant analysis showed that edible fraction, peel pH, pulp water content, and pulp total phenolics were among the most contributing attributes for the discrimination of the cultivar groups. With mean values ranging from 65.4 to 247.3 mg of gallic acid equivalents/100 g of fresh weight, the pulp total phenolics strongly differed between interspecific and monospecific cultivars within dessert and nonplantain cooking bananas. The results of the logistic regression revealed that the best models according to fitting parameters involved more than one physicochemical attribute. Interestingly, pulp and peel total phenolic contents contributed in the building up of these models.

**KEYWORDS:** *Musa sp. fruits, physicochemical analysis, total phenolic compounds, ripening stage, discriminant analysis, principal component analysis, logistic regression*

## INTRODUCTION

With a world production of more than 138 million tons in 2010, bananas (*Musa* sp. fruits) are the seventh most important food crop after maize, rice, wheat, potato, soybean, and cassava.[1] Although Asia is the continent of origin of both wild and cultivated *Musa* sp., this crop is now also widely cultivated in Latin America, Caribbean countries, and Africa, where their fruits contribute to food security and socio-economical life. Studies have shown that bananas are good sources of starch, fibers, minerals (potassium, magnesium, phosphorus, manganese), and vitamin $B_6$ for consumers.[2] Furthermore, bananas are a source of natural dietary antioxidants such as carotenoids and phenolic compounds, which exhibit health-promoting effects including antioxidant, anti-inflammatory, antibacterial, and anticancer activities.[3,4] Our recent study revealed that bananas are good sources of phenolic compounds, hydroxycinnamic acids, particularly ferulic acid-hexoside, and flavonol glycosides e.g. rutin dominating in the plantain pulp and peels, respectively.[5] Information about the nutrient composition of bananas is of major importance for breeders and programs of varietal dissemination.

Edible *Musa* sp. are characterized by a large diversity, which constitutes one of the most interesting property for breeders. Several field collections exhibiting *Musa* sp. diversity are hosted in Latin America, India, Asia, and Africa countries where they are managed for breeding.[6] *Musa* sp. genotypes are generally classified according to the consumption mode of the fruits (dessert or cooking bananas) and the constitution of their genome.[7,8] The wild diploid bananas are characterized by the presence of seeds in their pulps and include two main species *Musa acuminata* Colla (AA) and *Musa balbisiana* Colla (BB), which contributed to the major groups of edible bananas. Intra- and interspecific hybridizations between these wild species in nature gave rise to many seedless cultivars whose reproduction occurs by vegetative multiplication (rationing or suckering). These cultivars are diploids or triploids with different genomic constitutions composed of genome A or genomes A and B. According to molecular and cytological studies, most of the edible cultivars have the genomic constitutions AA, AB, AAA, AAB, or ABB.[9,10] Their peels are mostly green at harvest.

**Received:** May 9, 2014
**Revised:** July 22, 2014
**Accepted:** August 7, 2014
**Published:** August 7, 2014

ACS Publications © 2014 American Chemical Society



dx.doi.org/10.1021/jf5021939 | *J. Agric. Food Chem.* 2014, 62, 8705−8715

**Table 1. Description of *Musa* sp. Fruits Collected at Harvest[a]**

| groups based on the consumption mode | genomic constitution[b] | subgroup | name of the accessions | peel color at harvest | groups based on the consumption mode and the genomic constitution |
|---|---|---|---|---|---|
| dessert | AAA | Ibota | Yangambi km5 | green | D-A |
| | AAA | Ibota | Khom Bao | green | |
| | AAA | Red | Figue Rose Naine | red | |
| | AB | Ney Poovan | Figue Pome Ekona | green | D-AB |
| | AB | Ney Poovan | Safet Velchi | green | |
| | ABB | ABB ind. | Rana | green | |
| nonplantain cooking | AA | AAcv ind. | Kekiau | green | NPC-A |
| | AA | AAcv ind. | Tomolo | green | |
| | AAA | Lujugira | Mujuba | green | |
| | AAB | Laknao | Laknao | green | NPC-AB |
| | AAB | Maïa Maoli | Iho-U-Maohi | green | |
| | AAB | ABB ind. | Kupulik | green | |
| | ABB | Kalapua | Dwarf Kalapua | green | |
| | ABB | Pelipita | Pelipita. | green | |
| plantain cooking | AAB | Plantain | Mbeta 1 | green | PC-French[c] |
| | AAB | | Red Yade | green | |
| | AAB | | French Rouge 18 | green | |
| | AAB | | Ntie | green | |
| | AAB | | Rouge de Loum | green | |
| | AAB | | Banane Tigrée | green with black spots | |
| | AAB | | Kar Ngou | green with chestnut pigments | |
| | AAB | | French Sombre | green | |
| | AAB | | Meki | green | |
| | AAB | | Kelong Mekintu | green | |
| | AAB | plantain | Mbouroukou no. 1 | green yellowish | PC-Horn[c] |
| | AAB | | 3/4 Nain | green | |
| | AAB | | Batard | green | |
| | AAB | | 76−17 | green | |
| | AAB | | Niangafelo | red silver, | |
| | AAB | | Essang | green with chestnut pigments | |
| | AAB | | Soya | green with chestnut pigments | |
| | AAB | | Moto Ebanga | chimeric green white | |
| | AAB | | Ihitisim | green | |
| new hybrids | | secondary triploid hybrids derived from plantain (AAA/AAB | C 292 | green | unknown |
| | | | F 568 | green | |

[a]Abbreviations: cv, cultivar; ind, undetermined; D, dessert; NPC, nonplantain cooking; PC, plantain cooking. [b]A, B: genomic constitution of *Musa accuminata* and *Musa balbisiana* respectively. [c]French, Horn: agro-morphological character within plantain cooking indicating respectively the presence or the absence of the male bud at harvest.

Central Africa is considered as a secondary center of plantain (a type of cooking banana) diversity harboring a wide range of unique varieties.[11,12] In general, the presence or absence of the male bud at harvest is used to distinguish the two main types of plantain, namely, the French and the Horn plantains, respectively. There is also a wide diversity in fruit peel colors. Somatic mutations are likely to be responsible for the great morphological diversity observed in plantains.[13] Moreover, the breeders undertake crossings between *Musa* varieties including wild species and cultivars. This leads to the creation of hybrids with improved disease resistance such as CRBP 14, CRBP 39, FHIA 17, and FHIA 21, which contribute to the diversity observed in this group.[14]

Due to the large diversity of bananas, there is still a lack of information on the physicochemical characteristics of fruits of numerous varieties. Most of the studies focused on the export dessert banana "Grand Nain" (AAA). Investigations on plantain are often limited to their pulps. For instance, Gibert et al.[15] investigated the difference between dessert and cooking bananas based on some physicochemical characteristics of the

pulp and found that dry matter, edible fraction, pH, total ash, and total sugar can help to differentiate dessert, nonplantain cooking, and plantain cooking bananas. However, more information may emerge if the secondary metabolites as well as the overall physicochemical attributes of the fruit pulp and peel are also taken into account.

Edible *Musa* sp. are also characterized by the ripening process occurring during the storage. During ripening, the fruits undergo physicochemical changes associated with organoleptic and nutritional modifications. These changes have many implications on their uses in food processing. For instance, the quality of plantain banana chips and the functional properties of dessert banana flour vary according to the ripening stage of the raw material.[16−18] In field collections, postharvest characterization of the ripening stages are assessed on dessert and cooking bananas.[19] However, the identification of the fruit ripening stages is currently based on a subjective color scale, which is designated for dessert banana with green peels at harvest.[20] With regard to the large diversity of peel color among plantain cultivars, there is a need to predict the ripening stages of the fruits using quantitative attributes. A study on some physicochemical characteristics of plantain pulp and peel during ripening reported changes in edible fraction, pH, dry matter, and pulp soluble solids.[21] To our best knowledge, no attempt to predict the ripening stage from these postharvest physicochemical characteristics has been reported.

This study proposed multivariate analytical approaches to describe how some postharvest physicochemical characteristics can be used (i) to discriminate groups within the diverse *varieties* of *Musa* sp. and (ii) to predict the ripening stages in plantains.

## MATERIALS AND METHODS

**Plant Material.** The starting plant material consisted of 33 *Musa* genotypes from the germplasm collection of the African Research Centre on banana and plantain (CARBAP) in Njombe in the littoral region of Cameroon at 80 m above the sea level (Table 1).[22] This working collection was organized in six cultivar groups based on their consumption mode, genomic constitution and morphological characters. Each of the three consumption groups, which are dessert, nonplantain cooking, and plantain cooking bananas, were divided in two subgroups. For dessert and nonplantain cooking bananas, monospecific varieties were separated from interspecific varieties. The first group contained only the A genome (A group) whereas the other one was made of varieties containing both the A and B genomes (AB group). For the plantains, the two main phenotypic classes (French and Horn) were separated. In addition, two newly created plantain-like hybrids resistant to the black Sigatoka disease were also part of the study and constituted a separated group. Bunches were harvested at CARBAP in 2010 at physiological maturity according to the protocol described by Tchango, Achard and Ngalani.[23] For each genotype, two to three bunches from different plants were used.

At least 15 fruits were collected from the middle hands of each bunch and allowed to ripe at room temperature in cardboard containers. Dessert and plantain banana ripening stages have been defined on the basis of changes in peel colors according to the scale described by Soltani, Alimardani, and Omid.[20] The four ripening stages 1, 3, 5, and 7 assessed correspond to peel color being all green, greener than yellow, yellow with green ends, and yellow with brown speckles, respectively. For each ripening stage, 3 fruits were removed from the cardboard and weighted. Each fruit was cut on the length and across the width into four quarters. Diagonally opposite quarters were put together to form two groups. For each group, samples from the three fruits were pooled. The pulps and peels of one group were separately freeze-dried, ground, and then vacuum sealed in polypropylene plastic bags. The other group was used for the determination of color, edible fraction, peel thickness, total soluble solids, pH, and total ash content. The freeze-dried samples were transported to the laboratory (Louvain-La-Neuve, Belgium) and kept at −20 °C.

**Chemicals.** Gallic acid and Folin-Ciocalteu reagent (2 N) were purchased from Sigma (St Louis, MO). Pure acetone, glacial acetic acid, and sodium carbonate (purity ≥99.5) were respectively obtained from Prolabo (Fontenay-sous-bois, France), Fisher Scientific (Loughborough, U.K.), and Merck (Darmstadt, Germany).

**Physicochemical Analyses.** *Banana Peel and Pulp Color.* The color of peel and pulp was assessed at different ripening stages by a hand-held color reader (CR-14, Konica Minolta, Japan) displaying the CIE Yxy chromaticity coordinates. The recorded values were then transformed into C (chroma) and L (lightness) color indexes.[24]

*Edible Fraction and Peel Thickness.* Two quarters of each fruit were separately weighted, the peel was then separated from the pulp and weighted. Edible fraction (%) was calculated by dividing the pulp weight by the pulp and peel weight. Peel thickness was measured using a caliper, and the result was expressed in millimeters.

*Total Soluble Solids and pH.* Total soluble solids and pH were determined according to the methods described in the International Network of the Improvement of Banana and Plantain technical guidelines.[19] For each part of the fruit, a mixture of the sample in distilled water (1:3, w: w) was vigorously blended for 2 min. The mixture was filtered using a Whatman no. 1 paper and the refraction index was read using a visual hand-held refractometer. The total soluble solids were expressed in degrees Brix (°Bx). The pH was measured with a benchtop pH meter (Knick, Berlin, Germany).

*2.3.4. Water and Total Ash Contents.* The fresh samples of pulp and peel were separately analyzed for their water and ash contents according to the norms of AFNOR.[25] Water content was determined by oven drying for 24 h at 105 °C. The content of total ash composed of free minerals and mineral salts was determined by calcinating the dried samples at 550 °C during 24 h. The results were expressed in percentage of the fresh sample.

*Total Phenolic Content.* For each freeze-dried banana peel and pulp sample, 0.5 g were extracted with 10 mL of acetone/water/acetic acid (50:49:1). The mixture was vortexed for 1 min. and the extraction was carried out in a water bath under agitation at 40 °C for 1 h. The extract was centrifuged at 5000*g* for 20 min at 4 °C. The colorimetric method[26] for total phenolic content determination was then used as a measure of the reducing capacity of the sample.[27] For the calibration curve, 5 concentrations were prepared from a stock solution of gallic acid. The results were expressed in milligrams gallic acid equivalents (GAE)/100 g of fresh weight (FW).

**Statistical Analysis.** The statistical analysis of the data was performed by the JMP9.0 statistical discovery software from SAS and SAS entreprise guide 4.3.

*Discriminant Analysis.* A linear discriminant analysis[28] was performed to (i) compare the physicochemical profile of the six cultivar groups, and to (ii) assign each new hybrid fruit to one of the groups. To compare cultivar groups, the software displayed the scatterplot of the *Musa* sp. fruit scores and the loading plot of the physicochemical attributes. The loading plot reflected the relative contribution of physicochemical attributes to the separation of the groups. In order to identify to which cultivar group a new hybrid fruit sample is closest, classification functions were created for each group in the form

$$F = b_1x_1 + b_2x_2 + \ldots + b_nx_n + c \quad (1)$$

Each of the six classification functions were evaluated with the physicochemical attributes ($x$) of the hybrid fruit sample. This later was assigned to the group whose classification function yielded the highest value.

*Logistic Regression.* In order to predict the ripening stage of plantain cultivars according to physicochemical attributes, an ordinal logistic regression was performed. The ripening stage was considered as an ordinal response with 4 modalities. For each ripening stage, the software gave the cumulative logit($j$), which is the logarithmic function of the ratio between the cumulative probability $P(y \leq j)$ that a plantain

sample "$y$" is at a level less or equal to a given ripening stage "$j$" with $j$ = 1, 3, 5, or 7 and the probability that it is not $(1 - P(y \leq j))$. Its formula as adapted from Gillet, Brosteaux, and Palm[29] is written as follows:

$$\text{Logit}(j) = \ln \frac{P(y \leq j)}{1 - P(y \leq j)} = \beta_0 + \beta_1 X_1 + \beta_2 X_2 + \cdots + \beta_p X_p \quad (2)$$

In eq 2, $\beta_0$ is the constant, each of the $\beta_{(1\rightarrow p)}$ values stands for the coefficients related to each X physicochemical attribute. The model gives the coefficients for the first three ripening stages, the last one being used as the reference in the statistical procedure. The models were evaluated by the $R^2$ and the corrected Akaike information criterion (AICc), which measures the fit of the model.[30] Twelve plantain genotypes with a green peel color at stage 1 were used to build the models. Only models explaining at least 70% of the variability are presented. Three plantain genotypes (two with three biological replicates and one with two biological replicates) with green peel with chestnut pigments at stage 1 were used to investigate the abilities of the models to predict the ripening stages. To predict the ripening stage of a plantain sample $y$, the probability $P(y = j)$ for this sample to be at a ripening stage $j$ is estimated for each ripening stage and the sample is considered to be at the ripening stage that has the highest probability. For that, the cumulative probability $P(y \leq j)$ formula is first deduced from eq 2 as follows:

$$P(y \leq j) = \frac{e^{\text{logit}(j)}}{1 + e^{\text{logit}(j)}} \quad (3)$$

Cumulative probabilities are then calculated for ripening stages 1, 3, and 5 and probabilities $P(y = j)$ are deduced as follows:

$$P(y = 1) = P(y \leq 1) \quad (4)$$

$$P(y = 3) = P(y \leq 3) - P(y \leq 1) \quad (5)$$

$$P(y = 5) = P(y \leq 5) - P(y \leq 3) \quad (6)$$

$$P(y = 7) = 1 - P(y \leq 5) \quad (7)$$

## RESULTS AND DISCUSSION

**Physicochemical Composition of Cultivar Groups at Harvest.** *General Description.* Tables 2 and 3 present the results of the physicochemical composition of the seven groups of *Musa* sp. fruits. At harvest, the fruits were at the ripening stage 1.

Most of the physicochemical attributes studied varied according to the cultivar groups. Significant differences were observed for pulp color indexes L and C (chroma and lightness), edible fraction, peel thickness, pulp water content, pulp total soluble solids, pulp pH, and pulp total phenolic compounds. As regard the comparison between pulp and peel, the physicochemical attribute values were different except for total soluble solids and pH. The observations about the L index being lower in peel and the water content being higher in peel were also reported in the literature for dessert bananas.[31,32] The data showing that the total phenolic compounds were (1.5 to 2 times) higher in peel than in pulp also matched with a report published on total phenolic compounds in Malaysian bananas.[33]

Among the dessert bananas, the cultivar Yangambi km5 presented the highest content of pulp total phenolic compounds (306.4 mg GAE/100 g FW). The contents obtained for A dessert banana pulps were higher than the contents reported for the dessert banana Pisang Mas (35.9−72.2 mg GAE/100 g FW) by Alothman, Bhat, and Karim.[34] Peel total phenolic compound contents of A dessert bananas (252.1−383.5 mg GAE/100 g FW) were similar to those of the export dessert banana Grand Nain at a ripe stage (2.6−3.1 g GAE/100g dry weight ∼260−310 mg/100g FW) reported by González-Montelongo, Gloria Lobo, and González.[35] Surprisingly, the cultivar Pelipita from the AB nonplantain cooking banana group showed the highest pulp total phenolic compound values (319.5 ± 70.4 GAE/100 g FW) within our banana collection. A drastically lower value was reported by Ngoh Newilah et al.[36] for this genotype (46 μg GAE/100 g dry weight ∼0.02 mg GAE/100 g FW). This low value might have resulted from the fact that the samples were dried in oven, which might have provoked phenolic compound oxidation. The highest pulp total phenolic compound values of plantains were obtained for the French plantain Niangafelo (198.4 ± 28.9 mg GAE/100 g FW) and the Horn plantain Moto Ebanga (182.1 ± 27.4 mg GAE/100 g FW). These results show that bananas and plantains could be as important sources of phenolic compounds as other vegetables such as potato (3950 μg GAE/g dry weight ∼90.85 mg GAE/100 g FW),[37] bitter melon (143.6 ± 8.4 mg GAE/100 g FW), and beetroot (257.2 ± 0.7 mg GAE/100 g FW).[38]

*Discriminant Analysis.* A linear discriminant analysis was performed to point out the most relevant physicochemical attributes contributing to the differentiation between cultivar groups. Furthermore, this approach was also intended to help allocating each of the two new hybrids to one of the cultivar groups.

Figure 1 presents the scatterplot of the standardized discriminant scores (A) and the corresponding standardized scoring coefficients of the physicochemical attributes or loading plot (B). The 2 first discriminant functions (1 and 2) explain 79.23% of the variation between groups. These 2 first discriminant functions were found to be highly significant ($P$ < 0.0001). The matrix generated by the software indicated that the number of samples correctly classified in the groups accounted for 92.6% of the samples involved in this analysis. The scatterplot shows that the dessert banana groups are separated from the cooking banana groups along the function 1 axis. On this axis, peel pH, pulp water content, edible fraction and fruit mass have the higher scoring coefficients in absolute terms, meaning that they were mostly responsible for this differentiation. The two groups of dessert bananas (A and AB) are separated according to function 2 axis, where pulp total phenolic compounds have the highest scoring coefficient. Pulp total phenolic compounds appear therefore to have highly contributed to the differentiation between the dessert bananas containing only the A genome (247.3 ± 76.3 mg/100 g FW) and those containing both A and B genomes (103.7 ± 33.2 mg/100 g FW). The nonplantain cooking bananas also split on the second axis: the A nonplantain cooking group has considerably higher scores on the second axis than the AB nonplantain cooking group. Furthermore, the AB nonplantain cooking group partly overlaps with the French and Horn plantain cooking groups, suggesting close physicochemical characteristics.

The comparison of the loading and the score plots of Figure 1 indicates that dessert bananas had the highest values of peel pH, edible fraction, and pulp water content whereas AB nonplantain cooking bananas and plantain cooking bananas had the lowest values for these attributes. It also appears that AB dessert bananas had the highest edible fraction values and A dessert bananas had the highest pulp water content values. The fact that the pulp water content mean value of the A dessert

Table 2. Physicochemical Characteristics (L and C Indexes, Fruit Mass, Edible Fraction, Peel Thickness, and Water Content) of *Musa* sp. Fruits at Harvest[#]

| groups and accession names | peel L index | pulp L index | peel C index | pulp C index | fruit mass (g) | edible fraction (%) | peel thickness (mm) | peel water content (% FW) | pulp water content (% FW) |
|---|---|---|---|---|---|---|---|---|---|
| **D-A** | **50.1 ± 10.3$^{a}$** | **77.3 ± 2.1$^{ab}$** | **25.9 ± 6$^{a}$** | **28.4 ± 3.9$^{ab}$** | **126.9 ± 50.7$^{a}$** | **68.3 ± 1.8$^{abc}$** | **2.5 ± 0.5$^{ab}$** | **89.6 ± 1$^{a}$** | **74.2 ± 1.1$^{a}$** |
| Figue Rose Naine | 39 | 75.3 | 19.0 | 32.9 | 184.5 | 67.7 | 3.0 | 88.5 | 75.5 |
| Khom Bao | 59.4 ± 5.2 | 79.5 ± 1.5 | 28.5 ± 2.3 | 26.6 ± 2.4 | 107.0 ± 16.7 | 70.3 ± 2.2 | 2.3 ± 0.3 | 89.9 ± 0.2 | 73.9 ± 1.6 |
| Yangambi km5 | 51.8 | 77 | 30.1 | 25.7 | 89.0 | 66.8 | 2.2 | 90.3 | 73.3 |
| **D-AB** | **52.8 ± 3.8$^{a}$** | **80.3 ± 0.9$^{a}$** | **32.3 ± 1.7$^{a}$** | **24.4 ± 12.5$^{b}$** | **96.6 ± 40$^{a}$** | **76.2 ± 4$^{a}$** | **2.1 ± 0.7$^{b}$** | **89.1 ± 0.3$^{a}$** | **69.7 ± 5.3$^{ab}$** |
| Figue Pomme Ekona | 54.4 | 80.9 | 33.6 | 16.7 | 76.5 | 78.1 | 2.8 | 88.8 | 65.5 |
| Safet Velchi | 55.5 ± 3.2 | 80.8 ± 0.7 | 32.9 ± 2 | 17.7 ± 0.5 | 70.7 ± 1.4 | 78.7 ± 0.6 | 1.4 ± 0.1 | 89.4 ± 0.5 | 68.0 ± 1.4 |
| Rana | 48.5 | 79.3 | 30.3 | 38.9 | 142.7 | 71.6 | 2.2 | 89.0 | 75.7 |
| **NPC-A** | **46.8 ± 4.5$^{a}$** | **77.5 ± 3.4$^{ab}$** | **29.4 ± 2.1$^{a}$** | **38.0 ± 3.8$^{ab}$** | **188.3 ± 51.5$^{a}$** | **70.6 ± 3.7$^{ab}$** | **2.5 ± 0.3$^{ab}$** | **88.9 ± 1.1$^{a}$** | **69.0 ± 9.6$^{abc}$** |
| Kekiau | 45.7 ± 1.6 | 79.5 ± 2.9 | 31.5 ± 3.4 | 40.5 ± 3.8 | 206.6 ± 14.7 | 67.4 ± 2.2 | 2.6 ± 0.1 | 89.3 ± 0.7 | 62.8 ± 0.6 |
| Tomolo | 43 ± 1.3 | 79.4 ± 1.7 | 27.4 ± 6 | 39.8 ± 1.8 | 228.2 ± 42.9 | 69.6 ± 1.6 | 2.7 ± 0.3 | 89.7 ± 0.6 | 64.1 ± 1.6 |
| Mujuba | 51.7 | 73.5 | 29.4 | 33.6 | 130.1 | 74.6 | 2.2 | 87.6 | 80.1 |
| **NPC-AB** | **52.5 ± 2.9$^{a}$** | **75.1 ± 2.1$^{b}$** | **31.9 ± 3.2$^{a}$** | **37.7 ± 3.9$^{ab}$** | **210.3 ± 135.7$^{a}$** | **62.7 ± 3.9$^{bc}$** | **3.1 ± 0.4$^{a}$** | **87.3 ± 2.5$^{a}$** | **64.0 ± 4.6$^{bcd}$** |
| Dwarf Kalapua | 56.4 ± 4 | 76.4 ± 1.5 | 30.8 ± 5.8 | 33.3 ± 1.5 | 105.1 ± 17.6 | 56.3 ± 5.1 | 2.7 ± 0.2 | 84.7 ± 0.8 | 60.5 ± 1 |
| Pelipita | 48.3 ± 3.6 | 73.9 ± 2.1 | 27.2 ± 4 | 40.0 ± 4.5 | 130.2 ± 10 | 63.4 ± 1 | 3.0 ± 0.2 | 86.2 ± 1.1 | 59.4 ± 0.5 |
| Iho-U-Maohi | 53.7 ± 1.6 | 74.4 ± 1.8 | 34.6 ± 2.5 | 39.8 ± 1.9 | 166.9 ± 11.5 | 64.6 ± 3 | 3.0 ± 0.4 | 90.9 ± 0 | 69.8 ± 1.1 |
| Kupulik | 51.9 | 72. | 32.2 | 41.5 | 443.1 | 66.5 | 3.8 | 86.1 | 68.1 |
| Laknao | 52.1 ± 1.1 | 78 ± 1.6 | 34.9 ± 1 | 33.6 ± 1.4 | 206.4 ± 18.2 | 62.8 ± 1.1 | 2.9 ± 0.3 | 88.7 ± 1.1 | 62.4 ± 1.2 |
| **PC-French** | **50.4 ± 7$^{a}$** | **77.1 ± 1.4$^{ab}$** | **28.4 ± 7.4$^{a}$** | **39.6 ± 4.3$^{a}$** | **136.8 ± 28.4$^{a}$** | **61.7 ± 2.9$^{c}$** | **2.8 ± 0.2$^{ab}$** | **87.4 ± 1.8$^{a}$** | **61.4 ± 1.9$^{cd}$** |
| French Rouge 18 | 54.8 | 77 | 28.6 | 41.3 | 136.3 | 60.3 | 2.7 | 89.3 | 63.1 |
| Ntie | 49.9 | 76.4 | 26.8 | 41.8 | 171.4 | 61.3 | 3.2 | 87.7 | 61.3 |
| Mbeta 1 | 53.4 ± 1.5 | 79.5 ± 1.9 | 36.2 ± 3.4 | 38.1 ± 3.2 | 169.4 ± 1.5 | 67.2 ± 1.2 | 2.8 ± 0.3 | 89.3 ± 0.3 | 64.7 ± 2 |
| Rouge de Loum | 57.2 | 76.6 | 34.1 | 39.0 | 167.3 | 58.1 | 3.2 | 87.9 | 62.4 |
| Banane Tigree | 37 ± 2 | 74.3 ± 1.2 | 10.3 ± 1 | 43.7 ± 1.2 | 111.0 ± 6.7 | 59.8 ± 2.6 | 2.8 ± 0.2 | 86.2 ± 2.3 | 59.9 ± 2.2 |
| Kar Ngou | 43.6 ± 3 | 78.4 ± 1.9 | 25.0 ± 4.7 | 37.2 ± 1.3 | 107.0 ± 5.7 | 61.8 ± 1.7 | 3.0 ± 0.3 | 83.8 ± 0.9 | 58.0 ± 0.1 |
| French Sombre | 42.7 | 76.5 | 25.8 | 43.1 | 158.0 | 63.0 | 3.0 | 86.7 | 60.1 |
| Kelong Mekintu | 56.6 | 77.7 | 33.0 | 29.7 | 130.9 | 64.9 | 2.5 | 88.7 | 62.2 |
| Meki | 51.7 | 77.4 | 31.4 | 44.3 | 93.4 | 58.0 | 2.8 | 85.8 | 60.3 |
| Red Yade | 56.9 ± 1 | 76.6 ± 2.3 | 33.3 ± 3.5 | 37.8 ± 0.5 | 123.3 ± 25.3 | 62.8 ± 3.9 | 2.6 ± 0.1 | 88.5 ± 0.7 | 61.7 ± 1 |
| **PC-Horn** | **51.2 ± 12.1$^{a}$** | **76.2 ± 2$^{ab}$** | **27.2 ± 5.9$^{a}$** | **36.6 ± 6.8$^{ab}$** | **221.9 ± 83.2$^{a}$** | **64.8 ± 4.5$^{bc}$** | **3.1 ± 0.4$^{a}$** | **86.6 ± 2$^{a}$** | **60.8 ± 1.4$^{d}$** |
| Batard | 56.4 | 75.4 | 33.8 | 41.9 | 190.2 | 65.2 | 2.9 | 88.3 | 60.4 |
| 3/4 Nain | 55 ± 1.5 | 75.8 ± 1.4 | 33.4 ± 3.8 | 40.8 ± 0.8 | 296.7 ± 39 | 67.2 ± 3.9 | 3.4 ± 0.2 | 87.0 ± 1.2 | 61.3 ± 0.7 |
| Mbouroukou no. 1 | 63.9 ± 2.5 | 76.2 ± 1.8 | 24.3 ± 4.1 | 37.4 ± 1.4 | 292.2 ± 47 | 66.5 ± 2.8 | 3.6 ± 0.3 | 90.7 ± 1.3 | 63.8 ± 1.5 |
| 76−17 | 58 | 77.4 | 32.0 | 37.8 | 341.1 | 66.0 | 3.3 | 85.2 | 59.8 |
| Niangafelo | 25.3 ± 0.9 | 80.9 ± 0.7 | 17.5 ± 2.2 | 20.5 ± 1 | 107.0 ± 11.7 | 54.6 ± 1.6 | 3.2 ± 0.4 | 84.8 ± 1.5 | 60.6 ± 2.2 |
| Essang | 42.5 ± 5.1 | 79.7 ± 2 | 23.5 ± 5.3 | 36.1 ± 1.1 | 225.9 ± 56.1 | 67.2 ± 2.4 | 2.9 ± 0.2 | 84.9 ± 1 | 60.6 ± 1.7 |
| Moto Ebanga | 55.2 ± 3.9 | 75.6 ± 2.4 | 23.2 ± 3.5 | 38.1 ± 1.6 | 129.3 ± 12 | 68.9 ± 1.6 | 2.3 ± 0.2 | 85.6 ± 0.8 | 59.0 ± 0.7 |
| Ihitism | 53.3 | 76.809 | 29.8 | 40.2 | 192.5 | 62.7 | 3.1 | 86.3 | 60.5 |
| Hybrid | | | | | | | | | |
| C 292 | 53.9 ± 0.4 | 76 ± 2.1 | 34.0 ± 2.5 | 35.1 ± 1.6 | 208.4 ± 26.3 | 61.3 ± 0.7 | 3.1 ± 0.5 | 88.5 ± 0.5 | 69.3 ± 1.4 |
| F 568 | 50.3 ± 2.5 | 76.7 ± 0.7 | 30.0 ± 0.8 | 34.7 ± 2.1 | 114.2 ± 15.1 | 58.8 ± 1.7 | 2.8 ± 0.3 | 88.1 ± 1 | 69.3 ± 1.8 |

[#]See Table 1 for the significance of the group names. FW: fresh weight. For each cultivar, the value is the mean of two (standard deviation not shown) to three biological replicates, each in duplicate. Superscript a, b, and c result from the comparison of groups using Tukey's test. Groups connected by the same letter are not significantly different.



dx.doi.org/10.1021/jf5021939 | J. Agric. Food Chem. 2014, 62, 8705−8715

Table 3. Physicochemical Characteristics (Total Soluble Solids, pH, Total Ash, and Total Phenolic Compounds) of *Musa* sp. Fruits at Harvest[#]

| groups and accession names | peel total soluble solids (°Brix) | pulp total soluble solids (°Brix) | peel pH | pulp pH | peel total ash content (mg/100 g FW) | pulp total ash content (mg/100 g FW) | peel total phenolic compds. (mg/100 g FW) | pulp total phenolic compds. (mg/100 g FW) |
|---|---|---|---|---|---|---|---|---|
| **D-A** | **2.8 ± 0.6$^{bc}$** | **4.2 ± 1.3$^{a}$** | **6.1 ± 0.2$^{a}$** | **5.3 ± 0.1$^{b}$** | **1236.1 ± 103.5$^{a}$** | **854.6 ± 29.1$^{a}$** | **299.7 ± 7.8$^{a}$** | **247.3 ± 76.3$^{a}$** |
| Figue Rose Naine | 2.1 | 3.0 | 6.4 | 5.4 | 1355.1 | 860.5 | 252.1 | 161.2 |
| Khom Bao | 3.0 ± 0.1 | 4.0 ± 0.4 | 6.0 ± 0.2 | 5.3 ± 0 | 1167.5 ± 47.4 | 823.0 ± 35.1 | 263.5 ± 67.6 | 274.4 ± 22.3 |
| Yangambi km5 | 3.2 | 5.6 | 6.0 | 5.3 | 1185.6 | 880.3 | 383.5 | 306.4 |
| **D-AB** | **2.5 ± 0.3$^{c}$** | **3.5 ± 0.6$^{a}$** | **6.1 ± 0$^{a}$** | **5.8 ± 0.3$^{a}$** | **1558.1 ± 17.8$^{a}$** | **942.5 ± 101.6$^{a}$** | **224.9 ± 51.8$^{a}$** | **103.7 ± 33.2$^{b}$** |
| Figue Pomme Ekona | 2.4 | 2.9 | 6.1 | 6.1 | 1569.4 | 871.8 | 165.6 | 105.9 |
| Safet Velchi | 2.9 ± 0.6 | 3.5 ± 0.6 | 6.1 ± 0.3 | 5.8 ± 0.1 | 1567.4 ± 84.5 | 896.8 ± 50.9 | 247.5 ± 68.6 | 135.8 ± 20.7 |
| Rana | 2.2 | 4.2 | 6.1 | 5.4 | 1537.6 | 1059.0 | 261.6 | 69.5 |
| **NPC-A** | **3.5 ± 0.5$^{abc}$** | **4.1 ± 0.5$^{a}$** | **5.9 ± 0.7$^{a}$** | **6.1 ± 0.9$^{a}$** | **1544.5 ± 496.6$^{a}$** | **932.7 ± 115.1$^{a}$** | **186.6 ± 35.2$^{a}$** | **65.4 ± 23$^{b}$** |
| Kekiau | 3.7 ± 0.6 | 4.6 ± 0.4 | 6.2 ± 0.1 | 6.5 ± 0.3 | 1665.0 ± 258.6 | 933.5 ± 48.7 | 166.3 ± 32.8 | 83.2 ± 9.7 |
| Tomolo | 3.9 ± 0.7 | 4.1 ± 0.1 | 6.4 ± 0 | 6.7 ± 0 | 1969.8 ± 172 | 1047.3 ± 79.5 | 166.2 ± 43 | 73.7 ± 22.3 |
| Mujuba | 3.0 | 3.6 | 5.1 | 5.1 | 998.8 | 817.2 | 227.3 | 39.5 |
| **NPC-AB** | **3.8 ± 0.3$^{a}$** | **4.5 ± 0.5$^{a}$** | **6.0 ± 0.1$^{a}$** | **5.8 ± 0.3$^{a}$** | **1392.1 ± 115.5$^{a}$** | **890.7 ± 65.8$^{a}$** | **275.5 ± 159.9$^{a}$** | **146.8 ± 106.2$^{ab}$** |
| Dwarf Kalapua | 4.1 ± 0.3 | 5.1 ± 1.3 | 5.9 ± 0.2 | 6.1 ± 0.1 | 1376.9 ± 39.6 | 940.9 ± 25.3 | 341.0 ± 26 | 72.3 ± 3.4 |
| Pelipita | 4.0 ± 0.8 | 4.3 ± 0 | 6.1 ± 0.3 | 5.8 ± 0.4 | 1298.9 ± 48 | 789.1 ± 47.3 | 522.7 ± 31.3 | 319.5 ± 70.4 |
| Iho-U-Maohi | 3.4 ± 0.1 | 4.8 ± 0.5 | 5.7 ± 0.2 | 5.7 ± 0.1 | 1422.7 ± 57.7 | 863.6 ± 48 | 160.5 ± 30.7 | 54.3 ± 1 |
| Kupulik | 3.9 | 4.5 | 6.0 | 5.5 | 1288.7 | 947.6 | 222.1 | 168.1 |
| Laknao | 3.6 ± 0.6 | 3.8 ± 1.1 | 6.0 ± 0.4 | 6.1 ± 0.2 | 1573.3 ± 173.1 | 912.4 ± 34.4 | 131.4 ± 32.5 | 119.8 ± 32.6 |
| **PC-French** | **3.4 ± 0.5$^{ab}$** | **3.8 ± 0.4$^{a}$** | **5.8 ± 02$^{a}$** | **5.9 ± 0.2$^{a}$** | **1677.1 ± 325.3$^{a}$** | **947.1.0 ± 198.9$^{a}$** | **293.9 ± 120.3$^{a}$** | **132.7 ± 33$^{b}$** |
| French Rouge 18 | 3.1 | 4.1 | 5.8 | 5.7 | 1387.6 | 808.5 | 230.8 | 123.7 |
| Ntie | 3.2 | 3.6 | 6.0 | 5.9 | 1537.8 | 832.2 | 307.4 | 133.1 |
| Mbeta 1 | 3.8 ± 0.2 | 4.4 ± 0.5 | 5.4 ± 0.1 | 5.8 ± 0 | 1612.8 ± 116.9 | 923.4 ± 38.3 | 181.0 ± 140.7 | 154.5 ± 12 |
| Rouge de Loum | 3.2 | 3.5 | 5.9 | 5.8 | 1494.2 | 870.0 | 209.6 | 154.6 |
| Banane Tigree | 3.8 ± 0.4 | 3.8 ± 0.5 | 5.9 ± 0.1 | 6.0 ± 0.3 | 2546.1 ± 773.1 | 1498.9 ± 420.4 | 587.6 ± 290.5 | 163.4 ± 48.3 |
| Kar Ngou | 2.6 ± 0.4 | 3.0 ± 0.6 | 6.2 ± 0 | 6.3 ± 0.2 | 1674.7 ± 207.9 | 948.4 ± 55.1 | 303.4 ± 95.4 | 170.1 ± 39.6 |
| French Sombre | 4.1 | 4.0 | 5.7 | 6.2 | 1516.4 | 890.9 | 173.7 | 99.8 |
| Kelong Mekintu | 2.9 | 3.5 | 5.7 | 5.8 | 1602.4 | 940.7 | 290.3 | 136.3 |
| Meki | 3.5 | 3.9 | 5.6 | 5.7 | 1808.5 | 892.8 | 366.7 | 59.7 |
| Red Yade | 3.5 ± 0.3 | 4.3 ± 0.4 | 5.9 ± 0.1 | 5.8 ± 0.2 | 1590.4 ± 95.5 | 865.6 ± 56.1 | 288.4 ± 25.9 | 131.5 ± 21.5 |
| **PC-Horn** | **3.6 ± 0.4$^{ab}$** | **4 ± 0.4$^{a}$** | **5.7 ± 0.3$^{a}$** | **6 ± 0.2$^{a}$** | **1693.3 ± 157.1$^{a}$** | **943.2 ± 43.3$^{a}$** | **302.1 ± 94.6$^{a}$** | **153.9 ± 34$^{ab}$** |
| Batard | 3.4 | 4.2 | 5.5 | 5.7 | 1622.5 | 940.9 | 313.5 | 135.4 |
| 3/4 Nain | 3.8 ± 0.9 | 4.1 ± 0.5 | 5.6 ± 0.2 | 6.2 ± 0.4 | 1779.5 ± 134.5 | 956.6 ± 19.1 | 224.4 ± 54.2 | 152.1 ± 17.4 |
| Mbouroukou no. 1 | 2.9 ± 0.7 | 3.6 ± 0.7 | 5.8 ± 0.1 | 5.7 ± 0 | 1368.7 ± 84.3 | 1019.6 ± 35.5 | 127.2 ± 87.6 | 88.4 ± 28.5 |
| 76−17 | 3.5 | 3.5 | 6.1 | 6.0 | 1688.2 | 902.8 | 323.8 | 145.3 |
| Niangafelo | 4.3 ± 0.5 | 4.6 ± 0.4 | 5.6 ± 0.1 | 6.2 ± 0.2 | 1822.5 ± 239.1 | 893.5 ± 19.2 | 407.2 ± 81.8 | 198.4 ± 28.9 |
| Essang | 3.6 ± 1.3 | 3.8 ± 1.3 | 5.7 ± 0.2 | 6.0 ± 0.2 | 1656.0 ± 203 | 965.7 ± 33.3 | 262.5 ± 73.3 | 151.2 ± 31.7 |
| Moto Ebanga | 4.1 ± 0.2 | 4.5 ± 0.3 | 5.5 ± 0.1 | 6.1 ± 0.3 | 1882.2 ± 173.4 | 898.9 ± 21.1 | 401.1 ± 22.7 | 182.1 ± 27.4 |
| Ihitism | 3.3 | 3.4 | 6.1 | 6.0 | 1726.9 | 967.2 | 356.6 | 177.9 |
| **Hybrid** | | | | | | | | |
| C 292 | 3.2 ± 0.2 | 3.6 ± 0.3 | 5.8 ± 0.5 | 5.8 ± 0.2 | 1477.2 ± 204.4 | 1001.4 ± 9.5 | 167.6 ± 49.4 | 98.4 ± 15.6 |
| F 568 | 3.9 ± 0.9 | 3.9 ± 0.9 | 5.6 ± 0.2 | 5.6 ± 0.1 | 1347.3 ± 319.9 | 1176.0 ± 232.5 | 220.0 ± 24.1 | 164.3 ± 45.6 |

[#]FW: fresh weight. For each cultivar, the value is the mean of two (standard deviation not shown) to three biological replicates, each in duplicate. Superscript a, b, and c result from the comparison of groups using Tukey's test. Groups connected by the same letter are not significantly different.

bananas (74. Two ±1.1% FW) was higher than those of the plantain cooking bananas (61.4 ± 1.9% FW and 60.8% ± 1.4 FW for French plantain and Horn plantain cooking bananas, respectively) Table 2 is in agreement with the results obtained by Gibert et al.[15] According to the direction of the fruit mass vector, AB nonplantain and plantain cooking banana groups had the heaviest fruits. In addition, the highest mean value of pulp total phenolic compounds was observed for the A dessert banana group (247.3 ± 76.3 mg/100 g FW) whereas the lowest mean value was registered for the A nonplantain cooking banana group (65.4 ± 23 mg GAE/100 g FW).

Interestingly, this study shows that the content in pulp total phenolic compounds is one of the most important attributes, which has made the difference between both genomic constitutions (A and AB) within nonplantain cooking bananas and within dessert bananas.

Table 4 presents the nonstandardized coefficients of the estimated classification functions for the six cultivar groups. The two hybrid banana plant under investigation can then be classified by simply multiplying the values of the physicochemical attributes of their fruits with these coefficients and then taking the sum. Table 5 shows the results obtained for the three


dx.doi.org/10.1021/jf5021939 | J. Agric. Food Chem. 2014, 62, 8705−8715

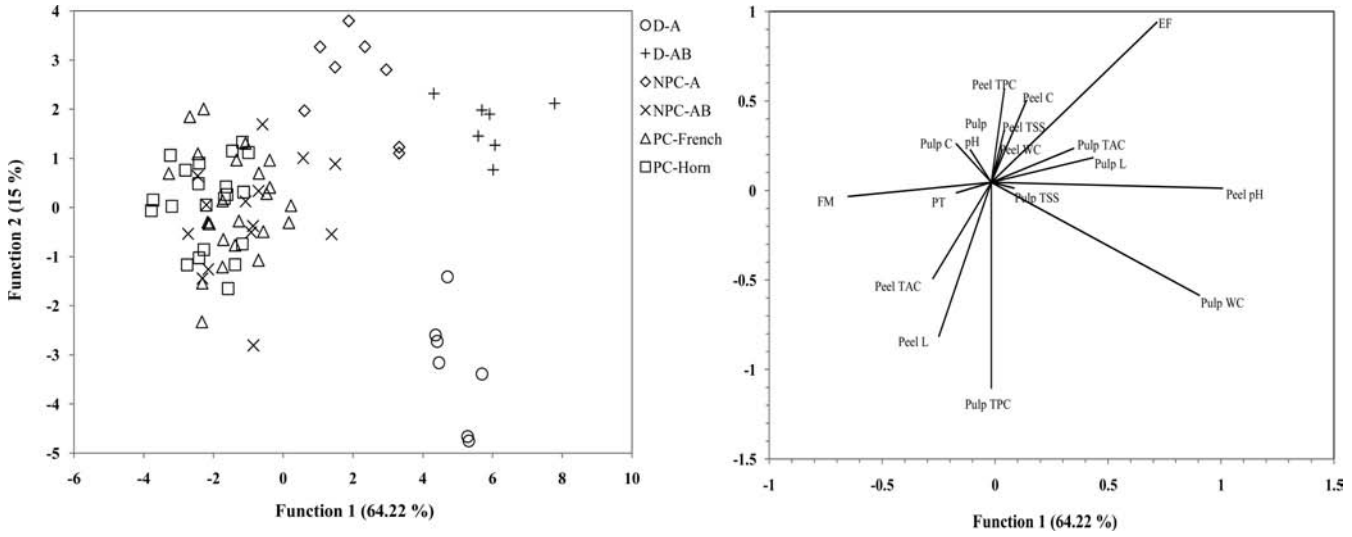


**Figure 1.** Scatterplot of fruit scores (A) and loading plot of the attribute scoring coefficients (B) from the linear discriminant analysis of cultivar groups at harvest. D, dessert; NPC, nonplantain cooking; PC, plantain cooking; L, lightness; C, chroma; FM, fruit mass; TSS, total soluble solids; TAC, total ash content; TPC, total phenolic compounds; EF, edible fraction; PT, peel thickness; WC, water content.

**Table 4. Coefficients of the Classification Functions of the Six Cultivar Groups: Two Groups of Dessert Bananas (D-A and D-AB), Two Groups of Non-Plantain Cooking Bananas (NPC-A and NPC-AB), and plantain cooking bananas (PC-French and PC-Horn)**

| | banana groups | | | | | |
|---|---|---|---|---|---|---|
| | dessert | | nonplantain cooking | | plantain cooking | |
| attributes | D-A | D-AB | NPC-A | NPC-AB | PC-French | PC-Horn |
| constant | −6149 | −6199 | −6092 | −5756 | −5768 | −5742 |
| pulp L index | 46.025 | 46.764 | 45.513 | 44.111 | 45.074 | 45.256 |
| peel L index | 1.764 | 1.250 | 1.229 | 1.479 | 1.584 | 1.690 |
| pulp C index | 7.235 | 7.187 | 7.581 | 7.279 | 7.576 | 7.391 |
| peel C index | −5.773 | −5.272 | −5.381 | −5.275 | −5.526 | −5.803 |
| fruit mass (g) | −0.646 | −0.666 | −0.625 | −0.598 | −0.612 | −0.577 |
| edible fraction (%) | 16.471 | 17.947 | 17.075 | 15.971 | 16.020 | 16.162 |
| peel thickness (mm) | 77.742 | 78.029 | 77.279 | 78.943 | 79.702 | 80.944 |
| pulp water content (% FW) | 23.642 | 22.400 | 22.308 | 21.587 | 21.304 | 21.015 |
| peel water content (% FW) | 40.304 | 40.437 | 40.951 | 40.353 | 40.382 | 40.283 |
| pulp total soluble solid (°Bx) | −15.451 | −14.873 | −16.142 | −15.996 | −16.850 | −15.741 |
| peel total soluble solid (°Bx) | 67.649 | 68.200 | 71.280 | 70.125 | 67.745 | 67.487 |
| pulp pH | 134.519 | 128.306 | 143.008 | 137.790 | 134.589 | 135.025 |
| peel pH | 183.918 | 187.257 | 175.114 | 168.686 | 162.929 | 158.509 |
| pulp total ash content (mg/100g FW) | 0.053 | 0.063 | 0.054 | 0.050 | 0.044 | 0.038 |
| peel total ash content (mg/100g FW) | −0.157 | −0.164 | −0.167 | −0.163 | −0.155 | −0.155 |
| pulp total phenolic compds. (mg/100 g FW) | −0.218 | −0.320 | −0.325 | −0.289 | −0.279 | −0.283 |
| peel total phenolic compds. (mg/100 g FW) | 0.722 | 0.741 | 0.745 | 0.734 | 0.727 | 0.735 |

**Table 5. Classification Functions Evaluated by Introducing the Physicochemical Attributes of Fruit Sample from Each Plant of the Two Hybrids in Equation 1[a]**

| hybrids | plant no. | D-A[b] | D-AB[b] | NPC-A[b] | NPC-AB[b] | PC-French[b] | PC-Horn[b] | closest match group | second closest group |
|---|---|---|---|---|---|---|---|---|---|
| C 292 | 1 | 5635.159 | 5624.706 | 5632.933 | **5643.053** | 5638.656 | 5629.607 | **AB-NPC** | PC-French |
| | 2 | 5808.170 | 5797.560 | 5819.661 | 5828.004 | **5828.487** | 5824.287 | **PC-French** | NPC-AB |
| | 3 | 5785.908 | 5770.814 | 5797.766 | **5807.890** | 5805.193 | 5803.327 | **AB-NPC** | PC-French |
| F 568 | 1 | 5805.211 | 5780.102 | 5792.958 | **5806.956** | 5804.187 | 5794.410 | **AB-NPC** | D-A |
| | 2 | 5838.463 | 5837.402 | 5855.108 | **5859.519** | 5852.975 | 5844.481 | **AB-NPC** | NPC-A |
| | 3 | 5805.542 | 5786.669 | 5802.703 | 5811.853 | **5815.021** | 5808.155 | **PC-French** | NPC-AB |

[a]The closest matches to the cultivar groups are indicated in bold. [b]A, B: genomic constitution of *Musa accuminata* and *Musa balbisiana*, respectively. D, dessert; NPC, nonplantain cooking; PC, plantain cooking. French, Horn: agro-morphological character within plantain cooking bananas, indicating respectively the presence or the absence of the male bud at harvest.


dx.doi.org/10.1021/jf5021939 | J. Agric. Food Chem. 2014, 62, 8705−8715

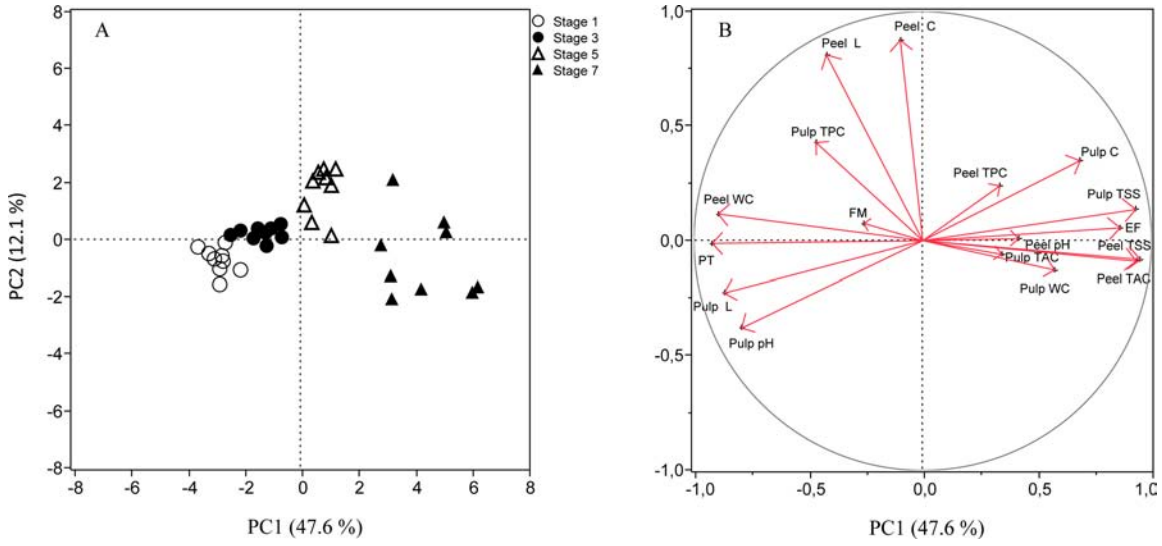


**Figure 2.** Scatterplot (A) and loading plot (B) of the principal component analysis performed on standardized data physicochemical tributes obtained from three plantain genotypes (Mbeta 1, Red Yade, and 3/4 Nain) at different ripening stages 1, 3, 5, and 7 ($n$ = 3). L, lightness; C, chroma; FM, fruit mass; TSS, total soluble solids; TAC, total ash content; TPC, total phenolic compounds; EF, edible fraction; PT, peel thickness; WC, water content.

plants of each of these two hybrids. It can be observed that the highest values correspond to AB nonplantain cooking (NPC-AB) and French plantain cooking groups (PC-French), which means that the hybrids appear closer to those groups. Interestingly, the two hybrids had in their family tree, monospecific (AA) and interspecific (AB) cooking bananas. In fact, their parents are also hybrids, obtained following two different crossings, one between the A nonplantain cooking banana Tomolo (AA) and the A cooking hybrid Crbp060 (AA), and another between the French plantain cooking banana Red Yade (AAB) and the wild species Calcutta 4 (AA) (which was shown to be close to the A dessert banana group, data not shown). This shows that the interspecific cooking banana physicochemical characters were dominant. However, for the hybrid F568, the plants nos. 1 and 2 also appear to be close to the A dessert group (D-A) and to the A nonplantain cooking group (NPC-A), respectively.

**Physicochemical Changes during the Ripening Process of Plantains.** *Description.* In order to study the evolution of the physicochemical attributes of plantains during ripening, we performed a principal component analysis on three cultivars, namely Mbeta 1, Red Yade, and 3/4 Nain. Stages 1, 3, 5, and 7 were evaluated. The results are presented as a scatterplot of the scores of the different ripening stages, and a loading plot of the attributes (Figure 2).

On the scatterplot, four clusters corresponding to each ripening stage can be observed. The four groups are separated along the principal component 1 (PC1) axis in an ascending order from the left to the right (Figure 2A). A simultaneous analysis of the vector positions of the attributes in the loading plots (Figure 2B) shows that the physicochemical attributes are distributed in three groups. Two of them are correlated with the ripening stage and negatively correlated with each other. The first group is positively correlated with the ripening stage and includes pulp and peel total soluble solids, peel total ash content, edible fraction and pulp C index, suggesting that these parameters increased during the ripening. Peel total phenolic compounds, pulp water content, pulp total ash content, and peel pH also appear positively correlated with the ripening stage but to a lesser extent. The second group consists of peel thickness, peel water content, pulp L index, and pulp pH, which are, on the other hand, negatively correlated with the ripening stage. The third group including peel C and peel L indexes and to a lesser extent pulp total phenolic compounds separated the ripening stage group 5 from the other ripening stage groups on the PC2 axis. This suggests that the values of these three attributes reached a maximum at stage 5 and then decreased.

Peel and pulp color changes associated with the ripening process could be described by the evolution of L and C indexes. The increase of peel lightness and chroma to a maximum level at stage 5 could express the change from the green color to the yellow color due to the chlorophyll degradation and the accumulation of carotenoids.[39] Their subsequent decrease could be related to the apparition of black spots that might involve enzymatic browning due to the activity of the polyphenol oxidase and of other oxidative enzymes.[39,40] In pulp, the decrease of lightness and the increase of chroma reflect the decrease of whiteness and the increase of the color intensity.

Changes in fruit firmness can be considered as another means by which the ripening is perceived. Fruit firmness was not measured in this study but it has been reported that the softening of the fruit results from the disruption of cell walls and the hydrolysis of starch under the actions of amylase and other enzymes.[39] In general terms, the ripening process in the pulp results in the release of water-soluble solids, which include proteins, minerals, and predominantly soluble sugars from the starch hydrolysis and are evaluated by the total soluble solid measurement. The subsequent osmotic transfer of water from the peel into the pulp may have resulted in the increase of pulp water content and pulp edible fraction.[41,42] A transfer of water and other volatile compounds (carbon dioxide, ethylene, and aroma) from the peel to the environment[31] has probably also contributed to the decrease of peel water content and peel thickness. The decrease of peel water content might have resulted in the increase of the peel total ash concentration.

A decrease of pulp pH was registered upon ripening, which fits with an increase of acidic taste. The pH decrease is believed


dx.doi.org/10.1021/jf5021939 | J. Agric. Food Chem. 2014, 62, 8705−8715

**Table 6. Models Proposed for the Prediction of the Ripening Stages of Plantains after Performing the Logistic Regression on Each Biological Replicate of 12 Genotypes[a]**

| | | prediction models | | | | prediction ability[b] | | | | |
|---|---|---|---|---|---|---|---|---|---|---|
| models | attributes involved | cumulative logits | $R^2$ | AICc criteria | $n^c$ | ripening stages | | | | $n$/stage[d] |
| | | | | | | 1 | 3 | 5 | 7 | |
| 1 | pulp TSS | $\text{logit}\begin{bmatrix}1\\3\\5\end{bmatrix} = \begin{bmatrix}6.94\\13.85\\27.23\end{bmatrix} - 1.48\ \text{pulp TSS}$ | 0.75 | 82.46 | 108 | 7 | 7 | 8 | 1 | 8 |
| 2 | pulp TSS, pulp pH, peel TAC, peel C | $\text{logit}\begin{bmatrix}1\\3\\5\end{bmatrix} = \begin{bmatrix}-7.20\\10.84\\42.7\end{bmatrix} - 2.20\ \text{pulp TSS} + 5.47\text{pulp pH} - 0.01\ \text{peel TAC} + 0.38\ \text{peel C}$ | 0.92 | 38.78 | 108 | 7 | 4 | 8 | 6 | 8 |
| 3 | pulp pH, peel TAC | $\text{logit}\begin{bmatrix}1\\3\\5\end{bmatrix} = \begin{bmatrix}-97.94\\-87.43\\-80.20\end{bmatrix} + 20.37\ \text{pulp pH} + 0.019\ \text{peel TAC} - 0.005\ \text{pulp pH·peel TAC}$ | 0.81 | 70.50 | 108 | 8 | 6 | 7 | 6 | 8 |
| 4 | pulp and peel L index, pulp and peel WC, PT | $\text{logit}\begin{bmatrix}1\\3\\5\end{bmatrix} = \begin{bmatrix}-125.35\\-116.8\\-103.7\end{bmatrix} + 0.96\ \text{pulp L} - 0.14\ \text{peel L} + 0.69\ \text{pulp WC} + 1.06\ \text{peel WC} + 3.76\ \text{PT}$ | 0.82 | 70.45 | 108 | 8 | 5 | 7 | 7 | 8 |
| 5 | peel TSS and peel TPC | $\text{logit}\begin{bmatrix}1\\3\\5\end{bmatrix} = \begin{bmatrix}33.67\\44.09\\65.20\end{bmatrix} - 6.72\ \text{peel TSS} - 0.022\ \text{peel TPC}$ | 0.88 | 23.30 | 36 | 5 | 1 | 1 | 6 | 6 |
| 6 | EF, pulp pH, pulp TPC | $\text{logit}\begin{bmatrix}1\\3\\5\end{bmatrix} = \begin{bmatrix}-71.14\\-66.21\\-47.61\end{bmatrix} - 0.86\text{EF} + 23.42\ \text{pulp pH} + 0.39\ \text{pulp TPC} - 0.074\ \text{pulp pH·pulp TPC}$ | 0.79 | 37.97 | 36 | 6 | 5 | 5 | 0 | 6 |

[a]Prediction abilities of the proposed equation on each biological replication of 3 genotypes characterized by a green peel with chestnut pigments are also presented. Abbreviations; TSS, total soluble solids; TAC, total ash content; TPC, total phenolic compounds; EF, edible fraction; PT, peel thickness; WC, water content; L, lightness; AICc, Akaike information criterion. [b]Number of samples determined to be at the corresponding ripening stage according to the corresponding prediction model. [c]Number of observations. Each observation represents one biological replicate of a cultivar, at one ripening stage. [d]Number of samples collected at each ripening stage according to the color scale.

to be associated with the accumulation of some organic acids such as malic acid.[43]

Pulp total phenolic compounds increased up to the ripening stage 5 and then decreased, whereas peel total phenolic compounds increased throughout the ripening process. This suggests a tissue specific regulation of the ripening process as mentioned by Bruno Bonnet et al.[44] and Inaba et al.[45] for *Musa* species. A different result was found by Ngoh Newilah et al.,[36] who obtained an increase in pulp total phenolic compounds of plantains from stage 1 to stage 7. During the ripening, it is generally reported that anthocyanin-rich fruits increase their content in total phenolic compounds, whereas many other fruits have their total phenolic compounds decreasing.[46]

The observed separation of the ripening stage groups suggests that, whatever the cultivar, a ripening stage could be characterized by a certain behavior of same physicochemical attributes. Under this hypothesis and considering the great importance of the identification of the ripening stage in food processing, physicochemical attributes were used to model the ripening stages.

*Modeling the Ripening Stages Using Logistic Regression.* Table 6 presents the proposed prediction equations in the form of the cumulative logit function as explained in the Materials and Methods section. The ability of those models to predict the ripening stages of three plantain genotypes are also presented. The number of well classified plantain samples over the total sample investigated at each ripening stage is reported. Each model presents the cumulative logit of each of the 3 first ripening stages, which have different constant values but the same coefficient per attribute. Lower AICc values indicate better fittings.

For each model, the involved attribute coefficients were found to be significant ($P < 0.05$) according to the likelihood-ratio $\chi$-square test. When performing stepwise regression control in the forward direction, pulp total soluble solids was the first attribute selected by the software and model 1 was proposed. This indicates that its contribution to the ripening was the most important. When the stepwise process ended, pulp pH, peel total ash content and peel C index were additionally selected. Model 2 was then proposed as the best model and was used as a reference. Its $R^2$ and AICc values were 0.92 and 38.78, respectively (Table 6).

We investigated many combinations of attributes to find other models with fitting parameters and prediction abilities similar to those of the reference model (model 2). Models 3 and 4 were found to be among the best. They had lower $R^2$ values (0.81 and 0.82, respectively) and higher AICc values (70.50 and 70.45, respectively) than model 2 but their

prediction abilities were close to those of model 2. They may offer an alternative when there is a lack of material needed to assess some attributes involved in model 2. Model 6, involving edible fraction, pulp pH, and pulp total phenolic compounds, had good fitting parameters when compared to models 3 and 4, and its prediction ability was almost similar to those of the model 1. Models 1 and 6 had acceptable prediction abilities up to stage 5 but were not effective to make the difference between stages 5 and 7.

All the models had ripening stage predictions below 100%. This supports the fact that the monitoring of the ripening stage based on the color scale and using a subjective assessment might lead to wrong classifications. Applying a model as a ripening stage control method, which uses objective parameters can increase the homogeneity within a ripening stage group and could be therefore relevant. Moreover, it is worth noting that the best models involved more than one physicochemical attribute, which stresses the importance of considering diverse attributes in the determination of the ripening stage of plantain.

## CONCLUSIONS

We aimed at investigating the involvement of some *Musa* sp. fruit postharvest physicochemical characteristics in the differentiation between diverse *Musa* sp. cultivars, as well as in the prediction of the plantain ripening stages. The discriminant analysis highlighted the importance of the edible fraction, the peel pH, the pulp water content, and the pulp total phenolic compounds in the distinction between cultivar groups at ripening stage 1. The great contribution of the pulp total phenolic compounds in the differentiation between interspecific and intraspecific groups within the dessert bananas and the nonplantain cooking bananas called for a deeper understanding of the specific phenolic composition. The physicochemical attributes considered in the present study did however not allow differentiating French and Horn plantain cooking bananas. They also showed that interspecific nonplantain cooking bananas are very close to plantain cooking bananas. The hybrids seemed to have physicochemical characteristics close to those of interspecific cooking bananas. This result seems to meet the breeder expectations who created these hybrids to be like plantain. It also emerged from this study that the use of logistic regression could be successfully applied in the control of the fruit ripening stages. The involvement of pulp total phenolic compounds in the model that had good evaluations according to $R^2$ and AICc criterion aroused the interest for monitoring the phenolic compound profiles during the ripening process. These results allow to consider applying the proposed analytical approaches to a whole collection such as that of the CARBAP. The genomic constitution in its entirety (ploidy level and composition in A and B genomes) will be thus taken into account for the characterization of *Musa* cultivars. This broadening of samples will also enhance the search of the ripening stage prediction models easily applicable to a wide range of cultivars.

## AUTHOR INFORMATION

### Corresponding Author

*Tel.: +352 470261 436. Email: andre@lippmann.lu.

### Funding

This study was partly funded by the CUI Programme of the Coopération Universitaire pour le Développement (CUD, Belgium).

### Notes

The authors declare no competing financial interest.

## ACKNOWLEDGMENTS

The authors thank the African Research Centre on Banana and Plantain (CARBAP) for providing banana cultivars and technical assistance in post-harvest handling.

## REFERENCES

(1) FAOSTAT: Food and Agriculture Organization Corporate Statistical Database. 2012. Available online: http://faostat.fao.org/site/567/DesktopDefault.aspx?PageID=567#ancor (accessed Oct. 12, 2013).

(2) Aurore, G.; Parfait, B.; Fahrasmane, L. Bananas, raw materials for making processed food products. *Trends Food Sci. Technol.* **2009**, *20*, 78−91.

(3) Someya, S.; Yoshiki, Y.; Okubo, K. Antioxidant compounds from bananas (Musa Cavendish). *Food Chem.* **2002**, *79*, 351−354.

(4) Guha, M.; Basuray, S.; Kumar Sinha, A. Preventive effect of ripe banana in the diet on Ehrlich's ascitic carcinoma cell induced malignant ascites in mice. *Nutr. Res. (N.Y.)* **2003**, *23*, 1081−1088.

(5) Tsamo, C. V. P.; Herent, M.-F.; Tomekpe, K.; Emaga, T. H.; Quetin-Leclercq, J.; Rogez, H.; Larondelle, Y.; Andre, C. Phenolic profiling in the pulp and peel of nine plantain cultivars (*Musa* sp.). *Food Chem.* **2015**, *167*, 197−204.

(6) Picq, C. *InfoMusa*; International Network for the Improvement of Banana and Plantain: Montpellier, France, 2005; Vol. *14*.

(7) Dufour, D.; Gibert, O.; Giraldo, A. s.; Sánchez, T.; Reynes, M.; Pain, J.-P.; González, A.; Fernández, A.; Díaz, A. Differentiation between Cooking Bananas and Dessert Bananas. 2. Thermal and Functional Characterization of Cultivated Colombian Musaceae (*Musa* sp.). *J. Agric. Food Chem.* **2009**, *57*, 7870−7876.

(8) de Jesus, O. N.; Silva, S. d. O. e.; Amorim, E. P.; Ferreira, C. F.; de Campos, J. M. S.; Silva, G. d. G.; Figueira, A. Genetic diversity and population structure of Musa accessions in ex situ conservation. *BMC Plant Biol.* **2013**, *13*, 41.

(9) Bakry, F.; Carreel, F.; Caruana, M.-L.; Côte, F. X. C.; Jenny, C.; Tézenas du Montcel, H. Les bananiers. *L'amélioration des Plantes Tropicales*; CIRAD: Montpellier, France, 1997.

(10) Venkatachalam, L.; Sreedhar, R. V.; Bhagyalakshmi, N. The use of genetic markers for detecting DNA polymorphism, genotype identification, and phylogenetic relationships among banana cultivars. *Mol. Phylogenet. Evol.* **2008**, *47*, 974−985.

(11) Crouch, H. K.; Crouch, J. H.; Madsen, S.; Vuylsteke, D. R.; Ortiz, R. Comparative analysis of phenotypic and genotypic diversity among plantain landraces (*Musa* spp., AAB group). *Theor. Appl. Genet.* **2000**, *101*, 1056−1065.

(12) Peraza-Echeverria, S.; Herrera-Valencia, V. A.; Kay, A.-J. Detection of DNA methylation changes in micropropagated banana plants using methylation-sensitive amplification polymorphism (MSAP). *Plant Science* **2001**, *161*, 359−367.

(13) Israeli, Y.; Ben-Bassat, D.; Reuveni, O. Selection of stable banana clones which do not produce dwarf somaclonal variants during in vitro culture. *Sci. Hortic.* **1996**, *67*, 197−205.

(14) Tomekpe, K.; Jenny, C.; Escalant, J.-V. A review of conventional improvement strategies for *Musa*. *InfoMusa* **2004**, *13*, 2−6.

(15) Gibert, O.; Dufour, D.; Giraldo, A. s.; Sánchez, T.; Reynes, M.; Pain, J.-P.; González, A.; Fernández, A.; Díaz, A. Differentiation between cooking bananas and dessert bananas. 1. Morphological and compositional characterization of cultivated colombian musaceae (*Musa* sp.) in relation to consumer preferences. *J. Agric. Food Chem.* **2009**, *57*, 7857−7869.

(16) Yomeni, M. O.; Njoukam, J.; Tchango Tchango, J. Influence of the stage of ripeness of plantains and some cooking bananas on the sensory and physicochemical characteristics of processed products. *J. Sci. Food Agric.* **2004**, *84*, 1069−1077.

(17) Alkarkhi, A. F. M.; Ramli, S. b.; Yong, Y. S.; Easa, A. M. Comparing physicochemical properties of banana pulp and peel flours prepared from green and ripe fruits. *Food Chem.* **2011**, *129*, 312−318.
(18) Bezerra, C. V.; Amante, E. R.; de Oliveira, D. C.; Rodrigues, A. M. C.; da Silva, L. H. M. Green banana (*Musa cavendishii*) flour obtained in spouted bed: Effect of drying on physicochemical, functional, and morphological characteristics of the starch. *Ind. Crops Prod.* **2013**, *41*, 241−249.
(19) Dadzie, B. K.; Orchard, J. E. *Routine Post-harvest Screening of Banana/Plantain Hybrids: Criteria and Methods*; INIBAP Technical Guidelines: International Plant Genetic Resources Institute: Rome, Italy, 1997.
(20) Soltani, M.; Alimardani, R.; Omid, M. Evaluating banana ripening status from measuring dielectric properties. *J. Food Eng.* **2011**, *105*, 625−631.
(21) Ngoh Newilah, G.; Tomekpe, K.; Fokou, E.; Etoa, F.-X. Effect of ripening on physicochemical composition of plantain cultivars and Musa hybrids grown in Cameroon. *Fresh Produce* **2011**, *5*, 61−68.
(22) Pretty, J. N.; Williams, S.; Toulmin, C. *Sustainable Intensification: Increasing Productivity in African Food and Agricultural Systems*; Taylor & Francis: New York, 2012.
(23) Tchango, J. T.; Achard, R.; Ngalani, J. A. Étude des stades de récolte pour l'exportation par bateau, vers l'Europe, de trois cultivars de plantains produits au Cameroun. *Fruits* **1999**, *54*, 215−224.
(24) Almela, L.; Javaloy, S.; Fernández-López, J.; Lôpez-Roca, J. Comparison between the tristimulus measurements Yxy and L*a*b* to evaluate the colour of young red wines. *Food Chem.* **1995**, *53*, 321−327.
(25) *Recueil de Normes Françaises des Produits Dérivés des Fruits et Légumes, Jus de Fruits*; AFNOR (Association Française de Normalization): Paris, 1982.
(26) Singleton, V.; Rossi, J. A. Colorimetry of total phenolics with phosphomolybdic−phosphotungstic acid reagents. *Am. J. Enol. Vitic.* **1965**, *16*, 144−158.
(27) Andre, C. M.; Ghislain, M.; Bertin, P.; Oufir, M.; del Rosario Herrera, M.; Hoffmann, L.; Hausman, J.-F.; Larondelle, Y.; Evers, D. Andean potato cultivars (*Solanum tuberosum* L.) as a source of antioxidant and mineral micronutrients. *J. Agric. Food Chem.* **2007**, *55*, 366−378.
(28) Alvin, C. R. *Methods of Multivariate Analysis*; 2nd ed.; John Wiley and Sons: New York, 2002.
(29) Gillet, A.; Brosteaux, Y.; Palm, R. Principaux modèles utilisés en regression logistique. *Biotechnol. Agrp. Soc. Environ.* **2011**, *15*, 425−433.
(30) Yanagihara, H.; Kamo, K.-i.; Imori, S.; Satoh, K. Bias-corrected AIC for selecting variables in multinomial logistic regression models. *Linear Algebra and its Applications* **2012**, *436*, 4329−4341.
(31) Kheng, T. Y.; Ding, P.; Abdul Rahman, N. A. Determination of optimum harvest maturity and physicochemical quality of Rastali banana (Musa AAB Rastali) during fruit ripening. *J. Sci. Food Agric.* **2012**, *92*, 171−176.
(32) Kulkarni, S.; Kudachikar, V. B.; Keshava Prakash, M. N. Studies on physicochemical changes during artificial ripening of banana (*Musa* sp.) variety 'Robusta'. *J. Food Sci. Technol.* **2011**, *48*, 730−734.
(33) Sulaiman, S. F.; Yusoff, N. A. M.; Eldeen, I. M.; Seow, E. M.; Sajak, A. A. B.; Supriatno; Ooi, K. L. Correlation between total phenolic and mineral contents with antioxidant activity of eight Malaysian bananas (*Musa* sp.). *J. Food Compos. Anal.* **2011**, *24*, 1−10.
(34) Alothman, M.; Bhat, R.; Karim, A. A. Antioxidant capacity and phenolic content of selected tropical fruits from Malaysia, extracted with different solvents. *Food Chem.* **2009**, *115*, 785−788.
(35) González-Montelongo, R.; Gloria Lobo, M.; González, M. Antioxidant activity in banana peel extracts: Testing extraction conditions and related bioactive compounds. *Food Chem.* **2010**, *119*, 1030−1039.
(36) Ngoh Newilah, G.; Brat, P.; Tomekpe, K.; Alter, P.; Fokou, E.; Etoa, F. Effect of ripening on total polyphenol contents of musa hybrids and cultivars grown in Cameroon. In *Acta Horticulturae, International Conference on Banana and Plantain in Africa*; Dubois, T., Hauser, S., Staver, C., Coyne, D., Eds.; International Society for Horticultural Science: Belgium, 2010; Vol. *879*; pp 413−418.
(37) Nayak, B.; Berrios, J. D. J.; Powers, J. R.; Tang, J.; Ji, Y. Colored potatoes (*Solanum tuberosum* L.) dried for antioxidant-rich value-added foods. *J. Food Process. Preserv.* **2011**, *35*, 571−580.
(38) Lin, J.-Y.; Tang, C.-Y. Determination of total phenolic and flavonoid contents in selected fruits and vegetables, as well as their stimulatory effects on mouse splenocyte proliferation. *Food Chem.* **2007**, *101*, 140−147.
(39) Happi Emaga, T.; Wathelet, B.; Paquot, M. Changements texturaux et biochimiques des fruits du bananier au cours de la maturation. Leur influence sur la préservation de la qualité du fruit et la maîtrise de la maturation. *Biotechnol. Agron. Soc. Environ.* **2008**, *12*, 89−98.
(40) Nguyen, T. B. T.; Ketsa, S.; van Doorn, W. G. Relationship between browning and the activities of polyphenoloxidase and phenylalanine ammonia lyase in banana peel during low temperature storage. *Postharvest Biol. Technol.* **2003**, *30*, 187−193.
(41) Charles, R. J.; Tung, M. A. Physical, rheological, and chemical properties of bananas during ripening. *J. Food Sci.* **1973**, *38*, 456−459.
(42) John, P.; Marchal, J. Ripening and biochemistry of the fruit. In *Bananas and Plantains*; Gowen, S., Ed.; Springer: Netherlands, 1995; pp 434−467.
(43) Ngoh Newilah, G.; Tomekpe, K.; Fokou, E.; Etoa, F.-X. Physicochemical changes during ripening of bananas grown in Cameroon. *Fresh Produce* **2009**, *3*, 64−70.
(44) Bruno Bonnet, C.; Hubert, O.; Mbeguie-A-Mbeguie, D.; Pallet, D.; Hiol, A.; Reynes, M.; Poucheret, P. Effect of physiological harvest stages on the composition of bioactive compounds in Cavendish bananas. *J. Zhejiang Univ., Sci., B* **2013**, *14*, 270−278.
(45) Inaba, A.; Liu, X.; Yokotani, N.; Yamane, M.; Lu, W.-J.; Nakano, R.; Kubo, Y. Differential feedback regulation of ethylene biosynthesis in pulp and peel tissues of banana fruit. *J. Exp. Bot.* **2007**, *58*, 1047−1057.
(46) Rogez, H.; Pompeu, D. R.; Akwie, S. N. T.; Larondelle, Y. Sigmoidal kinetics of anthocyanin accumulation during fruit ripening: A comparison between açai fruits (*Euterpe oleracea*) and other anthocyanin-rich fruits. *J. Food Compos. Anal.* **2011**, *24*, 796−800.

JOURNAL OF AGRICULTURAL AND FOOD CHEMISTRY

Article

pubs.acs.org/JAFC

# Influence of California-Style Black Ripe Olive Processing on the Formation of Acrylamide

Suthawan Charoenprasert and Alyson Mitchell*

Department of Food Science and Technology, University of California, Davis, California 95616, United States

**ABSTRACT:** Methods used in processing California-style black ripe olives generate acrylamide. California-style black ripe olives contain higher levels of acrylamide (409.67 ± 42.60−511.91 ± 34.08 $\mu$g kg$^{-1}$) as compared to California-style green ripe olives (44.02 ± 3.55−105.79 ± 22.01 $\mu$g kg$^{-1}$), Greek olives (<1.42 $\mu$g kg$^{-1}$), and Spanish olives (not detected), indicating that the higher temperatures used to sterilize the California-style green ripe and black ripe olives are required for acrylamide formation. Preprocessing brine storage influenced the formation of acrylamide in a time-dependent manner. Acrylamide increased during the first 30 days of storage. Longer brine storage times (>30 days) result in lower acrylamide levels in the finished product. The presence of calcium ions in the preprocessing brining solution results in higher levels of acrylamide in finished products. Air oxidation during lye processing and the neutralization of olives prior to sterilization significantly increase the formation of acrylamide in the finished products. Conversely, lye-processing decreases the levels of acrylamide in the final product. These results indicate that specific steps in the California-style black ripe olive processing may be manipulated to mitigate the formation of acrylamide in finished products.

**KEYWORDS:** *olive, Olea europaea, acrylamide, California-style black ripe olives*

## INTRODUCTION

Olive fruit is derived from a small evergreen tree in the family Oleaceae, genus *Olea*. California is the only U.S. state to commercially produce olives. About 50% of the production is destined for canning as in California-style black olives; another 46% is pressed into olive oil.[1] Raw olive fruit is very bitter due to the presence of high concentrations of phenolic compounds and in particular the *o*-diphenol oleuropein. Before olives can be consumed, they must be cured (processed) to remove the bitter components. There are numerous methods used worldwide to cure olives. One of the most popular is the California-style processing method created by Freda Ehmann in the 1890s.[2] To make California-style black ripe olives, the olives are picked green (unripe) and are cured by exposing them to a series of lye and oxygenated water baths over multiple days.[3] The main olive variety grown in California and used in the production of California-style black ripe olives is Manzanilla.[4−6] In 2012, canning olive production was 78,500 tons, of which 86% was Manzanilla olives.[6] Olives are harvested in California between September and November. Olives that cannot be processed directly after harvesting are stored in acidic brine solution (0.2−0.4% calcium chloride) to prevent the growth of spoilage organisms until they can be processed. During processing, the fresh or brine-stored olives are immersed in a 1−2% sodium hydroxide solution (lye) for 2−24 h over 3−7 consecutive days. During the intervals between lye treatments, the olives are suspended in water and air is bubbled through the tank to oxidize the olives and form the black color (air oxidation). These pigments, formed through oxidation and polymerization of *o*-diphenols (primarily hydroxytyrosol and caffeic acid), are not stable.[3] To prevent color deterioration, iron salts such as ferrous gluconate, ferrous sulfate, or ferrous lactate are added to fix the color. Olives are then neutralized with lactic acid or carbon dioxide, packed into cans in a sodium chloride solution, and sterilized. In the United States, olives are sterilized at 115.6 °C for 60 min or at 121.1 °C for 50 min.[2,3] A diagram of the steps involved in California-style black ripe olive processing is shown in Figure 1.

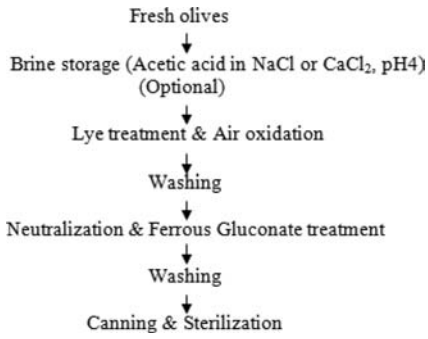


**Figure 1.** Processing diagram for the production of California-style black ripe olives.

Recently, the carcinogen acrylamide was found in California-style black ripe olives at relatively high concentrations (226−1925 $\mu$g kg$^{-1}$) as compared to other foods such as French fries (20−1325 $\mu$g kg$^{-1}$), baked goods (<364 $\mu$g kg$^{-1}$), and nut products (<457 $\mu$g kg$^{-1}$).[7] Acrylamide is classified as a probable human carcinogen (group 2A) by the International Agency for Research on Cancer on the basis of studies in laboratory animals.[8] In 2002, the Swedish National Food Administration and the University of Stockholm announced the finding of high

Received: May 13, 2014
Revised: August 6, 2014
Accepted: August 11, 2014
Published: August 11, 2014

ACS Publications © 2014 American Chemical Society



dx.doi.org/10.1021/jf5022829 | J. Agric. Food Chem. 2014, 62, 8716−8721

levels ($\mu$g kg$^{-1}$ to mg kg$^{-1}$) of acrylamide in foods cooked at elevated temperatures.[9] This finding led to worldwide concern and increased research activities investigating the formation and mitigation of acrylamide in foods.[9−14] Although the relevance to human health of dietary exposure to acrylamide is unclear, regulatory agencies such as the World Health Organization (WHO) continue to encourage food manufacturers to take measures to reduce acrylamide levels in processed foods.[15]

In general, acrylamide is formed through reactions between free amino acids and carbonyl compounds (e.g., reducing sugars) via the Maillard reaction at temperatures above 120 °C.[9−14] Stable isotope-labeling studies in potato-based foods and model systems indicate that the backbone of acrylamide arises from asparagine.[14] Alternative formation mechanisms have also been suggested to occur in lipid-rich foods.[16,17] For example, studies of model systems containing asparagine and unsaturated lipids demonstrate that the aldehydes and ketones, produced through the thermal degradation of lipids, can react with asparagine and lead to acrylamide formation.[16] Additionally, acrylamide was found to form through the reaction of acrolein and/or acrylic acid with ammonia.[16] Acrylic acid is generated from the oxidation of acrolein, a product of thermal degradation and/or oxidation of free fatty acids or glycerol.[18] In these cases, the backbone of acrylamide would arise from either acrylic acid or acrolein, and the amine group derived from the ammonia evolved from the thermal degradation of amino acids.[16]

The formation of acrylamide during California-style black ripe olive processing was studied by Casado and Montaño in 2008.[19] These studies demonstrated that there were undetectable amounts of acrylamide in the olives before sterilization, whereas the sterilized olives contained acrylamide ranging from 243.30 to 1349.00 $\mu$g kg$^{-1}$. This information suggests that acrylamide in California-style black ripe olives forms during sterilization. These studies also show very low concentrations (52.80−198.00 $\mu$g kg$^{-1}$) of asparagine in the nonsterilized olives and no correlation between the concentration of glucose and amino acids (both total and individual amino acids) and acrylamide formation.[19] More recently, using olive juice in a model system, Casado et al. proposed that peptides and proteins were responsible for acrylamide formation in sterilized olives and that the California-style black ripe olive processing method had no effect on acrylamide levels in the final products.[20]

To date, information on the mechanism of acrylamide formation in California-style black ripe olives is limited, and it remains unclear if acrylamide is formed through the California-style black ripe processing method or if it is an artifact of the sterilization process. Herein, we evaluate the effect of individual processing steps employed in the California-style black ripe olive processing method (i.e., brine storage, lye treatment, air oxidation, neutralization, and sterilization) on the formation of acrylamide to better understand the formation mechanism of acrylamide during processing and to provide information for mitigating acrylamide formation through processing.

## MATERIALS AND METHODS

**Reagents.** All reagents were of analytical grade unless otherwise stated. Acrylamide (99+%), $D_3$-Labeled acrylamide (2,3,3-$D_3$, 98.0%), and formic acid (∼98%) were purchased from Sigma-Aldrich (St. Louis, MO, USA). HPLC grade methanol and hexane were obtained from Fisher Scientific (Fair Lawn, NJ, USA).

**Olives.** To estimate acrylamide levels in various table olives, olives including Greek-style, Spanish-style, California-style black ripe, and California-style green ripe olives were studied. Three different commercial brands of each table olive style were purchased from local markets in at least triplicate over two years (2010 and 2014). A 15 kg sample of fresh and a 70 kg sample of brine-stored olives were kindly supplied by two independent commercial olive processors located in central California (processor A and processor B). These olives were graded as medium-sized Manzanilla harvested in 2009 and 2012. Olives represent pooled samples from numerous orchards. Directly after receipt of fresh olives, the processors prepared brine-stored olives and delivered both fresh and brine-stored olives to the University of California, Davis. Brine-stored olives were stored on site in brine for 6 months at room temperature before they were analyzed for acrylamide.

Graded medium-sized Manzanilla olives harvested in 2010 and 2011 were used to study the influence of the individual processing steps on acrylamide formation. A 30 kg sample of fresh and a 70 kg sample of brine-stored olives were also supplied by processors A and B and represent pooled samples from numerous orchards.

**Laboratory-Scale Models Mimicking California-Style Black Ripe Olive Processing.** A laboratory-scale model of the California-style black ripe olive processing method was developed for these studies. This model system enabled duplicate processing of small-scale samples (∼30 olives per sample). Briefly, olives were hand selected for no defect and placed into one of two sample chambers. The olives were exposed to a 1% sodium hydroxide solution for 5 h for lye processing. Next, the olives were rinsed and placed in fresh water for 19 h to remove residual sodium hydroxide. During this washing step, air was bubbled into the surrounding medium to oxidize olives. This lye−wash cycle was repeated for 4 days to allow sodium hydroxide to penetrate to the pit of the olive. A solution of 1% phenolphthalein in isopropanol was used to verify the penetration depth of the sodium hydroxide. After the final lye−wash, olives were treated with 0.15% ferrous gluconate solution for 4 h to fix the color. During the ferrous gluconate treatment, carbon dioxide gas was bubbled into the solution to neutralize olives and phenolphthalein solution was used to verify the pH of olives. When the pH was <8, the olives were rinsed and put into fresh water for 30 min to remove residual ferrous gluconate. Olives were then packed in a glass flask, which was filled with 2% sodium chloride. Finally, the olives were sterilized in an autoclave at a temperature of 127 °C for 30 min.

**Brine Storage.** To evaluate the influence of brining on acrylamide levels in the finished olive product, olives (harvested in 2010 and 2011) were stored in a standardized brine solution for 0−8 months at room temperature prior to processing as described above. Experiments were performed in duplicate. Preprocessing brine solutions reflected typical commercial brine solutions and were composed of calcium chloride (0.2−0.4%) and sodium benzoate (0.2−0.3%). The pH of the brine solutions was maintained at 3.7−4.0 with acetic acid. The influence of calcium chloride, sodium benzoate, or acetic acid was evaluated in olives harvested in 2011 from the two olive processors. This was achieved by omitting one of these individual components in three independent brine solutions and storing the olives in these solutions at room temperature for 3 months prior to processing as described above. The study was performed in duplicate.

**Effect of Lye, Air Oxidation, Ferrous Gluconate, Neutralization, and Sterilization.** Olives (harvested in 2010 from the two olive processors) were processed as described above. Individual processing parameters (i.e., air oxidation step, ferrous gluconate treatment, neutralization, and sterilization) were systematically omitted, and the levels of acrylamide were evaluated in the resulting products. The olives were stored in brine for 6 months prior to these studies. The studies were performed in duplicate.

**Analysis of Acrylamide.** *Preparation of Samples for Acrylamide Analysis.* Samples consisting of 30 g of olives were extracted with 60 mL of ultrapure water. A 1 mL aliquot of 4 ng mL$^{-1}$ of $D_3$-acrylamide was added to samples as an internal standard. The mixture was homogenized. Twenty-five grams of the mixture was collected, and 15 mL of hexane was added to remove oil and other nonpolar

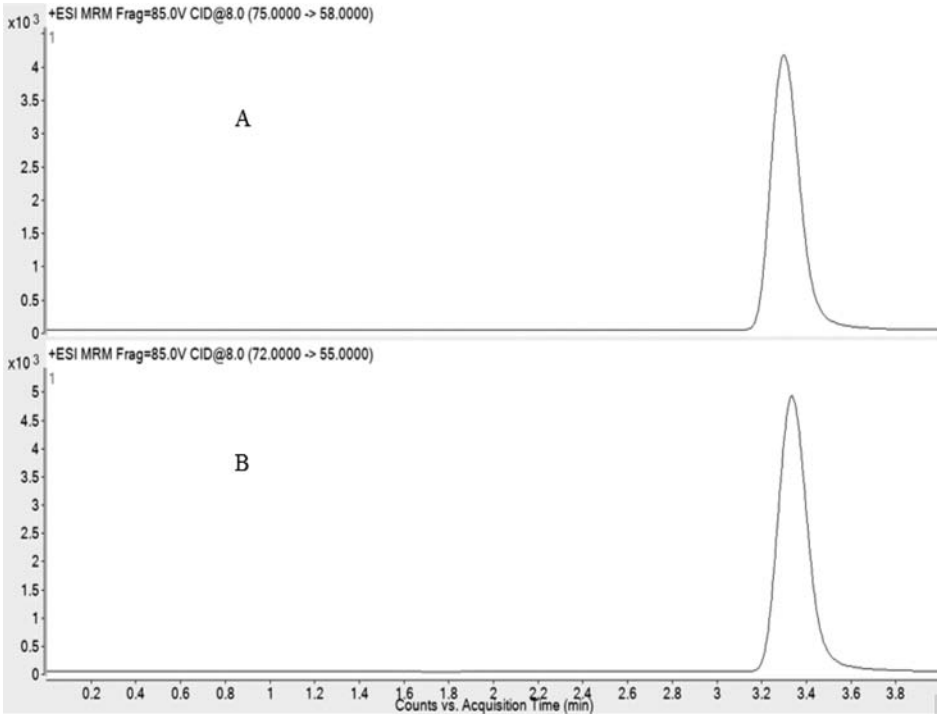


**Figure 2.** UHPLC-(ESI) MS/MS ion select chromatogram of $D_3$-labeled acrylamide (a) and acrylamide (b).

compounds. Then the mixture was centrifuged at 4000 rpm for 30 min. The aqueous layer was collected. Interfering compounds were removed, and sample was concentrated using solid phase extraction on a Strata-X-C cartridge (3 mL, 200 mg) preconditioned with two 1 mL aliquots of methanol, followed by two 1 mL aliquots of water at a flow rate of 2 mL $min^{-1}$. Acrylamide was eluted with 1 mL of 0.1% formic acid in water/methanol, 90:10, v/v. The eluted solution was collected and filtered through a 0.22 $\mu$m membrane prior to analysis by ultrahigh-pressure liquid chromatography electrospray ionization mass spectroscopy [UHPLC-(ESI)MS/MS].

*Acrylamide Analysis by UHPLC-(ESI)MS/MS.* Acrylamide was quantified in samples using a modified method of Zhang et al.[21] Samples were analyzed using an Agilent 1290 Infinity ultrahigh-pressure liquid chromatography (UHPLC) system coupled to an Agilent 6460 triple-quadrupole mass spectrometer interfaced with electrospray ionization (ESI) via jet stream technology (Agilent Technologies, Santa Clara, CA, USA). The UHPLC was equipped with a binary pump with integrated vacuum degasser (G4220A), an autosampler (G4226A), and a thermostated column compartment (G1316C). The olive extracts were separated on a Polaris C18-A column (2.0 × 150 mm, 3 $\mu$m, Agilent Technologies), and the column temperature was controlled at 30 °C. The mobile phase consisted of 0.1% formic acid in water (A) and methanol (B) as follows: 0% B, 0−1 min; 0−20% B, 1−2 min; 20% B, 2−4 min, at a flow rate of 0.2 mL/min. The column was re-equilibrated between injections for 4.5 min with 0.1% formic acid in water. The injection volume was 5 $\mu$L. To quantify acrylamide levels in olives, transition ions of $m/z$ 72 → 55 for acrylamide and $m/z$ 75 → 58 for $D_3$-labeled acrylamide were monitored. The UHPLC-(ESI)MS/MS was optimized using a fragmentor voltage of 85 V, a collision energy of 8 V, and a cell accelerator of 7 V in positive mode ESI. The drying gas temperature and flow rate were 300 °C and 5 L/min, respectively. The sheath gas temperature and flow rate were 400 °C and 11 L/min, respectively. The nebulizer gas pressure, nozzle voltage, and capillary voltage were 45 psi, 500, and 3000 V, respectively. The limit of detection (LOD) and the limit of quantification (LOQ) of this method were 0.71 and 1.42 $\mu$g $kg^{-1}$, respectively.

**Measurement of pH of Olives.** To measure the pH of olives, five olive fruits were homogenized and the pulp was filtered through cheesecloth. The pH was measured in the resulting olive juice using a SevenMulti pH meter (Mettler Toledo, Columbus, OH, USA).

**Statistical Analysis.** Means (duplicates or triplicates) of acrylamide concentrations in olives were statistically analyzed using one-way ANOVA followed by multiple-comparison test using Tukey (HSD). The difference among samples was at the 95% confidence level. ANOVA was performed using XLSTAT version 2013.

## ■ RESULTS AND DISCUSSION

The acrylamide concentrations of fresh, brine-stored, Greek-style, Spanish-style, California-style black ripe, and California-style green ripe olives were measured using UHPLC-(ESI)MS/MS monitoring transition ions of $m/z$ 72 → 55 for acrylamide and $m/z$ 75 → 58 for $D_3$-labeled acrylamide (Figure 2). The results are presented in Table 1. Acrylamide was undetected in fresh and brine-stored olives. Acrylamide levels in processed olives, over two harvest years, were not significantly different. Significant amounts of acrylamide were present in the California-style black ripe (409.67 ± 42.60−511.91 ± 34.08 $\mu$g $kg^{-1}$) and California-style green ripe olives (44.02 ± 3.55−105.79 ± 22.01 $\mu$g $kg^{-1}$) but not in the Greek-style or Spanish style olives. California-style green ripe olives are processed fresh (not brine stored) and are not subject to air oxidation or ferrous gluconate treatment. California-style black ripe and green ripe processing methods required the olives to be sterilized at temperatures >110 °C.[2,3] In contrast, Spanish- and Greek-style table olive processing methods preserve olives using additives and/or pasteurization at temperatures <65 °C.[2] These results are in agreement with those obtained from Casado and Montaño and indicate that sterilization plays an important role in the formation of acrylamide.[19] The difference in the levels of acrylamide found in the California-style black ripe and green ripe olives indicates that other processing steps (i.e., brine storage, air oxidation, and ferrous gluconate treatment) also influence the levels of acrylamide in the final

**Table 1. Acrylamide Levels in Fresh, Brine-Stored, Spanish-Style, Greek-Style, California-Style Black Ripe and California-Style Green Ripe Olives[a]**

| olive sample | acrylamide in olive ($\mu$g kg$^{-1}$) year 1 | year 2 |
|---|---|---|
| fresh | <0.71 | <0.71 |
| brine-stored | <1.42 | <0.71 |
| Spanish-style, brand A | <0.71 | <0.71 |
| Spanish-style, brand B | <0.71 | <0.71 |
| Spanish-style, brand C | <0.71 | <0.71 |
| Greek-style, brand D | <0.71 | <0.71 |
| Greek-style, brand E | <1.42 | <0.71 |
| Greek-style, brand F | <0.71 | <0.71 |
| California-style black ripe, brand G | 493.45ab ± 48.99 | 511.91a ± 34.08 |
| California-style black ripe, brand H | 419.61c ± 48.28 | 409.67c ± 42.60 |
| California-style black ripe, brand I | 499.84ab ± 12.07 | 458.66bc ± 29.82 |
| California-style green ripe, brand G | 44.02e ± 3.55 | 46.15 e ± 7.81 |
| California-style green ripe, brand H | 84.49de ±10.65 | 105.79d ± 22.01 |
| California-style green ripe, brand J | 50.41e ± 6.39 | 54.67e ± 7.81 |

[a]Results are mean values of three measurements. Means with different letters are significantly different at the 95% confidence level. There were 10 different commercial brands (A–J) used in the survey of acrylamide levels in olives. Fresh and brine-stored olives were received in 2009 and 2012. Commercial table olives (Greek-style, Spanish-style, California-style green, and California-style black ripe olives were purchased in 2010 and 2014.

product. Therefore, each of these parameters was evaluated independently as discussed below.

The influence of brining olives was evaluated by monitoring acrylamide in olives stored in brine over 8 months and processed into California-style black ripe olives. Acrylamide levels were lowest in processed fresh olives (95.85 ± 8.52–402.57 ± 12.07 $\mu$g kg$^{-1}$) as compared to processed brine-stored olives (408.96 ± 2.84–1135.29 ± 48.99 $\mu$g kg$^{-1}$). During storage, the acrylamide levels increased during the first month and then declined with increasing storage time (Figure 3). Acrylamide levels were highest in olives stored in brine for 1 month (590.01 ± 23.43–1135.29 ± 48.99 $\mu$g kg$^{-1}$). These data indicate that precursors of acrylamide formation either degrade

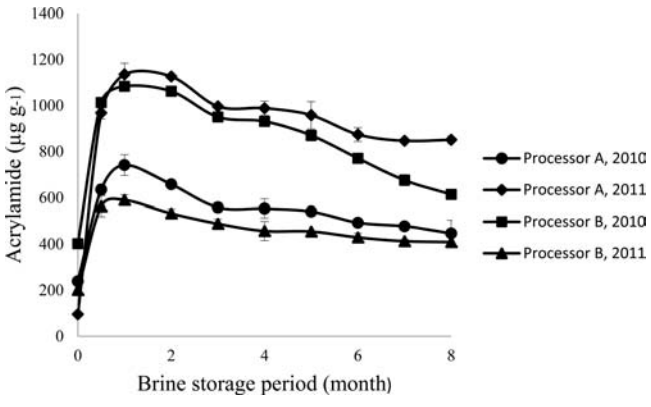


**Figure 3.** Effect of brine storage time (0–8 months) on acrylamide formation.

or diffuse into the surrounding medium during prolonged brine storage. This trend was observed in olives received from both olive processors and over the two harvest years (2010 and 2011). This result suggests that holding olives in brine may facilitate the reduction of acrylamide in final products.

The influence of the composition of preprocessing brine solutions was evaluated to identify relationships between individual brining components (i.e., calcium chloride, sodium benzoate, or acetic acid) and the formation of acrylamide (Table 2). The complete brine solution was composed of

**Table 2. Effect of Brine Composition on Acrylamide Formation in California-Style Black Ripe Olives[a]**

| brine composition | acrylamide ($\mu$g kg$^{-1}$) |
|---|---|
| sample a (complete brine) | 685.86 ± 26.98a |
| sample b (brine without sodium benzoate) | 642.55 ± 44.02a |
| sample c (brine without acetic acid) | 563.74 ± 36.21a |
| sample d (brine without calcium chloride) | 303.17 ± 43.31b |

[a]Means with different letters are significantly different at the 95% confidence level.

calcium chloride (0.2–0.4%) and sodium benzoate (0.2–0.3%) and acidified to a pH of 3.7–4.0 with acetic acid (sample a). The olives stored in brine solutions without added acidic acid (sample b) or sodium benzoate (sample c) did not differ significantly from the brine solution containing these compounds (sample a). However, the olives stored in the brine solution without added calcium chloride (sample d) had significantly lower levels of acrylamide in the finished products (303.17 ± 43.31 $\mu$g kg$^{-1}$). In general, calcium ions helps maintain structural firmness, stability of cell wall, and cell turgor of fruits by forming cross-linkages between pectin molecules, thereby strengthening and preventing the collapse of plant cells.[22,23] Our data suggest that calcium in the brine solutions helps retain precursors to acrylamide formation by improving cell wall integrity and that acrylamide levels in finished products may be reduced through the omission of calcium in brining solutions. The olives stored in the brine solution with no calcium chloride addition appeared to shrink to a greater degree than olives stored with calcium chloride during sterilization. Although it appears that acrylamide could be reduced through lowering the calcium content of the storage brine, consumer acceptance may be affected.

The influence of the individual processing steps involved in the production of California-style black ripe olives on acrylamide formation was evaluated and is given in Table 3. The levels of acrylamide in fully processed California-style black

**Table 3. Effect of Air Oxidation, Ferrous Gluconate Treatment, and Sterilization on Acrylamide Levels in Olives[a]**

| processing method | acrylamide ($\mu$g kg$^{-1}$) |
|---|---|
| complete (lye, air oxidation, ferrous gluconate, sterilization) | 569.42a ± 38.34 |
| no air oxidation (lye, ferrous gluconate, sterilization) | 310.27b ± 0.71 |
| no ferrous gluconate (lye, air oxidation, sterilization) | 545.99a ± 28.40 |
| no air oxidation or ferrous treatment (lye, sterilization) | 344.35b ± 14.91 |
| no sterilization (lye, air oxidation, ferrous gluconate) | 51.83c ± 12.78 |

[a]Means with different letters are significantly different at the 95% confidence level.


dx.doi.org/10.1021/jf5022829 | J. Agric. Food Chem. 2014, 62, 8716–8721

ripe olives (i.e., the olives that were subjected to lye hydrolysis, air oxidation, ferrous gluconate treatment, and sterilization) were the highest (569.42 ± 38.34 $\mu$g kg$^{-1}$). In comparison, olives processed without the air oxidation step had significantly lower levels of acrylamide (310.27 ± 0.71 $\mu$g kg$^{-1}$). Ferrous gluconate had no effect on acrylamide levels. Olives processed with no air oxidation or ferrous gluconate treatment (344.35 ± 14.91 $\mu$g kg$^{-1}$) were not significantly different from olives processed with no air oxidation (Table 3). Air oxidation significantly increases the formation of acrylamide during processing. Comparisons of the sterilized olives with non-sterilized olives demonstrate low levels of acrylamide (51.83 ± 12.781 $\mu$g kg$^{-1}$) in nonsterilized olives as compared with sterilized olives and confirmed that acrylamide forms during sterilization.

Lye processing was found to significantly decrease the levels of acrylamide (and/or its precursors) in finished California-style black ripe olives. The levels of acrylamide in fresh (11288.29 ± 5.68 $\mu$g kg$^{-1}$) or brine-stored olives (7694.27 ± 37.63 $\mu$g kg$^{-1}$) that were directly sterilized were 10 times greater than levels found in olives that underwent lye processing for 4 days (569.42 ± 38.34 $\mu$g kg$^{-1}$) prior to sterilization. This finding is in contrast to the results reported by Casado et al.,[20] who suggested that lye treatment did not affect acrylamide formation in olives. However, this difference may be explained by the use of olive juice in the Casado et al. study and the use of olive fruit in the current study.

Neutralization with carbon dioxide after lye treatment had a significant influence on the formation of acrylamide in olives (Table 4). The initial pH of the lye-treated olives was 9.76; after neutralization with carbon dioxide, the pH was reduced to 7.11. The lowest level of acrylamide (338.67 ± 9.23 $\mu$g kg$^{-1}$) was found in sterilized olives that were not previously neutralized with carbon dioxide, whereas the highest level of acrylamide (681.60 ± 11.36 $\mu$g kg$^{-1}$) was found in sterilized olives that had been neutralized. These results indicated that the formation of acrylamide in olives is pH dependent. This is in agreement with the results reported by Casado et al.[24]

**Table 4. Effect of Neutralization with Carbon Dioxide (pH) on Acrylamide Formation in California-Style Black Ripe Olives**[a]

| neutralization time (h) | measured pH | acrylamide ($\mu$g kg$^{-1}$) |
|---|---|---|
| 0 | 9.76 | 338.67d ± 9.23 |
| 1 | 8.61 | 437.36c ± 4.97 |
| 2 | 8.29 | 585.04b ± 0.71 |
| 3 | 7.65 | 591.43b ± 19.88 |
| 4 | 7.11 | 681.60a ± 11.36 |

[a]Means with different letters are significantly different at the 95% confidence level.

The studies described herein demonstrate that the formation of acrylamide is dependent upon the processing methods used in the production of table olives and that sterilization temperatures are required for the formation of acrylamide. Additionally, our results indicate that fresh olives contain precursors of acrylamide which either degrade and/or diffuse into surrounding medium during brine storage. Calcium ions in brine storage solutions appear to prevent the short-term diffusion of acrylamide and/or its precursor from olives into brine storage solutions. Longer term (>1 month) brine storage results in lower acrylamide levels in finished products. The observation that the air oxidation step results in increased levels of acrylamide in olives suggests that acrylamide precursors form via oxidation reactions during lye treatment and that these are converted into acrylamide during sterilization. Neutralization prior to sterilization increases acrylamide formation during sterilization, indicating that this is a pH-dependent process. These results suggest that employing small modifications during traditional processing methods (e.g., holding olives for longer periods in brining solutions, decreasing oxygen exposure time, reducing sterilization temperatures, etc.) may be useful in lowering acrylamide levels in finished table olive products.

Ongoing studies in our laboratory are focused on identifying the precursors of acrylamide in olives and determining the mechanism by which they form in olives.

## AUTHOR INFORMATION

### Corresponding Author

*(A.M.) Phone: (530) 752-7926. Fax: (530) 752-4759. E-mail: aemitchell@ucdavis.edu.

### Funding

We thank the California Olive Commission for kind financial support of this research.

### Notes

The authors declare no competing financial interest.

## ACKNOWLEDGMENTS

We thank Drs. Tomas Collins and Susan Ebeler of the University of California—Davis Food Safety and Measurement Facility for analytical and technical advice.

## REFERENCES

(1) Boriss, H. *Olive Profile*; Agricultural Issues Center, University of California, 2013; http://www.agmrc.org/commodities__products/fruits/olive-profile.

(2) Garrido Fernández, A.; Fernández Díez, M. J.; Adams, M. R. In *Table Olives, Production and Processing*; Chapman and Hall: London, UK, 1997; pp 10−367.

(3) Charoenprasert, S.; Mitchell, A. Factors influencing phenolic compounds in table olives (*Olea europaea*). *J. Agric. Food Chem.* **2012**, *60*, 7081−7095.

(4) California Department of Food and Agriculture. *California Olive Probability Survey Report*, 2011; California Agricultural Statistic Service, http://www.nass.usda.gov/Statistics_by_State/California/Publications/Fruits_and_Nuts/201108olvpb.pdf.

(5) California Department of Food and Agriculture. *California Olive Probability Survey Report*, 2012; California Agricultural Statistic Service, http://www.nass.usda.gov/Statistics_by_State/California/Publications/Fruits_and_Nuts/201208olvpb.pdf.

(6) California Department of Food and Agriculture. *California Table Olive Probability Survey Report*, 2013; California Agricultural Statistic Service, http://www.nass.usda.gov/Statistics_by_State/California/Publications/Fruits_and_Nuts/201308olvpb.pdf.

(7) U.S. Food and Drug Administration. *Survey Data on Acrylamide in Food: Individual Food Products*; U.S. Department of Health and Human Services, Center for Food Safety and Nutrition, 2006; http://www.fda.gov/food/foodborneillnesscontaminants/chemicalcontaminants/ucm053549.htm.

(8) IARC. *IARC Monographs on the Evolution of Carcinogenic Risks to Humans. Some Industrial Chemicals*; IARC: Lyon, France, 1994; Vol. 60, pp 389−434.

(9) Tareke, E.; Rydberg, P.; Karlsson, P.; Eriksson, S.; Tornqvist, M. Analysis of acrylamide, a carcinogen formed in heated foodstuffs. *J. Agric. Food Chem.* **2002**, *50*, 4998−5006.

(10) Schieberle, P.; Kohler, P.; Granvogl, M. New aspects on the formation and analysis of acrylamide. In *Chemistry and Safety of*

*Acrylamide in Food*; Friedman, M., Mottram, D., Eds.; Springer: New York, 2005; pp 223−233.
(11) Mottram, D. S.; Wedzicha, B. L.; Dodson, A. T. Acrylamide is formed in the Maillard reaction. *Nature* **2002**, *419*, 448−449.
(12) Stadler, R. H.; Robert, F.; Riediker, S.; Varga, N.; Davidek, T.; Devaud, S.; Goldmann, T.; Hau, J.; Blank, I. In-depth mechanistic study on the formation of acrylamide and other vinylogous compounds by the Maillard reaction. *J. Agric. Food Chem.* **2004**, *52*, 5550−5558.
(13) Yaylayan, V. A.; Wnorowski, A.; Perez Locas, C. Why asparagine needs carbohydrates to generate acrylamide. *J. Agric. Food Chem.* **2003**, *51*, 1753−1757.
(14) Zyzak, D. V.; Sanders, R. A.; Stojanovic, M.; Tallmadge, D. H.; Eberhart, B. L.; Ewald, D. K.; Gruber, D. C.; Morsch, T. R.; Strothers, M. A.; Rizzi, G. P.; Villagran, M. D. Acrylamide formation mechanism in heated foods. *J. Agric. Food Chem.* **2003**, *51*, 4782−4787.
(15) JECFA. *Joint FAO/WHO Expert Committee on Food Additives. Summary Report of 64th Meeting*; Rome, Italy, Feb 8−17, 2005.
(16) Ehling, S.; Hengel, M.; Shibamoto, T. Formation of acrylamide from lipids. In *Chemistry and Safety of Acrylamide in Food*; Friedman, M., Mottram, D., Eds.; Springer: New York, 2005; pp 223−233.
(17) Yasuhara, A.; Tanaka, Y.; Hengel, M.; Shibamoto, T. Gas chromatographic investigation of acrylamide formation in browning model systems. *J. Agric. Food Chem.* **2003**, *51*, 3999−4003.
(18) Skog, K., Alexander, J., Eds. *Acrylamide and Other Hazardous Compounds in Heat-Treated Foods*; CRC Press: Boca Raton, FL, USA, 2006; pp 1−14.
(19) Casado, F. J.; Montaño, A. Influence of processing conditions on acrylamide content in black ripe olive. *J. Agric. Food Chem.* **2008**, *56*, 2021−2027.
(20) Casado, F. J.; Montano, A.; Spitzner, D.; Carle, R. Investigations into acrylamide precursors in sterilized table olives: evidence of a peptic fraction being responsible for acrylamide formation. *Food Chem.* **2013**, *141*, 1158−1165.
(21) Zhang, G.; Huang, G.; Xiao, L.; Seiber, J.; Mitchell, A. E. Acrylamide formation in almonds (*Prunus dulcis*): influences of roasting time and temperature, precursors, varietal selection, and storage. *J. Agric. Food Chem.* **2011**, *59*, 8225−8232.
(22) Lamikanra, O. Enzymatic effects on flavor and texture of fresh-cut fruits and vegetables. In *Fresh-Cut Fruits and Vegetables Science, Technology and Market*; Lamikanra, O., Ed.; CRC Press: Boca Raton, FL, USA, 2002; pp 151−152.
(23) Monsalve-González, A.; Barbosa-Cánovas, G. V.; Swanson, B. G.; Cavalieri, R. P. Texture and structural changes in apples processed by combined methods. In *Innovations in Food Processing*; Gould, G. W., Ed.; CRC Press: Boca Raton, FL, USA, 2000; pp 193−204.
(24) Casado, F. J.; Sánchez, A. H.; Montaño, A. Reduction of acrylamide content of ripe olives by selected additives. *Food Chem.* **2010**, *119*, 161−166.

JOURNAL OF AGRICULTURAL AND FOOD CHEMISTRY

Article

pubs.acs.org/JAFC

# Characterization of Cuticle Composition after Cold Storage of "Celeste" and "Somerset" Sweet Cherry Fruit

Burcu Belge,[†,‡] Montserrat Llovera,[§] Eva Comabella,[†,‡] Ferran Gatius,[†] Pere Guillén,[†] Jordi Graell,[‡,∥] and Isabel Lara*[,†,‡]

[†]Departament de Química, [‡]Unitat de Postcollita-XaRTA, [§]Serveis Científico-Tècnics, [∥]Departament de Tecnologia d'Aliments, Universitat de Lleida, Alcalde Rovira Roure 191, 25198 Lleida, Spain

**ABSTRACT:** Cuticle composition and structure may be relevant factors affecting the storage potential of fruits, but very few studies have analyzed fruit cuticle composition from a postharvest perspective. In this work, the chemical composition of waxes and cutin (major cuticular components) was analyzed in cuticle samples isolated from "Celeste" and "Somerset" cherries (*Prunus avium* L.) after cold storage at 0 °C. Total cuticle amounts per surface unit ($\mu$g cm$^{-2}$) increased along with cold storage. The triterpene ursolic acid, the alkane nonacosane, linoleic acid, and $\beta$-sitosterol were the most abundant components of cuticular waxes, whereas cutin composition was dominated by $C_{18}$-type monomers. In spite of being comprised of similar chemical families, cultivar-related differences were found regarding the abundance and the evolution of some compound families during cold storage. To the best of our knowledge, this is the first report on changes in cuticle composition of sweet cherry during postharvest storage.

**KEYWORDS:** *cold storage, cuticle, cutin, Prunus avium L., postharvest, waxes*

## INTRODUCTION

The plant cuticle is a lipidic layer synthesized by the epidermis, which surrounds aerial, nonlignified organs, including fruits. Cuticles are composed mainly by cutin, a polyester polymer matrix rich in hydroxylated and epoxy-hydroxylated $C_{16}$ and $C_{18}$ fatty acids, embedded with amorphous waxes and a minor fraction of phenolics. The outer side of the cuticle is covered by epicuticular waxes, while in its inner side the cutin matrix mixes with polysaccharides from the epidermal cell walls.[1] Because the cuticle covers the epidermis of the fruit, it represents the first barrier against the abiotic and biotic conditions in which it develops. The composition and structure of this surface layer have a noticeable influence on the postharvest storage potential of fruits, inasmuch as it protects against transpirational water loss, mechanical injuries and microbial infections, and provides mechanical support.[2]

In spite of this relevance, there are few reports on cuticle modifications taking place along the life span of a fruit, which have often focused on physiological or morphological rather than on biochemical aspects. Some studies, though, have reported the evolution of the chemical composition of the cuticle during on-tree development of fruit,[3−9] and some genes putatively involved in the biosynthesis of cuticular wax and cutin components during fruit development have been identified.[10,11] Even more limited research attention has been apparently paid to the changes in fruit cuticle composition along its postharvest life. For apple, there seems to exist considerable cultivar-associated variability as to the progress of total wax amounts, properties, or chemical components during long-term cold storage[8,12] or in response to controlled atmosphere storage and subsequent shelf life.[13] The observations that 1-methylcyclopropene attenuated composition changes in cuticular waxes during storage of "Autumn Gold" and "Royal Gala" apples[14] and that exogenous ethylene induced structural and compositional changes in surface waxes of "Navelate" oranges[15] suggest that the biosynthesis of cuticular waxes in these fruit species might be under ethylene control.

Sweet cherry (*Prunus avium* L.) fruit is very perishable, owing to high respiration and water loss rates which favor rapid postharvest deterioration due to weight loss, detrimental effects on appearance, and increased susceptibility to infections and mechanical injuries, which notably restrict storage and shelf life potential. Postharvest quality of fruit produce is greatly impacted by cuticle composition, structure, and properties (reviewed in ref 2). Cuticles of sweet cherry fruit have been studied at commercial maturity[16] and during on-tree development regarding their chemical composition,[6] mechanical properties,[17] and frequency and distribution of microcracks.[18] However, no study has addressed the compositional changes in sweet cherry cuticles after harvest or during the refrigerated storage commonly used for its preservation. Therefore, the purpose of this work was to assess the evolution of the chemical constituents of the cuticle of two important cherry cultivars during cold storage.

## MATERIALS AND METHODS

**Plant Material, Assessment of Standard Quality, and Postharvest Handling.** Cherries (*Prunus avium* L. cv. "Celeste" and "Somerset") were hand-collected in 2011 (May 23rd and June 7th, respectively) from the same commercial orchard located in Corbins, in the area of Lleida (NE Spain), at marketable maturity according to the usual indices (size and color) in the producing area. Uniform, defect-free samples were selected and transported directly to the laboratory. Standard quality parameters were determined immediately thereafter in order to check adequate maturity of samples. Firmness was measured with a Durofel DFT 100 durometer (Agro-Technologie, Forges Les

Received: June 3, 2014
Revised: August 1, 2014
Accepted: August 4, 2014
Published: August 4, 2014

ACS Publications © 2014 American Chemical Society

Eaux, France) fitted with a 5.64 mm tip, on two opposite faces on the cheek region of 30 fruit, and results were expressed as Durofel units (1, no resistance, to 100, maximum resistance). For the assessment of juiciness, three replicate samples (10 fruit each) were stoned in each case and squeezed until no more juice was released. After filtration, the volume of juice recovered was measured and expressed as mL 100 $g^{-1}$ fresh weight. Soluble solids content (SSC) and titratable acidity (TA) were assessed in juice obtained as described above. SSC was determined with a hand-held refractometer (Atago, Tokyo, Japan), and results expressed as °Brix. For TA determination, 10 mL of juice were diluted in 10 mL of distilled water, and titrated with 0.1 M NaOH to pH 8.1; results were given as g malic acid $L^{-1}$. Skin color was determined at two opposite equatorial points of 30 fruit using a portable tristimulus colorimeter (Chroma Meter CR-200, Minolta Corp., Osaka, Japan), with CIE $D_{65}$ illuminant and 8 mm aperture diameter. Lightness ($L^*$) values were recorded, and hue angle was calculated from $a^*$ and $b^*$ parameters.

After quality assessments, fruits were stored at 0 °C and 92% relative humidity during 14 days followed by 3 days at 20 °C to simulate commercial shelf life. Skin samples were taken at harvest, upon removal from cold storage, and 3 days thereafter, and cuticles isolated and analyzed in triplicate as described below.

**Cuticle Isolation.** Exocarp segments were excised from the cheek region of 15 fruit using a cork borer (13 mm, i.d.). Four skin disks were so obtained from each individual fruit (5.31 $cm^2$ per fruit). Cuticular membranes (CM) were isolated enzymatically by incubation at 37 °C in 1.6 U $mL^{-1}$ cellulase and 100 U $mL^{-1}$ pectinase in 50 mM citrate buffer (pH 4.0) until no more material was released, in the presence of 1 mM $NaN_3$ to prevent microbial growth. After isolation, CM were washed in citrate buffer (50 mM, pH 4.0) at 37 °C until no material was left in suspension, thoroughly rinsed in distilled water in order to remove materials sorbed during isolation,[19] dried at 40 °C, and kept in hermetically capped vials until use. CM mass was determined gravimetrically and expressed per unit of fruit surface area ($\mu$g $cm^{-2}$) as well as on total fruit surface basis (mg $fruit^{-1}$). The reagents and standards used for the analysis of cuticular components were supplied by Sigma-Aldrich (Steinheim, Germany). All standards used were of analytical grade.

**Extraction and Analysis of Cuticular Wax Compounds.** Waxes were recovered from the 60 dry CM disks (a total of 79.64 $cm^2$ per cultivar and analysis date) obtained in each case. CM samples were dewaxed three times by shaking in $CHCl_3$ (1 mg sample $mL^{-1}$) 24 h at room temperature, followed by incubation (15 min) in an ultrasonic bath. After filtration, the chloroform extracts were pooled and concentrated using a rotary evaporator at 50 °C and the waxes transferred to a preweighed vial, dried under $N_2$ until complete dryness, and weighed in a microbalance for calculation of total wax yield ($\mu$g $cm^{-2}$). Free hydroxyl and carboxyl groups were converted respectively into their trimethylsilyl (TMSi) ethers and esters by derivatizing with *N*,*O*-bis(trimethylsilyl)trifluoroacetamide (BSTFA) in pyridine (2:1, v/v) for 15 min at 100 °C.

After derivatization, wax samples were added eicosane ($C_{20}$) and dotriacontane ($C_{32}$) as internal standards and injected (1 $\mu$L) in on-column mode into a gas chromatography−mass spectrometry (GC-MS) system for compound identification. A GC equipment (Agilent 7890A) coupled with a quadrupole mass selective detector (Agilent 5973N) was used for these analyses, equipped with a capillary column (BPX5, 30 m × 0.25 mm, 0.25 $\mu$m; SGE Europe Ltd., Milton Keynes, UK). Wax compounds were identified by comparing their retention indices with those of standards and by matching their electron ionization-mass spectra (EI-MS) (70 eV, $m/z$ 50−700) with those from the NIST 08 MS library. The oven was set at 50 °C (2 min), and the temperature was raised initially by 40 °C $min^{-1}$ to 200 °C, kept at 200 °C for 2 min, raised again by 3 °C $min^{-1}$ to 310 °C, and then kept constant at 310 °C for 30 min. Helium was used as the carrier gas (2 mL $min^{-1}$). Quantitative determination of wax compounds was carried out under the same chromatographic conditions using a GC system equipped with a flame ionization detector (FID). Data were expressed as relative %.

**Extraction and Analysis of Cutin Monomers.** Dewaxed cuticular membranes (DCM) were hydrolyzed in 3 mL of 1 M HCl in 100% MeOH and esterified in the same solvent for 2 h at 80 °C. After cooling, 2 mL of saturated NaCl was added to the methanolysate. The cutin monomers were extracted three times in 2 mL of hexane for 10 min, followed by thorough mixing and centrifugation at 20 °C. The monomer extracts were combined and evaporated to dryness in a $N_2$ steam. Cutin yields were determined gravimetrically as $\mu$g $cm^{-2}$. Dry cutin samples were derivatized with BSTFA for 15 min at 100 °C, then added heptadecanoate ($C_{17}$) and tricosanoate ($C_{23}$) as internal standards, and injected (1 $\mu$L) to GC-FID for quantitative determination.

Cutin compounds were identified by comparison with standards, and from their EI-MS spectra (70 eV, $m/z$ 50−700) after GC-MS analysis using the same GC-MS system as described in the previous section on wax analysis. The oven was set and held at 50 °C for 2 min, and then the temperature was raised to 250 °C by 10 °C $min^{-1}$, kept at 250 °C for 1 min, raised again by 3 °C $min^{-1}$ to 310 °C, and kept at that temperature for 20 min. The same chromatographic conditions were used for quantitative determination of cutin compounds by GC-FID. Results were expressed as relative %.

**Statistical Analysis.** A multifactorial design with storage and shelf life periods as factors was used to statistically analyze the results within each cultivar. All data were tested by analysis of variance (ANOVA) with the Minitab 16 program package, and means were separated by the Fisher's LSD test at $P \leq 0.05$.

## RESULTS AND DISCUSSION

The usual indicators of commercial quality show that samples were picked at marketable maturity according to the standards in the producing area (Table 1). Average weight and diameter at harvest were higher for "Somerset" than for "Celeste" fruit (Table 1). "Somerset" cherries were also firmer, juicier, and displayed higher SSC and TA values. Skin color of "Celeste" fruit was less red, but lighter, than that of "Somerset", as indicated by higher hue and lightness values.

**Table 1. Maturity and Quality Indicators of "Celeste" and "Somerset" Sweet Cherry Fruit at Commercial Harvest**

| parameter[a] | 'Celeste' | 'Somerset' |
|---|---|---|
| weight (g) | 9.02 b | 10.49 a |
| diameter (mm)[b] | 27.95 b | 30.73 a |
| firmness (Durofel units) | 77.67 a | 80.43 a |
| juiciness (mL 100 $g^{-1}$ FW) | 61.07 b | 65.37 a |
| SSC (°Brix) | 16.07 b | 19.43 a |
| TA (g $L^{-1}$) | 6.70 b | 7.32 a |
| hue (°) | 21.88 a | 16.97 b |
| lightness ($L^*$) | 33.51 a | 27.01 b |

[a]Values represent means of 30 or three (SSC, TA, juiciness) replicates. Mean values followed by a different lower-case letter within the same row are significantly different at $P \leq 0.05$ (LSD test). [b]Diameter is given as the average between the wider and the narrower sides of each fruit.

In addition to these differences in the usual quality indicators, both cultivars also differed in relation to cuticle amount recovered from fruit skin (Table 2). Cuticle yields ($\mu$g $cm^{-2}$) obtained from 60 skin disks were noticeably lower in "Celeste" than in "Somerset" fruit (100 vs 206 at harvest, respectively). Higher cuticle amounts per surface area might be indicative of thicker cuticles, but no measurements of cuticle thickness were undertaken in this study. Incidentally, weight loss and firmness changes after 3 days at 20 °C were more pronounced in "Celeste" than in "Somerset" samples (Table 3), showing a somewhat better conservation potential for "Somerset" fruit. However, published studies on the relevance of cuticle thickness for postharvest weight loss have reported contradictory results


dx.doi.org/10.1021/jf502650t | J. Agric. Food Chem. 2014, 62, 8722−8729

**Table 2. Total Amount of Cuticle Recovered, and Wax and Cutin Yields Obtained from "Celeste" and "Somerset" Sweet Cherries at Harvest and after Cold Storage[a]**

| | days at 0 °C + days at 20 °C | | | |
|---|---|---|---|---|
| | 0 + 0 | 0 + 3 | 14 + 0 | 14 + 3 |
| | **'Celeste'** | | | |
| cuticle amount (mg)[b] | 8.0 | 13.6 | 17.9 | 10.6 |
| cuticle yield ($\mu$g cm$^{-2}$) | 100.45 c | 170.77 b | 224.76 a | 133.10 bc |
| cuticle yield (mg/fruit) | 2.47 c | 4.19 b | 5.48 a | 2.30 c |
| wax yield ($\mu$g cm$^{-2}$) | 32.74 b | 37.13 a | 24.66 c | 24.90 c |
| wax yield (mg/fruit) | 0.80 b | 0.91 a | 0.60 c | 0.43 d |
| cutin yield ($\mu$g cm$^{-2}$) | 45.14 c | 38.29 d | 122.90 a | 82.45 b |
| cutin yield (mg/fruit) | 1.11 c | 0.94 c | 3.00 a | 1.42 b |
| wax (%) | 32.59 a | 21.74 b | 10.97 c | 18.71 bc |
| cutin (%) | 44.94 b | 22.42 c | 54.68 ab | 61.95 a |
| | **'Somerset'** | | | |
| cuticle amount (mg)[b] | 16.4 | 19.1 | 26.4 | 17.1 |
| cuticle yield ($\mu$g cm$^{-2}$) | 205.93 b | 239.83 b | 331.49 a | 214.72 b |
| cuticle yield (mg/fruit) | 6.11 b | 4.83 c | 7.47 a | 4.33 c |
| wax yield ($\mu$g cm$^{-2}$) | 47.51 b | 57.46 a | 33.91 c | 34.91 c |
| wax yield (mg/fruit) | 1.41 a | 1.16 b | 0.76 c | 0.70 c |
| cutin yield ($\mu$g cm$^{-2}$) | 84.53 c | 140.08 ab | 162.90 a | 105.86 bc |
| cutin yield (mg/fruit) | 2.51 bc | 2.82 b | 3.67 a | 2.14 c |
| wax (%) | 23.07 a | 23.96 a | 10.23 c | 16.26 b |
| cutin (%) | 41.05 b | 58.41 a | 49.14 ab | 49.30 ab |

[a]Yields and percentages represent means of three replicates. Mean values followed by a different lower-case letter within the same row are significantly different at $P \leq 0.05$ (LSD test). [b]Recovered from 60 skin discs (4 disks × 15 fruit), corresponding in total to 79.64 cm$^2$.

**Table 3. Some Physical Properties of "Celeste" and "Somerset" Sweet Cherries at Harvest and after Cold Storage[a]**

| | days at 0 °C + days at 20 °C | | | |
|---|---|---|---|---|
| | 0 + 0 | 0 + 3 | 14 + 0 | 14 + 3 |
| | **'Celeste'** | | | |
| firmness (Durofel units) | 77.7 a | 72.1 ab | 68.5 b | 69.9 b |
| weight loss (%) | – | 9.6 c | 15.8 b | 22.4 a |
| diameter (mm)[b] | 27.95 a | 27.94 a | 27.87 a | 23.43 b |
| fruit surface (cm$^2$/fruit)[c] | 24.54 a | 24.52 a | 24.40 a | 17.25 b |
| fruit volume (cm$^3$/fruit)[c] | 11.43 a | 11.42 a | 11.33 a | 6.73 b |
| | **'Somerset'** | | | |
| firmness (Durofel units) | 80.4 b | 77.2 b | 86.5 a | 82.1 ab |
| weight loss (%) | – | 2.4 c | 7.2 b | 15.4 a |
| diameter (mm)[b] | 30.73 a | 25.31 b | 26.79 b | 25.35 b |
| fruit surface (cm$^2$/fruit)[c] | 29.67 a | 20.12 c | 22.55 b | 20.19 c |
| fruit volume (cm$^3$/fruit)[c] | 15.19 a | 8.49 c | 10.07 b | 8.53 c |

[a]Values are the means of 30 replicates. Mean values followed by a different lower-case letter within the same row are significantly different at $P \leq 0.05$ (LSD test). [b]Diameter is given as the average between the wider and the narrower sides of each fruit. [c]Total surface and volume were estimated from the average diameter of each fruit assuming a spherical shape.

(reviewed in ref 2), and such a relationship has been actually shown in only a few instances.[20] The composition and/or structure of the fruit surface may be of more relevance for postharvest performance-related physiological traits.

**Cuticular Wax and Cutin Composition at Harvest.** Cutin and cuticular waxes were extracted from cuticles obtained enzymatically from fruit samples and analyzed chromatographically. In spite of being comprised of similar chemical families, both types of cuticular components showed cultivar-related differences in the specific composition and in the abundance of particular compounds. Noticeable differences in the total content of cuticular waxes and cutin were also observed between both cherry cultivars.

Total wax yields of fruit at harvest were around 33 ("Celeste") and 48 ("Somerset") $\mu$g cm$^{-2}$, corresponding to 33 and 23% of total cuticle material recovered, respectively. Triterpenes were the most abundant class of wax components in both cherry cultivars considered (Table 4), with ursolic acid as the dominating compound (49% and 47% of total waxes at harvest for "Celeste" and "Somerset", respectively). This is in accordance with an early report on "Bing" cherries.[16] The prevalence of ursolic acid agrees as well with a more recent investigation[6] in which cuticular wax composition was analyzed in four cherry cultivars ("Hedelfinger", "Kordia", "Sam", and "Van") during on-tree fruit development, although in that study the amount of triterpenes was found to account for up to 76% of total wax, which is higher than the levels observed in this work at harvest (55−57%). This difference was due to greater contents of ursolic acid (around 60%) because the relative amounts of oleanoic acid, the second triterpene in quantitative terms, were equivalent to those found in this study (7.5%).

Alkanes were the second most important class of wax components in quantitative terms, among which *n*-nonacosane ($C_{29}$) was the most abundant compound, followed by *n*-heptacosane ($C_{27}$) (Table 4), which is also consistent with previous observations.[6,16] However, "Somerset" cuticles were richer in alkanes than those obtained from "Celeste" fruit (roughly 15 vs 10% at harvest, correspondingly), particularly in those with longer chains ($C_{27}$ to $C_{31}$), and also contained higher percentages of phytosterols. In contrast, "Celeste" cuticles were richer in fatty acids than those of "Somerset" fruit, although in both cultivars linolenic acid predominated quantitatively among this type of wax components. Cuticular waxes of "Bing" cherries were also characterized to be rich in palmitic, stearic, oleic, and linoleic acids and to contain significant amounts of sitosterol.[16] None of these fatty acids, and only trace amounts of sitosterol, which are characteristic for membrane lipids, were found in a subsequent study,[6] leading to the suggestion that their presence in the previous report was due to the use of pressed, dehydrated fruit skins as the source of wax. Nevertheless, we wish to point out that we used enzymatically isolated cuticles herein as the source material for wax extraction. Therefore, presence of these compounds in the wax fraction is not likely to be artifactual but rather to be reflecting actual cultivar-related differences in cuticular wax composition.

Similarly to the observations for waxes, total cutin content was also higher in "Somerset" than in "Celeste" samples, expressed per unit surface area (85 vs 45 $\mu$g cm$^{-2}$, respectively) as well as on a whole fruit basis (2.5 vs 1.1 mg per fruit), even though it was a bit lower when expressed as a percentage over total cuticle yield (41 vs 45%) (Table 2). The analysis of cutin monomer composition revealed discrepancies with previous reports that the cutin fraction of mature "Kordia" fruit consisted mainly of $C_{16}$ (69.5%) and, to a much lesser extent, $C_{18}$ (19.4%) monomers.[6] In this work, in contrast, we found that the cutin fraction of "Celeste" and "Somerset" cherry fruit at harvest maturity was composed mainly of $C_{18}$ monomers (65.3%), comprising $\alpha$-monocarboxylic, $\alpha,\omega$-dicarboxylic, and $\omega$-hydroxylated acids (Table 5). The most abundant of these $C_{18}$ constituents were octadecane-1,18-dioic acid, 18-hydroxy-linoleic acid, 18-hydroxy-oleic acid, and oleic acid, whereas hexadecane-1,16-dioic


dx.doi.org/10.1021/jf502650t | J. Agric. Food Chem. 2014, 62, 8722−8729

**Table 4. Wax Constituents (Relative %) Identified in Cuticles of "Celeste" and "Somerset" Sweet Cherries at Harvest and after Cold Storage[a]**

| | days at 0 °C + days at 20 °C | | | |
|---|---|---|---|---|
| | 0 + 0 | 0 + 3 | 14 + 0 | 14 + 3 |
| | | **'Celeste'** | | |
| **triterpenes** | **57.28 b** | **65.73 a** | **67.3 a** | **69.22 a** |
| oleanolic acid | 7.76 b | 9.19 a | 9.68 a | 9.71 a |
| ursolic acid | 49.54 b | 56.55 a | 57.62 a | 59.51 a |
| **alkanes** | **10.28 b** | **12.91 a** | **12.27 a** | **12.33 a** |
| decane (C10) | 0.06 a | 0.04 b | 0.01c | 0.01 c |
| undecane (C11) | 0.03 a | 0.01 b | nd c | nd c |
| dodecane (C12) | 0.09 a | nd b | nd b | nd b |
| docosane (C22) | 0.03 b | 1.84 a | 0.01 b | 0.01 b |
| tricosane (C23) | 0.08 a | 0.03 b | 0.03 b | nd c |
| tetracosane (C24) | 0.22 a | 0.13 b | 0.02 c | 0.05 c |
| pentacosane (C25) | 0.33 a | 0.18 b | 0.14 b | 0.16 b |
| hexacosane (C26) | 0.33 a | 0.19 b | 0.13 b | 0.19 b |
| heptacosane (C27) | 1.18 c | 1.22 c | 1.35 b | 1.49 a |
| octacosane (C28) | 0.76 ab | 0.72 b | 0.72 b | 0.79 a |
| nonacosane (C29) | 5.96 c | 7.34 b | 8.51 a | 8.32 a |
| triacontane (C30) | 0.52 a | 0.49 b | 0.52 a | 0.53 a |
| hentriacontane (C31) | 0.66 d | 0.72 c | 0.83 a | 0.78 b |
| **fatty acids** | **13.03 a** | **7.29 b** | **3.43 c** | **2.56 c** |
| C16:0 | 1.06 a | 0.46 b | 0.18 b | 0.11 b |
| C17:0 | 0.09 a | 0.06 b | nd c | nd c |
| C18:0 | 1.27 a | 0.89 b | 0.76 b | 0.89 b |
| C18:1 (9) | 0.31 a | 0.21 b | 0.18 b | 0.15 b |
| C18:2 (9, 12) | 10.27 a | 5.66 b | 2.31 c | 1.41 c |
| *trans*-C18:2 (9,12) | 0.03 a | 0.01 b | 0.00 b | 0.00 b |
| **phytosterols** | **1.78 bc** | **2.11 ab** | **2.24 a** | **1.65 c** |
| campesterol | 0.83 a | 0.71 b | 0.76 ab | 0.72 b |
| *β*-sitosterol | 0.95 b | 1.40 a | 1.48 a | 0.93 b |
| **fatty alcohols** | **0.89 a** | **0.53 b** | **0.87 a** | **0.74 ab** |
| tricosanol (C23) | 0.34 a | 0.22 b | 0.34 a | 0.25 ab |
| tetracosanol (C24) | 0.14 a | 0.04 b | 0.19 a | 0.17 a |
| hexacosanol (C26) | 0.14 a | 0.05 b | 0.05 b | 0.04 b |
| octacosanol (C28) | 0.11 a | 0.07 b | 0.10 a | 0.11 a |
| triacontanol (C30) | 0.16 bc | 0.15 c | 0.19 a | 0.17 b |
| **identified wax** | **83.23 b** | **86.40 a** | **86.08 a** | **86.49 a** |
| **unidentified** | **16.77 a** | **13.60 b** | **13.92 b** | **13.51 b** |
| | | **'Somerset'** | | |
| **triterpenes** | **54.62 a** | **55.19 a** | **51.15 b** | **53.85 a** |
| oleanolic acid | 7.47 b | 7.39 b | 8.21 a | 7.68 b |
| ursolic acid | 47.15 a | 47.80 a | 42.94 b | 46.17 a |
| **alkanes** | **14.80 b** | **14.93 b** | **18.406 a** | **15.25 b** |
| decane (C10) | 0.07 a | 0.05 b | 0.06 ab | 0.06 ab |
| undecane (C11) | 0.03 a | 0.01 b | 0.02 ab | 0.01 b |
| docosane (C22) | 0.01 ab | 0.01 ab | 0.02 a | nd b |
| tricosane (C23) | 0.08 ab | 0.06 b | 0.13 a | 0.05 ab |
| tetracosane (C24) | 0.16 b | 0.11 b | 0.31 a | 0.12 b |
| pentacosane (C25) | 0.31 b | 0.21 b | 0.58 a | 0.27 b |
| hexacosane (C26) | 0.46 b | 0.30 b | 0.75 a | 0.34 b |
| heptacosane (C27) | 1.73 c | 1.75 c | 2.24 a | 1.99 b |
| octacosane (C28) | 1.15 b | 0.98 b | 1.47 a | 1.08 b |
| nonacosane (C29) | 8.94 c | 9.77 b | 10.68 a | 9.67 bc |
| triacontane (C30) | 0.81 ab | 0.69 b | 0.97 a | 0.71 b |
| hentriacontane (C31) | 1.05 b | 0.99 b | 1.23 a | 0.95 b |
| **fatty acids** | **7.58 a** | **7.01 ab** | **5.79 b** | **7.73 a** |
| C16:0 | 0.41 a | 0.33 ab | 0.20 b | 0.46 a |
| C17:0 | 0.06 a | 0.06 a | 0.02 b | 0.05 a |
| C18:0 | 1.20 b | 1.13 b | 1.18 b | 1.70 a |
| C18:1 (9) | 0.25 b | 0.24 b | 0.21 b | 0.36 a |


dx.doi.org/10.1021/jf502650t | J. Agric. Food Chem. 2014, 62, 8722−8729

**Table 4. continued**

| | days at 0 °C + days at 20 °C | | | |
|---|---|---|---|---|
| | 0 + 0 | 0 + 3 | 14 + 0 | 14 + 3 |
| | | 'Somerset' | | |
| C18:2 (9, 12) | 5.66 a | 5.25 a | 4.18 b | 5.16 a |
| **phytosterols** | **3.61 ab** | **3.01 b** | **4.82 a** | **2.91 b** |
| campesterol | 0.94 c | 1.07 b | 1.19 a | 1.12 ab |
| *β*-sitosterol | 2.67 ab | 1.94 b | 3.63 a | 1.79 b |
| **fatty alcohols** | **1.05 a** | **0.96 b** | **1.01** | **1.07** |
| tricosanol (C23) | 0.29 b | 0.23 b | 0.28 b | 0.46 a |
| tetracosanol (C24) | 0.21 a | 0.17 b | 0.06 c | 0.06 c |
| hexacosanol (C26) | 0.15 b | 0.17 a | 0.12 c | 0.12 c |
| octacosanol (C28) | 0.16 a | 0.15 ab | 0.16 a | 0.14 b |
| triacontanol (C30) | 0.24 b | 0.24 b | 0.39 a | 0.29 b |
| **identified wax** | **81.66 a** | **81.10 b** | **81.24 ab** | **80.83 b** |
| **unidentified** | **18.34 b** | **18.90 a** | **18.76 ab** | **19.17 a** |

[a]Values represent means of three replicates (nd, nondetectable). Mean values followed by a different lower-case letter within the same row are significantly different at $P \leq 0.05$ (LSD test).

acid predominated among the $C_{16}$-type monomers. Only minor quantitative differences in cutin composition were found between both cultivars considered at harvest, the main constituent compounds being the same. Because the procedures for cuticle isolation and cutin depolymerization were similar, the discrepancies with that report[6] may illustrate cultivar-related differences which should be explored in relation with their potential relevance for distinctive agronomic, physiological, and quality traits of each particular genotype, such as keeping potential, water loss rates or predisposition to cracking. For example, the prevalence of monohydroxylated monomers (Table 5) instead of di- and trihydroxy acids[6] may have consequences for the cross-linking of the cutin network. Although currently available information on the specific composition of fruit cuticles is limited, significant differences have been found among different cultivars of apple,[5,8,12,13,21] grape,[22−24] pepper,[25,26] persimmon,[27] or tomato mutants.[28−30] At least for apple, pepper, persimmon, and tomato, these differences appeared to be connected to relevant physiological traits related to cuticle functionality such as water loss rates or mechanical properties.

**Changes in Cuticular Wax and Cutin Composition after Harvest.** After harvest, fruit remained 3 days at 20 °C, after which the amount of cuticle per unit surface area and per fruit increased in "Celeste" (Table 2). While this could have arisen from decreased surface area leading to apparently higher cuticle yields per surface unit, data show that fruit diameter, surface, and volume were similar to those at harvest (Table 3). These data thus suggest that some deposition of cuticle material took place during that period. The physiological significance of this postharvest cuticle formation is unclear. Although cuticle deposition in sweet cherry is known to cease early during fruit development,[10] postharvest modifications in the regulation of cuticle-related metabolic pathways cannot be ruled out, as no postharvest studies on sweet cherry cuticles have been published to date. In contrast, CM mass per surface area did not change significantly in "Somerset" samples, and it was actually found to decrease when expressed on a whole fruit basis (Table 2), which suggests the existence of cultivar-related differences in cuticle dynamics.

Significantly higher wax yields in absolute terms ($\mu g\ cm^{-2}$) were observed in both cases. However, due to augmented cuticle amounts during the shelf life period, the percentage of cuticular waxes decreased ("Celeste") or remained unchanged ("Somerset"). The main difference between cultivars, though, was found for cutin yields, which decreased in both absolute and relative terms in "Celeste" fruit, while the opposite was observed for "Somerset" cherries (Table 2).

Detailed analysis of cuticle composition revealed different evolution of particular compounds after harvest. For example, in the case of "Celeste", the percentage of triterpenes and alkanes was higher after 3 days at 20 °C, while that of free fatty acids and alcohols decreased after the same period (Table 4). The decreased content of fatty acids could be related to increases in alkanes, which are believed to arise from fatty acid decarboxylation or fatty aldehyde decarbonylation (reviewed in ref 31). On the contrary, no significant differences in the percentage of the main wax compound families were found for "Somerset" cuticles (Table 4). However, triterpenes must have been also actively synthesized in this cultivar after harvest in order to keep pace with increased cuticle yields, as shown by clearly augmented amounts in quantitative terms (Figure 1). Some increase was also observed for alkane content in spite of unchanged alkane percentages over total waxes (Table 4). Little information has been published to date on postharvest changes in cuticular waxes, but epicuticular waxes increased in ripe "Navelate" oranges (*Citrus sinensis* L. Osbeck) kept at 22 °C for 14 days, this increase being accentuated in ethylene-treated fruit.[15] Formation of new waxes was suggested to serve protective purposes, covering stomata, cracks or areas lacking wax, and improving physical barriers against pathogen penetration.[15,32] Significant increases in the amount per surface unit of different classes of wax compounds have also been reported for "Jesca" peach fruit, likewise cherry a *Prunus* species,[33] accounting for augmented cuticle yields after harvest and suggestive of up-regulation of the biosynthetic pathways involved in cuticle biosynthesis.

In contrast to waxes, the percentages of particular cutin monomer types in fruit cuticles showed limited changes after shelf life at 20 °C, the only significant variations observed being restricted to some decline in monocarboxylic acids, particularly in "Somerset" samples (Table 5). Yet, some differences in the evolution of these compound families were found between both cultivars. For "Celeste", the content of hydroxy acids declined also in absolute terms (Figure 2A). In contrast, the observation of increased contents of dicarboxylic and hydroxy acids in cuticles of "Somerset" fruit after harvest (Figure 2B) suggests net biosynthesis taking place thereafter and accounting, at least

**Table 5. Cutin Constituents (Relative %) Identified in Cuticles of "Celeste" and "Somerset" Sweet Cherries at Harvest and after Cold Storage[a]**

| | days at 0 °C + days at 20 °C | | | |
|---|---|---|---|---|
| | 0 + 0 | 0 + 3 | 14 + 0 | 14 + 3 |
| | 'Celeste' | | | |
| **α-monocarboxylic acids** | **21.38 ab** | **15.52 bc** | **24.99 a** | **11.88 c** |
| C15:0 | nd b | nd b | 0.41 a | nd b |
| C16:0 | 3.72 ab | 2.70 b | 6.11 a | 2.17 b |
| C16:1 (9) | nd b | nd b | 0.50 a | 0.16 b |
| C18:0 | 0.99 a | 0.66 b | 1.03 a | 0.84 ab |
| C18:1 (9) | 11.53 a | 8.28 ab | 10.42 a | 4.73 b |
| C18:2 (9, 12) | 3.27 b | 2.68 b | 5.08 a | 2.20 b |
| C22 | 1.88 a | 1.21 b | 1.42 ab | 1.78 a |
| **α,ω-dicarboxylic acids** | **26.94 a** | **26.34 a** | **20.57 b** | **25.35 a** |
| 1,16-dioic $C_{16}$ | 7.67 a | 7.08 ab | 5.54 b | 8.10 a |
| 1,18-dioic $C_{18:1}$ | 18.05 a | 18.14 a | 14.06 c | 15.98 b |
| 1,18-dioic $C_{18:2}$ | 1.23 a | 1.13 ab | 0.96 b | 1.28 a |
| **hydroxyacids** | **35.90 a** | **37.38 a** | **28.30 c** | **31.24 b** |
| 2-OH $C_{16:0}$ | 0.70 ab | 0.50 b | 1.26 a | 0.21 b |
| 16-OH $C_{16:0}$ | 4.98 a | 4.89 a | 3.69 c | 4.29 b |
| 18-OH $C_{18:1}$ | 14.23 a | 14.92 a | 10.79 c | 12.68 b |
| 18-OH $C_{18:2}$ | 15.98 a | 17.07 a | 12.56 c | 14.06 b |
| **identified cutin** | **84.22 a** | **79.24 ab** | **75.32 b** | **68.47 c** |
| **unidentified** | **15.78 c** | **20.76 bc** | **24.68 b** | **31.53 a** |
| | 'Somerset' | | | |
| **α-monocarboxylic acids** | **22.38 b** | **19.24 c** | **27.64 a** | **26.91 a** |
| C16:0 | 3.64 bc | 3.06 c | 4.25 b | 5.31 a |
| C16:1 (9) | 0.21 b | 0.39 a | 0.35 a | 0.35 a |
| C18:0 | 1.12 c | 0.99 c | 1.36 b | 1.72 a |
| C18:1 (9) | 13.30 b | 11.11 b | 16.45 a | 12.01 b |
| C18:2 (9, 12) | 2.80 b | 2.19 b | 3.49 b | 6.23 a |
| C20:0 | nd c | nd c | 0.36 b | 0.43 a |
| C22:0 | 1.31 b | 1.50 c | 0.94 c | 0.86 c |
| C28:0 | nd | nd | nd | nd |
| C30:0 | nd b | nd b | 0.43 a | nd b |
| **α,ω-dicarboxylic acids** | **23.87 a** | **24.10 a** | **17.02 b** | **23.21 a** |
| 1,16-dioic $C_{16}$ | 6.27 ab | 6.72 a | 4.57 c | 5.65 b |
| 1,18-dioic $C_{18:1}$ | 16.30 a | 16.12 a | 11.51 b | 16.39 a |
| 1,18-dioic $C_{18:2}$ | 1.30 a | 1.26 a | 0.95 b | 1.17 a |
| **hydroxyacids** | **27.29 a** | **26.80 a** | **15.74 b** | **26.45** |
| 2-OH $C_{16:0}$ | 0.87 a | 0.73 ab | 1.31 a | nd b |
| 16-OH $C_{16:0}$ | 3.31 a | 3.02 a | 1.66 b | 3.37 a |
| 18-OH $C_{18:1}$ | 12.39 a | 11.94 a | 6.35 b | 12.52 a |
| 18-OH $C_{18:2}$ | 10.72 a | 11.10 a | 6.43 b | 10.55 a |
| **identified cutin** | **74.31 a** | **70.55 ab** | **66.47 b** | **77.63 a** |
| **unidentified** | **25.69 b** | **29.45 ab** | **33.53 a** | **22.37 b** |

[a]Values represent means of three replicates (nd, nondetectable). Mean values followed by a different lower-case letter within the same row are significantly different at $P \leq 0.05$ (LSD test).

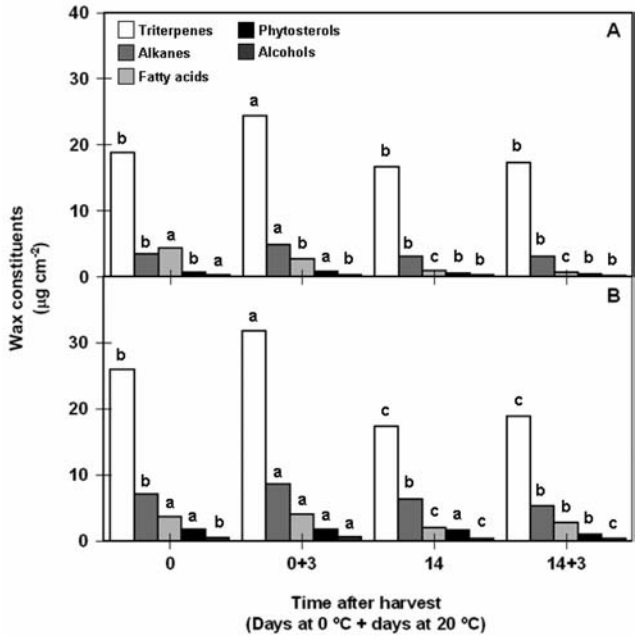


**Figure 1.** Amount ($\mu$g cm$^{-2}$) of the main classes of wax constituents identified in cuticles of "Celeste" (A) and "Somerset" (B) sweet cherries at harvest and after cold storage. For each class of wax constituents, values bearing different letters are significantly different at $P \leq 0.05$ (LSD test).

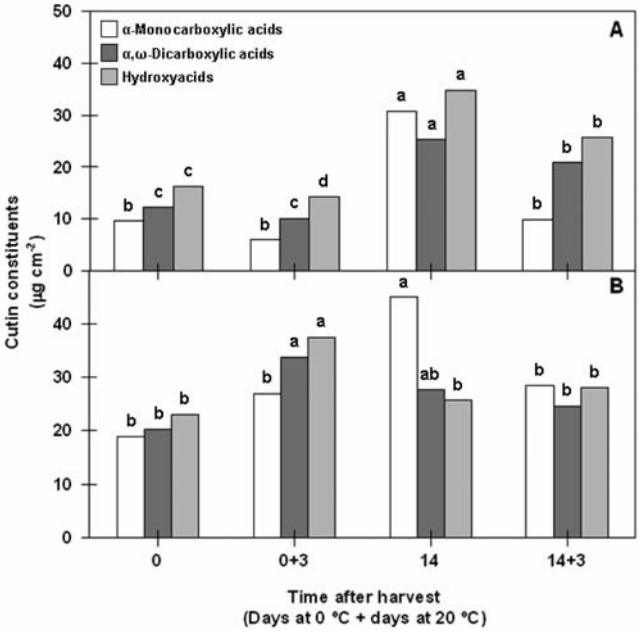


**Figure 2.** Amount ($\mu$g cm$^{-2}$) of the main types of cutin monomers identified in cuticles of "Celeste" (A) and "Somerset" (B) sweet cherries at harvest and after cold storage. For each type of cutin monomers, values bearing different letters are significantly different at $P \leq 0.05$ (LSD test).

partially, for the augment in cutin percentage over total cuticle material (Table 2). Differences in the postharvest evolution of particular types of cutin monomers also seem to exist between melting- and nonmelting-type peach genotypes.[33]

**Changes in Cuticular Wax and Cutin Composition after Cold Storage.** For both cultivars, the amount of cuticle per unit surface area and per total area increased after storage of fruit at 0 °C for 2 weeks, but decreased again during the subsequent 3 days of shelf life at 20 °C (Table 2), in parallel to lowered fruit surface and volume (Table 3). In the case of "Celeste", augmented cuticle yields after cold storage were detectable as soon as after only 7 days (data not shown). Total wax yield and wax percentage in both cultivars decreased significantly after keeping fruit at 0 °C for 14 days. In contrast, although cutin contents were higher in absolute terms than those at harvest (per surface unit as well as per fruit), the percentage over total cuticle amount remained the same owing to augmented cuticle yields per unit surface area (Table 2).


dx.doi.org/10.1021/jf502650t | J. Agric. Food Chem. 2014, 62, 8722−8729

Many metabolic processes in fruit are enhanced or redirected in response to low temperatures. Data shown herein put forward the possibility that cuticle formation is one of such processes. A few reports have described the changes in cuticular waxes after cold storage of apple[8,12−14] and shown considerable cultivar-associated variability for this fruit species. For instance, total wax contents after long-term cold storage were found to remain unchanged in "Sturmer" but to increase in "Granny Smith" and "Dougherty" apples,[12] while in contrast a sharp decline was observed for "Red Fuji" samples.[8] Changes in the composition of cuticular waxes during cold storage of apples were modulated in response to usual postharvest procedures such as controlled atmosphere storage[13] or 1-methylcyclopropene treatment.[8,14] However, we are not aware of any similar works for other fruit species. To the best of our knowledge, cutin changes after cold storage have not been previously reported for any fruit commodities either. We therefore analyzed the fate of wax and cutin components in cuticles isolated from "Celeste" and "Somerset" fruit kept at 0 °C. The modifications described below are indicative of intense alterations taking place in cuticle composition, and hence probably also in cuticle structure and properties, during cold storage.

The content of triterpenes ($\mu$g cm$^{-2}$) in cuticular waxes of "Celeste" fruit was unchanged after cold storage (Figure 1A). Still, owing to lower wax content in cuticles of cold-stored fruit as compared with values at harvest (roughly 25 vs 33 $\mu$g cm$^{-2}$, respectively), the percentage of triterpenes increased, ursolic and oleanoic acids representing approximately 58 and 10% of total waxes, in that order (Table 4). Although to a lower extent, some increase was also found in alkane percentage, particularly in that of *n*-nonacosane, the main alkane in quantitative terms, even though the absolute content was likewise unaffected (Figure 1A). Similar results were obtained for phytosterols, while in contrast the content of fatty acids decreased sharply, the main reduction being found for linoleic acid (Table 4). The total content of triterpenes after cold storage was also lower in cuticles of "Somerset" cherries, both in absolute (Figure 1B) and relative (Table 4) terms, while the percentage of alkanes and sterols increased. This is interesting in the light of previous suggestions that the waterproofing properties of fruit cuticles are defined primarily by the *n*-alkane components.[34] Reduced wax alkanes and enhanced triterpenoids would lead to increased content of amorphous waxes, thus impairing the transpiration barrier function of cuticles,[29] and in fact the ratio of alkanes to triterpenoids plus sterols has been found to correlate inversely with dehydration rates in pepper fruit.[26] Indeed, this ratio was 0.18 in "Celeste" and 0.33 in "Somerset", which would be consistent with the observation of higher weight loss rates for "Celeste" (15.8%) than for "Somerset" (7.2%) after cold storage (Table 3).

In relation to cutin monomers, some differences in the evolution of the content of particular compounds were also found between both cultivars considered. In "Celeste" samples, the percentage of monocarboxylic fatty acids was higher in fruit kept at 0 °C for 2 weeks, resulting from parallel increases in palmitic and linoleic acids (Table 5). However, the percentage of total fatty acids decreased again after 3 days of shelf life. In spite of a significant augment in the amount of $\alpha,\omega$-dicarboxylic and $\omega$-hydroxy acids per unit surface area (Figure 2), the percentage of these compounds (particularly those of the $C_{18}$-type) over total cutin mass decreased after cold storage. This is indicating that actual production of these cutin monomers must have taken place during the experimental period but that biosynthesis rates were not sufficient to keep pace with enhanced cuticle deposition (Table 2). This must have had consequences for cuticle structure and properties, as $\alpha,\omega$-diacid compounds are thought to be important for cross-linking of the cutin polymer.[35] In turn, the $\omega$-hydroxyl group in $\omega$-hydroxyacids is also necessary for the formation of the polymer.[36] Similar trends were observed in "Somerset" fruit for the evolution of the main types of cutin monomers, although some differences were found for particular compounds. For example, the content of oleic acid was higher after cold storage, in contrast with findings for "Celeste" fruit, and the increase in alkane content was also more perceptible (Table 5). Although the content of $\alpha,\omega$-dicarboxylic and $\omega$-hydroxy acids recovered after 3 days at 20 °C, the declining trend for the percentage of these families of cutin monomers along cold storage was accentuated in fruit kept at 0 °C for a longer period (data not shown), after which the contents of these compounds remained low. A little percentage of alkanes was noticed among the cutin constituents detected after cold storage, particularly for "Somerset" samples (data not shown). This may be an artifact representing wax constituents not completely released during the dewaxing procedure, which may have remained enclosed within the cutin matrix even though the chloroform extraction was repeated three times.

In summary, the most abundant components identified in cuticular waxes of "Celeste" and "Somerset" fruit agree with previous reports for other cherry cultivars,[6,16] but remarkable differences were found as to the main types of cutin monomers. These data suggest cultivar-related variability in the specific composition and in the abundance of particular compounds in cuticles of sweet cherry fruit. Such dissimilarities in the chemical composition of fruit cuticles and in their evolution during postharvest preservation of produce might account, at least partially, for some of the quality or storability characteristics of each cultivar, including weight loss, firmness, or susceptibility to infections or physiological disorders.[2] To the best of our knowledge, this is the first study reporting changes in cuticle composition of sweet cherry fruit during cold storage and one of the few works addressing postharvest modifications in the components of this outer layer of fruit surface. Further work on modifications in the relative amounts of the different cuticle components in response to internal and external factors will be required to shed light on the physiological consequences of these compositional changes, thus helping dissect the contribution of each particular compound family to the biological role of fruit cuticles.

## AUTHOR INFORMATION

### Corresponding Author

*Phone: +34 973 702526. E-mail: lara@quimica.udl.cat.

### Funding

B. Belge is the recipient of a FI-DGR grant from AGAUR (Generalitat de Catalunya). This work was supported through the AGL2010−14801/ALI project, funded by the Ministerio de Ciencia e Innovación (MICINN) of Spain.

### Notes

The authors declare no competing financial interest.

## ACKNOWLEDGMENTS

Fruit samples were provided by J. M. Camats (Cireres de Corbins Camats-Carpi).

## REFERENCES


(1) López-Casado, G.; Matas, A. J.; Domínguez, E.; Cuartero, J.; Heredia, A. Biomechanics of isolated tomato (*Solanum lycopersicum* L.) fruit cuticles: the role of the cutin matrix and polysaccharides. *J. Exp. Bot.* **2007**, *58*, 3875−3883.

(2) Lara, I.; Belge, B.; Goulao, L. F. The fruit cuticle as a modulator of postharvest quality. *Postharvest Biol. Technol.* **2014**, *87*, 103−112.

(3) Sala, J. M.; Lafuente, T.; Cuñat, P. Content and chemical composition of epicuticular wax of 'Navelina' oranges and 'Satsuma' mandarins as related to rindstaining of fruit. *J. Sci. Food Agric.* **1992**, *59*, 489−495.

(4) Comménil, P.; Brunet, L.; Audran, J. C. The development of the grape berry cuticle in relation to susceptibility to bunch rot disease. *J. Exp. Bot.* **1997**, *48*, 1599−1607.

(5) Belding, R. D.; Blankenship, S. M.; Young, E.; Leidy, R. B. Composition and variability of epicuticular waxes in apple cultivars. *J. Am. Soc. Hortic. Sci.* **1998**, *123*, 348−356.

(6) Peschel, S.; Franke, R.; Schreiber, L.; Knoche, M. Composition of the cuticle of developing sweet cherry fruit. *Phytochemistry* **2007**, *68*, 1017−1025.

(7) Kosma, D. K.; Parsons, E. P.; Isaacson, T.; Lü, S.; Rose, J. K. C.; Jenks, M. A. Fruit cuticle lipid composition during development in tomato ripening mutants. *Physiol. Plant.* **2010**, *139*, 107−117.

(8) Dong, X.; Rao, J.; Huber, D. J.; Chang, X.; Xin, F. Wax composition of 'Red Fuji' apple fruit during development and during storage after 1-methylcyclopropene treatment. *Hortic., Environ. Biotechnol.* **2012**, *53*, 288−297.

(9) Liu, D. C.; Zeng, Q.; Ji, Q. X.; Liu, C. F.; Liu, S. B.; Liu, Y. A comparison of the ultrastructure and composition of fruits' cuticular wax from the wild-type 'Newhall' navel orange (*Citrus sinensis* [L.] Osbeck cv. Newhall) and its glossy mutant. *Plant Cell Rep.* **2012**, *31*, 2239−2246.

(10) Alkio, M.; Jonas, U.; Sprink, T.; van Nocker, S.; Knoche, M. Identification of putative candidate genes involved in cuticle formation in *Prunus avium* (sweet cherry) fruit. *Ann. Bot.* **2012**, *110*, 101−112.

(11) Albert, Z.; Ivanics, B.; Molnár, A.; Miskó, A.; Tóth, M.; Papp, I. Candidate genes of cuticle formation show characteristic expression in the fruit skin of apple. *Plant Growth Regul.* **2013**, *70*, 71−78.

(12) Morice, I. M.; Shortland, F. B. Composition of the surface waxes of apple fruits and changes during storage. *J. Sci. Food Agric.* **1973**, *24*, 1331−1339.

(13) Veraverbeke, E. A.; Lammertyn, J.; Saevels, S.; Nicolaï, B. M. Changes in chemical wax composition of three different apple (*Malus domestica* Borkh.) cultivars during storage. *Postharvest Biol. Technol.* **2001**, *23*, 197−208.

(14) Curry, E. Effects of 1-MCP applied postharvest on epicuticular wax of apples (*Malus domestica* Borkh.) during storage. *J. Sci. Food Agric.* **2008**, *88*, 996−1006.

(15) Cajuste, J. F.; González-Candelas, L.; Veyrat, A.; García-Breijo, F. J.; Reig-Armiñana, J.; Lafuente, M. T. Epicuticular wax content and morphology as related to ethylene and storage performance of 'Navelate' orange fruit. *Postharvest Biol. Technol.* **2010**, *55*, 29−35.

(16) Markley, K. S.; Sando, C. E. The wax-like constituents of the cuticle of the cherry, *Prunus avium* L. *J. Biol. Chem.* **1937**, *119*, 641−645.

(17) Knoche, M.; Beyer, M.; Peschel, S.; Oparlakov, B.; Bukovac, M. J. Changes in strain and deposition of cuticle in developing sweet cherry fruit. *Physiol. Plant.* **2004**, *120*, 667−677.

(18) Peschel, S.; Knoche, M. Characterization of microcracks in the cuticle of developing sweet cherry fruit. *J. Am. Soc. Hortic. Sci.* **2005**, *130*, 487−495.

(19) Schönherr, J.; Riederer, M. Plant cuticles sorb lipophilic compounds during enzymatic isolation. *Plant Cell Environ.* **1986**, *9*, 459−466.

(20) Lownds, N. K.; Banaras, M.; Bosland, P. W. Relationships between postharvest water loss and physical properties of pepper fruit (*Capsicum annuum* L.). *HortScience* **1993**, *28*, 1182−1184.

(21) Belding, R. D.; Sutton, T. B.; Blankenship, S. M.; Young, E. Relationship between apple fruit epicuticular wax and growth of *Peltaster fructicola* and *Leptodontidium elatius*, two fungi that cause sooty blotch disease. *Plant Dis.* **2000**, *84*, 767−772.

(22) Radler, F. The main constituents of the surface waxes of varieties and species of the genus. *Vitis. Am. J. Enol. Vitic.* **1965**, *16*, 159−167.

(23) Radler, F.; Horn, D. H. S. The composition of grape cuticle wax. *Aust. J. Chem.* **1965**, *18*, 1059−1069.

(24) Casado, C. G.; Heredia, A. Structure and dynamics of reconstituted cuticular waxes of grape berry cuticle (*Vitis vinifera* L.). *J. Exp. Bot.* **1999**, *50*, 175−182.

(25) Kissinger, M.; Tuvia-Alkalai, S.; Shalom, Y.; Fallik, E.; Elkind, Y.; Jenks, M. A.; Goodwin, M. S. Characterization of physiological and biochemical factors associated with postharvest water loss in ripe pepper fruit during storage. *J. Am. Soc. Hortic. Sci.* **2005**, *130*, 735−741.

(26) Parsons, E. P.; Popopvsky, S.; Lohrey, G. T.; Lü, S.; Alkalai-Tuvia, S.; Perzelan, Y.; Paran, I.; Fallik, E.; Jenks, M. A. Fruit cuticle lipid composition and fruit post-harvest water loss in an advanced backcross generation of pepper (*Capsicum* sp.). *Physiol. Plant.* **2012**, *146*, 15−25.

(27) Tsubaki, S.; Ozaki, Y.; Yonemori, K.; Azuma, J. Mechanical properties of fruit-cuticular membranes isolated from 27 cultivars of *Diospyros kaki* Thunb. *Food Chem.* **2012**, *132*, 2135−2139.

(28) Leide, J.; Hildebrandt, U.; Reussing, K.; Riederer, M.; Vogg, G. The developmental pattern of tomato fruit wax accumulation and its impact on cuticular transpiration barrier properties: Effects of a deficiency in a *β*-ketoacyl-coenzyme A synthase (LeCER6). *Plant Physiol.* **2007**, *144*, 1667−1679.

(29) Isaacson, T.; Kosma, D. K.; Matas, A. J.; Buda, G. J.; He, Y.; Yu, B.; Pravitasari, A.; Batteas, J. D.; Stark, R. E.; Jenks, M. A.; Rose, J. K. C. Cutin deficiency in the tomato fruit cuticle consistently affects resistance to microbial infection and biomechanical properties, but not transpirational water loss. *Plant J.* **2009**, *60*, 363−377.

(30) Nadakuduti, S. S.; Pollard, M.; Kosma, D. K.; Allen, C.; Ohlrogge, J. B.; Barry, C. S. Pleoiotropic phenotypes of the sticky peel mutant provide new insight into the role of CUTIN DEFICIENT2 in epidermal cell function in tomato. *Plant Physiol.* **2012**, *159*, 945−960.

(31) Hannoufa, A.; McNevin, J.; Lemieux, B. Epicuticular waxes of *Eceriferum* mutants of *Arabidopsis thaliana*. *Phytochemistry* **1993**, *33*, 851−855.

(32) Dore, A.; Molinu, M. G.; Venditti, T.; D'Hallewin, G. Sodium carbonate induces crystalline wax generation, activates host-resistance, and increases imazalil level in rind wounds of oranges, improving the control of green mold during storage. *J. Agric. Food Chem.* **2010**, *58*, 7297−7304.

(33) Belge, B.; Llovera, M.; Comabella, E.; Graell, J.; Lara, I. Fruit cuticle composition of a melting and a nonmelting peach cultivar. *J. Agric. Food Chem.* **2014**, *62*, 3488−3495.

(34) Vogg, G.; Fischer, S.; Leide, J.; Emmanuel, E.; Jetter, R.; Levy, A. A.; Riederer, M. Tomato fruit cuticular waxes and their effect on transpiration barrier properties: functional characterization of a mutant deficient in a very-long-chain fatty acid *β*-ketoacyl-CoA synthase. *J. Exp. Bot.* **2004**, *55*, 1404−1410.

(35) Bonaventure, G.; Beisson, F.; Ohlrogge, J.; Pollard, M. Analysis of the aliphatic monomer composition of polyesters associated with *Arabidopsis* epidermis: occurrence of octadeca-*cis*-6,*cis*-9-diene-1,18-dioate as the major component. *Plant J.* **2004**, *40*, 920−930.

(36) Pollard, M.; Beisson, F.; Li, Y.; Ohlrogge, J. B. Building lipid barriers: biosynthesis of cutin and suberin. *Trends Plant Sci.* **2008**, *13*, 236−246.

JOURNAL OF AGRICULTURAL AND FOOD CHEMISTRY

Article

pubs.acs.org/JAFC

# Effect of the Biopolymer Mixing Ratio on the Formation of Electrostatically Coupled Whey Protein−κ- and ι-Carrageenan Networks in the Presence and Absence of Oil Droplets

Ricky S. H. Lam and Michael T. Nickerson*

Department of Food and Bioproduct Sciences, University of Saskatchewan, 51 Campus Drive, Saskatoon, Saskatchewan, Canada S7N 5A8

**ABSTRACT:** The rheological properties of 1.0% (w/w) whey protein isolate (WPI)−κ-/ι-carrageenan (CG) mixtures were investigated during a slow acidification process by glucono-δ-lactone from pH 7.00 to ∼4.20 as a function of biopolymer mixing ratio and in the presence and absence of oil droplets. In all cases, electrostatic coupled biopolymer and emulsion gel networks were formed at pH values corresponding to where attractive interactions between WPI and CG began. Formed WPI−CG complexes were found to be surface active, capable of lowering interfacial tension and forming viscoelastic interfacial films within emulsion-based systems. Both biopolymer and emulsion-based gels increased in strength and elasticity as the CG content increased, regardless of the type of CG present. However, WPI−ι-CG coupled networks were stronger than WPI−κ-CG networks, presumably due to the higher number of sulfate groups attracting the WPI molecules.

**KEYWORDS:** *emulsion, electrostatic coupled gel, coacervation, whey proteins, carrageenan*

## INTRODUCTION

Whey protein and carrageenan (CG) are commonly used as food ingredients in many applications (e.g., baked goods, beverages, desserts, confectionary and meat products) due to their gelling, emulsifying,or thickening abilities.[1] Whey proteins represent a mixture of proteins that are dominated by α-lactalbumin and β-lactoglobulin. These proteins have been intensively studied over the years for their functional attributes such as gelation[2−4] and their capacity to stabilize emulsions.[5−7] In contrast, carrageenan polysaccharides are extracted from red seaweeds (*Rhodophyta* species)[8] and consist of disaccharide repeating units composed of D-galactose and 3,6-anhydro-D-galactose residues, with one, two, or three sulfate groups associated each repeat unit for κ-, ι-, and λ-type carrageenans, respectively.[9] Although other minor types of CG have been identified by Knutsen and co-workers,[10] the present research will focus only on the κ- and ι-types due to their abilities to form strong gels.[11−13]

Mixtures of proteins and polysaccharides are known to undergo associative liquid/liquid phase separation (also known as complex coacervation) under conditions where biopolymers are oppositely charged and/or experiencing a significant amount of electrostatic attraction.[14] Whey protein−carrageenan mixtures have been explored previously in this respect by de Kruif and co-workers,[14] Weinbreck and co-workers,[9] and Stone and Nickerson.[15] During coacervation, the pH is lowered until a negatively charged protein (i.e., pH > p*I*) becomes neutral (i.e., at p*I*) and then positively charged (i.e., pH < p*I*), when it then can interact with a negatively charged polysaccharide. In the case of whey protein and CG, the initial interaction typically occurs at pH > p*I*, when both biopolymers carry similar net charges due to the interaction between CG and positively charged "patches" on a protein surface.[9] This initial interaction is denoted $pH_c$ and is evident by a slight increase in the absorption or light scattering in the protein−polysaccharide solution.[14] As the pH continues to decline, a sharp rise in the absorbance or light scattering of the biopolymer solution (designated $pH_{\phi 1}$) follows as the solution becomes turbid.[14] This sustained increase in absorbance and light scattering continues until a maximum is reached (designated $pH_{opt}$).[14] Beyond this point, continual acidification causes the complex to dissociate and dissolve.[14] The area of complex coacervation has been well studied with a number of reviews in the area.[14,16,17]

Recently, researchers have sought to use complexes as a means to stabilize emulsions.[18−24] Emulsions are formed when two immiscible liquids are mechanically agitated until one is dispersed as tiny droplets within the other. Because emulsions are thermodynamically unstable, amphiphilic biopolymers (e.g., proteins) can be used to inhibit emulsions from phase separation by reducing the surface tension between the droplets and the continuous solvent. Depending on the level of interactions, the biopolymers involved, and the processing conditions, systems may become stable or unstable. For instance, in dilute systems, the addition of a polysaccharide to a protein-stabilized oil droplet could lead to the formation of a viscoelastic bilayer where the polysaccharide complexes to the interfacial film, leading to increased emulsion stability[25] or causing instability via flocculation by the depletion interaction or bridging flocculation of neighboring droplets.[26] In more concentrated systems, various mixed protein−polysaccharide systems may take on a gel-like structure.[27] The nature of the gel may be considered as an "emulsion-filled protein gel, whereby oil droplets are simply encased within a gelled protein or a protein-stabilized emulsion gel", whereby the gel structure

Received: June 22, 2014
Revised: August 5, 2014
Accepted: August 7, 2014
Published: August 7, 2014

 © 2014 American Chemical Society  dx.doi.org/10.1021/jf5023669 | J. Agric. Food Chem. 2014, 62, 8730−8739

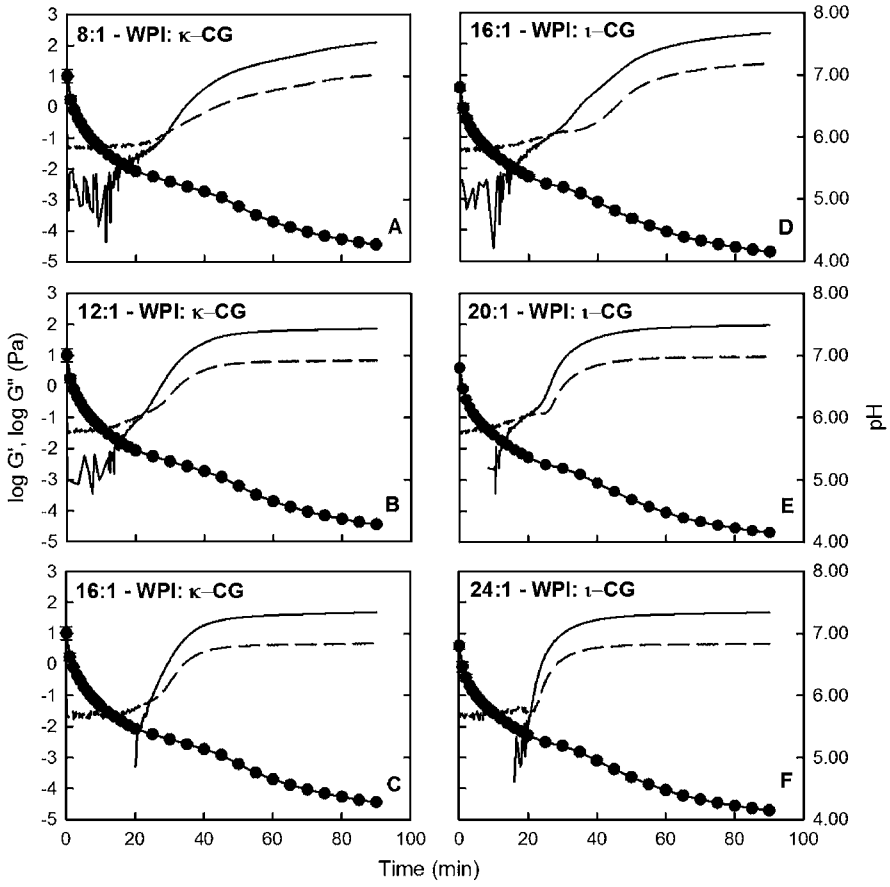


**Figure 1.** Dynamic viscoelastic storage ($G'$, solid line) and loss ($G''$, dashed line) moduli measured at 1 Hz with 1.0% constant strain for mixtures of WPI–$\kappa$-CG (A–C) and WPI–$\iota$-CG (D–F) at various mixing ratios as a function of pH (solid circles) and time (min). Each curve is the mean ± one standard deviation of three separate time sweep runs on separate samples. All solutions had a total biopolymer concentration of 1.0% (w/w) and were acidified using 0.5% (w/w) GDL.

consists of an interconnected flocculated network of oil droplets stabilized by an interfacial coacervate film.[27]

The inclusion of polysaccharides to protein-based emulsion systems has recently been researched as a means to reduce the oxidation of the emulsified oil for bioactive delivery[28] and for developing novel applications in controlled-release systems.[29] This body of work will continue to enhance our understanding of protein–polysaccharide interactions in emulsified systems.[30] The overall goal of the present study is to examine the underlying mechanisms driving the formation of electrostatically coupled biopolymer and emulsion gel networks, as a function of CG type ($\kappa$- and $\iota$-types) and mixing ratio between whey protein isolate (WPI) and the CG molecules. Stone and Nickerson investigated the formation of electrostatic complexes involving WPI and CG molecules as a function of CG type under dilute conditions (0.25% w/w) and reported the optimal mixing ratio to occur at a 12:1 ratio for WPI–$\kappa$-CG mixtures and at a 20:1 ratio for the WPI–$\iota$-CG system.[15] Information arising from this study will aid in controlling and optimizing their use in food or controlled delivery-type applications where gelation is important.

## MATERIALS AND METHODS

**Materials.** Whey protein isolate used in this study was generously donated by Davidson Foods International, Inc. (Le Sueur, MN, USA). The chemical composition of the commercial WPI powder was determined according to AOAC[31] methods; 925.10 (moisture), 923.03 (ash), 920.87 (crude protein), and 920.85 (lipid). Carbohydrate content was determined on the basis of present differential from 100%. The WPI powder was composed of 89.78% protein (%N × 6.38), 0.10% lipid, 4.92% moisture, 2.06% ash (including 0.08% $Ca^{2+}$, 0.01% $Mg^{2+}$, 0.02% $K^+$, and 0.66% $Na^+$), and 3.13% carbohydrate (wet basis). Carrageenan (CG) ($\kappa$- and $\iota$-) and glucono-$\delta$-lactone (GDL) were purchased from Sigma-Aldrich (Oakville, ON, Canada). For the two types of CG, the supplier information indicated that $\kappa$-CG was composed of 66.50% carbohydrate, 10.65% moisture, and 22.86% ash (including 2.4% $Ca^{2+}$, 0.16% $Mg^{2+}$, 5.4% $K^+$, 0.49% $Na^+$) and that $\iota$-CG contained 64.40% carbohydrate, 10.82% moisture, and 24.97% ash (including 3.4% $Ca^{2+}$, 0.18% $Mg^{2+}$, 3.2% $K^+$, 1.2% $Na^+$). Canola oil used in this study was purchased from a local supermarket. All other chemicals used in this study were of reagent grade and purchased through Sigma-Aldrich. The water used in this research was filtered using a Millipore Milli-Q water purification system (Millipore Corp., Milford, MA, USA). WPI and CG were used without further purification and were corrected for protein and polysaccharide content, respectively.

**Sample Preparation.** Biopolymer solutions (1.0% w/w biopolymer) were prepared by dispersing WPI and CG powders in water by mechanical stirring (500 rpm) at room temperature (21–23 °C) for 60 min. Afterward, 0.5% (w/w) of GDL was added to the biopolymer solution and stirred for 1 min prior to analysis to slowly acidify the solution. WPI and CG were mixed at ratios above and below the optimal ratio determined by Stone and Nickerson.[15] Mixing ratios of 8:1, 12:1, and 16:1 were tested for WPI–$\kappa$-CG, and ratios of 16:1, 20:1, and 24:1 were tested for WPI–$\iota$-CG. A total of 1.0% (w/w) biopolymer into the aqueous phase was used for all experiments. All WPI and CG powder weights used were corrected for both protein


dx.doi.org/10.1021/jf5023669 | J. Agric. Food Chem. 2014, 62, 8730–8739

and carbohydrate concentrations, respectively. Changes in pH upon GDL addition was monitored for each mixture using a Fisher Scientific Accumet pH meter equipped with an Ag/AgCl pH probe (Fisher Scientific, Ottawa, ON, Canada) over time.

*Emulsion Preparation.* Initially, biopolymer solutions were prepared as previously mentioned. Upon addition of the GDL, and equal ratio (1:1) of the aqueous biopolymer solution and canola oil was mixed to a total weight of 10 g. The mixture was subsequently homogenized at 7200 rpm for 5 min using an Omni Macro Homogenizer (Omni International Inc., Marietta, GA, USA) equipped with a 20 mm sawtooth generating probe.

**Interfacial Tension.** The interfacial tension for each WPI−CG mixture was measured using a Lauda TD 2 tensiometer (Lauda-Königshofen, Germany) equipped with a Du Nüoy ring (20 mm diameter). Within a 40 mm diameter glass sample cup, a 20 g biopolymer solution was added and then stirred for 1 min after the addition of 0.5% w/w GDL, followed by the immersion of the Du Nüoy ring and then the addition of the upper canola oil layer (20 g). The ring was then pulled upward to stretch the interface to measure the maximum force without breaking into the oil phase. Interfacial tension was measured over time (50 min) every 600 s, where the mean of three replicates ± one standard deviation was reported. Interfacial tension was calculated from the maximum force ($F_{max}$; units of mN; instrument measures mg × gravity) using equation 1)

$$\gamma = \frac{F_{max}}{4\pi R\beta} \quad (1)$$

where $\gamma$ is the interfacial tension (mN/m), $R$ is the radius of the ring (20 mm), and $\beta$ is a correction factor that depends on the dimensions of the ring and the density of the liquid involved.[32] All measurements are reported as the mean ± one standard deviation ($n$ = 3).

**Oscillatory Shear Deformation of the Bulk Solution.** Oscillatory shear deformation of the bulk biopolymer and emulsion solutions during a GDL acidification was monitored over time using an AR-G2 rheometer (TA Instruments, New Castle, DE, USA) equipped with a 40 mm diameter 2° acrylic cone. A time sweep was performed over a 90 min period to monitor changes in the dynamic storage ($G'$) and loss ($G''$) moduli. Measurements were made within the linear viscoelastic region at a frequency of 1 Hz every 10 s, where the maximum amplitude for strain was set at 1.0%. Following the time sweep, a frequency and strain sweep was performed on the same material to better characterize the formed gel network. During frequency sweeps, frequencies were increased continuously from 0.05 to 100 Hz with 15 points per logarithmic decade being captured, with maximum strain set at 1%. In contrast, strain sweeps were conducted by increasing the applied strain continuously from 0.01 to 500% with 15 data points per logarithmic decade captured at a frequency of 5 Hz. Each sample was prepared in triplicate.

**Oscillatory Shear Deformation at the Oil−Water Interface.** Interfacial oscillatory shear deformation was applied at the oil−water interface using the AR-G2 rheometer equipped with their interfacial bicone fixture. Interfacial oscillatory shear was performed in time sweep mode for 90 min at a frequency of 1 Hz and maximum strain set at 1.0%. Biopolymer solutions with GDL comprised the denser phase beneath the bicone, whereas canola oil comprised the less dense phase above the bicone. All measurements were made within the linear viscoelastic regimen. Each sample was prepared in triplicate.

## RESULTS AND DISCUSSION

**Formation of Electrostatic Coupled Biopolymer Networks.** The rheological properties of WPI−CG mixtures as a function of CG type and mixing ratio during a slow acidification from pH 7.00 to ∼4.20 using GDL are given in Figure 1. In all cases, gel-like properties ($G' > G''$) were evident once the solution pH was reduced to induce complexation between the WPI and CG molecules. In the absence of CG, WPI solutions did not exhibit gel-like properties (data not shown). In the case of the WPI−κ-CG mixture, the crossover point (denoted as the gel point[33]) of $G'$ with $G''$ was found to correspond to pH 5.37, 5.33, and 5.29 for the 16:1, 12:1, and 8:1 WPI−κ-CG mixing ratios, respectively (Figure 1a-c). The pI of WPI has been reported to be at pH 4.6,[34] suggesting that complexation is occurring where both biopolymers are carrying a negative net charge and most likely involve CG interactions with positively charged patches on the protein's surface.[9] At pH above the gel point, biopolymers were assumed to be cosoluble and noninteracting, leading to fluid-like flow behavior ($G' < G''$). Afterward, $G'$ increased substantially indicating a rise in network strength. In the case of the 8:1 mixing ratio, $G'$ approached a plateau regime whereas for the 12:1 and 16:1 ratio a plateau was reached (Figure 1A−C). The magnitude of $G'$ was found to increase as the CG concentration increased within the ratio, where $G'$ was found to be 45.4, 73.1, and 108.0 Pa for 16:1, 12:1, and 8:1 WPI−κ-CG mixing ratios, respectively (Table 1). It was hypothesized that the lower pH at the gel point for the 8:1 mixing ratio reflects a greater viscosity imparted by the higher CG content. Similarly, Perez and co-workers reported that an increase in polysaccharide content led to slower mobility of whey protein−polysaccharide complexes.[35] Therefore, it was hypothesized that the reduced mobility of WPI−CG complexes led to a slower gelation time due to the high viscosity imparted by the high CG content of the system. In the case of the WPI−ι-CG mixture, the gel point was found to correspond to pH 5.34, 5.34, and 5.20 for the 24:1, 20:1, and 16:1 mixing ratios, respectively (Figure 1D,E). A similar increase in the maximum $G'$ was seen with increasing CG content, where the magnitude was found at 52.9, 93.1, and 256.9 Pa for mixing ratios 24:1, 20:1, and 16:1, respectively (Table 1), suggesting it was following a similar mechanism of network formation.

**Table 1. Dynamic Storage ($G'$) and Loss ($G''$) Moduli for Electrostatic Coupled Networks Involving WPI−CG Mixtures As a Function of Mixing Ratio and in the Absence and Presence of Oil after a 90 min Time Sweep Measured at 1 Hz while a 1.0% Constant Strain Was Applied[a]**

| | biopolymer gel | | emulsion gel | |
|---|---|---|---|---|
| mixing ratio | $G'$ (Pa) | $G''$ (Pa) | $G'$ (Pa) | $G''$ (Pa) |
| **WPI−κ-Carrageenan** | | | | |
| 8:1 | 108.0 ± 15.6 | 10.0 ± 0.9 | 522.9 ± 49.8 | 67.5 ± 0.7 |
| 12:1 | 73.1 ± 2.2 | 6.9 ± 0.7 | 435.3 ± 16.2 | 54.5 ± 0.8 |
| 16:1 | 45.4 ± 6.8 | 4.5 ± 0.6 | 257.3 ± 28.5 | 36.2 ± 5.3 |
| **WPI−ι-Carrageenan** | | | | |
| 16:1 | 256.8 ± 29.8 | 26.6 ± 2.9 | 658.5 ± 60.0 | 91.4 ± 9.3 |
| 20:1 | 93.1 ± 1.6 | 9.1 ± 0.2 | 320.4 ± 17.4 | 45.9 ± 3.3 |
| 24:1 | 52.9 ± 12.5 | 5.1 ± 1.0 | 70.8 ± 16.6 | 15.8 ± 1.2 |

[a]All solutions had a total biopolymer concentration of 1.0% (w/w) and were acidified using 0.5% (w/w) GDL to pH 4.28 and 4.15 for the WPI−κ-CG and WPI−ι-CG mixtures, respectively. Data represent the mean value ± one standard deviation.

An increase in the $G'$ or the stiffness of the network has been previously reported by Tavares and co-workers, where the stiffness of whey protein−galactomannan networks was found with an increase in the polysaccharide content.[36] In the absence of CG, acidified WPI solutions did not form a network (data not shown). Therefore, it is assumed that the formation of WPI−CG networks is attributed to the formation of WPI−CG electrostatic complexes due to GDL acidification, which act as junction zones within the gel. Complex formation has been previously reported by others[9,14,15] and is a well-known

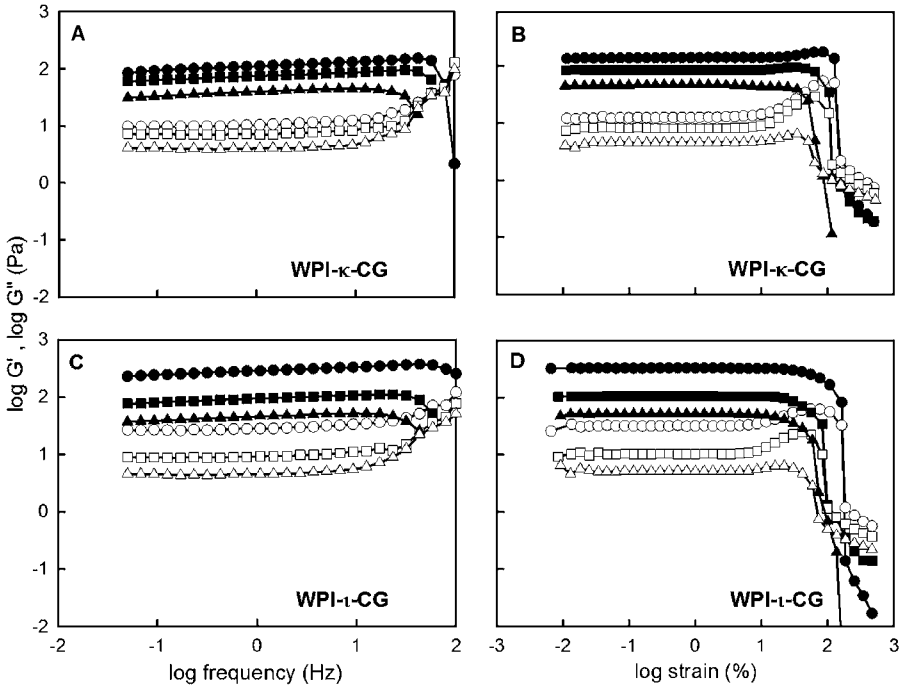


**Figure 2.** Dynamic viscoelastic storage ($G'$, solid symbols) and loss ($G''$, open symbols) moduli for mixtures of WPI−$\kappa$-CG (A, B) and WPI−$\iota$-CG (C, D) at various mixing ratios as a function of frequency (A, C) and strain (B, D). WPI−$\kappa$-CG (A, B) mixtures were mixed at ratios of 8:1 (circles), 12:1 (squares), and 16:1 (triangles), whereas WPI−$\iota$-CG (C, D) mixtures were mixed at 16:1 (circles), 20:1 (squares), and 24:1 (triangles). Each curve is representative of three separate sweep runs on separate samples. All solutions had a total biopolymer concentration of 1.0% (w/w) and were measured at a pH of 4.28 or 4.15 for WPI−$\kappa$-CG and WPI−$\iota$-CG mixtures, respectively.

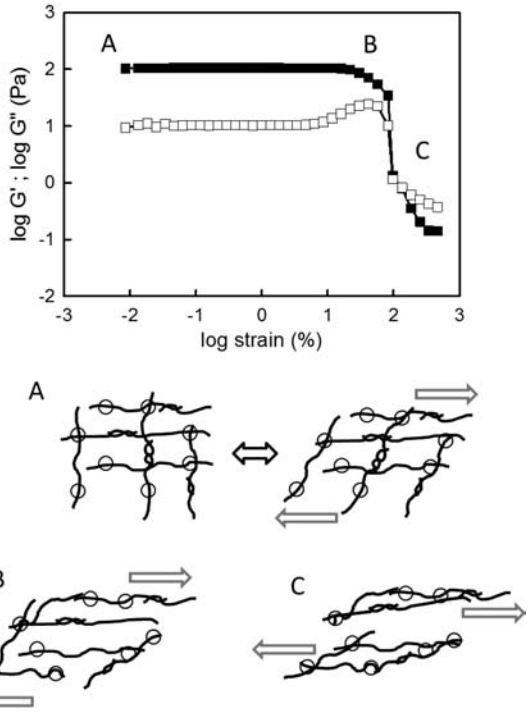


**Figure 3.** Schematic of a sample WPI−$\iota$-CG biopolymer gel at the ratio of 20:1 in response to strain ($G'$, solid symbols; $G''$, open symbols) where gelled networks composed of WPI (open circles) coupled with CG (lines) are elastic at low strains (A) and rearrange in their molecular bonding at higher strains (B), which leads to the breakdown of the network (C). The gray arrows indicate the direction of the applied shear.

phenomenon and therefore is beyond the scope of this paper. In part, coacervation requires the phase separation of the networks, where it is presumed that as proteins approach their p*I*, the precipitation of the proteins and their coacervation with polysaccharides enhance the strength of these networks. In a study of the effects of $\beta$-glucans complexed onto egg yolk stabilized oil-in-water emulsions, Santipanichwong and Suphantharika reported that insoluble $\beta$-glucans compared to soluble $\beta$-glucans exhibited a greater degree of structuring on their own.[37] To gain greater insights into the nature of these networks and to uncover their structural mechanism, they were physically characterized using frequency and strain sweeps.

Oscillatory frequency sweeps for both WPI−$\kappa$-CG and WPI−$\iota$-CG systems after the 90 min time sweep indicated that all materials exhibited gel-like features, regardless of the mixing ratio. Within this regimen, both moduli were slightly frequency dependent, and the magnitude of $G'$ was greater than that of $G''$ (Figure 2A,C). Without acidification, frequency sweeps of these WPI−CG biopolymer solutions were strongly frequency dependent, suggesting a noninteracting mixed biopolymer solution (data not shown). The slight dependence of these GDL acidified WPI−CG mixtures indicates a weak gel structure. Similarly, whey protein−galactomannan networks were also found to be slightly frequency dependent.[36]

Critical strains are helpful in characterizing the breakup of these gels under strain. In a previous study on pure CG gels, Azevedo and co-workers reported that in low ionic content CG mixtures, the critical strain was dependent on the CG content.[38] Similar to the present study, the critical strain decreases with increasing CG content.[38] CG content allowed for greater elasticity within these networks such that critical strains increased with CG content. Critical strain at break for WPI−$\kappa$-CG was found at ∼58.83, ∼73.41, and ∼116.4% for


dx.doi.org/10.1021/jf5023669 | J. Agric. Food Chem. 2014, 62, 8730−8739

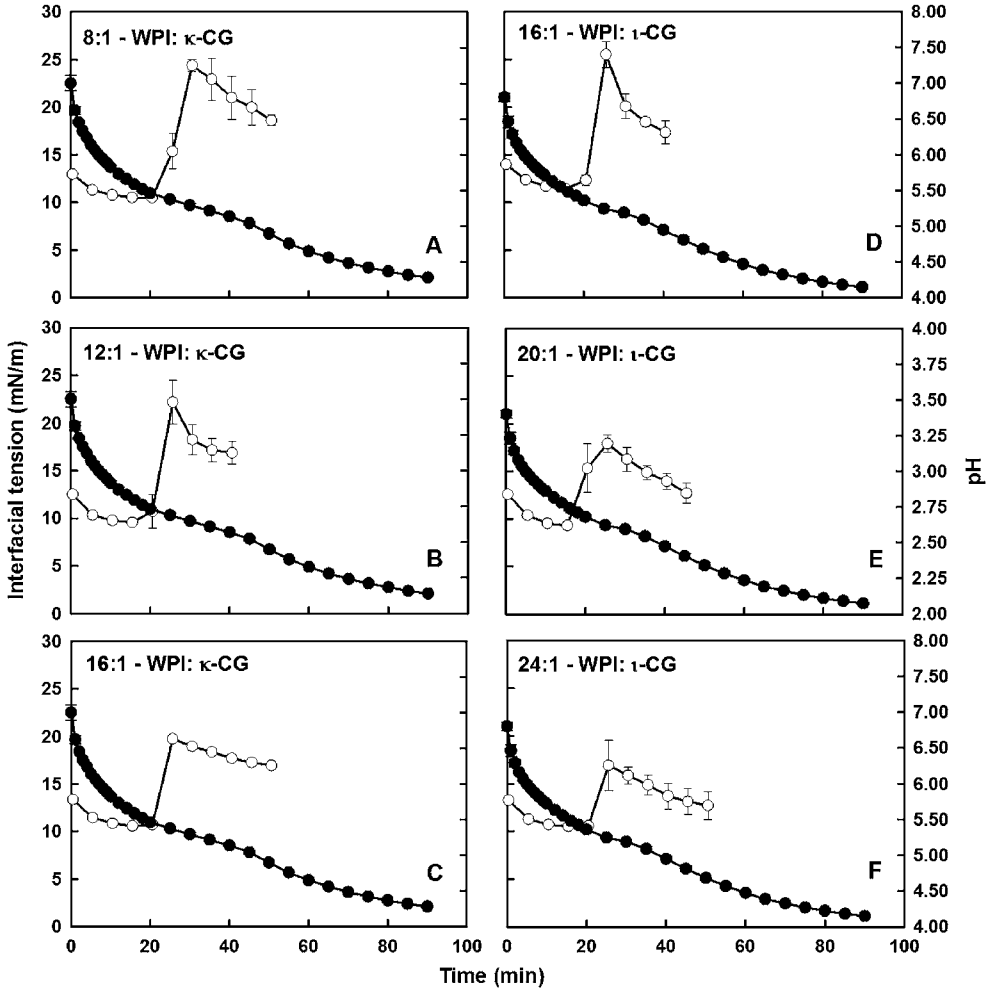


**Figure 4.** Interfacial properties of WPI/CG mixtures at the canola oil−water interface measured by interfacial tension (open circles) reported as the mean ± one standard deviation for mixtures of WPI−*κ*-CG (A−C) and WPI−*ι*-CG (D−F) at various mixing ratios as a function of pH (solid circles) and time (min). All solutions had a total biopolymer concentration of 1.0% (w/w) and were acidified using 0.5% (w/w) GDL.

mixing ratios of 16:1, 12:1, and 8:1, respectively, whereas for WPI−*ι*-CG, critical strain at the break occurred at ∼46.67, ∼74.52, and ∼98.25% for mixing ratios of 24:1, 20:1, and 16:1 respectively (Figure 2B,D). For both systems, the most elastic networks were formed at the highest CG content (i.e., lowest WPI/CG ratios). Networks were also more brittle (i.e., lower critical strain) when *κ*-CG was present relative to *ι*-CG, possibly due to its lower linear charge density, which reduces the number of potential bonds while allowing it to have greater conformational entropy (e.g., flexibility) and possibly more flexible cross-links between WPI molecules within the electrostatic coupled network. In contrast, *ι*-CG would have a higher number of sulfate groups present, leading to a stiffer polysaccharide molecule between the WPI molecules, which builds a stronger network.

The breakdown behavior in the strain sweep reveals the nature of these networks (Figure 2B,D) where the strain-independent behavior observed initially is a result of the elasticity exhibited by the network under low strains. At higher strains, the loss modulus increases slightly before decreasing along with the storage modulus. This strain behavior has been previously characterized as weak strain overshoot behavior by Hyun and co-workers.[39] In weak strain overshoot behavior, although frequency sweeps demonstrate gel-like behavior, their anionic polysaccharide (e.g., xanthan gum in a study by Hyun et al.[36] and CG in this study) was explained to possess large conformational entropy due to electrostatic repulsion within its structure.[39] This allows for alignment and association between biopolymers allowing for a network to form.[39] Hyun and co-workers later reported that weak strain overshoot behavior which results in a local $G''$ maximum is the result of junctions both breaking and forming new ones within the network under high strains.[40] Others have suggested that this localized $G''$ maximum is due to structural rearrangements due to the shear imposed onto the network.[41] Weak strain overshoot behavior was observed for all biopolymer networks formed with WPI−*ι*-CG mixtures and for WPI−*κ*-CG mixtures at a ratio of 16:1. In the case of WPI−*κ*-CG mixtures at ratios of 8:1 and 12:1, strong overshoot behavior was observed,[39] which is caused by the strong interactions formed by the interacting biopolymers. Under strong overshoot behavior, a local maximum for both $G'$ and $G''$ is observed before both rapidly decrease at higher strains. The decrease in both moduli is attributed to the breakdown of the network by shearing. This strain overshoot phenomenon is not unique to these WPI−CG systems but has also been previously reported in other associative biopolymer solutions.[42,43] WPI−CG networks within the present study are formed as a result of GDL acidification causing coacervation.


dx.doi.org/10.1021/jf5023669 | J. Agric. Food Chem. 2014, 62, 8730−8739

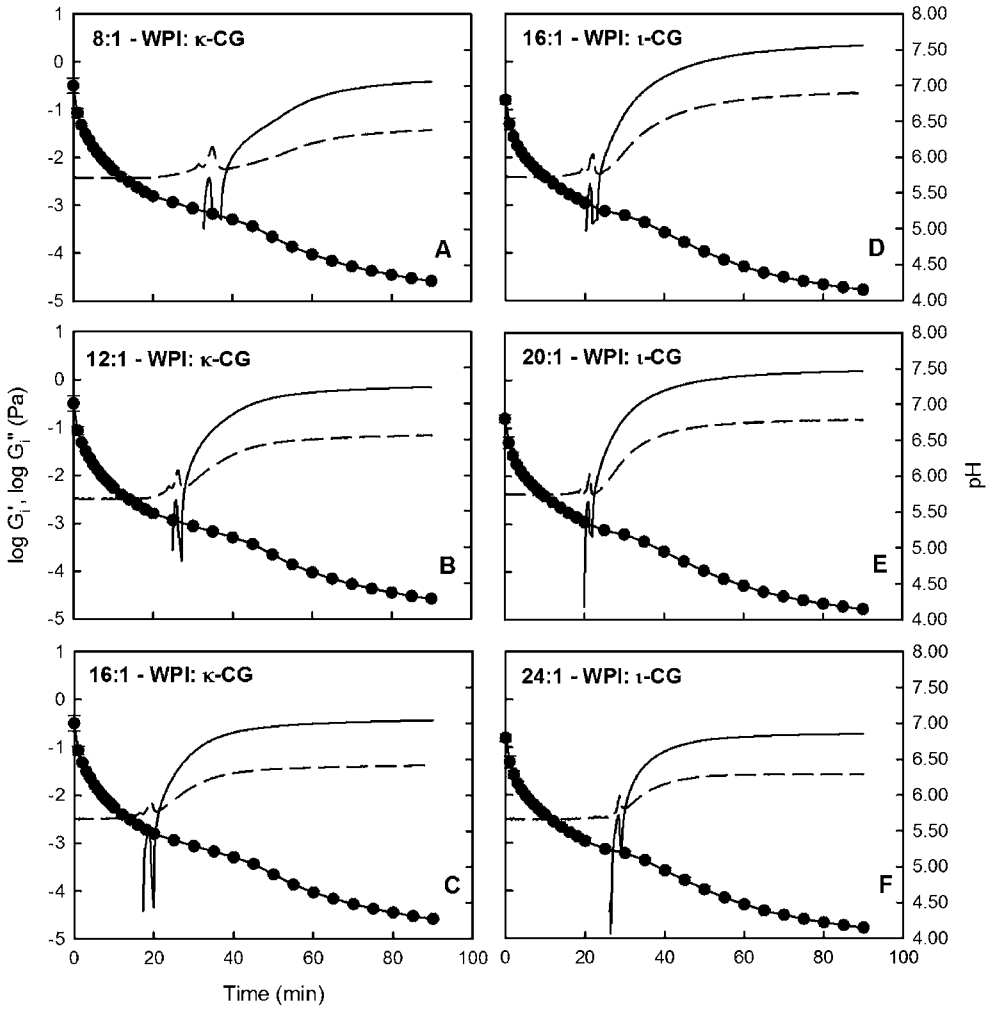


**Figure 5.** Interfacial rheological properties of WPI/CG mixtures at the canola oil−water interface measured by interfacial storage moduli (solid line) and interfacial loss moduli (dashed line) for mixtures of WPI−*κ*-CG (A−C) and WPI−*ι*-CG (D−F) at various mixing ratios as a function of pH (solid circles) and time (min). All solutions had a total biopolymer concentration of 1.0% (w/w) and were acidified using 0.5% (w/w) GDL.

The conformational entropy associated with CG allows for junction zones to be formed with either other CGs or WPIs present in solution (i.e., WPI−WPI, CG−CG, and WPI−CG interactions). These interactions, formed due to acidification over time, allow for a continuous network to be formed as captured by time sweeps under oscillatory stress measurements. Although a continuous network is formed, it is by no means uniform. Figure 3 provides a visual representation of the breakdown of networks under strain which are linked together via CG chains with other CG or WPI biopolymers. These networks are elastic under low-strain amplitudes (Figure 3A) but undergo stress overshoot behavior at higher strains (Figure 3B), which eventually leads to their breakdown (Figure 3C).

**Interfacial Properties of WPI−CG Complexes at the Water-and-Oil Interface.** Due to the amphiphilicity of WPI, the surface activity of WPI−CG mixtures during acidification was measured at the canola oil−water interface. In the absence of biopolymers, the interfacial tension between canola oil and water was found to be ∼28 mN/m, where the addition of WPI alone lowered the interfacial tension to ∼12 mN/m, where interfacial tension remains relatively constant between ∼10 and ∼12 mN/m for the duration for GDL acidification. Interfacial tension and interfacial rheology for WPI−CG mixtures as a function of mixing ratio during a slow acidification with GDL are given in Figures 4 and 5, respectively. Interfacial tension for all systems was found to decrease until reaching a pH where WPI and CG formed electrostatic complexes (Figures 4 and 5). This decline in tension is presumed to be caused by a highly surface active WPI molecule, which is presumed to be integrating alone into the interface rather than the CG molecule over this pH range (from 7.00 to 5.46 and 5.36 for WPI−*κ*-CG and WPI−*ι*-CG mixtures, respectively). At ∼20 min (pH 5.46 and 5.36 for WPI−*κ*-CG and WPI−*ι*-CG mixtures, respectively), a dramatic increase in tension was seen believed to be associated with the electrostatic interactions between WPI and CG. The rise in tension suggests that, possibly, WPI adhering to the interface is being pulled away by electrostatic attractive forces with CG molecules in solution, reducing its ability to lower the interfacial tension. Upon electrostatically interacting with CG molecules, WPI−CG complexes can readhere to the interface to form a stable film, to lower the interfacial tension once again. The decrease in interfacial tension can only be measured until ∼45 min/pH ∼5.00, after which the Du Nüoy ring punctures through the interface due to the formation of an electrostatic coupled gel network within the continuous phase, which would restrict the mobility of the interfacial film (Figure 4). However, it is presumed that free WPI and WPI−CG complexes not involved


dx.doi.org/10.1021/jf5023669 | J. Agric. Food Chem. 2014, 62, 8730−8739

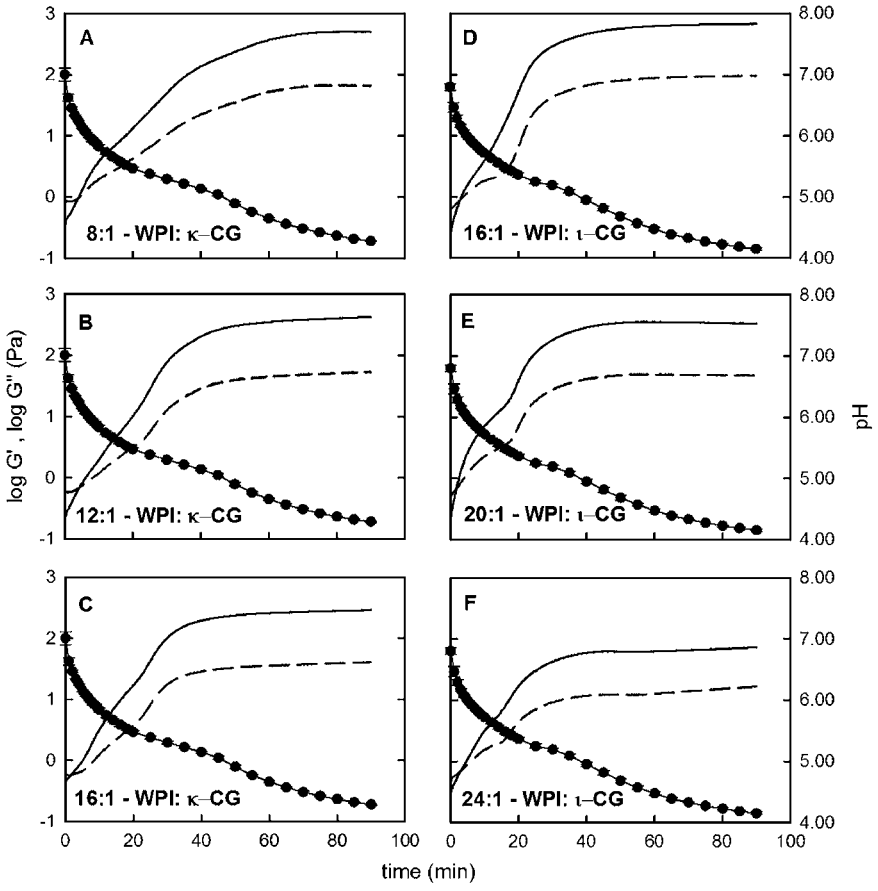


**Figure 6.** Dynamic viscoelastic storage ($G'$, solid line) and loss ($G''$, dashed line) moduli for 1:1 water/canola oil emulsions stabilized with WPI–$\kappa$-CG (A–C) and WPI–$\iota$-CG (D–F) at various mixing ratios measured at 1 Hz with 1.0% constant strain as a function of pH (solid circles) and time (min). Each curve is representative of three separate time sweep runs on separate samples. All solutions had a total biopolymer concentration of 1.0% (w/w) and were acidified using 0.5% (w/w) GDL.

within the network may still adhere to the interface to form a viscoelastic interfacial film.

The interfacial $G_i'$ and $G_i''$ values (Figure 5) within the pH range (7.00–5.41) where the two biopolymers were non-interacting (electrostatically) remained relatively constant. Because the interfacial tension decreased during this interval (Figure 4), it is possible that only WPI molecules were adhering to the oil–water interface. Near the time/pH corresponding to the rise in interfacial tension, small fluctuations or peaks in the $G_i'$ and $G_i''$ data were evident for all materials (Figure 5). These small peaks were found to be dependent upon the mixing ratio, suggesting they might be related to biopolymer interactions and complex formation. In the case of WPI–$\kappa$-CG mixtures, a small peak was observed in both $G_i'$ and $G_i''$ near pH ~5.22, ~5.33, and ~5.42 for the mixing ratios of 8:1, 12:1, and 16:1, respectively (Figure 5A–C). Similarly, for WPI–$\iota$-CG mixtures, a small peak was observed in both $G_i'$ and $G_i''$ within the pH range of ~5.37, ~5.33, and ~5.27 for the mixing ratios of 16:1, 20:1, and 24:1, respectively (Figure 5D,E). As the pH is reduced further, a rise in $G_i'$ values (i.e., so that they become greater than $G_i''$) occurs, until a plateau is reached corresponding to the formation of a viscoelastic interfacial film (Figure 3). For the WPI–$\kappa$-CG mixtures at pH ~4.2, the magnitude of $G_i'$ values was found to be 366.5, 729.6, and 424.2 mPa for the mixing ratios of 16:1, 12:1, and 8:1, respectively (Figure 5A–C), whereas for the WPI–$\iota$-CG mixtures at pH ~4.2, the magnitude of $G_i'$ values was found to be 173.6, 1358, and 2149 mPa for the mixing ratios of 24:1, 20:1, and 16:1, respectively (Figure 5D,E). Differences in the interfacial rheological properties of these two WPI–CG mixtures are attributed to the nature of their coacervation and their sensitivity toward changes in mixing ratio. Whereas WPI–$\kappa$-CG mixtures were reported by Stone and Nickerson to be sensitive toward changes in mixing ratio such that a peak optical density was reached when a 12:1 ratio was used, in contrast, WPI–$\iota$-CG mixtures were not found to be as sensitive to changes in mixing ratio, whereas at the ratio of 20:1 the optical density approached its plateau region.[15] This would account for the viscoelastic maxima at the interface observed for 12:1 WPI–$\kappa$-CG mixtures and the increasing moduli values observed as a function of CG content in WPI–$\iota$-CG mixtures.

**Formation of Electrostatically Coupled Biopolymer Emulsion Gels.** The rheological properties of WPI–CG mixtures as a function of CG type and mixing ratio during a slow acidification from pH 7.00 to ~4.20 using GDL, after being homogenized with canola oil to make an O/W emulsion, are given in Figure 6. For all materials, electrostatically coupled networks were formed as evident by a constant plateau region where $G'$ was greater than $G''$ (Figure 6). For both biopolymer mixtures, the magnitude of $G'$ at pH ~4.2 was found to increase as the mixing ratio decreased, corresponding to an increasing CG content indicating an increase in network strength (Figure 6). For instance, $G'$ was found to be 257.3, 435.3, and 522.9 Pa for the 16:1, 12:1, and 8:1 mixing ratios,


dx.doi.org/10.1021/jf5023669 | J. Agric. Food Chem. 2014, 62, 8730–8739

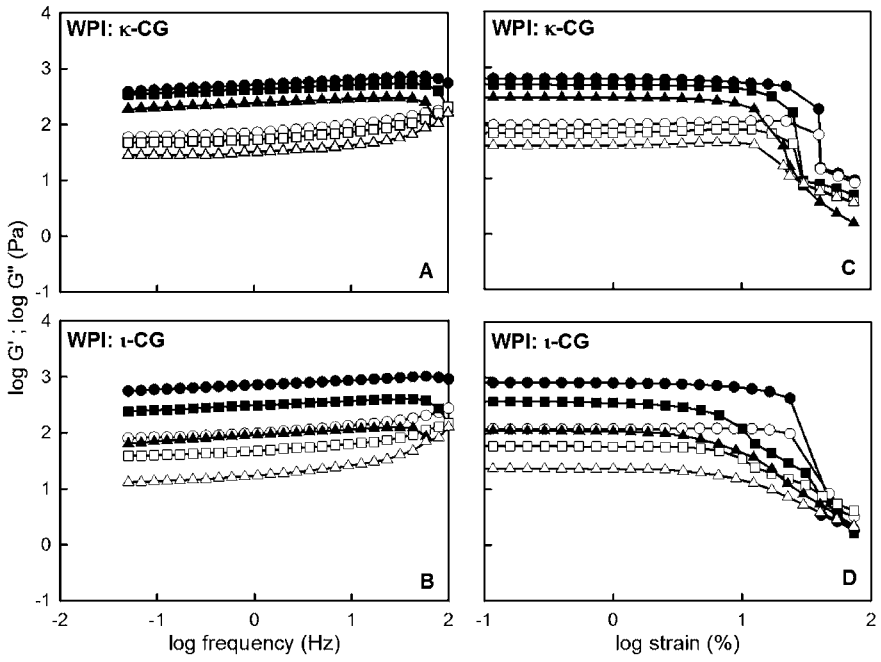


**Figure 7.** Dynamic viscoelastic storage ($G'$, solid symbols) and loss ($G''$, open symbols) moduli for 1:1 water/canola oil emulsions stabilized with WPI−κ-CG (A, C) and WPI−ι-CG (B, D) at various mixing ratios as a function of frequency (A, B) and strain (C, D). WPI−κ-CG (A, C) mixtures were mixed at ratios of 8:1 (circles), 12:1 (squares), and 16:1 (triangles), whereas WPI−ι-CG (B, D) were mixed at 16:1 (circles), 20:1 (squares), and 24:1 (triangles). Each curve is representative of three separate sweep runs on separate samples. All solutions had a total biopolymer concentration of 1.0% (w/w) and were measured at a pH of 4.28 or 4.15 for WPI−κ-CG and WPI−ι-CG mixtures, respectively.

respectively, for the WPI−κ-CG mixture (Table 1). Similarly, $G'$ was found to be 70.8, 320.4, and 658.5 Pa for the 24:1, 20:1, and 16:1 mixing ratios, respectively for the WPI−ι-CG mixture (Table 1). Similar to their biopolymer counterparts, CGs are known for their gelling ability and capacity to form coacervates with WPI. CGs are speculated to form bonds among themselves and with WPI. The conformational entropy associated with CGs allow for a greater number of bonds. It is presumed that three intermolecular interactions are present in this system: CG−CG, WPI−CG coacervate, and CG−CG. Therefore, an increase in CG content leads to better coverage of CG polymers throughout the solvent, leading to a greater number of junction zones and a stronger network. Therefore, the primary difference between mixtures containing κ-CG and ι-CG is that the latter contains a greater number of sulfated groups allowing for a greater number of bonds, leading to its comparatively stronger networks.

After the 90 min time sweep, the frequency and strain dependence of the viscoelastic moduli were measured to characterize these networks (Figure 7). For both the WPI−κ-CG and WPI−ι-CG mixtures, moduli were relatively frequency independent with $G' > G''$ (Figure 7A,B). The slight frequency dependence seen suggests that these networks may be considered as weak gels (Figure 7A,B). In the absence of acidification by GDL, these emulsions were found to be largely frequency dependent (data not shown). This suggests that the coacervation of WPI with CG led to the formation of a continuous gel-like network. Therefore, the strain response of these networks was captured to understand the nature of these networks to propose how these emulsion networks are structured.

Critical strain at the break was found to be ∼26.22, ∼17.77, and ∼8.83% for WPI−κ-CG with mixing ratios of 8:1, 12:1, and 16:1, respectively, and ∼27.35, ∼9.33, and ∼2.41% for WPI−ι-CG with mixing ratios of 16:1, 20:1, and 24:1, respectively (Figure 7C,D). Findings from this study indicate that as the CG content is higher (i.e., lower mixing ratios) within the sample, a more brittle network is formed. Compared to their biopolymer counterparts, these emulsion networks are much more brittle in nature. These emulsion networks were found to be elastic under low strain stresses and broke down when exposed to higher strains. These networks exhibited strain thinning behavior,[40] where structures within the network reorient in the direction of the applied strain. At higher strains, these networks begin to break in the direction of the applied strain and the viscous drag of the system decreases.[40] Beyond this point, increasing strains further break down the network.

Emulsion-based gels also were found to have higher network strength than the corresponding material in the biopolymer-only gels (Figures 1 and 6; Table 1). It is presumed that the greater stiffness of the network is attributed to the incompressibility of droplets and interdroplet interactions occurring within the continuous phase. The critical strains were found to increase with increasing CG content similar to the biopolymer-only networks; however, the strain needed for the emulsion-based gels to induce breakage was much less than the biopolymer gel counterparts, suggesting that they were more brittle in nature. These networks are more brittle in nature in part due to the presence of WPI−CG coacervates at the water−oil interface. Interfacial properties for WPI-CG coacervates reveal their ability to form a viscoelastic film at the water−oil interface. This does not fully explain why increasing CG content leads to stronger networks and does not explain why a similar trend was not observed in interfacial viscoelasticity. At interface, the rheological properties are sensitive to mixing ratio due to the limited space at the surface for bond formation, whereas in a continuous network, network strength is enhanced depending on the availability and


dx.doi.org/10.1021/jf5023669 | J. Agric. Food Chem. 2014, 62, 8730−8739

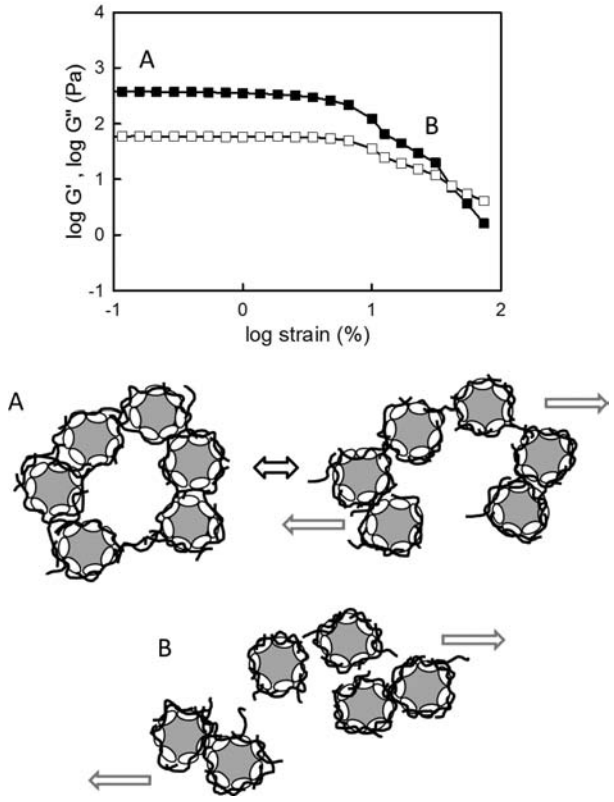


**Figure 8.** Schematic of a sample WPI–*ι*-CG emulsion gel at the biopolymer ratio of 20:1 and an aqueous/oil ratio of 1:1 in response to strain ($G'$, solid symbols; $G''$, open symbols) where the gelled network composed of WPI (open ovals) coupled with CG (lines) stabilizing oil droplets (gray circles) is elastic at low strains (A) and its breakdown at higher strains (B). The gray arrows indicate the direction of the applied shear.

opportunity to form bonds, which create junction zones that give the network strength.

In a study by Santipanichwong and Suphantharika, *β*-glucans were found to enhance the stability of egg yolk emulsions.[37] They were speculated to enhance emulsion stability by either increasing the viscosity of the continuous phase or creation of a three-dimensional network of flocculated droplets.[37] Similar to results reported here, frequency sweeps revealed that Santipanichwong and Suphantharika formed weak gels as well and that the addition of *β*-glucans to egg yolk emulsions had improved their creaming stability.[37] Furthermore, an addition of the polysaccharides to the emulsions had increased the storage modulus (i.e., stiffness) of the networks formed.[37] Kontogiorgos and co-workers, who also studied the influence of *β*-glucans on egg yolk stabilized emulsions, reported that the mechanism for stability depended on the molecular weight of the polysaccharide.[44] Polysaccharides containing lower molecular weights tended to form a network in the continuous phase, whereas higher molecular weight polysaccharides increased the viscosity of the continuous phase.[44] Therefore, enhanced emulsion stability in systems containing multiple biopolymers is reliant on the interactions between the biopolymers involved.

It is speculated that as WPI adheres to the water–oil interface, GDL acidification leads to a coacervate formed at the interface whereby the CG on the outside could bind and cause flocculation with other WPI or CG molecules bound to other droplets. This allows for a continuous network of droplets to form, which becomes the primary means for structuring these emulsion networks. Their brittleness may be attributed to the limited surface interactions between flocculated droplets. This reduces the number of available bonds between the biopolymers, which are needed to stabilize the network. A schematic of these emulsion systems is presented in Figure 8, which represents the breakdown of these emulsion networks under strain. It is speculated that any biopolymers not bound to the water–oil interface becomes available for interacting in the continuous phase, which provides additional strength to the network.

In conclusion, WPI–CG mixtures were found to form an electrostatically coupled continuous network during a slow acidification process using GDL. Networks formed with WPI–*ι*-CG complexes were found to be stronger than those with WPI–*κ*-CG. Although a similar mechanism is proposed for network formation, the difference is attributed to the number of sulfated bonds whereby *ι*-CG may form a greater number of bonds compared to *κ*-CG. Frequency sweeps determined that the networks formed were relatively frequency independent and gel-like. An increase in the CG content led to increased stiffness of these gels. Strain sweeps revealed that gels became increasingly elastic with rising CG levels within the mixing ratio. WPI–CG complexes were found to be surface active and capable of forming viscoelastic films at the water–oil interface. Furthermore, as WPI–CG formed electrostatic complexes, they had a profound impact on the interface, which was observed both by interfacial tension and by interfacial rheology. Due to the surface active properties of the WPI–CG complexes, they were used to stabilize the formed emulsions during gelation. Emulsion gels made with WPI–CG complexes were stiffer compared to their biopolymer counterparts but were comparatively much more brittle. The comparative difference in brittleness is attributed to the differences in the structure of these two networks. It is speculated that the large conformational entropy associated with CGs enabled their capacity to form a three-dimensionsal network as a biopolymer solution. Overall, the surface activity of WPI and their coacervation with CGs enabled a WPI-stabilized, flocculated emulsion interlinked by CGs.

## AUTHOR INFORMATION

### Corresponding Author

*(M.T.N.) Phone: (306) 966-5030. Fax: (306) 966-8898. E-mail: Michael.Nickerson@usask.ca.

### Funding

Financial support for this research was provided by the National Science and Engineering Research Council of Canada and the Canadian Dairy Commission (through scholarship support for R.S.H.L).

### Notes

The authors declare no competing financial interest.

## REFERENCES

(1) Mulvihill, D. M. Production, functional properties and utilization of milk protein products. In *Advanced Dairy Chemistry*, 1st ed.; Fox, P. F., Ed.; Elsevier Applied Science: London, UK, 1992; Vol. 1, p 781.

(2) Tang, Q. N.; McCarthy, O. J.; Munro, P. A. Gelling characteristics of egg-white, whey-protein concentrates, whey-protein isolate, and *β*-lactoglobulin. *J. Agric. Food Chem.* **1994**, *42*, 2126–2130.

(3) Elofsson, C.; Djmek, P.; Paulsson, M.; Burling, H. Characterization of a cold-gelling whey protein concentrate. *Int. Dairy J.* **1997**, *7*, 601–608.

(4) Gulzar, M.; Lechevalier, V.; Bouhallab, S.; Croguennec, T. The physicochemical parameters during dry heating strongly influence the gelling properties of whey proteins. *J. Food Eng.* **2012**, *112*, 296−303.
(5) Reiffers-Magnani, C. K.; Cuq, J. L.; Watzke, H. J. Depletion flocculation and thermodynamic incompatibility in whey protein stabilized O/W emulsions. *Food Hydrocolloids* **2000**, *14*, 521−530.
(6) Tcholakova, S.; Denkov, N. D.; Ivanov, I. B.; Campbell, B. Coalescence stability of emulsions containing globular milk proteins. *Adv. Colloid Interface Sci.* **2006**, *123*, 259−293.
(7) Manoi, K.; Rizvi, S. S. H. Emulsification mechanisms and characterizations of cold, gel-like emulsions produced from texturized whey protein concentrate. *Food Hydrocolloids* **2009**, *23*, 1837−1847.
(8) van de Velde, F.; Knutsen, S. H.; Usov, A. L.; Rollema, H. S.; Cerezo, A. S. $^{1}$H and $^{13}$C high resolution NMR spectroscopy of carrageenans: aplication in research in industry. *Trends Food Sci. Technol.* **2002**, *13*, 73−92.
(9) Weinbreck, F.; Nieuwenhuijse, H.; Robjijn, G. W.; de Kruif, C. G. Complexation of whey proteins with carrageenan. *J. Agric. Food Chem.* **2004**, *52*, 3550−3555.
(10) Knutsen, S. H.; Myladobodski, D. E.; Larsen, B.; Usov, A. I. A modified system of nomenclature for red algal galactans. *Bot. Mar.* **1994**, *37*, 163−169.
(11) Morris, E. R.; Rees, D. A.; Robinson, G. Cation-specific aggregation of carrageenan helicies − domain model of polymer gel structure. *J. Mol. Biol.* **1980**, *138*, 349−362.
(12) Rochas, C.; Rinaudo, M. Mechanism of gel formation in κ-carrageenan. *Biopolymers* **1984**, *23*, 735−745.
(13) Souza, H. K. S.; Hiliou, L.; Bastos, M.; Goncalves, M. P. Effect of molecular weight and chemical structure on thermal and rheological properties of gelling κ/ι-hybrid carrageenan solutions. *Carbohydr. Polym.* **2011**, *85*, 429−438.
(14) de Kruif, C. G.; Weinbreck, F.; de Vries, R. Complex coacervation of proteins and anionic polysaccharides. *Curr. Opin. Colloid Interface Sci.* **2004**, *9*, 340−349.
(15) Stone, A. K.; Nickerson, M. T. Formation and functionality of whey protein isolate-(κ-, ι-, and λ-type) carrageenan electrostatic complexes. *Food Hydrocolloids* **2012**, *27*, 271−277.
(16) Schmitt, C.; Sanchez, C.; Desobry-Banon, S.; Hardy, J. Structure and technofunctional properties of protein-polysaccharide complexes: a review. *Crit. Rev. Food Sci. Nutr.* **1998**, *38*, 689−753.
(17) Doublier, J. L.; Garnier, C.; Renard, D.; Sanchez, C. Protein-polysaccharide interactions. *Curr. Opin. Colloid Interface Sci.* **2000**, *5*, 202−214.
(18) Nakagawa, K.; Iwamoto, S.; Nakajima, M.; Shono, A.; Satoh, K. Microchannel emulsification using gelatin and surfactant-free coacervate microencapsulation. *J. Colloid Interface Sci.* **2004**, *278*, 198−205.
(19) Katona, J. M.; Sovilj, V. J.; Petrovic, L. B. Microencapsulation of oil by polymer mixture-ionic surfactant interaction induced coacervation. *Carbohydr. Polym.* **2010**, *79*, 563−570.
(20) Moschakis, T.; Murray, B. S.; Biliaderis, C. G. Modifications in stability and structure of whey protein-coated o/w emulsions by interacting chitosan and gum arabic mixed dispersions. *Food Hydrocolloids* **2010**, *24*, 8−17.
(21) Li, Y.; McClements, D. J. Inhibition of lipase-catalyzed hydrolysis of emulsified triglyceride ois by low-molecular weight surfactants under simulated gastrointestinal conditions. *Eur. J. Pharm. Biopharm.* **2011**, *79*, 423−431.
(22) Koupantsis, T.; Pavlidou, E.; Paraskevopoulou, A. Flavour encapsulation in milk proteins − CMC coacervate type complexes. *Food Hydrocolloids* **2014**, *37*, 134−142.
(23) Li, X.; Fang, Y.; Pilips, G. O.; Saphwan, A.-A. Improved sugar beet pectin-stabilized emulsions through complexation with sodium caseinate. *J. Agric. Food Chem.* **2013**, *61*, 1388−1396.
(24) Gao, Z.-M.; Yang, X.-Q.; Wu, N.-N.; Wang, L.-J.; Wang, J.-M.; Guo, J.; Yin, S.-W. Protein-based pickering emulsion and oil gel prepared by complexes of zein colloidal particles and stearate. *J. Agric. Food Chem.* **2014**, *62*, 2672−2678.
(25) Salminen, H.; Weiss, J. Electrostatic adsorption and stability of whey protein-pectin complexes on emulsion interfaces. *Food Hydrocolloids* **2014**, *35*, 410−419.
(26) Blijdenstein, T. B. J.; van Winden, A. J. M.; van Vliet, T.; van der Linden, E.; van Aken, G. A. Serum separation and structure of depletion- and bridging-flocculated emulsions: a comparison. *Colloid Surf., A* **2004**, *245*, 41−48.
(27) Dickinson, E. Emulsion gels: the structuring of soft solids with protein-stabilized oil droplets. *Food Hydrocolloids* **2012**, *28*, 224−241.
(28) Huang, P. H.; Lu, H. T.; Wang, Y. T.; Wu, M. C. Antioxidant activity and emulsion-stablizing effect of pectic enzyme treated pectin in soy protein isolate-stabilized oil/water emulsion. *J. Agric. Food Chem.* **2011**, *59*, 9623−9628.
(29) Liu, F.; Jiang, Y. F.; Du, B. J.; Chai, Z.; Jiao, T.; Zhang, C. Y.; Ren, F. Z.; Leng, X. J. Design and characterization of controlled-release edible packaging films prepared with synergistic whey-protein polysaccharide complexes. *J. Agric. Food Chem.* **2013**, *61*, 5824−5833.
(30) Zhu, D.; Damodaran, S.; Lucey, J. A. Physicochemical and emulsifying properties of whey protein isolate (WPI)-dextran conjugates produced in aqueous solution. *J. Agric. Food Chem.* **2010**, *58*, 2988−2994.
(31) Association of Official Analytical Chemists (AOAC). In *Official Methods of Analysis*, 17th ed.; AOAC: Washington, DC, USA, 2003.
(32) McClements, D. J. In *Food Emulsions: Principles, Practice and Techniques*, 2nd ed.; Taylor & Francis Group: Boca Raton, FL, USA, 2005; 632 pp.
(33) Winter, H. H.; Chambon, F. Analysis of linear viscoelasticity of a crosslinking polymer at the gel point. *J. Rheol.* **1986**, *30*, 367−392.
(34) Parris, N.; Baginski, M. A. A rapid method for the determination of whey-protein denaturation. *J. Dairy Sci.* **1991**, *74*, 58−64.
(35) Perez, A. A.; Carrara, C. R.; Sánchez, C. C.; Santiago, L. G.; Patino, J. M. R. Interfacial dynamic properties of whey protein concentrate/polysaccharide mixtures at neutral pH. *Food Hydrocolloids* **2009**, *23*, 1253−1262.
(36) Tavares, C.; Monteiro, S. R.; Moreno, N.; Lopes da Silva, J. A. Does the branching degree of galactomannans influence their effect on whey protein gelation? *Colloid Surf., A* **2005**, *270*−*271*, 213−219.
(37) Santipanichwong, R.; Suphantharika, M. Influence of different β-glucans on the physical and rheological properties of egg yolk stabilized oil-in-water emulsions. *Food Hydocolloids* **2009**, *23*, 1279−1287.
(38) Azevedo, G.; Bernardo, G.; Hilliou, L. NaCl and KCl phase diagrams of κ/ι-hybrid carrageenans extracted from *Mastocarpus stellatus*. *Food Hydrocolloids* **2014**, *37*, 116−123.
(39) Hyun, K.; Kim, S. H.; Ahn, K. H.; Lee, S. J. Large amplitude oscillatory shear as a way to classify the complex fluids. *J. Non-Newtonian Fluid Mech.* **2002**, *107*, 51−65.
(40) Hyun, K.; Wilhelm, M.; Klein, C. O.; Cho, K. S.; Nam, J. G.; Ahn, K. H.; Lee, S. J.; Ewoldt, R. H.; McKinley, G. H. A review of nonlinear oscillatory shear tests: analysis and application of large amplitude oscillatory shear (LAOS). *Prog. Polym. Sci.* **2011**, *36*, 1697−1753.
(41) Parthasarathy, M.; Klingenberg, D. J. Large amplitude oscillatory shear of ER suspensions. *J. Non-Newtonian Fluid Mech.* **1999**, *81*, 83−104.
(42) Tirtaatmadja, V.; Tam, K. C.; Jenkins, R. D. Superposition of oscillations on steady shear flow as a technique for investigating the structure of associative polymers. *Macromolecules* **1997**, *30*, 1426−1433.
(43) Tam, K. C.; Guo, L.; Jenkins, R. D.; Basset, D. R. Viscoelastic properties of hydrophobically modified alkali-soluble emulsions in salt solutions. *Polymer* **1999**, *40*, 6369−6379.
(44) Kontogiorgos, V.; Biliaderis, C. G.; Kiosseoglou, V.; Doxastakis, G. Stability and rheology of egg-yolk-stabilized concentrated emulsions containing cereal β-glucans of varying molecular size. *Food Hydrocolloids* **2004**, *18*, 987−998.

JOURNAL OF AGRICULTURAL AND FOOD CHEMISTRY

Article

pubs.acs.org/JAFC

# High Concentrations of Furan Fatty Acids in Organic Butter Samples from the German Market

Christine Wendlinger and Walter Vetter*

Institute of Food Chemistry (170b), University of Hohenheim, Garbenstraße 28, D-70599 Stuttgart, Germany

Supporting Information

**ABSTRACT:** Furan fatty acids (F-acids) are valuable antioxidants containing a furan moiety in the central part of the molecule. They occur in the lipids of different foodstuffs and plants, with grass being the main source for their presence in milk fat and butter. Because cows from organic farming receive higher portions of grass-based feed, it was tested whether organic butter samples ($n$ = 26) contain more F-acids than conventional ones ($n$ = 25) in Germany. For this purpose, samples were melted, and the lipid phase was separated and transesterified into methyl esters, which were enriched using silver ion chromatography and analyzed by GC-EI/MS in the selected ion monitoring (SIM) mode. Levels of F-acids in butter were higher in summer than in winter, and in both seasons, organic samples contained significantly higher levels of F-acids than conventional ones (one-way ANOVA: $p < 0.001$). Furthermore, the daily intake of F-acids via milk fat and other foodstuffs was calculated.

**KEYWORDS:** *furan fatty acids, organic butter, conventional butter, silver ion chromatography, daily intake*

## INTRODUCTION

Recent lipid research has shown that not only major fatty acids but also different classes of bioactive minor fatty acids, such as furan fatty acids (F-acids), contribute to the nutritional benefits of fats or oils.[1−3] F-acids are fatty acids containing a furan moiety in the central part of the acyl chain. The $\alpha$-position of the furan ring carries a carboxyalkyl chain typically with 7, 9, 11, or 13 carbons, and the $\alpha'$-position is substituted with a propyl or pentyl chain.[1] In addition, the $\beta$- and $\beta'$-positions may be substituted with one (methyl-substituted F-acids) or two methyl groups (dimethyl-substituted F-acids). F-acids are known to serve as hydroxyl and peroxyl radical scavengers and thus are able to protect polyunsaturated fatty acids from lipid peroxidation.[4,5] Furthermore, the anti-inflammatory activity of F-acids had been confirmed in vivo.[6] These natural antioxidants occur widely in foods including fish,[7−10] olive oil,[11] soybean oil,[12−14] rapeseed oil,[12] and butter.[15] Plants are able to synthesize F-acids from acetate, methionine, and oxygen from air, whereas F-acids in fish originate from the intake of algae and those in milk fat from the intake of grass and other plants by cows.[1] Concentrations of F-acids in butter ranged from 4.5 to 47.6 mg/100 g.[15,16] High amounts of F-acids also occurred in grass,[17] and because F-acids in milk fat originate from the cow's feed, we aimed to investigate whether there is a difference in the concentrations of F-acids in butter samples from organic and conventional farming due to higher proportions of pasture and hay fed in organic farming. For this purpose, F-acid methyl esters of 51 butter samples were enriched using silver ion microcolumn chromatography and analyzed by gas chromatography with mass spectrometry (GC-MS) operated in the selected ion monitoring (SIM) mode according to the method of Vetter et al.[16] On the basis of our results for butter and published concentrations of F-acids in other foodstuffs, we estimated the dietary daily intake of F-acids, as well as the corresponding share of milk fat in Germany.

## MATERIALS AND METHODS

**Samples.** Butter samples (26 organic and 25 conventional ones) were purchased from different supermarkets located in Stuttgart, Germany, between January 2012 and January 2014. Most of the samples originated from southwestern, southeastern, and northeastern Germany. Samples from summer and winter were included in the study. Information about the type of butter (sweet or sour cream), the farming system (organic or conventional), and the minimum durability dates (MDD) were provided on the packaging. Samples were assigned to winter/summer season by backdating MDD for 2 months to take into account the period from milking to the date printed as MDD on the label. The "summer" period was set from May to October and "winter" from November to April. This division resulted in four groups: winter conventional ($n$ = 14), winter organic ($n$ = 13), summer conventional ($n$ = 11), and summer organic ($n$ = 13).

**Chemicals and Standards.** Methanol and $n$-hexane (both of HPLC grade, ≥95% purity) were from Th. Geyer (Renningen, Germany). Sulfuric acid was from BASF (Ludwigshafen, Germany). Diethyl ether (for synthesis, ≥99%) and NaCl (≥99.5%) were from Carl Roth (Karlsruhe, Germany). Silica gel 60, $AgNO_3$, and myristic acid were from Sigma-Aldrich (Steinheim, Germany). The abbreviated nomenclature and preparation of the internal standard (IS) 10,13-epoxy-11-methyloctadeca-10,12-dienoic acid ethyl ester (9M5-EE) were according to Vetter et al.[16] Myristic acid ethyl ester (14:0-EE) was prepared by heating myristic acid with 1% sulfuric acid in ethanol.

**Sample Preparation and Transesterification.** Butter samples (~4 g) were melted at ~70 °C, and the supernatant clear lipid phase was separated (~2 g). For the formation of fatty acid methyl esters (FAME) about ~20 mg per sample was treated with 1.5 mL of 1% sulfuric acid in methanol in a small sealed tube at 80 °C for 1 h, which was shaken from time to time. Then, 1 mL of saturated aqueous NaCl solution and 1 mL of demineralized water were added, and FAME were extracted once using 2 mL of $n$-hexane.

Received: June 23, 2014
Revised: August 6, 2014
Accepted: August 7, 2014
Published: August 7, 2014

ACS Publications © 2014 American Chemical Society

**Enrichment of F-Acids by Silver Ion Micro Column Chromatography.** Silver ion microcolumn chromatography was performed according to the method of Vetter et al. with slight amendments.[16] In brief, an aliquot of the organic layer (~180−250 μL) was supplemented with 0.87 μg of the internal standard 9M5-EE, and the solution was placed on a Pasteur pipet (the tip was plugged with glass wool) containing ~0.6 g of 1% deactivated silica gel with 20% $AgNO_3$. Fraction 1 containing saturated and the majority of the monounsaturated fatty acids was eluted with 15 mL of *n*-hexane/diethyl ether (99.5:0.5, v/v). Fraction 2 containing F-acids was eluted with 15 mL of *n*-hexane/diethyl ether (97:3, v/v). Both fractions were individually evaporated at 38 °C by means of a gentle stream of nitrogen, the residue was transferred with *n*-hexane into a GC vial, and the volume of the solution was adjusted to 1 mL. Afterward, the second internal standard, 14:0-EE, was added, and the solution was analyzed by GC-MS. During the sample preparation, oxidation of F-acids was minimized by using amber glass and performing each step under the lowest possible lighting level.

**Gas Chromatography Coupled to Electron Ionization Mass Spectrometry (GC-EI/MS).** All analyses were carried out with a 5890 series II/5971A GC/MS system in combination with a 7673A autosampler (Hewlett-Packard/Agilent, Waldbronn, Germany). The carrier gas, helium (purity 5.0), was transported at a flow rate of 1 mL/min through two serially coupled 30 m columns (Rtx-2330, internal diameter = 0.25 mm, coated with 0.1 μm of 10% cyanopropylphenyl, 90% biscyanopropyl polysiloxane, Restek, Bellefonte, PA, USA). The GC oven program started at 60 °C for 1 min. It followed ramps of (i) 13 °C/min to 180 °C, (ii) 3 °C/min to 225 °C, and (iii) 20 °C/min to 250 °C. The final temperature was held for 5 min, and the solvent delay was set to 8 min. GC-MS measurements in the full scan mode covered *m/z* 50−500. In the SIM mode four ions (*m/z* 137, 151, 165, and 179) were measured throughout the run. Additionally, three further ions, divided into four time windows, were recorded: (I) 8−13 min, *m/z* 74, 88, 101; (II) 13−19.5 min, *m/z* 74, 294, 308; (III) 19.5−23 min, *m/z* 322, 336, 350; (IV) 23−31 min, *m/z* 364, 378, 392. Peak identification was carried out in the full scan mode, whereas quantification was performed in the SIM mode using 14:0-EE and 9M5-EE as internal standards.[16]

**Quantification Mode, Data Reporting, and Statistical Analysis.** The IS 9M5-EE was calibrated against 12,15-epoxy-13-methyleicosa-12,14-dienoic acid ethyl ester (11M5-EE) and 12,15-epoxy-13,14-dimethyleicosa-10,12-dienoic acid ethyl ester (11D5-EE). Because the peak areas at the same concentration did not deviate by more than 5%, 9M5-EE was used for the quantification of all F-acids as methyl esters. The quantitative results were further verified by standard addition experiments using 11D5-ME. All preparation steps were performed in duplicate, and for each sample mean values were calculated (individual values of replicates did not vary by more than 10%); the results were expressed as milligrams per 100 g of fat. The limit of quantification (LOQ) and the limit of detection (LOD) were 0.4 and 0.12 mg/100 g fat, respectively. For the calculation of total concentrations of F-acids in the samples, individual values below LOD were taken into account by using half the LOD (i.e., 0.06 mg/100 g fat). The F-acid concentrations were evaluated by one-way ANOVA as integrated in EXCEL. Significance was based on a probability of 0.05.

## RESULTS AND DISCUSSION

**F-Acid Variety and Pattern in Butter Samples.** Between two and six F-acids were detected by GC-MS in the 51 butter samples (Figure 1; Supporting Information Table S1). Highest concentrations were generally determined for 10,13-epoxy-11,12-dimethyloctadeca-10,12-dienoic acid (9D5) and 11D5, which represented 60−100% of the total amount of F-acids in the samples. A clear dominance of dimethyl-substituted F-acids (11D5 and 9D5) over methyl-substituted F-acids was also reported in previous studies.[15,16] These two major F-acids were partly accompanied by 11M5, 8,11-epoxy-9,10-dimethylhexadeca-8,10-dienoic acid (7D5), 9M5, and 14,17-epoxy-15,16-dimethyleicosa-14,16-dienoic acid (13D3). Depending on the abundance of the individual F-acids, most commonly four (7D5, 9M5, 9D5, and 11D5; 18 samples) or five (additionally 11M5; 17 samples) F-acids were present in the samples (Figure 1; Table S1). In five butter samples only two F-acids and in nine samples only three F-acids were detectable, whereas six F-acids were present in two cases (Figure 1; Table S1). A similar F-acid pattern was also reported in grass (blade).[16,17] Thus, it seems obvious that the occurrence of (especially dimethyl-substituted) F-acids in grass lipids and pasture was linked with the presence of F-acids in milk and butter fat.

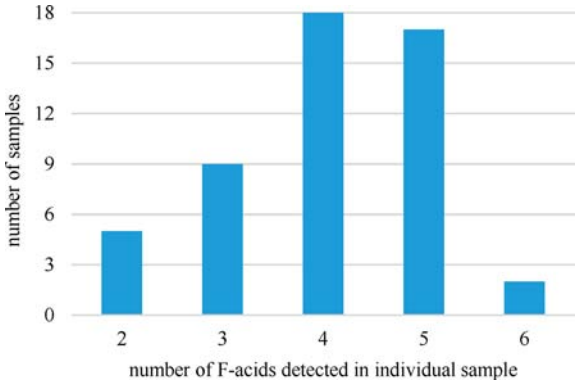


**Figure 1.** Frequency of the number of F-acids in butter samples from the German market.

**Concentrations of F-Acids in Organically or Conventionally Produced Butter Samples.** The total F-acid content in the samples ranged from 1.6 to 16.5 mg/100 g fat. Sweet cream and sour cream butter samples showed no difference in the F-acid pattern, yet the concentrations of F-acids were 3-fold lower than those reported by Guth and Grosch.[15] Concentrations of F-acids in organic butter samples (5.4−16.5 mg/100 g fat, $n = 26$) were significantly higher than in conventional samples (1.6−7.1 mg/100 g fat, $n = 25$) (one-way ANOVA: $p < 0.001$). The same result could be obtained by the sole evaluation of the summed concentration of 9D5 and 11D5 (one-way ANOVA: $p < 0.001$). However, 13 organic samples (all winter samples) with the lowest content of F-acids showed lower concentrations than the conventional sample with the highest F-acid content. This overlap did not allow unequivocally distinguishing organic from conventional butter samples.

Subsequently, the samples were further divided depending on the season into four groups (see Materials and Methods), that is, winter conventional ($n = 14$), winter organic ($n = 13$), summer conventional ($n = 11$), and summer organic ($n = 13$) (Table 1). Organic samples collected in summer (May−October) generally contained higher amounts of F-acids than samples from the winter months (November−April) (Table 1; one-way ANOVA: $p < 0.001$). Also, no overlap of the F-acid concentration range was observed for conventional samples collected in summer versus winter (Table 1; one-way ANOVA: $p < 0.001$). The widest ranges for F-acid concentrations were observed for conventional samples in winter and organic samples in summer, whereas ranges in organic butter samples collected in winter and conventional ones of the summer season were surprisingly small (Table 1). These wider ranges in the F-acid content could be due to a higher flexibility in the composition of the feed. Analysis of samples from the same producer in summer and winter showed the typical seasonal dependency of the F-acid concentrations. Accordingly, the


dx.doi.org/10.1021/jf502975b | J. Agric. Food Chem. 2014, 62, 8740−8744

**Table 1. F-Acid Concentrations in Butter Samples, Dependent on Season (Summer from May to October, Winter from November to April, According to the Backdated Minimum Durability Dates)**

| | winter samples (mg/100 g fat) | | summer samples (mg/100 g fat) | |
|---|---|---|---|---|
| F-acid | conventional ($n$=14) | organic ($n$=13) | conventional ($n$=11) | organic ($n$=13) |
| 7D5 | 0.1[a]–0.9 | 0.6–1.2 | 0.1[a]–1.1 | 0.7–2.2 |
| 9M5 | 0.1[a]–0.9 | 0.1[a]–1.2 | 0.1[a]–1.1 | 0.5–1.5 |
| 9D5 | 0.1[a]–1.9 | 1.7–2.5 | 1.7–2.6 | 1.7–5.6 |
| 11M5 | 0.1[a]–0.5 ($n$ = 1) | 0.1[a]–0.8 | 0.1[a]–0.6 | 0.1[a]–1.1 |
| 11D5 | 0.6–1.8 | 1.8–2.5 | 1.8–2.8 | 2.8–6.4 |
| 13D3 | 0.1[a] | 0.1[a] | 0.1[a]–0.4 ($n$ = 1) | 0.1[a]–0.4 ($n$ = 1) |
| Σ | 1.6–5.1 | 5.4–6.6 | 5.2–7.1 | 7.5–16.5 |
| mean (Σ) | 3.4 | 5.9 | 6.0 | 10.6 |
| median (Σ) | 3.4 | 6.0 | 6.0 | 9.5 |

[a]Values below LOQ were included to sum with 1/2 LOD (i.e., 0.06 mg/100 g fat).

processing technology of butter did not have a primary effect on the F-acid concentrations in butter. Moreover, the potential impact of the geographical origin of the milk samples was evaluated as follows. The four previously mentioned groups were further divided according to their geographical origins in southeastern, southwestern, and northeastern Germany. Irrespective of the sample group, the F-acid concentration ranges of the geographical groups were overlapping, and data analysis by one-way ANOVA did not show significant deviations ($p > 0.2$). Accordingly, organic or conventional farming systems could not be differentiated by their geographical position in Germany. However, by taking the season into account, it was possible to distinguish organic from conventional samples without exception (Figure 2).

Thus, the concentrations of F-acids may serve as a useful marker for the authentication of organic butter, especially in combination with other analytical markers such as the concentration of n-3 fatty acids,[18−21] the concentration and diastereomer ratio of phytanic acid,[22−25] the $\delta^{13}C$ values of milk fat,[26,27] or the fatty acid and triacylglycerol profiles.[28,29]

**Nutritional Intake of F-Acids in Germany.** Our data suggested that the intake of F-acids through milk and dairy products may vary up to the factor of 3, depending on the season and farming system (Table 1). From these findings we estimated the daily intake of F-acids by the consumption of milk and butter, as well as their percentage contribution of the nutritional intake.

The average daily milk fat intake in Germany was reported to be about 20−45 g per day.[30] On the basis of the mean values (Table 1), the daily intake of F-acids via milk fat amounted to 0.7−1.5 mg (full range, 0.3−2.3 mg; 1.1 mg mean of mean, which corresponds to 32.5 g milk fat) for conventional samples in winter, 1.2−2.7 mg (full range, 1.1−3.0 mg, mean of mean 1.9 mg) for organic samples in winter, 1.2−2.7 mg (full range, 1.0−3.2 mg, mean of mean 2.0 mg) for conventional samples in summer, and up to 2.1−4.8 mg (full range, 1.5−7.4 mg, mean of mean 3.4 mg) for organic ones in summer (Figure 3). Thus, the daily intake of F-acids via milk fat was highest for organic samples in summer.

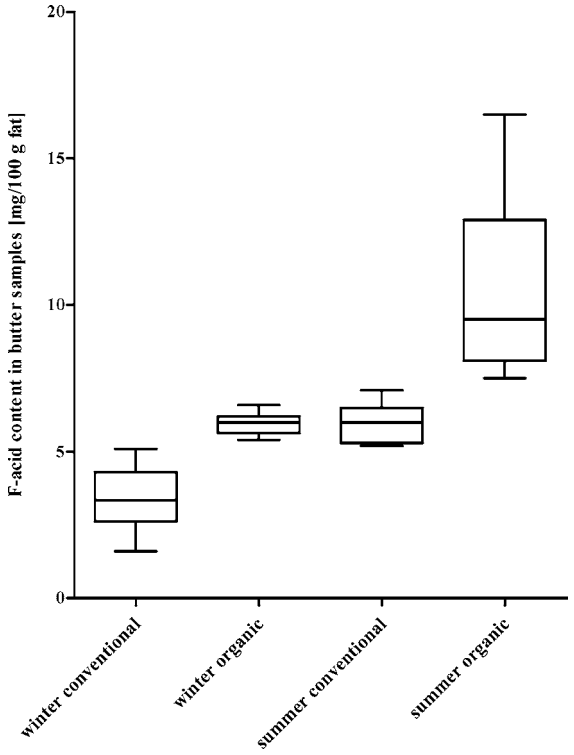


**Figure 2.** Concentration ranges of F-acids (mg/100 g fat) in organic and conventional butter samples collected in summer and winter in Germany.

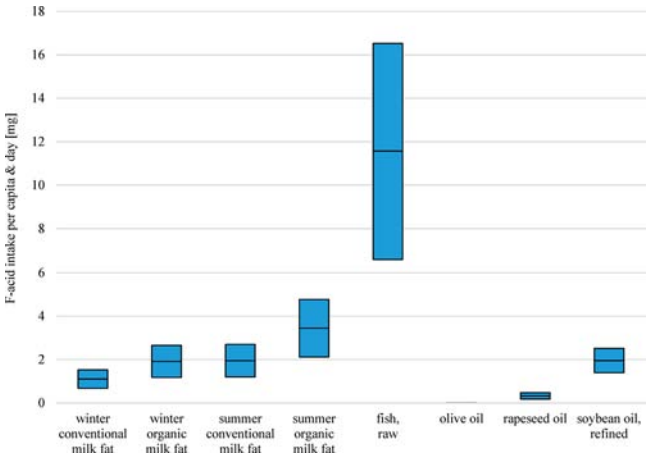


**Figure 3.** F-acid intake per capita and day (mg) from different food items in Germany with mean value (line in the middle) and minimum to maximum ranges.

According to national consumption data in Germany, the average per capita consumption of fish was about 40 g/day in 2012.[31] The intake of F-acids via fish was calculated on the basis of the six most popular fish species consumed in Germany: *Theragra chalcogramma*, Alaska pollock; *Clupea harengus*, herring; *Salmo salar*, salmon; *Thunnus*, tuna; *Pangasius hypophthalmus*, iridescent shark; and *Salmo trutta*, trout.[31] These six species contributed ∼80% to total fish consumption in Germany.[31] On the basis of these species, fish consumed in Germany contained an average of ∼8% lipids (weighted average). With an average F-acid content of 200 mg/100 g lipids (own determinations, data not shown) or 500 mg/100 g lipids (according to Pacetti et al.[10]), the daily intake of F-acids

by the consumption of fish accounted for ~6.6−16.5 mg (Figure 3). However, it should be noted that these values are calculated for raw fish and that cooking may result in lower F-acid contents due to their partial decomposition.

About 1.7 g of olive oil was consumed per capita and day in Germany in 2009.[32] According to Boselli et al. the average F-acid content in olive oil was about 2 mg/kg.[11] On the basis of these data, the daily F-acid intake through olive oil amounted to 0.003 mg. In Germany, the daily intake for rapeseed oil was 14 g and for soybean oil, 15 g, in 2009.[32] The average F-acid content was determined to be 1.3−3.4 mg/100 g in rapeseed oil, 26.3−42.4 mg/100 g in crude soybean oil, and 9.3−16.8 mg/100 g in refined soybean oil.[12] Thus, the F-acid intake via refined soybean oil, which is the primary source for human consumption, is much lower than the calculated values for crude soybean oil (Figure 3). Accordingly, the F-acid intake per capita and day would be 0.2−0.5 mg via rapeseed oil and 1.4−2.5 mg via refined soybean oil (Figure 3). Accordingly, the intake of F-acids by the consumption of vegetables and fruits is rather low.[1] However, plants are the origin of F-acids in both milk and fish.[1]

On the basis of these individual contributions of different foodstuffs to the overall nutritional daily intake of F-acids, it was apparent that intake based on raw fish represented the highest single source (Figure 3). Compared to fish, the F-acid intake via milk fat was relatively small for winter conventional samples (8 vs 77% from fish to the total F-acid intake), whereas organic samples milked during the summer had a larger share (20 vs 67% from fish to the total F-acid intake). By contrast, olive oil did not play any noticeable role in the dietary intake of F-acids in Germany. Even for Mediterranean diets with a per capita consumption for olive oil of about 38 g/day,[32] the F-acid intake would be only 0.08 mg/day, that is, <10% of the share of milk fat. The contribution of refined soybean oil to the daily intake of F-acids was between the intake via the consumption of conventionally produced milk fat in winter and organic milk fat in summer (Figure 3). Especially for persons who do not consume fish, milk fat represents a valuable source for the nutritional intake of F-acids.

## ■ ASSOCIATED CONTENT

### Supporting Information

Table S1: F-acid contents of all butter samples. This material is available free of charge via the Internet at http://pubs.acs.org.

## ■ AUTHOR INFORMATION


### Corresponding Author

*(W.V.) Phone: +49 711 459 24016. Fax: +49 711 459 24377. E-mail: walter.vetter@uni-hohenheim.de.


### Notes

The authors declare no competing financial interest.

## ■ ACKNOWLEDGMENTS

We are thankful to all colleagues from the Institute of Food Chemistry, University of Hohenheim, for providing butter samples.

## ■ REFERENCES


(1) Spiteller, G. Furan fatty acids: occurrence, synthesis, and reactions. Are furan fatty acids responsible for the cardioprotective effects of a fish diet? *Lipids* **2005**, *40*, 755−771.

(2) Pacetti, D.; Mozzon, M.; Lucci, P.; Frega, N. G. Bioactive fish fatty acids: health effects and their use as functional food ingredients. *Curr. Nutr. Food Sci.* **2013**, *9*, 283−297.

(3) Vetter, W.; Wendlinger, C. Furan fatty acids − valuable minor fatty acids in food. *Lipid Technol.* **2013**, *25*, 7−10.

(4) Okada, Y.; Kaneko, M.; Okajima, H. Hydroxyl radical scavenging activity of naturally occurring furan fatty acids. *Biol. Pharm. Bull.* **1996**, *19*, 1607−1610.

(5) Okada, Y.; Okajima, H.; Konishi, H.; Terauchi, M.; Ishii, K.; Liu, I.-M.; Watanabe, H. Antioxidant effect of naturally occurring furan fatty acids on oxidation of linoleic acid in aqueous dispersion. *J. Am. Oil Chem. Soc.* **1990**, *67*, 858−862.

(6) Wakimoto, T.; Kondo, H.; Nii, H.; Kimura, K.; Egami, Y.; Oka, Y.; Yoshida, M.; Kida, E.; Ye, Y.; Akahoshi, S.; Asakawa, T.; Matsumura, K.; Ishida, H.; Nukaya, H.; Tsuji, K.; Kan, T.; Abe, I. Furan fatty acid as an anti-inflammatory component from the green-lipped mussel *Perna canaliculus*. *Proc. Natl. Acad. Sci. U.S.A.* **2011**, *108*, 17533−17537.

(7) Glass, R. L.; Krick, T. P.; Eckhardt, A. E. New series of fatty acids in Northern Pike (*Esox lucius*). *Lipids* **1974**, *9*, 1004−1008.

(8) Gunstone, F. D.; Wijesundera, R. C.; Scrimgeour, C. M. The component acids of lipids from marine and freshwater species with special reference to furan-containing acids. *J. Sci. Food Agric.* **1978**, *29*, 539−550.

(9) Wahl, H. G.; Liebich, H. M.; Hoffmann, A. Identification of fatty acid methyl esters as minor components of fish oil by multidimensional GC-MSD: new furan fatty acids. *J. High Resolut. Chromatogr.* **1994**, *17*, 308−311.

(10) Pacetti, D.; Alberti, F.; Boselli, E.; Frega, N. G. Characterisation of furan fatty acids in Adriatic fish. *Food Chem.* **2010**, *122*, 209−215.

(11) Boselli, E.; Grob, K.; Lercker, G. Determination of furan fatty acids in extra virgin olive oil. *J. Agric. Food Chem.* **2000**, *48*, 2868−2873.

(12) Guth, H.; Grosch, W. Detection of furanoid fatty acids in soybean oil − cause for light-induced off-flavor. *Fett Wiss. Technol.* **1991**, *93*, 249−255.

(13) Wu, X.; Hammond, E. G.; White, P. J.; Fehr, W. Analysis of furanoid esters in soybean oil and the effect of variety and environment on furanoid ester content. *J. Am. Oil Chem. Soc.* **1997**, *74*, 1099−1103.

(14) Kao, J.-W.; Wu, X.; Hammond, E. G.; White, P. J. The impact of furanoid fatty acids and 3-methylnonane-2,4-dione on the flavor of oxidized soybean oil. *J. Am. Oil Chem. Soc.* **1998**, *75*, 831−835.

(15) Guth, H.; Grosch, W. Furan fatty acids in butter and butter oil. *Z. Lebensm. Unters. Forsch.* **1992**, *194*, 360−362.

(16) Vetter, W.; Laure, S.; Wendlinger, C.; Mattes, A.; Smith, A. W. T.; Knight, D. W. Determination of furan fatty acids in food samples. *J. Am. Oil Chem. Soc.* **2012**, *89*, 1501−1508.

(17) Hannemann, K.; Puchta, V.; Simon, E.; Ziegler, H.; Ziegler, G.; Spiteller, G. The common occurrence of furan fatty acids in plants. *Lipids* **1989**, *24*, 296−298.

(18) Slots, T.; Butler, G.; Leifert, C.; Kristensen, T.; Skibsted, L. H.; Nielsen, J. H. Potentials to differentiate milk composition by different feeding strategies. *J. Dairy Sci.* **2009**, *92*, 2057−2066.

(19) Ellis, K. A.; Innocent, G.; Grove-White, D.; Cripps, P.; McLean, W. G.; Howard, C. V.; Mihm, M. Comparing the fatty acid composition of organic and conventional milk. *J. Dairy Sci.* **2006**, *89*, 1938−1950.

(20) Collomb, M.; Bisig, W.; Bütikofer, U.; Sieber, R.; Bregy, M.; Etter, L. Fatty acid composition of mountain milk from Switzerland: comparison of organic and integrated farming systems. *Int. Dairy J.* **2008**, *18*, 976−982.

(21) Jahreis, G.; Fritsche, J.; Steinhart, H. Monthly variations of milk composition with special regard to fatty acids depending on season and farm management systems. Conventional versus ecological. *Fett/Lipid* **1996**, *98*, 356−359.

(22) Vetter, W.; Schröder, M. Concentrations of phytanic acid and pristanic acid are higher in organic than in conventional dairy products from the German market. *Food Chem.* **2010**, *119*, 746−752.

(23) Schröder, M.; Vetter, W. GC/EI-MS determination of the diastereomer distribution of phytanic acid in food samples. *J. Am. Oil Chem. Soc.* **2011**, *88*, 341−349.
(24) Baars, T.; Schröder, M.; Kusche, D.; Vetter, W. Phytanic acid content and SRR/RRR diastereomer ratio in milk from organic and conventional farms at low and high level of fodder input. *Org. Agric.* **2012**, *2*, 13−21.
(25) Che, B. N.; Kristensen, T.; Nebel, C.; Dalsgaard, T. K.; Hellgren, L. I.; Young, J. F.; Larsen, M. K. Content and distribution of phytanic acid diastereomers in organic milk as affected by feed composition. *J. Agric. Food Chem.* **2013**, *61*, 225−230.
(26) Molkentin, J. Authentication of organic milk using $\delta^{13}$C and the $\alpha$-linolenic acid content of milk fat. *J. Agric. Food Chem.* **2009**, *57*, 785−790.
(27) Kaffarnik, S.; Schröder, M.; Lehnert, K.; Baars, T.; Vetter, W. $\delta^{13}$C values and phytanic acid diastereomer ratios: combined evaluation of two markers suggested for authentication of organic milk and dairy products. *Eur. Food Res. Technol.* **2014**, *238*, 819−827.
(28) Capuano, E.; Van Der Veer, G.; Boerrigter-Eenling, R.; Elgersma, A.; Rademaker, J.; Sterian, A.; Van Ruth, S. M. Verification of fresh grass feeding, pasture grazing and organic farming by cows farm milk fatty acid profile. *Food Chem.* **2014**, *164*, 234−241.
(29) Capuano, E.; Boerrigter-Eenling, R.; Elgersma, A.; Van Ruth, S. M. Effect of fresh grass feeding, pasture grazing and organic/biodynamic farming on bovine milk triglyceride profile and implications for authentication. *Eur. Food Res. Technol.* **2014**, *238*, 573−580.
(30) Arnold, C.; Jahreis, G. Milk fat and health. *Ernaehr. -Umsch.* **2011**, *58*, 177−181.
(31) Fisch-Informationszentrum e.V. http://www.fischinfo.de/images/broschueren/book/Fischwirtschaft%20-%20Daten%20und%20Fakten%202013/index.html (accessed June 2014).
(32) FAOSTAT. http://faostat.fao.org/ (accessed June 2014).

JOURNAL OF AGRICULTURAL AND FOOD CHEMISTRY

Article

pubs.acs.org/JAFC

# Classification and Adulteration Detection of Vegetable Oils Based on Fatty Acid Profiles

Liangxiao Zhang,*[,†,∥,⊥] Peiwu Li,*[,†,§,∥,⊥] Xiaoman Sun,[†,⊥] Xuefang Wang,[†,⊥] Baocheng Xu,[†,⊥] Xiupin Wang,[†,⊥] Fei Ma,[†,‡,⊥] Qi Zhang,[†,‡,§] and Xiaoxia Ding[†,∥]

[†]Oil Crops Research Institute, Chinese Academy of Agricultural Sciences, Wuhan 430062, China

[‡]Key Laboratory of Biology and Genetic Improvement of Oil Crops, [§]Key Laboratory of Detection for Mycotoxins, [∥]Laboratory of Risk Assessment for Oilseeds Products (Wuhan), and [⊥]Quality Inspection and Test Center for Oilseeds Products, Ministry of Agriculture, Wuhan 430062, China

Supporting Information

**ABSTRACT:** The detection of adulteration of high priced oils is a particular concern in food quality and safety. Therefore, it is necessary to develop authenticity detection method for protecting the health of customers. In this study, fatty acid profiles of five edible oils were established by gas chromatography coupled with mass spectrometry (GC/MS) in selected ion monitoring mode. Using mass spectral characteristics of selected ions and equivalent chain length (ECL), 28 fatty acids were identified and employed to classify five kinds of edible oils by using unsupervised (principal component analysis and hierarchical clustering analysis), supervised (random forests) multivariate statistical methods. The results indicated that fatty acid profiles of these edible oils could classify five kinds of edible vegetable oils into five groups and are therefore employed to authenticity assessment. Moreover, adulterated oils were simulated by Monte Carlo method to establish simultaneous adulteration detection model for five kinds of edible oils by random forests. As a result, this model could identify five kinds of edible oils and sensitively detect adulteration of edible oil with other vegetable oils about the level of 10%.

**KEYWORDS:** *fatty acid profiles, adulteration identification, edible oil, GC/MS, chemometrics*

## INTRODUCTION

Edible vegetable oils are a kind of important food in our daily life, which provide human being with energy and nutritional components including but not limited to essential fatty acids, phytosterols, tocopherols, phenolic compounds, vitamins, and volatile organic compounds (VOC).[1,2] All over the world, palm, soybean, rapeseed, sunflower, and peanut oils are major cooking oil. Among them, palm and soybean oils possess the largest market share in vegetable oil consumption.[3] However, owing to pleasant flavor and nontransgenic merit, the proportion of peanut, rapeseed and sunflower oils gradually increase though their prices are higher than soybean and palm oils. Moreover, sesame oil is a high price edible vegetable oil, which is often used as a flavor enhancer in Asian countries. Ensuring the authenticity of food has been a problem for millennia.[4] Edible vegetable oil is also not an exception. As the same as adulteration of olive oil in western countries, adulteration in other high-price oils is still the biggest source of agricultural fraud problems. Therefore, it is a great demand for a reliable method to detect such adulterations.

The main compound in vegetable oil is triglyceride (~95%), which is composed of fatty acids.[5,6] Fatty acid profiles can serve as a characteristic of edible vegetable oil. Traditionally, only high-abundance fatty acids were analyzed and employed to classify edible vegetable oils. Recently, however, some common fatty acids (especially oleic acid) become a target of oilseed breeding, and the distribution of common fatty acids in different vegetable oils become increasingly overlapped. On the contrary, the low-abundance fatty acids are more specific to edible vegetable oils, such as erucic acid in rapeseed oil. Though these low-abundance fatty acids were not so attractive to nutritionist, they possess high sensitivity to adulteration identification of edible oils. The entire family of fatty acids, which is referred to as "fatty acidomics",[7] was therefore taken as a key marker and quality parameter of different oilseeds and their products.[8]

Fatty acids are usually analyzed by gas chromatography mass spectrometry (GC-MS) with derivatization[9] and routinely identified by comparing retention index (equivalent chain length, ECL[10]) with those of the authentic FAME standards and/or doing similarity search in reference mass spectra library.[11−13]

As the same as metabolomics, the multivariate chemometric methods are important to the application of fatty acid profiles. One often resorts to multivariate chemometric methods for fatty acids in edible oils, mainly including principal component analysis (PCA), hierarchical clustering analysis (HCA), soft independent modeling of class analogy (SIMCA), partial least-squares discriminant analysis (PLS-DA) and support vector machine (SVM).[14−16] As described by Ai et al.,[5] machine learning techniques of an ensemble of classification models are of particular interest. Among them, Random Forests (RF) is powerful to deal with multivariate classification,[17,18] in which, a

Received: March 8, 2014
Revised: July 29, 2014
Accepted: July 31, 2014
Published: July 31, 2014

ACS Publications © 2014 American Chemical Society

visual exploration of the proximity matrix could be obtained using the multidimensional scaling (MDS) technique to intuitively measure similarity between different samples. Besides, it can also provide a measurement for variable importance.

In this study, we developed a simultaneous adulteration detection method based on fatty acid profiles for vegetable edible oils and selected soybean, rapeseed, sunflower, peanut and sesame oils as target oils to illustrate and validate this method. First, fatty acid profiles of five main edible oils were established by GC-MS in selected ion monitoring mode. Using mass spectral characteristics of selected ions and equivalent chain length (ECL), fatty acids were identified and employed to classify five kinds of edible oils by using unsupervised (principal component analysis and hierarchical clustering analysis) and supervised (random forests) multivariate statistical methods. Moreover, since triacylglycerols are relatively stable and no chemical reaction happens when physical blend of vegetable oils, adulterated oils were simulated by adulterating the one oil with at least 10% of other four oils or mixtures thereof and employed to establish simultaneous adulteration detection model for five types of edible oils by random forests.

## 2. EXPERIMENTAL SECTION

**2.1. Materials and Regents.** To ensure that the oil samples could represent the actual status of edible oils, we adhere to the following sampling rules: (a) with respect to oil seeds selected for laboratory pressing, the oilseed samples were collected from the main produce areas of China; (b) the oilseeds were collected from farmers and local markets without considering their varieties. Totally, the 17 soybean samples, 75 peanut samples, 57 sunflower seed samples, 76 rapeseed samples, and 73 sesame samples were collected from different product areas. The detailed information was shown in Supporting Information Table S1. The seed oils were prepared by oil mill machinery (TZC-0502, Brand of TEN GUARD, China). Supelco 37 component FAME mix (No. 47885-U) was purchased from Sigma (St. Louis, MO, USA). 11-Octadecenoic acid (C18:1n-7, >97.0 purity) and 7-hexadecenoic acid methyl ester were purchased from Sigma (St. Louis, MO, USA).

**2.2. Experimental Procedure of Derivatization.** As described in the previous study,[19] 0.06 g of vegetable oil sample was diluted with 2 mL of a solvent of diethyl ether and petroleum ether (v/v 1:1), and 1 mL of 0.4 M KOH−$CH_3OH$ was added. Then, it was vortex-mixed for 30 s and placed at room temperature for 2.5 h, and then, 2 mL of redistilled water was added. It was then vortex-mixed and centrifuged at 4500 rpm for 2 min. The organic phase (200 $\mu$L) was collected and diluted by 800 $\mu$L of petroleum ether, prior to analysis by GC-MS.

**2.3. GC-MS Analysis.** The analyses were performed by Agilent GC-7890 gas chromatograph interfaced to a Agilent 5973 mass spectrometer. In the gas chromatography system, a fused silica capillary column DB-23 (30 m × 0.25 mm i.d. 0.15 $\mu$m film) (Agilent Technologies) was used. Helium (99.999% purity) was used as carrier gas at a flow-rate of 1.2 mL $min^{-1}$. The column was first set at 100 °C and held for 0.2 min, temperature was subsequently increased to 215 °C at the rate of 10 °C/min and held for 0.1 min, finally to 224 °C at the rate of 2 °C/min, which was held for an additional 0.2 min (total program time, 16.5 min). This is the optimum temperature programming for the conditions of both separation effect and run time. Mass spectrometric conditions were as follows: ionization mode: EI; electron energy 70 eV; temperatures of injector, ion-source and detector at 220, 250, and 150 °C, respectively. Solvent cut time was 3 min. Splitting ratio was 20:1. Selected ion monitoring (SIM) mode: $m/z$ 55, 67, 74 and 79.

**2.4. Identification of Fatty Acid Methyl Esters (FAME).** Identification of fatty acids in SIM mode was proposed in our pervious study.[19] The procedures mainly include (1) an automatic mass spectral search was conducted to identify straight saturated FAMEs and (2) the retention times of straight saturated FAMEs were used to calculate the ECLs of unsaturated FAMEs according to eq 1. If the retention times of interest were out of straight saturated FAMEs, extrapolation will be employed using retention times of two nearest straight saturated FAMEs; and (3) ECL of FAMEs in the sample were compared with those in freely available databases to identify the unsaturated FAMEs.[12,13]

$$\mathrm{ECL}(x) = n + \frac{RT(x) - RT(n)}{RT(n+1) - RT(n)} \quad (1)$$

where $n$ and $n + 1$ represent the numbers of carbons in the straight saturated FAME eluted immediately before and after the compound of interest, respectively.

Fatty acid percentage composition (percentage of peak area) was employed as quantitative results for edible oils.

**2.5. Multivariate Analysis.** Data matrix includes the relative content of fatty acids in edible oils. Data simulation of adulterated oils was conducted in Matlab 2011a for windows (The Mathworks, Natick, MA). Since the chemical properties of fatty acids and triacylglycerols are relatively stable, the fatty acid composition of blended oil equals to the summary of fatty acid composition of individual oils. To establish more precise adulteration detection model for five kinds of edible oils, two types of spurious edible oils were simulated by Monte Carlo method, including blending and adulterated oils. In this study, we defined the blended oil to mixing oil with random proportions of vegetable oils, while the adulterated oil was termed as spurious edible oil adulterated with low proportions of one or more than one vegetable oils. At first, 300 blended oils were simulated by blending five oils with random mixing proportions. In more details, for a blended oil, (1) random mixing proportions for five types of edible oils are created and then the sum of these proportions is normalized to unity; (2) one real edible oil of each type of edible oils is picked out at random; (3) fatty acid composition of this blended oil is calculated by weighted sum of five selected real oils; (4) repeat 1−3 for 300 times. For adulterated oils, one proportion of each kind of edible is set to 0.9 and other four proportions are created and the sum of these proportions is normalized to 0.1. Other procedures are the same with blended oils. For example, we could obtain an adulterated sesame oil sample by adding 10% content of soybean, peanut, sunflower, and rapeseed with random mixing proportions to 90% of sesame oil.

The data matrix was preprocessed through generalized log transformation and Pareto scaling (mean-centered and divided by the square root of standard deviation of each variable). As exploratory data analysis, principal component analysis (PCA) and hierarchical clustering analysis were employed to screen cluster of sampling and variable distribution in five groups. Then, the classification model for five kinds of edible oils was built by Random Forests. At last, the classification model for five types of edible oils and their blended and adulterated oils was also established by Random Forests. The model validation was conducted by OOB (out-of-bag) error in 3-fold cross validation.

Programs of automatic search tool for straight saturated FAMEs, and calculation of theoretical and experimental ECL were coded in Matlab 2011a for windows (The Mathworks, Natick, MA). Data preprocessing (Pareto scaling), Clustering (PCA and hierarchical clustering analysis) and classification (RF) were conducted by metabolomic data analysis tool of MetaboAnalyst 2.0.[20,21]

## 3. RESULTS AND DISCUSSION

**3.1. Identification and Quantitation of Fatty Acids in Five Types of Edible Oils.** In this study, fatty acidomics developed by GC/MS in SIM mode for classification and adulteration identification of edible vegetable oils. To detect more fatty acids in edible oils than the existing studies, selected ion monitoring mode (SIM) was used. The identification of FAMEs in samples was conducted using selected ions and retention indices (ECL).[13,19,22] At first, saturated FAMEs were automatically identified from background subtracted GC-MS data if the base peak of mass spectrum was at $m/z$ 74. Totally,

**Table 1. Identification and Relative Contents of Fatty Acids in Edible Vegetable Oils**

| fatty acids[a] | retention times | ECL | ECL in database[b] | soybean oil | peanut oil | sunflower oil | rapeseed oil | sesame oil |
|---|---|---|---|---|---|---|---|---|
| 12:0 | 5.75 | 12.00 | 12.00 | 0.0034 ± 0.0005 | 0.0021 ± 0.0012 | 0.0017 ± 0.0006 | 0.0134 ± 0.0024 | 0.0013 ± 0.0005 |
| 14:0 | 7.48 | 14.00 | 14.00 | 0.0566 ± 0.005 | 0.0303 ± 0.0061 | 0.0432 ± 0.006 | 0.049 ± 0.0045 | 0.0141 ± 0.0019 |
| 15:0 | 8.32 | 15.00 | 15.00 | 0.0106 ± 0.0009 | 0.0071 ± 0.0009 | 0.0104 ± 0.0012 | 0.0197 ± 0.0031 | 0.0014 ± 0.0002 |
| 15:1 n-5c | 8.66 | 15.41 | 15.42 | 0.0066 ± 0.0019 | 0.0036 ± 0.0033 | 0.0034 ± 0.001 | 0.0052 ± 0.0011 | 0.0038 ± 0.0024 |
| 16:0 | 9.14 | 16.00 | 16.00 | 12.5 ± 0.829 | 14.3 ± 0.703 | 5.93 ± 0.378 | 4.50 ± 0.430 | 10.5 ± 0.582 |
| 16:1 n-9c | 9.31 | 16.22 | 16.22 | 0.0074 ± 0.002 | 0.0214 ± 0.0026 | 0.0081 ± 0.0012 | 0.0216 ± 0.0035 | 0.0153 ± 0.0016 |
| 16:1 n-7c | 9.37 | 16.30 | 16.33 | 0.0352 ± 0.0053 | 0.0387 ± 0.0074 | 0.0286 ± 0.0079 | 0.1071 ± 0.0094 | 0.0621 ± 0.007 |
| 16:1 n-5c | 9.47 | 16.44 | **16.38** | 0.0089 ± 0.0012 | 0.0071 ± 0.0013 | 0.0022 ± 0.0005 | 0.0111 ± 0.0015 | 0.0049 ± 0.0008 |
| 16:2 n-5c | 9.68 | 16.70 | **16.68** | 0.0017 ± 0.0003 | 0.0013 ± 0.0003 | 0.0012 ± 0.0002 | 0.0459 ± 0.0059 | 0.0042 ± 0.0006 |
| 17:0 | 9.91 | 17.00 | 17.00 | 0.0739 ± 0.0063 | 0.063 ± 0.0107 | 0.0345 ± 0.0056 | 0.0291 ± 0.0037 | 0.0341 ± 0.0072 |
| 17:1 n-7c | 10.13 | 17.28 | 17.34 | 0.0221 ± 0.002 | 0.0183 ± 0.0045 | 0.0117 ± 0.003 | 0.0733 ± 0.0175 | 0.0119 ± 0.0026 |
| 16:3 n-3c | 10.54 | 17.88 | | 0.0201 ± 0.0032 | 0.0025 ± 0.0006 | 0.0079 ± 0.0021 | 0.0018 ± 0.0005 | 0.0033 ± 0.0009 |
| 18:0 | 10.67 | 18.00 | 18.00 | 4.32 ± 0.576 | 4.21 ± 0.5298 | 5.14 ± 0.705 | 2.34 ± 0.333 | 5.58 ± 0.503 |
| 18:1 n-9c | 10.87 | 18.29 | 18.27 | 16.2 ± 1.72 | 39.7 ± 3.15 | 16.4 ± 4.42 | 57.8 ± 10.1 | 33.2 ± 1.42 |
| 18:1 n-7c | 10.91 | 18.34 | 18.36 | 0.887 ± 0.0868 | 0.347 ± 0.132 | 0.310 ± 0.0332 | 2.17 ± 0.354 | 0.636 ± 0.0564 |
| 18:1 n-x | 11.15 | 18.68 | | 0.0281 ± 0.0037 | 0.0413 ± 0.0078 | 0.0289 ± 0.0063 | 0.0384 ± 0.007 | 0.0366 ± 0.005 |
| 18:2 n-6c | 11.23 | 18.80 | 18.76 | 55.6 ± 2.14 | 35.9 ± 3.17 | 70.9 ± 4.34 | 17.6 ± 2.16 | 48.9 ± 1.84 |
| 18:3 n-6c | 11.50 | 19.18 | 19.09 | 0.0702 ± 0.0099 | 0.0258 ± 0.004 | 0.0515 ± 0.0071 | 0.034 ± 0.0028 | 0.0278 ± 0.003 |
| 19:1 n-8 | 11.54 | 19.24 | **19.22** | 0.0045 ± 0.0014 | 0.0083 ± 0.0028 | 0.0058 ± 0.0019 | 0.0098 ± 0.0027 | 0.0038 ± 0.001 |
| 18:3 n-3c | 11.66 | 19.41 | 19.44 | 9.39 ± 1.37 | 0.0266 ± 0.0089 | 0.0547 ± 0.0105 | 7.81 ± 0.669 | 0.226 ± 0.0229 |
| 20:0 | 12.08 | 20.00 | 20.00 | 0.286 ± 0.0385 | 1.61 ± 0.158 | 0.241 ± 0.0207 | 0.5476 ± 0.1379 | 0.519 ± 0.0401 |
| 20:1 n-9c | 12.28 | 20.27 | 20.28 | 0.0772 ± 0.0093 | 0.466 ± 0.106 | 0.0596 ± 0.0062 | 2.47 ± 3.38 | 0.0826 ± 0.0042 |
| 20:2 n-6c | 12.69 | 20.81 | 20.84 | 0.0148 ± 0.0012 | 0.0096 ± 0.0024 | 0.0039 ± 0.0008 | 0.0653 ± 0.068 | 0.0097 ± 0.0017 |
| 21:0 | 12.84 | 21.00 | 21.00 | 0.0163 ± 0.0038 | 0.0122 ± 0.0014 | 0.0051 ± 0.0007 | 0.0104 ± 0.0024 | 0.0048 ± 0.0006 |
| 22:0 | 13.69 | 22.00 | 22.00 | 0.239 ± 0.0365 | 2.27 ± 0.402 | 0.582 ± 0.0587 | 0.163 ± 0.0724 | 0.0822 ± 0.0066 |
| 22:1 n-9c | 13.96 | 22.29 | 22.30 | 0.0033 ± 0.0027 | 0.0184 ± 0.0105 | 0.001 ± 0.0014 | 4.042 ± 8.43 | ND[c] |
| 23:0 | 14.63 | 23.00 | 23.00 | 0.0150 ± 0.0012 | 0.019 ± 0.0028 | 0.0145 ± 0.0024 | 0.0111 ± 0.003 | 0.0086 ± 0.0008 |
| 24:0 | 15.69 | 24.00 | 24.00 | 0.0444 ± 0.0062 | 0.826 ± 0.139 | 0.107 ± 0.0137 | 0.0698 ± 0.0299 | 0.0336 ± 0.0049 |

[a]Shorthand annotation according to *A*:*B* n-*i* z, where *A* is the number of carbon atoms in the fatty acid chain, *B* is the number of double bonds, *n*-*i* is the location of the double bond on the *i*th carbon−carbon bond, counting from the terminal methyl carbon toward the carbonyl carbon and z is the geometrical configuration expressed as c for cis and t for trans.[12] [b]Normal: ECL values in database in ref 13. Bold: ECL values in Chrombox database. Possible structure is deduced by mass spectral characteristics. [c]Not detected.

11 saturated FAMEs, 12:0, 14:0, 15:0, 16:0, 17:0, 18:0, 20:0, 21:0, 22:0, 23:0, and 24:0 included, were identified. Their retention times and relative abundances (RA) at *m*/*z* 55, 67, and 79 were then employed to validate whether saturated FAMEs are straight chain. The retention times of 11 straight saturated FAMEs were used to calculate the ECL values for other FAMEs. Identification of unsaturated FAMEs in the edible oils was conducted by searching their ECL values in the customized database constructed in the previous studies[13,14] for the FAME with the nearest ECL value as the candidate.

The threshold of difference between the experimental ECL and reference ECL in the database is set to 0.1. Using this method, as shown in Table 1, 17 unsaturated FAMEs were identified. Among them, 12 unsaturated FAMEs were validated by comparing the retention time and mass spectra with the authentic standards, while 3 unsaturated FAMEs were exploratively identified by searching freely available Chrombox database.[12] The other 2 unsaturated FAMEs were inferred to the type using their mass spectral characteristics. Totally, 28 FAMEs were identified and quantified, which are significantly higher than full scan mode (23 FAMEs).[5] Fatty acid composition of vegetable oils is described by percentage content of total amount of all fatty acids and shown in Table 1.

**3.2. Exploratory Data Analysis.** After determination and quantification of fatty acids in five vegetable oils, the data matrix of relative contents was preprocessed through generalized log transformation and Pareto scaling. In exploratory data analysis, principal component analysis (PCA) and hierarchical clustering analysis (HCA) were employed to screen cluster of sampling and fatty acid distribution in five groups. From the score plot obtained from PCA in Figure 1a, five kinds of edible oils were clearly classified into five groups, among which rapeseed and peanut oils are far from sunflower, sesame and soybean oils, respectively.

To investigate variable distribution in five groups, heat map of fatty acid profiles of five vegetable oils was illustrated. In heat map, the Euclidean distance was used for measuring the similarities using Wards' linkage by clustering to minimize the sum of squares of any two clusters. As shown in Figure 1b, the similar cluster analysis results were obtained as PCA. More importantly, we can find the fatty acids distribution in five groups from this heat map as follows: (a) soybean oils, relatively high content of 16:3 n-3, 17:0, and 18:3 n-6c (γ linolenic acid); (b) peanut oils, relatively high content of 20:0, 22:0, and 24:0; (c) rapeseed oils, relatively high content of 12:0, 16:1 n-5, 16:1 n-7, 17:1 n-7, 16:2 n-5, 18:1 n-7, 20:1 n-9, and 22:1 n-9; and (d) sunflower oils, the highest content of 18:2 n-6 (linoleic acid).

**3.3. Classification of Five Types of Edible Oils by Random Forests.** After exploratory data analysis, we can find that five kinds of vegetable oils could be clearly classified into five groups. To build classification model for five types of edible oils, an effective supervised multivariate statistical method of random forests (RF) was used. Random forests are a

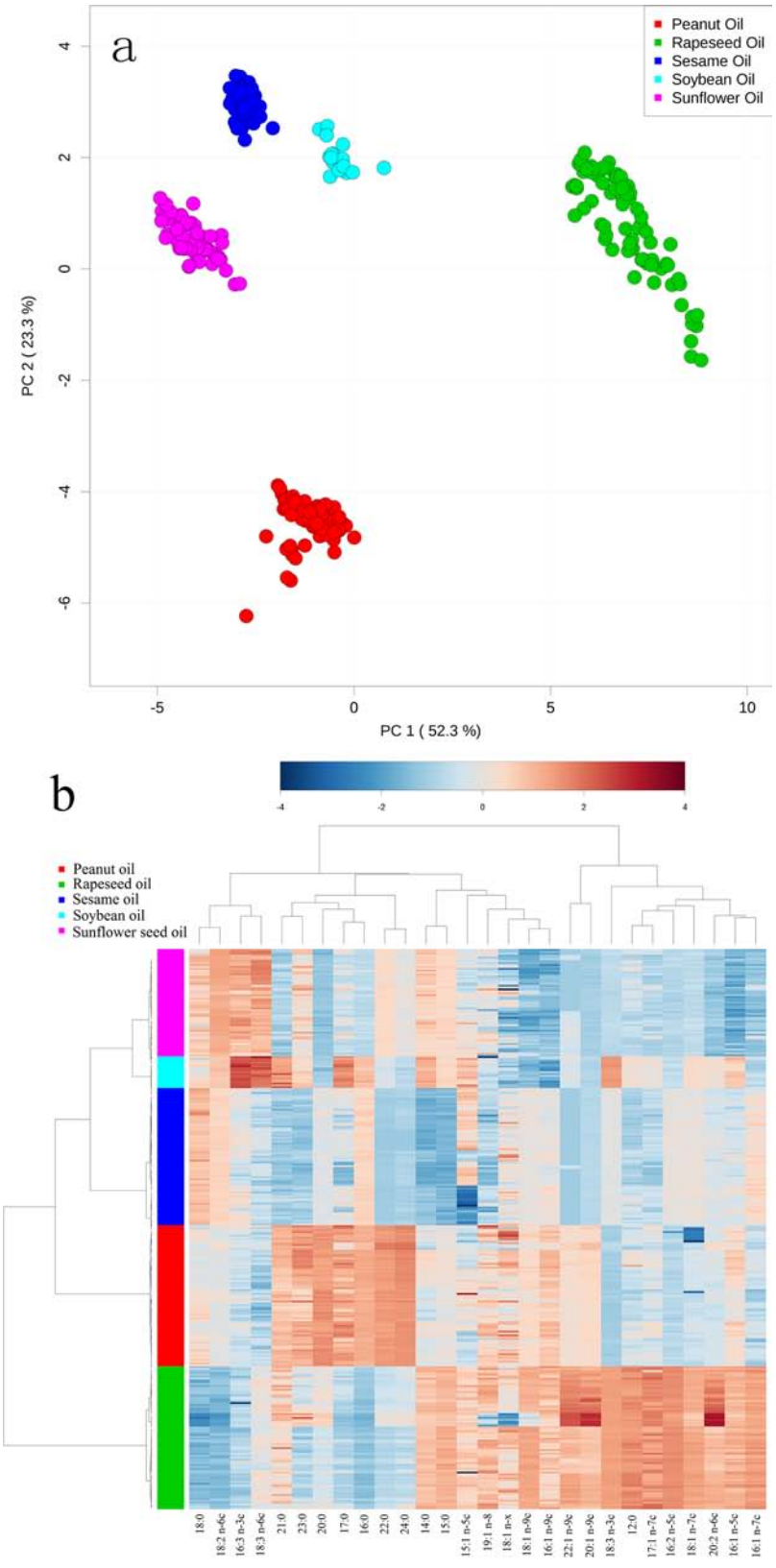


**Figure 1.** (a) Score plot between the first 2 PCs. (b) Heat map of five kinds of edible oils.

combination of tree predictors such that each tree depends on the values of a random vector sampled independently and with the same distribution for all trees in the forest.[23] The sample proximity matrix derived from these training trees is generated to collect the similarity information on the samples for classification of samples. Class prediction is based on the majority vote of the ensemble. Compared with other supervised multivariate statistical methods such as partial least-squares-discriminant analysis (PLS-DA) and support vector machine (SVM), random forests could be directly employed to


dx.doi.org/10.1021/jf501097c | J. Agric. Food Chem. 2014, 62, 8745−8751

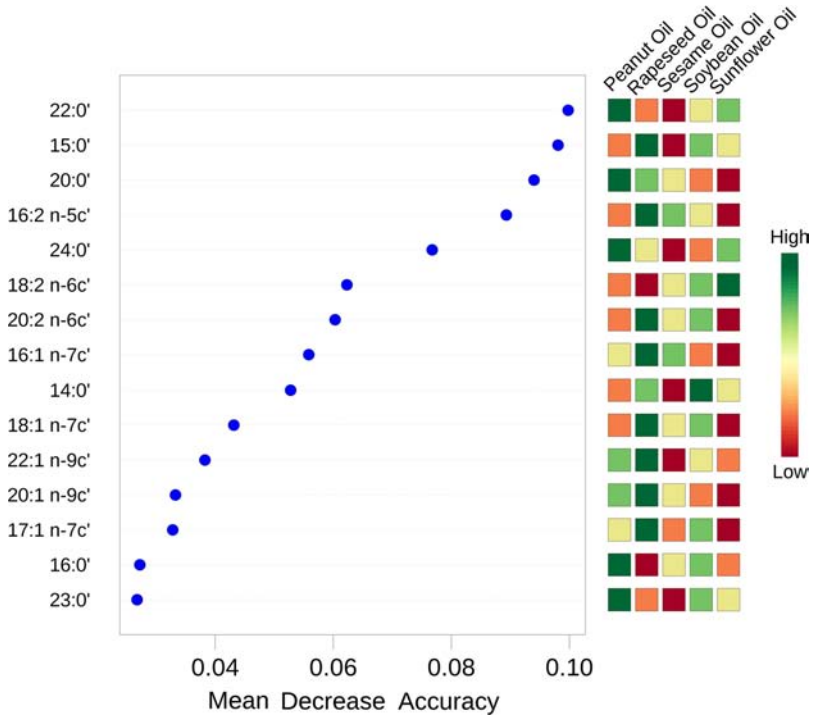


**Figure 2.** Significant features of five kinds of edible oils identified by Random Forest.

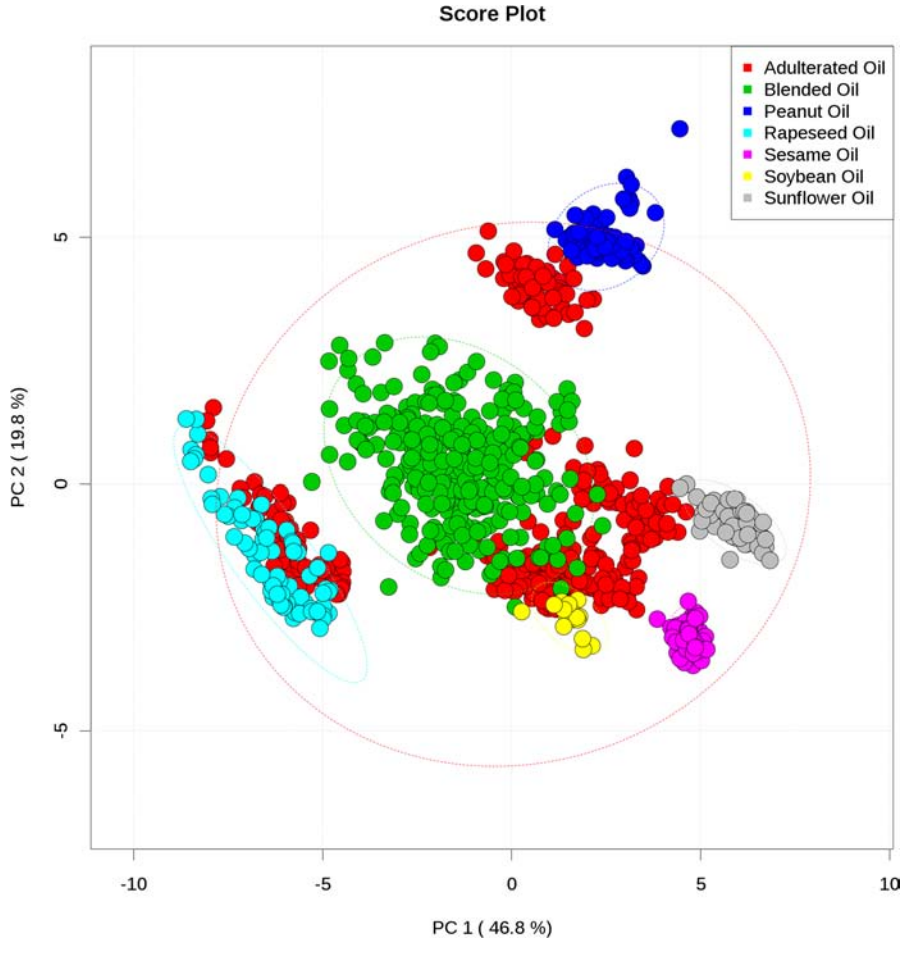


**Figure 3.** Score plot between the first 2 PCs for five kinds of edible oils and their blended/adulterated oils.


dx.doi.org/10.1021/jf501097c | J. Agric. Food Chem. 2014, 62, 8745−8751

Table 2. Random Forest Classification Performance

| | adulterated oil | blended oil | peanut oil | rapeseed oil | sesame oil | soybean oil | sunflower oil | class error |
|---|---|---|---|---|---|---|---|---|
| adulterated oil | 299 | 0 | 0 | 1 | 0 | 0 | 0 | 0.00 |
| blended oil | 0 | 300 | 0 | 0 | 0 | 0 | 0 | 0.00 |
| peanut oil | 0 | 0 | 75 | 0 | 0 | 0 | 0 | 0.00 |
| rapeseed Oil | 1 | 0 | 0 | 75 | 0 | 0 | 0 | 0.01 |
| sesame oil | 0 | 0 | 0 | 0 | 73 | 0 | 0 | 0.00 |
| soybean oil | 3 | 0 | 0 | 0 | 0 | 14 | 0 | 0.18 |
| sunflower oil | 0 | 0 | 0 | 0 | 0 | 0 | 57 | 0.00 |

multiclass classification. Furthermore, the RF classifier needs optimize only one parameter of the number of classification trees, which is relatively insensitive to predictive effect. In study, the number of classification trees is set to 500. During tree construction, about one-third of the samples are left out of the bootstrap sample. This out-of-bag (OOB) data is then used as test sample to obtain an unbiased estimate of the classification error (OOB error). From Figure 2a, it is found that the five errors decrease to zero after less than 20 trees. OOB error equals to 0 in the final classification model.

Random forests could provide the measure for variable importance. Figure 2b shows the contribution of each variable to the classification. According to the mean decrease, all important fatty acids except 18:2 n-6 (linoleic acid) and 16:0 (palmitic acid) are of low content. These results indicate that low abundant fatty acids might be more important to classification of five types of edible oils. Therefore, fatty acid profiles could reflect more information on fatty acids in edible oils, which benefit classification and adulteration identification.

**3.4. Adulteration Identification by Fatty Acid Profiles.** From the above analysis, it seems it is very easy to classify these five kinds of edible oils. Indeed, classification of commonly used edible oils is not hard thing by fatty acid analysis. However, classification of edible oils is not enough to ensure identity of edible oils. The most important thing is to identify adulteration of expensive oils with low price oils. Therefore, to test whether fatty acid profiles could serve adulteration detection, 300 blended oils were simulated by mixing five oils with random proportions, while, 60 adulterated oils were simulated by blending 10% content of other four oils with random proportions to 90% soybean, peanut, sunflower, rapeseed, and sesame oil, respectively. Then, the discriminative model for five pure oils and their blend and adulterated oils was built by RF after generalized log transformation and Pareto scaling. From Figure 3a, blend oils appear in the center of PCA score plot. It is found that fatty acid profiles could detect adulteration of peanut, sunflower and sesame oils with other vegetable oils about the level of 10%. For soybean and rapeseed oils, pure and adulterated oils are heavily overlapped.

Therefore, RF has been used to obtain high effective model. As shown in Figure 3b, except soybean oils, the OOB errors decrease to 0 or near 0 ($\leq$0.01) and the total OOB error is 0.00557. As illustrated in Table 2, peanut, sesame, and sunflower oils could completely separate from other oils and their blend and adulterated oils, respectively. Among them, peanut and sesame are key target of oil fraud in China market. Moreover, only one adulterated oil and one rapeseed oil were misidentified by RF model. The main reason is that fatty acids possess broad range, such as high and low erucic acid rapeseed. Thus, the rapeseed oil with 10% adulterated with other oils still stay at the space of rapeseed oils. However, only one rapeseed and one adulterated oils were misidentified. Finally, 3 out of 14 soybean oils were misidentified to be blend oils, suggesting more other parameter like phytosterol should be employed to assess the authenticity of soybean oils.[24] Fortunately, the soybean oil is the cheapest one in five types of edible oils, which has low risk to be adulterated.

From the above analysis, the established RF model could serve the authenticity assessment for four expensive oils. To validate the RF model, 16 real adulterated oils were physically blended. The blend proportions of these 16 adulterated oils were shown in Supporting Information Table S2. The results indicate that all of 16 blend oils could be identified as adulterated oil. Therefore, fatty acid profiles could be a good strategy to identify adulterated oils for edible oils. Compared with the pervious studies,[5,6,14] the adulteration detection method possess the following advantages: (1) it can simultaneously detect adulteration of more than one edible oils; (2) it can also detect the adulteration with more than one edible oils.

In conclusion, fatty acid profiles of five kinds of edible oils were established by GC-MS in SIM mode and employed to classify five types of edible oils with the help of multivariate statistical methods. The results indicate that fatty acid profiles of edible oils could completely classify the five kinds of edible oils into five groups and are therefore taken as markers of these four edible oils. Moreover, simulated data test indicate that fatty acid profiles could be used to detect adulterated by 10% or little more than 10% other oils for peanut, sunflower, rapeseed and sesame oil. The strategy of fatty acid profiles might be also useful to simultaneously identify the origin of various edible oils and detect suspected economically motivated the adulteration with more than one vegetable oils.

## ■ ASSOCIATED CONTENT

### Supporting Information

Additional information on detailed information on five types oil seeds (Table S1) and the blend proportions of 20 real adulterated oils (Table S2), cumulative error rates by Random Forest classification for five types of edible oils (Figure S1), five types of edible oils and their blended/adulterated oils (Figure S2). This material is available free of charge via the Internet at http://pubs.acs.org.

## ■ AUTHOR INFORMATION

### Corresponding Authors

*Phone: +86 27 86812943. E-mail: liangxiao_zhang@hotmail.com.

*E-mail: peiwuli@oilcrops.cn.

### Author Contributions

L.Z. and P.L. contributed equally to this study.

### Funding

This work was supported by the Project of National Science & Technology Pillar Plan (2012BAK08B03), the National Major

Project for Agro-product Quality & Safety Risk Assessment (GJFP2014006), the National Natural Science Foundation of China (21205118 and 31201447), the Special Fund for "Quality Inspection" Research in the Public Interest (2012104010-4), and the earmarked fund for China Agriculture research system (CARS-13).

### Notes

The authors declare no competing financial interest.

## ■ ACKNOWLEDGMENTS

The authors thank two anonymous reviewers for their insightful and detailed comments.

## ■ REFERENCES

(1) Cert, A.; Moreda, W.; Pérez, C. M. C. Chromatographic analysis of minor constituents in vegetable oils. *J. Chromatogr. A* **2000**, *881*, 131−148.
(2) Zhao, F.; Liu, J.; Wang, X.; Li, P.; Zhang, W.; Zhang, Q. Detection of adulteration of sesame and peanut oils via volatiles by GC×GC−TOF/MS coupled with principal components analysis and cluster analysis. *Eur. J. Lipid Sci. Technol.* **2013**, *115*, 337−347.
(3) Kabagambe, E. K.; Baylin, A.; Ascherio, A.; Campos, H. The Type of Oil Used for Cooking Is Associated with the Risk of Nonfatal Acute Myocardial Infarction in Costa Rica. *Nutr. Epidemiol.* **2005**, *135*, 2674−2679.
(4) Jeffrey, C. M.; Spink, J.; Lipp, M. Development and application of a database of food ingredient fraud and economically motivated adulteration from 1980 to 2010. *J. Food Sci.* **2012**, *77*, 118−126.
(5) Ai, F. F.; Bin, J.; Zhang, Z. M.; Huang, J. H.; Wang, J. B.; Liang, Y. Z.; Yu, L.; Yang, Z. Y. Application of random forests to select premium quality vegetable oils by their fatty acid composition. *Food Chem.* **2014**, *143*, 472−478.
(6) Yang, Y.; Ferro, M. D.; Cavaco, I.; Liang, Y. Z. Detection and identification of extra virgin olive oil adulteration by GC-MS combined with chemometrics. *J. Agric. Food Chem.* **2013**, *61*, 3693−3702.
(7) Wang, M.; Han, R. H.; Han, X. Fatty acidomics: Global analysis of lipid species containing a carboxyl group with a charge-remote fragmentation-assisted approach. *Anal. Chem.* **2013**, *85*, 9312−20.
(8) Bertrand, M. The new database seed oil fatty acids (SOFA). *Lipid Technol.* **2012**, *24*, 230−234.
(9) Drozd, J. Chemical derivatization in gas chromatography. *J. Chromatogr.* **1975**, *113*, 303−356.
(10) Miwa, T. K.; Mikolajczak, K. L.; Earle, F. R.; Wolff, L. A. Gas chromatographic characterization of fatty acids: Identification constants for mono- and dicarboxylic methyl esters. *Anal. Chem.* **1960**, *32*, 1739−1742.
(11) Härtig, C. Rapid identification of fatty acid methyl esters using a multidimensional gas chromatography-mass spectrometry database. *J. Chromatogr. A* **2008**, *1177*, 159−169.
(12) Wasta, Z.; Mjøs, S. A. A database of chromatographic properties and mass spectra of fatty acid methyl esters from omega-3 products. *J. Chromatogr. A* **2013**, *1299*, 94−102.
(13) Zhang, L. X.; Tan, B. B.; Zeng, M. M.; Lu, H. M.; Liang, Y. Z. Establishment of reliable mass spectra and retention indices library: Identification of fatty acids in human plasma without authentic standards. *Talanta* **2012**, *88*, 311−317.
(14) Diaz, T. G.; Meras, I. D.; Casas, J. S.; Franco, M. F. A. Characterization of virgin olive oils according to its triglycerides and sterols composition by chemometric methods. *Food Control* **2005**, *16*, 339−347.
(15) Li, C.; Yao, Y.; Zhao, G.; Cheng, W.; Liu, H.; Liu, C.; Shi, Z.; Chen, Y.; Wang, S. Comparison and Analysis of Fatty Acids, Sterols, and Tocopherols in Eight Vegetable Oils. *J. Agric. Food Chem.* **2011**, *59*, 12493−12498.
(16) Ruth, V. S. M.; Villegas, B.; Akkermans, W.; Rozijn, M.; Kamp, V. D. H.; Koot, A. Prediction of the identity of fats and oils by their fatty acid, triacylglycerol and volatile compositions using PLS-DA. *Food Chem.* **2010**, *118*, 948−955.
(17) Archer, K. J.; Kirnes, R. V. Empirical characterization of random forest variable importance measures. *Comput. Stat. Data Anal.* **2008**, *52*, 2249−2260.
(18) Rodriguez, G. V. F.; Ghimire, B.; Rogan, J.; Chica, O. M.; Rigol, S. J. P. An assessment of the effectiveness of a random forest classifier for land-cover classification. *ISPRS J. Photogramm. Remote Sens.* **2012**, *67*, 93−104.
(19) Zhang, L. X.; Li, P. W.; Sun, X. M.; Hu, W.; Wang, X. P.; Zhang, Q.; Ding, X. X. Untargeted fatty acid profiles based on the selected ion monitoring mode. *Anal. Chim. Acta* **2014**, *839*, 44−50.
(20) Xia, J.; Mandal, R.; Sinelnikov, I. V.; Broadhurst, D.; Wishart, D. S. MetaboAnalyst 2.0—A comprehensive server for metabolomic data analysis. *Nucleic Acids Res.* **2012**, *40*, 127−133.
(21) Xia, J.; Psychogios, N.; Young, N.; Wishart, D. S. MetaboAnalyst: A web server for metabolomic data analysis and interpretation. *Nucleic Acids Res.* **2009**, *37*, 652−660.
(22) Zhang, L. X.; Ji, B. B.; Tan, B. B.; Liang, Y. Z.; Liang, N. N.; Wang, X. L.; Dai, H. Identification of the composition of fatty acids in *Eucommia ulmoides* seed oil by fraction chain length and mass spectrometry. *Food Chem.* **2010**, *121*, 815−819.
(23) Breiman, L. Random forests. *Mach. Learn.* **2001**, *45*, 5−32.
(24) Xu, B. C.; Zhang, L. X.; Wang, H.; Luo, D. L.; Li, P. W. Characterization and authentication of four important edible oils using free phytosterol profiles established by GC-GC-TOF/MS. *Anal. Methods* **2014**, *6*, 6860−6870.

JOURNAL OF AGRICULTURAL AND FOOD CHEMISTRY

Article

pubs.acs.org/JAFC

Open Access on 07/31/2015

# Enhanced Sensitive Immunoassay: Noncompetitive Phage Anti-Immune Complex Assay for the Determination of Malachite Green and Leucomalachite Green

Jie-Xian Dong,[†,‡] Chao Xu,[†] Hong Wang,*[,†] Zhi-Li Xiao,[†] Shirley J. Gee,[‡] Zhen-Feng Li,[†] Feng Wang,[†] Wei-Jian Wu,[†] Yu-Dong Shen,[†] Jin-Yi Yang,[†] Yuan-Ming Sun,*[,†] and Bruce D. Hammock[‡]

[†]Guangdong Provincial Key Laboratory of Food Quality and Safety, South China Agricultural University, Guangzhou 510642, China

[‡]Department of Entomology and Nematology and UCD Comprehensive Cancer Center, University of California, Davis, California 95616, United States

Supporting Information

**ABSTRACT:** To develop a more sensitive immunoassay for malachite green (MG) and leucomalachite green (LMG), we identified the immunocomplex binding phage-borne peptides for use in the noncompetitive phage anti-immunocomplex assay (PHAIA). An anti-LMG monoclonal antibody (mAb) was used to select immunocomplex binding peptides from a circular random eight-amino-acid phage-displayed library. After three rounds of panning-elution, five peptides that bound the LMG−mAb immunocomplex were obtained. One of the phage-borne peptide clones that resulted in an assay with the highest sensitivity was chosen for further research. The concentration of LMG producing 50% of the saturated signal and the limit of detection of the assay were 7.02 and 0.55 ng/mL, respectively, with a linear range of 1.35 to 21.56 ng/mL. The PHAIA based on the same antibody was 16 times more sensitive compared to the competitive immunoassay. PHAIA was used to analyze LMG, MG, and two mixtures of spiked fish samples, with validation by high-performance liquid chromatography (HPLC) with fluorescence detector. Results showed a good correlation ($R^2_{LMG}$ = 0.9841; $R^2_{MG}$ = 0.993; $R^2_{Mixture}$ = 0.9903) between the data of PHAIA and HPLC, thus the assay was an efficient method for monitoring food safety.

**KEYWORDS:** *malachite green, leucomalachite Green, phage anti-immunocomplex assay*

## INTRODUCTION

The antimicrobial and antiparasitic triphenylmethane dye malachite green (MG) is widely used in aquaculture because it is active against skin flukes and gill flukes as well as protozoas and fungi.[1,2] MG is readily absorbed by fish, then metabolized to the colorless, lipophilic leucomalachite green (LMG).[3] Because both MG and LMG are suspected carcinogens, mutagens, and teratogens in humans, residues are not permitted in food of animal from many countries, including the United States, China, Canada, and the European Union (minimum required performance limit of 2 μg/kg).[4−6] Nevertheless, it is still used worldwide because it is cheap and effective. Therefore, a sensitive analytical method is needed to monitor its use in aquatic production.

Immunoassays can have a low limit of detection (LOD), which permits quantification at trace levels. It is a simple tool for detection and quantification of analytes, allowing relatively fast, high-throughput analysis.[7] According to the format, immunoassays fall into two main categories, competitive and noncompetitive assays. In theory, noncompetitive immunoassays are potentially superior to their competitive counterparts in term of precision, working range, sensitivity, and kinetics.[8] However, the noncompetitive assay are fundamental limited by the fact that the target antigen must have at least two epitopes, a drawback that essentially eliminates measurement of low molecular weight compounds. To overcome this limitation, several novel noncompetitive immunoassay approaches for small molecules have been proposed in the past few years. These were based on anti-idiotype antibody,[9,10] split recombinant variable region fragments of antibody,[11−15] and anti-metatype antibody.[16−18] It is quite difficult and time-consuming to prepare these antibodies requiring immunization with antibody or analyte−antibody complexes, making these methods rarely successful except in special cases. However, to circumvent the problems, the phage anti-immune complex assay (PHAIA) technology was developed for noncompetitive assays of small analytes. In this technique, selection of a phage-borne peptide from the phage-displayed library utilizes the analyte−antibody immune complex for selection. The phage clones, which recognize the immune complex instead of the free antibody, are the second binding reagents using an antiphage antibody coupled to horseradish peroxidase (HRP) to generate the signal. The noncompetitive PHAIA technology has been used in the detection of clomazone,[19] molinate and atrazine,[20] phenoxybenzoic acid,[21] and brominated diphenyl ether 47.[22] Significantly enhanced sensitivity was obtained compared to the chemically synthesized competing hapten-based enzyme-linked immunosorbent assays (ELISA).

So far, all of the immunoassays reported previously for MG and LMG are based on conventional competitive immunoassays.[23−27] To expand the sensitive immunoassay for MG and

Received: May 1, 2014
Revised: July 29, 2014
Accepted: July 30, 2014
Published: July 31, 2014

ACS Publications © 2014 American Chemical Society



dx.doi.org/10.1021/jf5019824 | J. Agric. Food Chem. 2014, 62, 8752−8758

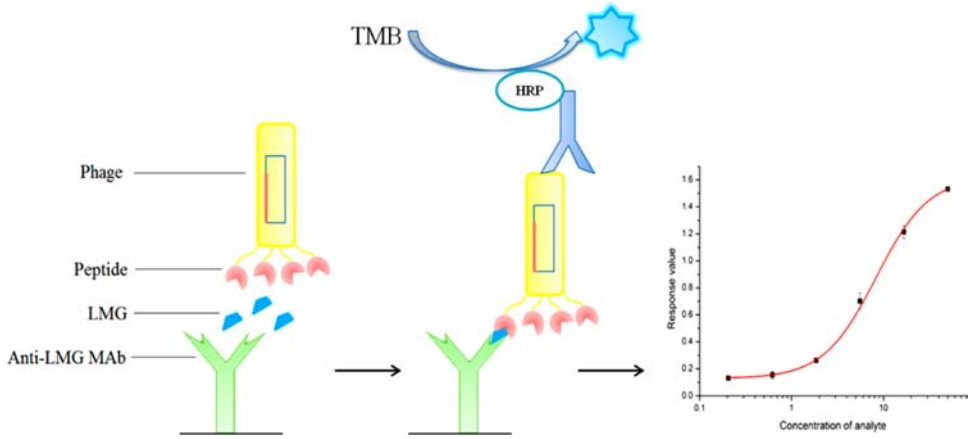


**Figure 1.** Schematic model of phage anti-immune complex assay (PHAIA). The peptide displayed on phage clones recognizes the immune complex to form the sandwich-model immunoassay. The detectable signal is amplified with antiphage antibody conjugated horseradish peroxidase(HRP), which catalyzes 3,3′,5,5′-tetramethylbenzidine(TMB) to produce a blue colored solution.

LMG, we developed the noncompetitive PHAIA with the anti-LMG monoclonal antibody (mAb), as shown in Figure 1. The phage-displayed peptides that were selective for the LMG-immunocomplex were chosen from the circular random eight-amino-acid library. One of the phage clones was used to establish noncompetitive immunoassays for quantitative estimation of MG and LMG in fish samples.

## MATERIALS AND METHODS

**Reagents.** All reagents were of analytical grade unless otherwise specified. MG, LMG, crystal violet (CV), leucocrystal violet (LCV), brilliant green (BG), parafuchsin (PA), methylene blue (MB), bovine serum albumin (BSA), ovalbumin (OVA), 3,3′,5,5′-tetramethylbenzidine (TMB), and protein A-based affinity columns to purify IgG were from Sigma Chemical Co. (St. Louis, MO, U.S.A.). Mouse anti-M13 mAb-HRP was obtained from GE Healthcare (Piscataway, NJ, U.S.A.). Polyethylene glycol 8000 (PEG 8000), Tween-20, tryptone, yeast extract, acetonitrile (ACN, HPLC grade), and dichloromethane (DCM) were obtained from Fisher Scientific Co. (Fair Lawn, NJ, U.S.A.). Bond Elut PRS columns were obtained from Agilent Technologies (Palo Alto, CA, U.S.A.). *Escherichia coli* (*E. coli*) ER2738 was obtained from Invitrogen Life Technologies (Carlsbad, CA, U.S.A.).

**Phage Displayed Peptide Library.** A random phage-displayed disulfide-constrained peptide library with an estimated diversity of $3.4 \times 10^{13}$ independent clones was constructed on the M13KE vector that expressed random peptide of eight amino acids.[28] These peptides are flanked by two cysteine residues and linked to the N terminus of the major pIII phage coat protein.

**Synthesis of Hapten and Production of Anti-LMG mAb.** 2-(3-(bis(4-(Dimethylamino)phenyl)methyl)phenoxy)-acetic acid (LMGH8) and LMGH8-BSA/OVA were synthesized and conjugated as described by Shen et al.[27] with 2-(3-formyl-phenoxy)acetic acid instead of 2-(4-formylphenoxy)acetic acid. The anti-LMG mAb was identified by competitive ELISA following immunization with LMGH8-BSA, cell fusion, hybridoma selection, ascites growth, and mAb purification processes, which were carried out as reported by Campbell.[29]

**Biopanning Procedure.** Two wells of a microtiter plate (Nunc-Immuno 96-MicroWell Plate) were coated with purified anti-LMG mAb (10 $\mu$g/mL) in 100 $\mu$L of 0.1 mol/L $NaHCO_3$ (pH 8.6) at 4 °C overnight. Two additional microtiter plates coated with 100 $\mu$L of 3% BSA and mAb, respectively, in 0.1 mol/L $NaHCO_3$ were used for preabsorption eliminating binding to BSA or mAb. Nonspecific binding was blocked by incubation with 300 $\mu$L of 0.1 mol/L $NaHCO_3$ containing 5 mg/mL BSA for 1 h at room temperature. Panning-elution was conducted by diluting the phage library ($1 \times 10^{10}$ pfu/mL) with phosphate-buffered saline (PBS). The diluted phage was then added to the BSA preabsorption plate. Following room temperature incubation for 1 h, the solution was transferred to a preabsorption plate containing mAb and incubated at room temperature for 1 h. Then, the unbound phage peptides were transferred into the other wells of the mAb coated plate that had been preincubated with 300 ng/mL LMG and washed seven times with PBS containing 0.1% (v/v) Tween-20 (PBST), followed by incubation at room temperature for 1 h. The wells were washed 10 times with PBST. The bound phage was eluted with 100 $\mu$L of 0.1 mol/L glycine-HCl (pH 2.2) per well and neutralized with 4.5 $\mu$L of 1 mol/L Tris (pH 9.0). After 10 min incubation, the elution solution was collected, and *E. coli* ER2738 was infected by adding the elution solution for amplification and titration. The amplified phage was used for a subsequent round of panning. The concentration of coating antibody was reduced to 5 and 1 $\mu$g/mL in the second and third rounds of panning. The ability to bind to the LMG−mAb immune complex was tested after three rounds of panning-elution selection. Individual plaques were picked from LB/IPTG/X-gal plates.

**Phage ELISA Screening.** A noncompetitive phage ELISA was set up to screen phage capable of binding the LMG immune complex. The microtiter plates were coated with the anti-LMG mAb or BSA and blocked as described before. Equal volumes of LMG solution (50 ng/mL) diluted with PBST were mixed with the culture of individual amplified phage clones. The mixture was then added to wells (100 $\mu$L/well) and incubated at room temperature for 1 h. After seven washes with PBST, 100 $\mu$L of a 1/5000 dilution of anti-M13 monoclonal labeled HRP was dispensed into each well. One hour later, the plates were washed another seven times, and 100 $\mu$L of peroxidase substrate, which contains 12.5 mL of 0.1 mol/L citrate acetate buffer with pH 5.5, 0.2 mL of TMB (6 mg/mL in dimethyl sulfoxide solution), and 0.1 mL of 1% $H_2O_2$, was added into each well. The enzymatic reaction was stopped with


dx.doi.org/10.1021/jf5019824 | J. Agric. Food Chem. 2014, 62, 8752−8758

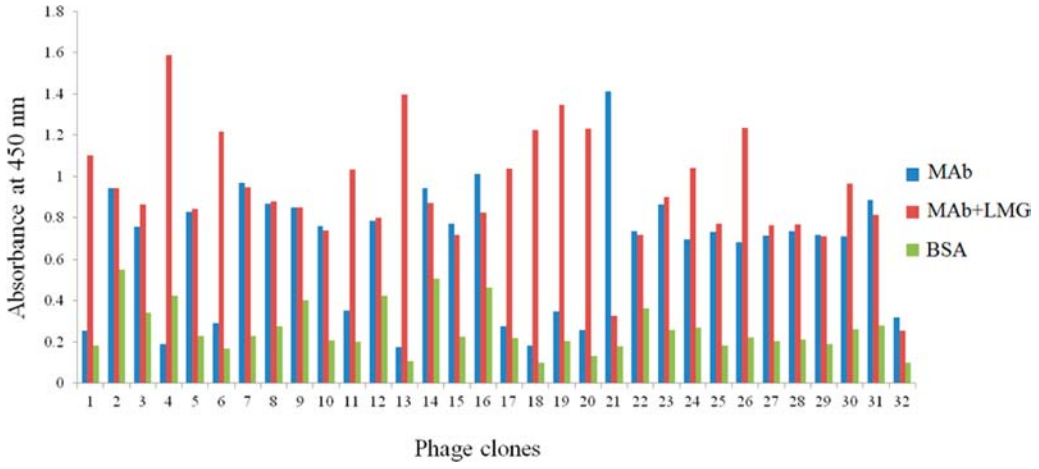


**Figure 2.** Screening of positive clones by noncompetitive phage ELISA. Clones 1, 4, 6, 11, 13, 17, 18, 19, 20 reacting specifically with the leucomalachite green-monoclonal antibody (LMG-mAb) immunocomplex showed little or negligible signal with the bovine serum albumin (BSA) or uncombined mAb.

50 $\mu$L of $H_2SO_4$ (4 mol/L) after 10 min, and the absorbance at 450 nm was recorded in a microtiter plate reader (Molecular Devices, Sunnyvale, CA, U.S.A.). The positive clones demonstrating high absorbance in wells coated with the immune complex and low absorbance in antibody or BSA-coated wells were selected and used for further analysis.

**DNA Sequencing and Analysis for the Positive Clones.** The positive clones as described above were further amplified and used for single-stranded DNA isolation as introduced in the Ph.D. peptide library kit instruction manual (New England Biolabs, Berverly, MA, U.S.A.). The product of phage DNA was submitted for DNA sequencing using the primer 96gIII (CCCTCATAGTTAGCGTAACG) (Division of Biological Sciences, Automated DNA Sequencing Facility, University of California, Davis, CA, U.S.A.). The program of DNAMAN 4.0 (Lynnon Biosoft, Quebec, Canada) was used to translate and align the amino acid residue sequences of the phage-display peptide from the inserted DNA sequences.

**Preparation of Purified Phage Suspensions.** Phage clones showing different amino acid residue sequences were selected and individually amplified as described above. After two steps of precipitation with PEG 8000-NaCl (20% (w/v) PEG-8000/2.5 mol/L NaCl), the phage particles were suspended with 0.5 mL of Tris-buffered saline (TBS, 50 mmol/L Tris-HCl, 150 mmol/L NaCl, pH 7.5) and stored at 4 °C.

**Noncompetitive Phage ELISA Protocol.** For checkerboard titration, 100 $\mu$L of various concentrations of the purified anti-LMG mAb (1 $\mu$g/mL, 0.5 $\mu$g/mL, 0.25 $\mu$g/mL, and 0.125 $\mu$g/mL) was used for coating as described before. The plates were blocked with 3% skim milk in PBS for 1 h at room temperature. After the plates were washed three times by PBST, the dilutions of purified phage suspensions were added to the mAb-coated wells in the presence or absence of LMG (50 ng/mL). Following the procedure of incubation, addition of anti-M13-HRP conjugate and color development as described in phage ELISA screening section, the concentration of coating antibody and phage particle combinations that resulted in an absorbance at about 1 were selected for the further assay.

After the confirmation of the coating antibody and phage particle dilutions, different concentrations of LMG (0−50 ng/mL in PBST solution) were mixed with equal volumes of phage to establish the noncompetitive standard curve for each clone.

**Cross-Reactivity Assay.** The specificity of the noncompetitive assay was evaluated by using some triphenylmethane analogues. We determined the average compound concentration corresponding to the midpoint of the curve (which corresponds to the concentration of analyte producing 50% saturation of the signal [$SC_{50}$]) and compared the values to the value from a standard curve for LMG run on the same plate. Cross-reactivity was calculated as follows: 100 × $SC_{50}$ (LMG)/$SC_{50}$ (cross-reactive compound).

**Matrix Effect and Assay Precision.** The PHAIA was used to detect MG and LMG in tilapia samples obtained from a local California market. Fish samples were minced and then homogenized. The homogenates (2.5 g) were spiked with MG, LMG, or the two-mixture standard solution (5, 10, or 20 ng/g). These samples stood for 5 min or more at room temperature prior to extraction. ACN (10 mL) was added and the sample was homogenized for 30 s at room temperature. Alumina (2.5 g) was added, and the samples were shaken for an additional 2 min. The samples were then centrifuged at 4000 rpm for 5 min and the supernatant was transferred to a clean tube. ACN (10 mL), 0.75 mL of hydroxylamine hydrochloride (20% mass ratio in deionized water), 1.25 mL of *p*-toluenesulfonic acid (0.05 mol/L), and 2.5 mL of ammonium acetate buffer (0.125 mol/L, pH 4.5) were used to re-extract the pellet. After shaking for 2 min, the samples were centrifuged again. Then, the supernatant was combined with the previous supernatant fraction. The extraction was repeated once more. Potassium borohydride (0.2 mol/L; 2.25 mL) was added to the supernatant fraction. After a 10 min incubation, DCM (5 mL) was added. These combined fractions were shaken vigorously for 15 s and centrifuged at 4000 rpm for 5 min. The lower organic layer was then transferred into a clean borosilicate glass tube and dried on a vacuum rotary evaporator at 45 °C. The dry residue was redissolved in 2.5 mL of ACN for solid-phase extraction.

The PRS solid phase extraction columns (Agilent Technologies, Palo Alto, CA, U.S.A.) were preconditioned with 5 mL of ACN. The sample extract was loaded onto the column followed by a 2 mL ACN wash. Two milliliters of the sample eluent solution (ACN/ammonium hydroxide, 90:10, v/v) was added to the column and the eluents were collected into a borosilicate glass tube. The extract was evaporated to dryness under a stream of nitrogen. Finally, the dry residue was

reconstituted and sonicated for 10 min in 2 mL of PBST for the noncompetitive PHAIA and HPLC analysis. The matrix effects determination was conducted according to the procedure described above using a pure extract to dilute the LMG.

**HPLC Analysis.** HPLC was carried out on an Agilent 1290 series HPLC system, equipped with an online-degasser, a binary pump, and an autosampler. A fluorescence detector (model G1321B, Agilent, U.S.A.) was adjusted at wavelengths of 265 and 360 nm for excitation and emission. The analysis procedure was run with an isocratic mobile phase consisting of ACN and 0.125 mol/L ammonium acetate (4:1, v/v) at a flow rate of 1.3 mL/min. A Phenomenex Luna 5 $\mu$m C18 column (250 mm × 4.6 mm; Torrance, CA, U.S.A.) was used. The injection volume was 20 $\mu$L.

## RESULTS AND DISCUSSION

**Purified Anti-LMG mAb Production and Identification.** A hybridoma 6D1 that stably secretes mAbs against LMG was obtained from ascites and purified by a protein A affinity column. The half inhibitory concentration ($IC_{50}$) of the purified mAb was determined to be 113.12 ng/mL by the indirect competitive ELISA.

**Screening of the Peptides by Phage ELISA.** In this study, we used the circular random eight-amino-acid library which was displayed on the pIII coat protein of filamentous phage. Compared with the other major coat protein, pVIII, pIII can tolerate the insertion of longer peptides because pIII is the longest coat protein and only 3−5 peptides copies are displayed.[30] We believed that the space between each peptide makes the immunocomplex more accessible for binding. The principle of noncompetitive immunoassay requires the phage-displayed peptides to recognize the antibody−analyte complex rather than any other part of antibody. After three rounds of panning, 32 clones were picked randomly and tested for binding to the anti-LMG mAb-coated wells in the presence or absence of LMG. Nine of 32 clones showed negligible binding to the uncombined antibody, although bounding specifically to the immunocomplex in the presence of 50 ng/mL LMG (Figure 2).

**Analysis of Positive Peptides Amino Acid Sequences.** After the isolation and sequencing of single stranded DNA from the positive phage clones, five different sequences were obtained (NCB1, NCB4, NCB6, NCB11, NCB13). The deduction of the amino acid sequences are shown in Table 1. The clones NCB 4, NCB 6, and NCB 13 shared the consensus motif of LPXHL, while HEXHXH was common to NCB1 and NCB11, where X represents any amino acid. The results indicated that the two motifs of LPXHL and HEXHXH contributed significantly to the LMG immune complex recognition.

**Table 1. Peptide Sequences Isolated with LMG Immunocomplex**

| phage clones | amino acid sequence |
|---|---|
| NCB-1 | C LNHEFHLHC (2) |
| NCB-4 | CT Y RLPLHLC (1) |
| NCB-6 | CTFTLPRHLC (1) |
| NCB-11 | CVPHEHHTHC (4) |
| NCB-13 | CLFTLPRHLC (1) |

**PHAIA for LMG.** The PHAIA sensitivity is associated with the concentration of coating mAb and the number of phage particles. To determine the optimal concentration of mAb and phage particles, a checkerboard procedure was performed for each clone. Serially diluted phage particles were added to the plates coated with purified antibody (1, 0.5, 0.25, and 0.125 $\mu$g/mL) in the absence or presence of LMG (50 ng/mL). The best results were obtained with antibody concentration of 0.5 $\mu$g/well and phage concentrations of $2.40 \times 10^{12}$ pfu/mL for clone NCB1, $1.20 \times 10^{12}$ pfu/mL for clone NCB4, and $1.27 \times 10^{12}$ pfu/mL for NCB13, whereas antibody concentrations of 0.25 $\mu$g/well and phage concentrations of $1.12 \times 10^{12}$ pfu/mL for clone NCB6, and $3.00 \times 10^{12}$ pfu/mL for clone NCB11, were identified (Figure S1−S5).

The assay with clone NCB1 demonstrated the highest sensitivity ($SC_{50}$ = 7.02 ng/mL), followed by clones NCB4, NCB13, NCB6, and NCB11 ($SC_{50}$ values of 8.39, 10.58, 13.00, and 16.15 ng/mL, respectively). For each of the five clones, standard curves were estimated using the optimized conditions. The noncompetitive standard curves are presented in Figure 3.

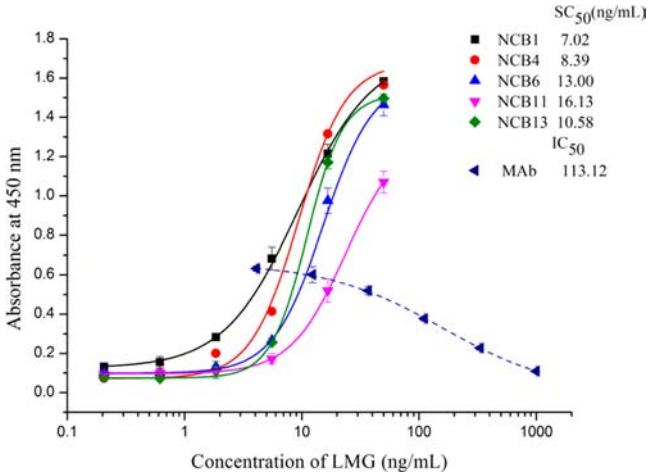


**Figure 3.** Noncompetitive ELISA for LMG performed with different phage-displayed peptide and competitive ELISA based on mAb for LMG. Results are the average of three replicates. The full lines are the standard curves of phage anti-immune complex assay. The dotted line is the inhibitory curve determined by competitive model. The 50% saturation of the signal ($SC_{50}$) and the half inhibitory concentration ($IC_{50}$) was calculated using a logistic plot equation with OriginPro 8.5 (OriginLab, Northampton, MA).

The linear range of NCB1 was 1.35 to 21.56 ng/mL. By altering the traditional competitive assay to the noncompetitive model, we improved the sensitivity of the assay by 16-fold using the same mAb. The sensitivity improvement is consistent with previously reported results.[19]

**Cross-Reactivity.** The cross reactivity of other structurally related compounds was determined to identify the specificity of the PHAIA, and the results are listed in Table 2. LCV and MG (6.89% and 2.93%, respectively) showed low cross-reactivity. The cross-reactivity was less than 0.01% for other compounds, similar to the competitive assay.

**Matrix Effect.** Due to the presence of the extraction agent, the sample component, and other ions, false positive or negative results from the matrix could be observed in the immunoassay. For the extraction of lipophilic LMG, it is necessary to minimize the matrix effect by using solid-phase extraction (SPE).[23] In our study, the maximum absorption with

**Table 2. Cross-Reactivity of LMG-PHAIA**[a]

| Analogues | Structure | Cross-reactivity(%) |
|---|---|---|
| LMG | 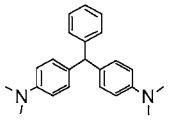 | 100 |
| MG | 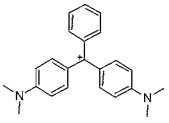 | 2.93 |
| LCV | 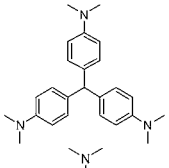 | 6.89 |
| CV | 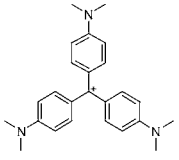 | <0.01 |
| BG | 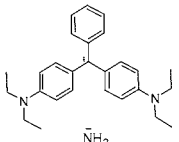 | <0.01 |
| PA | 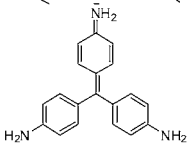 | <0.01 |
| MB | 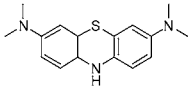 | <0.01 |

[a]The specificity was presented by cross-reactivity using the malachite green (MG), leucocrystal violet (LCV), crystal violet (CV), brilliant green (BG), parafuchsin (PA), methylene blue (MB).

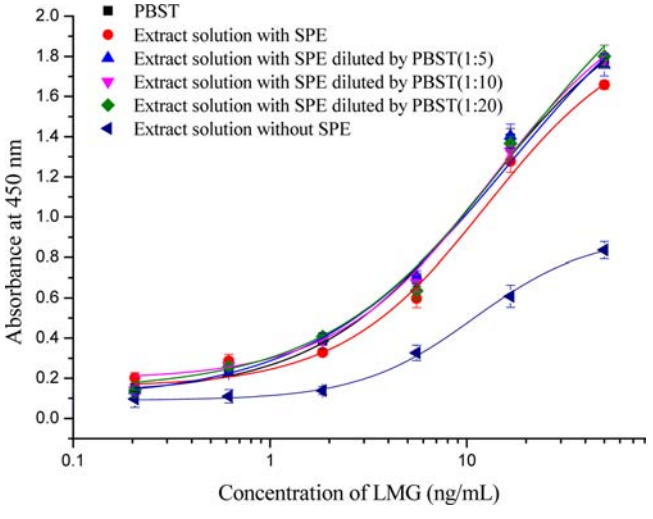


**Figure 4.** Standard curves of LMG in PBST and in sample extracts of different dilution with or without solid-phase extraction (SPE) ($n$ = 3). The matrix effect was studied by comparison of standard curves obtained in PBST, in sample extracts cleaned up with SPE of 1:1, 1:5, 1:10, 1:20 dilution, and in sample extracts without SPE.

**Table 3. Recovery of Spiked Fish Samples Determined by LMG-PHAIA ($n$ = 3)**

| analyte | spike level (ng/g) | mean ± SD (ng/g) | average recovery (%) | CV (%) |
|---|---|---|---|---|
| LMG | 0 | ND | | |
| | 5 | 3.77 ± 0.58 | 75.33 | 15.33 |
| | 10 | 8.20 ± 0.76 | 82.03 | 9.24 |
| | 20 | 17.60 ± 1.52 | 88.00 | 8.64 |
| MG | 0 | ND | | |
| | 5 | 4.14 ± 0.32 | 82.80 | 7.67 |
| | 10 | 8.07 ± 0.65 | 80.67 | 8.09 |
| | 20 | 16.89 ± 0.69 | 84.45 | 4.11 |
| LMG + MG(1:1) | 0 | ND | | |
| | 5 | 3.78 ± 0.56 | 75.60 | 14.82 |
| | 10 | 7.92 ± 0.74 | 79.20 | 9.29 |
| | 20 | 16.79 ± 1.01 | 83.93 | 5.99 |

ND means not detectable.

50 ng/mL LMG in 1:1, 1:5, 1:10, and 1:20 extract dilutions was 1.66 ± 0.02, 1.76 ± 0.06, 1.79 ± 0.03, and 1.80 ± 0.05 ($n$ = 3 per dilution), respectively, compared to 1.77 ± 0.02 in PBST (Figure 4). The $SC_{50}$ values were 8.09, 7.44, 7.64, and


dx.doi.org/10.1021/jf5019824 | J. Agric. Food Chem. 2014, 62, 8752−8758

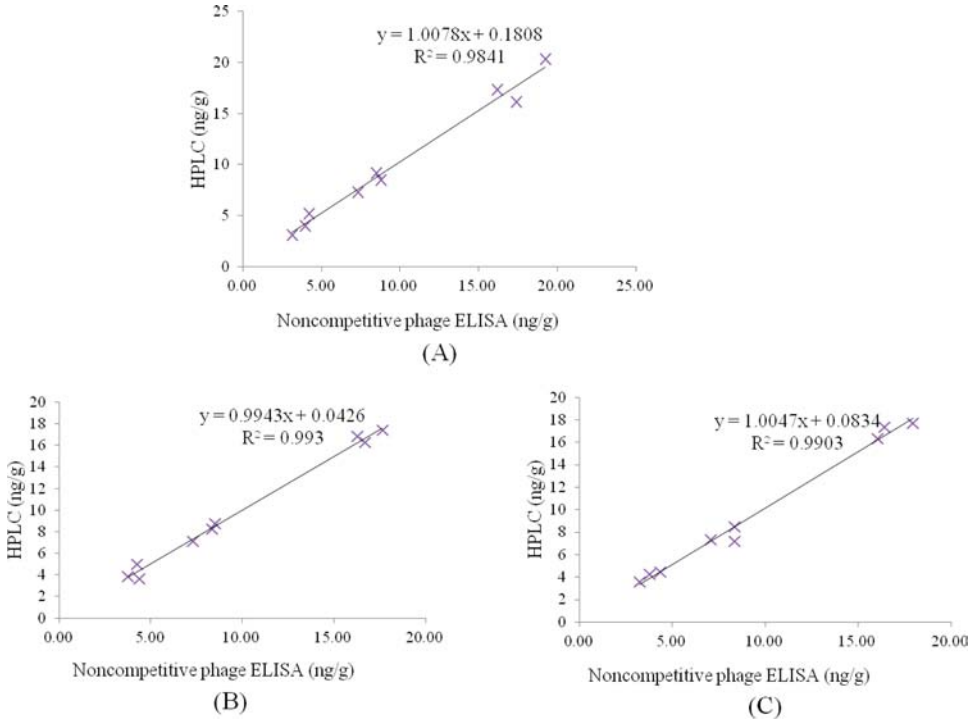


**Figure 5.** Correlation analysis between the PHAIA and HPLC ($n$ = 3). (A) Samples spiked with LMG. (B) Samples spiked with MG. (C) Sample spiked with a mixture LMG and MG (1:1). All the sample extracted by the same procedure were divided into two equal parts and tested by PHAIA and HPLC.

7.66 ng/mL compared with 7.37 ng/mL for PBST, indicating that the matrix effects of the three fish samples were completely eliminated after pretreatment by PRS solid phase extraction. Although the 1:10 dilution showed less matrix effect, the higher limit of quantitation makes it unattractive. Thus, LMG was extracted at a proportion of 1:5, and the extracts were diluted 5-fold with PBST to minimize matrix effects.

**Analysis of Spiked Samples by PHAIA and HPLC.** The accuracy and precision of the PHAIA format were evaluated by determination of MG and LMG in spiked fish samples as well as by spiking with the mixtures of the two analytes. The MG was reduced to LMG by potassium borohydride so that it could be detected by the specific anti-LMG mAb. As shown in Table 3, the mean recovery rate measured using the LMG-PHAIA standard curves were 75.33−88.00% for LMG, 80.67−84.45% for MG, and 75.60−83.93% for the LMG and MG mixture. The comparison of results with HPLC shown in Figure 5 indicated that good correlations were obtained at the 5, 10, and 20 ng/mL spiked levels.

The current work described a sensitive detection of MG and LMG using a noncompetitive PHAIA assay. The peptide-based sandwich can work as a simple method to convert competitive assays to more versatile noncompetitive formats for small molecules which will provide significantly improved sensitivity (~16-fold in this work) and more adaptable to other immunoassay detection systems. However, the biological *E. coli* infectivity of phage might be a concern in some laboratories and industry. Further research will focus on the novel phage-free peptide ELISA by using the chemical synthetic peptide or genetic fusion peptide.

## ■ ASSOCIATED CONTENT

### Ⓢ Supporting Information

Checkerboard assays of NCB1, NCB4, NCB6, NCB11, and NCB13 phage clones. Plates were coated with affinity-purified antibody at 1 μg/mL (a), 0.5 μg/mL (b), 0.25 μg/mL (c), and 0.125 μg/mL (d). This material is available free of charge via the Internet at http://pubs.acs.org.

## ■ AUTHOR INFORMATION

### Corresponding Authors

*E-mail: gzwhongd@163.com (H.W.). Tel.: (+86)-020-8528-3448.

*E-mail: ymsun@scau.edu.cn (Y.-M.S.).

### Funding

This work was supported by the National Natural Science Foundation of China, Grant (31271866), Provincial Natural Science Foundation of Guangdong, Grant (S2012010010323),Science and Technology Plan Projects in Guangdong Province (2012A020100002, 2010A020104004), National Institute of Environmental Health Science (NIEHS) Superfund Research Program Grant (P42 ES004699), the National Institute of Occupational Safety and Health (NIOSH) Western Center for Agricultural Health and Safety (U50 OH07550), and the Doctoral Innovation Program of Hopson Zhujiang Education Fund (H2011001).

### Notes

The authors declare no competing financial interest.

## ■ ABBREVIATIONS USED

ACN, acetonitrile; BG, brilliant green; BSA, bovine serum albumin; CV, crystal violet; DCM, dichloromethane; ELISA, enzyme-linked immunosorbent assays; HRP, horseradish peroxidase; $IC_{50}$, half inhibitory concentration; LCV, leucocrystal violet; LMG, leucomalachite green; LMGH8, 2-(3-(bis(4-(dimethylamino)phenyl)methyl)phenoxy)acetic acid; LOD, low limit of detection; mAb, monoclonal antibody; MB, methylene blue; MG, malachite green; OVA, ovalbumin; PA,

parafuchsin; PBS, phosphate-buffered saline; PBST, PBS containing 0.1% (v/v) Tween-20; PEG 8000, polyethylene glycol 8000; PHAIA, phage anti-immune complex assay; $SC_{50}$, concentration of analyte producing 50% saturation of the signal; TBS, Tris-buffered saline; TMB, 3,30,5,50-tetramethylbenzidine

## REFERENCES


(1) Willoughby, L. G.; Roberts, R. J. Towards strategic use of fungicides against *Saprolegnia parasitica* in salmonid fish hatcheries. *J. Fish. Dis.* **1992**, *15* (1), 1−13.

(2) Hecht, T.; Endemann, F. The impact of parasites, infections and diseases on the development of aquaculture in sub - Saharan Africa. *J. Appl. Ichthyol.* **1998**, *14* (3−4), 213−221.

(3) Plakas, S. M.; El Said, K. R.; Stehly, G. R.; Gingerich, W. H.; Allen, J. L. Uptake, tissue distribution, and metabolism of malachite green in the channel catfish (*Ictalurus punctatus*). *Can. J. Fish. Aquat. Sci.* **1996**, *53* (6), 1427−1433.

(4) Culp, S. J.; Blankenship, L. R.; Kusewitt, D. F.; Doerge, D. R.; Mulligan, L. T.; Beland, F. A. Toxicity and metabolism of malachite green and leucomalachite green during short-term feeding to Fischer 344 rats and B6C3$F_1$ mice. *Chem. Biol. Interact.* **1999**, *122* (3), 153−170.

(5) Mittelstaedt, R. A.; Mei, N.; Webb, P. J.; Shaddock, J. G.; Dobrovolsky, V. N.; McGarrity, L. J.; Morris, S. M.; Chen, T.; Beland, F. A.; Greenlees, K. J. Genotoxicity of malachite green and leucomalachite green in female Big Blue B6C3$F_1$ mice. *Mutat. Res.* **2004**, *561* (1), 127−138.

(6) Meyer, F. P.; Jorgenson, T. A. Teratological and other effects of malachite green on development of rainbow trout and rabbits. *Trans. Am. Fish. Soc.* **1983**, *112* (6), 818−824.

(7) Beier, R. C.; Stanker, L. H. Application of immunoassay for detection of antibiotics in foods and feed: a review. *Recent Res. Dev. Agric. Food Chem.* **2000**, *4* (1), 59−93.

(8) Jackson, T. M.; Ekins, R. P. Theoretical limitations on immunoassay sensitivity: current practice and potential advantages of fluorescent $Eu^{3+}$ chelates as non-radioisotopic tracers. *J. Immunol. Methods* **1986**, *87* (1), 13−20.

(9) He, J.; Liang, Y.; Fan, M.; Liu, X. Preparation of anti-idiotype antibodies of O, O-dimethyl organophosphorus pesticides by phage display technology. *Chin. J. Anal. Chem.* **2011**, *39* (2), 178−182.

(10) Niwa, T.; Kobayashi, T.; Sun, P.; Goto, J.; Oyama, H.; Kobayashi, N. An enzyme-linked immunometric assay for cortisol based on idiotype−anti-idiotype reactions. *Anal. Chim. Acta* **2009**, *638* (1), 94−100.

(11) Ihara, M.; Suzuki, T.; Kobayashi, N.; Goto, J.; Ueda, H. Open-sandwich enzyme immunoassay for one-step noncompetitive detection of corticosteroid 11-deoxycortisol. *Anal. Chem.* **2009**, *81* (20), 8298−8304.

(12) Lim, S.; Ichinose, H.; Shinoda, T.; Ueda, H. Noncompetitive detection of low molecular weight peptides by open sandwich immunoassay. *Anal. Chem.* **2007**, *79* (16), 6193−6200.

(13) Sakata, T.; Ihara, M.; Makino, I.; Miyahara, Y.; Ueda, H. Open sandwich-based immuno-transistor for label-free and noncompetitive detection of low molecular weight antigen. *Anal. Chem.* **2009**, *81* (18), 7532−7537.

(14) Suzuki, T.; Munakata, Y.; Morita, K.; Shinoda, T.; Ueda, H. Sensitive detection of estrogenic mycotoxin zearalenone by open sandwich immunoassay. *Anal. Sci.* **2007**, *23* (1), 65.

(15) Islam, K. N.; Ihara, M.; Dong, J.; Kasagi, N.; Mori, T.; Ueda, H. Direct construction of an open-sandwich enzyme immunoassay for one-step noncompetitive detection of thyroid hormone T4. *Anal. Chem.* **2011**, *83* (3), 1008−1014.

(16) Ullman, E. F.; Milburn, G.; Jelesko, J.; Radika, K.; Pirio, M.; Kempe, T.; Skold, C. Anti-immune complex antibodies enhance affinity and specificity of primary antibodies. *Proc. Natl. Acad. Sci. U.S.A.* **1993**, *90* (4), 1184−1189.

(17) Self, C. H.; Dessi, J. L.; Winger, L. A. High-performance assays of small molecules: enhanced sensitivity, rapidity, and convenience demonstrated with a noncompetitive immunometric anti-immune complex assay system for digoxin. *Clin. Chem.* **1994**, *40* (11), 2035−2041.

(18) Nagata, S.; Tsutsumi, T.; Yoshida, F.; Ueno, Y. A new type sandwich immunoassay for microcystin: production of monoclonal antibodies specific to the immune complex formed by microcystin and an anti-microcystin monoclonal antibody. *Nat. Toxins* **1999**, *7* (2), 49−55.

(19) Rossotti, M. A.; Carlomagno, M.; Gonzalez-Techera, A.; Hammock, B. D.; Last, J.; Gonzalez-Sapienza, G. Phage anti-immunocomplex assay for clomazone: two-site recognition increasing assay specificity and facilitating adaptation into an on-site format. *Anal. Chem.* **2010**, *82* (21), 8838−8843.

(20) González-Techera, A.; Vanrell, L.; Last, J. A.; Hammock, B. D.; González-Sapienza, G. Phage anti-immune complex assay: general strategy for noncompetitive immunodetection of small molecules. *Anal. Chem.* **2007**, *79* (20), 7799−7806.

(21) González-Techera, A.; Kim, H. J.; Gee, S. J.; Last, J. A.; Hammock, B. D.; González-Sapienza, G. Polyclonal antibody-based noncompetitive immunoassay for small analytes developed with short peptide loops isolated from phage libraries. *Anal. Chem.* **2007**, *79* (23), 9191−9196.

(22) Kim, H.; Rossotti, M. A.; Ahn, K. C.; González-Sapienza, G. G.; Gee, S. J.; Musker, R.; Hammock, B. D. Development of a noncompetitive phage anti-immunocomplex assay for brominated diphenyl ether 47. *Anal. Biochem.* **2010**, *401* (1), 38−46.

(23) Singh, G.; Koerner, T.; Gelinas, J.; Abbott, M.; Brady, B.; Huet, A.; Charlier, C.; Delahaut, P.; Benrejeb Godefroy, S. Design and characterization of a direct ELISA for the detection and quantification of leucomalachite green. *Food. Addit. Contam.* **2011**, *28* (6), 731−739.

(24) Xing, W.; He, L.; Yang, H.; Sun, C.; Li, D.; Yang, X.; Li, Y.; Deng, A. Development of a sensitive and group-specific polyclonal antibody-based enzyme-linked immunosorbent assay(ELISA) for detection of malachite green and leucomalachite green in water and fish samples. *J. Sci. Food Agric.* **2009**, *89* (13), 2165−2173.

(25) Oplatowska, M.; Connolly, L.; Stevenson, P.; Stead, S.; Elliott, C. T. Development and validation of a fast monoclonal based disequilibrium enzyme-linked immunosorbent assay for the detection of triphenylmethane dyes and their metabolites in fish. *Anal. Chim. Acta* **2011**, *698* (1), 51−60.

(26) Yang, M.; Fang, J.; Kuo, T.; Wang, D.; Huang, Y.; Liu, L.; Chen, P.; Chang, T. Production of antibodies for selective detection of malachite green and the related triphenylmethane dyes in fish and fishpond water. *J. Agric. Food Chem.* **2007**, *55* (22), 8851−8856.

(27) Shen, Y.; Deng, X.; Xu, Z.; Wang, Y.; Lei, H.; Wang, H.; Yang, J.; Xiao, Z.; Sun, Y. Simultaneous determination of malachite green, brilliant green and crystal violet in grass carp tissues by a broad-specificity indirect competitive enzyme-linked immunosorbent assay. *Anal. Chim. Acta* **2011**, *707* (1), 148−154.

(28) Wang, Y.; Wang, H.; Li, P.; Zhang, Q.; Kim, H. J.; Gee, S. J.; Hammock, B. D. Phage-displayed peptide that mimics aflatoxins and its application in immunoassay. *J. Agric. Food Chem.* **2013**, *61* (10), 2426−2433.

(29) Campbell, A. M. *Monoclonal Antibody Technology: The Production and Characterization of Rodent and Human Hybridomas*; Elsevier: Amsterdam, 2000.

(30) Cabilly, S. The basic structure of filamentous phage and its use in the display of combinatorial peptide libraries. *Mol. Biotechnol.* **1999**, *12* (2), 143−148.

JOURNAL OF AGRICULTURAL AND FOOD CHEMISTRY

Article

pubs.acs.org/JAFC

# Cadmium and Lead in Chocolates Commercialized in Brazil

Javier E. L. Villa, Rafaella R. A. Peixoto, and Solange Cadore*

Institute of Chemistry, University of Campinas, Post Office Box 6154, 13083-970 Campinas, São Paulo, Brazil

**ABSTRACT:** Cadmium (Cd) and lead (Pb) concentrations and their relationship to the cocoa content of chocolates commercialized in Brazil were evaluated by graphite furnace atomic absorption spectrometry (GF AAS) after microwave-assisted acid digestion. Several chemical modifiers were tested during method development, and analytical parameters, including the limits of detection and quantification as well as the accuracy and precision of the overall procedure, were assessed. The study examined 30 chocolate samples, and the concentrations of Cd and Pb were in the range of <1.7−107.6 and <21−138.4 ng/g, respectively. The results indicated that dark chocolates have higher concentrations of Cd and Pb than milk and white chocolates. Furthermore, samples with five different cocoa contents (ranging from 34 to 85%) from the same brand were analyzed, and linear correlations between the cocoa content and the concentrations of Cd ($R^2$ = 0.907) and Pb ($R^2$ = 0.955) were observed. The results showed that chocolate might be a significant source of Cd and Pb ingestion, particularly for children.

**KEYWORDS:** *chocolate, cadmium, lead, cocoa, GF AAS*

## INTRODUCTION

Chocolates are a type of food widely consumed around the world. The large consumption of chocolate is attributable mainly to its pleasant flavor and the feeling of well-being promoted by its ingestion,[1] which make it a very popular food among people of all ages, although children are often the major consumers.

The primary base of chocolate products is cocoa, the seed of the *Theobroma cacao* tree.[1−3] To be considered as chocolate, a food product must contain at least 25% cocoa solids or 20% cocoa butter.[4] According to the International Cocoa Organization, American production of cocoa beans accounts for approximately 16% of the worldwide production, and Brazil and Ecuador are the largest American producers.[5] In addition to being a large producer, Brazil is also an important market for cocoa derivatives. Dark, milk, and white are the main types of chocolates available on the Brazilian market, and the compositions of these varieties differ in terms of their cocoa solids, milk fat, and cocoa butter contents.[6]

Numerous studies have demonstrated that the ingestion of cocoa and its derivatives can benefit health, mainly because of the high levels of flavonoids and antioxidants present in cocoa-based foods.[2,7,8] This type of food may prevent harmful effects caused by free radicals in the human body, contributing to the reduction of cardiovascular disease and cancer risk.[9,10] In addition, cocoa and its derivatives are also an important source of essential inorganic constituents in the diet, such as Ca, P, Fe, Mg, Cu, Zn, K, and Mn.[2,11,12] However, the presence of potentially toxic elements has also been reported,[13−17] particularly lead and cadmium.[18,19]

The presence of lead in cocoa and its derivatives has been discussed for many years.[20] Although lead is naturally found in the environment, this element has no recognized function in the human body and is harmful even at trace levels. Once in the human body, lead can affect the metabolism of calcium and other essential nutrients by competing for binding sites in biological systems.[21,22] In adults, the primary symptoms of lead poisoning are abdominal pain, arthralgia, hypertension, headache, increased intracranial pressure, central nervous system dysfunction, anemia, and renal dysfunction. In children, the effects are more severe and are associated with long-term effects, such as growth failure, behavioral changes, language delay, and anemia.[23] Some studies have also noted a relationship between childhood exposure to lead and delayed intellectual development.[24−28]

Cadmium, another element that is potentially toxic at trace levels, is found in certain food crops grown in soils containing high levels of this element and is the major cause of non-workplace-related exposure to this element.[29] The presence of cadmium in the human body results in damage to several organs and can, thus, cause hepatic damage or kidney failure.[30,31] In addition, it may cause pneumonitis, destruction of mucous membranes, glomerular and tubular damage, testicular necrosis, estrogen-like effects, disruption of steroid-hormone synthesis, and numerous other harmful effects.[32]

Thus, controlling the cadmium and lead contents in chocolate products is a public health concern, especially because children are more susceptible to lead and cadmium poisoning through the consumption of chocolate products. However, the assessment of cadmium and lead concentrations in chocolate products remains an analytical challenge because of the complexity of the matrix. A successful approach must combine adequate sample treatment with a sensitive analytical technique.[1]

In this study, the concentrations of cadmium and lead found in different brands and types of chocolate bars available in the Brazilian market are presented. The relationship between lead and cadmium and the cocoa content of chocolates commercialized in Brazil were also evaluated.

**Received:** June 3, 2014
**Revised:** August 12, 2014
**Accepted:** August 15, 2014
**Published:** August 15, 2014

ACS Publications © 2014 American Chemical Society



dx.doi.org/10.1021/jf5026604 | *J. Agric. Food Chem.* 2014, 62, 8759−8763

## MATERIALS AND METHODS

**Chemicals.** Deionized water (Milli-Q system, 18.2 MΩ cm, Millipore, Bedford, MA) and analytical-grade reagents were used to prepare all solutions and standards. Nitric acid (65%) and hidrogen peroxide (30%, v/v) were purchased from Merck (Darmstadt, Germany). Pure argon (99.999%) purchased from White Martins (São Paulo, SP, Brazil) was used as purge and protective gas.

The palladium working solution (10 g/L) was purchased from PerkinElmer (Norwalk, CT). Magnesium nitrate was purchased from Merck (Darmstadt, Germany), and the corresponding working solution (10 g/L) was prepared by diluting an appropriate amount of the salt in ultrapure water. Ammonium dihydrogen phosphate was obtained from Fluka (Buch, Switzerland), and its working solution (100 g/L) was prepared by diluting the appropriate amount of the salt in deionized water.

The analyte solutions were prepared from 1000 mg/L standard solutions (Merck Darmstadt, Germany) in 0.2% (v/v) $HNO_3$. Appropriate dilutions were made from the standard solutions and stored in polyethylene flasks under refrigeration. All glass and quartz materials were treated with a 10% (v/v) $HNO_3$ solution for 24 h and then rinsed with deionized water prior to use.

**Instrumentation.** All measurements were carried out using an AAnalyst 600 atomic absorption spectrometer (PerkinElmer, Norwalk, CT) with Zeeman background correction that was equipped with a transversely heated graphite tube atomizer and an AS-800 autosampler. Electrodeless discharge lamps for Cd and Pb were operated at 230 and 440 mA, respectively. The selected wavelengths were 228.8 nm for Cd and 283.3 nm for Pb. Aliquots of 20 μL of the samples and calibration solutions were injected with 5 μL of chemical modifier directly into the graphite tube. Pure argon (99.999%) was used as the purge and protective gas. The optimum operating parameters for GF AAS are shown in Table 1.

**Table 1. Heating Programs for Cd and Pb Determination by GF AAS in Chocolate Samples Using 5 μg of Pd + 3 μg of $Mg(NO_3)_2$ and 3 μg of $Mg(NO_3)_2$ + 50 μg of $NH_4H_2PO_4$ as Chemical Modifiers**

| step | temperature (°C) | ramp (s) | hold (s) | argon flow rate (mL/min) |
|---|---|---|---|---|
| 1 | 110 | 5 | 20 | 250 |
| 2 | 130 | 5 | 30 | 250 |
| 3 | 600,[a] 850[b] | 10 | 20 | 250 |
| 4 | 1500,[a] 1600[b] | 0 | 5 | 0 |
| 5 | 2450 | 1 | 3 | 250 |

[a]Cadmium. [b]Lead.

**Certified Materials and Sample Collection.** Three certified reference materials (CRMs) from the National Institute of Standards and Technology (Gaithersburg, MD), specifically, corn bran (NIST 8433), wheat flour (NIST 1567a), and whole milk powder (NIST 8435), were used to verify the accuracy of the proposed method.

A total of 30 chocolate samples of different types (labeled by the manufacturers as white, milk, or dark chocolate) and brands (designated as brands A–K) were analyzed in this study. They were purchased in the local market of Campinas, State of São Paulo, Brazil, in the period of January–March 2014.

**Sample Treatment.** Sample treatment was performed using a microwave digestion system (ETHOS1, Milestone, Sorisole, Italy) equipped with closed polytetrafluoroethylene vessels and sensors for temperature and pressure control. Sample masses of 500 mg were accurately weighed into the closed vessels, and 1.5 mL of 30% (v/v) hydrogen peroxide and 6.5 mL of nitric acid at a concentration of 12, 9, 6, or 3 mol/L were subsequently added. The closed vessels were then placed inside the microwave oven, and the heating program was performed over six steps: (1) heat from room temperature to 80 °C in 3 min, (2) hold for 3 min at 80 °C, (3) heat from 80 to 140 °C in 3 min, (4) hold for 4 min at 140 °C, (5) heat from 140 to 200 °C in 8 min, and (6) hold for 16 min at 200 °C. After digestion, the resulting solutions were left to cool, transferred to individual 25.0 mL volumetric flasks, and diluted to the mark with deionized water.

A total organic carbon analyzer (TOC-VCPN, Shimadzu, Kyoto, Japan) was used to determine the residual carbon content (RCC). Acid–base titration of the digests was performed to determine the final acidities of the samples. The titrations were performed with a standard solution of sodium hydroxide (0.0989 mol/L) and phenolphthalein [1.0% (m/v) in ethanol].

**Validation Studies.** The method was validated by determining various figures of merit, such as the linearity, precision, accuracy, characteristic mass, and detection limit, as recommended by Welz and Sperling.[33] The accuracy of the method was evaluated using the following CRMs: corn bran (NIST 8433), wheat flour (NIST 1567a), and whole milk powder (NIST 8435). Furthermore, analyte addition and recovery experiments were performed for three different chocolate types at two concentration levels (0.2 and 0.5 μ/L for Cd and 1 and 4 μ/L for Pb) and in triplicate for each spiked level. The limits of detection (LOD) and quantitation (LOQ) of each analyte were also calculated.

## RESULTS AND DISCUSSION

**Sample Digestion.** The study of sample digestion procedures is an important topic for the improvement of analytical methods for the routine determination of trace elements in food materials. The sample decomposition using the minimal amount of reagents can offer advantages as reducing costs and the amounts of residue generated.[34−36] For this, the digestion procedure was evaluated at four different $HNO_3$ concentrations (12, 9, 6, and 3 mol/L) by comparing the RCCs and the residual acidities of the digests. The digestion solutions were free from solid residues when the nitric acid concentration was greater than 3 mol/L. The RCC for each

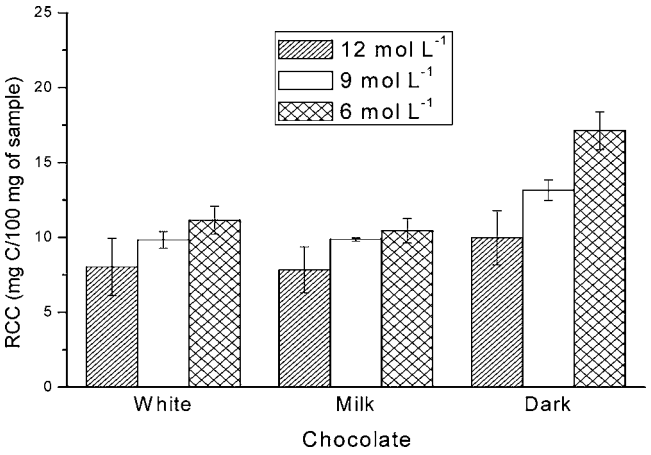


**Figure 1.** RCC in samples of each chocolate type digested using different nitric acid concentrations.

**Table 2. Pyrolysis Temperatures and Characteristic Masses ($m_o$) Obtained for Cd and Pb in a Sample of Dark Chocolate Using Different Chemical Modifiers**

| analyte | chemical modifier | $T_{pyrolysis}$ (°C) | $m_o$ (pg) |
|---|---|---|---|
| Cd | 10 μg of $NH_4H_2PO_4$ | 600 | 1.5 |
| | 3 μg of $Mg(NO_3)_2$ + 50 μg of $NH_4H_2PO_4$ | 700 | 1.5 |
| | 5 μg of Pd + 3 μg of $Mg(NO_3)_2$ | 600 | 1.4 |
| Pb | 10 μg of $NH_4H_2PO_4$ | 850 | 30.8 |
| | 3 μg of $Mg(NO_3)_2$ + 50 μg of $NH_4H_2PO_4$ | 850 | 31 |
| | 5 μg of Pd + 3 μg of $Mg(NO_3)_2$ | 1000 | 36.6 |


dx.doi.org/10.1021/jf5026604 | J. Agric. Food Chem. 2014, 62, 8759–8763

**Table 3. Determination of the Analytes in Standard Reference Materials**

| CRM | Cd (ng/g) | | Pb (ng/g) | |
|---|---|---|---|---|
| | certified value | found | certified value | found |
| corn bran | 12 ± 5 | 10 ± 2 | 140 ± 34 | 118 ± 12 |
| whole milk powder | nc[a] | | 110 ± 50 | 70 ± 9 |
| wheat flour | 26 ± 2 | 24.6 ± 0.5 | nc | |

[a]nc = not certified.

**Table 4. Recovery Results (%) for Cd and Pb in Spiked Samples ($n$ = 3)**

| chocolate type | Cd | | Pb | |
|---|---|---|---|---|
| | level 1 (0.2 μg/L) | level 2 (0.5 μg/L) | level 1 (1 μg/L) | level 2 (4 μg/L) |
| white | 93 ± 6 | 96 ± 4 | 92 ± 7 | 95 ± 3 |
| milk | 94 ± 6 | 92 ± 3 | 97 ± 5 | 99 ± 4 |
| dark | 96 ± 4 | 95 ± 5 | 102 ± 8 | 93 ± 3 |

**Table 5. Figures of Merit for the Determination of Cd and Pb in Chocolate**

| element | linear range (μg/L) | LOD (ng/g) | LOQ (ng/g) | $RSD_{repeat}$ (%) |
|---|---|---|---|---|
| Cd | 0.034−2 | 0.5 | 1.7 | 1.6 |
| Pb | 0.45−10 | 6.3 | 21 | 2.1 |

type of chocolate is shown in Figure 1, and the residual acidities of the digests prepared using nitric acid at 6, 9, and 12 mol/L ranged from 1 to 2.7 mol/L.

A concentration of 6 mol/L $HNO_3$ was used in subsequent experiments to digest 500 mg of chocolate, even though this condition presented the highest RCC value, considering that the technique of GF AAS has a pyrolysis step, which main function is to eliminate the matrix organic matter prior to the atomization. As already demonstrated, when using this technique, it is possible to do the introduction of samples with high contents of organic matter, including slurry and solid samples.[14,33]

**Optimization of the GF AAS Conditions.** Pyrolysis and atomization curves were established using the sample with the highest RCC (dark chocolate) to guarantee that the heating program would be adequate for all of the samples. The pyrolysis temperature and characteristic masses of Cd and Pb using different chemical modifiers are shown in Table 2. With respect to the chemical modifiers, the best detectability, analytical signal, and background signal for Cd determination were observed using 3 μg of $Mg(NO_3)_2$ + 5 μg of Pd, whereas the highest detectability and repeatability for Pb determination were observed when 3 μg of $Mg(NO_3)_2$ + 50 μg of $NH_4H_2PO_4$ was used.

**Analytical Features.** No chocolate reference material with certified Cd and Pb concentrations is currently available. However, three CRMs (NIST 8433, NIST 1567a, and NIST 8435) were used. The observed Cd and Pb concentrations were in agreement with the certified values at the 95% confidence level (Student's $t$ test); the results are shown in Table 3. Considering the analyte addition and recovery experiments, values ranging from 92 to 102% were obtained, as shown in Table 4.

The LOD and LOQ were calculated as $3S_{blank}/b$ and $10S_{blank}/b$,[33] respectively, where $S_{blank}$ is the standard deviation of 10 measurements of the blank and $b$ is the slope of the calibration curve. A further multiplication by a factor of 50, considering the mass of the sample (0.5 g) and the final volume of the solution (25 mL), allowed us to obtain the LOD and LOQ in ng/g. The repeatability was obtained by analyzing a control sample of dark chocolate 6 times within a short period of time.

The figures of merit for the determination of Cd and Pb are provided in Table 5.

**Table 6. Concentrations Found (ng/g) of Cd and Pb in Chocolates ($n$ = 3)**

| sample | type/brand | cocoa content (%) | Cd | Pb |
|---|---|---|---|---|
| 1 | white/A | ni[a] | <1.7 | <21 |
| 2 | white/B | ni | <1.7 | <21 |
| 3 | white/C | ni | <1.7 | <21 |
| 4 | white/D | ni | <1.7 | <21 |
| 5 | white/E | ni | <1.7 | <21 |
| 6 | white/F | ni | <1.7 | <21 |
| 7 | white/G | ni | <1.7 | <21 |
| 8 | milk/A | ni | 7.8 ± 1.4 | <21 |
| 9 | milk/B | ni | 12.3 ± 0.3 | <21 |
| 10 | milk/C | ni | 9.6 ± 1.1 | <21 |
| 11 | milk/D | ni | 8.7 ± 0.6 | <21 |
| 12 | milk/E | ni | 9.9 ± 0.5 | <21 |
| 13 | milk/G | ni | 9.7 ± 0.4 | <21 |
| 14 | milk/H | ni | 11.0 ± 0.3 | <21 |
| 15 | dark/A | 55 | 36.7 ± 1.0 | 138.4 ± 4.4 |
| 16 | dark/B | 60 | 38.0 ± 0.8 | 22.7 ± 2.7 |
| 17 | dark/C | 43 | 35.4 ± 1.2 | <21 |
| 18 | dark/E | 53 | 32.9 ± 2.3 | <21 |
| 19 | dark/G | 70 | 38.3 ± 0.5 | 44.8 ± 4.2 |
| 20 | dark/I | 75 | 107.6 ± 4.5 | 44.6 ± 2.7 |
| 21 | dark/J | 40 | 22.1 ± 0.4 | 59.5 ± 2.8 |
| 22 | dark/J | 70 | 40.0 ± 1.9 | 129.7 ± 6.9 |
| 23 | ni/A | 40 | 29.8 ± 0.7 | <21 |
| 24 | ni/B | 41 | 28.2 ± 0.3 | 39.1 ± 3.4 |
| 25 | ni/D | ni | 31.5 ± 0.7 | <21 |
| 26 | milk/K | 34 | 11.6 ± 1.0 | 27.0 ± 3.8 |
| 27 | milk/K | 41 | 14.4 ± 1.1 | 28.1 ± 3.1 |
| 28 | dark/K | 55 | 37.3 ± 0.9 | 39.5 ± 3.9 |
| 29 | dark/K | 70 | 48.5 ± 0.6 | 63.6 ± 3.7 |
| 30 | dark/K | 85 | 89.5 ± 2.3 | 73.8 ± 4.1 |

[a]ni = not informed.

**Analytical Determinations.** Cadmium and lead concentrations were determined in 30 chocolate samples of different types and brands using the proposed method. The results are shown in Table 6.

The concentrations of Cd and Pb found ranged between <1.7−107.6 and <21−138.4 ng/g, respectively, and the highest concentrations of Cd and Pb were found in dark chocolates. The results were in agreement with those found by Rehman et al.[13] (Cd and Pb ranged between 4.3 and 190 and between 29 and 1400 ng/g, respectively) and, in general, lower than those found by Dahiya et al.[18] (Cd and Pb ranged between 1 and 2730 and between 49 and 8040 ng/g, respectively).

The Cd and Pb concentrations of all of the samples analized in this work were below the maximum levels recommended by the Brazilian legislation,[37] the European Union,[38] and the Food and Agriculture Organization (FAO)/World Health Organization (WHO).[39] According to the U.S. Food and Drug Administration (FDA), the levels of Pb in candies must not exceed 100 ng/g. In this study, two samples of dark chocolates


dx.doi.org/10.1021/jf5026604 | J. Agric. Food Chem. 2014, 62, 8759−8763

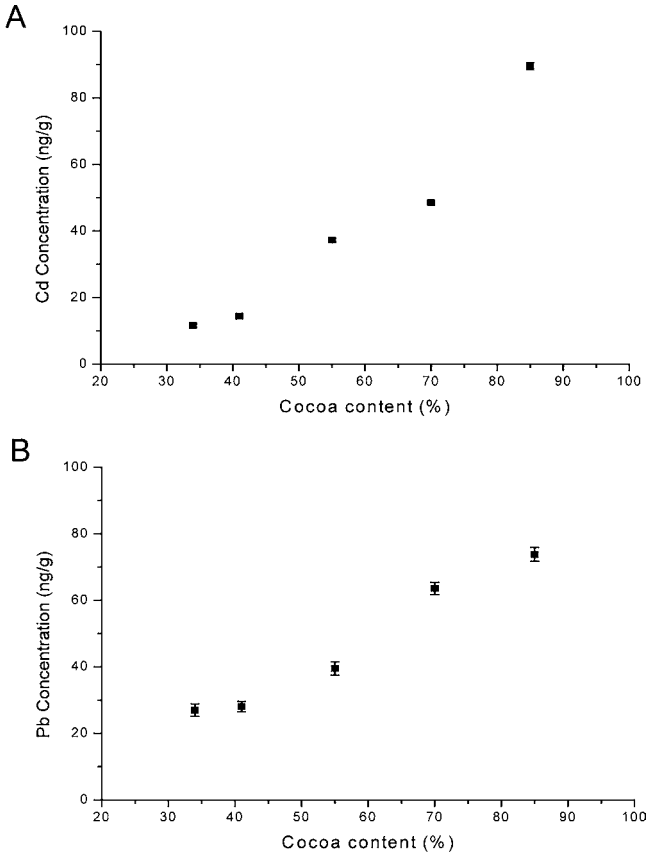


**Figure 2.** Correlation between the cocoa content (%) and the (A) cadmium and (B) lead concentrations.

have presented higher concentrations, what is already expected, considering that the cocoa liquor might be the principal source of lead.[40]

The provisional tolerable monthly intake (PTMI) for Cd recommended by the FAO/WHO is 25 $\mu$g/kg of body weight.[41] Considering an average weight of 15 kg for children and 70 kg for adults and a consumption of 10 g of chocolate per day, the maximum contribution for Cd was 8.6% of the PTMI for children and 1.8% for adults.

The European Union recommends a tolerable weakly intake (TWI) of 2.5 $\mu$g/kg of body weight for Cd,[42] and in this case, the maximum contribution was 20.1% of the TWI for children and 4.3% for adults. Thus, the dark chocolate consumption might be a significative source of Cd, especially for children.

Although the determination of the total concentrations allowed us to evaluate the maximum levels and tolerable intakes of Cd and Pb, it is important to point out that the evaluation of the risk assessment associated with the ingestion of metallic elements from a food matrix should estimate its bioaccessibility and bioavailability, considering that only a fraction of the ingested element is released from the food matrix into the gastrointestinal tract and is absorbed by humans to finally reach the bloodstream.[21,43,44]

With regard to the presence of Cd and Pb in chocolate samples, the possible sources of contamination include the raw materials used, the manufacturing processes, and the wrappers in which the chocolates are stored. As shown in Table 6, the concentrations of Cd and Pb in chocolates with the same cocoa content were slightly different depending upon the brand, which may be due to the different manufacturing processes used.

To evaluate the relationship between the cocoa content and the concentrations of Cd and Pb in chocolate, five samples with different cocoa contents (ranging from 34 to 85%) from the same brand were analyzed and the measured concentrations were plotted against the cocoa content. The results are shown in Figure 2.

According to the results, a linear correlation exists between the cocoa content and the concentrations of Cd ($R^2$ = 0.907) and Pb ($R^2$ = 0.955), which suggests that the main source of contamination of Cd and Pb in chocolates is the cocoa used in the manufacturing process.

## AUTHOR INFORMATION

### Corresponding Author

*Telephone: +55-19-3521-3125. Fax: +55-19-3521-3023. E-mail: cadore@iqm.unicamp.br.

### Funding

The authors gratefully acknowledge the Conselho Nacional de Desenvolvimento Científico e Tecnológico (CNPq), the Fundação de Amparo à Pesquisa do Estado de São Paulo (FAPESP/Process 2011/07759-7 and Process 2011/21023-3), and the Instituto Nacional de Ciências e Tecnologias Analíticas Avançadas (INCTAA) for their financial support.

### Notes

The authors declare no competing financial interest.

## REFERENCES

(1) Watson, R. R.; Preedy, V. R.; Zibadi, S. *Chocolate in Health and Nutrition*; Humana Press: London, U.K., 2013.

(2) Grivetti, L. I.; Shapiro, H. *Chocolate: History, Culture and Heritage*; Wiley: Hoboken, NJ, 2009.

(3) Lee, F. A. *Basic Food Chemistry*, 2nd ed.; The AVI Publishing Company: Westport, CT, 1983.

(4) Brazilian Health Surveillance Agency (ANVISA). *Technical Regulation for Chocolate and Cocoa Products*; http://www4.anvisa.gov.br/base/visadoc/CP/CP%5B8991-1-0%5D.PDF (accessed Aug 10, 2014).

(5) International Cocoa Organization (ICCO). *International Cocoa Agreements*; http://www.icco.org/about-us/international-cocoa-agreements/cat_view/30-related-documents/46-statistics-production.html (accessed Aug 10, 2014).

(6) Afoakwa, E. O.; Paterson, A.; Fowler, M. Factors influencing rheological and textural qualities in chocolate—A review. *Trends Food Sci. Technol.* **2007**, *18*, 290−298.

(7) Crozier, S. J.; Preston, A. G.; Hurst, J. W.; Payne, M. J.; Mann, J.; Hainly, L.; Miller, D. L. Cacao seeds are a "super fruit": A comparative analysis of various fruit powders and products. *Chem. Cent. J.* **2011**, *5*, N°5.

(8) Buitrago-Lopez, A.; Sanderson, J.; Johnson, L.; Warnakula, S.; Wood, A.; Angelantonio, E.; Franco, O. H. Chocolate consumption and cardiometabolic disorders: Systematic review and meta-analysis. *Br. Med. J.* **2011**, *343*, d4488.

(9) Fernandez-Murga, L.; Tarín, J. J.; García-Perez, M. A.; Cano, A. The impact of chocolate on cardiovascular health. *Maturitas* **2011**, *69*, 312−321.

(10) Yao, H.; Xu, W.; Shi, X.; Zhang, Z. Dietary flavonoids as cancer prevention agents. health. *J. Environ. Sci. Health, Part C: Environ. Carcinog. Ecotoxicol. Rev.* **2011**, *29*, 1−31.

(11) Peixoto, R. R. A.; Oliveira, A.; Cadore, S. Multielemental determinations in chocolate drink powder using multivariate optimization and ICP OES. *J. Agric. Food Chem.* **2012**, *60*, 8117−8122.

(12) Pedro, N. A. R.; Oliveira, E.; Cadore, S. Study of the mineral content of chocolate flavoured beverages. *Food Chem.* **2006**, *95*, 94−100.

(13) Rehman, S.; Husnain, S. M. Assessment of trace metal contents in chocolate samples by atomic absorption spectrometry. *J. Trace Elem. Anal.* **2013**, *1*, 1.
(14) Ieggli, C. V. S.; Bohrer, D.; Nascimento, P. C.; Carvalho, L. M.; Gobo, L. A. Determination of aluminum, copper and manganese content in chocolate samples by graphite furnace atomic absorption spectrometry using a microemulsion technique. *J. Food Compos. Anal.* **2011**, *24*, 465−468.
(15) Güldaş, M. Comparison of digestion methods and trace elements determination in chocolates with pistachio using atomic absoption spectrometry. *J. Food Nutr. Res.* **2008**, *47*, 92−99.
(16) Onianwa, P. C.; Adetola, I. G.; Iwegbue, C. M. A.; Ojo, M. F.; Tella, O. O. Trace heavy metals composition of some Nigerian beverages and food drinks. *Food Chem.* **1999**, *66*, 275−279.
(17) Yanus, R.; Sela, H.; Borojovich, E. J. C.; Zakon, Y.; Saphier, M.; Nikolski, A.; Gutflais, E.; Lorber, A.; Karpas, Z. Trace elements in cocoa solids and chocolate: A ICPMS study. *Talanta* **2014**, *119*, 1−4.
(18) Dahiya, S.; Karpe, R.; Hegde, A. G.; Sharma, R. M. Lead, cadmium and nickel in chocolates and candies from suburban areas of Mumbai, India. *J. Food Compos. Anal.* **2005**, *18*, 517−522.
(19) Jalbani, N.; Kazi, T. G.; Afridi, H. I.; Arain, M. B. Determination of toxic metals in different brand of chocolates and candies, marketed in Pakistan. *Pak. J. Anal. Environ. Chem.* **2009**, *10*, 48−52.
(20) Rankin, C. W.; Nriagu, J. O.; Aggarwal, J. K.; Arowolo, T. A.; Adebayo, K.; Flegal, A. R. Lead contamination in cocoa and cocoa products: Isotopic evidence of global contamination. *Environ. Health Perspect.* **2005**, *113*, 1344−1348.
(21) Cozzolino, S. M. F. *Biodisponibilidade de Nutrientes*, 2nd ed.; Manole: Barueri, Brazil, 2007.
(22) Mahaffey, K. R. Quantities of lead producing health effects in humans: Sources and bioavailability. *Environ. Health Perspect.* **1977**, *19*, 285−295.
(23) Needleman, H. Lead poisoning. *Annu. Rev. Med.* **2004**, *55*, 209−222.
(24) Dietrich, K. N. Environmental chemicals and child development. *J. Pediatr.* **1999**, *134*, 7−9.
(25) Bellinger, D. C.; Stiles, K. M.; Neddleman, H. L. Low-level lead exposure, intelligence and academic achievement: a long-term follow-up study. *Pediatrics* **1992**, *90*, 855−861.
(26) Baghurst, P. A.; McMichael, A. J.; Wigg, N. R.; Vimpani, G. V.; Robertson, E. F.; Roberts, R. J.; Tong, S. L. Environmental exposure to lead and children's intelligence at the age of seven years. *New Engl. J. Med.* **1992**, *327*, 1279−1284.
(27) Dietrich, K. N.; Berger, O. G.; Succop, P. A.; Hammond, P. B.; Bornschein, R. L. The developmental consequences of low to moderate prenatal and postnatal lead exposure: Intellectual attainment in the Cincinnati lead study cohort following school entry. *Neurotoxicol. Teratol.* **1993**, *15*, 37−44.
(28) Factor-Litvak, P.; Wasserman, G.; Kline, J. K.; Graziano, J. The Yugoslavia prospective study of environmental lead exposure. *Environ. Health Perspect.* **1999**, *107*, 9−15.
(29) Satarug, S.; Baker, J. R.; Unbenjapol, S.; Haswell-Elkins, M.; Reilly, P. E. B.; Williams, D. J.; Moore, M. R. A global perspective on cadmium pollution and toxicity in non-occupationally exposed population. *Toxicol. Lett.* **2003**, *137*, 65−83.
(30) Szefer, P.; Nriagu, J. O. *Mineral Components in Foods*; CRC Press: Boca Raton, FL, 2007.
(31) Järup, L.; Åkesson, A. Current status of cadmium as an environmental health problem. *Toxicol. Appl. Pharmacol.* **2009**, *238*, 201−208.
(32) Godt, J.; Scheidig, F.; Grosse-Siestrup, C.; Esche, V.; Brandenburg, P.; Reich, A.; Groneberg, D. A. The toxicity of cadmium and resulting hazards for human health. *J. Occup. Med. Toxicol.* **2006**, *1*, 22.
(33) Welz, B.; Sperling, M. *Atomic Absorption Spectrometry*, 3rd ed., Wiley-VCH: Weinheim, Germany, 1999.
(34) Demirel, S.; Tuzen, M.; Saracoglu, S.; Soylak, M. Evaluation of various digestion procedures for trace element contents of some food materials. *J. Hazard. Mater.* **2008**, *152*, 1020−1026.
(35) Castro, J. T.; Santos, E. C.; Santos, W. P. C.; Costa, L. M.; Korn, M.; Nóbrega, J. A.; Korn, M. G. A. A critical evaluation of digestion procedures for coffee samples using diluted nitric acid in closed vessels for inductively coupled plasma optical emission spectrometry. *Talanta* **2009**, *78*, 1378−1382.
(36) Gonzales, M. H.; Souza, G. B.; Oliveira, R. V.; Forato, L. A.; Nóbrega, J. A.; Nogueira, A. R. A. Microwave-assisted digestion procedures for biological samples with diluted nitric acid: Identification of reaction products. *Talanta* **2009**, *79*, 396−401.
(37) Brazilian Health Surveillance Agency (ANVISA). *Technical Regulation MERCOSUL on Maximum Inorganic Contaminants in Foods*; http://portal.anvisa.gov.br/wps/wcm/connect/8100bb8040eac2e8b590b79cca79f4cf/RDC+n%C2%BA+42_2013_final.pdf?MOD=AJPERES (accessed Aug 10, 2014).
(38) Commision Regulation (EU). *Maximum Levels of Cadmium in Foodstuffs*; http://eur-lex.europa.eu/legal-content/EN/TXT/PDF/?uri=CELEX:32014R0488&rid=1 (accessed Aug 10, 2014).
(39) Food and Agriculture Organization (FAO)/World Health Organization (WHO). *Drafts Standards for Chocolate and Chocolate Products. Joint FAO/WHO Standards Programme. CODEX Committee on Cocoa Products and Cocoa Chocolates, 19th Session, 3−5 October 2001, Fribourg, Switzerland, CX/CPC 01/3*; FAO/WHO: Rome, Italy, 2001.
(40) U.S. Food and Drug Administration (FDA). *Supporting Document for Recommended Maximum Level for Lead in Candy Likely to Be Consumed Frequently by Small Children*; http://www.fda.gov/Food/FoodborneIllnessContaminants/Metals/ucm172050.htm#lead (accessed Aug 10, 2014).
(41) Food and Agriculture Organization (FAO)/World Health Organization (WHO). *Working Document for Information and Use in Discussions Related to Contaminants and Toxins in the GSCTFF*; ftp://ftp.fao.org/codex/meetings/CCCF/cccf5/cf05_INF.pdf (accessed Aug 10, 2014).
(42) Commision Recommendation (EU). *On the Reduction of the Presence of Cadmium in Foodstuffs*; http://eur-lex.europa.eu/legal-content/EN/TXT/PDF/?uri=CELEX:32014H0193&from=DE (accessed Aug 10, 2014).
(43) Peixoto, R. R. A.; Mazon, E. A. M.; Cadore, S. Estimation of the bioaccessibility of metallic elements in chocolate drink powder using an in vitro digestion method and spectrometric techniques. *J. Braz. Chem. Soc.* **2013**, *24*, 884−890.
(44) Moreda-Piñero, J.; Moreda-Piñero, A.; Romarís-Hortas, V.; Moscoso-Pérez, C.; López-Mahía, P.; Muniategui-Lorenzo, S.; Bermejo-Barrera, P.; Prada-Rodríguez, D. In vivo and in vitro testing to assess the bioaccessibility and the bioavailability of arsenic, selenium and mercury species in food samples. *Trends Anal. Chem.* **2011**, *30*, 324−345.

JOURNAL OF AGRICULTURAL AND FOOD CHEMISTRY

Article

pubs.acs.org/JAFC

# Metabolite Profiling of Red and White Pitayas (*Hylocereus polyrhizus* and *Hylocereus undatus*) for Comparing Betalain Biosynthesis and Antioxidant Activity

Dong Ho Suh,[†] Sunmin Lee,[†] Do Yeon Heo,[†] Young-Suk Kim,[‡] Somi Kim Cho,[§] Sarah Lee,*[,†] and Choong Hwan Lee*[,†]

[†]Department of Bioscience and Biotechnology, Konkuk University, Seoul 143-701, Republic of Korea

[‡]Department of Food Science and Engineering, Ewha Womans University, Seoul 120-750, Republic of Korea

[§]Faculty of Biotechnology College of Applied Life Sciences, SARI, Jeju National University, Jeju 690-756, Republic of Korea

**ABSTRACT:** Metabolite profiling of red and white pitayas (*Hylocereus polyrhizus* and *Hylocereus undatus*) was performed using gas chromatography−time-of-flight−mass spectrometry and ultraperformance liquid chromatography−quadrupole-time-of-flight−mass spectrometry with multivariate analysis. Different species and parts of pitayas (red peel, RP; white peel, WP; red flesh, RF; and white flesh, WF) were clearly separated by partial least-squares discriminate analysis. Furthermore, betalain-related metabolites, such as betacyanins and betaxanthins, or their precursors were described on the basis of their metabolites. The results of antioxidant activity tests [1,1-diphenyl-2-picrylhydrazyl (DPPH), 2,2′-azinobis(3-ethylbenzothiazoline-6-sulfonic acid) diammonium salt (ABTS), and ferric reducing ability of plasma (FRAP)], total phenolic contents (TPC), total flavonoid contents (TFC), and total betacyanin contents (TBC) showed the following: RP ≥ WP > RF > WF. TPC, TFC, TBC, and betalain-related metabolites were higher in the peel than in the flesh and suggested to be the main contributors to antioxidant activity in pitayas. Therefore, peels as well as pulp of pitaya could beneficially help in the food industry.

**KEYWORDS:** *Hylocereus polyrhizus, Hylocereus undatus, metabolite profiling, GC−TOF−MS, UPLC−Q-TOF−MS, antioxidant activity, betalain biosynthesis pathway*

## INTRODUCTION

Pitayas, commonly known as dragon fruit, belong to the genus *Hylocereus* of the order Caryophyllales. The *Hylocereus* species originate from Latin America and West Indies and are cultivated in the tropical and subtropical regions worldwide. There are several types of pitayas, such as *Hylocereus undatus*, *Hylocereus polyrhizus*, and *Hylocereus megalanthus*. Among them, *H. undatus* and *H. polyrhizus* are the most widely cultivated[1] and have the same red fruit skin color but different flesh colors, white and red, respectively.

Recently, the interest in the natural pigments of plants has increased, because a natural source of pigments is considered nutritionally important in the food processing and pharmaceutical industries, particularly when, in the food industry, red pigments have been commonly used as food additives. Anthocyanins and carotenoids are mainly used, while betalains are less commonly used in food processing.[2] Pitayas contain two betalain pigments, namely, the red−violet betacyanins and yellow−orange betaxanthins.[3] These pigments are biosynthesized from tyrosine by enzymatic and spontaneous chemical reactions.[4] They are water-soluble nitrogen-containing pigments that also contain betalamic acid as the chromophore. Furthermore, betalain pigments have been studied for their antioxidant,[5−7] chemopreventive,[8] and anti-inflammatory activities.[9]

Metabolomics is used to compare the relative differences between biological samples based on their metabolites and changes in their environment. Metabolite analysis commonly involves the use of multiple experimental platforms, including nuclear magnetic resonance (NMR) and mass spectrometry (MS) coupled with separation techniques, such as gas chromatography (GC), liquid chromatography (LC), and capillary electrophoresis (CE).[10] These techniques produce large amounts of data and require data processing analyses, combined with multivariate analysis.[11] Data processing and data analyses affect the quality of metabolite identification and quantification. Data analyses include multivariate analysis, such as the clustering of metabolite profiles or discovering of important differences between groups of samples, which has been used in several previous studies. Metabolite profiling, short-term responses of rice leaves,[11] different-sized *Aloe vera*,[12] and Korean traditional meju during fermentation[13] were assessed using MS-based analysis.

The objective of this study was to investigate the different metabolites in red and white pitayas and compare their antioxidant activities [1,1-diphenyl-2-picrylhydrazyl (DPPH), 2,2′-azinobis(3-ethylbenzothiazoline-6-sulfonic acid) diammonium salt (ABTS), and ferric reducing ability of plasma (FRAP)], total phenolic contents (TPC), total flavonoid contents (TFC), and total betacyanin contents (TBC). Furthermore, we investigated the level of metabolites in the betalain biosynthesis pathway and tried to find major metabolites contributing to antioxidant activity.

**Received:** May 1, 2014
**Revised:** July 18, 2014
**Accepted:** August 7, 2014
**Published:** August 7, 2014

ACS Publications © 2014 American Chemical Society



dx.doi.org/10.1021/jf5020704 | *J. Agric. Food Chem.* 2014, 62, 8764−8771

## MATERIALS AND METHODS

**Chemicals and Reagents.** Methanol, acetonitrile, hexane, and water were purchased from Fisher Scientific (Pittsburgh, PA). Methoxyamine hydrochloride, *N*-methyl-*N*-(trimethylsilyl)-trifluoroacetamide (MSTFA), formic acid, pyridine, potassium persulfate, ABTS, DPPH, 6-hydroxy-2,5,7,8-tetramethylchromane-2-carboxylic acid (Trolox), 2,4,6-Tris(2-pyridyl)-striazine (TPTZ), iron(III) chloride hexahydrate, sodium acetate, acetic acid, sodium carbonate, sodium hydroxide, naringin, gallic acid, Folin and Ciocalteu's phenol reagent, diethylene glycol, and standard compounds were obtained from Sigma Chemical Co. (St. Louis, MO).

**Plant Materials.** Red and white pitayas (*H. polyrhizus* and *H. undatus*) were collected from a farm near Hallim Park, Jeju Island, in October 2007. All fruits were washed with distilled water and wiped with paper. Fruit was cut into two portions and separated into peel and flesh. Many seeds were embedded in the flesh. Pitaya samples were freeze-dried over 3 days and stored at below −20 °C before experiment. Four biological replications of each red and white pitaya sample were used in this study.

**Sample Preparation.** Freeze-dried samples were powdered using a mortar and pestle. Each ground sample (0.2 g) was extracted with 80% methanol by sonication for 30 min and then using a twist shaker (BioFree, Seoul, Korea) for 6 h at room temperature. After extraction, the extract was centrifuged at 5000 rpm for 15 min at 4 °C (Hettich Zentrifugen Universal 320, Tuttlingen, Germany). The supernatant was filtered through a 0.2 μm polytetrafluoroethylene (PTFE) filter and dried up using a speed vacuum concentrator (Biotron, Seoul, Korea). The final concentration of samples was 10 mg/mL with 80% methanol for ultraperformance liquid chromatography−quadrupole-time-of-flight−mass spectrometry (UPLC−Q-TOF−MS) and liquid chromatography−electrospray ionization−ion trap−tandem mass spectrometry (LC−ESI−IT−MS/MS) analyses. For gas chromatography−time-of-flight−mass spectrometry (GC−TOF−MS) analysis, the dried extracts had to undergo oximation and silylation. The dried extracts were oximated with 50 μL of methoxyamine hydrochloride in pyridine (20 mg/mL) for 90 min at 30 °C using a thermomixer (Eppendorf, Hamburg, Germany). After oximation, silylation was performed with 50 μL of MSTFA for 30 min at 37 °C using a thermomixer. Three analytical replications of each sample were used.

**GC−TOF−MS Analysis.** An Agilent 7890A GC system equipped with an Agilent 7693 autosampler (Agilent, Atlanta, GA) was coupled with a Pegasus HT TOF-MS (LECO Corp., St Joseph, MI). A Rtx-5MS capillary column (30 m × 0.25 mm × 0.25 μm particle size, Restek Corp., Bellefonte, PA) was used with a constant flow of 1.5 mL/min of helium. The front inlet and transfer line temperatures were set at 250 and 240 °C, respectively. The oven temperature was held at 75 °C for 2 min, followed by 300 °C from 2 to 17 min, with a 15 °C/min hold, and a final holding for 3 min. The electron ionization was set at 70 eV, and the mass spectra were recorded over the range of $m/z$ 50−600. A total of 1 μL of derivatized samples was injected into GC−TOF−MS with a split ratio of 20:1.

**UPLC−Q-TOF−MS and LC−ESI−IT−MS/MS Analyses.** UPLC−Q-TOF−MS analysis was performed using a Waters Micromass Q-TOF Premier with an UPLC Acquity system (Waters, Milford, MA) equipped with a binary solvent delivery system, an autosampler, and an ultraviolet (UV) detector. The column selected was an Acquity UPLC BEH $C_{18}$ column (100 mm × 2.1 mm × 1.7 μm particle size, Waters Corp.). The injection volume was 5 μL; the flow rate was 0.3 mL/min; and the column temperature was set at 37 °C. Elution conditions consisted of 0.1% formic acid in water (solvent A) and 0.1% formic acid in acetonitrile (solvent B). The initial condition was 5% solvent B for 1 min, gradually increasing to 100% over 9 min, maintained at 100% B for 1 min, and then decreased to 5% over 3 min. The total run time was 13 min. The Waters Q-TOF Premier (Micromass MS Technologies, Manchester, U.K.) MS data were collected in the range of $m/z$ 100−1000 within negative- and positive-ion modes. The source temperature was 100 °C, and the desolvation gas (nitrogen) was set to 600 L/h at a temperature of 200 °C; the cone gas (nitrogen) was set to 50 L/h. The capillary voltage and cone voltage were set at 2.5 kV and 50 V, respectively. Data were collected with a scan accumulation time of 0.2 s in the centroid mode. Leucine enkephalin (10 ppm) was used as the reference lock mass [$m/z$ 554.2615 (−) and 556.2771 (+)] at a flow rate of 10 μL/min.

LC−ESI−IT−MS/MS analysis was performed using a Varian 500-MS ion-trap mass spectrometer (Palo Alto, CA) equipped with a 212-LC binary solvent delivery system, an autosampler (Prostar 410), and a photodiode array detector (Prostar 335). The column selected was a Varian PurSuit XRs $C_{18}$ column (100 mm × 2.0 mm × 3 μm particle size) with a MetaGuard 2.0 PurSuit XRs $C_{18}$ guard column (Varian, Lake Forest, CA). The injection volume was 10 μL; the flow rate was 0.2 mL/min; and the column temperature was set at 40 °C. Elution conditions consisted of 0.1% formic acid in water (solvent A) and 0.1% formic acid in acetonitrile (solvent B). The initial condition was 10% solvent B for 2 min, which was increased to 40% solvent B at 10 min, then 70% solvent B at 20 min, and 90% solvent B at 25 min, after which was isothermally held for 5 min, and then decreased to 10% B, and maintained for 10 min. The total run time was 40 min. Mass spectra were acquired using electrospray ionization (ESI) over the range of $m/z$ 100−1000 within both negative- and positive-ion modes.

**Data Processing and Multivariate Analysis.** The GC−TOF−MS data were converted into NetCDF format (*.cdf) using the LECO ChromaTOF software (version 4.44, LECO Corp.). The UPLC−Q-TOF−MS data were analyzed with MassLynx software (version 4.1, Waters Corp.), and raw data files were converted to the NetCDF format (*.cdf) using the MassLynx DataBridge (version 4.1, Waters Corp.). After that, the MS data were processed using the MetAlign software package (http://www.metalign.nl) to obtain data containing retention times, normalized peak intensities, and accurate masses. The resulting data were exported to an Excel file, and statistical analysis was performed using SIMCA-P+ software (version 12.0, Umetrics, Umea, Sweden). Partial least-squares discriminant analysis (PLS-DA) was used to compare different metabolites of red and white pitaya samples. Differences in antioxidant activities, TPC, TFC, and TBC were tested by Duncan's multiple-range test using PASW Statistics (version 18.0, SPSS, Inc., Chicago, IL).

**Antioxidant Activity Tests.** The DPPH assay was carried out using the method by Dietz et al.,[14] with some modifications. Each pitaya extract (5 mg/mL, 20 μL) was combined with 180 μL of 0.2 mM DPPH in 80% methanol solution, and the reaction took place for 30 min at room temperature in the dark. Then, the samples were measured at 515 nm using a microplate reader (Thermo Electron, Spectronic Genesys 6, Madison, WI). The ABTS assay procedure followed the method by Roberta et al.,[15] with some modifications. The 7 mM ABTS solution was prepared by mixing with 2.45 mM potassium persulfate solution. Then, the ABTS solution reaction took place for 12 h at room temperature in the dark until it reached a stable state. The ABTS solution was diluted in deionized water to an absorbance of 0.7 (±0.02) at 734 nm. Each pitaya extract (5 mg/mL, 20 μL) was combined with 180 μL of 7 mM ABTS solution for 6 min at room temperature in the dark. After that, the samples were analyzed at 734 nm using a microplate reader. The FRAP assay was carried out using the modified procedure by Benzie and Strain et al.,[16] with some modifications. The FRAP solution, including 10 mM TPTZ and 20 mM ferric chloride, was diluted in 300 mM sodium acetate buffer (pH 3.6) at a ratio of 1:1:10. Each pitaya extract (5 mg/mL, 10 μL) was combined with 300 μL of FRAP solution, and the reaction took place for 6 min at room temperature in the dark. Then, the samples were analyzed at 593 nm using a microplate reader. All assays were performed in triplicate. For each antioxidant activity test, a Trolox aliquot was used to develop a 0.0156−0.5 mM standard curve, and all data were expressed as Trolox equivalents (mM).

**Determination of TPC, TFC, and TBC.** TPC and TFC were determined as described by Singleton et al.,[17] with some modifications. To measure TPC, 20 μL of each sample was combined with 100 μL of 0.2 N Folin and Ciocalteu's reagent placed in 96-well plates for 6 min at room temperature in the dark. Then, 80 μL of 7.5% sodium carbonate solution was added to the 96-well plate. The mixture was allowed to stand for 1 h at room temperature and analyzed at 750 nm using a microplate reader. The results are presented as the gallic acid

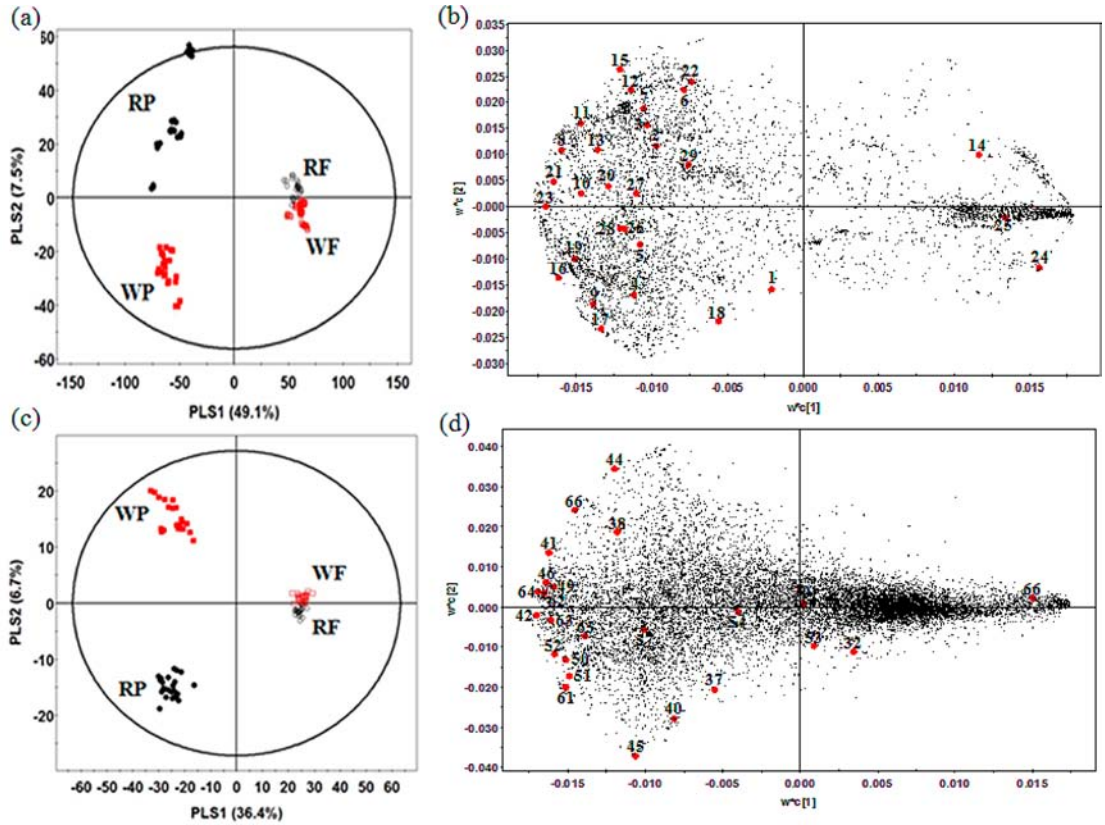


**Figure 1.** PLS-DA score plots and loading plots of red and white pitaya samples analyzed using (a and b) GC−TOF−MS and (c and d) UPLC−Q-TOF−MS. RF, red flesh; WF, white flesh; RP, red peel; and WP, white peel. Loading plot variable numbers are the same as the metabolite numbers shown in Tables 1 and 2.

equivalent concentration (31.25−500 ppm). TFC was measured as follows: 20 $\mu$L of 1 N NaOH, 180 $\mu$L of 90% diethylene glycol, and 20 $\mu$L of each sample were mixed and incubated for 60 min in the dark in 96-well plates. Then, the samples were analyzed at 450 nm using a microplate reader. The results are presented as the naringin equivalent concentration (15.625−200 ppm). TBC was measured using the method by Cai et al.,[18] with some modifications. The pitaya-dried extracts were calculated and expressed as betanin equivalents (mg/100 g of dried extract weight) using the following formula: concentration of betacyanins = $A_{538}(\mathrm{MW})V(\mathrm{DF}) \times 100/\varepsilon LW$, where $A_{538}$ is the absorbance at 538 nm ($\lambda_{max}$), MW = 550, $V$ is the dried extract solution volume (mL), DF is the dilution factor, $\varepsilon$ (molar extinction coefficient) = 65 000, $L$ (path length) = 1.0 cm, and $W$ is the dried extract weight (g). All assays were performed in triplicate.

## RESULTS AND DISCUSSION

**Metabolite Profiling of Red and White Pitaya Samples by GC−TOF−MS and UPLC−Q-TOF−MS.** Different species of pitaya samples were analyzed using GC−TOF−MS and UPLC−Q-TOF−MS with multivariate analyses. The characteristics of the data sets were represented using PLS-DA (Figure 1). The pitaya samples were separated using PLS-DA according to not only the different parts (peel and flesh) but also species (red and white). Metabolite profiling of the samples was used to investigate the different metabolites according to their species (red and white) and parts (peel and flesh). To discriminate significantly different metabolites between different parts and species, variable importance in projection (VIP) of >0.7 and $p$ value of <0.05 were used to select the variables in PLS-DA. The selected variables were identified and presented in loading plots (panels b and d of Figure 1).

According to GC−TOF−MS analysis, the PLS-DA score plot showed the separation of each sample with $R^2X$ = 0.693, $R^2Y$ = 0.98, and $Q^2$ = 0.971 (Figure 1a). The cross-validation results were $R^2Y$ intercept = 0.3687, $Q^2Y$ intercept = −0.464 18, and $p$ value < 0.05. The different parts of pitayas were separated using PLS 1 (49.1%), and the different species were separated using PLS 2 (7.5%). Different metabolites were identified on the basis of their retention times and mass fragmentation in comparison to standard compounds (Table 1). A total of 29 metabolites were present, including 15 amino acids and amines, 4 organic acids, 8 sugars and sugar alcohols, and 2 fatty acids. These metabolites were significantly distinguished between different parts, while ethanolamine (**3**), proline (**4**), serine (**6**), threonine (**7**), aspartic acid (**8**), $\gamma$-aminobutyric acid (GABA) (**9**), glutamic acid (**10**), phenylalanine (**11**), glutamine (**12**), tyrosine (**13**), L-DOPA (**14**), tryptophan (**15**), succinic acid (**16**), fumaric acid (**17**), malic acid (**18**), xylitol (**21**), rhamnose (**22**), and fucose (**23**) were separated on the basis of the species. Primary metabolites are directly involved in fruit growth, development, taste, and reproduction and are also important as the precursors of secondary metabolites.[4,19] In pitayas, several soluble sugars and organic acids affect fruit taste and, thereby, affect fruit quality. In particular, glucose, fructose, and citric acid mainly affected fruit taste.[20] Sugars, such as glucose and fructose, are associated with the sweet taste of fruits,[21] and citric acid is the major compound that contributes to fruit acidity.[22] Amino acids and amines are also responsible for fruit taste and, as betaxanthin precursors, are important for better understanding betalain biosynthesis.[4] Primary metabolites, such as amino acids, organic acids, and fatty acids, were


dx.doi.org/10.1021/jf5020704 | J. Agric. Food Chem. 2014, 62, 8764−8771

**Table 1. Different Metabolites in Red and White Pitayas Derived from the PLS-DA Model of the GC−TOF−MS Analysis**

| compound number | tR[a] (min) | metabolites[b] | MS fragment ion ($m/z$) | derivatized[c] |
|---|---|---|---|---|
| | | Amino Acids and Amines | | |
| **1** | 5.24 | alanine[d] | 73, 100, 116, 147 | TMS(X1) |
| **2** | 6.44 | valine[d] | 52, 73, 144, 147 | TMS(X3) |
| **3** | 6.94 | ethanolamine[d,e] | 59, 73, 86, 100, 147, 174 | TMS(X3) |
| **4** | 7.22 | proline[d,e] | 59, 73, 142, 143 | TMS(X3) |
| **5** | 7.34 | glycine[d] | 73, 100, 147, 245 | TMS(X3) |
| **6** | 7.84 | serine[d,e] | 73, 100, 147, 204, 218 | TMS(X3) |
| **7** | 8.09 | threonine[d,e] | 57, 73, 75, 101, 117, 147 | TMS(X3) |
| **8** | 9.22 | aspartic acid[d,e] | 73, 75, 100, 147, 232 | TMS(X3) |
| **9** | 9.30 | GABA[d,e] | 73, 75, 100, 147, 156, 174 | TMS(X3) |
| **10** | 10.01 | glutamic acid[d,e] | 73, 75, 128, 147, 156, 246 | TMS(X3) |
| **11** | 10.10 | phenylalanine[d,e] | 73, 75, 100, 147, 192, 218 | TMS(X2) |
| **12** | 11.17 | glutamine[d,e] | 73, 75, 147, 155, 156 | TMS(X3) |
| **13** | 12.33 | tyrosine[d,e] | 59, 73, 100, 103, 147, 218 | TMS(X3) |
| **14** | 13.38 | L-DOPA[d,e] | 59, 73, 100, 101, 133, 218, 219 | TMS(X6) |
| **15** | 14.11 | tryptophan[d,e] | 55, 73, 100, 116, 131, 202 | TMS(X3) |
| | | Organic Acids | | |
| **16** | 7.37 | succinic acid[d,e] | 55, 73, 75, 147, 247 | TMS(X2) |
| **17** | 7.66 | fumaric acid[d,e] | 58, 73, 75, 83, 147, 245 | TMS(X2) |
| **18** | 8.97 | malic acid[d,e] | 73, 101, 117, 133, 233, 245 | TMS(X3) |
| **19** | 11.52 | citric acid[d] | 73, 133, 147, 245, 273 | TMS(X4) |
| | | Sugars and Sugar Alcohols | | |
| **20** | 10.41 | arabinose[d] | 59, 73, 75, 103, 117, 147, 217 | TMS(X4) |
| **21** | 10.67 | xylitol[d,e] | 59, 73, 75, 103, 129, 147, 217 | TMS(X5) |
| **22** | 10.84 | rhamnose[d,e] | 73, 75, 103, 117, 129, 147, 217 | TMS(X4) |
| **23** | 10.91 | fucose[d,e] | 59, 73, 75, 86, 117, 147, 174 | TMS(X4) |
| **24** | 11.96 | fructose[d] | 59, 73, 75, 89, 103, 147, 217 | MeOX TMS(X5) |
| **25** | 12.26 | glucose[d] | 59, 73, 89, 103, 117, 129, 147, 319 | MeOX TMS(X5) |
| **26** | 12.50 | glucuronic acid[d] | 59, 73, 89, 133, 147, 160, 333 | TMS(X3) |
| **27** | 12.79 | gluconic acid[d] | 59, 73, 103, 117, 133, 147, 205, 217 | TMS(X5) |
| | | Fatty Acids | | |
| **28** | 14.09 | stearic acid[d] | 55, 75, 117, 129, 131 | TMS(X1) |
| **29** | 15.08 | oleamide[d] | 55, 75, 116, 128, 131, 144 | TMS(X1) |

[a]tR = retention time. [b]Metabolites = metabolites were identified using STD (standard compound) and selected according to VIP > 0.7 and $p$ value < 0.05. [c]Derivatized = TMS, trimethylsilyl; MeOX, methyloxime. [d]Different metabolites separated between peel and flesh from PLS-DA score plot by VIP 1. [e]Different metabolites between red and white pitayas derived from PLS-DA score plot by VIP 2.

relatively higher in the peel than in the flesh (Figure 2). The levels of organic acids, such as succinic acid (**16**), fumaric acid (**17**), malic acid (**18**), and citric acid (**19**), were higher in the peel, while the levels of fructose (**24**) and glucose (**25**) were higher in the flesh. In a previous study, fructose and glucose were the main sugars, and their levels were significantly high in pitaya flesh.[1] The fatty acids stearic acid (**28**) and oleamide (**29**) were detected, and their levels were higher in the peel than in the flesh, in both red and white pitaya. According to a study, red and white pitaya seed oils have essential fatty acids and two oleic acid isomers.[23] Essential fatty acids are important in that they are necessary fatty acids in animal metabolism and cannot be synthesized *in vivo*.[24]

In the UPLC−Q-TOF−MS analysis, the PLS-DA score plot showed the distribution of each pitaya sample (RP, WP, RF, and WF) with $R^2X$ = 0.479, $R^2Y$ = 0.982, and $Q^2$ = 0.959 (Figure 1c). The cross-validation results were $R^2Y$ intercept = 0.3716, $Q^2Y$ intercept = −0.291 94, and $p$ value < 0.05. Different parts and species were separated using PLS 1 (36.4%) and PLS 2 (6.7%), respectively. A total of 37 metabolites were tentatively identified using measured mass, retention time, elemental composition, i-FIT, $MS^n$ fragments, and $\lambda_{max}$ data obtained using UPLC−Q-TOF−MS and LC−ESI−MS/MS by standard compounds and references (Table 2). A total of 17 metabolites, including betanin (**30**), phyllocactin (**32**), betanidin (**38**), lampranthin II (**40**), tricarboxylated hylocerenin (**41**), decarboxylated neohylocerenin (**42**), dehydrogenated, decarboxylated neohylocerenin (**44**), neohylocerenin (**45**), miraxanthin V (**49**), 3-methoxytyramine−betaxanthin (**50**), phenylalanine−betaxanthin (**51**), portulacaxanthin II (**52**), dopamine (**53**), dopamine quinone (**54**), phlorizin (**60**), and two unknown metabolites (**61** and **62**) were significantly different between the parts (peel and flesh), whereas six metabolites, including bidecarboxylated hylocerenin (**46**), L-tryptophan (**57**), and four unknown metabolites (**63**−**66**), were significantly different between the species (red and white). Betalain-related metabolites were divided into three types, such as betacyanins, betaxanthins, and their precursors. Betalains have been important criteria for the classification of members of the order Caryophyllales. These pigments replace the anthocyanins in the plants of most families of Caryophyllales.[4] The structure of betacyanin showed the dihydropyridine moiety with some variations in the acyl groups and sugar moieties, while betaxanthin exhibited the same dihydropyridine moiety but showed conjugation with several amines and amino acids (Figure 3).[25] The maximum

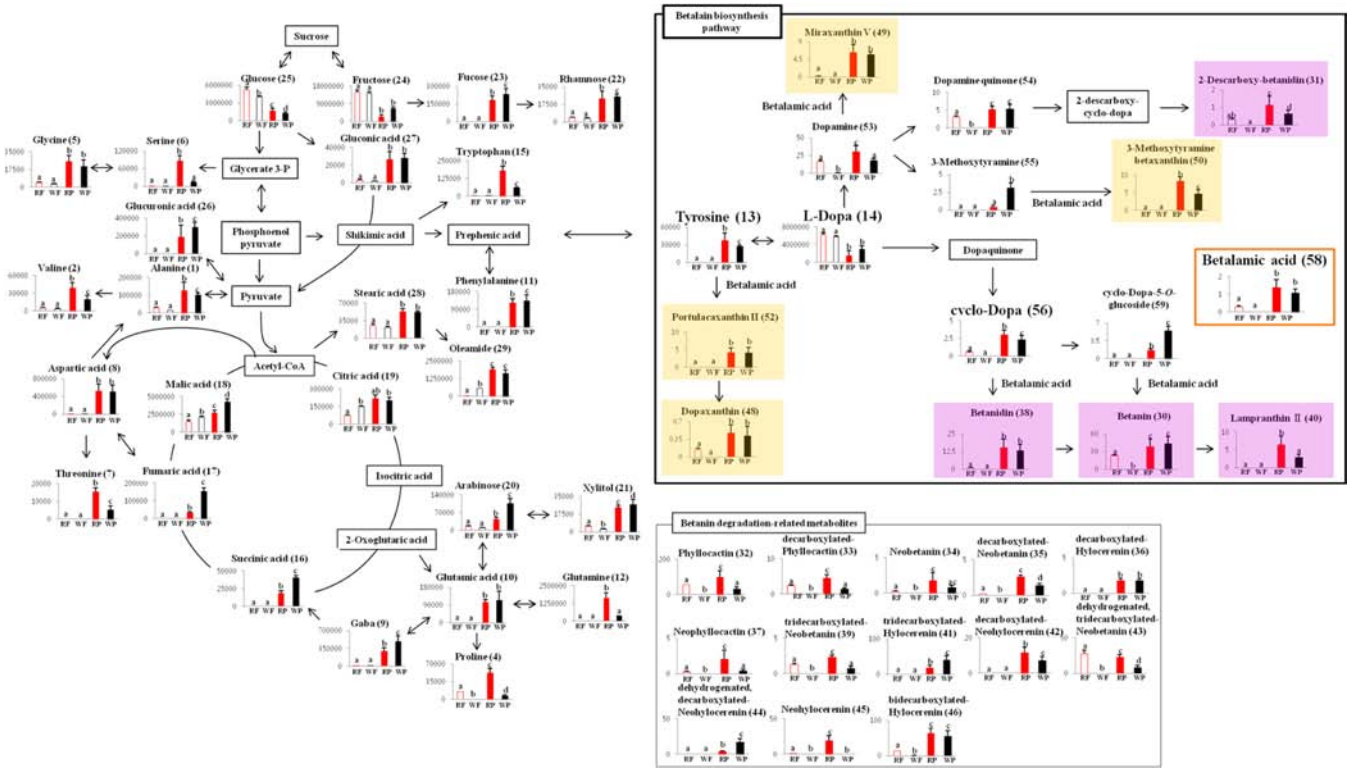


**Figure 2.** Betalain biosynthesis pathway and relative contents of metabolites in different pitaya samples. RF, red flesh; WF, white flesh; RP, red peel; and WP, white peel. The *y* axis of the histogram represents peak areas. Red−violet boxes are betacyanins, and yellow boxes are betaxanthins. Large characters represent the main betalain precursors. Different letters are significantly different by Duncan's multiple-range test. The pathway was modified from the KEGG database (http://www.genome.jp/kegg/).

absorption of betaxanthins varied between 460 and 480 nm, depending upon the structure of the amino acid compound. On the other hand, in comparison to betaxanthins, betacyanins showed a different maximum absorption shift of 50−70 nm because of the aromatic structure of cyclo-DOPA.[26]

**Comparison of Antioxidant Activity Tests (DPPH, ABTS, and DPPH), TPC, TFC, and TBC of Red and White Pitaya Samples.** Several assays, including the antioxidant activity tests (DPPH, ABTS, and FRAP), TPC, TFC, and TBC, were performed using both the red and white pitaya samples (Figure 4). The results of the antioxidant activity tests were as follows: RP ≥ WP > RF > WF. Similar results have been shown in other previous studies as well.[6,7,27] The TPC and TFC results were as follows: RP ≥ WP > RF > WF. The TPC and TFC of the peel of both red and white pitayas were approximately 2- and 3-fold higher than those of the flesh in red and white pitayas. The TBC result was as follows: RP > WP > RF > WF; this result reflects the sample pigment concentration. Pitayas have two betalain pigments, i.e., red−violet betacyanins and yellow−orange betaxanthins.[4] Betacyanins have antioxidant and radical-scavenging activities.[7,27] Furthermore, they contribute to certain oxidative, stress-related disorders.[7] Betaxanthins also have antioxidant activity and are used as food colorants and essential dietary amino acids by the simple technique of semi-synthesis.[28] Recently, several studies on the antioxidant activity of purified betalain-related compounds, such as betanin, decarboxylated betanin, neobetanin, betanidin, indicaxanthin, miraxanthin V, and 3-methoxytyramine−betaxanthin, were evaluated using the DPPH and ABTS assays in plants of the order Caryophyllales.[29−31] Furthermore, the antioxidant activity of betalain pigments has been shown to be higher than that of rutin, ascorbic acid, and catechin, which are known high antioxidant compounds.[32] Cai et al. discussed that betalain molecules were very good electron donors. The position of hydroxyl groups or glycosylation of betalain aglycones and numbers of hydroxyl (−OH) or imino (=NH) groups in the molecular structure led to higher antioxidant activity.[32] In this study, most of the betacyanins (**30**−**46**) were higher in the peel of both pitaya species than in their flesh (Figure 2). These data suggest that there are positive correlations between TPC, TFC, TBC, and betalain-related metabolites and antioxidant activity.

**Betalain Biosynthesis Pathway and Relative Contents of Metabolites in Different Pitaya Samples by GC−TOF−MS and UPLC−Q-TOF−MS Analyses.** To investigate the betalain biosynthesis pathway of different metabolites in red and white pitayas, betalain biosynthesis-related metabolites were obtained using GC−TOF−MS and UPLC−Q-TOF−MS analyses. Several metabolites were detected by target analysis for the supplemented betalain biosynthesis pathway. Each relative level of metabolites was represented by its peak area (Figure 2). According to Figure 2, betalain biosynthesis-related metabolites and their precursors were higher in the peel than in the flesh. To explain the betalain biosynthesis pathway in detail, we used tyrosine and L-DOPA because they are the two important precursors of betalain pigments.[4,33] L-DOPA is converted to betalamic acid, which is an important chromophore of both betacyanins and betaxanthins.[4] Cyclo-DOPA and its derivatives are essential to produce betacyanin. Betanidin, the aglycone of betanin, mediates condensation of cyclo-DOPA with betalamic acid.[4] According to the betanin (**30**) biosynthesized pathway in this study, in most of the


dx.doi.org/10.1021/jf5020704 | J. Agric. Food Chem. 2014, 62, 8764−8771

**Table 2. Metabolites in Red and White Pitayas Derived from the PLS-DA Model of the UPLC−Q-TOF−MS and LC−ESI−IT−MS/MS Analyses**

| compound number | tentative metabolites | UPLC−Q-TOF−MS tR[a] (min) | [M + H]$^+$ | elemental composition | i-FIT (norm) | LC−ESI−IT−MS/MS [M + H]$^+$ MS$^n$ fragments ($m/z$) | $\lambda_{max}$ | ID[b] |
|---|---|---|---|---|---|---|---|---|
| | | Betacyanins | | | | | | |
| **30** | betanin[c] | 2.52 | 551.15 | $C_{24}H_{27}N_2O_{13}$ | 2.1 | 389 | 534 | STD[37] |
| **31** | decarboxylated betanin[d] | 2.80 | 507.15 | $C_{23}H_{27}N_2O_{11}$ | 2.7 | | | ref 37 |
| **32** | phyllocactin[c] | 2.83 | 637.15 | $C_{27}H_{29}N_2O_{16}$ | 2.0 | 593, 551, 389 | 530 | ref 37 |
| **33** | decarboxylated phyllocactin[d] | 2.84 | 593.16 | $C_{26}H_{29}N_2O_{14}$ | 5.3 | 549, 389, 345 | 533 | ref 37 |
| **34** | neobetanin[d] | 2.87 | 549.13 | $C_{24}H_{25}N_2O_{13}$ | 3.3 | | | ref 37 |
| **35** | decarboxylated neobetanin[d] | 2.90 | 505.16 | $C_{23}H_{25}N_2O_{11}$ | 2.9 | 343, 299, 255 | 454 | ref 37 |
| **36** | decarboxylated hylocerenin[d] | 3.04 | 651.20 | $C_{29}H_{35}N_2O_{15}$ | 2.8 | | | ref 37 |
| **37** | neophyllocactin[c] | 3.09 | 635.14 | $C_{27}H_{27}N_2O_{16}$ | 3.1 | 591, 549, 387 | 484 | ref 37 |
| **38** | betanidin[c] | 3.98 | 389.14 | $C_{18}H_{17}N_2O_8$ | 0.3 | 343, 326, 297 | 538 | ref 38 |
| **39** | tridecarboxylated neobetanin[d] | 3.55 | 417.17 | $C_{21}H_{25}N_2O_7$ | 3.4 | | | ref 37 |
| **40** | lampranthin II[c] | 3.78 | 727.20 | $C_{34}H_{35}N_2O_{16}$ | 2.8 | | | ref 36 |
| **41** | tridecarboxylated hylocerenin[c] | 3.98 | 563.34 | $C_{27}H_{35}N_2O_{11}$ | 4.9 | | | ref 37 |
| **42** | decarboxylated neohylocerenin[c] | 4.09 | 649.33 | $C_{29}H_{33}N_2O_{15}$ | 4.4 | 631, 343, 299 | 452 | ref 37 |
| **43** | dehydrogenated,tridecarboxylated neobetanin[d] | 4.12 | 415.15 | $C_{21}H_{23}N_2O_7$ | 2.1 | | | ref 37 |
| **44** | dehydrogenated, decarboxylated neohylocerenin[c] | 4.18 | 647.16 | $C_{29}H_{31}N_2O_{15}$ | 4.1 | 341 | 410 | ref 37 |
| **45** | neohylocerenin[c] | 5.39 | 693.31 | $C_{30}H_{33}N_2O_{17}$ | 1.1 | 387, 343 | 491 | ref 37 |
| **46** | bidecarboxylated hylocerenin[e] | 9.72 | 607.26 | $C_{28}H_{34}N_2O_{13}$ | 1.8 | 563, 547, 461, 301 | 504 | ref 37 |
| | | Betaxanthins | | | | | | |
| **47** | indicaxanthin[d] | 2.58 | 309.11 | $C_{14}H_{17}N_2O_6$ | 3.1 | 292, 246 | 475 | ref 4 |
| **48** | dopaxanthin[d] | 2.74 | 391.11 | $C_{18}H_{19}N_2O_8$ | 2.0 | | | ref 27 |
| **49** | miraxanthin V[c] | 3.06 | 347.13 | $C_{17}H_{19}N_2O_6$ | 3.1 | | | ref 4 |
| **50** | 3-methoxytyramine−betaxanthin[c] | 3.49 | 361.14 | $C_{18}H_{21}N_2O_6$ | 2.4 | | 363 | ref 39 |
| **51** | phenylalanine−betaxanthin[c] | 3.76 | 359.12 | $C_{18}H_{19}N_2O_6$ | 1.7 | 315, 298 | 420 | ref 4 |
| **52** | portulacaxanthin II[c] | 3.86 | 375.12 | $C_{18}H_{19}N_2O_7$ | 4.7 | | | ref 4 |
| | | Betalain Precursors | | | | | | |
| **53** | dopamine[c] | 1.16 | 137.06 | $C_8H_{10}NO_2$ | 1.6 | | | ref 39 |
| **54** | dopamine quinone[c] | 1.18 | 152.06 | $C_8H_9O_2$ | 1.0 | | | ref 39 |
| **55** | 3-methoxytryamine[d] | 1.21 | 168.11 | $C_9H_{14}NO_2$ | 1.3 | | | ref 39 |
| **56** | cyclo-DOPA[d] | 1.69 | 196.09 | $C_9H_{10}NO_4$ | 2.0 | | | ref 40 |
| **57** | L-tryptophan[e] | 3.14 | 205.10 | $C_{11}H_{13}N_2O_2$ | 1.2 | | | ref 39 |
| **58** | betalamic acid[d] | 3.35 | 212.06 | $C_9H_{10}NO_5$ | 1.6 | | | ref 38 |
| **59** | cyclo-5-*O*-glucoside[d] | 3.72 | 358.12 | $C_{15}H_{20}NO_9$ | 3.1 | | | ref 38 |
| | | Flavonoids | | | | | | |
| **60** | phlorizin[c] | 4.24 | 437.14 | $C_{21}H_{25}O_{10}$ | 1.0 | | | ref 6 |
| | | Unknowns | | | | | | |
| **61** | NI[c,f] | 3.13 | 188.07 | | | | | |
| **62** | NI[c,f] | 6.85 | 409.16 | | | | | |
| **63** | NI[e,f] | 5.79 | 631.28 | | | 599, 441, 382, 368, 355 | 256 | |
| **64** | NI[e,f] | 6.84 | 425.14 | | | | | |
| **65** | NI[e,f] | 7.66 | 583.28 | | | | | |
| **66** | NI[e,f] | 9.33 | 228.23 | | | | | |

[a]tR = retention time. [b]ID = STD, standard compound; ref, reference. [c]Different metabolites separated between peel and flesh from PLS-DA score plot by VIP 1. [d]Targeted metabolites for the betalain biosynthesis pathway. [e]Different metabolites between red and white pitayas derived from PLS-DA score plot by VIP 2. [f]NI = not identified.

samples, the levels of betalain precursors and aglycone (**13**, **38**, **56**, and **58**), except that of L-DOPA (**14**), were as follows: RP ≥ WP > RF > WF. Several metabolites, such as betanin (**30**), decarboxylated betanin (**31**), phyllocactin (**32**), decarboxylated hylocerenin (**36**), neophyllocactin (**37**), tridecarboxylated neobetanin (**39**), dehydrogenated, decarboxylated neohylocerenin (**44**), bidecarboxylated hylocerenin (**46**), indicaxanthin (**47**), dopaxanthin (**48**), dopamine (**53**), dopamine quinone (**54**), and cyclo-5-*O*-glucoside (**59**), were not present in WF but were identified in other parts (RP, WP, and RF) because they were betalain-related metabolites or their precursors.

Betalamic acid was also condensed with amino acid or amine to give rise to a concentration of betaxanthins.[34] Amino acids, such as alanine, valine, proline, glycine, serine, glutamic acid, phenylalanine, glutamine, tyrosine, and tryptophan, are prerequisites for better understanding betaxanthin biosynthesis.[4] Betaxanthin was higher in the peel than in the flesh of both pitaya samples, because, together with betalamic acid, amino acids, such as alanine (**1**), valine (**2**), proline (**4**), glycine (**5**), serine (**6**), glutamic acid (**10**), phenylalanine (**11**), glutamine (**12**), tyrosine (**13**), and tryptophan (**15**), are condensed and may produce betaxanthins. Citric and ascorbic


dx.doi.org/10.1021/jf5020704 | J. Agric. Food Chem. 2014, 62, 8764−8771

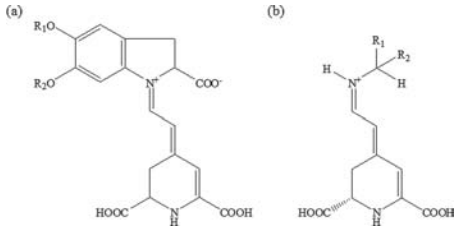

**Figure 3.** Two classes of betalains: (a) betacyanins and (b) betaxanthins. Both groups are condensation products from the precursor betalamic acid. R1 and R2 represent the functional groups (amino acids, amines, sugars, and decarboxyl sugars).

acids were higher in the peel than in the flesh of both pitaya samples. They are used as an additive for betalain stabilization in the food industry.[25,35] As a result, primary metabolites could help in understanding betalain biosynthesis-related metabolites as precursors and the stability of the betalain pigments and providing nutrient information on the different parts.

In conclusion, our study characterized different metabolites according to not only different species (red and white) but also different parts (peel and flesh) of pitayas by metabolite profiling (GC−TOF−MS and UPLC−Q-TOF−MS with multivariate analysis). Furthermore, through the MS-based metabolite profiling, we investigated the different metabolites and their relative contents in both red and white pitayas. The relative contents of primary and secondary metabolites within the betalain biosynthesis pathway were also explained. Thus, primary metabolite analysis could help in understanding betalain biosynthesis and the precursors and explaining the nutrient information on different parts of both pitaya species. Most of the betalain-related metabolites were significantly higher in the peel than in the flesh of pitayas. The results of the antioxidant activity tests (DPPH, ABTS, and DPPH), TPC, TFC, and TBC also showed higher metabolite contents in the peel than in the flesh of pitayas. As a result, betalain-related metabolites were suggested to be the main contributors to antioxidant activity in pitaya samples.

## AUTHOR INFORMATION


### Corresponding Authors

*Telephone: +82-2-444-4290. Fax: +82-2-455-4291. E-mail: ieesarah57@hotmail.com.

*Telephone: +82-2-2049-6177. Fax: +82-2-455-4291. E-mail: chlee123@konkuk.ac.kr.



### Funding

This study was supported by a National Research Foundation of Korea (NRF) grant funded by the Korea government (MEST 2013-A423-0061) and by a grant from the Next-Generation BioGreen 21 Program (SSAC, PJ00952004), Rural Development Administration, Republic of Korea.


### Notes

The authors declare no competing financial interest.

## REFERENCES


(1) Le Bellec, F.; Vaillant, F.; Imbert, E. Pitahaya (*Hylocereus* spp.): A new fruit crop, a market with future. *Fruits* **2006**, *61*, 237−250.

(2) Moreno, D. A.; García-Viguera, C.; Gil, J. I.; Gil-Izquierdo, A. Betalains in the era of global agri-food science, technology and nutritional health. *Phytochem. Rev.* **2008**, *7*, 261−280.

(3) Wybraniec, S.; Stalica, P.; Jerz, G.; Klose, B.; Gebers, N.; Winterhalter, P.; Sporna, A.; Szaleniec, M.; Mizrahi, Y. Separation of polar betalain pigments from cacti fruits of *Hylocereus polyrhizus* by ion-pair high-speed countercurrent chromatography. *J. Chromatogr. A* **2009**, *1216*, 6890−6899.

(4) Strack, D.; Vogt, T.; Schliemann, W. Recent advances in betalain research. *Phytochemistry* **2003**, *62*, 247−269.

(5) Vaillant, F.; Perez, A.; Davila, I.; Dornier, M.; Reynes, M. Colorant and antioxidant properties of red-purple pitahaya (*Hylocereus* sp.). *Fruits* **2005**, *60*, 3−12.

(6) Kim, H.; Choi, H.-K.; Moon, J. Y.; Kim, Y. S.; Mosaddik, A.; Cho, S. K. Comparative antioxidant and antiproliferative activities of red and white pitayas and their correlation with flavonoid and polyphenol content. *J. Food Sci.* **2011**, *76*, C38−C45.

(7) Tenore, G. C.; Novelino, E.; Basile, A. Nutraceutical potential and antioxidant benefits of red pitaya (*Hylocereus polyrhizus*) extracts. *J. Funct. Foods* **2012**, *4*, 129−136.

(8) Kapadia, G. J.; Azuine, M. A.; Sridhar, R.; Okuda, Y.; Tsuruta, A.; Ichiishi, E.; Mukainake, T.; Takasaki, M.; Konoshima, T.; Nishino, H.;


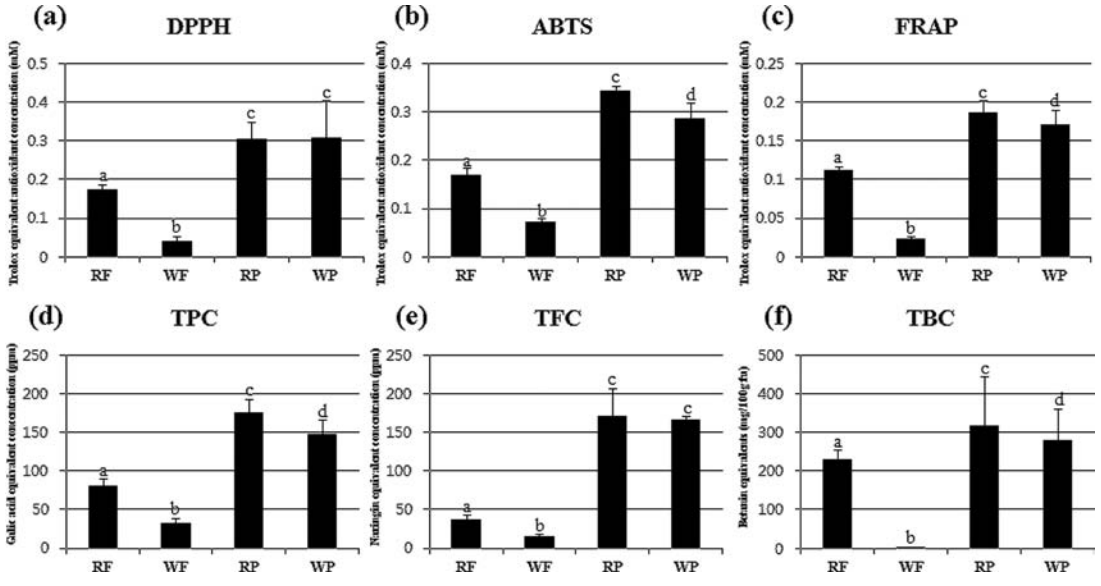


**Figure 4.** Antioxidant activity tests: (a) DPPH, (b) ABTS, (c) FRAP, (d) TPC, (e) TFC, and (f) TBC in the peel and flesh of different pitayas. RF, red flesh; WF, white flesh; RP, red peel; and WP, white peel. Different letters are significantly different by Duncan's multiple-range test.

Tokuda, H. Chemoprevention of DMBA-induced UV-B promoted, NOR-1-induced TPA promoted skin carcinogenesis, and DEN-induced phenobarbital promoted liver tumors in mice by extract of beetroot. *Pharmacol. Res.* **2003**, *47*, 141−148.
(9) Gentile, C.; Tesoriere, L.; Allegra, M.; Livrea, M. A.; D'Alessio, P. Antioxidant betalains from cactus pear (*Opuntia ficus indica*) inhibit endothelial ICAM-1 expression. *Ann. N. Y. Acad. Sci.* **2004**, *1028*, 481−486.
(10) Katajamaa, M.; Oresic, M. Data processing for mass spectrometry-based metabolomics. *J. Chromatogr. A* **2007**, *1158*, 318−328.
(11) Jung, E. S.; Lee, S.; Lim, S.-H.; Ha, S.-H.; Liu, K.-H.; Lee, C. H. Metabolite profiling of the short-term responses of rice leaves (*Oryza sativa* cv. Ilmi) cultivated under different LED lights and its correlations with antioxidant activities. *Plant Sci.* **2013**, *210*, 61−69.
(12) Lee, S.; Do, S. G.; Kim, S. Y.; Kim, J.; Jin, Y.; Lee, C. H. Mass spectrometry-based metabolite profiling and antioxidant activity of *Aloe vera* (*Aloe barbadensis* Miller) in different growth stages. *J. Agric. Food Chem.* **2012**, *60*, 11222−11228.
(13) Lee, S. Y.; Kim, H. Y.; Lee, S.; Lee, J. M.; Muthaiya, M. J.; Kim, B. S.; Oh, J. Y.; Song, C. K.; Jeon, E. S.; Ryu, H. S.; Lee, C. H. Mass spectrometry-based metabolite profiling and bacterial diversity characterization of Korean traditional meju during fermentation. *J. Microbiol. Biotechnol.* **2012**, *22*, 1523−1531.
(14) Dietz, B. M.; Kang, Y. H.; Liu, G.; Eggler, A. L.; Yao, P.; Chadwick, L. R.; Pauli, G. F.; Farnsworth, N. R.; Mesecar, A. D.; van Breemen, R. B.; Bolton, J. L. Xanthohumol isolated from *Humulus lupulus* inhibits menadione-induced DNA damage through induction of quinone reductase. *Chem. Res. Toxicol.* **2005**, *18*, 1296−1305.
(15) Re, R.; Pellegrini, N.; Proteggente, A.; Pannala, A.; Yang, M.; Rice-Evans, C. Antioxidant activity applying an improved ABTS radical cation decolorization assay. *Free Radical Biol. Med.* **1999**, *26*, 1231−1237.
(16) Benzie, I. F. F.; Strain, J. J. The ferric reducing ability of plasma (FRAP) as a measure of "antioxidant power": The FRAP assay. *Anal. Biochem.* **1996**, *239*, 70−76.
(17) Singleton, V. L.; Orthofer, R.; Lamuela-Raventos, R. M. Analysis of total phenols and other oxidation substrates and antioxidants by means of Folin−Ciocalteu reagent. *Methods Enzymol.* **1999**, *299*, 152−178.
(18) Cai, Y.; Sun, M.; Wu, H.; Huang, R.; Corke, H. Characterization and quantification of betacyanin pigments from diverse *Amaranthus* species. *J. Agric. Food Chem.* **1998**, *46*, 2063−2070.
(19) Carrari, F.; Fernie, A. R. Metabolic regulation underlying tomato fruit development. *J. Exp. Bot.* **2006**, *57*, 1883−1897.
(20) Etienne, C.; Rothan, C.; Moing, A.; Plomion, C.; Bodénès, C.; Svanella-Dumas, L.; Cosson, P.; Pronier, V.; Monet, R.; Dirlewanger, E. Candidate genes and QTLs for sugar and organic acid content in peach [*Prunus persica* (L.) Batsch]. *Theor. Appl. Genet.* **2002**, *105*, 145−159.
(21) Gomez, M.; Lajolo, F.; Cordenunsi, B. Evolution of soluble sugars during ripening of papaya fruit and its relation to sweet taste. *J. Food Sci.* **2002**, *67*, 442−447.
(22) Kafkas, E.; Kosar, M.; Turemis, N.; Baser, K. H. C. Analysis of sugars, organic acids and vitamin C contents of blackberry genotypes from Turkey. *Food Chem.* **2006**, *97*, 732−736.
(23) Ariffin, A. A.; Bakar, J.; Tan, C. P.; Rahman, R. A.; Karim, R.; Loi, C. C. Essential fatty acids of pitaya (dragon fruit) seed oil. *Food Chem.* **2009**, *114*, 561−564.
(24) Beare-Rogers, J.; Dieffenbacher, A.; Holm, J. V. Lexicon of lipid nutrition. *Pure Appl. Chem.* **2001**, *73*, 685−744.
(25) Moßhammer, M. R.; Rohe, M.; Stintzing, F. C.; Carle, R. Stability of yellow-orange cactus pear (*Opuntia ficus-indica*, [L.] Mill. Cv. 'Gialla') betalains as affected by the juice matrix and selected food additives. *Eur. Food Res. Technol.* **2007**, *225*, 21−32.
(26) Herbach, K. M.; Stintzing, F. C.; Carle, R. Betalain stability and degradation—structural and chromatic aspects. *J. Food Sci.* **2006**, *71*, R41−R50.
(27) Wu, L. C.; Hsu, H. W.; Chen, Y. C.; Chiu, C. C.; Lin, Y. I.; Ho, J. A. A. Antioxidant and antiproliferative activities of red pitaya. *Food Chem.* **2006**, *95*, 319−327.
(28) Leathers, R. R.; Davin, C.; Zryd, J. P. Betalain producing cell cultures of *Beta vulgaris* L. var. bikores monogerm (red beet). *In Vitro Cell. Dev. Biol. Plant* **1992**, *28*, 39−45.
(29) Wybraniec, S.; Starzak, K.; Skopinska, A.; Nemzer, B.; Pietrzkowski, Z.; Michałowski, T. Studies on nonenzymatic oxidation mechanisms in neobetanin, betanin, and decarboxylated betanins. *J. Agric. Food Chem.* **2013**, *61*, 6465−6476.
(30) Sekiguchi, H.; Ozeki, Y.; Sasaki, N. In vitro synthesis of betaxanthins using recombinant DOPA 4,5-dioxygenase and evaluation of their radical-scavenging activities. *J. Agric. Food Chem.* **2010**, *58*, 12504−12509.
(31) Gandía-Herrero, F.; Escribano, J.; García-Carmona, F. Structural implications on color, fluorescence, and antiradical activity in betalains. *Planta* **2010**, *232*, 449−460.
(32) Cai, Y.; Sun, M.; Corke, H. Antioxidant activity of betalains from plants of the Amaranthaceae. *J. Agric. Food Chem.* **2003**, *51*, 2288−2294.
(33) Gandía-Herrero, F.; García-Carmona, F. Biosynthesis of betalains: Yellow and violet plant pigments. *Trends Plant Sci.* **2013**, *18*, 334−343.
(34) Kugler, F.; Graneis, S.; Schreiter, P. P.-Y.; Stintzing, F. C.; Carle, R. Determination of free amino compounds in betalainic fruits and vegetables by gas chromatography with flame ionization and mass spectrometric detection. *J. Agric. Food Chem.* **2006**, *54*, 4311−4318.
(35) Kunnika, S.; Pranee, A. Influence of enzyme treatment on bioactive compounds and colour stability of betacyanin in flesh and peel of red dragon fruit *Hylocereus polyrhizus* (Weber) Britton and Rose. *Int. Food Res. J.* **2011**, *18*, 1437−1448.
(36) Kugler, F.; Stintzing, F. C.; Carle, R. Identification of betalains from petioles of differently colored Swiss Chard (*Beta vulgaris* L. ssp *cicla* [L.] Alef. Cv. Bright Lights) by high-performance liquid chromatography−electrospray ionization mass spectrometry. *J. Agric. Food Chem.* **2004**, *52*, 2975−2981.
(37) Wybraniec, S.; Mizrahi, Y. Generation of decarboxylated and dehydrogenated betacyanins in thermally treated purified fruit extract from purple pitaya (*Hylocereus polyrhizus*) monitored by LC−MS/MS. *J. Agric. Food Chem.* **2005**, *53*, 6704−6712.
(38) Herbach, K. M.; Stintzing, F. C.; Carle, R. Impact of thermal treatment on color and pigment pattern of red beet (*Beta vulgaris* L.) preparations. *J. Food Sci.* **2004**, *69*, C491−C498.
(39) Schliemann, W.; Cai, Y.; Degenkolb, T.; Schmidt, J.; Corke, H. Betalains of *Celosia argentea*. *Phytochemistry* **2001**, *58*, 159−165.
(40) Steiner, U.; Schliemann, W.; Böhm, H.; Strack, D. Tyrosinase involved in betalain biosynthesis of higher plants. *Planta* **1999**, *208*, 114−124.

JOURNAL OF AGRICULTURAL AND FOOD CHEMISTRY

Addition/Correction

pubs.acs.org/JAFC

# Correction to Optimization and Characterization of Curcumin Loaded in Octenylsuccinate Oat $\beta$-Glucan Micelles with an Emphasis on Degree of Substitution and Molecular Weight

Jia Liu, Fang Chen, Weina Tian, Yaqin Ma, Jing Li, and Guohua Zhao*

*J. Agric. Food Chem.* **2014**, *62* (30), 7532−7540. DOI: 10.1021/jf5014692

In Table 3, experiment values of no. 6 and no. 7 should be corrected as 0.40 ± 0.01 and 3.02 ± 0.16 $\mu$g/mg, respectively. The first sentence under Results and Discussion should cite Table 3.

**Published:** August 14, 2014

ACS Publications © 2014 American Chemical Society

JOURNAL OF AGRICULTURAL AND FOOD CHEMISTRY

Letter

pubs.acs.org/JAFC

# Delta 5 Fatty Acid Desaturase Upregulates the Synthesis of Polyunsaturated Fatty Acids in the Marine Diatom *Phaeodactylum tricornutum*

**ABSTRACT:** Microalgae are important primary producers in the marine ecosystem and excellent sources of lipids and other bioactive compounds. The marine diatom *Phaeodactylum tricornutum* accumulates eicosapentaenoic acid (EPA, 20:5n-3) as its major component of fatty acids. To improve the EPA production, delta 5 desaturase, which plays a role in EPA biosynthetic pathway, was characterized in *P. tricornutum*. An annotated delta 5 desaturase *PtD5b* gene was cloned and overexpressed in *P. tricornutum*. The transgene was integrated into the genome demonstrated by Southern blot, and the overexpression of *PtD5b* was verified by qPCR and Western blot analysis. Fatty acid composition exhibited a significant increase in the unsaturated fatty acids. Monounsaturated fatty acids (MUFA) and polyunsaturated fatty acids (PUFA) showed an increase of 75% and 64%, respectively. In particular, EPA showed an increase of 58% in engineered microalgae. Meanwhile, neutral lipid content showed an increase up to 65% in engineered microalgae. More importantly, engineered cells showed a similar growth rate with the wild type, thus keeping high biomass productivity. This work provides an effective way to improve the production of microalgal value-added bioproducts by metabolic engineering.

**KEYWORDS:** *microalga, polyunsaturated fatty acid, desaturase, lipid*

## INTRODUCTION

To meet the increasing demand for PUFA (polyunsaturated fatty acid) consumption from human nutrition and animal feed, microalgae, as the main natural producer of PUFAs, have been attracting much attention. The marine diatom *Phaeodactylum tricornutum*, which accumulates eicosapentaenoic acid (EPA, 20:5n-3) as its major component of fatty acids, has been tested for large scale production of EPA.[1] The content of PUFA is a critical criterion in industrial production, and an effective way is to create ideal strains by genetic modification of the biosynthetic pathway.[2] The desaturase and elongase were demonstrated by radiolabeled precursors to be involved in long chain PUFA biosynthetic pathways in the marine microalga *Pavlova lutheri*.[3] Δ5 desaturase, as a rate-limiting enzyme in the synthesis of PUFA, has been studied in some bacteria, fungi, and humans. A human Δ5 desaturase was expressed in Chinese hamster ovary cells and enabled the cells to convert 20:3(n-6) to 20:4(n-6).[4] *Saccharomyces cerevisiae* expressing a Δ5 desaturase from *Paramecium tetraurelia* successfully produced EPA.[5] Though Δ5 desaturase has been studied a great deal; however, so far few studies have focused on its role in PUFA accumulation in microalgae. The current study attempted to effectively improve PUFA accumulation in the diatom by overexpressing endogenous Δ5 desaturase.

## MATERIALS AND METHODS

**Diatom Cultures.** *Phaeodactylum tricornutum* Bohlin (CCMP2561) was used in this study. The diatom was grown in f/2-Si medium which was prepared as f/2 medium by omitting Si and sterilized with 0.22-$\mu$m filters (Millipore, USA). Cultures were grown at (21 ± 0.5 °C) in 15h/9h (light/dark). To detect the growth of microalgae, cells were counted with a hemacytometer.

**Cloning of PtD5b and Generation of Transgenic Diatoms.** An amino acid sequence homologous with putative PtD5b was searched by BLAST at NCBI (http://blast.ncbi.nlm.nih.gov/Blast/) and aligned with Clustal Omega (http://www.ebi.ac.uk/Tools/msa/clustalo/). The phylogenetic tree of PtD5b was constructed by using software MEGA. Genomic DNA of *P. tricornutum* was extracted with a HP Plant DNA Kit (Omega, USA). The full-length cDNA of Δ5 desaturase gene in *P. tricornutum* (*PtD5b*) (GenBank accession: XM_002182822.1) was amplified by PCR using primers: Pt61inf (5′-TTACAATCCAGTGGTACCATGGACGTGTCGTTACGGA-3′) and Pt62inf (5′-TTTTGTTCCAGGTGTTCCAATTTGGTAA-TTGCGTCC-3′). The PtD5b was cloned into plasmid pHY18 by infusion ligation, and the resultant plasmid was introduced into *P. tricornutum* by electroporation using Bio-Rad GenePulserXcell apparatus (Bio-Rad, USA) according to Niu et al.[6]

**Neutral Lipid Content and Fatty Acid Composition Analysis.** Neutral lipid content in diatom cells was analyzed by Nile red staining according to Yang et al. with modifications.[1] Cell cultures in the stationary phase were first treated with 20% DMSO for 20 min at room temperature. Then 30 $\mu$L of Nile red (0.1 mg/mL in acetone) was added to a 3 mL aliquot of pretreated cell culture in triplicates, mixed by rapid inversion, and incubated in darkness for 20 min at room temperature. The stained cells were transferred to a 96-well plate for the detection of fluorescence intensity with a F4600 microplate reader (Hitachi, Japan). The wavelengths used were the following: excitation at 530 nm and emission at 580 nm. The relative fluorescence intensity values provided a quantitative comparison of neutral lipid contents between samples. Total lipids of microalgae were extracted and analyzed by gas chromatography−mass spectrometry (GC−MS) according to Yang et al.[1] To determine the content of EPA and DHA at dry cell weight (DCW), 150 $\mu$L of *N*-nonadecyl ester (1 mg/mL) was added as an internal standard to the samples for analysis of fatty acid composition by gas chromatography−mass spectrometry (GC−MS). Fatty acid concentration ($C_{FA}$,mg/g) was calculated by comparing the peak area of fatty acid in the sample with the peak area of internal standard (*N*-nonadecyl ester) according to the following equation: $C_{FA} = A_S/A_{IS} \times C_{IS}/W_S$, where *A* indicates peak area; *C*, concentration; *W*, weight; IS, internal standard; S, sample.[7] Three parallely grown cultures were used for the above assays, and the results were tested by one-way ANOVA analysis and *t*-test.

**Detection of PtD5b Expression in Transgenic Microalgae by Molecular Approaches.** PtD5b mRNA expression was verified by

Received: July 4, 2014
Revised: August 10, 2014
Accepted: August 11, 2014
Published: August 11, 2014

ACS Publications © 2014 American Chemical Society



dx.doi.org/10.1021/jf5031086 | J. Agric. Food Chem. 2014, 62, 8773−8776

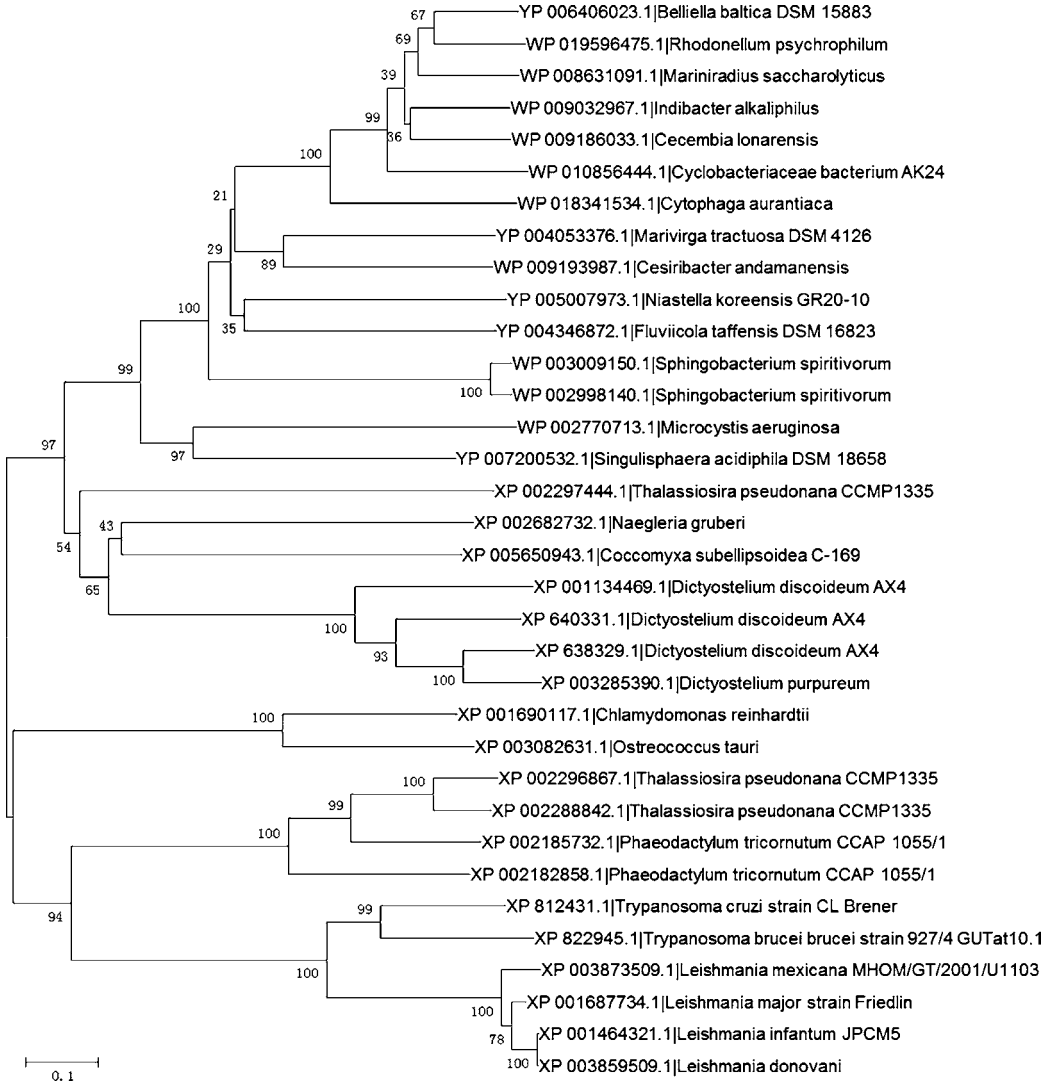


**Figure 1.** Phylogenetic relationships of PtD5b with related species. Amino acid sequences of fatty acid desaturases from various species retrieved from BLAST were analyzed with MEGA5.

quantitative real-time PCR (qPCR), and relative expression levels of PtD5b gene were calculated by normalization against the expression of *β*-actin. Primers used for qPCR were as follows: PtD5b (Forward primer: CATCACGGACCCAATCAATAC, Reverse primer: CGACGGACAATCTGGAAGAC); *β*-actin (Forward primer: AGGCAAAGCGTGGTGTTCTTA, Reverse primer: TCTGGGGAGCCTCAGTCAATA). To verify the foreign gene integration into the genome, Southern blot was performed with a fragment of CAT to prepare a DIG-labeled probe. PtD5b protein expression was detected by Western blot analysis using an anti-Myc antibody (Invitrogen). GAPDH was used as internal housekeeping control. Algal cell cultures in the stationary phase were used in the above assays.

## RESULTS AND DISCUSSION

**Prediction and Subcellular Localization of Δ5 Desaturase.** Phylogenetic tree of retrieved sequences homologous to the annotated *P. tricornutum* Δ5 desaturase (PtD5b) was initially constructed to verify its functional annotation. As shown in Figure 1, PtD5b had a close relationship with the other annotated Δ5 fatty acid desaturase (PtD5p) from *P. tricornutum* and that from the marine diatom *Thalassiosira pseudonana*,[8] and they were clustered into one group. PtD5b also exhibited a high homology with those Δ5 fatty acid desaturases from protozoa including *Trypanosoma* and *Leishmania* and microalgae species including *Chlamydomonas* and *Ostreococcus*.

Proteins are targeted to specific subcellular locations for their proper function.[9] According to software Target P ver1.1 (http://www.cbs.dtu.dk/services/TargetP/), a signal peptide was predicted in PtD5b (with a possibility of 0.318). According to software Cell-PLoc 2.0 (http://www.csbio.sjtu.edu.cn/bioinf/Cell-PLoc-2/), the subcellular localization of PtD5b was predicted to be the endoplasmic reticulum (ER). The most likely location was also predicted to be the ER (possibility of 77.8%) by software PSORT II, followed by the cytoplasm (11.1%) and the plasma membrane (11.1%). Taken together, PtD5b could be predicted to target to the ER.

**Growth and Neutral Lipid Analysis of Transgenic *Phaeodactylum tricornutum*.** The neutral lipid content was determined by Nile red fluorescence staining and indicated as the relative fluorescence intensity. As shown in Figure 2A, a significant increase of 24% in neutral lipid content was detected in transgenic line PtD5b-1 compared to the wild type ($P < 0.01$). A much more significant increase of 65% in neutral lipid content was detected in transgenic line PtD5b-2 ($P < 0.01$).


dx.doi.org/10.1021/jf5031086 | J. Agric. Food Chem. 2014, 62, 8773−8776

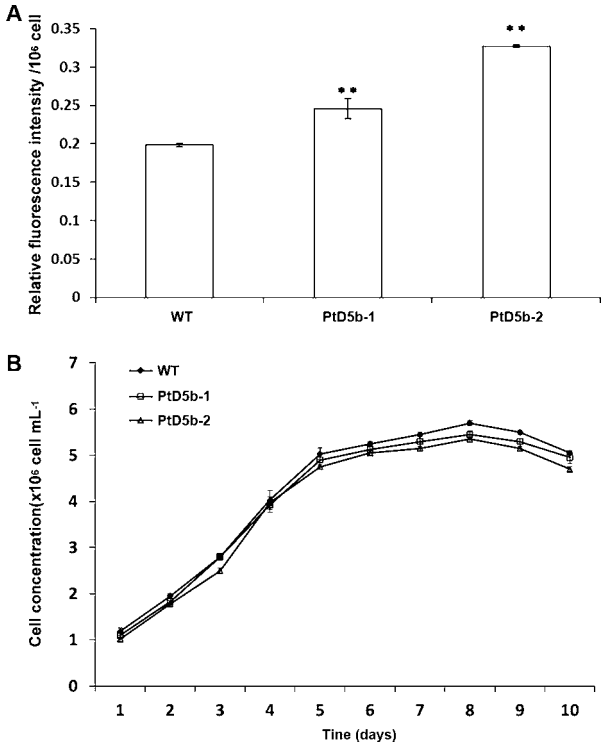


**Figure 2.** Neutral lipid content and growth of transgenic microalgae. a) Neutral lipid content. ** indicates extremely significant difference ($p < 0.01$). b) Growth curves.

The results demonstrated that overexpression of PtD5b could promote neutral lipid accumulation in *P. tricornutum*. This could be due to the overproduction of PUFA thus subsequently promoting the upstream biosynthetic pathways of fatty acids. The growth properties of transgenic cells were also examined. As shown in Figure 2B, transgenic and wild type microalgae showed quite similar growth curves. Cells started to reach the stationary phase at the sixth day after subculture. The results indicated that overexpression of PtD5b could induce the increase in neutral lipid content without compromising the growth properties.

**Fatty Acid Composition.** Marked changes in fatty acid composition were detected by GC-MS analysis in transgenic microalgae (Figure 3). Monounsaturated fatty acids (MUFAs) showed a significant increase of 75%, whereas polyunsaturated fatty acids (PUFAs) showed an increase of 64%. In particular, EPA (C20:5) showed an increase of 58% in transgenic microalgae, reaching up to 38.9 mg/g of dry cell weight. The results demonstrate that overexpression of PtD5b could successfully promote the synthesis of PUFAs. The proportions of saturated fatty acids (SFA) decreased by 16% in transgenic line PtD5b-1, suggesting that overexpressed PtD5b could redirect the flux of fatty acids toward the biosynthetic pathway of PUFA. Moreover, 0.44 mg/g DHA was detected in transgenic algae, while not detected in the wild type. Results implicated that *P. tricornutum* might lack suitable enzyme system or enough enzymatic activities of desaturase and/or elongase which are indispensable for the biosynthesis of DHA. Thus, further study is needed to investigate the key enzymes involved in DHA synthesis in *P. tricornutum*.

**Molecular Analysis of PtD5b Expression Transgenic Microalgae.** The transcript abundance of PtD5b in transgenic microalgae was determined by qPCR (Figure 4A). It showed a

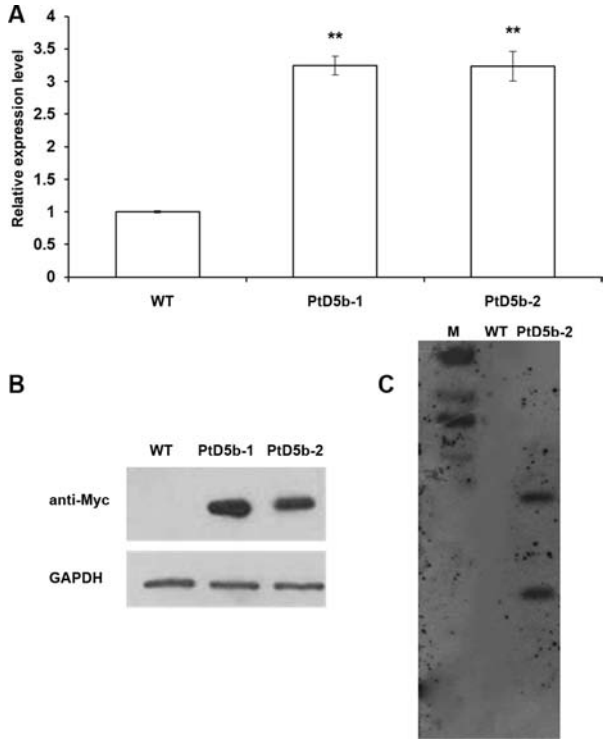


**Figure 4.** Molecular characterization of transgenic microalgae. a) Transcript abundance of PtD5b detected by qPCR analysis. ** indicates a significant difference between the wild type and PtD5b-transgenic microalgae ($p < 0.01$). b) Western blot analysis with an anti-Myc antibody. Actin was used as internal control. c) Southern blot analysis with a probe corresponding to 5′-CAT. Lane M, DNA marker.

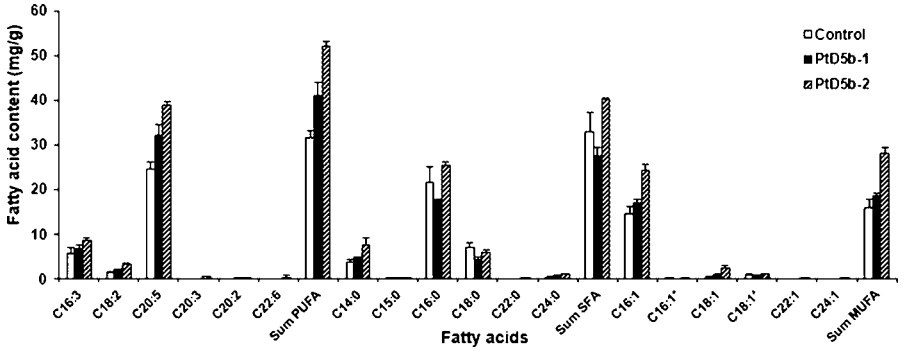


**Figure 3.** Fatty acid composition. Values indicate the dry cell weight content of fatty acids. * indicates the isomeride.


dx.doi.org/10.1021/jf5031086 | J. Agric. Food Chem. 2014, 62, 8773−8776

significant increase in the transgenic lines compared to the wild type, with a similar increase of 3.2-fold in both transgenic lines PtD5b-1 and PtD5b-2. The protein expression of introduced PtD5b in transgenic lines were detected by Western blot analysis with an anti-Myc antibody (Figure 4B). A specific cross-reacting band was present in transgenic lines, while no similar band was present in the wild type. These results indicated that the introduced PtD5b significantly increased both mRNA and protein expression of PtD5b.

Gene integration in the transgenic microalgae was verified by genomic Southern blot analysis in the overall better transgenic line PtD5b-2. As shown in Figure 4C, two hybridized bands detected with the CAT probe were present in the transgenic microalgae, whereas no band was present in wild type, demonstrating the integration of two copies of the transgene in the genome of transgenic line PtD5b-2.

In the current study, overexpression of PtD5b in *P. tricornutum* resulted in a significant increase in the unsaturated fatty acids. Further studies such as cotransformation of other key genes and transcriptional regulation can be conducted to achieve even higher PUFA productivity. This study has paved a way to engineer microalgae for sustainable production of value-added bioactive compounds.

**Kun-Tao Peng**[†]
**Cun-Ni Zheng**[†]
**Jiao Xue**[†]
**Xiao-Yan Chen**[†]
**Wei-Dong Yang**[†]
**Jie-Sheng Liu**[†]
**Weibin Bai**[§]
**Hong-Ye Li***[,†]

[†]Key Laboratory of Eutrophication and Red Tide Prevention of Guangdong Higher Education Institutes, College of Life Science and [§]Department of Food Science, Jinan University, Guangzhou, Guangdong 510632, China

## AUTHOR INFORMATION

### Corresponding Author

*Phone: 86-20-85228470. Fax: 86-20-85222720. E-mail: thyli@jnu.edu.cn.

### Funding

This work was supported by the National Science and Technology Support Program (2011BAD14B03) and the Fundamental Research Funds for the Central Universities (21610103).

### Notes

The authors declare no competing financial interest.

## REFERENCES

(1) Yang, Z. K.; Niu, Y. F.; Ma, Y. H.; Xue, J.; Zhang, M. H.; Yang, W. D.; Liu, J. S.; Lu, S. H.; Guan, Y.; Li, H. Y. Molecular and cellular mechanisms of neutral lipid accumulation in diatom following nitrogen deprivation. *Biotechnol. Biofuels* **2013**, *6*, 67.

(2) Li, H. Y.; Lu, Y.; Zheng, J. W.; Yang, W. D.; Liu, J. S. Biochemical and genetic engineering of PUFA biosynthesis in diatom. *Mar. Drugs* **2014**, *12* (1), 153−166.

(3) Guihéneuf, F.; Ulmann, L.; Mimouni, V.; Tremblin, G. Use of radiolabeled substrates to determine the desaturase and elongase activities involved in eicosapentaenoic acid and docosahexaenoic acid biosynthesis in the marine microalga *Pavlova lutheri*. *Phytochemistry* **2013**, *90*, 43−49.

(4) Cho, H. P.; Nakamura, M.; Clarke, S. D. Cloning, expression, and fatty acid regulation of the human Δ-5 desaturase. *J. Biol. Chem.* **1999**, *274*, 37335−37339.

(5) Tavares, S.; Grotkjær, T.; Obsen, T.; Haslam, R. P.; Napier, J. A.; Gunnarsson, N. Metabolic engineering of *Saccharomyces cerevisiae* for production of eicosapentaenoic acid, using a novel 5-desaturase from *Paramecium tetraurelia*. *Appl. Environ. Microbiol.* **2011**, *77* (5), 1854.

(6) Niu, Y. F.; Yang, Z. K.; Zhang, M. H.; Zhu, C. C.; Yang, W. D.; Liu, J. S.; Li, H. Y. Transformation of diatom *Phaeodactylum tricornutum* by electroporation and establishment of inducible selection marker. *Biotechniques* **2012**, DOI: 10.2144/000113881.

(7) Abdulkadir, S.; Tsuchiya, M. One-step method for quantitative and qualitative analysis of fatty acids in marine animal samples. *J. Exp. Mar. Biol. Ecol.* **2008**, *354*, 1−8.

(8) Domergue, F.; Lerchl, J.; Zähringer, U.; Heinz, E. Cloning and functional characterization of *Phaeodactylum tricornutum* front-end desaturases involved in eicosapentaenoic acid biosynthesis. *Eur. J. Biochem.* **2002**, *269*, 4105−4113.

(9) Glory, E.; Murphy, R. F. Automated subcellular location determination and high-throughput microscopy. *Dev. Cell* **2007**, *12*, 7−16.

JOURNAL OF AGRICULTURAL AND FOOD CHEMISTRY

Article

pubs.acs.org/JAFC

# Manganese Nanoparticles: Impact on Non-nodulated Plant as a Potent Enhancer in Nitrogen Metabolism and Toxicity Study both in Vivo and in Vitro

Saheli Pradhan,*[,†] Prasun Patra,[§] Shouvik Mitra,[†] Kushal Kumar Dey,[#] Sneha Jain,[†] Samapd Sarkar,[†] Shuvrodeb Roy,[†] Pratip Palit,[⊥] and Arunava Goswami[†]

[†]Biological Sciences Division, Indian Statistical Institute, 203 B.T. Road, Kolkata 700108, India

[§]Centre for Research in Nanoscience and Nanotechnology, University of Calcutta, Kolkata 700098, India

[#]Department of Statistics, University of Chicago, Chicago, Illinois 60637, United States

[⊥]Plant Physiology Section, Central Research Institute for Jute and Allied Fibers, Indian Council of Agricultural Research, Barrackpore, Kolkata 700120, India

Supporting Information

**ABSTRACT:** Mung bean plants were grown under controlled conditions and supplemented with macro- and micronutrients. The objective of this study was to determine the response of manganese nanoparticles (MnNP) in nitrate uptake, assimilation, and metabolism compared with the commercially used manganese salt, manganese sulfate (MS). MnNP was modulated to affect the assimilatory process by enhancing the net flux of nitrogen assimilation through NR-NiR and GS-GOGAT pathways. This study was associated with toxicological investigation on in vitro and in vivo systems to promote MnNP as nanofertilizer and can be used as an alternative to MS. MnNP did not impart any toxicity to the mice brain mitochondria except in the partial inhibition of complex II−III activity in ETC. Therefore, mitochondrial dysfunction and neurotoxicity, which were noted by excess usage of elemental manganese, were prevented. This is the first attempt to highlight the nitrogen uptake, assimilation, and metabolism in a plant system using a nanoparticle to promote a biosafe nanomicronutrient-based crop management.

**KEYWORDS:** *manganese nanoparticles, nitrogen metabolism, manganism, mitochondrial dysfunction*

## INTRODUCTION

Nitrogen assimilation is a vital process controlling plant growth and development. Plants biosynthesize both the suite of nitrogenous compounds that are present in all living organisms and many chemical species unique to plants. The most important and rate-limiting step is the assimilation of inorganic nitrogen into organic metabolites catalyzed by a series of enzymes through a high-flux process subjected to extensive regulation in all plants.[1] Nitrogen moves along a complex branching and merging pathway, which interacts at numerous sites with the carbon flow, pH regulation, and ions, assimilating flow at the cell within whole plant level. Superimposed on these metabolic fluxes, nitrate and nitrogen metabolism influences plant development and architecture including changes in root physiology, the timing of senescence, and flowering.[2] The largest requirement of nitrogen is the synthesis of amino acids, which function as the building blocks of proteins as well as precursors to many other metabolites. It is also prerequisite to nucleic acid, which is a cofactor to many physiological processes and a major component of chlorophyll.[3] In addition, several plant hormones contain nitrogen and/or nitrogenous precursors.[4] Plants can take up nitrogen from soil by roots in the form of nitrate ion ($NO_3^-$) and utilize it in nitrogen metabolism. Assimilation of $NO_3^-$ requires subsequent uptake, reduction, and conversion of $NO_3^-$ to ammonium ion ($NH_4^+$) and incorporation to organic compounds.[5] However, the availability of nutrients including nitrogen within the plant system is the limiting factor for its productivity. Henceforth, greater attention is demanded for crop improvement within the realm of nitrogen metabolism in both nodulated and non-nodulated plants. Presently several nanoparticles have been designed to work in agricultural industry by changing their size, shape, and surface functionality. Most of the works demonstrated the improvement of the biocidal activity of a compound so that it can break the resistance of pests and fungi,[6−9] whereas others showed detrimental roles in plant physiology and growth.[10,11] Little attention has been paid in crop improvement to modulating the structural or functional properties of existing plant nutrients for the atonement of plant nutritional deficiency. It has already been established that plant cells have the capacity to execute active transport of $NH_4^+$ during nitrogen assimilation. Some literature has shown that low availability of $NO_3^-$ concentration results from the decrease in the rate of nitrogen assimilation in acidic soil.[12] Meanwhile, manganese salt (Mn), as a fertilizer for nitrogen metabolism, has been used in acidic soil for many years, which also influences the assimilatory process as a cofactor.[13]

In this context, we introduce manganese nanoparticles (MnNP) within the framework that is already known to modulate the photochemical pathways in photosynthesis even better than its elemental/bulk counterpart.[14] MnNP increase the

Received: February 3, 2014
Accepted: August 15, 2014
Published: August 15, 2014

ACS Publications © 2014 American Chemical Society

activity of the electron transport chain by binding with the CP43 protein chain of photosystem II.[14] They also enhance the oxygen evolution process, being a part of the water splitting complex in light reaction of photosynthesis; as a consequence, photophosphorylation capacity is improved, too.[14] MnNP thus improve the photosynthetic ability of the plants, thereby producing more sugar, and can be useful in the agricultural sector for the improvement of plant productivity. As an afterthought, we have tried to investigate the route of nitrate uptake, assimilation, ammonium assimilation, and further downstream nitrogen metabolism in both source and sink tissues of legumes using MnNP to abate the problems of nitrogen metabolism. Thereafter, nitrogen reductase protein has been isolated from leaf tissue of treated plants followed by protein profiling and Western blot analysis to evaluate the mode of action of MnNP in accelerated nitrogen assimilation. Interestingly, MnNP are found to be more effective by both biochemical and molecular techniques in nitrogen assimilation and metabolism in contrast to their bulk counterpart, manganese sulfate (MS). To the best of our knowledge this is the first effort to use MnNP in the process of nitrogen metabolism for beneficial crop management study.

Mn is an essential trace element for human nutrition but also a toxicant at high concentration. Therefore, its biosafety impact has to be evaluated in light of in vivo experimentation for future research and development studies. As a consequence, MnNP have been injected intravenously to Swiss albino mice, and after 15 days of observation, the animals were sacrificed for biosafety studies following standard guidelines. Mn is also known to induce mitochondrial dysfunction and causes neurotoxicity, called manganism.[15] Manganism is characterized by neuropsychiatric symptoms and extrapyramidal dysfunction such as hypokinesia, rigidity, and tremor that often resembles Parkinson's disease.[16] Therefore, detailed toxicity profiling of MnNP is required related to mitochondrial dysfunction and neurotoxicity; as a result, the effect of MnNP in energy metabolism and ETC activity in isolated brain mitochondria has been assessed. Biosafety studies with newly synthesized engineered nanoparticles are important because they may be found to be hazardous for biological systems; if it is related to the agricultural sector, then it is necessarily obligatory to profile the entire biosafety experiments, which ensure the complete screening of the particles in mammalian systems. In a recent work MnNP have been found to decimate the level of dopamine, imparting mitochondrial dysfunctioning and generation of more ROS in vivo as a result of metal toxicity in PC-12 cells such as free $Mn2^{+}$ ions.[17] Besides, there are several studies on metal toxicity performed in cell lines[18−20] and mammalian systems[21−24] to access the biological importance and environmental hazard measurements. In our previous paper we have reported that our custom-made MnNP are biosafe on the basis of acute oral toxicity parameter, although detailed research is explicitly demanded for its future endeavor in agricultural sectors. Herein, histopathological analysis of MnNP-treated mice is performed after intravenous injection with emphasis on brain mitochondrial toxicity studies. A series of detailed in vitro and in vivo studies including studies on human lymphocytes, hemolysis, and murine model system with an emphasis on brain mitochondria has been carried out. Our studies reveal that severe toxicity symptoms are avoided in the treated sets with minor alterations noted in complex II−III activity in ETC. Excess oxidative stress, severe mitochondrial dysfunction, and neurotoxicity are avoided, thereby paving the way toward the development of a biosafe crop management study based on nitrogen assimilation and metabolism with the aid of MnNP.

## MATERIALS AND METHODS

**Characterization of MnNP.** Custom-made manganese nanoparticles were purchased from MK Implex, Canada. The surface morphology was determined by field emission scanning electron microscope (FESEM; FEI Quantum-200 MK-2), and particle size was observed through a transmission electron microscope (TEM) (JEOL 2010). Surface topology of MnNP was obtained using atomic force microscopy (AFM). Hydrodynamic size distribution was obtained by dynamic light scattering (DLS) spectroscopy.

**Experiments with Plant Model System.** Seeds of mung bean (*Vigna radiata*) were purchased from Berhampur Pulse and Oil Research Centre, West Bengal. These seeds were selected from Chaiti mung. Seeds were soaked in 5% sodium hypochloride solution for surface sterilization and imbibed with the treatment solutions (control; MnNP, 0.05, 0.1, 0.5, and 1 mg/L; MS, 0.05, 0.1, 0.5, and 1 mg/L) for a minimum of 4−6 h prior to germination for various analyses. After 24 h of germination, seeds were planted in pots filled with perlite supplemented with Hoagland's solution with or without manganese solution (control plants were treated without manganese solution) for 15 days in a growth cabinet (GC-300, Lab companion) with 14 h daytime temperature of 25 °C and night temperature of 20 °C at a relative humidity of 40−60% and a light intensity of 440 $\mu$mol/m$^2$/s. After 15 days of treatments, plants were uprooted and used to carry out further experiments.

**Preparation of Leaf and Root Enzyme Extract for the Assays of Nitrogen Metabolism.** Plant samples were ground with a ratio of 1:10 (w/v) in 50 mM phosphate buffer (pH 7.5) containing 2 mM EDTA, 1.5% (w/v) soluble casein, 2 mM DDT, and 1% (w/v) insoluble PVPP at cold. The homogenate was filtered and centrifuged at 3000*g* for 5 min. Supernatant was then centrifuged at 30000*g* for 20 min. The extract was then used for enzymatic assays.

*Determination of $NO_3^-$.* Enzyme extract was added to 10% salicyclic acid solution dissolved in 12 N sulfuric acid (w/v). $NO_3^-$ content was measured as described by Cataldo et al.[25] The results were expressed as micromoles per gram of fresh weight.

*Determination of Nitrate Reductase (NR) Activity.* The reaction mixture contained 100 mM phosphate buffer (pH 7.5), 100 mM $KNO_3$, 10 mM cysteine, 2 mM NADH, and enzyme extract. After 30 min of incubation at 30 °C, reaction was stopped by 1 M zinc acetate. The nitrite formed was determined at 540 nm after azocoupling with sulfanilamide and naphthylethylenediamine dihydrochloride. The NR activity was expressed as micromoles of $NO_2^-$ formed per gram fresh weight per hour.

*Determination of Nitrite Reduction (NiR) Activity.* The reaction mixture contained 50 mM phosphate buffer (pH 7.5), 20 mM $KNO_2$, 5 mM methyl viologen (MV), 300 mM $NaHCO_3$, and enzyme extract. After 30 min of incubation at 30 °C, NiR activity was determined by the disappearance of $NO_2^-$ from the reaction medium and expressed as micromoles of $NO_2^-$ per gram of fresh weight per hour.

*Determination of Glutamine Synthetase (GS) Activity.* Enzyme extract was mixed with the reaction mixture containing 100 mM phosphate buffer (pH 7.5), 4 mM EDTA, 1 M sodium glutamate, 450 mM $MgSO_4{\cdot}7H_2O$, 300 mM hydroxylamine, and 100 mM ATP. Two controls were prepared, one without glutamine and another without hydroxylamine, and all of the treatments were incubated for 30 min at 28 °C. The formation of glutamylhydroxamate was measured at 540 nm after complexing with acidified ferric chloride. GS activity was expressed as formed glutamylhydroxamate in grams of fresh weight per hour.

*Determination of NADH-Glutamate Synthase (GOGAT) Activity.* The reaction mixture contained 50 mM phosphate buffer (pH 7.5) with 0.1% (v/v) mercaptoethanol, 1 mM EDTA, 18.75 mM 2-oxoglutarate, 15 mM aminoxyacetate, 1.5 mM NADH, 75 mM L-glutamine, and enzyme extract. Two controls, without ketoglutarate and without glutamine, were used to correct for endogenous NADH oxidation. The decrease in absorbance was recorded for 5 min at 28 °C. The activity was expressed as micromoles of NAD per gram fresh weight per hour.

*SDS-PAGE and Western Blot of Isolated NR Protein.* NR protein was purified from mung bean leaves following a standard procedure.[26] NR protein was dissolved in a buffer containing 0.09% (w/v) *n*-decyl-β-D-maltopyranoside (β-DM), 20 mM NaCl, 70% (v/v) glycerol, and 20 mM HEPES (pH 7.5). After isolation of the protein, 12% SDS-PAGE was performed using a Bio-Rad protein gel apparatus, and subsequent Western blot analysis was also carried out by using NR antibody (Agrisera).

**Experiments with Mouse Model System.** Healthy young nulliparous, Swiss albino mice (average body weight = 20 g) of 8 weeks of age were kept in the animal house at 22 ± 2 °C), 60 ± 10% relative humidity, and 12 h light/dark cycle. The animals were kept in clean polypropylene cages and were provided with commercial rat pellet diet and deionized water. After 7 days of acclimatization, the mice were randomly assigned to control and treatment groups. There were five mice of each sex in each group. Water as control and MnNP as treatment were injected intravenously, and animals were weighed before and after the completion of the experiment. The animals were kept under close observation for 14 days. Skin and fur changes, eye secretion, and behavior patterns of the mice were observed. Special attention was paid to the clinical signs of toxicity including tremors, convulsions, salivation, nausea, vomiting, diarrhea, lethargy, etc. At the end of 14 days, they were sacrificed. Blood and serum from control and treated mice were analyzed for total count (TC), differential count (DC), platelet count (PLT), lactate dehydrogenase (LDH), creatinine, alkaline phosphatase (ALP), total protein (TP), cholesterol, triglyceride (TG), uric acid, blood urea nitrogen (BUN), serum glutamic oxaloacetic transaminase (SGOT), serum glutamic pyruvic transaminase (SGPT), and phosphorus. Brain, heart, lungs, liver, stomach, kidney, spleen, uterus, and testis were carefully removed and fixed in 10% formalin solution containing neutral phosphate-buffered saline (PBS). Thereafter, the organs were embedded in paraffin, stained with eosin−hematoxylin, and examined under a light microscope.

*Isolation of Mice Brain Mitochondria.* Mouse brain mitochondria (after 24 h of treatment) were isolated by a method based on differential centrifugation with digitonin treatment. The final mitochondrial pellet was suspended in isotonic buffer A (145 mM KCl, 50 mM sucrose, 1 mM EGTA, 1 mM magnesium chloride, 10 mM phosphate buffer, pH 7.4) and used immediately for the experiments related to measurement of membrane potential and phosphorylation capacity.[27] For the measurement of activity of respiratory complexes, the mitochondrial pellet was suspended in 50 mM phosphate buffer, pH 7.4, stored at 20 °C, and used within 3 days.

*Measurement of Transmembrane Potential of Mouse Brain Mitochondria.* Mitochondrial transmembrane potential was measured by using a mitochondrial membrane potential sensitive carbocyanine dye, 5,5′,6,6′-tetrachloro-1,10,3,30-tetraethylbenzamidazolocarbocyanine iodide (JC-1). When excited at 490 nm, the monomeric form of JC-1 had an emission maximum at 527 nm, but the aggregated form (J-aggregates) showed an emission maximum at 590 nm. Briefly, an aliquot of mitochondria (control or MnNP treated) was incubated at 37 °C for 30 min in isotonic buffer A containing 10 mM pyruvate, 10 mM succinate, and 1 mM ADP in the presence of 5 μM JC-1. At the end of the incubation, the dye-loaded mitochondria were collected by centrifugation and resuspended in the same buffer in appropriate dilution, followed by the measurement of fluorescence intensity ($\lambda_{ex}$ 490 nm, $\lambda_{em}$ 590 nm) in a spectrofluorometer.

*Measurement of Phosphate Utilization of Mitochondria.* In a total volume of 250 μL, an aliquot of 25 μL of mitochondrial suspension from control or MnNP-treated mitochondria was diluted into a medium containing 125 mM KCl, 75 mM sucrose, 0.1 mM EGTA, 1 mM $MgCl_2$, 10 mM HEPES, 2 mM phosphate, 0.3% bovine serum albumin, 0.5 mM ADP, 5 mM pyruvate, 10 mM succinate, and 10 mM glucose, followed by the immediate addition of 5 units of hexokinase, and the incubation was continued at 37 °C for 30 min. The incubation was terminated by the addition of 5% ice-cold trichloroacetic (TCA) acid, and the amount of inorganic phosphate was estimated spectrophotometrically. A 0 min sample was also assayed for inorganic phosphate content where hexokinase addition was immediately followed by treatment with 5% ice-cold TCA. Glucose and hexokinase in the reaction mixture acted as a trap for ATP to maintain the level of ADP in the system and also to prevent the release of free inorganic phosphate from ATP by the action of various phosphatases.

*Measurement of Respiratory Chain Activity of Isolated Brain Mitochondria after MnNP Treatment.* The activity of NADH−ferricyanide reductase (complex I) was assayed by using ferricyanide as the electron acceptor in a system containing 0.17 mM NADH, 0.6 mM ferricyanide, and Triton X-100 (0.1% v/v) in 50 mM phosphate buffer, pH 7.4, at 30 °C. The reaction was initiated by the addition of mitochondrial suspension (10−30 μg of protein) to the sample cuvette, and the rate of oxidation of NADH was measured by the decrease in absorbance at 340 nm.

The activity of succinate cytochrome *c* reductase (complex II−III) was assayed by following the succinate-supported reduction of ferricytochrome *c* to ferrocytochrome *c* at 550 nm in an assay mixture containing 100 mM phosphate buffer, 2 mM succinate, 1 mM KCN, 0.3 mM EDTA, and 1.2 mg/mL cytochrome *c* in a total volume of 1 mL. The reaction was initiated by adding mitochondrial suspension (10−30 μg) into the sample cuvette.

The activity of cytochrome *c* oxidase (complex IV) was assayed by measuring the rate of decrease in absorbance at 550 nm at room temperature following the oxidation of reduced cytochrome *c* (50 μM) in 10 mM phosphate buffer, pH 7.4. Ferricyanide (1 mM) was added to oxidize ferrocytochrome *c* in the blank cuvette and the reaction initiated in the sample cuvette by the addition of mitochondrial suspension (10−30 μg). The activity of the enzyme was calculated from the first-order rate constant.

*(a) Measurement of Mitochondrial Respiratory Control Ratio (RCR).* Polarographic study of oxygen consumption using freshly isolated mitochondria allows measurement of respiratory control ratios (RCR) calculated as the ratio of state III to state IV. The chamber of the oxygraph was filled with fresh respiratory buffer along with ADP, glutamate, pyruvate, maleate, succinate, and DNP. A low (state IV) oxygen consumption rate was achieved. After that, 100−200 nmol with or without treated mitochondria was added for inducing state III respiration. After 2 min, the data were recorded, and RCR was calculated accordingly.

*(b) Measurement of Reactive Oxygen Species (ROS).* ROS generation in treated and untreated brain was determined using the nitrotetrazolium blue (NBT) reduction assay.[28] The assay is based on the reduction of yellow water-soluble NBT powder to a blue insoluble substance upon reduction. The treated and control brains were incubated in NBT solution for 1 h. The reaction was stopped by the addition of acetic acid solution. After centrifugation (1 min, 12000*g*), intracellular reduced content was solubilized by adding 50% (v/v) acetic acid to the cell pellet followed by vortexing for 5 min. Cell debris was then pelleted, and the absorbance of the supernatant was determined at 595 nm using a UV−vis spectrophotometer.

*(c) Protein Estimation.* The protein was estimated after the membranes had been solubilized in 1% SDS according to Lowry's method.

**Experiments with Lymphocytes.** *Isolation of Lymphocyte from Blood.* Human peripheral blood was obtained by venipuncture from healthy volunteers into heparinized vacutainers. Lymphocytes were isolated from fresh blood according to the method of Boyum et al.[29] with some modifications using Histopaque.[30] The cells were washed with PBS and resuspended in RPMI-1640 medium at a concentration of $10^6$ cells $mol^{-1}$ for further use.

*Treatment of Lymphocytes.* Freshly isolated human lymphocytes were treated with different concentrations of MnNP and incubated for at least 3 h at 37 °C in RPMI-1640 medium. After incubation, cytotoxicity studies were carried out with treated lymphocytes.

*(a) Cell Proliferation Assay (WST).* The number of mononuclear cells remaining alive after reacting with the cellular mitochondrial dehydrogenase could be quantified by using a Biovision cell proliferation assay kit by measuring the absorbance of the dye solution at 440 nm. The formazan dye is produced by the breakdown of tetrazolium salt, and the amount of dye generated by the activity of dehydrogenase was directly proportional to the number of living cells.

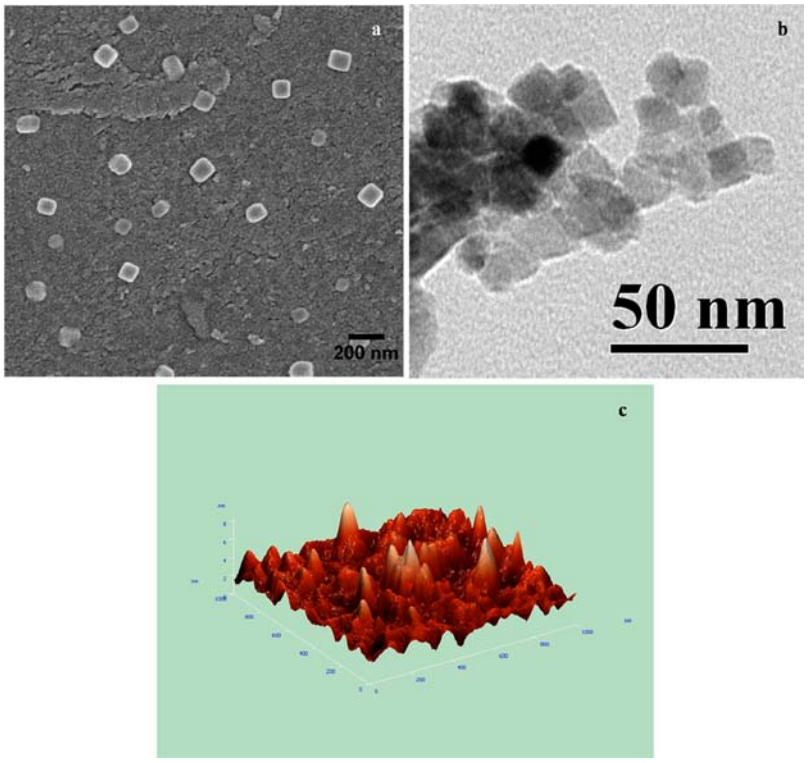


**Figure 1.** Characterization of MnNP: (a) FESEM image; (b) TEM image; (c) AFM micrograph of MnNP.

*(b) NO Content.* Measurement of NO involved a two-step process; in the first step, nitrate was converted to nitrite by nitrate reductase, and in the second step a deep purple azo compound was developed by Griess reagents, supplied externally to the system. The intensity of the azochromophore developed by this process could be measured spectroscopically to determine the amount of NO present in the samples.[31]

*(c) LDH Cytotoxicity Assay.* LDH cytotoxicity assay was performed using Cayman's LDH Cytotoxicity Assay Kit by reducing a tetrazolium salt to highly colored formazan, which absorbed strongly at 490−520 nm.

*(d) ROS/RNS Assay.* Total ROS/RNS generated within the treatments could be measured from fluorescence intensity. DCF could be used as standard, and the free radical content generated could be compared with the predetermined standard intensity using a Cell Biolab Assay Kit.

*Hemolysis.* To perform in vitro hemolysis experiments, human blood was centrifuged twice at 3000 rpm for 15 min to remove residual plasma from the erythrocyte-enriched fraction of blood. RBCs were washed three times with PBS, pH 7.4, and resuspended in the same buffer. Six hundred and ninety microliters of the above RBC stock was suspended with 10 $\mu$L of MnNP treatments (1, 10, and 25 mg/L) along with control, and then the volume was adjusted to 1.5 mL with PBS for each of the treatments. The cells were then centrifuged again at 3000 rpm for 15 min at 4 °C and washed three times with PBS before measurement at 540 nm in a UV−vis spectrophotometer.[32]

**Statistical Analysis.** We tested for the effect of MnNP and MS for different biochemical and biosafety features. For each of the biosafety experiments, we considered three levels of concentration of the nanoparticles, 1, 10, and 25 mg/L, and compared the effects of the various concentrations with respect to the control and also relative to each other. For each concentration in the design, we had three replicates and so, the total numbers of experiments conducted for a specific nanoparticle were $n = 12$ (3 replicates for the 4 levels: control and 1, 10, and 25 mg/L). Although the data size was small, from a biological point of view, normality of the replicate data for each experiment could be assumed. Because there were three replicates for each concentration, two errors were attached to each concentration with a total error degrees of freedom of 8. The degrees of freedom for the prediction space was (number of levels − 1) 3. Therefore, in an ANOVA table, we performed the $F_{3,8}$ distribution and calculated the $P$ value corresponding to this underlying distribution. In the case of biochemical assays of plants, four of each MnNP and MS concentrations were taken into account along with the control, so we had nine replicates altogether and for this case $n = 27$ (control, four concentrations of each MnNP and MS).

If the ANOVA $F$ test was found to be significant, then the next step would be to check which level significantly affected the response, thereby influencing the $F$ test to reject the null. This was achieved by using Tukey's post hoc called HSD (honestly significant difference) test. We used alphabetic labels to check if one level was significantly different from the previous one as concentrations of the nanoparticles were considered as ordered factors. We also observed the box plot response for various levels to get a better indicative picture.

## RESULTS

**Characterization of MnNP.** The morphology of MnNP was investigated by using FESEM and TEM images. Cubic-shaped MnNP of size around 20.88 ± 0.44 nm were more or less homogeneously distributed as revealed from FESEM (Figure 1a) and TEM (Figure 1b) images, respectively. It was previously mentioned that the surface of MnNP contained hydroxyl groups, which contributed to their hydrophilic character. Hydrophilic character was one of the key features of MnNP to study their interaction with plant systems.[14]Although due to the higher reactivity and oxophilicity of Mn,[33] synthesis of MnNP was quite difficult; however, these custom-made MnNP were stable for a long time. Hydrodynamic radius measurement revealed a hydrodynamic radius of around 101.5 ± 13.395 nm, which changed insignificantly over time (Supporting Information (SI) Figure S1). Surface topology of MnNP was obtained from an AFM micrograph (Figure 1c), which justified the average 10 point height of around 6 nm. Chemical purity of the nanoparticles was determined by EDX analysis (SI Figure S2), where Mn was the major component in the sample powder.

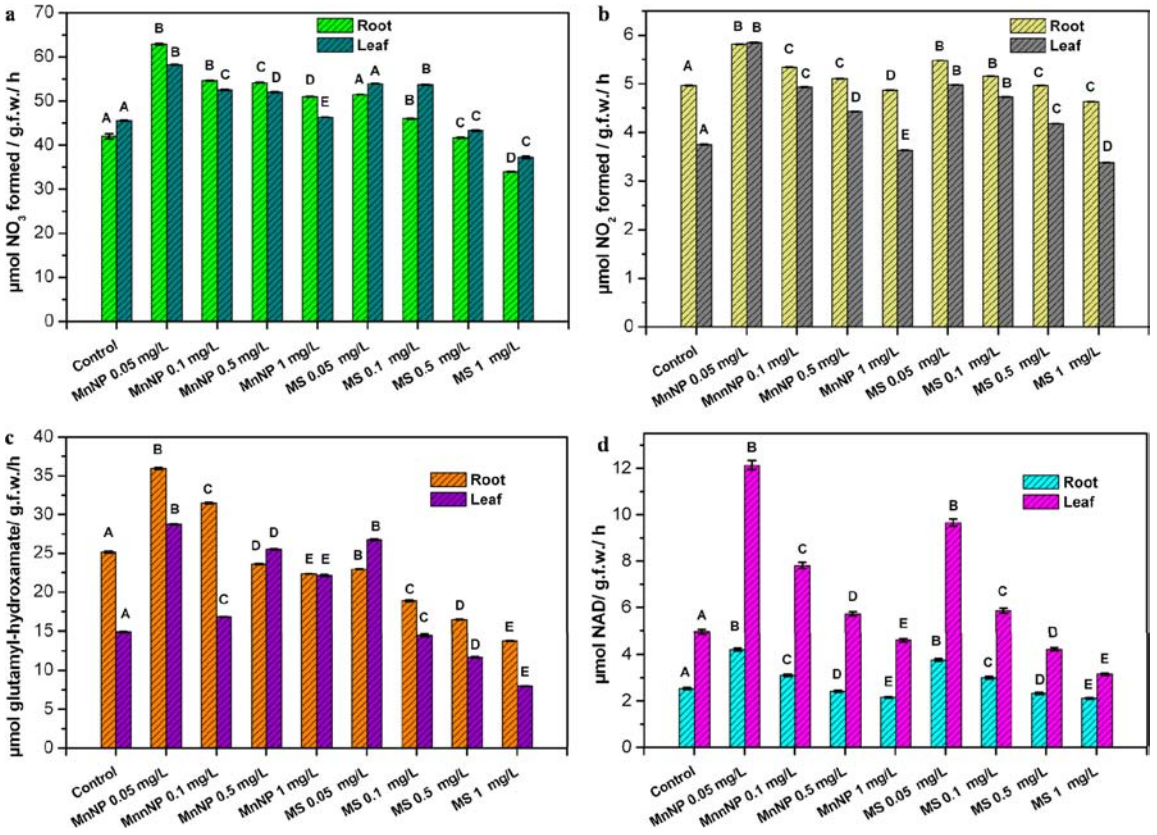


**Figure 2.** Effect of MnNP and MS on nitrogen metabolism of 15-day-treated mung bean plants. (a) NR activity. MnNP leaves: $F = 20.42$, $P < 0.0001$. MnNP roots: $F = 7.59$, $P < 0.01$. MS leaves: $F = 2.64$, $P < 0.1$. MS roots: $F = 8.18$, $P < 0.01$. (b) NiR activity. MnNP leaves: $F = 14.16$, $P < 0.01$. MnNP roots: $F = 8.83$, $P < 0.01$. MS leaves: $F = 19.95$, $P < 0.0001$. MS roots: $F = 8.09$. $P < 0.01$. (c) GS activity. MnNP leaves: $F = 39.21$, $P < 0.00001$. MnNP roots: $F = 23.66$, $P < 0.0001$. MS leaves: $F = 31.68$, $P < 0.0001$. MS roots: $F = 23.44$. $P < 0.0001$. (d) GOGAT activity. MnNP leaves: $F = 20.02$, $P < 0.0001$. MnNP roots: $F = 122.23$, $P < 0.0000001$. MS leaves: $F = 26.03$, $P < 0.0001$. MS roots: $F = 223.94$ $P < 0.000000001$. Within each type of treatment, mean data (±SE, $n = 3$) followed by the same upper case letter are not significantly different for a particular dose; within each dose, means followed by the same lower case letter are not significantly different (Tukey–Kramer HSD test).

Aqueous dispersion of MnNPs was fairly stable. No significant change in the hydrodynamic radius was noted up to 24 h under experimental condition. Even its XRD pattern was unchanged in aqueous dispersion after 24 h, which corroborated our previous report (SI Figure S3).[14] To produce some response in nitrogen assimilation and metabolism, MnNP should be bioavailable to the root system. In our previous study we have already demonstrated the bioavailability of MnNP in roots through confocal microscopy;[14] therefore, bioavailable MnNP on the root system could execute some response, which also triggered us to focus on a series of biochemical and molecular assays related to nitrogen assimilation and metabolism discussed below. Small-sized MnNP resulted in a better bioavailability with their nanosized effect, which was also consistent with the literature.

**Effect on Nitrogen Metabolism in Treated Plants.** The maximum $NO_3^-$ concentration was observed at the highest dose of MS in both root and leaf tissues, whereas a significant decrease in $NO_3^-$ concentration was noted in all of the MnNP-treated sets as shown in Figure S4 (SI). The amount of $NO_3^-$ present in the root was more than in the foliar tissue in all treatments. However, there were increases in both NR and NiR activities in root and leaf tissue of MnNP-treated plants in all treated sets, although the 0.05 mg/L MnNP dose was the most effective (Figure 2a,b). In non-nodulated plants activity of NR-NiR is the initial step for nitrogen metabolism, which is also a determining factor for the assimilation of inorganic nitrogen to organic metabolites in living tissues. Interestingly, $NO_3^-$ concentration in 0.05 mg/L MnNP treatment was lowest but NR and NiR activities were both maximum in the aforementioned dose. MnNP possibly influenced the process of enzymatic reduction during the course of assimilation; hence, NR and NiR activities were enhanced. The responses of GS and GOGAT, in the synthetic process of AA from the assimilated product of NR–NiR activities (Figure 2c,d), were similar. Maximum activity was found in 0.05 mg/L MnNP treatment in both root and leaf tissues, although functions of all of these enzymes were much greater in root tissue compared to foliar tissue. In all of the experiments, the highest doses of MS were found to be toxic to the plant tissues as expected.

Elevated NR activity was further confirmed by protein profiling and Western blot techniques shown in Figure S5 (SI). NR, a homodimer or homotetramer of 110 kDa protein, is present in shoot mesophyll cells and is tightly regulated to reduce nitrate to nitrite.[34] It plays a pivotal role in the nitrogen assimilatory pathway in plants. It was interesting to note that NR activity was increased biochemically; the result was further confirmed by SDS-PAGE and subsequent Western blot analysis of the protein. In both cases MnNP-treated plants showed enhanced activity with respect to control. This justified our hypothesis that MnNP modulated the activity of NR protein, the first assimilatory enzyme and also presumptive candidate responsible for nitrate inhibition step of nitrogen fixation. They bind to and inhibit nitrogenase and leghemoglobin,[35]


dx.doi.org/10.1021/jf502716c | J. Agric. Food Chem. 2014, 62, 8777–8785

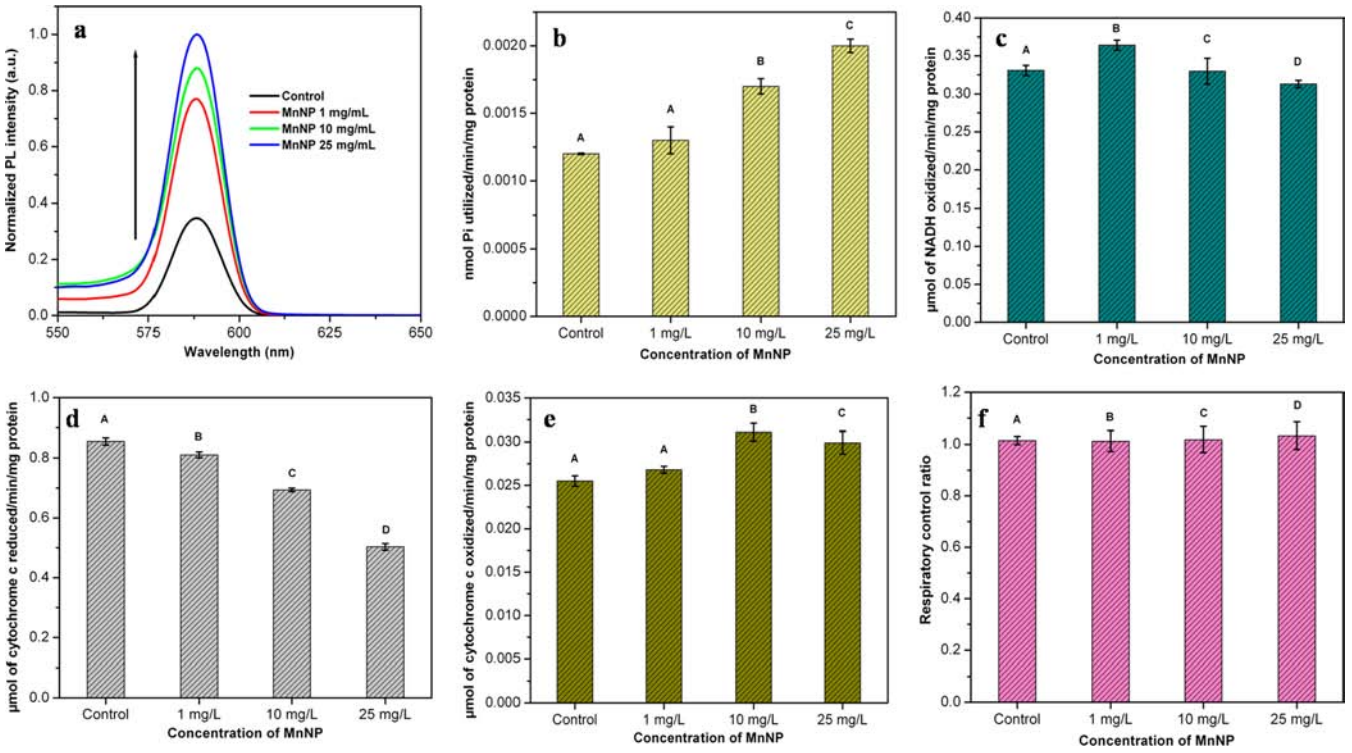


**Figure 3.** Effect of MnNP on mice brain mitochondria. (a) Mitochondrial membrane potential. (b) Inorganic phosphate utilization. $F = 76.18$, $P < 0.00001$. (c) Complex I activity. $F = 33.41$, $P < 0.0001$. (d) Complex II−III activity. $F = 746.35$, $P < 0.000000001$. (e) Complex IV activity. $F = 197.69$, $P < 0.0000001$. (f) RCR. $F = 43.07$, $P < 0.0001$. Within each type of treatment, mean data (±SE, $n = 3$) followed by the same upper case letter are not significantly different for a particular dose; within each dose, means followed by the same lower case letter are not significantly different (Tukey−Kramer HSD test).

simultaneously increasing the activities of all interlinked proteins in the course of nitrogen metabolism.

**Toxicity Study of MnNP with Mouse Model System.** MnNP was injected intravenously at different doses, and the mice were sacrificed after 15 days of observation. No significant changes were noted in general appearance or weight gain between control and treated mice during the observational period (SI Table 1). Treated animals did not show histological abnormalities except in brain tissue at very high doses (SI Figure S6), and even pathological changes (SI Table 2) were negligible. Thus, MnNP were considered to be safe at the recommended dosage after 15 days of treatment, which justified its biocompatibility for future perspectives. Anomalies in brain tissues at higher MnNP concentration forced us to conduct detailed brain mitochondrial assays as it might trigger manganism to the mammalian system. In all toxicity studies we have only accounted for MnNP, as MS is a known toxicant to mammalian systems at experimental doses according to the literature.[15,16]

**Experiments with Mouse Brain Mitochondria.** As shown in Figure 3a, there was a dose-dependent loss of mitochondrial membrane potential after MnNP treatment, although significant inhibition was observed at the highest dose of 25 mg/L. A gradual increase in inorganic phosphate utilization was observed in dose-dependent manner with MnNP treatment shown in Figure 3b. Complex I activity of treated brain mitochondria (Figure 3c) was not significantly altered, but the activities of complex II−III and complex IV were significantly increased at the highest dose of MnNP treatment (Figure 3d,e). MnNP at much higher doses might impair the activity of complex II−III and/or complex IV, resulting in a reduction in energy conversion through electron transport chain (ETC). RCR was left unaltered even after MnNP treatment, showing no negative influence in the respiratory process as shown in Figure 3f. However, more ROS were found to be generated at 25 mg/L MnNP treatment (Figure 4), whereas the lowest dose (1 mg/L) showed no significant change in ROS level with respect to control.

**Experiments with Lymphocyte and Hemolysis.** Figure 5a represents the cytotoxicity of mononuclear cells by MnNP treatment; minor alteration was noted in treated sets with respect

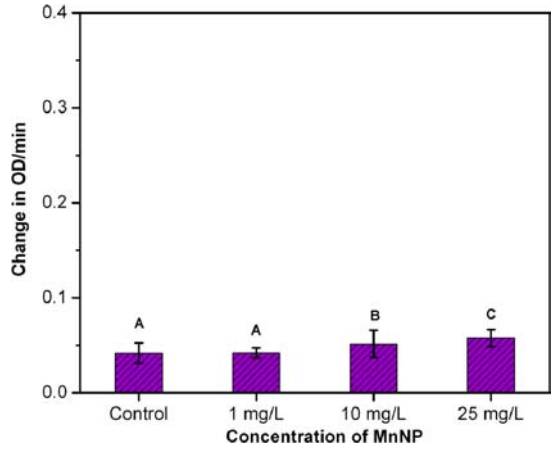


**Figure 4.** Effect of MnNP on ROS content of mice brain mitochondria: $F = 27.79$, $P = 0.0001$. Within each type of treatment, mean data (±SE, $n = 3$) followed by the same upper case letter are not significantly different for a particular dose; within each dose, means followed by the same lower case letter are not significantly different (Tukey−Kramer HSD test).


dx.doi.org/10.1021/jf502716c | J. Agric. Food Chem. 2014, 62, 8777−8785

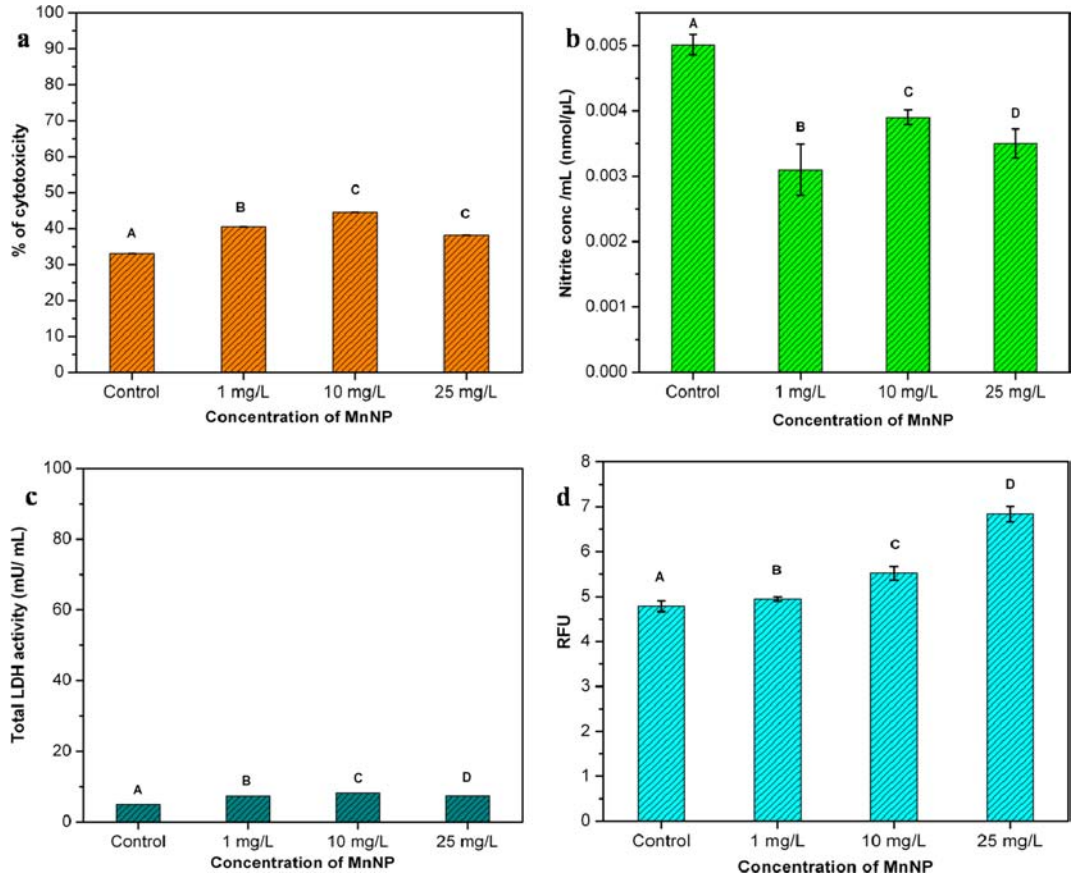


**Figure 5.** Effect of MnNP on human lymphocyte cells. (a) Cytotoxicity assay by WST method. $F = 10.57$, $P < 0.01$. (b) NO content. $F = 197.69$, $P < 0.000001$. (c) Cell viability assay by LDH method. $F = 10.57$, $P < 0.01$. (d) ROS generation. $F = 21.26$, $P < 0.001$. Within each type of treatment, mean data (±SE, $n = 3$) followed by the same upper case letter are not significantly different for a particular dose; within each dose means followed by the same lower case letter are not significantly different (Tukey–Kramer HSD test).

to control. Meanwhile, in the case of NO content (Figure 5b), LDH cell viability assay (Figure 5c), and ROS generation (Figure 5d), no significant alterations were noted between control and treated sets. Altogether MnNP did not impair dose-dependent cytotoxicity in any of the above-mentioned enzymatic assays expect in ROS content, although cytoxicity was seen at higher doses in treated lymphocytes. Similar results were noted in hemolysis experiments. No significant hemolysis was noted in any of the treated sets (SI Figure S7); the highest dose of MnNP treatment (25 mg/mL) exhibited 5.31% hemolysis, which was comparable with the control one (4.96%).

## DISCUSSION

This study revealed that MnNP might modulate the nitrogen metabolism process and thereby could be used as a suitable alternative for MS. MnNP, because of its size and properties, was absorbed readily by the root from soil and transported to the leaf, where it acted as a cofactor in the series of enzymatic reactions during the assimilation of nitrate salt into organic nitrogen compounds. That was probably the reason it did not participate in the process of $NO_3^-$ uptake and the level of $NO_3^-$ in the plant tissue was not influenced by uptake of MnNP. Nitrogen metabolism in plants is a linear pathway that involves the uptake and subsequent transport of nitrate within plant tissues, followed by nitrogen and ammonium assimilation and ultimately amino acid and protein synthesis. However, there had been complexities related to storage and remobilization of nitrate in different parts of the plants: de novo ammonium assimilation and its recycling in the course of photorespiration;[36] unpredictable interactions with carbon assimilatory pathways, which allowed malate to inhibit alkalization[37] and also 2-oxoglutarate to act as the primary acceptor of ammonium in GOGAT pathways.[38] These complexities made it difficult to develop new methodologies and innovations to enrich the status of nitrate assimilation within this complex biological network.

The first step in nitrogen metabolism was the reduction of $NO_3^-$ to $NO_2^-$ in the cytosol by NR. MnNP at all doses directly or indirectly increased NR activity in foliar tissue with respect to control, whereas no significant alterations were noted in root tissue even at the highest dose. Therefore, MnNP could influence the entry of $NO_3^-$ to the cells, resulting in the hyperpolarization of the plasma membrane. The influence of MnNP over NR activity was supported by biochemical and molecular techniques. Enhanced expression of NR protein after MnNP treatment with respect to the control validated our speculation that MnNP could enhance protein activity. This in turn improved nitrogen status in the mung bean crop. It might stimulate NR activity, which was further validated by the enhanced activity of NiR, an enzyme required for the conversion of $NO_2^-$ to $NH_4^+$ in the cytosol. Both NR and NiR were induced by the same factors, explaining their similar responses to the micronutrient treatments.

Plants assimilate inorganic nitrogen into nitrogen-transport amino acids (AAs), glutamate and glutamine, which are destined to transfer nitrogen from source to sink tissues and to build up reserves during periods of nitrogen availability for subsequent use in growth, defense, and reproductive processes. It also

decimated the level of ammonium toxicity. The immediate step thereafter was to convert $NH_4^+$ to amino acid with the help of glutamine synthetase (GS) and glutamate synthase (2-oxoglutarate aminotransferase, or GOGAT). These two very important enzymes are involved in the primary assimilation of inorganic nitrogen from soil along with reassimilation of free ammonium into the plants. GS catalyzed the ATP-dependent assimilation of $NH_4^+$ into glutamine using glutamate as a substrate. Mn is a known cofactor in this reaction, and thereby the presence of MnNP triggered more GS activity and also the activity of GOGAT. Because GOGAT was known to be stimulated by elevated plastid levels of glutamine during ammonium assimilation, GOGAT was required to produce 2-oxoglutamate, which ultimately produced dicarboxylic acids as carbon skeletons for glutamate, aspartate synthesis, and their corresponding amides. A couple of studies demonstrated the influence of high GS activity on vegetative growth and photosynthesis upliftment;[39] even earlier flower and seed development were also observed under accelerated GS activity.[40] MnNP triggered enhanced GS activity; thereby, it may function as an enzymatic cofactor in nitrogen assimilation in non-nodulated plants. It might work as a boon for agriculture as it was able to overcome the drawbacks of the commercially available MS salt at higher doses.

MnNP was already established as a micronutrient fertilizer over commercially available MS, but it was well recognized that excess use of Mn salt could induce manganism; therefore, the toxicity issues associated with MnNP could not be ruled out. As a consequence, we carried out a series of detailed toxicological evaluations on mononuclear cells and murine model system at relatively high dosages (1, 10, and 25 mg/mL) in contrast to the one used in nitrogen assimilation and metabolism. In murine model system MnNP was injected intravenously, and after 15 days of observation, mice were sacrificed for histopathological evaluation. From the results we confirmed that MnNP was biosafe for further implementation, although minor anomalies were noted in brain tissues. Therefore, we deliberately carried out a brain mitochondrial assay in the murine model system in light of manganism. The assays were carried out after 24 h of injection followed by isolation of brain tissues. In all of the experiments it was observed that 25 mg/L MnNP partially impaired the activity of complex II−III, but it had no effect in mitochondrial complex I, complex IV protein domains, and RCR activity. This justified that MnNP limited the efficiency of brain mitochondrial functions to some extent but did not hamper the entire physiological process. There was no loss of mitochondrial membrane potential at any of the dosages; increased phosphorylation capacity ensured no loss of phosphate utilization and hence ATP synthesis. The key function of the mitochondrial ETC was to supply reducing equivalents because the majority of electrons were provided by NADH. In our experiments, MnNP did not show any alteration in complex I activity of brain mitochondrial ETC like it did with its elemental counterpart. Therefore, MnNP could easily overcome the problem of inactivation of energy metabolism leading to mitochondrial dysfunction influenced by Mn salts. Partially inhibited complex II−III activity decreased electron transfer activity leading to ROS by leaking electrons from ETC complexes during respiration, particularly in complex III.

In addition, a detailed in vitro cytotoxicity experiment on human lymphocytes was carried out using MnNP of aforementioned dosages. No significant cytotoxic response was found in any of the treated sets with respect to control as noted from our detailed systematic evaluation. These results were consistent with the in vivo experiments mentioned earlier, which signified the biocompatibility of MnNP for biological perspectives. Interestingly, hemolysis experiments justified its biocompatibility as well, which also corroborated the results noted for mononuclear cells.

To the best of our knowledge, this is the first study in which MnNP has been used to enhance nitrogen metabolism in a plant model system. MnNP probably stimulated the activity of NR directly or indirectly as noted from biochemical and molecular techniques. They also enhanced the function of both GS and GOGAT enzyme activities, being an active cofactor in the biochemical reactions. They not only surpassed the difficulties raised due to low availability of inorganic ions during nitrogen assimilation but also alleviated enzymatic activities of the same physiological process. Hence, MnNP can be used as fertilizer for both carbon and nitrogen assimilatory processes. Biosafety experiments were carried out in both mouse and human mononuclear cells. Brain mitochondria of treated mice were isolated to check functional activities in respiration and energy production. Results demonstrated that MnNP were fairly biosafe, although minor toxic responses were noted at a very high dosage. We have good reason to believe that MnNP could be used as a fertilizer with great efficiency together with their biocompatibility relative to the commonly used salt counterpart, MS.

## ■ ASSOCIATED CONTENT

### Ⓢ Supporting Information

Additional figures and tables as noted in the text. This material is available free of charge via the Internet at http://pubs.acs.org.

## ■ AUTHOR INFORMATION

### Corresponding Author

*(S.P.) E-mail: saheli.pra@gmail.com.

### Funding

This work was generously supported by major grants from the Department of Biotechnology, government of India (DBT) (Grants BT/PR15217/NNT/28/506/2011-2015; BT/BIPP0439/11/10). We are grateful to the National Agricultural Innovation Project (ICAR) (Grant NAIP/Comp-4/C3004/2008-2014), the National Fund (Indian Council of Agricultural Research) (Grants NFBSFARA/GB-2019/2011−2015; NFBSFARA/CA-4-15/2013-14,,) and ISI plan project funds (2008−2013) for providing financial support. S.M. is thankful to CSIR, New Delhi, for SRF and P.P. is thankful to UGC-DSKPDF.

### Notes

The authors declare no competing financial interest.

## ■ ACKNOWLEDGMENTS

We acknowledge Ashim Dhar for his assistance during plant experiments.

## ■ REFERENCES

(1) Arnone, J. A.; Gordon, J. C. Effect of nodulation, nitrogen fixation and $CO_2$ enrichment on the physiology, growth and dry mass allocation of seedlings of *Alnus rubra* Bong. *New Phytol.* **1990**, *116*, 55−66.

(2) Hortensteiner, S.; Feller, U. Nitrogen metabolism and remobilization during senescence. *J. Exp. Bot.* **2002**, *53* (370), 927−937.

(3) Feller, U.; Fische, A. Nitrogen metabolism in senescing leaves. *Crit. Rev. Plant Sci.* **1994**, *13* (3), 241−273.

(4) Koch, K. Sucrose metabolism: regulatory mechanisms and pivotal roles in sugar sensing and plant development. *Curr. Opin. Plant Biol.* **2004**, *7*, 235−246.
(5) Robinson, S. A.; Slade, A. P.; Fox, G. G.; Phillips, R.; Ratcliffe, R. G.; Stewart, G. R. The role of glutamate dehydrogenase in plant nitrogen metabolism. *Plant Physiol.* **1991**, *95*, 509−516.
(6) Hänsch, R.; Mendel, R. R. Physiological functions of mineral micronutrients (Cu, Zn, Mn, Fe, Ni, Mo, B, Cl). *Curr. Opin. Plant Biol.* **2009**, *12* (3), 259−266.
(7) Patra, P.; Mitra, S.; Debnath, N.; Goswami, A. Biochemical-, biophysical-, and microarray-based antifungal evaluation of the buffer-mediated synthesized nano zinc oxide: an in vivo and in vitro toxicity study. *Langmuir* **2012**, *28* (49), 16966−16978.
(8) Pradhan, S.; Roy, I.; Lodh, G.; Patra, P.; Choudhury, S. R.; Samanta, A.; Goswami, A. Entomotoxicity and biosafety assessment of PEGylated acephate nanoparticles: a biologically safe alternative to neurotoxic pesticides. *J. Environ. Sci. Health., Part B* **2013**, *48*, 559−569.
(9) Debnath, N.; Das, S.; Seth, D.; Chandra, R.; Bhattacharya, S. C.; Goswami, A. Entomotoxic effect of silica nanoparticles against *Sitophilus oryzae* (L.). *J. Pest Sci.* **2011**, *84*, 99−105.
(10) Clément, L.; Hurel, C.; Marmier, N. Toxicity of $TiO_2$ nanoparticles to cladocerans, algae, rotifers and plants − effects of size and crystalline structure. *Chemosphere* **2013**, *90*, 1083−1090.
(11) Jośko, I.; Oleszczuk, P. Influence of soil type and environmental conditions on ZnO, $TiO_2$ and Ni nanoparticles phytotoxicity. *Chemosphere* **2013**, *92*, 91−99.
(12) Boer, W. D.; Kowalchuk, G. A. Nitrification in acid soils: micro-organisms and mechanisms. *Soil Biol. Biochem.* **2001**, *33* (7−8), 853−866.
(13) Jiang, W. Z. Mn use efficiency in different wheat cultivars. *Environ. Exp. Bot.* **2006**, *57* (1−2), 41−50.
(14) Pradhan, S.; Patra, P.; Das, S.; Chandra, S.; Mitra, S.; Dey, K. K.; Akbar, S.; Palit, P.; Goswami, A. Photochemical modulation of biosafe manganese nanoparticles on *Vigna radiata*: a detailed molecular, biochemical, and biophysical study. *Environ. Sci. Technol.* **2013**, *47* (22), 13122−13131.
(15) Wennberg, A.; Iregren, A.; Struwe, G.; Cizinsky, G.; Haqrnan, M.; Johansson, L. Manganese exposure in steel smelters a health hazard to the nervous system. *Scand. J. Work Environ. Health* **1991**, *17*, 255−262.
(16) Martin, C. J. Manganese neurotoxicity: connecting the dots along the continuum of dysfunction. *NeuroToxicology* **2006**, *27* (3), 347−349.
(17) Hussain, S. M.; Javorina, A. K.; Schrand, A. M.; Duhart, H. M.; Ali, S. F.; Schlager, J. J. The interaction of manganese nanoparticles with PC-12 cells induces dopamine depletion. *Toxicol. Sci.* **2006**, *92* (2), 456−463.
(18) Wang, J.; Rahman, M. F.; Duhart, H. M.; Newport, G. D.; Patterson, T. A.; Murdock, R. C.; Hussain, S. M.; Schlager, J. J.; Ali, S. F. Expression changes of dopaminergic system-related genes in PC12 cells induced by manganese, silver, or copper nanoparticles. *NeuroToxicology* **2009**, *30*, 926−933.
(19) Lanone, S.; Rogerieux, F.; Geys, J.; Dupont, A.; Maillot-Marechal, E.; Boczkowski, J.; Lacroix, G.; Hoet, P. Comparative toxicity of 24 manufactured nanoparticles in human alveolar epithelial and macrophage cell lines. *Part. Fibre Toxicol.* **2009**, *6*, 14.
(20) Limbach, L. K.; Wick, P.; Manser, P.; Grass, R. N.; Bruinink, A.; Stark, W. J. Exposure of engineered nanoparticles to human lung epithelial cells: influence of chemical composition and catalytic activity on oxidative stress. *Environ. Sci. Technol.* **2007**, *41* (11), 4158−4163.
(21) Gilad, A. A.; Walczak, P.; McMahon, M. T.; Na, H. B.; Lee, J. H.; An, K.; Hyeon, T.; Zijl, P. C. M.; Bulte, J. W. M. MR tracking of transplanted cells with "positive contrast" using manganese nanoparticles. *Magn. Reson. Med.* **2008**, *60* (1), 1−7.
(22) Hussain, S. M.; Hess, K. L.; Gearhart, J. M.; Geiss, K. T.; Schlager, J. J. In vitro toxicity of nanoparticles in BRL 3A rat liver cells. *Toxicol in Vitro* **2005**, *19* (7), 975−983.
(23) Yang, Z.; Liu, W.; Allaker, R. P.; Reip, P.; Oxford, J.; Ahmad, Z.; Ren, G. A review of nanoparticle functionality and toxicity on the central nervous system. *J. R. Soc. Interface* **2010**, *7*, S411−S422.
(24) Lee, Y. C.; Chen, D. Y.; Dodd, S. J.; Bouraoud, N.; Koretsky, A. P.; Krishnan, K. M. The use of silica coated MnO nanoparticles to control MRI relaxivity in response to specific physiological changes. *Biomaterials* **2012**, *3* (13), 3560−3567.
(25) Cataldo, D. A.; Haroon, M.; Schrader, L. E.; Young, V. L. Rapid colorimetric determination of nitrate in plant tissue by nitration of salicylic acid. *Commun. Soil Sci. Plant Anal.* **1975**, *6*, 71−80.
(26) Crawford, N. M.; Smith, M.; Bellissimo, D.; Davis, R. W. Sequence and nitrate regulation of the *Arabidopsis thaliana* mRNA encoding nitrate reductase, a metalloflavoprotein with three functional domains. *Proc. Natl. Acad. Sci. U.S.A.* **1988**, *85*, 5006−5010.
(27) Banerjee, K.; Sinha, M.; Pham, C. L. L.; Jana, S.; Chanda, D.; Cappai, R.; Chakrabarti, S. α-Synuclein induced membrane depolarization and loss of phosphorylation capacity of isolated rat brain mitochondria: implications in Parkinson's disease. *FEBS Lett.* **2010**, *584*, 1571−1576.
(28) Tian, J.; Fu, F.; Geng, M.; Jiang, Y.; Yang, J.; Jiang, W.; Wang, C.; Liu, K. Neuroprotective effect of 20(*S*)-ginsenoside $Rg_3$ on cerebral ischemia in rats. *Neurosci. Lett.* **2005**, *374* (2), 92−97.
(29) Boyum, A. Isolation of lymphocytes, granulocytes and macrophages. *Scand. J. Immunol.* **1976**, *5*, 9−15.
(30) Ghosh, M.; Bandyopadhyay, M.; Mukherjee, A. Genotoxicity of titanium dioxide ($TiO_2$) nanoparticles at two trophic levels: plant and human lymphocytes. *Chemosphere* **2010**, *81*, 1253−1262.
(31) Chatter, R.; Othman, R. B.; Rabhi, S.; Kladi, M.; Tarhouni, S.; Vagias, C.; Roussis, V.; Guizani-Tabbane, L.; Kharrat, R. In vivo and in vitro anti-inflammatory activity of neorogioltriol, a new diterpene extracted from the red algae *Laurencia glandulifera*. *Mar. Drugs* **2011**, *9*, 1293−1306.
(32) Mitra, S.; Subia, B.; Patra, P.; Chandra, S.; Debnath, N.; Das, S.; Banerjee, R.; Kundu, S. C.; Pramanik, P.; Goswami, A. Porous ZnO nanorod for targeted delivery of doxorubicin: in vitro and in vivo response for therapeautic applications. *J. Mater. Chem.* **2012**, *22*, 24145−24154.
(33) Bondi, J. F.; Oyler, K. D.; Ke, X.; Schiffer, P.; Schaak, R. E. Chemical synthesis of air-stable manganese nanoparticles. *J. Am. Chem. Soc.* **2009**, *131*, 9144−9145.
(34) Crawford, N. M. Nitrate: nutrient and signal for plant growth. *Plant Cell.* **1995**, *7*, 859−868.
(35) Carroll, B. J.; McNeil, D. L.; Gresshoff, P. M. Isolation and properties of soybean [*Glycine max* (L.) Merr.] mutants that nodulate in the presence of high nitrate concentrations. *Proc. Natl. Acad. Sci. U.S.A.* **1985**, *82*, 4162−4166.
(36) Stitt, M.; Muller, C.; Matt, P.; Gibon, Y.; Carillo, P.; Morcuende, R.; Scheible, W. R.; Krapp, A. Steps towards an integrated view of nitrogen metabolism. *J. Exp. Bot.* **2002**, *53* (370), 959−970.
(37) Tcherkez, G.; Hodges, M. How stable isotopes may help to elucidate primary nitrogen metabolism and its interaction with (photo) respiration in $C_3$ leaves. *J. Exp. Bot.* **2008**, *59* (7), 1685−1693.
(38) Müller, C.; Scheible, W. R.; Stitt, M.; Krapp, A. Influence of malate and 2-oxoglutarate on the NIA transcript level and nitrate reductase activity in tobacco leaves. *Plant Cell Environ.* **2001**, *24*, 191−203.
(39) Soussi, M.; Ocanã, A.; Lluch, C. Effects of salt stress on growth, photosynthesis and nitrogen fixation in chick-pea (*Cicer arietinum* L.). *J. Exp. Bot.* **1998**, *49* (325), 1329−1337.
(40) Murray, D. R. Changes in activities of enzymes of nitrogen metabolism in seedcoats and cotyledons during embryo development in pea seeds. *Plant Physiol.* **1980**, *66*, 782−786.

JOURNAL OF AGRICULTURAL AND FOOD CHEMISTRY

Article

pubs.acs.org/JAFC

# Effect of Second Cooling on the Chemical Components of Essential Oils from Orange Peel (*Citrus sinensis*)

Yulong Chen, Jijun Wu, Yujuan Xu,* Manqing Fu, and Gengsheng Xiao

Sericultural and Agro-Food Processing Research Institute, Guangdong Academy of Agricultural Sciences, Guangzhou 510610, People's Republic of China

**ABSTRACT:** A second cooling was added to the oil collectors of an improved Clevenger-type apparatus (ICT) to investigate the thermal reaction of essential oils from orange peel compared to a traditional Clevenger-type apparatus (CT). The results demonstrated the yield rate of essential oil from ICT was significantly higher ($p < 0.05$) than that from CT. The major components of the essential oils consisted of monoterpenes, such as *d*-limonene, *β*-myrcene, *β*-pinene, *γ*-terpinene, *α*-pinene. Interestingly, ICT prevented the thermal reaction—the transformation of *β*-myrcene to *β*-thujene—and reduced the oxidation on *α*-pinene and *β*-pinene of the essential oil in comparison to CT. In addition, the yield rate of *γ*-terpinene can also be improved via ICT compared to CT. Thus, ICT is an effective improvement to traditional CT.

**KEYWORDS:** *Clevenger-type apparatus, extraction, essential oil, thermal reaction*

## INTRODUCTION

The essential oils from various species of citrus can be used as ingredients for food flavor in, for example, beverages or ice cream, as well as materials in the fragrance industry.[1] Although the common way to get the essential oils is by cold pressing citrus peels, hydrodistillation is still adopted in some countries as an economical way to obtain the oils.[2]

The advantage of hydrodistilled extraction is evident. As a hydrodistillation of two mixed immiscible liquids, each exerts a vapor pressure, as if each liquid were pure.[3] The total vapor pressure of a boiling mixture is therefore equal to the sum of the partial pressures given by each of the individual components of the mixture. When the total vapor pressure reaches atmospheric pressure, the mixture starts to boil. This means that the boiling point of the mixture is reached at a lower temperature than the boiling points of the individual components. Therefore, hydrodistillation is able to separate volatile from nonvolatile components at a reduced boiling point, thus avoiding the high temperatures of boiling points.[4,5] Moreover, the displacement of atmospheric oxygen by steam, which protects compounds from oxidation, is another plus point of this method.[6] Thus, a Clevenger-type apparatus (CT), a popular method of hydrodistillation for the extraction of essential oils,[7] was employed in our research (Figure 1).

However, the drawback of this process is also obvious. As known, hydrolyzable compounds such as esters, as well as thermally labile components, may be decomposed during the distillation process.[3] In addition, partial loss of more polar constituents of the oil, due to their affinity for water, may also occur.[4,8] For this reason, the improved Clevenger-type apparatus (ICT) was used to avoid partial heat loss due to the volatilization of oils because the ICT equipment is modified with a water-cooled oil collector as the second cooling to reduce the temperature of the collector during hydrodistillation (Figure 1). This improvement has also been used in the extraction of essential oil of *Pericarpium Citri Reticulatae* in our laboratory.[9] In addition, the ICT equipment was used to tentatively determine other differences from CT due to overheating of oils, such as the degradation of volatile and thermolabile compounds and the formation of artifacts.

The orange (*Citrus sinensis*) is widely grown in China, and the peel of the orange, as one of the byproducts of orange processing, can be used for the extraction of oil. Although some modified CTs were used in the literature,[10,11] few studies demonstrated the difference between CT and ICT. Thus, the focus of this study was on the variation of chemical compositions of the essential oils isolated from orange peels by CT and ICT. Through the research, evidence of the advantage of ICT was found in comparison with CT. Accordingly, the research can supply an improved classical extraction method of essential oils, which possesses not only the interest of solvent inertness and nontoxicity but also more effective fractionation at moderate temperatures.[12]

## MATERIALS AND METHODS

**Chemicals.** Homologous series of $C_6$−$C_{22}$ *n*-alkanes were purchased from Sigma Chemical Co. (St. Louis, MO, USA). Reference chemicals such as *d*-limonene and *γ*-terpinene were obtained from Aladdin Chemistry Co., Ltd. (Shanghai, China). Other reference chemicals, such as *β*-myrcene, *α*-caryophyllene, *α*-pinene, decanal, and *p*-menth-1-en-8-ol, were supplied by College of Food Science and Technology, Huazhong Agricultural University (Wuhan, China).

**Plant Materials.** Orange peel (*C. sinensis*) was purchased from Guangxi province, China. The specimens were dried in the sun to constant weight, ground to a fine powder, and stored in waterproof bags at 4 °C before use.

**Isolation of the Essential Oils.** One hundred grams of dried and ground powder (80 mesh) from orange peel was hydrodistilled with 400 g of water for 2 h, using a CT[7] and an ICT (Figure 1), respectively. When using a CT, the distilled essential oil mixed with vapor is condensed by the top condenser and dropped into the

Received: March 7, 2014
Revised: June 17, 2014
Accepted: June 18, 2014
Published: June 19, 2014

ACS Publications © 2014 American Chemical Society



dx.doi.org/10.1021/jf501079r | J. Agric. Food Chem. 2014, 62, 8786−8790

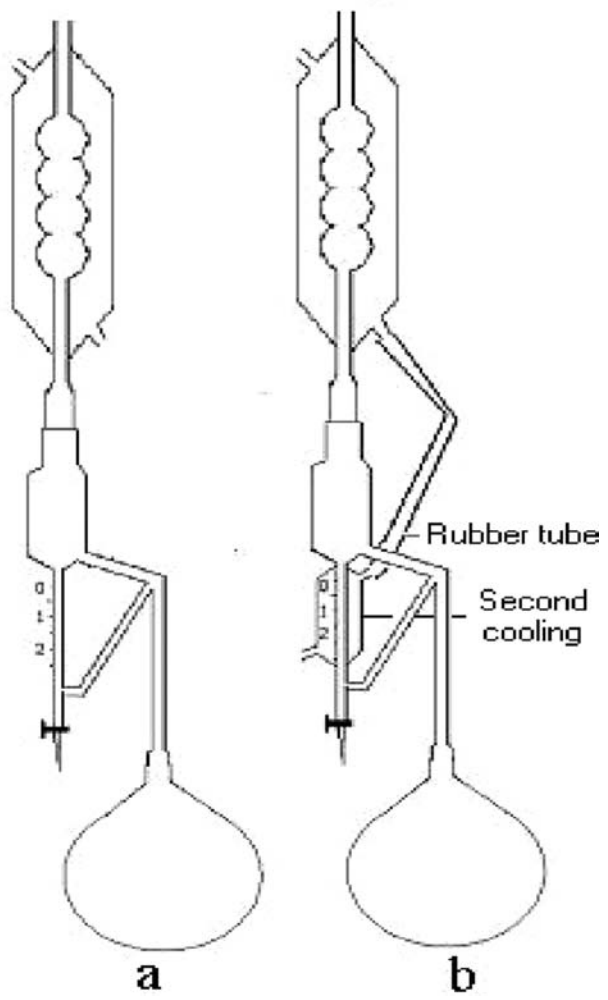


**Figure 1.** Improved (b) and conventional (a) Clevenger-type apparatus.

essential oil collector. Superficial essential oil is obtained after the water in the collector is drained. When a second condenser is added to the essential oil collector of a CT, the improved apparatus, namely, ICT, becomes different. The second condenser is linked with the top condenser with a rubber pipe. When cooling, running water first enters the second condenser and then goes out of the top condenser. Different from a CT, the distilled essential oil is first condensed by the top condenser and dropped into the essential oil collector and then cooled again by the second condenser. Anhydrous sodium sulfate was used to dry the distilled essential oils. After filtering, the oils were stored in sealed vials at 4 °C for further analyses. This experiment was performed in triplicate.

**Analysis of Gas Chromatography (GC).** A PerkinElmer (Norwalk, CT, USA) gas chromatograph model 8700 equipped with a flame ionization detector (FID) and an HP-Wax bonded polyethylene glycol capillary column (30 m × 0.25 mm, film thickness = 0.25 μm; Agilent Technologies, Little Falls, CA, USA) was employed to analyze the essential oils. Injector and detector temperatures were 220 and 250 °C, respectively. Column temperature was set from 50 to 230 °C at a rate of 5 °C/min and, lower and upper temperatures were maintained for 4 and 5 min, respectively. Helium was regarded as carrier gas at a flow rate of 1.0 mL $min^{-1}$. When a sample of 10 μL was injected, split mode (split ratio, 1:30) was adopted. All quantifications were finished using a built-in data-handling program provided by the manufacturer of the gas chromatograph. The quantification of compositions was reported using a relative percentage of the total peak area.

**Analysis of Gas Chromatography–Mass Spectrometry (GC-MS).** The essential oil was analyzed using an Agilent Technologies 6890N network gas chromatographic (GC) system, equipped with an Agilent Technologies 5975B inert XL mass selective detector and an Agilent Technologies 7683B series autoinjector to obtain the qualitative GC-MS results. Chromatographic conditions were set the same as described above. An electron ionization mode with an ionization energy of 70 eV was used for MS detection. Injector and MS transfer line temperatures were 220 and 250 °C, respectively.

**Compound Identification.** The identification of the essential oil constituents was performed by comparison of their retention indices relative to ($C_6$–$C_{22}$) *n*-alkanes, published data, and spectra of authentic compounds. Moreover, compounds were further identified and authenticated by comparing their MS data to the NIST mass spectral library and published mass spectra.[13]

**Statistical Analysis.** SAS 8.1 (SAS Institute Inc., Cary, NC, USA) was used to analyze the data. A variance analysis (ANOVA) was followed by an analysis of least significant difference ($p < 0.05$) among means by Duncan's multiple-range test.

## RESULTS AND DISCUSSION

**Yield Rates of the Essential Oils.** In Table 1, the yield rate of essential oils from ICT (ca. 1.98%) is significantly higher than that of CT (ca. 1.00%) ($p < 0.05$). As the second condenser was added to the collector of essential oil, the temperature of the essential oil in the collector of ICT was lower than that of CT. This result is in line with our previous report.[9] On the contrary, in the process of CT extraction, the collector of oil is connected to the bottom of the CT, which is being heated by steamed vapor; the temperature of the collector is nearly similar to that of the CT bottom. Thus, the temperature of the essential oil in the collector of the CT is higher than that of the ICT and, therefore, the volatilization of essential oils was accelerated. As a result, the yield rate of essential oil extracted from ICT was greatly increased in comparison with CT.

**Main Compositions.** The compositions of essential oils from CT and ICT methods were different (Figure 2; Table 1). The major ingredients of essential oils from the hydrodistilled method are *d*-limonene, γ-terpinene, β-thujene, *p*-cymene, β-myrcene, α-pinene, β-pinene, and (+)-4-carene. These components are similar to the result from *Pericarpium Citri Reticulatae* essential oil.[9] According to Yang et al.,[14] essential oil of citrus fruit waste contained limonene (80.51%), γ-terpinene (6.80%), *p*-cymene (4.02%), β-myrcene (1.59%), α-pinene (1.02%), and α-terpinolene (0.56%). Although the major components of the oils are not completely the same as found by Yang et al.,[14] *d*-limonene and γ-terpinene are predominant constituents in the orange essential oils. This result is in accord with the literature.[15,16] *d*-Limonene and γ-terpinene are monocyclic terpenes that are consumed by humans predominantly as an ingredient of traditional foods such as citrus fruits, carrots, coffee, orange, and nutmeg.

To our best knowledge, the monoterpenes and monoterpenoids, comprising the most important class of terpenic compounds, have been best investigated. This class is further subcategorized as these molecules reveal various structures and diversity of internal C,C linkage.[17,18] Subclasses are classified according to the similarity of molecular structures of compounds in this class. Accordingly, citral, nerol, and myrcene are regarded as the 3, 6-dimethyloctane subclass, whereas limonene, pulegone, and menthol are the *p*-menthane subclass.[19] Therefore, the major components of the essential oils extracted from orange peel consisted of monoterpenes,

**Table 1. Chemical Composition of Orange Peel Essential Oils from CT and ICT**

| peak | compound | RI[b] | relative contents[a] (%) ICT | relative contents[a] (%) CT | method of identification[c] |
|---|---|---|---|---|---|
| 1 | α-pinene | 1019 | 2.02 ± 0.04b | 2.48 ± 0.06a | c, d, e |
| 2 | β-pinene | 1105 | 1.21 ± 0.05b | 1.32 ± 0.04a | c, d |
| 3 | β-thujene | 1159 | 2.78 ± 0.03b | 5.42 ± 0.14a | c, d |
| 4 | β-myrcene | 1162 | 2.18 ± 0.02 | nd[d] | c, d, e |
| 5 | *d*-limonene | 1195 | 64.15 ± 0.92a | 65.62 ± 0.93a | c, d, e |
| 6 | γ-terpinene | 1258 | 10.28 ± 0.21a | 9.87 ± 0.16b | c, d, e |
| 7 | *p*-cymene | 1274 | 2.32 ± 0.12a | 2.23 ± 0.10a | c, d |
| 8 | (+)-4-carene | 1285 | 0.82 ± 0.05a | 0.80 ± 0.04a | c, d |
| 9 | α-cubebene | 1487 | 0.13 ± 0.01a | 0.13 ± 0.00a | c, d |
| 10 | decanal | 1495 | 0.31 ± 0.02a | 0.28 ± 0.02a | c, d, e |
| 11 | linalool | 1547 | 0.66 ± 0.04a | 0.52 ± 0.02b | c, d |
| 12 | β-elemene | 1583 | 0.31 ± 0.00a | 0.25 ± 0.01a | c, d |
| 13 | *p*-menth-1-en-4-ol | 1597 | 0.58 ± 0.03a | 0.55 ± 0.03a | c, d |
| 14 | 2,6-octadiene, 2,6-dimethyl- | 1649 | 0.13 ± 0.01a | 0.12 ± 0.01a | c, d |
| 15 | α-caryophyllene | 1657 | 0.16 ± 0.01a | 0.15 ± 0.01a | c, d, e |
| 16 | *p*-menth-1-en-8-ol | 1693 | 0.68 ± 0.05a | 0.61 ± 0.06a | c, d, e |
| 17 | nerol acetate | 1721 | 0.47 ± 0.03a | 0.43 ± 0.00a | c, d |
| 18 | α-farnesene | 1746 | 0.68 ± 0.04a | 0.61 ± 0.03a | c, d |
| 19 | geraniol ester | 1752 | 0.70 ± 0.03a | 0.69 ± 0.03a | c, d |
| 20 | D-citronellol | 1766 | 0.20 ± 0.00a | 0.15 ± 0.01a | c, d |
| 21 | *p*-mentha-1,8-dien-6-ol | 1859 | 0.15 ± 0.01a | 0.12 ± 0.01a | c, d |
| 22 | *p*-thymol | 2197 | 0.22 ± 0.03a | 0.16 ± 0.00b | c, d |
| total | | | 91.14 | 92.51 | |
| yield rates (%) | | | 1.98 ± 0.10a | 1.00 ± 0.07b | |

[a]Values are means ± standard deviation of three separate experiments. Different letters (a, b) in a row indicate significant differences ($p < 0.05$). [b]RI, retention index. [c]c, identification using retention index; d, identification by comparing with mass spectra; e, identification using authentic compounds. [d]nd, not detected.

including *d*-limonene, β-myrcene, α-pinene, γ-terpinene, and β-pinene.

**Comparison of Components of Essential Oils.** Both β-thujene and β-myrcene were found in the oil from ICT, whereas only β-thujene was detected in the oil from CT (Figure 2; Table 1). Interestingly, the relative content of β-thujene in the oil from CT was almost the sum of the relative contents of β-thujene and β-myrcene in the oil from ICT. Because β-thujene and β-myrcene are isomers, β-myrcene can be changed into β-thujene via electrocyclic reaction and rearrangement under long duration of high temperature in the oil collector of the CT (Figure 3). With regard to the CT, when the mixture of steam and oil was first condensed into the oil collector, the oil was still affected by the heating. Accordingly, it is postulated that CT may be involved in the thermal reaction that turned β-myrcene into β-thujene in the process of oil extraction. Various papers in the literature have reported thermal rearrangements of small molecules.[20,21] The dienes bearing internal C═C bonds are prone to thermal rearrangement.[22] Thus, thermal rearrangement of β-myrcene is prone to happen as the molecule has intramolecular C═C bonds. β-Myrcene is first rearranged into an intermediate, and then the intermediate is cyclized via intramolecular reaction under the condition of heating.[19,23] Ultimately, the cyclized molecule is thermally induced and rearranged, leading to β-thujene by isomerization[19] (Figure 3). On the contrary, the unsaturated monoterpene β-thujene can also undergo the reverse transformation: ring opening via 1, j-H shift reaction,[20,22] turning into an acyclic monoterpene.

As known, the relative contents of α-pinene and β-pinene in the oil from ICT were significantly lower ($p < 0.05$) than those from CT. The result indicates that CT extraction can obviously promote the formation of α-pinene and β-pinene in comparison with ICT. In the process of extraction of oils, the difference of CT and ICT is attributed to the different collectors. Because the CT oil was heated at the higher temperature of the collector over ICT, greater amounts of α-pinene and β-pinene in the oil of CT may be produced through thermal reaction, in which the transformation of other ingredients can be achieved. On the other hand, α-pinene and β-pinene, as bicyclic monoterpenes, can be also formed via electrocyclic reaction of monoterpenes. This conclusion has been reported. Mcgraw et al.[24] have found that part of α-pinene has been rearranged or oxidized in the presence of air at temperatures of 90−130 °C. The products included β-pinene, α-pinene oxide, etc. The thermal rearrangement of β-pinene produces limonene, myrcene, and ψ-limonene.[19] Obviously, the different colors of oils from CT and ICT can also be observed in our experiment. The phenomenon is in accord with the report that the color of orange oils obtained by hydrodistillation was observed to deepen, expressing the composition change of isolated orange oils.[25] This further confirmed the postulated fact that ICT could effectively reduce the thermal reaction of monoterpenes in the oil.

γ-Terpinene is one of the major constituents in the orange essential oils. The concentration of γ-terpinene from ICT is 10.28%, which is significantly higher ($p < 0.05$) than that (9.87%) from CT (Table 1). This indicates that ICT can also benefit the extraction of γ-terpinene to avoid its loss. The

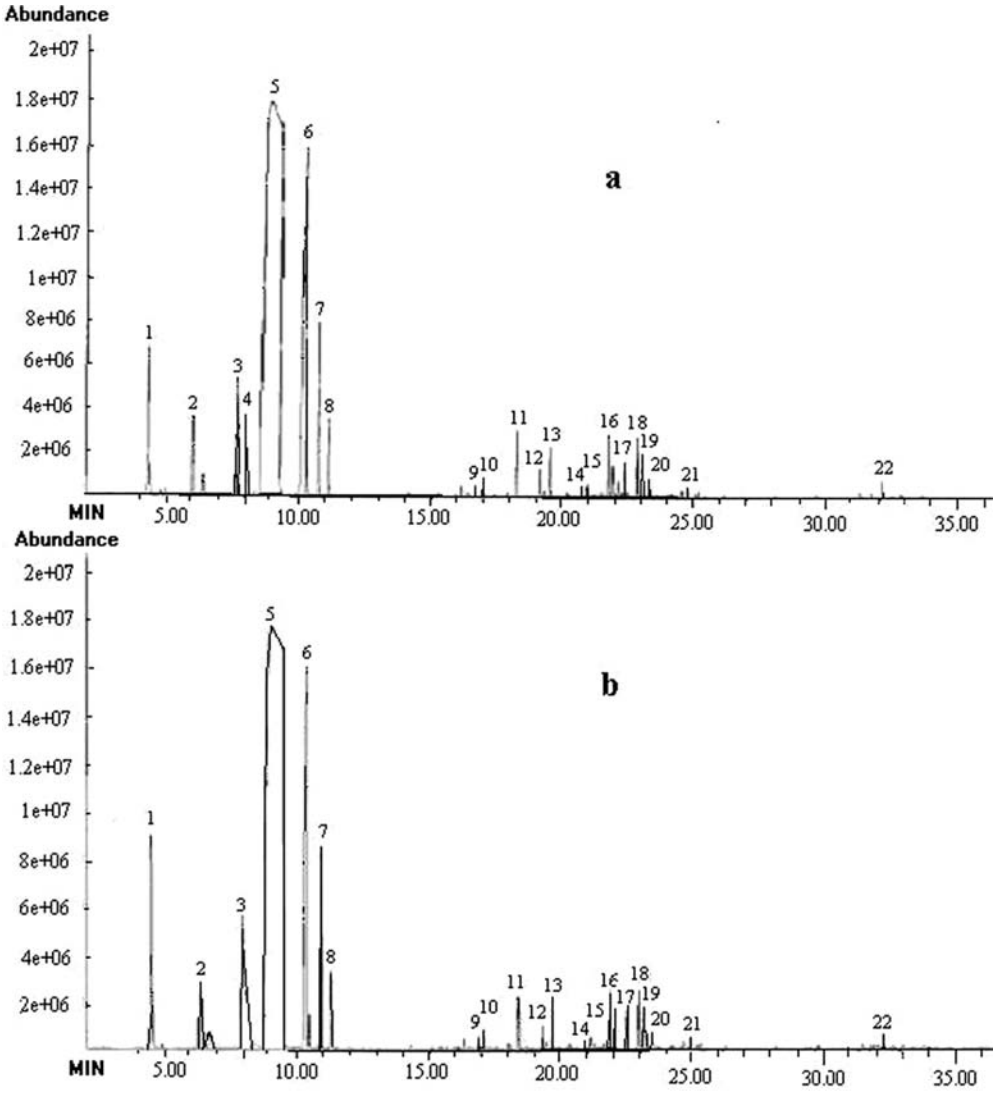


**Figure 2.** GC chromatograms of essential oils of orange peel from hydrodistilled methods: (a) ICT; (b) CT. Component numbers of chromatograms are from Table 1.

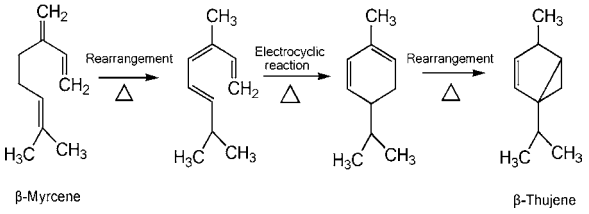


**Figure 3.** Possible pathway of $\beta$-thujene formation from $\beta$-myrcene.

cooling collector of essential oils in ICT can markedly reduce volatilization of $\gamma$-terpinene. Maybe ICT can also reduce the formation of other compounds from $\gamma$-terpinene[26] in comparison with CT.

In general, as a cooling collector was added the CT, the low temperature of the oil collector in ICT can significantly increase the yield rates of essential oils ($p < 0.05$) compared to CT. In addition, ICT avoided the transformation of $\beta$-myrcene to $\beta$-thujene, improved the yield rate of $\gamma$-terpinene, and reduced the thermal reaction on $\alpha$-pinene and $\beta$-pinene of oil in comparison to CT. Thus, ICT is an effective improvement to traditional CT.

## AUTHOR INFORMATION


### Corresponding Author

*(Y.X.) Phone: + 86 20 37219162. Fax: + 86 20 87236354. E-mail: xyj6510@126.com.



### Funding

We are very grateful for the financial support from the key projects in key fields of Guangdong Province, China (Grants 2007A020901004 and 2009B020311008).


### Notes

The authors declare no competing financial interest.

## REFERENCES


(1) Raeissi, S.; Diaz, S.; Espinosa, S.; Peters, C. J.; Brignole, E. A. Ethane as an alternative solvent for supercritical extraction of orange peel oils. *J. Supercrit. Fluids* **2008**, *45*, 306−313.

(2) Dugo, G.; Di Giacomo, A. In *Citrus—The Genus Citrus; Essential Oil Production*; Taylor Francis Publishing: London, UK, 2002; pp 115−140.

(3) Houghton, P. J.; Raman, A. *Laboratory Handbook for Fractionation of Natural Extracts*; Chapman and Hall: London, UK, 1998; 199 pp.

(4) Baker, G. R.; Lowe, R. F.; Southwell, I. A. Comparison of oil recovered from tea tree by ethanol extraction and steam distillation. *J. Agric. Food Chem.* **2000**, *48*, 4041−4043.
(5) Donelian, A.; Carlson, L. H. C.; Lopes, T. J.; Machado, R. A. F. Comparison of extraction of patchouli (*Pogostemon cablin*) essential oil with supercritical $CO_2$ and by steam distillation. *J. Supercrit. Fluids* **2009**, *48*, 15−20.
(6) Krell, E. *Handbook of laboratory Distillation: Techniques and Instrumentation in Analytical Chemistry*, 2nd ed.; Elsevier Scientific Publishing: Amsterdam, The Netherlands, 1982; Vol. 2.
(7) Clevenger, J. F. Apparatus for the determination of volatile oil. *J. Am. Pharm. Assoc.* **1928**, *17*, 345.
(8) Masango, P. Cleaner production of essential oil by steam distillation. *J. Clean. Prod.* **2004**, *13*, 833−839.
(9) Gao, B.; Chen, Y. L.; Zhang, M. W.; Xu, Y. J.; Pan, S. Y. Chemical composition, antioxidant and antimicrobial activity of *Pericarpium Citri Reticulatae* essential oil. *Molecules* **2011**, *16*, 4082−4096.
(10) Ferhat, M. A.; Meklati, B. Y.; Smadja, J.; Chemat, F. An improved microwave Clevenger apparatus for distillation of essential oils from orange peel. *J. Chromatogr., A* **2006**, *1112*, 121−126.
(11) Skaltsa, H. D.; Demetzos, C.; Lazari, D.; Sokovic, M. Essential oil analysis and antimicrobial activity of eight *Stachys* species from Greece. *Phytochemistry* **2003**, *64*, 743−752.
(12) Temelli, F.; Chen, C. S.; Braddock, R. J. Supercritical fluid extraction in citrus oil processing. High-pressure $CO_2$ system concentrates aroma and flavor compounds in citrus oils. *Food Technol.* **1988**, *42*, 145−150.
(13) Adam, R. P. *Identification of Essential Oils Components by Gas Chromatography/Quadrupole Mass Spectroscopy*; Allured Publishing: Carol Stream, IL, USA, 2001.
(14) Yang, E. J.; Kim, S. S.; Oh, T. H.; Baik, J. S.; Lee, N. H.; Hyun, C. G. Essential oil of citrus fruit waste attenuates LPS-induced nitric oxide production and inhibits the growth of skin pathogens. *Int. J. Agric. Biol.* **2009**, *11*, 791−794.
(15) Elson, C. E.; Yu, S. G. The chemoprevention of cancer by mevalonate-derived constituents of fruits and vegetables. *J. Nutr.* **1994**, *124*, 607−614.
(16) Lota, M.; De Rocca Serra, D.; Tomi, F.; Casanova, J. Chemical variability of peel and essential oils of 15 species of mandarins. *Biochem. Syst. Ecol.* **2001**, *29*, 77−104.
(17) Eggersdorfer, M. *Ullmann's Encyclopedia of Industrial Chemistry*, 6th ed.; Wiley-VCH: Weinheim, Germany, 2002; Vol. 35, pp 653−671.
(18) Erman, W. F. Studies in organic chemistry. *Chemistry of the Monoterpenes: An Encyclopedic Handbook, Parts A and B*; Dekker: New York, 1985.
(19) Stolle, A.; Ondruschka, B.; Hopf, H. Thermal rearrangements of monoterpenes and monoterpenoids. *Helv. Chim. Acta* **2009**, *92*, 1673−1719.
(20) Goldschmidt, Z.; Crammer, B. Vinylcyclopropane rearrangements. *Chem. Soc. Rev.* **1988**, *17*, 229−267.
(21) Leber, P. A.; Baldwin, J. E. Thermal [1,3]carbon sigmatropic rearrangements of vinylcyclobutanes. *Acc. Chem. Res.* **2002**, *35*, 279−287.
(22) Gajewski, J. J. *Hydrocarbon Thermal Isomerizations*, 2nd ed.; Elsevier: London, UK, 2004.
(23) Hoffmann, R.; Woodward, R. B. The conservation of orbital symmetry. *Acc. Chem. Res.* **1968**, *1*, 17−22.
(24) Mcgraw, G. W.; Hemingway, R. W.; Ingram, L. L., Jr.; Canady, C. S.; Mcgraw, W. B. Thermal degradation of terpenes: camphene, $\Delta^3$-carene, limonene, and $\alpha$-terpinene. *Environ. Sci. Technol.* **1999**, *33*, 4029−4033.
(25) Rezzoug, S.-A.; Louka, N. Thermomechanical process intensification for oil extraction from orange peels. *Innovative Food Sci. Emerging. Technol.* **2009**, *10*, 530−536.
(26) Aschmann, S. M.; Arey, J.; Atkinson, R. Formation of *p*-cymene from OH + $\gamma$-terpinene: H-atom abstraction from the cyclohexadiene ring structure. *Atmos. Environ.* **2011**, *45*, 4408−4411.

JOURNAL OF AGRICULTURAL AND FOOD CHEMISTRY

Article

pubs.acs.org/JAFC

# A Novel Fluorescent Conjugate Applicable To Visualize the Translocation of Glucose−Fipronil

Jie Wang,[†,‡,§] Zhiwei Lei,[†,‡,§] Yingjie Wen,[†,‡] Genlin Mao,[†,‡] Hanxiang Wu,[†,‡] and Hanhong Xu*[,†,‡]

[†]State Key Laboratory for Conservation and Utilization of Subtropical Agro-bioresources and [‡]Key Laboratory of Natural Pesticide and Chemical Biology, Ministry of Education, South China Agricultural University, Guangzhou, 510642, Guangdong China

Supporting Information

**ABSTRACT:** The ability to visualize the movement of glycosyl insecticides contributes to learning their translocation and distribution in plants. In our present work, a novel fluorescent glucose−fipronil conjugate *N*-[3-cyano-1-[2,6-dichloro-4-(trifluoromethyl)phenyl]-4-[(trifluoromethyl)sulfinyl]-1*H*-pyrazol-5-yl]-1-(2-[*N*-(7-nitrobenz-2-oxa-1,3-diazol-4-yl)amino]-2-deoxy-β-D-glucopyranosyl)-1*H*-1,2,3-triazole-4-methanamine (2-NBDGTF), was obtained via click chemistry. Disk uptake experiments showed that an active carrier-mediated system was involved in the 2-NBDGTF uptake process. Meanwhile, 2-NBDGTF exhibited comparable phloem mobility with GTF in castor bean seedlings. Visualization of 2-NBDGTF uptake and transport experiment showed that this fluorescent glucose−fipronil conjugate could be loaded into sieve tubes after transiting through epidermal cells and mesophyll cells and then translocate from cotyledon to hypocotyl via phloem in castor bean seedlings. The results above determined that it is a promising fluorescence tagging approach for revealing the activities of glycosyl insecticides and 2-NBDGTF is a reasonable and feasible fluorescent surrogate of GTF for tracing the distribution of glucose−fipronil conjugates.

**KEYWORDS:** *visualization, carrier-mediated, phloem mobility, fluorescence tagging, castor bean*

## INTRODUCTION

Insecticides with phloem mobility are desirable for controlling piercing and sucking insects as well as vascular insects in agriculture. Despite the positive implications of such insecticides, only a few phloem mobile or ambimobile insecticides are currently available. An optional strategy used in developing phloem-mobile pesticides is to chemically modify parent pesticides. Such modifications include sugar conjugation, acid functionalization, and formation of quaternary salts from the parent pesticides.[1] The addition of carboxyl groups to immobile or poorly mobile pesticides has proven to be an efficient method of imparting phloem mobility to parent pesticides.[2,3] The conjugation of parent pesticides to endogenous substances, such as amino acids and monosaccharides, is another approach that is used for developing propesticides with phloem mobility.[4,5]

In our previous work, we demonstrated that the glucose−fipronil conjugate *N*-[3-cyano-1-[2,6-dichloro-4-(trifluoromethyl)phenyl]-4-[(trifluoromethyl)sulfinyl]-1*H*-pyrazol-5-yl]-1-(β-D-glucopyranosyl)-1*H*-1,2,3-triazole-4-methanamine (GTF) exhibits moderate phloem mobility in the phloem of castor bean seedlings.[6] That the hydroxyl of the monosaccharide significantly affects the phloem mobility of the monosaccharide−fipronil conjugates was also demonstrated using castor bean seedlings.[7] Additionally, the uptake and transport of GTF within castor bean seedlings demonstrated the involvement of an active carrier-mediated mechanism.[8] Despite the progress made in this field, the uptake mechanisms of GTF analogues and the distribution within plants remain unknown. The ability to visualize GTF analogues within plants has great potential for addressing these questions.

Fluorescence tagging techniques are promising approaches to trace uptake pathways, transport routes, and distributions of xenobiotics within plants. Compared with radiolabeling techniques, which have been widely used to investigate the uptake and translocation of xenobiotics,[9,10] fluorescence tagging offers both high spatial and temporal resolution. Moreover, the use of fluorescence tagging could provide dynamic and real-time information on xenobiotics at the cellular level. In order to visualize transport of xenobiotics within plants, several studies were performed using various fluorescent dyes with similar physicochemical properties.[11,12] Recently, fluorescently labeled plant hormones were used to reveal the distribution and signaling receptor of hormones within plants.[13,14]

To visualize the uptake activity and translocation of GTF analogues in plants, a novel fluorescently labeled GTF derivative was synthesized with the modification of an NBD moiety at the C-2 position of the glucose−fipronil conjugate (Figure 1). The uptake mechanism and the phloem mobility of

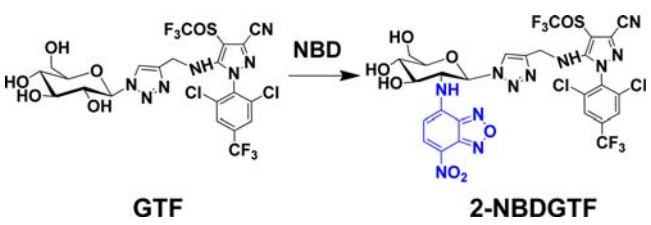


**Figure 1.** Structures of GTF and 2-NBDGTF.

**Received:** April 29, 2014
**Accepted:** August 18, 2014
**Published:** August 18, 2014

ACS Publications © 2014 American Chemical Society

**Scheme 1. Synthesis of 2-NBDGTF; Reaction conditions: 1.1 $CF_3COOC_2H_5$, $Et_3N$, MeOH; 1.2 $SnCl_4$, $TMSN_3$, $CH_2Cl_2$; 1.3 $CuSO_4{\cdot}5H_2O$, sodium ascorbate; 1.4 MeOH, NaOMe; 1.5 1M NaOH; 1.6 NBD-Cl, $K_2CO_3$, MeOH**

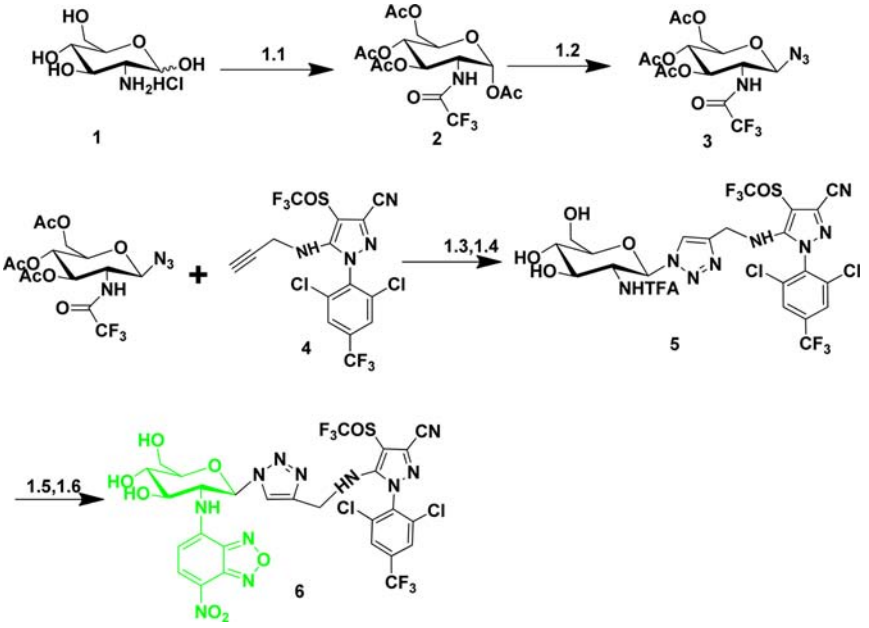


2-NBDGTF were investigated to prove that the fluorescent glucose−fipronil derivative 2-NBDGTF is a reasonable fluorescent GTF surrogate. Then 2-NBDGTF was used to visualize the movement of GTF analogues within castor bean seedlings using confocal laser scanning microscopy.

## MATERIALS AND METHODS

**General Information.** Reagents and anhydrous solvents were used directly. Melting points were determined on an FP62 digital micro melting point apparatus; data were left uncorrected. NMR spectra were obtained from a Bruker AV-600 instrument. Deuterated solvents were obtained from Cambridge Isotope Laboratories (Andover, MA). $CD_3OD$ and $CDCl_3$ solvent peaks (3.31 and 7.26 ppm for 1H; 49.0 and 77.0 ppm for 13C, respectively) were used as internal chemical shift references. The mass spectra (MS) of new compounds were obtained by Bruker maXis with an electrospray ionization (ESI) spectrometer. Silica gel was used for column chromatography. GTF was prepared according to our previously described procedure.[6] The compounds to be added to the incubation medium were purchased from Sigma [carbonyl cyanidem-chlorophenylhy-drazone (CCCP)] and Aladdin (phloridzin, MES, and mannitol).

**Chemicals (Scheme 1).** *1,3,4,6-Tetra-O-acetyl-2-deoxy-2-trifluoroacetamido-α-D-glucopyranoside (2).* 2-Deoxy-2-trifluoroacetamido-D-glucopyranose (2 g, 7.24 mmol) was dissolved in pyridine (15 mL) and acetic anhydride (5 mL). The reaction mixture was kept at room temperature overnight and poured into ice water and stirred for 1 h. The mixture was extracted with dichloromethane, and the organic layer was washed with 1 M HCl and saturated aqueous $NaHCO_3$ and dried on $Na_2SO_4$. The solution was concentrated and purified by silica gel column chromatography to obtain a light yellow solid. Slightly yellow solid: yield 78%; mp 123.5 °C; $^1$H NMR (600 MHz, $CDCl_3$) $\delta$ 6.27 (d, $J$ = 3.9 Hz, 1H), 5.32 (br,1H), 5.22 (dd, $J$ = 10.0 Hz, 10.0 Hz, 1H), 4.44 (m, 1H), 4.28 (dd, $J$ = 12.0 Hz, 4.2 Hz, 1H), 4.07 (dd, $J$ = 12.0, 2.2 Hz, 1H), 4.04 (m, 1H), 2.19 (s, 3H), 2.09 (s, 3H), 2.06 (s, 3H), 2.05 (s, 3H); $^{13}$C NMR (150 MHz, $CDCl_3$) $\delta$ 171.8, 170.6, 169.0, 168.2, 157.7, 116.7, 89.4, 69.8, 69.8, 67.0,61.3, 52.2, 20.7, 20.6, 20.5, 20.4; ESI-MS, $m/z$ 442.2 $[M - H]^-$.

*3,4,6-Tetra-O-acetyl-2-trifluoroacetamido-2-deoxy-β-D-glucopyranosyl Azide (3).* Compound **2** (170 mg, 0.384 mmol) and azidotrimethylsilane (TMS-$N_3$, 56 μL, 0.423 mmol) were dissolved in anhydrous $CH_2Cl_2$ (5 mL), and $SnCl_4$ (45 μL, 0.384 mmol) was added dropwise. The resulting mixture was stirred at room temperature until TLC indicated the disappearance of starting material (about 2 h). The mixture was extracted with $CH_2Cl_2$ (3 × 20 mL) and then washed with $NaHCO_3$ (3 × 20 mL) and water (20 mL). The organic layer was dried ($Na_2SO_4$) and filtered, and the solvent was evaporated under reduced pressure. The residue was purified by flash chromatography (petroleum ether:ethyl acetate = 2:1) to give **3**. Needle solid: yield 75%; $^1$H NMR (600 MHz, $CDCl_3$) $\delta$ 7.17 (d, $J$ = 8.8 Hz, 1H), 5.39−5.27 (m, 1H), 5.10 (t-like, $J$ = 9.7 Hz, 1H), 4.81 (d, $J$ = 9.2 Hz, 1H), 4.28 (dd, $J$ = 12.5, 5.0 Hz, 1H), 4.20 (dd, $J$ = 12.5, 2.2 Hz, 1H), 4.03 (dd, $J$ = 19.7, 9.4 Hz, 1H), 3.88 (ddd, $J$ = 10.0, 4.9, 2.3 Hz, 1H), 2.10 (s, 3H), 2.04 (s, 3H), 2.03 (s, 3H); $^{13}$C NMR (150 MHz, $CDCl_3$) $\delta$ 171.41, 170.95, 169.49, 157.78, 115.61, 87.82, 74.14, 71.72, 68.30, 61.96, 54.35, 20.81, 20.67, 20.46.

*N-[3-Cyano-1-[2,6-dichloro-4-(trifluoromethyl)phenyl]-4-[(trifluoromethyl)sulfinyl]-1H-pyrazol-5-yl]-1-(2-trifluoroacetamido-2-deoxy-β-D-glucopyranosyl)-1H-1,2,3-triazole-4-methanamine (5).* Fipronil-alkyne **4** (474 mg, 1 mmol) was added to a vigorously stirred suspension of compound **2** (426 mg, 1 mmol) in 3 mL of *tert*-butyl alcohol. The reaction was initiated by the addition of a solution of $CuSO_4{\cdot}5H_2O$ (100 mg, 0.4 mmol) and sodium ascorbate (173 mg, 0.8 mmol) in distilled water (3 mL). The deep yellow suspension was stirred vigorously at 50 °C for 3 h. Distilled water (10 mL) was added, and the aqueous layer was extracted with chloroform (10 mL × 3). The combined organic extracts were washed with aqueous sodium hydrogen carbonate and brine, dried with sodium sulfate, filtered, and evaporated in vacuo. The crude compound was added to a solution of sodium methoxide in dry methanol (0.05 M, 15 mL). The resultant solution was stirred for 30 min at room temperature. The mixture was neutralized with Amberlite IR 120 ($H^+$) resin and filtered, and the filtrate was then evaporated. The residues were purified by column chromatography to obtain compound **5**. White solid: yield 78%; $^1$H NMR (600 MHz, MeOD) $\delta$ 8.12 (s, 1H), 8.09* (s, 1H), 8.06 (dd, $J$ = 7.6, 6.3 Hz, 2H), 5.88 (d, $J$ = 5.7 Hz, 1H), 5.86* (d, $J$ = 5.7 Hz, 1H), 4.64 (d, $J$ = 4.1 Hz, 1H), 4.62* (d, $J$ = 4.1 Hz, 1H), 4.45 (d, $J$ = 2.3 Hz, 1H), 4.43* (d, $J$ = 2.3 Hz, 1H), 4.30 (t, $J$ = 7.3 Hz, 1H), 4.27* (t, $J$ = 7.3 Hz, 1H), 3.92 (t-like, 1H), 3.90 (t-like, 1H), 3.84−3.73 (m, 2H), 3.63−3.55 (m, 2H); $^{13}$C NMR (150 MHz, MeOD) $\delta$ 157.93, 150.54, 144.27, 136.57, 136.45, 134.68, 126.63, 126.54, 126.44, 124.42, 123.12, 121.47, 116.66, 114.76, 110.79, 96.26, 85.99, 79.92, 79.90*, 73.76, 73.66*, 69.88, 69.88*, 60.77, 60.74*, 55.75, 55.65*, 39.66, 39.59* (*enantiomer); ESI-MS, $m/z$ 807.4 $[M - H]^-$.


dx.doi.org/10.1021/jf502838m | J. Agric. Food Chem. 2014, 62, 8791−8798

*N-[3-Cyano-1-[2,6-dichloro-4-(trifluoromethyl)phenyl]-4-[(trifluoromethyl)sulfinyl]-1H-pyrazol-5-yl]-1-(2-[N-(7-nitrobenz-2-oxa-1,3-diazol-4-yl)amino]-2-deoxy-β-D-glucopyranosyl)-1H-1,2,3-triazole-4-methanamine (**6**).* Compound **5** (774 mg, 1 mmol) was dissolved in 1 M NaOH (5 mL) and was stirred for 5 h. The mixture was extracted with ethyl acetate, dried on $Na_2SO_4$, and filtered, and the filtrate was evaporated. The residue and $K_2CO_3$ (140 mg, 2.5 mmol) were suspended in methanol (3 mL), and the reaction mixture was cooled to 0 °C on an ice bath. To the suspension was added in small portions NBD-Cl (300 mg, 1.5 mmol), and the reaction mixture was kept at room temperature for another 12 h. Solvent was evaporated under reduced pressure, and the crude product was purified by TLC. Red brown solid: yield 68%; $^1$H NMR (600 MHz, MeOD) $\delta$ 8.40 (d, $J$ = 8.8 Hz, 1H), $\delta$ 8.40* (d, $J$ = 8.8 Hz, 1H), 8.20 (s, 1H), 8.17* (s, 1H), 7.96 (m, 2H), 6.46 (d, $J$ = 8.8 Hz, 1H), 6.43* (d, $J$ = 8.8 Hz, 1H), 6.01* (d, $J$ = 9.5 Hz, 1H), 5.99* (d, $J$ = 9.5 Hz, 1H), 4.60 (s-like, 1H), 4.51 (dd, $J$ = 16.5, 4.86 Hz, 1H), 4.30 (dd, $J$ = 16.5, 9 Hz, 1H), 3.95 (dd, $J$ = 12.1, 3.8 Hz, 1H), 3.96* (dd, $J$ = 12.1, 3.8 Hz, 1H), 3.91−3.85 (m, 1H), 3.81 (dd, $J$ = 12.1, 7.7 Hz, 1H), 3.81* (dd, $J$ = 12.1, 7.4 Hz, 1H), 3.70−3.65 (m, 2H); $^{13}$C NMR (150 MHz, MeOD) $\delta$ 151.7, 146.2, 145.72, 145.5, 145.2, 137.8, 137.7, 137.6*, 136.2, 136.0, 135.9, 127.9, 127.8, 127.8, 124.5, 123.5, 123.3, 122.6, 112.1, 112.0, 97.4, 81.4, 77.5, 77.2*, 71.1, 62.2, 56.0, 40.7, 40.5* (*enantiomer); ESI-MS, $m/z$ 842.0499 $[M + H]^+$, 840.0331 $[M - H]^-$.

**Plant Materials.** Castor bean seeds (No. 9) were obtained from the Agricultural Science Academy of Zibo Shandong China. The seeds were treated and grown as previously described.[8] Six day old seedlings were selected for the further experiments.

**Uptake by *Ricinus communis* Foliar Disks.** Disks were obtained and treated with incubation medium containing 20 mM MES (pH 5.6), 250 mM mannitol, 0.25 mM $MgCl_2$, and 0.5 mM $CaCl_2$ as described formerly.[8,15] Then the disks were transferred to the incubation medium supplemented with 2-NBDGTF to perform the time-course uptake experiment and to investigate the concentration dependence of 2-NBDGTF uptake. Disks were incubated with incubation medium, pH ranging from 4.0 to 8.0, to investigate the pH dependence, and treated at 4 or 28 °C to examine the temperature effect on the 2-NBDGTF uptake. For the inhibition experiments, the disks were preincubated with 50 μM CCCP, 1 mM phloridzin, 1 mM GTF, and 2 mM monosaccharide (glucose, xylose, arabinose, mannose, and galactose) in the incubation medium for 30 min, respectively. Then the disks were coincubated with 50 μM 2-NBDGTF and these substrates for 1 h. Incubation was run under mild agitation on a reciprocal shaker at 28 °C. After the total incubation period, the disks were rinsed using the incubation solution three times to remove the residuals. Then the disks were freeze-dried using liquid nitrogen and then ground with 10 mL of methanol and ultrasonically treated for 30 min. The extract solutions were centrifuged at 12000 rpm/min for 10 min and then filtered with 0.22 μm filter. Then the extract solution was analyzed by HPLC system (Shimadzu, Japan).

**Phloem Sap Collection.** As described previously,[6] the cotyledons, from which the endosperm had been removed, were incubated in the buffer solution containing test compound 2-NBDGTF at a 100 μM concentration. GTF synthesized in our previous work was set as the positive control in this experiment. The roots of seedlings were immersed in 0.5 mM $CaCl_2$ solution. After 1 h of incubation, the hypocotyl was severed in the hook region for phloem exudation. The interval of phloem sap collection was 1 h, and the duration was 5 h. The collected phloem sap was quantified by an HPLC system after dilution with pure water (phloem sap/pure water, 1/4, v/v).

**Visualization of Cotyledon Uptake and Translocation of 2-NBDGTF in *R. communis* Seedlings.** Visualization of uptake and translocation of 2-NBDGTF was investigated using 6 day old castor bean seedlings as described in our previous work.[16] After treatment with 100 μM 2-NBDGTF incubation solution, cotyledons and stems were excised at 1 h, 2 h, and 3 h and washed thoroughly with incubation solution to remove the residual conjugate. Freehand cross sections of midveins and petioles were taken from the treated cotyledons, and sections of hypocotyl were immediately taken above the hook. Then sections were observed with confocal laser scanning microscopy (Zeiss LSM780, Germany) directly. Photos of at least five sections from each treatment were taken with a 10× or 20× Plan-Apochromat (0.8 M27) objective using an argon laser with 488 nm excitation and 500−535 nm emission filter.

**Determination of 2-NBDGTF.** Disk extracts and phloem sap were analyzed using an HPLC system (Shimadzu, Japan) equipped with a LC-20A fluorescence detector. The fluorescence detection conditions of 2-NBDGTF were excitation at 470 nm and emission at 530 nm. The determination of GTF was performed with a HP 1100 (Agilent) HPLC system. Separations were made with a C8 reversed-phase column. The solvent system consisted of acetonitrile and water (60:40, v/v). The injection volume was 10 μL, and the flow rate was 1 mL/min. The calibration curve of 2-NBDGTF (ranging from 1 μM to 100 μM, $r$ = 0.999) and GTF (ranging from 2.5 μM to 100 μM, $r$ = 0.998) was linear.

The presence of 2-NBDGTF in disk extracts and phloem sap was further identified by HPLC−HRMS (high resolution mass spectrometry) (Bruker maXis, Germany) using electrospray ionization. The mass spectrometer was operated in the positive electrospray ionization mode ($ESI^+$). The HPLC system was an Agilent 1290 Infinity LC system which was equipped with a diode array detector. The operating conditions of the HPLC were the same as described above.

**Physicochemical Properties.** Physicochemical properties [molecular mass (MW), ionization constant in aqueous solution ($pK_a$), octanol/water partitioning coefficient (log $K_{ow}$)] of GTF and 2-NBDGTF were predicted using ACD LogD suite version 14.0 software. The chemical structures of conjugates 2-NBDGTF and GTF are shown in Figure 1, and the physicochemical properties of 2-NBDGTF are summarized in Table 1. The excitation and emission fluorescence spectra are shown in Figure 2.

**Table 1. Properties of the Tested Conjugates[a]**

| properties | GTF | 2-NBDGTF |
|---|---|---|
| mol wt | 680.4 | 842.5 |
| LogP | 2.06 | 3.31 |
| $pK_a$ | 12.8 ± 0.7 (acid) | 12.8 ± 0.7 (acid) |

[a]The value of log $K_{ow}$ and $pK_a$ of GTF and 2-NBDGTF were predicted by ACD Laboratories Percepta program, version 14.0. Log $K_{ow}$ and $pK_a$ value was classic value.

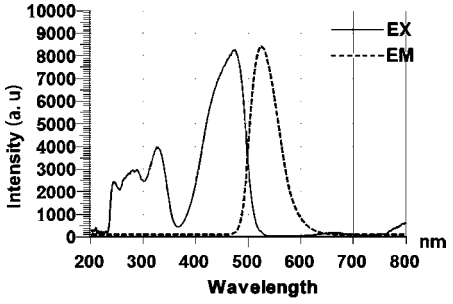


**Figure 2.** Excitation and emission fluorescence spectra of fluorescent conjugate 2-NBDGTF. The maximum fluorescence excitation wavelength was at 470 nm, and the maximum emission wavelength was at 530 nm.

## RESULTS AND DISCUSSION

**Synthesis of 2-NBDGTF.** As outlined in Scheme 1, glucosamine hydrochloride was chosen as starting material, and the amino group was protected by the trifluoroacetyl group to obtain compound **2**. Reaction of compound **2** and TMS-$N_3$ in the presence of $SnCl_4$ afforded compound **3**.[17] Compound **5** was synthesized via click chemistry by introducing an azide group or an alkyne moiety to the corresponding compounds **3**

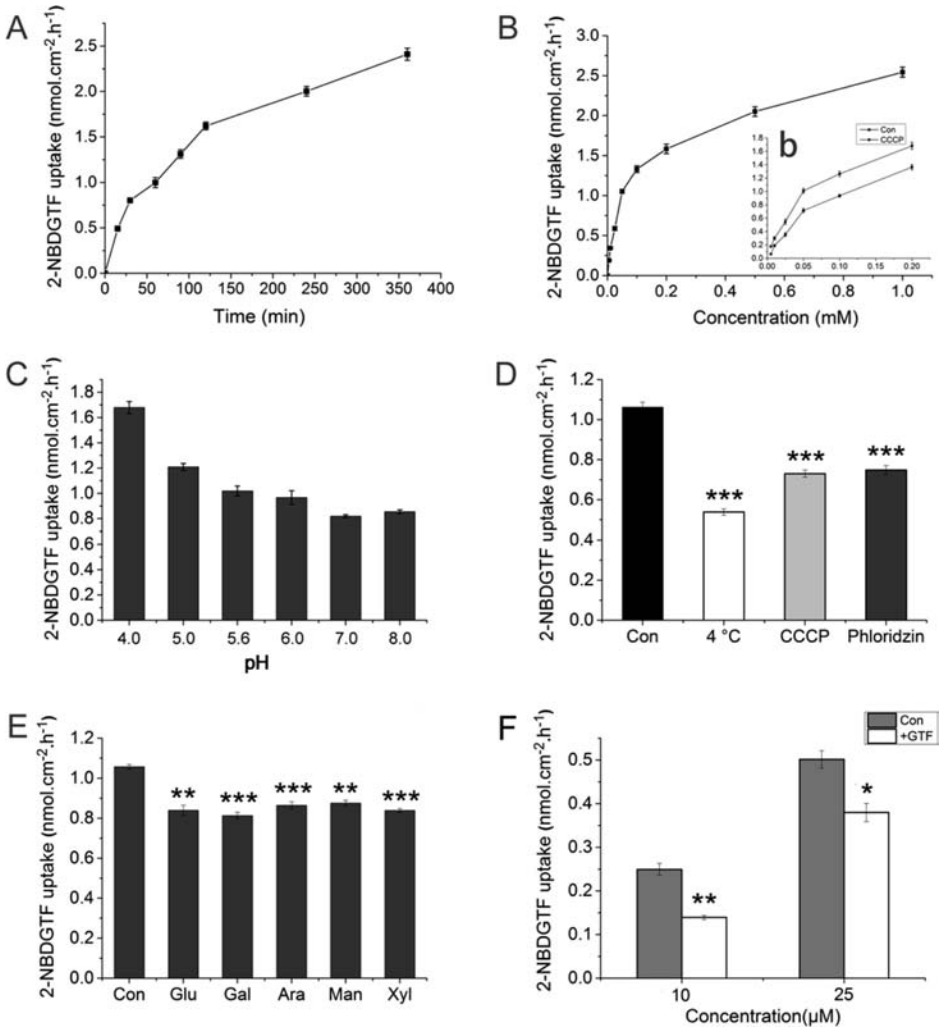


**Figure 3.** Uptake of 2-NBDGTF by cotyledon disks obtained from castor bean seedlings. (A) Time course of 2-NBDGTF uptake by disks. Disks were incubated in a buffered solution containing 50 $\mu$M 2-NBDGTF at pH 5.6. Shown are the averages of 12 disks ± SE ($n$ = 4). (B) Concentration dependence of 2-NBDGTF uptake. Disks were incubated in a buffered solution at pH 5.6 containing 2-NBDGTF concentration ranged from 0.005 mM to 1 mM. Disks coincubated with 50 $\mu$M CCCP were set as the complementary set (b). Each point was the mean of 12 disks ± SE ($n$ = 6). (C) pH dependence of 2-NBDGTF uptake by disks. Each bar represents the mean of 12 disks ± SE ($n$ = 4). (D) Effect of low temperature (4 °C) and inhibitor (50 $\mu$M CCCP and 1 mM phloridzin) on the 2-NBDGTF uptake. Each bar represents the mean of 12 disks ± SE ($n$ = 5). (E) Effect of 2 mM monosaccharides on the uptake of 50 $\mu$M 2-NBDGTF at pH 5.6. Data are mean of 12 disks ± SE ($n$ = 4). (F) Effect of 1 mM GTF on the uptake of 2-NBDGTF. Shown are the averages of 12 disks ± SE ($n$ = 4). Statistical analysis was performed using the ANOVA test, and Dunnett's test was used to analyze differences in the mean of each group with control group. *, $p < 0.05$; **, $p < 0.01$; ***, $p < 0.001$.

and **4**. NaOMe/MeOH was used to remove the acetyl and trifluoroacetyl groups. However, the trifluoroacetyl group remained intact after reaction to get compound **5**. The trifluoroacetyl group was finally deprotected with 1 M NaOH solution and then reacted with NBD-Cl to obtain target product 2-NBDGTF.

All products were identified by $^{1}$H and $^{13}$C NMR spectroscopy and mass spectrometry. The $^{1}$H NMR spectra of these compounds are complicated because fipronil has a symmetrical sulfoxide and forms two enantiomers.[18,19] Their configurations were confirmed on the basis of a chemical shift, coupling constants, and band shape of H-1. For example, the NMR signals of product 2-NBDGTF were immediately measured after the dissolution of the glucosyl conjugates in denatured methanol.

The doublet, observed at 6.01 and $J_{1,2}$ = 9.5 Hz, was assigned to H-1 of the $\beta$-D-pyranose anomer. The synthesized compound $C_{27}H_{19}Cl_2F_6N_{11}O_8S$ (2-NBDGTF) was further identified by HRMS-ESI analysis (calculated for 2-NBDGTF $[M + H]^+$, 842.0420; found, 842.0499;). From these results, the synthesized product was identified as 2-NBDGTF.

**The Foliar Disk Uptake of 2-NBDGTF Is Carrier-Mediated.** When castor bean foliar disks were incubated with buffer solution supplemented with 50 $\mu$M 2-NBDGTF at pH 5.6 for up to 360 min, the rate of 2-NBDGTF uptake increased rapidly and almost linearly during the 120 min incubation period and then decreased until 360 min (Figure 3A). The results suggested that the uptake of 2-NBDGTF will reach equilibrium rapidly with increasing incubation times.

To investigate the concentration dependence of 2-NBDGTF uptake, castor bean foliar disks were incubated with buffer solution supplemented with 2-NBDGTF at concentrations ranging from 0.005 to 1 mM for 1 h. Concentration dependence data clearly show that there were two components involved in 2-NBDGTF uptake. The first component is a saturable component that occurs between 0.005 and 0.2 mM,


dx.doi.org/10.1021/jf502838m | J. Agric. Food Chem. 2014, 62, 8791−8798

suggesting that part of 2-NBDGTF uptake is carrier-mediated at low concentrations. The second component is a roughly linear component at higher concentrations, indicating the existence of passive diffusion (Figure 3B). Upon cotreatment with 50 $\mu$M CCCP, which is widely utilized in studies of transmembrane transport to dissipate the proton motive force,[8,15,20] the saturable component of 2-NBDGTF uptake appeared to be apparently inhibited (Figure 3b). To study the pH effect of incubation medium on 2-NBDGTF uptake, the disks were incubated with different pH buffer solution (pH ranging from 4.0 to 8.0). The results showed that uptake of 2-NBDGTF was sensitive to pH changes in the incubation medium. The uptake of 2-NBDGTF apparently increased with decreasing incubation pH, and the reduction of pH from 8.0 to 4.0 increased the uptake of 2-NBDGTF approximately 2-fold (Figure 3C). The results above confirmed that 2-NBDGTF uptake in lower concentrations is proton motive force dependent.

To further understand the uptake mechanism, the effect of temperature on 2-NBDGTF uptake was investigated. The uptake of 2-NBDGTF maintained at low temperature (4 °C) was reduced about 47% compared with normal incubation conditions (28 °C), suggesting that the 2-NBDGTF uptake machinery is energy dependent (Figure 3D). Phloridzin is an inhibitor of the sodium-linked glucose transporters,[21] and it is also used as an inhibitor of plant hexose transporter.[22,23] When treated with 1 mM phloridzin or 50 $\mu$M CCCP alone, the 2-NBDGTF uptake was remarkably decreased about 29% and 31%, respectively (Figure 3D). The results suggested that the 2-NBDGTF uptake machinery is also sensitive to phloridzin.

To clarify the competitive inhibition of substrates, the effect of monosaccharides on the uptake of 2-NBDGTF was investigated. At 2 mM concentration, both monosaccharides significantly inhibited 2-NBDGTF uptake by 10−15% (Figure 3E). In the case of the CCCP-sensitive component of the conjugate, the influx was only about 31% of the total uptake when the disks were incubated with 50 $\mu$M 2-NBDGTF. At 2 mM concentrations, these monosaccharides led to a 0.05 mM 2-NBDGTF uptake of the CCCP sensitive component, totaling 30−50%. In addition, the effect of GTF on 2-NBDGTF uptake was also evaluated. When treated with 1 mM GTF, the uptake of 2-NBDGTF was dramatically reduced about 42% at 10 $\mu$M and 24% at 25 $\mu$M, respectively (Figure 3F). The results above suggested that both monosaccharides and GTF exhibited strong competition with the uptake of 2-NBDGTF.

The characteristics of carrier-mediated transport mainly include that it is concentration dependent (saturable), subject to inhibition, more structure specific compared to passive transport, and cell type specific, which requires expression of the transporter.[24] In the present research, the disk results showed that the uptake of 2-NBDGTF was concentration dependent, energy dependent, and subject to CCCP and phloridzin inhibition and involved competitive inhibition of monosaccharides. Besides, GTF exhibited strong competition with the uptake of 2-NBDGTF. Altogether, these disk uptake results demonstrated the involvement of a carrier-mediated system in the 2-NBDGTF uptake process.

**Phloem Sap Determination of 2-NBDGTF.** Castor bean seedling is an ideal system to identify endogenous molecules moving in sieve tubes[25,26] and to evaluate phloem systemicity of xenobiotics.[27] Thanks to the cotyledon epidermis being thin and highly permeable and making contact with the external space directly, the system could respond to incubation with solutes readily. Therefore, the castor bean seedling system is employed to evaluate phloem mobility of 2-NBDGTF in the present work.

When the cotyledons were incubated in buffer solution containing 100 $\mu$M 2-NBDGTF, the conjugate was clearly detected in the phloem sap. Time-course experimental results indicated that the concentrations of 2-NBDGTF in the phloem sap increased almost linearly during the experimental period, which is consistent with GTF (Figure 4). The measured 2-

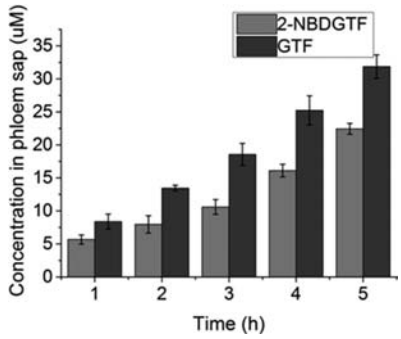


**Figure 4.** Time course of the concentration of conjugates 2-NBDGTF and GTF in *R. communis* phloem sap. The cotyledons were incubated in a buffered solution containing 100 $\mu$M 2-NBDGTF or GTF at pH 5.0. The hook of the hypocotyl was severed after 1 h incubation, and then the sap was collected per hour during 5 h. Each bar represents the mean of 12 plants ± SE, $n$ = 4.

NBDGTF concentrations in the phloem sap were 5.68 ± 0.69 $\mu$M, 10.61 ± 1.11 $\mu$M, and 22.45 ± 0.83 $\mu$M (mean ± SE) at 1 h, 3 h, and 5 h, respectively. These values represent GTF concentrations in the phloem sap of 0.68-fold, 0.64-fold, and 0.70-fold, respectively. The results showed that 2-NBDGTF exhibited comparable phloem mobility with GTF in castor bean seedlings.

Moreover, the fluorescent glucose−fipronil conjugate present in the foliar disk extracts and phloem sap at 5 h was further identified by HPLC−HRMS (high resolution mass spectrometry) analysis. Calculated for 2-NBDGTF ($C_{27}H_{19}Cl_2F_6N_{11}O_8S$) was $[M + H]^+$ 842.0420; and the found mass $[M + H]^+$ of 2-NBDGTF in disk extracts was 842.0482 (Supporting Information, Figure 1B) and in phloem sap was 842.0480 (Supporting Information, Figure 1D), respectively. These results established that it was the intact molecule that was detected in the disk extracts and phloem sap, indicating that the fluorescent molecule 2-NBDGTF was relatively stable during the experimental period.

The "Kleier model" was widely employed to predict the mobility of xenobiotics based on the physicochemical properties (log $P$ and p$K_a$).[3,28] Taking the given physicochemical properties into consideration, 2-NBDGTF is a compound ranging into the non-phloem-mobile area which is similar to GTF (Figure 5). However, 2-NBDGTF presented comparable phloem mobility with GTF in castor bean seedlings. Most xenobiotics fitted well into this model except for some xenobiotics whose transport was carrier-mediated. This inconsistency between the predicting results and phloem mobility test confirmed that 2-NBDGTF was an exception to the "Kleier model" and the involvement of a carrier-mediated system in the uptake process.

Introduction of fluorophores will inevitably bring some changes to physicochemical properties of the parent com-


dx.doi.org/10.1021/jf502838m | J. Agric. Food Chem. 2014, 62, 8791−8798

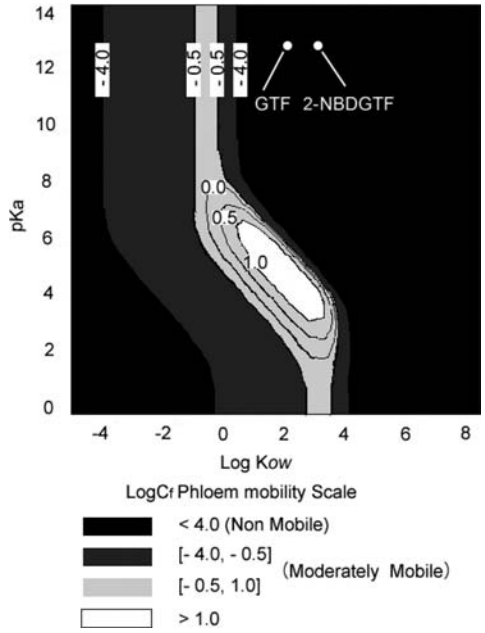


**Figure 5.** Prediction of phloem mobility of GTF and 2-NBDGTF using Kleier map;[1,32] log $K_{ow}$ and p$K_a$ values were calculated by ACD Laboratories Percepta program version 14.0.

pounds, including enlarging the molecular weight, increasing the octanol/water partitioning coefficient value, etc., which is consequently to have some effects on the parent compound characteristics. Compared with fluorescein (Fl) and Alexa Fluor 647 (AF), which have been employed successfully to label the gibberellins and castasterone,[13,14] NBD is a fluorophore with lower molecular weight and good cell permeability and thus has been widely utilized to label the glucose. The fluorescent conjugate of glucose 2-NBDG, fluorescently modified with a small fluorescent moiety NBD of glucose at the C-2 position, has been employed as a fluorescent glucose replacement and widely used to monitor the cellular glucose uptake activity.[29,30] It seems that the effect of the fluorescent tag NBD on the parent conjugate is tolerable. In comparison with GTF, 2-NBDGTF is indeed a compound with larger MW, and higher log *P* and HBA value (Table 1). Our results showed that the fluorescent conjugate 2-NBDGTF retained the carrier-mediated uptake mechanism and moderate phloem mobile property of GTF. Hence, 2-NBDGTF is regarded as a reasonable fluorescent surrogate of GTF and is believed to be capable of revealing the movement of glucose−fipronil analogues within plants.

**Visualization of Uptake and Transport of 2-NBDGTF in Castor Bean Seedlings.** The visualization of uptake and transport of 2-NBDGTF within castor bean seedlings was performed using confocal laser scanning microscopy (CLSM). The CLSM observation results showed the presence of remarkable fluorescence in epidermal cells and mesophyll cells (Figure 6B) of the midveins of the cotyledons treated with 2-NBDGTF for 1 h. Moreover, enormous fluorescence was observed present in the phloem. *Ricinus* is a symplastic−apoplastic loader, meaning that endogenous molecules from the seedling endosperm or incubation solution found in the phloem sap via the symplastic pathway may originate from the transfer cells of the lower epidermis. These molecules may have also been taken up directly from the phloem apoplast.[26,27] The observed results of the presence of remarkable

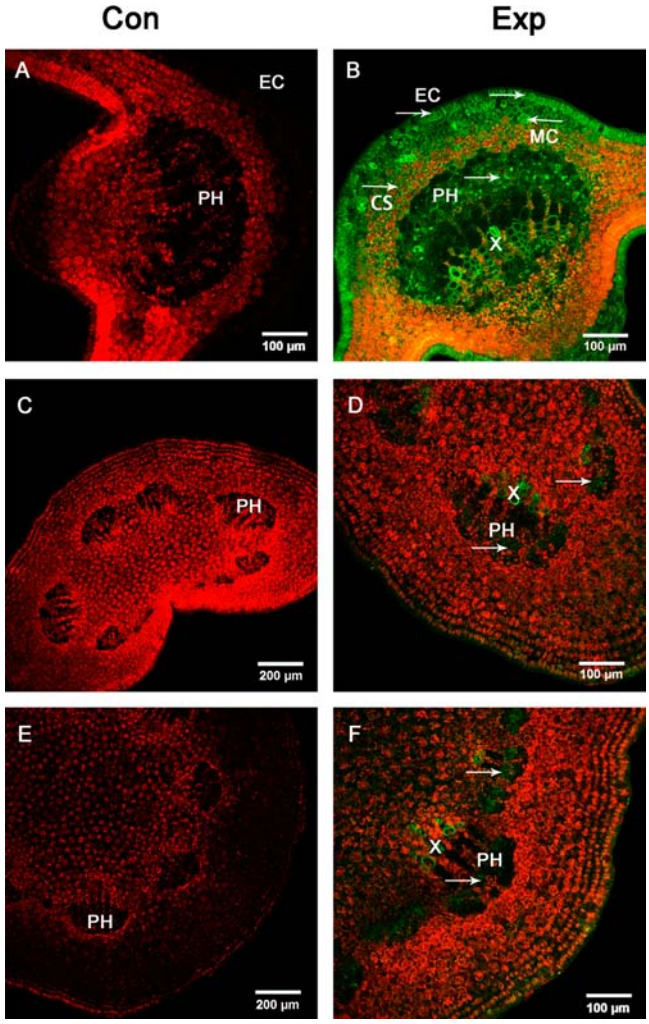


**Figure 6.** Representative fluorescence photographs of six day old caster bean seedlings: The cotyledons were incubated in a buffered solution containing 100 $\mu$M 2-NBDGTF. (A, B) Cross sections of midveins of cotyledons, (C, D) cross sections of petioles of cotyledons, and (E, F) cross sections of hypocotyl of caster bean seedlings. All photos were observed by confocal laser scanning microscope (Zeiss780, Germany). No significant fluorescence was observed in the mesophyll cells or phloem of control set (A, C, E). The presence of fluorescent xenobiotics was indicated by arrowheads. EC: epidermal cells. CS: cell wall space. MC: mesophyll cells. PH: phloem. X: xylem.

fluorescence in epidermal cells and mesophyll cells obtained using 2-NBDGTF suggest that cotyledons could take up 2-NBDGTF from the medium readily via lower epidermal cells. The cotyledons could then load the 2-NBDGTF into sieve tubes from the apoplast after transission through mesophyll cells in an indirect apoplasmic loading process or via plasmodesmata after uptake by mesophyll cells in a symplasmic loading process. The obvious fluorescence observed in the cell wall and intercellular space (Figure 6B) suggests that cotyledons may load 2-NBDGTF into sieve tubes directly via an apoplasmic loading pathway. The observed results show that the loading pathway of 2-NBDGTF is consistent with the phloem loading pathway of sucrose in *Ricinus* cotyledons.[26]

After a 2 h incubation, intense fluorescence was also detected in the phloem of cotyledon petiole (Figure 6D), signifying that the 2-NBDGTF efflux can rapidly export via the phloem of the

cotyledon petiole. Intense fluorescence was also observed in the phloem of the hypocotyls after receiving 3 h of treatment (Figure 6F). These results indicate that 2-NBDGTF is phloem mobile and can translocate at a distance (from cotyledon to hypocotyl) via phloem.

The cells of 6 day old *Ricinus* seedling cotyledons appear as meristematic cells with well-developed organelles lacking large central vacuoles.[31] Fluorescence present in epidermal and mesophyll cells was homogeneously distributed in the cytoplasm, but was not caused by the compartmentation trapping by the vacuole. Alternatively, the intense fluorescence present in the xylem of the treated cotyledons was likely caused by the direct loading into the vessels. The fluorescence observed in the xylem of petioles and hypocotyls may be the result of lateral diffusion during phloem translocation and the adsorption of the lipophilic xenobiotic on lignins.

Since 2-NBDGTF was stable in the phloem during the experimental period, the fluorescence observed in the epidermal cells, mesophyll cells, and phloem could reflect the distribution of 2-NBDGTF, which would in turn reveal the distribution of GTF within plants. Accumulation spots of 2-NBDGTF likely represent the tissue sites of GTF, meaning that GTF was also loaded into the sieve tubes after transiting through epidermal cells and mesophyll cells along a symplastic−apoplastic loading route and was able to translocate at a distance (from cotyledon to hypocotyl) via phloem within seedlings.

In conclusion, a fluorescent glucose−fipronil conjugate was obtained via click chemistry. The uptake of disks of 2-NBDGTF was demonstrated to involve a carrier-mediated uptake process, and the phloem mobility in castor bean seedlings was comparable with GTF. Visualization of 2-NBDGTF movement showed that this fluorescent glucose−fipronil conjugate could be loaded into sieve tubes after transiting through epidermal cells and mesophyll cells and translocate at a distance via phloem within seedlings. From this information, 2-NBDGTF was determined to be a reasonably fluorescent surrogate of GTF and capable of revealing the movement of GTF analogues. The wide utilization of 2-NBDG provides us a substantial belief that 2-NBDGTF is a promising fluorescent conjugate. Moreover, this fluorescently labeled approach presents a great potential for revealing the activities of other glucose insecticides in plants.

## ■ ASSOCIATED CONTENT

### Supporting Information

HPLC and mass spectra analysis of fluorescent molecule present in disk extracts and phloem sap from 2-NBDGTF treated caster bean seedlings. This material is available free of charge via the Internet at http://pubs.acs.org.

## ■ AUTHOR INFORMATION


### Corresponding Author

*E-mail: hhxu@scau.edu.cn. Tel: +86-20-85285127. Fax: +86-20-38604926.

### Author Contributions

§Authors contributed equally to this work.



### Funding

This research was supported by the National Natural Science Foundation of China (Grant No. 31171886) and The Doctor Science Research Foundation of the Education Ministry of China (Grant No. 2011440411002)


### Notes

The authors declare no competing financial interest.

## ■ REFERENCES


(1) Kleier, D. A. Phloem mobility of xenobiotics. V. Structural requirements for phloem-systemic pesticides. *Pestic. Sci.* **1994**, *42* (1), 1−11.

(2) Hsu, F. C.; Sun, K.; Kleier, D. A.; Fielding, M. J. Phloem mobility of xenobiotics VI. Preparation of a phloem-mobile pro-nematocide based on oxamyl, exhibiting root-specific activation in transgenic tobacco. *Pestic. Sci.* **1995**, *44*, 9−19.

(3) Chollet, J. F.; Rocher, F.; Jousse, C.; Delétage-Grandon, C.; Bashiardes, G.; Bonnemain, J. L. Synthesis and phloem mobility of acidic derivatives of the fungicide fenpiclonil. *Pest Manage. Sci.* **2004**, *60*, 1063−1072.

(4) Chollet, J.; Deletage, C.; Faucher, M.; Miginiac, L.; Bonnemain, J. Synthesis and structure-activity relationships of some pesticides with an alpha-amino acid function. *Biochim. Biophys. Acta* **1997**, *1336* (2), 331−341.

(5) Qin, P.; Wang, J.; Wang, H.; Wen, Y.; Lu, M.; Li, Y.; Xu, Y.; Xu, H. Synthesis of Rotenone-O-monosaccharide derivatives and their phloem mobility. *J. Agric. Food Chem.* **2014**, *62* (20), 4521−4527.

(6) Yang, W.; Wu, H.; Xu, H.; Hu, A.; Lu, M. Synthesis of glucose-fipronil conjugate and its phloem mobility. *J. Agric. Food Chem.* **2011**, *59*, 12534−12542.

(7) Yuan, J.; Wu, H.; Lu, M.; Song, G.; Xu, H. Synthesis of a series of monosaccharide-fipronil conjugates and their phloem mobility. *J. Agric. Food Chem.* **2013**, *61*, 4236−4241.

(8) Wu, H. X.; Yang, W.; Zhang, Z.; Huang, T.; Yao, G.; Xu, H. Uptake and phloem transport of glucose-fipronil conjugate in *Ricinus* communis involve a carrier-mediated mechanism. *J. Agric. Food Chem.* **2012**, *60*, 6088−6094.

(9) Aajoud, A.; Raveton, M.; Azrou-Isghi, D.; Tissut, M.; Ravanel, P. How can the fipronil insecticide access phloem? *J. Agric. Food Chem.* **2008**, *56* (10), 3732−3737.

(10) Alsayeda, H.; Pascal-Lorber, S.; Nallanthigal, C.; Debrauwer, L.; Laurent, F. Transfer of the insecticide [14C] imidacloprid from soil to tomato plants. *Environ. Chem. Lett.* **2008**, *6* (4), 229−234.

(11) Liu, Z. Q.; Gaskin, R. E. Visualisation of the uptake of two model xenobiotics into bean leaves by confocal laser scanning microscopy: diffusion pathways and implication in phloem translocation. *Pest Manage. Sci.* **2004**, *60* (5), 434−439.

(12) Wright, K. M.; Horobin, R. W.; Oparka, K. J. Phloem mobility of fluorescent xenobiotics in Arabidopsis in relation to their physicochemical properties. *J. Exp. Bot.* **1996**, *47* (304), 1779−1787.

(13) Shani, E.; Weinstain, R.; Zhang, Y.; Castillejo, C.; Kaiserli, E.; Chory, J.; Tsien, R. Y.; Estelle, M. Gibberellins accumulate in the elongating endodermal cells of Arabidopsis root. *Proc. Natl. Acad. Sci. U.S.A.* **2013**, *110* (12), 4834−4839.

(14) Irani, N. G.; Di Rubbo, S.; Mylle, E.; Van den Begin, J.; Schneider-Pizoń, J.; Hniliková, J.; Šíša, M.; Buyst, D.; Vilarrasa-Blasi, J.; Szatmári, A. M.; et al. Fluorescent castasterone reveals BRI1 signaling from the plasma membrane. *Nat. Chem. Biol.* **2012**, *8* (6), 583−589.

(15) Delétage-Grandon, C.; Chollet, J. F.; Faucher, M.; Rocher, F.; Komor, E.; Bonnemain, J. L. Carrier-mediated uptake and phloem systemy of a 350-Dalton chlorinated xenobiotic with an $\alpha$-amino acid function. *Plant Physiol.* **2001**, *125*, 1620−1632.

(16) Lei, Z.; Wang, J.; Mao, G.; Wen, Y.; Xu, H. Phloem mobility and translocation of fluorescent conjugate containing glucose and NBD in castor bean (*Ricinus* communis). *J. Photochem. Photobiol., B* **2014**, *132*, 10−16.

(17) Cagnoni, A. J.; Varela, O.; Gouin, S. G.; Kovensky, J.; Uhrig, M. L. Synthesis of multivalent glycoclusters from 1-Thio-$\beta$-d-galactose and their inhibitory activity against the $\beta$-Galactosidase from E. coli. *J. Org. Chem.* **2011**, *76* (9), 3064−3077.

(18) Teicher, H. B.; Kofoed Hansen, B.; Jacobsen, N. Insecticidal activity of the enantiomers of fipronil. *Pest Manage. Sci.* **2003**, *59* (12), 1273−1275.

(19) Zhao, Q.; Li, Y.; Xiong, L.; Wang, Q. Design, synthesis and insecticidal activity of novel phenylpyrazoles containing a 2, 2, 2-trichloro-1-alkoxyethyl moiety. *J. Agric. Food Chem.* **2010**, *58* (8), 4992−4998.
(20) Hu, A.; Yang, W.; Xu, H. Novel fluorescent conjugate containing glucose and NBD and its carrier-mediated uptake by tobacco cells. *J. Photochem. Photobiol., B* **2010**, *101* (3), 215−223.
(21) Ehrenkranz, J. R.; Lewis, N. G.; Ronald Kahn, C.; Roth, J. Phlorizin: a review. *Diabetes/Metab. Res. Rev.* **2005**, *21* (1), 31−38.
(22) Etxeberria, E.; Gonzalez, P.; Tomlinson, P.; Pozueta-Romero, J. Existence of two parallel mechanisms for glucose uptake in heterotrophic plant cells. *J. Exp. Bot.* **2005**, *56* (417), 1905−1912.
(23) Stubbs, V.; Standing, D.; Knox, O.; Killham, K.; Bengough, A. G.; Griffiths, B. Root border cells take up and release glucose-C. *Ann. Bot.* **2004**, *93* (2), 221−224.
(24) Sugano, K.; Kansy, M.; Artursson, P.; Avdeef, A.; Bendels, S.; Di, L.; Ecker, G. F.; Faller, B.; Fischer, H.; Gerebtzoff, G.; Lennernaes, H.; Senner, F. Coexistence of passive and carrier-mediated processes in drug transport. *Nat. Rev. Drug Discovery* **2010**, *9* (8), 597−614.
(25) Kallarackal, J.; Orlich, G.; Schobert, C.; Komor, E. Sucrose transport into the phloem of *Ricinus communis* L. seedlings as measured by the analysis of sieve-tube sap. *Planta* **1989**, *177* (3), 327−335.
(26) Orlich, G.; Komor, E. Phloem loading in *Ricinus* cotyledons: sucrose pathways via the mesophyll and the apoplasm. *Planta* **1992**, *187* (4), 460−474.
(27) Rocher, F.; Chollet, J. F.; Legros, S.; Jousse, C.; Lemoine, R.; Faucher, M.; Bush, D. R.; Bonnemain, J. L. Salicylic acid transport in *Ricinus communis* involves a pH-dependent carrier system in addition to diffusion. *Plant Physiol.* **2009**, *150* (4), 2081−2091.
(28) Rocher, F.; Chollet, J. F.; Jousse, C.; Bonnemain, J. L. Salicylic acid, an ambimobile molecule exhibiting a high ability to accumulate in the phloem. *Plant Physiol.* **2006**, *141* (4), 1684−1693.
(29) Yoshioka, K.; Takahashi, H.; Homma, T.; Saito, M.; Oh, K.; Nemoto, Y.; Matsuoka, H. A novel fluorescent derivative of glucose applicable to the assessment of glucose uptake activity of Escherichia coli. *Biochim. Biophys. Acta* **1996**, *1289* (1), 5−9.
(30) Zou, C.; Wang, Y.; Shen, Z. 2-NBDG as a fluorescent indicator for direct glucose uptake measurement. *J. Biochem. Biophys. Methods* **2005**, *64* (3), 207−215.
(31) Komor, E.; Orlich, G.; Bauer-Ruckdeschel, H. Relationship between apoplastic nutrient concentrations and the long-distance transport of nutrients in the *Ricinus communis* L. seedling. In *The Apoplast of Higher Plants: Compartment of Storage, Transport and Reactions*; Springer: The Netherlands, 2007; pp 231−249.
(32) Kleier, D. A. Phloem Mobility of Xenobiotics I. Mathematical model unifying the weak acid and intermediate permeability theories. *Plant Physiol.* **1988**, *86* (3), 803−810.

JOURNAL OF AGRICULTURAL AND FOOD CHEMISTRY

Article

pubs.acs.org/JAFC

# Small Changes Result in Large Differences: Discovery of (−)-Incrustoporin Derivatives as Novel Antiviral and Antifungal Agents

Aidang Lu,*[,†] Jinjin Wang,[‡] Tengjiao Liu,[‡] Jian Han,[†] Yinhui Li,[†] Min Su,[†] Jianxin Chen,*[,†] Hui Zhang,[§] Lizhong Wang,[§] and Qingmin Wang*[,§]

[†]School of Marine Science and Engineering and [‡]School of Chemical Engineering, Hebei University of Technology, Tianjin 300130, China

[§]State Key Laboratory of Elemento-Organic Chemistry, Research Institute of Elemento-Organic Chemistry, Nankai University, Tianjin 300071, China

Supporting Information

**ABSTRACT:** On the basis of the structure of natural product (−)-incrustoporin (**1**), a series of lactone compounds **4a**−**i** and **5a**−**i** were designed and synthesized from nitroolefin. The antiviral and antifungal activities of these compounds were evaluated in vitro and in vivo. The small changes between **4** and **5** at the 3,4-position result in large differences in bioactivities. Compounds **4** exhibited significantly higher antiviral activity against tobacco mosaic virus (TMV) than dehydro compounds **5**. However, the antifungal activity of **4** is relatively lower than that of **5**. Compounds **4a**, **4c**, and **4i** with excellent in vivo anti-TMV activity emerged as new antiviral lead compounds. Compounds **5d**−**g** showed superiority over the commercial fungicides chlorothalonil and carbendazim against *Cercospora arachidicola* Hor at 50 mg $kg^{-1}$. The present study provides fundamental support for the development and optimization of (−)-incrustoporin derivatives as potential inhibitors of plant virus and pathogenic fungi.

**KEYWORDS:** *2,5-dihydrofuran-2-ones, (−)-incrustoporin derivatives, anti-TMV, antifungal activity*

## INTRODUCTION

Plant diseases are caused primarily by fungal and bacterial pathogens, leading to severe losses for agriculture and horticulture crop production worldwide, and constitute a great threat to global food security.[1] The yield of major food and cash crops was reduced nearly 20% by pathogenic fungi.[2] Plant viral diseases, known as "plant cancer", are serious threats after fungal diseases. They cause a variety of detrimental effects, and usually the infected plants are more susceptible to damage by pests and pathogens. Tobacco mosaic virus (TMV), one of the most well-studied plant viruses, is known to infect more than 400 plant species belonging to 36 families, such as tobacco, tomato, potato, and cucumber. It is found that in certain fields 90−100% of the plants show mosaic or leaf necrosis by harvesting time.[3]

Many of the currently available antifungal and antiviral agents have several drawbacks, such as pesticide related toxicity, severe pesticide resistance, and serious pesticide interactions.[4−7] Therefore, there is a growing need to develop new antifungal agents to effectively control these agricultural diseases.

Using natural products as lead compounds to develop new pesticides with novel structures and mechanisms is one of the most effective pesticide design methods.[8,9] (−)-Incrustoporin (**1**, Figure 1), isolated from *Incrustoporia carneola* (Bres.) Ryv. (Basidiomycetes) by Zapf in 1995,[10] is found to possess antifungal activity against a wide array of pathogenic fungi (*Candida albicans* strains, *Candida krusei*, *Candida glabrata*, and so on).[11−17] Biological screening has revealed that the endocyclic double bond is necessary for the antifungal effect, and the substitution of the C(3)-aryl ring with halogens could boost their antifungal activity. The preparation of (−)-incrustoporin and its derivatives has been reported by Mori,[18] Rossi,[19] Wu,[20] Fontes,[21] Oh,[22] and Fernandes[23] successively. Until now, most of the studies about (−)-incrustoporin and its derivatives were focused on antifungal activity against a panel of human pathogenic fungi; there have been no reports about the antiviral activity against TMV and only a few reports about antifungal activity against plant pathogenic fungi.[10]

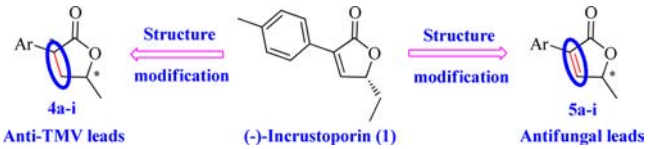


**Figure 1.** Design of (−)-incrustoporin derivatives **4a**−**i** and **5a**−**i**.

In the process of developing new potent plant virus inhibitors, phenanthroindolizidine alkaloids,[24] phenanthroquinolizidine alkaloids,[25] and β-carboline alkaloids[26] have been found to have good anti-TMV activity. As a continued work, 3-aryl-5-methyl-γ-butyrolactones **4** and 3-aryl 5-methyl-2,5-dihydrofuran-2-ones **5** were designed, synthesized from nitroolefin on the basis of the structure of the natural product (−)-incrustoporin (**1**). Their antiviral activity against TMV and

Received: June 27, 2014
Revised: August 2, 2014
Accepted: August 13, 2014
Published: August 13, 2014

 © 2014 American Chemical Society 

antifungal activity against plant pathogenic fungi were systematically investigated for the first time.

## MATERIALS AND METHODS

**Instruments.** The melting points of the products were determined on an X-4 binocular microscope (Gongyi Yuhua Instrument Co., China) and were not corrected. NMR spectra were acquired with a Bruker 400 MHz (100 MHz for $^{13}C$) instrument at room temperature. Chemical shifts were measured relative to residual solvent peaks of $CDCl_3$ as internal standards ($^1H$, $\delta$ = 7.26 ppm; $^{13}C$, $\delta$ = 77.0 ppm). The following abbreviations were used to designate chemical shift multiplicities: s, singlet; d, doublet; t, triplet; m, multiplet; and bs, broad singlet. All first-order splitting patterns were assigned on the basis of multiplet appearance. Splitting patterns that could not be easily interpreted were designated multiplet (m) or broad (br). Enantiomeric excesses were determined with an HP1-100 instrument (chiral column; mobile phase of hexane/2-propanol). HRMS data were recorded with a Varian QFT-ESI instrument. Analytical TLC was performed on silica gel GF 254. Column chromatographic purification was performed using silica gel. All reagents were of analytical reagent grade or chemically pure and purified prior to use when necessary. The $\beta$-nitrostyrene **2a**−**i** were prepared according to the literature.[27] (*S*)-**3d** were prepared according to our previously reported procedure.[28]

**General Experimental Procedures.** *General Procedures for the Preparation of Intermediate **3a**−**i**.*[29] To a mixture of $CHCl_3$ (10 mL), $Et_3N$ (20−30 mol %), and acetone (40.0 mmol, 3 mL) was added the corresponding nitroolefin (4.0 mmol) followed by (±)-proline (20−30 mol %), and the resulting mixture was stirred at room temperature until TLC indicated the reaction was complete. The reaction mixture was evaporated under vacuum, and the residue was dissolved in $CH_2Cl_2$ (30 mL). The mixture was treated with 1 M HCl (20 mL) solution, the layers were separated, and the aqueous layer was extracted several times with $CH_2Cl_2$, dried with anhydrous $MgSO_4$, and evaporated. The pure products **3a**−**g** were obtained by recrystallization from methanol. **3h** and **3i** were purified by column chromatography on silica gel (100−200 mesh, petroleum ether/ethyl acetate = 5:1).

*(±)-5-Nitro-4-phenylpentan-2-one (**3a**):* white solid; 92% yield; mp 110−112 °C (lit.[30] 110−112 °C); $^1H$ NMR $\delta$ 2.12 (s, 3 H), 2.92 (d, *J* = 6.8 Hz, 2 H), 4.01 (quintet, *J* = 7.2 Hz, 1 H), 4.60 (dd, *J* = 8.0 and 12.4 Hz, 1 H), 4.70 (dd, *J* = 6.8 and 12.4 Hz, 1 H), 7.22 (d, *J* = 7.6 Hz, 2 H), 7.27−7.35 (m, 3 H); $^{13}C$ NMR $\delta$ 205.4, 138.8, 129.0, 127.9, 127.3, 79.4, 46.1, 40.0, 30.4.

*(±)-5-Nitro-4-(p-tolyl)pentan-2-one (**3b**):* white solid; 93% yield; mp 68−70 °C (lit.[30] 70−72 °C); $^1H$ NMR $\delta$ 2.11 (s, 3 H), 2.31 (s, 3 H), 2.89 (d, *J* = 6.8 Hz, 2 H), 3.97 (quintet, *J* = 7.2 Hz, 1 H), 4.58 (dd, *J* = 7.6 and 12.4 Hz, 1 H), 4.66 (dd, *J* = 7.2 and 12.4 Hz, 1 H), 7.09 (d, *J* = 8.0 Hz, 2 H), 7.13 (d, *J* = 8.0 Hz, 2 H); $^{13}C$ NMR $\delta$ 205.5, 137.6, 135.7, 129.7, 127.2, 79.6, 46.2, 38.7, 30.4, 21.0.

*(±)-4-(4-Fluorophenyl)-5-nitropentan-2-one (**3c**):* white solid; 97% yield; mp 100−103 °C (lit.[31] 102.0−104.9 °C); $^1H$ NMR $\delta$ 2.12 (s, 3 H), 2.89 (d, *J* = 6.8 Hz, 2 H), 3.40 (quintet, *J* = 7.2 Hz, 1 H), 4.58 (dd, *J* = 7.6 and 12.0 Hz, 1 H), 4.66 (dd, *J* = 6.4 and 12.4 Hz, 1 H), 6.99−7.03 (m, 2 H), 7.17−7.20 (m, 1 H); $^{13}C$ NMR $\delta$ 205.1, 163.4, and 161.0 ($J_{C-F}$ = 245.2 Hz), 134.6 and 134.6 ($J_{C-F}$ = 3.2 Hz), 129.1 and 129.0 ($J_{C-F}$ = 7.9 Hz), 116.1 and 115.9 ($J_{C-F}$ = 21.5 Hz), 79.4, 46.2, 38.3, 30.4.

*(±)-4-(4-Chlorophenyl)-5-nitropentan-2-one (**3d**):* white solid; 93% yield; mp 75−77 °C (lit.[30] 89−91 °C); $^1H$ NMR $\delta$ 2.13 (s, 3 H), 2.89 (d, *J* = 7.2 Hz, 2 H), 3.99 (quintet, *J* = 7.2 Hz, 1 H), 4.58 (dd, *J* = 8.0 and 12.4 Hz, 1 H), 4.66 (dd, *J* = 6.8 and 12.4 Hz, 1 H), 7.16 (d, *J* = 8.4 Hz, 2 H), 7.30 (d, *J* = 8.4 Hz, 2 H); $^{13}C$ NMR $\delta$ 205.0, 137.3, 133.8, 129.3, 128.8, 79.2, 46.0, 38.4, 30.4.

*(±)-4-(2,4-Dichlorophenyl)-5-nitropentan-2-one (**3e**):* white solid; 83% yield; mp 52−54 °C (lit.[30] 48−50 °C); $^1H$ NMR $\delta$ 2.17 (s, 3 H), 2.91−3.08 (m, 2 H), 4.40 (quintet, *J* = 6.4 Hz, 1 H), 4.73 (d, *J* = 6.4 Hz, 2 H), 7.14 (d, *J* = 8.0 Hz, 1 H), 7.22 (d, *J* = 8.0 Hz, 1 H), 7.42 (s, 1 H); $^{13}C$ NMR $\delta$ 205.0, 134.6, 134.4, 134.2, 130.2, 129.3, 127.7, 77.1, 44.2, 35.3, 30.2.

*(±)-4-(4-Bromophenyl)-5-nitropentan-2-one (**3f**):* white solid; 92% yield; mp 78−80 °C (lit.[31] 103.4−106.5 °C); $^1H$ NMR $\delta$ 2.13 (s, 3 H), 2.89 (d, *J* = 6.8 Hz, 2 H), 3.98 (quintet, *J* = 6.8 Hz, 1 H), 4.58 (dd, *J* = 8.0 and 12.4 Hz, 1 H), 4.67 (dd, *J* = 6.8 and 12.4 Hz, 1 H), 7.10 (d, *J* = 7.6 Hz, 2 H), 7.45 (d, *J* = 7.6 Hz, 2 H); $^{13}C$ NMR $\delta$ 205.0, 137.8, 132.1, 129.1, 121.8, 79.0, 45.8, 38.4, 30.3.

*(±)-5-Nitro-4-(4-(trifluoromethyl)phenyl)pentan-2-one (**3g**):* yellow oil; 96% yield; $^1H$ NMR $\delta$ 2.14 (s, 3 H), 2.93 (d, *J* = 7.2 Hz, 2 H), 4.09 (quintet, *J* = 7.2 Hz, 1 H), 4.63 (dd, *J* = 8.0 and 12.8 Hz, 1 H), 4.71 (dd, *J* = 6.4 and 12.4 Hz, 1 H), 7.35 (d, *J* = 8.0 Hz, 2 H), 7.59 (d, *J* = 8.0 Hz, 1 H); $^{13}C$ NMR $\delta$ 204.7, 143.0, 130.4, and 130.1 ($J_{C-F}$ = 32.6 Hz), 127.9, 126.1 ($J_{C-F}$ = 3.4 Hz), 125.2 and 122.5 ($J_{C-F}$ = 270.4 Hz), 78.9, 45.8, 38.7, 30.3.

*(±)-4-(Furan-2-yl)-5-nitropentan-2-one (**3h**):* brown solid; 88% yield; mp 47−49 °C (lit.[30] 48−49 °C); $^1H$ NMR $\delta$ 2.15 (s, 3 H), 2.84−2.99 (m, 2 H), 4.08 (quintet, *J* = 6.8 Hz, 1 H), 4.61−4.70 (m, 2 H), 6.12 (d, 1 H, *J* = 3.2 Hz), 6.27 (m, 1 H), 7.32 (s, 1 H); $^{13}C$ NMR $\delta$ 205.1, 151.7, 142.3, 110.5, 107.1, 77.0, 43.5, 32.9, 30.2.

*(±)-5-Nitro-4-(thiophen-2-yl)pentan-2-one (**3i**):* brown solid; 88% yield; mp 35−37 °C (lit.[30] 37−38 °C); $^1H$ NMR $\delta$ 2.17 (s, 3 H), 2.98 (d, *J* = 7.2 Hz, 2 H), 4.32 (quintet, *J* = 6.8 Hz, 1 H), 4.63 (dd, *J* = 7.2 and 12.4 Hz, 1 H), 4.70 (dd, *J* = 6.4 and 12.4 Hz, 1 H), 6.91−6.95 (m, 2 H), 7.20 (dd, *J* = 1.2 and 5.2 Hz, 1 H); $^{13}C$ NMR $\delta$ 205.0, 141.5, 127.1, 125.6, 124.7, 79.7, 46.8, 34.5, 30.3.

*General Synthetic Procedures for Intermediate **4a**−**i** (Diastereomers of **4a**−**g** Shown as A and B, Respectively).*[32] $NaBH_4$ (0.19 g, 5 mmol) was added to a solution of **3a**−**i** (5 mmol) in MeOH/$CH_2Cl_2$ (v/v = 1:1, 10 mL) at 0 °C. The mixture was stirred for 15 min at the same temperature, and $H_2O$ (10 mL) was added. After evaporation of the methanol under reduced pressure, HCl (aq) 1 M (10 mL) was added, and the aqueous phase was extracted with $CH_2Cl_2$ (3 × 15 mL). The combined organic layers were dried over $MgSO_4$ and evaporated to afford the expected nitroalcohol, which was redissolved in DMSO (8.5 mL). Sodium nitrite (0.80 g, 12.75 mmol) and acetic acid (1.7 mL, 42.5 mmol) were then added, and the solution was stirred at room temperature overnight and at 40 °C for 6 h. The mixture was allowed to cool, and HCl (aq) 1 M (50 mL) was added. The aqueous phase was extracted with $CH_2Cl_2$ (3 × 50 mL). The organic layers were combined, dried over $MgSO_4$, and evaporated under vacuum to afford the γ-butyrolactones **4a**−**i**, which were then purified by flash column chromatography on silica gel (100−200 mesh, petroleum ether/ethyl acetate = 12:1).

*3-Phenyl-5-methyltetrahydrofuran-2-one (**4a**):* colorless oil (lit.[13] colorless oil); yield 60%; $^1H$ NMR **A**/**B** = 1.7:1, **A** $\delta$ 1.43 (d, *J* = 6.4 Hz, 3 H), 2.28−2.35 (m, 1 H), 2.47−2.54 (m, 1 H), 3.90 (dd, *J* = 7.2 and 9.2 Hz, 1 H), 4.73−4.81 (m, 1 H), 7.25−7.29 (m, 5 H); **B** $\delta$ 1.46 (d, *J* = 6.4 Hz, 3 H), 1.93−2.02 (m, 1 H), 2.71−2.77 (m, 1 H), 3.86 (dd, *J* = 8.8 and 12.8 Hz, 1 H), 4.56−4.61 (m, 1 H), 7.32−7.36 (m, 5 H); $^{13}C$ NMR **A** $\delta$ 177.3, 137.2, 129.0, 128.2, 127.7, 75.0, 45.7, 37.9, 21.0; **B** $\delta$ 177.0, 136.7, 128.8, 128.2, 127.6, 75.0, 47.7, 39.8, 20.8.

*3-(4-Methylphenyl)-5-methyltetrahydrofuran-2-one (**4b**):* white crystals; yield 60%; mp 46−48 °C (lit.[13] colorless oil); $^1H$ NMR **A**/**B** = 1.5:1, **A** $\delta$ 1.45 (d, *J* = 6.4 Hz, 3 H), 2.29−2.36 (m, 1 H), 2.48−2.55 (m, 1 H), 3.89 (dd, *J* = 7.6 and 9.2 Hz, 1 H), 4.75−4.83 (m, 1 H), 7.16 (m, 4 H); **B** $\delta$ 1.49 (d, *J* = 6.0 Hz, 3 H), 1.96−2.04 (m, 1 H), 2.72−2.79 (m, 1 H), 3.85 (dd, *J* = 7.2 and 11.2 Hz, 1 H), 4.57−4.65 (m, 1 H), 717 (m, 4 H); $^{13}C$ NMR **A** $\delta$ 177.5, 137.3, 134.0, 129.7, 127.5, 75.2, 45.3, 38.0, 21.1, 21.1; **B** $\delta$ 177.2, 137.3, 133.5, 129.5, 128.0, 75.0, 47.4, 39.9, 21.1, 20.9.

*3-(4-Fluorophenyl)-5-methyltetrahydrofuran-2-one (**4c**):* yellow solid; yield 53%; mp 36−38 °C (lit.[13] 33−35 °C); $^1H$ NMR **A**/**B** = 3.7:1, **A** $\delta$ 1.46 (d, *J* = 6.4 Hz, 3 H), 2.33−2.39 (m, 1 H), 2.48−2.55 (m, 1 H), 3.92 (t, *J* = 8.8 Hz, 1 H), 4.78−4.83 (m, 1 H), 7.05 (m, 2 H), 7.26 (m, 2 H); **B** $\delta$ 1.51 (d, *J* = 6.0 Hz, 3 H), 1.95−2.04 (m, 1 H), 2.75−2.82 (m, 1 H), 3.89 (dd, *J* = 8.8 and 12.4 Hz, 1 H), 4.61−4.66 (m, 1 H), 7.15 (m, 2 H), 7.26 (m, 2 H); $^{13}C$ NMR **A** $\delta$ 176.9, 160.9, and 163.3 ($J_{C-F}$ = 244.9 Hz), 132.6 and 132.7 ($J_{C-F}$ = 3.2 Hz), 129.2 and 129.3 ($J_{C-F}$ = 8.0 Hz), 115.7 and 115.9 ($J_{C-F}$ = 21.5 Hz), 75.0, 44.7, 37.7, 20.9; **B** $\delta$ 176.6, 160.9, and 163.3 ($J_{C-F}$ = 241.4 Hz), 132.15

and 132.18 ($J_{C-F}$ = 3.1 Hz), 129.6 and 129.7 ($J_{C-F}$ = 8.1 Hz), 115.5 and 115.8 ($J_{C-F}$ = 21.5 Hz), 74.9, 46.9, 36.7, 20.7.

*3-(4-Chlorophenyl)-5-methyltetrahydrofuran-2-one (**4d**):* white crystals; yield 68%; mp 40−42 °C (lit.[13] 38−40 °C); $^1$H NMR **A**/**B** = 1:1.1, **A** $\delta$ 1.46 (d, $J$ = 6.4 Hz, 3 H), 2.32−2.39 (m, 1 H), 2.47−2.54(m, 1 H), 3.91 (t, $J$ = 8.4 Hz, 1 H), 4.76−4.83 (m, 1 H), 7.21 (d, $J$ = 3.6 Hz, 2 H), 7.33 (d, $J$ = 8.4 Hz, 2 H); **B** $\delta$ 1.50 (d, $J$ = 6.0 Hz, 3 H), 1.94−2.03 (m, 1 H), 2.74−2.81 (m, 1 H), 3.87 (dd, $J$ = 8.4 and 12.4 Hz, 1 H), 4.58−4.67 (m, 1 H), 7.23 (d, $J$ = 3.6 Hz, 2 H), 7.33 (d, $J$ = 8.4 Hz, 2 H); $^{13}$C NMR **A** $\delta$ 177.4, 136.1, 134.3, 129.8, 129.8, 75.8, 45.6, 38.4, 21.7; **B** $\delta$ 177.1, 135.6, 134.3, 130.2, 129.7, 75.7, 47.7, 40.3, 21.5.

*(3S,5R)-3-(4-Chlorophenyl)-5-methyltetrahydrofuran-2-one ((3S,5R)-**4d**):* white crystals; yield 55%; mp 38−40 °C; $^1$H NMR $\delta$ 1.47 (d, $J$ = 6.4 Hz, 3 H), 2.32−2.39 (m, 1 H), 2.48−2.55 (m, 1 H), 3.91 (t, $J$ = 9.2 Hz, 1 H), 4.76−4.84 (m, 1 H), 7.22 (d, $J$ = 8.4 Hz, 2 H), 7.33 (d, $J$ = 8.4 Hz, 2 H); $^{13}$C NMR $\delta$ 176.6, 135.4, 133.6, 129.1, 129.1, 75.1, 44.9, 37.7, 21.0.

*(3S,5S)-3-(4-Chlorophenyl)-5-methyltetrahydrofuran-2-one ((3S,5S)-**4d**):* white crystals; yield 63%; mp 38−40 °C; $^1$H NMR $\delta$ 1.51 (d, $J$ = 6.4 Hz, 3 H), 1.94−2.04 (m, 1 H), 2.75−2.81 (m, 1 H), 3.88 (dd, $J$ = 8.4 and 12.8 Hz, 1 H), 4.59−4.68 (m, 1 H), 7.23 (d, $J$ = 8.4 Hz, 2 H), 7.34 (d, $J$ = 8.4 Hz, 2 H); $^{13}$C NMR $\delta$ 176.4, 134.9, 133.6, 129.5, 129.0, 75.0, 47.0, 39.6, 20.8.

*3-(2,4-Dichlorophenyl)-5-methyltetrahydrofuran-2-one (**4e**):* yellow solid; yield 64%; mp 41−43 °C (lit.[13] 45−47 °C); $^1$H NMR **A**/**B** = 3:1, **A** $\delta$ 1.48 (d, $J$ = 6.4 Hz, 3 H), 2.39−2.43 (m, 2 H), 4.27 (t, $J$ = 9.2 Hz, 1 H), 4.76−4.84 (m, 1 H), 7.19 (d, $J$ = 8.4 Hz, 1 H), 7.27 (d, $J$ = 7.6 Hz, 1 H), 7.43 (s, 1 H); **B** $\delta$ 1.51 (d, $J$ = 6.4 Hz, 3 H), 1.87−1.96 (m, 1 H), 2.81−2.87 (m, 1 H), 4.26 (t, $J$ = 9.2 Hz, 1 H), 4.66−4.71 (m, 1 H), 7.23−7.28 (m, 2 H), 7.42 (s, 1 H); $^{13}$C NMR **A** $\delta$ 176.2, 134.7, 134.2, 134.0, 130.1, 129.8, 127.7, 75.1, 43.4, 37.1, 21.1; **B** $\delta$ 175.7, 134.8, 134.2, 133.4, 130.6, 129.7, 127.8, 75.3, 45.5, 38.9, 20.8.

*3-(4-Bromophenyl)-5-methyltetrahydrofuran-2-one (**4f**):* yellow solid; yield 52%; mp 47−49 °C (lit.[13] 52−53 °C); $^1$H NMR **A**/**B** = 1:1.3, **A** $\delta$ 1.44 (d, $J$ = 6.4 Hz, 3 H), 2.30−2.37 (m, 1 H), 2.45−2.52 (m, 1 H), 3.88 (t, $J$ = 8.8 Hz, 1 H), 4.73−4.81 (m, 1 H), 7.14 (d, $J$ = 2.8 Hz, 2 H), 7.47 (d, $J$ = 8.4 Hz, 2 H); **B** $\delta$ 1.48 (d, $J$ = 6.0 Hz, 3 H), 1.91−2.00 (m, 1 H), 2.72−2.78 (m, 1 H), 3.84 (dd, $J$ = 8.4 and 12.4 Hz, 1 H), 4.56−4.61 (m, 1 H), 7.17 (d, $J$ = 2.8 Hz, 2 H), 7.47 (d, $J$ = 8.4 Hz, 2 H); $^{13}$C NMR **A** $\delta$ 176.6, 136.0, 132.0, 129.4, 121.6, 75.1, 44.9, 37.6, 21.0; **B** $\delta$ 176.3, 135.5, 131.9, 129.8, 121.6, 75.0, 47.1, 39.5, 20.8.

*3-(4-Trifluoromethylphenyl)-5-methyltetrahydrofuran-2-one (**4g**):* white crystals; yield 65%; mp 75−77 °C (lit.[13] 88−89 °C); $^1$H NMR **A**/**B** = 1:5.5, **A** $\delta$ 1.49 (d, $J$ = 6.4 Hz, 3 H), 2.37−2.46 (m, 1 H), 2.53−2.60 (m, 1 H), 4.00 (dd, $J$ = 8.8 and 12.8 Hz, 1 H), 4.81−4.85 (m, 1 H), 7.42−7.44 (m, 2 H), 7.62−7.64 (m, 2 H); **B** $\delta$ 1.53 (d, $J$ = 6.0 Hz, 3 H), 1.99−2.08 (m, 1 H), 2.79−2.85 (m, 1 H), 3.97 (dd, $J$ = 8.8 and 12.8 Hz, 1 H), 4.63−4.71 (m, 1 H), 7.42−7.44 (m, 2 H), 7.62−7.64 (m, 2 H); $^{13}$C NMR **A** $\delta$ 176.4, 140.9, 130.5, and 129.5 ($J_{C-F}$ = 109.1 Hz), 128.2, 126.0 ($J_{C-F}$ = 3.4 Hz), 125.3, 75.2, 45.3, 37.5, 21.0; **B** $\delta$ 176.1, 140.4, 130.1, and 129.8 ($J_{C-F}$ = 32.5 Hz), 128.6, 125.8 ($J_{C-F}$ = 3.3 and $J_{C-F}$ = 7.3 Hz), 125.4 and 122.7 ($J_{C-F}$ = 270.7 Hz), 75.2, 47.4, 39.5, 20.8.

*3-(Furan-2-yl)-5-methyltetrahydrofuran-2-one (**4h**):* yellow oil; yield 43%; $^1$H NMR $\delta$ 1.45 (d, $J$ = 6.4 Hz, 3 H), 2.20−2.27 (m, 1 H), 2.60−2.66 (m, 1 H), 3.99 (dd, $J$ = 6.0 and 9.2 Hz, 1 H), 4.80−4.88 (m, 1 H), 6.27 (d, $J$ = 3.2 Hz, 1 H), 6.34 (dd, $J$ = 1.6 and 3.2 Hz, 1 H), 7.37 (d, 1 H, $J$ = 1.6 Hz); $^{13}$C NMR $\delta$ 174.7, 149.4, 142.6, 110.6, 107.5, 76.0, 40.4, 35.4, 20.9.

*3-(Thiophen-2-yl)-5-methyltetrahydrofuran-2-one (**4i**):* yellow oil; yield 52%; $^1$H NMR $\delta$ 1.49 (d, $J$ = 6.0 Hz, 3 H), 2.05−2.14 (m, 1 H), 2.84−2.91 (m, 1 H), 4.14 (dd, $J$ = 8.8 and 12.8 Hz, 1 H), 4.60−4.68 (m, 1 H), 6.99−7.02 (m, 2 H), 7.25−7.27 (m, 1 H); $^{13}$C NMR $\delta$ 175.5, 138.2, 127.0, 125.8, 125.1, 75.2, 42.8, 39.6, 20.8.

*General Procedures for the Preparation of Furanones **5a**−**5i**.*[13] Butyllithium (11.0 mmol) was added to a solution of diisopropylamine (10.6 mmol) in dry THF (30 mL) at 0 °C under $N_2$. After 30 min, the LDA solution was cooled to −60 °C, and a solution of a saturated lactone (**4a**−**i**) (10.0 mmol) in THF (5 mL) was added. The reaction temperature was maintained at −60 °C for 30 min, and a solution of phenylselenenyl chloride (15.0 mmol) in THF (10 mL) was added. The resultant mixture was slowly warmed to room temperature, diluted with ethyl acetate (50 mL), washed with saturated aqueous $NH_4Cl$, dried over $Na_2SO_4$, and concentrated. The crude phenylselanyl derivative was rapidly purified by column chromatography and dissolved in $CHCl_3$ (20 mL), and then *m*-CPBA (15.0 mmol) was added to the solution in several portions at 0 °C. The reaction mixture was then stirred for 2 h at room temperature or until TLC indicated the reaction was complete. A further portion of $CHCl_3$ (10 mL) was added along with 5% aqueous $Na_2CO_3$ (20 mL). The layers were separated, and the organic phase was washed with 5% aqueous $Na_2CO_3$ (20 mL), dried over $Na_2SO_4$, and evaporated. Products **5a**−**i** were purified by column chromatography on silica gel (100−200 mesh, petroleum ether/ethyl acetate = 15:1) and were obtained with overall yields in the range 31−51% over two steps.

*3-Phenyl-5-methyl-2,5-dihydrofuran-2-one (**5a**):* white solid; yield 40%; mp 49−51 °C (lit.[13] 45−46 °C); $^1$H NMR $\delta$ 1.52 (d, $J$ = 6.8 Hz, 3 H), 5.15 (qd, $J$ = 6.4 and 13.2 Hz, 1 H), 7.40−7.43 (m, 3 H), 7.55 (s, 1 H), 7.85 (d, $J$ = 6.4 Hz, 2 H); $^{13}$C NMR $\delta$ 171.8, 149.2, 131.3, 129.5, 129.3, 128.7, 127.1, 76.8, 19.2; HRMS (ESI) calcd for $C_{11}H_{10}O_2$ $(M + H)^+$ 175.0754, found 175.0756.

*3-(4-Methylphenyl)-5-methyl-2,5-dihydrofuran-2-one (**5b**):* white solid; yield 39%; mp 53−54 °C (lit.[13] 55−57 °C); $^1$H NMR $\delta$ 1.50 (d, $J$ = 6.8 Hz, 3 H), 2.37 (s, 3 H), 5.14 (qd, $J$ = 6.8 and 13.6 Hz, 1 H), 7.22 (d, $J$ = 8.0 Hz, 2 H), 7.49 (s, $J$ = 2.0 Hz, 1 H), 7.75 (d, $J$ = 8.0 Hz, 1 H); $^{13}$C NMR $\delta$ 171.9, 148.1, 139.4, 131.2, 129.4, 126.9, 126.7, 76.7, 21.4, 19.2; HRMS (ESI) calcd for $C_{12}H_{12}O_2$ $(M + H)^+$ 189.0910, found 189.0912.

*3-(4-Fluorophenyl)-5-methyl-2,5-dihydrofuran-2-one (**5c**):* white solid; yield 32%; mp 71−73 °C (lit.[13] 81−83 °C); $^1$H NMR $\delta$ 1.52 (d, 3 H, $J$ = 6.8 Hz), 5.16 (m, 1 H), 7.08−7.13 (m, 2 H), 7.51 (d, 1 H, $J$ = 2.0 Hz), 7.85−7.88 (m, 2 H); $^{13}$C NMR $\delta$ 171.6, 164.5, and 162.1 ($J_{C-F}$ = 248.1 Hz), 148.5, 130.4, 129.1, and 129.0 ($J_{C-F}$ = 8.3 Hz), 125.69 and 125.66 ($J_{C-F}$ = 2.9 Hz), 115.8 and 115.6 ($J_{C-F}$ = 21.6 Hz), 76.7, 19.1; HRMS (ESI) calcd for $C_{11}H_9FO_2$ $(M + H)^+$ 193.0659, found 193.0661.

*3-(4-Chlorophenyl)-5-methyl-2,5-dihydrofuran-2-one (**5d**):* white solid; yield 31%; mp 101−102 °C (lit.[13] 99−101 °C); $^1$H NMR $\delta$ 1.51 (d, $J$ = 6.8 Hz, 3 H), 5.15 (qd, $J$ = 6.4 and 13.2 Hz, 1 H), 7.36 (d, $J$ = 8.0 Hz, 2 H), 7.56 (s, 1 H), 7.80 (d, $J$ = 8.4 Hz, 1 H); $^{13}$C NMR $\delta$ 171.5, 149.5, 135.26, 130.1, 128.9, 128.4, 128.0, 76.9, 19.1; HRMS (ESI) calcd for $C_{11}H_9ClO_2$ $(M + H)^+$ 209.0364, found 209.0362.

*(R)-3-(4-Chlorophenyl)-5-methyl-2,5-dihydrofuran-2-one (**5d**):* white solid; yield 51%; $[\alpha]_D^{20}$ = −15.5° (*c* 1.0, $CHCl_3$); mp 38−40 °C; $^1$H NMR $\delta$ 1.51 (d, $J$ = 6.4 Hz, 3 H), 5.15 (qd, $J$ = 6.4 and 12.8 Hz, 1 H), 7.38 (d, $J$ = 7.6 Hz, 2 H), 7.55 (s, 1 H), 7.81 (d, $J$ = 7.6 Hz, 1 H); $^{13}$C NMR $\delta$ 171.4, 149.2, 135.4, 130.3, 128.9, 128.4, 127.9, 76.8, 19.1; HRMS (ESI) calcd for $C_{11}H_9ClO_2$ $(M + H)^+$ 209.0364, found 209.0367; HPLC analysis (Chiralpak OJ-H column, hexane/2-propanol = 98:2, flow rate = 1.0 mL/min, wavelength = 254 nm) $t_R$ = 57.23 (minor) and 68.66 min (major), 56% ee.

*3-(2,4-Dichlorophenyl)-5-methyl-2,5-dihydrofuran-2-one (**5e**):* yellow oil; yield 42%; 47−49 °C; $^1$H NMR $\delta$ 1.55 (d, $J$ = 7.2 Hz, 3 H), 5.23 (qd, $J$ = 6.8 and 13.6 Hz, 1 H), 7.32 (dd, $J$ = 6.4 and 8.4 Hz, 1 H), 7.47 (d, $J$ = 2.0 Hz, 1 H), 7.66 (d, $J$ = 8.4 Hz, 1 H), 7.78 (d, $J$ = 1.2 Hz, 1 H); $^{13}$C NMR $\delta$ 171.4, 154.9, 135.3, 133.9, 131.6, 130.0, 128.3, 127.3, 126.9, 77.4, 19.0; HRMS (ESI) calcd for $C_{11}H_8Cl_2O_2$ $(M + H)^+$ 242.9974, found 242.9975.

*3-(4-Bromophenyl)-5-methyl-2,5-dihydrofuran-2-one (**5f**):* white solid; yield 44%; mp 103−104 °C (lit.[13] 105−106 °C); $^1$H NMR $\delta$ 1.52 (d, $J$ = 6.8 Hz, 3 H), 5.15 (qd, $J$ = 6.8 and 13.6 Hz, 1 H), 7.54−7.56 (m, 3 H), 7.75 (d, $J$ = 8.4 Hz, 2 H); $^{13}$C NMR $\delta$ 171.4, 149.4, 131.9, 130.4, 128.6, 128.4, 123.7, 76.9, 19.1; HRMS (ESI) calcd for $C_{11}H_9BrO_2$ $(M + H)^+$ 252.9859, found 252.9854.

*3-(4-Trifluoromethylphenyl)-5-methyl-2,5-dihydrofuran-2-one (**5g**):* white solid; yield 43%; mp 88−90 °C (lit.[13] 91−93 °C); $^1$H NMR $\delta$ 1.55 (d, $J$ = 6.8 Hz, 3 H), 5.20 (qd, $J$ = 6.8 and 13.6 Hz, 1 H), 7.66 (s, 1 H), 7.67 (d, $J$ = 8.8 Hz, 2 H), 8.00 (d, $J$ = 8.1 Hz, 2 H); $^{13}$C

NMR $\delta$ 171.14, 150.96, 132.91, 131.3, and 130.9 (d, $J_{C-F}$ = 32.4 Hz), 130.3, 127.4, 125.6 (q, $J_{C-F}$ = 3.2 and $J_{C-F}$ = 7.1 Hz), 125.3, 77.0, 19.0; HRMS (ESI) calcd for $C_{12}H_9F_3O_2$ $(M + H)^+$ 243.0627, found 243.0624.

*3-(Furan-2-yl)-5-methyl-2,5-dihydrofuran-2-one (**5h**):* colorless oil; yield 36%; $^1$H NMR $\delta$ 1.49 (d, $J$ = 6.4 Hz, 3 H), 5.18 (qd, $J$ = 6.4 and 12.8 Hz, 1 H), 6.47 (s, 1 H), 7.13 (s, 1 H), 7.41(s, 1 H), 7.47 (s, 1 H); $^{13}$C NMR $\delta$ 170.1, 145.3, 144.2, 143.6, 123.0, 111.8, 111.1, 77.1, 19.2; HRMS (ESI) calcd for $C_9H_8O_3$ $(M + H)^+$ 165.0546, found 165.0542.

*3-(Thiophen-2-yl)-5-methyl-2,5-dihydrofuran-2-one (**5i**):* colorless oil; yield 38%; $^1$H NMR $\delta$ 1.51 (d, $J$ = 6.8 Hz, 3 H), 5.17 (qd, $J$ = 6.8 and 13.6 Hz, 1 H), 7.09 (t, $J$ = 3.6 Hz, 1 H), 7.38 (d, $J$ = 5.2 Hz, 1 H), 7.75 (d, $J$ = 3.2 Hz, 1 H); $^{13}$C NMR $\delta$ 170.9, 145.2, 131.5, 127.8, 127.5, 127.2, 126.3, 77.4, 19.2; HRMS (ESI) calcd for $C_9H_8SO_2$ $(M + H)^+$ 181.0318, found 181.0316.

**Biological Assay.** All bioassays were performed on representative test organisms reared in the laboratory. Percentage mortalities were evaluated according to a percentage scale of 0−100, in which 0 indicates no activity and 100 indicates total kill.

*Antiviral Biological Assay.* The procedure of purifying TMV and the method to test the anti-TMV activity of the synthesized compounds were the same with those reported previously in the literature.[24,25]

*Antifungal Biological Assay.* The detailed assay method to test the antifungal activity of the synthesized compounds was described in the literature.[33]

## RESULTS AND DISCUSSION

**Chemistry.** *Synthesis of Compounds **5a−i**.* Compounds **5a−i** were synthesized according to procedures in Figure 2.

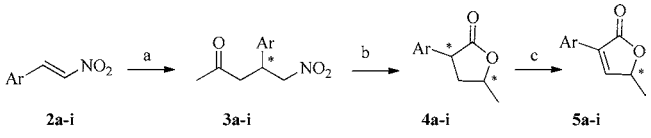


a: acetone, (± )-proline, $Et_3N$, $CH_2Cl_2$, rt;
b: 1)$NaBH_4$, $CH_3OH$, $CH_2Cl_2$, rt; 2)$NaNO_2$, AcOH, DMSO, 40 °C;
c: 1)LDA, THF, PhSeCl; 2) m-CPBA, $CHCl_3$

**a**: Ar = Ph; **b**: 4-$MeC_6H_4$; **c**: 4-$FC_6H_4$; **d**: 4-$ClC_6H_4$; **e**: 2,4-$Cl_2C_6H_3$; **f**: 4-$BrC_6H_4$; **g**: 4-$CF_3C_6H_4$; **h**: 2-furyl; **i**: thienyl

**Figure 2.** Synthesis of (−)-incrustoporin derivatives **4a−i** and **5a−i**.

Under the catalysis of proline, acetone reacted with different nitroolefins to give corresponding adducts **3a−i** in high yield (83−97%). Via reactions of reduction, oxidation, and intramolecular esterification successively, **3a−i** were converted to corresponding 3-aryl-5-methyl-$\gamma$-butyrolactone **4a−i**.[32] Finally, the double bond was introduced by enolization of the lactones **4a−i** followed by treatment with phenylselenenyl chloride, oxidation, and spontaneous selenoxide elimination to yield the target compounds **5a−i**.[13]

*Synthesis of the Compound (R)-**5d**.* To explore the effect of chirality at C(5) on biological activity, (*R*)-**5d** was prepared from (*S*)-**3d** by using the method shown in Figure 2. (3*S*,5*RS*)-**4**, obtained via reactions of reduction, oxidation, and intramolecular esterification of (*S*)-**3d**, were separated by column chromatography to give (3*S*,5*R*)-**4d** and (3*S*,5*S*)-**4d** with excellent diastereoselective (*trans*/*cis* = 23:1 and 1:15, respectively) determined by $^1$H NMR analysis. Their absolute configurations were confirmed by spectroscopic data ($^1$H NMR, $^{13}$C NMR) and single-crystal X-ray diffraction analysis (Figure 3). Unfortunately, (*R*)-**5d** was obtained with moderate enantioselectivities (56% ee) under the above reaction conditions from (3*S*,5*R*)-**4d**, and (*R*)-**5d** was obtained with enantioselectivities (16% ee) from (3*S*,5*S*)-**4d**.

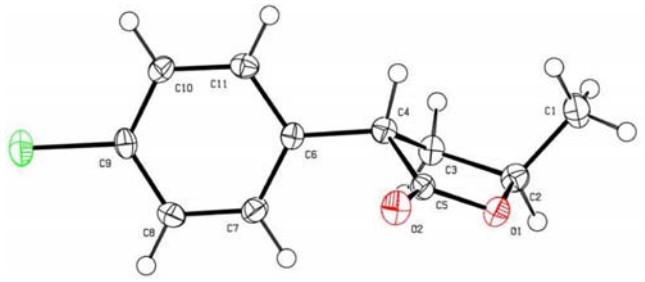


**Figure 3.** ORTEP drawing of compound (3*S*,5*R*)-**4d** (CCDC 1009910).

**Phytotoxic Activity.** Compounds **4a−i** and **5a−i** were first tested for their phytotoxic activity against the test plant. The results indicated that compounds **4a−i** showed no phytotoxic activity at 500 $\mu$g mL$^{-1}$. However, dehydro compounds **5a−g** displayed phytotoxic activity to tobacco (*Nicotiana tabacum* var. Xanthi nc), so the antiviral activity of **5a−g** was not tested at 500 $\mu$g mL$^{-1}$.

**Antiviral Activity.** The anti-TMV activity of compounds **4a−i** and **5a−i** was tested. The commercial plant virucide ribavirin was used as the control.

*In Vitro Anti-TMV Activity.* The in vitro antiviral assay results of all of the synthesized compounds are listed in Table 1. As the control, ribavirin exhibited a 41% inhibitory effect at 500 $\mu$g mL$^{-1}$, whereas most of the synthesized compounds **4a−i** exhibited higher antiviral activity than ribavirin; especially compound **4i** with 61% inhibitory effect emerged as a new lead compound for anti-TMV research. When the concentration was lowered to 100 $\mu$g mL$^{-1}$, compounds **4c**, (3*S*,5*R*)-**4d**, **4i**, and **5i** displayed nearly equal or higher inhibitory effect than that of ribavirin. To investigate the influence of chirality at C(5) and C(3) on the anti-TMV activity, compounds (3*S*,5*R*)-**4d**, (3*S*,5*S*)-**4d**, and (3*RS*, 5*RS*)-**4d** (or **4d** for short) were tested, which exhibited 48, 43, and 40% inhibitory effect at 500 $\mu$g mL$^{-1}$, respectively. The bioassay results also showed that the (3*S*, 5*R*) configuration is the preferred antiviral configuration for 3-aryl-5-methyl-$\gamma$-butyrolactone [(3*S*,5*R*)-**4d** > (3*S*,5*S*)-**4d** > **4d**].

As shown in Table 1, most of the compounds **4a−i** displayed good in vitro activity against TMV; however, almost all of the compounds **5a−i** displayed phytotoxic activity against the test plant at 500 $\mu$g mL$^{-1}$. Therefore, compounds **4a−i** were bioassayed further to investigate their antiviral activity in vivo.

*In Vivo Anti-TMV Activity.* As shown in Table 2, most of the compounds also displayed higher in vivo activity than that of the ribavirin. **4i** showed the best in vivo anti-TMV activity (inactivation activity = 52% at 500 $\mu$g mL$^{-1}$ and 20% at 100 $\mu$g mL$^{-1}$; curative activity = 57% at 500 $\mu$g mL$^{-1}$ and 30% at 100 $\mu$g mL$^{-1}$; and protection activity = 56% at 500 $\mu$g mL$^{-1}$ and 28% at 100 $\mu$g mL$^{-1}$), which is significantly higher than that of ribavirin (inactivation activity = 40% at 500 $\mu$g mL$^{-1}$ and 12% at 100 $\mu$g mL$^{-1}$; curative activity = 37% at 500 $\mu$g mL$^{-1}$ and 14% at 100 $\mu$g mL$^{-1}$; and protection activity = 40% at 500 $\mu$g mL$^{-1}$ and 17% at 100 $\mu$g mL$^{-1}$).

Unlike in vitro antiviral assay results, **4d** displayed higher in vivo activity than that of (3*S*,5*R*)-**4d** and (3*S*,5*S*)-**4d** (in vivo activity: **4d** > (3*S*,5*R*)-**4d** > (3*S*,5*S*)-**4d**), except for the protection effect of (3*S*,5*R*)-**4d**.

**Table 1. In Vitro Antiviral Activity of Compounds 4a−i and 5a−i against TMV**

| compd | concn ($\mu$g mL$^{-1}$) | inhibition rate[a] (%) | compd | concn ($\mu$g mL$^{-1}$) | inhibition rate[a] (%) |
|---|---|---|---|---|---|
| **4a** | 500 | 46 ± 1 | **5a** | 500 | NT |
| | 100 | 8 ± 1 | | 100 | 0 |
| **4b** | 500 | 38 ± 2 | **5b** | 500 | NT |
| | 100 | 0 | | 100 | 5 ± 1 |
| **4c** | 500 | 53 ± 1 | **5c** | 500 | NT |
| | 100 | 16 ± 2 | | 100 | 9 ± 1 |
| **4d** | 500 | 40 ± 2 | **5d** | 500 | NT |
| | 100 | 5 ± 1 | | 100 | 0 |
| (3*S*,5*R*)-**4d** | 500 | 48 ± 2 | (*R*)-**5d** | 500 | NT |
| | 100 | 20 ± 1 | | 100 | 6 ± 1 |
| (3*S*,5*S*)-**4d** | 500 | 43 ± 2 | **5e** | 500 | NT |
| | 100 | 0 | | 100 | 0 |
| **4e** | 500 | 45 ± 1 | **5f** | 500 | NT |
| | 100 | 0 | | 100 | 0 |
| **4f** | 500 | 46 ± 2 | **5g** | 500 | NT |
| | 100 | 0 | | 100 | 0 |
| **4g** | 500 | 43 ± 1 | **5h** | 500 | 37 ± 1 |
| | 100 | 0 | | 100 | 0 |
| **4h** | 500 | 35 ± 2 | **5i** | 500 | 38 ± 2 |
| | 100 | 0 | | 100 | 10 ± 1 |
| **4i** | 500 | 61 ± 1 | ribavirin | 500 | 41 ± 2 |
| | 100 | 27 ± 1 | | 100 | 10 ± 1 |

[a]Average of three replicates. All results are expressed as mean ± SD. NT, not tested.

**Table 2. In Vivo Antiviral Activity of Compounds 4a−i against TMV**

| compd | concn ($\mu$g mL$^{-1}$) | inactivation effect[a] (%) | curative effect[a] (%) | protection effect[a] (%) |
|---|---|---|---|---|
| **4a** | 500 | 50 ± 1 | 55 ± 2 | 58 ± 1 |
| | 100 | 19 ± 3 | 20 ± 1 | 22 ± 1 |
| **4b** | 500 | 35 ± 1 | 33 ± 3 | 47 ± 1 |
| | 100 | 0 | 0 | 0 |
| **4c** | 500 | **48** ± 2 | **57** ± 1 | **60** ± 2 |
| | 100 | 25 ± 2 | 27 ± 1 | 21 ± 1 |
| **4d** | 500 | 43 ± 1 | 51 ± 2 | 47 ± 1 |
| | 100 | 15 ± 1 | 19 ± 1 | 11 ± 1 |
| (3*S*,5*R*)-**4d** | 500 | 42 ± 1 | 40 ± 3 | 50 ± 1 |
| | 100 | 13 ± 1 | 9 ± 1 | 18 ± 1 |
| (3*S*,5*S*)-**4d** | 500 | 30 ± 2 | 41 ± 1 | 46 ± 2 |
| | 100 | 0 | 0 | 10 ± 1 |
| **4e** | 500 | 38 ± 2 | 34 ± 2 | 44 ± 1 |
| | 100 | 0 | 0 | 0 |
| **4f** | 500 | 46 ± 1 | 43 ± 1 | 34 ± 1 |
| | 100 | 14 ± 2 | 9 ± 2 | 0 |
| **4g** | 500 | 42 ± 1 | 35 ± 1 | 39 ± 2 |
| | 100 | 0 | 0 | 16 ± 1 |
| **4h** | 500 | 31 ± 2 | 39 ± 2 | 47 ± 1 |
| | 100 | 0 | 11 ± 2 | 0 |
| **4i** | 500 | **52** ± 2 | **57** ± 1 | **56** ± 2 |
| | 100 | 20 ± 1 | 30 ± 2 | 28 ± 1 |
| ribavirin | 500 | 40 ± 2 | 37 ± 1 | 40 ± 2 |
| | 100 | 12 ± 1 | 14 ± 1 | 17 ± 1 |

[a]Average of three replicates. All results are expressed as mean ± SD.

Introduction of a methyl or trifluoromethyl group at the 4-position of the phenyl ring dramatically decreased inhibition effect (in vivo activity: **4a** > **4g** > **4b**). Compounds **4d−f** containing halogen atoms such as chlorine and bromine on the phenyl ring also exhibited lower inhibitory effect than that of **4a**. However, 4-fluorophenyl-substituted compound **4c** gave relatively higher activity (48, 57, and 60% at 500 $\mu$g mL$^{-1}$).

Compound **4h** containing a furan ring at C(3) exhibited a lower activity than the others, whereas **4i** containing a thiofuran ring was the optimal compound for anti-TMV research.

**Fungicidal Activity.** The fungicidal activities of compounds **4a−i** and **5a−i** were investigated. The commercial fungicides chlorothalonil, carbendazim, and azoxystrobin were used as the controls.

*In Vitro Fungicidal Activity.* The target compounds **5** and **4** were evaluated for their in vitro antifungal activity on 14 kinds of plant fungi at 50 mg kg$^{-1}$ (Table 3). Unlike the antiviral activity, saturated lactones **4** displayed moderate fungicidal activity, whereas most of the unsaturated lactones **5** exhibited excellent fungicidal activity against the tested fungi, which indicated that the small changes between **4** and **5** at the 3,4-position result in large differences in bioactivities. Compound **5g**, containing a trifluoromethyl group at the 4-position of phenyl ring, exhibited broad-spectrum and good fungicidal activity against 13 kinds of fungi. Compounds **5d−g** exhibited higher fungicidal activity than chlorothalonil and carbendazim against *C.H* (*Cercospora arachidicola* Hori) at 50 mg kg$^{-1}$. Some of these compounds selectively exhibited fungicidal activity to certain fungi. For example, the inhibitory effect of compound **5b** (against *Rhizoctonia solani*), compound **5c−d** (against *Sclerotinia sclerotiorum*), and **5d−g** (against *Cercospora arachidicola* Hori, *Rhizoctonia cerealis*, *Rhizoctonia solani*, *Botrytis cinerea*) were >90%, which is much higher than that for other fungi.

The fungicidal activities of compound **5b** (against *Rhizoctonia solani*) and compounds **5d−g** (against *Cercospora arach-idicola* Hori, *Rhizoctonia cerealis*, *Rhizoctonia solani*, *Botrytis cinerea*) were also excellent at 25 mg kg$^{-1}$ (>70%, except for **5g** against *Rhizoctonia cerealis*). Compounds (*R*)-**5d** and **5g** exhibited >50% inhibition rate against *Rhizoctonia solani* at 6.25 mg kg$^{-1}$ (Table 4).


dx.doi.org/10.1021/jf503060k | J. Agric. Food Chem. 2014, 62, 8799−8807

**Table 3. Fungicidal Activity of the Compounds 4a−i and 5a−i against 14 Kinds of Fungi**

| | fungicidal activity (%)[a]/50 mg kg$^{-1}$ | | | | | | | | | | | | | |
|---|---|---|---|---|---|---|---|---|---|---|---|---|---|---|
| compd | *F.C*[b] | *C.H*[b] | *P.P*[b] | *A.S*[b] | *F.G*[b] | *F.M*[b] | *S.S*[b] | *P.C*[b] | *R.C*[b] | *B.M*[b] | *W.A*[b] | *P.I*[b] | *R.S*[b] | *B.C*[b] |
| **4a** | 26 ± 1 | 8 ± 1 | 46 ± 2 | 35 ± 1 | 17 ± 2 | 18 ± 1 | 55 ± 2 | 19 ± 1 | 21 ± 1 | 29 ± 2 | 39 ± 1 | 19 ± 1 | 44 ± 2 | 57 ± 1 |
| **4b** | 26 ± 1 | 15 ± 2 | 69 ± 1 | 41 ± 1 | 41 ± 2 | 18 ± 1 | 82 ± 2 | 38 ± 1 | 58 ± 2 | 12 ± 1 | 50 ± 1 | 19 ± 2 | 74 ± 1 | 47 ± 1 |
| **4c** | 26 ± 1 | 23 ± 2 | 54 ± 2 | 41 ± 1 | 24 ± 3 | 18 ± 1 | 73 ± 1 | 29 ± 2 | 79 ± 1 | 35 ± 2 | 28 ± 1 | 44 ± 2 | 82 ± 1 | 86 ± 1 |
| **4d** | 26 ± 2 | 23 ± 1 | 77 ± 1 | 41 ± 2 | 35 ± 1 | 36 ± 1 | 64 ± 2 | 43 ± 2 | 58 ± 1 | 47 ± 1 | 33 ± 2 | 31 ± 1 | 64 ± 2 | 33 ± 1 |
| (3*S*,5*R*)-**4d** | 32 ± 1 | 23 ± 1 | 39 ± 1 | 29 ± 3 | 21 ± 1 | 18 ± 2 | 55 ± 2 | 43 ± 1 | 21 ± 2 | 29 ± 2 | 39 ± 1 | 25 ± 1 | 33 ± 3 | 81 ± 1 |
| (3*S*,5*S*)-**4d** | 37 ± 3 | 23 ± 1 | 46 ± 1 | 41 ± 1 | 24 ± 1 | 18 ± 1 | 55 ± 1 | 48 ± 1 | 26 ± 1 | 24 ± 1 | 22 ± 1 | 13 ± 1 | 62 ± 1 | 71 ± 1 |
| **4e** | 37 ± 1 | 31 ± 1 | 15 ± 2 | 35 ± 1 | 38 ± 2 | 36 ± 1 | 46 ± 2 | 43 ± 1 | 37 ± 2 | 41 ± 1 | 50 ± 1 | 38 ± 2 | 59 ± 1 | 71 ± 3 |
| **4f** | 53 ± 2 | 46 ± 2 | 92 ± 1 | 41 ± 3 | 45 ± 1 | 18 ± 4 | 82 ± 1 | 48 ± 4 | 90 ± 1 | 35 ± 3 | 39 ± 3 | 31 ± 1 | 85 ± 3 | 86 ± 1 |
| **4g** | 32 ± 1 | 8 ± 1 | 46 ± 1 | 35 ± 2 | 10 ± 1 | 36 ± 2 | 73 ± 1 | 38 ± 1 | 68 ± 3 | 29 ± 1 | 33 ± 2 | 19 ± 1 | 33 ± 2 | 67 ± 3 |
| **4h** | 32 ± 2 | 8 ± 1 | 62 ± 3 | 24 ± 1 | 17 ± 1 | 18 ± 2 | 27 ± 1 | 33 ± 2 | 37 ± 1 | 18 ± 2 | 28 ± 1 | 6 ± 1 | 36 ± 2 | 57 ± 1 |
| **4i** | 32 ± 1 | 8 ± 2 | 62 ± 1 | 29 ± 2 | 24 ± 1 | 9 ± 1 | 64 ± 2 | 24 ± 1 | 26 ± 2 | 18 ± 1 | 33 ± 2 | 6 ± 1 | 8 ± 1 | 24 ± 1 |
| **5a** | 26 ± 1 | 31 ± 2 | 62 ± 1 | 41 ± 2 | 52 ± 1 | 36 ± 2 | 82 ± 1 | 38 ± 3 | 79 ± 2 | 29 ± 1 | 33 ± 1 | 31 ± 1 | 85 ± 2 | 71 ± 1 |
| **5b** | 37 ± 1 | 46 ± 1 | 31 ± 2 | 53 ± 1 | 69 ± 1 | 9 ± 2 | 73 ± 1 | 38 ± 1 | 58 ± 3 | 47 ± 1 | 39 ± 1 | 25 ± 1 | **95** ± 1 | 81 ± 1 |
| **5c** | 32 ± 3 | 54 ± 1 | 31 ± 4 | 41 ± 1 | 38 ± 3 | 18 ± 1 | 91 ± 2 | 38 ± 1 | 32 ± 3 | 29 ± 1 | 39 ± 3 | 13 ± 1 | 90 ± 2 | 86 ± 1 |
| **5d** | 74 ± 1 | 85 ± 3 | 92 ± 1 | 77 ± 1 | 59 ± 2 | 46 ± 1 | 91 ± 2 | 81 ± 1 | **95** ± 2 | 59 ± 1 | 61 ± 1 | 31 ± 2 | **97** ± 1 | 91 ± 1 |
| (R)-**5d** | 42 ± 1 | **100** | 85 ± 2 | 77 ± 1 | 59 ± 2 | 36 ± 2 | 91 ± 1 | 67 ± 1 | **95** ± 2 | 53 ± 1 | 67 ± 2 | 44 ± 1 | **100** | **100** |
| **5e** | 68 ± 2 | **100** | 92 ± 1 | 88 ± 1 | 55 ± 1 | 55 ± 1 | 46 ± 3 | 62 ± 1 | **95** ± 2 | 76 ± 2 | 83 ± 1 | 56 ± 3 | **97** ± 1 | 95 ± 2 |
| **5f** | 42 ± 1 | 92 ± 2 | 77 ± 1 | 82 ± 2 | 52 ± 1 | 46 ± 3 | 91 ± 1 | 57 ± 2 | **95** ± 1 | 35 ± 1 | 44 ± 2 | 38 ± 1 | 95 ± 2 | 91 ± 1 |
| **5g** | 47 ± 2 | **100** | 92 ± 3 | 88 ± 1 | 41 ± 1 | 82 ± 3 | 82 ± 1 | 81 ± 1 | **95** ± 1 | 88 ± 2 | 83 ± 1 | 69 ± 2 | **100** | **95** ± 1 |
| **5h** | 16 ± 1 | 0 | 62 ± 1 | 47 ± 1 | 14 ± 2 | 18 ± 1 | 36 ± 1 | 24 ± 2 | 37 ± 1 | 35 ± 1 | 33 ± 2 | 19 ± 1 | 0 | 86 ± 2 |
| **5i** | 32 ± 2 | 8 ± 1 | 62 ± 3 | 35 ± 1 | 38 ± 2 | 27 ± 1 | 73 ± 2 | 14 ± 1 | 79 ± 1 | 35 ± 1 | 50 ± 2 | 25 ± 1 | 69 ± 1 | 48 ± 1 |
| chlorothalonil[c] | 100 | 73 ± 1 | 100 | 73 ± 2 | <50 | 100 | <50 | 100 | 100 | 91 ± 1 | 91 ± 2 | 86 ± 1 | 100 | 100 |
| carbendazim[c] | <50 | <50 | <50 | <50 | 100 | <50 | 100 | <50 | 100 | 100 | 100 | 100 | 100 | <50 |

[a]Average of three replicates. All results are expressed as mean ± SD. [b]F.C, *Fusarium oxysporum* f. sp. *cucumeris*; C.H, *Cercospora arachidicola* Hori; P.P, *Physalospora piricola*; A.S, *Alternaria solani*; F.G, *Fusarium graminearum*; F.M, *Fusarium moniliforme*; S.S, *Sclerotinia sclerotiorum*; P.C, *Phytophthora capsici*; R.C, *Rhizoctonia cerealis*; B.M, *Bipolaris maydis*; W.A, watermelon anthracnose; P.I,*Phytophthora infestans*; R.S, *Rhizoctonia solani*; B.C, *Botrytis cinerea*. [c]The commercial agricultural fungicides were used for comparison of antifungal activity.



dx.doi.org/10.1021/jf503060k | J. Agric. Food Chem. 2014, 62, 8799−8807

**Table 4. Fungicidal Activity of the Selected Compounds**

| compd | concn ($\mu$g mL$^{-1}$) | inhibition rate[a](%) C.H | R.C | R.S | B.C |
|---|---|---|---|---|---|
| **5b** | 25.00 | NT | NT | 73 ± 2 | NT |
| **5c** | 25.00 | NT | NT | 69 ± 1 | NT |
| **5d** | 25.00 | 75 ± 1 | 74 ± 2 | **96** ± 1 | 88 ± 2 |
| | 12.50 | NT | NT | 77 ± 1 | NT |
| | 6.25 | NT | NT | 10 ± 1 | NT |
| (*R*)-**5d** | 25.00 | 88 ± 2 | 76 ± 1 | **100** | 88 ± 1 |
| | 12.50 | NT | NT | 77 ± 3 | NT |
| | 6.25 | NT | NT | 72 ± 1 | NT |
| **5e** | 25.00 | 88 ± 1 | 91 ± 2 | **94** ± 1 | **94** ± 2 |
| | 12.50 | NT | NT | 85 ± 3 | 80 ± 1 |
| | 6.25 | NT | NT | 59 ± 1 | 61 ± 1 |
| **5f** | 25.00 | 75 ± 1 | 71 ± 1 | 92 ± 2 | 88 ± 1 |
| | 12.50 | NT | NT | 46 ± 1 | NT |
| | 6.25 | NT | NT | 8 ± 1 | NT |
| **5g** | 25.00 | 88 ± 2 | 55 ± 1 | **98** ± 1 | 82 ± 2 |
| | 12.50 | NT | NT | 74 ± 3 | NT |
| | 6.25 | NT | NT | 0 | NT |
| chlorothalonil[b] | 25.00 | NT | NT | NT | 96 ± 2 |
| | 12.50 | NT | NT | NT | 89 ± 2 |
| | 6.25 | NT | NT | NT | 82 ± 1 |
| carbendazim[b] | 25.00 | NT | 100 | 100 | NT |
| | 12.50 | NT | 97 ± 2 | 97 ± 1 | NT |
| | 6.25 | NT | 94 ± 1 | 67 ± 3 | NT |

[a]Average of three replicates. All results are expressed as mean ± SD. NT, not tested. [b]The commercial agricultural fungicides were used for comparison of antifungal activity.

*In Vivo Fungicidal Activity.* Compounds **4a−i** and **5a−i** were evaluated in a series of in vivo fungicidal tests. The pathogens tested in this screen were *Puccinia sorghi* on corn, *Puccinia triticina* on wheat, *Blum eria graminis* f. sp.*tritici* on wheat, *Sclerotinia sclerotiorum* on rape, *Rhizoctonia solani* on rice, *Botrytis cinerea on* cucumber, and *Corynespora cassiicola* on cucumber with protection. The resulting data (Table 5) revealed that compounds **5a−i** displayed a degree of in vivo fungicidal activity. Compounds **5b−d** with ≥60% inhibitory effect against *Puccinia sorghi* on corn emerged as new antifungal lead compounds.

In summary, a series of lactone compounds **4a−i** and **5a−i** were designed and synthesized on the basis of the structure of natural product (−)-incrustoporin (**1**) and characterized by $^1$H NMR and mass spectroscopy. Their antiviral activity against TMV and antifungal activity against 14 fungi were systematically evaluated. The bioassay results showed that the small changes between **4** and **5** at the 3,4-position result in large differences in bioactivities. 3-Aryl-5-methyl-$\gamma$-butyrolactone **4** exhibited good to excellent anti-TMV activity, and some of the compounds displayed higher antiviral activity than commercial ribavirin. Especially, the inactivation, curative, and protection activities of compound **4i** (52, 57, and 56%, respectively, at 500 $\mu$g mL$^{-1}$) were much higher than those of ribavirin (40, 37, and 40% at 500 $\mu$g mL$^{-1}$). Compounds **5** exhibited good fungicidal activity; especially (*R*)-**5d** displayed excellent fungicidal activity both in vitro and in vivo. To our knowledge, this is the first report on 3-aryl-5-methyl-$\gamma$-butyrolactone and 3-aryl-5-methyl-2,5-dihydrofuran-2-one as potential disease control agents against tobacco mosaic virus and plant pathogenic fungi.

**Table 5. In Vivo Fungicidal Activity of the Compounds 4a−i and 5a−i against Seven Kinds of Fungi**

| compd | inhibition rate (%)[a]/200 mg kg$^{-1}$ P.S[b] | P.T[b] | B.G[b] | S.S[b] | R.S[b] | B.C[b] | C.C[b] |
|---|---|---|---|---|---|---|---|
| **4a** | 0 | 0 | 10 ± 1 | 7 ± 2 | 3 ± 1 | 11 ± 1 | 13 ± 3 |
| **4b** | 0 | 0 | 10 ± 1 | 11 ± 3 | 6 ± 2 | 15 ± 2 | 13 ± 1 |
| **4c** | 0 | 0 | 0 | 6 ± 1 | 5 ± 1 | 11 ± 4 | 6 ± 2 |
| **4d** | 0 | 0 | 20 ± 2 | 15 ± 2 | 23 ± 1 | 22 ± 3 | 11 ± 3 |
| (3*S*,5*R*)-**4d** | 0 | 10 ± 1 | 20 ± 2 | 7 ± 2 | 3 ± 1 | 15 ± 2 | 11 ± 1 |
| (3*S*,5*S*)-**4d** | 0 | 0 | 0 | 7 ± 1 | 16 ± 2 | 11 ± 1 | 22 ± 3 |
| **4e** | 0 | 10 ± 1 | 20 ± 2 | 18 ± 2 | 5 ± 1 | 11 ± 1 | 6 ± 1 |
| **4f** | 0 | 0 | 0 | 7 ± 1 | 10 ± 2 | 22 ± 3 | 22 ± 1 |
| **4g** | 0 | 0 | 0 | 6 ± 1 | 5 ± 1 | 6 ± 1 | 6 ± 1 |
| **4h** | 0 | 0 | 10 ± 2 | 9 ± 1 | 5 ± 1 | 7 ± 2 | 11 ± 2 |
| **4i** | 0 | 0 | 0 | 18 ± 3 | 5 ± 1 | 6 ± 1 | 15 ± 1 |
| **5a** | 10 ± 1 | 10 ± 2 | 20 ± 1 | 6 ± 1 | 10 ± 1 | 11 ± 1 | 13 ± 1 |
| **5b** | **60** ± 1 | 0 | 0 | 11 ± 1 | 23 ± 4 | 11 ± 1 | 26 ± 2 |
| **5c** | **70** ± 2 | 0 | 0 | 40 ± 2 | 56 ± 1 | 56 ± 2 | 41 ± 1 |
| **5d** | **60** ± 3 | 20 ± 1 | 0 | 19 ± 1 | 13 ± 1 | 13 ± 1 | 18 ± 1 |
| (*R*)-**5d** | **85** ± 1 | 10 ± 1 | 30 ± 2 | 22 ± 3 | 18 ± 1 | 22 ± 2 | 22 ± 1 |
| **5e** | 10 ± 1 | 20 ± 2 | 20 ± 1 | 22 ± 1 | 10 ± 1 | 11 ± 1 | 11 ± 1 |
| **5f** | 30 ± 3 | 0 | 0 | 11 ± 1 | 10 ± 3 | 11 ± 1 | 16 ± 1 |
| **5g** | 0 | 10 | 0 | 22 ± 2 | 10 ± 1 | 9 ± 1 | 17 ± 1 |
| **5h** | 0 | 10 | 0 | 11 ± 1 | 10 ± 1 | 37 ± 4 | 11 ± 1 |
| **5i** | 0 | 0 | 0 | 15 ± 1 | 6 ± 1 | 22 ± 2 | 11 ± 1 |
| azoxystrobin[c] | 100 | 100 | 100 | 83 ± 2 | 81 ± 1 | 82 ± 3 | 75 ± 2 |

[a]Average of five replicates. All results are expressed as mean ± SD. [b]P.S, *Puccinia sorghi* (corn protection); P. T, *Puccinia triticina* (wheat protection); B. G, *Blum eria graminis* f. sp. *tritici* (wheat protection); S.S, *Sclerotinia sclerotiorum* (rape protection); R.S, *Rhizoctonia solani* (rice protection); B.C, *Botrytis cinerea* (cucumber protection); C.C, *Corynespora cassiicola* (cucumber protection). [c]The commercial agricultural fungicide was used for comparison of antifungal activity. The dilution of azoxystrobin is 1000 times.


dx.doi.org/10.1021/jf503060k | J. Agric. Food Chem. 2014, 62, 8799−8807

Further studies on mode of action are currently underway in our laboratories.

## ■ ASSOCIATED CONTENT

### Supporting Information

$^{1}$H and $^{13}$C NMR and HRMS spectra of compounds **3**, **4**, **5** and HPLC chromatograms of (*R*)-**5d**. This material is available free of charge via the Internet at http://pubs.acs.org.

## ■ AUTHOR INFORMATION


### Corresponding Authors

*(A.L.) E-mail: luaidang@hebut.edu.cn. Phone: 0086-22-60202241, ext. 205. Fax: 0086-22-60204274.

*(J.C.) E-mail: chjx2000@gmail.com. Phone: 0086-22-60202241, ext. 215. Fax: 0086-22-60204274.

*(Q.W.) E-mail: wangqm@nankai.edu.cn. Phone: 0086-22-23503952. Fax: 0086-22-23503952



### Funding

This study was supported by Natural Science Fund of China (21302038, 21276063, and 51309074), Natural Science Fund of Hebei Province (B2013202237), PCSIRT (IRT1059), and Support Program for Hundred Excellent Innovation Talents from the Universities of Hebei Province (CPRC013).


### Notes

The authors declare no competing financial interest.

## ■ REFERENCES


(1) Wilson, R. A.; Talbot, N. J. Fungal physiology − a future perspective. *Microbiology (Reading, U.K.)* **2009**, *155*, 3810−3815.

(2) Chattapadhyay, T. K.; Dureja, P. Antifungal activity of 4-methyl-6-alkyl-2*H*-pyran-2-ones. *J. Agric. Food Chem.* **2006**, *54*, 2129−2133.

(3) Ritzenthaler, C. Resistance to plant viruses: old issue, new answer. *Curr. Opin. Biotechnol.* **2005**, *16*, 118−122.

(4) Liu, C. L. *Pesticide in the World: Fungicide*; Chemical Industry Press: Beijing, China, 2006; pp 1−492.

(5) Song, B. A.; Yang, S.; Jin, L. H. *New Heterocyclic Pesticide: Fungicide*; Chemical Industry Press: Beijing, China, 2009; pp 1−473.

(6) Song, B. A.; Yang, S.; Jin, L. H.; Bhadury, P. S. *Environment-Friendly Anti-plant Viral Agents*; Chemical Industry Press (Beijing) and Springer Press: Beijing, China, 2009; pp 1−305.

(7) Xu, H.; Fan, L. L. Antifungal agents. Part 4: Synthesis and antifungal activities of novel indole[1,2-*c*]-1,2,4-benzotriazine derivatives against phytopathogenic fungi in vitro. *Eur. J. Med. Chem.* **2011**, *46*, 364−369.

(8) Qian, X. H.; Lee, P. W.; Cao, S. China: Forward to the green pesticides via a basic research program. *J. Agric. Food Chem.* **2010**, *58*, 2613−2623.

(9) Newman, D. J.; Cragg, G. M. Natural products as sources of new drugs over the 30 years from 1981 to 2010. *J. Nat. Prod.* **2012**, *75*, 311−335.

(10) Zapf, S.; Anke, T.; Sterner, O. Incrustoporin, a new antibiotic from *Incrustoporia carneola* (Bres.) Ryv. (Basidiomycetes). *Acta Chem. Scand.* **1995**, *49*, 233−234.

(11) Kuneš, J.; Balšánek, V.; Pour, M.; Buchta, V. Synthesis and antifungal activity evaluation of 3-hetaryl-2,5-dihydrofuran-2-ones. An unusual fragmentation of the oxazole ring via 2,3-selenoxide shift. *Collect. Czech. Chem. Commun.* **2001**, *66*, 1809−1830.

(12) Pour, M.; Špulák, M.; Buchta, V.; Kubanová, P.; Opršalová, M.; Wsól, V.; Fáková, H.; Koudelka, P.; Pourová, H.; Schiller, R. 3-Phenyl-5-acyloxymethyl-2*H*,5*H*-furan-2-ones: synthesis and biological activity of a novel group of potential antifungal drugs. *J. Med. Chem.* **2001**, *44*, 2701−2706.

(13) Pour, M.; Špulák, M.; Balšánek, V.; Kuneš, J.; Kubanová, P.; Buchta, V. Synthesis and structure−antifungal activity relationships of 3-aryl-5-alkyl-2,5-dihydrofuran-2-ones and their carbanalogues: further refinement of tentative pharmacophore group. *Bioorg. Med. Chem.* **2003**, *11*, 2843−2866.

(14) Pour, M. Giberelity, nakienony a inkrustoporiny: radosti a strasti syntéz malých, vysoce funkcionalizovaných molekul. *Chem. Listy* **2003**, *97*, 1061−1069.

(15) Vale-Silva, L. A.; Buchta, V.; Vokurková, D.; Pour, M. Investigation of the mechanism of action of 3-(4-bromophenyl)-5-acyloxymethyl-2,5-dihydrofuran-2-one against *Candida albicans* by flow cytometry. *Bioorg. Med. Chem. Lett.* **2006**, *16*, 2492−2495.

(16) Nobilis, M.; Pour, M.; Šenel, P.; Pavlík, J.; Kuneš, J.; Opršalová, M.; Kolářová, L.; Holčapek, M. Metabolic profiling of a potential antifungal drug, 3-(4-bromophenyl)-5-acetoxymethyl-2,5-dihydrofuran-2-one, in mouse urine using high-performance liquid chromatography with UV photodiode-array and mass spectrometric detection. *J. Chromatogr., B* **2007**, *853*, 10−19.

(17) Šenel, P.; Tichotová, L.; Votruba, I.; Buchta, V.; Špulák, M.; Kuneš, J.; Nobilis, M.; Krenk, O.; Pour, M. Antifungal 3,5-disubstituted furanones: from 5-acyloxymethyl to 5-alkylidene derivatives. *Bioorg. Med. Chem.* **2010**, *18*, 1988−2000.

(18) Yajima, A.; Mori, K. Synthesis of both the enantiomers of incrustoporin, an antibiotic from *Incrustoporia carneola*. *Liebigs Ann.* **1996**, *1996*, 1091−1093.

(19) Rossi, R.; Bellina, F.; Biagetti, M.; Mannina, L. Enantioselective synthesis of (*R*)-incrustoporin, an antibiotic isolated from *Incrustoporia carneola*. *Tetrahedron: Asymmetry* **1999**, *10*, 1163−1172.

(20) Yu, Q.; Liu, J. F.; Wu, Y. L. Total synthesis of (−)-incrustoporin. *J. Asian Nat. Prod. Res.* **1999**, *1*, 183−188.

(21) Fontes, M.; Verdaguer, X.; Solà, L.; Vidal-Ferran, A.; Reddy, K. S.; Riera, A.; Pericàs, M. A. Addition of diethylzinc to dicobalt hexacarbonyl complexes of $\alpha,\beta$-acetylenic aldehydes with virtually complete enantioselectivity. A formal synthesis of (+)-incrustoporin. *Org. Lett.* **2002**, *4*, 2381−2383.

(22) Oh, C. H.; Park, S. J.; Ryu, J. H.; Gupta, A. K. Regioselective Pd-catalyzed alkylative lactonizations of 4-hydroxy-2-alkynecarboxylates with organoboronic acids. *Tetrahedron Lett.* **2004**, *45*, 7039−7042.

(23) Fernandes, R. A.; Patil, P. H.; Chowdhury, A. K. Ring-closing metathesis enabled efficient synthesis of $\gamma$-butenolide antifungal agent (−)-incrustoporin and its analogues. *Asian J. Org. Chem.* **2014**, *3*, 58−62.

(24) Wang, Z. W.; Wei, P.; Wang, L. Z.; Wang, Q. M. Design, synthesis, and anti-tobacco mosaic virus (TMV) activity of phenanthroindolizidines and their analogues. *J. Agric. Food Chem.* **2012**, *60*, 10212−10219.

(25) Wang, Z. W.; Feng, A.; Cui, M.; Liu, Y.; Wang, L.; Wang, Q. M. First discovery and structure-activity relationship study of phenanthroquinolizidines as novel antiviral agents against tobacco mosaic virus (TMV). *PLoS One* **2012**, *7*, No. e52933.

(26) Song, H. J.; Liu, Y. X.; Liu, Y. X.; Wang, L. Z.; Wang, Q. M. Synthesis and antiviral and fungicidal activity evaluation of $\beta$-carboline, dihydro-$\beta$-carboline, tetrahydro-$\beta$-carboline alkaloids, and their derivatives. *J. Agric. Food Chem.* **2014**, *62*, 1010−1018.

(27) Kuster, G. J. T.; Steeghs, R. H. J.; Scheeren, H. W. Novel five/five- and six/five-membered bicyclic nitroso acetals from high-pressure-promoted cyclisation reactions of *p*-methoxybenzyl vinyl ether, 1-nitro-2-heteroaryl ethenes, and mono- and disubstituted olefins. *Eur. J. Org. Chem.* **2001**, *2001*, 553−560.

(28) Lu, A. D.; Liu, T.; Wu, R. H.; Wang, Y. M.; Wu, G. P.; Zhou, Z. H.; Fang, J. X.; Tang, C. C. A recyclable organocatalyst for asymmetric Michael addition of acetone to nitroolefins. *J. Org. Chem.* **2011**, *76*, 3872−3879.

(29) Sakthivel, K.; Notz, W.; Bui, T.; Barbas, C. F. Amino acid catalyzed direct asymmetric Aldol reactions: a bioorganic approach to catalytic asymmetric carbon−carbon bond-forming reactions. *J. Am. Chem. Soc.* **2001**, *123*, 5260−5267.

(30) Lu, A. D.; Liu, T.; Wu, R. H.; Wang, Y. M.; Zhou, Z. H.; Wu, G. P.; Fang, J. X.; Tang, C. C. Highly enantioselective Michael addition of acetone to nitro olefins catalyzed by chiral bifunctional primary amine-thiophosphoramide catalyst. *Eur. J. Org. Chem.* **2010**, *2010*, 5777−5781.

(31) Mei, K.; Jin, M.; Zhang, S. L.; Li, P.; Liu, W. J.; Chen, X. B.; Xue, F.; Duan, W. H.; Wang, W. Simple cyclohexanediamine-derived primary amine thiourea catalyzed highly enantioselective conjugate addition of nitroalkanes to enones. *Org. Lett.* **2009**, *11*, 2864−2867.
(32) Palomo, C.; Vera, S.; Mielgo, A.; Gómez-Bengoa, E. Highly efficient asymmetric Michael addition of aldehydes to nitroalkenes catalyzed by a simple *trans*-4-hydroxyprolylamide. *Angew. Chem., Int. Ed.* **2006**, *45*, 5984−5987.
(33) Zhao, H. P.; Liu, Y. X.; Cui, Z. P.; Beattie, D.; Gu, Y. C.; Wang, Q. M. Design, synthesis, and biological activities of arylmethylamine substituted chlorotriazine and methylthiotriazine compounds. *J. Agric. Food Chem.* **2011**, *59*, 11711−11717.

JOURNAL OF AGRICULTURAL AND FOOD CHEMISTRY

Article

pubs.acs.org/JAFC

# Stabilization of the Potent Odorant 2-Acetyl-1-pyrroline and Structural Analogues by Complexation with Zinc Halides

Ming-Chih Fang[†] and Keith R. Cadwallader*[,‡]

[†]Taiwan Food and Drug Administration, 161-2 Kunyang Street, Nangang District, Taipei City, Taiwan 115

[‡]Department of Food Science and Human Nutrition, University of Illinois, 1302 West Pennsylvania Avenue, Urbana, Illinois 61801, United States

**ABSTRACT:** 2-Acetyl-1-pyrroline (2AP) and the structurally similar compounds 6-acetyl-2,3,4,5-tetrahydropyridine (ATHP, along with its tautomer 6-acetyl-1,2,3,4-tetrahydropyridine), 2-propionyl-1-pyrroline (2PP), and 2-acetyl-2-thiazoline (2A2T) are well-known potent odorants in various food products. However, due to the highly unstable nature of these compounds, especially 2AP and ATHP, they are scarcely used commercially in flavor formulations. A novel and attractive method for the stabilization of these potent odorants in dry powder form is presented. Coordination of 2AP, ATHP, 2PP, and 2A2T to zinc ions ($ZnI_2$, $ZnBr_2$, or $ZnCl_2$) resulted in the formation in high yields of stable crystalline complexes, which upon hydration release the free odorant. Infrared spectroscopy was used to study the coordination complexes. 2AP contains donor atoms, which coordinate (with covalent character) through both the heterocyclic nitrogen and carbonyl oxygen atoms to the zinc ion. This is also the case for ATHP and 2PP, but not for 2A2T, because the sulfur group in 2A2T provides a third possible donor site. Stability studies showed that the 2AP-$ZnI_2$ complex (with 14% loading) maintained >94% retention of 2AP after 3 months of storage at ambient temperature in a dry environment. Meanwhile, the ATHP−$ZnI_2$ complex was similarly stable and retained 89% of the ATHP after 3 months of storage. This stabilization technology may enable the commercial use of this powerful aroma compound as a flavoring agent.

**KEYWORDS:** *2-acetyl-1-pyrroline, 6-acetyl-2,3,4,5-tetrahydropyridine, complexation, stabilization, zinc*

## INTRODUCTION

2-Acetyl-1-pyrroline (2AP) was first identified in cooked rice[1] and was regarded as the most powerful odorant among all rice volatiles identified.[2] 2AP, with an odor threshold of 0.1 $\mu g\ L^{-1}$ in water,[1] dominates the structurally related analogues 6-acetyl-2,3,4,5-tetrahydropyridine (ATHP, including the tautomer 6-acetyl-1,2,3,4-tetrahydropyridine), 2-propionyl-1-pyrroline (2PP), and 2-acetyl-2-thiazoline (2A2T), all of which possess roasted, cracker-like, and popcorn-like aroma notes and are also important odorants in numerous food products.[3]

The specialty fragrant or aromatic rice varieties contain high levels of 2AP. In an effort to boost the production of 2AP, the gene linked to the accumulation of 2AP in fragrant rice has been identified[4] and later transferred into nonaromatic rice varieties, which enabled them to accumulate greater levels of 2AP.[5] 2AP is of potential commercial interest to the flavor industry because of its pleasant and characteristic flavor. However, the highly unstable nature of the compound has hindered its widespread commercial use. In popcorn 2AP decreased by about 80% during room temperature storage for 1 week in polyethylene bags.[6] In raw aromatic rice, the concentration of 2AP was shown to diminish by about half its original content after 3 months.[7] Pure 2AP turns red and degrades in 10 min while standing at ambient temperature. The instability of 2AP has been postulated to occur via a polymerization reaction.[1] The cyclic imine of 1-pyrroline was shown to form trimers during workup, which then undergo condensation with neighboring molecules to form polymeric products.[8]

Some efforts have been made to increase the stability of 2AP. Duby et al.[9] patented a process for encapsulation of 2AP with $\beta$-cyclodextrin ($\beta$-CD); however, 2AP (10% loading) was decomposed by 91% after 13 days of storage at 20 °C. At a loading of 1%, 2AP decomposed by 99% after 110 days of storage. Additional efforts to stabilize 2AP were made by Srinivas et al.[10] through encapsulation, where gum acacia and/or starch were applied to form a stabilized dry powder; however, no proven stability was demonstrated. In another study, a crude extract from pandan leaves served as a natural source of 2AP, which was mixed with $\beta$-CD to form a powder. However, no storage stability data were reported to demonstrate the effectiveness of this approach.[11] In a different study 2AP was maintained at a level of 70% after 72 days of storage at ambient temperature when encapsulated at very low loading (0.003%) in a gum acacia/maltodextrin matrix.[12] 2AP can be stabilized by chemical means, such as the addition of an acetal protection group. The synthesis of 6-acetyl-1-isopropyl-1,2,3,4-tetrahydropyridine and 6-(1,1-diethoxyethyl)-2,3,4,5-tetrahydropyridine after purification by preparative gas chromatography provided the more stable acetal and enol ether derivatives of ATHP.[13]

Previous attempts to stabilize 2AP suffer to some extent from at least one of the following three deficiencies: (1) stability of 2AP was either not mentioned or was insufficiently studied; (2)

Received: April 28, 2014
Revised: August 5, 2014
Accepted: August 6, 2014
Published: August 6, 2014

ACS Publications © 2014 American Chemical Society



dx.doi.org/10.1021/jf5020186 | J. Agric. Food Chem. 2014, 62, 8808−8813

low loadings of 2AP were used; and (3) 2AP was only stable during storage at low temperature (4 and −20 °C). In this study, a novel and attractive stabilization method is described. The compound 2AP is coordinated as a ligand onto a zinc halide, thus forming a powdered stable complex. Complexes of 2AP, as well as some other acylheterocyclic compounds, such as 2PP, ATHP, 2A2T, 2-acetylpyrazine (APra), 2-acetylpyridine (APri), and 2-acetylthiazole (ATz), can be prepared with $ZnI_2$, $ZnBr_2$, and $ZnCl_2$ in a similar manner. The chemical characteristics of these complexes and the stability of the 2AP−$ZnI_2$ complex during storage are described.

## MATERIALS AND METHODS

**Chemicals.** 2-Acetyl-2-thiazoline (2A2T), 2-acetylthiazole (ATz), 2-acetylpyridine (APri), 2-acetylpyrazine (APra), piperidine, pyrrolidine, 2,4,6-trimethylpyridine, nonane, zinc chloride (1.0 M solution in diethyl ether), zinc bromide, iodomethane, bromoethane, magnesium (turnings), zinc (dust, <10 μm), iodine, boric acid, zincon monosodium salt, silver nitrate, potassium cyanide, *tert*-butanol, triethylamine, and sodium methoxide (25 wt % in methanol) were purchased from Sigma-Aldrich (St. Louis, MO, USA). 2A2T was purified by precipitating out impurities in anhydrous diethyl ether and by subsequent distillation in vacuo. Zinc iodide was prepared by stirring zinc and iodine in anhydrous diethyl ether for 3 days. Anhydrous diethyl ether and methylene chloride were obtained from Fisher Scientific (Fair Lawn, NJ, USA). 2AP (yield = 10% from pyrrolidine; purity = 91% after vacuum distillation, by GC-FID) and ATHP (yield = 5% from piperidine; purity = 83% after vacuum distillation, by GC-FID, with two tautomers, 6-acetyl-2,3,4,5-tetrahydropyridine and 6-acetyl-1,2,3,4-tetrahydropyridine, at a ratio of 7:3) were synthesized using published methods.[14−16] 2PP was prepared by reacting 2-cyano-1-pyrroline with ethylmagnesium bromide in diethyl ether, by following closely the published procedure for the synthesis of 2-acetyl-1-pyrroline (yield = 4% from pyrrolidine; purity = 72% after vacuum distillation, by GC-FID).[15] 2-Ethyl-1-pyrroline was synthesized as described by Fuganti et al.[17]

**General Procedure for the Preparation of 2AP−Zinc Halide Complexes and Other Acylheterocyclic Complexes.** An anhydrous etheric solution of 2AP or other acylheterocyclic compound listed in Table 1 (1 mmol in 10 mL ether) was added to $ZnI_2$, $ZnBr_2$, or $ZnCl_2$ in anhydrous diethyl ether (0.1M) in a 50 mL centrifuge tube cooled in an ice−water bath with good stirring and nitrogen purging for 1 min. During addition, a significant amount of precipitate was observed. The reaction mixture was stored at −20 °C for 5 min and then centrifuged (3000*g*, 3 min) to isolate the precipitate. The precipitate was washed with fresh anhydrous diethyl ether (10 mL × 3) and then collected. Solvent was removed by gentle purging with nitrogen to obtain a fine powdered 2AP zinc halide complex, which was stored at −20 °C in a vial equipped with a PTFE-lined silicon cap.

**Content of an Acylheterocyclic Compound in the Complex.** 2AP or other acylheterocyclic zinc complex (5−10 mg) was placed in a 1.5 mL vial, then 0.5 mL of aqueous phosphate buffer (50 mM, pH 7) was added (this solution turned cloudy/white because of the insoluble metal content). Subsequent extraction was conducted via addition of methylene chloride (0.5 mL) containing an internal standard (2,4,6-trimethylpyridine, 1.00 mg $mL^{-1}$) to form a mixture. This mixture was vigorously shaken by hand for 1 min and then centrifuged (3000*g*, 5 min). The solvent layer was recovered and dried over sodium sulfate prior to GC analysis. Pure 2AP (91%) or other acylheterocyclic compound was prepared in phosphate buffer and extracted with methylene chloride following the above procedure to generate a response factor for each acylheterocyclic compound against the internal standard. The content of each acylheterocyclic compound in its respective complex was calculated using the following equation:

$$\text{loading (\%)} = \text{peak area of 2AP/peak area of 2,4,6-timethylpyridine} \times \text{concentration of 2,4,6-trimethylpyridine (mg mL}^{-1}\text{)} \times 0.5\ \text{mL} \times \text{response factor/sample weight (mg)} \times 100\%$$

**Stability of 2AP with Zinc Iodide in Solution.** 2AP (2.00 mg $mL^{-1}$) in pentane (1 mL) and $ZnI_2$ in diethyl ether solution (0.2M, 0.2 mL) were combined with 8 mL of methylene chloride (containing nonane as internal standard at 1.00 mg $mL^{-1}$) in a 10 mL volumetric flask and the volume immediately made up to the mark with methylene chloride to form a solution. The solution was incubated at room temperature for a period of 20 h, during which time the 2AP content was periodically monitored by transferring a 0.5 mL aliquot of the solution into a 1.5 mL vial followed by the addition of 0.5 mL of a quenching solution (phosphate buffer, 50 mM, pH 7) to form a mixture. The mixture was shaken and centrifuged (3000*g*, 5 min), and the solvent layer was immediately analyzed by GC. To check the stability of the quenched 2AP extract, the initial sample (time zero, quenched immediately after $ZnI_2$ addition) was held at room temperature and analyzed periodically by GC for up to 20 h. To serve as a control, a separate 2AP solution that did not contain $ZnI_2$ was also stored at room temperature and monitored periodically during this same time period.

**Gas Chromatography (GC).** GC was performed using either a (1) 6890N GC/5973N mass selective detector (MSD; Agilent Technologies Inc., Palo Alto, CA, USA) equipped with a fused-silica capillary column (Stabilwax, 30 m × 0.25 mm × 0.25 μm film thickness; or Rtx-5, 15 m × 0.32 mm × 0.5 μm film thickness; Restek, Bellefonte, PA, USA) or (2) 5890 series II GC equipped with a split/splitless injector, flame ionization detector (FID), and HP-1 column (30m × 0.32 mm × 0.25 μm film thickness, Agilent). Helium was the carrier at a constant flow of 1 mL/min. The injector was held at 250 °C in the split mode. GC oven temperature was programmed from 50 to 225 °C at 10 °C/min with initial and final hold times of 5 and 20 min, respectively. Other conditions for the MSD were as follows: MSD interface temperature, 260 °C; ionization energy, 70 eV; mass range, 35−350 amu; EM voltage, Autotune +165 V; scan rate, 4.45 scans/s.

**Determination of the Zinc Content.** Zinc content was measured spectrophometrically using a published procedure.[18] A sample of 2AP−zinc halide or other complex (5−10 mg) was diluted in water (pH 2, adjusted using HCl) in a 25 mL volumetric flask. A 70 μL aliquot of this solution and 100 μL of Zincon dye (1.6 mM; 37 mg Zincon in 1 mL of NaOH (1M) followed by dilution into 50 mL of water) and 3 mL of borate buffer (53 mM, pH 9.0) were then combined in a test tube. After incubation of this solution for 5 min, absorbance was measured at 620 nm using a Lambda 1050 UV/vis/NIR spectrophotometer (PerkinElmer Inc., Shelton, CT, USA). A six-point calibration plot was constructed from a dilution series of a zinc stock solution (100 mg of zinc dust in 1 mL of HCl for 4 h prior to dilution to 1 L).

**Infrared Spectra.** Infrared spectra of 2AP and the other acylheterocyclic compounds as well their zinc halide complexes were recorded using a Spectrum 100 FT-IR (PerkinElmer Inc., Waltham, MA, USA) with attenuated total reflectance (ATR) accessory (resolution = 4 $cm^{-1}$, 4 scans/spectra, range = 500−4000 $cm^{-1}$). Liquid samples were analyzed in neat form. Solid complexes were applied directly to the diamond ATR top plate.

**Stabilities of 2AP and ATHP Zinc Iodide Complexes in Dry Powder Form.** 2AP−$ZnI_2$ complex (5−10 mg) was stored in sealed (PTFE-lined silicon cap) 1.5 mL glass vials at 25, 10, or −20 °C. ATHP−$ZnI_2$ complex was stored at 25 °C. The residual 2AP or ATHP in each complex was monitored during a 3 month storage period as previously described.

## RESULTS AND DISCUSSION

**Complexation of 2AP and Other Heterocyclic Compounds to Zinc Halides.** The addition of anhydrous $ZnI_2$ to an anhydrous solution of 2AP in diethyl ether caused a


dx.doi.org/10.1021/jf5020186 | J. Agric. Food Chem. 2014, 62, 8808−8813

Table 1. Yield, Color, Stoichiometry, and Component Analyses of Acylheterocyclic−Zinc Halide Complexes

| compound | yield[a] (%) | color | stoichiometry[b] ($n$) | found (calcd) (%, $n$ = 2, mean ± SD) | |
|---|---|---|---|---|---|
| | | | | heterocyclic | zinc halide |
| $ZnI_2$(2-acetyl-1-pyrroline)$_n$ | 62 | pale yellow | 1 | 29 ± 1 (26) | 73 ± 2 (74) |
| $ZnBr_2$(2-acetyl-1-pyrroline)$_n$ | 96 | white | 1 | 35 ± 1 (33) | 672 ± 2 (67) |
| $ZnCl_2$(2-acetyl-1-pyrroline)$_n$ | 86 | white | 1 | 50 ± 5 (45) | 52 ± 0 (55) |
| $ZnI_2$(2-propionyl-1-pyrroline)$_n$ | 32 | orange | 1 | 23 ± 1 (28) | 76 ± 2 (72) |
| $ZnBr_2$(2-propionyl-1-pyrroline)$_n$ | 49 | pale yellow | 1 | 31 ± 3 (36) | 65 ± 5 (64) |
| $ZnCl_2$(2-propionyl-1-pyrroline)$_n$ | 60 | pale yellow | 1 | 46 ± 2 (48) | 53 ± 3 (52) |
| $ZnI_2$(2-acetyl-2-thiazoline)$_n$ | 90 | yellow | 2/3 | 25 ± 2 (21) | 77 ± 5 (79) |
| $ZnBr_2$(2-acetyl-2-thiazoline)$_n$ | 95 | white | 2/3 | 33 ± 1 (28) | 72 ± 2 (72) |
| $ZnCl_2$(2-acetyl-2-thiazoline)$_n$ | 98 | pale yellow | 2/3 | 47 ± 11 (39) | 61 ± 2 (61) |
| $ZnI_2$(6-acetyl-2,3,4,5-tetrahydropyridine)$_n$[c] | 59 | yellow | 1 | 16 ± 9 (28) | 71 ± 11 (72) |
| $ZnBr_2$(6-acetyl-2,3,4,5-tetrahydropyridine)$_n$ | 71 | pale yellow | 1 | 30 ± 5 (36) | 68 ± 1 (64) |
| $ZnCl_2$(6-acetyl-2,3,4,5-tetrahydropyridine)$_n$ | 100 | pale yellow | 1 | 35 ± 9 (48) | 56 ± 6 (52) |
| $ZnI_2$(2-acetylpyridine)$_n$ | 102 | white | 2 | 42 ± 2 (43) | 59 ± 1 (57) |
| $ZnBr_2$(2-acetylpyridine)$_n$ | 97 | white | 2 | 52 ± 2 (52) | 51 ± 7 (48) |
| $ZnCl_2$(2-acetylpyridine)$_n$ | 101 | white | 2 | 58 ± 2 (64) | 36 ± 0 (36) |
| $ZnI_2$(2-acetylpyrazine)$_n$ | 74 | orange | 2/3 | 25 ± 0 (20) | 79 ± 8 (80) |
| $ZnBr_2$(2-acetylpyrazine)$_n$ | 93 | white | 2/3 | 30 ± 2 (27) | 73 ± 1 (73) |
| $ZnCl_2$(2-acetylpyrazine)$_n$ | 91 | white | 2/3 | 37 ± 1 (37) | 65 ± 5 (63) |
| $ZnI_2$(2-acetylthiazole)$_n$ | 40 | pale yellow | 1 | 27 ± 0 (29) | 72 ± 1 (72) |
| $ZnBr_2$(2-acetylthiazole)$_n$ | 76 | white | 1 | 36 ± 0 (36) | 64 ± 1 (64) |
| $ZnCl_2$(2-acetylthiazole)$_n$ | 103 | white | 1 | 47 ± 2 (48) | 54 ± 1 (52) |

[a]Yield = $W/(\mathrm{mM} \times \mathrm{MW} \div n) \times 100\%$ [$W$ = amount (mg) of obtained complex; mM = amount (mM) of starting acylheterocyclic compound; MW = molecular weight of complex (base on the formula in this table)]. [b]Proposed stoichiometry. [c]6-Acetyl-2,3,4,5-tetrahydropyridine plus its tautomer 6-acetyl-1,2,3,4-tetrahydropyridine.

yellowish precipitate to form immediately. This reaction mixture was incubated in the freezer for 5 min and then triturated with fresh anhydrous diethyl ether to remove excess $ZnI_2$ and other impurities from the 2AP−$ZnI_2$ complex. A fine powder, pale yellow in color, was obtained after collecting the precipitate and purging with nitrogen gas. The free 2AP ligand could be freed from the powdered 2AP−$ZnI_2$ complex via hydration with water, in which case a white cloudy metallic substance also appeared at neutral pH and the yellow color faded immediately, indicating the loss of the complex structure. GC-MS analysis of a methylene chloride extract of this aqueous mixture yielded a main peak (recovery = 54−111%, by GC-FID) with a mass spectrum and retention index in agreement with those of authentic 2AP.

One possible explanation for the stabilization effect observed could be through the coordination of the ring nitrogen and carbonyl oxygen atoms of the compound to the zinc ion. Coordination of 2AP with other zinc salts such as $ZnBr_2$ and $ZnCl_2$ acts in a similar fashion.

**Stoichiometry of Complex Formation.** Table 1 shows the yields, color, proposed stoichiometry, and component analysis of 2AP-$ZnI_2$, 2AP-$ZnBr_2$, 2AP-$ZnCl_2$, and 17 other acylheterocyclic−zinc halide complexes. Contents of acylheterocyclic compounds and zinc halide in the various complexes were determined by GC and spectrophotometric analyses, respectively. The theoretical loadings of 2AP were 26, 33, and 45% in the $ZnI_2$, $ZnBr_2$, and $ZnCl_2$ complexes, respectively. We found the content of 2AP was 29, 35, and 50% in the $ZnI_2$, 2AP−$ZnBr_2$, and 2AP-$ZnCl_2$ complexes, respectively, indicating a one-to-one stoichiometry of 2AP to zinc halide in the complexes. Similar results were observed for the complexes of 2PP and ATz for which the same molar ratios were found between the metal and heterocyclic ligands. For APri, ATz, and APra more complex stoichiometries were observed with 2, 2/3, and 2/3 of the acylheterocyclic molecules, respectively, binding to the zinc halides. For ATHP, lower loadings were observed for its complexes compared to the theoretical values. For example, only 16% ATHP was recovered from ATHP−$ZnI_2$. However, the theoretical recovery was 28%. This could be due to the great instability of ATHP, which may have degraded during the complexation step. Higher recoveries might be obtained by optimizing the method of preparation. Due to poor recovery of ATHP, only the zine contents were used to determine the proposed stoichiometry of the ATHP-zinc halide complexes.

Zinc halide was postulated to have two binding sites in its complex;[19] however, due to its flexible coordination, four or even six chelate rings have also been reported.[20] Because 2AP, 2PP, and ATHP contained two donor atoms (a nitrogen and a carbonyl oxygen), they were postulated to form one-to-one metal−ligand complexes. However, although APri contained two donors as well, it was found to form bivalent metal complexes[21] and, accordingly, the APri−zinc complexes were found to have four binding sites. 2A2T and APra were believed to form $(ZnX_2)_3L_2$ complexes (where X = I, Br, or Cl; L = 2A2T or APra ligands) because both had three possible donor sites (nitrogen, carbonyl, and sulfur atoms for 2A2T; two nitrogens and one carbonyl for APra). However, the same rule did not apply to ATz, for which a one-to-one stoichiometry was observed for the complexes even though ATz contains three donor atoms. The same ligands or structurally similar ligands that link to the zinc halide may have various coordinations. For example, pyrazine−$ZnBr_2$ could yield two reversible coordination polymers, (pyrazine)$_2$−$ZnBr_2$, which forms 2D regular square-grid coordinations, and pyrazine−$ZnBr_2$, which forms a zigzag chain polymer with a network having an octahedral center.[22] Further work such as elemental analysis or X-ray diffraction may be useful in elucidating the complex multi-


dx.doi.org/10.1021/jf5020186 | J. Agric. Food Chem. 2014, 62, 8808−8813

**Table 2. Infrared Spectral Assignment of Acylheterocyclic Compounds and Their Zinc Complexes**

| compound | carbonyl vibration ($cm^{-1}$) free ligand | $ZnI_2$ complex | $ZnBr_2$ complex | $ZnCl_2$ complex | peak shape |
|---|---|---|---|---|---|
| 2-acetyl-1-pyrroline | 1695 | 1627 | 1630 | 1633 | broadened, split |
| 2-propoinyl-1-pyrroline | 1698 | 1647 | 1640 | 1642 | |
| 6-acetyl-2,3,4,5-tetrahydropyridine | 1695, 1666 | 1632 | 1635 | 1637 | |
| 2-acetyl-2-thiazoline | 1700 | 1694 | 1696 | 1702 | broadened, split |
| 2-acetylthiazole | 1682 | 1656 | 1654 | 1655 | |
| 2-acetylpyrazine | 1688 | 1674 | 1673 | 1675 | split |
| 2-acetylpyridine | 1696 | 5659 | 1672 | 1676 | split |

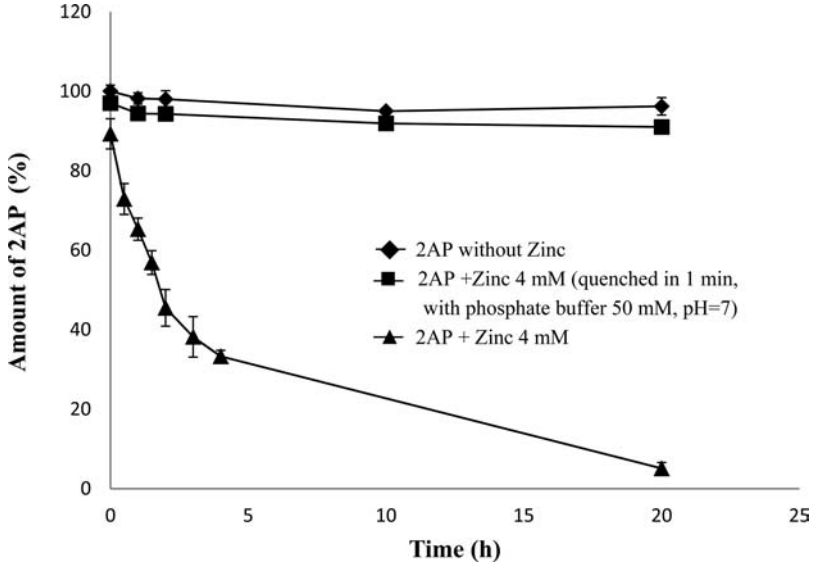


**Figure 1.** 2-Acetyl-1-pyrroline (2AP) degradation in methylene chloride solution in the presence of zinc iodide (mean ± SD, $n$ = 2).

dimensional structures of the acylheterocyclic−zinc ion complexes or even to correct the proposed stoichiometry. However, this was beyond the scope of the present study.

**Infrared Spectra and Nature of Coordination.** The infrared spectra of the Zn(II)−acylheterocyclic complexes were recorded in the range 4000−400 $cm^{-1}$, but only the 2000−600 $cm^{-1}$ region was considered. The carbonyl (C═O) band assignments for the complexes are given in Table 2. It was observed that the carbonyl vibration shifted to lower wavenumbers for the complexes as compared to their free ligands, indicating the existence of a coordination complex. This was observed for all complexes except for those of 2A2T. For example, 2AP produced a very strong absorption around 1695 $cm^{-1}$, which was attributed to C═O stretching. The corresponding bends shifted to the lower wavenumbers at 1627, 1630, and 1633 $cm^{-1}$ for its $ZnI_2$, 2AP−$ZnBr_2$, and 2AP−$ZnCl_2$ complexes, respectively. This provides evidence for coordination through the carbonyl oxygen. In addition, the broadened bandwidth at around 1695 $cm^{-1}$ in the complexes may be considered as further evidence for metal chelation.[23] The heterocyclic ring nitrogen was suggested to undergo bond formation with the metal, thus increasing the dipolar contribution of $C{=}N^+$.[21] Bands at 1632 or 1619 $cm^{-1}$ may be assigned as ring nitrogen vibration. However, the C—C vibration occurred at around 1600−1650 $cm^{-1}$ with broad and split or multipeak shapes, which always overlapped the nitrogen (C—N═C) region, which made it more difficult to determine the coordination between the metal and ring nitrogen. We believed nitrogen was involved in coordination because many heterocyclic−metal complexes containing only nitrogen and carbon have been previously observed, including (1-pyrroline)$_2$−$ZnI_2$,[19] (pyridine)$_2$−$ZnCl_2$, (pyridine)$_6$−$CdCl_2$,[24] pyrazine−$ZnBr_2$,[22] and (2-ethyl-1-pyrroline)$_2$−$ZnI_2$, which was observed in our laboratory.

For ATHP, the carbonyl vibration located at 1695 and 1666 $cm^{-1}$ for the free ligand shifted upon O-complexation to lower wavenumbers of 1632, 1635, and 1637 $cm^{-1}$ in its $ZnI_2$, 2AP−$ZnBr_2$, and 2AP−$ZnCl_2$ complexes, respectively. The two bands for ATHP indicated the carbonyl groups of two tautomers. However, there was only one band observed in their complexes, which suggested a single stable ATHP−zinc halide complex was constructed. However, for 2A2T complexes, the differences between coordinated and noncoordinated carbonyl groups was evidenced by only the broadening and splitting of this band, which was located at around 1700 $cm^{-1}$. A strong C═N stretching band at 1592 $cm^{-1}$[25] shifted to lower wavenumbers at 1574, 1576, and 1576 $cm^{-1}$ for its $ZnI_2$, $ZnBr_2$, and $ZnCl_2$ complexes, respectively, apparently indicating N coordination.

**Unstable Nature of 2AP.** It was observed that 2AP−$ZI_2$ complex solutions prepared in polar solvents, such as methanol, acetone, dimethyl sulfoxide (DMSO), propylene glycol, or glycerin, turned red immediately, which is indicative of 2AP polymerization; however, solutions of the free 2AP ligand in these solvents remained colorless or pale yellow. We suggest that zinc ion may catalyze the polymerization of 2AP, because 2AP alone in these solvents was relatively stable but was unstable in the presence of zinc ion. The 2AP−$ZnI_2$ complex in tetrahydrofuran (THF), chloroform, and methylene chloride


dx.doi.org/10.1021/jf5020186 | J. Agric. Food Chem. 2014, 62, 8808−8813

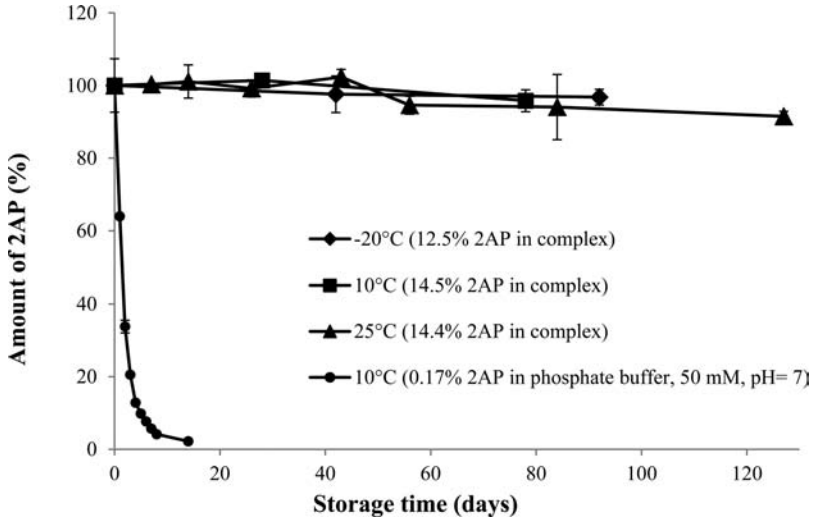


**Figure 2.** Stability of 2-acetyl-1-pyrroline (2AP) and its zinc iodide complex during storage at various temperatures (mean ± SD, $n$ = 2).

(polarity = 3−4) was yellow in color and turned red gradually. A sticky dark red material that adhered to the wall of the beaker was observed due to the poor solubility of the 2AP polymer in solvents of intermediate polarity. 2AP−$ZnI_2$ complex did not go into solution in nonpolar solvents, such as pentane, benzene, and diethyl ether, and the complex remained as a stable, solid powder that did not undergo zinc-mediated polymerization.

To study the zinc-mediated deterioration, 2AP in methylene chloride was added to $ZnI_2$ (4 mM), which caused the solution to turn red. A quenching solution (phosphate buffer, 50 mM, pH 7, 0.5 mL) was added to the methylene chloride solution prior to GC analysis, which not only inhibited zinc-mediated polymerization but also minimized the chromatographic interference caused by zinc. The results showed 2AP decayed by 70% in 4 h (Figure 1) in the presence of zinc ion. However, when a 2AP/zinc ion solution was treated with the above-mentioned quenching solution within 1 min 2AP was retained at 97% and remained stable throughout a 20 h period. The quenching solution acted to remove the zinc ion from methylene chloride, and thus 2AP was relatively stable in the zinc free solvent. The results indicated the zinc ion catalyzed the deterioration of 2AP in methylene chloride in the absence of the quenching solution.

**Stability of 2AP Zinc Iodide Complex.** The tendency of metal−ligand coordination complexes to form can be applied for the protection of unstable compounds, such as the stabilization of 1-pyrroline as a stable crystalline complex with zinc ion.[19,26] In the present study, the stability of 2AP−$ZnI_2$ complex was studied over a period of 3 months. A 0.17% aqueous solution of 2AP (pH 7) showed an 80% reduction after 3 days and a 90% reduction after 5 days. However, the 2AP complex stored at three different temperatures showed significantly increased stability (Figure 2). As expected, lower temperature storage was found to favor stability. During storage at −20 °C the 2AP content was retained by 97% in the complex (2AP content = 12.5%) after 92 days of storage. About 96% retention was observed after 78 days of storage when the 2AP complex (14.5% 2AP) was stored at 10 °C. Meanwhile, in a moisture-free environment 2AP (14.4% complex) declined by only 6% after 3 months of storage at 25 °C. The ATHP−$ZnI_2$ complex was similarly stable, and only 11% of the ATHP was lost after 3 months of storage at 25 °C under anhydrous conditions (Figure 3).

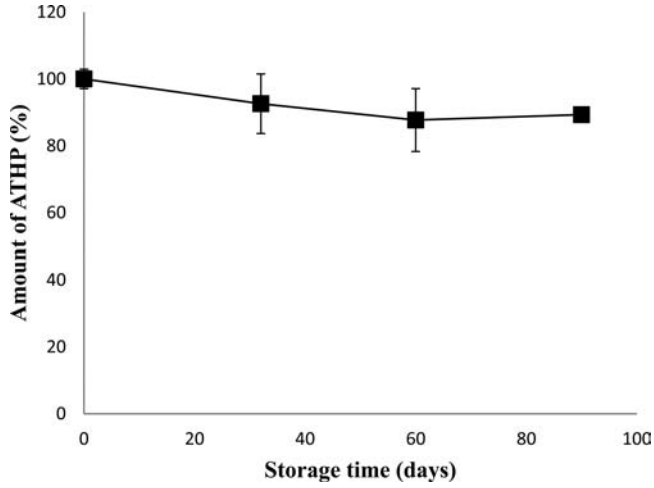


**Figure 3.** Stability of ATHP (sum of tautomers)-zine iodide complex stored at 25 °C (mean ± SD, $n$ = 2).

The results of the present study demonstrate that complexation of 2AP with $ZnI_2$ forms a stable, solid complex in powder form. This complex is stable at ambient temperature (only 6% reduction during 3 months of storage at 25 °C), which may enable its use as a flavoring agent. When this complex is applied to foods, the temperature, moisture, and other possible food matrix components may influence its stability. Therefore, an appropriate package or encapsulation technology, such as dispersion in an edible oil or lipid, or wax encapsulation is suggested to protect the complex from moisture and from interactions with other food components. It may be preferable to prepare complexes with $ZnCl_2$ because it has GRAS status. It is hoped that this novel stabilization process can enable the practical use of the labile, yet powerful, flavor compound 2-acetyl-1-pyrroline and its analogues as flavoring agents.

## AUTHOR INFORMATION

### Corresponding Author

*(K.R.C.) Phone: (217) 333-5803. Fax: (217) 333-1875. E-mail: cadwlldr@illinois.edu.

### Notes

The authors declare no competing financial interest.

## REFERENCES


(1) Buttery, R. G.; Ling, L. G.; Juliano, B. O. 2-Acetyl-1-pyrroline: an important aroma component of cooked rice. *Chem. Ind.* **1982**, *12*, 958−959.

(2) Buttery, R. G.; Turnbaugh, L. G.; Ling, L. C. Contribution of volatiles to rice aroma. *J. Agric. Food Chem.* **1983**, *36*, 1006−1009.

(3) Adams, A.; De Kimpe, N. Chemistry of 2-acetyl-1-pyrroline, 6-acetyl-1,2,3,4-tetrahydropyridine, 2-acetyl-2-thiazoline, and 5-acetyl-2,3-dihydro-4*H*-thiazine: extraordinary Maillard flavor compounds. *Chem. Rev.* **2006**, *106*, 2299−2319.

(4) Bradbury, L. M.; Fitzgerald, T. L.; Henry, R. J.; Jin, Q.; Waters, D. L. The gene for fragrance in rice. *Plant Biol. J.* **2005**, *3*, 363−370.

(5) Vanavichit, A.; Tragoonrung, S.;Toojinda, T.; Wanchana, S.; Kamolsukyunyong, W. Transgenic rice plants with reduced expression of Os2AP and elevated levels of 2-acetyl-1-pyrroline. U.S. Patent 7319181, 2008.

(6) Schieberle, P. Quantitation of important roast-smelling odorants in popcorn by stable isotope dilution assays and model studies on flavor formation during popping. *J. Agric. Food Chem.* **1995**, *43*, 2442−2448.

(7) Widjaja, R.; Craske, J. D.; Wootton, M. Changes in volatile components of paddy, brown and white fragrant rice during storage. *J. Sci. Food Agric.* **1996**, *71*, 218−224.

(8) Fuhlhage, D. W.; Vander Werf, C. A. Studies on the formation and reaction of 1-pyrroline. *J. Am. Chem. Soc.* **1958**, *80*, 6249−6254.

(9) Duby, P.; Huynh-Ba, T. Preparation of 2-acetyl-1-pyrroline compositions. U.S. Patent 5512290, 1996.

(10) Srinivas, P.; Sulochanamma, G.; Raghavan, B.; Gurudutt, K. N. Process for the stabilization of 2-acetyl-1-pyrroline, the basmati rice flavorant. U.S. Patent Appl. 2006/0147596, 2006.

(11) Andreas, D.; Gerhard, K.; Hens, K.; Mee Yin, T. Novel pandan extract articles in powder form and process for the production thereof. U.S. Patent 20120213904 A1, 2012.

(12) Apintanapong, M.; Noomhorm, A. The use of spray dring to microencapsulate 2-acetyl-1-pyrroline, a major flavor component of aromatic rice. *Int. J. Food Sci. Technol.* **2003**, *38*, 95−102.

(13) De Kimpe, N.; Stevens, C. V.; Keppens, M. A. Synthesis of 2-acetyl-1-pyrroline, the principal rice flavor component. *J. Agric. Food Chem.* **1993**, *41*, 1458−1461.

(14) De Kimpe, N.; Stevens, C. A convenient synthesis of 6-acetyl-1,2,3,4-tetrahydropyridine, the principle bread flavor component. *J. Org. Chem.* **1993**, *58*, 2904−2906.

(15) De Kimpe, N.; Stevens, C. Syntheses of the principal bread flavor component, 6-acetyl-1,2,3,4-tetrahydropyridine, and acetal protected precursors. *Tetrahedron* **1995**, *8*, 2387−2402.

(16) De Kimpe, N.; Keppens, M. Novel syntheses of the major flavor components of bread and cooked rice. *J. Agric. Food Chem.* **1996**, *44*, 1515−1519.

(17) Fuganti, C.; Gatti, F. G.; Serra, S. A general method for the synthesis of the most powerful naturally occurring Maillard flavors. *Tetrahedron* **2007**, *63*, 4762−4767.

(18) Säbel, C. E.; Meureuther, J. E.; Siemann, S. A spectrophotometric method for the determination of zinc, copper, and cobalt ions in metalloproteins using zincon. *Anal. Biochem.* **2010**, *397*, 218−226.

(19) Baxter, G.; Melville, J. C.; Robins, D. J. Stabilisation of 3,4-dihydro-2*H*-pyrrole (1-pyrroline) by complexation with zinc iodide. *Synlett* **1991**, 359−360.

(20) Erxleben, A. Structures and properties of zinc(II) coordination polymers. *Coord. Chem. Rev.* **2003**, 203−228.

(21) Kidani, Y.; Noji, M.; Koike, H. Studies of bivalent metal complexes of 2-acetylpyridine. *Bull. Chem. Soc. Jpn.* **1975**, *48*, 239−244.

(22) Bourne, S. A.; Kilkenny, M.; Nassimbeni, L. R. One- and two-dimensional coordination polymers of zinc(II) with pyrazine. Solid state reactions and decomposition kinetics of the interconversion reactions. *J. Chem. Soc., Dalton Trans.* **2001**, *8*, 1176−1179.

(23) Singh, N. P.; Singh, J. Magnetic and spectroscopic studies of the synthesized metal complexes of bis(pyridine-2-carbo)hydrazine and their antimicrobial studies. *E−J. Chem.* **2002**, *9*, 1835−1842.

(24) Mason, R. B.; Mathews, J. H. Equilibrium in the systems: zinc chloride-pyridine; and cadmium chloride-pyridine. *J. Phys. Chem.* **1925**, *29*, 1178−1183.

(25) Doornbos, T.; Peer, H. G. Synthesis of 2-acyl-2-thiazolines. *Recl. Trav. Chim. Pay-Bas* **1972**, *91*, 711−728.

(26) Freer, A. A.; McDermott, G.; Melville, J. C.; Robins, D. Structure of diiodobis(1-pyrroline) zinc(II). *Acta Crystallogr.* **1993**, *c49*, 2115−2117.

Fernandez-Gonzales et al. evaluated molecularly imprinted sol−gel materials for the detection of nafcillin.[13] For the β-lactam antibiotic cephalexin, MIPs were synthesized and evaluated by Guo and He.[14] Skudar et al. produced MIPs for penicillin V and oxacillin. However, the developed MIPs also possessed an affinity for other antibiotics of the β-lactam group.[15] Cederfur et al. synthesized MIPs for benzylpenicillin using a molecularly imprinted polymer library.[10] Caro et al. developed two MIPs using tetracycline and oxytetracycline as template molecules.[16] Zhang et al. investigated the use of MIPs for the determination of benzylpenicillin in milk, but their detection limit was only 1 mg/kg.[17] Kempe et al. tested the influence of salt ions on the binding properties of MIPs and applied this to benzylpenicillin in milk.[18] The recoveries obtained amounted to 87%, but the control polymer showed also a high recovery of 73%, indicating a high level of nonspecific binding. Finally, Guardia et al. developed molecularly imprinted sol−gel materials for the determination of nafcillin in milk-based products, and a detection limit of 13.2 mg/kg was obtained.[19] Several MIPs for the detection of other antibiotics in different fields have been developed: for example, trace analysis of quinolones in eggs,[20] determination of nitroimidazoles and fluoroquinolones in egg-based products,[21,22] extraction of sulfonamides from honey,[23] and determination of sulfonamides in pork and chicken.[24] Even MIPs for extraction of several antibiotics from complex matrices are already commercially available.

In this study, MIPs were developed through suspension polymerization for application in an SPE procedure for the detection of benzylpenicillin in milk, which has a maximal residue level (MRL) of 4 μg/kg.

Binding properties (cross-reactivity, recoveries, number of binding sites, etc.) were evaluated via binding experiments. The MIPs were validated in acetonitrile and then in a milk matrix, where the limit of detection (LOD) and limit of quantitation (LOQ) were determined. Finally, the molecularly imprinted solid-phase extraction (MISPE) procedure was compared (Pearson correlation) with a traditional sample preparation method performed in an accredited laboratory.

## MATERIALS AND METHODS

**Solvents and Solid Reagents.** All products [benzylpenicillin, nafcillin, piperacillin, ampicillin, amoxicillin, oxacillin, cloxacillin, dicloxacillin, cephalexin, cephapirin, sulfadiazin, oxytetracycline, methacrylic acid, trimethylolpropane methacrylate, ethylene glycol dimethacrylate, and azobis(isobutyronitrile)] were purchased from Sigma-Aldrich (St. Louis, MO), except for acetonitrile (AcN), formic acid, and methanol (MeOH), which were purchased from Biosolve (Valkenswaard, The Netherlands). Water ($H_2O$) was purified by a Millipore (Billerica, MA) Milli-Q gradient system to high-performance liquid chromatography (HPLC) grade.

**Standard Solutions of the Antibiotics.** Analytical standards were dissolved at a concentration of 1 mg/mL (stock solutions) in a 1/1 (v/v) AcN/$H_2O$ mixture. The working standard solutions were made by dilution with AcN. The stock solutions were kept at −20 °C, and the working solutions were freshly prepared before use.

**Apparatus.** A shaker (Bühler, Hechingen, Germany), a centrifuge (model 4K15, Sigma, Osterode am Harz, Germany), a vortex mixer (Scientific Industries, Bohemia, NY), and a vacuum manifold (Varian, Palo Alto, CA) were used during the experiments and sample preparation. A high-performance liquid chromatograph combined with a mass spectrometer was used for the detection and quantification of benzylpenicillin. The high-performance liquid chromatographic−tandem mass spectrometry (LC−MS/MS) system consisted of a LC system (Alliance, Waters, Milford, MA) with a model 2695 separation module coupled to a quattro LCZ tandem quadrupole mass spectrometer (Micromass, Altrincham, U.K.) equipped with a z-spray electrospray ion interface or an Acquity Ultra Performance liquid chromatograph (Waters) coupled to a Xevo TQ mass spectrometer (Waters) also equipped with a z-spray system. The mass spectrometers were fully controlled by MASSLYNX version 4.0 or 4.1 (Waters). The separations on the LC system were conducted on an Xterra MS $C_{18}$ column [Waters, 5 μm, 150 mm × 2.1 mm (inside diameter)] protected with an Alltima $C_{18}$ guard column [Alltech, Deerfield, IL, 5 μm, 7.5 mm × 2.1 mm inside diameter)]. The ultra performance liquid chromatography (UPLC) separations were performed on a Waters UPLC BEH $C_{18}$ column [Waters, 1.7 μm, 100 mm × 2.1 mm (inside diameter)].

**Synthesis of the MIP for Benzylpenicillin.** Benzylpenicillin (2 mmol or 0.7 g), methacrylic acid (16 mmol or 1.4 g), trimethylolpropane methacrylate (7 mmol or 2.4 g) or ethylene glycol dimethacrylate (7 mmol or 1.4 g), and azobis(isobutyronitrile) (0.4 mmol or 0.07 g) were dissolved in 6 mL of AcN (bulk polymerization) or in 70 mL of AcN (suspension polymerization). These solutions were polymerized for 20 h in a water bath at 75 °C under nitrogen saturation. After the MIP had been dried in an oven at 60 °C for 48 h, the template molecule was washed out with a MeOH/$H_2O$ mixture [95/5 (v/v)] according to the Soxhlet principle.

**Equilibrium Binding Experiments in Acetonitrile or Milk Extracts.** Ten milligrams of MIP or NIP was incubated on a shaker for 4 h in 1 mL of AcN or milk extract containing different amounts of benzylpenicillin. For the binding experiments in AcN, the following protocol was used. First, the solution was centrifuged for 15 min at 4302*g*, after which 500 μL of the supernatant was dried at 60 °C under a flow of nitrogen. Then, the residue was redissolved in 1 mL of a 1/1 (v/v) AcN/$H_2O$ mixture and 1 mL of internal standard (containing 1 μg/mL nafcillin or piperacillin solution in AcN). This solution was filtered through a syringe-driven filter unit with a pore size of 0.22 μm (Millipore, Bedford, MA) and analyzed via LC−MS/MS. The protocol for the binding experiments in milk extracts was similar. These binding experiments were used for the evaluation of the binding capacities, the determination of the cross reactivity, and the Scatchard analysis of the developed MIP.

**Extraction of Bound Benzylpenicillin from a Previously Used MIP or NIP.** The suspension of 10 mg of MIP or NIP in 1 mL of AcN containing 5 μg of benzylpenicillin used for the equilibrium binding experiments was passed through a syringe-driven filter unit with a pore size of 0.22 μm (Millipore). A light vacuum (maximum of 0.17 bar) was produced, and the solvent that came through the filter was analyzed using LC−MS/MS as fraction 1 using the same preparative steps described above (see Equilibrium Binding Experiments in Acetonitrile or Milk Extracts). The vial used during the equilibrium binding experiment was rinsed with AcN to pass the total amount of MIP or NIP used during the binding experiment through the filter unit. Again a light vacuum was developed, and the collected solvent was analyzed as fraction 2. The total amount of MIP or NIP on the filter was then washed with MeOH to recover the bound benzylpenicillin. This was repeated in fractions of 1 mL. These fractions (3−6) were also analyzed using LC−MS/MS. These tests were performed to prove the reversibility of the binding of benzylpenicillin to the MIP or NIP.

**Extraction of the Milk Samples.** The blank milk samples were skimmed (centrifugation at 3399*g* for 10 min). An equal amount of AcN was added to the skimmed milk sample together with NaCl (0.2 g/mL). After the solution had been mixed with a vortex mixer and centrifuged for 10 min at 3399*g*, a portion of the supernatant was evaporated and spiked with different concentrations of benzylpenicillin, dissolved in AcN, before application to the MIP or NIP.

**MISPE and Non-molecularly Imprinted Solid-Phase Extraction (NISPE) for the Analysis of AcN Solutions or Milk Samples.** An empty SPE cartridge was packed with 50 mg of the (non)imprinted polymer. The polymers were packed between two glass wool frits and washed with 50 mL of MeOH and 15 mL of a MeOH/$H_2O$ mixture [95/5 (v/v)] to remove the remaining benzylpenicillin after Soxhlet treatment. The last 5 mL was collected and analyzed by HPLC−MS/MS to rule out template bleeding.

Before the sample was loaded, the polymers were conditioned with 5 mL of a MeOH/AcN mixture [50/50 (v/v)] to remove the remaining impurities. Next, the AcN solution or the extract of the milk sample was loaded onto the MIP dissolved in 5 mL of AcN. The loading was followed by a washing step with 2 mL of AcN, and finally, the MIP was treated with 6 mL of a MeOH/$H_2O$ mixture [50/50 (v/v)] to elute the benzylpenicillin. This eluent was collected, dried at 60 °C under a flow of nitrogen, and redissolved in 1 mL of a 1/1 (v/v) water/acetonitrile mixture and 1 mL of internal standard (containing 1 μg/mL piperacillin solution in acetonitrile). This solution was filtered through a syringe-driven filter unit with a pore size of 0.22 μm (Millipore) and analyzed using LC−MS/MS.

**Validation Study in Acetonitrile and Milk.** The validation of the performance of the MIP is based on the criteria mentioned in EU Commission Decision 2002/657/EG. Solutions of AcN and spiked milk sample extracts were percolated through the MIP and NIP. The experiments were performed in triplicate, and the recovery was calculated. The recovery is expressed in percent, i.e., the amount of benzylpenicillin obtained after the cleanup step (over MIP or NIP) in relation to the amount of benzylpenicillin added to the AcN solution or milk extract. The goal of the study is to validate the MIP cleanup procedure and not the extraction protocol. That is why we chose to spike the milk samples after extraction to prevent variations originating from the extraction step. Validation of the developed method (including extraction and cleanup step) was conducted during the analysis of contaminated milk samples (see below). The precision was evaluated by calculating the standard deviation for the three experiments executed on different days. The LOD and LOQ were calculated using a calibration curve and the equations

$$\mathrm{LOD} = 3 \times \frac{\mathrm{SEB}}{M}$$

$$\mathrm{LOQ} = 6 \times \frac{\mathrm{SEB}}{M}$$

where SEB is the standard error value on the intercept of the calibration curve and $M$ the slope of the calibration curve.

**Analysis of Contaminated Milk Samples.** To evaluate the implementation of the developed MIP as an SPE sorbent, the concentration of benzylpenicillin present in contaminated milk samples was determined. The results were compared with those obtained after the execution of the traditional protocol (extraction with AcN) for the determination of benzylpenicillin in milk samples in a Beltest-accredited laboratory.

**Liquid Chromatography.** The HP liquid chromatographic separation of benzylpenicillin was performed at room temperature on a $C_{18}$ column. Mobile phase A consisted of $H_2O$ and phase B AcN. In both phases, 0.1% formic acid was added to increase the ionization efficiency. To increase the separation capacity and to decrease the retention times, gradient elution was applied. The gradient program was as follows: 100% A (from 0 to 0.5 min), 100 to 55% A and 45% B (from 0.5 to 0.6 min), 55% A and 45% B to 35% A and 65% B (from 0.6 to 8.5 min), 35% A and 65 to 100% B (from 8.5 to 8.6 min), 100% B (from 8.6 to 18.6 min), 100% B to 100% A (from 18.6 to 20.0 min), and 100% A (from 20.0 to 30.0 min) to re-equilibrate. Before the start of the analyses, the column was conditioned with 100% A until the pressure was stable for at least 15 min. The flow rate was 0.25 mL/min, and a volume of 40 μL of sample extract was injected into the LC−MS/MS apparatus.

The UPLC separation was conducted on a Waters HPLC BEH $C_{18}$ column held at 30 °C. The injection volume was set at 10 μL and the eluent flow at 0.40 mL/min. Mobile phase A consisted of a $H_2O$/AcN mixture [95/5 (v/v)] with 0.3% acetic acid and phase B an AcN/$H_2O$ mixture [95/5 (v/v)] with 0.3% acetic acid. Gradient elution was applied here, as well. The gradient program was as follows: 100% A (from 0 to 2 min), 100 to 70% A and 30% B (from 2 to 8 min), 70% A and 30 to 100% B (from 8 to 12 min), 100% B (from 12 to 13 min), 100% B to 100% A (from 13 to 13.01 min), and 100% A (from 13.01 to 14.6 min) to re-equilibrate. Before the start of the analysis, the column was conditioned with 100% A until the pressure was stable for at least 15 min.

**Mass Spectrometry.** The method and optimized $ESI^+$ mass spectrometric conditions described by Daeseleire et al.[25] for detecting penicillins in milk were used. The data obtained were analyzed using MassLynx version 4.0 or 4.1 (Waters).

**Statistical Analysis.** To test the influence of the applied cross-linker on the polymerization yield, one-way analysis of variance (ANOVA) was conducted. A Sheffé post hoc test was performed. In addition, one-way ANOVA was used to determine the effect of the application of NIP and MIP on the binding capacity toward benzylpenicillin.

SAS version 9.4 (SAS Institute Inc., Cary, NC) was used for all analyses. Significant differences were assumed when $p < 0.05$.

## RESULTS AND DISCUSSION

This study builds upon the literature.[14,15] Our experiments for the production of MIPs used benzylpenicillin as the template molecule, methacrylic acid (MAA) as the monomer, trimethylolpropane methacrylate (TRIM) or ethylene glycol dimethacrylate (EDMA) as the cross-linker, and AcN as the solvent. The MIP was produced through polymerization using azobis(isobutyronitrile) (AIBN) as the heat-induced initiator.

The first step was to select the most suitable polymerization technique for the production of MIPs for benzylpenicillin (bulk polymerization vs suspension polymerization). The initial screening tests we performed indicated that the latter technique generated the best results in terms of higher production yields (data not shown) and the more refined way of working that could be applied, i.e., no grinding and sieving required. Second, using the selected suspension polymerization technique, the possible effect of the selected cross-linker on the polymerization yield was evaluated. EDMA and TRIM were selected as bi- and trifunctional cross-linkers, respectively (Table 1).

**Table 1. Effects of Cross-Linker Type on Polymerization Yield (expressed in percent)**

| applied cross-linker | batch 1 | batch 2 | batch 3 | mean | standard deviation |
|---|---|---|---|---|---|
| TRIM | 81.0 | 90.1 | 89.0 | 86.7 | 5.0 |
| TRIM blank | 94.0 | 89.3 | 90.1 | 91.1 | 2.5 |
| EDMA | 78.0 | 81.3 | 80.9 | 80.1 | 1.8 |
| EDMA blank | 80.8 | 78.8 | 79.3 | 79.6 | 1.0 |

The yields of the MIPs produced using TRIM as a cross-linker were higher, although not significantly so ($p > 0.05$) (Table 1). The higher yields can most likely be explained by the differences in the number of reactive functional groups between EDMA (bifunctional) and TRIM (trifunctional). On the basis of these data, we decided to continue all further experimental work using TRIM as the cross-linker.

After optimization of the template/functional monomer/cross-linker molar ratio, the composition applied for the development of a benzylpenicillin selective MIP was as follows: benzylpenicillin (2 mmol), MAA (16 mmol), TRIM (7 mmol), and AIBN (0.4 mmol) dissolved in 70 mL of AcN. Using this formulation, the MIP produced was visualized by scanning electron microscopy (SEM). Uniformly sized microspheres were obtained by applying the suspension polymerization method (Figure 1). The microspheres had an average size of 1.2 μm.

To determine the binding specificity of the developed MIP for benzylpenicillin in AcN, we first performed an equilibrium

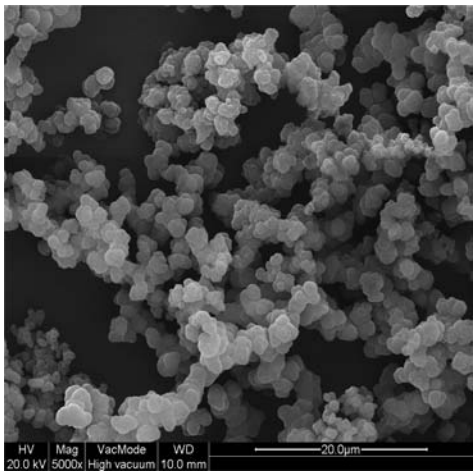


**Figure 1.** Size of benzylpenicillin selective MIP as visualized by SEM.

experiment by comparing the produced MIP and NIP. The obtained results of three independently performed equilibrium binding studies show a statistically significant ($p < 0.01$) difference in binding capacity between the MIP or NIP and benzylpenicillin (68.3 ± 3.1 or 13.2 ± 8.2%, respectively). This represented the first convincing proof that the developed MIP possessed a high affinity for benzylpenicillin.

The reversibility of the binding of benzylpenicillin to the MIP or NIP was proven by washing out the MIP or NIP used during an equilibrium binding experiment. The amounts of benzylpenicillin detected in the different fractions are expressed in relation to that of an internal standard (nafcillin). The experiments were executed in duplicate, and the results (Table 2) clearly show that the total amount of benzylpenicillin (5 μg) used to execute the binding experiment is recovered. This indicates the total reversibility of the binding of benzylpenicillin to the MIP or NIP. The observation that more than half of the benzylpenicillin (fractions 1 and 2) is not retained by the MIP sorbent is in contradiction with the observations in all other experiments and can be explained by the excess of benzylpenicillin present in the solution used during this experiment (5 ppm), resulting in a large amount of benzylpenicillin that was not specifically bound to the MIP.

**Table 2. Results of the Recovery of Benzylpenicillin out of MIP or NIP of an Equilibrium Binding Experiment**

| benzylpenicillin/nafcillin ratio | MIP (first experiment) | MIP (second experiment) | NIP (first experiment) | NIP (second experiment) |
|---|---|---|---|---|
| fraction 1[a] | 0.530 | 0.541 | 1.177 | 1.168 |
| fraction 2[a] | 0.506 | 0.514 | 0.735 | 0.735 |
| fraction 3[b] | 0.758 | 0.774 | 0.044 | 0.067 |
| fraction 4[b] | 0.004 | 0.003 | 0.003 | 0.007 |
| fraction 5[b] | 0.000 | 0.000 | 0.001 | 0.001 |
| fraction 6[b] | 0.001 | 0.002 | 0.001 | 0.003 |
| sum fractions | 1.799 | 1.834 | 1.961 | 1.981 |
| standard 5 μg of benzylpenicillin | 1.805 | 1.805 | 1.805 | 1.805 |

[a]Collected fractions when rinsing the used MIP or NIP. [b]Collected fractions when washing out the used MIP or NIP to recover the bound benzylpenicillin.

The next step in evaluating the binding characteristics of the MIP was to test the cross-reactivity of the developed MIP or NIP with respect to structural analogues of benzylpenicillin. This was done by performing the equilibrium binding experiments in AcN with solutions containing seven molecules belonging to the group of the β-lactam antibiotics (benzylpenicillin is one of them). The selected molecules included ampicillin, amoxicillin, oxacillin, cloxacillin, dicloxacillin, cephalexin, and cephapirin. In addition, one molecule of the group of sulfonamides (sulfadiazin) and one of the group of the tetracyclines (oxytetracycline) were also included. All equilibrium binding tests were repeated three times (Table 3).

**Table 3. Results of the Cross-Reactivity Tests for the Developed NIP**

| % binding components | first test | second test | third test | mean | standard deviation |
|---|---|---|---|---|---|
| benzylpenicillin | 3.8 | 16.9 | 18.8 | 13.17 | 8.17 |
| ampicillin | 92.0 | 91.0 | 94.0 | 92.33 | 1.53 |
| amoxicillin | 94.5 | 94.2 | 91.5 | 93.40 | 1.65 |
| oxacillin | 11.0 | 14.6 | 11.0 | 12.20 | 2.08 |
| cloxacillin | –[a] | 32.2 | 12.3 | 22.25 | 14.07 |
| dicloxacillin | 11.0 | 3.9 | 12.9 | 9.27 | 4.74 |
| cephalexin | 72.1 | 68.0 | 71.0 | 70.37 | 2.12 |
| cephapirin | 90.2 | 94.9 | 93.1 | 92.73 | 2.37 |
| sulfadiazine | 6.0 | 5.0 | 10.7 | 7.23 | 3.04 |
| oxytetracycline | 73.1 | 86.3 | 87.3 | 82.23 | 7.93 |
| benzylpenicillin | 66.9 | 71.8 | 66.1 | 68.27 | 3.09 |
| ampicillin | 99.1 | 98.6 | 99.2 | 98.97 | 0.32 |
| amoxicillin | 99.6 | 99.6 | 98.8 | 99.33 | 0.46 |
| oxacillin | 63.5 | 61.2 | 58.5 | 61.07 | 2.50 |
| cloxacillin | 50.3 | 51.6 | 43.6 | 48.50 | 4.29 |
| dicloxacillin | 33.8 | 45.9 | 46.2 | 41.97 | 7.07 |
| cephalexin | 97.1 | 97.2 | 93.5 | 95.93 | 2.11 |
| cephapirin | 97.4 | 99.4 | 99.6 | 98.80 | 1.22 |
| sulfadiazin | 15.6 | –[a] | 21.7 | 18.65 | 4.31 |
| oxytetracycline | 87.8 | 94.2 | 91.5 | 91.17 | 3.21 |

[a]Results not included because of problems with the internal standard.

The results of the tests for both the NIP and the MIP clearly show that the compounds included in this study can be classified into three separate groups. A first group showed binding efficiencies of >90% for the MIP and >70% for the NIP (ampicillin, amoxicillin, cephalexin, cephaphirin, and oxytetracycline). A second group showed binding percentages between 42 and 68% for the MIP and between 10 and 22% for the NIP (oxacillin, cloxacillin, and dicloxacillin). The last group showed binding degrees of <20% for the MIP and <10% for the NIP (sulfadiazin).

These results can be explained by comparing the chemical structures of the substances included in the cross-reactivity test (see Figure 2). For the substances of group I, very high binding efficiencies were observed for the MIP and the NIP. This can most likely be attributed to the oppositely charged MIP and template molecule. The template contains an amino group that is protonated under the experimental conditions (pH 6.34), while the methacrylic acid from the MIP or NIP has a negative charge at this pH value. This most likely results in a strong electrostatic attraction between both compounds. The substances of group II possess a structure analogous to that of benzylpenicillin. The only difference among the molecules oxacillin, cloxacillin, and dicloxacillin is the number of chlorine substituents. As we anticipated, the binding efficiency decreased as the number of chlorine atoms increased, because of the

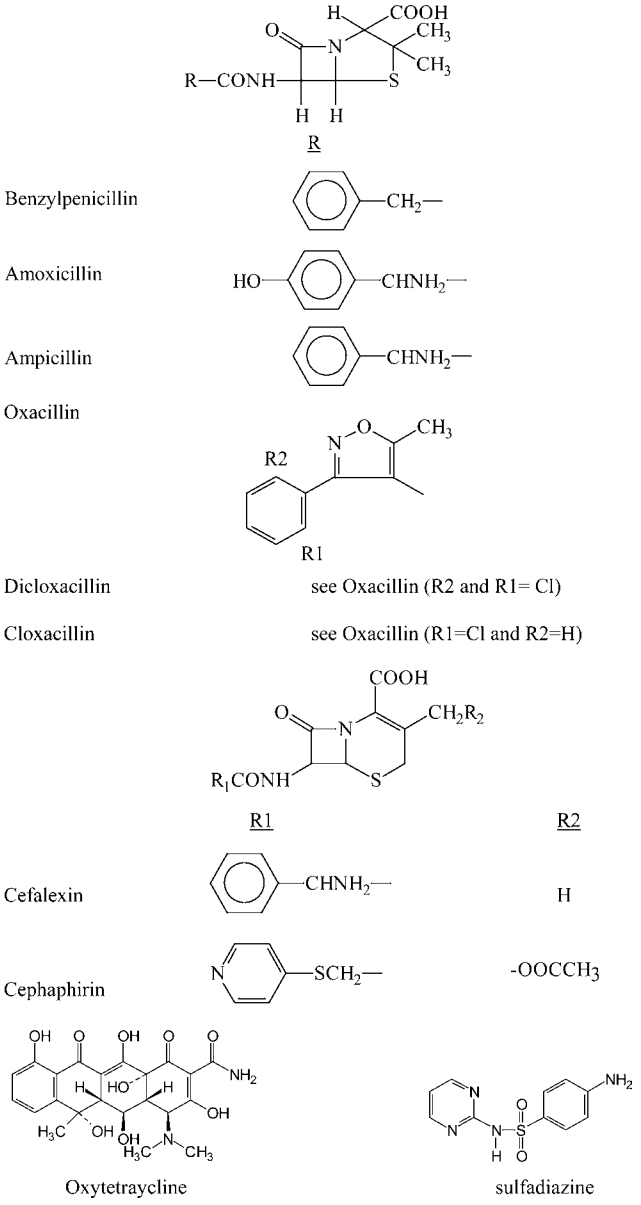


**Figure 2.** Structures of the substances tested in the cross-reactivity test.

increasing sterical effects with an increasing number of chlorine atoms. Members of group III possessed a low binding efficiency because of the absence of chemical structural similarities between sulfadiazin and benzylpenicillin. These observed cross-reactivities will not interfere with the results of our proposed analysis protocol, because the purification step with the developed MIP (MISPE) is followed by a LC−MS/MS analysis, which makes it possible to focus on specific substances. This makes it impossible for the "cross-reactivity" compounds to interfere. This approach can even be an advantage because these cross-reactivity compounds can be detected using the same cleanup step.

Three independent binding equilibrium experiments were also performed to assess the binding affinity of benzylpenicillin for the imprinted particles. The binding isotherm was determined in a concentration range of 0.0015−0.0299 μmol/mL (0.5−10 mg/kg) benzylpenicillin (Figure 3).

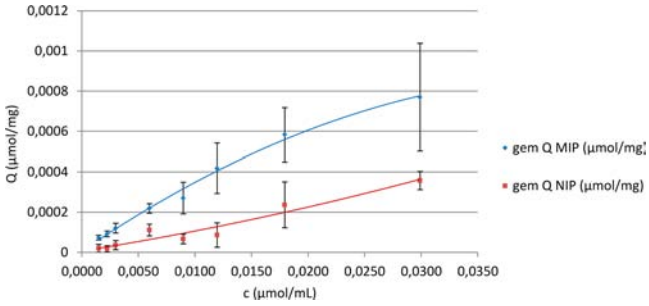


**Figure 3.** Binding isotherms of benzylpenicillin on the MIP and the NIP.

We observed that the amount of benzylpenicillin bound to the MIP and the NIP at equilibrium increased along with the initial concentration of benzylpenicillin and that the amount of benzylpenicillin bound to the MIP was larger than the amount bound to the NIP (the degree of difference depends on the initial concentration), which indicates high-affinity binding by the imprinted binding sites.

The binding affinity can be calculated from the Scatchard equation:

$$\frac{Q}{[\mathrm{PenG}]} = \frac{Q_{\max} - Q}{K_D}$$

where $Q$ is the amount of benzylpenicillin bound to 1 mg of MIP or NIP at equilibrium, [PenG] is the free analyte concentration at equilibrium, $Q_{max}$ is the maximal number of binding sites, and $K_D$ is the equilibrium dissociation constant of the binding sites. The units of $Q$ and $K_D$ are micromoles per milligram and micromoles per milliliter, respectively.

The Scatchard plot (Figure 4) shows that the binding sites in the MIP are heterogeneous, while those of the NIP are

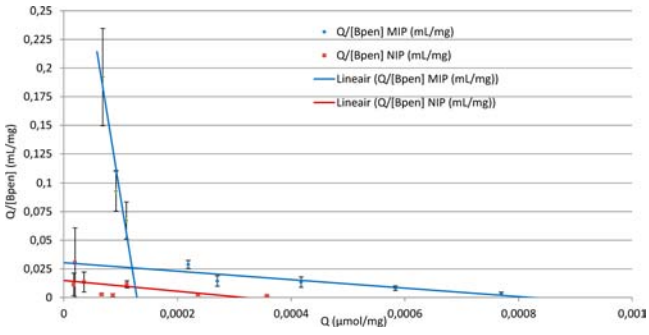


**Figure 4.** Scatchard plot for benzylpenicillin on the MIP and the NIP.

homogeneous. Analysis of the plot gives the linear regression equations of the high- and low-affinity binding sites in the MIP: $Q/[\mathrm{PenG}] = -3061Q + 0.394$, and $Q/[\mathrm{PenG}] = -36.96Q + 0.0303$.

With these equations, $K_D$ and $Q_{max}$ can be calculated. For the high-affinity binding sites, $K_D$ and $Q_{max}$ amounted to 0.33 μmol/L and 0.13 μmol/g, respectively, while for the low-affinity binding sites, the values were found to be 27.1 μmol/L and 0.82 μmol/g, respectively. The homogeneous binding sites of the NIP had $K_D$ and $Q_{max}$ values of 21.3 μmol/L and 0.32 μmol/g, respectively.

The explanation of these findings lies in the synthesis of the imprinted polymers according to the noncovalent method, thus exhibiting heterogeneous binding sites because of the


dx.doi.org/10.1021/jf502331h | J. Agric. Food Chem. 2014, 62, 8814−8821

incomplete association between the benzylpenicillin and methacrylic acid molecules. Specific binding sites are the result of this association, but because of its incompleteness, the polymer also shows nonspecific binding sites. Therefore, only a small number of the binding sites in the MIP are tailor-made in shape and size for the template benzylpenicillin.

The last part of the evaluation of the binding characteristics was the development and validation of a protocol for the application of the MIP in a molecularly imprinted solid-phase extraction (MISPE). The AcN solutions analyzed were fortified with 1, 2, 3, 4, 6, 8, and 10 μg of benzylpenicillin/kg. These concentrations were chosen around the MRL value in milk of 4 μg/kg. The results of the MISPE experiments are listed in Table 4. The experiments were repeated three times.

**Table 4. Recovery of Benzylpenicillin after Cleanup of Acetonitrile Solutions using the MIP (MISPE) and the NIP (NISPE)**

| | recovery [% ($n$ = 3)] | |
|---|---|---|
| spiking level (μg/kg) | MISPE | NISPE |
| 1 | 94.9 ± 3.5 | 14.6 ± 12.9 |
| 2 | 94.9 ± 1.0 | 12.0 ± 10.7 |
| 3 | 83.8 ± 11.1 | 4.5 ± 2.3 |
| 4 | 89.6 ± 3.2 | 4.5 ± 4.0 |
| 6 | 91.8 ± 5.0 | 6.6 ± 2.9 |
| 8 | 92.8 ± 4.1 | 4.8 ± 1.1 |
| 10 | 92.3 ± 5.2 | 5.0 ± 1.4 |

In addition to a satisfying level of precision, a significant difference in binding between MIP and NIP (up to 88%) was observed. We can also conclude that the recovery percentages are independent of the spiking level, because no significant differences were observed between the results obtained with the MIP and the NIP.

To validate these results, a validation study was conducted in AcN at three spiking levels (2, 4, and 6 μg/kg). The study was repeated on three separate days. At each spiking level, five samples were spiked and analyzed. Standard deviations were calculated to evaluate the precision (Table 5).

**Table 5. Recovery of Benzylpenicillin during the Validation Study in Acetonitrile Solutions Spiked at Three Levels Using MISPE and NISPE**

| | recovery [μg/kg ($n$ = 5)] | |
|---|---|---|
| spiking level (μg/kg) | MISPE | NISPE |
| 2 | 1.91 ± 0.13 | 0.04 ± 0.31 |
| | 2.06 ± 0.22 | 0.00 ± 0.19 |
| | 2.19 ± 0.29 | 0.43 ± 0.11 |
| 4 | 4.18 ± 0.64 | 0.14 ± 0.31 |
| | 4.24 ± 0.34 | 0.41 ± 0.38 |
| | 4.30 ± 0.12 | 0.19 ± 0.57 |
| 6 | 6.64 ± 1.20 | 0.00 ± 0.36 |
| | 6.32 ± 0.64 | 0.31 ± 0.43 |
| | 6.07 ± 0.90 | 0.44 ± 1.17 |
| | average recovery [% ($n$ = 15)] | |
| spiking level (μg/kg) | MISPE | NISPE |
| 2 | 102.7 ± 12.0 | 7.5 ± 14.5 |
| 4 | 105.9 ± 10.0 | 6.2 ± 10.7 |
| 6 | 105.7 ± 15.3 | 0.0 ± 16.4 |

The results confirm the conclusions from the recovery experiments in AcN, i.e., a good precision and a significant difference in binding between the MIP and the NIP. Individual differences of up to 100% can be perceived between the MIP and the NIP. Additionally, we can conclude that 100% of the benzylpenicillin in the AcN solutions can be recovered using MISPE.

After the validation of the MISPE protocol, the MIP was applied in a milk matrix. First, the MIP in MISPE for milk samples was validated. Subsequently, naturally contaminated samples were analyzed, and the results were compared with the results obtained by a traditional sample preparation.

Analogous with the validation study in AcN, the validation study in a milk matrix was conducted, at three spiking levels (2, 4, and 6 μg/kg). The study was repeated on three days, and at each spiking level, five samples were spiked and analyzed. Standard deviations were calculated to evaluate the precision (Table 6).

**Table 6. Recovery of Benzylpenicillin during the Validation Study in Milk Extracts Spiked at Three Levels Using MISPE and NISPE**

| | recovery [μg/kg ($n$ = 5)] | |
|---|---|---|
| spiking level (μg/kg) | MISPE | NISPE |
| 2 | 1.67 ± 0.40 | 0.37 ± 0.16 |
| | 1.71 ± 0.26 | 0.00 ± 0.07 |
| | 1.62 ± 0.09 | 0.39 ± 0.10 |
| 4 | 3.47 ± 0.51 | 0.00 ± 0.30 |
| | 3.85 ± 0.16 | 0.00 ± 0.16 |
| | 3.28 ± 0.42 | 0.00 ± 0.11 |
| 6 | 4.57 ± 0.25 | 0.00 ± 0.27 |
| | 5.39 ± 0.28 | 0.00 ± 0.48 |
| | 5.77 ± 0.36 | 0.30 ± 0.43 |
| | average recovery [% ($n$ = 15)] | |
| spiking level (μg/kg) | MISPE | NISPE |
| 2 | 83.2 ± 13.5 | 11.4 ± 12.3 |
| 4 | 88.3 ± 11.1 | 0.0 ± 4.9 |
| 6 | 87.3 ± 9.8 | 0.0 ± 9.1 |

The results show high recoveries (up to 88%) using MISPE for the cleanup of spiked milk extracts, while the use of NISPE resulted in low recoveries between 0 and 11%. We can thus conclude that significant differences in cleanup performances between MIP and NIP can be obtained when used in SPE analysis. The MIP developed by Kempe et al.[18] to detect benzylpenicillin in milk also showed recoveries of up to 87%, but the control polymer also showed very high recovery percentages (73%), indicating a large contribution of nonspecific binding between the template molecule and the sorbent.

Intriguingly, the recoveries obtained after MISPE were in accordance with the criteria set by the EC (Commission Decision 2002/657/EC): for benzylpenicillin levels between 1 and 10 μg/kg, recoveries between 70 and 110% should be achieved. This demonstrates the potential for implementation of the imprinted polymer in the cleanup of benzylpenicillin-contaminated milk samples.

Comparison of Tables 5 and 6 reveals that the milk matrix interfered with the performance of the MIP (in AcN average recoveries are obtained up to 100%, while in milk extract up to 88%). Despite the preparatory steps of the milk samples, the


dx.doi.org/10.1021/jf502331h | J. Agric. Food Chem. 2014, 62, 8814−8821

somewhat lower recoveries can most likely be explained by the interference of matrix factors such as lactose, which were not eliminated during the pretreatment of the samples. We would expect even larger differences if the fat molecules and proteins had not been removed, because the cavities in the used MIP would be less accessible and there would be a greater risk of obstruction of the MIP. For this reason, a defatting and deproteinating step is common in the analysis of antibiotics or other components in milk samples.[26,27]

The LOD and LOQ obtained for the MISPE analysis of milk extracts spiked with benzylpenicillin are 0.51 and 1.02 μg/kg, respectively. These values are very low compared with the LOD of the MIP developed by Guardia et al.[19] to determine naficillin in milk-based products (13.2 mg/kg).

These results indicate that the MIP developed in our study is an appropriate sorbent for the detection and quantification of low concentrations of benzylpenicillin in milk samples.

The same conclusion could also be drawn from the results of the analysis of positive samples. The contamination level of the samples ranged between 3 and 20 μg/kg. The samples were analyzed using MISPE and the classic sample preparation applied in a Beltest-accredited laboratory at the Institute for Agricultural and Fisheries Research (ILVO) (Table 7). The Pearson correlation between the MISPE results and the results of the accredited classic analyses was calculated. An excellent correlation of 0.989 was obtained.

**Table 7. Results of the Analysis of Positive Milk Samples Using MISPE and a Classical Sample Preparation Step**

| | [benzylpenicillin] (μg/kg) | |
|---|---|---|
| sample number | MIP | classic cleanup |
| 13/4102 | 17.36 | 15.29 |
| 13/5312 | 9.77 | 9.96 |
| 13/1022 | 4.04 | 3.32 |
| 13/0206 | 9.58 | 8.37 |
| Pearson correlation, 0.989 | | |

These results confirm that the implementation of molecularly imprinted polymers during the cleanup step is a good alternative for the determination of benzylpenicillin in milk matrices and makes it possible to detect concentrations of benzylpenicillin in milk samples at a level 8 times lower than the MRL. However, direct application of the milk sample on the MISPE cartridge would offer a real advantage to the accredited classic analysis, which is therefore the subject of further research. Because of the risk of obstruction of the used MIP sorbent during the cleanup step, it may be necessary to remove certain matrix components or to add clarifying agents during a short preparation step to make the milk filterable. Possible strategies include a decreaming step to remove the fat molecules, the use of Carrez clarification solutions I and II (Boehringer Mannheim Biochemica[28]), or the use of clarifying agents such as L-NRS (Reybroeck et al.[29]), Somex A (Meyer et al.[30]), or Enliten (Technical Bulletin Enliten ATP assay system bioluminescence detection kit for ATP measurement, Promega).

## AUTHOR INFORMATION


### Corresponding Author

*Telephone: +32-9-272-30-45. Fax: +32-9-272-30-01. E-mail: geert.vanroyen@ilvo.vlaanderen.be.



### Funding

This work was partially sponsored by the Federal Public Service of Health, Food Chain Safety and Environment (Contract RF 6178).


### Notes

The authors declare no competing financial interest.

## ACKNOWLEDGMENTS

We thank Tim De Cock, Marijke Hunninck, and Evy Maseman for their assistance during the experiments and the analysis of the samples. We also thank Petra De Neve and Patricia Van Herreweghe (†) for their assistance with the analysis of the samples.

## REFERENCES


(1) Seiffert, S. N.; Hilty, M.; Perreten, V.; Endimiani, A. Extended-spectrum cephalosporin-resistant gram-negative organisms in livestock: An emerging problem for human health? *Drug Resist. Updates* **2013**, *16*, 22−45.

(2) Smet, A.; Martel, A.; Persoons, D.; Dewulf, J.; Heyndrickx, M.; Herman, L.; Haesebrouck, F.; Butaye, P. Broad-spectrum β-lactamases among Enterobacteriaceae of animal origin: Molecular aspects, mobility and impact on public health. *FEMS Microbiol. Rev.* **2010**, *34*, 295−316.

(3) Reybroeck, W.; Daeseleire, E. Invloed bewaring op antibioticaresiduen in melk. Heranalyse positieve stalen & identificatie van remstoffen verantwoordelijk voor een ongunstig resultaat bij de officiële kwaliteitsbepaling van melk: Resultaten. ILVO: Melle, Belgium, 2003; pp 20.

(4) Martin-Esteban, A. Molecularly imprinted polymers: New molecular recognition materials for selective solid-phase extraction of organic compounds. *Fresenius' J. Anal. Chem.* **2001**, *370*, 795−802.

(5) Svensson, J.; Nicholls, I. A. On the thermal and chemical stability of molecularly imprinted polymers. *Anal. Chim. Acta* **2001**, *435*, 19−24.

(6) Haupt, K. Molecularly imprinted polymers: The next generation. *Anal. Chem.* **2003**, *75*, 376A−383A.

(7) Andersson, L. I. Molecular imprinting: Developments and applications in the analytical chemistry field. *J. Chromatogr., B* **2000**, *745*, 3−13.

(8) Nilsson, J.; Spegel, P.; Nilsson, S. Molecularly imprinted polymer formats for capillary electrochromatography. *J. Chromatogr., B* **2004**, *804*, 3−12.

(9) Ye, L.; Cormack, P. A. G.; Mosbach, K. Molecular imprinting on microgel spheres. *Anal. Chim. Acta* **2001**, *435*, 187−196.

(10) Cederfur, J.; Pei, Y.; Zihui, M.; Kempe, M. Synthesis and screening of a molecularly imprinted polymer library targeted for penicillin G. *ACS Comb. Sci.* **2003**, *5*, 67−72.

(11) Guzman-Vazquez de Prada, A.; Martinez-Ruiz, P.; Reviejo, A. J.; Pingarrón, J. M. Solid-phase molecularly imprinted on-line preconcentration and voltammetric determination of sulfamethazine in milk. *Anal. Chim. Acta* **2003**, *539*, 125−132.

(12) Guzman-Vazquez de Prada, A.; Reviejo, A. J.; Pingarrón, J. M. A method for the quantification of low concentration sulfamethazine residues in milk based on molecularly imprinted clean-up and surface preconcentration at a Nafion-modified glassy carbon electrode. *J. Pharm. Biomed. Anal.* **2006**, *40*, 281−286.

(13) Fernandez-Gonzalez, A.; Badia Laino, R.; Diaz-Garcia, M. E.; Guardia, L.; Viale, J. Assessment of molecularly imprinted sol-gel materials for selective room temperature phosphorescence recognition of nafcillin. *J. Chromatogr., B* **2004**, *804*, 247−254.

(14) Guo, H. S.; He, X. U. Study of the binding characteristics of molecular imprinted polymer selective for cefalexin in aqueous media. *Fresenius' J. Anal. Chem.* **2000**, *368*, 461−465.

(15) Skudar, K.; Brüggemann, O.; Wittelsberger, A.; Ramström, O. Selective recognition and separation of β-lactam antibiotics using molecularly imprinted polymers. *Anal. Commun.* **1999**, *36*, 327−331.

(16) Caro, E.; Marcé, R. M.; Cormack, P. A. G.; Sherrington, D. C.; Borrull, F. Synthesis and application of an oxytetracycline imprinted polymer for the solid-phase extraction of tetracycline antibiotics. *Anal. Chim. Acta* **2005**, *552*, 81−86.
(17) Zhang, J.; Wang, H.; Liu, W.; Bai, L.; Ma, N.; Lu, J. Synthesis of molecularly imprinted polymer for sensitive penicillin determination in milk. *Anal. Lett.* **2008**, *41*, 3411−3419.
(18) Kempe, H.; Kempe, M. Influence of salt ions on binding to molecularly imprinted polymers. *Anal. Bioanal. Chem.* **2010**, *396*, 1599−1606.
(19) Guardia, L.; Badia, R.; Diaz-Garcia, M. E. Molecularly imprinted sol-gels for nafcillin determination in milk-based products. *J. Agric. Food Chem.* **2007**, *55*, 566−570.
(20) Blasco, C.; Pico, Y. Development of an improved method for trace analysis of quinolones in eggs of laying hens and wildlife species using molecularly imprinted polymers. *J. Agric. Food Chem.* **2012**, *60*, 11005−11014.
(21) Mohamed, R.; Mottier, P.; Treguier, L.; Richoz-Payot, J.; Yilmaz, E.; Tabet, J.-C.; Guy, P. A. Use of molecularly imprinted solid-phase extraction sorbent for the determination of four 5-nitro-imidazoles and three of their metabolites from egg-based samples before tandem LC-ESIMS/MS. *J. Agric. Food Chem.* **2008**, *56*, 3500−3508.
(22) Liu, S.; Yan, H.; Wang, M.; Wang, L. Water-compatible molecularly imprinted microspheres in pipette tip solid-phase extraction for simultaneous determination of five fluoroquinolones in eggs. *J. Agric. Food Chem.* **2013**, *61*, 11974−11980.
(23) Chen, L.; Zhang, X.; Sun, L.; Xu, Y.; Zeng, Q.; Wang, H.; Xu, H.; Yu, A.; Zhang, H.; Ding, L. Fast and selective extraction of sulfonamides from honey based on magnetic molecularly imprinted polymer. *J. Agric. Food Chem.* **2009**, *57*, 10073−10080.
(24) He, J.; Wang, S.; Fang, G.; Huaping, Z.; Zhang, Y. Molecularly imprinted polymer online solid-phase extraction coupled with high-performance liquid chromatography-UV for the determination of three sulfonamides in pork and chicken. *J. Agric. Food Chem.* **2008**, *56*, 2919−2925.
(25) Daeseleire, E.; De Ruyck, H.; Van Renterghem, R. Confirmatory assay for the simultaneous detection of penicillins and cephalosporins in milk using liquid chromatography/tandem mass spectrometry. *Rapid Commun. Mass Spectrom.* **2000**, *14*, 1404−1409.
(26) Wang, J. Analysis of Antibiotics in Milk and its Products. In *Handbook of Dairy Food Analysis*, 1st ed.; Nollet, L. M. L., Toldra, F., Eds.; CRC Press: Boca Raton, FL, 2010; Vol. *1*, pp 900.
(27) Richardson, G. H. Dairy Products. In *AOAC Official Methods of Analysis*, 15th ed.; Helrich, K., Ed.; Association of Official Analytical Chemists, Inc.: Arlington, VA, 1990; Vol. *2*, pp 1298.
(28) *Methods of Enzymatic Bioanalysis and Food Analysis Using Test Combinations*; Boehringer Mannheim Biochemical: Basel, Switzerland, 1995; pp 157.
(29) Reybroeck, W.; Schram, E. Improved filtration method to assess bacteriological quality of raw milk based on bioluminescence of adenosine triphosphate. *Neth. Milk Dairy J.* **1995**, *49*, 1−14.
(30) Meyer, M. J.; Schmidt, K. A.; Shirley, J. E.; Sukup, D. Assessment of mastitic infection in bovine milk using ATP bioluminescence. *Dairy Day* **1998**, 32−35.

$Fe_3O_4$ microspheres (MFMs) sorbents for SPE has not been reported.

Rhei Radix et Rhizoma, the root or rhizome of perennial herbaceous plant *Rheum palmatum* L., *Rheum tanguticum* Maxim. ex Balf., or *Rheum officinale* Baill., is not only consumed as a health food supplement in China or other countries, but it also represents one of the most popular medicinal herbs used in clinical practice for the treatment of blood stagnation syndrome as well as a purgative agent. Recent publications have demonstrated that anthraquinone derivatives were thought to be the major active components responsible for the pharmacological activities and therapeutic efficacy.[24] In this study, the use of IL-coated MFMs sorbents combined with ultraperformance liquid chromatography (UPLC) was developed to preconcentrate and determine the anthraquinones in dietary supplements, namely, aloe emodin, rhein, emodin, chrysophanol, and physcion. Furthermore, various parameters, including IL type, concentration of ILs and MFMs, diluent pH, and concentration of acetic acid in eluent were optimized in detail. The experimental results indicated that the established method was reliable and feasible for the analysis of real rhubarb samples.

## MATERIALS AND METHODS

**Reagents and Standards.** 1-Dodecyl-3-methylimidazolium bromide ($[C_{12}mim]Br$), 1-dodecyl-3-methylimidazolium chloride ($[C_{12}mim]Cl$), 1-butyl-3-methylimidazolium tetrafluoroborate ($bminBF_4$), and 1-butyl-3-methylimidazolium polystyrenesulfonate (bminPSSA) were purchased from Shanghai Cheng Jie Chemical Co., Ltd. (Shanghai, China). Methanol (HPLC grade) was supplied by Sigma-Aldrich Shanghai Trading Co., Ltd. (Shanghai, China). Purified water was obtained from Hangzhou Wahaha Group Co., Ltd. (Hangzhou, China). All other chemicals and reagents were of analytical grade and were used without further purification.

The investigated standards, including emodin, rhein, aloe emodin, and physcion, were purchased from Shanghai Winherb Medical Technology Co., Ltd. (Shanghai, China). Chrysophanol was obtained from the National Institute for the Control of Pharmaceutical and Biological Products (Beijing, China). The purity of each standard was higher than 98%, and their structures are shown in Figure 1. The herb and granules of Rhei Radix et Rhizoma were collected from the local drugstore (Hangzhou, China).

**UPLC Analysis.** The separation and quantitation of anthraquinones was accomplished using UPLC with ultraviolet (UV) detection (Waters Co., Milford, MA, U.S.A.) with solvent A (0.1% formic acid, v/v) and B (methanol) at a flow rate of 0.5 mL $min^{-1}$ as eluents. The gradient eluent program was as follows: 0−1 min, 25%−30% B; 1−3 min, 30%−45% B; 3−5 min, 45%−60% B; 5−7 min, 60%−80% B; 7−8 min, 80%−100% B; 8−8.5 min, 100%−100% B. An Acquity UPLC BEH $C_{18}$ analytical column (1.7 $\mu$m, 2.1 mm × 50 mm) was supplied by Waters Co. During the separation, the injection volume was 1 $\mu$L for standards and sample solutions. UV detection was performed at a wavelength of 254 nm.

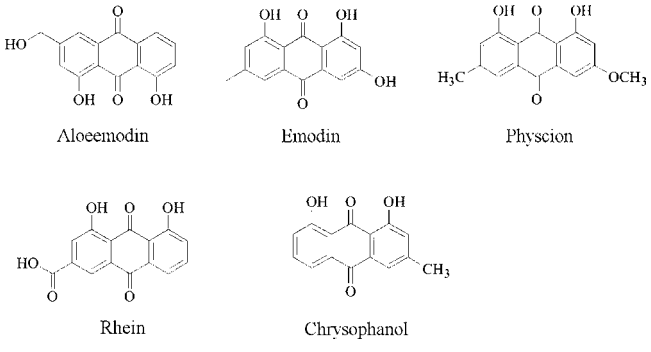


**Figure 1.** Chemical structures of the five compounds investigated.

**Preparations of Standard Solution and Sample Solutions.** Standard solutions of emodin (500 $\mu$g $mL^{-1}$), rhein (250 $\mu$g $mL^{-1}$), aloe emodin (500 $\mu$g $mL^{-1}$), physcion (250 $\mu$g $mL^{-1}$), and chrysophanol (500 $\mu$g $mL^{-1}$) were prepared in methanol and then diluted to the appropriate concentration using pure water prior to MSPE.

Rhei Radix et Rhizoma sample was prepared according to the approach described in the Chinese Pharmacopoeia 2010 without any modifications. First, a 0.15 g sample of powdered rhubarb herb was extracted with methanol (25 mL) by refluxing for 60 min. Next, the solution was cooled to room temperature, and the weight lost was compensated with methanol in the extraction process. After shaking and filtering, 5 mL of filtrate was transferred to a small flask and evaporated to dryness. The residue was redissolved in 10 mL of 8% HCl and then sonicated at 100 W (40 kHz) for 2 min. Next, 10 mL of chloroform was added in acidified solution. The solution was refluxed for 60 min and allowed to cool. The mixture was then transferred to a separating funnel and extracted three times with 10 mL of chloroform, and the combined solutions were dried to a residue under reduced pressure. The residue was dissolved with methanol and transferred to a 10 mL volumetric flask, and methanol was added to the mark. The rhubarb granules were prepared using the same method.

**Preparation of MFMs.** Monodispersed $Fe_3O_4$ microspheres of average size were synthesized according to previous reports.[25,26] For a typical synthesis of $Fe_3O_4$ microspheres, $FeCl_3$ (0.406 g) and NaAc (1.026 g) were dissolved in 49.02 mL of ethylene glycol and 0.98 mL of water. After vigorous stirring of the mixture for 8 h, the homogeneous solution was transferred to a Teflon-lined stainless-steel autoclave (100 mL in volume), sealed, and heated to 200 °C. After a 12 h reaction period, the autoclave was cooled to room temperature. The obtained $Fe_3O_4$ microspheres were washed with ethanol and water and then dried in a vacuum for 12 h. Finally, the resulting $Fe_3O_4$ MMNPs were stored at 25 °C before being used for the following MSPE process.

**Material Characterization.** Transmission electron microscope (TEM) (Zeiss Supra 55, Oberkochen, Germany) was used to obtain the micrographs of MFMs (100 kV), which were used to characterize their particle size and morphology.

**MSPE Procedure.** The extraction procedure, elaborately depicted in Figure 2, was as follows. First, 20 $\mu$L of the standard/sample solutions was homogeneously mixed with 6.6 mg $mL^{-1}$ MFMs and 0.32 mg $mL^{-1}$ $[C_{12}mim]Cl$ dispersions in a 1.5 mL Eppendorf tube. Subsequently, 1000 $\mu$L of purified water was slowly added to the tube, and the mixture was vortexed for 10 s at fast speed before being allowed to stand for 5 min. A magnet was deposited outside the bottom of the centrifuge tube for 1 s to separate the $Fe_3O_4$-retrieval anthraquinone sorbents from the sample solution. Next, the supernatant was decanted, and each of the target analytes was eluted from the sorbents using 200 $\mu$L of methanol (containing 1% acetic acid). The collected eluents (eluted thrice, yielding


dx.doi.org/10.1021/jf502323f | J. Agric. Food Chem. 2014, 62, 8822−8829

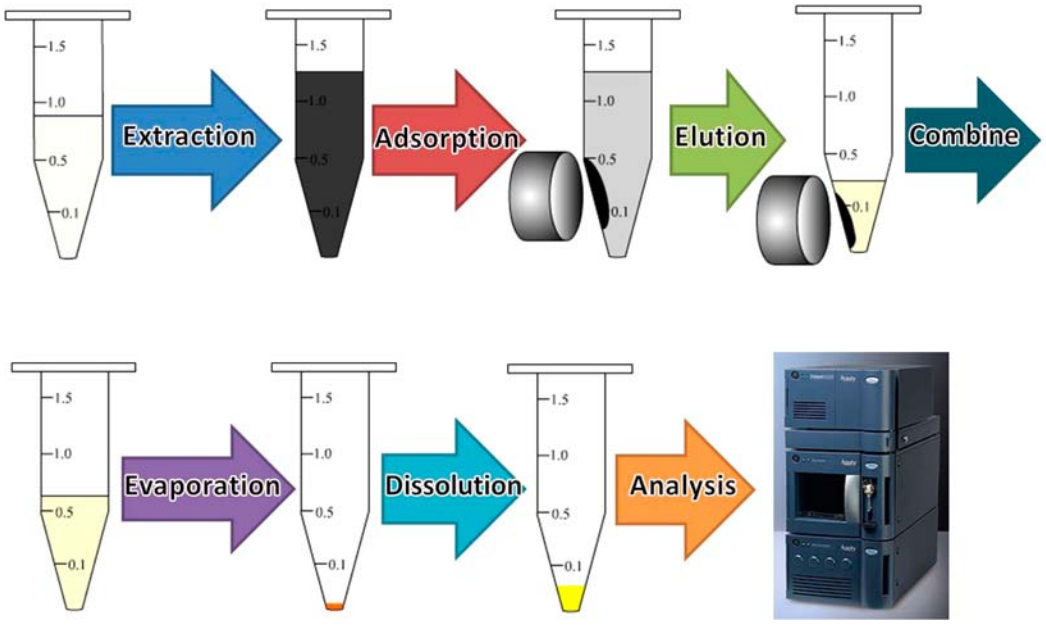


**Figure 2.** Schematic of the magnetic SPE process using IL-functionalized MFMs.

600 μL) were transferred to a new Eppendorf tube and then evaporated to dryness in an 80 °C water bath. The residues were redissolved with 50 μL of methanol, sonicated at 100 W (40 kHz) for 2 min, and then centrifuged at 13 000 rpm for 5 min. Finally, 1 μL of the standard or sample solution of interest was injected into UPLC for identification and quantification of the anthraquinones.

## RESULTS AND DISCUSSION

**Characterization of MFMs.** The morphology and size of MFMs were characterized by TEM with 200 nm (A), 100 nm (B), and 50 nm (C) in scale bars. As indicated from the TEM image (Figure 3), the sample consisted of a large quantity of tiny primary $Fe_3O_4$ nanocrystals with an average size of 100 nm. In addition, the uniform shape and hierarchical structure of mesoporous $Fe_3O_4$ were observed from Figure 3. When the nanocrystals were used as building blocks, they were assembled into a mesoporous structure. It was obvious that the TEM image confirmed the loosely packed character with lots of void space between microspheres.

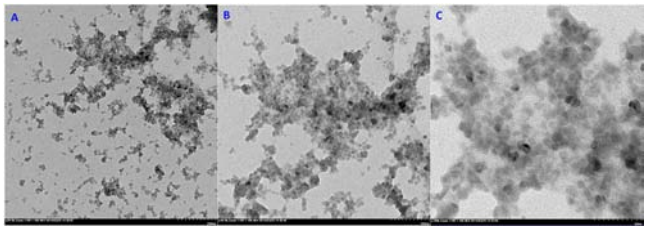


**Figure 3.** TEM image of MFMs with 200 nm (A), 100 nm (B), and 50 nm (C) in scale bars.

To achieve the best extraction efficiency of MSPE for the target analytes, several variables, including IL type, concentration of ILs and MFMs, diluent pH, and concentration of acetic acid in the eluent, were investigated in depth in the optimization process following a univariate method.

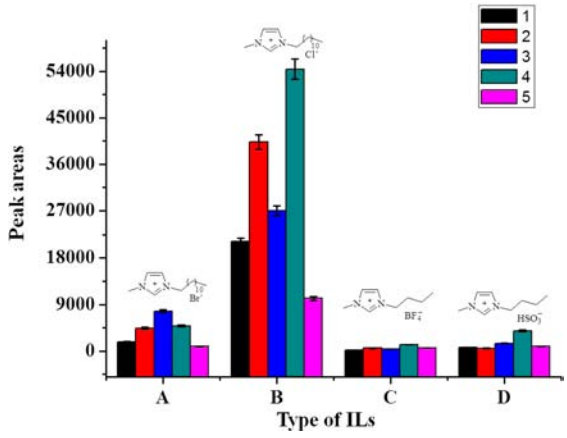


**Figure 4.** IL selection. Extraction conditions: sample volume, 1230 μL; spiked working solution, 20 μL; IL concentration, 0.32 mg $mL^{-1}$; MFMs concentration, 6.6 mg $mL^{-1}$; pH, 11. Desorption conditions: 200 μL of methanol (containing 1.0% acetic acid), thrice. Types of ILs: (A) $[C_{12}mim]Br$, (B) $[C_{12}mim]Cl$, (C) $bminBF_4$, (D) bminPSSA. Peak identification: 1, aloe emodin; 2, rhein; 3, emodin; 4, chrysophanol; 5, physcion.

**Selection of ILs.** The principal aims of this study were to investigate the unique characteristics of an adsorbent comprising MFMs and ILs in dispersion and to select a suitable type of IL for the preparation of dispersants. To this end, four types of ILs ($[C_{12}mim]Br$, $[C_{12}mim]Cl$, $bminBF_4$, and bminPSSA) containing different inorganic anions were selected in this work. For all IL species investigated, a good dispersion was achieved by adding MFMs to the IL solutions. The dispersions, which were optically inhomogeneous at the microcosmic level, exhibited more intense UV absorption with increasing IL alkyl chain length. As shown in Figure 4, a significantly higher extraction efficiency was obtained by mixing with long-chain ILs ($[C_{12}mim]Br$, $[C_{12}mim]Cl$) in the magnetic functionalization process than when using short-aliphatic-chain ILs ($bminBF_4$ and bminPSSA). This may due to the following. (a) The long-alkyl-chain ILs possessed surface-

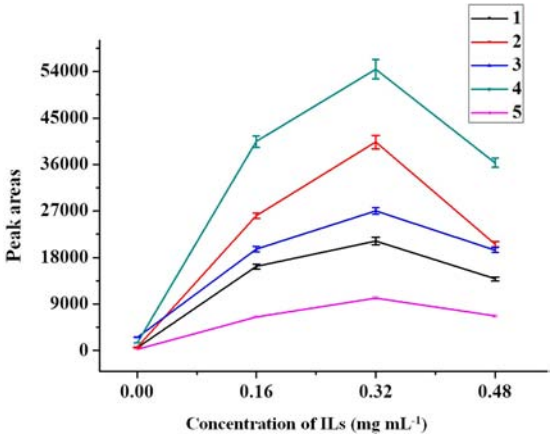


**Figure 5.** Effect of IL concentration on the extraction of five compounds. Extraction conditions: sample volume, 1230 $\mu$L; spiked working solution, 20 $\mu$L; MFMs concentration, 6.6 mg mL$^{-1}$; pH, 11; [$C_{12}$mim]Cl concentration, 0–0.48 mg mL$^{-1}$. Peak identification: 1, aloe emodin; 2, rhein; 3, emodin; 4, chrysophanol; 5, physcion. The other conditions were the same as in Figure 4.

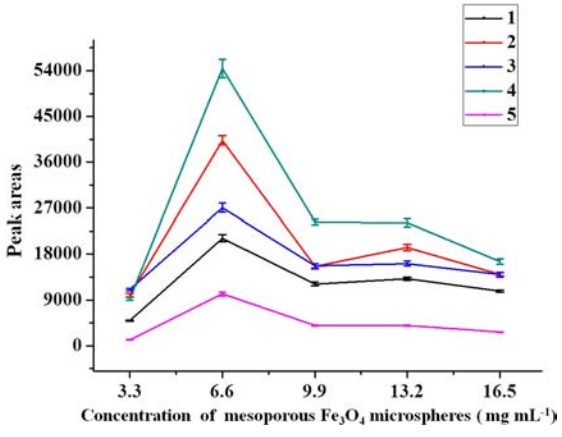


**Figure 6.** Influence of MFMs concentration on the extraction of five compounds. Extraction conditions: sample volume, 1230 $\mu$L; spiked working solution, 20 $\mu$L; [$C_{12}$mim]Cl concentration, 0.32 mg mL$^{-1}$; pH, 11; MFMs concentration, 3.3–16.5 mg mL$^{-1}$. Peak identification: 1, aloe emodin; 2, rhein; 3, emodin; 4, chrysophanol; 5, physcion. The other conditions were the same as in Figure 4.

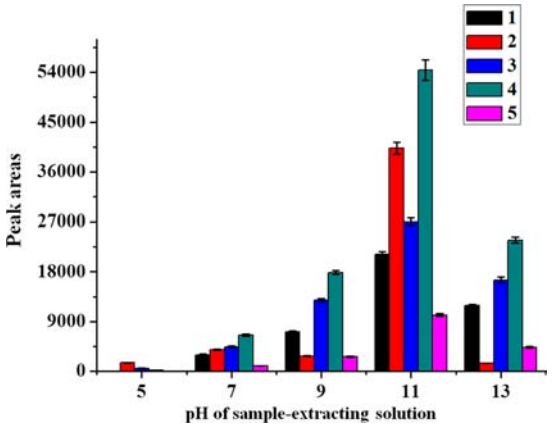


**Figure 7.** Influence of pH on the extraction of five compounds. Extraction conditions: sample volume, 1230 $\mu$L; spiked working solution, 20 $\mu$L; [$C_{12}$mim]Cl concentration, 0.32 mg mL$^{-1}$; MFMs concentration, 6.6 mg mL$^{-1}$; pH, 5–13. Peak identification: 1, aloe emodin; 2, rhein; 3, emodin; 4, chrysophanol; 5, physcion. The other conditions were the same as in Figure 4.

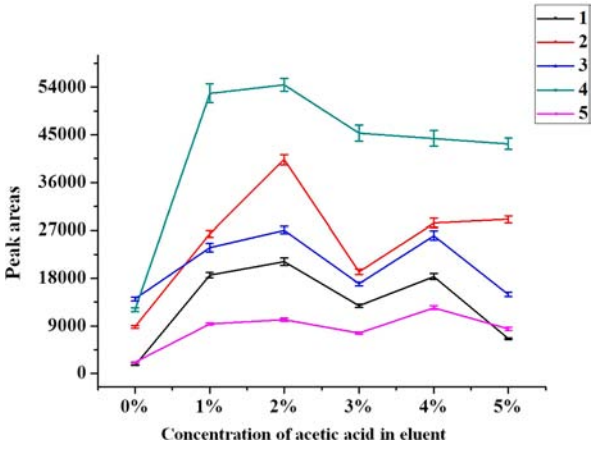


**Figure 8.** Effect of acetic acid concentration on the extraction of five compounds. Extraction conditions: sample volume, 1230 $\mu$L; spiked working solution, 20 $\mu$L; [$C_{12}$mim]Cl concentration, 0.32 mg mL$^{-1}$; MFMs concentration, 6.6 mg mL$^{-1}$; pH, 11. Desorption conditions: 200 $\mu$L of methanol (containing 0%–5% acetic acid), thrice. Peak identification: 1, aloe emodin; 2, rhein; 3, emodin; 4, chrysophanol; 5, physcion.

active characteristics similar to conventional cationic surfactants and may be amphiphilic when dissolved in water.[27] Moreover, the IL with longer alkyl chains at the cation featured a higher distribution ratio in the functionalization process. (b) Imidazolium-based ILs with longer alkyl side chains strengthened the directionality of hydrogen bonds and other weak forces (e.g., van der Waals),[28] which provided a greater interaction with MFMs and target analytes. In addition, the application of [$C_{12}$mim]Cl-functionalized magnetic dispersion achieved the optimum UV absorption due to the stronger conjugated and inductive effect induced by the chloride anions. It also can be clearly seen that the addition of four ILs in MSPE ultimately yielded yellow liquids. Among these ILs, the deepest color was observed using [$C_{12}$mim]Cl dispersion. The results indicated that [$C_{12}$mim]Cl employed in functional magnetic materials indeed had a significant effect on the extraction of analytes in the types of ILs investigated. Therefore, [$C_{12}$mim]Cl was selected as the optimal IL and used in further study.

**Effect of IL Concentration.** The IL concentration generally has a strong effect on the extraction efficiency and the site of action of target compounds. During the optimization of the method, the effect of IL concentration was evaluated at concentrations ranging from 0 to 0.48 mg mL$^{-1}$. The results indicated that when the concentration of [$C_{12}$mim]Cl in the dispersions increased from 0 to 0.32 mg mL$^{-1}$, the detected anthraquinone peak areas greatly improved by factors of 20 to 60 (Figure 5). It was also apparent that the maximum adsorption of target analytes was obtained with 0.32 mg mL$^{-1}$ of [$C_{12}$mim]Cl in the dispersion. However, further increasing the concentration of ILs to 0.48 mg mL$^{-1}$ resulted in serious deterioration of the extraction efficiency, although the dispersion of the sample was good for high IL concentrations, indicating that the partition of the analytes between the sorbents and aqueous phase was reduced. Additionally, the yellow color of the solutions was observed in the final step of the extraction process, especially when 0.32 mg mL$^{-1}$


dx.doi.org/10.1021/jf502323f | J. Agric. Food Chem. 2014, 62, 8822–8829

**Table 1. Linear Regression Data and Precision of Investigated Compounds**

| | | | | precision (RSD%) | | | |
|---|---|---|---|---|---|---|---|
| | | linear range | | intraday ($n$ = 6) | | interday ($n$ = 3) | |
| analytes | calibration curves | ($\mu$g mL$^{-1}$) | $r^2$ | peak area | retention time | peak area | retention time |
| aloe emodin | $y$ = 278813$x$− 2683.5 | 0.0122−1.2200 | 0.9995 | 0.10 | 0.30 | 1.11 | 0.66 |
| rhein | $y$ = 480700$x$ − 213.04 | 0.0115−1.1500 | 0.9994 | 0.25 | 0.27 | 1.12 | 0.60 |
| emodin | $y$ = 596132$x$ − 1846.2 | 0.0084−0.8400 | 0.9998 | 0.20 | 0.24 | 1.03 | 0.48 |
| chrysophanol | $y$ = 151816$x$ − 2730.5 | 0.0245−2.4500 | 0.9997 | 0.23 | 0.22 | 1.19 | 0.43 |
| physcion | $y$ = 119604$x$ − 2919.1 | 0.0219−2.1900 | 0.9998 | 0.11 | 0.18 | 0.95 | 0.34 |

**Table 2. Repeatability, Limits of Detection (LODs), Limits of Quantitation (LOQs), and Recovery of Investigated Compounds**

| | repeatability | | LOD | LOQ | recovery |
|---|---|---|---|---|---|
| | (RSD%) $n$ = 3 | | (ng mL$^{-1}$) | (ng mL$^{-1}$) | % |
| analytes | peak area | retention time | | | |
| aloe emodin | 3.08 | 0.44 | 1.1 | 3.8 | 89.25 |
| rhein | 2.21 | 0.46 | 0.6 | 2.1 | 92.66 |
| emodin | 1.82 | 0.28 | 0.4 | 1.4 | 95.32 |
| chrysophanol | 3.55 | 0.27 | 1.5 | 4.9 | 90.22 |
| physcion | 4.32 | 0.21 | 2.8 | 9.4 | 96.48 |

[$C_{12}$mim]Cl was added into the MFMs dispersion. The overall results indicated that the extraction efficiency was significantly improved by various interactions between the ions themselves,[1,29,30] such as van der Waals forces, electrostatic interactions, and hydrogen bonding. As a result, 0.32 mg mL$^{-1}$ [$C_{12}$mim]Cl was chosen in this experiment.

**Influence of MFMs Concentration.** The concentration of MFMs is also a vital parameter for magnetic SPE, as it is directly related to the extraction efficiency of the tested analytes. In this study, to investigate the adsorption capacity of MFMs and to choose the optimal content, 0.32 mg mL$^{-1}$ ILs and 20 $\mu$L of rhubarb-herb-extracting solution were added into diluents containing MFMs ranging in concentration from 3.3 to 16.5 mg mL$^{-1}$. As illustrated in Figure 6, the adsorption capacity sharply increased with the MFMs concentration up to 6.6 mg mL$^{-1}$ but then decreased significantly when 9.9 mg mL$^{-1}$ MFMs was used in the dispersion, decreasing the efficiency of the magnetic SPE. Furthermore, the UV absorption of the five compounds remained substantially unchanged as the MFMs concentration increased from 9.9 to 16.5 mg mL$^{-1}$. These observations demonstrated that the capacity of MFMs adsorbing compounds was saturated, and it was difficult to elute more analytes from the sorbent in the presence of high concentrations of MFMs in dispersions. According to the above results, 6.6 mg mL$^{-1}$ was selected as the optimal MMNP concentration and employed in the following studies.

**Effect of pH.** The pH of the sample-extracting solution played an important role in the extraction process, as it determined the type of compounds present and the state of the ILs. Additionally, it was a critical parameter for the MSPE method optimization. In the experiment, the pH of the sample solution was adjusted using 1 M phosphoric acid or 1 M sodium hydroxide to values ranging from 5 to 13. The effect of pH on the extraction efficiency of the analytes is shown in Figure 7. It was apparent that with the increment of pH values from 5 to 11, the magnitude of the extracted peak areas of the target compounds was progressively increased, especially in the

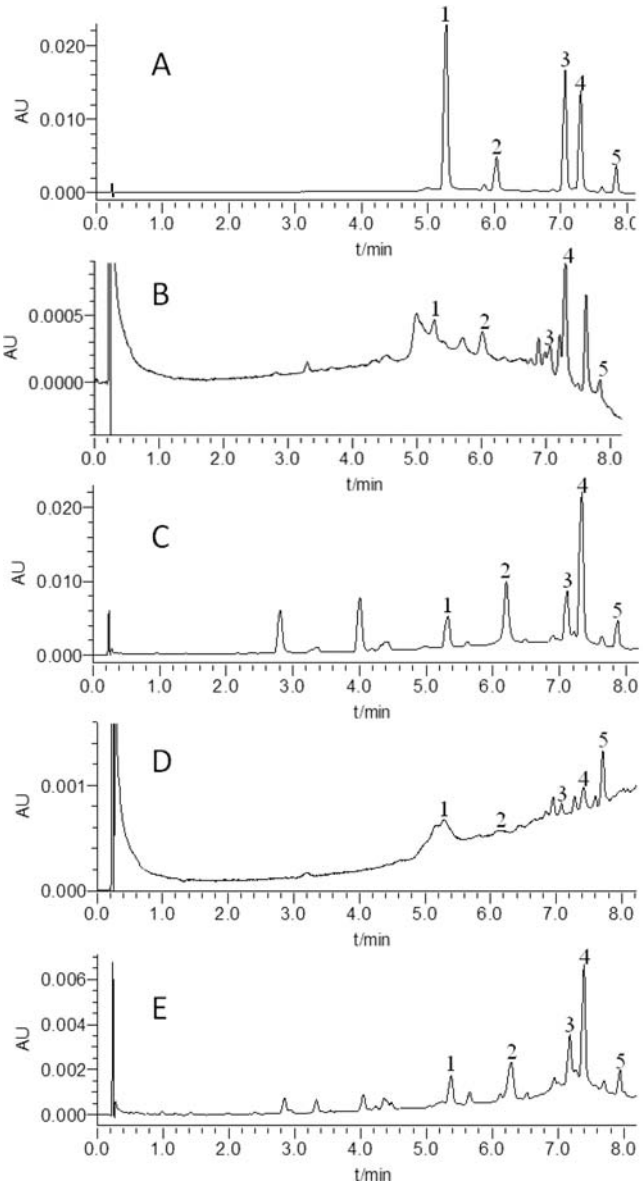


**Figure 9.** Chromatograms obtained from the analysis of (A) standard solutions, (B) Radix et Rhizoma Rhei sample (sample solution, 20 $\mu$L; extraction volume, 1230 $\mu$L) using the unenriched method, (C) Radix et Rhizoma Rhei extracted by IL coated MFMs SPE under optimum conditions, (D) Radix et Rhizoma Rhei granule sample (sample solution, 20 $\mu$L; sample volume, 1230 $\mu$L) using the unenriched method, (E) Radix et Rhizoma Rhei granules extracted by IL-coated MFMs SPE under optimum conditions. Peak identification: 1, aloe emodin; 2, rhein; 3, emodin; 4, chrysophanol; 5, physcion.


dx.doi.org/10.1021/jf502323f | J. Agric. Food Chem. 2014, 62, 8822−8829

Table 3. Comparison of Proposed Extraction Procedure with Other Published Methods for the Extraction of Anthraquinones

| sorbent[a] | extraction method[b] | instrumental technique[c] | sample volume (mL) | LODs (ng/mL) | recovery (%) | analysis time (min) | reference |
|---|---|---|---|---|---|---|---|
| $C_{18}$ | SPE | HPLC-UV | 4 | 230−4610 | 81.2−106 | 45 | 32 |
| CTAB-SCMNPs | magnetic-SPE | HPLC-FLD | 0.1−1 | 0.2−10 | 92.8−109.9 | 20 | 33 |
| CTAB-MNPs | magnetic-SPE | HPLC-DAD | 0.02 | 2.6−6.6 | 96.7−106.6 | 50 | 34 |
| IL-MFMFMs | magnetic-SPE | UPLC-UV | 0.02 | 0.4−2.8 | 89.25−96.48 | 8 | this work |

[a]CTAB-SCMNPs, cetyltrimethylammonium bromide−silica-coated magnetic nanoparticles; CTAB-MNPs, cetyltrimethylammonium bromide-magnetic nanoparticles; IL-MFMFMs, ionic-liquid-micelle-functionalized mesoporous $Fe_3O_4$ microspheres. [b]SPE, solid-phase extraction; magnetic-SPE, magnetic solid-phase extraction. [c]HPLC-UV, high-performance liquid chromatography-ultraviolet; HPLC-FLD, high-performance liquid chromatography-fluorescence detection; HPLC-DAD, high-performance liquid chromatography-diode array detection; UPLC-UV, ultraperformance liquid chromatography-ultraviolet.

case of the absorption of rhein (peak 2) and chrysophanol (peak 4). This result is ascribed to the presence of the hydroxyl groups (OHs) in the molecular structures of anthraquinones. The lone-pair electrons exposed in OHs could interact with the $\pi$ electrons in the imidazole structure of IL-coated MFMs, which increased the extraction efficiency of the target analytes. However, the peak areas of the analytes greatly decreased when the pH value increased to 13, indicating that stronger alkalinity of the solution resulted in more difficult desorption of target analytes from functionalized magnetic materials. This finding may imply that the enrichment effect was strongly pH dependent. As a result, a pH of 11 was found to be optimal.

**Concentration of Acetic Acid in the Eluent.** After the IL-coated MFMs and extracted compounds were separated from the aqueous phase, an elution procedure with an organic solvent was required to remove the target compounds from the sorbents. On the basis of our experience and the nature of the desorption solvent, methanol was chosen as an eluent. In addition, the eluent efficiency of methanol was investigated by adding from 0% to 5% acetic acid to adjust the eluent pH. Initially, poor extraction efficiencies were obtained, and the aloe emodin and physcion signals (peaks 1 and 5) were extremely weak (Figure 8) in pure methanol. The extraction efficiency then improved as the acetic acid concentration increased from 1% to 2%. However, when larger volumes of acetic acid (from 3% to 5%) were applied, the peak areas of the five compounds decreased sharply. This may be due to the decreased hydrogen bonding, ionic interactions, and solubilities between the analytes and eluent.[31,34] Thus, based on the above observations, 2% acetic acid in methanol was chosen as the optimal eluent.

**Validation of the Proposed Method.** Once optimized, the proposed process was analytically characterized in terms of linearity, precision, repeatability, limits of detection (LODs), limits of quantification (LOQs), and recovery. The calibration curves were established using five target compounds at concentrations ranging from 0.0084 to 2.4537 $\mu$g mL$^{-1}$. The results summarized in Tables 1 and 2 indicate good linearity over the concentration range investigated, and the correlation coefficients of determination ($r^2$) were all greater than 0.9994. To confirm the repeatability, five different working solutions prepared from rhubarb samples using MSPE were analyzed, and the RSDs of peak areas and retention times were found to be lower than 4.32% and 0.46%, respectively. The intra- and interday precision of the proposed method were also calculated as the RSD among concentrations in the middle of the linear range. As listed in Table 1, the RSDs of the peak areas and retention times based on six replicated injections for interday precision were in the range of 0.95%−1.19% and 0.18%−0.30%, respectively. For the intraday precision test, the peak areas and retention times were less than 0.25% and 0.66%, respectively. The LOD values calculated based on a signal-to-noise ratio (S/N) of 3 ranged from 0.0004 to 0.0028 $\mu$g mL$^{-1}$. Using an S/N ratio of 10, the LOQ values of these analytes were 0.0014−0.0094 $\mu$g mL$^{-1}$. Good recoveries were obtained by IL-coated MFMs SPE, ranging from 89.25% to 96.48%. The results indicated that the proposed method could provide good qualitative results for the analysis of the target analytes.

**Sample Analysis.** The optimized IL-based MFMs SPE coupled with UPLC method was applied to the extraction of anthraquinones in dietary supplements collected from a local drugstore. Figure 9 presents representative chromatograms of the standards (Figure 9A) and extracted samples (Figure 9B−E) under the determined optimal conditions. Without the sample pretreatment step (Figure 9B,D), five anthraquinones were not obviously detected by UPLC (below the LOQ of the method) in rhubarb herb and rhubarb granules. On the other hand, target compounds were notably determined using magnetic SPE (Figure 9C,E) without any interference. It was observed that the obtained extraction efficiency of the samples using magnetic SPE was remarkably greater, and the enrichment factors for all analytes were in the range from 23 (for physcion) to 60 (for emodin). The rhubarb herb and rhubarb granules contained 0.0146 mg g$^{-1}$ and 0.0071 mg g$^{-1}$ aloe emodin, 0.0089 mg g$^{-1}$ and 0.0047 mg g$^{-1}$ rhein, 0.0056 mg g$^{-1}$ and 0.0024 mg g$^{-1}$ emodin, 0.1411 mg g$^{-1}$ and 0.0692 mg g$^{-1}$ chrysophanol, and 0.0334 mg g$^{-1}$ and 0.0227 mg g$^{-1}$ physcion, respectively. It was obvious that the contents of anthraquinones in the rhubarb granules were much lower than those in the rhubarb herb, which may due to the complexity of the production process. The experimental results clearly indicated that the proposed method was a useful tool for the analysis of multiple ingredients in real plant samples.

**Comparison with Other Methods.** Table 3 presents a comparison of the proposed method with other counterparts based on the use of SPE. The comparison is performed on the basis of some operational (sample volume, sorbent) and analytical (LODs, recovery, and analysis time) properties. In the majority of the cases, the extraction method is performed using the principles of magnetic SPE. Our proposal provides low LODs (0.4−2.8 ng/mL) for target analytes by using the lowest amount of sample volume, which is comparable with the HPLC-FLD method. Moreover, the recoveries are comparable with the other counterparts, requiring a shorter analysis time. In summary, IL-MFMFMs can be considered as a promising alternative for the extraction of phytochemical compounds.

In conclusion, a novel IL-coated MFMs SPE method coupled with UPLC was developed for the preconcentration of five anthraquinones in dietary supplements. The contents of target

components were successfully determined with satisfactory precision, recovery, and repeatability. Compared with traditional extraction modes, this proposed method has the advantages of simplicity, rapidity, ease of operation, and environmental-friendliness. Therefore, IL-functionalized MFMs SPE could have high analytical potential for the extraction of other analytes from complex plant samples.

## AUTHOR INFORMATION


### Corresponding Author

*E-mail: caojun91@163.com. Fax: +86 571 2886 7909. Tel.: +86 571 2886 7909.

### Author Contributions

§S.-S.H., W.C., H.-B.D., and J.-H.D. contributed equally to this work.



### Funding

This study was supported by General Program of National Natural Science Foundation of China (No. 81274065), Research on Public Welfare Technology Application Projects of Zhejiang Province (No. 2014C37069), Changjiang Scholars and Innovative Research Team in Chinese University (IRT 1231), Young and Middle-Aged Academic Leaders of Hangzhou (2013−45), Scientific Research Foundation of Hangzhou Normal University (2011QDL33), and the New-Shoot Talents Program of Zhejiang province (2013R421044, 2014R421019).


### Notes

The authors declare no competing financial interest.

## REFERENCES


(1) Reyes-Gallardo, E. M.; Lasarte-Aragonés, G.; Lucena, R.; Cárdenas, S.; Valcárcel, M. Hybridization of commercial polymeric microparticles and magnetic nanoparticles for the dispersive micro-solid phase extraction of nitroaromatic hydrocarbons from water. *J. Chromatogr. A* **2013**, *1271*, 50−55.

(2) Wang, Y. G.; Ren, J. W.; Liu, X. H.; Wang, Y. Q.; Guo, Y.; Guo, Y. L.; Lu, G. Z. Facile synthesis of ordered magnetic mesoporous gamma-$Fe_2O_3/SiO_2$ nanocomposites with diverse mesostructures. *J. Colloid Interface Sci.* **2008**, *326*, 158−165.

(3) Mashhadizadeh, M. H.; Karami, Z. Solid phase extraction of trace amounts of Ag, Cd, Cu, and Zn in environmental samples using magnetic nanoparticles coated by 3-(trimethoxysilyl)-1-propantiol and modified with 2-amino-5-mercapto-1,3,4-thiadiazole and their determination by ICP-OES. *J. Hazard. Mater.* **2011**, *190*, 1023−1029.

(4) Lasarte-Aragonés, G.; Lucena, R.; Cárdenas, S.; Valcárcel, M. Effervescence assisted dispersive liquid-liquid microextraction with extractant removal by magnetic nanoparticles. *Anal. Chim. Acta* **2014**, *807*, 61−66.

(5) Mashhadizadeh, M. H.; Amoli-Diva, M.; Pourghazi, K. Magnetic nanoparticles solid phase extraction for determination of ochratoxin A in cereals using high-performance liquid chromatography with fluorescence detection. *J. Chromatogr. A* **2013**, *1320*, 17−26.

(6) Liu, X. D.; Yu, Y. J.; Li, Y.; Ning, S. L.; Liu, T. T.; Li, F. J.; Duan, G. L. Restricted access magnetic core-mesoporous shell microspheres with $C_8$-modified interior pore-walls for the determination of diazepam in rat plasma by LC-MS. *Talanta* **2013**, *106*, 321−327.

(7) Liu, H.; Lin, C.; Ma, Z.; Yu, H. B.; Zhou, S. H. Gold nanoparticles on mesoporous $SiO_2$-coated magnetic $Fe_3O_4$ spheres: a magnetically separatable catalyst with good thermal stability. *Molecules* **2013**, *18*, 14258−14267.

(8) Joshi, M. D.; Steyer, D. J.; Anderson, J. L. Evaluating the complexation behavior and regeneration of boron selective glucaminium-based ionic liquids when used as extraction solvents. *Anal. Chim. Acta* **2012**, *740*, 66−73.

(9) Ho, T. D.; Zhang, C.; Hantao, L. W.; Anderson, J. L. Ionic liquids in analytical chemistry: fundamentals, advances, and perspectives. *Anal. Chem.* **2014**, *86*, 262−285.

(10) Alothman, Z. A.; Yilmaz, E.; Habila, M.; Shabaka, A.; Soylak, M. Ligandless temperature-controlled ionic liquid-phase microextraction of lead(II) ion prior to its determination by FAAS. *Microchim Acta* **2013**, *180*, 669−674.

(11) Liang, R.; Bao, Z.; Su, B.; Xing, H.; Yang, Q.; Yang, Y.; Ren, Q. Feasibility of Ionic Liquids as Extractants for Selective Separation of Vitamin D3 and Tachysterol3 by Solvent Extraction. *J. Agric. Food Chem.* **2013**, *61*, 3479−3487.

(12) Yilmaz, E.; Soylak, M. Ionic liquid-linked dual magnetic microextraction of lead(II) from environmental samples prior to its micro-sampling flame atomic absorption spectrometric determination. *Talanta* **2013**, *116*, 882−886.

(13) Bwambok, D. K.; Thuo, M. M.; Atkinson, M. B. J.; Mirica, K. A.; Shapiro, N. D.; Whitesides, G. M. Paramagnetic ionic liquids for measurements of density using magnetic levitation. *Anal. Chem.* **2013**, *85*, 8442−8447.

(14) Laremore, T. N.; Zhang, F. M.; Linhardt, R. J. Ionic liquid matrix for direct UV-MALDI-TOF-MS analysis of dermatan sulfate and chondroitin sulfate oligosaccharides. *Anal. Chem.* **2007**, *79*, 1604−1610.

(15) Cao, J.; Li, P.; Yi, L. Ionic liquids coated multi-walled carbon nanotubes as a novel pseudostationary phase in electrokinetic chromatography. *J. Chromatogr. A* **2011**, *1218*, 9428−9434.

(16) Shao, Y. F.; Yan, B.; Li, Q. P. Magnetic Mesoporous Silica Nanosphere Supported Europium(III) Tetrakis(β-diketonate) Complexes with Ionic Liquid Compounds as Linkers. *Eur. J. Inorg. Chem.* **2013**, *3*, 381−387.

(17) Li, X. S.; Wu, J. H.; Zhao, Y.; Zhang, W. P.; Gao, Q.; Guo, L.; Yuan, B. F.; Feng, Y. Q. Preparation of magnetic polymer material with phosphate group and its application to the enrichment of phosphopeptides. *J. Chromatogr. A* **2011**, *1218*, 3845−3853.

(18) He, H.; Yuan, D. H.; Gao, Z. Q.; Xiao, D. L.; He, H.; Dai, H.; Peng, J.; Li, N. Mixed hemimicelles solid-phase extraction based on ionic liquid-coated Fe3O4/SiO2 nanoparticles for the determination of flavonoids in bio-matrix samples coupled with high performance liquid chromatography. *J. Chromatogr. A* **2014**, *1324*, 78−85.

(19) Qing, L. S.; Xue, Y.; Liu, Y. M.; Liang, J.; Xie, J.; Liao, X. Rapid magnetic solid-phase extraction for the selective determination of isoflavones in soymilk using baicalin-functionalized magnetic nanoparticles. *J. Agric. Food Chem.* **2013**, *61*, 8072−8078.

(20) Wang, L.; Zang, X. H.; Chang, Q. Y.; Zhang, G. J.; Wang, C.; Wang, Z. Determination of triazole fungicides in vegetable samples by magnetic solid-phase extraction with graphene-coated magnetic nanocomposite as adsorbent followed by gas chromatography−mass spectrometry detection. *Food Anal. Methods* **2014**, *7*, 318−325.

(21) Li, N.; Qi, L.; Shen, Y.; Li, Y. P.; Chen, Y. Amphiphilic block copolymer modified magnetic nanoparticles for microwave-assisted extraction of polycyclic aromatic hydrocarbons in environmental water. *J. Chromatogr. A* **2013**, *1316*, 1−7.

(22) Farré, M.; Sanchís, J.; Barceló, D. Analysis and assessment of the occurrence, the fate and the behavior of nanomaterials in the environment. *TrAC, Trends Anal. Chem.* **2011**, *30*, 517−527.

(23) Han, Q.; Wang, Z.; Xia, J.; Chen, S.; Zhang, X.; Ding, M. Facile and tunable fabrication of Fe3O4/graphene oxide nanocomposites and their application in the magnetic solid-phase extraction of polycyclic aromatic hydrocarbons from environmental water samples. *Talanta* **2012**, *101*, 388−395.

(24) Wang, G. Y.; Chen, F. F.; Shi, Y. P. Ultra-performance LC-photodiode array-eλ-ESI-MS/MS screening method for the detection of radical-scavenging natural antioxidants fromRadix et Rhizoma Rhei. *J. Sep. Sci.* **2011**, *34*, 268−277.

(25) Xuan, S. H.; Wang, F.; Lai, J. M. Y.; Sham, K. W. Y.; Wang, Y. X. J.; Lee, S. F.; Yu, J. C.; Cheng, C. H. K.; Leung, K. C. F. Synthesis of biocompatible, mesoporous Fe3O4 nano/microspheres with large surface area for magnetic resonance imaging and therapeutic applications. *ACS Appl. Mater. Interfaces* **2011**, *3*, 237−244.

(26) Zhang, D. P.; Lu, C. H.; Ni, Y. R.; Xu, Z. Z.; Zhang, W. B. Effect of water on size-controllable synthesis of mesoporous Fe3O4 microspheres and their applications in waste water treatment. *CrystEngComm* **2013**, *15*, 4755−4764.
(27) Jungnickel, C.; Łuczak, J.; Ranke, J.; Fernández, J. F.; Müller, A.; Thöming, J. Micelle formation of imidazolium ionic liquids in aqueous solution. *Colloids Surf., A* **2008**, *316*, 278−284.
(28) Greaves, T. L.; Drummond, C. J. Solvent nanostructure, the solvophobic effect and amphiphile self-assembly in ionic liquids. *Chem. Soc. Rev.* **2013**, *42*, 1096−1120.
(29) Galán-Cano, F.; Alcudia-León, M. d. C.; Lucena, R.; Cárdenas, S.; Valcárcel, M. Ionic liquid coated magnetic nanoparticles for the gas chromatography/mass spectrometric determination of polycyclic aromatic hydrocarbons in waters. *J. Chromatogr. A* **2013**, *1300*, 134−140.
(30) Hu, S. S.; Yi, L.; Li, X. Y.; Cao, J.; Ye, L. H.; Cao, W.; Da, J. H.; Dai, H. B.; Liu, X. J. Ionic liquid-based one-step micellar extraction of multiclass polar compounds from hawthorn fruits by ultrahigh-performance liquid chromatography coupled with quadrupole time-of-flight tandem mass spectrometry. *J. Agric. Food Chem.* **2014**, *62*, 5275−5280.
(31) Bouri, M.; Gurau, M.; Salghi, R.; Cretescu, I.; Zougagh, M.; Rios, Á. Ionic liquids supported on magnetic nanoparticles as a sorbent preconcentration material for sulfonylurea herbicides prior to their determination by capillary liquid chromatography. *Anal. Bioanal. Chem.* **2012**, *404*, 1529−1538.
(32) Fernand, V. E.; Dinh, D. T.; Washington, S. J.; Fakayode, S. O.; Losso, J. N.; van Ravenswaay, R. O.; Warner, I. M. Determination of pharmacologically active compounds in root extracts of *Cassia alata* L. by use of high performance liquid chromatography. *Talanta* **2008**, *74*, 896−902.
(33) Zhu, L.; Pan, D.; Ding, L.; Tang, F.; Zhang, Q. L.; Liu, Q.; Yao, S. Z. Mixed hemimicelles SPE based on CTAB-coated Fe3O4/SiO2NPs for the determination of herbal bioactive constituents from biological samples. *Talanta* **2010**, *80*, 1873−1880.
(34) Zhang, H. F.; Shi, Y. P. Pretreatment properties of CTAB coated $Fe_3O_4$ nanoparticle mixed hemimicelle sorbents for the analysis of herbal medicine samples. *Curr. Anal. Chem.* **2012**, *8*, 150−158.

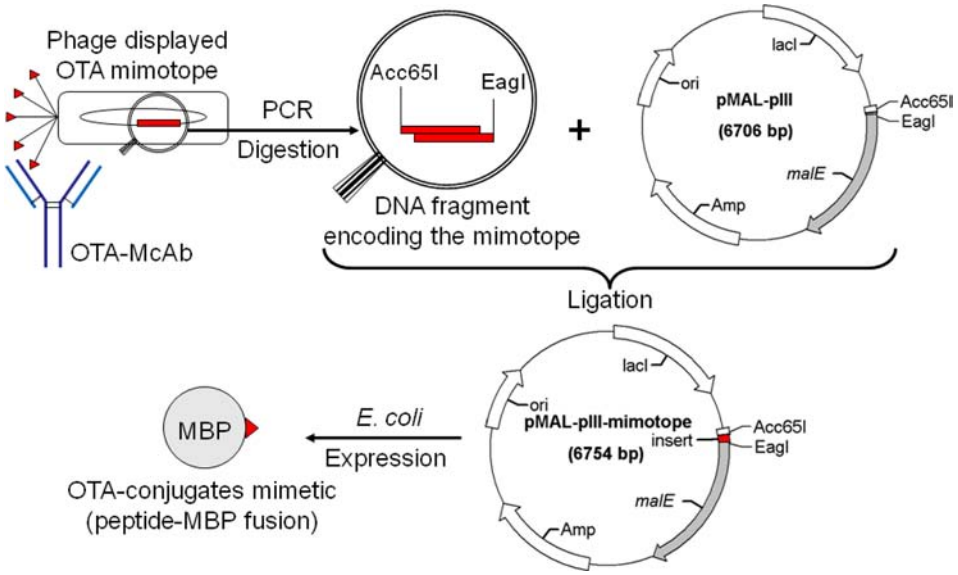


**Figure 1.** Schematic presentation of the construction of expression plasmid for mimetic OTA conjugate.

mL.[26] Nevertheless, current research concerning the mimotope is usually based on the phage serving as a competitive antigen, and there are few reports of mimotopes used as a coating antigen in quantitative immunoassay.

In addition to using mimotopes in the form of phage-displayed peptides, the chemosynthetic peptide has also been employed as a substitute for mycotoxin conjugate in immunoassays.[27−29] The chemosynthetic peptide allows precise control of peptide concentration and conformation, with a simple molecular weight and structure, and thus is conducive to analyzing the peptide structure−function relationship. However, the problem of environmental pollution and high cost during the chemosynthesis of peptide conjugate chemosynthesis is still inevitable.

We have previously reported ochratoxin A (OTA) mimotopes selected from a second-generation peptide library.[30] Here, using OTA as a model analyte, substitutes for OTA conjugates were produced by genetically fusing OTA mimotopes to a maltose binding protein (MBP) and expressed in *Escherichia coli* cells. The resulting peptide−MBP fusion proteins (mimetic OTA conjugate), which are "cloneable" homogeneous and OTA-free products, worked successfully in quantitative and qualitative immunoassays for measuring OTA in cereals and would facilitate standardization of immunoassays for mycotoxin OTA.

## MATERIALS AND METHODS

**Chemicals and Reagents.** Mycotoxin ochratoxin A, aflatoxin $B_1$ ($AFB_1$), zearalenone (ZEN), citrinin (CIT), and horseradish peroxidase (HRP)-conjugated goat anti-mouse antibody were obtained from Sigma (St. Louis, MO, USA). Phage particles displaying OTA mimotopes (named L12-204, L12-206, L12-214, L12-311, L12-314, L12-317, and L12-330), anti-OTA monoclonal antibody (OTA-McAb), and OTA conjugated with ovalbumin (OTA−OVA) were previously prepared in our laboratory.[30,31] Anti-MBP Tag mouse monoclonal antibody was purchased from CWBIO (Beijing, China). 3,3′-Diaminobenzidine (DAB) substrate was purchased from Bio Basic Inc. (Toronto, ON, Canada). SuperSignal ELISA Pico chemiluminescent substrate was obtained from Thermo Scientific (Waltham, MA, USA). Polyvinylidene fluoride (PVDF) membrane was purchased from Millipore Co. (Bedford, MA, USA). The *p*MAL-pIII vector, restriction enzymes *Acc*65I and *Eag*I, and amylose resin were purchased from New England Biolabs, Inc. (Beverly, MA, USA). Taq polymerase, minibest DNA fragment purification kit, and T4 DNA ligase were purchased from TaKaRa (Dalian, China). Commercial ELISA kit for OTA was purchased from Defeng (Taiyuan, China). All inorganic chemicals and organic solvents were of reagent grade.

**Construction of Expression Plasmid for Mimetic OTA Conjugate.** An expression plasmid was constructed aiming to reproducibly prepare mimetic OTA conjugate (peptide−MBP fusion protein). The schematic diagram of constructing expression plasmid is presented in Figure 1. First, phage particles displaying OTA mimotopes were used for single-stranded phage DNA isolation and purification as described by He et al.[25] Then phage DNA fragment encoding the selected OTA mimotope was amplified by polymerase chain reaction (PCR) using the forward primer (5′-CAT GCC CGG GTA CCT TTC TAT TCT C-3′) and reverse primer (5′-CCC TCA TAG TTA GCG TAA CG-3′). The PCR was performed in a total volume of 100 μL (containing 200 μM each dNTP, 100 nM each forward and reverse primer, 1 U TaKaRa Taq, and 1 μL of single-stranded phage DNA; 95 °C for 30 s, 55 °C for 30 s, and 72 °C for 30 s, cycled 30 times). PCR product was purified using a DNA fragment purification kit (Tiangen, Beijing, China) and then digested with *Acc*65I and *Eag*I restriction enzymes (37 °C for 5 h). After the digested DNA fragment was purified by 8% polyacrylamide gel electrophoresis (PAGE), it was ligated into an *Acc*65I and *Eag*I-digested vector pMAL-pIII and transformed into *E. coli* TB1. The constructed expression plasmid was extracted from the transformants and sequenced as described previously.[32]

**Preparation and Characterization of Mimetic OTA Conjugate.** After the construction of expression plasmid, the mimetic OTA conjugate (peptide−MBP fusion protein) was prepared through the technique of protein engineering. Initially, expression plasmid was transformed to *E. coli* TB1 cells and cultured in LB medium (containing 0.2% glucose and 100 μg/mL ampicillin) at 37 °C by shaking (250 rpm) to $OD_{600}$ ∼0.5. The culture was then induced with 0.4 mM isopropyl-*β*-D-thiogalactopyranoside (IPTG) and shaken at 25 °C for 16 h. After that, the periplasmic fusion proteins were extracted by osmotic shock as described previously.[33] Following the preparation of the cold osmotic shock fluid, the OTA conjugates mimetics were purified by amylose affinity chromatography.[33] Afterward, a Western blot analysis was carried out to validate the mimetic OTA conjugates according to the protocol described previously.[32]

**Chemiluminescent Immunoassay Established with Mimetic OTA Conjugate.** A quantitative chemiluminescent enzyme-linked immunoassay (CLEIA) for OTA was developed with mimetic OTA conjugate. Briefly, purified mimetics (diluted in PBS, pH 7.4) was


dx.doi.org/10.1021/jf5028922 | J. Agric. Food Chem. 2014, 62, 8830−8836

coated in microplate wells for 2 h at 37 °C and blocked for 1 h at 37 °C with 3% skim milk in PBS. The plate was washed three times with PBST. Afterward, 50 μL of anti-OTA monoclonal antibody (OTA-McAb) (diluted in PBS, pH 7.4) was added in the coated wells in the presence of 50 μL of sample extracted solution or OTA standard solution at 37 °C for 30 min. The plate was then washed three times, and 100 μL of a 1:2000 dilution of HRP-conjugated goat anti-mouse antibody was added to the wells for 30 min at 37 °C. The peroxidase activity was finally developed with 100 μL of chemiluminescent substrate, and chemiluminescent intensity was measured by a luminescence reader (Thermo Scientific). To measure the optimized dilution of the immunoassay reagents, a checkerboard assay was conducted by using different dilutions of mimetics and anti-OTA-McAb in advance. To compare the performance as coating antigen in immunoassay, chemosynthetic OTA−OVA conjugates and phage particles (OTA mimotope displays on phage) were also coated in microplate wells, respectively, and tested as above-described in CLEIA procedures.

**Qualitative Immunoassay Based on Mimetic OTA Conjugate.** A qualitative dot immunoassay was also developed using mimetic OTA conjugate. The procedure was performed as follows: A 0.45 μm PVDF membrane marked with 7 mm × 7 mm squares was soaked with methanol at room temperature for 10 s and placed on a drenched filter paper as previously described.[31] Then 3 μL of serial dilutions of mimetic OTA conjugate in PBS was spotted onto the squares and incubated at 37 °C for 2 h. After washing with PBST, the membrane was blocked by soaking in 3% skimmed milk in PBS for 30 min. After rinsing in PBST, 7 mm squares were cut, dried, and stored at 4 °C until used.

After the preparation of mimetics-spotted membrane, the assay was performed as follows: Membrane strips were soaked in 10% (v/v) methanol−PBS spiked with sample extracts or various concentrations of OTA and containing the appropriate dilution of OTA-McAb, incubated for 15 min at room temperature. After washing with PBST, the strips were incubated for 15 min in a dilution solution of HRP-conjugated goat anti-mouse antibody, washed, and incubated with TMB substrate. The membrane was rinsed with tap water, and the color intensity of the OTA-positive control and sample test zones was visually compared to that of the OTA-negative control (which has the most intense color).

**Validation of Mimetic OTA Conjugate-Based Immunoassay.** Validation of the mimetic OTA conjugate-based immunoassay was performed by analyzing the reproducibility and by determining the OTA concentrations in spiked cereal samples and incurred samples.

For the determination of reproducibility, CLEIAs were performed using the mimetic OTA conjugate produced within one batch (intra-assay) and three batches (interassay), respectively. Then the coefficients of variation (CVs) of the $IC_{50}$ of the calibration curves for intra- and interassays were calculated.

To measure the recovery of OTA, OTA-negative samples (corn, rice, and wheat samples) confirmed by HPLC (<0.6 μg/kg) were spiked with OTA at various concentrations, respectively. Both OTA-negative samples and spiked samples were extracted as described below: 5 g of finely ground samples mixed with 10 mL of methanol/water (50:50, v/v) was ultrasonically extracted for 20 min; after centrifuging, the supernatant was diluted 5-fold with PBS for the dot immunoassay analysis or diluted 5-fold with PBS and subsequently diluted 4-fold with PBS containing 10% methanol for the CLEIA analysis. As to the analysis of incurred samples, cereals and feedstuffs were prepared as above.

## RESULTS AND DISCUSSION

**Production and Characterization of Mimetic OTA Conjugate.** Phage single-stranded DNA fragment isolated from seven selected OTA mimotopes (L12-204, L12-206, L12-214, L12-311, L12-314, L12-317, and L12-330) were PCR amplified, respectively (Figure 2A), and digested by *Eag*I and *Acc*65I (Figure 2B). As to the vector of *p*MAL-pIII, it was digested with the same enzymes and isolated by 8% agarose gel

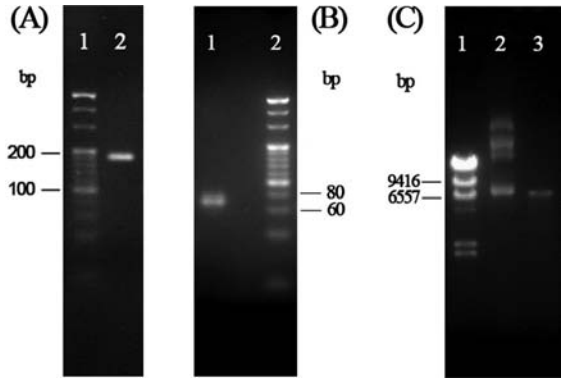


**Figure 2.** Agarose gel electrophoresis of the results for PCR and digestion: (A) PCR product of DNA fragment (182 bp) that encodes the OTA mimotope (L12-206, others not shown;. (B) DNA fragment (68 bp) digested with restriction enzymes *Acc*65I and *Eag*I; (C) vector pMAL-pIII (6.7 kb) before (lane 2) and after (lane 3) digestion with the same restriction enzymes.

electrophoresis (6.7 kb) (Figure 2C). Seven expression plasmids of mimetic OTA conjugate were constructed and confirmed by sequencing, respectively (data of DNA sequencing is available in the Supporting Information Figure S1).

The constructed expression plasmids were transformed into *E. coli* TB1 cells, and peptide−MBP fusion proteins (mimetic OTA conjugate) were expressed by IPTG inducing. An orthogonal experiment was implemented to analyze the effect of IPTG concentration, induction temperature, and time, which showed that the optimal fusion protein expression was induced with 0.4 mM IPTG at 25 °C for 16 h. As shown in the results of SDS-PAGE and Western blot, the purified mimetic OTA conjugates (named L12-204−MBP, L12-206−MBP, L12-214−MBP, L12-311−MBP, L12-314−MBP, L12-317−MBP, and L12-330−MBP, respectively) all ran as a single band at the predicted molecular mass (calculated as 44 kDa for the 1:1 fusion of peptide and MBP) and specifically bind to the anti-MBP antibody (Figure 3).

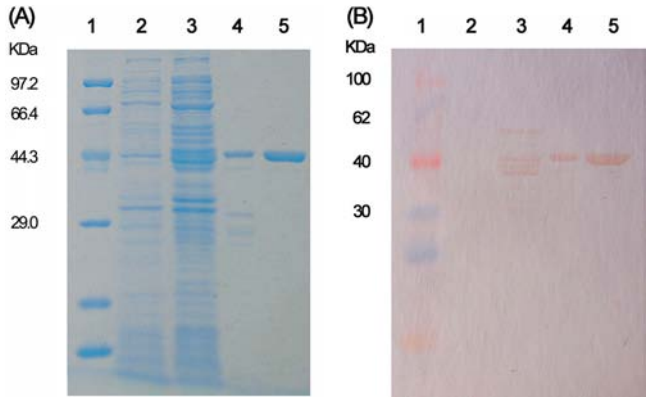


**Figure 3.** (A) SDS-PAGE and (B) Western blot of expression of mimetic OTA conjugate (L12-206−MBP, others not shown). Blots were stained with Coomassie brilliant blue or probed with anti-MBP mouse monoclonal antibody. Lanes: 2, whole-cell extract harvested immediately prior to IPTG induction or, 3, 16 h after IPTG induction; 4, osmotic shock supernatant; 5, purified L12-206−MBP by amylose affinity chromatography.


dx.doi.org/10.1021/jf5028922 | J. Agric. Food Chem. 2014, 62, 8830−8836

**Chemiluminescent Immunoassay for OTA Using Mimetic OTA Conjugate.** Competitive inhibition curves of chemiluminescent immunoassay based on mimetic OTA conjugate (L12-204−MBP, L12-206−MBP, L12-214−MBP, L12-311−MBP, L12-314−MBP, L12-317−MBP,and L12-330−MBP) were established, respectively, and the sensitivity of immunoassay was determined. Among the seven mimetic-based inhibition curves, the $IC_{50}$ values were 1.23 ± 0.11, 0.88 ± 0.05, 1.62 ± 0.12, 1.92 ± 0.17, 1.30 ± 0.06, 1.54 ± 0.12, and 1.30 ± 0.10 ng/mL, respectively (Figure 4A, the value is the average of five replicates ± standard deviation). According to the cross-reactivity test, no reaction with mycotoxin $AFB_1$, ZEN, or CIT was found in mimetic-based chemiluminescent immunoassay (Figure 4B). Among the seven curves, inhibition curves established with L12-206−MBP revealed the highest sensitivity; the $IC_{50}$ was 0.82 ng/mL, and linearity ranged (20−80% inhibition of the maximal chemiluminescent intensity) from 0.31 to 2.17 ng/mL (Figure 4C, the value is the average of three replicates). For comparison, the value of $IC_{50}$ and working range for conventional OTA−OVA cojugate -based immunoassay were 0.90 and 0.21−3.88 ng/mL; the competitive inhibition curves between the OTA−OVA conjugate and mimetic OTA conjugate had no significant difference. However, the phage-displayed OTA mimotope-based immunoassay did not exhibit a typical sigmoid curve; with the addition of OTA standard, the chemiluminescent intensity did not decrease for the phage-displayed peptide-coated microwells (Figure 4C), which indicated that phage-displayed mimotopes of OTA are not adaptable for polystyrene microwells directly serving as coating antigens in quantitative immunoassays.

The influences of buffer ionic strength and pH were investigated to evaluate the effect on mimetic-based immunoassay for OTA. The appropriate buffer ionic strength was tested with 5, 10, 25, and 50 mM methanol−PBS (Figure 5A). According to the result, ionic strength between 10 and 50 mM has little significant influence on the assay. Taking both $IC_{50}$ and $RLU_{max}/IC_{50}$ into consideration, optimized performance was achieved at 10 mM. At the optimal ionic strength, the pH effect was investigated between 6.0 and 9.0 (Figure 5B). The result suggests the best performance at pH 7.4 when the $RLU_{max}/IC_{50}$ was the highest. In addition, methanol that affects antigen−antibody interaction is generally utilized as OTA solvent and extraction agent; the proper content of methanol was estimated using OTA prepared in various concentrations of (5, 10, 20, and 40%, v/v). The relative luminescent intensity declined and $IC_{50}$ increased significantly when methanol concentration was >10%. The highest $RLU_{max}/IC_{50}$ and the lowest $IC_{50}$ were observed at 10% methanol−PBS (Figure 5C).

**Qualitative Immunoassay Based on the Mimetic OTA Conjugate.** After being employed in the quantitative immunoassay, the mimetic OTA conjugate (L12-206−MBP) was also utilized to develop a qualitative dot immunoassay to visually detect OTA without instrumentation. A checkerboard assay was performed by using different dilutions of immunoreagents (mimetic OTA conjugate and OTA-McAb). The selected mimetic OTA conjugate diluted to 10, 25, 50, and 100 μg/mL and OTA-McAb diluted to 1:500, 1:1000, 1:2000, and 1:4000 were tested, respectively. The assay incubated with 100 μg/mL mimetic OTA conjugate and 1:2000 dilution of OTA-McAb for 15 min was chosen to be the minimum concentration of immunoreagents for a clear and sufficient intensity of spot (Figure 6A). Increasing the incubation time beyond 15 min did not increase the spot color intensity (data not shown).

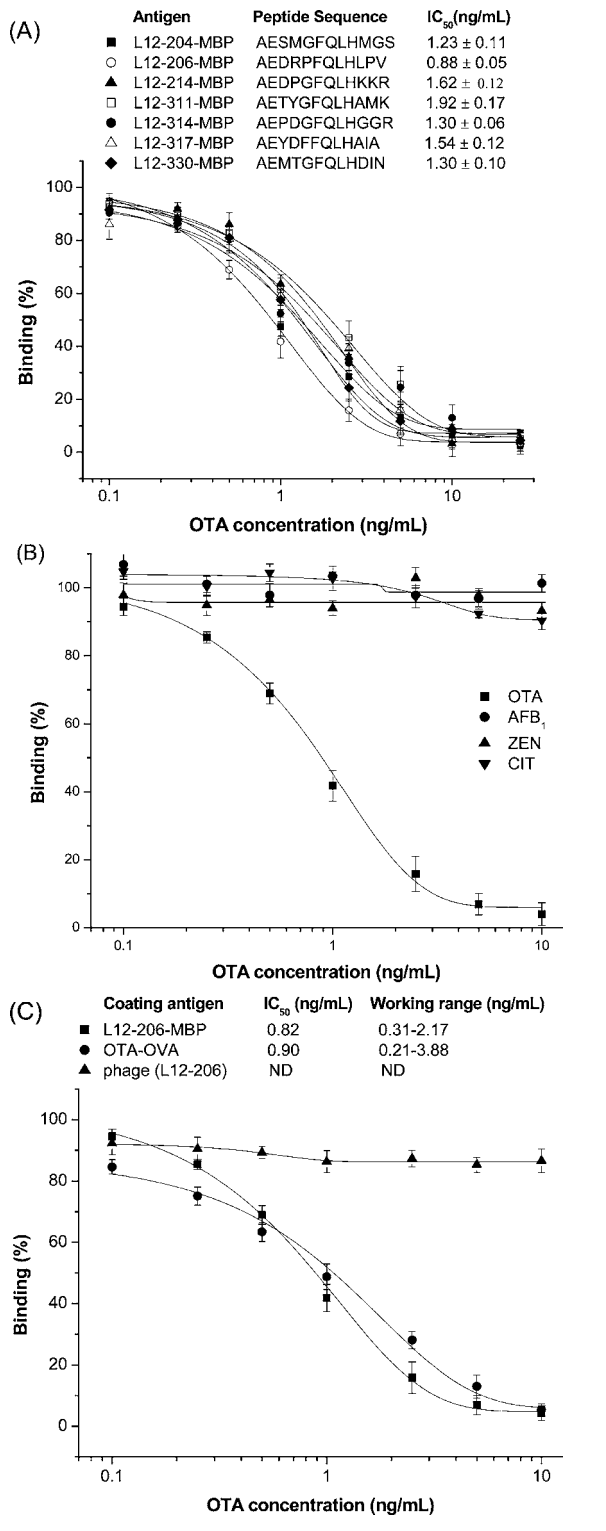


**Figure 4.** (A) Dose−response curves of the CLEIAs for OTA established with seven mimetic OTA conjugates (L12-204−MBP, L12-206−MBP, L12-214−MBP, L21-311−MBP, L12-314−MBP, L12-317−MBP, and L12-330−MBP. The value is the average of five replicates ± standard deviation. (B) Cross-reactivity of the mimetic OTA conjugate (L12-206−MBP)-based CLEIA toward mycotoxin OTA, $AFB_1$, ZEN, and CIT. (C) Dose−response curves of the CLEIAs using the mimetic OTA conjugate (L12-206−MBP, 5 μg/mL), OTA−OVA conjugate (2 μg/mL) and phage (L12-206, 2.5 × $10^8$ pfu/mL) as coating antigens, respectively. The vertical bars indicate the standard deviation ($n$ = 3).


dx.doi.org/10.1021/jf5028922 | J. Agric. Food Chem. 2014, 62, 8830−8836

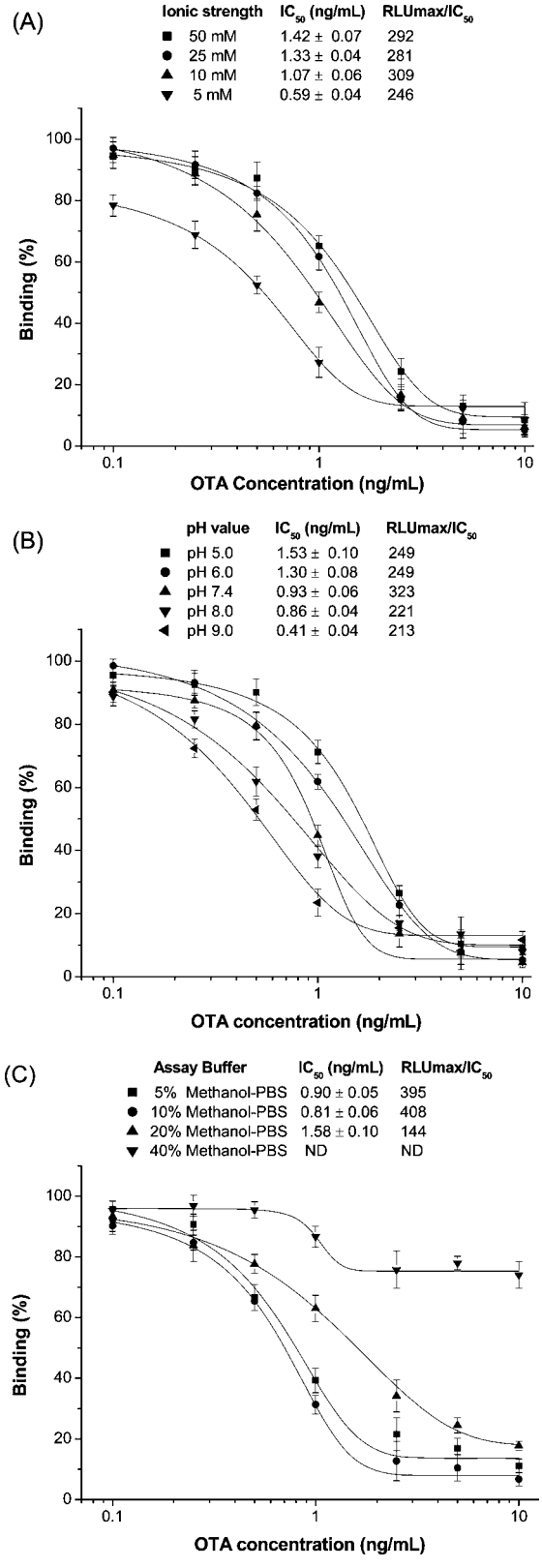


**Figure 5.** (A) Ionic strength, (B) pH, and (C) methanol effects on the performance of the mimetic OTA conjugate-based chemiluminescent ELISA. Each experiment was implemented in triplicate, and the means of the triplicates are plotted (error bars represent the standard deviation).

To visually evaluate the cutoff levels (the lowest concentration of OTA able to achieve 100% inhibition and therefore

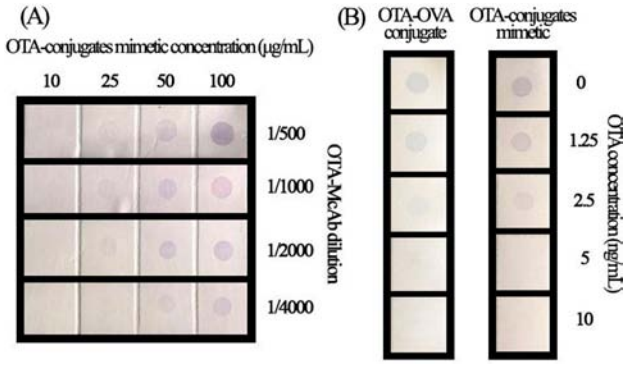


**Figure 6.** OTA−OVA conjugates and mimetic OTAconjugate-based dot immunoassays: (A) mimetic OTA conjugate (ranging from 10 to 100 μg/mL) spotted onto PVDF membranes incubated with different dilutions of OTA−McAb (ranging from 1/500 to 1/4000); (B) evaluation of the cutoff level (smallest amount of OTA able to achieve 100% inhibition and therefore no spot color development) of the dot immunoassay assessed visually. Mimetic OTA conjugate and conventional OTA−OVA conjugates were applied to the assay as coating antigen, and OTA levels (0, 1.25, 2.5, 5.0,10 ng/mL) were analyzed, respectively.

no color development) of the mimetic OTA conjugate-based dot immunoassay, OTA was analyzed at different concentrations (0, 1.25, 2.5, 5.0, 10 ng/mL). As presented in Figure 6B, the intensity of the spot decreased with increasing OTA concentration, and no spot color development on the membrane was obtained when the OTA standard concentration rose beyond 5.0 ng/mL. The cutoff level of the mimetic OTA conjugate-based dot immunoassay was 5.0 ng/mL, which was equal to that of the OTA−OVA conjugate-based dot immunoassay (thecutoff level was 5.0 ng/mL, Figure 6B).

**Validation Studies.** The validation of the CLEIA based on the mimetic OTA conjugate (L12-206−MBP) was carried out by measuring the OTA recovery and reproducibility. Table 1 shows the recoveries of OTA added to corn, rice, and wheat samples analyzed by three methods. In the first two assays (CLEIAs set up with both the mimetic OTA conjugate and OTA−OVA), the spiked and detected OTA contents were in accord with each other. The recovery of cereals spiked with 10−100 μg/kg OTA ranged from 82.6 to 134.0% determined by the mimetic OTA conjugate-based CLEIA and from 90.2 to 132.0% by conventional OTA−OVA-based assay. In the case of the dot immunoassay, a clear dot was observed for adding cereals OTA <50 μg/kg, but no dot appeared for OTA ≥50 μg/kg.

As for the reproducibility, it is evaluated by determining the CVs of the $IC_{50}$ of the calibration curves. The CV was 5.3% for intra-assay and 10.4% for interassay, respectively. Furthermore, the mimetic OTA conjugate kept at −20 °C until use for 1 year remained effective, indicating the stable performance of the mimetic OTA conjugate-based immunoassay (data not shown).

Twenty samples of cereal and feedstuffs purchased from the Chinese market were analyzed using mimetic OTA conjugate-based CLEIA, dot immunoassay, and commercial ELISA kit for OTA, respectively. Among the 20 samples, 5 were positively detected by CLEIA and commercial ELISA kit (their limits of detection were both 5.0 μg/kg). The results obtained from CLEIA and commercial ELISA kits were in agreement with each other. However, no positive sample was detected by dot immunoassay because of its cutoff level (50 μg/kg), higher than


dx.doi.org/10.1021/jf5028922 | J. Agric. Food Chem. 2014, 62, 8830−8836

**Table 1. Recoveries of OTA Added to Corn, Rice, and Wheat Samples in Determinations Performed by CLEIAs and Dot Immunoassay Based on OTA−OVA Conjugate and Mimetic OTA Conjugate**

| | | mimetic OTA conjugate-based CLEIA ($n$ = 3) | | | OTA−OVA conjugate-based CLEIA ($n$ = 3) | | | |
|---|---|---|---|---|---|---|---|---|
| matrix | spiked ($\mu$g/kg) | detected ($\mu$g/kg) | recovery (%) | RSD (%) | detected ($\mu$g/kg) | recovery (%) | RSD (%) | mimetic OTA conjugate-based dot immunoassay ($n$ = 3) |
| corn | 10 | 10.2 ± 0.7 | 102.0 ± 7.0 | 6.9 | 9.8 ± 0.6 | 98.0 ± 6.0 | 6.1 | −[a] − − |
| | 20 | 26.7 ± 1.8 | 133.5 ± 9.0 | 6.7 | 22.7 ± 1.0 | 113.5 ± 5.0 | 4.4 | − − − |
| | 50 | 41.3 ± 3.4 | 82.6 ± 6.8 | 8.2 | 46.0 ± 3.6 | 92.0 ± 7.2 | 7.8 | +[b] + − |
| | 100 | 92.3 ± 5.2 | 92.3 ± 5.2 | 5.6 | 98.2 ± 6.3 | 98.2 ± 6.3 | 6.4 | + + + |
| rice | 10 | 13.4 ± 0.8 | 134.0 ± 8.0 | 6.0 | 12.7 ± 0.7 | 127.0 ± 7.0 | 5.5 | − − − |
| | 20 | 19.2 ± 1.8 | 96.0 ± 9.0 | 9.4 | 23.0 ± 1.1 | 115.0 ± 5.5 | 4.8 | − − − |
| | 50 | 51.1 ± 3.4 | 102.2 ± 6.8 | 6.7 | 48.2 ± 2.9 | 96.4 ± 5.8 | 6.0 | + + ±[c] |
| | 100 | 89.3 ± 6.5 | 89.3 ± 6.5 | 7.3 | 90.2 ± 6.0 | 90.2 ± 6.0 | 6.7 | + + + |
| wheat | 10 | 12.5 ± 0.9 | 125.0 ± 9.0 | 7.2 | 13.2 ± 1.2 | 132.0 ± 12.0 | 9.1 | − − − |
| | 20 | 23.3 ± 1.9 | 116.5 ± 9.5 | 8.2 | 20.6 ± 2.1 | 103.0 ± 10.5 | 10.2 | − − − |
| | 50 | 51.2 ± 2.4 | 102.4 ± 4.8 | 4.7 | 54.5 ± 1.3 | 109.0 ± 2.6 | 2.4 | + + + |
| | 100 | 97.0 ± 4.5 | 97.0 ± 4.5 | 4.6 | 93.2 ± 6.2 | 93.2 ± 6.2 | 6.7 | + + + |

[a]Negative, an obvious dot was observed. [b]Positive, no dot was observed. [c]Negative/positive, an unclear dot was observed.

the OTA concentration in contaminated samples (data are available in the Supporting Information, Table S1).

In conclusion, we described a new approach for developing coating antigen mimetics in immunoassay. The conventional antigen, OTA conjugates, was replaced with mimetic OTA conjugate (peptide−MBP fusion protein). This fusion protein mimics the reaction between the OTA and antibody and serves as a substitute for the OTA conjugates in immunoassays. These peptide−MBP fusion proteins (mimetic OTA conjugate) are cloneable and homogeneous products expressed from constructed express plasmids, which can be prepared reproducibly in large scale and with low cost. The peptide−MBP fusion protein provides practical sensitivity, specificity, and reliability in the standard qualitative and quantitative immunoassays.

## ■ ASSOCIATED CONTENT

### Supporting Information

Figure S1 and Table S1. This material is available free of charge via the Internet at http://pubs.acs.org.

## ■ AUTHOR INFORMATION


### Corresponding Author

*(Q.H.) Phone:+86-791-8830 5177. E-mail: heqinghua@ncu.edu.cn.



### Funding

This work was supported financially by grants from the National Natural Science Funds (Grants NSFC-31360386, NSFC-31201360, and NSFC-31171696), the Jiangxi Province Key Technology R&D Program (Grant 2014BBG70090), the Natural Science Foundation of Jiangxi, China (Grant 20132BAB214005), and the Education Department of Jiangxi Province (Grant GJJ13095).


### Notes

The authors declare no competing financial interest.

## ■ REFERENCES


(1) Kabak, B.; Dobson, A. D. W.; Var, I. Strategies to prevent mycotoxin contamination of food and animal feed: a review. *Crit. Rev. Food Sci. Nutr.* **2006**, *46*, 593−619.

(2) Ibáñez-Vea, M.; González-Peñas, E.; Lizarraga, E.; López de Cerain, A. Co-occurrence of aflatoxins, ochratoxin A and zearalenone in barley from a northern region of Spain. *Food Chem.* **2012**, *132*, 35−42.

(3) Trucksess, M. W.; Giler, J.; Young, K.; White, K. D.; Page, S. W. Determination and survey of ochratoxin A in wheat, barley, and coffee − 1997. *J. AOAC Int.* **1999**, *82*, 85−89.

(4) Zachariasova, M.; Dzuman, Z.; Veprikova, Z.; Hajkova, K.; Jiru, M.; Vaclavikova, M.; Pospichalova, M.; Florian, M.; Hajslova, J. Occurrence of multiple mycotoxins in European feedingstuffs, assessment of dietary intake by farm animals. *Anim. Feed Sci. Technol.* **2014**, *193*, 124−140.

(5) Commission Regulation (EC) No. 1881/2006 of 19 December 2006 setting maximum levels for certain contaminants in foodstuffs. *Off. J. Eur. Union* **2006**, *L364*, 5−24.

(6) Shephard, G. S.; Kimanya, M. E.; Kpodo, K.; Gnonlonfin, B.; Gelderblom, W. C. A. The risk management dilemma for fumonisin mycotoxins. *Food Control* **2013**, *34*, 596−600.

(7) Kim, N. Y.; Lee, I.; Ji, G. E. Reliable and simple detection of ochratoxin and fumonisin production in black *Aspergillus*. *J. Food Prot.* **2014**, *4*, 653−658.

(8) Wen, J.; Kong, W.; Hu, Y.; Wang, J.; Yang, M. Multi-mycotoxins analysis in ginger and related products by UHPLC-FLR detection and LC-MS/MS confirmation. *Food Control* **2014**, *43*, 82−87.

(9) Rodriguez-Carrasco, Y.; Font, G.; Manes, J.; Berrada, H. Determination of mycotoxins in bee pollen by gas chromatography-tandem mass spectrometry. *J. Agric. Food Chem.* **2013**, *61* (8), 1999−2005.

(10) Rossi, C. N.; Takabayashi, C. R.; Ono, M. A.; Saito, G. H.; Itano, E. N.; Kawamura, O.; Hirooka, E. Y.; Ono, E. Y. S. Immunoassay based on monoclonal antibody for aflatoxin detection in poultry feed. *Food Chem.* **2012**, *132*, 2211−2216.

(11) Shim, W. D.; Kim, K. Y.; Chung, D. H. Development and validation of a gold nanoparticle immunochromatographic assay (ICG) for the detection of zearalenone. *J. Agric. Food Chem.* **2009**, *57* (8), 4035−4041.

(12) Meneely, J. P.; Ricci, F.; van Egmond, H. P.; Elliott, C. T. Current methods of analysis for the determination of trichothecene mycotoxins in food. *TrAC, Trends Anal. Chem.* **2011**, *30*, 192−203.

(13) Basova, E. V.; Goryacheva, I. Y.; Rusanova, T. V.; Burmistrova, N. A.; Dietrich, R.; Martlbauer, E.; Detavernier, C.; Van Peteghem, C.; De Saeger, S. An immunochemical test for rapid screening of zearalenone and T-2 toxin. *Anal. Bioanal. Chem.* **2010**, *397*, 55−62.

(14) Pulli, T.; Höyhtyä, M.; Söderlund, H.; Takkinen, K. One-step homogeneous immunoassay for small analytes. *Anal. Chem.* **2005**, *77*, 2637−2642.
(15) He, J.; Fan, M.; Liang, Y.; Liu, X. Application of anti-idiotype antibody in small molecules immunoassay. *Chin. J. Anal. Chem.* **2010**, *38*, 1366−1370.
(16) Xiao, H.; Clarke, J. R.; Marquardt, R. R.; Frohlich, A. A. Improved methods for conjugating selected mycotoxin to carrier proteins and dextran for immunoassays. *J. Agric. Food Chem.* **1995**, *43*, 2092−2097.
(17) Chen, F. S.; Zhou, Q.; Lou, X. C.; Li, S. Q.; Wang, A. H.; Lu, L. Preparation and application of aflatoxin $B_1$ anti-idiotype antibody II. *Mycosystema* **2004**, *23*, 280−285.
(18) Wang, Y.; Li, P.; Majkova, Z.; Bever, C. R. S.; Kim, H. J.; Zhang, Q.; Dechant, J. E.; Gee, S. J.; Hammock, B. D. Isolation of alpaca anti-idiotypic heavy-chain single-domain antibody for the aflatoxin immunoassay. *Anal. Chem.* **2013**, *85* (17), 8298−8303.
(19) Yuan, Q.; Pestka, J. J.; Hespenheide, B. M.; Kuhn, L. A.; Linz, J. E.; Hart, L. P. Identification of mimotope peptides which bind to the mycotoxin deoxynivalenol-specific monoclonal antibody. *Appl. Environ. Microbiol.* **1999**, *65*, 3279−3286.
(20) Chanh, T. C.; Rappocciolo, G.; Hewetson, J. F. Monoclonal anti-idiotype induces protection against the cytotoxicity of the trichothecene mycotoxin T-2. *J. Immunol.* **1990**, *144*, 4721−4728.
(21) Khoobdel, M.; Nayeri Fasaei, B.; Zahraei Salehi, T.; Khosravi, M.; Taheri, M.; Koochakzadeh, A.; Masihipour, B.; Motedayen, M. H.; Akbari, S. The productionof monovalent and anti-idiotype antivenom against *Mesobuthus eupeus* (Scorpionida: Buthidae) venom in rabbits. *Toxicon* **2013**, *76*, 44−49.
(22) Liu, R.; Xu, L.; Qiu, X.; Chen, X.; Deng, S.; Lai, W.; Xu, Y. An immunoassay for determining aflatoxin B1 using a recombinant phage as a nontoxic coating conjugate. *J. Food Saf.* **2012**, *32*, 318−325.
(23) He, Q.; Xu, Y.; Zhang, C.; Li, Y.; Huang, Z. Phage-borne peptidomimetics as immunochemical reagent in dot-immunoassay for mycotoxin zearalenone. *Food Control* **2014**, *39*, 56−61.
(24) Guo, J.; Xu, Y.; Huang, Z.; He, Q.; Liu, S. Development of an immunoassay for rapid screening of vardenafil and its potential analogues in herbal products based on a group specific monoclonal antibody. *Anal. Chim. Acta* **2010**, *658*, 197−203.
(25) He, Q.; Xu, Y.; Huang, Y.; Liu, R.; Huang, Z.; Li, Y. Phage displayed peptides that mimic zearalenone and its application in immunoassay. *Food Chem.* **2011**, *126*, 1312−1315.
(26) Wang, Y.; Wang, H.; Li, P.; Zhang, Q.; Kim, H. J.; Gee, S. J.; Hammock, B. D. Phage displayed peptide that mimics aflatoxins and its application in immunoassay. *J. Agric. Food Chem.* **2013**, *61*, 2426−2433.
(27) Lai, W.; Fung, D. Y. C.; Xu, Y.; Liu, R.; Xiong, Y. Development of a colloidal gold strip for rapid detection of ochratoxin a with mimotope peptide. *Food Control* **2009**, *20*, 791−795.
(28) Liu, R.; Yu, Z.; He, Q.; Xu, Y. An immunoassay for ochratoxin A without the mycotoxin. *Food Control* **2007**, *18*, 872−877.
(29) Liu, X.; Xu, Y.; He, Q.; He, Z.; Xiong, Z. Application of mimotope peptides of fumonisin B1 in peptide ELISA. *J. Agric. Food Chem.* **2013**, *61*, 4765−4770.
(30) He, Z.; He, Q.; Xu, Y.; et al. Ochratoxin A mimotope from second-generation peptide library and its application in immunoassay. *Anal. Chem.* **2013**, *85*, 10304−10311.
(31) He, Q.; Xu, Y.; Wang, D.; Kang, M.; Huang, Z.; Li, Y. Simultaneous multiresidue determination of mycotoxins in cereal samples by polyvinylidene fluoride membrane based dot immunoassay. *Food Chem.* **2012**, *134*, 507−512.
(32) Sambrook, J.; Fritsch, E. F.; Maniatis, T. *Molecular Cloning: A Laboratory Manual*, 2nd ed.; Cold Spring Harbor Laboratory Press: Cold Spring Harbor, NY, USA, 1989.
(33) Zwick, M. B.; Bonnycastle, L. L. C.; Noren, K. A.; Venturini, S.; Leong, E.; Barbas, C. F.; Noren, C. J.; Scott, J. K. The maltose-binding protein as a scaffold for monovalent display of peptides derived from phage libraries. *Anal. Biochem.* **1998**, *264*, 87−97.

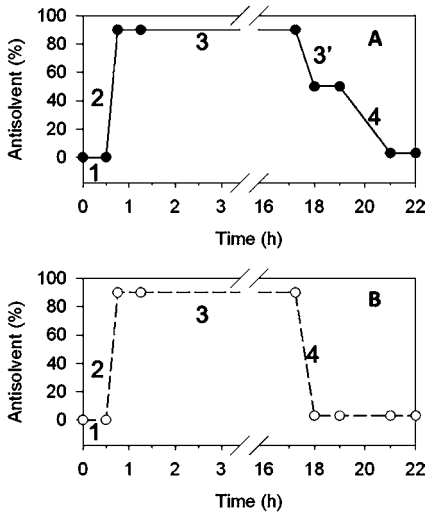


**Figure 1.** Change in antisolvent content during the preparation of protein nanoparticles. Steps 1, 2, 3, and 4 represent dispersion, desolvation, cross-linking, and evaporation, respectively. Compared to the conventional method (B), a new step (3′) was added between steps 3 and 4 in the new method (A) to lower the antisolvent content to 40−60% before evaporation.

Meanwhile, lower levels of glutaraldehyde were applied for preparing BLG nanoparticles with higher curcumin/BLG ratios. This was inspired by a series of recent studies on epigallocatechin gallate (EGCG)-loaded protein nanoparticles.[27,28] As suggested by these studies, protein aggregated into nanoparticles in the presence of polyphenols such as EGCG, and these particles remained stable without additional cross-linkers. The strong interaction between protein and polyphenols, including hydrogen bonding and $\pi-\pi$ interaction,[29] made EGCG a possible cross-linker surrogate. Likewise, if the target compound (e.g., resveratrol or curcumin) shows certain similarity in the structure and protein affinity with EGCG, the dose of glutaraldehyde could be lowered accordingly. An excessive dose of glutaraldehyde may not only cause higher toxicity but also lead to lower LE, considering that excessive cross-linking by both glutaraldehyde and the phenol might cause extensive formation of insoluble complexes.

It should be pointed out that great efforts have been made to seek alternative cross-linkers (e.g., genipin and transglutaminase) for the preparation of protein network structures, such as protein oligomers or hydrogels.[30−32] However, with regard to protein nanoparticles, glutaraldehyde remains the major cross-linking agent. This is probably because nanoparticles are compact assemblies of proteins that are very close to each other. Glutaraldehyde is a relatively small molecule, which can easily approach the functional groups (primary amino groups which is likely to be exposed at the surface of proteins) on protein nanoparticles. Other cross-linkers, such as transglutaminase, are relatively bulky molecules that are difficult to react with the required functional groups due to the steric hindrance. By replacing glutaraldehyde partially with phenolic compounds such as CUR, one may achieve a satisfactory cross-linking effect while reducing the toxicity of the final product.

In this study, BLG was chosen as a model protein to implement these strategies. BLG is the major component of whey protein and a natural carrier for various lipophilic nutrients.[33,34] Curcumin as an antioxidant[35] and chemopreventive[36] compound was selected as a model nutraceutical to be incorporated. According to previous literature (excluding those studies that might have counted coprecipitated curcumin molecules as encapsulated ones), the LE of curcumin-loaded protein nanoparticles varied from 2 to 5%.[3,9,12,37,38] The binding between curcumin and BLG nanoparticles in different water−acetone binary systems was first assessed by investigating the distribution of curcumin in different phases. The optimal acetone content before evaporation was then determined on the basis of the result. The effect of glutaraldehyde level and curcumin loading on the LE was also investigated. The formed nanoparticles were characterized for their size, surface charge, and morphology. Finally, because BLG is known for its remarkable resistance against pepsin and moderate digestibility by trypsin,[39] the nanoparticles were anticipated to show controlled-release property, that is, minimal and maximal release in the stomach and small intestine, respectively. Therefore, the nanoparticles were studied for their integrity as well as releasing profile in PBS and simulated gastric/intestinal fluids.

## MATERIALS AND METHODS

**Materials.** Bovine BLG (90% purity), pepsin (3200−4500 units/mg), trypsin (10000 BAEE units/mg), and curcumin (98% purity) were purchased from Sigma-Aldrich (St. Louis, MO, USA). Simulated gastric and intestinal fluids (abbreviated SGF and SIF, respectively) were obtained from Ricca Chemical (Arlington, TX, USA). All other chemicals (acetone, glutaraldehyde, buffers, etc.) were of analytical grade.

**Preparation of Curcumin-Loaded BLG Nanoparticles.** BLG nanoparticles were prepared by desolvation method[5] with several modifications. The whole process was undertaken in the dark under constant stirring (800 rpm). BLG was dissolved in deionized water at 10 mg/mL, and curcumin was dispersed in acetone at 4 mg/mL. Both dispersions were equilibrated for 1 h. To 2 mL of BLG dispersion was added dropwise 3 mL of pure acetone, after which an appropriate amount of curcumin solution was introduced to achieve predetermined curcumin/protein ratios (5, 10, and 15%, w/w, same hereinafter). Additional pure acetone was then added to a total volume of 20 mL. After 30 min of equilibration, glutaraldehyde (5 mg/mL aqueous solution) was introduced as a cross-linker. Theoretically, each milligram of BLG needs 40 $\mu$g of glutaraldehyde for stoichiometric cross-linking.[33] This ratio is defined as 100% glutaraldehyde equivalent, and three levels of glutaraldehyde (25, 50, and 100% equivalent) were applied in this study. After 16 h of cross-linking, aliquots of 2 mL were withdrawn and mixed with 4 mL of aqueous acetone. The composition of the aqueous acetone was designed so that the final acetone content ranged from 30 to 90% (v/v, same hereinafter) after mixing. After 1 h of equilibration, the acetone was evaporated mildly at room temperature under reduced pressure using a VWR Symphony vacuum oven (VWR International, Radnor, PA, USA). The pressure was first kept to $5 \times 10^4$ Pa for 20 min to remove dissolved air and then maintained at $4 \times 10^3$ Pa until all acetone was removed. This procedure typically lasted for 2−3 h, and additional water was then supplemented to achieve a final volume of 6 mL. The dispersion (defined as the "final dispersion") was stored at 4 °C for subsequent assays. The initial and final pH values of the dispersions ranged from 7.2 to 7.6.

**Quantitative Analysis of Free and Bound Curcumin.** Following the procedures described above, BLG−curcumin nanoparticles were prepared in 90% acetone, cross-linked using 100% equivalent of glutaraldehyde, and mixed with aqueous acetone to achieve various acetone contents. After equilibration for 1 h, the dispersion was centrifuged (9000*g*, 15 min, room temperature). The insoluble curcumin was recovered in the precipitate and dissolved in pure acetone, whereas the supernatant was subjected to dialysis centrifugation (5000*g*, 30 min, room temperature) using a Macrosep centrifuge tube (MW cutoff 10 kDa; Pall Corp., Ann Arbor, MI, USA).

A preliminary study was conducted with 90% aqueous acetone containing 1 mg/mL curcumin. More than 90% of the dissolved curcumin was able to pass the dialysis membrane and recovered in the filtrate. The filtrate containing freely dissolved (nonbound) curcumin was recovered and diluted with acetone. Both dispersions mentioned above were further diluted with acetone, so that the final water content in the mixture was <1%. The resultant mixtures were then measured for their absorbance at 426 nm by a DU-730 UV−vis spectrophotometer (Beckman Coulter Inc., Fullerton, CA, USA). The percentages of insoluble and dissolved curcumin were calculated using an established standard curve ($R^2$ = 0.9991), and the ratio of BLG nanoparticle-bound curcumin was derived by subtracting these two proportions from 100%.

**Characterization of Curcumin-Loaded BLG Nanoparticles.** Freshly prepared "final dispersions" of curcumin-loaded BLG nanoparticles were subjected to the following measurements.[33] The particle size and count rate were determined by dynamic laser scattering (DLS) using a BI-200 SM Goniometer version 2 (Brookhaven Instrument Corp., Holtsville, NY, USA) equipped with a 35 mW He−Ne laser beam. No dilution was undertaken prior to the assays. Two separate measurements were carried out on each sample to obtain accurate results. For count rate determination, the aperture pinhole size was fixed at 400 $\mu$m. To measure the particle size, appropriate aperture sizes were chosen to achieve a count rate between 100 and 300 kcps (kilo counts per second, same hereinafter). The obtained data were analyzed using the Cumulant algorithm, and the quadratic mean particle size ($z$-average size) was reported.

The electrophoretic mobility of nanoparticle dispersions was determined by laser Doppler velocimetry using a Nano ZS90 Zetasizer (Malvern, UK). Each sample was measured three times, and at least 12 runs were performed per measurement. The data were then converted to zeta potentials using the Smoluchowski model.

The structure of curcumin-loaded BLG nanoparticles was investigated by Fourier-transform infrared (FT-IR) analysis. Samples (3−5 mg) were freeze-dried and mounted onto a Jasco FT/IR 4100 spectrometer (Jasco Inc., Easton, MD, USA). The infrared transmittance was recorded at wavenumbers between 1000 and 4000 $cm^{-1}$ with a resolution of 4 $cm^{-1}$. At least 100 scans were undertaken for each sample. The spectra were averaged, smoothed, and corrected for their baselines using the Spectra Manager software (Jasco Inc.).

The morphology of nanoparticles was observed under scanning electron microscopy (SEM). Approximately 40 $\mu$L of the dispersion (after evaporation and water supplementation) was cast dried on an aluminum pan, mounted on a conductive carbon tape, coated with gold/platinum using a sputter coater (Hummer XP, Anatech, Union City, CA, USA), and observed under SEM (Hitachi SU-70, Pleasanton, CA, USA). Representative images were reported.

**Determination of Encapsulation Efficiency (EE) and Loading Efficiency (LE).** The EE of curcumin-loaded nanoparticles was determined as follows.[9] After evaporation and water supplementation as described under Preparation of Curcumin-Loaded BLG Nanoparticles, the final dispersions were allowed to stand at room temperature for 1 h and then centrifuged at 9000$g$ for 30 min. The insoluble curcumin was recovered from the precipitate and dissolved in pure acetone. The supernatant was subjected to dialysis centrifugation as was discussed under Quantitative Analysis of Free and Bound Curcumin, and the free curcumin was collected in the filtrate. The two parts of curcumin were diluted with acetone and measured for their absorbance at 426 nm, which was converted to the curcumin content using the same standard curve as described before. The EE was calculated as follows:

$$\mathrm{EE} = 100 - \frac{\text{amount of precipitated curcumin}}{\text{total amount of curcumin}} \times 100 \quad (1)$$

In addition, after the dialysis centrifugation mentioned above, the retentate containing the curcumin-encapsulated nanoparticles was collected and lyophilized. The dry nanoparticles were weighed, and the LE was calculated as follows:

$$\mathrm{LE} = \frac{\text{weight of encapsulated curcumin}}{\text{total weight of nanoparticles}} \times 100 \quad (2)$$

**In Vitro Release of Curcumin in Different Buffering Systems.** *Release in PBS.* Samples prepared with the following parameters were chosen for in vitro release study: curcumin loading of 5, 10, and 15% (w/w), initial acetone content of 90%, pre-evaporation acetone content of 50%, and glutaraldehyde levels that resulted in optimal EE for each curcumin loading ratio. Samples were taken after evaporation but prior to supplementation of water. All buffers used in this section contained 5 mg/mL Tween 20. Unless specified, the PBS used in this section was at pH 7.2 and 0.1 mol/L.

Two milliliters of the above-mentioned samples was mixed with 2 mL of PBS (pH 7.2, 0.2 mol/L). After incubation at 37 °C for 30 min, the mixture was injected into a sealed dialysis tube (MW cutoff 10 kDa), which was then placed in a flask containing 60 mL of PBS (preheated at 37 °C). The flask was then incubated in a reciprocal shaking bath (Thermo Scientific, Odessa, TX, USA) at 37 °C under constant shaking at 120 rpm. At predetermined time intervals, aliquots of 2 mL were withdrawn from the flask and diluted with an appropriate amount of PBS. The resultant dispersion was measured for its absorbance at 426 nm, which was converted to the mass of released curcumin using a linear standard curve ($R^2$ = 0.9993). After each measurement, 2 mL of fresh PBS was added to the flask to maintain sink condition. The kinetic release profile of curcumin was plotted as a function of time and curve fitted to the first-order kinetic model

$$C = C_0 + k \ln t \quad (3)$$

where $C$ indicates the cumulative percentage of released curcumin, $C_0$ represents the initial percentage of curcumin present in the buffer, and $t$ stands for time.

*Release in SGF and SIF.* The nanoparticle dispersion with a curcumin loading of 10% was chosen for this study. Two milliliters of the sample was incubated at 37 °C and then diluted with 8 mL of two preheated buffers: SGF-2 (commercial SGF, adjusted to pH 2.0, added with pepsin at a BLG/pepsin ratio of 100:1, w/w) or SGF-5 (same as SGF-2 except that the pH was adjusted to 5.0). These buffers mimicked the gastric environment at fasting and fed states, respectively.[40] After mixing, 0.5 mL of the dispersion was withdrawn immediately, diluted with 2.0 mL of PBS, and then subjected to dialysis centrifugation (5000$g$, 30 min) using a Macrosep centrifuge tube (MW cutoff 100 kDa; Pall Corp.). The filtrate containing released curcumin was diluted appropriately with PBS before spectrophotometric measurement at 426 nm. The absorbance was converted to the amount of released curcumin as described before. Meanwhile, the above-mentioned mixture was incubated at 37 °C in the reciprocal shaking bath (120 rpm), and aliquots of 0.5 mL were withdrawn and measured as mentioned above at predetermined time intervals. Fresh SGF was supplemented after each measurement to maintain sink condition.

On the other hand, another batch of the nanoparticle dispersions were mixed with SGF and digested for 60 min at 37 °C in the reciprocal shaking bath. The digesta was diluted with PBS and centrifuged as mentioned above, and the retentate containing intact nanoparticles was supplemented with PBS to 2 mL. The dispersion was incubated at 37 °C for 15 min and then mixed with 8 mL of preheated SIF (commercial SIF with added trypsin at a BLG/trypsin ratio of 100:1, w/w). Immediately after mixing, 0.5 mL of the dispersion was withdrawn and subjected to dialysis centrifugation (5000$g$, 45 min, 4 °C), after which the filtrate was diluted with PBS and measured as discussed before. Similar procedures were followed to determine the percentage of released curcumin at desired time intervals, and fresh SIF was supplemented to maintain sink condition. The combined kinetic release profile of curcumin in SGF and SIF was plotted against time.

**In Vitro Disintegration of BLG Nanoparticles.** The nanoparticle dispersion with a curcumin loading of 10% was chosen for this study. Digestion in SGF was carried out following the same procedure as described in the previous section. Digestion in SIF was initiated by diluting the nanoparticle dispersion directly with SIF, without prior

treatment with SGF. This was because the nanoparticles were either largely degraded (at pH 2.0) or intact (at pH 5.0), as indicated by the particle sizes, count rates, and size distribution profiles observed at these two pH values. At desired time intervals, samples were withdrawn, diluted with PBS and then measured for their particle sizes and count rates.

**Statistics.** All measurements were performed in triplicates. The results were expressed as means ± standard error. The data were subjected to analysis of variance followed by Tukey's test with an experimental confidence level of $\alpha = 0.10$ using SAS 9 software (SAS Institute Inc., Cary, NC, USA).

## RESULT AND DISCUSSION

**Binding of Curcumin to BLG Nanoparticles as a Function of Acetone Content.** In a water/acetone binary system containing BLG nanoparticles, curcumin molecules may exist in three forms: insoluble curcumin that was found in the precipitate, dissolved curcumin that was collected in the filtrate, and BLG-bound curcumin molecules obtained in the retentate. Figure 2 shows the distribution of curcumin in the nanoparticle dispersion as a function of acetone content. The data were obtained after rapidly diluting the cross-linked dispersion with appropriate water/acetone mixtures. As can be seen, the percentage of free curcumin increased significantly at acetone content >30% (v/v, same hereinafter). Similar results were obtained from a relevant study on BLG monomers,[41] which reported that the secondary structure and the capability of binding retinol were decreased in 30% or higher concentration of ethanol. The results from previous and current studies suggested weak interaction between curcumin and BLG nanoparticles.

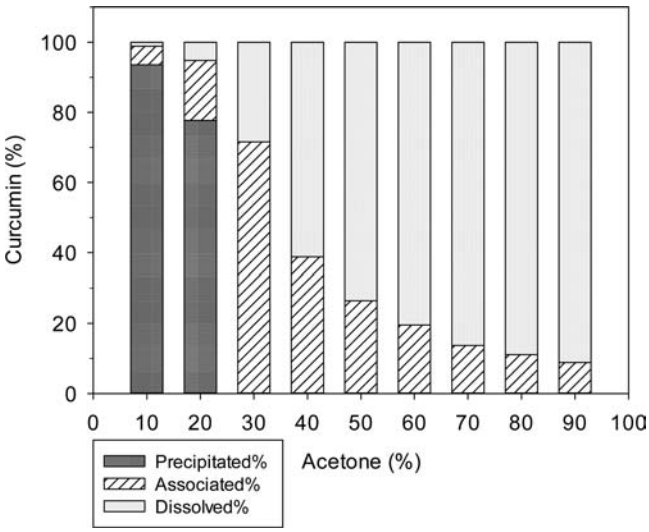


**Figure 2.** Effect of acetone content on the distribution of curcumin in BLG nanoparticle dispersion. The nanoparticles were cross-linked with 100% equivalent of glutaraldehyde.

On the other hand, >80% of curcumin molecules were detected in the precipitate in the presence of 10−20% acetone. This was probably because (1) curcumin as a hydrophobic compound exhibits low solubility in 10−20% acetone and (2) most protein molecules were partly or fully folded, so that there were insufficient hydrophobic sites that associated with curcumin.[9] It was noteworthy that previous studies on BLG monomers[41,42] showed considerable binding to ligands (such as retinol) at low organic solvent concentrations (such as 10−20% ethanol). However, the native binding sites on BLG were limited, and the ligand/BLG ratio in our study was much higher than that of the previous study (equimolar, which was translated to a weight ratio of 1.4%). In addition, most of these ligand-binding sites lost their activity at high level of organic solvents during the preparation of nanoparticles.[43] Therefore, the curcumin−BLG association involved in our study might have taken place mostly on the hydrophobic sites exposed by desolvation,[9] rather than the native binding sites. As acetone content decreased rapidly from 90 to 20%, these sites were possibly buried inside the protein molecules. In addition, the solubility of curcumin was greatly reduced as the acetone content decreased to 20%. As a result, the originally dissolved curcumin molecules might not be able to establish strong association with BLG before extensive precipitation occurred.

In 30% acetone, a considerable percentage (71.5%) of curcumin molecules was found to associate with BLG. This phenomenon was possibly ascribed to two factors. First, the high polarity of 30% acetone compared to 90% acetone drove more curcumin molecules to associate with other hydrophobic molecules, to minimize their contact with water. Second, a greater number of hydrophobic sites in BLG molecules were exposed in 30% acetone than in 20% acetone,[9] which enabled the association and stabilization of more curcumin molecules. Such association might have been relatively strong, so that the majority of originally dissolved curcumin molecules were converted into the bound form without significant precipitation.

On the basis of the dependence of curcumin distribution on acetone content, it can be inferred that the evaporation process during which the acetone content decreases continuously may be critical for the encapsulation of curcumin. We hypothesized that the LE of BLG nanoparticles might be improved by lowering the acetone content from 90 to 30−50% after cross-linking and equilibrating the dispersion for a period of time to allow sufficient curcumin−BLG binding. Thereafter, the dispersion should be evaporated mildly, so that the acetone content could be maintained slightly above 30% for maximal time before declining gradually to lower levels. This hypothesis will be tested in the next section.

**Effect of Acetone Content and Glutaraldehyde Level on EE.** Figure 3 depicts the EE of curcumin-loaded BLG nanoparticles as a function of acetone content (before evaporation, same in this section) and glutaraldehyde level. In general, lower EE was observed as the curcumin content increased. In addition, regardless of the curcumin/BLG weight ratio and the glutaraldehyde concentration, a V-shaped dependence of EE on acetone content was observed, with the highest EE achieved in the presence of 40−50% acetone. At 90% acetone, the LE was only 3.6 and 2.3% for the nanoparticles mixed with 10 and 15% curcumin, respectively. These values increased to 5.3 and 3.4% in the presence of 30% acetone, and they increased more significantly to 9.1 and 10.9% when the acetone content was adjusted to 50%. The low LE at 90% acetone could be ascribed to two factors. First, as discussed in the previous section, the majority of curcumin molecules existed in the freely dissolved form in 90% acetone. Due to the high acetone concentration in the bulk dispersion, the evaporation might have proceeded rapidly, leading to a sudden decrease in the local acetone concentration on the surface of the dispersion. Such a phenomenon resulted in a marked increase in local solvent polarity, which drove free curcumin molecules to precipitate rapidly without establishing a

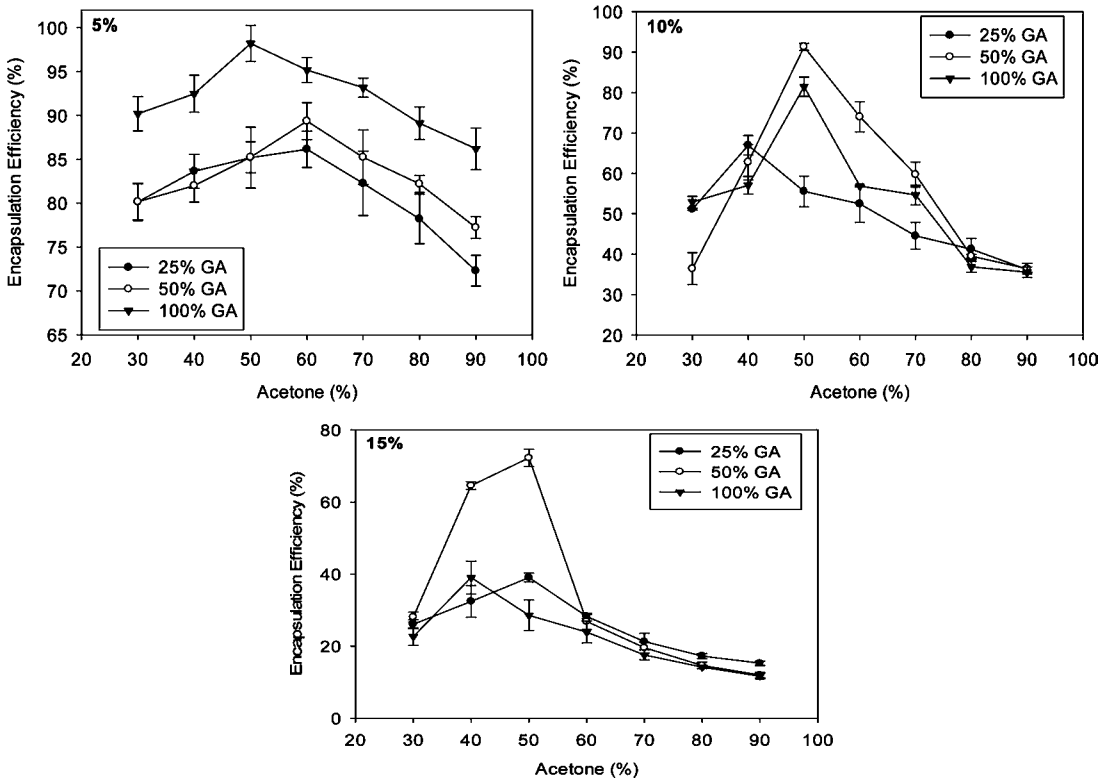


**Figure 3.** Effect of acetone and glutaraldehyde content on the EE of BLG−curcumin nanoparticles at three curcumin−BLG mixing ratios, 5, 10, and 15%.

**Table 1. Particle Sizes and Count Rates of Curcumin-Loaded BLG Nanoparticles**[a]

| | | before evaporation | | after evaporation | | |
|---|---|---|---|---|---|---|
| GA % | CUR % | PS (nm) | CR (kcps) | PS′ (nm) | CR′ (kcps) | CR′/CR (%) |
| 25 | 0 | 61.3 ± 2.5 b | 135.7 ± 7.9 cd | 251.2 ± 12.5 a | 28.3 ± 3.9 f | 20.8 ± 1.7 e |
| 25 | 5 | 62.4 ± 1.7 b | 171.6 ± 9.2 b | 262.9 ± 10.4 a | 48.7 ± 2.8 e | 28.4 ± 1.2 e |
| 25 | 15 | 64.2 ± 3.4 ab | 164.3 ± 10.1 b | 104.0 ± 9.8 d | 106.9 ± 2.7 c | 65.1 ± 3.4 c |
| 50 | 0 | 77.5 ± 3.1 a | 144.8 ± 3.5 cd | 269.0 ± 11.7 a | 73.5 ± 4.5 d | 50.8 ± 2.2 d |
| 50 | 5 | 66.5 ± 2.6 ab | 133.4 ± 4.7 cd | 271.5 ± 15.6 a | 92.6 ± 3.2 c | 69.4 ± 2.5 c |
| 50 | 15 | 76.9 ± 1.9 a | 214.4 ± 7.2 a | 123.7 ± 9.4 d | 153.1 ± 7.1 a | 71.4 ± 2.7 c |
| 75 | 0 | 74.3 ± 4.6 a | 176.6 ± 6.4 b | 226.3 ± 3.6 b | 127.3 ± 4.1 b | 72.1 ± 3.1 c |
| 75 | 5 | 77.2 ± 3.1 a | 126.0 ± 5.8 d | 158.1 ± 11.5 c | 100.2 ± 3.2 c | 79.5 ± 2.0 bc |
| 75 | 15 | 63.9 ± 2.6 ab | 144.8 ± 8.2 c | 119.1 ± 2.4 d | 144.7 ± 4.5 a | 100.0 ± 1.2 a |
| 100 | 0 | 74.6 ± 3.5 a | 133.8 ± 9.1 cd | 104.6 ± 7.4 d | 97.9 ± 2.1 c | 73.5 ± 0.3 c |
| 100 | 5 | 76.0 ± 4.2 a | 154.5 ± 4.4 c | 68.0 ± 3.9 e | 150.7 ± 6.8 a | 97.5 ± 1.2 a |
| 100 | 15 | 70.1 ± 1.9 a | 145.8 ± 3.2 cd | 63.1 ± 2.2 e | 122.0 ± 2.4 b | 83.7 ± 1.4 b |

[a]GA, glutaraldehyde dose (in % equivalent); CUR, curcumin/BLG weight ratio; PS, particle size; CR, count rate. Data with different letters showed significant difference ($n = 3$, $P < 0.05$).

strong association with BLG nanoparticles. Second, a higher acetone percentage suggested a lower content of water and consequently a lower volume in the final dispersion. For instance, the final volume of a 6 mL water/acetone mixture was 3 or 0.6 mL if its initial acetone content was 50 or 90%, respectively. As a result, dispersion with 90% acetone content underwent more significant increase in the concentration of curcumin and BLG. This might have led to more extensive aggregation and precipitation as a result of intermolecular attraction.

For the samples containing 30% acetone, the curcumin−BLG interaction was maximal as shown in the previous section. However, after evaporation began, the acetone content was lowered immediately to critical values (≤20%) that favored the precipitation of curcumin, and such a condition was maintained virtually during the whole process of evaporation. As a result, the EE values obtained from these samples were also not satisfactory, although they were generally higher than those achieved by samples with 80−90% acetone.

When the acetone content of the nanoparticle dispersion was adjusted to 50%, a relatively large number of curcumin molecules were bound to BLG nanoparticles, as is shown in Figure 2. During the slow evaporation process, the acetone content of the dispersion was maintained for a considerable period of time in an optimal range (30−50%) where maximal curcumin−BLG association was observed. In addition, the mild evaporation led to a gradual increase in solvent polarity, which served as a driving force for dissolved curcumin to associate


dx.doi.org/10.1021/jf503199g | J. Agric. Food Chem. 2014, 62, 8837−8847

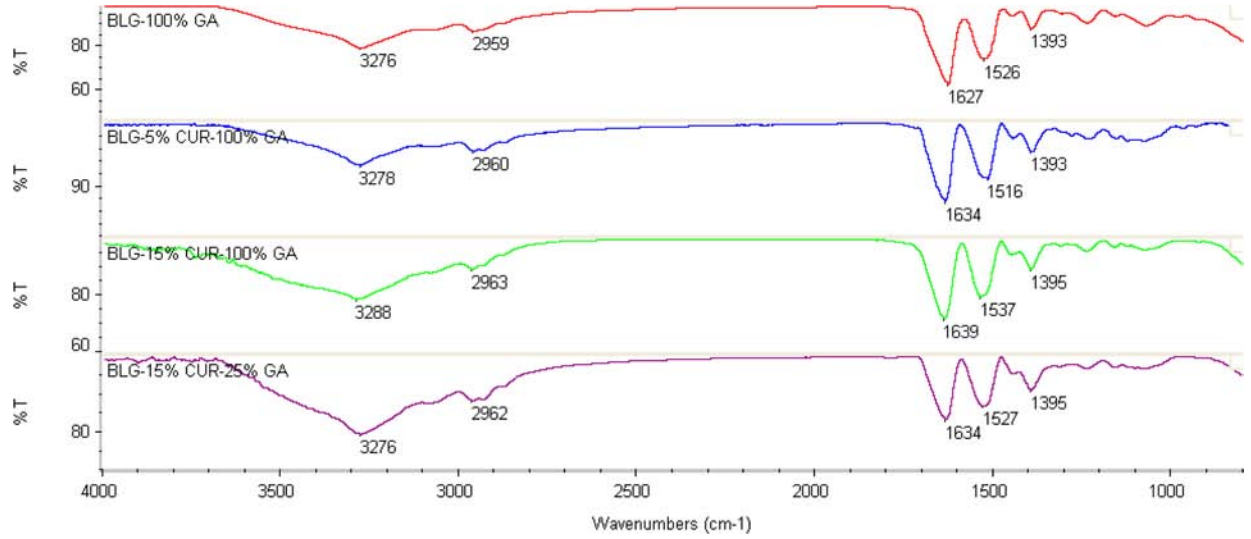


**Figure 4.** FT-IR spectra of empty BLG nanoparticles and BLG/CUR nanoparticles with different CUR/BLG weight ratios and glutaraldehyde (GA) doses.

**Table 2. Characteristics of Curcumin-Loaded BLG Nanoparticles**[a]

| CUR (%) | acetone[b] (%) | GA (% equivalent) | particle size (nm) | polydispersity (dimensionless) | ZP (mV) | EE % | LE % |
|---|---|---|---|---|---|---|---|
| 0 | 50 | 100 | 85.4 ± 6.7 d | 0.127 ± 0.025 b | −44.7 ± 1.4 ab | | |
| 5 | 50 | 100 | 164.4 ± 8.5 c | 0.187 ± 0.034 ab | −46.6 ± 2.8 a | 98.2 ± 1.4 a | 4.9 ± 0.1 b |
| 10 | 50 | 50 | 186.1 ± 13.7 b | 0.201 ± 0.023 a | −42.1 ± 1.6 b | 91.3 ± 5.2 b | 9.1 ± 0.5 a |
| 15 | 50 | 50 | 213.9 ± 8.2 a | 0.202 ± 0.017 a | −42.4 ± 1.9 b | 72.2 ± 4.6 c | 10.9 ± 0.7 a |

[a]CU, curcumin/BLG weight ratio; GA, glutaraldehyde; ZP, zeta potential. Data with different letters showed significant difference ($n = 3$, $P < 0.05$). [b]The percentages represented the acetone content before evaporation.

with BLG nanoparticles.[7,9] These factors resulted in minimal precipitation and maximum protein binding of curcumin, both of which contributed to higher EE.

Besides acetone content, the glutaraldehyde level also played a critical role in the EE of BLG nanoparticles (Figure 3). At 5% curcumin loading, the EE increased gradually as the glutaraldehyde level increased from 25 to 100% equivalent. Glutaraldehyde acts as a cross-linker that hardens the structure of nanoparticles via intermolecular amide bonds.[44] Higher glutaraldehyde concentration was beneficial for maintaining the compact structure of curcumin-loaded BLG nanoparticles, thus preventing the release and precipitation of curcumin molecules.[9] As the content of curcumin increased to 10 and 15%, however, the highest EE was observed when 50% equivalent of glutaraldehyde was applied. In fact, flocculation occurred probably as a result of excessive cross-linking at a glutaraldehyde level of 100% and a curcumin/BLG ratio of ≥15%, resulting in low EE under these conditions (data not shown).

On the basis of these results, adjustment of acetone content was critical for achieving optimal LE and EE. In addition, a lower glutaraldehyde dose could be applied to BLG nanoparticles with higher curcumin loading. This result further suggested that toxic cross-linkers such as glutaraldehyde could be partly replaced by natural phenolic compounds. Further studies need to be carried out to test this hypothesis.

**Evidence for the Cross-Linking Effect of Curcumin.** To confirm the role of curcumin as a partial cross-linking agent, we measured the particle sizes and count rates of a series of samples containing different amounts of curcumin as well as glutaraldehyde. The rationale of this experiment was that well-cross-linked nanoparticles are able to maintain their shape and size. Therefore, the average size and count rate of their dispersion after the evaporation of acetone should be similar to those before evaporation.[3,9] As shown in Table 1, the dispersions with higher glutaraldehyde levels (e.g., 100%) showed less significant change in the particle sizes after evaporation. In addition, the ratio of count rate after evaporation to that before evaporation was significantly higher for the samples with higher glutaraldehyde contents. These phenomena provided indirect evidence of the cross-linking effect of glutaraldehyde. On the other hand, at any given glutaraldehyde level, the dispersions with higher curcumin-to-BLG weight ratios exhibited less significant change in the particle size and count rate after evaporation. This was especially remarkable at the 25% glutaraldehyde level, when the sample with 15% curcumin exhibited a much higher retention in count rate (65%) compared to that containing no curcumin (21%). These results shed some light on the possible cross-linking effect of phenolic compounds such as curcumin.

The interaction between phenols and proteins has been extensively studied in the past decades. Although the exact mechanism has not been fully established, it is generally recognized that hydrogen bonding, hydrophobic interaction, and $\pi-\pi$ stacking[29,45] were involved in the complexation between these two types of compounds. In this study, FT-IR was applied to investigate the possible mechanisms involved in the cross-linking role of curcumin. Figure 4 shows the FT-IR spectra of BLG nanoparticles containing different contents of curcumin and glutaraldehyde. The amide I (1627 $cm^{-1}$, C═O stretching) and amide II bands (1526 $cm^{-1}$, N—H bending and C—N stretching) in empty BLG nanoparticles shifted


dx.doi.org/10.1021/jf503199g | J. Agric. Food Chem. 2014, 62, 8837−8847

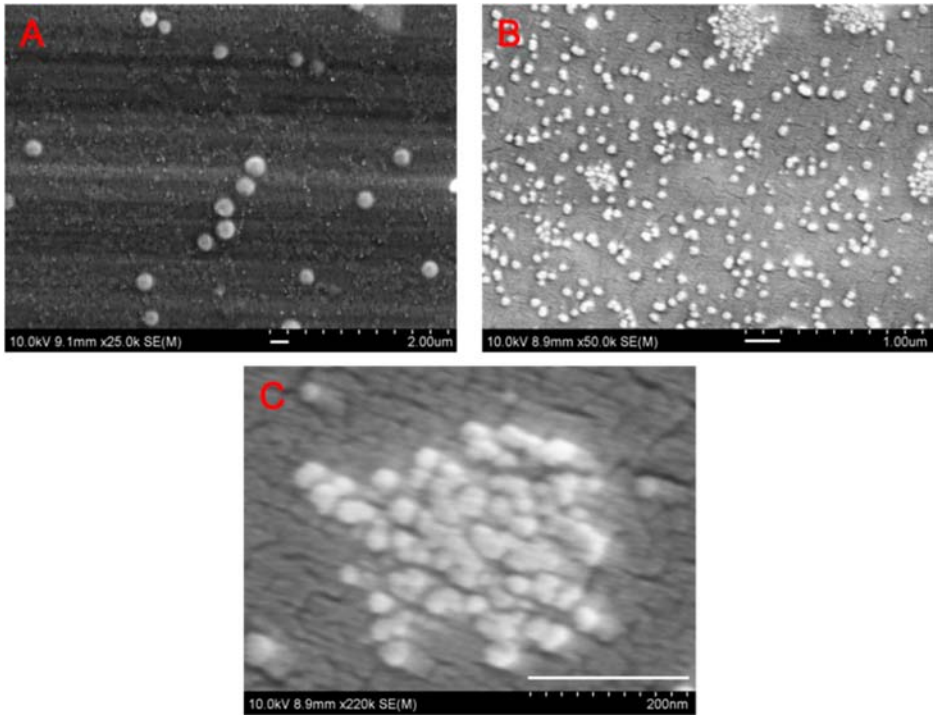


**Figure 5.** SEM images of curcumin-loaded BLG nanoparticles: (A) coexistence of larger and smaller particles; (B, C) larger particles might be the assembly of smaller ones. All images were acquired from the same sample. White bars represent 200 nm.

significantly in the presence of 5 or 15% curcumin, suggesting the possible involvement of the backbone carbonyl and/or amino groups in the BLG−curcumin interaction.[9] Furthermore, the wide band occurring at 3276 $cm^{-1}$ (O−H stretching) exhibited a marked increase in its intensity in the presence of curcumin. This phenomenon suggested the extensive involvement of hydrogen bonding in the curcumin-loaded nanoparticles.[14] Interestingly, at 15% curcumin/BLG ratio, the sample with 25% glutaraldehyde exhibited a significantly higher absorbance at 3276 $cm^{-1}$ than that with 75% glutaraldehyde. This was confirmed by analyzing the relative percentage of areas of these two peaks (data not shown). This difference implied that more hydrogen bonds were formed between BLG and curcumin to stabilize the complex nanoparticles at low glutaraldehyde levels. Further studies need to be conducted to test this hypothesis.

**Characterization of Curcumin-Loaded BLG Nanoparticles.** Table 2 summarizes the properties of curcumin-loaded BLG nanoparticles. For each curcumin loading ratio, the formula (shown in Table 2) yielding the highest EE was chosen for subsequent evaluation. The nanoparticles exhibited an average size of 164−184 nm, with highly negative zeta potential. These properties were favorable for the dispersion stability of the formed particles. The polydispersity of the samples fell in the range of 0.100−0.250, indicating a relatively narrow size distribution. The difference in the zeta potentials for BLG nanoparticles with 5 and 10% curcumin loading was statistically significant, and it was probably due to the consumption of the cationic amine groups in BLG molecules by different amounts of glutaraldehyde.[9] The EE decreased with increasing curcumin/BLG ratio, but the LE kept increasing and reached 10.9% at the curcumin/BLG ratio of 15%. This value was considerably higher than those for a number of protein-based nanoparticles and comparable to some synthetic polymeric encapsulation systems, which were summarized in the Introduction.

Figure 5 shows the morphology of curcumin-loaded BLG nanoparticles observed under SEM. Because no significant difference was observed among the BLG nanoparticles with different curcumin/BLG weight ratios, only the images corresponding to 10% curcumin loading are presented. The particle appeared approximately spherical and exhibited a smooth surface. Two major groups of particles were identified from the image: larger particles with an average size of around 200 nm (Figure 5A) and smaller ones showing diameters of 40−50 nm (Figure 5B). Figure 5C demonstrates that the former type of particles was possibly assembled from the latter ones. Such aggregates might have existed in the nanoparticle dispersion before drying, because their size was comparable to the average size in dispersions obtained by DLS.

**In Vitro Release of Curcumin from BLG Nanoparticles.** Figure 6A shows the release of curcumin from BLG nanoparticles in a PBS/Tween 20 system. The three formulas (one for each curcumin loading ratio) shown in the previous section were chosen for this study. It is noteworthy that curcumin degrades rapidly in PBS, but its stability could be greatly improved in the presence of nonionic surfactants such as Tween 20.[46] Regardless of the curcumin loading ratio, the releasing profile showed satisfactory fit with the first-order kinetic model (Table 3). This result suggested that the release of curcumin was controlled by its dissociation from the porous polymer matrix.[47] Possible reasons why the release rate for nanoparticles with low curcumin loading was higher than that with high curcumin loading were as follows: (1) the particles with higher curcumin loading exhibited greater sizes, and their specific surface area was hence lower; (2) the solubility of curcumin in the PBS/Tween 20 system is a constant in a given environment, and the dissolution of curcumin was slowed as its concentration approached the equilibrium value; and (3) higher

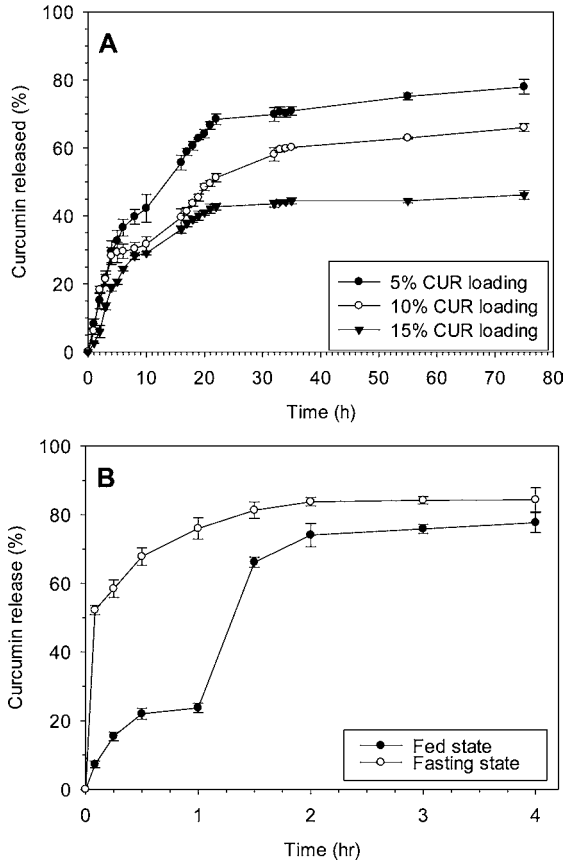


**Figure 6.** Time-dependent release of curcumin from BLG nanoparticles in (A) PBS/Tween 20 and (B) simulated gastrointestinal environment.

**Table 3. Curve Fitting of Curcumin Release Profile from BLG Nanoparticles**

| CUR[a] (%) | $C_0$ (in percentage) | $k$ | $R^2$ |
|---|---|---|---|
| 5 | 4.43 | 18.63 | 0.979 |
| 10 | 4.95 | 14.41 | 0.970 |
| 15 | 2.62 | 11.76 | 0.965 |

[a]CUR, curcumin/BLG weight ratio.

loading indicated higher concentration of curcumin accumulated in the outer buffer, which slowed the diffusion of curcumin through the dialysis membrane. Further study needs to be conducted to validate these hypotheses.

The release of curcumin in SGF and SIF is shown in Figure 6B. Our preliminary results indicated overlapping releasing patterns for nanoparticles with 5, 10, and 15% curcumin loadings (data not shown). Hence, only the releasing profile for nanoparticles with 10% curcumin loading is presented. The release in SGF was investigated at two different pH values: pH 2, which represents the gastric condition in the fasting state; and pH 5, which corresponds to the fed state.[40] After 1 h of digestion, the mixture was transferred to SIF to determine the release profile under simulated intestinal conditions. It was noteworthy that >70% of encapsulated curcumin was released in SGF at pH 2 (Figure 6B). This result is unexpected because BLG is known for its remarkable resistance against peptic digestion,[39] and it was anticipated to prevent curcumin from being released in the stomach. We hypothesized from this result that the BLG nanoparticles were actually decomposed in SGF at pH 2, although the individual BLG monomers remained intact. This hypothesis will be tested and discussed in the next section.

When dispersed in SGF at pH 5 (Figure 6B), the BLG nanoparticles exhibited a significantly lower rate of release than at pH 2, with only 24% of encapsulated curcumin being released in 1 h. This phenomenon could be explained by two reasons. First, pepsin tends to be much less active at pH 5 than at pH 2. Second, BLG exhibits an isoelectric point at around pH 5; therefore, the nanoparticles formed with BLG tended to form large agglomerates that were more resistant to peptic digestion. As a result, the curcumin molecules were more compactly encapsulated at pH 5 than at pH 2, leading to a lower release rate.

After being transferred to SIF (Figure 6B), the remaining curcumin molecules continued to be released from the nanoparticles. This was probably due the degradation of residual BLG nanoparticles as well as the monomers, because of the known capability of trypsin to digest BLG.[39] The significant difference in the releasing pattern of dispersions previously treated at pH 2 and 5 was probably due to the different residual concentrations of curcumin after the first digestion step. At the end of the two-step digestion, 70−80% of curcumin was recovered from the two buffers (SGF and SIF). On the basis of these results, BLG nanoparticles might not be suitable for the controlled release of curcumin in the fasting state, but they could release curcumin in a controlled and sustained manner if administered during the fed state.

**Disintegration of BLG Nanoparticles in Different Buffers.** We further investigated the disintegration of BLG nanoparticles in different buffers. The formula with 10% curcumin loading was chosen for this section. When incubated in SGF at pH 2 (Figure 7A), BLG nanoparticles exhibited a two-stage pattern of degradation. In the first 30 min, they showed a constant average size while the count rate decreased continuously. These data suggested that, despite the decrease in number, there still existed a considerable number of BLG nanoparticles that maintained their size and probably morphology.[9] Thereafter, a rapid increase in the average size was observed, together with a slow decrease in the count rate. A possible explanation for this trend was that the majority of smaller particles (around 160 nm) were decomposed by pepsin after 30 min, but some larger aggregates remained intact. As a result, the average size shifted markedly to higher values, whereas the count rate declined only mildly because larger particles contributed much more significantly to the count rate than did smaller ones.[5,9] This was supported by the fact that the polydispersity index increased gradually from 0.177 (uniform distribution, Figure 8A) to 0.855 (broad distribution, Figure 8B), because of the increase in the relative content of larger particles. The data on size distribution obtained by DLS (Figure 8) also supported the disintegration of BLG nanoparticles.

Intriguingly, BLG nanoparticles were susceptible to peptic digestion, considering that BLG itself is resistant against pepsin. Previous literature on BLG−EGCG nanoparticles[28] showed that BLG molecules remained intact after 120 min of peptic digestion (as evidenced by SDS-PAGE). The same results were obtained in our preliminary study. However, that study did not indicate whether BLG maintained the morphology as spherical aggregates. On the basis of the findings from previous and current studies, we deduced that the intermolecular amide bonds produced by glutaraldehyde, instead of the original

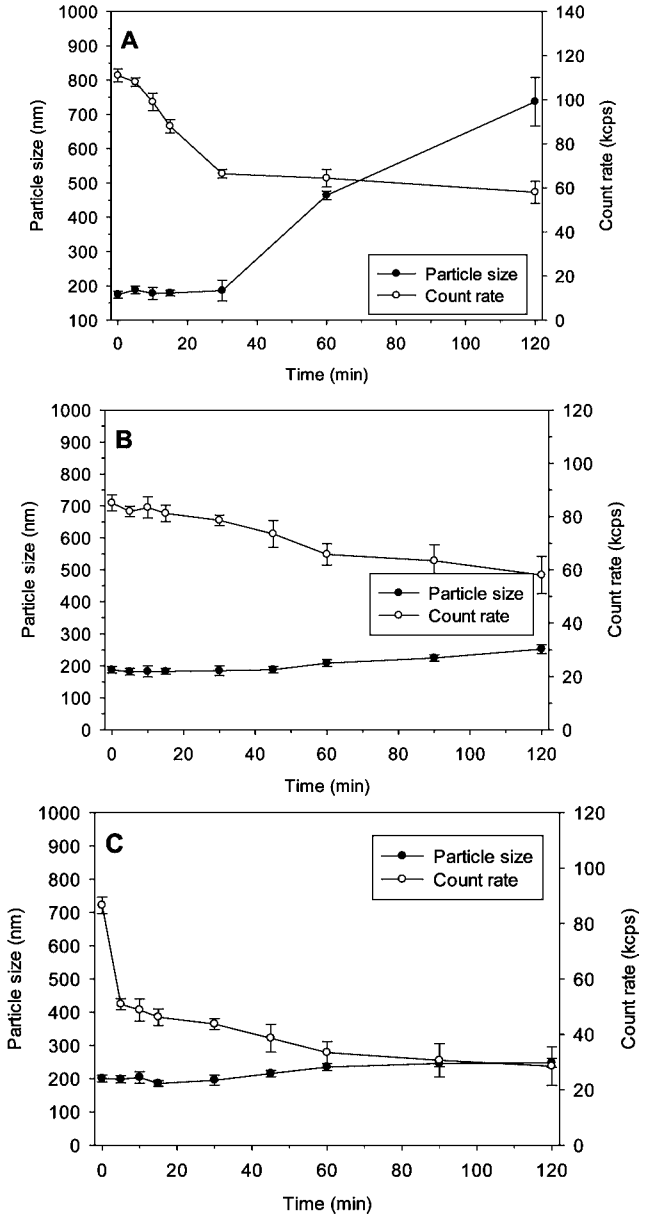


**Figure 7.** Time-dependent disintegration of curcumin-loaded BLG nanoparticles in (A) SGF at pH 2, (B) SGF at pH 5, and (C) SIF.

peptide bonds within BLG molecules, might be more prone to peptic digestion, and the breakage of these bonds might be responsible for particle disintegration. Our follow-up study (unpublished data) showed that nanoparticles prepared with cationized BLG (CBLG) exhibited remarkable resistance to pepsin, although this protein showed virtually the same resistance against pepsin as native BLG. Because CBLG contains abundant modified amine groups that could also be cross-linked by glutaraldehyde,[33,48] it is likely that the different conformations of glutaraldehyde-induced amide bonds in native and cationized BLG dictated the particle digestibility. Another relevant study using turbidity also pointed out cross-linked BLG nanoparticles could be digested by pepsin, but the time needed for complete degradation was as long as 7 h.[49] The discrepancy between that and our study may be ascribed to the use of different enzyme activities and different measuring techniques (turbidity versus DLS measurement). However, that

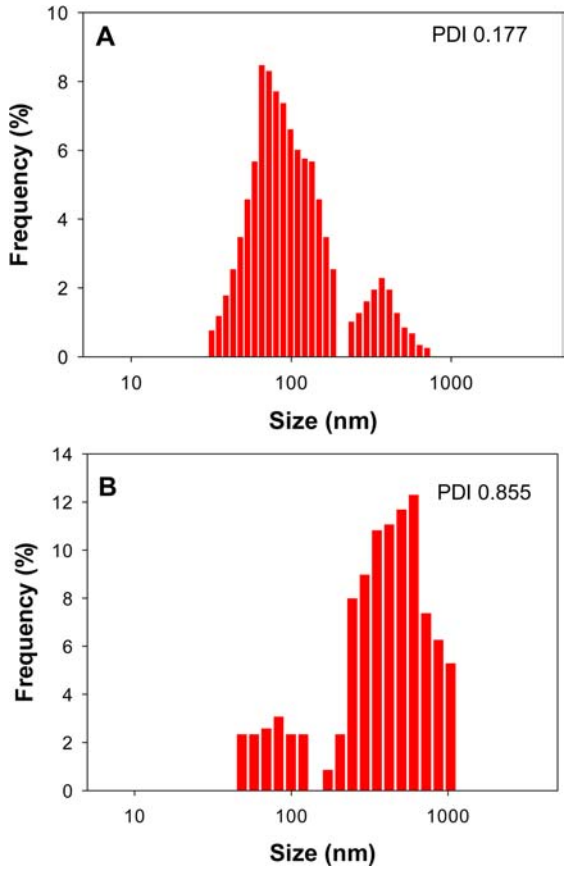


**Figure 8.** Intensity-based size distribution of CUR–BLG nanoparticle dispersions before (A) and after (B) digestion in SGF (pH 2, containing pepsin).

study was consistent with the present one in that proteins with poor digestibility can assemble into digestible nanoparticles.

On the contrary, the degradation of BLG nanoparticles proceeded at a much lower rate in SGF at pH 5 than at pH 2 (Figure 7B). During the experiment that lasted for 2 h, the average particle size did not show any significant change, whereas the count rate decreased by only 24%. The polydispersity remained stable at 0.127–0.159 during the digestion (Suppporting Information Table S1), which also suggested the stability of the nanoparticles. These results were consistent with the slow release of curcumin as indicated in the previous section. Lower activity of pepsin and the agglomeration of BLG at this pH were possible reasons for this difference, as discussed before.

When the particles were incubated with SIF, the particles were more rapidly digested, as was indicated by the sharp decrease in the count rate (Figure 7C). As discussed before, trypsin shows a higher capacity to digest BLG,[39] which was probably the main reason for the rapid digestion of BLG nanoparticles. Interestingly, the average size was kept steady at around 200 nm, a trend that was different from the situation in SGF at pH 2.0. The polydispersity index varied from 0.135 to 0.164 without any significant difference (Supporting Information Table S1). This result suggested that trypsin could not only break down smaller nanoparticles but also disintegrate larger aggregates. In the follow-up study that lasted for 4 h, a very low count rate (<10 kcp) was detected (data not shown) in SIF, suggesting that BLG nanoparticles were nearly completely decomposed.


dx.doi.org/10.1021/jf503199g | J. Agric. Food Chem. 2014, 62, 8837–8847

In summary, the encapsulation and releasing processes of curcumin-loaded BLG nanoparticles were systematically investigated. The association between BLG nanoparticles and curcumin was affected significantly by the content of antisolvents such as acetone. Therefore, adjustment of acetone to moderate values (40−50%) followed by mild evaporation led to a remarkable improvement in EE and LE. In addition, the optimal dose of glutaraldehyde decreased at higher curcumin loadings, which suggested that curcumin could replace part of the toxic cross-linkers and aid the maintenance of particle structure. The nanoparticles formed through the optimized procedure showed average sizes between 164 and 214 nm, high zeta potential of −42 mV, and loading efficiency of at most 11%. Moreover, this study suggested that proteins that are resistant to peptic digestion could form nanoparticles that were digestible by pepsin at pH 2, probably because of the breakage of amide bonds formed with glutaraldehyde. As a result, no controlled release of curcumin was observed under simulated fasting condition. However, satisfactory controlled release was achieved under simulated fed condition, that is, digestion in SGF at pH 5 and then in SIF. The conclusions from this study may apply not only to the curcumin−BLG system but also to a wide array of encapsulation systems consisting of a water-soluble protein encapsulant and a hydrophobic target compound. Therefore, this study provides insight into the assembly and disassembly of protein nanoparticles, and it may shed some light on the development of encapsulating systems with satisfying LE and reduced toxicity.

## ■ ASSOCIATED CONTENT

### Supporting Information

Supplemental Table S1 describes the polydispersity index (PDI) of curcumin-loaded BLG nanoparticles in different digestive fluids (SGF at pH 2 and 5, as well as SIF) as a function of timel these data were obtained by DLS as introduced under Characterization of Curcumin-Loaded BLG Nanoparticles. This material is available free of charge via the Internet at http://pubs.acs.org.

## ■ AUTHOR INFORMATION

### Corresponding Author

*(Q.W.) Phone: (301) 405-8421. Fax: (301) 314-3313. E-mail: wangqin@umd.edu.

### Notes

The authors declare no competing financial interest.

## ■ ACKNOWLEDGMENTS

We appreciate the support of the Maryland NanoCenter of the University of Maryland in scanning electron microscopy.

## ■ REFERENCES

(1) Chen, L. Y.; Remondetto, G. E.; Subirade, M. Food protein-based materials as nutraceutical delivery systems. *Trends Food Sci. Technol.* **2006**, *17*, 272−283.

(2) Jahanshahi, M.; Babaei, Z. Protein nanoparticle: a unique system as drug delivery vehicles. *Afr. J. Biotechnol* **2008**, *7*, 4926−4934.

(3) Teng, Z.; Luo, Y.; Wang, T.; Zhang, B.; Wang, Q. Development and application of nanoparticles synthesized with folic acid conjugated soy protein. *J. Agric. Food Chem.* **2013**, *61*, 2556−2564.

(4) Zhang, J.; Liang, L.; Tian, Z.; Chen, L.; Subirade, M. Preparation and in vitro evaluation of calcium-induced soy protein isolate nanoparticles and their formation mechanism study. *Food Chem.* **2012**, *133*, 390−399.

(5) Weber, C.; Coester, C.; Kreuter, J.; Langer, K. Desolvation process and surface characterisation of protein nanoparticles. *Int. J. Pharm.* **2000**, *194*, 91−102.

(6) Paik, S.-Y.-R.; Nguyen, H. H.; Ryu, J.; Che, J.-H.; Kang, T. S.; Lee, J. K.; Song, C. W.; Ko, S. Robust size control of bovine serum albumin (BSA) nanoparticles by intermittent addition of a desolvating agent and the particle formation mechanism. *Food Chem.* **2013**, *141*, 695−701.

(7) Luo, Y.; Teng, Z.; Wang, Q. Development of zein nanoparticles coated with carboxymethyl chitosan for encapsulation and controlled release of vitamin $D_3$. *J. Agric. Food Chem.* **2012**, 836−843.

(8) Zhong, Q.; Jin, M. Zein nanoparticles produced by liquid-liquid dispersion. *Food Hydrocolloids* **2009**, *23*, 2380−2387.

(9) Teng, Z.; Luo, Y. C.; Wang, Q. Nanoparticles synthesized from soy protein: preparation, characterization, and application for nutraceutical encapsulation. *J. Agric. Food Chem.* **2012**, *60*, 2712−2720.

(10) Patel, A. R.; Bouwens, E. C. M.; Velikov, K. P. Sodium caseinate stabilized zein colloidal particles. *J. Agric. Food Chem.* **2010**, *58*, 12497−12503.

(11) Zhang, Y.; Niu, Y.; Luo, Y.; Ge, M.; Yang, T.; Yu, L. L.; Wang, Q. Fabrication, characterization and antimicrobial activities of thymol-loaded zein nanoparticles stabilized by sodium caseinate-chitosan hydrochloride double layers. *Food Chem.* **2014**, *142*, 269−275.

(12) Patel, A.; Hu, Y. C.; Tiwari, J. K.; Velikov, K. P. Synthesis and characterisation of zein-curcumin colloidal particles. *Soft Matter* **2010**, *6*, 6192−6199.

(13) Luo, Y.; Wang, T.; Teng, Z.; Chen, P.; Sun, J.; Wang, Q. Encapsulation of indole-3-carbinol and 3,3′-diindolylmethane in zein/carboxymethyl chitosan nanoparticles with controlled release property and improved stability. *Food Chem.* **2013**, *139*, 224−230.

(14) Teng, Z.; Luo, Y.; Wang, Q. Carboxymethyl chitosan-soy protein complex nanoparticles for the encapsulation and controlled release of vitamin D3. *Food Chem.* **2013**, *141*, 524−532.

(15) Prajakta, D.; Ratnesh, J.; Chandan, K.; Suresh, S.; Grace, S.; Meera, V.; Vandana, P. Curcumin loaded pH-sensitive nanoparticles for the treatment of colon cancer. *J. Biomed. Nanotechnol.* **2009**, *5*, 445−455.

(16) Maham, A.; Tang, Z. W.; Wu, H.; Wang, J.; Lin, Y. H. Protein-based nanomedicine platforms for drug delivery. *Small* **2009**, *5*, 1706−1721.

(17) Kumari, A.; Yadav, S. K.; Yadav, S. C. Biodegradable polymeric nanoparticles based drug delivery systems. *Colloids Surf., B* **2010**, *75*, 1−18.

(18) Wang, L.; Dong, J.; Chen, J.; Eastoe, J.; Li, X. Design and optimization of a new self-nanoemulsifying drug delivery system. *J. Colloid Interface Sci.* **2009**, *330*, 443−448.

(19) Luo, Y.; Teng, Z.; Wang, X.; Wang, Q. Development of carboxymethyl chitosan hydrogel beads in alcohol-aqueous binary solvent for nutrient delivery applications. *Food Hydrocolloids* **2013**, *31*, 332−339.

(20) Hu, D.; Lin, C.; Liu, L.; Li, S.; Zhao, Y. Preparation, characterization, and in vitro release investigation of lutein/zein nanoparticles via solution enhanced dispersion by supercritical fluids. *J. Food Eng.* **2012**, *109*, 545−552.

(21) Luo, Y.; Teng, Z.; Wang, Q. Development of zein nanoparticles coated with carboxymethyl chitosn for encapsulation and controlled release of vitamin D3. *J. Agric. Food Chem.* **2012**, *60*, 836−843.

(22) Chen, J.; Zheng, J.; McClements, D. J.; Xiao, H. Tangeretin-loaded protein nanoparticles fabricated from zein/$\beta$-lactoglobulin: preparation, characterization, and functional performance. *Food Chem.* **2014**, *158*, 466−472.

(23) Maghsoudi, A.; Shojaosadati, S. A.; Farahani, E. V. 5-Fluorouracil-loaded BSA nanoparticles: formulation optimization and in vitro release study. *AAPS PharmSciTech* **2008**, *9*, 1092−1096.

(24) Jithan, A. V.; Madhavi, K.; Madhavi, M.; Prabhakar, K. Preparation and characterization of albumin nanoparticles encapsulating curcumin intended for the treatment of breast cancer. *Int. J. Pharm. Invest.* **2011**, *1*, 119.

(25) Shaikh, J.; Ankola, D. D.; Beniwal, V.; Singh, D.; Kumar, M. N. V. Nanoparticle encapsulation improves oral bioavailability of curcumin by at least 9-fold when compared to curcumin administered with piperine as absorption enhancer. *Eur. J. Pharm. Sci.* **2009**, *37*, 223−230.
(26) Jordan, S. L.; Russo, M. R.; Blessing, R. L.; Theis, A. B. Inactivation of glutaraldehyde by reaction with sodium bisulfite. *J. Toxicol. Environ. Health* **1996**, *47*, 299−309.
(27) Zhou, H.; Sun, X.; Zhang, L.; Zhang, P.; Li, J.; Liu, Y.-N. Fabrication of biopolymeric complex coacervation core micelles for efficient tea polyphenol delivery via a green process. *Langmuir* **2012**, *28*, 14553−14561.
(28) Shpigelman, A.; Cohen, Y.; Livney, Y. D. Thermally-induced β-lactoglobulin-EGCG nanovehicles: loading, stability, sensory and digestive-release study. *Food Hydrocolloids* **2012**, *29*, 57−67.
(29) Van Buren, J. P.; Robinson, W. B. Formation of complexes between protein and tannic acid. *J. Agric. Food Chem.* **1969**, *17*, 772−777.
(30) Kirchmajer, D. M.; Watson, C. A.; Ranson, M.; Panhuis, M. i. h. Gelapin, a degradable genipin cross-linked gelatin hydrogel. *RSC Adv.* **2013**, *3*, 1073−1081.
(31) Lorenzen, P. C.; Schlimme, E.; Roos, N. Crosslinking of sodium caseinate by a microbial transglutaminase. *Food/Nahrung* **1998**, *42*, 151−154.
(32) Elzoghby, A. O.; Helmy, M. W.; Samy, W. M.; Elgindy, N. A. Novel ionically crosslinked casein nanoparticles for flutamide delivery: formulation, characterization, and in vivo pharmacokinetics. *Int. J. Nanomed.* **2013**, *8*, 1721.
(33) Teng, Z.; Li, Y.; Luo, Y.; Zhang, B.; Wang, Q. Cationic β-lactoglobulin nanoparticles as a bioavailability enhancer: protein characterization and particle formation. *Biomacromolecules* **2013**, *14*, 2848−2856.
(34) Kontopidis, G.; Holt, C.; Sawyer, L. Invited review: β-lactoglobulin: binding properties, structure, and function. *J. Dairy Sci.* **2004**, *87*, 785−796.
(35) Sharma, O. P. Antioxidant activity of curcumin and related compounds. *Biochem. Pharmacol.* **1976**, *25*, 1811−1812.
(36) Goel, A.; Aggarwal, B. B. Curcumin, the golden spice from Indian saffron, is a chemosensitizer and radiosensitizer for tumors and chemoprotector and radioprotector for normal organs. *Nutr. Cancer* **2010**, *62*, 919−930.
(37) Sneharani, A. H.; Karakkat, J. V.; Singh, S. A.; Rao, A. G. A. Interaction of curcumin with β-lactoglobulin-stability, spectroscopic analysis, and molecular modeling of the complex. *J. Agric. Food Chem.* **2010**, *58*, 11130−11139.
(38) Podaralla, S.; Averineni, R.; Alqahtani, M.; Perumal, O. Synthesis of novel biodegradable methoxy poly(ethylene glycol)-zein micelles for effective delivery of curcumin. *Mol. Pharm.* **2012**, *9*, 2778−2786.
(39) Otte, J.; Zakora, M.; Qvist, K. B.; Olsen, C. E.; Barkholt, V. Hydrolysis of bovine β-lactoglobulin by various proteases and identification of selected peptides. *Int. Dairy J.* **1997**, *7*, 835−848.
(40) Fotaki, N.; Vertzoni, M. Biorelevant dissolution methods and their applications in in vitro-in vivo correlations for oral formulations. *Open Drug Delivery J.* **2010**, *4*, 2−13.
(41) Dufour, E.; Haertl, T. Alcohol-induced changes of β-lactoglobulin-retinol-binding stoichiometry. *Protein Eng.* **1990**, *4*, 185−190.
(42) Dufour, E.; Genot, C.; Haertlé, T. β-Lactoglobulin binding properties during its folding changes studied by fluorescence spectroscopy. *Biochim. Biophys. Acta, Protein Struct. Mol. Enzymol.* **1994**, *1205*, 105−112.
(43) Sneharani, A. H.; Karakkat, J. V.; Singh, S. A.; Rao, A. G. A. Interaction of curcumin with β-lactoglobulin: stability, spectroscopic analysis, and molecular modeling of the complex. *J. Agric. Food Chem.* **2010**, *58*, 11130−11139.
(44) Marty, J. J.; Oppenheim, R. C.; Speiser, P. Nanoparticles − a new colloidal drug delivery system. *Pharm. Acta Helv.* **1978**, *53*, 17−23.
(45) Siebert, K. J.; Troukhanova, N. V.; Lynn, P. Y. Nature of polyphenol-protein interactions. *J. Agric. Food Chem.* **1996**, *44*, 80−85.
(46) Tonnesen, H. H.; Karlsen, J. Studies on curcumin and curcuminoids. VI. Kinetics of curcumin degradation in aqueous solution. *Z. Lebensm. Unters. Forsch.* **1985**, *180*, 402−404.
(47) Dash, S.; Murthy, P. N.; Nath, L.; Chowdhury, P. Kinetic modeling on drug release from controlled drug delivery systems. *Acta Polym. Pharm.* **2010**, *67*, 217−223.
(48) Teng, Z.; Li, Y.; Niu, Y.; Xu, Y.; Yu, L.; Wang, Q. Cationic β-lactoglobulin nanoparticles as a bioavailability enhancer: comparison between ethylenediamine and polyethyleneimine as cationizers. *Food Chem.* **2014**, *159*, 333−342.
(49) Ko, S.; Gunasekaran, S. Preparation of sub-100-nm β-lactoglobulin (BLG) nanoparticles. *J. Microencapsul.* **2006**, *23*, 887−898.

**Table 1. Composition of the Root Essential Oils of *Angelica dahurica* (Ad) and *A. pubescentis* (Ap)**

| RRI[a] | compound | Ad (%) | Ap (%) | identification method[b] |
|---|---|---|---|---|
| 1032 | α-pinene | 46.3 | 37.6 | $t_R$, MS |
| 1035 | α-thujene | 0.6 | 0.5 | $t_R$, MS |
| 1048 | 2-methyl-3-buten-2-ol | 0.5 | | MS |
| 1076 | camphene | 0.2 | 1.8 | $t_R$, MS |
| 1100 | undecane | | 0.3 | $t_R$, MS |
| 1093 | hexanal | | 0.1 | $t_R$, MS |
| 1118 | β-pinene | 2.5 | 2.2 | $t_R$, MS |
| 1132 | sabinene | 9.3 | 0.3 | $t_R$, MS |
| 1159 | δ-3-carene | | 0.4 | MS |
| 1174 | myrcene | 5.5 | 0.7 | $t_R$, MS |
| 1194 | heptanal | 0.1 | | $t_R$, MS |
| 1203 | limonene | 1.0 | 8.7 | $t_R$, MS |
| 1218 | β-phellandrene | 1.8 | 3.8 | $t_R$, MS |
| 1280 | *p*-cymene | 3.3 | 11.6 | $t_R$, MS |
| 1296 | octanal | 0.2 | | $t_R$, MS |
| 1300 | tridecane | | 0.3 | $t_R$, MS |
| 1384 | α-pinene oxide | | 0.2 | MS |
| 1398 | 2-nonanone | | 0.2 | MS |
| 1429 | perillen | 0.1 | | MS |
| 1455 | *p*-cresyl methyl ether | | 0.7 | MS |
| 1471 | 2-nonylacetate | | 0.2 | MS |
| 1479 | δ-elemene | 0.3 | | MS |
| 1492 | cyclosativene | | 0.1 | MS |
| 1496 | 2-decanone | | 0.2 | MS |
| 1499 | α-campholene aldehyde | | 0.2 | MS |
| 1504 | daucene | | 0.1 | MS |
| 1521 | 2-nonanol | | 0.7 | MS |
| 1571 | *trans*-*p*-menth-2-en-1-ol | | 0.1 | MS |
| 1586 | pinocarvone | 0.1 | 0.5 | $t_R$, MS |
| 1591 | bornyl acetate | | 1.2 | $t_R$, MS |
| 1594 | *trans*-β-bergamotene | 0.1 | | MS |
| 1600 | β-elemene | 1.6 | 0.2 | $t_R$, MS |
| 1604 | thymol methyl ether | | 0.5 | $t_R$, MS |
| 1611 | terpinen-4-ol | 4.9 | | $t_R$, MS |
| 1614 | carvacrol methyl ether | | 1.0 | $t_R$, MS |
| 1620 | selina-5,11-diene | 0.2 | | MS |
| 1638 | *cis*-*p*-menth-2-en-1-ol | 0.1 | 0.2 | MS |
| 1668 | (*Z*)-β-farnesene | 0.1 | 0.3 | MS |
| 1669 | sesquisabinene | | 0.5 | MS |
| 1670 | *trans*-pinocarveol | 0.2 | 0.3 | MS |
| 1688 | selina-4,11-diene | 0.5 | | MS |
| 1690 | cryptone | 2.5 | 6.7 | MS |
| 1725 | verbenone | 0.4 | 0.3 | MS |
| 1740 | valencene | | 0.2 | MS |
| 1741 | β-bisabolene | 0.1 | | MS |
| 1742 | β-selinene | 0.1 | 0.3 | MS |
| 1744 | α-selinene | 0.1 | | MS |
| 1745 | selina-4(15),7(11)-diene | tr[c] | | MS |
| 1758 | *cis*-piperitol | tr | | MS |
| 1786 | *ar*-curcumene | | 0.2 | MS |
| 1802 | cumin aldehyde | 0.2 | 0.8 | $t_R$, MS |
| 1804 | myrtenol | 0.1 | 0.2 | MS |
| 1811 | *p*-mentha-1,3-dien-7-al | | 0.1 | MS |
| 1814 | *p*-mentha-1,5-dien-7-ol | tr | | MS |
| 1823 | *p*-mentha-1(7),5-dien-2-ol | | 0.1 | MS |
| 1845 | *trans*-carveol | | 0.1 | $t_R$, MS |
| 1849 | cuparene | 0.2 | | MS |
| 1854 | germacrene-B | 0.1 | | MS |
| 1864 | *p*-cymen-8-ol | tr | | $t_R$, MS |
| 1973 | 1-dodecanol | 5.2 | | $t_R$, MS |
| 2008 | caryophyllene oxide | 0.6 | | $t_R$, MS |
| 2071 | humulene epoxide II | tr | 0.1 | $t_R$, MS |
| 2077 | 1-tridecanol | 2.0 | | $t_R$, MS |
| 2113 | cumin alcohol | 0.3 | 1.3 | $t_R$, MS |
| 2144 | spathulenol | 0.2 | | MS |
| 2232 | α-bisabolol | | tr | MS |
| 2232 | 4-isopropylphenol | | 0.1 | MS |
| 2269 | guaia-6,10(14)-dien-4β-ol | 0.5 | | MS |
| | total | 92.1 | 86.2 | |

[a]RRI, relative retention indices calculated against *n*-alkanes; % calculated from FID data. [b]Identification method: $t_R$, identification based on the retention times ($t_R$) of genuine standard compounds on the HP Innowax column; MS, identification was performed on the basis of computer matching of the mass spectra with those of the Wiley and MassFinder libraries and comparison with literature data. [c]tr, <0.01.

received greater attention as natural sources of potentially useful biopesticides targeting a diversity of pests including plant pathogens, *Varroa* mites, cockroaches, mosquitoes, stored-product insects, and house flies.[4,6−16]

*Angelica dahurica* (Fisch. Ex Hoffm.) Benth. & Hook. and *Angelica pubescentis* Maxim. are well-known in TCM, and their roots are recorded as Baizhi and Duhuo, respectively, in the Chinese pharmacopoeia.[17] Both *Angelica* roots have a long history of use in Asian countries. *A. dahurica* roots have been used for the treatment of headache, rhinitis, nose problems, skin problems,[18−23] and toothache.[17,24,25] *A. pubescentis* roots have been used for the treatment of rheumatoid arthritis, headache, paralysis,[17,24] and insomnia.[17,26] The pharmacological activities associated with *A. dahurica* include antibacterial, antifebrile, analgesic, and antispasmodic,[17,27] and those for *A. pubescentis* include antibacterial, analgesic, antirheumatic, antispasmodic, antifungal, and antitumor.[17,28−30]

As part of our research program aimed at the identification of new natural-based insecticides and fungicides, we previously investigated two *Angelica* essential oils for their antifungal activity.[4] In our previous study, *A. sinensis* root oil showed good antifungal activity against three *Colletotrichum* species; however, *A. archangelica* root oil did not show any antifungal activity.[4] The bioassay-guided isolation was followed, and the active compound (*Z*)-ligustilide was isolated. This compound also demonstrated potent biting deterrent activity against *Aedes aegypti* and *Anopheles stephensi*.[4] In a continuing effort to investigate new alternative biopesticides from other *Angelica* species, *A. dahurica* and *A. pubescentis* root essential oils from China were explored in the current study for their pest management properties. Both *Angelica* essential oils were analyzed by gas chromatography (GC) with a flame ionization detector (FID) and gas chromatography−mass spectrometry (GC-MS) using an Agilent GC-mass selective detector (MSD) system. In addition, a nuclear molecular marker to distinguish between these two *Angelica* species was also investigated.


dx.doi.org/10.1021/jf5024752 | J. Agric. Food Chem. 2014, 62, 8848−8857

## MATERIALS AND METHODS

**Chemicals.** Myrcene (CAS Registry No. 123-35-3), 1-tridecanol (CAS Registry No. 112-70-9), 1-dodecanol (CAS Registry No. 112-53-8), thymol methyl ether (CAS Registry No. 1076-56-8), carvacrol methyl ether (CAS Registry No. 6379-73-3), *p*-cymene (CAS Registry No. 99-87-6), (−)-terpinen-4-ol (CAS Registry No. 20126-76-5), and (+)-terpinen-4-ol (CAS Registry No. 2438-10-0) were purchased from Sigma-Aldrich (St. Louis, MO, USA). Sabinene (CAS Registry No. 3387-41-5) was purchased from ChromaDex (Irvine, CA, USA). Fungicide standards benomyl, cyprodinil, azoxystrobin, and captan were purchased from Chem Service, Inc. (West Chester, PA, USA).

**Plant Material.** *A. dahurica* and *A. pubescentis* roots were purchased from Beijing Heng Yu Hua Kang Pharmaceutical Co., Ltd. Species were identified by Professor Dr. Yu-Ning Yan, School of Chinese Materia Medica, Beijing University of Chinese Medicine, Beijing, China. Voucher specimens of these samples (No. 20 and 21) were deposited at the Herbarium of the Faculty of Pharmacy, Anadolu University, Eskisehir, Turkey. For the molecular analysis, additional samples of *Angelica* species were chosen: *A. acutiloba* 2935; *A. gigas* 2944, and *A. sinensis* 14427. Vouchers 2935 and 2944 were from the repository at the National Center for Natural Products (NCNPR), The University of Mississippi, University, MS, USA. Voucher 14427 was deposited at the Herbarium of the Faculty of Pharmacy, Anadolu University.

**Isolation of the Essential Oils.** Air-dried roots of *A. dahurica* and *A. pubescentis* were water distilled for 3 h using a Clevenger-type apparatus to produce essential oils at yields of 0.45 and 0.65%, respectively.

**Gas Chromatography (GC) and Gas Chromatography−Mass Spectrometry (GC-MS) Conditions.** The *A. dahurica* and *A. pubescentis* root oils were analyzed by GC-FID and GC-MS using an Agilent GC-mass selective detector (MSD) system. The GC-MS analyses were carried out with an Agilent 5975 GC-MSD system. An Innowax fused silica capillary column (60 m × 0.25 mm, 0.25 μm film thickness) was used with helium as the carrier gas (0.8 mL/min). The oven temperature was kept at 60 °C for 10 min, then programmed to 220 °C at a rate of 4 °C/min, then maintained constant at 220 °C for 10 min, and finally programmed to 240 °C at a rate of 1 °C/min. The injector temperature was set at 250 °C. The split flow was adjusted at 50:1. Mass spectra were recorded at 70 eV over the mass range $m/z$ 35−450.

The GC analyses were performed using an Agilent 6890N GC system. The FID detector temperature was set to 300 °C, and the same operational conditions were used with a duplicate of the same column employed in GC-MS analyses. Simultaneous autoinjection was done to obtain equivalent retention times. Relative percentages of the separated compounds were calculated from integration of the peak areas in the GC-FID chromatograms (Table 1).

Identification of essential oil components was accomplished by comparison of retention times with authentic samples or by comparison of their relative retention index (RRI) to a series of *n*-alkanes.[31,32] Computer matching for identification was accomplished with commercial mass spectral libraries (Wiley GC/MS Library, MassFinder 3 Library) and with an in-house "Baser Library of Essential Oil Constituents", which includes over 3200 genuine compounds with MS and retention data from pure standard compounds and components of known oils as well as MS literature data.[33,34]

**DNA Extraction and ITS Amplification from Plant Tissue.** DNA from *Angelica* species (dried root/rhizome) was extracted with a DNeasy Plant Mini Kit (Qiagen Inc., Valencia, CA, USA). The ITS region (internal transcribed spacer region, consisting of 18S rRNA gene, partial sequence; internal transcribed spacer 1, 5.8S rRNA gene; internal transcribed spacer 2, complete sequence; and 28S rRNA gene, partial sequence) was amplified from genomic DNA using the forward primer ITS1 (5′-TCCGTAGGTGAACCTGCGG-3′) and ITS4 (5′-TCCTCCGCTTATTGATATGC-3′).[35] PCR amplifications were carried out in a 50 μL reaction mixture containing 1× PCR reaction buffer, 0.2 mM dNTP mixture, 0.2 μM of each forward and reverse primer, 1.5 mM $MgCl_2$, and 2 U of Platinum Taq DNA Polymerase (Invitrogen, Carlsbad, CA, USA). The PCR program consisted of one initial denaturation step at 96 °C for 3 min followed by 35 cycles at 96 °C for 30 s, 50 °C for 30 s, and 72 °C for 2 min, with a final extension at 72 °C for 7 min. PCR products were cut with one of the restriction endonucleases, *Cac*8I, *Hae*III, *Rsa*I, or *Sau*96I (New England Biolabs, Ipswich, MA, USA), without prior purification or precipitation.[36] In brief, 2 μL of the appropriate restriction buffer and 5−10 units of restriction enzyme *Cac*8I, *Hae*III, *Rsa*I, or *Sau*96I (New England Biolabs) were added to 20 μL of PCR product and incubated at 37 °C for 15 h, followed by 60 °C for 10 min to inactivate the enzyme. PCR and restriction reactions were run in an M&J Research Gradient Cycler PTC-225. After amplification and restriction, an aliquot was analyzed by electrophoresis on a 1−2% TAE agarose gel and visualized under UV light. The PCR products were compared to the molecular size standard 1 kb plus DNA ladder (Invitrogen).

**Antifungal Bioassay against Plant Pathogens.** The antifungal assay was carried out by using the direct bioautography bioassays against *Colletotrichum acutatum*, *Colletotrichum fragariae*, and *Colletotrichum gloeosporioides*, and the detailed assay procedures were described previously.[4,8−10,14,15] Fungal growth inhibition was evaluated 4−5 days after treatment by measuring zone diameters. Conidia were harvested from 7−10-day-old cultures by flooding plates with 5 mL of sterile distilled water, and conidia concentrations were determined photometrically from a standard curve based on the percent transmittance (%T) at 625 nm. Suspensions were then adjusted with sterile distilled water to a concentration of $1.0 \times 10^5$ conidia/mL.[4−8,14,15] The essential oils of *A. dahurica* and *A. pubescentis* were applied at 80 and 160 μg/spot in *n*-hexane onto a silica plate. To detect biological activity directly on the TLC plate, silica gel plates were sprayed with one of the three spore suspensions adjusted to a final concentration of $3.0 \times 10^5$ conidia/mL with liquid potato dextrose broth (PDB, Difco) and 0.1% Tween-80. Using a 50 mL chromatographic sprayer, each TLC plate with a fluorescent indicator (250 μm, silica gel GF Uniplate, Analtech, Inc., Newark, DE, USA) was sprayed lightly (to a damp appearance) three times with the conidial suspension. Inoculated plates were then placed in a 30 × 13 × 7.5 cm moisture chamber (398 °C, 100% relative humidity, Pioneer Plastics, Inc., Dixon, KY, USA) and incubated in a growth chamber at 24 °C and a 12 h photoperiod under 60 ± 5 μmols $m^{-2}$ $s^{-1}$ light. Inhibition of fungal growth was measured 4 days after treatment. The sensitivity of each fungal species to each test compound was determined by comparing sizes of inhibitory zones. Clear zones of fungal growth inhibition on the TLC plate indicated the presence of antifungal constituents in each extract. Antifungal metabolites were readily located on the plates by visually observing clear zones where the active compounds inhibited fungal growth. Fungicide standards of benomyl, cyprodinil, azoxystrobin, and captan were used as positive controls at 1.16, 0.9, 1.61, and 1.2 μg, respectively, in 95% EtOH.

**Insects.** *Ae. aegypti* L. used in these studies were from a laboratory colony maintained at the Mosquito and Fly Research Unit at the Center for Medical, Agricultural and Veterinary Entomology, USDA-ARS, Gainesville, FL, USA.[37] For biting deterrence bioassays, pupae were maintained in the laboratory at 27 ± 2 °C and 60 ± 10% relative humidity (RH), and 7−15 d-old adult females were used. For repellent activity, pupae were maintained in the laboratory at 28 ± 1 °C and 30−60% RH, and the resulting adult females aged 5−9 days were selected from the stock cages by a hand-draw box.[38] For larval bioassays, the eggs were hatched and the larvae were maintained at a temperature of 27 ± 2 °C and 60 ± 10% RH in a photoperiod regimen of 12/12 h (L/D). Adults of azalea lace bug, *Stephanitis pyrioides* (Scott), were collected by using electric aspirators (Hausherr's Machine Works, Tom's River, NJ, USA) from bouquets of azalea terminals (*Rhododendron* species). These plants were constantly maintained in plant growth chambers (Percival Scientific, Perry, IA, USA) at a temperature of 27 °C and 65% RH with a photoperiod of 14/10 L/D.

**Mosquito Biting Bioassay.** Experiments were conducted by using a six-celled in vitro Klun and Debboun (K&D) module bioassay system, developed by Klun et al.,[39] for quantitative evaluation of biting deterrent properties of candidate compounds. Briefly, the assay system

consists of a 6-well reservoir with each of the 3 × 4 cm wells containing 6 mL of blood. As described by Ali et al.,[8] a feeding solution consisting of CPDA-1 and ATP was used instead of blood. Green fluorescent tracer dye (www.blacklightworld.com) was used to determine the feeding by the females. *A. dahurica* and *A. pubescentis* root essential oils and some of their pure compounds were tested in this study. Treatments of essential oils were applied at 10 $\mu g/cm^2$, and DEET (97%, *N*, *N*-diethyl-*m*-toluamide) (Sigma-Aldrich, St. Louis, MO, USA) at 4.8 $\mu g/cm^2$ was used as positive control. All of the treatments were freshly prepared in molecular biology grade 100% ethanol (Fisher Scientific Chemical Co., Fair Lawn, NJ, USA) at the time of bioassay. The temperature of the solution in the reservoirs was maintained at 37.5 °C by continuously passing warm water through the reservoir using a circulatory bath. The reservoirs were covered with a layer of collagen membrane (Devro, Sandy Run, SC, USA). The test compounds were randomly applied to six 4 × 5 cm areas of organdy cloth and positioned over the membrane-covered CPDA-1 + ATP solution with a Teflon separator placed between the treated cloth and the 6-cell module to prevent contamination of the module. A 6-cell module containing five female mosquitoes per cell was positioned over cloth treatments covering the six CPDA-1 + ATP solution membrane wells, and trap doors were opened to expose the treatments to these females. The number of mosquitoes biting through cloth treatments in each cell was recorded after a 3 min exposure, and mosquitoes were prodded back into the cells to check the actual feeding. Mosquitoes were squashed, and the presence or absence of green fluorescent tracer dye in the gut was used as an indicator of feeding. A replicate consisted of six treatments: four test oils/compounds, DEET (a standard biting deterrent), and ethanol-treated organdy as solvent control. Two sets of five replications each with five females per treatment were conducted on two different days using a newly treated organdy and a new batch of females in each replication. Treatments were replicated 10 times.

**Mosquito Repellent Bioassay.** Repellency was determined as the minimum effective dosage (MED), which is the minimum threshold surface concentration necessary to prevent mosquitoes from biting through the treated surface.[40] Approximately 500 (±10%) mosquitoes were collected and loaded into a test cage (size of 45 cm × 37.5 cm × 35 cm) and held in the cage for 25 (±2.5) min before initiating repellency assays. Serial dilutions were then made such that the concentrations on the cloth for the remaining 1 mL of solution were 1.5, 0.75, 0.375, 0.094, 0.047, 0.023, and 0.011 $mg/cm^2$. Each concentration was tested to determine the point at which the repellent failed for each of the volunteers in the study; this concentration was averaged and reported. Each test was conducted by having a volunteer affix the treated cloth onto a plastic sleeve to cover a 32 $cm^2$ window previously cut into the sleeve. Each of the volunteers wore this sleeve/cloth assembly above a nylon stocking covering their arm, with their hands protected by a glove.[41] The arm with the sleeve/cloth assembly was inserted into a cage, where approximately 500 female *Ae. aegypti* mosquitoes (aged 6−10 days) had been preselected as host-seeking using a draw box.[38] Failure of the repellent treatment was 1% bite through; that is, the volunteer received five bites through the cloth over the sleeve window in the 1 min assay. There were three human volunteers in this study, and all three provided written informed consent to participate in this study as part of a protocol (636-2005) approved by the University of Florida Human Use Institutional Review Board (IRB-01).

**Larval Bioassay.** Bioassays were conducted to test *A. dahurica* and *A. pubescentis* root essential oils and some of their pure compounds for larvicidal activity against 1-day-old *Ae. aegypti* larvae by using the bioassay system described by Pridgeon et al.[42] Five 1-day-old *Ae. aegypti* larvae were added in a droplet of water to each well of 24-well plates (BD Labware, Franklin Lakes, NJ, USA) by use of a disposable 22.5 cm Pasteur pipet. Fifty microliters of larval diet [2% slurry of 3:2 beef liver powder (Now Foods, Bloomingdale, IL, USA) and brewer's yeast (Lewis Laboratories Ltd., Westport, CT, USA)] was added to each well by using a Finnpipette stepper (Thermo Fisher, Vantaa, Finland). All chemicals tested were diluted in dimethyl sulfoxide (DMSO). Eleven microliters of the test chemical was added to the labeled wells, whereas 11 $\mu L$ of DMSO was added to control treatments. After the treatment application, the plates were swirled in clockwise and counterclockwise motions, front to back, and side to side five times to ensure even mixing of the chemicals. Larval mortality was recorded 24 and 48 h post treatment. Larvae that showed no movement in the well after manual disturbance of water were recorded as dead. Permethrin (46.1% cis −53.2% trans, Chemical Service, West Chester, PA, USA) was used as positive control. Five concentrations ranging between 300 and 6.25 ppm were used in each treatment to obtain a range of mortality between 0 and 100. Treatments were replicated 10 times for each oil or pure compound.

**Data Analyses.** The parameter of proportion not biting (PNB) mosquitoes was calculated as described earlier by Ali et al.[43] The K&D module bioassay system can handle only four treatments along with negative and positive controls at the one setup experiment. To make direct comparisons among more than four test compounds and to compensate for variation in overall response among replicates, the biting deterrent activity was quantified as the biting deterrence index (BDI). BDIs were calculated using the formula

$$[\mathrm{BDI}_{i,j,k}] = \left[\frac{\mathrm{PNB}_{i,j,k} - \mathrm{PNB}_{c,j,k}}{\mathrm{PNB}_{d,j,k} - \mathrm{PNB}_{c,j,k}}\right]$$

where $\mathrm{PNB}_{i,j,k}$ denotes the proportion of females not biting when exposed to test compound $i$ for replication $j$ and day $k$ ($i$ = 1−4, $j$ = 1−5, $k$ = 1−2), $\mathrm{PNB}_{c,j,k}$ denotes the proportion of females not biting the solvent control $c$ for replication $j$ and day $k$ ($j$ = 1−5, $k$ = 1−2), and $\mathrm{PNB}_{d,j,k}$ denotes the proportion of females not biting in response to DEET $d$ (positive control) for replication $j$ and day $k$ ($j$ = 1−5, $k$ = 1−2). This formula makes an adjustment for interday variation in response and incorporates information from the solvent control as well as the positive control. A BDI value of 0 indicates an effect similar to that of ethanol, whereas a value significantly greater than 0 indicates biting deterrent effect relative to ethanol. BDI values not significantly different from 1 are statistically similar to DEET. BDI values were analyzed using SAS Proc ANOVA [single factor: test compound (fixed)],[44] and means were separated using the Ryan−Einot−Gabriel−Welsch multiple-range test. To determine whether confidence intervals include the values of 0 or 1 for treatments, Scheffe's multiple-comparison procedure with the option of CLM was used in SAS. $LC_{50}$ values for larvicidal data were calculated by using SAS, Proc Probit. Control mortality was corrected by using Abbott's formula.[45] Toxicity was compared among treatments based on nonoverlapping 95% CI.[46]

**Adulticidal Activity against Azalea Lace Bug.** Bioassay and statistical methods follow those of Sampson et al.,[12,13] with some modifications. For these bioassays, *A. dahurica* and *A. pubescentis* essential oils as well as five chemical constituents [*p*-cymene, carvacrol methyl ether (CME), (+)-terpinen-4-ol, (−)-terpinen-4-ol, thymol methyl ether (TME)] were tested against adult azalea lace bug at a single dose of 10000 ppm (1% oil). In addition, *Angelica sinensis* and *Angelica archangelica* essential oils from our previous study[6] were also included to identify chemical diversity and activity relationship. Mortality data for lace bugs exposed to the two isomers of terpinen-4-ol were combined before analysis (total $n$ = 16). Selection of 10000 ppm as our trial dose was based on standard evaluation methods used for essential oil-based insecticides such as Ecotrol and previous bioassay results with other essential oils.[12−15] Oil emulsions were freshly prepared using DMSO as a solvent and a 10% aqueous solution of DMSO as the solvent's control. Positive controls used for evaluating *Angelica* spp. included 1% emulsions of two essential oils that are currently commercialized as insecticides and acaricides (*Chenopodium ambrosioides* (Requiem EC, AgraQuest, Inc., Davis CA, USA) and azadirachtin (ChemService, Inc.). Twenty microliters of each treatment and control emulsions was pipetted into individual plastic wells of a standard 96-well microtiter plate in a randomized complete block design. To prevent bugs from drowning in residual fluid, an absorbent disk of Whatman no. 2 filter paper was placed at the bottom of each well. Three adult azalea lace bugs were transferred from their holding vials to treatments and control wells. Mortality data were recorded by observing lace bugs under a dissecting microscope at 1 h intervals for 5 h at 21 °C. Lace bugs that remained motionless in the well after

manual disturbance with a probe were recorded as dead. Between observations, bugs were kept at 23 °C in a separate growth chamber.

## RESULTS AND DISCUSSION

Water-distilled essential oils from roots of *A. dahurica* and *A. pubescentis* were analyzed by GC-FID and GC-MS systems. The components identified are given in Table 1 with their relative percentages. Forty-three compounds were characterized in the oil of *A. dahurica*, making up 92.1% of the oil. Forty-six compounds were identified in the oil of *A. pubescentis*, representing 86.2% of the oil. The oil of *A. dahurica* was characterized with $\alpha$-pinene (46.3%), sabinene (9.3%), myrcene (5.5%), and 1-dodecanol (5.2%) as major constituents. $\alpha$-Pinene (37.6%), *p*-cymene (11.6%), limonene (8.7%), cryptone (6.7%), and $\beta$-phellandrene (3.8%) were characterized as main compounds in the oil of *A. pubescentis*. Both *Angelica* species were mainly rich in monoterpene hydrocarbons in our study. Tetradecanol (19.4%), limonene (15.3%), $\delta$-3-carene (11.0%), 1-dodecanol (5.8%), and $\alpha$-pinene (3.9%) were reported as major compounds of *A. dahurica* root oil.[47] $\delta$-3-Carene (9.0%), $\beta$-phellandrene (8.4%), $\alpha$-bisabolol (6.0%), and *m*-cymene (5.0%) were found as the main components in *A. pubescentis* radix oil.[48] The observed differences in the constituents of these two *Angelica* essential oils even collected inside the same country may be due to different environmental and harvesting season of the plants.

The coding ribosomal 18S, 5.8S, and 28S RNA genes are highly conserved, but the regions that separate them (internal spacer) are variable in length and nucleotide sequence. The diversity of the spacer region can be used as an identification basis.[49,50] In addition to the chemical profiling, a PCR–restriction fragment length polymorphism (PCR-RFLP) method was applied on the internal transcribed spacer region (ITS) using *Cac*8I, *Hae*III, *Rsa*I, or *Sau*96I restriction endonucleases to help distinguish between *A. dahurica* and *A. pubescentis*, *A. acutiloba*, *A. gigas*, and *A. sinensis*. Using the ITS primers, a single fragment of >600 bp was produced from all of the analyzed samples. PCR products were digested with restriction endonucleases *Cac*8I, *Hae*III, *Rsa*I, and *Sau*96I. A RFLP was observed from almost all of the samples analyzed (Figure 1). The digestion showed that *Cac*8I, *Rsa*I, or *Sau*96I produced polymorphic patterns that distinguished the *A. dahurica* from the *A. pubescentis* sample and from the other analyzed *Angelica* samples (*A. acutiloba*, *A. gigas*, and *A. sinensis*). A powerful tool for plant material identification, the PCR-RFLP approach was also successfully employed for the identification of plant materials such as *Bursaphelenchus* species[49] and for the discrimination of *Mitragyna* species[50] and the parasitic nematode *Anisakis* species.[51]

To discover natural product fungicides, essential oils of *A. dahurica* and *A. pubescentis* were evaluated for antifungal activity using direct bioautography assays leading to the discovery of promising antifungal compounds against three *Colletotrichum* species, which cause anthracnose diseases of strawberry.[4,8−10,14,15] The *A. pubescentis* essential oil demonstrated clear zones (2.83 ± 0.29 mm) against plant pathogens *C. acutatum*, *C. fragariae*, and *C. gloeosporioides* at 160 $\mu$g/spot, whereas the *A. dahurica* essential oil did not show antifungal activity at the same concentration (Figure 2). Antifungal activity was evident by the presence of clear zones with a dark background where fungal mycelia or reproductive stroma were not present on the TLC plates. *A. pubescentis* essential oil demonstrated weaker antifungal activity compared to the positive control captan. The commercial fungicide captan, which is a well-known multisite inhibitor fungicide standard, showed clear inhibitory zones of 18.67 ± 1.53 mm at 1.2 $\mu$g concentration. The TLC profile of *A. pubescentis* in *n*-hexane/diethyl ether (8:2, v/v) was subsequently tested against three *Colletotrichum* species to identify the active inhibitory zones. The minor polar compounds appeared to be responsible for antifungal activity (Figure 3).

BDI values representing the biting deterrent activity of *A. dahurica* and *A. pubescentis* root essential oils against *Ae. aegypti* are given in Figure 4. Both *Angelica* oils were tested at 10 $\mu$g/cm$^2$, and *A. dahurica* oil demonstrated slightly higher biting deterrent activity than *A. pubescentis*, but both were less active than DEET. Therefore, we selected possible active compounds that were present in *A. dahurica* oil but not present in the *A.*

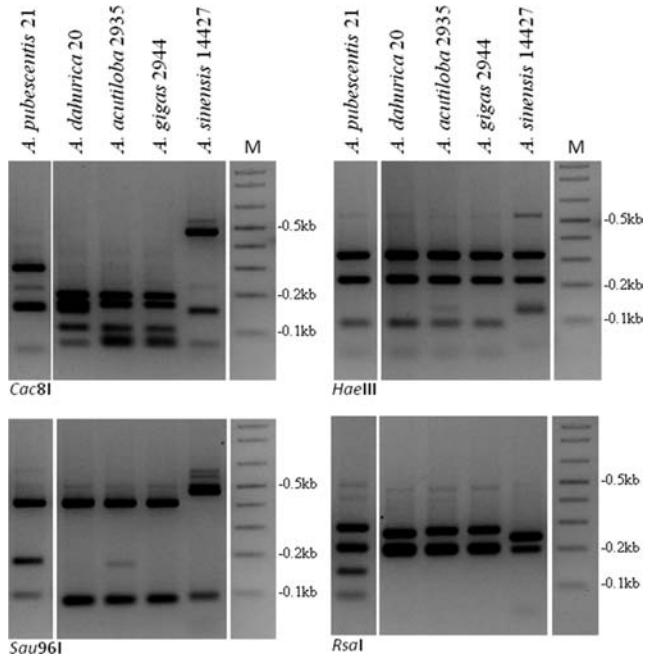


**Figure 1.** Agarose gel image of digested ITS PCR products with various restriction endonucleases (PCR-RFLP analysis). A different RFLP was observed from almost all of the samples analyzed. *A. dahurica* can be distinguished from *A. pubescentis* or any of the tested *Angelica* samples by cutting the amplified ITS region with *Cac*8I, *Rsa*I, or *Sau*96I. M = molecular size standard; fragment sizes are given in kilo base pairs (kb).

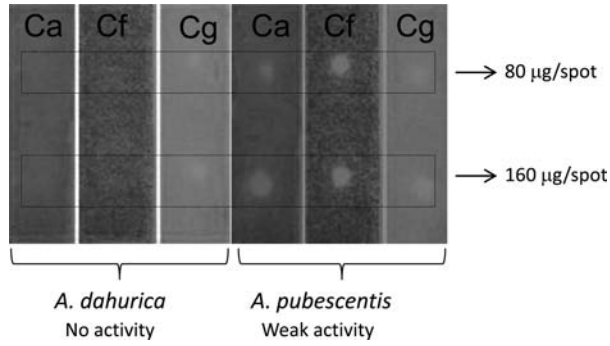


**Figure 2.** Bioautography of *A. dahurica* and *A. pubescentis* essential oils at 80 and 160 mg/spot against *C. acutatum* (Ca), *C. fragariae* (Cf), and *C. gloeosporioides* (Cg). Clear inhibitory zones indicate the antifungal activity.


dx.doi.org/10.1021/jf5024752 | J. Agric. Food Chem. 2014, 62, 8848−8857

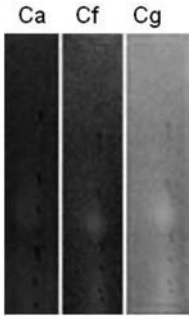


**Figure 3.** 1D-bioautography of *A. pubescentis* essential oil against *C. acutatum* (Ca), *C. fragariae* (Cf), and *C. gloeosporioides* (Cg) in *n*-hexane/diethyl ether (8:2, v/v) at 160 μg/spot concentration. The *A. pubescentis* essential oil showed weak antifungal activity with the diffuse zones against all three *Colletotrichum* species.

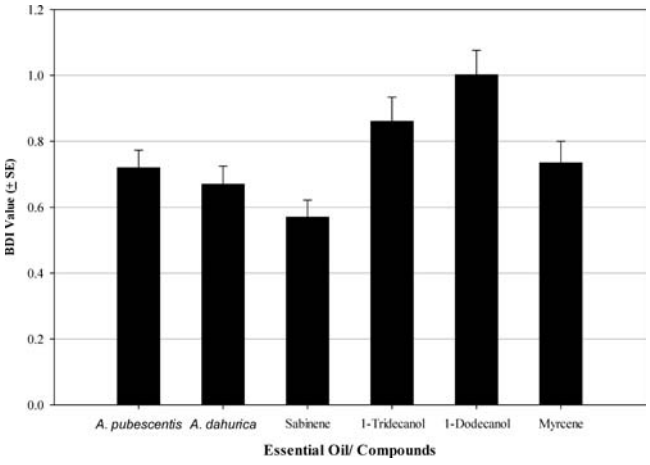


**Figure 4.** Mean biting deterrent index (BDI) value of *Angelica* species and active pure compounds. Essential oils were evaluated at 10 μg/cm$^2$ and the pure compounds were tested at 25 nmol/cm$^2$. DEET at 25 nmol/cm$^2$ was used as a positive control.

*pubescentis* oil. The major compound, α-pinene, and its β isomer, β-pinene, showed in our previous paper low biting deterrent activity at 25 nmol/cm$^2$.[52] The other monoterpene hydrocarbons sabinene and myrcene were present in higher concentration in *A. dahurica* oil than in *A. pubescentis* oil. Myrcene showed higher biting deterrence activity than sabinene, and the activity was similar to that of *A. dahurica* oil (Figure 4). We previously tested (+)- and (−)-terpinen-4-ol for biting deterrent activity, and both enantiomers showed biting deterrent activity greater than that of the solvent control.[53] Two aliphatic alcohols, 1-dodecanol and 1-tridecanol, that were present only in *A. dahurica* oil were individually tested for their biting deterrent activity. On the basis of 95% CI values, 1-dodecanol (C12:0) and 1-tridecanol (C13:0) at 25 nmol/cm$^2$ showed biting deterrent activity similar to that of DEET, whereas all the other compounds, such as sabinene and myrcene, were lower than 1-dodecanol and 1-tridecanol. In our research group it was previously reported that carboxylic acid forms of these alcohols, dodecanoic acid (C12:0) and tridecanoic acid (C13:0) showed higher BDI than other short- and long-chain fatty acids.[43] It appears that the number of carbons in the aliphatic compounds influences the biting deterrent activity. These two aliphatic alcohols (1-dodecanol and 1-tridecanol) may not be active at the concentrations present in the *A. dahurica* oil, and, although they are not also present in *A. pubescentis* essential oil, the activity of these oils may be due to the combined effect of all the compounds present in the complex oil. Active biting deterrent compounds 1-dodecanol and 1-tridecanol were also tested in cloth patch assays. 1-Tridecanol showed positive repellency in the cloth patch bioassay, with a minimum effective dosage (MED) of 0.086 ± 0.089 mg/cm$^2$ as compared to that of DEET, 0.007 ± 0.003 mg/cm$^2$, whereas 1-dodecanol did not show repellency at the maximum dose of 0.375 mg/cm$^2$.

Essential oils of *A. dahurica* and *A. pubescentis* did not show any larvicidal activity against 1-day-old *Ae. aegypti* larvae at the highest screening dose of 125 ppm. The pure compounds 1-dodecanol and 1-tridecanol demonstrated good larvicidal activity, with $LC_{50}$ values of 2.1 (1.8−2.3) and 5.2 (4.7−5.7) ppm, respectively. Myrcene showed weak toxicity with a $LC_{50}$ value of 120.3 (103.6−141.9) ppm, whereas sabinene killed only 40% of the larvae at the highest screening dose of 100 ppm (Table 2). Therefore, dose response bioassays were not necessary for sabinene. The $LC_{50}$ value of permethrin, which was used as positive control, was 0.0034 ppm against *Ae. aegypti*. In a previous study, 1-dodecanol was reported to have larvicidal activity against *Ae. aegypti* and *Ae. scutellaris* at low doses,[54] and both dodecanol and tridecanol exhibited good toxicity against first instar *Culex tartalis* larvae.[55] Sinniah has suggested that aliphatic alcohols can act as irritants, so they can break down the cellular structure to cause the death of larvae.[54]

The azalea lace bug *S. pyrioides* is a major leaf pest of azalea plants in commercial nurseries and residential landscapes. Foliar injury inflicted by this insect is mostly cosmetic and appears as black ovipositional scabs, leaf stippling, and leaf chlorosis. However, if there is no early control for lace bug feeding, leaf chlorosis induced by unrestricted herbivory can lead to necrosis, leaf abscission, and, in severe cases, plant death. Azalea lace bugs are difficult to control. Adult females protect their offspring by laying eggs underneath leaves and

**Table 2. Toxicity of Essential Oils of *A. dahurica* and *A. pubescentis* Essential Oils and Active Biting Deterrent Compounds from *A. dahurica* Oil against 1-Day-Old *Aedes aegypti* Larvae**

| compound/oil | $LC_{50}$ | (95% CI)[a] | $LC_{90}$ | (95% CI)[a] | $\chi^2$ | DF[b] |
|---|---|---|---|---|---|---|
| 1-tridecanol | 2.1 | (1.8−2.3) | 3.8 | (3.2−4.7) | 66.1 | 47 |
| 1-dodecanol | 5.2 | (4.7−5.7) | 7.5 | (6.7−8.9) | 46.2 | 38 |
| myrcene | 120.3 | (103.6−141.9) | 273.5 | (214.5−411.5) | 46.1 | 28 |
| sabinene | *c* | | | | | |
| *A. dahurica* oil | *d* | | | | | |
| *A.pubescentis* oil | *d* | | | | | |

[a]$LC_{50}$ and $LC_{90}$ values are given in ppm (95% confidence interval). [b]DF refers to degree of freedom. [c]Killed 40% of the larvae at the highest dose of 100 ppm. [d]No larvicidal mortality at the maximum dose of 125 ppm.

**Table 3. Insecticidal Bioassays for the Essential Oils (in a DMSO Emulsion) of Four *Angelica* Species, Five of Their Chemical Constituents, Three Positive Controls [*Chenopodium ambrosioides*, Malathion (Baseline), Azadirachtin], and a Negative Control (DMSO) Topically Applied to Adult Azalea Lace Bugs *Stephanitis pyrioides***

| treatment | insect toxicity rating[a] | *n* | estimate ± SEM | *t* | *P* |
|---|---|---|---|---|---|
| azadirachtin[b] | 1 | 5 | 0.427 ± 0.051 | 8.43 | 0.0001 |
| terpinen-4-ol | 1 | 16 | 0.390 ± 0.034 | 11.24 | 0.0001 |
| *A. dahurica* oil | 2 | 10 | 0.294 ± 0.040 | 7.41 | 0.0001 |
| thymol methyl ether | 2 | 8 | 0.227 ± 0.043 | 5.32 | 0.0001 |
| *C. ambrosioides*[b] | 2 | 10 | 0.167 ± 0.040 | 4.22 | 0.0001 |
| *A. sinensis* | 2 | 8 | 0.111 ± 0.043 | 2.59 | 0.0097 |
| malathion[b] | 3 | 17 | 0.000 ± 0.000 | | |
| *A. pubescentis* oil | 4 | 10 | −0.133 ± 0.040 | −3.34 | 0.0009 |
| carvacrol methyl ether | 4 | 8 | −0.172 ± 0.043 | −4.04 | 0.0001 |
| *A. archangelica* oil | 4 | 10 | −0.273 ± 0.040 | −6.86 | 0.0001 |
| *p*-cymene | 5 | 8 | −0.548 ± 0.043 | −12.82 | 0.0001 |
| DMSO | 5 | 27 | −0.544 ± 0.031 | −17.62 | 0.0001 |
| exposure time | | 669 | | 28.43 | 0.0001 |

[a]Insect toxicity rankings based on *t* comparisons and Tukey's HSD test ($P < 0.05$; 1, active; 5, least active). [b]Malathion, azadirachtin, and *C. ambrosioides* extract were used as positive controls for testing the relative biological activity of the other materials. Malathion served as the baseline control.

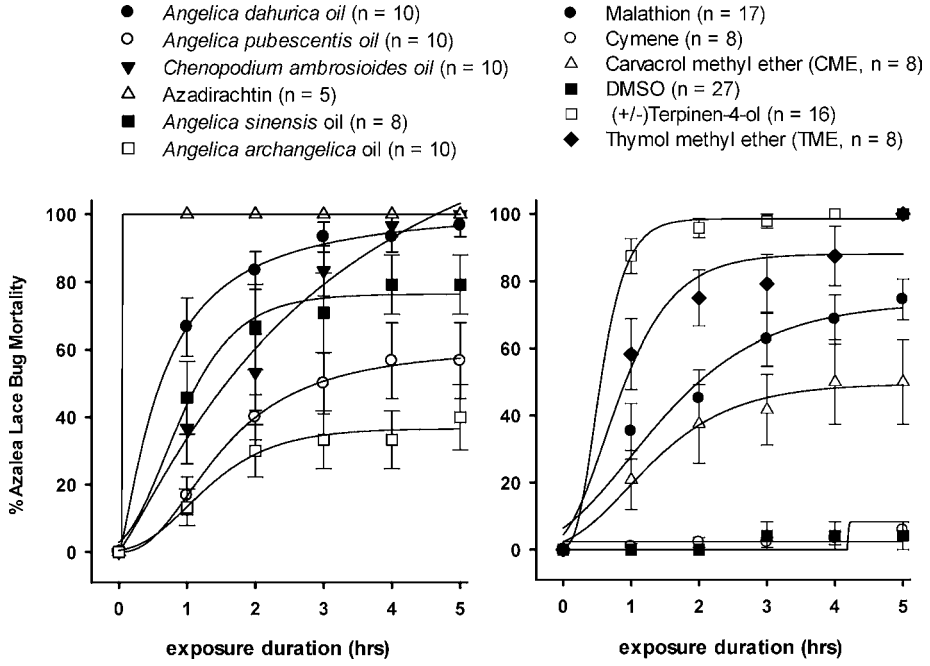


**Figure 5.** Azalea lace bug *S. pyrioides* mortality during 5 h of exposure to 1% emulsions of root essential oils from *Angelica dahurica*, *A. pubescentis*, *A. sinensis*, and *A. archangelica*, four constituent compounds of *A. dahurica* and *A. pubescentis* (*p*-cymene, carvarol methyl ether, thymol methyl ether, and terpinen-4-ol), and three insecticide standards (azadirachtin, *C. ambrosioides* oil, and malathion).

covering them with a hard fecal dome. Such egg-laying behaviors minimize an immature bug's exposure to natural enemies and water-soluble insecticides.[15] Natural oil-based insecticides, such as those based on extracts of the terpenoid-rich *Angelica* species and *Chenopodium ambrosioides*, show promise for development into commercial products for the control of highly gregarious insect herbivores such as *S. pyrioides*. Four *Angelica* essential oils (*A. dahurica*, *A. pubescentis*, *A. sinensis*, and *A. archangelica*) were then tested in insecticidal bioassays against *S. pyrioides* with *A. sinensis* and *A. archangelica* oils originating from the mosquito study[4] to compare their insecticidal activity. *A. sinensis* oil was composed of 81% phthalides, whereas *A. archangelica* included 72% monoterpene hydrocarbons.[4] There was good chemical diversity between these two species, which helped reveal their insecticidal activity results. Azalea lace bugs were most susceptible to emulsions of azadirachtin, in particular to the *Angelica* component terpinen-4-ol. Adult lace bugs exposed to these two compounds suffered 100% mortality within the first 4 h of exposure (Table 3; Figure 5). In fact, *A. dahurica* and *A. sinensis* essential oils compared favorably with the active ingredients of the two broad-spectrum commercial biopesticides azadirachtin and *Chenopodium* oil. *A. dahurica* oil was as bioactive as azadirachtin in killing nearly 100% of azalea lace bugs within 5 h (Table 3; Figure 5). Oils from *A. dahurica*, *A. sinensis*, and *C. ambrosioides* were more lethal to bugs than malathion. The other two TCM plant species tested (*A. pubescentis* and *A. archangelica*), which were high in monoterpene hydrocarbons (65 and 72%, respectively),


dx.doi.org/10.1021/jf5024752 | J. Agric. Food Chem. 2014, 62, 8848−8857

were less toxic than malathion and other essential oil extracts assessed, and they were only weakly active against lace bugs. *p*-Cymene was relatively nontoxic to lace bugs and can be associated with mortality rates no greater than those induced by the DMSO control. Although we did not test the bioactivity of *Angelica*'s major promising component, $\alpha$-pinene, both species had roughly the same proportion of this molecule. Therefore, *A. dahurica*'s greater toxicity to lace bugs may originate from the presence of terpinen-4-ol, which at a concentration of 1% can kill >85% adult *S. pyrioides* within the first hour of exposure and all bugs within 4 h of exposure. Conversely, the weaker activity of *A. pubescentis* oil may stem from its higher concentration of the relatively nontoxic monoterpene hydrocarbons. It was also interesting to see that two phenolic compounds, thymol methyl ether and carvacrol methyl ether, showed different levels of toxicity against azalea lace bugs. The position of functional group plays an important role in this insecticidal activity. Myrcene and sabinene were present in higher concentration here than in *A. pubescentis* oil. Higher proportions of 1-dodecanol and 1-tridecanol in *A. dahurica* oil may also contribute to its potency; however, these compounds remain to be bioassayed against *S. pyrioides*.

As a conclusion, in this study, *A. dahurica* and *A. pubescentis* essential oils were evaluated for the first time for detailed antifungal and insecticidal activity. The diverse chemical characteristics between these two species play important roles for their biological activity. The 1D-TLC bioautography of *A. dahurica* and *A. pubescentis* oils proved that monoterpene hydrocarbons are not antifungal. Therefore, the antifungal activity of *A. pubescentis* observed in this study might be related to the presence of polar compounds such as cryptone and cumin alcohol or due to possible synergistic effects of the oil's minor compounds. Terpenoid substances, however, are naturally involved in antibiosis, many being potent antifeedents or insecticides. Monoterpene hydrocarbons are significantly less active in the insecticidal activity against *Ae. aegypti* or *S. pyrioides*. Multiple modes of action enhance pesticidal efficacy. With *A. dahurica* rich in alcohols and *A. sinensis* rich in phthalides, the chemical diversity within this genus offers promise as novel sources of broad-spectrum insecticides capable of quick knockdown of small arthropod pests. They compare favorably with the bioactivity of the active ingredients of commercially available botanical pesticide (*C. ambrosioides*). Terpinen-4-ol appears to be the leading active compound in *A. dahurica* root oil. Aliphatic alcohols play an important role in mosquito control, with the chain length and the degree of unsaturation important factors for bioactivity. Plants contain fatty alcohols with carbon numbers ranging from C6 to C16, which are important features for future tests for biting deterrent, repellent, and larvicidal activity against *Ae. aegypti*. Using the PCR-RFLP method, we were able to distinguish between *A. dahurica* and *A. pubescentis* samples, which can be a feasible method for the identification and authentication of *Angelica* samples.

## AUTHOR INFORMATION


### Corresponding Author

*(N.T.) E-mail: ntabanca@olemiss.edu.



### Funding

This study was supported in part by USDA-ARS Grant 56-6402-1-612 and a Deployed War-Fighter Protection research program grant funded by the U.S. Department of Defense through the Armed Forces Pest Management Board and the Food and Drug Administration, Grant 300 212 193G.


### Notes

The authors declare no competing financial interest.

## ACKNOWLEDGMENTS


We thank J. L. Robertson, R. Pace, M. Ruscoe, Dr. V. Raman, Dr. J. U. Rehman, Dr. V. Joshi, Dr. Maia Tsikolia, Natasha M. Agramonte, Nathan Newlon, and Greg Allen for performing bioassays and for their technical support and Dr. James J. Becnel, Mosquito and Fly Research Unit, Center for Medical, Agricultural and Veterinary Entomology, USDA-ARS, Gainesville, FL, USA, for supplying *Ae. aegypti* eggs. We thank Dr. Jon F. Parcher, National Center for Natural Products Research, The University of Mississippi, University, MS, USA, for English grammar corrections and suggestions.


## REFERENCES


(1) Li, B.; Xu, X.; Wang, X.; Yu, H.; Li, X.; Tao, W.; Wang, Y.; Yang, L. A systems biology approach to understanding the mechanisms of action of Chinese herbs for treatment of cardiovascular disease. *Int. J. Mol. Sci.* **2012**, *13*, 13501−13520.

(2) Ganzera, M. Recent advancements and applications in the analysis of Traditional Chinese Medicines. *Planta Med.* **2009**, *75*, 776−783.

(3) Xie, P. S.; Leung, A. Y. Understanding the traditional aspect of Chinese medicine in order to achieve meaningful quality control of Chinese material medica. *J. Chromatogr., A* **2009**, *1216*, 1933−1940.

(4) Wedge, D. E.; Klun, J. A.; Tabanca, N.; Demirci, B.; Ozek, T.; Baser, K. H.C.; Liu, Z.; Zhan, S.; Cantrell, C. L.; Zhan, J. Bioactivity-guided fractionation and GC/MS fingerprinting *Angelica sinensis* and *A. archangelica* root components for antifungal and mosquito deterrent activity. *J. Agric. Food Chem.* **2009**, *57*, 464−470.

(5) Gao, F.; Hu, Y.; Fang, G.; Yang, G.; Xu, Z.; Dou, L.; Chen, Z.; Fan, G. Recent developments in the field of the determination of constituents of TCMs in body fluids of animals and human. *J. Pharm. Biomed.* **2014**, *87*, 241−260.

(6) Tabanca, N.; Wang, M.; Avonto, C.; Chittiboyina, A. G.; Parcher, J. F.; Carroll, J. F.; Kramer, M.; Khan, I. A. Bioactivity-guided investigation of geranium essential oils as natural tick repellents. *J. Agric. Food Chem.* **2012**, *61*, 4101−4107.

(7) Tabanca, N.; Bernier, U. R.; Ali, A.; Wang, M.; Demirci, B.; Blythe, E. K.; Khan, S. I.; Baser, K. H. C.; Khan, I. A. Bioactivity-guided investigation of two *Monarda* essential oils as repellents of yellow fever mosquito *Aedes aegypti*. *J. Agric. Food Chem.* **2013**, *61*, 8573−8580.

(8) Ali, A.; Tabanca, N.; Demirci, B.; Baser, K. H. C.; Ellis, J.; Gray, S.; Lackey, B. R.; Murphy, C.; Khan, I. A.; Wedge, D. E. Composition, mosquito larvicidal, biting deterrent and antifungal activity of essential oils of different plant parts of *Cupressus arizonica* var. *glabra* (Sudw.) Little ('Carolina Sapphire'). *Nat. Prod. Commun.* **2013**, *8*, 257−260.

(9) Tabanca, N.; Bernier, U. R.; Tsikola, M.; Becnel, J. J.; Sampson, B. J.; Werle, C.; Demirci, B.; Baser, K. H. C.; Blythe, E. K.; Pounders, C.; Wedge, D. E. *Eupatorium capillifolium* essential oil: chemical composition, antifungal activity, and insecticidal activity. *Nat. Prod. Commun.* **2010**, *5*, 1409−1415.

(10) Tabanca, N.; Wedge, D. E.; Wang, X.; Demirci, B.; Baser, K. H. C.; Zhou, L.; Cutler, S. J. Chemical composition and antifungal activity of *Angelica sinensis* essential oil against three *Colletotrichum* species. *Nat. Prod. Commun.* **2008**, *3*, 1073−1078.

(11) Carroll, J. F.; Tabanca, N.; Kramer, N.; Elejalde, N. M.; Wedge, D. E.; Bernier, U. R.; Coy, M.; Becnel, J. J.; Demirci, B.; Baser, K. H. C.; Zhang, J.; Zhang, S. Essential oils of *Cupressus funebris, Juniperus communis,* and *J. chinensis* (Cupressaceae) as repellents against ticks (Acari: Ixodidae) and mosquitoes (Diptera: Culicidae) and as toxicants against mosquitoes. *J. Vector Ecol.* **2011**, *36*, 258−268.

(12) Sampson, B. J.; McLaughlin, J. L.; Wedge, D. E. Evaluating the extract of the paw paw tree extract as a botanical insecticide. *Arthropod Manage. Tests* **2003**, *28*, L5.
(13) Sampson, B. J.; Tabanca, N.; Kirimer, N.; Demirci, B.; Baser, K. H. C.; Khan, I. A.; Spiers, J. M.; Wedge, D. E. Insecticidal activity of 23 essential oils and their major compounds against adult *Aphis pseudobrassicae* (Davis) (Aphididae: Homoptera). *Pest Manage. Sci.* **2005**, *61*, 1122−1128.
(14) Wedge, D. E.; Tabanca, N.; Sampson, B. J.; Werle, C. T.; Demirci, B.; Baser, K. H. C.; Nan, P.; Duan, J.; Liu, Z. Antifungal and insecticidal activity from two *Juniperus* essential oils. *Nat. Prod. Commun.* **2009**, *4*, 123−127.
(15) Sakhanokho, H. F.; Sampson, B. J.; Tabanca, N.; Wedge, D. E.; Demirci, B.; Baser, K. H. C.; Bernier, U. R.; Tsikolia, M.; Agramonte, N. M.; Becnel, J.; Chen, J.; Rajasekaran, K.; Spiers, J. M. Chemical composition, antifungal and insecticidal activities of *Hedychium* essential oils. *Molecules* **2013**, *18*, 4308−4327.
(16) Gupta, A.; Sharma, S.; Naik, S. N. Biopesticidal value of selected essential oils against pathogenic fungus, termites and nematodes. *Int. Biodeter. Biodegr.* **2011**, *65*, 703−707.
(17) *The Pharmacopoeia Commission of P.R. China*; Chemical Industry Press: Beijing, China, 2010; pp 97 and 246.
(18) Zhang, J. R.; Xu, D. S.; Liu, L.; Jin, P. G. Effect and clinical application of radix *Angelicae Duhuricae*. *Shanghai J. TCM* **2013**, *47*, 82−83.
(19) Qiu, M. S.; Xu, M.; Chen, J. C.; Zhang, Q.; Peng, H. C.; Zhang, Y. Y.; Yang, M. Y. To observe the effect of *Angelica dahurica* combined with conventional medicine on the treatment of rheumatoid anthritis. *Rheum. Arthrit.* **2012**, *2*, 15−18.
(20) Yang, Z. B. The syndrome differentiation and treatment of headache during spring. *Bei Fang Yao Xue* **2013**, *10*, 56.
(21) Ji, Y. X.; Yu, M. The treatment of Xin Fang Bai Zhi decoction on 52 cases of allergic sinusitis. *Shi Yong Zhong Yi Yao Za Zhi* **2013**, *29*, 38.
(22) Yang, P. F.; Wang, S. N. Review of TCM mask in treating chloasma. *Clin J. Chinese Med.* **2013**, *5*, 116−118.
(23) Li, G. X.; Fa, L. L. The treatment of drying up in hands and feet with a self-made plaster of Chinese herbs. *Zhong Guo Min Jian Liao Fa* **2013**, *21*, 56.
(24) Lee, M. Y.; Seo, C. S.; Lee, J. A.; Lee, N. H.; Kim, J. H.; Ha, H.; Zhen, M. S.; Son, J. K.; Shin, H. K. Anti-asthmatic effects of *Angelica dahurica* against ovalbumin-induced airway inflammation via upregulation of heme oxygenase-1. *Food Chem. Toxicol.* **2011**, *49*, 829−837.
(25) Seo, W. D.; Kim, J. Y.; Ryu, H. W.; Kim, J. H.; Han, S. I.; Ra, J. E.; Seo, K. H.; Jang, K. C.; Lee, J. H. Identification and characterization of coumarins from the roots of *Angelica dahurica* and their inhibitory effects against cholinesterase. *J. Funct. Foods* **2013**, *5*, 1421−1431.
(26) Zaugg, J.; Eickmeier, E.; Rueda, D. C.; Hering, S.; Hamburher, M. HPLC-based activity profiling of *Angelica pubescens* roots for new positive GABAA receptor modulators in *Xenopus oocytes*. *Fitoterapia* **2011**, *82*, 434−440.
(27) Lechner, D.; Stavri, M.; Oluwatuyi, M.; Pereda-Miranda, R.; Gibbons, S. The anti-staphylococcal activity of *Angelica dahurica* (Bai Zhi). *Phytochemistry* **2004**, *65*, 331−335.
(28) Qiu, M. S.; Chen, J. C.; Xu, Z. X.; Zhang, Y. Y.; Jiang, Y. F.; Peng, H. C. Effect of Du-Huo on collagen induced arthritis in rats. *Zhong Yi Zheng-Gu* **2012**, *24*, 6−8.
(29) Zhao, D.; Zhang, X. D.; Hao, H. G.; Hu, Y.; Sun, D.; Li, H. Y.; Yang, J. X. Study on neural protective function of duhuo experimental allergic encephalomyelitis. *Chin Med. J. Res. Prac.* **2013**, *27*, 31−33.
(30) Lin, L.; Qian, X. P.; Liu, B. R. Research progress on the chemical constituents and the anti-tumor activity of *Angelica pubescitis*. *Xian Dai Zhong Liu Yi Xue* **2011**, *19*, 373−376.
(31) McLafferty, F. W.; Stauffer, D. B *The Wiley/NBS Registry of Mass Spectral Data*; J. Wiley and Sons: New York, 1989.
(32) Joulain, D.; König, W. A.; Hochmuth, D. H. Terpenoids and related constituents of essential oils. *Library of MassFinder 3.0*; Hamburg Germany, 2004.
(33) Joulain, D.; König, W. A. *The Atlas of Spectra Data of Sesquiterpene Hydrocarbons*; E.B.-Verlag: Hamburg, Germany, 1998.
(34) ESO. *The Complete Database of Essential Oils*; Boelens Aroma Chemical Information Service: Huizen, The Netherlands, 2000.
(35) White, T. J.; Bruns, T.; Lee, S.; Taylor, J. W. Amplification and direct sequencing of fungal ribosomal RNA genes for phylogenetics. In *PCR Protocols: A Guide to Methods and Applications*; Innis, M. A., Gelfand, D. H., Sninsky, J. J., White, T. J., Eds.; Academic Press: New York, 1990; pp 315−322.
(36) Turbett, G. R.; Sellner, L. N. Digestion of PCR and RT-PCR products with restriction endonucleases without prior purification or precipitation. *Promega Notes Magazine 60*; 1996; p 23, http://www.promega.com/pnotes/60/6079_23/6079_23_core.pdf.
(37) Pridgeon, J. W.; Meepagala, K. M.; Becnel, J. J.; Clark, G. G.; Pereira, R. M.; Linthicum, K. J. Structure-activity relationships of 33 piperidines as toxicants against female adults of *Aedes aegypti* (Diptera: Culicidae). *J. Med. Entomol.* **2007**, *44*, 263−269.
(38) Posey, K. H.; Schreck, C. E. An airflow apparatus for selecting female mosquitoes for use in repellent and attraction studies. *Mosquito News* **1981**, *41*, 566−568.
(39) Klun, J. A.; Kramer, M.; Debboun, M. A new *in vitro* bioassay system for discovery of novel human-use mosquito repellents. *J. Am. Mosq. Control Assoc.* **2005**, *21*, 64−70.
(40) U.S. Department of Agriculture. Repellent activity of compounds submitted by Walter Reed Army Institute of Research. Part 1. Protection time and minimum effective dosage against *Aedes aegypti* mosquitoes. *Technical Bulletin 1549*; 1977.
(41) Katritzky, A. R.; Wang, Z.; Slavov, S.; Dobchev, D.; Hall, C. D.; Tsikolia, M.; Bernier, U. R.; Elejalde, N. M.; Clark, G. G.; Linthicum, K. J. Novel carboxamides as potential mosquito repellents. *J. Med. Entomol.* **2010**, *47*, 924−938.
(42) Pridgeon, J. W.; Becnel, J. J.; Clark, G. G.; Linthicum, K. J. A high-throughput screening method to identify potential pesticides for mosquito control. *J. Med. Entomol.* **2009**, *46*, 335−341.
(43) Ali, A.; Cantrell, C. L.; Bernier, U. R.; Duke, S. O.; Schneider, J. C.; Agramonte, N. M.; Khan, I. *Aedes aegypti* (Diptera: Culicidae) biting deterrence: structure activity relationship of saturated and unsaturated fatty acids. *J. Med. Entomol.* **2013**, *49*, 1370−1378.
(44) SAS Institute. *SAS OnlineDoc*, version 9.2; SAS Institute: Cary, NC, USA, 2007.
(45) Abbott, W. S. A method of computing the effectiveness of an insecticide. *J. Econ. Entomol.* **1925**, *18*, 265−267.
(46) Savin, N. E.; Robertson, J. L.; Jacqueline, L.; Russell, R. M. A critical evaluation of bioassay in insecticide research: likelihood ratio tests of dose-mortality regression. *Bull. Entomol. Soc. Am.* **1977**, *23*, 257−266.
(47) Zhao, A.; Yang, X.; Yang, X.; Tao, H.; Yu, J.; Wang, W. GC-MS analysis of chemical components of volatile oil from root of *Angelica dahurica*. *Yaowu Fenxi Zazhi* **2012**, *32*, 763−768.
(48) Liu, Y. X.; TaoH, Y.; Yang, Z.; Shiying, Z. GC-MS analysis of essential oils from *Angelica pubescens*. *Zhongguo Zhongyao Zazhi* **2006**, *31*, 663−666.
(49) Han, H.; Han, B. Y.; Jin, Y.; Chung, J.; Shin, S. C. A Simple PCR-RFLP for identification of *Bursaphelenchus* species collected from Korea. *Plant Pathol. J.* **2008**, *24*, 159−163.
(50) Sukrong, S.; Zhu, S.; Ruangrungsi, N.; Phadungcharoen, T.; Palanuvej, C.; Komatsu, K. Molecular analysis of the genus *Mitragyna* existing in Thailand based on rDNA ITS sequences and its application to identify a narcotic species: *Mitragyna speciosa*. *Biol. Pharm. Bull.* **2007**, *30*, 1284−1288.
(51) D'Amelio, S.; Mathiopoulos, K. D.; Santos, C. P.; Pugachev, O. N.; Webb, S. C.; Picanco, M.; Paggi, L. Genetic markers in ribosomal DNA for the identification of members of the genus *Anisakis* (Nematoda: Ascaridoidea) defined by polymerase chain reaction-based restriction fragment length polymorphism. *Int. J. Parasitol.* **2000**, *30*, 223−226.
(52) Abbas, A.; Tabanca, N.; Kurkcuoglu, M.; Duran, A.; Blythe, E. K.; Khan, I. A.; Baser, K. H. C. Chemical composition, larvicidal and biting deterrent activity of essential oils of two subspecies of

*Tanacetum argenteum* (Lam.) Willd and individual constituents against *Aedes aegypti* (L) (Diptera: Culicidae). *J. Med. Entomol.* **2014**, *51*, 824−830.

(53) Tabanca, N.; Avonto, C.; Wang, M.; Parcher, J. F.; Ali, A.; Demirci, B.; Khan, I. A. Comparison of chemical composition and mosquito activity of *Umbellularia californica* and *Laurus nobilis* leaf essential oils and the active compounds against *Aedes aegypti*. *J. Agric. Food Chem.* **2013**, *61*, 12283−12291.

(54) Sinniah, B. Insecticidal effect of aliphatic alcohols against aquatic stages of *Aedes* mosquitoes. *Trans. R. Soc. Trop. Med. Hyg.* **1983**, *77*, 35−38.

(55) Hammond, D. G.; Kubo, I. Structure-activity relationship of alkanols as mosquito larvicides with novel findings regarding their mode of action. *Bioorg. Med. Chem.* **1999**, *7*, 271−278.

confined to its bionomics, nutritional and functional components, and cultivation.[20] To our knowledge, there are as yet no reports about the hepatoprotective effect of polysaccharides from *R. vinosa* against $CCl_4$-induced hepatotoxicity in rats. Hence, in this study, we used in vitro biochemical tests and an in vivo mouse model of $CCl_4$ intoxication to investigate the activities of *R. vinosa* water-soluble and alkali-soluble polysaccharides. Our data demonstrate that they elicited pronounced antioxidant and hepatoprotective effects, suggesting that the mushroom can be used as a functional food additive for hepatoprotection.

## MATERIALS AND METHODS

**Mushroom and Chemicals.** Dried fruiting bodies of the mushroom *R. vinosa* Lindblad were collected from Fujian province in China. The diagnostic kits for assaying activities of aspartate aminotransferase (AST), alanine aminotransferase (ALT), malondialdehyde (MDA), superoxide dismutase (SOD), and glutathione peroxidase (GSH-Px) were purchased from Nanjing Jiancheng Bioengineering Institute (Nanjing, China). Ascorbic acid, linoleic acid, 1,1-diphenyl-2-picrylhydrazyl (DPPH), and monosodium salt of (2-pyridyl)-5,6-diphenyl-1,2,4-triazine-4′4″-disulfonic acid (ferrozine) were purchased from Sigma-Aldrich (Steinheim, Germany). All other chemicals were of analytical grade and purchased from Beijing Chemical Co. (Beijing, China).

**Extraction and Isolation of Polysaccharides.** The polysaccharides of *R. vinosa* were isolated by employing a previously described procedure.[21,22] Briefly, dried fruiting bodies of the mushroom (100 g) were crushed into powder by using a disintegrator. The powder was extracted twice with 95% ethanol (2 L) for 2 h to remove lipid, and the residue was extracted with 10 volumes of water (w/v) at 90 °C for 6 h. The supernatant was obtained after centrifugation (9000*g*, 4 °C, 10 min), and then the residue was extracted with 0.5 M NaOH solution at room temperature for 5 h. The extract was concentrated 10-fold and precipitated with ethanol (1:4, v/v) at 4 °C overnight. The precipitate was collected by centrifugation and deproteinated by employing the Sevage method.[23] Finally, the deproteinated supernatant was extensively dialyzed against distilled water and lyophilized to give crude *R. vinosa* polysaccharides (cRVLWP/cRVLAP). cRVLWP/cRVLAP was dissolved in distilled water, then applied to a 5 cm × 20 cm column of DEAE-cellulose (Sigma, USA), and eluted at a flow rate of 3.0 mL/min with distilled water. The eluent was concentrated, lyophilized, and then subjected to gel filtration on a Superdex 75 HR 10/30 column (GE Healthcare) in 0.15 M $NH_4HCO_3$ buffer (pH 8.5). The eluent was collected automatically, and carbohydrates were determined by the authrone−sulfuric acid colorimetric method.[24] The main fraction was pooled and lyophilized to yield RVLWP/RVLAP, which were used for further study.

**Preliminary Characterization of RVLWP/RVLAP.** Total carbohydrate content of the polysaccharide was determined by using the authrone−sulfuric acid colorimetric method, with glucose as the standard.[24] The protein content in polysaccharide was measured by using Bradford's method.[25] UV absorption was determined with a UV−visible spectrophotometer (Thermo Scientific, USA) in the range of 200−400 $cm^{-1}$.[23,26]

Gel filtration on an FPLC-Superdex 75 column, which had been calibrated with a molecular mass marker, was conducted to determine the molecular masses of RVLWP and RVLAP.

The monosaccharide compositions of RVLWP/RVLAP were analyzed by ion exchange chromatography on a Dionex ICS-5000 HPIC system (Thermo Scientific, USA). RVLWP/RVLAP was hydrolyzed with 2 M trifluoroacetic acid (TFA) (2 mL) at 110 °C for 4 h. After removal of TFA with methanol, the hydrolyzed product was dissolved in distilled water. The supernatant was filtered through a 0.22 μm nylon membrane (MSI, Westborough, MA, USA), and 10 μL of the filtrate was injected into the Dionex CarboPac PA-200 anion exchange column (3 mm × 250 mm), eluted with 1 mM NaOH solution. The flow rate was 0.45 mL/min, and the column temperature was 30 °C. Sugar identification was done by comparison with reference sugars (D-glucose, D-galactose, L-arabinose, and L-fucose).

**Analysis of Antioxidant Activities in in Vitro Systems.** *DPPH Radical Scavenging Activity.* The activity was measured by using the method reported by Cheng et al.[27] with slight modifications. Briefly, 200 μL of different concentrations (0−5 mg/mL) of the sample were added to 600 μL of DPPH solution (0.004% in methanol solution). The mixture was shaken thoroughly and allowed to stand at room temperature in the dark for 30 min. The absorbance was measured at 517 nm. The scavenging percentage was calculated by using the equation

$$\text{scavenging of DPPH radical (\%)} = (A_{\text{control}} - A_{\text{sample}})/A_{\text{control}} \times 100$$

where $A_{\text{control}}$ is the absorbance of control (water used instead of sample) and $A_{\text{sample}}$ is the absorbance in the presence of the sample.

*Inhibitory Effect on Lipid Peroxidation.* The inhibitory effect on lipid peroxidation was determined in accordance with the conjugated diene method but with some modifications.[28] Samples at different concentrations (0−5 mg/mL) were prepared and incubated with 500 μL of linoleic acid emulsion (10 mM) in 0.2 M sodium phosphate buffer (pH 6.5) for 15 h at 37 °C. Then 1.5 mL of 60% methanol in deionized water was added, and the absorbance of the mixture was measured at 234 nm. The inhibitory effect on lipid peroxidation was calculated according to the formula

$$\text{inhibition of lipid peroxidation (\%)} = (A_{\text{control}} - A_{\text{sample}})/A_{\text{control}} \times 100$$

where $A_{\text{control}}$ is the absorbance of the control sample (water used instead of sample) and $A_{\text{control}}$ is the absorbance in the presence of the tested sample. Ascorbic acid was used for comparison.

*Hydrogen Peroxide Scavenging Activity.* The ability to scavenge hydrogen peroxide ($H_2O_2$) was determined according to the reported method,[1] with minor modifications. The reaction mixture was composed of 200 μL of phosphate buffer (0.1 M, pH 7.4), 40 μL of $H_2O_2$ solution (0.3%), and 100 μL of RVLWP/RVLAP solution (0−5 mg/mL). Absorbance of the reaction mixture at 234 nm was determined after 10 min. Ascorbic acid was used as a reference compound. The scavenging of $H_2O_2$ was expressed as

$$\text{scavenging of } H_2O_2\ (\%) = (A_{\text{control}} - A_{\text{sample}})/A_{\text{control}} \times 100$$

where $A_{\text{control}}$ and $A_{\text{sample}}$ are the absorbance readings of the control group (water used instead of sample) and sample group at 234 nm, respectively.

*Reducing Power.* The reducing power was determined according to the method reported[29] with some modifications. Different concentrations of 1 mL of sample (0−5 mg/mL) were mixed with 1 mL of phosphate buffer (0.2 M, pH 6.6) and 1 mL of potassium ferricyanide (0.1%). The mixtures were incubated at 50 °C for 20 min. Trichloroacetic acid solution (1 mL, 10%) was added to the mixture, which was then centrifuged at 3000 rpm for 10 min. The upper layer of the solution (1 mL) was mixed with 1 mL of distilled water and 0.2 mL of ferric chloride (0.3%), and the absorbance was measured at 700 nm. All assays were carried out in triplicate. Ascorbic acid was used as a positive control at the same concentration.

*Ferrous Ion Chelating Activity.* For each sample, the chelating effect on $Fe^{2+}$ ions was measured according to the reference method[30] with some modifications. Briefly, the reaction mixture, containing 200 μL of sample (0−5 mg/mL), 10 μL of ferrous chloride ($FeCl_2$), 40 μL of ferrozine solution (5 mM), and 550 μL of distilled water, was shaken well and incubated for 10 min at room temperature. The absorbance of the mixture was determined at 562 nm. A lower absorbance indicated stronger chelating activity. Ethylenediaminetetraacetic acid disodium salt (EDTA·2Na) was used as a positive control in the present study. The $Fe^{2+}$ chelating activity was calculated according to the formula


dx.doi.org/10.1021/jf502632c | J. Agric. Food Chem. 2014, 62, 8858−8866

$$Fe^{2+}\text{chelating activity } (\%) = (A_{control} - A_{sample})/A_{control} \times 100$$

where $A_{control}$ is the absorbance of the control sample (water used instead of sample) and $A_{sample}$ is the absorbance in the presence of tested sample.

**Animal Experiments.** *Animals.* Male Kunming mice (weighing 18−22 g) were provided by Xinglong Experimental Animal Breeding Factory in Haidian District, Beijing, China. The animals were allowed to acclimatize for 7 days to conditions in the animal room and were maintained on standard pellet diet and water ad libitum at a temperature of 20−25 °C under a 12 h light/dark cycle throughout the experiment. All experiments were performed in accordance with the Regulations of Experimental Animal Administration issued by the State Committee of Science and Technology of the People's Republic of China.

*In Vivo Hepatoprotective Activity.* The mice were randomly allocated into seven groups (I−VII) of eight animals each: I, control; II, $CCl_4$; III, bifendate (200 mg/kg + $CCl_4$); IV, RVLWP (100 mg/kg + $CCl_4$); V, RVLWP (200 mg/kg + $CCl_4$); VI, RVLAP (100 mg/kg + $CCl_4$); and VII, RVLAP (200 mg/kg + $CCl_4$). In the normal control group and $CCl_4$-intoxicated group, animals were given a single dose of distilled water (0.2 mL, ig) once daily. The positive control group was treated with bifendate (200 mg/kg in 0.5% sodium carboxymethyl cellulose, ig) once daily for 10 days. In the four experimental groups, the mice were pretreated with RVLWP and RVLAP (100 and 200 mg/kg, ig) once daily for 10 consecutive days. On the 11th day, all mice except those in the normal control group were given a $CCl_4$/peanut oil mixture (1%, 5 mL/kg, ig) 2 h after the last administration, whereas the normal control group received peanut oil alone.[31−33] All animals were sacrificed by anesthesia 16 h after $CCl_4$ administration. The livers perfused with saline were dissected and processed immediately for further analysis.

*Biochemical Assays.* After blood collection, serum was obtained by centrifugation at 5000 rpm for 10 min. The activities of the enzymes ALT and AST were measured with commercially available diagnostic kits, and the results were expressed as units per liter (IU/L).

The liver was excised, weighed, and homogenized (10% w/v) in ice-cold physiological saline. The homogenate was centrifuged (8000*g*, 4 °C, 10 min), and the supernatant obtained was stored at −20 °C. The activities of hepatic superoxide dismutase (SOD), glutathione peroxidase (GSH-Px), and malondialdehyde (MDA) and hepatic protein concentrations were assayed using commercially available diagnostic kits. The activities of SOD, GSH-Px, and MDA were normalized with reference to protein, and the results were expressed in units per milligram of protein, units per milligram of protein, and nanomoles per milliggram of protein, respectively. The hepatosomatic index (HI) was calculated according to the following formula: HI = liver weight/body weight × 1000%.

*Histopathological Study on the Liver.* Tissue samples were taken immediately from the liver and fixed in 10% buffered formalin, dehydrated in alcohol, and embedded in paraffin. Sections of 4−5 $\mu$m thickness were cut and stained with hematoxylin-eosin. For evaluation of morphological changes, the slides were examined under the microscope. Finally, the images were examined (× 400 magnification) and evaluated for pathological changes.

*Acute Toxicity Study.* Male Kunming mice were randomly divided into five groups of eight animals each. In the control group, mice were given distilled water by gavage. In the experimental group, mice were given RVLWP and RVLAP (500 and 1000 mg/kg, respectively). The animals were observed continuously in the first 24 h for any gross behavioral changes and toxic symptoms in the first 48 h for mortality.

**Statistical Analysis.** All data are presented as the mean ± standard deviation (SD) from three independent experiments. Significant differences among the groups were determined by one-way ANOVA using the IBM SPSS Statistical software (version 20) package program. $p < 0.05$ was considered to be statistically significant.

## RESULTS

**Isolation and Characterization of Polysaccharides.** RVLWP and RVLAP were isolated from *R. vinosa* through hot water extraction followed by 0.5 M NaOH extraction, ethanol precipitation, deproteinization, and lyophilization. As a result, the yields of RVLWP and RVLAP attained approximately 2.67 and 3.19% of dried *R. vinosa* fruiting bodies by weight, respectively. The extracts were further fractionated on a DEAE-cellulose column and then on a Superdex 75 HR 10/30 column. The main eluted fraction named RVLWP/RVLAP was collected for further structural characterization and bioactivity assay.

The chemical compositions of the purified polysaccharides were determined as shown in Table 1. The total carbohydrate contents of RVLWP and RVLAP were 96.7 and 97.3%, respectively. The negative results in Bradford's test and the lack of absorption at either 280 or 260 nm in the UV−visible spectrum indicated that RVLWP/RVLAP contained no protein or nucleic acid.[22] As can be seen from Table 1, RVLWP was mainly composed of glucose and galactose in a molar ratio of 41.69:2.51. RVLAP consisted of glucose, galactose, and fructose with a molar ratio of 63.93:1.3:0.18. The average molecular weights of RVLWP and RVLAP were $8.71 \times 10^4$ and $10.72 \times 10^4$ Da, respectively.

**Table 1. Compositions and Molecular Weights of RVLWP and RVLAP**

| sample | RVLWP | RVLAP |
|---|---|---|
| carbohydrate (wt %) | 96.7 | 97.3 |
| protein (wt %) | 0 | 0 |
| galactose (mol %) | 2.51 | 1.3 |
| arabinose (mol %) | 0 | 0.18 |
| glucose (mol %) | 41.69 | 63.93 |
| molecular weight (Da) | $8.71 \times 10^4$ | $10.72 \times 10^4$ |

**In Vitro Antioxidant Activity.** To analyze the antioxidant activities of RVLWP/RVLAP in vitro, five parameters were monitored, and the results are as follows.

*DPPH Radical Scavenging Activity.* The DPPH radical scavenging activities of RVLWP, RVLAP, and ascorbic acid are presented in Figure 1A. It was observed that the DPPH radical scavenging effects of the samples increased dose-dependently. At the higher concentration (5 mg/mL) of RVLWP and RVLAP, respectively, 85.89 and 52.53% of DPPH radicals were scavenged. The antioxidant activity of the water-extracted polysaccharide, RVLWP ($IC_{50}$ = 1.55 ± 0.04 mg/mL), was higher than that of RVLAP ($IC_{50}$ = 3.37 ± 0.21 mg/mL) at the tested concentration as determined by the DPPH radical scavenging assay.

*Inhibitory Effect on Lipid Peroxidation.* The abilities of RVLWP, RVLAP, and ascorbic acid to inhibit lipid peroxidation are presented in Figure 1B. Using the conjugated diene method, RVLWP, RVLAP, and ascorbic acid ($IC_{50}$ = 0.12 ± 0.048 mg/mL), all when tested at 1 mg/mL, elicited respectively 64.39, 54.72, and 87.24% inhibition of lipid peroxidation. The results demonstrated that RVLWP ($IC_{50}$ = 0.52 ± 0.095 mg/mL) and RVLAP ($IC_{50}$ = 0.86 ± 0.043 mg/mL) manifested potent activity in inhibiting linoleic acid peroxidation.

*Hydrogen Peroxide Scavenging Activity.* The abilities of RVLWP and RVLAP to scavenge hydrogen peroxide are shown

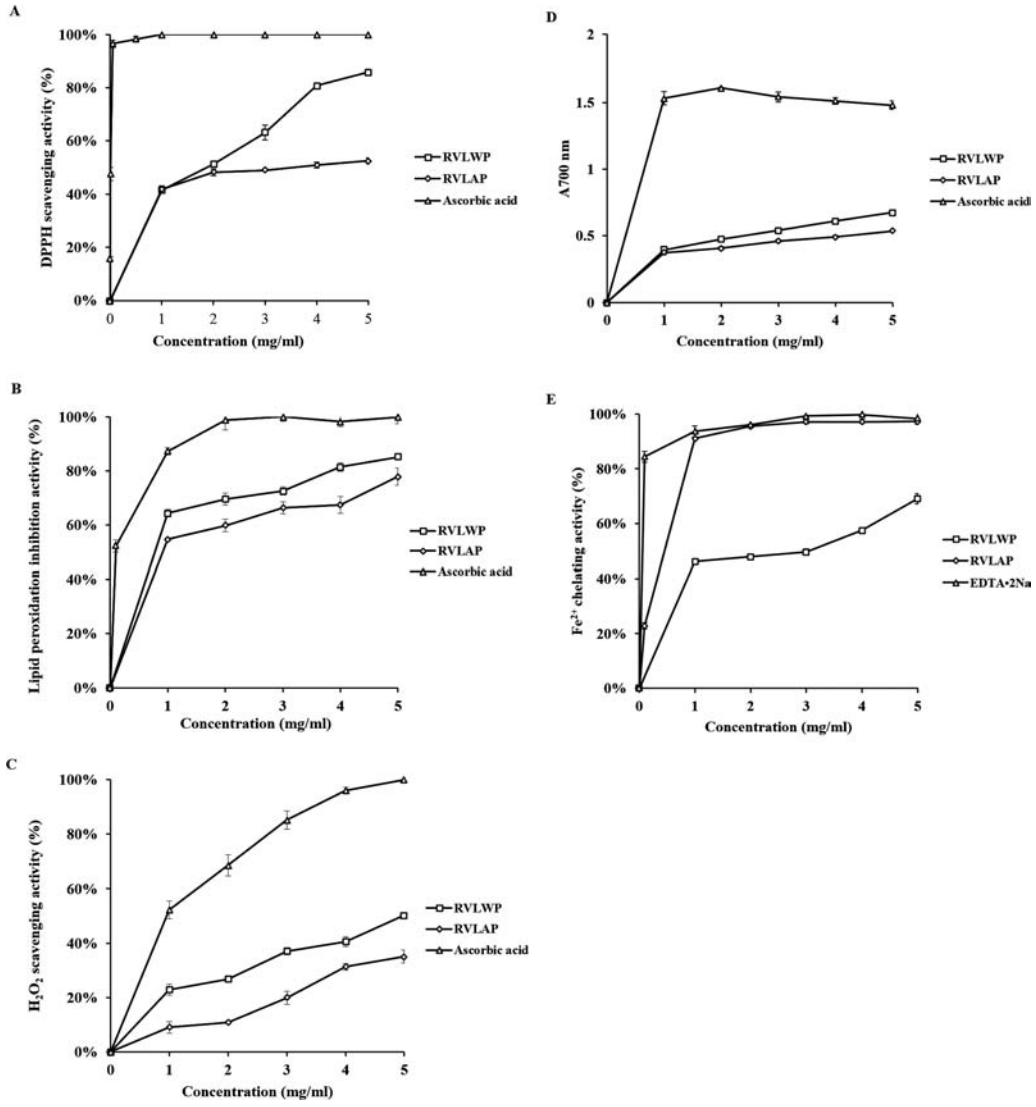


**Figure 1.** Antioxidant activities of RVLWP and RVLAP: (A) scavenging of DPPH radicals; (B) inhibitory effect on lipid peroxidation; (C) hydrogen peroxide scavenging activity; (D) reducing power; (E) $Fe^{2+}$ ion chelating activity. The values are representative of three separate experiments.

**Table 2. Effects of RVLWP and RVLAP on Body Weight, Liver Weight, and Hepatosomatic Index (HI) in $CCl_4$-Treated Mice[a]**

| treatment | dose (RVLWP/RVLAP) (mg/kg) | body wt (g) | liver wt (g) | HI (%) |
|---|---|---|---|---|
| normal control | | 29.13 ± 3.22 | 1.23 ± 0.20 | 42.24 ± 2.87 |
| $CCl_4$ only | | 29.07 ± 1.50 | 1.54 ± 0.09## | 53.25 ± 3.48### |
| $CCl_4$ + bifendate | 200 | 29.86 ± 1.10 | 1.39 ± 0.12** | 46.66 ± 4.12*** |
| $CCl_4$ + RVLWP | 100 | 27.37 ± 1.44 | 1.36 ± 0.09** | 49.55 ± 2.27* |
| $CCl_4$ + RVLWP | 200 | 27.97 ± 2.32 | 1.35 ± 0.11** | 48.23 ± 1.83** |
| $CCl_4$ + RVLAP | 100 | 28.17 ± 2.71 | 1.41 ± 0.24* | 49.71 ± 4.68* |
| $CCl_4$ + RVLAP | 200 | 27.52 ± 1.67 | 1.35 ± 0.18** | 49.04 ± 4.38* |

[a]Mice were randomized into seven groups as follows: control group (normal control), $CCl_4$ intoxication ($CCl_4$ only group), pretreatment with bifendate at 200 mg/kg plus $CCl_4$ intoxication ($CCl_4$ + bifendate group), pretreatment with RVLWP at 100 mg/kg plus $CCl_4$ intoxication ($CCl_4$ + RVLWP group), pretreatment with RVLWP at 200 mg/kg plus $CCl_4$ intoxication ($CCl_4$ + RVLWP group), pretreatment with RVLAP at 100 mg/kg plus $CCl_4$ intoxication ($CCl_4$ + RVLAP group), pretreatment with RVLAP at 200 mg/kg plus $CCl_4$ intoxication ($CCl_4$ + RVLAP group). $CCl_4$-induced hepatotoxic mice were given a $CCl_4$/peanut oil mixture (1%, 5 mL/kg, ig), whereas the normal control group received peanut oil alone. The values are reported as the mean ± SD of eight mice per group: ###, $p < 0.001$ compared with normal control; ***, $p < 0.001$, **, $p < 0.01$, and *, $p < 0.05$ compared with the $CCl_4$ group.

in Figure 1C and compared with that of ascorbic acid. All samples demonstrated a dose-dependent $H_2O_2$ scavenging activity. When the concentration of the samples tested was raised from 1 to 5 mg/mL, the percentages of $H_2O_2$ scavenged increased from 22.91 to 50.23% for RVLWP and from 8.97 to 35.03% for RVLAP. Ascorbic acid scavenged 52.28% $H_2O_2$ at 1 mg/mL. Compared with ascorbic acid ($IC_{50}$ = 1.28 ± 0.04 mg/mL), RVLWP ($IC_{50}$ = 6.07 ± 0.24 mg/mL) and RVLAP ($IC_{50}$


dx.doi.org/10.1021/jf502632c | J. Agric. Food Chem. 2014, 62, 8858−8866

= 9.23 ± 0.54 mg/mL) exhibited moderate $H_2O_2$ scavenging activity.

*Reducing Power.* As shown in Figure 1D, RVLWP and RVLAP brought about reduction of the $Fe^{3+}/K_3Fe(CN)_6$ complex to $Fe^{2+}$ ions and, consequently, the $Fe^{2+}$ ions could be monitored by measurement of the enhanced formation of Perl's Prussian blue at 700 nm.[31] In the concentration range of 1−5 mg/mL, a concentration-dependent effect was discernible. At 5 mg/mL, RVLWP and RVLAP exhibited reducing powers of 0.67 and 0.54, respectively. The data presented here indicate that both RVLWP and RVLAP have potential to be exploited as strong antioxidants, albeit somewhat inferior to the reference ascorbic acid in antioxidant capacity.

*Ferrous Ion Chelating Activity.* Figure 1E shows the $Fe^{2+}$ ion chelating activity of RVLWP and RVLAP when compared to the standard, EDTA·2Na ($IC_{50}$ < 0.1 mg/mL). The $Fe^{2+}$ ion chelating activity of RVLWP and RVLAP increased with concentration. The percentage of $Fe^{2+}$ ions chelated by RVLWP, RVLAP, and EDTA·2Na was respectively 69.08, 97.28, and 98.38% at a concentration of 5 mg/mL. The present results demonstrated that RVLWP ($IC_{50}$ = 1.86 ± 0.0036 mg/mL) and RVLAP ($IC_{50}$ = 0.22 ± 0.0057 mg/mL) elicited strong activity in chelating $Fe^{2+}$ ions.

**Animal Experiments.** *Effects of Polysaccharides on Body Weight, Liver Weight, and HI in Mice.* Table 2 shows the changes in body weight, liver weight, and HI of different groups of experimental mice. The liver weight and HI of the mice increased significantly after $CCl_4$ treatment when compared to the normal control (#, $p$ < 0.01; #, $p$ < 0.001). However, the $CCl_4$-induced increases in the liver weight and HI could be mitigated by pretreatment with RVLWP and RVLAP at two different doses (100 and 200 mg/kg), similar to results of pretreatment with the positive control bifendate at a dose of 200 mg/kg (*, $p$ < 0.01; *, $p$ < 0.001, respectively). These results are in agreement with a previous study.[31] The body weights of the experimental groups did not show statistically significant differences compared with the normal control group.

*Effects of Polysaccharides on AST, ALT, MDA, GSH-Px, and SOD Activities.* Several enzymes in serum such as AST and ALT were used as biochemical markers for early acute hepatic damage. As displayed in Figure 2, $CCl_4$ treatment significantly increased the activities of AST and ALT in serum. When compared with the normal control group, mice treated with $CCl_4$ alone showed acute liver damage as evidenced by a significant rise in the serum activities of AST and ALT (both with #, $p$ < 0.001), which are indicators of hepatocyte damage and loss of functional integrity. Interestingly, pretreatment with RVLWP and RVLAP significantly suppressed elevations in the serum levels of AST (∗, $p$ < 0.05) and ALT (∗, $p$ < 0.05), especially at the dose of 200 mg/kg (∗, $p$ < 0.01). The results signified that supplementation with RVLWP and RVLAP could depress the serum activities of AST and ALT in $CCl_4$-intoxicated mice and appeared to be protective in undermining the deleterious effect of $CCl_4$. Bifendate (positive control) at a dose of 200 mg/kg demonstrated the most significant hepatoprotective effect (∗, $p$ < 0.001).

In this study, the product of membrane lipid peroxidation (MDA) was also examined. As illustrated in Figure 3A, $CCl_4$ treatment significantly raised the hepatic level of MDA (#, $p$ < 0.001). RVLWP and RVLAP at 100 and 200 mg/kg significantly suppressed the level of MDA in a dose-dependent manner. Bifendate-treated mice also manifested a significant

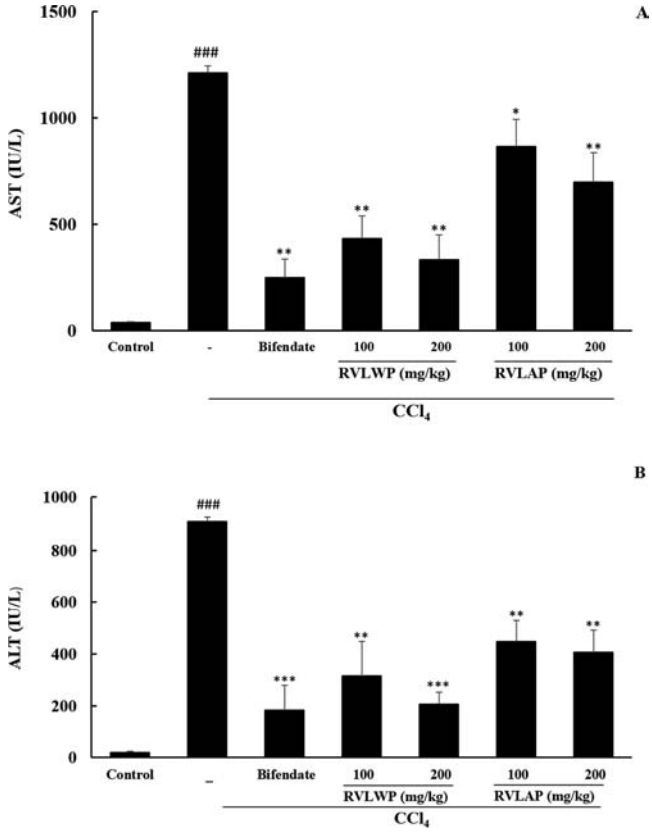


**Figure 2.** Effects of RVLWP and RVLAP on the activities of serum AST (A) and ALT (B) in $CCl_4$-treated mice. The values are reported as the mean ± SD of eight mice per group: (###)$p$ < 0.001 compared with normal control; (∗∗∗) $p$ < 0.001, (∗∗) $p$ < 0.01, and (∗)$p$ < 0.05 compared with the $CCl_4$-treated group.

decline in hepatic MDA compared to $CCl_4$-treated mice (∗, $p$ < 0.001).

The hepatic activities of GSH-Px and SOD in experimental animals are shown in Figure 3B, C. When compared to the normal control group, the acute administration of $CCl_4$ to mice induced characteristic hepatotoxicity that affected the antioxidant parameters of liver tissue, as indicated by a significant decrease in SOD and GSH-Px levels (#, $p$ < 0.001). The $CCl_4$-induced decrement was dose-dependently attenuated by pretreatment with RVLWP and RVLAP at 100 mg/kg (∗, $p$ < 0.05) and 200 mg/kg (∗, $p$ < 0.01). When tested at a dose of 200 mg/kg, bifendate as a positive control also effectively protected against the fall in hepatic activities of GSH-Px and SOD (∗, $p$ < 0.001).

*Liver Histopathological Study.* In the current study, histopathological observation of the liver was performed to corroborate the evidence from biochemical analyses. In comparison with the cellular architecture of hepatic tissue from the normal control group (Figure 4A), acute administration of $CCl_4$ to mice induced extensive liver damage characterized by moderate to severe cellular degeneration, hepatocyte necrosis, and lipid droplet accumulation (Figure 4B). However, bifendate pretreatment effectively protected against $CCl_4$-induced liver damage (Figure 4C). Likewise, RVLWP and RVLAP pretreatment ameliorated liver damage, as evidenced by a diminution of necrotic zones and attenuation of lipid droplet accumulation (Figure 4D−G). This finding was


dx.doi.org/10.1021/jf502632c | J. Agric. Food Chem. 2014, 62, 8858−8866

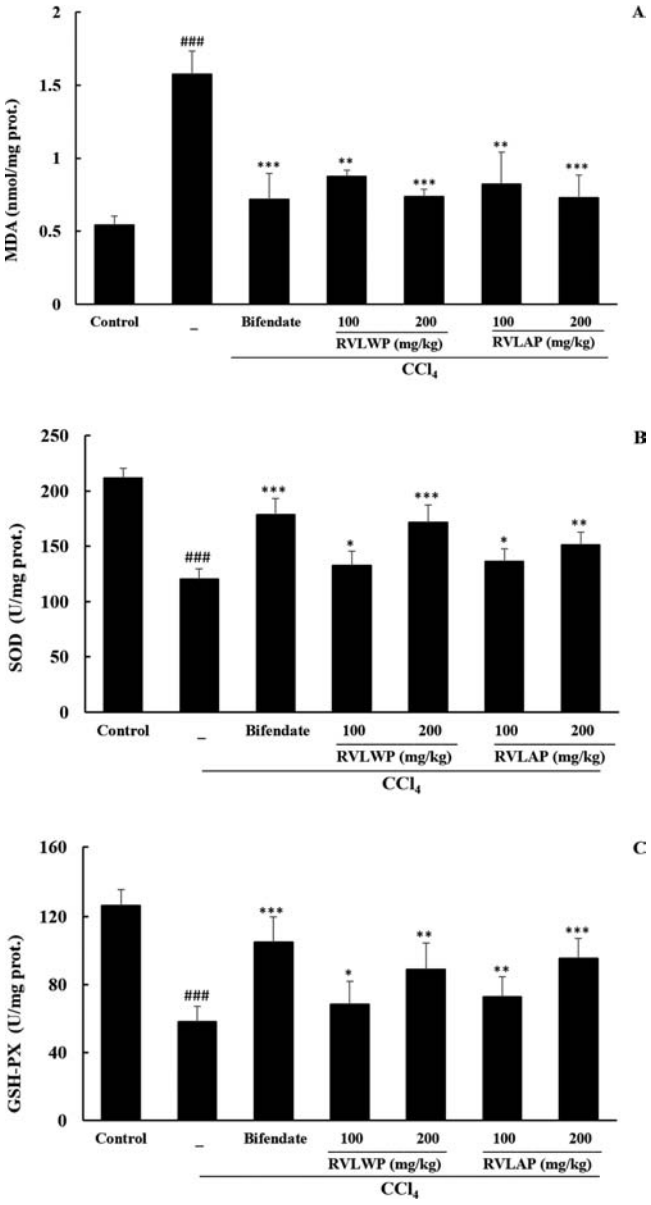


**Figure 3.** Effects of RVLWP and RVLAP on (A) hepatic MDA content, (B) hepatic GSH-Px activity, and (C) hepatic SOD activity in $CCl_4$-treated mice. The values are reported as the mean ± SD of eight mice per group: (###) $p < 0.001$ compared with normal control; (***) $p < 0.001$, (**) $p < 0.01$, and (*) $p < 0.05$ compared with the $CCl_4$-treated group.

consistent with the levels of serum and hepatic enzyme markers.

*Acute Toxicity Study.* In the acute toxicity studies, RVLWP and RVLAP exhibited no toxicity in experimental mice. No mortality occurred within 48 h either in the control or in the treated group. No gross behavioral abnormalities were detected in the treated mice during the first 24 h.

## ■ DISCUSSION

Metabolism of chemicals takes place largely in the liver, which accounts for the organ's susceptibility to metabolism-dependent injury.[31,34,35] Many compounds, including clinically useful therapeutic drugs, can cause cellular damage in the liver through metabolic activation of chemicals to highly reactive compounds such as free radicals, ensuing in oxidative stress.[3]

Hence, it is possible to limit oxidative tissue injury and hence prevent disease progression by employing antioxidant defense supplements. Some of the natural polysaccharide-containing extracts from plants and fungi possess free radical scavenging activities.[9,19,36] In our study, the antioxidant effects of water-soluble and alkali-soluble polysaccharides from *R. vinosa* Lindblad were determined using enzymatic and nonenzymatic methods under in vivo and in vitro conditions.

The DPPH-based assay system is a rapid and efficient method for measuring the free radical scavenging activities of antioxidants. In this assay, the absorbance decreases due to a color change from deep violet to colorless as the radical is scavenged by RVLWP/RVLAP. DPPH radical is characterized as a stable free radical and can accept an electron or a hydrogen radical to become a stable diamagnetic molecule. To our knowledge, cysteine, glutathione, ascorbic acid, and aromatic amines could reduce and decolorize DPPH by virtue of their hydrogen-donating ability.[37] Similarly, in this investigation, RVLWP and RVLAP exhibited significant dose-dependent DPPH radical scavenging activities. Thus, the results implied that RVLWP/RVLAP might also, like the antioxidants cysteine, glutathione, and ascorbic acid and aromatic amines, act as an electron or a hydrogen donor to scavenge DPPH radicals.

Lipid peroxidation is a complicated process involving the interaction of oxygen-derived free radicals with polyunsaturated fatty acids, resulting in a variety of highly reactive electrophilic aldehydes.[38] In this study, a well-known polyunsaturated fatty acid, linoleic acid, was oxidized in a water emulsion. Peroxyl ($LOO^{\bullet}$) and alkoxyl ($LOS^{\bullet}$) radicals, the products of linoleic acid oxidation, form pre-existing lipid peroxide (LOOH) to initiate lipid peroxidation.[39,40] Antioxidants could inhibit lipid peroxidation by scavenging lipid-derived radicals ($LOO^{\bullet}$ or $LOS^{\bullet}$).[41,42] As observed in this investigation, RVLWP and RVLAP displayed significant activity in combatting the peroxidation of linoleic acid, indicating that these polysaccharides can serve as good antioxidants.

The measurement of $H_2O_2$ scavenging activity is one of the useful methods for determining the ability of antioxidants to lower the level of pro-oxidants such as $H_2O_2$.[43] Hydrogen peroxide causes toxicity to cells because it depletes antioxidants and produces strand breaks in DNA and oxidative degradation of most biological macromolecules such as lipids, proteins, carbohydrates, and nucleic acids.[44] At the concentration of 5 mg/mL, the percentage inhibition of RVLWP and RVLAP on $H_2O_2$ observed was 50.23 and 35.03%, respectively. The present results disclosed that RVLWP and RVLAP evinced moderate dose-dependent $H_2O_2$ scavenging activity.

The reducing power of a compound may serve as an indicator of its potential antioxidant activity.[45] It has also been reported that the reducing properties were generally associated with the presence of reductones.[46] Our results suggest that RVLWP and RVLAP have moderate but concentration-dependent reducing power. They might play a role as hydrogen donors and could react with free radicals to stabilize and terminate radical chain reactions.

$Fe^{2+}$ chelation might ensue in important antioxidative effects by retarding metal-catalyzed oxidation.[47] Some transition metals could trigger free radical reactions to magnify the cellular damage. Among the transition metals, Fe is known as the most important pro-oxidant due to its high reactivity. The ferrous state of iron can stimulate lipid oxidation by generating reactive free radicals via the Fenton reaction.[48,49] RVLAP showed stronger activity than RVLWP in chelating ferrous ions

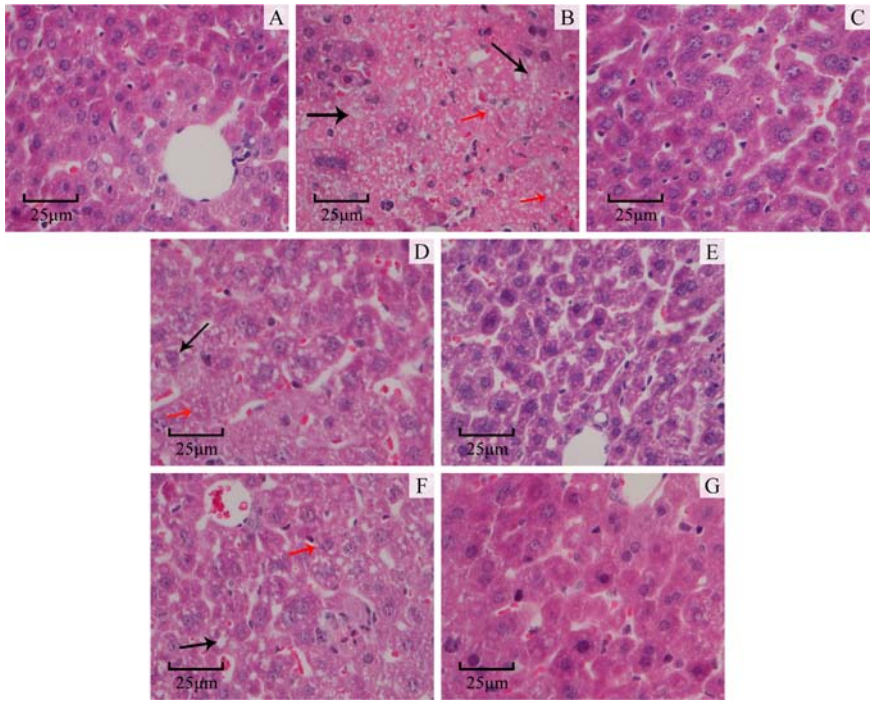


**Figure 4.** Effects of RVLWP and RVLAP on liver as disclosed by morphological analysis (×400 H&E staining): (A) normal control group; (B) $CCl_4$-intoxicated group; (C) bifendate positive control group (200 mg/kg) + $CCl_4$; (D) RVLWP (100 mg/kg) + $CCl_4$; (E) RVLWP (200 mg/kg) + $CCl_4$; (F) RVLAP (100 mg/kg) + $CCl_4$; (G) RVLAP (200 mg/kg) + $CCl_4$. Black arrows indicate necrotic zones; red arrows indicate lipid droplet accumulation.

and at 1 mg/mL concentration had a closer $Fe^{2+}$ chelating activity to that of EDTA·2Na. The chelating effect of RVLWP and RVLAP might be partly due to the presence of $Fe^{2+}$ chelating groups in their structure.

Tsiapali et al. proposed a model for the antioxidant ability of carbohydrate polymers.[42,50] They demonstrated that the antioxidant effect of glucans and nonglucan polymers, which are significantly better free radical scavengers than monosaccharides, does not correlate with the type of intrachain linkages, molecular weight, or degree of polymer branching, but rather with the monosaccharide composition of the polymer. The weak activity of monosaccharides is attributed to abstraction of the anomeric hydrogen and the enhanced activity of the polymers to the greater ease of abstraction of anomeric hydrogen from one of the internal monosaccharide units rather than from the reducing end. RVLWP and RVLAP were mainly composed of glucose and galactose. The higher antioxidant ability of RVLWP than of RVLAP is likely due to more facile anomeric hydrogen abstraction than RVLAP.

Many studies have shown that the hepatoprotective effects may be associated with an antioxidant capacity to scavenge ROS.[51] The present study was undertaken to evaluate the hepatoprotective effects of RVLWP/RVLAP on $CCl_4$-induced oxidative stress in the liver of Kunming mice. Bifendate (biphenyldicarboxylate) is a synthetic hepatoprotective agent derived from Schisandrin C. It is active against a variety of hepatotoxins and has been used as a curative agent for the treatment of hepatitis with minimal observable side effects at the prescribed dosage. Many authors considered bifendate as a hepatoprotective agent against drug-induced liver injuries in animals.[52] In this study, bifendate was utilized as a positive control medicine for exploring the hepatoprotective effect of water-soluble and alkali-soluble polysaccharides from *R. vinosa* (RVLWP and RVLAP).

The serum levels of AST and ALT have been used as biochemical markers for acute liver damage.[53] When liver cells are damaged, these enzymes leak into the bloodstream from the liver tissue and produce markedly heightened serum levels.[54] Our results demonstrate that $CCl_4$ administration causes severe acute liver damage as evidenced by a dramatic rise of the serum levels of AST and ALT. It has been reported that the leakage of large quantities of enzymes into the bloodstream was associated with massive centrilobular necrosis, ballooning degeneration, and cellular infiltration of the liver.[51,55] Our results demonstrate that $CCl_4$ administration causes severe acute liver damage as evidenced by a dramatic rise of the serum levels of AST and ALT. The suppression of AST and ALT activities brought about by RVLWP/RVLAP indicates stabilization of plasma membrane as well as repair of hepatic tissue damage caused by $CCl_4$. This hepatoprotective effect was also confirmed by the histopathological observations of diminished necrotic zones and lipid droplet accumulation.

$CCl_4$-mediated hepatotoxicity arises from the cytochrome P450-catalyzed biotransformation of $CCl_4$ to the trichloromethyl free radicals ($^{\bullet}CCl_3$), which is further converted to the highly reactive trichloromethylperoxy radicals ($CCl_3OO^{\bullet}$) capable of bombarding biomolecules, thus engendering lipid peroxidation and depletion of the antioxidant enzymes and eventually liver damage.[31] MDA is widely used as a marker of lipid peroxidation and oxidative stress.[56] Enhanced hepatic MDA levels reflect a causal role of lipid peroxidation in $CCl_4$-induced liver damage. Our results revealed that pretreatment with RVLWP and RVLAP significantly reversed these deleterious changes. This effect might, at least in part, be derived from the capability of RVLWP/RVLAP to scavenge ROS. Free radical scavenging enzymes such as SOD and GSH-Px are in the first line of defense against oxidative injury. The status of these antioxidant enzymes is an appropriate indirect

way to assess the pro-oxidant−antioxidant status in tissues.[47] SOD and GSH-Px catalyze, respectively, reduction of the superoxide radical ($O^{2-}$) into $H_2O_2$ and $O_2$, and reduction of $H_2O_2$ to $H_2O$ and $O_2$, thereby preventing the formation of hydroxyl radicals.[27,47,53] The results of the present study showed that the activities of SOD and GSH-Px in the livers of $CCl_4$-treated mice were suppressed compared with normal control mice, indicating escalated oxidative damage to the liver. However, pretreatment with RVLWP and RVLAP could notably restore the levels of SOD and GSH-Px in the livers of $CCl_4$-treated mice, implying that RVLWP/RVLAP exerted a substantial protective effect against $CCl_4$-induced acute hepatotoxicity in mice.

A review of the recent literature revealed that the hepatoprotective activities of a diversity of extracts and compounds were related to antioxidant and free radical scavenging activities.[53−56] Likewise, the hepatoprotective effect of water-soluble and alkali-soluble polysaccharides from *R. vinosa* might be a consequence of their free radical scavenging effect, antioxidant activity and inhibitory action on lipid peroxidation. The anticoagulant activities of different sea cucumber polysaccharides are probably related to monosaccharide composition and sulfate content.[57] Hence, it is likely that the physicochemical differences between RVLWP and RVLAP may account for the observation that the former appeared to have higher activity. In conclusion, the wild edible mushroom *R. vinosa* has shown to be an excellent source of antioxidant and hepatoprotective polysaccharides, which could be developed as a natural functional food ingredient or a novel nutraceutical to enhance health.

## AUTHOR INFORMATION


### Corresponding Authors

*(H.W.) Phone: 86-10-62732578. E-mail: hxwang@cau.edu.cn. *(T.B.N.) Phone: 852-3943-6872. E-mail: b021770@mailserv.cuhk.edu.hk



### Funding

This work was financially supported by China Agriculture Research System (CARS24).


### Notes

The authors declare no competing financial interest.

## REFERENCES


(1) Ganie, S. A.; Haq, E.; Masood, A.; Hamid, A.; Zargar, M. A. Antioxidant and protective effect of ethyl acetate extract of podophyllum hexandrum rhizome on carbon tetrachloride induced rat liver injury. *Evidence-Based Complement. Alternat. Med.* **2011**, *2011*, No. 238020.

(2) Saha, D.; Paul, S. Evaluation of antioxidant and free radical scavenging activities of different fractions of *Pterospermum suberifolium* leaf extract. *Thai J. Pharm. Sci.* **2014**, *38*, 28−35.

(3) Kepekci, R. A.; Polat, S.; Celik, A.; Bayat, N.; Saygideger, S. D. Protective effect of *Spirulina platensis* enriched in phenolic compounds against hepatotoxicity induced by $CCl_4$. *Food Chem.* **2013**, *141* (3), 1972−1979.

(4) Muriel, P.; Rivera-Espinoza, Y. Beneficial drugs for liver diseases. *J. Appl. Toxicol.* **2008**, *28* (2), 93−103.

(5) Wang, H.; Ng, T. B.; Ooi, V. E. C. Lectins from mushrooms. *Mycol. Res.* **1998**, *102* (8), 897−906.

(6) Chang, S. T.; Buswell, J. A. Mushroom nutriceuticals. *World J. Microbiol. Biotechnol.* **1996**, *12* (5), 473−476.

(7) Guillamon, E.; Garcia-Lafuente, A.; Lozano, M.; D'Arrigo, M.; Rostagno, M. A.; Villares, A.; Martinez, J. A. Edible mushrooms: role in the prevention of cardiovascular diseases. *Fitoterapia* **2010**, *81* (7), 715−723.

(8) Lindequist, U.; Niedermeyer, T. H.; Julich, W. D. The pharmacological potential of mushrooms. *Evidence-Based Complement. Alternat. Med.* **2005**, *2* (3), 285−299.

(9) Li, X.; Wang, Z.; Wang, L.; Walid, E.; Zhang, H. *In vitro* antioxidant and anti-proliferation activities of polysaccharides from various extracts of different mushrooms. *Int. J. Mol. Sci.* **2012**, *13* (5), 5801−5817.

(10) Han, X. Q.; Chan, B. C.; Yu, H.; Yang, Y. H.; Hu, S. Q.; Ko, C. H.; Dong, C. X.; Wong, C. K.; Shaw, P. C.; Fung, K. P.; Leung, P. C.; Hsiao, W. L.; Tu, P. F.; Han, Q. B. Structural characterization and immuno-modulating activities of a polysaccharide from *Ganoderma sinense*. *Int. J. Biol. Macromol.* **2012**, *51* (4), 597−603.

(11) Ma, L.; Chen, H.; Dong, P.; Lu, X. Anti-inflammatory and anticancer activities of extracts and compounds from the mushroom *Inonotus obliquus*. *Food Chem.* **2013**, *139* (1−4), 503−508.

(12) Giavasis, I. Bioactive fungal polysaccharides as potential functional ingredients in food and nutraceuticals. *Curr. Opin. Biotechnol.* **2014**, *26*, 162−173.

(13) Vaz, J. A.; Barros, L.; Martins, A.; Santos-Buelga, C.; Vasconcelos, M. H.; Ferreira, I. C. F. R. Chemical composition of wild edible mushrooms and antioxidant properties of their water soluble polysaccharidic and ethanolic fractions. *Food Chem.* **2011**, *126* (2), 610−616.

(14) Yu, J.; Cui, P. J.; Zeng, W. L.; Xie, X. L.; Liang, W. J.; Lin, G. B.; Zeng, L. Protective effect of selenium-polysaccharides from the mycelia of *Coprinus comatus* on alloxan-induced oxidative stress in mice. *Food Chem.* **2009**, *117* (1), 42−47.

(15) Wang, J.; Wang, Y.; Liu, X.; Yuan, Y.; Yue, T. Free radical scavenging and immunomodulatory activities of *Ganoderma lucidum* polysaccharides derivatives. *Carbohydr. Polym.* **2013**, *91* (1), 33−38.

(16) Cha, J. Y.; Ahn, H. Y.; Cho, Y. S.; Je, J. Y. Protective effect of cordycepin-enriched *Cordyceps militaris* on alcoholic hepatotoxicity in Sprague-Dawley rats. *Food Chem. Toxicol.* **2013**, *60*, 52−57.

(17) Wu, M. F.; Hsu, Y. M.; Tang, M. C.; Chen, H. C.; Chung, J. G.; Lu, H. F.; Lin, J. P.; Tang, N. Y.; Yeh, C.; Yeh, M. Y. *Agaricus blazei* Murill extract abrogates $CCl_4$-induced liver injury in rats. *In Vivo* **2011**, *25*, 35−40.

(18) Gan, D.; Ma, L.; Jiang, C.; Wang, M.; Zeng, X. Medium optimization and potential hepatoprotective effect of mycelial polysaccharides from *Pholiota dinghuensis* Bi against carbon tetrachloride-induced acute liver injury in mice. *Food Chem. Toxicol.* **2012**, *50* (8), 2681−2688.

(19) Soares, A. A.; de Sa-Nakanishi, A. B.; Bracht, A.; da Costa, S. M.; Koehnlein, E. A.; de Souza, C. G.; Peralta, R. M. Hepatoprotective effects of mushrooms. *Molecules* **2013**, *18* (7), 7609−7630.

(20) Wang, Q.; Shi, M. Present and future of *Russula* in China. *Edible Fungi China* **2004**, *24*, 10−12.

(21) Ding, X.; Zhu, F.; Gao, S. Purification, antitumour and immunomodulatory activity of water-extractable and alkali-extractable polysaccharides from *Solanum nigrum* L. *Food Chem.* **2012**, *131* (2), 677−684.

(22) Sun, Y.; Sun, T.; Wang, F.; Zhang, J.; Li, C.; Chen, X.; Li, Q.; Sun, S. A polysaccharide from the fungi of Huaier exhibits anti-tumor potential and immunomodulatory effects. *Carbohydr. Polym.* **2013**, *92* (1), 577−582.

(23) Miao, S.; Mao, X.; Pei, R.; Miao, S.; Xiang, C.; Lv, Y.; Yang, X.; Sun, J.; Jia, S.; Liu, Y. Antitumor activity of polysaccharides from *Lepista sordida* against laryngocarcinoma *in vitro* and *in vivo*. *Int. J. Biol. Macromol.* **2013**, *60*, 235−240.

(24) Bao, X.; Yuan, H.; Wang, C.; Liu, J.; Lan, M. Antitumor and immunomodulatory activities of a polysaccharide from *Artemisia argyi*. *Carbohydr. Polym.* **2013**, *98* (1), 1236−1243.

(25) Shen, H.; Tang, G.; Zeng, G.; Yang, Y.; Cai, X.; Li, D.; Liu, H.; Zhou, N. Purification and characterization of an antitumor polysaccharide from *Portulaca oleracea* L. *Carbohydr. Polym.* **2013**, *93* (2), 395−400.

(26) Chen, X.; Nie, W.; Fan, S.; Zhang, J.; Wang, Y.; Lu, J.; Jin, L. A polysaccharide from *Sargassum fusiforme* protects against immunosuppression in cyclophosphamide-treated mice. *Carbohydr. Polym.* **2012**, *90* (2), 1114−1119.
(27) Cheng, N.; Ren, N.; Gao, H.; Lei, X.; Zheng, J.; Cao, W. Antioxidant and hepatoprotective effects of *Schisandra chinensis* pollen extract on $CCl_4$-induced acute liver damage in mice. *Food Chem. Toxicol.* **2013**, *55*, 234−240.
(28) Tseng, Y. H.; Yang, J. H.; Mau, J. L. Antioxidant properties of polysaccharides from *Ganoderma tsugae*. *Food Chem.* **2008**, *107* (2), 732−738.
(29) Estevinho, L.; Pereira, A. P.; Moreira, L.; Dias, L. G.; Pereira, E. Antioxidant and antimicrobial effects of phenolic compounds extracts of Northeast Portugal honey. *Food Chem. Toxicol.* **2008**, *46* (12), 3774−3779.
(30) Dinis, T. C. P.; Madeira, V. M. C.; Almeida, L. M. Action of phenolic derivatives (acetaminophen, salicylate, and 5-aminosalicylate) as inhibitors of membrane lipid peroxidation and as peroxyl radical scavengers. *Arch. Biochem. Biophys.* **1994**, *315* (1), 161−169.
(31) Lu, X.; Zhao, Y.; Sun, Y.; Yang, S.; Yang, X. Characterisation of polysaccharides from green tea of Huangshan Maofeng with antioxidant and hepatoprotective effects. *Food Chem.* **2013**, *141* (4), 3415−3423.
(32) Ma, L.; Gan, D.; Wang, M.; Zhang, Z.; Jiang, C.; Zeng, X. Optimization of extraction, preliminary characterization and hepatoprotective effects of polysaccharides from *Stachys floridana* Schuttl. ex Benth. *Carbohydr. Polym.* **2012**, *87* (2), 1390−1398.
(33) Wang, D.; Zhao, Y.; Jiao, Y.; Yu, L.; Yang, S.; Yang, X. Antioxidative and hepatoprotective effects of the polysaccharides from *Zizyphus jujube* cv. Shaanbeitanzao. *Carbohydr. Polym.* **2012**, *88* (4), 1453−1459.
(34) Altas, S.; Kizil, G.; Kizil, M.; Ketani, A.; Haris, P. I. Protective effect of Diyarbakir watermelon juice on carbon tetrachloride-induced toxicity in rats. *Food Chem. Toxicol.* **2011**, *49* (9), 2433−2438.
(35) Simeonova, R.; Vitcheva, V.; Kondeva-Burdina, M.; Krasteva, I.; Manov, V.; Mitcheva, M. Hepatoprotective and antioxidant effects of saponarin, isolated from *Gypsophila trichotoma* Wend. on paracetamol-induced liver damage in rats. *BioMed Res. Int.* **2013**, *2013*, No. 757126.
(36) Dang, Z.; Feng, D.; Liu, X.; Yang, T.; Guo, L.; Liang, J.; Liang, J.; Hu, F.; Cui, F.; Feng, S. Structure and antioxidant activity study of sulfated acetamido-polysaccharide from *Radix Hedysari*. *Fitoterapia* **2013**, *89*, 20−32.
(37) Qiao, D.; Ke, C.; Hu, B.; Luo, J.; Ye, H.; Sun, Y.; Yan, X.; Zeng, X. Antioxidant activities of polysaccharides from *Hyriopsis cumingii*. *Carbohydr. Polym.* **2009**, *78* (2), 199−204.
(38) Reed, T. T. Lipid peroxidation and neurodegenerative disease. *Free Radical Biol. Med.* **2011**, *51* (7), 1302−1319.
(39) Davies, S. S.; Guo, L. Lipid peroxidation generates biologically active phospholipids including oxidatively N-modified phospholipids. *Chem. Phys. Lipids* **2014**, *181*, 1−33.
(40) Püssa, T.; Raudsepp, P.; Toomik, P.; Pällin, R.; Mäeorg, U.; Kuusik, S.; Soidla, R.; Rei, M. A study of oxidation products of free polyunsaturated fatty acids in mechanically deboned meat. *J. Food Compos. Anal.* **2009**, *22* (4), 307−314.
(41) Bajpai, V. K.; Sharma, A.; Kang, S. C.; Baek, K. H. Antioxidant, lipid peroxidation inhibition and free radical scavenging efficacy of a diterpenoid compound sugiol isolated from *Metasequoia glyptostroboides*. *Asian Pac. J. Trop. Med.* **2014**, *7* (1), 9−15.
(42) Kozarski, M.; Klaus, A.; Niksic, M.; Jakovljevic, D.; Helsper, J. P. F. G.; Van Griensven, L. J. L. D. Antioxidative and immunomodulating activities of polysaccharide extracts of the medicinal mushrooms *Agaricus bisporus*, *Agaricus brasiliensis*, *Ganoderma lucidum* and *Phellinus linteus*. *Food Chem.* **2011**, *129* (4), 1667−1675.
(43) Pázdzioch-Czochra, M.; Widénska, A. Spectrofluorimetric determination of hydrogen peroxide scavenging activity. *Anal. Chim. Acta* **2002**, *452*, 177−184.
(44) Özyürek, M.; Bektaşoğlu, B.; Güçlü, K.; Güngör, N.; Apak, R. A novel hydrogen peroxide scavenging assay of phenolics and flavonoids using cupric reducing antioxidant capacity (CUPRAC) methodology. *J. Food Compos. Anal.* **2010**, *23* (7), 689−698.
(45) Liu, X.; Sun, Z.; Zhang, M.; Meng, X.; Xia, X.; Yuan, W.; Xue, F.; Liu, C. Antioxidant and antihyperlipidemic activities of polysaccharides from sea cucumber *Apostichopus japonicus*. *Carbohydr. Polym.* **2012**, *90* (4), 1664−1670.
(46) Li, X. L.; Zhou, A. G.; Li, X. M. Inhibition of *Lycium barbarum* polysaccharides and *Ganoderma lucidum* polysaccharides against oxidative injury induced by $\gamma$-irradiation in rat liver mitochondria. *Carbohydr. Polym.* **2007**, *69* (1), 172−178.
(47) Sabir, S. M.; Ahmad, S. D.; Hamid, A.; Khan, M. Q.; Athayde, M. L.; Santos, D. B.; Boligon, A. A.; Rocha, J. B. T. Antioxidant and hepatoprotective activity of ethanolic extract of leaves of *Solidago microglossa* containing polyphenolic compounds. *Food Chem.* **2012**, *131* (3), 741−747.
(48) Sun, Y. X.; Kennedy, J. F. Antioxidant activities of different polysaccharide conjugates (CRPs) isolated from the fruiting bodies of *Chroogomphis rutilus* (Schaeff.: Fr.) O. K. Miller. *Carbohydr. Polym.* **2010**, *82* (2), 510−514.
(49) Yuan, J. F.; Zhang, Z. Q.; Fan, Z. C.; Yang, J. X. Antioxidant effects and cytotoxicity of three purified polysaccharides from *Ligusticum chuanxiong* Hort. *Carbohydr. Polym.* **2008**, *74* (4), 822−827.
(50) Tsiapali, E.; Whaley, S.; Kalbfleisch, J.; Ensley, H. E.; Browder, I. W.; Williams, D. L. Glucans exhibit weak antioxidant activity, but stimulate macrophage free radical activity. *Free Radical Biol. Med.* **2001**, *30*, 393−402.
(51) Huang, G. J.; Deng, J. S.; Huang, S. S.; Shao, Y. Y.; Chen, C. C.; Kuo, Y. H. Protective effect of antrosterol from *Antrodia camphorata* submerged whole broth against carbon tetrachloride-induced acute liver injury in mice. *Food Chem.* **2012**, *132* (2), 709−716.
(52) Pan, S. Y.; Yang, R.; Dong, H.; Yu, Z. L.; Ko, K. M. Bifendate treatment attenuates hepatic steatosis in cholesterol/bile salt- and high-fat diet-induced hypercholesterolemia in mice. *Eur. J. Pharmacol.* **2006**, *552* (1−3), 170−175.
(53) Jiang, C.; Xiong, Q.; Gan, D.; Jiao, Y.; Liu, J.; Ma, L.; Zeng, X. Antioxidant activity and potential hepatoprotective effect of polysaccharides from *Cyclina sinensis*. *Carbohydr. Polym.* **2013**, *91* (1), 262−268.
(54) Kasdallah-Grissa, A.; Mornagui, B.; Aouani, E.; Hammami, M.; El May, M.; Gharbi, N.; Kamoun, A.; El-Fazaa, S. Resveratrol, a red wine polyphenol, attenuates ethanol-induced oxidative stress in rat liver. *Life Sci.* **2007**, *80* (11), 1033−1039.
(55) Tung, Y. T.; Wu, J. H.; Huang, C. C.; Peng, H. C.; Chen, Y. L.; Yang, S. C.; Chang, S. T. Protective effect of *Acacia confusa* bark extract and its active compound gallic acid against carbon tetrachloride-induced chronic liver injury in rats. *Food Chem. Toxicol.* **2009**, *47* (6), 1385−1392.
(56) You, Y.; Yoo, S.; Yoon, H. G.; Park, J.; Lee, Y. H.; Kim, S.; Oh, K. T.; Lee, J.; Cho, H. Y.; Jun, W. *In vitro* and *in vivo* hepatoprotective effects of the aqueous extract from *Taraxacum officinale* (dandelion) root against alcohol-induced oxidative stress. *Food Chem. Toxicol.* **2010**, *48* (6), 1632−1637.
(57) Luo, L.; Wu, M.; Xu, L.; Lian, W.; Xiang, J.; Lu, F.; Gao, N.; Xiao, C.; Wang, S.; Zhao, J. Comparison of physicochemical characteristics and anticoagulant activities of polysaccharides from three sea cucumbers. *Mar. Drugs* **2013**, *11* (2), 399−417.

phenylacetophenone (BDK), methanol, sodium hydroxide, and sodium chloride were from Beijing Chemical Works (Beijing, China). All agents were of analytical grade.

**Preparation of MB−PAA and PAA Superabsorbent Composite.** A certain amount of AA was neutralized in an ice bath with 20 wt % NaOH solution in a 500 mL glass beaker with constant stirring until 85% neutralization degrees of AA solution was obatined. Certain amounts of MB, MBA (0.02 g $mL^{-1}$), APS, and BDK (0.05 g $mL^{-1}$) (the mass ratio of AA, MB, MBA, APS, and BDK was 100:40:0.12:0.40:0.25) were added to 2.0 mL of prepared AA solutions in 50 mL glass beakers, and the mixtures were treated ultrasonically for 1 min. Then, the homogeneous mixtures were exposed under a UV lamp (1000 W) for 5 min. (The self-regulated UV irradiation system consisted of an iron box containing a UV lamp with a wavelength of 365 nm.) The distance between the light source and the reaction mixtures was 37 cm. After complete polymerization, the resulting products were immersed in methanol to remove water-soluble oligomer, un-cross-linked polymer, and unreacted monomer. Finally, the gels were dried in an oven to a constant weight (at 70 °C) and pulverized through 80, 60, and 20 mesh steel screens. The particles obtained were used to determine the effect of grain diameter on water absorbency, and 80 mesh particles were used in the rest of the experiments. PAA was prepared using the above method, except without MB.

**Water Absorbency Measurement.** The swelling characteristics of the prepared hydrogel were measured via gravimetric analysis. Approximately 0.10 g of hydrogel was immersed in 500 mL of distilled water at room temperature (25 °C) at different intervals ($t$; 5, 10, 15, 20, 25, 30, 40, 50, 60, 120, 150, 200, 240, 300 min). The swollen sample was filtered through a 100 mesh nylon bag to separate unabsorbed water and then weighed. The water absorbency of hydrogel ($Q_t$; g $g^{-1}$) was calculated by using the equation

$$Q_t = \frac{m_t - m_0}{m_0} \quad (1)$$

where $m_0$ (g) and $m_t$ (g) are the weights of the samples in the dry state and the swollen state at a certain time, respectively. Water absorbency in salt solutions was tested in the same way, and $Q_e$ is defined as the water absorbency at the equilibrium swelling state. All of the experiments were performed in triplicate, and the results were averaged.

**Water Retention Measurement.** The percentage of water retention (WR) was determined under high temperature and high pressure. A certain quantity of water-swollen gel ($M_0$) was centrifuged at 6000 rpm (centrifugal radius is 8.6 cm) or heated at 60 °C in an air oven for different intervals ($t$; min), respectively. Then the quantity of remaining gel was weighed and denoted by $M_t$. The WR of the sample was calculated according to eq 2:

$$\mathrm{WR}\ (\%) = \frac{M_t}{M_0} \times 100 \quad (2)$$

**Characterization.** A scanning electron microscope (SEM) (Shimadzu SSX-550, Japan) was used to analyze the morphology of the samples. Before the test, all samples were sprayed with gold by using an ETD-2000 autosputter coater (Beijing, China) for 2 min (with a current of 4 mA). A Fourier transform infrared spectrometer (Shimadzu, 1.50SU1, Japan) was used to record the vibration in functional groups of the samples (spectral range from 4000 to 400 $cm^{-1}$ and data averaged over 20 scans). Thermal gravimetric analysis (TGA) was carried out by using a PerkinElmer Pyris 1 TGA (Boston, MA, USA) from 25 to 850 °C at a heating rate of 10 °C $min^{-1}$ under a flowing nitrogen atmosphere. A Techcomp CT14D centrifuge (Shanghai, China) was used to calculate WR.

## RESULTS AND DISCUSSION

**Hydrogel Preparation.** The proposed mechanism for chemically cross-linking reactions of MB−PAA is outlined in Figure1. First, initiators decomposed into sulfate and benzoyl

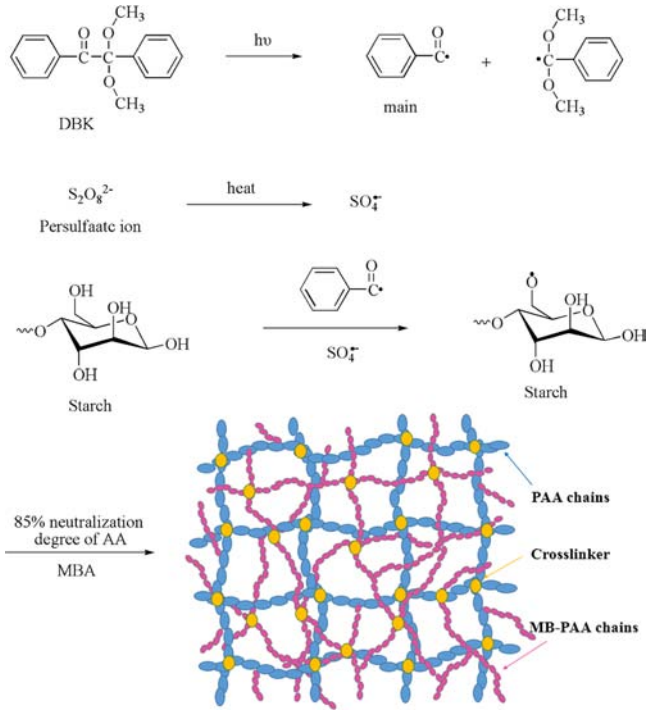


**Figure 1.** Proposed reaction mechanism for the synthesis of MB−PAA.

radicals under UV irradiation. Second, the radicals extracted hydrogen from the hydroxyl group of the active ingredients in MB to form alkoxy radicals on the substrate. Then the monomer molecules became acceptor of the radicals, resulting in chain initiation and thereafter themselves became free radical donors to neighboring molecules, which led to the growth of polymer chains. Finally, the end vinyl groups of the cross-linker (MBA) reacted with the polymer chains during chain propagation. In this way a cross-linked structure combined with network structure was formed gradually.[27]

**Characterization of Materials.** *Elemental Analysis.* Elemental analysis of MB, PAA, and MB−PAA is shown in Table 1. Compared with PAA, C content in MB−PAA

**Table 1. Elemental Analysis of MB, PAA, and MB−PAA**

| sample | C (%) | N (%) | H (%) |
|---|---|---|---|
| MB | 45.91 | 1.98 | 7.084 |
| PAA | 34.16 | 0.13 | 4.859 |
| MB−PAA | 35.32 | 0.33 | 5.126 |

increased from 34.16 to 35.32%, N content increased from 0.13 to 0.33%, and H content increased from 4.859 to 5.126%. This was because that C content in MB (45.91%) was approximately 10% higher than in PAA, and the polysaccharide molecules with relatively high carbon contents in MB reacted with the monomer molecules and changed the polymer chains. Meanwhile, part of the nitrogen-containing compound such as protein in MB was added to polymer chains; thus, for the above reasons, the contents of C, N, and H are increased.

*Morphology.* The SEM images revealed the morphology of the employed MB, PAA, and MB−PAA (Figure 2a−c). As can be seen, MB showed a lamellar and loose morphology. PAA displayed a tight, smooth, and porous surface. However, MB−PAA exhibited a comparatively coarse, loose, and porous


dx.doi.org/10.1021/jf5021279 | J. Agric. Food Chem. 2014, 62, 8867−8874

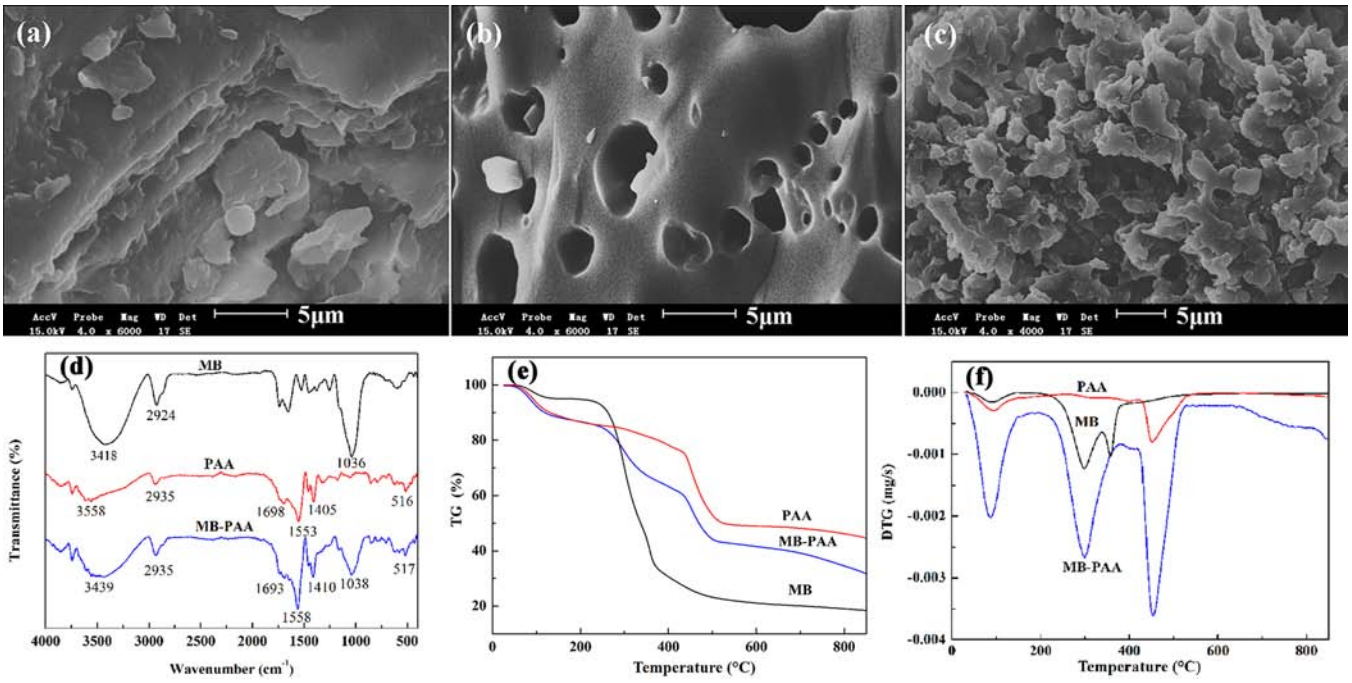


**Figure 2.** SEM micrographs of (a) MB, (b) PAA, and (c) MB−PAA; (d) FTIR spectra of MB, PAA, and MB−PAA; (e) TG curves of MB, PAA, and MB−PAA; (f) DTG curves of MB, PAA, and MB−PAA.

surface, which combined the characteristics of both MB and PAA. The morphology of MB−PAA illustrates that the starch particles were added to polymer chains and many irregular aggregates were formed during the copolymerization reaction. The larger specific surface area of MB−PAA led to a larger contact area with the solution than that of PAA, which facilitated the permeation of water into the polymeric network.[28]

*FITR Spectroscopy.* The FTIR spectra of the MB, PAA, and MB−PAA are shown in Figure 2d. In the spectrum of MB, the absorption bands at 3418 and 2924 $cm^{-1}$ were due to the stretching vibrations of the hydroxyl group (OH) and C−H, respectively. The band at 1036 $cm^{-1}$ was related to −CH−O−CH stretching vibration.[29] The three bands were all characteristic absorptions of starch structures. In the spectrum of PAA, the bands at 3558, 2935, 1698, and 1405 $cm^{-1}$ were assigned to the stretching vibrations of O−H and N−H, C−H, CO−NH, and symmetric stretching of $-COO^-$, respectively. The band at 1553 $cm^{-1}$ was due to the C═O asymmetric stretching of $-COO^-$ and amide II stretching.[30] Compared with the spectrum of PAA, the absorption peaks of MB−PAA revealed some changes. The absorption band at 3439 $cm^{-1}$, which corresponded to stretching vibrations of O−H and N−H groups, showed a major shift, and the peaks at 1693 $cm^{-1}$ (CO—NH), 1558 $cm^{-1}$ (C═O asymmetric stretching of $-COO^-$ and amide II stretching), and 1410 $cm^{-1}$ (symmetric stretching of $-COO^-$) showed a slight shift. They were due to the chemical interaction of MB with the copolymer. Furthermore, an additional absorption peak at 1038 $cm^{-1}$ (−CH−O−CH stretching vibration) was observed,[31] providing evidence of functional groups of MB grafting to PAA during the polymerization.

*Thermal Properties.* The TG/DTG curves of MB, PAA, and MB−PAA are presented in Figure 2e,f. The TG curve of MB exhibited four steps, 25−138, 138−333, 333−530, and 530−850 °C, with weight losses of 4.83, 43.60, 29.20, and 3.92%, respectively. Meanwhile, three peaks in the DTG curve at about 90, 298, and 358 °C corresponded to the first three stages, which represented the maximum decomposition speeds. The PAA had a four-step thermogram, 25−150, 150−415, 415−558, and 558−850 °C, with weight losses of 11.11, 11.84, 27.82, and 4.69%, respectively. Compared with PAA, the TG curves of MB−PAA also had four stages, but the various stages of weightlessness showed large differences. Similar to PAA, the first stage occurring before 159 °C (11.97% weight loss) was due to the loss of absorbed moisture.[28] The major weight loss, 23.12%, occurred in the second stage from 159 to 379 °C; this was assigned to splitting of the starch structure, chain scission eliminating CO and $CO_2$, and the formation of carbonaceous residues.[31] At this stage, the decomposition rate was much faster than that of PAA, which was due to the rapid degradation of MB. The 21.97% weight loss occurring between 379 and 530 °C was the contribution of the elimination of the water molecule from the two neighboring carboxylic groups of the polymer chains with the formation of anhydride, main-chain decomposition of the polymer, and destruction of cross-linked network structure.[32] The last weight loss (11.27%) region occurring from 530 to 850 °C was associated with the further decomposition or degradation of residual organic matter at high temperatures. Ultimately, the weight of the residual sample was 31.67% [less than that of PAA (44.57%) but more than that of MB (18.45%)]; this was attributed to part of the decomposition products and inorganic salts. The TG/DTG results confirmed that chemical reaction between MB and AA occurred, and the incorporation of MB reduced the thermal stability of MB−PAA.

**Water Retention.** The water retention capacity was determined under the condition of centrifugal separation (6000 rpm) and high-temperature drying (60 °C). The results are shown in Figure 3a, which indicates that the WR maintained 39 and 0.5% after centrifugation for 60 min and drying for 70 h, respectively. van der Waal's forces and the hydrogen-bonding interaction between the superabsorbent and


dx.doi.org/10.1021/jf5021279 | J. Agric. Food Chem. 2014, 62, 8867−8874

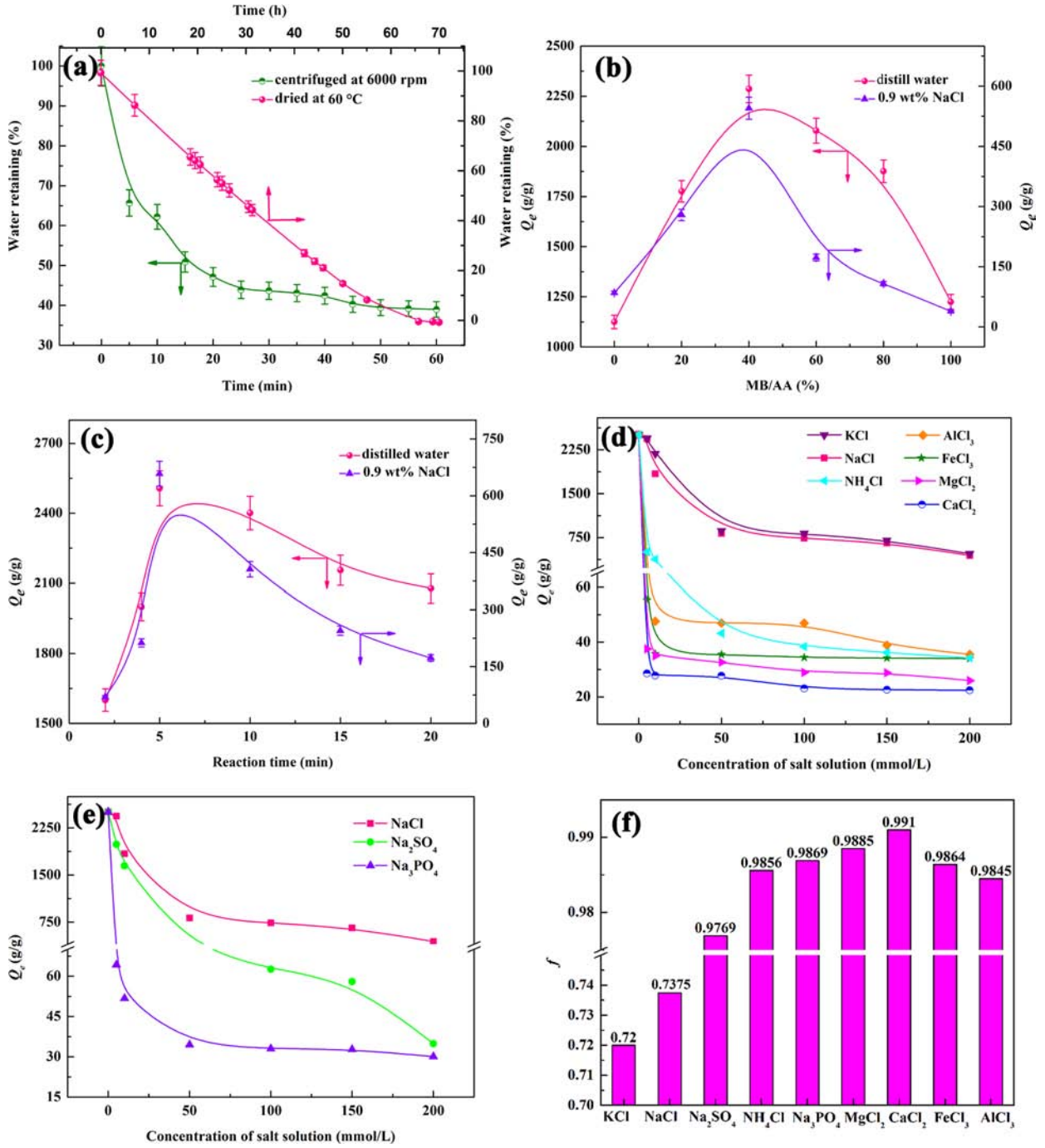


**Figure 3.** (a) Water-retaining capacity of MB−PAA centrifuged at 6000 rpm and dried at 60 °C; effect of (b) maize bran content on AA and (c) reaction time on water absorbency; water absorbency of superabsorbent hydrogel in (d) KCl, NaCl, $NH_4Cl$, $CaCl_2$, $MgCl_2$, $FeCl_3$ and $AlCl_3$ and (e) NaCl, $Na_2SO_4$, and $Na_3PO_4$ aqueous solutions; (f) salt sensitivity factor of various salts at a concentration of 150 mmol $L^{-1}$.

water molecules directly affected the water retention performance of the absorbent resin.[33] The substantial carboxylate groups contained in MB−PAA made the chemical interaction stronger, which could improve the WR. From the centrifugation curve, it can be seen that in the first 20 min, the curve showed a sharp decline, whereas 20 min later, the water retention went down slowly. The reasons for this phenomenon were that, initially, more weak absorption water contained in the gel was more easily broken free, and with the passage of the centrifugation time, the relative proportion of strong absorption water increased, leading to a relatively slow dehydration. The drying curve showed similar properties, but the changes in the rate of water loss were not so obvious. This indicates that the water-absorbing resin was more sensitive to pressure than to temperature. The obtained good water absorbency and retention properties would allow for a further development of the material, such as in agricultural, forestry, and horticulture applications as a water-retaining agent in arid soils.

**Swelling Behavior.** *Effect of Maize Bran Content.* The effect of the weight ratio of MB to AA on the water absorbency was studied. It is observed from Figure 3b that with an increase in content of MB, water absorbency increased to 2286 g $g^{-1}$ in


dx.doi.org/10.1021/jf5021279 | J. Agric. Food Chem. 2014, 62, 8867−8874

distilled water and to 545 g $g^{-1}$ in 0.9 wt % NaCl solution and then decreased (reaction conditions, AA/MBA/APS/BDK = 100:0.2:0.3:0.75; reaction time, 20 min; neutralization degree of AA, 85%). A number of hydrophilic functional groups (−OH, $-NH_2$, and −COOH) are contained in MB, which could react with the monomer and enhance the water absorbency. The ratio of MB was from 0 to 40%, because of the introduction of these hydrophilic groups, and the polymeric network was enhanced and the water absorption increased. When the amount of MB exceeded the best quantity, the water absorbency was reduced. This phenomenon may be due to the conformation of more cross-linking points in the polymeric network; this would lead to an excessive increase in the cross-linking density of the superabsorbent hydrogel. Moreover, too much MB may have resulted in a relative ratio reduction in hydrophilic groups, such as −OH, −COOH, $-NH_2$, and $-COO^-$, in the superabsorbent composite. The above two causes decreased the water absorbency.[34]

*Effect of Reaction Time.* As shown in Figure 3c, the water absorbency in distilled water increased from 2 to 5 min and then decreased from 5 to 20 min (reaction conditions, AA/MBA/APS/BDK/MB = 100:0.2:0.3:0.75:40; neutralization degree of AA, 85%). The water absorbency in 0.9 wt % NaCl solution exhibited a similar trend. The maximum absorbency (2507 g $g^{-1}$ in distilled water and 658 g $g^{-1}$ in 0.9 wt % NaCl solution) was observed at 5 min. On the one hand, a short reaction time resulted in incomplete polymerization and a short polymer chain, which were not conducive to water absorption; on the other hand, too long an irradiation time caused an increase in polymer cross-linking degree, and many branched chains were formed in the network structure, which tangled with each other and produced small holes in three-dimensional networks, which obstructed the expansion of the polymer.[35] Therefore, both of these resulted in a low water absorbency.

*Effect of Various Cations.* The characteristics of external solution such as salt concentration and ionic valence greatly influence the swelling behavior of the superabsorbent polymers. To achieve a comparative measure of sensitivity of the hydrogels to the kind of aqueous fluid, a dimensionless salt sensitivity factor ($f$) for 150 mmol $L^{-1}$ salt solution was calculated by using the equation[29]

$$f = 1 - \frac{Q_s}{Q_d} \tag{3}$$

where $Q_s$ and $Q_d$ are the swelling in salt solution and in deionized water, respectively.

The effect of the ionic strength on the water absorbency can be expressed by Flory's equation[32]

$$Q^{5/3} \approx \frac{(i/2V_uI^{1/2})^2 + (1/2 - x_1)/V_1}{v_e/V_0} \tag{4}$$

where $Q$ is water absorbency, $i/V_u$ is the charge density of polymer, $I$ is the ionic strength of solution, $(1/2 - x_1)/V_1$ is the polymer−solvent affinity, and $v_e/V_0$ is the cross-linking density.

The effect of various ions on water absorbency can be concluded from Figure 3d and Table 2. Three conclusions were obtained from Figure 3d; first, the water absorbency was appreciably decreased as the salt concentration of the solutions increased from 0 to 50 mmol $L^{-1}$ and gently decreased in the concentration >50 mmol $L^{-1}$. This was because, for ionic hydrogels, the additional cations causing an anion−anion electrostatic repulsion, leading to a reduced osmotic pressure difference between the external solution and the polymer network, resulted in decrreased swelling.[36] Second, the order of water absorbency of the hydrogel in the chloride salt solutions was KCl > NaCl > $NH_4Cl$ > $AlCl_3$ > $FeCl_3$ > $MgCl_2$ > $CaCl_2$ when the solution concentrations were <50 mmol $L^{-1}$. We found that hydrogels were hard and very rubbery after swelling in $MgCl_2$ and $CaCl_2$ solution. In contrast, they exhibited lower strength in other solutions. This may be due to the ionic cross-linking of the polymer particles; different ions affected the cross-linking density differently, which influenced the gel strength to different degrees. The effects of seven cationic on the swelling were in the order $K^+ > Na^+ > NH_4^+ > Al^{3+} > Fe^{3+} > Mg^{2+} > Ca^{2+}$, but $Al^{3+} > NH_4^+$ when the concentration was >50 mmol $L^{-1}$. The curves of water absorbency for monovalent metal cationic salt solution were gentler than those for divalent and trivalent cationic salt solutions. This was because the polyvalent metal ion would form complexes with the carboxylate group and the solutions had higher ionic strength. As shown in Table 2, the ionic strength of 150 mmol $L^{-1}$ salt solution was trivalent cationic > divalent cationic > monovalent cationic. According to eq 4, when the ionic strength of saline solution increased, the water absorbency decreased. Interestingly, the water absorbencies in $AlCl_3$ and $FeCl_3$ solution were better than in $MgCl_2$ and $CaCl_2$ solutions, whereas their ionic strength was higher (Table 2). This may be due to divalent and trivalent cations affecting the charge density of polymer in different degrees, being greater for trivalent cations, leading to stronger water absorbency. Third, we found that the larger the radius of monovalent metal cations, the greater was the water absorption capacity ($K^+ > Na^+$), and the less the radius of the same polyvalent monatomic cation, the larger the water absorbency ($Mg^{2+} > Ca^{2+}$ and $Al^{3+} > Fe^{3+}$). Moreover, the water absorbency decreased more in polyatomic monovalent cationic ($NH_4^+$) solution than in single atom monovalent cationic ($K^+$ and $Na^+$) solutions. The sensitivity of the gel to various cations was $K^+ < Na^+ < NH_4^+ < Al^{3+} < Fe^{3+} < Mg^{2+} < Ca^{2+}$ at a concentration of 150 mmol $L^{-1}$ (Figure 3f).

**Table 2. Effect of Salt Solutions on Water Absorption**

| solution (150 mmol $L^{-1}$) | ionic strength[a] (mol-ion $dm^{-3}$) | $Q_e$ (g $g^{-1}$) |
|---|---|---|
| KCl | 0.15 | 702.0 |
| NaCl | 0.15 | 658.0 |
| $NH_4Cl$ | 0.15 | 36.2 |
| $CaCl_2$ | 0.45 | 22.6 |
| $MgCl_2$ | 0.45 | 28.8 |
| $FeCl_3$ | 0.90 | 34.2 |
| $AlCl_3$ | 0.90 | 38.9 |
| $Na_2SO_4$ | 0.45 | 58.0 |
| $Na_3PO_4$ | 0.90 | 32.8 |

[a] $I = 0.5\sum(C_iZ_i^2)$, where $I$, $C_i$, and $Z_i$ are the ionic strength, the ionic concentration, and the charge on each individual ion, respectively.

*Effect of Various Anions.* Figure 3e shows the effects of monovalent ($Cl^-$), divalent ($SO_4^{2-}$), and trivalent anions ($PO_4^{3-}$) with $Na^+$ on water absorbency of the superabsorbent composite. The water absorbency showed the tendency $Cl^- > SO_4^{2-} > PO_4^{3-}$. This may be due to the ionic strength $Na_3PO_4$ > $Na_2SO_4$ > NaCl. These results indicate that trivalent anion and divalent anion salt solutions showed a larger influence on water absorbency. The sensitivity factors of $Na_3PO_4$, $Na_2SO_4$, and NaCl were 0.9869, 0.9769, and 0.7375, respectively (Figure 3f). The sensitivity of the gel to multivalent anions was much

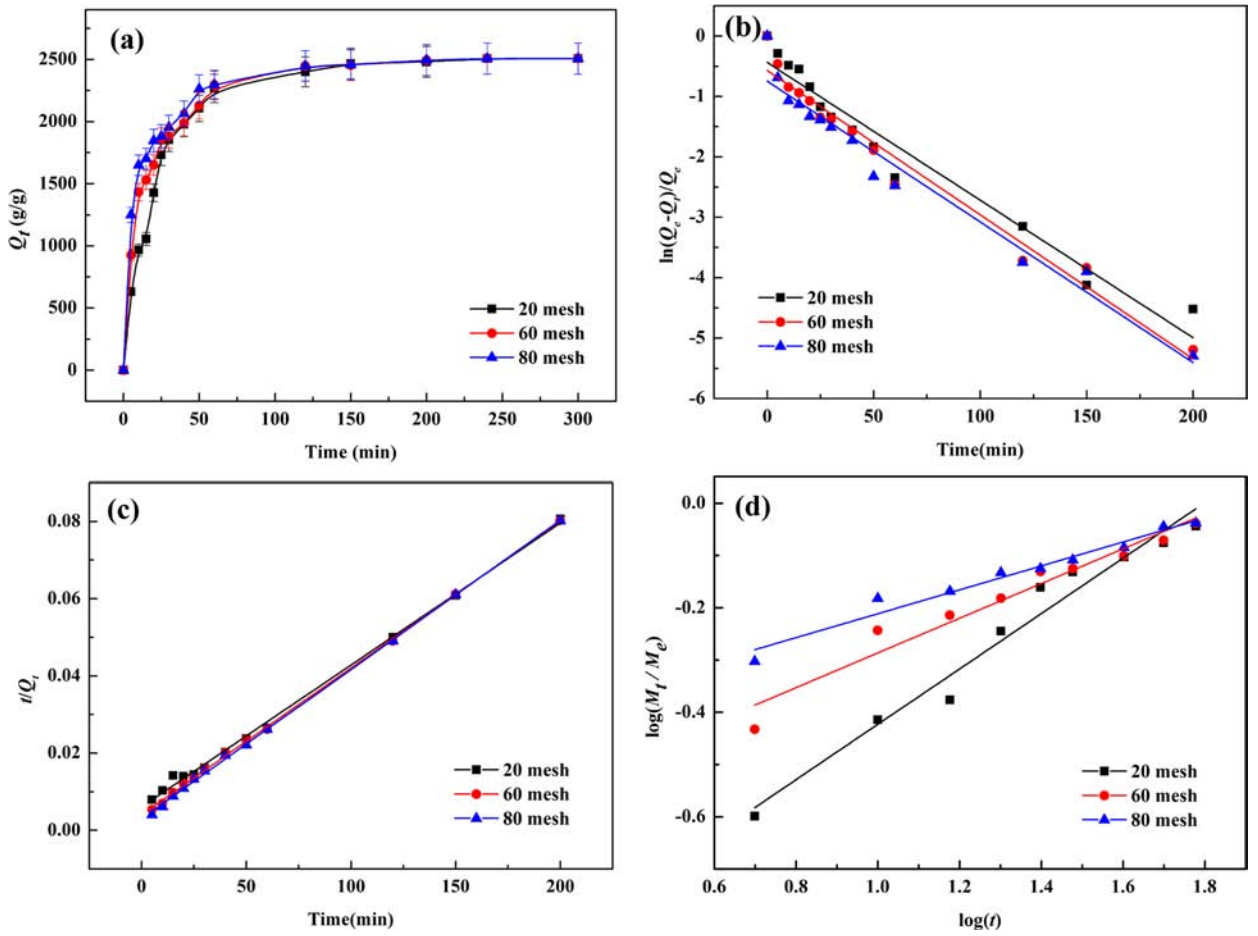


**Figure 4.** (a) Swelling behavior of different hydrogel particle sizes in distilled water absorbency; (b) pseudo-first-order kinetic model; (c) pseudo-second-order kinetic model; (d) water diffusion behavior for different hydrogel particle sizes.

**Table 3. Kinetic Parameters for the Water Absorbency of MB−PAA in Distilled Water**

| | | pseudo-first-order swelling kinetic | | | pseudo-second-order swelling kinetic | | |
|---|---|---|---|---|---|---|---|
| sample (mesh) | $Q_{e,exp}$ (g g$^{-1}$) | $R^2$ | $K_1$ (min$^{-1}$) | $Q_{e,cal}$ (g g$^{-1}$) | $R^2$ | $K_2$ ($10^{-5}$ g g$^{-1}$ min$^{-1}$) | $Q_{e,cal}$ (g g$^{-1}$) |
| 20 | 2507 | 0.9516 | 0.0228 | 1618 | 0.9974 | 2.63 | 2720 |
| 60 | 2507 | 0.9659 | 0.0239 | 1416 | 0.9994 | 3.96 | 2629 |
| 80 | 2507 | 0.9554 | 0.0233 | 1188 | 0.9994 | 5.29 | 2588 |

larger than that to monovalent anions at the same concentration.

*Effect of Hydrogel Particle Size.* To study the effect of particle size of the hydrogel on water absorbency, composite hydrogel particles with different granularities were examined. Figure 4a shows the influence of the hydrogel particle size on water absorbency at different times. It is clear that the hydrogel particle size had a significant influence on water absorbency before equilibrium and had almost no impact on the equilibrium water absorbency. Smaller particles had a larger water absorption rate before equilibrium, particularly at the first 20 min. This was because the smaller particles had a greater surface area, leading to a larger contact area and a higher water absorbency.[8] The process of water absorption (80 mesh) consisted of three steps: (1) 0−10 min, a rapid increase phase, in which the water absorption rate was fastest and up to 39% of equilibrium absorption capacity; (2) 10−120 min, a slower increase phase, for which the contribution to equilibrium absorption was approximately 59%; (3) 120−300 min, an equilibrium phase, when absorption remained almost constant. The other two (60 mesh and 20 mesh) had similar swelling processes.

**Kinetic Analysis.** *Swelling Kinetics in Distilled Water.* To investigate the kinetic mechanism, the pseudo-first-order and pseudo-second-order models were adopted to fit the experimental data. The pseudo-first-order swelling kinetic model is based on the approximation that the absorption rate relates to the quantity of unoccupied sites. The model[9,37] can be expressed in eq 5:

$$\ln(Q_e - Q_t) = \ln Q_e - K_1 t \quad (5)$$

The pseudo-second-order swelling kinetic model is deduced on the basis of the concept that the absorption relates to the squared product of the difference between the number of available equilibrium absorptive sites and that of occupied sites. The model[38,39] is expressed in eq 6

$$\frac{t}{Q_t} = \frac{1}{K_2 Q_e^{\,2}} + \frac{t}{Q_e} \quad (6)$$


dx.doi.org/10.1021/jf5021279 | J. Agric. Food Chem. 2014, 62, 8867−8874

where $Q_e$ (g g$^{-1}$) is the equilibrium water absorbency, $Q_t$ (g g$^{-1}$) is water absorbency at contact time $t$ (min), and $K_1$ (min$^{-1}$) and $K_2$ (g g$^{-1}$ min$^{-1}$) are the rate constants.

Panels b and c of Figure 4 are the pseudo-first-order and pseudo-second-order plots. The values of $K_1$, $K_2$, and $Q_{e,cal}$ along with those of the correlation coefficient ($R^2$) are summarized in Table 3. On the basis of the values of the correlation coefficient ($R^2$), the experimental data fit better with the pseudo-second-order swelling kinetic than with the pseudo-first-order swelling kinetic. In addition, the $Q_{e,cal}$ values as obtained from the pseudo-first-order swelling kinetic model appeared to be largely different from the experimental data, and the values from the pseudo-second-order swelling kinetic model were very close to the experimentally observed values. Therefore, the swelling process in distilled water followed the pseudo-second-order swelling kinetic model better.

*Diffusion Kinetics in Distilled Water.* The diffusion behavior of water into polymers networks was analyzed using the empirical equation[10]

$$\log(M_t/M_e) = \log(k) + n\log(t) \quad (7)$$

where $M_t$ and $M_e$ are the mass of water absorbency at time $t$ (min) and at equilibrium, respectively. $k$ is a characteristic constant of the polymer, and $n$ is a diffusional exponent. From the slope and intercept of the plot of $\log(M_t/M_e)$ versus $\log(t)$, the kinetic parameters $n$ and $k$ were calculated. The results are presented in Figure 4d and Table 4. According to the classification of the diffusion mechanism, at a value of $n < 0.5$, the rate of water moving into the polymer is dominated by a Fickian diffusion mechanism. At $n > 0.5$, it conforms to the non-Fickian diffusion mechanism, in which the relaxation rate was greater than or equal to the water diffusion rate. Therefore, it complied with a non-Fickian diffusion mechanism at the particle size of 20 mesh and corresponded to a Fickian diffusion mechanism at 60 and 80 mesh. We believed that the smaller particles had a relatively larger contact area with the liquid, making easier the macromolecular chain relaxation, the relaxation rate being greater than the water diffusion rate.[10]

**Table 4. Diffusion Parameters and the Correlation Coefficients for the Water Diffusion of MB−PAA in Distilled Water**

| sample (mesh) | $R^2$ | $n$ | $k$ |
|---|---|---|---|
| 20 | 0.9648 | 0.5301 | 0.1114 |
| 60 | 0.9446 | 0.3320 | 0.2408 |
| 80 | 0.9624 | 0.2287 | 0.3630 |

## ■ ASSOCIATED CONTENT

### Supporting Information

Figure S1: Effect of (a) neutralization degree of AA, (b) cross-linker content, (c) water-soluble initiator content, and (d) photoinitiator content on water absorbency of the superabsorbent polymer. The factors of neutralization degree of AA, weight ratio of cross-linker, initiator content to AA and reaction time on water absorbency had been studied. The optimized synthetic conditions were identified. This material is available free of charge via the Internet at http://pubs.acs.org.

## ■ AUTHOR INFORMATION


### Corresponding Author

*(J.L.) E-mail: jfli@jlu.edu.cn. Phone: 0431-85168470-4. Fax: 0431-85168470-4.



### Funding

This work was financially supported by the Basic Research Program of Jilin Provincial Science and Technology Department (20130102040JC) and Changchun Science and Technology Project (13NK01).


### Notes

The authors declare no competing financial interest.

## ■ ACKNOWLEDGMENTS


We thank the Jilin Provincial Science and Technology Department and the Changchun Science and Technology Department.


## ■ ABBREVIATIONS USED

SAP, superabsorbent polymers; MB, maize bran; AA, acrylic acid; BDK, 2,2-dimethoxy-2-phenylacetophenone; APS, ammonium persulfate; MBA, *N*,*N*′-methylenebis(acrylamide); MB−PAA, maize bran−poly(acrylic acid); PAA, poly(acrylic acid); FTIR, Fourier transform infrared radiation; SEM, scanning electron microscopy; TG/DTG, thermogravimetry

## ■ REFERENCES


(1) Jin, S.; Yue, G.; Feng, L.; Han, Y.; Yu, X.; Zhang, Z. Preparation and properties of a coated slow-release and water-retention biuret phosphoramide fertilizer with superabsorbent. *J. Agric. Food Chem.* **2010**, *59*, 322−327.

(2) Bansiwal, A. K.; Rayalu, S. S.; Labhasetwar, N. K.; Juwarkar, A. A.; Devotta, S. Surfactant-modified zeolite as a slow release fertilizer for phosphorus. *J. Agric. Food Chem.* **2006**, *54*, 4773−4779.

(3) Teodorescu, M.; Lungu, A.; Stanescu, P. O.; Neamţu, C. Preparation and properties of novel slow-release NPK agrochemical formulations based on poly(acrylic acid) hydrogels and liquid fertilizers. *Ind. Eng. Chem. Res.* **2009**, *48*, 6527−6534.

(4) Esteves, L. P. Superabsorbent polymers: on their interaction with water and pore fluid. *Cement Concrete Composites* **2011**, *33*, 717−724.

(5) Singh, B.; Sharma, V. Influence of polymer network parameters of tragacanth gum-based pH responsive hydrogels on drug delivery. *Carbohydr. Polym.* **2014**, *101*, 928−940.

(6) Loo, S.-L.; Fane, A. G.; Lim, T.-T.; Krantz, W. B.; Liang, Y.-N.; Liu, X.; Hu, X. Superabsorbent cryogels decorated with silver nanoparticles as a novel water technology for point-of-use disinfection. *Environ. Sci. Technol.* **2013**, *47*, 9363−9371.

(7) Kabiri, K.; Omidian, H.; Zohuriaan-Mehr, M. J.; Doroudiani, S. Superabsorbent hydrogel composites and nanocomposites: a review. *Polym. Compos.* **2011**, *32*, 277−289.

(8) Li, D.; Zhang, X.; Simon, G. P.; Wang, H. Forward osmosis desalination using polymer hydrogels as a draw agent: Influence of draw agent, feed solution and membrane on process performance. *Water Res.* **2013**, *47*, 209−215.

(9) Liu, D.; Li, Z.; Li, W.; Zhong, Z.; Xu, J.; Ren, J.; Ma, Z. Adsorption behavior of heavy metal ions from aqueous solution by soy protein hollow microspheres. *Ind. Eng. Chem. Res.* **2013**, *52*, 11036−11044.

(10) Witono, J. R.; Noordergraaf, I. W.; Heeres, H. J.; Janssen, L. P. B. M. Water absorption, retention and the swelling characteristics of cassava starch grafted with polyacrylic acid. *Carbohydr. Polym.* **2014**, *103*, 325−332.

(11) Zhang, J.; Liu, R.; Li, A.; Wang, A. Preparation, swelling behaviors, and slow-release properties of a poly(acrylic acid-*co*-acrylamide)/sodium humate superabsorbent composite. *Ind. Eng. Chem. Res.* **2005**, *45*, 48−53.

(12) Wang, Y.; Liu, M.; Ni, B.; Xie, L. κ-Carrageenan−sodium alginate beads and superabsorbent coated nitrogen fertilizer with slow-release, water-retention, and anticompaction properties. *Ind. Eng. Chem. Res.* **2011**, *51*, 1413−1422.
(13) Demitri, C.; Scalera, F.; Madaghiele, M.; Sannino, A.; Maffezzoli, A. Potential of cellulose-based superabsorbent hydrogels as water reservoir in agriculture. *Int. J. Polym. Sci.* **2013**, DOI: 10.1155/2013/435073.
(14) Sawut, A.; Yimit, M.; Sun, W.; Nurulla, I. Photopolymerisation and characterization of maleylatedcellulose-*g*-poly(acrylic acid) superabsorbent polymer. *Carbohydr. Polym.* **2014**, *101*, 231−239.
(15) Xie, L.; Lü, S.; Liu, M.; Gao, C.; Wang, X.; Wu, L. Recovery of ammonium onto wheat straw to be reused as a slow-release fertilizer. *J. Agric. Food Chem.* **2013**, *61*, 3382−3388.
(16) Yang, Y.; Tong, Z.; Geng, Y.; Li, Y.; Zhang, M. Biobased polymer composites derived from corn stover and feather meals as double-coating materials for controlled-release and water-retention urea fertilizers. *J. Agric. Food Chem.* **2013**, *61*, 8166−8174.
(17) Xie, L.; Liu, M.; Ni, B.; Wang, Y. Utilization of wheat straw for the preparation of coated controlled-release fertilizer with the function of water retention. *J. Agric. Food Chem.* **2012**, *60*, 6921−6928.
(18) Hussain, Y. A.; Liu, T.; Roberts, G. W. Synthesis of cross-linked, partially neutralized poly(acrylic acid) by suspension polymerization in supercritical carbon dioxide. *Ind. Eng. Chem. Res.* **2012**, *51*, 11401−11408.
(19) Wan, T.; Huang, R.; Zhao, Q.; Xiong, L.; Qin, L.; Tan, X.; Cai, G. Synthesis of wheat straw composite superabsorbent. *J. Appl. Polym. Sci.* **2013**, *130*, 3404−3410.
(20) Ge, H.; Pang, W.; Luo, D. Graft copolymerization of chitosan with acrylic acid under microwave irradiation and its water absorbency. *Carbohydr. Polym.* **2006**, *66*, 372−378.
(21) Lin, C.-x.; Zhan, H.-y.; Liu, M.-h.; Fu, S.-y.; Huang, L.-h. Rapid homogeneous preparation of cellulose graft copolymer in BMIMCL under microwave irradiation. *J. Appl. Polym. Sci.* **2010**, *118*, 399−404.
(22) Bardajee, G. R.; Hooshyar, Z.; Zehtabi, F.; Pourjavadi, A. A superabsorbent hydrogel network based on poly((2-dimethylaminoethyl)methacrylate) and sodium alginate obtained by gamma-radiation: synthesis and characterization. *Iran. Polym. J.* **2012**, *21*, 829−836.
(23) Zhang, S.; Wang, W.; Wang, H.; Qi, W.; Yue, L.; Ye, Q. Synthesis and characterisation of starch grafted superabsorbent via 10MeV electron-beam irradiation. *Carbohydr. Polym.* **2014**, *101*, 798−803.
(24) El Salmawi, K. M.; Ibrahim, S. M. Characterization of superabsorbent carboxymethylcellulose/clay hydrogel prepared by electron beam irradiation. *Macromol. Res.* **2011**, *19*, 1029−1034.
(25) El-Mohdy, H. L. A.; Safrany, A. Preparation of fast response superabsorbent hydrogels by radiation polymerization and crosslinking of *N*-isopropylacrylamide in solution. *Radiat. Phys. Chem.* **2008**, *77*, 273−279.
(26) Shi, X.; Wang, W.; Wang, A. Synthesis and enhanced swelling properties of a guar gum-based superabsorbent composite by the simultaneous introduction of styrene and attapulgite. *J. Polym. Res.* **2011**, *18*, 1705−1713.
(27) Rashidzadeh, A.; Olad, A.; Salari, D.; Reyhanitabar, A. On the preparation and swelling properties of hydrogel nanocomposite based on sodium alginate-*g*-poly(acrylic acid-*co*-acrylamide)/clinoptilolite and its application as slow release fertilizer. *J. Polym. Res.* **2014**, *21*, 1−15.
(28) Yadav, M.; Singh, S. K.; Rhee, K. Y. Synthesis of partially hydrolyzed graft copolymer (H-*Ipomoea hederacea* seed gum-*g*-polyacrylonitrile). *Carbohydr. Polym.* **2013**, *95*, 471−478.
(29) Akar, E.; Altinisik, A.; Seki, Y. Preparation of pH- and ionic-strength responsive biodegradable fumaric acid crosslinked carboxymethyl cellulose. *Carbohydr. Polym.* **2012**, *90*, 1634−1641.
(30) Wan, T.; Huang, R.; Zhao, Q.; Xiong, L.; Luo, L.; Tan, X.; Cai, G. Synthesis and swelling properties of corn stalk-composite superabsorbent. *J. Appl. Polym. Sci.* **2013**, *130*, 698−703.
(31) Anirudhan, T. S.; Rejeena, S. R.; Tharun, A. R. Investigation of the extraction of hemoglobin by adsorption onto nanocellulose-based superabsorbent composite having carboxylate functional groups from aqueous solutions: kinetic, equilibrium, and thermodynamic profiles. *Ind. Eng. Chem. Res.* **2013**, *52*, 11016−11028.
(32) Bao, Y.; Ma, J.; Li, N. Synthesis and swelling behaviors of sodium carboxymethyl cellulose-*g*-poly(AA-*co*-AM-*co*-AMPS)/MMT superabsorbent hydrogel. *Carbohydr. Polym.* **2011**, *84*, 76−82.
(33) Patra, T.; Pal, A.; Dey, J. A smart supramolecular hydrogel of *Nα*-(4-*n*-alkyloxybenzoyl)-L-histidine exhibiting pH-modulated properties. *Langmuir* **2010**, *26*, 7761−7767.
(34) Zhang, M.; Cheng, Z.; Liu, M.; Zhang, Y.; Hu, M.; Li, J. Synthesis and properties of a superabsorbent from an ultraviolet-irradiated waste nameko mushroom substrate and poly(acrylic acid). *J. Appl. Polym. Sci.* **2014**, http://onlinelibrary.wiley.com/doi/10.1002/app.40471/full.
(35) Liu, J.; Li, Q.; Su, Y.; Yue, Q.; Gao, B.; Wang, R. Synthesis of wheat straw cellulose-*g*-poly(potassium acrylate)/PVA semi-IPNs superabsorbent resin. *Carbohydr. Polym.* **2013**, *94*, 539−546.
(36) Zhao, Y.; Su, H.; Fang, L.; Tan, T. Superabsorbent hydrogels from poly(aspartic acid) with salt-, temperature- and pH-responsiveness properties. *Polymer* **2005**, *46*, 5368−5376.
(37) Evren, M.; Acar, I.; Guclu, K.; Guclu, G. Removal of $Cu^{2+}$ and $Pb^{2+}$ ions by *N*-vinyl 2-pyrrolidone/itaconic acid hydrogels from aqueous solutions. *Can. J. Chem. Eng.* **2014**, *92*, 52−59.
(38) Ho, Y. S.; McKay, G. Pseudo-second order model for sorption processes. *Process Biochem.* **1999**, *34*, 451−465.
(39) Singh, T.; Singhal, R. Reuse of a waste adsorbent poly(AAc/AM/SH)-Cu superabsorbent hydrogel, for the potential phosphate ion removal from waste water: matrix effects, adsorption kinetics, and thermodynamic studies. *J. Appl. Polym. Sci.* **2013**, *129*, 3126−3139.

Table 1. Composition of Whole Grain Barley Samples

| variety | crop year | ear type[a] | starch (% db[b]) | protein (% db) | β-glucan (% db) | raw fat (% db) | ash (% db) |
|---|---|---|---|---|---|---|---|
| **feed type varieties** | | | | | | | |
| Pilvi | 2006 | 6r | 67.8 | 11.7 | 3.4 | 3.0 | 2.8 |
| | 2007 | 6r | 67.9 | 11.5 | 2.9 | 2.9 | 2.9 |
| Vilde | 2006 | 6r | 67.8 | 10.6 | 4.3 | 3.0 | 2.9 |
| | 2007 | 6r | 65.0 | 11.2 | 3.8 | 3.0 | 2.7 |
| Voitto | 2006 | 6r | 71.8 | 9.7 | 3.9 | 3.2 | 2.4 |
| | 2007 | 6r | 69.5 | 9.7 | 3.3 | 3.0 | 2.7 |
| **malting type varieties** | | | | | | | |
| Saana | 2006 | 2r | 66.3 | 12.5 | 4.8 | 3.2 | 2.4 |
| | 2007 | 2r | 64.9 | 12.3 | 4.0 | 3.0 | 2.6 |
| Scarlett | 2006 | 2r | 65.2 | 12.5 | 5.5 | 2.9 | 2.2 |
| | 2007 | 2r | 64.8 | 11.8 | 5.1 | 3.0 | 2.4 |
| SW Makof | 2006 | 2r | 65.9 | 12.0 | 4.3 | 3.6 | 2.4 |
| | 2007 | 2r | 66.5 | 11.8 | 3.1 | 3.0 | 2.6 |
| **waxy variety** | | | | | | | |
| Magdalena | 2006 | 2r | 61.2 | 12.3 | 5.7 | 3.0 | 2.6 |
| | 2007 | 2r | 62.9 | 11.7 | 4.6 | 3.2 | 2.8 |
| $u^c$ | | | 5.6 | 0.9 | 0.1 | 0.2 | 0.1 |

[a]2r, 2-row; 6r, 6-row. [b]Dry basis. [c]Standard uncertainty corresponding to one standard deviation.

selected, and associations between the chemical composition, structure, and processing behavior were studied.

## MATERIALS AND METHODS

**Barley Material.** The barley material consisted of 14 lots representing seven spring barley cultivars: three 6-row feed type varieties (Pilvi, Vilde, Voitto), three 2-row malting type varieties (Saana, Scarlett, SW Makof), and one 2-row waxy barley variety (Magdalena). Each variety was grown in the same field in Hauho (southern Finland, 60°48′ N, 23°30′ E) in 2006 and 2007. The preceding crop was the same for all lots. Fertilizer (N, K) was placed in the seed bed at sowing. Samples of 6-row and 2-row barley were from the separate trials in which 50 and 80 kg N/ha were applied, respectively. Weeds and plant diseases were controlled with herbicides and fungicides.

**Composition Analysis.** Moisture, protein, lipids, and ash contents were analyzed using methods described in Nordlund et al.[15] Starch quantification was carried out in triplicate using an enzymatic–spectrophotometric method.[16] β-Glucan contents were determined in triplicate with a fluorometric method based on Calcofluor binding, according to the protocol recommended by the European Brewing Convention (Analytica-EBC: 3.10.2).[17]

**Milling.** Whole-grain barley samples were milled with a fine impact mill (100 UPZ-lb, Hosokawa Alpine, Augsburg, Germany) with stainless steel pin disk grinders using maximum speed (17700 rpm; tip speed 180 m/s) for the pin disk. Particle size distributions of pin-milled and two commercial barley flours were determined in triplicate using a set of 11 sieves with apertures from 1250 to 75 μm.

**Water Uptake during Malting and Friability of Malts.** Sixty gram lots of barley were malted in duplicate using a Joe White micromalting unit (Joe White Maltings Pty. Ltd., Adelaide, Australia). Malting consisted of steeping for a total of 48 h (8 h wet, 16 h dry, 8 h wet, 16 h dry) at 14 °C, germination for 5 days at 15 °C, and kilning for 19 h to a final temperature of 80 °C. Water uptake during malting was measured by weighing the duplicate grain lots after 24, 48, and 72 h of malting. Distribution of water in endosperm was determined according to the method described in detail in Holopainen et al.[14] For this purpose, grain samples were taken after steeping or 48 h of malting. Grains were classified into four groups based on the proportion of hydrated endosperm.

The friability of the malt samples was determined using the EBC method (Analytica-EBC: 4.15)[17] optimized for smaller sample size according to Holopainen et al.[14] using a malt with friability of 84.9 as a standard. The analysis was performed in triplicate for each sample. Due to down-scaling of the standard procedure, the numerical values for friability are not directly comparable to the standard EBC method, but results describe the relative friability of the samples assayed.

**Localization of Grain Components by an Abrasive Method.** To study the localization of β-glucan, total protein, and hordeins, grain batches of 100 g were pearled using a custom-made barley dehuller-pearler (VTT Technical Research Centre of Finland). The grain material was pearled for 60 s four times consecutively. This resulted in grain samples with 13–17, 21–24, 29–33, and 35–40% of the outer layers removed. Protein and β-glucan contents of the pearled grains were determined in triplicate as described above.

For localization of salt-soluble proteins and hordeins, the amounts of these protein fractions were analyzed from both intact and pearled barley kernels. Protein fractions were extracted from 150 mg of ground grain in triplicate using a modified Osborne fractionation method described in Holopainen et al.[11] with the following modifications: a protease inhibitor tablet (Complete Mini, Roche) was added into 0.5 M sodium chloride solution, and the extractions with 0.5 M sodium chloride, water, and 50% (v/v) 1-propanol were carried out with constant shaking at room temperature.

Protein contents of these extracts were determined with a 2D Quant protein kit (Amersham Biosciences). NaCl extracts containing albumins and globulins were analyzed as such. Two hundred microliters of the 1-propanol- and the 1-propanol+dithiothreitol (DTT)-soluble hordein fractions were precipitated in 4 volumes of acetone at −20 °C and resuspended in 100 μL of rehydration solution containing 7 M urea, 2 M thiourea, and 0.5% (v/v) Triton-X-100 (BDH, Dorset, UK) prior to protein assay. The total hordein content per dry matter of barley was defined as the sum of the two hordein extracts.

For SDS-PAGE, a 25 μL aliquot of each triplicate 1-propanol- or 1-propanol+DTT-soluble hordein fraction was precipitated as described above and resuspended in 40 μL of sample buffer (62.5 mM Tris-HCl buffer (pH 6.8), 20% (v/v) glycerol, 2.0% (v/v) SDS, 0.05% (w/v) bromophenol blue, and 5% (v/v) mercaptoethanol) for 16 h at 4 °C. Samples were then boiled for 3 min, centrifuged (20800*g*, 10 min, 4 °C) and separated in 12% Tris-borate gels (pH 8.9) using 0.125 M Tris-borate with 0.1% (v/v) SDS (pH 8.9) as a running buffer.[18] Gels were rinsed, stained with Coomassie Brilliant Blue G 250 (Fluka, Buchs, Switzerland), and fixed according to the method of Neuhoff et al.[19] using ethanol instead of methanol in both staining and washing solutions. After fixation, gels were scanned with GS-710 calibrated

Table 2. Correlations between Barley Grain Components and Grain Processing Parameters Calculated as Spearman Correlation Coefficients ($n$ = 14)

| | starch | protein | $\beta$-glucan | raw fat | ash |
|---|---|---|---|---|---|
| **grain components** | | | | | |
| starch | 1.00 | | | | |
| protein | −0.74**[a] | 1.00 | | | |
| $\beta$-glucan | −0.63* | 0.48 | 1.00 | | |
| raw fat | 0.12 | 0.00 | 0.07 | 1.00 | |
| ash | 0.03 | −0.33 | −0.53 | −0.31 | 1.00 |
| **proportion of size fractions of whole grain flour** | | | | | |
| >633 $\mu$m | −0.55* | 0.24 | 0.48 | −0.16 | 0.09 |
| 355−<633 $\mu$m | −0.80** | 0.50 | 0.81** | −0.05 | −0.19 |
| 180−<355 $\mu$m | −0.23 | 0.02 | 0.45 | −0.23 | −0.07 |
| 132−<180 $\mu$m | 0.81** | −0.61* | −0.58* | 0.23 | 0.05 |
| 95−<132 $\mu$m | 0.86** | −0.46 | −0.66* | −0.05 | 0.05 |
| 75−<95 $\mu$m | 0.41 | 0.06 | −0.39 | 0.39 | −0.11 |
| <75 $\mu$m | 0.23 | −0.19 | −0.63* | −0.07 | 0.30 |
| **water uptake from the beginning of malting** | | | | | |
| 24 h | 0.36 | −0.37 | −0.68* | −0.41 | 0.41 |
| 48 h | 0.41 | −0.37 | −0.61* | −0.41 | 0.25 |
| 72 h | 0.11 | −0.38 | −0.52 | −0.39 | 0.49 |
| **distribution of water in grains after 48 h of malting** | | | | | |
| 0−25% | 0.18 | −0.25 | −0.19 | 0.09 | 0.37 |
| 25−50% | −0.25 | 0.13 | 0.42 | −0.27 | −0.24 |
| 50−75% | 0.33 | −0.14 | −0.51 | 0.23 | 0.22 |
| 75−100% | −0.05 | 0.17 | −0.10 | 0.27 | −0.11 |
| **modification during malting** | | | | | |
| friability | 0.62* | −0.33 | −0.42 | 0.29 | −0.36 |

[a]Significance level: *, $p < 0.05$; **, $p < 0.01$.

imaging densitometer (Bio-Rad Laboratories, Hercules, CA, USA). B, C, and D hordeins separated in the gels were quantified using QuantityOne software (Bio-Rad) based on the band intensity and protein content of the hordein extracts. The average content of each hordein fraction and their relative proportions were calculated on the basis of the results of three replicate extracts.

**Statistical Analysis.** The results were calculated as averages of the replicates. The results of the composition analysis, excluding $\beta$-glucan contents, were presented with the standard uncertainty corresponding to one standard deviation calculated from the extended uncertainty of measurement of each validated method. For the $\beta$-glucan results, respective standard uncertainty was calculated from the 95% confidence interval. For the water uptake results, pooled standard deviations were calculated on the basis of two replicate micromaltings. When applicable, the results were examined statistically using correlation analysis and analysis of variance (ANOVA) with Tukey's honestly significant difference posthoc test (IBM SPSS Statistics software for Windows v20.0; IBM Corp., Somers, NY, USA).

## RESULTS AND DISCUSSION

**Composition of Different Barley Lots.** For comparison with processing properties, the chemical composition of the barley samples was analyzed (Table 1). The starch contents varied from 61.2 to 71.8%, and the feed varieties had somewhat higher contents (65.0−71.8%) compared to other samples. The starch contents of the feed varieties were higher than reported earlier, which may be explained by their lower nitrogen fertilizer application rate in this study.[20−22] The lower starch content of the waxy barley variety in comparison to the other varieties is in accordance with earlier literature.[21,22]

Protein contents of the samples ranged from 9.7 to 12.5% (Table 1). The variation in protein content was a little lower compared to the data of Holtekjølen et al.,[22] which included 29 hulled barley samples with protein contents from 8.4 to 14.5%. In the current study, lower nitrogen application to feed varieties resulted in lower protein contents compared to the malting type varieties. Higher protein contents of the malting barley varieties were most likely due to unrealized yield potential resulting in excessive nitrogen availability.

The variation in $\beta$-glucan content (2.9−5.7%; Table 1) was consistent with results published earlier.[23,24] Both genotype and growing conditions are known to influence $\beta$-glucan content.[23,25,26] The 6-row ear type and waxy barley varieties have been associated with low and high contents of $\beta$-glucan, respectively,[23,27] and similar results were obtained in the current study. In addition to genotypic association, each cultivar showed also crop year dependency, the $\beta$-glucan contents of each variety being substantially higher in 2006 than in 2007. The ranges of raw fat and ash contents were similar to those reported earlier.[20,28]

The correlation coefficients calculated between the main grain components showed significant negative correlations between starch and protein contents as well as starch and $\beta$-glucan contents (Table 2; $p < 0.01$ and $p < 0.05$, $n$ = 14). Both of these correlations are in line with earlier studies (e.g., Holtekjølen et al.[22]). Protein and $\beta$-glucan contents did not show a positive correlation as in previous studies.[22] Raw fat and ash contents showed no significant correlations with other components. Overall, the compositional variation in the sample set used was considered to be adequate and suitable for further investigation of the relationship between composition and processing behavior of grains.

**Association of Milling Behavior with Grain Composition.** The dissociation of endosperm into flour particles was studied by analyzing particle size distribution of flours produced by pin milling. All of the studied barley samples yielded flour

Table 3. Cumulative Particle Size Distribution of Flours Calculated as Averages of Triplicate Sieving Tests

| | | proportion of particles (% w/w) smaller than | | | | | |
|---|---|---|---|---|---|---|---|
| variety | crop year | 633 μm | 355 μm | 180 μm | 132 μm | 95 μm | 75 μm |
| **feed/starch type varieties** | | | | | | | |
| Pilvi | 2006 | 97.5 bcd[a] | 87.6 fg | 65.7 de | 57.9 ef | 46.9 b | 5.8 efgh |
| | 2007 | 96.9 bcd | 87.0 ef | 67.1 e | 59.8 g | 49.4 de | 6.5 h |
| Vilde | 2006 | 97.8 cd | 88.0 fg | 66.5 e | 58.1 f | 47.1 bc | 4.7 defg |
| | 2007 | 97.8 cd | 86.9 def | 65.0 de | 57.3 ef | 49.0 cde | 10.8 i |
| Voitto | 2006 | 97.8 cd | 88.3 fg | 67.0 e | 58.2 fg | 46.5 b | 4.1 bcde |
| | 2007 | 96.4 b | 86.1 cde | 65.1 de | 57.3 ef | 47.6 bcd | 4.2 cdef |
| **malting type varieties** | | | | | | | |
| Saana | 2006 | 97.5 bcd | 85.4 c | 63.6 cd | 56.3 de | 46.9 b | 3.0 abcd |
| | 2007 | 97.0 bcd | 85.5 cd | 65.1 de | 57.4 ef | 47.4 bc | 4.8 efgh |
| Scarlett | 2006 | 96.7 bc | 81.1 b | 57.8 b | 51.2 c | 42.6 a | 2.6 abc |
| | 2007 | 97.8 cd | 85.5 cde | 62.8 c | 55.3 d | 46.1 b | 4.2 cdef |
| SW Makof | 2006 | 97.1 bcd | 85.0 c | 66.5 e | 58.8 fg | 50.6 ef | 5.9 fgh |
| | 2007 | 97.9 d | 88.5 g | 69.8 f | 62.4 h | 51.8 f | 6.2 gh |
| **waxy variety** | | | | | | | |
| Magdalena | 2006 | 92.9 a | 72.3 a | 51.7 a | 46.8 a | 41.9 a | 1.6 a |
| | 2007 | 96.7 b | 80.4 b | 55.8 b | 49.0 b | 42.2 a | 2.4 ab |
| **commercial barley flours** | | | | | | | |
| flour I | | 99.9 | 98.0 | 80.9 | 71.7 | 63.7 | 5.9 |
| flour II | | 99.8 | 91.2 | 55.5 | 46.3 | 39.2 | 3.7 |

[a]Different letters indicate statistically significant difference ($p < 0.05$) between samples based on Tukey's HSD test.

with similar, bimodal particle size distribution with peaks at 75−95 and 250−355 μm (data not shown). However, certain differences between samples were observed in the cumulative particle size distributions (Table 3). The results were comparable to particle size distribution of commercial barley flours available in Finland. Compared to other samples, the milling of the grains of waxy variety Magdalena resulted in coarser flour containing significantly fewer particles smaller than 132 μm ($p < 0.05$, $n = 3$). Excluding samples of Voitto, each variety produced finer flour from the 2007 crop than from the 2006 crop. This difference was observed at least in one of the cumulative proportions of particles smaller than 132 μm ($p < 0.05$, $n = 3$). Nair et al.[31] have shown that the flours produced from harder grains contain more particles >106 μm than the flours from grains with softer structure. Therefore, the grains from crop 2006 may have been harder compared to those grown in 2007.

For examination of the effect of composition on milling properties, particle size distributions of flours were compared with the results of composition analysis. The composition analysis had revealed that starch content correlated negatively with protein and β-glucan contents, which, however, were not positively correlated with each other (Table 2). It was therefore considered reasonable to examine associations of starch with β-glucan content and protein content separately. Higher starch and lower protein and β-glucan contents were significantly linked to a higher fragility of the grain as indicated by the increased formation of flour particles of size from 132 to 180 μm upon milling (Table 2). Also, the proportion of the finer flour particles (from 95 to 132 μm) correlated positively with starch content and negatively with β-glucan content. Negative correlations were observed between the proportion of coarser flour particles (from 355 to 633 μm) and starch and β-glucan contents. Moreover, negative correlations were found between the proportion of the finest flour and β-glucan content as well as between the proportion of the coarsest flour and starch content. These results suggest that starch, protein, and β-glucan contents each affect the dissociation of the endosperm into flour particles.

The current results are consistent with the previous findings that starch content correlates negatively and β-glucan content positively with milling energy and kernel hardness.[4,8,29,30] Additionally, finer flours are produced from softer grains.[31] The more fragile structure of the grains with higher starch content could be a consequence of their lower β-glucan content (Table 2). The lower β-glucan content might indicate thinner cell walls and/or larger cell size causing a more easily breakable endosperm. Accordingly, thicker cell walls have been associated with hard-structured, steely barley grains.[10] However, varieties representing both low and high β-glucan levels showed crop year-related differences in flour coarseness, indicating that also factors besides β-glucan content affected grain milling properties and the hardness of grains. This is in line with the fact that a relationship between β-glucan content and grain hardness has not been found in all studies.[30,32]

In the sample set studied, also a lower protein content (associated with higher starch content) was linked to higher grain fragility in milling. Accordingly, protein content correlates positively with grain hardness.[3,29] Protein influences grain hardness via two mechanisms, both related to the dissociation of starch granules from the protein matrix during milling. First, a discontinuous or less compact protein matrix surrounding the starch granules is associated with softer grain structure.[3,10] Second, limited adhesion of protein to starch granules has been linked to a more fragile endosperm structure.[9,10] A correlation between protein content and milling energy or grain hardness has, however, not been observed in all studies, probably because grain hardness is associated also with β-glucan content, as described above.[4,30,32] It can be concluded therefore that barley grain composition greatly defines its milling properties, although the structure of endosperm must also be considered.

**Association of Water Uptake and Endosperm Modification with Grain Composition.** Water uptake was monitored during malting by measuring the increase in the

water content of the grains (Table 4). Water uptake was faster in the samples grown in 2007 than in the samples of 2006. This

**Table 4. Water Uptake of Barley Grains Measured as Water Content at 24, 48, and 72 h from the Beginning of Malting and the Friability of Final Malts[a]**

| | | water content from beginning of malting (%; w/w) | | | |
|---|---|---|---|---|---|
| variety | crop year | 24 h | 48 h | 72 h | friability[b] (%) |
| **feed type varieties** | | | | | |
| Pilvi | 2006 | 38.2 | 44.4 | 45.1 | 63.3 c[c] |
| | 2007 | 42.4 | 46.4 | 46.8 | 65.2 cd |
| Vilde | 2006 | 38.2 | 43.9 | 45.3 | 68.3 de |
| | 2007 | 42.6 | 47.1 | 47.2 | 73.3 fg |
| Voitto | 2006 | 38.6 | 44.6 | 45.1 | 80.4 ij |
| | 2007 | 42.2 | 47.7 | 47.9 | 89.1 l |
| **malting type varieties** | | | | | |
| Saana | 2006 | 38.3 | 44.8 | 44.8 | 78.1 hi |
| | 2007 | 42.1 | 46.7 | 47.0 | 74.8 fgh |
| Scarlett | 2006 | 36.6 | 44.3 | 45.1 | 71.0 ef |
| | 2007 | 38.7 | 44.4 | 45.2 | 76.0 ghi |
| SW Makof | 2006 | 36.0 | 42.6 | 45.1 | 85.7 kl |
| | 2007 | 38.6 | 44.4 | 45.4 | 83.3 jk |
| **waxy variety** | | | | | |
| Magdalena | 2006 | 35.0 | 41.7 | 45.2 | 41.3 a |
| | 2007 | 37.7 | 43.9 | 45.9 | 51.2 b |
| $s_p$[d] | | 0.8 | 0.5 | 0.3 | |

[a]Results on water uptake are expressed as means of two replicate malting lots and friability values as averages of triplicate analyses. [b]Relative value of friability. [c]Different letters indicate statistically significant difference ($p < 0.05$; $n = 3$) between samples based on Tukey's HSD test. [d]Pooled standard deviation.

difference in water uptake was observed in all varieties after 24 and 48 h of malting, except for samples of Scarlett, in which there was no difference between the crop years at the 48 h time point. After the first day of germination (72 h from the beginning of malting), all of the samples had reached at least a water content of 45%, which is considered optimal for germination. Distribution of water in the grains was analyzed after 48 h of malting (Figure 1). By that time point, hydration had proceeded further in the samples of Vilde, Voitto, Scarlett, and Magdalena grains from the 2007 crop compared to those from 2006. This difference was observed in the proportion of grains having 50−75 and/or 75−100% of endosperm hydrated. In addition, the water content of grains after 24 and 48 h of malting correlated positively with the proportion of grains having 50−75% of endosperm hydrated after 48 h of malting ($p < 0.05$, $n = 14$, data not shown).

Similarly to the results of Gamlath et al.,[4] hydration of the grains at the time points of 24 and 48 h correlated negatively with $\beta$-glucan content (Table 2; $p < 0.05$, $n = 14$). Due to higher $\beta$-glucan content, grains grown in 2006 may have had a harder structure, which is known to be negatively correlated with water uptake.[3] However, $\beta$-glucan did not explain all of the variation observed in the extent of hydration, and no significant correlations between the distribution of water and grain composition were observed (Table 2). Therefore, water uptake was probably regulated also by packing or distribution of components in the endosperm rather than by the chemical composition only, as shown by, for example, Brennan et al.[33]

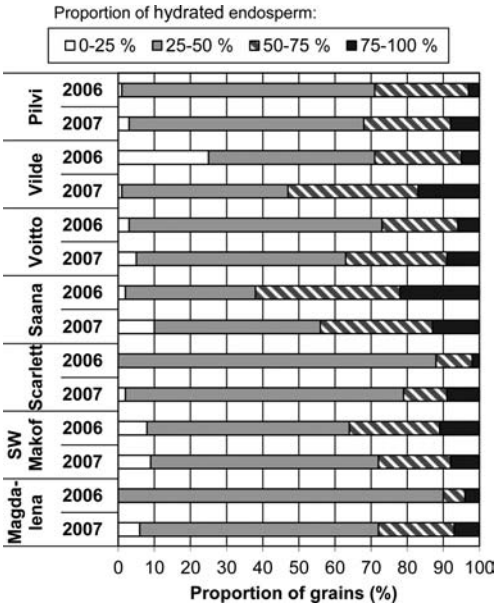


**Figure 1.** Distribution of water in barley grains after 48 h of malting. Results are based on 100 grains/sample.

and Chandra et al.[3] Although the steeping phase in the malting process represents a discontinuous hydration method, the effect of $\beta$-glucan content on water uptake observed in this study is likely to be applicable to other procedures requiring entry of water into grain.

The extent of endosperm modification during malting was determined by analyzing friability, the tendency of the endosperm to break into flour in a specified milling process. The higher the friability value, the more extensively the endosperm has been modified during malting, mostly with respect to degradation of cell walls and protein matrix.[34,35] Quite large variation in the friability values was observed among the barley samples in this study (Table 4). Malts of the samples of malting type variety SW Makof and feed variety Voitto were the most friable. SW Makof is known to have high activities of hydrolyzing enzymes, leading to release of high concentrations of fermentable sugars for distilling processes. The lower friability values of the other malting barley varieties were explained by high protein contents, which are known to cause insufficient modification.[36] The good modification of the Voitto samples was likely a consequence of low protein content.

The samples of waxy barley variety Magdalena had the lowest friability values (Table 4; $p < 0.05$, $n = 3$). This variety also showed high water uptake as mentioned above. The rapid hydration of waxy barley grains has been linked to starch composition, as low-amylose starch is known to differ from regular barley starch with respect to its physicochemical properties.[37,38] Although water uptake is a fundamental requirement for endosperm modification by enabling the synthesis and activity of hydrolyzing enzymes, fast hydration does not necessarily ensure good friability. Modification is also greatly dependent on hydrolytic enzyme activities not analyzed in this study.[33] Enzyme activities, the rate of enzyme activation, and the accessibility of the substrate to the enzyme may vary due to genetic background.[24,33]

Starch content correlated positively with friability (Table 2; $p < 0.05$, $n = 14$). Due to the inverse relationship of starch and protein contents of the grains, higher starch content could be associated with higher modification because of a more easily


dx.doi.org/10.1021/jf500857e | J. Agric. Food Chem. 2014, 62, 8875−8882

hydrolyzed, less dense protein matrix surrounding starch granules.[3] No significant correlation between protein content and friability was found. A negative association between protein content and friability is usually observed in studies of malting barley varieties and feed-type varieties.[11,33,36,39] The lack of correlation may be due to different nitrogen application given to 2-row and 6-row barley varieties.

The association between crop year and friability was not consistent; friability was higher in 2007 samples except for those of Pilvi, Saana, and SW Makof. This was probably due to varietal differences related, for example, to enzymatic hydrolysis of the endosperm during germination. Furthermore, no direct correlation was found between barley $\beta$-glucan content and friability in this study, although $\beta$-glucan content has been linked to grain hardness, which is known to correlate negatively with endosperm modification and friability.[29,30] In the case of $\beta$-glucan, the role of enzyme action during germination is significant, and the amount of $\beta$-glucan left in barley malt has been shown to correlate more strongly with friability than the $\beta$-glucan content of unmalted barley.[40]

**Association of Grain Processing Behavior with Localization of $\beta$-Glucan, Total Protein, and Hordeins.** The distribution of different components within the grain was examined by progressively pearling grains of the varieties Scarlett and Vilde from crop years 2006 and 2007 and analyzing the composition of the pearled kernels. In all samples, protein content decreased gradually toward the center of the grain at pearling rates >15% (Figure 2a). $\beta$-Glucan, in turn, was enriched in the remaining kernel up to a pearling rate of 30%. Similar changes in the protein and $\beta$-glucan contents of the pearled kernels have been linked to removal of the protein-rich aleurone layer and enrichment of subaleurone and starchy endosperm cell walls rich in $\beta$-glucan.[38,41] Grains of Scarlett samples had consistently higher contents of protein and $\beta$-glucan in the endosperm at all pearling rates compared to samples of Vilde, indicating a less fragile endosperm structure, which may explain the coarser flour produced from sample lots of Scarlett. Higher protein contents in the endosperm of grains of Scarlett samples were probably a consequence of the higher nitrogen fertilizer application given for this cultivar. The distribution of total protein or $\beta$-glucan showed no clear association with water uptake or friability.

The decrease in concentrations of water- and salt-soluble proteins (globulins and albumins) was more pronounced toward the center of the grain relative to the total protein content (Figure 2b). Hordein was rather evenly distributed in the grains of Scarlett samples, but in the grains of Vilde samples it decreased at the pearling rates of 20−30% (Figure 2c). Distribution of these protein fractions is in line with the known location of hordeins in the subaleurone and starchy endosperm cells and globulins and albumins in the aleurone layer.[42] Clear correlations between the distribution of these protein fractions and processing behavior including milling, water uptake, and friability were not observed.

Hordeins were extracted from whole and pearled grains sequentially in 50% (v/v) 1-propanol first without and thereafter with DTT for the reduction of interchain disulfide bonds of B and D hordein aggregates (Table 5). Irrespective of the pearling rate, most of the hordeins were monomeric B and C hordeins. Some C hordein was extracted after reduction, showing its entrapment among the aggregated B and D hordeins. The inner endosperm (pearling rate approximately 30%) of Vilde and Scarlett grown in 2007 contained

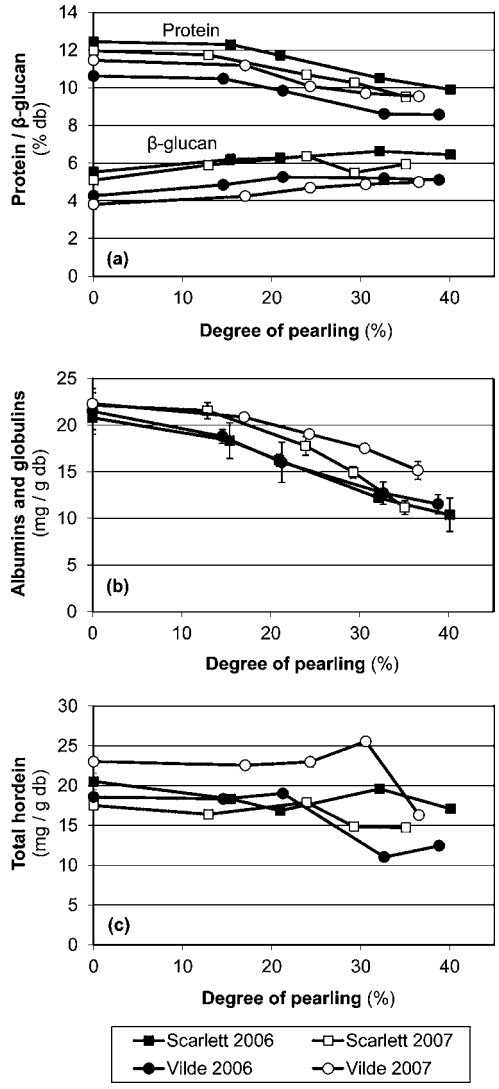


**Figure 2.** Effect of pearling on content of (a) protein and $\beta$-glucan, (b) water- and salt-soluble proteins or albumins and globulins, and (c) total hordeins in barley grains. Analyses and extractions were performed in triplicate. Error bars indicate the 95% confidence intervals ($n$ = 3).

proportionally less 1-propanol-soluble C hordein and more 1-propanol+DTT-soluble B, C, and D hordeins in the endosperm compared to the samples harvested in 2006 (Table 5; $p < 0.05$, $n$ = 3). Moreover, 1-propanol+DTT-soluble B hordein was more concentrated in the peripheral endosperm in the grains of both varieties grown in 2006.

Both the hordein localization and $\beta$-glucan content in the grains of Scarlett and Vilde were associated with the crop year, suggesting that their formation during grain filling could be affected by similar environmental conditions. Furthermore, distribution of hordein fractions and $\beta$-glucan was associated with processability in the samples of these two cultivars. In both cases there was a lower $\beta$-glucan content, localization of aggregated hordeins (with entrapped C hordein) within the more central endosperm, and nonentrapped C hordein located less deeply. These characteristics correlated positively with the proportion of fine flour after milling, water uptake after 24 h of malting, and proportion of hydrated endosperm after 48 h of malting and friability.


dx.doi.org/10.1021/jf500857e | J. Agric. Food Chem. 2014, 62, 8875−8882

**Table 5. Proportions of 1-Propanol- and 1-Propanol+DTT-Soluble B, C, and D Hordeins of Total Hordein Content in Intact and Gradually Pearled Grains of Cultivars Scarlett and Vilde Grown in 2006 and 2007.[a]**

| | | pearling rate | | | |
|---|---|---|---|---|---|
| sample | intact grains | 13−17% | 21−24% | 29−33% | 35−40% |
| **1-propanol-soluble hordeins** | | | | | |
| *B hordein (% (w/w db) of total hordein)* | | | | | |
| Scarlett 2006 | 40.2 a[b] | 42.3 ab | 48.2 d | 49.0 d | 46.8 cd |
| Scarlett 2007 | 41.6 a | 45.0 bc | 46.9 cd | 48.6 d | 49.7 d |
| Vilde 2006 | 40.1 a | 41.2 ab | 46.9 c | 62.6 e | 55.8 d |
| Vilde 2007 | 39.8 a | 40.4 a | 42.5 b | 46.3 c | 54.1 d |
| *C hordein (% (w/w db) of total hordein)* | | | | | |
| Scarlett 2006 | 34.1 bc | 37.9 d | 44.5 e | 43.8 e | 42.8 e |
| Scarlett 2007 | 30.6 a | 32.8 ab | 35.1 bcd | 36.2 cd | 36.6 cd |
| Vilde 2006 | 18.4 a | 20.3 b | 23.2 c | 29.3 d | 27.6 d |
| Vilde 2007 | 21.9 bc | 20.6 b | 22.0 bc | 23.2 c | 28.5 d |
| *D hordein (% (w/w db) of total hordein)* | | | | | |
| Scarlett 2006 | 0.6 a | 0.5 a | 0.7 a | 0.8 a | 0.7 a |
| Scarlett 2007 | 0.4 a | 0.4 a | 0.5 a | 0.6 a | 0.8 a |
| Vilde 2006 | 1.0 a | 1.1 ab | 1.1 ab | 1.6 b | 1.2 ab |
| Vilde 2007 | 0.8 a | 0.6 a | 0.6 a | 1.1 ab | 0.8 a |
| **1-propanol+DTT-soluble hordeins** | | | | | |
| *B hordein (% (w/w db) of total hordein)* | | | | | |
| Scarlett 2006 | 15.8 h | 10.7 f | 3.5 a | 3.0 a | 4.6 b |
| Scarlett 2007 | 17.2 i | 13.0 g | 9.5 e | 7.7 d | 6.3 c |
| Vilde 2006 | 31.3 f | 26.9 d | 20.0 c | 4.3 a | 10.3 b |
| Vilde 2007 | 28.9 e | 29.5 ef | 26.1 d | 20.8 c | 11.8 b |
| *C hordein (% (w/w db) of total hordein)* | | | | | |
| Scarlett 2006 | 4.7 e | 3.9 de | 1.3 a | 1.3 a | 1.9 ab |
| Scarlett 2007 | 4.6 e | 3.4 d | 3.2 cd | 2.4 bc | 2.4 bc |
| Vilde 2006 | 3.1 cd | 3.3 cd | 2.8 cd | 0.6 a | 1.5 ab |
| Vilde 2007 | 3.3 cd | 3.5 d | 3.0 cd | 2.6 c | 1.7 b |
| *D hordein (% (w/w db) of total hordein)* | | | | | |
| Scarlett 2006 | 4.7 cd | 4.7 cd | 1.7 a | 2.1 a | 3.2 b |
| Scarlett 2007 | 5.6 e | 5.3 de | 4.8 cde | 4.6 cd | 4.2 c |
| Vilde 2006 | 6.1 c | 7.1 c | 6.0 c | 1.6 a | 3.6 ab |
| Vilde 2007 | 5.3 bc | 5.3 bc | 5.9 c | 6.1 c | 3.1 ab |

[a]Values are expressed as means of triplicate hordein extractions. [b]Proportions of the same variety followed by different letters differ significantly from each other ($p < 0.05$) based on Tukey's HSD test.

Although the effect of hordein localization and $\beta$-glucan content on processing behavior cannot be fully separated on the basis of the current results, several earlier studies suggest that hordeins influence grain properties. For example, the concentration of aggregated B hordein in the peripheral endosperm has been associated with impaired malting quality,[43] and the deeper localization of C hordein entrapped by aggregated B and D hordeins improved water uptake during steeping.[14] Moreover, this minor proportion of C hordein might assist hydration and modification, restricting the aggregation of B hordein or changing the number and orientation of disulfide bonds between aggregated hordeins.[12,44] The nonentrapped C hordein, representing the majority of the C hordein, could in turn limit water uptake and endosperm modification on the basis of its hydrophobic structure, effect on endosperm hardness, and slow hydrolysis during malting.[44−46] Hordeins could also influence milling properties, because steely grains, which generally produce coarser flour upon milling, are rich in C hordein.[31,45] Therefore, a lower proportion of nonentrapped C hordein within the central starchy endosperm could be expected to facilitate dissociation of the protein matrix and starch granules into finer flour particles. However, the more specific mechanisms by which the degree of hordein aggregation affects properties of barley endosperm such as dissociation of flour particles, hydration, or modification during germination are not known.

This study has shown that the processing properties (milling behavior, water uptake, and modification) of barley grains are associated not only with their main constituents (starch and protein) but also with $\beta$-glucan content. The distribution of hordein within the grain could also contribute to grain structure and processing performance. These results further indicate that understanding the role and biochemical action of macromolecules located inside cells, as well as macromolecules that make up cell walls, is necessary to accurately predict the functional performance of individual lots of barley grains.

## AUTHOR INFORMATION


### Corresponding Author

*(U.R.M.H.) Phone: +358-20-722-4488; Fax: +358-20-722-7071. E-mail: ulla.holopainen@vtt.fi.

### Present Address

⊥(P.L.) Senson Oy, P.O. Box 94, FI-15141 Lahti, Finland.



### Funding

This work was performed within projects financed by the Finnish Ministry of Agriculture and Forestry and the Academy of Finland.


### Notes

The authors declare no competing financial interest.

## ACKNOWLEDGMENTS


Agricultural Foundation of Trade K-maatalous Experimental Farm is thanked for supplying the barley material. Dr. Brian Gibson is acknowledged for a critical reading of the manuscript. Tarja Wikström and Eero Mattila are gratefully thanked for technical assistance.


## REFERENCES


(1) Wood, P. Cereal $\beta$-glucans in diet and health. *J. Cereal Sci.* **2007**, *46*, 230−238.

(2) Evers, T.; Millar, S. Cereal grain structure and development: some implications for quality. *J. Cereal Sci.* **2002**, *36*, 261−284.

(3) Chandra, G. S.; Proudlove, M. O.; Baxter, E. D. The structure of barley endosperm − an important determinant of malt modification. *J. Sci. Food Agric.* **1999**, *79*, 37−46.

(4) Gamlath, J.; Aldred, G. P.; Panozzo, J. F. Barley (1→3; 1→4)-$\beta$-glucan and arabinoxylan content are related to kernel hardness and water uptake. *J. Cereal Sci.* **2008**, *47*, 365−371.

(5) Shewry, P. R. Plant storage proteins. *Biol. Rev. Camb. Philos. Soc.* **1995**, *70*, 375−426.

(6) Shewry, P. R. Barley seed storage proteins structure, synthesis, and deposition. In *Nitrogen Metabolism of Plants*; Pilbeam, D. J., Mengel, K., Eds.; Oxford University Press: Oxford, UK, 1992; pp 201−227.

(7) Fincher, G. B.; Stone, B. A. Cell walls and their components in cereal grain technology. *Adv. Cereal Sci. Technol.* **1986**, *8*, 207−295.

(8) Izydorczyk, M. S.; Dexter, J. E.; Desjardins, R. G.; Rossnagel, B. G.; Lagasse, S. L.; Hatcher, D. W. Roller milling of Canadian hull-less barley: optimization of roller milling conditions and composition of mill streams. *Cereal Chem.* **2003**, *80*, 637−644.

(9) Brennan, C. S.; Harris, N.; Smith, D.; Shewry, P. R. Structural differences in the mature endosperms of good and poor malting barley cultivars. *J. Cereal Sci.* **1996**, *24*, 171−177.
(10) Nair, S.; Knoblauch, M.; Ullrich, S. E.; Baik, B. K. Microstructure of hard and soft kernels of barley. *J. Cereal Sci.* **2011**, *54*, 354−362.
(11) Holopainen, U. R. M.; Wilhelmson, A.; Salmenkallio-Marttila, M.; Peltonen-Sainio, P.; Rajala, A.; Reinikainen, P.; Kotaviita, E.; Simolin, H.; Home, S. Endosperm structure affects the malting quality of barley (*Hordeum vulgare* L.). *J. Agric. Food Chem.* **2005**, *53*, 7279−7287.
(12) Molina-Cano, J. L.; Ramo, T.; Ellis, R. P.; Swanston, J. S.; Bain, H.; Uribe-Echeverria, T.; Perez-Vendrell, A. M. Effect of grain composition on water uptake by malting barley: a genetic and environmental study. *J. Inst. Brew.* **1995**, *101*, 79−83.
(13) Molina-Cano, J. L.; Sopena, A.; Polo, J. P.; Bergareche, D.; Moraleho, M. A.; Swanston, J. S.; Glidewell, S. M. Relationships between barley hordeins and malting quality in a mutant of cv. Triumph. II. Genetic and environmental effects on water uptake. *J. Cereal Sci.* **2002**, *36*, 39−50.
(14) Holopainen, U. R. M.; Wilhelmson, A.; Home, S.; Poutanen, K.; Shewry, P. R. Day-length effects on protein localization affect water absorption in barley (*Hordeum vulgare*) grains. *J. Sci. Food Agric.* **2012**, *92*, 2944−2951.
(15) Nordlund, E.; Heiniö, R.-L.; Viljanen, K.; Pihlava, J.-M.; Lehtinen, P.; Poutanen, K. Flavour and stability of rye grain fractions in relation to their chemical composition. *Food Res. Int.* **2013**, *54*, 48−56.
(16) Bach Knudsen, K. E.; Åman, P.; Eggum, B. O. Nutritive value of Danish-grown barley varieties, I, carbohydrates and other major constituents. *J. Cereal Sci.* **1987**, *6*, 173−186.
(17) European Brewing Convention. *Analytica-EBC*; Fachverlag Hans Carl: Nürnberg, Germany, 2007.
(18) Laemmli, U. K. Cleavage of structural proteins during the assembly of the head of bacteriophage T4. *Nature* **1970**, *227*, 680−685.
(19) Neuhoff, V.; Arold, N.; Taube, D.; Ehrhardt, W. Improved staining of proteins in polyacrylamide gels including isoelectric focusing gels with clear background at nanogram sensitivity using Coomassie Brilliant Blue G250 and R250. *Electrophoresis* **1988**, *9*, 255−262.
(20) Åman, P.; Hesselman, K.; Tilly, A. C. The variation in chemical composition of Swedish barleys. *J. Cereal Sci.* **1985**, *3*, 73−77.
(21) Oscarsson, M.; Parkkonen, T.; Autio, K.; Åman, P. Composition and microstructure of waxy, normal and high amylose barley samples. *J. Cereal Sci.* **1997**, *26*, 259−264.
(22) Holtekjølen, A. K.; Uhlen, A. K.; Bråthen, E.; Sahlstrøm, S.; Knutsen, S. H. Contents of starch and non-starch polysaccharides in barley varieties of different origin. *Food Chem.* **2006**, *94*, 348−358.
(23) Lehtonen, M.; Aikasalo, R. $\beta$-Glucan in two- and six-rowed barley. *Cereal Chem.* **1987**, *64* (3), 191−193.
(24) Kato, T.; Sasaki, A.; Takeda, G. Genetic variation of $\beta$-glucan contents and $\beta$-glucanase activities in barley, and their relationships to malting quality. *Breed. Sci.* **1995**, *45*, 471−477.
(25) Perez-Vendrell, A. M.; Brufau, J.; Molina-Cano, J. L.; Francesch, M.; Guasch, J. Effects of cultivar and environment on $\beta$-(1,3)-(1,4)-D-glucan content and acid extract viscosity of Spanish barleys. *J. Cereal Sci.* **1996**, *23*, 285−292.
(26) Zhang, G.; Chen, J.; Wang, J.; Ding, S. Cultivar and environmental effects on (1→3; 1→4)-$\beta$-D-glucan and protein content in malting barley. *J. Cereal Sci.* **2001**, *34*, 295−301.
(27) Ajithkumar, A.; Andersson, R.; Christerson, T.; Åman, P. Amylose and $\beta$-glucan content of new waxy barleys. *Starch* **2005**, *57*, 235−239.
(28) Andersson, A. A. M.; Lampi, A. M.; Nyström, M.; Piironen, V.; Li, L.; Ward, J. L.; Gebruers, K.; Courtin, C. M.; Delcour, J. A.; Boros, D.; Fraś, A.; Dynkowska, W.; Rakszegi, M.; Bedő, Z.; Shewry, P. R.; Åman, P. Phytochemical and dietary fiber components in barley varieties in the HEALTHGRAIN Diversity screen. *J. Agric. Food Chem.* **2008**, *56*, 9767−9776.
(29) Henry, R. J.; Cowe, I. A. Factors influencing the hardness (milling energy) and malting quality of barley. *J. Inst. Brew.* **1990**, *96*, 135−136.
(30) Psota, V.; Vejražka, K.; Faměra, O.; Hrčka, M. Relationship between grain hardness and malting quality of barley (*Hordeum vulgare* L.). *J. Inst. Brew.* **2007**, *113*, 80−86.
(31) Nair, S.; Ullrich, S. E.; Baik, B. K. Association of barley kernel hardness with physical grain traits and food processing parameters. *Cereal Chem.* **2011**, *88* (2), 147−152.
(32) Nair, S.; Ullrich, S. E.; Blake, T. K.; Cooper, B.; Griffey, C. A.; Hayes, P. M.; Hole, D. J.; Horsley, R. D.; Obert, D. E.; Smith, K. P.; Muehlbauer, G. J.; Baik, B. K. Variation in kernel hardness and associated traits in U.S. barley breeding lines. *Cereal Chem.* **2010**, *87* (5), 461−466.
(33) Brennan, C. S.; Amor, M. A.; Harris, N.; Smith, D.; Cantrell, I.; Griggs, D.; Shewry, P. R. Cultivar differences in modification patterns of protein and carbohydrate reserves during malting of barley. *J. Cereal Sci.* **1997**, *26*, 83−93.
(34) Chapon, L.; Maucourt, J. M.; Gobert, J. P. The friabilimeter, an apparatus for objective measurement of malt friability. *Monatsschr. Brau.* **1979**, *32*, 160−167.
(35) Darlington, H. F.; Palmer, G. H. Homogeneity of the friable flour of malting barley. *J. Inst. Brew.* **1996**, *102*, 179−182.
(36) Agu, R. C.; Palmer, G. H. The effect of nitrogen level on the performance of malting barley varieties during germination. *J. Inst. Brew.* **2001**, *107*, 93−98.
(37) Vasanthan, T.; Bhatty, R. S. Physicochemical properties of small- and large-granule starches of waxy, regular, and high-amylose barleys. *Cereal Chem.* **1996**, *72* (2), 199−207.
(38) Klamczynski, A.; Baik, B. K.; Czuchajowska, Z. Composition, microstructure, water imbibition, and thermal properties of abraded barley. *Cereal Chem.* **1998**, *75* (5), 677−685.
(39) Fox, G.; Kelly, A.; Bowman, J.; Inkerman, A.; Poulsen, D.; Henry, R. Is malting barley better feed for cattle than feed barley? *J. Inst. Brew.* **2009**, *115* (2), 95−104.
(40) Henry, R. J. Changes in $\beta$-glucan and other carbohydrate components of barley during malting. *J. Sci. Food Agric.* **1988**, *42* (4), 333−341.
(41) Marconi, E.; Graziano, M.; Cubadda, R. Composition and utilization of barley pearling by-products for making functional pastas rich in dietary fiber and $\beta$-glucans. *Cereal Chem.* **2000**, *77* (2), 133−139.
(42) Yupsanis, T.; Burgess, S. R.; Jackson, P. J.; Shewry, P. R. Characterisation of the major protein component from aleurone cells of barley (*Hordeum vulgare* L.). *J. Exp. Bot.* **1990**, *41*, 385−392.
(43) Millet, M. O.; Montembault, A.; Autran, J. C. Hordein composition differences in various anatomical regions of the kernel between two different barley types. *Sci. Aliments* **1991**, *11*, 155−161.
(44) Skerritt, J. H.; Janes, P. W. Disulphide-bonded "gelprotein" aggregates in barley, quality related differences in composition and reductive dissociation. *J. Cereal Sci.* **1992**, *16*, 219−235.
(45) Ferrari, B.; Baronchelli, M.; Stanca, A. M.; Gianinetti, A. Constitutive differences between steely and mealy barley samples associated with endosperm modification. *J. Sci. Food Agric.* **2010**, *90*, 2105−2113.
(46) Bénétrix, F.; Sarrafi, A.; Autran, J. C. Effects of genotype and nitrogen nutrition on protein aggregates in barley. *Cereal Chem.* **1994**, *71* (1), 75−82.

furosine levels (0.91 mg/kg) in a dry dog food, providing evidence that at least FL can be found in pet foods.[13] As pet animals usually consume processed foods throughout their lives, chronic ingestion of advanced MRPs could induce long-term effects on pet health.

The aim of this study was to quantitate key MRPs in commercial pet foods to calculate the daily intake of MRPs in pet animals. The MRP data were subjected to multivariate analysis to identify diet formulation factors such as processing type, animal species, life stage, and nutrient composition that could affect the variation in MRP concentrations in these foods.

## MATERIALS AND METHODS

**Materials.** L-Lysine monohydrochloride (Fluka, Buchs, Switzerland), furosine dihydrochloride, ε-*N*-carboxymethyl-L-lysine, lysinoalanine (PolyPeptide Group, Strasbourg, France), and 5-hydroxymethyl-2-furaldehyde (Sigma-Aldrich, Steinheim, Germany) were used as external chemical standards. External standards of all other amino acids were purchased from Serva Electrophoresis (Heidelberg, Germany). Other chemicals of analytical grade were nonafluoropentanoic acid (NFPA) (Fluka), barium hydroxide octahydrate and trichloroacetic acid (TCA) (Merck, Darmstadt, Germany), hydrochloric acid 37% (HCl) and *O*-methylisourea hemi sulfate (OMIU) (Sigma-Aldrich), water, acetonitrile (ACN), and methanol (UPLC-MS, Biosolve BV, Valkenswaard, The Netherlands), and buffers for amino acid analyses (Frank Gutjar Chromatographie, Balingen, Germany).

**Diets and Sample Preparation.** A sample set was created containing 153 extruded, canned, and pelleted pet foods commercially available on the Dutch market. Pet food types were categorized according to species (dog or cat) and life stage (junior and adult). From each category in the sample set, five pet foods (single batch) were randomly selected, resulting in a selection of 50 foods. In addition, 11 extruded dry foods for growing dogs and 6 extruded dry foods for growing cats were obtained from Australia, Brazil, China, Germany, Mexico, Thailand, the United Kingdom, and the United States. This results in a total of 67 foods that were included in the study. The moist canned foods were freeze-dried, and all of the foods were ground to pass through a 1 mm sieve in a centrifugal mill (Retsch ZM100, Retsch BV, Ochten, The Netherlands). All samples were stored in airtight plastic containers at 4 °C prior to analyses.

**Proximate Analyses.** Dry matter (DM) and crude ash contents were determined by drying to a constant weight at 103 °C (ISO 6496, 1999) and combustion at 550 °C (ISO 5984, 2002), respectively. Crude protein (CP; N × 6.25) was determined using the Dumas method (AOAC 990.03), and crude fat (CFat) was gravimetrically determined after hydrolysis with HCl and extraction with light petroleum ether (boiling point 40−60 °C; ISO 6492, 1999). Crude fiber (CFiber) was gravimetrically determined as the remaining insoluble organic fraction after acid and alkaline digestion (ISO 6865, 2000). All analyses were performed in duplicate. The content of nitrogen-free extract (NFE, g/kg DM) of foods was calculated as described by eq 1, and metabolizable energy (ME, in kJ "as is") content was calculated using predictive equations for ME (eq 2, 3, 4, and 5).[14]

$$\text{NFE (g/kg DM)} = 1000 - \text{CFat} - \text{CP} - \text{crude ash} - \text{CFiber} \quad (1)$$

$$\text{Dogs: ME (kJ "as is")} = \text{digestible energy (DE, kJ)} - (4.35 \times g\ \text{CP})$$

$$\text{Cats: ME (kJ "as is")} = (\text{DE, kJ}) - (3.22 \times g\ \text{CP}) \quad (2)$$

$$\text{DE (kJ)} = \text{gross energy (GE, kJ)} \times \text{energy digestibility (\%)}/100 \quad (3)$$

$$\text{Dogs: energy digestibilty (\%)} = 91.2 - (1.43 \times \%\ \text{CFiber in DM})$$

$$\text{Cats: energy digestibilty (\%)} = 87.9 - (0.88 \times \%\ \text{CFiber in DM}) \quad (4)$$

$$\text{GE (kJ)} = (23.85 \times \text{g CP}) + (39.33 \times g\ \text{CFat}) + (17.15 \times (\text{g NFE} + g\ \text{CFiber})) \quad (5)$$

**Amino Acid Analyses.** Samples were defatted by extraction with light petroleum ether without acid hydrolysis (ISO 6492, 1999) and ground using a mixer mill (Retsch MM2000, Retsch BV). Total lysine (TL) was analyzed using traditional amino acid analysis and represents both reactive as well as unreactive lysine that reverts back to reactive lysine during acid hydrolysis. Amino acids including TL were determined according to the method of Hendriks et al.[15] Samples (5 mg) were hydrolyzed using 1 mL of 6 M HCl during 23 h at 110 °C in glass tubes that were sealed under vacuum. The tubes were opened, norleucine was added as an internal standard, and the tubes were dried under vacuum (Savant SpeedVac Plus, SC210A). The dried pellet was redissolved in 2 mL of loading buffer (0.1 M sodium acetate; pH 2.2). Amino acids were separated by ion exchange chromatography using a Biochrom 20 AA analyzer (Biochrom, Cambridge, UK) and analyzed by postcolumn derivatization with ninhydrin, using photometric detection at 570 nm. Reactive lysine (RL) was measured using the OMIU procedure that transforms RL into homoarginine through a guanidination reaction. OMIU-RL was determined according to the method of Moughan and Rutherfurd.[16] Samples (5 mg) were incubated during 7 days with 1 mL of OMIU to convert all lysine with a free ε-amino group into homoarginine. Homoarginine was measured in the dried sample according to the amino acid analysis procedure described previously. The amount of OMIU-RL was calculated from the molar amount of homoarginine and the molecular weight of lysine. All analyses were performed in duplicate. The ratio between TL and OMIU-RL was calculated using eq 6.

$$\text{RL/TL ratio} = \text{OMIU} - \text{reactive lysine/total lysine} \quad (6)$$

**RP-UPLC-MS.** The MRPs furosine (as an indirect measurement for FL, see below), CML, HMF, and the cross-linked amino acid LAL were analyzed. Defatted samples (10 mg) were hydrolyzed according to the amino acid analysis procedure described previously. The samples were redissolved in 2 mL of 5 mM NFPA and filtered (0.2 μm) into vials for RP-UPLC-MS analysis. Because HMF is not stable during acid hydrolysis, the sample preparation was performed according to the method of Ameur et al.[17] For this, 10 mg of defatted sample was dissolved in 1 mL of Milli-Q and 250 μL of 40% TCA. The sample was stirred for 5 min and centrifuged for 5 min at 9000*g*. Then, 800 μL of the supernatant was separated, dried under vacuum (Savant SpeedVac Plus, SC210A), redissolved in 1 mL of 5 mM NFPA, and filtered (0.2 μm) into vials for RP-UPLC-MS analysis.

Samples were analyzed using an Acella RP-UHPLC system (Thermo Scientific, San Jose, CA, USA). Samples (5 μL) were injected on an Acquity UPLC BEH C18 column (2.1 × 150 mm, 1.7 μm particle size; Waters, Milford, MA, USA) with an Acquity UPLC BEH C18 Vanguard precolumn (2.1 × 5 mm, 1.7 μm particle size; Waters) housed in a column oven at 40 °C. The mobile phases were eluent A, 5 mM NFPA in Milli-Q water, and eluent B, 100% ACN. The flow rate was 300 μL/min. The following elution profile was used: 0−11 min, eluent B linear gradient from 20 to 24%; 11−12 min, eluent B linear gradient from 24 to 100%; 12−17 min, eluent B isocratic on 100%; 17−18 min, eluent B linear gradient from 100 to 20%; 18−25 min, eluent B isocratic on 20%.

Mass spectrometric (MS) data were obtained by analyzing the eluate on a Thermo Scientific LTQ-Velos Pro equipped with an HESI-MS probe coupled to the RP-UHPLC; 300 μL/min of the flow from the RP-UHPLC was directed to the MS. Nitrogen was used as sheath gas and as auxiliary gas. Data were collected in positive ionization mode with selected reaction monitoring (SRM); for details, see Table

1. Data-dependent $MS^n$ analyses were performed with a normalized collision energy of 35%. Settings were optimized using "LTQ tune plus" (Velos Pro 2.7, Thermo Scientific) via automatic tuning using standard stock solutions. The capillary temperature was 300 °C, the source heater 230 °C, and the source voltage 3.0 kV. Compounds were quantified by reference to an external standard calibration curve by plotting MS area ratio in base peak SRM against amount ratio using external standard concentrations of 0.1, 0.05, 0.01, 0.005, 0.001, 0.005, and 0.0001 mg/mL. Data acquisition and reprocessing was done with Xcalibur 2.1 software (Thermo Scientific).

**Table 1. Selected Reaction Monitoring Conditions**

| compound | parent mass (Da) | fragment mass (Da) | range ($m/z$) |
|---|---|---|---|
| furosine | 255 | 130 | 127.50−132.50 |
| carboxymethyllysine | 205 | 130 | 127.50−132.50 |
| hydroxymethylfurfural | 127 | 108 | 106.50−111.50 |
| lysinoalanine | 234 | 198 | 195.50−200.50 |

Furosine is an indirect measurement of FL; during acid hydrolysis in 6 M HCl, peptide-bound FL is transformed into approximately 32% furosine, 56% regenerated (unreactive) lysine, and 16% pyridosine.[18] RL can be calculated using this furosine procedure. FL, regenerated lysine, and FUR-RL were calculated using eqs 7, 8, and 9, respectively.[18,19]

$$\text{FL (g/kg DM)} = \text{furosine (g/kg DM)}/(32/100) \quad (7)$$

$$\text{regenerated (unreactive) lysine (g/kg DM)} = \text{FL (g/kg DM)} \times (56/100) \quad (8)$$

$$\text{FUR-RL (g/kg DM)} = \text{total lysine (g/kg DM)} - \text{regenerated lysine (g/kg DM)} \quad (9)$$

**Statistical Analyses.** Statistical analyses were performed using SAS 9.2 for Windows (SAS Institute, Cary, NC, USA). Data analysis to identify factors associated with variation in dietary MRPs was performed by ANOVA using the GLMSELECT procedure. CML and HMF were square root transformed, and FL was logarithmically transformed (Ln) to attain normal distribution of the residuals evaluated with the Sharpiro−Wilk test. Using stepwise regression and the Schwarz Bayesian information criteria, the best model explaining the variance of the dependent variables FL, CML, HMF, and LAL was selected. The following independent variables were used: animal species (dog, cat), processing type (extruded, canned, pelleted), life stage (adult, junior), DM (in g/kg), CP, CFat, CFiber, crude ash, NFE (g/kg DM). Correlations were assessed by use of the Pearson correlation method. Regressions were assumed significant when $P < 0.05$.

## RESULTS AND DISCUSSION

**Proximate Composition of Commercially Available Pet Foods.** The selected commercial pet foods differed considerably in proximate composition and ME content (Table 2). With regard to animal species, cat foods contain, on average, higher CP and CFat but lower DM and lower CFiber and NFE contents on a DM basis compared to corresponding dog foods. This result could be expected as cats require more protein and fat for growth and maintenance compared to dogs.[14] Crude ash content was comparable among foods in the category animal species. For processing type, canned foods contain on average more crude ash, CP, and CFat on a DM basis compared to extruded and pelleted foods. The lower CFiber and NFE contents of the canned foods are due to little or no inclusion of starch sources in the latter foods. In the category life stage, foods formulated for animals at different life stages did not differ in proximate composition. However, nutrient composition can vary within this category; CP contents, for example, varied considerably in extruded adult dog foods (range 211−445 g/kg DM), canned junior dog foods (range 364−710 g/kg DM), canned adult dog foods (range 294−591 g/kg DM), and canned adult cat foods (range 489−712 g/kg DM). The mean NFE content was higher in pelleted dog foods than in extruded dog and cat foods, with the latter foods showing larger ranges in NFE contents.

**Reactive Lysine Content of Commercially Available Pet Foods.** The mean values for TL and RL of the commercial pet foods are shown in Table 3. RL contents met the minimal lysine requirements for dogs and cats; however, levels could be at risk of not meeting lysine requirements in weaning diets for growing dogs as described in Van Rooijen et al.[12] To estimate the extent to which the MR affected the RL content of pet foods, two procedures (OMIU or FUR method) were applied to analyze the RL contents. The two methods showed a strong correlation ($r = 0.98$; $P < 0.0001$). The mean RL content of the pet foods was lower compared to the mean TL content regardless of the procedure that was used to measure RL, with some samples having equal OMIU-RL and TL values. Except for the canned dog diets, mean OMIU-RL values were lower than FUR-RL values. A difference between OMIU-RL and FUR-RL was also reported using corn distillers' dried grains with solubles.[19] The regenerated (unreactive) lysine calculated from the furosine procedure originates specifically from the Amadori compound,[18] and the FUR-RL calculation assumes that the remaining lysine is reactive. The conversion factors used in the furosine calculation are uncertain as these depend on the origin of the Amadori compound and the hydrolysis conditions.[18,20] The OMIU-RL calculated using the OMIU procedure measures the actual amount of free $\varepsilon$-amino groups when complete conversion occurs of lysine to homoarginine. Why the difference between OMIU-RL and FUR-RL is reversed when canned pet foods are analyzed is unknown. The analyzed concentration of RL can be affected by the measuring procedure, and it is important to take into account using either of the two procedures to measure RL.

The RL/TL ratio is often used as an indication of lysine damage during processing. Pelleted dog foods had the lowest mean RL/TL ratio (0.85), compared to extruded (0.89) and canned (0.97) dog foods and extruded (0.93) and canned (0.90) cat foods, respectively (Table 3).[12] Using OMIU-RL, the lowest RL/TL ratio was 0.67 and was found in an extruded junior cat food. The reported mean and minimal RL/TL ratios of the foods were higher compared to previous studies. Rutherfurd et al.[10] reported mean RL/TL ratios of 0.51 (minimum 0.38, maximum 0.61) for canned cat foods and of 0.59 (minimum 0.51, maximum 0.80) for dry cat foods. Williams et al.[9] reported mean RL/TL ratios of 0.85 (minimum 0.44, maximum 1.06) for adult dog foods and of 0.75 (minimum 0.47, maximum 0.98) for foods for growing dogs. It is, however, known that depending on the extent of the MR, some lysine may be converted to compounds that do not revert back to lysine during acid hydrolysis, thus reducing the total lysine content of the food. The RL/TL ratio, therefore, is valid when the RL/TL ratio of the unprocessed ingredient mixture is known, but is not suitable as an indicator of advanced MRPs that could have formed in processed pet foods.

**Presence of Common Markers of the Maillard Reaction.** The current study is the first to quantitate levels

**Table 2. Proximate Composition and Metabolizable Energy Content of 67 Commercial Pet Foods Categorized by Animal Species, Processing Type, and Life Stage (Mean ± Standard Error of the Mean, g/kg Dry Matter unless Defined Differently)[a]**

| | | dog | | | | | | cat | | | |
|---|---|---|---|---|---|---|---|---|---|---|---|
| | | extruded | | canned | | pelleted | | extruded | | canned | |
| component | | junior | adult | junior | adult | junior | adult | junior | adult | junior | adult |
| dry matter | mean | 922 ± 2.0 | 922 ± 4.2 | 231 ± 18.0 | 204 ± 16.4 | 909 ± 5.6 | 906 ± 6.3 | 940 ± 4.2 | 939 ± 6.4 | 241 ± 18.4 | 181 ± 4.8 |
| (g/kg "as is") | range | 908−938 | 910−932 | 187−296 | 169−259 | 900−931 | 885−922 | 919−972 | 915−949 | 198−296 | 168−196 |
| crude protein | mean | 302 ± 8.7 | 297 ± 39.8 | 513 ± 57.4 | 483 ± 56.6 | 260 ± 9.6 | 261 ± 9.9 | 394 ± 12.3 | 334 ± 9.2 | 701 ± 30.2 | 619 ± 39.1 |
| | range | 205−354 | 211−445 | 364−710 | 294−591 | 229−280 | 246−300 | 352−494 | 311−366 | 590−758 | 489−712 |
| crude fat | mean | 160 ± 8.6 | 132 ± 15.7 | 224 ± 26.7 | 222 ± 24.2 | 155 ± 12.1 | 92 ± 12 | 167 ± 11.8 | 179 ± 20.8 | 247 ± 15.5 | 239 ± 19.0 |
| | range | 107−210 | 98−190 | 158−309 | 165−276 | 116−188 | 63−128 | 119−240 | 115−233 | 217−300 | 198−303 |
| crude ash | mean | 74 ± 3.8 | 75 ± 6.2 | 105 ± 9.0 | 101 ± 16.7 | 78 ± 3.0 | 80 ± 3.6 | 83 ± 4.5 | 75 ± 7.6 | 90 ± 14.8 | 114 ± 8.4 |
| | range | 52−118 | 58−96 | 74−127 | 43−133 | 69−88 | 73−93 | 59−110 | 55−101 | 44−124 | 91−139 |
| crude fiber | mean | 18 ± 0.6 | 25 ± 1.3 | 11 ± 0.9 | 15 ± 2.5 | 22 ± 2.7 | 26 ± 2.3 | 16 ± 1.2 | 19 ± 3.7 | 10 ± 3.9 | 10 ± 3.4 |
| | range | 15−24 | 22−29 | 8−14 | 11−25 | 12−28 | 21−33 | 8−22 | 12−29 | 2−24 | 4−22 |
| nitrogen-free extract[b] | mean | 447 ± 14.8 | 472 ± 60.0 | 163 ± 55.9 | 181 ± 88.3 | 485 ± 21.0 | 541 ± 21.0 | 341 ± 22.5 | 393 ± 23.4 | 19 ± 19.2 | 50 ± 38.3 |
| | range | 342−595 | 240−577 | 0−341 | 0−482 | 443−558 | 467−589 | 168−426 | 320−466 | 0−96 | 0−199 |
| metabolizable energy[c] | mean | 16 ± 0.2 | 16 ± 0.3 | 5 ± 0.4 | 4 ± 0.3 | 16 ± 0.3 | 15 ± 0.2 | 17 ± 0.3 | 17± 0.6 | 5 ± 0.4 | 4 ± 0.1 |
| (MJ/kg "as is") | range | 15−17 | 15−16 | 3−6 | 3−5 | 15−17 | 14−15 | 16−19 | 15−18 | 4−6 | 3−4 |

[a] $n = 5$, except for extruded junior dog foods ($n = 16$) and extruded junior cat foods ($n = 11$). [b] Calculated as (g/DM) 1000 − crude fat − crude protein − crude ash − crude fiber. [c] Calculated using predictive equations for ME.[14]



dx.doi.org/10.1021/jf502064h | J. Agric. Food Chem. 2014, 62, 8883−8891

**Table 3. Total Lysine (TL), *O*-Methylisourea Reactive Lysine (OMIU-RL), Reactive Lysine Calculated Using the Furosine Method (FUR-RL), RL/TL Ratio, and Maillard Reaction Products Fructoselysine (FL), Carboxymethyllysine (CML), Hydroxymethylfurfural (HMF), and the Cross-Linked Amino Acid Lysinoalanine (LAL) of 67 Commercial Pet Foods Categorized by Animal Species, Processing Type, and Life Stage (Mean ± Standard Error of the Mean, g/kg Dry Matter unless Defined Differently)[a]**

| | | dog | | | | | | cat | | | |
|---|---|---|---|---|---|---|---|---|---|---|---|
| | | extruded | | canned | | pelleted | | extruded | | canned | |
| variable | | junior | adult | junior | adult | junior | adult | junior | adult | junior | adult |
| TL | mean | 13.7 ± 0.9 | 14.5 ± 3.0 | 28.4 ± 5.0 | 24.2 ± 3.2 | 12.7 ± 0.9 | 11.6 ± 0.8 | 17.4 ± 1.4 | 16.4 ± 1.6 | 44.3 ± 3.7 | 36.5 ± 2.5 |
| | range | 8.08−24.12 | 9.08−26.04 | 19.42−44.88 | 16.27−32.83 | 10.62−15.70 | 10.17−14.44 | 12.51−28.00 | 12.50−20.24 | 36.19−55.09 | 27.42−40.80 |
| OMIU-RL[b] | mean | 11.9 ± 0.9 | 13.2 ± 2.8 | 27.1 ± 4.5 | 23.9 ± 3.6 | 10.9 ± 0.8 | 9.9 ± 0.8 | 15.0 ± 1.1 | 15.9 ± 1.8 | 40.7 ± 4.9 | 32.1 ± 2.2 |
| | range | 6.63−20.43 | 7.09−23.38 | 18.74−41.54 | 13.45−32.64 | 9.13−13.58 | 8.59−12.88 | 11.86−23.20 | 11.73−20.08 | 30.60−52.87 | 25.63−36.82 |
| FUR-RL[c] | mean | 13.3 ± 1.0 | 14.1 ± 3.0 | 26.2 ± 4.8 | 21.7 ± 2.8 | 11.9 ± 1.2 | 11.5 ± 0.8 | 16.9 ± 1.4 | 15.9 ± 1.6 | 41.3 ± 4.1 | 34.1 ± 2.4 |
| | range | 7.73−23.95 | 8.83−25.75 | 16.06−40.84 | 14.77−28.32 | 8.35−15.53 | 10.08−14.26 | 11.90−27.33 | 12.28−19.60 | 34.14−53.88 | 25.50−38.51 |
| RL/TL[d] | mean | 0.87 ± 0.02 | 0.90 ± 0.03 | 0.96 ± 0.02 | 0.98 ± 0.04 | 0.86 ± 0.02 | 0.84 ± 0.01 | 0.88 ± 0.03 | 0.97 ± 0.02 | 0.91 ± 0.05 | 0.88 ± 0.02 |
| | range | 0.77−0.99 | 0.78−0.97 | 0.92−1.03 | 0.83−1.10 | 0.78−0.94 | 0.81−0.89 | 0.67−0.98 | 0.91−1.03 | 0.75−1.03 | 0.82−0.93 |
| FL[e] | mean | 0.58 ± 0.04 | 0.71 ± 0.19 | 4.00 ± 1.26 | 4.46 ± 0.94 | 1.48 ± 0.71 | 0.21 ± 0.05 | 0.80 ± 0.08 | 0.73 ± 0.18 | 5.38 ± 1.67 | 4.30 ± 0.35 |
| | range | 0.30−0.82 | 0.38−1.44 | 1.57−7.21 | 2.67−8.06 | 0.31−4.05 | 0.11−0.33 | 0.42−1.19 | 0.38−1.32 | 2.15−11.45 | 3.43−5.15 |
| CML[f] | mean | 11.23 ± 0.66 | 15.40 ± 1.31 | 29.88 ± 7.39 | 36.50 ± 6.00 | 24.39 ± 4.63 | 16.07 ± 2.15 | 10.87 ± 0.82 | 13.25 ± 2.81 | 38.76 ± 4.11 | 41.61 ± 5.65 |
| | range | 7.75−16.67 | 13.24−20.22 | 12.27−50.61 | 20.42−54.69 | 16.00−40.30 | 11.99−21.58 | 7.72−17.26 | 6.01−20.72 | 27.40−51.65 | 26.74−60.54 |
| HMF | mean | 0.65 ± 0.06 | 1.11 ± 0.27 | 1.79 ± 0.59 | 1.70 ± 0.33 | 0.92 ± 0.21 | 1.40 ± 0.26 | 0.64 ± 0.08 | 0.47 ± 0.07 | 1.24 ± 0.37 | 0.93 ± 0.12 |
| | range | 0.33−1.25 | 0.27−1.92 | 0.34−2.82 | 1.33−3.02 | 0.52−1.70 | 0.91−2.38 | 0.27−1.02 | 0.24−0.64 | 0.07−2.29 | 0.59−1.24 |
| LAL[f] | mean | 7.76 ± 0.63 | 6.41 ± 1.19 | 5.80 ± 0.64 | 7.64 ± 1.06 | 6.14 ± 0.89 | 10.24 ± 1.82 | 5.55 ± 0.78 | 7.23 ± 0.82 | 6.77 ± 1.41 | 7.32 ± 1.29 |
| | range | 4.25−12.95 | 3.15−9.33 | 4.05−7.45 | 3.49−9.49 | 4.12−8.54 | 6.31−16.11 | 1.39−9.49 | 5.09−10.02 | 1.59−9.69 | 4.22−11.63 |

[a] $n = 5$, except for extruded junior dog foods ($n = 16$) and extruded junior cat foods ($n = 11$). [b] Reactive lysine analyzed using the *O*-methylisourea procedure. [c] Reactive lysine analyzed using the furosine procedure; calculated as total lysine − regenerated lysine.[19] [d] Ratio, calculated as reactive lysine/total lysine (TL and RL in g/kg dry matter). [e] Calculated as furosine/(32/100).[18] [f] In mg/kg dry matter.



dx.doi.org/10.1021/jf502064h | J. Agric. Food Chem. 2014, 62, 8883−8891

of various MRPs in commercial pet foods. High variation in MRP content was seen between as well as within processing type. Canned pet foods contained on average the most FL, CML, and HMF followed by pelleted and extruded foods (FL, 4534, 844, 706; CML, 37, 20, 12; HMF, 1417, 1161, 715 mg/kg DM, respectively; Table 3). However, when expressed on an "as is" basis, canned pet foods contain the lowest CML and HMF contents. In dry dog foods, the mean contents of FL, CML, and HMF were higher in pellets than in extrudates (FL, 844 vs 646 mg/kg DM; CML, 20 vs 13 mg/kg DM; HMF, 1161 vs 880 mg/kg DM, respectively). The HMF content in pelleted dog foods is much higher than previously reported in a pelleted piglet starter diet (16.66 mg/kg).[21] For LAL, the means are comparable between processing types. The only study to date focusing on MRP content in pet foods reported a FL content of 2840 mg/kg "as is" in one dry dog food.[13] This level is twice as high as the highest level for the dry extruded dog foods in the present study (1440 mg/kg DM), but not as high as the highest level for pelleted junior dog foods (4050 mg/kg DM). No data are available for comparison of the CML, HMF, and LAL in pet foods. However, several studies are available that evaluated these advanced MRPs in human food items. CML concentrations in human foods were found to range between 0.1 and 68.7 mg/kg in meat and fish products, between 1.0 and 423.9 mg/kg in meat dishes, between 7.6 and 54.2 mg/kg in cereals, and between 0.5 and 39.4 mg/L in infant formulas.[22−27] The manner of processing has an influence on the level of CML; raw minced beef contained less CML (0.7 mg/kg) than boiled and fried minced beef (5.0 and 11.2 mg/kg CML, respectively).[28] Increasing CML levels with increasing severity of processing was also found in roasted beef joint (1.5, 2.5, and 4.2 mg/kg for rare, medium-rare, and well-done, respectively)[22] and chicken breast (3.8, 4.6, 5.1, and 23.9 mg/kg, for boiled, roasted, fried, and casseroled breast, respectively). HMF levels in human foods were found in the ranges of 91.3−3060 mg/kg in instant coffee (values for ground roasted coffee beans were found within this range),[29−31] 6.6−241 mg/kg in breakfast cereals,[32] 0.2−69 mg/kg in white bread,[31,33] 0.5−74.6 mg/kg in cookies,[17] and 0.2−34.7 mg/L in infant formulas.[34−37] LAL levels of 10−70 mg/kg for baby food, 200−300 mg/kg for cereal products, 150−920 mg/kg for dry infant formulas, and 140−540 mg/kg for meat products were reported in human foods.[3] However, Raymond[38] reported lower levels for LAL, 0−70 mg/kg for ready-to-eat cereals, 0 mg/kg for pasta, 0−50 mg/kg for infant formula, 0 mg/kg for prepared meat, and 0−120 mg/kg for canned fish. The CML, HMF, and LAL levels of the analyzed pet foods are within the range reported for human foods (Table 3).

**Daily Intake of Common Markers of the Maillard Reaction.** On the basis of the MRPs and the calculated ME contents of the pet foods, daily MRP intake can be estimated. A 20 kg adult dog having a daily energy requirement of 5.15 MJ ME[14] would ingest 0.50 mg CML and 34.58 mg HMF/kg body weight (BW)$^{0.75}$/day when eating an extruded diet with an average content of 3.83 and 266.00 mg CML and HMF/4.18 MJ ME (Figure 1). An adult cat (4 kg) with a daily energy requirement of 1.06 MJ ME[14] would ingest 0.28 mg CML and 10.90 mg HMF/kg BW$^{0.75}$/day when consuming an extruded diet with an average of 3.12 and 121.80 mg CML and HMF/4.18 MJ ME. For canned and pelleted diets, these values were even higher (Figure 1). Limited estimates are available for humans, and these may be influenced by country, region, social class, and age. For Spanish adolescents, a mean daily intake of

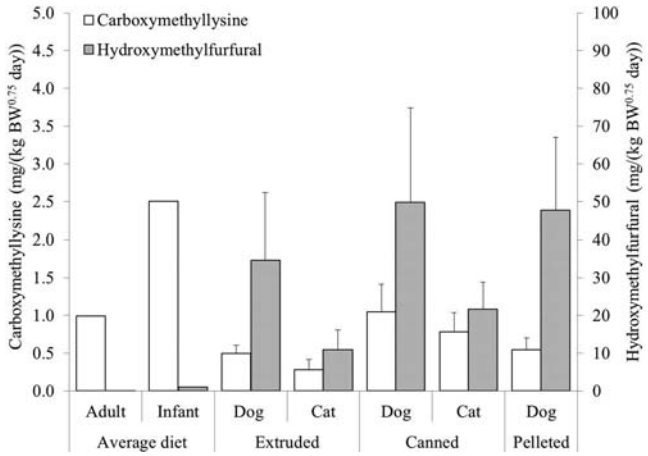


**Figure 1.** Estimated daily intake (mg/kg body weight (BW)$^{0.75}$) of carboxymethyllysine and hydroxymethylfurfural of a 70 kg adult human consuming a standard Western diet,[22,31,32,39] a 6 kg human infant consuming 1 L of an average infant formula,[23−27,34−37] and a 20 kg adult dog and a 4 kg adult cat fed either an extruded, canned, or pelleted diet for adult dogs and cats at maintenance (using a standard daily energy requirement[14]) containing an average ± standard deviation content of carboxymethyllysine and hydroxymethylfurfural as reported in the current study.

0.99 mg CML/kg BW$^{0.75}$ (70 kg BW) was estimated.[39] The CML content in infant formulas was quantified in five studies. Assuming a daily intake of 1 L for a 6 kg infant, daily CML intake ranges from 0.49 to 39.38 mg corresponding to mean values of 1.23, 3.69, 4.60, 4.75, and 33.77 mg.[23−27] For HMF, the mean intake for adult humans in three different studies was 5.08, 5.56, and 10 mg per day,[31,32,39] resulting in an average daily intake of 0.28 mg HMF/kg BW$^{0.75}$. HMF levels in infant formulas range from 0.158 to 34.7 mg/L,[34−37] resulting in average daily values of 0.16, 0.32, 0.38, and 13.9 mg/L. This results in an average daily intake of 0.96 mg HMF/kg BW$^{0.75}$. Compared to the calculated average for human adults, dogs may ingest up to 122 times more HMF when consuming an average extruded dog food (Figure 1). In addition, dogs may ingest up to 36 times more HMF compared to human infants fed infant formula. Cats consuming an average extruded cat food may ingest up to 38 times more HMF compared to adult humans and 11 times more HMF compared to human infants. Dogs and cats fed canned and pelleted diets are more likely to ingest higher amounts of HMF and CML compared to animals that are fed an extruded diet. No data are available regarding the average daily intake of LAL in humans. Both CML and HMF from consumed foods can cross the intestinal wall and enter the circulation. In rats, dietary HMF has been shown to be rapidly absorbed, metabolized into 5-hydroxymethyl-2-furoic acid and *N*-(5-hydroxymethyl-2-furoyl)glycine as main metabolites, and 70−82% of the ingested HMF is excreted via the urine within 48 h.[40] No evidence for prolonged accumulation in body tissues was observed. No adverse effects regarding acute and subacute toxicity in rats and mice ingesting HMF concentrations of 80−100 mg/kg body weight was reported.[41] In humans, intake of dietary CML resulted in an increase in circulatory CML concentration.[42] In rats, approximately 26−29% of the ingested CML was excreted in the urine, whereas in humans 14% of ingested dietary CML was excreted in urine.[8,43] Around 50% of the ingested CML was not recovered, and it is unknown if it is deposited in organs, degraded by colonic

**Table 4. Linear Regression Coefficients Animal Species, Life Stage, Processing Type, Proximate Composition (g/kg Dry Matter unless Defined Differently) on Fructoselysine (FL),[a] Carboxymethyllysine (CML), Hydroxymethylfurfural (HMF), and Lysinoalanine (LAL) in 67 Commercial Pet Foods (g/kg Dry Matter; Estimate ± Standard Error)**

| variable | Ln(FL) ($R^2$ = 0.70) | Sqrt(CML) ($R^2$ = 0.73) | Sqrt(HMF) ($R^2$ = 0.48) | LAL ($R^2$ = 0.00) |
|---|---|---|---|---|
| intercept | 8.29 ± 0.13 | 7.04 ± 0.93 | 59.15 ± 7.07 | 7.03 ± 0.33 |
| animal species | –[b] | – | – | – |
| dog | | | | |
| cat | | | | |
| processing type[c] | | | | – |
| extruded | 1.84 ± 0.17 | 5.93 ± 2.7 | −24.91 ± 3.40 | |
| canned | 0 | 0 | 0 | |
| pelleted | 2.25 ± 0.22 | 6.85 ± 2.64 | −22.79 ± 4.57 | |
| life stage | – | – | – | – |
| adult | | | | |
| junior | | | | |
| dry matter (g/kg) | – | −0.01 ± 0.004 | – | – |
| crude protein | – | – | −0.05 ± 0.01 | – |
| crude fat | – | 0.006 ± 0.002 | – | – |
| crude fiber | – | – | 0.35 ± 0.17 | – |
| crude ash | – | – | – | – |
| NFE[d] | – | – | – | – |
| RMSE[e] | 0.59 | 0.73 | 7.29 | 2.72 |

[a]Calculated as furosine/(32/100).[18] [b]–, no significant correlation. [c]Extruded pet foods $n$ = 37, canned pet foods $n$ = 20, pelleted pet foods $n$ = 10. [d]NFE, nitrogen-free extract calculated as 1000 − crude fat − crude protein − crude ash − crude fiber. [e]RMSE, root mean squared error.

microbiota, or metabolized. Whether the MRPs in pet foods are absorbed and excreted when consumed, and subsequently add to the endogenous AGE load in dogs and cats, remains to be investigated.

**Dietary Factors Associated with the Occurrence of the Maillard Reaction.** Dietary factors associated with variation in advanced MRP content of pet foods are shown in Table 4. The levels of MRPs in pet foods were not related to animal species or life stage; however, type of pet food shows a correlation for FL, CML, and HMF (Table 4). The processing conditions between pelleting, extrusion, and canning differ considerably. Extruded kibbles are processed at temperatures of 80−200 °C for 10−270 s under high pressure.[44] Canned foods are heated until the center of the can reaches temperatures of 121 °C for >10 min to sterilize the product.[45] Pelleted foods are relatively mildly heat treated using temperatures of 60−90 °C for 30−45 s.[46] In addition, pet food ingredients can be extensively processed (i.e., rendered, cooked, dried, and/or ground) before inclusion. Depending on the severity of the processing, the MR progresses through several stages of the reaction. Overall, pelleted foods contain more CML and HMF compared to extruded foods (and canned foods when expressed on an "as is" basis). This result is unexpected considering the rather mild heat treatment used during pelleting compared to extrusion conditions. Because of this mild heat treatment, ingredients used during pelleting are often preprocessed. Carbohydrate sources, for example, are often pretreated as pelleting processing temperatures and residence times are not sufficiently high to fully gelatinize the starch in the raw ingredients during processing.[47] It could, therefore, be that the MRP contents in pellets mainly originate from the preprocessed ingredients rather than de novo formation due to the processing itself. Analyses of ingredients and food mixtures prior to processing are required to confirm this hypothesis. LAL content in pet foods is comparable between processing types and is not associated with type of processing. With regard to the chemical composition, CML was associated with CFat content. Besides the MR, lipid peroxidation during processing results in the intermediate glyoxal, which can react with lysine to form CML.[48] Next to the association with CFat, CML content showed a strong correlation with FL content ($r$ = 0.78; $P$ < 0.0001), which reflects the formation of CML from FL via an oxidation pathway.[49] HMF was associated with a decreased CP content and increased CFiber content. CML is moderately correlated to HMF ($r$ = 0.45; $P$ = 0.0001). The MR pathways that result in the formation of CML and HMF are different but apparently occur in a certain ratio during the processing of pet foods. No factor was associated with the content of LAL in the analyzed pet foods.

In conclusion, this study demonstrates that pet foods do contain Maillard reaction products. Type of processing seems to be a key factor for the concentration of FL, CML, and HMF, with on average higher amounts in wet canned pet foods than in dry extruded or pelleted pet foods (DM basis). LAL contents were similar for wet canned and dry pet foods. Further research is required to determine the contribution of pet food processing and the use of processed ingredients in the observed concentrations of Maillard reaction products in pet foods. Average daily intake of MRPs in pet animals can be higher compared to limited adult human and infant data. As commercial pet foods are most often the only source of food for dogs and cats, future research focus should be on the bioavailability and long-term health implications of MRP consumption by dogs and cats.

## ■ ASSOCIATED CONTENT

### Supporting Information

Table S1. Amino acid composition of 67 commercial pet foods categorized by animal species, processing type, and life stage. This material is available free of charge via the Internet at http://pubs.acs.org.

## AUTHOR INFORMATION


### Corresponding Author

*(G.B.) Mail: De Elst 1, 6708 WD, Wageningen, The Netherlands. Phone: +31 317 482982. Fax: +31 317 483962. E-mail: guido.bosch@wur.nl.


### Author Contributions

All authors contributed fundamentally to the present manuscript. C.v.R. contributed to all facets including data collection, calculations, and writing the initial manuscript. Other authors contributed to study design, data interpretation, and manuscript preparation.


### Funding

The project for which this work was conducted is jointly financed by the European Union, European Regional Development Fund, and The Ministry of Economic Affairs, Agriculture and Innovation, Peaks in the Delta, the Municipality of Groningen, the Province of Groningen, and MARS Petcare as well as the Dutch Carbohydrate Competence Center (CCC WP 5). MARS Petcare was involved in study design, data interpretation, and manuscript preparation. All other funders had no role in the design, analysis, or writing of this paper.


### Notes

The authors declare the following competing financial interest(s): Lucille Alexander is an employee of Mars Petcare.

## ACKNOWLEDGMENTS

We thank Michel Breuer and Edwin Bakx for their assistance during the analyses.

## ABBREVIATIONS USED

ACN, acetonitrile; AGEs, advanced glycation end-products; BW, body weight; CML, *ε-N*-carboxymethyllysine; CFat, crude fat; CFiber, crude fiber; CP, crude protein; DM, dry matter; FL, fructoselysine; HCl, hydrochloric acid; HMF, (5-hydroxymethyl)-2-furfural; LAL, lysinoalanine; ME, metabolizable energy; MR, Maillard reaction; MRPs, Maillard reaction products; MS, mass spectrometric; NFE, nitrogen-free extract; NFPA, nonafluoropentanoic acid; OMIU, *O*-methylisourea; RL, reactive lysine; SEM, standard error of the mean; SRM, selected reaction monitoring; TCA, trichloroacetic acid; TL, total lysine

## REFERENCES


(1) Hodge, J. E. Dehydrated foods − chemistry of browning reactions in model systems. *J. Agric. Food Chem.* **1953**, *1*, 928−943.

(2) Finot, P. A. The absorption and metabolism of modified amino acids in processed foods. *J. AOAC Int.* **2005**, *88*, 894−903.

(3) Friedman, M. Chemistry, biochemistry, nutrition, and microbiology of lysinoalanine, lanthionine, and histidinoalanine in food and other proteins. *J. Agric. Food Chem.* **1999**, *47*, 1295−1319.

(4) Erbersdobler, H. F.; Somoza, V. Forty years of furosine − forty years of using Maillard reaction products as indicators of the nutritional quality of foods. *Mol. Nutr. Food Res.* **2007**, *51*, 423−430.

(5) Thorpe, S. R.; Baynes, J. W. Maillard reaction products in tissue proteins: new products and new perspectives. *Amino Acids* **2003**, *25*, 275−281.

(6) Van Rooijen, C.; Bosch, G.; Van der Poel, A. F. B.; Wierenga, P. A.; Alexander, L.; Hendriks, W. H. The Maillard reaction and pet food processing: effects on nutritive value and pet health. *Nutr. Res. Rev.* **2013**, *26*, 130−148.

(7) Förster, A.; Kühne, Y.; Henle, T. Studies on absorption and elimination of dietary Maillard reaction products. *Ann. N.Y. Acad. Sci.* **2005**, *1043*, 474−481.

(8) Delgado-Andrade, C.; Tessier, F. J.; Niquet-Leridon, C.; Seiquer, I.; Pilar Navarro, M. Study of the urinary and faecal excretion of $N^{\varepsilon}$-carboxymethyllysine in young human volunteers. *Amino Acids* **2012**, *43*, 595−602.

(9) Williams, P. A.; Hodgkinson, S. M.; Rutherfurd, S. M.; Hendriks, W. H. Lysine content in canine diets can be severely heat damaged. *J. Nutr.* **2006**, *136*, 1998S−2000S.

(10) Rutherfurd, S. M.; Rutherfurd-Markwick, K. J.; Moughan, P. J. Available (ileal digestible reactive) lysine in selected pet foods. *J. Agric. Food Chem.* **2007**, *55*, 3517−3522.

(11) Tran, Q. D.; van Lin, C. G. J. M.; Hendriks, W. H.; van der Poel, A. F. B. Lysine reactivity and starch gelatinization in extruded and pelleted canine diets. *Anim. Feed Sci. Technol.* **2007**, *138*, 162−168.

(12) Van Rooijen, C.; Bosch, G.; Van der Poel, A. F. B.; Wierenga, P. A.; Alexander, L.; Hendriks, W. H. Reactive lysine content in commercially available pet foods. *J. Nutr. Sci.* **2014**.

(13) Chiang, G. H. A simple and rapid high-performance liquid chromatographic procedure for determination of furosine, lysine-reducing sugare derivative. *J. Agric. Food Chem.* **1983**, *31*, 1373−1374.

(14) NRC. *Nutrient Requirements of Dogs and Cats*; National Academy Press: Washington, DC, USA, 2006.

(15) Hendriks, W. H.; Moughan, P. J.; Tarttelin, M. F. Gut endogenous nitrogen and amino acid excretions in adult domestic cats fed a protein-free diet or an enzymatically hydrolyzed casein-based diet. *J. Nutr.* **1996**, *126*, 955−962.

(16) Moughan, P. J.; Rutherfurd, S. M. A new method for determining digestible reactive lysine in foods. *J. Agric. Food Chem.* **1996**, *44*, 2202−2209.

(17) Ameur, L. A.; Trystram, G.; Birlouez-Aragon, I. Accumulation of 5-hydroxymethyl-2-furfural in cookies during the backing process: validation of an extraction method. *Food Chem.* **2006**, *98*, 790−796.

(18) Krause, R.; Knoll, K.; Henle, T. Studies on the formation of furosine and pyridosine during acid hydrolysis of different Amadori products of lysine. *Eur. Food Res. Technol.* **2003**, *216*, 277−283.

(19) Pahm, A. A.; Pedersen, C.; Stein, H. H. Application of the reactive lysine procedure to estimate lysine digestibility in distillers dried grains with solubles fed to growing pigs. *J. Agric. Food Chem.* **2008**, *56*, 9441−9446.

(20) Giménez, E. C.; Bénet, T.; Spack, L. The uncertainty in the calculation of the amount of blocked and reactive lysine in milk products, as determined by the furosine method. *Accredit. Qual. Assur.* **2004**, *9*, 605−614.

(21) Delgado-Andrade, C.; Rufián-Henares, J. A.; Nieto, R.; Aguilera, J. F.; Pilar Navarro, M.; Seiquer, I. Does the pelleting process affect the nutritive value of a pre-starter diet for suckling piglets? *Ex vivo* studies on mineral absorption. *J. Sci. Food Agric.* **2010**, *90*, 898−905.

(22) Hull, G. L. J.; Woodside, J. V.; Ames, J. M.; Cuskelly, G. J. $N^{\varepsilon}$-(carboxymethyl)lysine content of foods commonly consumed in a Western style diet. *Food Chem.* **2012**, *131*, 170−174.

(23) Birlouez-Aragon, I.; Pischetsrieder, M.; Leclère, J.; Morales, F. J.; Hasenkopf, K.; Kientsch-Engel, R.; Ducauze, C. J.; Rutledge, D. Assessment of protein glycation markers in infant formulas. *Food Chem.* **2004**, *87*, 253−259.

(24) Dittrich, R.; Hoffmann, I.; Stahl, P.; Müller, A.; Beckmann, M. W.; Pischetsrieder, M. Concentrations of $N^{\varepsilon}$-carboxymethyllysine in human breast milk, infant formulas, and urine of infants. *J. Agric. Food Chem.* **2006**, *54*, 6924−6928.

(25) Šebeková, K.; Saavedra, G.; Zumpe, C.; Somoza, V.; Klenovicsová, K.; Birlouez-Aragon, I. Plasma concentration and urinary excretion of $N^{\varepsilon}$-(carboxymethyl) lysine in breast milk- and formula-fed infants. *Ann. N.Y. Acad. Sci.* **2008**, *1126*, 177−180.

(26) Fenaille, F.; Parisod, V.; Visani, P.; Populaire, S.; Tabet, J.-C.; Guy, P. A. Modifications of milk constituents during processing: a preliminary benchmarking study. *Int. Dairy J.* **2006**, *16*, 728−739.

(27) Delatour, T.; Hegele, J.; Parisod, V.; Richoz, J.; Maurer, S.; Steven, M.; Buetler, T. Analysis of advanced glycation endproducts in dairy products by isotope dilution liquid chromatography−electrospray tandem mass spectrometry. The particular case of carboxymethyllysine. *J. Chromatogr., A* **2009**, *1216*, 2371−2381.

(28) Assar, S. H.; Moloney, C.; Lima, M.; Magee, R.; Ames, J. M. Determination of $N^{\varepsilon}$-carboxymethyllysine in food systems by ultra

performance liquid chromatography-mass spectrometry. *Amino Acids* **2009**, *36*, 317−326.
(29) Arribas-Lorenzo, G.; Morales, F. J. Estimation of dietary intake of 5-hydroxymethylfurfural and related substances from coffee to Spanish population. *Food Chem. Toxicol.* **2010**, *48*, 644−649.
(30) Murkovic, M.; Pichler, N. Analysis of 5-hydroxymethylfurfual in coffee, dried fruits and urine. *Mol. Nutr. Food Res.* **2006**, *50*, 842−846.
(31) Husøy, T.; Haugen, M.; Murkovic, M.; Jöbstl, D.; Stølen, L. H.; Bjellaas, T.; Rønningborg, C.; Glatt, H.; Alexander, J. Dietary exposure to 5-hydroxymethylfurfural from Norwegian food and correlations with urine metabolites of short-term exposure. *Food Chem. Toxicol.* **2008**, *46*, 3697−3702.
(32) Rufián-Henares, J. A.; de la Cueva, S. P. Assessment of hydroxymethylfurfural intake in the Spanish diet. *Food Addit. Contam.* **2008**, *25*, 1306−1312.
(33) Ramírez-Jiménez, A.; Guerra-Hernández, E.; García-Villanova, B. Browning indicators in bread. *J. Agric. Food Chem.* **2000**, *48*, 4176−4181.
(34) Chávez-Servín, J. L.; Castellote, A. I.; López-Sabater, M. C. Evolution of potential and free furfural compounds in milk-based infant formula during storage. *Food Res. Int.* **2006**, *39*, 536−543.
(35) Guerra-Hernandez, E.; Leon Gomez, C.; Garcia-Villanova, B.; Corzo Sanchez, N.; Romera Gomez, J. M. Effect of storage on non-enzymatic browning of liquid infant milk formulae. *J. Sci. Food Agric.* **2002**, *82*, 587−592.
(36) Albalá-Hurtado, S.; Veciana-Nogués, M. T.; Izquierdo-Pulido, M.; Vidal-Carou, M. C. Determination of free and total furfural compounds in infant milk formulas by high-performance liquid chromatography. *J. Agric. Food Chem.* **1997**, *45*, 2128−2133.
(37) Morales, F. J.; Jiménez-Pérez, S. Hydroxymethylfurfural determination in infant milk-based formulas by micellar electrokinetic capillary chromatography. *Food Chem.* **2001**, *72*, 525−531.
(38) Raymond, M. L. Studies concerning the determination of lysinoalanine in food proteins. *J. Food Sci.* **1980**, *45*, 56−59.
(39) Delgado-Andrade, C.; Seiquer, I.; Navarro, M. P.; Morales, F. J. Maillard reaction indicators in diets usually consumed by adolescent population. *Mol. Nutr. Food Res.* **2007**, *51*, 341−351.
(40) Godfrey, V. B.; Chen, L. J.; Griffin, R. J.; Lebetkin, E. H.; Burka, L. T. Distribution and metabolism of (5-hydroxymethyl)furfural in male F344 rats and B6C3F1 mice after oral administration. *J. Toxicol. Environ. Health A* **1999**, *57*, 199−210.
(41) Abraham, K.; Gürtler, R.; Berg, K.; Heinemeyer, G.; Lampen, A.; Appel, K. E. Toxicology and risk assessment of 5-hydroxymethylfurfural in food. *Mol. Nutr. Food Res.* **2011**, *55*, 667−678.
(42) Uribarri, J.; Cai, W.; Sandu, O.; Peppa, M.; Goldberg, T.; Vlassara, H. Diet-derived advanced glycation end products are major contributors to the body's AGE pool and induce inflammation in healthy subjects. *Ann. N.Y. Acad. Sci.* **2005**, *1043*, 461−466.
(43) Ames, J. M. Evidence against dietary advanced glycation endproducts being a risk to human health. *Mol. Nutr. Food Res.* **2007**, *51*, 1085−1090.
(44) Crane, S. W.; Cowell, C. S.; Stout, N. P.; Moser, E. A.; Millican, J.; Romano, P.; Crane, S. E. Chapter 8. Commercial pet foods. In *Small Animal Clinical Nutrition*, 5th ed.; Hand, M. S., Thatcher, C. D., Remillard, R. L., Roudebush, P., Novotny, B. J., Eds.; Mark Morris Institute: Topeka, KS, USA, 2010; pp 156−190.
(45) Hendriks, W. H.; Emmens, M. M.; Trass, B.; Pluske, J. R. Heat processing changes the protein quality of canned cat foods as measured with a rat bioassay. *J. Anim. Sci.* **1999**, *77*, 669−676.
(46) Thomas, M.; Van Zuilichem, D. J.; Van der Poel, A. F. B. Physical quality of pelleted animal feed. 2. Contribution of processes and its conditions. *Anim. Feed. Sci. Technol.* **1997**, *64*, 173−192.
(47) Svihus, B.; Uhlen, A. K.; Harstad, O. M. Effect of starch granule structure, associated components and processing on nutritive value of cereal starch: a review. *Anim. Feed Sci. Technol.* **2005**, *122*, 303−320.
(48) Wells-Knecht, K. J.; Zyzak, D. V.; Litchfield, J. E.; Thorpe, S. R.; Baynes, J. W. Mechanism of autoxidative glycolysation: Identification of glyoxal and arabinose as intermediates in the autoxidative modification of proteins by glucose. *Biochemistry* **1995**, *34*, 3702−3709.
(49) Ahmed, M. U.; Frye, E. B.; Degenhardt, T. P.; Thorpe, S. R.; Baynes, J. W. $N^{\varepsilon}$-(Carboxyethyl)lysine, a product of the chemical modification of proteins by methylglyoxal, increases with age in human lens proteins. *Biochem. J.* **1997**, *324*, 565−570.

oxygen through the barrel depends on the permeability of the wood used, its thickness, and the oxygen concentration difference between both sides. Thus, the rate of gas diffusion $dV/dt$ can be calculated by Fick's law, where $V$ is the volume of oxygen diffused, $t$ is time, $\mu$ is permeability, $d$ is the thickness of the stave, $\Delta P$ is the difference in the partial pressure of the gas, and $A$ is area. Thus, oxygen transfer rates (OTRs) of up to 2.2 mL/L per month (37 mg/L per year) are theoretically justified.[5]

$$\frac{dV}{dt} = \mu A \times \frac{\Delta P}{d}$$

In this work, results are shown from studying the OTRs of barrels by measuring the temporal variations in oxygen in the barrel. A system was used to measure dissolved oxygen in liquids without altering the environment. To date, different authors who have studied oxygen supply to wine in oak barrels have measured the processes at one point during aging (6 months) and have extrapolated this value to obtain annual data without considering possible changes in the rate of oxygen supply with time. This work demonstrates a more realistic approach to what (until now) has been called the OTR, which studies the dynamics of oxygen supply to wine in barrels with aging time. This study focused on the importance of the type of wood of the barrel (American oak, *Quercus alba*; and French oak, *Quercus petraea*), as well as the aging time of the wine, during 1 year of study.

Overall, the oxygen permeability of the barrels was modified by aging time. Thus, 50% of the total oxygen was received by the wine within the first 4 months of the 1 year aging period.

## MATERIALS AND METHODS

**Oak Barrels.** The characteristics of the 12 Bordeaux barrels (225 L) that were used in this study are presented in Table 1. This experiment was conducted in three parts. First, the dissolved oxygen gradient in the liquid within the barrel was studied (B0, Table 1). Next, OTRs were assessed for new American oak (B1–B8, Table 1) and French oak (B9–B12, Table 1) barrels. Finally, four of the new barrels from the same American oak cooperage (B5–B8, Table 1) that were previously analyzed in part 2 were systematically analyzed for 12 months. This trial made it possible to determine the kinetic variations of oxygen infiltration into the barrel with time and to establish the annual OTR.

**Table 1. Characteristics of Tested American and French Oak Barrels with Medium Toast**

| cooperage | origin[a] | barrel | grain |
|---|---|---|---|
| C1 | American | B0 | fine |
| C1 | American | B1 | medium |
| C1 | American | B2 | medium |
| C1 | American | B3 | medium |
| C1 | American | B4 | medium |
| C1 | American | B5 | fine |
| C1 | American | B6 | fine |
| C1 | American | B7 | fine |
| C1 | American | B8 | fine |
| C2 | French | B9 | fine |
| C2 | French | B10 | fine |
| C2 | French | B11 | fine |
| C2 | French | B12 | fine |

[a]Origin according to cooperage information.

**Dissolved Oxygen (DO) Distribution Measurements of a Model Wine in the Barrel.** To determine the oxygen distribution within the liquid in the barrel, it was important to guarantee that no wine compounds were consuming oxygen. Thus, a model wine (pure water and ethanol at 15% v/v, pH 3.5) was chosen without oxygen scavengers to monitor the formation and evolution of DO gradients. In addition, an oxygen mass balance was conducted to determine the OTR.

The temperature of the fluid inside the barrel was measured on different days at the eight different depths of the DO probes to verify that no temperature gradient occurred (Figure 1). Thus, oxygen gradient tests were conducted in the synthetic wine. During the tests with the model wine in a climatically controlled cellar, the room temperature was maintained at 15 ± 1 °C and the humidity was maintained at 65–75% to mimic the common hydrothermal properties of the air in actual cellars. During the first part of the study, eight independent channels were used to measure the DO evolution simultaneously during the test. The DO concentrations were measured with eight optical probes that were immersed at different depths (Table 2) inside the oak barrel (Figure 1). These probes were equipped with a luminescent sensor on their extremity. The luminescent systems selected for this work were of the Oxy-trace (PreSens GmbH, Germany) series and worked with the PSt6 (detection limit = 1 ppb, 0–4.2% oxygen) trace oxygen sensor coating type as described in previous studies.[6] Eight submergible oxygen probes were monitored with two OXY-4 trace transmitters (PreSens GmbH) that were connected to a PC.

During the second and third parts of this study, two optical fibers with submergible probes were placed in each of the barrels through the silicone bung to obtain simultaneous continuous measurements from the four barrels. The study of the equations representing DO evolution enables selection of two probes, of the eight placed to measure it, of which average measurements are representative of the whole barrel DO average.

The oxygen systems were calibrated in a tonometer[7] by using the conventional two-point calibration method in the synthetic wine that was saturated with nitrogen (cal 0). A calibration gas mixture of 2.001% (±0.5% rel) pure oxygen gas in nitrogen (9.55% air saturation) was used as the second calibration standard (Carburos Metálicos, Spain). Both gases were sparged into the tonometer for 10 min at 15 ± 0.01 °C until stable conditions were achieved by a Julabo FP40-ME thermostatic bath (Seelbach, Germany). For more details regarding the calibration procedure, please see ref 6.

**Measurement Conditions.** Prior to use, the barrels were washed to remove toasting powder before filling with the model wine. Four sintered stainless steel diffusers were placed inside each barrel. Each diffuser had a pore size of 1 $\mu$m and was connected to a nitrogen line to displace DO from the model wine until it reached DO concentrations between 0.01 and 0.1 hPa. This process was performed before each test for 12 h to prevent overflow of the barrels. Because the solubility of oxygen is almost half the solubility of nitrogen in synthetic wine, nitrogen was selected in this study (Henry's constant for oxygen in ethanol–water mixtures at a mole fraction of 0.15 = $k_H$atm ($O_2$, 20 °C) = 23900; $k_H$atm ($N_2$, 20 °C) = 42600).[8]

Once readings from the submergible probes showed stable values in the absence of dissolved oxygen, the barrels were completely filled with the deoxygenated solution and a modified expandable silicone bung, similar to those used in cooperage to test the barrels, was inserted. This bung was modified to weld on it a multiple optical fiber feed for the eight optical fibers in test 1 (B1, Table 1) or for the two optical fibers (the rest of the tests) for the submergible oxygen probes that were introduced to each barrel. Each test lasted for 18–24 days. The lengths of the tests were dependent on the rate of oxygen entry into the barrels because the upper limit of the experiment was determined by the measurement range of the probes that were equipped with the PSt6 sensors (DO partial pressure of 0–41.4 hPa). When the DO variations in the model wine were measured within the barrel, the DO concentrations increased because DO was not consumed. This procedure would prevent the necessity of maintaining normal operating conditions in which the oxygen concentration gradient or

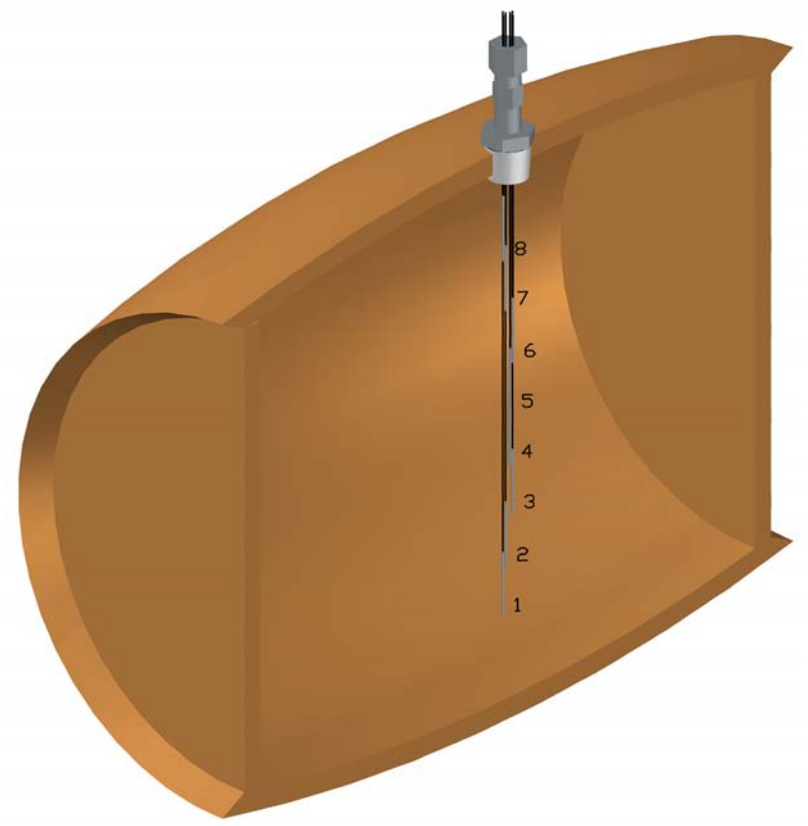


**Figure 1.** Distribution of the eight probes inside the barrel.

**Table 2. Comparison of the Regressions Obtained for the Dissolved Oxygen Measurements at Different Points of the Oak Barrel**

| | regression | *p* value |
|---|---|---|
| probes on the bottom | | |
| mean position 4 (390)[a] | $y = 8.4463 + 1.8978x$ | 0.0000 |
| mean position 3 (468) | $y = 22.4746 + 2.1405\ x$ | 0.5248 |
| mean position 2 (546) | $y = 17.4114 + 2.3545x$ | 0.0097 |
| mean position 1 (624) | $y = 21.4754 + 2.3692x$ | 0.0000 |
| mean 4 down probes ($DO_{1-4}$) | $y = 8.4463 + 1.8978x$ | |
| probes on the top | | |
| mean position 8 (78) | $y = 39.149 + 1.3879x$ | 0.0000 |
| mean position 7 (156) | $y = 30.1094 + 1.6414x$ | 0.5098 |
| mean position 6 (234) | $y = 17.4726 + 2.3628x$ | 0.0000 |
| mean position 5 (312) | $y = 37.5691 + 3.0842x$ | 0.0000 |
| mean 4 up probes ($DO_{5-8}$) | $y = 31.1665 + 1.71061x$ | |
| comparison of means | | |
| mean 3−7 probes ($DO_{3-7}$) | $y = 26.292 + 1.8909x$ | 0.8285 |
| mean 8 probes ($DO_{1-8}$) | $y = 26.5456 + 2.0382x$ | |

[a]Distance from the bung (in mm) is given in parentheses.

$pO_2$ in and out of the barrel remains constant due to oxygen consumption by the wine. Normally, the barrel's volume is so large that the $pO_2$ of the permeated gas remains negligibly small ($pO_2$ inside ≤5% $pO_2$ in the atmosphere) even upon reaching steady-state permeation. The $pO_2$ was measured with time in a previously oxygen-evacuated barrel that contained the model wine to maintain an initial $pO_2$ between 0.01 and 0.1 kPa.[9] The slope of the resulting oxygen evolution represents the flux of oxygen that permeates the liquid in the barrel from the atmosphere, or the $pO_2$ as a function of time. All $pO_2$ measurements were corrected to compensate for any interference by ethanol according to the model developed in previous studies.[10] Henry's law was applied to evaluate the oxygen concentration in milligrams per liter. In addition, the solubility of oxygen in hydroalcoholic mixtures was used[11] to avoid underestimation of the readings when the solubility of oxygen in water is used.[12]

After completion of each test, the barrels were not emptied and the model wine was degassed according to the previously described procedure. The microbiological analysis of the liquid confirmed the absence of microorganisms, probably due to the characteristic toasting process of oak wood barrels in cooperage. Thus, this liquid does not consume oxygen, which makes it suitable for the next test. By not emptying the barrel, the kinetics of the model wine absorption through the wood are not altered, and the humidity of the barrel oak staves is maintained. To test each barrel further, the same initial preparation procedure was applied. After all of the oxygen was displaced, DO measurements began again with the system of submergible probes.

**Oxygen Transfer Rate.** The OTR of barrels is usually expressed in milligrams per liter per year.[3,13] However, given the importance of time in studying the kinetics of oxygen entry, oxygen transfer is expressed as micrograms per liter per day.

The daily increase of oxygen within each barrel was determined by considering the mean values that were obtained from the two probes that were installed in each barrel. Daily values were added to determine the cumulative concentrations of DP that reached the model wine in each barrel for each day of the test. At this point, it is important to use a liquid that does not consume oxygen, has the same pH and ethanol content as wine, and allows for oxygen mass balance calculations. By using the model wine in the measurements, the OTR could be calculated because there were no compounds to consume the oxygen. The potential roles that the compounds in the wood would have in oxygen consumption[14,15] are considered in these trials, which allowed the determination of the true OTR of wine barrels.

**Statistical Analysis.** Regression analysis was conducted in the Statgraphics Centurion XVI statistics software (version XVI; StatPoint Inc., USA). Multiple regression analysis was used to compare the differences between the regression lines that were obtained from measuring the DO concentrations at different points in the oak barrel.

**Table 3. Regression Lines Obtained for the Dissolved Oxygen Measurements during the First Weeks of Aging in the Studied Barrels (B1−B12)**

| | B1 | B2 | B3 | B4 | mean |
|---|---|---|---|---|---|
| American medium grain | $y = 226.37x^{0.7176}$ | $y = 113.5x^{0.9605}$ | $y = 139.63x^{0.9522}$ | $y = 167.7x^{0.8927}$ | $y = 164.14x^{0.8630}$ |
| | $R^2 = 0.9403$ | $R^2 = 0.9789$ | $R^2 = 0.9608$ | $R^2 = 0.9779$ | $R^2 = 0.9757$ |
| | B5 | B6 | B7 | B8 | mean |
| American fine grain | $y = 162.72x^{0.8401}$ | $y = 177.07x^{0.7879}$ | $y = 180.34x^{0.8054}$ | $y = 122.15x^{0.9559}$ | $y = 161.3x^{0.8414}$ |
| | $R^2 = 0.9767$ | $R^2 = 0.9682$ | $R^2 = 0.9579$ | $R^2 = 0.9751$ | $R^2 = 0.9751$ |
| | B9 | B10 | B11 | B12 | mean |
| French fine grain | $y = 98.33x^{0.9083}$ | $y = 188.44x^{0.6731}$ | $y = 200.92x^{0.6505}$ | $y = 198.77x^{0.6963}$ | $y = 170.61x^{0.7204}$ |
| | $R^2 = 0.9717$ | $R^2 = 0.9812$ | $R^2 = 0.9781$ | $R^2 = 0.9589$ | $R^2 = 0.9781$ |

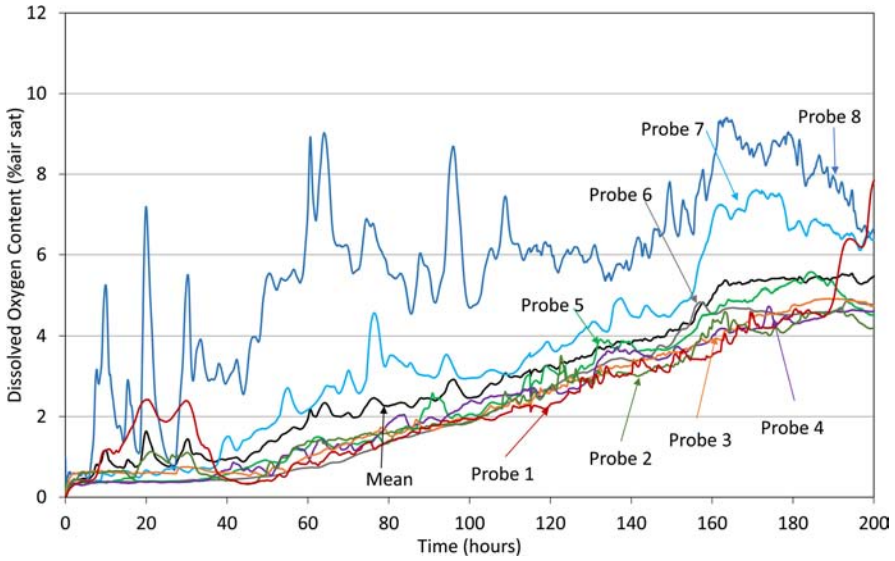


**Figure 2.** Measured dissolved oxygen (% air saturation) at each of the eight probes placed inside the barrel when no vacuum was generated inside the barrel.

The regression lines for the DO measurements with aging were conducted in Excel 2013 (Microsoft Office Professional Plus 2013) and are shown in Tables 2 and 3.

## RESULTS AND DISCUSSION

**Oxygen Distribution in the Barrel.** Figure 1 shows the arrangement of the eight probes within the barrel. Simultaneous measurements of DO within the barrels were used to determine the oxygen distribution inside the barrels. Measurements were conducted for 200 h, and the accumulated DO content is expressed in percent air saturation. The amount of DO read by the probes decreased as the distance from the bung increased (Figure 2). The highest DO concentrations were found at the top of the barrel (measured with probes 5, 6, 7, and 8), and the DO concentrations decreased with increasing distance from the bung. Lower DO concentrations were observed at the bottom of the barrel (measured with probes 4, 3, 2, and 1). Therefore, a high to low concentration gradient formed from the top to the bottom of the barrel.

Due to liquid losses, gaseous headspace rapidly forms near the bung. This space contains air with 21% oxygen, which diffuses into the wine through its surface and produces a decreasing gradient of DO with barrel depth.[16] These results agree with the results of Vivas and Glories,[17,18] who emphasized that the DO concentrations in wine oak barrels differed with distance from the bung. Thus, oxygen levels were much greater at 10 cm from the bung than at the center or bottom of the barrel. This result was observed in barrels after 1, 3, and 4 years of use.

The results indicated that the position of the dissolved oxygen probe is critical when evaluating DO throughout the entire barrel. Therefore, measurements must be made at representative points throughout the barrel. To reduce the number of probes required for an OTR assessment, the number of measurement points in each barrel was reduced from eight to two while accounting for the geometry of the barrel. By using the average of two representative DO measurements to represent the DO concentrations of an entire barrel, four barrels were monitored simultaneously in the second and third parts of the study.

To select two of the eight positions, a comparative study using equations that represented the evolution of DO at each submergible probe within the barrel was conducted. The equations that describe the DO variations with time in the bottom of the barrel (probes 1, 2, 3, and 4) and the mean of the four probes ($DO_{1-4}$) are provided in Table 2. In addition, Table 2 contains the $p$ values that were obtained by comparing the equations for each probe with the equation that was determined for the average of the four probes, which were representative of the DO evolution in the lower half of the barrel. The DO concentrations measured by probe 3 were not significantly different from the average DO ($p = 0.5248$, Table 2) concentrations. Thus, the position of probe 3 was selected as a representative measuring point for the lower half of the barrel.


dx.doi.org/10.1021/jf502333d | J. Agric. Food Chem. 2014, 62, 8892−8899

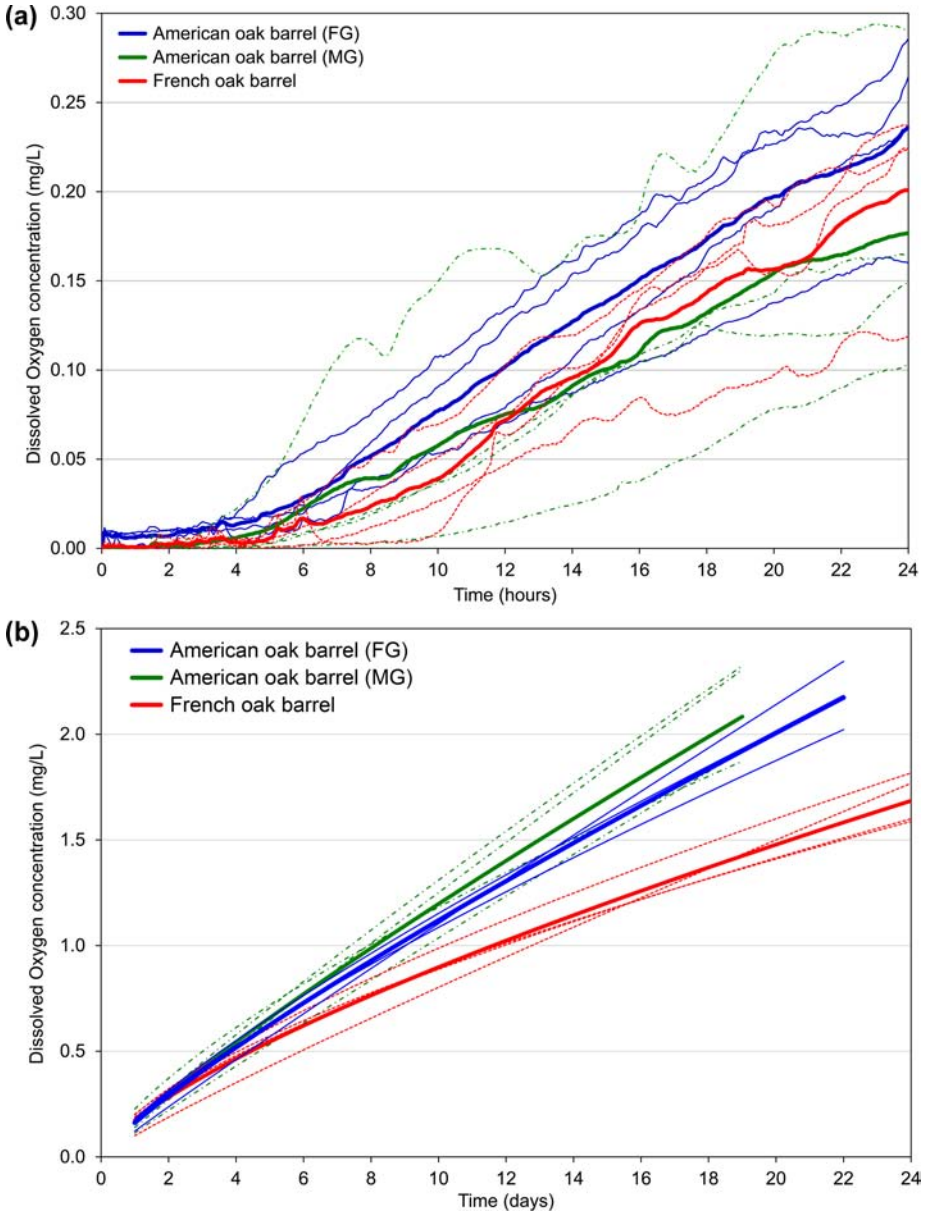


**Figure 3.** (a) Dissolved oxygen concentrations ($\mu$g/L) during the first 24 h; (b) fitted curves of the dissolved oxygen concentrations ($\mu$g/L) in the first few weeks. Measurements were taken in 12 American medium grain (MG) and fine grain (FG) and French oak barrels.

A similar analysis of the equations that describe DO variations with time at the top of the barrel (probes 5, 6, 7, and 8) was conducted. This analysis indicated that the equation describing the average DO evolution at probe 7 yielded results that were statistically equivalent to those obtained from the equation that described the mean values for probes 5, 6, 7, and 8 ($DO_{5-8}$) ($p$ = 0.5089). A comparative analysis between the equations that represented the average DO evolution at all eight probes ($DO_{1-8}$) and the average DO evolution at probes 3 and 7 ($DO_{3-7}$) was conducted. This comparison indicated that no statistically significant differences occurred between these equations ($p$ = 0.8285). Thus, the positions of probes 3 and 7 were used to represent the evolution of DO within each barrel.

**Kinetics of Oxygen Entry into the Barrels.** Figure 3a shows oxygen entry into the 12 American (B1−B8) and French (B9−B12) oak barrels during the first day expressed as accumulated DO concentration in milligrams per liter. The oxygen entry profiles in the American and French oak were not significantly different. However, the American oak barrels provided higher oxygen concentrations during the first 10 h than the French oak ones.

The initial oxygen contribution differs depending on the characteristics of the barrel and represents an extra oxygen input in addition to that produced during wine transport and barrel filling. The initial oxygen contributions were 230 and 281 $\mu$g/L for the fine- and medium-grain American oak barrels and 238 $\mu$g/L for the French oak barrels, respectively. Subsequently, oxygen entry was monitored in each of the studied barrels for 3 weeks. Figure 3b shows the accumulated oxygen trends between 18 and 23 days for the 12 studied American and French oak barrels. The oxygen provided from the initial degassing of the wood, the joints between the staves (gaps), and the permeability to oxygen of the wood was greater in the medium- and fine-grain American oak barrels than in the French oak barrels.

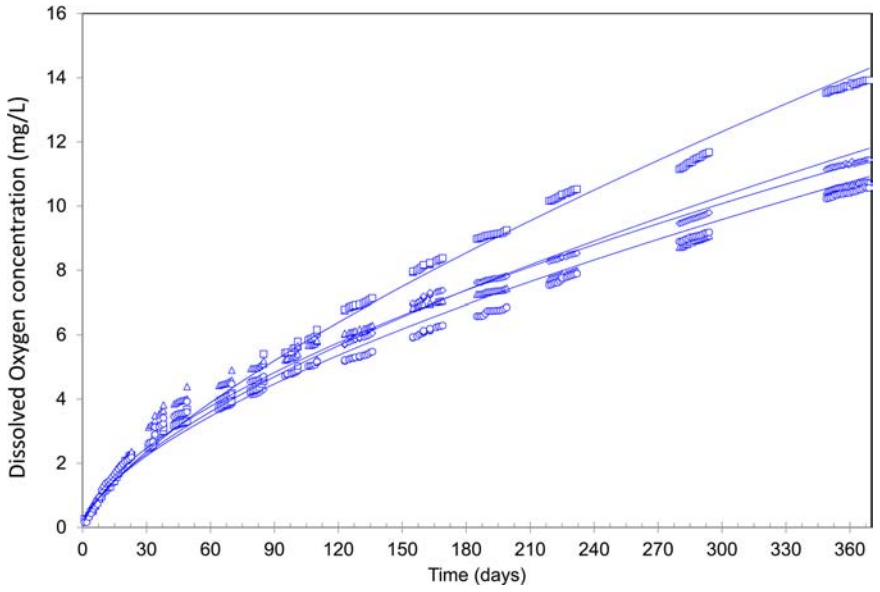


**Figure 4.** Fitted curves of the total dosed dissolved oxygen ($\mu$g/L) concentrations for 1 year in the four fine-grain American oak barrels.

Relative to the French oak barrels, these results indicated that the wine in the medium- and fine-grain American oak barrels would receive 30 and 10% more oxygen, respectively, during aging. This difference was maintained throughout the study. These differences were mainly explained by the initial contributions that resulted from wood degassing during the first few days. In addition, this result is easily explained by the different types of treatment that each type of oak receives in cooperage. American oak has a high rate of tyloses, which allows sawing the logs to obtain the staves without any leakage problems.[14,19] In contrast, French oak has a low rate of tyloses, which requires splitting the logs open into a series of sections (quarters), which are worked into staves by following the rays of the wood. The medullary rays in French oak are mainly parallel to the face of the stave in contact with the wine, which slows the wood degassing process. In contrast, sawing American oak does not guarantee parallel arrangement, which favors the release of air from the wood because the wine can access deeper layers of the staves. Tylosis itself facilitates this process because it is permeable to oxygen but not liquids.[19]

The oxygen entry trends were very similar for the analyzed barrels during the first few weeks of the experiment (Table 3). The kinetics of oxygen entry into the barrels with time followed the potential line $y = ax^b$. Here, $a$ is a constant that varies from 113 to 226 for medium-grain American barrels, from 122 to 180 for fine-grain American barrels, and from 98 to 201 for French barrels. In addition, $b$ represents the mathematical power of the aging time (ranging from 0.72 to 0.96 for medium-grain American barrels, from 0.79 to 0.96 for fine-grain American barrels, and from 0.65 to 0.91 for French barrels).

The regression equations that described oxygen entry in the 12 barrels followed a $t^{0.5}$ trend that was inverse to the equation defining wood impregnation[19] ($y = 0.63t^{-0.5}$). According to this author, liquid impregnation resembles a linear function of the square root of time during the first kinetics phase and is characteristic of liquid impregnation in wood. Subsequently, deceleration occurs because the wood is heterogeneous regarding stave thickness and consists of layers (early wood and late wood) of different thicknesses and characteristics.

The importance of wood moisture content for allowing oxygen permeation has already been evaluated by Vivas et al.[13] These authors showed that dry wood is 20−100 times more permeable to oxygen than wet wood. Other authors have emphasized the importance of wood moisture contents in the radial transport of oxygen in oak[21] and have highlighted how wood can be modeled as a porous solid in which the porosity is occupied by air when the wood is dry or below its fiber saturation point (FSP). However, these pore spaces are occupied by free water when the moisture content is greater than the FSP, which would decrease the oxygen permeability of the wood. These results are based on the diffusion coefficients of oxygen in air ($1.95 \times 10^{-5}$ m$^2$/s) and water ($2.0 \times 10^{-9}$ m$^2$/s) at 20 °C and 101.3 kPa.[20] Thus, $O_2$ diffusion is approximately $10^4$ times slower in water than in air. The movement of $O_2$ in water is extremely retarded by the interactions of $O_2$ with $H_2O$ molecules (hydrogen bonding).[22] The diffusion coefficient for oxygen in ethanol has been reported as $DO_2 = 2.64 \times 10^{-9}$ m$^2$/s at 303 K. At 293 K, the diffusion coefficient for oxygen in ethanol was estimated as $2.1 \times 10^{-9}$ m$^2$/s (by assuming that the diffusion coefficient for ethanol follows the same temperature dependence as the diffusion coefficient for water). This hypothesis was formulated because the temperature dependencies of the water and ethanol viscosities are nearly the same.[23]

Even though coopers assign importance to the type of grain, no significant differences were observed between the fine-grain and medium-grain American oak barrels. However, the fine-grain barrels provided more oxygen to the model wine during the first few hours as the wood degassed and began to moisten. This result agrees with the results described by Vivas et al.,[13] who found that fine-grain French oak (*Q. petraea*) was more permeable to oxygen than medium-grain French oak when analyzing small pieces of dry wood with varying thicknesses (2, 4, 8, and 12 mm). Here, the permeation of oxygen through the wood and the gaps was evaluated (i.e., the full barrel was analyzed). Consequently, the results were not maintained throughout this study, as previously described.[13] This observation potentially resulted from wetting the wood, which changed the oxygen permeability. In addition, the

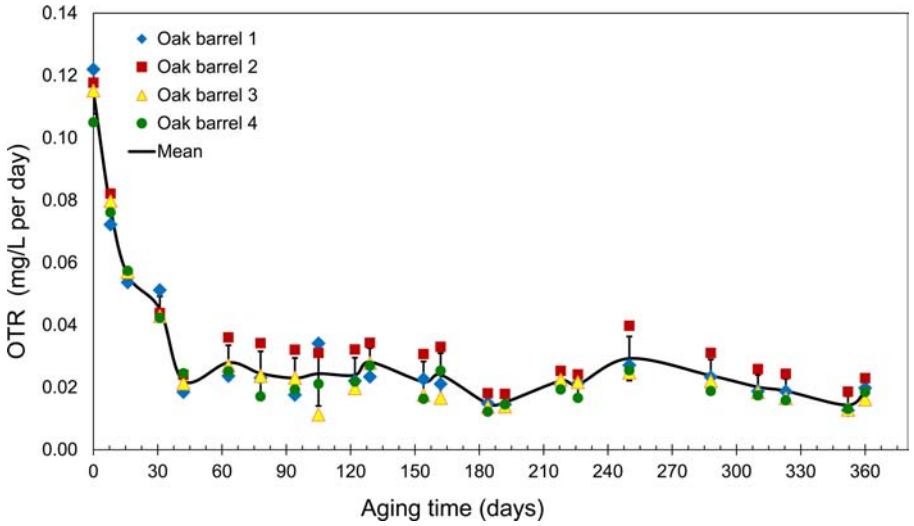


**Figure 5.** Oxygen transfer rate (mg/L per day) in the tested fine-grain American oak barrels.

entry of oxygen through the gaps is not the same in all barrels. Three weeks after filling the barrels, the medium-grain American oak barrels resulted in slightly higher average oxygen doses in the model wine relative to the oxygen doses observed in the fine-grain American oak barrels (Figure 3b).

**Annual Rate of Oxygen Entry into the Barrels.** The tests that were performed for the 12 barrels indicated that the oxygen supply decreases as the barrel is moistened. This phenomenon was mentioned previously and described by Sorz and Hietz.[21] These authors indicated that increases in wood moisture were responsible for the decreasing permeability of wood to oxygen because atmospheric oxygen diffuses better through dry wood.

To evaluate the overall rate of oxygen entry into moist oak barrels, the initial analysis was extended from 3 weeks (conducted for eight barrels) to 12 months in the remaining four barrels. In this experiment, aging was monitored for 1 year in the four fine-grain American oak barrels (B5, B6, B7, and B8) under the previously described conditions.

Figure 4 shows the evolution of the cumulative daily intake throughout the year, which was calculated by adding the oxygen contributions that were evaluated in successive tests for 12 months as described under Materials and Methods. Analysis of the cumulative daily intake for 12 months indicated that the observed trend during the first few weeks continued throughout the entire year of aging. In addition, the DO content decreased following the first 3−4 weeks.

Figure 4 shows the evolution of the accumulated oxygen that was dosed by each of the studied barrels throughout the year. The previously described equations correspond to the first few weeks and were modified by defining a constant $a$ that varied from 206 to 309 and a potential gaining time of $b$ that varied from 0.61 to 0.71. These results indicated that the actual rate of oxygenation per year is much lower than the rate that was estimated during the first weeks of testing. Therefore, it is important to test the evolution of oxygen entry kinetics for 1 year. Specifically, the daily average dose throughout the year was 32 $\mu$g/L (B5 = 31.1 $\mu$g/L, B6 = 38 $\mu$g/L, B7 = 30 $\mu$g/L, and B8 = 28.7 $\mu$g/L). Therefore, after the first month of aging, the fine-grain American oak barrels continued to provide the wine with between 28.7 and 38 $\mu$g/L oxygen daily for the remainder of the year. These levels can vary for different types of aged wine because precipitation, condensation, and the polymerization of phenols, salts, and other compounds in wine can block the wood and the gaps and decrease the rate of oxygen entry.[18] Prolonged barrel use progressively blocks the wall of the wood and diminishes the DO content.

According to these results, the total dose of oxygen that wine would receive in a fine-grain American oak barrel was calculated as 11.62 mg/L per year.

These results were significantly lower than the results that were published by other authors who measured oxygen entry into new barrels. For example, Riberau-Gayon[1] observed an oxygen entry rate of 15−20 mL/L per year, and Vivas and Glories[2] observed an oxygen entry rate of 20 mg/L per year in two new Limousin barrels from central France. In these studies, the sulfate formed from $SO_2$ in solution inside the barrel was evaluated at 6 months. Thus, these results did not assess the entire year of oxygen entry into the barrels. Instead, these results were obtained from theoretical approaches or were extrapolated from 6 months of aging data at different times of the year. The methodologies of these studies may explain the high rates of oxygen entry postulated by these authors when considering OTR as a constant rate with time and without considering the influences of the progressively increasing wood moisture contents with decreasing OTR.

The results obtained are also lower than those estimated by Kelly and Wolan.[5] These authors treated the wood as a semipermeable membrane that allowed for oxygen diffusion according to Fick's law. On the basis of their calculations, the maximum amount of oxygen that could enter a barrel is 26 mL/L per year. However, this approach is erroneous because wood is a porous membrane that does not always function the same. Specifically, the moisture content of wood can modify its properties and oxygen permeability.

On the basis of the annual dose results of oxygen in the four barrels in the third part of this study, the percentage of daily oxygen intake for each barrel was calculated relative to the oxygen that was supplied throughout the year (which is considered to be 100%). On average, the fine-grain American oak barrels supply wine with 7% of the total yearly oxygen within the first week. After a month, 23% of the total oxygen (B5 = 22.63%, B6 = 17.90%, B7 = 28.72%, and B8 = 25.06%) was supplied. Finally, 4 months (120 days) was required to

dose the wine with 50% of the total oxygen received in a year. These results suggest that adding wine to new barrels before the filling or development of young oak wine (which corresponds with maintaining these wines in new barrels for 2−4 months) reduces the potential for barrel oxygenation. For example, if barrels are used for 2−4 months for one batch of wine and are used for 9 months for a second batch of wine, the latter receives only 50% of the potential oxygen that these barrels would provide in a year.

Figure 5 shows the annual evolution of the daily measured oxygen permeability rates for the four fine-grain American oak barrels. The results show that the daily rate fell significantly in the first few months before stabilizing for the remainder of the year. In addition, a simple visual analysis indicates that a kinetics study is necessary to establish the annual rate of oxygen supply to wine in oak barrels.

These results can be used to extrapolate the behaviors and annual rate calculations for the other eight studied barrels between 19 and 24 days during the second phase of the study. After approximately 3 weeks, the oxygen received by the wine in a barrel represents 17−20% of the total oxygen that will be received in a year (observed in fine-grain American oak barrels and valid for medium-grain American and French oak barrels). Thus, these results could be extracted and the annual oxygen entry rates could be calculated for the barrels that were analyzed in phase 2. For the medium-grain American oak barrels, it took 19 days to dose B1 = 1.81 mg/L, B2 = 1.84 mg/L, B3 = 2.07 mg/L, and B4 = 2.10 mg/L with 17.3% of the total yearly oxygen dose. Therefore, these barrels would provide an average of 11.3 mg/L per year (B1 = 10.46 mg/L, B2 = 10.64 mg/L, B3 = 11.96 mg/L, and B4 = 12.14 mg/L) of oxygen to aged wine French oak barrels measured after 24 days (B9 = 1.61 mg/L, B10 = 1.63 mg/L, B11 = 1.59 mg/L, and B12 = 1.82 mg/L). Thus, the annual rate of supply for these barrels was 8.18 mg/L per year (B9 = 7.93 mg/L, B10 = 8.01 mg/L, B11 = 7.81 mg/L, and B12 = 8.97 mg/L per year).

In summary, this paper was the first to analyze the kinetics of oak barrel oxygen permeability for 1 year to establish the kinetics of the annual OTR of a barrel. The results of this study indicated that the American oak barrels resulted in greater oxygen doses than the French oak barrels. In addition, different wood grains (fine and medium) did not significantly affect the oxygenation rates of the barrels.

## AUTHOR INFORMATION


### Corresponding Author

*(I.N.) E-mail: inevares@iaf.uva.es.



### Funding

This work was financed by the Ministerio de Ciencia e Innovación (AGL2011-26931) from Spain.


### Notes

The authors declare no competing financial interest.

## ACKNOWLEDGMENTS

We acknowledge Carlos González Muñoz for data acquisition. We express great appreciation to Tonelería Victoria and Radoux for their generous collaboration.

## REFERENCES


(1) Ribereau-Gayon, J. *Contribution à l'étude des oxydations et réductions dans les vins*. Thesis, Université de Bordeaux, France, 1933.

(2) Vivas, N.; Glories, Y. Modélisation et calcul du bilan des apports d'oxygène au cours de l'élevage des vins rouges. II. Les apports liés au passage d'oxygène au travers de la barrique. *Prog. Agric. Vitic.* **1997**, *114*, 315−316.

(3) Peterson, R. Research note: formation of reduced pressure in barrels during wine aging. *Am. J. Enol. Vitic.* **1976**, *27*, 80−81.

(4) Singleton, V. L. Maturation of wines and spirits: comparisons, facts, and hypotheses. *Am. J. Enol. Vitic.* **1995**, *46*, 98−115.

(5) Kelly, M.; Wollan, D. Micro-oxygenation of wine in barrels. *Aust. N. Z. Grapegrower Winemaker* **2003**, *473A*, 29−32.

(6) Nevares, I.; del Alamo, M.; Gonzalez-Muñoz, C. Dissolved oxygen distribution during micro-oxygenation. Determination of representative measurement points in hydroalcoholic solution and wines. *Anal. Chim. Acta* **2010**, *660*, 232−239.

(7) Proctor, K. G.; Bohlen, H. G. Tonometer for calibration and evaluation of oxygen microelectrodes. *J. Appl. Physiol.* **1979**, *46*, 1016−1018.

(8) Tokunaga, J. Solubilities of oxygen, nitrogen, and carbon dioxide in aqueous alcohol solutions. *J. Chem. Eng. Data* **1975**, *20*, 41−46.

(9) Piringer, O. G.; Baner, A. L. *Plastic Packaging Materials for Food: Barrier Function, Mass Transport, Quality Assurance, and Legislation*; Wiley-VCH: Weinheim, Germany, 2000.

(10) del Alamo-Sanza, M.; Pando, V.; Nevares, I. Investigation and correction of the interference of ethanol, sugar and phenols on dissolved oxygen measurement in wine. *Anal. Chim. Acta* **2014**, *809*, 162−173.

(11) Mejane, J. V.; Debailleul, M.; Lecerf, J. Étude sur la solubilité de l'oxygène dans l'alcool. *Ind. Aliment. Agric.* **1973**, *90*, 719−727.

(12) Nevares, I.; del Alamo Sanza, M.; Waters, E.; Day, M. La medida del oxígeno disuelto en vino y mostos. Concentración o presión parcial? Estado actual del conocimiento. In *XIII Congreso Latinoamericano de Viticultura y Enología*, Santiago de Chile, Nov 21−23, 2011.

(13) Vivas, N.; Debèda, H.; Ménil, N.; Vivas de Gaulejac, N.; Nonier, M. Mise en évidence du passage de l'oxygène au travers des douelles constituant les barriques par l'utilisation d'un dispositif original de mesure de la porosité du bois. Premiers résultats. *Sci. Aliment.* **2003**, *23*, 655−678.

(14) Feuillat, F. *Contribution à l'étude des phénomènes d'échanges bois/vin/atmosphère à l'aide d'un "fût" modèle. Relations avec l'anatomie du bois de chêne (*Quercus robur* L., *Quercus petraea* Liebl.)*. Thesis, Ecole Nationale du Génie Rural des Eaux et des Forêts, Nancy, France, 1996.

(15) Vivas, N.; Saint-Cricq de Gaulejac, N. The useful lifespan of new barrels and risk related to the use of old barrels. *Aust. N. Z. Wine Ind.* **1999**, *14*, 37−45.

(16) Moutounet, M.; Mazauric, J. P.; Saint-Pierre, B.; Hanocq, J. F. Gaseous exchange in wines stored in barrel. *J. Sci. Technol. Tonnellerie* **1998**, *4*, 131−145.

(17) Vivas, N.; Glories, Y. Les phénomènes d'oxydoréduction liés à l'elevage en barriques des vins rouges: aspects technologiques. *Rev. Fr. Oenol.* **1993**, *33*, 33−38.

(18) Vivas, N. The quality of oak wood and its use for the vinification and ageing of wine. *J. Sci. Technol. Tonnellerie* **1995**, 9−16.

(19) Feuillat, F.; Huber, F.; Keller, R. Relation between the porosity of oak-wood, *Quercus robur* L. and *Quercus petraea* Liebl., and variability of several physical and anatomical characteristics, with regard to cooperage. *Rev. Fr. Oenol.* **1993**, *142*, 1−15.

(20) Stamm, A. Penetration of hardwoods by liquids. *Wood Sci. Technol.* **1973**, *7*, 285−296.

(21) Sorz, J.; Hietz, P. Gas diffusion through wood: implications for oxygen supply. *Trees − Struct. Funct.* **2006**, *20*, 34−41.

(22) Mugnai, S.; Mancuso, S. Oxygen transport in the sapwood of trees. In *Waterlogging Signalling and Tolerance in Plants*; Mancuso, S., Shabala, S., Eds.; Springer: Berlin, Germany, 2010; pp 61−75.

(23) Kruk, N. N. Fluorescence quenching of water-soluble porphyrins by molecular oxygen. *J. Appl. Spectrosc.* **2008**, *75*, 174−180.

## MATERIALS AND METHODS

**Materials.** BC (≥97.0%, UV), β-lactoglobulin, dextran (MW 69800), FITC−dextran (MW 4000), pepsin, and trypsin were purchased from Sigma-Aldrich (St. Louis, MO, USA). Transwell permeable supports (polycarbonate membrane, pore size = 0.4 μm, area = 4.2 $cm^2$) were obtained from Millipore Corp. (Billerica, MA, USA). Dulbecco's modified Eagle's medium (DMEM) (containing 4.5 g/L D-glucose and GlutaMAX), penicillin and streptomycin (100×), fetal bovine serum (FBS), TrypLE Select, Hanks' balanced salt solution (HBSS), and phosphate buffer solution (PBS) (10×) were purchased from GIBCO (Grand Island, NY, USA). The human colon carcinoma cell lines (Caco-2 cells, ATCC, Manassas, VA, USA) were grown in DMEM. Cells after 100−120 passages were used for this study. All other chemicals and reagents used were of HPLC grade and obtained from Sigma-Aldrich. Ultrapure water (18 mΩ) was supplied by a Milli-Q apparatus (Millipore Corp.).

**Methods.** *Preparation of Glycation Conjugates.* BLG−dextran conjugates were prepared according to the method published by Liu et al. with minor changes.[13] Solutions containing 1% BLG and 1% dextran were hydrated overnight in ultrapure water. The solutions were adjusted to pH 7 and lyophilized. The powders were incubated for 24, 48, and 72 h, respectively, at 60 °C and 79% relative humidity in an incubator to produce the glycated dextran. The samples were then collected and stored at −20 °C for further use.

*Characterization of Maillard-Based Conjugates. (a) Sodium Dodecyl Sulfate−Polyacrylamide Gel Electrophoresis (SDS-PAGE).* A 4−20% gradient polyacrylamide gel was prepared in-house for SDS-PAGE. Five microliters of sample (protein content = 5 mg/mL) was mixed with 5 μL of ultrapure water and 10 μL of 2× SDS sample buffer (100 mM Tris-HCl, pH 6.8, 4% SDS, 0.2% bromophenol blue, 20% glycerol, and 200 mM 2-mercaptoethanol) and then heated for 5 min at 95 °C. Fifteen microliters of each sample was loaded to a designated well for electrophoresis at 120 V with a Tris−HEPES−SDS running buffer (100 mM Tris, 100 mM HEPES, 3 mM SDS, pH 8.0). The gel was stained using the Colloidal Coomassie G-250 Staining protocol.[14] The stained gel was scanned with an ImageQuant LAS 4000digital imaging system (GE Healthcare, Piscataway, NJ, USA). EZ-Run Rec protein ladder (10−200 kDa) was obtained from Fisher BioReagents.

*(b) Circular Dichroism (CD).* A J-815 CD spectrometer (Jasco, Tokyo, Japan) was used to analyze the conformational changes of the protein after glycation in the wavelength range of 195−260 nm using a cell with a 2.0 mm path length. Samples were prepared with 10 mM PB (pH 7.0) at a protein concentration of 0.2 mg/mL. Scanning was performed at 50 nm/min at 20 °C. CD spectra were collected 10 times for each sample and displayed as mean residue ellipicity (degrees·$cm^2$/dmol) using 113 for the average number of amino acid residues per molecule of BLG.

*(c) Degree of Glycation (DG).* The DG was determined from the analysis of the free amino groups in BLG and conjugates. The level of free amino groups in the BLG−dextran conjugates was determined according to the trinitrobenzenesulfonic acid (TNBS) method.[8] In brief, BLG and conjugates dispersions (protein content = 1.0%, w/w) were prepared in 50 mM phosphate buffer (pH 8.5) containing 50 mM NaCl. One milliliter of a 0.1% (w/v) TNBS solution was thoroughly mixed with 1 mL of protein dispersion, and the resultant mixtures were incubated in a 50 °C water bath for 2 h in the dark and then cooled to room temperature. One milliliter of 10% SDS and 0.5 mL of 1.0 M HCl were added to the protein mixtures. The absorbance was measured at 335 nm. The degree of glycation was determined as

$$\mathrm{DG}\ (\%) = ((A_0 - A_s)/A_0) \times 100\%$$

where $A_0$ is the absorbance of the sample without glycation and $A_s$ is the absorbance of the sample after glycation.

*BC-Loaded Nanoparticle Preparation.* Native BLG or the 72 h glycated BLG−dextran was dispersed (1.0%, w/w) in ultrapure water at pH 7.0 containing 0.02 wt % sodium azide as antimicrobial agent. The dispersions were stirred for 2 h at room temperature, and then 0.1% BC (w/w) solutions were prepared in ethyl acetate. BC-loaded nanoparticles were prepared according to the method described by Tan and Nakajima[15] with minor changes. Water (100 mL) was saturated with 8.3 g of ethyl acetate[16] prior to formulating the protein solution to prevent precipitation of BC during homogenization. The BC in ethyl acetate solution was combined with the ethyl acetate saturated protein solution at a ratio of 1:9. The mixtures were homogenized for 10 min at 8000 rpm using an Ultra-Turrax homogenizer (T25, Ika-Werke, Staufen, Germany) to form a coarse emulsion before additional homogenization using a two-stage valve homogenizer (APV-1000 high-pressure homogenizer, Wilmington, MA, USA) for one cycle at 70 MPa. After the homogenization, ethyl acetate was removed from the emulsions on a rotary evaporator at 40 °C. The residual ethyl acetate was determined by headspace gas chromatography and found to be <0.001% (data not shown).

*Nanoparticle Characterization.* The characteristics of BC-loaded nanoparticle solutions were determined by measuring the mean particle diameter, diameter distribution, and ζ-potential of nanoparticles by dynamic light scattering technique using a Malvern Zetasizer (Nano-ZS; Malvern Instruments, Worcestershire, UK). Refractive indices of 1.47 for BC and 1.33 for ultrapure water were used. To reduce multiple scattering effects, the nanoparticle dispersions were diluted 100 times with ultrapure water and the pH was adjusted to 7.0 prior to acquiring triplicate measurements.

The BC contents of the nanoparticles were determined by HPLC. The content of free BC suspended in aqueous phase was extracted with *n*-hexane. The total BC in aqueous phase was obtained by demulsification−extraction with ethanol and *n*-hexane. The BC content in nanoparticles was obtained by subtracting free BC from total BC. The encapsulation efficiency (EE) and the loading capacity (LC) were calculated using the following equations:

$$\mathrm{EE} = \text{BC quantity encapsulated in nanoparticles} / \text{BC quantity in total nanoparticles solution} \times 100\%$$

$$\mathrm{LC} = \text{BC quantity encapsulated in nanoparticles} / \text{quantity of total nanoparticles} \times 100\%$$

*Transmission Electron Microscopy (TEM).* TEM was used to observe the shape of the formed nanoparticles and to confirm diameter by dynamic light scattering. Samples were prepared by the conventional negative-staining method. Nanoparticles were placed on copper grids and negatively stained with 2% (w/v) phosphotungstic acid for several minutes at room temperature. Grids bearing nanoparticles were analyzed with a Hitachi H-700 transmission electron microscope (Hitachi, Tokyo, Japan).

*Stability in Different pH Condition.* The influence of pH on the mean particle diameter of nanoparticles was evaluated. The pH of nanoparticle solutions was adjusted with HCl or NaOH from pH 2.0 to 7.0, and the prepared samples were kept for 4 h at room temperature before particle characterization analysis. The mean particle diameter, diameter distribution, and ζ-potential of nanoparticles by dynamic light scattering technique using a Malvern Zetasizer were determined as described previously.

*Release of BC-Loaded Nanoparticles in Vitro.* Two proteases were used to study the release of BC-loaded nanoparticles in vitro to simulate gastric and intestinal digestive environments. The gastric stage digestion was simulated by suspending 2 mg/mL of BC nanoparticle powder in 0.1 M HCl, adjusting to pH 2, and treating with pepsin solution (pH 2.0, 1 mg/mL) while stirring at 250 rpm at 37 °C. An aliquot of reactant was removed, and the hydrolysis was terminated by adjusting the pH at several time intervals during 120 min of digestion time. The released BC was extracted with *n*-hexane. The BC content was determined by the HPLC method described below. The intestinal protein hydrolysis was simulated by trypsin digestion in 0.1 M PBS (pH 7.0, 1 mg/mL) at 37 °C.

*MTT Cytotoxicity Assay.* Cell viability after treatment with BLG or BLG−dextran nanoparticles was determined by the MTT (3-(4,5-dimethylthiazol-2-yl)-2,5-diphenyltetrazolium bromide) assay. The MTT assay measures the activity of cellular enzymes by the reduction

of MTT to its insoluble purple formazan form.[1] Caco-2 cells were incubated in DMEM containing 10% FBS, 1× nonessential amino acid (NAA), and 1× penicillin and streptomycin. Caco-2 cells in DMEM were seeded at a density of $1.2 \times 10^5$ cells/well onto tissue-treated 96-well plates and incubated (Sanyo, Osaka, Japan) at 37 °C in an atmosphere of 95% humidified air−5% $CO_2$. After 2 days of incubation, the medium was discharged, and 100 μL of BC-loaded nanoparticles diluted with DMEM at different protein concentrations (0.1−10.0 mg $mL^{-1}$) was added to the wells. After 24 h of incubation at 37 °C, the nanoparticles containing medium were replaced with 100 μL of DMEM containing MTT (10 μL, 5 mg $mL^{-1}$ in 1× PBS, pH 7.2) and incubated for 2 h at 37 °C. Finally, the supernatant was removed and 100 μL of dimethyl sulfoxide (DMSO) added. The absorbance of each well was measured with a Multilabel microplate counter (Victor$^3$, PerkinElmer, Waltham, MA, USA) at 570 nm. Cell viability was calculated by the percentage of absorbance relative to control (treated with DMEM only).

*Caco-2 Cell Monolayer Incubation.* Caco-2 cells were incubated (Sanyo) in DMEM containing 10% FBS, 1× nonessential amino acid (NAA), and 1× penicillin and streptomycin at 37 °C in an atmosphere of 95% humidified air and 5% $CO_2$ onto transwell permeable supports (Millipore), with membrane area of 4.2 $cm^2$, in 6-well plates. Caco-2 cells were seeded at a density of $1.2 \times 10^5$ cells $well^{-1}$. The medium was changed every second day. Transport experiments were performed at 21−28 days. Before BC transport experiment, both the trans-epithelial electrical resistance (TER) value and the apparent permeation rate of the paracellular permeation marker ($P_{app}$, FITC−dextran) were measured to ensure the integrity of Caco-2 cell monolayers. In this study, after 3 weeks of incubation, the TER was measured with an Evohm2 epithelial voltmeter (World Precision Instruments, Sarasota, FL, USA) and was >350 Ω $cm^2$; the $P_{app}$ of 1 mg/mL FITC−dextran detected with a Multilabel microplate counter (Victor$^3$, PerkinElmer) at an excitation wavelength of 487 nm and an emission of 518 nm was $(4.3 \pm 1.1) \times 10^{-8}$ cm $s^{-1}$. Both the TER, which was higher than reported values (260 ± 65 Ω $cm^2$),[17] and $P_{app}$, which was lower than reported values, indicated that the Caco-2 cell monolayers were confluent and suitable for permeation study.

*BC Transport with Caco-2 Monolayers.* The Caco-2 monolayers were washed with DMEM three times. Both BLG and BLG−dextran conjugate-encapsulated BC nanoparticles were diluted in DMEM to a final BC concentration of 20 μg $mL^{-1}$. Free BC in THF/DMSO (1:1, v/v) after dilution in DMEM (20 μg $mL^{-1}$) was used as control. One and a half milliliters of the BC-encapsulated nanoparticle and control solution was added to separate inserts. The medium in the basal side was sampled at several time intervals, extracted with solvent, and analyzed for BC content by HPLC (procedure given below).

The TER was also measured at several time intervals (0, 0.5, 1, 2, 3, and 4 h) to measure the integrity of Caco-2 monolayers.

The apparent permeability coefficient ($P_{app}$, cm $s^{-1}$) was calculated using the equation

$$P_{app} = (dQ/dt)(1/(AC_0))$$

where $dQ/dt$ is the permeability rate (μg $s^{-1}$), $A$ is the surface area of the filter ($cm^2$), and $C_0$ is the initial concentration in the donor chamber (μg $mL^{-1}$).

*Extraction and Quantification of BC.* BC was extracted from the nanoparticles with 3 mL of ethanol/*n*-hexane (1:2, v/v) three times. The hexane extracts were combined and brought up to 10 mL for HPLC analysis. Five microliters of 5 μg/mL *trans*-β-apo-8′-carotenal (internal standard) in ethanol was added to 1.0 mL samples. The transport samples (1.0 mL) were extracted three times with 3 mL of ethanol/*n*-hexane (1:2, v/v). Organic fractions were removed and combined with transfer pipets, and the extract was dried under a stream of nitrogen gas at 40 °C. The BC extract was dissolved in 0.1 mL of methanol/dichloromethane (1:1, v/v) containing 0.1% BHT for HPLC analysis. The recovery of *trans*-β-apo-8′-carotenal was >94%.

HPLC quantification of BC was performed using an Agilent 1100 HPLC system with a DAD UV−vis absorption detector (Agilent, Santa Clara, CA, USA), according to the published method.[2] BC quantitation range (0.1−100 ug $mL^{-1}$) was established for HPLC analysis of BC in nanoparticles and in Caco-2 cell transport. A polymeric $C_{30}$ reverse-phase analytical column (250 × 4.6 mm i.d., 5 μm, YMC, Inc., Wilmington, NC, USA) was used to separate BC with a flow rate of 1 mL $min^{-1}$ at room temperature. The guard column was a reverse-phase $C_{18}$ column (50 × 3.0 mm i.d., 5 μm, YMC, Inc.). The injection volume was 20 μL, and the detection wavelength was 450 nm. The chromatography conditions were as follows: solvent A, methanol/acetonitrile/$H_2O$ (84:14:2, v/v/v); solvent B, dichloromethane. The solvent gradient program was 80% A/20% B at 0 min and was changed linearly to 45% A/55% B in 15 min, maintained for 5 min, and followed by a linear return to 80% A/20% B at 25 min.

*Statistics.* All experiments were performed at least three times and were reported as the mean ± standard deviation. The data were analyzed by analysis of variance (ANOVA) using the SPSS 17.0 package (IBM, Armonk, NY, USA). Duncan's multiple-range test was used to determine significant differences of the mean values ($P < 0.05$).

## RESULTS AND DISCUSSION

**BLG Glycation.** *SDS-PAGE.* The characterization of BLG glycation products was determined by SDS-PAGE. The bands corresponding to native BLG, BLG glycation with dextran for 24, 48, and 72 h, and BLG heated for 72 h under reducing conditions are shown in Figure 1. One obvious band

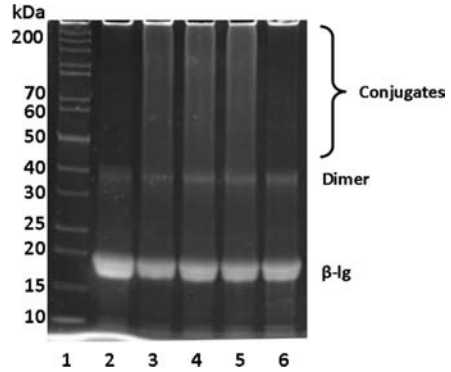


**Figure 1.** SDS-PAGE analysis under reducing conditions of BLG and BLG−dextran conjugates. Lanes: 1, protein markers; 2, native BLG; 3, 4, and 5, BLG−dextran conjugates treated by glycation for 24, 48, and 72 h, respectively; 6, BLG treated for 72 h (control).

corresponding to BLG was found at about 18 kDa.[18] Small amounts of BLG dimers are observed at about 40 kDa. There appears to be a slight decrease in intensity of the BLG band after heating for 72 h (control), but no absorption in the 40−200 kDa range. After glycation with dextran for 24, 48, and 72 h, smeared zones were formed between 50 and 200 kDa. Dextran-glycated ovalbumin[19] show similar smeared zones. Carbohydrate staining but not protein staining confirmed glycation by SDS-PAGE of gelatin.[20] In this study the smeared zone densities appear to become more intense with increasing treatment time (from 24 to 72 h), suggesting that more conjugates were formed. The TNBS assay shows that the extent of glycation increased from 6.7 to 14.5% with increasing treatment time (from 24 to 72 h) (Table 1). The SDS-PAGE and TNBS results confirm that BLG−dextran conjugates were formed by dry-heating.

*CD.* Changes in the secondary structure of BLG after glycation by the much larger dextran molecule were determined by far-UV CD spectroscopy (Figure 2). The negative peak at 216 nm indicates that BLG is rich in β-sheet secondary

**Table 1. Degree of Glycation of BLG and the Conjugates**

| sample | degree of glycation (%) |
|---|---|
| BLG native | 0 |
| BLG−dextran conjugates (24 h) | 6.7 ± 1.5 |
| BLG−dextran conjugates (48 h) | 9.4 ± 2.0 |
| BLG−dextran conjugates (72 h) | 14.5 ± 1.7 |
| BLG control | 0 |

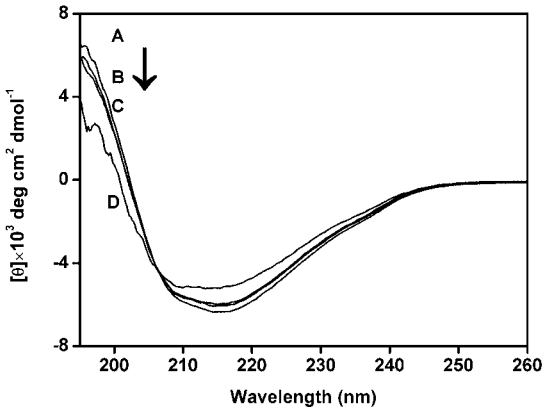


**Figure 2.** Far-UV CD spectra (195−260 nm) of BLG native (A) and BLG−dextran conjugates treated by glycation for 24 h (B), 48 h (C), and 72 h (D).

structure.[21] The mean residue ellipticity was decreased slightly by 72 h of Maillard-based reaction (Figure 2). The secondary structure composition of native BLG and BLG−dextran conjugates was calculated according to DichroWeb online (Table 2). The composition of native BLG in this study was α-helix, 9.3%; β-sheet, 39.5%; turn, 22.5%; and unordered, 27%; whereas BLG was reported to have 15% α-helix, 50% β-sheet, and 15−20% reverse turn.[22] The differences may be due to the different sources of BLG and different curve fitting analysis programs.[23] SELCON3 was used in this study. After glycation, the α-helix and β-sheet structure increased, whereas the turn and unordered structure slightly decreased. The highly ordered structure content (α-helix + β-sheet) was increased slightly by 4.5, 4.1, and 2.9%, corresponding to 24, 48, and 72 h of incubation time, compared to native BLG. Levels of 40−75% glycosylation of kidney bean vicilin with glucose by large molar excess of glucose resulted in marked shifts in wavelength and ellipticity in the CD spectra.[24] However, no significant change of secondary structure compositions was reported by Enomoto et al. after glycation with maltopentaose and phosphorylation with pyrophosphate.[21] In this study the small changes may be due to the low degree of glycosylation.[24]

**Table 2. Secondary Structure Composition of Native BLG and BLG−Dextran Conjugates[a]**

| sample | incubation time (h) | α-helix (%) | β-sheet (%) | turns (%) | unordered (%) |
|---|---|---|---|---|---|
| native BLG | | 9.3 | 39.5 | 22.5 | 27 |
| BLG−dextran | 24 | 11 | 40 | 21.7 | 26 |
| BLG−dextran | 48 | 10.6 | 40.2 | 21.4 | 25.8 |
| BLG−dextran | 72 | 10.1 | 40.1 | 21.1 | 26.2 |

[a]The secondary structure composition was calculated from far-UV CD spectra data using DichroWeb online (http://dichroweb.cryst.bbk.ac.uk/html/home.shtml).

*Characterization of BC Nanoparticles.* BC-loaded nanoparticles were encapsulated with native BLG and BLG−dextran conjugates (72 h) (the conjugates used below were all conjugates after 72 h of incubation) by the homogenization−evaporation method.[1] The characteristics of both nanoparticles are shown in Table 3. There were no significant differences in particle diameter. The unimodal particle diameter distributions of BLG and BLG−dextran-conjugated nanoparticles are shown in Figure 3. Both polydispersity index (PDI) values were below 0.200, indicating a narrow particle size distribution. The BC nanoparticles were spherically shaped, approximately 50 nm in diameter, confirming light scattering results, and uniformly dispersed (Figure 3). Although similar in diameter, the BC nanoparticles' ζ-potential values were different. Glycation with dextran significantly decreased the apparent ζ-potential from −32.9 ± 0.8 mV for native BLG to −14.0 ± 0.7 mV for BLG−dextran ($P < 0.05$). Although only a fraction (∼15%) of the BLG was glycated, Lesmes and McClements have suggested that steric barriers may screen the positively charged surface from the continuous phase.[12] The encapsulation efficiency of BC was 98.6 and 98.4% for native BLG and BLG−dextran conjugates, respectively, and the loading capacity was 1.07 and

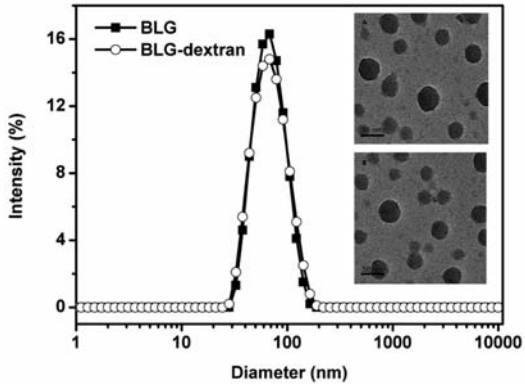


**Figure 3.** Particle diameter distributions of BLG and BLG−dextran conjugate (72 h)-encapsulated BC loaded nanoparticles (1.0% protein content, w/w) and (inset) transmission electron micrographs of BC-loaded nanoparticles prepared with BLG (A) and BLG−dextran conjugates (B), respectively, at a final protein concentration of 1% (w/w). Scale bar indicates 50 nm.

**Table 3. Mean Particle Diameter (Z-Average), Polydispersity Index (PDI), ζ-Potential, Loading Efficiency, and Loading Capacity of BC-Encapsulated BLG and BLG−Dextran (72 h) Nanoparticles[a]**

| nanoparticle | Z-average (nm) | PDI | ζ-potential | encapsulation efficiency (%) | loading capacity (%) |
|---|---|---|---|---|---|
| BLG | 66.6 ± 1.2 | 0.178 ± 0.035 | −32.9 ± 0.8 | 98.6 ± 1.0 | 1.07 ± 0.02 |
| BLG−dextran | 68.2 ± 2.9 | 0.171 ± 0.034 | −14.0 ± 0.7 | 98.4 ± 1.2 | 1.06 ± 0.03 |

[a]Data are expressed as the mean ± STD.

1.06% for native BLG and BLG−dextran conjugate, respectively.

*pH Stability against Aggregation.* Protein-based nanoparticles may flocculate or aggregate around their isoelectric point,[12,25−27] leading to increased particle size[28] and restricting their application in food systems, especially in mildly acidic beverages, such as juice, yogurt, and functional beverages. The glycation of lysine groups by the Maillard reaction to reduce the number of basic groups and increase steric hindrance by the use of large carbohydrates was used to overcome this problem. In this study, both native BLG and BLG−dextran conjugate-based BC nanoparticles were exposed to pH 2−7 (Figure 4). The

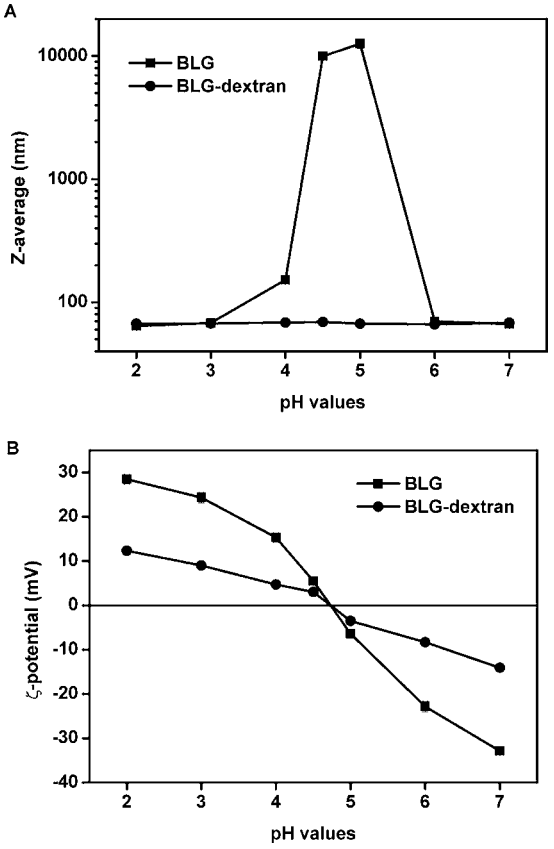


**Figure 4.** Effects of pH (2.0−7.0) on mean particle diameter (A) and ζ-potential (B) of BC-loaded nanoparticles stabilized by native BLG or BLG−dextran conjugates.

diameters of native BLG nanoparticles were stable at pH 2.0−3.0 and 6.0−7.0, but the particle diameters increased significantly to 152, 9964, and 12619 nm for pH 4.0−5.0 (Figure 4A). The large particle size about the isoelectric point suggests that the nanoparticles were strongly flocculated. Nanoparticles encapsulated by BLG−dextran conjugates did not show changes in particle diameter under the same pH conditions. The lack of aggregation and ζ-potential data support the role of steric hindrance by dextran at the interface to prevent nanoparticle flocculation or aggregation and separation of the protein surface from the continuous media.[12,19,27]

*BC Release during in Vitro Digestion.* As shown in Figure 5A, after 120 min of digestion by pepsin at pH 2.0, 6.2 and 5.4% of BC were released from BLG and BLG−dextran nanoparticles, respectively. Native BLG is resistant to proteolysis by pepsin at pH 2.0[6,29] because the peptic cleavage

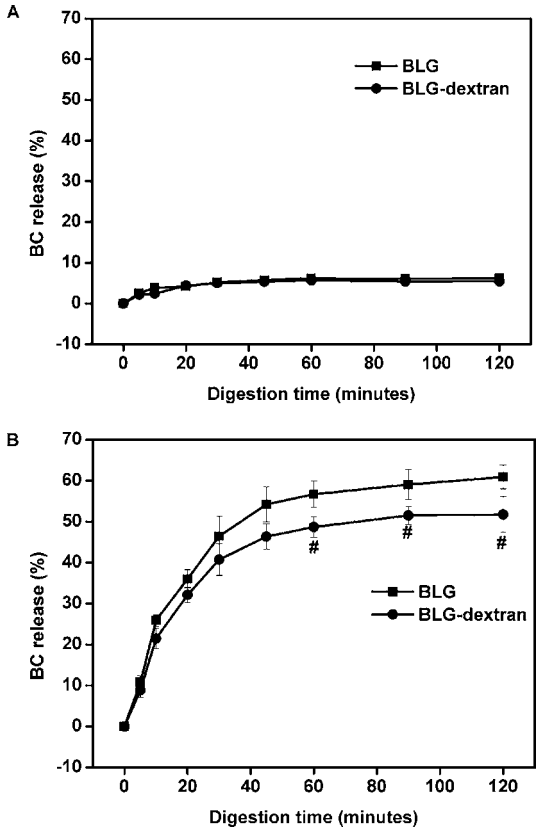


**Figure 5.** In vitro release of BC in nanoparticles encapsulated with native BLG or BLG−dextran conjugates treated with pepsin (1.0 mg/mL) and trypsin (1.0 mg/mL) at simulated gastrointestinal juice (A, pepsin at pH 2.0; B, trypsin at pH 7.0). (#) Significant ($P < 0.05$) difference.

sites are in the interior of the protein and inaccessible for hydrolysis.

BC-loaded nanoparticles were digested with trypsin (Figure 5B). Note that chymotrypsin was not used in intestinal digestion. It is possible that the combined use of trypsin−chymotrypsin could change the release rate of BC encapsulated either in BLG or BLG−dextran nanoparticles. The release of BC from native BLG nanoparticles was relatively rapid during the first 30 min, and 46.4% BC was released, whereas only 40.7% was released for BLG−dexran conjugates, suggesting BC release was prevented by glycation. After 120 min of trypsin digestion, 60.9 and 51.8% BC were released from native BLG nanoparticles and BLG−dextran nanoparticles ($P < 0.05$), respectively (Figure 5B). There are at least two possible explanations. First, the proteolysis of glycated Lys and Arg residues of BLG was largely reduced.[9,29,30] Alternatively, glycation by the large dextran used in this study sterically hindered access of the enzyme to the BLG at the surface of the nanoparticles.[12,31]

*Cell Toxicity of BC-Loaded Nanoparticles.* The viability of Caco-2 cells treated with BC-loaded nanoparticles was evaluated after the MTT assay as previously described (Figure 6).[1] The cell viability after treatment with native BLG-based nanoparticles, at protein contents of 5 and 10 mg/mL, was greater than 98 and 91 ± 2%, respectively, indicating that native BLG-based nanoparticles were nontoxic and biocompatible.

There are concerns about the health risks and benefits of the intake of Maillard reaction or glycation products.[32,33] The


dx.doi.org/10.1021/jf502639k | J. Agric. Food Chem. 2014, 62, 8900−8907

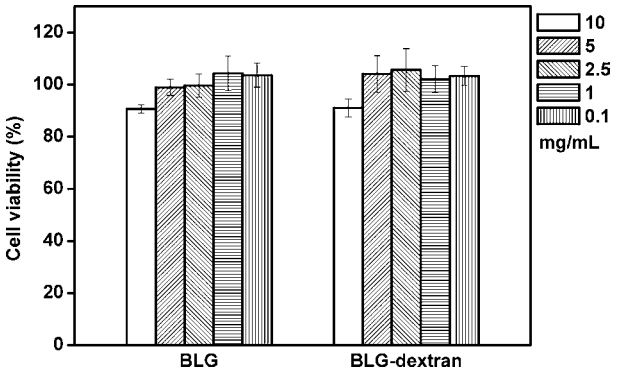


**Figure 6.** In vitro cytotoxicity of BC-loaded nanoparticles encapsulated with native BLG or BLG−dextran conjugates at different protein concentrations on Caco-2 cells measured by MTT assay. Cell viability is expressed as the mean ± STD ($n$ = 3).

results of the MTT cell viability assay of Maillard-based conjugate nanoparticles were similar to that of native BLG-based nanoparticles even at 10 mg/mL (91 ± 3%), indicating that glycation did not induce toxicity. The results above clearly showed both native BLG and BLG−dextran conjugate-based nanoparticles are safe and may be useful for BC carriers.

*Transport in Caco-2 Cells.* The uptake of lipophilic carotenoids was studied in Caco-2 cell monolayers, a model for intestinal absorption.[34−36] Caco-2 monolayers were grown to confluence, and there were no differences in TER in cells treated with free BC or BC-loaded nanoparticles (data not shown). The transport of BC into the cells was proportional to the incubation time (Figure 7A). The cumulative transport, $P_{app}$, of free BC (control, suspended in THF/DMSO) was (2.3 ± 0.5) × $10^{-7}$, whereas $P_{app}$ values for native BLG and BLG−dextran conjugate nanoparticles were (3.5 ± 0.3) × $10^{-6}$ and (3.4 ± 0.3) × $10^{-6}$, respectively ($P$ < 0.05) (Figure 7B). Compared to free BC (control), the $P_{app}$ was significantly increased by 15.4- and 14.5-fold for native BLG and BLG−dextran conjugates, respectively. The results showed that the bioavailability of carotenoids can be significantly improved by nanoencapsulation with proteins. The cellular uptake of nanoparticles is believed to occur by endocytosis. There were three main endocytic pathways: clathrin-mediated endocytosis, lipid raft/caveolae-mediated endocytosis, and macropinocytosis.[37,38] Conner et al. suggested that nanoparticles with mean diameters between 60 and 70 nm were mainly transported through lipid raft/caveolae-mediated endocytosis.[37] After internalization, the BC nanoparticles are then intracellularly transported from endosome to lysosomes. Nanoparticles were excreted from lysosomes to basolateral compartments by exocytosis.[39,40] According to a recently published paper, Golgi was involved in the nanoparticle exocytosis.[38] There were no differences in the permeability rate between native BLG and BLG−dextran conjugates ($P$ > 0.05), which indicated that polysaccharide molecules on the surface of nanoparticles had no adverse effects on bioavailability.

In conclusion, we prepared BLG glycated to very large dextran molecules. Although only about 15% of the BLG was glycated, agglomeration and ζ-potential were consistent with steric hindrance. BLG−dextran conjugated nanoparticles improved the stability in simulated gastrointestinal environment around the isoelectric point (pH 4.0−5.0) to control the release of encapsulated BC. Neither native BLG nor BLG−dextran-conjugated nanoparticles affected Caco-2 cell viability.

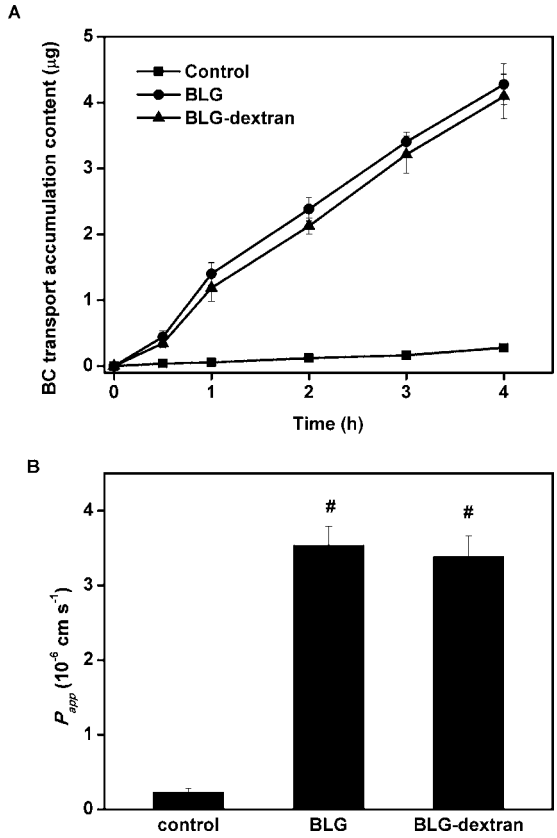


**Figure 7.** Accumulation transport (A) and apparent permeability coefficient ($P_{app}$) (B) of BC by Caco-2 cell monolayers incubated with BC THF/DMSO suspension, native BLG-stabilized BC-loaded nanoparticles, and BLG−dextran conjugate-stabilized BC-loaded nanoparticles at a BC concentration of 20 μg/mL. Values are expressed as the mean ± STD ($n$ = 3). (#) Significant ($P$ < 0.05) difference.

Transport of BC by BLG and BLG−dextran-conjugated nanoparticles increased about 15 times compared to that of free BC. The results found in this study can be used in better designing carotenoid delivery systems.

## AUTHOR INFORMATION

### Corresponding Author

*(F.Z.) Phone: +86-510-85197876. Fax: +86-510-85197876. E-mail: fzhong@jiangnan.edu.cn.

### Funding

This work was financially supported by National 125 Program 2011BAD23B02, 2013AA1022207; NSFC 31171686; NSF-Jiangsu-BK2012556; 111 Project B07029; PCSIRT0627 and JUSRP11422.

### Notes

The authors declare no competing financial interest.

## ABBREVIATIONS USED

BC, β-carotene; BLG, β-lactoglobulin; WPI, whey protein isolate; PDI, polydispersity index; MTT, 3-(4,5-dimethylthiazol-2-yl)-2,5-diphenyltetrazolium bromide; DMEM, Dulbecco's modified Eagle medium; THF, tetrahydrofuran; DMSO, dimethyl sulfoxide; SDS-PAGE, sodium dodecyl sulfate−polyacrylamide gel electrophoresis; CD, circular dichroism

## REFERENCES


(1) Yi, J.; Lam, T. I.; Yokoyama, W.; Cheng, L. W.; Zhong, F. Cellular uptake of β-carotene from protein stabilized solid lipid nanoparticles prepared by homogenization−evaporation method. *J. Agric. Food Chem.* **2014**, *62*, 1096−1104.

(2) Yi, J.; Li, Y.; Zhong, F.; Yokoyama, W. The physicochemical stability and in vitro bioaccessibility of β-carotene in oil-in-water sodium caseinate emulsions. *Food Hydrocolloids* **2014**, *35*, 19−27.

(3) He, W.; Tan, Y. N.; Tian, Z. Q.; Chen, L. Y.; Hu, F. Q.; Wu, W. Food protein-stabilized nanoemulsions as potential delivery systems for poorly water-soluble drugs: preparation, in vitro characterization, and pharmacokinetics in rats. *Int. J. Nanomed.* **2011**, *6*, 521−533.

(4) Mao, L. K.; Xu, D. X.; Yang, J.; Yuan, F.; Gao, Y. X.; Zhao, J. Effects of small and large molecule emulsifiers on the characteristics of β-carotene nanoemulsions prepared by high pressure homogenization. *Food Technol. Biotechnol.* **2009**, *47*, 336−342.

(5) Qian, C.; Decker, E. A.; Xiao, H.; McClements, D. J. Physical and chemical stability of β-carotene-enriched nanoemulsions: influence of pH, ionic strength, temperature, and emulsifier type. *Food Chem.* **2012**, *132*, 1221−1229.

(6) Reddy, I. M.; Kella, N. K. D.; Kinsella, J. E. Structural and conformational basis of the resistance of β-lactoglobulin to peptic and chymotryptic digestion. *J. Agric. Food Chem.* **1988**, *36*, 737−741.

(7) Teng, Z.; Li, Y.; Luo, Y.; Zhang, B.; Wang, Q. Cationic β-lactoglobulin nanoparticles as a bioavailability enhancer: protein characterization and particle formation. *Biomacromolecules* **2013**, *14*, 2848−2856.

(8) Li, Y.; Zhong, F.; Ji, W.; Yokoyama, W.; Shoemaker, C. F.; Zhu, S.; Xia, W. Functional properties of Maillard reaction products of rice protein hydrolysates with mono-, oligo- and polysaccharides. *Food Hydrocolloids* **2013**, *30*, 53−60.

(9) Liu, G.; Zhong, Q. Thermal aggregation properties of whey protein glycated with various saccharides. *Food Hydrocolloids* **2013**, *32*, 87−96.

(10) Wooster, T. J.; Augustin, M. A. β-Lactoglobulin−dextran Maillard conjugates: their effect on interfacial thickness and emulsion stability. *J. Colloid Interface Sci.* **2006**, *303*, 564−572.

(11) Corzo-Martínez, M.; Soria, A. C.; Belloque, J.; Villamiel, M.; Moreno, F. J. Effect of glycation on the gastrointestinal digestibility and immunoreactivity of bovine β-lactoglobulin. *Int. Dairy J.* **2010**, *20*, 742−752.

(12) Lesmes, U.; McClements, D. J. Controlling lipid digestibility: response of lipid droplets coated by β-lactoglobulin-dextran Maillard conjugates to simulated gastrointestinal conditions. *Food Hydrocolloids* **2012**, *26*, 221−230.

(13) Liu, G.; Zhong, Q. Glycation of whey protein to provide steric hindrance against thermal aggregation. *J. Agric. Food Chem.* **2012**, *60*, 9754−9762.

(14) Dyballa, N.; Metzger, S. Fast and sensitive colloidal Coomassie G-250 staining for proteins in polyacrylamide gels. *J. Vis. Exp.* **2009**, DOI: 10.3791/1431.

(15) Tan, C. P.; Nakajima, M. β-Carotene nanodispersions: preparation, characterization and stability evaluation. *Food Chem.* **2005**, *92*, 661−671.

(16) Altshuller, A. P.; Everson, H. E. The solubility of ethyl acetate in water. *J. Am. Chem. Soc.* **1953**, *75*, 1727−1727.

(17) Hubatsch, I.; Ragnarsson, E. G. E.; Artursson, P. Determination of drug permeability and prediction of drug absorption in Caco-2 monolayers. *Nat. Protoc.* **2007**, *2*, 2111−2119.

(18) Chen, Y.-j.; Liang, L.; Liu, X.-m.; Labuza, T. P.; Zhou, P. Effect of fructose and glucose on glycation of β-lactoglobulin in an intermediate-moisture food model system: analysis by liquid chromatography−mass spectrometry (LC−MS) and data-independent acquisition LC−MS (LC−MSE). *J. Agric. Food Chem.* **2012**, *60*, 10674−10682.

(19) Li, Z.; Gu, L. Fabrication of self-assembled (−)-epigallocatechin gallate (EGCG) ovalbumin−dextran conjugate nanoparticles and their transport across monolayers of human intestinal epithelial Caco-2 cells. *J. Agric. Food Chem.* **2014**, *62*, 1301−1309.

(20) Zhou, H.; Sun, X.; Zhang, L.; Zhang, P.; Li, J.; Liu, Y.-N. Fabrication of biopolymeric complex coacervation core micelles for efficient tea polyphenol delivery via a green process. *Langmuir* **2012**, *28*, 14553−14561.

(21) Enomoto, H.; Li, C.-P.; Morizane, K.; Ibrahim, H. R.; Sugimoto, Y.; Ohki, S.; Ohtomo, H.; Aoki, T. Glycation and phosphorylation of β-lactoglobulin by dry-heating: effect on protein structure and some properties. *J. Agric. Food Chem.* **2007**, *55*, 2392−2398.

(22) Creamer, L. K.; Parry, D. A. D.; Malcolm, G. N. Secondary structure of bovine β-lactoglobulin B. *Arch. Biochem. Biophys.* **1983**, *227*, 98−105.

(23) Greenfield, N. J. Using circular dichroism spectra to estimate protein secondary structure. *Nat. Protoc.* **2007**, *1*, 2876−2890.

(24) Tang, C.-H.; Sun, X.; Foegeding, E. A. Modulation of physicochemical and conformational properties of kidney bean vicilin (phaseolin) by glycation with glucose: implications for structure−function relationships of legume vicilins. *J. Agric. Food Chem.* **2011**, *59*, 10114−10123.

(25) Diftis, N. G.; Biliaderis, C. G.; Kiosseoglou, V. D. Rheological properties and stability of model salad dressing emulsions prepared with a dry-heated soybean protein isolate−dextran mixture. *Food Hydrocolloids* **2005**, *19*, 1025−1031.

(26) Evans, M.; Ratcliffe, I.; Williams, P. A. Emulsion stabilisation using polysaccharide−protein complexes. *Curr. Opin. Colloid Interface Sci.* **2013**, *18*, 272−282.

(27) Wong, B. T.; Day, L.; Augustin, M. A. Deamidated wheat protein−dextran Maillard conjugates: effect of size and location of polysaccharide conjugated on steric stabilization of emulsions at acidic pH. *Food Hydrocolloids* **2011**, *25*, 1424−1432.

(28) Charoen, R.; Jangchud, A.; Jangchud, K.; Harnsilawat, T.; Naivikul, O.; McClements, D. J. Influence of biopolymer emulsifier type on formation and stability of rice bran oil-in-water emulsions: whey protein, gum arabic, and modified starch. *J. Food Sci.* **2011**, *76*, E165−E172.

(29) Luz Sanz, M.; Corzo-Martínez, M.; Rastall, R. A.; Olano, A.; Moreno, F. J. Characterization and in vitro digestibility of bovine β-lactoglobulin glycated with galactooligosaccharides. *J. Agric. Food Chem.* **2007**, *55*, 7916−7925.

(30) Wang, W.; Zhong, Q. Properties of whey protein−maltodextrin conjugates as impacted by powder acidity during the Maillard reaction. *Food Hydrocolloids* **2014**, *38*, 85−94.

(31) Mun, S.; Decker, E.; Park, Y.; Weiss, J.; McClements, D. J. Influence of interfacial composition on in vitro digestibility of emulsified lipids: potential mechanism for chitosan's ability to inhibit fat digestion. *Food Biophys.* **2006**, *1*, 21−29.

(32) Ames, J. M. Evidence against dietary advanced glycation endproducts being a risk to human health. *Mol. Nutr. Food Res.* **2007**, *51*, 1085−1090.

(33) Somoza, V. Five years of research on health risks and benefits of Maillard reaction products: an update. *Mol. Nutr. Food Res.* **2005**, *49*, 663−672.

(34) Claudie, D.-m.; Alexandrine, D.; Bertrand, C.; Franck, T.; Marie-Josephe, A. Citrus flavanones enhance carotenoid uptake by intestinal Caco-2 cells. *Food Funct.* **2013**, *4*, 1625−1631.

(35) During, A.; Harrison, E. H. An in vitro model to study the intestinal absorption of carotenoids. *Food Res. Int.* **2005**, *38*, 1001−1008.

(36) Sy, C.; Gleize, B.; Dangles, O.; Landrier, J.-F.; Veyrat, C. C.; Borel, P. Effects of physicochemical properties of carotenoids on their bioaccessibility, intestinal cell uptake, and blood and tissue concentrations. *Mol. Nutr. Food Res.* **2012**, *56*, 1385−1397.

(37) Conner, S. D.; Schmid, S. L. Regulated portals of entry into the cell. *Nature* **2003**, *422*, 37−44.

(38) He, B.; Lin, P.; Jia, Z.; Du, W.; Qu, W.; Yuan, L.; Dai, W.; Zhang, H.; Wang, X.; Wang, J.; Zhang, X.; Zhang, Q. The transport mechanisms of polymer nanoparticles in Caco-2 epithelial cells. *Biomaterials* **2013**, *34*, 6082−6098.

(39) Chiu, Y.-L.; Ho, Y.-C.; Chen, Y.-M.; Peng, S.-F.; Ke, C.-J.; Chen, K.-J.; Mi, F.-L.; Sung, H.-W. The characteristics, cellular uptake and

intracellular trafficking of nanoparticles made of hydrophobically-modified chitosan. *J. Controlled Release* **2010**, *146*, 152−159.
(40) Roger, E.; Lagarce, F.; Garcion, E.; Benoit, J.-P. Biopharmaceutical parameters to consider in order to alter the fate of nanocarriers after oral delivery. *Nanomedicine* **2010**, *5*, 287−306.

body weight (bw) per day. The toxin was also evaluated by the Scientific Committee on Food, which proposed that exposure should be below 5 ng/kg (bw) per day.[21] The Joint FAO/WHO Expert Committee for Food Additives (JECFA) reconfirmed the provisional tolerable weekly intake (PTWI) of OTA as 100 ng $kg^{-1}$ $week^{-1}$.[22] At present, the International Office of Vine and Wine (OIV) is considering the application of a limit of 2 μg/kg OTA for wine;[23] however, there is no regulation or limit standards with respect to OTA in wine from China currently. In 2013, Zhang et al.[24] analyzed a total of 119 wines, which were obtained from four major regions around China from 1999 to 2009; the OTA levels ranged from <0.1 to 5.65 μg/L, with an average concentration of 2.18 μg/L. However, other results showed the OTA content of Chinese wine at levels of 0−0.94 μg/kg ($n$ = 100) and 0.02−1.18 μg/L ($n$ = 105),[11,25] far below the research of Zhang. Among the reasons for the difference, sample mode, sample types, and determination method were the main factors. Therefore, the OTA level of Chinese wine should be further generally surveyed and analyzed with a reasonable sampling scheme and accurate determination method.

As an important factor, very sensitive analytical methods for OTA detection are needed. The most common analytical method for OTA determination in foodstuff is HPLC coupled to fluorescence detection.[26,27] Other methods, such as photodiode array detection (LC-DAD)[28] or mass spectrometry (LC-MS) and tandem MS (LC-MS/MS),[29] have also been established. Alternative applied techniques are thin layer chromatography (TLC),[30] gas chromatography coupled with MS (GC-MS),[31] and fluorescence polarization immunoassay.[32] Also, capillary electrophoresis (CE) with UV−vis detection has also been proposed for the determination of OTA in wine.[33] As for the sample preparation, more extraction and cleanup methods for the determination of OTA have been reported. Most of them are based on immunoaffinity columns (IACs) to higher cleanup and sample purification. However, this methodology is high-cost and tedious. Solid-phase extraction (SPE),[26] liquid−liquid extraction (LLE),[34] and SPE with molecular imprinted polymers (MISPE) in different matrices,[35] have been also used for the determination of OTA. The stability of OTA during its extraction using microwave-assisted extraction (MAE), PLE, ultrasound-assisted and magnetic stirring-assisted extraction,[36] and dispersive liquid−liquid microextraction (DLLME)[37] has also been evaluated in the determination of OTA in wine.

In the present study, OTA contents were analyzed from a large number of Chinese wine samples, which were from the main producing areas and different production years and varieties, using the SPE method in combination with HPLC-FLD (better resolution, lower detection limits, and lower solvent consumption). Then, OTA exposure assessment of Chinese wine consumers was analyzed with a point evaluation model based on a wine consumption survey in China, which was also in great accordance with the literature,[11,20] and by the daily intake (DI) of OTA from the wine consumption data provided by the invited participants to the comparison of the DI of OTA from analysis of the wine consumption data. Although maximum limits of OTA content have been applied to some foods, no limit or regulation currently exists for OTA in Chinese wines so far. The results of this study will provide essential data for establishing the maximum limit of OTA in Chinese wine.

## MATERIALS AND METHODS

**Samples.** A total of 223 samples were obtained from wine manufacturers of the major wine-producing areas of China: Shandong, Hebei, Tianjin, Beijing, Xinjiang, Gansu, and Yunnan (all of Chinese wine in circulation was manufactured in these areas). The samples include 183 red wines and 40 white wines. All samples have different origins, years, cultivars, and types, which can represent the real status of Chinese wine sufficiently.

**Chemicals.** Acetonitrile, methanol, methanoic acid, and other chemical reagents were all of HPLC grade and were supplied by Merck (Darmstadt, Germany). The standard of OTA (≥98% (HPLC) was also purchased from Sigma. Analytically pure phosphoric acid and potassium hydroxide were also used, and double-distilled water was used in all experiments. Stock standard solutions of 100 mg/mL OTA were prepared in methanol. Working standard solutions were prepared daily by diluting the stock solution with methanol/water (98:2, v/v). All working standard solutions were stored at 4 °C in the dark. Anion-exchange SPE columns (150 mg/mL Agela Technologies, China) were used for cleanup.

Extract solutions were prepared from 0.1 M KOH/ethanol/water (2:60:38, v/v/v). The concentrations of potassium hydroxide solution used were 10 and 0.1 M, respectively.

**Apparatus.** Purification and determination of the preconcentration of OTA prior to quantitative analyses were performed using the Waters 2695 HPLC (Waters, Milford, MA, USA) and the Waters 2475 FLD. Chromatography software (Empower; Waters) was used to collect and process the chromatographic data. Separation was performed on a C18 analytical column (5 μm, 250 × 4.6 mm, Waters, Atlantis T3).

**Sample Pretreatment.** The anion-exchange SPE column was used for cleanup following this procedure: First, 6 mL of extract solution was added into 10 mL of sample, which was shaken in a vortex device and then adjusted to pH 8−9 with 10 mol/L potassium hydroxide solution. After activation and conditioning of the cartridges by rinsing with 5 mL of methanol and 3 mL of extract solution, the prepared sample was then added to the SPE column at a flow of 1−2 drops per second. Third, 3 mL of a mixture of acetonitrile/water/0.1 M KOH (50:47:3, v/v/v) was used to wash the SPE column using the same flow rate. Fourth, 1.2 mL of double-distilled water was added to remove neutral and basic interferences. Finally, the OTA of the wine was eluted using 5 mL of a mixture of methanol/acetonitrile/methanoic acid/water (40:50:5:5, v/v/v/v) at the rate of 1 drop per second, and the eluate was collected in a glass test tube. The eluate was evaporated to dryness at 45 °C with nitrogen and dissolved again immediately in 0.5 mL of the HPLC mobile phase (A/B = 1:1, v/v) and kept at 4 °C until the HPLC analysis.

**HPLC Analysis.** The fluorescence detector (Waters 2475) was set at excitation and emission wavelengths of 333 and 443 nm, respectively. A C18 column (5 mm, 250 m × 4.6 mm) at 30 °C and mobile phase A and B solutions composed of phosphate solution adjusted to pH 2.5 by the addition of 5% phosphate and acetonitrile, at a flow rate of 1 mL $min^{-1}$, were used to separate the OTA. The gradient elution program started with a linear gradient from 12 to 20% acetonitrile in 10 min, followed by a 2 min linear gradient from 20 to 30% acetonitrile, a 7 min linear gradient from 30 to 50% acetonitrile, was maintained at 50% acetonitrile isocratic until 30 min, followed by a 1 min linear gradient from 50 to 100% acetonitrile then maintained at 100% acetonitrile isocratic until 39 min, and then finally returned to the initial conditions; the column was re-equilibrated with the initial mobile phase composition for 15 min. The injection volume was set to 10 μL.

**Method Validation.** A five-point calibration curve of OTA was created for quantification of the following concentrations: 0.5, 1.0, 2.0, 5.0, and 10.0 μg/L. Every level was injected three replicates to acquire the mean value of the area. The calibration curve was derived by plotting concentrations as a function of peak area of OTA, which resulted in a good linear regression. Reproducibility of the results was investigated by injecting three replicates of the same sample on seven different days and on the same day seven times.

**Wine Consumption Data.** A questionnaire method was further used to collect quantitative survey data related to wine consumption. A total of 1268 completed questionnaire surveys about the amount and frequency of consumption of wine were obtained. Wine consumers between 18 and 60 years old were invited to fill in the wine consumption questionnaire survey; people who never drink wine were excluded. The survey was carried out in the major wine-producing areas, main cities, and bars of China, including ordinary citizens, winery staff, company executives, etc. It may represent the consumption of wine by residents of China comprehensively. The weekly wine consumption equals the average amount of wine drunk per time multiplied by the frequency of wine consumption per week.

**Risk Assessment.** Previous exposure assessments had been based on a deterministic approach (point estimate) or on the estimation of the empirical probability for consumers to exceed the toxicological reference value.[53,54] In both cases, various levels of consumption were combined with the mean concentrations of OTA in wine. Two mathematical approaches of the point evaluation and the Monte Carlo assessment model were combined to perform the risk assessment of OTA in the present study according to eq 1

$$y = xc/w \quad (1)$$

where $y$ is the DI value of OTA (ng/kg bw), $x$ is the food consumption (g day$^{-1}$), $c$ is the concentration level of OTA in wine (ng g$^{-1}$), and $w$ is body weight (kg).

## RESULTS AND DISCUSSION

**Quality Control.** A high correlation coefficient ($R^2$ = 0.9999) was obtained for the tested interval, and the linear regression equation was $Y = 2883.2x - 293.64$. The standard deviation of the slope and intercept were 9.91and 3.59 ($n$ = 3), respectively, which meet requirements of methodology absolutely. The relative standard deviations (RSDs) of both the intraday and interday precision were 5.8 and 12.6%, respectively.

As shown in Table 1, average recoveries of OTA were 94.47% and the RSD was 4.03%. These results demonstrate

**Table 1. OTA Recovery and Relative Standard Deviations (RSDs) ($n$ = 3)**

| sample | wine OTA content (μg/L) | lead spiked (μg/L) | determined result (μg/L) | recovery (%) | mean recovery (%) | RSD (%) |
|---|---|---|---|---|---|---|
| white wine | 0.13 | 0.05 | 0.177 | 94.00 | | |
| | | 0.10 | 0.225 | 95.00 | | |
| | | 0.20 | 0.326 | 98.00 | | |
| | | 0.40 | 0.541 | 102.75 | | |
| | | | | | 97.47 | 4.03 |
| red wine | 0.36 | 0.05 | 0.406 | 92.00 | | |
| | | 0.15 | 0.504 | 96.00 | | |
| | | 0.40 | 0.758 | 99.50 | | |
| | | 0.80 | 1.180 | 102.50 | | |

that this method is suitable and efficient for analyzing OTA content. The recovery range fell within the guidelines for acceptable recovery limits of the Association of Analytical Chemists (AOAC) and the Codex Alimentarius: 70−125% at the 10 ng/mL level (AOAC) and 70−110% at the 10−100 ng/mL level and 60−120% at the 1−10 ng/mL level (Codex Alimentarius).[38]

As shown in Figure 1, the peak of OTA in standard and sample was symmetrical with good separation at 32 min, but there weas no peak for free-OTA sample. The retention time of OTA in another HPLC method was less than this method, and the minimum was approximately 5 min;[39,46,48] however, every method has a different mobile phase and pretreatment method. Moreover, the pretreatment method was immunoadsorption or the sample also needed to derive in another method. All of them would increase the cost. For anion-exchange/reversed-phase cleanup, Reinsch et al. determined OTA in wine by LC-MS, and the retention time was about 9.5 min.[40]

The limit of detection (LOD) was obtained using free-OTA wine samples spiked with OTA at low concentration levels at a signal-to-noise (S/N) ratio of 3. The LOD and the limit of quantification (LOQ) (normally based on S/N = 10) were 0.01 and 0.03 μg/L, respectively. As can be seen, the sensitivity of the method allowed the quantification of OTA at concentrations much lower than the maximum level established for wine samples.[41]

**General Investigation.** The LOQ of the established HPLC-FLD method was 0.03 μg/L for the determination of OTA in Chinese wine, and the concentration of OTA in the analyte-free wine was recorded as 0.015 μg/L (half of the LOQ), which was used for the risk assessment. The maximum concentration of OTA in wine was 0.98 μg/L. The mean concentration of OTA in all samples was 0.146 μg/L; the $P_{50}$ and $P_{95}$ values were 0.510 and 0.767 μg/L, respectively. The OTA level was lower than that found (from <0.1 to 5.65 μg/L) by Zhang[24] in 2013, but similar to the research (0.02−1.18 μg/L) of Wu[25] and Han (0−0.94 μg/L).[11] The mean of OTA concentration in white wine was 0.05 μg/L, lower than in red wine (0.17 μg/L) (Table 2), which was similar to other research in Chinese wine.[11,25,42] In Europe, the OTA content in wine production generally varies between 0.01 and 15.60 μg/kg, with a mean of 0.357 μg/kg. In addition, the means were 0.159 and 0.453 μg/kg in white wine and red wine, respectively.[19] Red wine generally contains higher OTA than white wine. This fact evidences a clear relationship between the maceration of the must with grape skins and OTA solubilization in the must. That is because dark grape skins are easily infected by mycete, and grape skins are sometimes discarded in the brewing process of white wine.[43] The survey results showed that OTA contamination in Chinese wine was lower than in European wine reported by European studies.[44−47] Furthermore, the incidence (45.2%) studied in this paper was higher than reported by Han et al. (35%) of Shanghai and Wu et al. (17.6%, 2011; 11.8%, 2012) of China,[11,25,42] but similar to the results reported by Solfrizzo.[48]

As listed in Figure2, the highest mean OTA concentration was observed in wine from Henan province (0.24 μg/L), whereas the lowest mean value was observed in Jilin (0.07 μg/L). The considerable climatic differences, related to geographic regions, have also an influence on OTA occurrence in wine. The means of southern and northern Europe were 0.181 and 0.636 μg/kg, respectively.[4,49,50] The distribution trend was just like results of Chinese wine.[24,25] Italian and Spanish surveys confirm that OTA levels were high in wines produced in areas with warm climatic conditions, suggesting that OTA production could be due to fungi belonging to the genus *Aspergillus*.[6,51,52]

**Consumption Survey.** There were 1268 questionnaires finished during June−August 2011, and 948 questionnaires had been confirmed as valid by logic questions in 1268 questionnaires (effective rate of 74.76%). After collection of the questionnaires, there were 607 males and 341 females. The average weights of the males and females were calculated as 64 and 56 kg, respectively. The ages of the participants registered were in the range of 18−60 years old, and the ages between 30

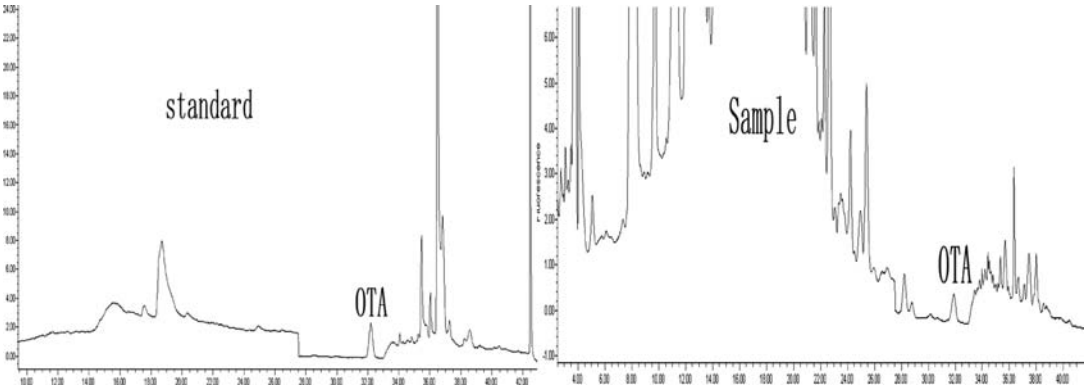


**Figure 1.** HPLC chromatograms: left, OTA standards; right, wine sample.

**Table 2. OTA Levels of Wine Samples and Consumption Analysis**

| | OTA levels of wine | | | |
|---|---|---|---|---|
| | all wines ($\mu$g/L) | red wine ($\mu$g/L) | white wine ($\mu$g/L) | wine consumption (mL/week/person) |
| *n* | 223 | 183 | 40 | 948 |
| mean | 0.15 | 0.17 | 0.05 | 342.3 |
| median | 0.08 | 0.09 | 0.01 | 116.7 |
| minimum | 0.00 | 0.00 | 0.00 | 0.0 |
| maximum | 0.98 | 0.20 | 0.36 | 7000.0 |
| $P_{95}$ | 0.51 | 0.59 | 0.22 | 1400.0 |
| $P_{97.5}$ | 0.75 | 0.79 | 0.36 | 1750.0 |

and 40 were the maximum proportion with 38%. As Table 3 shows, the weekly wine consumption of the Chinese population was statistically analyzed on the basis of these questionnaires. The median, mean, and $P_{95}$ values were 116.7, 342.3, and 1400 mL/week, respectively. The statistical result was higher than the values surveyed by Su[20] in China from 1989 to 2006 and quantitative assessment of risk associated with OTA (mean = 2.8 ± 5.8 g/day, $P_{90}$ 38.8 g/day) on the adult inhabitants in Shanghai of China by Han.[11]

**Exposure Assessment.** Statistical results show that the weight of 71% of consumers surveyed was between 45 and 75 kg, and the average weights of the maled and femaled were calculated as 64 and 56 kg, respectively. The weight distribution of the surveyed population was in close proximity with 60 kg, which was used to carry out the assessment in international organizations. Therefore, consumers with 60 kg weight were used as reference.

According to these data, the intake of OTA for the average adult consumer varies between 0.86 and 1.08 ng/kg bw/week. These data indicate that the intake of OTA for consumers of higher consumption ranges from 4.38 to 5.54 ng/kg bw/week (Table 3). As shown in Figure 3, there were different exposures of OTA in wine of different provinces. The exposure levels of Henan, Hebei, and Gansu were higher than those in Yannan, Xinjiang, and Ningxia. The dietary intake of OTA except for consumers reporting higher consumption was low, which had been higher than 5% PTWI (100 ng/kg/week) by the JECFA.

In conclusion, an exposure assessment of OTA in wine was conducted to evaluate the potential health risks of the estimated dietary exposure in comparison with the PTWI of OTA recommended by the JECFA. The results suggested that dietary intake of OTA had very low health risks in wine except for high percentile (97.5) consumers. Nonetheless, on the basis of the exposure assessment, the suggested safe limit value of OTA for Chinese wine was suggested to be 2.0 $\mu$g/kg. Not only was this

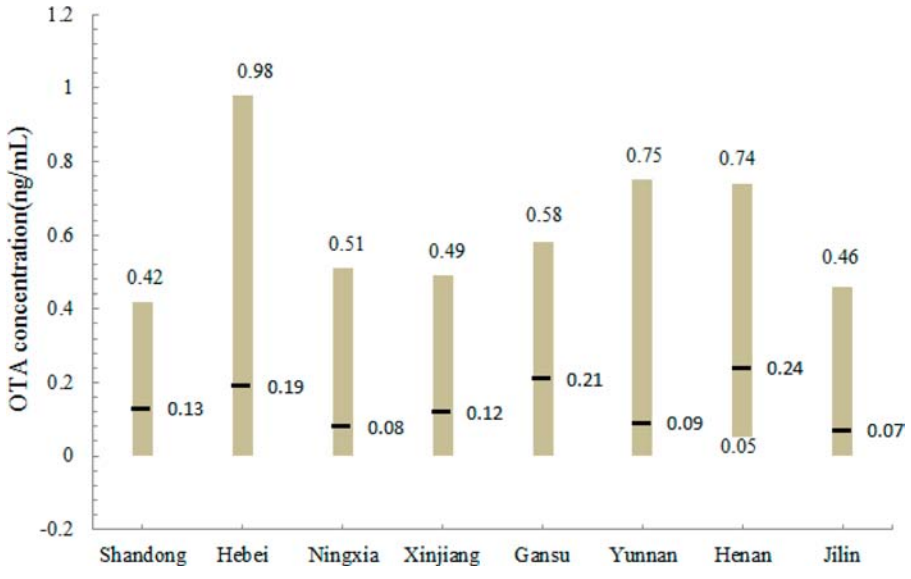


**Figure 2.** OTA levels of wine from different wine-producing areas.


dx.doi.org/10.1021/jf500713x | J. Agric. Food Chem. 2014, 62, 8908−8913

**Table 3. Estimated Intake of Ochratoxin A in Consumers of Mean Percentile (Average Wine Consumption) and Consumers of High Percentile (97.5 Percentile Wine Consumption) from Wine**

| wine consumption (mL/week/person) | | OTA in wine ($\mu$g/L) | | | intake of OTA (ng kg$^{-1}$ week$^{-1}$) | | | |
|---|---|---|---|---|---|---|---|---|
| | | | | | mean (wine consumption) | | $P_{97.5}$ (wine consumption) | |
| mean | $P_{97.5}$ | mean1* | mean2* | range | mean1 | mean2 | mean1 | mean2 |
| 342.3 | 1750 | 0.15 | 0.19 | ND−0.98 | 0.86 | 1.08 | 4.38 | 5.54 |

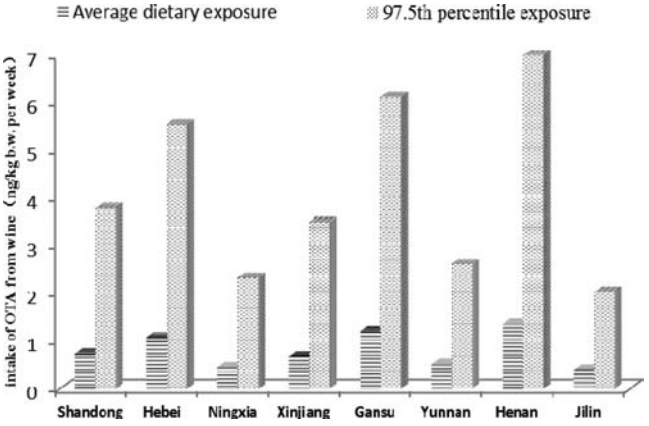


**Figure 3.** Dietary exposure to OTA in mean consumption (average consumption) and higher consumption (97.5 percentile consumption in consumers only) from different provinces in China.

limit consistent with OIV international limit standards, but it also protects the rapid and healthy development of the Chinese wine industry.

## AUTHOR INFORMATION


### Corresponding Authors

*(Q.D.Z.) E-mail: zhongqiding@163.com.

*(Y.N.W) E-mail: wuyongning@cfsa.net.cn.



### Funding

The work was supported by the Quality Inspection of Public Welfare Project (Item 201210104), the National Food Safety Standards Project (Item SPAQ- 2011-33), and the MOH Key Lab of Food Safety Risk Assessment (No. 201401).


### Notes

The authors declare no competing financial interest.

## REFERENCES


(1) Kuiper, G. T.; Scott, P. M. Risk assessment of the mycotoxin ochratoxin A. *Biomed. Environ. Sci.* **1989**, *2*, 179−248.

(2) Tarín, A.; Rosell, M. G.; Guardino, X. Use of high performance liquid chromatography to assess airborne mycotoxins aflatoxins and ochratoxin A. *J. Chromatogr., A* **2004**, *1047*, 235−240.

(3) Majerus, P.; Otteneder, H. Detection and occurrence of ochratoxin A in wine and grape juice. *Dsch. Lebensm.-Rundsch.* **1996**, *92*, 388−390.

(4) Zimmerli, B.; Dick, R. Ochratoxin A in table wine and grape juice: occurrence and risk assessment. *Food Additi. Contam.* **1996**, *13*, 655−668.

(5) Ospita, M.; Cazabeil, J. M.; Betbeder, A. M.; Tricard, C.; Creppy, E.; Medina, B. L'Ochratoxine A dans les vins. *Oenologie* **1998**, *169*, 16−19.

(6) Battilani, P.; Languasco, L.; Pietri, A.; Bertuzzi, T.; Giorni, P. Ochratoxin A in grape and wine: causes and conditions of production. *J. Plant Pathol.* **2000**, 553−555.

(7) Battilani, P.; Giorni, P.; Bertuzzi, T.; Pietri, A. Preliminary results on ochratoxin A production by fungi invading grape berries.In *Proceedings of the 11th Congress of Mediterranean Phytopathological Union and 3rd Congress of Sociedade Portuguesa de Fitopatologia' Evora Portugal*, 2001; pp 120−122

(8) Abarca, M. L.; Accensi, F.; Bragulat, M. R.; Cabañes, F. J. Current importance of ochratoxin A-producing *Aspergillus* spp. *J. Food Prot.* **2001**, *64*, 903−906.

(9) Bellí, N.; Marín, S.; Sanchis, V.; Ramos, A. J. Ochratoxin A (OTA) in wines, musts and grape juices: occurrence, regulations and methods of analysis. *Food Sci. Technol. Int.* **2002**, *8* (6), 325−335.

(10) Battilani, P.; Magan, N.; Logrieco, A. European research on ochratoxin A in grapes and wine. *Int. J. Food Microbiol.* **2006**, *111*, S2−S4.

(11) Han, Z.; Nie, D. X.; Yang, X. L.; Wang, J. H. Quantitative assessment of risk associated with dietary intake of mycotoxin ochratoxin A on the adult inhabitants in Shanghai city of P.R. China. *Food Control* **2013**, *32*, 490−495.

(12) IARC. Evaluation of carcinogenic risks of chemical to humans. *IARC Monograph on Some Naturally-Occurring Substances: Food Items and Constituents. Heterocyclic Aromatic Amines and Mycotoxins*; IARC: Lyon, France, 1993; pp 359−362.

(13) Haighton, L. A.; Lynch, B. S.; Magnuson, B. A.; Nestmann, E. R. A reassessment of risk associated with dietary intake of ochratoxin A based on a lifetime exposure model. *Crit. Rev. Toxicol.* **2012**, *42* (2), 147−168.

(14) Walker, R. Risk assessment of ochratoxin: current views of the European Scientific Committee on Food, the JECFA and the Codex Committee on Food Additives and Contaminants. *Adv. Exp. Med. Biol.* **2002**, *504*, 249−255.

(15) Coronel, M. B.; Marín, S.; Cano-Sancho, G.; Ramos, A. J.; Sanchis, V. Exposure assessment to ochratoxin A in Catalonia (Spain) based on consumption of cereals, nuts, coffee, wine, and beer. *Food Addit. Contam.: Part A* **2012**, *29* (6), 979−993.

(16) Coronel, M. B.; Sanchis, V.; Ramos, A. J.; Marin, S. Assessment of the exposure to ochratoxin A in the province of Lleida, Spain. *Food Chem. Toxicol.* **2009**, *47* (11), 2847−2852.

(17) Kuiper-Goodman, T.; Hilts, C.; Billiard, S. M.; Kiparissis, Y.; Richard, I. D. K.; Hayward, S. Health risk assessment of ochratoxin A for all age-sex strata in a market economy. *Food Additi. Contam.: Part A* **2010**, *27* (2), 212−240.

(18) Iavicoli, I.; Brera, C.; Carelli, G.; Caputi, R.; Marinaccio, A.; Marinaccio, M. External and internal dose in subjects occupationally exposed to ochratoxin A. *Int. Arch. Occup. Environ. Health* **2002**, *75* (6), 381−386.

(19) EU Commission. *Assessment of Dietary intake of Ochratoxin A by the Population of EU Member States*; Report of experts participating in Task 3.2.7; 2002.

(20) Su, C.; Zhang, B.; Wang, H. J.; Du, W. W. The status and trend of cereal consumption among Chinese adults in nine provinces (municipality) from 1989 to 2006. *Zhonghua Yu Fang Yi Xue Za Zhi* **2011**, *45* (9), 798−801.

(21) EC. *Opinion on Ochratoxin A*; European Commission report, Scientific Committee on Food, 1998.

(22) JECFA. Evaluation of certain mycotoxins in food: 56th report of the joint FAO/WHO Expert Committee on Food Additives, 2002.

(23) OIV. Maximum acceptable limits of various substances contained in wine, OIV-MA-C1-01, 2011; available at http://www.oiv.int/oiv/files/OIV-MA-C1-01._EN.pdf.

(24) Zhang, X.; Chen, L.; Li, J.; Zhu, B.; Ma, L. Occurrence of ochratoxin A in Chinese wines: influence of local meteorological parameters. *Eur. Food Res. Technol.* **2013**, *236* (2), 277−283.

(25) Wu, J. W.; Tan, Y. F.; Wang, Y. Q.; Xu, Q. Occurrence of ochratoxin A in wine and beer samples from China. *Food Addit. Contam., Part B: Surveillance* **2011**, *4* (1), 52−56.
(26) González-Peñas, E.; Leache, C.; López de Cerain, A.; Lizarraga, E. Comparison between capillary electrophoresis and HPLC-FL for ochratoxin A quantification in wine. *Food Chem.* **2006**, *97*, 349−354.
(27) Hernández, M. J.; García-Moreno, M. V.; Durán, E.; Guillén, D.; Barroso, C. G. Validation of two analytical methods for the determination of ochratoxin A by reversed-phased high-performance liquid chromatography coupled to fluorescence detection in musts and sweet wines from Andalusia. *Anal. Chim. Acta* **2006**, *566*, 117−121.
(28) Soleas, G. J.; Yan, J.; Goldberg, D. M. Assay of ochratoxin A in wine and beer by high-pressure liquid chromatography photodiode array and gas chromatography mass selective detection. *J. Agric. Food Chem.* **2011**, *49*, 2733−2740.
(29) Zöllner, P.; Mayer-Helm, B. Trace mycotoxin analysis in complex biological and food matrices by liquid chromatography−atmospheric pressure ionization mass spectrometry. *J. Chromatogr., A* **2006**, *1136*, 123−169.
(30) Welke, J. E.; Hoeltz, M.; Dottori, H. A.; Noll, I. B. Determination of ochratoxin A in wine by high-performance thin-layer chromatography using charged coupled device. *J. Braz. Chem. Soc.* **2010**, *21*, 441−446.
(31) Olsson, J.; Borjesson, T.; Lundstedt, T.; Schnurer, J. Detection and quantification of ochratoxin A and deoxynivalenol in barley grains by GC−MS and electronic nose. *Int. J. Food Microbiol.* **2002**, *72*, 203−214.
(32) Zezza, F.; Longobardi, F.; Pascale, M.; Eremin, S. A.; Visconti, A. Fluorescence polarization immunoassay for rapid screening of ochratoxin A in red wine. *Anal. Bioanal. Chem.* **2009**, *395*, 1317−1323.
(33) Almeda, S.; Arce, L.; Valcárcel, M. Combined use of supported liquid membrane and solid-phase extraction to enhance selectivity and sensitivity in capillary electrophoresis for the determination of ochratoxin A in wine. *Electrophoresis* **2009**, *29*, 1573−1581.
(34) González-Osnaya, L.; Soriano, J. M.; Moltó, J. C.; Mañes, J. Simple liquid chromatography assay for analyzing ochratoxin A in bovine milk. *Food Chem.* **2008**, *108*, 272−276.
(35) Yu, J. C. C.; Lai, E. P. C. Molecularly imprinted polymers for ochratoxin A extraction and analysis. *Toxins* **2010**, *2*, 1536−1553.
(36) Liazid, A.; Palma, M.; Brigui, J.; Barroso, C. G. Investigation on ochratoxin A stability using different extraction techniques. *Talanta* **2007**, *71*, 976−980.
(37) Arroyo-Manzanares, N.; Gámiz-Gracia, L.; García-Campana, A. M. Determination of ochratoxin A in wines by capillary liquid chromatography with laser induced fluorescence detection using dispersive liquid−liquid microextraction. *Food Chem.* **2012**, *135*, 368−372.
(38) Trucksess, M. W.; Weaver, C. M.; Oles, C. J.; Fry, F. S.; Noonan, G. O.; Betz, J. M.; Reader, J. I. Determination of aflatoxins B1, B2, G1, and G2 and ochratoxin A in ginseng and ginger by multitoxin immunoaffinity column cleanup and liquid chromatographic quantitation: collaborative study. *J. AOAC Int.* **2008**, *91* (3), 511−523.
(39) González-Peñas, E.; Leache, C.; Viscarret, M.; Pérez de Obanos, A.; Araguás, C.; López de Cerain, A. Determination of ochratoxin A in wine using liquid-phase microextraction combined with liquid chromatography with fluorescence detection. *J. Chromatogr., A* **2004**, *1025*, 163−168.
(40) Reinsch, M.; Topfer, A.; Lehmann, A.; Nehls, I. Determination of ochratoxin A in wine by liquid chromatography tandem mass spectrometry after combined anion-exchange/reversed-phase clean-up. *Anal. Bioanal. Chem.* **2005**, *381*, 1592−1595.
(41) European Commission. Commission Regulation (EC) No. 1881/2006 of 19 December 2006 setting maximum levels for certain contaminants in foodstuffs. *Off. J. Eur. Union* **2006**, *L364*, 5−24.
(42) Wu, J.; Tan, Y.; Wang, Y.; Xu, R. Occurrence of ochratoxin A in grain and manufactured food products in China detected by HPLC with fluorescence detection and confirmed by LC-ESI-MS/MS. *Mycopathologia* **2012**, *173* (2−3), 199−205.
(43) Paola, B.; Amedeo, P. Ochratoxin A in grapes and wine. *Eur. J. Plant Pathol.* **2002**, *108*, 639−643.
(44) Burdaspal, P. A.; Legarda, T. M. Ochratoxin A in wines and grape products originating from Spain and other European countries. *Alimentaria* **1999**, *36*, 107−113.
(45) Majerus, P.; Bresch, H.; Otteneder, H. Ochratoxin A in wines, fruit juices and seasonings. *Arch. Lebensmittelhyg.* **2000**, *51*, 95−97.
(46) Markaki, P.; Delpont, B. C.; Grosso, F.; Dragacci, S. Determination of ochratoxin A in red wine and vinegar by immunoaffinity high-pressure liquid chromatography. *J. Food Prot.* **2001**, *64*, 533−537.
(47) Pietri, A.; Bertuzzi, T.; Pallaroni, L.; Piva, G. Occurrence of ochratoxin A in Italian wines. *Food Addit. Contam.* **2001**, *18*, 647−654.
(48) Solfrizzo, M.; Panzarini, G.; Visconti, A. Determination of ochratoxin A in grapes, dried vine fruits, and winery byproducts by high-performance liquid chromatography with fluorometric detection (HPLC-FLD) and immunoaffinity cleanup. *J. Agric. Food Chem.* **2008**, *56* (23), 11081−11086.
(49) Otteneder, H.; Majerus, P. Occurrence of ochratoxin A (OTA) in wines:influence of the type of wine and its geographical origin. *Food Addit. Contam.* **2000**, *17* (9), 793−798.
(50) Valero, A.; Marín, S.; Ramos, A. J.; Sanchis, V. Survey: Ochratoxin A in European special wines. *Food Chem.* **2008**, *108*, 593−599.
(51) Pietri, A.; Bertuzzi, T.; Pallaroni, L.; Piva, G. Occurrence of ochratoxin A in Italian wines. *Food Addit. Contam.* **2001**, *18*, 647−654.
(52) Belli, N.; Mitchell, D.; Marín, S.; Alegre, I.; Ramos, A. J.; Magan, N.; Sanchis, V. Ochratoxin A-producing fungi in Spanish wine grapes and their relationship with meteorological conditions. *Eur. J. Plant Pathol.* **2005**, *113*, 233−239.
(53) Lammerding, A. M.; Fazil, A. Hazard identification and exposure assessment for microbial food safety risk assessment. *Int. J. Food Microbiol.* **2000**, *58*, 147−157.
(54) Counil, E.; Verger, P.; Volatier, J.-L. Fitness-for-purpose of dietary survey duration: a case-study with the assessment of exposure to ochratoxin A. *Food Chem. Toxicol.* **2006**, *4* (44), 499−509.

Table 1. Antimicrobial Activity of β-CD/EO in CS Films[a]

| EO | concentration (%) | *E. coli* | *S. typhimurium* | *S. aureus* | *L. monocytogenes* |
|---|---|---|---|---|---|
| CIN | 0 | 0.51 ± 0.06 d | 0.69 ± 0.12 e | 0.82 ± 0.12 d | 0.71 ± 0.04 e |
| | 0.25 | 1.28 ± 0.12 c | 0.94 ± 0.01 d | 1.54 ± 0.25 c | 0.87 ± 0.02 d |
| | 0.5 | 1.59 ± 0.03 b,c | 1.19 ± 0.02 c | 1.78 ± 0.04 b | 0.97 ± 0.06 c |
| | 0.75 | 1.79 ± 0.21 a,b | 1.42 ± 0.27 b | 1.83 ± 0.14 b | 1.13 ± 0.04 b |
| | 1 | 2.11 ± 0.19 a | 1.88 ± 0.03 a | 2.52 ± 0.07 a | 1.31 ± 0.14 a |
| CAR | 0 | 0.51 ± 0.06 b | 0.69 ± 0.12 c | 0.82 ± 0.12 d | 0.71 ± 0.04 e |
| | 0.25 | 1.38 ± 0.13 a | 0.87 ± 0.06 b,c | 1.58 ± 0.15 c | 0.88 ± 0.02 d |
| | 0.5 | 1.99 ± 0.54 a | 1.08 ± 0.35 b,c | 2.01 ± 0.24 b | 0.97 ± 0.08 c |
| | 0.75 | 2.08 ± 0.52 a | 1.31 ± 0.11 a,b | 2.24 ± 0.29 b | 1.18 ± 0.04 b |
| | 1 | 2.24 ± 0.13 a | 1.82 ± 0.56 a | 2.78 ± 0.11 a | 1.30 ± 0.14 a |
| EUG | 0 | 0.51 ± 0.06 e | 0.69 ± 0.12 c | 0.82 ± 0.12 e | 0.71 ± 0.04 d |
| | 0.25 | 1.07 ± 0.03 d | 0.43 ± 0.12 b | 1.48 ± 0.12 d | 0.70 ± 0.04 d |
| | 0.5 | 1.35 ± 0.01 c | 0.61 ± 0.05 b | 1.65 ± 0.03 c | 0.74 ± 0.07 c |
| | 0.75 | 1.51 ± 0.03 b | 0.75 ± 0.14 b | 1.75 ± 0.11 b | 0.76 ± 0.07 b |
| | 1 | 1.69 ± 0.04 a | 1.13 ± 0.04 a | 2.04 ± 0.03 a | 0.81 ± 0.01 a |

[a]Within each column and for each essential oil, means having the same letters are not significantly different ($p > 0.05$) from each other.

plasticizing agent, and CAR, CIN, and EUG, which are antimicrobial agents, were purchased from Fisher Scientific, Inc. (Pittsburgh, PA). All other chemicals and solvents were of analytical grade.

**Preparation of Essential Oils and β-CD Complex.** The complex of β-CD and essential oils (β-CD/EO) was prepared using a co-precipitation method described by Ayala-Zavala et al.,[14] with minor modification. Briefly, 5 g (± 0.01) of β-CD was dissolved in 100 mL of an ethanol/distilled water (1:2, v/v) mixture and maintained at 60 ± 2 °C on a hot plate. After cooling the β-CD solution to 40 ± 2 °C, a portion of 0.5 g of EO dissolved in ethanol (1:1, v/v) was then slowly added to the solution with continuous agitation. The resultant mixture was treated by ultrasonic cleaners at 90 W for 4 h. The final solution was maintained overnight at 4 °C. The cold precipitated β-CD/EO complex was recovered by vacuum filtration. The precipitate was washed twice with 30% ethanol solution to clear EO, which was absorbed on the surface of β-CD and dried in a vacuum oven at 40 °C for 4 h until the weight was kept constant. The final dry complex powders were stored in an airtight glass desiccator at room temperature for further analysis.

**Film Preparation.** The edible films were prepared by dissolving 1% (w/v) of CS in a 1% acetic acid solution and stirred, at room temperature, until CS was completely dissolved. Glycerol at 30% (w/w of CS) was added as a plasticizer. Films without β-CD/EO were designated as the control sample. To make the antimicrobial films, a constant amount (150 mL) of the film solutions with varying concentrations of β-CD/EO (0.25, 0.5, 0.75, and 1%) were spread in a glass plate (200 × 200 $mm^2$) and dried at 35 ± 2 °C in an incubator (New Brunswick Scientific Excella E24, Fisher Scientific, Inc., Pittsburgh, PA). The films were removed from the glass plate with a thin spatula and conditioned at 23 ± 2 °C and 50 ± 2% relative humidity (RH) before running further tests.[15]

**Bacterial Strains and Cultures.** Four types of bacterial strains, *E. coli* ATCC 25922 and *S. typhimurium* ATCC 19585 were used representing Gram-negative bacteria. *Staphylococcus aureus* NCTC 8325 and *L. monocytogenes* ATCC 23074 were used representing Gram-positive bacteria. They were incubated in nutrient broth media at 37 °C for 24 h.

**Antimicrobial Activity.** Antimicrobial properties of the crafted films were determined by the log reduction method, with a slight modification.[16] Briefly, culture medium broth was inoculated with 1% suspension of bacteria. The bacterial concentration in the seeding culture was approximately 6 × $10^8$ colony forming units (CFU)/mL. Serial dilutions of the suspension were performed, and the optical density values were tested to achieve a standard curve. Square film pieces (20 × 20 $mm^2$) were sterilized and introduced into a test tube containing 5 mL of fresh suspension of bacteria and incubated at 37 °C for 24 h. The optical density of culture media was measured at 620 nm using a PerkinElmer HTS 7000 Bio Assay reader, and cell concentrations were determined. All samples/standards were run in triplicate.

**Film Thickness (FT).**[17] FT was measured with a 0−25 mm dial thickness gauge with an accuracy of ± 0.01 mm in five random locations for each film. The average was calculated for mechanical properties, water vapor permeability (WVP), and oxygen permeability.

**Mechanical Properties.** Tensile strength (TS) and elongation at break (EB) tests were performed at room temperature (23 ± 2 °C) using a universal testing machine [PARAM XLW (B) Auto Tensile Tester, Jinan, China] according to the standard testing method ASTM D882-01. Sample films, previously equilibrated at 23 ± 2 °C and 50 ± 2% RH, were cut into strips 15 mm wide and 130 mm long. Five specimens from each film were tested. The initial grip separation and mechanical crosshead speed were set at 80 mm and 50 mm/min, respectively.[18]

TS[19] was calculated using the following equation:

$$TS = F_{max}/A$$

where $F_{max}$ is the maximum load (N) needed to pull the sample apart and $A$ is the cross-sectional area ($m^2$) of the samples.

EB (%) was calculated using the following equation:

$$EB = (L/80) \times 100$$

where $L$ is the film elongation (mm) at the moment of rupture and 80 is the initial grip length (mm) of samples.

**WVP.** The WVP of the films was determined by a WVP tester (PERME TSY-TIL, Labthink Instruments Co., Ltd., Jinan, China) according to the standard testing method ASTM E-96-95. Test cups were $^2/_3$ filled with distilled water. The circular sample was tightly covering the cup. The different water vapor pressures between the inside and outside of the cup causes the water vapor diffusion through the sample. Water vapor transmission rates were determined at 23 ± 2 °C and 50 ± 2% RH using saturated salt solutions of $MgCl_2$. The weight of the cups was measured at 1 h intervals for 24 h to determine the water vapor transmission rate and transmission coefficient. For each sample, at least five replicates were tested.

**Statistical Analysis.** Analysis of variance (ANOVA) was carried out by SPSS software (version 17). A significance level was set at 0.05.

## RESULTS AND DISCUSSION

**Antimicrobial Activity.** The antimicrobial activity of β-CD/EO in CS films against *E. coli*, *S. typhimurium*, *S. aureus*, and *L. monocytogenes* was tested, and the results are shown in Table 1. The CS films incorporated with different concentrations of β-CD/EO significantly improved the antimicrobial activities of the CS film against all of the tested bacteria ($p <$


dx.doi.org/10.1021/jf5027873 | J. Agric. Food Chem. 2014, 62, 8914−8918

0.05). The log reduction increases with the increase of the β-CD/EO concentration, which illustrates the antimicrobial activity of β-CD/EO.

The results show that the log reductions for β-CD/CIN CS and β-CD/CAR CS films were higher than β-CD/EUG CS films. The β-CD/CIN CS films at 1% CIN could reduce the number of *E. coli* and *S. aureus* up to 2.11 and 2.52 logs, respectively. The β-CD/CAR CS films showed the best inhibition to *S. aureus*, and the log reduction of it was about 3. β-CD/CAR CS films were able to inhibit *E. coli* and *S. aureus* growth significantly.

Essential oils capable of preventing the growth of foodborne bacteria have been well-documented.[7] Studies have shown that essential oils are able to disrupt and penetrate the lipid structure of the cell membrane and the mitochondrial membrane, leading to the disruption of the cell membrane, cytoplasmatic leakage, cell lysis, and eventually, cell death.[20] It has been suggested that the antimicrobial activity of essential oils may be related to their involvement with enzymatic reactions, which regulate wall synthesis.[21] The lipophilic properties of essential oil components might have also aided its ability to penetrate the plasma membrane.[22] The observations made with light microscopy are in accordance with previous studies, in which essential oils of aromatic plants caused morphological alterations on the fungal hyphae.[21]

The antibacterial activities of CIN, EUG, and CAR against *E. coli* were compared in a previous study, and the minimum inhibitory concentrations (MIC) of CIN and CAR were 400 mg/L; however, MIC of EUG was 1600 mg/L, indicating that EUG has weaker antimicrobial activity against *E. coli*.[23] It is possible that this resulted from the lower aqueous solubility of EUG that would prevent maximum contact with the pathogens in solution.[24] CIN may act upon the pathogens without being fully released from the inclusion complex.[25] The inhibition zones of CAR and EUG against *S. typhimurium* were larger than *L. monocytogenes* indicating that *L. monocytogenes* was more resistant to CAR and EUG than *S. typhimurium*.[24] *E. coli*, *L. monocytogenes*, and *S. typhymurium* were destroyed completely by four essential oils at concentrations of ≤ 0.8% (v/v), whereas *S. aureus* was destroyed completely by 26 essential oils at concentrations of ≤ 0.4% (v/v), demonstrating that *S. aureus* was the most sensitive bacteria to essential oils.[26] Our results shown in Table 1 are in agreement with those results.

The β-CD/EO complexes were shown to be able to inhibit *Salmonella enterica* and *Listeria innocua* at low active compound concentrations, and the MIC values for free essential oils, such as EUG and CIN, were significantly higher than β-CD/EO complexes ($p < 0.05$), which is probably due to the increased water solubility of β-CD/EO complexes that led to increased contact between pathogens and essential oils, thus improving the antimicrobial activity of EO at lower concentrations of active compound.[11] The cinnamon bark and clove bud extract β-CD complexes were the most powerful antimicrobials, despite showing the lowest entrapment efficiencies among the oils.[11] Results suggest that the application of these antimicrobial complexes in food systems may be effective at inhibiting pathogens.

Furthermore, the films showed a higher effectiveness against *S. aureus* compared to *E. coli* and *S. typhimurium*, which may be due to the characteristic difference of the outer membrane between Gram-positive bacteria and Gram-negative bacteria.[27] It was reported that Gram-negative bacteria were more resistant to the essential oils.[6] However, *L. monocytogenes* (Gram-positive bacteria) was more resistant than other bacteria tested, which is in agreement with the previous work.[24]

**Mechanical Properties.** The results of TS and EB are shown in Figures 1 and 2. The effect on these properties of the type and concentration of β-CD/EO in CS films were evaluated.

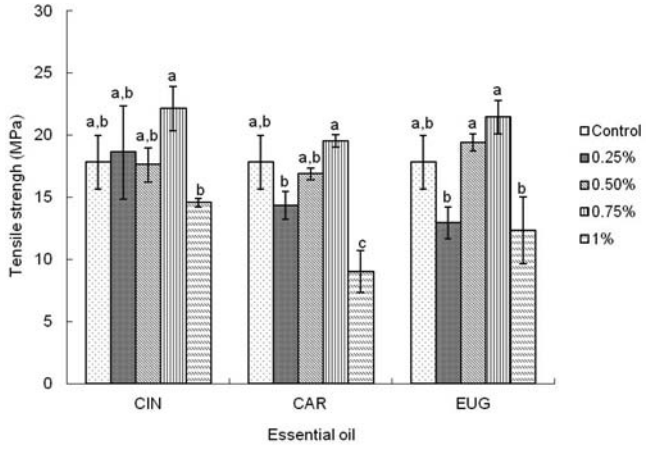


**Figure 1.** TS of β-CD/EO in CS films at four different concentrations (0.25, 0.5, 0.75, or 1%) of β-CD/EO (CIN, CAR, or EUG) were incorporated into 1% chitosan solution, and the one without β-CD/EO was taken as the control.

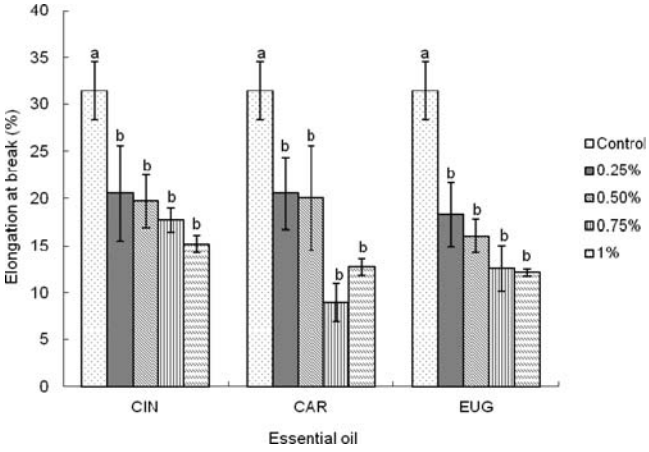


**Figure 2.** EB of β-CD/EO in CS films at four different concentrations (0.25, 0.5, 0.75, or 1%) of β-CD/EO (CIN, CAR, or EUG) were incorporated into 1% chitosan solution, and the one without β-CD/EO was taken as the control.

The CS control film had TS and EB values of 17.82 ± 3.75 MPa and 31.46 ± 5.31%, respectively (Figures 1 and 2). These values are comparable to the previous reports with TS and EB in the range of 12−20 MPa and 17−42%, respectively.[28] The addition of β-CD/EO to the CS films produced changes in their mechanical properties. The films exhibited the highest TS when the concentration of β-CD/EO was 0.75% (Figure 1). However, the EB was significantly ($p < 0.05$) reduced by the incorporation of β-CD/EO at all four concentrations. The EB values of the films decreased significantly ($p < 0.05$) with increasing β-CD/EO concentrations (Figure 2).

The TS and EB of CS films are affected by the type of CS used, the presence of glycerol, and the temperature during film drying.[29] Interestingly, the incorporation of 0.75% β-CD/EO


dx.doi.org/10.1021/jf5027873 | J. Agric. Food Chem. 2014, 62, 8914−8918

into CS films significantly increased the TS of the films with 1% β-CD/EO ($p < 0.05$). The addition of a relatively lower dose of β-CD/EO (0.75%) exhibited the highest TS among the films, which could be attributed to the formation of intermolecular hydrogen bonding between $NH_3^+$ of the CS backbone and $OH^-$ of β-CD/EO.[30] The intermolecular hydrogen bonding between CS and β-CD/EO could enhance the cross-linkage, which decreases the molecular mobility and the free volume of CS.[31] This phenomenon was reported by other researchers in similar systems. For example, the cross-linking of microcrystalline wheat-bran cellulose and soy protein isolate films resulted in an increased TS because of the enhancement of the structural bonds in the polymer network.[32] However, when the added concentration of β-CD/EO is higher than 0.75%, the TS of the resulting films decreased with increasing the β-CD/EO concentration. It is possible that the excessive β-CD/EO could aggregate and destroy the inner structure of β-CD/EO and the CS matrix.

The decrease of EB values in β-CD/EO in CS films indicated that β-CD/EO acted as fillers for the CS matrix, decreasing the strain of the films. The incorporation of β-CD/EO into the CS film resulted in a strong reaction between fillers and matrix, which decreased EB by the motion restriction of the matrix.[10] It has been reported that the filler cellulose whiskers produce a significant decrease in the EB of CS films, indicating that the strong interactions between matrix and filler restricted the motion of the matrix.[33]

**WVP.** The effect of different concentrations of EO on the resistance to permeability of water vapor was evaluated for the films, and the results are presented in Figure 3.

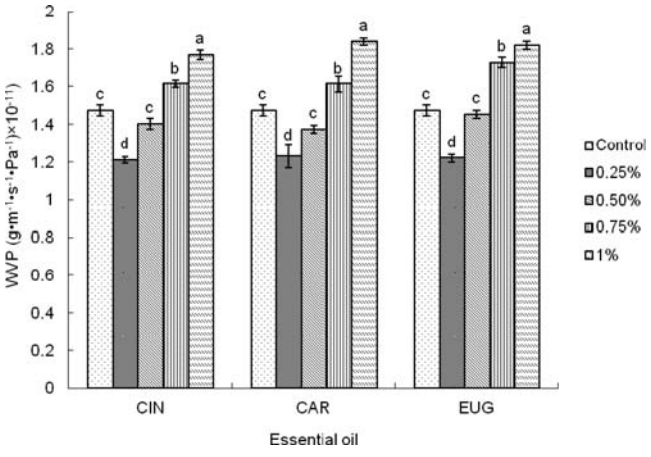


**Figure 3.** WVP of β-CD/EO in CS films at four different concentrations (0.25, 0.5, 0.75, or 1%) of β-CD/EO (CIN, CAR, or EUG) were incorporated into 1% chitosan solution, and the one without β-CD/EO was taken as the control.

The presence of a lower concentration of β-CD/EO in the CS matrix resulted in an improvement in the water vapor barrier property. The WVP value was $1.22 \times 10^{-11}$ and $1.40 \times 10^{-11}$ g m$^{-1}$ s$^{-1}$ Pa$^{-1}$ when the concentration of β-CD/EO was 0.25 and 0.5%, respectively. The WVP values of the films decreased significantly ($p < 0.05$) with increasing β-CD/EO concentrations when added β-CD/EO was below 0.5%, which could be because the presence of β-CD/EO appeared to produce an antiplasticizing effect on the film, as reported after the incorporation of fillers in polymers.[10] β-CD/EO interactions and the structural rigidity of β-CD/EO could create steric hindrance and decrease segmental mobility, restricting water vapor diffusion between the CS matrix and β-CD/EO. The fillers provide an excellent water vapor barrier property because they contain a large number of hydrogen bonds between the matrix, which has a strong holding property to keep water trapped and prevent water diffusion through the films,[32] thus reducing WVP values.

However, when the concentration of β-CD/EO was higher than 0.5%, the WVP of the film increased ($p < 0.05$), which may be related to the excessive β-CD/EO scattered in the film, which subsequently decreased the intermolecular forces between polymer chains and increased the free volume and segmental motions.[34]

In conclusion, it was shown that incorporation of low amounts of β-CD/EO in the CS film significantly improves its antimicrobial properties. The mechanical properties of films incorporated with β-CD/EO in CS were confirmed to be at least as effective for active food packaging as films without the additional incorporation of β-CD/EO in CS. The interaction between CS and β-CD/EO could improve tensile strength of the CS films. The CS films with a lower concentration of β-CD/EO improved the barrier properties by reducing WVP. Because of the antimicrobial, mechanical, and physical properties, the films developed could be used as functional food packaging.

## AUTHOR INFORMATION

### Corresponding Author

*Telephone: +1-313-577-3444. Fax: +1-313-577-8616. E-mail: kzhou@wayne.edu.

### Funding

The authors recognize and appreciate the financial support from Wayne State University Rumble Fellowship.

### Notes

The authors declare no competing financial interest.

## REFERENCES

(1) Gutierrez-Larrainzar, M.; Rua, J.; Caro, I.; de Castro, C.; de Arriaga, D.; Garcia-Armesto, M. R.; del Valle, P. Evaluation of antimicrobial and antioxidant activities of natural phenolic compounds against foodborne pathogens and spoilage bacteria. *Food Control* **2012**, *26*, 555−563.

(2) Abdollahi, M.; Rezaei, M.; Farzi, G. Improvement of active chitosan film properties with rosemary essential oil for food packaging. *Int. J. Food Sci. Technol.* **2012**, *47*, 847−853.

(3) Guillier, L.; Nazer, A. I.; Dubois-Brissonnet, F. Growth response of *Salmonella typhimurium* in the presence of natural and synthetic antimicrobials: Estimation of MICs from three different models. *J. Food Prot.* **2007**, *70*, 2243−2250.

(4) Pelissari, F. M.; Grossmann, M. V.; Yamashita, F.; Pineda, E. A. Antimicrobial, mechanical, and barrier properties of cassava starch−chitosan films incorporated with oregano essential oil. *J. Agric. Food Chem.* **2009**, *57*, 7499−7504.

(5) Wang, S.; Zhu, H. P.; Ge, Y.; Qiao, H. Current status and management of chemical residues in food and ingredients in China. *Trends Food Sci. Technol.* **2009**, *20*, 425−434.

(6) Smith-Palmer, A.; Stewart, J.; Fyfe, L. Antimicrobial properties of plant essential oils and essences against five important food-borne pathogens. *Lett. Appl. Microbiol.* **1998**, *26*, 118−122.

(7) Friedman, M.; Henika, P. R.; Mandrell, R. E. Bactericidal activities of plant essential oils and some of their isolated constituents against *Campylobacter jejuni*, *Escherichia coli*, *Listeria monocytogenes*, and *Salmonella enterica*. *J. Food Prot.* **2002**, *65*, 1545−1560.

(8) Lopez-Mata, M. A.; Ruiz-Cruz, S.; Silva-Beltran, N. P.; Ornelas-Paz, J. D.; Zamudio-Flores, P. B.; Burruel-Ibarra, S. E. Physicochem-

ical, antimicrobial and antioxidant properties of chitosan films incorporated with carvacrol. *Molecules* **2013**, *18*, 13735−13753.
(9) Rezaei, M.; Ojagh, S. M.; Razavi, S. H.; Hosseini, S. M. H. Development and evaluation of a novel biodegradable film made from chitosan and cinnamon essential oil with low affinity toward water. *J. Biotechnol.* **2010**, *150*, S573−S573.
(10) Higueras, L.; Lopez-Carballo, G.; Cerisuelo, J. P.; Gavara, R.; Hernandez-Munoz, P. Preparation and characterization of chitosan/HP-β-cyclodextrins composites with high sorption capacity for carvacrol. *Carbohydr. Polym.* **2013**, *97*, 262−268.
(11) Hill, L. E.; Gomes, C.; Taylor, T. M. Characterization of β-cyclodextrin inclusion complexes containing essential oils (*trans*-cinnamaldehyde, eugenol, cinnamon bark, and clove bud extracts) for antimicrobial delivery applications. *LWT—Food Sci. Technol.* **2013**, *51*, 86−93.
(12) Uekama, K.; Hirayama, F.; Irie, T. Cyclodextrin drug carrier systems. *Chem. Rev.* **1998**, *98*, 2045−2076.
(13) Qi, Z. H.; Hedges, A. R. Use of cyclodextrins for flavors. *Flavor Technol.* **1995**, *610*, 231−243.
(14) Ayala-Zavala, J. F.; Soto-Valdez, H.; Gonzalaz-Leon, A.; Alvarez-Parrilla, E.; Martin-Belloso, O.; Gonzalez-Aguilar, G. A. Microencapsulation of cinnamon leaf (*Cinnamomum zeylanicum*) and garlic (*Allium sativum*) oils in β-cyclodextrin. *J. Inclusion Phenom. Macrocyclic Chem.* **2008**, *60*, 359−368.
(15) Krishna, M.; Nindo, C. I.; Min, S. C. Development of fish gelatin edible films using extrusion and compression molding. *J. Food Eng.* **2012**, *108*, 337−344.
(16) Ravishankar, S.; Zhu, L. B.; Olsen, C. W.; McHugh, T. H.; Friedman, A. Edible apple film wraps containing plant antimicrobials inactivate foodborne pathogens on meat and poultry products. *J. Food Sci.* **2009**, *74*, M440−M445.
(17) Tifft, E. C.; Moffa, P. E.; Richardson, S. L.; Field, R. I. Enhancement of high-rate disinfection by sequential addition of chlorine and chlorine dioxide. *J.—Water Pollut. Control Fed.* **1977**, *49*, 1652−1658.
(18) Ghasemlou, M.; Khodaiyan, F.; Oromiehie, A. Physical, mechanical, barrier, and thermal properties of polyol-plasticized biodegradable edible film made from kefiran. *Carbohydr. Polym.* **2011**, *84*, 477−483.
(19) Errampalli, D.; Peters, R. D.; MacIsaac, K.; Darrach, D.; Boswall, P. Effect of a combination of chlorine dioxide and thiophanate-methyl pre-planting seed tuber treatment on the control of black scurf of potatoes. *Crop Prot.* **2006**, *25*, 1231−1237.
(20) Kalemba, D.; Kunicka, A. Antibacterial and antifungal properties of essential oils. *Curr. Med. Chem.* **2003**, *10*, 813−829.
(21) Soylu, E. M.; Kurt, S.; Soylu, S. In vitro and in vivo antifungal activities of the essential oils of various plants against tomato grey mould disease agent *Botrytis cinerea*. *Int. J. Food Microbiol.* **2010**, *143*, 183−189.
(22) Pauli, A.; Knobloch, K. Inhibitory effects of essential oil components on growth of food-contaminating fungi. *Z. Lebensm.-Unters. Forsch.* **1987**, *185*, 10−13.
(23) Pei, R. S.; Zhou, F.; Ji, B. P.; Xu, J. Evaluation of combined antibacterial effects of eugenol, cinnamaldehyde, thymol, and carvacrol against *E. coli* with an improved method. *J. Food Sci.* **2009**, *74*, M379−M383.
(24) Kim, J. M.; Marshall, M. R.; Wei, C. Antibacterial activity of some essential oil components against 5 foodborne pathogens. *J. Agric. Food Chem.* **1995**, *43*, 2839−2845.
(25) Hedges, A. R.; Shieh, W. J.; Sikorski, C. T. Use of cyclodextrins for encapsulation in the use and treatment of food-products. In *Encapsulation and Controlled Release of Food Ingredients*; Risch, S. J., Reineccius, G. A., Eds.; American Chemical Society (ACS): Washington, D.C., 1995; ACS Symposium Series, Vol. *590*, Chapter 6, pp 60−71.
(26) Oussalah, M.; Caillet, S.; Saucier, L.; Lacroix, M. Inhibitory effects of selected plant essential oils on the growth of four pathogenic bacteria: *E. coli* O157: H7, *Salmonella typhimurium*, *Staphylococcus aureus* and *Listeria monocytogenes*. *Food Control* **2007**, *18*, 414−420.
(27) Ramos, O. L.; Santos, A. C.; Leao, M. V.; Pereira, J. O.; Silva, S. I.; Fernandes, J. C.; Franco, M. I.; Pintado, M. E.; Malcata, F. X. Antimicrobial activity of edible coatings prepared from whey protein isolate and formulated with various antimicrobial agents. *Int. Dairy J.* **2012**, *25*, 132−141.
(28) Vargas, M.; Albors, A.; Chiralt, A.; Gonzalez-Martinez, C. Characterization of chitosan−oleic acid composite films. *Food Hydrocolloids* **2009**, *23*, 536−547.
(29) Pereda, M.; Amica, G.; Marcovich, N. E. Development and characterization of edible chitosan/olive oil emulsion films. *Carbohydr. Polym.* **2012**, *87*, 1318−1325.
(30) Sun, Y.; Liu, Y.; Li, Y. Z.; Lv, M. Z.; Li, P. W.; Xu, H. L.; Wang, L. Preparation and characterization of novel curdlan/chitosan blending membranes for antibacterial applications. *Carbohydr. Polym.* **2011**, *84*, 952−959.
(31) Pasanphan, W.; Chirachanchai, S. Conjugation of gallic acid onto chitosan: An approach for green and water-based antioxidant. *Carbohydr. Polym.* **2008**, *72*, 169−177.
(32) Wang, Z.; Sun, X. X.; Lian, Z. X.; Wang, X. X.; Zhou, J.; Ma, Z. S. The effects of ultrasonic/microwave assisted treatment on the properties of soy protein isolate/microcrystalline wheat-bran cellulose film. *J. Food Eng.* **2013**, *114*, 183−191.
(33) Li, Q.; Zhou, J. P.; Zhang, L. N. Structure and properties of the nanocomposite films of chitosan reinforced with cellulose whiskers. *J. Polym. Sci., Part B: Polym. Phys.* **2009**, *47*, 1069−1077.
(34) Sothornvit, R.; Krochta, J. M. Plasticizer effect on mechanical properties of β-lactoglobulin films. *J. Food Eng.* **2001**, *50*, 149−155.

JOURNAL OF AGRICULTURAL AND FOOD CHEMISTRY

Addition/Correction

pubs.acs.org/JAFC

# Correction to Quantifying the Contribution of Grape Hexoses to Wine Volatiles by High-Precision [U$^{13}$C]-Glucose Tracer Studies

Mark A. Nisbet, Herbert J. Tobias, J. Thomas Brenna, Gavin L. Sacks,* and Anna Katharine Mansfield

*J. Agric. Food Chem.* **2014**, *62* (28), 6820−6827. DOI: 10.1021/jf500947x

The following funding was mistakenly omitted from the original publication:

## AUTHOR INFORMATION

### Funding

This work was supported by NIH Grant RR031264 and the National Institute of Food and Agriculture (NIFA)−Cornell Federal Formula Funds Grant Program.

**Published:** August 25, 2014

ACS Publications © 2014 American Chemical Society

still possible that lower short-term levels can occur in air downwind of treatment sites from multiple field sources over a fumigation season.

This paper reports on a rugged and sensitive field sampling and analysis procedure for assessing MIC air concentrations in residential air. We also report for the first time on observed MIC air concentrations that were concurrently monitored with MITC during a period of metam soil fumigations near a residential area in southern Franklin county, Washington state, USA. Understanding the combined contributions of MITC with MIC will be important especially to residential communities existing in close proximity to where agricultural soil fumigations occur.

## MATERIALS AND METHODS

**MIC Air Sampling.** A batch (~30 g) of XAD-7 medium-polarity polymeric adsorbent (XAD7HP; Sigma-Aldrich) was washed and drained several times by swirling with excess pesticide grade acetonitrile (Fisher). The final rinse was vacuum filtered until the adsorbent was dry and flowable. Three milliliter portions of the dry adsorbent (ca. 1.12 g by weight) were each packed into separate 5 $cm^3$ plastic Bond Elut reservoirs containing a porous frit at the tip end (Agilent) and capped with a plug of glass wool. Using a syringe, 80 $\mu$L of 1-(2-pyridyl)piperazine (1-2PP, 98%; Sigma-Aldrich) was dissolved in 20 mL of pesticide grade methylene chloride (Fisher), yielding a concentration of ~4.3 mg/mL. The 1-2PP solution was transferred to the reservoir of the cartridge-coating apparatus (Figure 1). The free end of the flexible tubing extending from the bottom of the reservoir was attached to the tip end of a cartridge containing XAD-7, and the cartridge was lowered to allow the 1-2PP solution to flood the cartridge up to the glass wool plug. The cartridge was then raised to drain the solution. This was repeated three times. The coated cartridge was then transferred to a vacuum source for air-drying (~1 h for each cartridge). Each dry, coated cartridge was wrapped in aluminum foil and stored under refrigeration (1–7 °C) in an amber screw-cap jar. The cartridges were prepared no more than 5 days prior to use in the field.

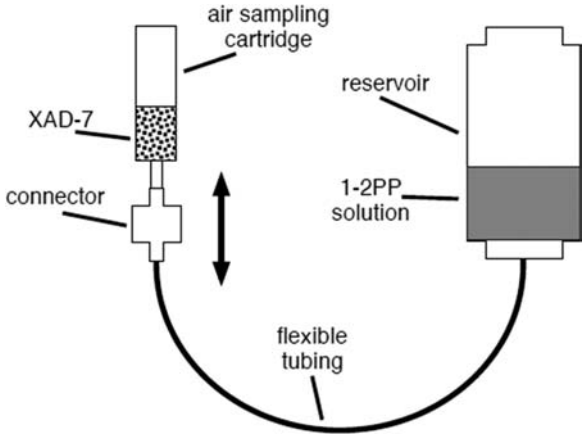


**Figure 1.** XAD-7 cartridge coating apparatus.

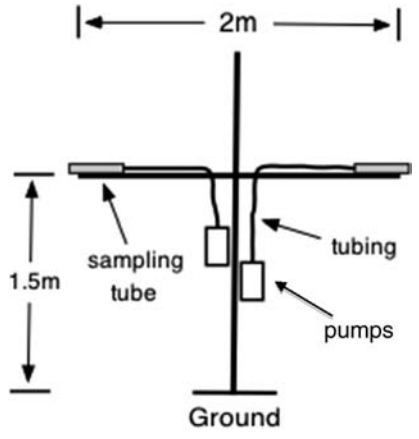


**Figure 3.** MIC air sampling mast.

**MIC Residential Air Monitoring.** MIC receptor stations were set up at three separate sampling sites, two in yards of single-family homes and one at an outdoor commercial building location (site 1). All were bordered by agricultural land (Figure 2, sites 1, 3, and 5). These sampling locations have been routinely used for past MITC area-wide assessments in this residential area.[20,21] The site 3 location consisted of

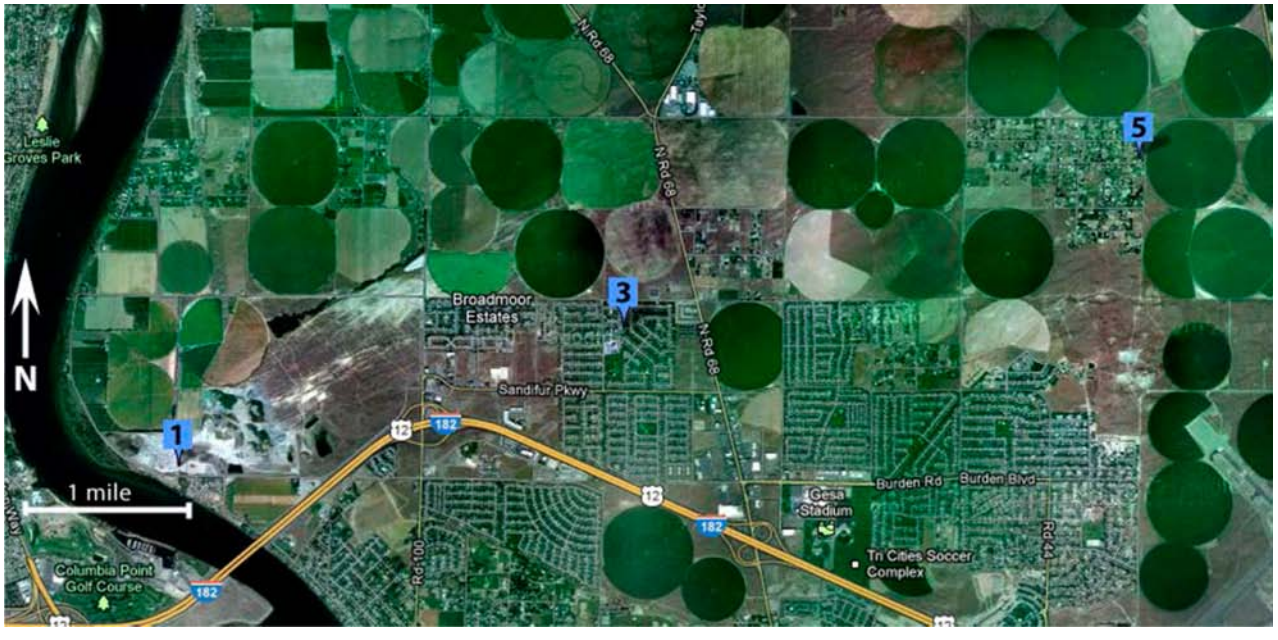


**Figure 2.** 2012 MIC residential sampling site map (southern Franklin county, Washington state, USA).

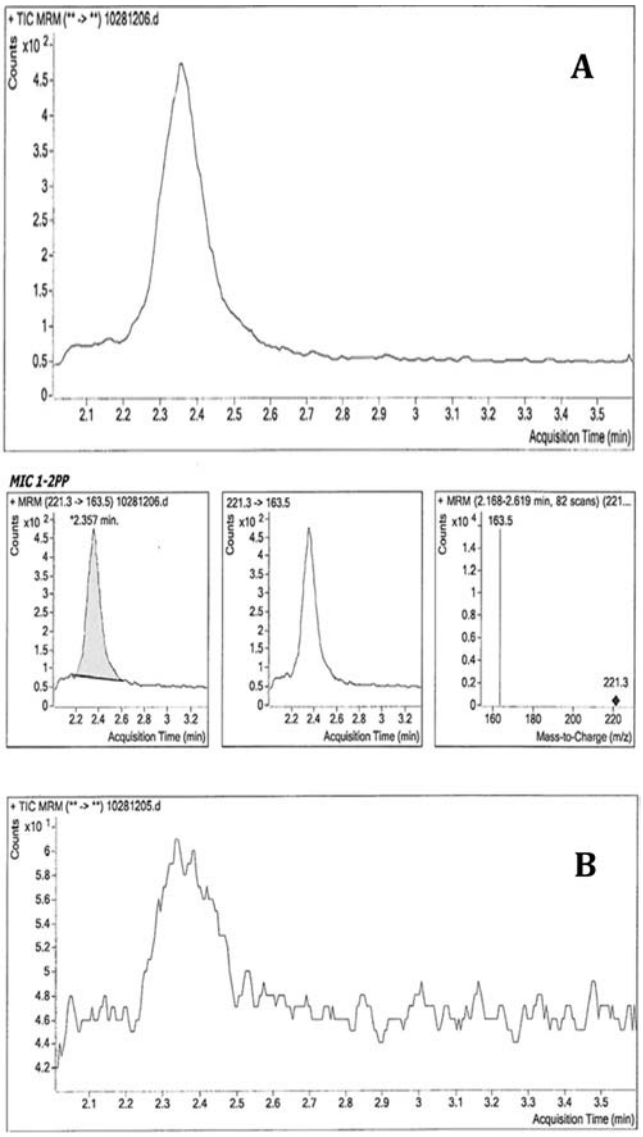


**Figure 4.** LC-MS/MS chromatograms of MIC-1-2PP derivative (10 ng/mL, A) and a blank cartridge (B).

a collocated duplicate cartridge sampling system that served to corroborate capture efficiency among the collocated cartridges. Each station consisted of a 2 m horizontal metal rod attached to a vertical rod at 1.5 m above the ground to sample air at a child's approximate breathing zone level (Figure 3). Sampling cartridges were attached horizontally to the end(s) of the horizontal bar and the cartridges were connected to tubing attached to portable pumps (model 224 PCXR8; SKC) preset to a flow rate of ca. 450 mL/min. Rotameter flow meters were used to measure actual start and stop flows. The cartridges were operated for 4 h and then wrapped in foil and transported on ice packs to the laboratory where they were stored under refrigeration (1−7 °C) to await analysis.

Field fortification (FF) samples were included on each day of air sampling. For field fortifications, the intakes of coated XAD-7 cartridges were spiked with a known amount of MIC and placed on a sampling mast located at a site remote from the metam applications. Air was sampled through the FF cartridges, and corresponding field control cartridges to sample background air, at ca. 500 mL/min for 4 h (0.12 $m^3$ total volume). Additionally, to verify sample integrity during transport and storage, spiked trip blank (STB) and trip blank (TB) samples accompanied each day of sampling. STB cartridges were fortified with MIC and stored in an ice-packed cooler throughout all six 4 h sampling intervals (24 h). The TB and STB samples were momentarily deployed on a pump without flow and immediately removed to simulate sampling procedures for the other cartridges. The TB and STB samples were analyzed with the field samples.

Fortification solutions of MIC (99%; ChemService) in methylene chloride (at 1, 10, and 500 $\mu$g/mL) were used for the laboratory and field cartridge fortifications. The concentrations of these solutions were verified against standards of the MIC-1-2PP-substituted urea derivative by spiking cartridges with the fortification solutions and then recovering the MIC-1-2PP derivative.

The MIC-1-2PP derivative was prepared for use as an analytical standard according to the guidelines of OSHA method 54, section 3.3.1.[22] One-tenth of a gram of MIC was dissolved in 25 mL of methylene chloride. This solution was slowly added to a dilute solution of 1-2PP in methylene chloride with stirring. The mixture was stirred for an hour and then evaporated to <10 mL. The remaining methylene chloride solution was added dropwise to hexane, resulting in the precipitation of the MIC-1-2PP derivative. The precipitate was dried and weighed for a stock solution of MIC-1-2PP in acetonitrile (0.5 mg/mL). From this stock, standards of the MIC-1-2PP derivative were prepared to bracket the range of concentrations expected in the air samples (1, 2, 5, 10, 20, and 40 ng/mL). All standard and fortification solutions were stored in a freezer at ca. −15 °C.

**Sample Analysis.** The amounts of MIC-1-2PP derivative in the samples were determined using an Agilent 1200 HPLC coupled to an Agilent 6460 triple-quadrupole mass spectrometer (LC-MS/MS) equipped with a positive atmospheric pressure chemical ionization (APCI) interface. The contents of each air-sampling cartridge were emptied into separate 25 mL screw-cap tubes, and each was extracted with 10 mL of acetonitrile by vortexing periodically for an hour. A 1−2 mL aliquot from each tube was filtered through 0.2 $\mu$m Teflon filters, 5 $\mu$L portions of filtrate were then injected onto an Eclipse XDB-C18 column (4.6 mm × 50 mm; Agilent), and the analyte was eluted with a 15:85 water/methanol mobile phase at 0.3 mL/min. The $m/z$ 221 → 163.5 transition was used for quantitation. Prior to the analysis of any samples, the working method was validated by fortifying and recovering MIC from treated XAD-7 cartridges. The method was validated in triplicate at three concentration levels,10 ng, 50 ng, and 6 $\mu$g of MIC, on-cartridge. Figure 4 shows example chromatograms of the MIC-1-2PP derivative and a 1-2PP-coated XAD-7 cartridge blank. Analyte retention time was ca. 2.4 min. The low-end fortification (10 ng of MIC on-cartridge) was designated as the method's limit of quantification (mLOQ). The method's limit of detection (mLOD) was empirically estimated to be roughly half of the mLOQ, or 5 ng MIC on-cartridge, due to a low-level but consistent background interference in the control samples.

Each laboratory analytical set (ca. 8 field cartridges) included a blank cartridge and an MIC laboratory-fortified cartridge (at various concentrations) with the field samples. The recovery fortification sample was prepared by injecting a known volume of MIC fortification solution into a 1-2PP-coated XAD-7 cartridge. For each analytical set, percent recovery for the fortified sample was calculated after the average peak area of the corresponding control sample had been subtracted. At least four external standards were used to generate the linear regression curve. All field samples were analyzed within 5 days of collection.

## RESULTS AND DISCUSSION

**MIC Cartridge Performance and Quality Control.** The successful sampling of gaseous MIC in air was made possible by the rapid reaction of MIC with 1-2PP. As an electrophile, MIC reacts with the nucleophilic cyclic amine of 1-2PP to form the urea derivative according to the following equation:

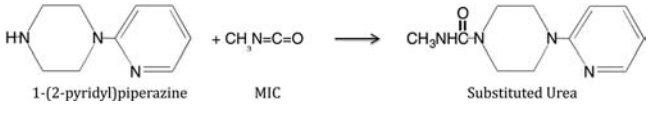



dx.doi.org/10.1021/jf501696a | J. Agric. Food Chem. 2014, 62, 8921−8927

**Table 1. Quality Control Validation and Recovery Information**

| | | | | |
|---|---|---|---|---|
| **Method Validation** | | | | |
| fortification level | recovery[a] % | | | |
| 0.01 $\mu$g | 84 | 89 | 72 | av validation recovery |
| 0.05 $\mu$g | 78 | 85 | 95 | ($n$ = 9) |
| 6.0 $\mu$g | 71 | 78 | 78 | 81 ± 8% |
| **Field Cartridge Fortifications (FF)** | | | | |
| sample ID | fortification level ($\mu$g) | recovery[a] % | | |
| FF-XAD-X-8 | 0.10 | 82 | | av recovery |
| FF-XAD-Y-4 | 0.05 | 80 | | ($n$ = 3) |
| FF-XAD-Z-4 | 0.50 | 77 | | 80 ± 3% |
| **Spike Trip Fortifications (STB)** | | | | |
| sample ID | fortification level ($\mu$g) | recovery[a] % | | |
| STB-X-XAD | 0.10 | 64 | | av recovery |
| STB-Y-XAD | 0.05 | 109 | | ($n$ = 3) |
| STB-Z-XAD | 0.50 | 69 | | 81 ± 25% |
| **Analytical Set Laboratory Cartridge Fortifications** | | | | |
| fortification level | av recovery[a] % | | | |
| 0.05 $\mu$g | 81 ± 7 ($n$ = 4) | | | total av recovery |
| 0.10 $\mu$g | 90 ± 16 ($n$ = 5) | | | ($n$ = 10) |
| 0.50 $\mu$g | 108 ($n$ = 1) | | | 88 ± 14% |

[a]Recoveries are corrected for controls.

Our sampling method was a modification of OSHA Method 54.[22] The OSHA method minimum quantitation level was reported to be about 4.8 $\mu$g/m$^3$ for a sample collection volume of no more than 15 L at 50 mL/min through tubes of 120 mg of XAD-7 coated with 1-2PP. For this study, our goal was to capture MIC on-cartridge during 4 h of air sampling at a flow rate of about 500 mL/min (~0.12 m$^3$ total volume) with minimal breakthrough. Therefore, we increased the amounts of the XAD-7 adsorbent (~1.1 g) and 1-2PP (4−5 mg/XAD-7 cartridge), allowing for ~10 times higher sampling flow rates. Compared to OSHA Method 54, the modified higher sampling volume cartridge, coupled with the use of positive APCI LC-MS/MS, resulted in an appreciable 60-fold increase in sensitivity for the MIC-1-2PP derivative.

The modified cartridge design and sampling method were validated in triplicate at 10 ng, 50 ng, and 6 $\mu$g of MIC spiked to the 3 mL 1-2PP-coated XAD-7 cartridges (Table 1). These levels were equivalent to air concentrations of 0.08 , 0.42, and 50 $\mu$g/m$^3$, respectively, based on air sampling rates of 500 mL/min for 4 h. From this, a mLOQ was established at 0.08 $\mu$g/m$^3$ with a mLOD of 0.05 $\mu$g/m$^3$. Subsequent to the cartridge validation, a breakthrough test was conducted to examine retention of MIC-1-2PP on the sampling media. Three prepared cartridges were spiked with 50 ng of MIC and attached to air sampling pumps for 5 h at ca. 500 mL/min air flow (0.15 m$^3$ total sampling volume) at ambient room temperature. The breakthrough sample recoveries ranged from 106 to 118% with an average recovery of 112 ± 6% ($n$ = 3).

Table 1 provides field fortification recoveries and also reports recoveries for spiked trip MIC-1-2PP cartridges that accompanied the three sampling day shipments. Laboratory recoveries of the MIC-1-2PP derivative prepared with each analytical set are also reported in Table 1. We also examined if MITC in the ambient residential air could in itself result in an increase of the MIC-1-2PP derivative. Here, a separate validation was performed with replicate 1-2PP XAD-7 control cartridges and control cartridges separately fortified at various concentrations with MITC. A slight 2.5% signal enhancement corresponding to MIC-1-2PP was estimated for the replicated spiked MITC cartridges compared to the blank control cartridges. This estimated level of response was within method and instrument errors. All residential air monitoring data are reported without recovery correction.

Table 2 provides 4 h TWA MIC air concentrations along with 4 h TWA MITC air concentration data that were concurrently determined at the three-receptor locations during this 2012 study. Although the focus of this investigation was MIC, MITC air concentrations were concurrently gathered with the MIC data to examine the combined presence of these metam products in residential air (Table 2 and Figure 5). The

**Table 2. Measured Methyl Isocyanate (MIC) and Methyl Isothiocyanate (MITC) in Residential Air**

| | | MIC ($\mu$g/m$^3$) | | | | MITC ($\mu$g/m$^3$) | | | |
|---|---|---|---|---|---|---|---|---|---|
| interval | time | site 1 | site 3-L | site 3-R | site 5 | site 1 | site 3-L | site 3-R | site 5 |
| Oct 22 | 7:00−11:00 a.m. | 0.46 | 0.74 | 0.78 | 0.90 | 1.44 | 4.90 | 5.10 | 13.2 |
| Oct 22 | 11:00 a.m.−3:00 p.m. | 0.24 | −[a] | 0.64 | 0.82 | 0.82 | 4.55 | 4.83 | − |
| Oct 22 | 3:00−7:00 p.m. | 3.08 | 4.35 | 2.54 | 3.74 | − | 1.54 | 1.69 | 3.93 |
| Oct 22 | 7:00−11:00 p.m. | 1.66 | 2.65 | 4.24 | 3.70 | 1.07 | 1.26 | 1.38 | 6.29 |
| Oct 22−23 | 11:00 p.m.−3:00 a.m. | 1.20 | 0.52 | 0.19 | 0.61 | 2.89 | 3.22 | 3.38 | 1.67 |
| Oct 23 | 3:00−7:00 a.m. | 1.18 | 0.67 | 2.17 | 1.85 | 12.3 | 4.23 | 2.47 | 4.09 |
| Oct 24 | 7:00−11:00 a.m. | 1.19 | 0.58 | 0.53 | 0.32 | 0.66 | 7.80 | 8.13 | 3.95 |
| Oct 24 | 11:00 a.m.−3:00 p.m. | 0.27 | 0.42 | 0.38 | 0.34 | 0.67 | 2.51 | 2.52 | 2.68 |
| Oct 24 | 3:00−7:00 p.m. | 0.19 | 0.47 | 0.48 | 0.18 | 0.79 | 7.27 | 7.64 | 1.29 |
| Oct 24 | 7:00−11:00 p.m. | 0.21 | 0.35 | 0.29 | 0.23 | 0.57 | 4.35 | 4.47 | 1.76 |
| Oct 24−25 | 11:00 p.m.−3:00 a.m. | 2.38 | 1.82 | 2.27 | 0.92 | 0.65 | 1.10 | 1.13 | 21.7 |
| Oct 25 | 3:00−7:00 a.m. | 0.55 | 0.63 | 0.57 | 0.86 | 12.2 | 14.9 | 15.6 | 18.9 |
| Oct 26 | 7:00−11:00 a.m. | 0.14 | 0.12 | 0.13 | 0.14 | 0.91 | 2.41 | 1.11 | 1.67 |
| Oct 26 | 11:00 a.m.−3:00 p.m. | − | 0.15 | 0.14 | 0.15 | 0.94 | 1.21 | − | 1.76 |
| Oct 26 | 3:00−7:00 p.m. | 0.16 | 0.14 | − | 0.15 | 0.65 | 0.81 | 0.82 | 1.47 |
| Oct 26 | 7:00−11:00 p.m. | 0.11 | 0.11 | 0.13 | 0.15 | 0.59 | 0.70 | − | 0.90 |
| Oct 26−27 | 11:00 p.m.−3:00 a.m. | − | 0.14 | 0.11 | 0.20 | 0.62 | 0.70 | 0.72 | 0.70 |
| Oct 27 | 3:00−7:00 a.m. | 0.19 | 0.16 | 0.26 | 0.172 | 1.67 | 3.10 | 3.29 | 3.13 |

[a]Air sampling device failure.

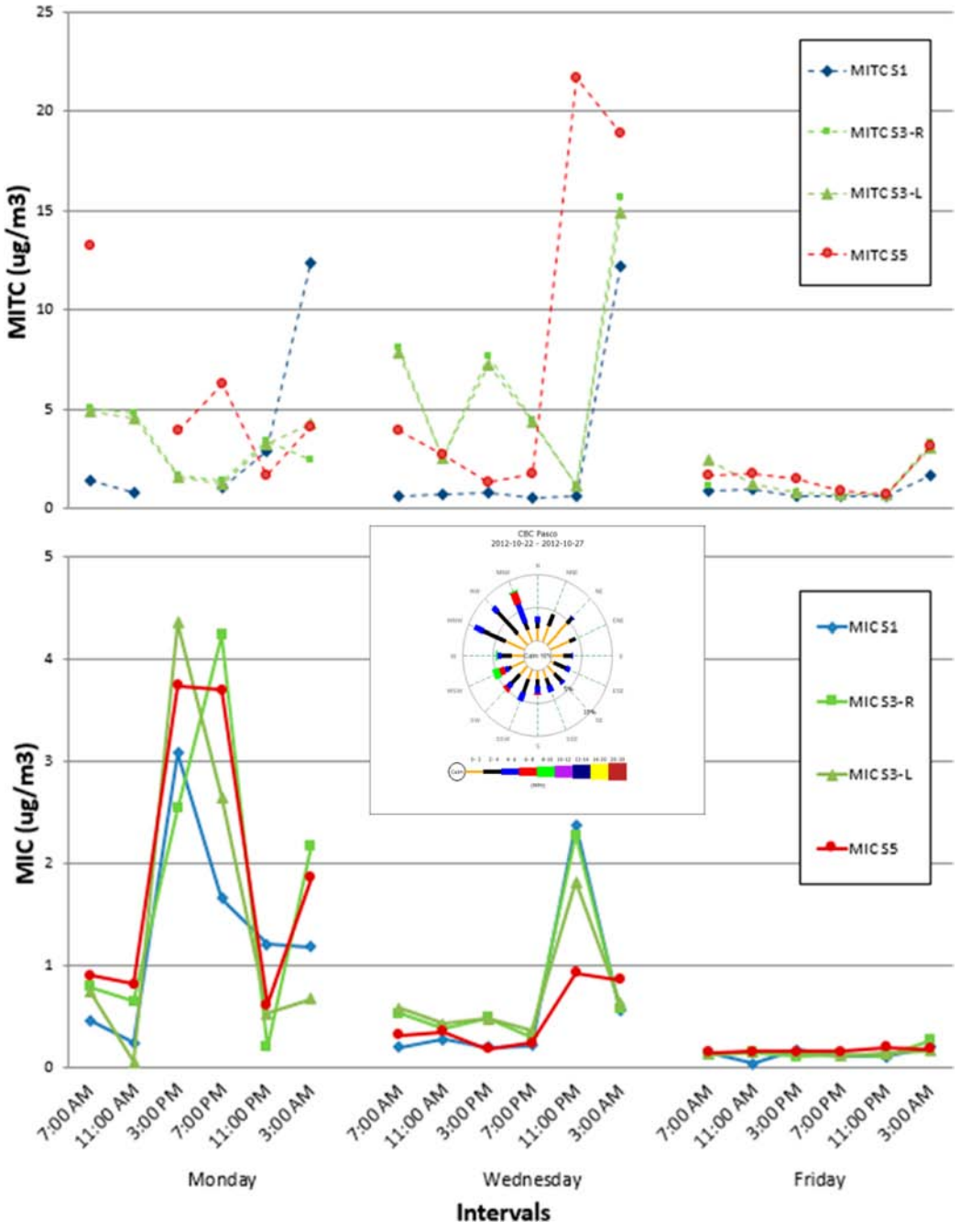


**Figure 5.** Four-hour time-weighted average MIC and MITC air concentrations (week of October 22−27, 2012). Columbia Basin College meteorological windrose was provided by WSU-AgWeather Net, Prosser, WA, USA.

analytical method for quantifying MITC was previously developed and validated in our facility for a 2005 residential air monitoring study.[20] This method was adapted from a California Department of Pesticide Regulation method and relied on solvent extracting MITC from activated charcoal using an 80:20 proportion, respectively, of ethyl acetate to carbon disulfide followed by sonication and microfiltration.[23] MITC air concentrations were determined by gas chromatography with nitrogen phosphorus detection (GC-NPD). Details of this companion 2012 MITC air monitoring assessment can be found in Hastings and Hebert.[24]

The MIC-1-2PP derivative was observed in 68 of the 72 air samples giving equivalent MIC concentrations that were greater than the mLOQ (0.08 $\mu g/m^3$), from 0.11 $\mu g/m^3$ to a maximum of 4.4 $\mu g/m^3$. The maximum was observed in the afternoon on Monday, October 22, 2012 (Table 2 and Figure 5). MIC residues at the other two receptor locations, although lower, were also elevated during that time interval, and all concentrations gradually decreased through the evening hours (Figure 5). Wednesday, October 24, was the last day water was supplied to this irrigation district for conducting center pivot metam fumigations. MIC and MITC concentrations were evident on this day but were appreciably lower soon after irrigation cutoff as can be seen for Friday, October 26 (Figure 5). This pattern of increasing fumigant air concentrations just before irrigation cutoff has been consistently observed for MITC in residential air in this basin.[20,21,24]

MITC was usually higher in the early morning hours (Figure 5). Some of the higher MIC residues were observed in outdoor residential air during the mid-to-late afternoon sampling period. These higher concentrations may be attributed to the reported short 12−16 h atmospheric half-life for the conversion of MITC to MIC.[14,15] MIC, although of higher volatility, is appreciably less reactive toward hydroxyl radical oxidation, with a reported gas-phase half-life of 66 h.[15] Given that MITC can transform to less reactive MIC in the presence of atmospheric oxidants and sunlight, the measured residential air concentrations reasonably confirm that MIC, along with MITC, will be present in air during soil fumigation. In 1995, a near-field shank fumigation air study by the California Air Resources Board also observed MIC from 0.21 to 5.8 $\mu g/m^3$ (12 h TWA samples), with concurrent measurements of MITC from 0.24 to 250 $\mu g/m^3$.[19] These earlier MITC to MIC near-field fumigation conversion observations taken over a 3 day application period are in agreement with our 2012 residential air study observations.

We observed measurable MIC concentrations in >90% of residential air samples. Of the 68 confirmed measurements, 15 (22%) were above CalEPA's chronic inhalation reference level of 1 $\mu g/m^3$, with some several times greater than this level, but were about $^1/_{10}$ of the REL/PEL of 50 $\mu g/m^3$ for an 8 h work shift. The CalEPA reference level is not a direct indicator of risk but rather a reference point to gauge potential effects. For short-term exposures greater than the reference exposure level, the potential for adverse health effects increases.

South Franklin county, Washington, USA, continues to undergo rapid residential and commercial expansion onto large production rotational potato, corn, wheat, and alfalfa crop circle systems (each circle ca. 48−64 ha). This study was initiated to address public health agency concerns that earlier reported 2005−2008 MITC residential air concentrations could also result in significant MIC air contributions during periods of active soil fumigation.[20,21] These earlier air monitoring studies indicated that MITC air concentrations were uniformly distributed throughout this basin and intermittently exceeded EPA regulatory acute [67 $\mu g/m^3$ (1−8 h)] and short-term (15 $\mu g/m^3$ over a 24 h period) inhalation exposure levels of concern (LOC). In 2008, stagnant air/inversion conditions just before the irrigation district's water cutoff date contributed to MITC residential air levels exceeding the EPA acute LOC on 3 days, with a 4 h TWA observed maximum air concentration of 650 $\mu g/m^3$. The EPA short-term MITC LOC threshold was exceeded on 20% of the days monitored.[21] On the basis of the reported daytime high rate of oxidative conversion of MITC to MIC,[14,15] 2008 MITC levels could have potentially led to MIC air concentrations greater than the REL/PEL of 50 $\mu g/m^3$, suggesting that monitoring of MIC is warranted.

In 2012, windy conditions from early October through irrigation cutoff resulted in fewer soil fumigations occurring than in previous monitoring years (personal communications with Washington State Department of Agriculture). Although many soil fumigations were delayed by growers to spring 2013, the 2012 MITC emission profile does show consistency in seasonal trends with previous 2005, 2007, and 2008 monitoring seasons, with higher MITC concentrations during the peak period of fall soil fumigation 1 week before irrigation water cutoff (Figure 5).

Traditionally, metam applications in Franklin county, WA, USA, have been performed mid-September to late October by center-pivot surface chemigation, which typically led to MITC levels much greater than those resulting from soil-incorporated shank injection.[9] As of winter 2012, the EPA Office of Pesticide Programs adopted mitigation measures to increase protections for agricultural workers and bystanders.[10] It is anticipated that this adoption of fumigation field edge set back distances (buffers) based on field size, application method, and rate will shift practices away from traditional surface-applied center-pivot chemigation to soil-incorporated shank injection. This transition will be especially significant in reducing MITC emissions in potato-growing regions in close proximity to residential communities, commercial development, and difficult-to-evacuate zones.

Metam product labels now specify that fumigant shank injection can be conducted at a minimum 8 cm depth from the soil surface. The high porosity and low organic content of soils typically found in field crop production agriculture in the inner Pacific Northwest will remain favorable to high MITC emission rates,[25] especially at very shallow shank depths. Because prescribed buffer zone specifications allow large potato field shank fumigations to occur in close proximity to homes and residential communities (ca. 8−20 m), there continues to be concern among public health officials that shallow depth metam soil incorporation can result in appreciable MITC off-target movement and bystander/residential exposure. Evaluating first-hand the impact of changing fumigation practices driven by recent metam 2012 label changes will remain important for confirming that there is a substantial reduction in MITC with associated MIC emissions at the rural−urban interface over the entire soil fumigation season.

## AUTHOR INFORMATION

### Corresponding Author

*(V.R.H.) Phone: (509) 372-7393. E-mail: vhebert@tricity.wsu.edu.

### Funding

We acknowledge funding provided by EPA Region 10.

### Notes

The authors declare no competing financial interest.

## ACKNOWLEDGMENTS

We acknowledge the valuable assistance of Cynthia Lopez and Barbara Morrissey from the Washington State Department of Health.

## REFERENCES

(1) Grube, A.; Donaldson, D.; Kiely, T.; Wu, L. Pesticides industry sales and usage: 2006 and 2007 market estimate. U.S. EPA, Office of Chemical Safety and Pollution Prevention, Office of Pesticide Programs, Biological and Economic Analysis Division, Washington, DC, USA, 2011; http://www.epa.gov/opp00001/pestsales/.

(2) Pest Management Strategic Plan for Pacific Northwest Potato Production-REVISION (issued July 13, 2007). Summary of a workshop Boise, ID, Feb 16−20, 2002; revision workshop Pocatello, ID, 2007, Jan 26, 2006.

(3) Smelt, J. H.; Leistra, M. Conversion of metham-sodium to methyl isothiocyanate and basic data on the behavior of methyl isothiocyanate in soil. *Pestic. Sci.* **1974**, *5*, 401−407.

(4) Worthington, E. A.; Wade, E. A. Henry's Law coefficients of chloropicrin and methyl isothiocyanate. *Atmos. Environ.* **2007**, *41*, 5510−5515.

(5) Leistra, M.; Crum, S. J. H. Emission of methyl isothiocyanate to the air after application of metham-sodium to greenhouse soil. *Water, Air, Soil Pollut.* **1990**, *50*, 109−121.

(6) Van den Berg, F. Measured and computed concentrations of methyl isothiocyanate in the air around fumigated fields. *Atmos. Environ.* **1992**, *27A*, 63−71.
(7) Van den Berg, F.; Smelt, J. H.; Boesten, J. J. T. I.; Teunissen, W. Volatilization of methyl isothiocyanate from soil after application of metam-sodium with two techniques. *J. Environ. Qual.* **1999**, *28*, 918−928.
(8) Seiber, J. N.; Woodrow, J. E.; Krieger, R. I.; Dinoff, T. Determination of ambient MITC residues in indoor and outdoor air in townships near fields treated with metam-sodium. Department of Pesticide Regulation, Sacramento, CA, USA. Pesticide Registration Document 50150-151, Record 170403, 1999.
(9) Littke, M.; LePage, J.; Hebert, V. Comparison of field methyl isothiocyanate flux following Pacific Northwest surface-applied and ground-incorporated fumigation practices. *Pest Manage. Sci.* **2013**, *69* (5), 620−626.
(10) Amended Reregistration Eligibility Decision (RED) for Methyldithiocarbamate Salts − Metam Sodium/Potassium and MITC May 2009; EPA 738-R-09-310, 231 pp.
(11) Alvarez, R. A.; Moore, C. B. Quantum yield for production of CH3NC in the photolysis of $CH_3NCS$. *Science* **1994**, *263*, 205−207.
(12) Cal DPR. Evaluation of methyl isothiocyanate as a toxic air contaminant; Part A − Environmental Fate. TAC-2002-01A, 2002; 127 pp.
(13) Geddes, J. D.; Miller, G. C.; Taylor, G. E., Jr. Gas phase photolysis of methyl isothiocyanate. *Environ. Sci. Technol.* **1995**, *29*, 2590−2594.
(14) Sommerlade, R.; Ekici, P.; Parlar, H. Gas phase reaction of selected isothiocyanates with OH radicals using a smog chamber-mass analyzer system. *Atmos. Environ.* **2006**, *40*, 3306−3315.
(15) Lu, Z.; Hebert, V.; Miller, G. Gas-phase reaction of methyl isothiocyanate and methyl isocyanate with hydroxyl radicals under static relative rate conditions. *J. Agric. Food Chem.* **2014**, *62*, 1792−1795.
(16) Mishra, P. K.; Samaarth, R. M.; Pathal, N.; Jain, S. K.; Banerjee, S.; Muudar, K. K. Bhopal gas tragedy: review of clinical and experimental findings after 25 years. *Int. J. Occup. Med. Enviro. Health* **2009**, *22* (3), 198−202.
(17) California Environmental Protection Agency (CalEPA). *Technical Support Document for the Determination of Noncancer Chronic Reference Exposure Levels*; Draft for Public Comment; Office of Environmental Health Hazard Assessment: Berkeley, CA, USA, 1997.
(18) U.S. EPA. Methyl isocyanate. Technology transfer network-air toxics website; http://www.epa.gov/ttn/atw/hlthef/methylis.html#ref1 (accessed March 23, 2014).
(19) California Air Resources Board. Ambient Air Monitoring for MIC and MITC after Soil Injection Application of Metam Sodium in Kern County during August 1995. C94-046A, May 20, 1997; Air Resources Board, State of California: Sacramento, CA, USA, 1997.
(20) Merriman, J.; Hebert, V. R. Methyl isothiocyanate residential community air assessment; South Franklin County, Washington. *Bull. Environ. Contam. Toxicol.* **2007**, *78* (1), 17−21.
(21) LePage, J.; Gross, A.; Hebert, V. *MITC Residential Community Air Assessment*; Franklin County, WA, USA, 2008; FEQL 1008, 98 pp; http://www.doh.wa.gov/DataandStatisticalReports/EnvironmentalHealth/Pesticides/AirMonitoringStudy.aspx (accessed March 23, 2014).
(22) Burright, D.; Lee, D. OSHA method 54, https://www.osha.gov/dts/sltc/methods/organic/org054/org054.html, April 1985 (accessed March 6, 2014).
(23) California Department of Pesticide Regulation. Air monitoring for methyl isothiocyanate during a sprinkler application of metam-sodium; Report EH 94-02, 1994.
(24) Hastings, N.; Hebert, V. *MITC Residential Community Air Assessment*; FEQL-0412 MITC; Franklin County, WA, USA, 2012; 77 pp, http://feql.wsu.edu.
(25) Yates, S. R.; Wang, D.; Papiernik, S. K.; Gan, J. Predicting pesticide volatilization from soils. *Environmetrics* **2002**, *13*, 569−578, DOI: 10.1002/env.542.

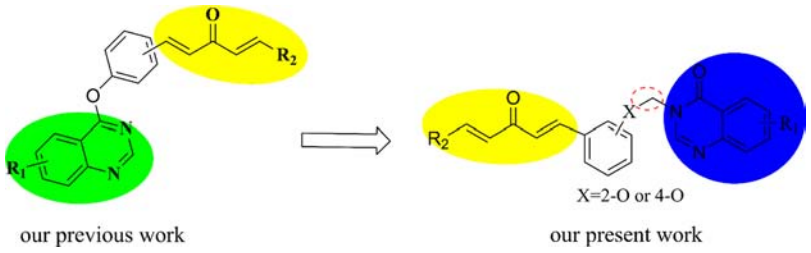


**Figure 1.** Design of the title compounds.

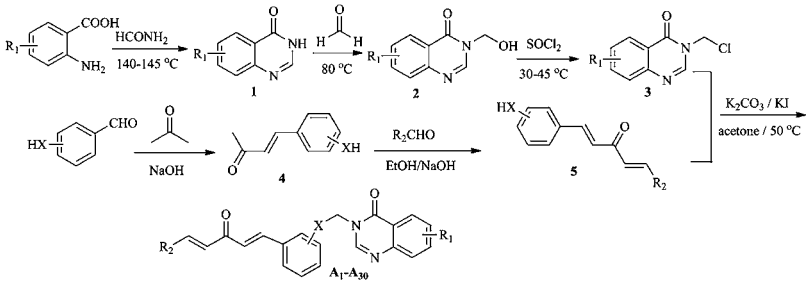


$A_1$:$R_1$=H $R_2$=Ph X=2-O; $A_2$:$R_1$=H $R_2$=4-Cl-Ph X=2-O; $A_3$:$R_1$=H $R_2$=2-F-Ph X=2-O;
$A_4$:$R_1$=8-CH3 $R_2$=Ph X=2-O; $A_5$:$R_1$=H $R_2$=2-$OCH_3$-Ph X=2-O; $A_6$:$R_1$=H $R_2$=4-C$(CH_3)_3$-Ph X=2-O;
$A_7$:$R_1$=H $R_2$=3-$NO_2$-Ph X=4-O; $A_8$:$R_1$=H $R_2$= 4-F-Ph X=2-O; $A_9$:$R_1$=H $R_2$=4-F-Ph X=4-O;
$A_{10}$:$R_1$=H $R_2$=furan-2-yl X=2-O; $A_{11}$:$R_1$=H $R_2$=4-$CH_3$-Ph X=2-O; $A_{12}$:$R_1$=8-$CH_3$ $R_2$=thiophen-2-yl X= 2-O;
$A_{13}$:$R_1$=8-$CH_3$ $R_2$=thiophen-2-yl X=4-O; $A_{14}$:$R_1$=H $R_2$=furan-2-yl X=4-O; $A_{15}$:$R_1$=8-$CH_3$ $R_2$=2-Cl-5-$NO_2$-Ph X=2-O;
$A_{16}$:$R_1$=H $R_2$=4-methylthiazol-5-yl X=2-O; $A_{17}$:$R_1$=H $R_2$=thiophen-2-yl X=2-O; $A_{18}$:$R_1$=H $R_2$=thiophen-2-yl X=4-O;
$A_{19}$:$R_1$=H $R_2$=4-$OCH_3$-Ph X=4-O; $A_{20}$:$R_1$=H $R_2$=2-$CF_3$-Ph X=2-O; $A_{21}$:$R_1$=H $R_2$=2,4-di-$OCH_3$-Ph X=4-O;
$A_{22}$:$R_1$=8-$CH_3$ $R_2$=2,4-di-$OCH_3$-Ph X=4-O; $A_{23}$:$R_1$=8-$CH_3$ $R_2$=pyrid-2-yl X=4-O; $A_{24}$:$R_1$=8-$CH_3$ $R_2$=2,4-di-$OCH_3$-Ph X=2-O;
$A_{25}$:$R_1$=8-$CH_3$ $R_2$=3,4-di-$OCH_3$-Ph X=4-O; $A_{26}$:$R_1$=H $R_2$=3,4-di-$OCH_3$-Ph X=4-O; $A_{27}$:$R_1$=H $R_2$=4-$OCH_3$-Ph X=2-O;
$A_{28}$:$R_1$=8-$CH_3$ $R_2$=2-$OCH_3$-Ph X=2-O; $A_{29}$:$R_1$=H $R_2$=3,4,5-tri-$OCH_3$-Ph X=4-O; $A_{30}$:$R_1$=H $R_2$=3,4,5-tri-$OCH_3$-Ph X=2-O.

**Figure 2.** Synthesis of the title compounds $A_1$–$A_{30}$.

Our research showed that 4(3*H*)-quinazolinone derivatives possess excellent anti-TMV activities. The third position of 4(3*H*)-quinazolinones is particularly an active site. Futhermore, 1,4-pentadien-3-one belongs to natural product derivatives, which exhibits outstanding antiviral bioactivity. However, no study has investigated 4(3*H*)-quinazolinone derivatives containing 1,4-pentadien-3-one moieties to date. In this study, we incorporated a 1,4-pentadien-3-one unit to the backbone of 4(3*H*)-quinazolinone, which may result in 4(3*H*)-quinazolinone derivatives with good antiviral activity. The 4(3*H*)-quinazolinone analogues $A_1$ to $A_{30}$ were designed and synthesized, and their antiviral activities against TMV were evaluated (Figure 1). The biological assay revealed that some of the title compounds displayed moderate to good antiviral activity. For example, the title compounds $A_5$, $A_{12}$, $A_{25}$, and $A_{27}$ showed superior curative activities against TMV in vivo relative to the commercial agricultural antiviral agent ningnanmycin. To the best of our knowledge, this study is the first to report the synthesis and antiviral activity of 3-((2-((1*E*,4*E*)-3-oxo-5-arylpenta-1,4-dien-1-yl)phenoxy)methyl)-4(3*H*)-quinazolinone derivatives.

## MATERIALS AND METHODS

**Equipment.** The melting points of the products were determined under an XT-4 binocular microscope (Beijing Tech Instrument Co., China) and were left untouched. IR spectra were recorded on a Bruker VECTOR 22 spectrometer in a KBr disk. $^1$H and $^{13}$C nuclear magnetic resonance (NMR) (solvent $CDCl_3$ or DMSO-$d_6$) spectra were obtained on a JEOL-ECX500 NMR spectrometer at room temperature using tetramethylsilane as an internal standard. Elemental analysis was performed through an Elementar Vario-III CHN analyzer. Analytical thin-layer chromatography (TLC) was conducted on silica gel GF254 (400 mesh). TLC purification was conducted using silica gel. All reagents and reactants were purchased from commercial suppliers and were analytical reagent grade or chemically pure. All solvents were dried, deoxygenated, and redistilled prior to use.

**General Procedure for Preparation of the Key Intermediates.** 3-Chloromethyl-4(3*H*)-quinazolinone and 3-chloromethyl-8-methyl-4(3*H*)-quinazolinone were prepared according to the literature.[32] (*E*)-4-(2-Hydroxyphenyl)-3-butylene-2-one and (*E*)-4-(4-hydroxyphenyl)-3-butylene-2-one were prepared according to a previous report.[33] Intermediate **5** was prepared following reported methods.[34]

**General Procedure for Preparation of the Title Compounds $A_1$ to $A_{30}$.** Figure 2 shows the synthesis of the target compounds $A_1$ to $A_{30}$. A 50 mL round-bottomed flask equipped with a magnetic stirrer was charged with intermediates **3** (2.62 mmol) and **5** (1.31 mmol), acetone (50 mL), and $K_2CO_3$ (5.24 mmol). The flask was stirred at room temperature for 10 min, after which KI (1.31 mmol) was added. The resulting mixture was refluxed and stirred at 56 °C for 5 to 10 h. TLC was used to monitor the progress of the reaction. After the reaction was completed (as indicated by TLC), the solvent was removed under depressurization, and the residue was dissolved with $CH_2Cl_2$. The crude product was then separated through TLC purification using silica gel. The solid was recrystallized from dichloromethane/petroleum ether (2:1, v/v) to obtain the title compounds $A_1$ to $A_{30}$ at 25% to 55% yields. The experimental protocols show the physical characteristics, IR, $^1$H NMR, $^{13}$C NMR, and elemental analysis data for all the synthesized compounds. The data for compound $A_5$ are shown below, and the data for compounds $A_1$ to $A_{30}$ are shown in the Supporting Information.

*3-((2-((1E,4E)-5-(2-Methoxyphenyl)-3-oxopenta-1,4-dien-1-yl)-phenoxy)methyl)-4(3H)-quinazolinone ($A_5$).* Yellow solid: mp 170 to 173 °C; yield, 54.0%; IR (KBr, $cm^{-1}$) $\nu$ 3444.9 (amidic N−CH−N), 2948.8−2879.3 (C−H), 1660.7 (CH═CH−C═O), 1610.6 (C═O of Qu-ring), 1457.4−1598.2 (C═C and benzene and Qu-ring), 1298.1 (C−N), 1228.7 (C−O), 1159.4 (−O−$CH_3$); $^1$H NMR (500 MHz, $CDCl_3$) $\delta$ 8.31(d, $J$ = 8.05 Hz, 1H, Qu-5-H), 8.17 (s, 1H, Qu-2-H), 8.02 (d, $J$ = 16.05 Hz, 2H, −O−Ph−CH═, ═CH−Ar), 7.76 (t, $J_1$


dx.doi.org/10.1021/jf502162y | J. Agric. Food Chem. 2014, 62, 8928−8934

**Table 1. Physical and Analytical Data of Synthesized Compounds $A_1$−$A_{30}$[a]**

| Compd. | 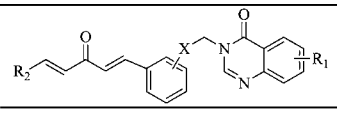 | | | Molecular Formula/M.W | M.p./°C | Yield [a]/% | Elemental Analysis/%: Found/Calcd. | | |
|---|---|---|---|---|---|---|---|---|---|
| | $R_1$ | $R_2$ | X | | | | C | H | N |
| $A_1$ | H | Phenyl | 2-O | $C_{26}H_{20}N_2O_3$ (408.4) | 174-176 | 48.6 | 76.45/76.37 | 4.94/4.54 | 6.86/6.92 |
| $A_2$ | H | 4-Clphenyl | 2-O | $C_{26}H_{19}ClN_2O_3$ (442.9) | 195-197 | 39.6 | 70.51/70.33 | 4.32/4.43 | 6.33/6.20 |
| $A_3$ | H | 2-Fphenyl | 2-O | $C_{26}H_{19}FN_2O_3$ (426.4) | 142-144 | 44.7 | 73.23/73.00 | 4.49/4.67 | 6.57/6.07 |
| $A_4$ | 8-$CH_3$ | Phenyl | 2-O | $C_{27}H_{22}N_2O_3$ (422.5) | 162-164 | 38.7 | 76.76/76.63 | 5.25/5.20 | 6.63/6.98 |
| $A_5$ | H | 2-$OCH_3$phenyl | 2-O | $C_{27}H_{22}N_2O_4$ (438.5) | 170-173 | 54.0 | 73.96/73.46 | 5.05/5.09 | 6.39/6.36 |
| $A_6$ | H | 4-$C(CH_3)_3$phenyl | 2-O | $C_{30}H_{28}N_2O_3$ (464.5) | 158-160 | 47.6 | 77.56/77.19 | 6.08/5.83 | 6.03/6.05 |
| $A_7$ | H | 3-$NO_2$phenyl | 4-O | $C_{26}H_{19}N_3O_5$ (453.4) | 223-225 | 26.9 | 68.87/68.45 | 4.22/4.00 | 9.27/9.64 |
| $A_8$ | H | 4-Fphenyl | 2-O | $C_{26}H_{19}FN_2O_3$ (426.1) | 205-207 | 35.8 | 73.23/73.61 | 4.49/4.69 | 6.57/6.34 |
| $A_9$ | H | 4-Fphenyl | 4-O | $C_{26}H_{19}FN_2O_3$ (426.1) | 211-213 | 32.3 | 73.23/73.52 | 4.49/4.66 | 6.57/6.36 |
| $A_{10}$ | H | 2-furyl | 2-O | $C_{24}H_{18}N_2O_4$ (398.4) | 146-148 | 57.5 | 72.35/72.12 | 4.55/4.61 | 7.03/7.08 |
| $A_{11}$ | H | 4-$CH_3$phenyl | 2-O | $C_{27}H_{22}N_2O_3$ (422.2) | 160-162 | 48.8 | 76.76/76.26 | 5.25/5.53 | 6.63/6.37 |
| $A_{12}$ | 8-$CH_3$ | 2-thiophenyl | 2-O | $C_{25}H_{20}N_2O_3S$(428.5) | 151-153 | 51.6 | 70.07/70.38 | 4.70/4.56 | 6.54/6.29 |
| $A_{13}$ | 8-$CH_3$ | 2-thiophenyl | 4-O | $C_{25}H_{20}N_2O_3S$ (428.5) | 194-195 | 42.0 | 70.07/70.29 | 4.70/4.68 | 6.54/6.39 |
| $A_{14}$ | H | 2-furyl | 4-O | $C_{24}H_{18}N_2O_4$ (398.4) | 156-158 | 44.1 | 72.35/72.43 | 4.55/4.86 | 7.03/7.01 |
| $A_{15}$ | 8-$CH_3$ | 2-Cl-5-$NO_2$phenyl | 2-O | $C_{27}H_{20}ClN_3O_5$ (501.9) | 207-209 | 27.7 | 64.61/64.29 | 4.02/4.37 | 8.37/8.21 |
| $A_{16}$ | H | 4-methylthiazol-5-yl | 2-O | $C_{24}H_{19}N_3O_3S$ (429.5) | 198-200 | 53.3 | 67.12/67.02 | 4.46/4.50 | 9.78/9.80 |
| $A_{17}$ | H | 2-thiophenyl | 2-O | $C_{24}H_{18}N_2O_3S$ (414.5) | 159-161 | 53.4 | 69.55/69.22 | 4.38/4.40 | 6.76/6.75 |
| $A_{18}$ | H | 2-thopenyl | 4-O | $C_{24}H_{18}N_2O_3S$ (414.5) | 162-164 | 47.9 | 69.55/69.10 | 4.38/4.53 | 6.76/6.70 |
| $A_{19}$ | H | 4-$OCH_3$phenyl | 4-O | $C_{27}H_{22}N_2O_4$ (438.5) | 219-221 | 43.5 | 73.96/73.53 | 5.06/5.08 | 6.39/6.41 |
| $A_{20}$ | H | 2-$CF_3$phenyl | 2-O | $C_{27}H_{19}F_3N_2O_3$ (476.4) | 137-139 | 28.8 | 68.05/67.90 | 4.02/3.99 | 5.88/5.76 |
| $A_{21}$ | H | 2,4-di-$OCH_3$phenyl | 4-O | $C_{28}H_{24}N_2O_5$ (468.5) | 165-167 | 44.9 | 71.78/71.68 | 5.16/5.47 | 5.98/6.02 |
| $A_{22}$ | 8-$CH_3$ | 2,4-di-$OCH_3$phenyl | 4-O | $C_{29}H_{26}N_2O_5$ (482.5) | 185-187 | 40.7 | 72.18/72.50 | 5.43/5.76 | 5.81/5.47 |
| $A_{23}$ | 8-$CH_3$ | 2-pyridyl | 4-O | $C_{26}H_{21}N_3O_3$ (423.5) | 194-196 | 42.5 | 73.74/73.44 | 5.00/4.59 | 9.92/10.03 |
| $A_{24}$ | 8-$CH_3$ | 2,4-di-$OCH_3$phenyl | 2-O | $C_{29}H_{26}N_2O_5$ (482.5) | 190-192 | 57.7 | 72.18/72.45 | 5.43/5.08 | 5.81/5.59 |
| $A_{25}$ | 8-$CH_3$ | 3,4-di-$OCH_3$phenyl | 4-O | $C_{29}H_{26}N_2O_5$ (482.2) | 142-143 | 49.2 | 72.18/72.53 | 5.43/5.27 | 5.81/5.39 |
| $A_{26}$ | H | 3,4-di-$OCH_3$phenyl | 4-O | $C_{28}H_{24}N_2O_5$ (482.5) | 178-180 | 52.1 | 71.78/71.37 | 5.16/5.54 | 5.98/6.00 |
| $A_{27}$ | H | 4-$OCH_3$phenyl | 2-O | $C_{27}H_{22}N_2O_4$ (438.5) | 154-156 | 50.5 | 73.96/73.57 | 5.06/5.39 | 6.39/6.53 |
| $A_{28}$ | 8-$CH_3$ | 2-$OCH_3$phenyl | 2-O | $C_{28}H_{24}N_2O_4$ (452.5) | 142-144 | 48.8 | 74.32/73.78 | 5.35/5.56 | 6.19/6.48 |
| $A_{29}$ | H | 3,4,5-tri-$OCH_3$phenyl | 4-O | $C_{29}H_{26}N_2O_6$ (498.5) | 180-182 | 49.0 | 69.87/69.63 | 5.26/5.67 | 5.62/5.27 |
| $A_{30}$ | H | 3, 4,5-tri-$OCH_3$phenyl | 2-O | $C_{29}H_{26}N_2O_6$ (498.5) | 134-135 | 53.6 | 69.87/69.69 | 5.26/5.52 | 5.62/5.34 |

[a]The reaction was performed according to the general experimental program. X = 2-O or 4-O.

= 6.85 Hz, J2 = 8.60 Hz, 1H, Qu-7-H), 7.70 (d, $J$ = 8.00 Hz, 1H, Ph−6−H), 7.66 (d, $J$ = 8.00 Hz, 1H, Ar-6-H), 7.62 (d, $J$ = 7.45 Hz, 1H, Qu-8-H), 7.50 (t, $J_1$ = 6.85 Hz, $J_2$ = 8.05 Hz, 1H, Qu−6−H), 7.39−7.36 (m, 2H, Ph-4-H, Ar-4-H), 7.23 (d, $J$ = 8.05 Hz, 1H, Ph-3-H), 7.13−7.06 (m, 3H, −O−Ph−CH═CH−, −CH═CH−Ar, Ph-5-H), 6.99 (t, $J_1$ = $J_2$ = 7.45 Hz, 1H, Ar-5-H), 6.93 (d, 1H, $J$ = 8.60 Hz, Ar-3-H), 6.06 (s, 2H, $-CH_2-$), 3.90 (s, 3H, $OCH_3$−2−Ar); $^{13}$C NMR (125 MHz, $CDCl_3$) $\delta$ 189.47, 160.61, 158.57, 154.58, 147.67, 145.10, 138.57, 136.79, 134.93, 131.75, 131.71, 128.81, 128.47, 127.77, 127.13, 126.97, 125.91, 125.84, 123.74, 123.48, 121.73, 120.74, 115.31, 111.11, 73.22, 55.49. Anal. Calcd for $C_{27}H_{22}N_2O_4$ (438.5): C, 73.46; H, 5.09; N, 6.36. Found: C, 73.96; H, 5.05; N, 6.39.

**Antiviral Biology against TMV.** *Purification of TMV.* Using the Gooding method,[35] the virus was multiplied in *N. tabacum* cv. K326 and purified. The absorbance values were estimated at 260 nm using an ultraviolet spectrophotometer.

$$\text{virus concn} = (A_{260} \times \text{dilution ratio})/E_{1\text{cm}}^{0.1\%,260\text{nm}}$$

*Half-Leaf Method Protective Effects of Title Compounds against TMV in Vivo.* The compound solution was smeared on the left side of growing *N. tabacum* L. leaves of the same age. The solvent was smeared on the right side of the leaves to serve as the control. The leaves, which were previously scattered with silicon carbide, were inoculated with the virus after 12 h using a brush dipped in $6 \times 10^{-3}$ mg/mL TMV and subsequently washed with water and rubbed softly along the nervature once or twice. The local lesions that appeared 3 to 4 d after the inoculation were counted.[36,37] Three replications were reproduced for each compound.

*Inactivation Effects of Title Compounds on TMV in Vivo.* The virus was inhibited after it was mixed with a compound solution of the same volume for 30 min. The right side of the *N. tabacum* L. leaves was then inoculated with the solvent and virus mixture for control. All of the leaves were previously scattered with silicon carbide. The number of local lesions was recorded 3 to 4 d after the inoculation.[37] Three replications were reproduced for each compound.

*Curative Effects of Title Compounds against TMV in Vivo.* Growing *N. tabacum* L. leaves of the same age were selected. The leaves were inoculated with TMV (concentration of $6 \times 10^{-3}$ mg/mL) by dipping and brushing the whole leaves, which were previously scattered with silicon carbide. The leaves were then washed with water after inoculation for 0.5 h. The compound solution was smeared on the left side of the leaves, and the solvent was smeared on the right side for control. The number of local lesions was counted and recorded 3 to 4 d after the inoculation.[37] Three replications were reproduced for each compound. The inhibitory rate of the compound was calculated according to the following formula ("av" means average):


dx.doi.org/10.1021/jf502162y | J. Agric. Food Chem. 2014, 62, 8928−8934

**Table 2. Inhibitory Effect of the Title Compounds against TMV in Vivo at 500 μg/mL**

| Compd. | 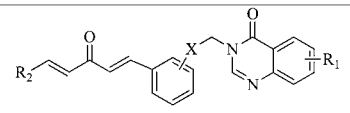 | | | Curative activity (%)[a] | Inactivation activity (%)[a] | Protection activity (%)[a] |
|---|---|---|---|---|---|---|
| | $R_1$ | $R_2$ | X | | | |
| $A_1$ | H | Ph | 2-O | 43.9±0.8 | 82.6±2.5 | 23.6±2.2 |
| $A_2$ | H | 4-Cl-Ph | 2-O | 36.3±2.9 | 88.4±1.3 | 49.8±1.8 |
| $A_3$ | H | 2-F-Ph | 2-O | 48.1±2.1 | 90.2±1.7 | 26.6±3.5 |
| $A_4$ | 8-$CH_3$ | Ph | 2-O | 46.5±1.6 | 82.2±2.5 | 49.2±2.4 |
| $A_5$ | H | 2-$OCH_3$-Ph | 2-O | 64.3±1.1 | 82.0±1.6 | 54.4±2.1 |
| $A_6$ | H | 4-$C(CH)_3$-Ph | 2-O | 28.8±1.0 | 87.5±0.1 | 56.5±0.7 |
| $A_7$ | H | 3-$NO_2$-Ph | 4-O | 46.2±2.3 | 45.8±1.2 | 18.9±1.9 |
| $A_8$ | H | 4-F-Ph | 2-O | 45.8±1.4 | 83.0±2.0 | 68.7±1.8 |
| $A_9$ | H | 4-F-Ph | 4-O | 23.5±1.0 | 64.6±1.2 | 42.5±4.1 |
| $A_{10}$ | H | furan-2-yl | 2-O | 49.9±1.3 | 91.9±0.8 | 66.9±1.9 |
| $A_{11}$ | H | 4-$CH_3$-Ph | 2-O | 29.6±2.8 | 81.5±3.1 | 54.2±2.6 |
| $A_{12}$ | 8-$CH_3$ | thiophen-2-yl | 2-O | 63.5±2.7 | 89.2±2.5 | 55.8±1.9 |
| $A_{13}$ | 8-$CH_3$ | thiophen-2-yl | 4-O | 26.5±3.4 | 75.1±3.6 | 59.1±0.9 |
| $A_{14}$ | H | furan-2-yl | 4-O | 12.7±2.0 | 85.1±2.1 | 63.1±2.4 |
| $A_{15}$ | 8-$CH_3$ | 2-Cl-5-$NO_2$-Ph | 2-O | 43.6±1.5 | 72.9±4.1 | 39.0±0.4 |
| $A_{16}$ | H | 4-methylthiazol-5-yl | 2-O | 50.1±1.2 | 89.3±0.2 | 71.7±3.0 |
| $A_{17}$ | H | thiophen-2-yl | 2-O | 34.0±3.1 | 83.7±1.2 | 64.6±2.1 |
| $A_{18}$ | H | thiophen-2-yl | 4-O | 34.6±1.5 | 50.0±4.8 | 54.7±2.4 |
| $A_{19}$ | H | 4-$OCH_3$-Ph | 4-O | 21.9±1.9 | 78.3±0.8 | 20.0±2.3 |
| $A_{20}$ | H | 2-$CF_3$-Ph | 2-O | 29.0±2.3 | 75.8±3.3 | 24.0±2.6 |
| $A_{21}$ | H | 2, 4-di-$OCH_3$-Ph | 4-O | 35.0±2.8 | 83.2±2.0 | 47.9±3.9 |
| $A_{22}$ | 8-$CH_3$ | 2, 4-di-$OCH_3$-Ph | 4-O | 48. 9±0.9 | 84.7±0.7 | 48.0±1.4 |
| $A_{23}$ | 8-$CH_3$ | pyrid-2-yl | 4-O | 51.9±1.1 | 81.4±0.2 | 24.1±0.8 |
| $A_{24}$ | 8-$CH_3$ | 2, 4-di-$OCH_3$-Ph | 2-O | 36.2±0.8 | 86.1±1.8 | 30.3±0.6 |
| $A_{25}$ | 8-$CH_3$ | 3, 4-di-$OCH_3$-Ph | 4-O | 69.0±0.3 | 64.6±4.8 | 66.5±0.8 |
| $A_{26}$ | H | 3, 4-di-$OCH_3$-Ph | 4-O | 57.7±1.8 | 87.8±0.5 | 34.4±1.8 |
| $A_{27}$ | H | 4-$OCH_3$-Ph | 2-O | 64.7±3.2 | 82.1±1.6 | 52.6±3.3 |
| $A_{28}$ | 8-$CH_3$ | 2-$OCH_3$-Ph | 2-O | 59.4±2.4 | 90.0±2.5 | 47.0±2.1 |
| $A_{29}$ | H | 3, 4, 5-tri-$OCH_3$-Ph | 4-O | 40.3±4.5 | 91.2±0.4 | 71.6±2.8 |
| $A_{30}$ | H | 3, 4, 5-tri-$OCH_3$-Ph | 2-O | 57.0±3.4 | 47.0±4.1 | 51.7±1.6 |
| Ningnanmycin[b] | | | | 58.4±0.9 | 95.8±1.4 | 68.4±2.2 |

[a]Average of three replicates. [b]The commercial, agricultural, and antiviral product ningnanmycin was used for comparison of activity. X = 2-O or 4-O.

$$\text{inhibition rate (\%)} = [(\text{av local lesion no. of control (not treated with compd)} - \text{av local lesion no. smeared with drugs})/\text{av local lesion no. of control (not treated with compd)}] \times 100\,\%$$

## RESULTS AND DISCUSSION

**Chemistry.** Figure 2 shows the summary of the synthetic route designed for the 4(3*H*)-quinazolinone analogues. The starting materials were substituted with 2-aminobenzoic acid, formamide, salicylaldehyde, hydroxybenzaldehyde, and acetone. The substituted *o*-aminobenzoic acid was allowed to react with formamide for 4.5 h at 140 to 145 °C to obtain the intermediate 4(3*H*)-quinazolinone **1**, and then with 37% formaldehyde for 5 h at 80 °C to obtain the intermediate substituted 3-hydroxymethyl-4(3*H*)-quinazolinone **2**. The substituted 3-chloromethyl-4(3*H*)-quinazolinone **3** was prepared by chlorination reaction with $SOCl_2$ in 1,4-dioxane. Intermediates **5a** to **5m** were obtained through the condensation of the (*E*)-4-(2-hydroxyphenyl)-3-butene-2-ones and (*E*)-4-(4-hydroxyphenyl)-3-butene-2-ones with the substituted aldehydes in ethanol for 12 h at room temperature. The title compounds 4(3*H*)-quinazolinone derivatives ($A_1$−$A_{30}$) were synthesized by the etherification reaction of intermediates **5** and **3** with $K_2CO_3$/KI in acetone refluxed at 56 °C for 5 to 10 h. The final step of the reaction yielded some by-products. The purification compound obtained by the TLC and recrystallization methods involved the loss of some products. Thus, the yield of the title compounds is low. All compounds were confirmed by spectroscopic data and elemental analysis.

Table 1 shows the structures of all the compounds confirmed through IR, $^1$H NMR, and $^{13}$C NMR spectral and elemental analyses. The IR spectra of the title products $A_1$ to $A_{30}$ exhibited characteristic absorption bands at 3421 to 3460 $cm^{-1}$, which indicate the presence of amidic N−CH−N. The stretching frequency at 1690 to 1650 $cm^{-1}$ was assigned to C═O vibrations. The characteristic absorptions at 1491 to 1620


dx.doi.org/10.1021/jf502162y | J. Agric. Food Chem. 2014, 62, 8928−8934

$cm^{-1}$ and 1219 to 1316 $cm^{-1}$ were attributed to the presence of C═C and C−O−C groups, respectively. $^1H$ NMR indicated that all of the phenyl protons had multiplets at 7.50 to 6.71 ppm. The main characteristic of the $^1H$ NMR spectra for the compound was the presence of a high-frequency downfield singlet $\delta_H$ 8.18−8.62 for N−C−H protons. N−$CH_3$ absorption peaks showed a singlet at 2.56 ppm to 3.87 ppm. The chemical shifts at nearly 188.00 ppm, 71.81 to 73.75 ppm, and 17.35 to 17.42 ppm in $^{13}C$ NMR also confirmed the presence of C═O, $-CH_2-$, and $-CH_3$, respectively.

**Antiviral Activity Screening of Title Compounds against TMV in Vivo.** The antiviral tests of $\mathbf{A_1}$ to $\mathbf{A_{30}}$ against TMV were conducted, and the results are summarized in Table 2. Most of the title compounds generally exhibited good antiviral activity against TMV in vivo, and some of them even showed higher antiviral activity than the control ningnanmycin. Our results indicated that compounds $\mathbf{A_5}$, $\mathbf{A_{12}}$, $\mathbf{A_{25}}$, and $\mathbf{A_{27}}$ exhibited higher curative activity than ningnanmycin, with values of 64.3%, 63.5%, 69.0%, and 64.7% at 500 $\mu$g/mL, respectively. The other compounds showed moderate curative activities at 500 mg/L. Among these compounds, $\mathbf{A_8}$, $\mathbf{A_{10}}$, $\mathbf{A_{14}}$, $\mathbf{A_{16}}$, $\mathbf{A_{17}}$, $\mathbf{A_{25}}$, and $\mathbf{A_{29}}$ exhibited significant protective effects against TMV and produced relatively high inhibitory activities with values of 68.7%, 66.9%, 63.1%, 71.7%, 64.6%, 66.5%, and 71.6% at 500 $\mu$g/mL, respectively. These values are similar to those of ningnanmycin (68.4%) against TMV at 500 $\mu$g/mL. Compounds $\mathbf{A_2}$, $\mathbf{A_3}$, $\mathbf{A_5}$, $\mathbf{A_6}$, $\mathbf{A_{10}}$, $\mathbf{A_{12}}$, $\mathbf{A_{14}}$, $\mathbf{A_{16}}$, $\mathbf{A_{24}}$, $\mathbf{A_{28}}$, and $\mathbf{A_{29}}$ inactivated efficacy at 88.4%, 90.2%, 87.5%, 91.9%, 89.2%, 85.1%, 89.3%, 86.1%, 87.8%, 90.0%, and 91.2%, respectively. These compounds exhibited slightly lower inactivation activities than ningnanmycin (95.8%) at 500 $\mu$g/mL.

Based on previous bioassays, all the test compounds showed moderate to excellent activity against plant viruses (TMV). Table 3 lists the $EC_{50}$ values of some of the synthesized compounds. In short, the $EC_{50}$ values of about 18 compounds with inhibition rate higher than 40% were obtained. Compounds $\mathbf{A_5}$, $\mathbf{A_{12}}$, $\mathbf{A_{25}}$, and $\mathbf{A_{27}}$ exhibited remarkable curative effects against TMV, with $EC_{50}$ values of 132.25, 138.01, 156.10, and 135.89 $\mu$g/mL, respectively. These values indicate stronger curative activity against the tested virus of the compounds than those of the commercial agent ningnanmycin ($EC_{50}$ = 281.22 $\mu$g/mL). However, the $EC_{50}$ values of the others are higher than that of ningnanmycin. The results show that their anti-TMV activities are very good. These findings suggest that these compounds can be used as lead structures in discovering new antiviral agents.

**Antiviral Activity and Structure Activity Relationship against TMV.** Some of the compounds showed potential potency against TMV. Various 1,4-pentadien-3-one substituent groups were introduced into the 4(3*H*)-quinazolinone ring system to establish a structure−activity relationship based on the experimental data. Ningnanmycin, a commercially available plant virucide in China, was used as control. Most of the final compounds showed low to high antiviral activities against TMV at 500 $\mu$g/mL. Several title compounds showed comparably good activities relative to ningnanmycin. When $R_1$ was H and $R_2$ was substituted with 2-methoxyphenyl, 2-furyl, 4-methylthiazol-5-yl, or 3,4,5-trimethoxyphenyl groups, the corresponding target compounds exhibited excellent activity against TMV. The relationships of the antiviral activities to different $R_1$ and $R_2$ were deduced, as shown by the activity values in Table 2. The strongest curative activity against TMV was observed when $R_1$ was H and $R_2$ was changed to 2-methoxyphenyl, thiophen-2-yl, 3,4-dimethoxyphenyl, or 4-methoxyphenyl groups. Some of the title compounds were as potent as ningnanmycin. When $R_1$ was H and $R_2$ was substituted with 2-fluorophenyl, 4-methylthiazol-5-yl or 3,4,5-trimethoxyphenyl groups, the target compounds exhibited remarkable protective activities against TMV that surpassed those of ningnanmycin. Compounds $\mathbf{A_3}$, $\mathbf{A_{10}}$, $\mathbf{A_{28}}$, and $\mathbf{A_{29}}$ displayed good inactivation activities. The inactivation activities of these compounds were further investigated at various concentrations, using ningnanmycin as commercial control. The presence of 2-fluorophenyl, 2-furyl, 2-methoxyphenyl, or 3,4,5-trimethoxyphenyl groups in a compound effectively improved the antiviral activity of the compound more than that of other groups.

**Table 3. $EC_{50}$ Values of Some Compounds against TMV in Vivo**

| Compd. | 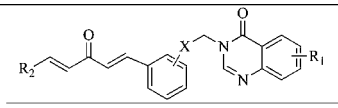 | | | $EC_{50}$ ($\mu$g/mL)[a] |
|---|---|---|---|---|
| | $R_1$ | $R_2$ | X | |
| $A_1$ | H | Ph | 2-O | 529.03±3.4 |
| $A_3$ | H | 2-F-Ph | 2-O | 484.09±2.8 |
| $A_4$ | 8-$CH_3$ | Ph | 2-O | 496.40±1.7 |
| $A_5$ | H | 2-$OCH_3$ | 2-O | 132.25±2.5 |
| $A_7$ | H | 3-$NO_2$-Ph | 4-O | 478.58±2.9 |
| $A_8$ | H | 4-F-Ph | 2-O | 502.64±1.6 |
| $A_{10}$ | H | furan-2-yl | 2-O | 356.34±3.5 |
| $A_{12}$ | 8-$CH_3$ | thiophen-2-yl | 2-O | 138.01±2.3 |
| $A_{15}$ | 8-$CH_3$ | 2-Cl-5-$NO_2$-Ph | 2-O | 509.87±2.1 |
| $A_{16}$ | H | 4-methylthiazol-5-yl | 2-O | 323.76±4.8 |
| $A_{22}$ | 8-$CH_3$ | 2, 4-di-$OCH_3$-Ph | 4-O | 345.15±5.3 |
| $A_{23}$ | 8-$CH_3$ | pyrid-2-yl | 4-O | 318.43±1.5 |
| $A_{25}$ | 8-$CH_3$ | 3, 4-di-$OCH_3$-Ph | 4-O | 156.10±2.6 |
| $A_{26}$ | H | 3, 4-di-$OCH_3$-Ph | 4-O | 298.44±3.2 |
| $A_{27}$ | 8-$CH_3$ | 4-$OCH_3$-Ph | 2-O | 135.59±2.9 |
| $A_{28}$ | 8-$CH_3$ | 2-$OCH_3$-Ph | 2-O | 289.35±1.4 |
| $A_{29}$ | H | 3, 4, 5-tri-$OCH_3$-Ph | 4-O | 564.25±1.2 |
| $A_{30}$ | H | 3, 4, 5-tri-$OCH_3$-Ph | 2-O | 300.18±3.1 |
| Ningnanmycin[b] | | | | 281.22±2.0 |

[a]Average of three replicates. [b]The commercial, agricultural, and antiviral product ningnanmycin was used for comparison of activity.

In summary, 4(3*H*)-quinazolinone analogues containing a 1,4-pentadien-3-one moiety were prepared in moderate yield and evaluated for their antiviral activities against TMV. Some of the synthesized compounds exhibited moderate to excellent antiviral activity in vivo. The preliminary structure−activity relationships established the importance of the presence of a 1,4-pentadien-3-one moiety in the 4(3*H*)-quinazolinone component in obtaining title compounds with the desired antiviral activity. Compounds $\mathbf{A_5}$, $\mathbf{A_{12}}$, $\mathbf{A_{25}}$, and $\mathbf{A_{27}}$ possessed appreciable curative bioactivities against TMV in vivo, and such bioactivities were superior to those of ningnanmycin. Therefore, based on the antiviral studies on the biological efficacies, crop safety, and toxicities of these compounds, they can be considered for further development as a new class of tobacco protection agents.


dx.doi.org/10.1021/jf502162y | J. Agric. Food Chem. 2014, 62, 8928−8934

## ■ ASSOCIATED CONTENT

### Supporting Information

Results of our physical analyses and the data on the synthesis and characterization of target compounds $\mathbf{A_1}$ to $\mathbf{A_{30}}$. This material is available free of charge via the Internet at http://pubs.acs.org.

## ■ AUTHOR INFORMATION


### Corresponding Author

*Phone: +86(851)362-0521. Fax: +86(851)362-2211. E-mail: songbaoan22@yahoo.com.



### Funding

The authors gratefully acknowledge the National Natural Science Foundation of China (Nos. 21132003 and 21362004).


### Notes

The authors declare no competing financial interest.

## ■ ABBREVIATIONS USED

TLC, thin layer chromatography; $EC_{50}$, 50% effective concentration; $^1$H NMR, $^1$H nuclear magnetic resonance; $^{13}$C NMR, $^{13}$C nuclear magnetic resonance; TMV, tobacco mosaic virus; CMV, cucumber mosaic virus

## ■ REFERENCES


(1) Li, Y. M.; Wang, L. H.; Li, S. L.; Chen, X. Y.; Shen, Y. M.; Zhang, Z. K.; He, H. P.; Xu, W. B.; Shu, Y. L.; Liang, G. D.; Fang, R. X.; Hao, X. J. Seco-pregnane steroids target the subgenomic RNA of alphavirus-like RNA viruses. *Proc. Natl. Acad. Sci. U.S.A.* **2007**, *104*, 8083−8088.

(2) Qian, X. H.; Lee, P. W.; Cao, S. China: Forward to the green pesticides via a basic research program. *J. Agric. Food Chem.* **2010**, *58*, 2613−2623.

(3) Seiber, J. N. Sustainability and agricultural and food chemistry. *J. Agric. Food Chem.* **2011**, *59*, 1−21.

(4) Deng, W. B.; Hu, H. Z.; Chen, J. R.; Yu, M. Q. Biological activity of Ningnanmycin on tobacco mosaic virus. *Chin. J. Appl. Environ. Biol.* **2004**, *10*, 695−698.

(5) Zhang, Z. K.; Ouyang, M. A.; Wu, Z. J.; Lin, Q. Y.; Xie, L. H. Structure-activity relationship of triterpenes and triterpenoid glycosides against tobacco mosaic virus. *Planta Med.* **2007**, *73*, 1457−1463.

(6) Wu, Z. J.; Ouyang, M. A.; Wang, C. Z.; Zhang, Z. K. Six new triterpenoid saponins from the leaves of *Ilex oblonga* and their inhibitory activities against TMV replication. *Chem. Pharm. Bull.* **2007**, *55*, 422−427.

(7) Yan, X. H.; Chen, J.; Di, Y. T.; Fang, X.; Dong, J. H.; Sang, P.; Wang, Y. H.; He, H. P.; Zhang, Z. K.; Hao, X. J. Anti-tobacco mosaic virus (TMV) quassinoids from *Brucea javanica* (L.) Merr. *J. Agric. Food Chem.* **2010**, *58*, 1572−1577.

(8) Chen, J.; Yan, X. H.; Dong, J. H.; Sang, P.; Fang, X.; Di, Y. T.; Zhang, Z. K.; Hao, X. J. Tobacco mosaic virus (TMV) inhibitors from Picrasma quassioides Benn. *J. Agric. Food Chem.* **2009**, *57*, 6590−6595.

(9) Wu, Z. J.; Ouyang, M. A.; Wang, C. Z.; Zhang, Z. K.; Sheng, J. G. Anti-tobacco mosaic virus (TMV) triterpenoid saponins from the leaves of Ilex oblonga. *J. Agric. Food Chem.* **2007**, *55*, 1712−1717.

(10) Li, Y. T.; Hao, X. J.; Li, S. F.; He, H. P.; Yan, X. H.; Chen, Y. D.; Dong, J. H.; Zhang, Z. K.; Li, J. H. Eudesmanolides from Wedelia trilobata (L.) Hitchc. as potential inducers of plant systemic acquired resistance. *J. Agric. Food Chem.* **2013**, *61*, 3884−3890.

(11) Ge, Y. H.; Liu, K. X.; Zhang, J. X.; Mu, S. Z.; Hao, X. J. The limonoids and their antitobacco mosaic virus (TMV) activities from Munronia unifoliolata Oliv. *J. Agric. Food Chem.* **2012**, *60*, 4289−4295.

(12) Wang, Z. W.; Wei, P.; Xu, X. Z.; Liu, Y. X.; Wang, L. Z.; Wang, Q. M. Design, synthesis, and antiviral activity evaluation of phenanthrene-based antofine derivatives. *J. Agric. Food Chem.* **2012**, *60*, 8544−8551.

(13) Wang, Z. W.; Wei, P.; Wang, L. Z.; Wang, Q. M. Design, synthesis, and anti-tobacco mosaic virus (TMV) activity of phenanthroindolizidines and their analogues. *J. Agric. Food Chem.* **2012**, *60*, 10212−10219.

(14) Wang, Z. W.; Wang, L.; Ma, S.; Liu, Y. X.; Wang, L. Z.; Wang, Q. M. Design, synthesis, antiviral activity, and SARs of 14-aminophenanthroindolizidines. *J. Agric. Food Chem.* **2012**, *60*, 5825−5831.

(15) Song, H. J.; Liu, Y. X.; Liu, Y. X.; Wang, L. Z.; Wang, Q. M. Synthesis and antiviral and fungicidal activity evaluation of $\beta$-carboline, dihydro-$\beta$-carboline, tetrahydro-$\beta$-carboline alkaloids, and their derivatives. *J. Agric. Food Chem.* **2014**, *62*, 1010−1018.

(16) Su, B.; Chen, F. Z.; Wang, L. Z.; Wang, Q. M. Design, synthesis, antiviral activity, and structure-activity relationships (SARs) of two types of structurally novel phenanthroindo/quinolizidine analogues. *J. Agric. Food Chem.* **2014**, *62*, 1233−1239.

(17) An, T. Y.; Huang, R. Q.; Yang, Z.; Zhang, D. K.; Li, G. R.; Yao, Y. C.; Gao, J. Alkaloids from *Cynanchum komarovii* with inhibitory activity against the tobacco mosaic virus. *Phytochemistry* **2001**, *58*, 1267−1269.

(18) Wang, Q. M.; Yao, Y. C.; Huang, R. Q.; Fan, Z. J.; Li, G. R.; Yu, X. S. Antiviral activity of antofine from *Cynanchum komarovii*. *Agrochemicals* **2007**, *46*, 425−427.

(19) Wang, Q. M.; Wang, K. L.; Wu, M.; Li, Z.; Wang, Z. W.; Su, B.; Hu, Y. N.; Liu, Y. X.; Huang, R. Q. Application of tylophorine-like alkaloid organic acid salt derivative to prepare the pesticide formulations for preventing and controlling plant diseases. CN 101875657, CAN 154:3276, 2010.

(20) Kim, M. K.; Choi, G. J.; Lee, H. S. Fungicidal property of curcuma longa L. rhizome-derived curcumin against phytopathogenic fungi in a greenhouse. *J. Agric. Food Chem.* **2003**, *51*, 1578−1581.

(21) Wang, Z. N.; Hu, D. Y.; Song, B. A.; Yang, S.; Jin, L. H.; Xue, W. Synthesis and biological activity of 1,5-bis(substituted pyrazol-4-yl)-1,4-pentadien-3-one derivatives. *Chin. J. Org. Chem.* **2009**, *29*, 1412−1418.

(22) Qiu, Q. J.; Xue, W.; Lu, P.; Wang, Z. C.; Wei, X. Synthesis of oxime esters of curcumin derivatives and their anti-CMV activities. *Chin. J. Synth. Chem.* **2011**, *19*, 36−40.

(23) Luo, H.; Liu, J. J.; Jin, L. H.; Hu, D. Y.; Chen, Z.; Yang, S.; Wu, J.; Song, B. A. Synthesis and antiviral bioactivity of novel (1*E*,4*E*)-1-aryl-5-(2-(quinazolin-4-yloxy)phenyl)-1,4-pentadien-3-one derivatives. *Eur. J. Med. Chem.* **2013**, *3*, 662−669.

(24) Ashis, K. N.; Subarna, G.; Ranadhir, C. Antibacterial activity of some 3-(arylideneamino)-2-phenylquinazoline-4(3*H*)-ones: synthesis and preliminary QSAR studies. *Molecules* **2007**, *12*, 2413−2426.

(25) Kumar, K. S.; Ganguly, S.; Veerasamy, R. Synthesis, antiviral activity and cytotoxicity evaluation of Schiff bases of some 2-phenyl quinazoline-4(3*H*)-ones. *Eur. J. Med. Chem.* **2010**, *45*, 5474−5479.

(26) Koepfli, J. B.; Mead, J. F.; Brockman, J. A. J. *J. Am. Chem. Soc.* **1947**, *69*, 1837.

(27) Ding, M. W.; Yang, S. J.; Chen, Y. F. Synthesis and fungicidal activities of 2-alkoxy-3*H*-quinazolin-4-ones. *Chin. J. Org. Chem.* **2004**, *24*, 923−926.

(28) Gao, X. W.; Cai, X. J.; Yan, K.; Song, B. A.; Gao, L. L.; Chen, Z. Synthesis and antiviral bioactivities of 2-aryl- or 2-methyl-3-(substituted-benzalamino)-4(3*H*)-quinazolinone derivatives. *Molecules* **2007**, *12*, 2621−2642.

(29) Gao, X. W.; Cai, X. J.; Yan, K.; Gao, L. L.; Wang, H. Y.; Chen, Z.; Song, B. A. Synthesis and anti-tobacco mosaic virus activity of 4(3*H*)-quinazolinone Schiff base. *Chin. J. Org. Chem.* **2008**, *28*, 1785−1791.

(30) Ouyang, G. P.; Zhang, P. Q.; Xu, G. F.; Song, B. A.; Yang, S.; Jin, L. H.; Xue, W.; Hu, D. Y.; Lu, P.; Chen, Z. Synthesis and antifungal bioactivities of 3-alkylquinazolin-4-one derivatives. *Molecules* **2006**, *11*, 383−392.

(31) Wang, X.; Li, P.; Li, Z. N.; Yin, J.; He, M.; Xue, W.; Chen, Z. W.; Song, B. A. Synthesis and bioactivity evaluation of novel arylimines containing a 3-aminoethyl-2-[(*p*-trifluoromethoxy)anilino]-4(3*H*)-quinazolinone moiety. *J. Agric. Food. Chem.* **2013**, *61*, 9575−9582.

(32) Liu, G.; Song, B. A.; Sang, W. J.; Yang, S.; Jin, L. H.; Ding, X. Synthesis and bioactivity of N-aryl-4-aminoquinazoline compounds. *Chin. J. Org. Chem.* **2004**, *10*, 1296−1299.
(33) Mc Gookin, A.; Heilbron, I. M. CCLXXV.—The isomerism of the styryl alkyl ketones. Part I. The isomerism of 2-hydroxystyryl methyl ketone. *J. Chem. Soc. Trans.* **1924**, *125*, 2099−2105.
(34) Li, S. B.; Hu, D. Y.; Song, B. A.; Yang, S.; Jin, L. H.; Xue, W.; Zeng, S.; Wang, J.; Chen, Z.; Lu, P.; Zhou, X.; Fan, L. E. Synthesis and antifungal activity of novel 1,5-diphenyl-1,4-pentadien-3-one oxime esters. *Chin. J. Org. Chem.* **2008**, *28*, 311−316.
(35) Gooding, G. V., Jr.; Hebert, T. T. A simple technique for purification of tobacco mosaic virus in large quantities. *Phytopathology* **1967**, *57*, 1285−1287.
(36) Fan, Z. J.; Shi, Z. G.; Zhang, H. K.; Liu, X. F.; Bao, L. L.; Ma, L.; Zuo, X.; Zheng, Q. X.; Mi, N. Synthesis and biological activity evaluation of 1,2,3-thiadiazole derivatives as potential elicitors with highly systemic acquired resistance. *J. Agric. Food Chem.* **2009**, *57*, 4279−4286.
(37) Song, B. A.; Zhang, H. P.; Wang, H.; Yang, S.; Jin, L. H.; Hu, D. Y.; Pang, L. L.; Xue, W. Synthesis and antiviral activity of novel chiral cyanoacrylate derivatives. *J. Agric. Food. Chem.* **2005**, *53*, 7886−7891.

Table 1. Names, Molecular Formulas, Weights, and Structures, and LC−MS Parameters of Mycotoxins and [$^{13}$C]-IS

| Mycotoxins | Molecular formula | Molecular weight | Molecular stucture | RT (min) | MRM transitions* | DP (eV) | CE (eV) | CXP (eV) |
|---|---|---|---|---|---|---|---|---|
| Aflatoxin $B_1$ | $C_{17}H_{12}O_6$ | 312.1 | 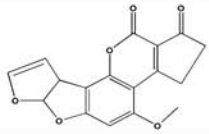 | 7.0 | 313.1→**241.0**/285.0 | 86/106 | 55/37 | 14/8 |
| [$^{13}C_{17}$]-aflatoxin $B_1$ | $^{13}C_{17}H_{12}O_6$ | 329.1 | | 7.0 | 330.1→**255.2**/301.0 | 86/106 | 55/37 | 14/8 |
| Aflatoxin $B_2$ | $C_{17}H_{14}O_6$ | 314.1 | 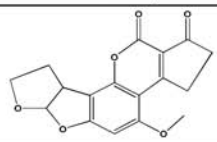 | 6.5 | 315.2→**287.1**/259.1 | 91/91 | 39/45 | 16/14 |
| [$^{13}C_{17}$]-aflatoxin $B_2$ | $^{13}C_{17}H_{14}O_6$ | 331.1 | | 6.5 | 332.0→**303.2**/273.1 | 91/91 | 39/45 | 16/14 |
| Aflatoxin $G_1$ | $C_{17}H_{12}O_7$ | 328.1 | 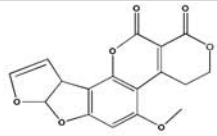 | 5.9 | 328.8→**243.2**/200.0 | 86/86 | 41/99 | 14/10 |
| [$^{13}C_{17}$]-aflatoxin $G_1$ | $^{13}C_{17}H_{12}O_7$ | 345.1 | | 5.9 | 345.8→**257.1**/124.2 | 86/86 | 41/99 | 14/10 |
| Aflatoxin $G_2$ | $C_{17}H_{14}O_7$ | 330.1 | 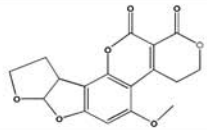 | 5.4 | 331.2→**313.0**/245.0 | 111/111 | 36/49 | 18/20 |
| [$^{13}C_{17}$]-aflatoxin $G_2$ | $^{13}C_{17}H_{14}O_7$ | 347.1 | | 5.4 | 348.0→**330.0**/259.0 | 111/111 | 36/49 | 18/20 |
| Deoxynivalenol | $C_{15}H_{20}O_6$ | 296.1 | 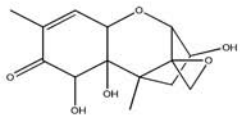 | 3.2 | 297.0→**249.0**/231.2 | 71/61 | 17/21 | 44/22 |
| [$^{13}C_{15}$]-deoxynivalenol | $^{13}C_{15}H_{20}O_6$ | 311.2 | | 3.2 | 312.0→**263.0**/345.2 | 71/61 | 17/21 | 44/22 |
| Fumonisin $B_1$ | $C_{34}H_{59}NO_{15}$ | 721.4 | 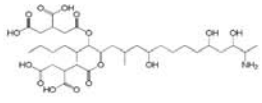 | 9.3 | 722.5→**352.5**/334.5 | 111/111 | 53/57 | 10/54 |
| [$^{13}C_{34}$]-fumonisin $B_1$ | $^{13}C_{34}H_{59}NO_{15}$ | 755.5 | | 9.3 | 756.4→**374.5**/356.4 | 111/111 | 53/57 | 10/54 |
| Fumonisin $B_2$ | $C_{34}H_{59}NO_{14}$ | 705.4 | 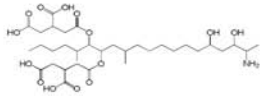 | 9.9 | 706.3→**336.3**/318.3 | 106/106 | 55/59 | 10/20 |
| [$^{13}C_{34}$] fumonisin $B_2$ | $^{13}C_{34}H_{59}NO_{14}$ | 739.5 | | 9.9 | 740.3→**358.4**/340.5 | 106/106 | 55/59 | 10/20 |
| Fumonisin $B_3$ | $C_{34}H_{59}NO_{14}$ | 705.4 | 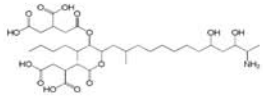 | 9.7 | 706.3→**336.3**/318.3 | 106/106 | 55/59 | 10/20 |
| [$^{13}C_{34}$]- fumonisin $B_3$ | $^{13}C_{34}H_{59}NO_{14}$ | 739.5 | | 9.7 | 740.5→**358.4**/340.4 | 106/106 | 55/59 | 10/20 |
| Ochratoxin A | $C_{20}H_{18}ClNO_6$ | 403.1 | 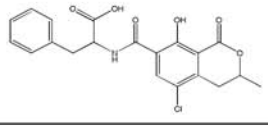 | 9.5 | 404.0→**239.0**/102.0 | 66/66 | 41/101 | 16/16 |
| [$^{13}C_{20}$]-ochratoxin A | $^{13}C_{20}H_{18}ClNO_6$ | 423.1 | | 9.5 | 424.1→**250.1**/110.1 | 66/66 | 41/101 | 16/16 |
| T-2 toxin | $C_{24}H_{34}O_9$ | 466.2 | 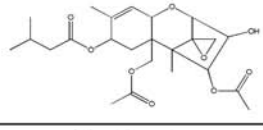 | 9.4 | 484.3→**215.2**/185.1 | 57/57 | 29/33 | 17/11 |
| [$^{13}C_{24}$]-T-2 toxin | $^{13}C_{24}H_{34}O_9$ | 490.3 | | 9.4 | 508.3→**229.2**/198.2 | 57/57 | 29/33 | 17/11 |
| Zearalenone | $C_{18}H_{22}O_5$ | 318.1 | 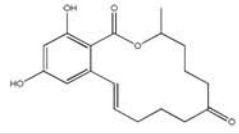 | 9.8 | 317.0→**175.0**/130.0 | -100/-100 | -38/-48 | -10/-10 |
| [$^{13}C_{18}$]-Zearalenone | $^{13}C_{18}H_{22}O_5$ | 336.2 | | 9.8 | 337.2→**185.0**/140.0 | -100/-100 | -38/-48 | -10/-10 |

matrices and minimize or correct matrix suppression from coeluted matrix components in the electrospray ionization (ESI) source.[22−24] However, optimization of extraction conditions is time-consuming and may be matrix and mycotoxin dependent. As a result a single extraction method may not be applicable to all food/feed matrices.[25] In addition, ESI-based LC−MS/MS analysis of mycotoxins is prone to matrix suppression. Despite extensive cleanup using immunoaffinity cartridges, matrix-matched calibration was still required for quantitation.[26] Although dilution could alleviate matrix suppression, dilution factors still have to be determined on a case by case basis.[27] Standard addition is feasible for


dx.doi.org/10.1021/jf503943r | J. Agric. Food Chem. 2014, 62, 8935−8943

samples containing a single mycotoxin, but preparation of fortified samples is very complex for samples with multiple mycotoxins with significantly different concentrations.

Isotope dilution mass spectrometry has been used for the quantitative analysis of elements and chemicals in biological, environmental, and food samples.[28−30] This mass spectrometry approach is based on the fortification of samples with isotope labeled internal standards (IS) (e.g., [$^{13}$C]-IS) prior to sample preparation or instrumental analysis. The target analytes and fortified IS have the same or similar physicochemical properties, which results in identical recoveries and MS responses. By measuring the relative response ratio between a target analyte and its corresponding labeled IS, signal variations caused by sample loss or ionization suppression are corrected as the relative response ratio would remain constant.

Stable isotope dilution would be a viable approach for multimycotoxin analysis in challenging matrices such as animal feed, cereal/grain-based baby formula, dry botanicals, and spices. To eliminate matrix interferences and achieve satisfactory recoveries of target mycotoxins, one often has to perform laborious matrix/mycotoxin-dependent cleanup or prepare matrix-matched calibration standards for quantitation. In theory, the application of stable isotope dilution should be instrument-, matrix-, and mycotoxin-independent, as long as the target mycotoxin and the corresponding labeled internal standard could be detected. This way, sample preparation and quantitation would be significantly simplified and developed stable isotope dilution methods could be expanded to other matrices of interest. Furthermore, a developed stable isotope dilution method could be easily shared by laboratories using different LC−MS instruments. Although using [$^{13}$C]-mycotoxins as IS would simplify the analysis of multimycotoxins in food/feed, researchers have only tested the applicability and benefits of this approach in a few food and feed matrices.[31−33] The application of stable isotope dilution has not been a well-establish practice among mycotoxin laboratories due to the lack of commercially available isotope labeled internal standards. Recently, certified isotope labeled mycotoxins can be obtained from various commercial sources. The increasing sensitivity of LC−MS makes it more cost-effective to use these labeled internal standards because only a small amount of the labeled standards is required to be used. To take advantage of the available isotope labeled mycotoxins and the sensitivity of today's LC−MS, we used stable isotope dilution and LC−MS for multimycotoxin analysis in milk, milk-based infant formula, and food grade gums.[34,35] The aim of this work was to further assess the applicability of the stable isotope dilution mass spectrometry approach using important but more challenging matrices, animal feeds and cereal-based baby foods, for the determination of aflatoxin $B_1$, $B_2$, $G_1$, and $G_2$, deoxynivalenol, fumonisin $B_1$, $B_2$, and $B_3$, ochratoxin A, T-2 toxin, and zearalenone. Although the FDA has only established action or advisory levels for aflatoxins, deoxynivalenol, and fumonisins, we also included ochratoxin A, T-2 toxin, and zearalenone for exploratory purposes. Our method consisted of simple extraction and filtration steps. Quantitation for all target mycotoxins was achieved without using matrix-matched calibration.

## MATERIALS AND METHODS

**Chemicals and Materials.** Aflatoxins $B_1$, $B_2$, $G_1$, and $G_2$; deoxynivalenol; fumonisins $B_1$, $B_2$, and $B_3$; ochratoxin A; T-2 toxin; and zearalenone standards were purchased in neat form from Romer Laboratories, Inc. (Union, MO). Stable isotope labeled internal standards, [$^{13}C_{17}$]-aflatoxin $B_1$ (500 ng/mL), [$^{13}C_{17}$]-aflatoxin $B_2$ (500 ng/mL), [$^{13}C_{17}$]-aflatoxin $G_1$ (500 ng/mL), [$^{13}C_{17}$]-aflatoxin $G_2$ (500 ng/mL), [$^{13}C_{15}$]-deoxynivalenol (25,000 ng/mL), [$^{13}C_{34}$]-fumonisin $B_1$ (25,000 ng/mL), [$^{13}C_{34}$]-fumonisin $B_2$ (10,000 ng/mL), [$^{13}C_{34}$]-fumonisin $B_3$ (10,000 ng/mL), [$^{13}C_{20}$]-ochratoxin A (10,000 ng/mL), [$^{13}C_{24}$]-T-2 toxin (25,000 ng/mL), and [$^{13}C_{18}$]-zearalenone (25,000 ng/mL) were purchased from Romer Laboratories, Inc. (Union, MO). The names, molecular formulas, weights, structures, and LC−MS parameters of mycotoxins are included in Table 1.

Two European reference materials, ERM-BE375 (low level aflatoxins in compound feeding stuff) and ERM-BE376 (high level aflatoxins in compound feeding stuff), were purchased from Analytical Reference Materials International (Golden, CO). Dry cat (2)/dog food (2) and animal feed samples (10) and grain/rice/oatmeal-based baby formulas (17) were purchased from local stores in the Washington, DC, metropolitan area or other commercially available sources. Animal feeds are cotton seed meal, DDGs, hog, fish, and sheep feed. The dry cat/dog foods are mix of chicken meal, dried veggies/fruits, oat, rice, and grain. Fat, protein, fiber, vitamins, and minerals are listed as major ingredients on the labels. Baby food samples are rice, grain, or oatmeal-based cereal. Milk is not listed as one of the ingredients for these baby foods.

LC grade acetonitrile, methanol, water, and MS grade formic acid and ammonium formate were purchased from Fisher Scientific (Pittsburgh, PA). Amicon Ultra-4 centrifugal filters with Ultracel-3 membrane (3 kDa) were purchased from EMD Millipore (Billerica, MA).

**Stock and Calibration Solutions.** Stock standard solutions of aflatoxins $B_1$, $B_2$, $G_1$, and $G_2$; deoxynivalenol; fumonisins $B_1$, $B_2$, and $B_3$; ochratoxin A; T-2 toxin; and zearalenone were prepared by dissolving each mycotoxin (5.0 ± 0.1 mg) in 25.00 mL of acetonitrile in volumetric flasks. Three working solutions containing these mycotoxins (A, B, C), were prepared by diluting and pipetting an appropriate amount of each individual stock standard solution to a 10 mL volumetric flask and bringing it up to volume with acetonitrile/water (1:1, v/v). Stock solutions and working standard solutions used in this study were stored in the dark at −20 °C. In working solution A, concentrations of the mycotoxins were prepared as follows: 1,000 ng/mL for aflatoxins $B_1$, $B_2$, $G_1$, and $G_2$; 20,000 ng/mL for deoxynivalenol and fumonisins $B_1$, $B_2$, and $B_3$; 10,000 ng/mL for ochratoxin A; and 20,000 ng/mL for T-2 toxin and zearalenone. Working solution B consisted of 200 ng/mL of aflatoxins $B_1$, $B_2$, $G_1$, and $G_2$; 4,000 ng/mL of deoxynivalenol and fumonisins $B_1$, $B_2$, and $B_3$; 2,000 ng/mL of ochratoxin A; and 4,000 ng/mL of T-2 toxin and zearalenone. Working solution C consisted of 40 ng/mL of aflatoxins $B_1$, $B_2$, $G_1$, and $G_2$; 1,000 ng/mL of deoxynivalenol and fumonisins $B_1$, $B_2$, and $B_3$; 400 ng/mL of ochratoxin A; and 800 ng/mL of T-2 toxin and zearalenone. Calibration solutions were prepared from the working standard solutions by a series of dilutions on the day of experiment.

A mixed [$^{13}$C]-IS solution was prepared by mixing an appropriate amount of each [$^{13}$C]-IS in a 5 mL volumetric flask and bringing it up to volume with acetonitrile/water (1/1, v/v). The final concentrations were 100 ng/mL for [$^{13}C_{17}$]- aflatoxin $B_1$, [$^{13}C_{17}$]- aflatoxin $B_2$, [$^{13}C_{17}$]- aflatoxin G1, and [$^{13}C_{17}$]- aflatoxin $G_2$; 2,000 ng/mL for [$^{13}C_{15}$]-deoxynivalenol, [$^{13}C_{34}$]- fumonisin $B_1$, [$^{13}C_{34}$]- fumonisin $B_2$, and [$^{13}C_{34}$]- fumonisin $B_3$; 500 ng/mL for [$^{13}C_{20}$]-ochratoxin A; and 1,000 ng/mL for [$^{13}C_{24}$]-T-2 toxin and [$^{13}C_{18}$]-zearalenone.

**Sample Preparation and Recovery Studies.** Samples were homogenized with dry ice in a Robot Coupe blender (Ridgeland, MS) to a powdery consistency and then put into polypropylene freezer bags and stored at −20 °C. The bags were not immediately sealed to allow residual carbon dioxide to sublime. Ground samples (0.5 ± 0.01 g) were weighed into 15 mL disposable glass vials with solid green melamine cap and PTFE liner (Sigma, St. Louis) and then fortified with 50 μL of [$^{13}$C]-IS solution, prior to extraction This way the fortified standard would go through the sample preparation and instrumental analysis as the target mycotoxin and the signal variation of target mycotoxin caused by sample preparation or matrix suppression could be offset by monitoring the relative response

Table 2. Estimated Matrix-Dependent LOQs (ng/g)

| mycotoxin | animal feed | cat food | dog food | grain based | rice based | oatmeal based | std solns |
|---|---|---|---|---|---|---|---|
| aflatoxin $B_1$ | 0.1 | 0.10 | 0.10 | 0.03 | 0.02 | 0.03 | 0.1 |
| aflatoxin $B_2$ | 0.1 | 0.1 | 0.1 | 0.1 | 0.03 | 0.03 | 0.04 |
| aflatoxin $G_1$ | 0.1 | 0.2 | 0.2 | 0.04 | 0.1 | 0.03 | 0.04 |
| aflatoxin $G_2$ | 0.1 | 0.3 | 0.4 | 0.1 | 0.1 | 0.1 | 0.1 |
| deoxynivalenol | 8.3 | 3.2 | 4.3 | 3.7 | 4.3 | 2.6 | 3.4 |
| fumonisin $B_1$ | 6.6 | 4.1 | 5.3 | 3.0 | 3.8 | 3.5 | 1.4 |
| fumonisin $B_2$ | 5.9 | 3.1 | 3.4 | 2.7 | 4.8 | 4.3 | 0.7 |
| fumonisin $B_3$ | 5.4 | 4.7 | 5.3 | 4.6 | 3.3 | 4.0 | 1.9 |
| ochratoxin A | 1.3 | 1.1 | 1.2 | 0.7 | 0.4 | 0.7 | 0.5 |
| T-2 toxin | 3.3 | 4.1 | 3.7 | 4.6 | 2.6 | 3.0 | 1.6 |
| zearalenone | 1.3 | 2.2 | 5.2 | 1.8 | 1.4 | 0.4 | 1.0 |

between the mycotoxin and the corresponding [$^{13}$C]-IS. The glass vials were capped, placed on a shaker with pulsation (Glas-Col, Terre Haute, IN, USA), and shaken for 10 min at a speed set to 50 and pulsation frequency set at 30−35 pulsations/min. After the addition of 5.0 mL of acetonitrile/water (50:50, v/v), the vials were shaken again for 15 min at a speed set to 50 and pulsation frequency set at 30−35 pulsations/min. A 2.0 mL aliquot of the sample was transferred to an Amicon Ultra-4 centrifugal filter with Ultracel-3 membrane (molecular weight cutoff value of 3 kDa) and centrifuged for 30 min at 4500 rpm (4200*g*). The aliquots of the resulting filtrates were transferred into autosampler vials with polypropylene cap and PTFE/silicone septa for LC−MS/MS analysis. Recovery studies were carried out using dry cat/dog food, animal feed, and grain/oatmeal/rice-based infant formula at three fortification levels (Tables 3, 4). The prepared working solution A, B, or C (25 $\mu$L for baby foods and 50 $\mu$L for dry cat/dog food and animal feed) and IS solution (50 $\mu$L) were added to samples and then prepared following the extraction, centrifugation, and filtration procedures described above. At each fortification concentration, samples were prepared in quadruplicate. No mycotoxins were detected in blank samples used for recovery studies.

Quantitation was performed using solvent only calibration standards. The concentration of each target mycotoxin was determined using the peak area ratio of response of the mycotoxin to that of the corresponding [$^{13}$C]-IS, and calculating the concentration by preparing a calibration curve using the peak area ratios of solvent-only calibration standards to that of the same [$^{13}$C]-IS. Each calibration curve consisted of multiple calibration standards and was constructed using least-squares regression. Recoveries were calculated using the formula "detected concentration/fortified concentration × 100%".

**Matrix-Dependent Limit of Detection and Quantitation.** The matrix-dependent limits of detection and quantitation (LOD and LOQ) for each analyte were obtained by following the U.S. Environmental Protection Agency's (EPA) protocol.[36] The matrix-dependent LOD was determined by analyzing ten replicates of matrix-matched calibration standards prepared by fortifying 5.0 mL of blank matrix with 25 and 50 $\mu$L of working solution C. The mean and standard deviations (SD) of each target mycotoxin were obtained from the ten replicates. The method-dependent LOD was calculated using the formula LOD = 2.821 × SD (critical $t_{0.01}$ = 2.821 for degree of freedom (df) of 9). The corresponding method dependent LOQ was calculated as 3 × LOD. At the determined LODs the confirmation transitions were detectable.

**Matrix Effects.** Calibration standards at multiple concentrations were prepared in the extraction solvent, and the blank baby food, dry cat/dog food, and animal feed extracts were prepared following sample preparation procedures. [$^{13}$C]-IS (5.0 $\mu$L) was fortified into each calibration standard (0.5 mL) prior to LC−MS/MS analysis. Matrix-matched and solvent calibration curves for all mycotoxins were established with coefficients of correlation ($r^2$) >0.99, including aflatoxins $B_1$, $B_2$, $G_1$, and $G_2$ (0.05−25 ng/mL); deoxynivalenol and fumonisins $B_1$, $B_2$, and $B_3$ (5.0−500 ng/mL); ochratoxin A (1.0−250 ng/mL); and T-2 toxin and zearalenone (2.5−250 ng/mL). A slope ratio of a pair of matrix-matched and solvent calibration curves was used to suggest ionization suppression. It is worth noting that only in-depth statistical analysis could determine whether two slopes are different.

**LC−MS/MS Conditions.** All sample analyses were performed on a Shimadzu Prominence/20 series (Columbia, MD) liquid chromatograph coupled with an Applied Biosystems (Forest City, CA) 6500 quadrupole linear ion trap (QTrap) mass spectrometer equipped with an electrospray ionization (ESI) interface source. LC separation was achieved using a Phenomenex Kinetex XB-C18 LC column (100 mm × 2.1 mm i.d., 2.6 $\mu$m) and a 10 × 2.1 mm guard cartridge (Torrance, CA). The LC mobile phases consist of 10 mM ammonium formate/0.1% formic acid/water (A) and 10 mM ammonium formate/0.1% formic acid/methanol (B). Gradient elution at 0.3 mL/min flow rate started at 5% B, was ramped to 40% B in 2 min via linear gradient mode and then to 100% B by 9 min via exponential gradient mode (pump B curves 3 to 6), was held for 2.5 min, and was changed to 5% B at 12 min. Total run time was 15 min including 3 min of column conditioning time. Injection volume was 10 $\mu$L, and the column temperature was 40 °C. Ionization source dependent parameters were set as follows: curtain gas (CUR), 30 psi; ion spray voltage, 4,500 V for the positive mode and −4,500 V for the negative mode; nitrogen collision gas (CAD), medium; source temperature (TEM), 500 °C; ion source gases 1 and 2 (GS1 and GS2), each at 60 psi. Resolutions at Q1 and Q3 were set to unit.

Two MRM transitions of each [$^{13}$C]-labeled or native mycotoxin were determined in a previous study[34,35] or generated using direct infusion. All native mycotoxins and [$^{13}$C]-IS were monitored in polarity switching ionization mode. Switching time was 20 ms, scan time was 0.2 s, and the scheduled MRM window was set to 30 s. Zearalenone and [$^{13}$C]-zearalenone were analyzed in the negative mode, and the other mycotoxins and [$^{13}$C]-IS were analyzed in the positive mode. Nitrogen gas (99% purity) was used in the ESI source and the collision cell. The identification of target mycotoxins was based on two specific MRM transitions. Retention time, values of DP, CE, and CXP, and the two selected MRM transitions are listed in Table 1.

## RESULTS AND DISCUSSION

**MS/MS Optimization.** One of the limitations associated with MS/MS analysis is that it is difficult to predict whether a selected MRM transition will be free from coextracted/eluted matrix interferences from food or feed samples. The molecular ions ($[M + H]^+$ or $[M - H]^-$) for all target myxotoxins and [$^{13}$C]-mycotoxins in full-scan MS experiments were determined using positive or negative ionization mode. For each analyte, the two most intense fragments (MRM transitions) were generated and selected using MRM compound optimization tuning. Because these transitions were determined using solvent-only standards, it is possible that MRM transitions may be suppressed due to matrix interferences compromising the sensitivity and specificity needed to identify and quantitate

**Table 3. Recoveries (%) in Grain/Rice/Oatmeal-Based Baby Foods**[a]

| mycotoxin | fortification (ng/g) | grain based | rice based | oatmeal based | av | fortification (ng/g) | grain based | rice based | oatmeal based | ave | fortification (ng/g) | grain based | rice based | oatmeal based | av |
|---|---|---|---|---|---|---|---|---|---|---|---|---|---|---|---|
| aflatoxin $B_1$ | 2 | 104(2) | 103(2) | 101(2) | 103(2) | 10 | 100(2) | 97(2) | 97(2) | 98(2) | 50 | 97(3) | 98(1) | 97(3) | 97(2) |
| aflatoxin $B_2$ | 2 | 101(2) | 100(4) | 99(3) | 100(3) | 10 | 97(2) | 96(2) | 94(4) | 96(3) | 50 | 96(4) | 97(1) | 97(1) | 97(2) |
| aflatoxin $G_1$ | 2 | 105(5) | 106(1) | 107(3) | 106(3) | 10 | 102(3) | 101(3) | 101(1) | 101(2) | 50 | 101(3) | 104(1) | 101(1) | 102(2) |
| aflatoxin $G_2$ | 2 | 104(10) | 106(6) | 104(5) | 104(6) | 10 | 99(3) | 100(4) | 93(3) | 97(4) | 50 | 98(3) | 96(5) | 96(5) | 97(4) |
| deoxynivalenol | 50 | 120(8) | 84(25) | 110(4) | 105(19) | 200 | 106(4) | 96(10) | 94(8) | 99(9) | 1000 | 115(9) | 106(8) | 110(12) | 110(10) |
| fumonisin $B_1$ | 50 | 92(13) | 101(22) | 102(9) | 98(15) | 200 | 75(9) | 106(13) | 82(9) | 88(19) | 1000 | 93(17) | 116(6) | 100(7) | 103(14) |
| fumonisin $B_2$ | 50 | 87(10) | 70(9) | 81(8) | 79(12) | 200 | 82(10) | 76(12) | 74(4) | 77(10) | 1000 | 102(8) | 95(5) | 91(15) | 103(14) |
| fumonisin $B_3$ | 50 | 95(9) | 76(21) | 111(2) | 94(19) | 200 | 78(9) | 74(8) | 71(13) | 75(10) | 1000 | 84(16) | 76(10) | 97(16) | 85(17) |
| ochratoxin A | 20 | 96(3) | 97(4) | 97(5) | 96(4) | 100 | 102(4) | 100(5) | 104(5) | 102(5) | 500 | 100(1) | 103(3) | 105(2) | 102(3) |
| T-2 toxin | 40 | 99(19) | 114(17) | 85(18) | 100(28) | 200 | 80(5) | 91(13) | 84(7) | 85(10) | 1000 | 92(14) | 83(17) | 80(8) | 85(14) |
| zearalenone | 40 | 108(10) | 108(4) | 101(7) | 106(7) | 200 | 101(2) | 102(4) | 102(3) | 102(3) | 1000 | 100(2) | 98(2) | 100(4) | 99(2) |

[a]Each recovery reported as mean (RSD)%. In each matrix, recovery was calculated as the mean value of 4 replicates. Average (av) recovery at each fortification concentration was reported as the mean of the 12 replicates.



**Table 4. Recoveries (%) in Dry Cat/Dog Food and Animal Feed**[a]

| mycotoxin | fortification (ng/g) | animal feed | cat food | dog food | av | fortification (ng/g) | animal feed | cat food | dog food | av | fortification (ng/g) | animal feed | cat food | dog food | av |
|---|---|---|---|---|---|---|---|---|---|---|---|---|---|---|---|
| aflatoxin $B_1$ | 4 | 113(1) | 99(4) | 101(3) | 104(7) | 20 | 104(3) | 101(1) | 100(5) | 102(3) | 100 | 106(4) | 103(2) | 103(3) | 104(3) |
| aflatoxin $B_2$ | 4 | 106(3) | 101(2) | 98(5) | 102(5) | 20 | 101(3) | 102(1) | 102(5) | 102(3) | 100 | 103(3) | 100(2) | 100(2) | 101(3) |
| aflatoxin $G_1$ | 4 | 102(2) | 95(3) | 96(4) | 98(5) | 20 | 101(3) | 99(3) | 99(6) | 100(4) | 100 | 103(1) | 97(5) | 100(2) | 100(4) |
| aflatoxin $G_2$ | 4 | 74(9) | 101(12) | 93(6) | 89(16) | 20 | 74(3) | 115(9) | 101(3) | 97(19) | 100 | 71(9) | 108(4) | 104(8) | 94(20) |
| deoxynivalenol | 100 | 112(5) | 90(6) | 71(4) | 91(20) | 400 | 114(10) | 101(4) | 89(7) | 102(13) | 2000 | 90(10) | 105(5) | 102(9) | 99(10) |
| fumonisin $B_1$ | 100 | 105(9) | 74(11) | 86(23) | 88(20) | 400 | 75(7) | 93(11) | 111(5) | 93(18) | 2000 | 101(4) | 105(16) | 117(7) | 108(11) |
| fumonisin $B_2$ | 100 | 106(4) | 83(5) | 100(8) | 96(12) | 400 | 85(5) | 94(9) | 106(2) | 95(11) | 2000 | 104(6) | 91(8) | 97(15) | 97(11) |
| fumonisin $B_3$ | 100 | 102(3) | 101(27) | 77(19) | 95(21) | 400 | 87(4) | 100(12) | 96(15) | 94(12) | 2000 | 106(5) | 85(4) | 98(21) | 96(15) |
| ochratoxin A | 40 | 81(4) | 108(3) | 117(4) | 102(16) | 200 | 96(6) | 98(3) | 100(3) | 98(4) | 1000 | 99(2) | 100(4) | 104(1) | 101(3) |
| T-2 toxin | 80 | 113(10) | 87(12) | 84(11) | 96(17) | 400 | 88(14) | 102(7) | 110(16) | 100(15) | 2000 | 83(14) | 120(6) | 119(10) | 107(19) |
| zearalenone | 80 | 110(5) | 75(9) | 72(5) | 86(22) | 400 | 93(2) | 103(4) | 97(10) | 98(7) | 2000 | 96(2) | 111(7) | 105(4) | 104(8) |

[a]Each recovery reported as mean (RSD)%. In each matrix, recovery was calculated as the mean value of 4 replicates. Average (av) recovery at each fortification concentration was reported as the mean of the 12 replicates.

dx.doi.org/10.1021/jf503943r | J. Agric. Food Chem. 2014, 62, 8935−8943

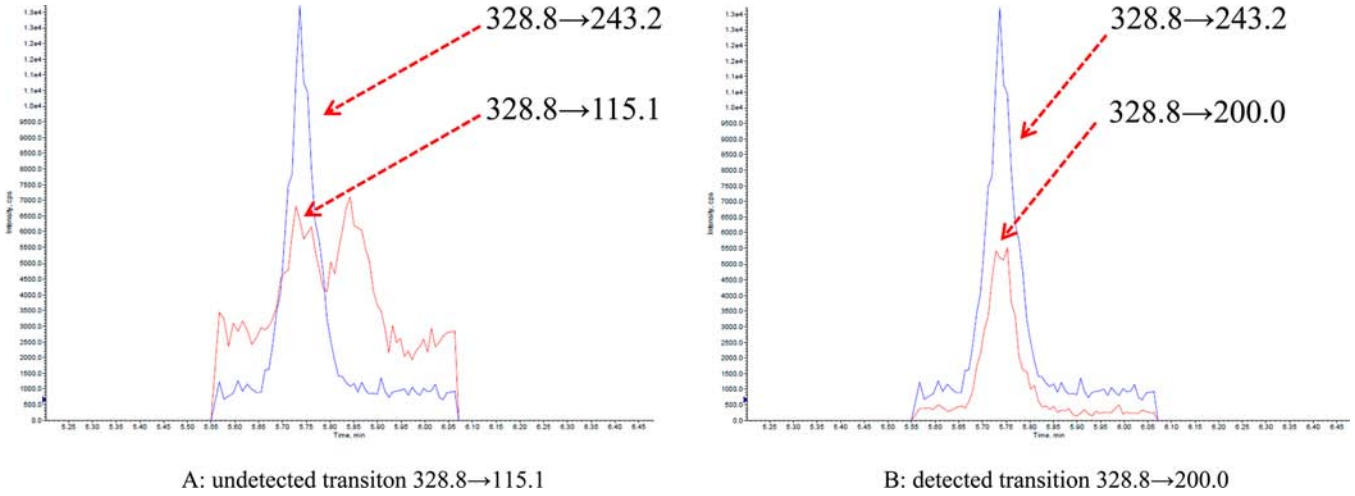


**Figure 1.** Using a different MRM transition for aflatoxin $G_1$ to avoid interference in animal feed samples. A: Undetected transition (328.8 → 115.1) due to interference. B: Detected transition (328.8 → 200.0).

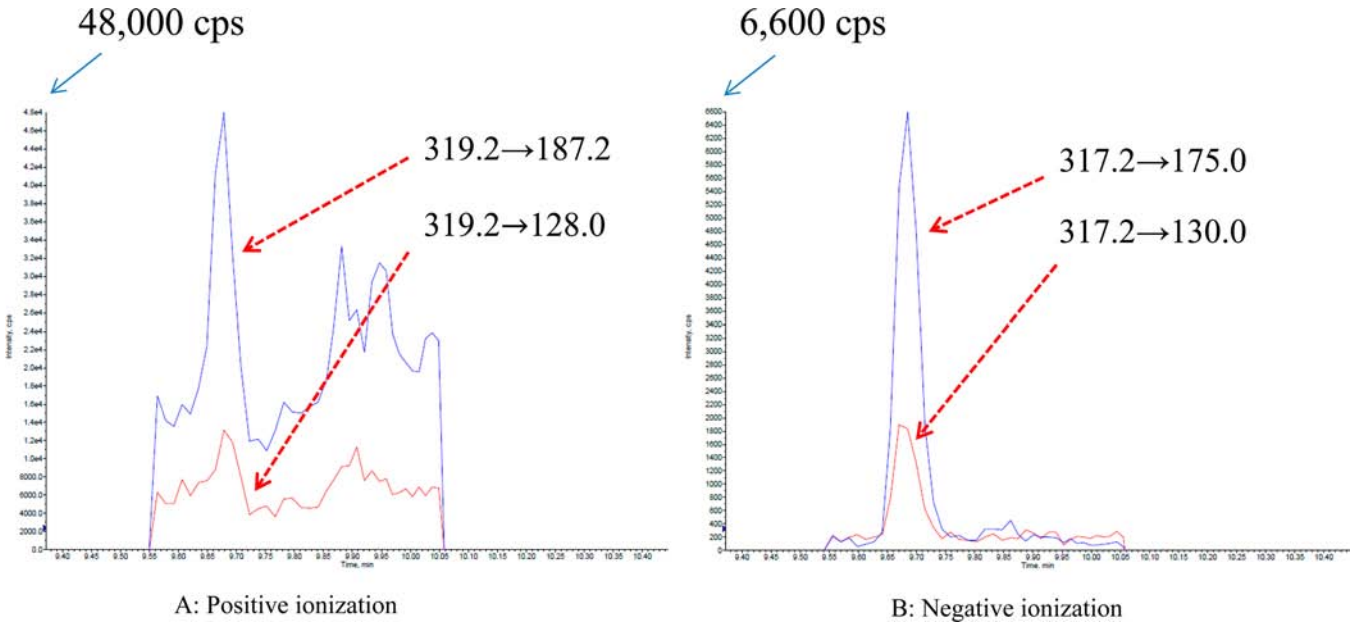


**Figure 2.** Using negative ionization to achieve better S/N for zearalenone (100 ng/g) in animal feed samples. A: Extracted ion chromatogram in positive ionization mode. B: Extracted ion chromatogram in negative ionization mode.

mycotoxins. This is especially true in complex matrices prepared without using extensive sample cleanup. In the course of developing the method, some MRM transitions such as 319.2 $m/z$ → 128.0 $m/z$ of zearalenone and 328.8 $m/z$ → 115.1 $m/z$ of aflatoxin $G_1$ became difficult to monitor in some animal feed samples, though they worked well in solvent or baby food matrices. Because of this, the method was modified to use different MRM transitions (328.8 $m/z$ → 200.0 $m/z$) for aflatoxin $G_1$ and using negative ionization mode to monitor zearalenone. This modification allowed the two mycotoxins to be unambiguously identified in animal feed samples. Figure 1 shows that the new transition (328.8 $m/z$ → 200.0 $m/z$) of aflatoxin $G_1$ can be clearly detected in the same animal feed samples. Under positive ionization mode, the absolute signal intensity of zearalenone is higher than that under negative ionization mode, but the sensitivity (single-to-noise ratio) was offset by the corresponding high background noise caused by coeluted matrix components. The second transition was barely detected. Switching to negative ionization mode produced a much cleaner background, and even though the absolute signal intensity of zearalenone decreased, the resulting signal-to-noise became sufficient for identification and quantitation (Figure 2).

**Matrix Effects.** For this study slope ratios between matrix-matched calibration curves and solvent calibration curves were used to graphically suggest matrix effects in the test samples. If the suppression or enhancement is marginal, the ratio (matrix-matched/solvent-only standard) would equal or be very close to 1.00; if there is severe suppression/enhancement, the ratio would deviate from one. Specifically, using [$^{13}$C]-IS, the ratios of the 11 mycotoxins in the six tested matrices center toward 1.00, ranging from 0.86 (aflatoxin $G_2$ in animal feed extract) to 1.09 (ochratoxin A in grain-based baby food extract) as illustrated in Figure 3. As previously discussed, [$^{13}$C]-IS and the unlabeled mycotoxins undergo the same ionization conditions, and therefore the coeluted matrix components have the same impact on a target mycotoxin and its [$^{13}$C]-IS during ionization.


dx.doi.org/10.1021/jf503943r | J. Agric. Food Chem. 2014, 62, 8935−8943

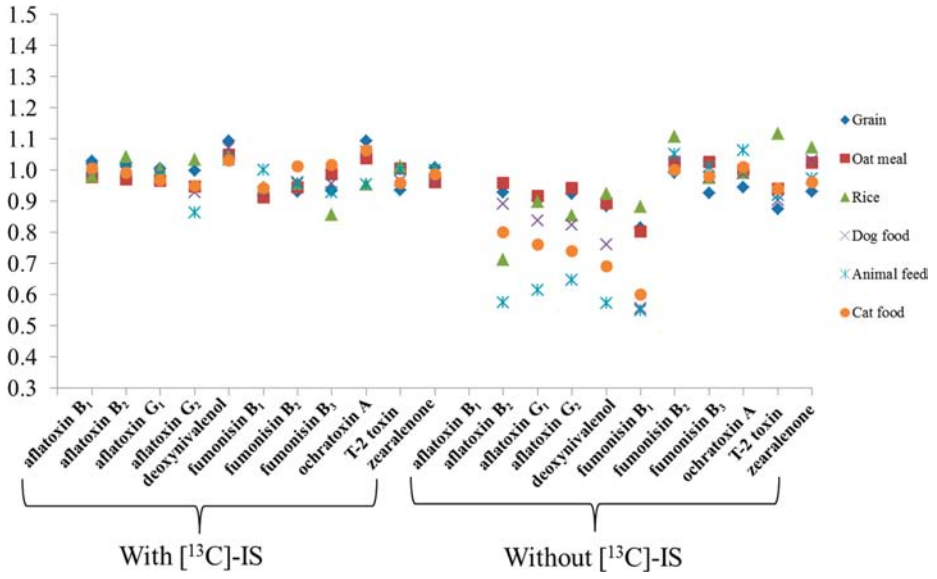


**Figure 3.** Slope ratios of matrix-matched and solvent calibration curves used to suggest matrix effects in baby food and animal feed matrices.

Therefore, if a calibration curve is established using relative responses of the mycotoxin and [$^{13}$C]-IS, the matrix suppression would be corrected. True matrix suppression or enhancement on the calibration curves can only be demonstrated by statistically evaluating the difference between the slopes and using the standard error of the slopes. However, here we have calculated a slope ratio to graphically suggest matrix effects in the different test samples (Figure 3). For example, without using [$^{13}$C]-aflatoxin $B_1$, the average slope ratio of aflatoxin $B_1$ in the six matrices is 0.81 with a RSD of 18%; while using [$^{13}$C]-aflatoxin $B_1$, the average ratio is 1.01 with a RSD of 2%. The same pattern is clearly observed for the other mycotoxins. These results emphasize the unpredictable and complex nature of matrix suppressions that would affect quantitation in the course of LC−MS/MS analysis, although it is well-known that matrix suppressions are determined by various factors such as physicochemical properties of target matrices and mycotoxin, sample preparation procedures, LC separation conditions, and MS ionization. There are no universal sample cleanup procedures, LC separation programs, or ionization sources that can eliminate/separate coeluted matrix interferences for these target mycotoxins. A common practice is to use matrix-matched calibration standards. It would be a heavy burden for researchers to find blank matrices and prepare matrix-matched calibration standards when analyzing multiple mycotoxins in a wide range of matrices, which has been the bottleneck for routine mycotoxin analysis that compromises sample throughput and increases labor cost per sample. Obviously, the use of [$^{13}$C]-IS eliminated the need for matrix-matched calibration standards for quantitation in this study, achieving satisfactory accuracy and precision in an efficient manner. If such a practice could be adopted for routine mycotoxin analysis, the corresponding sample throughput would be improved with ensured data quality.

**Matrix-Dependent LOQs and Recovery Studies.** It is important to determine the LODs/LOQs in an objective manner by factoring in the impact of matrix interferences and background noise. Whether the stable isotope dilution approach can be successfully applied for mycotoxin analysis is determined by the detectability of the native mycotoxins and their [$^{13}$C]-IS. Therefore, we chose to use the matrix-matched calibration standards at realistic low concentrations to estimate the instrument LODs/LOQs. This way we would be able to find out the instrument performance in terms of the sensitivity in the presence of matrix components without overestimating or underestimating the sensitivity of the 11 target mycotoxins. Generally, LODs and LOQs are estimated using signal-to-noise (S/N) ratio (e.g., LOD = 3 × S/N and LOQ = 10 × S/N), but in extracted ion chromatograms, there is little or no background noise, making it difficult to accurately assess the sensitivity of target mycotoxins. Based on a well-established EPA protocol,[36] the LOQs of the 11 mycotoxins were determined by measuring the standard deviations of repeat injections of matrix-matched calibration standards at low concentrations. The LOQs were statistically estimated using a predefined confidence interval (e.g., 99%). Estimated LOQs ranged from 0.02 ng/g (aflatoxin $B_1$ in rice-based baby food) to 8.3 ng/g (deoxynivalenol in animal feed) (Table 2).

The major interferences in cereal-based baby food and animal feed matrices could be fat, proteins, and fibers. Complete separation of target mycotoxins with low concentrations from these matrix components would require extraction, solvent exchange, defatting, and extensive cleanup procedures. The diversity of physicochemical properties of the 11 target mycotoxins further complicates the selection of extraction and cleanup procedures.[13,14,37] Because quantitation was achieved based on the relative response between fortified [$^{13}$C]-IS and mycotoxins, only a simple dilution and filtration was used to prepare our samples. As long as a fortified [$^{13}$C]-IS and its native counterpart reached equilibration in extraction solvent and sample, the accuracy and precision would be maintained.[28] Recoveries at three fortification concentrations in the six selected matrices are listed in Tables 3 and 4. The majority of the recoveries are in the range of 70−120% with RSDs less than 20%. Obviously, using [$^{13}$C]-IS enabled us to achieve the confidence in quantitative analysis via a simple sample preparation. It is worth noting that at the lowest fortification concentration, 4 ng/g, aflatoxin $G_2$'s recoveries in all pet food and feed matrices are just around 70%, which is much lower than those of the other three aflatoxins. It is speculated that the ion suppression caused the signal intensity of aflatoxin $G_2$ to approach the detection limit, leading to the


dx.doi.org/10.1021/jf503943r | J. Agric. Food Chem. 2014, 62, 8935−8943

Table 5. Detected Mycotoxins in Animal Feed Samples (Av ± SD[a], ng/g)

| mycotoxin | cattle feed | cat food | cotton seed meal | DDGs | fish feed | hog feed | poultry feed | sheep feed |
|---|---|---|---|---|---|---|---|---|
| aflatoxin $B_1$ | <LOQ | 5 ± 0.1 | 0.3 ± 0.02 | 5.0 ± 0.2 | 3.0 ± 0.1 | 0.3 ± 0.01 | 0.3 ± 0.02 | 0.4 ± 0.02 |
| aflatoxin $B_2$ | | 1 ± 0.1 | | | 0.3 ± 0.01 | | | |
| aflatoxin $G_1$ | | | | | | | | |
| aflatoxin $G_2$ | | | | | | | | |
| deoxynivalenol | 1779 ± 77 | | 496 ± 65 | 2732 ± 446 | 78 ± 24 | 2247 ± 330 | 62 ± 6 | 1242 ± 79 |
| fumonisin $B_1$ | 214 ± 26 | <LOQ | 184 ± 51 | 2280 ± 288 | 116 ± 6 | 354 ± 30 | 180 ± 22 | 65 ± 4 |
| fumonisin $B_2$ | 51 ± 2 | | 48 ± 10 | 358 ± 29 | 28 ± 1 | 112 ± 5 | 39 ± 8 | 23 ± 2 |
| fumonisin $B_3$ | 35 ± 4 | | 19 ± 4 | 139 ± 28 | 16 ± 2 | 35 ± 1 | | 9 ± 1 |
| ochratoxin A | | <LOQ | 2.0 ± 0.4 | 5 ± 1 | <LOQ | | | 1 ± 0.1 |
| T-2 toxin | 67 ± 26 | | 6 ± 1 | 34 ± 3 | 15 ± 4 | 10 ± 2 | | |
| zearalenone | 66 ± 30 | | 14 ± 2 | 109 ± 8 | 65 ± 6 | 71 ± 7 | | 15 ± 1 |

[a]Average of three replicates; nondetected mycotoxins were left blank.

low recoveries. Further studies need to be conducted to better understand the observation.

**Sample Analysis.** Two reference materials (animal feed) were analyzed to demonstrate the accuracy of the stable isotope dilution and LC−MS/MS method. In sample ERM-BE375, aflatoxins $B_1$ and $B_2$ were detected at 2.4 ± 0.2 ng/g (reference value: 2.6 ± 0.4 ng/g) and <LOQ (reference value: 0.2 ± 0.04 ng/g). Aflatoxins $G_1$ and $G_2$ (reference values: 0.4 ± 0.1 and <0.2 ng/g) were not detected. The current FDA action concentration for aflatoxins is 20 ng/g, and so we did not further modify our method to be able to detect aflatoxin $G_1$ or $G_2$ at these sub ng/g concentrations. The performance of the method was ensured with the detection of [$^{13}$C]-aflatoxins $B_1$, $B_2$, $G_1$, and $G_2$ around 0.5 ng/g in the same sample. For sample ERM-BE376, the detected concentrations of aflatoxins $B_1$, $B_2$, and $G_1$ were 11.8 ± 1.0 ng/g (reference value: 12.9 ± 1.8 ng/g), 0.69 ± 0.1 (0.68 ± 0.1 ng/g), and 4.9 ± 0.3 ng/g (reference value: 5.2 ± 0.8 ng/g). Aflatoxin $G_2$ was not detected, and no reference value was provided.

Previous studies have reported the presence of various mycotoxins in baby foods.[15,38] In order to determine applicability, the method was used to analyze market samples of baby food and animal feed (Table 5) as described in the Materials and Methods. In the 10 domestic grain/oatmeal/rice-based baby food samples, no mycotoxins were detected. Deoxynivalenol was detected in 4 out of the 7 rice/corn-based baby food samples collected from foreign countries, ranging from 46 ± 10 to 877 ± 57 ng/g (mean ± SD, $n$ = 3). Trace amounts of aflatoxin $B_1$, ochratoxin A, and zearalenone were detected in the foreign baby food samples as well, but the corresponding concentrations are lower than the method LOQs. Co-occurrence of multiple mycotoxins (including aflatoxins, fumonisins, and zearalenone) was observed in 2 of the 7 foreign baby food samples. No reported concentrations were above the FDA action or advisory concentrations. Mold contamination in rice and corn has been a persistent health issue, so it is not surprising to detect deoxynivalenol, fumonisins, or the other mycotoxins in related food products.

Multiple mycotoxins were detected in every animal feed or feed ingredient sample analyzed in this study. Except for aflatoxins $G_1$ and $G_2$, the other 9 mycotoxins were detected ranging from <LOQ to 5 ng/g for aflatoxin $B_1$, 0.3−1 ng/g for aflatoxin $B_2$, 62−2732 ng/g for deoxynivalenol, <LOQ to 2280 ng/g for fumonisin $B_1$, <LOQ to 5 ng/g for ochratoxin A, 6−67 ng/g for T−2 toxin, and 14−109 ng/g for zearalenone. The formulations of animal feed are complex and diverse,[18,39] and some of the major ingredients used for animal feed, such as distiller's dry grains (DDGs) or cotton seed meal, are prone to mold contamination.[20,40] Although the individual concentration of each detected mycotoxin is lower than FDA action or advisory levels, the health effects, if any, associated with cocontamination, additive toxicity, or other synergic effects of these mycotoxins in feeds are poorly understood.

In summary, a stable isotope dilution and LC−ESI-MS/MS method was developed that allowed for the simultaneous quantification of 11 mycotoxins of regulatory significance for the purpose of screening for these toxic compounds in cereal-based baby foods, dry cat/dog food, and animal feeds. Validation parameters were established in accordance with FDA method validation guidelines for sensitivity, accuracy, precision, and recovery. The method was applied to certified animal feed reference materials as well as baby food and feed samples collected from markets, showing that the method achieved identification and quantitation in a quick, easy, and reliable manner without using extensive sample cleanup or matrix-matched calibration. The method could be modified for application to other food matrices. Further applications of this stable isotope dilution mass spectrometry method for the analysis of multiple mycotoxins in other food matrices such as spices and dry botanicals are currently under way.

## AUTHOR INFORMATION


### Corresponding Author

*Tel: 240-402-2318. E-mail: kai.zhang@fda.hhs.gov.


### Notes

The authors declare no competing financial interest.

## REFERENCES


(1) Fink-Gremmels, J. Mycotoxins in cattle feeds and carry-over to dairy milk: A review. *Food Addit. Contam., Part A* **2008**, *25*, 172−180.

(2) Miller, J. D., Trenholm, H. L., Eds. Myotoxins in Grain. Compounds Other Than Aflatoxins, 2nd ed.; Eagan Press: St. Paul, MN, 1997.

(3) Sweeney, M. J.; Dobson, A. D. W. Mycotoxin production by *Aspergillus, Fusarium* and *Penicillium* Species. *Int. J. Food Microbiol.* **1998**, *43*, 141−158.

(4) Newberne, P. M. Mycotoxins: toxicity, carcinogenicity, and the influence of various nutritional conditions. *Environ. Health Perspect.* **1974**, *9*, 1−32.

(5) Stoev, S. D. Food Safety and Increasing Hazard of Mycotoxin Occurrence in Foods and Feeds. *Crit. Rev. Food Sci. Nutr.* **2013**, *53*, 887−901.

(6) Marin, S.; Ramos, A. J.; Cano-Sancho, G.; Sanchis, V. Mycotoxins: occurrence, toxicology, and exposure assessment. *Food Chem. Toxicol.* **2013**, *60*, 218−237.

(7) FAO 2004. Food and Agriculture Organization of the United Nations, Worldwide regulations for mycotoxins in food and feed 2003. FAO Food and Nutrition Paper.
(8) FDA Compliance Program Guidance Manual. Chapter 07 – Molecular Biology and Natural Toxins – Mycotoxins in Domestic and Imported Foods. http://www.fda.gov/downloads/Food/ComplianceEnforcement/ucm073294.pdf. Feed Contaminants Program. http://www.fda.gov/downloads/AnimalVeterinary/GuidanceComplianceEnforcement/ComplianceEnforcement/UCM113409.pdf. (Accessed February 28, 2014.)
(9) Bennett, A. G.; Nelsen, T. C.; Miller, B. M. Enzyme-linked immunosorbent assay for detection of zearalenone in corn, wheat, and pig feed: collaborative study. *J. AOAC Int.* **1994**, *77*, 1500–1505.
(10) Gimeno, A. Thin layer chromatographic determination of aflatoxins, ochratoxins, sterigmatocystin, zearalenone, citrinin, T-2 toxin, diacetoxyscirpenol, penicillic acid, patulin, and penitrem A. *J. Assoc. Off. Anal. Chem.* **1979**, *62*, 579–585.
(11) Stroka, J.; von Holst, C.; Anklam, E.; Reutter, M. Immunoaffinity Column Cleanup with Liquid Chromatography Using Post-Column Bromination for Determination of Aflatoxin B1 in Cattle Feed: Collaborative Study. *J. AOAC Int.* **2003**, *86*, 1179–1186.
(12) Brera, C.; Debegnach, F.; De Santis, B.; Pannunzi, E.; Berdini, C.; Prantera, E.; Gregori, E.; Miraglia, M. Simultaneous determination of aflatoxins and ochratoxin A in baby foods and paprika by HPLC with fluorescence detection: a single-laboratory validation study. *Talanta* **2010**, *83*, 1442–1446.
(13) *AOAC 994.08. Official Methods of Analysis of AOAC International*, 17th ed.; AOAC: Washington, DC, 2000; Chapter 49, pp 26–27.
(14) Romer, T. R. Use of small charcoal/alumina cleanup columns in determination of trichothecene mycotoxins in foods and feeds. *J. Assoc. Off. Anal. Chem.* **1986**, *69*, 699–703.
(15) Lombaert, G. A.; Pellaers, P.; Roscoe, V.; Mankotia, M.; Neil, R.; Scott, P. M. Mycotoxins in infant cereal foods from the Canadian retail market. *Food Addit. Contam.* **2003**, *20*, 494–504.
(16) Tavares, A. M.; Alvito, P.; Loureiro, S.; Louro, H.; Silva, M. J. Multi-mycotoxin determination in baby foods and in vitro combined cytotoxic effects of aflatoxin $M_1$ and ochratoxin A. *World Mycotoxin J.* **2013**, *6*, 375–388.
(17) Juan, C.; Raiola, A.; Mañes, J.; Ritien, A. Presence of mycotoxin in commercial infant formulas and baby foods from Italian market. *Food Control.* **2014**, *39*, 227–236.
(18) Wood, G. E. Mycotoxins in foods and feeds in the United States. *J. Anim. Sci.* **1992**, *70*, 3941–3949.
(19) Streit, E.; Schatzmayr, G.; Tassis, P.; Tzika, E.; Marin, D.; Taranu, I.; Tabuc, C.; Nicolau, A.; Aprodu, I.; Puel, O.; Oswald, I. P. Current situation of mycotoxin contamination and co-occurrence in animal feed–focus on Europe. *Toxins* **2012**, *4*, 788–809.
(20) Streit, E.; Schwab, C.; Sulyok, M.; Naehrer, K.; Krska, R.; Schatzmayr, G. Multi-Mycotoxin Screening Reveals the Occurrence of 139 Different Secondary Metabolites in Feed and Feed Ingredients. *Toxins* **2013**, *5*, 504–523.
(21) Sulyok, M.; Krska, R.; Schuhmacher, R. A liquid chromatography/tandem mass spectrometric multi-mycotoxin method for the quantification of 87 analytes and its application to semi-quantitative screening of moldy food samples. *Anal. Bioanal. Chem.* **2007**, *389*, 1509–1523.
(22) Spanjer, M. C.; Rensen, P. M.; Scholten, J. M. LC-MS/MS multi-method for mycotoxins after single extraction, with validation data for peanut, pistachio, wheat, maize, cornflakes, raisins and figs. *Food Addit. Contam., Part A* **2008**, *25*, 472–489.
(23) Mol, H. G.; Plaza-Bolaños, P.; Zomer, P.; de Rijk, T. C.; Stolker, A. A.; Mulder, P. P. Toward a generic extraction method for simultaneous determination of pesticides, mycotoxins, plant toxins, and veterinary drugs in feed and food matrixes. *Anal. Chem.* **2008**, *80*, 9450–9499.
(24) Liao, C. D.; Wong, J. W.; Zhang, K.; Hayward, D. G.; Lee, N. S.; Trucksess, M. W. Multi-mycotoxin analysis of finished grain and nut products using high-performance liquid chromatography-triple-quadrupole mass spectrometry. *J. Agric. Food Chem.* **2013**, *61*, 4771–4782.
(25) Marschik, S.; Hepperle, J.; Lauber, U.; Schnaufer, R.; Maier, S.; Kühn, C.; Schwab-Bohnert, G. Extracting fumonisins from maize: efficiency of different extraction solvents in multi-mycotoxin analytics. *Mycotoxin Res.* **2013**, *29*, 119–129.
(26) Lattanzio, V. M. T.; Solfrizzo, M.; Powers, S.; Visconti, A. Simultaneous determination of aflatoxins, ochratoxin A and *Fusarium* toxins in maize by liquid chromatography/tandem mass spectrometry after multitoxin immunoaffinity cleanup. *Rapid Commun. Mass Spectrom.* **2007**, *21*, 3253–3261.
(27) Stahnke, H.; Kittlaus, S.; Kempe, G.; Alder, L. Reduction of matrix effects in liquid chromatography–electrospray ionization–mass spectrometry by dilution of the sample extracts: how much dilution is needed? *Anal. Chem.* **2012**, *84*, 1474–1482.
(28) Fassett, J. D.; Powell, L. J.; Moore, L. J. Determination of iron in serum and water by resonance ionization isotope dilution mass spectrometry. *Anal. Chem.* **1984**, *56*, 2228–2233.
(29) Krynitsky, A. J.; Niemann, R. A.; Nortrup, D. A. Determination of perchlorate anion in foods by ion chromatography-tandem mass spectrometry. *Anal. Chem.* **2004**, *76*, 5518–5522.
(30) Hao, C.; Zhao, X.; Tabe, S.; Yang, P. Optimization of a multiresidual method for the determination of waterborne emerging organic pollutants using solid-phase extraction and liquid chromatography/tandem mass spectrometry and isotope dilution mass spectrometry. *Environ. Sci. Technol.* **2008**, *42*, 4068–4075.
(31) Li, W.; Herrman, T. J.; Dai, S. Y. Determination of aflatoxins in animal feeds by liquid chromatography/tandem mass spectrometry with isotope dilution. *Rapid Commun. Mass Spectrom.* **2011**, *25*, 1222–1230.
(32) Varga, E.; Glauner, T.; Köppen, R.; Mayer, K.; Sulyok, M.; Schuhmacher, R.; Krska, R.; Berthiller, F. Stable isotope dilution assay for the accurate determination of mycotoxins in maize by UHPLCMS/MS. *Anal. Bioanal. Chem.* **2012**, *402*, 2675–2686.
(33) Al-Taher, F.; Banaszewski, K.; Jackson, L.; Zweigenbaum, J.; Ryu, D.; Cappozzo, J. Rapid method for the determination of multiple mycotoxins in wines and beers by LC-MS/MS using a stable isotope dilution assay. *J. Agric. Food Chem.* **2013**, *61*, 2378–2384.
(34) Zhang, K.; Wong, J. W.; Hayward, D. G.; Vaclavikova, M.; Liao, C. D.; Trucksess, M. W. Determination of mycotoxins in milk-based products and infant formula using stable isotope dilution assay and liquid chromatography tandem mass spectrometry. *J. Agric. Food Chem.* **2013**, *61*, 6265–6273.
(35) Zhang, K.; Wong, J. W.; Jia, Z.; Vaclavikova, M.; Trucksess, M. W.; Begley, T. H. Screening multimycotoxins in food-grade gums by stable isotope dilution and liquid chromatography/tandem mass spectrometry. *J. AOAC Int.* **2014**, *97* (3), 889–895.
(36) Title 40. Protection of the Environment. Part 136. Guidelines establishing test procedures for the analysis of pollutants. *Appendix B: Definition and Procedure for the Determination of the Method Detection Limit Revision 1.11*; Code of Federal Regulations; U.S. Government Printing Office: Washington, DC, 2010.
(37) D'Arco, G.; Fernández-Franzón, M.; Damiani, P.; Mañes, J. Analysis of fumonisins B1, B2 and B3 in corn-based baby food by pressurized liquid extraction and liquid chromatography/tandem mass spectrometry. *J. Chromatogr. A* **2008**, *1209*, 188–194.
(38) Trucksess, M. W.; Dombrink-Kurtzman, M. A.; Tournas, V. H.; White, K. D. Occurrence of aflatoxins and fumonisins in Incaparina from Guatemala. *Food Addit. Contam.* **2002**, *19*, 671–675.
(39) Zhang, Y. H.; Caupert, J. Survey of Mycotoxins in U.S. Distiller's Dried Grains with Solubles from 2009 to 2011. *J. Agric. Food Chem.* **2012**, *60*, 539–543.
(40) Sapkota, A. R.; Lefferts, L. Y.; McKenzie, S.; Walker, P. What Do We Feed to Food-Production Animals? A Review of Animal Feed Ingredients and Their Potential Impacts on Human Health. *Environ. Health Perspect.* **2007**, *115*, 663–670.

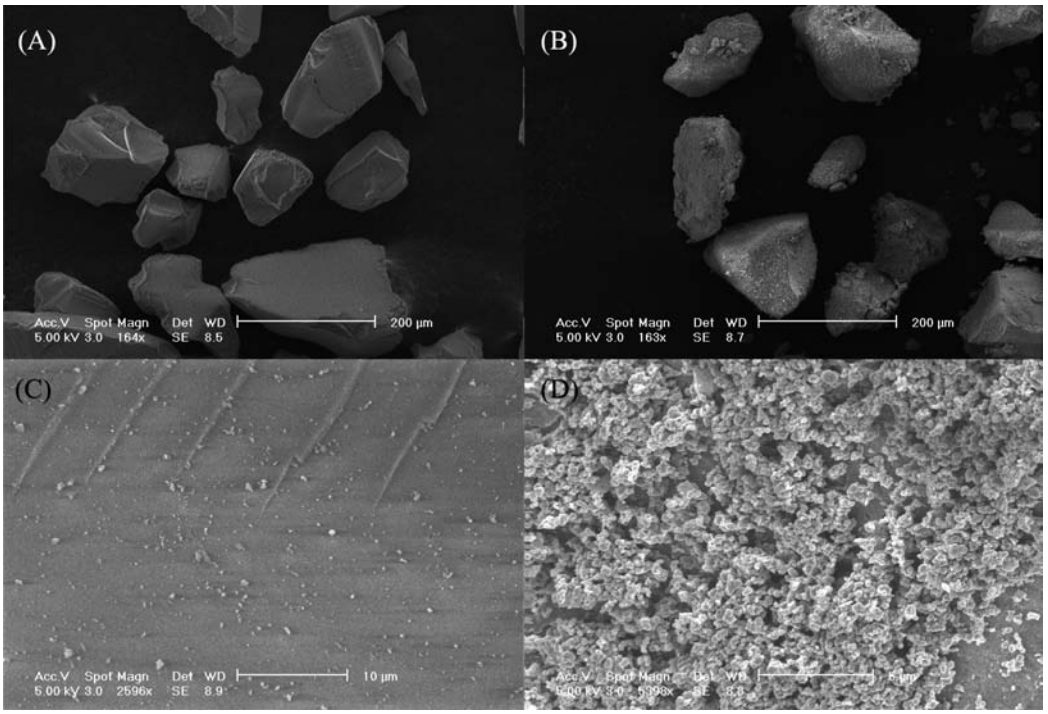


**Figure 1.** SEM images of (A) $SiO_2$, (B) $TiO_2/SiO_2$ composites, (C) expanded view of $SiO_2$, and (D) expanded view of $TiO_2/SiO_2$ composites.

(GC), coupling with a flame ionization detector (FID) or mass spectrometer (MS).[14−16] $^{31}P$ NMR spectroscopy was reported to be convenient for the routine analysis of phospholipids from biological sources.[17] Along with the rapid development of soft ionization techniques, such as electrospray ionization (ESI) or matrix-assisted laser desorption and ionization time-of-flight (MALDI-TOF), mass spectrometry also became applicable to lipid analysis.[18,19] Han et al. developed a multidimensional mass spectrometry (MDMS)-based shotgun lipidomics method for comprehensively profiling lipids in biological samples.[20] Verardo et al. used HILIC and MS for the determination of phospholipids in virgin olive oil.[21] Jackson et al. successfully employed MALDI-TOF/MS and MALDI ion mobility (IM)-TOF/MS for direct analysis of phospholipids in rat brain tissue.[22]

In this study, we aimed to establish an efficient method for selective extraction of phospholipids from a complex shrimp waste sample (cephalothorax). Titania-coated silica ($TiO_2/SiO_2$) core−shell composites were synthesized and used as the sorbent for homemade solid-phase extraction (SPE) cartridge. The eluates were analyzed by a hydrophilic interaction chromatography (HILIC) coupled with quadrupole time-of-flight tandem mass spectrometry (QTOF/MS/MS).

## MATERIALS AND METHODS

**Chemicals and Regents.** Phospholipid standards, including phosphatidylcholine (PC, 14:0/14:0), phosphatidylethanolamine (PE, 15:0/15:0), phosphatidylinositol (PI, 16:0/16:0), and phosphotidylserine (PS, 14:0/14:0), were obtained from Avanti Polar Lipids, Inc. (Alabaster, AL) and prepared in solvents to a final concentration of 1 $\mu g\ mL^{-1}$. Titanium butoxide, chloroform, ethanol, and methanol were purchased from Fisher Scientific (Waltham, MA). Titanium dioxide and silica were purchased from Aladdin (Shanghai, China). Water with a resistivity of 18 MΩ cm was purified by a Milli-Q system from Millipore (Billerica, MA). Other chemicals and solvents were in the highest quality without additional purification unless specified otherwise.

**$TiO_2/SiO_2$ Synthesis.** $TiO_2/SiO_2$ composite was synthesized through a water-vapor-induced internal hydrolysis method with modification. Briefly, 3.5 g of titanium butoxide was dissolved in 14 mL of ethanol. The mixture was sealed, vortexed, and heated to 60 °C. A mass of 8 g of silica was added to the mixture under stirring until dryness. The obtained solid material was stored at 100 °C for 6 h. Afterward, 1 g of titania-precursor-loaded silica was placed in an open glass vial and kept inside an autoclave containing 20 mL of water at 60 °C for 5 h. Subsequently, the power was dried completely at room temperature and calcined under air at 500 °C for 5 h. Finally, 10 wt % $TiO_2/SiO_2$ composites were obtained.

**Sample Preparation.** Fresh shrimp was collected from a local market and well-stored at −20 °C in the Laboratory of Natural Products, City University of Hong Kong. The cephalothorax of shrimp was separated from muscles, rinsed with cold distilled water, and homogenized. A mass of 0.1 g of shrimp waste sample was accurately weighted, placed in a 5 mL polytetrafluoroethylene tube, mixed with 2 mL of $CHCl_3$/MeOH (2:1, v/v) solution, and extracted by an ultrasonic cleaning device for 15 min. Then, a potion of 2 mL of water was added, and the sample tube was centrifuged at 8000*g* for 10 min. The lower organic phase was recovered, and the aqueous phase was re-extracted with 2 mL of $CHCl_3$ for another 2 times, as described before. The collected organic phase were combined and evaporated under nitrogen flow. To minimize the risk of oxidation of the polyunsaturated fatty acids or lipid hydrolysis during the process of isolation, it is always recommended that the extractions process of lipids should be completed at a low temperature (4 °C) as soon as possible after collecting the cephalothorax of shrimp from a living shrimp body.

**SPE Procedure.** A mass of 150 mg of $TiO_2/SiO_2$ composite was packed into a 1 mL syringe. Polypropylene materials were set as frits at both sides to hold the sorbent (a bed of 0.6 cm height of $TiO_2/SiO_2$ was obtained). Before use, the homemade SPE cartridge was preconditioned and activated by washing with 3.0 mL of methanol and water (pH 5), respectively. The crude extract was loaded on and passed through the cartridge at a flow rate of 0.2 mL $min^{-1}$. Then, the cartridge was washed with 10% aqueous methanol to remove the matrix. After that, the analytes retained on the SPE sorbent were eluted with 1 mL of mixture of chloroform and methanol (1:2). The


dx.doi.org/10.1021/jf503040p | J. Agric. Food Chem. 2014, 62, 8944−8951

eluent was dried and redissolved in aqueous methanol for HILIC–QTOF/MS.

**HILIC–QTOF/MS Analysis.** Liquid chromatographic experiments were on an Agilent 1100 LC system, equipped with a quaternary pump and degasser, thermostatic autosampler (4 °C), and column compartment (50 °C). A YMC Triart diol HILIC column (4.6 × 250 mm, 3 μm) was employed for the chromatographic separation. The column was operated under gradient conditions with mobile phase A, 53 mM formic acid in ACN (pH ca. 4.0–4.5), and mobile phase B, 60 mM ammonium formate and 53 mM formic acid in water (pH ca. 3.6). The binary gradient program consisted of 0–15 min, 2% A (and 98% B); 15–60 min, from 2 to 40% A; 60–70 min, 40% A; and 70–80 min, from 40 to 2% A. The flow rate was set at 200 μL $min^{-1}$.

QTOF/MS was performed using a QSTAR mass spectrometer (AB Sciex, Foster City, CA) equipped with a TurboIonSpray source. Mass calibration and optimization of instrumental parameters were performed using a mixture of phospholipid standards dissolved in methanol at a flow rate of 10 μL $min^{-1}$. The TurboIonSpray source worked in negative-ion and full-spectrum mode. Mass spectra were acquired over the $m/z$ 400–2000 range at a scan rate of 1 s per spectrum. The optimized parameters were as follows: declustering potential (DP), 50 V; focusing potential (FP), 200 V; turbo ionspray voltage, 4500 V; declustering potential 2 (DP2), 10 V; gas source 1 (GS1), 50 psi; gas source 2 (GS2), 45 psi; curtain gas (CUR), 40 psi; and temperature (TEM), 400 °C. A collision energy (CE) of 20 V was applied to obtain MS/MS spectrum for the product ion scan (PIS). All of the acquisition and data analyses were performed using Analyst QS version 2.0 (AB Sciex, Foster City, CA).

## RESULTS AND DISCUSSION

**Characterization of $TiO_2/SiO_2$ Composites.** The scanning electron microscopy (SEM) characteristic of the silica gel and $TiO_2/SiO_2$ composites are shown in Figure 1. Before titania coating, the surface of silica gel was smooth and solid, as shown in panels A and B of Figure 1. After synthesis, a porous surface could be clearly observed (Figure 1C), and the shell was constructed by numerous $TiO_2$ microspheres (Figure 1D). All of these characteristics indicated that the $TiO_2/SiO_2$ composites were potential sorbents for selective enrichment and separation of phospholipids from the shrimp waste sample.

**SPE Parameter Optimization.** The efficiency of sample preparation and the cleanness of phospholipid extracts depend upon the factors of the SPE procedure, including sample loading, matrix washing, and analyte recovering. Therefore, the $TiO_2/SiO_2$-based SPE optimization was carried out by sequential selection of the pH conditions of the loading solvent, the polarity of the washing solvent, and the type and amount of eluting solvents, to achieve extracts with the highest recovery and the lowest amount of the matrix effect. The optimization experiments were performed using homemade SPE tubes packing with $TiO_2/SiO_2$ core–shell composites and a standard solution containing PC (14:0/14:0), PE (15:0/15:0), PI (16:0/16:0), and PS (14:0/14:0) at a concentration of 1000 ng $mL^{-1}$ each in methanol.

The retention behavior of phospholipids on $TiO_2/SiO_2$ composites is governed by their chemical properties and ionization state. Therefore, the pH value of loading solvents is important for the quantitative recoveries of phospholipids during the SPE procedure by influence of the interaction between the phospholipids and $TiO_2/SiO_2$ composites. There are studies reporting that phosphonate and phosphate moieties confer high affinity to $TiO_2$ under acidic pH, and the most favorable bonding mode is bidentate, involving two oxygen atoms in each bond.[23] Consequently, the adsorption capability of $TiO_2/SiO_2$ composites was tested by varying the pH from 2 to 9. The results were depicted in Figure 2A, and it can be found that the acidic condition is obviously better than the alkaline condition. The recoveries of the four standards decreased dramatically when the pH was increased to 8. Meanwhile, an extreme acidic condition is also not applicable because the signals of phospholipids are unstable and suppressed in the negative-ion mode. Finally, pH 5 was used, and maximal peak areas are acquired.

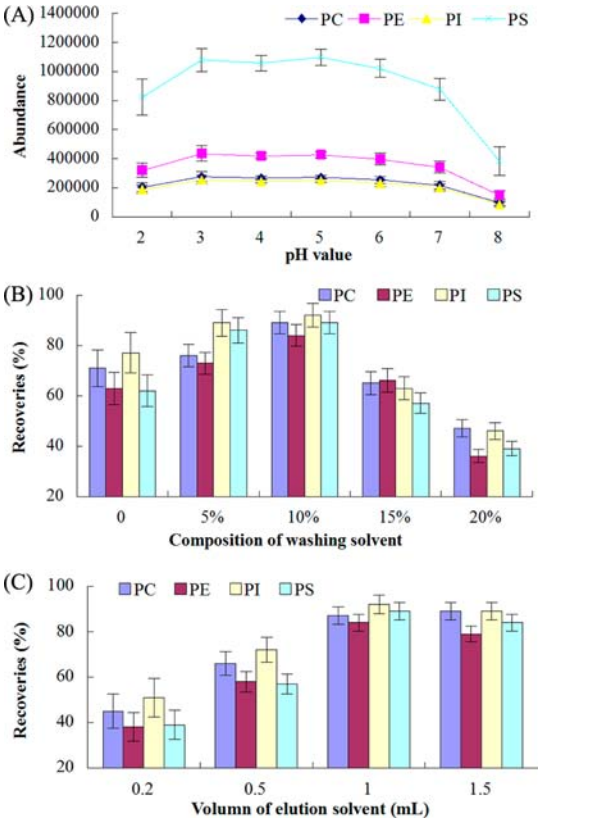


**Figure 2.** (A) Signal abundance of phospholipid standards PC (14:0/14:0), PE (15:0/15:0), PI (16:0/16:0), and PS (14:0/14:0) under different pH of loading solvents. Recoveries of phospholipid standards when the (B) polarity of the washing solvent and (C) type and amount of eluting solvents were varied. The standard solution, containing PC (14:0/14:0), PE (15:0/15:0), PI (16:0/16:0), and PS (14:0/14:0) at a concentration of 1000 ng $mL^{-1}$ each, was freshly prepared in methanol.

Given that the constitutes in the cephalothorax of shrimp are quite complex and they may easily influence the ionization efficiency of phospholipids in the ESI source, the polarity of the washing solvent was studied by varying the organic modifier from 0 to 20% methanol. It can be seem from Figure 2B that the recoveries of the four phospholipid standards increased gradually when the concentration of the organic modifier was raised from 0 to 10%. It indicated that some interfering matrix could be efficiently removed by the washing solvent. However, if the proportion of methanol was further increased to 15% or even 20%, the recoveries of phospholipids were decreased significantly. Finally, 10% aqueous methanol was chosen as the washing solvent.

After washing the $TiO_2/SiO_2$ SPE cartridge, the target analytes need to be eluted out using elution solvent with an appropriate amount. The elution solvents are characterized by their polarity and elution strength for a specific sorbent, and the

**Table 1. Method Linearity, LOD, LOQ, Precision, and Recovery at Three Different Concentrations for $TiO_2/SiO_2$ Composite-Based SPE Coupled with HILIC−QTOF/MS Analysis of Phospholipid Standards**

| | | | | | | RSD | | recovery | | |
|---|---|---|---|---|---|---|---|---|---|---|
| analyte | calibration curve | $R^2$ | linearity range[a] | LOD[a] | LOQ[a] | intraday (%) | interday (%) | low | middle | high |
| PC 14:0/14:0 | $y = 6.3 \times 10^6 x - 29680$ | 0.9975 | 0.37−200 | 0.12 | 0.37 | 4.3 | 5.8 | 102.4 | 98.3 | 82.3 |
| PE 15:0/15:0 | $y = 1.1 \times 10^7 x + 12658$ | 0.9974 | 0.71−200 | 0.23 | 0.71 | 4.7 | 6.1 | 89.6 | 94.5 | 90.7 |
| PI 16:0/16:0 | $y = 5.0 \times 10^7 x + 24805$ | 0.9978 | 0.45−100 | 0.14 | 0.45 | 5.2 | 6.4 | 87.3 | 97.8 | 74.2 |
| PS 14:0/14:0 | $y = 2.1 \times 10^7 x + 98919$ | 0.9964 | 0.78−500 | 0.25 | 0.78 | 6.3 | 8.1 | 96.5 | 101.6 | 81.8 |

[a]In units of $\mu g\ mL^{-1}$.

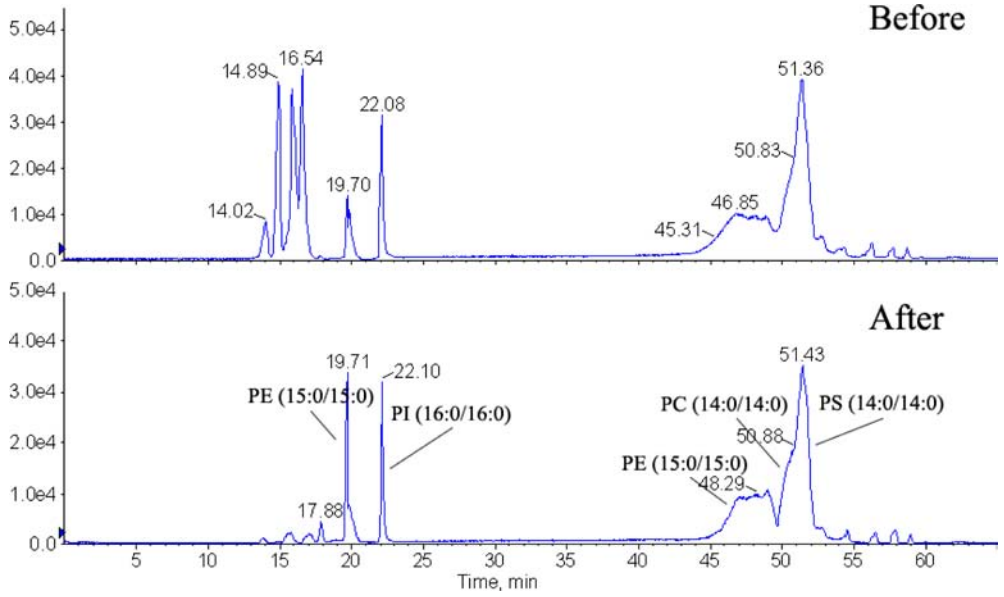


**Figure 3.** HILIC−QTOF/MS chromatograms relevant to the extract of shrimp waste using the (A) Bligh & Dyer method and (B) $TiO_2/SiO_2$ microsphere-based SPE method.

most suitable solvent was selected by testing a variety of solvents, including methanol, acetonitrile, and mixtures of chloroform and methanol (2:1, 1:1, and 1:2, v/v). During the study, it was found that a mixture of chloroform and methanol (1:2, v/v) can recover almost all of the phospholipids from the SPE sorbent, while the other solvent systems did not perform so well. After that, the optimum volume was tested by varying it from 0.2 to 1.5 mL. The results were demonstrated in Figure 2C, and it showed that the recoveries of phospholipid standards climbed up gradually and reached the highest value when 1.0 mL of elution solvent was used. Finally, 1.0 mL of chloroform/methanol (1:2, v/v) was used as the elution solvent.

**HILIC−QTOF/MS Development.** Prior to the application of the $TiO_2/SiO_2$ core−shell composite-based SPE for the determination of each phospholipid species in the cephalothorax of shrimp by HILIC−QTOF/MS, the following performance studies were implemented, including linearity, limit of detection (LOD) and limit of quantification (LOQ), accuracy and precision, and recovery. The method linearity (peak area versus concentration) was evaluated to overcome ion suppression/enhancement, matrix effects and variations caused by instrument parameters, sample preparations, and injections. A linear matrix-matched calibration model was used on the basis of the analysis of the data with six levels of concentration by linear regression with intercepts and $1/x$ weighting factor. All of the compounds displayed good linearity in selected concentration ranges (Table 1). The correlation coefficients ($R^2$) of the calibration curves were in the range between 0.9964 and 0.9978 ($n = 6$), which indicated good linearity between the peak area ($y$) and investigated compound concentration ($x$, ng $mL^{-1}$). LOD and LOQ were calculated on the basis of the signal-to-noise ratio (S/N = 3 for LOD and S/N = 10 for LOQ) on the mass spectrograms of the tested waste samples. The results (Table 1) showed that the LOD and LOQ were less than 0.25 and 0.78 $\mu g\ mL^{-1}$, which indicated enough sensitivity for conducting the determination process. Accuracy and precision were expressed in terms of repeatability by running seven extracts of shrimp waste samples on a single day (intraday), and reproducibility was quantified using five replicate samples spiked at the same levels on five different days (interday). Three replicates were performed at each spiking level to determine the relative standard deviation (RSD). The RSD of intra- and interday accuracy for the four phospholipid standards in shrimp waste extracts were in the ranges of 4.3−6.3 and 5.8−8.1%, respectively. These data indicated that the repeatability, intermediate precision, and bias values of the assay are regarded as quite satisfactory. The performance of recovery was determined on the basis of the ratio of the measured concentration/fortified level × 100% at low, middle, and high different levels. The results of recoveries ranging from 74.2 to 102.4% (Table 1). It suggested that all of the phospholipid standards could be recovered well at low and medium concentration levels. However, when a high concentration of analytes was injected, the recoveries were easily influenced because of the MS/in-source fragmentation, leading to the cross-effect of phospholipids during ionization.


dx.doi.org/10.1021/jf503040p | J. Agric. Food Chem. 2014, 62, 8944−8951

Table 2. Probable Attribution of Molecular Species and Their Contents in Shrimp Waste (Cephalothorax)

| | PC | | PE | | PI | | PS | |
|---|---|---|---|---|---|---|---|---|
| sn-1/sn-2[a] | $[M + HCOO]^-$ | abundance[b] | $[M - H]^-$ | abundance | $[M - H]^-$ | abundance | $[M - H]^-$ | abundance |
| *a*16:0/18:3[c] | ud[d] | ud | 698.58 | 0.35 ± 0.02 | ud | ud | ud | ud |
| *a*16:1/20:5 | ud | ud | 720.56 | 3.84 ± 0.18 | ud | ud | ud | ud |
| *a*16:0/20:5 | ud | ud | 722.58 | 0.91 ± 0.05 | ud | ud | ud | ud |
| *a*18:0/18:3 | ud | ud | 726.61 | 0.57 ± 0.23 | ud | ud | ud | ud |
| 16:1/20:5 | ud | ud | 734.58 | 0.80 ± 0.05 | ud | ud | 778.63 | 1.44 ± 0.06 |
| *a*16:0/20:5 | 810.64 | 0.73 ± 0.03 | ud | ud | ud | ud | ud | ud |
| 16:0/20:5 | 824.62 | 5.21 ± 0.23 | 736.57 | 0.71 ± 0.48 | 855.57 | 0.19 ± 0.06 | 780.64 | 0.03 ± 0.00 |
| 16:0/20:4 | 826.63 | 1.63 ± 0.11 | ud | ud | 857.57 | 0.11 ± 0.04 | ud | ud |
| 18:1/18:2 and 18:0/18:3 | 828.65 | 1.16 ± 0.09 | ud | ud | ud | ud | ud | ud |
| 18:0/18:2 | 830.66 | 7.26 ± 0.32 | ud | ud | ud | ud | 786.64 | 0.29 ± 0.01 |
| 18:0/18:1 | 832.68 | 3.16 ± 0.11 | ud | ud | ud | ud | 788.66 | 0.41 ± 0.03 |
| *a*16:1/22:6 | ud | ud | 746.58 | 2.64 ± 0.12 | ud | ud | 790.63 | 0.17 ± 0.01 |
| *a*16:0/22:6 and *a*18:1/20:5 | 836.65 | 4.20 ± 0.19 | 748.58 | 37.8 ± 2.57 | ud | ud | 792.64 | 0.12 ± 0.01 |
| *a*16:0/22:5 and *a*18:0/20:5 | 838.65 | 4.17 ± 0.18 | 750.6 | 8.05 ± 0.66 | 869.55 | 0.05 ± 0.01 | 794.65 | 0.12 ± 0.01 |
| *a*18:0/20:4 | 840.66 | 0.59 ± 0.06 | 752.62 | 0.27 ± 0.04 | ud | ud | ud | ud |
| 18:3/20:5 | ud | ud | ud | ud | ud | ud | 802.63 | 6.31 ± 0.42 |
| 16:1/22:6 | 848.62 | 3.84 ± 0.15 | 760.58 | 0.69 ± 0.08 | 879.61 | 0.03 ± 0.00 | 804.64 | 15.88 ± 0.89 |
| 16:0/22:6 | 850.62 | 48.07 ± 3.11 | 762.57 | 10.06 ± 0.74 | 881.59 | 0.24 ± 0.02 | 806.66 | 3.52 ± 0.20 |
| 16:0/22:5 and 18:0/20:5 | 852.64 | 32.88 ± 2.86 | 764.59 | 6.24 ± 0.48 | 883.6 | 4.52 ± 0.31 | 808.61 | 1.50 ± 0.06 |
| 16:0/22:4 or 18:0/20:4 | 854.66 | 4.17 ± 0.22 | 766.61 | 1.24 ± 0.65 | 885.61 | 1.68 ± 0.22 | 810.61 | 1.10 ± 0.04 |
| 16:0/22:3 or 18:0/20:3 | 856.69 | 0.62 ± 0.04 | ud | ud | 887.66 | 0.04 ± 0.01 | ud | ud |
| 18:0/20:2 | 858.7 | 0.46 ± 0.06 | ud | ud | ud | ud | ud | ud |
| 18:0/20:1 | ud | ud | ud | ud | ud | ud | 816.66 | 0.33 ± 0.01 |
| 18:0/20:0 | ud | ud | ud | ud | ud | ud | 818.68 | 0.43 ± 0.01 |
| *a*18:1/22:6 | ud | ud | 774.61 | 9.50 ± 0.36 | ud | ud | ud | ud |
| *a*18:0/22:6 | 864.67 | 0.86 ± 0.09 | 776.62 | 3.10 ± 0.17 | ud | ud | 820.69 | 0.10 ± 0.01 |
| *a*18:0/22:4 | ud | ud | ud | ud | ud | ud | 824.65 | 0.26 ± 0.01 |
| 20:5/20:5 | ud | ud | ud | ud | ud | ud | 826.64 | 0.89 ± 0.04 |
| 18:3/22:6 | ud | ud | ud | ud | ud | ud | 828.65 | 1.76 ± 0.05 |
| 18:2/22:6 | 874.63 | 2.22 ± 0.12 | 786.58 | 0.47 ± 0.02 | ud | ud | 830.66 | 7.20 ± 0.45 |
| 18:1/22:6 | 876.65 | 3.25 ± 0.15 | 788.6 | 0.91 ± 0.05 | ud | ud | 832.68 | 2.43 ± 0.18 |
| 18:0/22:6 | 878.66 | 1.93 ± 0.06 | 790.61 | 1.99 ± 0.14 | ud | ud | 834.62 | 0.57 ± 0.03 |
| 20:5/22:6 | ud | ud | 808.57 | 0.30 ± 0.21 | ud | ud | ud | ud |

[a]Fatty acid chain constituents (sn-1/sn-2) were confirmed by $MS^2$ analysis and referred to other results already published. [b]The concentration data of phospholipids are shown as the mean and standard deviation (SD) ($n$ = 6). [c]In the notation *a*16:0/18:3, *a* means alkyl linkage (1-*O*-alkyl or plasmanyl). [d]ud stands for undetected.

**Analysis of Phospholipids in Shrimp Waste.** The well-optimized strategy, $TiO_2/SiO_2$ composite-based SPE and liquid chromatography−tandem mass spectrometry (LC−MS/MS), was then applied to shrimp waste samples (*L. vannamei*). The chromatograms of lipid extracts before and after SPE purification were recorded in Figure 3. As shown, many peaks could be observed in the chromatogram of crude lipid extract (Figure 3A). After the mass spectra were checked, many of them, especially the four significant peaks in the retention time window from 14 to 18 min, could be regarded as interferences, because no unique fragments can be observed in their MS/MS spectrum, for example, $+m/z$ 184 (PC), $-m/z$ 196 (PE), $-m/z$ 241 (PI), etc. The results were further confirmed by $MS^2$ analysis. The complexity of the crude lipid extract could be attributed to the composition of the cephalothorax of shrimp, which comprised almost all of the organs, such as the brain, stomach, heart, and glands. Meanwhile, the extraction solvent, a mixture of chloroform and methanol, can dissolve a wide range of compounds, such as lipids, carbohydrates, organometallic compounds, and even some environmental contaminants. After SPE purification, the chromatogram (Figure 3B) became much cleaner and the non-phospholipid peaks were well-reduced. In addition, the intensity of the peak at 19.7 min was enhanced, and the resolution between two adjacent peaks in the retention time window from 45 to 53 min was improved as well. The results indicated that the $TiO_2/SiO_2$ core−shell composite-based SPE cartridge is efficient in selectively extracting phospholipids from the crude lipid mixture. Meanwhile, the well-purified phospholipid sample could be separated on a diol column and detected by a mass spectrometer with enhanced signal intensity and resolution.

The identity of each peak in the chromatogram (Figure 3B) was characterized by comparing their retention time to that of phospholipid standards and analyzing the mass spectra based on our experience. The fraction of PC class is eluated at ca. 50.5 min in the mass range from $m/z$ 800 to 900, and it was half-overlapped with the fraction of PS class, which is eluated at ca. 51.5 min in the mass range from $m/z$ 750 to 850. Fortunately, the overlap will not interfere with the calculation of the content of each phospholipid species, because they can be well-determined using an extracted-ion chromatogram (XIC). For PE class, two peaks could be observed in the chromatogram (at ca. 19.7 and 48.3 min, in the mass range from $m/z$ 680 to 820),


dx.doi.org/10.1021/jf503040p | J. Agric. Food Chem. 2014, 62, 8944−8951

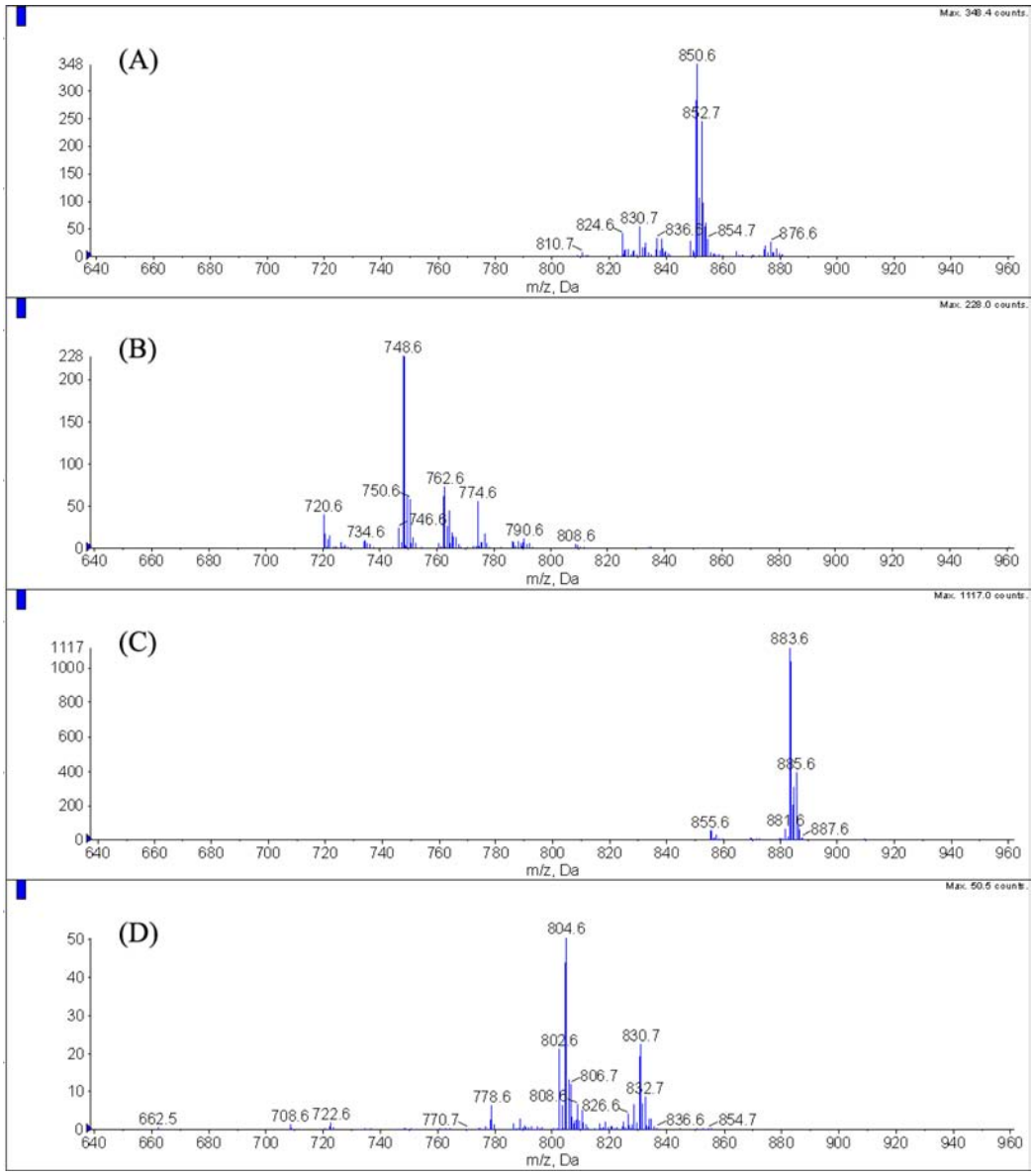


**Figure 4.** MS spectra of phospholipid classes: (A) PC, (B) PE, (C) PI, and (D) PS.

and the mass spectrum of these two peaks was identical. It was speculated that there were two states of PE molecules when they were dissolved in the acidic mobile phase, and the retention behavior of these two states of PE molecules was different. After evaporation and charging in the ESI source, the PE molecules became uniform, that is, $[PE - H]^-$. In fact, this phenomenon also could be found in another publication.[24] The PI class was eluated at a retention time of 22.1 min in the mass range from $m/z$ 850 to 900, with a sharp and symmetrical peak.

Identification of individual molecular species of each phospholipid class was based on the expected retention time and mass spectrum. The information on fatty acyl chain constituents (sn-1/sn-2) was obtained using $MS^2$ data, aided with the lipid map database and other results already published.[25] The characteristics of all of the detected phospholipids were summarized in Table 2. It is worth mentioning that, in the negative-ion mode, the species of PE, PI, and PS were all detected as $[M - H]^-$ ions, while the PC class was detected as formate adducts $[M + HCOO]^-$ because of the choline group at the polar head. Meanwhile, some minor peaks of $[M - 15]^-$ could also be observed in the mass spectrum of PC, resulting from the loss of the methyl group of choline. In this study, a total of 69 phospholipid species were detected and analyzed, including 20 PC species, 20 PE species, 8 PI species, and 21 PS species. Figure 4 demonstrated the mass spectra of the four phospholipid classes. The mass spectrum of PC species is shown in Figure 4A. All of the peaks were formate adducts in the mass range from $m/z$ 800 to 900. The most abundant peaks were $m/z$ 850.6 and 852.7, which were elucidated as [PC 16:0/22:6 + HCOO]$^-$ and [PC 18:0/20:5 + HCOO]$^-$, respectively. The others were also identified, and their sn-2 acyl chain proved to be unsaturated or polyunsaturated, such as 18:1, 18:2, 20:5, and 22:6. Besides, another sample injection was conducted under the same conditions but in positive-ion mode. All of the above-described PC species could be well-observed as protonated ions $[M + H]^+$ (data not shown), which well-confirmed the characteristics of PC species. PE species were quite diverse and mainly located in the mass range from $m/z$ 700 to 820, as shown in Figure 4B. A total of 20 PE species were successfully detected. The


dx.doi.org/10.1021/jf503040p | J. Agric. Food Chem. 2014, 62, 8944−8951

dominant ion at $m/z$ 748.6 was identified as [PE $a$18:1/20:5 − H]$^-$, where the symbol $a$ stands for alkyl linkage (1-$O$-alkyl or plasmanyl). Ions of $m/z$ 720.6, 750.6, 762.6, and 774.7 were also significant, and they were corresponding to [PE $a$16:1/20:5 − H]$^-$, [PE $a$18:0/20:5 − H]$^-$, [PE 18:1/20:5 − H]$^-$, and [PE $a$18:1/22:6 − H]$^-$, respectively. The mass spectrum of the PI class is shown in Figure 4C. Actually, not many PI species could be found, and only 6 species were detected, with a mass-to-charge ratio ranging from $m/z$ 850 to 900. The peak at $m/z$ 883.6 ([PI 16:0/22:5 − H]$^-$ and [PI 18:0/20:5 − H]$^-$) was the dominant ion, accompanied with some minor peaks, such as 855.6 ([PI 16:0/22:4 − H]$^-$). PS is also an important phospholipid class in the cephalothorax of shrimp (Figure 4D), and a total of 21 PS species were detected and elucidated, as summarized in Table 2. The most significant peaks were at $m/z$ 802.6, 804.6, and 830.6, and their structures were speculated to be PS 18:3/20:5, PS 16:1/22:6, and PS 18:2/22:6, respectively. In general, the phospholipids extracted from the cephalothorax of shrimp are diverse and concentrated in polyunsaturated fatty acyl chains at the sn-2 position, such as 18:3 [$\alpha$-linolenic acid (ALA)], 20:5 (EPA), and 22:6 (DHA), which are important for normal metabolism but cannot be synthesized by the human body. The phospholipid species in the cephalothorax of shrimp are very similar to that of other aquatic products, such as shark liver and Pacific oyster.[26,27]

Determination of phospholipids in the cephalothorax of shrimp was conducted on the basis of an external calibration model. The total contents of PC, PE, PI, and PS classes were calculated to be 1264.1, 904.4, 68.6, and 134.5 $\mu$g g$^{-1}$, respectively. As expected, PC was the most abundant class in the cephalothorax of shrimp, amounting to almost 53.3% of the total. PE is a close second, whose proportion is as much as 38.1%. The percentages of PI and PE are relatively lower, accounting for 2.9 and 5.7%, respectively. The content of each phospholipid species was determined using the normalization method. The principle is that the ionization efficiency of different covalently linked compounds in the ESI source depends upon the dipole potentials of each analyte. For phospholipids, the headgroup component contributes to the dominant dipole of the molecules, while other dipole components are neglectable. Therefore, the ionization efficiency of different naturally occurring phospholipid species is essentially identical within experimental error after correction for $^{13}$C isotope effects.[20] On the basis of that, all of the molecular species were quantitatively analyzed and listed in Table 2. The major phospholipid species of each class were PC 16:0/22:6 (480.7 $\mu$g g$^{-1}$), $a$PE 18:1/20:5 (378.0 $\mu$g g$^{-1}$), PI 18:0/20:5 (45.2 $\mu$g g$^{-1}$), and PS 16:1/22:5 (47.6 $\mu$g g$^{-1}$), and the proportions in their corresponding classes are 38.0, 41.8, 66.0, and 35.4%, respectively. The contents of phospholipid-containing saturated acyl chains (SAC), monounsaturated acyl chains (MUAC), and polyunsaturated acyl chains (PUAC) were depicted in Figure 5. It is obvious that the proportion of PUAC phospholipids takes as much as half of the total phospholipids. MUAC phospholipids were abundant in PE (33.8%) and PS (22.7%) classes. SAC phospholipids could be frequently found in PC (45.1%) and PI (49.8%) classes. It is well-known that polyunsaturated fatty acids (PUFAs) and monounsaturated fatty acids (MUFAs) are beneficial to human health. For example, PUFAs lower heart attacks and cardiovascular disease, while MUFAs reduce low-density lipoprotein (LDL) cholesterol but increase high-density lipoprotein (HDL) cholesterol. The high content of PUAC

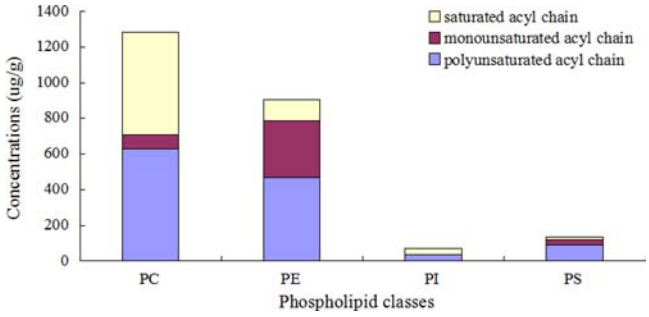


**Figure 5.** Content of SAC phospholipids, MUAC phospholipids, and PUAC phospholipids of each phospholipid class in the extract of shrimp waste.

phospholipids and MUAC phospholipids makes the shrimp waste an excellent recourse for industrial use.

**Method Comparison.** Most lipid extraction methods are designed for extracting the crude lipid mixture, while the method for selective extraction of phospholipids is still quite limited. It is reported that hybrid SPE−precipitation (hybrid SPE−PPT) and the $TiO_2$-based $\mu$SPE method can well remove the interferences and retain the phospholipids.[13,28] Unfortunately, the recovery information on these two techniques was not mentioned in the literature. As we known, the consumable materials of hybrid SPE−PPT are very expensive. On the other hand, $TiO_2$ is easily dispersed in the solvent; thus, it is unsuitable to be used directly as a sorbent of SPE. Montanari et al. introduced a supercritical carbon dioxide (SC-$CO_2$) method for selective extraction of phospholipids from soybeans.[29] However, its recovery of total phospholipids was only 74.8%, which is lower than that of the $TiO_2/SiO_2$-based SPE method (~90%). In summary, $TiO_2/SiO_2$-based SPE is a cost-effective and efficient method for selective extraction of phospholipids.

In conclusion, a $TiO_2/SiO_2$-based SPE method was successfully employed for selective extraction of phospholipids from shrimp waste (cephalothorax) samples. Under the optimized conditions, the interfering matrix is removed and the phospholipids are well-recovered. After that, a HILIC−QTOF/MS method was developed and fully validated to achieve baseline separation of phospholipid classes and characterization the distinctive phospholipid profile. As a result, a total of 69 phospholipid species were successfully identified and determined in shrimp waste. It is found that there is a great amount of phospholipids in shrimp waste, most of which contain PUAC, such as 18:3 (ALA), 20:5 (EPA), and 22:6 (DHA). Further effort will put in investigating the recycle of $TiO_2/SiO_2$ composite-based SPE cartridge. Preparative and process chromatography $TiO_2/SiO_2$ composites will also be studied for expanding the production and industrial application.

## AUTHOR INFORMATION

### Corresponding Author

*Telephone: +852-27887746. Fax: +852-27887406. E-mail: bhhonyun@cityu.edu.hk.

### Funding

Qing Shen thanks the School of Graduate Studies (SGS) Committee of City University of Hong Kong for granting a Ph.D. studentship and partial financial support from a Research Grants Council (RGC) grant (Grant 7002872) for the purchase of consumable materials.

### Notes

The authors declare no competing financial interest.

## ■ ABBREVIATIONS USED

PC, phosphatidylcholine; PE, phosphatidylethanolamine; PI, phosphatidylinositol; PS, phosphotidylserine; $SiO_2/TiO_2$, titania-coated silica; B&D, Bligh & Dyer; HILIC, hydrophilic interaction chromatography; QTOF/MS, quadrupole time-of-flight/mass spectrometry

## ■ REFERENCES


(1) Cullis, P. R.; de Kruijff, B. Lipid polymorphism and the functional roles of lipids in biological membranes. *Biochim. Biophys. Acta, Rev. Biomembr.* **1979**, *559*, 399−420.

(2) Gordon, B. R.; Parker, T. S.; Levine, D. M.; Feuerbach, F.; Saal, S. D.; Sloan, B. J.; Chu, C.; Stenzel, K. H.; Parrillo, J. E.; Rubin, A. L. Neutralization of endotoxin by a phospholipid emulsion in healthy volunteers. *J. Infect. Dis.* **2005**, *191*, 1515−1522.

(3) Küllenberg, D.; Taylor, L. A.; Schneider, M.; Massing, U. Health effects of dietary phospholipids. *Lipids Health Dis.* **2012**, *11*, 3−19.

(4) Zimman, A.; Chen, S. S.; Komisopoulou, E.; Titz, B.; Martinez-Pinna, R.; Kafi, A.; Berliner, J. A.; Graeber, T. G. Activation of aortic endothelial cells by oxidized phospholipids: A phosphoproteomic analysis. *J. Proteome Res.* **2010**, *9*, 2812−2824.

(5) Wyban, J. Domestication of pacific white shrimp revolutionizes aquaculture. *Global Aquacult. Advocate* **2007**, *July/August*, 42−44.

(6) Balogun, A. M.; Akegbejo-Samsons, Y. Waste yield, proximate and mineral composition of shrimp resources of Nigeria's coastal waters. *Bioresour. Technol.* **1992**, *40*, 157−161.

(7) Folch, J.; Lees, M.; Sloane-Stanley, G. H. A simple method for the isolation and purification of total lipids from animal tissues. *J. Biol. Chem.* **1957**, *226*, 497−509.

(8) Cequier-Sánchez, E.; Rodríguez, C.; Ravelo, A. G.; Zárate, R. Dichloromethane as a solvent for lipid extraction and assessment of lipid classes and fatty acids from samples of different natures. *J. Agric. Food Chem.* **2008**, *56*, 4297−4303.

(9) Qiao, L.; Roussel, C.; Wan, J.; Yang, P.; Girault, H. H.; Liu, B. Specific on-plate enrichment of phosphorylated peptides for direct MALDI-TOF MS analysis. *J. Proteome Res.* **2007**, *6*, 4763−4769.

(10) Shen, Q.; Dong, W.; Yang, M.; Baibado, J. T.; Wang, Y.; Alqouqa, I.; Cheung, H. Lipidomic study of olive fruit and oil using $TiO_2$ nanoparticle based matrix solid-phase dispersion and MALDI-TOF/MS. *Food Res. Int.* **2013**, *54*, 2054−2061.

(11) Cantin, G. T.; Shock, T. R.; Park, S. K.; Madhani, H. D.; Yates, J. R., III Optimizing $TiO_2$-based phosphopeptide enrichment for automated multidimensional liquid chromatography coupled to tandem mass spectrometry. *Anal. Chem.* **2007**, *79*, 4666−4673.

(12) Lu, Z.; Duan, J.; He, L.; Hu, Y.; Yin, Y. Mesoporous $TiO_2$ nanocrystal clusters for selective enrichment of phosphopeptides. *Anal. Chem.* **2010**, *82*, 7249−7258.

(13) Calvano, C. D.; Jensen, O. N.; Zambonin, C. G. Selective extraction of phospholipids from dairy products by micro-solid phase extraction based on titanium dioxide microcolumns followed by MALDI-TOF-MS analysis. *Anal. Bioanal. Chem.* **2009**, *394*, 1453−1461.

(14) Sinanoglou, V. J.; Kokkotou, K.; Fotakis, C.; Strati, I.; Proestos, C.; Zoumpoulakis, P. Monitoring the quality of $\gamma$-irradiated macadamia nuts based on lipid profile analysis and chemometrics. Traceability models of irradiated samples. *Food Res. Int.* **2014**, *60*, 38−47.

(15) Lucci, P.; Pacetti, D.; Calzuola, I.; Marsili, V.; Perni, S.; Giavarini, F.; Frega, N. G.; Gianfranceschi, G. L. Characterization of phospholipid molecular species and peptide molecules in wheat sprout hydroalcoholic extract. *J. Agric. Food Chem.* **2013**, *61*, 11453−11459.

(16) Tzompa-Sosa, D. A.; Yi, L.; van Valenberg, H. J. F.; van Boekel, M. A. J. S.; Lakemond, C. M. M. Insect lipid profile: Aqueous versus organic solvent-based extraction methods. *Food Res. Int.* **2014**, *62*, 1087−1094.

(17) Meneses, P.; Glonek, T. High resolution $^{31}$P NMR of extracted phospholipids. *J. Lipid Res.* **1998**, *29*, 679−689.

(18) Shen, Q.; Dong, W.; Yang, M.; Li, L.; Cheung, H.; Zhang, Z. Lipidomic fingerprint of almonds (*Prunus dulcis* L. cv Nonpareil) using $TiO_2$ nanoparticle based matrix solid-phase dispersion and MALDI-TOF/MS and its potential in geographical origin verification. *J. Agric. Food Chem.* **2013**, *61*, 7739−7748.

(19) Calvano, C. D.; De Ceglie, C.; Aresta, A.; Facchini, L. A.; Zambonin, C. G. MALDI-TOF mass spectrometric determination of intact phospholipids as markers of illegal bovine milk adulteration of high-quality milk. *Anal. Bioanal. Chem.* **2013**, *405*, 1641−1649.

(20) Han, X.; Gross, R. W. Shotgun lipidomics: electrospray ionization mass spectrometric analysis and quantitation of cellular lipidomes directly from crude extracts of biological samples. *Mass Spectrom. Rev.* **2005**, *24*, 367−412.

(21) Verardo, V.; Gómez-Caravaca, A. M.; Montealegre, C.; Segura-Carretero, A.; Caboni, M. F.; Fernández-Gutiérrez, A.; Bendini, A. Optimization of a solid phase extraction method and hydrophilic interaction liquid chromatography coupled to mass spectrometry for the determination of phospholipids in virgin olive oil. *Food Res. Int.* **2013**, *54*, 2083−2090.

(22) Jackson, S. N.; Wang, H. Y.; Woods, A. S.; Ugarov, M.; Egan, T.; Schultz, J. A. Direct tissue analysis of phospholipids in rat brain using MALDI-TOF/MS and MALDI-ion mobility-TOF/MS. *J. Am. Soc. Mass Spectrom.* **2005**, *16*, 133−138.

(23) Engholm-Keller, K.; Larsen, M. R. Titaniumdioxide as chemo-affinity chromatographic sorbent of biomolecular compounds applications in acidic modification specific proteomics. *J. Proteomics* **2011**, *75*, 317−328.

(24) Zhu, C.; Dane, A.; Spijksma, G.; Wang, M.; van der Greef, J.; Luo, G.; Hankemeier, T.; Vreeken, R. J. An efficient hydrophilic interaction liquid chromatography separation of 7 phospholipid classes based on a diol column. *J. Chromatogr. A* **2012**, *1220*, 26−34.

(25) Shen, Q.; Wang, Y.; Gong, L.; Guo, R.; Dong, W.; Cheung, H. Shotgun lipidomics strategy for fast analysis of phospholipids in fisheries waste and its potential in species differentiation. *J. Agric. Food Chem.* **2012**, *60*, 9384−9393.

(26) Chen, S.; Belikova, N. A.; Subbaiah, P. V. Structural elucidation of molecular species of pacific oyster ether amino phospholipids by normal-phase liquid chromatography/negative-ion electrospray ionization and quadrupole/multiple-stage linear ion-trap mass spectrometry. *Anal. Chim. Acta* **2012**, *735*, 76−89.

(27) Chen, S.; Li, K. W. Mass spectrometric identification of molecular species of phosphatidylcholine and lysophosphatidylcholine extracted from shark viscera. *J. Agric. Food Chem.* **2007**, *55*, 9670−9677.

(28) Ferreiro-Vera, C.; Priego-Capote, F.; Luque de Castro, M. D. Comparison of sample preparation approaches for phospholipids profiling in human serum by liquid chromatography−tandem mass spectrometry. *J. Chromatogr. A* **2012**, *1240*, 21−28.

(29) Montanari, L.; Fantozzi, P.; Snyder, J. M.; King, J. W. Selective extraction of phospholipids from soybeans with supercritical carbon dioxide and ethanol. *J. Supercrit. Fluids* **1999**, *14*, 87−93.

of type 1 diabetes. Moreover, insulin is also the only drug that triggers insulin signaling pathway via binding to IR.

*Momordica charantia* Linn. (MC) is a common vegetable that displays antidiabetic potential.[8−12] In a previous study, we have demonstrated that an aqueous extract of MC stimulates the insulin signaling pathway and displays a hypoglycemic effect in mice. By proteomic and docking analyses, we have found that trypsin inhibitor might interact with IR.[13] Trypsin inhibitor, also named as bitter gourd trypsin inhibitor or MC trypsin inhibitor, has been isolated from MC, and its amino acid sequences have been identified.[14] Trypsin inhibitor consists of 68 amino acid residues and inhibits not only trypsin but also subtilisin Carlsberg. In this study, we renamed this protein as MC IR-binding protein (mcIRBP) because of its novel function on glucose homeostasis. The physical and functional interactions between mcIRBP and IR were clearly elucidated here. Recombinant mcIRBP was purified from *Escherichia coli* (*E. coli*) overexpression system. The physical and functional interactions between mcIRBP and IR were analyzed by photo-cross-linking coupled with mass spectrometry (MS), IR-binding assay, and IR kinase activity assay. Furthermore, the hypoglycemic effect and mechanism of mcIRBP were evaluated in normal and type 1 diabetic mice. Our data showed that mcIRBP bound to the sites different from the insulin-binding sites on IR and consequently enhanced the uptake of glucose in cells and the clearance of glucose in mice.

## MATERIALS AND METHODS

**Chemicals.** Chemicals, unless indicated, were purchased from Sigma (St. Louis, MO). SuperScript III, RPMI-1640, and Dulbecco's modified Eagle's medium (DMEM) were purchased from Invitrogen (Carlsbad, CA). Fetal bovine serum (FBS) and calf serum were purchased from Hyclone (Logan, UT). [$^{125}$I]Insulin, [$\gamma$-$^{32}$P]ATP, and 2-[1,2-$^{3}$H(N)]-deoxy-D-glucose were purchased from PerkinElmer (Boston, MA). Rabbit monoclonal antibodies against IR, phospho-IR, phosphoinositide-dependent kinase 1 (PDK1), phospho-PDK1, Akt, phospho-Akt (Ser473), and phospho-Akt (Thr308) were purchased from Cell Signaling (Beverly, MA). Mouse monoclonal antibody against $\beta$-actin was purchased from Santa Cruz (Dallas, TX).

**Cloning of mcIRBP Gene.** To clone the mcIRBP cDNA, total RNA was extracted from MC, reverse transcribed by SuperScript III, and amplified with P1 (5′-GATCAAGCTTATGTGTCAGGGGA-AGTCGTCGTGGCCGCAG-3′) and M1 (5′-GATCGAGCTCT-CAACCGATGGTGGGGGGGCGGGCGACGAT-3′) primers. The resulting 216-bp mcIRBP cDNA fragment was inserted into *Hin*dIII and *Sac*I sites of pBluescript II KS(−) vector to create pBKS-mcIRBP. pBKS-mcIRBP was further amplified with P2 (5′-GATCACATGTG-TCAGGGGAAGTCGTCGTGG-3′) and T7 (5′-AATACGACTCA-CTATAG-3′) primers. The 242-bp mcIRBP cDNA fragment was then inserted into *Nco*I and *Sac*I sites of pET-28a(+) vector to create pET-mcIRBP (Figure 1A). The plasmid DNA, which was created in this study, was confirmed as an in-frame construction by sequencing. The template sequences for primer design are originated from GenBank (accession number: 2111250B). The protein sequences of mcIRBP have been deposited in GenBank (accession number: AGU04661.1).

**Expression and Purification of Recombinant mcIRBP.** Recombinant mcIRBP was expressed in *E. coli* BL21(DE3) pLysS strain, which was transformed with pET-mcIRBP. Expression and purification of recombinant mcIRBP were performed as described previously.[15] Molecular mass of mcIRBP was analyzed by sodium dodecyl sulfate polyacrylamide gel electrophoresis (SDS−PAGE), and the concentration of mcIRBP was quantified by a Bradford method (Bio-Rad, Hercules, CA).

**Photo-Cross-Linking Coupled with MS.** Photoinduced cross-linking was performed as described previously.[16] Briefly, mcIRBP was mixed with IR in a molar ratio of 10:1 in 10 mM sodium phosphate buffer (pH 7.4). To a total volume of 18 $\mu$L of protein solution were

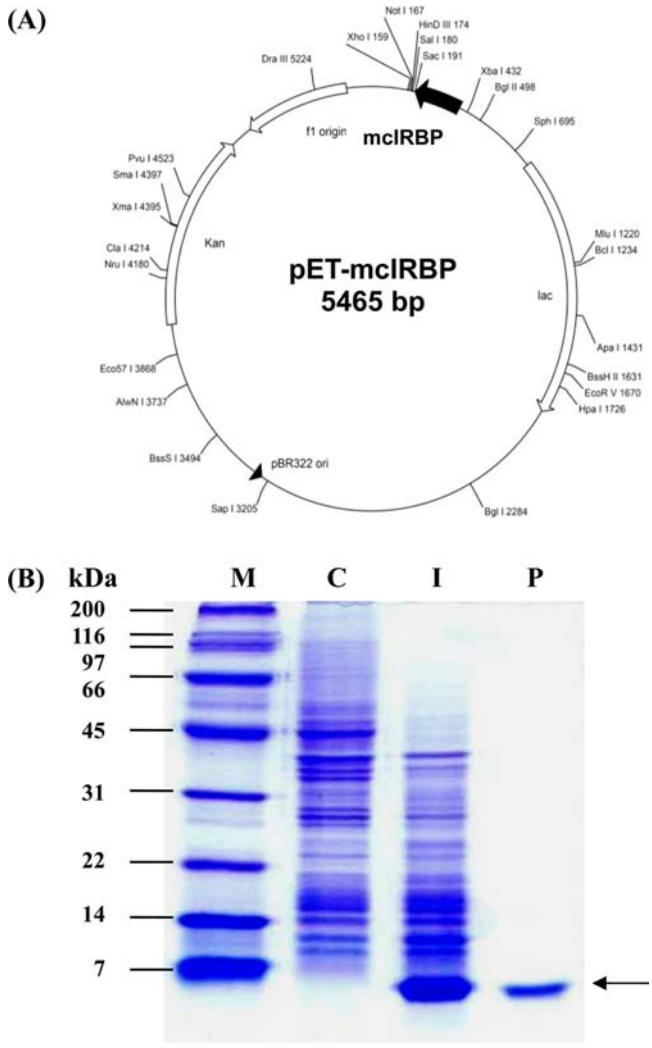


**Figure 1.** Cloning, expression, and purification of recombinant mcIRBP. (A) Map of pET-mcIRBP. The diagram represents the location of mcIRBP gene in the pET-28a(+) vector. Closed arrow represents mcIRBP gene. (B) SDS−PAGE analysis. The preparations of uninduced *E. coli* containing pET-mcIRBP (lane C), isopropyl-$\beta$-D-thiogalactoside-induced *E. coli* containing pET-mcIRBP (lane I), and purified mcIRBP (lane P) were analyzed by 15% SDS−PAGE and stained by Coomassie Brilliant Blue. The molecular masses of protein standards (lane M) are shown at the left. Recombinant mcIRBP is indicated by the arrow.

then added 1 $\mu$L of tris(bipyridyl)Ru(II) (RuBpy) solution (1 mM RuBpy in 10 mM sodium phosphate buffer, pH 7.4) and 1 $\mu$L of ammonium persulfate (APS) solution (20 mM APS in 10 mM sodium phosphate buffer, pH 7.4). The reaction mixture was exposed to ultraviolet light for 30 s and quenched by adding 1 $\mu$L of 1 M dithiothreitol. Protein solution was further identified using an Ultimate capillary liquid chromatography system (LC Packings, Amsterdam, The Netherlands) coupled to a QSTARXL quadrupole-time-of-flight MS (Applied Biosystem/MDS Sciex, Foster City, CA).

**Docking Calculations.** The PatchDock was used for the prediction of ligand-binding sites.[17] The PDB files of IR (PDB code 3LOH), mcIRBP (PDB code 1VBW), and insulin (PDB code 1JCO) were obtained from Protein Data Bank (http://www.rcsb.org/pdb/). The PDBQ files of these proteins were derived from PDB2PQR version 1.8 (http://nbcr-222.ucsd.edu/pdb2pqr_1.8/).[18]

**Cell Culture.** IM-9 myeloma cells, HepG2 hepatocytes, and 3T3-L1 preadipocytes were purchased from Bioresource Collection Research Center (Hsinchu, Taiwan). IM-9 cells were maintained in


dx.doi.org/10.1021/jf5002099 | J. Agric. Food Chem. 2014, 62, 8952−8961

RPMI-1640 supplemented with 10% FBS. HepG2 cells were maintained in DMEM supplemented with 10% FBS. 3T3-L1 preadipocytes were maintained in DMEM supplemented with 10% heat-inactivated calf serum. All cell lines were incubated at 37 °C in a humidified atmosphere containing 5% $CO_2$.

**IR-Binding Assays.** The binding of mcIRBP to IR was measured by IR-binding assay, IR kinase activity assay, and enzyme-linked immunosorbent assay (ELISA). IR-binding assay was performed as described previously.[19] Briefly, IM-9 cells ($1.2 \times 10^6$ cells/mL) were incubated with different amounts of mcIRBP for 15 min at 25 °C. $^{125}$I-labeled insulin (60,000 cpm/mL of cells) was then added and incubated for 90 min at 16 °C. Cells were centrifuged at 3000*g* for 10 min, and the supernatant containing unbound ligands was removed. The radioactivity of cell pellet containing bound $^{125}$I-labeled insulin was measured by scintillation counter (Beckman Coulter, Fullerton, CA).

IR kinase activity assay was performed as described previously.[13] Briefly, mixtures containing IR and various amounts of mcIRBP in kinase buffer (25 mM HEPES, pH 7.6, 25 mM $MgCl_2$, 100 $\mu$M ATP, 100 $\mu$M sodium orthovanadate, 2.5 mg/mL poly(Glu,Tyr), 25 $\mu$Ci/mL [$\gamma$-$^{32}$P]ATP) were incubated at 30 °C for 10 min and spotted on chromatography papers. Poly(Glu,Tyr) was precipitated on papers by soaking papers in 10% trichloroacetic acid solution, and the radioactivity incorporated into the precipitated poly(Glu,Tyr) was counted by scintillation counter.

For ELISA, HepG2 cells were treated with various amounts of mcIRBP, incubated at 37 °C for 10 min, and solubilized in lysis buffer (1% NP-40, 20 mM Tris-HCl, pH 8.0, 137 mM NaCl, 10% glycerol, 2 mM EDTA, 1 mM sodium orthovanadate, 10 $\mu$g/mL aprotinin, 10 $\mu$g/mL leupeptin) on ice for 15 min. After the centrifugation at 2000*g* for 5 min, the supernatant was collected, and the protein concentration was quantified. ELISA was performed with the DuoSet IC Human Phospho-IR set (R&D Systems, Minneapolis, MN). Briefly, microtiter plates (MaxiSorp, Nunc, Denmark) were coated with antibody against phospho-IR at 4 °C overnight, incubated with cellular proteins (250 $\mu$g) at room temperature for 2 h, and then incubated with horseradish peroxidase-conjugated antibody against phospho-tyrosine at room temperature for 2 h. Following four washes, chromogenic substrate tetramethylbenzidine was added, incubated at room temperature for 20 min, and stopped with 2 N $H_2SO_4$. The absorbance at 450 nm was measured in an ELISA plate reader.

**Western Blot Analysis.** HepG2 cells were cultured in 25 cm$^2$ flasks, treated with various amounts of mcIRBP for 30 min, collected using cell scrapers, and lysed with sample buffer (62.5 mM Tris-HCl, pH 6.8, 2% SDS, 10% glycerol, 50 mM dithiothreitol). HepG2 cells were also treated with LY294002 (50 $\mu$M) to block the PI3K activity. Proteins (10 $\mu$g) were separated by 10% SDS−PAGE and transferred electrophoretically to nitrocellulose membranes. Membranes were then probed with anti-IR, anti-phospho-IR, anti-PDK1, anti-phospho-PDK1, anti-Akt, anti-phospho-Akt (Ser473), anti-phospho-Akt (Thr308), and anti-$\beta$-actin antibodies. The bound antibody was detected with horseradish peroxidase-conjugated anti-rabbit antibody followed by chemiluminescence and X-ray film exposure.

**Adipocyte Differentiation and Glucose Uptake Assay.** The differentiation of 3T3-L1 preadipocytes was induced by the addition of 0.5 mM 3-isobutyl-1-methylxanthine, 0.5 $\mu$M dexamethasone, 10 $\mu$g/mL insulin, and 10% FBS in DMEM for 3 days. The aforementioned medium was then replaced with 10% FBS/DMEM containing 10 $\mu$g/mL insulin. After another 3 days, the medium was subsequently replaced with fresh culture medium (10% FBS/DMEM), which was changed every 2 days until the cells were fully differentiated, judged by oil red O staining. Fully differentiated 3T3-L1 adipocytes were used for glucose uptake assay. Glucose uptake assay was performed as previously described.[20] Briefly, 3T3-L1 adipocytes were cultured in 24-well plates. After a 4.5 h starvation, adipocytes were incubated in Krebs−Ringer bicarbonate buffer (118 mM NaCl, 4.7 mM KCl, 1.3 mM $CaCl_2$, 1.2 mM $MgSO_4$, 1.2 mM $Na_2HPO_4$, 2% bovine serum albumin, 0.5 mM glucose, 25 mM $NaHCO_3$, pH 7.4) without or with various amounts of mcIRBP for 30 min at 37 °C. [$^3$H]-2-Deoxy-D-glucose (0.1 $\mu$Ci) was then added to adipocytes and incubated for another 10 min. Finally, cells were solubilized in 0.1% SDS and the radioactivity uptaken by cells was measured by scintillation counter.

**Animals.** BALB/c mice were obtained from National Laboratory Animal Center (Taipei, Taiwan). Mouse experiments were conducted under ethics approval from China Medical University Animal Care and Use Committee (Permit Number: 101-188-N). Type I diabetic mice were induced by streptozotocin.[21] Briefly, male BALB/c mice (6 weeks old) were injected intraperitoneally with streptozotocin (200 mg/kg in 200 $\mu$L of normal saline). Two weeks later, mice were bled via tail veins after 4 h starvation, and the blood glucose was measured by glucose oxidase method using a glucometer (ACCU-CHEK Advantage, Roche Diagnostics, Basel, Switzerland).

**Glucose Tolerance Assay.** Normal and type I diabetic mice were fasted for 18 and 4 h, respectively. mcIRBP (2.5 nmol/kg) was then given intraperitoneally 15 min before intraperitoneal administration of glucose solution (4 g/kg for normal mice and 1 g/kg for diabetic mice).[22] Blood samples were collected from tails at 15 min before and at 15, 30, 60, 90, 120, 150, 180, 240, and 270 min after glucose challenge. Blood glucose was measured by glucose oxidase method using a glucometer. Data were also expressed as area under the curve (AUC). Mice were sacrificed 5 h after glucose challenge, and muscles were collected for microarray analysis.

**Microarray Analysis.** Five hours after glucose challenge, mice were sacrificed and muscle tissues were collected for microarray analysis. Total RNAs were extracted from muscle tissues using RNeasy Mini kit (Qiagen, Valencia, CA). Total RNA from three mice was pooled, and three microarray replicates for each pooled RNA were performed. Microarray analysis was performed as described previously.[23−25] Briefly, fluorescence-labeled RNA targets were hybridized to Mouse Whole Genome OneArray (Phalanx Biotech Group, Hsinchu, Taiwan). The Cy5 fluorescent intensity of each spot was analyzed by Genepix 4.1 software (Molecular Devices, Sunnyvale, CA). The signal intensity of each spot was corrected and further normalized by R program in the limma package.[26] Fold changes of genes were calculated by dividing the normalized signal intensities of genes in mcIRBP-treated tissues by those in untreated tissues. We used the geneSetTest function to test which biological pathways were affected by mcIRBP. This function computes a *p*-value to test the hypothesis that the selected genes in a pathway tend to be differentially expressed. Kyoto Encyclopedia of Genes and Genomes pathways (http://www.genome.jp/kegg/pathway.html) was extracted and used for this analysis. Microarray data are MIAME compliant, and raw data have been deposited in the Gene Expression Omnibus (accession number: GSE39689).

**Statistical Analysis.** Data were presented as mean ± standard error. Student's *t* test was used for comparisons between two experiments. A value of $p < 0.05$ was considered statistically significant.

## RESULTS

**Expression and Purification of mcIRBP.** In our previous study, we identified a trypsin inhibitor, named as mcIRBP here, that might interact with IR. The mcIRBP gene was therefore amplified by PCR and cloned for expression. mcIRBP was expressed and purified from *E. coli* BL21 (DE3) pLysS strain, which was transformed with pET-mcIRBP. After the induction with isopropyl-$\beta$-D-thiogalactoside, mcIRBP with molecular mass of approximately 7 kDa was observed by SDS−PAGE analysis (Figure 1B). The amount of purified mcIRBP recovered was approximately 2 mg per 100 mL of bacterial culture.

**Analysis of the Physical Interaction between IR and mcIRBP.** Photo-cross-linking coupled with MS was performed to analyze the physical interaction between IR and mcIRBP. mcIRBP was cross-linked with IR by ultraviolet light oxidized $Ru^{2+}$, and the cross-linked proteins were further identified by LC-MS/MS. We mixed mcIRBP and IR in the molar ratio of 1:1 and 10:1 and found that the cross-linking efficiency at 10:1

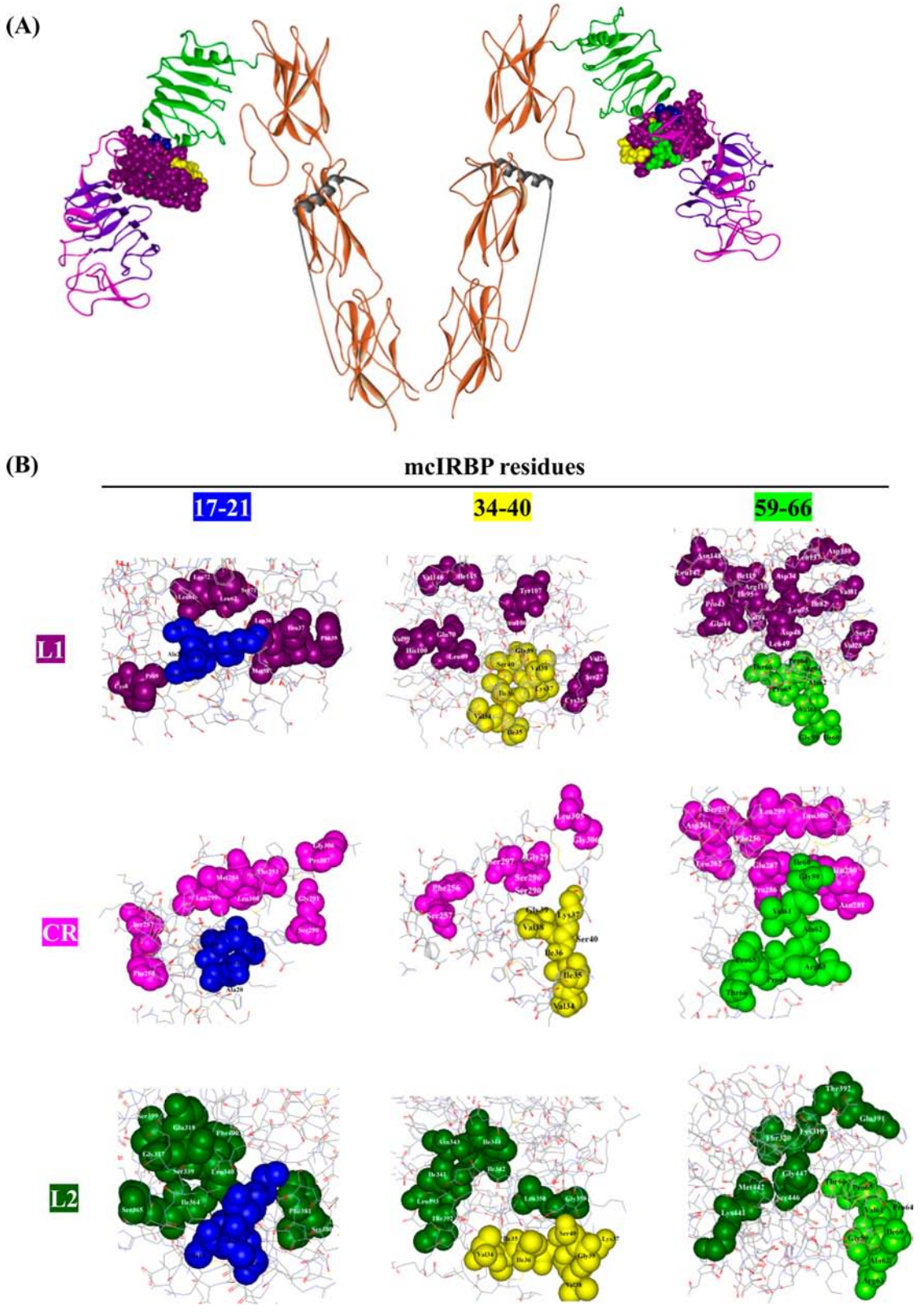


**Figure 2.** Physical interaction between mcIRBP and IR. (A) Docking structure of IR and mcIRBP. The IR ectodomain monomer is shown in a schematic presentation. L1, CR, L2, fibronectin domains, and $\alpha$-CT segment are colored purple, pink, green, orange, and gray, respectively. mcIRBP is shown in an atomic sphere representation. The 17−21, 34−40, and 59−66 amino acid residues of mcIRBP are colored blue, yellow, and light green, respectively. The remaining regions of mcIRBP are colored violet. (B) Close-up view of mcIRBP complexes with IR. The 17−21, 34−40, and 59−66 amino acid residues of mcIRBP and the amino acid residues located on L1, CR, and L2 regions of IR are shown in atomic sphere representations. The remaining regions of mcIRBP and IR are represented by stick styles.


dx.doi.org/10.1021/jf5002099 | J. Agric. Food Chem. 2014, 62, 8952−8961

was better (data not shown). A total of 2,731 peptide fragments was identified by MS/MS, and 1,518 fragments were chosen after excluding the repeated fragments. We further picked up the fragments that had ≥3 consecutive amino acid sequences of mcIRBP on the central region and ≥2 consecutive amino acid sequences of IR on either terminus. A total of 146 fragments fulfilling aforementioned criteria were selected. We found that three regions located on 17−21, 34−40, and 59−66 residues of mcIRBP physically interacted with the amino acid residues located on leucine-rich repeat domains and cysteine-rich (CR) region of IR.

We further built the docking structures of IR and mcIRBP based on photo-cross-linking data. As shown in Figure 2A, the crystal structure of IR ectodomain monomer formed an inverted "V" layout of which one side consists of leucine-rich repeat domains (L1 and L2) and CR region, and another side is composed of fibronectin domains and $\alpha$-CT segment. mcIRBP interacted with L1/CR/L2 segments on IR, and the docking score between mcIRBP and IR was 14,636. In comparison with mcIRBP, insulin, as expected, interacted with the $\alpha$-CT segment on IR, with a docking score of 14,134 (Supporting Information, Figure S1).[27] Close-up view of mcIRBP and IR showed that three regions located on 17−21, 34−40, and 59−66 residues of mcIRBP were close to the amino acid residues located on the L1, CR, and L2 regions of IR (Figure 2B). These data suggested that mcIRBP was a novel IRBP that bound to the sites different from the insulin-binding sites on IR.

We analyzed the binding behavior of mcIRBP on IR by incubating cells with various amounts of mcIRBP, radioisotope-labeled insulin (hot insulin), and/or non-radioisotope-labeled insulin (cold insulin). As shown in Figure 3A, when more hot insulin was added to a fixed amount of IR, an increasing fraction of IR was occupied by hot insulin. However, when more cold insulin was added to a fixed amount of IR and hot insulin, a decreasing fraction of IR was occupied by hot insulin (Figure 3B). These results indicated that cold insulin competed with hot insulin and blocked the insulin-binding sites on IR. Then, we measured the IR-binding behavior of mcIRBP by incubating IM-9 cells with various amounts of mcIRBP and 6 pM of hot insulin. As shown in Figure 3C, an increasing fraction of IR was occupied by hot insulin when an increasing amount of mcIRBP was added to a fixed amount of IR and hot insulin. These data suggested that mcIRBP bound to a site other than the insulin-binding sites on IR and enhanced the binding of hot insulin to IR. However, the amount of bound hot insulin in the presence of 10 nM mcIRBP was dramatically decreased by the addition of an excessive amount (1 $\mu$M) of cold insulin, suggesting that the mcIRBP-dependent enhancement of insulin binding on IR was specifically blocked and abolished by cold insulin. These results indicated that mcIRBP might bind to the allosteric site of IR and further enhance the effectivity of IR on the insulin binding.

**mcIRBP Enhanced the Kinase Activity and Autophosphorylation of IR.** IR is a transmembrane protein that exhibits tyrosine kinase activity. Insulin binding to IR stimulates the intrinsic tyrosine kinase activity, leading to the autophosphorylation of IR.[6] Therefore, we analyzed the kinase activity of IR by kinase activity assay and evaluated the level of autophosphorylated IR by ELISA. Figure 4A shows that the addition of insulin stimulated the kinase activity of IR by (7.35 ± 0.89)-fold. mcIRBP also enhanced the kinase activity of IR in a dose-dependent manner. Moreover, the maximal enhancement [(5.87 ± 0.45)-fold] of kinase activity was achieved in the

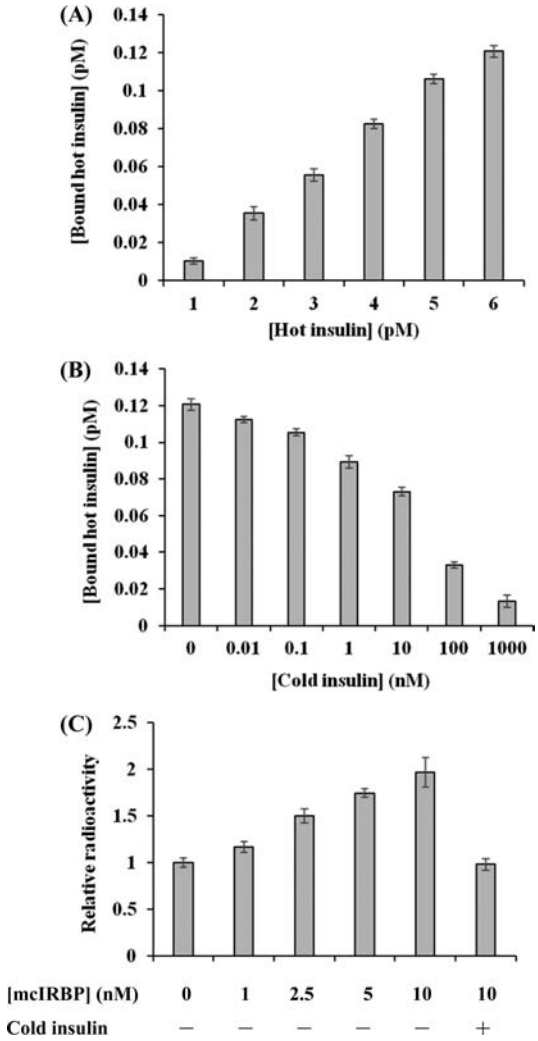


**Figure 3.** IR-binding assay of mcIRBP. IM-9 cells were treated with various amounts of $^{125}$I-labeled insulin (A), 6 pM $^{125}$I-labeled insulin and various amounts of insulin (B), or various amounts of mcIRBP, 6 pM $^{125}$I-labeled insulin, and/or 1 $\mu$M insulin (C). The reaction was incubated for 90 min at 16 °C, and the radioactivity of bound $^{125}$I-labeled insulin was counted by scintillation counter. Values are mean ± standard error ($n$ = 3).

presence of 5 $\mu$M mcIRBP. Figure 4B shows that insulin increased the level of phosphorylated IR in HepG2 cells, as compared with mock. mcIRBP significantly stimulated the autophosphorylation of IR in a dose-dependent manner. Moreover, the maximal increase [(1.31 ± 0.03)-fold] of phosphorylated IR was achieved by 5 $\mu$M mcIRBP. These findings indicated that mcIRBP bound to IR, activated the kinase activity of IR, and sequentially stimulated the autophosphorylation of IR.

**mcIRBP Affected IR/PI3K/Akt Signaling Pathway.** We further performed Western blot to analyze the IR-downstream signaling pathway affected by mcIRBP. As shown in Figure 5A, insulin and mcIRBP stimulated the phosphorylation of IR, which was consistent with aforementioned data (Figure 4). Insulin enhanced the phosphorylations of PDK1 and Akt at Ser473 and Thr308, as compared with mock. mcIRBP also increased the amounts of phosphorylated PDK1 and Akt in a dose-dependent manner. However, LY294002, a PI3K inhibitor, inhibited the mcIRBP-induced phosphorylation of

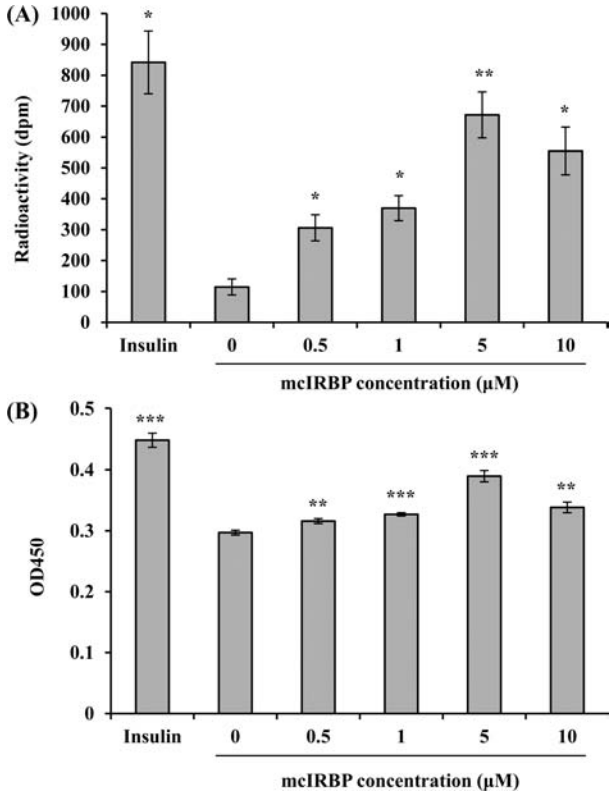


**Figure 4.** Effect of mcIRBP on the kinase activity and autophosphorylation of IR. (A) Kinase activity assay. IR was mixed with 0.5 $\mu$M insulin or various amounts of mcIRBP in the presence of [$\gamma$-$^{32}$P]ATP and poly(Glu,Tyr). The radioactivity (dpm) incorporated into the precipitated poly(Glu,Tyr) was counted by scintillation counter. (B) ELISA. HepG2 cells were treated with 0.5 $\mu$M insulin or various amounts of mcIRBP. Ten minutes later, cellular proteins were collected and the phosphorylated IR was quantitated by ELISA. Values are mean ± standard error ($n$ = 3). *$p$ < 0.05, **$p$ < 0.01, ***$p$ < 0.001, compared with no treatment.

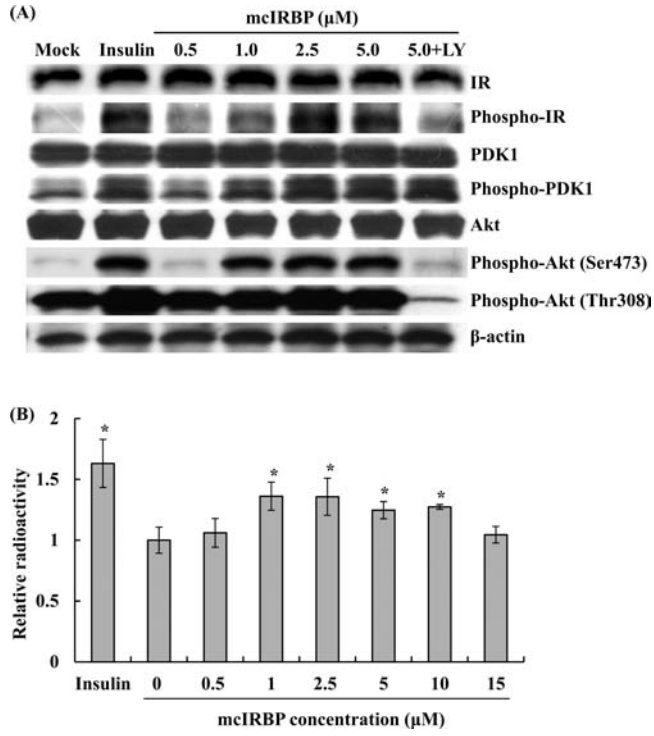


**Figure 5.** Effect of mcIRBP on the insulin signaling pathway in HepG2 cells and the glucose uptake of 3T3-L1 adipocytes. (A) Western blot. HepG2 cells were treated with 1 $\mu$M insulin or various amounts of mcIRBP for 30 min. LY294002 (50 $\mu$M) was used to inhibit PI3K activity. IR, phosphorylated IR, PDK1, phosphorylated PDK1, Akt, phosphorylated Akt (Ser473), and phosphorylated Akt (Thr308) were then detected by Western blot and visualized by chemiluminescence. Similar results are obtained in three independent experiments. Photos are representative images. (B) Glucose uptake assay. Fully differentiated 3T3-L1 adipocytes were treated with 1 nM insulin or various amounts of mcIRBP. Thirty minutes later, [$^3$H]-2-deoxy-D-glucose was added and the radioactivity uptaken by cells was counted. Data are expressed as relative radioactivity, which is presented as the comparison with the radioactivity relative to mock. Values are mean ± standard error ($n$ = 3). *$p$ < 0.05, compared with mock.

Akt. These findings suggested that mcIRBP bound to IR, stimulated the kinase activity of IR, and sequentially activated the PI3K/PDK1/Akt pathway.

**mcIRBP Stimulated the Uptake of Glucose in 3T3-L1 Adipocytes.** PI3K has a pivotal role in the metabolic action of insulin. Activation of PI3K stimulates the activation of Akt and subsequently stimulates the translocation of GLUT4 to the cell surface, a crucial event for glucose uptake by skeletal muscle and fat.[28] Therefore, we further evaluated the effect of mcIRBP on glucose uptake in 3T3-L1 adipocytes. As shown in Figure 5B, insulin and mcIRBP significantly enhanced the uptake of glucose in 3T3-L1 by (1.63 ± 0.20)-fold and (1.36 ± 0.12)-fold, respectively. The enhancement displayed a dose-dependent manner, and the maximal enhancement was achieved by 1 $\mu$M mcIRBP. These data suggested that mcIRBP bound to IR, stimulated PI3K/PDK1/Akt pathway, and, in turn, increased the uptake of glucose in adipocytes.

**mcIRBP Displayed the Hypoglycemic Effect in Normal and Diabetic Mice.** To analyze whether mcIRBP was capable of lowering the blood glucose levels in sera, we evaluated the hypoglycemic effect of mcIRBP by glucose tolerance assay in normal and diabetic mice. As shown in Figure 6, fasting blood glucose levels of normal and diabetic mice were approximately 40 mg/dL and 450 mg/dL, respectively. After glucose challenge, the blood glucose concentrations were dramatically increased at 30 min. The mock group displayed a poor glucose clearance, while intraperitoneal administration of mcIRBP resulted in a more rapid clearance of glucose in both normal and diabetic mice. The AUC was significantly decreased by 20.9 ± 3.2% and 10.8 ± 3.6% in mcIRBP-treated normal and diabetic mice, respectively. The AUC was significantly decreased by 34.7 ± 2.1% in insulin-treated diabetic mice. These data indicated that mcIRBP exhibited hypoglycemic effects in mice.

**Signal Transduction Pathways of mcIRBP on Glucose Metabolism in Normal and Diabetic Mice.** Microarray analysis was performed to investigate whether insulin signaling pathway and glucose metabolism were affected by mcIRBP in mice. Although muscle and adipose tissues are dominant tissues for glucose uptake, we chose muscle tissues only to analyze the gene expression profiles affected by mcIRBP because of the similar pathway pattern between muscle and adipose tissues in our previous study.[13] In a total of 29,922 genes, 636 and 1,523 genes with fold changes ≥2 or ≤−2 in normal and diabetic mice, respectively, were selected and tested for the biological pathways by geneSetTest function. Top 20 upregulated and downregulated genes are listed in Table S1 and Table S2 (Supporting Information). A total of 108 pathways and 95


dx.doi.org/10.1021/jf5002099 | J. Agric. Food Chem. 2014, 62, 8952−8961

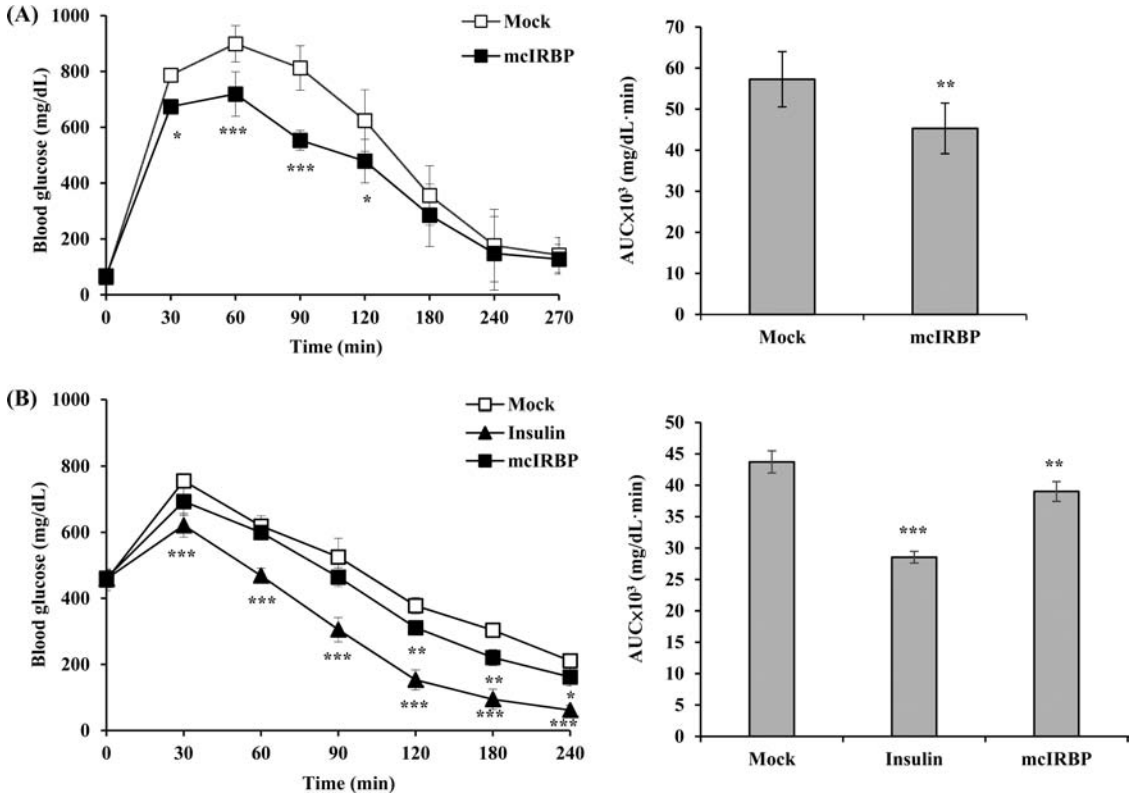


**Figure 6.** Hypoglycemic effects of mcIRBP in normal and type 1 diabetic mice by glucose tolerance assay. Normal (A) and type 1 diabetic mice (B) were administrated mcIRBP (2.5 nmol/kg) or insulin (2.5 nmol/kg) intraperitoneally. Fifteen minutes later, glucose was administrated intraperitoneally, blood samples were collected at intervals, and blood glucose levels were measured by the glucometer. AUC of glucose tolerance assay is shown at the right. Values are mean ± standard error ($n$ = 6). *$p$ < 0.05, **$p$ < 0.01, ***$p$ < 0.001, compared with mock.

pathways was significantly affected by mcIRBP in normal and diabetic mice, respectively (Supporting Information, Table S3 and Table S4). The information on genes for each of the significant pathways listed in Table S3 and Table S4 (Supporting Information) is shown in Table S5 and Table S6 (Supporting Information), respectively. As shown in Table 1, insulin signaling pathway and glucose metabolism, such as glycolysis/gluconeogenesis, citrate cycle, pentose phosphate pathway, and pyruvate metabolism, were significantly regulated by mcIRBP in both normal and diabetic mice. Moreover, PPAR signaling pathway, adipocytokine signaling pathway, leptin signaling pathway, and fatty acid metabolism were also significantly regulated by mcIRBP. These findings suggested that administration of mcIRBP triggered the insulin signaling pathway and subsequently affected the glucose and lipid metabolism in mice.

## DISCUSSION

In this study, we identified that a novel protein, mcIRBP, from MC directly bound to IR and triggered the insulin signaling transduction pathway in vitro and in vivo. Recently, the interaction of insulin with its primary binding site on IR was reported.[27] IR is a disulfide-linked homodimer, and each IR monomer contains two different insulin binding sites. Insulin binds asymmetrically to two different sites in IR dimer via bivalent growth hormone-receptor-binding mechanism.[29] The primary binding site with high affinity is located on both the $\alpha$-CT segment of one IR monomer and the central $\beta$-sheet of L1 of another IR monomer. The second site is located on both fibronectin domains and L2 segment of each IR monomer.

**Table 1. Pathways Significantly Affected by mcIRBP in Normal and Diabetic Mice**

| | $p$ value[b] (obsd/total[c]) for mcIRBP-treated mice | | obsd/total[c] for insulin-treated tissue | |
|---|---|---|---|---|
| pathway[a] | normal | diabetic | human skeletal muscle[d] | L6 skeletal muscle cells[e] |
| insulin signaling pathway | $4.06 \times 10^{-7}$ (16/132) | $2.48 \times 10^{-6}$ (24/132) | 4/132 | 29/132 |
| PPAR signaling pathway | $1.02 \times 10^{-10}$ (23/72) | $6.92 \times 10^{-7}$ (26/72) | 2/72 | 2/72 |
| adipocytokine signaling pathway | 0.000898 (11/69) | 0.000173 (14/69) | 1/69 | 11/69 |
| leptin signaling pathway | 0.000206 (6/25) | 0.000448 (11/25) | 1/25 | 0/25 |
| glycolysis/ gluconeogenesis | $2.27 \times 10^{-6}$ (15/54) | $3.53 \times 10^{-5}$ (19/54) | 5/54 | 3/54 |
| citrate cycle | $6.86 \times 10^{-6}$ (5/26) | $1.80 \times 10^{-9}$ (17/26) | 0/26 | 0/26 |
| pentose phosphate pathway | 0.000209 (11/25) | 0.000516 (6/25) | 3/25 | 3/25 |
| pyruvate metabolism | 0.001912 (10/39) | $2.06 \times 10^{-7}$ (19/39) | 2/39 | 0/39 |
| fatty acid metabolism | $4.57 \times 10^{-7}$ (11/42) | $5.61 \times 10^{-8}$ (23/42) | 2/42 | 0/42 |

[a]Pathways associated with glucose and lipid metabolism are shown. [b]$p$ values were calculated by the geneSetTest function implemented in the limma package. [c]Obsd/total means the number of selected genes/ the number of total genes in this pathway. [d]Microarray data were cited from Rome et al.[39] [e]Microarray data were cited from Di Camillo et al.[40]

Docking structure of IR and insulin in this study displayed that insulin interacted with two different sites with different docking scores on IR, as described previously.[27] Analysis of the physical interaction between IR and mcIRBP by docking and photo-cross-linking showed that mcIRBP interacted with L1/CR/L2 region on IR, on opposite site of the primary binding site of insulin on IR. Moreover, IR-binding assay showed that the binding behavior of mcIRBP and insulin on IR was cooperative. These data suggested that mcIRBP was a novel IR-binding protein that bound to the sites different from the insulin-binding sites on IR. Additionally, IR is a tyrosine kinase and, in the basal state, the kinase domain of IR is wrapped up by the juxtamembrane regions proximal to the catalytic domain. Upon binding to insulin, rearrangement within the ectodomain of IR results in the removal of the juxtamembrane region, the release of tyrosine kinase domain, and the *trans*-phosphorylation of IR.[30] Binding of mcIRBP to IR might induce the conformational change and release the kinase domain. This might explain why the incubation of mcIRBP and IR in tubes resulted in the activation of tyrosine kinase activity of IR.

IR significantly plays an important role in glucose homeostasis. Upon binding to insulin, tyrosine kinase activity of IR is activated, leading to the activation of PI3K/Akt and the subsequent translocation of GLUT4. Defects in the IR-mediated signaling pathways in tissues from diabetic patients or animal models also emphasize the importance of the IR pathway in the regulation of glucose metabolism.[6,29] In this study, we found that mcIRBP bound to IR, affected IR/PI3K/Akt pathway and, in turn, stimulated glucose uptake in 3T3-L1 cells. The hypoglycemic mechanism of mcIRBP was similar to that of insulin but was different from those of other glucose-lowering agents. For example, thiazolidinediones, such as troglitazone, rosiglitazone, and pioglitazone, bind to PPAR-$\gamma$, resulting in the enhancement of fatty acid storage, the increase of adiponectin levels, and the subsequent reduction of insulin resistance. Biguanides, such as metformin, improve insulin sensitivity and lower blood glucose levels mainly through the activation of AMP-activated protein kinase pathway.[7] In addition, some compounds exhibit hypoglycemic effects by affecting the PI3K/Akt pathway. For example, herbal compounds, such as ginsenoside Rb1, 6-gingerol, tea catechins, honokiol, and embelin, stimulate the phosphorylations of PI3K and Akt, leading to the translocation of GLUT4.[31−34] Cellular proteins, such as nexillin (a cardiomyopathy-associated F-actin binding protein), apelin (a cytokine mainly secreted by adipocytes), and obestatin (ghrelin gene-derived peptide), affect glucose homeostasis by activating the PI3K/Akt pathway.[35−38] However, none of these compounds or proteins targets to IR even though they activated the PI3K/Akt pathway. These data suggested the unique mechanism of mcIRBP on the regulation of glucose homeostasis. Furthermore, mcIRBP stimulated the phosphorylation of Akt proteins at both Ser473 and Thr308. Because mammalian target of rapamycin complex 2 (mTORC2) induces the phosphorylation of Akt at Ser473 and PDK1 activates Akt activity by phosphorylating Akt at Thr308,[28] we suggested that mcIRBP might also activate mTORC2 activity downstream from IR. In addition, in Figure 5A, we found that PI3K inhibitor LY294002 inhibited mcIRBP-induced phosphorylation of IR. Previous study indicates that PTP1B is a protein tyrosine phosphatase that negatively regulates insulin sensitivity by dephosphorylating the IR. However, phosphorylation of PTP1B by Akt negatively modulates its phosphatase activity and impairs it ability to dephosphorylate IR.[39] Because LY294002 inhibits PI3K and PI3K-downstream Akt activities, we proposed that the decreased amount of phosphorylated IR in the presence of insulin resulted from the increased amount of unphosphorylated PTP1B.

The hypoglycemic effect of mcIRBP was analyzed by glucose tolerance assays in normal and diabetic mice. The AUC was significantly decreased by 20.9% in mcIRBP-treated normal mice, while the AUC was significantly decreased by 10.8% and 34.7% in diabetic mice treated with mcIRBP and insulin, respectively. Although the hypoglycemic effects of mcIRBP and insulin displayed a significant manner, mcIRBP was less effective than insulin in blood glucose-lowering ability. Photo-cross-linking assay suggested that mcIRBP interacted with L1/CR/L2 region on IR, on opposite site of the primary binding site of insulin on IR. IR-binding assay further showed that mcIRBP cooperated with insulin for binding to IR. Therefore, we proposed that the mcIRBP-binding site on IR was minor, in comparison with primary insulin-binding site on IR, in stimulating the IR signaling pathway and subsequently the clearance of glucose. That might explain why the blood glucose-lowering ability of mcIRBP was less effective than that of insulin.

We performed microarray analysis to study gene expression profiles of mcIRBP in normal and diabetic mice. Microarray profiles of insulin in human skeletal muscle and rat L6 skeletal muscle myoblasts have been reported.[40,41] Their data show that insulin regulates several genes involved in intermediary and energy metabolism, transcriptional and translational regulation, cell cycle, cytoskeleton, vesicle traffic, and immune response. By pathway analysis, we found the consistency of gene expression profiling between mcIRBP and insulin. Among mcIRBP-regulated pathways, the majority of pathway was associated with glucose, lipid, and energy metabolism. There were 20 and 45 differentially expressed genes in insulin-treated human skeletal muscle and insulin-stimulated rat skeletal muscle myoblasts, respectively, involved in glucose and lipid metabolism pathways (Table 1). The dominant affected pathway in insulin-treated human skeletal muscle, insulin-stimulated rat skeletal muscle myoblasts, and mcIRBP-treated mouse muscle was insulin signaling pathway. Moreover, pathways involved in transcriptional and translational regulation, such as ribosome, proteasome, RNA polymerase, SNARE, and protein transport, were affected by mcIRBP. Cell cycle- and cytoskeleton-associated pathways, such as tight junction, focal adhesion, cell cycle, regulation of actin cytoskeleton, gap junction, apoptosis, and cell adhesion molecules, were also regulated by mcIRBP. Additionally, mcIRBP significantly affected four immune response-associated pathways, namely, complement and coagulation cascades, leukocyte transendothelial migration, antigen processing and presentation, and Toll-like receptor signaling pathway, and five signaling pathways, namely, PPAR, insulin, adipocytokine, mitogen-activated protein kinase, and gonadotropin-releasing hormone signaling pathways (Supporting Information, Table S3 and Table S4). These findings suggested that although mcIRBP bound to the sites different from the insulin-binding sites on IR, mcIRBP stimulated the similar biological pathways as insulin in mice.

In conclusion, our findings suggested that mcIRBP was a novel IR-binding polypeptide that bound to the sites different from the insulin-binding sites on IR. After binding to IR, mcIRBP activated IR-downstream signaling transduction path-

way, regulated genes involved in glucose and lipid metabolism, and, in turn, enhanced the glucose uptake in cells and the clearance of glucose in normal and diabetic mice.

## ■ ASSOCIATED CONTENT

### Supporting Information

Figure depicting docking structure of IR and insulin and tables of the top 20 upregulated and downregulated genes by mcIRBP in normal mice and diabetic mice, pathways significantly affected by mcIRBP in normal mice and type 1 diabetic mice, information of genes for each of the significant pathways affected by mcIRBP in normal mice and type 1 diabetic mice. This material is available free of charge via the Internet at http://pubs.acs.org.

## ■ AUTHOR INFORMATION

### Corresponding Author

*Department of Microbiology, China Medical University, 91 Hsueh-Shih Road, Taichung 40402, Taiwan. Tel: +886 4 22053366 ext 2163. Fax: +886 4 22053764. E-mail: cyhsiang@mail.cmu.edu.tw.

### Author Contributions

‡These authors contributed equally to this work.

### Funding

This work was supported by grants from National Research Program for Biopharmaceuticals (NSC101-2325-B-039-007, NSC102-2325-B-039-007, and MOST103-2325-B-039-002), Ministry of Science and Technology (NSC101-2320-B-039-034-MY3, NSC101-3114-Y-466-002, NSC102-2632-B-039-001-MY3, and MOST103-2815-C-039-044-B), Council of Agriculture (103AS-14.3.2-ST-a1), China Medical University (CMU101-S-21, CMU101-AWARD-09, CMU102-NSC-04, and CMU103-SR-44), and CMU under the Aim for Top University Plan of the Ministry of Education, Taiwan.

### Notes

The authors declare no competing financial interest.

## ■ ABBREVIATIONS USED

APS, ammonium persulfate; AUC, area under the curve; CR, cysteine-rich; DMEM, Dulbecco's modified Eagle's medium; ELISA, enzyme-linked immunosorbent assay; *E. coli*, *Escherichia coli*; FBS, fetal bovine serum; GLUT4, glucose transporter 4; IR, insulin receptor; IRBP, IR-binding protein; mTORC2, mammalian target of rapamycin complex 2; MS, mass spectrometry; MC, *Momordica charantia* Linn.; PPAR, peroxisome proliferator-activated receptors; PI3K, phosphoinositide-3-kinase; PDK1, phosphoinositide-dependent kinase 1; SDS−PAGE, sodium dodecyl sulfate polyacrylamide gel electrophoresis

## ■ REFERENCES

(1) Wild, S.; Roglic, G.; Green, A.; Sicree, R.; King, H. Global prevalence of diabetes: estimates for the year 2000 and projection for 2030. *Diabetes Care* **2004**, *27*, 1047−1053.

(2) Kaul, K.; Tarr, J. M.; Ahmad, S. I.; Kohner, E. M.; Chibber, R. Introduction to diabetes mellitus. *Adv. Exp. Med. Biol.* **2012**, *771*, 1−11.

(3) The Diabetes Control and Complications Trial Research Group. The effect of intensive treatment of diabetes on the development and progression of long-term complications in insulin-dependent diabetes mellitus. *N. Engl. J. Med.* **1993**, *329*, 977−986.

(4) Cleary, P. A.; Orchard, T. J.; Genuth, S.; Wong, N. D.; Detrano, R.; Backlund, J. Y.; Zinman, B.; Jacobson, A.; Sun, W.; Lachin, J. M.; Nathan, D. M. DCCT/EDIC Research Group. The effect of intensive glycemic treatment on coronary artery calcification in type 1 diabetic participants of the Diabetes Control and Complications Trial/Epidemiology of Diabetes Interventions and Complications (DCCT/EDIC) Study. *Diabetes* **2006**, *55*, 3556−3565.

(5) UK Prospective Diabetes Study (UKPDS) Group. Intensive blood-glucose control with sulphonylureas or insulin compared with conventional treatment and risk of complications in patients with type 2 diabetes (UKPDS 33). *Lancet* **1998**, *352*, 837−853.

(6) Saltiel, A. R.; Kahn, C. R. Insulin signalling and the regulation of glucose and lipid metabolism. *Nature* **2001**, *414*, 799−806.

(7) Powers, A. C. Diabetes mellitus. In *Harrison's principles of internal medicine*; Longo, D. L., Fauci, A. S., Kasper, D. L., Hauser, S. L., Jameson, J. L., Loscalzo, J., Eds.; The McGraw-Hill Companies, Inc.: New York, 2012; pp 2275−2304.

(8) Broadhurst, C. L.; Polansky, M. M.; Anderson, R. A. Insulin-like biological activity of culinary and medicinal plant aqueous extracts *in vitro*. *J. Agric. Food Chem.* **2000**, *48*, 849−852.

(9) Horax, R.; Hettiarachchy, N.; Over, K.; Chen, P.; Gbur, E. Extraction, fractionation and characterization of bitter melon seed proteins. *J. Agric. Food Chem.* **2010**, *58*, 1892−1897.

(10) Hsu, C.; Hsieh, C. L.; Kuo, Y. H.; Huang, C. J. Isolation and identification of cucurbitane-type triterpenoids with partial agonist/antagonist potential for estrogen receptors from *Momordica charantia*. *J. Agric. Food Chem.* **2011**, *59*, 4553−4561.

(11) Chaturvedi, P. Antidiabetic potentials of *Momordica charantia*: multiple mechanisms behind the effects. *J. Med. Food* **2012**, *15*, 101−107.

(12) Wang, X.; Sun, W.; Cao, J.; Qu, H.; Bi, X.; Zhao, Y. Structures of new triterpenoids and cytotoxicity activities of the isolated major compounds from the fruit of *Momordica charantia* L. *J. Agric. Food Chem.* **2012**, *60*, 3927−3933.

(13) Lo, H. Y.; Ho, T. Y.; Lin, C.; Li, C. C.; Hsiang, C. Y. *Momordica charantia* and its novel polypeptide regulate glucose homeostasis in mice via binding to insulin receptor. *J. Agric. Food Chem.* **2013**, *61*, 2461−2468.

(14) Miura, S.; Funatsu, G. Isolation and amino acid sequences of two trypsin inhibitors from the seeds of bitter gourd (*Momordica charantia*). *Biosci., Biotechnol., Biochem.* **1995**, *59*, 469−473.

(15) Chen, J. C.; Ho, T. Y.; Chang, Y. S.; Wu, S. L.; Li, C. C.; Hsiang, C. Y. Identification of *Escherichia coli* enterotoxin inhibitors from traditional medicinal herbs by *in silico*, *in vitro*, and *in vivo* analyses. *J. Ethnopharmacol.* **2009**, *121*, 372−378.

(16) Rahimi, F.; Maiti, P.; Bitan, G. Photo-induced cross-linking of unmodified proteins (PICUP) applied to amyloidogenic peptides. *J. Visualized Exp.* **2009**, *23*, 1071.

(17) Schneidman-Duhovny, D.; Inbar, Y.; Nussinov, R.; Wolfson, H. J. PatchDock and SymmDock: servers for rigid and symmetric docking. *Nucleic Acids Res.* **2005**, *33*, W363−W367.

(18) Dolinsky, T. J.; Nielsen, J. E.; McCammon, J. A.; Baker, N. A. PDB2PQR: an automated pipeline for the setup, execution, and analysis of Poisson-Boltzmann electrostatics calculations. *Nucleic Acids Res.* **2004**, *32*, W665−W667.

(19) Gauguin, L.; Delaine, C.; Alvino, C. L.; McNeil, K. A.; Wallace, J. C.; Forbes, B. E.; De Meyts, P. Alanine scanning of a putative receptor binding surface of insulin-like growth factor-I. *J. Biol. Chem.* **2008**, *283*, 20821−20829.

(20) Chen, C. C.; Hsiang, C. Y.; Chiang, A. N.; Lo, H. Y.; Li, C. I. Peroxisome proliferator-activated receptor gamma transactivation-mediated potentation of glucose uptake by Bai-Hu-Tang. *J. Ethnopharmacol.* **2008**, *118*, 46−50.

(21) Hayashi, K.; Kojima, R.; Ito, M. Strain differences in the diabetogenic activity of streptozotocin in mice. *Biol. Pharm. Bull.* **2006**, *29*, 1110−1119.

(22) Zhao, L.; Ye, H.; Li, D.; Lao, X.; Li, J.; Wang, Z.; Xiao, L.; Wu, Z.; Huang, J. Glucagon-like peptide-1(1−37) can enhance blood glucose homeostasis in mice. *Regul. Pept.* **2012**, *178*, 1−5.

(23) Li, C. C.; Hsiang, C. Y.; Lo, H. Y.; Pai, F. T.; Wu, S. L.; Ho, T. Y. Genipin inhibits lipopolysaccharide-induced acute systemic

inflammation in mice as evidenced by nuclear factor-κB bioluminescent imaging-guided transcriptomic analysis. *Food Chem. Toxicol.* **2012**, *50*, 2978−2986.
(24) Li, C. C.; Lo, H. Y.; Hsiang, C. Y.; Ho, T. Y. DNA microarray analysis as a tool to investigate the therapeutic mechanisms and drug development of Chinese medicinal herbs. *BioMedicine* **2012**, *2*, 10−16.
(25) Hsiang, C. Y.; Lo, H. Y.; Huang, H. C.; Li, C. C.; Wu, S. L.; Ho, T. Y. Ginger extract and zingerone ameliorated trinitrobenzene sulfonic acid-induced colitis in mice via modulation of nuclear factor-κB activity and interleukin-1β signaling pathway. *Food Chem.* **2013**, *136*, 170−177.
(26) Smyth, G. K. Limma: linear models for microarray data. In *Bioinformatics and computational biology solutions using R and bioconductor*; Gentleman, R., Carey, V., Dudoit, S., Irizarry, R., Huber, W., Eds.; Springer: New York, 2005; pp 397−420.
(27) Menting, J. G.; Whittaker, J.; Margetts, M. B.; Whittaker, L. J.; Kong, G. K.; Smith, B. J.; Watson, C. J.; Záková, L.; Kletvíková, E.; Jiráček, J.; Chan, S. J.; Steiner, D. F.; Dodson, G. G.; Brzozowski, A. M.; Weiss, M. A.; Ward, C. W.; Lawrence, M. C. How insulin engages its primary binding site on the insulin receptor. *Nature* **2013**, *493*, 241−245.
(28) Schultze, S. M.; Hemmings, B. A.; Niessen, M.; Tschopp, O. PI3K/AKT, MAPK and AMPK signalling: protein kinases in glucose homeostasis. *Expert Rev. Mol. Med.* **2012**, *14*, e1.
(29) De Meyts, P. Insulin and its receptor: structure, function and evolution. *Bioessays* **2004**, *26*, 1351−1362.
(30) Ward, C. W.; Lawrence, M. C. Similar but different: ligand-induced activation of the insulin and epidermal growth factor receptor families. *Curr. Opin. Struct. Biol.* **2012**, *22*, 360−366.
(31) Shang, W.; Yang, Y.; Zhou, L.; Jiang, B.; Jin, H.; Chen, M. Ginsenoside Rb1 stimulates glucose uptake through insulin-like signaling pathway in 3T3-L1 adipocytes. *J. Endocrinol.* **2008**, *198*, 561−569.
(32) Choi, S. S.; Cha, B. Y.; Iida, K.; Sato, M.; Lee, Y. S.; Teruya, T.; Yonezawa, T.; Nagai, K.; Woo, J. T. Honokiol enhances adipocyte differentiation by potentiating insulin signaling in 3T3-L1 preadipocytes. *J. Nat. Med.* **2011**, *65*, 424−430.
(33) Chakraborty, D.; Mukherjee, A.; Sikdar, S.; Paul, A.; Ghosh, S.; Khuda-Bukhsh, A. R. [6]-Gingerol isolated from ginger attenuates sodium arsenite induced oxidative stress and plays a corrective role in improving insulin signaling in mice. *Toxicol. Lett.* **2012**, *210*, 34−43.
(34) Wang, C. H.; Lin, W. D.; Bau, D. T.; Chou, I. C.; Tsai, C. H.; Tsai, F. J. Appearance of acanthosis nigricans may precede obesity: An involvement of the insulin/IGF receptor signaling pathway. *BioMedicine* **2013**, *3*, 82−87.
(35) Gandhi, G. R.; Stalin, A.; Balakrishna, K.; Ignacimuthu, S.; Paulraj, M. G.; Vishal, R. Insulin sensitization via partial agonism of PPARγ and glucose uptake through translocation and activation of GLUT4 in PI3K/p-Akt signaling pathway by embelin in type 2 diabetic rats. *Biochim. Biophys. Acta* **2013**, *1830*, 2243−2255.
(36) Zhu, S.; Sun, F.; Li, W.; Cao, Y.; Wang, C.; Wang, Y.; Liang, D.; Zhang, R.; Zhang, S.; Wang, H.; Cao, F. Apelin stimulates glucose uptake through the PI3K/Akt pathway and improves insulin resistance in 3T3-L1 adipocytes. *Mol. Cell. Biochem.* **2011**, *353*, 305−313.
(37) Granata, R.; Gallo, D.; Luque, R. M.; Baragli, A.; Scarlatti, F.; Grande, C.; Gesmundo, I.; Córdoba-Chacón, J.; Bergandi, L.; Settanni, F.; Togliatto, G.; Volante, M.; Garetto, S.; Annunziata, M.; Chanclón, B.; Gargantini, E.; Rocchietto, S.; Matera, L.; Datta, G.; Morino, M.; Brizzi, M. F.; Ong, H.; Camussi, G.; Castaño, J. P.; Papotti, M.; Ghigo, E. Obestatin regulates adipocyte function and protects against diet-induced insulin resistance and inflammation. *FASEB J.* **2012**, *26*, 3393−3411.
(38) Lee, A.; Hakuno, F.; Northcott, P.; Pessin, J. E.; Rozakis Adcock, M. Nexilin, a cardiomyopathy-associated F-actin binding protein, binds and regulates IRS1 signaling in skeletal muscle cells. *PLoS One* **2013**, *8*, e55634.
(39) Ravichandran, L. V.; Chen, H.; Li, Y.; Quon, M. J, Phosphorylation of PTPB1 at Ser(50) by Akt impairs its ability to dephosphorylate the insulin receptor. *Mol. Endocrinol.* **2001**, *15*, 1768−1780.
(40) Rome, S.; Clément, K.; Rabasa-Lhoret, R.; Loizon, E.; Poitou, C.; Barsh, G. S.; Riou, J. P.; Laville, M.; Vidal, H. Microarray profiling of human skeletal muscle reveals that insulin regulates approximately 800 genes during a hyperinsulinemic clamp. *J. Biol. Chem.* **2003**, *278*, 18063−18068.
(41) Di Camillo, B.; Irving, B. A.; Schimke, J.; Sanavia, T.; Toffolo, G.; Cobelli, C.; Nair, K. S. Function-based discovery of significant transcriptional temporal patterns in insulin stimulated muscle cells. *PLoS One* **2012**, *7*, e32391.

models.[3,23,24] However, most studies on soybean and skin inflammation were performed using an atopic dermatitis (AD) model for human AD, the NC/Tnd mouse model.[25,26] Research on the effect of soybean on UVB-induced skin inflammation and skin photoaging has been focused on the topical application of isoflavone extract and anthocyanins prior to UVB irradiation of hairless mice.[27,28] Despite being considered a good dietary supplement, there is no report on anti-inflammatory effects of soybean long-term supplementation in UVB-treated animal models.

Fermentation is widely used in food processing. Fermentation is defined as the conversion of carbohydrates to alcohols and carbon dioxide or organic acids using yeasts, bacteria, or a combination of both. Through the process of fermentation, daidzin and genistin in soybean are converted into daidzein, and genistein, which have been shown to protect against UV-induced photodamage in human skin fibroblast cells.[4] Based on these previous reports, we investigated the anti-inflammatory effects of long-term dietary supplementation with fermented soybean in UVB-induced skin photodamage in hairless mice. Additionally, we compared the effectiveness of soybean (S) and fermented soybean (FS) long-term dietary supplementation in relieving skin inflammation pain caused by UVB irradiation in hairless mice.

## MATERIALS AND METHODS

**Chemicals.** Dulbecco's modified Eagle's medium (DMEM), fetal bovine serum (FBS), and penicillin streptomycin were purchased from Gibco BRL (Grand Island, NY, USA). 3-(4,5-Dimethylthiazol-2-yl)-2,5-diphenyltetrazolium bromide (MTT), dimethyl sulfoxide (DMSO), and a Masson's trichrome stain kit were purchased from Sigma-Aldrich (St. Louis, MO, USA). ELISA assay kits to measure levels of IL-16 were purchased from R&D Systems (R&D Systems, Inc., Minneapolis, MN, USA).

**Standard and Sample Preparation.** Daidzin, daidzein, genistin, and genistein were purchased from Sigma-Aldrich (St. Louis, MO). The standard stock solutions were prepared by dissolving 1 mg of each compound in 1 mL of methanol and stored at −20 °C. Soybean was supplied by Aqua Green Technology Co., Ltd. (Jeju, South Korea) in February 2012. A voucher specimen was deposited in the herbarium at the R&D Center of SEMPIO Food Company (Seoul, South Korea). Soybean was stored at −4 °C during the preparation. Soybean was roasted at 100 °C and ground prior to lyophilization. *Aureobasidium pullulans* (KCCM 12017) was purchased from the Korean Culture Center of Microorganisms (Seoul, South Korea) and *Pichia jadinii* (KFCC 11487P) was obtained from SEMPIO Food Company.

**Fermentation Conditions.** Fermented soybean was prepared according to a previously described method by Cho et al.[29] Briefly, synthetic medium containing soybean (40 g/L), 1.0 g/L ammonium nitrate, 0.5 g/L dipotassium phosphate, 0.1 g/L magnesium sulfate, and 1.0 g/L sodium chloride was autoclaved at 121 °C for 15 min. The two yeast cultures (*A. pullulans* and *P. jadinii*) were inoculated into a synthetic medium containing soybean in a 5-L bioreactor. The synthetic medium was incubated at 30 °C with shaking at 20*g* for 48 h. The samples were then sterilized at 121 °C for 10 min to prevent contamination, after which they were freeze-dried and stored at −18 °C. The yield of the fermented sample was 90%.

**HPLC Analysis.** The HPLC analysis was carried out on a Waters system (Waters Corp., Milford, MA), consisting of a separation module (e2695) with an integrated column heater, an autosampler, and a photodiode array detector (2998). UV absorbance was monitored at 200−400 nm. Quantification was carried out by integration of the peak areas at 254 nm. The injection volume was 10 μL. A column (J'shpere ODS-H80, 250 mm × 4.6 mm; particle size, 4 μm; YMC Co. Ltd., Japan) was installed in a column oven and maintained at 40 °C.[28] The mobile phase was composed of water containing 1% acetic acid (solvent A) and acetonitrile (solvent B). The flow rate was 1.0 mL/min. The gradient was 0.0 min, 8% B; 3.5 min, 15% B; 12.0 min, 17% B; 23.0 min, 24% B; 28.0 min, 50% B; 33.0 min, 100% B; 38.0 min, 100% B; and 40.0 min, 8% B. The re-equilibration time between runs was 20 min.

**Cell Culture.** Normal human dermal fibroblasts (NHDFs) were purchased from ScienCell Research Laboratories (CA, USA). Human keratinocytes (HaCaT) were supplied by professor Tae-Yoon Kim. These cells were grown in DMEM supplemented with 10% FBS, 100 U/mL of penicillin, and 100 U/mL of streptomycin at 37 °C, in a 5% $CO_2$ humidified atmosphere.

**Co-cultivation of NHDF and HaCaT Cells and Treatment of UVB.** NHDF and HaCaT cells were cocultivated according to a previously described method with some modifications.[30] Fibroblast NHDF cells were seeded at $6 \times 10^4$ cells/mL in 40 mm cell culture dishes. And it was incubated in a DMEM culture medium. After 24 h, keratinocyte HaCaT cells ($6 \times 10^4$ cells/mL) were added to the NHDF cultures in the DMEM culture medium. After 24 h, the cell mixture was washed with PBS and was treated with 100 mJ/cm$^2$ of UVB irradiation under a BLX-312 UV irradiation system (Vilber Lourmat, Marne-La-Vallée, France). The cell mixture was washed with PBS and changed into fresh serum-free medium. The cell mixture was then treated 10 μM of diadzin, daidzein, genistin, and genistin and incubated at 37 °C in a humidified air atmosphere in the presence of 5% $CO_2$ for 72 h. Finally, conditioned medium and cells were harvested for the ELISA assay and Western blot analysis, respectively.

**Animals.** Seven-week-old albino and hairless male mice (SKH:HR-1) (20−27 g; $n$ = 40) were obtained from Japan SLC, Inc. (Hamamatsu, Japan). The experimental protocol for this study was approved by the Institutional Animal Care and Use Committee of Kyunghee University (KHUASP (SU)-12-09). Mice were housed in a temperature- and humidity-controlled room (22 ± 1 °C, 60 ± 5% humidity) with 12 h light/dark cycles. After a week of quarantine, mice were randomly divided into 4 groups with 10 mice/cage and acclimated. During the experimental period, access to food and water was provided *ad libitum*.

**UVB Exposure to Hairless Mice.** The UV source was supplied by a closely spaced array of five Sankyo Denki sunlamps, which have an irradiance peak at 310 nm (Kanagawa, Japan). Bulbs were positioned 15 cm above the mice. Irradiance (0.1 mW/cm$^2$) was measured with an IL1700 Research Radiometer (International Light, Inc., Newburyport, MA) equipped with a UVB sensor. Mice were exposed to 100 mJ/cm$^2$ UVB radiation (minimal erythemal dose) every day for the first week, and at 200 mJ/cm$^2$ three times per week thereafter for 11 weeks. UVB irradiation was applied to the dorsal skin of mice.

**Diet.** Forty hairless male mice were randomly assigned to four groups of ten mice per cage: (a) normal (N) (control diet only), (b) control (C) (UVB irradiation + control diet), (c) soybean (S) 2.5% (UVB irradiation + diet containing 2.5% soybean), and (d) fermented soybean (FS) 2.5% (UVB irradiation + diet containing 2.5% fermented soybean). All the mice were fed solid formula feed. Animals in each group received the experimental diets for 8 weeks concurrently with the UVB irradiation regimen. Dietary sources were provided (500 g/cage) every week. To calculate the feed intake, we measured the weight of the remaining feed each week. The animals were allowed free access to food and water. The body weight of mice was measured once a week.

**Histological Skin Analysis.** The animals were euthanized after the final UVB exposure, and biopsies were obtained from the dorsal skin. Biopsies were fixed in 4% paraformaldehyde for 24 h and embedded in paraffin. Four-micrometer-thick sections were stained with hematoxylin for 10 min, washed, and then stained with eosin for 2 min. After washing with water, the slides were gradually dehydrated in 50%, 70%, 90%, and 100% ethanol. For immunohistochemistry, the sections were incubated in 0.1% protease in PBS for antigen retrieval. Then the sections were incubated in 3% $H_2O_2$ in PBS for 10−15 min to block endogenous peroxidase activity. The sections were then incubated with 2% normal horse serum in PBS for 20 min to block nonspecific binding of secondary immunoglobulin. After blocking, the sections were incubated with primary antibody CD11b and iNOS (Cell Signaling Technology, Danvers, MA). After washing in PBS, the

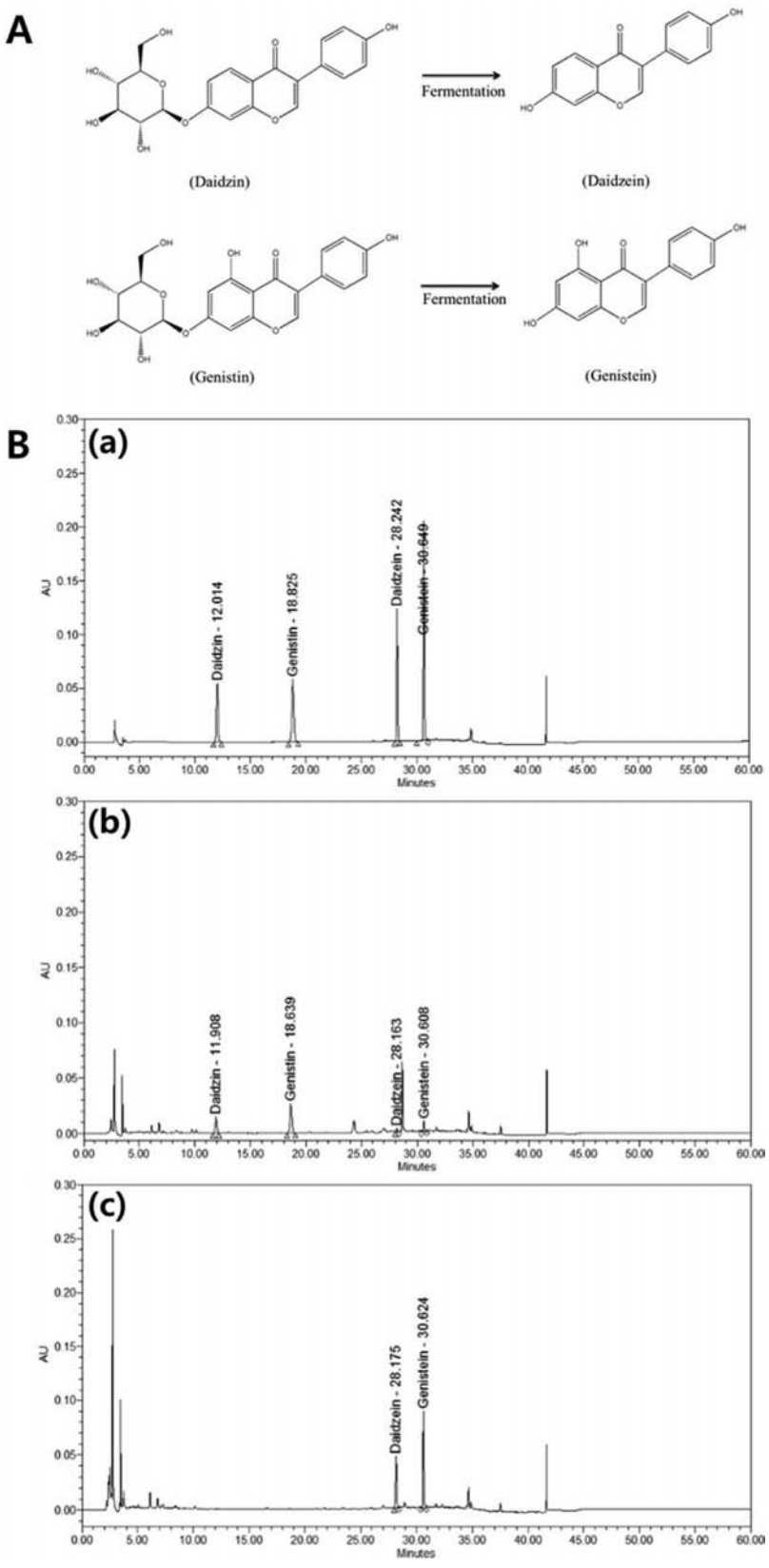


**Figure 1.** (A) Bioconversion of soy isoflavones by fermentation process. (B) Representative HPLC chromatogram of soybean: standard (a); soybean (b); fermented soybean (c).

slides were incubated in Vectastain ABC reagent (Vector Laboratory, Piscataway, NJ) for 1 h. The color was developed with 3,3′-diaminobenzidine (DAB). Images were recorded using a Zeiss inverted microscope connected to a digital CCD camera (Axiocam, Zeiss, Oberko, Germany). For immunohistofluorescence analysis, the method is the same as above up to the blocking step. Then slides were


dx.doi.org/10.1021/jf5018252 | J. Agric. Food Chem. 2014, 62, 8962−8972

incubated in COX-2 antibodies (Cell Signaling Technology, Danvers, MA) at 4 °C for overnight. After a wash with PBS, the sections were incubated with FTIC-conjugated secondary antibodies (Santa Cruz Biotechnology Inc., CA). Nuclei were counterstained with 4′,6-diamidino-2-phenylindole (DAPI). The sections were then observed under a Zeiss LSM 700 confocal microscope (Carl Zeiss, Oberkochen, Germany).

**Western Blot Analysis.** Western blotting was performed using cells and skin tissue lysates. Following treatment, cells and tissues were harvested and washed in PBS. Tissue samples were homogenized with lysis buffer containing 50 mM Tris-Cl, pH 8.0, 0.1% SDS, 150 mM NaCl, 1% NP-40, 0.02% sodium azide, 0.5% sodium deoxycholate, 100 Pg/mL PMSF, 1 pg/mL aprotinin, and a phosphatase inhibitor. The lysates were then subjected to centrifugation at 12,000*g* for 20 min. Cells and tissue lysates were analyzed in triplicate. Protein concentrations were measured using the Bradford reagent (Bio-Rad, Hercules, CA) with bovine serum albumin as the standard. Cells and skin tissue lysates containing equal amounts of total protein were separated on 10% or 12% SDS-PAGE gels and then transferred to a nitrocellulose membrane (Amersham Pharmacia Biotech, UK). Next, the membranes were blocked with a solution containing 5% nonfat milk in TBST for 1 h at room temperature and then incubated overnight with a primary antibody at 4 °C. The membranes were then washed three times with TBST and incubated with secondary antibodies (Santa Cruz Biotechnology Inc., CA) for 1 h at room temperature. Finally, the immune complexes were detected with a chemidoc XRS+ imaging system (Bio-Rad, CA). Densitometry analysis of the bands was performed using imagequant TL version 8.1 (GE Healthcare, Madison, WI).

**Statistical Analysis.** All experiments were carried out in triplicate. The data are expressed as means ± standard deviation (SD). Statistical comparisons between different treatment groups were performed using one-way analysis of variance (ANOVA) with Tukey' multiple comparisons test. The level of statistical significance was set at $*P < 0.05$, $**P < 0.01$, and $***P < 0.001$.

## RESULTS

**Soybean and Fermented Soybean Isoflavonoid Content.** Daidzin and genistin were converted into daidzein and genistein by a fermentation process in soybean (Figure 1A).[31] Daidzin, daizein, genistin, and genistein contents in soybean and fermented soybean were measured by HPLC. The retention time of each compound is presented in Figure 1. The linearity of each compound was calculated using three concentrations of each specific compound. The daidzin, daidzein, genistin, and genistein contents in soybean were 0.1197, 0.0053, 0.2220, and 0.0170 μg/mg, respectively. The daidzein and genistein contents in fermented soybean were 0.1870 and 0.2083 μg/mg, respectively (Table 1). Daidzin and genistin peaks were not detected in fermented soybean (Figure 1B). Our HPLC results confirmed the significant bioconversion of the isoflavonoidal glycosides into their corresponding aglycone types in fermented soybean.

**Table 1. Isoflavone Content (μg/mg) in Soybean and Fermented Soybean**

| | $r^2$ | soybean | fermented soybean |
|---|---|---|---|
| Daidzin | 0.9997 | 0.1197 ± 0.0008 | - |
| Daidzein | 0.9997 | 0.0053 ± 0.0003 | 0.1870 ± 0.0020 |
| Genistin | 0.9997 | 0.2220 ± 0.0002 | |
| Genistein | 0.9998 | 0.0170 ± 0.0001 | 0.2083 ± 0.0021 |

**Daidzein and Genistein Inhibited IL-6 and Phosphorylation of MAPK Signaling in HaCaT Keratinocytes and NHDF Fibroblasts Coculture Systems.** We confirmed that diadzein and genistein are major isoflavones of fermented soybean (Figure 1). To investigate the anti-inflammatory activities of these two compounds, we used coculture systems with keratinocytes and fibroblasts. These different cells were grown in a single dish. When the cell mixtures were treated with 100 mJ/cm$^2$ of UVB irradiation, they were mildly damaged. The cell viability of UVB treated control cells was decreased by 76.6% ± 1.3% compared with UVB nontreated normal cells (Figure 2B). When the cell mixtures were treated with 10 μM of daidzin, daidzein, genistin, and genistein, there was no effect on cell viability in UVB treated cells (Figure 2A, B).

UVB irradiation stimulated the cell mixture. As a result, secretion of pro-inflamatory cytokines increased. We measured two major pro-inflamatory cytokines: interleukin-6 (IL-6) and tumor necrosis factor-α (TNF-α). The concentration of IL-6 was higher in the conditioned medium of the UVB control group compared with the normal group. Although the difference was not statistically significant, we confirmed the inhibitory effect of daidzein and genistein on IL-6 production (Figure 2C). TNF-α was not detected in conditioned medium (data not shown).

We investigated the MAPK signaling cascade, which is known to regulate inflammation. All compounds (daidzin, daidzein, genistin, and genistein) inhibited UVB-induced phosphorylation of ERK (Figure 2E). In particular, genistein inhibited phosphorylation of p38, ERK, and JNK (Figure 2D–F). Moreover, the inhibitory activity of genistein was significantly different for genistin and genistein (Figure 2D, E)

**Measurement of Food Efficiency Ratio.** There was no significant difference in the average body weight among the four groups of mice after 12 weeks. The groups did not differ significantly in their food efficiency ratios (Figure 3C).

**FS Dietary Supplementation Improved UVB-Induced Skin Erythema and Inflammation.** Mouse dorsal skin physiological changes were recorded after dietary supplementation with S or FS, and after 12 weeks of UVB irradiation. Prolonged skin exposure to UVB leads to skin inflammation erythema and epidermal thickness. In our study, the group FS presented a decrease in UVB-induced erythema (Figure 4A). In addition, the thickness of the epidermis in the UVB treated control group was significantly larger than the normal group. However, this increase in epidermal thickness was lower in the S (79.4 ± 0.8%) and the FS (83.4 ± 0.8%) group (Figure 4B, C).

Our histological analysis indicated that UVB radiation induced typical skin inflammation in hairless mice. Prolonged exposure to UVB increased the macrophage population in the upper dermis and epidermis (Figure 4D). Scoring of the four groups was done by Dr. Young Lyun Oh, who is a pathologist at SMC, Korea, based on our H&E staining analysis. The inflammation score was classified as either 0, +, ++, or +++. The score "0" indicates no inflammation, and the number of + symbols indicates the degree of inflammation. Therefore, "+++" represents severe skin inflammation. Group N had a score of "0" and group C was "+++", group S was "+," and group FS was "0−+." Inflammatory symptoms such as intrahorn and subepithelial vacuolization were observed in group C. However, these symptoms were not observed in other groups. Based on immunohistochemical analysis, the population of CD11b$^+$ macrophages was significantly reduced in the group FS compared with the control group (Figure 4D). Particularly,


dx.doi.org/10.1021/jf5018252 | J. Agric. Food Chem. 2014, 62, 8962−8972

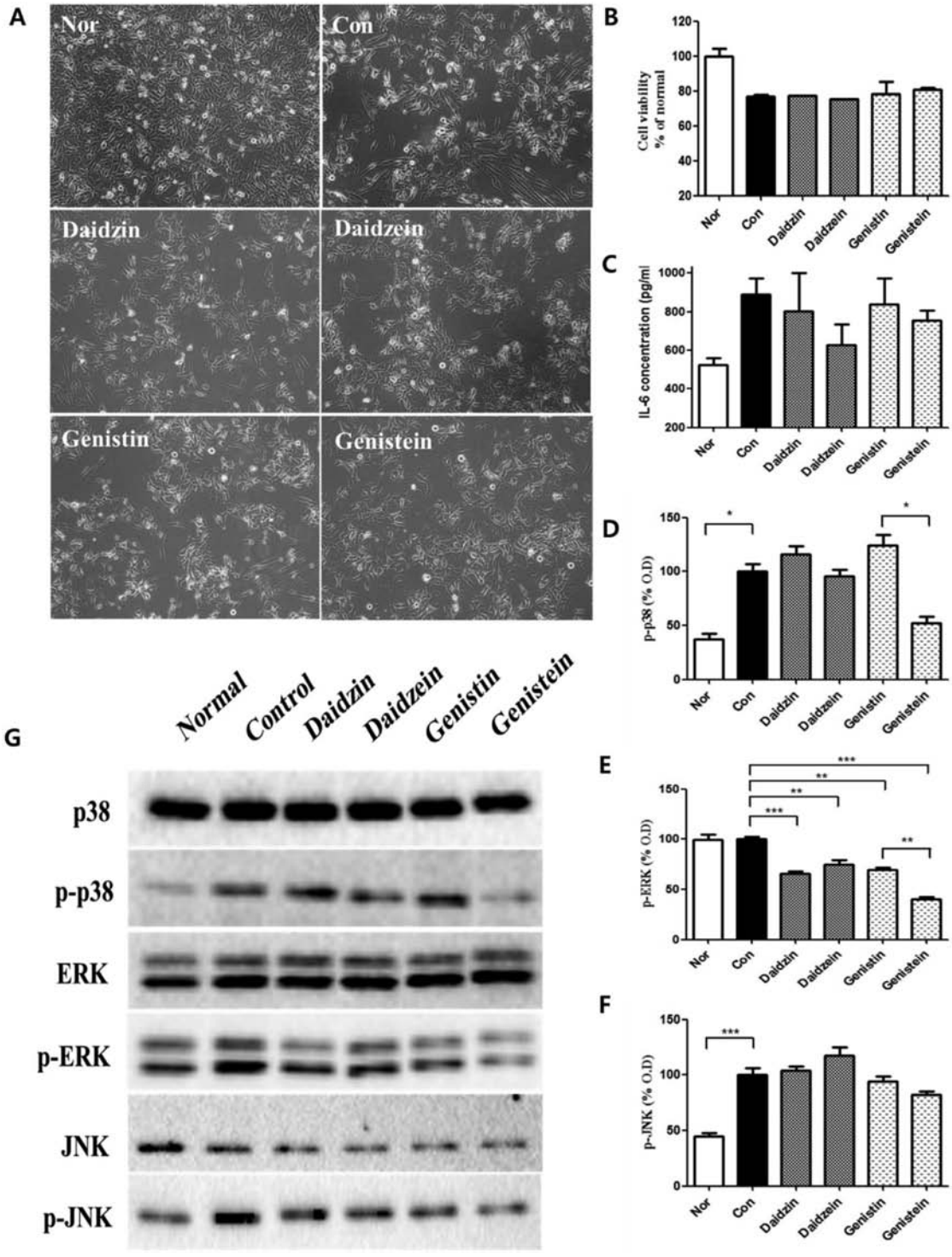


**Figure 2.** Effect of Daidzin, Daidzein, Genistin, and Genistein on the production of IL-6 and MAPK signaling in a UV-irradiated HaCaT and NHDF coculture. NHDF cells and HaCaT cells were grown in the same dish (1:1 cellular mixture). After treatment with 10 $\mu$M of each of the four compounds for 72 h, cells were observed using an Olympus CKX-41 microscope (×100 in bright field) (A) and cell viability was measured by an MTT assay (B). Conditioned medium was cultivated and the IL-6 concentration was measured (C). For Western blot analysis, the mixtures were treated with 100 mJ/cm$^2$ of UVB irradiation and 10 $\mu$M of each of the four compounds, treated at the same time. After 1 h, the mixture cells were harvested and the protein levels were measured (D−G). *$P$ < 0.05, **$P$ < 0.01, and ***$P$ < 0.001 indicate statistically significant differences.

the anti-inflammatory effect was more intense in group FS than in group S.

**FS Inhibits iNOS and COX-2 Expression.** In the immunohistological analysis, group C showed a marked increase in iNOS expression, especially in the epidermis (Figure 5A). We also confirmed the increase in iNOS expression in group C by Western blot analysis (Figure 5B). Interestingly, dietary supplementation with S and FS inhibited the protein expression of iNOS at 70.3% ± 7.0% and 7.7% ± 0.4%, respectively ($p$ < 0.05) (Figure 5C). The increase of COX-2 expression in group C (Figure 6A) was inhibited by


dx.doi.org/10.1021/jf5018252 | J. Agric. Food Chem. 2014, 62, 8962−8972

A

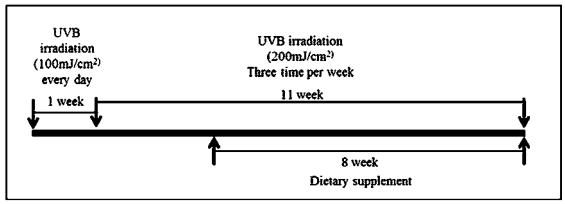


B

Composition of diet (g/kg Dry diet)

| | Experimental groups | | | |
|---|---|---|---|---|
| | N (n=10) | C (n=10) | S (n=10) | FS (n=10) |
| Casein | 200 | 200 | 200 | 200 |
| L-Cystine | 3 | 3 | 3 | 3 |
| Maltodextrin 10 | 132 | 132 | 132 | 132 |
| Surcrose | 100 | 100 | 100 | 100 |
| Cellulose | 50 | 50 | 50 | 50 |
| Soybean Oil | 70 | 70 | 70 | 70 |
| T-Butylhydrozuinone | 70 | 70 | 70 | 70 |
| Mineral Mix | 35 | 35 | 35 | 35 |
| Vitamin Mix | 10 | 10 | 10 | 10 |
| Choline Bitartrate | 2.5 | 2.5 | 2.5 | 2.5 |
| Corn Starch | 397 | 397 | 372 | 372 |
| S (soybean) | - | - | 25 | - |
| FS (fermented soybean) | - | - | - | 25 |

C

Food efficiency ratio of experimental groups

| | Dietary group[a] | | | |
|---|---|---|---|---|
| | N | C | S | FS |
| FER[b] | 0.094±0.017 | 0.098±0.017 | 0.095±0.018 | 0.096±0.020 |

**Figure 3.** (A) Experimental design of the animal study procedures. (B) Composition of diet. (C) Food efficiency ratio during the 8 week intervention. [a]Group N: hairless mice fed control diet only; group C: UVB-irradiated hairless mice fed control diet; groups S: UVB-irradiated hairless mice fed diets containing 2.5% soybean; groups FS: UVB-irradiated hairless mice fed diets containing 2.5% fermented soybean. [b]FER (food efficiency rate) = gain of body weight (g)/amount of food intake (g). Values are mean ± SEM ($n$ = 10). Means with different letters differ by $P < 0.05$.

long-term dietary supplementation with S and FS by 26.9% ± 0.4% and 21.2% ± 0.3%, respectively ($p < 0.05$) (Figure 6B, C).

**FS Regulates MAPK Signaling in the Skin Dermis of UVB-Irradiated Hairless Mice.** The UVB-induced inflammatory responses were remarkably reduced by FS long-term treatment. To evaluate the FS anti-inflammatory mechanism on UVB-induced skin inflammation, we investigated the MAPK signaling pathways in the skin dermis by Western blot analysis. UVB radiation increased the phosphorylation of p38, ERK, JNK, and c-Jun in the skin.[1,10] As shown in Figure 7, phosphorylation of p38, ERK, JNK, and c-Jun was increased in UVB-irradiated skin dermis. In contrast, long-term FS treatment significantly inhibited the phosphorylation of MAPK (p-p38, 61.3 ± 0.5%; p-ERK, 78.9 ± 3.3%; p-JNK, 14.4 ± 0.5%; and p-c-Jun, 37.6 ± 0.6%) (Figure 7B–E).

## DISCUSSION

Dietary supplements such as vitamins, minerals, or essential fatty acids have been reported to restore damaged skin.[21,32] Particularly, dietary supplements can help control skin aging as well as inflammation and hyperpigmentation due to overexposure to UVR. However, there is only a paucity of evidence in the literature; therefore, in depth studies are required. Natural and functional food sources will allow the development of nutraceutical and cosmeceutical treatments for skin photodamage. Evidence suggests that soybeans containing isoflavones may be useful for the regulation of skin problems.[33−35] However, no report is available on the anti-inflammatory effect of long-term soybean dietary supplementation on skin inflammation in UVB-irradiated animals. First, we chose the safest and potential soybean as a natural source of functional food for the regulation of photoinduced skin inflammation. Raw soybeans are rich in soyasaponins and isoflavonol glycosides. Namely, soybeans generally contain more isoflavonol glycosides, such as daidzin, genistin, and glycitin, than aglycone type, such as daidzein, genistein, and glycitein.[36] Because long-term use of soybean may be associated with allergic reactions involving rash, itching, food protein-induced enterocolitis, constipation, bloating, and nausea,[20,21] long-term dietary supplementation is difficult to achieve. Although natural products have many great benefits as dietary supplements, there are some limits in terms of efficacy and side effects. In an attempt to increase the efficacy of soybean supplementation, we established an optimal fermentation process design. The strategy included fermentation optimization using a mixed native yeast culture composed of *Pichia jadinii* and *Aureobasidium pullulans*. The optimization standards were based on isoflavonoid glycoside contents and efficacy as well as flavor and taste. Our goal was to increase the efficiency and activity as well as the flavor and taste compared to raw soybeans. In fact, several studies have already reported that biological activities of natural products might be improved by fermentation. Kim et al. reported that fermented red ginseng showed higher antiobesity effect on obesity-mediated metabolic disorders than nonfermented red ginseng.[37] Our recent study proved the enhanced antiphotoaging activity of *Opuntia ficus-indica* by fermentation using two species of yeast, *Pichia jadinii* and *Aureobasidium pullulans*.[29] For this reason, we designed a powerful strategy, such as soybean fermentation with *Pichia jadinii* and *Aureobasidium pullulans*. Based on our HPLC analysis, we found that FS contained only aglycone type. Isoflavone glycosides were not detected in FS. Soy isoflavone aglycones were increased through the fermentation process, which converts glucosides into aglycone by deconjugation of the glycosyl group of a glycoside (Figure 1).[31] According to several studies, daidzein and genistein show higher bioavailability and bioactivity than daidzin and genistin. Iovine et al. reported that daidzein and genistein present synergic effects on UVB-mediated DNA damage.[4] In fact, aglycones may be absorbed faster and better than glucosides in the human body.[38] In conclusion, this fermented soybean may be biochemically and technically superior to its raw material.

Dermatitis is a representative problem that is related to skin inflammation. Chronic and overexposure to UVR can induce photosensitivity and photoallergy, which can subsequently lead to phototoxic dermatitis. Particularly, UVB is a potent factor, which induces skin inflammation. Our histological data indicate that the UVB-irradiated group typically showed severe inflammation of the intrahorn. Other groups previously reported that UVB radiation triggered skin inflammation by inflammatory cellular infiltration into the upper dermis and epidermis.[39] We also confirmed inflammatory cellular infiltration in the skin dermis of the UVB-induced group (Figure 4).

Macrophages, important inflammatory cells, are involved in the initiation of inflammation by the production of various proinflammatory mediators such as nitric oxide (NO) and prostaglandins (PGs). The production of NO and PGs are

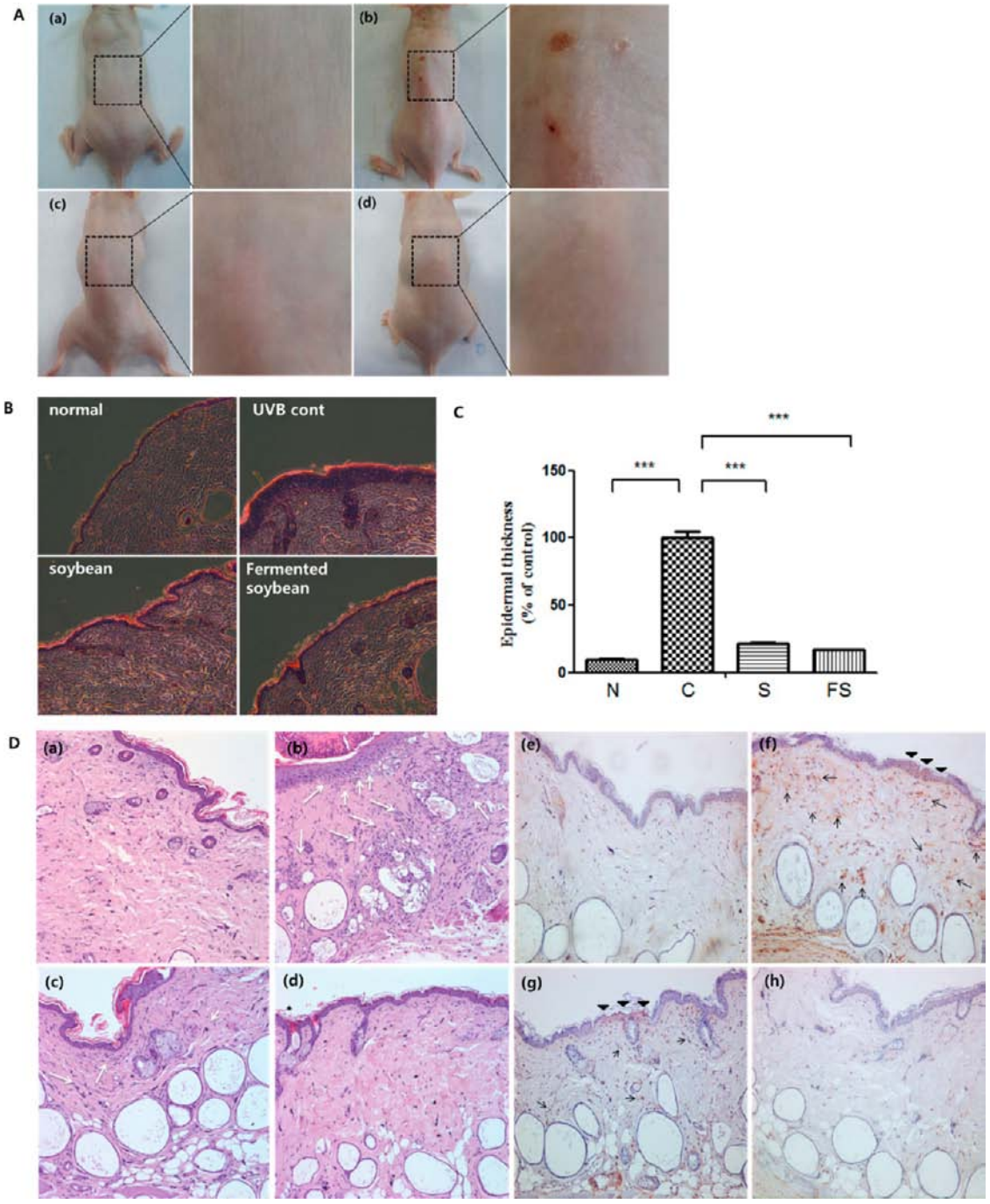


**Figure 4.** (A) Effects of S and FS on the histology of UVB irradiated hairless mouse skin. (B) Representative features of hairless mice dorsal skin: Group N with no UVB irradiation (a), group C with UVB irradiation (b), group S with UVB irradiation and soybean supplementation (c), and group FS with UVB irradiation and fermented soybean supplementation (d) were recorded using a digital camera (Samsung, Korea). H&E staining (magnification 200×). (C) Measurement of epidermal thickness. (D) Analysis of inflammatory infiltration of macrophages using the marker CD11b in hairless mouse skin after UVB irradiation. White arrows indicate infiltrating inflammatory cells in H&E stained tissue (magnification 200×). Black arrows and arrowhead indicate $CD11b^{+}$ macrophage cells (magnification 200×). Group N with no UVB irradiation (a, e), group C with UVB irradiation (b, f), group S (c, g), group FS (d, h).

regulated by iNOS and COX-2 enzymes, respectively.[40,41] Thus, overexpression of COX-2 in the skin may result in edema and epidermal hyperplasia.[28,42] Our immunohistological study indicated that UVB overexposure increased iNOS and COX-2 expression in the dermal cells of the dorsal skin (Figures 5 and 6). Interestingly, a dietary supplement of FS significantly decreased iNOS and COX-2 expression in the skin. Recent studies report a link between iNOS, COX-2, and photoinflammation in mouse skin. In particular, the up-regulation of COX-2 is often accompanied by overexpression of iNOS.[43] In conclusion, FS inhibited both iNOS and COX-2 expression in dermal skin. FS ameliorated skin inflammation by UVB irradiation, which regulates MAPK signaling. Furthermore, activation of MAPK can cause the induction of iNOS and COX-2 expression and, consequently, may induce skin cancer.[44]


dx.doi.org/10.1021/jf5018252 | J. Agric. Food Chem. 2014, 62, 8962−8972

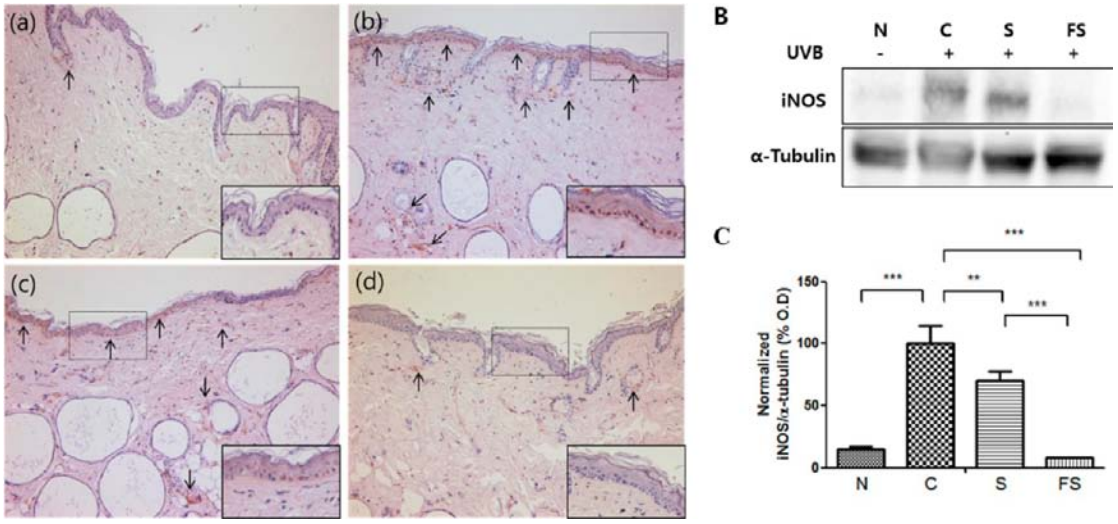


**Figure 5.** (A) Effects of S and FS on iNOS expression in the skin. Representative immunohistochemical images show that iNOS (brown color) is expressed. Nuclei were counterstained with hematoxylin (magnification 200×). Black arrows indicate iNOS expressed cells: group N (a), group C (b), group S (c), and group FS (d). (B) Western blot analysis of iNOS in skin lysates. (C) The protein expression of iNOS was normalized to the band corresponding to $\alpha$-tubulin. $^{**}P < 0.01$ and $^{***}P < 0.001$ indicate statistically significant differences.

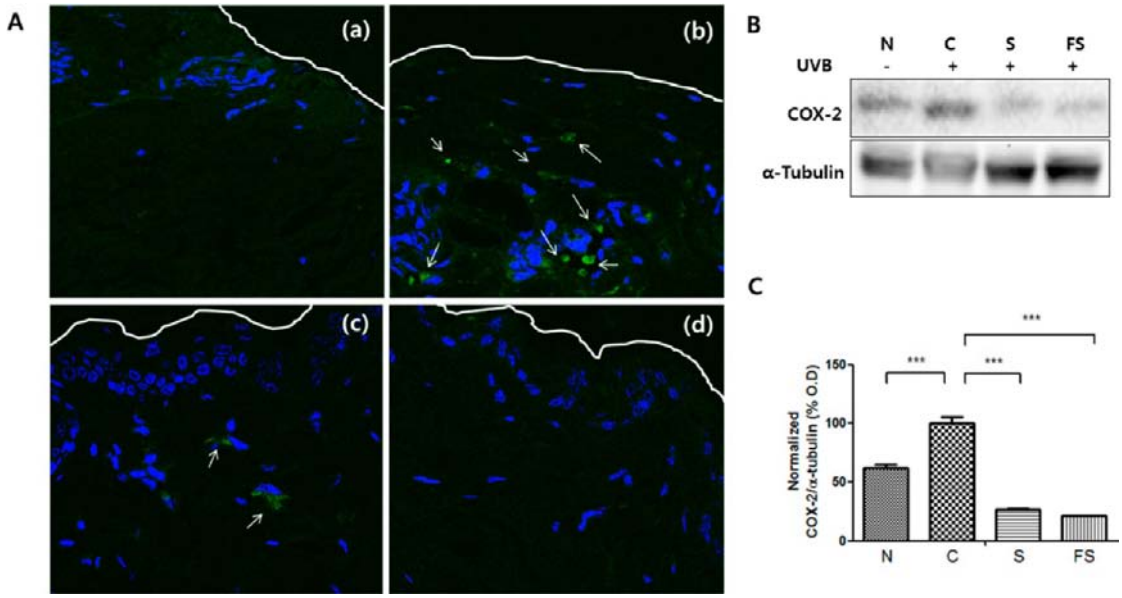


**Figure 6.** (A) Effects of S and FS on COX-2 expression in the skin. Representative immunohistochemical images show that COX-2 (green staining) is expressed. Nuclei were counterstained using DAPI (blue staining) (magnification 400×). White arrows indicate COX-2 expression; group N (a), group C (b), group S (c), and group FS (d). (B) Western blot analysis of COX-2 in skin lysates. (C) The protein expression of COX-2 was normalized to the band corresponding to $\alpha$-tubulin. $^{*}P < 0.05$ and $^{**}P < 0.01$ indicate statistically significant differences.

UVB-induced skin inflammation is usually conducted under acute UV exposure conditions in *in vivo* models.[10,45,46] After 24 h of UVB exposure, inflammatory signaling was significantly changed. Kim et al. reported that phosphorylation of p38 MAPK was increased by UVB exposure in a time dependent manner at 24 h. Thus, their studies support that p38 MAPK plays an important role in UVB-induced inflammatory responses in the skin of SKH-1 hairless mice.[47] Generally, recovery from skin inflammation is easy and spontaneous in acute UVB exposure models. Therefore, identifying the anti-inflammatory effects of a product in acute conditions can be challenging. In this study, we focused on chronic skin inflammation, which is induced after long-term UVB exposure (12 weeks). From our results, we showed that chronic skin inflammation by UVB exposure significantly changed the MAPK signaling pathway. Soybean inhibited the UVB-induced activation of p38, JNK, and c-JUN. Furthermore, FS was more effective in inhibiting p-JNK activation than S. Raw soybean had no effect on the regulation of ERK, but FS treatment strongly affected ERK phosphorylation in the dorsal skin. Thus, the anti-inflammatory effect of FS on UVB-induced skin inflammation could mainly be attributed to the regulation of MAPK signaling. However, additional studies on fermented and raw soybean are warranted to confirm these results. Based on our HPLC data, the chemical patterns of FS were different from that of raw soybean in the polar region, distinguishing the isoflavonoid region. Further studies are required to definitively identify the most biologically active component in FS. Our


dx.doi.org/10.1021/jf5018252 | J. Agric. Food Chem. 2014, 62, 8962−8972

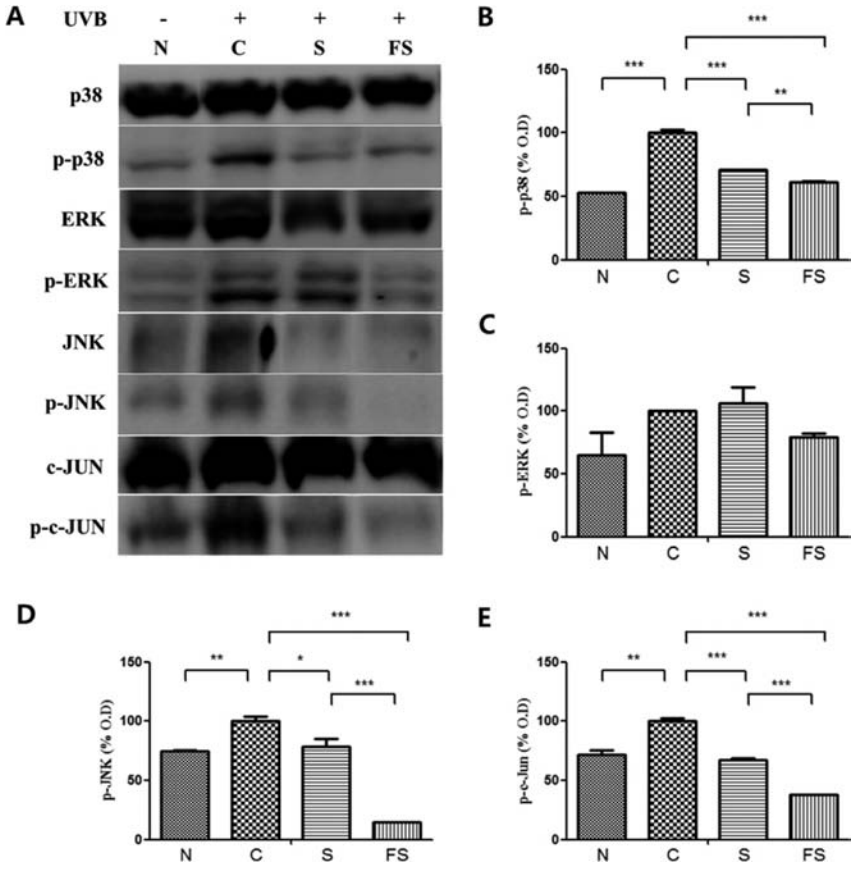


**Figure 7.** Effects of S and FS on UVB-induced MAPK signaling in skin lysates by Western blot and densitometric analysis. Forty micrograms of total protein from the tissue lysates were used for Western blot analysis. Significance was determined using a one-way ANOVA followed by a Tukey's multiple comparison test. $^{*}P < 0.05$, $^{**}P < 0.01$, and $^{***}P < 0.001$ indicate statistically significant differences.

study only investigated the efficacy of fermented soybean in resolving chronic skin inflammation. However, our findings indicate that future research on the use of natural resources such as soybean in the treatment of chronic skin inflammation may be promising.

In conclusion, this study provides meaningful evidence that long-term dietary supplementation with isoflavone-rich, fermented soybean improves skin inflammation induced by chronic exposure to UVB. We suggest that natural fermented soybean will be a safe, potential functional food for skin inflammation due to photodamage.

## AUTHOR INFORMATION

### Corresponding Author

*Tel: +82-32-899-6411, Fax: +82-32-899-8962, E-mail: sunnykim@gachon.ac.kr.

### Funding

This research was supported by Korea Institute of Planning and Evaluation for Technology in Food, Agriculture, Forestry and Fisheries (iPET, 311035-03-1-HD110), and a grant from the Next-Generation BioGreen 21 Program (No.PJ009511), Rural Development Administration, Republic of Korea.

### Notes

The authors declare no competing financial interest.

## ABBREVIATIONS USED

UV, ultraviolet; UVR, ultraviolet radiation; UVB, ultraviolet B; S, soybean; FS, fermented soybean; ROS, reactive oxygen species; MAPK, mitogen-activated protein kinase; ERK, extracellular signal-regulated kinase; JNK, c-Jun amino-terminal kinase; COX-2, cyclooxygenase-2; iNOS, inducible nitric oxide synthase; TNF-$\alpha$, tumor necrosis factor-$\alpha$; MMP, metalloproteinase; AD, atopic dermatitis; YM, yeast mold; DAPI, 4′,6-diamidino-2-phenylindole; SD, standard deviation; ANOVA, analysis of variance

## REFERENCES

(1) Dickinson, S. E.; Olson, E. R.; Zhang, J.; Cooper, S. J.; Melton, T.; Criswell, P. J.; Casanova, A.; Dong, Z.; Hu, C.; Saboda, K.; Jacobs, E. T.; Alberts, D. S.; Bowden, G. T. p38 MAP kinase plays a functional role in UVB-induced mouse skin carcinogenesis. *Mol. Carcinog.* **2011**, *50*, 469−78.

(2) Katiyar, S.; Elmets, C. A.; Katiyar, S. K. Green tea and skin cancer: photoimmunology, angiogenesis and DNA repair. *J. Nutr. Biochem.* **2007**, *18*, 287−96.

(3) Chen, N.; Scarpa, R.; Zhang, L.; Seiberg, M.; Lin, C. B. Nondenatured soy extracts reduce UVB-induced skin damage via multiple mechanisms. *Photochem. Photobiol.* **2008**, *84*, 1551−9.

(4) Iovine, B.; Iannella, M. L.; Gasparri, F.; Monfrecola, G.; Bevilacqua, M. A. Synergic Effect of Genistein and Daidzein on UVB-Induced DNA Damage: An Effective Photoprotective Combination. *J. Biomed. Biotechnol.* **2011**, *2011*, 692846.

(5) Morch, C. D.; Gazerani, P.; Nielsen, T. A.; Arendt-Nielsen, L. The UVB cutaneous inflammatory pain model: a reproducibility study in healthy volunteers. *Int. J. Physiol. Pathophysiol. Pharmacol.* **2013**, *5*, 203−15.

(6) Ryser, S.; Schuppli, M.; Gauthier, B.; Hernandez, D. R.; Roye, O.; Hohl, D.; German, B.; Holzwarth, J. A.; Moodycliffe, A. M. UVB-induced skin inflammation and cutaneous tissue injury is dependent

on the MHC class I-like protein, CD1d. *J. Invest. Dermatol.* **2014**, *134*, 192−202.
(7) Shibata, A.; Nakagawa, K.; Yamanoi, H.; Tsuduki, T.; Sookwong, P.; Higuchi, O.; Kimura, F.; Miyazawa, T. Sulforaphane suppresses ultraviolet B-induced inflammation in HaCaT keratinocytes and HR-1 hairless mice. *J. Nutr. Biochem.* **2010**, *21*, 702−9.
(8) Honda, K. S. HIV and skin cancer. *Dermatol. Clin.* **2006**, *24*, 521−30 , vii..
(9) Wolnicka-Glubisz, A.; Damsker, J.; Constant, S.; Corn, S.; De Fabo, E.; Noonan, F. Deficient inflammatory response to UV radiation in neonatal mice. *J. Leukoc. Biol.* **2007**, *81*, 1352−61.
(10) Lee, J. K.; Ko, S. H.; Ye, S. K.; Chung, M. H. 8-Oxo-2′-deoxyguanosine ameliorates UVB-induced skin damage in hairless mice by scavenging reactive oxygen species and inhibiting MMP expression. *J. Dermatol. Sci.* **2013**, *70*, 49−57.
(11) Kaminska, B. MAPK signalling pathways as molecular targets for anti-inflammatory therapy—from molecular mechanisms to therapeutic benefits. *Biochim. Biophys. Acta* **2005**, *1754*, 253−62.
(12) Debacq-Chainiaux, F.; Leduc, C.; Verbeke, A.; Toussaint, O. UV, stress and aging. *Dermatoendocrinol* **2012**, *4*, 236−40.
(13) Schonthaler, H. B.; Guinea-Viniegra, J.; Wagner, E. F. Targeting inflammation by modulating the Jun/AP-1 pathway. *Ann. Rheum. Dis.* **2011**, *70* (Suppl 1), i109−12.
(14) Koistinaho, M.; Kettunen, M. I.; Goldsteins, G.; Keinanen, R.; Salminen, A.; Ort, M.; Bures, J.; Liu, D.; Kauppinen, R. A.; Higgins, L. S.; Koistinaho, J. Beta-amyloid precursor protein transgenic mice that harbor diffuse A beta deposits but do not form plaques show increased ischemic vulnerability: role of inflammation. *Proc. Natl. Acad. Sci. U. S. A.* **2002**, *99*, 1610−5.
(15) Velasquez, M. T.; Bhathena, S. J. Role of dietary soy protein in obesity. *Int. J. Med. Sci.* **2007**, *4*, 72−82.
(16) Roghani, M.; Vaez Mahdavi, M. R.; Jalali-Nadoushan, M. R.; Baluchnejadmojarad, T.; Naderi, G.; Roghani-Dehkordi, F.; Taghi Joghataei, M.; Kord, M. Chronic administration of daidzein, a soybean isoflavone, improves endothelial dysfunction and attenuates oxidative stress in streptozotocin-induced diabetic rats. *Phytother. Res.* **2013**, *27*, 112−7.
(17) Lee, Y. K.; Park, O. J. Soybean isoflavone genistein regulates apoptosis through NF-kappaB dependent and independent pathways. *Exp. Toxicol. Pathol.* **2013**, *65*, 1−6.
(18) Kanamoto, Y.; Yamashita, Y.; Nanba, F.; Yoshida, T.; Tsuda, T.; Fukuda, I.; Nakamura-Tsuruta, S.; Ashida, H. A black soybean seed coat extract prevents obesity and glucose intolerance by up-regulating uncoupling proteins and down-regulating inflammatory cytokines in high-fat diet-fed mice. *J. Agric. Food Chem.* **2011**, *59*, 8985−93.
(19) Rebholz, C. M.; Reynolds, K.; Wofford, M. R.; Chen, J.; Kelly, T. N.; Mei, H.; Whelton, P. K.; He, J. Effect of soybean protein on novel cardiovascular disease risk factors: a randomized controlled trial. *Eur. J. Clin. Nutr.* **2013**, *67*, 58−63.
(20) Sudel, K. M.; Venzke, K.; Mielke, H.; Breitenbach, U.; Mundt, C.; Jaspers, S.; Koop, U.; Sauermann, K.; Knussman-Hartig, E.; Moll, I.; Gercken, G.; Young, A. R.; Stab, F.; Wenck, H.; Gallinat, S. Novel aspects of intrinsic and extrinsic aging of human skin: beneficial effects of soy extract. *Photochem. Photobiol.* **2005**, *81*, 581−7.
(21) Kim, S. Y.; Kim, S. J.; Lee, J. Y.; Kim, W. G.; Park, W. S.; Sim, Y. C.; Lee, S. J. Protective effects of dietary soy isoflavones against UV-induced skin-aging in hairless mouse model. *J. Am. Coll. Nutr.* **2004**, *23*, 157−62.
(22) Nizamutdinova, I. T.; Kim, Y. M.; Chung, J. I.; Shin, S. C.; Jeong, Y. K.; Seo, H. G.; Lee, J. H.; Chang, K. C.; Kim, H. J. Anthocyanins from black soybean seed coats stimulate wound healing in fibroblasts and keratinocytes and prevent inflammation in endothelial cells. *Food Chem. Toxicol.* **2009**, *47*, 2806−12.
(23) Choi, Y. H.; Lim, H.; Heo, M. Y.; Kwon, D. Y.; Kim, H. P. Anti-inflammatory activity of the ethanol extract of Chungkukjang, Korean fermented bean: 5-lipoxygenase inhibition. *J. Med. Food* **2008**, *11*, 539−43.
(24) Chiu, T. M.; Huang, C. C.; Lin, T. J.; Fang, J. Y.; Wu, N. L.; Hung, C. F. In vitro and in vivo anti-photoaging effects of an isoflavone extract from soybean cake. *J. Ethnopharmacol.* **2009**, *126*, 108−13.
(25) Matsuda, A.; Tanaka, A.; Pan, W.; Okamoto, N.; Oida, K.; Kingyo, N.; Amagai, Y.; Xia, Y.; Jang, H.; Nishikawa, S.; Kajiwara, N.; Ahn, G.; Ohmori, K.; Matsuda, H. Supplementation of the fermented soy product ImmuBalance effectively reduces itching behavior of atopic NC/Tnd mice. *J. Dermatol. Sci.* **2012**, *67*, 130−9.
(26) Burks, A. W.; Williams, L. W.; Thresher, W.; Connaughton, C.; Cockrell, G.; Helm, R. M. Allergenicity of peanut and soybean extracts altered by chemical or thermal denaturation in patients with atopic dermatitis and positive food challenges. *J. Allergy Clin. Immunol.* **1992**, *90*, 889−97.
(27) Tsoyi, K.; Park, H. B.; Kim, Y. M.; Chung, J. I.; Shin, S. C.; Lee, W. S.; Seo, H. G.; Lee, J. H.; Chang, K. C.; Kim, H. J. Anthocyanins from black soybean seed coats inhibit UVB-induced inflammatory cylooxygenase-2 gene expression and PGE2 production through regulation of the nuclear factor-kappaB and phosphatidylinositol 3-kinase/Akt pathway. *J. Agric. Food Chem.* **2008**, *56*, 8969−74.
(28) Huang, C. C.; Hsu, B. Y.; Wu, N. L.; Tsui, W. H.; Lin, T. J.; Su, C. C.; Hung, C. F. Anti-photoaging effects of soy isoflavone extract (aglycone and acetylglucoside form) from soybean cake. *Int. J. Mol. Sci.* **2010**, *11*, 4782−95.
(29) Cho, D. W.; Kim, D. E.; Lee, D. H.; Jung, K. H.; Hurh, B. S.; Kwon, O. W.; Kim, S. Y. Metabolite profiling of enzymatically hydrolyzed and fermented forms of Opuntia ficus-indica and their effect on UVB-induced skin photoaging. *Arch. Pharm. Res.* **2014**, *37*, 1159.
(30) Ries, C.; Popp, T.; Egea, V.; Kehe, K.; Jochum, M. Matrix metalloproteinase-9 expression and release from skin fibroblasts interacting with keratinocytes: Upregulation in response to sulphur mustard. *Toxicology* **2009**, *263*, 26−31.
(31) Rekha, C. R.; Vijayalakshmi, G. Bioconversion of isoflavone glycosides to aglycones, mineral bioavailability and vitamin B complex in fermented soymilk by probiotic bacteria and yeast. *J. Appl. Microbiol.* **2010**, *109*, 1198−208.
(32) Shibata, A.; Nakagawa, K.; Kawakami, Y.; Tsuzuki, T.; Miyazawa, T. Suppression of gamma-tocotrienol on UVB induced inflammation in HaCaT keratinocytes and HR-1 hairless mice via inflammatory mediators multiple signaling. *J. Agric. Food Chem.* **2010**, *58*, 7013−20.
(33) Polito, F.; Marini, H.; Bitto, A.; Irrera, N.; Vaccaro, M.; Adamo, E. B.; Micali, A.; Squadrito, F.; Minutoli, L.; Altavilla, D. Genistein aglycone, a soy-derived isoflavone, improves skin changes induced by ovariectomy in rats. *Br. J. Pharmacol.* **2012**, *165*, 994−1005.
(34) Lee, D. E.; Lee, K. W.; Byun, S.; Jung, S. K.; Song, N.; Lim, S. H.; Heo, Y. S.; Kim, J. E.; Kang, N. J.; Kim, B. Y.; Bowden, G. T.; Bode, A. M.; Lee, H. J.; Dong, Z. 7,3′,4′-Trihydroxyisoflavone, a metabolite of the soy isoflavone daidzein, suppresses ultraviolet B-induced skin cancer by targeting Cot and MKK4. *J. Biol. Chem.* **2011**, *286*, 14246−56.
(35) Huang, Z. R.; Hung, C. F.; Lin, Y. K.; Fang, J. Y. In vitro and in vivo evaluation of topical delivery and potential dermal use of soy isoflavones genistein and daidzein. *Int. J. Pharm.* **2008**, *364*, 36−44.
(36) Chiou, R. Y.; Cheng, S. L. Isoflavone transformation during soybean koji preparation and subsequent miso fermentation supplemented with ethanol and NaCl. *J. Agric. Food Chem.* **2001**, *49*, 3656−60.
(37) Kim, C. M.; Yi, S. J.; Cho, I. J.; Ku, S. K. Red-koji fermented red ginseng ameliorates high fat diet-induced metabolic disorders in mice. *Nutrients* **2013**, *5*, 4316−32.
(38) Iovine, B.; Iannella, M. L.; Gasparri, F.; Giannini, V.; Monfrecola, G.; Bevilacqua, M. A. A comparative analysis of the photo-protective effects of soy isoflavones in their aglycone and glucoside forms. *Int. J. Mol. Sci.* **2012**, *13*, 16444−56.
(39) Wolnicka-Glubisz, A.; De Fabo, E.; Noonan, F. Functional melanocortin 1 receptor Mc1r is not necessary for an inflammatory response to UV radiation in adult mouse skin. *Exp. Dermatol.* **2013**, *22*, 226−8.

(40) Lamon, B. D.; Upmacis, R. K.; Deeb, R. S.; Koyuncu, H.; Hajjar, D. P. Inducible nitric oxide synthase gene deletion exaggerates MAPK-mediated cyclooxygenase-2 induction by inflammatory stimuli. *Am. J. Physiol. Heart Circ. Physiol.* **2010**, *299*, H613−23.
(41) Au, R. Y.; Al-Talib, T. K.; Au, A. Y.; Phan, P. V.; Frondoza, C. G. Avocado soybean unsaponifiables (ASU) suppress TNF-alpha, IL-1beta, COX-2, iNOS gene expression, and prostaglandin E2 and nitric oxide production in articular chondrocytes and monocyte/macrophages. *Osteoarthritis Cartilage* **2007**, *15*, 1249−55.
(42) Hsu, C. H.; Ho, Y. S.; Lai, C. S.; Hsieh, S. C.; Chen, L. H.; Lin, E.; Ho, C. T.; Pan, M. H. Hexahydro-beta-acids potently inhibit 12-O-tetradecanoylphorbol 13-acetate-induced skin inflammation and tumor promotion in mice. *J. Agric. Food Chem.* **2013**, *61*, 11541−9.
(43) Yoshida, E.; Watanabe, T.; Takata, J.; Yamazaki, A.; Karube, Y.; Kobayashi, S. Topical application of a novel, hydrophilic gamma-tocopherol derivative reduces photo-inflammation in mice skin. *J. Invest. Dermatol.* **2006**, *126*, 1633−40.
(44) Wolfle, U.; Esser, P. R.; Simon-Haarhaus, B.; Martin, S. F.; Lademann, J.; Schempp, C. M. UVB-induced DNA damage, generation of reactive oxygen species, and inflammation are effectively attenuated by the flavonoid luteolin in vitro and in vivo. *Free Radical Biol. Med.* **2011**, *50*, 1081−93.
(45) Li, S.; Zhu, F.; Zykova, T.; Kim, M. O.; Cho, Y. Y.; Bode, A. M.; Peng, C.; Ma, W.; Carper, A.; Langfald, A.; Dong, Z. T-LAK cell-originated protein kinase (TOPK) phosphorylation of MKP1 protein prevents solar ultraviolet light-induced inflammation through inhibition of the p38 protein signaling pathway. *J. Biol. Chem.* **2011**, *286*, 29601−9.
(46) Wang, Y.; Zhang, X.; Lebwohl, M.; DeLeo, V.; Wei, H. Inhibition of ultraviolet B (UVB)-induced c-fos and c-jun expression in vivo by a tyrosine kinase inhibitor genistein. *Carcinogenesis* **1998**, *19*, 649−54.
(47) Kim, A. L.; Labasi, J. M.; Zhu, Y.; Tang, X.; McClure, K.; Gabel, C. A.; Athar, M.; Bickers, D. R. Role of p38 MAPK in UVB-induced inflammatory responses in the skin of SKH-1 hairless mice. *J. Invest. Dermatol.* **2005**, *124*, 1318−25.

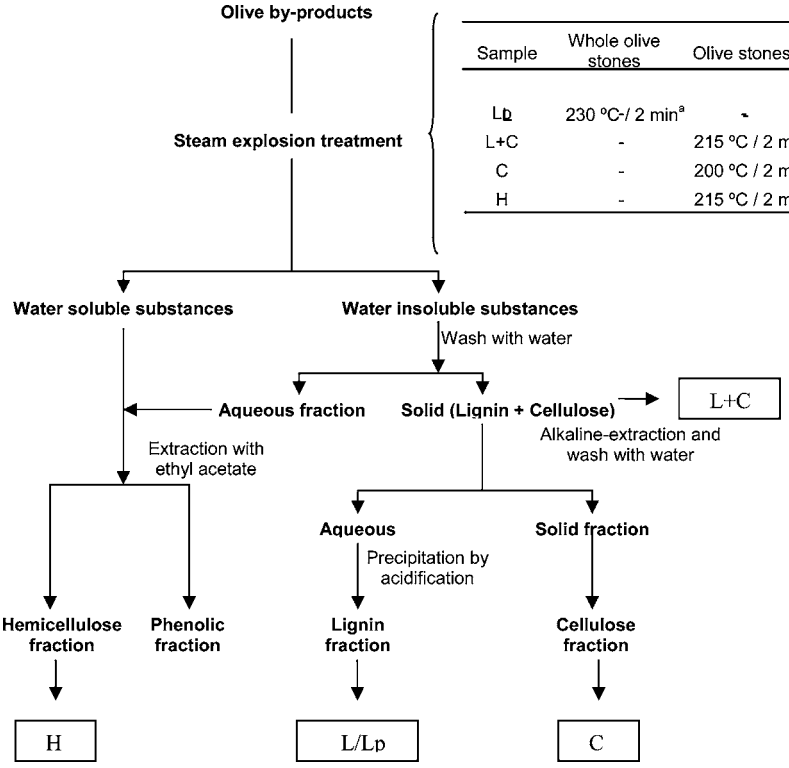


| Sample | Whole olive stones | Olive stones | Olive cake |
|---|---|---|---|
| Lp | 230 °C-/ 2 min[a] | - | 200 °C-/ 2 min |
| L+C | - | 215 °C / 2 min | - |
| C | - | 200 °C / 2 min | - |
| H | - | 215 °C / 2 min | - |

**Figure 1.** Scheme of the fractionation treatments of whole olive stones (stone and seed), olive stones (seed husks fragments), and olive cake (residual seed husks, seed, pulp, and peel) after steam explosion pretreatment. [a]Previous impregnation with dilute solution of strong mineral acid.

and antioxidant properties. In a previous study, low-molecular-weight phenols solubilized by the steam pretreatment were characterized.[5] The present study is focused on the residual insoluble material, polyphenolic polymerized and strongly bound to cell wall components that were extractable with an alkaline solution post-treatment. This aromatic (phenolic) polymer was dissolved in an alkali solution, probably as occurs in alkali-extracted lignin with a stable colloid structure by the negative charge (electrostatic interactions) due to the phenolic hydroxyl and carboxyl groups in the alkaline medium, which precipitated when the solution was changed to an acidic pH.[12] In addition, the lignin, an amorphous polyphenol of high molecular weight, can vary in structure according to their method of extraction and their plant source. Therefore, the properties and health benefits of the lignin will depend on the used lignocellulosic material, in this case olive stones and olive cake. The uses of fiber from new origins will probably widen the field of application for dietary fiber.

The aim of this work was the fractionation of olive stones (whole and fragmented, without seeds) and olive cake by a two-stage process based on a previous work,[3] involving a steam explosion pretreatment and alkaline solution post-treatment. Each fraction enriched in cellulose, hemicelluloses, and lignin was characterized and investigated for the potential use of these polymers. We highlight their physicochemical and functional properties, with special focus on bile acid binding and the glucose retardation index, using in vitro studies.

## MATERIALS AND METHODS

**Raw Material.** Whole olive stones were obtained from pitted table olives and, following incubation in an air stove at 30 °C, rubbed vigorously on filter paper to remove any loosely adhering pulp tissue.

The fragments of olive stones (seed husks) with an average length of 2−6 mm were supplied by an oil extraction plant (Oleícola el Tejar, Córdoba, Spain). The husks (9% moisture) were obtained from olive pomace after separating peel, pulp, and seeds.

Olive cake was also supplied as pellets by Oleícola el Tejar. The olive cake, which included the residual olive stone, was subjected to vibratory ball milling before determination of its chemical composition.

**Steam Explosion and Fractionation.** Steam explosion was carried out using a 2 L pilot-scale reactor, with a maximum operating pressure of 4.12 MPa, equipped with a ball valve opening. All experiments were carried out with samples of 100 g (dry weight). The samples were steamed at various temperatures for 2 min, prior to rapid decompression (explosion). Lignin was isolated from whole olive stone with a treatment at 230 °C/2 min (with acid), the lignin fraction from olive cake was obtained at 200 °C/2 min, the fractions of lignin + cellulose and hemicellulose were obtained at 215 °C/2 min from olive stone, and cellulose was isolated from olive stone at 200 °C/2 min.

One treatment (whole olive stones) was carried out with previous impregnation with an acid solution (0.1% $H_2SO_4$ w/v) for a period of 1 h under vacuum (to remove the air from the material and facilitate the penetration of acid through the structural matrix). The material was drained in a sieve and rinsed thoroughly with distilled water to remove all traces of acid, prior to loading into the steam reactor.

After steam explosion (Figure 1), the sample was vacuum filtered through Albet filter paper (weight, 73 g/cm$^2$; Albet, Barcelona, Spain) in a Buchner funnel. The residue was washed three times with 500 mL of distilled water for 30 min at 60 °C and filtered to remove the water-soluble fraction. The filtrate was concentrated to 250−300 mL by rotary evaporation at 40 °C. The aqueous concentrate was continuously extracted for 5−6 h with ethyl acetate (refluxed at 77 °C). The aqueous and organic phases were rotary evaporated under vacuum at 40 °C for several hours to remove all traces of ethyl acetate. The aqueous phase was freeze-dried (fraction H). The water-insoluble material (fraction L+C) was extracted with 0.5 M NaOH (250 mL) for 15 min at room temperature to remove the lignin from the cellulose residue. The residual solid was thoroughly washed with warm water until all traces of alkali were removed or brought to a neutral pH (fraction C). The dissolved lignin was acidified with 5 M $H_2SO_4$ to pH


dx.doi.org/10.1021/jf502062b | J. Agric. Food Chem. 2014, 62, 8973−8981

2−3. The precipitate was centrifuged, washed to neutral pH, and freeze-dried (fraction L).

**Ultraviolet Spectroscopy.** The ultraviolet spectra of samples were recorded at a concentration of 0.0027% in methanol on a UV−vis Hewlett-Packard (Waldbronn, Germany), model 8452 A.

To study the difference in spectra, $\Delta\varepsilon_i$, 10 mg of lignin was dissolved in 25 mL of dioxane/water (9:1). The neutral solution was prepared by diluting 3 mL of this solution in 25 mL of dioxane. The alkaline solution was prepared by the addition of 100 mg of NaOH. The alkaline-neutral difference spectra were determined by running the alkali solution against the neutral solution.

**Infrared Spectroscopy.** Infrared spectra were recorded on a Bio-Rad FTS 7PC using KBr disks. Lignin (1 mg) was mixed and thoroughly ground with 300 mg of KBr to reduce particle size and to obtain a uniform dispersion of the sample in the disks. The conditions of analysis were as follows: resolution, 8 $cm^{-1}$; co-adding 250 scans; frequency range, 400−4000 $cm^{-1}$.

**Analytical Method.** Moisture, fat, and ash contents were determined according to the AOAC method.[13] The uronic acids were estimated according to the *m*-hydroxydiphenyl method described by Blumenkrantz and Asboe-Hansen.[14] Total phenolic content was determined by the Folin−Ciocalteu spectrophotometric method and expressed as grams of gallic acid equivalents.[15]

The content of water-soluble low-molecular-weight sugars was determined by analysis with trifluoroacetic acid (TFA) hydrolysis (2 N TFA at 121 °C for 1 h) prior to reduction, acetylation, and analysis by gas chromatography.[16] Inositol was used as an internal standard. The chromatographic conditions applied were described by Lama-Muñoz et al.[17]

Klason lignin was determined gravimetrically.[18] The $\alpha$-cellulose determination of the insoluble fraction was carried out from bleached cellulose, which was extracted with 17.5% NaOH, and the residue was measured gravimetrically.[3] The hemicelluloses were determined as the difference between bleached cellulose and $\alpha$-cellulose. Bleached cellulose was prepared by sodium chlorite delignification.[19]

**Functional Properties.** *Water/Oil-Holding Capacity (WHC/OHC).* These properties were determined by centrifugation using the method described by Fuentes-Alventosa et al.[20] The OHC was determined under the same conditions as the WHC using soybean oil (0.92 g/mL density) and was expressed as grams of oil retained per gram of sample.

*Emulsification Activity (EA) and Emulsion Stability (ES).* EA and ES were evaluated in duplicate using the method of Betancur-Ancona et al.[21] EA was expressed as the volume of the emulsified layer as a percentage of the volume of the entire layer in the centrifuge tube. ES was determined using the prepared emulsions heated at 80 °C for 30 min. The emulsion was cooled to room temperature and centrifuged at 1200*g* for 5 min in a Sorvall RT 6000D (DuPont, Mechelen, Belgium). ES was expressed as the percentage of the remaining emulsified layer volume of the original emulsion volume.

*Binding of Bile Acid (BA).* The capacity of the fractions for binding BA in vitro was evaluated following the method described by Camire and Dougherty[8] with some modifications. Binding for each fraction was estimated from the change in BA concentration on exposure of the solution to the soluble fiber during an in vitro digestion process, which included an acidic digestion of the sample at pH 2, followed by pancreatic digestion. The individual BAs cholic acid (CA), deoxycholic acid (DCA), and chenodeoxycholic acid (CDCA) (Sigma, St. Louis, MO, USA) were selected for analysis. The results obtained for each sample of isolated pectin were compared with the results obtained for cholestyramine resin (Sigma C 4650), cellulose (Macherey Nagel, GmbH & Co. KG), and commercial pectin from citrus peel (Sigma P 9135).

*(a) In Vitro Digestion Procedure.* Each BA was dissolved in 0.1 M $NaHCO_3$ to make a 31.25 mM BA solution, which, in the final mixture, will be in a range of BA concentration close to the human body concentration in the final mixture (1.5−7 mM). One hundred milligrams of sample, pectin, cholestyramine, and cellulose were added to each tube (50 mL plastic centrifuge tubes) in triplicate. The individual sample without BA was used as a blank, and a tube for reagents including BA but without sample was considered as 100% of BA concentration. Samples were digested in 1 mL of 0.01 M HCl for 1 h at 37 °C in a shaking water bath (P-Selecta Unitronic 320 OC). After this acidic incubation, which simulated gastric digestion, the sample was neutralized with 0.1 M NaOH to pH 7.0. To each test sample was added 4 mL of BA solution. For the sample blank, 4 mL of $NaHCO_3$ was added without bile acid. After the addition of 5 mL of porcine pancreatin (activity equivalent 8 × USP) with a concentration of 10 mg/mL in 0.01 M buffer phosphate, pH 7.0, the tubes were incubated for 1 h at 37 °C in a shaking water bath. The mixtures were centrifuged for 10 min at 1120*g* in a Sorvall RT 6000D (DuPont). The supernatants were transferred to new tubes. An additional 5 mL of phosphate buffer was used to rinse out the incubation tube, which was vortexed and centrifuged as before, and the supernatants were combined.

*(b) Bile Acid Analysis.* BA was analyzed by a colorimetric method (a modified Pettenkofer reaction) that was described by Boyd et al.[22] One hundred microliters of supernatant (samples, blank, and standards of individual BAs) was collected and heated for 1 h at 137 °C, after the addition of 5 mL of sulfuric acid (70%). Five minutes later 1 mL of a freshly prepared solution of furfural (0.25%) was also added. The solutions were thoroughly mixed after each addition. A pink color appears, which takes 60 min to reach maximum intensity. The readings were made at the absorption maximum of 490 nm in an iMark microplate absorbance reader (Bio-Rad, Hercules, CA, USA), and the values were determined from the obtained standard curve. The ranges for the different standards were 0−30 $\mu$g for CA, 0−750 $\mu$g for DCA, and 0−750 $\mu$g for CDCA. Binding capacity was expressed as millimolar bile acid per 100 mg of fraction and was calculated from the decrease in BA concentration (mM) in the test solution after exposure to 100 mg of added fraction.

*Glucose Dialysis Retardation Index (GDRI).* GDRI was determined as described by Fuentes-Alventosa et al.[20] Samples of 400 mg were thoroughly hydrated with 15 mL of distilled water containing 30 mg of glucose and stirring during 1 h. Then samples were transferred to a dialysis bag (12000 MWCO, Sigma Chemical Co.). Each bag, blank of sample (with sample, without glucose), and a control bag (with glucose, but without sample) were put into a reservoir containing 400 mL of distilled water and held in a thermostatic water bath at 37 °C for 1 h with constant shaking. At 10 min intervals, 0.5 mL of dialysate was collected, and the glucose concentration was determined spectrophotometrically by using the anthrone method.[23]

$$\mathrm{GDRI} = 100 - \left(\frac{\text{total glucose diffused sample}}{\text{total glucose diffused control}} \times 100\right)$$

**Statistical Analysis.** Results were expressed as mean values ± standard deviations. To assess differences in the composition and functional characteristics among the different isolated fractions, a sample comparison was performed using Statgraphics Plus program version 2.1. A multivariate analysis of variance (ANOVA), followed by Duncan's comparison test, was performed. The level of significance used was $p < 0.05$.

## RESULTS AND DISCUSSION

**Chemical Characterization of the Main Fraction Obtained after Steam Explosion Pretreatment.** Table 1 shows the operation conditions of steam explosion carried out for each of the samples used in the present work. These samples were chosen by the best yield and/or the more representative chemical composition of hemicelluloses, cellulose, and lignin from pretreated whole olive stones (stone and seed), fragmented olive stones (seed husks), or olive cake (byproduct derived from olive oil extraction by a continuous triphasic extraction system, with seed husks, seed, pulp, and peel) as was described in previous works.[3−5] The lignocellulosic olive byproduct materials were treated in a steam explosion reactor, with or without a previous impregnation with a dilute

**Table 1. Composition and Recovery Yield of the Water-Insoluble and Soluble Fraction (Sample L+C; Sample H[a]) and Composition of Water-and-Alkali-Insoluble Fraction (Sample C) of Steam-Exploded Olive Stones at 215 and 200 °C during 2 min, Respectively**

| sample | | g/100 g dry weight of initial material |
|---|---|---|
| L+C | water-soluble substance | 27.5 |
| | insoluble fraction sample (L+C) | 54.1 |
| | lignin alkali-extracted (L) | 13.3 |
| | insoluble (C) | 48.8 |
| C | bleached cellulose | 68.8 ± 2.5 |
| | $\alpha$-cellulose | 60.7 ± 1.5 |
| | hemicellulose[b] | 8.1 ± 0.9 |
| | Klason lignin | 35.7 ± 0.8 |
| H | total sugar[c] | 61.03 ± 5.02 |
| | rhamnose | 0.28 ± 0.01 |
| | arabinose | 2.24 ± 0.23 |
| | xylose | 55.35 ± 4.5 |
| | mannose | 0.44 ± 0.06 |
| | galactose | 1.62 ± 0.03 |
| | glucose | 1.10 ± 0.01 |
| | uronic acids | 2.52 ± 0.06 |
| | polyphenols | 2.91 ± 0.34 |
| | ash | 4.02 ± 0.02 |
| | other compounds[d] | 29.6 ± 0.25 |

[a]aAfter steam explosion of olive stone at 215 °C/2 min, and after ethyl acetate extraction. [b]Hemicellulose was determined by difference between bleached cellulose and $\alpha$-cellulose. [c]Sugar determined by 2 N trifluoroacetic acid (TFA) hydrolysis at 120 °C for 2 h prior to gas chromatography derivatization to alditol acetates. [d]Quantified by difference (100% − known compounds).

solution of strong mineral acid, followed by fractionation (Figure 1). The major part of hemicelluloses (sample H) and a small part of lignin become soluble in the aqueous phase and can be separated from the remaning lignin and cellulose insoluble material (sample L+C). Lignin was recovered from the insoluble material by an alkaline extraction followed by acid precipitation (sample L), resulting in a cellulose fraction (sample C) and the remaining lignin and hemicellulose.

The maximum yield of lignin from whole olive stones was achieved at 230 °C/2 min with acid impregnation (sample L). A fraction of lignin was also obtained from olive cake steam-treated at 200 °C/2 min (sample Lp). These milder conditions (lower temperature and no acid impregnation) were chosen to avoid the autohydrolysis of the residual fragment of olive stones present in the olive cake, obtaining the lignin from the pulp only. The lignin recovered by alkali extraction followed by acid precipitation from steam-exploded olive stones was a de-etherified lignin with an extensive cleavage of $\beta$-aryl ether linkages, similar to exploded hardwood lignin.[3] However, the "lignin" obtained by alkaline delignification from steam-exploded olive cake did not resemble a true lignin. The parenchymal cells of olive fruit pulp are scarcely lignified,[24] and the "lignin" is composed mostly of condensed and polymerized polyphenols and other polymers, with variable levels of polymerization during the processing of the olive cake. Studies on ultraviolet and infrared spectroscopy of both extracted and autohydrolyzed lignin were followed to match the difference in functional groups. The two lignin fractions (L and Lp) exhibited the basic UV spectra typical of lignin (Figure 2a), with an absorption maximum around 240 nm and a second maximum at 280 nm, associated with a nonconjugated phenolic group (aromatic ring), and a slight shoulder at 340−350 nm. The difference spectra, obtained by subtracting the spectra of the alkaline lignin from the neutral lignin (ionization difference, $\Delta\varepsilon_i$) are shown in Figure 2b. The two lignins (lignin from whole olive stones, L, and lignin from olive cake, Lp) were found to have three characteristic maximums at 254−256, 298−300, and 360−370 nm in their ultraviolet ionization spectrum, which indicate that both contain phenolic hydroxyls conjugated to the $\alpha$ carbonyl group, carbon−carbon double bonds, or biphenyl group.[25] A list of previously reported absorption coefficients $E(\%_{cm})$ from steam-exploded olive stones at various wavelengths in the 260−350 nm region[3] showed similar absorption coefficients to guaicyl-syringyl lignin of hardwoods, in contrast to the results for exploded olive cake lignin with

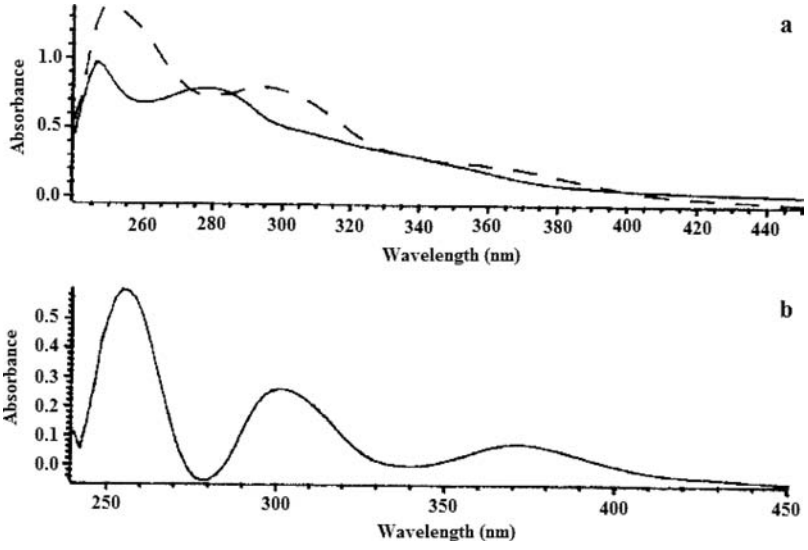


**Figure 2.** (a) Ultraviolet spectrum for alkaline (dash line) and neutral solution (solid line) of alkali-extracted lignin from steam-exploded olive cake (sample Lp); (b) alkaline-neutral difference spectra, ultraviolet ionization, $\Delta\varepsilon_i$.

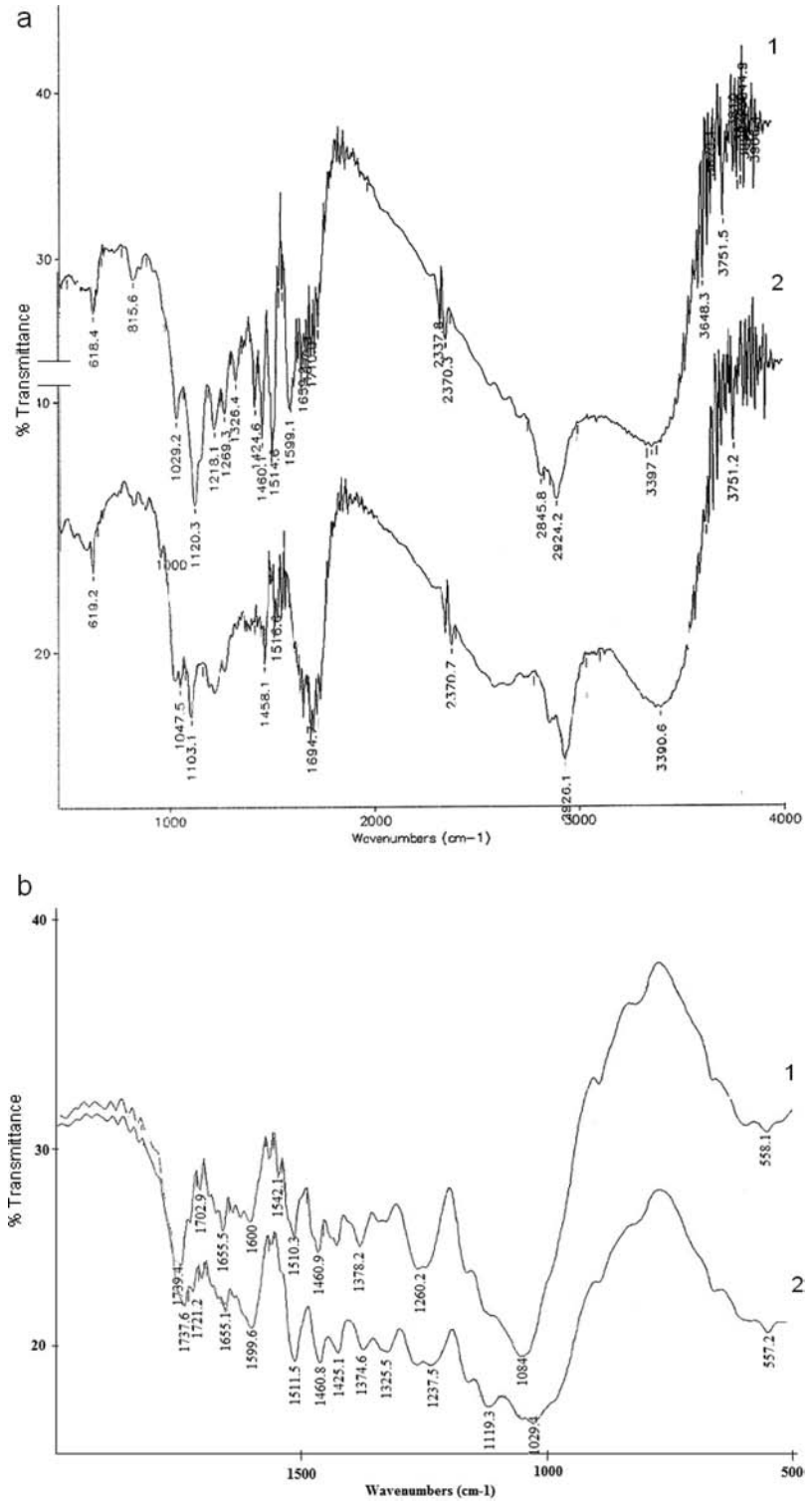


**Figure 3.** (a) Infrared spectra of alkali-extracted lignin (1) from steam-exploded whole olive stones (sample L) and (2) from steam-exploded olive cake (sample Lp); (b) infrared spectra of (1) milled and steam-untreated olive stones and (2) insoluble fraction isolated from steam-exploded olive stones (sample L+C).

very low absorption coefficients. The lignin isolated from steam-exploded olive stones showed a typical infrared lignin spectrum of guaicyl-syringyl lignin (Figure 3a1), with a characteristic lignin band in the region 1327−815 $cm^{-1}$ due to aromatic ether ring breathing and aromatic C−H deformation of the syringyl and guaicyl units.[26] In both lignin samples, a wide absorption band focused at 3396 $cm^{-1}$, originated from the OH− stretching vibration in the aromatic and aliphatic OH group, and a band at 2926 $cm^{-1}$, from the C−H stretching, were present. In addition, the occurrence of obvious aromatic skeleton vibration bands at 1600, 1515, and 1460 $cm^{-1}$ confirmed the presence of "lignin bands" in both alkaline-extractable lignins, although in the case of lignin from olive cake, a lower intensity relative to other bands indicates a


dx.doi.org/10.1021/jf502062b | J. Agric. Food Chem. 2014, 62, 8973−8981

Table 2. Functional Properties of the Main Components of the Olive Stones and Olive Cake Byproducts Fractionated by Steam Explosion Pretreatment Combined with Alkali Delignification and Comparison with Commercial Citrus Pectin: Water-Holding Capacity (WHC), Oil-Holding Capacity (OHC), Emulsification Activity (EA), and Emulsion Stability (ES)

| | WHC (g water holding/g sample) | OHC (g oil holding/g sample) | EA (emulsion vol/total vol) | ES (%) |
|---|---|---|---|---|
| citrus pectin | 10.35 ± 0.24 | 2.59 ± 0.19 | 64.58 ± 2.95 | 100 ± 0.01 |
| sample L | 3.18 ± 0.25 | 3.37 ± 0.06 | 44.96 ± 3.76 | 81.36 ± 1.21 |
| sample Lp | 6.00 ± 0.27 | 2.28 ± 0.21 | 5.71 ± 0.96 | 50.01 ± 5.35 |
| sample L+C | 6.73 ± 0.77 | 2.73 ± 0.28 | 13.55 ± 0.35 | 75.02 ± 0.35 |
| sample C | 4.69 ± 0.46 | 2.86 ± 0.02 | 33.97 ± 0.91 | 83.33 ± 7.86 |
| sample H | 4.63 ± 0.76 | 1.97 ± 0.69 | 32.18 ± 1.63 | 94.44 ± 7.86 |

smaller content of aromatic ring. However, the lignin fraction isolated from olive cake showed some significant differences (Figure 3a2), with a strong multiple and broad absorption band between 1736 and 1675 $cm^{-1}$ attributed to conjugated/unconjugated carbonyl groups, carboxylic acid, and ester, indicating the presence of hemicelluloses, and a conjugated aryl carbonyl group, absent in the lignin of olive stone. These results confirm that the lignin fraction isolated from olive stones had a typical exploded hardwood lignin structure, distinguishable from steamed olive cake lignin, although with the presence of certain similar functional groups.

The water-insoluble fraction (sample L+C) was recovered from olive stone steam-treated at 215 °C/2 min (with previous acid impregnation) prior to alkali extraction, and the overall yield represents a recovery of total solid matter, including $\alpha$-cellulose and lignin (Table 1). However, the efficiency of the process is more associated with the extent of transformation in the substrate. Because the steam explosion results in the hydrolysis of the major part of the hemicelluloses and a small part of the lignin remains soluble in the aqueous fraction, a residue of $\alpha$-cellulose and lignin remains. In these conditions the material defibrates efficiently and then favors the release of lignin in the alkaline solution to achieve a maximum yield of lignin fraction, which then falls gradually with the severity of treatment.[3] The infrared spectra of the insoluble fraction isolated from steam-exploded olive stones was compared to the initial olive stone, which was milled and steam-untreated (Figure 3b1,b2). The relative intensities of the bands for aromatic skeleton vibration assigned at 1600, 1510, and 1425 $cm^{-1}$ were rather similar in milled and steam-pretreated samples, indicating a similar core structure of the lignins.[27,28] However, it appears that olive stone exhibited considerable changes following steam explosion, with the disappearance or decrease in characteristic absorption peaks of hemicelluloses. A wide absorption band focused on the ester group at 1740 $cm^{-1}$ with another at 1240 $cm^{-1}$, and it is also possible to relate the enhancement of the cellulose peaks at 1120 and 1030 $cm^{-1}$ to the disappearance of the characteristic vibration at 1080 and 1047 $cm^{-1}$ of the C−O stretching bands of hemicelluloses.

Cellulose was the major component in the insoluble water fraction of olive stones after the steam explosion (200 °C/2 min) and alkali extraction of lignin (sample C), in which the remaining lignin (36%) and hemicellulose (8%) were present (Table 1).

The water-soluble fraction obtained after extraction by ethyl acetate for a selected sample of olive stones steam-extracted at 215 °C/2 min was rich in hemicelluloses (sample H). The main components were carbohydrates (61%) from polysaccharides extracted from the cell wall with quite different structures (xylans, arabinoxylan, xyloglucan; Table 1), although a substantial portion of the water-soluble material produced during the pretreatment (30%) was not identified.[4] This may be explained by the high percentage of chemical transformation and by the condensation reaction between carbohydrates, their degradation products, and the phenol derived from lignin degradation.[29]

**Functional Properties: WHC, OHC, EA, and ES.** The functional properties of the fractions obtained by steam explosion and alkali delignification of olive byproducts were compared to those of commercial citrus pectin (Table 2). Citrus pectin showed significantly the highest WHC (10.3 g water/g sample), which is an important property of dietary fiber (related to soluble fiber) to absorb and retain water. WHC is an important quality from both a physiological and a technological point of view, increasing the bulk volume of food and modifying the viscosity and texture of formulated products in addition to reducing calories.[30] Sample L+C had significantly the highest WHC, compared to samples C and L, with a value similar to that of sample Lp. Becausee WHC is related to soluble dietary fiber content, the low WHC of sample H could be attributed to the degradation or changes in the structure of some fiber components by heating, leading to a loss of ability to retain water in the fiber.

Ingredients with a high OHC allowed for the stabilization of high-fat food products and emulsions, facilitating the solubilization or dispersion of two immiscible liquids.[31] The mechanism of oil adsorption is not well characterized, but a high OHC could be related to a high pectin content. The OHC of the fiber fraction studied varied between 2.0 and 3.4 g oil/g dry matter for samples H and L, respectively. Although the values obtained for commercial citrus pectin were low, higher levels were found in the literature for dietary fiber from asparagus byproducts (around 7.5−8 g/g dry matter), with high contents in insoluble fiber, 51−67 and 8.3−11% of soluble fiber.[20]

To evaluate the functionality of these samples as emulsifier agents, the EA and ES were studied. Citrus pectin had the highest EA value, 64.6%, despite the fact that the OHC of commercial pectin was lower, followed by sample L with a value around 45%. The other samples could not be considered as good emulsifiers as their EAs were <50%.[32] However, almost all of the samples showed good emulsification stability (75−100%) after the emulsion had been heated at 80 °C for 30 min. Despite the low emulsifying capacity and stability indices, the use of the material obtained may stabilize foods with a high percentage of fat and emulsion as noted by Borchani et al.[33] for date fiber concentrates with an EA below 13%.

**In Vitro BA Binding.** The in vitro digestion procedure used in this study was designed to mimic aspects of the human digestion system, including acid digestion of a sample at pH 2 followed by a pancreatine digestion at pH 7.[8] Three of the major BAs present in human bile were individually used for the

binding assays. Cholic acid (CA) and chenodeoxycholic acid (CDCA) are the two primary BAs secreted by the liver. Deoxycholic acid (DCA) is one of the secondary BAs formed through the transformation of primary acid by intestinal bacteria. Secondary acids are thought to be involved in the etiology and development of colorectal cancer.[34]

The samples prepared from olive stones and olive cake byproducts on dry matter were compared to the BA binding of citrus pectin, cholestyramine, a well-known BA binding anionic resin, and the negative control, commercial cellulose (Figure 4a–c). The results obtained for cholestyramine (which bound 6.7, 12.7, and 6.4 mM CA, DCA, and CDCA per 100 mg of sample, equal to 81.8, 96.6, and 91.8% of the total added BA) and cellulose (which bound only 0.08, 1.12, and 0.59 mM CA, DCA, and CDCA in 100 mg of sample, or 1.0, 9.6, and 7.6% of the total added BAs) are similar to previously published results.[7] The BA binding values of the material fractionated from different steam explosion treatments of olive byproducts were in the range of 0.6–7.7 mM/100 mg of sample depending on the type of BA. The sample rich in lignin from olive stones, sample L, bound similar amounts of the secondary bile acid, DCA, as citrus pectin (8.5 mM DCA per 100 mg), a dietary fiber component that is known to interact with bile acids.[35] However, it is noteworthy that the BA binding values of sample L, as well as sample Lp, were significantly higher for the two primary bile acids, CA and CDCA, than those of citrus pectin. These results are in agreement with the fact that lignin is another of the dietary fiber components that interacts with BA.[36] The CA and CDCA binding of samples H, C, and L+C were not statistically different and had slightly lower values than those determined for citrus pectin. Although the mechanism of interaction with BA is currently not fully understood, the structural parameter of the different polymers extracted from olive byproducts may influence this interaction. It is remarkable that the fraction of the olive stone rich in lignin (sample L) behaves similarly to cholestyramine, commonly used in the treatment of hypercholesterolemia. However, the lignin within the matrix of cellulose (sample L+C) showed a very small capacity for adsorption, not being statistically different from the fraction rich in cellulose (sample C) in the case of CA and CDCA, and in the case of DCA even lower than sample C, with values similar to the cellulose negative control. The fiber fractions studied, except samples L+C and Lp, showed higher percentages of bile acid binding with DCA (secondary BA) than with CDCA and CA (primary BAs). This was similar to results obtained by other authors who showed that BA adsorption decreases with the hydroxyl groups' increment in steroid nuclei.[37] In the case of the fraction of lignin from olive cake, sample Lp, with a composition somewhat different from that of a true lignin, a more substantial difference in BA binding between primary and secondary BAs was seen that may be related to the polymer's structure or composition.

A comparison of these results with those from previous studies on lignin[8] and other dietary fibers[7,9] shows a high bile acid binding capacity of primary and secondary acids, especially for sample L with CA, which points to their possible health-promoting activity. The captation of bile acid in the organism cause its excretion in the feces. The continued depletion of bile acid in this way appears to be related with the levels of reduced serum cholesterol, thereby reducing the risk of cardiovascular disease.[38] This binding to bile salts (carcinogenic agents) also causes a reduction of the excessive level of bile in the colon, thus reducing the risk of developing cancer in the intestine.[9]

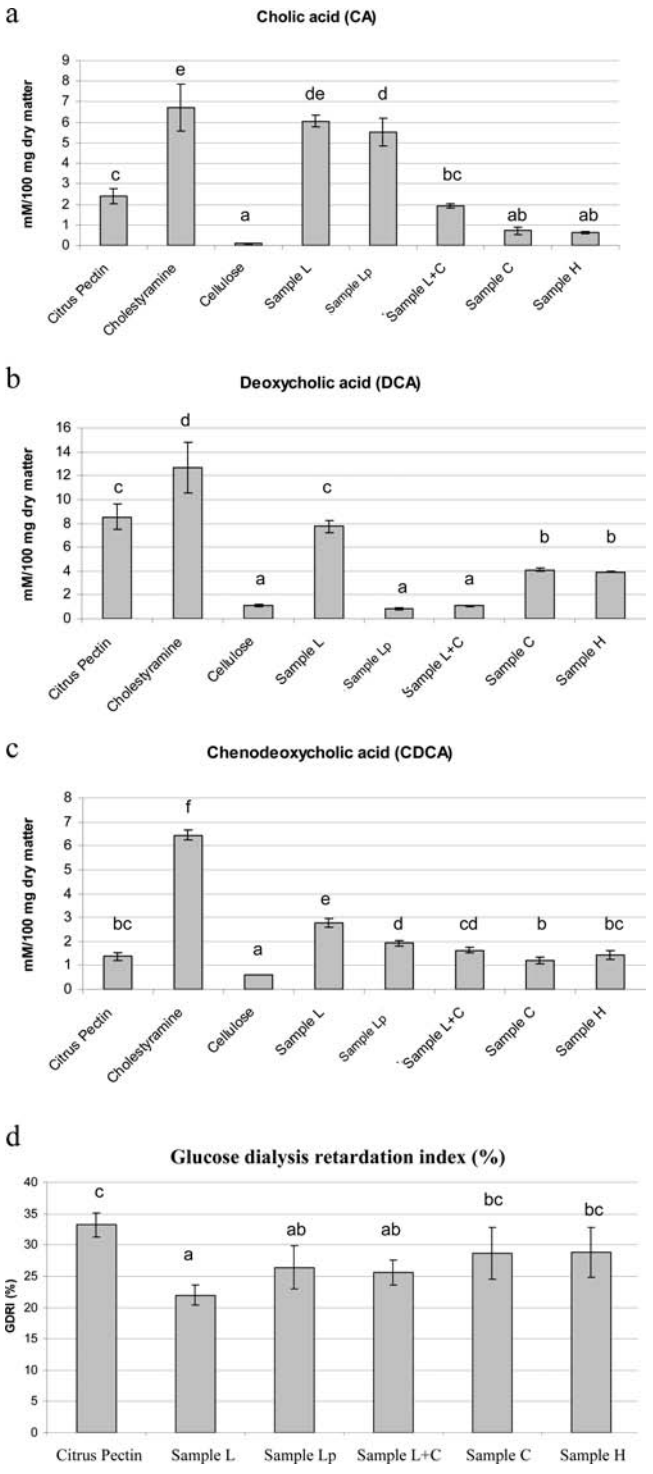


**Figure 4.** In vitro bile acid binding ability of olive stones and olive cake byproducts fractionated by steam explosion pretreatment combined with alkali delignification, compared to cholestyramine, cellulose, citrus, and pectin (a–c); (d) glucose dialysis retardation index (%) of the samples prepared from olive stones and olive cake byproducts steam-exploded on in vitro glucose diffusion, compared to citrus pectin. Data are presented as the means of three replicates ± SDs. Different letters indicate significantly different results ($p < 0.05$).

**Glucose Dialysis Retardation Index (GDRI).** The GDRI is a useful in vitro index to predict the effect that fiber has on the delay of glucose absorption in the gastrointestinal tract.[10] The GDRI phenomenon seems to be related to the soluble


dx.doi.org/10.1021/jf502062b | J. Agric. Food Chem. 2014, 62, 8973–8981

dietary fiber and uronic acid contents of insoluble fiber, although other authors have pointed to the relationship between the internal structure and surface properties of fiber and glucose diffusion.[39]

In Figure 4d the graphs for GDRI are presented. The results showed that both factors, composition and internal structure, could probably modulate this functional property, because values ranged from 22 to 29% for very different composition and nature of samples. The citrus pectin tested presented the highest value of GDRI (34%), although without significant differences between the sample of soluble fiber (sample H) or insoluble fiber (sample C).

The results obtained for the different components of olive stones and olive cake fractionated by steam explosion pretreatment combined with alkali delignification were similar to those reported in the literature for mango peel (21%),[9] artichoke fiber (27%),[39] and carambola pomace (25%),[40] lower than for fiber from asparagus byproduct (48%)[19] yet higher than those reported for wheat bran (5.3%).[41]

**General Comments.** The processing of olive byproducts obtained from olive oil extraction (fragmented olive stones and olive cake) and pitted table olives (whole olive stones) by steam explosion pretreatment/alkali delignification allowed for the fractionation of the three main polymers present in the lignocellulosic matrix with a reasonable yield and purity. This study showed that the pretreatment converted the hemicelluloses into a water-soluble fraction (sample H) rich in carbohydrates. The resulting insoluble material (sample L+C) was characterized by the spectroscopy method and compared with the material without steam explosion (ball-milled material). As such, we showed that the hemicelluloses were autohydrolyzed and the material had undergone important structural modifications during the steam explosion treatment. The cellulose was associated with a high proportion of lignin, which was partially recovered by alkaline extraction followed by acid precipitation (sample L), although some remains in the cellulose-rich fraction (sample C).

The functional properties were analyzed, and the fractions were found to have a WHC similar to those described for other agricultural byproducts, with an average OHC. The in vitro studies showed an important activity of bile acid binding for the lignin fraction from olive stones (sample L). This lignin fraction bound significantly more bile acid than any other fraction, with values similar to those for cholestyramine, especially when CA was tested. For the alkaline-extractable fraction from olive cake and subsequent precipitate by acid solution (sample Lp), substantially different UV and IR spectra were obtained from those of guaicyl-syringyl lignin of olive stones; the binding values were also significantly higher than those of the rest of the fractions, except for DCA. Therefore, both lignin fractions (L and Lp) could contribute to the reduction of serum cholesterol levels and a decreased risk of bowel cancer. Furthermore, the GDRI is a useful predictor of the in vitro health-promoting properties of the fractions and showed that the water-soluble fraction (sample H) and the fraction rich in cellulose (sample C) had high activities similar to those of pectin and other agricultural byproducts. These results would suggest the suitability of these fractions, extracted from olive byproducts, for incorporation as low-calorie bulk ingredients in high-fiber foods to lower postprandial serum glucose levels.

## AUTHOR INFORMATION


### Corresponding Author

*(J.F.-B.) Phone: 34-954691054. Fax 34-954691262. E-mail: jfbg@cica.es.



### Funding

Funding was received from the Ministerio de Economía y Competitividad of Spain and cofunded by European Social Fund (ESF) (Project AGL2013-48291-R). F.R.-S. received funding from the Spanish JAE-PRE program (CSIC-ESF) and G.R.-G. received funding from Spanish Ramón y Cajal program (RYC-2012-10456 contract) of Ministerio de Economía y Competitividad.


### Notes

The authors declare no competing financial interest.

## REFERENCES


(1) Valiente, C.; Arrigoni, E.; Esteban, R.; Amadó, R. Chemical composition of olive by-product and modifications through enzymatic treatments. *J. Sci. Food Agric* **1995**, *69*, 27−32.

(2) Heredia, A.; Guillén, R.; Fernández-Bolaños, J.; Rivas, M. Olives stone as a source of fermentable sugars. *Biomass* **1987**, *14*, 143−148.

(3) Fernández-Bolaños, J.; Felizón, B.; Guillén, R.; Jiménez, A.; Heredia, A. Characterization of lignin steam-exploded olive stones and the cellulose residue. *Bioresour. Technol.* **1999**, *68*, 121−132.

(4) Fernández-Bolaños, J.; Felizón, B.; Heredia, A.; Rodríguez, R.; Guillén, R.; Jiménez, A. Steam-explosion of olive stones: hemicellulose solubilisation and enhancement of enzymatic hydrolysis of cellulose. *Bioresour. Technol.* **2001**, *79*, 53−61.

(5) Felizón, B.; Fernández-Bolaños, J.; Heredia, A.; Guillén, R. Steam-explosion pretreatment of olive cake. *J. Am. Oil Chem. Soc.* **2000**, *77*, 15−22.

(6) Rodríguez, R.; Jiménez, A.; Fernández-Bolaños, J.; Guillén, R.; Heredia, A. Dietary fibre from vegetable products as source of functional ingredients. *Trends Food Sci. Technol.* **2006**, *17*, 3−15.

(7) Kim, H. J.; White, P. J. In vitro bile-acid binding and fermentation of high, medium, and low molecular weight $\beta$-glucan. *J. Agric. Food Chem.* **2010**, *58*, 628−634.

(8) Story, J. A.; Kritchevsky, D. Comparison of the binding of various bile acids and bile salts in vitro by several types of fiber. *J. Nutr.* **1976**, *106*, 1292−1294.

(9) Camire, M. E.; Dougherty, M. P. Raisin dietary fibre composition and in vitro bile acid bindig. *J. Agric. Food Chem.* **2003**, *51*, 834−837.

(10) Larrauri, J. A.; Goñi, I.; Martín-Carrón, N.; Rupérez, P.; Saura-Calixto, F. Measurement of health-promoting properties in fruit dietary fibres: antioxidant capacity, fermentability and glucose retardation index. *J. Sci. Food Agric* **1996**, *71*, 515−519.

(11) Aguedo, M.; Kohnen, S.; Rabetafika, N.; Bossche, S. V.; Sterckx, J.; Blecker, C.; Beauve, C.; Paquot, M. Composition of by-products from cooked fruit processing and potential use in food products. *J. Food Compos. Anal.* **2012**, *27*, 61−69.

(12) Wang, G.; Chen, H. Fractionation of alkali-extracted lignin from steam-exploded stalk by gradient acid precipitation. *Sep. Purif. Technol.* **2013**, *105*, 98−105.

(13) AOAC. *Official Methods of AnalysisFood Composition*, 15th ed.; Gaithersburg, MD, USA, 1990; Vol. 1, pp 915−919.

(14) Blumenkrantz, N.; Asboe-Hansen, G. New method for quantitative determination of uronic acids. *Anal. Biochem.* **1973**, *54*, 484−489.

(15) Singleton, V. L.; Rossi, J. A., Jr. Colorimetry of total phenolics with phosphomolybdic-phosphotungstic acid reagents. *Am. J. Enol. Vitic.* **1965**, *16*, 144−158.

(16) Englyst, H. N.; Cummings, J. H. Simplified method for the measurement of total non-starch polysaccharides by gas-liquid chromatography of constituent sugars as aditol acetates. *Analyst* **1984**, *109*, 937−942.

(17) Lama-Muñoz, A.; Rodríguez-Gutiérrez, G.; Rubio-Senent, F.; Fernández-Bolaños, J. Production, characterization and isolation of

neutral and pectic oligosaccharides with low molecular weights from olive by-products thermally treated. *Food Hydrocolloids* **2012**, *28*, 92−104.
(18) Fengel, D.; Weggener, G. *Wood-Chemistry, Ultrastructure and Reactions*; De Gruyter: Berlin, Germany, 1984; pp 92−95.
(19) Browning, B. L. *Methods of Wood Chemistry*; Wiley Interscience: New York, 1967; Vol. II.
(20) Fuentes-Alventosa, J. M.; Rodríguez-Gutiérrez, G.; Jaramillo-Carmona, S.; Espejo-Calvo, J. A.; Rodríguez-Arcos, R.; Fernández-Bolaños, J.; Guillén-Bejarano, R.; Jiménez-Araujo, A. Effect of extraction method on chemical composition and functional characteristics of high dietary fibre powders obtained from asparagus by-products. *Food Chem.* **2009**, *119*, 665−671.
(21) Betancur-Ancona, D.; Peraza-Mercado, G.; Moguel-Ordoñez, Y.; Fuertes-Blanco, S. Physicochemical characterization of lima bean (*Phaseolus lunatus*) and jack bean (*Canavalia ensiformis*) fibrous residues. *Food Chem.* **2004**, *84*, 287−295.
(22) Boyd, G. S.; Eastwood, M. A.; MacLean, N. Bile acids in the rat: studies in experimental occlusion of the bile duct. *J. Lipid Res.* **1966**, *7*, 83−93.
(23) Dische, Z. Color reactions of carbohydrates. In *Methods in Carbohydrates Chemistry*; Whistler, R. L., Wolfram, M. L., Eds.; Academic Press: New York, 1962; pp 477−512.
(24) Jiménez, A.; Guillén, R.; Fernández-Bolaños, J.; Heredia, A. Cell wall composition of olives. *J. Food Sci.* **1994**, *59*, 1192−1201.
(25) Chua, M. G. S.; Wayman, M. Characterization of autohydrolysis aspen (*P. tremuloides*) lignin. Part 3. Infrared and ultraviolet studies of extracted autohydrolysis lignin. *Can. J. Chem.* **1979**, *57*, 2603−2611.
(26) Thring, R. W.; Chornet, E.; Bouchard, J.; Vidal, P. F.; Overend, R. P. Characterization of lignin residues derived from the alkaline hydrolysis of poplar cell wall components. *Anim. Feed Sci. Technol.* **1990**, *32*, 235−242.
(27) Marchessault, R. H.; Coulombe, S.; Morikawa, H. Characterization of aspen exploded wood lignin. *Can. J. Chem.* **1982**, *60*, 2372−2382.
(28) Reeves, J. B., III. Infrared spectroscopic studies on forage and by-product fibre fractions and lignin determination residues. *Vib. Spectrosc.* **1993**, *5*, 303−310.
(29) Kuznetsov, B. N.; Efrenov, A. A.; Levdanskii, V. A.; Kuznetosova, S. A.; Polezhayeva, N. I.; Shikina, T. A.; Krotova, I. V. The use of non-isobaric pre-hydrolysis for the isolation of organic compounds from wood and bark. *Bioresour. Technol.* **1996**, *58*, 181−188.
(30) Rodríguez, R.; Jiménez, A.; Fernández-Bolaños, J.; Guillén, R.; Heredia, A. Dietary fibre from vegetable products as source of functional ingredients. *Trends Food Sci. Technol.* **2006**, *17*, 3−15.
(31) Grigelmo-Miguel, N.; Gorinstein, S.; Martín-Belloso, O. Characterisation of peach dietary fibre concentrate as a food ingredient. *Food Chem.* **1999**, *65*, 175−181.
(32) Abdul-Hamid, A.; Luan, Y. S. Functional properties of dietary fibre prepared from defatted rice bran. *Food Chem.* **2000**, *68*, 15−19.
(33) Borchani, C.; Besbes, S.; Masmoudi, M.; Bouaziz, M. A.; Blecker, C.; Attia, H. Influence of oven-drying temperature on physicochemical and functional properties of date fibre concentrates. *Food Bioprocess Technol.* **2012**, *5*, 1541−1551.
(34) Baijal, P. K.; Fitzpatrick, D. W.; Bird, R. P. Comparative effects of secondary bile acids, deoxycholic and lithocholic acids, on aberrant crypt foci growth in the postinitiation phases of colon carcinogenesis. *Nutr. Cancer* **1998**, *31*, 81−89.
(35) Sayar, S.; Jannink, J. L.; White, P. J. In vitro bile acid binding of flours from oat lines varying in percentage and molecular weight distribution of $\beta$-glucan. *J. Agric. Food Chem.* **2005**, *53*, 8797−8803.
(36) Kosikova, B.; Slamenova, D.; Mikulasova, M.; Horvathova, E.; Labaj, J. Reduction of carcinogenesis by bio-based lignin derivatives. *Biomass Bioenergy* **2002**, *23*, 153−159.
(37) Drzikova, B.; Dongowski, G.; Gebhardt, E.; Habel, A. The composition of dietary fibre-rich extrudates from oat affects bile acids binding and fermentation in vitro. *Food Chem.* **2005**, *90*, 181−192.
(38) Eastwood, M. A.; Hamilton, D. Studies on the adsorption of bile salts to non-absorbed components of diet. *Biochim. Biophys. Acta* **1968**, *152*, 165−173.
(39) López, G.; Ros, G.; Rincón, F.; Periago, M. J.; Martínez, M. C.; Ortuño, J. Relationship between physical and hydration properties of soluble and insoluble fibre of artichoke. *J. Agric. Food Chem.* **1996**, *44*, 2773−2778.
(40) Chau, C.-F.; Chen, C.-H.; Lin, C.-Y. Insoluble fiber-rich fraction derived from *Averrhoa caramola*: hypoglycemic effects determined by *in vitro* methods. *LWT−Food Sci. Technol.* **2004**, *37*, 331−335.
(41) Adiotomre, J.; Eastwood, M. A.; Edwards, C. A.; Brydon, W. G. Dietary fibre: in vitro methods that anticipate nutrition and metabolic activity in human. *Am. J. Clin. Nutr.* **1990**, *52*, 128−134.

Table 1. Effect of Different Domestic Cooking Methods on Proximate Composition of Sweet Potato Leaves (g/100 g DW)[a]

| cooking method | crude protein | crude fat | crude fiber | ash |
|---|---|---|---|---|
| raw | 24.04 ± 0.08e | 4.39 ± 0.12b | 11.33 ± 0.46b | 7.84 ± 0.62b |
| boiling | 25.56 ± 0.05d | 3.19 ± 0.14cd | 10.47 ± 0.11cd | 7.44 ± 0.01b |
| steaming | 28.66 ± 0.14b | 3.32 ± 0.12c | 10.41 ± 0.25cd | 8.16 ± 0.01ab |
| microwaving | 28.11 ± 0.13c | 2.90 ± 0.06d | 10.05 ± 0.08d | 8.17 ± 0.12ab |
| baking | 29.56 ± 0.28a | 3.38 ± 0.11c | 10.96 ± 0.06bc | 8.82 ± 0.01a |
| frying | 17.11 ± 0.07f | 42.92 ± 0.12a | 20.51 ± 0.19a | 4.67 ± 0.09c |

[a]Values are means ± SD of three determinations. Cooking methods that were not significantly different are assigned the same letter ($p > 0.05$).

## MATERIALS AND METHODS

**Plant Materials.** Fresh sweet potato leaves (cv. Pushu 53, a popular leaf-vegetable sweet potato cultivar in mainland China) were obtained from the Academy of Agricultural and Forestry Sciences in Hebei Province, China. All sweet potatoes were planted with standard production practices at the experimental farm of the Academy of Agricultural and Forestry Sciences in Shijiazhuang city, Hebei province, at the beginning of June 2013. The average temperatures during the growth period of 2013 were as follows: June, 26 °C; July, 26 °C; August, 31 °C; September, 23 °C; and October, 12 °C. The leaves were collected in the middle of August.

**Cooking Methods.** The sweet potato leaves were thoroughly cleaned with tap water and wiped with tissue paper. Eighteen hundred grams was taken and divided into six portions (300 g for each application). One portion was retained raw; the others were cooked in five different methods (reported by Perla et al.,[4] Palermo et al.,[11] and Tudela et al.[12] with slight modification) in triplicate, as given below.

For boiling, sweet potato leaves (100 g) were cooked in a stainless steel pan for 2 min after distilled water (500 mL) had come to a boil. For steaming, sweet potato leaves (100 g) were placed on tray in a steam cooker (Supor Co., Ltd., Hangzhou, Zhejiang, China) covered with a lid and steamed over boiling water for 2 min under atmospheric pressure. For microwave cooking, sweet potato leaves (100 g) were placed in a glass dish and cooked in a commercial 1000 W microwave oven for 2 min. For baking, sweet potato leaves (100 g) were baked at 204 °C for 2 min in a commercial oven after the oven had come to the prescribed temperature. For frying, sweet potato leaves (100 g) were cooked in a stainless steel pan for 2 min after corn oil (50 mL) had come to 180 °C. The treated and raw samples were freeze-dried and ground in a commercial grinder and stored at −20 °C in sealed aluminum bags until analyzed.

**Proximate Composition.** Ash, crude fat, and crude protein contents were determined according to AOAC methods.[13] Ash content was determined by weighing leaf samples before and after heat treatment (550 °C for 12 h). Crude fat content was determined according to AOAC method 960.39. Crude protein was assessed by the micro-Kjeldahl method, with a nitrogen to protein conversion factor of 6.25 (AOAC method 976.05).

Crude fiber was determined according to ISO method 5498:1981.[14] First, a sample of leaf powder was boiled in 0.255 M sulfuric acid for 30 min. The resulting insoluble residue was filtered, washed, and boiled in 0.313 M sodium hydroxide. After the sample had been filtered and washed, it was dried at 130 ± 2 °C for 2 h. Weight loss was determined at 350 ± 25 °C. Crude fiber content was expressed relative to the dry weight (DW) of leaf powder.

**Total Polyphenol Content (TPC).** TPC was measured by using the Folin−Ciocalteu method.[15] Briefly, 1 g of leaf powder was extracted with 20 mL of 70% (v/v) ethanol for 30 min at 50 °C and subjected to ultrasonic wave treatment. Following centrifugation at 5000*g* for 10 min at 4 °C, the residue was re-extracted twice with 70% ethanol as described above. The supernatants were pooled, concentrated in a rotary evaporator, and freeze-dried, thereby obtaining a crude extract. The crude extract was dissolved in 100 mL of distilled water; an aliquot (0.5 mL) was mixed with 1.0 mL of Folin−Ciocalteu reagent (Sigma-Aldrich, Inc., St. Louis, MO, USA), previously diluted 10 times, and allowed to react at 30 °C for 30 min. Subsequently, 2.0 mL of saturated $Na_2CO_3$ (10%, w/v) was added to the mixture. Following 30 min, absorbance was measured at 736 nm in a UV1101 spectrophotometer (Hitachi, Japan). A calibration curve consisting of chlorogenic acid (CHA) standards (Sigma-Aldrich, Inc.), ranging from 0.02 to 0.10 mg/mL, was prepared. The linear regression equation was $y = 8.7671x + 0.0068$ and $R^2 = 0.9994$. TPC of sweet potato leaves was calculated according to the following equation and expressed as milligrams per gram on a DW basis (mg/g DW).

$$\mathrm{TPC} = (A - 0.0068)/8.7671 \times V/M$$

$A$ is the absorbance, $V$ is the volume of the crude extract diluent (mL), and $M$ is the mass of the tested sweet potato leaf powder on a DW basis (g).

**Antioxidant Activity.** Antioxidant activity of sweet potato leaf powder samples was determined by using the ORAC assay, as reported by Blasa et al.[16] Briefly, 1 g of leaf powder sample was extracted with 20 mL of 70% (v/v) ethanol for 30 min at 50 °C and subjected to ultrasonic wave treatment. Following centrifugation at 5000*g* for 10 min at 4 °C, the residue was re-extracted twice with 70% ethanol as described above. The supernatants were pooled, concentrated in a rotary evaporator, and freeze-dried, thereby obtaining a crude extract. The assay was carried out using a microplate reader (Chameleon, Hidex, Turku, Finland) equipped with a temperature-controlled incubation chamber and an automatic injection pump. Incubator temperature was set at 37 °C. The reaction mixture for hydrophilic assay was the following: 200 μL of 0.096 μM fluorescein sodium salt in 0.075 M sodium phosphate buffer (pH 7.0) and 20 μL of sample or Trolox. A calibration curve was made each time with the standard Trolox (100, 50, 25 μM). The blank was 0.075 M sodium phosphate buffer (pH 7.0). The reaction was initiated with 40 μL of 0.33 M AAPH. Fluorescence was read at 485 nm excitation and 520 nm emission until complete extinction. ORAC values were expressed as micrograms of Trolox equivalents (TE) per milligram DW of sweet potato leaves and were the means ± standard deviation (SD) of three analyses.

**Quantification of Phenolic Compounds by RP-HPLC.** Phenolic compounds in sweet potato leaf extract were evaluated by reversed-phase high-performance liquid chromatography (RP-HPLC, Agilent Technologies, Palo Alto, CA, USA). Detection and quantification were carried out with a four-channel gradient pump, a diode array detector, a column heater, a degasser, and an autosampler (Agilent Technologies). Separations were conducted at 30 °C on an Agilent ZORBAX Eclips Plus C-18 reversed-phase column (150 mm × 4.6 mm length, 5 μm particle size). The mobile phases were (A) 0.1% (w/v) phosphoric acid solution and (B) acetonitrile. Flow rate was 1.0 mL/min. For analysis, 2 mg of dry sweet potato leaf extract was dissolved in 10 mL of 80% (v/v) methanol, and the injection volume of the sample solution was 20 μL. The gradient program was as follows: from 20 to 65% B from 0 to 15 min, from 65 to 80% B from 15 to 15.1 min, and 80% B maintained from 15.1 to 20 min. Spectral data from 200 to 800 nm were recorded, and the polyphenol chromatograms were monitored at 326 nm. Rutin, quercetin, caffeic acid, 3-*O*-caffeoylquinic acid, 4-*O*-caffeoylquinic acid, 5-*O*-caffeoylquinic acid, 3,4-di-*O*-caffeoylquinic acid, 3,5-di-*O*-caffeoylquinic acid, 4,5-di-*O*-caffeoylquinic acid, and 3,4,5-tri-*O*-caffeoylquinic acid (Sigma-Aldrich, Inc.) were used as standards. Identification and quantitative analysis were done by comparison with standards. The amount of each phenolic compound was expressed as milligrams per gram of sweet potato leaves (DW).

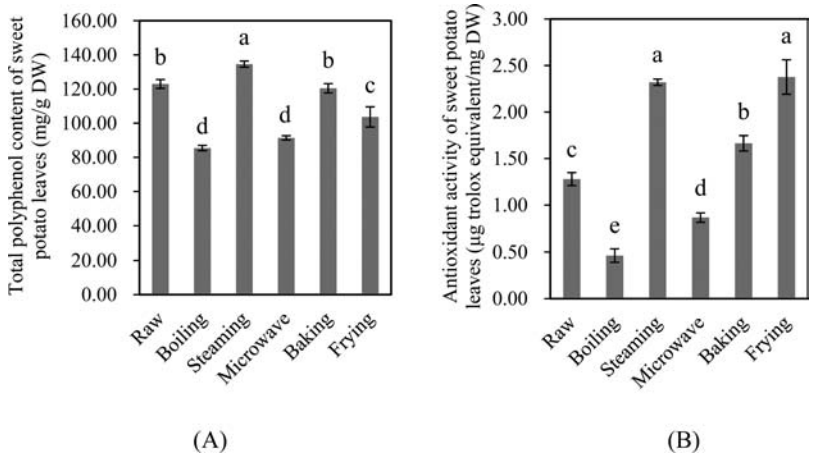


**Figure 1.** Effect of different domestic cooking methods on total polyphenol content (A) and antioxidant activity (B) of sweet potato leaves. Values are means ± SD of three determinations. Cooking methods that were not significantly different are assigned the same letter ($p > 0.05$).

**Table 2. Retention Time, Maximum Absorbance, and Linear Calibration Curves of Phenolic Compounds Found in Sweet Potato Leaves**

| peak | retention time (min) | HPLC-DAD $\lambda_{max}$ (nm) | identity | linear calibration curve | $R^2$ |
|---|---|---|---|---|---|
| 1 | 1.47 | 326 | 5-*O*-caffeoylquinic acid | $y = 11.372x - 0.428$ | 0.996 |
| 2 | 1.91 | 326 | 3-*O*-caffeoylquinic acid | $y = 9.909x + 0.286$ | 0.999 |
| 3 | 2.10 | 326 | 4-*O*-caffeoylquinic acid | $y = 25.894x - 17.128$ | 0.998 |
| 4 | 2.92 | 326 | caffeic acid | $y = 28.183x - 1.211$ | 0.999 |
| 5 | 4.16 | 326 | 4,5-di-*O*-caffeoylquinic acid | $y = 9.208x - 7.244$ | 0.998 |
| 6 | 4.54 | 326 | 3,5-di-*O*-caffeoylquinic acid | $y = 18.056x - 18.405$ | 0.998 |
| 7 | 4.88 | 326 | 3,4-di-*O*-caffeoylquinic acid | $y = 15.353x - 12.021$ | 0.998 |
| 8 | 6.87 | 326 | 3,4,5-tri-*O*-caffeoylquinic acid | $y = 6.218x - 5.158$ | 0.995 |

**Statistical Analyses.** The results were expressed as means ± SD of three replicates. Statistical analyses were performed using SAS version 8.1 software (SAS Institute Inc., Cary, NC, USA). Statistical significance was set at $p < 0.05$.

## RESULTS AND DISCUSSION

**Proximate Composition.** The effect of cooking methods on proximate composition of sweet potato leaves is shown in Table 1. Compared with the crude protein content in raw sweet potato leaves, boiling, steaming, microwaving, and baking increased crude protein content significantly, whereas frying decreased crude protein content significantly ($p < 0.05$). The possible reason was that, in the processes of boiling, steaming, and baking, other constituents, for example, fat and fiber, were partially lost or destroyed, resulting in the relative increase of protein content in sweet potato leaves; in contrast, the absorption of fat through frying caused an increase of dry matter, resulting in the relative decrease of protein content in sweet potato leaves.

Compared with the crude fat content in raw sweet potato leaves, the crude fat contents of sweet potato leaves cooked by boiling, steaming, microwaving, and baking were decreased significantly, whereas frying increased crude fat content significantly ($p < 0.05$). During boiling, steaming, and microwaving treatments, volatile and water-soluble fatty acids would be partialy lost or destroyed, which induced the decrease of fat content in sweet potato leaves. Fried samples had a higher level of fat than raw or other cooked samples, mainly due to the absorption of fat by the sweet potato leaves. Similar findings were already reported by Donya et al., who investigated the effects of cooking methods on the proximate composition of bitter melon vegetable and found that the fat content of fried sample increased from 3.6 to 67%, because frying resulted in the expulsion of water and the absorption of fat.[17] Fillion and Henry have already reported that the initial composition of the food (water and fat content) has a great effect on fat uptake during frying, and plant foods, which initially have high water and low fat contents, will absorb a large amount of frying fat.[18]

There was no significant difference between the crude fiber content of raw sweet potato leaves and that of baked sweet potato leaves. Compared with raw sweet potato leaves, boiling, steaming, and microwaving decreased the crude fiber content of sweet potato leaves significantly, whereas frying increased the crude fiber content significantly ($p < 0.05$). It was suggested that boiling caused a great loss of water-soluble dietary fiber. Although sweet potato leaves were not exposed to water, a large amount of cytochylema would flow out during steaming and microwaving treatments, causing the loss of water-soluble dietary fiber. In contrast, fried samples had a higher level of fiber than raw or other cooked samples. Murniece et al. investigated the nutritional composition and energy content of several varieties of potatoes prepared by traditional cooking methods and got the similar result we did, that the fiber content of deep-fat-fried samples was higher than that of uncooked samples.[19] The possible reason was that frying could lead to structural damage of vegetable cells to maximum extent, inducing great loss of other liposoluble constituents in sweet potato leaves; as a result, the fiber content was relatively increased.

The ash content of sweet potato leaves cooked by boiling, steaming, and microwaving did not show significant difference when compared with that of raw sweet potato leaves. Baking

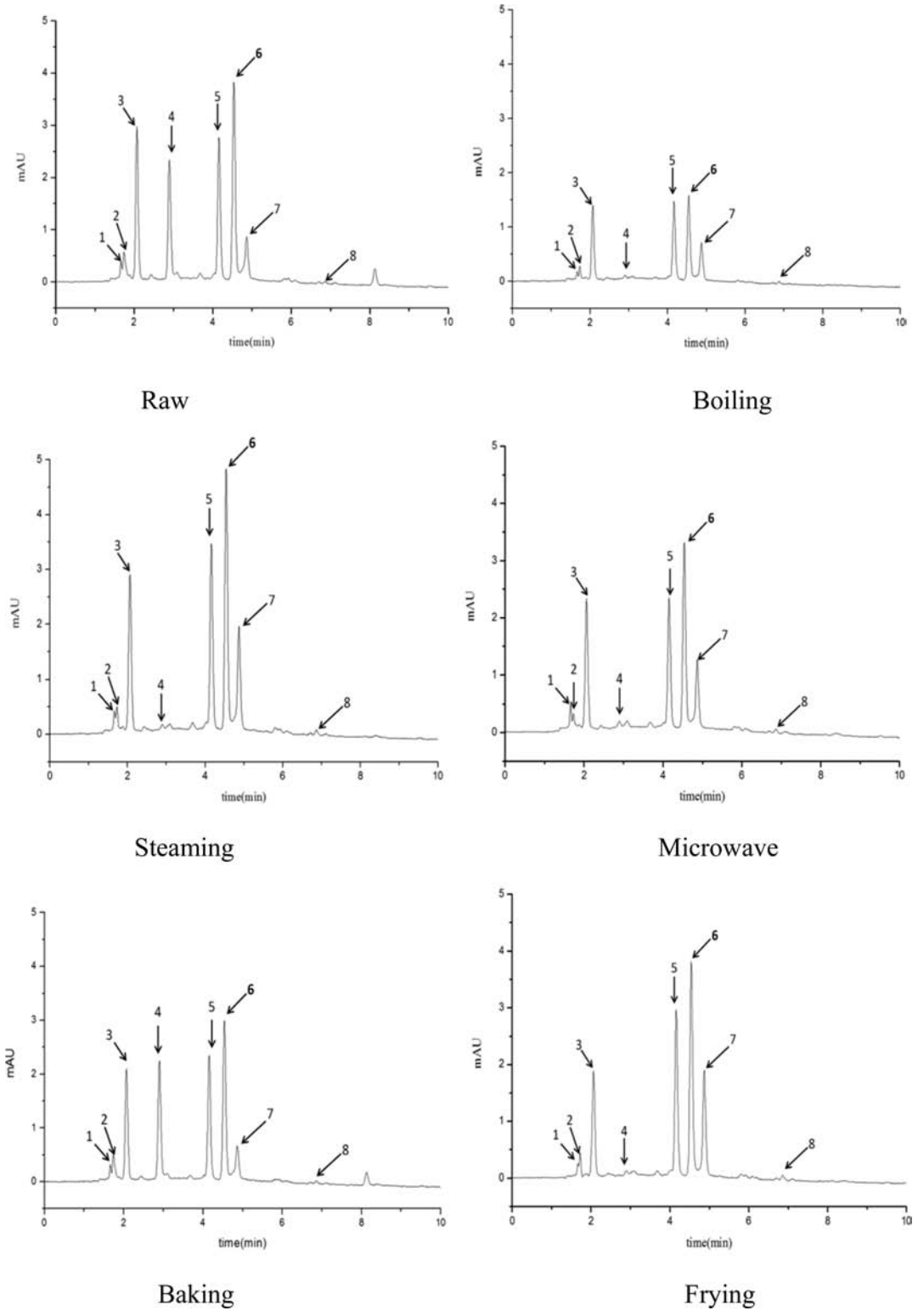


**Figure 2.** Chromatograms of phenolic standards and sweet potato leaf extracts at 326 nm in HPLC. The identities of the compounds identied by numbered peaks are given in Table 2.

increased the ash content of sweet potato leaves significantly, whereas frying decreased the ash content significantly ($p < 0.05$). Our results were very different from those reported by Gidamis et al., who investigated the effect of traditional cooking methods on nutrient contents in young *Moringa* leaves and immature pods and found a significant reduction of ash content as the result of cooking.[20] Baking caused the least loss of ash, compared to other cooking treatments. Besides, baking induced greater loss of other constituents, for example, fat, from raw sweet potato leaves, resulting in the relative increase of ash content. On the contrary, inorganic solids partly flowed out from sweet potato leaf cells during frying treatment, causing the decrease of ash content.


dx.doi.org/10.1021/jf502328d | J. Agric. Food Chem. 2014, 62, 8982−8989

Table 3. Contents of Individual Phenolic Compounds in Sweet Potato Leaves Treated by Different Domestic Cooking Methods (mg/g of DW)[a]

| identity | cooking methods | | | | | |
|---|---|---|---|---|---|---|
| | raw | boiling | steaming | microwaving | baking | frying |
| 5-*O*-caffeoylquinic acid | 2.58 ± 0.16a | 1.55 ± 0.11d | 1.93 ± 0.16c | 2.63 ± 0.22a | 2.25 ± 0.05b | 1.76 ± 0.00cd |
| 3-*O*-caffeoylquinic acid | 3.06 ± 0.31a | 1.16 ± 0.35c | 1.63 ± 0.25b | 1.14 ± 0.12c | 3.06 ± 0.06a | 1.32 ± 0.06bc |
| 4-*O*-caffeoylquinic acid | 13.55 ± 1.36ab | 11.20 ± 0.00c | 14.67 ± 0.33a | 13.17 ± 0.45b | 13.53 ± 0.52b | 12.86 ± 0.19b |
| caffeic acid | 4.62 ± 0.81b | 0.62 ± 0.00c | 0.75 ± 0.04c | 0.74 ± 0.02c | 5.80 ± 0.59a | 0.75 ± 0.02c |
| 4,5-di-*O*-caffeoylquinic acid | 27.23 ± 2.28ab | 19.60 ± 0.13c | 29.84 ± 2.88a | 24.28 ± 1.47b | 30.10 ± 3.81a | 30.04 ± 0.54a |
| 3,5-di-*O*-caffeoylquinic acid | 25.02 ± 1.26ab | 18.09 ± 0.07c | 26.96 ± 2.53a | 23.14 ± 1.09b | 26.01 ± 2.80ab | 25.90 ± 0.38ab |
| 3,4-di-*O*-caffeoylquinic acid | 14.18 ± 0.44b | 12.90 ± 0.04c | 17.71 ± 1.16a | 14.91 ± 0.60b | 14.38 ± 1.04b | 18.32 ± 0.08a |
| 3,4,5-tri-*O*-caffeoylquinic acid | 10.68 ± 0.00c | 10.84 ± 0.00bc | 11.08 ± 0.17a | 10.81 ± 0.03c | 11.07 ± 0.28ab | 11.11 ± 0.10a |
| sum of phenolic compounds | 100.92 ± 6.62a | 75.95 ± 0.30b | 104.58 ± 7.52a | 90.82 ± 4.01ab | 106.21 ± 9.04a | 102.07 ± 0.82a |

[a]Values are means ± SD of three determinations. Cooking methods that were not significantly different are assigned the same letter ($p > 0.05$).

**Total Polyphenols.** Figure 1A shows the effect of cooking methods on TPC of sweet potato leaves. Compared with raw sweet potato leaves, the TPC of sweet potato leaves cooked by boiling, microwaving, and frying decreased significantly, whereas steaming increased the TPC of sweet potato leaves significantly ($p < 0.05$). There was no significant difference between the TPC of raw and baked sweet potato leaves. An increase of 9.44% in TPC was observed after steaming, whereas decreases of 30.51, 25.70, and 15.73% was noted after boiling, microwaving, and frying, respectively. The changes in TPC agreed with the findings of Wachtel-Galor et al., who investigated the effect of cooking on TPC in cauliflower and found that steaming showed the highest TPC (an increase of 45%), followed by boiling (a loss of 4%), and microwaving (a loss of 39%) showed the lowest value.[21] On the other hand, Pellegrini et al. found that oven steaming was the most disadvantageous method for cooking fresh Brussels sprouts.[6] The effect of cooking depends on several factors, such as the cooking procedure, degree of heating, leaching into the cooking medium, solvent used for extraction, pH, and surface area exposed to water and oxygen.[21] For example, Roy et al. investigated the effect of water temperature (50−100 °C) and cooking time (10, 30, 75 min) on TPC in cabbage and found a decrease of TPC as temperature and cooking duration increased.[22] Besides, different plants contain various compounds, some of which are thermally labile and some are not and, therefore, the same cooking method may have different effects on different types of plants.[23] In this study, the depletion of TPC in sweet potato leaves after boiling, microwaving, and frying could be due to phenolic breakdown during cooking.[24] For steaming and baking, the basis of the increased or unchanged TPC in sweet potato leaves could not be categorically stated; however, it could be attributed to the possible breakdown of complex structures liberating individual phenolics and/or phenolic degradation products, which could also react with the Folin−Ciocalteu reagent.[25]

**Antioxidant Activity.** The effect of cooking method on antioxidant activity of sweet potato leaves is shown in Figure 1B. The antioxidant activity of raw sweet potato leaves was 1.28 ± 0.07 μg Trolox equiv/mg, DW. Compared with raw sweet potato leaves, the antioxidant activity of sweet potato leaves cooked by boiling and microwaving was decreased significantly, whereas that of sweet potato leaves cooked by steaming, baking, and frying was increased significantly ($p < 0.05$). Decreases of 63.82 and 32.35% in antioxidant activity were noted after boiling and microwaving, respectively, which was in agreement with the loss of TPC in sweet potato leaves. Price et al. found that only 18% of TPC was retained in broccoli after boiling, the rest being largely leached into cooking water,[26] which supported the data in this study and suggested that boiling caused a decrease of antioxidant activity of sweet potato leaves. The lower antioxidant activity of microwaved samples was perhaps due to a greater thermal effect, rather than the microwaving per se.[21] In contrast, increases of 81.40, 30.09, and 85.82% in antioxidant activity were observed after steaming, baking, and frying, respectively, which was not in accordance with the changes of TPC in sweet potato leaves. This was perhaps due to the production of other redox-active secondary plant metabolites or breakdown products, but was highly likely to be related to the more efficient release of other antioxidants from intracellular proteins, changes in plant cell wall structure, and matrix modifications.[27]

**Quantification of Phenolic Compounds by RP-HPLC.** It is obvious that the TPC measured by the Folin−Ciocalteu method does not give a full picture of the qualification or quantification of the phenolic compounds in the sweet potato leaf extracts. Therefore, the phenolic compounds in the sweet potato leaf extracts cooked by different methods were determined by the HPLC method, and the HPLC results are presented in Table 2 and Figure 2. Eight phenolic compounds, 5-*O*-caffeoylquinic acid, 3-*O*-caffeoylquinic acid, 4-*O*-caffeoylquinic acid, caffeic acid, 4,5-di-*O*-caffeoylquinic acid, 3,5-di-*O*-caffeoylquinic acid, 3,4-di-*O*-caffeoylquinic acid, and 3,4,5-tri-*O*-caffeoylquinic acid, were identified by comparison with the retention times and UV spectra of authentic standards analyzed under identical conditions, whereas the quantitative data were calculated from their respective regression equations.

On the basis of the plots of the peak area ($y$) versus concentration ($x$, mg/g, DW), the regression equations of the eight phenolic compounds detected in sweet potato leaves and their correlation coefficients ($R^2$) were obtained and are shown in Table 2. The contents of individual phenolic compounds in sweet potato leaves treated by different cooking methods are shown in Table 3. In a comparison of the amounts of the eight phenolic compounds present in raw sweet potato leaves, 4,5-di-*O*-caffeoylquinic acid > 3,5-di-*O*-caffeoylquinic acid > 3,4-di-*O*-caffeoylquinic acid > 4-*O*-caffeoylquinic acid > 3,4,5-tri-*O*-caffeoylquinic acid > caffeic acid > 3-*O*-caffeoylquinic acid > 5-*O*-caffeoylquinic acid.

For 5-*O*-caffeoylquinic acid, boiling, steaming, baking, and frying decreased its content significantly, whereas microwaving did not cause a significant change. For 3-*O*-caffeoylquinic acid, boiling, steaming, microwaving, and frying induced significant losses, whereas baking did not change its content significantly.


dx.doi.org/10.1021/jf502328d | J. Agric. Food Chem. 2014, 62, 8982−8989

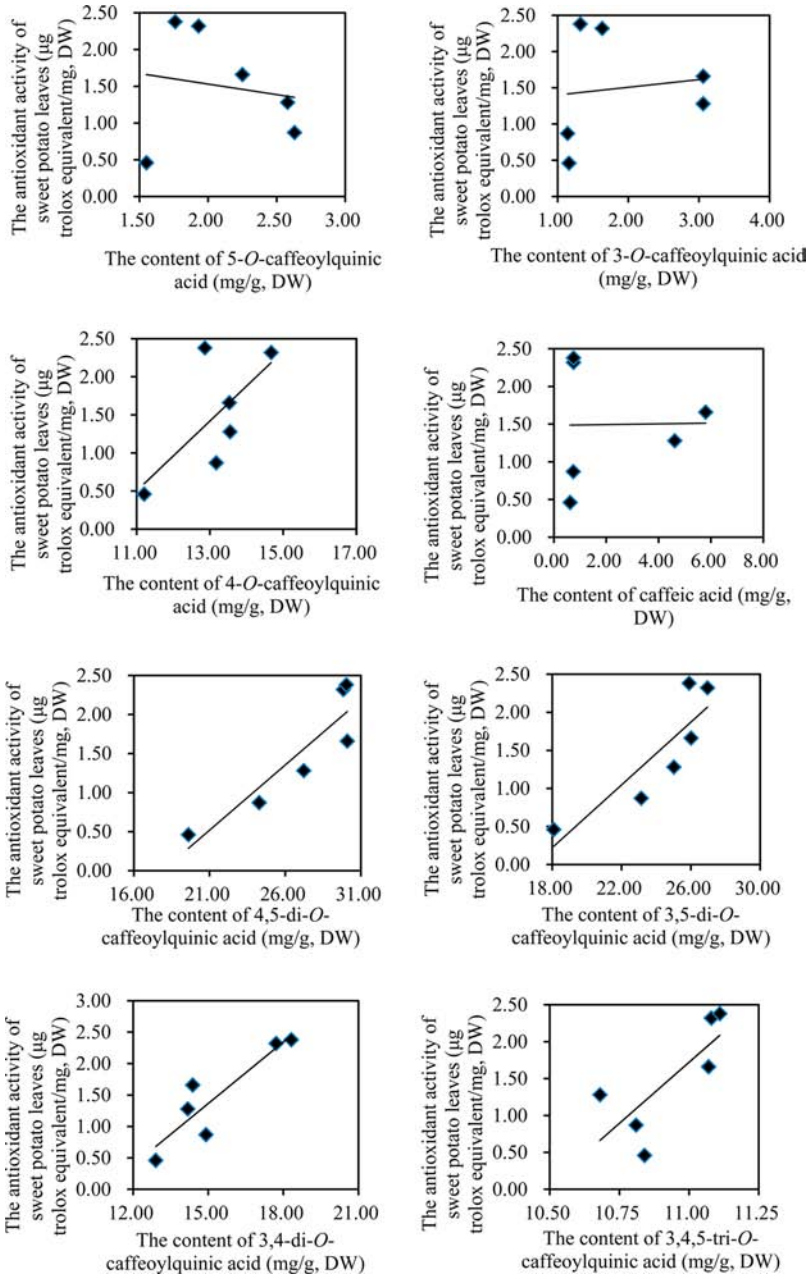


**Figure 3.** Correlation between the content of (a) 5-*O*-caffeoylquinic acid content and antioxidant activity ($R = -0.16433$; $p = 0.7557$); (b) 3-*O*-caffeoylquinic acid content and antioxidant activity ($R = 0.12552$; $p = 0.8127$); (c) 4-*O*-caffeoylquinic acid content and antioxidant activity ($R = 0.67485$; $p = 0.1414$); (d) caffeic acid content and antioxidant activity ($R = 0.01559$; $p = 0.9766$); (e) 4,5-di-*O*-caffeoylquinic acid content and antioxidant activity ($R = 0.90926$; $p = 0.0120$); (f) 3,5-di-*O*-caffeoylquinic acid content and antioxidant activity ($R = 0.86450$; $p = 0.0263$); (g) 3,4-di-*O*-caffeoylquinic acid content and antioxidant activity ($R = 0.90267$; $p = 0.0137$); and (h) 3,4,5-tri-*O*-caffeoylquinic acid content and antioxidant activity ($R = 0.76352$; $p = 0.0773$) of sweet potato leaves treated by different domestic cooking methods.

4-*O*-Caffeoylquinic acid was the most abundant monocaffeoylquinic acid in sweet potato leaves, and among the used cooking methods, only boiling decreased its content significantly. For caffeic acid, baking increased its content significantly, whereas the rest of the cooking methods caused significant losses of caffeic acid. Wang and Ho reported that during thermal treatment, the hydrolysis of chlorogenic acid could produce caffeic acid,[28] but our result was not in accordance with it, suggesting that boiling, steaming, microwaving, and frying induced the leaching out or degradation of caffeic acid. Guillot et al. reported that under mild pyrolysis caffeic acid could be degraded into tetraoxygenated 1,3-*cis*- and 1,3-*trans*-phenylindane isomers, which showed comparable antioxidant activity and were 8-fold more active than butylated hydroxytoluene (BHT),[29] and this might make some contribution to the relatively high antioxidant activity of steamed and fried sweet potato leaves. 4,5-Di-*O*-caffeoylquinic acid was the most abundant dicaffeoylquinic acid in sweet potato leaves, and only boiling induced significant loss of 4,5-di-*O*-caffeoylquinic acid. For 3,5-di-*O*-caffeoylquinic acid, only boiling decreased its content significantly. For 3,4-di-*O*-caffeoylquinic acid, steaming and frying increased its content significantly, whereas boiling decreased its content significantly. For 3,4,5-tri-*O*-caffeoylquinic acid, steaming, baking, and frying induced significant increases,


dx.doi.org/10.1021/jf502328d | J. Agric. Food Chem. 2014, 62, 8982−8989

whereas there were no significant differences between raw and other treated sweet potato leaves. The above-mentioned results indicated that most of the individual phenolic compounds measured by HPLC in sweet potato leaves showed the same general trend in their content, that is, decreases after boiling and better retention after other cooking methods. Especially, there is a common point for steamed and fried sweet potato leaves that the contents of both 3,4-di-*O*-caffeoylquinic acid and 3,4,5-tri-*O*-caffeoylquinic acid increased significantly compared with raw samples, which is in accordance with the trend of antioxidant activity, indicating that 3,4-di-*O*-caffeoylquinic acid and 3,4,5-tri-*O*-caffeoylquinic acid might be the main contributor to the antioxidant activity of sweet potato leaves. A sum of individual phenolic compounds detected by HPLC of 100.92 mg/g DW was obtained for raw sweet potato leaves. In steamed sweet potato leaves, the sum of individual phenolic compounds was 104.58 mg/g DW, 3.63% more than for raw samples. This value is far from the increase in antioxidant activity of 81.4% of steamed samples. The same trend could be seen for baked sweet potato leaves and fried ones. This result demonstrated a production of antioxidant compounds other than polyphenols. The interesting fact that has to be more pointed out is that these substances do not react in the Folin−Ciocalteu system, because in Figure 1A, only a slight increase of TPC has been detected in steamed sweet potato leaves in comparison with raw sweet potato leaves. It is very hard to identify which individual phenolic compound was the biggest contributor to the antioxidant activity of sweet potato leaves. Palermo et al. found that different cooking treatments caused an increase in total antioxidant activity of artichokes and ascribed this increase to the increase of 5-*O*-caffeoylquinic and 1,5-di-*O*-caffeoylquinic acid.[11] However, our result was very different from theirs. To tell the relationship between individual phenolic compounds and antioxidant activity of sweet potato leaves clearly, we analyzed the correlation between the content of individual phenolic compounds and antioxidant activity of sweet potato leaves by Pearson test using SAS version 8.1 software (Figure 3). 4,5-Di-*O*-caffeoylquinic acid showed the biggest correlation coefficient, followed by 3,4-di-*O*-caffeoylquinic acid, 3,5-di-*O*-caffeoylquinic acid, 3,4,5-tri-*O*-caffeoylquinic acid, 4-*O*-caffeoylquinic acid, 3-*O*-caffeoylquinic acid, caffeic acid, and 5-*O*-caffeoylquinic acid. Therefore, the antioxidant activity of sweet potato leaves could be mainly attributed to the increases in the contents of 4,5-di-*O*-caffeoylquinic acid, 3,4-di-*O*-caffeoylquinic acid, 3,5-di-*O*-caffeoylquinic acid, and 3,4,5-tri-*O*-caffeoylquinic acid. The antioxidant activity of phenolics compounds is mainly due to redox properties, which allow them to act as reducing agents, hydrogen donors, singlet oxygen quenchers, heavy metal chelators, and hydroxyl radical quenchers.[30] The di- and tricaffeoylquinic acids have more hydroxyl groups in their molecular structure,[31] making them more active than monocaffeoylquinic acids.

The TPC calculated from the data obtained by HPLC analysis was lower than that estimated by using the Folin−Ciocalteu method. One of the possible reasons is that the Folin−Ciocalteu method suffers from a number of interfering substances [particularly sugars, aromatic amines, sulfur dioxide, ascorbic acid and other enediols and reductones, organic acids, and Fe(II)].[32] Another possible reason is the limitation of individual phenolic compounds used as standard.[33]

In conclusion, sweet potato leaves are good sources of protein, fiber, and minerals, and the polyphenols therein are important antioxidants. Understanding the antioxidant activity of sweet potato leaves can help human beings enhance antioxidant intake, and this work must consider the effects of cooking on antioxidant activity. The results presented here clearly demonstrated that cooking could make the antioxidant activity of cooked sweet potato leaves quite different from that of the uncooked leaves. This was perhaps due to a variety of effects, including damage, flowing out, and transformation of the constituents in sweet potato leaves. In this study, steaming was found to retain or enhance TPC and antioxidant activity of sweet potato leaves best, followed by frying, baking, microwaving, and then boiling. Cooking in water seemed to cause a leakage of polyphenols into the cooking water. The correlation between the content of individual phenolic compounds and antioxidant activity suggested that the antioxidant activity of sweet potato leaves could be mainly attributed to 4,5-di-*O*-caffeoylquinic acid, 3,4-di-*O*-caffeoylquinic acid, 3,5-di-*O*-caffeoylquinic acid, and 3,4,5-tri-*O*-caffeoylquinic acid.

## AUTHOR INFORMATION

### Corresponding Author

*(T.M.) Phone: (+86) 10 62815541. Fax: (+86) 10 62815541. E-mail: mutaihua@126.com.

### Funding

This research was supported by Earmarked Fund for the China Agriculture Research System (CARS-11-B-19).

### Notes

The authors declare no competing financial interest.

## ACKNOWLEDGMENTS

We are grateful to the Academy of Agricultural and Forestry Sciences in Hebei Province for providing the sweet potato leaves used in this study.

## ABBREVIATIONS USED

CHA, chlorogenic acid; CHAE, chlorogenic acid equivalents; RP-HPLC, reversed-phase high-performance liquid chromatography; SD, standard deviation; TE, Trolox equivalents; TPC, total polyphenol content

## REFERENCES

(1) Gharras, H. E. Polyphenols: food sources, properties and applications-a review. *Int. J. Food Sci. Technol.* **2009**, *44*, 2512−2518.

(2) Rehman, Z. U.; Islam, M.; Shah, W. H. Effect of microwave and conventional cooking on insoluble dietary fibre components of vegetables. *Food Chem.* **2003**, *80*, 237−240.

(3) Zhang, D.; Hamauzu, Y. Phenolics, ascorbic acid, carotenoids and antioxidant activity of broccoli and their changes during conventional and microwave cooking. *Food Chem.* **2004**, *88*, 503−509.

(4) Perla, V.; Holm, D. G.; Jayanty, S. S. Effects of cooking methods on polyphenols, pigments and antioxidant activity in potato tubers. *LWT−Food Sci. Technol.* **2012**, *45*, 161−171.

(5) Oboh, G. Effect of blanching on the antioxidant properties of some tropical green leafy vegetables. *LWT−Food Sci. Technol.* **2005**, *38*, 513−517.

(6) Pellegrini, N.; Chiavaro, E.; Gardana, C.; Mazzeo, T.; Contino, D.; Gallo, M.; et al. Effect of different cooking methods on color, phytochemical concentration, and antioxidant capacity of raw and frozen *Brassica* vegetables. *J. Agric. Food Chem.* **2010**, *58*, 4310−4321.

(7) An, L. V.; Frankow-Lindberg, B. E.; Lindberg, J. E. Effect of harvesting interval and defoliation on yields and chemical composition of leaves, stems and tubers of sweet potato (*Ipomoea batatas* L. (Lan.)) plant parts. *Field Crop Res.* **2003**, *82*, 49−58.

(8) Johnson, M.; Pace, R. D. Sweet potato leaves: properties and synergistic interactions that promote health and prevent disease. *Nutr. Rev.* **2010**, *68*, 604−615.
(9) Sun, H. N.; Mu, T. H.; Xi, L. X.; Zhang, M.; Chen, J. W. Sweet potato (*Ipomoea batatas* L.) leaves as nutritional and functional foods. *Food Chem.* **2014**, *156*, 380−389.
(10) Taira, J.; Taira, K.; Ohmine, W.; Nagata, J. Mineral determination and anti-LDL oxidation activity of sweet potato (*Ipomoea batatas* L.) leaves. *J. Food Compos. Anal.* **2013**, *29*, 117−125.
(11) Palermo, M.; Colla, G.; Barbieri, G.; Fogliano, V. Polyphenol metabolite profile of artichoke is modulated by agronomical practices and cooking method. *J. Agric. Food Chem.* **2013**, *61*, 7960−7968.
(12) Tudela, J. A.; Cantos, E.; Espín, J. C.; Tomás-Barberán, F. A.; Gil, M. I. Induction of antioxidant flavonol biosynthesis in fresh-cut potatoes. Effect of domestic cooking. *J. Agric. Food Chem.* **2002**, *50*, 5925−5931.
(13) AOAC (Association of Analytical Chemists). *Official Methods of Analysis*, 17th ed.; AOAC International: Gaithersburg, MD, USA, 2000.
(14) ISO (International Standards Organization). ISO 5498:1981. Determination of crude fibre content, general method; ISO: Geneva, Switzerland, 1981.
(15) Yoshimoto, M.; Yahara, S.; Okuno, S.; Islam, M. S.; Ishiguro, K.; Yamakawa, O. Antimutagenicity of mono-, di-, and tricaffeoylquinic acid derivatives isolated from sweet potato (*Ipomoea batatas* L.) leaf. *Biosci., Biotechnol., Biochem.* **2002**, *66*, 2336−2341.
(16) Blasa, M.; Angelino, D.; Gennari, L.; Ninfali, P. The cellular antioxidant activity in red blood cells (CAA-RBC): a new approach to bioavailability and synergy of phytochemicals and botanical extracts. *Food Chem.* **2011**, *125*, 685−691.
(17) Donya, A.; Hettiarachchy, N.; Liyanage, R.; Lay, J.; Chen, P.; Jalaluddin, M. Effects of processing methods on the proximate composition and momordicosides K and L content of bitter melon vegetable. *J. Agric. Food Chem.* **2007**, *55*, 5827−5833.
(18) Fillion, L.; Henry, C. J. K. Nutrient losses and gains during frying: a review. *Int. J. Food Sci. Nutr.* **1998**, *49*, 157−168.
(19) Murniece, I.; Karklina, D.; Galoburda, R.; Santare, D.; Skrabule, I.; Costa, H. S. Nutritional composition of freshly harvested and stored Latvian potato (*Solanum tuberosum* L.) varieties depending on traditional cooking methods. *J. Food Compos. Anal.* **2011**, *24*, 699−710.
(20) Gidamis, A. B.; Panga, J. T.; Sarwatt, S. V.; Chove, B. E.; Shayo, N. B. Nutrient and antinutrient contents in raw and cooked young leaves and immature pods of *Moringa oleifera*, Lam. *Ecol. Food Nutr.* **2003**, *42*, 399−411.
(21) Wachtel-Galor, S.; Wong, K. W.; Benzie, I. F. F. The effect of cooking on *Brassica* vegetables. *Food Chem.* **2008**, *110*, 706−710.
(22) Roy, M. K.; Takenaka, M.; Isobe, S.; Tsushida, T. Antioxidant potential, anti-proliferative activities, and phenolic content in water-soluble fractions of some commonly consumed vegetables: effects of thermal treatment. *Food Chem.* **2007**, *103*, 106−114.
(23) Bernhardt, S.; Schlich, E. Impact of different cooking methods on food quality: retention of lipophilic vitamins in fresh and frozen vegetables. *J. Food Eng.* **2006**, *77*, 327−333.
(24) Padda, M. S.; Picha, D. H. Phenolic composition and antioxidant capacity of different heat-processed forms of sweet potato cv. 'Beauregard'. *Int. J. Food Sci. Technol.* **2008**, *43*, 1404−1409.
(25) Lutz, M.; Henríquez, C.; Escobar, M. Chemical composition and antioxidant properties of mature and baby artichokes (*Cynara scolymus* L.), raw and cooked. *J. Food Compos. Anal.* **2011**, *24*, 49−54.
(26) Price, K. R.; Casuscelli, F.; Colquhoun, I. J.; Rhodes, M. J. C. Composition and content of flavonol glycosides in broccoli florets (*Brassica olearacea*) and their fate during cooking. *J. Sci. Food Agric.* **1998**, *77*, 468−472.
(27) Rechkemmer, G. Nutritional aspects. In *Thermal Processing of Food: Potential Health Benefits and Risks*; Deutsche Forschungsgemeinschaft (DFG); Wiley-VCH Verlag: Weinheim, Germany, 2007; DOI: 10.1002/9783527611492.ch5.
(28) Wang, Y.; Ho, C. T. Polyphenolic chemistry of tea and coffee: a century of progress. *J. Agric. Food Chem.* **2009**, *57*, 8109−8114.
(29) Guillot, F. L.; Malnoë, A.; Stadler, R. H. Antioxidant properties of novel tetraoxygenated phenylindan isomers formed during thermal decomposition of caffeic acid. *J. Agric. Food Chem.* **1996**, *44*, 2503−2510.
(30) Kaur, C.; Kapoor, H. C. Anti-oxidant activity and total phenolic content of some Asian vegetables. *Int. J. Food Sci. Technol.* **2002**, *37*, 153−161.
(31) Zheng, W.; Clifford, M. N. Profiling the chlorogenic acids of sweet potato (*Ipomoea batatas*) from China. *Food Chem.* **2008**, *106*, 147−152.
(32) Prior, R. L.; Wu, X.; Schaich, K. Standardized methods for the determination of antioxidant capacity and phenolics in foods and dietary supplements. *J. Agric. Food Chem.* **2005**, *53*, 4290−4302.
(33) Sagdic, O.; Ozturk, I.; Ozkan, G.; Yetim, H.; Ekici, L.; Yilmaz, M. T. RP-HPLC−DAD analysis of phenolic compounds in pomace extracts from five grape cultivars: evaluation of their antioxidant, antiradical and antifungal activities in orange and apple juices. *Food Chem.* **2011**, *126*, 1749−1758.

cancer,[10] breast cancer,[11] leukemia,[12] and lung cancer.[13] In our previous studies, PGG suppresses the functions of ER$\alpha$ by lysosome-dependent depletion and modulating the ErbB/PI3K/Akt pathway in hormone-dependent breast cancer cells.[14] Moreover, PGG exerts an anti-invasive effect in androgen-independent prostate cancer by controlling MMP-9 expression through the suppression of the EGFR/JNK pathway and suppresses bone metastasis in nude mice treated with intratibial injection of prostate cancer (PC-3) cells.[15]

We still need to establish a comprehensive method to study how PGG affects EGF-induced prostate cancer bone metastasis. Therefore, we utilized 2D-PAGE and MALDI-TOF to analyze the effect of PGG treatment on EGF-induced prostate cancer bone metastasis. Our results showed that PGG suppressed EGF-induced eIF3i expression through inhibition of the PI3K/AKT/mTOR pathway. Therefore, EGF-induced eIF3i expression played an important role in prostate cancer bone metastasis.

## MATERIALS AND METHODS

**Materials and Antibodies.** PGG was isolated from the leaves of *Macaranga tanarins* (L.) as described previously.[16] The purity was determined by HPLC to be approximately 99%. For treatment of cells, PGG was dissolved in dimethyl sulfoxide (DMSO) as a stock solution. The final DMSO added to cell culture medium was below 0.1%. EGF, LY294002, PD98059, SB203580, and SP600125 were obtained from Sigma (St. Louis, MO, USA). Antiphospho-ERK1/2 (Thr 202/Tyr 204) and ERK1/2 were from Upstate Biotechnology, Inc. (Lake Placid, NY, USA). Antibodies against p-Akt (Ser473), Akt, p-p38, p38, JNK, and p-JNK were from Cell Signaling (Beverly, MA, USA). Antibodies for $\beta$-actin, eIF3i, p-PI3K, PI3K, p-mTOR, mTOR, p-4EBP1, and 4EBP1 were purchased from Santa Cruz Biotechnology, Inc. (Santa Cruz, CA, USA). Anti-mouse and anti-rabbit antibodies conjugated to horseradish peroxidase were also obtained from Santa Cruz Biotechnology, Inc.

**Cell Cultures.** PC-3 cells were obtained from the American Type Culture Collection (Rockville, MD, USA). PC-3 cells were cultured in RPMI 1640 supplemented with 10% fetal bovine serum (FBS) and 1% penicillin–streptomycin in a 5% $CO_2$ atmosphere at 37 °C.

**Two-Dimensional Gel Electrophoresis (2-DE).** In the first dimension, isoelectric focusing (IEF) was done with commercially available preformed immobilized pH gradients (IPGs) (linear pH gradient 3–10, 13 cm). The gels were rehydrated overnight by placing the strips gel-side-down in sample-containing rehydration solution in an IPGphor strip holder and covering them with mineral oil. IEF was conducted using an IPGphore IEF System (Amersham Pharmacia Biotech, Piscataway, NJ, USA) with a three-phase program. The first phase was set at 500 V for 1 h, the second phase was set at 1000 V for 1 h, and the final phase was a linear gradient spanning from 8000 to 16000 V for 2 h. Before second-dimensional electrophoresis, the IPG gel strips were incubated at room temperature for 15 min in equilibration solution (50 mM Tris-HCl, pH 8.8, 6 M urea, 2% SDS, 30% glycerol) containing 1% DTT and then in equilibration solution containing 2.5% iodoacetamide for 5 min. The gels were then submitted to a second dimension run on a Hoefere SE 600 (Amersham Pharmacia Biotech), at 4 °C, on running 12.5% SDS-PAGE gels (16 × 15 cm), without stacking gels. The IPG gel strips were embedded on top of the gels with 1% agarose. Electrophoresis was conducted at 30 mA/gel for 5 h. The 2-D polyacrylamide gels were stained with CBB. Protein p*I* and $M_w$, respectively, were assigned by calibration of 2-D PAGE gels with carbamylyte p*I* calibration markers and molecular weight markers (Amersham Pharmacia Biotech). On 2-DE, only those significantly and consistently altered protein spots in at least two independent experiments (over 2-fold up- or down-regulation) were selected for analysis by MALDI-TOF. Protein spots were quantified using ImageMaster 2D Elite software (Amersham Pharmacia Biotech).

**In-Gel Digestion.** Protein spots excised from the CBB-stained gel were destained in microtubes with 0.2 mL of acetonitrile (ACN) for 15 min and dried completely in a centrifugal evaporator. The dried gels were rehydrated on ice for 45 min with a digestion buffer composed of 0.04 mg/mL of modified trypsin (Promega, Madison, WI, USA) in 0.005% zwittergent 3-16 and 50 mM $NH_4HCO_3$. After removal of excess solution, proteins were further digested at 37 °C for 15 h. The resultant peptides were extracted with 5% ACN in 5% formic acid, desalted, and concentrated using in-tip reversed phase resin (Zip tip C18; Millipore, Bedford, MA, USA).

**Western Blotting.** Western Blot was done as described previously.[17] After treatment, cells were harvested, washed twice with cold PBS, and then lysed in gold lysis buffer. A total of 50 $\mu$g of protein was separated by SDS-PAGE and transferred to the PVDF membrane. The filters were probed with appropriate primary antibodies. Reactive bands were visualized using an enhanced chemiluminescence system (Amersham Biosciences, Arlington Heights, IL, USA).

**Tranfection.** One day before transfection, $2 \times 10^5$ cells without serum and antibiotics were plated in six-well plates. Starved PC-3 cells were grown to 90% confluence and transfected on the following day by Lipofectamine 2000 (Invitrogen, Carlsbad, CA, USA) and premixed plasmid DNA with OPTI-MEM (GIBCO) for 5 min and then added to each well. After 24 h of incubation, the transfection was completed.

**Reverse Transcription Real-Time Quantitative PCR.** Total RNA was extracted from cancer cells using a TRIzol kit (MDBio, Taipei, Taiwan). The reverse transcription was carried out using 2 $\mu$g of total RNA that was reversely transcribed into complementary DNA using oligo (dT) primer by Superscript RT (Invitrogen, Burlington, ON, Canada). qPCR assays were performed with a StepOne-Plus sequence detection system in triplicate. The cycling conditions were 10 min of polymerase activation at 95 °C followed by 40 cycles at 95 °C for 15 s and 60 °C for 60 s. Data were analyzed by relative quantification normalized with GAPDH gene.

**Cell Invasion Assay.** A Boyden chamber (8 $\mu$m pore size) was used for in vitro invasion assay. Cells ($1 \times 10^5$) in medium containing 0.5% serum were seeded in the upper chamber, and 15% FBS was added to the medium in the lower chamber as a chemoattractant. For invasion assays, the upper side of the filter was covered with Matrigel (Collaborative Research, Inc., Boston, MA, USA). After 24 h for invasion assays, cells on the upper side of the filter were removed, and cells that remained adherent to the underside of membrane were fixed in 4% formaldehyde and stained with Hoechst 33342 dye. Ten contiguous fields of each sample were examined using a microscope

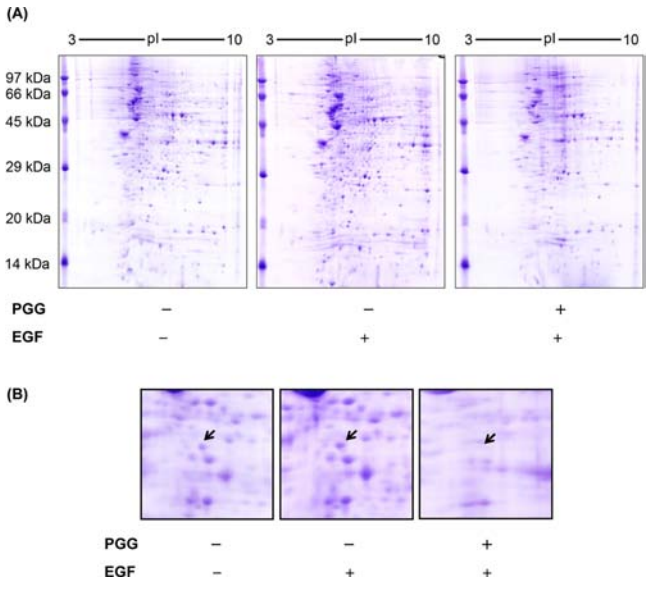


**Figure 1.** Proteomics analysis: (A) representative 2-DE gel images from PC-3 cells pretreated with/without 10 $\mu$M PGG for 1 h and then added to 25 ng/mL EGF for 24 h; (B) magnified regions of identified differently expressed protein spots. Spots within the arrow were identified as differently expressed eIF3i proteins.

**Table 1. Six Proteins Were Identified during EGF-Stimulated Expression and Reduced by PGG Treatment**

| spot | protein | accession no. | mass (Da) | predicted p*I* | expression change fold | | |
|---|---|---|---|---|---|---|---|
| | | | | | PC-3 | PC-3 + EGF | PC-3 + EGF + PGG |
| 68 | heat shock 70 kDa protein 4 | 38327039 | 95127 | 5.11 | 1 | 6.31291 | 0.689115 |
| 266 | heterogeneous nuclear ribonucleoprotein L | 11527777 | 64617 | 8.49 | 1 | 2.46426 | 0 |
| 447 | annexin VII isoform 1 | 4502111 | 50569 | 6.25 | 1 | 3.98495 | 1.09136 |
| 642 | eukaryotic translation initation factor 3, subunit 2 | 4503513 | 36878 | 5.38 | 1 | 3.11322 | 0 |
| 1021 | prenylcysteine oxidase-like OS | 31543181 | 54809 | 6.81 | 1 | 3.97152 | 0 |
| 1127 | exosome component 2 | 126541113 | 30552 | 66.2 | 1 | 2.65663 | 0.983926 |

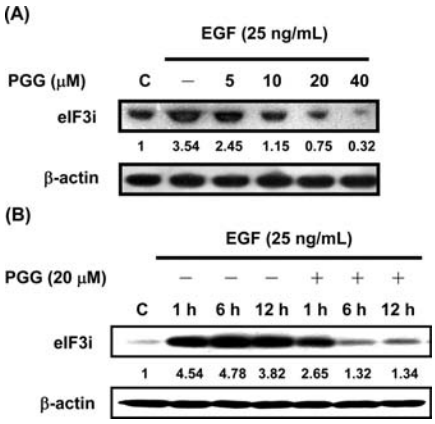


**Figure 2.** PGG blocked EGF-induced eIF3i expression in PC-3 cells. (A) PC-3 cells were pretreated with DMSO (control) or increasing PGG concentrations (5−40 $\mu$M) for 1 h prior to EGF stimulation (25 ng/mL) for 24 h. (B) PC-3 cells were incubated with DMSO (control) or 20 $\mu$M PGG for 1, 6, or 12 h prior to EGF stimulation (25 ng/mL) for 24 h. The cells were then harvested and lysed for the detection of eIF3i and $\beta$-actin. Western blot data presented are representative of those obtained in at least three separate experiments. Immunoblots were quantified, and relative expression to control is indicated.

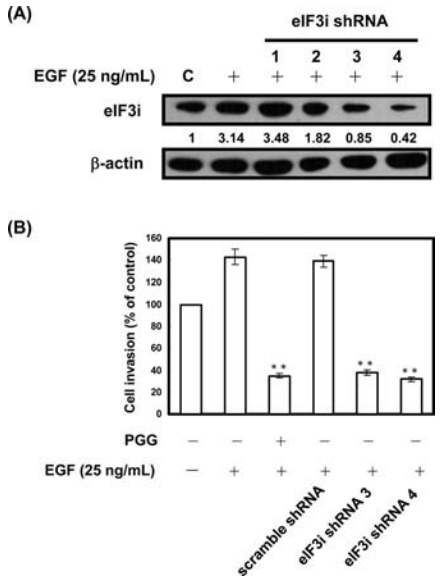


**Figure 3.** shRNA knockdown of eIF3i revealed a critical role for EGF-induced prostate cancer cells invasion. (A) PC-3 cells were transfected with eIF3i shRNA and then stimulated with EGF (25 ng/mL) for 24 h. The cells were then harvested and lysed for the detection of eIF3i and $\beta$-actin. Western blot data presented are representative of those obtained in at least three separate experiments. Immunoblots were quantified, and relative expression to control is indicated. (B) Invasion ability of P-C3 cells transfected with scramble shRNA or eIF3i shRNA and then stimulated with EGF (25 ng/mL) for 24 h. Data represent means ± SEM ($n$ = 3). Asterisks indicate $P < 0.01$ compared with PC-3 cells stimulated with EGF. Two independent clones are shown, as indicated.

and a 40× objective to obtain a representation of the number of cells that had invaded across the membrane.

## RESULTS

**Proteomic Profile of EGF-Induced Prostate Cancer Cells Treated with or without PGG.** Our previous studies showed that PGG could suppress prostate cancer cell (PC-3) bone metastasis by transcriptionally repressing EGF-inducing MMP-9 expression.[15] However, the protein expression profile of EGF-induced prostate cancer cells treated with PGG was not investigated. We utilized 2D-PAGE and MALDI-TOF to analyze the differences of protein expression profile between EGF-induced prostate cancer cells treated with or without PGG. In 2D-PAGE, the protein spots were clearly visualized, with around 1400 protein spots on each gel (Figure 1A). The protein expression profile of PC-3 cells treated with neither EGF nor PGG was used as a control. PC-3 cells were pretreated without and with 10 $\mu$M PGG for 1 h and then added to 25 ng/mL EGF for 24 h. Six proteins were identified during EGF-stimulated expression and reduced by PGG treatment (Table 1). The eukaryotic translation initiation factor 3 subunit 2 (eIF3i) was one of these six proteins (Figure 1B).

**PGG Suppressed EGF-Induced eIF3i Expression in PC-3 Cells.** To further confirm whether PGG could suppress EGF-induced eIF3i expression, Western blotting was performed. PC-3 cells were pretreated with indicated concentrations of PGG for 1 h prior to stimulation with EGF. Figure 2A showed that PGG inhibited EGF-induced eIF3i expression in a dose-dependent manner. To address this time-dependent pretreatment effect, we pretreated PC-3 cells with 20 $\mu$M PGG for various periods of time from 1 to 12 h prior to EGF addition. As shown in Figure 2B, 20 $\mu$M PGG exerted its inhibitory effect on EGF-induced eIF3i expression in a time-dependent manner. Our data suggested that PGG inhibited EGF-induced eIF3i expression in PC-3 cells.

**EGF-Induced eIF3i Expression Involved in Prostate Cancer Cell Bone Metastasis.** PGG suppressed EGF-induced prostate cancer cell bone metastasis and also decreased EGF-induced expression of eIF3i. To understand the biological functions of eIF3i involved in EGF-induced prostate cancer cells invasion, we employed the loss-of-function approach, that is, by knocking down the expression level of eIF3. We transiently transfected PC-3 cells with four shRNA clones specifically targeting eIF3i (Figure 3A). Clones 3 and 4 were good enough for reducing EGF-induced eIF3i expression in PC-3 cells. Subsequently, we examined the effect of EGF-induced eIF3i expression involved in PC-3 cell invasion. The results showed


dx.doi.org/10.1021/jf502447e | J. Agric. Food Chem. 2014, 62, 8990−8996

that PGG suppressed EGF-induced invasion in PC-3 cells. Moreover, down-regulation of EGF-induced eIF3i expression resulted in significant reduction of PC-3 cells' invasive ability (Figure 3B). The studies indicated that PGG suppressed EGF-induced prostate cancer cell bone metastasis through the down-regulation of eIF3i.

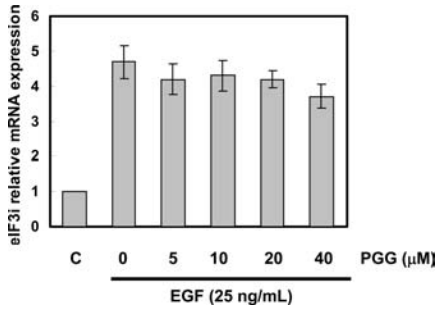


**Figure 4.** PGG does not inhibit EGF-induced eIF3i mRNA expression. PC-3 cells were pretreated with DMSO (control) or increasing PGG concentrations (5−40 $\mu$M) for 1 h prior to EGF stimulation (25 ng/mL) for 24 h. Real-time PCR analysis was employed on total mRNA. Data represent means ± SEM ($n$ = 3).

**PGG Did Not Suppress EGF-Induced eIF3i mRNA Expression in PC-3 Cells.** To investigate whether the suppression of EGF-induced eIF3i expression by PGG was due to reduced eIF3i mRNA expression, real-time PCR analysis was employed. As shown in Figure 4, the results showed that EGF-induced eIF3i mRNA expression. However, PGG did not repress EGF-induced eIF3i mRNA expression in a dose-dependent manner (Figure 4). The data suggested that PGG did not modulate EGF-induced eIF3i expression at the transcriptional level.

**PGG Suppressed EGF-Induced eIF3i Expression through the Inhibition of PI3K Signaling Pathway.** EGF signaling activates multiple important pathways such as RAS/mitogen-activated protein kinase (MAPK) and phosphatidylinositol 3-kinase (PI3K)-Akt.[3] To confirm which pathways participated in EGF-induced eIF3i expression, we examined the phosphorylation state of p38, JNK, PI3K, and ERK by Western blotting. As shown in Figure 5A, 25 ng/mL EGF activated the phosphorylation of p38, JNK, PI3K, and ERK, and PGG inhibited EGF-induced PI3K/JNK/p38 phosphorylation. We also use ERK inhibitor (PD98059), PI3K inhibitor (LY294002), JNK (SP600125), and p38 inhibitor (SB203580) to further

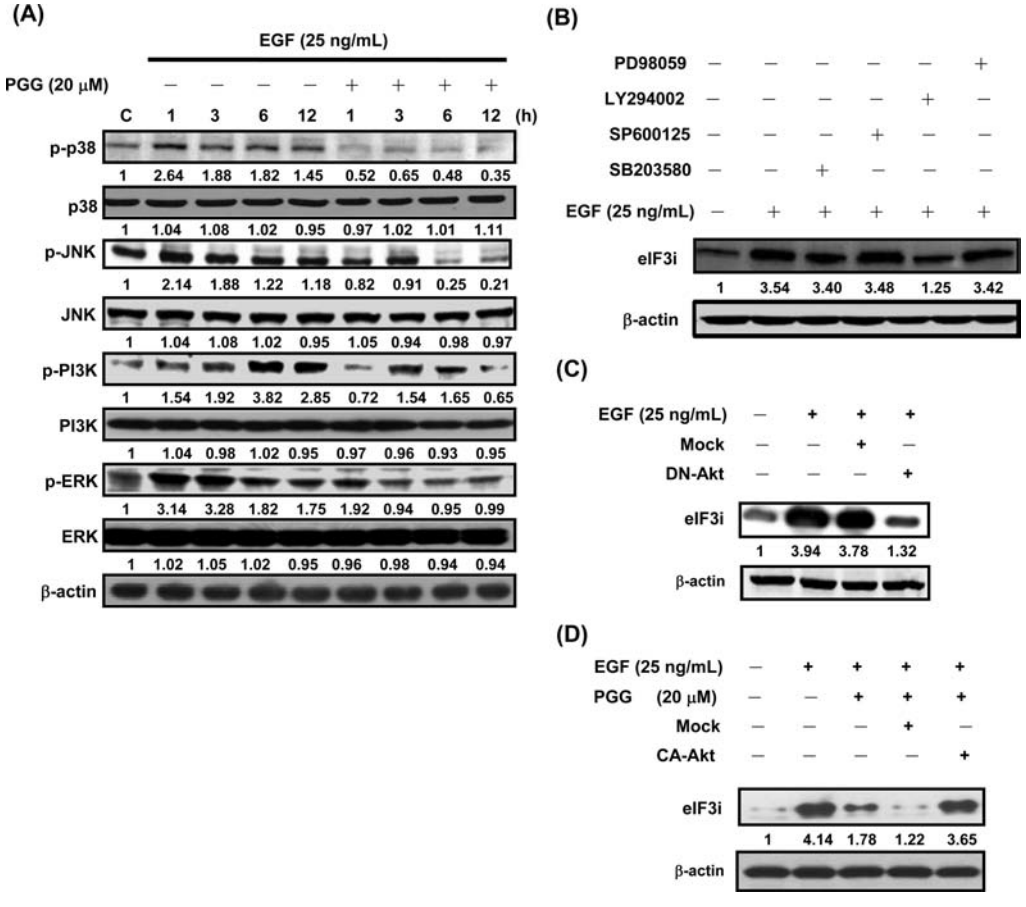


**Figure 5.** PGG inhibited EGF-induced eIF3i expression through inhibition of the PI3K signaling pathway. (A) PC-3 cells were preincubated in the presence or absence of 20 $\mu$M PGG for 1 h prior to EGF stimulation (25 ng/mL) for various times. The cells were then harvested and lysed for the detection of p-p38, p38, p-JNK, JNK, p-PI3K, PI3K, p-ERK, ERK, and $\beta$-actin. (B) PC-3 cells were pretreated with 20 $\mu$M PGG, PI3K inhibitor (40 $\mu$M LY294002), JNK inhibitor (20 $\mu$M SP600125), or p38 inhibitor (30 $\mu$M SB203580) for 1 h and then treated with EGF (25 ng/mL) for 24 h. (C) PC-3 cells were transfected with 50 nmol/L DN-Akt or mock. Twenty-four hours after transfection, cells were incubated with EGF (25 ng/mL) for 24 h. The cells were then harvested and lysed for the detection of eIF3i and $\beta$-actin. (D) PC-3 cells were transfected with 50 nmol/L CA-Akt or mock. Twenty-four hours after transfection, they were preincubated in the presence or absence of 20 $\mu$M PGG for 1 h prior to EGF stimulation (25 ng/mL) for 24 h. The cells were then harvested and lysed for the detection of eIF3i and $\beta$-actin. Western blot data presented are representative of those obtained in at least three separate experiments. Immunoblots were quantified, and relative expression to control is indicated.


dx.doi.org/10.1021/jf502447e | J. Agric. Food Chem. 2014, 62, 8990−8996

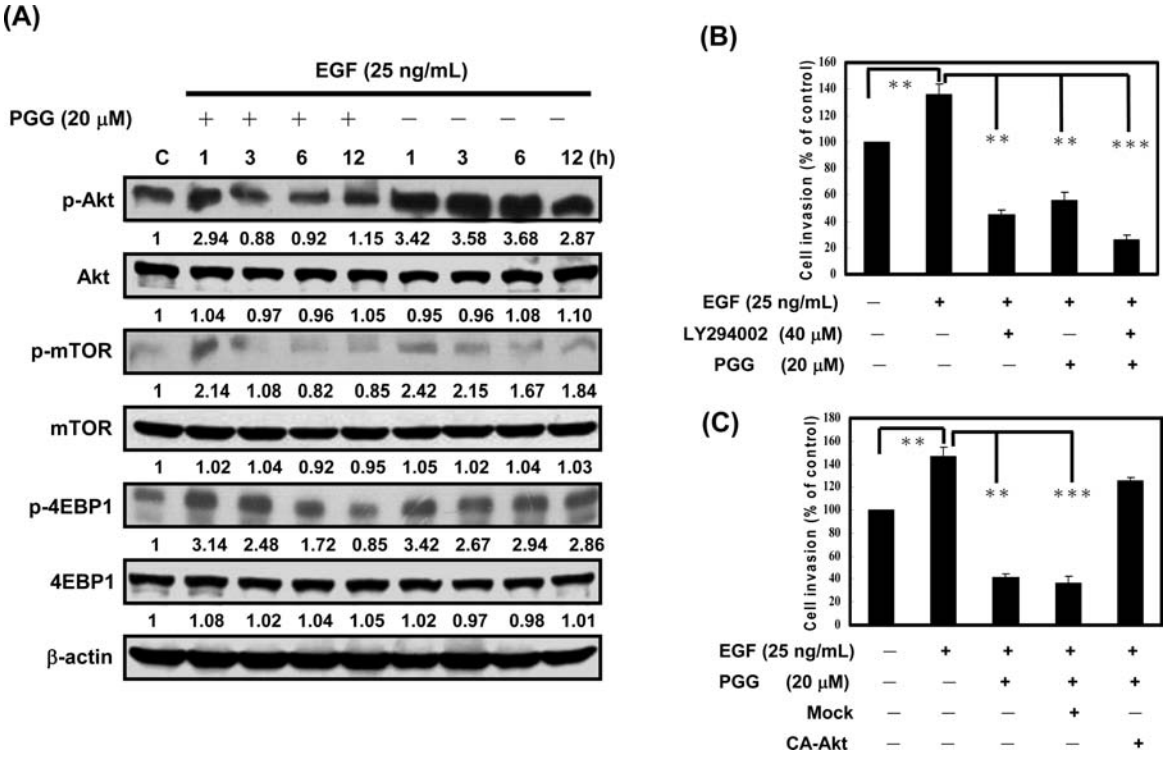


**Figure 6.** PGG reduced EGF-induced eIF3i expression through the PI3K/AKT/mTOR pathway. (A) PC-3 cells were preincubated in the presence or absence of 20 $\mu$M PGG for 1 h prior to EGF stimulation (25 ng/mL) for various times. The cells were then harvested and lysed for the detection of p-AKT, AKT, p-mTOR, mTOR, p-4EBP1, 4EBP1, eIF3i, and $\beta$-actin. Western blot data presented are representative of those obtained in at least three separate experiments. Immunoblots were quantified, and relative expression to control is indicated. (B) PC-3 cells were pretreated with 20 $\mu$M PGG or 40 $\mu$M LY294002 or a combination of 40 $\mu$M LY294002 and 20 $\mu$M PGG for 1 h and then treated with EGF for 24 h, and then cell invasion was determined. Data represent means ± SEM ($n$ = 3). An asterisk indicates that the values are significantly different (**, $P < 0.01$; ***, $P < 0.001$). (C) PC-3 cells were transfected with 50 nmol/L CA-Akt or mock. Twenty-four hours after transfection, cells were preincubated in the presence or absence of 20 $\mu$M PGG for 1 h prior to EGF stimulation (25 ng/mL) for 24 h, and then cell invasion was determined. Data represent means ± SEM ($n$ = 3). An asterisk indicates that the values are significantly different (**, $P < 0.01$; ***, $P < 0.001$).

investigate which signaling pathways are involved in EGF-induced eIF3i expression. Interestingly, only pretreatment with PI3K inhibitor (LY294002) could abolish EGF-induced eIF3i expression in PC-3 cells (Figure 5B). To further investigate which signaling pathways are involved in EGF-induced eIF3i expression, we performed an Akt inhibition experiment using dominant negative Akt (DN-Akt). The result showed that DN-Akt abolished EGF-induced eIF3i expression in PC-3 cells (Figure 5C). To test whether PI3K was involved in PGG-inhibited EGF-induced eIF3i expression, we performed an Akt-overexpression experiment using constitutively active Akt (CA-Akt). The result showed that CA-Akt abolished the ability of PGG-inhibited EGF-induced eIF3i expression (Figure 5D). The results suggested that the inhibition of PI3K signaling pathway was involved in PGG-suppressed EGF-induced eIF3i expression.

**PGG Suppressed EGF-Induced eIF3i Expression through Inhibition of the PI3K/AKT/mTOR Pathway.** The PI3K/AKT/mammalian target of rapamycin (mTOR) signaling pathway is a master regulator of protein translation and plays important roles in other biological processes, such as cancer cell invasion.[18] Our data showed that EGF-induced eIF3i expression was completely suppressed by PI3K inhibitor (Figure 5B) and PGG could decrease PI3K phosphorylation (Figure 5A). We further confirmed whether PGG inhibited EGF-induced eIF3i expression through inhibition of the PI3K/AKT/mTOR pathway. Our results demonstrated that PGG inhibited the EGF-induced phosphorylation of AKT, mTOR, and its downstream 4EBP1 (Figure 6A). To understand whether PGG inhibited EGF-induced prostate cancer cell invasion via the PI3K/Akt/mTOR pathway, a cell invasion assay was employed. Figure 6B shows that EGF-induced cell migration was significantly inhibited by pretreatment with 40 $\mu$M LY294002. In the cotreatment of LY294002 (40 $\mu$M) and PGG (20 $\mu$M), EGF-induced cell invasion was more potent than pretreatment with LY294002 or PGG alone. Moreover, our result showed that CA-Akt abolished the ability of PGG-inhibited EGF-induced cell invasion (Figure 6C). The data suggested that PGG suppressed EGF-induced eIF3i expression through the inhibition of protein translation.

## ■ DISCUSSION

EGF signaling stimulates prostate cancer cell bone metastasis directly by increasing cancer cell proliferation and indirectly by engaging bone stromal cell in metastasis-promoting activities. In this study we verified the differences of protein expression profile between EGF-induced prostate cancer cell bone metastasis treated with or without PGG using a 2-DE-based proteomic approach. Six proteins differentially expressed by EGF stimulation but reduced by PGG treatment were successfully identified. Among them, prenylcysteine oxidase was involved in the cellular metabolism of prenylcysteines,[19] heterogeneous nuclear ribonucleoprotein L[20] and exosome component 2[21] were RNA-binding proteins, and eIF3i was involved in the translation process.[6] Interestingly, we found that EGF-induced


dx.doi.org/10.1021/jf502447e | J. Agric. Food Chem. 2014, 62, 8990−8996

eIF3i expression and was reduced by PGG treatment in androgen-independent prostate cancer cell lines (PC-3).

Recent studies suggest that aberrant mRNA and protein levels of several eIF3 subunits have been detected in several different cancers. Most eIF3 subunits (a, b, c, h, and i) are oncogenic. Deregulation of these oncogenic eIF3 subunits will cause abnormal gene expression, leading to altered cell growth and possibly cancer. For example, eIF3a was overexpressed in human cancers of the lung,[22] stomach,[23] breast,[24] and cervix.[25] eIF3b expression was related to human prostate and bladder cancer prognosis and was required for tumor growth.[26] The down-regulation of eIF3c decreased the global protein synthesis and mediated G0/G1 or G2/M arrest in a tissue-dependent manner, which led to a reduction in cell proliferation and eventually to cancer cell death.[27] In colorectal cancer, an elevated level of the *eIF3h* gene was found.[28]

eIF3i was overexpressed in human colon cancer, head and neck cancer, breast cancer, hepatocellular carcinoma, neuroblastoma, and melanoma, suggesting that eIF3i overexpression might be an oncogenic factor.[6,8,29] Clearly, deregulation of eIF3i can contribute to tumorigenesis, but its oncogenic mechanisms remain unknown. To our best knowledge, our studies are the first to report that eIF3i participates in EGF-induced prostate cancer cell bone metastasis. To support this conclusion, we transiently transfected PC-3 cells with eIF3i shRNA, and our results showed that down-regulation of EGF-induced eIF3i expression resulted in a significant reduction of PC-3 cells' invasive ability (Figure 3B). Further studies using in vivo animal models are needed to demonstrate the participation of eIF3i in EGF-induced prostate cancer bone metastasis.

PGG has been shown to exhibit antiprostate cancer effects. Our previous study showed that PGG suppressed in vivo invasion and xenograft growth in nude mice with intratibially injected PC-3 human prostate cancer cells.[15] Recently, Hu et al. have shown that PGG could serve as a multitargeting agent for the chemoprevention and therapy of prostate cancer.[30] Lee et al. reported the inhibitory effect of PGG on the androgen receptor (AR) signaling pathway in human prostate cancer LNCaP cells.[31] Moreover, treatment with subapoptotic doses of PGG induced S phase arrest, whereas apoptotic doses of PGG induced not only S phase arrest but also G1 phase arrest in prostate cancer cells.[32] Overall, these data supported the potential role of PGG as a novel therapeutic or chemopreventive agent for prostate cancer. However, these effects need to be validated in vivo.

In the present study, we first evaluated the effects of PGG on EGF-induced eIF3i expression in PC-3 cells. Our study showed that EGF-induced eIF3i expression could be effectively blocked by PGG. Pretreatment with PGG blocked EGF-induced eIF3i expression. How PGG affects these changes remains to be determined. To further delineate the molecular mechanism of PGG in inhibiting EGF-induced eIF3i expression, related pathways were investigated. In the study, both MAPK and PI3K/AKT signaling pathways were investigated in PGG-treated PC-3 cells. Our experiments showed that PGG significantly decreased the PI3K/AKT pathway in PC-3 cells. Park et al. revealed that PGG inhibits hypoxia-induced transcriptional activation, mRNA expression, and protein accumulation of HIF-1$\alpha$ and its downstream signaling to VEGF and PI3K/AKT/mTOR pathway in LNCaP prostate cancer cells.[33] On the basis of these findings, PGG may be an ideal inhibitor for the PI3K/AKT signaling pathway.

## AUTHOR INFORMATION


### Corresponding Author

*(T.-D.W.) Mail: Department of Biological Science and Technology, College of Life Sciences, China Medical University, No. 91 Hsueh-Shih Road, Taichung, Taiwan 40402, ROC. Phone: (886)-4-2205-3366, ext. 2509. Fax: (886)-4-2207-0465. E-mail: tdway@mail.cmu.edu.tw.



### Funding

This study was supported by E-Da Hospital Grant EDAHP102010 and EDAHP103054. We also acknowledge support (in part) by a grant from the Department of Health (Taiwan), China Medical University Hospital Cancer Research Center of Excellence (DOH100-TD-C-111-005).


### Notes

The authors declare no competing financial interest.

## ABBREVIATIONS USED

DMSO, dimethyl sulfoxide; EGF, epidermal growth factor; EGFR, epidermal growth factor receptor; eIF, eukaryotic initiation factor; FBS, fetal bovine serum; MAPK, mitogen-activated protein kinase; MTT, 3-(4,5-dimethylthiazol-2-yl)-2,5-diphenyl tetrazolium bromide; mTOR, mammalian target of rapamycin; PGG, penta-*O*-galloyl-$\beta$-D-glucose; PI3K, phosphatidylinositol 3-kinase

## REFERENCES


(1) Siegel, R.; Naishadham, D.; Jemal, A. Cancer statistics, 2013. *CA Cancer J. Clin.* **2013**, *63*, 11−30.

(2) Coleman, R. E. Clinical features of metastatic bone disease and risk of skeletal morbidity. *Clin. Cancer Res.* **2006**, *12*, 6243s−6249s.

(3) Lu, X.; Kang, Y. Epidermal growth factor signaling and bone metastasis. *Br. J. Cancer* **2010**, *102*, 457−461.

(4) Kingsley, L. A.; Fournier, P. G.; Chirgwin, J. M.; Guise, T. A. Molecular biology of bone metastasis. *Mol. Cancer Ther.* **2007**, *6*, 2609−2617.

(5) Bilanges, B.; Stokoe, D. Mechanisms of translational deregulation in human tumors and therapeutic intervention strategies. *Oncogene* **2007**, *26*, 5973−5990.

(6) Qi, J.; Dong, Z.; Liu, J.; Zhang, J. T. EIF3i promotes colon oncogenesis by regulating COX-2 protein synthesis and $\beta$-catenin activation. *Oncogene* **2013**, 1−8.

(7) Ahlemann, M.; Zeidler, R.; Lang, S.; Mack, B.; Münz, M.; Gires, O. Carcinoma-associated eIF3i overexpression facilitates mTOR-dependent growth transformation. *Mol. Carcinog.* **2006**, *45*, 957−967.

(8) Wang, Y. W.; Lin, K. T.; Chen, S. C.; Gu, D. L.; Chen, C. F.; Tu, P. H.; Jou, Y. S. Overexpressed-eIF3I interacted and activated oncogenic Akt1 is a theranostic target in human hepatocellular carcinoma. *Hepatology* **2013**, *58*, 239−250.

(9) Zhang, J.; Li, L.; Kim, S. H.; Hagerman, A. E.; Lu, J. Anti-cancer, anti-diabetic and other pharmacologic and biological activities of penta-galloyl-glucose. *Pharm. Res.* **2009**, *26*, 2066−2080.

(10) Hu, H.; Lee, H. J.; Jiang, C.; Zhang, J.; Wang, L.; Zhao, Y.; Xiang, Q.; Lee, E. O.; Kim, S. H.; Lu, J. Penta-1,2,3,4,6-*O*-galloyl-$\beta$-D-glucose induces p53 and inhibits STAT3 in prostate cancer cells in vitro and suppresses prostate xenograft tumor growth in vivo. *Mol. Cancer Ther.* **2008**, *7*, 2681−2691.

(11) Yu, W. S.; Jeong, S. J.; Kim, J. H.; Lee, H. J.; Song, H. S.; Kim, M. S.; Ko, E.; Lee, H. J.; Khil, J. H.; Jang, H. J.; Kim, Y. C.; Bae, H.; Chen, C. Y.; Kim, S. H. The genome-wide expression profile of 1,2,3,4,6-penta-*O*-galloyl-$\beta$-D-glucose-treated MDA-MB-231 breast cancer cells: molecular target on cancer metabolism. *Mol. Cells* **2011**, *32*, 123−132.

(12) Kwon, T. R.; Jeong, S. J.; Lee, H. J.; Lee, H. J.; Sohn, E. J.; Jung, J. H.; Kim, J. H.; Jung, D. B.; Lu, J.; Kim, S. H. Reactive oxygen species-mediated activation of JNK and down-regulation of DAXX are

critically involved in penta-*O*-galloyl-*β*-D-glucose-induced apoptosis in chronic myeloid leukemia K562 cells. *Biochem. Biophys. Res. Commun.* **2012**, *424*, 530−537.
(13) Huh, J. E.; Lee, E. O.; Kim, M. S.; Kang, K. S.; Kim, C. H.; Cha, B. C.; Surh, Y. J.; Kim, S. H. Penta-*O*-galloyl-*β*-D-glucose suppresses tumor growth via inhibition of angiogenesis and stimulation of apoptosis: roles of cyclooxygenase-2 and mitogen-activated protein kinase pathways. *Carcinogenesis* **2005**, *26*, 1436−1445.
(14) Hua, K. T.; Way, T. D.; Lin, J. K. Pentagalloylglucose inhibits estrogen receptor alpha by lysosome-dependent depletion and modulates ErbB/PI3K/Akt pathway in human breast cancer MCF-7 cells. *Mol. Carcinog.* **2006**, *45*, 551−560.
(15) Kuo, P. T.; Lin, T. P.; Liu, L. C.; Huang, C. H.; Lin, J. K.; Kao, J. Y.; Way, T. D. Penta-*O*-galloyl-*β*-D-glucose suppresses prostate cancer bone metastasis by transcriptionally repressing EGF-induced MMP-9 expression. *J. Agric. Food Chem.* **2009**, *57*, 3331−3339.
(16) Yokozawa, T.; Chung, H. Y.; Oura, H.; Nonaka, G.; Nishioka, I. Isolation of a renal function-facilitating constituent from the Oriental drug, salviae miltiorrhizae radix. *Nippon Jinzo Gakkaishi* **1989**, *31*, 1091−1098.
(17) Chen, W. C.; Lai, Y. A.; Lin, Y. C.; Ma, J. W.; Huang, L. F.; Yang, N. S.; Ho, C. T.; Kuo, S. C.; Way, T. D. Curcumin suppresses doxorubicin-induced epithelial-mesenchymal transition via the inhibition of TGF-*β* and PI3K/AKT signaling pathways in triple-negative breast cancer cells. *J. Agric. Food Chem.* **2013**, *61*, 11817−11824.
(18) Arcaro, A.; Guerreiro, A. S. The phosphoinositide 3-kinase pathway in human cancer: genetic alterations and therapeutic implications. *Curr. Genomics* **2007**, *8*, 271−306.
(19) Tschantz, W. R.; Digits, J. A.; Pyun, H. J.; Coates, R. M.; Casey, P. J. Lysosomal prenylcysteine lyase is a FAD-dependent thioether oxidase. *J. Biol. Chem.* **2001**, *276*, 2321−2324.
(20) Zhang, W.; Zeng, F.; Liu, Y.; Zhao, Y.; Lv, H.; Niu, L.; Teng, M.; Li, X. Crystal structures and RNA-binding properties of the RNA recognition motifs of heterogeneous nuclear ribonucleoprotein L: insights into its roles in alternative splicing regulation. *J. Biol. Chem.* **2013**, *288*, 22636−22649.
(21) Schneider, C.; Anderson, J. T.; Tollervey, D. The exosome subunit Rrp44 plays a direct role in RNA substrate recognition. *Mol. Cell* **2007**, *27*, 324−331.
(22) Yin, J. Y.; Shen, J.; Dong, Z. Z.; Huang, Q.; Zhong, M. Z.; Feng, D. Y.; Zhou, H. H.; Zhang, J. T.; Liu, Z. Q. Effect of eIF3a on response of lung cancer patients to platinum-based chemotherapy by regulating DNA repair. *Clin. Cancer Res.* **2011**, *17*, 4600−4609.
(23) Chen, G.; Burger, M. M. p150 overexpression in gastric carcinoma: the association with p53, apoptosis and cell proliferation. *Int. J. Cancer* **2004**, *112*, 393−398.
(24) Olson, J. E.; Wang, X.; Goode, E. L.; Pankratz, V. S.; Fredericksen, Z. S.; Vierkant, R. A.; Pharoah, P. D.; Cerhan, J. R.; Couch, F. J. Variation in genes required for normal mitosis and risk of breast cancer. *Breast Cancer Res. Treat.* **2010**, *119*, 423−430.
(25) Dellas, A.; Torhorst, J.; Bachmann, F.; Bänziger, R.; Schultheiss, E.; Burger, M. M. Expression of p150 in cervical neoplasia and its potential value in predicting survival. *Cancer* **1998**, *83*, 1376−1383.
(26) Wang, H.; Ru, Y.; Sanchez-Carbayo, M.; Wang, X.; Kieft, J. S.; Theodorescu, D. Translation initiation factor eIF3b expression in human cancer and its role in tumor growth and lung colonization. *Clin. Cancer Res.* **2013**, *19*, 2850−2860.
(27) Emmanuel, R.; Weinstein, S.; Landesman-Milo, D.; Peer, D. eIF3c: a potential therapeutic target for cancer. *Cancer Lett.* **2013**, *336*, 158−166.
(28) Tomlinson, I.; Webb, E.; Carvajal-Carmona, L.; Broderick, P.; Kemp, Z.; Spain, S.; Penegar, S.; Chandler, I.; Gorman, M.; Wood, W.; Barclay, E.; Lubbe, S.; Martin, L.; Sellick, G.; Jaeger, E.; Hubner, R.; Wild, R.; Rowan, A.; Fielding, S.; Howarth, K.; CORGI Consortium; Silver, A.; Atkin, W.; Muir, K.; Logan, R.; Kerr, D.; Johnstone, E.; Sieber, O.; Gray, R.; Thomas, H.; Peto, J.; Cazier, J. B.; Houlston, R. A genome-wide association scan of tag SNPs identifies a susceptibility variant for colorectal cancer at 8q24.21. *Nat. Genet.* **2007**, *39*, 984−988.
(29) Ahlemann, M.; Zeidler, R.; Lang, S.; Mack, B.; Münz, M.; Gires, O. Carcinoma-associated eIF3i overexpression facilitates mTOR-dependent growth transformation. *Mol. Carcinog.* **2006**, *45*, 957−967.
(30) Hu, H.; Lee, H. J.; Jiang, C.; Zhang, J.; Wang, L.; Zhao, Y.; Xiang, Q.; Lee, E. O.; Kim, S. H.; Lü, J. Penta-1,2,3,4,6-*O*-galloyl-*β*-D-glucose induces p53 and inhibits STAT3 in prostate cancer cells in vitro and suppresses prostate xenograft tumor growth in vivo. *Mol. Cancer Ther.* **2008**, *7*, 2681−2691.
(31) Lee, H. H.; Ho, C. T.; Lin, J. K. Theaflavin-3,3′-digallate and penta-*O*-galloyl-*β*-D-glucose inhibit rat liver microsomal 5*α*-reductase activity and the expression of androgen receptor in LNCaP prostate cancer cells. *Carcinogenesis* **2004**, *25*, 1109−1118.
(32) Hu, H.; Zhang, J.; Lee, H. J.; Kim, S. H.; Lu, J. Penta-*O*-galloyl-*β*-D-glucose induces S- and G(1)-cell cycle arrests in prostate cancer cells targeting DNA replication and cyclin D1. *Carcinogenesis* **2009**, *30*, 818−823.
(33) Park, K. Y.; Lee, H. J.; Jeong, S. J.; Lee, H. J.; Kim, H. S.; Kim, S. H.; Lim, S.; Kim, H. C.; Lü, J.; Kim, S. H. 1,2,3,4,6-Penta-*O*-galloyl-*β*-D-glucose suppresses hypoxia-induced accumulation of hypoxia-inducible factor-1*α* and signaling in LNCaP prostate cancer cells. *Biol. Pharm. Bull.* **2010**, *33*, 1835−1840.

extract, 20 g of sucrose, 1 g of peptone, and 20 g of agar in 1 L of distilled water). The plates were incubated aerobically in a chamber for 72 h at 28 ± 0.5 °C, and colonies were transferred and purified on new MEA mediums to obtain pure cultures.

The fungal strain was differentiated by the morphological characteristics according to the manual description by Cappuccino and Sherman. Genomic DNA was extracted, and the internal transcribed spacer (ITS) region sequence was amplified using the universal primers ITS1 and ITS4. Then, the sequence was submitted to GenBank (accession number KJ490634) and analyzed by BLAST search with reference sequences. Phylogenetic analysis was performed by neighbor joining in MEGA 5.0 with 1000 bootstrap replicates. The strain was deposited at China Center for Type Culture Collection (CCTCC) as M2013257.

**Fermentation.** The strain was cultured on MEA medium at 28 ± 0.5 °C for 3 days until the colony emerged. Then, pieces of fresh mycelium were inoculated into 250 mL Erlenmeyer flasks each containing 100 mL of malt-extract (ME) liquid medium, after 2 days of incubation at 28 ± 0.5 °C on rotary shakers at 150 rpm. A 20 mL suspension of the strain was transferred as seed into 1 L Erlenmeyer flasks each containing 500 mL of ME liquid medium. The flask cultures were incubated at 28 ± 0.5 °C for 7 days.

**Phytogrowth Inhibitory Bioassay of Ethyl Acetate Extracts.** The phytotoxic effects of the ethyl acetate extracts of ZS07 were evaluated on radicle growth of *A. retroflexus* L., and selected crops (*Brassica campestris* L., *Glycine max*, *Lycopersicon esculentum* Mill., and *Capsicum annuum*) were easily affected by *A. retroflexus* L. on the base of a Petri dish bioassay.[14] Briefly, seeds were first pretreated with sodium hypochlorite (1%) and washed with sterile distilled water before germination. Then, 25 pregerminated seeds were placed in 9 cm diameter Petri dishes on filter paper disks imbibed with 5.0 mL sample solution (100 μg/mL). To avoid the toxic effect of solvents, filter papers were placed in a cabinet to evaporate the solvent. Subsequently, 5.0 mL of distilled water was added to each Petri dish. 2,4-Dichlorophenoxyacetic acid (2,4-D) was used as the positive control, and three replicates were prepared for each sample. Dishes were then kept in a growth chamber at 25 °C under continuous light. After 2 days, the root length were measured and compared to the proper untreated control. The inhibition percent[15] was calculated using the formula below

$$\text{inhibition}\ (\%) = (L_{\text{control}} - L_{\text{treatment}})/L_{\text{control}} \times 100$$

where $L_{\text{control}}$ is the radicle length of seedlings in the control and $L_{\text{treatment}}$ is the radicle length of seedlings treated.

**Isolation and Characterization of Secondary Metabolites.** A total of 40 L of fermentation broth was filtered and extracted 3 times with an equal volume of EtOAc at room temperature. The solvent was then removed *in vacuo* to give a crude extract (3.0 g). The extract was subjected to a silica gel column eluting with a stepwise gradient of $CH_2Cl_2$/MeOH (100:0−100:4, v/v) to afford four fractions (Fr-1−Fr-4). Fr-1 was further chromatographed over silica gel ($CH_2Cl_2$/MeOH, 100:0−100:2) to give five subfractions (R1−R5). Compound **2** (30 mg) was crystallized from the MeOH solution of subfraction R2. The remaining fractions of R4 and R5 were combined and purified by Sephadex LH-20 using a $CH_2Cl_2$/MeOH mixture (1:1) as the eluent to give compound **6** (3 mg). Fr-2 ($CH_2Cl_2$/MeOH, 100:1) was repeatedly purified on Sephadex LH-20 (MeOH) and detected by thin-layer chromatography (TLC) to yield compound **4** (6 mg). Fr-3 ($CH_2Cl_2$/MeOH, 100:2) was also loaded onto a Sephadex LH-20 column (MeOH) to give compounds **3** (35 mg), **5** (5 mg), and **1** (50 mg).

Structural identifications of the secondary metabolites were made by the spectroscopic analysis. $^1$H nuclear magnetic resonance (NMR), $^{13}$C NMR, and distortionless enhancement by polarization transfer (DEPT) spectra were measured with a Bruker AVANCE-400 (Bruker, Switzerland) spectrometer at 400 MHz, and chemical shifts were reported as parts per million ($\delta$) by referring to the solvent signals and tetramethylsilane (TMS) as internal standards. $^1$H and $^{13}$C NMR assignments were supported by the $^1$H−$^1$H correlation spectroscopy (COSY), heteronuclear multiple-quantum coherence (HMQC), and heteronuclear multiple-bond correlation (HMBC) experiments. The electrospray ionization mass spectrometry (ESI−MS) spectra were acquired on a Mariner Mass 5304 instrument.

**Phytogrowth Inhibitory Bioassay of Metabolites.** The phytotoxic effects of compounds **1**−**4** were evaluated on radicle growth of *A. retroflexus* L., as described above. Concentrations of compounds **1**−**4** at 1, 10, and 100 μg/mL were prepared with acetone. Then, 5.0 mL of varying concentration solution was applied to each Petri dish. After the solvent was evaporated, 5.0 mL of distilled water was added to the Petri dish before the sowing of pregerminated 25 seeds of *A. retroflexus* L. Root length were measured, and 2,4-D was used as the positive control.

**Detection of Antibacterial Activity.** The disc diffusion method was employed for the determination of antibacterial activity of the bioactive metabolites. Bacterial strains *Escherichia coli* (ATCC 8739), *Bacillus subtilis* (ATCC 6633), *Staphylococcus aureus* (ATCC 6538), and *Salmonella typhimurium* [CMCC(B) 50115] were cultured overnight at 37 °C in Mueller Hinton broth (MHB), and then a 0.2 mL suspension of the tested microorganisms ($1.0 \times 10^8$ cfu/mL) were spread on the solid media plates. Filter paper disks containing 5 μL of each metabolite solution (6 mg/mL) were applied to the surface of agar plates. The plates were incubated at 37 °C for 18 h. The diameters of the inhibition zones were measured, and average diameter values were calculated for each compound. All tests were performed in triplicate. The minimum inhibitory concentrations (MICs) of purified compounds against bacteria were determined using the microbroth dilution method[16] in disposable 96-well microtiter dishes. A stock solution of each sample was prepared at a concentration of 200 μg/mL in MHB [supplemented with 1% dimethyl sulfoxide (DMSO) and 4% Tween 80, v/v], which was further 2-fold diluted and micropipetted separately into individual microplate wells (100 μL/well) with a series of concentrations ranging from 100 to 0.78 μg/mL. Then, a standard amount of the tested microbes ($1.0 \times 10^6$ cfu/mL) were added per well and incubated 24 h at 37 °C for *E. coli*, *S. aureus*, *B. subtilis*, and *S. typhimurium*. The antibacterial activity was evaluated by comparing to a control well containing culture broth and microorganisms without the compound. The MIC was defined as the minimum concentration of compounds at which the bacterial growth was inhibited, as indicated by the absence of turbidity. Each test was performed in duplicate, and gentamicin served as the reference compound.

## RESULTS AND DISCUSSION

**Identification of the Fungus.** Morphological characteristics of the fungus were observed in potato dextrose agar (PDA) medium. The colonies were slow growing at first, becoming floccose with age and purple in color. Reddish purple appeared in the reverse of the colony when aerial mycelium reached the edge of the medium. Sporulation started early in aerial mycelium. Microconidia were produced in false head and variable in shape. Conidiophores originated erect from the substrate, sympodially branched and bearing nearly cylindrical monophialides. The isolated fungus would be located in the Liseola section and showed high similarity in morphology with *Fusarium*. Phylogenetic taxonomy with sequence alignment of ITS rDNA of the fungus was performed with MEGA 5.0 software. The phylogenetic tree (Figure 1) indicated that the title fungus was closely related to *Fusarium proliferatum* (FJ648201), with the ITS sequence similarity of 99.5%. In combination with the morphological characteristics, the fungus was identified as *F. proliferatum*.

**Phytotoxic Activity of the Ethyl Acetate Extracts.** A Petri dish bioassay was used to evaluate the phytotoxic activities of ethyl acetate extract from *F. proliferatum* against the radicle growth of *A. retroflexus* L. and selected crops. The results (Figure 2) indicated that the crude extract showed selectivity greater than 2 times for weed over the tested crop. Under the concentration of 100 μg/mL, the crude extract produced

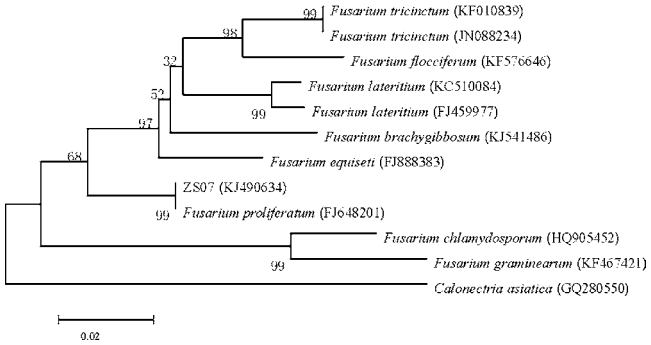


**Figure 1.** Phylogenetic tree of the fungus ZS07 based on the 5.8S rDNA sequences.

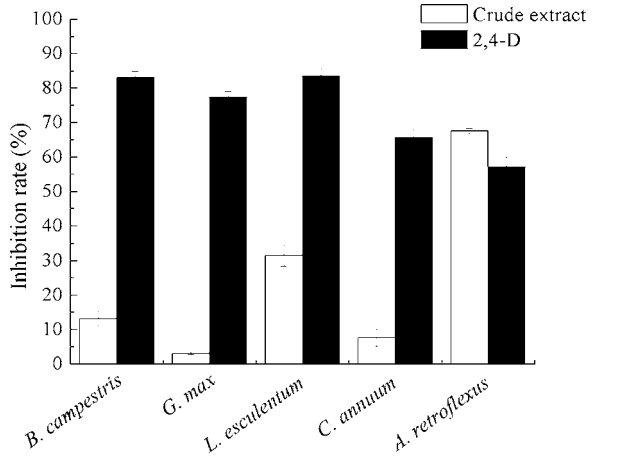


**Figure 2.** Phytotoxic effects of the crude extract of ZS07 on the radicle growth of *A. retroflexus* L. and tested crops (100 $\mu$g/mL).

significant inhibition against the radicle growth of *A. retroflexus* L. with the inhibition rate of 67.6%, while it produced weak inhibition against the radicle growth of *B. campestris* L., *G. max*, *L. esculentum* Mill., and *C. annuum* with the inhibition rate of less than 35%. Our research provided evidence that the extract of *F. proliferatum* showed good selective phytotoxic activities for *A. retroflexus* L.

**Identification of Active Compounds.** Bioassay-guided fractionation of the constituents in the ethyl acetate extract of *F. proliferatum* ZS07 yielded a novel derivate **2** and five known active metabolites (Figure 3).

Compound **2** was obtained as an orange powder, and its molecular formula $C_{19}H_{16}O_7$ was deduced from high-resolution

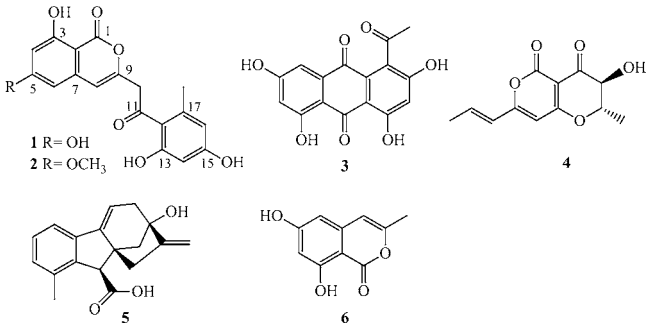


**Figure 3.** Chemical structures of secondary metabolites **1**–**6** of *F. proliferatum* ZS07.

(HR)-ESI–MS ($m/z$ 379.0789 $[M + Na]^+$, calcd for $C_{19}H_{16}O_7Na$, 379.0794), which was consistent with the $^1H$ and $^{13}C$ NMR data. The $^1H$ NMR (Table 1) of compound **2**

**Table 1. $^1H$ and $^{13}C$ NMR Data of Compound 2 in DMSO-$d_6$**

| position | $\delta_H$, mult. ($J$ in Hz) | $\delta_C$ |
|---|---|---|
| 1 | | 165.7 |
| 2 | | 99.6 |
| 3 | | 163.0 |
| 4 | 6.55, d (2.3) | 101.1 |
| 5 | | 167.0 |
| 6 | 6.63, s | 101.9 |
| 7 | | 139.7 |
| 8 | 6.62, d (2.3) | 107.2 |
| 9 | | 152.9 |
| 10 | 4.14, s | 48.4 |
| 11 | | 199.7 |
| 12 | | 119.2 |
| 13 | | 158.5 |
| 14 | 6.23, d (2.3) | 100.7 |
| 15 | | 160.5 |
| 16 | 6.13, d (2.3) | 110.0 |
| 17 | | 139.7 |
| 18 | 2.14, s | 20.8 |
| 3-OH | 10.96, s | |
| 5-$OCHH_3$ | 3.87, s | 56.4 |
| 13-OH | 10.26, s | |
| 15-OH | 9.79, s | |

indicated the presence of the 1,3-disubstituted benzene ring ($\delta_H$ 6.13, $J$ = 2.3 Hz; $\delta_H$ 6.23, $J$ = 2.3 Hz), one methoxyl ($\delta_H$ 3.87), one methyl ($\delta_H$ 2.14), and one methylene ($\delta_H$ 4.14). Three proton signals at $\delta_H$ 10.96, 10.26, and 9.79 were assigned to hydroxy groups because no HMQC correlation was observed. The $^1H$ and $^{13}C$ NMR data were similar to those of SMA93 (**1**),[17] except the substituent at position 5 in compound **2** appeared to be $OCH_3$, which was corresponding to the increase in molecular weight of compound **2** by 14 amu compared to compound **1**. This was further confirmed by the HMBC correlation of MeO-5 to C-5 ($\delta_C$ 167.0). Further confirmation was achieved by the HMBC correlation of H-4 to C-2 ($\delta_C$ 99.6), C-3 ($\delta_C$ 163.0), C-5, and C-6 ($\delta_C$ 101.9); H-6 to C-2, C-5, C-7 ($\delta_C$ 139.7), and C-8 ($\delta_C$ 107.2); H-10 to C-8, C-9 ($\delta_C$ 152.9), and C-11 ($\delta_C$ 199.7); H-14 to C-12 ($\delta_C$ 119.2), C-13 ($\delta_C$ 158.5), C-15 ($\delta_C$ 160.5), and C-16 ($\delta_C$ 110.0); H-16 to C-12, C-14 ($\delta_C$ 100.7), and C-17 ($\delta_C$ 139.7); and H-18 to C-16 and C-17. Thus, the structure of compound **2** was determined as an O-methylated derivative of compound **1**.

The other secondary metabolites were identified as rhodolamprometrin (**3**),[18,19] radicinin (**4**),[3] dehydroallogibberic acid (**5**),[20,21] and 3-methyl-6,8-dihydroxyisocoumarin (**6**),[22] by spectroscopic data analyses and comparison of their or derivative data in the literature.

The genus of *Fusarium* species was well-known to produce a variety of secondary metabolites. Previous investigations led to the isolation of several compounds, such as toxic fumonisins,[23,24] mycotoxins,[25] antibiotic and insecticidal beauvericin,[26] histone deacetylase (HDAC) inhibitor apicidin,[27] and other compounds related to the precursors.[19] However, to the best of our knowledge, it was the first report that the new polyketide **2** and the following metabolites **1** and **3**–**5** were isolated from the

title strain *F. proliferatum* ZS07, a fungus residing in the gut of long-horned grasshoppers.

**Phytotoxic Activity of the Bioactive Metabolites.** Compounds **1**−**4** were assayed for their ability to inhibit radicle growth of *A. retroflexus* L. using a Petri dish bioassay. The result (Figure 4) showed that compound **2** was very active

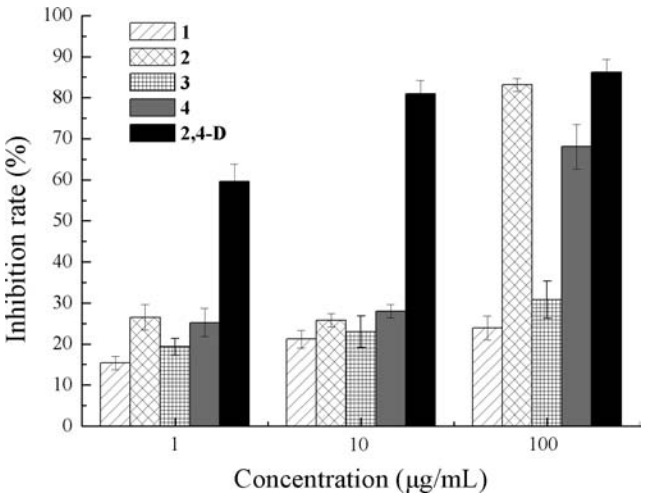


**Figure 4.** Phytotoxic effects of compounds **1**−**4** on radicle growth of *A. retroflexus* L.

to reduce radicle growth of *A. retroflexus* L. under the concentration of 100 μg/mL. With a little morphological alterations of the radicle, the relative inhibition rate of compound **2** was 83.0%, which was comparable to that of positive 2,4-D with the inhibition rate of 86.4%. Compound **4** showed moderate phytotoxic activity with the inhibition rate of 65.2% at the concentration of 100 μg/mL. However, compounds **2** and **4** showed weak inhibitory effect in a low concentration. No obvious inhibitory effects were displayed by the compounds **1** and **3** in this bioassay.

**Antibacterial Activity of the Bioactive Metabolites.** The disc diameters of zone of inhibition (ZOI) and MIC values of compounds **1**−**5** against different bacteria were presented in Table 2. The results showed that compound **3** had the greatest antibacterial effect against *B. subtilis* with ZOI of 24.8 mm and MIC value of 3.13 μg/mL, which were comparable to those of referenced gentamicin with the ZOI and MIC value of 25.6 mm and 3.13 μg/mL, respectively. Similar to the inhibition zone result of 19.5 mm, compound **1** possessed moderate antibacterial effect against *B. subtilis* with MIC value of 6.20 μg/mL, followed by the new derivate **2** with MIC value of 12.50 μg/mL. The replacement of the phenolic hydroxyl group by one methoxy group in the phenolic nucleus of compound **1** resulted in the weaker antibacterial activity for *B. subtilis*, which was in agreement with the earlier postulate.[28] Compounds **4** and **5** inhibited the growth of *B. subtilis* in disc diffusion tests, but the MIC values of them were not detected in the concentrations of 100 μg/mL. Similarly, compounds **1**−**3** possessed weak antibacterial activities against *S. aureus* in disc diffusion tests, but no inhibition was found in the MIC test. The remaining microorganisms *E. coli* and *S. typhimurium* were not susceptible to all compounds.

**Table 2. ZOI (mm) and MIC (μg/mL) of Compounds 1−5 against the Tested Bacteria**

| | *B. subtilis* | | *S. aureus* | |
|---|---|---|---|---|
| compound | ZOI[a] | MIC | ZOI | MIC |
| **1** | 19.5 ± 0 | 6.20 | 11.7 ± 0.5 | >100 |
| **2** | 13.8 ± 0.6 | 12.50 | 8.4 ± 0.4 | >100 |
| **3** | 24.8 ± 0.6 | 3.13 | 8.0 ± 0 | >100 |
| **4** | 6.6 ± 0 | >100 | NI[b] | >100 |
| **5** | 9.2 ± 0.6 | >100 | NI | >100 |
| GEN[c] | 25.6 ± 0.5 | 3.13 | 30.0 ± 0 | 3.13 |

[a]ZOI = zone of inhibition; results were presented as the mean ± standard deviation for triplicate experiments. [b]NI = not inhibited. [c]GEN = gentamicin, 30 μg/disc.

In summary, we identified one new polyketide together with five known compounds from a fungus *F. proliferatum* ZS07. The new polyketone **2** and the known compound **4** attenuated the radicle growth of *A. retroflexus* L., and for the first time, we found that compounds **1** and **3** possessed potent or moderate antibacterial activity against *B. subtilis in vitro*. These results suggested that the compounds **1**−**4** have some potential as agents for weeds and pathogenic bacteria control. Further studies will be carried out to better understand the mechanism of action associated with phytotoxic and antibacterial effects. In addition, the discovery of our study provided additional evidence that uninvestigated habitats, just like the title strain, may inspire the discovery of chemical agents with interesting biological activity.

## AUTHOR INFORMATION

### Corresponding Author

*Telephone: +86-579-8228-6419. Fax: +86-579-8228-2269. E-mail: ylzhang@zjnu.cn.

### Author Contributions

[†]Shuai Li and Ming-Wei Shao contributed equally to this work.

### Funding

This work was co-financed by the National Natural Science Foundation of China (NSFC) (21002092 and 21272215) and the Open Project of the State Key Laboratory of Pharmaceutical Biotechnology in Nanjing University (KF-GN-201411).

### Notes

The authors declare no competing financial interest.

## REFERENCES

(1) Oerke, E. C. Crop losses to pests. *J. Agric. Sci.* **2006**, *144*, 31−43.
(2) Baucom, R. S.; Holt, J. S. Weeds of agricultural importance: Bridging the gap between evolutionary ecology and crop and weed science. *New Phytol.* **2009**, *184*, 741−743.
(3) Zhang, Y. L.; Kong, L. C.; Jiang, D. H.; Yin, C. P.; Cai, Q. M.; Chen, Q.; Zheng, J. Y. Phytotoxic and antifungal metabolites from *Curvularia* sp. FH01 isolated from the gut of *Atractomorpha sinensis*. *Bioresour. Technol.* **2011**, *102*, 3575−3577.
(4) Petroski, R. J.; Stanley, D. W. Natural compounds for pest and weed control. *J. Agric. Food Chem.* **2009**, *57*, 8171−8179.
(5) Barton, A. F.; Dell, B.; Knight, A. R. Herbicidal activity of cineole derivatives. *J. Agric. Food Chem.* **2010**, *58*, 10147−10155.
(6) Demirci, F.; Guven, K.; Demirci, B.; Dadandi, M. Y.; Baser, K. H. C. Antibacterial activity of two *Phlomis* essential oils against food pathogens. *Food Control* **2008**, *19*, 1159−1164.
(7) Oroojalian, F.; Kasra-Kermanshahi, R.; Azizi, M.; Bassami, M. R. Phytochemical composition of the essential oils from three Apiaceae species and their antibacterial effects on food-borne pathogens. *Food Chem.* **2010**, *120*, 765−770.

(8) Negi, P. S. Plant extracts for the control of bacterial growth: Efficacy, stability and safety issues for food application. *Int. J. Food Microbiol.* **2012**, *156*, 7−17.
(9) Galvez, A.; Lucas-Lopez, R.; Abriouel, H. Application of bacteriocins in the control of foodborne pathogenic and spoilage bacteria. *Crit. Rev. Biotechnol.* **2008**, *28*, 125−152.
(10) Xiao, J.; Zhang, Q.; Gao, Y. Q.; Tang, J. J.; Zhang, A. L.; Gao, J. M. Secondary metabolites from the endophytic *Botryosphaeria dothidea* of *Melia azedarach* and their antifungal, antibacterial, antioxidant, and cytotoxic activities. *J. Agric. Food Chem.* **2014**, *62*, 3584−3590.
(11) Zhang, Y. L.; Ge, H. M.; Zhao, W.; Dong, H.; Xu, Q.; Li, S. H.; Li, J.; Zhang, J.; Song, Y. C.; Tan, R. X. Unprecedented immunosuppressive polyketides from *Daldinia eschscholzii*, a mantis associated fungus. *Angew. Chem., Int. Ed.* **2008**, *120*, 5907−5910.
(12) Colman, D. R.; Toolson, E. C.; Takacs-Vesbach, C. D. Do diet and taxonomy influence insect gut bacterial communities? *Mol. Ecol.* **2012**, *21*, 5124−5137.
(13) Mathew, G. M.; Ju, Y. M.; Lai, C. Y.; Mathew, D. C.; Huang, C. C. Microbial community analysis in the termite gut and fungus comb of *Odontotermes formosanus*: The implication of *Bacillus* as mutualists. *FEMS Microbiol. Ecol.* **2012**, *79*, 504−517.
(14) Silva, M. P.; Piazza, L. A.; López, D.; López Rivilli, M. J.; Turco, M. D.; Cantero, J. J.; Tourn, M. G.; Scopel, A. L. Phytotoxic activity in *Flourensia campestris* and isolation of (−)-hamanasic acid A as its active principle compound. *Phytochemistry* **2012**, *77*, 140−148.
(15) Tsao, R.; Romanchuk, F. E.; Peterson, C. J.; Coats, J. R. Plant growth regulatory effect and insecticidal activity of the extracts of the tree of heaven (*Ailanthus altissima* L.). *BMC Ecol.* **2002**, *2*, 1−6.
(16) Wang, L.; Yang, X.; Qin, P.; Shan, F.; Ren, G. Flavonoid composition, antibacterial and antioxidant properties of tartary buckwheat bran extract. *Ind. Crop Prod.* **2013**, *49*, 312−317.
(17) Ma, S. M.; Zhan, J. X.; Xie, X. K.; Watanabe, K.; Tang, Y.; Zhang, W. J. Redirecting the cyclization steps of fungal polyketide synthase. *J. Am. Chem. Soc.* **2008**, *130*, 38−39.
(18) Betina, V.; Sedmera, P.; Vokoun, J.; Podoji, M. Anthraquinone pigments from a conidiating mutant of *Trichoderma viride*. *Experientia* **1986**, *42*, 196−197.
(19) Zhan, J.; Burns, A. M.; Liu, M. X.; Faeth, S. H.; Gunatilaka, A. L. Search for cell motility and angiogenesis inhibitors with potential anticancer activity: Beauvericin and other constituents of two endophytic strains of *Fusarium oxysporum*. *J. Nat. Prod.* **2007**, *70*, 227−232.
(20) Cross, B. E.; Galt, R. H. B.; Hanson, J. R.; Curtis, P. J.; Grove, J. F.; Morrison, A. New metabolites of *Gibberella fujikuroi*. Part II. The isolation of fourteen new metabolites. *J. Chem. Soc.* **1963**, 2937−2943.
(21) Cross, B. E.; Markwell, R. E. New metabolites of *Gibberella fujikuroi*. Part XVIII. 4b*β*,7-Dihydroxy-1-methyl-8-methylenegibba-1,3,4a(10a)-trien-10-one. *J. Chem. Soc. C* **1971**, 2980−2983.
(22) Kumagai, H.; Amemiya, M.; Naganawa, H.; Sawa, T.; Ishizuka, M.; Takeuchi, T. Biosynthesis of antitumor antibiotic, cytogenin. *J. Antibiot.* **1994**, *47*, 440−446.
(23) Musser, S. M.; Eppley, R. M.; Mazzola, E. P. Identification of an N-acetyl keto derivative of fumonisin $B_1$ in corn cultures of *Fusarium proliferatum*. *J. Nat. Prod.* **1995**, *58*, 1392−1397.
(24) Moretti, A.; Susca, A.; Mulé, G.; Logrieco, A. F.; Proctor, R. H. Molecular biodiversity of mycotoxigenic fungi that threaten food safety. *Int. J. Food Microbiol.* **2013**, *167*, 57−66.
(25) Desjardins, A. E.; Manandhar, H. K.; platiner, R. D.; Manandhar, G. G.; Poling, S. M.; Maragos, C. M. *Fusarium* species from nepalese rice and production of mycotoxins and gibberellic acid by selected species. *Appl. Environ. Microbiol.* **2000**, *66*, 1020−1025.
(26) Gupta, S.; Krasnoff, S. B.; Underwood, N. L.; Renwick, J. A. A.; Roberts, D. W. Isolation of beauvericin as an insect toxin from *Fusarium semitectum* and *Fusarium moniliforme* var. *subglutinans*. *Mycopathologia* **1991**, *115*, 185−189.
(27) Whitt, J.; Shipley, S. M.; Newman, D. J.; Zuck, K. M. Tetramic acid analogues produced by coculture of *Saccharopolyspora erythraea* with *Fusarium pallidoroseum*. *J. Nat. Prod.* **2014**, *77*, 173−177.
(28) Kim, J. H.; Park, E. S.; Shim, J. H.; Kim, M. N.; Moon, W. S.; Chung, K. H.; Yoon, J. S. Antimicrobial activity of *p*-hydroxyphenyl acrylate derivatives. *J. Agric. Food Chem.* **2004**, *52*, 7480−7483.

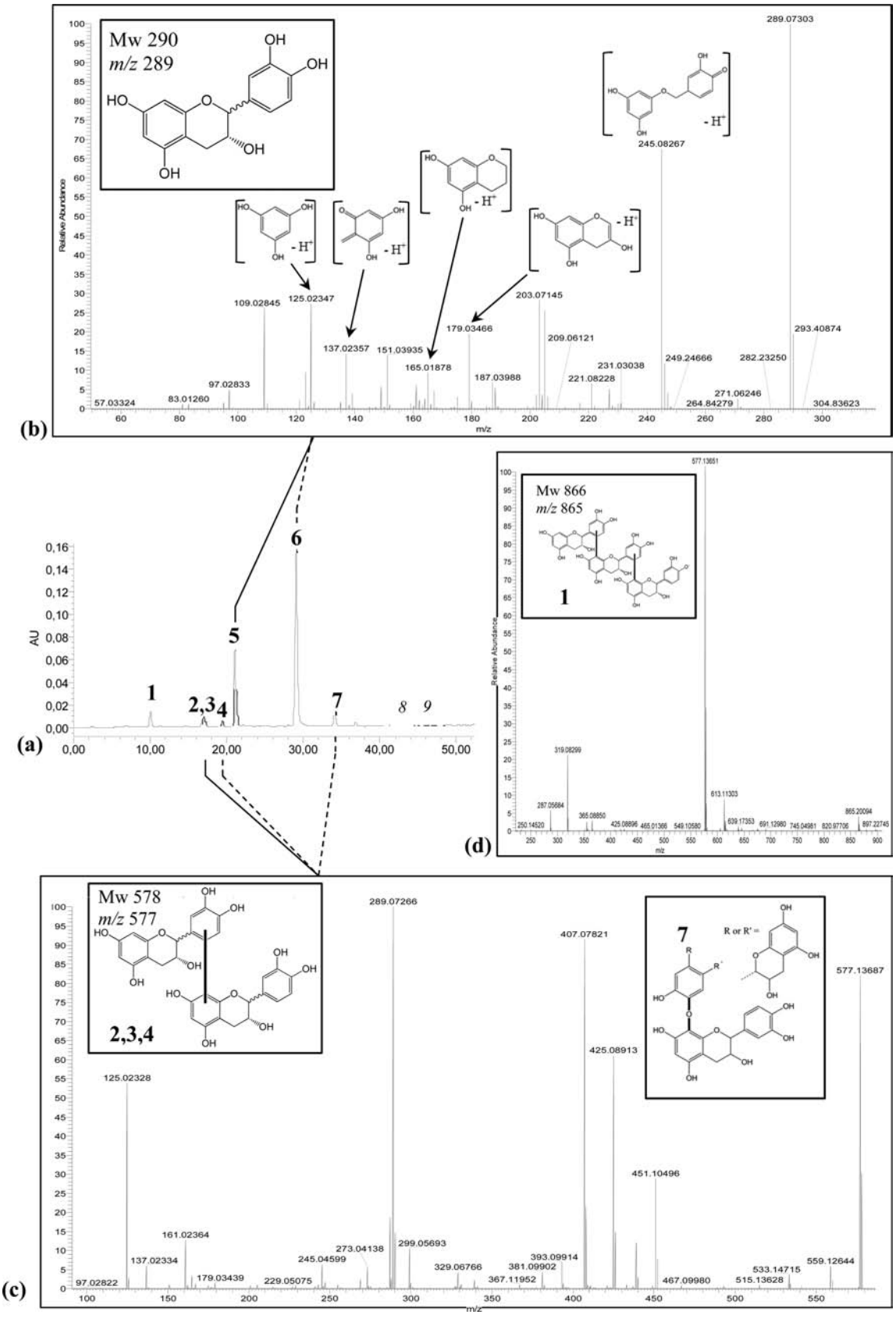


**Figure 1.** (a) RP-HPLC-UV chromatogram (280 nm) of (−)-epicatechin heated at 60 °C for 12 h in aqueous media. ESI(−)HRMS/MS spectra at (b) $m/z$ 289 ± 0.1 (compounds **5** and **6**), (c) 577 ± 0.1 (compounds **2**, **3**, **4** and **7**), and (d) $m/z$ 865 ± 0.1. The bold lines in the molecule indicate that the precise position of the chemical bonds is not known. The dotted lines indicate that these compounds gave an HRMS/MS spectrum very similar to that here displayed.


dx.doi.org/10.1021/jf502016z | J. Agric. Food Chem. 2014, 62, 9002−9016

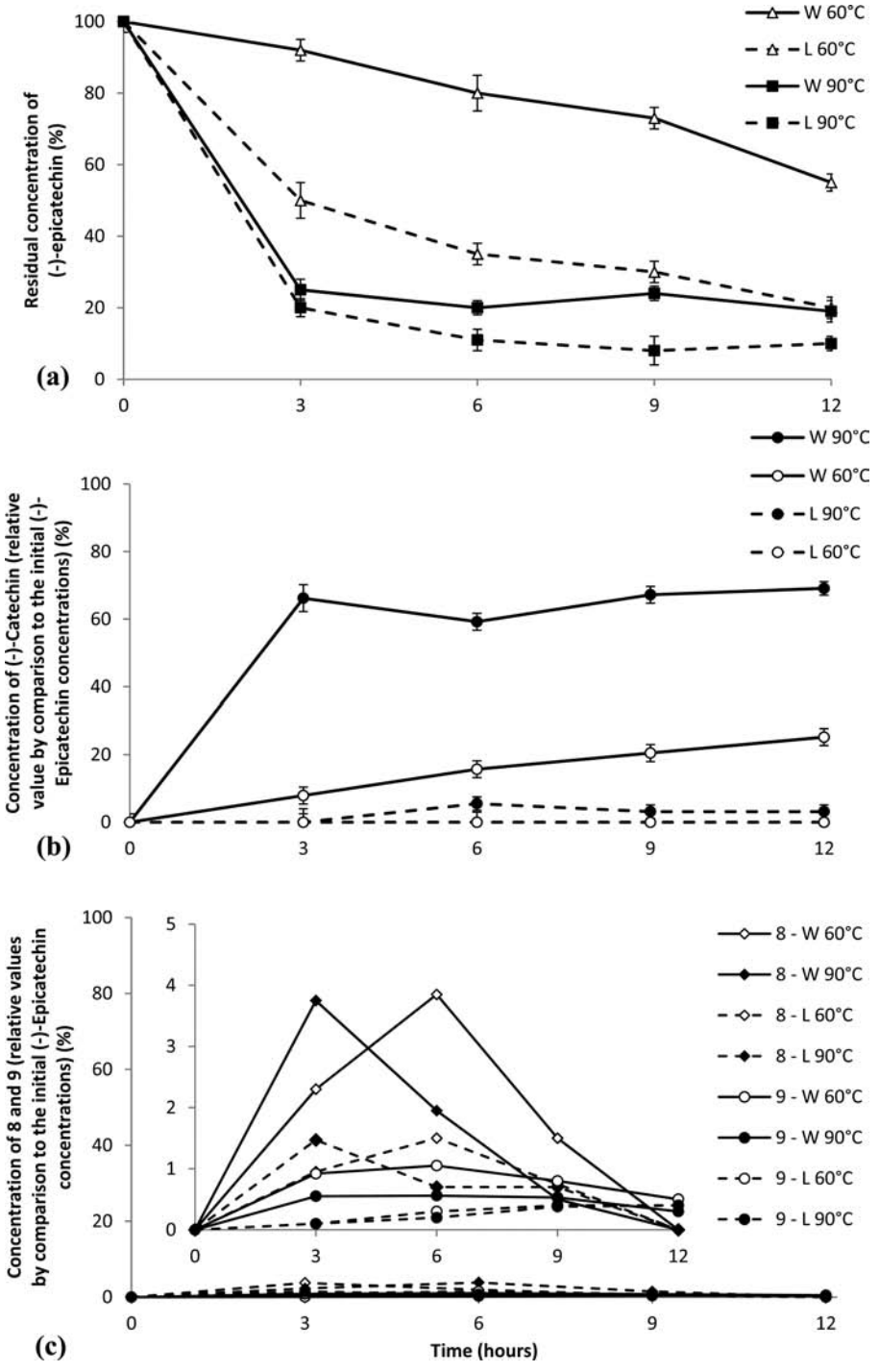


**Figure 2.** Evolution of the (−)-epicatechin model medium at 60 and 90 °C: (a) degradation of (−)-epicatechin; (b) synthesis of (−)-catechin; (c) synthesis of compounds **8** and **9**. Quantitation is in epicatechin equivalents by ESI(−)-MS/MS. Standard deviation was <5%.

supplied by VWR (Leuven, Belgium). Formic acid (99%) was obtained from Acros Organic (Geel, Belgium). (−)-Epicatechin (98%), (+)-catechin (98%), caffeine, and theobromine (>99%) were supplied by Sigma-Aldrich (Bornem, Belgium). (−)-Epicatechin-4$\beta$-8-(−)-epicatechin (B2, 90%), (−)-epicatechin-2*O*-7,4$\beta$-8-(−)-epicatechin (A2, 99%), and kaempferol (>90%) were obtained from Extrasynthese (Genay, France). (−)-Epicatechin-4$\beta$-8-(−)-epicatechin-4$\beta$-8-(−)-epicatechin (C1, 99%) and (−)-epicatechin-4$\beta$-8-(+)-catechin (B1, 99%) were supplied by PhytoLab GmbH & Co. KG (Vestenbergsgreuth, Germany). Aqueous solutions were made with Milli-Q (Millipore, Bedford, MA, USA) water (resistance = 18 m$\Omega$). Cocoa butter, sugar, and lecithin were obtained from Belcolade (Puratos Group, Erembodegem, Belgium).

**Cocoa and Chocolate Samples.** Ecuadorian National cocoa beans (before and after roasting for 30 min at 150 °C) and derived chocolate (72% cacao, conching step of 12 h at 75 °C) were provided by the chocolate factory Pierre Marcolini (Brussels, Belgium).

**Preparation of Model Media.** Aqueous model media were obtained by diluting (−)-epicatechin or B2 at a concentration of 1000 mg/L in ultrapure water (stock solution of 10000 mg/L prepared in methanol). Lipidic model media contained sugar (59.7% w/w), cocoa butter (39.8% w/w), and lecithin (0.5% w/w, addition after 6 h) and (−)-epicatechin or B2 (1000 mg/L). All media were treated in duplicates at 60 or 90 °C, and samples were taken at 0, 3, 6, 9, and 12 h.

**Extraction of Flavan-3-ols from Lipidic Model Systems.** This method has been adapted from the one developed in our laboratory for

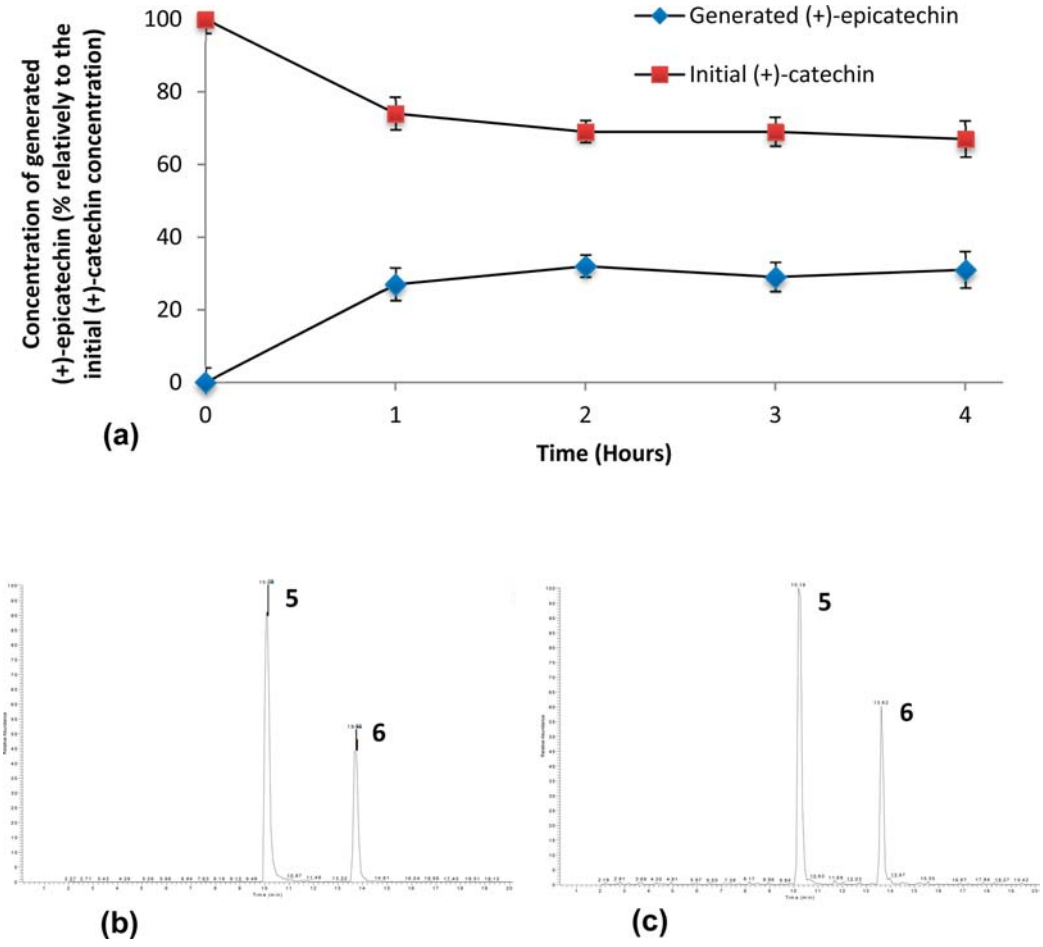


**Figure 3.** (a) Evolution of the (+)-catechin model medium at 90 °C. (b, c) RP-HPLC-MS chromatograms obtained after 12 h at 90 °C, from the (+)-catechin or (−)-epicatechin aqueous model media, respectively.

the analysis of flavan-3-ols in chocolate.[14] All extraction steps have been done in duplicate.

*Lipid Removal.* Lipidic model systems (500 mg) were introduced into a centrifugal vial. By successive 10 min extractions, lipids were removed with 3 × 1.5 mL diethyl ether at room temperature under gentle stirring. At the end of each step, the sample was centrifuged for 10 min at 2500*g*, and the supernatant was eliminated. After the last step, the powder was dried under vacuum to get rid of residual solvent.

*Flavan-3-ol Extraction.* Defatted samples were extracted three times with 3 mL of acetone/water/acetic acid (70:28:2, v/v/v), each time for 1 h under shaking at room temperature. After each extraction, the suspension was centrifuged for 10 min at 2500*g*, and the supernatant was collected. The combined supernatants were concentrated by rotary evaporation to obtain ∼3 mL of extract, and residual particles were removed by filtration.

*Solid-Phase Extraction Purification Step.* To purify the flavan-3-ol extract, a 360 mg C18 Sep-Pak cartridge (Waters, Millipore) was preconditioned with 10 mL of methanol and 20 mL of water. The extract was loaded on the cartridge, and sugars were removed with 5 mL of water. Flavan-3-ols were finally eluted with 5 mL of acetone/water/acetic acid (70:28:2, v/v/v). The eluates were concentrated by rotary evaporation (<40 °C) and freeze-dried. The extract was dissolved in methanol and stored under nitrogen at −80 °C in the dark until used.

**Extraction of Flavan-3-ols from Cocoa and Chocolate.** The method was close to the one used here above for model systems. Seven grams of cocoa beans or chocolate was defatted by diethyl ether (3 × 50 mL) at room temperature under gentle stirring. After centrifugation, samples were dried under vacuum. Defatted samples spiked with 500 μL of kaempferol at 10000 mg/L in methanol (used as internal standard; 714 mg/kg if calculated in beans) were extracted with 3 × 50 mL of acetone/water/acetic acid (70:28:2, v/v/v) and purified on a 10 g C18 Sep-Pak cartridge (Waters, Millipore) preconditioned with 200 mL of methanol and 300 mL of water. The samples were finally eluted with 50 mL of acetone/water/acetic acid (70:28:2, v/v/v), concentrated by rotary evaporation/ and freeze-dried.

**RP-HPLC-DAD-ESI(−)-MS/MS Quantitation of Flavan-3-ols.** Quantitations were performed on a C18 Kinetex column (150 × 2.1 mm, 2.6 μm) (Phenomenex, Torrance, CA, USA) using a linear gradient from A (water containing 1% acetonitrile and 2% formic acid) to B (acetonitrile containing 2% formic acid). Gradient elution was as follows: from 97% A to 91% in 5 min, from 91 to 85% in 25 min, from 85 to 64% in 35 min, from 64 to 10% in 10 min, and isocratic for 20 min at a flow rate of 200 μL/min. Five microliters of the sample was injected in duplicates onto the column kept at 20 °C. A SpectraSystem equipped with an AS3000 autosampler and a P4000 quaternary pump was used. The system was controlled with Xcalibur software version 1.2 (Thermo Fisher Scientific, Austin, TX, USA). Flavan-3-ols were monitored from 200 to 800 nm with a UV6000LP diode array detector. Mass spectra were acquired using an LCQ ion trap mass spectrometer equipped with an ESI source (ThermoFisher). Collision-induced dissociation spectra were recorded at a relative collision energy of 30, 35, and 40%, respectively, for singly charged $[M - H]^{-1}$ ions of monomers ($m/z$ 289), dimers ($m/z$ 577, 575, and 573), and trimers ($m/z$ 865). The ESI inlet conditions were as follows: source voltage, 4.9 kV; capillary voltage, −4 V; capillary temperature, 200 °C; and sheath gas, 39 psi. For ESI(−)-MS/MS semiquantitation in cocoa beans and chocolate (kaempferol used as internal standard), a relative recovery factor = 1 was applied for all compounds. Flavan-3-ol monomers were quantitated according to the calibration curve of (−)-epicatechin (0, 10, 25, 50, 100 mg/L, $R^2$ = 0.99648), procyanidins B2 and B5 with the one of B2


dx.doi.org/10.1021/jf502016z | J. Agric. Food Chem. 2014, 62, 9002−9016

**Table 1. Polyphenols Detected in the (−)-Epicatechin Model Media**[a]

| Peak n°, name and formula | Rt [min] (relative retention time) | $[M-H]^{-1}$ | MS/MS ions m/z (%) | Suspected structure |
|---|---|---|---|---|
| **1** Chemical trimer ($C_{45}H_{38}O_{18}$) | 10.0 (0.34) | 865 | 577.1 (100) 319.1 (23) 613.1 (11) 287.1 (8) | *** 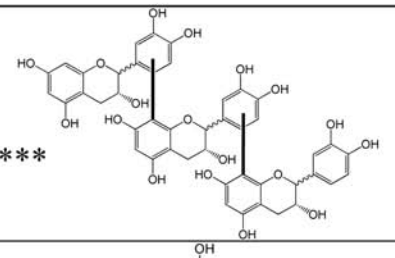 |
| **2,3,4** Chemical dimer ($C_{30}H_{26}O_{12}$) | 16.8 19.3 (0.57) (0.65) | 577 | 393.2 (100) 559.1(94) 425.1 (57) 439.1 (50) | ** 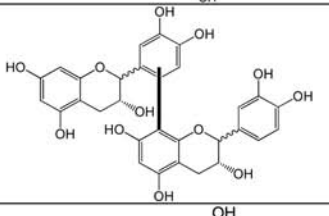 |
| **5** (-)-Catechin ($C_{15}H_{14}O_6$) | 21.2 (0.72) | 289 | 245.1 (100), 205.1 (34), 179.1 (12) | * 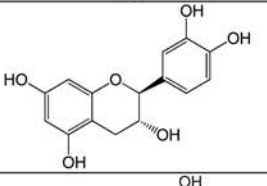 |
| **6** (-)-Epicatechin ($C_{15}H_{14}O_6$) | 29.6 (1.00) | 289 | 245.1 (100), 205.1 (34), 179.1 (12) | * 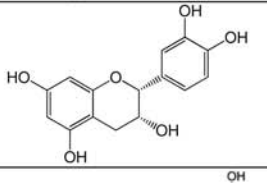 |
| **7** Chemical dimer ($C_{30}H_{26}O_{12}$) | 34.0 (1.15) | 577 | 393.2 (100) 559.1(94) 425.1 (57) 439.1 (50) | *** 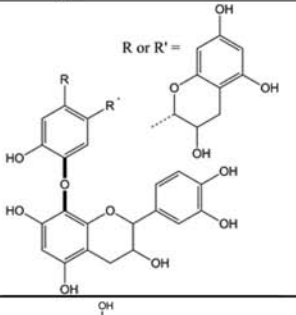 |
| **8** Dehydrodiepicatechin A (epicatechin-catechin) ($C_{30}H_{24}O_{12}$) | 53.1 (1.79) | 575 | 449.1 (100), 423.0 (75), 539.2 (28), 289.1 (22), 407.1 (20), 557.1 (13) | *** 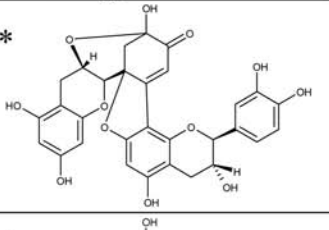 |
| **9** Dehydrodiepicatechin A (epicatechin-epicatechin) ($C_{30}H_{24}O_{12}$) | 58.0 (1.95) | 575 | 449.1 (100), 423.0 (75), 539.2 (28), 289.1 (22), 407.1 (20), 557.1 (13) | *** 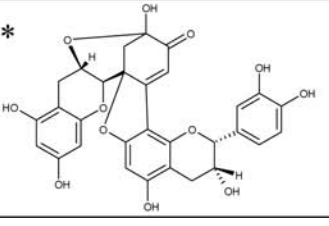 |

[a]Rt = retention time. * Comparison with purified commercial standards (retention time and ESI(−)-HRMS/MS spectra). ** From refs 38 and 42 and ESI(−)-HRMS/MS. *** From refs 21 and 42 and ESI(−)-HRMS/MS.


dx.doi.org/10.1021/jf502016z | J. Agric. Food Chem. 2014, 62, 9002−9016

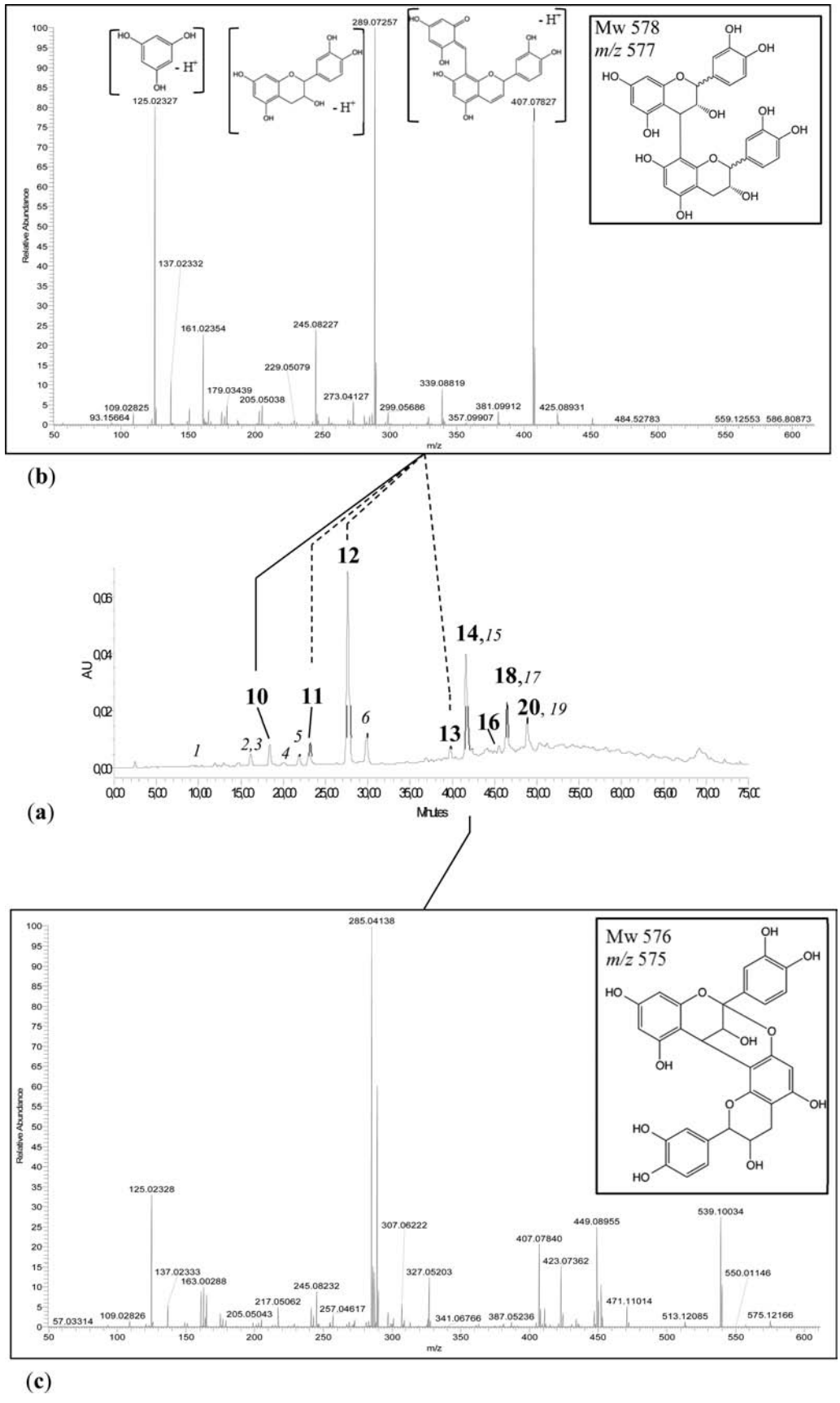


**Figure 4.** (a) RP-HPLC-UV chromatogram (280 nm) of procyanidin B2 heated at 60 °C for 12 h in aqueous media. ESI(−)HRMS/MS spectra at (b) $m/z$ 577 ± 0.1 (peaks 10−13) and (c) 575 ± 0.1 (peak 14). The dotted lines indicate that these compounds gave an HRMS/MS spectrum very similar to that here displayed.


dx.doi.org/10.1021/jf502016z | J. Agric. Food Chem. 2014, 62, 9002−9016

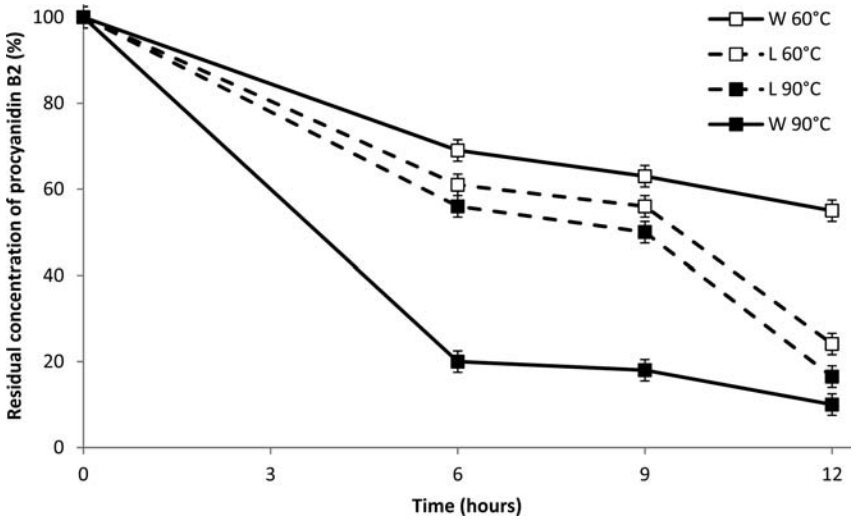


**Figure 5.** Evolution at 60 and 90 °C of the procyanidin B2 model medium. Quantitation was in B2 equivalents by ESI(−)-MS/MS. Standard deviation was <5%.

(0, 10, 25, 50, 100 mg/L, $R^2$ = 0.99831), and C1 with itself (0, 10, 25, 50, 100 mg/L, $R^2$ = 0.99873). No extraction was applied on aqueous model systems. For the lipidic model systems, a theoretical recovery factor of 100% was also used (relative values by comparison to the initial concentrations).

**HRMS/MS Identification.** High-resolution MS/MS spectra were obtained by connecting the same colomn with the same elution program to an Exactive system composed of Accela LC coupled to the Orbitrap mass spectrometer and controlled with Xcalibur software version 2.0.7 (Thermo Fisher Scientific). The ESI inlet conditions were as follows: sheet gas flow rate, 70; auxiliary gas flow rate, 5; sweep gas flow rate, 0; spray voltage, 3.50 kV; capillary temperature, 320 °C; S-lens level, 80%; heater temperature, 50 °C.

## RESULTS AND DISCUSSION

The stability of (−)-epicatechin and procyanidin B2 was monitored by investigating model media after 0, 3, 6, 9, and 12 h at 60 and 90 °C. After a first series of experiments conducted in water (W; extraction steps here not required before HPLC separation), lipidic media (L) were also investigated. As for typical Belgian consumer chocolates,[47] the lipidic medium was composed of 59.7% (w/w) saccharose and 39.8% (w/w) cocoa butter spiked at midtime with lecithin (0.5%). Lecithin is often added in the last part of the conching process chocolate (heat treatment of 6−18 h at 60−90 °C) to improve rheological properties (0.1% of lecithin provides a similar effect as 1% cocoa butter).

**Monitoring (−)-Epicatechin Degradation in Aqueous Medium.** As depicted in Figure 1a, eight new peaks were detected in the aqueous (−)-epicatechin medium heated for 12 h at 60 °C (six at 280 nm and two at 410 nm). Most of them were already apparent after 3 h, especially when the temperature was increased to 90 °C (73% loss of (−)-epicatechin after 3 h at 90 °C versus only 11% loss at 60 °C; solid lines in Figure 2a).

The epimerization of (−)-epicatechin (peak 6) to (−)-catechin (peak 5, Figure 1a,b) accounted for 25% of the degradation of the monomer at 60 °C and even reached 70% at 90 °C (Figure 2b). Of course, catechin can also epimerize to epicatechin, but as depicted in Figure 3, because of lesser steric hindrance, catechin epimerization is less favored ((+)-catechin used in this experiment). Thus, whatever the initial epimer used, an equilibrium between epicatechin and catechin is reached before 3 h at 90 °C, with the same final ratio close to 70:30 in favor of catechin (Figure 3). At 60 °C, on the other hand, (−)-epicatechin remained the major monomer in epicatechin-spiked medium after 12 h (Figure 1a).

Although not found in the 280 nm UV chromatogram (peaks 8 and 9 in Figure 1a), two yellow-orange compounds clearly appeared at 410 nm during (−)-epicatechin degradation, explaining the observed color of the medium (Figure 2c). Dehydrodi(epi)catechins A, previously described in a model medium[21] and in 5-day-stored beer[5] as arising through (+)-catechin degradation, eluted at the corresponding retention times (structures detailed in Table 1).

Three "chemically derived" dimers similar to the dehydrodi-(epi)catechin B4 described by Guyot et al.[21] and Sun and Miller[38] in model apple media were evidenced at 280 nm (peaks 2, 3, and 4, Figure 1a). They are here referred to as "chemical dimers" because contrary to native flavan-3-ols, the interflavan linkage is always created between aromatic rings. The formulas of these chemical dimers were confirmed by high-resolution mass spectrometry ($C_{30}H_{26}O_{12}$ experimental $m/z$ = 577.13687; theoretical $m/z$ 577.13460; $\delta$ 3.93). In all three ESI(−)-HRMS/MS spectra (Figure 1c), the characteristic $m/z$ peak = 393.09914 ($C_{21}H_{12}O_{16}$, not found for the natural procyanidin B2, Figure 4b) was evidenced, allowing further differentiation between "natural" (C4−C8 or C4−C6 linkages) and "chemical" (C2′−C8 or C6′−C8) dimers in complex media. Due to different possible structures that cannot be distinguished by HRMS/MS, the bold lines drawn in Table 1 and Figure 1 do not specify the precise position of the chemical bonds. Also worth stressing is the presence of compound **7**, which elutes much later than compounds **2**, **3**, and **4**, but with exactly the same mass spectrum (Figure 1c). We suspect it could be another chemical dimer, dehydrodi(epi)catechin B (Table 1), previously described by Guyot et al.[21] and Poupard[42] (same theoretical $m/z$ 577.13460). All four compounds together account for <6%.

A trimer (peak 1; $C_{45}H_{38}O_{18}$, experimental $m/z$ 865.20094; theoretical $m/z$ 865.19854; $\delta$ 2.77) was also detected at 280 nm and suspected to have arisen through addition of a "chemical dimer" to an oxidized monomer (Figure 1d). The commercial C1 trimer eluted 13.3 min after compound **1** by RP-HPLC (RT = 23.3 and 10 min, respectively). Only trimers containing (+)- or (−)-catechin units could elute before catechin.[49] Therefore, we


dx.doi.org/10.1021/jf502016z | J. Agric. Food Chem. 2014, 62, 9002−9016

**Table 2. Characterization of the Degradation Products in the Procyanidin B2 Model Media**

| Peak n°, name and formula | Rt (min) (relative retention time ) | $[M-H]^{-1}$ | MS/MS ions m/z (%) | Structure |
|---|---|---|---|---|
| **1** Chemical trimer ($C_{45}H_{38}O_{18}$) | 10.0 (0.34) | 865 | 577.1 (100) 319.1 (23) 613.1 (11) 287.1 (8) | *** 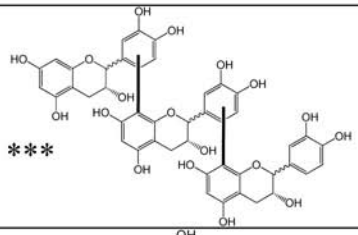 |
| **2,3,4** Chemical dimer ($C_{30}H_{26}O_{12}$) | 16.8 19.3 (0.57) (0.65) | 577 | 393.2 (100) 559.1(94) 425.1 (57) 439.1 (50) | ** 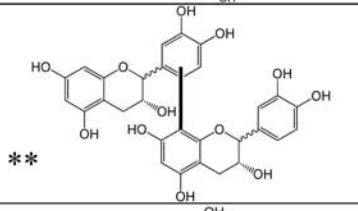 |
| **10** B2 epimer ($C_{30}H_{26}O_{12}$) | 18.5 (0.62) | 577 | 425.1 (100), 451.1 (65), 407.2 (47), 289.1 (28) | **** 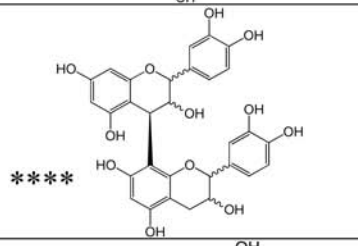 |
| **5** (-)-Catechin ($C_{15}H_{14}O_6$) | 21,2 (0.72) | 289 | 245.1 (100), 205.1 (34), 179.1 (12) | * 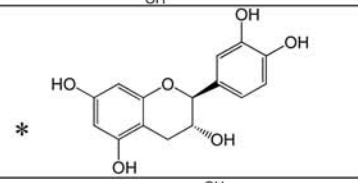 |
| **11** B2 epimer ($C_{30}H_{26}O_{12}$) | 23.3 (0.78) | 577 | 425.1 (100), 451.1 (65), 407.2 (47), 289.1 (28) | **** 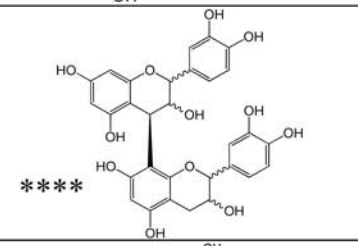 |
| **12** Procyanidin B2 ($C_{30}H_{26}O_{12}$) | 27.8 (0. 94) | 577 | 425.1 (100), 451.1 (65), 407.2 (47), 289.1 (28) | * 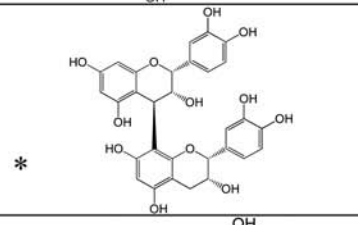 |
| **6** (-)-Epicatechin ($C_{15}H_{14}O_6$) | 29.6 (1.00) | 289 | 245.1 (100), 205.1 (34), 179.1 (12) | * 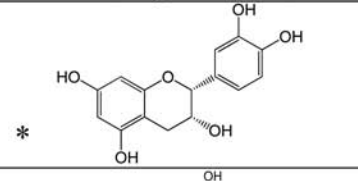 |
| **13** B2 epimer ($C_{30}H_{26}O_{12}$) | 39.8 (1.34) | 577 | 425.1 (100), 451.1 (65), 407.2 (47), 289.1 (28) | **** 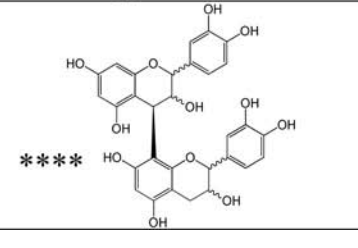 |


dx.doi.org/10.1021/jf502016z | J. Agric. Food Chem. 2014, 62, 9002−9016

**Table 2. continued**

| Peak n°, name and formula | Rt (min) (relative retention time ) | $[M-H]^{-1}$ | MS/MS ions m/z (%) | Structure |
|---|---|---|---|---|
| **14** A2 ($C_{30}H_{24}O_{12}$) | 41.9 (1.42) | 575 | 449.1 (100), 539.2 (47), 423.1 (42), 289.1 (30), 407.2 (15), 557.1 (14) | 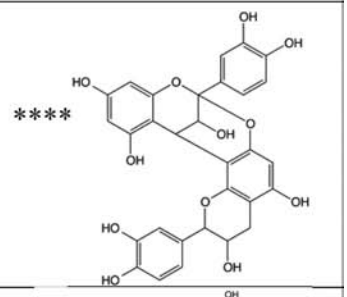 |
| **15** Oxidized A2 epimer ($C_{30}H_{22}O_{12}$) | 42.3 (1.43) | 573 | 285.1 (100), 125.1 (75), 555.1 (40), 161.1 (31) 423.1 (23) | 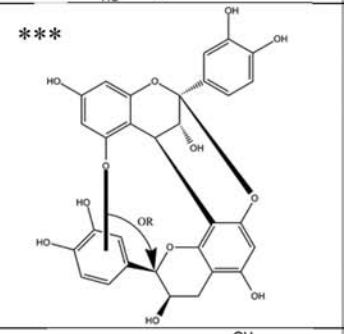 |
| **16** $A_2$ Epimer ($C_{30}H_{24}O_{12}$) | 45.5 (1.54) | 575 | 449.1 (100), 539.2 (47), 423.1 (42), 289.1 (30), 407.2 (15), 557.1 (14) | 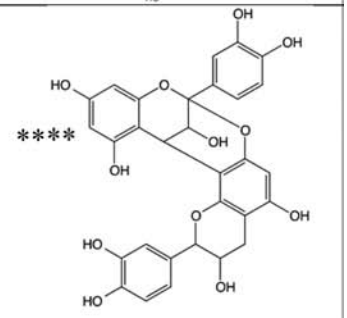 |
| **17** Oxidized A2 epimer ($C_{30}H_{22}O_{12}$) | 46.7 (1.58) | 573 | 285.1 (100), 125.1 (75), 555.1 (40), 161.1 (31) 423.1 (23) | 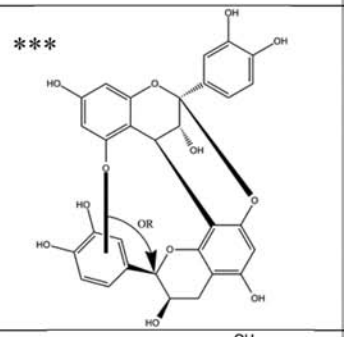 |
| **18** A2 epimer ($C_{30}H_{24}O_{12}$) | 46.2 (1.56) | 575 | 449.1 (100), 423.0 (75), 539.2 (28), 289.1 (22), 407.1 (20), 557.1 (13) | 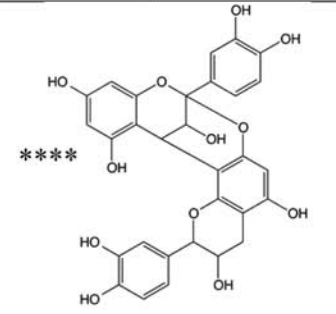 |


dx.doi.org/10.1021/jf502016z | *J. Agric. Food Chem.* 2014, 62, 9002−9016

**Table 2. continued**

| Peak n°, name and formula | Rt (min) (relative retention time ) | $[M-H]^{-1}$ | MS/MS ions m/z (%) | Structure |
|---|---|---|---|---|
| **19** Oxidized A2 epimer ($C_{30}H_{22}O_{12}$) | 46.7 (1.58) | 573 | 285.1 (100), 125.1 (75), 555.1 (40), 161.1 (31) 423.1 (23) | *** 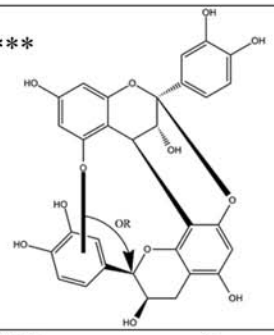 |
| **20** A2 epimer ($C_{30}H_{24}O_{12}$) | 48.7 (1.56) | 575 | 449.1 (100), 423.0 (75), 539.2 (28), 289.1 (22), 407.1 (20), 557.1 (13) | *** **** 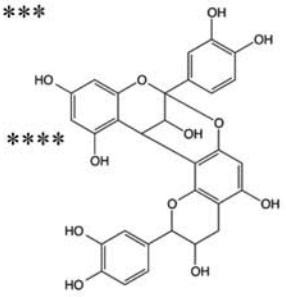 |
| **21**[a] Chemical trimer ($C_{45}H_{38}O_{18}$) | 28.1 (0.95) | 865 | 864.2 (100) 865.2 (50) 846.2 (30) 820.3 (20 | 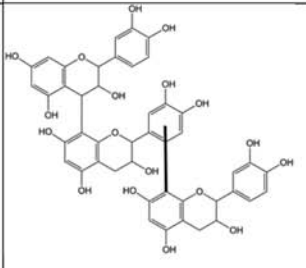 or 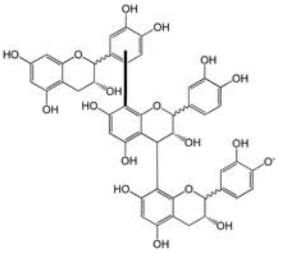 |

[a]Trimer only observed in the medium containing both (−)-epicatechin and procyanidin B2 * Comparison with purified commercial standards (retention time and ESI(−)-HRMS/MS spectra). ** From refs 38 and 42 and ESI(−)-HRMS/MS. *** From refs 21 and 42 and ESI(−)-HRMS/MS. **** Similitudes with the ESI(−)-HRMS/MS of a commercial epimer.

suspect that peak 1 could be a chemical trimer containing one to three units of (−)-catechin.

**Monitoring Procyanidin B2 Degradation in Aqueous Medium.** Figures 4 and 5 show that procyanidin B2 (peak 12) was also degraded in aqueous medium, especially at 90 °C, and yielded a large number of derived compounds (Table 2). Again, epimerization was found to occur, leading to three peaks (10, 11, and 13) in addition to B2 (12), all with an ESI(−)-HRMS/MS spectrum identical to that of the native dimer (epimers commercially unavailable) (Figure 4b). Those epimers are (−)-epicatechin-4$\beta$-8-(−)-catechin, (−)-catechin-4$\beta$-8-(−)-epicatechin, and (−)-catechin-4$\beta$-8-(−)-catechin. In B2 equivalents, none of them exceeded 5% of the initial procyanidin B2 concentration. Compound **10** could be suspected to coelute with commercially available procyanidin B1 [(−)-epicatechin-4$\beta$-8-(+)-catechin]. Our gradient elution applied on the C18 column was able to differentiate the natural procyanidin B1 from the suspected (−)-epicatechin-4$\beta$-8-(−)-catechin epimer, called here "B1-like" (elution of compound **10** 0.6 min after B1; data not shown). It was nonetheless impossible in our model medium to create B1 that includes a (+)-catechin moiety in its structure.


dx.doi.org/10.1021/jf502016z | J. Agric. Food Chem. 2014, 62, 9002−9016

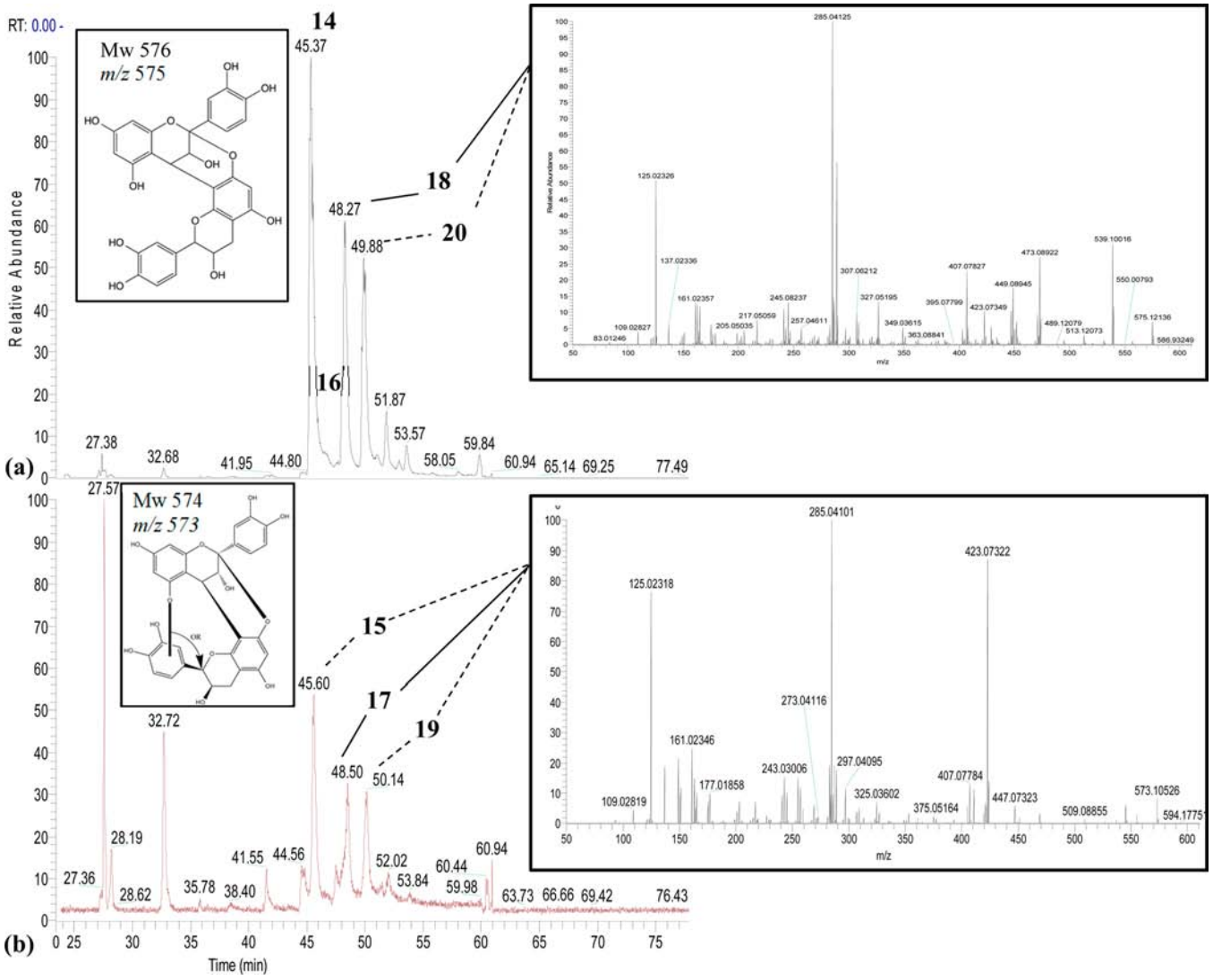


**Figure 6.** RP-HPLC-ESI(−)-HRMS/MS chromatogram of B2 heated at 90 °C for 12 h in aqueous media: (a) $m/z$ 575 ± 0.1; (b) $m/z$ 573 ± 0.1. The bold lines in the molecule indicate that the precise position of the chemical bonds is not known. The dotted lines indicate that these compounds gave an HRMS/MS spectrum very similar to that here displayed.

Depolymerization and further epimerization also generated some peaks [all discussed here above in relation to Figure 1): (−)-epicatechin (peak 6), (−)-catechin (peak 5), and dehydrodiepicatechins A (peaks 8 and 9, resolved only at 410 nm). The aqueous B2-containing media were, as expected, slightly yellow after degradation at 60 °C and red-brown at 90 °C. Only 50 mg/L (−)-epicatechin and (−)-catechin were observed after 12 h at 90 °C, accounting for <5% of the initial procyanidin B2 (1000 mg/L).

No trimer (**1**) was detectable on the UV chromatogram (Figure 4a). Yet traces were found by selecting $m/z$ 865 at the mass detector (fragmentation similar to that of compound **1** in the epicatechin model system). These results are in line with those previously published by Vidal et al.[7]

Procyanidin A2 (compound **14**, Figure 4a,c) was also produced from B2 (detectable only at 90 °C). Poupard et al.[42] also evidenced A2 in apple juice media. Three analogues (**16**, **18**, and **20**) with the same mass spectrum (Figure 6a) were found in lower amounts. They are suspected to be three A2 epimers ($C_{30}H_{24}O_{12}$: experimental $m/z$ for **18** 575.12136; theoretical $m/z$ 575.11950; $\delta$ 3.23). These compounds can undergo further oxidation leading to compounds **15**, **17**, and **19** ($C_{30}H_{22}O_{12}$: experimental $m/z$ for **17** 573.10526; theoretical $m/z$ 573.10385; $\delta$ 2.46 ppm; Figure 6b). The position of the third interunit linkage must still be determined.

**Comparison between Aqueous and Lipidic Media.** (−)-Epicatechin degradation at 60 °C proved much faster in lipidic medium (dotted lines in Figure 2a, 11% loss after 3 h in water versus 50% in cocoa butter). This contrasted with the epimerization pathway, an important degradation pathway in aqueous medium, which proved to be much slower in lipidic medium (<5% after 12 h at 90 °C, Figure 2b). Epimerization of epicatechin involves the breaking of the C-ring, leading to a radicalar intermediate. The higher efficiency of epimerization in the aqueous medium is most probably explained by the higher relative stability of this intermediate in an aqueous environment.

In contrast to (−)-catechin, dehydrodi(epi)catechins A were formed more quickly in lipidic medium and obviously much more quickly at higher temperature (Figure 2c). Yet none of the studied modalities allowed generating more than the equivalent of 4% of the epicatechin initially present. The "chemical" dimers (**2**, **3**, and **4**), intermediate compounds involved in the reaction


dx.doi.org/10.1021/jf502016z | J. Agric. Food Chem. 2014, 62, 9002−9016

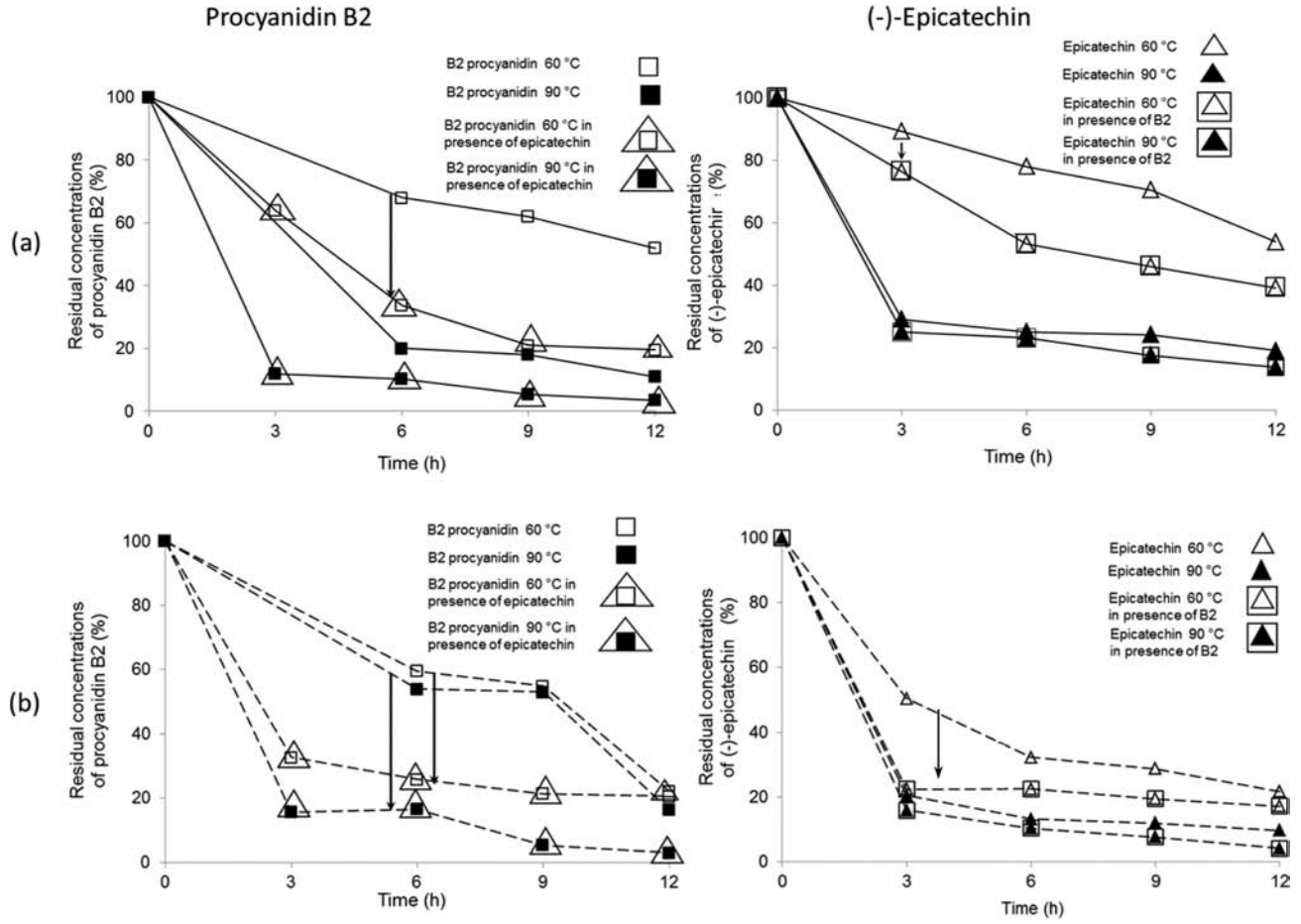


**Figure 7.** Comparison of the evolution at 60 and 90 °C of (−)-epicatechin and procyanidin B2 in (a) aqueous and (b) lipidic media, pure or mixed together. Quantitation was by ESI(−)-MS/MS. Standard deviation was <5%.

forming the dehydrodi(epi)catechins A, were found in both media, but in lower amounts in the lipidic environment.

Dimer B2 also behaved differently in the fatty environment. At 90 °C, B2 was degraded more slowly in the lipidic medium, although the two systems showed similar residual concentrations after 12 h (Figure 5). At 60 °C on the other hand, as previously seen for the monomer, the procyanidin B2 concentration decreased more rapidly in lipidic medium than in water (78% degradation versus 42%, after 12 h at 60 °C) (Figure 5).

**Synergy between Monomers and Dimers.** To determine whether a monomer might influence the degradation of the dimer or vice versa, aqueous and lipidic model media containing (−)-epicatechin and procyanidin B2 together (1000 mg/L each) were analyzed.

As depicted in Figure 7, the presence of the monomer was found to strongly accelerate degradation of the dimer, in both aqueous (Figure 7a) and lipidic (Figure 7b) media (e.g., 34% residual procyanidin B2 for the aqueous medium after 6 h at 60 °C in the presence of monomer versus 68% in its absence).

Likewise, the degradation rate of (−)-epicatechin was influenced, at least at 60 °C, by the presence of procyanidin B2. After 3 h, the residual concentrations of (−)-epicatechin were significantly lower in the presence of the dimer (76% in water and 22% in lipidic medium) than in its absence (89% in water and 50% in lipidic medium, coefficient of variation below 5% for our data). Epimerization, in contrast, was 10% less efficient than in the media containing only the monomer. At 90 °C, the (−)-epicatechin degradation rate was not significantly influenced by the presence of procyanidin B2.

As depicted in Figure 8a,b, in addition to the previously described "chemical" trimer **1**, a new trimer (**21**) emerged in this mixed medium, with a retention time of 28.1 min (HRMS/MS confirmation of $C_{45}H_{38}O_{18}$: experimental $m/z$ 865.20094; theoretical $m/z$ 865.19854; $\delta$ 2.77). Most probably, this was due to polymerization of an oxidized monomer with the natural dimer (both at 60 and at 90 °C). Not present for the natural C1 trimer (Figure 8c), the $m/z$ 319 fragment was found for both chemical trimers. Further investigations are required to reveal their accurate structure.

**Occurrence of Native Flavan-3-ol Degradation Products in Roasted Cocoa and Chocolate.** As depicted in Figure 9, unroasted Ecuadorian cocoa beans (Figure 9a) contained (−)-epicatechin (1523 mg/kg, **6**) and very little catechin (77 mg/kg, **5**), procyanidins B2 (561 mg/kg, **12**), B5 (397 mg/kg), and C1 (309 mg/kg). As expected, high temperature during roasting (30 min at 150 °C) significantly decreased the amount of natural monomer (−51% epicatechin), dimers (−50% B2 and −57% B5), and trimer (−81% C1). On the other hand, degradation through conching (12 h at 75 °C) was moderate except for the monomer (−53% epicatechin, −12% dimer B2, −8% dimer B5, and −9% trimer C1, taking into account the 72% cocoa content in the resulting chocolate). Of course, due to the presence of various higher oligomers in cocoa (not detectable in our RP-HPLC chromatograms), part of the "natural" monomers and


dx.doi.org/10.1021/jf502016z | J. Agric. Food Chem. 2014, 62, 9002−9016

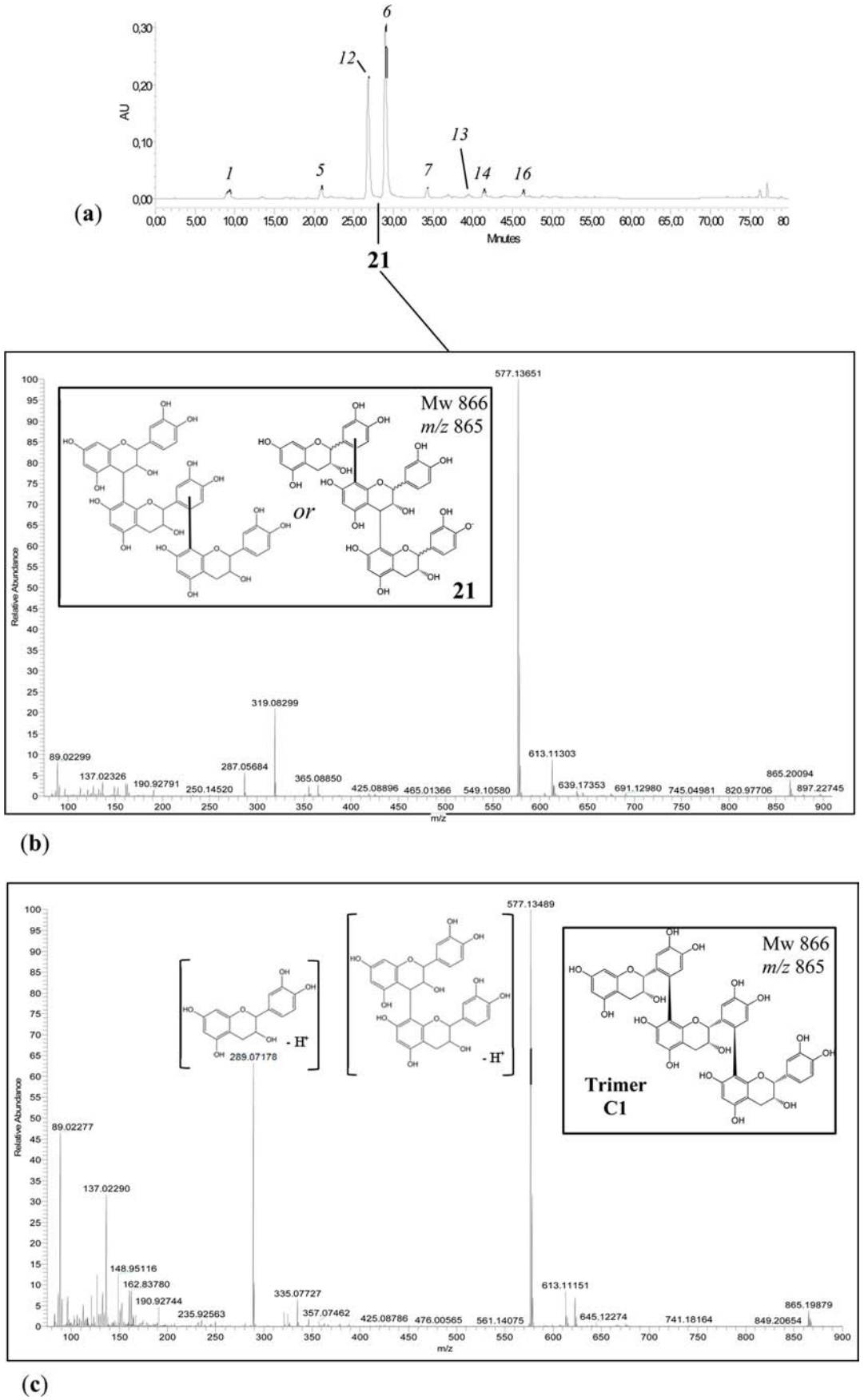


**Figure 8.** (a) RP-HPLC-UV chromatogram (280 nm) of B2 heated at 60 °C for 12 h in aqueous media in the presence of (−)-epicatechin and ESI(−)HRMS/MS spectra of (b) compound **21** and (c) the natural procyanidin C1.


dx.doi.org/10.1021/jf502016z | *J. Agric. Food Chem.* 2014, 62, 9002−9016

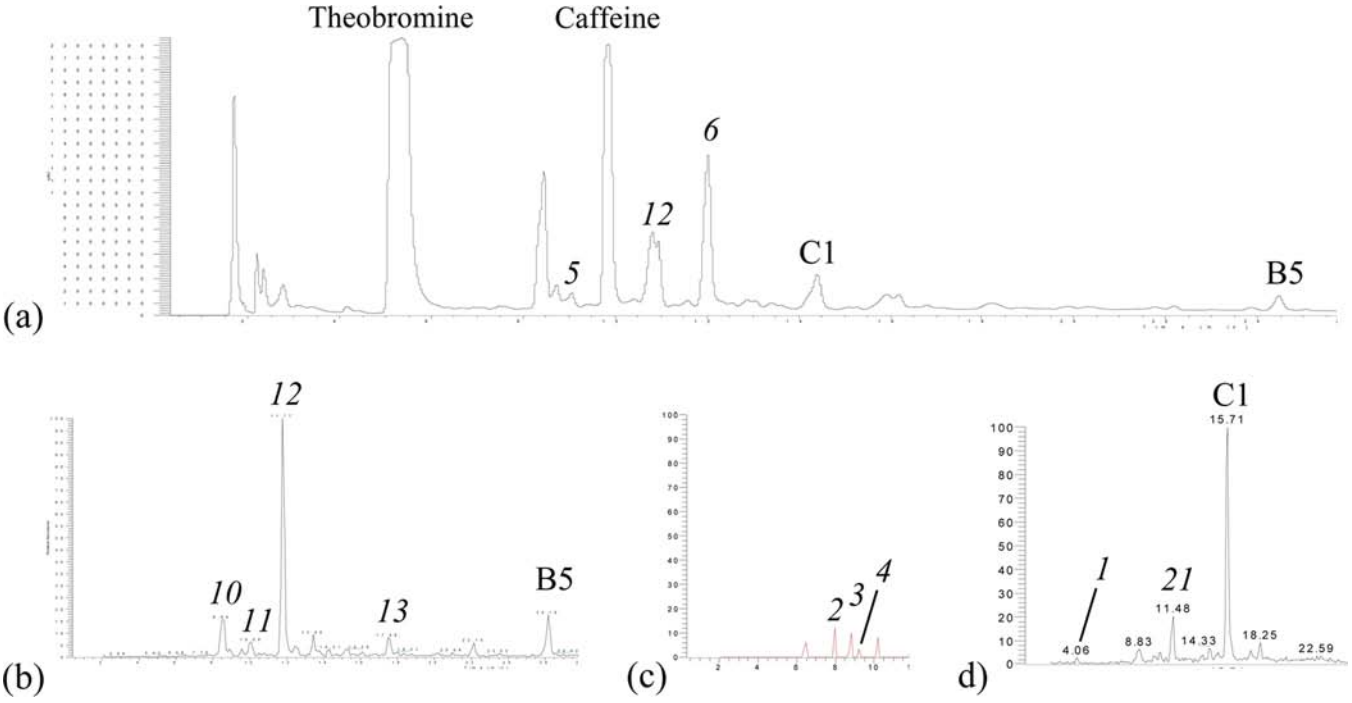


**Figure 9.** (a) RP-HPLC-UV(280 nmm) chromatogram of the polyphenolic extract issued from unroasted cocoa beans. (b–d) RP-HPLC-MS/MS chromatograms of the extract issued from the corresponding roasted cocoa beans at (b) $m/z$ 577, (c) $m/z$ 577 → 393, and (d) $m/z$ 865.

dimers found in roasted cocoa beans could also be issued from depolymerization.

Most of the degradation products evidenced in our model media have been found in the roasted cocoa beans (Figure 9b,c) as well as in chocolate. Epimerization of (−)-epicatechin significantly occurred through roasting, as shown by the epicatechin/catechin ratios of 19.8 and 5.2 before and after roasting, respectively. B2 epimers (peaks 10, 11, and 13) were also formed (observed only by MS/MS on $m/z$ 577, Figure 9b). Epimerization was revealed to be less efficient during chocolate conching (the epicatechin/catechin ratio remained close to 5 in the derived chocolate).

Compounds **2**, **3**, and **4**, all three suspected to be "chemical" newly formed dimers, were absent in unroasted beans but were evidenced after heat treatment (Figure 9c; selection of the specific fragment 393 issued from $m/z$ 577). In the same way, **1** and **21** suspected to be "chemical" trimers were detectable after roasting (Figure 9d). To our best knowledge, this is the first work that states the presence of chemical oligomers in processed cocoa.

The "chemical" dimers and oligomers produced during cocoa processing still require deeper investigations (detailed structure, antioxidant capacity, bioavailability, etc.). The further step of this research will be to optimize the roasting and conching temperature programs to maximize the content of bioavailable antioxidant polyphenols.

## AUTHOR INFORMATION

### Corresponding Author

*(S.C.) E-mail: sonia.collin@uclouvain.be. Fax: +32 10 47 21 78. Phone: +32 10 47 29 13.

### Notes

The authors declare no competing financial interest.

## REFERENCES

(1) Counet, C.; Ouwerx, C.; Rosoux, D.; Collin, S. Relationship between procyanidin and flavour contents of cocoa liquors from different origins. *J. Agric. Food Chem.* **2004**, *52*, 6243–6249.

(2) Cooper, K. A.; Campos-Giménez, E.; Jiménez Alvarez, D.; Nagy, K.; Donovan, J. L.; Williamson, G. Rapid reversed phase ultra-performance liquid chromatography analysis of the major cocoa polyphenols and inter-relationships of their concentrations in chocolate. *J. Agric. Food Chem.* **2007**, *55*, 2841–2847.

(3) Othman, A.; Jalil, A. M. M. J.; Weng, K. K.; Ismail, A.; Ghani, N. A.; Adenan, I. Epicatechin content and antioxidant capacity of cocoa beans from four different countries. *Afr. J. Biotechnol.* **2010**, *9*, 1052–1059.

(4) Li, H.-J.; Deinzer, M. L. Structural identification and distribution of proanthocyanidins in 13 different hops. *J. Agric. Food Chem.* **2006**, *54*, 4048–4056.

(5) Callemien, D.; Collin, S. Involvement of flavanoids in beer color instability during storage. *J. Agric. Food Chem.* **2007**, *55*, 9066–9073.

(6) Jerkovic, V.; Callemien, D.; Collin, S. Determination of stilbenes in hop pellets from different cultivars. *J. Agric. Food Chem.* **2005**, *53*, 4202–4206.

(7) Vidal, S.; Cartalade, D.; Souquet, J.-M.; Fulcrand, H.; Cheynier, V. Changes in proanthocyanidin chain length in winelike model solutions. *J. Agric. Food Chem.* **2002**, *50*, 2261–2266.

(8) Awika, J. M.; Dykes, L.; Gu, L.; Rooney, L. W.; Prior, R. L. Processing of sorghum (*Sorghum bicolor*) and sorghum products alters procyanidin oligomer and polymer distribution and content. *J. Agric. Food Chem.* **2003**, *51*, 5516–5521.

(9) Bröhan, M.; Jerkovic, V.; Wilmotte, R.; Collin, S. Catechins and derived procyanidins in red and white sorghum. Contribution of them to the antioxidant activity. *J. Inst. Brew.* **2011**, *117*, 600–607.

(10) Tsao, R.; Yang, R.; Xie, S.; Sockovie, E.; Khanizadeh, S. Which polyphenolic compounds contribute to the total antioxidant activities of apple? *J. Agric. Food Chem.* **2005**, *53*, 4989–4995.

(11) Katalini, V.; Milos, M.; Modun, D.; Musi, I.; Boban, M. Antioxidant effectiveness of selected wines in comparison with (+)-catechin. *Food Chem.* **2004**, *86*, 593–600.

(12) Kang, K. W.; Oh, S. J.; Ryu, S. Y.; Song, G. Y.; Kim, B.-H.; Kang, J. S.; Kim, S. K. Evaluation of the total oxy-radical scavenging capacity of catechins isolated from green tea. *Food Chem.* **2010**, *121*, 1089–1094.

(13) Dong, X.-Q.; Zou, B.; Zhang, Y.; Ge, Z.-Z.; Du, J.; Li, C.-M. Preparation of A-type proanthocyanidin dimers from peanut skins and persimmon pulp and comparison of the antioxidant activity of A-type and B-type dimers. *Fitoterapia* **2013**, *91*, 182–139.

(14) Counet, C.; Collin, S. Effect of the number of flavanol units on the antioxidant activity of procyanidin fractions isolated from chocolate. *J. Agric. Food Chem.* **2003**, *51*, 6816−6822.
(15) Liégeois, C.; Lermusieau, G.; Collin, S. Measuring antioxidant efficiency of wort, malt, and hops against the 2,2′-azobis(2-amidinopropane) dihydrochloride-induced oxidation of an aqueous dispersion of linoleic acid. *J. Agric. Food Chem.* **2000**, *48*, 1129−1134.
(16) Taubert, D.; Roesen, R.; Lehmann, C.; Jung, N.; Schömig, E. Effects of low habitual cocoa intake on blood pressure and bioactive nitric oxide. *JAMA, J. Am. Med. Assoc.* **2007**, *298*, 49−60.
(17) McShea, A.; Ramiro-Puig, E.; Munro, S. B.; Casadesus, G.; Castell, M.; Smith, M. A. Clinical benefit and preservation of flavonols in dark chocolate manufacturing. *Nutr. Rev.* **2008**, *66*, 630−641.
(18) Misnawi Jinap, S.; Jamilah, B.; Nazamid, S. Sensory properties of cocoa liquor as affected by polyphenol concentration and duration of roasting. *Food Qual. Pref.* **2004**, *15*, 403−409.
(19) Soares, S.; Kohl, S.; Thalmann, S.; Mateus, N.; Meyerhof, W.; De Freitas, V. Different phenolic compounds activate distinct human bitter taste receptors. *J. Agric. Food Chem.* **2013**, *61*, 1525−1533.
(20) Thorngate, J. H.; Noble, A. C. Sensory evaluation of bitterness and astringency of 3*R*-(−)-epicatechin and 3*S*-(+)-catechin. *J. Sci. Food Agric.* **1995**, *67*, 531−535.
(21) Guyot, S.; Vercauteren, J.; Cheynier, V. Structural determination of colourless and yellow dimers resulting from (+)-catechin coupling catalysed by grape polyphenoloxidase. *Phytochemistry* **1996**, *42*, 1279−1288.
(22) Poupard, P.; Guyot, S.; Bernillon, S.; Renard, C. M. G. C. Characterisation by liquid chromatography coupled to electrospray ionisation ion trap mass spectrometry of phloroglucinol and 4-methylcatechol oxidation products to study the reactivity of epicatechin in an apple juice model system. *J. Chromatogr., A* **2008**, *1179*, 168−181.
(23) Stark, T.; Hofmann, T. Structures, sensory activity, and dose/response functions of 2,5-diketopiperazines in roasted cocoa nibs (*Theobroma cacao*). *J. Agric. Food Chem.* **2005**, *53*, 7222−7231.
(24) Serra Bonvehi, J.; Ventura Coll, F. Evaluation of bitterness and astringency of polyphenolic compounds in cocoa powder. *Food Chem.* **1997**, *60*, 365−370.
(25) Rouseff, R. L. Bitterness in food products: an overview. *Dev. Food Sci.* **1990**, *25*, 1−14.
(26) Carillo, L. C.; Londoño-Londoño, J.; Gil, A. Comparison of polyphenol, methylxanthines and antioxidant activity in *Theobroma cacao* beans from different cocoa-growing areas in Colombia. *Food Res. Int.* **2014**, *60*, 273−280.
(27) Jerkovic, V.; Nguyen, F.; Timmermans, A.; Collin, S. Comparison of procedures for resveratrol analysis in beer. Assessment of stilbenoids stability through wort fermentation and beer aging. *J. Inst. Brew.* **2008**, *114*, 143−149.
(28) Jerkovic, V.; Collin, S. Fate of resveratrol and piceid through different hop. Processings and storage times. *J. Agric. Food Chem.* **2008**, *56*, 584−590.
(29) Fuleki, T.; Ricardo-Da-Silva, J. M. Effects of cultivar and processing method on the contents of catechins and procyanidins in grape juice. *J. Agric. Food Chem.* **2003**, *51*, 640−646.
(30) Khanal, R. C.; Howard, L. R.; Brownmiller, C. R.; Prior, R. L. Influence of extrusion processing on procyanidin composition and total anthocyanin contents of blueberry pomace. *J. Food Sci.* **2009**, *74*, 52−58.
(31) Yue, X.; Xu, Z. Changes of anthocyanins, anthocyanidins, and antioxidant activity in bilberry extract during dry heating. *J. Food Sci.* **2008**, *73*, 494−499.
(32) Mulinacci, N.; Ieri, F.; Giaccherini, C.; Innocenti, M.; Andrenelli, L.; Canova, G.; Saracchi, M.; Casiraghi, M. C. Effect of cooking on the anthocyanins, phenolic acids, glycoalkaloids, and resistant starch content in two pigmented cultivars of *Solanum tuberosum* L. *J. Agric. Food Chem.* **2008**, *56*, 11830−11837.
(33) Sadilova, E.; Carle, R.; Stintzing, F. C. Thermal degradation of anthocyanins and its impact on color and in vitro antioxidant capacity. *Mol. Nutr. Food Res.* **2007**, *51*, 1461−1471.
(34) Hamauzu, Y.; Kume, C.; Yasui, H.; Fujita, T. Reddish coloration of Chinese quince (*Pseudocydonia sinensis*) procyanidins during heat treatment and effect on antioxidant and antiinfluenza viral activities. *J. Agric. Food Chem.* **2007**, *55*, 1221−1226.
(35) Hong, Y.-J.; Barrett, D. M.; Mitchell, A. E. Liquid chromatography/mass spectrometry investigation of the impact of thermal processing and storage on peach procyanidins. *J. Agric. Food Chem.* **2004**, *52*, 2366−2371.
(36) Dueñas, M.; Fulcrand, H.; Cheynier, V. Formation of anthocyanin−flavanol adducts in model solutions. *Anal. Chim. Acta* **2006**, *563*, 15−25.
(37) Osman, A. M.; Wong, K. K. Y.; Fernyhough, A. The laccase/ABTS system oxidizes (+)-catechin to oligomeric products. *Enzyme Microb. Technol.* **2007**, *40*, 1272−1279.
(38) Sun, W.; Miller, J. M. Tandem mass spectrometry of the B-type procyanidins in wine and B-type dehydrodicatechins in an autoxidation mixture of (+)-catechin and (−)-epicatechin. *J. Mass Spectrom.* **2003**, *38*, 438−446.
(39) Guyot, S.; Marnet, N.; Laraba, D.; Sanoner, P.; Drilleau, J. F. Reversed-phase HPLC following thiolysis for quantitative estimation and characterization of the four main classes of phenolic compounds in different tissue zones of a french cider apple variety (*Malus domestica* var. Kermerrien). *J. Agric. Food Chem.* **1998**, *46*, 1698−1705.
(40) Guyot, S.; Marnet, N.; Sanoner, P.; Drilleau, J. F. Variability of the polyphenolic composition of cider apple (*Malus domestica*) fruits and juices. *J. Agric. Food Chem.* **2003**, *51*, 6240−6247.
(41) Contreras-Domínguez, M.; Guyot, S.; Marnet, N.; Le Petit, J.; Perraud-Gaime, I.; Roussos, S.; Augur, C. Degradation of procyanidins by *Aspergillus fumigatus*: identification of a novel aromatic ring cleavage product. *Biochimie* **2006**, *88*, 1899−1908.
(42) Poupard, P. Oxydation des procyanidines en solution modèle jus de pomme: caractérisation structurale des produits et études des propriétés tannantes. Thesis, Université de Rennes 1, France, 2008.
(43) Totlani, V. M.; Peterson, D. G. Epicatechin carbonyl-trapping reactions in aqueous Maillard systems: identification and structural elucidation. *J. Agric. Food Chem.* **2006**, *54*, 7311−7318.
(44) Di Mattia, C.; Martuscelli, M.; Sacchetti, G.; Scheirlinck, I.; Beheydt, B.; Mastrocola, D.; Pittia, P. Effect of fermentation and drying on procyanidins, antiradical activity and reducing properties of cocoa beans. *Food Bioprocess Technol.* **2013**, *6*, 3420−3432.
(45) Afoakwa, E. O.; Quao, J.; Takrama, F. S.; Budu, A. S.; Saalia, F. K. Changes in total polyphenols, *o*-diphenols and anthocyanin concentrations during fermentation of pulp pre-conditioned cocoa (*Theobroma cacao*) beans. *Int. Food Res. J.* **2012**, *19*, 1071−1077.
(46) Kothe, L.; Zimmermann, B. F.; Galensa, R. Temperature influences epimerization and composition of flavanol monomers, dimers and trimers during cocoa bean roasting. *Food Chem.* **2013**, *141*, 3656−3663.
(47) Miller, K. B.; Hurst, W. J.; Payne, M. J.; Stuart, D. A.; Apgar, J.; Sweigart, D. S.; Ou, B. Impact of alkalization on the antioxidant and flavanol content of commercial cocoa powders. *J. Agric. Food Chem.* **2008**, *56*, 8527−8533.
(48) Beheydt, B.; Ouwerx, C.; Collin, S.; Deledicque, C.; Nguyen, F. Method to increase the antioxidant activity of chocolate. PCT/EP2007/058533, 2007.
(49) Collin, S.; Callemien, D.; Nizet, S. Extraction et analyse des polyphénols. In *Polyphénols et Procédés − Transformation des Polyphénols au Travers des Procédés Appliqués à l'agro-alimentaire*; Collin, S., Crouzet, J., Eds.;Tec & Doc Lavoisier: Paris, France, 2011.

antioxidant capacity of methanolic-water okara extracts was examined.[16] It is clear that many food items have insoluble components that cannot be solubilized without altering their molecular nature by chemical or enzymatic treatments.[25,26] However, the insoluble components are not necessarily chemically inert. The contribution of insoluble matter to total antioxidant capacity is especially high for cereal-based and dietary-fiber-rich foods.[27] So far, the total antioxidant capacity of both soluble and insoluble components of okara has not been reported.

The mineral content in okara is relatively well researched. Okara contains macro- and microelements that increase its nutritional value.[1,3,28,29] Mateos-Aparicio et al.[28] emphasize that within the group of macroelements potassium is the main mineral, whereas iron is the predominant microelement. In the literature there are no data on the contents of Cd, Co, Cr, and Pb in okara, although the amounts of these microelements in foods are strictly limited.[30]

Lipoxygenase (Lox) is an important bioactive protein in soybean. This enzyme catalyzes the addition of molecular oxygen to polyunsaturated molecules containing a *cis*,*cis*-1,4-pentadiene structure to pentadienyl and further results in a pentadienyl radical intermediate, which could interact with other lipids to form many other derivatives such as aldehydes and ketones.[11] Because of this activity of Lox, sensory characteristics of soy foods are significantly affected. Lox produces off-flavors in soybeans by hydroperoxidation of fatty acids and by interaction with protein in flours, concentrates, and isolates.[31] The undesirable flavors, characterized as beany, green, grassy, painty, astringent, and bitter, reduce acceptance of soy foods by many consumers who may prefer a bland flavor in soy products. Nowadays, efforts are made to produce soy foods with more efficient Lox inactivation because in this way the off-flavor in soy foods could be eliminated.[32]

Traditionally prepared soy milk has beany and painty flavors owing to lipid oxidation catalyzed by Lox during soaking and grinding. In Western societies, this flavor is unacceptable for most consumers. A steam infusion cooking process, known as hydrothermal cooking (HTC), was developed to produce soy milk continuously from ground full-fat soybeans. During HTC processing the temperature is higher and the processing time shorter than for conventional methods. HTC-processed soy milk had less beany flavor because of the much shorter time for Lox activity and because steam flashing stripped volatiles. The process also increased recoveries of dry matter and protein in the soy milk from 60 and 70% for traditional soy milk to 87 and 90%, respectively.[33] Characteristics with advantages over conventionally processed soy milk have been demonstrated by physical and chemical analyses of hydrothermally cooked soy milk.[33] Hydrothermal cooking results in an acceptable decrease in activities of trypsin inhibitors[7] as well as in levels of lysinoalanine and browning products. However, previous papers have not documented the nutritional performance in mineral element content of hydrothermally processed okara. Also, total antioxidant capacity arising from both soluble and insoluble matters of okara has not been studied.

Therefore, the aim of this study was to assess the influence of a pilot plant method that uses high-pressure hydrothermal conditions on mineral composition and antioxidative capacity as well as lipoxygenase activity in okara produced from different soybean genotypes. The results obtained in this study would complement our previous work on bioactive proteins and nutritional properties of okara produced by this proccess.[2,7]

## MATERIALS AND METHODS

**Materials.** For okara preparation six commercial soybean genotypes grown in field conditions were used: ZPS-015 (0 maturity group), Krajina (00 maturity group), Novosađanka and Balkan (I maturity group), and Nena and Lana (II maturity group). Three genotypes (Lana, Nena, and ZPS-015) were selected by the Maize Research Institute Zemun Polje (Belgrade, Serbia) and the others (Novosadjanka, Krajina, and Balkan) by the Institute of Field and Vegetable Crops (Novi Sad, Serbia). All of the genotypes were of food grade and were characterized by high protein content in grain.

**Okara Processing.** Okara was made on the pilot plant scale using the production method that includes HTC[34] for soy milk preparation, as modified by Stanojevic et al.[35] Briefly, soybeans were soaked for 14 h in water at 5−7 °C. Soaked beans were ground and cooked by steam injection system at 1.8 bar/110 °C/8 min (SoyaCow VS 30/40, model SM-30, Russia). Thereafter, the slurry was filtered to separate soy milk from okara.

**Sodium Dodecyl Sulfate−Polyacrylamide Gel Electrophoresis (SDS-PAGE).** The soybean powder and defatted raw okara were prepared for SDS-PAGE analyses according to the method of Stanojevic et al.[7] Briefly, the soybean powder and raw okara were defatted using hexane. Thereafter, proteins were extracted for 120 min at room temperature with 0.03 M Tris-HCl buffer, pH 8.00, which contained 0.01 M $\beta$-mercaptoethanol. For defatted soy flour, the sample to buffer ratio was 1:20; for okara, the sample to buffer ratio was 1:10. The mixture was centrifuged at 7558*g* for 15 min at room temperature. The protein extracts were diluted with sample buffer (pH 6.80) to a concentration of 2 mg/mL, then heated at 90 °C for 5 min, and cooled to room temperature.

Dissociating electrophoresis for all samples was performed according to the Fling and Gregerson[36] procedure, as modified by Stanojevic et al.,[2,7] using 5% (w/v) (pH 6.80) stacking and 12.5% (w/v) separating gels (pH 8.85). Briefly, 25 $\mu$L of sample containing 0.05 mg of protein was loaded onto each well, and then the gels were run at 80 mA per gel for 6 h in a buffer solution (pH 8.30). The gels were fixed for 50 min, stained with 0.23% (w/v) Coomassie brilliant blue R-250, and destained with 8% (v/v) acetic acid and 18% (v/v) ethanol. Molecular weight markers that were used were phosphorylase B (94 kDa), bovine albumin (67 kDa), ovoalbumin (43 kDa), carbonic anhydrase (30 kDa), trypsin inhibitor (20.1 kDa), and $\alpha$-lactalbumin (14.4 kDa) (Pharmacia, Uppsala, Sweden).

**Densitometric Analysis.** All gels were destained, then scanned, and subsequently analyzed by SigmaGel software version 1.1 (Jandel Scientific, San Rafael, CA, USA). Quantitative analysis of each identified polypeptide was calculated as the percentage of the respective area with respect to total area of the densitogram.

**Lipoxygenase Activity.** The Lox (EC 1.13.11.12) was extracted from fresh okara with 5 volumes (w/v) of 0.2 M sodium phosphate buffer (pH 6.5) at 4 °C for 120 min. Supernatant obtained by centrifugation at 10000*g* for 10 min was used to measure the activity of Lox I. The reaction was carried out at 25 °C in a quartz cuvette with a 1.0 cm light path. The assay mixture contained 0.060 mL of 10 mM linoleate substrate and 0.1 mL of the extract in 2.440 mL of 0.2 M borate buffer, pH 9.0. The initial rate of the absorbance changes at 234 nm ($\varepsilon = 2.5 \times 10^4$ $M^{-1}$ $cm^{-1}$) was recorded, and the activity of Lox I was expressed in micromoles of conjugated diene formed per minute and per gram of dry matter.[37]

**Total Antioxidant Capacity.** The antioxidant capacity was measured by QUENCHER method described by Serpen et al.[27] using 7 mM aqueous solution of 2,2-azinobis(3-ethyl-benothiazoline-6-sulfonic acid) (ABTS). Radical cation was generated by reacting ABTS stock solution with 2.45 mM potassium persulfate (final concentration), and the mixture was kept in the dark at room temperature for 12−16 h before use. The working solution of $ABTS^{\bullet+}$ was obtained by diluting the stock solution with water/ethanol (50:50, v/v). Finely ground sample (10 mg) was mixed with 20 mL of $ABTS^{\bullet+}$ working solution, and the mixture was vigorously shaken for 25 min. After centrifugation at 10000*g* for 5 min, the absorbance was recorded at 734 nm. The total antioxidant capacity was expressed as Trolox

equivalent antioxidant capacity (TEAC) in millimoles of Trolox per kilogram of dry matter.

**Mineral Content.** The mineral content in fresh okara was analyzed by atomic absorption spectroscopy (AAS) (Varian Spectra AA 220). The microelement Fe, Mn, Cu, Zn, Cr, Pb, Co, and Cd contents in okara were analyzed after the destruction in concentrated $HNO_3$ and $HClO_4$ with the addition of 33% $H_2O_2$ by wet ashing.[38] Contents of Ca and Mg in okara were detected after the destruction with concentrated acids $HNO_3$ and HCl by dry ashing.[39] Contents of P, K, and Na in okara were determined after the destruction with concentrated acids $H_2SO_4$ and $HClO_4$ by dry ashing. Phosphorus was determined by the colorimetric method, whereas K and Na were determined by the flame-photometry method.[39]

**Other Analyses.** Total nitrogen content in okara was determined by using the micro-Kjeldahl method,[40] and protein content was calculated (N × 6.25). Ash content was calculated from the weight of okara after burning at 550 °C for 2 h in a muffle furnace.[41] Okara moisture and volatiles were determined according to standard AACC procedures.[42] The pH of a 1:10 okara water suspension (w/v) was measured using a Consort-C931 pH meter (Belgium) with automatic temperature compensation.

**Statistical Analysis.** Data were assessed by analysis of variance (ANOVA) using the Statistical software version 7.0 (StatSoft Co., Tulsa, OK, USA). The Tukey multiple-range test was used to separate means, and significance was accepted at $p < 0.05$. Regression analyses were also carried out. The different parameters were correlated with each other by Pearson two-tailed significance correlation at the $p < 0.05$ level. The experiments were performed in triplicate.

## RESULTS AND DISCUSSION

**Lipoxygenase Content and Activity.** The sensory quality of soy foods is limited by the soybean's content of Lox. By SDS-PAGE analysis of investigated soybean genotypes and okara extractable protein composition, we registered the presence of Lox (Figures 1 and 2); the first significant single broad band

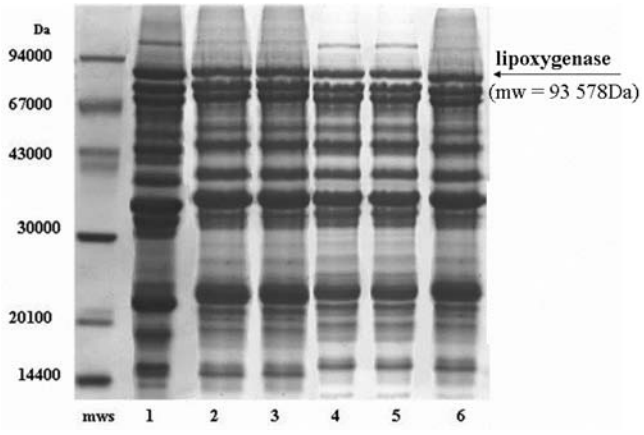


**Figure 1.** SDS-PAGE analysis of protein composition in soybeans from investigated genotypes. Lanes: mws, molecular weight standards; 1, Lana; 2, Krajina; 3, Novosadjanka; 4, Balkan; 5, Nena; 6, ZPS-015.

corresponds to lipoxygenase. Soybeans have three Lox isoforms (Lox-I, Lox-II, and Lox-III), which have homologous sequences and MW of about 96 kDa.[43,44] According to the results of densitometric analysis (Table 1) all genotypes had very similar contents of Lox, which ranged from 4.32 to 5.62% of total extractable proteins. Nowadays, lipoxygenase-free soy genotypes have been developed. Soy milk made from lipoxygenase-free soybeans has a less beany aroma, a less beany flavor, and less astringency and was rated darker and more yellow than that made from soybeans synthesizing lipoxygenase.[12] In addition to

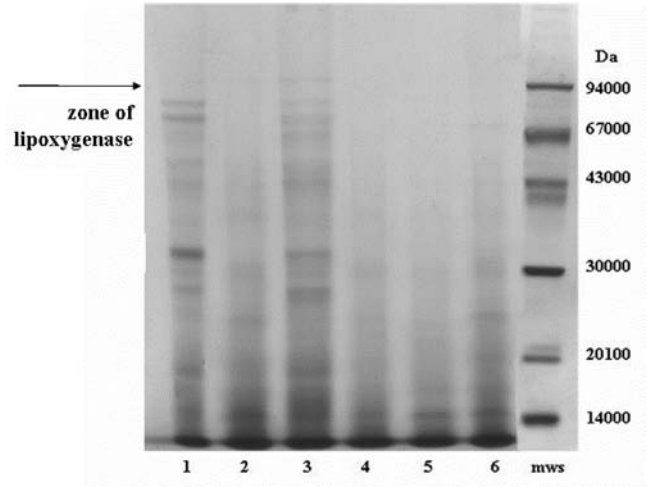


**Figure 2.** SDS-PAGE analysis of protein composition in okara from investigated genotypes. Lanes: mws, molecular weight standards; 1, Nena; 2, Krajina; 3, Novosadjanka; 4, Balkan; 5, Lana; 6, ZPS-015.

**Table 1. Lipoxygenase Content of Soybeans and Okara from Investigated Genotypes**[a]

| | % extractable protein | |
|---|---|---|
| genotype | soybean | okara |
| Nena | 4.95 ± 0.04 c | 0.21 ± 0.001 c |
| Krajina | 5.42 ± 0.03 b | 0.31 ± 0.003 b |
| Novosadjanka | 5.11 ± 0.02 bc | 0.54 ± 0.002 a |
| Balkan | 4.32 ± 0.01 d | 0.03 ± 0.000 d |
| ZPS-015 | 5.51 ± 0.03 ab | 0.05 ± 0.000 d |
| Lana | 5.62 ± 0.04 a | 0.19 ± 0.002 c |

[a]Means in the same column with different letters are significantly different ($p < 0.05$).

the development of lipoxygenase-free soy genotypes, there is permanent striving to reduce the content or activity of this enzyme by technological process.[32] Our results showed that thermal/pressure treatment applied to soybeans was sufficient to get such a result in okara. When compared to soybeans, the applied treatment significantly reduced Lox content in okara (0.03−0.54%; Table 1). This result was expected because the denaturation temperature of Lox is at 69−74 °C,[45] and the applied temperature in the production of okara was 110 °C. We did not register a significant correlation between the content of Lox in soybean and in okara ($r = 0.21$; Table 2). This indicates that the content of this enzyme in okara significantly depended on the technological process but not on soybean genotype.

On the basis of this very low Lox content in okara, a very low activity of this enzyme was expected. Our results confirmed that applied thermal/pressure treatment was sufficient to inactivate Lox activity in okara. Because the most stable isomer is Lox-I, we registered only its activity. Because of its stability, most kinetic, structural, and spectroscopic studies have involved this isoform.[43] Okara Lox-I activity was registered in traces (0.004−0.007 $\mu$mol $g^{-1}$ $min^{-1}$; Table 3). The okara's pH value might contribute to such low Lox-I activity. Okara pH was from 6.88 to 7.04 (Table 4), whereas the value for the optimum activity of Lox-I is about 9.0.[44] These results suggested that the applied thermal/pressure treatment produced okara with very low Lox content and activity. Therefore, when used for the preparation of food, this okara would not give undesirable sensory effects.


dx.doi.org/10.1021/jf501800s | J. Agric. Food Chem. 2014, 62, 9017−9023

**Table 2. Correlation Coefficients**

| relationship | $r$ |
|---|---|
| soybean Lox[a] content/okara Lox content | 0.21 |
| okara Lox content/okara Lox activity | 0.99[b] |
| okara ash content/okara K content | 0.11 |
| okara ash content/okara P content | −0.25 |
| okara ash content/okara Ca content | −0.50 |
| okara ash content/okara Mg content | −0.30 |
| okara ash content/okara Na content | −0.40 |
| okara ash content/okara N content | 0.06 |
| okara ash content/okara Fe content | −0.54 |
| okara ash content/okara Cu content | −0.37 |
| okara ash content/okara Mn content | −0.30 |
| okara ash content/okara Zn content | 0.15 |
| okara ash content/okara Cr content | 0.73 |
| okara ash content/okara Pb content | 0.14 |

[a]Lox, lipoxygenase; [b]Significant at $p < 0.05$.

Literature data show that the correlation between Lox content in soybeans and respective enzymatic activity was positive but not significant ($r = 0.57$, $p < 0.05$).[11] On the contrary, our results showed very strong correlation ($r = 0.99$; Table 2) between okara Lox content and activity. This indicates that the most stable isoform of this enzyme survived the heat/pressure treatment that resulted in the proportional relationship between Lox content and activity.

**Total Antioxidant Capacity.** To examine the influence of the applied heat/pressure treatment on okara total antioxidant capacity arising from both soluble and solid okara particles, we implemented the direct procedure developed by Serpen et al.[27] to include the activity arising from insoluble matter. According to our results (Table 3), very high values of okara antioxidant capacity were registered. The lowest antioxidant capacity was found for genotype Lana (19.06 mmol Trolox $kg^{-1}$ dm) and the highest for genotype Novosadjanka (29.36 mmol Trolox $kg^{-1}$ dm). Other genotypes had very similar antioxidant capacities ranging from 23.31 to 29.31 mmol Trolox $kg^{-1}$ dm. When compared to raw soybeans. the antioxidant capacity of okara was decreased by around 34−58%. When compared with the published results for different foods, our values are higher than for oat flour or breakfast cereals.[27] Our results are similar to the antioxidant capacity of pumpkin or beet and much higher than those of broccoli, tomato, onion, or carrot.[46] Registered okara antioxidant capacity is more than twice higher than the antioxidant capacity of green beans, a plant belonging to the same family of legumes as soybeans.[46] Registered antioxidant activity certainly contributed to the functional value of fresh okara.

**Content of Mineral Elements.** The okara ash content of only 3.50−4.25% suggested that during production minerals of the soybeans mainly found their way into the soymilk, Table 5. Osthoff et al.[47] have come to the same conclusion. This result is in agreement with literature data.[1,28,29,47] Total ash content in okara was not significantly correlated with the content of certain mineral elements Table 2. Smith and Circle[48] pointed out direct dependence of ash and phosphorus contents in soybeans, but this was not the case with the investigated okara ($r = -0.25$; $p = 0.05$; Table 2). We have registered a slightly higher correlation coefficient between the okara ash content and calcium, iron, and chrome contents, but they were not in significant dependence (Table 2). This result of correlation analysis showed that the content of total minerals could not indicate a trend change in the content of certain mineral elements. Smith and Circle[48] noted that the mineral compositions of soybeans vary depending on the origin of the crop or the specific cultivar. Our results have shown that there were differences in the content of certain mineral components of the okara from different genotypes. However, these differences were not for all mineral elements statistically significant (e.g., P, Na). These results of statistical analysis suggest that the technological process of okara production has a much greater influence on mineral composition of okara than soybean genotype.

With the exception of nitrogen, within the group of macroelements, potassium was the main mineral in the okara (1.04−1.21 g/100 g dm), approximately 2 times higher than the amount of phosphorus (0.45−0.50 g/100 g dm; Table 5). Calcium also appeared in significant amounts (0.26−0.39 g/100 g dm). Okara contains significant amount of dietary fiber (54.3%).[28] Van der Rietet et al.[29] indicated a possible association of calcium, potassium, phosphorus, and sodium with the fiber. Because of this, it is possible that these elements are bound for fiber and remain in okara, thus comprising its nutritional value. In addition, nondigestible polysaccharides can positively affect the absorption of calcium.[50] Jiménez-Escrig et al.[20] evaluated the metabolism of calcium, magnesium, and zinc in rats fed a diet supplemented with okara, and a significant enhancement on the absorption of calcium was found. In addition, literature data indicate that okara contains very small amounts of phytic acid (0.5−1.2%).[29] Van der Riet et al.[29] note that phytic acid largely remains in tofu. Phytic acid is nutritionally significant because of its potential to chelate essential dietary minerals such as calcium and zinc.[49] Due to the low phytic acid content, and hence the lower chelating capacity, calcium remained in available form.

Iron is the predominant microelement ranging from 5.45 to 10.95 mg/100 g dm, whereas the manganese content is very similar in all samples (1.43−1.85 mg/100 g dm; Table 5).

**Table 3. Lipoxygenase (Lox-I) Activities and Antioxidant Capacity[a]**

| | lipoxygenase activity ($\mu$mol $g^{-1}$ $min^{-1}$) | antioxidant capacity (mmol Trolox equiv $kg^{-1}$ dm) | |
|---|---|---|---|
| genotype | okara | beans | okara |
| Nena | 0.005 ± 0.00 a | 63.47 ± 2.17 a | 26.57 ± 0.26 b |
| Krajina | 0.006 ± 0.00 a | 38.99 ± 1.24 e | 23.31 ± 1.07 c |
| Novosadjanka | 0.007 ± 0.00 a | 58.42 ± 2.11 b | 29.36 ± 1.22 a |
| Balkan | 0.004 ± 0.00 a | 42.19 ± 0.56 d | 27.84 ± 1.32 ab |
| ZPS-015 | 0.004 ± 0.00 a | 36.92 ± 0.79 d | 19.06 ± 0.24 d |
| Lana | 0.005 ± 0.00 a | 49.05 ± 2.09 c | 29.31 ± 0.71 a |

[a]Values are given on a moisture-free, full-fat basis. Means in the same column with different letters are significantly different ($p < 0.05$).

**Table 4. Some Characteristics of Raw Okara (Percent)[a]**

| genotype | total proteins[bb] | ash[b] | moisture | pH |
|---|---|---|---|---|
| Nena | 30.89 ± 1.37 a | 3.50 ± 0.00 b | 79.19 ± 1.82 | 7.04 ± 0.04 |
| Krajina | 32.06 ± 0.03 a | 3.50 ± 0.08 b | 83.63 ± 1.15 | 6.93 ± 0.02 |
| Novosadjanka | 32.06 ± 0.42 a | 4.25 ± 0.29 a | 75.00 ± 1.10 | 6.93 ± 0.03 |
| Balkan | 27.81 ± 0.11 b | 4.00 ± 0.00 ab | 79.76 ± 1.85 | 6.96 ± 0.05 |
| ZPS-015 | 28.12 ± 0.61 b | 3.50 ± 0.00 a | 73.68 ± 1.18 | 7.01 ± 0.06 |
| Lana | 27.44 ± 1.57 b | 3.75 ± 0.09 ab | 76.86 ± 1.85 | 6.88 ± 0.07 |

[a]Values are given on a moisture-free, full-fat basis. [b]Means in the same column with different letters are significantly different ($p < 0.05$).

**Table 5. Content of Mineral Elements in Raw Okara[a]**

| | Nena | Krajina | Novosadjanka | Balkan | ZPS-015 | Lana |
|---|---|---|---|---|---|---|
| | | | **Macroelements (g/100 g dry matter)[b]** | | | |
| K | 1.04 ± 0.01 c | 1.08 ± 0.03 bc | 1.04 ± 0.03 c | 1.21 ± 0.07 a | 1.01 ± 0.04 c | 1.15 ± 0.04 ab |
| P | 0.46 ± 0.00 a | 0.50 ± 0.02 a | 0.50 ± 0.01 a | 0.46 ± 0.01 a | 0.48 ± 0.01 a | 0.45 ± 0.02 a |
| Ca | 0.28 ± 0.00 c | 0.32 ± 0.01 b | 0.26 ± 0.01 c | 0.30 ± 0.01 cb | 0.39 ± 0.01 a | 0.33 ± 0.01 b |
| Mg | 0.11 ± 0.00 b | 0.14 ± 0.00 a | 0.13 ± 0.01 ab | 0.11 ± 0.00 b | 0.15 ± 0.00 a | 0.13 ± 0.00 ab |
| Na | 0.01 ± 0.00 a | 0.02 ± 0.00 a | 0.01 ± 0.00 a | 0.01 ± 0.00 a | 0.02 ± 0.00 a | 0.02 ± 0.00 a |
| N | 4.94 ± 0.02 a | 5.13 ± 0.05a | 5.13 ± 0.06 a | 4.45 ± 0.02 b | 4.50 ± 0.09 b | 4.39 ± 0.05 b |
| | | | **Microelements (mg/100g dry matter)[b]** | | | |
| Fe | 7.05 ± 0.08 c | 10.95 ± 0.10 a | 5.45 ± 0.06 d | 7.80 ± 0.05 bc | 7.20 ± 0.02 c | 9.03 ± 0.04 b |
| Cu | 1.70 ± 0.08 a | 0.78 ± 0.05 d | 0.70 ± 0.00 d | 1.10 ± 0.00 b | 0.90 ± 0.08 c | 0.78 ± 0.05 d |
| Mn | 1.58 ± 0.05 b | 1.50 ± 0.08 b | 1.43 ± 0.05 b | 1.45 ± 0.01 b | 1.52 ± 0.05 b | 1.85 ± 0.01 a |
| Zn | 5.53 ± 0.08 b | 2.15 ± 0.08 c | 1.93 ± 0.05 c | 7.97 ± 0.01 a | 1.67 ± 0.05 c | 1.50 ± 0.08 c |
| | | | **Microelements (mg/kg dry matter)[b]** | | | |
| Cd | nd[c] | nd | nd | nd | nd | nd |
| Co | nd | nd | nd | nd | nd | nd |
| Cr | 0.43 ± 0.02 e | 1.13 ± 0.10 b | 2.04 ± 0.07 a | 0.91 ± 0.04 c | 0.62 ± 0.05 d | 0.46 ± 0.07 e |
| Pb | 3.04 ± 0.10 b | 2.78 ± 0.27 b | 3.19 ± 0.41 ab | 3.47 ± 0.30 a | 3.07 ± 0.26 b | 3.04 ± 0.11 b |

[a]Values are given on a moisture-free, full-fat basis. [b]Means in the same row with different letters are significantly different ($p < 0.05$). [c]nd, not detected.

Legumes are generally rich in iron; nevertheless, the bioavailability of this microelement is low, and therefore its value as a source of iron is diminished. The content of zinc significantly depended on the soybean genotype (1.50−7.97 mg/100 g dm). Zinc bioavailability is relatively good in legumes, approximately 25% from the zinc intake;[50] however, there is no evidence of an increase of zinc absorption in rats fed diets supplemented with okara during 4 weeks.[20] Copper is in low amount in all of the samples (0.70−1.70 mg/100 g dm; Table 5). Okara micro- and macroelements present similar values in this study as those given by Van der Riet et al.[29]

Because the plant material may contain harmful substances, we examined the contents of Cd, Co, Cr, and Pb in okara produced from the investigated genotypes using hydrothermal processes. The content of these microelements in raw okara is presented in Table 5. Our results have shown that chromium (0.43−2.04 mg/kg dm) and lead (2.78−3.47 mg/kg dm) were both registered in okara (Table 5). In the literature there are no data on the content of these microelements in okara, but our results indicated their presence in very low amounts, and therefore their content should be controlled in food and feed products. According to the FAO/WHO Expert Committee on food additives,[30] acceptable daily intakes (ADI) of these elements are for Cr, 200 μg/daily, and for Pb, 214 μg/daily. Okara is considered to be a functional food, a rich natural source of nutritional ingredients. Okara is mainly incorporated into baked goods to enhance their dietary fiber and protein contents. New bakery products such as cakes and cookies fortified with high amounts of okara have been developed. The best scores for sensory characteristics were given to cookies prepared with the addition of 60%[9] and 70%[8] okara. If we calculate the daily intake of both of these harmful elements for the consumption of 100 g of cakes, our results suggest that the lead content can be problematic in biscuits containing 70% okara, because the result was on the border or slightly increased than the allowable value for Pb (Table 6). These results suggest that the content of potentially harmful microelements should be controlled when okara is incorporated in foods and feeds.

**Table 6. Daily Intake (Micrograms per Day) of Microelements in the Consumption of 100 g of Biscuits with Okara Different Content**

| | with 60% okara | | with 70% okara | |
|---|---|---|---|---|
| genotype | Cr | Pb | Cr | Pb |
| Nena | 25.50 | 212.80 | 29.70 | 259.53 |
| Krajina | 76.55 | 166.95 | 79.10 | 194.78 |
| Novosadjanka | 122.25 | 191.55 | 142.63 | 223.47 |
| Balkan | 54.75 | 208.05 | 63.87 | 242.72 |
| ZPS-015 | 37.05 | 184.05 | 43.23 | 214.72 |
| Lana | 27.30 | 182.55 | 31.85 | 212.97 |

The investigated samples of okara bear no health risk regarding the contents of Cd and Co as these elements were below the limit of detection. Accumulation and translocation of Cd and Co as well as other toxic metals by plants depends not only of their content in soil but also on soil characteristics such as pH and its granulometric composition as well as organic


dx.doi.org/10.1021/jf501800s | J. Agric. Food Chem. 2014, 62, 9017−9023

matter content, etc., which all influence the availability of these metals to plants.[51] The fact that Cd and Co were not detected points out favorable conditions that were present in the soil where soybeans were grown.

In summary, the investigated soybean genotypes all produced okara containing very similar concentrations of Lox with Lox-I activity only in traces. Therefore, this okara would not produce undesirable effects on the sensory characteristics of foods. No significant correlation between the content of Lox in soybean and in okara was registered, thus indicating that the content of this enzyme in okara depended more on the technological process than on soybean genotypes. There was very strong correlation between okara Lox content and activity. Registered total antioxidant activity (soluble and insoluble components) certainly contributed to the nutritional value of raw okara. The minerals of the soybeans mainly found their way into the soy milk. The value of total mineral content could not indicate a trend change in the content of particular mineral elements. Potassium was the main macroelement in okara, approximately 2 times higher than phosphorus. Calcium also appeared in significant amounts. Iron was the predominant microelement, whereas the manganese contents were very similar in all samples. The content of zinc significantly depended on the soybean genotype. As the presence of some potentially harmful microelements was registered, their contents should be controlled in products intended for consumption. Finally, we can summarize that HTC treatment opens the way to a more effective use of okara as a plant source of nutritionally valuable minerals and antioxidants that could be used as feed or in food fortification.

## AUTHOR INFORMATION

### Corresponding Author

*(S.P.S.) Phone: +381 11 2615 315, ext. 358. Fax: +381 11 2199 711. E-mail: sladjas@agrif.bg.ac.rs.

### Funding

We are grateful to the Serbian Ministry of Education, Science and Technological Development for financial support (Project TR 31022) and EU FP7 Project Grant Agreement 316004 (REGPOT-AREA).

### Notes

The authors declare no competing financial interest.

## ACKNOWLEDGMENTS

We are indebted to the Maize Research Institute, Zemun Polje, Serbia, and the Institute of Field and Vegetable Crops, Novi Sad, Serbia, for providing soybean genotypes.

## REFERENCES

(1) O'Toole, D. K. Characteristics and use of okara, the soybean residue from soy milk production: a review. *J. Agric. Food Chem.* **1999**, *47*, 363−371.

(2) Stanojevic, S. P.; Barac, M. B.; Pesic, M. B.; Vucelic-Radovic, B. V. Composition of proteins in okara as a byproduct in hydrothermal processing of soymilk. *J. Agric. Food Chem.* **2012**, *60*, 9221−9228.

(3) Khare, S. K.; Jha, K.; Gandhi, A. P. Citric acid production from okara (soy-residue) by solid-state fermentation. *Bioresour. Technol.* **1995**, *54*, 323−325.

(4) Vishwanathan, H. K.; Singh, V.; Subramanian, R. Influence of particle size on protein extractability from soybean and okara. *J. Food Eng.* **2011**, *102*, 240−246.

(5) Peñalvo, L. J.; Castilho, C. M.; Silveira, M. I. N.; Matallana, M. C.; Torija, M. E. Fatty acid profile of traditional soymilk. *Eur. Food Res. Technol.* **2004**, *219*, 251−253.

(6) Waliszewski, K. N.; Pardio, V.; Carreon, E. Physicochemical and sensory properties of corn tortillas made from nixtamalized corn flour fortified with spent soymilk residue (okara). *J. Food Sci.* **2002**, *67* (8), 3149−3197.

(7) Stanojevic, S.; Barac, M.; Pesic, M.; Jankovic, V.; Vucelic-Radovic, B. Bioactive proteins and energy value of okara as a byproduct in hydrothermal processing of soymilk. *J. Agric. Food Chem.* **2013**, *61*, 9210−9219.

(8) Xie, M.; Huff, H.; Hsieh, F.; Mustapha, A. Puffing of okara/rice blends using a rice cake machine. *J. Food Sci.* **2008**, *73* (8), 341−348.

(9) Sinha, L. K.; Khare, S. K.; Jha, K. Studies on okara fortified biscuits: preparation and nutritional evaluation. *J. Dairying, Foods Home Sci.* **1995**, *14*, 91−94.

(10) Barać, M.; Stanojević, S.; Pesic, M. Biologically active components of soy bean − a review. *Acta Periodica Technol.* **2005**, *36*, 155−169.

(11) Žilić, M. S.; Barać, B. M.; Pešić, B. M.; Mladenović-Drinić, D. S.; Ignjatović-Micić, D. D.; Srebrić, M. Characterization of proteins from kernel of different soybean varieties. *J. Sci. Food Agric.* **2010**, *91*, 60−67.

(12) Torres-Penaranda, V. A.; Reitmeier, A. C.; Wilson, A. L.; Fehr, R. W.; Narvel, M. J. Sensory characteristics of soymilk and tofu made from lipoxygenase-free and normal soybeans. *J. Food Sci.* **1998**, *63* (6), 1084−1087.

(13) Wolf, W. J. Physical and chemical properties of soybean proteins. *J. Am. Oil Chem. Soc.* **1977**, *54*, 112−117.

(14) Finkel, T.; Holbrook, N. J. Oxidants, oxidative stress and the biology of ageing (review). *Nature* **2000**, *408*, 239−247.

(15) Moure, A.; Cruz, J. M.; Franco, D.; Dominguez, J. M.; Sineiro, J.; Dominiguez, H.; Nunez, M. J.; Parajo, J. C. Natural antioxidants from residual sources (review). *Food Chem.* **2001**, *72*, 145−171.

(16) Amin, I.; Mukhrizah, O. Antioxidant capacity of methanolic and water extracts prepared from food-processing by-products. *J. Sci. Food Agric.* **2006**, *86* (5), 778−784.

(17) Yokomizo, A.; Takenaka, Y.; Takenaka, T. Antioxidative activity of peptides prepared from okara protein. *Food Sci. Technol. Res.* **2002**, *8* (4), 357−359.

(18) Mateos-Aparicio, I.; Mateos-Peinado, C.; Jiméz-Escrig, A.; Rupéz, P. Multifunctional antioxidant activity of polysaccharide fractions from the soybean byproduct okara. *Carbohydr. Polym.* **2010**, *82*, 245−250.

(19) Jiménez-Escrig, A.; Alaiz, M.; Vioque, J.; Rupérez, P. Health-promoting activities of ultra-filtered okara protein hydrolysates released by in vitro gastrointestinal digestion: identification of active peptide from soybean lipoxygenase. *Eur. Food Res. Technol.* **2010**, *230*, 655−663.

(20) Jiménez-Escrig, A.; Tenorio, M. D.; Espinosa-Martos, I.; Rupérez, P. Health-promoting effects of a dietary fiber concentrate from the soybean byproduct okara in rats. *J. Agric. Food Chem.* **2008**, *56*, 7495−7501.

(21) Zhou, K.; Yu, L. Antioxidant properties of bran extracts from Trego wheat grown at different locations. *J. Agric. Food Chem.* **2004**, *52*, 1112−1117.

(22) Martinez-Tome, M.; Murcia, M.; Frega, N.; Ruggieri, S.; Jimenez, A. M.; Roses, F. Evaluation of antioxidant capacity of cereal brans. *J. Agric. Food Chem.* **2004**, *52*, 4690−4699.

(23) Zhu, P. Y.; Fan, F. J.; Cheng, Q.; Li, T. L. Improvement of the antioxidant activity of chinese traditional fermented okara (Meitauza) using *Bacillus subtilis* B2. *Food Control* **2008**, *19*, 654−661.

(24) Tan, S. T.; Nagendra, P. K.; Amin, I. Antioxidant capacity, phenolics and isoflavones in soybean by-products. *Food Chem.* **2010**, *123*, 583−589.

(25) Adom, K.; Sorrells, M.; Liu, R. Phytochemical profiles and antioxidant activity of wheat varieties. *J. Agric. Food Chem.* **2003**, *51*, 7825−7834.

(26) Bonoli, M.; Verardo, V.; Marconi, E.; Caboni, M. Antioxidant phenols in barley (*Hordeum vulgare* L.) flour: comparative spectrophotometric study among extraction methods of free and bound phenolic compounds. *J. Agric. Food Chem.* **2004**, *52*, 5195−5200.
(27) Serpen, A.; Gökmen, V.; Pellegrini, N.; Fogliano, V. Direct measurement of the total antioxidant capacity of cereal products. *J. Cereal Sci.* **2008**, *48*, 816−820.
(28) Mateos-Aparicio, I.; Redondo-Cuenca, A.; Villanueva-Suarez, M. J.; Zapata-Revilla, M. A.; Tenorio-Sanz, M. D. Pea pod, broad bean pod and okara, potential sources of functional compounds. *LWT−Food Sci. Technol.* **2010**, *43*, 1467−1470.
(29) Van der Riet, W. B.; Wight, A. W.; Cilliers, J.J. L.; Datel, J. M. Food chemical investigation of tofu and its byproduct okara. *Food Chem.* **1989**, *34*, 193−202.
(30) FAO/WHO Expert Committee on food additives: summary and conclusions. In *53rd Meeting*; Roma, Italy, June 1−10, 1990.
(31) Rackis, J. J.; Sessa, D. J.; Honig, D. H. Flavor problems of vegetable food proteins. *J. Am. Oil Chem. Soc.* **1979**, *56*, 262−271.
(32) Van der Ven, C.; Matser, M. A.; Master, M. A.; Van den Berg, W. R. Inactivation of soybean trypsin inhibitors and lipoxygenase by high-pressure processing. *J. Agric. Food Chem.* **2005**, *53*, 1087−1092.
(33) Johnson, L. A.; Deyoe, C. W.; Hoover, W. J. Yield and quality of soymilk processed by steam-infusion cooking. *J. Food Sci.* **1981**, *46*, 239−243.
(34) Wang, C.; Johnson, A. L.; Wilson, A. L. Calcium coagulation properties of hydrothermally processed soymilk. *J. Am. Oil Chem. Soc.* **2003**, *80* (12), 1225−1229.
(35) Stanojevic, P. S.; Barac, B. M.; Pesic, B. M.; Vucelic-Radovic, V. B. Assessment of soy genotype and processing method on quality of soybean tofu. *J. Agric. Food Chem.* **2011**, *59* (13), 7368−7376.
(36) Fling, S. P.; Gregerson, D. S. Peptide and protein molecular weight determination by electrophoresis using a high-molarity Tris-buffer system without urea. *Anal. Biochem.* **1986**, *155*, 83−88.
(37) Axelrod, B.; Cheesbrough, T. M.; Laakso, S. Lipoxygenase from soybeans. *Methods Enzymol.* **1981**, *71*, 441−451.
(38) Jones, B. J.; Case, W. V. Sampling, handling and analyzing plant tissue samples. In *Soil Testing and Plant Analysis*; Westerman, L. R., Ed.; SSSA Book Series 3; Soil Science Society of America: Madison, WI, USA, 1990; pp 404−409.
(39) Jones, B. J. Plant analysis. In *Laboratory Guide for Conducting Soil Tests and Plant Analysis*; CRC Press: London, UK, 2001; pp 203−207.
(40) Crude protein-micro Kjeldahl method (AACC method 46-13). In *Approved Methods of the AACC*, 10th ed.; AACC International: St. Paul, MN, USA, 2000; Vol. II.
(41) *Official Methods of Analysis*, 14th ed.; Association of Official Analytical Chemists: Arlington, VA, USA, 1984.
(42) Moisture and volatile matter in soy flours (AACC method 44-31). In *Approved Methods of the AACC*, 10th ed.; AACC International: St. Paul, MN, USA, 2000; Vol. II.
(43) Schenk, G.; Neidig, M.; Zhou, J.; Holman, T. R.; Solomon, E. I. Spectroscopic characterization of soybean lipoxygenase-1 mutants: the role of second coordination sphere residues in the regulation of enzyme activity. *Biochemistry* **2003**, *42*, 7294−7302.
(44) Kumar, V.; Rani, A.; Tindwani, C.; Jain, M. Lipoxygenase isozymes and trypsin inhibitor activities in soybean as influenced by growing location. *Food Chem.* **2003**, *83*, 79−83.
(45) Lopez, P.; Burgos, J. Lipoxygenase inactivation by manothermosonication: effects of sonication physical parameters, pH, KCl, sugars, glycerol, and enzyme concentration. *J. Agric. Food Chem.* **1995**, *43* (3), 620−625.
(46) Pellegrini, N.; Serafini, M.; Colombi, B.; Del Rio, D.; Salvatore, S.; Bianchi, M.; Brighenti, F. Total antioxidant capacity of plant foods, beverages and oils consumed in Italy assessed by three different in vitro assays. *J. Nutr.* **2003**, *133* (9), 2812−2819.
(47) Osthoff, G.; Hugo, A.; Van Wyk, P.; de Wit, M.; Meyer, S. Characterization of a spray-dried soymilk powder and changes observed during storage. *Food Sci. Technol. Int.* **2010**, *16* (2), 169−178.
(48) Smith, K. A.; Circle, S. J. Chemical composition of the seed. In *Soybeans: Chemistry and Technology*; Smith, K. A., Circle, S. J., Eds.; AVI Publishing: Westport, CT, USA, 1972; Vol. 1, pp 61−92.
(49) Forbeas, R. M.; Erdman, J. W.; Parker, H. M.; Kondo, H.; Ketelsen, S. M. Bioavailability of zinc in coagulated soyprotein (tofu) to rats and effect of dietary calcium at a constant phytate: zinc ratio. *J. Nutr.* **1983**, *113*, 205−210.
(50) Sandström, B.; Almgren, A.; Kivistö, B.; Cederblad, A. Effect of protein level and protein source on zinc absorption in humans. *J. Nutr.* **1989**, *119*, 48−53.
(51) Kabata-Pendias, A. *Trace Elements in Soils and Plants*, 4th ed.; CRC Press, Taylor and Francis Group: Boca Raton, FL, USA, 2011.

**Table 1. Validation Data of UPLC-MS Quantitative Method for Eight Saponins**

| | | | | precision (RSD%) ($n$ = 6) | | | | | |
|---|---|---|---|---|---|---|---|---|---|
| marker | regression eq | linearity ($\mu$g/mL) | $r^2$ | intraday | interday | repeatability | recovery rate (%) | LOD ($\mu$g/mL) | LOQ ($\mu$g/mL) |
| $R_1$ | $y$ = 132995$x$ + 4969.8 | 0.125−10 | 0.9998 | 1.99 | 1.25 | 2.25 | 98.66 (1.81)[a] | 0.005 | 0.021 |
| $Rg_1$ | $y$ = 125416$x$ − 6776.7 | 0.125−10 | 0.9998 | 1.28 | 1.99 | 1.08 | 99.10 (2.90) | 0.004 | 0.024 |
| Re | $y$ = 148540$x$ + 15054 | 0.125−10 | 0.9995 | 2.67 | 2.18 | 2.11 | 103.03 (2.22) | 0.005 | 0.017 |
| $Rb_1$ | $y$ = 64969$x$ − 4164.7 | 0.125−10 | 0.9997 | 2.31 | 2.60 | 1.72 | 99.65 (3.29) | 0.015 | 0.054 |
| $Rb_2$ | $y$ = 116356$x$ − 5883 | 0.125−10 | 0.9997 | 2.87 | 1.68 | 3.84 | 99.06 (3.43) | 0.011 | 0.029 |
| $Rb_3$ | $y$ = 134365$x$ − 851 | 0.05−4 | 0.9999 | 3.00 | 3.44 | 1.61 | 97.7 (1.26) | 0.008 | 0.025 |
| Rc | $y$ = 122449$x$ − 500.33 | 0.05−4 | 0.9999 | 2.18 | 2.21 | 2.79 | 99.62 (2.70) | 0.008 | 0.026 |
| Rd | $y$ = 152720$x$ − 6790.6 | 0.125−10 | 0.9999 | 2.41 | 1.22 | 2.97 | 101.65 (1.60) | 0.006 | 0.021 |

[a]The values in the parentheses are the RSDs of six replicated determinations of recovery rate.

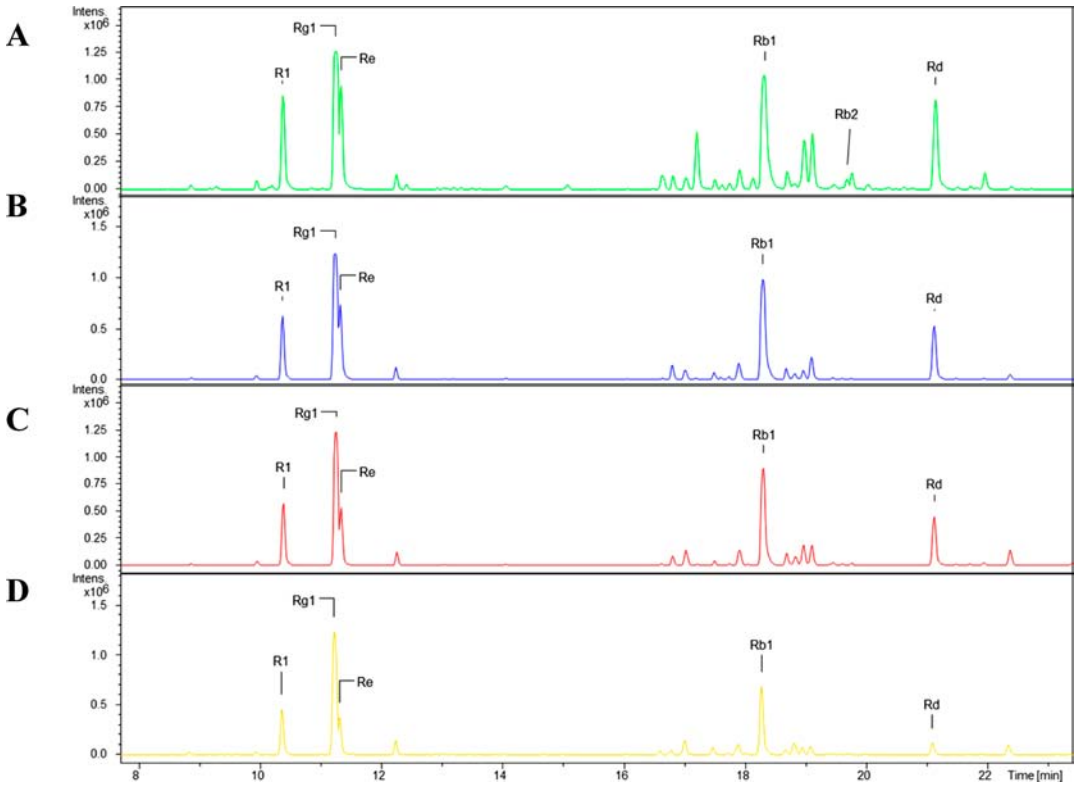


**Figure 1.** Total ion chromatogram (TIC) of rhizome (A), main root, (B) branch root (C), and fibrous root (D) of *Panax notoginseng*.

number of quantified saponins is still quite limited. (2) Metabolite profiling by using UPLC-ESI-MS has been applied for evaluating the chemical characteristics of different parts of *P. notoginseng*, that is, flower, leaf, seed, rhizome, and main root,[19,39,40] or raw notoginseng and steamed notoginseng.[40] However, this approach is still not well applied for the examination of different underground parts of *P. notoginseng*. Especially, comparison among the four parts of notoginseng by using a metabolomics approach is absent. (3) Comparison was often made among the different parts sampled from roots of diverse origin (e.g, roots collected from different regions or collected at different seasons). However, the different origin itself might introduce significant variation in the content of chemical constituents. As such, the "real" variation resulting from biosynthesis in different portions of the root might be compromised by the origin-derived variation.

Therefore, we herein conducted a quantitative comparison on the different parts derived from the whole root of *P. notoginseng* collected from the major production region of notoginseng, Wenshan city, Yunnan province. Eight dammarane-type saponins were quantitatively compared by using the validated UPLC-Q-TOF MS method. Commercial samples of individual parts of notoginseng were also analyzed to verify the chemical difference. A nontargeted metabolomics approach was subsequently applied for discrimination of different parts of the root. This combinative comparison approach facilitated an overall evaluation of chemical difference among these closely related samples.

## MATERIALS AND METHODS

**Plant Materials.** Twelve batches of the whole root of *P. notoginseng* (3 years) were collected from the wholesale markets of Wenshan, Yunnan province, China, in December 2008. For each batch of the root, three to five of the whole roots were divided into rhizome, main root, branch root, and fibrous root. The obtained individual parts were then mixed to yield the representative portion of each batch. The yield of each part from the whole root was measured to be 15% (rhizome), 66% (main root), 18% branch root, and 2% (fibrous root) on average. Commercial samples of individual parts of notoginseng were also collected from the markets of Wenshan during 2006−2008, including


dx.doi.org/10.1021/jf502214x | J. Agric. Food Chem. 2014, 62, 9024−9034

**Table 2. Potential Marker Compounds Responsible for Differentiation of Rhizome, Main Root, Branch Root, and Fibrous Root of *Panax notoginseng***

| no. | identificaton | VIP | $t_R$ (min) | calcd mass | measured mass | error (ppm) | ion species | molecular formula | fragment ($m/z$) |
|---|---|---|---|---|---|---|---|---|---|
| 1 | ginsenoside $Rb_1$ | 22.67 | 18.26 | 1153.6011 | 1153.6003 | −0.7 | $[M + HCOO]^-$ | $C_{54}H_{92}O_{23}$ | 1107.5952 $[M - H]^-$, 945.5421 $[M - H - Glc]^-$, 783.4901 $[M - H - 2Glc]^-$, 621.4370 $[M - H - 3Glc]^-$, 459.3851 $[M - H - 4Glc]^-$ |
| 2 | malonyl-ginsenoside $Rb_1$ | 17.71 | 18.64 | 1193.5961 | 1193.6004 | 3.6 | $[M - H]^-$ | $C_{57}H_{94}O_{26}$ | 1149.6009 $[M - H - CO_2]^-$, 1107.5986 $[M - H - malonyl]^-$, 1089.5857 $[M - H - malonyl - H_2O]^-$, 945.5532 $[M - H - malonyl - Glc]^-$, 927.5230 $[M - H - malonyl - Glc - H_2O]^-$, 825.4972 $[M - H - CO_2 - 2Glc]^-$, 783.4871 $[M - H - malonyl - 2Glc]^-$, 621.4402 $[M - H - malonyl - 3Glc]^-$ |
| 3 | ginsenoside Rd | 16.77 | 21.20 | 991.5483 | 991.5482 | −0.1 | $[M + HCOO]^-$ | $C_{48}H_{82}O_{18}$ | 945.5423 $[M - H]^-$, 783.4901 $[M - H - Glc]^-$, 765.4788 $[M - H - Glc - H_2O]^-$, 621.4374 $[M - H - 2Glc]^-$, 603.4284 $[M - H - 2Glc - H_2O]^-$, 459.3844[M-H-3Glc]$^-$ |
| 4 | ginsenoside $Rg_1$ | 14.03 | 11.22 | 845.4904 | 845.4913 | 1 | $[M + HCOO]^-$ | $C_{42}H_{72}O_{14}$ | 799.4825 $[M - H]^-$, 637.4316 $[M - H - Glc]^-$, 619.4183 $[M - H - Glc\text{-}H_2O]^-$, 475.3796 $[M - H - 2Glc]^-$, 457.3689 $[M - H - 2Glc - H_2O]^-$ |
| 5 | notoginsenoside K | 11.94 | 22.36 | 991.5483 | 991.5509 | 2.6 | $[M + HCOO]^-$ | $C_{48}H_{82}O_{18}$ | 945.5419 $[M - H]^-$, 783.4870 $[M - H - Glc]^-$, 765.4788 $[M - H - Glc - H_2O]^-$, 621.4356 $[M - H - 2Glc]^-$, 603.4214 $[M - H - 2Glc - H_2O]^-$, 459.3840 $[M - H - 3Glc]^-$ |
| 6 | notoginsenoside $R_1$ | 11.89 | 10.34 | 977.5327 | 977.5291 | −3.7 | $[M + HCOO]^-$ | $C_{47}H_{80}O_{18}$ | 931.5278 $[M - H]^-$, 799.4845 $[M - H - Xyl]^-$, 781.4743 $[M - H - Xyl - H_2O]^-$, 769.4744 $[M - H - Glc]^-$, 751.4629 $[M - H - Glc - H_2O]^-$, 637.4324 $[M - H - Xyl - Glc]^-$, 619.4220 $[M - H - Xyl - Glc - H_2O]^-$, 475.3797 $[M - H - Xyl - 2Glc]^-$ |
| 7 | notoginsenoside $Rw_1$ | 11.69 | 17.17 | 947.5221 | 947.5199 | −2.3 | $[M + HCOO]^-$ | $C_{46}H_{78}O_{17}$ | 901.5160 $[M - H]^-$, 769.4766 $[M - H - Xyl]^-$, 637.4311 $[M - H - 2Xyl]^-$, 475.3794 $[M - H - 2Xyl - Glc]^-$ |
| 8 | ginsenoside $Rb_2$ | 9.43 | 19.60 | 1123.5906 | 1123.5945 | 3.4 | $[M + HCOO]^-$ | $C_{53}H_{90}O_{22}$ | 1077.5861 $[M - H]^-$, 945.5278 $[M - H - Xyl]^-$, 915.5379 $[M - H - Glc]^-$, 783.4869 $[M - H - Xyl - Glc]^-$, 765.4677 $[M - H - Xyl - Glc - H_2O]^-$, 621.4399 $[M - H - Xyl - 2Glc]^-$, 603.4351 $[M - H - Xyl - 2Glc - \text{-}H_2O]^-$, 459.3876 $[M - H - Xyl - 3Glc]^-$ |
| 9 | malonyl-ginsenoside Rd | 9.07 | 21.91 | 1031.5432 | 1031.5465 | 3.2 | $[M - H]^-$ | $C_{51}H_{84}O_{21}$ | 987.5508 $[M - H - CO_2]^-$, 945.5399 $[M - H - malonyl]^-$, 927.5307 $[M - H - malonyl - H_2O]^-$, 783.5049 $[M - H - malonyl - Glc]^-$ |
| 10 | ginsenoside Re | 8.65 | 11.30 | 991.5483 | 991.5509 | 2.6 | $[M + HCOO]^-$ | $C_{48}H_{82}O_{18}$ | 945.5430 $[M - H]^-$, 799.4834 $[M - H - Rha]^-$, 783.4900 $[M - H - Glc]^-$, 765.4793 $[M - H - Glc - H_2O]^-$, 637.4323 $[M - H - Rha - Glc]^-$, 619.4214 $[M - H - Rha - Glc - H_2O]^-$, 475.3792 $[M - H - Rha - 2Glc]^-$ |
| 11 | ginsenoside $Rg_3$ | 8.47 | 24.84 | 829.4955 | 829.4989 | 4.1 | $[M + HCOO]^-$ | $C_{42}H_{72}O_{13}$ | 783.4896 $[M - H]^-$, 621.4426 $[M - H - Glc]^-$, 603.4216 $[M - H - Glc - H_2O]^-$, 459.3803 $[M - H - 2Glc]^-$ |
| 12 | notoginsenoside $R_4$/ ginsenoside $Ra_3$ | 6.04 | 17.45 | 1239.6374 | 1239.6379 | −2.46 | $[M - H]^-$ | $C_{59}H_{100}O_{27}$ | 1107.5934 $[M - H - Xyl]^-$, 1089.5813 $[M - H - Xyl - H_2O]^-$, 1077.5904 $[M - H - Glc]^-$, 945.5438 $[M - H - Xyl - Glc]^-$, 915.5320 $[M - H - 2Glc]^-$, 783.4890 $[M - H - Xyl - 2Glc]^-$, 765.4824 $[M - H - Xyl - 2Glc - \text{-}H_2O]^-$, 621.4360 $[M - H - Xyl - 3Glc]^-$ |
| 13 | notoginsenoside $R_2$/ ginsenoside $F_5$/ ginsenoside La | 5.88 | 18.09 | 815.4798 | 815.4792 | 0.95 | $[M + HCOO]^-$ | $C_{41}H_{70}O_{13}$ | 769.4728 $[M - H]^-$, 637.4318 $[M - H - Xyl]^-$, 475.3783 $[M - H - Xyl - Glc]^-$ |
| 14 | notoginsenoside Fa/ notoginsenoside $R_4$/ ginsenoside $Ra_3$ | 5.59 | 16.77 | 1239.6374 | 1239.6399 | 1.19 | $[M - H]^-$ | $C_{59}H_{100}O_{27}$ | 1107.6014 $[M - H - Xyl]^-$, 1077.5904 $[M - H - Glc]^-$, 945.5473 $[M - H - Xyl - Glc]^-$, 927.5299 $[M - H - Xyl - Glc - H_2O]^-$, 783.489 $[M - H - Xyl - 2Glc]^-$, 765.4788 $[M - H - Xyl - 2Glc - \text{-}H_2O]^-$ |
| 15 | floralginsenoside E/ floralginsenoside F | 5.51 | 4.92 | 861.4853 | 861.4848 | 0.59 | $[M + HCOO]^-$ | $C_{42}H_{72}O_{15}$ | 815.4779 $[M - H]^-$, 653.4239 $[M - H - Glc]^-$, 635.4188 $[M - H - Glc - H_2O]^-$, 491.3739 $[M - H - 2Glc]^-$ |
| 16 | ginsenoside Rc | 5.36 | 18.97 | 1077.5852 | 1077.5851 | 0.68 | $[M - H]^-$ | $C_{53}H_{90}O_{22}$ | 945.5278 $[M - H - Xyl]^-$, 915.5383 $[M - H - Glc]^-$, 783.4916 $[M - H - Xyl - Glc]^-$, 765.4830 $[M - H - Xyl - Glc - H_2O]^-$, 621.4399 $[M - H - Xyl - 2Glc]^-$, 603.4351 $[M - H - Xyl - 2Glc\text{-}H_2O]^-$, 459.3876 $[M - H - Xyl - 3Glc]^-$ |
| 17 | notoginsenoside I | 4.76 | 17.58 | 568.2989 | 568.2970 | −3.3 | $[M - H + HCOO]^{2-}$ | $C_{54}H_{92}O_{22}$ | 1091.5981 $[M - H]^-$, 929.5497 $[M - H - Glc]^-$, 767.4939 $[M - H - 2Glc]^-$, 605.4420 $[M - 2H - 3Glc]^-$ |
| 18 | 10-hydroxy-4,6-decadiy-noic acid | 4.74 | 3.56 | 503.1770 | 503.1764 | 1.19 | $[M - H]^-$ | $C_{22}H_{32}O_{13}$ | 503.1769 $[M - H]^-$, 341.1234 $[M - H - Glc]^-$ |
| 19 | ginsenoside Rf/ginseno-side la/ginsenoside lb/ notoginsenoside U | 4.62 | 16.60 | 845.4904 | 845.4898 | 0.91 | $[M + HCOO]^-$ | $C_{42}H_{72}O_{14}$ | 799.4825 $[M - H]^-$, 637.4316 $[M - H - Glc]^-$, 475.3796 $[M - H - 2Glc]^-$ |
| 20 | notoginsenoside $R_2$/ ginsenoside $F_5$/ ginsenoside La | 3.98 | 16.98 | 815.4798 | 815.482 | 2.7 | $[M + HCOO]^-$ | $C_{41}H_{70}O_{13}$ | 769.4728 $[M - H]^-$, 637.4318 $[M - H - Xyl]^-$, 619.4202 $[M - H - Xyl - H_2O]^-$, 475.3783 $[M - H - Xyl - Glc]^-$, 457.643 $[M - H - Xyl - Glc - H_2O]^-$ |



dx.doi.org/10.1021/jf502214x | J. Agric. Food Chem. 2014, 62, 9024−9034

**Table 2. continued**

| no. | identificaton | VIP | $t_R$ (min) | calcd mass | measured mass | error (ppm) | ion species | molecular formula | fragment ($m/z$) |
|---|---|---|---|---|---|---|---|---|---|
| 21 | notoginsenoside Fa/ notoginsenoside $R_4$/ ginsenoside $Ra_3$ | 3.69 | 18.24 | 1239.6374 | 1239.6375 | 0.84 | $[M - H]^-$ | $C_{59}H_{100}O_{27}$ | 1107.5901 $[M - H - Xyl]^-$, 1089.5897 $[M - H - Xyl - H_2O]^-$, 945.5394 $[M - H - Xyl - Glc]^-$, 783.4790 $[M - H - Xyl - 2Glc]^-$, 765.4824 $[M - H - Xyl - 2Glc - -H_2O]^-$, 621.4331 $[M - H - Xyl - 3Glc]^-$, 459 $[M - H - Xyl - 4Glc]^-$ |
| 22 | ginsenoside $Ra_1$/ ginsenoside $Ra_2$/ notoginsenoside Fc /notoginsenoside $FP_2$ | 3.32 | 19.02 | 1209.6274 | 1209.629 | 0.69 | $[M - H]^-$ | $C_{58}H_{98}O_{26}$ | 1077.5815 $[M - H - Xyl]^-$, 945.5171 $[M - H - Xyl - Ara]^-$, 915.5203 $[M - H - Xyl - Glc]^-$, 783.4702 $[M - H - Xyl - Ara - Glc]^-$, 621.4456 $[M - H - Xyl - Ara - 2Glc]^-$, 459.4373 $[M - H - Xyl - Ara - 3Glc]^-$ |
| 23 | notoginsenoside A/ koryoginsenoside $Rg_2$ | 3.22 | 12.88 | 584.2938 | 584.2926 | −2.2 | $[M - H + HCOO]^{2-}$ | $C_{54}H_{92}O_{24}$ | 1123.5821 $[M - H]^-$, 961.5508 $[M - H - Glc]^-$, 799.4908 $[M - H - 2Glc]^-$, 561.2922 $[M - 2H]^{2-}$ |
| 24 | ginsenoside $Rg_2$ | 2.61 | 17.86 | 829.4955 | 829.4969 | 1.7 | $[M + HCOO]^-$ | $C_{42}H_{72}O_{13}$ | 783.4896 $[M - H]^-$, 637.4303 $[M - H - Rha]^-$, 619.4279 $[M - H - Rha - H_2O]^-$, 475.3790 $[M - H - Rha - Glc]^-$, 457.3690 $[M - H - Rha - Glc - H_2O]^-$ |
| 25 | ginsenoside $Rh_1$ | 2.47 | 17.85 | 683.4376 | 683.4345 | 4.5 | $[M + HCOO]^-$ | $C_{36}H_{62}O_9$ | 637.4318 $[M - H]^-$, 475.3770 $[M - H - Glc]^-$ |
| 26 | panaxoside C | 2.30 | 20.73 | 975.5534 | 975.5544 | 0.81 | $[M + HCOO]^-$ | $C_{48}H_{82}O_{17}$ | 929.5470 $[M - H]^-$, 767.4978 $[M - H - Glc]^-$ |
| 27 | 20-glucoginsenoside Rf/ floralginsenoside La/ floralginsenoside Lb | 2.28 | 23.66 | 961.5378 | 961.5380 | 0.03 | $[M - H]^-$ | $C_{48}H_{82}O_{19}$ | 799.4854 $[M - H - Glc]^-$, 781.4751 $[M - H - Glc - H_2O]^-$, 637.4334 $[M - H - 2Glc]^-$, 619.4242 $[M - H - 2Glc - H_2O]^-$, 475.3794 $[M - H - 3Glc]^-$ |
| 28 | 6,20-di-*O*-*β*-D-glucopyranoside | 2.28 | 11.23 | 843.4748 | 843.4740 | 2.25 | $[M + HCOO]^-$ | $C_{42}H_{70}O_{14}$ | 797.4710 $[M - H]^-$, 635.4210 $[M - H - Glc]^-$ |
| 29 | notoginsenoside J | 2.17 | 2.85 | 879.4959 | 897.4953 | 1.07 | $[M + HCOO]^-$ | $C_{42}H_{74}O_{16}$ | 833.5020 $[M - H]^-$, 671.4385 $[M - H - Glc]^-$ |
| 30 | notoginsenoside D/ notoginsenoside T | 2.06 | 18.27 | 1371.6802 | 1371.6806 | 1.05 | $[M - H]^-$ | $C_{64}H_{108}O_{31}$ | 685.3421 $[M - 2H]^{2-}$, 619.3171 $[M - 2H - Xyl]^{2-}$, 553.7970 $[M - 2H - 2Xyl]^{2-}$ |
| 31 | vinaginsenoside $R_{20}$/ ginsenoside III | 1.89 | 13.28 | 1005.5276 | 1005.5266 | 1.45 | $[M + HCOO]^-$ | $C_{48}H_{80}O_{19}$ | 959.5205 $[M - H]^-$, 797.4775 $[M - H - Glc]^-$, 635.4040 $[M - H - 2Glc]^-$, 473.3665 $[M - H - 3Glc]^-$ |
| 32 | notoginsenoside H | 1.87 | 4.55 | 993.5276 | 993.5285 | 0.93 | $[M - H]^-$ | $C_{48}H_{82}O_{21}$ | 947.5253 $[M - H]^-$, 785.4690 $[M - H - Glc]^-$, 767.4594 $[M - H - Glc - H_2O]^-$, 653.4277 $[M - H - Xyl - Glc]^-$, 635.4162 $[M - H - Xyl - Glc - H_2O]^-$, 491.3763 $[M - H - Xyl - 2Glc]^-$ |



dx.doi.org/10.1021/jf502214x | J. Agric. Food Chem. 2014, 62, 9024−9034

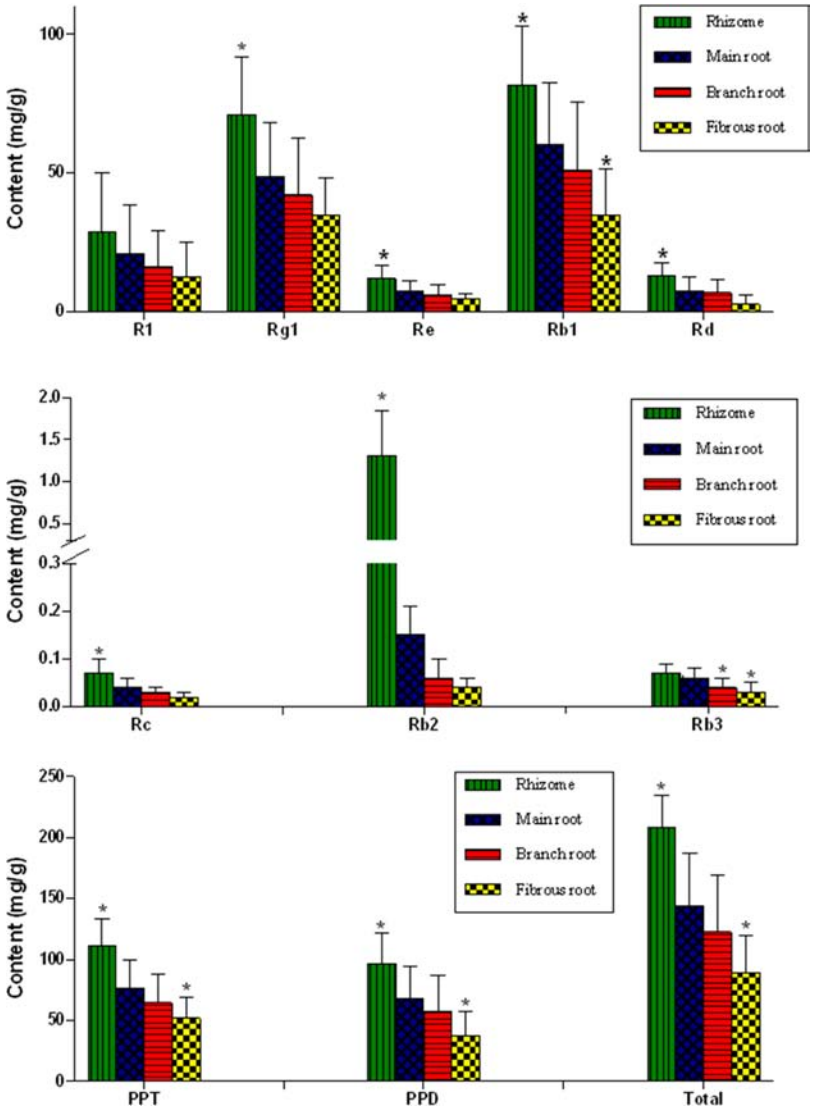


**Figure 2.** Contents of eight dammarane-type saponins and total saponins in rhizome, main root, branch root, and fibrous root of *P. notoginseng*. Each bar represents the mean ± SD ($n$ = 12). (∗) $p < 0.05$, one-way ANOVA (compared with main root).

four batches of rhizome; main roots with growing years of 3 years (four batches), 4 years (two batches), and 5 years (two batches); four batches of main root without growing year information; four batches of branch root; and six batches of fibrous root.

**Chemicals.** Notoginsenoside $R_1$ and ginsenoside $Rg_1$ (purity > 98%) were purchased from Kunming Zhongzheng Biotech Co., Ltd. (Kunming, China); ginsenosides Re, $Rb_1$, $Rb_2$, $Rb_3$, Rc, and Rd (each purity > 98%) were purchased from Chengdu Scholar Biotech Co., Ltd. (Chengdu, China). HPLC grade methanol and acetonitrile were purchased from Anaqua Chemicals Supply Inc., Ltd. (Houston, TA, USA), and distilled water was purified by a Milli-Q system (Millipore).

**Preparation of Standard and Sample Solution.** Stock solutions of notoginsenoside $R_1$ and ginsenosides $Rg_1$, Re, $Rb_1$, $Rb_2$ and Rd in 70% methanol were diluted to a series of working solutions (0.125, 0.625, 1.25, 2.5, 5, and 10 μg/mL), whereas those of ginsenosides $Rb_3$ and Rc were diluted to yield working solutions of 0.05, 0.25, 0.5, 1, 2, and 4 μg/mL.

Sample solutions were prepared following the procedures developed in our previous studies.[41,42] Briefly, 200 mg of powdered samples of each representative part was accurately weighed into a PTFE-stopped tube and sonicated with 10 mL of 70% methanol for 1 h. The mixture was centrifuged, and the supernatant was collected and then diluted by 200- and 4-fold for the quantitation of major ginsenosides ($R_1$, $Rg_1$, Re, $Rb_1$, Rd, and $Rb_2$) and minor ginsenosides ($Rb_3$ and Rc), respectively. All samples were filtered through a 0.2 μm filter before analysis.

**LC-MS Analysis.** LC-MS was performed using a Waters Acquity UPLC system (Waters, Milford, MA, USA) coupled to a Bruker MicroTOF mass spectrometer with an ESI source (Bruker, Bremen, Germany). All of the operation, acquisition, and data analysis were operated by Hystar software (Bruker). MS/MS experiments were carried out on an Agilent 1290 infinity UHPLC system (Santa, Clara, CA, USA) coupled with an Agilent 6550 QTOF.

Chromatographic separation was performed on an Acquity UPLC BEH $C_{18}$ column (2.1 mm × 100 mm, 1.7 μm). The mobile phase consisted of 0.1% formic acid in water (A) and 0.1% formic acid in acetonitrile (B), with a flow rate of 0.35 mL/min. The following gradient was used: 0−23 min, 10−40% B; 23−27 min, 40−85% B; 27−29 min, 85−100% B; 29−32 min, 100% B; 32−36 min, 10% B. The column was maintained at 40 °C, and the injection volume of each sample was 1 μL.

The mass spectrometer was operated in the negative mode with a scanning range of $m/z$ 100−3000. The optimized mass conditions were as follows: drying gas ($N_2$) flow rate, 8 L/min; drying gas temperature, 180 °C; capillary voltage, 4500 V; nebulizing gas ($N_2$) pressure, 2.5 bar; end plate offset, −500 V. The following ions were extracted for the quantitative analysis of different compounds: $m/z$ 977.5 ($[M + HCOO]^-$, notoginsenoside $R_1$), $m/z$ 845.5 ($[M + HCOO]^-$, ginsenoside $Rg_1$), $m/z$ 991.5 ($[M + HCOO]^-$, ginsenosides


dx.doi.org/10.1021/jf502214x | J. Agric. Food Chem. 2014, 62, 9024−9034

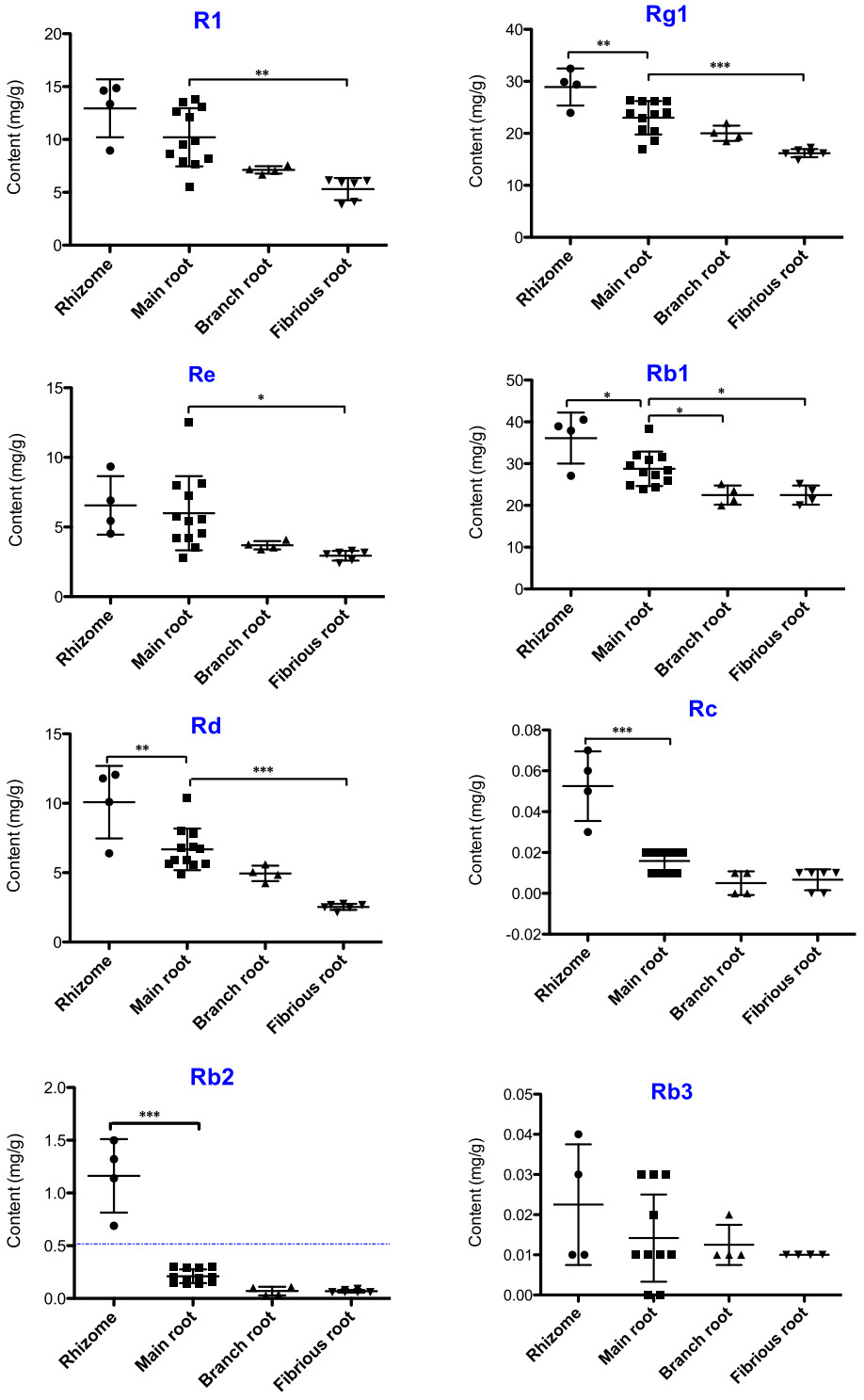


**Figure 3.** Contents of eight dammarane-type saponins in the commercial sample of rhizome ($n$ = 4), main root ($n$ = 12), branch root ($n$ = 4), and fibrous root ($n$ = 6) of *P. notoginseng*. (*) $p < 0.05$, (**) $p < 0.01$, (***) $p < 0.001$, one-way ANOVA (compared with main root).

Re and Rd), $m/z$ 1153.5 ($[M + HCOO]^-$, ginsenoside $Rb_1$), $m/z$ 1123.5 ($[M + HCOO]^-$, ginsenosides $Rb_2$, $Rb_3$, and Rc).

**Method Validation for Quantitation.** The calibration curve ($y = a + bx$) for each ginsenoside was constructed by plotting the peak area against concentration, and the linearity was verified by correlation coefficients ($r^2$). The lower limit of detection (LOD) and lower limit of quantification (LOQ) were determined on the basis of response at signal-to-noise ratios (S/N) of 3 and 10, respectively. The precision was determined by intra- and interday variations. The intraday precision was performed by six replicate analyses of a mixed standard solution within a day, and the interday precision was carried out by analyzing the same mixed standard solution on five consecutive days. The repeatability was evaluated by carrying out six replicate analyses of the same sample. The recovery test was performed by spiking a sample with the mixed standards, and the recovery rate was calculated by using the following formula: recovery rate (%) = (observed amount − original amount)/spiked amount × 100%. Variations were expressed as relative standard deviations (RSD%).

**Multivariate Analysis.** The UPLC-Q-TOF MS data of different parts of notoginseng were first exported as cdf format. The peak


dx.doi.org/10.1021/jf502214x | J. Agric. Food Chem. 2014, 62, 9024−9034

finding, alignment, and filtering of raw data were preprocessed by MassLynx V4.1 (Waters, Milford, MA, USA). The parameters were set as the following conditions: retention time of 2−27 min, mass range of 100−1500 Da, mass tolerance of 0.05 Da. The resulting three-dimensional matrix using retention time, mass to charge ratio, and intensities of all detected peaks were tabulated and exported for subsequent analysis. Principal component analysis (PCA), partial least squares discriminate analysis (PLS-DA), and orthogonal partial least squares discriminate analysis (OPLS-DA) were performed by using SIMCA 13.0 software (Umetrics, Umea, Sweden). Components that played important roles in differentiation were picked out according to the variable importance in the projection (VIP) value.

## RESULTS AND DISCUSSION

**Method Validation for Quantitation.** All calibration curves showed good linearity ($r^2$ > 0.999). The LOD ranged from 0.0038 to 0.0146 μg/mL, and the LOQ ranged from 0.0171 to 0.0541 μg/mL. The calibration curves, correlation coefficients, LOD, and LOQ of each compound are given in Table 1. The UPLC-Q-TOF MS method showed good precision for the quantitation of the eight saponins with intra- and interday variations of 1.28−3.00 and 1.22−3.44% and repeatability variations of 1.08−3.84%. The overall recoveries ranged from 97.70 to 103.03%, with variations of 1.60−3.46% (Table 1). These results demonstrated that the established UPLC-Q-TOF MS method was sensitive, accurate (with recovery accuracy within the criteria of 95−105%), and precise (with precision of <5%) and thereby appropriate for the quantitative analyses of notoginsenoside $R_1$ and ginsenosides $Rg_1$, Re, $Rb_1$, $Rb_2$, $Rb_3$, Rc, and Rd in different parts of notoginseng.

**Quantitative Comparison of Different Parts of Notoginseng.** The contents of chemical constituents are always influenced by various factors such as the place of origin, the growing year, and the harvesting season. To evaluate the variation of ginsenosides inherently associated with the different parts of the root, we specially collected the whole root for the comparative study. The qualitative results revealed quite similar content distribution of eight dammarane-type saponins in different parts of the root (Figure 1). As can be seen in Table 1, in all parts of the root, ginsenosides $Rb_1$ and $Rg_1$ were shown to be the most abundant ginsenosides, both accounting for >20% of the total saponins (Table 2). Notoginsenoside $R_1$ was less abundant than $Rg_1$ and $Rb_1$, but with great variation among individual samples in both absolute content and relative composition of the total amount of saponins. Content of ginsenosides Re and Rd also varied greatly among individual samples, but their percentage in the total amount of saponins remained at about 1−10% in most portion samples of the root, whereas ginsenosides $Rb_2$, Rc, and $Rb_3$ were minor constituents in all parts of the root (Supporting Information, Table S1). In commercial samples, similar patterns were observed for all individual parts of notoginseng (Figure 3).

Among different parts of the root, the content of each saponin was always the highest in rhizome, followed by main root and branch root, and then fibrous root. This observation was consistent with previous studies.[24,39,43] Individually, except for notoginsenoside $R_1$, contents of all ginsenosides in rhizome were significantly higher than those in main root (Figure 2), among which $Rb_2$ was the most important ginsenoside as featured by up to 8-fold content in rhizome of that in main root (Figure 2). The higher content of each saponin in rhizome accumulatively led to the significantly higher content of subtotal PPD-type and PPT-type ginsenosides, as well as the content of total saponins than that in main root (Figure 2). On average,

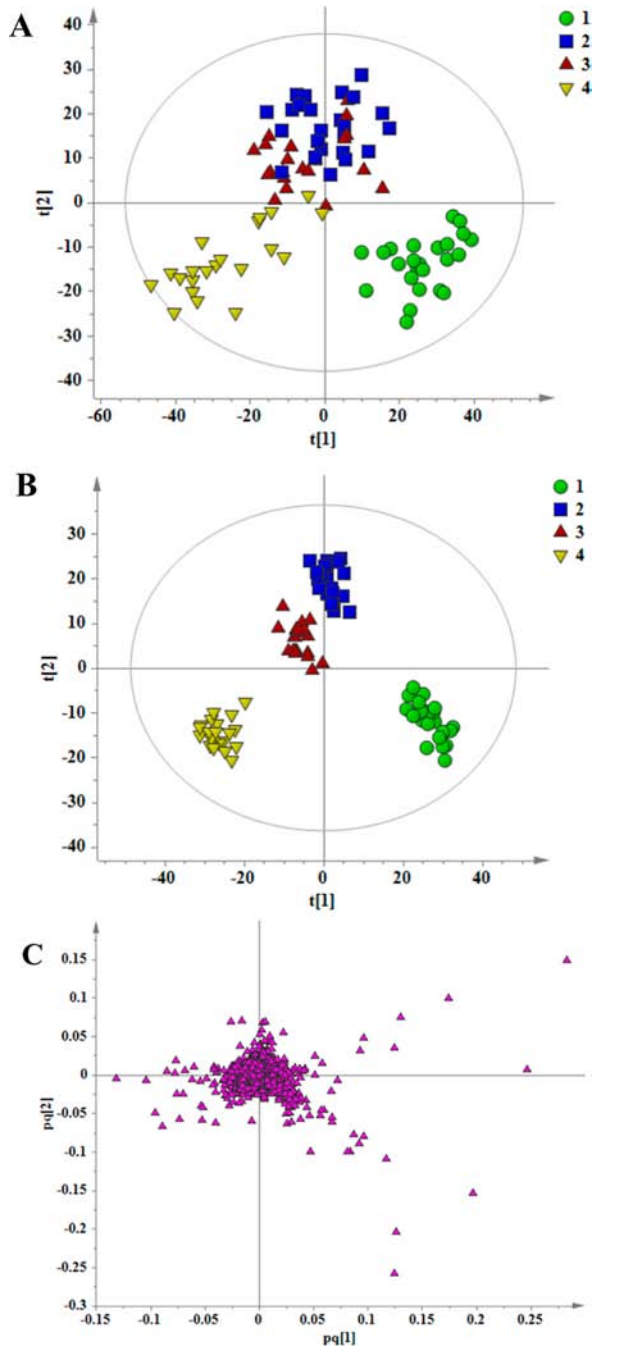


**Figure 4.** PLS-DA scores plot (A), OPLS-DA scores plot (B), and loading plot (C) of UPLC-Q-TOF MS data of rhizome (1), main root (2), branch root (3), and fibrous root (4) of *P. notoginseng*.

the content of total ginsenosides in rhizome is about 20−60% higher than that in main root and about 50−90% higher than that in branch root. The higher saponin content, together with the considerable biomass of the rhizome (about 15% of the whole root), supported the utilization of rhizome as the raw material for manufacturing ginsenoside-based products.

The contents of all eight ginsenosides in branch root appear to be lower than that in main root, but statistical significance for such difference was not observed ($p$ value > 0.05). Moreover, in PLS-DA scores plot (Figure 4A), branch root is almost superimposed with main root but separated from rhizome and fibrous root. In OPLS-DA scores plot, branch root is separated


dx.doi.org/10.1021/jf502214x | J. Agric. Food Chem. 2014, 62, 9024−9034

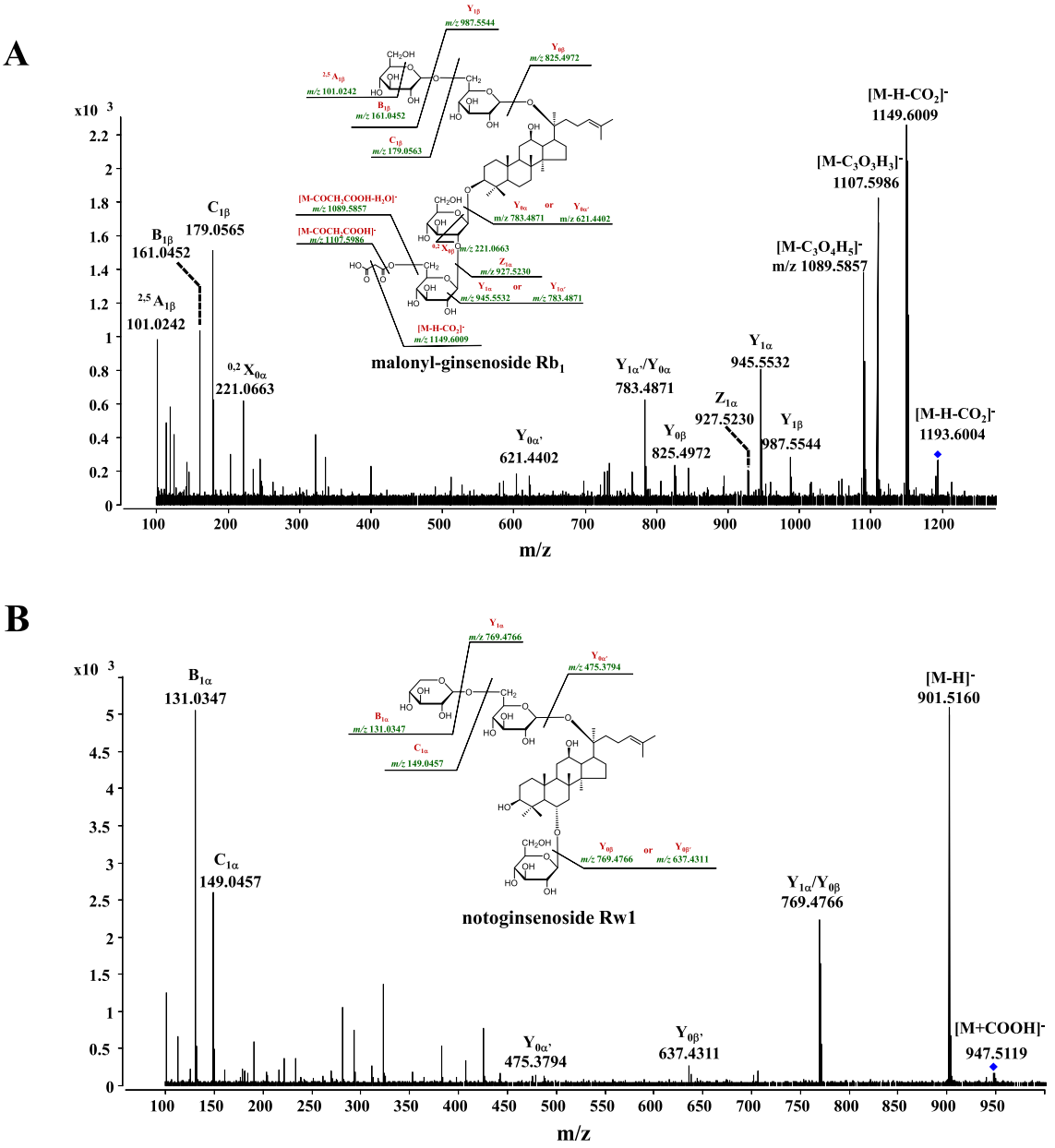


**Figure 5.** Targeted MS/MS of representative markers (A, malonyl ginsenoside $Rb_1$; B, notginsenoside $Rw_1$) contributing to the differentiation of different parts of notoginseng. Nomenclature of the fragments was assigned according to a systematic nomenclature for carbohydrate fragmentations.[46]

from main root but still very close to the main root in the space. These results indicated an overall similar chemical profile of branch root with main root, therefore supporting the equivalent usage of branch root and main root as indicated in "Chinese Pharmacopeia".

In commercial unassorted samples, the content of individual saponins in the rank order of rhizome > main root ≥ branch root > fibrous root was also observed, demonstrating this is an overall pattern of saponin distribution in different parts of notoginseng. Consistent with that revealed in whole root-derived samples, significant differences in the content of ginsenosides $Rg_1$, $Rb_1$, Rd, Rc, and $Rb_2$ between rhizome and main root were observed, despite the great intragroup variation (Figure 3). In addition, significant difference in the contents of $R_1$, $Rg_1$, Re, and $Rb_1$ between main root and fibrous root were observed. Most notable is the significantly different contents of $Rb_2$ in rhizome and other parts (Figure 3). It has been found that the content of $Rb_2$ in rhizome was >0.5 mg/g in all samples, whereas the contents in other parts were all <0.3 mg/g and mostly <0.2 mg/g. This evidence facilitated 0.5 mg/g of $Rb_2$ as a threshold value for the discrimination of rhizome and other parts of notoginseng.

**Multivariate Analysis of Different Parts of Notoginseng.** Untargeted metabolomics has the ability to profile diverse classes of metabolites and thereby has been widely used for comparing the overall metabolic composition between samples.[44] Among the techniques used for untargeted metabolomics, UPLC-Q-TOF MS has been especially widely utilized for profiling metabolites due to its superiority in high-resolution mass, precision, and sensitivity. In the current study, >15000 ions were achieved in the UPLC-Q-TOF MS data of notoginseng. Analysis results of these ions were exported for subsequent multivariate analysis by using SIMCA 13.0. As


dx.doi.org/10.1021/jf502214x | J. Agric. Food Chem. 2014, 62, 9024−9034

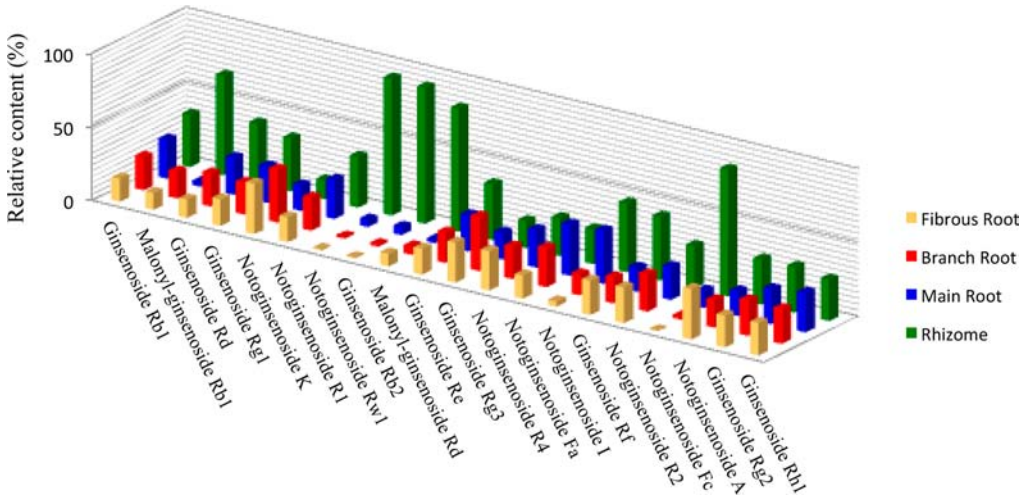


**Figure 6.** Relative contents of 20 marker compounds in different parts of notoginseng. To compare the level of individual markers between different parts, the content of each marker compound was normalized as a relative content, which was calculated by using the following equation: relative content = content in individual part/sum of the contents in four parts × 100%.

shown in Figure 4A, separation of rhizome, fibrous root, and main/branch root can be observed in the PLS-DA plots. $Q^2$, the parameter that estimates how well the model predicts $Y$, was calculated to be 63.8% (five significant components, $R^2Y$ = 91.2%) for this PLS-DA model, suggesting the good predictive capacity of the model. To minimize any effects of nonrelevant metabolite variability, OPLS-DA analyses were also carried out to identify the differences between groups (Figure 4B). Consistent with the results obtained from quantitative analysis, branch root and main root were very close in the OPLS-DA plot, indicating high similarity of the two parts. In a loading plot, the ions farthest away from the main cluster of ions possess the higher VIP value and play more important roles in the differentiation. As shown in Figure 4C, a number of ions were distant from the main cluster and were identified as the marker ions. These marker ions were identified according to the accurate mass, retention time, and targeted MS/MS data. Figure 5 represents examples for the identification of potential markers by MS/MS data. A list of the identified marker ions is shown in Table 2, which included both major and minor constituents in notoginseng. This result suggested ginsenosides Rf, $Rg_1$, Re, $Rg_2$, $Rh_1$, $Rb_1$, $Rb_2$, Rd, and $Rg_3$ and notoginsenosides A, Fa, Fc, I, K, $R_1$, $R_2$, $R_4$, and $Rw_1$, as well as malonyl-ginsenosides $Rb_1$ and Rd were the major potential marker compounds responsible for differentiation of rhizome, main root, branch root, and fibrous root of *P. notoginseng*.

The relative contents of the first 20 potential marker compounds in each part of notoginseng were then compared on the basis of their peak areas. As shown in Figure 6, notoginsenosides Fc and $Rw_1$, malonyl-ginsenoside Rd, and ginsenoside $Rb_2$ were found to present in rhizome at significantly higher content than in other parts. It is worth pointing out that both quantitative and multivariate analyses showed that the content of ginsenoside $Rb_2$ was much higher in rhizome than in other parts of notoginseng. This implied the potential marker compounds identified from the multivariate analysis were instructive.

In the current study, quantitative comparison by using a validated UPLC-Q-TOF MS method and metabolite profiling approach was combinatively employed for evaluating the similarities and differences among rhizome, main root, branch root, and fibrous root of *P. notoginseng*. Both quantitative analysis and metabolite profiling study suggested that rhizome was significantly different from the other parts. It contained the highest contents of individual saponin and total saponins, clearly suggesting the suitability of this part as the raw material for the manufacture of ginsenoside-based products. The chemical compositions of the main root and branch root are quite similar and thereby can be utilized equivalently. The fibrous root also showed a clear separation from the other parts and contained the lowest content of saponins. The multivariate study suggested that notoginsenosides Fc and $Rw_1$, malonyl-ginsenoside Rd, and ginsenoside $Rb_2$ could be potential chemical markers for discrimination of different parts of notoginseng. Because processing (e.g., steaming) and transformation in the gastrointestinal tract would further introduce chemical diversity of saponins,[32,45] chemical differences among individual parts of notoginseng might be amplified or become more complicated after processing or oral consumption. Overall, our work represents the first comprehensive study dealing with four parts of notoginseng by using an approach integrating quantitative and qualitative comparison. The result is of importance for the appraisal of the chemical characteristics of different parts of notoginseng and provides chemical evidence for the rational application of each part of notoginseng.

## ■ ASSOCIATED CONTENT

### Ⓢ Supporting Information

Table S1. This material is available free of charge via the Internet at http://pubs.acs.org.

## ■ AUTHOR INFORMATION

### Corresponding Authors

*(L.L.) Phone: +853-8897 2077. Fax: +853-2882 7222. E-mail: lliu@must.edu.mo. Mail: State Key Laboratory of Quality Research in Chinese Medicine, Macau University of Science and Technology, Taipa, Macau, 999078, China.

*(Z.-H.J.) Phone: +853-8897 2777. Fax: +853-2882 5886. E-mail: zhjiang@must.edu.mo. Mail: State Key Laboratory of Quality Research in Chinese Medicine, Macau Institute for

Applied Research in Medicine and Health, Macau University of Science and Technology, Taipa, Macau, 999078, China.

### Funding

This project is sponsored by the Macao Science and Technology Development Fund, Macau Special Administrative Region (066/2011/A3 to J.-R.W.) and the National Institutes of Health (AT005522-03).

### Notes

The authors declare no competing financial interest.

## REFERENCES

(1) Gao, B.; Huang, L.; Liu, H.; Wu, H.; Zhang, E.; Yang, L.; Wu, X.; Wang, Z. Platelet P2Y(1)(2) receptors are involved in the haemostatic effect of notoginsenoside Ft1, a saponin isolated from *Panax notoginseng*. *Br. J. Pharmacol.* **2014**, *171*, 214−223.

(2) Que, W.; Liao, L.; Li, Y. Traditional Chinese medicinal composition with analgesic and hemostatic effects. CN1961912A, 2007.

(3) Li, B.; Wang, Y.; Zuo, W.; Hong, W.; Meng, T.; Xiao, N. A water-soluble hemostatic gauze prepared from *Panax notoginseng* having function of activating blood and promoting healing, and its preparation. CN103623458A, 2014.

(4) Han, J. B.; Hua, Y. Q.; Chen, L. Y.; Liu, L. M. Advances in smoothened-targeting therapies for pancreatic cancer: implication for drug discovery from herbal medicines. *J. Chin. Integr. Med.* **2012**, *10*, 256−263.

(5) He, N. W.; Zhao, Y.; Guo, L.; Shang, J.; Yang, X. B. Antioxidant, antiproliferative, and pro-apoptotic activities of a saponin extract derived from the roots of *Panax notoginseng* (Burk.) F.H. Chen. *J. Med. Food* **2012**, *15*, 350−359.

(6) Ng, T. B. Pharmacological activity of sanchi ginseng (*Panax notoginseng*). *J. Pharm. Pharmacol.* **2006**, *58*, 1007−1019.

(7) Yoshikawa, M.; Murakami, T.; Ueno, T.; Yashiro, K.; Hirokawa, N.; Murakami, N.; Yamahara, J.; Matsuda, H.; Saijoh, R.; Tanaka, O. Bioactive saponins and glycosides. VIII. Notoginseng (1): new dammarane-type triterpene oligoglycosides, notoginsenosides-A, -B, -C, and -D, from the dried root of *Panax notoginseng* (Burk.) F.H. Chen. *Chem. Pharm. Bull. (Tokyo)* **1997**, *45*, 1039−1045.

(8) Yoshikawa, M.; Morikawa, T.; Kashima, Y.; Ninomiya, K.; Matsuda, H. Structures of new dammarane-type triterpene saponins from the flower buds of *Panax notoginseng* and hepatoprotective effects of principal ginseng saponins. *J. Nat. Prod.* **2003**, *66*, 922−927.

(9) Chan, R. Y.; Chen, W. F.; Dong, A.; Guo, D.; Wong, M. S. Estrogen-like activity of ginsenoside Rg1 derived from *Panax notoginseng*. *J. Clin. Endocrinol. Metab.* **2002**, *87*, 3691−3695.

(10) Konoshima, T.; Takasaki, M.; Tokuda, H. Anti-carcinogenic activity of the roots of *Panax notoginseng*. II. *Biol. Pharm. Bull.* **1999**, *22*, 1150−1152.

(11) Wang, C. Z.; Yuan, C. S. Potential role of ginseng in the treatment of colorectal cancer. *Am. J. Chin. Med.* **2008**, *36*, 1019−1028.

(12) Yang, J. M.; Lu, F. H.; Jin, S. K.; Sun, S. W.; Zhao, Y. X.; Wang, S. J.; Zhou, X. H. [A cohort study on the predictive value of factors influencing cardio-cerebro vascular death among people over 40 years of age]. *Zhonghua Liu Xing Bing Xue Za Zhi* **2007**, *28*, 119−122.

(13) Mao, Q.; Li, Y.; Li, S.-L.; Yang, J.; Zhang, P.-H.; Wang, Q. Chemical profiles and anticancer effects of saponin fractions of different polarity from the leaves of *Panax notoginseng*. *Chin. J. Nat. Med.* **2014**, *12*, 30−37.

(14) Dong, H.; Bai, L. P.; Wong, V. K.; Zhou, H.; Wang, J. R.; Liu, Y.; Jiang, Z. H.; Liu, L. The in vitro structure-related anti-cancer activity of ginsenosides and their derivatives. *Molecules* **2011**, *16*, 10619−10630.

(15) Ruan, J. Q.; Leong, W. I.; Yan, R.; Wang, Y. T. Characterization of metabolism and in vitro permeability study of notoginsenoside R1 from Radix Notoginseng. *J. Agric. Food Chem.* **2010**, *58*, 5770−5776.

(16) Cui, H.; Zhang, C.; Lin, H.; Lu, W.; Cheng, H.; Wang, J. [Determination of effective components in different positions of *Panax notoginseng* by HPLC]. *Zhongyaocai* **2009**, *32*, 1810−1813.

(17) Liu, J. H.; Lee, C. S.; Leung, K. M.; Yan, Z. K.; Shen, B. H.; Zhao, Z. Z.; Jiang, Z. H. Quantification of two polyacetylenes in Radix Ginseng and roots of related *Panax* species using a gas chromatography-mass spectrometric method. *J. Agric. Food Chem.* **2007**, *55*, 8830−8835.

(18) Kim, D. H. Chemical diversity of *Panax ginseng*, *Panax quinquifolium*, and *Panax notoginseng*. *J. Ginseng Res.* **2012**, *36*, 1−15.

(19) Wan, J.-B.; Zhang, Q.-W.; Hong, S.-J.; Li, P.; Li, S.-P.; Wang, Y.-T. Chemical investigation of saponins in different parts of *Panax notoginseng* by pressurized liquid extraction and liquid chromatography-electrospray ionization-tandem mass spectrometry. *Molecules* **2012**, *17*, 5836−5853.

(20) Yamada, Y.; Yuasa, Y.; Udaka, Y.; Takeuchi, K. Quality estimation by the head number of Tienchi ginseng. *Igaku to Seibutsugaku* **1998**, *137*, 145−150.

(21) Zhang, C.; Bao, J.; Li, X.; Zheng, Y. HPLC determination of the amount of ginsenosides in different parts of *Panax ginseng* C. A. Mey. and *P. quinquefolius* L. and *P. notoginseng* (burk) F. H. Chen. *Yaowu Fenxi Zazhi* **2005**, *25*, 1190−1194.

(22) Wang, D.; Zhu, H.; Chen, K.; Xu, M.; Zhang, Y.; Yang, C. Saponin accumulation in the seedling root of *Panax notoginseng*. *Chin. Med.* **2011**, *6* (5), No. http://www.cmjournal.org/content/6/1/5.

(23) Wang, D.; Li, H.; Chen, K.; Zhang, Y.; Yang, C. HPLC comparative analysis of ginsenoside saponins in different underground parts of *Panax notoginseng*. *Yunnan Zhiwu Yanjiu* **2005**, *27*, 685−690, 694.

(24) Jia, X.-H.; Wang, C.-Q.; Liu, J.-H.; Li, X.-W.; Wang, X.; Shang, M.-Y.; Cai, S.-Q.; Zhu, S.; Komatsu, K. Comparative studies of saponins in 1−3-year-old main roots, fibrous roots, and rhizomes of *Panax notoginseng*, and identification of different parts and growth-year samples. *J. Nat. Med.* **2013**, *67*, 339−349.

(25) Wang, J. R.; Yamasaki, Y.; Tanaka, T.; Kouno, I.; Jiang, Z. H. Dammarane-type triterpene saponins from the flowers of *Panax notoginseng*. *Molecules* **2009**, *14*, 2087−2094.

(26) Yoshikawa, M.; Morikawa, T.; Yashiro, K.; Murakami, T.; Matsuda, H. Bioactive saponins and glycosides. XIX. Notoginseng (3): immunological adjuvant activity of notoginsenosides and related saponins: structures of notoginsenosides-L, -M, and -N from the roots of *Panax notoginseng* (Burk.) F. H. Chen. *Chem. Pharm. Bull. (Tokyo)* **2001**, *49*, 1452−1456.

(27) Zhou, J.; Wu, M. Z.; Taniyasu, S.; Besso, H.; Tanaka, O.; Saruwatari, Y.; Fuwa, T. Dammarane-saponins of Sanchi ginseng, roots of *Panax notoginseng* (Burk.) F.H. Chen (Araliaceae): structures of new saponins, notoginsenosides-R1 and -R2, and identification of ginsenosides-Rg2 and -Rh1. *Chem. Pharm. Bull.* **1981**, *29*, 2844−2850.

(28) Komakine, N.; Okasaka, M.; Takaishi, Y.; Kawazoe, K.; Murakami, K.; Yamada, Y. New dammarane-type saponin from roots of *Panax notoginseng*. *J. Nat. Med.* **2006**, *60*, 135−137.

(29) Qiu, L.; Jiao, Y.; Huang, G.-K.; Xie, J.-Z.; Miao, J.-H.; Yao, X.-S. New dammarane-type saponins from the roots of *Panax notoginseng*. *Helv. Chim. Acta* **2014**, *97*, 102−111.

(30) Fu, H.-Z.; Zhong, R.-J.; Zhang, D.-M.; Wang, D. A new protopanaxadiol-type ginsenoside from the roots of *Panax notoginseng*. *J. Asian Nat. Prod. Res.* **2013**, *15*, 1139−1143.

(31) Pei, Y.; Du, Q.; Liao, P. Y.; Chen, Z. P.; Wang, D.; Yang, C. R.; Kitazato, K.; Wang, Y. F.; Zhang, Y. J. Notoginsenoside ST-4 inhibits virus penetration of herpes simplex virus in vitro. *J. Asian Nat. Prod. Res.* **2011**, *13*, 498−504.

(32) Liao, P. Y.; Wang, D.; Zhang, Y. J.; Yang, C. R. Dammarane-type glycosides from steamed notoginseng. *J. Agric. Food Chem.* **2008**, *56*, 1751−1756.

(33) Xie, Y. Y.; Luo, D.; Cheng, Y. J.; Ma, J. F.; Wang, Y. M.; Liang, Q. L.; Luo, G. A. Steaming-induced chemical transformations and holistic quality assessment of red ginseng derived from *Panax ginseng* by means of HPLC-ESI-MS/MS(n)-based multicomponent quantification fingerprint. *J. Agric. Food Chem.* **2012**, *60*, 8213−8224.

(34) Qin, F.; Yu, S.; Gao, Y.; Zheng, Y. Simultaneous determination of ginsenoside Rg1 and ginsenoside Re in total saponins of fibrous

roots of *Panax notoginseng* by HPLC-MS/MS. *Zhongguo Yaofang* **2010**, *21*, 2922−2924.
(35) Jiang, Y.; Wang, Q.; Ma, S.; Dang, X. Quantitative determination of saponins in the root of *Panax* pseudo-ginseng var. notoginseng by HPLC-ELSD and UV spectrophotometry. *Zhongcaoyao* **2000**, *31*, 737−739.
(36) Wang, X.; Ni, J.; Guo, Y. Quantitative determination of ginsenoside Rg1 and Rb1 in Radix Notoginseng. *Beijing Zhongyiyao Daxue Xuebao* **2000**, *23*, 38−40.
(37) Lang, W.; Lou, Z.; But, P. P. High-performance liquid chromatographic analysis of ginsenosides in *Panax ginseng*, *P. quinquefolium*, and *P. notoginseng*. *J. Chin. Pharm. Sci.* **1993**, *2*, 133−143.
(38) Wan, X.-q.; Xia, B.-h.; Lou, Z.-h.; Peng, Y.-s.; Gong, Y.-c.; Wu, Y.-y. Determination of saponins in different processed products of *Panax notoginseng*. *Zhonghua Zhongyiyao Zazhi* **2011**, *26*, 841−843.
(39) Dan, M.; Xie, G.; Gao, X.; Long, X.; Su, M.; Zhao, A.; Zhao, T.; Zhou, M.; Qiu, Y.; Jia, W. A rapid ultra-performance liquid chromatography-electrospray ionisation mass spectrometric method for the analysis of saponins in the adventitious roots of *Panax notoginseng*. *Phytochem Anal.* **2009**, *20*, 68−76.
(40) Toh, D. F.; New, L. S.; Koh, H. L.; Chan, E. C. Ultra-high performance liquid chromatography/time-of-flight mass spectrometry (UHPLC/TOFMS) for time-dependent profiling of raw and steamed *Panax notoginseng*. *J. Pharm. Biomed. Anal.* **2010**, *52*, 43−50.
(41) Hu, P.; Luo, G. A.; Wang, Q.; Zhao, Z. Z.; Wang, W.; Jiang, Z. H. The retention behavior of ginsenosides in HPLC and its application to quality assessment of Radix Ginseng. *Arch. Pharm. Res.* **2009**, *32*, 667−676.
(42) Wang, J. R.; Leung, C. Y.; Ho, H. M.; Chai, S.; Yau, L. F.; Zhao, Z. Z.; Jiang, Z. H. Quantitative comparison of ginsenosides and polyacetylenes in wild and cultivated American ginseng. *Chem. Biodivers.* **2010**, *7*, 975−983.
(43) Dong, T. T. X.; Cui, X. M.; Song, Z. H.; Zhao, K. J.; Ji, Z. N.; Lo, C. K.; Tsim, K. W. K. Chemical assessment of roots of *Panax notoginseng* in China: regional and seasonal variations in its active constituents. *J. Agric. Food Chem.* **2003**, *51*, 4617−4623.
(44) Clarke, J. D.; Alexander, D. C.; Ward, D. P.; Ryals, J. A.; Mitchell, M. W.; Wulff, J. E.; Guo, L. Assessment of genetically modified soybean in relation to natural variation in the soybean seed metabolome. *Sci. Rep.* **2013**, *3*, 3082.
(45) Wang, J. R.; Yau, L. F.; Zhang, R.; Xia, Y.; Ma, J.; Ho, H. M.; Hu, P.; Hu, M.; Liu, L.; Jiang, Z. H. Transformation of ginsenosides from notoginseng by artificial gastric juice can increase cytotoxicity toward cancer cells. *J. Agric. Food Chem.* **2014**, *62*, 2558−2573.
(46) Domon, B.; Costello, C. E. A systematic nomenclature for carbohydrate fragmentations in FAB-MS/MS spectra of glycoconjugates. *Glycoconjugate J.* **1988**, *5*, 397−409.

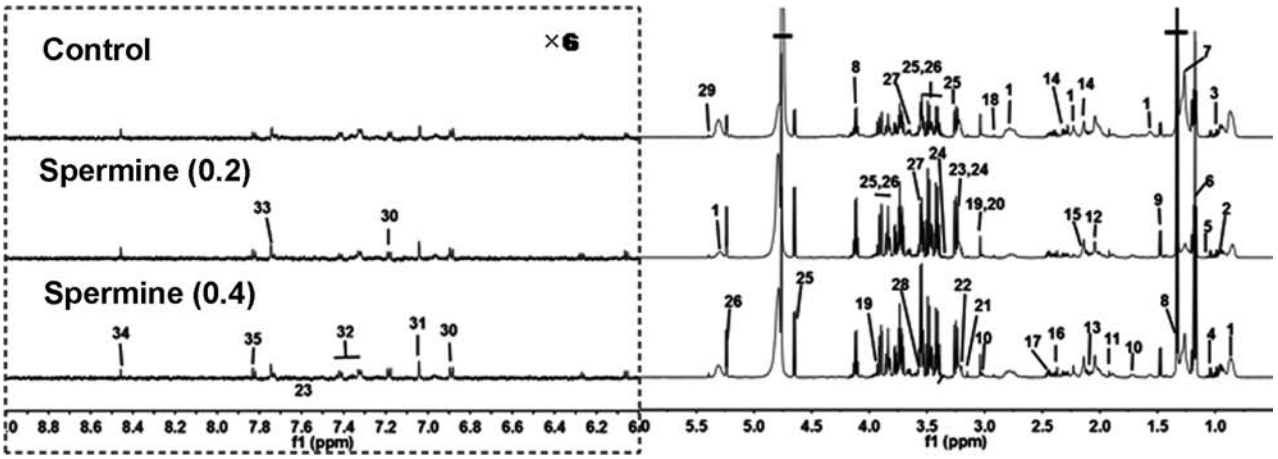


**Figure 1.** Typical one-dimensional $^1$H NMR spectra of plasma metabolites taken from the control and spermine (0.2 and 0.4 $\mu$mol/g BW) groups. The region of $\delta$ 6.0−9.0 was magnified 6 times compared with the corresponding region of $\delta$ 0.5−6.0 for clarity. A total of 34 metabolites were unambiguously assigned. The chemical shifts and peak multiplicities of these metabolites are given in Table 1.

response of animal or human biological systems to spermine supplementation.

To explore the molecular mechanisms of the role of spermine in ameliorating weaning stress, variations in the plasma metabolome were examined by using a metabolomic strategy. Plasma is a complex mixture of many constituents, and the $^1$H NMR spectra of plasma from animals under similar physiological conditions are reproducible. Each peak in the $^1$H NMR spectra of plasma is accurately correlated with the hydrogen atom of different metabolic chemicals. The relative signal intensity of each peak represents the contents of each component detected in the samples compared with the control. The metabolic profiles of spermine supplementation in rats can improve the current understanding of the association between metabolites and spermine supplementation, provide clues on the correlation between the metabolite and nutritional biochemical mechanisms of spermine, and create baseline data for future metabolomic experiments on spermine metabolism. This approach is also potentially valuable to the study of spermine metabolism and the search for other relationships between spermine administration and health or disease risk. This study would help define the effects of metabolic modifiers and the refinement of nutritional requirements. This should allow for the better formulation of nutritional support for growth and health. This experiment aims to examine the effect of spermine administration on the plasma compositions of rats by employing an explorative metabolomic approach via $^1$H NMR spectroscopy and chemometrics.

## MATERIALS AND METHODS

**Animal Experiment and Sample Collection.** The protocol used in this study was approved by the Animal Care and Use Committee of the Animal Nutrition Institute of Sichuan Agricultural University and was conducted according to the *Guide for the Care and Use of Laboratory Animals* of the National Research Council. A total of 18 19-day-old male Sprague−Dawley rats weighing 38−54 g were habituated in individual metabolic cages and were allowed to acclimatize for 1 day. The rats received intragastric administration of either 0.2 or 0.4 $\mu$mol/g body weight (BW) of spermine (Sigma Chemical Co., St. Louis, MO, USA) or saline (control) once a day for 3 days. Six rats were allocated for each group. Blood samples were collected (9:00 a.m.) from the eye after anesthesia with ether and were placed into Eppendorf tubes that contain sodium heparin 48 h after the last spermine administration. Centrifugation at 3500*g* for 10 min at 4 °C was performed on whole blood samples to obtain plasma. All plasma samples were stored at −80 °C pending NMR spectroscopic analysis. The dosage selected for this study was based on a prior experiment.[10,16] The rats were allowed ad libitum access to food and drinking water. Temperatures between 22 and 25 °C, a cycle of 12 h light/12 h dark, and humidity from 50 to 70% were maintained throughout the study. Clinical observations were made during the experimental period.

**Sample Preparation and NMR Spectroscopy.** Plasma samples were thawed from −80 °C. Six hundred and thirty microliters of plasma samples was mixed with 70 $\mu$L of Anachro certified DSS standard solution containing 99.9% v/v $D_2O$ (for field frequency lock purposes), 0.2% w/v $NaN_3$ (for inhibiting bacterial growth), and 4.08 mM DSS as a reference at 0 ppm (Anachro Technology Co., Ltd. Wuhan, China). After vortexing and centrifugation at 12000 rpm for 10 min (4 °C), 550 $\mu$L of the samples was placed into 5 mm NMR tubes for NMR analysis.

The proton NMR spectra of the plasma samples were achieved at 300 K on a Bruker Avance II 600 MHz spectrometer (Bruker Biospin, Rheinstetten, Germany) operating at a $^1$H frequency of 600.13 MHz with broadband-observe probe. A water-presaturated Carr−Purcell−Meiboom−Gill pulse sequence (recycle delay−90°−$(\tau-180°-\tau)_n$−acquisition) was used to attenuate the NMR signals from macromolecules. A spin−spin relaxation delay ($2n\tau$) of 76.8 ms and a spin−echo delay $\tau$ of 400 $\mu$s were employed. A 90° pulse was set to 13.7 $\mu$s with a recycle delay of 2 s and acquisition time of 2.56 s. A total of 32 transients were collected into 49178 data points for each spectrum with a spectral width of 15 ppm. For assignment purposes, $^1$H−$^1$H correlation spectroscopy and $^1$H−$^1$H total correlation spectroscopy were acquired for selected samples.

**NMR Spectroscopic Processes and Analysis.** Before Fourier transformation, the free induction decays were multiplied by an exponential window function with a 1 Hz line-broadening factor. All NMR spectra were then manually phase- and baseline-corrected. The plasma spectral region $\delta$ 0.5−9.0 was integrated into regions with equal widths of 0.002 ppm by using Mestrenova 8.1.2 software (Mestrelab Research S.L., Spain). Plasma chemical shifts were referenced to the peak of the methyl proton of L-lactate at $\delta$ 1.33. The ethanol signals from the process of blood collection were carefully excluded together with the regions containing urea and $H_2O$ signals to obtain only the endogenous metabolite changes induced by spermine exposure. This treatment helps avoid any contributions of ethanol, urea, and $H_2O$ to intergroup differentiations. In the plasma spectra, the discarded regions contain $\delta$ 4.19−5.23 and $\delta$ 5.40−6.80 for $H_2O$ and urea, and $\delta$ 1.16−1.19 and $\delta$ 3.60−3.62 for ethanol. Subsequently, each integral region was normalized to the total sum of all integral regions for each spectrum prior to pattern recognition analysis.

**Table 1. $^1$H NMR Data for Metabolites in Rat Plasma**

| key | metabolite | moieties | $\delta$ $^1$H (ppm) and multiplicity |
|---|---|---|---|
| 1 | lipid | $CH_3(CH_2)_n$, $CH_3CH_2CH_2C{=}$, $(CH_2)_n$, $CH_2CH_2CO$, $CH_2C{=}C$, $CH_2CO$, $C{=}CCH_2C{=}C$, $-CH{=}CH-$ | 0.84(t), 0.89(t), 1.28(m), 1.58(m), 2.01(m), 2.24(m), 2.76(m), 5.30(m) |
| 2 | isoleucine | $\alpha$CH, $\beta$CH, $\beta CH_3$, $\gamma CH_2$, $\delta CH_3$ | 3.68(d), 1.99(m), 1.01(d), 1.26(m), 1.47(m), 0.94(t) |
| 3 | leucine | $\alpha$CH, $\beta CH_2$, $\gamma$CH, $\delta CH_3$ | 3.73(t), 1.72(m), 1.72(m), 0.96(d), 0.97(d) |
| 4 | valine | $\alpha$CH, $\beta$CH, $\gamma CH_3$ | 3.62(d), 2.28(m), 0.99(d), 1.04(d) |
| 5 | propionate | $CH_3$, $CH_2$ | 1.08(t), 2.18(q) |
| 6 | ethanol | $CH_3$, $CH_2$ | 1.18(t), 3.55(q) |
| 7 | 3-hydroxybutyrate | $\alpha CH_2$, $\beta$CH, $\gamma CH_3$ | 2.28(dd), 2.42(dd), 4.16(m), 1.20(d) |
| 8 | lactate | $\alpha$CH, $\beta CH_3$ | 4.13(q), 1.33(d) |
| 9 | alanine | $\alpha$CH, $\beta CH_3$ | 3.77(q), 1.48(d) |
| 10 | lysine | $\alpha$CH, $\beta CH_2$, $\gamma CH_2$, $\varepsilon CH_2$ | 3.76(t), 1.91(m), 1.48(m), 1.72(m), 3.01(t) |
| 11 | acetate | $CH_3$ | 1.92(s) |
| 12 | *N*-acetyl glycoprotein | $CH_3$ | 2.04(s) |
| 13 | *O*-acetyl glycoprotein | $CH_3$ | 2.08(s) |
| 14 | glutamate | $\alpha$CH, $\beta CH_2$, $\gamma CH_2$ | 3.75(m), 2.12(m), 2.35(m) |
| 15 | methionine | $\alpha$CH, $\beta CH_2$, $\gamma CH_2$, S-$CH_3$ | 3.87(t), 2.16(m), 2.65(t), 2.14(s) |
| 16 | pyruvate | $CH_3$ | 2.37(s) |
| 17 | glutamine | $\alpha$CH, $\beta CH_2$, $\gamma CH_2$ | 3.78(m), 2.14(m), 2.45(m) |
| 18 | trimethylamine | $CH_3$ | 2.92(s) |
| 19 | creatine | $CH_3$, $CH_2$ | 3.04(s), 3.93(s) |
| 20 | creatinine | $CH_3$, $CH_2$ | 3.04(s), 4.05(s) |
| 21 | malonate | $CH_2$ | 3.45(s) |
| 22 | choline | $OCH_2$, $NCH_2$, $N(CH_3)_3$ | 4.07(t), 3.53(t), 3.20(s) |
| 23 | glycerolphosphocholine | $CH_3$, $\beta CH_2$, $\alpha CH_2$ | 3.22(s), 3.69(t), 4.33(t) |
| 24 | phosphorylcholine | $N(CH_3)_3$, $OCH_2$, $NCH_2$ | 3.22(s), 4.21(t), 3.61(t) |
| 25 | $\beta$-glucose | 1-CH, 2-CH, 3-CH, 4-CH, 5-CH, 6-CH | 4.65(d), 3.25(dd), 3.49(t), 3.41(dd), 3.46(m), 3.73(dd), 3.90(dd) |
| 26 | $\alpha$-glucose | 1-CH, 2-CH, 3-CH, 4-CH, 5-CH, 6-CH | 5.24(d), 3.54(dd), 3.71(dd), 3.42(dd), 3.84(m), 3.78(m) |
| 27 | *myo*-inositol | 1,3-CH, 2-CH, 5-CH, 4,6-CH | 3.60(dd), 4.06(t), 3.30(t), 3.63(t) |
| 28 | glycine | $CH_2$ | 3.58(s) |
| 29 | allantoin | CH | 5.40(s) |
| 30 | tyrosine | 2,6-CH, 3,5-CH | 7.20(dd), 6.91(d) |
| 31 | 1-methylhistidine | 4-CH, 2-CH | 7.05(s), 7.78(s) |
| 32 | phenylalanine | 2,6-CH, 3,5-CH, 4-CH | 7.32(m), 7.42(m), 7.37(m) |
| 33 | 3-methylhistidine | 4-CH, 2-CH | 7.07(s), 7.67(s) |
| 34 | formate | CH | 8.46(s) |
| 35 | unknown | | 7.83 (d) |



dx.doi.org/10.1021/jf500882t | J. Agric. Food Chem. 2014, 62, 9035−9042

Multivariate data analysis was performed on normalized NMR data sets with the software package SIMCA-P+ (version 11.0, Umetrics, Sweden). Principal component analysis (PCA) was performed on the data set to examine group clustering and to find possible outliers. The results were viewed in the form of score plots, where each point represented an individual sample, and loading plots, where each coordinate represented one NMR spectral region. Projection to latent structure−discriminant analysis (PLS-DA) and orthogonal projection to latent structure−discriminant analysis (OPLS-DA) were performed by using the NMR data (scaled to unit variance) as the *X*-matrix and the class information as the *Y*-matrix.[17] The quality of the model was evaluated by the parameters $R^2X$, representing the total explained variation, and $Q^2$, standing for the model predictability. The models were validated by using a 7-fold cross-validation method and a permutation test.[18,19] A model was considered significant if the $Q^2$ value was significant ($P < 0.05$) through permutation. The OPLS-DA models were interpreted by coefficient-coded loading plots. The loadings were backtransformed in Excel (Microsoft, USA) and plotted with the color-coded absolute coefficient values ($|r|$) of the variables in MATLAB (The Mathworks Inc., Natwick, MA, USA; version 7.1).[18] In these loading plots, the warm-colored (e.g., red) variables contributed more to intergroup differentiation than cool-colored (e.g., blue) variables. In the current study, appropriate correlation coefficients were used as the cutoff values (depending upon the number of animals used for each group) for the statistical significance based on the discrimination significance ($P < 0.05$). These coefficients were determined by using Pearson's product-moment correlation coefficient.[18]

## RESULTS AND DISCUSSION

**$^1$H NMR Spectra of Plasma Samples.** Figure 1 demonstrates the representative $^1$H NMR spectra of rat plasma from the control and spermine-treated groups. NMR signals were assigned to specific metabolites for $^1$H NMR resonances (Table 1). The spectra of the plasma samples mainly contained resonances from glucose, lactate, lipids, choline metabolites, and a series of amino acids.

**Multivariate Data Analysis of NMR Data.** PCA was initially performed on plasma spectral data. Two principal components were calculated for the treatment groups, with 55.8 and 12.9% of the variables explained by PC1 and PC2, respectively. PCA results (Figure 2A) showed that separation were absent in the metabolic plasma profiles of rats from the treatment and control groups. Moreover, PLS-DA was conducted on the plasma spectra of the spermine-treated and control groups. The score plots clearly highlighted three clusters corresponding to the three groups (Figure 2B). Furthermore, the plasma metabolic changes in the rats from the spermine-treated and control groups were analyzed by using OPLS-DA. The corresponding coefficient analysis demonstrated that spermine (0.2 μmol/g BW) significantly increased the plasma levels of 1-methylhistidine, 3-hydroxybutyrate, alanine, glutamine, glycerolphosphocholine (GPC), phosphorylcholine, *myo*-inositol, phenylalanine, tyrosine, valine, trimethylanine, and α-glucose compared with the control group ($P < 0.05$; Table 2 and Figure 3B). Spermine (0.4 μmol/g BW) significantly increased the plasma levels of 1-methylhistidine, alanine, formate, glutamate, glutamine, GPC, phosphorylcholine, lysine, lipid, phenylalanine, tyrosine, trimethylanine, α-glucose, and β-glucose compared with the control groups ($P < 0.05$; Table 2 and Figure 3A). Furthermore, spermine (0.4 μmol/g BW) significantly decreased the plasma levels of 3-hydroxybutyrate, acetate, choline, lactate, and *myo*-inositol and increased the plasma levels of glutamine compared with the spermine-treated (0.2 μmol/g BW) groups ($P < 0.05$; Table 2 and Figure 3C).

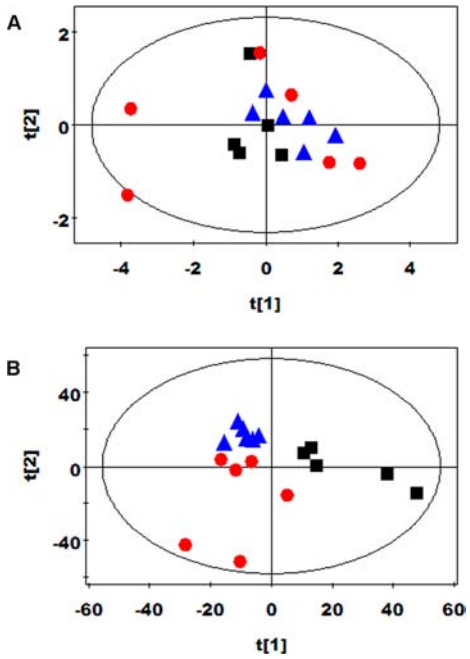


**Figure 2.** PCA score plots ($R^2X = 0.865$, $Q^2 = 0.638$; A) and PLS-DA score plots ($R^2X = 0.639$, $R^2Y = 0.987$, $Q^2 = 0.537$; B) based on the $^1$H NMR spectra of 48 h plasma metabolites taken from the spermine-treated groups (0.2 (red circles) and 0.4 μmol/g BW (blue triangles)) and the control group (black squares). One sample from the control group was excluded because of hemolysis.

**Spermine Supplementation Induces Alterations to Cell Membrane Metabolism and Lipid Metabolism.** Spermine supplementation can alter cell membrane metabolism. Phosphorylcholine and GPC are essential elements for the structural integrity of cell membranes and play critical roles in cell metabolism and signaling processes.[20,21] In this study, plasma phosphorylcholine and GPC levels were increased by spermine ingestion. Spermine supplementation can enhance intestinal maturation (data not shown). Therefore, the structural integrity of the cell membrane is ameliorated. Moreover, spermine supplementation can alter lipid metabolism. GPC synthesis in mammalian and bacterial cells occurs with choline.[22] GPC acts as an inhibitor of lysophospholipase, which catalyzes the hydrolysis of physiologically important lysophospholipid substrates (containing lysophosphatidic acid and sphingosine 1-phosphate). These lipids play a critical role in cellular signaling and nutrient metabolism regulation.[23] The plasma concentrations of *myo*-inositol were increased in response to spermine supplementation. This carbocyclic polyol provides the structural basis for many secondary messengers (e.g., inositol phosphates, phosphatidylinositol, and phosphatidylinositol phosphate) in eukaryotic cells.[24] Therefore, inositol is linked to the regulation of intracellular calcium (Ca) concentrations, insulin signal transduction, gene expression, and fatty acid oxidation.[24,25] This result is in agreement with a previous study that shows that spermine enhances electrogenic $Ca^{2+}$ uptake and increases mitochondrial $Ca^{2+}$ retention.[26] Phosphorylcholine is an essential component for the assembly and secretion of very-low-density lipoproteins in the liver, and an increased level of phosphorylcholine can cause high lipid transfer into the blood. This result is in agreement with that of

**Table 2. OPLS-DA Coefficients, *P* Values, and Main Functions Derived from the NMR Data of 48 h Plasma Metabolites Obtained from the (A) Control Group and Spermine-Treated Groups ((A) 0.2 and (B) 0.4 μmol/g BW)**

| | OPLS-DA coefficient ($r$)[a] | | | *P* value[b] | | | |
|---|---|---|---|---|---|---|---|
| metabolite | B (vs A) | C (vs A) | C (vs B) | B (vs A) | C (vs A) | C (vs B) | main functions |
| 1-methylhistidine (31) | 0.912 | 0.91 | – | <0.01 | <0.01 | 0.782 | protein metabolism |
| 3-hydroxybutyrate (33) | 0.882 | – | −0.863 | <0.01 | 0.779 | <0.01 | providing fuel for vital organs |
| lactate (8) | – | – | −0.719 | 0.360 | 0.260 | <0.05 | energy metabolism |
| acetate (11) | – | – | −0.708 | 0.489 | 0.125 | <0.05 | microbial metabolite |
| choline (22) | – | – | −0.757 | 0.616 | 0.081 | <0.05 | essential elements for the structural integrity of cell membranes and lipid metabolism |
| glycerolphosphocholine (23) | 0.783 | 0.876 | – | <0.01 | <0.01 | 0.848 | |
| phosphorylcholine (24) | 0.804 | 0.782 | – | <0.01 | <0.01 | 0.420 | |
| alanine (9) | 0.806 | 0.884 | – | <0.01 | <0.01 | 0.218 | glucose−alanine cycle metabolism |
| α-glucose (26) | 0.786 | 0.758 | −0.708 | <0.01 | <0.01 | 0.135 | |
| β-glucose (25) | – | 0.867 | −0.767 | <0.05 | <0.01 | 0.434 | |
| lysine (10) | – | 0.879 | – | <0.05 | <0.01 | 0.416 | protein synthesis and cell growth |
| phenylalanine (32) | 0.865 | 0.789 | −0.751 | <0.01 | <0.05 | 0.224 | |
| tyrosine (30) | 0.815 | 0.794 | −0.767 | <0.01 | <0.05 | 0.391 | |
| glutamate (14) | – | 0.765 | – | 0.07 | <0.05 | 0.554 | |
| glutamine (17) | 0.798 | 0.758 | 0.782 | <0.01 | <0.05 | <0.05 | protein synthesis, maintenance of gut barrier function, and intestinal cell proliferation and differentiation |
| *myo*-inositol (27) | 0.758 | – | −0.771 | <0.01 | <0.05 | <0.01 | structural basis for many secondary messengers |
| lipid (1) | – | 0.857 | – | 0.08 | <0.01 | 0.09 | lipid metabolism |
| valine (4) | 0.853 | – | – | <0.01 | <0.05 | 0.135 | energy-generating amino acid |
| trimethylamine (18) | 0.899 | 0.833 | – | <0.01 | <0.01 | 0.497 | microbial metabolites |
| formate (34) | – | 0.844 | – | <0.05 | <0.05 | 0.726 | |
| unknown (35) | 0.798 | – | – | 0.192 | 0.774 | 0.120 | |

[a]Correlation coefficients: positive and negative signs indicate positive and negative correlation in the concentrations, respectively. The correlation coefficient of $|r| > 0.755$ (for B vs A and C vs A) or 0.707 (for C vs B) was used as the cutoff value. "'−'" means the correlation coefficient $|r|$ is <0.755 (for B vs A and C vs A) or <0.707 (for C vs B). [b]Normalized integral of metabolites in the spectrum (normalized to 100). Integrals of the altered metabolites were analyzed statistically using one-way analysis of variance (ANOVA) of SPSS 17.0 software (SPSS Inc., Chicago, IL, USA). Date sets were further analyzed using post hoc tests (least significant difference, LSD) for multiple comparisons to determine the statistical differences between groups. *P* values are significant at the <0.05 or <0.01 level, and *P* values are not significant at >0.05.

the present study. GPC and phosphorylcholine also have critical roles in lipid cholesterol transport and metabolism.[21] Furthermore, ketone body production (e.g., acetone, 3-hydroxybutyrate, and acetoacetate) provides fuel for vital organs (e.g., heart, brain), thus increasing the chance of survival from metabolic problems. Acetoacetate and 3-hydroxybutyrate are products of fatty acid oxidation in the liver, and their ratios are useful indicators of the mitochondrial redox state. Spermine supplementation increased 3-hydroxybutyrate concentrations but did not change acetoacetate concentrations in plasma, thus decreasing the acetoacetate to 3-hydroxybutyrate ratio. This result suggests the decreased oxidized state of cells, which can be given by the decreased oxidation of fatty acids. Collectively, spermine supplementation can alter cell membrane and lipid metabolism.

**Spermine Intakes Cause Changes in Glucose−Alanine Cycle Metabolism.** The spermine-treated group exhibited a significant increase of plasma glucose and alanine levels compared with the control group. Glucose is a major energy substrate that plays a role in animal growth and development. Alanine is an important participant and regulator in glucose metabolism. Alanine levels are correlated with blood sugar levels in both diabetes and hypoglycemia, and alanine alleviates both severe hypoglycemia and ketosis in diabetes. Alanine is an important amino acid for lymphocyte reproduction and immunity.[27] These findings suggest that spermine supplementation can affect the glucose−alanine cycle metabolism.

**Spermine Supplementation Alters Amino Acid Metabolism.** Spermine exposure can alter amino acid metabolism. In this study, spermine decreased urinary *N*-acetylglutamate levels (data not shown). Urea plays an important role in the metabolism of nitrogen-containing compounds. *N*-Acetylglutamate is necessary for the normal functioning of the urea cycle, and variations in its concentration affect the urea production rate and other urea synthesis substrates.[28] The increase of blood urea nitrogen is related to the decrease of *N*-


dx.doi.org/10.1021/jf500882t | J. Agric. Food Chem. 2014, 62, 9035−9042

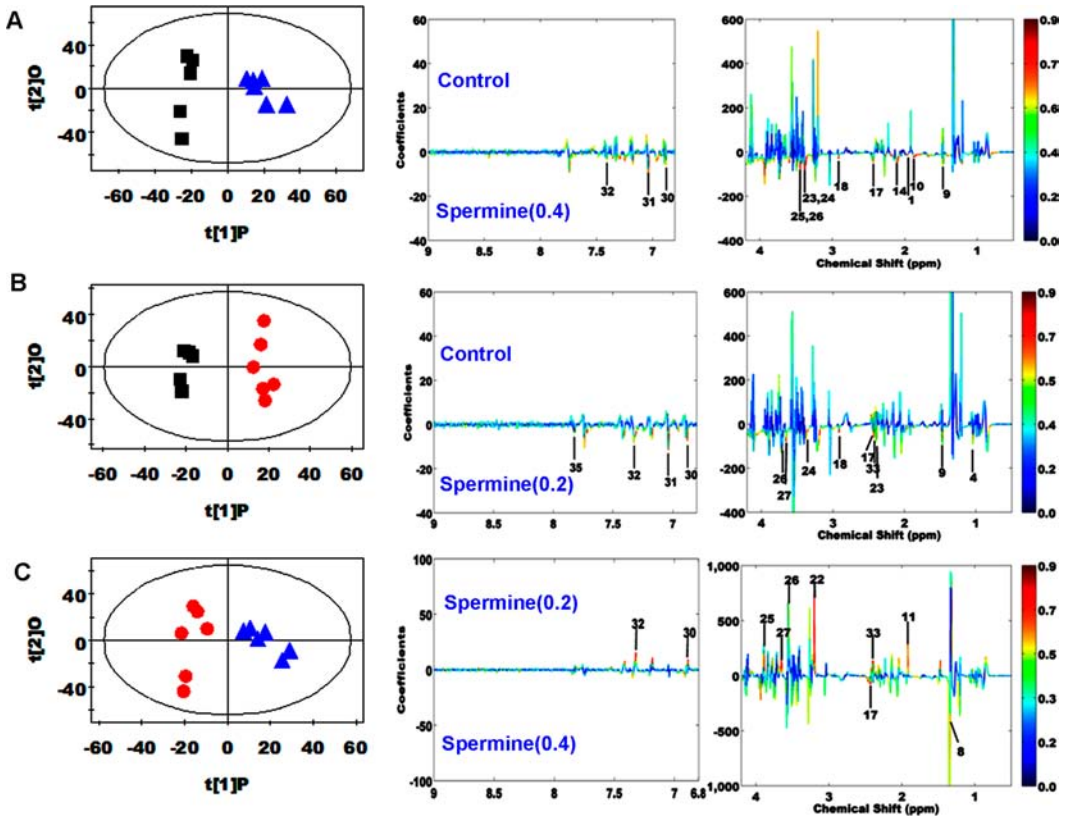


**Figure 3.** OPLS-DA score plots (left panel) and the corresponding coefficient loading plots (right panel) derived from the $^{1}$H NMR spectra of 48 h plasma metabolites obtained from the spermine-treated group (0.2 (red circles) and 0.4 $\mu$mol/g BW (blue triangles)) and the control (black squares) groups (A, $R^2X = 0.397$, $Q^2 = 0.327$; B, $R^2X = 0.294$, $Q^2 = 0.457$; C, $R^2X = 0.364$, $Q^2 = -0.0257$). One sample from the control group was excluded because of hemolysis. The color scale in the coefficient plot shows the significance of metabolite variation between the spermine (0.2 and 0.4 $\mu$mol/g BW) and control groups.

acetylglutamate, thus indicating that urea production is modulated by *N*-acetylglutamate. Amino acids in the intestine increased during protein synthesis to promote intestinal maturation, thus leading to increased levels of amino acids present in plasma. The other possible reason is that spermine-induced energy expenditure may also lead to elevated consumptions of amino acids as an energy source. Our results demonstrated that the levels of branched-chain amino acids (BCAAs) were increased by spermine supplementation. BCAAs are known as key metabolites involved in protein synthesis and cell growth. BCAAs are some of the most efficient energy-generating amino acids in mammals. The increase of BCAA may further indicate increased energy expenditure during intestinal maturation. In the present study, we observed an increase in the levels of plasma tyrosine by spermine supplementation. This result is in accordance with the increase of phenylalanine levels in plasma because phenylalanine is the precursor for the amino acid tyrosine. This result also agrees with that of previous study; that is, spermine supplementation can ameliorate protein synthesis.[29] Moreover, we observed an increase in the levels of plasma lysine, glutamate, and glutamine; this result agrees with the role of spermine in increasing protein synthesis in rats.[29] Glutamine can activate signaling pathways to enhance protein synthesis, thus influencing animal growth and development. Glutamine is the principal carrier of nitrogen in the body and is an important energy source for many cells. A significant body of evidence links glutamine-enriched diets with intestinal effects. Glutamine aids in the maintenance of gut barrier function and intestinal cell proliferation and differentiation, as well as the reduction of septic morbidity and irritable bowel syndrome symptoms.[6,30] The possible explanation for the increase in glutamine is that the structural integrity of the cell membrane is ameliorated. Taken together, spermine ingestion can change amino acid metabolism.

**Spermine Supplementation Results in Changes in Gut Microbiota Functions.** A novel and unexpected finding from this work is that plasma formate and nitrogenous compounds (trimethylamine) were increased. Plasma formate and trimethylamine are microbial metabolites of carbohydrates and amino acids, which are probably produced in the lumen of the small and large intestines.[31,32] Intestinal microbes convert dietary nondigestible fibers into short-chain fatty acids and other nutrients that can be used by the mammalian host as energy sources or as precursors for fatty acid synthesis.[33] The introduction of spermine supplementation into the mammalian system may disrupt baseline mammalian-to-microbe behavior, thereby leading to a disruption in microbial populations and metabolism. Changes in these metabolites may be caused by the reduced number and/or altered activity of intestinal microorganisms. An in vitro experiment has showed that spermine supplementation can inhibit some microbes, thus leading to a decrease in microbe number and/or metabolic activity.[34] A decrease in the number of intestinal bacteria is believed to be consistent with decreased fat accretion,[35] although the underlying mechanisms are still unknown.

In conclusion, our results provide the metabolic processes associated with spermine supplementation in modulating

weaning stress, including cell membrane metabolism, lipid metabolism, glucose−alanine cycle metabolism, amino acid metabolism, and gut microbiota metabolism, which have important implications in nutritional research in infants. This study also highlights the potential for the development of a metabolomic strategy in probing the effects of nutritional intervention in a mammalian system. To the best of our knowledge, this is the first study to identify systematically the expressed metabolites in plasma from spermine supplementation. Future studies may be directed toward a mechanistic understanding of the effects of spermine on animal tissue intermediary metabolism.

## AUTHOR INFORMATION


### Corresponding Author

*(G.L.) Mail: Institute of Animal Nutrition, Sichuan Agricultural University and Key Laboratory for Animal Disease-Resistance Nutrition of China Ministry of Education, Chengdu 611130, Sichuan, China. Phone: +86-28-86291256. E-mail: okliugm@gmail.com, liugm@sicau.edu.cn.



### Funding

The investigation received financial support from the National Natural Science Foundation of China (No. 31301986), the Research Foundation of Education Bureau of Sichuan Province (No. 11ZB061), the Ministry of Education Chunhui Project of China (No. Z2010092), and the Specific Research Supporting Program for Discipline Construction in Sichuan Agricultural University.


### Notes

The authors declare no competing financial interest.

## ACKNOWLEDGMENTS

We thank all of the study participants for their ongoing assistance.

## ABBREVIATIONS USED

PCA, principal component analysis; PLS-DA, projection to latent structure−discriminant analysis; OPLS-DA, orthogonal projection to latent structure−discriminant analysis; GPC, glycerolphosphocholine; BCAAs, branched-chain amino acids

## REFERENCES


(1) Moeser, A. J.; Ryan, K. A.; Nighot, P. K.; Blikslager, A. T. Gastrointestinal dysfunction induced by early weaning is attenuated by delayed weaning and mast cell blockade in pigs. *Am. J. Physiol. Gastrointest. Liver Physiol.* **2007**, *293*, G413−G421.

(2) Smith, F.; Clark, J. E.; Overman, B. L.; Tozel, C. C.; Huang, J. H.; Rivier, J. E.; Blikslager, A. T.; Moeser, A. J. Early weaning stress impaires development of mucosal barrier function in the porcine intestine. *Am. J. Physiol. Gastrointest. Liver Physiol.* **2010**, *298*, G352−G363.

(3) Lallès, J. P.; Bosi, P.; Smidt, H.; Stokes, C. R. Weaning − a challenge to gut physiologists. *Livest. Sci.* **2007**, *108*, 82−93.

(4) Pluske, J. R.; Hampson, D. J.; Williams, I. H. Factors influencing the structure and function of the small intestine in the weaned pig: a review. *Livest. Prod. Sci.* **1997**, *51*, 215−236.

(5) He, Q.; Tang, H.; Ren, P.; Kong, X.; Wu, G.; Yin, Y.; Wang, Y. Dietary supplementation with L-arginine partially counteracts serum metabonome induced by weaning stress in piglets. *J. Proteome Res.* **2011**, *10*, 5214−5221.

(6) Wang, J.; Chen, L.; Li, P.; Li, X.; Zhou, H.; Wang, F.; Li, D.; Yin, Y.; Wu, G. Gene expression is altered in piglet small intestine by weaning and dietary glutamine supplementation. *J. Nutr.* **2008**, *138*, 1025−1032.

(7) Dufour, C.; Dandrifosse, G.; Forget, P.; Vermesse, F.; Romain, N.; Lepoint, P. Spermine and spermidine induce intestinal maturation in the rat. *Gastroenterology* **1988**, *95*, 112−116.

(8) ter Steege, J. C.; Buurman, W. A.; Forget, P. P. Spermine induces maturation of the immature intestinal immune system in neonatal mice. *J. Pediatr. Gastroenterol. Nutr.* **1977**, *25*, 332−340.

(9) Peulen, O.; Pirlet, C.; Klimek, M.; Goffinet, G.; Dandrifosse, G. Comparison between the natural postnatal maturation and the spermine-induced maturation of the rat intestine. *Arch. Physiol. Biochem.* **1998**, *106*, 46−55.

(10) Deloyer, P.; Peulen, O.; Dandrifosse, G. Intestinal effects of long-lasting spermine ingestion by suckling rats. *Exp. Physiol.* **2005**, *90*, 901−908.

(11) Kaouass, M.; Deloyer, P.; Wery, I.; Dandrifosse, G. Analysis of structural and biochemical events occurring in the small intestine after dietary polyamine ingestion in suckling rats. *Dig. Dis. Sci.* **1996**, *41*, 1434−1444.

(12) Wéry, I.; Deloyer, P.; Dandrifosse, G. Effects of a single dose of orally-administered spermine on the intestinal development of unweaned rats. *Arch. Physiol. Biochem.* **1996**, *104*, 163−172.

(13) Peulen, O.; Denis, G.; Defresne, M. P.; Dandrifosse, G. Spermine-induced alteration of small intestine in suckling rat: involvement of apoptosis or $Zn^{2+}$ enzymes? *Dig. Dis. Sci.* **2001**, *46*, 2490−2498.

(14) Xiao, Y. P.; Wu, T. X.; Sun, J. M.; Yang, L.; Hong, Q. H.; Chen, A. G.; Yang, C. M. Response to dietary L-glutamine supplementation in weaned piglets: a serum metabolomic comparison and hepatic metabolic regulation analysis. *J. Anim. Sci.* **2012**, *90*, 4421−4430.

(15) Wang, Y.; Holmes, E.; Tang, H.; Lindon, J. C.; Sprenger, N.; Turini, M. E.; Bergonzelli, G.; Fay, L. B.; Kochhar, S.; Nicholson, J. K. Experimental metabonomic model of dietary variation and stress interactions. *J. Proteome Res.* **2006**, *5*, 1535−1542.

(16) Gréco, S.; Niepceron, E.; Hugueny, I.; George, P.; Louisot, P.; Biol, M. C. Dietary spermidine and spermine participate in the maturation of galactosyltransferase activity and glycoprotein galactosylation in rat small intestine. *J. Nutr.* **2001**, *131*, 1890−1897.

(17) Trygg, J.; Wold, S. Orthogonal projections to latent structures (O-PLS). *J. Chemom.* **2002**, *16*, 119−128.

(18) Cloarec, O.; Dumas, M. E.; Trygg, J.; Craig, A.; Barton, R. H.; Lindon, J. C.; Nicholson, J. K.; Holmes, E. Evaluation of the orthogonal projection on latent structure model limitations caused by chemical shift variability and improved visualization of biomarker changes in $^{1}H$ NMR spectroscopic metabonomic studies. *Anal. Chem.* **2005**, *77*, 517−526.

(19) Lindgren, F.; Hansen, B.; Karcher, W.; Sjöström, M.; Eriksson, L. Model validation by permutation tests: applications to variable selection. *J. Chemom.* **1996**, *10*, 521−532.

(20) Klein, J. Membrane breakdown in acute and chronic neurodegeneration: focus on choline-containing phospholipids. *J. Neural Transm.* **2000**, *107*, 1027−1063.

(21) Zeisel, S. H.; Blusztajn, J. K. Choline and human nutrition. *Annu. Rev. Nutr.* **1994**, *14*, 269−296.

(22) Burt, C. T.; Ribolow, H. Glycerol phosphorylcholine (GPC) and serine ethanolamine phosphodiester (SEP): evolutionary mirrored metabolites and their potential metabolic roles. *Comp. Biochem. Physiol. Biochem. Mol. Biol.* **1994**, *108*, 11−20.

(23) Tokumura, A. Metabolic pathways and physiological and pathological significances of lysolipid phosphate mediators. *J. Cell Biochem.* **2004**, *92*, 869−881.

(24) Di Paolo, G.; De Camilli, P. Phosphoinositides in cell regulation and membrane dynamics. *Nature* **2006**, *443*, 651−657.

(25) Siddiqui, R. A.; Harvey, K. A.; Zaloga, G. P. Modulation of enzymatic activities by n-3 polyunsaturated fatty acids to support cardiovascular health. *J. Nutr. Biochem.* **2008**, *19*, 417−437.

(26) Rottenberg, H.; Marbach, M. Regulation of $Ca^{2+}$ transport in brain mitochondria. I. The mechanism of spermine enhancement of $Ca^{2+}$ uptake and retention. *Biochim. Biophys. Acta* **1990**, *1016*, 77−86.

(27) Felig, P. The glucose-alanine cycle. *Metabolism* **1973**, *22*, 179−207.

(28) Meijer, A. J.; Verhoeven, A. J. *N*-Acetylglutamate and urea synthesis. *Biochem. J.* **1984**, *56*, 559−560.
(29) Igarashi, K.; Kashiwagi, K. Polyamines: mysterious modulators of cellular functions. *Biochem. Biophys. Res. Commun.* **2000**, *271*, 559−564.
(30) Wu, G.; Meier, S. A.; Knabe, D. A. Dietary glutamate supplementation prevents jejunal atrophy in weaned pigs. *J. Nutr.* **1996**, *126*, 2578−2584.
(31) Rezzi, S.; Ramadan, Z.; Fay, L. B.; Kochhar, S. Nutritional metabonomics: applications and perspectives. *J. Proteome Res.* **2007**, *6*, 513−525.
(32) Tannock, G. W. A special fondness for lactobacilli. *Appl. Environ. Microbiol.* **2004**, *70*, 3189−3194.
(33) Ley, R. E.; Turnbaugh, P. J.; Klein, S.; Gordon, J. I. Microbial ecology: human gut microbes associated with obesity. *Nature* **2006**, *444*, 1022−1023.
(34) Kwon, D.; Lu, C. Polyamine effects on antibiotic susceptibility in bacteria. *Antimicrob. Agents Chemother.* **2007**, *51*, 2070−2077.
(35) Turnbaugh, P. J.; Ley, R. E.; Mahowald, M. A.; Magrini, V.; Mardis, E. R.; Gordon, J. I. An obesity-associated gut microbiome with increased capacity for energy harvest. *Nature* **2006**, *444*, 1027−1031.

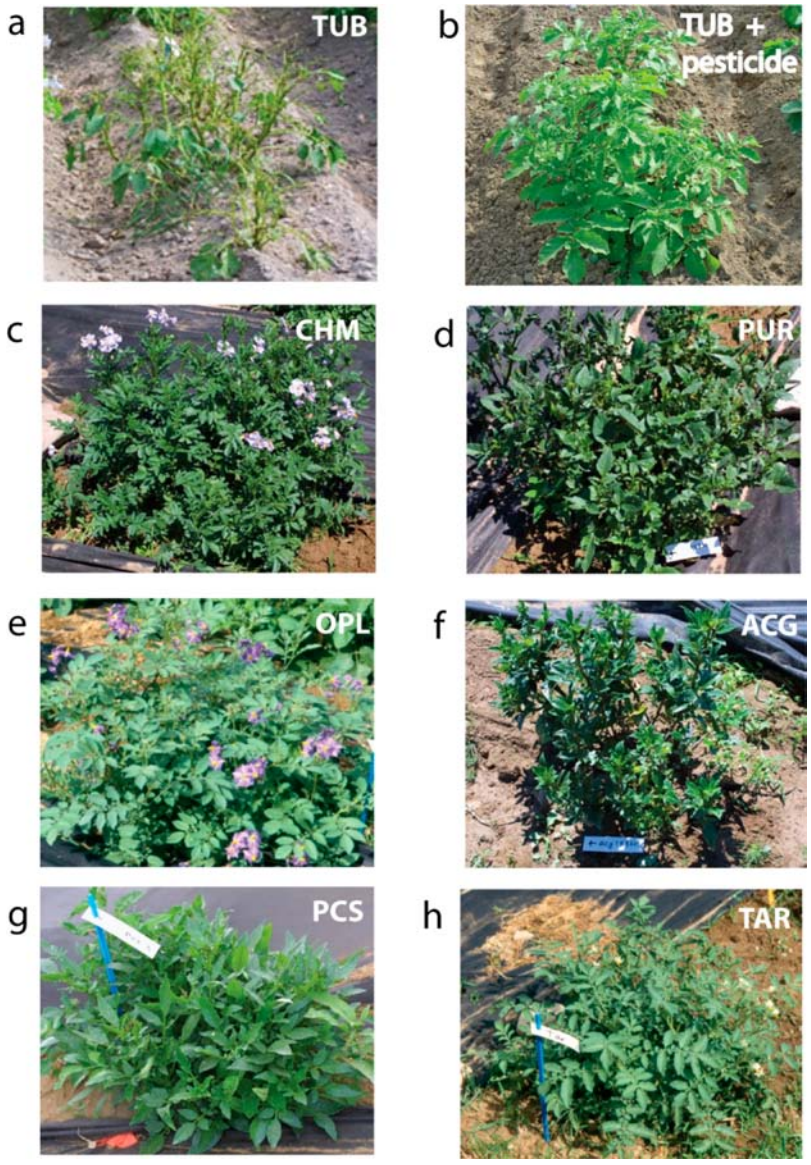


**Figure 1.** *Solanum* plants grown in the field: (a) *S. tuberosum* cv. Shepody (TUB); (b) *S. tuberosum* cv. Shepody treated with imidacloprid (TUB + pesticide); (c) *S. chomatophilum* (CHM); (d) *S. oplocense* (OPL); (e) *S. paucissectum* (PCS); (f) *S. piurae* (PUR); (g) *S. acroglossum* (ACG); (h) *S. tarijense* (TAR). Plants were grown in the absence of imidacloprid pesticide treatment except as indicated.

in the greenhouse in pots with potting mix and weekly fertilizer application of 20−20−20. Sampling of foliage was done on fully grown plants at 12 weeks after planting. The apical leaflets from five leaves for each plant were pooled in 15 mL conical tubes and flash frozen in liquid nitrogen. Samples were stored at −80 °C prior to extraction. A minimum of three replicate plants were sampled for all species.

**Growth of Plants in the Field.** Four plants from each wild *Solanum* species and *S. tuberosum* were grown in pots in the greenhouse in May 2008 and transplanted to a field at the Potato Research Centre 4 weeks after planting. The field was not treated with pesticide to allow for CPB infestation. For comparison, *S. tuberosum* was also planted in a field with imidacloprid (Admire) pesticide treatment in the soil prior to planting and two foliar treatments in July. The presence/absence of CPB and defoliation was noted during July and August, and photographs were taken.

**Extraction.** The frozen foliar samples were ground into a fine powder using a mortar and pestle while immersed in liquid nitrogen. One hundred milligrams of frozen ground tissue was placed in a 1.5 mL polyethylene screw-cap tube and kept frozen in a liquid nitrogen holding station (SPEX Sampleprep, Metuchen, NJ, USA) until all samples were ground. The ground powder was extracted with 400 μL of extraction solution (92% methanol, 0.1% formic acid LC-MS grade v/v) (Sigma-Aldrich, Oakville, ON, Canada). The samples were briefly vortexed and placed on ice until all samples were prepared. Samples were then sonicated in a Branson sonicator bath for 15 min and filtered through a 0.2 μm syringe filter into an LC-MS autosampler vial. Sample dilutions were optimized to ensure peak intensities were in the linear range and to avoid detector saturation. Wild *Solanum* and *S. tuberosum* samples were diluted 4-fold with extraction buffer. The samples were allowed to equilibrate at 23 °C in the dark for 1 h prior to analysis and were maintained under these conditions for the duration of the LC-MS analysis.

**UPLC-qTOF-MS.** Metabolite analysis was carried out using Acuity ultraperformance liquid chromatography− Xevo quadrupole time-of-flight mass spectrometry (UPLC-qTOF-MS) (Waters, Milford, MA, USA). Using a 5 μL loop, 0.75 μL injections were made for all samples in the study. The same volume of test mixture (rutin hydrate, caffeic acid, benzoic acid, *p*-coumaric acid, quercetin, L-phenylalanine, resveratrol, ferulic acid, L-tryptophan, sinapic acid, naringenin, *trans*-cinnamic acid, and isorhamnetin) (Sigma-Aldrich) was injected. All components of the test mixture were present at approximately 35 μg/mL in 60:40 acetonitrile/water v/v. All chromatographic separations


dx.doi.org/10.1021/jf502508y | J. Agric. Food Chem. 2014, 62, 9043−9055

were carried out on a 1 mm × 100 mm BEH C18 reverse phase column. The mobile phase was composed of LC-MS grade water with 0.1% formic acid (phase A) and LC-MS grade acetonitrile with 0.1% formic acid (phase B). The linear gradient consisted of six segments as follows: initial segment, 95% A, 5% B; 13:33 min, 25% A, 75% B; 13:53 min, 5% A, 95% B; 18:00 min, 5% A, 95% B; 18:01 min, 95% A, 5% B; and 20:00 min, 95% A, 5% B. The flow rate was 45.0 μL/min for all segments. The autosampler bed was maintained at 23 °C and the column at 35 °C. Samples were injected in a randomized fashion. Each sample was injected in triplicate with the exception of the test mixture which was injected after every six samples to evaluate the stability of retention time and mass accuracy over the duration of the experiment. Mass spectrometry data were collected over the duration of the LC ramp from 0 to 800 s. Mass-to-charge ratios ($m/z$) between 100 and 1500 were detected by electrospray ionization in positive ionization mode. A lockmass solution of dilute leucine enkephalin (LE) in acetonitrile/water (50:50 v/v) was introduced via the lockspray probe at 25 μL/min as directed by the MS manufacturer.

**Data Processing.** Mass spectrometry data were processed using Waters Markerlynx XS software. The UPLC-MS data were detected and noise-reduced in both the UPLC and MS domains such that only true analytical peaks were further processed by the software. Each peak was a feature that was identified using the chromatographic retention time from the chromatogram and $m/z$ of the positive molecular ion. The molecular ion adduct most commonly observed was $[M + H]^+$. No retention time correction was used as retention time stability was sufficient for UPLC. Quantification of peak intensity was done by integrating peaks with a mean retention time in the window of 100−800 s. The retention time window was selected on the basis of visual evaluation of chromatograms to exclude column void and washout. Features were tentatively assigned compound identities through matching $m/z$ against theoretical masses of compounds in the MetLin (http://metlin.scripps.edu/metabo_search_alt2.php) and KNApSAcK v1.200.3 (http://kanaya.naist.jp/KNApSAcK/) databases. Metabolites present in plant species with molecular masses within 6 ppm of the features were listed.

**Statistical Analysis.** The Multi-Experiment Viewer (MeV 4.7.4) software (http://www.tm4.org/mev/) was used for statistical analysis of the data. Samples for the biological replicates for each species were each injected three times for each species. The data was $\log_{10}$ transformed after adding $1 \times 10^{-12}$ to all data to remove zeros. The $\log_{10}$-transformed peak intensity data for all of the features were averaged for each of the species, and hierarchical clustering of the *Solanum* species was done using Euclidean distance. Additionally, one-way analysis of variance (ANOVA) was used to find features with variation between species at $p \leq 0.01$. Bonferroni correction was applied. The null hypothesis tested was that there were no differences between the mean peak intensities between species; the alternative hypothesis was that there were differences between species. The features with significant species variation were further analyzed. The untransformed peak intensity data for these features were averaged and further filtered as follows: (a) features with average peak intensity 100-fold increased in each of the wild species over *S. tuberosum* and with a minimum untransformed peak intensity of 10 in at least two wild species; (b) features with peak intensity data 100-fold increase in *S. tuberosum* over all of the wild species and with a minimal untransformed peak intensity of 10 in *S. tuberosum*.

## RESULTS AND DISCUSSION

**Comparative Analysis of Wild Species and *S. tuberosum*.** Studies have shown that the wild species *S. acroglossum*, *S. tarijense*, *S. chomatophilum*, *S. oplocense*, *S. paucisectum*, and *S. piurae* have CPB resistance.[17,18,23,24] These wild species along with *S. tuberosum* were grown in the field in the absence of the pesticide imidacloprid. CPB defoliation was observed on *S. tuberosum* in the absence (Figure 1a), but not in the presence, of imidacloprid (Figure 1b). The wild species showed low levels of defoliation in the field without imidacloprid (Figure 1c−h), which concurs with previous observations.[17,18,23,24] An objective of the study was to find metabolites that can be used as markers for screening CPB resistance in potato germplasm grown in greenhouses. Therefore, comparative analysis of foliar metabolites in *S. tuberosum* and the wild species was done with greenhouse-grown plants. The total ion chromatograph of extracted metabolites in positive ionization mode (Figure 2) and processed peak intensity data (Supporting Information Table S1) demonstrated metabolite variation between species.

The *Solanum* species were grouped using hierarchical clustering of all feature peak intensities from Table S1 (Figure

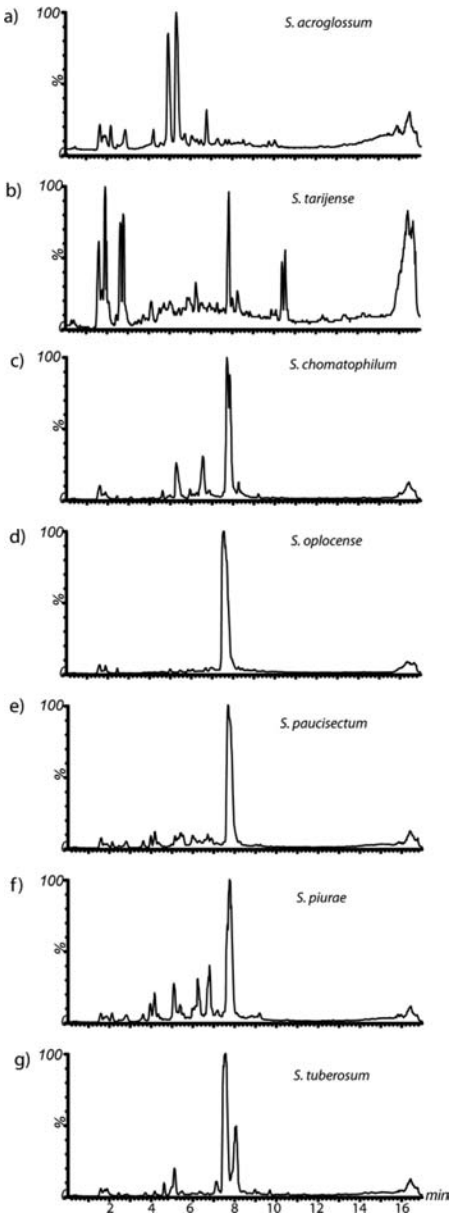


**Figure 2.** Total ion chromatograms for (a) *S. acroglossum* (4.87\307.1725), (b) *S. tarijense* (1.89\121.0636), (c) *S. chomatophilum* (7.56\1046.5571), (d) *S. oplocense* (7.56\1046.5571), (e) *S. paucisectum* (7.56\1046.5571), (f) *S. piurae* (7.77\578.4045), and (g) *S. tuberosum* (7.60\868.5004). The base peak features are given in parentheses. One hundred percent peak intensity for each was set at the intensity of the base peak. Each chromatogram is for a single representative sample for each species.


dx.doi.org/10.1021/jf502508y | J. Agric. Food Chem. 2014, 62, 9043−9055

3). *S. tuberosum* was found to be the most distant from the other species. *S. chomatophilum* and *S. oplocense* were found to

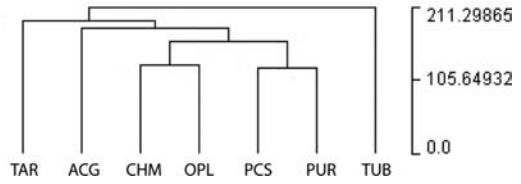


**Figure 3.** Hierarchical clustering of species based on metabolite profiles. TUB, *S. tuberosum* cv. Shepody; CHM *S. chomatophilum*; OPL, *S. oplocense*; PCS, *S. paucissectum*; PUR, *S. piurae*; ACG, *S. acroglossum*; TAR, *S. tarijense*. The scale is the Euclidean distance.

be closely related as were *S. paucisectum* and *S. piurae*. *S. acroglossum* and *S. tarijense* were more distant from these wild species. The results from hierarchical clustering were compared to published taxonomic groupings for species. All of the species studied were members of *Solanum* section Petota Dumortier, including *S. tuberosum*. Using morphological and genetic markers *S. piurae*, *S. acroglossum*, *S. paucisectum*, and, more recently *S. chomatophilum* were all placed in series Piurana.[25] Interestingly, our results showed that *S. acroglossum* did not cluster with the other three species on the basis of foliar metabolite profiles. *S. tarijense* has been recently found to be synonymous with *S. berthaultii*.[26] *S. tarijense* and *S. berthaultii* were designated as belonging to series Tuberosa III and Yungasensa by Hawkes. *S. oplocense* is part of the series Tuberosa, and more recently this species has been classified as belonging to the *S. brevicaule* complex, which encompasses some 20 species.[27] The clustering of metabolites places *S. oplocense* close to the Piurana species *S. chomatophilum* and, to a lesser extent, *S. paucisectum* and *S. piurae*. The results show that metabolite diversity occurs within a taxonomic grouping, and similarities occur between species described as more distantly related. Chemotaxonomic analysis of sapogenins from wild *Solanum* species also demonstrated clustering of species not found to be grouped together taxonomically.[28] Variability between accessions of the same species was also noted.

**Glycoalkaloid Variation between Species.** Features with $m/z$ corresponding to known glycoalkaloids found in *S. tuberosum* and other *Solanum* species[7−10] were identified from Table S1 and are listed in Table 1. The glycoalkaloid peaks in the chromatographic spectra were found at retention times between 7.00 and 8.50 min. The major peaks for *S. tuberosum*, *S. chomatophilum*, *S. oplocense*, *S. paucisectum*, and *S. piurae* were glycoalkaloids (Figure 2 and Table 1). *S. tarijense* and *S. acroglossum* had major peaks outside the range for glycoalkaloids (Figure 2) and lower levels of known glycoalkaloids (Table 1). *S. acroglossum*, in particular, did not have high peak intensity in the range between 7.00 and 8.50 min. The total peak intensity for all features across all species was similar (Table S1). The differences were in the distribution of peaks in the spectra (Figure 2).

The feature 8.05\852.514 had a $m/z$ that was a match with chaconine. 8.05\852.514 was barely detectable in the wild species but had high levels of production in *S. tuberosum*. Solanine, the other glycoalkaloid found in *S. tuberosum*, was a match with 7.60\868.5004 and had high peak intensity *S. tuberosum* but not the wild species (Table 1). These results were similar to those reported by others.[7,9] The assignment of chaconine and solanine was also verified using standards (data not shown). 7.60\868.5004 could also be assigned to $\beta$-solamarine, solamargine and leptinine I; however, these glycoalkloids were not found to be at high levels in *S. tuberosum* by others.[7,9] These glycoalkaloids could also be assigned to features 8.32\868.5086 and 7.96\868.5099, which were not found at high levels in *S. tuberosum*, consistent with published studies.[7,9] Feature 7.46\884.5049 had an $m/z$ that matched glycoalkaloids leptinine II, solasonine, and solamarine. Table 1 shows that 7.46\884.5049 was found at high levels in *S. tuberosum*, which was not consistent with published information showing that these glycoalkaloids were not found in *S. tuberosum*.[8] An alternative explanation is that 7.46\884.5049 is the $[M + CH_3OH + H]^+$ molecular ion adduct of chaconine (theoretical mass of 884.5366), which can form in positive ionization mode in ESI. Assignment of the feature to the $[M + CH_3OH + H]^+$ adduct would concur with the high levels in *S. tuberosum* observed for 7.46\884.5049. *S. oplocense* had the next highest intensity for 7.46\884.5049 followed by four other wild species at lower levels (Table 1).

The remaining glycoalkloids in Table 1 were all not detectable in *S. tuberosum* but were produced in wild species. Feature 7.56\1046.5571 was found in the largest number of wild species (four) and was assigned to the glycoalkaloid dehydrocommersonine, which had been previously characterized from *S. oplocense*.[29−31] The peak intensity for dehydrocommersonine was highest in *S. oplocense* and was the highest peak intensity of all the features in any species. High levels were also found in *S. paucisectum*, *S. chomatophilum*, and *S. piurae*. Feature 7.94\1034.5581 was assigned to tomatine, which is a tomato glycoalkaloid associated with CPB resistance.[11] It was detectable in *S. piurae* at lower levels than dehydrocommersonine and was at very low levels in *S. chomatophilum*. Removal of the xylose sugar converts tomatine to $\beta$-tomatine. The feature 7.80\902.5148 had a $m/z$ matching $\beta$-tomatine and, like tomatine, was also found in *S. piurae* and *S. chomatophilum*. The feature 7.73\1064.568 was assigned to the glycoalkloid neotomatine, which had highest levels in *S. piurae* followed by *S. chomatophilum* and very low detection in *S. paucisectum*. 7.72\1016.5479 was assigned to dehydrodemissine, which was previously described in *Solanum commeronii* Dun ex. Poir.[32] Dehydrodemissine was found in *S. piurae* at levels over 300-fold lower than dehydrocommersonine. 8.01\1018.5629 and 6.92\1032.5429 were assigned to glycoalkaloids demissine and dehydrotomatine, respectively. These glycoalkloids had very low peak intensities.

The chemical structures of chaconine and solanine were compared with glycoalkaloids from the wild species. Figure 4 shows that the glycoalkaloids found in *S. tuberosum* had triose sugar side chains compared to wild species, where there were tetrose side chains. The results suggest that the larger tetrose side chain glycoalkaloids were associated with resistance to CPB. These findings correlate with studies showing that CPB has a preference for potato over tomato, which produces the tetrose glycoalkaloid tomatine.[33] Other studies have shown that decreasing the sugar side chain on glycoalkaloids reduces their toxicity[34] and capacity to disrupt membranes.[35]

**Non-glycoalkaloid Metabolites Associated with CPB Resistance.** Previous studies on *S. berthaultii* have demonstrated that resistance was associated with glandular trichomes.[16] However, it was also observed that CPB feeding remains low in *S. tarijense* after the mechanical removal of trichomes, indicating that there are other components of the leaf involved in resistance.[36] Our observations indicate that *S.*

**Table 1. Glycoalkaloids**[a]

| feature ID | glycoalkaloid | formula | theor mass[b] | Δ ppm | ACG | TAR | CHM | OPL | PCS | PUR | TUB |
|---|---|---|---|---|---|---|---|---|---|---|---|
| 8.05\852.514 | chaconine | $C_{45}H_{73}NO_{14}$ | 852.5104 | 4 | 0 | 0 | 0.0054 | 0 | 0.0008 | 0.1038 | 1266.9750 |
| 7.60\868.5004 | solanine | $C_{45}H_{73}NO_{15}$ | 868.5053 | 5 | 0 | 0 | 0.0691 | 0.0009 | 0.0041 | 0.1245 | 2135.0593 |
| | β-solamarine | $C_{45}H_{73}NO_{15}$ | | 5 | | | | | | | |
| | solamargine | $C_{45}H_{73}NO_{15}$ | | 5 | | | | | | | |
| | leptinine I | $C_{45}H_{73}NO_{15}$ | | 5 | | | | | | | |
| 8.32\868.5086 | solanine | $C_{45}H_{73}NO_{15}$ | 868.5053 | 3 | 0 | 0 | 0.0231 | 0.0709 | 0.0098 | 0 | 17.5432 |
| | β-solamarine | $C_{45}H_{73}NO_{15}$ | | 3 | | | | | | | |
| | solamargine | $C_{45}H_{73}NO_{15}$ | | 3 | | | | | | | |
| | leptinine I | $C_{45}H_{73}NO_{15}$ | | 3 | | | | | | | |
| 7.96\868.5099 | solanine | $C_{45}H_{73}NO_{15}$ | 868.5053 | 5 | 0.0085 | 0 | 0 | 0.0033 | 0 | 0 | 532.7175 |
| | β-solamarine | $C_{45}H_{73}NO_{15}$ | | 5 | | | | | | | |
| | solamargine | $C_{45}H_{73}NO_{15}$ | | 5 | | | | | | | |
| | leptinine I | $C_{45}H_{73}NO_{15}$ | | 5 | | | | | | | |
| 8.54\884.5002 | leptinine II | $C_{45}H_{73}NO_{16}$ | 884.5002 | 0 | 0.0056 | 0.0068 | 0 | 0 | 0 | 0.0020 | 7.8517 |
| | solasonine | $C_{45}H_{73}NO_{16}$ | | 0 | | | | | | | |
| | solamarine | $C_{45}H_{73}NO_{16}$ | | 0 | | | | | | | |
| 7.46\884.5049 | leptinine II | $C_{45}H_{73}NO_{16}$ | 884.5002 | 5 | 0 | 0.0042 | 10.0907 | 70.9600 | 10.5427 | 4.6792 | 1320.1321 |
| | solasonine | $C_{45}H_{73}NO_{16}$ | | 5 | | | | | | | |
| | solamarine | $C_{45}H_{73}NO_{16}$ | | 5 | | | | | | | |
| | chaconine | $C_{45}H_{73}NO_{14}$ | 884.5366[c] | 35 | | | | | | | |
| 7.80\902.5148 | β-tomatine | $C_{45}H_{75}NO_{17}$ | 902.5108 | 4 | 0 | 0 | 7.2080 | 0.0592 | 49.6026 | 26.4639 | 0 |
| 7.72\1016.5479 | dehydrodemissine | $C_{50}H_{81}NO_{20}$ | 1016.5425 | 5 | 0.0025 | 0.0050 | 7.8641 | 0 | 0.5620 | 14.4214 | 0.0076 |
| 8.01\1018.5629 | demissine | $C_{50}H_{83}NO_{20}$ | 1018.5581 | 4 | 0.0058 | 0.0170 | 2.0795 | 1.6633 | 2.4713 | 0 | 0 |
| 6.92\1032.5429 | dehydrotomatine | $C_{50}H_{81}NO_{21}$ | 1032.5374 | 5 | 0.0062 | 0.0117 | 0 | 0 | 0.0104 | 4.7287 | 0.0013 |
| 7.94\1034.5581 | tomatine | $C_{50}H_{83}NO_{21}$ | 1034.5531 | 4 | 0.0147 | 0 | 0.8863 | 0 | 1.3943 | 89.0285 | 0.0691 |
| 7.56\1046.5571 | dehydrocommersonine | $C_{51}H_{83}NO_{21}$ | 1046.5531 | 3 | 0 | 0 | 858.3495 | 2445.9540 | 947.8109 | 266.7079 | 0 |
| 7.73\1064.568 | neotomatine | $C_{51}H_{85}NO_{22}$ | 1064.5636 | 4 | 0 | 0.0096 | 153.6252 | 0 | 187.6920 | 558.2309 | 0 |

[a]Metabolites with $m/z$ matching with known glycoalkaloids are shown. The feature ID is the retention time\$m/z$ combination. Compounds in the MetLin database that matched the $m/z$ are listed along with their molecular formulas and theoretical mass of the $[M + H]^+$ molecular ion. Differences between $m/z$ of the feature and theoretical masses of matching compounds are indicated as Δ ppm. TUB, *S. tuberosum* cv. Shepody; CHM, *S. chomatophilum*; OPL, *S. oplocense*; PCS, *S. paucissectum*; PUR,*S. piurae*; ACG, *S. acroglossum*; TAR, *S. tarijense*. The average Markerlynx processed peak intensity across the replicates for each species is presented. [b]Theoretical mass is for the $[M + H]^+$ molecular ion unless otherwise indicated. [c]Theoretical mass is for the $[M + CH_3OH + H]^+$ molecular ion.



dx.doi.org/10.1021/jf502508y | J. Agric. Food Chem. 2014, 62, 9043−9055

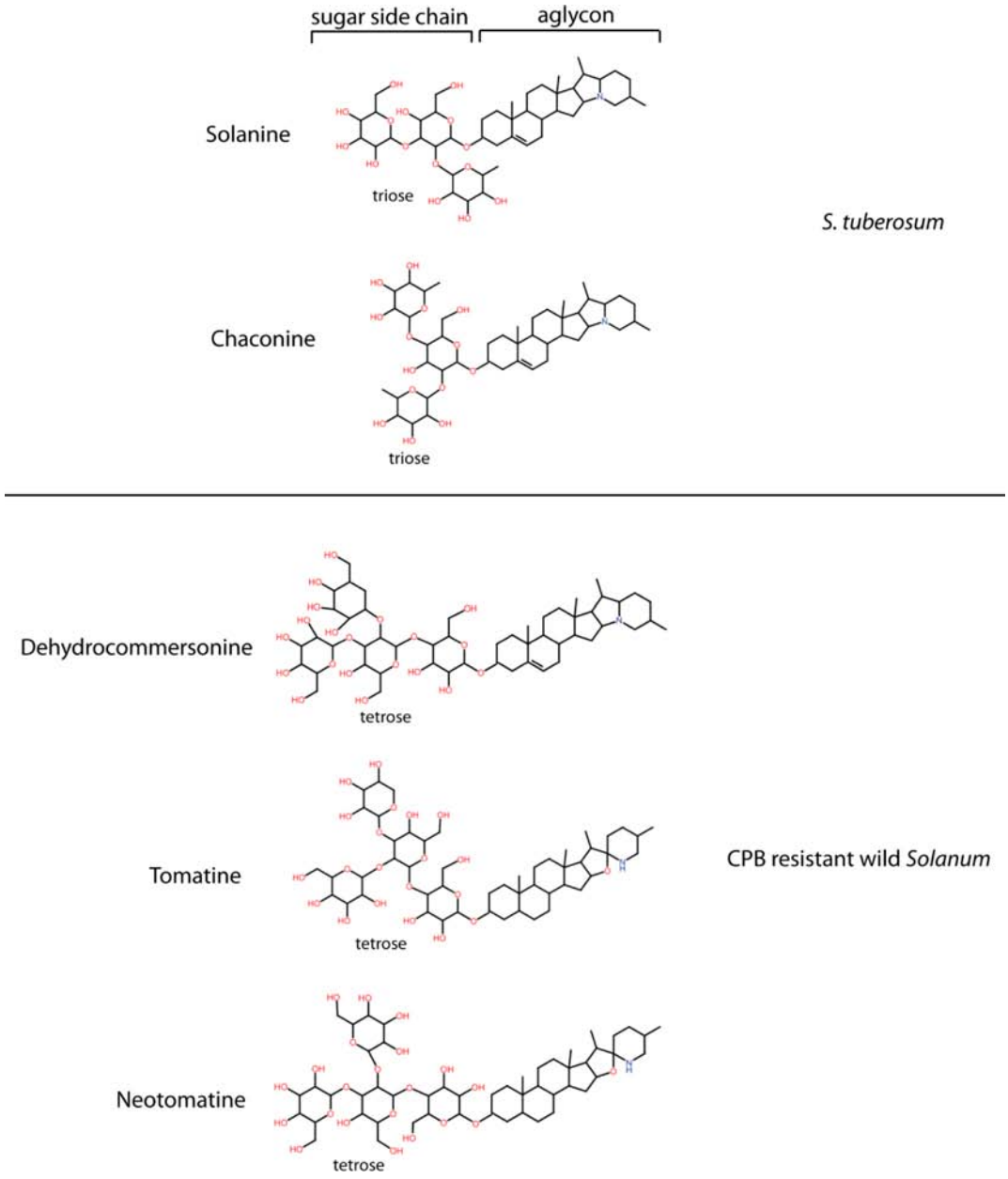


**Figure 4.** Chemical structures of glycoalkaloids. Chaconine and solanine were produced in *S. tuberosum*; dehydrocommersonine, tomatine, and neotomatine were produced in the CPB-resistant wild *Solanum* species. Triose and tetrose sugar side chains are indicated.

*acroglossum* did not have trichomes, which agrees with previous descriptions of the species as glabrous.[37] Hence, resistance in *S. acroglossum* is not associated with high levels of either glycoalkaloids or trichomes. An analysis of foliar metabolites shared between the wild species in the study but not *S. tuberosum* was done to identify non-glycoalkaloid and non-trichome metabolites associated with resistance to CPB. An ANOVA analysis was done to find features with significant variation between the species. Eight hundred and sixty-seven features had significant variation in peak intensity between the species (see Supporting Information Table S2). The 867 features were screened to identify features with peak intensities 100 times increased over *S. tuberosum* for all of the wild species (Table 2). Additionally, features had to have untransformed peak intensities of at least 10 in two of the wild species. The criteria were used to select for features highly associated with CPB resistance and to eliminate features that were produced at very low levels or only in a single wild species. Features 3.60\163.0387 and 4.02\163.0393 had an $m/z$ that was matched to hydroxycoumarin. This feature was present in all of the wild species. There are six isomers of hydroxycoumarin, each with the hydroxyl group in a different position. 7-Hydroxycoumarin or umbelliferone is a precursor to other coumarins, including bergamottin, which is ovicidal to CPB.[38] 4-Hydroxycoumarin itself can act as a blood anticoagulant in humans but is often used as a precursor for synthesis of more powerful anticoagulants such as warfarin.[39] Derivatives of 4-hydroxycoumarin also have larvicidal activity against *Aedes aegyti*.[40] Hydroxycoumarin produced in the wild species may directly affect CPB or may be a common precursor to other metabolites that are antifeedants.

5.80\319.0417 was assigned to 3-deoxy-D-*manno*-octulosonate 8-phosphate (KDOP). Plants synthesize KDOP for polysaccharide cross-links of pectin.[41] KDOP is a precursor


dx.doi.org/10.1021/jf502508y | J. Agric. Food Chem. 2014, 62, 9043−9055

**Table 2. Metabolites Increased in All Wild Species over *S. tuberosum*[a]**

| feature ID | putative ID | formula | theor mass $[M + H]^+$ | Δ ppm | ACG | TAR | CHM | OPL | PCS | PUR | TUB |
|---|---|---|---|---|---|---|---|---|---|---|---|
| 7.84\145.0502 | 3-hexenedioic acid<br>allylmalonic acid<br>(*E*)-3-methylglutaconic acid<br>(*E*)-hex-2-enedioic acid<br>2,3-dimethylmaleate<br>methylitaconate<br>2-methyleneglutarate<br>triacetate, 2-hydroxy-2-(hydroxymethyl)-2*H*-pyran-3(6*H*)-one<br>1,5-Aanhydro-4-deoxy-D-*glycero*-hex-3-en-2-ulose<br>1,5-anhydro-4-deoxy-D-*glycero*-hex-1-en-3-ulose<br>2*E*-methylglutaconic acid<br>3-hydroxyadipic acid 3,6-lactone<br>dimethyl fumarate<br>ethyl hydrogen fumarate<br>(*E*)-2-methylglutaconic acid | $C_6H_8O_4$ | 145.0502 | 4 | 0.3426 | 2.2907 | 37.2655 | 1.8167 | 21.5554 | 80.3951 | 0 |
| 3.60\163.0387 | 3-hydroxycoumarin<br>7-hydroxycoumarin<br>umbelliferone<br>7-hydroxy-2*H*-chromen-2-one<br>4-hydroxycoumarin<br>5-hydroxycoumarin<br>8-hydroxycoumarin<br>6-hydroxycoumarin | $C_9H_6O_3$ | 163.0387 | 1 | 1.4602 | 30.7208 | 16.5359 | 7.8594 | 60.0625 | 50.8605 | 0 |
| 4.02\163.0393 | 3-hydroxycoumarin<br>7-hydroxycoumarin<br>umbelliferone<br>7-hydroxy-2*H*-chromen-2-one<br>4-hydroxycoumarin<br>5-hydroxycoumarin<br>8-hydroxycoumarin<br>6-hydroxycoumarin | $C_9H_6O_3$ | 163.0393 | 2 | 49.8817 | 141.2625 | 40.4365 | 19.9633 | 98.6877 | 95.3974 | 0 |
| 4.84\177.0546 | herniarin<br>7-methoxychromon E<br>2-propenal, 3-(1,3-benzodioxol-5-yl)-<br>1,3,8-naphthalenertriol<br>4-methylumbelliferone<br>10-hydroxy-8*E*-decene-2,4,6-triynoic acid<br>10-hydroxy-2,8-decadiene-4,6-diynoic acid<br>1,4,5-naphthalenetriol | $C_{10}H_8O_3$ | 179.0473 | 0 | 180.2685 | 8.7228 | 19.7829 | 0.5979 | 2.3425 | 6.9256 | 0 |



dx.doi.org/10.1021/jf502508y | J. Agric. Food Chem. 2014, 62, 9043−9055

**Table 2. continued**

| feature ID | putative ID | formula | theor mass $[M + H]^+$ | Δ ppm | ACG | TAR | CHM | OPL | PCS | PUR | TUB |
|---|---|---|---|---|---|---|---|---|---|---|---|
| | 7-hydroxy-6-methyl-2*H*-1-benzopyran-2-one<br>3-(3,4-methylenedioxyphenyl)propenal | | | | | | | | | | |
| 3.61\251.1384 | *N*,*N*-diisopropyl-3-nitrobenzamide<br>NH-Phe(NMe)-Gly-OMe<br>heptabarbital<br>4-coumaroyl-2-hydroxyputrescine<br>caffeoylputrescine | $C_{13}H_{18}N_2O_3$ | 250.1317 | 2 | 0.6402 | 0.0380 | 28.6526 | 8.1334 | 105.1551 | 88.2894 | 0 |
| 6.71\261.1699 | unknown | | | | 472.2803 | 0.1759 | 0.0594 | 19.1877 | 110.2894 | 152.1236 | 0 |
| 5.80\319.0417 | 3-deoxy-D-*manno*-octulosonate 8-phosphate | $C_8H_{15}O_{11}P$ | 319.0425 | 2 | 14.6945 | 0.2787 | 0.1642 | 13.5001 | 0.2783 | 3.1046 | 0 |
| 2.11\399.0485 | unknown | | | | 64.7065 | 0.0079 | 0.0013 | 1.3982 | 16.4110 | 7.6426 | 0 |
| 7.81\400.3566 | demissidine<br>oblonginine<br>veramiline | $C_{27}H_{45}NO$ | 400.3574 | 1 | 0.0183 | 0.2617 | 163.9837 | 35.2965 | 169.8858 | 65.2168 | 0 |
| 7.78\416.3512 | tomatidine<br>soladucidine | $C_{27}H_{45}NO_2$ | 415.3450 | 2 | 0.0280 | 0.0306 | 123.9308 | 13.9041 | 121.7996 | 315.8535 | 0 |
| 7.83\459.2213 | marioside | $C_{22}H_{34}O_{10}$ | 459.2225 | 2 | 0.5093 | 417.1292 | 1.0307 | 12.4345 | 1.6100 | 0.0918 | 0 |
| 5.50\470.2281 | unknown | | | | 0.0691 | 0.0536 | 0.1472 | 27.8406 | 231.5718 | 45.4547 | 0 |
| 7.84\534.7624 | unknown | | | | 4.0082 | 3.7564 | 6.1707 | 92.9919 | 40.1914 | 45.4547 | 0 |
| 7.80\562.4093 | unknown | | | | 0.0350 | 1.6845 | 493.5220 | 87.1664 | 492.2046 | 188.1997 | 0 |
| 6.81\576.3895 | unknown | | | | 0.0257 | 0.0141 | 5.3507 | 15.1207 | 7.4583 | 128.4867 | 0 |
| 7.63\576.3906 | unknown | | | | 0.0310 | 0.0255 | 63.2127 | 4.9227 | 51.6607 | 263.4704 | 0 |
| 7.77\578.4045 | unknown | | | | 0.0500 | 0.0794 | 316.2244 | 37.9129 | 306.7277 | 766.7678 | 0 |
| 6.11\592.3855 | unknown | | | | 0.0045 | 0.0120 | 32.1651 | 1.0518 | 11.2982 | 11.3511 | 0 |
| 5.99\933.2699 | pelargonidin 3-*O*-[2-*O*-(6-*O*-(*E*)-feruloyl-*β*-D-glucopyranosyl)-*β*-D-glucopyranoside]-5-*O*-(*β*-D-glucopyranoside)<br>pelargonidin 3-*O*-[6-*O*-(*E*)-feruloyl-2-*O*-*β*-D-glucopyranosyl-*β*-D-glucopyranoside]-5-*O*-(*β*-D-glucopyranoside)<br>peonidin 3-*p*-coumarylsophoroside-5-glucoside<br>peonidin 3-caffeylrutinoside-5-glucoside<br>petanin<br>isovitexin 2′′-*O*-(6′′′-(*E*)-feruloyl)glucoside 4′-*O*-glucoside<br>kaempferol 3-neohesperidoside-7-(2′′-ferulylglucoside)<br>kaempferol 3-[2Gal-(6′′′-feruloylglucosyl)robinobioside]<br>petunidin-3-(*p*-coumaroyl)-rutinoside-5-glucoside | $C_{43}H_{48}O_{23}$ | 933.2659 | 4 | 81.7991 | 0.4922 | 5.6224 | 27.5091 | 49.0876 | 169.9223 | 0 |



dx.doi.org/10.1021/jf502508y | J. Agric. Food Chem. 2014, 62, 9043−9055

Table 2. continued

| feature ID | putative ID | formula | theor mass $[M + H]^+$ | Δ ppm | ACG | TAR | CHM | OPL | PCS | PUR | TUB |
|---|---|---|---|---|---|---|---|---|---|---|---|
| | amurenoside A | | | | | | | | | | |
| | amurenoside B | | | | | | | | | | |
| 7.60\1062.5525 | unknown | | | | 0.0028 | 0.0156 | 43.2917 | 0.4790 | 30.6382 | 95.5583 | 0 |

[a]The feature ID is the retention time\$m/z$ combination. Compounds in the MetLin database that matched the $m/z$ are listed along with their molecular formulas and theoretical mass of the $[M + H]^+$ molecular ion. Differences between $m/z$ of the feature and theoretical masses of matching compounds are indicated as Δ ppm. TUB, *S. tuberosum* cv. Shepody; CHM, *S. chomatophilum*; OPL, *S. oplocense*; PCS, *S. paucissectum*; PUR, *S. piurae*; ACG, *S. acroglossum*; TAR, *S. tarijense*. The average MarkerLynx processed peak intensity across the replicates for each species is presented.

for KDO, which is component of rhamnogalactouronan II, a borate-binding cross-linked component of pectin in cell walls.[42] *S. acroglossum* and *S. oplocense* produce the highest levels of KDOP among the species. The results suggest that these two species may have altered cell wall structures.

7.81\400.3566 was assigned to demissidine, a glycoalkaloid aglycon; additionally, the feature could also be assigned to veramiline, an alkaloid with the same chemical formula. The levels were highest in *S. chomatophilum* and *S. piurae*. Demissidine could be a fragment ion of the glycocoalkaloid demissine, which was detected in *S. chomatophilum* and *S. paucisectum* at low levels (Table 1). Demissine is the major glycoalkloid of *Solanum demissum* Lindl., another species with resistance to CPB, and is an antifeedant for CPB.[43] However, the feature identified as demissine, 8.01\1018.5629, had a retention time slower than 7.81\400.3566, which is inconsistent with a parent molecular ion for a demissidine aglycon fragment ion. It is possible that demissidine serves as an aglycon to an unknown glycoalkaloid.

Tomatidine and soladucidine were aglycons that were both assigned to 7.78\416.3512. Tomatine, a glycoalkaloid with a tomatidine aglycon, was identified as feature 7.94\1034.5581 (Table 1). However, 7.94\1034.5581 had a slower retention time than 7.78\416.3512, indicating that 7.78\416.3512 was unlikely a fragment ion. Alternatively, 7.78\416.3512 may be the aglycon of an unknown glycoalkaloid. It is also possible that 7.78\416.3512 is an unknown non-glycoalkaloid metabolite with a mass similar to that of tomatidine and soladucidine.

7.83\459.2213 was assigned to marioside, a norcarotane sesquiterpene glucoside found in ferns.[44] This metabolite had high peak intensity in *S. tarijense*. There is very little information on the biological functions of marioside. 7.84\145.0502 and 4.84\177.0546 were assigned to multiple metabolites that were not previously associated with plant insect interactions.

5.99\933.2699 had highest peak intensity in *S. piurae* followed by *S. acroglossum*. 5.99\933.2699 had a large number of $m/z$ matches in the chemical databases. Chief among these metabolites were anthocyanins and other flavonoid glycosides in the phenylpropanoid biosynthetic pathway. 3.61\251.1384 was assigned to the polyamine-conjugated phenylpropanoid, caffeyolputrescine, in addition to other metabolites. Phenylpropanoids have been noted for their role in plant defense against pathogens, herbivores, and environmental stress. The loss of flavonoids in tomatoes was associated with increased herbivory by coleopterans.[45] Increased expression of phenylpropanoid biosynthetic enzyme genes were also noted with CPB herbivory.[46] The results of the current study demonstrate that phenylpropanoids were increased in CPB-resistant wild species. Flavonoids also have health benefits for humans,[47] as opposed to glycoalkaloids that are toxic.[5]

Several of the features in Table 2 were unknowns with no metabolites in the MetLin and KNApSAcK databases with matching masses.

**Metabolites Increased in *S. tuberosum*.** The metabolites with increased levels in *S. tuberosum* relative to the wild species would not be associated with CPB resistance. Metabolites highly enriched in *S. tuberosum* over each of the wild species were screened by selecting features with 100-fold increased peak intensity in *S. tuberosum* over each of the wild species (Table 3). Features with $m/z$ matching chaconine and solanine, the two major glycoalkaloids for *S. tuberosum*,[8] were found, which concurs with the analysis of glycoalkloids (Table 1).

**Table 3. Metabolites Increased in *S. tuberosum* over All Wild Species[a]**

| feature ID | putative ID | formula | theor mass $[M + H]^+$ | Δ ppm | ACG | TAR | CHM | OPL | PCS | PUR | TUB |
|---|---|---|---|---|---|---|---|---|---|---|---|
| 4.89\229.0674 | unknown | | | | 0 | 0.0252 | 0.0023 | 0.0080 | 0.0070 | 0.0035 | 10.4685 |
| 7.98\398.3406 | solanidine | $C_{27}H_{43}NO$ | 398.3417 | 2 | 0 | 0 | 3.9729 | 34.8602 | 0.5949 | 0 | 185.0466 |
| | verazine | | | | | | | | | | |
| | epi-verazine | | | | | | | | | | |
| | iso-shinonomenine | | | | | | | | | | |
| | shinonomenine | | | | | | | | | | |
| | veralinine | | | | | | | | | | |
| | veralomidine | | | | | | | | | | |
| 11.34\411.0882 | newbouldiaquinone A | $C_{25}H_{14}O_6$ | | 4 | 0 | 0.0311 | 0.0127 | 0 | 0.0070 | 0.0091 | 10.7033 |
| 7.95\445.7395 | unknown | | | | 0.0034 | 0.0022 | 0 | 0.0042 | 0.0013 | 0 | 38.4241 |
| 7.42\453.7369 | unknown | | | | 0 | 0.0117 | 0 | 0 | 0.7788 | 0.0051 | 82.5877 |
| 11.34\587.2077 | blestrianol C | $C_{37}H_{30}O_7$ | 587.2064 | 2 | 0.0054 | 0.0078 | 0.0107 | 0 | 0.0020 | 0.0039 | 11.5610 |
| 8.08\850.5003 | unknown | | | | 0 | 0.0093 | 0 | 0 | 0 | 0 | 31.1549 |
| 8.05\852.514 | chaconine | $C_{45}H_{73}NO_{14}$ | 852.5104 | 4 | 0 | 0 | 0.0054 | 0 | 0.0007 | 0.1038 | 1266.9750 |
| 7.94\866.4931 | unknown | | | | 0 | 0.0029 | 0 | 0.0145 | 0 | 0 | 15.2681 |
| 7.00\866.4934 | unknown | | | | 0 | 0.0039 | 0 | 0.0019 | 0.0020 | 0 | 15.1389 |
| 9.14\867.479 | sansevistatin 1 | $C_{45}H_{70}O_{16}$ | 867.4737 | 6 | 0 | 0 | 0.0009 | 0 | 0 | 0 | 28.6052 |
| | malonylsaikosaponin A | | | | | | | | | | |
| | malonylsaikosaponin D | | | | | | | | | | |
| 9.10\868.4968 | unknown | | | | 0.0112 | 0 | 0.0012 | 0 | 0 | 0 | 10.2539 |
| 7.60\868.5004 | solanine | $C_{45}H_{73}NO_{15}$ | 868.5053 | 5 | 0 | 0 | 0.0692 | 0.0010 | 0.0038 | 0.1245 | 2135.0590 |
| | solamargine | | | | | | | | | | |
| | $\beta$-solamarine | | | | | | | | | | |
| | solanelagnin | | | | | | | | | | |
| | solanidine 3-*O*-[$\alpha$-L-rhamnopyranosyl-(1→2)[$\beta$-D-glucopyranosyl-(1→4)]-$\beta$-D-glucopyranoside | | | | | | | | | | |
| | leptinine I | | | | | | | | | | |
| 8.32\868.5086 | solanine | $C_{45}H_{73}NO_{15}$ | 868.5053 | 5 | 0 | 0 | 0.0231 | 0.0709 | 0.0098 | 0 | 17.5432 |
| | solamargine | | | | | | | | | | |
| | $\beta$-solamarine | | | | | | | | | | |
| | solanelagnin | | | | | | | | | | |
| | solanidine 3-*O*-[$\alpha$-L-rhamnopyranosyl-(1→2)[$\beta$-D-glucopyranosyl-(1→4)]-$\beta$-D-glucopyranoside | | | | | | | | | | |
| | leptinine I | | | | | | | | | | |
| 7.96\868.5099 | solanine | $C_{45}H_{73}NO_{15}$ | 868.5053 | 5 | 0.0085 | 0 | 0 | 0.0033 | 0 | 0 | 532.7175 |
| | solamargine | | | | | | | | | | |
| | $\beta$-solamarine | | | | | | | | | | |



dx.doi.org/10.1021/jf502508y | J. Agric. Food Chem. 2014, 62, 9043−9055

**Table 3. continued**

| feature ID | putative ID | formula | theor mass $[M + H]^+$ | Δ ppm | ACG | TAR | CHM | OPL | PCS | PUR | TUB |
|---|---|---|---|---|---|---|---|---|---|---|---|
| | solanelagnin | | | | | | | | | | |
| | solanidine 3-*O*-[α-L-rhamnopyranosyl-(1→2)[β-D-glucopyranosyl-(1→4)]-β-D-glucopyranoside | | | | | | | | | | |
| | leptinine I | | | | | | | | | | |
| 7.59\874.2084 | unknown | | | | 0 | 0.0094 | 0 | 0.0059 | 0.0006 | 0.0014 | 11.7016 |
| 7.56\874.5895 | unknown | | | | 0.0068 | 0 | 0 | 0 | 0.0022 | 0.0006 | 11.3667 |
| 7.52\877.0086 | unknown | | | | 0.0089 | 0 | 0 | 0.0033 | 0.0007 | 0 | 26.4519 |
| 8.99\883.4724 | unknown | | | | 0 | 0 | 0.0159 | 0 | 0.0006 | 0.0034 | 42.0095 |
| 10.54\885.4881 | diosgenin 3-[glucosyl-(1→4)-rhamnosyl-(1→4)-glucoside] | $C_{45}H_{72}O_{17}$ | 885.4842 | 4 | 0 | 0 | 0.0117 | 0.0066 | 0.0050 | 0.0013 | 11.1546 |
| | deltonin | | | | | | | | | | |
| | gracillin | | | | | | | | | | |
| | polypodoside A | | | | | | | | | | |
| | β-chacotriosyllilagen | | | | | | | | | | |
| | graecunin G | | | | | | | | | | |
| | melongoside H | | | | | | | | | | |
| | orbiculatoside B | | | | | | | | | | |
| | spiroconazole A | | | | | | | | | | |
| | anguivioside A | | | | | | | | | | |
| | lyconoside II | | | | | | | | | | |
| | shatavarin VII | | | | | | | | | | |
| | pennogenin 3-*O*-β-chacotrioside | | | | | | | | | | |
| | mubenoside A | | | | | | | | | | |

[a]The feature ID is the retention time*m/z* combination. Compounds in the MetLin database that matched the *m/z* are listed along with their molecular formulas and theoretical mass of the $[M + H]^+$ molecular ion. Differences between *m/z* of the feature and theoretical masses of matching compounds are indicated as Δ ppm. TUB, *S. tuberosum* cv. Shepody; CHM, *S. chomatophilum*; OPL, *S. oplocense*; PCS, *S. paucissectum*; PUR, *S. piurae*; ACG, *S. acroglossum*; TAR, *S. tarijense*. The average Markerlynx processed peak intensity across the replicates for each species is presented.



dx.doi.org/10.1021/jf502508y | J. Agric. Food Chem. 2014, 62, 9043−9055

Metabolites from other organisms that had the same $m/z$ as solanine, chaconine, and solanidine that were found in the MetLin database are also shown in Table 3. These metabolites are less likely to occur in *S. tuberosum*.

Feature 11.34\411.0882 had a $m/z$ that matched to newbouldiaquinone A, a metabolite from the medicinal plant *Newbouldia laevis* that is a naphthoquinone−anthroquinone coupled pigment.[48] 11.34\587.2077 was matched with blestrianol C, a biphenanthrene isolated from the tubers of the orchid *Bletillla striata*.[49] Alternatively, the latter two features may be derived from the same unknown metabolite as they share the same retention time, indicating that 11.34\411.0882 could be a fragment ion of 11.34\587.2077. 9.14\867.479 and 10.54\885.4881 were assigned to several metabolites with structures corresponding to steroidal glycoside saponins.[50] 11.34\411.0882, 11.34\587.2077, 9.14\867.479, and 10.54\885.4881 were found at lower levels in *S. tuberosum* compared with glycoalkaloids.

In summary, the comparative analysis of wild species with CPB resistance against CPB-susceptible *S. tuberosum* done in this study has resulted in the identification of several metabolites correlated with resistance. Glycoalkaloids solanine and chaconine were found to be unique to *S. tuberosum*, whereas glycoalkaloids with tetrose side chains dehydrocommersonine, tomatine, and neotomatine were associated with CPB-resistant species *S. oplocense*, *S. paucisectum*, *S. chomatophilum*, and *S. piurae*. This study has added to the evidence that tetrose side chain glycoalklaoids are associated with CPB resistance. The results can also be applied to the development of selection methods for CPB-resistant breeding material derived from intercrosses of *S. tuberosum* with species enriched in tetrose glycoalkaloids. For example, a high ratio of tetrose glycoalkaloids to solanine and/or chaconine can be used to select for CPB resistance. Non-glycoalkaloids hydroxycoumarin and phenylpropanoid metabolites were also found increased in all wild species and have also application as markers for CPB resistance.

## ■ ASSOCIATED CONTENT

### Supporting Information

Table S1: Peak intensity data for all replicates. Table S2: Averaged peak intensities of features with significant species variation in ANOVA. This material is available free of charge via the Internet at http://pubs.acs.org.

## ■ AUTHOR INFORMATION


### Corresponding Author

*(H.H.T.) E-mail: Helen.Tai@agr.gc.ca. Phone: (506) 460-4519. Fax: (506) 460-4377.



### Funding

The work was funded by Agriculture and Agri-Food Canada Agricultural Bioproducts Innovation Program and the Developing Innovative Agri-products program.


### Notes

The authors declare no competing financial interest.

## ■ ACKNOWLEDGMENTS

We thank Charlotte Davidson and Catherine Clark, who provided technical assistance.

## ■ REFERENCES


(1) McLeod, C.; Tolman, J. H. Evaluation of losses in potatoes. In *Potato Pest Management in Canada*, Proceedings of a Symposium on Improving Potato Pest Protection, Fredericton, NB; Boiteau, G., Singh, R. P., Parry, R. H., Eds.; New Brunswick Department of Agriculture: Fredericton, N. B., 1987; pp 363−373.

(2) Hare, J. D. Ecology and management of the Colorado potato beetle. *Annu. Rev. Entomol.* **1990**, *35*, 81−100.

(3) Pelletier, Y. Recognition of conspeciflc eggs by female Colorado potato beetles (Coleoptera: Chrysomelidae). *Environ. Entomol.* **1995**, *24*, 875−878.

(4) Pelletier, Y.; King, R. R. Semiochemicals and potato pests: review and perspective for crop protection. In *Potato Pest Management in Canada*, Proceedings of a Symposium on Improving Potato Pest Protection, Fredericton, NB; Boiteau, G., Singh, R. P., Parry, R. H., Eds.; New Brunswick Department of Agriculture: Fredericton, N. B., 1987; pp 146−172.

(5) Mensinga, T. T.; Sips, A. J.; Rompelberg, C. J.; van Twillert, K.; Meulenbelt, J.; van den Top, H. J.; van Egmond, H. P. Potato glycoalkaloids and adverse effects in humans: an ascending dose study. *Regul. Toxicol. Pharmacol.* **2005**, *41*, 66−72.

(6) Ginzberg, I.; Tokuhisa, J.; Veilleux, R. Potato steroidal glycoalkaloids: biosynthesis and genetic manipulation. *Potato Res.* **2009**, *52*, 1−15.

(7) Friedman, M. Potato glycoalkaloids and metabolites: roles in the plant and in the diet. *J. Agric. Food Chem.* **2006**, *54*, 8655−8681.

(8) Shakya, R.; Navarre, D. A. LC-MS analysis of solanidane glycoalkaloid diversity among tubers of four wild potato species and three cultivars (*Solanum tuberosum*). *J. Agric. Food Chem.* **2008**, *56*, 6949−6958.

(9) Kozukue, N.; Yoon, K.-S.; Byun, G.-I.; Misoo, S.; Levin, C. E.; Friedman, M. Distribution of glycoalkaloids in potato tubers of 59 accessions of two wild and five cultivated *Solanum* species. *J. Agric. Food Chem.* **2008**, *56*, 11920−11928.

(10) Mweetwa, A. M.; Hunter, D.; Poe, R.; Harich, K. C.; Ginzberg, I.; Veilleux, R. E.; Tokuhisa, J. G. Steroidal glycoalkaloids in *Solanum chacoense*. *Phytochemistry* **2012**, *75*, 32−40.

(11) Barbour, J. D.; Kennedy, G. G. Role of steroidal glycoalkaloid α-tomatine in host-plant resistance of tomato to colorado potato beetle. *J. Chem. Ecol.* **1991**, *17*, 989−1005.

(12) Rangarajan, A.; Miller, A. R.; Veilleux, R. E. Leptine glycoalkaloids reduce feeding by Colorado potato beetle in diploid *Solanum* sp. hybrids. *J. Am. Soc. Hortic. Sci.* **2000**, *125*, 689−693.

(13) Carter, C. D.; Gianfagna, T. J.; Sacalis, J. N. Sesquiterpenes in glandular trichomes of a wild tomato species and toxicity to the Colorado potato beetle. *J. Agric. Food Chem.* **1989**, *37*, 1425−1428.

(14) King, R. R.; Pelletier, Y.; Singh, R. P.; Calhoun, L. A. 3,4-Di-*O*-isobutyryl-6-*O*-caprylsucrose: the major component of a novel sucrose ester comples from the type B glandular trichomers of *Solanum berthaultii* Hawkes (PI473340). *J. Chem. Soc., Chem. Commun.* **1986**, 1078−1079.

(15) Sabotič, J.; Smid, I.; Gruden, K.; Gašparič, M. B.; Koruza, K.; Petek, M.; Pohleven, J.; Brzin, J.; Janko, K.; Zel, J. Inhibition of the growth of Colorado potato beetle larvae by macrocypins, protease inhibitors from the parasol mushroom. *J. Agric. Food Chem.* **2013**, *61*, 12499−12509.

(16) Pelletier, Y.; Smilowitz, Z. Effect of trichome B exudate of *Solanum berthaultii* Hawkes on consumption by the Colorado potato beetle, *Leptinotarsa decemlineata* (Say). *J. Chem. Ecol.* **1990**, *16*, 1547−1555.

(17) Jansky, S. H.; Simon, R.; Spooner, D. M. A test of taxonomic predictivity: resistance to the Colorado potato beetle in wild relatives of cultivated potato. *J. Econ. Entomol.* **2009**, *102*, 422−431.

(18) Pelletier, Y.; Tai, G. C. C. Genotypic variability and mode of action of Colorado potato beetle (Coleoptera: Chrysomelidae) resistance in seven *Solanum* species. *J. Econ. Entomol.* **2001**, *94*, 572−578.

(19) Yencho, G. C.; Tingey, W. M. Glandular trichomes of *Solanum berthaultii* alter host preference of the Colorado potato beetle, *Leptinotarsa decemlineata*. *Entomol. Exp. Appl.* **1994**, *70*, 217−225.
(20) Sanford, L.; Kowalski, S.; Ronning, C.; Deahl, K. Leptines and other glycoalkaloids in tetraploid *Solanum tuberosum* × *Solanum chacoense*; $F_2$ hybrid and backcross families. *Am. J. Potato Res.* **1998**, *75*, 167−172.
(21) Alyokhin, A.; Baker, M.; Mota-Sanchez, D.; Dively, G.; Grafius, E. Colorado potato beetle resistance to insecticides. *Am. J. Potato Res.* **2008**, *85*, 395−413.
(22) Kempel, A.; Schädler, M.; Chrobock, T.; Fischer, M.; van Kleunen, M. Tradeoffs associated with constitutive and induced plant resistance against herbivory. *Proc. Natl. Acad. Sci. U.S.A.* **2011**, *108*, 5685−5689.
(23) Pelletier, Y.; Clark, C.; Tai, G. C. Resistance of three wild tuber-bearing potatoes to the Colorado potato beetle. *Entomol. Exp. Appl.* **2001**, *100*, 31−41.
(24) Pelletier, Y.; Grondin, G.; Maltais, P. Mechanism of resistance to the Colorado potato beetle in wild *Solanum* species. *J. Econ. Entomol.* **1999**, *92*, 708−713.
(25) Ames, M.; Spooner, D. M. Phylogeny of *Solanum* series Piurana and related species in *Solanum* section Petota based on five conserved ortholog sequences. *Taxon* **2010**, *59*, 1091−1101.
(26) Spooner, D. M.; Fajardo, D.; Bryan, G. J. Species limits of *Solanum berthaultii* Hawkes and *S. tarijense* Hawkes and the implications for species boundaries in *Solanum* Sect. Petota. *Taxon* **2007**, *56*, 987−999.
(27) Cataldi, T. R. I.; Lelario, F.; Bufo, S. A. Analysis of tomato glycoalkaloids by liquid chromatography coupled with electrospray ionization tandem mass spectrometry. *Rapid Commun. Mass Spectrom.* **2005**, *19*, 3103−3110.
(28) Herz, W.; Wahlberg, I.; Stevens, C. S.; Kalyanaraman, P. S. Three new 5,10-epoxygermacranolides from *Liatris chapmanii* and *Liatris gracilis*. *Phytochemistry* **1975**, *14*, 1803−1808.
(29) Sinden, S. L.; Sanford, L. L.; Deahl, K. L. Segregation of leptine glycoalkaloids in *Solanum chacoense* bitter. *J. Agric. Food Chem.* **1986**, *34*, 372−377.
(30) King, R. R.; Calhoun, L. A. Complete $^{1}H$ and $^{13}C$ NMR spectral assignments for the glycoalkaloid dehydrocommersonine. *Magn. Reson. Chem.* **2012**, *50*, 627−631.
(31) De Koeyer, D.; Pelletier, Y.; Murphy, A.; Embleton, J.; Clark, C. Allaby, S. Breeding for resistance to Colorado potato beetle using a wild potato species. In *Northeast Potato Technology Forum Proceedings*, Bangor, ME; Northeast Potato Technology Forum: Bangor, ME, 2009; pp 30.
(32) Vázquez, A.; González, G.; Ferreira, F.; Moyna, P.; Kenne, L. Glycoalkaloids of *Solanum commersonii* Dun. ex Poir. *Euphytica* **1997**, *95*, 195−201.
(33) Weber, D. C.; Drummond, F. A.; Ferro, D. N. Recruitment of Colorado potato beetles (Coleoptera: Chrysomelidae) to solanaceous hosts in the field. *Environ. Entomol.* **1995**, *24*, 608−622.
(34) Rayburn, J. R.; Bantle, J. A.; Friedman, M. Role of carbohydrate side chains of potato glycoalkaloids in developmental toxicity. *J. Agric. Food Chem.* **1994**, *42*, 1511−1515.
(35) Keukens, E. A. J.; de Vrije, T.; Fabrie, C. H. J. P.; Demel, R. A.; Jongen, W. M. F.; de Kruijff, B. Dual specificity of sterol-mediated glycoalkaloid induced membrane disruption. *Biochim. Biophys. Acta* **1992**, *1110*, 127−136.
(36) Pelletier, Y.; Dutheil, J. Behavioural responses of the Colorado potato beetle to trichomes and leaf surface chemicals of Solanum tarijense. *Entomol. Exp. Appl.* **2006**, *120*, 125−130.
(37) Ochoa, C. M. *The Potatoes of South America: Peru, Part 1: The Wild Species*; International Potato Centre (CIP): Lima, Peru, 2004.
(38) Berenbaum, M. Coumarins. In *Herbivores: Their Interactions with Secondary Plant Metabolites*, 2nd ed.; Rosenthal, G. A., Berenbaum, M., Eds.; Academic Press: San Diego, CA, USA, 1991; pp 221−244.
(39) Au, N.; Rettie, A. E. Pharmacogenomics of 4-hydroxycoumarin anticoagulants. *Drug Metab. Rev.* **2008**, *40*, 355−375.
(40) Jung, J. C.; Moon, H. I. Larvicidal activity of 4-hydroxycoumarin derivatives against *Aedes aegypti*. *Pharm. Biol.* **2011**, *49*, 190−193.
(41) Doong, R. L.; Ahmad, S.; Jensen, R. A. Higher plants express 3-deoxy-D-*manno*-octulosonate 8-phosphate synthase. *Plant Cell. Env.* **1991**, *14*, 113−120.
(42) O'Neill, M. A.; Ishii, T.; Albersheim, P.; Darvill, A. G. Rhamnogalacturonan II: structure and function of a borate cross-linked cell wall pectic polysaccharide. *Annu. Rev. Plant Biol.* **2004**, *55*, 109−139.
(43) Sanford, L. L.; Cantelo, W. W. Larval development rate and mortality of Colorado potato beetle on detached leaves of wild-Solanum species. *Am. Potato J.* **1989**, *66*, 575−582.
(44) Cui, C. B.; Tezuka, Y.; Kikuch, T.; Nakano, H.; Tamaoki, T.; Park, J. H. Constituents of a fern, *Davallia mariesii* Moore. Isolation and identification of a novel norcarotane sequiterpene glycoside, a chromone glucuronide, and two epicatechin glycosides. *Chem. Pharm. Bull. (Tokyo)* **1992**, *40*, 2035−2040.
(45) Kang, J.-H.; McRoberts, J.; Shi, F.; Moreno, J. E.; Jones, A. D.; Howe, G. A. The flavonoid biosynthetic enzyme chalcone isomerase modulates terpenoid production in glandular trichomes of tomato. *Plant Physiol.* **2014**, *164*, 1161−1174.
(46) Lawrence, S. D.; Novak, N. G.; Ju, C. J. T.; Cooke, J. E. K. Examining the molecular interaction between potato (*Solanum tuberosum*) and Colorado potato beetle *Leptinotarsa decemlineata*. *Botany* **2008**, *86*, 1080−1091.
(47) Yao, L. H.; Jiang, Y. M.; Shi, J.; Tomas-Barberan, F. A.; Datta, N.; Singanusong, R.; Chen, S. S. Flavonoids in food and their health benefits. *Plant Foods Hum. Nutr.* **2004**, *59*, 113−122.
(48) Eyong, K. O.; Folefoc, G. N.; Kuete, V.; Beng, V. P.; Krohn, K.; Hussain, H.; Nkengfack, A. E.; Saeftel, M.; Sarite, S. R.; Hoerauf, A. Newbouldiaquinone A: a naphthoquinone-anthraquinone ether coupled pigment, as a potential antimicrobial and antimalarial agent from *Newbouldia laevis*. *Phytochemistry* **2006**, *67*, 605−609.
(49) Bai, L.; Kato, T.; Inoue, K.; Yamaki, M.; Takagi, S. Blestrianol A, B and C, biphenanthrenes from *Bletilla striata*. *Phytochemistry* **1991**, *30*, 2733−2735.
(50) Rao, A. V.; Gurfinkel, D. M. The bioactivity of saponins: triterpenoid and steroidal glycosides. *Drug Metab. Drug Interact.* **2000**, *17*, 211−235.

JOURNAL OF AGRICULTURAL AND FOOD CHEMISTRY

Addition/Correction

pubs.acs.org/JAFC

# Correction to Synthesis and Application of $^{13}$C-Labeled 2-Acetyl-4-((1*R*,2*S*,3*R*)-1,2,3,4-tetrahydroxybutyl)imidazole (THI), an Immunosuppressant Observed in Caramel Food Colorings

Paul W. Elsinghorst,* Marion Raters, Anna Dingel, Jochen Fischer, and Reinhard Matissek

*J. Agric. Food Chem.* **2013**, *61* (31), 7494−7499. DOI:10.1021/jf4026772

The $^{13}$C NMR assignments for carbon C-2 of both tautomeric forms of compounds **4** and **5** should read (p 7496) as follows:

Compound **4** $^{13}$C NMR (DMSO-$d_6$) (tautomer A (minor)) $\delta$ 25.3 (C-2′), 63.5 (d, $J$ = 40 Hz, C-4″), 64.9 (dd, $J$ = 42, 54 Hz, C-1″), 71.4 (dd, $J$ = 42 Hz, C-3″), 73.9 (dd, $J$ = 43 Hz, C-2″), 128.1 (d, $J$ = 63 Hz, C-5), 139.4 (dd, $J$ = 61 Hz, C-4), 144.5 (C-2), 188.5 (C-1′); (tautomer B (major)) $\delta$ 25.5 (C-2′), 63.7 (d, $J$ = 41 Hz, C-4″), 67.3 (ddd, $J$ = 3.5, 40, 60 Hz, C-1″), 71.4 (dd, $J$ = 42 Hz, C-3″), 73.9 (dd, $J$ = 43 Hz, C-2″), 119.2 (dd, $J$ = 4.5, 65 Hz, C-5), 143.9 (C-2), 147.0 (dd, $J$ = 63 Hz, C-4), 188.5 (C-1′).

Compound **5** $^{13}$C NMR (DMSO-$d_6$) (tautomer A (minor)) $\delta$ 25.3 (C-2′), 63.5 (C-4″), 64.9 (C-1″), 71.4 (C-3″), 73.9 (C-2″), 128.1 (C-5), 139.4 (C-4), 144.5 (C-2), 188.5 (C-1′); (tautomer B (major)) $\delta$ 25.5 (C-2′), 63.7 (C-4″), 67.3 (C-1″), 71.4 (C-3″), 73.9 (C-2″), 119.2 (C-5), 143.9 (C-2), 147.0 (C-4), 188.5 (C-1′).

**Published:** August 27, 2014

ACS Publications © 2014 American Chemical Society

JOURNAL OF AGRICULTURAL AND FOOD CHEMISTRY

Addition/Correction

pubs.acs.org/JAFC

# Correction to Chemical Compositional, Biological, and Safety Studies of a Novel Maple Syrup Derived Extract for Nutraceutical Applications

Yan Zhang, Tao Yuan, Liya Li, Pragati Nahar, Angela Slitt, and Navindra P. Seeram*

*J. Agric. Food Chem.* **2014**, *62* (28), 6687−6698. DOI: 10.1021/jf501924y

In the next to last line of the abstract, "consumption (by HepG2 cells)" should be replaced by "levels (in HepG2 cells)".

**Published:** September 2, 2014

ACS Publications © 2014 American Chemical Society

automated, dynamic in-syringe liquid-phase microextraction, which was more efficient for extracting pesticides from water samples.[28] Several studies have employed low-density solvents as substitutes for toxic halogenated solvents. These developments widened the selection of solvents available for DLLME and extended its application.[17,29−34]

Ultrasound-assisted emulsification microextraction (USAEME) for DLLME has also been developed to improve the generation of droplets with or without using dispersive solvent.[34−38] Another alternative to ultrasound assistance is the use of surfactants. As some surfactants are just soluble in an organic solvent and some are just water-soluble, their presence improves the generation of fine droplets in DLLME.[39−41] However, high concentrations of surfactants are generally required to disperse the extraction solvents. Water with a low concentration of surfactant in dispersed solvent-assisted emulsion dispersive liquid−liquid microextraction (WLSSAE-DLLME) was developed recently,[42,43] which used in combination with an improved solvent collection system (ISCS) avoids the problems associated with DLLME to analyze water samples.[33]

In the present study, WLSSAE coupled with gas chromatography−mass spectrometry (GC-MS) was developed to analyze six fungicides in wine samples. The accuracy, precision, linearity, enrichment factor (EF), and LOD of WLSSAE in the analysis of wine samples were evaluated and tested.

## MATERIALS AND METHODS

**Reagents and Samples.** All solvents and chemicals used in the study were of analytical grade. Cyprodinil (CYP), procymidone (PRC), fludioxonil (FLD), flusilazole (FLU), benalaxyl (BEN), tebuconazole (TEB), anthracene-$d_{10}$ (ANT-$d_{10}$; internal standard), 1-heptanol, 1-octanol, 1-nonanol, Triton X-114, Triton X-100, Tween 80, and Tween 60 were purchased from Sigma-Aldrich (St. Louis, MO, USA). Methanol (liquid chromatography (LC)-MS grade) was obtained from J. T. Baker (Phillipsburg, NJ, USA). Acetone (LC grade) and sodium chloride were purchased from Merck (Darmstadt, Germany). Deionized water (DI water) was obtained by using a Milli-Q reagent water system (Millipore, Milford, MA, USA).

Stock solutions of each fungicide and of ANT-$d_{10}$ were prepared by dissolving each in methanol to obtain a 1000 mg $L^{-1}$ solution, which was then stored at 4 °C. Standard working solutions and ANT-$d_{10}$ solution were prepared by diluting each stock solution with methanol to 10 mg $L^{-1}$. Each sample solution was prepared by spiking pure water with 10 and 5 $\mu$g $L^{-1}$ fungicide and ANT-$d_{10}$. Two kinds of white wine and one kind of red wine made in California (USA) were purchased from a local supermarket (Hsinchu, Taiwan). All wine samples contained 12% alcohol. The samples were filtered through 0.45 $\mu$m membrane filters from Millipore (Bedford, MA, USA) and then stored at 4 °C overnight before analysis.

**Instrumentation.** To separate the aqueous and organic phases, microtubes that were designed in-house (15 × 3 mm; inner diameter, 1.8 mm; total volume, 38 $\mu$L; Qing-Fa Co., Hsinchu, Taiwan) were used in the ISCS system. A CN-2200 centrifuge (Hsiantai Machinery Industry, Taipei, Taiwan) and a miVac DUC-12060-C00 centrifuge (Stockholm, Sweden) were used in the study.

Analyses were carried out by using a 6850 Agilent Technologies gas chromatograph (Wilmington, DE, USA) with a split/splitless injector operated at 300 °C and a single quadrupole (Agilent Technologies mass detector 5975B). The splitless time was 1 min. The flow rate of helium was 1.0 mL $min^{-1}$. A 30 m DB-5MS UI-fused silica capillary column (0.25 mm i.d., 0.25 $\mu$m film thickness; J&W Scientific, Folsom, CA, USA) was employed in the determination of fungicides. The temperature of the column was initially held at 100 °C, raised to 250 °C at 35 °C $min^{-1}$, held at 250 °C for 3 min, raised to 300 °C at 10 °C $min^{-1}$, and then held at 300 °C for 1 min. The carrier gas was helium (purity = 99.9995%), which was further purified by passage through a helium gas purifier (Agilent Technologies model RMSH-2). The temperature of the GC-MS transfer line was 280 °C, 230 °C for ion source, and 150 °C for quadrupoles. A mass detector in the electron impact mode (70 eV) was used. Spectra were scanned over the $m/z$ range of 50−400 to confirm the retention times of the analytes. Selected ion monitoring mode (SIM) was applied for the determination of fungicides. In the determination of fungicides, two or three ions were selected in Table 1.

**Table 1. Retention Time and $m/z$ Values Selected for SIM Mass Detection**

| compd | retention time (min) | selected ions ($m/z$) |
|---|---|---|
| ANT-$d_{10}$ | 4.96 | 187, 188, and 189 |
| CYP | 5.87 | 210, 214, and 225 |
| PRC | 6.07 | 96, 283, and 285 |
| FLD | 6.61 | 182 and 248 |
| FLU | 6.76 | 206, 233, and 234 |
| BEN | 7.78 | 91, 148, and 206 |
| TEB | 8.22 | 120, 250, and 252 |

**Extraction Procedure.** A diagram of the WLSSAE procedure is shown in our previously published work.[42] A 5 mL portion of the blank white wine and DI water (1:1, v/v) spiked with analytes at 5 $\mu$g $L^{-1}$ were transferred to a 10 mL conical-bottom glass centrifuge tube. A mixture of 12 $\mu$L of extraction solvent (1-octanol) and 240 $\mu$L of water containing 10 mg $L^{-1}$ Triton X-100 (dispersed solvent) was transferred to an Eppendorf tube. A 500 $\mu$L syringe (Reno, NV, USA) was used to pump the mixture back and forth four times within 10 s, and then a cloudy emulsion was formed. This emulsion was then injected into the sample solution. After centrifugation for 5 min at 5000 rpm, an organic droplet formed on the surface of the solution. The phase separation after DLLME of white and red wines is also shown in ref [44]. The floating phase, which had a volume of approximately 3.0 ± 0.5 $\mu$L, was hard to withdraw into a microsyringe. Therefore, the mixture of the floating phase and aqueous solution was first transferred to a in-house-designed microtube (15 × 3 mm). After centrifugation for 1 min, the organic phase was collected from the upper portion of the microtube by using a 10 $\mu$L microsyringe and then injected into the GC-MS system. The ambient temperature was 25 °C.

## RESULTS AND DISCUSSION

**Impact of Solvent on Extraction Efficiency.** The selection of extraction solvent is important in maximizing the extraction efficiency. The solvents should be immiscible with

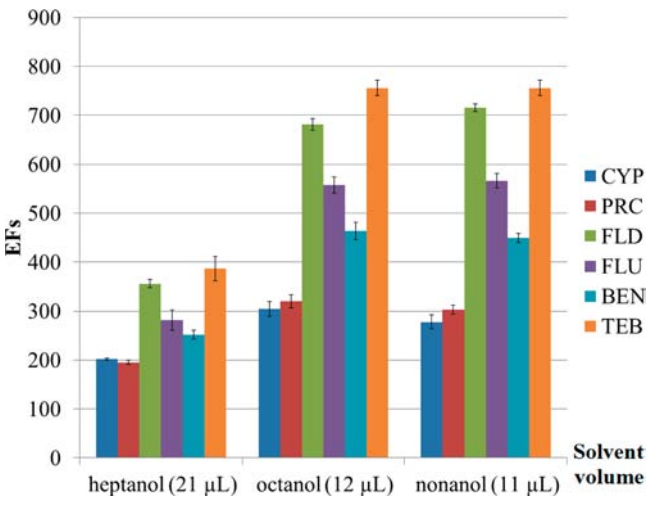


**Figure 1.** Effect of the type of extraction solvent ($n$ = 3). Samples were spiked with 5 $\mu$g $L^{-1}$ of each analyte. Extraction conditions: dispersed solvent volume, 240 $\mu$L; surfactant, 1 mg $L^{-1}$ Triton X-100.


dx.doi.org/10.1021/jf5036096 | J. Agric. Food Chem. 2014, 62, 9059−9065

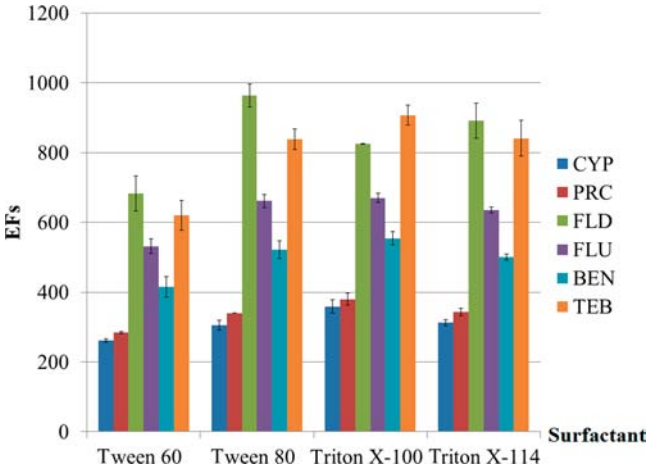


**Figure 2.** Effect of the type of surfactant for the first extraction solvent ($n$ = 3). Samples were spiked with 5 $\mu$g $L^{-1}$ of each analyte. Extraction conditions: extraction solvent, 1-octanol; volume, 12 $\mu$L; dispersed solvent volume, 240 $\mu$L; concentration of the surfactant, 1 mg $L^{-1}$.

water and have low toxicity, and analytes should be highly soluble in such solvents. To apply the above conditions, alcohols 1-heptanol, 1-octanol, and 1-nonanol were tested. To consistently collect 3.0 $\mu$L of the floating organic phase, various amounts of extraction solvent (21 $\mu$L of 1-heptanol, 12 $\mu$L of 1-octanol, and 11 $\mu$L of 1-nonanol) had to be combined with 240 $\mu$L of Triton X-100 (1 mg $L^{-1}$) in a microsyringe.[43] The mixture was subsequently injected into the sample solution. The results are shown in Figure 1. The experiment revealed that 1-octanol had better EFs than those of the other solvents; it was thus chosen as the extraction solvent for use in subsequent experiments.

**Type of Surfactant.** The selection of surfactant is crucial to the success of the proposed method. As surfactants are soluble in the extraction solvent and in water, they are commonly used to improve the dispersion of extraction solvents. A surfactant with high hydrophilic−lipophilic balance (HLB) has higher hydrophilicity. When the HLB value of a surfactant is between 12 and 16, the surfactant is considered as an oil-in-water emulsifier. Two kinds of well-known polyoxyethylene-type nonionic surfactants, Tween and Triton (Figure 2), were studied. The HLBs of Tween 60, Tween 80, Triton X-100, and Triton X-114 are 14.9, 15.0, 13.4, and 12.3, respectively. Compared with other surfactants, using Triton-X-100 resulted in higher EFs for five of six compounds, especially for BEN and TEB, which had lower extraction efficiency. On the basis of the experimental results, Triton X-100, which had better extraction efficiency and precision for most fungicides, was selected as the dispersed solvent.

**Volume of Extraction Solvent.** Different volumes of the extraction solvent (12, 14, 16, and 18 $\mu$L) were tested. When the solvent volume was <12 $\mu$L, the amount of organic phase was insufficient for analysis. As the volume of the extraction solvent increased, the volume of the floating phase increased accordingly. This resulted in dilution of the extractants. The EFs were maximal when the solvent volume was 12 $\mu$L. Hence, 12 $\mu$L was selected as the volume of extraction solvent.

**Concentration of Surfactant.** The concentration of surfactant in aqueous solution plays an important role in effective extraction. The influence of the Triton X-100 concentration was investigated by studying the results obtained with concentrations of 1, 5, 10, and 50 mg $L^{-1}$. At >50 mg $L^{-1}$ surfactant, the solution was still an emulsion after centrifugation. The floating phase could not be collected. Therefore, the maximum concentration of surfactant used was 50 mg $L^{-1}$. When the concentration of

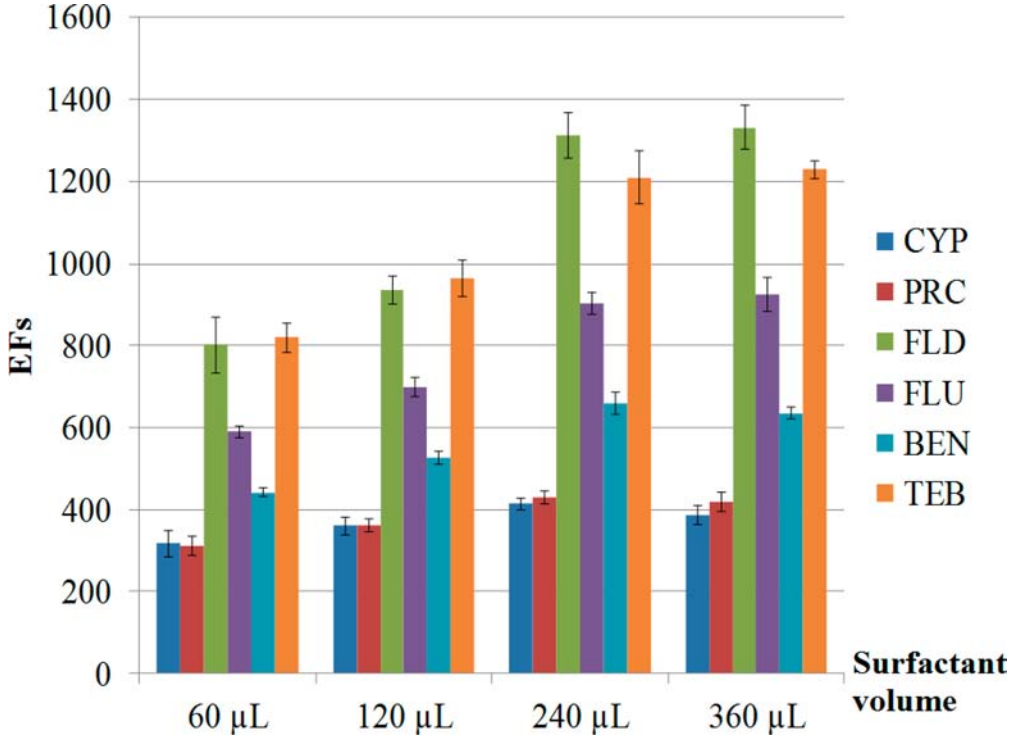


**Figure 3.** Effect of the volume of the surfactant ($n$ = 3). Samples were spiked with 5 $\mu$g $L^{-1}$ of each analyte. Extraction conditions: extraction solvent, 1-octanol; volume, 12 $\mu$L; dispersed solvent, Triton X-100; concentration, 10 mg $L^{-1}$.


dx.doi.org/10.1021/jf5036096 | J. Agric. Food Chem. 2014, 62, 9059−9065

**Table 2. Linearity, EFs, LODs, and Precision of Blank White and Red Wines**

| | linearity[a] ($n$ = 3, $\mu$g L$^{-1}$) | | $R^2$ | | EFs[b] | | LOD[c] ($\mu$g L$^{-1}$) | | LOQ[d] ($\mu$g L$^{-1}$) | | RSD[e] (%) intraday, $n$ = 7 | | RSD[e] (%) interday, $n$ = 6 | |
|---|---|---|---|---|---|---|---|---|---|---|---|---|---|---|
| compd | white | red | white | red | white | red | white | red | white | red | white | red | white | red |
| CYP | 0.05−100 | 0.05−100 | 0.9996 | 0.9997 | 414 | 349 | 0.021 | 0.036 | 0.072 | 0.121 | 7.2 | 2.3 | 11.2 | 3.3 |
| PRC | 0.05−100 | 0.10−100 | 0.9999 | 0.9998 | 430 | 328 | 0.018 | 0.092 | 0.061 | 0.306 | 6.1 | 8.9 | 10.1 | 14.1 |
| FLD | 0.1−100 | 0.05−100 | 0.9978 | 0.9977 | 1313 | 796 | 0.026 | 0.035 | 0.088 | 0.116 | 8.8 | 1.7 | 9.3 | 3.4 |
| FLU | 0.05−100 | 0.05−100 | 0.9995 | 0.9984 | 904 | 505 | 0.013 | 0.020 | 0.044 | 0.069 | 4.4 | 0.9 | 4.3 | 5.6 |
| BEN | 0.1−100 | 0.05−100 | 0.9998 | 0.9999 | 659 | 416 | 0.020 | 0.051 | 0.066 | 0.173 | 6.6 | 5.4 | 9.7 | 12.6 |
| TEB | 0.05−100 | 0.50−100 | 0.9999 | 0.9996 | 1210 | 911 | 0.016 | 0.155 | 0.053 | 0.517 | 5.3 | 12.7 | 7.9 | 13.6 |

[a]Blank white and red wine samples spiked with 0.05, 0.1, 0.5, 1, 5, 10, 50, and 100 $\mu$g L$^{-1}$. [b]Blank white and red wine samples spiked with 5 $\mu$g L$^{-1}$, $n$ = 3. [c]LODs were determined as 3 times the standard deviation obtained from seven replicate runs of blank white wine samples spiked with 0.1 $\mu$g L$^{-1}$ of each fungicide. [d]LOQs were determined as 10 times the standard deviation obtained from seven replicate runs of blank white and red wine samples spiked with 0.1 $\mu$g L$^{-1}$ of each fungicide. [e]Blank wine samples were spiked with 0.5 $\mu$g L$^{-1}$.

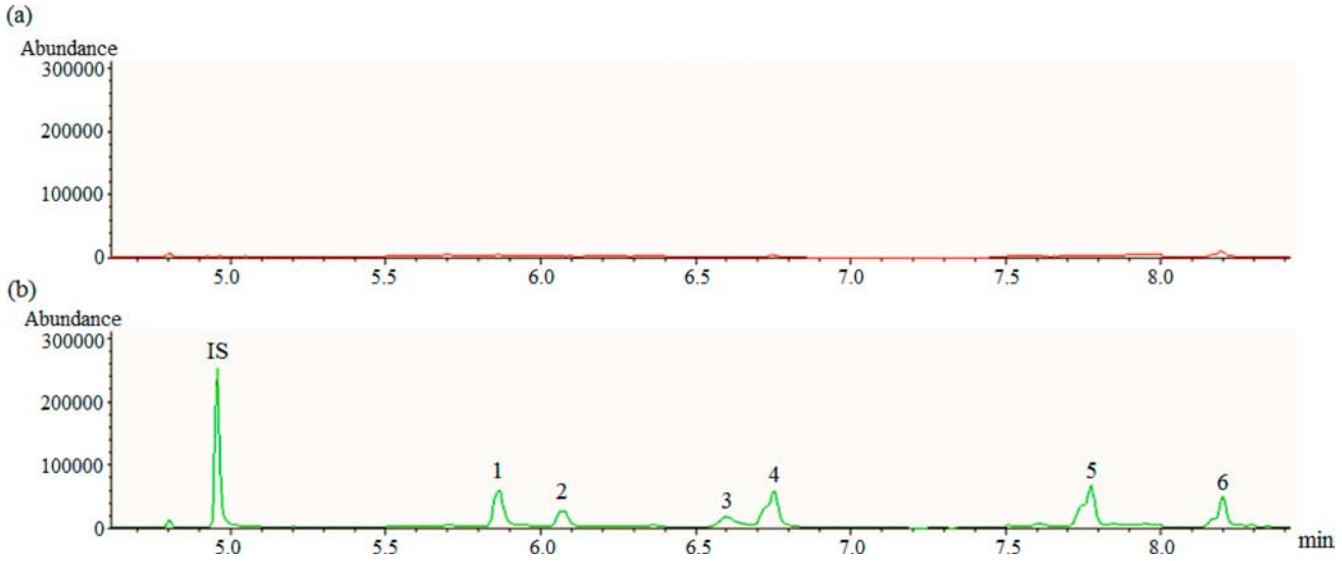


**Figure 4.** GC-MS selected ion chromatograms for the analysis of (a) white wine sample and (b) sample spiked with 5 $\mu$g L$^{-1}$ fungicides: IS, ANT-$d_{10}$; 1, CYP; 2, PRC; 3, FLD; 4, FLU; 5, BEN; 6, TEB.

surfactant in the aqueous solution was increased from 0 to 10 mg L$^{-1}$, the extraction EF was significantly improved. However, EFs declined slightly upon spiking with >10 mg L$^{-1}$ Triton X-100. Evidently, higher concentrations of Triton X-100 increased the solubility of analytes in the aqueous solutions, resulting in lower EFs. The optimal surfactant concentration in the aqueous solution was therefore 10 mg L$^{-1}$.

**Volume of the Surfactant Solution.** To investigate the impact of the volume of the aqueous solution, different volumes of aqueous solution (60, 120, 240, and 360 $\mu$L) containing 10 mg L$^{-1}$ Triton X-100 were evaluated (Figure 3). When the volume of aqueous solution was changed from 60 to 240 $\mu$L, the EFs were increased. On the other hand, the EFs decreased when the volume of aqueous solution was increased from 240 to 360 $\mu$L. Therefore, the volume of aqueous solution was fixed at 240 $\mu$L. The surfactant concentration was approximately equivalent to 0.48 mg L$^{-1}$ in the total volume (5 mL) of the sample solution.

**Quantitative Aspects.** The linearity obtained by using 12 $\mu$L of 1-octanol was evaluated under optimum conditions. Calibration curves were constructed by analyzing solutions of white and red wines with DI water (1:1, v/v) at concentrations of 0.05, 0.1, 0.5, 1, 5, 10, 50, and 100 $\mu$g L$^{-1}$. Curves for all fungicides have coefficients of determination ($R^2$) >0.9977. Data on the linear range (LR), $R^2$, LOD, limit of quantification (LOQ), precision (as relative standard deviation, RSD), and EF are summarized in Table 2. $R^2$ values of the calibration curves are in the range of 0.9977−0.9999, indicating high linearity within the concentration range used for each analyte. The LODs were calculated as 3 times the standard deviation of seven replicate runs of blank white and red wines spiked with low concentrations of the analytes. LODs for determination of fungicides in the blank wine samples differed substantially and ranged from 0.013 to 0.155 $\mu$g L$^{-1}$. Intra- and interday RSDs for determination of the analytes ranged from 0.9 to 12.7% and from 3.4 to 14.1%, respectively.

**Application in the Analysis of Wine Samples.** To demonstrate the capability of WLSSAE, the procedure was applied to the analysis of fungicides in white wine and red wine samples. The results show that the analyzed samples were free of fungicides (Figure 4). FLU, BEN, and TEB have a broad shoulder (Figure 4b), which might result from the surfactant partially extracted into the 1-octanol phase or from matrix effect of the samples. The wine samples were spiked with the analytes at 0.5, 5, and 50 $\mu$g L$^{-1}$ levels. The absolute recovery (AR) was defined as the percentage of the total analyte ($n_0$) that was extracted into the floating organic phase ($n_{org}$).

$$AR = n_{org}/n_0 \times 100$$


dx.doi.org/10.1021/jf5036096 | J. Agric. Food Chem. 2014, 62, 9059−9065

**Table 3. Accuracy, Absolute Recoveries (AR), Relative Recoveries (RR), and Precision (RSD) of Fungicides in Spiked White and Red Wines**

| | | white wine ($n$ = 3) | | | | red wine ($n$ = 3) | | | |
|---|---|---|---|---|---|---|---|---|---|
| WLSSAE | spiked concn ($\mu$g L$^{-1}$) | calcd concn ($\mu$g L$^{-1}$) | AR (%) | RR (%) | RSD (%) | calcd concn ($\mu$g L$^{-1}$) | AR (%) | RR (%) | RSD (%) |
| CYP | 0.5 | 0.44 | 52 | 88 | 4.2 | 0.48 | 56 | 96 | 4.2 |
| | 5 | 4.7 | 30 | 94 | 3.6 | 5.1 | 32 | 101 | 4.3 |
| | 50 | 44.1 | 34 | 88 | 1.9 | 47.0 | 37 | 94 | 7.1 |
| PRC | 0.5 | 0.47 | 43 | 93 | 6.6 | 0.44 | 40 | 88 | 1.9 |
| | 5 | 4.3 | 32 | 86 | 2.2 | 4.1 | 30 | 81 | 4.2 |
| | 50 | 45.5 | 37 | 91 | 2.7 | 45.0 | 37 | 90 | 4.2 |
| FLD | 0.5 | 0.45 | 76 | 90 | 5.9 | 0.55 | 92 | 109 | 2.6 |
| | 5 | 6.2 | 81 | 120 | 2.4 | 5.5 | 75 | 110 | 3.0 |
| | 50 | 54.3 | 81 | 108 | 3.2 | 52.0 | 78 | 104 | 1.0 |
| FLU | 0.5 | 0.47 | 78 | 94 | 2.7 | 0.42 | 69 | 84 | 7.2 |
| | 5 | 4.3 | 63 | 86 | 5.8 | 4.2 | 61 | 84 | 4.6 |
| | 50 | 42.4 | 64 | 84 | 2.1 | 41.0 | 62 | 82 | 2.2 |
| BEN | 0.5 | 0.49 | 54 | 97 | 1.0 | 0.44 | 49 | 87 | 6.3 |
| | 5 | 4.1 | 34 | 81 | 8.9 | 4.2 | 35 | 83 | 4.3 |
| | 50 | 42.2 | 38 | 84 | 1.6 | 41.0 | 37 | 82 | 5.8 |
| TEB | 0.5 | 0.52 | 83 | 104 | 4.1 | 0.54 | 85 | 107 | 2.5 |
| | 5 | 5.1 | 67 | 102 | 5.4 | 4.9 | 64 | 97 | 4.9 |
| | 50 | 43.5 | 72 | 87 | 2.6 | 43.5 | 72 | 87 | 4.3 |

**Table 4. Comparison of WLSSAE with Other Methods for Analysis of Fungicides in Wine**

| separation/detection methods | sample | extraction solvent ($\mu$L) | dispersive agent ($\mu$L) | extraction time (min) | linear range ($\mu$g L$^{-1}$) | LOD ($\mu$g L$^{-1}$) | ref |
|---|---|---|---|---|---|---|---|
| SPE/LC-MS[a] | wine | | | 20 | 0.2−2000 | 0.06−0.51 | 24 |
| BA$\mu$E-LD/GC-MS[b] | water/wine | methanol (750) + acetonitrile (750) | | 255 | 0.04−1.6 | 0.004−0.030 | 25 |
| DLLME-SFO/GC-MS[c] | wine | 1-undecanol (50) | acetone (500) | 1 | 1−300 | 0.06−0.90 | 17 |
| UASEME-SFO/HPLC-DAD[d] | water/wine | 1-undecanol (30) | Tween 80 (10 mmol L$^{-1}$, 24 $\mu$L) | 1 | 5−1000 | 1.2−4.7 | 38 |
| WLSSAE[e] | wine | 1-octanol (12) | Triton X-100 (10 mg L$^{-1}$, 240 $\mu$L) | few seconds | 0.05−100 | 0.013−0.026 | this work |

[a]Solid phase extraction/liquid chromatography quadrupole time-of-flight tandem mass spectrometry. [b]Bar adsorptive microextraction combined with liquid desorption/gas chromatography−mass spectrometry. [c]Dispersive liquid−liquid microextraction based on solidification of floating organic drop/gas chromatography−mass spectrometry. [d]Ultrasound-assisted surfactant-enhanced emulsification microextraction/high-performance liquid chromatography with diode array detection. [e]Water with low concentration of surfactant in dispersed solvent-assisted emulsion dispersive liquid−liquid microextraction.

ARs were between 30 and 83% for white wine and between 30 and 92% for red wine. The relative recovery (RR) is defined by the following equation:

$$RR = [(C_{found} - C_{real})/C_{added}] \times 100$$

$C_{found}$, $C_{real}$, and $C_{added}$ are defined as the concentration of analyte after addition of a known amount of standard in the real sample, the concentration of analyte in the real sample, and the concentration of known amount of standard that was spiked to the real sample, respectively. RRs were between 81 and 108% for white wine and between 81 and 110% for red wine. RSDs for the determination of the analytes ranged from 1.0 to 8.9% for white wine and from 1.0 to 7.2% for red wine (Table 3). This shows that after the wine samples were diluted with DI water there was no significant matrix effect using WLSSAE.

In Table 4, the performance of WLSSAE is compared with that of other extraction techniques for the determination of fungicides in wine. The results indicate that the proposed method is sensitive and applicable to the analysis of fungicides at trace levels. The method requires a very short extraction time (a few seconds) and 12 $\mu$L of extraction solvent only, in contrast to other methods.

To extract fungicides from wine samples through the ISCS technique, 0.48 mg L$^{-1}$ of surfactants was required in using water with low concentration of surfactant as dispersed solvent. The results suggest that high EFs were achieved in a few seconds. The approach afforded high repeatability and high recovery within a short extraction time. WLSSAE employed a few microliters of low-toxicity, halogen-free organic solvents to extract fungicides in wine samples. The analysis had a wide linear range and low LODs, as well as high precision, EFs, and RRs. The LODs were much lower than the tolerance of procymidone in wine prescribed by the FDA.[16] The method is a desirable application for the separation and preconcentration of fungicides at trace levels in wine samples.


dx.doi.org/10.1021/jf5036096 | J. Agric. Food Chem. 2014, 62, 9059−9065

## AUTHOR INFORMATION


### Corresponding Authors

*(P.-S.C.) Phone: +886-2-2312-3456, ext. 65495. E-mail: paishanchen@ntu.edu.tw.

*(S.-D.H.) Phone:+886-937997973. E-mail: sdhuang@mx.nthu.edu.tw.

### Author Contributions

‖W.-C.T and S.-P.C. contributed equally to this work.



### Funding

This study was supported by the Ministry of Science and Technology of Taiwan (NSC 99-2113-M-007-004-MY3).

### Notes

The authors declare no competing financial interest.


## REFERENCES


(1) Kamrin, M. A. *Pesticides Profiles: Toxicity, Environmental Impact, and Fate*; CRC Press: Boca Raton, FL, USA, 1997.

(2) Pose-Juan, E.; Rial-Otero, R.; Martínez-Carballo, E.; López-Periago, E.; Simal-Gándara, J. Determination of metalaxyl and identification of adjuvants in wettable powder pesticide technical formulas. *Anal. Bioanal. Chem.* **2009**, *394*, 1535−1544.

(3) González-Rodríguez, R. M.; Cancho-Grande, B.; Simal-Gándara, J. Decay of fungicide residues during vinification of white grapes harvested after the application of some new active substances against downy mildew. *Food Chem.* **2011**, *125*, 549−560.

(4) Rial Otero, R.; Cancho Grande, B.; Arias Estévez, M.; López Periago, E.; Simal Gándara, J. Procedure for the measurement of soil inputs of plant-protection agents washed off through vineyard canopy by rainfall. *J. Agric. Food Chem.* **2003**, *51*, 5041−5046.

(5) Noguerol-Pato, R.; González-Rodríguez, R. M.; González-Barreiro, C.; Cancho-Grande, B.; Simal-Gándara, J. Influence of tebuconazole residues on the aroma composition of Mencía red wines. *Food Chem.* **2011**, *124*, 1525−1532.

(6) Teixeira, M. J.; Aguiar, A.; Afonso, C. M. M.; Alves, A.; Bastos, M. M. S. M. Comparison of pesticides levels in grape skin and in the whole grape by a new liquid chromatographic multiresidue methodology. *Anal. Chim. Acta* **2004**, *513*, 333−340.

(7) González-Rodríguez, R. M.; Cancho-Grande, B.; Torrado-Agrasar, A.; Simal-Gándara, J.; Mazaira-Pérez, J. Evolution of tebuconazole residues through the winemaking process of Mencía grapes. *Food Chem.* **2009**, *117*, 529−537.

(8) González-Rodríguez, R. M.; Cancho-Grande, B.; Simal-Gándara, J. Efficacy of new commercial formulations to control downy mildew and dissipation of their active fungicides in wine after good agricultural practices. *J. Sci. Food Agric.* **2009**, *89*, 2625−2635.

(9) Cabras, P.; Angioni, A. Pesticide residues in grapes, wine, and their processing products. *J. Agric. Food Chem.* **2000**, *48*, 967−973.

(10) Fernandez, M. J.; Oliva, J.; Barba, A.; Camara, M. A. Fungicide dissipation curves in winemaking processes with and without maceration step. *J. Agric. Food Chem.* **2005**, *53*, 804−811.

(11) Ruediger, G. A.; Pardon, K. H.; Sas, A. N.; Godden, P. W.; Pollnitz, A. P. Removal of pesticides from red and white wine by the use of fining and filter agents. *Aust. J. Grape Wine Res.* **2004**, *10*, 8−16.

(12) González-Rodríguez, R. M.; Noguerol-Pato, R.; González-Barreiro, C.; Cancho-Grande, B.; Simal-Gándara, J. Application of new fungicides under good agricultural practices and their effects on the volatile profile of white wines. *Food Res. Int.* **2011**, *44*, 397−403.

(13) González-Álvarez, M.; González-Barreiro, C.; Cancho-Grande, B.; Simal-Gándara, J. Impact of phytosanitary treatments with fungicides (cyazofamid, famoxadone, mandipropamid and valifenalate) on aroma compounds of Godello white wines. *Food Chem.* **2012**, *131*, 826−836.

(14) Commission Regulation No. 459/2010 of 27 May, 2010, European Union.

(15) http://www.fda.gov.tw/TC/index.aspx.

(16) *Code of Federal Regulations*, Title 40, Parts 180, USA, 2003.

(17) Rodriguez-Cabo, T.; Rodriguez, I.; Ramil, M.; Cela, R. Dispersive liquid-liquid microextraction using non-chlorinated, lighter than water solvents for gas chromatography mass spectrometry determination of fungicides in wine. *J. Chromatogr., A* **2011**, *1218*, 6603−6611.

(18) Vaquero-Fernandez, L.; Sanz-Asensio, J.; Fernandez-Zurbano, P.; Sainz-Ramirez, M.; Lopez-Alonso, M.; Epifanio-Fernandez, S. I.; Martinez-Soria, M. T. Development of a liquid-liquid extraction method for the determination of pyrimethanil, metalaxyl, dichlofluanid and penconazol during the fermentative process of must by GC-NPD. *J. Sci. Food Agric.* **2009**, *89*, 750−757.

(19) Moeder, M.; Bauer, C.; Popp, P.; van Pinxteren, M.; Reemtsma, T. Determination of pesticide residues in wine by membrane-assisted solvent extraction and high-performance liquid chromatography-tandem mass spectrometry. *Anal. Bioanal. Chem.* **2012**, *403*, 1731−1741.

(20) Martins, J.; Esteves, C.; Limpo-Faria, A.; Barros, P.; Ribeiro, N.; Simoes, T.; Correia, M.; Delerue-Matos, C. Analysis of six fungicides and one acaricide in still and fortified wines using solid-phase microextraction-gas chromatography/tandem mass spectrometry. *Food Chem.* **2012**, *132*, 630−636.

(21) López-Fernández, O.; Rial-Otero, R.; González-Barreiro, C.; Simal-Gándara, J. Surveillance of fungicidal dithiocarbamate residues in fruits and vegetables. *Food Chem.* **2012**, *134*, 366−374.

(22) Montes, R.; Rodriguez, I.; Ramil, M.; Rubi, E.; Cela, R. Solid-phase extraction followed by dispersive liquid-liquid microextraction for the sensitive determination of selected fungicides in wine. *J. Chromatogr., A* **2009**, *1216*, 5459−5466.

(23) Lagunas-Allue, L.; Sanz-Asensio, J.; Martinez-Soria, M. T. Optimization and validation of a simple and fast method for the determination of fungicides in must and wine samples by SPE and GC/MS. *J. AOAC Int.* **2012**, *95*, 1511−1519.

(24) Fontana, A. R.; Rodriguez, I.; Ramil, M.; Altamirano, J. C.; Cela, R. Solid-phase extraction followed by liquid chromatography quadrupole time-of-flight tandem mass spectrometry for the selective determination of fungicides in wine samples. *J. Chromatogr., A* **2011**, *1218*, 2165−2175.

(25) Almeida, C.; Nogueira, J. M. F. Comparison of the selectivity of different sorbent phases for bar adsorptive microextraction − application to trace level analysis of fungicides in real matrices. *J. Chromatogr., A* **2012**, *1265*, 7−16.

(26) Rezaee, M.; Assadi, Y.; Milani Hosseini, M. R.; Aghaee, E.; Ahmadi, F.; Berijani, S. Determination of organic compounds in water using dispersive liquid-liquid microextraction. *J. Chromatogr., A* **2006**, *1116*, 1−9.

(27) Khalili Zanjani, M. R.; Yamini, Y.; Shariati, S.; Jönsson, J. A. A new liquid-phase microextraction method based on solidification of floating organic drop. *Anal. Chim. Acta* **2007**, *585*, 286−293.

(28) Lee, J.; Lee, H. K. Fully automated dynamic in-syringe liquid-phase microextraction and on-column derivatization of carbamate pesticides with gas chromatography/mass spectrometric analysis. *Anal. Chem.* **2011**, *83*, 6856−6861.

(29) Zacharis, C. K.; Tzanavaras, P. D.; Roubos, K.; Dhima, K. Solvent-based de-emulsification dispersive liquid-liquid microextraction combined with gas chromatography-mass spectrometry for determination of trace organochlorine pesticides in environmental water samples. *J. Chromatogr., A* **2010**, *1217*, 5896−5900.

(30) Shi, Z. G.; Lee, H. K. Dispersive liquid-liquid microextraction coupled with dispersive $\mu$-solid-phase extraction for the fast determination of polycyclic aromatic hydrocarbons in environmental water samples. *Anal. Chem.* **2010**, *82*, 1540−1545.

(31) Farajzadeh, M. A.; Seyedi, S. E.; Shalamzari, M. S.; Bamorowat, M. Dispersive liquid-liquid microextraction using extraction solvent lighter than water. *J. Sep. Sci.* **2009**, *32*, 3191−3200.

(32) Chen, H.; Chen, R. W.; Li, S. Q. Low-density extraction solvent-based solvent terminated dispersive liquid-liquid microextraction combined with gas chromatography-tandem mass spectrometry for the determination of carbamate pesticides in water samples. *J. Chromatogr., A* **2010**, *1217*, 1244−1248.

(33) Chang, C.-C.; Wei, S.-Y.; Huang, S.-D. Improved solvent collection system for a dispersive liquid-liquid microextraction of organochlorine pesticides from water using low-density organic solvent. *J. Sep. Sci.* **2011**, *34*, 837−843.
(34) Saleh, A.; Yamini, Y.; Faraji, M.; Rezaee, M.; Ghambarian, M. Ultrasound-assisted emulsification microextraction method based on applying low density organic solvents followed by gas chromatography analysis for the determination of polycyclic aromatic hydrocarbons in water samples. *J. Chromatogr., A* **2009**, *1216*, 6673−6679.
(35) Regueiro, J.; Llompart, M.; Garcia-Jares, C.; Garcia-Monteagudo, J. C.; Cela, R. Ultrasound-assisted emulsification-microextraction of emergent contaminants and pesticides in environmental waters. *J. Chromatogr., A* **2008**, *1190*, 27−38.
(36) Fontana, A. R.; Wuilloud, R.; Martinez, L. D.; Altamirano, J. C. Simple approach based on ultrasound-assisted emulsification-microextraction for determination of polibrominated flame retardants in water samples by gas chromatography-mass spectrometry. *J. Chromatogr., A* **2009**, *1216*, 147−153.
(37) Liang, P.; Wang, F.; Wan, Q. Ionic liquid-based ultrasound-assisted emulsification microextraction coupled with high performance liquid chromatography for the determination of four fungicides in environmental water samples. *Talanta* **2013**, *105*, 57−62.
(38) You, X.; Wang, S.; Liu, F.; Shi, K. Ultrasound-assisted surfactant-enhanced emulsification microextraction based on the solidification of a floating organic droplet used for the simultaneous determination of six fungicide residues in juices and red wine. *J. Chromatogr., A* **2013**, *1300*, 64−69.
(39) Sarafraz Yazdi, A.; Es'haghi, Z. Surfactant enhanced liquid-phase microextraction of basic drugs of abuse in hair combined with high performance liquid chromatography. *J. Chromatogr., A* **2005**, *1094*, 1−8.
(40) Wu, Q.; Chang, Q.; Wu, C.; Rao, H.; Zeng, X.; Wang, C.; Wang, Z. Ultrasound-assisted surfactant-enhanced emulsification microextraction for the determination of carbamate pesticides in water samples by high performance liquid chromatography. *J. Chromatogr., A* **2010**, *1217*, 1773−1778.
(41) Cheng, J.; Matsadiq, G.; Liu, L.; Zhou, Y. W.; Chen, G. Development of a novel ultrasound-assisted surfactant-enhanced emulsification microextraction method and its application to the analysis of eleven polycyclic aromatic hydrocarbons at trace levels in water. *J. Chromatogr., A* **2011**, *1218*, 2476−2482.
(42) Li, Y.; Chen, P.-S.; Huang, S.-D. Water with low concentration of surfactant in dispersed solvent-assisted emulsion dispersive liquid-liquid microextraction for the determination of organochlorine pesticides in aqueous samples. *J.Chromatogr., A* **2013**, *1300*, 51−57.
(43) Tseng, W.-C.; Chen, P.-S.; Huang, S.-D. Optimization of two different dispersive liquid-liquid microextraction methods followed by gas chromatography-mass spectrometry determination for polycyclic aromatic hydrocarbons (PAHs) analysis in water. *Talanta* **2014**, *120*, 425−432.
(44) Chen, P.-S.; Haung, W.-Y.; Huang, S.-D. Analysis of triazine herbicides using an up-and-down-shaker-assisted dispersive liquid−liquid microextraction coupled with gas chromatography−mass spectrometry. *J. Chromatogr., B* **2014**, *955−956*, 116−123.

Table 1. Sampling Sites and Characterization of the Soils Studied

| | | particle size | | | | | | |
|---|---|---|---|---|---|---|---|---|
| no. | soil site[a] | sand | silt | clay | soil texture | pH[b] | Corg(%)[c] | biomass C (mg/kg)[d] |
| alk-1 | Haozhou | 39.7 | 50.3 | 10.0 | silt loam | 8.29 | 1.68 | 213 |
| alk-2 | Guiyang | 16.8 | 72.5 | 10.7 | silt loam | 7.73 | 3.49 | 218 |
| neut-3 | Jilin | 25.5 | 68.4 | 6.1 | silt loam | 7.22 | 2.12 | 178 |
| ac-4 | Hangzhou | 10.8 | 80.1 | 9.1 | silt | 5.65 | 5.56 | 236 |
| ac-5 | Haikou | 58.1 | 32.7 | 9.2 | sandy loam | 5.01 | 0.26 | 26.4 |

[a]The cities in China. [b]Suspension of soil in water, 1:2.5 (w/w). [c]Following the potassium dichromate volumetric method. [d]Following the fumigation−extraction method.

enantiomeric proportion of various enantiomeric compositions thus far. Moreover, microorganisms in soils are considered as the main cause of enantioselective processes,[25−28] and enantiomeric degradation constantly changes due to soils with different microbial communities. Our study systematically investigated the selective degradations of two enantiomers in indoxacarb concentrate (2.33S/1R) and in its racemate (1S/1R) in five soils to determine the differences between the racemate and concentrate with respect to enantiomer degradation (In this article, mixtures of the two enantiomers enriched with the S-enantiomer (S/R = 2.33:1) are called concentrate). We also investigated the degradation of pure *R*-indoxacarb and pure *S*-indoxacarb applied to five soils. The steric configuration of *S*-(+)-indoxacarb and *R*-(−)-indoxacarb was first confirmed here by X-ray diffraction. The results provide new aspects of the enantioselective behavior of indoxacarb, which should be considered to achieve better understanding of the profiles and fate of chiral pesticides in the environment.

## MATERIALS AND METHODS

**Chemicals and Reagents.** The analytical standard of racemic indoxacarb was purchased from Dr. Ehrenstorfer GmbH. Indoxacarb powder enriched with the *S*-enantiomer (2.33S/1R, 97.3% purity) was provided by Yancheng Limin Agrochemical Co., Ltd. (Jiangsu, China). The two indoxacarb enantiomers were prepared by semipreparative high-performance liquid chromatography (HPLC) in our laboratory.[29] HPLC-grade *n*-hexane and isopropanol (IPA) were purchased from Jiangsu Hanbang Science and Technology Co., Ltd. (Jiangsu, China). All other chemicals and solvents used were of analytical grade and purchased from commercial sources.

**Single-Crystal X-ray Investigation of Enantiopure *S*-Indoxacarb and Enantiopure *R*-Indoxacarb.** The stereochemical configuration was determined using X-ray diffraction. Diffraction patterns were obtained at 293 K with a Bruker SMART II diffractometer using Mo-K$\alpha$ radiation ($\lambda$ = 0.71073 Å) under $\varphi-\omega$ scan. Empirical absorption correction (SADABS) was applied to raw intensities. The structures were determined by direct methods (SHELXS-97) and refined by full matrix least-squares procedures on $F^2$ in the anisotropic approximation for all of the atoms except hydrogen. The absolute configurations were determined by anomalous dispersion effects and corresponding calculations of Flack's absolute structure parameters.[30]

**Soil Samples.** Five soil samples representing different physicochemical properties and climatic environments were collected at 0 to 10 cm plow layer from geographically distinct regions of China (Haozhou city, Anhui Province, Northern China; Guiyang City, Guizhou Province, Southwest China; Jilin city, Jilin Province, Northern China; Hangzhou city, Zhejiang Province, Southeastern China; and Haikou City, Hainan Province, Southern China). No indoxacarb was found at detectable levels in soils. After collection, the soil samples were air-dried at room temperature, homogenized, passed through a 2 mm sieve, and then stored in the dark until use within a few days. Details about soil sites and specific physicochemical characteristics (particle size, texture, pH, and organic carbon) are presented in Table1.

**Incubation of Indoxacarb Concentrate (2.33S/1R) and Racemate (1S/1R) in Soils.** Separate incubation experiments with indoxacarb concentrate and with racemate compounds in five soils were conducted in 50 mL of polypropylene centrifuge tubes covered with aluminum foil. Before pesticide treatment, the soils were preincubated in the dark at 25 ± 2 °C for 7 days to activate the soil microorganisms. The soil sample (5.0 g, dry weight equivalent) was treated with 50 $\mu$g of indoxacarb (50 $\mu$L 1000 $\mu$g/mL stock solution in acetone) and then air-dried for 30 min before homogenization. The soil samples were then rehydrated by adding 1.2 mL of purified water [approximately 60% of the field holding capacity (w/w)] and incubated at 25 °C in the dark. The samples were weighed regularly, and purified water was added to the samples to compensate for water loss during the entire experiment. Triplicate samples were removed from each treatment at different time intervals (0, 1, 3, 5, 7, 10, 14, 21, 33, and 51 d) and immediately transferred into a freezer (−20 °C).

**Incubation of Enantiopure *R*-(−)- and *S*-(+)-Indoxacarb.** Separation of the two pure indoxacarb enantiomers is necessary to understand the differences in their dissipation behaviors and detect potential enantiomerization of indoxacarb. Separate incubations were conducted with the enantiopure *R*-(−)- and *S*-(+)-indoxacarb in five soils. The tested soils were fortified with the pure enantiomers at the 10 $\mu$g/g level and incubated in the same way as the other soil experiments.

**Incubation of Indoxacarb Racemate (1S/1R) or Concentrate (2.33S/1R) in Soils under Sterilized Conditions.** To determine whether the enantioselective degradation was a result of microbially mediated transformations, portions of the 5.0 g soil set in 50 mL polypropylene centrifuge tubes were sterilized with the use of an autoclave (twice) at 121 °C for 40 min with 24 h intervals to eliminate microbial activity. In a biologically clean workbench, the sterilized samples were treated with 50 $\mu$g of indoxacarb racemate or concentrate (50 $\mu$L of a 1000 $\mu$g/mL stock solution in acetone). After eliminating the acetone by air-drying for 20 min, 1.2 mL of sterile water was added to the samples. The samples were then sealed with a stopper and membrane to maintain sterile conditions. The samples were incubated at 25 °C in the dark. Three or two replicate samples were removed from each treatment at different time intervals (0, 5, 10, 20, 40, 60, and 93 d) and immediately transferred to a freezer (−20 °C).

**Extraction of Soil Samples.** Three replicate samples were removed from each treatment at different time intervals after pesticide addition and immediately transferred into a freezer (−20 °C) to stop dissipation. For extraction, 25 mL of methanol/water (6:4, v/v) was added into a 50 mL polypropylene centrifuge tube containing 5 g (dry weight basis) of incubated soil sample. The sample was ultrasonically extracted for 20 min and centrifuged at 6000 rpm for 5 min. The extract was transferred to a 150 mL separatory funnel. The extraction was repeated by adding 15 mL of methanol/water (6:4, v/v) to the 50 mL polypropylene centrifuge tube. The tube was then stirred for 30 s on a vortex mixer and centrifuged at 6000 rpm for 5 min. The extracts were combined in the 150 mL separatory funnel and extracted two times using 40 mL of dichloromethane. Afterward, the organic phase (dichloromethane) was collected, concentrated to dryness, and reconstituted with 1.0 mL of methanol. Each sample was filtered


dx.doi.org/10.1021/jf5018803 | J. Agric. Food Chem. 2014, 62, 9066−9072

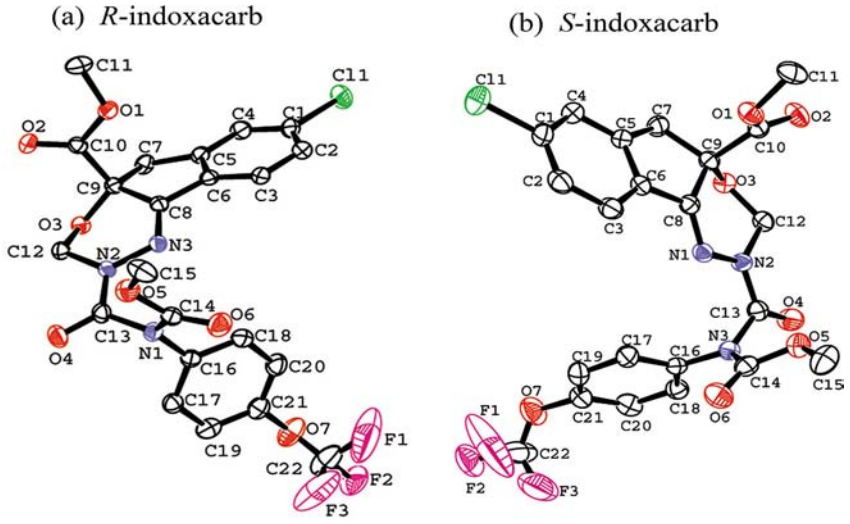


**Figure 2.** Stereoview of the indoxacarb enantiomers ($C_{22}H_{17}ClF_3N_3O_7$, M.W. = 527.83) (a) *R*-indoxacarb and (b) *S*-indoxacarb.

through a 0.45 $\mu$m nylon membrane filter and analyzed by HPLC (20 $\mu$L final extract).

**Instrumental Conditions (Enantioselective HPLC Analysis of Indoxacarb).** HPLC analysis of racemic indoxacarb was performed using an Agilent 1200 series apparatus composed of a quaternary pump, an autosampler, a diode array detector, a vacuum degasser, a column oven, and Agilent Chemstation software. The chiral analytical column amylose tris(3,5-dimethylphenyl carbamate) immobilized on silica-gel (Chiralpak IA) was purchased from Daicel (Tokyo, Japan). The dimensions of the column were 250 mm × 4.6 mm i.d., and it was packed with 5 $\mu$m particles.

The samples were analyzed using a mixture of *n*-hexane/isopropanol (70:30 v/v) at 1.0 mL/min flow rate on a Chiralpak IA column. The UV detection wavelength was 310 nm, and the temperature for separation was 30 °C. Under the selected conditions, the R-(−)-enantiomer eluted before the S-(+)-enantiomer.

**Method Validation.** A series of rac-indoxacarb standard solutions (0.25, 2.5, 5, 50, and 100 $\mu$g/mL) was prepared for HPLC analysis to determine the linearity of the method and quantify the analyte. The obtained regression equations and respective correlation coefficients were $A = 44.3880C - 1.8603$ ($R^2 = 0.9999$) for the R-(−)-enantiomer and $A = 43.325x + 2.9917$ ($R^2 = 0.9999$) for the S-(+)-enantiomer. A series of blank samples fortified with rac-indoxacarb at 0.1, 1.0, and 10 mg/kg was prepared for method validation and analyzed by the described procedure. The recovery and precision data for the samples in five soils are summarized in Table S2 (Supporting Information). For indoxacarb enantiomers, the recovery ranges in low, intermediate, and high spiked levels were 86.1−98.3, 86.3−99.2, and 95.5−103%, respectively, and each recovery value was acceptable for enantiomer determination. The limit of quantitation (LOQ) for each indoxacarb enantiomer was 0.05 $\mu$g/g in soil samples based on the acceptable RSDs of 5.14% to 10.2% for the two enantiomers. The limit of detection (LOD), defined as the concentration that produces a signal-to-noise (S/N) ratio of 3, was estimated to be 0.01 $\mu$g/g for each enantiomer by analyses of spiked samples at low concentration levels.

**Kinetic Analysis and Calculation.** The kinetic study of indoxacarb in soil was performed by plotting the residue concentration against time, and the corresponding rate constants $k$ for the *S*-(+)-enantiomer and *R*-(−)enantiomer were calculated using the first-order kinetic eq 1 by regression analysis; the half-life ($t_{1/2}$) was determined using eq 2.

$$C_t = C_0 e^{-kt} \quad (1)$$

$$t_{1/2} = \ln 2/k \quad (2)$$

where $C_0$ is the initial concentration ($\mu$g/g) of the enantiomer, $C_t$ is its concentration ($\mu$g/g) at time $t$ (d), and $k$ is the degradation rate constant.

The enantiomer fraction (EF) was used to express enantioselectivity as defined by the equation EF = peak area of the (+)-enantiomer/[(+)-enantiomer + (−)-enantiomer]. EF values ranged from 0 to 1, with an EF value of 0.50 indicating a racemic mixture and EF value of 0.70 indicating indoxacarb enriched with the S-enantiomer (2.33S:1R).

Enantioselectivity (ES), which reflects the overall trend in enantioselective dissipation, was defined as ES = $(k_S - k_R)/(k_S + k_R)$ in a previous study,[31] where $k_S$ is the degradation rate constant of *S*-indoxacarb, and $k_R$ is the degradation rate constant of *R*-indoxacarb. Positive values ($0 < ES \leq 1$) indicate a more rapid degradation of the S-enantiomer, whereas negative values ($-1 \leq ES < 0$) indicate a more rapid dissipation of the R-enantiomer. Dissipation is not enantioselective at an ES value of 0, whereas degradation is fully enantioselective at an ES value of 1.

## RESULTS AND DISCUSSION

**Absolute Configuration Assignment.** Individual enantiomers with enantio purity >99.0% were obtained by enantioselective separation of the indoxacarb racemate using semipreparative HPLC.[29] Single crystals of enantiopure *S*-indoxacarb and enantiopure *R*-indoxacarb were obtained by recrystallization from dimethyl sulfoxide and ethanol mixture at room temperature.

The molecular structures of *R*-indoxacarb and *S*-indoxacarb are illustrated in Figure 2, and the crystallographic data are summarized in Table S1, Supporting Information. Both compounds crystallize in the monoclinic crystal system in space group *C*2, and absolute structure parameters are −0.09 (13) and 0.10 (15), respectively. On the basis of these results, the first eluted enantiomer on the Chiralpak IA column was confirmed as the R-enantiomer followed by *S*-indoxacarb. The complete set of experimental and computational data was deposited in the Cambridge Crystallographic Data Center (CCDC# 911685 for *S*-indoxacarb and CCDC# 921088 for *R*-indoxacarb).

Melting points were measured on a Tech X-4 melting point apparatus, and optical rotations were measured on a WZZ-ZS automatic polarimeter, and they were not corrected. The isolated enantiomers were characterized as follows: *R*-indoxacarb, $[\alpha]_D^{20} = -68.4$ (menthol) and mp 86 to 89 °C;


dx.doi.org/10.1021/jf5018803 | J. Agric. Food Chem. 2014, 62, 9066−9072

Table 2. Kinetic Data for Dissipation of the Two Enantiomers of Indoxacarb Concentrate (2.33S/1R) in Soils

| soil no. | soil origins | enantiomer | regressive function | $R^2$ | $t_{1/2}$ (d) | ES[a] |
|---|---|---|---|---|---|---|
| alk-1 | Haozhou | R-(−) | $C = 2.8216\ e^{-0.0687t}$ | 0.9840 | 10.1 | 0.095 |
| | | S-(+) | $C = 6.5825\ e^{-0.0829\ t}$ | 0.9803 | 8.36 | |
| alk-2 | Guiyang | R-(−) | $C = 2.8029\ e^{-0.0696\ t}$ | 0.9923 | 9.96 | 0.245 |
| | | S-(+) | $C = 6.7152\ e^{-0.1148\ t}$ | 0.9931 | 6.04 | |
| neut-3 | Jilin | R-(−) | $C = 2.9329\ e^{-0.0621t}$ | 0.9880 | 11.2 | −0.365 |
| | | S-(+) | $C = 6.1897\ e^{-0.0289\ t}$ | 0.9845 | 24.0 | |
| ac-4 | Hangzhou | R-(−) | $C = 3.0604\ e^{-0.0928\ t}$ | 0.9731 | 7.47 | −0.001 |
| | | S-(+) | $C = 7.2715\ e^{-0.0926\ t}$ | 0.9691 | 7.49 | |
| ac-5 | Haikou | R-(−) | $C = 2.7473\ e^{-0.0378\ t}$ | 0.9719 | 18.3 | −0.306 |
| | | S-(+) | $C = 7.0256e^{-0.0201\ t}$ | 0.9861 | 34.5 | |

[a]Enantioselectivity.

Table 3. Kinetic Data for Dissipation of the Two Enantiomers of Indoxacarb (1S/1R) in Soils

| soil no. | soil origins | enantiomer | regressive function | $R^2$ | $t_{1/2}$ (d) | ES[a] |
|---|---|---|---|---|---|---|
| alk-1 | Haozhou | R-(−) | $C = 4.9338\ e^{-0.0630\ t}$ | 0.9604 | 11.0 | 0.121 |
| | | S-(+) | $C = 5.0758\ e^{-0.0803t}$ | 0.9658 | 8.63 | |
| alk-2 | Guiyang | R-(−) | $C = 4.8370\ e^{-0.0677\ t}$ | 0.9958 | 10.2 | 0.207 |
| | | S-(+) | $C = 4.6104\ e^{-0.1030t}$ | 0.9876 | 6.72 | |
| neut-3 | Jilin | R-(−) | $C = 5.1290\ e^{-0.0526\ t}$ | 0.9779 | 13.2 | −0.251 |
| | | S-(+) | $C = 4.9289\ e^{-0.0315t}$ | 0.9855 | 22.0 | |
| ac-4 | Hangzhou | R-(−) | $C = 5.3632e^{-0.0883t}$ | 0.9696 | 7.85 | −0.005 |
| | | S-(+) | $C = 5.4033\ e^{-0.0874\ t}$ | 0.9706 | 7.93 | |
| ac-5 | Haikou | R-(−) | $C = 4.7060\ e^{-0.0308t}$ | 0.8796 | 22.5 | −0.222 |
| | | S-(+) | $C = 5.2248\ e^{-0.0196t}$ | 0.9292 | 35.4 | |

[a]Enantioselectivity.

and *S*-indoxacarb, $[\alpha]_D^{20}$ = +69.4 (menthol) and mp 88 to 90 °C.

**Degradation of Indoxacarb Concentrate (2.33S/1R) in Soil.** The degradation of the two enantiomers in the indoxacarb concentrate (2.33S/1R) followed first-order kinetics (Table 2 and Figure S1, Supporting Information), with $R^2$ values of 0.9691 to 0.9931, which indicated acceptable linearity. Half-lives ($t_{1/2}$) in the two alkaline soils (alk-1 and alk-2) were about 10.1 and 9.96 days for *R*-(−)-indoxacarb and 8.36 and 6.04 days for *S*-(+)-indoxacarb. This finding suggests that the two enantiomers degraded selectively in weakly alkaline soil and that the (*S*)-(+)-indoxacarb was preferentially degraded. The corresponding ES values were 0.095 and 0.245. The half-lives ($t_{1/2}$) of the two enantiomers were 11.2 and 24.0 d in neutral soil (neut-3). In soil neut-3, the degradation rates varied by a factor of 2, and the ES value of −0.365 indicates that (*R*)-(−)-indoxacarb was preferentially degraded. Furthermore, the two enantiomers display different degradation trends in the two acid soils (ac-4 and ac-5). In soil ac-4, the half-lives ($t_{1/2}$) of the two enantiomers were almost equal at 7.47 and 7.49 d. The ES value was −0.001; thus, the degradations of the two enantiomers was not selective. In soil ac-5, the half-lives ($t_{1/2}$) of the two enantiomers were 18.3 and 34.5 d, with an ES value of −0.306. This result indicates that (*R*)-(−)-indoxacarb was preferentially degraded.

**Degradation of Indoxacarb Racemate (1S/1R) in Soil.** The degradation of the two enantiomers in the indoxacarb racemate (1S/1R) followed first-order kinetics (Table 3 and Figure S2, Supporting Information), with $R^2$ values of 0.8796 to 0.9958. In addition to a half-life of 35.4 d of *S*-(+)-indoxacarb in soil ac-5, the other half-lives were similar to the results studied by Li et al.[16] and Sun et al.,[20] which were less than 23 d. Table 3 presents the statistically significant differences in the degradation half-life of the two enantiomers in the two weakly alkaline soils (alk-1 and alk-2) at 2.37 and 3.48 d, respectively. The corresponding ES values were 0.121 and 0.207, thus suggesting that the two enantiomers degraded selectively in weakly alkaline soil and that the (*S*)-(+)-indoxacarb was preferentially degraded. It is also consistent with the findings with the concentrate. In the neutral soil (neut-3), the half-lives ($t_{1/2}$) of the two enantiomers were 13.2 and 22.0 d. In soil neut-3, the ES value was −0.251, and (*R*)-(−)-indoxacarb was preferentially degraded. The degradation trends of the two enantiomers differed in acid soils ac-4 and ac-5. In soil ac-4, the half-lives ($t_{1/2}$) of two enantiomers were almost equal at 7.93 and 7.85 d, and the ES value was −0.005. Thus, the degradations of the two enantiomers were not selective. In soil ac-5, the half-lives ($t_{1/2}$) of two enantiomers were 22.5 and 35.4 d. The corresponding ES value was −0.222, thereby indicating that the (*R*)-(−)-indoxacarb was preferentially degraded. Only one alkaline soil and one acid soil were selected for enantioselective degradation of indoxacarb racemate by Sun et al.[20] Our result was consistent with the result reported by Sun et al. that *S*-(+)-indoxacarb degraded faster than *R*-(−)-indoxacarb in alkaline soil. In one of the acid soils (ac-5), our result was consistent with the result reported by Sun et al. that *R*-(−)-indoxacarb degraded faster than *S*-(+)-indoxacarb in acid soil. In the other acid soil (ac-4) in our study, the two enantiomers were nonselective.

**Comparison of Racemate (1S/1R) and Concentrate (2.33S/1R) in Terms of Selective Degradation.** With the indoxacarb racemate, *S*-(+)-indoxacarb was preferentially degraded in the two alkaline soils (alk-1 and alk-2). Thus, the amount of *S*-(+)-indoxacarb residue was lower than that of *R*-(−)-indoxacarb residue in the soil. As a result, the soil was enriched in *R*-(−)-indoxacarb. With the indoxacarb concen-


dx.doi.org/10.1021/jf5018803 | J. Agric. Food Chem. 2014, 62, 9066−9072

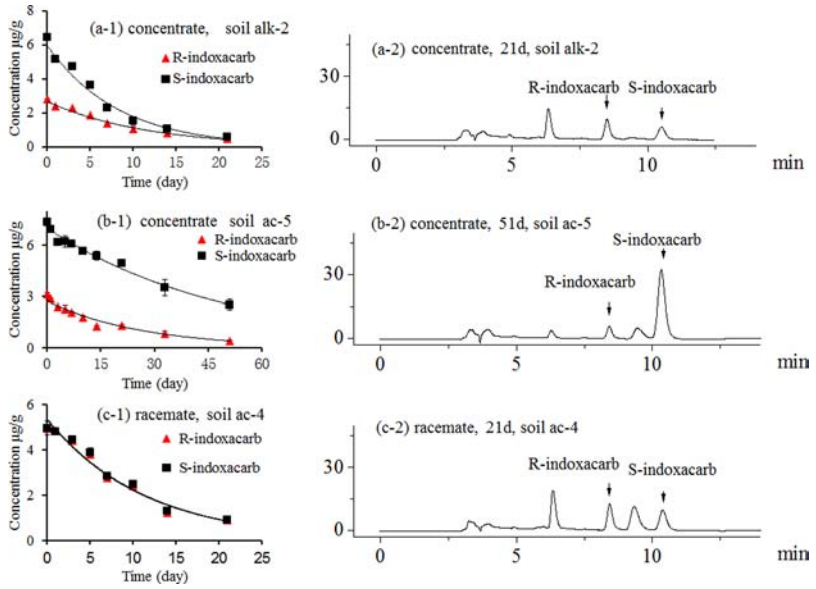


**Figure 3.** (a-1) Concentration−time curves and (a-2) chromatograms of indoxacarb concentrate (2.33S/1R) in soil alk-2 after 21d. (b-1) Concentration−time curves and (b-2) chromatograms of indoxacarb concentrate (2.33S/1R) in soil ac-5 after 51d. (c-1) Concentration−time curves and (c-2) chromatograms of indoxacarb racemate (1S/1R) in soil ac-4 after 21d.

**Table 4. Kinetic Data for Dissipation of Pure *S*-Indoxacarb and Pure *R*-Indoxacarb in Soils**

| soil no. | soil origins | enantiomer | regressive function | $R^2$ | $t_{1/2}$ (d) |
|---|---|---|---|---|---|
| alk-1 | Haozhou | pure R-(−) | $C = 8.6953\ e^{-0.0742t}$ | 0.9870 | 9.34 |
| | | pure S-(+) | $C = 8.5341\ e^{-0.0846t}$ | 0.9930 | 8.19 |
| alk-2 | Guiyang | pure R-(−) | $C = 7.6505\ e^{-0.0806t}$ | 0.9916 | 8.60 |
| | | pure S-(+) | $C = 7.819e^{-0.1668t}$ | 0.9859 | 4.16 |
| neut-3 | Jilin | pure R-(−) | $C = 8.7672\ e^{-0.0853t}$ | 0.9380 | 8.13 |
| | | pure S-(+) | $C = 9.000e^{-0.0287t}$ | 0.9480 | 24.2 |
| ac-4 | Hangzhou | pure R-(−) | $C = 9.4875e^{-0.0929t}$ | 0.9732 | 7.46 |
| | | pure S-(+) | $C = 9.5389e^{-0.0815t}$ | 0.9664 | 8.50 |
| ac-5 | Haikou | pure R-(−) | $C = 9.8631e^{-0.0386t}$ | 0.9970 | 18.0 |
| | | pure S-(+) | $C = 10.4155e^{-0.0171t}$ | 0.9836 | 40.5 |

trate, the *S*-(+)-indoxacarb was also preferentially degraded in the two alkaline soils. Therefore, the difference between the R-(−)- and S-(+)-residues in soil was reduced. As depicted in Figure 3a, the amount of *S*-(+)-indoxacarb was 2.33 times that of the *R*-(−)-indoxacarb at 0 d when the indoxacarb concentrate was added into soil alk-2. At 21 d, however, the amount of *S*-(+)-indoxacarb was only 0.90 times that of the *R*-(−)-indoxacarb. In soils neut-3 and ac-5, the directions of selective degradation in indoxacarb racemate and concentrate were the same. In these soils, the *R*-(−) indoxacarb was preferentially degraded in both racemate and concentrate enantiomers. Consequently, the soil was enriched in *S*-(+)-indoxacarb and S-(+)-residue was significantly more abundant than R-(−) residue, as shown in Figure 3b. In soil ac-4, the degradations of the two enantiomers in both racemate and concentrate were not selective, and the degradation rates of S-(+) and R-(−) were similar, as presented in Figure 3c. The ES values of the racemate and the concentrate varied greatly; these values indicated the degree of selective difference. In soil alk-1, the ES value was 0.095 in the concentrate, and it was 0.121 in the racemate, indicating the selective degradations of enantiomers differ more in the racemate than in the concentrate. In three of the soils (alk-2, neut-3, and ac-5), the ES values were 0.245, −0.365, and −0.306 in the concentrate, respectively, and were 0.207, −0.251, and −0.222 in the racemate, respectively, which showed the selective degradations of enantiomers varied more in the concentrate than in the racemate. Overall, the results indicate that the directions of selective degradation of the enantiomers in the concentrate are analogous to directions in the racemate for all five soil types.

**Degradation of Enantiopure Indoxacarb in Soil.** The determination of samples of separate incubations with enantiopure *R*-(−)- and *S*-(+)-indoxacarb is necessary to understand the differences in their dissipation behaviors and detect potential enantiomerization of the compound. We therefore conducted separate incubations with enantiopure *R*-(−)- and *S*-(+)-indoxacarb in all soils. As exhibited in Table 4, the half-lives ($t_{1/2}$) of pure *R*-(−)-indoxacarb and pure *S*-(+)-indoxacarb were 9.34 and 8.19 d in soil alk-1, and 8.60 and 4.16 d in soil alk-2, which was similar to the directions of enantioselective degradation in the concentrate and the racemate, namely, *S*-(+)-indoxacarb degraded faster than *R*-(−)-indoxacarb. The half-lives ($t_{1/2}$) of pure *R*-(−)-indoxacarb and pure *S*-(+)-indoxacarb were 8.13 and 24.2 d in soil neut-3, and 18.0 and 40.5 d in soil ac-5, respectively. The degradation rate of the pure *R*-(−)-indoxacarb was higher than that of pure *S*-(+)-indoxacarb, as with the directions of enantioselective degradation in the concentrate and the racemate in soils neut-3 and ac-5.


dx.doi.org/10.1021/jf5018803 | J. Agric. Food Chem. 2014, 62, 9066−9072

Table 5. Enantiomer Fraction (EF) of Indoxacarb upon Degradation in Sterilized Soil Samples ($n$ = 3 or 2)[a]

| time (d) | EF (soil alk-1) | EF (soil alk-2) | EF (neut-3) | EF (soil ac-4) | EF (soil ac-5) |
|---|---|---|---|---|---|
| 0 | 0.500 ± 0.001 | 0.500 ± 0.001 | 0.498 ± 0.002 | 0.500 ± 0.001 | 0.704 ± 0.003 |
| 5 | 0.499 ± 0.001 | 0.500 ± 0.001 | 0.498 ± 0.002 | 0.496 ± 0.005 | 0.707 ± 0.001 |
| 10 | 0.498 ± 0.001 | 0.500 ± 0.001 | 0.498 ± 0.002 | 0.499 ± 0.001 | 0.708 ± 0.004 |
| 20 | 0.498 ± 0.003 | 0.497 ± 0.001 | 0.497 ± 0.003 | 0.499 ± 0.001 | 0.705 ± 0.012 |
| 40 | 0.498 ± 0.004 | 0.496 ± 0.001 | 0.506 ± 0.014 | 0.499 ± 0.001 | 0.696 ± 0.001 |
| 60 | 0.494 ± 0.002 | 0.494 ± 0.001 | 0.492 ± 0.004 | 0.496 ± 0.001 | 0.696 ± 0.002 |
| 93 | 0.483 ± 0.013 | 0.494 ± 0.008 | 0.495 ± 0.001 | 0.499 ± 0.001 | 0.708 ± 0.001 |

[a]Values represent the mean ± SD ($n$ = 3 or 2).

These results differed from the degradation study of enantiopure indoxacarb by Sun et al. that showed conversion between *R*-(−)-indoxacarb and *S*-(+)-indoxacarb in soils.[20] However, no enantiomerization was observed in our study. The current experiment results show that neither (*S*)-(+)-indoxacarb nor (*R*)-(−)-indoxacarb convert directly; both enantiomers are configurationally stable in the selected soils.

**Degradation of Indoxacarb Racemate (or Concentrate) in Soils under Sterile Conditions.** No significant difference in enantioselectivity was found for indoxacarb racemate (or concentrate) degradation in five soils under sterile conditions, the degradation rates of *S*-(+)- and *R*-(−)-indoxacarb were the same. The concentrations of the two enantiomers of indoxacarb in sterile soils were determined. The EF values of indoxacarb in sterile soils were approximately 0.50 (for the racemate) and 0.70 (for the concentrate) before, during, and after incubation (Table 5). In sterilized soils, indoxacarb enantiomers showed slow dissipation rates. The spiked concentrations dissipated 73%, 84%, 18%, 13%, and 24% in soils alk-1, alk-2, neut-3, ac-4, and ac-5, respectively, after 93 d of incubation. The results indicated that the biological process by microorganisms played important roles in the enantioselective degradation of indoxacrb, consistent with the other studies about many chiral chemicals in soils.[20,25−28] The correlation between enantioselectivity and microbial biomass carbon was considered. However, we observed no clear linear relationship between the selective degradation of indoxacarb and soil microbial biomass. Incubation conditions in different types of soils from various locations may have affected the makeup of microorganisms and hence influenced the rate and direction of the observed enantioselectivity.

**Relationship between the Selective Degradation of Indoxacarb and Soil Properties.** The selective degradation of indoxacarb concentrate (or racemate) varies across the five selected soils. In the two alkaline soils, with positive ES values, the degradation rate of the (*S*)-(+)-indoxacarb was faster than that of the (*R*)-(−)-indoxacarb. In two other soils, one acid and one neutral, with negative ES values, the degradation rate of the (*R*)-(−)-indoxacarb was faster than that of the (*S*)-(+)-indoxacarb. In the other acid soil, the degradation rates of enantiomers were similar and are not selective. Hence, its ES value was 0. The activity and types of soil microorganisms were affected by pH level, organic substances in soil, and soil texture. Therefore, the correlation between ES value and pH was considered, along with that between organic substances and the content of sand and clay and silt in soil. However, we observed no clear linear relationship between the selective degradation of indoxacarb and soil properties. Combined with the results of previous research of indoxacarb in soils,[16,20] we believed the selectivity may vary with different soils, which contained different microorganisms affected by the collective soil environment.

In conclusion, we investigated the enantioselective degradation of the indoxacarb concentrate (2.33S/1R) and racemate (1S/1R) in five types of soil using a chiral Chiralpak IA column under normal-phase conditions. We initially determined the absolute configuration of indoxacarb enantiomers based on single-crystal X-ray diffraction. We found that the directions of selective degradation of the enantiomers in the concentrate are analogous to directions in the racemate for all five soil types. Even in the five soils, the degradation of enantiopure *R*-(−)- and *S*-(+)-indoxacarb was similar to the directions of enantioselective degradation in the concentrate and racemate. As our study shows, enantioselective degradation and soil properties such as pH level, organic substances, and soil texture were not linearly correlated.

## ■ ASSOCIATED CONTENT

### Supporting Information

Crystallographic data and the recovery and precision data in five soils, and concentration of the indoxacarb concentrate (2.33S/1R), racemate (1S/1R), and enantiopure indoxacarb in five soils versus incubation time. This material is available free of charge via the Internet at http://pubs.acs.org.

## ■ AUTHOR INFORMATION

### Corresponding Author

*Tel: +86 851 362-0521. Fax: +86 851 362-2211. E-mail: songbaoan22@yahoo.com.

### Funding

We thank the National Natural Science Foundation of China (No. 21367007) and the Special Fund for Agro-scientific Research in the Public Interest (No. 201203022) for financial support.

### Notes

The authors declare no competing financial interest.

## ■ REFERENCES

(1) Zhou, Y.; Li, L.; Lin, K. D.; Zhu, X. P.; Liu, W. P. Enantiomer separation of triazole fungicides by high-performance liquid chromatography. *Chirality* **2009**, *21*, 421−427.

(2) Sekhon, B. S. Chiral pesticides. *J. Pest. Sci.* **2009**, *34*, 1−12.

(3) McCann, S. F.; Annis, G. D.; Shapiro, R.; Piortowshi, D. W.; Lahm, G. P.; Long, J. K. The discovery of indoxacarb: oxadiazines as a new class of pyrazoline-type insecticides. *Pest Manage. Sci.* **2001**, *57*, 153−164.

(4) Liu, W. P.; Gan, J. Y.; Shneak, D.; Jury, W. A. Enantioselectivity in environmental safety of current chiral insecticides. *Proc. Natl. Acad. Sci. U.S.A.* **2004**, *102* (70), 1−706.

(5) Liu, W. P.; Gan, J. Y.; Lee, S.; Werner, I. Isomer selectivity in aquatic toxicity and biodegradation of bifenthrin and permethrin. *Environ. Toxicol. Chem.* **2005**, *24*, 1861−1866.

(6) Peng, X.; Liu, D. H.; Diao, J. L.; Lu, D. H.; Zhou, Z. Q. Enantioselective acute toxicity and bioaccumulation of benalaxyl in earth-worm (*Eisenia fedtia*). *J. Agric. Food Chem.* **2009**, *57*, 8545−8549.
(7) Li, L.; Zhou, S. S.; Jin, L. X.; Zhang, C.; Liu, W. P. Enantiomeric separation of organophosphorus pesticides by high-performance liquid chromatography, gas chromatography and capillary electrophoresis and their applications to environmental fate and toxicity assays. *J. Chromatogr. B* **2010**, *878*, 1264−1276.
(8) Xu, P.; Diao, J. L.; Liu, D. H.; Zhou, Z. Q. Enantioselective bioaccumulation and toxic effects of metalaxyl in earthworm *Eisenia foetida*. *Chemosphere* **2011**, *83*, 1074−1079.
(9) Faller, J.; Huhnerfuss, H.; Konig, W. A. Do marine bacteria degrade α-hexachlorocyclohexane stereoselectivity. *Environ. Sci. Technol.* **1991**, *25*, 676−678.
(10) Buerge, I. J.; Poiger, T.; Muller, M. D.; Buser, H. R. The chiral herbicide beflubutamid (II): enantioselective degradation and enantiomerization in soil, and formation/ degradation of chiral metabolites. *Environ. Sci. Technol.* **2003**, *37*, 2668−2674.
(11) Chen, S.; Liu, W. Enantioselective degradation of metalaxyl in anaerobic activated sewage sludge. *Bull. Environ. Contam. Toxicol.* **2009**, *82*, 327−331.
(12) Zhang, Y. F.; Liu, D. H.; Diao, J. L.; He, Z. Y.; Zhou, Z. Q.; Wang, P.; Li, X. F. Enantioselective environmental behavior of the chiral herbicide fenoxaprop-ethyl and its chiral metabolite fenoxaprop in soil. *J. Agric. Food. Chem.* **2010**, *58*, 12878−12884.
(13) Celis, R.; Gámiz, B.; Adelino, M. A.; Hermosín, M. C.; Cornejo, J. Environmental behavior of the enantiomers of the chiral fungicide metalaxyl in Mediterranean agricultural soils. *Sci. Total Environ.* **2013**, *444*, 288−297.
(14) Campbell, S.; Chen, L.; Yu, J.; Li, Q. X. Adsorption and analysis of the insecticides thiamethoxam and indoxacarb in Hawaiian soils. *J. Agric. Food Chem.* **2005**, *53*, 5373−5376.
(15) Zhou, F.; Li, P. Study on degradation dynamics of indoxacarb in the soil. *Environ. Sci. Technol.* **2008**, *33*, 58−61.
(16) Li, X.; Liu, Y.; Liu, S.; Hu, C.; Bai, L.; Gao, B.; Jiang, H. Enantioselective degradation of indoxacarb enantiomers in soils. *Environ. Chem. (in Chinese)* **2012**, *31*, 1262−1267.
(17) Dewey, K. A.; Gaw, S. K.; Northcott, G. L.; Lauren, D. R.; Hackenburg, S. The effects of copper on microbial activity and the degradation of atrazine and indoxacarb in a New Zealand soil. *Soil Biol. Biochem.* **2012**, *52*, 64−74.
(18) Sun, D.; Qiu, J.; Wu, Y.; Liang, H.; Liu, C.; Li, L. Enantioselective degradation of indoxacarb in cabbage and soil under field conditions. *Chirality* **2012**, *24*, 628−633.
(19) Peng, X.; Gong, D. Residual dynamics of indoxacarb in paddy field. *Agrochemicals (in Chinese)* **2013**, *52*, 284−286.
(20) Sun, D.; Pang, J.; Qiu, J.; Li, L.; Liu, C. Enantioselective degradation and enantiomerization of Indoxacarb in Soil. *J. Agric. Food Chem.* **2013**, *61*, 11273−11277.
(21) Urvashi, J. G.; Sahoo, S. K.; Kaur, S.; Battu, R. S.; Singh, B. Estimation of indoxacarb residues by QuEChERS technique and its degradation pattern in cabbage. *Bull. Environ. Contam. Toxicol.* **2012**, *88*, 372−376.
(22) Zhang, X.; Luo, F.; Chen, Z.; Liu, G.; Lou, Z.; Wang, F.; Wu, L. Residue determination of epoxiconazole, indoxacarb and difenoconazole in tea, tea infusion and soil using ultra high performance liquid chromatography coupled with tandem mass spectrometry. *Chin. J. Anal. Chem.* **2013**, *41*, 215−222.
(23) Wang, H.; Dong, F.; Li, Y.; Chen, X.; Cheng, Y.; Xiang, W.; Zheng, Y. Enantioselective determination of the insecticide indoxacarb in cucumber and tomato by chiral liquid chromatography-tandem mass spectrometry. *Chirality* **2013**, *25*, 350−354.
(24) Zhang, K. K.; Hu, D. Y.; Zhu, H. J.; Yang, J. C.; Song, B. A. Enantioselective degradation of Dufulin in four types of soil. *J. Agric. Food Chem.* **2014**, *62*, 1771−1776.
(25) Diao, J.; Lv, C.; Wang, X.; Dang, Z.; Zhu, W.; Zhou, Z. Influence of soil properties on the enantioselective dissipation of the herbicide lactofen in soils. *J. Agric. Food Chem.* **2009**, *57*, 5865−5871.
(26) Li, Z.; Zhang, Z.; Zhang, L.; Leng, L. Isomer- and enantioselective degradation and chiral stability of fenpropathrin and fenvalerate in soils. *Chemosphere* **2009**, *76*, 509−516.
(27) Li, Z. Y.; Zhang, Y. C.; Li, Q. L.; Wang, W. X.; Li, J. Y. Enantioselective degradation, abiotic racemization, and chiral transformation of triadimefon in soils. *Environ. Sci. Technol.* **2011**, *45*, 2797−2803.
(28) Xu, Y. X.; Zhang, H.; Zhuang, S. L.; Yu, M.; Xiao, H.; Qian, M. R. Different enantioselective degradation of Pyraclofos in soils. *J. Agric. Food Chem.* **2012**, *60*, 4173−4178.
(29) Zhang, Y.; Zhang, K.; Song, B.; Ling, H.; Li, Z.; Li, M.; Hu, D. Enantiomeric separation of indoxacarb on an amylose-based chiral stationary phase and its application in study of indoxacarb degradation in water. *Biomed. Chromatogr.* **2014**, DOI: 10.1002/bmc.3178.
(30) Flack, H. D. On enantiomorph-polarity estimation. *Cryst.* **1983**, *A39*, 876−881.
(31) Buser, H. R.; Müller, M. D. Environmental behavior of acetamide pesticide stereoisomers. 2. Stereo- and enantioselective degradation in sewage sludge and soil. *Environ. Sci. Technol.* **1995**, *29*, 2031−2037.

identify different cultivation locations of eight wolfberry samples.[8] Although HPLC−UV fingerprints were obtained, no compositional information was related to the clustering tree. The mass spectrometric technique offers mass-to-charge ratio measurements that generally furnished greater specificity for differentiation and component characterization than the UV fingerprints. Bondia-Pons et al. applied ultraperformance liquid chromatography coupled with mass spectrometry (UPLC−MS) with partial least-squares-discriminant analysis (PLS-DA) to differentiate the geographic origin of wolfberries.[20] However, samples from only three origins (Tibet, Northern China, and Mongolia) were analyzed. It is interesting to test whether the UPLC−MS and FIMS may be applied to differentiate Chinese wolfberries produced in Ningxia and other locations, or the different wolfberry cultivars from a selected growing region.

In this study, the PLS-DA of UPLC−MS and FIMS fingerprints was tested for possible differentiation of Chinese wolfberries produced in Ningxia from those grown in other locations. The PLS-DA was also utilized to possibly distinguish the four wolfberry cultivars grown in Ningxia. The prediction accuracies for both approaches were calculated. In addition, the phytochemical compositions of the wolfberries were examined. The results from this study may serve as a scientific foundation for the authentication of Chinese wolfberries.

## MATERIALS AND METHODS

**Materials and Reagents.** Twenty-nine wolfberry samples harvested in 2012 were obtained from Professor Jinming Gao at Shaanxi Engineering Center of Bioresource Chemistry & Sustainable Utilization, College of Science, Northwest A&F University. The sample set included 19 Ningxia (NX) wolfberry samples and 10 samples from five other provinces of China, including three Inner Mongolia (IM), three Qinghai (QH), two Gansu (GS), one Hebei (HB), and one Xinjiang (XJ) samples, respectively. All samples were *L. barbarum* fruits, except that one was *Lycium ruthenicum* Murr. fruits from QH. Out of all 19 NX samples, the cultivars of 16 NX *L. barbarum* fruit were recorded, including five NX wolfberry No. 1 (NX1), five NX wolfberry No. 4 (NX4), two NX wolfberry No. 5 (NX5), and four NX wolfberry No. 7 (NX7) samples. Three other samples had no cultivar information and were removed in the statistical analysis related to wolfberry cultivars. The fruits were air-dried immediately after harvest and stored in zip-lock plastic bags at −20 °C. Deionized water was obtained using a Milli-Q purification system (Millipore Laboratory, Bedford, MA, USA). The HPLC grade methanol and acetonitrile were purchased from Merck (Darmstadt, Germany). The high-performance liquid chromatographic grade formic acid was purchased from Sigma-Aldrich (St. Louis, MO, USA). The analytical grade ethanol was purchased from Yangyuan Chemical (Changshu, Jiangsu, China). Other chemicals or solvents were of the highest commercial grade and used without further purification.

**Instrumentation.** A Precellys 24 Dual homogenizer (Bertin Technologies, Bretonneux, France) was used for sample homogenization. A KH7200 sonicator was used for sonication during sample extraction (Kunshan Hechuang Ultrasonic Corporation, Kunshan, Jiangsu, China). UPLC−MS analysis was performed by an Acquity UPLC coupled with a Xevo G2 quadrupole time-of-flight (QTOF) mass spectrometer (Waters, Milford, MA, USA).

**Sample Preparation.** The dried fruits (dry weight: 0.512 ± 0.010 g) were placed in a 7 mL homogenizing tube with 1 mL of deionized water. The homogenization was performed twice at a speed of 5500 rpm. Each cycle lasted for 20 s with a 5 s hold time between cycles. Then 4 mL of analytical grade ethanol was added. The extraction was performed at ambient temperature for 30 min using 80% (v/v) ethanol under sonication. After the mixture was centrifuged at 3901*g* for 5 min, 1 mL of supernatant was transferred to a clean tube, and the solvent was removed with nitrogen flow. The extract was redissolved in 1 mL of 50% acetonitrile (v/v) with sonication at ambient temperature for 5 min, and then centrifuged at 13400*g* for 10 min to remove the nondissolvable impurities. The supernatant was subjected to UPLC−MS and FIMS analysis.

**Ultraperformance Liquid Chromatography−Mass Spectrometry (UPLC−MS).** An Acquity UPLC BEH C18 column (2.1 mm i.d. × 100 mm, 1.7 $\mu$m) attached with a VanGuard precolumn (2.1 mm i.d. × 5 mm, 1.7 $\mu$m) (Waters, Milford, MA, USA) was used. A binary solvent system of 0.1% (v/v) formic acid in deionized water (solvent A) and 0.1% (v/v) formic acid in acetonitrile (solvent B) was used. It has been studied that the addition of formic acid as a mobile phase modifier would reduce peak tailing and improve the performance of separation for flavonoids and phenolic acids, the major functional components of wolfberries.[21] The gradient elution program was 0−8 min, 10−100% B with a concave (curve parameter was 8); 8−13 min, 100% B; 13−15 min, 100−10% B with a linear gradient; and 15−16.5 min, 10% B. The column temperature was 40 °C, and the flow rate was 0.4 mL/min.

Based on the previous liquid chromatography−mass spectrometry (LC−MS) studies of Chinese wolfberries, the negative ion mode was better at characterizing the major functional components such as flavonoids and phenolic acids in wolfberries than the positive ion mode.[20,21] The electrospray ionization (ESI) source was operated under the negative ion mode without applying collision energy. The capillary voltage was 2.5 kV, and the cone voltage was 40 V. The ionization temperature was 120 °C, and desolvation temperature was 250 °C. The sodium formate (0.34 g/L in 90% isopropanol, v/v) was used for QTOF-MS startup calibration under the same ESI conditions for sample measurement, and leucine enkephalin (2 mg/L in 50% acetonitrile, v/v) was used for QTOF-MS lockspray calibration. The sodium formate was introduced prior to the ESI interface during the startup calibration. The mass spectra from 0.5 to 8.5 min were recorded. Two channels of MS measurements were recorded. The first channel was for the data collection of MS signals ranging from 100 to 1500 Da without collision energy. The second channel offered additional fragmentation information for the compound identification, which collected mass fragments of 100 to 1000 Da with a 35 eV collision energy. The scanning speed was 0.3 s/scan. Each sample was injected in triplicate by a sequence of random block design. Three blocks were injected sequentially, and each block contained a replicate of 29 samples in a randomized order. The methanol blank solution was injected at the beginning and the end of each block to reduce sample cross-contaminations. The entire UPLC−MS sequence ran for two consecutive days.

**Flow Injection Mass Spectrometry (FIMS).** The same MS instrumentation and method were applied in FIMS fingerprinting as that described in the UPLC−MS analysis section, without the UPLC column. The solvent was 0.1% (v/v) formic acid in 50% acetonitrile:-water (v/v). The solvent pH was 3.0 with a flow rate of 0.5 mL/min. The MS signals from 100 to 1000 Da were collected from 0 to 0.5 min after injection.

**Data Analysis.** The peak areas and PLS-DA plots were calculated using the Waters MarkerLynx software (version 4.1). For UPLC−MS data, the component peaks were extracted with a chromatogram mass window of 0.01 Da, and a retention time window of 0.2 min. Twenty characteristic peaks appearing in all NX samples were selected manually, in addition with five characteristic peaks in QH sample to validate peak selection. For each FIMS spectrum, peaks were extracted by a mass window of 1 Da. The peak areas and FIMS spectra were preprocessed by dividing the mass of each sample weighed before homogenization, followed by the autoscaling transformation, i.e., each feature was subtracted by its mean value, and divided by their standard deviation. The number of classes was 2 for wolfberries produced in NX and other locations. When differentiating NX cultivars, the number of classes was 4.

The bootstrapped Latin partition[22] of 10 bootstraps and 5-fold Latin partition was applied for validation to evaluate the model prediction power. The bootstrapping applied resampling, and achieved multiple evaluations with a statistical power similar to permutation. Also, Latin partition is an improved method derived from cross-

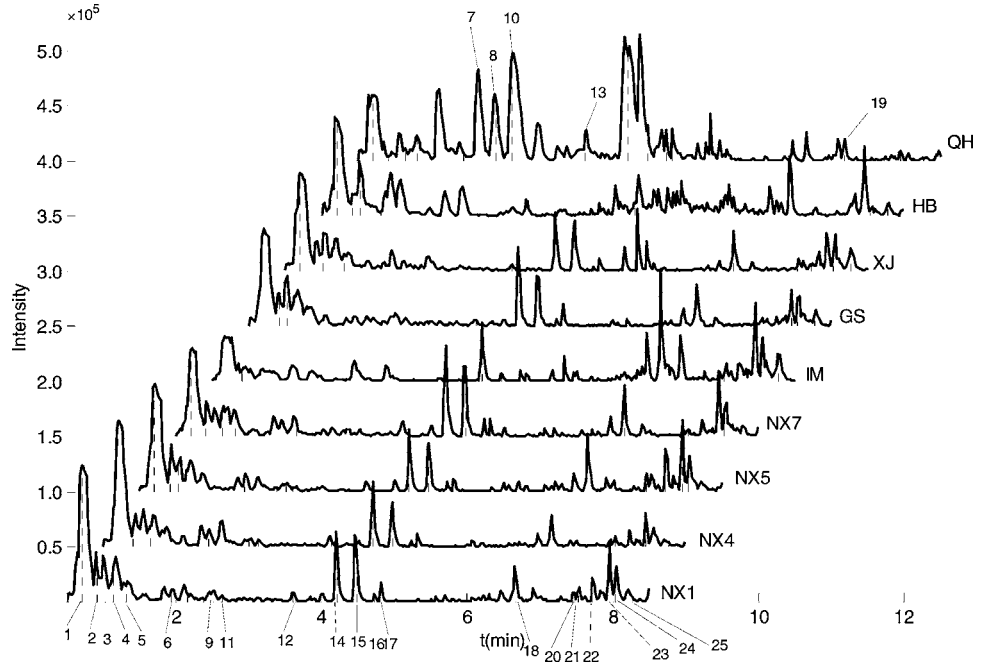


**Figure 1.** UPLC−MS base peak chromatograms of Chinese wolfberries. QH, HB, XJ, GS, and IM represent samples from Qinghai, Hebei, Xinjiang, Gansu, and Inner Mongolia, respectively. NX1, NX4, NX5, and NX7 represent Ningxia (NX) wolfberry No. 1, No. 4, No. 5, and No. 7 cultivars, respectively.

validation, in which the ratio between different classes is maintained. The validation result was reported as the percentage of correct predictions to reflect the prediction accuracy. Afterward, a two-way analysis of variance (ANOVA) was applied to determine whether the prediction models were statistically different from each other. In addition, the average regression coefficients of PLS-DA could be plotted with confidence intervals. Positive and negative coefficients represent the relationships of the peaks to different classes. The importance of each peak could be quantified by the absolute magnitude of each regression coefficient. The peak would be insignificant for classification, if the confidence interval crossed zero. The PLS-DA model validation and ANOVA were performed by an in-house program using MATLAB R2013b (The MathWorks, Natick, MA, USA). The number of latent variables to build the PLS-DA model is an important parameter that affects its prediction ability. If the number of latent variables is too large, overfitting may occur, and underfitting may occur otherwise. The optimized number of latent variables was determined by achieving the best mean prediction accuracy when applying the same bootstrapped Latin partition procedure (10 bootstraps and 5-fold Latin partition) on each training partition in the validation process. The algorithm of PLS was the nonlinear iterative partial least-squares (NIPALS), and the binary encoding was applied to handle the multiclass problem.

## RESULTS AND DISCUSSION

**UPLC−MS Chromatograms.** Figure 1 reports the representative UPLC−MS base peak chromatograms of the nine Chinese wolfberry extracts. The base peak chromatogram plots the intensity of the most abundant ion, the base peak intensity, in each MS scan. More components can be observed in the base peak chromatograms than in the total ion chromatogram, because the base peak intensity is less influenced by noise than the total intensity. The peak profiles of a sample from QH significantly differed from samples grown in other locations. This probably was because this QH sample was a wild grown *Lycium* species (*L. ruthenicum*), which has a unique composition according to a previous study.[23] Besides location and genotype, significant differences in the chemical composition could occur due to planting season, or the interactions between factors such as season and location, or season and genotype. Peaks 7, 8, 10, 13, and 19 were the typical components in this QH sample. Peaks 13 and 19 were tentatively identified as quercetin-di(rhamno)-hexoside and cirsimaritin. The overall profiles of HB were also different from the NX samples. This result was consistent with a previous UPLC−UV fingerprinting study in which HB samples furnished the largest dissimilarity compared to other samples from eight locations.[8] However, it was difficult to predict the growing location of a commercial wolfberry sample based only on direct observation of its base peak chromatogram. For all NX wolfberries, most of the peaks were identical except for variations in their relative concentrations. This observation was consistent with the previous genetic diversity studies on NX wolfberry cultivars that demonstrated high genetic similarities of NX wolfberries,[24] indicating a challenging objective to distinguish the cultivars by manually inspecting the chromatogram.

**Differentiating Samples from Ningxia and Other Locations by UPLC−MS Peak Areas.** Figure 2A depicts the PLS-DA scores plot of the UPLC−MS for the 29 wolfberry samples using the peak areas of 20 and 5 peaks selected from NX and the wild grown QH sample, respectively. Most samples from NX were separated from the samples grown in other locations regardless of cultivar differences.

Figure 1 demonstrated that the wolfberry samples from locations outside NX may contain many characteristic components to help differentiation. However, it is not possible to perform an exhaustive compositional analysis on all species of *Lycium*. Consequently, it should be verified that 20 primary peaks selected from NX samples alone was adequate for differentiation. Comparing the PLS-DA scores plots which included (Figure 2A) or excluded (Figure 2B) peaks 7, 8, 10, 13, and 19 that were only detected in wild grown QH samples, a similar clustering trend was observed. In both plots, the wild


dx.doi.org/10.1021/jf502156n | J. Agric. Food Chem. 2014, 62, 9073−9080

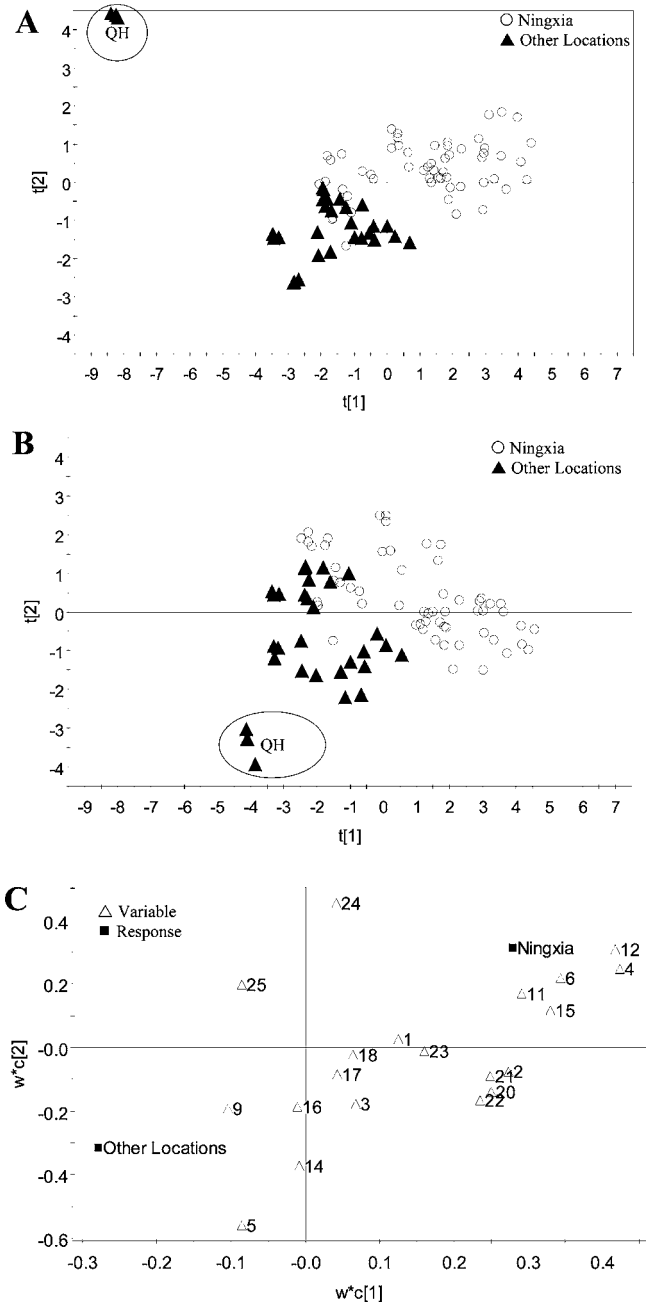


**Figure 2.** PLS-DA scores and loading plots differentiating wolfberries produced in NX and other locations using UPLC−MS peak areas: (A) the scores plot by 20 and 5 peaks respectively selected from NX and wild grown Qinghai (QH) sample; (B) the scores plot by 20 peaks only selected from NX samples; and (C) the corresponding loading plot of B. In both A and B, the wild grown QH sample is circled.

grown QH samples were away from all other samples and respectively positioned at the top-left and bottom-left corners. As a result, any peaks observed only in non-NX samples were excluded for further analysis.

The loading plot (Figure 2C) reflects the importance of each compound for each data cluster. The closer a peak was to the respective sample response, the more characteristic it was in that class of sample. It can be observed that peaks 4, 6, 11, 12, and 15 were mainly related to NX samples. According to the tentative identification by QTOF-MS, peaks 4 and 6 were glycosides of coumaric acid; peak 11 was scopoletin; and peak 12 was 1,3-dihydro-2-benzofuran. In addition, 18 components were tentatively identified according to the high-resolution measurements with QTOF-MS (Table 1). The phenolic acids including quercetin-rhamno-dihexoside, quercetin-di(rhamno)-hexoside, quercetin-3-*O*-rutinoside, kaempferol-3-*O*-rutinoside, and isorhamnetin-3-*O*-rutinoside were consistent with the findings of a previous study using a liquid chromatography with ultraviolet detection.[21] Citric acid, citric acid glycoside, coumaric acid glycoside, ferulic acid glycoside, scopoletin glycoside, isocoumaran, trihydroxy octadecenoic acid, dihydroxy octadecadienoic acid, hydroperoxy octadecatrienoic acid, dihydroxy octadecadienoic acid, and hydroxy linoleic acid were not reported in wolfberry previously.

**Differentiating Cultivars from a Selected Location by UPLC−MS Peak Areas.** With the application of PLS-DA on the subset of 16 NX samples, different cultivars were also separated into distinctive clusters (Figure 3A). Data points representing NX1 were located in the center of the plot, indicating that less characteristic components were extracted compared to the other three cultivars. Because NX1 was the earliest commercial breed of NX wolfberry cultivar, all other cultivars from NX were developed from NX1. The cultivation process led to the occurrences of characteristic components and variations in concentrations. The locations of peaks differed in Figure 2C, suggesting a different component profile of NX cultivars as compared to the fruits outside NX province. Specifically, peak 21 (tentatively identified as hydroperoxy octadecatrienoic acid) and peaks 12, 16, and 18 (tentatively identified as 1,3-dihydro-2-benzofuran, kaempferol-3-*O*-rutinoside, and trihydroxy octadecenoic acid, respectively) were respectively related to NX5 and NX7. The loading plots (Figures 2C and 3B) clearly demonstrated UPLC−MS advantages in discovering the relationships between phytochemical compounds and different sample classes, with the trade-off of analysis time. The PCA was also performed. Similar clustering trends could be observed by comparing Figures 2B and 3A with the principal component scores plots (Figures S1 and S2 in the Supporting Information). As a supervised method, the PLS-DA achieved better separations between different sample classes than PCA.

**FIMS Fingerprints.** FIMS fingerprinting is a novel technique without chromatographic separation. It is suitable for a high-throughput assay of food materials. In the present study, FIMS fingerprinting was compared to the conventional UPLC−MS base peak fingerprints under the same instrumentation configurations. Nine representative FIMS fingerprints were plotted in Figure 4. Distinctively unique patterns of wild grown QH and HB samples were observed in Figure 4, in good agreement with the chromatograms obtained by UPLC−MS (Figure 1). The peaks at $m/z$ 191.0192 and 191.0555 were tentatively identified as citric acid and scopoletin, respectively. The peaks at $m/z$ 111.0082 and 133.0136 were tentatively identified as the fragments of citric acid, which were consistent with the UPLC−MS measurements of peak 1 (Table 1).

**Differentiating Samples from Ningxia and Other Locations by FIMS Fingerprints.** Figure 5 is the PLS-DA plot to differentiate samples from Ningxia and other locations by their FIMS fingerprints. The scores plots (Figure 5A) indicated a similar clustering trend as the UPLC−MS plots (Figure 2B). The wild grown QH samples presented in Figure 5A were located at the bottom of the plot away from the other samples, consistent with the FIMS fingerprints in Figure 4 and the scores plot of Figure 2B. There were many variables in the


dx.doi.org/10.1021/jf502156n | J. Agric. Food Chem. 2014, 62, 9073−9080

**Table 1. Tentatively Identified Compounds by UPLC−MS[a]**

| | $t_R$ (min) | compound | formula | $[M-H]^-$ exptl | $[M-H]^-$ theor | fragment ions and formula |
|---|---|---|---|---|---|---|
| 1 | 0.71 | citric acid | $C_6H_8O_7$ | 191.0187 | 191.0192 | 111.0088 ($C_5H_3O_3^-$),[b] 133.0127 ($C_4H_5O_5^-$)[b] |
| 2 | 0.92 | citric acid glycoside | $C_{39}H_{55}O_{17}$ | 794.3354 | 794.3361 | 191.0191 ($C_6H_7O_7^-$), 470.2286 ($C_{27}H_{34}O_7^-$),[b] 632.2822 ($C_{33}H_{44}O_{12}^-$) |
| 3 | 1.03 | unknown | $C_{46}H_{53}O_{12}$ | 796.3470 | 796.3459 | 634.2954 ($C_{40}H_{42}O_7^-$), 472.2437 ($C_{27}H_{34}O_7^-$) |
| 4 | 1.15 | coumaric acid glycoside | $C_9H_8O_3$ | 163.0393 | 163.0395 | 353.0867 ($C_{16}H_{17}O_9^-$) |
| 5 | 1.32 | quercetin-rhamno-dihexoside | $C_{33}H_{40}O_{21}$ | 771.1987 | 771.1984 | 301.0364 ($C_{15}H_9O_7^-$),[b] 609.1465 ($C_{27}H_{29}O_{16}^-$)[b] |
| 6 | 1.95 | coumaric acid glycoside | $C_{15}H_{17}O_8$ | 325.0928 | 325.0923 | 163.0397 ($C_9H_7O_3^-$) |
| 7 | 2.16 | unknown | $C_{27}H_{37}O_7$ | 472.2447 | 472.2461 | 228.1711 ($C_{13}H_{24}O_3^-$)[b], 308.1979 ($C_{18}H_{28}O_4^-$)[b], 350.2081 ($C_{20}H_{30}O_5^-$)[b] |
| 8 | 2.39 | unknown | $C_{27}H_{35}O_7$ | 470.2290 | 470.2305 | 135.0450 ($C_8H_7O_2^-$),[b] 291.1702 ($C_{21}H_{23}O^-$),[b] 334.1760 ($C_{19}H_{26}O_5^-$)[b] |
| 9 | 2.51 | ferulic acid glycoside | $C_{10}H_{10}O_4$ | 193.0500 | 193.0501 | 355.1003 ($C_{16}H_{19}O_9^-$) |
| 10 | 2.62 | unknown | $C_{27}H_{35}O_7$ | 470.2281 | 470.2305 | 135.0448 ($C_8H_7O_2^-$),[b] 291.1712 ($C_{21}H_{23}O^-$),[b] 334.1774 ($C_{19}H_{26}O_5^-$)[b] |
| 11 | 2.64 | scopoletin | $C_{10}H_8O_4$ | 191.0340 | 191.0344 | nd |
| 12 | 3.62 | 1,3-dihydro-2-benzofuran (isocoumaran) | $C_8H_8O$ | 119.0495 | 119.0497 | nd |
| 13 | 3.64 | quercetin-di(rhamno)-hexoside | $C_{33}H_{40}O_{20}$ | 755.2031 | 755.2035 | nd |
| 14 | 4.21 | quercetin-3-*O*-rutinoside (rutin) | $C_{27}H_{30}O_{16}$ | 609.1456 | 609.1456 | 300.0274 ($C_{15}H_8O_7^-$)[b] |
| 15 | 4.48 | unknown | $C_8H_{14}O$ | 245.0926 | 245.0966 | 203.1826 ($C_{16}H_{11}^-$) |
| 16 | 4.73 | kaempferol-3-*O*-rutinoside | $C_{27}H_{30}O_{15}$ | 593.1519 | 593.1506 | 285.0311 ($C_{15}H_9O_6^-$) |
| 17 | 4.81 | isorhamnetin-3-*O*-rutinoside | $C_{28}H_{32}O_{16}$ | 623.1610 | 623.1612 | 315.0501 ($C_{16}H_{11}O_7^-$) |
| 18 | 6.66 | trihydroxy octadecenoic acid | $C_{18}H_{34}O_5$ | 329.2320 | 329.2328 | nd |
| 19 | 7.18 | cirsimaritin | $C_{17}H_{14}O_6$ | 313.0714 | 313.0712 | 253.0509 ($C_{15}H_9O_4^-$), 283.0970 ($C_{17}H_{15}O_4^-$) |
| 20 | 7.47 | dihydroxy octadecadienoic acid | $C_{18}H_{32}O_4$ | 311.2224 | 311.2222 | 293.2123 ($C_{18}H_{29}O_3^-$) |
| 21 | 7.53 | hydroperoxy octadecatrienoic acid | $C_{18}H_{30}O_4$ | 309.2058 | 309.2066 | nd |
| 22 | 7.72 | dihydroxy octadecadienoic acid | $C_{18}H_{32}O_4$ | 311.2220 | 311.2220 | nd |
| 23 | 7.95 | hydroxy linoleic acid | $C_{18}H_{32}O_3$ | 295.2271 | 295.2273 | nd |
| 24 | 8.03 | unknown | $C_{48}H_{78}O_{10}$ | 814.5580 | 814.5595 | 566.3455 ($C_{31}H_{50}O_9^-$), 506.3423 ($C_{29}H_{46}O_7^-$), 293.2114 ($C_{18}H_{29}O_3^-$) |
| 25 | 8.27 | unknown | $C_{34}H_{44}O_9$ | 595.2890 | 595.2907 | 241.0114 ($C_{13}H_5O_5^-$),[b] 279.2318 ($C_{18}H_{31}O_2^-$)[b] |

[a] $t_R$, retention time; exp $[M-H]^-$ and theor $[M-H]^-$ were experimental and theoretical $m/z$ of molecular ions, respectively; nd, not detected; the formulas were determined by achieving the smallest mass error between theoretical and experimental $m/z$, taking the fragment ions into consideration; [b] The fragment ions observed in the second mass spectral channel.

loading plots (Figure 5B), but few $m/z$ peaks could be related to differentiation by the FIMS fingerprints. For the FIMS method, the PCA was not able to effectively differentiate the production location (Figures S3 in the Supporting Information).

**Differentiating Cultivars from a Selected Location by FIMS Fingerprints.** Figure 6A is the PLS-DA scores plot to differentiate cultivars of a selected location. Different cultivars were separated, except NX1 and NX4 were overlapped. This was probably due to the greatest similarity between NX1 and NX4, compared with other cultivars. This close relationship was also observed in the loading plot in Figure 6B. Similar to Figure 5B, the extraction of characteristic components was relatively difficult due to the large amount of variables in the FIMS fingerprints. Compared with the conventional chromatographic methods, the FIMS fingerprinting reduced the analysis time significantly while retaining enough information for differentiation. On the other hand, the UPLC−MS method has advantages in providing detailed component information. The PCA results indicated less degree of separation between the cultivars (Figure S4 in the Supporting Information), compared to the PLS-DA scores plot (Figure 6A).

**Partial Least-Squares-Discriminant Analysis (PLS-DA) Validation.** A quantitative evaluation of the accuracies for differentiation is necessary since there were no definite boundaries between different classes of samples in the scores plots for both UPLC−MS and FIMS fingerprints (Figures 2, 3, 5, and 6). The PLS-DA with bootstrapped Latin partition was applied as a classifier to achieve the automatic prediction. Table 2 is the validation result. The FIMS fingerprinting yielded 71% averaged prediction accuracy when differentiating the NX cultivars, since the autoscaling data transformation elevated noise in the FIMS spectra, especially when handling the multiclass problem. For UPLC−MS, because the peak-selection step ensured the removal of most noises, the averaged prediction accuracy did not decrease with the application of autoscaling. The scaling step was removed and the model was re-evaluated afterward for differentiating the NX cultivars using FIMS fingerprints. To achieve an unbiased spectrometric comparison to the predictions, the total ion spectra (TIS) obtained from UPLC−MS by averaging all MS spectra from 100 to 1000 Da across retention times were also evaluated. The autoscaling was also applied to TIS because the spectrometric noise was reduced by signal averaging. All prediction accuracies were above 90%. The TIS and UPLC−MS achieved higher prediction accuracies than the FIMS fingerprinting method. The two-way ANOVA was performed on the prediction accuracies. The result indicated that the prediction accuracies using UPLC−MS, TIS, or FIMS methods were statistically different at a 95% confidence level. The results proved the


dx.doi.org/10.1021/jf502156n | J. Agric. Food Chem. 2014, 62, 9073−9080

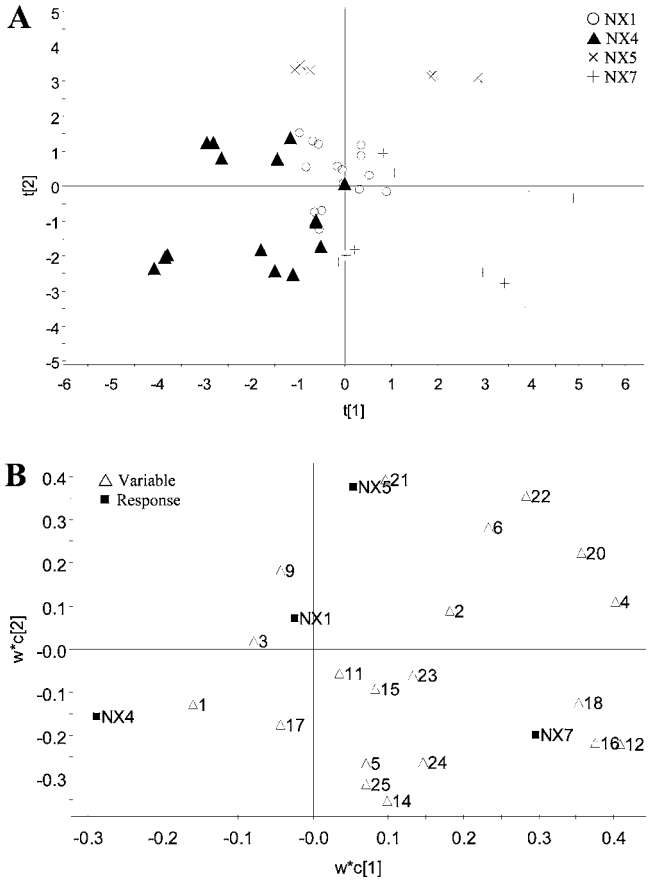


**Figure 3.** PLS-DA scores (A) and loading (B) plots differentiating NX cultivars using UPLC−MS peak areas. NX1, NX4, NX5, and NX7 respectively represent NX wolfberry No. 1, No. 4, No. 5, and No. 7 cultivars, respectively.

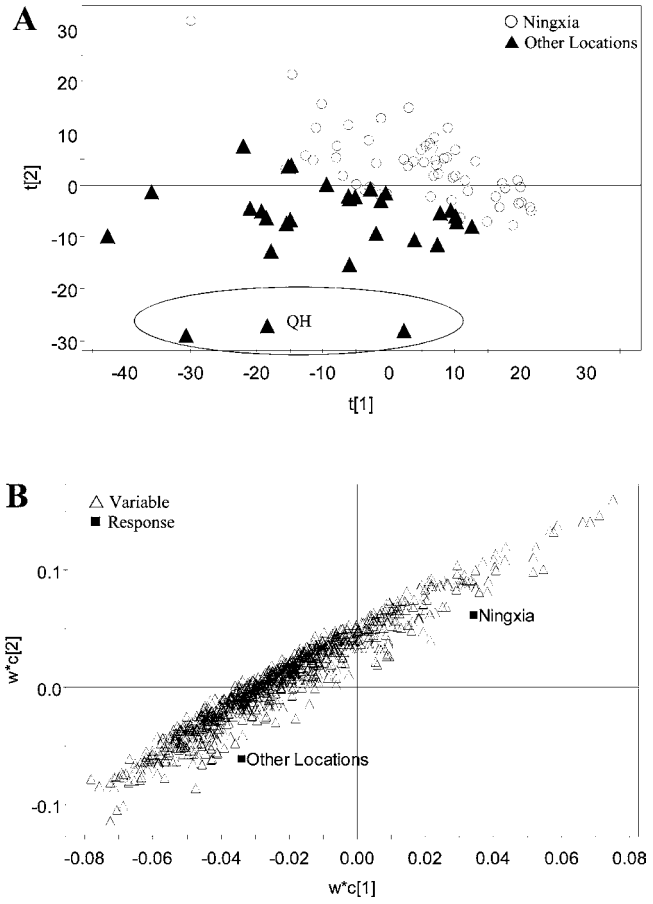


**Figure 5.** PLS-DA scores (A) and loading (B) plots differentiating wolfberries produced in NX and other locations using FIMS fingerprints. In A, the wild grown QH sample is circled.

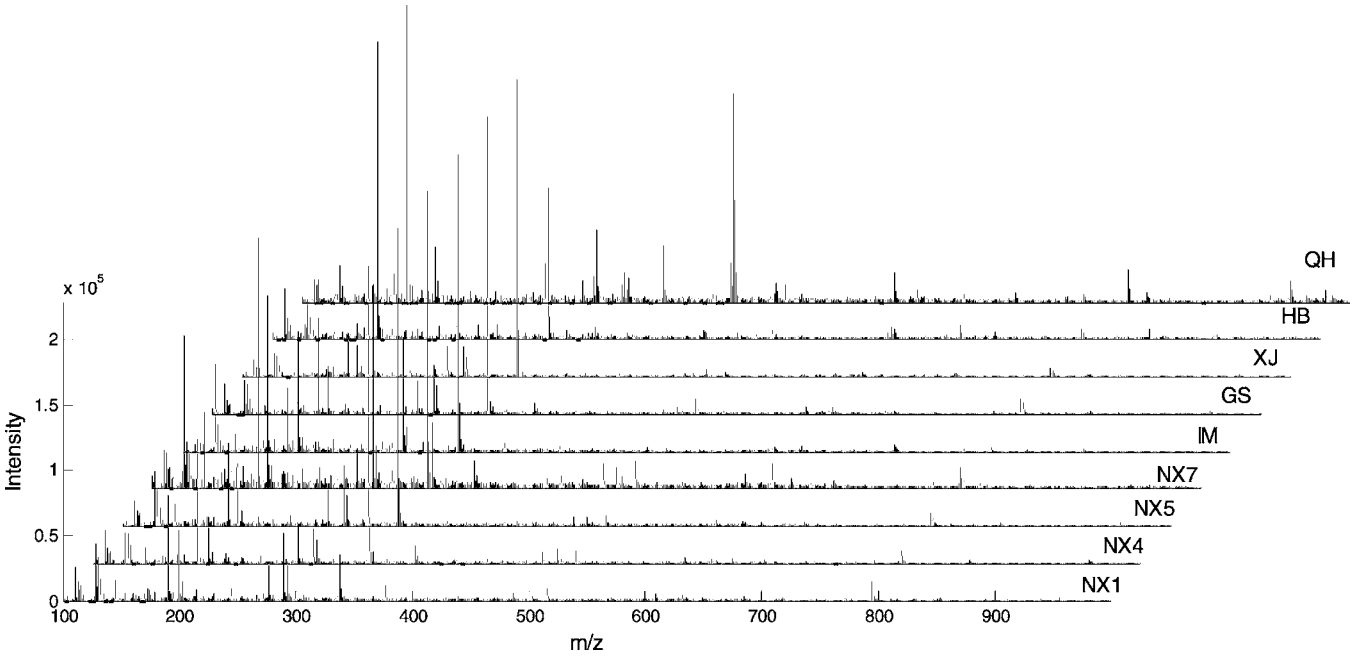


**Figure 4.** FIMS fingerprints of Chinese wolfberries. QH, HB, XJ, GS, and IM represent samples from Qinghai, Hebei, Xinjiang, Gansu, and Inner Mongolia, respectively. NX1, NX4, NX5, and NX7 respectively represent NX wolfberry No. 1, No. 4, No. 5, and No. 7 samples, respectively.


dx.doi.org/10.1021/jf502156n | J. Agric. Food Chem. 2014, 62, 9073−9080

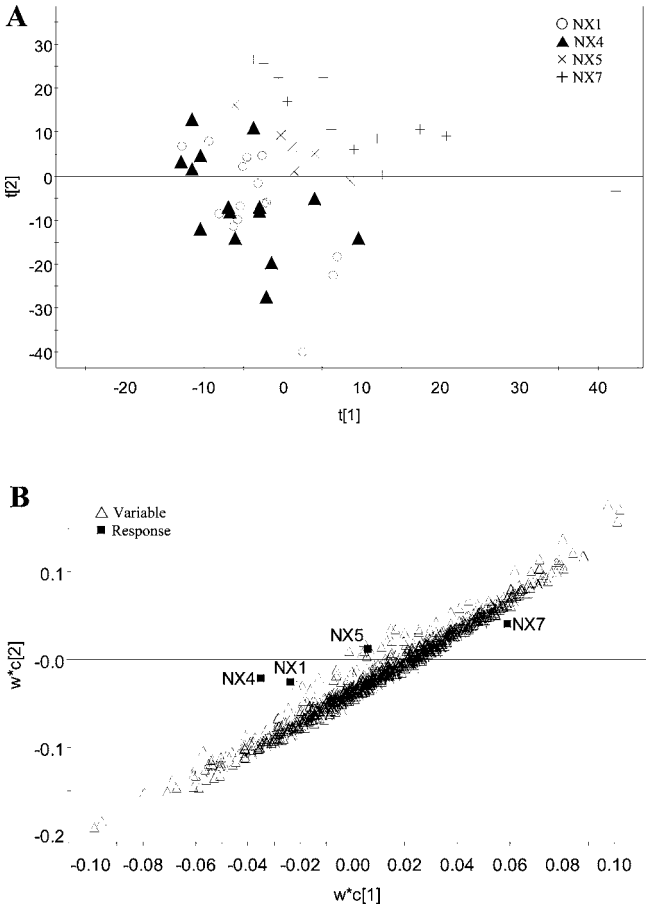


**Figure 6.** PLS-DA scores (A) and loading (B) plots differentiating NX cultivars using FIMS fingerprints. NX1, NX4, NX5, and NX7 respectively represent NX wolfberry No. 1, No. 4, No. 5, and No. 7 samples, respectively.

**Table 2. Statistical Validation Results of PLS-DA Classification Model by Bootstrapped Latin Partition[a]**

| | | UPLC−MS | TIS | FIMS |
|---|---|---|---|---|
| cultivation location | APA (%) | 94 ± 3 | 97 ± 2 | 93 ± 4 |
| | nLVs | 17 ± 1 | 51 ± 10 | 47 ± 12 |
| NX cultivar | APA (%) | 93 ± 6 | 95 ± 4 | 91 ± 4[b] |
| | nLVs | 16 ± 2 | 28 ± 3 | 25 ± 8 |

[a]The deviations were reported as 95% confidence interval; APA, averaged prediction accuracy; nLVs, number of latent variables. [b]Calculated by the mean-centering preprocessing method.

effectiveness of the PLS-DA projection plots as a convenient visualization technique for the differentiation. In addition, the average regression coefficients with confidence limits from all the latent variables in the PLS-DA model were calculated and plotted (Figure S5−S8 in the Supporting Information). Each extracted chromatographic peak or $m/z$ measurement can be estimated for its statistical significance in the PLS-DA model for each class of sample. For example, in Figure S8 in the Supporting Information, peaks of $m/z$ 792 and 794 were positively related to cultivars NQ1 and NQ7, and negatively related to cultivars NQ4 and NQ5.

In summary, the UPLC−MS chromatogram and the FIMS fingerprints combined with PLS-DA projection plots were quantitatively validated for their potential utilization in differentiating wolfberries from Ningxia and other locations, as well as the different cultivars grown at a selected location. Compared with each other, FIMS fingerprinting has advantages in reducing the analysis time significantly, and UPLC−MS offers more information when relating the differentiation model to chemical compositions. Both methods could be developed for the quality assurance, quality control, and authentication of wolfberry and wolfberry-containing foods.

## ■ ASSOCIATED CONTENT

### Supporting Information

Principal component scores plots and PLS-DA model regression coefficients. This material is available free of charge via the Internet at http://pubs.acs.org.

## ■ AUTHOR INFORMATION

### Corresponding Author

*Tel: (86)-21-3420-5828. Fax: (86)-21-3420-4107. E-mail: liangli.yu@sjtu.edu.cn.

### Funding

This work was supported by National High Technology Research and Development Program of China (Grant Nos. 2013AA102202; 2013AA102207); a special fund for Agro-scientific Research in the Public Interest (Grant No. 201203069); and SJTU startup fund for young talent (Grant No. 13X100040047), and SJTU 985-III disciplines platform and talent fund (Grants TS0414115001; TS0320215001).

### Notes

The authors declare no competing financial interest.

## ■ ACKNOWLEDGMENTS

Prof. Jinming Gao at Shaanxi Engineering Center of Bioresource Chemistry & Sustainable Utilization, College of Science, Northwest A&F University, is thanked for kindly providing us the wolfberry samples for this study.

## ■ REFERENCES

(1) Zhang, X.; Li, Y.; Cheng, J.; Liu, G.; Qi, C.; Zhou, W.; Zhang, Y. Immune activities comparison of polysaccharide and polysaccharide-protein complex from *Lycium barbarum* L. *Int. J. Biol. Macromol.* **2014**, *65*, 441−445.

(2) Qian, J.; Liu, D.; Huang, A. The efficiency of flavonoids in polar extracts of *Lycium chinense* Mill fruits as free radical scavenger. *Food Chem.* **2004**, *87*, 283−288.

(3) Wang, C.; Chang, S.; Stephen Inbaraj, B.; Chen, B. Isolation of carotenoids, flavonoids and polysaccharides from *Lycium barbarum* L. and evaluation of antioxidant activity. *Food Chem.* **2010**, *120*, 184−192.

(4) Stephen Inbaraj, B.; Lu, H.; Hung, C.; Wu, W.; Lin, C.; Chen, B. Determination of carotenoids and their esters in fruits of *Lycium barbarum* Linnaeus by HPLC−DAD−APCI−MS. *J. Pharm. Biomed. Anal.* **2008**, *47*, 812−818.

(5) Chang, R.; So, K. Use of anti-aging herbal medicine, *Lycium barbarum*, against aging-associated diseases. What do we know so far? *Cell. Mol. Neurobiol.* **2008**, *28*, 643−652.

(6) Wang, P. *Wolfberry industrial competitiveness of Zhongning Ningxia*; Northwest A&F University: Yangling, Shaanxi, China, 2013.

(7) Moore, J.; Luther, M.; Cheng, Z.; Yu, L. Effects of baking conditions, dough fermentation, and bran particle size on antioxidant properties of whole-wheat pizza crusts. *J. Agric. Food. Chem.* **2009**, *57*, 832−839.

(8) Li, X.; Li, R.; Xiang, H.; Zhao, Z.; Liu, X. Study on quality evaluation of *Lycium chinense* from different areas by HPLC fingerprint and cluster analysis. *Mod. Food Sci. Technol.* **2012**, *28*, 1251−1253.

(9) Whent, M.; Hao, J.; Slavin, M.; Zhou, M.; Song, J.; Kenworthy, W.; Yu, L. Effect of genotype, environment, and their interaction on

chemical composition and antioxidant properties of low-linolenic soybeans grown in Maryland. *J. Agric. Food. Chem.* **2009**, *57*, 10163−10174.
(10) Xie, Z.; Liu, W.; Huang, H.; Slavin, M.; Zhao, Y.; Whent, M.; Blackford, J.; Lutterodt, H.; Zhou, H.; Chen, P.; Wang, T. T. Y.; Wang, S.; Yu, L. Chemical composition of five commercial *Gynostemma pentaphyllum* samples and their radical scavenging, antiproliferative, and anti-inflammatory properties. *J. Agric. Food. Chem.* **2010**, *58*, 11243−11249.
(11) Zheng, G.; Zheng, Z.; Xu, X.; Hu, Z. Variation in fruit sugar composition of *Lycium barbarum* L. and *Lycium chinense* Mill. of different regions and varieties. *Biochem. Syst. Ecol.* **2010**, *38*, 275−284.
(12) Zhao, L.; Qiu, Z.; Narasimhamoorthy, B.; Greaves, J. Development of a rapid, high-throughput method for quantification of zeaxanthin in Chinese wolfberry using HPLC−DAD. *Ind. Crop Prod.* **2013**, *47*, 51−57.
(13) Chen, P.; Harnly, J. M.; Lester, G. E. Flow injection mass spectral fingerprints demonstrate chemical differences in Rio Red grapefruit with respect to year, harvest time, and conventional versus organic farming. *J. Agric. Food. Chem.* **2010**, *58*, 4545−4553.
(14) Gao, B.; Lu, Y.; Qin, F.; Chen, P.; Shi, H.; Charles, D.; Yu, L. Differentiating organic from conventional peppermints using chromatographic and flow injection mass spectrometric (FIMS) fingerprints. *J. Agric. Food. Chem.* **2012**, *60*, 11987−11994.
(15) Lu, Y.; Gao, B.; Chen, P.; Charles, D.; Yu, L. Characterisation of organic and conventional sweet basil leaves using chromatographic and flow-injection mass spectrometric (FIMS) fingerprints combined with principal component analysis. *Food Chem.* **2014**, *154*, 262−268.
(16) Zhao, Y.; Niu, Y.; Xie, Z.; Shi, H.; Chen, P.; Yu, L. Differentiating leaf and whole-plant samples of di- and tetraploid *Gynostemma pentaphyllum* (Thunb.) Makino using flow-injection mass spectrometric fingerprinting method. *J. Funct. Foods* **2013**, *5*, 1288−1297.
(17) Wang, Z.; Chen, P.; Yu, L.; Harrington, P. d. B. Authentication of organically and conventionally grown basils by gas chromatography/mass spectrometry chemical profiles. *Anal. Chem.* **2013**, *85*, 2945−2953.
(18) Wang, Z.; Harrington, P. Feature selection of gas chromatography/mass spectrometry chemical profiles of basil plants using a bootstrapped fuzzy rule-building expert system. *Anal. Bioanal. Chem.* **2013**, *405*, 9219−9234.
(19) Yao, X.; Peng, Y.; Zhou, Q.; Xiao, P.; Sun, S. Distinction of eight *Lycium* species by Fourier-transform infrared spectroscopy and two-dimensional correlation IR spectroscopy. *J. Mol. Struct.* **2010**, *974*, 161−164.
(20) Bondia-Pons, I.; Savolainen, O.; Törrönen, R.; Martinez, J. A.; Poutanen, K.; Hanhineva, K. Metabolic profiling of Goji berry extracts for discrimination of geographical origin by non-targeted liquid chromatography coupled to quadrupole time-of-flight mass spectrometry. *Food Res. Int.* **2014**, *63* (part B), 132−138.
(21) Stephen Inbaraj, B.; Lu, H.; Kao, T.; Chen, B. Simultaneous determination of phenolic acids and flavonoids in *Lycium barbarum* Linnaeus by HPLC−DAD−ESI-MS. *J. Pharm. Biomed. Anal.* **2010**, *51*, 549−556.
(22) Harrington, P. Statistical validation of classification and calibration models using bootstrapped Latin partitions. *TrAC, Trends Anal. Chem.* **2006**, *25*, 1112−1124.
(23) Zheng, J.; Ding, C.; Wang, L.; Li, G.; Shi, J.; Li, H.; Wang, H.; Suo, Y. Anthocyanins composition and antioxidant activity of wild *Lycium ruthenicum* Murr. from Qinghai-Tibet Plateau. *Food Chem.* **2011**, *126*, 859−865.
(24) Shang, J.; Si, B. Genetic diversity analysis of four domestic of *Lycium barbarum* L. *J. Anhui Agric. Sci.* **2010**, *38*, 2801−2802.

samples has been detected using HPLC,[18,19] GLC,[20] GC headspace,[21] GC-MS,[22] and spectrophotometric methods[23,24] or FTIR.[25]

Another approach, mostly used in industry, is basic titration, again based on the methanol release from ester induced by the basic environment.[26,27]

Methods combining both acetic acid and methanol determination are limited. There have been attempts measuring both using HPLC[18,19] or GC-MS[22] for the detection after saponification. No methods were found allowing the simultaneous detection of methylation, acetylation, and feruloylation degree of pectin. Ferulic acid in pectin was generally determined by spectroscopic methods[28] or HPLC-UV methods.[29]

NMR was extensively used to study pectin and, more in general, food carbohydrates at a structural level,[30] whereas the application of this technique as a quantitative analytical tool in carbohydrate determination is still limited, despite its huge possibilities.[31]

With regard to the determination of the degree of esterification in pectin by NMR, few studies can be found in the literature,[32−34] and only two papers report the simultaneous measurement of the methylation and acetylation degrees of pectin by NMR.[35,36] In most of these studies, the NMR analysis is performed on intact pectin and the degree of methylation is based on the integration of the signals of the protons adjacent to the carboxylate in free or esterified form. However, the determination of the methylation degree of intact pectin is affected by difficulties related to the low spectral resolution due to the gelling properties of pectin. In fact, in an attempt to reduce the poor resolution, all of the NMR experiments reported in the literature are registered at high temperatures (60−90 °C). The low spectral resolution leads to an enlargement and a deviation from the Lorentzian form of the NMR signals, which become more difficult to integrate, thus affecting the error of the measurement. Bedouet et al.[36] explored the possibility to determine acetylation and methylation degrees of pectin by $^1$H NMR measurement after saponification of pectic material directly in the NMR tube. However, also in this case experiments were performed at 80 °C, due to the known jellying properties of pectin also after saponification. Neumuller et al.[37] proposed a quantitative NMR-based method to determine phenoyl and acetyl esters of different polysaccharides as corn fiber and potato starch after saponification. The method was in good agreement with a conventional HPLC analyses, with the advantage of significantly reduced analysis time.

Here, we suggest a simpler method for the simultaneous detection of methylation, acetylation, and feruloylation degrees of pectin, which consists of an easy preparation of the sample for $^1$H NMR analysis by performing an alkaline saponification (Figure 1) on the pectin isolated from the food sources. This step allows very resolved NMR spectra to be obtained at room temperature, where the peaks of methanol, acetic acid, and ferulic acid can easily be integrated and quantified with respect to the amount of pectin.

## MATERIALS AND METHODS

**Materials and Chemicals.** Standard of pectin from citrus peel, deuterium oxide, 3-(trimethylsilyl)propionate-$d_4$ (TSP), methanol, acetic acid, ferulic acid, galacturonic acid, sulfamic acid, potassium hydroxide, sodium tetraborate, *m*-hydroxydiphenyl, sodium hydroxide, *trans*-1,2-diaminocyclohexane-*N*,*N*,*N*′,*N*′-tetraacetic acid (CDTA), phenol, 4-(2-hydroxyethyl)piperazine-1-ethanesulfonic acid (HEPES), dimethyl sulfoxide, porcine pancreatic α-amylase, and sulfuric acid, of analytical grade were purchased from Sigma-Aldrich (Taufkirchen, Germany).

Three samples of pectin with different methylation degrees determined by titration were provided by Silvaextracts (Cuneo, Italy) as freeze-dried powders. Sugar beet flakes, pea hulls, olive pomace, grape pomace, and apple cake were provided by IGV (Nuthetal, Germany) as part of the NOSHAN EU project.

**Methods of Analysis.** *Extraction of Soluble Pectic Polysaccharides by a Chelating Agent Solution.* The isolation of cell wall was performed following the instructions of Melton and Smith[38] for samples containing starch. To inactivate enzymes, the samples were homogenized (Ultraturrax T-50 basic, IKA-Werke, Staufen im Breisgau, Germany; 2−3 min, 4000 rpm) with 80% phenol−0.5 M HEPES buffer (w/v). Soluble cell matrix contents were solubilized by 50 mM HEPES buffer (pH 6.7) and separated by centrifuge (Eppendorf AG, Hamburg, Germany; 20 min, 3220*g*, RT, HDPE centrifuge bottles). The pellet was treated (incubation for 6 and 24 h) with DMSO 90% (v/v) and further incubated for 1 h at 40 °C with 200 U of porcine pancreatic α-amylase stabilized by 20 mM HEPES buffer with 20 mM $CaCl_2$ (pH 6.9), to remove starch. Cell walls were treated twice (6 and 12 h) with 50 mM CDTA in 50 mM potassium acetate buffer (pH 6.5). The supernatants were separated by centrifuge, combined, and dialyzed with 0.1 M ammonium acetate buffer (pH 6.5, 1 day, three changes, 4 °C) followed by $H_2O$ (3 days, three changes at 4 °C). All samples were freeze-dried and stored at −18 °C.

*Galacturonic Acid Determination.* The galacturonic acid content was determined with *m*-hydroxydiphenyl as described by Melton and Smith[39] using galacturonic acid as standard. Pectin samples were hydrolyzed using 1 mL × 2 concentrated sulfuric acid, mixed, and cooled in an ice bath. Bidistilled water, 0.5 and 5 mL, was added, respectively, centrifuged (Eppendorf 5810R, Eppendorf, Augsburg, Germany), and the supernatant was used for spectrophotometric measurements (UV−vis Lambda BIO 20 spectrophotometer, PerkinElmer, Waltham, MA, USA). To 400 μL of supernatant or standard were added 40 μL of 4 M sulfamic acid/potassium sulfamate solution (pH 1.6) and 2.4 mL of 75 mM sodium tetraborate/sulfuric acid solution. The mixture was heated (100 °C) for 20 min and then cooled. To the sample control was added 80 μL of 0.5% NaOH to determine the sugar coloring. To the sample and standard was added 80 μL of 8.8 mM *m*-hydroxydiphenyl in 0.5% NaOH. The absorbance was measured after 10 min of incubation time at 525 nm against a water blank.

*Methylation, Acetylation, and Feruloylation Degree.* Pectic polysaccharides were incubated (2 h, room temperature) with 1 mL of 0.4 M NaOH in $D_2O$ and 0.1 mL of internal standard (TSP, 0.2 mg/mL in $D_2O$). The supernatant was centrifuged (Centrifuge Eppendorf 5810R, Eppendorf, Augsburg, Germany), clarified (nylon syringe filter system, 0.4 μm), and transferred in NMR tubes. $^1$H NMR spectra were acquired on a Varian-Inova 600 MHz spectrometer, equipped with a triple-resonance inverse probe (HCN), operating at 599.736 MHz for proton. Spectra were collected at 298 K, with 32K complex points, using a 90° pulse length. Sixty-four scans were acquired with a spectral width of 7196.8 Hz, an acquisition time of 2.53, and a relaxation delay (d1) of 5 s. The experiments were carried out with water suppression by low-power selective water signal presaturation during 5 s of the relaxation delay. The accuracy of the quantitative data was assured by the relaxation delay, determined by the longitudinal relaxation time (T1) measurements, which is set in order to allow the complete relaxation of the nuclei. The T1 time was determined by the T1 inversion recovery pulse sequence consisting of a 180° pulse followed by a variable delay ($\tau$), a 90° pulse, and an acquisition.

The NMR spectra were processed by MestreC software. The spectra were Fourier transformed with FT size of 64K and 0.2 Hz line-broadening factor, phased and baseline corrected, and referenced to the TSP peak (0 ppm). The quantitative determination of acetic acid, methanol, and ferulic acid was obtained by manual integration of the

corresponding signals (1.920 ppm for acetic acid, 3.358 ppm for methanol, and 6.233 ppm for ferulic acid) and comparison with the TSP area. Integrals were converted in mass value (mg) according to the following formula, as previously reported.[40]

$$A\ x \times \frac{\mathrm{EW}\ x}{\mathrm{mg}\ x} = A\ \mathrm{TSP} \times \frac{\mathrm{EW\ TSP}}{\mathrm{mg\ TSP}}$$

$A\ x$ is the spectral area of the analyte, $A$ TSP is the spectral area of the internal standard, EW $x$ is the equivalent weight of the analyte, EW TSP is the equivalent weight of the internal standard, and EW = (molecular weight/number of hydrogens in the signal).

Through the content of methanol and the content of galacturonic acid, the degree of methylation (or acetylation/feruloylation) was calculated, using the following equation:

$$\text{degree of methylation} = \frac{\text{mol of methanol}}{\text{mol of galacturonic acid}} \times 100\%$$

*Linearity, Limit of Detection, and Limit of Quantification.* The linearity of the method was checked at a range between 0.1 mM (detection limit) and 100 mM for each analyte. Three replicates were performed for each concentration. Each solution was subjected to the entire experimental protocol. The limit of detection (LOD) and the limit of quantification (LOQ) were calculated utilizing the S/N ratio methods, based on the determination of the peak to peak noise.[41] LOD and LOQ were therefore calculated as the minimum concentrations producing a recognizable peak with a signal-to-noise ratio of, respectively, 3.3 or 10.

*Accuracy, Precision, Recovery, and Robustness of the Method.* The accuracy of the analyte's recovery was determined by assaying samples with known concentrations of methanol, acetic acid, and ferulic acid, both as pure compounds and as spiked matrix. Accuracy was determined by the following equation: accuracy = $(p^2 + b^2)^{1/2}$, where $p$ is precision and $b$ is the bias (difference between NMR value and the true or "accepted" value). Precision was evaluated both intraday and interday (intermediate precision), and the data were compared after three consecutive analyses (intraday) and from data obtained over a 15 day period (interday). The precision was expressed as coefficient of variation (CV%). Recovery of analytes was determined by spiking a sample of sugar beet pectin with pure compounds. The evaluation of robustness was performed by varying two parameters of the analytical procedure as hydrolyzing volume and time of hydrolysis.

## RESULTS AND DISCUSSION

**Development and Optimization of the Sample Preparation.** The proposed method involves pectin saponification (Figure 1) followed by separation of the polysaccharidic component by filtration and direct $^1$H NMR analysis at room temperature. The filtration step is necessary to eliminate from the solution the de-esterified polysaccharidic polymers. In fact, preliminary tests aiming to evaluate the possibility of analyzing directly the solution after saponification showed that pectin gave very poorly resolved spectra, also when de-esterified. For this reason, in the method we proposed, the polysaccharidic components were separated by filtration prior to NMR analysis. In a previous paper,[36] the authors determined the acetylation and methylation degree of pectin by $^1$H NMR measurement of the product of in-tube saponification of pectic material, and in an attempt to reduce the poor resolution of pectin solutions, NMR experiments were registered at high temperatures (80 °C). However, from a technical point of view, 80 °C is the maximum permitted temperature for many common NMR probes, thus limiting the applicability of the methods. Moreover, this approach is not optimal when the goal is the accurate determination of methanol, because at high temperatures a repartition of methanol in the headspace of the NMR tube may occur, and this might represent a delicate point that affects the robustness of the procedure.

The method proposed was initially tested on a standard of pectin sample, namely, citrus peel pectin with a declared methylation degree of 63−66%. To obtain satisfactory efficiency, the effect of the main variables involved in the hydrolysis of pectin, time of hydrolysis and volume of NaOH in $D_2O$, were varied to determine the optimal conditions allowing the complete reaction. Variable volumes of NaOH in $D_2O$ (1, 2, and 3 mL) and different incubation times (30, 60, 120, and 180 min) were tested. The results were evaluated by applying two-way ANOVA at a $p$ level of 0.05, considering also the interactions of the two factors. ANOVA results showed that the incubation time had a significant effect in enhancing the hydrolysis degree ($p$ = 0.007), whereas the NaOH in $D_2O$ volume and the interactions among the parameters were not found to be significant ($p$ = 0.079 and $p$ = 0.629, respectively). The incubation times of 30 and 60 min gave results significantly different from those obtained with incubation times of 120 and 180 min (as determined by post hoc Tukey-HSD tests). Thus, the use of 1 mL of NaOH in $D_2O$, to avoid deuterated solvent consumption, and 120 min of incubation, to minimize analysis time, was chosen in the final method.

**Method Validation.** The optimized method was subjected to validation in terms of precision, accuracy, linearity, detection and quantitation limits, repeatability, reproducibility, recovery, and robustness following recommendations of the International Conference on Harmonization (ICH (2005)): validation of analytical procedures, text and methodology; harmonized tripartite guideline, Q2(R1)). The validation tests were performed on a pure solution of methanol, acetic acid, and ferulic acid.

To determine the accuracy and precision of the methanol, acetic acid, and ferulic acid analysis by $^1$H NMR, a solution containing all of the analytes was obtained by weighing the compounds and dissolving them in the hydrolyzing solution (1 mL of 0.4 M NaOH in $D_2O$ and 0.1 mL of 0.2 mg/mL TSP in $D_2O$ as internal standard) and analyzed by $^1$H NMR in the experimental conditions previously reported. The same solution was used to spike a real matrix of sugar beet pectin. Measured results of the standard solution were in agreement with the amounts weighed in the range of concentrations of 0.1−100 mM, a range that corresponds with the final in-tube concentration of the analytes in real samples of pectin. Linearity was demonstrated in the same range. The instrumental quantification limit (LOQ, signal-to-noise ratio >10) in the experimental conditions reported was about 0.1 mM for methanol and acetic acid and 0.2 mM for ferulic acid, whereas the LOD was obtained at 0.03 mM for methanol and acetic acid and at 0.05 mM for ferulic acid (S/N ratio 3.3).

Standard solutions were also subjected to the entire experimental protocol to verify eventual loss of methanol and acetic acid during the various steps of sample preparation. Results are reported in Table 1 as precision, bias, and accuracy. A spiked matrix (sugar beet) was also analyzed, and the corresponding recoveries are reported in Table 1.

**Reproducibility and Robustness of the Method.** To determine the interday reproducibility, a pectin standard, after the first measurement, was kept refrigerated and reanalyzed by $^1$H NMR spectrometer after 3, 7, and 14 days. On each day three repetitions of the experiment were performed. The data were treated with one-way ANOVA for each analyte, and the results showed that no significant differences had arisen in the


dx.doi.org/10.1021/jf502679s | J. Agric. Food Chem. 2014, 62, 9081−9087

**Table 1. Precision (Percent; Standard Deviation), Accuracy, Bias, and Recovery of the NMR Measurement of Methanol, Acetic Acid, and Ferulic Acid**

| | methanol | acetic acid | ferulic acid |
|---|---|---|---|
| precision (CV%)[a] | 2.22 | 1.94 | 2.01 |
| bias[a] | 0.024 | 0.093 | 0.002 |
| accuracy[a] | 2.22 | 1.94 | 2.00 |
| recovery %[b] | 93 ± 2 | 96 ± 2 | 90 ± 2 |

[a]Calculated on a standard solution subjected to the entire experimental protocol. [b]Calculated on sugar beet pectin spiked with standard solution and subjected to the entire experimental protocol.

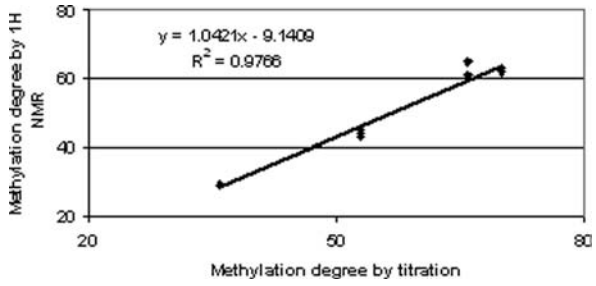


**Figure 2.** Correlation observed between the results obtained from the titration method and the $^1$H NMR-based method for citrus peel pectin methylation degree.

time interval under study. The coefficients of variation (CV) calculated on all 12 data (3 repetitions for 4 days) were 2.4% for acetic acid and 2.5% for methanol.

The data obtained from method optimization trials were analyzed to test the robustness of the method: the non-significant effect of the hydrolyzing agent volume and of hydrolysis time in the range of 120−180 min, as reported above, demonstrated that the method is robust to the variation of these factors. In this case the CV% calculated for methanol was 3.9%.

**Comparison of $^1$H NMR-Based Method and Titration Method.** The method was applied to three commercial pectin samples from citrus peel with different values of methylation, certified by the producer (Silvaextracts) and determined by titration. The titration method[26] is based on the determination of the ratio between the volume of NaOH used for the titration of the carboxylic groups "covered" by methyl groups ($V_2$) on the sum of $V_2$ + the volume of NaOH used for the titration of free carboxylic groups ($V_1$).

$$\text{degree of methylation} = \frac{V_2}{V_1 + V_2} \times 100\%$$

Results obtained by the proposed $^1$H NMR method (determined in triplicate) compared to the values provided are shown in Table 2.

The values determined are in line with the data provided by Silvaextracts. The correlations between couples of data were obtained by applying the regression analysis and are shown in Figure 2 for methylation degree. A good correlation ($R^2$ = 0.9766) was obtained. It can be observed that in general data from NMR were lower than those obtained by titration. The differences between the two methods can be ascribed to interfering substances present in pectin able to react with the sodium hydroxide, thus "inflating" the methylation degree. Also, similar differences between the method of titration and saponification combined with HPLC were reported previously.[18,19] The method here presented, based on the actual visualization of methanol and acetic acid, is expected to be more accurate.

As compared to the HPLC methods reported in the literature, the $^1$H NMR-based method here proposed presents the advantages of reduced time of analysis and the possibility to obtain in a single analysis data on methylation, acetylation, and feruloylation, which generally require separate chromatographic analyses. Another important advantage is that NMR allows absolute quantitative data to be obtained, avoiding the need of reference compounds and calibration curves.

**Analysis of Real Samples.** The validated method was applied to samples of soluble pectin extracted by chelating agent solutions from different food waste sources: sugar beet flakes, apple cake, pea hulls, olive pomace, and grape pomace. Figures 3 and 4 show the $^1$H NMR spectra for sugar beet flakes and olive pomace. $^1$H NMR spectra show the optimal resolution of methanol, acetic acid, and ferulic acid, which can be easily detected and quantified in samples of various origins. It is worth noting that besides signals of methanol and acetic acid, it is possible to detect in the spectra some other minor signals (evidenced in the spectra enlargements) that correspond to other chemical molecules linked to the pectin backbone. In the case of pectin originating from sugar beet, the main minor signals are in the aromatic zone and can be attributed to ferulic acid analogues.

The degree of methylation, acetylation, and feruloylation determined in the samples of industrial byproducts having variable levels of esterification degrees are reported in Table 3. Feruloylation degree is expressed with respect to galacturonic acid to make the data compatible with methylation and acetylation, even if ferulic acid in pectin can be linked also to arabinose side chains.

Results showed that, as expected, methanol is the main compound linked via ester bond to the pectin backbone. Sugar beet flakes and pea hulls contain also a significant amount of acetic esters, whereas ferulic acid esters were detected only in sugar beet.

**Table 2. Methylation and Acetylation Degree (Mole Percent of Galacturonic Acid) of Standard Citrus Peel Pectin Determined by Titration or $^1$H NMR**

| | standard[a] | | low methylation degree[b] | | medium methylation degree[b] | | high methylation degree[b] | |
|---|---|---|---|---|---|---|---|---|
| | titration | $^1$H NMR | titration | $^1$H NMR | titration | $^1$H NMR | titration | $^1$H NMR |
| galacturonic acid | 75 | 77 ± 1[c] | 80.8 | 85 ± 2[c] | 86.2 | 81.8 ± 0.3[c] | 84.4 | 78 ± 3[c] |
| methylation degree | 63−66 | 61.1 ± 0.4 | 36.1 | 29.1 ± 0.2 | 53.5 | 44 ± 1 | 69.5 | 62.4 ± 0.4 |
| acetylation degree | nd | 1.0 ± 0.1 | nd | 0.10 ± 0.01 | nd | 0.40 ± 0.01 | nd | 2.4 ± 0.1 |

[a]Citrus peel pectin purchased from Sigma-Aldrich. [b]Citrus peel pectin provided by Silvaextract. [c]Galacturonic acid content (%) determined by colorimetric method.


dx.doi.org/10.1021/jf502679s | J. Agric. Food Chem. 2014, 62, 9081−9087

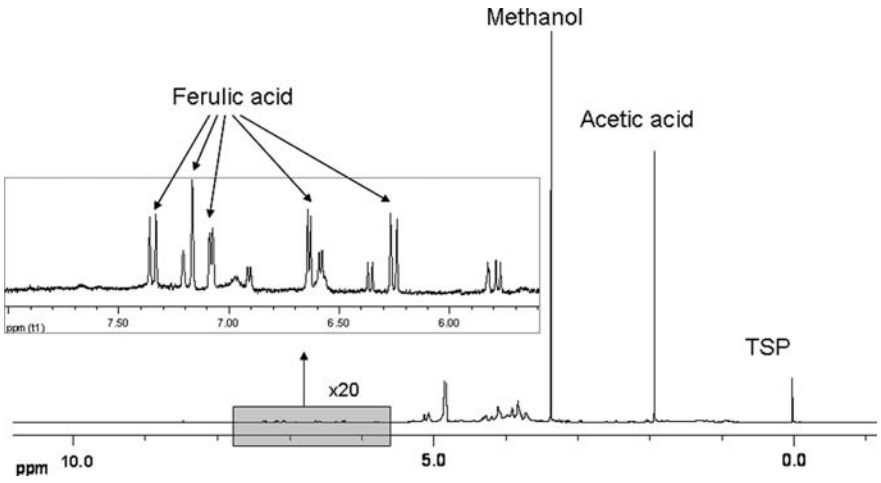


**Figure 3.** [1]H NMR spectrum of pectin sample (source: sugar beet flakes). Experimental conditions are reported under Materials and Methods.

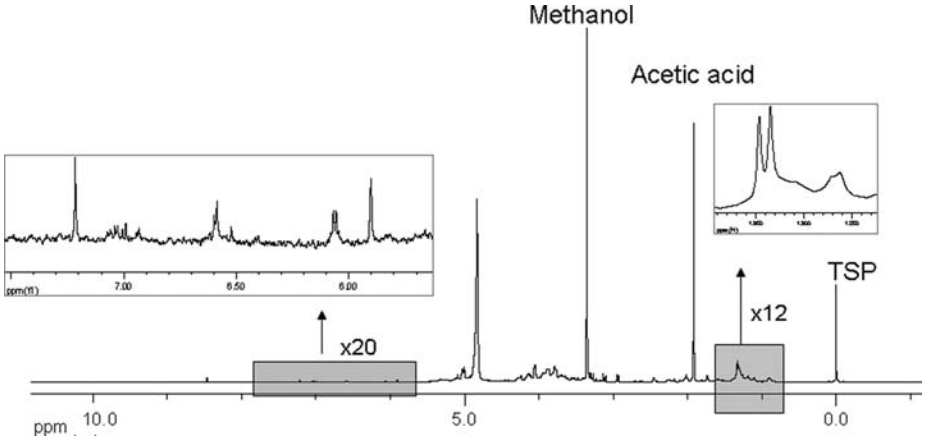


**Figure 4.** [1]H NMR spectrum of pectin sample (source: olive pomace). Experimental conditions are reported under Materials and Methods.

**Table 3. Galacturonic Acid Content (Percent) and Methylation, Acetylation, and Feruloylation Degrees (Mole Percent of Galacturonic Acid) of Some Industrial Byproducts Determined by NMR[a]**

| | galacturonic acid content | methylation degree | acetylation degree | feruloylation degree |
|---|---|---|---|---|
| sugar beet flakes | 67.1 ± 0.9 | 29.1 ± 0.8 | 18.0 ± 0.5 | 0.268 ± 0.001 |
| pea hulls | 44.6 ± 0.8 | 29.83 ± 0.03 | 10.5 ± 0.9 | nd |
| apple cake | 40.8 ± 0.5 | 40 ± 1 | 5.6 ± 0.1 | nd |
| olive pomace | 72 ± 1 | 10.5 ± 0.5 | 7.5 ± 0.1 | nd |
| grape pomace | 89 ± 2 | 5.0 ± 0.2 | 1.0 ± 0.1 | nd |

[a]Galacturonic acid content was determined spectrophotometrically.

The values determined for pea hull sample using our method are in line with the values obtained by similarly extracted pectic polysaccharides of this byproduct reported previously[42] (methylation degree of 24%).

For sugar beet samples, lower values for methylation degree were observed with respect to the data published by Renard and Thibault[43] (29.1% for our sample vs 52%). This can be attributed to the different sample origins: the current sample was dried sugar beet flakes, whereas the sample analyzed by Renard and Thibault[43] was fresh sugar beet pulp. This indicates that the process of drying sugar beet pulp to obtain flakes can actually lower the degree of methylation. The same behavior is also observed by comparing the feruloylation degree obtained (0.2%) that is lower with respect to previously published data.[28]

The method is currently being applied to a wide number of different food and byproduct samples, showing that it is suitable for all food matrices.

The overall data demonstrate that the quantitative [1]H NMR methodology proposed can be considered a high-throughput analysis that combines the determination of methylation, acetylation, and also feruloylation degree of pectin using a small sample amount and short preparation time. Furthermore, the method can be applied to pectic polysaccharides originating from a wide range of sources and having very different physical properties. It can detect small amounts of methanol, acetic acid, and ferulic acid.

The method is expected to be more accurate with respect to titration in determining the methylation degree without confusing it with other esterified forms present in pectin and also offers the advantage to obtain structural information on other compounds possibly linked via ester bond to pectin.


dx.doi.org/10.1021/jf502679s | J. Agric. Food Chem. 2014, 62, 9081−9087

## AUTHOR INFORMATION


### Corresponding Author

*(A.C.) Mail: Department of Food Science, University of Parma, Parco Area delle Scienze 17A, 43124 Parma, Italy. Phone: +39 0521 905407. Fax: +39 0521 905472. E-mail: augusta.caligiani@unipr.it.



### Funding

The research leading to these results has received funding from the European Union, Seventh Framework Program (FP7/2007-2013), under Grant Agreement 312140 (Functional and Safe Feed from Food Waste − NOSHAN).


### Notes

The authors declare no competing financial interest.

## REFERENCES


(1) Ridley, B. L.; O'Neill, M. A.; Mohnen, D. Pectins: structure, biosynthesis, and oligogalacturonide-related signaling. *Phytochemistry* **2001**, *57*, 929−967.

(2) Voragen, A. G. J.; Coenen, G. J.; Verhoef, R. P.; Schols, H. A. Pectin, a versatile polysaccharide present in plant cell walls. *Struct. Chem.* **2009**, *20*, 263−275.

(3) Saulnier, L.; Thibault, J. F. Ferulic acid and diferulic acids as components of sugar-beet pectins and maize bran heteroxylans. *J. Sci. Food Agric.* **1999**, *79*, 396−402.

(4) Fry, S. Phenolic components of the primary cell wall. *Biochem. J.* **1982**, *203*, 493−504.

(5) Renard, C.; Champenois, Y.; Thibault, J. F. Characterisation of the extractable pectins and hemicelluloses of the cell wall of glasswort *Salicornia ramosissima*. *Carbohydr. Polym.* **1993**, *22*, 239−245.

(6) Endreß, H. U.; Rentschler, C. Chances and limits for the use of pectin as emulsifier. *Eur. Food Drink Rev.* **1999**, 49−53.

(7) Krall, S.; McFeeters, R. Pectin hydrolysis: effect of temperature, degree of methylation, pH, and calcium on hydrolysis rates. *J. Food Chem.* **1998**, *46*, 1311−1315.

(8) van Buggenhout, S.; Sila, D.; Duvetter, T.; van Loey, A.; Hendrickx, M. Pectins in processed fruits and vegetables: Part III. Texture engineering. *Compr. Rev. Food Sci. Food Saf.* **2009**, *8*, 105−117.

(9) Yoo, S. H.; Fishman, M. L.; Hotchkiss, A. T.; Lee, H. G. Viscometric behavior of high-methoxy and low-methoxy pectin solutions. *Food Hydrocolloids* **2006**, *1*, 62−67.

(10) May, C. Industrial pectins: sources, production and applications. *Carbohydr. Polym.* **1990**, *12*, 79−99.

(11) Pippen, E.; McCready, R.; Owens, H. Gelation properties of partially acetylated pectin. *J. Am. Chem. Soc.* **1950**, *2*, 813−816.

(12) Renard, C.; Jarvis, M. C. Acetylation and methylation of homogalacturonans 2. Effect on ion-binding properties and conformations. *Carbohydr. Polym.* **1999**, *39*, 209−216.

(13) Dea, I.; Madden, J. Acetylated pectic polysaccharides of sugar beet. *Food Hydrocolloids* **1986**, *1*, 71−88.

(14) Leroux, J.; Langendorff, V.; Schick, G.; Vaishnav, V.; Mazoyer, J. Emulsion stabilizing properties of pectin. *Food Hydrocolloids* **2003**, *4*, 455−462.

(15) Siew, C. K.; Williams, P. A. Role of protein and ferulic acid in the emulsification properties of sugar beet pectin. *J. Agric. Food Chem.* **2008**, *56*, 4164−4171.

(16) Wicker, L.; Kim, Y.; Kim, M. J.; Thirkield, B.; Lin, Z.; Jung, J. Pectin as a bioactive polysaccharide − extracting tailored function from less. *Food Hydrocolloids* **2014**, DOI: 10.1016/j.foodhyd.2014.01.002.

(17) Sila, D.; van Buggenhout, S.; Duvetter, T.; Fraeye, I.; de Roeck, A.; van Loey, A.; Hendrickx, M. Pectins in processed fruits and vegetables. Part II − Structure-function relationships. *Compr. Rev. Food Sci. Food Saf.* **2009**, *8*, 86−104.

(18) Voragen, A.; Schols, H. A.; Pilnik, W. Determination of the degree of methylation and acetylation of pectins by h.p.l.c. *Food Hydrocolloids* **1986**, *1*, 65−70.

(19) Levigne, S.; Thomas, M.; Ralet, M. C.; Quemener, B.; Thibault, J. F. Determination of the degrees of methylation and acetylation of pectins using a C18 column and internal standards. *Food Hydrocolloids* **2002**, *16*, 547−550.

(20) McFeeters, R.; Armstrong, S. Measurement of pectin methylation in plant cell walls. *Anal. Biochem.* **1984**, *139*, 212−217.

(21) Huisman, M.; Oosterveld, A.; Schols, H. Fast determination of the degree of methyl esterification of pectins by head-space GC. *Food Hydrocolloids* **2004**, *4*, 665−668.

(22) Savary, B. J.; Nuñez, A. Gas chromatography−mass spectrometry method for determining the methanol and acetic acid contents of pectin using headspace solid-phase microextraction and stable isotope dilution. *J. Chromatogr., A* **2003**, *1*−*2*, 151−159.

(23) Klavons, J.; Bennett, R. Determination of methanol using alcohol oxidase and its application to methyl ester content of pectins. *J. Food Chem.* **1986**, *34*, 597−599.

(24) Anthon, G. E.; Barrett, D. M. Comparison of three colorimetric reagents in the determination of methanol with alcohol oxidase. Application to the assay of pectin methylesterase. *J. Agric. Food Chem.* **2004**, *12*, 3749−3753.

(25) Gnanasambandam, R.; Proctor, A. Determination of pectin degree of esterification by diffuse reflectance Fourier transform infrared spectroscopy. *Food Chem.* **2000**, *68*, 327−332.

(26) Mizote, A.; Odagiri, H.; Thei, K.; Tanaka, K. Determination of residues of carboxylic acids (mainly galacturonic acid) and their degree of esterification in industrial pectins by colloid titration with Cat-Floc. *Analyst* **1975**, *100*, 822−826.

(27) Schultz, T. H. Determination of the degree of esterification of pectin. In *Methods in Carbohydrate Chemistry*; Whistler, R. L., Ed.; Academic Press: New York, 1965; Vol. V, 189 pp.

(28) Synytsya, A.; Copikova, J.; Jankovska, P.; Matejka, P.; Machovic, V. Spectroscopic estimation of feruloyl groups in sugar beet pulp and pectin. *Int. Sugar J.* **2003**, *105*, 481−488.

(29) Jankovska, P.; Copikova, J.; Synytsya, A. The determination of ferulic acid in sugar beet pulp. *Czech J. Food Sci.* **2001**, *19*, 143−147.

(30) Cheng, H. N.; Neiss, T. G. Solution NMR spectroscopy of food polysaccharides. *Polym. Rev.* **2012**, *52*, 81−114.

(31) Simmler, C.; Napolitano, J. G.; McAlpine, J. B.; Chen, S. N.; Pauli, G. F. Universal quantitative NMR analysis of complex natural samples. *Curr. Opin. Biotechnol.* **2014**, *25*, 51−59.

(32) Grasdalen, H.; Bakóy, O. E.; Larsen, B. Determination of the degree of esterification and the distribution of methylated and free carboxyl groups in pectins by $^{1}$H-NMR spectroscopy. *Carbohydr. Res.* **1988**, *184*, 183−191.

(33) Rosenbohm, C.; Lundt, I.; Christensen, T.; Young, N. Chemically methylated and reduced pectins: preparation, characterisation by $^{1}$H NMR spectroscopy, enzymatic degradation, and gelling properties. *Carbohydr. Res.* **2003**, *7*, 637−649.

(34) Kostálová, Z.; Hromádková, Z.; Ebringerová, A. Structural diversity of pectins isolated from the Styrian oil-pumpkin (*Cucurbita pepo* var. *styriaca*) fruit. *Carbohydr. Polym.* **2013**, *93*, 163−171.

(35) Renard, C.; Jarvis, M. C. Acetylation and methylation of homogalacturonans. 1: Optimization of the reaction and characterisation of the products. *Carbohydr. Polym.* **1999**, *39*, 201−207.

(36) Bedouet, L.; Courtois, B.; Courtois, J. Rapid quantification of *O*-acetyl and *O*-methyl residues in pectin extracts. *Carbohydr. Res.* **2003**, *338*, 379−383.

(37) Neumuller, K. G.; Carvalho de Souza, A.; Van Rijn, J.; Appeldoorn, M. M.; Streekstra, H.; Schols, H. A.; Gruppen, H. Fast and robust method to determine phenoyl and acetyl esters of polysaccharides by quantitative $^{1}$H NMR. *J. Agric. Food Chem.* **2013**, *61*, 6282−6287.

(38) Melton, L.; Smith, B. Isolation of plant cell walls and fractionation of cell wall polysaccharides. In *Current Protocols in Food Analytical Chemistry*; Wiley: Hoboken, NJ, USA, 1991; unit E 3.1.1−3.1.22.

(39) Melton, L.; Smith, B. Determination of the uronic acid content of plant cell walls using a colorimetric assay. In *Current Protocols in*

*Food Analytical Chemistry*; Wiley: Hoboken, NJ, USA, 1991; unit E 3.3.1−3.3.3.

(40) Caligiani, A.; Acquotti, D.; Palla, G.; Bocchi, V. Identification and quantification of the main organic components of vinegars by high resolution $^{1}$H NMR spectroscopy. *Anal. Chim. Acta* **2007**, *585*, 110−119.

(41) Apostol, I.; Miller, K. J.; Ratto, J.; Kelner, D. N. Comparison of different approaches for evaluation of the detection and quantitation limits of a purity method: a case study using a capillary isoelectrofocusing method for a monoclonal antibody. *Anal. Biochem.* **2009**, *385*, 101−106.

(42) Weightman, R.; Renard, C.; Thibault, J. F. Structure and properties of the polysaccharides from pea hulls. Part 1: Chemical extraction and fractionation of the polysaccharides. *Carbohydr. Polym.* **1994**, *24*, 139−148.

(43) Renard, C.; Thibault, J. F. Structure and properties of apple and sugar-beet pectins extracted by chelating agents. *Carbohydr. Res.* **1993**, *244*, 99−114.

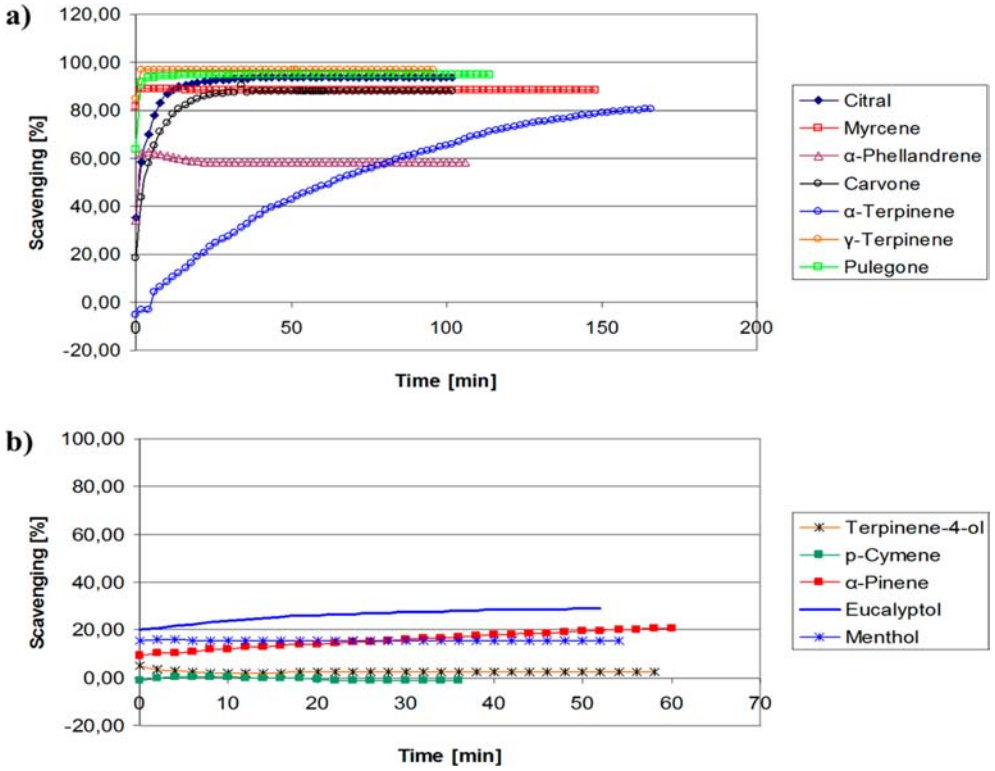


**Figure 1.** Free radical scavenging activity toward DPPH•, in methanol, for (a) monoterpenes with conjugated $\pi$ bonds and (b) monoterpenes lacking conjugated double bonds.

obtained from Polish Reagents (Gliwice, Poland). All solvents were of analytical purity grade.

**DPPH• Radical Scavenging Assay.** The radical scavenging activity of the analyzed compounds was determined spectrophotometrically by using the DPPH• assay.[12−15] Absorbance was measured by a Genesys 20 UV−vis spectrophotometer (Thermo Fisher Scientific, Waltham, MA, USA) in a 1 cm quartz cell. DPPH• solution was prepared by mixing 0.004 g ($10^{-5}$ mol) of DPPH• with 100 mL of each of the five solvents used in the study: methanol, 2-butanone, ethyl acetate, chloroform, and *n*-heptane. The concentration of the resulting solution was 0.1 mM. Fresh reagent was always prepared prior to analysis. A reference sample was prepared by mixing 2.5 mL of DPPH• (0.1 mM) with 0.7 mL of appropriate solvent. Afterward, each of the examined compounds was mixed with DPPH• solution. For each sample, the same amount (0.003 mol) of the compound was added to 2.5 mL of 0.1 mM DPPH• solution (the exact volumes of all liquid compounds and the weighed amounts of thymol and menthol are given in all tables in the Supporting Information). To obtain the exact volume for each of the measurements, the samples were made up to 3.2 mL volume, with the use of proper solvent. The samples were prepared with the same molar ratio of DPPH• to terpene. The loss of DPPH• absorbance was measured in the excess of examined compounds. Each measurement was repeated three times at 517 nm at room temperature. The final result is the average of three replicates. Free radical scavenging activity was calculated as a percentage of DPPH• decoloration according to the formula

$$\text{scavenging}\,\% = 100 \times (A_{\text{blank}} - A_{\text{sample}}/A_{\text{blank}}) \quad (1)$$

where $A_{\text{blank}}$ is the absorbance of the sample except tested substances and $A_{\text{sample}}$ is the absorbance of the sample with a tested compound.

**DPPH• Radical Scavenging Assay in the Presence of Silver Nitrate.** To check the influence of double bonds on the DPPH• scavenging activity of terpenes, a test with $AgNO_3$ was performed. Silver ions are known to form stable complexes with dienes. A reference sample was prepared by mixing 2.5 mL of DPPH• (0.1 mM) in methanol with 0.003 mol of $AgNO_3$ dissolved in a 1.2 mL of mixture of 0.4 mL of distilled water and 0.8 mL of methanol. Tested samples were prepared by mixing the proper volume of monoterpene containing 0.003 mol of the compound, with $AgNO_3$ (0.003 mol) solution in 0.5 mL of 70% aqueous methanol. After 2 min, 2.5 mL of DPPH• in methanol (0.1 mM) was added to the mixture, and the volume was always made up to 3.7 mL with methanol. The activity of tested samples was compared to the activity of samples that contained a proper amount of methanol instead of $AgNO_3$ solution. For each sample, the absorbance was measured at 517 nm directly after mixing. The measurements were repeated three times. Free radical scavenging activity was calculated according to eq 1.

**Statistical Analysis.** All of the experiments were performed in triplicate, and the data are presented as mean values (±standard deviation values are given in the Supporting Information).

## RESULTS AND DISCUSSION

In the attempt to develop a pharmacophore model of monoterpene chain-breaking antioxidant, the experiments aimed at identification of structural elements responsible for free radical scavenging activity. The literature broadly covers the problem of polyphenols' structure−activity relationships; however, in the case of monoterpenes such data are scarce, and no evidence has been delivered at to which part of the molecule is responsible for direct antioxidant activity or for its enhancement. Twenty compounds (17 monoterpnes, 1 sesquiterpene, 1 monoterpenic phenol, and 1 phenyl propanoid) commonly present in essential oils were used in the study.

The loss of DPPH• absorbance was read in the presence of an excess of the analyzed compounds. The DPPH•/analyte molar ratio was kept constant for all of the analyzed compounds. Keeping this ratio constant was crucial to give the possibility to properly compare the activity of individual analytes (the amount of moles of all the studied terpenoids, which reacted with DPPH•, was equal). In the literature equal


dx.doi.org/10.1021/jf502857s | J. Agric. Food Chem. 2014, 62, 9088−9094

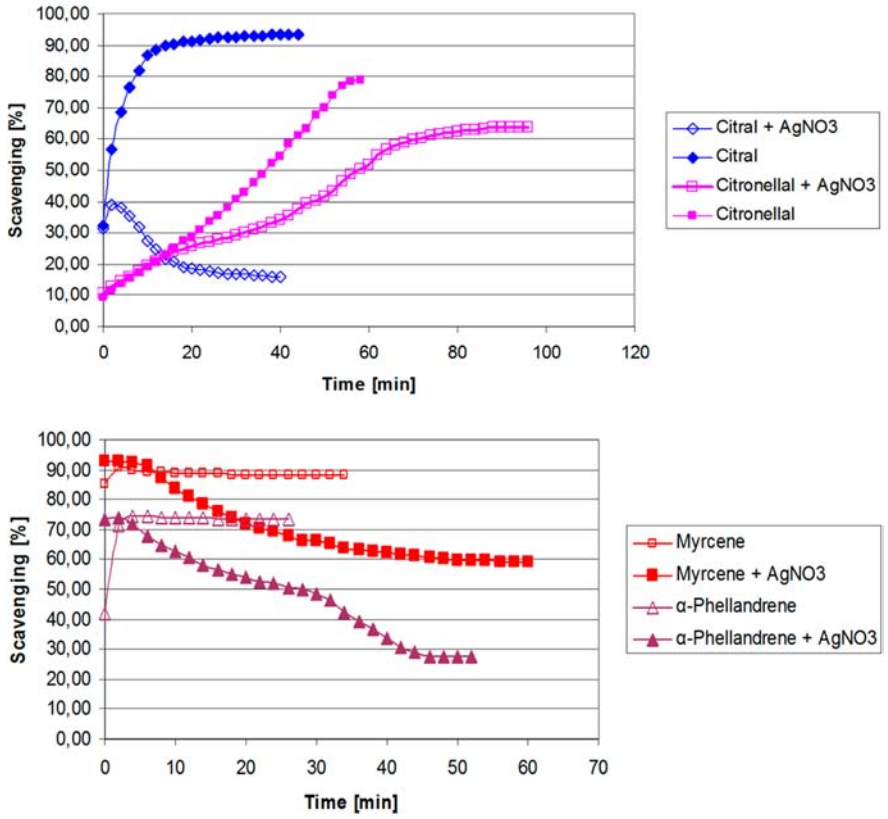


**Figure 2.** Influence of silver nitrate addition on free radical scavenging activity of selected monoterpenes. For experimental details, please refer to Materials and Methods.

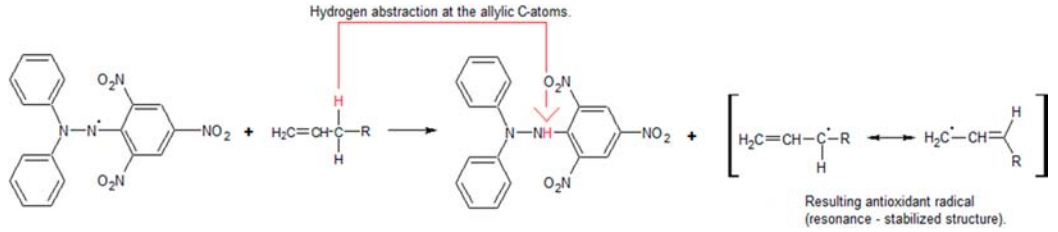


**Figure 3.** Proposed reaction mechanism between DPPH• and monoterpenes possessing conjugated double bonds.

volumes of liquid terpenes are usually added to DPPH• without taking into account that these volumes refer to different amounts of moles.

The radical scavenging activity of terpenoids was expressed as the percentage quenching of DPPH• radical.[8] The absorbance was read every 2 min from the beginning of the reaction until a plateau was reached. In the literature the activity of individual compounds is compared, for example, after 5 or 30 min.[8,12−15] However, the reaction of each free radical scavenger with DPPH• may be different, even among the compounds characterized with potent free radical scavenging activity, as can be seen for several terpenoids in Figure 1. The following terpenes have been found inactive or of weak activity in methanol (insoluble hydrocarbons are not taken into consideration): α-pinene, *p*-cymene, eucalyptol, menthol, and terpinene-4-ol (see Figure 1b). Another group of compounds has been found to scavenge DPPH• radical very quickly, reaching plateau values after several minutes: citral, carvone, myrcene, γ-terpinene, and pulegone. α-Terpinene and α-phellandrene, although found active in methanol, exerted lower scavenging activity when compared to the aforementioned five very active monoterpenes (see Figure 1a).

All of the analyzed compounds that were found to scavenge DPPH• free radical possessed a double bond in their molecule. Terpenes with conjugated double bonds quickly scavenged DPPH• radical, reaching plateau values within minutes, as seen in Figure 1a. To check the influence of blocking π bonds on monoterpenes' free radical scavenging activity, another test was performed. The π bonds were blocked with the use of silver ions as the Ag(I)−diene complexes are easily formed.[31] As can be seen in Figure 2, addition of silver nitrate leads to the decrease of chain-breaking antioxidant activity of terpenes. The decrease is more significant for terpenoids possessing conjugated double bonds (citral, myrcene, α-phellandrene) than for those without conjugation of double bonds, for example, citronellal. It can be concluded that π bonds are responsible for the chain-breaking antioxidant activity of terpenes. It has been proved, for the first time, that blocking conjugated double bonds leads to inhibition of the chain-breaking antioxidant activity of terpenes, which proves


dx.doi.org/10.1021/jf502857s | J. Agric. Food Chem. 2014, 62, 9088−9094

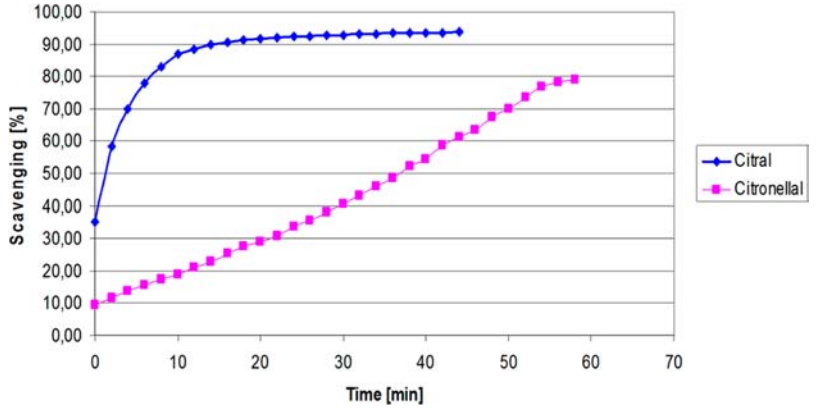


**Figure 4.** Comparison of free radical scavenging activity of two monoterpenes with very similar structures (citral, with conjugated double bonds; and citronellal, without conjugated double bonds) toward DPPH• in methanol.

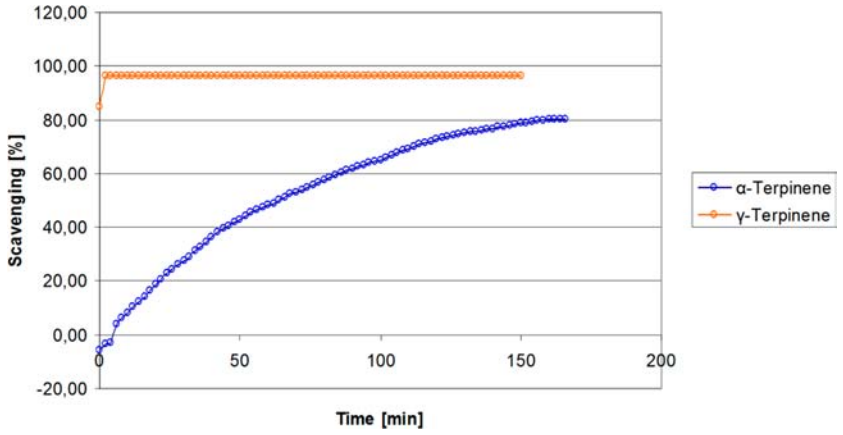


**Figure 5.** Comparison of free radical scavenging activity of $\alpha$- and $\gamma$-terpinene toward DPPH• in methanol.

conjugated $\pi$ bonds are essential for the free radical scavenging activity of monoterpenes.

To explain the influence of conjugated double bonds on terpenes' chain-breaking antioxidant activity, the possible reaction mechanism with DPPH• is proposed, as seen in Figure 3. Terpenes may lose allylic hydrogen atoms (C−H allylic bond dissociation energy = 364 kJ/mol, compared to those of alkylic C−H bonds = 410 kJ/mol and vinylic C−H bonds = 452 kJ/mol) and neutralize a radical, as also postulated by Öztürk.[28] In the presence of free radical scavenger DPPH• is reduced to hydrazine, and resulting antioxidant radical is formed. The resulting antioxidant radical may either propagate or terminate radical chain reaction. To be an effective direct antioxidant, a new radical, formed in the reaction with DPPH•, should not propagate the chain reaction. The resulting antioxidant radical should be unreactive to terminate radical chain reaction quickly. The reaction of DPPH• with conjugated double-bond terpenes results in the formation of resonance-stabilized structure. The stabilization is associated with the charge delocalization over the whole molecule, possibly due to the presence of conjugation of $\pi$ bonds (Figure 3).

The following terpenes have been characterized with potent chain-breaking antioxidant activity, as they quickly terminated radical chain reaction in methanol (Figure 1a): citral, pulegone, $\gamma$-terpinene, carvone, and myrcene. The influence of conjugated double bonds on terpene's activity can be easily noted when two monoterpenes, with very similar structures, are compared, for example, citral and citronellal (Figure 4). The only difference between these two structures is the presence of a conjugated double bond (additional $\pi$ bond) in citral. However, this small difference leads to a substantial change of citral chain-breaking antioxidant activity in comparison to the activity of citronellal.

Quite surprising were the results obtained for terpinenes: $\alpha$-terpinene, possessing conjugated $\pi$ bonds in its structure, was a less potent free radical scavenger than $\gamma$-terpinene (Figure 5). In the literature $\gamma$-terpinene has been defined as a very effective antioxidant with the possibility to easily lose allylic hydrogen atoms in the 3- and 6-positions (1,4-cyclohexadiene derivative).[28] In the case of $\alpha$-terpinene (1,3-cyclohexadiene derivative) allylic H atoms are at the 5- and 6-positions. Therefore, it may be postulated that in case of cyclic monoterpenes, containing double bonds, the 1,4-cyclohexadiene moiety enhances their free radical scavenging activity. The spare electron of the resulting antioxidant is better delocalized over the whole molecule when double bonds are between the C1−C2 and C4−C5 atoms. This effect can be compared to a similar good resonance stabilization of radicals formed in the reaction between DPPH• and hydroquinone (benzene-1,4-diol) derivatives.[6] Further studies with the use of terpenes containing 1,4-cyclohexadiene moiety (of natural and synthetic origin) can be performed to provide additional proof. Generally, terpenes, which quickly lead to stable (plateau) radical scavenging activity values, can be considered as good free radical scavengers, as they terminate radical chain reaction. Those that form non-resonance-stabilized radicals, in the


dx.doi.org/10.1021/jf502857s | J. Agric. Food Chem. 2014, 62, 9088−9094

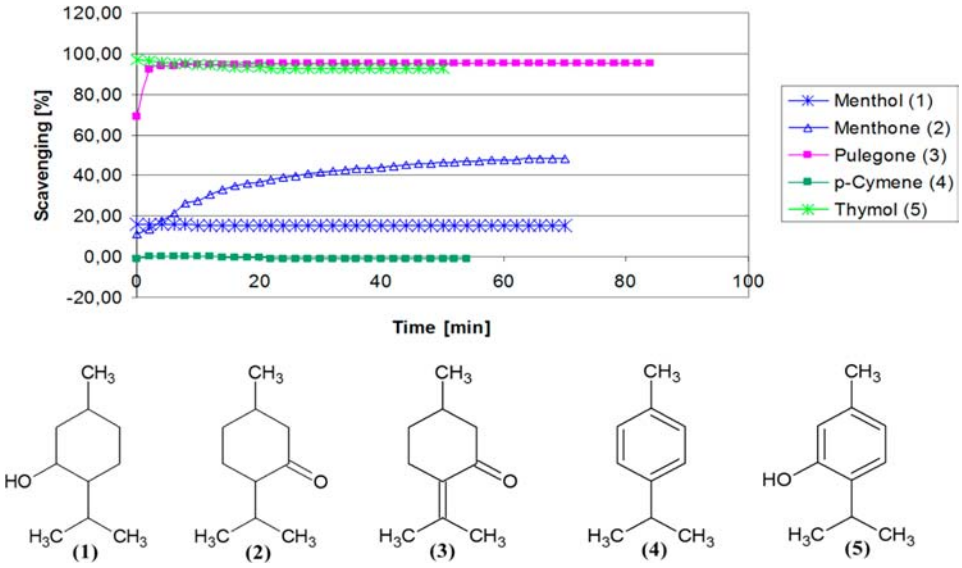


**Figure 6.** Comparison of free radical scavenging activity of selected monoterpenes and thymol, as influenced by their structures.

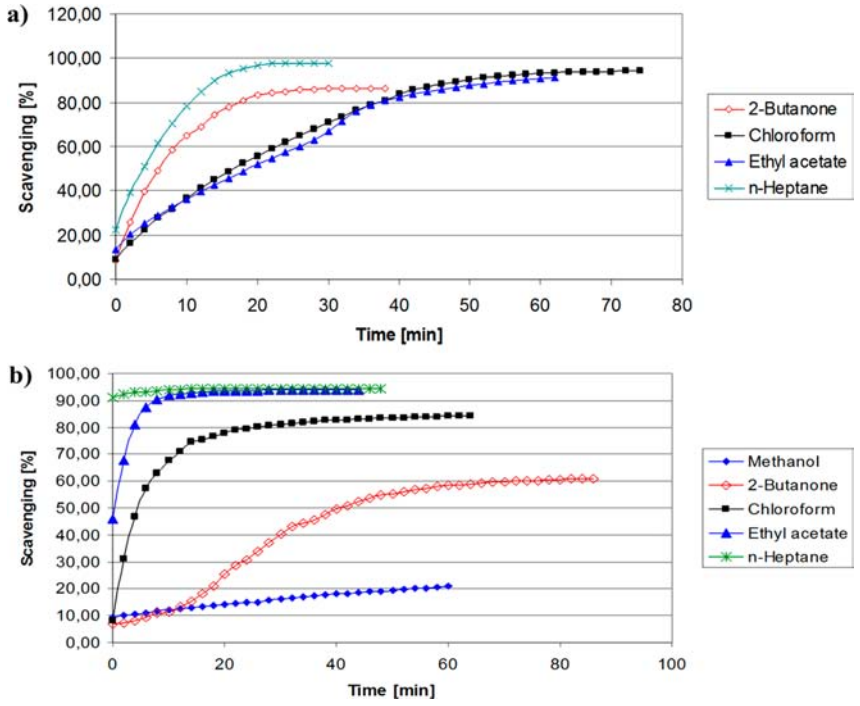


**Figure 7.** Influence of solvent type, used in the DPPH• assay, on free radical scavenging activity of two exemplary monoterpenes: (a) ocimene and (b) $\alpha$-pinene.

reaction with DPPH•, for example, citronellal (a molecule without $\pi$ bond conjugation), may propagate radical reactions and may not be regarded as efficient free radical scavengers.

To grasp the idea of how the molecular structure influences direct antioxidant activity of common terpenes, the activities of selected terpenes and thymol have been compared (Figure 6). Monoterpenes without a $\pi$ bond, for example, menthol, do not exert free radical scavenging activity in the DPPH• assay. When one double bond appears in the molecule, DPPH• scavenging ability increases, as, for example, for menthone. Compounds with two double bonds, as already explained, quickly terminate radical chain reaction and can be considered as potent free radical scavengers, for example, pulegone. Direct antioxidant activity disappears when a diene molecule is replaced by an aromatic ring, as was observed for *p*-cymene. A molecule regains its activity when a hydroxyl group appears, as, for example, in thymol.

In the last part of the experiment, the activity of the analyzed compounds was investigated in a set of five solvents, representing a continuous scale of polarity: *n*-heptane, chloroform, ethyl acetate, 2-butanone, and methanol (Figure 7). The first stimulus to measure the activity of compounds in the above-mentioned solvents was due to terpenes' solubility problems in DPPH• methanolic solution. The other one was related to the fact that the reaction environment, for example, the polarity of solvent, was found to influence the antioxidant activity of fragrance phenols.[13] Less polar terpenes, for example, myrcene, $\alpha$-pinene, farnesene, and ocimene, were characterized


dx.doi.org/10.1021/jf502857s | J. Agric. Food Chem. 2014, 62, 9088−9094

with better antioxidant activity in nonpolar solvents than in polar ones, which is the opposite of the results obtained for monoterpenic phenols. Hydrogen bond accepting solvents (HBA) (ketones, esters, ethers) formed hydrogen bonds with phenols' hydroxyl groups, making them less accessible to DPPH$^{\bullet}$. For terpenes, another mechanism may be suspected, as hydrogen abstraction from phenols is due to the presence of hydroxyl groups, which may form hydrogen bonds with HBA solvents. As the free radical scavenging activity of terpenes is due to $\pi$ bonds, therefore HBA solvents will not decrease the activity of terpenes as substantially as in the case of phenols. The results presented in Figure 7 clearly show that the free radical scavenging activity of terpenes depends on the solvent type used in the study. It is well seen with the example of $\alpha$-pinene, which quickly reaches scavenging activity plateau values in *n*-heptane, although $\alpha$-pinene possesses only one $\pi$ bond. This compound is a representative of bicyclic monoterpenes. Further studies are required to study the aforementioned phenomenon. It may be concluded that compounds exerting potent free radical scavenging activity in nonpolar solvents may act as efficient antioxidants in lipophilic end-use products, whereas those active in a polar environment may be efficient in scavenging free radicals in polar end-use products' media.

The presented results should stimulate additional research in the field of terpenoid antioxidants. Further studies may consider the influence of different substituents on the exerted activity, for example, for chemically modified structures. As interesting results have been obtained for $\alpha$-pinene, in nonpolar solvents, the analysis of a broader group of bicyclic monoterpenes may provide interesting data. In nature, individual terpenes are found in complex mixtures; therefore, synergistic and antagonistic interactions should be considered. Structure−activity relationships for terpenes may also be checked with other antioxidant tests, for example, ABTS$^{\bullet+}$, $\beta$-carotene assays, and other methods measuring antioxidant activity.

## ■ ASSOCIATED CONTENT

### Ⓢ Supporting Information

Tables presenting scavenging activity results obtained for all of the analyzed compounds in five different solvents. This material is available free of charge via the Internet at http://pubs.acs.org.

## ■ AUTHOR INFORMATION


### Corresponding Author

*(L.M.C.) Phone: +48 81756 4837. Fax: +48 81535 7378. E-mail: lukecarpenter@poczta.onet.pl.



### Funding

This work was supported by the TEAM research subsidy from the Foundation for Polish Science.


### Notes

The authors declare no competing financial interest.

## ■ REFERENCES


(1) Peñuelas, J.; Munné-Bosch, S. Isoprenoids: an evolutionary pool for photoprotection. *Trends Plant Sci.* **2005**, *10*, 166−169.

(2) Peñuelas, J.; Llusiá, J.; Asensio, D.; Munné-Bosch, S. Linking isoprene with plant thermotolerance, antioxidants and monoterpene emissions. *Plant Cell Environ.* **2005**, *28*, 278−286.

(3) Perwez Hussain, S.; Hofseth, L. J.; Harris, C. C. Radical causes of cancer. *Nat. Rev. Cancer* **2003**, *3*, 276−285.

(4) Uttara, B.; Singh, A. V.; Zamboni, P.; Mahajan, R. T. Oxidative stress and neurodegenerative diseases: a review of upstream and downstream antioxidant therapeutic options. *Curr. Neuropharmacol.* **2009**, *7*, 65−74.

(5) Graßmann, J. Terpenoids as plant antioxidants. *Vitam. Horm.* **2005**, *72*, 505−535.

(6) Kancheva, V. D. Phenolic antioxidants − radical-scavenging and chain-breaking activity: a comparative study. *Eur. J. Lipid Sci.* **2009**, *111*, 1072−1089.

(7) Rice-Evans, C. A.; Miller, N. J.; Paganga, G. Structure-antioxidant activity relationships of flavonoids and phenolic acids. *Free Radical Biol. Med.* **1996**, *20*, 933−956.

(8) Burda, S.; Oleszek, W. Antioxidant and antiradical activities of flavonoids. *J. Agric. Food Chem.* **2001**, *49*, 2774−2779.

(9) Ordoudi, S. A.; Tsimidou, M. Z.; Vafiadis, A. P.; Bakalbassis, E. G. Structure-DPPH$^{\cdot}$ scavenging activity relationships: parallel study of catechol and guaiacol acid derivatives. *J. Agric. Food Chem.* **2006**, *54*, 5763−5768.

(10) Ciesla, L.; Kowalska, I.; Oleszek, W.; Stochmal, A. Free radical scavenging activities of polyphenolic compounds isolated from *Medicago sativa* and *Medicago truncatula* assessed by means of thin-layer chromatography DPPH$^{\bullet}$ rapid test. *Phytochem. Anal.* **2013**, *24*, 47−52.

(11) Kowalska, I.; Jedrejek, D.; Ciesla, L.; Pecio, L.; Masullo, M.; Piacente, S.; Oleszek, W.; Stochmal, A. Isolation, chemical and free radical scavenging characterization of phenolics from *Trifolium scabrum* L. aerial parts. *J. Agric. Food Chem.* **2013**, *61*, 4417−4423.

(12) Mishra, K.; Ojha, H.; Chaudhury, N. K. Estimation of antiradical properties of antioxidants using DPPH$^{\bullet}$ assay: a critical review and results. *Food Chem.* **2012**, *130*, 1036−1043.

(13) Marteau, C.; Nardello-Rataj, V.; Favier, D.; Aubry, J.-M. Dual role of phenols as fragrances and antioxidants: mechanism, kinetics and drastic solvent effect. *Flavour Fragrance J.* **2013**, *28*, 30−38.

(14) Kedare, S. B.; Singh, R. P. Genesis and development of DPPH method of antioxidant assay. *J. Food Sci. Technol.* **2011**, *48*, 412−422.

(15) Sharma, O. P.; Bhat, T. K. DPPH antioxidant assay revisited. *Food Chem.* **2009**, *113*, 1202−1205.

(16) Foti, M.; Ruberto, G. Kinetic solvent effects on phenolic antioxidants determined by spectrophotometric measurements. *J. Agric. Food Chem.* **2001**, *49*, 342−348.

(17) Foti, M. C.; Daquino, C.; Mackie, I. D.; DiLabio, G. A.; Ingold, K. U. Reaction of phenols with the 2,2-diphenyl-1-picrylhyrazyl radical. Kinetics and DFT calculations applied to determine ArO-H bond dissociation enthalpies and reaction mechanism. *J. Org. Chem.* **2008**, *73*, 9270−9282.

(18) Bertalanič, L.; Košmerl, T.; Poklar Ulrih, N.; Cigić, B. Influence of solvent composition on antioxidant potential of model polyphenols and red wines determined with 2,2-diphenyl-1-picrylhydrazyl. *J. Agric. Food Chem.* **2012**, *60*, 12282−12288.

(19) Bietti, M.; Salamone, M.; DiLabio, G. A.; Jockusch, S.; Turro, N. J. Kinetic solvent effects on hydrogen abstraction from phenol by the cymyloxyl radical. Toward an understanding of the role of protic solvents. *J. Org. Chem.* **2012**, *77*, 1267−1272.

(20) Prevc, T.; Šegatin, N.; Poklar Ulrih, N.; Cigić, B. DPPH assay of vegetable oils and model antioxidants in protic and aprotic solvents. *Talanta* **2013**, *109*, 13−19.

(21) Litwinienko, G.; Ingold, K. U. Solvent effects on the rates and mechanism of reaction of phenols with free radicals. *Acc. Chem. Res.* **2007**, *40*, 222−230.

(22) Dawidowicz, A. L.; Olszowy, M. Mechanism change in estimating of antioxidant activity of phenolic compounds. *Talanta* **2012**, *97*, 312−317.

(23) Ciesla, L.; Kryszen, J.; Stochmal, A.; Oleszek, W.; Waksmundzka-Hajnos, M. Approach to develop a standardized TLC-DPPH$^{\bullet}$ test for assessing free radical scavenging properties of selected phenolic compounds. *J. Pharm. Biomed. Anal.* **2012**, *70*, 126−135.

(24) González-Burgos, E.; Gómez-Serranillos, M. P. Terpene compounds in nature: a review of their potential antioxidant activity. *Curr. Med. Chem.* **2012**, *19*, 5319−5341.

(25) Ciesla, L. Thin-layer chromatography with biodetection for the search of new potential drugs to treat neurodegenerative diseases − state of the art and future perspectives. *Med. Chem.* **2012**, *8*, 102−111.
(26) Ciesla, L.; Kryszen, J.; Stochmal, A.; Oleszek, W.; Waksmundzka-Hajnos, M. Low-temperature thin-layer chromatography preliminary bioautographic tests for detection of free radical scavengers and acetylcholinesterase inhibitors in volatile samples. *J. Planar Chromatogr. − Modern TLC* **2012**, *25*, 225−231.
(27) Choi, H.-S.; Song, H. S.; Ukeda, H.; Sawamura, M. Radical-scavenging activities of citrus essential oils and their components: detection using 1,1-diphenyl-2-picrylhydrazyl. *J. Agric. Food Chem.* **2000**, *48*, 4156−4161.
(28) Öztürk, M. Anticholinesterase and antioxidant activities of Savoury (*Satureja thymbra* L.) with identified major terpenes of the essential oil. *Food Chem.* **2012**, *134*, 48−54.
(29) Kivrak, I.; Duru, M. E.; Öztürk, M.; Mercan, N.; Harmandar, M.; Topçu, G. Antioxidant, anticholinesterase and antimicrobial constituents from the essential oil and ethanol extract of *Salvia potentillifolia*. *Food Chem.* **2009**, *116*, 470−479.
(30) Foti, M. C.; Ingold, K. U. Mechanism of inhibition of lipid peroxidation by γ-terpinene, an unusual and potentially useful hydrocarbon antioxidant. *J. Agric. Food Chem.* **2003**, *51*, 2758−2765.
(31) Bera, M.; Roy, S. Silver(I)-diene complexes as versatile catalysts for the C-arylation of *N*-tosylaziridines: mechanistic insight from in situ diagnostics. *J. Org. Chem.* **2010**, *13*, 4402−4412.

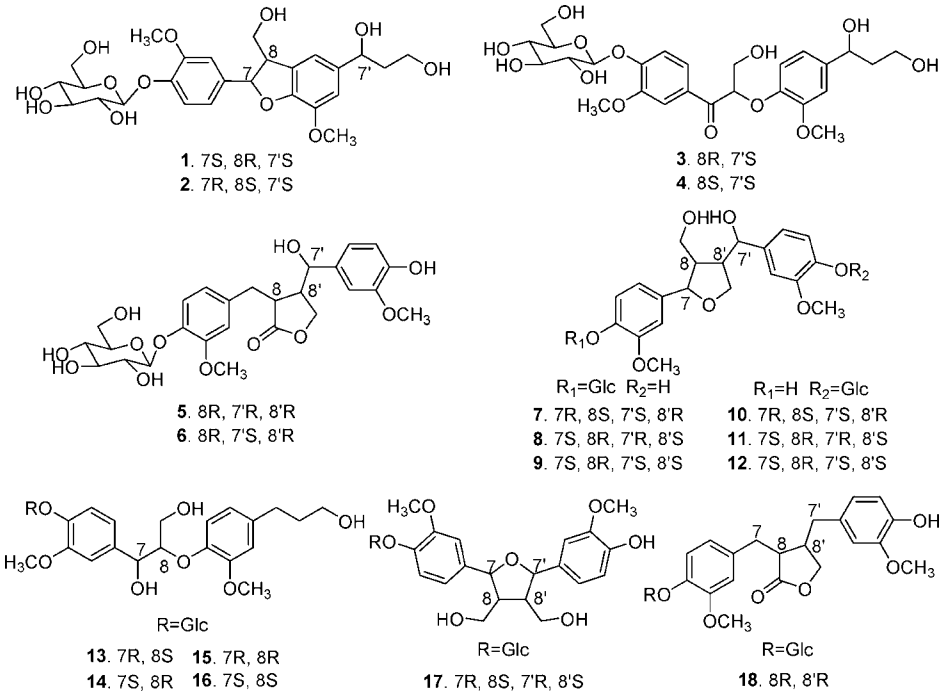


**Figure 1.** Structures of compounds **1**−**18**.

**Table 1. $^1$H NMR Data (500 MHz, DMSO-$d_6$) for Compounds 1−6**

| position | 1 | 2 | 3 | 4 | 5 | 6 |
|---|---|---|---|---|---|---|
| 2 | 6.96 d (2.0) | 6.96 d (2.0) | 7.57 d (2.0) | 7.56 d (2.0) | 6.65 d (2.0) | 6.65 d (2.0) |
| 5 | 7.06 d (8.5) | 7.06 d (8.5) | 7.18 d (8.5) | 7.18 d (8.5) | 6.96 d (8.5) | 6.92 d (8.0) |
| 6 | 6.84 dd (8.5, 2.0) | 6.84 dd (8.5, 2.0) | 7.75 dd (8.5, 2.0) | 7.75 dd (8.5, 2.0) | 6.57 dd (8.5, 2.0) | 6.53 dd (8.0, 2.0) |
| 7 | 5.49 d (6.5) | 5.49 d (6.5) | | | 2.70 dd (13.5, 6.5) | 2.86 overlap |
| | | | | | 2.49 overlap | 2.49 dd (15.5, 7.5) |
| 8 | 3.42 m | 3.43 m | 5.58 t (5.0) | 5.59 t (5.0) | 2.84 dt (8.5, 6.0) | 2.86 overlap |
| 9 | 3.73 m | 3.72 m | 3.88 m | 3.88 m | | |
| | 3.63 m | 3.61 m | | | | |
| 2′ | 6.83 d (2.0) | 6.82 brs | 6.92 brs | 6.92 brs | 6.78 d (2.0) | 6.81 d (2.0) |
| 5′ | | | 6.68 overlap | 6.69 overlap | 6.72 d (8.5) | 6.72 d (8.0) |
| 6′ | 6.81 d (2.0) | 6.82 brs | 6.68 overlap | 6.69 overlap | 6.66 dd (8.5, 2.0) | 6.69 dd (8.0, 2.0) |
| 7′ | 4.57 m | 4.57 m | 4.53 t (5.0) | 4.53 t (5.0) | 4.34 t (5.0) | 4.55 t (5.0) |
| 8′ | 1.75 m | 1.75 m | 1.71 m | 1.71 m | 2.46 m | 2.49 overlap |
| | 1.68 m | 1.68 m | 1.64 m | 1.64 m | | |
| 9′ | 3.48 m | 3.48 m | 3.46 m | 3.46 m | 4.01 t (8.5) | 3.94 m |
| | 3.44 m | 3.44 m | 3.39 m | 3.39 m | 4.13 t (8.5) | |
| 1″ | 4.88 d (7.5) | 4.88 d (7.5) | 5.08 d (7.5) | 5.08 d (7.5) | 4.83 d (7.5) | 4.83 d (7.5) |
| 2″ | 3.24 m | 3.24 m | 3.28 m | 3.28 m | 3.24 m | 3.24 m |
| 3″ | 3.28 m | 3.28 m | 3.39 m | 3.39 m | 3.26 m | 3.26 m |
| 4″ | 3.15 m | 3.15 m | 3.17 m | 3.17 m | 3.15 m | 3.15 m |
| 5″ | 3.26 m | 3.26 m | 3.28 m | 3.28 m | 3.28 m | 3.28 m |
| 6″ | 3.65 m | 3.65 m | 3.67 m | 3.67 m | 3.66 brd (11.5) | 3.66 brd (11.5) |
| | 3.42 m | 3.42 m | 3.46 m | 3.46 m | 3.45 dt (11.5, 6.0) | 3.45 dt (11.5, 6.0) |
| 3-$CH_3O$ | 3.75 s | 3.75 s | 3.81 s | 3.81 s | 3.71 s | 3.70 s |
| 3′-$CH_3O$ | 3.78 s | 3.78 s | 3.74 s | 3.73 s | 3.73 s | 3.73 s |

raphy was performed on a macroporous adsorption resin (HP-20) column (10 L). After eluting with $H_2O$ (20 L), the adsorbed constituents were eluted with 15% ethanol (20 L), 30% ethanol (20 L), 50% ethanol (20 L), 70% ethanol (20 L), and 95% ethanol (10 L). The 30% ethanol part (86.4 g) was subjected to flash chromatography elution with $H_2O$−MeOH (from 100:0 to 0:100) in gradient to yield 13 fractions (fractions A−M).

Fraction D was further chromatographed over Sephadex LH-20 and eluted with MeOH−$H_2O$ (from 0:100 to 100:0) to give 12 fractions (fractions D-1−12). Fractions D-5 and D-6 were obtained with the mobile phase of MeOH−$H_2O$ (0:100), and fraction D-8 was obtained with the mobile phase of MeOH−$H_2O$ (10:90). Fraction D-5 was purified using reversed-phase preparative HPLC with MeOH−$H_2O$ (25:75) as the mobile phase at a flow rate of 5 mL/min to give **17** (22 mg, 55 min). Fraction D-6 was purified using reversed-phase preparative HPLC with MeOH−$H_2O$ (25:75) as the mobile phase at a flow rate of 5 mL/min to give **7** (16 mg, 48 min) and **8** (19 mg, 44 min). Using the same method as that used for fraction D-6, **1** (24 mg,


dx.doi.org/10.1021/jf501859x | J. Agric. Food Chem. 2014, 62, 9095−9102

Table 2. $^{13}$C NMR Data (125 MHz, DMSO-$d_6$) for Compounds 1−12

| position | 1 | 2 | 3 | 4 | 5 | 6 | 7 | 8 | 9 | 10 | 11 | 12 |
|---|---|---|---|---|---|---|---|---|---|---|---|---|
| 1 | 135.5 | 135.5 | 129.0 | 129.0 | 131.6 | 131.5 | 133.5 | 133.4 | 133.8 | 136.5 | 136.6 | 136.8 |
| 2 | 110.4 | 110.5 | 111.7 | 111.6 | 113.9 | 114.1 | 110.6 | 110.6 | 110.9 | 110.8 | 110.8 | 110.6 |
| 3 | 149.0 | 149.0 | 148.7 | 148.7 | 148.6 | 148.5 | 147.4 | 147.4 | 147.4 | 148.8 | 148.8 | 148.7 |
| 4 | 146.2 | 146.2 | 151.1 | 151.1 | 145.3 | 145.3 | 145.8 | 145.8 | 145.6 | 145.7 | 145.7 | 145.6 |
| 5 | 115.4 | 115.4 | 114.2 | 114.3 | 115.1 | 115.0 | 115.1 | 115.1 | 115.1 | 115.0 | 115.1 | 115.0 |
| 6 | 117.9 | 118.0 | 122.9 | 122.9 | 121.4 | 121.5 | 118.9 | 119.0 | 118.9 | 118.4 | 118.4 | 118.2 |
| 7 | 86.7 | 86.7 | 195.5 | 195.5 | 33.7 | 34.2 | 83.4 | 83.4 | 82.8 | 83.3 | 83.3 | 82.7 |
| 8 | 53.6 | 53.6 | 81.7 | 81.6 | 45.9 | 45.0 | 53.9 | 54.0 | 51.9 | 54.1 | 54.1 | 52.1 |
| 9 | 63.2 | 63.2 | 62.6 | 62.6 | 178.7 | 178.8 | 61.6 | 61.6 | 60.4 | 61.8 | 61.8 | 60.6 |
| 1′ | 140.0 | 139.9 | 140.1 | 140.2 | 134.5 | 134.1 | 138.4 | 138.3 | 138.3 | 135.6 | 135.6 | 135.5 |
| 2′ | 114.2 | 114.2 | 110.3 | 110.4 | 110.1 | 110.2 | 111.1 | 111.0 | 110.4 | 110.8 | 110.8 | 110.7 |
| 3′ | 143.3 | 143.3 | 148.9 | 148.9 | 147.5 | 147.4 | 148.7 | 148.7 | 148.7 | 147.4 | 147.4 | 147.3 |
| 4′ | 146.2 | 146.2 | 145.6 | 145.6 | 145.7 | 145.7 | 145.8 | 145.8 | 145.8 | 145.7 | 145.7 | 145.5 |
| 5′ | 128.5 | 128.6 | 114.1 | 114.2 | 115.1 | 115.0 | 114.9 | 114.7 | 114.7 | 114.9 | 114.9 | 115.1 |
| 6′ | 110.1 | 110.2 | 117.6 | 117.5 | 118.3 | 118.4 | 119.4 | 119.0 | 118.7 | 119.2 | 119.2 | 119.1 |
| 7′ | 69.8 | 69.8 | 69.4 | 69.3 | 72.3 | 72.5 | 74.8 | 74.9 | 73.7 | 74.9 | 74.9 | 73.9 |
| 8′ | 42.7 | 42.6 | 42.4 | 42.4 | 42.7 | 42.4 | 50.6 | 50.6 | 49.3 | 50.7 | 50.7 | 49.4 |
| 9′ | 58.2 | 58.2 | 58.1 | 58.1 | 67.7 | 68.2 | 69.5 | 69.4 | 69.5 | 69.6 | 69.6 | 69.7 |
| 1″ | 100.1 | 100.2 | 99.4 | 99.4 | 100.2 | 100.2 | 100.7 | 100.2 | 100.2 | 100.2 | 100.2 | 100.2 |
| 2″ | 73.2 | 73.2 | 73.1 | 73.1 | 73.3 | 73.3 | 73.3 | 73.3 | 73.3 | 73.3 | 73.3 | 73.3 |
| 3″ | 77.0 | 77.1 | 77.2 | 77.2 | 77.0 | 77.0 | 77.1 | 77.0 | 77.0 | 77.1 | 77.1 | 77.1 |
| 4″ | 69.8 | 69.7 | 69.6 | 69.6 | 69.7 | 69.7 | 69.7 | 69.7 | 69.7 | 69.7 | 69.7 | 69.7 |
| 5″ | 76.9 | 76.9 | 76.9 | 76.9 | 76.9 | 76.9 | 76.9 | 76.9 | 76.9 | 76.9 | 76.9 | 76.9 |
| 6″ | 60.7 | 60.7 | 60.6 | 60.6 | 60.7 | 60.7 | 60.7 | 60.7 | 60.7 | 60.7 | 60.7 | 60.7 |
| 3-$CH_3O$ | 55.7 | 55.8 | 55.6 | 55.6 | 55.7 | 55.6 | 55.7 | 55.7 | 55.6 | 55.7 | 55.7 | 55.6 |
| 3′-$CH_3O$ | 55.8 | 55.8 | 55.6 | 55.6 | 55.7 | 55.6 | 55.8 | 55.7 | 55.7 | 55.7 | 55.7 | 55.7 |

42 min), **2** (27 mg, 46 min), and **3** (11 mg, 36 min) were isolated from fraction D-8.

Fraction F was subjected to flash chromatography elution with $H_2O$−MeOH (from 100:0 to 0:100) in gradient to yield 10 fractions (fractions F-1−10). Fraction F-3 was obtained with the mobile phase of MeOH−$H_2O$ (10:90), and was further purified using reversed-phase preparative HPLC with MeOH−$H_2O$ (27:73) as the mobile phase at a flow rate of 5 mL/min to give **4** (33 mg, 31 min) and **10** (20 mg, 47 min). Fraction F-5 was obtained with the mobile phase of MeOH−$H_2O$ (20:80), and was subjected to chromatography over Sephadex LH-20 with $H_2O$ as the mobile phase to give **9** (15 mg) and **13** (27 mg). Fractions F-6 and F-7 were obtained with the mobile phase of MeOH−$H_2O$ (30:70). Fraction F-6 was chromatographed over Sephadex LH-20 with $H_2O$ elution to give **15** (31 mg). Fraction F-7 was purified using reversed-phase preparative HPLC with MeOH−$H_2O$ (30:70) as the mobile phase at a flow rate of 5 mL/min to give **14** (19 mg, 55 min) and **16** (21 mg, 51 min).

Fraction H was subjected to flash chromatography elution with $H_2O$−MeOH in gradient to yield 12 fractions (fractions H-1−12). Fraction H-5 was obtained with the mobile phase of MeOH−$H_2O$ (20:80), and was further purified by reversed-phase preparative HPLC with MeOH−$H_2O$ (30:70) as the mobile phase at a flow rate of 5 mL/min to give **5** (18 mg, 33 min) and **11** (10 mg, 39 min). Fraction H-6 was obtained with the mobile phase of MeOH−$H_2O$ (30:70), and was purified using reversed-phase preparative HPLC with MeOH−$H_2O$ (30:70) as the mobile phase at a flow rate of 5 mL/min to give **6** (13 mg, 35 min) and **12** (14 mg, 37 min). Fraction K was chromatographed over Sephadex LH-20 with $H_2O$ elution to give **18** (106 mg). The structures of compounds **1**−**18** are shown in Figure 1.

*Spectral Data. (7S,8R,7′S)-Dihydrodehydrodiconiferyl Alcohol-7′-hydroxy-4-O-β-D-glucopyranoside (**1**).* White amorphous powder; soluble in water or methanol; $[\alpha]^{20}_D$ −32.8° (*c* 0.07, MeOH); CD (MeOH) $\lambda_{max}$ ($\Delta\varepsilon$) 292 (+0.53), 245 (+0.81), 226 (−1.59) nm; IR $\nu_{max}$ 3384, 2933, 1601, 1518, 1464, 1335, 1268, 1136, 1076, 859, 803 cm$^{-1}$; $^1$H NMR (DMSO-$d_6$, 500 MHz) data, see Table 1; $^{13}$C NMR (DMSO-$d_6$, 125 MHz) data, see Table 2; (+)-HRESIMS *m*/*z* 561.1954 (calcd for $C_{26}H_{34}O_{12}Na$, 561.1942).

*(7R,8S,7′S)-Dihydrodehydrodiconiferyl Alcohol-7′-hydroxy-4-O-β-D-glucopyranoside (**2**).* White amorphous powder; soluble in water or methanol; $[\alpha]^{20}_D$ −40.3° (*c* 0.07, MeOH); CD (MeOH) $\lambda_{max}$ ($\Delta\varepsilon$) 282 (−1.11), 243 (−1.79), 217 (+1.06) nm; IR $\nu_{max}$ 3423, 2928, 1601, 1516, 1464, 1334, 1266, 1139, 1076, 897, 805 cm$^{-1}$; $^1$H NMR (DMSO-$d_6$, 500 MHz) data, see Table 1; $^{13}$C NMR (DMSO-$d_6$, 125 MHz) data, see Table 2; (+)-HRESIMS *m*/*z* 561.1951 (calcd for $C_{26}H_{34}O_{12}Na$, 561.1942).

*(8R,7′S)-4,9,7′,9′-Tetrahydroxy-3,3′-dimethoxyl-7-oxo-8−4′-oxyneolignan-4-O-β-D-glucopyranoside (**3**).* White amorphous powder; soluble in water or methanol; $[\alpha]^{20}_D$ −31.4° (*c* 0.07, MeOH); CD (MeOH) $\lambda_{max}$ ($\Delta\varepsilon$) 331 (−0.95), 266 (+1.99), 231 (−1.53) nm; IR $\nu_{max}$ 3342, 2933, 1676, 1593, 1512, 1421, 1267, 1137, 1076, 889, 801 cm$^{-1}$; $^1$H NMR (DMSO-$d_6$, 500 MHz) data, see Table 1; $^{13}$C NMR (DMSO-$d_6$, 125 MHz) data, see Table 2; (+)-HRESIMS *m*/*z* 577.1900 (calcd for $C_{26}H_{34}O_{13}Na$, 577.1892).

*(8S,7′S)-4,9,7′,9′-Tetrahydroxy-3,3′-dimethoxyl-7-oxo-8−4′-oxyneolignan-4-O-β-D-glucopyranoside (**4**).* White amorphous powder; soluble in water or methanol; $[\alpha]^{20}_D$ −44.8° (*c* 0.07, MeOH); CD (MeOH) $\lambda_{max}$ ($\Delta\varepsilon$) 346 (+0.29), 299 (−1.26), 259 (−2.54) nm; IR $\nu_{max}$ 3331, 2926, 1677, 1593, 1512, 1420, 1267, 1137, 1076, 883, 800 cm$^{-1}$; $^1$H NMR (DMSO-$d_6$, 500 MHz) data, see Table 1; $^{13}$C NMR (DMSO-$d_6$, 125 MHz) data, see Table 2; (+)-HRESIMS *m*/*z* 577.1905 (calcd for $C_{26}H_{34}O_{13}Na$, 577.1892).

*(8R,7′R,8′R)-4,4′,7′-Trihydroxy-3,3′-dimethoxyl-9-oxo Dibenzylbutyrolactone Lignan-4-O-β-D-glucopyranoside (**5**).* White amorphous powder; soluble in water or methanol; $[\alpha]^{20}_D$ −26.7 (*c* 0.07, MeOH); CD (MeOH) $\lambda_{max}$ ($\Delta\varepsilon$) 278 (−0.83), 229 (−7.37) nm; IR $\nu_{max}$ 3386, 2916, 1757, 1601, 1514, 1453, 1423, 1385, 1269, 1227, 1157, 1076, 860, 821 cm$^{-1}$; $^1$H NMR (DMSO-$d_6$, 500 MHz) data, see Table 1; $^{13}$C NMR (DMSO-$d_6$, 125 MHz) data, see Table 2; (+)-HRESIMS *m*/*z* 559.1787 (calcd for $C_{26}H_{32}O_{12}Na$, 559.1786).

*(8R,7′S,8′R)-4,4′,7′-Trihydroxy-3,3′-dimethoxyl-9-oxo Dibenzylbutyrolactone Lignan-4-O-β-D-glucopyranoside (**6**).* White amorphous powder; soluble in water or methanol; $[\alpha]^{20}_D$ −33.9° (*c* 0.07, MeOH); CD (MeOH) $\lambda_{max}$ ($\Delta\varepsilon$) 307 (−1.09), 225 (−10.79) nm; IR $\nu_{max}$ 3369, 2922, 1755, 1599, 1514, 1453, 1423, 1388, 1269, 1227,


dx.doi.org/10.1021/jf501859x | J. Agric. Food Chem. 2014, 62, 9095−9102

Table 3. $^1$H NMR Data (500 MHz, DMSO-$d_6$) for Compounds 7−12

| position | 7 | 8 | 9 | 10 | 11 | 12 |
|---|---|---|---|---|---|---|
| 2 | 6.87 brs | 6.86 brs | 6.85 brs | 6.92 d (2.0) | 6.92 d (2.0) | 6.91 d (2.0) |
| 5 | 6.72 overlap | 6.72 overlap | 6.71 overlap | 7.03 d (8.5) | 7.02 d (8.5) | 7.03 d (8.0) |
| 6 | 6.72 overlap | 6.72 overlap | 6.71 overlap | 6.83 dd (8.5, 2.0) | 6.83 dd (8.5, 2.0) | 6.83 dd (8.0, 2.0) |
| 7 | 4.46 d (8.0) | 4.45 d (8.0) | 4.51 d (7.0) | 4.51 d (8.5) | 4.51 d (8.5) | 4.55 d (8.5) |
| 8 | 2.14 m | 2.13 m | 1.73 m | 2.14 m | 2.14 m | 1.73 m |
| 9 | 3.48 m | 3.45 m | 3.14 m | 3.47 m | 3.47 m | 3.14 m |
| | | | 3.07 m | | | 3.07 m |
| 2′ | 6.96 d (2.0) | 6.97 d (2.0) | 6.87 d (2.0) | 6.90 brs | 6.90 brs | 6.80 d (2.0) |
| 5′ | 7.03 d (8.0) | 7.02 d (8.5) | 6.98 d (8.5) | 6.72 overlap | 6.72 overlap | 6.67 d (8.0) |
| 6′ | 6.84 dd (8.0, 2.0) | 6.82 dd (8.5, 2.0) | 6.72 overlap | 6.72 overlap | 6.72 overlap | 6.61 dd (8.0, 2.0) |
| 7′ | 4.41 dd (8.5, 2.5) | 4.39 dd (8.5, 2.5) | 4.37 dd (7.5, 4.5) | 4.33 dd (9.0, 2.5) | 4.34 d (8.5) | 4.30 dd (8.5, 4.5) |
| 8′ | 2.45 m | 2.45 m | 2.38 m | 2.42 m | 2.42 m | 2.36 m |
| 9′ | 3.60 m | 3.59 m | 4.07 m | 3.60 m | 3.60 m | 4.07 m |
| | 3.49 m | 3.49 m | 3.72 m | 3.50 m | 3.50 m | 3.74 m |
| 1″ | 4.87 d (7.5) | 4.87 d (7.5) | 4.84 d (7.5) | 4.88 d (7.5) | 4.88 d (7.5) | 4.87 d (7.5) |
| 2″ | 3.25 m | 3.25 m | 3.26 m | 3.25 m | 3.24 m | 3.25 m |
| 3″ | 3.29 m | 3.28 m | 3.28 m | 3.29 m | 3.29 m | 3.29 m |
| 4″ | 3.16 m | 3.16 m | 3.15 m | 3.16 m | 3.15 m | 3.15 m |
| 5″ | 3.27 m | 3.27 m | 3.27 m | 3.28 m | 3.26 m | 3.27 m |
| 6″ | 3.67 m | 3.65 m | 3.66 m | 3.68 m | 3.68 m | 3.67 m |
| | 3.46 m | 3.44 m | 3.44 m | 3.45 m | 3.44 m | 3.44 m |
| 3-$CH_3O$ | 3.77 s | 3.77 s | 3.72 s | 3.76 s | 3.76 s | 3.72 s |
| 3′-$CH_3O$ | 3.76 s | 3.75 s | 3.75 s | 3.75 s | 3.75 s | 3.75 s |

1157, 1073, 857, 823 cm$^{-1}$; $^1$H NMR (DMSO-$d_6$, 500 MHz) data, see Table 1; $^{13}$C NMR (DMSO-$d_6$, 125 MHz) data, see Table 2; (+)-HRESIMS $m/z$ 559.1798 (calcd for $C_{26}H_{32}O_{12}Na$, 559.1786).

*(7R,8S,7′S,8′R)-4,9,4′,7′-Tetrahydroy-3,3′-dimethoxy-7,9′-epoxylignan-4′-O-β-D-glucopyranoside (7).* White amorphous powder; soluble in water or methanol; $[\alpha]_{20}^{D}$ −85.1° ($c$ 0.07, MeOH); CD (MeOH) $\lambda_{max}$ ($\Delta\varepsilon$) 277 (−1.84), 231 (−5.34) nm; IR $\nu_{max}$ 3344, 2926, 1602, 1514, 1462, 1388, 1269, 1159, 1073, 858, 814 cm$^{-1}$; $^1$H NMR (DMSO-$d_6$, 500 MHz) data, see Table 3; $^{13}$C NMR (DMSO-$d_6$, 125 MHz) data, see Table 2; (+)-HRESIMS $m/z$ 561.1945 (calcd for $C_{26}H_{34}O_{12}Na$, 561.1942).

*(7S,8R,7′R,8′S)-4,9,4′,7′-Tetrahydroy-3,3′-dimethoxy-7,9′-epoxylignan-4′-O-β-D-glucopyranoside (8).* White amorphous powder; soluble in water or methanol; $[\alpha]^{20}_{D}$ +74.6° ($c$ 0.06, MeOH); CD (MeOH) $\lambda_{max}$ ($\Delta\varepsilon$) 285 (+0.45), 235 (+2.26) nm; IR $\nu_{max}$ 3381, 2927, 1602, 1514, 1463, 1425, 1268, 1159, 1073, 859, 815 cm$^{-1}$; $^1$H NMR (DMSO-$d_6$, 500 MHz) data, see Table 3; $^{13}$C NMR (DMSO-$d_6$, 125 MHz) data, see Table 2; (+)-HRESIMS $m/z$ 561.1956 (calcd for $C_{26}H_{34}O_{12}Na$, 561.1942).

*(7S,8R,7′S,8′S)-4,9,4′,7′-Tetrahydroy-3,3′-dimethoxy-7,9′-epoxylignan-4′-O-β-D-glucopyranoside (9).* White amorphous powder; soluble in water or methanol; $[\alpha]^{20}_{D}$ +29.9° ($c$ 0.07, MeOH); CD (MeOH) $\lambda_{max}$ ($\Delta\varepsilon$) 281 (+0.88), 234 (+1.19) nm; IR $\nu_{max}$ 3374, 2937, 1601, 1514, 1463, 1424, 1268, 1157, 1076, 859, 821 cm$^{-1}$; $^1$H NMR (DMSO-$d_6$, 500 MHz) data, see Table 3; $^{13}$C NMR (DMSO-$d_6$, 125 MHz) data, see Table 2; (+)-HRESIMS $m/z$ 561.1946 (calcd for $C_{26}H_{34}O_{12}Na$, 561.1942).

*(7R,8S,7′S,8′R)-4,9,4′,7′-Tetrahydroy-3,3′-dimethoxy-7,9′-epoxylignan-4-O-β-D-glucopyranoside (10).* White amorphous powder; soluble in water or methanol; $[\alpha]^{20}_{D}$ −84.2° ($c$ 0.08, MeOH); CD (MeOH) $\lambda_{max}$ ($\Delta\varepsilon$) 278 (−1.17), 229 (−5.75) nm; IR $\nu_{max}$ 3372, 2888, 1601, 1514, 1463, 1427, 1268, 1159, 1076, 860, 818 cm$^{-1}$; $^1$H NMR (DMSO-$d_6$, 500 MHz) data, see Table 3; $^{13}$C NMR (DMSO-$d_6$, 125 MHz) data, see Table 2; (+)-HRESIMS $m/z$ 561.1948 (calcd for $C_{26}H_{34}O_{12}Na$, 561.1942).

*(7S,8R,7′R,8′S)-4,9,4′,7′-Tetrahydroy-3,3′-dimethoxy-7,9′-epoxylignan-4-O-β-D-glucopyranoside (11).* White amorphous powder; soluble in water or methanol; $[\alpha]^{20}_{D}$ +74.5° ($c$ 0.06, MeOH); CD (MeOH) $\lambda_{max}$ ($\Delta\varepsilon$) 291 (+1.14), 237 (+3.73) nm; IR $\nu_{max}$ 3370, 2925, 1601, 1514, 1462, 1427, 1269, 1159, 1074, 860, 817 cm$^{-1}$; $^1$H NMR (DMSO-$d_6$, 500 MHz) data, see Table 3; $^{13}$C NMR (DMSO-$d_6$, 125 MHz) data, see Table 2; (+)-HRESIMS $m/z$ 561.1954 (calcd for $C_{26}H_{34}O_{12}Na$, 561.1942).

*(7S,8R,7′S,8′S)-4,9,4′,7′-Tetrahydroy-3,3′-dimethoxy-7,9′-epoxylignan-4-O-β-D-glucopyranoside (12).* White amorphous powder; soluble in water or methanol; $[\alpha]^{20}_{D}$ +55.2° ($c$ 0.06, MeOH); CD (MeOH) $\lambda_{max}$ ($\Delta\varepsilon$) 281 (+0.61), 231 (+1.92) nm; IR $\nu_{max}$ 3372, 2933, 1601, 1514, 1463, 1426, 1269, 1157, 1076, 859, 820 cm$^{-1}$; $^1$H NMR (DMSO-$d_6$, 500 MHz) data, see Table 3; $^{13}$C NMR (DMSO-$d_6$, 125 MHz) data, see Table 2; (+)-HRESIMS $m/z$ 561.1952 (calcd for $C_{26}H_{34}O_{12}Na$, 561.1942).

*Enzymatic Hydrolysis of 1−12.* Compound **1** (6.0 mg) was dissolved in 0.1 M acetate buffer (3.0 mL). The reaction mixture was added to cellulase (9.0 mg, Sigma-Aldrich, St. Louis, MO) and left at 38 °C for 2 h. The solution was then transferred to a liquid−liquid extractor and extracted with $CHCl_3$. The aqueous fraction was subjected to silica gel thin layer chromatography (TLC) [$CHCl_3$−MeOH−$H_2O$ (7:3:1)] to show the presence of D-glucose ($R_f$ = 0.16). The organic layer was evaporated in vacuo and purified using reversed-phase preparative HPLC with MeOH−$H_2O$ (45:55) as the mobile phase to give **1a** (3 mg), which was identified using NMR. Hydrolysis of **2**−**12** and sugar identification were performed according to the procedure described for **1**.

*Hepatoprotective Effects on Cytotoxicity Induced by D-Galactosamine in HL-7702 Cells.* Compounds **1**−**18** were tested for hepatoprotective effects using an MTT assay in HL-7702 cells. Each cell suspension containing 1 × 10$^{-5}$ cells in 1 mL of Dulbecco's modified Eagle's medium containing fetal calf serum (10%), penicillin (100 units/mL), and streptomycin (100 μg/mL) was placed in a 96-well microplate and precultured for 24 h at 37 °C under a 5% $CO_2$ atmosphere. Fresh medium containing bicyclol and the test samples was added, and the cells were cultured for 1 h. The cultured cells were exposed to 25 mM D-galactosamine for 24 h. The medium was then replaced with fresh medium containing 0.5 mg/mL MTT. After incubation of 4 h, the medium was removed, and DMSO was added to dissolve formazan crystals. The optical density (OD) of the formazan solution was measured using a microplate reader at 492 nm.

Inhibition (%) was calculated using the following formula:

$$\text{inhibition (\%)} = [(OD_{sample} - OD_{control})/(OD_{normal} - OD_{control})] \times 100$$


dx.doi.org/10.1021/jf501859x | J. Agric. Food Chem. 2014, 62, 9095−9102

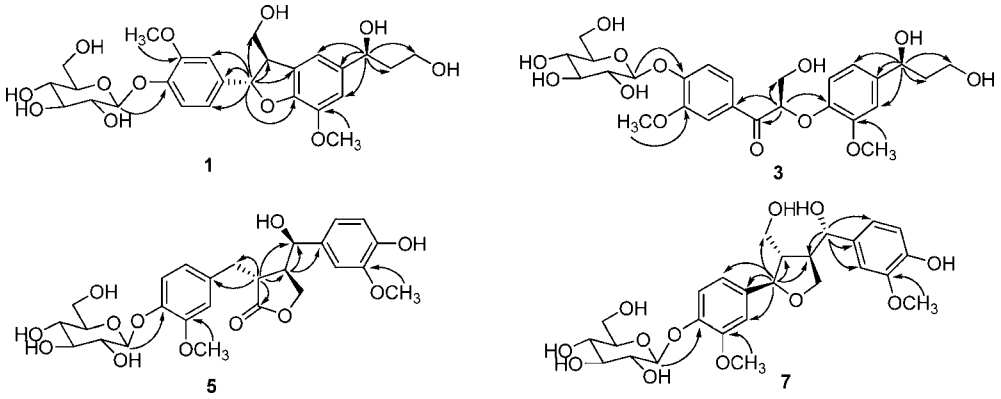


**Figure 2.** Key HMBC correlations of compounds **1**, **3**, **5**, and **7**.

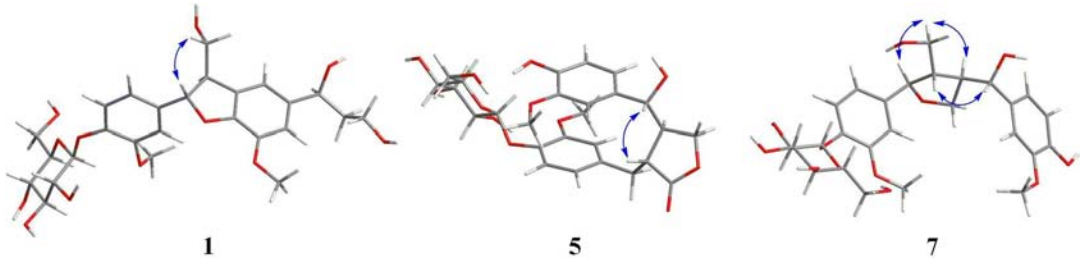


**Figure 3.** Key ROESY correlations of compounds **1**, **5**, and **7**.

## RESULTS AND DISCUSSION

A previous study has shown strong inhibitory effects of two tetrahydrofuranoid lignans, taxiresinol and (7′*R*)-7′-hydroxytaxiresinol, on the elevation of serum levels of tumor necrosis factor-alpha (TNF-$\alpha$) by D-galactosamine/LPS toxication.[10] Furthermore, these two lignans protected hepatocytes from cytotoxicity induced by D-galactosamine/TNF-$\alpha$ in primary cultured mouse hepatocytes. Therefore, in the present study, all isolated compounds were tested for hepatoprotective effects on D-galactosamine-induced cytotoxicity in HL-7702 hepatic cells. Compounds **1**, **2**, **7**−**12**, and **17** showed significantly stronger hepatoprotective activity than the positive control bicyclol at a concentration of $1 \times 10^{-5}$ M. Analysis of structure−activity relationships revealed that the tetrahydrofuran ring in lignan glucosides might contribute to the hepatoprotective activity.

**Structure Elucidation.** Compound **1** was obtained as a white powder, and its molecular formula was determined to be $C_{26}H_{34}O_{12}$ on the basis of HRESIMS findings at *m*/*z* 561.1954 $[M + Na]^+$. The $^1$H NMR spectrum of **1** (see Table 1) revealed an ABX system aromatic ring [$\delta$ 7.06 (1H, d, $J$ = 8.5 Hz), 6.96 (1H, d, $J$ = 2.0 Hz), 6.84 (1H, dd, $J$ = 8.5, 2.0 Hz)] and a 1,3,4,5-tetra-substituted aromatic ring [$\delta$ 6.83 (1H, d, $J$ = 2.0 Hz), 6.81 (1H, d, $J$ = 2.0 Hz)] in the downfield region. $^1$H NMR spectrum analysis revealed two methoxy groups at $\delta$ 3.78 (3H, s) and 3.75 (3H, s) and a glucopyranosyl anomeric proton at $\delta$ 4.88 (1H, d, $J$ = 7.5 Hz). Additionally, the $^1$H NMR spectrum revealed a methylene group at $\delta$ 1.75 (1H, m) and 1.68 (1H, m); two oxymethylene protons at $\delta$ 3.73 (1H, m), 3.63 (1H, m), 3.48 (1H, m), and 3.44 (1H, m); two oxymethine protons at $\delta$ 5.49 (1H, d, $J$ = 6.5 Hz) and 4.57 (1H, m); and a methine proton at $\delta$ 3.42 (1H, m).

The $^{13}$C NMR spectrum of **1** (see Table 2) showed 26 carbon signals, of which eight could be assigned to a glucose unit ($\delta$ 100.1, 77.0, 76.9, 73.2, 69.8, 60.7) and two methoxy groups ($\delta$ 55.8, 55.7), and the remaining 18 carbons could be assigned to a lignan skeleton.[11] In the heteronuclear multiple-bond correlation (HMBC) spectroscopy spectrum (see Figure 2), the correlation peaks of H-7 resonated at $\delta$ 5.49 with C-1, C-2, C-6, C-8, C-9, C-4′, and C-5′, and H-7′ resonated at $\delta$ 4.57 with C-1′, C-2′, C-6′, C-8′, and C-9′, which confirmed the benzofuran-type lignan of **1**. A detailed HMBC spectrum analysis revealed the positions of two methoxy groups located at C-3 and C-3′, respectively. Furthermore, the glucose unit was connected at C-4, according to the correlation from anomeric proton H-1″ resonated at $\delta$ 4.88 to C-4; **1** was hydrolyzed with cellulase to yield **1a** and D-glucose, which was identified by TLC analysis. The $\beta$ form of glucose was determined by the presence of an anomeric proton at $\delta$ 4.88 (1H, d, $J$ = 7.5 Hz, H-1″). On the basis of the above analysis, the planar structure of **1** was defined as dihydrodehydrodiconiferyl alcohol-7′-hydroxy-4-*O*-$\beta$-D-glucopyranoside.

The relative configuration of H-7 and H-8 in **1** was defined as *trans* from the characteristic correlation peak of H-7 with H-9 in the ROESY spectrum (see Figure 3). The positive Cotton effects at 245 and 292 nm in the CD spectrum revealed the 7*S*,8*R* configuration for **1**.[11] A positive Cotton effect at 346 nm in the $Rh_2(OCOCF_3)_4$-induced CD spectrum indicated the 7′*S* configuration for **1a**.[12] Thus, compound **1** was defined as (7*S*,8*R*,7′*S*)-dihydrodehydrodiconiferyl alcohol-7′-hydroxy-4-*O*-$\beta$-D-glucopyranoside.

Compound **2** had the same molecular formula as **1**, which was determined from HRESIMS at *m*/*z* 561.1951 $[M + Na]^+$. Its NMR data (Tables 1 and 3) were almost identical to those of compound **1**, which indicated that compound **2** had the same planar structure as **1**. The absolute configurations for C-7, C-8, and C-7′ of **2** were identified by the same method as that used for **1**. In the ROESY experiment, the correlation peak of H-7 with H-9 determined the *trans* configuration of H-7 and H-8 in **2**. The 7*R*,8*S* configuration for **2** was confirmed by the negative Cotton effects at 243 and 282 nm in the CD spectrum.


dx.doi.org/10.1021/jf501859x | J. Agric. Food Chem. 2014, 62, 9095−9102

Hydrolysis of **2** with cellulase yielded **2a** and D-glucose, which was identified by comparison with the D-glucose standard in TLC analysis. The absolute configuration for C-7′ in **2a** was defined as *S* based on a positive Cotton effect at 350 nm in the $Rh_2(OCOCF_3)_4$-induced CD spectrum. Therefore, compound **2** was defined as (7*R*,8*S*,7′*S*)-dihydrodehydrodiconiferyl alcohol-7′-hydroxy-4-*O*-*β*-D-glucopyranoside.

Compound **3** exhibited the molecular formula $C_{26}H_{34}O_{13}$, as determined using HRESIMS at *m*/*z* 577.1900 $[M + Na]^+$. The $^1H$ NMR spectrum (see Table 1) of **3** showed six aromatic proton signals at *δ* 7.75 (1H, dd, *J* = 8.5, 2.0 Hz), 7.57 (1H, d, *J* = 2.0 Hz), 7.18 (1H, d, *J* = 8.5 Hz), 6.92 (1H, brs), 6.68 (1H, overlap), and 6.68 (1H, overlap), revealing the presence of two ABX system aromatic rings. In addition, the $^1H$ NMR spectrum revealed two methoxy groups at *δ* 3.81 (3H, s) and 3.74 (3H, s) and a glucopyranosyl anomeric proton at *δ* 5.08 (1H, d, *J* = 7.5 Hz). In the $^{13}C$ NMR spectrum (see Table 2), apart from two methoxy carbons and a glucose unit, the remaining 18 skeleton carbon signals suggested that the aglycone of **3** was also a lignan. In the HMBC spectrum (see Figure 2), the characteristic correlation of H-8 at *δ* 5.58 with C-4′ at *δ* 145.6 indicated that **3** was an 8-*O*-4′ neolignan. The correlation peaks of two methoxy groups at *δ* 3.81 and 3.74 with C-3 and C-3′ confirmed that the linkage position of these methoxy groups was at C-3 and C-3′, respectively. The correlation of H-1″ (*δ* 5.08) with C-4 (*δ* 151.1) indicated that the linkage point of the glucose unit was at C-4. On the basis of the above data, **3** was defined as 4,9,7′,9′-tetrahydroxy-3,3′-dimethoxyl-7-oxo-8−4′-oxyneolignan-4-*O*-*β*-D-glucopyranoside.

To designate the absolute configuration of C-8 and C-7′ in compound **3**, CD exciton chirality and the $Rh_2(OCOCF_3)_4$-induced CD spectrum were assayed. Cellulase hydrolysis of **3** resulted in **3a** and D-glucose. A negative exciton-split Cotton effect at 332 nm (Δ*ε* −0.05) and 261 nm (Δ*ε* +0.07) in **3a** exhibited in the CD spectrum indicated that the two transition dipole moments of the chromophores (benzoyl moiety and benzene moiety) were oriented in an anticlockwise manner (see Supporting Information Figure S26). Thus, the absolute configuration of C-8 was assigned as 8*R*. Moreover, the positive Cotton effects at 328 and 374 nm in the $Rh_2(OCOCF_3)_4$-induced CD spectrum indicated the 7′*S* configuration for **3a**. From the above analysis, **3** was defined as (8*R*,7′*S*)-4,9,7′,9′-tetrahydroxy-3,3′-dimethoxyl-7-oxo-8−4′-oxyneolignan-4-*O*-*β*-D-glucopyranoside (**3**).

Compound **4**, a white powder, had the same molecular formula ($C_{26}H_{34}O_{13}Na$, *m*/*z* 577.1905) as **3**. The UV, IR, and NMR spectroscopy data of **4** indicated that it was an 8-*O*-4′ system neolignan and an optical isomer of **3**. Cellulase hydrolysis of **4** resulted in **4a** and D-glucose. In the CD spectrum, a positive exciton-split Cotton effect at 332 nm (Δ*ε* +0.04) and 265 nm (Δ*ε* −0.06) caused by the exciton coupling of the benzoyl and benzene chromophores indicated the 8*S* configuration of **4a** (see Supporting Information Figure S35). In the $Rh_2(OCOCF_3)_4$-induced CD experiment, a positive Cotton effect at 367 nm indicated the 7′*S* configuration for **4a**. Thus, compound **4** was defined as (8*S*,7′*S*)-4,9,7′,9′-tetrahydroxy-3,3′-dimethoxyl-7-oxo-8−4′-oxyneolignan-4-*O*-*β*-D-glucopyranoside (**4**).

Compound **5** had the molecular formula $C_{26}H_{32}O_{12}$ (*m*/*z* 559.1787 for $C_{26}H_{32}O_{12}Na$ in HRESIMS), and exhibited hydroxyl (3386 $cm^{-1}$), carbonyl (1757 $cm^{-1}$), and phenyl (1601 and 1514 $cm^{-1}$) groups in the IR spectrum. The $^1H$ NMR spectrum (see Table 1) showed two sets of ABX system aromatic rings [*δ* 6.96 (1H, d, *J* = 8.5 Hz), 6.78 (1H, d, *J* = 2.0 Hz), 6.72 (1H, d, *J* = 8.5 Hz), 6.66 (1H, dd, *J* = 8.5, 2.0 Hz), 6.65 (1H, d, *J* = 2.0 Hz), and 6.57 (1H, dd, *J* = 8.5, 2.0 Hz)]. In addition, two methylene protons [*δ* 2.70 (1H, dd, *J* = 13.5, 6.5), 2.49 (1H, overlap), 4.13 (1H, t, *J* = 8.5), 4.01 (1H, t, *J* = 8.5)], three methane protons [*δ* 4.34 (1H, t, *J* = 5.0), 2.84 (1H, dt, *J* = 8.5, 6.0), 2.46 (1H, m)], two methoxy groups [*δ* 3.73(3H, s), 3.71 (3H, s)], and a glucopyranosyl anomeric proton [*δ* 4.83 (1H, d, *J* = 7.5 Hz)] were observed in the upfield region. The $^{13}C$ NMR spectrum of **5** revealed 26 carbon resonances (Table 2) corresponding to the glucose unit, two methoxy groups, and two C6−C3 units. These data indicated that **5** was a dibenzylbutyrolactone lignan with substitution of two methoxy groups and a glucose unit.

In the HMBC spectrum (see Figure 2), correlation peaks from H-8 to C-1, C-7, C-9, C-7′, C-8′, and C-9′, from H-8′ to C-1′, C-7′, C-9′, C-7, C-8, and C-9, from $OCH_3$-3/3′ to C-3/3′, and from H-1″ to C-4 confirmed the dibenzylbutyrolactone skeleton of **5**, as well as the location of two methoxy groups and a glucose unit. The ROESY correlation (see Figure 3) from H-8 to H-7′ determined the *trans* configuration of H-8/8′. The 8*R*,8′*R* configuration was verified by the negative Cotton effect at 229 nm in the CD spectrum.[13] **5** was hydrolyzed with cellulase to yield **5a**, which was treated with $Rh_2(OCOCF_3)_4$ at room temperature. A negative Cotton effect at 340 nm in the $Rh_2(OCOCF_3)_4$-induced CD spectrum indicated the 7′*R* configuration for **5a**. Thus, compound **5** was defined as (7′*R*)-hydroxy matairesinol-4-*O*-*β*-D-glucopyranoside.

Compound **6**, an optical isomer of **5**, displayed spectroscopic data features that were almost identical to those of **5**. In the ROESY spectrum, the correlation peak of H-8/H-7′ was uncertain because of the overlap between H-8 and H-7a; therefore, the DMSO-$d_6$ was replaced with $CD_3OD$. 1D NMR data assignments were completed by comprehensive analysis of the 2D NMR data in $CD_3OD$. The chemical shift of H-8 was separated with H-7a in the $^1H$ NMR spectrum. The relative configuration of H-8/8′ was determined to be *trans* by the unambiguous correlation peak of H-8 with H-7′ in the ROESY spectrum. In combination with the negative Cotton effect at 225 nm in the CD spectrum, the absolute configuration of C-8 and C-8′ was established as 8*R*,8′*R*. Using the same method as that used for **5**, the 7′*S* configuration was determined. Thus, **6** was defined as (7′*S*)-hydroxy matairesinol-4-*O*-*β*-D-glucopyranoside.

Compound **7** was obtained as a white powder with a molecular formula of $C_{26}H_{34}O_{12}$, on the basis of HRESIMS at *m*/*z* 561.1945 $[M + Na]^+$ (calculated for $C_{26}H_{34}O_{12}Na$, *m*/*z* 561.1942). In the $^1H$ NMR spectrum (see Table 3), two sets of ABX system aromatic rings [*δ* 7.03 (1H, d, *J* = 8.0 Hz), 6.96 (1H, d, *J* = 2.0 Hz), 6.87 (1H, brs), 6.84 (1H, dd, *J* = 8.0, 2.0 Hz), 6.72 (1H, overlap), and 6.72 (1H, overlap)], together with two methine protons at *δ* 2.45 (1H, m), 2.14 (1H, m), two oxymethine protons at *δ* 4.46 (1H, d, *J* = 8.0 Hz), 4.41 (1H, dd, *J* = 8.5, 2.5 Hz), two oxymethylene protons at *δ* 3.60 (1H, m), 3.49 (1H, m), 3.48 (2H, m), two methoxy groups at *δ* 3.77 (3H, s), 3.76 (3H, s), and a glucopyranosyl anomeric proton at *δ* 4.87 (1H, d, *J* = 7.5 Hz), were observed. The $^{13}C$ NMR spectrum (see Table 2) showed 26 carbon signals, consisting of two methoxy carbon signals, six carbon signals of a glucose unit, and 18 skeleton carbon signals of two C6−C3 units. These spectroscopic data were very similar to those of lanicepsides A, which was isolated from *Saussurea laniceps*.[14] In the HMBC spectrum (see Figure 2), the correlation peaks of H-7 at *δ* 4.46


dx.doi.org/10.1021/jf501859x | J. Agric. Food Chem. 2014, 62, 9095−9102

with C-1, C-2, C-6, C-8, C-9, C-8′, and C-9′, and of H-7′ at $\delta$ 4.41 with C-1′, C-2′, C-6′, C-8′, C-9′, and C-8 helped verify that **7** was a tetrahydrofuranoid lignan. The location of the glucose unit was determined to be at C-4′ from the correlation of H-1″ with C-4′ in the HMBC spectrum. All of the above data indicated the same planar structure for **7** as for lanicepsides A.

The spectroscopic data of compounds **8** and **9** were in agreement with those of **7**, which indicated that these two compounds were optical isomers of **7**. The absolute configurations of these three compounds were determined by the ROESY spectrum, CD spectrum, and $Rh_2(OCOCF_3)_4$-induced CD assay. In the ROESY spectrum (see Figure 3), the correlation peaks of H-7/H-9, H-8/H-7′, and H-8′/H-9 helped confirm the *trans* configurations of H-7/H-8 and H-8/H-8′ in **7**, **8**, and **9**. In the CD spectrum, a negative Cotton effect at 230 nm indicated the 8*S* configuration for **7**.[15] Moreover, positive Cotton effects at 235 and 234 nm indicated the 8*R* configuration for **8** and **9**.[16] From the above analysis, the absolute configurations of C-7, C-8, and C-8′ for these compounds were determined as 7*R*,8*S*,8′*R* (**7**), 7*S*,8*R*,8′*S* (**8**), and 7*S*,8*R*,8′*S* (**9**).

To determine the absolute configuration at C-7′, the $Rh_2(OCOCF_3)_4$-induced CD assay was performed; **7** was hydrolyzed with cellulase to yield **7a**, which was treated with $Rh_2(OCOCF_3)_4$ at room temperature. A positive Cotton effect at 371 nm in the $Rh_2(OCOCF_3)_4$-induced CD spectrum indicated the 7′*S* configuration of **7a**. The absolute configurations of C-7′ in **8** and **9** were confirmed using the same method as that used for **7**. A negative Cotton effect at 350 nm for **8a** and a positive Cotton effect at 350 nm for **9a** indicated the 7′*R* and 7′*S* configurations, respectively. From the above analysis, compounds **7**−**9** were defined as (7*R*,8*S*,7′*S*,8′*R*)-4,9,4′,7′-tetrahydroy-3,3′-dimethoxy-7,9′-epoxylignan-4′-*O*-$\beta$-D-glucopyranoside (**7**), (7*S*,8*R*,7′*R*,8′*S*)-4,9,4′,7′-tetrahydroy-3,3′-dimethoxy-7,9′-epoxylignan-4′-*O*-$\beta$-D-glucopyranoside (**8**), and (7*S*,8*R*,7′*S*,8′*S*)-4,9,4′,7′-tetrahydroy-3,3′-dimethoxy-7,9′-epoxylignan-4′-*O*-$\beta$-D-glucopyranoside (**9**).

The molecular formulas of compounds **10**, **11**, and **12** were determined to be $C_{26}H_{34}O_{12}$ from HRESIMS ion *m*/*z* of 561.1948 $[M + Na]^+$, 561.1954 $[M + Na]^+$, and 561.1952 $[M + Na]^+$, respectively. The UV, IR, and NMR spectroscopic data of **10**−**12** were almost identical to those of compounds **7**−**9**. In comprehensive analysis of the ROESY and HMBC spectra of **10**−**12**, the correlation peak of H-1″ with H-5 in the ROESY spectrum, and with C-4 in the HMBC spectrum, indicated that the glucose unit was located at C-4. The absolute configurations of these three compounds were established using the same methods as those used for **7**−**9**. Compounds **10**−**12** were identified as (7*R*,8*S*,7′*S*,8′*R*)-4,9,4′,7′-tetrahydroy-3,3′-diethoxy-7,9′-epoxylignan-4-*O*-$\beta$-D-glucopyranoside (**10**), (7*S*,8*R*,7′*R*,8′*S*)-4,9,4′,7′-tetrahydroy-3,3′-dimethoxy-7,9′-epoxylignan-4-*O*-$\beta$-D-glucopyranoside (**11**), and (7*S*,8*R*,7′*S*,8′*S*)-4,9,4′,7′-tetrahydroy-3,3′-dimethoxy-7,9′-epoxylignan-4-*O*-$\beta$-D-glucopyranoside (**12**).

On the basis of MS data, NMR data, and comparison with literature, known compounds (see Figure 1) were identified as (7*R*,8*S*)-7,9,9′-trihydroxy-3,3′-dimethoxy-8-*O*-4′-neolignan-4-*O*-$\beta$-D-glucopyranoside (**13**),[17] (7*S*,8*R*)-7,9,9′-trihydroxy-3,3′-dimethoxy-8-*O*-4′-neolignan-4-*O*-$\beta$-D-glucopyranoside (**14**),[17] (7*R*,8*R*)-7,9,9′-trihydroxy-3,3′-dimethoxy-8-*O*-4′-neolignan-4-*O*-$\beta$-D-glucopyranoside (**15**),[17] (7*S*,8*S*)-7,9,9′-trihydroxy-3,3′-dimethoxy-8-*O*-4′-neolignan-4-*O*-$\beta$-D-glucopyranoside (**16**),[17] (7*R*,7′*R*,8*S*,8′*S*)-(+)-neo-olivil-4-*O*-$\beta$-D-glucopyranoside (**17**),[18] and arctiin (**18**).[19]

**Cytotoxic Activity.** In previous studies, arctigenin, the main component of Arctii Fructus, inhibited proliferation of and promoted apoptosis in SMMC-7721 human hepatocellular carcinoma cells.[9] To clarify whether lignan glucosides in Arctii Fructus have cytotoxic activity, all of the isolated compounds were tested for cytotoxic activity using an MTT assay in HCT-8, Bel-7402, BGC-823, A549, and A2780 cells. All of the tested compounds exhibited no significant cytotoxicity in cell model systems. Analysis of structures indicated that the glucose moiety in lignans may have reduced cytotoxic activity.

**Hepatoprotective Activity.** Compounds **1**−**18** were tested for hepatoprotective activities against D-galactosamine-induced toxicity in HL-7702 cells. Compounds **1**, **2**, **7**−**12**, and **17** showed stronger hepatoprotective activities than that shown by the positive control bicyclol at a concentration of $1 \times 10^{-5}$ M. Among them, compounds **1** and **2** reduced D-galactosamine-induced damage in HL-7702 cells (cell survival rate of 51%) with 79% and 71% inhibition, respectively, while the positive control bicyclol gave a 61.0% inhibition. Meanwhile, compounds **7**−**12** and **17** had 61−70% inhibition. From the above experimental data, only benzofuran-type neolignans and tetrahydrofuranoid lignans showed hepatoprotective activity. Tetrahydrofuran rings in lignans might contribute to the hepatoprotective activity observed. Furthermore, compounds **1** and **2**, which owned benzofuran rings, revealed stronger hepatoprotective activities than those of compounds **7**−**12** and **17**, which owned tetrahydrofuran rings.

In conclusion, we conducted a phytochemical investigation of Arctii Fructus, from which a series of 12 novel 7′-hydroxy lignan glucosides were isolated, along with six known lignan glucosides. To determine the absolute configurations for chiral carbons, the ROESY assay was combined with the CD exciton chirality method and $Rh_2(OCOCF_3)_4$-induced CD spectrum analysis. Further investigation of the in vitro bioactivities of **1**−**18** revealed that some compounds showed significantly stronger hepatoprotective activities than that shown by the positive control bicyclol. The structure−activity relationships revealed that the tetrahydrofuran ring in lignan glucosides might contribute to the hepatoprotective activity observed. These results provide additional phytochemical and bioactive information on Arctii Fructus, which is widely used in traditional Chinese medicine.

## ■ ASSOCIATED CONTENT

### Supporting Information

NMR, IR, MS, and CD spectra of compounds **1**−**12**. This material is available free of charge via the Internet at http://pubs.acs.org.

## ■ AUTHOR INFORMATION


### Corresponding Author

*Tel.: +86 10 63165231. Fax: 86-10-63017757. E-mail: pczhang@imm.ac.cn.



### Funding

This research was supported by the Nation Science and Technology Project of China (no. 2012ZX09301002-002).


### Notes

The authors declare no competing financial interest.

## ■ ACKNOWLEDGMENTS

We thank Ying-hong Wang for NMR measurements.

## ■ REFERENCES

(1) Matsumoto, T.; Hosono-Nishiyama, K.; Yamada, H. Antiproliferative and apoptotic effects of butyrolactone lignans from Arctium lappa on leukemic cells. *Planta Med.* **2006**, *72*, 276−278.
(2) Xu, Z. H.; Wang, X.; Zhou, M.; Ma, L.; Deng, Y.; Zhang, H.; Zhao, A.; Zhang, Y.; Jia, W. The antidiabetic activity of total lignan from Fructus Arctii against alloxan-induced diabetes in mice and rats. *Phytother. Res.* **2008**, *22*, 97−101.
(3) Kim, J. H.; Bae, J. T.; Song, M. H.; Lee, G. S.; Choe, S. Y.; Pyo, H. B. Biological activities of Fructus Arctii fermented with the basidiomycete Grifola frondosa. *Arch. Pharm. Res.* **2010**, *33*, 1943−1951.
(4) Hayashi, K.; Narutaki, K.; Nagaoka, Y.; Hayashi, T.; Uesato, S. Therapeutic effect of arctiin and arctigenin in immunocompetent and immunocompromised mice infected with influenza A virus. *Biol. Pharm. Bull.* **2010**, *33*, 1199−1205.
(5) Yang, Y. N.; Zhang, F.; Feng, Z. M.; Jiang, J. S.; Zhang, P. C. Two new neolignan glucosides from Arctii Fructus. *J. Asian Nat. Prod. Res.* **2012**, *14*, 981−985.
(6) Park, S. Y.; Hong, S. S.; Han, X. H.; Hwang, J. S.; Lee, D.; Ro, J. S.; Hwang, B. Y. Lignans from Arctium lappa and their inhibition of LPS-induced nitric oxide production. *Chem. Pharm. Bull.* **2007**, *55*, 150−152.
(7) Liu, J. Y.; Cai, Y. Z.; Wong, R. N.; Lee, C. K.; Tang, S. C.; Sze, S. C.; Tong, Y.; Zhang, Y. Comparative analysis of caffeoylquinic acids and lignans in roots and seeds among various Burdock (Arctium lappa) genotypes with high antioxidant activity. *J. Agric. Food Chem.* **2012**, *60*, 4067−4075.
(8) Kravtsova, S. S.; Khasanov, V. V. Lignans and fatty-acid composition of Arctium lappa seeds. *Chem. Nat. Compd.* **2011**, *47*, 800−801.
(9) Zheng, G. C.; Wang, B.; Qian, C. J. Effect and mechanism of proliferation and apoptosis induced by arctigenin in human hepatocellular carcinoma SMMC-7721 cell. *Shandong Med. J.* **2011**, *51*, 13−15.
(10) Nguyen, N. T.; Banskota, A. H.; Tezuka, Y.; Le Tran, Q.; Nobukawa, T.; Kurashige, Y.; Sasahara, M.; Kadota, S. Hepatoprotective effect of taxiresinol and (7′*R*)-7′-hydroxytaxiresinol on D-galactosamine and lipopolysaccharide-induced liver injury in mice. *Planta Med.* **2004**, *70*, 29−33.
(11) Yang, Y. N.; Liu, Z. Z.; Feng, Z. M.; Jiang, J. S.; Zhang, P. C. Lignans from the root of *Rhodiola crenulata*. *J. Agric. Food Chem.* **2012**, *60*, 964−972.
(12) Frelek, J.; Klimek, A.; Ruskowska, P. Dinuclear transition metal complexes as auxiliary chromophores in chiroptical studies on bioactive compounds. *Curr. Org. Chem.* **2003**, *7*, 1081−1104.
(13) Luo, S. Q.; Lin, L. Z.; Cordell, G. A. Lignan glucosides from *Bupleurum wenchuanense*. *Phytochemistry* **1993**, *33*, 193−196. Macías, F. A.; López, A.; Varela, R. M.; Torres, A.; Molinillo, J. M. G. Bioactive Lignans from a Cultivar of *Helianthus annuus*. *J. Agric. Food Chem.* **2004**, *52*, 6443−6447.
(14) Zhou, Z. W.; Yin, S.; Wang, X. N.; Fan, C. Q.; Li, H.; Yue, J. M. Two new lignan glycosides from *Saussurea laniceps*. *Helv. Chim. Acta* **2007**, *90*, 951−956.
(15) Tezuka, Y.; Morikawa, K.; Li, F.; Auw, L.; Awale, S.; Nobukawa, T.; Kadota, S. Cytochrome P450 3A4 inhibitory constituents of the wood of *Taxus yunnanensis*. *J. Nat. Prod.* **2011**, *74*, 102−105.
(16) Lee, J.; Seo, E. K.; Jang, D. S.; Ha, T. J.; Kim, J. P.; Nam, J. W.; Bae, G.; Lee, Y. M.; Yang, M. S.; Kim, J. S. Two new stereoisomers of neolignan and lignan from the flower buds of *Magnolia fargesii*. *Chem. Pharm. Bull.* **2009**, *57*, 298−301.
(17) Huo, C. H.; Liang, H.; Zhao, Y. Y.; Wang, B.; Zhang, Q. Y. Neolignan glycosides from *Symplocos caudata*. *Phytochemistry* **2008**, *69*, 788−795.
(18) Kikuchi, M.; Kikuchi, M. Studies on the constituents of *Swertia japonica* MAKINO II. On the structures of new glycosides. *Chem. Pharm. Bull.* **2005**, *53*, 48−51.
(19) Rahman, M. M. A.; Dewick, P. M.; Jackson, D. E.; Lucas, J. A. Lignans of *Forsythia Intermedia*. *Phytochemistry* **1990**, *29*, 1971−1980.

**Table 1. List of Ester Compounds Tested**

| Alcohol moieties | Acid moieties: Isobutyric acid[a] (-IB) | 2-Methylbutyric acid[b] (-2MB) | Isovaleric acid[c] (-IV) | 3-Methyl-2-butenoic acid[d] (-IP) | Angelic acid[e] | Tiglic acid[f] |
|---|---|---|---|---|---|---|
| Isobutyl (IB-) | 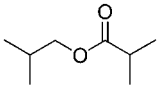 IB-IB Y; 88.5%, P; 98.8% | 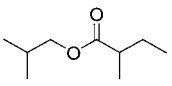 IB-2MB Y; 77.2%, P; 99.0% | 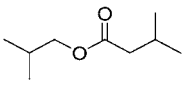 IB-IV Y; 79.7%, P; 98.8% | 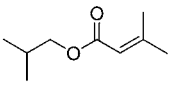 IB-IP Y; 92.6%, P; 96.2% | 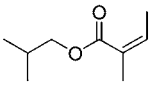 IB-A[g] TCI, P: 98% | - |
| 2-Methylbutyl (2MB-) | 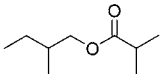 2MB-IB Y; 80.4%, P; 97.5% | 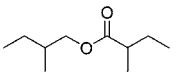 2MB-2MB Y; 91.9%, P; 99.0% | 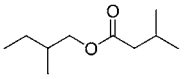 2MB-IV Y; 99.7%, P; 97.5% | 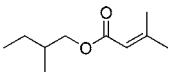 2MB-IP Y; quant., P; 95.1% | 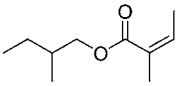 2MB-A Y; 54.0%, P; >99% | - |
| 3-Methylbutyl (3MB-) | 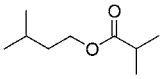 3MB-IB Y; 87.8%, P; 98.5% | 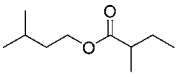 3MB-2MB Y; 87.2%, P; 99.0% | 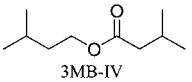 3MB-IV Y; 85.5%, P; 99.0% | 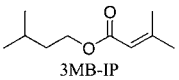 3MB-IP Y; quant., P; 96.3% | 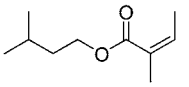 3MB-A[g] TCI, P: 99% | 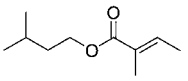 3MB-T Y; 78.0%, P; 99.0%; |
| 3-Methyl-2-butenyl (IP-) | 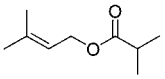 IP-IB Y; 99.0%, P; 99.0% | 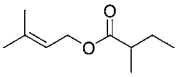 IP-2MB Y; 88.5%, P; 99.0% | 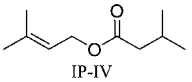 IP-IV Y; quant., P; 98.6% | 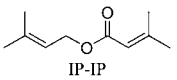 IP-IP Y; 97.9%, P; 95.9% | - | - |
| Butyl (C4-) | 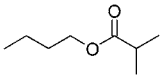 C4-IB Y; 85.8%, P;98.2% | 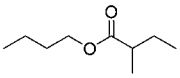 C4-2MB Y; 69.6%, P; 99.0% | 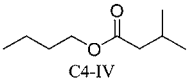 C4-IV Y; quant., P; 99.9% | 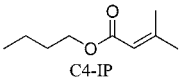 C4-IP Y; 96.8%, P; 96.2% | - | - |
| Pentyl (C5-) | 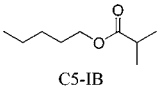 C5-IB Y; 99.0%, P; 99.0% | 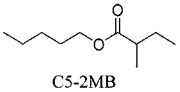 C5-2MB Y; 95.9%, P; 99.0% | 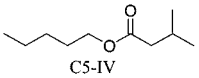 C5-IV Y; 95.6%, P; 99.9% | 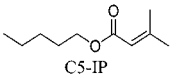 C5-IP Y; 99.7%, P; 96.3% | - | - |

[a,c,d]These compounds were synthesized following synthetic method A with isobutyl chloride, isovaleryl chloride, and 3,3-dimethylacryloyl chloride, respectively. [b,e,f]These compounds were synthesized following synthetic method B with the corresponding acids (see first footnote). [g]These compounds were purchased from Tokyo Chemical Industry. Y: yield (by isolation), P: purity (determined by GC).

(purity: 98%) and 3-methylbutyl angelate (i.e., = isoamyl angelate; purity, 99%) were purchased from Tokyo Chemical Industry (Tokyo, Japan).

**Instrumental Analysis.** Gas chromatography (GC) analysis was performed using an Agilent 6890N equipped a DB-1MS column (30 m × 0.25 mm i.d., 0.25 $\mu$m film thickness; J&W Scientific, Folsom, CA). GC-mass spectrometry (GC-MS) analysis was performed on an Agilent 7980A coupled with a 5975C mass selective detector (MSD). A DB-5MS (30 m × 0.25 mm i.d., 0.25 $\mu$m film thickness; J&W Scientific, Folsom, CA) was used for the separation of the analytes. The oven temperature was programmed as 40 °C for 1 min, then raised to 250 °C at 6 °C/min, and the temperature held for 4 min. Purities of synthesized compounds were checked by GC. NMR spectra were taken on a Varian UI500 spectrometer ($^1$H; 500 MHz, $^{13}$C; 125 MHz) using TMS in $CDCl_3$ as an internal standard at the Korea Basic Science Institute (Seoul, Korea). Infrared (IR) spectra were recorded on a Nicolet FT-IR spectrometer (Thermo Fisher Scientific Inc.). The structure was confirmed by comparison of its mass spectrum with data from the NIST mass spectrum library, IR data, and the NMR spectrum.

**Synthesis of Esters.** The esters listed in Table 1 were synthesized using two different procedures (i.e., methods A and B). In method A, the desired esters were synthesized with their corresponding alcohols and acyl chlorides. Briefly, a solution of alcohol (1.0 equiv) and acyl chloride (1.5 equiv) in $CH_2Cl_2$, pyridine (1.5 equiv), and a catalytic amount of DMAP were added at 0 °C. After 30 min of stirring at 0 °C, the solution was stirred for 2 h at room temperature. The solution was diluted with ether, and the organic phase was washed with 2 N HCl, water, and brine and then dried. After the solvent was removed, the residue was distilled and subjected to silica gel chromatography to give the desired ester (5% ether in hexane fraction). In method B, the esters were synthesized with their corresponding alcohols and acids, DMAP and DCC, following the method by Neises and Steglich.[19] Alcohol (2.0 equiv), acid (1.0 equiv), and DMAP (1.6 equiv) were dissolved in $CH_2Cl_2$ at 0 °C. DCC (2.2 equiv) was added to the solution over a 4 min period. The solution was stirred for 30 min at 0 °C and then for 3 h at room temperature. The precipitate was removed by filtration; the filtrate was diluted with ether and then worked up. The purification procedure was the same as that in method A.

Isobutyl isobutanoate (IB-IB): GC-MS, $m/z$ (%); 129 (0.1, $M^+-CH_3$), 101 (7.2), 89 (27.4), 71 (100.0), 56 (39.8).

2-Methylbutyl isobutanoate (2MB-IB): GC-MS, $m/z$ (%); 129 (0.5, $M^+-CH_2CH_3$), 101 (5.8), 89 (8.9), 71 (100.0), 70 (63.7), 55 (17.8).

3-Methylbutyl isobutanoate (3MB-IB): GC-MS, $m/z$ (%); 143 (0.2, $M^+-CH_3$), 115 (6.0), 101 (2.4), 89 (21.1), 71 (80.0), 70 (100.0), 55 (35.2).

3-Methyl-2-butenyl isobutanoate (IP-IB): GC-MS, $m/z$ (%); 156 (2.1, $M^+$), 113 (1.1), 85 (3.5), 71 (46.1), 69 (100.0), 68 (78.4), 67 (74.6), 53 (38.1).

Butyl isobutanoate (C4-IB): GC-MS, $m/z$ (%); 115 (0.6, $M^+-CH_2CH_3$), 101 (6.5), 89 (85.9), 71 (100), 57 (38.7), 56 (44.6).

Pentyl isobutanoate (C5-IB): GC-MS, $m/z$ (%); 129 (0.4, $M^+-CH_2CH_3$), 115 (2.4), 101 (3.4), 89 (77.7), 71 (80.6), 70 (48.1), 55 (20.6), 43 (100.0).

Isobutyl 2-methylbutanoate (IB-2MB): GC-MS, $m/z$ (%); 143 (0.2, $M^+-CH_3$), 130 (4.5), 115 (3.2), 103 (36.7), 85 (78.9), 74 (12.0), 57 (100.0), 56 (42.0).

2-Methylbutyl 2-methylbutanoate (2MB-2MB): GC-MS, $m/z$ (%); 143 (0.5 $M^+-CH_2CH_3$), 103 (14.9), 85 (100.0), 71 (24.7), 70 (86.5), 57 (92.2), 55 (25.4).


dx.doi.org/10.1021/jf503631e | J. Agric. Food Chem. 2014, 62, 9103−9108

3-Methylbutyl 2-methylbutanoate (3MB-2MB): GC-MS, *m/z* (%). 157 (0.3, $M^+-CH_3$), 144 (1.1), 129 (2.9), 115 (2.2), 103 (20.8), 85 (42.9), 70 (100.0), 57 (62.9), 55 (31.1).

3-Methyl-2-butenyl 2-methylbutanoate (IP-2MB): GC-MS, *m/z* (%): 170 (2.1, $M^+$), 103 (1.4), 85 (25.0), 74 (18.0), 69 (100.0), 68 (76.7), 67 (75.1), 57 (71.7), 53 (42.1).

Butyl 2-methylbutanoate (C4-2MB): GC-MS, *m/z* (%); 143 (0.2, $M^+-CH_3$), 130 (5.5), 115 (1.9), 103 (78.7), 85 (61.9), 74 (20.8), 57 (100.0), 56 (41.0).

Pentyl 2-methylbutanoate (C5-2MB): GC-MS, *m/z* (%); 172 (0.1, $M^+$), 144 (3.5), 115 (5.1), 103 (100.0), 85 (60.6), 74 (20.1), 71 (10.4), 70 (45.0), 57 (77.6), 56 (10.0), 55 (22.5).

Isobutyl isovalerate (IB-IV): GC-MS, *m/z* (%) 158 (0.08, $M^+$), 143 (0.1), 128 (1.5), 115 (3.6), 103 (22.0), 85 (100.0), 73 (2.1), 60 (13.7), 57 (74.3).

2-Methylbutyl isovalerate (2MB-IV): GC-MS, *m/z* (%) 172 (0.4, $M^+$), 142 (0.8), 115 (4.1), 103 (8.3), 85 (100.0), 71 (23.6), 70 (66.2), 57 (44.0), 55 (16.7).

3-Methylbutyl isovalerate (3MB-IV): GC-MS, *m/z* (%) 157 (0.2, $M^+$-$CH_3$), 142 (0.1), 115 (3.2), 103 (14.9), 85 (56.8), 71 (29.7), 70 (100.0), 57 (34.1), 55 (28.2).

3-Methyl-2-butenyl isovalerate (IP-IV): GC-MS, *m/z* (%) 170 (1.6, $M^+$), 128 (1.0), 110 (0.5), 103 (1.8), 85 (69.6), 69 (82.5), 68 (100.0), 67 (92.1), 60 (38.0), 57 (65.1), 53 (45.6).

Butyl isovalerate (C4-IV): GC-MS, *m/z* (%) 158 (0.1, $M^+$), 143 (0.2), 116 (5.0), 103 (69.1), 87 (20.9), 85 (100.0), 73 (1.5), 60 (24.1), 57 (74.3), 56 (68.0)

Pentyl isovalerate (C5-IV): GC-MS, *m/z* (%) 170 (0.1, $M^+$), 157 (0.2), 130 (3.4), 115 (6.6), 103 (89.1), 85 (100.0), 71 (16.9), 70 (85.7), 61(14.7), 60 (18.3), 57 (55.9), 55 (26.3).

Isobutyl 3-methyl-2-butenoate (IB-IP): GC-MS, *m/z* (%) 156 (1.7, $M^+$), 156 (1.7), 141 (0.2), 126 (0.1), 113 (0.5), 101 (16.8), 100 (36.8), 99 (0.3), 83 (100.0), 73 (0.4), 67 (0.8), 57 (10.6), 55 (19.7).

2-Methylbutyl 3-methyl-2-butenoate (2MB-IP): GC-MS, *m/z* (%) 170 (0.7, $M^+$), 155 (0.1), 113 (0.5), 101 (16.4), 100 (34.7), 83 (100.0), 70 (17.2), 67 (1.0), 55 (25.6).

3-Methylbutyl 3-methyl-2-butenoate (3MB-IP): GC-MS, *m/z* (%) 170 (3.0, $M^+$), 155 (0.3), 113 (0.4), 101 (23.9), 100 (42.2), 83 (100.0), 82 (10.3), 71 (19.6), 70 (23.2), 67 (2.2), 55 (40.7).

3-Methyl-2-butenyl 3-methyl-2-butenoate (IP-IP): GC-MS, *m/z* (%) 168 (0.7, $M^+$), 153 (0.7), 109 (6.9), 100 (42.2), 95 (0.8), 83 (43.3), 77 (1.4), 69 (24.6), 68 (69.6), 67 (100.0), 55 (10.4), 53 (60.9).

Butyl 3-methyl-2-butenoate (C4-IP): GC-MS, *m/z* (%) 156 (7.5, $M^+$), 141 (0.9), 113 (0.6), 101 (19.3), 100 (57.2), 85 (11.1), 83 (100.0), 82 (19.6), 55 (25.6).

Pentyl 3-methyl-2-butenoate (C5-IP): GC-MS, *m/z* (%) 170 (5.4, $M^+$), 155 (0.4), 101 (32.1), 100 (68.9), 83 (100.0), 82 (17.3), 71 (3.2), 70 (5.6), 55 (33.8).

2-Methylbutyl angelate (2MB-A): GC-MS, *m/z* (%) 170 (1.6, $M^+$), 100 (100.0), 83 (90.0), 71 (23.4), 70 (21.9), 55 (85.4). IR (neat, $cm^{-1}$), 3005 (w), 2980 (s), 1710 (s), 1670 (m), 1220 (s), 1160 (s), 850 (s).

3-Methylbutyl tiglate (3MB-T): $^1$H NMR (ppm), $\delta$ 0.936 (6H, d, $J$ = 6.5), 1.567 (2H, dt, $J$ = 7, 6.5), 1.722 (1H, nonet, $J$ = 6.5), 1.785 (3H, dq, $J$ = 7, 1.5), 1.829 (3H, quin., $J$ = 1.5), 4.159 (2H, t, $J$ = 7), 6.840 (1H, qq, $J$ = 7, 1.5); $^{13}$C NMR (ppm), $\delta$ 12.03 ($CH_3$), 14.13 ($CH_3$), 22.52 ($CH_3$ × 2), 25.22 (CH), 37.47 ($CH_2$), 63.07 ($CH_2$), 128.83 (=C), 136.79 (=CH), 168.22 (O=C). IR (neat, $cm^{-1}$), 2980 (s), 2105 (m), 1710 (s), 1670 (m), 1280 (s), 1110 (s), 730 (s).

**Nematicidal Activity.** To test the nematicidal activity of ester compounds, test compounds were suspended in ethanol (100 mg/mL). Test solutions (1 $\mu$L) were placed in the wells of a 96-well plate (Falcon, USA) containing 50−150 nematodes (mixture of juvenile and adult nematodes, male−female−juvenile ≈1:1:2) in 99 $\mu$L of water. Thus, the total volume of the solution in each well was 100 $\mu$L, and the concentration of the test ester compounds was 1 mg/mL. As a control, four wells were treated with ethanol (1 $\mu$L) in the same volume as the test samples. In four adjacent wells (i.e., in a column) on the plate, nematodes were treated with the ester compounds, and a set of treatment samples was placed in the wells of every second column. The entire completely experiment was repeated four times. The order of the ester compounds was randomly determined. The tested plates were stored under a 14:10 h (light−dark) regime at 25 ± 1 °C and 60% relative humidity. Nematode mortality was recorded after 48 h of treatment as follows: 10 $\mu$L of the test suspension was transferred to 100 $\mu$L of fresh water with a micropipette. Ten minutes after transfer, nematode mortality was observed under a microscope. Nematodes were classified as dead if their bodies were motionless and straightened. The mortality of termites was transformed to the arcsine square root values for analysis of variance (ANOVA). Mean values for treatment data were compared and separated by Scheffé's test.[20] Five chemicals (i.e., isobutyl 2-methylbutanoate, 3-methylbutyl 2-methylbutanoate, 3-methyl-2-butenyl 2-methylbutanoate, 3-methylbutyl tiglate, and pentyl 2-methylbutanoate) that showed strong nematicidal activity at a concentration of 1 mg/mL against the pine wood nematode were chosen for testing at a lower concentration. These chemicals were serially diluted with ethanol to obtain four different concentrations; the final concentrations were 0.250, 0.125, 0.0625, and 0.03125 mg/mL for pentyl 2-methylbutanoate; 0.125, 0.0625, 0.03125, and 0.015625 mg/mL for isobutyl 2-methylbutanoate, 3-methylbutyl 2-methylbutanoate, and 3-methyl-2-butenyl 2-methylbutanoate; and 0.0625, 0.03125, 0.015625, and 0.0078125 mg/mL for 3-methylbutyl tiglate. The $LC_{50}$ was estimated by probit analysis.[20]

## RESULTS AND DISCUSSION

The nematicidal activity of the ester compounds is shown in Table 2. Among the ester compounds tested, isobutyl 2-methylbutanoate, 3-methylbutyl 2-methylbutanoate, and 3-methylbutyl tiglate showed 100% nematicidal activity against the pine wood nematode at a concentration of 1 mg/mL. The nematicidal activities of 3-methyl-2-butenyl 2-methylbutanoate and pentyl 2-methylbutanoate were 98.73% and 97.63% against the pine wood nematode at a concentration of 1 mg/mL, respectively. The nematicidal activities of the other ester compounds were <11%. The nematicidal activities of isobutyl 2-methylbutanoate, 3-methylbutyl 2-methylbutanoate, 3-methylbutyl tiglate, 3-methyl-2-butenyl 2-methylbutanoate, and pentyl 2-methylbutanoate, which showed strong nematicidal activities at a 1 mg/mL concentration, were also tested at a lower concentration (Table 3). The $LC_{50}$ values of 3-methylbutyl tiglate, isobutyl 2-methylbutanoate, 3-methylbutyl 2-methylbutanoate, 3-methyl-2-butenyl 2-methylbutanoate, and pentyl 2-methylbutanoate were 0.0218, 0.0284, 0.0326, 0.0402, and 0.0480 mg/mL, respectively. Nematicidal activities of many phytochemicals from essential oils have been reported.[9−17] Choi et al.[9] reported that $LC_{50}$ values of thymol, carvacrol, citral, citronellol, and citronellal were 0.119, 0.125, 0.187, 0.245, and 0.321 mg/mL, respectively. Some natural ester compounds tested in this study have been reported as the main compounds of certain plant essential oils.[21,22] Isobutyl angelate was the most abundant compound identified in *Chamaemelum nobile* plant essential oil, followed by 2-methylbutyl angelate, isobutyl isobutyrate, methyl 2-methylbuyrate, prenyl acetate, 2-methylbutyl 2-methylbutyrate, and 2-methylbutyl acetate.[21] Mierendorff et al.[22] reported that the main compounds of *Eriocephalus punctulatus* were 2-methylbutyl isobutanoate (21.2%), 2-methylbutyl 2-methylbutanoate (5.6%), isobutyl isobutanoate (5.3%), and linalyl acetate (4.4%). Bail et al.[21] reported the antimicrobial activities of some ester compounds identified in *Chamaemelum nobile* plant essential oils. Seo et al.[23] reported the fumigant toxicities of some ester compounds derived from *E. punctulatus* and *C. mobile* plant essential oils against Japanese termites (*Reticulitermes speratus*); however, there have been no reports on the nematicidal activities of the natural ester

**Table 2. Nematicidal Activity of Ester Compounds against Pine Wood Nematode, *B. xylophilus***

| ester compounds | mortality (%, mean ± S.E., $N = 4$)[a] |
|---|---|
| isobutyl isobutanoate (IB-IB) | 0b[b] |
| isobutyl 2-methylbutanoate (IB-2MB) | 100a |
| isobutyl isovalerate (IB-IV) | 0b |
| isobutyl 3-methyl-2-butenoate (IB-IP) | 0.68 ± 1.35b |
| isobutyl angelate (IB-A) | 9.5 ± 15.08b |
| 2-methylbutyl isobutanoate (2MB-IB) | 0.63 ± 1.25b |
| 2-methylbutyl 2-methylbutanoate (2MB-2MB) | 0b |
| 2-methylbutyl isovalerate (2MB-IV) | 1.05 ± 1.26b |
| 2-methylbutyl 3-methyl-2-butenoate (2MB-IP) | 0.65 ± 1.30b |
| 2-methylbutyl angelate (2MB-A) | 9.0 ± 5.15b |
| 3-methylbutyl isobutanoate (3MB-IB) | 0b |
| 3-methylbutyl 2-methylbutanoate (3MB-2MB) | 100a |
| 3-methylbutyl isovalerate (3MB-IV) | 0b |
| 3-methylbutyl 3-methyl-2-butenoate (3MB-IP) | 0.58 ± 1.15b |
| 3-methylbutyl angelate (3MB-A) | 10.6 ± 9.06b |
| 3-methylbutyl tiglate (3MB-T) | 100a |
| 3-methyl-2-butenyl isobutanoate (IP-IB) | 4.3 ± 2.84b |
| 3-methyl-2-butenyl 2-methylbutanoate (IP-2MB) | 98.73 ± 0.85a |
| 3-methyl-2-butenyl isovalerate (IP-IV) | 5.63 ± 1.8b |
| 3-methyl-2-butenyl 3-methyl-2-butenoate (IP-IP) | 8.08 ± 2.65b |
| butyl isobutanoate (C4-IB) | 1.5 ± 3.0b |
| butyl 2-methylbutanoate (C4-2MB) | 0b |
| butyl isovalerate (C4-IV) | 1.2 ± 1.47b |
| butyl 3-methyl-2-butenoate (C4-IP) | 1.48 ± 1.81b |
| pentyl isobutanoate (C5-IB) | 0.5 ± 1.0b |
| pentyl 2-methylbutanoate (C5-2MB) | 97.63 ± 2.06a |
| pentyl isovalerate (C5-IV) | 0b |
| pentyl 3-methyl-2-butenoate (C5-IP) | 0.55 ± 1.1b |
| control | 0b |
| | $F_{28,87} = 485.72$, $p < 0.0001$ |

[a]1 mg/mL concentration. [b]Means within a column followed by same letters are not significantly different (Scheffe's test).

**Table 3. $LC_{50}$ Values of Five Active Ester Compounds against Pine Wood Nematode, *B. xylophilus***

| compounds | $LC_{50}$ (mg/mL) | slope | 95% cl[a] | $\chi^2$ |
|---|---|---|---|---|
| isobutyl 2-methylbutanoate | 0.0284 | 4.25 ± 0.37 | 0.0258−0.0311 | 1.11 |
| 3-methylbutyl 2-methylbutanoate | 0.0326 | 3.86 ± 0.32 | 0.0295−0.0359 | 7.83 |
| 3-methylbutyl tiglate | 0.0218 | 4.13 ± 0.33 | 0.0199−0.0239 | 2.71 |
| 3-methyl-2-butenyl 2-methylbutanoate | 0.0402 | 4.55 ± 0.37 | 0.0368−0.0439 | 0.12 |
| pentyl 2-methylbutanoate | 0.0480 | 2.81 ± 0.27 | 0.0413−0.0545 | 5.66 |

[a]Confidence limit.

compounds utilized in the current study against the pine wood nematode.

Among the ester compounds tested in the current study, there was a significant difference in nematicidal activity against the pine wood nematode. The nematicidal activities of the ester compounds with 2-methylbutyric acid moiety, such as isobutyl 2-methylbutanoate, 3-methylbutyl 2-methylbutanoate, 3-methyl-2-butenyl 2-methylbutanoate, and pentyl 2-methylbutanoate, were stronger than those of the other ester compounds, except 3-methylbutyl tiglate. This result indicates that the 2-methylbutyric acid moiety may play an important role in nematicidal activity against the pine wood nematode. Specific functional groups in the chemical structure are closely related to the nematicidal activity against the pine wood nematode.[9,16] Choi et al.[9] investigated the nematicidal activities of monoterpenoids typically found in plant essential oils and found that chemicals belonging to the phenols, alcohols, and aldehydes were generally more toxic than the other monoterpenoid groups such as the ketones and hydrocarbons. Park et al.[16] compared the nematicidal activities of eugenol, methyl eugenol, isoeugenol, methyl isoeugenol, and acetyl eugenol and insisted that a functional group at the C1 position of the benzene ring was very important for nematicidal activity.

There was a significant difference in nematicidal activities among the ester compounds with a 2-methylbutyric acid moiety. Nematicidal activities of isobutyl 2-methylbutanoate, 3-methylbutyl 2-methylbutanoate, 3-methyl-2-butenyl 2-methylbutanoate, and pentyl 2-methylbutanoate were strong; however, 2-methylbutyl 2-methylbutanoate and butyl 2-methylbutanoate did not show nematicidal activity against the pine wood nematode. Grodnitzky and Coats[24] investigated the QSAR of monoterpenoids against the house fly, *Musca domestica*. They insisted that the optimum shape and size of monoterpenoids was necessary to fit into a site of toxic action. Seo et al.[25] studied the structure−activity relationship of aliphatic compounds for nematicidal activity against the pine wood nematode. There was a significant difference in nematicidal activity according to chain length. Among the aliphatic compounds belonging to the alkanols and 2*E*-alkenols, compounds with a $C_9$−$C_{11}$ chain length showed strong nematicidal activity when compared to the other compounds with different chain lengths. In the case of the 2*E*-alkenals and alkanoic acids groups, compounds with $C_8$−$C_9$ and $C_9$−$C_{10}$ chain lengths, respectively, showed strong nematicidal activity; however, compounds with $C_{12}$−$C_{14}$ chain lengths showed weak nematicidal activity against the pine wood nematode. The current study is in accordance with a previous study, indicating that an optimum shape and size of chemicals are necessary for the nematicidal activity against the pine wood nematode.

*α,β*-Unsaturated carbonyl compounds such as citral, 2-decenal, *trans*-cinnamate, and 2*E*-alkenal were reported to be responsible for nematicidal activities against the pine wood nematode.[9,13,14,25] Ester compounds with 3-methyl-2-butenoic acid, angelic acid, and tiglic acid moiety provide *α,β*-unsaturated carbonyl structure, but only 3-methylbutyl tiglate showed strong nematicidal activity. The relationship between nematicidal activity and *α,β*-unsaturated carbonyl structure was not clarified in the current study.

The structure−activity relationships of the *cis*- and *trans*-isomers of various compounds have been well-studied. Park et al.[26] reported that the insecticidal activity of *cis*-asarone was stronger than that of *trans*-asarone against *Sitophilus oryzae*, *Callosobruchus chinensis*, and *Lasioderma serricorene*. Lee et al.[27] also reported that the insecticidal activity of *cis*- and *trans*-asarone were different against *Nilaparvata lugens* (Homoptera: Delphacidae) and *Plutella xylostella* (Lepidoptera: Yponomeutoidae). Park et al.[16] reported that the nematicidal activity of geranial was ∼4.3 times stronger than that of neral, a


dx.doi.org/10.1021/jf503631e | J. Agric. Food Chem. 2014, 62, 9103−9108

geometrical isomer of geranial. In the current study, there was a difference in the nematicidal activity of two geometrical isomers—3-methylbutyl angelate and 3-methylbutyl tiglate. The nematicidal activity of 3-methylbutyl tiglate was much stronger than that of 3-methylbutyl angelate. The current study and previous studies indicate that the position of the substituent in the geometrical isomer is very important for nematicidal or insecticidal activities.

Clarifying the mode of action for active compounds is of practical importance for nematode control because it provides valuable information for developing the most appropriate methods for delivery. Lei et al.[28] reported that the nematicidal activity of thymol and carvacrol against two nematodes, *Caenorhabditis elegans* and *Ascaris suum*, might be mediated through a tyramine receptor (TyrR). Recently, Kang et al.[29] investigated the inhibition activities of phytochemicals from plant essential oils against acetylcholinesterases of the pine wood nematode. They reported that (+)-α-pinene, (−)-α-pinene, 3-carene, *o*-anisaldehyde, coniferyl alcohol, and *cis*-nerolidol showed inhibition activities against acetylcholinesterases of the pine wood nematode. Kang et al.[30] also reported the inhibition of acetylcholinesterase and glutathione *S*-transferase of the pine wood nematode by aliphatic compounds. They found that the nematicidal activity of the 2*E*-alkenal compounds is related to the inhibition of BxACE (*B. xylophilus* acetylcholinesterase); however, ester compounds tested in the current study did not show inhibition activity against BxACE (data not shown here). Moreover, the exact mode-of-action for ester compounds used in current study remains unclear.

In conclusion, natural ester compounds such as isobutyl 2-methylbutanoate, 3-methylbutyl 2-methylbutanoate, 3-methylbutyl tiglate, 3-methyl-2-butenyl 2-methylbutanoate, 3-methyl-2-butenyl 2-methylbutanoate, and pentyl 2-methylbutanoate showed very strong nematicidal activity against the pine wood nematode. We also investigated the structure−activity relationship of natural ester compounds and their analogues. For the practical use of these ester compounds as novel nematicides, further studies investigating systemic action, phytotoxicity, mode-of-action, and formulation for improving nematicidal potency and stability are necessary.

## AUTHOR INFORMATION


### Corresponding Author

*Telephone: +82-2-880-4751; fax: +82-2-873-3560; e-mail: parkik1@snu.ac.kr.


### Author Contributions

S.-M.S. and J.K. contributed equally to this work.

### Notes

The authors declare no competing financial interest.

## REFERENCES


(1) Zhao, B. G.; Futai, K.; Sutherland, J. R.; Takeuchi, Y. *Pine Wilt Disease*; Springer: Japan, 2008; p 459.

(2) Yi, C. K.; Byun, B. H.; Park, J. D.; Yang, S. I.; Chang, K. H. First finding of the pine wood nematode, *Bursaphelenchus xylophilus* (Steiner et Buhrer) Nickle and its insect vector in Korea. *Res. Rep. For. Res. Inst.* **1989**, *38*, 141−149.

(3) Lee, S. M.; Chung, Y. J.; Moon, Y. S.; Lee, S. G.; Lee, D. W.; Choo, H. Y.; Lee, C. K. Insecticidal activity and fumigation conditions of several insecticides against Japanese pine sawyer (*Monochamus alternates*) larvae. *J. Kor. For. Soc.* **2003**, *92*, 191−198.

(4) Korea Forest Service. *Guideline for the control of forest diseases and insect pests*; Korea Forest Service: Daejeon, Republic of Korea, 2013; p 325.

(5) Kwon, T. S.; Shin, J. H.; Lim, J. H.; Kim, Y. K.; Lee, E. J. Management of pine wilt disease in Korea through preventative silvicultural control. *For. Ecol. Manag.* **2011**, *261*, 562−569.

(6) Pruett, S. B.; Myers, L. P.; Keil, D. E. Toxicology of metam sodium. *J. Toxicol. Environ. Health B* **2001**, *4*, 207−222.

(7) Beketov, M. A.; Liess, M. Acute and delayed effects of the neonicotinoid insecticide thiacloprid on seven freshwater arthropods. *Environ. Toxicol. Chem.* **2008**, *27*, 461−470.

(8) Cônsoli, F. L.; Parra, J. R. P.; Hassan, S. A. Side-effects of insecticides used in tomato fields on the egg parasitoid *Trichogramma pretiosum* Riley (Hym., Trichogrammatidae), a natural enemy of *Tuta absoluta* (Meyrick) (Lep., Gelechiidae). *J. Appl. Ent.* **1998**, *122*, 43−47.

(9) Choi, I. H.; Kim, J.; Shin, S. C.; Park, I. K. Nematicidal activity of monoterpenoids against the pine wood nematode (*Bursaphelenchus xylophilus*). *Russ. J. Nematol.* **2007**, *15*, 35−40.

(10) Choi, I. H.; Park, J. Y.; Shin, S. C.; Park, I. K. Nematicidal activity of medicinal plant extracts and two cinnamates isolated *Kaempferia galanga* L. (Proh Hom) against the pine wood nematode, *Bursaphelenchus xylophilus*. *Nematology* **2006**, *8*, 359−365.

(11) Choi, I. H.; Shin, S. C.; Park, I. K. Nematicidal activity of onion (*Allium cepa*) oil and its components against the pine wood nematode (*Bursaphelenchus xylophilus*). *Nematology* **2007**, *9*, 231−235.

(12) Kim, E.; Park, I. K. Nematicidal activity of Korean domestic plant extracts against the pine wood nematode, *Bursaphelenchus xylophilus*. *Nematology* **2011**, *13*, 377−380.

(13) Kim, J.; Seo, S. M.; Lee, S. G.; Shin, S. C.; Park, I. K. Nematicidal activity of plant essential oils and components from coriander (*Coriandrum sativum*), Oriental sweetgum (*Liquidambar orientalis*), and valerian (*Valeriana wallichii*) essential oils against pine wood nematode (*Bursaphelenchus xylophilus*). *J. Agric. Food Chem.* **2008**, *56*, 7316−20.

(14) Kim, J.; Seo, S. M.; Park, I. K. Nematicidal activity of plant essential oils and components from *Gaultheria fragrantissima* and *Zanthoxylum alatum* against the pine wood nematode, *Bursaphelenchus xylophilus*. *Nematology* **2011**, *13*, 87−93.

(15) Kong, J. O.; Park, I. K.; Choi, K. S.; Shin, S. C.; Ahn, Y. J. Nematicidal and Propagation Activities of Thyme Red and White Oil Compounds toward *Bursaphelenchus xylophilus* (Nematoda: Parasitaphelenchidae). *J. Nematol.* **2007**, *39*, 237−42.

(16) Park, I. K.; Kim, J.; Lee, S. G.; Shin, S. C. Nematicidal activity of plant essential oils and components from ajowan (*Trachyspermum ammi*), allspice (*Pimenta dioica*) and litsea (*Litsea cubeba*) essential oils against pine wood nematode (*Bursaphelenchus xylophilus*). *J. Nematol.* **2007**, *39*, 275−279.

(17) Park, I. K.; Park, J. Y.; Kim, K. H.; Choi, K. S.; Choi, I. H.; Kim, C. S.; Shin, S. C. Nematicidal activity of plant essential oils and components from garlic (*Allium sativum*) and cinnamon (*Cinnamomum verum*) oils against the pinewood nematode (*Bursaphelenchus xylophilus*). *Nematology* **2005**, *7*, 767−774.

(18) Chawla, M. L.; Prasad, S. K. Techniques in nematology. II. Comparative efficiency of sampling tools and nematode extraction methods. *Ind. J. Nematol.* **1975**, *4*, 115−123.

(19) Neises, B.; Steglich, W. Esterification of carboxylic acids with dicyclohexylcarbodiimide/4-dimethylaminopyridine: *tert*-Butyl ethyl fumarate. *Org. Synth. Coll.* **1990**, *7*, 93−94.

(20) SAS Institute. *SAS/STAT User's Guide*, Version 9.1.3; SAS Institute: Cary, NC. 2004.

(21) Bail, S.; Buchbauer, G.; Jirovetz, L.; Denkova, Z.; Slavchev, A.; Stoyanova, A.; Schmidt, E.; Geissler, M. Antimicrobial activities of roman chamomile oil from France and its main compounds. *J. Essential Oil Res.* **2009**, *21*, 283−286.

(22) Mierendorff, H. G.; Stahl-Biskup, E.; Posthumus, M. A.; van Beek, T. A. Composition of commercial cape chamomile oil (*Eriocephalus punctulatus*). *Flavour Frag. J.* **2003**, *18*, 510−514.

(23) Seo, S. M.; Kim, J.; Kang, J.; Koh, S. H.; Ahn, Y. J.; Kang, K. S.; Park, I. K. Fumigant toxicity and acetylcholinesterase inhibitory

activity of 4 Asteraceae plant essential oils and their constituents against Japanese termite (*Reticulitermes speratus* Kolbe). *Pestic. Biochem. Physiol.* **2014**, *113*, 55−61.
(24) Grodnitzky, J. A.; Coats, J. R. QSAR evaluation of monoterpenoids' insecticidal activity. *J. Agric. Food Chem.* **2002**, *50*, 4576−4580.
(25) Seo, S. M.; Kim, J.; Kim, E.; Park, H. M.; Kim, Y. J.; Park, I. K. Structure-activity relationship of aliphatic compounds for nematicidal activity against pine wood nematode (*Bursaphelenchus xylophilus*). *J. Agric. Food Chem.* **2010**, *58*, 1823−1827.
(26) Park, C.; Kim, S. I.; Ahn, Y. J. Insecticidal activity of asarone identified *in Acorus gramineus* rhizome against three coleopteran stored-product insects. *J. Stored Prod. Res.* **2003**, *39*, 333−342.
(27) Lee, H. K.; Park, C.; Ahn, Y. J. Insecticidal activities of asarones identified in *Acorus gramineus* rhizome against *Nilaparvata lugens* (Homoptera: Delphacidae) and *Plutella xylostella* (Lepidoptera: Yponomeutoidae). *Appl. Entomol. Zool.* **2002**, *37*, 459−464.
(28) Lei, J.; Leser, M.; Enan, E. Nematicidal activity of two monoterpenoids and SER-2 tyramine receptor of *Caenorhabditis elegans*. *Biochem. Pharmacol.* **2010**, *79*, 1062−1071.
(29) Kang, J. S.; Kim, E.; Lee, S. H.; Park, I. K. Inhibition of acetylcholinesterases of the pine wood nematode, *Bursaphelenchus xylophilus*, by phytochemicals from plant essential oils. *Pestic. Biochem. Physiol.* **2013**, *105*, 50−56.
(30) Kang, J. S.; Moon, Y. S.; Lee, S. H.; Park, I. K. Inhibition of acetylcholinesterases and glutathione S-transferase of pinewood nematode (*Bursaphelenchus xylophilus*) by aliphatic compounds. *Pestic. Biochem. Physiol.* **2013**, *105*, 184−188.

(OXPHOS) machinery. Reprogramming energy metabolism has been demonstrated to be a cancer hallmark.[14] Most cancer cells exhibit high glycolysis capacity and low mitochondrial respiration even in the presence of oxygen, which is recognized as the "Warburg effect". Compelling evidence suggests that the Warburg effect might result from mitochondrial dysfunction, activation oncogenes (e.g., Ras and Myc), oncogenic alterations (e.g., c-myc and p53), or environmental stresses (e.g., hypoxia and inflammation).[15] Recent studies demonstrate that glycolysis not only generates ATP but also provides carbon-containing intermediates (such as pyruvate and glucose-6-phosphate) for cancer progression. These intermediates can be diverted to amino acid and ribose for nucleotide to supply the nutrients that the fast-growing cancer cells need. In addition, the over-expression of glycolysis in cancer cells will produce a lot of lactate, which can acidify the tumor microenvironment.[16] The acidity of the microenvironment has been reported to promote cancer metastasis, which is probably mediated by pH-dependent activation of proteases, such as MMPs and cathepsins, that degrade the tumor extracellular matrix.[17] Thus, targeting both mitochondrial OXPHOS and glycolysis to selective inhibition of energy metabolism of cancer cells may be an attractive strategy for the treatment of metastatic cancer.

Butein (3,4,2′,4′-tetrahydroxychalcone) is a chalcone derivative extracted from the heartwood of *Dalbergia odoriferau*. Butein can also be identified in the barks of *Rhus verniciflua* and *Semecarpus anacardiu*.[18] The extract of natural chalcone butein has been found with reported benefits including antioxidant, anti-inflammatory, and antirestenosis activities.[19−21] Emerging studies have shown that butein exhibits an antiangiogenesis property and antiproliferation and apoptotic effects against numerous lines of cancer cells.[22−25] However, the effects of butein on cancer metastasis and the energy metabolism of cancer cells are not fully understood. The purpose of this study was to determine the antimetastatic effect and mechanism of butein in vitro and in vivo.

## MATERIALS AND METHODS

**Materials.** Butein was purchased from Extrasynthese Corp. (Genay, France). Crystal violet and other chemicals were obtained from Sigma-Aldrich (St. Louis, MO, USA). Rabbit monoclonal antibodies specific for p-ERK1/2, ERK1/2, and p-p70S6K, as well as mouse monoclonal antibody specific for p-IκBα, were obtained from Cell Signaling Technologies (Boston, MA, USA). Rabbit monoclonal antibodies specific for p-Akt, Akt, p-mTOR, p-NF-κB/p65, MMP-9, and GAPDH were obtained from Epitomics (Burlingame, CA, USA). Anti-mouse and anti-rabbit IgG-conjugated horseradish peroxidase and rabbit polyclonal antibody specific for uPA were obtained from Santa Cruz Biotechnology (Santa Cruz, CA, USA). Dulbecco's modified Eagle's medium (DMEM), fetal bovine serum (FBS), and other cell culture reagents were purchased from Gibco (Grand Island, NY, USA).

**Cell Culture.** The human hepatocellular carcinoma (HCC) cell line SK-Hep-1 was purchased from American Type Culture Collection (ATCC, Manassas, VA, USA). SK-Hep-1 cells were maintained in humidified air containing 5% $CO_2$ at 37 °C with DMEM containing 10% FBS, penicillin (100 units/mL), streptomycin (100 μg/mL), and L-glutamine (2 mM).

**In Vitro Metastasis Analysis.** Cell invasion and migration assays were performed using Transwell inserts (Corning, Corning, NY, USA) to assess in vitro metastasis of cancer cells. For invasion assay, filters were precoated with 30 μL of Matrigel (BD Biosciences, Bedford, MA, USA) for 30 min. Approximately $5 \times 10^4$ cells in 100 μL of serum-free medium were placed in the upper chamber, and 500 μL of the same medium containing 10% FBS in the absence or presence of butein was placed in the lower chamber in both invasion and migration assays. After 12 h of treatment, cells on the upper side of the filters were mechanically removed by cotton-tipped swabs, then cells on the lower side were fixed in methanol for 15 min and stained with 0.05% crystal violet for 15 min. The invaded or migrated cells were photographed and quantified by counting the number of stained cells under a microscope.

**In Vivo Metastasis Analysis.** The chorioallantoic membrane (CAM) intravasation model was performed to evaluate tumor cell metastasis as described previously.[26] After treatment with butein for 12 h, surviving cells ($10^6$ cells) were collected and resuspended in 50 μL of serum-free DMEM and inoculated onto the CAM of a 9-day-old chick embryo, in which an artificial air sac was created (designated "upper CAM"). After 48 h of incubation, the lower half of the CAM (designated "lower CAM") was removed and stored frozen at −80 °C. Genomic DNA of the frozen tissue was purified from lower CAM by the DNA Isolation Kit. To determine human cells in the chick tissues, the primers specific for human *alu* sequence (5′-ACGCCTGTAATCCCAGCACTT-3′/5′-TCGCCCAGGCTGGAGTGCA-3′) were used to amplify the human *alu* repeats present in genomic DNA that was isolated from chick tissues. A quantitative measure of amplifiable chick DNA was examined by amplification of chick GAPDH genomic DNA sequence with chGAPDH primers (5′-GAGGAAAGGTCGCCTGGTGGATCG-3′/5′-GGTGAGGACAAGCAGTGAGGAACG-3′). The cycling conditions were 10 min of polymerase activation at 95 °C followed by 30 cycles at 95 °C for 30 s, 58 °C for 45 s, and 72 °C for 45 s and a final incubation at 72 °C for 10 min. Finally, PCR products were conducted on the agarose gel and visualized using ethidium bromide.

**Cell Viability Analysis.** Cells ($10^4$ cells/well) were incubated in 96-well plates. After 24 h of incubation, the culture medium was removed and treated with butein for 12 or 24 h. Then, cell survival was determined using the MTT colorimetric assay. The absorbance at 550 nm was measured using a FlexStation 3 microplate reader (Molecular Devices, Sunnyvale, CA, USA).

**MMP-9 and uPA Activity Assay.** After treatment, the medium was collected and stored at −80 °C. Then, MMP-9 and uPA activities in the medium were determined and quantified using MMP-9 and uPA ELISA kits (R&D Systems, Minneapolis, MN, USA).

**Western Blot Analysis.** The cellular lysates were prepared according our previous instruction.[27] Proteins were resolved by 8−12% sodium dodecyl sulfate−polyacrylamide gel electrophoresis and immunoblotted with specific primary antibodies. Then, the blots were subsequently incubated with the secondary antibody, and the signals were determined using the chemiluminescent assay kit (Amersham, Buckinghamshire, UK).

**RT-PCR Analysis.** Total RNA was extracted from cells by using a TRIzol kit (MDBio Inc., Taipei, Taiwan). First-strand cDNA was synthesized with random primer and moloney murine leukemia virus reverse transcriptase (M-MLV RT). The primer sequences used for amplification were listed as follows: MMP-9, 5′-TGGGCTACGTGACCTATGAC-3′/5′- CAAAGGTGAGAAGAGAGGGC-3′; uPA, 5′-AGAATTCTACCGACTATCTC-3′/5′- ATTCTCTTCCTTGGTGTGAC-3′; PAI, 5′-TGGTTCTGCCCAAGTTCTCC-3′/5′-GACAGCTGTGGATGAGGAGG-3′; uPAR, 5′- CCGAGGTTGTGTGTGGGTTA-3′/5′-ATGCATTCGAGGTAACGGCT-3′; TIMP-1, 5′-TTGGCTTCTGCACTGATGGT-3′/5′-TAAATGTCCACGCTAGGGGC-3′; GAPDH, 5′-TGATGACATCAAGAAGGTGGTGAAG-3′/5′-TCCTTGGAGGCCATGTGGGCCAT-3′. The cycling conditions were 5 min of polymerase activation at 94 °C followed by 30 cycles at 94 °C for 1 min, 60 °C for 1 min, and 72 °C for 1 min and a final incubation at 72 °C for 10 min. The PCR products were separated on the agarose gel and visualized using ethidium bromide.

**Bioenergetic Function Analysis.** The XF24 Analyzer (Seahorse Bioscience, North Billerica, MA, USA) was used to determine the bioenergetic metabolism of cancer cells. Cells ($2 \times 10^4$ cells/well) were seeded in an XF24 24-well plate and were allowed to grow for 1 day. Culture medium was next replaced 1 h prior to measurement by the assay medium that contained unbuffered DMEM with or without butein and incubated in a 37 °C incubator for 30 min to stabilize the pH and temperature. Then, the plate was transferred into the incubation chamber of the XF24 Analyzer for real-time determination of the oxygen consumption rate (OCR) and extracellular acidification rate (ECAR).

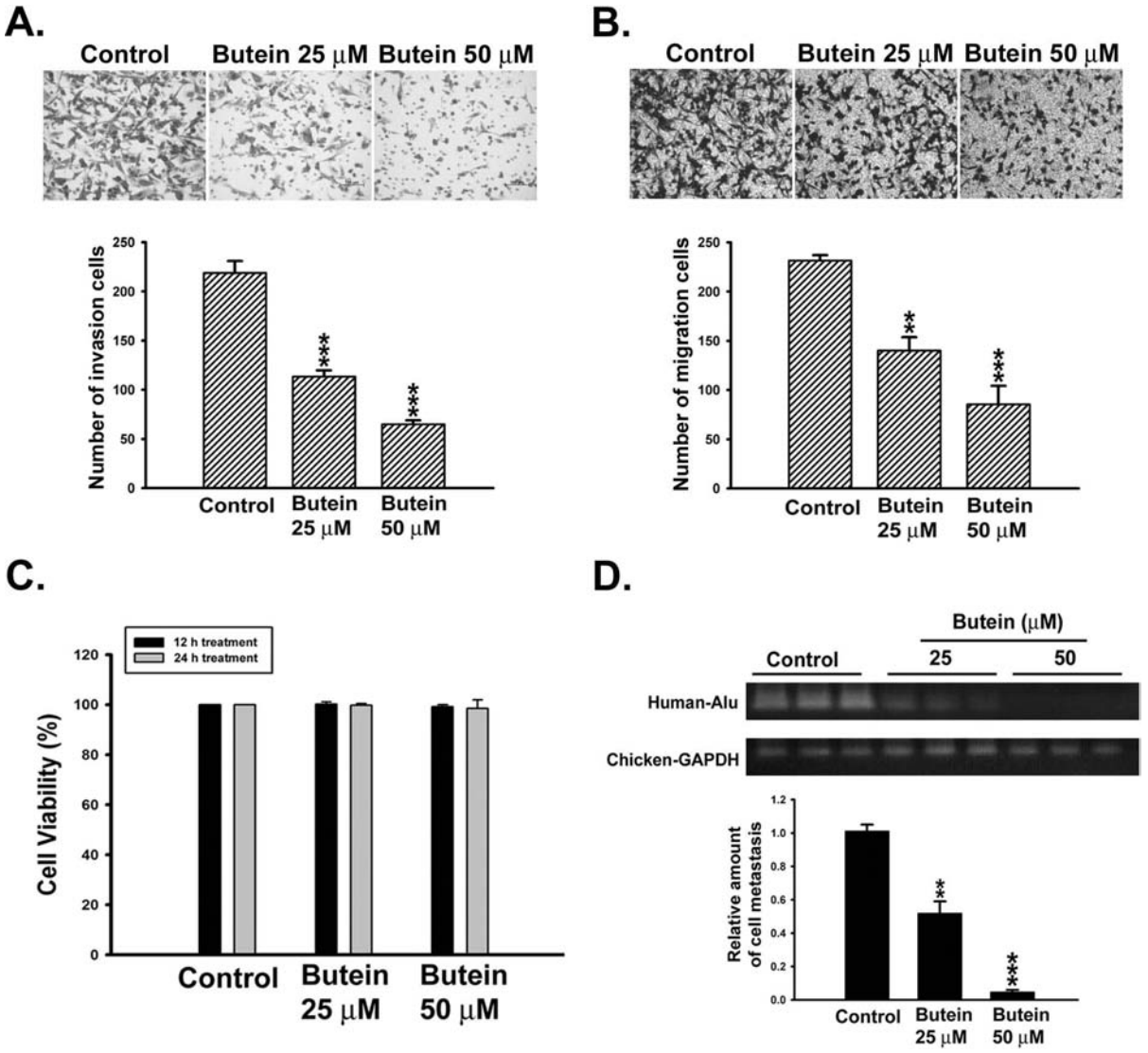


**Figure 1.** Effect of butein on cancer metastasis in vitro and iv vivo. SK-Hep-1 cells were seeded onto the upper chamber consisting of 8 mm pore size filters and then treated with the indicated concentration of butein for 12 h in medium containing 10% FBS as a chemoattractant in the lower chamber for the analysis of cell invasion (A) and migration (B). (C) SK-Hep-1 cells were treated with the indicated concentrations of butein for 12 and 24 h in medium containing 10% FBS, and the cell viability was determined using the MTT assay. (D) SK-Hep-1 cells were treated with the indicated concentrations of butein for 12 h and then subjected to CAM-intravasation assay coupled with the Alu PCR-based assay. The cancer cells in the chick embryo lower CAM were determined using PCR of the human genome-specific Alu sequence with chick GAPDH specific primers as the control. The quantitative detection for the relative amount of cell metastasis was represented and normalized against chick GAPDH. Data are expressed as the mean ± SEM of four independent experiments. (**) $p < 0.01$ and (***) $p < 0.001$ compared with the control group.

The program Seahorse of the XF24 Analyzer was set according to the manufacturer's protocol, and the data were represented in picomoles per minute per $10^4$ cells for OCR and in milli-pH units per minute per $10^4$ cells for ECAR to allow comparison between independent experiments.

**ATP Content Assay.** The intracellular ATP level was measured by Luminescent ATP Detection Assay (Abcam, Cambridge, UK). After treatment, 50 $\mu$L of detergent was added to 100 $\mu$L of medium in each well to release the intracellular ATP. Half of the mixture was then transferred into a black 96-well plate containing 50 $\mu$L of substrate solution, and the luminescence intensity was measured using FlexStation 3 (Molecular Devices).

**Reporter Gene Assay.** Transfection was performed using Lipofectmine 2000 (Invitrogen, Carlsbad, CA, USA) according to the manufacturer's protocol. Cells were cotransfected with NF-$\kappa$B promoter plasmid (pNF-$\kappa$B-Luc) and *Renilla* luciferase reporter vector (phRG-TK). After 24 h of transfection, cells were treated with butein for 12 h. Cell extracts were then prepared, and the activities of firely and *Renilla* luciferases were measured by DLR assay system (Promega, Madison, WI, USA) using FlexStation 3 (Molecular Devices).

**Statistics.** Data are presented as the mean ± standard error of mean (SEM). Statistical analyses of data were done with one-way ANOVA followed by Student's *t* test. The difference is significant if the *p* value is <0.05.

## RESULTS

**Butein Inhibits Cancer Metastasis without Cytotoxicity.** We first applied a Transwell chamber assay to explore the antimetastatic effect of butein in vitro. As shown in Figure 1A,B, butein significantly inhibited both invasion and migration of hepatocellular carcinoma SK-Hep-1 cells in a concentration-dependent manner after 12 h of treatment. We next examined the cytotoxicity of butein by the MTT assay. Butein did not inhibit cell viability at 12 h. The cytotoxicity of butein was limited even


dx.doi.org/10.1021/jf502370c | J. Agric. Food Chem. 2014, 62, 9109−9117

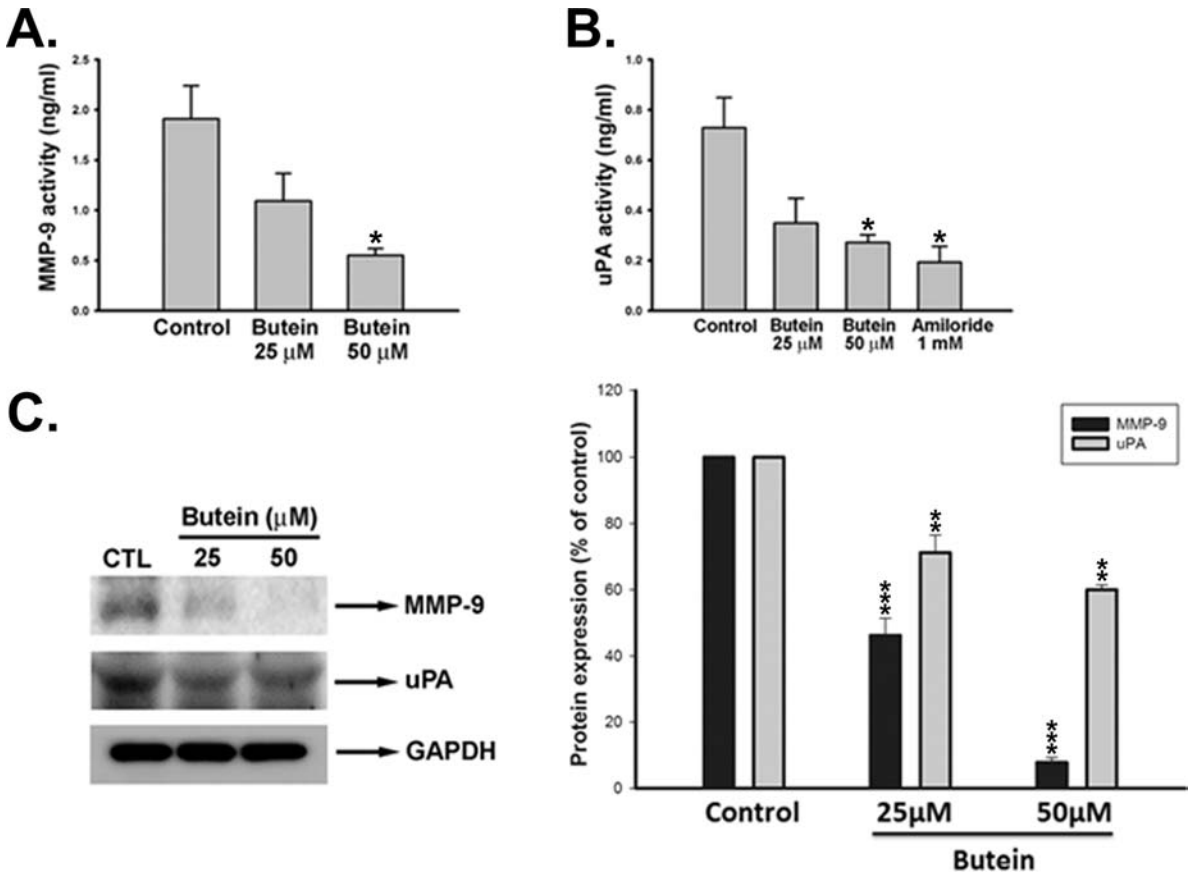


**Figure 2.** Effect of butein on the enzyme activity and protein expression of MMP-9 and uPA. SK-Hep-1 cells were treated with the indicated concentration of butein for 12 h in medium containing 10% FBS. Then each conditioned medium was collected and subjected to ELISA for analysis of proteolytic activities of MMP-9 (A) and uPA (B). Total cell lysates were corrected for the detection of MMP-9 and uPA protein expression by Western blot analysis (C). The quantitative densitometry of the relative level of protein was performed with Image-Pro Plus. Data are expressed as the mean ± SEM of three independent experiments. (∗) $p < 0.05$, (∗∗) $p < 0.01$, and (∗∗∗)$p < 0.001$ compared with the control group.

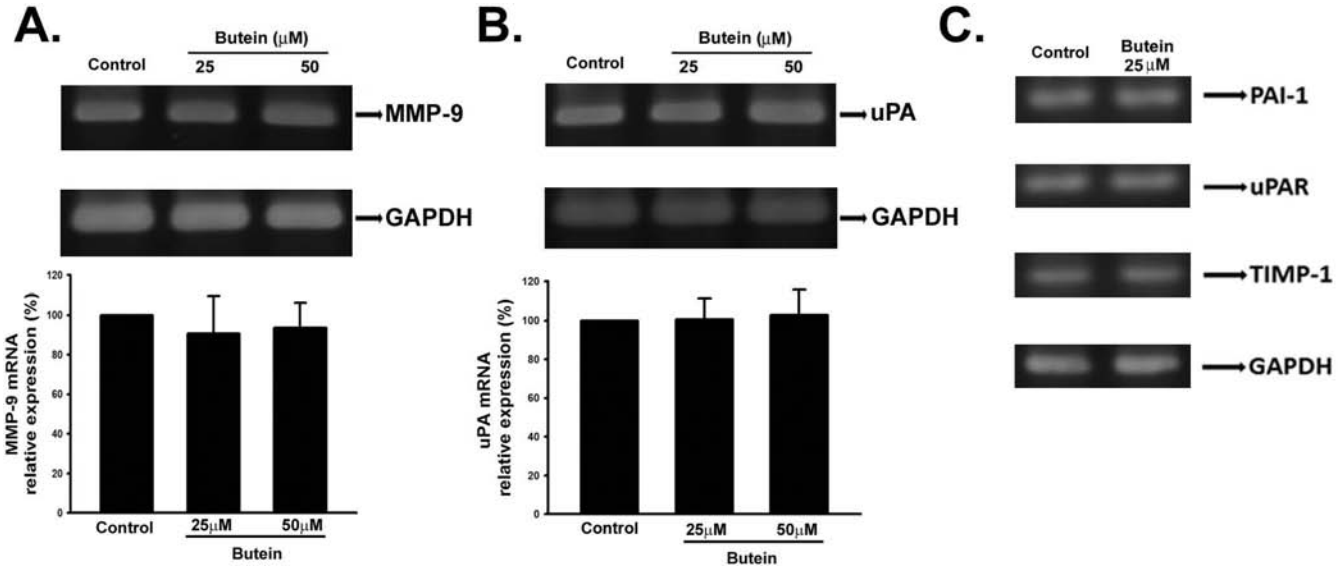


**Figure 3.** Effect of butein on the mRNA expression of MMP-9 and uPA. SK-Hep-1 cells were treated with the indicated concentration of butein for 6 h. The mRNA level of MMP-9 (A), uPA (B), and PAI-1, uPAR, and TIMP-1 (C) was determined using reverse RT-PCR. The quantitative densitometry of the relative level of mRNA was performed with Image-Pro Plus. Data are expressed as the mean ± SEM of four independent experiments.

under the long-term (24 h) treatment (Figure 1C). Our results demonstrate that the inhibitory effect of butein on cell invasion and migration is not due to its cytotoxicity. To investigate whether butein affects cancer metastasis in vivo, we performed a metastatic animal model by CAM-intravasation assay. SK-Hep-1 cells were treated with butein for 12 h before being seeded on the


dx.doi.org/10.1021/jf502370c | J. Agric. Food Chem. 2014, 62, 9109−9117

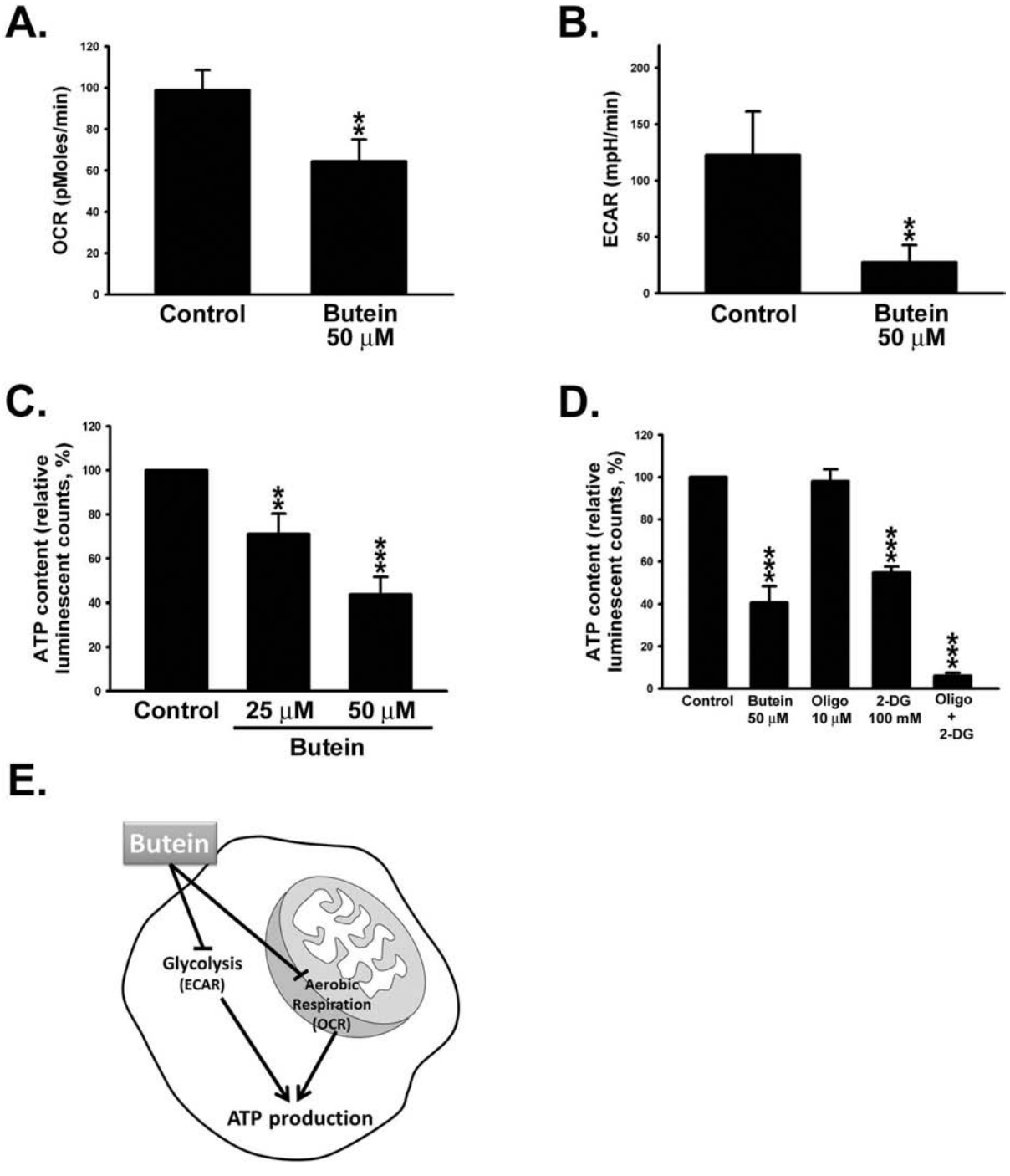


**Figure 4.** Effect of butein on the changes of bioenergetics. SK-Hep-1 cells were treated without or with butein (50 $\mu$M) for 2 h, and the OCR (A) and ECAR (B) were determined using Seahorse XF24 analyzer. Cells were treated with the indicated concentration of butein for 6 h, and the ATP production was examined by ATP content assay (C). In addition, cells were exposed to oligomycin (Oligo), 2-deoxyglucose (2-DG), or oligomycin combined with 2-DG to validate the effect of butein on ATP production in SK-Hep-1 cells (D). Data are expressed as the mean ± SEM of four independent experiments. (**) $p < 0.01$ and (***)$p < 0.001$ compared with the control group. (E) Schematic presentation of butein-mediated bioenergetics modulation. Butein inhibits ATP production through suppression of mitochondrial respiration and glycolysis on cancer cells.

upper CAM. Following 48 h of incubation, cells invading the lower CAM were determined by PCR for human *Alu* gene (h-Alu) and then normalized to chick GAPDH. We found that butein repressed the metastasis of SK-Hep-1 cells, which was in accordance with the results from the Trasnwell chamber assay (Figure 1D). Collectively, our findings indicate that noncytotoxic concentrations of butein significantly inhibit cancer metastasis in vitro and in vivo.

**Butein Inhibits MMP-9 and uPA Expression and Activity without Repressing Their mRNA Expression.** MMP-9 and uPA are the key enzymes participating in cell migration and invasion as well as metastasis.[2] We next investigated the molecular targets of butein-mediated inhibition of the invasive phenotype of SK-Hep-1 cells by determining the involvement of MMP-9 and uPA. ELISA was used to examine the effects of butein on MMP-9 and uPA enzyme activities. The data


dx.doi.org/10.1021/jf502370c | J. Agric. Food Chem. 2014, 62, 9109−9117

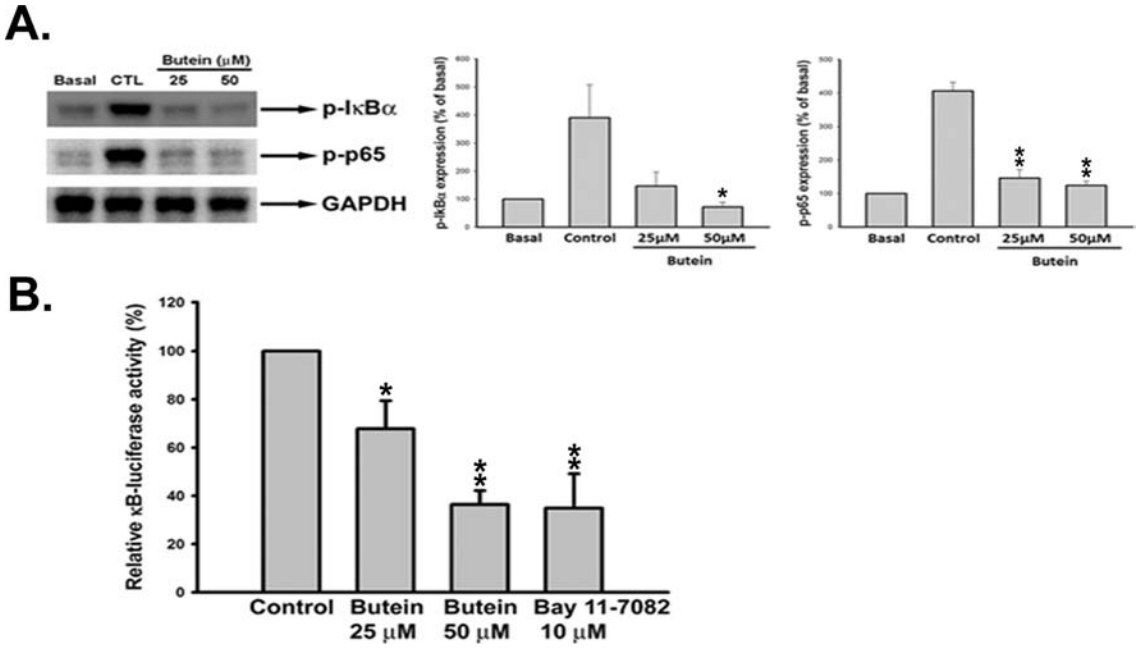


**Figure 5.** Effect of butein on NF-$\kappa$B activation. (A) Serum-starved cells were treated with vehicle (basal) or 10% FBS in the absence (control) or presence the indicated concentration of butein for 15 min. Cells were harvested and lysed for the detection of p-I$\kappa$B$\alpha$ and p-p65 by Western blot analysis. The quantitative densitometry of the relative level of protein was performed with Image-Pro Plus. (B) Cells cotransfected with pNF-$\kappa$B-Luc and phRG-TK vector were treated with butein (25, 50 $\mu$M) or BAY 11-7082 (10 $\mu$M) in medium containing 10% FBS. After 12 h of treatment, the promoter luciferase activities were detected using a luminometer. Data are expressed as the mean ± SEM of three independent experiments. (*) $p < 0.05$ and (**) $p < 0.01$ compared with the control group.

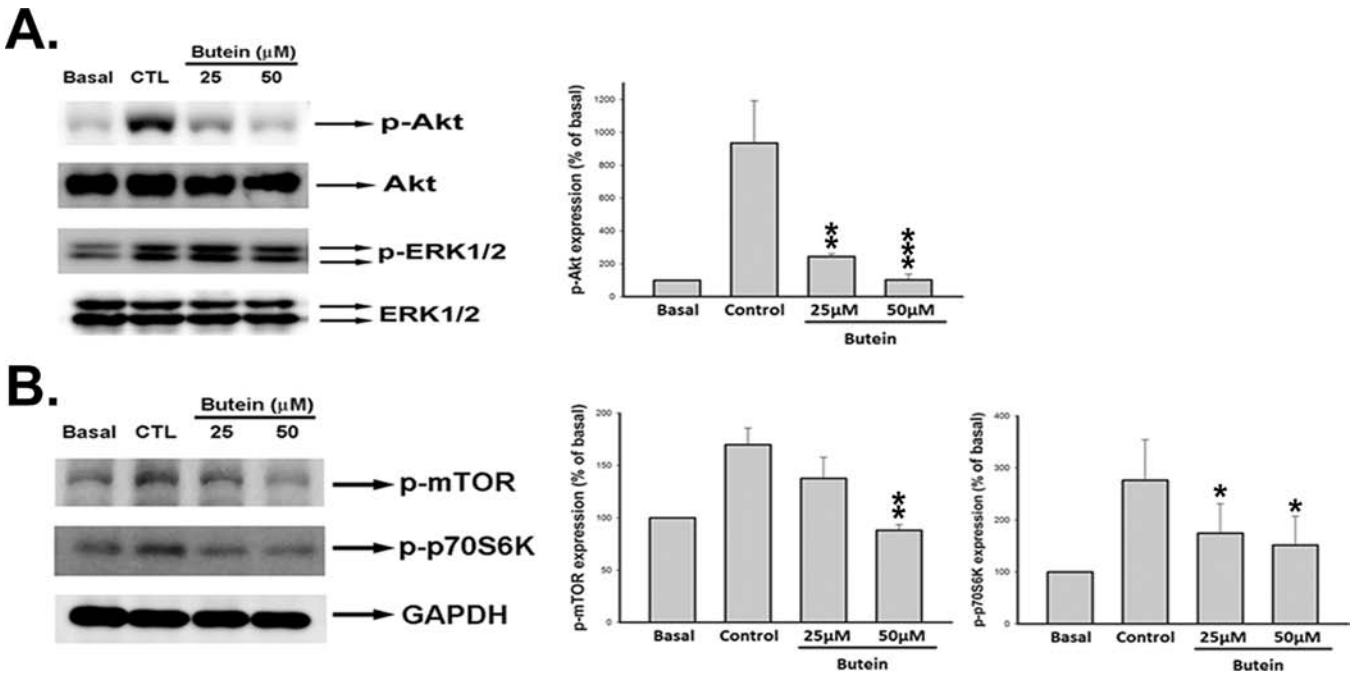


**Figure 6.** Effect of butein on Akt/mTOR/p70S6K translational signaling pathway. Serum-starved cells were treated with vehicle (basal) or 10% FBS in the absence (control) or presence of the indicated concentration of butein for 15 min. Cells were harvested and lysed for the detection of p-Akt and p-ERK1/2 (A) or p-mTOR and p-p70S6K (B) by Western blot analysis. The quantitative densitometry of the relative level of protein was performed with Image-Pro Plus. Data are expressed as the mean ± SEM of four independent experiments. (*) $p < 0.05$, (**) $p < 0.01$, and (***) $p < 0.001$ compared with the control group.

showed that butein dramatically repressed both MMP-9 and uPA activities (Figure 2A,B). Amiloride was used as a positive control for suppressing uPA activity. We further found that treatment with butein for 12 h caused the concentration-dependent inhibition of MMP-9 and uPA protein expression (Figure 2C). However, butein did not affect the mRNA expression of MMP-9 and uPA at the earlier time point (6 h) (Figure 3A,B). We then investigated whether butein inhibits TIMP-1 and PAI-1, which are MMP-9 and uPA endogenous inhibitors, respectively. It turned out that butein did not repress the mRNA expression of


dx.doi.org/10.1021/jf502370c | J. Agric. Food Chem. 2014, 62, 9109−9117

TIMP-1 and PAI-1. We also found that butein did not repress the mRNA expression of uPAR, which is a uPA receptor (Figure 3C). These results suggest that TIMP-1, PAI-1, and uPAR are not molecular targets of butein-mediated antimetastatic effect. Butein may suppress cancer metastasis through inhibition of MMP-9 and uPA proteolytic activities at the translational level.

**Butein Inhibits ATP Synthesis through Suppression of OXPHOS and Glycolysis.** Deregulated energetics is a property of most cancer cells. Aerobic glycolysis and mitochondrial oxidative biogenesis can produce the intracellular ATP that cells need.[13] Here, we further evaluated the impact of butein on energy metabolism of cancer cells. We evaluated the oxidative metabolism by measuring the oxygen consumption rate (OCR) and aerobic glycolysis by measuring the extracellular acidification rate (ECAR) after treatment of butein for 2 h using the Seahorse Bioscience XF24 cellular bioenergetics analyzer platform. As shown in Figure 4A, SK-Hep-1 cells treated with butein exhibited significantly reduced OCR compared with the respective control. Additionally, butein also markedly suppressed ECAR in SK-Hep-1 cells (Figure 4B). To understand if the inhibition of OCR and ECAR is correlated with energy levels, the intracellular ATP content was measured in butein-treated cells. We found that butein decreased the ATP production in a concentration-dependent manner (Figure 4C). To validate butein-mediated ATP reduction, mitochondrial OXPHOS inhibitor oligomycin and glycolysis inhibitor 2-deoxyglucose (2-DG) were used as positive controls in ATP content analysis. The results showed that oligomycin did not affect the intracellular ATP content, but 2-DG significantly inhibited the ATP production (Figure 4D). Moreover, the combination of oligomycin and 2-DG induced a dramatic reduction of ATP content. These results suggest that butein may repress ATP production and block cancer metastasis by suppressing both oxidative and glycolytic metabolism.

**Butein Inhibits NF-κB and Akt/mTOR/p70S6K Signaling Pathways.** We then investigated the signaling pathway underlying the butein-mediated antimetastasis property. It has been reported that butein inhibits the NF-κB activation pathway to exhibit antitumor and anti-inflammatory activities.[18] As shown in Figure 5A, treatment of 10% FBS for 15 min potently increased the phosphorylation of IκBα and p65, and butein significantly suppressed FBS-induced IκBα and p65 phosphorylation. Additionally, a NF-κB binding site-driven luciferase activity assay was carried out to confirm this result. We found that FBS-induced κB-luciferase activity was attenuated by butein (Figure 5B). A selective NF-κB inhibitor (BAY 11-7082) was used as the positive control. Because butein does not inhibit the transcription of MMP-9 and uPA, we next investigated whether the translational machinery was involved in butein-regulated protein inhibition of MMP-9 and uPA. Our data indicated that butein significantly decreased the phosphorylation of Akt, but did not decrease the phosphorylation of ERK1/2 in SK-Hep-1 cells (Figure 6A). The important downstream effector of PI3K/Akt pathway termed mTOR is recognized to modulate the translational machinery by inducing p70S6K phosphorylation.[28] Herein we investigated whether butein regulated these signaling pathways in SK-Hep-1 cells. As shown in Figure 6B, 10% FBS dramatically increased the phosphorylation of mTOR and p70S6K. Butein inhibited the phosphorylation of mTOR and its downstream effector p70S6K in a concentration-dependent manner. On the basis of these finding, we suggest butein may repress MMP-9 and uPA proteolytic activities and subsequently inhibit cancer metastasis via the Akt/mTOR/p70S6K translational signaling pathway.

## DISCUSSION

Metastasis is one of the most deadly steps in cancer progression, and the acquisition of the ability to invade surrounding tissue is one of the most important prerequisites for cancer cells to undergo metastasis.[1,2] The development of promising therapeutic agents against cancer invasion and metastasis is urgently needed. This study showed that butein, a naturally occurring chalcone derivative, significantly inhibited invasion and migration of cancer cells without acting in a cytotoxic fashion (Figure 1A−C). It has been reported that butein decreased cell growth, migration, and invasion of SK-Hep-1 cells.[25] Those results showed that butein inhibited migration and invasion at concentrations of 50 and 75 μM with 24 and 48 h of treatment; under this condition butein also dramatically induced cell death in SH-Hep-1 cells. These data indicate that the finding of butein-mediated inhibitory effects on cancer migration and invasion is due to its cytotoxicity. As compared with the Ma et al. study, our experiments provided promising evidence for the anti-invasive function of butein. Here, we demonstrated that butein exhibited an anti-invasive property at low concentration (25 and 50 μM) under short-term treatment (12 h) without inducing significant cell death of SK-Hep-1 cells. Notably, we found that butein significantly attenuated the metastasis of SK-Hep-1 cells using an in vivo CAM-intravasation model. The chicken CAM assay is one of the models for evaluating angiogenesis. Several innovative studies have established the chicken embryo as a useful model to investigate cancer metastasis.[26,29] Our results showed that butein induced a concentration-dependent inhibition of the intravasation of cancer cells in chick embryo CAM (Figure 1D). Taken together, we demonstrate that noncytotoxic concentrations of butein exert the antimetastatic effect in vitro and in vivo, suggesting butein may be a potential therapeutic agent worthy of further development for cancer treatment.

MMP-9 and uPA are two crucial matrix-degrading proteases in the progression of cancer invasion. They enable cancer cells to decompose and escape from the ECM of the primary tumor site and undergo the invasion−metastasis cascade.[4,11] Here, we found that butein markedly inhibited both MMP-9 and uPA enzyme activities (Figure 2). Moreover, butein repressed the protein expressions of MMP-9 and uPA without altering the mRNA level of MMP-9 and uPA (Figure 3). Several studies have shown that targeting and blocking the expression of MMP-9 or uPA profoundly suppressed the invasion of cancer cells.[30,31] Furthermore, in vivo evidence from the chicken CAM assay showed that u-PA and MMPs are interdependent and play the important role in the intravasation of cancer cells.[26] Thus, we suggest that butein may reduce cancer metastasis through suppression of MMP-9 and uPA. Because butein caused the inhibition of MMP-9 and uPA proteolytic activities at the translation level, we examined the translational signaling pathway in butein-treated cells. The translation of protein from mRNA is modulated by many signaling pathways. Among these pathways, Akt/mTOR translational machinery is the most intensively studied pathway.[32] Emerging evidence indicates that mTOR controls cap-dependent mRNA translation by activation of its downstream p70S6K and 4E-BP1. Importantly, the mTOR signaling pathway is commonly up-regulated in various tumor cells and is a potential target for cancer therapy.[28,33] Herein we demonstrated that butein dramatically blocked the phosphorylation of Akt, mTOR, and p70S6K, which could repress the recruitment of signals needed for protein translation of MMP-9 and uPA (Figure 6). Previous papers showed that activation of

the mTOR pathway can promote the synthesis of MMP-9 and uPA.[34−36] Our previous study also indicated that butein inhibited angiogenesis through the Akt/mTOR translational pathway in human endothelial progenitor cells.[22] Collectively, these results demonstrate the antimetastatic effect of butein may be through down-regulation of MMP-9 and uPA regulated by Akt/mTOR/p70S6K translational machinery.

Glycolysis and mitochondrial oxidative phosphorylation are the major sources of cellular energy. Deregulated cellular energetics is now recognized as an emerging hallmark of cancer.[15] The Warburg effect or aerobic glycolysis is characterized by increased glucose uptake, lactate export, and extracellular acidification of cancer cells to acquire energy, even in the presence of oxygen. Aerobic glycolysis is predominately up-regulated in cancer cells and contributes to tumor growth and aggressiveness through acidification of the extracellular environment.[14] However, the modulation of butein on energy metabolism of cancer cells has not been well explored. The present study demonstrated that suppression of glycolytic and oxidative metabolism by butein resulted in the reduction of ATP contents in SK-Hep-1 cells, although cell viability was not affected (Figure 4). In addition, we found that glycolysis inhibitor 2-DG but not OXPHOS inhibitor oligomycin reduced ATP production in SK-Hep-1 cells. Wu et al. have shown that the cellular ATP content was nearly unchanged by oligomycin in H460 and A549 cells, suggesting that glycolytic ATP generation was sufficient to maintain the energy balance.[37] On the other hand, 2-DG markedly decreased ATP production in both cell lines, indicating these cancer cells were intimately dependent on the glycolysis pathway to generate ATP. Here, we showed that SK-Hep-1 cells exhibited a dependency on glycolysis for bioenergetics. This extremely high glycolysis activity of SK-Hep-1 cells may be associated with its highly invasive characteristic. Several findings demonstrated that the inhibition of glycolysis can indeed repress the invasion and metastasis of cancer cells.[38] Extracellular acidity is the important constituent of the invasive microenvironment that promotes cancer progression. Thus, we suggest that butein may partly suppress cancer metastasis by down-regulating ATP synthesis via glycolytic and oxidative metabolism. It has been reported that mTOR is a direct sensor of intracellular ATP concentration. The phosphorylation of mTOR can also be affected by intracellular ATP levels. An enzyme kinetics study shows that the Michaelis constant ($K_m$) of mTOR for ATP is about 1 mM, whereas most protein kinases have $K_m$ values for ATP of 10−20 $\mu$M, indicating that there is a tighter positive correlation between the phosphorylation level of mTOR and the concentration of ATP than for other kinases.[39] Therefore, butein-mediated ATP reduction may repress mTOR signaling and its downstream cascades in cancer cells.

Earlier studies have shown that the activity of transcription factor NF-$\kappa$B is responsible for the transcription of MMP-9 and uPA.[40] Butein can suppress the transcription activity of NF-$\kappa$B to block cancer progression.[18] Our data also demonstrated that NF-$\kappa$B activation was attenuated by butein (Figure 5). However, butein did not affect the mRNA levels of MMP-9 and uPA, indicating butein may inhibit cancer metastasis through suppression of MMP-9 and uPA via a NF-$\kappa$B-independent pathway. In conclusion, this study provides evidence that butein may inhibit Akt/mTOR/p70S6K translational machinery, leading to down-regulation of MMP-9 and uPA, and subsequently exhibit the antimetastatic effect. We demonstrate for the first time that butein may alter oxidative and glycolytic metabolism to suppress ATP-dependent cancer metastasis. The detailed mechanism between butein-mediated bioenergetics modulation and the antimetastasis property needs to be investigated in the future.

## AUTHOR INFORMATION


### Corresponding Author

*(S.-W.W.) Mail: Department of Medicine, Mackay Medical College, No. 46, Sec. 3, Zhongzheng Rd., Sanzhi Dist., New Taipei City, Taiwan. Phone: 886-2-26360303, ext. 1219. Fax: 886-2-26361295. E-mail: shihwei@mmc.edu.tw.

### Author Contributions

‖Shih-Chia Liu and Ching-Hu Chung contributed equally to this work.


### Author Contributions

Chih-Hsin Tang and Shih-Wei Wang conceived and designed the experiments. Shih-Chia Liu, Chi Chen, and Ching-Hu Chung performed the experiments. Jen-Kun Cheng, Yu-Wei Lai, Hui-Lung Sun, and Chieh-Yu Peng analyzed the data. Po-Chuan Wang and Nan-Lin Wu contributed reagents/materials/analysis tools. Shih-Chia Liu and Shih-Wei Wang wrote the manuscript.


### Funding

This work was supported by grants from the National Science Council of Taiwan (NSC 101-2320-B-715−002 -MY3), Mackay Medical College (MMC-981A05), and Mackay Memorial Hospital (MMH-MM-10303; MMH-HB-10201).


### Notes

The authors declare no competing financial interest.

## ABBREVIATIONS USED

ATP, adenosine triphosphate; CAM, chorioallantoic membrane; ECAR, extracellular acidification rate; mTOR, mammalian target of rapamycin; MTT, 3-(4,5-dimethylthiazol-2-yl)-2,5-diphenyl tetrazolium bromide; MMP-9, matrix metalloproteinase-9; uPA, urokinase plasminogen activator; OCR, oxygen consumption rate; p70S6K, 70 kDa ribosomal protein S6 kinase; NF-$\kappa$B, nuclear factor kappa-light-chain-enhancer of activated B cells

## REFERENCES


(1) Jemal, A.; Bray, F.; Center, M. M.; Ferlay, J.; Ward, E.; Forman, D. Global cancer statistics. *CA Cancer J. Clin* **2011**, *61*, 69−90.

(2) Chaffer, C. L.; Weinberg, R. A. A perspective on cancer cell metastasis. *Science* **2011**, *331*, 1559−1564.

(3) Deryugina, E. I.; Quigley, J. P. Matrix metalloproteinases and tumor metastasis. *Cancer Metastasis Rev.* **2006**, *25*, 9−34.

(4) Gialeli, C.; Theocharis, A. D.; Karamanos, N. K. Roles of matrix metalloproteinases in cancer progression and their pharmacological targeting. *FEBS J.* **2011**, *278*, 16−27.

(5) Dass, K.; Ahmad, A.; Azmi, A. S.; Sarkar, S. H.; Sarkar, F. H. Evolving role of uPA/uPAR system in human cancers. *Cancer Treat. Rev.* **2008**, *34*, 122−136.

(6) Sasaki, M.; Kashima, M.; Ito, T.; Watanabe, A.; Izumiyama, N.; Sano, M.; Kagaya, M.; Shioya, T.; Miura, M. Differential regulation of metalloproteinase production, proliferation and chemotaxis of human lung fibroblasts by PDGF, interleukin-1$\beta$ and TNF-$\alpha$. *Mediators Inflamm.* **2000**, *9*, 155−160.

(7) Cho, A.; Graves, J.; Reidy, M. A. Mitogen-activated protein kinases mediate matrix metalloproteinase-9 expression in vascular smooth muscle cells. *Arterioscler. Thromb. Vasc. Biol.* **2000**, *20*, 2527−2532.

(8) St-Pierre, Y.; Couillard, J.; Van Themsche, C. Regulation of MMP-9 gene expression for the development of novel molecular targets against cancer and inflammatory diseases. *Expert Opin. Ther. Targets* **2004**, *8*, 473−489.

(9) Ulisse, S.; Baldini, E.; Sorrenti, S.; D'Armiento, M. The urokinase plasminogen activator system: a target for anti-cancer therapy. *Curr. Cancer Drug Targets* **2009**, *9*, 32−71.
(10) Harbeck, N.; Kates, R. E.; Gauger, K.; Willems, A.; Kiechle, M.; Magdolen, V.; Schmitt, M. Urokinase-type plasminogen activator (uPA) and its inhibitor PAI-I: novel tumor-derived factors with a high prognostic and predictive impact in breast cancer. *Thromb. Haemostasis* **2004**, *91*, 450−456.
(11) Zheng, Q.; Tang, Z. Y.; Xue, Q.; Shi, D. R.; Song, H. Y.; Tang, H. B. Invasion and metastasis of hepatocellular carcinoma in relation to urokinase-type plasminogen activator, its receptor and inhibitor. *J. Cancer Res. Clin. Oncol.* **2000**, *126*, 641−646.
(12) Zhang, Y.; Guan, X. Y.; Dong, B.; Zhao, M.; Wu, J. H.; Tian, X. Y.; Hao, C. Y. Expression of MMP-9 and WAVE3 in colorectal cancer and its relationship to clinicopathological features. *J. Cancer Res. Clin. Oncol.* **2012**, *138*, 2035−2044.
(13) Lee, H. C.; Wei, Y. H. Mitochondrial biogenesis and mitochondrial DNA maintenance of mammalian cells under oxidative stress. *Int. J. Biochem. Cell Biol.* **2005**, *37*, 822−834.
(14) Kroemer, G.; Pouyssegur, J. Tumor cell metabolism: cancer's Achilles' heel. *Cancer Cell* **2008**, *13*, 472−482.
(15) Hanahan, D.; Weinberg, R. A. Hallmarks of cancer: the next generation. *Cell* **2011**, *144*, 646−674.
(16) Koukourakis, M. I.; Giatromanolaki, A.; Harris, A. L.; Sivridis, E. Comparison of metabolic pathways between cancer cells and stromal cells in colorectal carcinomas: a metabolic survival role for tumor-associated stroma. *Cancer Res.* **2006**, *66*, 632−637.
(17) Lardner, A. The effects of extracellular pH on immune function. *J. Leukocyte Biol.* **2001**, *69*, 522−530.
(18) Pandey, M. K.; Sandur, S. K.; Sung, B.; Sethi, G.; Kunnumakkara, A. B.; Aggarwal, B. B. Butein, a tetrahydroxychalcone, inhibits nuclear factor (NF)-κB and NF-κB-regulated gene expression through direct inhibition of IκBα kinase β on cysteine 179 residue. *J. Biol. Chem.* **2007**, *282*, 17340−17350.
(19) Chen, Y. N.; Huang, T. F.; Chang, C. H.; Hsu, C. C.; Lin, K. T.; Wang, S. W.; Peng, H. C.; Chung, C. H. Antirestenosis effect of butein in the neointima formation progression. *J. Agric. Food Chem.* **2012**, *60*, 6832−6838.
(20) Cheng, Z. J.; Kuo, S. C.; Chan, S. C.; Ko, F. N.; Teng, C. M. Antioxidant properties of butein isolated from *Dalbergia odorifera*. *Biochim. Biophys. Acta* **1998**, *1392*, 291−299.
(21) Lee, S. H.; Seo, G. S.; Sohn, D. H. Inhibition of lipopolysaccharide-induced expression of inducible nitric oxide synthase by butein in RAW 264.7 cells. *Biochem. Biophys. Res. Commun.* **2004**, *323*, 125−132.
(22) Chung, C. H.; Chang, C. H.; Chen, S. S.; Wang, H. H.; Yen, J. Y.; Hsiao, C. J.; Wu, N. L.; Chen, Y. L.; Huang, T. F.; Wang, P. C.; Yeh, H. I.; Wang, S. W. Butein inhibits angiogenesis of human endothelial progenitor cells via the translation dependent signaling pathway. *Evidence-Based Complement. Altern. Med.: eCAM* **2013**, *2013*, No. 943187.
(23) Chua, A. W.; Hay, H. S.; Rajendran, P.; Shanmugam, M. K.; Li, F.; Bist, P.; Koay, E. S.; Lim, L. H.; Kumar, A. P.; Sethi, G. Butein downregulates chemokine receptor CXCR4 expression and function through suppression of NF-κB activation in breast and pancreatic tumor cells. *Biochem. Pharmacol.* **2010**, *80*, 1553−1562.
(24) Moon, D. O.; Kim, M. O.; Lee, J. D.; Choi, Y. H.; Kim, G. Y. Butein suppresses c-Myc-dependent transcription and Akt-dependent phosphorylation of hTERT in human leukemia cells. *Cancer Lett.* **2009**, *286*, 172−179.
(25) Ma, C. Y.; Ji, W. T.; Chueh, F. S.; Yang, J. S.; Chen, P. Y.; Yu, C. C.; Chung, J. G. Butein inhibits the migration and invasion of SK-HEP-1 human hepatocarcinoma cells through suppressing the ERK, JNK, p38, and uPA signaling multiple pathways. *J. Agric. Food Chem.* **2011**, *59*, 9032−9038.
(26) Kim, J.; Yu, W.; Kovalski, K.; Ossowski, L. Requirement for specific proteases in cancer cell intravasation as revealed by a novel semiquantitative PCR-based assay. *Cell* **1998**, *94*, 353−362.
(27) Wang, S. W.; Wu, H. H.; Liu, S. C.; Wang, P. C.; Ou, W. C.; Chou, W. Y.; Shen, Y. S.; Tang, C. H. CCL5 and CCR5 interaction promotes cell motility in human osteosarcoma. *PLoS One* **2012**, *7*, No. e35101.
(28) Mamane, Y.; Petroulakis, E.; LeBacquer, O.; Sonenberg, N. mTOR, translation initiation and cancer. *Oncogene* **2006**, *25*, 6416−6422.
(29) Yang, S. F.; Yang, W. E.; Kuo, W. H.; Chang, H. R.; Chu, S. C.; Hsieh, Y. S. Antimetastatic potentials of flavones on oral cancer cell via an inhibition of matrix-degrading proteases. *Arch. Oral Biol.* **2008**, *53*, 287−294.
(30) Huang, H. Y.; Jiang, Z. F.; Li, Q. X.; Liu, J. Y.; Wang, T.; Zhang, R.; Zhao, J.; Xu, Y. M.; Bao, W.; Zhang, Y.; Jia, L. T.; Yang, A. G. Inhibition of human breast cancer cell invasion by siRNA against urokinase-type plasminogen activator. *Cancer Invest.* **2010**, *28*, 689−697.
(31) Kunigal, S.; Lakka, S. S.; Gondi, C. S.; Estes, N.; Rao, J. S. RNAi-mediated downregulation of urokinase plasminogen activator receptor and matrix metalloprotease-9 in human breast cancer cells results in decreased tumor invasion, angiogenesis and growth. *Int. J. Cancer* **2007**, *121*, 2307−2316.
(32) Hay, N.; Sonenberg, N. Upstream and downstream of mTOR. *Genes Dev.* **2004**, *18*, 1926−1945.
(33) Hay, N. The Akt-mTOR tango and its relevance to cancer. *Cancer Cell* **2005**, *8*, 179−183.
(34) Wang, C. H.; Cao, G. F.; Jiang, Q.; Yao, J. TNF-α promotes human retinal pigment epithelial (RPE) cell migration by inducing matrix metallopeptidase 9 (MMP-9) expression through activation of Akt/mTORC1 signaling. *Biochem. Biophys. Res. Commun.* **2012**, *425*, 33−38.
(35) Busch, S.; Renaud, S. J.; Schleussner, E.; Graham, C. H.; Markert, U. R. mTOR mediates human trophoblast invasion through regulation of matrix-remodeling enzymes and is associated with serine phosphorylation of STAT3. *Exp. Cell Res.* **2009**, *315*, 1724−1733.
(36) Murooka, T. T.; Rahbar, R.; Platanias, L. C.; Fish, E. N. CCL5-mediated T-cell chemotaxis involves the initiation of mRNA translation through mTOR/4E-BP1. *Blood* **2008**, *111*, 4892−4901.
(37) Wu, M.; Neilson, A.; Swift, A. L.; Moran, R.; Tamagnine, J.; Parslow, D.; Armistead, S.; Lemire, K.; Orrell, J.; Teich, J.; Chomicz, S.; Ferrick, D. A. Multiparameter metabolic analysis reveals a close link between attenuated mitochondrial bioenergetic function and enhanced glycolysis dependency in human tumor cells. *Am. J. Physiol. Cell Physiol.* **2007**, *292*, C125−C136.
(38) Sottnik, J. L.; Lori, J. C.; Rose, B. J.; Thamm, D. H. Glycolysis inhibition by 2-deoxy-D-glucose reverts the metastatic phenotype in vitro and in vivo. *Clin. Exp. Metastasis* **2011**, *28*, 865−875.
(39) Dennis, P. B.; Jaeschke, A.; Saitoh, M.; Fowler, B.; Kozma, S. C.; Thomas, G. Mammalian TOR: a homeostatic ATP sensor. *Science* **2001**, *294*, 1102−1105.
(40) Kong, D.; Li, Y.; Wang, Z.; Banerjee, S.; Sarkar, F. H. Inhibition of angiogenesis and invasion by 3,3′-diindolylmethane is mediated by the nuclear factor-κB downstream target genes MMP-9 and uPA that regulated bioavailability of vascular endothelial growth factor in prostate cancer. *Cancer Res.* **2007**, *67*, 3310−3319.

would exhibit a better affinity with lipophilic membrane constituents of drug target cells.[8] This property would make from ascorbyl derivatives good candidates to be used in pharmaceutical and cosmetic lipophilic formulations.[9] The interest in new compounds with antimicrobial properties has been revived because of current problems associated with the use of antibiotics.[10] Aissa et al.[11] have synthesized a large series of tyrosyl esters with increasing lipophilicity using lipase of *Candida antarctica*. The authors showed that the parent tyrosol does not have any effect on various pathogenic bacteria. However, tyrosyl esters and especially medium chain tyrosyl derivatives exhibited an antimicrobial activity against staphylococcus strains.

In the wake of resistance to pentavalent antimonial drugs, new therapeutic alternatives are desirable.[12] Hence, it is of interest to analyze the performance of the amphiphilic ascorbyl derivatives and study the relationship between their structure and their antileishmanial activity.

Based on the above-mentioned information, a large series of ascorbyl fatty acid esters with increasing lipophilicity was synthesized by the direct esterification of ascorbic acid with various fatty acids using *Staphylococcus xylosus* immobilized onto silica aerogel produced in our laboratory as catalyst and evaluated for their antioxidant, emulsifying, and antimicrobial activity against several pathogenic strains and their antileishmanial effects on both cutaneous (*Leishmania major*) and visceral parasites (*Leishmania infantum*). Finally, the interaction of the ester derivatives with a mimetic phospholipid film mixture was evaluated using a monomolecular film technique.

## 2. MATERIALS AND METHODS

**2.1. Materials.** Ascorbic acid was purchased from Bio Basic Inc. (Switzerland); chloroform and methanol were purchased from Scharlau (Spain); acetonitrile and acetic acid from Pharmacia (Uppsala, Sweden); caprylic, capric, lauric, palmitic, stearic, and oleic acids and 2-methyl-2-propanol from Fluka (Germany); 4,5-dimethylthiazol-2-yl-2,5-diphenyltetrazolium bromide (MTT) and 2,2-diphenyl-1-picrylhydrazyl (DPPH) were purchased from Fluka (Switzerland); BHT (purity ≥99%), α-tocopherol (purity ≥96%) and arabic gum (purity 99%) from Sigma; soya lecithin (verolec F-62) was purchased from LASENOR. EggPC, cholesterol, phosphatidylethanolamine (PE), phosphatidylglycerol (PG), and sphingolipid (SL) were purchased from Avanti. The egg-yolk lecithin was extracted from fresh egg yolks using a modified method described by Palacios and Wang.[13] The purity of egg-yolk lecithin was checked by TLC. *Staphylococcus xylosus* lipase was produced as described by Mosbah et al.[14] Enzyme immobilization was made onto silica aerogel as previously described by Kharrat et al.[15]

**2.2. Methods.** *2.2.1. Esterification Reactions.* Ascorbyl lipophilic esters (Asc-$C_2$ to Asc-$C_{18:1}$) were prepared by direct esterification between ascorbic acid (Asc) and various fatty acids in screw-capped flasks. Asc (8 mg/mL) was dissolved in 2-methyl-2-propanol to an acetonitrile volume ratio of 0.2 (3 mL of total volume). The fatty acid concentration was adjusted to obtain an ascorbic acid/fatty acid molar ratio of eight. The mixture was stirred at 45 °C in an orbital shaker at 220 rpm and in the presence of *Staphylococcus xylosus* lipase immobilized onto silica aerogel (600 IU). Control reactions in the absence of lipase were also carried out parallelly. Aliquots from the mixture reaction were withdrawn after 72 h of incubation and filtered to be used for HPLC analysis. The conversion yield of ascorbyl derivatives was calculated as the ratio of the number of moles of ascorbic acid converted per the total number of moles of ascorbic acid. All experiments were performed in triplicate. Study has been selected from five microorganism lipases produced in our laboratory. This enzyme presented the higher yield conversion (data not shown).

*2.2.2. Purification and Identification of Ascorbyl Esters.* The reaction mixture resulting from the esterification of ascorbic acid with different fatty acids contains a mixture of ascorbic acid ester and residual substrates. After enzyme removal by centrifugation at 8000 rpm for 15 min, the solvent (2-methyl-2-propanol) was evaporated at 45 °C under vacuum and the synthesized ester was purified as follows: 100 mg of target product was taken up in 2 mL of chloroform. The purification of esters was achieved by chromatography on a silica gel 60 column (Merck) (25 cm × 2 cm) according to Aissa et al.[16] The column was previously equilibrated in chloroform. Elution was carried out using chloroform/methanol/acetic acid mixtures (78:18:4). The collected solvent fractions were analyzed by TLC. The spots were identified under evaporated iodine. Purified fractions were pooled and solvents evaporated at 45 °C under vacuum. Final purity of the products obtained was checked using LC/MS analysis.

*2.2.3. HPLC Analysis.* The identification and conversion yields of ascorbyl derivatives were carried out by HPLC analysis (Ultimate 3000, Dionex, Germany). The HPLC system was equipped with a pump (LPG-3400SD), column oven, and diode-array UV−vis detector (DAD-3000RS). The output signal of the detector was recorded using Dionex Chromeleon chromatography Data System. Separation was executed on an Inertsil ODS-4 C-18 column (5 μm, 4.6 mm × 250 mm; Shimpack) maintained at 30 °C. The flow rate used was 1.5 mL/min, and the detection UV wavelength was set at 254 nm. The used mobile phase was 0.05% acetic acid in water (A) versus 0.1% acetic acid in acetonitrile (B) for a total running time of 12 min, and the following proportions of solvent (B) were used for elution: 0−3 min, 10−30%; 3−5 min, 30−90%; 5−10 min, 90%; and 10−12 min, 90−10%.

*2.2.4. LC−-MS/MS Analysis.* An analytical LC−UV−MS/MS analysis was performed on a Phenomenex Luna C18 (2) column (150 × 4.6 mm i.d., 5 μm particle size), using a 1 mL/min linear mobile phase gradient of 20−50% aqueous MeOH (containing 1% HOAc) in 30 min, and mass spectra were recorded by a Thermo Scientific "LCQ Classic" ion trap mass spectrometer fitted with an ESI source. Accurate mass measurements were performed on Finnigan MAT900 XLT or Thermo Scientific LTQ Orbitrap XL mass spectrometers in negative and positive ESI mode.

*2.2.5. NMR and FT-IR Experiments.* $^1$H and $^{13}$C NMR spectra were recorded in deuterated chloroform ($CDCl_3$) on a Bruker TOPSPIN spectrometer operating at 400 MHz. IR spectra were recorded on FT/IR-410 (JASCO).

Asc-C10: $^1$H NMR (400 MHz, $CDCl_3$): 4.25 (2H ($H_{1'}$), d); 3.85 (1H ($H_{2'}$), dd); 4.35 (1H ($H_{3'}$), d); 4.27 (1H ($H_{7'}$), s); 4.9 (1H ($H_{8'}$), s); 5.19 (1H ($H_{9'}$), s); 2.3 (2H ($H_2$), t, $-CH_2CO$); 1.6 (2H ($H_3$), m); 1.3 (nH ($H_4$−$H_9$), m, $(CH_2)_6$); 0.9 (3H ($H_{10}$), t, $CH_3$).

$^{13}$C NMR (400 MHz, $CDCl_3$): 14.08 ($C_{10}$), 22.68 ($C_3$), 24.74−33.81 ($C_4$−$C_9$), 34.11 ($C_2$), 64.16 ($C_{1'}$), 67.47 ($C_{2'}$), 130.16 ($C_{4'}$), 130.88 ($C_{5'}$), 153.05 ($C_{3'}$), 172.48 ($C_{6'}$, C═O); 178.35 ($C_1$, C═O).

IR (liquid) cm$^{-1}$: 3108−3023 (HO-Ø), 2905 (C−H), 1700 (C═O), 1200− 1350 ($CH_2$) stretching, 1100 (C−O).

*2.2.6. Antioxidant Activity.* The free radical scavenging activity of Asc and its derivatives was determined using the method of Brand-Williams et al. with a little modification.[17] An aliquot of ethanol absolute solution (0.1 mL) containing different concentrations (1:2 serial dilutions from the initial sample) of Asc and its esters was added to 3.9 mL of DPPH solution (0.06 mM in ethanol). The mixture was vortexed vigorously and incubated at room temperature (25 °C) in darkness for 60 min, and then the absorbance was read at 517 nm against ethanol blank using a spectrophotometer (Uvi Light XT5).

The $IC_{50}$ values denote the concentration of tested compounds, which is required to scavenge 50% of DPPH free radicals. The corresponding inhibition percentages were calculated according to the following equation:

$$\text{radical scavenging activity (\%)} = \frac{(A_{\text{blank}} - A_{\text{sample}})}{A_{\text{sample}}} \times 100$$

where $A_{\text{blank}}$ is the absorbance of the control (prepared in the same manner without test compound), and $A_{\text{sample}}$ is the absorbance of the


dx.doi.org/10.1021/jf5029398 | J. Agric. Food Chem. 2014, 62, 9118−9127

**Table 1. Conversion Yields of the Ascorbyl Derivatives and Physicochemical Parameters of Ascorbic Acid and Its Esters Related to Their Lipophilicity**

| compounds | abbreviations | radicals | conversion yield (%) | characteristics | MW (g/mol)[a] | miLogP[a] | $t_R$[b] (min) | $IC_{50}$[c] (μg/mL) |
|---|---|---|---|---|---|---|---|---|
| ascorbic acid | Asc | $C_6H_8O_6$ | | white solid | 176.124 | −1.402 | 1.990 | 2.010 ± 0.085 |
| ascorbyl acetate | Asc-$C_2$ | $-CH_3$ | 82.57 ± 2.32 | yellow slimy oil | 218.161 | −0.698 | 3.540 | 3.435 ± 0.091 |
| ascorbyl caprylate | Asc-$C_8$ | $-C_7H_{15}$ | 68.21 ± 2.75 | yellow slimy oil | 302.323 | 2.243 | 6.627 | 3.515 ± 0.084 |
| ascorbyl caprate | Asc-$C_{10}$ | $-C_9H_{19}$ | 59.39 ± 2.30 | white amorphous solid | 330.377 | 3.253 | 7.807 | 3.215 ± 0.078 |
| ascorbyl laurate | Asc-$C_{12}$ | $-C_{11}H_{23}$ | 58.24 ± 2.72 | white amorphous solid | 358.431 | 4.263 | 8.372 | 3.355 ± 0.092 |
| ascorbyl palmitate | Asc-$C_{16}$ | $-C_{15}H_{31}O$ | 52.86 ± 2.71 | white amorphous solid | 414.539 | 6.284 | 9.537 | 3.205 ± 0.088 |
| ascorbyl stearate | Asc-$C_{18:0}$ | $-C_{17}H_{35}O$ | 42.08 ± 1.62 | white amorphous solid | 442.593 | 7.295 | 11.392 | 3.310 ± 0.099 |
| ascorbyl oleate | Asc-$C_{18:1}$ | $-C_{17}H_{33}O$ | 40.96 ± 1.07 | yellow oil | 440.577 | 6.809 | 9.743 | 2.980 ± 0.085 |
| α-tocopherol | | $C_{29}H_50O_2$ | | yellow viscous liquid | 430.717 | 9.043 | | 5.760 ± 0.028 |
| BHT | | $C_{15}H_{24}O$ | | white solid | 220.356 | 5.435 | | 7.265 ± 0.064 |

[a]miLogP and MW values calculated using Molinspiration program. [b]Retention time from HPLC. [c]Antioxidant activity of ascorbic acid and their fatty acid esters determined by the DPPH method.

test compound. Ascorbic acid, butylated hydroxytoluene (BHT), and α-tocopherol were used as standard control. The values are presented as the means of triplicate analyses.

*2.2.7. Lipophilicity Evaluation.* The partition coefficients (miLogP) values and the molecular weight of ascorbyl esters were calculated using Molinspiration software (available online at www.molinspiration.com). The lipophilic character of ascorbyl esters was evaluated as described by Viskupicova et al.[18]

*2.2.8. Measurement of Conjugated Diene (CD) and Triene (CT).* The effect of ascorbyl esters on the oxidative state of oil was evaluated by the measuring of conjugated diene (CD) and conjugated triene (CT) as previously described by Della et al.[19] Oxidation was induced during 20 days by storing soya oil at 70 °C. Every 2 days, the absorbance was measured at 232 nm (for CD) and 270 nm (for CT), using hexane as a blank. All measurements were performed in triplicate. BHT and α-tocopherol were used as standard control.

*2.2.9. Emulsifying Activity.* The ability of the purified ascorbyl esters to form oil-in-water (o/w) emulsions against soya oil was determined using the method described by Gutierrez et al.[20] Activities were compared under neutral (0.1 M phosphate-buffered saline, pH 7), acidic (0.1 M sodium acetate buffer, pH 4), and basic (0.1 M Tris-HCl buffer, pH 8.5) conditions. 5 mL of buffer was vortexed for 2 min at 2200 rpm with 0.8 mL of soya oil containing 0.02% (w/v) of each emulsifier. The turbidity of the lower aqueous layer was measured using a spectrophotometer at 540 nm. All measurements were carried out in triplicate, and the mean values of the triplicates were reported with standard error. Egg-yolk lecithin, soya lecithin, and Arabic gum were used as commercial emulsifiers.

*2.2.10. Determination of the Minimum Inhibitory Concentration (MIC) and the Minimum Bactericidal Concentration (MBC).* The antibacterial activities of Asc, Asc + FAs (separated substrates taken together at the same concentration), and ascorbyl derivatives were tested against several bacteria strains using Luria broth (LB) medium. The minimum inhibitory concentration (MIC) values, which correspond to the lowest compound concentration that completely inhibits the growth of microorganisms, were determined by a microwell dilution method as previously described by Eloff[21] using 3-(4,5-dimethylthiazol-2-yl)-2,5-diphenyltetrazolium bromide (MTT). The inoculum of each bacterium was prepared, and the suspensions were adjusted to $10^7$ CFU/mL. All the compounds were dissolved in 100% ethanol, and then dilution series were prepared in a 96-well plate, ranging from 3.125 μg/mL to 4 mg/mL. Each well of the microplate contained 175 μL of the growth medium, 5 μL of inoculum, and 20 μL of the diluted sample extract. Ethanol was used as a negative control. The plates were incubated at 37 °C for 24 h, and then 40 μL of MTT, at a final concentration of 0.5 mg/mL freshly prepared in sterile water, was added to each well and incubated for 30 min. The change to purple color indicated that the bacteria were biologically active. The MIC was taken where no change of MTT color was observed in the well.

To determine the minimum bactericidal concentration (MBC), a liquid portion from each well that showed no change in color will be placed on solid LB and incubated at 37 °C for 24 h. The lowest concentration that yielded no growth after this subculturing will be taken as the MBC.[22] All experiments were made in duplicate. Several bacterial strains were used: i.e., *Bacillus cereus* (*BC*), *Bacillus subtilis* (*BS*), *Staphylococcus aureus* (*Sa*), *Staphylococcus epidermidis* (*SEp*), *Enterococcus faecalis* (*EF*), *Enterococcus faecium* (*EFa*), *Enterobacter cloacae* (*EC*), *Micrococcus luteus* (*ML*), *Brevibacterium flavum* (*BF*), *Pseudomonas aeruginosa* (*Ps*), *Salmonella typhimurium* (*STyphi*), *Klebsielle pneumonia* (*KP*), *Echerichia coli* (*Ecoli*), and *Staphylococcus xylosus* (*Sx*).

*2.2.11. Leishmanicidal Activity.* (These experiments have been performed in the Pasteur Institute of Tunis (Tunisia)). *L. major* (MHOM/TN/95/GLC94)[23] and *L. infantum* (MHOM/TN/94/LV50)[24] strains isolated from Tunisian patients were used within this study. Promastigotes were cultured in solid medium at 26 °C during 6 days. They must be in their infective metacyclic forms as mentioned by Aissa et al.[11] The effects of ascorbyl derivatives on *Leishmania* promastigotes were evaluated by the MTT assay as described by Dutta et al.[25] Parasites ($10^7$ parasites/well in the complete medium) were incubated for 24 h in the presence of serially diluted concentrations of ascorbyl derivatives (ranging from 25 to 400 μg/mL).[11] After this treatment, microtiter plates were centrifuged at 1700*g* for 10 min and supernatants were removed and replaced with the same volume of 1 mg/mL of MTT freshly dissolved in PBS. Plates were then incubated overnight at room temperature. After centrifugation at 2500*g*, formazan salt formed inside the parasite mitochondria was solubilized by discarding supernatants and adding SDS 10% for 2 h at 37 °C in the dark. Absorbance was measured at 540 nm using an ELISA plate reader. Negative controls were conducted without addition of ascorbyl derivative solutions. Each assay was performed in duplicate.

*2.2.12. Monolayer Study of the Ascorbyl Derivatives.* Experiments were carried out on KSV 2200 Baro-stat equipment as described by Aissa et al.[11] A Teflon trough was equipped with two hydrophilic Delrin barriers (symmetric compression) and a Wilhelmy plate as a surface-pressure sensor. Software KSV 2200 was used to control the experiments. Before each utilization, the Teflon trough was cleaned and brushed in the presence of distilled ethanol, subsequently washed again with tap water, and finally rinsed with double-distilled water. The aqueous subphase (buffer A) was composed of 10 mM Tris−HCl, pH 8, 100 mM NaCl, 21 mM $CaCl_2$, and 1 mM EDTA. Buffer was prepared with double-distilled water and filtered through a 0.45 μM Millipore filter. Residual surface active impurities were removed before each assay by sweeping and suction of the surface.[26]

*2.2.13. Measurement of the Ascorbyl Derivatives Penetration into Mixture Film Monolayer.* The surface pressure increase, due to the penetration of the ascorbyl derivatives into a mixture film monolayer, was measured in a cylindrical trough drilled into a Teflon block (surface area 17.42 $cm^2$, total volume 15 mL). The aqueous

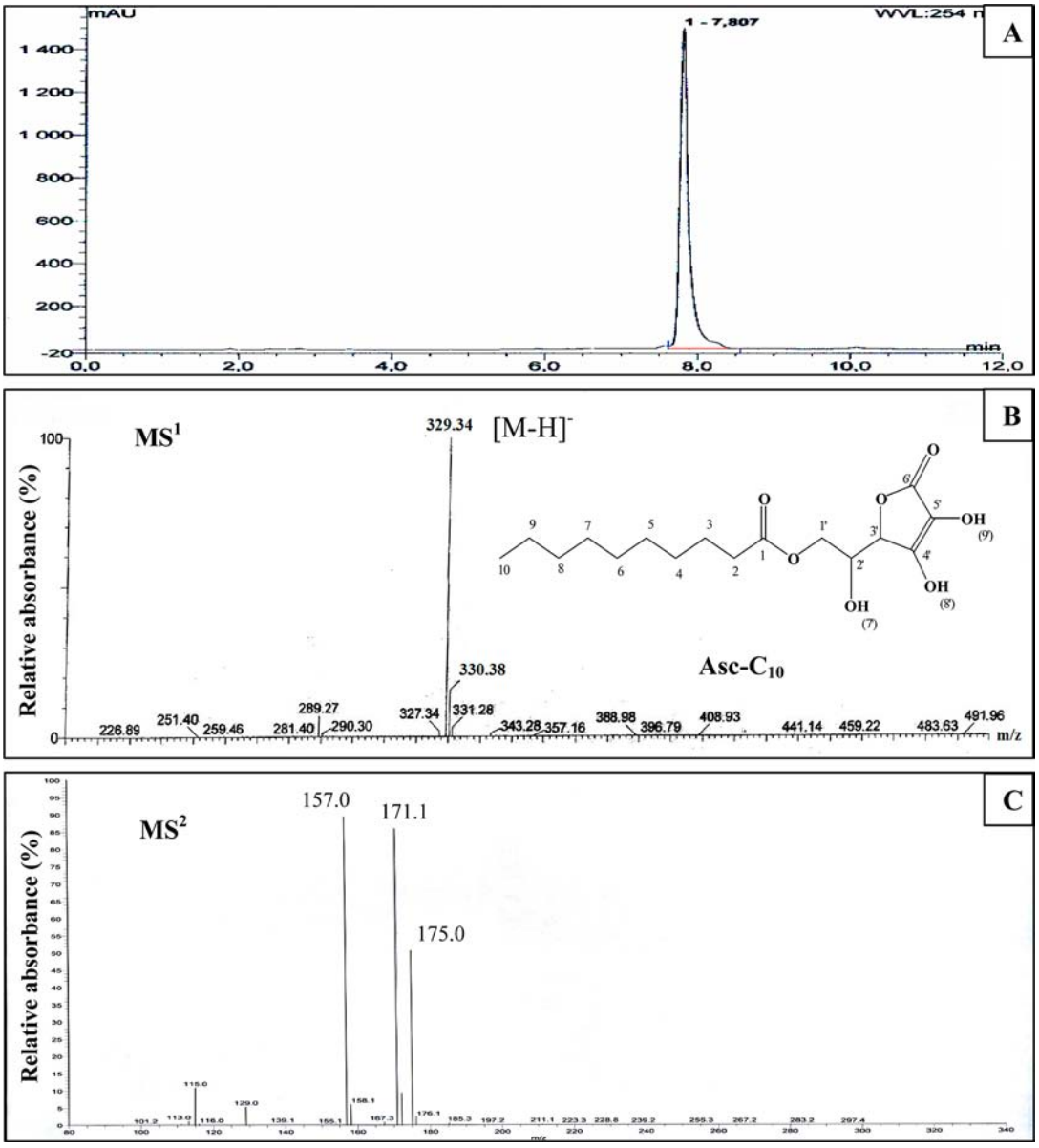


**Figure 1.** (A) HPLC profile of ascorbyl caprate (Asc-$C_{10}$) after biosynthesis and purification. The biosynthesis reaction of ascorbic acid with capric acid (ascorbic acid/fatty acid molar ratio of eight) was catalyzed by *Staphylococcus xylosus* lipase immobilized onto silica aerogel at 45 °C and 220 rpm in 2-methyl-2-propanol to acetonitrile volume ratio of 0.2 (72 h). HPLC analysis was carried out on a C-18 column by gradient elution using acidified water and acetonitrile at a flow rate of 1.5 mL/min. (B) $MS^1$ spectra of purified ascorbyl caprate (Asc-$C_{10}$). (C) $MS^2$ spectra of purified ascorbyl caprate (Asc-$C_{10}$).

subphase (buffer A) was stirred continuously at 250 rpm with a magnetic rod. The critical surface pressures were determined as described previously.[27] A sample of Asc or synthesized ester solution (0.5 $\mu$M) was injected with a Hamilton microsyringe, under a monomolecular film of mixture film spreads at an initial surface pressure ($\pi_i$) ranging from 4 to 37 mN/m. To mimic the lipidic components of leishmania membrane, a mixture of phospholipids was used, containing 40% EggPC, 30% cholesterol, 10% phosphatidylethanolamin (PE), 10% phosphatidylglycerol (PG) and 10% sphingolipid (SL).[28]

*2.2.14. Statistical Analysis.* All analyses were carried out in triplicate. Results were expressed as mean values ± standard deviation (SD) ($n$ = 3). The differences were calculated using one-way analysis of variance (ANOVA), and statistically significant differences were reported at $P < 0.05$. Data analysis was carried out using the SPSS 10.0 software.

## 3. RESULTS AND DISCUSSION

**3.1. Enzymatic Synthesis and Characterization of Ascorbyl Fatty Acid Esters.** A chemoselective enzymatic esterification was used to synthesize lipophilic ascorbyl ester derivatives (Asc-$C_2$ to Asc-$C_{18:1}$). Several solvents such as hexane, chloroform, acetone, and toluene were used as reaction media. However, among all these organic solvents tested, only cosolvent 2-methyl-2-propanol/acetonitrile was suitable for this esterification reaction.

The conversion yields calculated after 72 h of incubation using lipase from *Staphylococcus xylosus* immobilized onto silica aerogel as a catalyst are presented in Table 1. As it can be seen, the highest ester synthesis yield was obtained when using short acyl chain ester Asc-$C_2$. For medium and long chain esters (Asc-$C_8$ to Asc-$C_{18:1}$), the conversion yield decreased


dx.doi.org/10.1021/jf5029398 | J. Agric. Food Chem. 2014, 62, 9118−9127

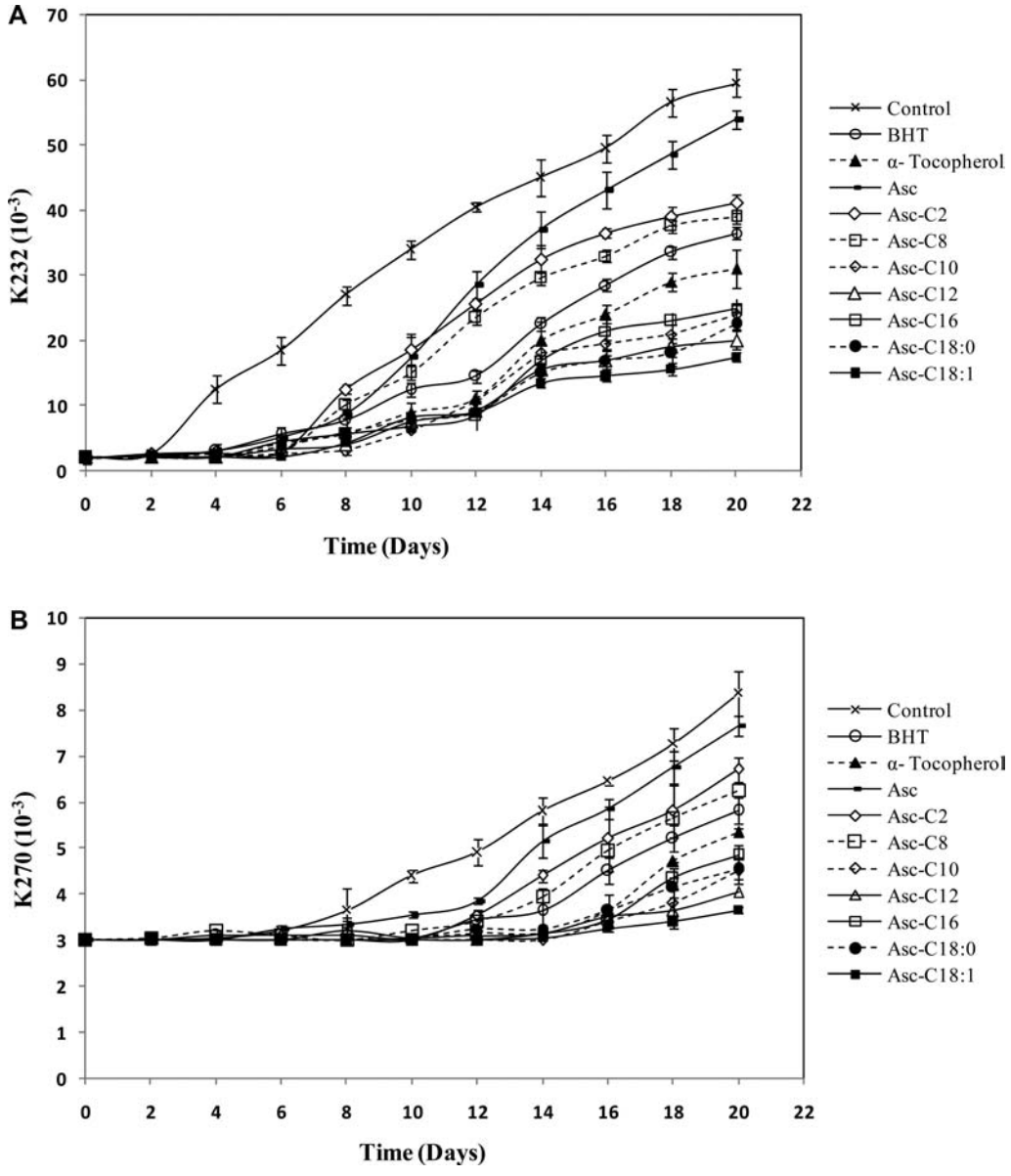


**Figure 2.** Antioxidant activities of ascorbyl ester derivatives (Asc-$C_2$ to Asc-$C_{18:1}$) tested by the measurement of conjugated diene (A) and conjugated triene (B) of refined soy oil during storage at 70 °C. For each test, negative and positive controls using BHT and $\alpha$-tocopherol were run in parallel. Values are mean ± SD ($n$ = 3) of three determinations.

progressively with the increase of the acyl chain length (Table 1) although *Staphylococcus xylosus* lipase hydrolyzes triacylglycerols without significant chain length preference.[14]

These results are in line with those observed previously by Aissa et al.[16] The fatty acid unsaturation seems to affect the synthesis yield. In fact, the ester conversion yield reached 52.86% with ascorbyl palmitate and decreased to 40.96% of ascorbyl oleate when using oleic acid as acyl donor. Our observations are in agreement with those described by Selmi et al.[29] They concluded that the increase of the unsaturation number is responsible for the lower rate of triacylglycerol synthesis using immobilized *Rhizomucor miehei* lipase. These results are however in contradiction with those described by Song et al.,[30] which showed that $C_{18}$ unsaturated FAs gave better conversion yield as compared to $C_{18}$ saturated FAs using Novozym 435 as catalyst. These contradictions between these findings could be attributed to the nature of the lipase used and the composition of the reaction medium (solvent, water content, substrate chemistry) or the operating conditions.[31,32]

**3.2. Purification and Identification of Ascorbyl Fatty Acid Esters.** The purification of each ascorbyl ester was achieved by chromatography on a silica gel 60 column according to Aissa et al.[16] as described above in Materials and Methods. The purity of these products was then checked via HPLC analysis (Figure 1A); their retention time is mentioned in Table 1. RMN, $MS^1$, and IR analysis were used to identify the purified products.

As shown in Figure 1B, $MS^1$ analysis in the negative mode of pure Asc-$C_{10}$, taken as a typical compound, exhibited a molecular ion at $m/z$ = 329.34 $[M - H]^-$ attributed to the molecular weight of calculated ester using Molinspiration software (330.37 g/mol) shown in Table 1.

The $MS^2$ experiments focusing on the fragment generated from the peak in $m/z$ = 329.34 $[M - H]^-$ revealed a fragment corresponding to the pseudo molecular ion at $m/z$ = 171.1


dx.doi.org/10.1021/jf5029398 | J. Agric. Food Chem. 2014, 62, 9118−9127

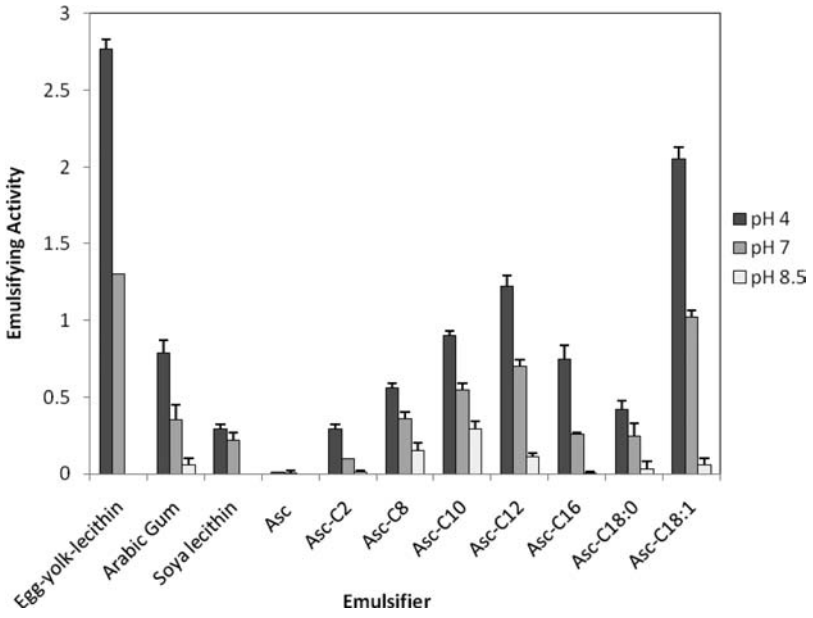


**Figure 3.** Emulsifying activity at pH 4, pH 7, and pH 8.5 of ascorbic acid and its derivatives (Asc-$C_2$ to Asc-$C_{18:1}$). The activity reflects the capacity of the emulsifier to form soya oil-in-water emulsions. Egg-yolk lecithin, arabic gum, and soya lecithin were used as control emulsifiers. Values are mean ± SD ($n$ = 3) of three determinations.

attributed to capric acid and $m/z$ = 175.0 attributed to ascorbic acid ion. The ion at $m/z$ = 157 was formed by the cleavage of the capric acid and neutral losses of $H_2O$ linked to the ascorbic acid (Figure 1C).

**3.3. Antioxidant Activity.** Ascorbic acid exhibits low solubility and stability in the lipophilic media, which can limit its efficient use in these conditions. Hence, the lipophilic derivatives of Asc and, in particular, long acyl chain esters, would exhibit a better affinity with lipophilic matrices. Being a lipophilic compound may improve its solubility as well as maintain or enhance its radical scavenging capacity.[16,32] This property would make ascorbyl derivatives strong candidates for pharmaceutical and cosmetic lipophilic formulation.

The antioxidant efficiency of ascorbic acid was checked after lipophilization using DPPH in an ethanolic medium, a rapid and sensitive scavenging test. As indicated in Table 1, ascorbic acid and its synthesized esters were shown to be strong DPPH radical scavengers. Esterification of Asc-$C_2$ to Asc-$C_{18:0}$ seems to slightly affect the radical-scavenging potential. All ascorbyl derivatives exhibited a high antioxidant activity with an $IC_{50}$ varying between 3 and 3.5 $\mu$g/mL, which are near the $IC_{50}$ value of ascorbic acid (2.01 $\mu$g/mL). Moreover, the antioxidant effect of ascorbic acid and its derivatives was twice as efficient as the known synthetic antioxidants such as BHT and $\alpha$-tocopherol. These results are, however, in contradiction with those described by Burham et al.,[33] who showed that ascorbic acid exhibited a higher antioxidant activity than ascorbyl palmitate and pure palm-based ascorbyl esters. The radical-scavenging capacity of ascorbic acid and its derivatives can be explained by the number and position of hydrogen-donating groups (OH) in hydroxyl headgroup.[32]

**3.4. Ascorbyl Ester Derivatives Effect on Oil Oxidative Stability.** The effect of lipophilic ascorbyl derivatives on the oxidative stability of oils was determined by the measurement of conjugated diene (CD) and triene (CT). Ascorbic acid and its acyl esters (Asc-$C_2$ to Asc-$C_{18:1}$) were added to refined soy oil. CD and CT of the different preparations were measured upon 20 days storage at 70 °C in the open air (Figures 2A and 2B). The CD and CT determine the primary products of oil oxidation.[34] A remarkable increase in the CD and CT of refined soya oil was observed. As shown in Figures 2A and 2B, the addition of ascorbyl derivatives, as antioxidants, prevented oil oxidation as well as BHT and $\alpha$-tocopherol. Interestingly, the protective effect against oxidation by ascorbyl derivatives was higher than that of Asc and increased with the fatty acid chain length. However, Asc, Asc-$C_2$, and Asc-$C_8$ derivatives displayed the lowest protective effect of soya oil against oxidation. Based on the increasing trend of miLogP values (Table 1), it seems that ascorbyl esters having a high lipophilicity (miLogP higher than 3.2) display the best antioxidant capacities. Ascorbyl derivatives, the amphiphilic natural antioxidants, could be used for increasing protection of target lipids from oxidation such as skin creams, facial treatments (acne or wrinkle removers), bath oils, sunscreens, preshave, and makeup.

**3.5. Emulsifying Activity.** Today, more than ever, a large amount of surfactant is required for a microemulsion system used for pharmaceutical/cosmetic purposes.[35] However, a surfactant may exhibit undesirable effects like skin irritation, allergy, etc. when used excessively. Therefore, one must choose materials that are biocompatible, nontoxic, and clinically acceptable and use emulsifiers in an appropriate concentration range that will result in mild and nonaggressive micro-emulsions.[35] The excipients generally regarded as safe (GRAS) are being increasingly preferred. For these reasons, the ability of purified ascorbic acid derivatives to emulsify soya oil in water was tested. The emulsifying capacity of the different ascorbyl derivatives was determined under acidic, neutral, and basic conditions. Arabic gum, soya lecithin, and egg-yolk-lecithin were taken as control emulsifiers since they are the most important hydrocolloid ingredients in the formulation of many food products. Based on average results provided in acidic, neutral, and basic pH conditions presented in Figure 3, the ascorbyl derivatives produced emulsifying activities that were significantly different from those of control. In fact, apart from Asc and Asc-$C_2$, all ascorbyl derivatives (Asc-$C_8$ to Asc-$C_{18:1}$) produced a significantly higher emulsifing activity than


dx.doi.org/10.1021/jf5029398 | J. Agric. Food Chem. 2014, 62, 9118−9127

**Table 2. Minimum Inhibitory Concentration and Minimum Bactericidal Concentration of Ascorbyl Ester Derivatives on Bacteria**

| bacteria strain | Gram | concentration (mg/mL) | | | | | | | | |
|---|---|---|---|---|---|---|---|---|---|---|
| | | Asc | (Asc + $C_8$)[a] | Asc-$C_8$ | (Asc + $C_{10}$)[a] | Asc-$C_{10}$ | (Asc + $C_{12}$)[a] | Asc-$C_{12}$ | (Asc + $C_{18:1}$)[a] | Asc-$C_{18:1}$ |
| (A) Minimum Inhibitory Concentration | | | | | | | | | | |
| *Bacillus cereus* | + | >4 | 2 | 1 | 2 | 0.5 | 1 | 0.125 | 2 | 1 |
| *Bacillus subtilis* | + | >4 | 2 | 1 | 2 | 0.25 | 1 | 0.125 | 1 | 0.5 |
| *Staphylococcus aureus* | + | >4 | 2 | 0.5 | 2 | 0.25 | 2 | 0.062 | 1 | 0.25 |
| *Staphylococcus xylosus* | + | >4 | 2 | 0.5 | 2 | 0.25 | 2 | 0.062 | 1 | 0.25 |
| *Staphylococcus epidermidis* | + | >4 | 2 | 0.5 | 2 | 0.25 | 2 | 0.062 | 1 | 0.25 |
| *Enterobacter cloacae* | − | >4 | 2 | 1 | 2 | 0.5 | 2 | 0.25 | 2 | 0.5 |
| *Salmonella typhimurium* | − | >4 | 2 | 1 | 2 | 0.25 | 2 | 0.25 | 2 | 0.5 |
| *Klebsielle pneumoniae* | − | >4 | 2 | 1 | 2 | 0.5 | 2 | 0.125 | 2 | 1 |
| *Escherchia coli* | − | >4 | 4 | 2 | 4 | 1 | 2 | 0.5 | 2 | 0.5 |
| (B) Minimum Bactericidal Concentration | | | | | | | | | | |
| *Bacillus cereus* | + | >4 | 4 | 2 | 4 | 0.5 | 2 | 0.25 | 4 | 2 |
| *Bacillus subtilis* | + | >4 | 4 | 2 | 4 | 0.5 | 2 | 0.25 | 4 | 2 |
| *Staphylococcus aureus* | + | >4 | 2 | 1 | 2 | 0.25 | 1 | 0.125 | 2 | 0.5 |
| *Staphylococcus xylosus* | + | >4 | 2 | 1 | 2 | 0.25 | 1 | 0.125 | 2 | 0.5 |
| *Staphylococcus epidermidis* | + | >4 | 2 | 1 | 4 | 0.5 | 1 | 0.125 | 2 | 0.5 |
| *Enterobacter cloacae* | − | >4 | 4 | 2 | 4 | 0.5 | 2 | 0.5 | >4 | 1 |
| *Salmonella typhimurium* | − | >4 | 4 | 2 | 4 | 0.5 | 4 | 0.25 | >4 | 1 |
| *Klebsielle pneumoniae* | − | >4 | 4 | 2 | 4 | 1 | 4 | 0.25 | >4 | 2 |
| *Escherchia coli* | − | >4 | 4 | 2 | 4 | 1 | 4 | 0.5 | >4 | 2 |

[a]Taken together at the same concentration.

**Table 3. $IC_{50}$ Activities of Ascorbic Acid and Its Acyl Chain Derivatives against *L. major* and *L. infantum* Parasite Species Evaluated by the MTT Assay**

| | $IC_{50}$ (μg/mL) | | | | | | | |
|---|---|---|---|---|---|---|---|---|
| | Asc | Asc-$C_2$ | Asc-$C_8$ | Asc-$C_{10}$ | Asc-$C_{12}$ | Asc-$C_{16}$ | Asc-$C_{18:0}$ | Asc-$C_{18:1}$ |
| *L. major* | *a* | *a* | *a* | 217.74 ± 13.33 | 196.26 ± 10.53 | *a* | *a* | 154.23 ± 12.41 |
| *L. infantum* | *a* | *a* | *a* | 347.12 ± 12.32 | 284.80 ± 20.33 | *a* | *a* | 205.81 ± 14.35 |

[a]Without effect up to 400 μg/mL.

arabic gum and soya lecithin, but lower than egg-yolk lecithin. Comparable results were obtained by Kuwabara et al.,[36] who demonstrated that caproyl and lauroyl L-ascorbates are useful emulsifiers for emulsions. In addition, under acidic conditions, the emulsifying activities of all ascorbyl esters were significantly higher compared to those measured under basic or neutral conditions (Figure 3). Among all the tested derivatives, Asc-$C_{18:1}$ was found to be the most potent as emulsifier.

**3.6. Determination of the Minimum Inhibitory Concentration (MIC) and the Minimum Bactericidal Concentration (MBC).** The antibacterial activity of Asc, FAs, Asc + FAs, and the synthesized esters (Asc-$C_2$ to Asc-$C_{18:1}$) was checked against Gram-positive (*Bacillus cereus* (*BC*), *Bacillus subtilis* (*BS*), *Brevibacterium flavum* (*BF*), *Micrococcus luteus* (*ML*), *Staphylococcus xylosus* (*Sx*), *Staphylococcus aureus* (*Sa*), *Staphylococcus epidermidis* (*SEp*), *Enterococcus faecalis* (*EF*), and *Enterococcus faecium* (*EFa*)) and Gram-negative (*Enterobacter cloacae* (*EC*), *Pseudomonas aeruginosa* (*Ps*), *Salmonella typhimurium* (*STyphi*), *Klebsielle pneumonia* (*KP*), and *Echerichia coli* (*Ecoli*)) bacteria by the determination of MIC and MBC values. As can be seen from Table 2, sections A and B, ascorbic acid does not show any inhibitory or bactericidal effect up to a concentration of 4 mg/mL. Compared to Asc and mixed solution of Asc + FAs, synthesized ester exhibits the most effect against the bacteria tested, in particular Gram (+) ones. In fact, with Gram (+) bacteria, MIC values ranged from 0.0625 to 2 mg/mL and the MBC values are between 0.500 and 4 mg/mL, while Gram (−) bacteria appear to be less sensitive to the tested compounds. Previous studies reported that Gram (−) bacteria presented lower sensitivity than Gram (+) bacteria to various polyphenols.[37] This higher resistance may be related to minor differences present in the outer membrane in the cell wall composition.[37] As it can be seen from Table 2, panel A, MIC and MBC values showed that ascorbyl derivatives exhibit a similar or a slightly higher inhibitory activity and more bactericidal effect against Gram (+) bacteria than the separated substrates (Asc + FAs). These results indicate that we have significantly enhanced the antimicrobial activity of the ascorbic acid after esterification. These findings are in agreement with those of Aissa et al.,[11] who showed that only medium chain tyrosyl esters had an antibacterial activity especially against *Staphylococcus* strains.

These results could be explained by their hydrophobicity, which may allow them to partition the lipids of the bacterial cell membrane, making them more permeable and leading to ion leakage and other cell constituents.[38] The authors suggested that these compounds could be able to infiltrate the cell and interact with some metabolic mechanisms, which allowed us to show their bacteriostatic effect.

**3.7. Antileishmanial Activity.** Ascorbic acid and its lipophilic derivatives were screened for their leishmanicidal activity. Screening was carried out using two *Leishmania* species: *L. major* GLC94[23] and *L. infantum* LV50.[24] As shown in Table 3, only Asc-$C_{10}$, Asc-$C_{12}$, and Asc-$C_{18:1}$ ascorbyl


dx.doi.org/10.1021/jf5029398 | J. Agric. Food Chem. 2014, 62, 9118−9127

derivatives were effective against both *Leishmania* species, while either ascorbic acid or Asc-$C_2$, Asc-$C_8$, Asc-$C_{16}$, and Asc-$C_{18:0}$ derivatives had no leishmanicidal activity up to 400 $\mu$g/mL. Interestingly, the three effective derivatives showed a higher activity against *L. major* promastigotes compared to that obtained against *L. infantum* promastigote. Indeed, $IC_{50}$ values were approximately two times higher against the former than the latter. This indicates that *L. major* parasites are more sensitive to these compounds than *L. infantum* ones. Asc-$C_{18:1}$, the most effective derivative, showed an $IC_{50}$ of 154.23 $\mu$g/mL and 205.81 $\mu$g/mL against *L. major* and *L. infantum*, respectively. Also, Asc-$C_{12}$ showed a moderate activity of 196.262 $\mu$g/mL and 284.8 $\mu$g/mL against *L. major* and *L. infantum*, respectively. Finally, Asc-$C_{10}$ was the less active compound of the three derivatives, which showed an $IC_{50}$ of 217.74 $\mu$g/mL and 347.12 $\mu$g/mL against the dermotropic and the viscerotropic strain, respectively. These results are in line with those observed previously by Aissa et al.,[11] who showed that the medium chain tyrosyl esters had an antileishmanial effect. However, for our case, the most effective derivative was ascorbyl oleate (Asc-$C_{18:1}$). These results could be attributed to the nature of the hydroxyl headgroup of ascorbic acid and besides their amphiphilicity degree.

**3.8. Interactions of Ascorbyl Derivatives with Mixture Film Monolayer.** In order to study the influence of the length and the nature of the ascorbyl derivatives acyl chain on the esters adsorption properties, their critical surface pressures ($\pi_c$) were compared using a mixture film monolayer, containing the principal components of leishmania membranes: 40% EggPC, 30% cholesterol, 10% phosphatidylethanolamine (PE), 10% phosphatidylglycerol (PG), and 10% sphingolipid (SL).[28]

The maximum surface pressure increase was determined at different initial pressures ($\pi_i$) of mixture film ranging from 5 to 40 mN/m (Figure 4). The critical surface pressure ($\pi_c$) for each ester was estimated by the linear extrapolation of the experimental curves at zero surface pressure increase. A critical pressure for penetration ($\pi_c$) may thus be defined; it corresponds to the extrapolated value of initial beyond which there is no increase in surface pressure. The value of the maximum surface pressure increase ($\Delta\pi_{max}$) reached at equilibrium (around 40 min after the injection of the ascorbyl derivative in the aqueous subphase) was determined and plotted as a function of $\pi_i$ (Figure 4). For all ascorbyl derivatives, a general trend was observed: the higher the $\pi_i$, the lower the interaction of the ascorbyl derivatives with the monolayer because of the higher packing of phospholipids. Asc, Asc-$C_2$, and Asc-$C_8$ cannot interact with the mixture film (data not shown). It can be seen from Table 4 that all ascorbyl esters

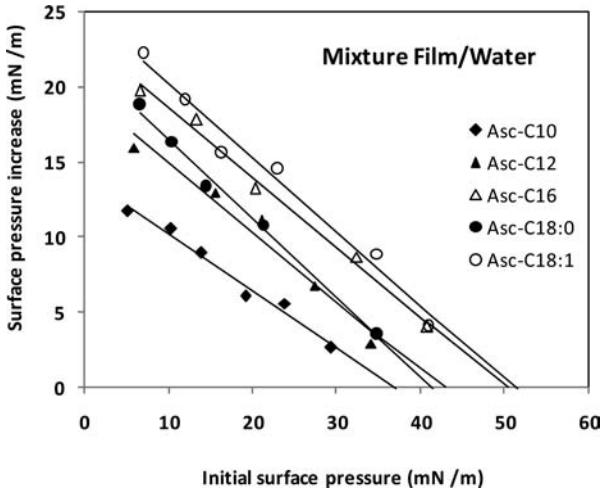


**Figure 4.** Maximal increase in surface pressure after ascorbyl derivative injection with respect to the initial surface pressure of mixture films (40% PC, 30% cholesterol, 10% SL, 10% PG, 10% PE) spread in a cylindrical Teflon trough (volume, 15 mL; surface, 17.42 $cm^2$). Final ascorbyl derivative concentration, 0.5 $\mu$M. Buffer, 10 mM Tris−HCl, pH 8.0, 100 mM NaCl, 21 mM $CaCl_2$, and 1 mM EDTA.

**Table 4. Critical Surface Pressure ($\pi_c$) of the Ascorbic Acid and Ascorbyl Acyl Esters**

| compounds | $\pi_c$ (mixture film) (mN/m) |
|---|---|
| Asc | 0 |
| Asc-$C_2$ | 0 |
| Asc-$C_8$ | 0 |
| Asc-$C_{10}$ | 36.96 |
| Asc-$C_{12}$ | 42.07 |
| Asc-$C_{16}$ | 50.06 |
| Asc-$C_{18:0}$ | 41.30 |
| Asc-$C_{18:1}$ | 50.74 |

(Asc-$C_{10}$ to Asc-$C_{18:1}$) could interact with the mimetic membrane of leishmania. The critical surface pressures ($\pi_c$) of these esters on mixture film monolayer range from 36.96 mN/m to 50.74 mN/m (Table 4). Mottola et al.[39] showed that the Asc-$C_{16}$ is an anionic amphiphilic molecule, which allowed them to penetrate phospholipid monolayers. These results are in line with those observed previously by Aissa et al.,[16] who showed that the medium and long chain tyrosyl esters could interact with biological membrane. We can also notice that unsaturation in the acyl chain (Asc-$C_{18:1}$) seems to strengthen its interaction with the mixture film. In fact, the critical surface pressures of Asc-$C_{18:1}$ and Asc-$C_{18:0}$ are 50.74 mN/m and 41.30 mN/m, respectively (Table 4). Makyla and Paluch[40] demonstrated that the presence of the unsaturated fatty acid in cholesterol/DPPC mixed monolayer makes the membrane more fluid. Asc-$C_{16:0}$ and Asc-$C_{18:0}$ showed an interaction with the mimetic membrane model but not an antileishmanial activity. This result could be explained by the self-aggregation and the reduced mobility of long saturated ascorbyl derivatives in the aqueous phase of the parasite culture medium as it was hypothesized by Laguerre et al.[41] In light of these results, if one takes the $\pi_c$ as a threshold value to appreciate the capacity of the ascorbyl esters to penetrate mixture film monolayers, we can tentatively conclude that the medium and long chain ascorbyl esters (Asc-$C_{10}$ to Asc-$C_{18:1}$) could interact efficiently with a biological membrane, characterized by a surface pressure between 25 and 35 mN/m.[42]

In conclusion, from all the tested derivatives, only medium and unsaturated ascorbyl derivatives (Asc-$C_{10}$, Asc-$C_{12}$, and Asc-$C_{18:1}$) exhibited potent antimicrobial and antileishmanial activities. These amphiphilic antioxidants could be used as membrane-perturbing surfactants in clinical applications such as for dermatological and pharmacological uses.

## AUTHOR INFORMATION

### Corresponding Author

*Laboratoire de Biochimie et de Génie Enzymatique des Lipases, ENIS, Université de Sfax, Route de Soukra, 1173 Sfax, Tunisia. Tel/fax: + 21674675055. E-mail: ytgargouri@yahoo.fr.

### Funding

This work received financial support from the Ministry of Higher Education and Scientific Research in Tunisia.

### Notes

The authors declare no competing financial interest.

## ■ ACKNOWLEDGMENTS

This work represents a part of the thesis of N.K. The authors would like to thank Pr. Sofiane Bezzine (ENIS, Sfax-Tunisia) for his generous gift of bacterial strains. We are grateful to Pr. Verger Robert and Pr. Pierre Villeneuve for their fruitful discussion. We are grateful to Pr. Bejaoui Hafedh (FSS, Sfax-Tunisia) for his help with English. Parasite experiments were partially supported by NIH/NIAID/DMID Grant Number 5P50AI074178 to LTCII.

## ■ REFERENCES

(1) Timm-Heinrich, M.; Nielsen, N. S.; Xu, X.; Jacobsen, C. Oxidative stability of structured lipids containing C18:0, C18:1, C18:2, C18:3 or CLA in sn2-position as bulk lipids and in milk drinks. *Innovative Food Sci. Emerging Technol.* **2004**, *5*, 249−61.

(2) Guillèn, M. D.; Ruiz, A. Study by means of H-1 nuclear magnetic resonance of the oxidation process undergone by edible oils of different natures submitted to microwave action. *Food Chem.* **2006**, *96* (4), 665−674.

(3) Lanigan, R. S.; Yamarik, T. A. Final report on the safety assessment of BHT. *Int. J. Toxicol.* **2002**, *21*, 19−94.

(4) Kurl, S.; Tuomainen, T. P.; Laukkanen, J. A.; Nyyssonen, L. T.; Sivenius, J.; Salonen, J. T. Plasma vitamin C modifies the association between hypertension and risk of stroke. *Stroke* **2002**, *33*, 1568−1573.

(5) Linster, C. L.; Van Schaftingen, E. Vitamin C. Biosynthesis, recycling and degradation in mammals. *FEBS J.* **2007**, *274*, 1−22.

(6) Haizhen, Z.; Yu, Z.; Fengxia, L.; Xiaomei, B.; Zhaoxin, L.; Hongmei, J. N. Optimized enzymatic synthesis of ascorbyl esters from lard using *Novozym* 435 in co-solvent mixtures. *J. Mol. Catal. B: Enzym.* **2011**, *69*, 83−176.

(7) Adamczak, M.; Bornscheuer, U. T. Improving ascorbyl oleate synthesis catalyzed by *Candida antarctica* lipase B in ionic liquids and water activity control by salt hydrates. *Process Biochem.* **2009**, *44*, 257−261.

(8) Naidu, K. A.; Richard, C. K.; Naidu, A. K.; Coppola, D. Antiproliferative and Proapoptotic effect of ascorbyl stearate in human pancreatic cancer cells: Association with decreased expression of insulin-like growth factor receptor-1. *Dig. Dis. Sci.* **2003**, *48*, 230−237.

(9) Fragopoulou, E.; Nomikos, T.; Karantonis, H. C.; Apostolakis, C.; Pliakis, E.; Samiotaki, M.; Panayotou, G.; Antonopoulou, S. Biological activity of acetylated phenolic compounds. *J. Agric. Food Chem.* **2007**, *55*, 80−89.

(10) Voravuthikunchai, S. P.; Sririrak, T.; Limsuwan, S.; Supawita, T.; Iida, T.; Honda, T. Inhibitory Effects of Active Compounds from *Punica granatum* Pericarp onVerocytotoxin Productionby Enterohemorrhagic *Escherichia coli* O157:H7. *J. Health Sci.* **2005**, *51*, 590−596.

(11) Aissa, I.; Sghair, R. M.; Bouaziz, M.; Laouini, D.; Sayadi, S.; Gargouri, Y. Synthesis of lipophilic tyrosyl esters derivatives and assessment of their antimicrobial and antileishmania activities. *Lipids Health Dis.* **2012**, 11−13.

(12) Sen, R.; Chatterjee, M. Plant derived therapeutics for the treatment of Leishmaniasis. *Phytomedicine* **2011**, *18* (12), 1056−1069.

(13) Palacios, L. E.; Wang, T. Extraction of egg-yolk lecithin. *J. Am. Oil Chem. Soc.* **2005**, *82*, 565−569.

(14) Mosbah, H.; Sayari, A.; Mejdoub, H.; Dhouib, H.; Gargouri, Y. Biochemical and molecular characterization of *Staphylococcus xylosus* lipase. *Biochim. Biophys. Acta* **2005**, *1723*, 282−291.

(15) Kharrat, N.; Ben Ali, Y.; Marzouk, S.; Gargouri, Y.; Châabouni-Karra, M. Immobilization of *Rhizopus oryzae* Lipase on silica aerogels by adsorption: Comparaison with the free enzyme. *Process Biochem.* **2011**, *46*, 1083−1089.

(16) Aissa, I.; Leclaire, J.; Ben Ali, Y.; Frikha, F.; Gargouri, Y. Monolayer properties of synthesized tyrosyl esters. *J. Mol. Catal. B: Enzym.* **2012 b**, *83*, 125−130.

(17) Brand-Williams, W.; Cuvelier, M.; Berset, C. Use of a free radical method to evaluate antioxidant activity. *Lebensm.-Wiss. Technol.* **1995**, *28*, 25−30.

(18) Viskupicova, J.; Danihelova, M.; Ondrejovic, M.; Liptaj, T.; Sturdik, E. Lipophilic rutin derivatives for antioxidant protection of oil-based foods. *Food Chem.* **2010**, *123*, 45−50.

(19) Sin, D. W. M.; Wong, Y. C.; Mak, C. Y.; Sze, S. T.; Yao, W. Y. Determination of five phenolic antioxidants in edible oils: Method validation and estimation of measurement uncertainty. *J. Food Compos. Anal.* **2006**, *19*, 784−791.

(20) Gutierrez, T.; Shimmield, T.; Haidon, C.; Black, K.; Green, D. H. Emulsifying and Metal Ion Binding Activity of a Glycoprotein Exopolymer Produced by *Pseudomonas sp.* Strain TG12. *Appl. Environ. Microbiol.* **2008**, *74*, 4867−4876.

(21) Eloff, J. N. A sensitive and quick microplate method to determine the minimal inhibitory concentration of plant extracts for bacteria. *Planta Med.* **1998**, *64*, 711−713.

(22) Okore, V. C. Evaluation of chemical antimicrobial agents. Bacterial resistance to antimicrobial agents. *Pharmaceutical Microbiology*; El'Demark publishers: Nsukka, 2005; pp 55−120.

(23) Kebaier, C.; Louzir, H.; Chenik, M.; Ben Salah, A.; Dellagi, K. Heterogeneity of wild Leishmania major isolates in experimental murine pathogenicity and specific immune response. *Infect. Immun.* **2001**, *69*, 4906−4915.

(24) Aoun, K.; Bouratbine, A.; Harrat, Z.; Belkaied, M. Bel hadj Ali S. Particular profile of the zymodemes of *Leishmania infantum* causing visceral leishmaniasis in Tunisia. *Bull. Soc. Pathol. Exot.* **2001**, *94*, 375−377.

(25) Dutta, A.; Bandyopadhyay, S.; Mandal, C.; Chatterjee, M. Development of a modified MTT assay for screening antimonial resistant field isolates of Indian visceral Leishmaniasis. *Int. J. Parasitol.* **2005**, *54*, 119−122.

(26) Verger, R.; de Haas, G. H. Enzyme reactions in a membrane model. 1: A new technique to study enzyme reactions in monolayers. *Chem. Phys. Lipids* **1973**, *10*, 127−136.

(27) Piéroni, G.; Gargouri, Y.; Sarda, L.; Verger, R. Interactions of lipases with lipid monolayers. Facts and fictions. *Adv. Colloid Interface Sci.* **1990**, *32*, 341−378.

(28) Zhang, K.; Beverley, S. M. Phospholipid and sphingolipid metabolism in Leishmania. *Mol. Biochem. Parasitol.* **2010**, *170*, 55−64.

(29) Selmi, B.; Gontier, E.; Ergan, F.; Thomas, D. Effect of fatty acid chain length and unsaturation number on triglyceride synthesis catalyzed by immobilized lipase in solvent-free medium. *Enzyme Microb. Technol.* **1998**, *23*, 182−186.

(30) Song, Q. X.; Zhao, Y.; Xu, W. Q.; Zhou, W. Y.; Wei, D. Z. Enzymatic synthesis of L-ascorbyl linoleate in organic media. *Bioprocess Biosyst. Eng.* **2006**, *28*, 211−215.

(31) Lecomte, J.; López Giraldo, L. J.; Laguerre, M.; Baréa, B.; Villeneuve, P. Synthesis, characterization and free radical scavenging properties of rosmarinic acid fatty esters. *J. Am. Oil Chem. Soc.* **2010**, *87*, 615−620.

(32) Laguerre, M.; López Giraldo, L. J.; Lecomte, J.; Figueroa-Espinoza, M. C.; Baréa, B.; Weiss, J.; Decker, E. A.; Villeneuve, P. Chain length affects antioxidant properties of chlorogenate esters in emulsion: the cutoff theory behind the polar paradox. *J. Agric. Food Chem.* **2009**, *57*, 11335−11342.

(33) Burham, H.; Abdul Rasheed, R.; Ainaa, G.; Noorullhamezon, M. N.; Suzaini, B.; Sidek, H. Enzymatic synthesis of palm-based ascorbyl esters. *J. Mol. Catal. B: Enzym.* **2009**, *58*, 153−157.

(34) Shahidi, F.; Zhong, Y. Lipid Oxidation: Measurement Methods. *Bailey's Industrial Oil and Fat Products*, 6th ed., 6 volume set; **2005**; pp 357−385.

(35) Azeem, A.; Rizwan, M.; Farhan, J. A.; Khan Zeenat, I.; Khar Roop, K.; Aqil, M.; Talegaonkar, S. Emerging Role of Microemulsions in Cosmetics. *Recent Pat. Drug Delivery Formulation* **2008**, *2*, 275−289.
(36) Kuwabara, K. O.; Watanabe, Y.; Adachi, S.; Nakanishi, K.; Matsuno, R. Emulsifier properties of saturated acyl l-ascorbates for preparation of O/W emulsions. *Food Chem.* **2003**, *82*, 191−194.
(37) Taguri, T.; Tanaka, T.; Kouno, I. Antimicrobial activity of 10 different plant polyphenols against bacteria causing food-borne disease. *Biol. Pharm. Bull.* **2004**, *27*, 1965.
(38) Ultee, A.; Bennik, M. H. J.; Moezelaar, R. The phenolic hydroxyl group of carvacrol is essential for action against the food-borne pathogen *Bacillus cereus*. *Appl. Environ. Microbiol.* **2002**, *68*, 1561−1568.
(39) Mottola, M.; Wilke, N.; Benedini, L.; Oliveira, R. G.; Fanani, M. L. Ascorbyl palmitate interaction with phospholipid monolayers: electrostatic and rheological preponderancy. *Biochim. Biophys. Acta* **2013**, *1828*, 2496−2505.
(40) Makyla, K.; Paluch, M. The linoleic acid influence on molecular interactions in the model of biological membrane. *Colloids Surf., B* **2009**, *71*, 59−66.
(41) Laguerre, M.; Bayrasy, C.; Lecomte, J.; Chabi, B.; Decker, E. A.; Wrutniak-Cabello, C.; Cabello, G.; Villeneuve, P. How to boost antioxidants by lipophilization? *Biochimie* **2013**, *95*, 20−26.
(42) Sanchez-Martin, M. J.; Haro, I.; Alsina, M. A.; Busquets, M. A.; Pujol, M. A Langmuir monolayer study of the interaction of E1 (145−162) Hepatitis G virus peptide with phospholipid membranes. *J. Phys. Chem. B* **2010**, *114*, 448−456.

previous studies, the grafting substitution by chemical reagents is also limited. The reported maximum grafting ratio of GA onto CS was 128.3 mg GA equivalents (GAE)/g via free radicals generated by ascorbic acid and the hydrogen peroxide-mediated method.[19] For 1-ethyl-3-(3′-dimethylaminopropyl) carbodiimide/*N*-hydroxysuccinimide (EDC/NHS)-mediated activated ester method, the maximum grafting ratio of GA onto CS was only about 65 mg GAE/g CS.[31] Furthermore, the rheological potential of GA-grafted-CS (GA-*g*-CS) compared to free GA has seldom been studied. Therefore, the objectives of this work are to establish an efficient method to graft large amounts of GA onto CS and to study the influence of grafted GA on CS, especially the antioxidant activities and rheological properties. In the present study, a new synthetic method to implant GA to CS with significantly improved graft ratio was developed, in which CS was dissolved, assisted with hydroxybenzotriazole (HOBt), and the synthesized GA-*g*-CS was characterized by UV−vis spectroscopy and proton nuclear magnetic resonance ($^1$H NMR) spectroscopy. Then, GA-*g*-CS with different degrees of substitution were prepared and investigated systematically with various in vitro antioxidant assays, including assays of scavenging activities on 2,2-diphenyl-1-picrylhydrazyl (DPPH), superoxide, and 2,2′-azino-bis(3-ethylbenzothiazoline-6-sulfonic acid) (ABTS) free radicals, reducing power, chelating power, inhibition of lipid peroxidation, ferric reducing antioxidant potential, and $\beta$-carotene-linoleic acid assay. Finally, the viscosities of GA-*g*-CS with different grafting ratios were investigated.

## MATERIALS AND METHODS

**Materials and Reagents.** CS (viscosity-average molecular weight ~$1.5 \times 10^5$, degree of deacetylation ≥90.0%), EDC hydrochloride (EDC-HCl), Folin-Ciocalteau reagent were purchased from Kayon Biological Technology Co., Ltd. (Shanghai, China). GA, nitrotetrazolium blue (NBT) chloride, and HOBt were obtained from Sinopharm Chemical Reagent Co., Ltd. (Shanghai, China). DPPH, $\beta$-carotene, linoleic acid, ABTS, phenazine methosulfate (PMS), 2,4,6-tris(2-pyridyl)-*s*-triazine (TPTZ) were purchased from Sigma Chemical Co. (St. Louis, MO). Ferrozine (3-(2-pyridyl)-5,6-diphenyl-1,2,4-triazine-*p*,*p*′-disulfonic acid monosodium salt) was purchased from Aladdin Industrial Inc. (Shanghai, China). Reduced nicotinamide adenine dinucleotide disodium salt (NADH) was purchased from Roche Ltd. (Basel, Switzerland). Deuterium oxide ($D_2O$) and acetic acid-$d_4$ ($CD_3COOD$) for NMR were purchased from J&K Scientific Ltd. (Beijing, China). All of other reagents were of analytical grade.

**Synthesis of GA-*g*-CS.** The synthesis of GA-*g*-CS was performed based on the reported one-pot method[32] with some modifications. CS (0.303 g, 1.85 mmol) was stirred in deionized water (30.0 mL) with HOBt (0.282 g, 1.85 mmol) overnight until a clear solution was obtained. GA (0.311 g, 1.85 mmol) was introduced into the CS solution followed by the dropwise addition of an alcoholic solution of EDC-HCl (0.355 g, 1.85 mmol, 2.0 mL). The reaction was carried out for 24 h in ambient temperature and atmosphere. The resultant liquid was poured into dialysis tubes (MWCO 3500 Da) and dialyzed against deionized water for 48 h with eight changes of deionized water. The resulting solution was lyophilized to afford solid copolymer of GA-*g*-CS. Thin layer chromatography (TLC) was performed to verify whether free GA was removed from the product of GA-*g*-CS. Briefly, silica plates with applied CS, GA, and GA-*g*-CS were developed with acetic acid−water−*n*-butanol (v/v/v, 1:4:5) as the mobile phase at laboratory temperature. After development and air-drying, the spots on the silica plate were detected by using iodine vapor. Blank CS, acting as a control, was prepared in the same conditions but in the absence of GA. GA-*g*-CS with different substitutions of GA, named as GA-*g*-CS I, II, and III, were prepared by changing the ratio of GA and EDC.

**Characterization of GA-*g*-CS.** Structural characterization of GA-*g*-CS was performed by UV−vis and NMR analysis. The UV−vis spectra were determined by a UV-2600 spectrophotometer (Shimadzu, Kyoto, Japan) by scanning from 200 to 600 nm. $^1$H NMR spectra were recorded at 25 °C with samples dissolved in $CD_3COOD/D_2O$ (v/v, 1%) by using AVANCE III 500 MHz NMR Spectrometer (Bruker, Switzerland).

**Determination of Phenolic Content.** Phenolic content was determined according to the previous reported method.[33] Briefly, 0.5 mL of GA-*g*-CS solution was mixed with 1.0 mL of Folin-Ciocalteau reagent for 5 min in the dark, followed by the addition of 2.0 mL 20% sodium carbonate ($Na_2CO_3$) solution. The mixture was shaken and kept at 30 °C for 1 h, absorbance (Abs) of which was measured at 747 nm by using a 722S Visible Spectrophotometer (Shnghai Jinghua Science & Technology Instruments Co., Ltd., China). GA was used as a standard. The grafting ratios of GA-*g*-CS were expressed as milligram GAE per gram of copolymer (mg GAE/g).

**Assay of Antioxidant Activity of GA-*g*-CS in Vitro.** *Assay of Scavenging Activity on DPPH Free Radicals.* DPPH free radicals scavenging activity was determined according to the reported procedure[34] with slight modifications. Briefly, GA, CS, and GA-*g*-CS (I, II, and III) were homogeneously dispersed in deionized water for preparation of a series of concentrations (0.125, 0.25, 0.5, 1.0, 1.5, and 2.0 mg/mL). The solutions were pipetted into a 96-well plate (50 $\mu$L/well), and to each well, 200 $\mu$L of methanolic DPPH solution (0.4 mM) was added and mixed. After a 30 min reaction at room temperature in the dark, the Abs at 517 nm was measured by a microplate reader (BioTek Instruments Inc., Winooski, VT).

$$\text{DPPH free radicals scavenging activity (\%)} = \left(1 - \frac{\text{Abs}_1 - \text{Abs}_2}{\text{Abs}_0}\right) \times 100$$

where $Abs_0$ is the Abs of the control (water instead of sample), $Abs_1$ is the Abs of the sample, and $Abs_2$ is the Abs of the sample under identical conditions as $Abs_1$ with methanol instead of DPPH solution.

*Evaluation of Reducing Power.* Reducing powers of the samples were determined by the previously described method[35] with some modifications. The reactions were carried out in 96-well microplates, each well of which contained a mixture of 50 $\mu$L of sample solution, sodium phosphate buffer (PBS, 0.2 M, pH 6.6), and $K_3Fe(CN)_6$ solution (1%, w/v), and were incubated at 50 °C for 20 min. After the addition of 50 $\mu$L of trichloroacetic acid (10%, w/v) and 30 $\mu$L of $FeCl_3$ (0.1%, w/v), the Abs was measured at 700 nm.

$$\text{reducing power} = \text{Abs}_1 - \text{Abs}_2$$

where $Abs_1$ is the Abs of sample and $Abs_2$ is the Abs of the sample under identical conditions as $Abs_1$ with water instead of $FeCl_3$ solution only.

*Assay of Scavenging Activity on Superoxide Radicals.* Superoxide radicals scavenging activities of the samples were evaluated according to the literature[35] with some modifications. NADH, NBT, and PMS were diluted in PBS (0.1 M, pH 7.4). The mixture of 50 $\mu$L of sample, NADH (468 mM), NBT (156 mM), and PMS (60 mM) was added in the well of the microplate and incubated at 25 °C for 5 min, and then the Abs was measured at 560 nm.

$$\text{superoxide radicals scavenging activity (\%)} = \left(1 - \frac{\text{Abs}_1 - \text{Abs}_2}{\text{Abs}_0}\right) \times 100$$

where $Abs_0$ is the Abs of the control (water instead of sample solution), $Abs_1$ is the Abs of the sample, and $Abs_2$ is the Abs of the sample under identical conditions as $Abs_1$ with 0.1 M phosphate buffer instead of NBT solution.

*Assay of Metal Chelating Ability.* The metal chelating ability for $Fe^{2+}$ was tested according to the reported method[34] with some

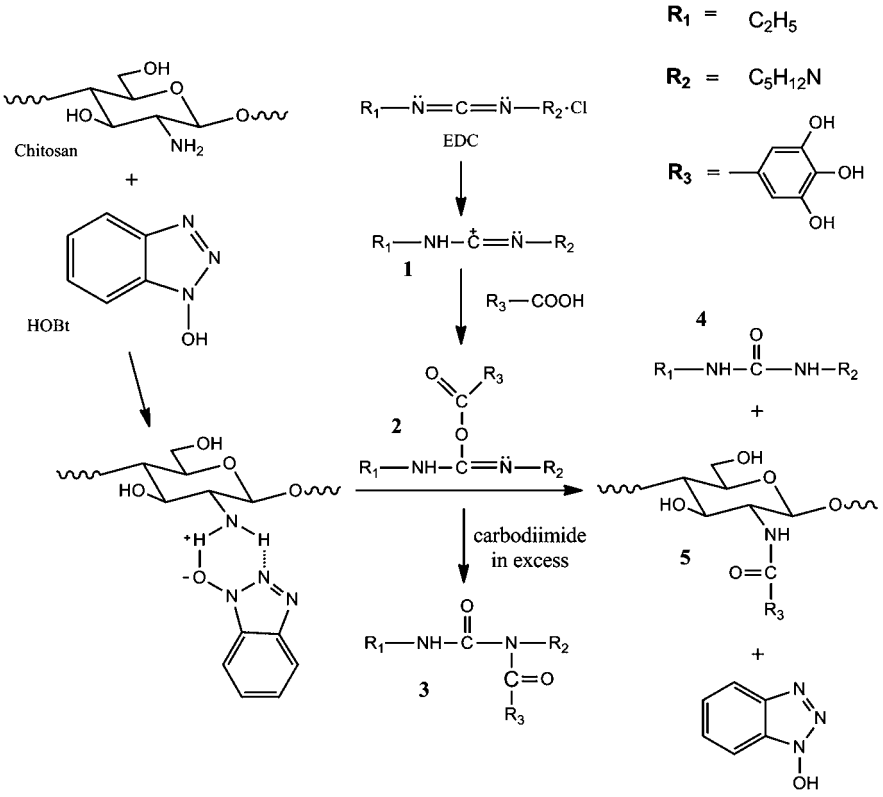


**Figure 1.** Proposed mechanism for grafting gallic acid onto chitosan.

modifications. Briefly, 50 $\mu$L of sample, 30 $\mu$L of $FeCl_2$ (0.3 mM), and 120 $\mu$L of ferrozine (0.3 mM) solutions were mixed and incubated at 25 °C for 10 min, and then Abs at 562 nm was determined.

$$\text{chelating activity (\%)} = \left(1 - \frac{\text{Abs}_1 - \text{Abs}_2}{\text{Abs}_0}\right) \times 100$$

where $Abs_0$ is the Abs of the control (water instead of sample), $Abs_1$ is the Abs of the sample, and $Abs_2$ is the Abs of the sample under identical conditions as $Abs_1$ with deionized water instead of $FeCl_2$ solution.

*Assay of Lipid Peroxidation Inhibition.* The lipid peroxidation inhibitory effect was determined by thiobarbituric acid reactive substances (TBARS) assay.[34] First, 1.0 g of mouse liver was homogenated in 100.0 mL purified water to afford lipid-rich media. Then, 0.2 mL of sample was mixed with 1.0 mL of liver homogenate, and 50 $\mu$L $FeCl_2$ solution (0.1 mM) and $H_2O_2$ (0.1 mM) were added. After incubation at 37 °C for 1 h, the peroxidizing reaction was quenched by the addition of 0.3 mL of trichloroacetic acid (20%, w/v) and thiobarbituric acid (0.8%, w/v). The resulting mixture was incubated at 100 °C for 15 min and then centrifuged (4000 rpm, 10 min), and 200 $\mu$L of the supernatant was added to the well of the 96-well microplate. Abs was measured at 532 nm.

$$\text{lipid peroxidation inhibitory effect (\%)} = \left(1 - \frac{\text{Abs}_1 - \text{Abs}_2}{\text{Abs}_0}\right) \times 100$$

Where $Abs_0$ is the Abs of the control (water instead of sample), $Abs_1$ is the Abs of the sample, and $Abs_2$ is the Abs of the sample only (water instead of liver homogenate).

*Assay of Total Antioxidant Capacity.* The ferric reducing antioxidant potential (FRAP) was used to determine the total antioxidant capacity according to the previous procedure[34] with some modifications. The FRAP working solution was obtained by mixing 100.0 mL of sodium acetic buffer (0.3 M, pH 3.6), 10.0 mL of TPTZ (10 mM, dissolved in 40 mM HCl), and 10.0 mL of $FeCl_3$ solution (20 mM) together. The mixture containing 40 $\mu$L of sample and 200 $\mu$L of FRAP solution was incubated at 25 °C for 10 min, and the Abs was detected at 593 nm.

*Assay of Scavenging Activity on ABTS Free Radicals.* The preformed radicals of ABTS were generated by oxidation of ABTS (7.0 mM) with potassium persulfate ($K_2S_2O_8$, 4.95 mM) for 12 h in the dark at room temperature.[33] After generation, ABTS was diluted with PBS (0.2 M, pH 7.4) to an appropriate concentration, affording the working solution. The Abs of a mixture of a 20 $\mu$L sample and a 200 $\mu$L working solution was measured at 734 nm.

$$\text{ABTS free radicals scavenging activity (\%)} = \left(1 - \frac{\text{Abs}_1 - \text{Abs}_2}{\text{Abs}_0}\right) \times 100$$

where $Abs_0$ is the Abs of the control (water instead of sample), $Abs_1$ is the Abs of the sample, and $Abs_2$ is the Abs of the sample only (PBS instead of ABTS).

*β-Carotene-Linoleic Acid Assay.* GA-*g*-CS inhibiting peroxidation in a linoleic acid model was determined by a β-carotene bleaching test[15] with some modifications. Briefly, 2.0 mL of β-carotene solution (1.0 mg/mL in chloroform) was added to 40 mg of linoleic acid and 400 mg of Tween 20. The mixture was evaporated by a rotary evaporator at 40 °C to remove chloroform. After that, the mixture was immediately diluted with 200.0 mL of distilled water and followed by ultrasonication to form an emulsion. The emulsion (1.25 mL) was transferred to the microcentrifuge tube containing 50 $\mu$L of sample. The tubes were then shaken gently and incubated at 45 °C for 1 h. The Abs of resulting liquid was measured at 470 nm by using the microplate reader.

$$\text{antioxidant activity (\%)} = \left(1 - \frac{\text{Abs}_0 - \text{Abs}_{60}}{\text{Abs}_0^0 - \text{Abs}_{60}^0}\right) \times 100$$

where $Abs_0$ and $Abs_0^0$ are the Abs measured at the initial incubation time for samples and control, respectively, whereas $Abs_{60}$ and $Abs_{60}^0$ are


dx.doi.org/10.1021/jf503207s | J. Agric. Food Chem. 2014, 62, 9128−9136

the Abs of the samples and control, respectively, after incubation for 60 min.

**Analysis of Rheological Property.** Rheological behavior of sample was measured on a MCR 301 Rheometer (Anton Paar GmbH, Austria) at a temperature of 20 °C. The samples, CS and GA-*g*-CS (I, II, and III), were dissolved in acetic acid solution (v/v, 1%) to a concentration of 1% (m/v). The viscosity was measured as a function of increasing shear rate, varying from 2 to 256 $s^{-1}$. The viscosity at every point was recorded five times, and each sample was tested in triplicate.

**Statistical Analysis.** Data were expressed as the mean ± standard deviation (SD) of triplicates. The least significant difference (LSD), Duncan's multiple range test, and one-way analysis of variance (ANOVA) were used for multiple comparisons by SPSS 16.0. The difference was considered to be statistically significant if $p < 0.05$.

## RESULTS AND DISCUSSION

**Synthesis of GA-*g*-CS.** CS was chosen as the polymeric backbone to synthesize the biomaterial containing the antioxidant groups of GA since it is natural, edible, and biocompatible and processes the amino groups of which can be grafted onto easily. For the grafting reaction, CS is generally dissolved in acetic acid solution. In the present study, however, CS was dissolved with the assistance of HOBt. As we know, HOBt is an organic compound used as a racemization suppressor and also for improving the yield in peptide synthesis. There are relatively intense hydrogen bonds or even ionic bonds between the amino groups of CS and the hydroxyl groups of HOBt.[36] The transparence in the mixture of CS and HOBt means it is possible to modify CS in an aqueous system without the organic solvent, avoiding the side reactions resulting from the presence of acetic acid. As a result, CS was efficiently conjugated with GA in the present study via a water-soluble carbodiimide conjugating agent.[37] The detailed reaction mechanism is depicted in Figure 1. EDC was protonated by HCl coexisting in the carbodiimide conjugating reagent, forming carbocation **1** that further reacted with the carboxyl group of GA to form *O*-acylisourea **2**. In order to avoid the hydrolyzation of EDC to urea **4**, EDC was dissolved in ethanol and added slowly into the solution of CS-HOBt and GA. When EDC was in excess, *N*-acylurea **3** could be by-produced. Herein, the presence of HOBt in combination with EDC is designed to reduce **3** and also to improve the reaction rate.[32] The conjugation might occur at C-2 of CS to afford amide or at C-3 and C-6 of CS to afford ester linkages. Although the hydroxyl group is reactive, the reaction at C-3 can be omitted due to the steric hindrance.[32] HOBt and byproduct urea **4** were removed from the resulting solution by dialysis against water. It has been reported that the binding constant ($K$) of HOBt with CS is 112.32 L/mol,[38] which means HOBt may be present a little in the resulting product. The absence of HOBt in the target copolymer **5** was confirmed by $^1$H NMR.

**Characterization of GA-*g*-CS.** The UV−vis spectra of GA, CS, and GA-*g*-CS (I, II and III) are displayed in Figure 2. During 240 to 500 nm, CS showed no absorption peak, and GA exhibited two characteristic absorption bands at 212 and 262 nm, respectively, assigned to the $\pi$-system of the benzene ring. In the spectra of GA-*g*-CS (I, II, and III), it was found that the UV−vis absorption peak at 262 nm shifted toward a longer wavelength (272 nm). It is consistent with the reported result for GA-*g*-carboxymethyl CS.[14] The results indicated that GA was successfully grafted onto CS.[2] The red shift might be attributed to the smaller amount of energy required for the

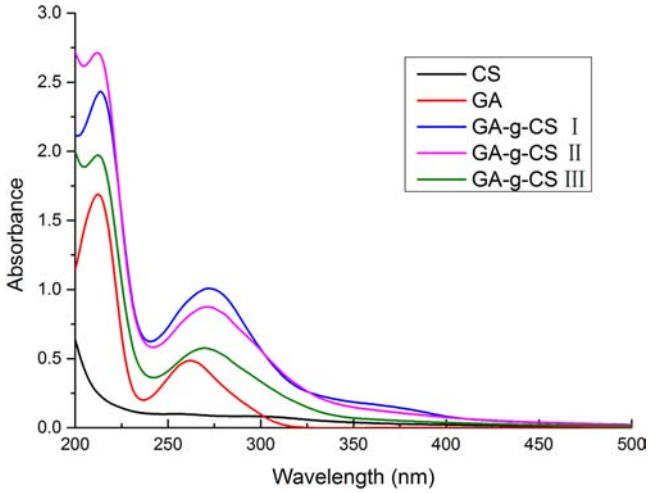


**Figure 2.** UV−vis spectra of chitosan (CS), gallic acid (GA), and GA grafted CS (GA-*g*-CS I, II, and III).

$\pi-\pi^*$ transition due to the longer conjugated system brought by the covalent linkage of GA with CS.

Further characterization of GA-*g*-CS was performed by $^1$H NMR. As shown in Figure 3, GA showed only one peak at 7.1 ppm (H-a of benzene ring). CS exhibited a single peak at 3.1 ppm (H-2), multiple peaks at 3.6−3.9 ppm (H-3 to H-6), a small peak at 4.6 ppm (H-1), and a single peak at 2.0 ppm, representing the three protons of the *N*-acetyl group. The spectrum of GA-*g*-CS contained all the peaks of CS, and a new peak at around 7.1 ppm originated from GA, confirming again the successful grafting of GA onto CS. In addition, the peaks at 7.4−8.0 ppm, the signals of HOBt, did not appear in the spectrum, assuring that there was no HOBt remaining in the copolymer.

The substitution of GA on CS could be evaluated by determining the phenolic groups of GA-*g*-CS. In the Folin-Ciocalteu reaction, phenolic compounds undergo a complex redox reaction with phosphotungstic and phosphomolybdic acids.[39] The transfer of electrons at basic pH reduces the phosphomolybdic/phosphotungstic acid complexes to form chromogens, and then the color is developed. For GA-*g*-CS I, II, and III, these values were 209.9 ± 2.0, 117.8 ± 1.3, and 99.6 ± 0.7 mg GAE/g of dry copolymers, respectively. Interestingly, the 209.9 mg GAE/g copolymer is the highest substitution ratio of GA grafted onto CS among those that have been reported so far. As the reason, it might be due to the use of HOBt that resulted in more efficient grafting than traditional ways. In addition, it is meaningful to express the antioxidant potential in terms of phenolic content, since the activity of GA-*g*-CS conjugate is mainly originated from the phenolic groups in the polymeric backbone.

**Antioxidant Activity of GA-*g*-CS.** CS has been exploited as a natural macromolecular antioxidant recently. However, three main obstacles including the poor solubility, chemical inertness based on the strong inter- and intramolecular hydrogen bonds network, and poor H atom-donating ability have to be overcome. Introduction of GA onto CS gives a solution to such problems, and GA-*g*-CS has been synthesized as a novel potential polysaccharide antioxidant.[40] The antioxidant activities of compounds are attributed to various mechanisms, such as breaking radical chain, prevention of introduction of initiating radicals, hindering metal-catalyzed initiation reactions, decomposition of lipid hydroperoxides,


dx.doi.org/10.1021/jf503207s | J. Agric. Food Chem. 2014, 62, 9128−9136

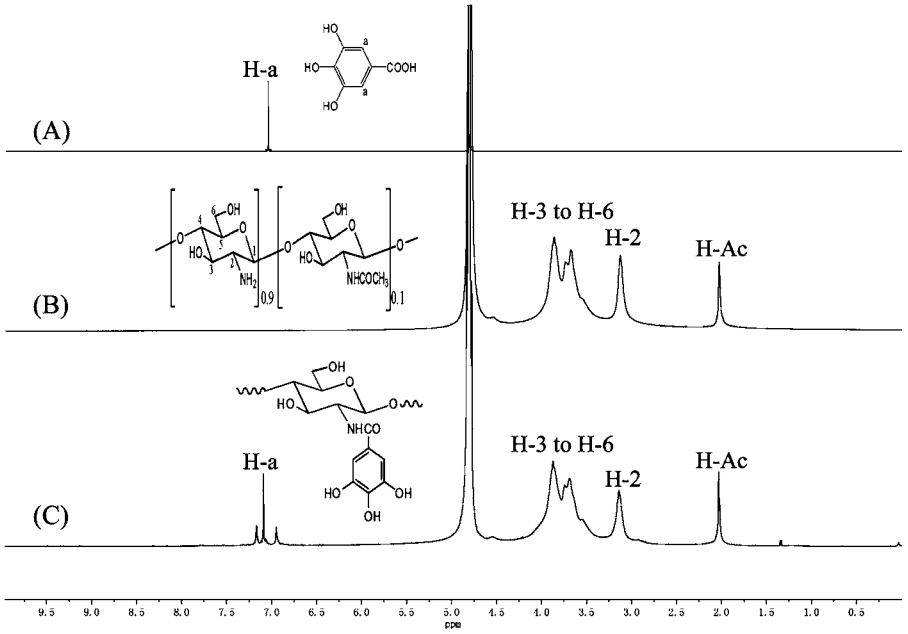


**Figure 3.** $^{1}$H NMR spectra of (A) gallic acid, (B) chitosan, and (C) GA grafted CS (GA-*g*-CS).

singlet oxygen quenching, oxygen scavenging, and blocking the prooxidant effects by binding certain proteins containing catalytic metal sites.[41] Therefore, various in vitro chemical-based assays, such as assays of oxygen radical absorbance capacity (ORAC), scavenging activity on DPPH free radicals, and ferric reducing capacity, have been developed to determine antioxidant activity. Furthermore, a single in vitro chemical method is not enough to evaluate and compare their antioxidant properties by considering the complexity involved in their in vivo mechanisms of action.

The results of antioxidant assays are displayed in Figure 4. The results showed that the antioxidant ability decreased in the order of GA-*g*-CS I, GA-*g*-CS II, GA-*g*-CS III, and CS. Obviously, GA-*g*-CS showed great antioxidant potential. In addition, the antioxidant capacities of all samples were well-correlated with the increase of concentrations and the amount of GA grafted onto the backbone.

The DPPH and ABTS free radicals have been widely used for testing the preliminary radical scavenging capacity of plant extracts or antioxidant compounds. The DPPH and ABTS free radical scavenging activities of GA-*g*-CS are shown in Figure 4 (panels A and B), respectively. The results of the two assays were presented in a similar manner that the scavenging activities of samples decreased in order of GA, GA-*g*-CS I, GA-*g*-CS II, GA-*g*-CS III, and CS at a low concentration corresponding to the quantities of GA contained, and there was no significant difference between the scavenging activities of GA-*g*-CS and GA at high concentrations.

Superoxide radical, arising from the addition of one electron to dioxygen either through metabolic processes or following oxygen activation by physical irradiation, is considered as the primary reactive oxygen species (ROS). It can interact with other molecules to generate secondary ROS either directly or prevalently through enzyme- or metal-catalyzed processes, including hydroxyl radical, $H_2O_2$, and singlet oxygen.[42] The superoxide radical scavenging activities of CS, GA-*g*-CS, and GA are shown in Figure 4C. All the samples exhibited scavenging activities on superoxide radicals. The scavenging abilities of all the three GA-*g*-CS were above 80%, and GA-*g*-CS I was equal to GA ($p > 0.05$) at a concentration of 2.0 mg/mL.

The reducing power of a compound is a significant index of its potential antioxidant activity. As shown in Figure 4D, the reducing power of all samples increased with concentrations. The reducing power of GA-*g*-CS I was stronger than GA-*g*-CS II and GA-*g*-CS III ($p < 0.05$) and equal to GA at high concentrations (>1.0 mg/mL).

Metal ion chelating activity plays a vital role in antioxidant mechanism since transition metals are known to catalyze the formation of ROS and aggravate oxidative stress.[43] The $Fe^{2+}$ chelating ability was determined by measuring the iron-ferrozine complex, and the results are summarized in Figure 4E. GA-*g*-CS showed much higher metal chelating activity than GA and CS. Especially, GA-*g*-CS I and GA-*g*-CS II showed stronger chelating capacity than GA-*g*-CS III ($p < 0.05$), except at a low concentration (0.125 mg/mL). Phenolics grafted onto CS lead to an exponential increase in iron-chelating ability and open a novel strategy for the development of a new generation of CS-based chelating therapeutic polymers for iron overload.[44]

Lipids, especially polyunsaturated fatty acids in the cell membrane, are vulnerable to both enzymes and nonenzymatic oxidants and are readily oxidized by free radicals, leading to membrane damage and eventually to various disorders and diseases.[45] Antioxidant may directly react with initiator radicals or lipid peroxides involved in lipid peroxidation processes, and it may also inhibit the formation of active radicals. As shown in Figure 4F, the lipid peroxidation inhibition effect of GA-*g*-CS was about 50% at a high concentration, much higher than CS ($p < 0.05$) but lower than GA ($p < 0.05$). And the inhibition increased with the elevation of concentration.

The $\beta$-Carotene–linoleic acid system is a rapid method for evaluation of antioxidants developed by Marco.[46] In this method, the linoleic acid free radical formed attacks the highly unsaturated $\beta$-carotene molecules and rapidly bleached the orange color of $\beta$-carotene in the absence of an antioxidant.[47] The lowest $\beta$-carotene discoloration rate exhibited the highest antioxidant activity. The inhibition effect of GA-*g*-CS was


dx.doi.org/10.1021/jf503207s | J. Agric. Food Chem. 2014, 62, 9128–9136

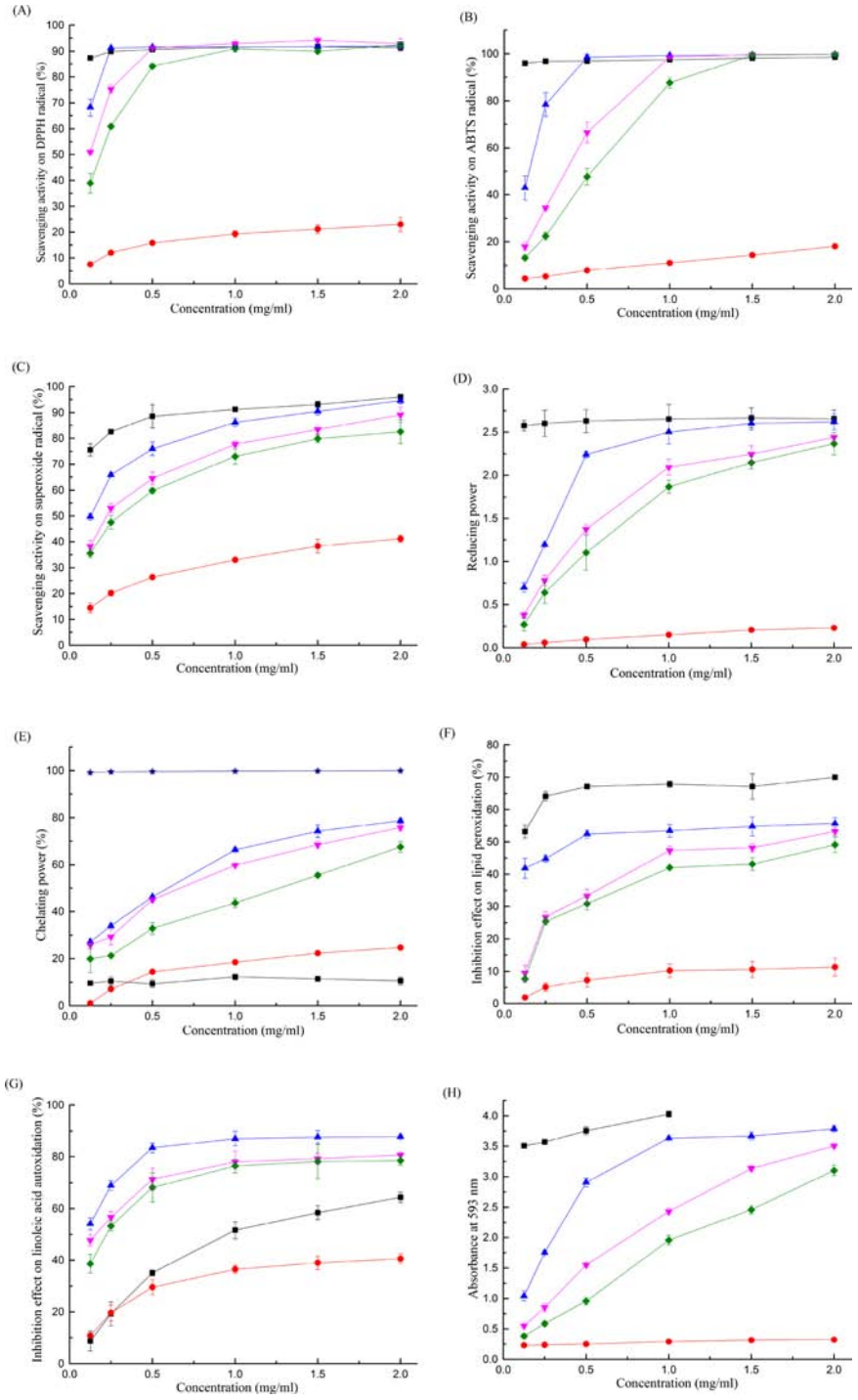


**Figure 4.** Scavenging activities on (A) 2,2-diphenyl-1-picrylhydrazyl (DPPH) radical, (B) 2,2′-azino-bis(3-ethylbenzothiazoline-6-sulfonic acid) (ABTS) radical, and (C) superoxide radical. (D) reducing power, (E) chelating power, (F) lipid peroxidation, (G) linoleic acid autoxidation inhibition effect, and (H) total antioxidant capacity of gallic acid (GA, ■), chitosan (CS, red ●), GA-*g*-CS I (blue ▲), GA-*g*-CS II (pink ▼), GA-*g*-CS III (green ◆), ethylene diamine tetraacetic acid (EDTA, blue ★). Data are presented as means ± SD of triplicates.

around 80% at 1.0 mg/mL (Figure 4G), higher than that of CS ($p < 0.05$) and notably even much better than GA ($p < 0.05$).

The FRAP assay is based on the ability of antioxidant compounds to reduce complex (Fe (III)-TPTZ) to (Fe (II)-TPTZ) that gives a blue color. The results of the FRAP assay are presented in Figure 4H. The activities increased in order of CS, GA-*g*-CS III, GA-*g*-CS II, GA-*g*-CS I, and GA ($p < 0.05$), related to the reductant (GA) content of the sample.

The assays used in the present study can roughly be classified into two types, depending upon the reactions involved: assays based on hydrogen atom transfer (HAT) reactions and the ones based on electron transfer (ET) reactions.[48] The ET-based assays included the total phenol assay by Folin-Ciocalteu reagent, DPPH and ABTS radicals scavenging assays, reducing power, and total antioxidant potential assays with FRAP. The antioxidant activities measured by these assays are correlated with the reducing agent present in samples, the GA grafted


dx.doi.org/10.1021/jf503207s | J. Agric. Food Chem. 2014, 62, 9128−9136

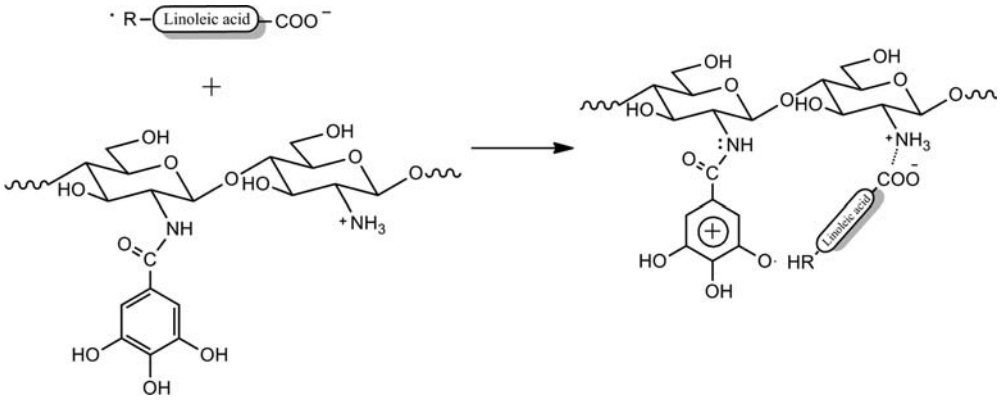


**Figure 5.** Proposed interaction between gallic acid–chitosan and free linoleic acid radicals.

onto CS in our case. It could easily be understood that the antioxidant potential obtained from these assays decreased in the order of GA, GA-*g*-CS I, GA-*g*-CS II, GA-*g*-CS III and CS, which was associated with concentration of sample.

CS showed little antioxidant potential in our assays. However, previous studies reported that CS dissolved with acetic acid, HOBt, thiamine pyrophosphate (CS-TPP), and the ethylenediaminetetraacetic acid (CS-EDTA) solution possessed superoxide and hydroxyl radicals scavenging abilities.[49] It was supposed that the antioxidant capacity of CS dissolved in pure water was suppressed due to its limited solubility.

Notably, GA-*g*-CS showed stronger antioxidant activity than GA in the *β*-carotene-linoleic acid assay. *β*-Carotene-linoleic assay, different from DPPH assay, is a HAT-based antioxidant assay. It was observed that the extract of mushroom with great antioxidant potential in the DPPH assay did not perform well in *β*-carotene-linoleic acid assay, as variation of phenolic contents did not directly influence the antioxidant activity in the *β*-carotene-linoleic acid assay.[50] During the oxidation in this model, an atom of hydrogen is abstracted from the active bis-allylic methylene group of linoleic acid located at C-11 between two double bonds and then the formed pentadienyl free-radical attacks highly unsaturated *β*-carotene molecules in an effort to reacquire a hydrogen atom. As the *β*-carotene molecules lose their conjugation, the carotenoids lose their characteristic orange color in the absence of an antioxidant.[51] It has been reported that CS could absorb fatty acids by electrostatic interaction,[52] and the antioxidant activity of phenolic compounds depends on various structural features such as the O–H bond dissociation energy, resonance delocalization of the phenoxyl radical, and the steric hindrance due to bulky groups substituting hydrogen in the aromatic ring.[53] Considering that, we hypothesize that the interaction between GA-*g*-CS and linoleic acid radicals could occur as illustrated in Figure 5, GA-*g*-CS attracting linoleic acid radicals by electrostatic affinity and quenching them with the GA groups rapidly. Furthermore, grafting GA onto CS developed amide linkages that enlarged the conjugated system of GA and contributed to an increase in electron donating groups, making GA-*g*-CS more stable than free GA. We suppose that GA-*g*-CS with swelling macromolecular structure could capture the linoleic acid free radicals, while small molecule GA could not. Linoleic acid radicals had larger size and had more potential for interacting with CS than superoxide radicals so that they were more easily captured. Those might be the reasons why GA-*g*-CS exhibited higher free radical scavenging ability than GA in the *β*-carotene-linoleic acid assay.

**Rheological Property of GA-*g*-CS.** The flow curves of CS and GA-*g*-CS are shown in Figure 6. It was observed that GA-*g*-

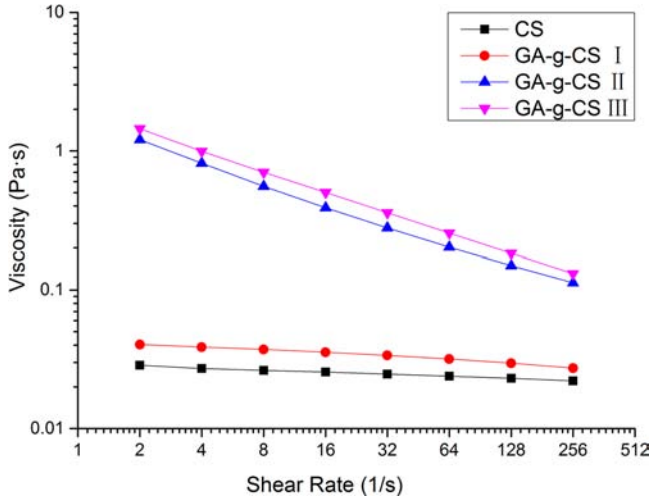


**Figure 6.** Viscosity of chitosan (CS) and gallic acid (GA) grafted CS (GA-*g*-CS I, II, and III).

CS (I, II, and III) was more viscous than plain CS significantly ($p < 0.05$). The viscosity of GA-*g*-CS decreased in order of GA-*g*-CS III, GA-*g*-CS II, GA-*g*-CS I, and CS, and the viscosity of GA-*g*-CS III was 50 times higher than that of CS at 2 $s^{-1}$ and 5 times higher at 256 $s^{-1}$. Similar phenomenon had also been found in natural macromolecules. The polysaccharide-containing ferulic acid extracted from the seeds of *Plantago asiatica* L. exhibited much higher apparent viscosity compared to that of the polysaccharide depleted ferulic acid.[54] Additionally, arabinoxylan samples with different ferulic acid contents had been employed to obtain gels by enzymatic covalent cross-linking of the phenolic acid.[55] For GA-*g*-CS, the grafting of GA onto CS provides the possibility that links the different GA-*g*-CS macromolecular chains by the formation of phenolic dimers or trimers and even the covalent junction between GA and amino group from glucosamine residue. The new bonds may lead to larger molecular weight, longer chain length, and a more viscous solution. Therefore, it was hypothesized that the high viscosity of GA-*g*-CS was attributed to the covalent cross-linking junctions produced by the oxidation of GA groups.

For GA-*g*-CS (I, II and III), the viscosity of the sample decreased with the increase of the substituting degree. The GA-*g*-CS III with a substituting degree of 99.6 mg GAE/g of dry


dx.doi.org/10.1021/jf503207s | J. Agric. Food Chem. 2014, 62, 9128–9136

copolymers appeared more viscous than both the plain CS and copolymer with a higher degree of substitution (I or II). A similar tendency was also observed in GA-gelatin. The gel strength and modulus of viscosity ($G''$) increased with increasing GA concentration up to 20 mg/g dry gelatin and then decreased at further elevated GA concentrations.[56] The results indicated that the viscosity of GA-*g*-CS was related to the grafting amount of GA.

The introduction of GA onto CS takes many properties to GA-*g*-CS copolymer. On one hand, GA may reduce the intra- and intermolecular hydrogen bond networks and eliminate crystal structure, but on the other, the grafting provides the sites to form covalent bonds and further affects the solubility and rheological property of CS. A balance may be achieved by regulating the grafted amount of GA. As the previous study suggested, GA-*g*-CS of a certain substitution was more soluble than plain CS, and higher substitution led to higher solubility in some range.[13] In addition, reacting conditions, especially the oxygen content and pH, could be the main factors contributing to the oxidative polymerization of the copolymer. GA-*g*-CS with a different viscoelastic property and gelling capacity could be obtained by controlling oxidative conditions.[55] The results suggest that GA-*g*-CS possesses the potential to be employed as thickener or gel-forming material in food industries.

In conclusion, GA-*g*-CS with GA grafted up to 209.9 mg/g of the copolymer, strong antioxidant activity, and an adjustable rheological property was synthesized and characterized in the present study. The results suggested that high content of GA could be easily grafted onto CS by the developed one-pot method with EDC and HOBt. GA-*g*-CS, possessing the advantages of both GA and CS, showed greater antioxidant potential and stronger antioxidant power than GA in the $\beta$-carotene-linoleic acid assay. It was the first time to observe that polyphenol-polysaccharide conjugate exhibited stronger antioxidant power than its corresponding polyphenol. In addition, GA grafted onto CS altered the rheological property of the biopolymer, making GA-*g*-CS with a higher viscosity than plain CS, which could be adjustable through modifying the amount of grafted GA. Our present study developed a novel approach to synthesize GA-*g*-CS that could be explored as promising biomaterials in food industries.

## AUTHOR INFORMATION

### Corresponding Author

*E-mail: zengxx@njau.edu.cn. Tel: +86-25-84396791.

### Funding

This work was supported by Project Funded by the Priority Academic Program Development of Jiangsu Higher Education Institutions (PAPD).

### Notes

The authors declare no competing financial interest.

## REFERENCES

(1) Bhattacharya, A.; Misra, B. N. Grafting: A versatile means to modify polymers - Techniques, factors and applications. *Prog. Polym. Sci.* **2004**, *29*, 767−814.

(2) Spizzirri, U. G.; Iemma, F.; Puoci, F.; Cirillo, G.; Curcio, M.; Parisi, O. I.; Picci, N. Synthesis of antioxidant polymers by grafting of gallic acid and catechin on gelatin. *Biomacromolecules* **2009**, *10*, 1923−1930.

(3) Prodpran, T.; Benjakul, S.; Phatcharat, S. Effect of phenolic compounds on protein cross-linking and properties of film from fish myofibrillar protein. *Int. J. Biol. Macromol.* **2012**, *51*, 774−782.

(4) Aewsiri, T.; Benjakul, S.; Visessanguan, W.; Eun, J. B.; Wierenga, P. A.; Gruppen, H. Antioxidative activity and emulsifying properties of cuttlefish skin gelatin modified by oxidised phenolic compounds. *Food Chem.* **2009**, *117*, 160−168.

(5) Ihara, N.; Schmitz, S.; Kurisawa, M.; Chung, J. E.; Uyama, H.; Kobayashi, S. Amplification of inhibitory activity of catechin against disease-related enzymes by conjugation on poly($\varepsilon$-lysine). *Biomacromolecules* **2004**, *5*, 1633−1636.

(6) Chung, J. E.; Kurisawa, M.; Uyama, H.; Kobayashi, S. Enzymatic synthesis and antioxidant property of gelatin-catechin conjugates. *Biotechnol. Lett.* **2003**, *25*, 1993−1997.

(7) Shiu, J. C.; Ho, M. H.; Yu, S. H.; Chao, A. C.; Su, Y. R.; Chen, W. J.; Chiang, Z. C.; Yang, W. P. Preparation and characterization of caffeic acid grafted chitosan/CPTMS hybrid scaffolds. *Carbohydr. Polym.* **2010**, *79*, 724−730.

(8) Zhang, X. Q.; Do, M. D.; Casey, P.; Sulistio, A.; Qiao, G. G.; Lundin, L.; Lillford, P.; Kosaraju, S. Chemical cross-linking gelatin with natural phenolic compounds as studied by high-resolution NMR spectroscopy. *Biomacromolecules* **2010**, *11*, 1125−1132.

(9) Spizzirri, U. G.; Parisi, O. I.; Iemma, F.; Cirillo, G.; Puoci, F.; Curcio, M.; Picci, N. Antioxidant-polysaccharide conjugates for food application by eco-friendly grafting procedure. *Carbohydr. Polym.* **2010**, *79*, 333−340.

(10) Spizzirri, U. G.; Altimari, I.; Puoci, F.; Parisi, O. I.; Iemma, F.; Picci, N. Innovative antioxidant thermo-responsive hydrogels by radical grafting of catechin on inulin chain. *Carbohydr. Polym.* **2011**, *84*, 517−523.

(11) Ren, J. M.; Li, Q.; Dong, F.; Feng, Y.; Guo, Z. Y. Phenolic antioxidants-functionalized quaternized chitosan: Synthesis and antioxidant properties. *Int. J. Biol. Macromol.* **2013**, *53*, 77−81.

(12) Puoci, F.; Morelli, C.; Cirillo, G.; Curcio, M.; Parisi, O. I.; Maris, P.; Sisci, D.; Picci, N. Anticancer activity of a quercetin-based polymer towards HeLa cancer cells. *Anticancer Res.* **2012**, *32*, 2843−2847.

(13) Pasanphan, W.; Chirachanchai, S. Conjugation of gallic acid onto chitosan: An approach for green and water-based antioxidant. *Carbohydr. Polym.* **2008**, *72*, 169−177.

(14) Yu, S. H.; Mi, F. L.; Pang, J. C.; Jiang, S. C.; Kuo, T. H.; Wu, S. J.; Shyu, S. S. Preparation and characterization of radical and pH-responsive chitosan-gallic acid conjugate drug carriers. *Carbohydr. Polym.* **2011**, *84*, 794−802.

(15) Curcio, M.; Puoci, F.; Iemma, F.; Parisi, O. I.; Cirillo, G.; Spizzirri, U. G.; Picci, N. Covalent insertion of antioxidant molecules on chitosan by a free radical grafting procedure. *J. Agric. Food Chem.* **2009**, *57*, 5933−5938.

(16) Cho, Y. S.; Kim, S. K.; Ahn, C. B.; Je, J. Y. Preparation, characterization, and antioxidant properties of gallic acid-grafted-chitosans. *Carbohydr. Polym.* **2011**, *83*, 1617−1622.

(17) Casettari, L.; Gennari, L.; Angelino, D.; Ninfali, P.; Castagnino, E. ORAC of chitosan and its derivatives. *Food Hydrocolloids* **2012**, *28*, 243−247.

(18) Vittorio, O.; Cirillo, G.; Iemma, F.; Di Turi, G.; Jacchetti, E.; Curcio, M.; Barbuti, S.; Funel, N.; Parisi, O. I.; Puoci, F.; Picci, N. Dextran-catechin conjugate: A potential treatment against the pancreatic ductal adenocarcinoma. *Pharm. Res.* **2012**, *29*, 2601−2614.

(19) Liu, J.; Lu, J. F.; Kan, J.; Jin, C. H. Synthesis of chitosan-gallic acid conjugate: Structure characterization and in vitro anti-diabetic potential. *Int. J. Biol. Macromol.* **2013**, *62*, 321−329.

(20) Eom, T. K.; Ryu, B.; Lee, J. K.; Byun, H. G.; Park, S. J.; Kim, S. K. $\beta$-Secretase inhibitory activity of phenolic acid conjugated chitooligosaccharides. *J. Enzyme Inhib. Med. Chem.* **2013**, *28*, 214−217.

(21) Lee, D. S.; Je, J. Y. Gallic acid-grafted-chitosan inhibits foodborne pathogens by a membrane damage mechanism. *J. Agric. Food Chem.* **2013**, *61*, 6574−6579.

(22) Rinaudo, M. Chitin and chitosan: Properties and applications. *Prog. Polym. Sci.* **2006**, *31*, 603−632.

(23) No, H. K.; Meyers, S. P.; Prinyawiwatkul, W.; Xu, Z. Applications of chitosan for improvement of quality and shelf life of foods: A review. *J. Food Sci.* **2007**, *72*, R87−R100.

(24) Shi, C. M.; Zhu, Y.; Ran, X. Z.; Wang, M.; Su, Y. P.; Cheng, T. M. Therapeutic potential of chitosan and its derivatives in regenerative medicine. *J. Surg. Res.* **2006**, *133*, 185−192.
(25) Prabaharan, M.; Mano, J. F. Chitosan derivatives bearing cyclodextrin cavities as novel adsorbent matrices. *Carbohydr. Polym.* **2006**, *63*, 153−166.
(26) Kumar, M. N. V. R.; Muzzarelli, R. A. A.; Muzzarelli, C.; Sashiwa, H.; Domb, A. J. Chitosan chemistry and pharmaceutical perspectives. *Chem. Rev.* **2004**, *104*, 6017−6084.
(27) Bozic, M.; Strancar, J.; Kokol, V. Laccase-initiated reaction between phenolic acids and chitosan. *React. Funct. Polym.* **2013**, *73*, 1377−1383.
(28) Jus, S.; Stachel, I.; Fairhead, M.; Meyer, M.; Thony-Meyer, L.; Guebitz, G. M. Enzymatic cross-linking of gelatine with laccase and tyrosinase. *Biocatal. Biotransform.* **2012**, *30*, 86−95.
(29) Liu, Y.; Sakai, S.; Taya, M. Impact of the composition of alginate and gelatin derivatives in bioconjugated hydrogels on the fabrication of cell sheets and spherical tissues with living cell sheaths. *Acta Biomater.* **2013**, *9*, 6616−6623.
(30) Verma, S.; Singh, A.; Mishra, A. Gallic acid: Molecular rival of cancer. *Environ. Toxicol. Pharmacol.* **2013**, *35*, 473−485.
(31) Schreiber, S. B.; Bozell, J. J.; Hayes, D. G.; Zivanovic, S. Introduction of primary antioxidant activity to chitosan for application as a multifunctional food packaging material. *Food Hydrocolloids* **2013**, *33*, 207−214.
(32) Fangkangwanwong, J.; Akashi, M.; Kida, T.; Chirachanchai, S. One-pot synthesis in aqueous system for water-soluble chitosan-graft-poly(ethylene glycol) methyl ether. *Biopolymers* **2006**, *82*, 580−586.
(33) Liu, L.; Sun, Y.; Laura, T.; Liang, X.; Ye, H.; Zeng, X. Determination of polyphenolic content and antioxidant activity of kudingcha made from *Ilex kudingcha* C.J. Tseng. *Food Chem.* **2009**, *112*, 35−41.
(34) Liu, J.; Luo, J.; Ye, H.; Sun, Y.; Lu, Z.; Zeng, X. *In vitro* and *in vivo* antioxidant activity of exopolysaccharides from endophytic bacterium *Paenibacillus polymyx*a EJS-3. *Carbohydr. Polym.* **2010**, *82*, 1278−1283.
(35) Liu, J.; Luo, J.; Ye, H.; Sun, Y.; Lu, Z.; Zeng, X. Production, characterization and antioxidant activities in vitro of exopolysaccharides from endophytic bacterium *Paenibacillus polymyxa* EJS-3. *Carbohydr. Polym.* **2009**, *78*, 275−281.
(36) Opanasopit, P.; Techaarpornkul, S.; Rojanarata, T.; Ngawhirunpat, T.; Ruktanonchai, U. Nucleic acid delivery with chitosan hydroxybenzotriazole. *Oligonucleotides* **2010**, *20*, 127−136.
(37) Fangkangwanwong, J.; Akashi, M.; Kida, T.; Chirachanchai, S. Chitosan-hydroxybenzotriazole aqueous solution: A novel water-based system for chitosan functionalization. *Macromol. Rapid Commun.* **2006**, *27*, 1039−1046.
(38) Dai, B.; Peng, M.; Chen, Q. Interaction between chitosan and 1-hydroxybenzotriazole studied by NMR spectroscopy. *Chin. J. Magn. Reson.* **2008**, *4*, 453−460.
(39) Siripatrawan, U.; Harte, B. R. Physical properties and antioxidant activity of an active film from chitosan incorporated with green tea extract. *Food Hydrocolloids* **2010**, *24*, 770−775.
(40) Pasanphan, W.; Buettner, G. R.; Chirachanchai, S. Chitosan gallate as a novel potential polysaccharide antioxidant: An EPR study. *Carbohydr. Res.* **2010**, *345*, 132−140.
(41) Frankel, E. N.; Meyer, A. S. The problems of using one-dimensional methods to evaluate multifunctional food and biological antioxidants. *J. Sci. Food Agric.* **2000**, *80*, 1925−1941.
(42) Valko, M.; Leibfritz, D.; Moncol, J.; Cronin, M. T. D.; Mazur, M.; Telser, J. Free radicals and antioxidants in normal physiological functions and human disease. *Int. J. Biochem. Cell Biol.* **2007**, *39*, 44−84.
(43) Lu, J. M.; Lin, P. H.; Yao, Q. Z.; Chen, C. Y. Chemical and molecular mechanisms of antioxidants: Experimental approaches and model systems. *J. Cell. Mol. Med.* **2010**, *14*, 840−860.
(44) Brzonova, I.; Steiner, W.; Zankel, A.; Nyanhongo, G. S.; Guebitz, G. M. Enzymatic synthesis of catechol and hydroxyl-carboxic acid functionalized chitosan microspheres for iron overload therapy. *Eur. J. Pharm. Biopharm.* **2011**, *79*, 294−303.
(45) Niki, E. Biomarkers of lipid peroxidation in clinical material. *Biochim. Biophys. Acta, Gen. Subj.* **2014**, *1840*, 809−817.
(46) Marco, G. J. A rapid method for evaluation of antioxidants. *J. Am. Oil Chem. Soc.* **1968**, *45*, 594−598.
(47) Abdille, M. H.; Singh, R. P.; Jayaprakasha, G. K.; Jena, B. S. Antioxidant activity of the extracts from *Dillenia indica* fruits. *Food Chem.* **2005**, *90*, 891−896.
(48) Huang, D. J.; Ou, B. X.; Prior, R. L. The chemistry behind antioxidant capacity assays. *J. Agric. Food Chem.* **2005**, *53*, 1841−1856.
(49) Charernsriwilaiwat, N.; Opanasopit, P.; Rojanarata, T.; Ngawhirunpat, T. In vitro antioxidant activity of chitosan aqueous solution: Effect of salt form. *Trop. J. Pharm. Res.* **2012**, *11*, 235−242.
(50) Vieira, P. A. F.; Gontijo, D. C.; Vieira, B. C.; Fontes, E. A. F.; de Assuncao, L. S.; Leite, J. P. V.; Oliveira, M. G. D.; Kasuya, M. C. M. Antioxidant activities, total phenolics and metal contents in *Pleurotus ostreatus* mushrooms enriched with iron, zinc or lithium. *LWT−Food Sci. Technol.* **2013**, *54*, 421−425.
(51) Amarowicz, R.; Pegg, R. B.; Rahimi-Moghaddam, P.; Barl, B.; Weil, J. A. Free-radical scavenging capacity and antioxidant activity of selected plant species from the *Canadian prairies*. *Food Chem.* **2004**, *84*, 551−562.
(52) Xia, W.; Liu, P.; Zhang, J.; Chen, J. Biological activities of chitosan and chitooligosaccharides. *Food Hydrocolloids* **2011**, *25*, 170−179.
(53) Adelakun, O. E.; Kudanga, T.; Parker, A.; Green, I. R.; le Roes-Hill, M.; Burton, S. G. Laccase-catalyzed dimerization of ferulic acid amplifies antioxidant activity. *J. Mol. Catal. B: Enzym.* **2012**, *74*, 29−35.
(54) Yin, J. Y.; Nie, S. P.; Li, J.; Li, C.; Cui, S. W.; Xie, M. Y. Mechanism of interactions between calcium and viscous polysaccharide from the seeds of *Plantago asiatica* L. *J. Agric. Food Chem.* **2012**, *60*, 7981−7987.
(55) Carvajal-Millan, E.; Landillon, V.; Morel, M. H.; Rouau, X.; Doublier, J. L.; Micard, V. Arabinoxylan gels: Impact of the feruloylation degree on their structure and properties. *Biomacromolecules* **2005**, *6*, 309−317.
(56) Yan, M. Y.; Li, B. F.; Zhao, X.; Yi, J. B. Physicochemical properties of gelatin gels from walleye pollock (*Theragra chalcogramma*) skin cross-linked by gallic acid and rutin. *Food Hydrocolloids* **2011**, *25*, 907−914.

reaction. Concretely, Demuth et al.[12] and Côté et al.[14,17] showed isomaltulose to be a moderate acceptor for glucansucrases, and only the corresponding trisaccharide acceptor product could be structurally characterized as isomaltotriulose following transglucosylation reaction catalyzed by an alternansucrase from *L. mesenteroides* NRRL B-21297.[17] However, the rest of the acceptor products were neither structurally characterized nor quantified. Finally, isomaltotriulose was also detected in trace amounts in broths of dextran-producing cultures of *Streptococcus bovis* containing sucrose as substrate.[20]

In this work the efficient enzymatic synthesis of a homologous series of isomaltulose-derived oligosaccharides catalyzed by a dextransucrase from *L. mesenteroides* B-512F, as well as their comprehensive NMR structural characterization, is reported.

## MATERIALS AND METHODS

**Chemicals, Reagents, Standards, and Enzymes.** Fructose, glucose, sucrose, maltotriose, maltotetraose, maltopentaose, and maltohexaose were purchased from Sigma-Aldrich (Steinheim, Germany), whereas isomaltulose was bought from Carbosynth (Compton, UK). Acetonitrile (HPLC grade) was obtained from Lab-scan (Gliwice, Poland) and deuterium oxide from Merck Millipore (Darmstadt, Germany). Ultrapure water quality (18.2 MΩ cm) with 1−5 ppb of total organic carbon (TOC) and <0.001 EU $mL^{-1}$ pyrogen levels was produced in-house using a laboratory water purification Milli-Q Synthesis A10 system from Millipore (Billerica, MA, USA). Purified dextransucrase (EC 2.4.1.5) from *L. mesenteroides* B-512F was purchased from CRITT Bio-Industries (Toulouse, France). Specific activity was 0.4 U $mg^{-1}$, where 1 unit is the amount of enzyme required to transfer 1 μmol of glucose per minute, with 100 g sucrose $L^{-1}$ as the substrate in 20 mM sodium acetate buffer (pH 5.2) with 10 mg $L^{-1}$ $CaCl_2$ at a working temperature of 30 °C. All other chemicals were of analytical grade and commercially available.

**Enzymatic Synthesis of Isomaltulose-Derived Oligosaccharides.** Oligosaccharide synthesis was carried out by transglucosylation reaction catalyzed by dextransucrase from *L. mesenteroides* B-512F (0.8 U $mL^{-1}$) at 30 °C in 20 mM sodium acetate buffer with 0.34 mM $CaCl_2$ (pH 5.2) in the presence of 250 g $L^{-1}$ sucrose (donor) and 250 g $L^{-1}$ isomaltulose (acceptor). The reaction was allowed to proceed up to 48 h, and aliquots were repeatedly taken from the reaction mixture at suitable time intervals (1, 3, 5, 8, 24, and 48 h). The enzyme was inactivated by heating at 100 °C for 5 min, and inactivated samples were then 40-fold diluted with acetonitrile/water (50:50, v/v), filtered using a 0.45 μm syringe filter (Symta, Madrid, Spain), and analyzed by liquid chromatography with a refractive index detector (LC-RID). All enzymatic syntheses were carried out in triplicate.

**Chromatographic Determination of Carbohydrates by Liquid Chromatography with Refractive Index Detector.** The progress of the synthesis process of isomaltulose-derived oligosaccharides was monitored by LC-RID on an Agilent Technologies 1220 Infinity LC System 1260 RID (Boeblingen, Germany). The separation of carbohydrates was carried out with an analytical Zorbax $NH_2$ column (150 × 4.6 mm, 5 μm particle size) and an analytical Zorbax $NH_2$ guard column (12.5 × 4.6 mm, 5 μm particle size) (Agilent Technologies) using isocratic elution with acetonitrile/water at 75:25 or 70:30 (v/v) as the mobile phase to quantify mono- and disaccharides or oligosaccharides, respectively, and at a flow rate of 1.0 mL $min^{-1}$ for 60 min. Injection volume was 50 μL (750 μg of total carbohydrates). Data acquisition and processing were performed using Agilent ChemStation software (Agilent Technologies).

Carbohydrates in the reaction mixtures were identified by comparing their retention times with those of standard sugars. Quantitative analysis was performed by the external standard method, using calibration curves in the range of 0.1−5 mg $mL^{-1}$ for fructose, glucose, sucrose, isomaltulose, maltotriose, maltotetraose, maltopentaose, and maltohexaose. Individual maltodextrins were used to quantify the isomaltulose-derived oligosaccharides with the same degree of polymerization (DP). Maltohexaose was also used for the quantification of oligosaccharides with DP above 6. All analyses were carried out in triplicate. Determination coefficients obtained from these calibration curves, which were linear over the range studied, were high ($R^2 > 0.999$). Reproducibility of the method was estimated on the basis of the intraday and interday precision, calculated as the relative standard deviation (RSD) of concentrations of oligosaccharide standards obtained in $n \geq 6$ independent measurements, obtaining RSD values below 10% in all cases.

**Purification and Structural Characterization of the Isomaltulose-Derived Oligosaccharides by Nuclear Magnetic Resonance (NMR).** Isomaltulose-derived oligosaccharides from DP3 to DP7 were isolated and purified by LC-RID from sucrose/isomaltulose mixtures after 24 h of transglucosylation reaction and using a semipreparative column Kromasil (100-$NH_2$) column (250 × 10 mm, 5 μm particle size) (Akzo Nobel, Brewster, NY, USA). Thus, 500 μL of reaction mixtures (7.5 mg of total carbohydrates) was repeatedly eluted with acetonitrile/water (70:30, v/v) as the mobile phase at a flow rate of 5 mL $min^{-1}$, and fractions corresponding to the main synthesized oligosaccharide were manually collected, pooled, evaporated in a rotatory evaporator R-200 (Büchi, Flawil, Switzerland) below 25 °C/ and freeze-dried for their subsequent characterization.

Structure elucidation of the purified oligosaccharides was accomplished by NMR. NMR spectra were recorded at 298 K, using $D_2O$ as solvent, on a Varian System 500 NMR spectrometer ($^1H$ 500 MHz, $^{13}C$ 125 MHz) equipped with a 5 mm HCN cold probe. Chemical shifts of $^1H$ ($\delta_H$) and $^{13}C$ ($\delta_C$) in parts per million were determined relative to an external standards of sodium [2,2,3,3-$^2H_4$]-3-(trimethylsilyl)propanoate in $D_2O$ ($\delta_H$ 0.00) and 1, 4-dioxane ($\delta_C$ 67.40) in $D_2O$, respectively. One-dimensional (1D) NMR experiments ($^1H$ and $^{13}C$) were performed using standard Varian pulse sequences. Two-dimensional (2D) ($^1H$, $^1H$) NMR experiments [gradient correlation spectroscopy (gCOSY) and total correlation spectroscopy (TOCSY)] were carried out with the following parameters: delay time of 1 s, spectral width of 1675.6 Hz in both dimensions, 4096 complex points in t2, 4 transients for each of 128 time increments, and linear prediction to 256. The data were zero-filled to 4096 × 4096 real points. 2D ($^1H-^{13}C$) NMR experiments [gradient heteronuclear single-quantum coherence (gHSQC) and gradient heteronuclear multiple-bond correlation (gHMBC)] used the same $^1H$ spectral window, a $^{13}C$ spectral window of 30165 Hz, 1 s of relaxation delay, 1024 data points, and 128 time increments, with a linear prediction to 256. The data were zero-filled to 4096 × 4096 real points. Typical numbers of transients per increment were 4 and 16, respectively.

## RESULTS

The optimal conditions, that is, pH, temperature, enzyme charge, and concentration ratio of donor/acceptor, for the transglucosylation activity of dextransucrase in acceptor reactions using disaccharides as lactose or lactulose were previously established by Díez-Municio et al.[21,22] On the basis of these reaction conditions, the enzymatic synthesis was monitored by LC-RID as a function of time. Figure 1, which depicts a typical chromatogram obtained after 48 h of transglucosylation reaction of isomaltulose, shows a series of oligosaccharide acceptor products with DP values ranging from 3 to 9 resolved in 60 min using an isocratic elution with acetonitrile/water 70:30 (v/v). Sucrose and isomaltulose could not be well resolved under these chromatographic conditions, and a mobile phase composition with a weaker elution strength (i.e., acetonitrile/water 75:25, v/v) was used to quantify mono- and disaccharides (chromatograms not shown).

As indicated in Table 1, sucrose was readily hydrolyzed throughout the enzymatic reaction and only 3.5% remained after 48 h, whereas fructose was progressively released as the sucrose hydrolysis advanced. Concomitantly, only traces of

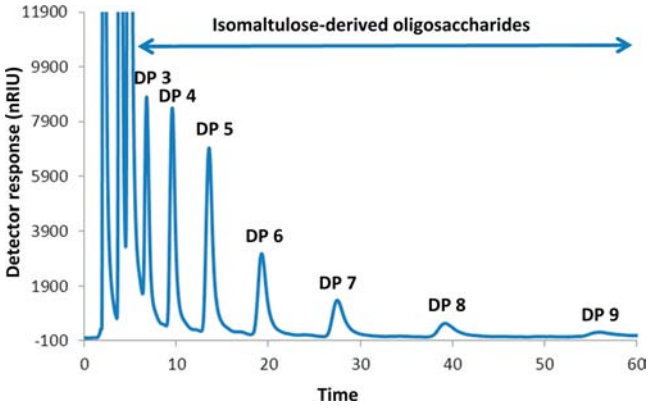


**Figure 1.** LC-RID profile of transglucosylation reaction with 250 g isomaltulose $L^{-1}$ and 250 g sucrose $L^{-1}$ as initial substrates and catalyzed by dextransucrase from *Leuconostoc mesenteroides* B-512F (0.8 U $mL^{-1}$) at 30 °C, in 20 mM sodium acetate buffer at pH 5.2, for 48 h. DP, degree of polymerization.

glucose could be detected, whereas isomaltulose content substantially decreased, which was indicative of the efficient transfer of glucose moieties as well as of the capacity of isomaltulose to act as acceptor. With regard to oligosaccharide acceptor products, the isomaltulose-derived trisaccharide was the predominant acceptor product during the first 8 h of reaction, whereas at 24 and 48 h of reaction the most abundant oligosaccharides were the tetrasaccharide and the pentasaccharide acceptor products, respectively (Table 1). Overall, the maximum formation of isomaltulose-derived oligosaccharides was obtained after 24−48 h of reaction by producing 101.6−104 g $L^{-1}$, which is equivalent to a yield of 41−42% (in weight with respect to the initial amount of isomaltulose).

Figure 2 shows the evolution of each individual oligosaccharide acceptor product expressed as percent of the total carbohydrate composition (including fructose, sucrose, and isomaltulose). The maximum relative percentage of the trisaccharide reached a plateau from the fifth hour of reaction, and this was kept until the end of the reaction, whereas the tetrasaccharide reached a plateau at 24 h and the pentasaccharide exhibited a moderate increase between 24 and 48 h of reaction. In contrast, hexa-, hepta-, octa-, and nonasaccharides were initially detected at 3, 5, 8, and 24 h of reaction, respectively, and did not reach a maximum formation at 48 h of reaction. This behavior clearly indicated that oligosaccharide acceptor products of low molecular weight could in turn act as an acceptor for further transglucosylation, thus yielding a homologous series of oligosaccharide products with an elongated chain.

To comprehensively characterize the synthesized oligosaccharides as well as to confirm the enzyme mechanism in the synthesis of oligosaccharides, the resulting carbohydrate mixture obtained after 24 h of reaction was repeatedly analyzed using a semipreparative LC column to purify the oligosaccharides with DP ranging from 3 to 7. These isolated oligosaccharides (structures DP3, DP4, DP5, DP6, and DP7, respectively; Figure 3) were then fully characterized by 1D ($^1$H and $^{13}$C) and 2D ($^1$H, $^1$H and $^1$H, $^{13}$C) NMR experiments (gCOSY, TOCSY, multiplicity-edited gHSQC, and gHMBC). $^1$H and $^{13}$C NMR chemical shifts observed are summarized in Table 2.

These compounds showed duplicate NMR signals in 1D $^1$H and $^{13}$C NMR spectra, indicating the presence of two quite

**Table 1. Carbohydrate Composition (Grams per Liter) Determined by LC-RID and Produced upon Transglucosylation of the Reaction Mixture Using 250 g $L^{-1}$ Sucrose (Donor) and 250 g $L^{-1}$ Isomaltulose (Acceptor) as Starting Substrates**

| | | | | isomaltulose-derived oligosaccharides | | | | | | | |
|---|---|---|---|---|---|---|---|---|---|---|---|
| time (h) | fructose | sucrose | isomaltulose | DP3 | DP4 | DP5 | DP6 | DP7 | DP8 | DP9 | total oligosaccharide |
| 0 | 0.0 | 247.4 ± 1.3[a] | 261.2 ± 11.2 | 0.0 | 0.0 | 0.0 | 0.0 | 0.0 | 0.0 | 0.0 | 0.0 |
| 1 | 30.7 ± 4.4 | 158.6 ± 6.6 | 198.8 ± 11.0 | 12.3 ± 1.5 | 5.6 ± 0.2 | 1.4 ± 0.1 | 0.0 | 0.0 | 0.0 | 0.0 | 19.3 |
| 3 | 81.3 ± 0.3 | 156.6 ± 9.6 | 176.2 ± 13.4 | 18.2 ± 0.9 | 13.3 ± 0.9 | 7.1 ± 0.9 | 4.3 ± 0.7 | 0.0 | 0.0 | 0.0 | 42.9 |
| 5 | 110.7 ± 14.0 | 125.8 ± 1.5 | 165.1 ± 24.1 | 21.8 ± 1.6 | 19.6 ± 1.1 | 13.9 ± 1.0 | 7.9 ± 0.2 | 6.0 ± 0.5 | 0.0 | 0.0 | 69.2 |
| 8 | 134.2 ± 8.6 | 98.6 ± 13.5 | 154.8 ± 14.6 | 20.7 ± 0.5 | 19.2 ± 0.0 | 14.8 ± 0.2 | 8.3 ± 0.2 | 5.1 ± 0.3 | 3.7 ± 0.3 | 0.0 | 71.8 |
| 24 | 216.3 ± 4.1 | 23.8 ± 1.4 | 119.6 ± 16.9 | 20.8 ± 0.6 | 24.1 ± 0.2 | 23.9 ± 1.7 | 14.4 ± 0.7 | 9.4 ± 0.6 | 5.8 ± 0.3 | 3.2 ± 0.1 | 101.6 |
| 48 | 210.4 ± 10.2 | 8.9 ± 0.4 | 94.4 ± 10.2 | 18.8 ± 0.6 | 22.1 ± 0.8 | 24.0 ± 0.7 | 15.3 ± 0.1 | 11.4 ± 0.2 | 7.3 ± 0.3 | 5.1 ± 0.1 | 104.0 |

[a]Standard deviation ($n$ = 3).


dx.doi.org/10.1021/jf5033735 | J. Agric. Food Chem. 2014, 62, 9137−9144

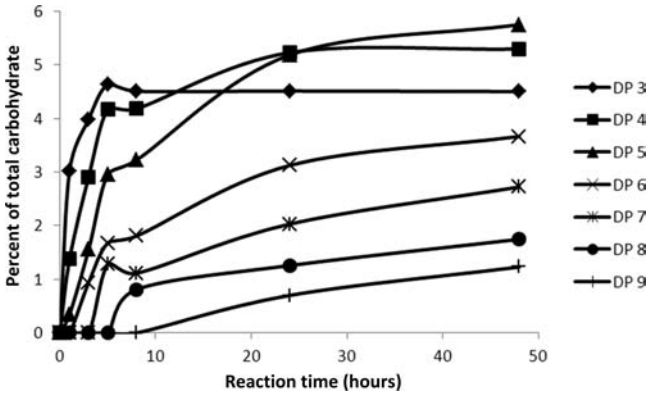


**Figure 2.** Isomaltulose-derived oligosaccharide synthesis during the time course of the transglucosylation reaction performed at 30 °C at an initial concentration of 250 g isomaltulose $L^{-1}$ with 250 g sucrose $L^{-1}$ and 0.8 U $mL^{-1}$ enzyme in 20 mM sodium acetate buffer at pH 5.2. DP, degree of polymerization.

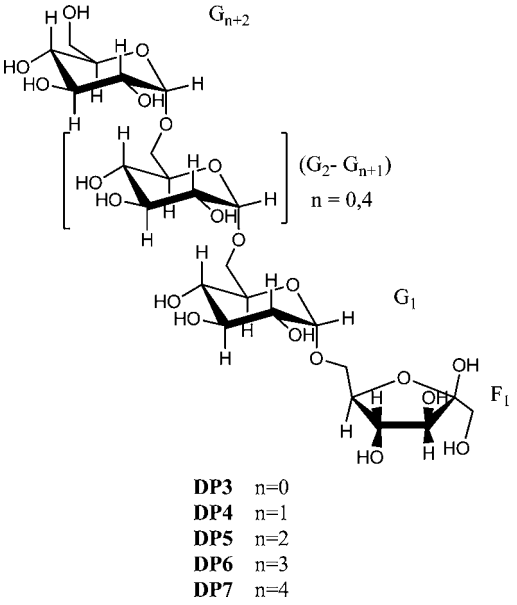


**Figure 3.** Structures of the isomaltulose-derived oligosaccharides from DP3 to DP7.

different populated isomers at room temperature, probably due to an anomeric mixture of $\beta$- and $\alpha$-fructose anomers. Structural determinations were performed on the major isomer for all structures.

The 1D $^{13}C$ spectrum of DP3 showed a major set of signals corresponding to 18 carbons including 3 anomeric carbons ($\delta$ 102.31, 98.95, and 98.40), indicative of the presence of a trisaccharide with 3 hexose sugars in its structure. A multiplicity-edited gHSQC spectrum was used to link the carbon signals to the corresponding proton resonances, so the anomeric carbon at $\delta$ 98.95 correlated with an $\alpha$-anomeric proton at $\delta$ 4.98 ($J$(H1,H2) = 3.8 Hz) and the anomeric carbon at $\delta$ 98.40 correlated with an $\alpha$-anomeric proton at $\delta$ 4.95 ($J$(H1,H2) = 3.8 Hz). The anomeric carbon at $\delta$ 102.31 was a quaternary carbon. In addition, four methylene carbons at $\delta$ 68.61, 66.12, 63.22, and 61.05 were identified. Careful analysis of the 2D gCOSY and TOCSY spectra revealed the $^1H$ signals of two units of glucopyranose and a unit of fructofuranose (Figure 3). To assign the configuration of each anomeric center, the values of the vicinal coupling constants for the glucopyranose anomeric protons and the $^{13}C$ chemical shift values of the fructofuranose anomeric carbons were used.[23] These results were consistent with the structure of a trisaccharide with the presence of two $\alpha$-D-glucopyranose residues ($G_1$ and $G_2$) and as the reducing terminal unit $F_1$ a fructose residue in the form of a furanosyl ring with $\beta$ and $\alpha$ forms in a 3:1 ratio. The position of glycosidic linkages was analyzed as follows: gHMBC experiment showed correlations between the anomeric proton of $G_1$ (4.98 ppm) and C-6 of the terminal fructose $F_1$ (68.61 ppm), between the anomeric carbon of $G_1$ (98.95 ppm) and the methylene H6 protons of the terminal fructose $F_1$ (3.88, 3.70 ppm), between the anomeric proton of $G_2$ (4.95 ppm) and C-6 of $G_1$ (66.12 ppm), and between the anomeric carbon of $G_2$ (98.40 ppm) and the methylene H6 protons of $G_1$ (3.97, 3.76 ppm). Finally, the major isomer of compound DP3 was identified as $\alpha$-D-glucopyranosyl-(1→6)-$\alpha$-D-glucopyranosyl-(1→6)-$\beta$-D-fructofuranoside, commonly called isomaltotriulose.

The 1D $^1H$ NMR spectrum of DP4 showed three resonances in the anomeric region, and besides the 1D $^{13}C$ NMR spectrum showed a major set of signals corresponding to 24 carbons including 4 anomeric carbons ($\delta$ 102.31, 98.94, 98.35, and 98.32), indicative of the presence of a tetrasaccharide. Careful analysis of the 2D gCOSY and TOCSY spectra revealed the $^1H$ signals of three units of glucopyranose and a unit of fructofuranose. To assign the configuration of each glucopyranose, the values of $^3J$(H1,H2) coupling constants (3.8, 3.8, and 3.8 Hz) were used. Following the same procedure used for the trisaccharide, using multidimensional solution NMR and $^{13}C$ chemical shift comparison (Figure 4), the major isomer of compound DP4 was identified as $\alpha$-D-glucopyranosyl-(1→6)-$\alpha$-D-glucopyranosyl-(1→6)-$\alpha$-D-glucopyranosyl-(1→6)-$\beta$-D-fructofuranoside.

1D $^1H$ NMR spectra of DP5, DP6, and DP7 showed one, two, and three additional doublets in the anomeric region, respectively. Likewise, the corresponding 1D $^{13}C$ NMR spectra showed five ($\delta$ 102.32, 98.95, 98.35, 98.34, and 98.24), six ($\delta$ 102.31, 98.94, 98.35, 98.34, 98.29, and 98.27), and seven anomeric carbons ($\delta$ 102.31, 98.94, 98.35, 98.34, 98.29, 98.28, and 98.27), consistent with the presence of a penta-, hexa-, and heptasaccharide, respectively. Following the same procedure as for DP3, compound DP5 was identified as $\alpha$-D-glucopyranosyl-(1→6)-$\alpha$-D-glucopyranosyl-(1→6)-$\alpha$-D-glucopyranosyl-(1→6)-$\alpha$-D-glucopyranosyl-(1→6)-$\beta$-D-fructofuranoside, compound DP6 as $\alpha$-D-glucopyranosyl-(1→6)-$\alpha$-D-glucopyranosyl-(1→6)-$\alpha$-D-glucopyranosyl-(1→6)-$\alpha$-D-glucopyranosyl-(1→6)-$\alpha$-D-glucopyranosyl-(1→6)-$\beta$-D-fructofuranoside, and compound DP7 as $\alpha$-D-glucopyranosyl-(1→6)-$\alpha$-D-glucopyranosyl-(1→6)-$\alpha$-D-glucopyranosyl-(1→6)-$\alpha$-D-glucopyranosyl-(1→6)-$\alpha$-D-glucopyranosyl-(1→6)-$\alpha$-D-glucopyranosyl-(1→6)-$\beta$-D-fructofuranoside.

## DISCUSSION

This work describes the efficient synthesis of a homologous series of 6-*O*-$\alpha$-glucosylated isomaltuloses with DP ranging from 3 to 9 by transferring the glucosyl moiety from sucrose to the C-6 of the nonreducing end of isomaltulose. To the best of our knowledge, this paper contains the first structural NMR data of isomaltulose-derived oligosaccharides from DP4 to DP7. Côté et al.[17] previously published the NMR shifts for the isomaltulose trisaccharide product derived from a transglucosylation reaction catalyzed by an alternansucrase from *L.*


dx.doi.org/10.1021/jf5033735 | J. Agric. Food Chem. 2014, 62, 9137−9144

Table 2. $^{1}H$ (500 MHz) and $^{13}C$ (125 MHz) NMR Spectral Data for Isomaltulose-Derived Oligosaccharides from DP3 to DP7[a]

| structure | position | $G_{n+2}$ | | $G_2$–$G_{n+1}$ | | $G_1$ | | $F_1$ | |
|---|---|---|---|---|---|---|---|---|---|
| | | $\delta_H$ | $\delta_C$ | $\delta_H$ | $\delta_C$ | $\delta_H$ | $\delta_C$ | $\delta_H$ | $\delta_C$ |
| DP3 ($n$ = 0) | 1 | 4.95 (3.8) | 98.40 | | | 4.98 (3.8) | 98.95 | 3.57, 3.54 | 63.22 |
| α-D-glucopyranosyl-(1→6)-α-D-glucopyranosyl-(1→6)-β-D-fructofuranoside | 2 | 3.57 | 72.06 | | | 3.55 | 71.93 | | 102.31 |
| | 3 | 3.73 | 73.64 | | | 3.71 | 73.92 | 4.19 | 75.83 |
| | 4 | 3.43 | 70.09 | | | 3.51 | 70.05 | 4.11 | 75.15 |
| | 5 | 3.73 | 72.42 | | | 3.89 | 70.96 | 3.97 | 79.43 |
| | 6 | 3.85, 3.77 | 61.05 | | | 3.97, 3.76 | 66.12 | 3.88, 3.70 | 68.61 |
| DP4 ($n$ = 1) | 1 | 4.97 (3.8) | 98.32 | 4.97 (3.8) | 98.35 | 4.99 (3.8) | 98.94 | 3.59, 3.54 | 63.22 |
| α-D-glucopyranosyl-(1→6)-α-D-glucopyranosyl-(1→6)-α-D-glucopyranosyl-(1→6)-β-D-fructofuranoside | 2 | 3.57 | 72.08 | 3.57 | 71.96 | 3.57 | 71.93 | | 102.31 |
| | 3 | 3.73 | 73.68 | 3.73 | 73.94 | 3.73 | 73.92 | 4.20 | 75.83 |
| | 4 | 3.43 | 70.10 | 3.52 | 70.08 | 3.52 | 70.08 | 4.12 | 75.15 |
| | 5 | 3.73 | 72.42 | 3.91 | 70.84 | 3.91 | 70.90 | 3.98 | 79.43 |
| | 6 | 3.85, 3.77 | 61.05 | 3.99, 3.77 | 66.19 | 3.99, 3.77 | 66.11 | 3.88, 3.71 | 68.61 |
| DP5 ($n$ = 2) | 1 | 4.97 (3.8) | 98.28 | 4.97 (3.8) | 98.34, 98.35 | 4.99 (3.8) | 98.95 | 3.58, 3.53 | 63.23 |
| α-D-glucopyranosyl-(1→6)-α-D-glucopyranosyl-(1→6)-α-D-glucopyranosyl-(1→6)-α-D-glucopyranosyl-(1→6)-β-D-fructofuranoside | 2 | 3.57 | 72.08 | 3.57 | 71.99, 71.97 | 3.57 | 71.93 | | 102.32 |
| | 3 | 3.73 | 73.68 | 3.73 | 73.96, 73.95 | 3.73 | 73.95 | 4.20 | 75.82 |
| | 4 | 3.43 | 70.15 | 3.52 | 70.09, 70.09 | 3.52 | 70.09 | 4.12 | 75.14 |
| | 5 | 3.73 | 72.42 | 3.91 | 70.85, 70.78 | 3.91 | 70.89 | 3.98 | 79.44 |
| | 6 | 3.85, 3.77 | 61.05 | 3.99, 3.77 | 66.18, 66.18 | 3.99, 3.77 | 66.10 | 3.89, 3.72 | 68.61 |
| DP6 ($n$ = 3) | 1 | 4.97 (3.8) | 98.29 | 4.97 (3.8) | 98.35, 98.34, 98.27 | 4.99 (3.8) | 98.94 | 3.58, 3.55 | 63.23 |
| α-D-glucopyranosyl-(1→6)-α-D-glucopyranosyl-(1→6)-α-D-glucopyranosyl-(1→6)-α-D-glucopyranosyl-(1→6)-α-D-glucopyranosyl-(1→6)-β-D-fructofuranoside | 2 | 3.57 | 72.07 | 3.57 | 71.99, 71.99, 71.96 | 3.57 | 71.93 | | 102.31 |
| | 3 | 3.73 | 73.67 | 3.73 | 73.98, 73.95, 73.95 | 3.73 | 73.95 | 4.20 | 75.83 |
| | 4 | 3.43 | 70.13 | 3.52 | 70.13, 70.08, 70.08 | 3.52 | 70.08 | 4.12 | 75.14 |
| | 5 | 3.73 | 72.42 | 3.91 | 70.84, 70.77, 70.76 | 3.91 | 70.89 | 3.98 | 79.43 |
| | 6 | 3.85, 3.77 | 61.05 | 3.99, 3.77 | 66.17, 66.17, 66.13 | 3.99 3.77 | 66.10 | 3.89, 3.71 | 68.60 |
| DP7 ($n$ = 4) | 1 | 4.97 (3.8) | 98.29 | 4.97 (3.8) | 98.35, 98.34, 98.28, 98.27 | 4.99 (3.8) | 98.94 | 3.58, 3.55 | 63.22 |
| α-D-glucopyranos yl-(1→6)-α-D-glucopyranosyl-(1→6)-α-D-glucopyranosyl-(1→6)-α-D-glucopyranosyl-(1→6)-α-D-glucopyranosyl-(1→6)-α-D-glucopyranosyl-(1→6)-β-D-fructofuranoside | 2 | 3.57 | 72.07 | 3.57 | 71.99, 71.99, 71.99, 71.96 | 3.57 | 71.93 | | 102.31 |
| | 3 | 3.73 | 73.67 | 3.73 | 73.98, 73.98, 73.95, 73.95 | 3.73 | 73.95 | 4.20 | 75.83 |
| | 4 | 3.43 | 70.13 | 3.52 | 70.13, 70.08, 70.08, 70.08 | 3.52 | 70.08 | 4.12 | 75.14 |
| | 5 | 3.73 | 72.42 | 3.91 | 70.84, 70.78, 70.77, 70.77 | 3.91 | 70.89 | 3.98 | 79.43 |
| | 6 | 3.85, 3.77 | 61.05 | 3.99, 3.77 | 66.17, 66.17, 66.13, 66.13 | 3.99, 3.77 | 66.10 | 3.89, 3.71 | 68.66 |

[a]Chemical shifts ($\delta$) and coupling constants ($J$ in hertz, in parentheses).

*mesenteroides* NRRL B-21297. Also, Seo et al.[24] identified isomaltulose and the corresponding 6-O-α-glucosylated isomaltuloses of DP3, DP4, and DP5, which were produced in minor amounts when dextransucrase was used to hydrolyze concentrated sucrose solutions, although in that case, the authors used a combination of enzymatic approaches and MALDI-TOF MS analysis.

The formation of α-(1→6) glucosidic bonds is in good agreement with the reaction mechanism described for the dextransucrase from *L. mesenteroides* NRRL B-512F, which catalyzes the formation of the polysaccharide dextran with 95% of α-(1→6)-linked glucan and 5% of α−(1→3) branch linkages. In addition, the bond formed during the acceptor reaction is normally an α-(1→6) glucosidic linkage.[10,25,26] As an example, this was the case for maltose, which gave rise to a series of seven homologous acceptor products having isomaltodextrin residues attached to the C-6 of the nonreducing glucosyl residue of maltose.[16] However, some exceptions have been described for this enzyme as was the case of the main production of 2-α-glucosyl-cellobiose, 2-α-glucosyl-lactose, or lactulosucrose through the formation of an α-(1→2) glucosidic linkage to the reducing end of cellobiose, lactose, or lactulose, respectively.[21,22,27]

Elegant works led by Robyt and coauthors determined that at high sucrose concentrations (≥200 mM) in the presence of equimolar amounts of suitable acceptors, dextransucrase tends to catalyze the synthesis of negligible amounts of dextran but does catalyze large amounts of acceptor products.[28−30] Our data confirmed this observation and revealed the suitability of isomaltulose as acceptor to yield around 42% of oligosacchar-


dx.doi.org/10.1021/jf5033735 | J. Agric. Food Chem. 2014, 62, 9137−9144

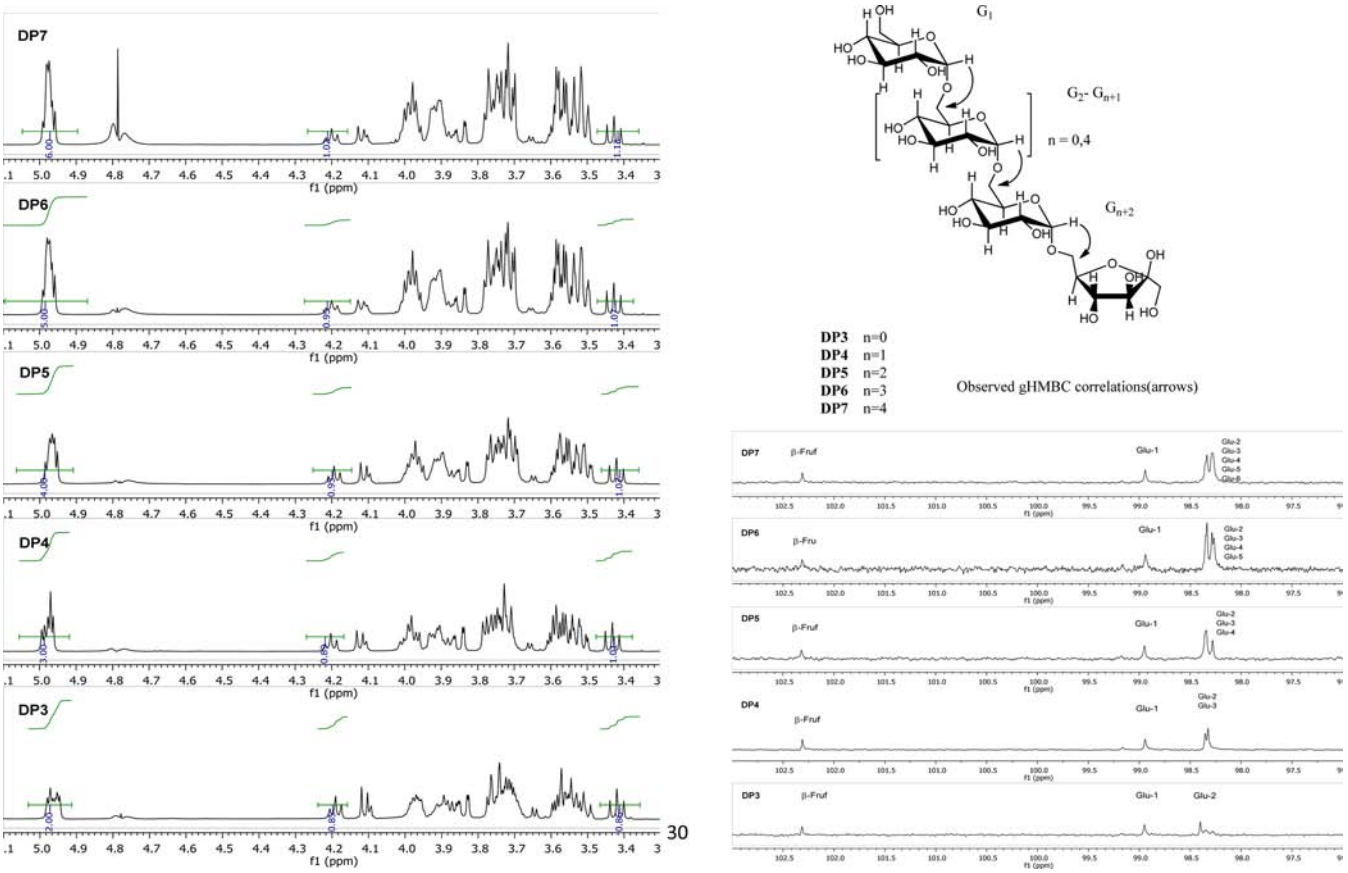


**Figure 4.** One-dimensional NMR spectra of isomaltulose-derived oligosaccharides from DP3 to DP7 at 500 MHz in $D_2O$. Data represent $^{1}H$ (left) and $^{13}C$ (right) anomeric region spectra.

ides after 24 h of reaction using equimolar amounts of sucrose and isomaltulose (Table 1). Likewise, the progress of the content of the acceptor products throughout the enzymatic reaction (Figure 2) as well as their characterized structures indicated the ability of the acceptor products to also serve as acceptors to give oligosaccharides of higher DP, thus yielding a homologous series of isomaltulose-derived oligosaccharides of decreasing amounts as DP increase (Table 1).

The produced isomaltulose-derived oligosaccharides can be considered as IMOs in the strict sense because they are linked by only α-(1→6) bonds. In addition, bearing in mind that isomaltulose is the core structure, these oligosaccharides could possess a series of bioactive properties based on isomaltulose functionality. In this sense, Seo et al.[24] synthesized a series of oligosaccharides from high concentrations of sucrose (2.5−4 M) using a dextransucrase prepared from a mutant *L. mesenteroides* strain. Among these oligosaccharides, low levels (between 2.7 and 3.7%) of 6-O-α-glucosylated isomaltuloses of DP3, DP4, and DP5 were present. These authors reported that the mixture of oligosaccharides effectively inhibited the formation of insoluble glucan by *Streptococcus sobrinus*, which plays an important role in the etiology of dental caries, suggesting their potential use as anticariogenic sucrose substitute. Interestingly, Kashimura et al.[31] demonstrated that isomaltulose and its hydrogenated disaccharide products, which were also linked through an α-(1→6) glucosyl bond, that is, α-*O*-D-glucopyranosyl-1,6-D-sorbitol and α-*O*-D-glucopyranosyl-1,6-D-mannitol, competitively inhibited rat small intestinal α-glucosidases (sucrase, maltase, and glucoamylase) and reduced the rate of hydrolysis of sucrose and other α-glucosylsaccharides such as maltose, dextrin, or soluble starch. Considering that maltitol, a disaccharide alcohol with an α-(1→4) glucosyl linkage, did not exert inhibitory effects, these authors suggested that the inhibitory action of isomaltulose and its derivatives could be related to the α-(1→6) glucosyl linkage. Given that the rates of hydrolysis of isomaltulose[3] and its hydrogenated derivatives are low in the small intestine,[32] they could contribute to reduce glycemic and insulinemic responses following their ingestion. In fact, there is solid scientific evidence that points out isomaltulose as an efficient low-glycemic sweetener with the capacity to reduce the speed of digestion and absorption, resulting in lower postprandial blood glucose.[33−40] In this context, and given that the isomaltulose-derived oligosaccharides described in the current work possess an α-1,6 glucosyl linkage as a unique structural bond, it will be of interest to investigate their role in glycemic control.

Considering their inhibitory action on small intestinal α-glucosidases and reduced absorption, IMO-like structures might have the ability to reach the large intestine, at least partially, intact.[8] Nevertheless, IMOs do not conform strictly to the nondigestibility criterion as they could be hydrolyzed by the membrane-bound isomaltase and maltase−glucoamylase enzymatic complexes in the small intestine, despite not all IMO species being digested at the same rate.[41] In this context, composition and dosage in the diet should be key parameters for the prebiotic potential of IMOs[8] and, consequently, additional studies on the effect of isomaltulose-derived oligosaccharides on the modulation of both the composition and activity of the gut microbiota should be warranted. In this sense, some in vivo studies carried out in humans have

provided evidence on the prebiotic effect after IMO administration in adults and elderly individuals.[42,43] Furthermore, Yen et al.[44] also observed an improvement in bowel movement in chronically constipated elderly subjects, as well as a beneficial effect on blood cholesterol levels after long-term supplementation (8 weeks) of IMOs.

To conclude, this paper reports the efficient enzymatic synthesis of a homologous series (DP3−DP9) of 6-O-α-glucosylated oligosaccharides derived from the transglucosylation reaction of isomaltulose catalyzed by a *L. mesenteroides* B-512F dextransucrase (EC 2.4.1.5). According to the oligosaccharide structures elucidated using a comprehensive NMR approach, these isomaltulose-derived oligosaccharides are consecutively elongated by the addition of glucose moieties linked by α-(1→6) glycosidic bonds at the nonreducing glucose residue while they keep the fructose unit at the reducing end. By having isomaltulose as the core structure and the α-(1→6) linkage as a unique structural feature, these IMO-like structures could possess appealing bioactive properties, which might warrant their potential use as functional ingredients. The reported enzymatic synthesis offers a good yield of isomaltulose-derived oligosaccharides, as well as provides a relatively noncomplex carbohydrate mixture that should make easier their purification for further investigation of their functional properties.

## ■ ASSOCIATED CONTENT

### Supporting Information

Figures S1−S12. This material is available free of charge via the Internet at http://pubs.acs.org.

## ■ AUTHOR INFORMATION


### Corresponding Author

*(F.J.M.) Phone: +34 91 0017948. E-mail: javier.moreno@csic.es.



### Funding

This work has been financed by Projects AGL2011-27884 from Ministerio de Ciencia e Innovación and ALIBIRD 2009/AGR-1469 from Comunidad de Madrid.


### Notes

The authors declare no competing financial interest.

## ■ REFERENCES


(1) Lina, B. A. R.; Jonker, D.; Kozianowski, G. Isomaltulose (Palatinose®): a review of biological and toxicological studies. *Food Chem. Toxicol.* **2002**, *40*, 1375−1381.

(2) Pszczola, D. E. Sweeteners for the 21st century. *Food Technol.* **2008**, *62* (11), 49−57.

(3) Sentko, A. Innovative low-glycaemic carbohydrates: an update. *Nutrafoods* **2013**, *12*, 127−135.

(4) O'Neill, J. Health trends in snack and breakfast foods: how prebiotics play a starring role. *Cereal Foods World* **2011**, *56*, 232−234.

(5) EFSA NDA Panel (EFSA Panel on Dietetic Products, Nutrition and Allergies). Scientific Opinion on the substantiation of health claims related to the sugar replacers xylitol, sorbitol, mannitol, maltitol, lactitol, isomalt, erythritol, D-tagatose, isomaltulose, sucralose and polydextrose and maintenance of tooth mineralisation by decreasing tooth demineralisation (ID 463, 464, 563, 618, 647, 1182, 1591, 2907, 2921, 4300), and reduction of post-prandial glycaemic responses (ID 617, 619, 669, 1590, 1762, 2903, 2908, 2920) pursuant to Article 13(1) of Regulation (EC) No. 1924/2006. *EFSA J.* **2011**, *9* (4), 2076.

(6) U.S. Food and Drug Administration.. 21 CFR 101.80 Food Labeling: health claims; dietary noncariogenic carbohydrate sweeteners and dental caries. *Fed. Regist.* **2008**, *73*, 30299−30301.

(7) Moynihan, P. J. Update on the nomenclature of carbohydrates and their dental effects. *J. Dent.* **1998**, *26*, 209−218.

(8) Goffin, D.; Delzenne, N.; Blecker, C.; Hanon, E.; Deroanne, C.; Paquot, M. Will isomalto-oligosaccharides, a well-established functional food in Asia, break through the European and American market? The status of knowledge on these prebiotics. *Crit. Rev. Food Sci. Nutr.* **2011**, *51*, 394−409.

(9) Jeanes, A. R.; Haynes, W. C.; Wilham, C. A.; Rankin, J. C.; Melvin, E. H.; Austin, M. J.; Cluskey, J. E.; Fisher, B. E.; Tsuchiya, H. M.; Rist, C. E. Characterization and classification of dextrans from ninety six strains of bacteria. *J. Am. Chem. Soc.* **1954**, *76*, 5041−5052.

(10) Robyt, J. F.; Ecklund, S. H. Relative, quantitative effect of acceptors in the reaction of *Leuconostoc mesenteroides* dextransucrase. *Carbohydr. Res.* **1983**, *121*, 279−286.

(11) Paul, F.; Oriol, E.; Auriol, D.; Monsan, P. Acceptor reaction of a highly purified dextran sucrase with maltose and oligosaccharides. Application to the synthesis of controlled-molecular-weight dextrans. *Carbohydr. Res.* **1986**, *149*, 433−441.

(12) Demuth, K.; Jordening, H. J.; Buchholz, K. Oligosaccharide synthesis by dextransucrase: new unconventional acceptors. *Carbohydr. Res.* **2002**, *337*, 1811−1820.

(13) Plou, F. J.; Martin, M. T.; Gomez de Segura, A.; Alcalde, M.; Ballesteros, A. Glucosyltransferases acting on starch or sucrose for the synthesis of oligosaccharides. *Can. J. Chem.−Rev. Can. Chim.* **2002**, *80*, 743−752.

(14) Côté, G. L.; Holt, S. M.; Miller-Fosmore, C. Prebiotic oligosaccharides via alternansucrase acceptor reactions. In *Oligosaccharides in Food and Agriculture*; Eggleston, G., Côté, G. L., Eds.; ACS Symposium Series 849; American Chemical Society: Washington, DC, USA, 2003; pp 77−89.

(15) Goffin, D.; Wathelet, B.; Blecker, C.; Deroanne, C.; Malmendier, Y.; Paquot, M. Comparison of the glucooligosaccharide profiles produced from maltose by two different transglucosidases from *Aspergillus niger*. *Biotechnol. Agron. Soc. Environ.* **2010**, *14*, 607−616.

(16) Fu, D.; Robyt, J. F. Acceptor reactions of maltodextrins with *Leuconostoc-mesenteroides* B-512FM dextransucrase. *Arch. Biochem. Biophys.* **1990**, *283*, 379−387.

(17) Côté, G. L.; Sheng, S.; Dunlap, C. A. Alternansucrase acceptor products. *Biocatal. Biotransform.* **2008**, *26*, 161−168.

(18) Dobruchowska, J. M.; Gerwig, G. J.; Kralj, S.; Grijpstra, P.; Leemhuis, H.; Dijkhuizen, L.; Kamerling, J. P. Structural characterization of linear isomalto-/malto-oligomer products synthesized by the novel GTFB 4,6-α-glucanotransferase enzyme from *Lactobacillus reuteri* 121. *Glycobiology* **2012**, *22*, 517−528.

(19) Dobruchowska, J. M.; Meng, X. F.; Leemhuis, H.; Gerwig, G. J.; Dijkhuizen, L.; Kamerling, J. P. Gluco-oligomers initially formed by the reuteransucrase enzyme of *Lactobacillus reuteri* 121 incubated with sucrose and malto-oligosaccharides. *Glycobiology* **2013**, *23*, 1084−1096.

(20) Bourne, E. J.; Weigel, H.; Hutson, D. H. Oligosaccharides in dextran-producing cultures of *Streptococcus bovis*. *Biochem. J.* **1961**, *79*, 549−553.

(21) Díez-Municio, M.; Montilla, A.; Jimeno, M. L.; Corzo, N.; Olano, A.; Moreno, F. J. Synthesis and characterization of a potential prebiotic trisaccharide from cheese whey permeate and sucrose by *Leuconostoc mesenteroides* dextransucrase. *J. Agric. Food Chem.* **2012**, *60*, 1945−1953.

(22) Díez-Municio, M.; Herrero, M.; Jimeno, M. L.; Olano, A.; Moreno, F. J. Efficient synthesis and characterization of lactulosucrose by *Leuconostoc mesenteroides* B-512F dextransucrase. *J. Agric. Food Chem.* **2012**, *60*, 10564−10571.

(23) Jarrell, H. C.; Conway, T. F.; Moyna, P.; Smith, I. Manifestation of anomeric form, ring structure, and linkage in the $^{13}$C-N.M.R. spectra of oligomers and polymers containing D-fructose: maltulose, isomaltulose, sucrose, leucrose, 1-kestose, nystose, inulin, and grass levan. *Carbohydr. Res.* **1979**, *76*, 45−57.

(24) Seo, E. S.; Nam, S. H.; Kang, H. K.; Cho, J. Y.; Lee, H. S.; Ryu, H. W.; Kim, D. Synthesis of thermo- and acid-stable novel

oligosaccharides by using dextransucrase with high concentration of sucrose. *Enzyme Microb. Technol.* **2007**, *40*, 1117−1123.
(25) Heincke, K.; Demuth, B.; Jördening, H.-J.; Buchholz, K. Kinetics of the dextransucrase acceptor reaction with maltose: experimental results and modeling. *Enzyme Microb. Technol.* **1999**, *24*, 523−534.
(26) Côté, G. L.; Cormier, R. S.; Vermillion, K. E. Glucansucrase acceptor reactions with D-mannose. *Carbohydr. Res.* **2014**, *387*, 1−3.
(27) Yamauchi, F.; Ohwada, Y. Synthesis of oligosaccharides by growing culture of *Leuconostoc mesenteroides*. Part IV. Oligosaccharide formation in the presence of various types of glucobioses as acceptors. *Agric. Biol. Chem.* **1969**, *33*, 1295−1300.
(28) Tanriseven, A.; Robyt, J. F. Interpretation of dextransucrase inhibition at high sucrose concentrations. *Carbohydr. Res.* **1993**, *245*, 97−104.
(29) Su, D. L.; Robyt, J. F. Control of the synthesis of dextran and acceptor-products by *Leuconostoc-mesenteroides* B-512FM dextransucrase. *Carbohydr. Res.* **1993**, *248*, 339−348.
(30) Robyt, J. F. Mechanisms in the glucansucrase synthesis of polysaccharides and oligosaccharides from sucrose. *Adv. Carbohydr. Chem. Biochem.* **1995**, *51*, 133−168.
(31) Kashimura, J.; Nagai, Y.; Goda, T. Inhibitory action of palatinose and its hydrogenated derivatives on the hydrolysis of $\alpha$-glucosylsaccharides in the small intestine. *J. Agric. Food Chem.* **2008**, *56*, 5892−5895.
(32) Goda, T.; Takase, S. N. Hydrolysis of $\alpha$-D-glucopyranosyl-1,6-sorbitol and $\alpha$-D-glucopyranosyl-1,6-mannitol by rat intestinal disaccharidases. *J. Nutr. Sci. Vitaminol.* **1988**, *34*, 131−140.
(33) Arai, H.; Mizuno, A.; Sakuma, M.; Fukaya, M.; Matsuo, K.; Muto, K.; Sasaki, H.; Matsuura, M.; Okumura, H.; Yamamoto, H.; Taketani, Y.; Doi, T.; Takeda, E. Effects of a palatinose-based liquid diet (Inslow) on glycemic control and the second-meal effect in healthy men. *Metab., Clin. Exp.* **2007**, *56*, 115−121.
(34) van Can, J. G.; Ijzerman, T. H.; van Loon, L. J.; Brouns, F.; Blaak, E. E. Reduced glycaemic and insulinaemic responses following isomaltulose ingestion: implications for postprandial substrate use. *Br. J. Nutr.* **2009**, *102*, 1408−1413.
(35) Häberer, D.; Thibault, L.; Langhans, W.; Geary, N. Beneficial effects on glucose metabolism of chronic feeding of isomaltulose versus sucrose in rats. *Ann. Nutr. Metab.* **2009**, *54*, 75−82.
(36) Lansink, M.; van Laere, K. M.; Vendrig, L.; Rutten, G. E. Lower postprandial glucose responses at baseline and after 4 weeks use of a diabetes-specific formula in diabetes type 2 patients. *Diabetes Res. Clin. Pract.* **2011**, *93*, 421−429.
(37) Bracken, R. M.; Page, R.; Gray, B.; Kilduff, L. P.; West, D. J.; Stephens, J. W.; Bain, S. C. Isomaltulose improves glycemia and maintains run performance in type 1 diabetes. *Med. Sci. Sports Exercise* **2012**, *44*, 800−808.
(38) van Can, J. G.; van Loon, L. J.; Brouns, F.; Blaak, E. E. Reduced glycaemic and insulinaemic responses following trehalose and isomaltulose ingestion: implications for postprandial substrate use in impaired glucose-tolerant subjects. *Br. J. Nutr.* **2012**, *108*, 1210−1217.
(39) Brunner, S.; Holub, I.; Theis, S.; Gostner, A.; Melcher, R.; Wolf, P.; Amann-Gassner, U.; Scheppach, W.; Hauner, H. Metabolic effects of replacing sucrose by isomaltulose in subjects with type 2 diabetes: a randomized double-blind trial. *Diabetes Care* **2012**, *35*, 1249−1251.
(40) König, D.; Theis, S.; Kozianowski, G.; Berg, A. Postprandial substrate use in overweight subjects with the metabolic syndrome after isomaltulose (Palatinose) ingestion. *Nutrition* **2012**, *28*, 651−656.
(41) Tovar, J.; Rascón, A. Starch hydrolysis products with physiological activity in humans. In *Food Oligosaccharides: Production, Analysis and Bioactivity*; Moreno, F. J., Sanz, M. L., Eds.; IFT Press Series; Wiley-Blackwell: Chichester, UK, 2014; pp 107−117.
(42) Kohmoto, T.; Fukui, F.; Takaku, H.; Machida, Y.; Arai, M.; Mitsuoka, T. Effect of isomaltooligosaccharides on human fecal flora. *Bifidobact. Microflora* **1988**, *7*, 61−69.
(43) Kaneko, T.; Kohmoto, T.; Kikuchi, H.; Shiota, M.; Iino, H.; Mitsuoka, T. Effects of isomaltooligosaccharides with different degrees of polymerization on human fecal bifidobacteria. *Biosci., Biotechnol., Biochem.* **1994**, *58*, 2288−2290.
(44) Yen, C. H.; Tseng, Y. H.; Kuo, Y. W.; Lee, M. C.; Chen, H. L. Long-term supplementation of isomalto-oligosaccharides improved colonic microflora profile, bowel function, and blood cholesterol levels in constipated elderly people − a placebo-controlled, diet-controlled trial. *Nutrition* **2011**, *27*, 445−450.

Keratin, the major protein in poultry feathers, hairs, and horns of animals, was water-stable and biocompatible and could be a promising biomaterial for medical applications. Keratin has molecular structures similar to collagen, the prominent protein in native extracellular matrices (ECMs). Furthermore, tripeptides "Arg-Gly-Asp" (RGD) and "Leu-Asp-Val" (LDV) existing in keratin molecules could bind with cell surface ligands and promote cell adhesion on keratin-based materials.[21] In addition, because of the highly cross-linked molecular structures attributed to the 7% cysteine in the amino acid components,[21] keratin might not suffer from poor water stability, the prominent problem that restricted biomedical applications of many proteins.

Because of its intrinsic water stability, keratin is advantageous over other proteins as nanoparticles. As a satisfactory biomaterial,[22] keratin was used to coat silver nanoparticles to improve their water stability.[23] Keratin has been fabricated into microparticles[24] and nanoparticles with polyethylene glycol grafting or using toxic solvent.[25] A better method should be developed, and the biodistribution should be investigated for drug delivery purposes.

## MATERIALS AND METHODS

**Materials.** Chicken feather barbs were provided by Featherfiber Corporation, Nixa, MO. Sodium bisulfite (98.0%), sodium hydroxide, hydrochloric acid, and ethylene glycol were purchased from AMRESCO LLC, Solon, OH. Purity of chemicals was considered in all of the calculations of concentrations.

**Preparation of Nanoparticles.** Chicken feathers were washed with reflux of ethanol in a Soxhlet extractor for 12 h to remove lipid and other impurities, followed by rinsing in distilled water 3 times to remove water-soluble impurities. After drying under 50 °C, the cleaned chicken feathers were hydrolyzed using 0.1 M sodium hydroxide at a ratio of 15:1 with sodium bisulfite (30% on weight of feathers) for 2 h at 80 °C. Hydrochloric acid was added to precipitate hydrolyzed feather keratin. The dispersion was centrifuged at 8000 rcf for 20 min, and subsequently, the obtained precipitated keratin was washed using distilled water 3 times. The feather keratin was dried under 50 °C and pulverized into powder.

To prepare nanoparticles, the obtained keratin powder was dissolved in ethylene glycol at designated concentrations (1, 2, 3, 4, 5, 10, and 20%, w/w) under room temperature. To precipitate keratin microparticles, ethylene glycol solution of keratin was added to distilled water with a weight ratio of keratin/water at 1:500. To further break the keratin microparticles into nanoparticles, 30 min of ultrasonication was applied using an ultrasonic processor (VCX 500:500 W, Sonics & Materials, Newton, CT) with an amplitude of vibration at 40%. At last, the dispersion of keratin nanoparticles were dialyzed (molecular weight cutoff of 7000) against distilled water for 4 days to remove ethylene glycol. The concentration of the keratin nanoparticles was adjusted via evaporation under reduced pressure.

**Size Measurement via Dynamic Light Scattering.** The sizes and $\zeta$ potential of keratin nanoparticles were measured on a Delsa Nano C particle analyzer (Beckman Coulter, Inc., Brea, CA) at least 1 h after particle formation. Sodium hydroxide and hydrochloric acid were used to adjust pH values of the dispersion to study the effects of pH on the size and surface charge of keratin nanoparticles. At least three measurements from separate samples were performed for each condition, and the average and standard deviation of the data are reported.

**Transmission Electron Microscopy (TEM).** Nanoparticle dispersion was placed on the copper mesh, dried, and then observed under a transmission electron microscope (Hitachi H7500 transmission electron microscope, Hitachi, Inc., Parlin, NJ).

**Crystallinity Analysis.** An X-ray diffraction (XRD) study was carried out on raw chicken feathers and freeze-dried keratin nanoparticles. The data were obtained using a Rigaku SmartLab X-ray diffractometer with Bragg–Brentano parafocusing geometry, a diffracted beam monochromator, and a conventional copper target X-ray tube set ($\lambda$ = 1.54 Å) to 40 kV and 44 mA at 26 °C. Diffraction intensities were recorded with $2\theta$ ranging from 3° to 40° at a scan speed of 0.02°/s.

**Stability of the Nanoparticles.** To evaluate the dimensional stability, physiological conditions of pH 7 and 37 °C and pH 6 and 37 °C and storage conditions of pH 2 and 4 °C were used to store the keratin nanoparticle dispersion with a concentration of 1 wt %. At designated time points, sizes of keratin nanoparticles were measured in the particle size analyzer. Three samples were measured for each condition to obtain average and standard deviation.

***In Vitro* Study.** To evaluate the biocompatibility, dispersion of keratin nanoparticles (10% on weight of the medium) was added to Dulbecco's modified low-glucose Eagle's medium (DMEM, Sigma-Aldrich, St. Louis, MO). NIH 3T3 mouse fibroblast cells (ATCC CRL-1658, Manassas, VA) with a seeding density of $1 \times 10^5$ cells/mL were cultured in humidified 5% $CO_2$ at 37 °C for 5 days. After every 24 h, the metabolic activity of the cells were analyzed using the MTS assay (Promega, Madison, WI) according to standard procedures with a multi-well plate Multiskan reader (Thermo Scientific, Waltham, MA). To prepare control samples, aliquots of distilled water with the same volume of keratin nanoparticle dispersion were added to the cell culture medium. For each data point, 6–9 replication experiments were conducted. Cells cultured in DMEM without keratin nanoparticles were used as a control.

***In Vivo* Study.** Biodistribution of keratin nanoparticles in mice was studied. The nanoparticles were first labeled with fluorescein isothiocyanate (FITC, Sigma-Aldrich, St. Louis, MO) in dimethyl sulfoxide (DMSO) with the addition of pH 9.5 carbonate–bicarbonate buffer in the dark. Free FITC was removed after dialyzed against distilled water for 4 days. The concentration of the FITC–keratin dispersion was readjusted to 100 mg/mL via evaporation under reduced pressure.

Mice were injected intravenously with 0.17 mL of dispersion of keratin nanoparticles (1%, w/w) every 24 h for up to 5 days. The mice were sequentially sacrificed 24 h after injection for up to 5 days. Mice sacrificed after the first 24 h had one injection of the nanoparticles; mice sacrificed after 48 h had two injections; etc. At the required time, mice were euthanized using $CO_2$ to collect the major organs, including liver, kidney, spleen, heart, and lungs. Organs stored in RPMI solution at 4 °C were analyzed in 5 h after collection. All experiments were carried out according to the Institutional Animal Care and Use Committee (IACUC)-approved protocol, and two mice were sacrificed for each time point.

The organ tissues were minced using a 70 $\mu$m cell strainer (Falcon, Tewksbury, MA) to obtain single-cell suspension in RPMI solution. For each organ, an aliquot of 500 $\mu$L of cell suspension was measured on the flow cytometer (BD Accuri, Franklin Lakes, NJ). The population of single cells was defined in a plot of 90° side scattering (SSC) versus forward scattering (FSC), and the percentage of nanoparticle-loaded cells was counted by measuring the fluorescence signal in the green fluorescence channel (FL1).

**Statistical Analysis.** All of the data obtained were analyzed by the one-way analysis of variance with the Scheffé test with a confidence interval of 95%. For characterizations of keratin nanoparticles, at least four specimens were measured or analyzed for each sample under one treatment. A statistically significant difference was indicated with a $p$ value smaller than 0.05. The data in the figures labeled with different numbers or characters indicated significant differences among different conditions.

## RESULTS AND DISCUSSION

**Characterizations of Keratin Nanoparticles.** Morphologies of the nanoparticles were shown in the TEM image in Figure 1. The dark shade indicated that the particles had solid structures. The particle sizes varied from around 50 to 130 nm. The sizes of keratin nanoparticles made them not easily being immediately filtered via kidney, because it has been reported

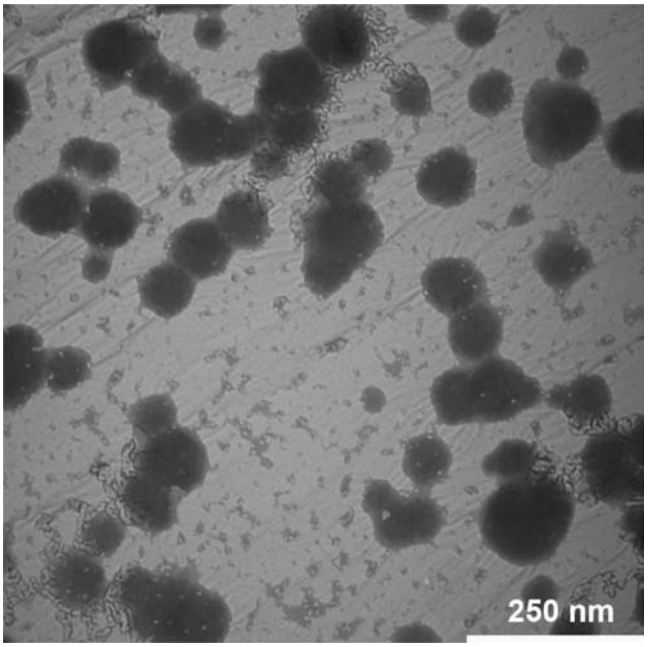


**Figure 1.** Morphologies of keratin nanoparticles in a TEM image showing the diameters from 50 to 130 nm and solid structures.

that nanoparticles with diameters smaller than 5.5 nm could be completely removed from the blood and then body.[26]

Figure 2 shows that the particle sizes obtained from particle analyzer measurement did not change significantly as the keratin concentration increased from 1 to 5% and then increased significantly from less than 100 nm to larger than 350 nm. The average diameter of 70 nm measured using the particle size analyzer was consistent with the results of TEM observation, as shown in Figure 1. A lower concentration of keratin resulted in less polypeptides that could wrap on keratin nanoparticles to increase the particle size. However, agglomeration tended to occur while the keratin concentration increased.

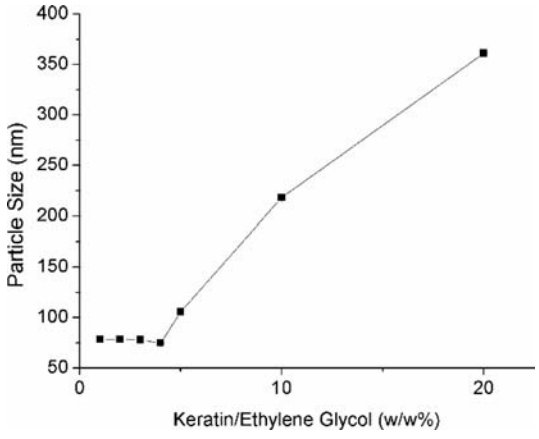


**Figure 2.** Effect of keratin/ethylene glycol ratio on the particle sizes of keratin nanoparticles. Keratin was dissolved in ethylene glycol at concentrations of 1, 2, 3, 4, 5, 10, and 20% based on the weight of ethylene glycol.

Figure 3 demonstrates that the hydrolyzed keratin had an isoelectric point (PI) of around 4.4 and a strong net surface charge at high or low pH values. $\zeta$ potential of keratin nanoparticles could increase to higher than 50 mV at pH below 3. A negative charge was shown on the keratin particles at pH values above 6.0, and the $\zeta$ potential decreased to −60 mV when pH was around 10. The range of surface charge variation reached 120 mV (from 60 to −60 mV) as pH varied from 2.0 to 12.0. The net charge on keratin nanoparticles was much higher than nanoparticles from other proteins, indicating higher potential for keratin to attract adsorbates with opposite charges.[27] Therefore, keratin nanoparticles may serve as good adsorbents to both positively or negatively charged substances.

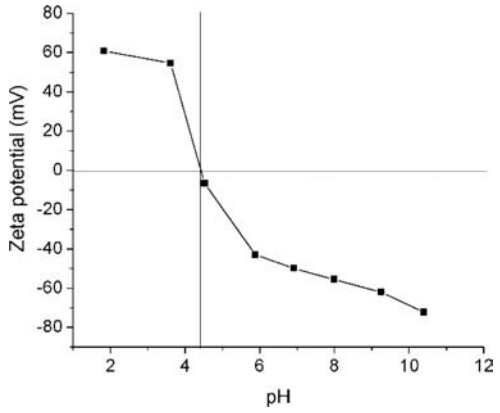


**Figure 3.** $\zeta$ potential of keratin nanoparticles. Sodium hydroxide solution and hydrochloric acid solution were used to adjust pH values of the keratin dispersion before ultrasonication. The nanoparticles were stabilized for 1 h before measurement.

Figure 4 shows the wide-angle XRD profiles of raw chicken feathers and dry keratin nanoparticles. For both samples, a prominent $2\theta$ peak at 20° and a minor peak at 9° indicated a typical diffraction pattern of $\alpha$-keratin with crystalline spacings of 4.4 and 9.8 Å, respectively. The proportion of the $2\theta$ peak at 20° increased and that of $2\theta$ peaks at 9° decreased after dissolution and precipitation of keratin, inferring that raw feathers had a larger amount of more tightly packed crystals than regenerated keratin nanoparticles. A certain degree of damage might occur to the original molecular structures during preparation of nanoparticles.

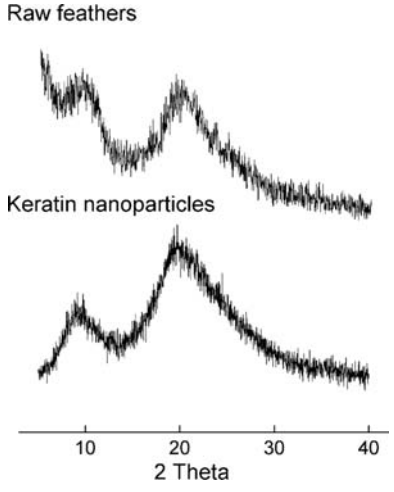


**Figure 4.** XRD spectrogram of keratin nanoparticles and raw feathers.

**Stability of Keratin Nanoparticles.** Figure 5 shows that the sizes of keratin nanoparticles increased from 75 to 130 nm as pH increased from 2 to 5 and then decreased from 130 nm


dx.doi.org/10.1021/jf502242h | J. Agric. Food Chem. 2014, 62, 9145−9150

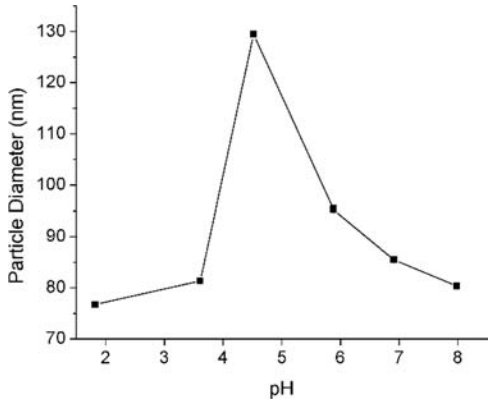


**Figure 5.** Effect of pH on the particle sizes of keratin nanoparticles. Sodium hydroxide solution and hydrochloric acid solution were added to the dispersion before ultrasonication to adjust pH values of the keratin dispersion. The nanoparticles were stabilized for 1 h before measurement.

to less than 85 nm as pH decreased from 5 to 8. The keratin nanoparticles had large diameters at pH similar to pI, because lower surface charge reduced electrical repulsion among nanoparticles and, thus, induced aggregation of small nanoparticles into larger nanoparticles. However, under physiological pH of 7.4 and storage pH of 2, keratin nanoparticles did not show hydrodynamic diameters larger than 100 nm.

Figure 6 indicated that keratin nanoparticles increased in the first 8 h and stabilized for up to 50 h when stored in phosphate-

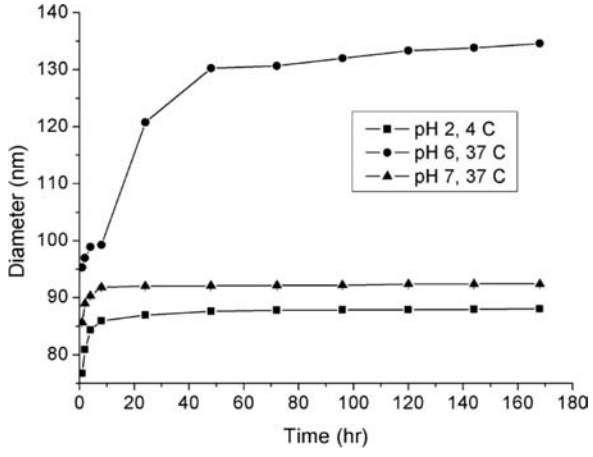


**Figure 6.** Influence of pH and temperature on the sizes of the keratin nanoparticles between 0 and 170 h. The diameters of keratin nanoparticles increased rapidly during the first 10 h and became stable at pH 2 under 4 °C and pH 7 under 37 °C.

buffered saline (PBS) medium. Keratin nanoparticles were highly stable at pH 2 under 4 °C, moderately stable at pH 7 under 37 °C, but unstable at pH 6 under 37 °C. Instability of the nanoparticles at a higher temperature should be due to the higher mobility, and therefore, chances of collision between particles could lead to agglomeration. Under the same temperature, pH 6 was closer to pH 4.5 compared to pH 7, suggesting weaker electrostatic repulsion among the keratin nanoparticles, as indicated in Figure 2, and therefore, better stability was seen at pH 7. However, even under high temperatures at pH 6, the diameters of keratin nanoparticles were still below 150 nm, indicating that the nanoparticles had remarkable water stability. The intrinsically high cross-linking degree of keratin might contribute to the water stability of the keratin nanoparticles.[27]

***In Vitro* Study for Biocompatibility.** The effects of keratin nanoparticles on cell growth and proliferation *in vitro* are shown in Figure 7. Cells in the culture medium containing keratin

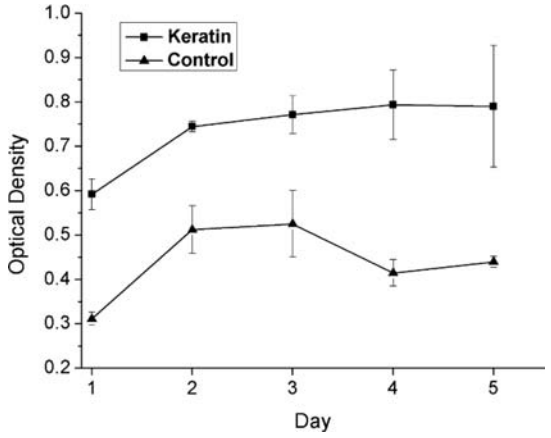


**Figure 7.** Comparison of the optical densities of mouse fibroblast cells with and without nanoparticles based on the MTS assay. The cells were cultured at 37 °C for 5 days.

nanoparticles showed continued proliferation of cells from day 1 to day 5, while the cells in culture medium without any additional additives showed maximum population on days 2 and 3, followed with a decrease on days 4 and 5. Keratin nanoparticles could hydrolyze into peptides and amino acids in the culture medium that could act as a nutrient to support cell growth, leading to higher proliferation.

***In Vivo* Study for Biodistribution.** As shown in Figure 8, keratin nanoparticles were predominantly found in the kidneys,

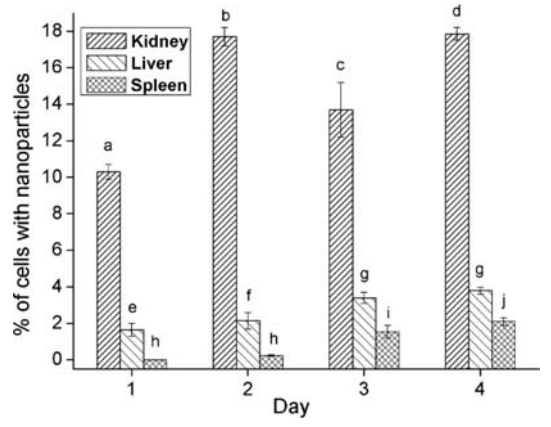


**Figure 8.** Comparison of the percentage of cells containing nanoparticles detected in kidneys, liver, and spleen in mice using flow cytometer after 1, 2, 3, and 4 days of injection. The uptake of nanoparticles did not increase continuously in kidneys but increased gradually in liver and spleen.

followed by liver and spleen in mice. The amount of nanoparticles in kidneys was not affected by dosage, while the amount of the nanoparticles in liver and spleen gradually increased as the dosage increased. Nanoparticles with diameters up to about 5.5 nm could be completely filtered by kidneys.[28] Keratin nanoparticles had significantly larger average diameter


dx.doi.org/10.1021/jf502242h | J. Agric. Food Chem. 2014, 62, 9145−9150

and were probably trapped in the kidneys before they were degraded into diameters smaller than 5.5 nm. The undegraded particles are removed via hepatic clearance through liver, which clears nanoparticles in the range of 10−20 nm.[29] Therefore, considerable amounts of nanoparticles were also found in the liver. Fewer nanoparticles could reach the spleen after being accumulated or filtered in the kidneys and liver. Successive injections were made every 24 h to ensure that sufficient nanoparticles were available to reach the targeted organs. After multiple injections, the amount of nanoparticles did not change significantly in kidneys. However, the quantity of nanoparticles slightly increased in liver and spleen in 2 days but also leveled off at the third and fourth days. The phenomenon suggested that the keratin nanoparticles could effectively degrade in the body. Keratin nanoparticles could be effective drug delivery vehicles to target kidney and liver for sustained release.

Cross-linking degrees of proteins might markedly affect the biodistribution of nanoparticles in different organs. Nanoparticles from highly cross-linked keratin with 7% cysteine[30] showed a similarly high content of accumulation in kidneys compared to those from other highly cross-linked protein, such as wheat glutenin.[31] However, nanoparticles from zein with a trace content of cysteine among its amino acids[32] were mainly found in liver.[33] In nature, keratin is a protein that takes a considerably long time to degrade because of the cross-linked structure. Even with partially destroyed physical structures, as indicated by the XRD results in Figure 4, the remaining cross-linkage still might render the keratin nanoparticles stable at physiological pH, as shown in Figure 6. It could be inferred that the cross-linking degree of proteins might have major effects on the water stability and enzymatic degradation rate of nanoparticles in physiological environments and, thus, might influence the biodistribution of protein nanoparticles.

In this research, the highly cross-linked keratin was developed into nanoparticles at around 70 nm via a phase separation and ultrasonication method. The influence of conditions, such as ratios of keratin/ethylene glycol and pH of dispersion on the particle sizes, was investigated. The isoelectric point of keratin was around pH 4.4. The keratin nanoparticles were highly stable after stored in physiological pH of 7 and storage condition of pH 2. The *in vitro* study indicated that keratin nanoparticles supported the attachment and proliferation of fibroblast cells. After injection into mice, it was found that up to 18% of the cells in kidneys and 4% of the cells in liver of mice were penetrated by the keratin nanoparticles. In summary, keratin nanoparticles could be potential vehicles for efficient drug delivery in treatments of livestock diseases.

## AUTHOR INFORMATION


### Corresponding Author

*Telephone: +001-402-472-5197. Fax: +001-402-472-0640. E-mail: yyang2@unl.edu.



### Funding

This research was financially supported by the Agricultural Research Division at the University of Nebraska—Lincoln, the United States Department of Agriculture (USDA) Hatch Act, the Multistate Research Project S-1054 (NEB 37-037), the Nebraska Environmental Trust (13-142), and the Key Scientific and Technological Projects of Science and Technology Commission of Shanghai Municipality (12JC1400300). Financial support provided to Zhen Shi through the Program for Changjiang Scholars and Innovative Research Team in University (IRT1135) at Jiangnan University, the Scientific Support Program of Jiangsu Province (BE2011404), the Graduate Student Innovation Plan of Jiangsu Province (CX10B_222Z), and the Doctor Candidate Foundation of Jiangnan University (JUDCF10004) is also thankfully acknowledged.

### Notes

The authors declare no competing financial interest.

## ACKNOWLEDGMENTS

The authors thank Dr. Han Chen for his help in TEM and Zhuanzhuan Ma for her help in XRD.


## REFERENCES


(1) Iyer, A. K.; Khaled, G.; Fang, J.; Maeda, H. Exploiting the enhanced permeability and retention effect for tumor targeting. *Drug Discovery Today* **2006**, *11*, 812−818.

(2) Sunkara, B. K.; Misra, R. D. K. Enhanced antibactericidal function of $W^{4+}$-doped titania-coated nickel ferrite composite nanoparticles: A biomaterial system. *Acta Biomater.* **2008**, *4*, 273−283.

(3) Huang, H.; Yuan, Q.; Shah, J. S.; Misra, R. D. K. A new family of folate-decorated and carbon nanotube-mediated drug delivery system: synthesis and drug delivery response. *Adv. Drug Delivery Rev.* **2011**, *63*, 1332−1339.

(4) Zhang, J.; Misra, R. D. K. Magnetic drug targeting carrier encapsulated with thermosensitive smart polymer: Core−shell nanoparticle carrier and drug release response. *Acta Biomater.* **2007**, *3*, 838−850.

(5) Xu, W.; Yang, Y. Drug release and its relationship with kinetic and thermodynamic parameters of drug sorption onto starch acetate fibers. *Biotechnol. Bioeng.* **2010**, *105*, 814−822.

(6) Yang, S.-T.; Wang, X.; Jia, G.; Gu, Y.; Wang, T.; Nie, H.; Ge, C.; Wang, H.; Liu, Y. Long-term accumulation and low toxicity of single-walled carbon nanotubes in intravenously exposed mice. *Toxicol. Lett.* **2008**, *181*, 182−189.

(7) Nel, A.; Xia, T.; Mädler, L.; Li, N. Toxic potential of materials at the nanolevel. *Science* **2006**, *311*, 622−627.

(8) Zhen, X.; Wang, X.; Xie, C.; Wu, W.; Jiang, X. Cellular uptake, antitumor response and tumor penetration of cisplatin-loaded milk protein nanoparticles. *Biomaterials* **2013**, *34*, 1372−1382.

(9) Elzoghby, A. O.; Abo El-Fotoh, W. S.; Elgindy, N. A. Casein-based formulations as promising controlled release drug delivery systems. *J. Controlled Release* **2011**, *153*, 206−216.

(10) Teng, Z.; Li, Y.; Luo, Y.; Zhang, B.; Wang, Q. Cationic $\beta$-lactoglobulin nanoparticles as a bioavailability enhancer: Protein characterization and particle formation. *Biomacromolecules* **2013**, *14*, 2848−2856.

(11) Ding, D.; Zhu, Z.; Liu, Q.; Wang, J.; Hu, Y.; Jiang, X.; Liu, B. Cisplatin-loaded gelatin-poly(acrylic acid) nanoparticles: Synthesis, antitumor efficiency in vivo and penetration in tumors. *Eur. J. Pharm. Biopharm.* **2011**, *79*, 142−149.

(12) Xu, H.; Jiang, Q.; Reddy, N.; Yang, Y. Hollow nanoparticles from zein for potential medical applications. *J. Mater. Chem.* **2011**, *21*, 18227−18235.

(13) Elzoghby, A. O. Gelatin-based nanoparticles as drug and gene delivery systems: Reviewing three decades of research. *J. Controlled Release* **2013**, *172*, 1075−1091.

(14) Luo, Y.; Teng, Z.; Wang, T. T.; Wang, Q. Cellular uptake and transport of zein nanoparticles: Effects of sodium caseinate. *J. Agric. Food Chem.* **2013**, *61*, 7621−7629.

(15) Elzoghby, A. O.; Saad, N. I.; Helmy, M. W.; Samy, W. M.; Elgindy, N. A. Ionically-crosslinked milk protein nanoparticles as flutamide carriers for effective anticancer activity in prostate cancer-bearing rats. *Eur. J. Pharm. Biopharm.* **2013**, *85*, 444−451.

(16) Pawar, S. N.; Edgar, K. J. Alginate derivatization: A review of chemistry, properties and applications. *Biomaterials* **2012**, *33*, 3279−3305.

(17) Hennink, W.; Van Nostrum, C. Novel crosslinking methods to design hydrogels. *Adv. Drug Delivery Rev.* **2012**, *64*, 223−236.
(18) Jiang, Q.; Reddy, N.; Yang, Y. Cytocompatible cross-linking of electrospun zein fibers for the development of water-stable tissue engineering scaffolds. *Acta Biomater.* **2010**, *6*, 4042−4051.
(19) Xu, H.; Cai, S.; Sellers, A.; Yang, Y. Electrospun ultrafine fibrous wheat glutenin scaffolds with three-dimensionally random organization and water stability for soft tissue engineering. *J. Biotechnol.* **2014**, *184*, 179−186.
(20) Xu, H.; Cai, S.; Sellers, A.; Yang, Y. Intrinsically water-stable electrospun three-dimensional ultrafine fibrous soy protein scaffolds for soft tissue engineering using adipose derived mesenchymal stem cells. *RSC Adv.* **2014**, *4*, 15451−15457.
(21) Xu, H.; Cai, S.; Xu, L.; Yang, Y. Water-stable three-dimensional ultrafine fibrous scaffolds from keratin for cartilage tissue engineering. *Langmuir* **2014**, *30*, 8461−8470.
(22) Arai, K.; Naito, S.; Dang, V. B.; Nagasawa, N.; Hirano, M. Crosslinking structure of keratin. VI. Number, type, and location of disulfide crosslinkages in low-sulfur protein of wool fiber and their relation to permanent set. *J. Appl. Polym. Sci.* **1996**, *60*, 169−179.
(23) Reichl, S. Films based on human hair keratin as substrates for cell culture and tissue engineering. *Biomaterials* **2009**, *30*, 6854−6866.
(24) Martin, J. J.; Cardamone, J. M.; Irwin, P. L.; Brown, E. M. Keratin capped silver nanoparticles—Synthesis and characterization of a nanomaterial with desirable handling properties. *Colloids Surf., B* **2011**, *88*, 354−361.
(25) Pedram Rad, Z.; Tavanai, H.; Moradi, A. Production of feather keratin nanopowder through electrospraying. *J. Aerosol Sci.* **2012**, *51*, 49−56.
(26) Li, Q.; Zhu, L.; Liu, R.; Huang, D.; Jin, X.; Che, N.; Li, Z.; Qu, X.; Kang, H.; Huang, Y. Biological stimuli responsive drug carriers based on keratin for triggerable drug delivery. *J. Mater. Chem.* **2012**, *22*, 19964−19973.
(27) Choi, H. S.; Liu, W.; Misra, P.; Tanaka, E.; Zimmer, J. P.; Ipe, B. I.; Bawendi, M. G.; Frangioni, J. V. Renal clearance of quantum dots. *Nat. Biotechnol.* **2007**, *25*, 1165−1170.
(28) Xu, H.; Zhang, Y.; Jiang, Q.; Reddy, N.; Yang, Y. Biodegradable hollow zein nanoparticles for removal of reactive dyes from wastewater. *J. Environ. Manage.* **2013**, *125*, 33−40.
(29) Katoh, K.; Tanabe, T.; Yamauchi, K. Novel approach to fabricate keratin sponge scaffolds with controlled pore size and porosity. *Biomaterials* **2004**, *25*, 4255−4262.
(30) Xu, H.; Yang, Y. Controlled de-cross-linking and disentanglement of feather keratin for fiber preparation via a novel process. *ACS Sustainable Chem. Eng.* **2014**, *2*, 1404−1410.
(31) Reddy, N.; Shi, Z.; Xu, H.; Yang, Y. Development of wheat glutenin nanoparticles and their biodistribution in mice. *J. Biomed. Mater. Res., Part A* **2014**, DOI: 10.1002/jbm.a.35302.
(32) Gianazza, E.; Viglienghi, V.; Righetti, P. G.; Salamini, F.; Soave, C. Amino acid composition of zein molecular components. *Phytochemistry* **1977**, *16*, 315−317.
(33) Lai, L. F.; Guo, H. X. Preparation of new 5-fluorouracil-loaded zein nanoparticles for liver targeting. *Int. J. Pharm.* **2011**, *404*, 317−323.

Materials Inc., Newtown, CT, USA; 750 W power output with frequency of 20 kHz ± 50 Hz) using a sonication probe of 13 mm tip diameter for 5 min with on/off pulse of 5 s. The cell lysate was then clarified by centrifugation at 11627*g* for 20 min. The processing temperature was maintained at 4 °C throughout. Subsequently, the crude extract was concentrated by acetone precipitation (1:1, v/v) and purified by Q-Sepharose anion-exchange chromatography (column dimensions, 8 cm × 1.5 cm; flow rate, 3 mL/min) using 10 mM Tris-HCl buffer (pH 9.0). Protein was eluted with a 0.1−3 M NaCl gradient. Five milliliter fractions were collected, and their protein content (at 280 nm) and GGT activity (at 410 nm) were determined.

**GGT Assay.** GGT assay was performed according to the method described by Ikeda.[16] One milliliter of reaction volume contained 1 mM γ-glutamyl-*p*-nitroanilide hydrochloride (γ-GpNA), 10 mM glycylglycine (excluded in hydrolytic reactions), and appropriately diluted enzyme. Unless otherwise indicated, GGT assay was performed in 50 mM Tris-HCl buffer (pH 9.0) at 60 °C for 5 min. Reaction was stopped by adding 100 μL of 3 M acetic acid, and the activity was monitored by measuring hydrolyzed γ-GpNA at 410 nm. One enzyme unit was defined as the amount of enzyme required to release 1 μmol of *p*-nitroaniline per minute under standard assay conditions.

End product inhibition was studied by adding L-theanine (10−40 mM) to the reaction while the GGT assay was performed and monitoring the change in transpeptidase activity.

**Electrophoresis, Western Blotting, and Activity Staining.** SDS-PAGE of purified rBLGGT along with the crude enzyme was carried out according to the procedure of Laemmli[17] to determine the molecular mass and subunit composition of the enzyme. A 12% (v/v) resolving gel stacked with a 5% (v/v) stacking gel was run at 20 mA for approximately 1 h using a Bio-Rad power pac. Gels were then stained with 0.25% (w/v) Coomassie Brilliant blue R-250 at mild shaking and destained thereafter.

Western blot analysis was done by transferring the protein to a PVDF membrane (Bio-Rad). The membrane was then blocked for 1 h in 3% (w/v) BSA prepared in 1× PBS and thereafter incubated with 1:5000 streptactin antibody conjugated with horseradish peroxidase (HRP) for 1 h on mild shaking at room temperature. Subsequently, the membrane was washed with 0.05% (v/v) Tween-20 in 1× PBS. The protein band was then visualized using diaminobenzidine (DAB, 0.1% w/v) solution prepared in hydrogen peroxide.

Native PAGE (10% v/v) was prepared, and purified rBLGGT was loaded in two wells of the gel along with native molecular markers and was run at 20 mA for 1 h. Thereafter, one of the lanes containing rBLGGT sample was sliced using a scalpel and subjected to activity staining, whereas the remaining gel was stained with 0.25% (w/v) Coomassie Brilliant blue R-250 to analyze the molecular mass of the native protein.

For acitivity staining, the gel piece was first equilibrated at 50 mM Tris-HCl buffer (pH 9.0) for 10 min and then placed over an agar plate containing the substrates (γ-GpNA and glycylglycine). Gel was incubated at 45 °C until the yellow color of *p*-nitroaniline appeared. To intensify the stain, gel was further treated with *N*-(1-naphthyl)-ethylenediamine employing the method described previously.[18]

**Biochemical Characterization of rBLGGT.** *Effect of pH and Temperature.* GGT assay was performed at various pH values (5.0−12.0), using universal pH buffer (Britton−Robinson buffer) to determine the effect of pH on transpeptidase activity. pH stability was studied by preincubating the enzyme at pH 5.0−12.0 (10 mM) for 1 h and then performing the assay under standard conditions. The effect of temperature on enzyme activity and stability was determined by incubating the reaction at various temperatures ranging from 40 to 80 °C. All of the experiments were performed in triplicate. Relative and residual enzyme activities were plotted, and the activity obtained under standard assay conditions was regarded as 100%.

Steady-state kinetics of purified rBLGGT was performed with various concentrations of γ-GpNA ranging from 0.016 to 0.2 mM at its optimal pH and temperature. The $K_m$ and $V_{max}$ values were calculated using a Lineweaver−Burk plot (graph was plotted using Systat Software, Inc., SigmaPlot for Windows).

*Substrate Specificity for γ-Glutamyl Acceptors.* Substrate specificity of rBLGGT toward various amino acids as γ-glutamyl acceptors, namely, alanine, threonine, leucine, methionine, phenylalanine, glycine, asparagine, isoleucine, tryptophan, glutamine, glutamic acid, aspartic acid, serine, histidine, valine, arginine, and lysine, was studied considering activity with glycylglycine, as an acceptor, as 100%.

*Effect of Metal Ions and Inhibitors.* The effect of various metal ions on enzyme activity was studied by pre-incubating the enzyme in the respective metal ion solution (pH 9.0) for 5 min and then performing the assay as mentioned. Enzyme was investigated for nine different metal ions, namely, $Co^{2+}$, $Cu^{2+}$, $Ca^{2+}$, $Cd^{2+}$, $Mn^{2+}$, $Mg^{2+}$, $Ni^{2+}$, $Zn^{2+}$, and $Pb^{2+}$, at a final concentration of 5 mM in the reaction. The influence of various inhibitors, for example, phenylmethanesulfonyl fluoride (PMSF), *N*-bromosuccinamide (NBS), bromoacetic acid, ethylenediaminetetraacetic acid (EDTA), β-mercaptoethanol, idoacetamide, sodium azide, iodoacetic acid, dithiothreitol, and 1,10-phenanthroline, on GGT activity was also investigated along with some specific inhibitors of GGT such as 6-diazo-5-oxo-L-norleucine (DON) and azaserine.

**Theanine Biosynthesis: Optimization of Reaction Parameters.** Initially, theanine synthesis was determined in a 5 mL reaction containing 20 mM L-glutamine (donor) and 200 mM ethylamine (acceptor) at pH 9.0 and 37 °C using 0.4 U/mL rBLGGT for a period of 6 h to select an appropriate time for further optimization. Reactions were stopped by an equal volume of 0.5% (v/v) trifluoroacetic acid (TFA) and were then filtered through a 0.2 μm filter. The products were analyzed with a Shimadzu high-performance liquid chromatograph (HPLC) equipped with a $C_{18}$ reverse phase column (Luna 5 μm C18 (2); dimensions, 250 × 4.6 mm). L-Theanine was detected according to the method of Zhang[19] with a few modifications in the mobile phase: 0.05% (v/v) TFA in water; flow rate, 0.5 mL/min; oven temperature, 40 °C. UV−vis absorbance detection was done at 203 nm without any derivatization, and the L-theanine peak was identified by running commercial standards. However, a measurable amount of L-theanine was obtained within 1 h of the reaction; thus, further parameters, such as the concentrations of donor, acceptor, and enzyme, were optimized using a one variable at a time approach for a 1 h reaction at pH 9.0 and 37 °C.

**One Variable at a Time Approach.** Ethylamine concentration was varied from 40 to 400 mM in a reaction containing 20 mM L-glutamine and 0.4 U/mL rBLGGT in the above specified conditions. Similarly, L-glutamine (10−100 mM) was varied at a constant concentration of ethylamine (200 mM) and rBLGGT (0.4 U/mL). The effect of enzyme concentration was also studied in reactions containing 40 mM L-glutamine and 200 mM ethylamine at pH 9.0 and 37 °C by varying its concentration from 0.1 to 1.0 U/mL. All of the reactions were done in triplicate, and theanine yield was determined after 1 h of incubation according to the method described above.

**Statistical Approach: Response Surface Methodology (RSM).** The interaction pattern of three main components of L-theanine synthesis reaction, namely, L-glutamine ($X_1$), ethylamine ($X_2$), and rBLGGT ($X_3$), was studied by employing RSM strategy. The experiment was designed using the Box−Behnken model following Design Expert software (version 6.0.10). Each of the independent variables was studied at three different coded levels of −1, 0, and +1, resulting in 17 sets of experiments (5 replications of the central run). The actual and coded forms with respect to the full experimental plan of all three variables are listed in Table 1. L-Theanine yield ($Y_1$) and percent conversion ($Y_2$) of L-glutamine to L-theanine were taken as the two responses for this study. All of the reactions were performed in 50 mM Tris-HCl buffer (pH 9.0) and were incubated at 37 °C for 4 h. A second-

**Table 1. Experimental Ranges and Levels of the Three Independent Variables Used in RSM in Terms of Actual and Coded Factors**

| variable | actual | coded | actual | coded | actual | coded |
|---|---|---|---|---|---|---|
| L-glutamine (mM) | 20 | −1 | 80 | 0 | 140 | +1 |
| ethylamine (mM) | 200 | −1 | 400 | 0 | 600 | +1 |
| rBLGGT (U/mL) | 0.5 | −1 | 1.0 | 0 | 1.5 | +1 |

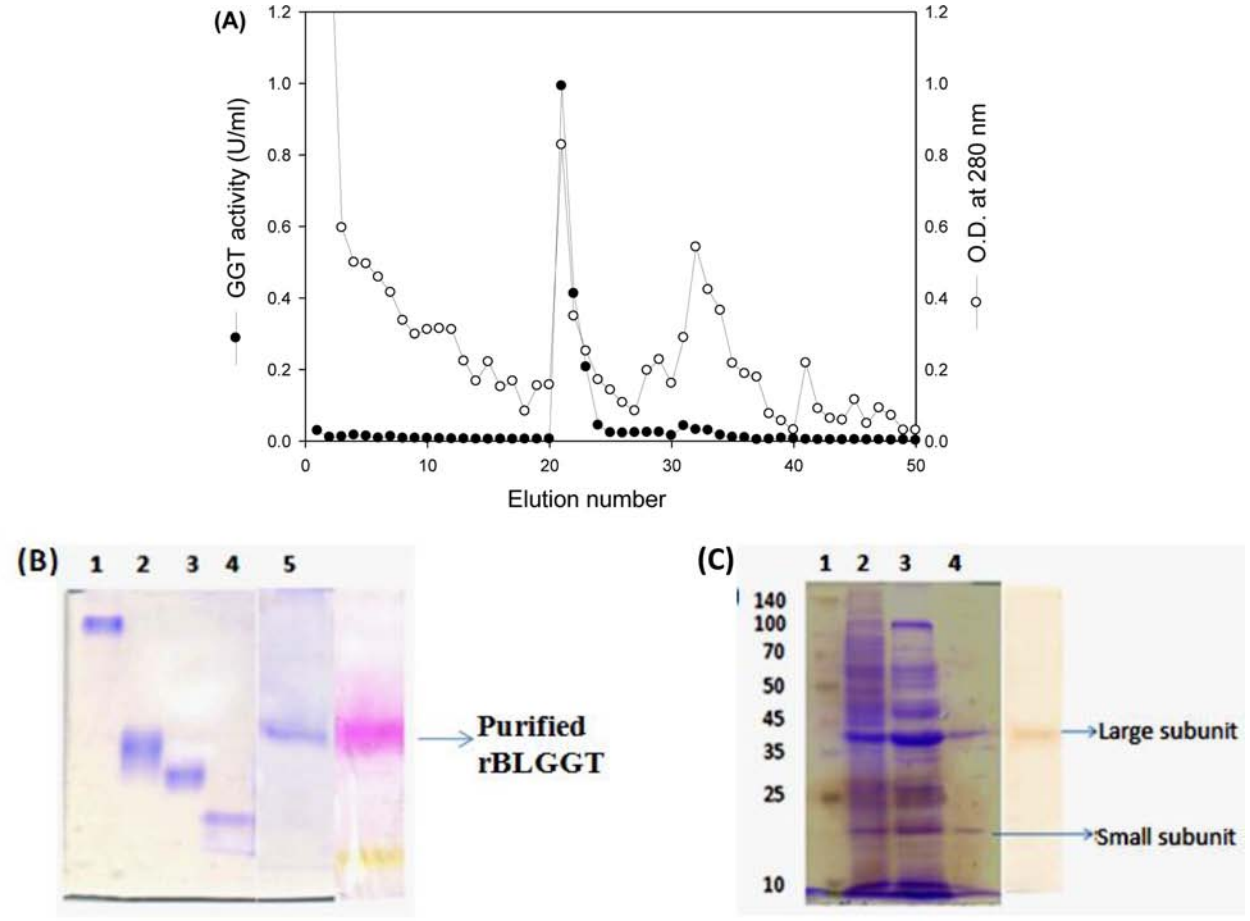


**Figure 1.** (A) Elution profile of rBLGGT from Q-Sepharose fast flow column pre-equilibrated with 10 mM, pH 9.0, Tris-Cl buffer (fractions 21, 22, and 23 were pooled together for biochemical characterization). (B) Native-PAGE (lane 5) and zymogram of purified rBLGGT (native protein markers used; lanes: 1, catalase, 240 kDa; 2, bovine albumin, 67 kDa; 3, egg albumin, 43 kDa; 4, trypsin soybean inhibitor, 20.1 kDa). (C) SDS-PAGE and Strep-tag Western blot of rBLGGT (lanes: 1, SDS protein marker; 2, crude cell lysate; 3, acetone precipitated fraction; 4, purified rBLGGT).

degree polynomial equation was generated using a modified quadratic model

$$Y_{1or2} = \beta_0 + \beta_1 X_1 + \beta_2 X_2 + \beta_3 X_3 + \beta_{11} X_1^2 + \beta_{22} X_2^2 + \beta_{33} X_3^2 + \beta_{12} X_1 X_2$$

where $\beta_0$ is the constant coefficient, $\beta_1$, $\beta_2$, and $\beta_3$ are linear, $\beta_{11}$, $\beta_{22}$, and $\beta_{33}$ are quadratic, and $\beta_{12}$ is the interaction coefficient.

**Statistical Analyses.** RSM results were analyzed by performing an analysis of variance (ANOVA) test. *F* value and Prob > *F* generated by ANOVA were used to determine the statistical significance of the regression coefficients. Also, the model applicability was assessed by observing the values of $R^2$, adjusted $R^2$, and the coefficient of variance. Subsequently, the model was validated by setting up 10 random experiments (9 within the design space and 1 beyond), and the results thus obtained were checked against their predicted values.

**Enzyme Immobilization.** rBLGGT was immobilized by entrapping the enzyme in calcium alginate beads. Acetone-precipitated enzyme (9.0 U/mL) was added to an equal volume of 6% (w/v) sodium alginate and mixed thoroughly, resulting in a 3% (w/v) sodium alginate enzyme mixture. Beads were prepared by adding the above mixture dropwise to a 0.2 M $CaCl_2$ solution at 4 °C. Beads were left in the $CaCl_2$ solution for 3 h at 4 °C for hardening, subsequently washed with ultrapure water, and air-dried. GGT activity retained in the beads as compared to the free enzyme was estimated by hydrolytic assay using oxidized glutathione (GSSG) as substrate.

A 10 mM stock solution of GSSG was prepared in 50 mM Tris-HCl buffer (pH 9.0). GGT assay of free as well as immobilized enzyme was done using GSSG as substrate for hydrolytic reaction. Enzyme units were calculated by monitoring the decrease in substrate concentration with time, and thus units were defined as micromoles of GSSG utilized per minute under standard assay conditions. GSSG peak was analyzed on HPLC using the same protocol as employed for theanine detection.

Assuming equal distribution of the enzyme in the beads, theanine synthesis reaction was carried out by adding calcium alginate beads equivalent to 1.0 U/mL in 50 mL of reaction volume and was kept at 37 °C and 100 rpm for 4 h. Reaction was repeated five times by harvesting the beads from the previous reaction. Subsequently, the reaction was scaled up to 1 L.

**Purification of L-Theanine.** A 50 mL reaction under optimized conditions was set up and terminated by lowering its pH to 3.0 by adding 3% (v/v) HCl solution. Batch purification was done by adding 10 g of Dowex 50W X 8 hydrogen form resin to the reaction vessel and kept at mild shaking (50 rpm) for 10 min at room temperature. The vessel was then allowed to stand for 10 min so that the resin settled at the bottom and was separated by decantation. L-Theanine was then eluted with 5 volumes of ammonia−water (pH 11.6; pH was adjusted by diluting 30% (v/v) ammonium hydroxide solution with ultrapure water), five times. Each fraction was analyzed on HPLC. Resin was regenerated using 2% (v/v) sulfuric acid and ultrapure water.

The fraction containing purified theanine was then lyophilized and compared with the commercial standards on HPLC. $^1$H NMR analysis was done by dissolving 10 mg of the sample in 500 $\mu$L of $D_2O$ followed by analysis on a Bruker Avance 400 MHz spectrophotometer at the University Science Instrumentation Centre (USIC), University of Delhi, with TMS as internal standard. $^1$H NMR was done as single pulse (1D) at 23.7 °C, and acquisition duration and relaxation delay were 1.37 and 4 s per scan, respectively, with a pulse angle of 45°.


dx.doi.org/10.1021/jf5022913 | J. Agric. Food Chem. 2014, 62, 9151−9159

## RESULTS AND DISCUSSION

**Purification and Characterization of rBLGGT.** rBLGGT was purified by Q-Sepharose ion-exchange chromatography, and the active fraction was eluted in 0.3 M NaCl (Figure 1A) with a yield of 28.8% and a specific activity of 4.58 U/mg (Table 2). The purity of the enzyme was checked with native-PAGE gel, which showed a single band of around 64 kDa. Activity staining was done to check the enzyme activity of the corresponding band (Figure 1B).

**Table 2. Purification Summary of rBLGGT**

| step | total protein (mg) | total activity (U) | specific activity (U/mg) | yield (%) | purification fold |
|---|---|---|---|---|---|
| cell lysate | 125 | 55.75 | 0.446 | 100 | 1.0 |
| acetone precipitated | 7.8 | 29.64 | 3.80 | 53.1 | 8.5 |
| Q-Sepharose ion-exchange purified (0.3 M fraction)[a] | 3.5 | 16.06 | 4.588 | 28.8 | 10.2 |

[a]Acetone-precipitated fraction was purified in two lots from Q-Sepharose fast flow column.

rBLGGT is a heterodimeric protein, which was confirmed by SDS-PAGE gel (Figure 1C). The apparent molecular masses of large and small subunits were approximately 42 and 22 kDa, respectively. The molecular masses of GGTs from other microbial sources range from 50 to 63 kDa, with variable sizes of large subunits, whereas the molecular masses of small subunits were almost constant.[20,21]

*Biochemical Characterization.* rBLGGT exhibited maximum activity at pH 9.0 and a temperature of 60 °C, similar to wild enzyme (Figure 2A,B). However, wild GGT showed a steep fall in activity when the pH was increased to 10.0, whereas rBLGGT retained around 60% of its activity until pH 11.0. GGTs from *Bacillus* sp. have been reported to work at alkaline pH ranging from 8.0 to 10.0, but there is a wide range (37−62 °C) with respect to temperature optima.[21] rBLGGT was stable in a broad pH range of 6.0−12.0, following almost the same pattern as wild type (Figure 2C). During temperature stability experiments it was observed that the enzyme was stable at 40 °C up to 3 h, whereas at 50 °C enzyme activity decreased gradually with a $t_{1/2}$ of 56 min. On the contrary, wild GGT was found to be more stable with a $t_{1/2}$ of 192 min at 50 °C (Figure 2D and Figure S2 in the Supporting Information). rBLGGT was found to be stable for 3 months at 4 °C and for 1 week at 37 °C.

Steady state kinetics of rBLGGT revealed a $K_m$ value of 45 $\mu$M against $\gamma$-GpNA, whereas that of wild GGT was 84 $\mu$M (Supporting Information Figure S3). This difference in $K_m$ values could be attributed to some conformational changes incurred by the recombinant protein while attaining its tertiary

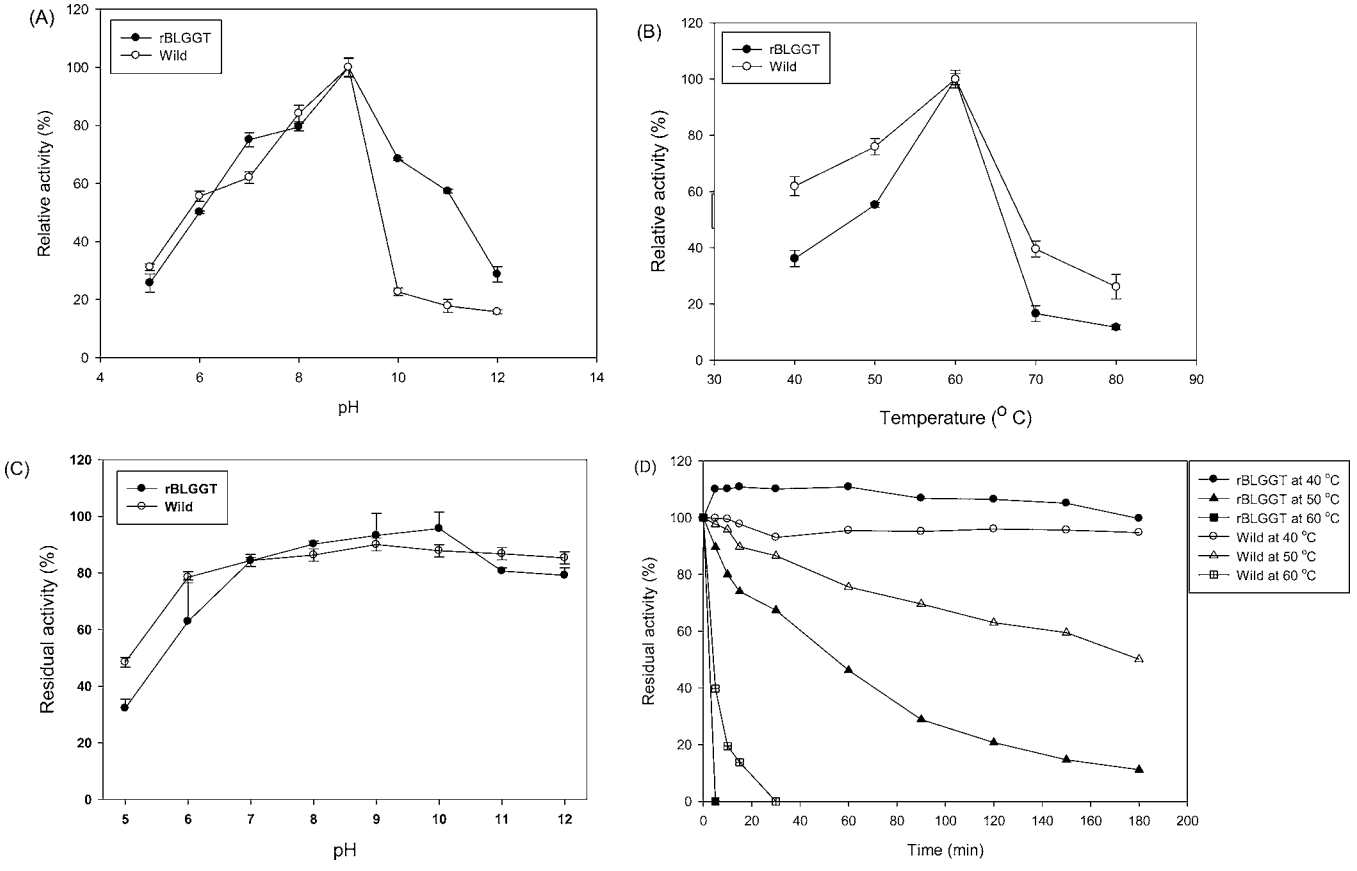


**Figure 2.** (A) Effect of pH on rBLGGT activity. For pH optimization GGT assay was performed in different pH buffers (5.0−12.0) at 60 °C. rBLGGT activity of 0.53 U/mL at 60 °C was taken as 100%. All reactions were done in triplicate. (B) Effect of temperature on BLGGT activity. GGT assay was performed by incubating the reaction at specific temperatures (40−80 °C) for 5 min. (C) rBLGGT stability in different pH buffers. Enzyme was preincubated in different pH buffers (5−12; 10 mM) for 1 h, and then GGT assay was performed at pH 9.0 and 60 °C. (D) Determination of temperature stability of rBLGGT. Enzyme was preincubated at different temperatures, and then GGT assay was performed under standard conditions after every 30 min interval. At 60 °C enzyme stability was checked for 5 min intervals. rBLGGT was also compared with wild GGT form *B. licheniformis* ER-15 for pH and temperature optima and stability (0.37 U/mL of wild GGT under standard conditions was taken as 100%).


dx.doi.org/10.1021/jf5022913 | J. Agric. Food Chem. 2014, 62, 9151−9159

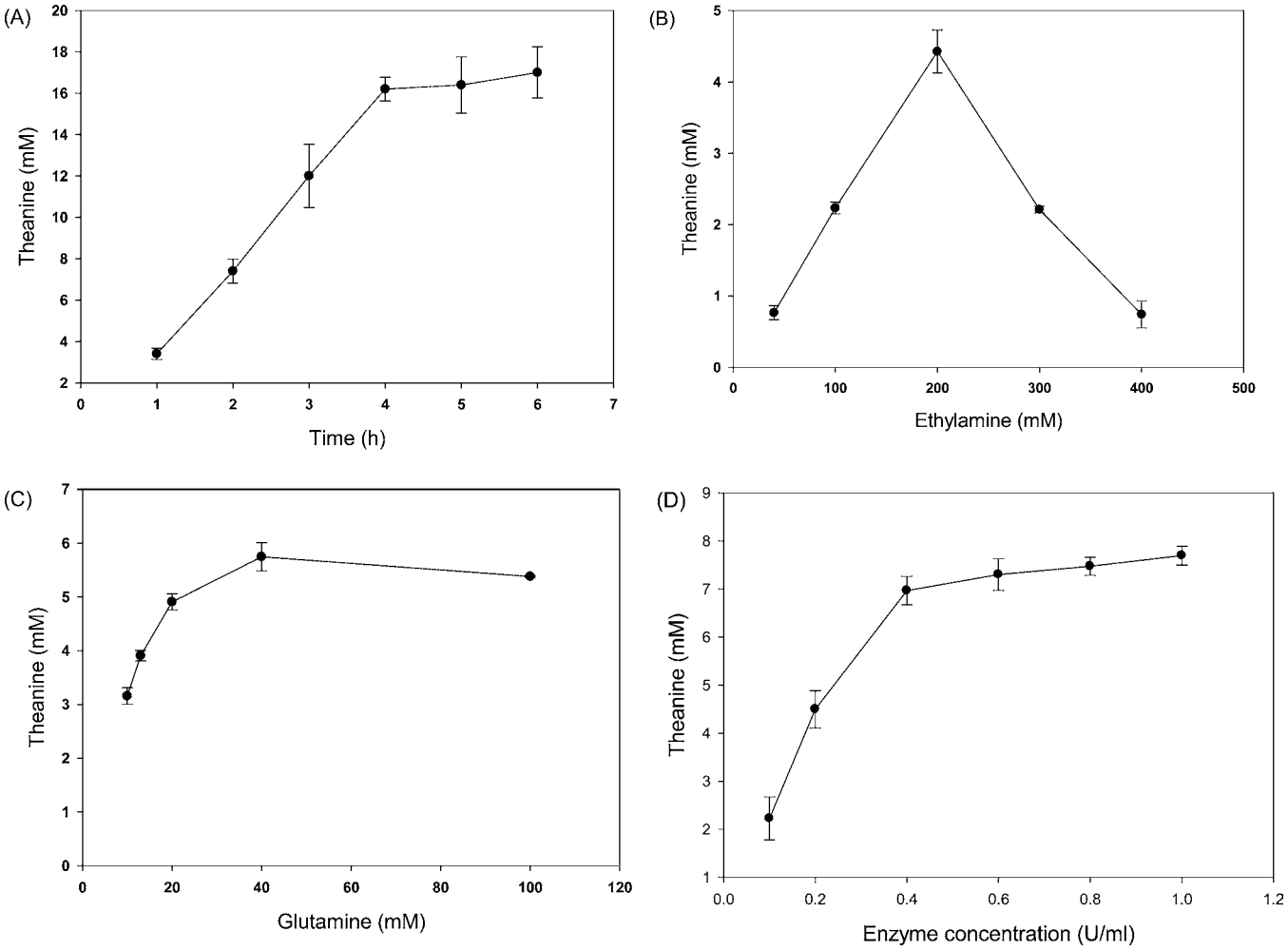


**Figure 3.** (A) Time profile for L-theanine synthesis (reaction containing 20 mM L-glutamine, 200 mM ethylamine, and 0.4 U/mL BLGGT in Tris-Cl, pH 9.0, buffer (50 mM), kept at 37 °C). (B) Optimization of acceptor concentration by a one variable at time approach (L-glutamine was kept constant at 20 mM. (C) Effect of L-glutamine concentration (ethylamine concentration was kept constant at 200 mM). (D) Optimization curve of enzyme concentration for theanine synthesis (5 mL reaction containing 40 mM L-glutamine and 200 mM ethylamine). All of the above reactions were done in triplicate and were carried out at 37 °C and pH 9.0 for 1 h.

structure. The affinity of rBLGGT for γ-GpNA as substrate is around 2 times that of *B. licheniformis* ATCC 27811 GGT,[20] whereas the $K_m$ of *B. subtilis* SK11.004 GGT has been reported to be 7500 μM.[21]

Inhibition studies of rBLGGT and the wild type revealed that the two amino acids, namely, serine and tryptophan, are of utmost importance with respect to its activity as the enzyme is strongly inhibited by PMSF and NBS, which correlates with the previously reported results of Inoue et al.,[22] wherein it has been shown that N-terminal threonine residue is crucial for both autocatalysis and activity of the enzyme. Although inhibition with NBS supports the hypothesis of Shuai et al.,[21] complete inhibition of both the enzymes by GGT specific inhibitors such as DON and azaserine confirmed the nature of the enzymes as γ-glutamyl transferases (Supporting Information Figure S4). Metal ion inhibition studies demonstrated some contrasting features between the recombinant and wild enzymes. rBLGGT inhibition was observed with $Zn^{2+}$, $Mn^{2+}$, $Ni^{2+}$, and $Pb^{2+}$ metal ions, whereas there was apparently no change in GGT activity in the presence of $Mg^{2+}$, $Ca^{2+}$ $Cu^{2+}$, and $Cd^{2+}$ ions. On the other hand, wild-type GGT showed more sensitivity toward all of the metal ions used. Moreover, complete inhibition of the wild type was observed in the presence of $Co^{2+}$, whereas rBLGGT retained around 80% of the activity (Supporting Information Figure S5). rBLGGT was also inhibited by ethylene glycol tetraacetic acid (EGTA) with 37% residual activity, which was completely regained in the presence of $Ca^{2+}$ or $Mg^{2+}$ but not with $Cd^{2+}$ metal ions; similar observations were also reported previously in the case of GGT from *B. licheniformis*.[20] Inhibition with EGTA was not observed in case of wild- type.

Substrate specificity of rBLGGT with various amino acids as γ-glutamyl acceptors was analyzed, and it showed >50% transpeptidase activity with most of the amino acid acceptors, whereas serine, alanine, and aspartic acid were weak acceptors. With respect to substrate specificity, rBLGGT showed a behavior highly similar to that of its wild counterpart Supporting Information Figure S6). High substrate specificity of rBLGGT makes the enzyme a good choice for synthesizing γ-glutamyl compounds. There are a very few reports of GGTs from *Bacillus* sp. having >50% transpeptidase activity with respect to monomers.[23,24]

**Theanine Synthesis.** Various parameters affecting the conversion of L-theanine from L-glutamine were investigated. L-Theanine was quantified using HPLC, where theanine eluted in a linear fashion in the range from 0.25 to 2 mM between 10.8 and 11.4 min using 0.05% (v/v) TFA as a mobile phase. This is the


dx.doi.org/10.1021/jf5022913 | J. Agric. Food Chem. 2014, 62, 9151−9159

**Table 3. Box−Behnken Design and the Results along with the Variance Analysis for the Selected Quadratic Model[a]**

(A)

| | | | | theanine yield (mM) | | % conversion | |
|---|---|---|---|---|---|---|---|
| run | L-glutamine (mM) | ethylamine (mM) | rBLGGT (U/mL) | actual | predicted | actual | predicted |
| 1 | 0 | −1 | +1 | 17.09 | 21.99 | 21.36 | 28.84 |
| 2 | −1 | 0 | −1 | 2.45 | 4.04 | 12.24 | 31.45 |
| 3 | 0 | −1 | −1 | 12.31 | 15.75 | 15.38 | 10.19 |
| 4 | +1 | −1 | 0 | 10.41 | 5.49 | 7.43 | 7.54 |
| 5 | 0 | +1 | +1 | 68.88 | 60.88 | 86.1 | 85.59 |
| 6 | +1 | 0 | −1 | 31.02 | 26.32 | 22.16 | 9.92 |
| 7 | 0 | 0 | 0 | 65.63 | 63.42 | 82.04 | 79.27 |
| 8 | −1 | +1 | 0 | 17.18 | 22.1 | 85.92 | 85.82 |
| 9 | +1 | +1 | 0 | 56.27 | 59.7 | 40.19 | 42.59 |
| 10 | 0 | 0 | 0 | 62.51 | 63.42 | 78.13 | 79.27 |
| 11 | +1 | 0 | +1 | 26.37 | 32.56 | 18.83 | 28.57 |
| 12 | 0 | 0 | 0 | 58.42 | 63.42 | 73.03 | 79.27 |
| 13 | −1 | −1 | 0 | 1.95 | −1.47 | 9.77 | 7.38 |
| 14 | 0 | +1 | −1 | 54.97 | 54.64 | 68.71 | 66.93 |
| 15 | −1 | 0 | +1 | 13.36 | 10.28 | 66.82 | 50.11 |
| 16 | 0 | 0 | 0 | 67.12 | 63.42 | 83.9 | 79.27 |
| 17 | 0 | 0 | 0 | 63.41 | 63.42 | 79.26 | 79.27 |

(B)

| | response | |
|---|---|---|
| ANOVA values | theanine yield | % conversion |
| $F$ value | 45.38 | 18.48 |
| $P > F$ | <0.0001 | 0.0001 |
| mean | 37.02 | 50.08 |
| $R^2$ | 0.9724 | 0.9350 |
| adjusted $R^2$ | 0.9510 | 0.8844 |
| coefficient of variance | 15.30 | 21.67 |
| adequate precision | 16.700 | 10.536 |

[a]Actual values are the average of the values obtained from three independent experiments.

modification of the method reported by Zhang et al.[19] where the pH of the mobile phase was adjusted to 3.0 using formic acid instead of TFA. Generally, theanine is detected by reverse phase HPLC equipped with fluorescence detectors using pre- or post-column derivatization,[25−27] but simple methods are also available that are free from reagent interference and cumbersome processing of the samples.

L-Theanine biosynthesis was carried out at pH 9.0 and 37 °C throughout the study. Although the temperature optimum of rBLGGT is 60 °C, by keeping in mind the lower boiling point of ethylamine (bp = 20 °C), synthesis was done at 37 °C.

During time profiling 16 mM theanine was obtained using 20 mM L-glutamine and detectable amounts of L-theanine can be obtained within 1 h (Figure 3A). Therefore, further parameters were studied for 1 h of reaction using a one variable at a time approach.

The substrate ratio was taken into consideration because it has been reported that the donor to acceptor ratio plays a significant role in transpeptidation reactions carried out by GGTs.[28] It is known that GGTs catalyze three different reactions, depending on the substrates availability, namely, transpeptidation, hydrolysis, and autotranspeptidation. Therefore, initially, ethylamine (acceptor) concentration was standardized in the ratios of 1:2, 1:5, 1:10, 1:15, and 1:20 in the presence of 20 mM L-glutamine. Maximum yield of 4.5 mM was achieved when the donor to acceptor ratio was 1:10 within 1 h (Figure 3B). Subsequently, the donor concentration was optimized keeping ethylamine constant at 200 mM, and the optimal ratio obtained was 1:5, that is, 40 mM L-glutamine and 200 mM ethylamine with 5.7 mM theanine yield (Figure 3C). This is in agreement with a previous study[14] in which a lower ratio of 1:2.5 was reported for *Bacillus subtilis* GGT but a higher ratio was needed for GGTs from *E. coli*.[11−15] This shows that GGTs from *Bacillus* sp. are better transpeptidases with respect to ethylamine as an acceptor.

Enzyme concentration was optimized to be 0.5 U/mL as no significant increase in theanine yield was observed when the enzyme concentration was increased from 0.4 to 0.6 U/mL (Figure 3D). With further increase in the enzyme concentration (1.2 U/mL), byproduct formation was observed, which shows that at higher concentrations, enzyme also catalyzes side reactions such as hydrolysis and autotranspeptidation (Supporting Information Figure S7). Subsequently, the time kinetics revealed that 33 mM theanine yield could be obtained within 4 h, which was 2 times the initial yield (Figure 5). Around 80% conversion of L-glutamine to L-theanine could be achieved in a reaction consisting of 40 mM L-glutamine, 200 mM ethylamine, and 0.5 U/mL rBLGGT at pH 9.0 and 37 °C within 4 h, in contrast to previous studies in which a similar conversion has been reported in >6 h[29] except for GGT from *B. subtilis*[14] where 94% conversion has been reported in 4 h.

Statistical optimization was employed using Box−Behnken design. The actual and predicted values for both of the responses, L-theanine yield (mM) and percent conversion of L-glutamine to L-theanine, are listed in Table 3A. ANOVA studies revealed the model to be significant with $F$ values of 45.38 ($P > F < 0.0001$) and 18.48 ($P > F = 0.0001$) for the former and the latter,


dx.doi.org/10.1021/jf5022913 | J. Agric. Food Chem. 2014, 62, 9151−9159

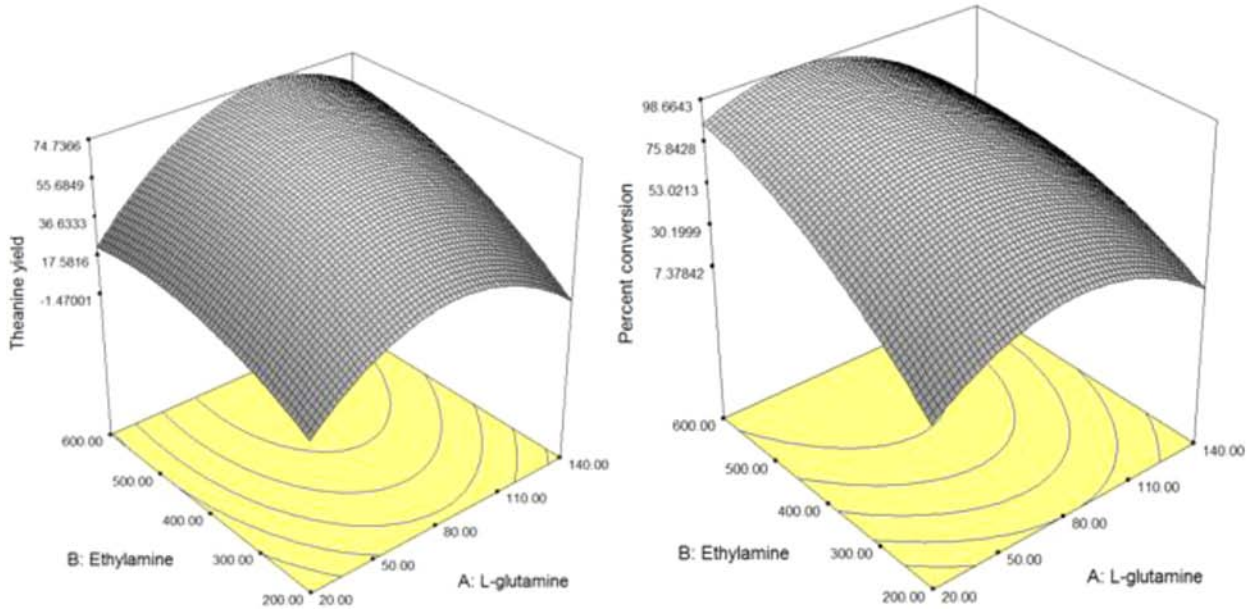


**Figure 4.** 3D plot for L-theanine yield (mM) and percent conversion of L-glutamine to L-theanine: effect of L-glutamine and ethylamine concentrations at a constant concentration of rBLGGT (1 U/mL).

respectively. Also, the adjusted $R^2$ values were in good agreement with the predicted $R^2$ for both responses (Table 3B). Thus, it can be concluded that the empirical model fits the experimental values very well. On the basis of the regression analyses the following equations were generated for $Y_1$ and $Y_2$:

$$\text{theanine yield } (Y_1) = 63.42 + 11.14X_1 + 19.44X_2 + 3.12X_3 - 30.99X_1^2 - 10.97X_2^2 - 14.13X_3^2 + 7.66X_1X_2$$

$$\%\ \text{conversion } (Y_2) = 79.27 - 10.77X_1 + 28.37X_2 + 9.33X_3 - 30.66X_1^2 - 12.78X_2^2 - 18.60X_3^2 - 10.85X_1X_2$$

$X_1$, $X_2$, and $X_3$ are three independent variables included in the study. The interacting parameters, $X_{13}$ and $X_{23}$, were found to be insignificant and thus excluded from the model.

From analysis of the interaction plots (Figure 4), it can be observed that on increasing the ethylamine concentration, yield as well as the percent conversion for L-theanine also increases at a constant concentration of L-glutamine and rBLGGT, whereas on increasing L-glutamine at a constant concentration of ethylamine, a decrease in percent conversion was observed. This could be attributed to either overcrowding of the active sites of rBLGGT or end product inhibition. However, with increasing enzyme, no benefit regarding percent conversion was encountered. Therefore, end product inhibition studies were carried out and a gradual decrease in enzyme activity was observed when the theanine concentration was increased from 10 to 40 mM during the GGT assay (Supporting Information Figure S8). The model was validated by conducting a set of 10 random experiments (9 within and 1 outside the design space), and the results were found to be in good agreement with the predicted values (Supporting Information Table S1).

Thus, following RSM a maximum of 85−87% conversion of L-glutamine to L-theanine was obtained with the total theanine yield of 68−70 mM in a reaction containing 80 mM L-glutamine, 600 mM ethylamine, and 1 U/mL rBLGGT at pH 9.0 and 37 °C within 4 h, which is nearly 4.25-fold the initial yield. rBLGGT enzyme concentration used in the current study is higher than in earlier studies[14] because the enzyme has a temperature optimum of 60 °C and retains only 30% of its activity at 37 °C (Figure 2B).

Furthermore, to make the reaction cost-effective, rBLGGT was immobilized by entrapment method using calcium alginate beads. Enzyme activity was retained at a level of 40−50% after entrapment as assessed by GGT assay using GSSG as substrate (retention time = 25 min). Immobilization had no effect on pH and temperature optima of the enzyme, whereas the thermal stability of the enzyme was enhanced with >80% activity at 60 °C until 15 min, in contrast to free rBLGGT that lost its activity at 60 °C within 5 min (Supporting Information Figure S9).

Under optimized conditions 84% conversion was achieved using immobilized enzyme in 50 mL of reaction volume within 4 h, which was scaled up to 1 L with similar yields (Figure 5). Beads were reused for five times with >90% efficiency retained up to the third cycle.

More than 90% of pure L-theanine was recovered by using the method of Zhu et al.[30] with a few modifications. The purification was done in batch, and theanine was eluted using ammonia−water at pH 11.6 instead of pH 11.3. The purified fractions were then subjected to lyophilization, and finally a white theanine powder was obtained.

The purity of the final product was assessed by HPLC (see Supporting Information Figure S10), and it was >95% pure. L-Theanine was further identified by $^1$H NMR analysis (see Supporting Information Figure S10).

Finally, through this process 35.2 g of theanine was obtained in three cycles of 1 L each. A brief comparison with the previously optimized methods for the synthesis of L-theanine using γ-glutamyl transpeptidase from various sources is listed in Table 4. This is the first report of the synthesis of L-theanine from *B. licheniformis* GGT. To date only *E. coli* and *B. subtilis* GGTs have been explored with 80−95% conversion efficiency. *B. subtilis* GGT has been reported to convert 94% L-glutamine to L-theanine within 4 h[14] in contrast to rBLGGT (84%), but the


dx.doi.org/10.1021/jf5022913 | J. Agric. Food Chem. 2014, 62, 9151−9159

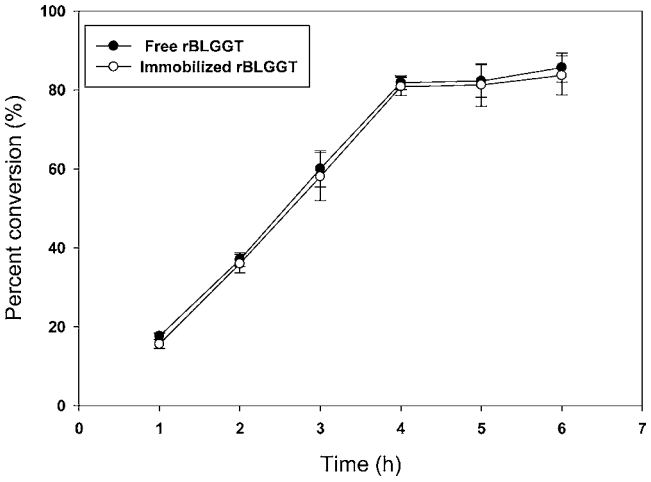


**Figure 5.** Time profiling of theanine synthesis using free and immobilized enzyme. After all of the reaction conditions had been optimized, time was again standardized for 50 mL of reaction using free and immobilized enzyme.

overall yield was less, as only 20 mM L-glutamine was used in that study. However, higher L-glutamine (or other γ-glutamyl donors) concentration (100−300 mM) in the case of *E. coli* GGTs resulted in higher yields, but accordingly high donor to acceptor ratios (1:7.5 or 1:10) and longer reaction times (8−24 h) were required to achieve >80% conversion. Thus, rBLGGT can be employed for the enzymatic synthesis of L-theanine with appreciable catalytic efficiency.

Stereoselective synthesis of L-theanine with appreciable yields can thus be obtained from enzymatic reactions, as documented in Table 4. Also, *Bacillus* GGTs have been demonstrated to provide higher conversion rates as well as least reaction times. Thus, scaling up of the process, for L-theanine synthesis, at the industrial level could be achieved using *B. licheniformis* GGT. In contrast to natural extraction and chemical synthesis processes for L-theanine production, enzymatic synthesis has many advantages such as lower reaction time, high specificity, and higher yields. However, for such large-scale productions enzyme could be a limiting factor; therefore, now more emphasis should be given to increasing the enzyme production and immobilization. Reusability of the enzyme is one the most important parameters that should be focused on to make the process more cost-effective.

## ■ ASSOCIATED CONTENT

### Supporting Information

Figures S1−S9 and Tables S1 and S2. This material is available free of charge via the Internet at http://pubs.acs.org.

## ■ AUTHOR INFORMATION

### Corresponding Author

*(R.G.) Phone: +91-11-24111933. Fax: +91-11-24115270. E-mail: ranigupta15@rediffmail.com.

### Funding

We thank the Ministry of Food Processing Industries (MoFPI) for financial assistance. S.B. thanks DST-INSPIRE for a fellowship.

### Notes

The authors declare no competing financial interest.

## ■ ACKNOWLEDGMENTS

We thank the University of Delhi for facilities.

## ■ ABBREVIATIONS AND NOMENCLATURE

rBLGGT:recombinant γ-glutamyl transpeptidase from *Bacillus licheniformis* ER-15
SDS-PAGE:sodium dodecyl sulfate−polyacrylamide gel electrophoresis
$K_m$:substrate concentration at which the reaction rate is half of $V_{max}$
$V_{max}$:maximum rate achieved by the system, at maximum (saturating) substrate concentrations
FDA:U.S. Food and Drug Administration
L- and D-form:levorotatory and dextrorotatory
ATP:adenosine triphosphate
GGT:γ-glutamyl transpeptidase
LB:Luria−Bertani
SRL:Sisco Research Laboratory Pvt. Ltd.
IPTG:isopropyl-β-D-thiogalactopyranoside
NaCl:sodium chloride
γ-GpNA:γ-glutamyl-*p*-nitroanilide hydrochloride
PVDF:polyvinylidene difluoride
BSA:bovine serum albumin
PBS:phosphate buffer saline

**Table 4. Comparative Analysis of the Methods Available for Enzymatic Synthesis of L-Theanine Using GGT from Various Sources**

| γ-glutamyl donor used | enzyme | donor concn (mM) | acceptor (ethylamine) concn (mM) | conditions | time (h) | conversion (%) | ref |
|---|---|---|---|---|---|---|---|
| L-glutamine | recombinant *B. licheniformis* GGT (BLGGT) | 80 | 600 | pH 9.0, 37 °C | 4 | ≥84 | current study |
| | recombinant *E. coli* GGT | 200 | 1500 | pH 10.0, 37 °C | 5 | 60 | Suzuki et al.[11] |
| | *Bacillus subtilis* GGT | 20 | 50 | pH 10.0, 37 °C | 4 | 94 | Shuai et al.[14] |
| | recombinant *E. coli* GGT | 267 | 2000 | pH 10.5, 37 °C | 24 | 80 | Wang et al.[15] |
| glutamic acid γ-methyl ester (GAME) | immobilized *E. coli* cells | 300 | 3000 | pH 10.0, 50 °C | 18 | 87.2 (after 6 uses) | Zhang et al.[13] |
| | *E. coli* cells | 100 | 1000 | pH 10.0, 45 °C | 8 | 95 | Zhang et al.[13] |
| γGpNA | recombinant *E. coli* GGT | 5 | 50 | pH 9.0, 37 °C | 6 | 93 | Zhang et al.[29] |

HRP:horseradish peroxidase
DAB:diaminobenzidine
PMSF:phenylmethylsulfonyl fluoride
NBS:*N*-bromosuccinamide
EDTA:ethylenediaminetetraacetic acid
DON:6-diazo-5-oxo-L-norleucine
HPLC:high-performance liquid chromatography
TFA:trifluoroacetic acid
UV−vis:ultraviolet−visible
HCl:hydrochloric acid
$^1$H NMR:nuclear magnetic resonance with respect to hydrogen-1 nuclei
$D_2O$:heavy water
TMS:tetramethylsilane
kDa:kilodalton
EGTA:ethylene glycol tetraacetic acid

## REFERENCES


(1) Voung, Q. V.; Bowyer, M. C.; Roach, P. D. L-Theanine: properties, synthesis and isolation from tea. *J. Sci. Food Agric.* **2011**, *91*, 1931−1939.

(2) Huber, L. G. Green tea catechins and L-theanine in integrative cancer care: a review of the research. *Altern. Complement. Ther.* **2003**, *9*, 294−298.

(3) Liu, Q.; Duan, H.; Luan, J.; Yagasaki, K.; Zhang, G. Effects of theanine on growth of human lung cancer and leukemia cells as well as migration and invasion of human lung cancer cells. *Cytotechnology* **2009**, *59*, 211−217.

(4) Kim, T.; Lee, Y. K.; Park, S. G.; et al. L-Theanine, an amino acid in green tea, attenuates *β*-amyloid-induced cognitive dysfunction and neurotoxicity: reduction in oxidative damage and inactivation of ERK/p38 kinase and NF-*κ*B pathways. *Free Radical Biol. Med.* **2009**, *47*, 1601−1610.

(5) Lichtenstein, N. Preparation of *γ*-alkylamides of glutamic acid. *J. Am. Chem. Soc.* **1942**, *64*, 1021−1022.

(6) Gu, H.; Jiang, Y.; Wang, J. A practical synthesis of ethyl L-glutamine (L-theanine). *Org. Prep. Proced. Int.* **2004**, *36*, 182−185.

(7) Tachiki, T.; Suzuki, H.; Wakisaka, S.; Yano, T.; Tochikura, T. Production of *γ*-glutamylmethylamide and *γ*-glutamylethylamide by coupling of baker's yeast preparations and bacterial glutamine synthetase. *J. Gen. Appl. Microbiol.* **1986**, *32*, 545−548.

(8) Tachiki, T.; Yamada, T.; Mizuno, K.; Ueda, M.; Shiode, J. I.; Fukami, H. *γ* -Glutamyl transfer reactions by glutaminase from *Pseudomonas nitroreducens* IFO 12 694 and their application for the syntheses of theanine and *γ*-glutamylmethylamide. *Biosci., Biotechnol., Biochem.* **1998**, *62*, 1279−1283.

(9) Itoh, T.; Hoshikawa, Y.; Matsuura, S.; Mizuguchi, J.; Arafune, H.; Hanaoka, T.; Mizukami, F.; Hayashi, A.; Nishihara, H.; Kyotani, T. Production of L-theanine using glutaminase encapsulated in carbon-coated mesoporous silica with high pH stability. *Biochem. Eng. J.* **2012**, *68*, 207−214.

(10) Liu, B.; Li, P.; Zhang, C.; Wang, Y.; Zhao, Y. S. Theanine synthesized by immobilizing *Pseudomonas nitroreducens* LY in nano-fibrous membranes. *Process Biochem.* **2010**, *45*, 1330−1333.

(11) Suzuki, H.; Izuka, S.; Miyakawa, N.; Kumagai, H. Enzymatic production of theanine, an 'umami' component of tea, from glutamine and ethylamine with bacterial *γ*-glutamyltranspeptidase. *Enzyme Microb. Technol.* **2002**, *31*, 884−889.

(12) Zhang, F.; Zheng, Q. Z.; Jiao, Q. C.; Liu, J. Z.; Zhao, G. H. Enzymatic synthesis of theanine from glutamic acid *γ*-methyl ester and ethylamine by immobilized *Escherichia coli* cells with *γ*-glutamyltranspeptidase activity. *Amino Acids* **2010**, *39*, 1177−1182.

(13) Zhang, F.; Zheng, Q. Z.; Jiao, Q. C.; Liu, J. Z.; Zhao, G. H. Synthesis of theanine from glutamic acid *γ*-methyl ester and ethylamine catalyzed by *Escherichia coli* having *γ*-glutamyltranspeptidase activity. *Biotechnol. Lett.* **2010**, *32*, 1147−1150.

(14) Shuai, Y.; Zhang, T.; Jiang, B.; Mu, W. Development of efficient enzymatic production of theanine by *γ*-glutamyltranspeptidase from a newly isolated strain of *Bacillus subtilis*, SK11.004. *J. Sci. Food Agric.* **2010**, *90*, 2563−2567.

(15) Wang, Q.; Min, C.; Zhu, F.; Xin, Y.; Zhang, S.; Luo, L.; Yin, Z. Production of bioactive *γ*-glutamyl transpeptidase in *Escherichia coli* using SUMO fusion partner and application of the recombinant enzyme to L-theanine synthesis. *Curr. Microbiol.* **2011**, *62*, 1535−1541.

(16) Ikeda, Y.; Taniguchi, N. *γ*-Glutamyl transpeptidase activity assay. *Curr. Protoc. Toxicol.* **2001**, *5*, 6.6.1−6.6.8.

(17) Laemmli, U. K. Cleavage of structural proteins during the assembly of the head of bateriophage T4. *Nature* **1970**, *227*, 680−685.

(18) Rajput, R.; Verma, V. V.; Chaudhary, V.; Gupta, R. A hydrolytic *γ*-glutamyl transpeptidase from thermo-acidophilic archaeon *Picrophilus torridus*: binding pocket mutagenesis and transpeptidation. *Extremophiles* **2013**, *17*, 29−41.

(19) Zhang, Y.; Chen, B.; Huang, Z.; Shi, Z. Preparative isolation and purification of L-theanine by HPLC. *J. Liq. Chromatogr. Relat. Technol.* **2005**, *27*, 875−884.

(20) Lin, L. L.; Chou, P. R.; Hua, Y. W.; Hsu, W. H. Overexpression, one-step purification, and biochemical characterization of a recombinant *γ*-glutamyltranspeptidase from *Bacillus licheniformis*. *Appl. Microbiol. Biotechnol.* **2006**, *73*, 103−112.

(21) Shuai, Y.; Zhang, T.; Mu, W.; Jiang, B. Purification and characterization of *γ*-glutamyltranspeptidase from *Bacillus subtilis* SK11.004. *J. Agric. Food Chem.* **2011**, *59*, 6233−6238.

(22) Inoue, M.; Hiratake, J.; Suzuki, H.; Kumagai, H.; Sakata, K. Identification of catalytic nucleophile of *Escherichia coli* *γ*-glutamyltranspeptidase by *γ*-monofluorophosphono derivative of glutamic acid: N-terminal Thr-391 in small subunit is the nucleophile. *Biochemistry* **2000**, *39*, 7764−7771.

(23) Hwang, S.-Y.; Ryang, J.-H.; Lim, W.-J.; Yoo, I.-D.; Oishi, K. Purification and properties of *γ*-glutamyl transpeptidase from *Bacillus* sp. KUN-17. *J. Microbiol. Biotechnol.* **1996**, *6*, 238−244.

(24) Moallic, C.; Dabonne, S.; Colas, B.; Sine, J. P. Identification and characterization of a *γ*-glutamyl transpeptidase from a thermo-alcalophile strain of *Bacillus pumilus*. *Protein J.* **2006**, *25*, 391−397.

(25) Zhu, X.; Chen, B.; Ma, M.; Luo, X.; Zhang, F.; Yao, S.; Wan, Z.; Yang, D.; Hang, H. Simultaneous analysis of theanine, chlorogenic acid, purine alkaloids and catechins in tea samples with the help of multi-dimension information of on-line high performance liquid chromatography/electrospray-mass spectrometry. *J. Pharm. Biomed. Anal.* **2004**, *34*, 695−704.

(26) Ying, Y.; Ho, J. W.; Chen, Z. Y.; Wang, J. Analysis of theanine in tea leaves by HPLC with fluorescence detection. *J. Liq. Chromatogr. Relat. Technol.* **2005**, *28*, 727−737.

(27) Thippeswamy, R.; Gouda, K. G. M.; Rao, D. H.; Martin, A.; Gowda, L. R. Determination of theanine in commercial tea by liquid chromatography with fluorescence and diode array ultraviolet detection. *J. Agric. Food Chem.* **2006**, *54*, 7014−7019.

(28) Tate, S. S.; Meister, A. *γ*-Glutamyl transpeptidase: catalytic, structural and functional aspects. *Mol. Cell. Biochem.* **1981**, *39*, 357−368.

(29) Zhang, H.; Zhang, W.; Wang, Z.; Zhan, Y.; Xu, L.; Liu, J.; Liu, Q.; Jiao, Q. Enzymatic synthesis of theanine with*Escherichia coli* *γ*-glutamyltranspeptidase from a series of *γ*-glutamyl anilide substrate analogues. *Biotechnol. Bioprocess Eng.* **2013**, *18*, 358−364.

(30) Zhu, S.; Wang, H. X.; Chen, S. W.; Dai, J. Study on adsorption and separation of theanine by ion exchange. *Food Sci.* **2007**, *9*, 148−153.

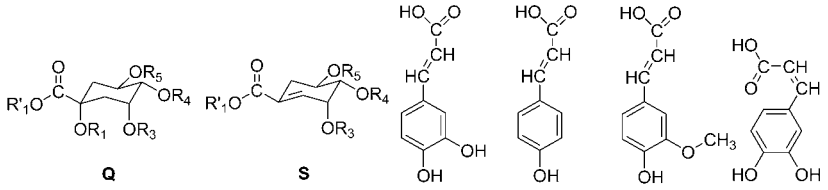


| Number | Name and abbreviation | Q | | | | | S | | |
|---|---|---|---|---|---|---|---|---|---|
| | | $R_1$ | $R_3$ | $R_4$ | $R_5$ | $R'_1$ | $R_3$ | $R_4$ | $R_5$ |
| 1 | 1-*O*-caffeoylquinic acid (1-CQA) | C | H | H | H | - | - | - | - |
| 2 | 3-*O*-caffeoylquinic acid (3-CQA) | H | C | H | H | - | - | - | - |
| 3 | 5-*O*-caffeoylquinic acid (5-CQA) | H | H | H | C | - | - | - | - |
| 4 | 4-*O*-caffeoylquinic acid (4-CQA) | H | H | C | H | - | - | - | - |
| 5 | 1,3-di-*O*-caffeoylqunic acid (1,3-diCQA) | C | C | H | H | - | - | - | - |
| 6 | 1,4-di-*O*-caffeoylqunic acid (1,4-diCQA) | C | H | C | H | - | - | - | - |
| 7 | 1,5-di-*O*-caffeoylqunic acid (1,5-diCQA) | C | H | H | C | - | - | - | - |
| 8 | 3,4-di-*O*-caffeoylqunic acid (3,4-diCQA) | H | C | C | H | - | - | - | - |
| 9 | 3,5-di-*O*-caffeoylqunic acid (3,5-diCQA) | H | C | H | C | - | - | - | - |
| 10 | 4,5-di-*O*-caffeoylqunic acid (4,5-diCQA) | H | H | C | C | - | - | - | - |
| 11 | 1-*O*-*p*-coumaroylqunic acid (1-*p*CoQA) | *p*Co | H | H | H | - | - | - | - |
| 12 | 3-*O*-*p*-coumaroylqunic acid (3-*p*CoQA) | H | *p*Co | H | H | - | - | - | - |
| 13 | 5-*O*-*p*-coumaroylqunic acid (5-*p*CoQA) | H | H | H | *p*Co | - | - | - | - |
| 14 | 4-*O*-*p*-coumaroylqunic acid (4-*p*CoQA) | H | H | *p*Co | H | - | - | - | - |
| 15 | 1,3-di-*O*-*p*-coumaroylqunic acid (1,3-di*p*CoQA) | *p*Co | *p*Co | H | H | - | - | - | - |
| 16 | 1,4-di-*O*-*p*-coumaroylqunic acid (1,4-di*p*CoQA) | *p*Co | H | *p*Co | H | - | - | - | - |
| 17 | 1,5-di-*O*-*p*-coumaroylqunic acid (1,5-di*p*CoQA) | *p*Co | H | H | *p*Co | - | - | - | - |
| 18 | 3,4-di-*O*-*p*-coumaroylqunic acid (3,4-di*p*CoQA) | H | *p*Co | *p*Co | H | - | - | - | - |
| 19 | 3,5-di-*O*-*p*-coumaroylqunic acid (3,5-di*p*CoQA) | H | *p*Co | H | *p*Co | - | - | - | - |
| 20 | 4,5-di-*O*-*p*-coumaroylqunic acid (4,5-di*p*CoQA) | H | H | *p*Co | *p*Co | - | - | - | - |
| 21 | 1-*O*-feruloylquinic acid (1-FQA) | F | H | H | H | - | - | - | - |
| 22 | 3-*O*-feruloylquinic acid (3-FQA) | H | F | H | H | - | - | - | - |
| 23 | 5-*O*-feruloylquinic acid (5-FQA) | H | H | H | F | - | - | - | - |
| 24 | 4-*O*-feruloylquinic acid (4-FQA) | H | H | F | H | - | - | - | - |
| 25 | 1,3-di-*O*-feruloylqunic acid (1,3-diFQA) | F | F | H | H | - | - | - | - |
| 26 | 1,4-di-*O*-feruloylqunic acid (1,4-diFQA) | F | H | F | H | - | - | - | - |
| 27 | 1,5-di-*O*-feruloylqunic acid (1,5-diFQA) | F | H | H | F | - | - | - | - |
| 28 | 3,4-di-*O*-feruloylqunic acid (3,4-diFQA) | H | F | F | H | - | - | - | - |
| 29 | 3,5-di-*O*-feruloylqunic acid (3,5-diFQA) | H | F | H | H | - | - | - | - |
| 30 | 4,5-di-*O*-feruloylqunic acid (4,5-diFQA) | H | H | F | F | - | - | - | - |
| 36 | 1-*O*-caffeoyl-1,5-quinide (1-CQL) | C | H | H | L | - | - | - | - |
| 37 | 3-*O*-caffeoyl-1,5-quinide (3-CQL) | H | C | H | L | - | - | - | - |
| 38 | 4-*O*-caffeoyl-1,5-quinide (4-CQL) | H | H | C | L | - | - | - | - |
| 39 | 5-*O*-*p*-coumaroyl-methylquinate | H | H | H | *p*Co | Me | - | - | - |
| 40 | 5-*O*-caffeoyl-methylquinate | H | H | H | C | Me | - | - | - |
| 41 | 5-*O*-caffeoylshikimic acid (5-CSA) | - | - | - | - | - | H | H | C |
| 42 | *cis*-5-*O*-caffeoylshikimic acid (5-*cis*-CSA) | - | - | - | - | - | H | H | *cis*-C |
| 43 | 4,5-di-*O*-caffeoylshikimic acid (4,5-diCSA) | - | - | - | - | - | H | C | C |
| 44 | 3,5-di-*O*-caffeoylshikimic acid (4,5-diCQA) | - | - | - | - | - | C | H | C |
| 45 | 3,4,5-tri-*O*-caffeoylshikimic acid (3,4,5-triCSA) | - | - | - | - | - | C | C | C |
| 46 | 3,4-di-*O*-caffeoyl-1,5-quinide (3,4-diCQL) | H | C | C | L | - | - | - | - |
| 47 | *cis*-1-*O*-caffeoylquinic acid (1-*cis*-CQA) | *cis*-C | H | H | H | - | - | - | - |
| 48 | *cis*-4-*O*-caffeoylquinic acid (4-*cis*-CQA) | H | H | *cis*-C | H | - | - | - | - |

Q- quinic acid, C- caffeic acid, *p*Co- *p*-coumaric acid, F- ferulic acid, L- lactone, Me- methyl

**Figure 1.** Structures of mono- and dicaffeoylquinic, *p*-coumaroylquinic, and feruloylquinic acids.

reflux in an acid−water solution including two water addition products. This study only incorporated 5-CQA, and the brewing time was not in line with common consumer practice. No comprehensive mechanistic study has been previously reported that investigated the intra- versus intermolecular acyl migration under different conditions incorporating all major commercially available regioisomers of mono- and dicaffeoyl chlorogenic acids. Most importantly, data on acyl migration under roasting conditions are absent from the literature.

The complexity in the data interpretation for the structural analyses of the CGAs present in the roasted coffee melanoidins arises from the regio- and stereoisomeric compounds in the natural sources. For this reason, model roasting experiments on the commercially available mono- and dicaffeoylquinic acids were attempted in the present work to study the trans-


dx.doi.org/10.1021/jf5017384 | J. Agric. Food Chem. 2014, 62, 9160−9170

formations taking place in CGAs during the early roasting stages. Also, isomerization (acyl migration) was induced by both basic hydrolysis and simple hydrolysis (brewing) in these reference standards to observe the isomeric transformations on the basis of relative quantitation. Recently, tandem mass spectrometry has allowed accurate structural assignment and identification of the CGA regioisomers. The advantage of multidimensional specificity of LC-MS$^n$ enabled isomeric resolution and relative quantitation of the early roasting transformations in the CGAs.[13]

## MATERIALS AND METHODS

**Chemicals and Materials.** All of the chemicals (analytical grade) were purchased from Sigma-Aldrich (Bremen, Germany). Commercially available mono- and dicaffeoylquinic acids such as 5-*O*-caffeoylquinic acid (**3**), 3-*O*-caffeoylquinic acid (neo-chlorogenic acid) (**2**), 4-*O*-caffeoylquinic acid (crypto-chlorogenic acid) (**4**), 1,3-di-*O*-caffeoylquinic acid (cynarin) (**5**), 3,4-di-*O*-caffeoylquinic acid (**8**), 3,5-di-*O*-caffeoylquinic acid (**9**), and 4,5-di-*O*-caffeoylquinic acid (**10**) were purchased from PhytoLab GmbH & Co. KG (Vestenbergsgreuth, Germany).

**Hydrolysis by Tetramethylammonium Hydroxide (TMAH).** All seven CGA reference standards were treated with aqueous TMAH (25 g/L). Each sample was diluted by 5 mL of aqueous TMAH and stirred at room temperature. The pH of the mixture was observed to be around 12. One milliliter of solution from each sample was taken out at 2, 5, 10, 30, and 60 min time intervals. Each sample was saturated with brine and extracted twice with ethyl acetate. Combined organic layers were concentrated in vacuo, and each sample was prepared in 1 mL of methanol for analysis by LC-MS*n* for intramolecular acyl migration.

To study the intermolecular acyl migration (crossover experiment), 5-CQA (25 mg, 0.07062 mmol) was added to a round-bottom flask containing ferulic acid (13.7 mg, 0.07062 mmol). Five milliliters of 10 times diluted (25 g/L) TMAH was added to the flask, and the mixture was stirred at room temperature. One milliliter samples were taken from the flask at 2, 5, 10, 15, and 30 min time intervals. Each sample was saturated with brine and extracted twice with ethyl acetate. The combined organic layers were concentrated in vacuo, and each sample was prepared in methanol to be analyzed by LC-MS*n*. The same procedure was repeated with *p*-coumaric acid (11.57 mg, 0.07062 mmol) and 5-CQA (25 mg, 0.07062 mmol).

**Model Roasting.** All seven CGA reference standards were heated at 180 °C for 12 min separately to study the intramolecular acyl migration. Equimolar quantities of 5-CQA with *p*-coumaric acid and 5-CQA with ferulic acid were heated together at 180 °C for 12 min to study the intermolecular acyl migration (crossover experiment). All of the samples were heated in a Buechi Glass Oven B-585 and prepared in 1 mL of methanol for LC-MS*n* analysis.

**Brewing of CGAs (2−5 and 8−10).** Commercially available chlorogenic acid standards (each sample 500 μg) were infused in 3 mL of hot water each and stirred for 5 h under reflux. The pH of each sample was determined to be 5 with a pH meter. The solvent was removed under low pressure, and the samples were dissolved in 1 mL of MeOH and used for LC-MS$^n$.

**LC-MS$^n$.** The 1100 series LC equipment (Agilent, Bremen, Germany) comprised a binary pump, an autosampler with a 100 μL loop, and a DAD detector with a light-pipe flow cell (recording at 254 and 320 nm and scanning from 200 to 600 nm). This was interfaced with an ion-trap mass spectrometer fitted with an HCT Ultra ESI source (Bruker Daltonics, Bremen, Germany) operating in full scan, auto MS$^n$ mode to obtain fragment ion $m/z$. Tandem mass spectra were acquired in auto MS$^n$ mode (smart fragmentation) using a ramping of the collision energy. Maximum fragmentation amplitude was set to 1 V, starting at 30% and ending at 200%. The MS operating conditions (negative mode) had been optimized using 5-caffeoylquinic acid with a capillary temperature of 365 °C, a dry gas flow rate of 10 L/min, and a nebulizer pressure of 10 psi.

**HPLC.** Separation was achieved on a 150 × 3 mm i.d., 5 μm diphenyl column, with a 5 mm × 3 mm i.d. guard column (Varian, Darmstadt, Germany). Alternatively, separation was also achieved on a 250 mm × 3 mm i.d., 5 μm, C18-amide column, with a 5 mm × 3 mm i.d. guard column of the same material (Varian) for the cases of hydrolysis (brewing) of reference standard experiments. Solvent A was water/formic acid (1000:0.05, v/v), and solvent B was methanol. Solvents were delivered at a total flow rate of 500 μL/min. The gradient profile was from 10 to 70% B linearly in 60 min followed by 10 min isocratic and a return to 10% B at 90 and 10 min isocratic to re-equilibrate.

**Preliminary Assessment of Data.** All of the data for the chlorogenic acids use the recommended IUPAC numbering system;[14] the same numbering system was adopted for chlorogenic acids, their *cis*-isomers, their acyl migration isomers, and water addition products (Figure 1). The relative concentrations of the transformed products are expressed here in terms of the peak areas obtained in their UV chromatograms assuming the relative response factor in UV close to 1, based on identical absorptivity of all mono CGAs.[13,15] In the tables and figures, the peak area values are stated accordingly.

## RESULTS AND DISCUSSION

**Intramolecular Acyl Migration: Hydrolysis by TMAH of 2−5 and 8−10.** The most common CGAs in the green coffee bean, **2**−**5** and **8**−**10**, were selected and subjected to aqueous TMAH, with samples taken at intervals from 2 to 60 min. Samples were directly analyzed by LC-MS with compound identification and assignment achieved through comparison of retention times and fragment spectra.[2,18−23] Relative or absolute quantitation was carried out using HPLC-UV traces monitoring cinnamoyl absorption at 320 nm. The concentration of the samples was chosen to be sufficiently low (1−1.5 mg/mL) to prevent intermolecular acyl migration or transesterification, yet corresponding to typical coffee brew CGA levels (around 200 mg/cup = 1 mg/mL), therefore allowing observation of intramolecular acyl migration exclusively. In the hydrolysis of 3-CQA (**2**), 5-CQA (**3**), and 4-CQA (**4**), all of the other monoacyl derivatives were identified during the hydrolysis except for 1-CQA (**1**). Also, we did not observe the formation of any diacyl derivatives in the hydrolysis of the monoacyl quinic acids. This observation confirms that the acyl migration we observed in this study was in fact an intramolecular process. Figure 2 represents the UV chromatograms of the 5-CQA in basic solution at different time intervals. It should be noted that the UV response in mono- and diacylquinic acids has been used in the past as a reliable relative response factor.[1] Hanson et al.[16] used radiolabeled quinic acid to investigate the acyl migration pathway in cinnamoylqunic acids; in accordance with these findings, we assumed that the mechanism of the acyl migration follows the 1,2-*ortho*-ester intermediate formation. This assumption is also supported by the study of Xie et al.[17] The transformations of 5-CQA (**3**), 4-CQA (**4**), and 3-CQA (**2**) with time are presented in Figure 3. From the results, we can conclude that 5-CQA is much more stable than 4-CQA and 3-CQA, and the order of the stability is **5** > **4** > **3** in terms of the hydrolysis of the caffeoyl ester. This stability was observed to provide resistance to decomposition, thus allowing 5-CQA to form the acyl migrated products over longer hydrolysis durations. On the other hand, with 3-CQA being the least stable of the three monoacylquinic acids, it decomposes to form caffeic acid and quinic acid even before acyl migration takes place.

Considering the mechanism of the acyl migration proceeding through an 1,2-*ortho*-ester intermediate formation as 5-CQA ⇋ 4-CQA ⇋ 3-CQA, the reverse equilibrium, through which the

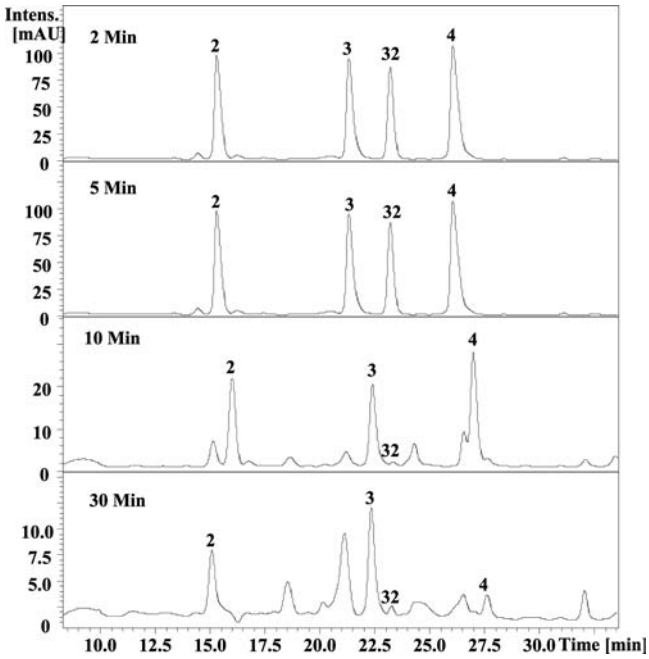


**Figure 2.** UV chromatograms (318−322 nm) at 2, 5, 10, and 30 min of basic hydrolysis of 5-CQA.

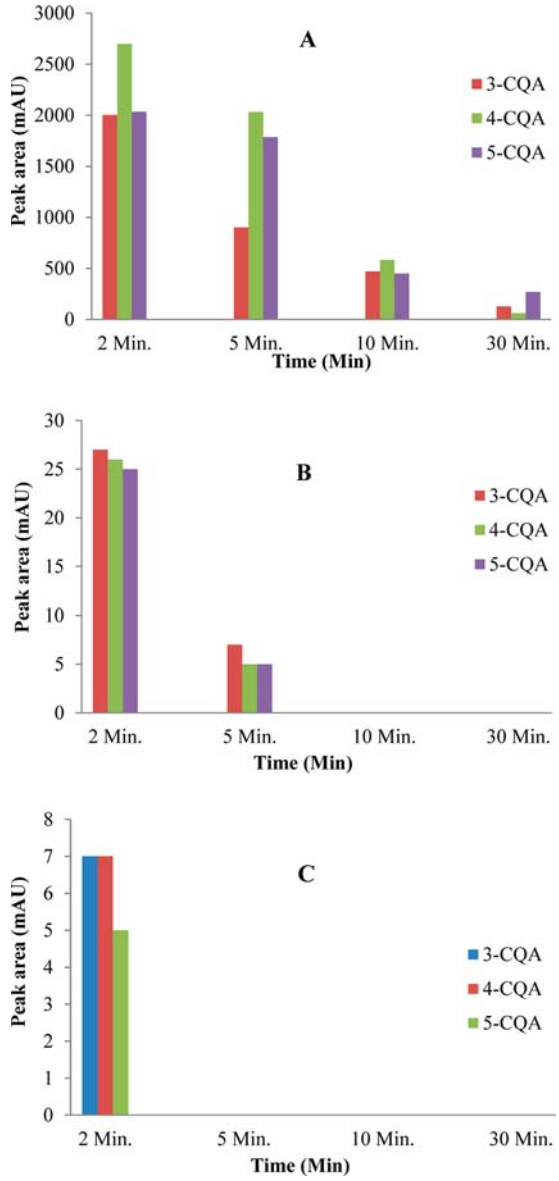


**Figure 3.** Amount of transformation products after basic hydrolysis for different time intervals of (A) 5-CQA, (B) 4-CQA, and (C) 3-CQA.

migrated acyl group reverts to its original position, appears to be slower. It is difficult to comment on the thermodynamic equilibrium of the acyl migration because of the ongoing simultaneous ester hydrolysis competing with the acyl migration process.

The equilibrium between 3-CQA (**2**) and 4-CQA (**4**) is readily achieved because the *ortho*-ester intermediate is more stable due to the *cis* geometry (Figure 4). Compound **2** shows a tendency to hydrolyze to generate caffeic acid and quinic acid rather than to undergo acyl migration, presumably due to the 1,3-*syn*-diaxial arrangement between the $C_1$ hydroxyl group and the $C_3$ ester. The hydrogen bonding between $C_1$−OH and the carbonyl oxygen on the ester on $C_3$ results in steric hindrance, preventing nucleophilic attack on the carbonyl carbon by the $C_4$ hydroxyl group, and facilitates the hydrolysis of the ester bond, thus dissociating the caffeoyl moiety in basic conditions. At the same time this hydrogen bonding presumably activates the ester at $C_3$ for hydrolytic cleavage.

Similar to monocaffeoyl derivatives, dicaffeoylquinic acids were subjected to aqueous TMAH treatment and analyzed in the same manner. Previous studies have shown that 1,5-diCQA (**7**) was converted into 1,3-diCQA (**5**) and 5-CQA (**3**) rapidly and extensively by TMAH treatment within 1 min of hydrolysis.[18,19] In the present study, however, basic hydrolysis of 1,3-diCQA (**5**) did not show any presence of 1,5-diCQA (**7**) or 1,4-diCQA (**6**). 1,3-DiCQA (**5**) decomposed largely into 1-CQA (**1**) rather than 3-CQA (**2**) in the ratio 2.2:1 after 2 min of base treatment. 1,3-DiCQA (**5**) did not transform preferably into 3,5-diCQA (**9**), whereas 3,4-diCQA (**8**) and 4,5-diCQA (**10**) were formed in very small quantities from (**5**) (Figure 5). 1-CQA (**1**) was found to be present entirely as a decomposition product of 1,5-diCQA (**7**) or 1,4-diCQA (**6**) or 1,3-diCQA (**5**) rather than a product of acyl migration as it was not observed as an acyl migration product of any other mono- or diacylated substrates; this fact also supports the *ortho*-ester propagation of acyl migration process. Moreover, this observation confirms the hydrolytic lability of the esters in the 3-acylated position.

In the case of hydrolysis of 4,5-diCQA (**10**), we observed that 4,5-diCQA transformed mainly into 3,4-diCQA (**8**) after 2 min of base treatment. Additionally, CQAs, in particular 5-CQA (**3**), 4-CQA (**4**), and 3-CQA (**2**), were observed after 2 min of reaction time. This trend continued for 5 min during the base treatment, after which all of the CGA derivatives were completely decomposed. 3,4-DiCQA (**8**) was observed to be the least stable isomer during the base treatment study. At 2 min, **8** was found to be in equilibrium with 3,5-diCQA (**9**); however, after 5 min of treatment, 3,5-diCQA (**9**) was observed to display a slightly larger peak area than 3,4-diCQA (**8**). 3-CQA (**2**) was not observed in any sample throughout the duration of the base treatment of 3,4-diCQA due to its tendency to decompose rapidly by hydrolysis.

Observations based on the results from the base treatment on 3,5-diCQA (**9**) were quite distinctive. After 5 min, 3,5-diCQA (**9**) was observed to possess surprising stability to the


dx.doi.org/10.1021/jf5017384 | J. Agric. Food Chem. 2014, 62, 9160−9170

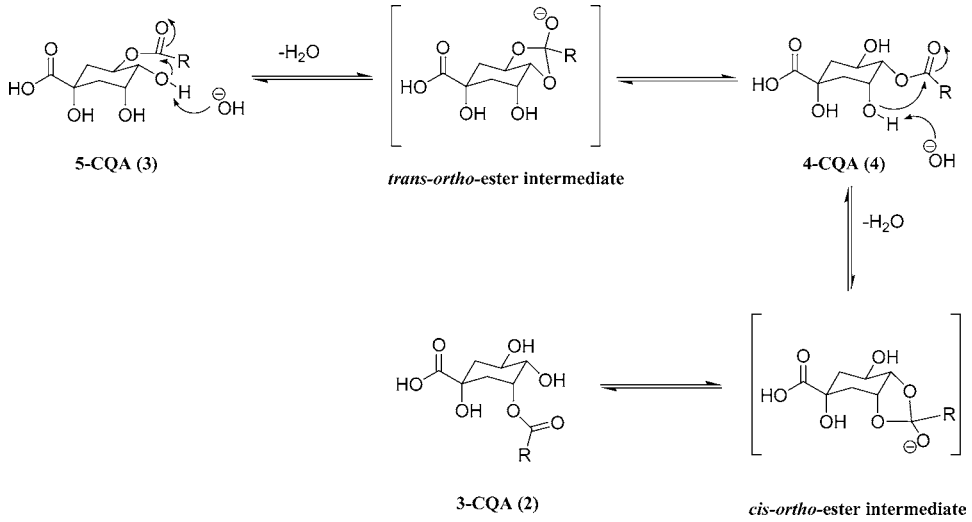


**Figure 4.** Mechanism of the acyl migration through an *ortho*-ester intermediate formation.

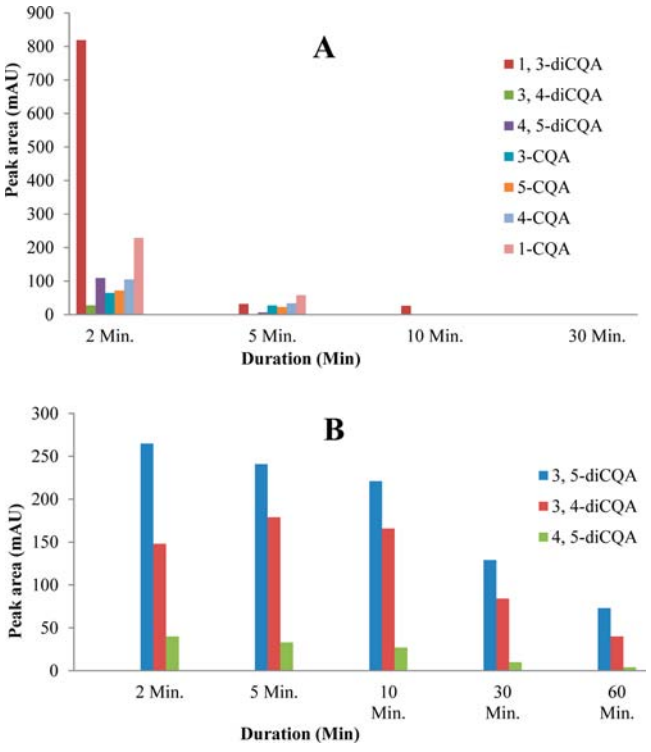


**Figure 5.** Amount of the transformation products after basic hydrolysis for different time intervals of (A) 1,3-diCQA and (B) 3,5-diCQA.

hydrolysis of the ester as we did not detect any of the mono-CQA derivatives even after 60 min of base treatment (Figure 5). 3,5-DiCQA (**9**) transformed mainly into 3,4-diCQA (**8**) followed by 4,5-diCQA (**10**). The ratio of **9**:**8**:**10** remained approximately constant throughout the 60 min of base treatment.

**Intermolecular Acyl Migration (Transesterification): Hydrolysis by TMAH (Crossover Experiment).** In these experiments, we investigated intermolecular acyl migration by carrying out crossover experiments, in which 5-CQA was reacted with the free acids such as ferulic and *p*-coumaric acids at 1:1 stoichiometry in the presence of a base. The change of substituents hereby allows easy identification of products by LC-MS based on the *m*/*z* value of the pseudomolecular ions of the products. The intermolecular acyl migration was found to be simultaneously competing with intramolecular acyl migration as well as hydrolysis of the CQA. The products identified in the reaction of 5-CQA with ferulic acid and *p*-coumaric acid at 2, 5, 10, 15, and 30 min of crossover experiment are summarized in Table 1. Along with the transesterification products of 5-CQA and respective free acid, formation of the *cis*-cinnamoyl isomers was also observed in ferulic, caffeic, and *p*-coumaric acids. All products were identified according to the fragmentation schemes reported previously.[18−21]

In the case of the base treatment of an equimolar mixture of *p*-coumaric acid and 5-CQA (**3**), the intramolecular acyl migration within 5-CQA seemed to be dominating the hydrolysis and the intermolecular acyl migration. According to the peak areas observed, the formation of the intermolecular acyl migrated species (transesters) was found to be least favored (Figure 6). For example, 3-CQA (**2**), 5-CQA (**3**), and 4-CQA (**4**) formed predominantly over caffeic acid (**32**) during 2 min of TMAH treatment of 5-CQA. *p*-Coumaric acid (**33**) did not esterify with the quinic acid generated from the hydrolysis of the 5-CQA (**3**) after 2 min; hence, no *p*-coumaroylquinic acids were observed. However, after 5 min of base treatment, the first transesterification product appeared in the form of 4-*p*CoQA (**14**), and after 10 min, both 5-*p*CoQA (**13**) and 4-*p*CoQA (**14**) were observed. Unfortunately, due to very low concentration, we could not compare the peak areas of compounds **13** and **14** in the UV chromatogram and hence cannot comment on the kinetics of the acyl migration. Although it was clear that 4-*p*CoQA (**14**) was formed earlier than 5-*p*CoQA (**13**), it was not obvious whether **13** was an acyl migration product of **14**. Formation of intramolecular acyl migration products takes place according to the conclusions established earlier in this study. After 2 min, the rate of hydrolysis of 5-CQA was very low and the amounts of 3-CQA (**2**), 5-CQA (**3**), and 4-CQA (**4**) were the highest. Between 5 and 10 min of basic hydrolysis, equilibrium was reached where 5-CQA was found to be the predominant isomer. Formation of the *cis*-cinnamoyl derivatives supposedly follows a water addition−elimination pathway to the double bond in the cinnamoyl moiety during the basic hydrolysis as described earlier.[25]

When an equimolar mixture of ferulic acid (**31**) and 5-CQA (**3**) was treated with base, we observed three regioisomers of


dx.doi.org/10.1021/jf5017384 | J. Agric. Food Chem. 2014, 62, 9160−9170

**Table 1. Compounds Identified after Base Treatment of CGA with *p*-Coumaric Acid and CGA with Ferulic Acid for Various Time Intervals**

| 5-CQA + *p*-coumaric acid | | | | 5-CQA + ferulic acid | | | |
|---|---|---|---|---|---|---|---|
| reaction time (min) | product no. | RT (min) | *m/z* (M − H) | reaction time (min) | product no. | RT (min) | *m/z* (M − H) |
| 2 | **33** | 26.70 | 162.6 | 2 | **31** | 27.3 | 192.6 |
| | **32** | 19.30 | 178.6 | | **34** | 29.6 | 192.6 |
| | **37** | 25.70 | 334.8 | | **22** | 19.2 | 366.7 |
| | **38** | 29.40 | 334.9 | | **23** | 24.1 | 366.9 |
| | **2** | 11.50 | 352.8 | | **24** | 26.4 | 366.9 |
| | **3** | 17.10 | 352.8 | | **47** | 3.0 | 352.8 |
| | **4** | 20.80 | 352.8 | | **2** | 11.2 | 352.9 |
| | | | | | **48** | 13.1 | 352.8 |
| 5 | **37** | 25.80 | 335.0 | | **3** | 16.9 | 352.8 |
| | **38** | 29.80 | 335.1 | | **4** | 20.5 | 352.8 |
| | **14** | 27.60 | 337.0 | | **37** | 23.6 | 334.9 |
| | **1** | 10.70 | 353.1 | | **38** | 25.7 | 334.9 |
| | **2** | 12.10 | 353.0 | | **32** | 7.4 | 178.6 |
| | **3** | 17.30 | 353.1 | | **35** | 19.2 | 178.6 |
| | **4** | 21.70 | 353.1 | | | | |
| | **40** | 30.60 | 367.1 | 5 | **23** | 26.9 | 367.1 |
| | **32** | 19.50 | 178.6 | | **40** | 28.7 | 367.1 |
| | **33** | 26.60 | 162.6 | | **1** | 11.10 | 353.1 |
| | | | | | **37** | 25.9 | 335.1 |
| 10 | **2** | 12.20 | 353.1 | | **38** | 29.6 | 335.1 |
| | **37** | 25.90 | 335.1 | | **2** | 12.5 | 353.1 |
| | **38** | 29.80 | 335.0 | | **3** | 17.7 | 353.0 |
| | **1** | 10.80 | 353.1 | | **4** | 22.2 | 353.0 |
| | **3** | 17.50 | 353.0 | | **49** | 30.8 | 529.0 |
| | **4** | 21.90 | 353.1 | | | | |
| | **33** | 26.40 | 162.9 | 10 | **37** | 25.9 | 335.1 |
| | **40** | 30.60 | 367.1 | | **1** | 10.9 | 353.0 |
| | **13** | 24.30 | 336.8 | | **2** | 12.2 | 353.0 |
| | **14** | 28.40 | 337.0 | | **3** | 17.6 | 353.0 |
| | **32** | 19.70 | 178.6 | | **4** | 22.1 | 353.1 |
| | | | | | **23** | 26.8 | 367.1 |
| 15 | **38** | 29.80 | 335.1 | | **40** | 28.9 | 367.1 |
| | **2** | 12.40 | 353.1 | | **49** | 31.0 | 529.0 |
| | **3** | 17.70 | 353.0 | | | | |
| | **32** | 19.60 | 178.9 | 15 | **37** | 26.2 | 335.1 |
| | **4** | 22.00 | 352.8 | | **2** | 12.4 | 353.0 |
| | | | | | **3** | 17.7 | 353.0 |
| 30 | **3** | 18.00 | 353.1 | | **4** | 22.3 | 353.1 |
| | **4** | 22.60 | 352.8 | | **23** | 27.2 | 367.1 |
| | **33** | 26.60 | 162.9 | | **40** | 28.9 | 367.1 |
| | | | | | **49** | 31.2 | 529.0 |
| | | | | | | | |
| | | | | 30 | **40** | 28.9 | 367.1 |
| | | | | | **3** | 18.0 | 353.0 |

feruloylquinic acid resulting from intermolecular transesterification: 3-FQA (**22**), 5-FQA (**23**), and 4-FQA (**24**).[22] The peak area of compounds **22**−**24** is very low compared to the intramolecular acyl migration products formed in this experiment; hence, they do not appear in the plot shown in Figure 6. The same was not observed in the case of the *p*-coumaric acid experiment. After 2 min, 3-FQA (peak area = 3215) was formed predominantly over 5-FQA and 4-FQA. 5-FQA (**23**) and 4-FQA (**24**) showed negligible peak areas. Only 5-FQA remained stable enough to be detected after 10 and 15 min of basic hydrolysis. After 30 min, all of the transesters and the substrate 5-CQA were found to be decomposed completely as we could identify caffeic acid only. Formation of 3-FQA was found to be kinetically favored. This was found to be consistent with the fact that during the first few minutes of the base treatment of 5-CQA to study intramolecular acyl migration, 3-CQA dominates the acyl migration product spectrum. We also identified *cis*-1-*O*-caffeoylquinic acid (**47**) in the extracted ion chromatogram (EIC) of *m/z* 353 and the UV chromatogram on the basis of its early elution and fragmentation (Figure 7).[23] Similar to 1- *cis*-CQA (**47**), 4-*cis*-CQA (**48**) was also identified as another isomerized caffeoylquinic acid derivative, both of which are assumed to be formed by an addition elimination of the water molecule across the double bond in caffeic acid. 4-*cis*-CQA (**48**) was observed to be in equilibrium with 4-*trans*-CQA (**4**) after 2 min, but with an increase in the reaction time only


dx.doi.org/10.1021/jf5017384 | J. Agric. Food Chem. 2014, 62, 9160−9170

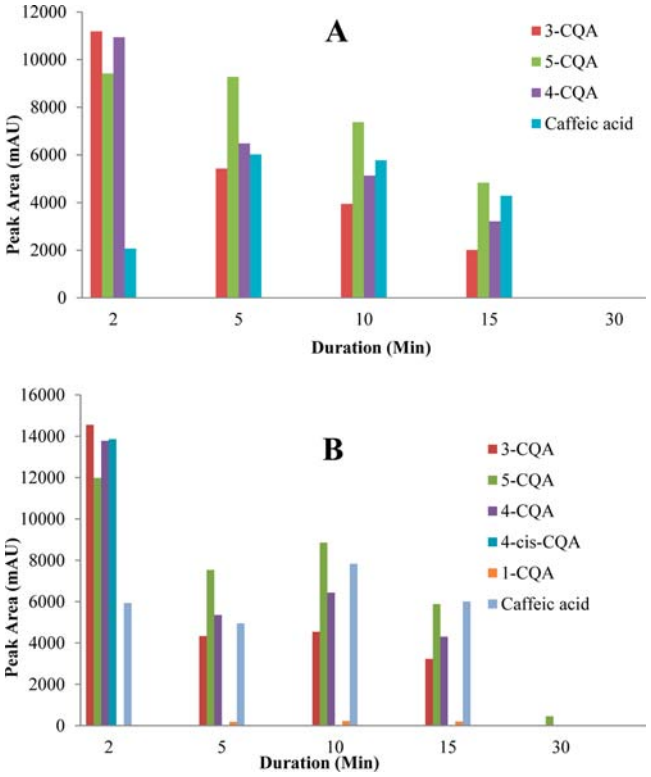


**Figure 6.** Comparison between the peak areas of compounds formed during TMAH treatment of (A) 5-CQA (**3**) with *p*-coumaric acid (*p*CoA) and (B) 5-CQA with ferulic acid (FA).

4-CQA was observed to survive the base treatment. Unexpectedly, we identified two chlorogenic acid lactones as minor by products, namely, 3-CQL (**37**) and 4-CQL (**38**) in this sample. Under basic conditions the dehydrated product of caffeoylquinic acid must be in continuous equilibrium with caffeoylquinic acid. A single heterodiacyl chlorogenic acid was observed in the chromatogram in the form of caffeoyl-feruloylquinic acid (**49**) after 5−15 min of basic hydrolysis (Figure 6). Figure 7 shows the fragmentation pathway for compound (**49**), in which it loses the ferulic acid moiety and undergoes simultaneous dehydration to give *m*/*z* 335 as a base peak in $MS^2$. Furthermore, in $MS^3$ the dehydrated caffeoylquinic acid entity undergoes decarboxylation to give a base peak at *m*/*z* 291 and also shows the presence of ferulic acid as a secondary peak at *m*/*z* 193. This fragmentation pathway for a caffeoyl-feruloylquinic acid was found to be inconsistent with the fragmentation pathways of 1-caffeoyl-3-feruloylquinic acid, 3-feruloyl-5-caffeoylquinic acid, *cis*-4-feruloyl-5-caffeoylquinic acid, 4-feruloyl-5-caffeoylquinic acid, 4-caffeoyl-5-feruloylquinic acid, and *cis*-3-feruloyl-5-caffeoyl-quinic acid previously reported by Jaiswal et al.[21] Hence, the regiochemistry of the acyl groups in caffeoyl-feruloylquinic acid (**49**) remains unknown.

**Intramolecular Acyl Migration: Model Roasting of 2−5 and 8−10.** Compounds 3-CQA (**2**), 5-CQA (**3**), 4-CQA (**4**), 1,3-diCQA (**5**), 3,4-diCQA (**8**), 3,5-diCQA (**9**), and 4,5-diCQA (**10**) were heated at 180 °C for 12 min separately to study the intramolecular acyl migration in the absence of solvents in conditions closely mimicking coffee roasting. From the data summarized in Table 2, we clearly see that only 4-CQA (**4**), 3,4-diCQA (**8**), and 3,5-diCQA (**9**) undergo transformations to generate various dehydrated products mainly in

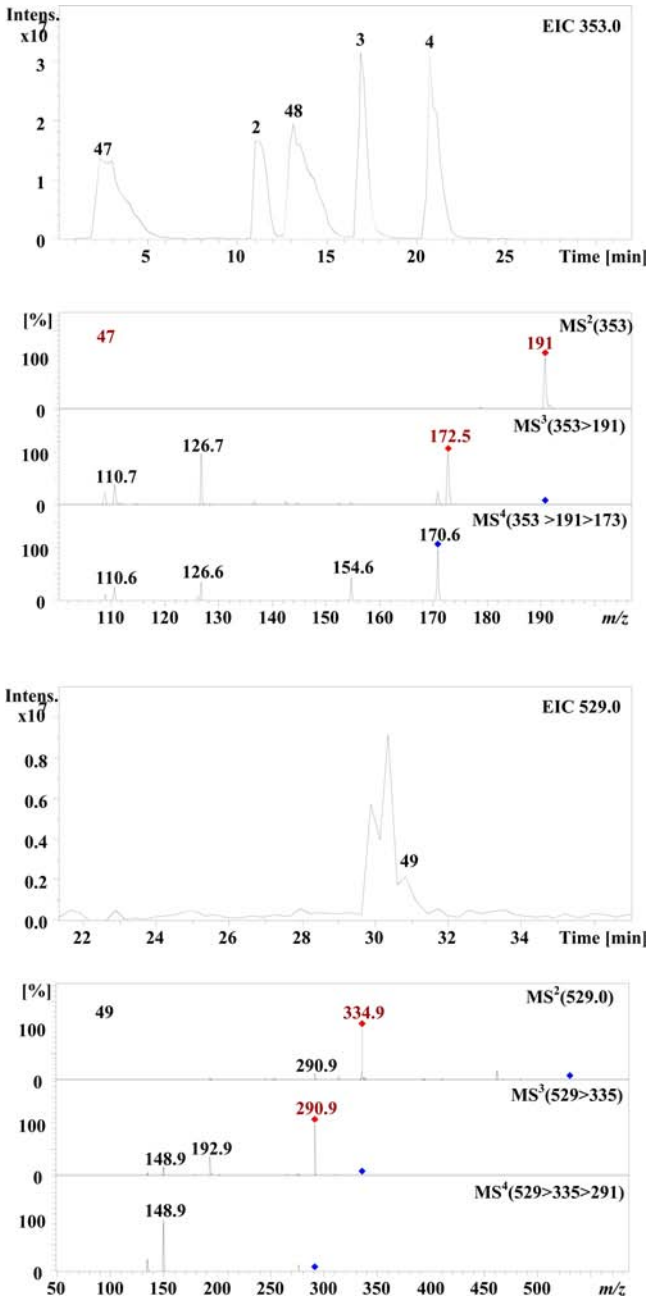


**Figure 7.** EIC and fragmentation patterns for 1-*cis*-caffeoylquinic acid (**47**) at *m*/*z* 353 and caffeoyl-feruloylquinic acid (**49**) at *m*/*z* 529 in transesterification induced by TMAH.

the form of caffeoylquinic acid lactones. In the case of monoacylated chlorogenic acid reference standards, only 4-CQA undergoes acyl migration with simultaneous dehydration. 3-CQL (**37**) was found to be the predominant transformation product in the heat treatment of 4-CQA. 5-Caffeoyshikimic acid was also identified but was found to be the least favored dehydration product after 4-CQL. In this experiment, we observed that 3-CQL (**37**) was forming predominantly over 4-CQL (**38**) irrespective of the substrate, possibly because of the additional stability gained by the equatorial position that 3-CQL assumes in the inverted chair conformation required for stereoelectronic reasons for lactonization. Therefore, we suggest that the dehydration processes such as lactone and shikimic acid formation at the quinic acid moiety follow acyl


dx.doi.org/10.1021/jf5017384 | J. Agric. Food Chem. 2014, 62, 9160−9170

**Table 2. Compounds Identified after Heating (Model Roasting) Reference Standards**

| starting material | compound | product | RT (min) | peak area (UV) |
|---|---|---|---|---|
| **3** | 5-CQA | **3** | 23.7 | 11035 |
| **2** | 3-CQA | **2** | 18.9 | 6034 |
| **4** | 4-CQA | **37** | 31.8 | 2418 |
| | | **38** | 35.1 | 1543 |
| | | **41** | 32.9 | 396 |
| | | **47** | 44.9 | 210 |
| | | **48** | 52.3 | 197 |
| | | **52** | 46.3 | 80 |
| | | **48** | 49.5 | 521 |
| **5** | 1,3-diCQA | **5** | 30.2 | 16245 |
| **8** | 3,4-diCQA | **37** | 31.7 | 98 |
| | | **38** | 35.2 | 74 |
| | | **46** | 51.2 | 7099 |
| | | **46**-*cis* | 52.4 | 896 |
| **9** | 3,5-diCQA | **46** | 56.2 | 3034 |
| | | **46**-*cis* | 56.9 | 119 |
| **10** | 4,5-diCQA | **10** | 46.3 | 26560 |

migration; that is, in the simulated roasting environment, acyl migration takes place before dehydration at the quinic acid moiety. Additionally, lactonization dominates over the alternative shikimate formation in the model roasting of all substrates (Table 2). 1,3-DiCQA (**5**) did not undergo noticeable transformation by the heat treatment, whereas 3,4-diCQA (**8**) generated most of the transformation products among all four di-CQAs. It is likely that the observed products 3-CQL (**37**) and 4-CQL (**38**) resulting from 3,4-diCQA (**8**) were formed by lactonization and loss of one of the two acyl moieties following the order of the processes as dissociation first and dehydration at the quinic acid moiety later, attributed to the fact that both of the caffeoyl lactones possess similar peak areas. 3,4-Di-*O*-caffeoyl-1,5-quinide (**46**) was preferably formed in the heat treatment of 3,4-diCQA. The presence of the two different peaks eluting at 51.2 and 52.4 min having the same fragmentation pattern as 3,4-diCQL (**46**) suggested the presence of a *cis* isomer of compound **46** (Figure 8). Both isomers of 3,4-diCQL (**46**) generate a base peak at $m/z$ 335 with virtually nonexistent secondary peaks confirming the regiochemistry of 3,4-diCQL.

Among the unchanged substrates throughout the heat treatment at 180 °C for 12 min, such as 5-CQA, 3-CQA, 1,3-diCQA, and 4,5-diCQA, the stability of 5-CQA (**3**) and 1,3-diCQA (**5**) to high temperatures was confirmed by heating them at 200 °C for 10 min.

**Transesterification (Intermolecular Acyl Migration): Model Roasting (Crossover Experiment).** In these sets of experiments, we explored the possibilities of transesterification or intermolecular acyl migration by carrying out crossover experiments in which 5-CQA was subjected to heat treatment in the presence of free acids such as ferulic acid and *p*-coumaric acid at 1:1 stoichiometry. In the first case an equimolar mixture of *p*CoA and 5-CQA (**3**) was heated. It was observed that 5-CQA (**3**) mostly remained unchanged by the heat treatment

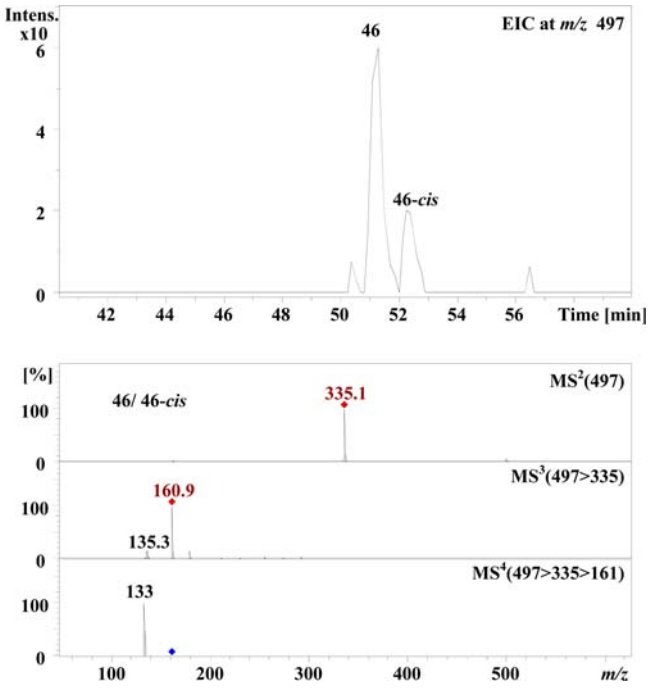


**Figure 8.** EIC and fragmentation patterns for the ion at $m/z$ 497 observed during model roasting.

with the peak area corresponding to 5-CQA accounting for 5 times the peak area of all the transformation products combined (Table 3). Again, caffeoylquinic acid lactones

**Table 3. Compounds Identified after Heating (Model Roasting) of 5-CQA (3) with *p*-Coumaric Acid and 5-CQA (3) with Ferulic Acid**

| 5-CQA (3) and *p*-coumaric acid | | | 5-CQA (3) and ferulic acid | | |
|---|---|---|---|---|---|
| product no. | RT (min) | peak area | product no. | RT (min) | peak area |
| **37** | 25.9 | 1093 | **37** | 26.0 | 484 |
| **38** | 29.6 | 1538 | **38** | 29.4 | 535 |
| **14** | 28.0 | 330 | **3** | 16.8 | 44224 |
| **47** | 36.9 | 145 | **2** | 12.2 | 45 |
| **52** | 39.8 | 642 | **4** | 21.9 | 421 |
| **52** | 41.6 | 2137 | **23** | 26.8 | 484 |
| **3** | 17.5 | 30503 | **47** | 36.8 | 176 |
| | | | **52** | 39.9 | 138 |
| | | | **52** | 41.9 | 500 |

dominated as the main transformation products. Because it was established earlier by Clifford et al.[3] that acyl migration takes place before dehydration in chlorogenic acid when there is still some water present in the sample, it can be assumed that the 5-acyl group migrates to positions $C_3$ and $C_4$ first and then both products undergo dehydration to yield the corresponding lactones in the form of 3-CQL and 4-CQL. 4-CQL (**38**) was formed in larger quantities if compared to 3-CQL (**37**). Only a single transesterification product was identified in the form of 4-*p*CoQA (**14**), which formed during model roasting (Table 3 and Figure 8). It is speculated that the formation of the 1,5-quinide takes place earlier, making $C_5$ on quinic acid unavailable for the possible condensation with *p*-coumaric acid; hence, we do not observe 5-*p*CoQA (**13**) but 4-*p*CoQA (**14**).


dx.doi.org/10.1021/jf5017384 | J. Agric. Food Chem. 2014, 62, 9160−9170

Model roasting experiment between 5-CQA (**3**) and ferulic acid (**31**) generated a larger number of transformation products compared to the number of transformation products detected from the same experiment with *p*CoA (**33**) and 5-CQA (**3**). A similar trend in terms of the number of transformed products was observed in the crossover experiment by TMAH treatment. The list of the transformation products in this experiment looks very similar to the list in Table 3. An additional two products are found to be the acyl migration products of 5-CQA. The acyl group in 5-CQA (**3**) was found to presumably migrate intramolecularly to produce 3-CQA (**2**) and 4-CQA (**4**), but the corresponding caffeoyllactones 3-CQL (**37**) and 4-CQL (**38**) were formed in greater quantity. The ratio of 3-CQL (**37**) to 3-CQA (**2**) was 11:1, whereas the ratio of 4-CQL (**38**) to 4-CQA (**4**) was found to be 1:1.3 because 4-CQL formed in higher quantity if compared to 3-CQL judged by comparison of the corresponding peak areas (Table 3). In this experiment it was observed that 5-CQA (**3**) remained unchanged by the heat treatment to an even greater extent than in previous experiments because the peak area under 5-CQA alone is >16 times the sum of peak areas of all the transformation products combined (Table 3). 5-FQA (**23**) was formed in considerable quantity, confirming intermolecular acyl migration between ferulic acid and 5-CQA (**3**) (Figure 9).

**Intramolecular Acyl Migration: Brewing of CGAs.** In these experiments we investigated acyl migration products of mono- and diacyl CGAs (**2**−**5** and **8**−**10**) formed during the brewing process (Table 4). Typically, the pH of a coffee brew is between 4.7 and 5.1. In our case the pH of the model brew was measured at 5.0. We observed that hot water also serves as a reactive reagent rather than just as a simple solvent in coffee brewing, similar to previous work on tea fermentation, where water was shown to be the key reagent in thearubigin formation.[24] Apart from the acyl migration products and *trans*−*cis* isomerization (*cis*-caffeoylquinic acids) products, the resulting chromatograms showed transformation products referred to here as hydroxy-dihydrocaffeoylquinic acids arising

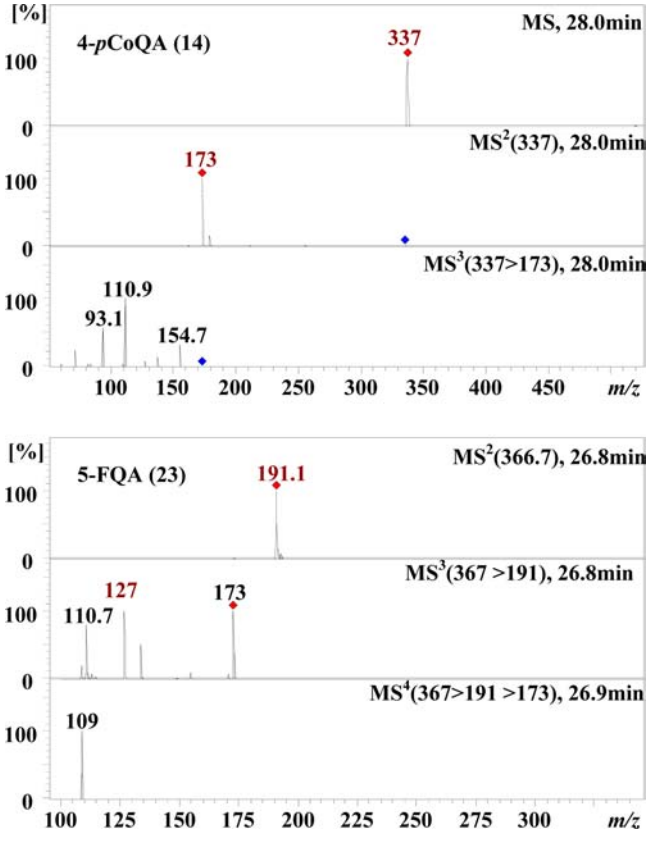


**Figure 9.** $MS^3$ and $MS^4$ of 4-*p*CoQA (**14**) and 5-FQA (**23**), respectively, observed during crossover experiment by model roasting.

**Table 4. Compounds Identified after Hydrolysis of Reference Standards (Brewing of CGAs)**

| starting material | product name | RT (min) | peak area (UV) |
|---|---|---|---|
| 5-CQA (**3**) | 5-CQA | 20.1 | 17610 |
| | *cis*-5-CQA | 23.0 | 347 |
| | 5-hCQA I | 7.3 | NA[a] |
| | 5-hCQA II | 7.9 | NA |
| 4-CQA (**4**) | 3-CQA | 13.1 | 17576 |
| | 4-CQA | 20.6 | 6098 |
| | *cis*-3-CQA | 11.9 | 17 |
| | *cis*-4-CQA | 16.5 | 179 |
| | 4-hCQA I | 6.9 | NA |
| | 4-hCQA II | 7.9 | NA |
| 3-CQA (**2**) | 3-CQA | 13.1 | 639 |
| | 4-CQA | 20.6 | 954 |
| | *cis*-3-CQA | 11.9 | 150 |
| | 3-hCQA I + II | 5.6 | 17 |
| 1, 3-diCQA (**5**) | 1, 3-diCQA | 22.9 | 3422 |
| 3, 4-diCQA (**8**) | 3,4-diCQA | 35.2 | 2558 |
| | *cis*-4,5-diCQA I | 38.0 | 99 |
| | 4,5-diCQA | 36.9 | 520 |
| | *cis*-3,4-diCQA I | 34.2 | 393 |
| | *cis*-3,4-diCQA II | 35.9 | 345 |
| | 3-CQA | 12.3 | 20 |
| | 4-CQA | 19.3 | 27 |
| | 5-CQA | 15.6 | 2 |
| | 3-C-4-hCQA | 26.4 | 57 |
| 3, 5-diCQA (**9**) | 3,4-diCQA | 36.5 | 1406 |
| | 3,5-diCQA | 37.3 | 1057 |
| | 4,5-diCQA | 41.4 | 1107 |
| | 3-C-5-hCQAI | 23.8 | 14 |
| | 3-hC-5-CQA I | 27.8 | 22 |
| | 3-hC-*cis*-5-CQA | 28.3 | 4 |
| | 3-hC-5-CQA II | 31.7 | 4 |
| | 3-CQA | 12.9 | 80 |
| | 5-CQA | 20.3 | 126 |
| 4, 5-diCQA (**10**) | 3,4-diCQA | 43.7 | 1825 |
| | 3,5-diCQA | 42.6 | 512 |
| | 4,5-diCQA | 45.7 | 2148 |
| | *cis*-4,5-diCQA I | 47.2 | 36 |
| | *cis*-4,5-diCQA II | 52.0 | 7 |
| | 3-CQA | 16.8 | 19 |
| | 4-CQA | 27.9 | 14 |
| | 5-CQA | 23.1 | 18 |
| | 4-hC-5-CQA | 34.7 | 18 |
| | 3-hC-5-CQA II | 35.5 | 18 |
| | 3-C-5-hCQA II | 63.1 | 23 |

[a]NA, insignificant peak area.


dx.doi.org/10.1021/jf5017384 | J. Agric. Food Chem. 2014, 62, 9160−9170

through conjugate addition of a water molecule to the olefinic cinnamoyl moiety.[25]

Similar to the model roasting experiment, 5-CQA (**3**) did not show any acyl migrated products in hydrolysis (brewing). The acyl moiety in 4-CQA (**4**) and 3-CQA (**2**) did not migrate to $C_5$ of the quinic acid, but acyl moiety interchange between $C_3$ and $C_4$ was observed due to the stability of the *ortho*-ester intermediate arising from the *cis* geometry (Figure 4). Acyl migration to $C_5$ from $C_3$ and $C_4$ was found to be highly pH dependent as we only observed it in the case of basic hydrolysis.

Cynarin (1,3-diCQA) did not show any transformation products under acidic brewing conditions after 5 h of reflux. Among the remaining diacylated reference standards, 3,4-diacylated esters were preferably formed irrespective of the substrate. This observation can possibly be attributed to the fact that the parallel aromatic rings allow for $\pi-\pi$ stacking interactions providing added stability to the 3,4-diCQA in the minimum energy chair conformation of qunic acid moiety. By comparing the peak areas in the UV chromatogram it was observed that the decomposition of the di-CQAs to produce mono-CQAs was taking place in minute quantity as compared to the basic hydrolysis experiment to study intermolecular acyl migration. In the case of monoacylated chlorogenic acids, up to 1.5−2.0% of the chlorogenic acids were transformed into their hydroxylated derivatives and the diacylated chlorogenic acids up to 4−4.5% if the relative peak areas in EIC are considered.[25] However, their peak areas in UV chromatograms were found to be negligible. The structures for the water addition compounds can be found in our previous publication[25] and are not further commented on here.

In this work we investigated acyl migration under three conditions relevant to the processing of coffee, aqueous basic and acidic and dry roasting conditions. Under all three conditions acyl migration was observed, however, dominating only as a pathway under aqueous basic conditions. Under aqueous acidic and dry roasting conditions acyl migration products were in contrast observed as minor products. Acyl migration in aqueous solution is under typical chlorogenic acid concentrations in a coffee brew predominantly a reversible intramolecular process, showing a strong pH dependency. We could furthermore show that the acyl migration phenomena occurs in dry roasting before dehydration takes place in the quinic acid moiety. Acyl migration is facilitated in the presence of the liquid media, as the esters present on the $C_3$ position of the quinic acid are prone to hydrolysis of the ester bond, rather than undergoing acyl migration in any experimental condition. In crossover experiments (TMAH and model roasting), 5-CQA (**3**) ferulic acid compared to *p*-coumaric acid showed increased reactivity generating a large number of transesterification products. A significant proportion of 3-CQA and 4-CQA quantities and their derivatives in a cup of coffee must be assumed to be a result of acyl migration occurring in roasting and brewing processes originating from 5-CQA.

## ■ ASSOCIATED CONTENT

### Supporting Information

Table S1 and Figures S1 and S2. This material is available free of charge via the Internet at http://pubs.acs.org.

## ■ AUTHOR INFORMATION

### Corresponding Author

*(N.K.) Phone: 49 421 200 3120. Fax: 49 421 200 3229. E-mail: n.kuhnert@jacobs-university.de.

### Funding

We gratefully acknowledge financial support from Kraft Food (now Mondelez International) and Jacobs University Bremen gGmbH.

### Notes

The authors declare no competing financial interest.

## ■ ACKNOWLEDGMENTS

We acknowledge support from Dr. Frank Ullrich during the project. Furthermore, we acknowledge excellent technical support by Anja Müller.

## ■ REFERENCES

(1) Clifford, M. N. Chlorogenic acids and other cinnamates − nature, occurrence, dietary burden, absorption and metabolism. *J. Sci. Food Agric.* **2000**, *80*, 1033−1043.

(2) Jaiswal, R.; Matei, M. F.; Golon, A.; Witt, M.; Kuhnert, N. Understanding the fate of chlorogenic acids in coffee roasting using mass spectrometry based targeted and non-targeted analytical strategies. *Food Funct.* **2012**, *3*, 976−984.

(3) Crozier, A.; Jaganath, I. B.; Clifford, M. N. Dietary phenolics: chemistry, bioavailability and effects on health. *Nat. Prod. Rep.* **2009**, *26*, 1001−1043.

(4) Farah, A.; De Paulis, T.; Trugo, L. C.; Martin, P. R. Effect of roasting on the formation of chlorogenic acid lactones in coffee. *J. Agric. Food Chem.* **2005**, *53*, 1505−1513.

(5) Kweon, M. H.; Hwang, H. J.; Sung, H. C. Identification and antioxidant activity of novel chlorogenic acid derivatives from bamboo (*Phyllostachys edulis*). *J. Agric. Food Chem.* **2001**, *49*, 4646−4655.

(6) Wang, G.; Shi, L.; Ren, Y.; Liu, Q.; Liu, H.; Zhang, R.; Li, Z.; Zhu, F.; He, P.; Tang, W.; Tao, P.; Li, C.; Zhao, W.; Zuo, J. Anti-hepatitis B virus activity of chlorogenic acid, quinic acid and caffeic acid in vivo and in vitro. *Antiviral Res.* **2009**, *83*, 186−190.

(7) Hemmerle, H.; Burger, H.; Below, P.; Schubert, G.; Rippel, R.; Schindler, P. W.; Paulus, E.; Herling, A. W. Chlorogenic acid and synthetic chlorogenic acid derivatives: novel inhibitors of hepatic glucose-6-phosphate translocase. *J. Med. Chem.* **1997**, *40*, 137−145.

(8) Robinson, W. E.; Reinecke, M. G.; Abdel-Malek, S.; Jia, Q.; Chow, S. A. Inhibitors of HIV-1 replication that inhibit HPV integrase. *Proc. Natl. Acad. Sci. U.S.A.* **1996**, *93*, 6326−6331.

(9) Kwon, H. C.; Jung, C. M.; Shin, C. G.; Lee, J. K.; Choi, S. U.; Kim, S. Y.; Lee, K. R. A new caffeoyl quinic acid from Aster scaber and its inhibitory activity against human immunodeficiency virus-1 (HIV-1) integrase. *Chem. Pharm. Bull.* **2000**, *48*, 1796−1798.

(10) Clifford, M. N.; Kellard, B.; Birch, G. G. Characterisation of chlorogenic acids by simultaneous isomerisation and transesterification with tetramethylammonium hydroxide. *Food Chem.* **1989**, *33*, 115−123.

(11) Clifford, M. N.; Kellard, B.; Birch, G. G. Characterization of caffeoylferuloylquinic acids by simultaneous isomerization and trans-esterification with tetramethylammonium hydroxide. *Food Chem.* **1989**, *34*, 81−88.

(12) Dawidowicz, A. L.; Typek, R. Thermal stability of 5-*O*-caffeoylquinic acid in aqueous solutions at different heating conditions. *J. Agric. Food Chem.* **2010**, *58*, 12578−12584.

(13) Trugo, L. C.; Macrae, R. A study of the effect of roasting on the chlorogenic acid composition of coffee using HPLC. *Food Chem.* **1984**, *15*, 219−227.

(14) Anonymous IUPAC Commission on the Nomenclature of Organic Chemistry (CNOC) and IUPAC-IUB Commission on Biochemical Nomenclature (CBN).. Nomenclature of cyclitols. Recommendations, 1973. *Biochem. J.* **1976**, *153*, 23−31.

(15) Clifford, M. N.; Williams, T.; Bridson, D. Chlorogenic acids and caffeine as possible taxonomic criteria in *Coffea* and *Psilanthus*. *Phytochemistry* **1989**, *28*, 829−838.

(16) Hanson, K. R. Chlorogenic acid biosynthesis. Chemical synthesis and properties of the mono-*O*-cinnamoylquinic acids. *Biochemistry* **1965**, *4*, 2719−2731.
(17) Xie, C.; Yu, K.; Zhong, D.; Yuan, T.; Ye, F.; Jarrell, J. A.; Millar, A.; Chen, X. Investigation of isomeric transformations of chlorogenic acid in buffers and biological matrixes by ultraperformance liquid chromatography coupled with hybrid quadrupole/ion mobility/orthogonal acceleration time-of-flight mass spectrometry. *J. Agric. Food Chem.* **2011**, *59*, 11078−11087.
(18) Clifford, M. N.; Johnston, K. L.; Knight, S.; Kuhnert, N. Hierarchical scheme for LC-MS$^n$ identification of chlorogenic acids. *J. Agric. Food Chem.* **2003**, *51*, 2900−2911.
(19) Clifford, M. N.; Knight, S.; Kuhnert, N. Discriminating between the six isomers of dicaffeoylquinic acid by LC-MS$^n$. *J. Agric. Food Chem.* **2005**, *53*, 3821−3832.
(20) Jaiswal, R.; Matei, M. F.; Ullrich, F.; Kuhnert, N. How to distinguish between cinnamoylshikimate esters and chlorogenic acid lactones by liquid chromatography-tandem mass spectrometry. *J. Mass Spectrom.* **2011**, *46*, 933−942.
(21) Jaiswal, R.; Sovdat, T.; Vivan, F.; Kuhnert, N. Profiling and characterization by LC-MS$^n$ of the chlorogenic acids and hydroxycinnamoylshikimate esters in Mate (*Ilex paraguariensis*). *J. Agric. Food Chem.* **2010**, *58*, 5471−5484.
(22) Kuhnert, N.; Jaiswal, R.; Matei, M. F.; Sovdat, T.; Deshpande, S. How to distinguish between feruloyl quinic acids and isoferuloyl quinic acids by liquid chromatography/tandem mass spectrometry. *Rapid Commun. Mass Spectrom.* **2010**, *24*, 1575−1582.
(23) Clifford, M. N.; Kirkpatrick, J.; Kuhnert, N.; Roozendaal, H.; Salgado, P. R. LC-MS$^n$ analysis of the *cis* isomers of chlorogenic acids. *Food Chem.* **2008**, *106*, 379−385.
(24) Kuhnert, N.; Drynan, J. W.; Obuchowicz, J.; Clifford, M. N.; Witt, M. Mass spectrometric characterization of black tea thearubigins leading to an oxidative cascade hypothesis for thearubigin formation. *Rapid Commun. Mass Spectrom.* **2010**, *24*, 3387−3404.
(25) Matei, M. F.; Jaiswal, R.; Kuhnert, N. Investigating the chemical changes of chlorogenic acids during coffee brewing: conjugate addition of water to the olefinic moiety of chlorogenic acids and their quinides. *J. Agric. Food Chem.* **2012**, *60*, 12105−12115.

cytokines) in macrophages stimulated with LPS have not yet been investigated. The aim of this study was to determine the effects on these mediators and cytokines and possible regulation mechanisms of 6-DG in LPS-treated macrophages.

## MATERIALS AND METHODS

**Reagents.** LPS (*Escherichia coli* O26:B6), negative control esiRNA (EHURLUC), and STAT1 esiRNA (EMU071921) were all purchased from Sigma Chemical (St. Louis, MO, USA). All other chemical buffers and reagents were purchased at the highest commercial purity and quality possible.

**DG Purification Procedures.** The rhizomes (25.6 kg) of *Z. officinale* were chipped and air-dried and extracted repeatedly with $CHCl_3$ (50 L × 4) at room temperature. The combined $CHCl_3$ extracts (896.5 g) were then evaporated and further separated into 20 fractions by column chromatography on silica gel (3.8 kg, 70−230 mesh) with *n*-hexane/chloroform/methanol. Fraction 8 (81.2 g), eluted with chloroform/methanol (60:1), was next subjected to silica gel CC (chloroform/methanol (100:1)) and yielded 6-DG (163 mg). The other fractions were further processed for other components unrelated to this study. The identity and purity of 6-DG were confirmed by NMR and HPLC.[20,22,23]

**Cytotoxicity.** The cytotoxic properties were evaluated in an Alamar Blue assay. Briefly, 200 μL of 10% Alamar Blue reagent (Serotec, BUF012B) was added into medium, $2 \times 10^4$ cells/200 μL/well, the cells of which were pretreated with indicated concentrations of 6-DG 30 min before stimulation with LPS (100 ng/mL) for 24 h. Cells were incubated with Alamar Blue reagent (37 °C, 5% $CO_2$) for 4 h, and the colorimetric readings were evaluated with the ELISA plate reader at 570 and 600 nm.

**Cell Culture.** RAW 264.7 cells, derived from murine macrophages, were obtained from the Bioresource Collection and Research Center (BCRC 60001). RAW 264.7 cells were cultured in DMEM (with 10% heat-inactivated fetal bovine serum, 100 U/mL penicillin, 100 μg/mL streptomycin, 25 g/mL amphotericin B, and 2 mM L-glutamine, all purchased from Biological Industries (Kibbutz Beit Haemek, Israel)). Various concentrations of 6-DG were dissolved in DMSO.

**Nitrite Quantification.** The nitrite concentration in the supernatant was measured as an indicator of NO production, determined by Griess Reagent System (G2930, Promega Biotech Co., Ltd., Madison, WI, USA) according to the manufacturer protocols. The cells ($4 \times 10^5$ cells/mL) were pretreated with indicated concentrations of 6-DG for 30 min before stimulation with LPS (100 ng/mL) for 24 h.

**Extraction of Cytosol, Nuclear, and Total Proteins of RAW 264.7 Cells.** RAW 264.7 cells were plated at a density of $5 \times 10^6$ cells in each 6 cm dish. Cells were pretreated with 25 μM 6-DG and harvested protein of cytosol and Nuclear at 15, 30, 60, 120 min after stimulation with LPS. Buffer A (10 mM HEPES (pH 7.9), 10 mM KCl, 1.5 mM $MgCl_2$, 10 mM DTT, 4% 25× protease inhibitors (PI), 0.375% NP-40 in $ddH_2O$) and buffer C (20 mM HEPES, 400 mM NaCl, 1 mM EDTA, 1 mM EGTA, 10 mM DTT, 4% 25× PI in $ddH_2O$) were prepared immediately before use. The supernatant was removed and followed by two washings of 1× PBS. Then 300 μL of buffer A was added into each dish and ensuring that buffer A covered cells completely. Ten minutes later, the edges of the dish were knocked to allow cells to shed from the bottom of dish, and then a scraper was used to collect cells. After 10 s of vortex mixing, the cytosol extract was prepared by 1 min centrifugation at 10000*g*. The resulting pellet contained the nuclear extract. The pellet was washed twice with 1× PBS, then 100 μL of buffer C was added into each sample, and the nuclear envelope was broken by using a stir bar for 20 min. Nuclear extracts were prepared by 10 min centrifugation at 10000*g*. All above procedures should be performed on ice. In addition, total proteins were extracted from RAW 264.7 cells with RIPA buffer,[23] and the protein concentration was measured using the bicinchoninic acid assay (BCA) (Thermo Fisher Scientific, Rockford, IL, USA).

**Reverse Transcription (RT) PCR.** Total RNA was isolated from RAW 264.7 cells using an RNAspin Mini RNA isolation kit according to the manufacturer's instructions (GE Healthcare, 25-0500-71). The level of iNOS, COX-2, or GAPDH mRNA expression was assessed by RT-PCR. Briefly, total RNA (2 mg) was reverse-transcribed into cDNA using random primers (Promega, C1181) and oligo-dT (Promega, C1101) DNA amplification in 20 cycles of iNOS, 94 °C for 30 s, 60.5 °C for 40 s, and 72 °C for 30 s, followed by a 2 min extension at 72 °C. The thermal cycle conditions of COX-2 were 20 cycles of amplification (94 °C for 30 s, 52 °C for 40 s, 72 °C for 30 s, and 72 °C for 2 min). DNA amplification of GAPDH thermal cycle condition was 94 °C for 30 s, 56 °C for 40 s, and 72 °C for 30 s, followed by a 2 min extension at 72 °C. The PCR products were separated by electrophoresis on a 1.5% agarose gels and visualized by SYBR Safe DNA Gel Stain (Invitrogen, S33102).

The amplification of GAPDH acted as an internal control for sample loading. PCR was performed using the following primers:

iNOS forward primer, 5′-CCCTTCCGAAGTTTCTGGCAG-CAGC-3′′ reverse primer, 5′-GGCTGTCAGAGAGCCTCGTGG-CTTTGG-3′.

COX-2 forward primer, 5′-CATTGATGGTGGCTGTTTTG-3′; reverse primer, 5′-GTTGCTGGGGGAAGAAATGT-3′.

GAPDH forward primer, 5′-TCCACCACCCTGTTGCTGTA-3′; reverse primer, 5′-ACCACAGTCCATGCCATCAC-3′.

**Western Blotting.** Western blotting was performed as mentioned previously.[23] Briefly, equal amounts of total proteins were resolved by 10% SDS−polyacrylamide gel and transferred onto polyvinylidene difluoride membranes. The membrane was blocked for 30 min at room temperature with blocking buffer (20 mM Tris-HCl, pH 7.4, 125 mM NaCl, 0.2% Tween 20, 2% BSA, and 0.1% sodium azide). Antibodies were all purchased from Cell Signaling Technology, except iNOS (610432, BD PharMingen, San Diego, CA, USA), tubulin (sc-5286, Santa Cruz), GAPDH (MAB374, Millipore), and Lamin B (sc-6216, Santa Cruz). The membrane was then incubated with the primary antibody of COX-2, iNOS p-Erk1/2 (9100), Erk (4695), p-p38 (9215S), p-38 (9212), p-JNK (9250), JNK (9258S), p-c-Jun (9164), c-Fos (2250), p-IκB (9246), p-p65 (3033S), STAT1 (9172), p-STAT1 (9171), STAT3 (4904), p-STAT3 (9134), p-JAK2 (3776), tubulin, GAPDH, or Lamin B overnight. The membrane was incubated with blocking buffer and primary antibody overnight at 4 °C. The membranes were subsequently probed with anti-mouse (sc-2005, Santa Cruz) or anti-rabbit (7074, Cell Signaling) or anti-goat IgG (81-1620, Zymed) antibody conjugated to horseradish peroxidase and visualized using enhanced chemiluminescence (ECL, Amersham). The densities of the bands were quantitated with the GelPro 32 analysis program.

**Transient Cell Transfection and Luciferase Assay.** Transfection of RAW 264.7 cells was performed with TurboFect Transfection Reagent (Thermo Scientific) according to the manufacturer's instructions. Briefly, cells were plated onto 60 mm dish at a density of $2 \times 10^6$ cells/dish for 18−24 h and then transfected with 5 mg of pNF-kB-luc or p-AP-1-luc plasmid, cells were cultured for 24 h and then reseed cell onto 24-well plate at a density of $2 \times 10^5$ cells/plate overnight, then pretreated with 6-DG for 30 min before 100 ng/mL LPS treatment. Cells were harvested after 6 h, and luciferase activity was assessed using the Luciferase reporter assay system (Promega) according to manufacturer's instructions.

**Enzyme-Linked Immunosorbent Assay (ELISA).** RAW 264.7 cells were plated at a density of $4 \times 10^5$ cells per well in 12-well plates. Cells were pretreated with different concentrations of 6-DG, and the supernatants were collected 24 h later after stimulation with LPS. The amounts of various proteins were measured by ELISA kits for IL-10 (eBioscience; 88-104-88), IL-6 (eBioscience; 88-7064-88), IL-6 (eBioscience; 88-7064-88), IL-1β (eBioscience; 88-7013-88), TNF-α (eBioscience; 88-7324-88), and PGE2 (R&D Systems; KGE004), respectively. Each assay was performed in duplicate.

**Electroporation.** Negative control esiRNA and STAT1 esiRNA were transfected into RAW 264.7 cells by using Amaxa Nucleofector (Lonza), following the manufacturer's protocol (Nucleofector solution V, Nucleofector program D-032), respectively, with 1.5 ng of esiRNA/$2 \times 10^6$ cells. Cells were incubated at 37 °C for 24 h. Cells were then

pretreated with 25 $\mu$M 6-DG 30 min before stimulation with 100 ng/mL LPS, and the supernatant was harvested after 24 h.

**Statistical Analysis.** All assays were performed in triplicate, and the mean values were calculated. The data were subjected to analysis of variance (ANOVA), and Student's $t$ tests were used to assess differences between means. Significant differences were concluded at a level of $p < 0.05$.

## RESULTS

**6-DG Has an Unapparent Toxicity and Suppresses iNOS in RAW 264.7 Stimulated with LPS.** To investigate the cell toxicity of 6-DG (Figure 1), four indicated concentrations (5, 10, 25, and 50 $\mu$M) were selected to treat macrophages stimulated with LPS, as shown in Figure 2A. The cell toxicity of 6-DG was determined by Alamar Blue assay and showed there was no significant difference between these four concentrations compared to the vehicle. Results revealed that pretreatment with 25 and 50 $\mu$M 6-DG was more efficient in the attenuation of LPS-induced iNOS protein expression than post-treated 6-DG. However, no suppression effect was found in the group with 6-DG post-treatment after LPS given (Figure 2B,C). 6-DG treatment for 48 h alone has no effect on the cell viability of RAW 264.7 cells at different concentrations, as shown in Figure 2D.

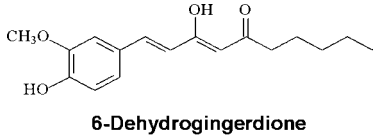


**Figure 1.** Chemical structure of 6-DG.

**6-DG Down-regulates the IKK-NF-$\kappa$B Pathway To Inhibit the Expression of p-p38.** When LPS stimulates macrophages, MAPK pathways are reported to regulate the transcription factor NF-$\kappa$B and AP-1 (c-Jun/c-Fos).[9] Western blotting data demonstrated that pretreatment with 6-DG (25 $\mu$M) down-regulates the phosphorylation of both p38 and I$\kappa$B induced by LPS for 30 min and inhibits the expression of p-p65 induced by LPS for 15 min, but will up-regulate the phosphorylation of JNK induced by LPS for 10 min. There was no effect on p-Erk, p-c-Jun, or c-Fos expression induced by LPS (Figure 3). 6-DG significantly suppressed the NF-$\kappa$B signaling pathway (Figure 3C) but had little effect on the AP-1 signaling pathway (Figure 3D). According to a past study, p38 MAPK regulates the LPS-induced NF-$\kappa$B activation pathway through two different mechanisms that contribute to the phosphorylation of I$\kappa$B-$\alpha$ or p65 NF-$\kappa$B.[24] It may be concluded that 6-DG might down-regulate both I$\kappa$B and p65 phosphorylation by attenuating the phosphorylation of p38 (Figure 3A,B).

**6-DG Inhibits LPS-Induced Nitrite and PGE2 Production via the Suppression of iNOS and COX-2 Expression.** COX-2 and iNOS play the key roles in the production of PGE2 and NO during inflammation, and COX-2 and iNOS inhibitors block their synthesis.[6,13] Our PCR data revealed that

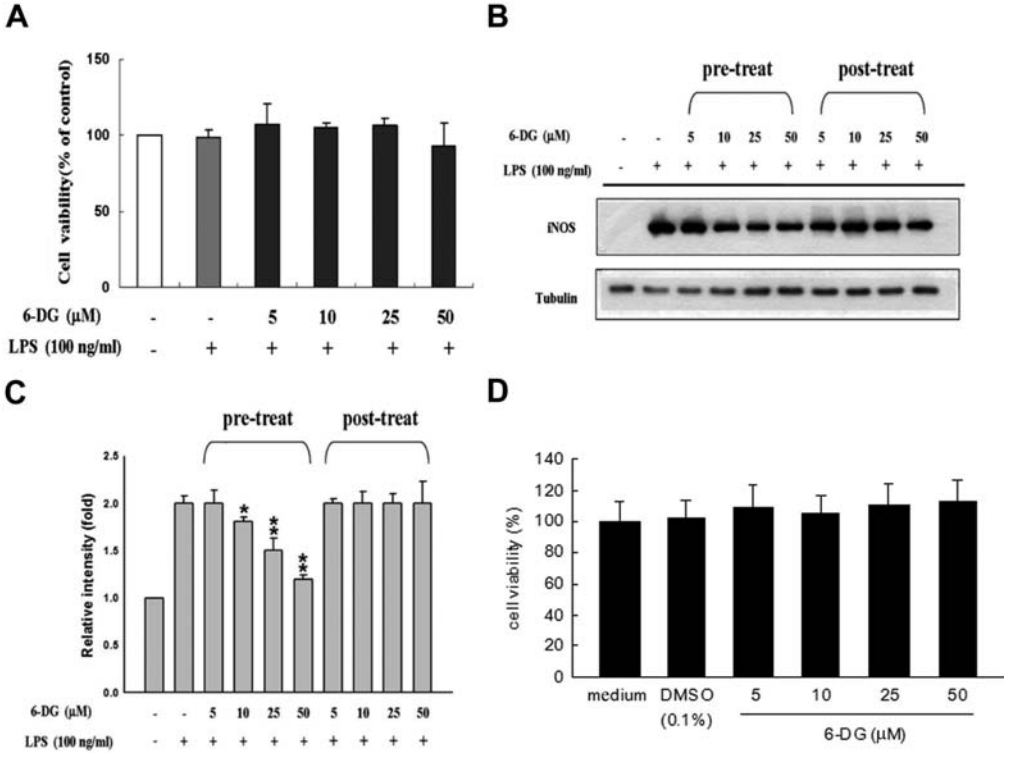


**Figure 2.** Effect of 6-DG treatment in RAW 264.7 stimulated with LPS. (A) Effects of 6-DG in cell viability. Cells were pretreated with 6-DG for 30 min in various concentrations (5, 10, 25, and 50 $\mu$M) before being stimulated with LPS (100 ng/mL) for 24 h and then measured by Alamar Blue assay. Data are expressed as the mean ± SD of three independent experiments. (B) Different treatment conditions: pretreatment where 6-DG was administered 30 min before LPS and post-treatment where 6-DG was administered 30 min after LPS treatment. (C) Corresponding quantification data of iNOS protein levels. (D) 6-DG treatment for 48 h alone to examine the cell viability in RAW 264.7. Results show the mean ± SD of three experiments. (*) $p < 0.05$ and (**) $p < 0.001$ versus LPS treatment, by Student's $t$ test, $n = 3-5$. The relative intensity was normalized to tubulin and relative to the control.


dx.doi.org/10.1021/jf501665v | J. Agric. Food Chem. 2014, 62, 9171−9179

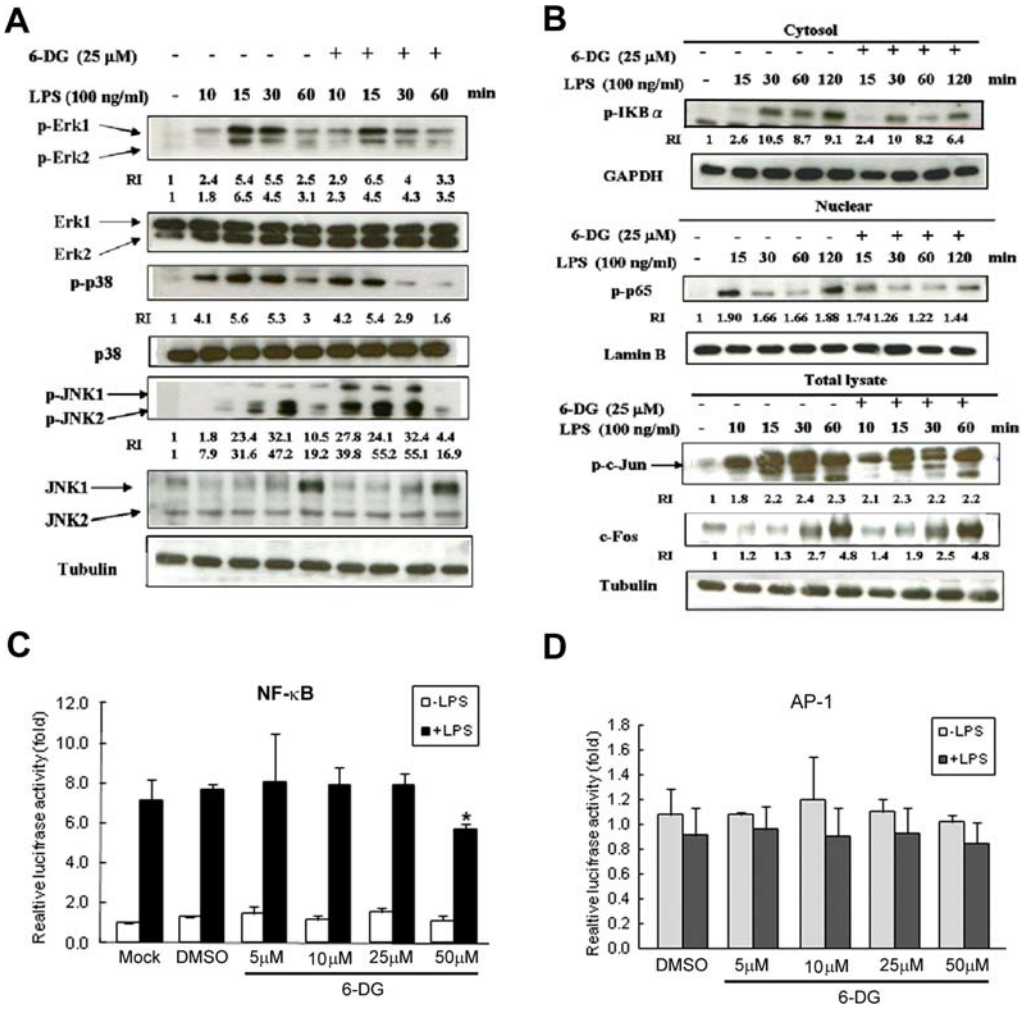


**Figure 3.** Effects of 6-DG on LPS-induced phosphorylation and the MAPK and Ikk-NFκB pathway. (A) Western blot analysis of the phosphorylation of Erk, p38, and JNK expression induced by LPS. Cells were pretreated with 25 μM 6-DG for 30 min, and the total protein was harvested at four different time points (10, 15, 30, and 60 min) after stimulation with LPS (100 ng/mL). (B) Western blot analysis of the phosphorylation of p65 NF-κB, and IκBα induced by LPS. Cells were pretreated with 25 μM 6-DG for 30 min, and cytosol and nuclear extract were harvested at four different time points (15, 30, 60, and 120 min) after stimulation with LPS (100 ng/mL). Expression levels of p-c-Jun and c-Fos were determined by Western blot analysis. Cells were pretreated with 25 μM 6-DG for 30 min, and total protein was harvested at four different time points (10, 15, 30, and 60 min) after stimulation with LPS (100 ng/mL). RAW 264.7 macrophages were transfected with the luciferase reporter pAP-1-luc (C) and pNF-κB-luc (D). Twenty-four hours after transfection, cells were pretreated with 6-DG for 30 min and then exposed to LPS (100 ng/mL) at the indicated concentrations. After 6 h, the luciferase activity was determined. (*) $p < 0.05$ versus LPS treatment group. Bars represent the mean ± SD of three independent experiments. All intensity of results was normalized to internal control and relative to the control. These experiments were repeated three times with similar results.

pretreatment with 5, 10, 25, and 50 μM 6-DG could inhibit the RNA expression of both COX-2 and iNOS induced by LPS (Figure 4A). Western blotting results indicated that pretreatment with 10, 25, and 50 μM 6-DG can inhibit the protein production of both COX-2 and iNOS induced by LPS (Figure 4B). Furthermore, pretreatment with 5, 10, 25, and 50 μM 6-DG significantly down-regulated the production of both NO and PGE2 induced by LPS (Figure 4C,D).

**6-DG Suppresses LPS-Induced TNFα, IL-6, IL-1β, and IL-10 Production.** In patients with sepsis, plasma concentrations of TNF-α, IL-1β, IL-6, and IL-10 were significantly higher in nonsurvivors than in survivors.[3] According to our ELISAs, pretreatment with 25 and 50 μM 6-DG was found to significantly inhibit the production of TNF-α, IL-6, and IL-10 in RAW 264.7 macrophages through LPS simulation (Figure 5A,C,D), and pretreatment with 5, 10, 25, and 50 μM 6-DG could inhibit the secretion of IL-1β induced by LPS (Figure 5B).

**6-DG Inhibited STAT3-Mediated Genes through Elevating the p-STAT1/p-STAT3 Ratio.** A past study indicated that LPS-stimulated macrophages could activate JAK2, STAT1, and STAT3.[25] Many studies revealed that the JAK−STAT pathway is one of the main pathways that regulated cytokine gene expression. Western blotting data showed that pretreatment with 25 μM 6-DG can decrease the phosphorylation of both JAK2 and STAT3 (ser) after stimulation with 100 ng/mL LPS as shown in (Figure 6A). Reversely, pretreatment with 25 μM 6-DG enhanced the expression of p-STAT1 (Figure 6A). There were no changes of these three total protein levels.

STAT1 and STAT3 mutually inhibited one another, and another study indicated that STAT1 levels and activity increased in the absence of STAT3.[26−28] Our results revealed


dx.doi.org/10.1021/jf501665v | J. Agric. Food Chem. 2014, 62, 9171−9179

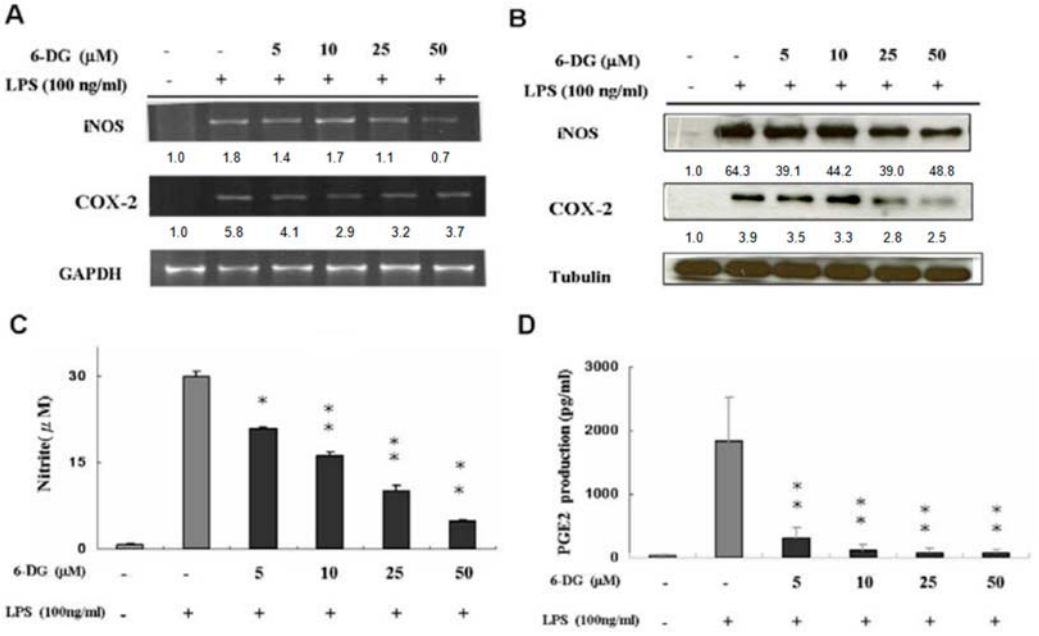


**Figure 4.** Effects of 6-DG on LPS-induced iNOS, COX-2, NO, and PGE2 expression and production in RAW 264.7 cells. (A) RAW 264.7 cells were treated with the indicated concentration of 6-DG for 30 min followed by LPS (100 ng/mL) for 3 h. RT-PCR analysis of the expression of iNOS and COX-2 was performed. Intensities of the bands for iNOS and COX-2 were normalized to GAPDH and relative to the control. (B) RAW 264.7 cells were treated with the indicated concentration of 6-DG for 30 min followed by LPS (100 ng/mL) for 6 h. Western blot analysis of the expressions of iNOS and COX-2 was performed. The intensities of the bands for iNOS and COX-2 were normalized to tubulin and relative to the control. (C) RAW 264.7 cells were pretreated with the indicated concentration of 6-DG for 30 min followed by LPS (100 ng/mL) for 24 h. Griess reagent assay analysis of the production of nitrite was performed. (D) RAW 264.7 cells were treated with the indicated concentration of 6-DG for 30 min followed by LPS (100 ng/mL). PGE2 assay analysis of the production of PGE2 was performed. Results show the mean ± SD of three experiments. (∗) $p < 0.05$ and (∗∗)$p < 0.001$ versus LPS treatment, by Student's $t$ test, $n = 3–6$. These experiments were repeated three times with similar results.

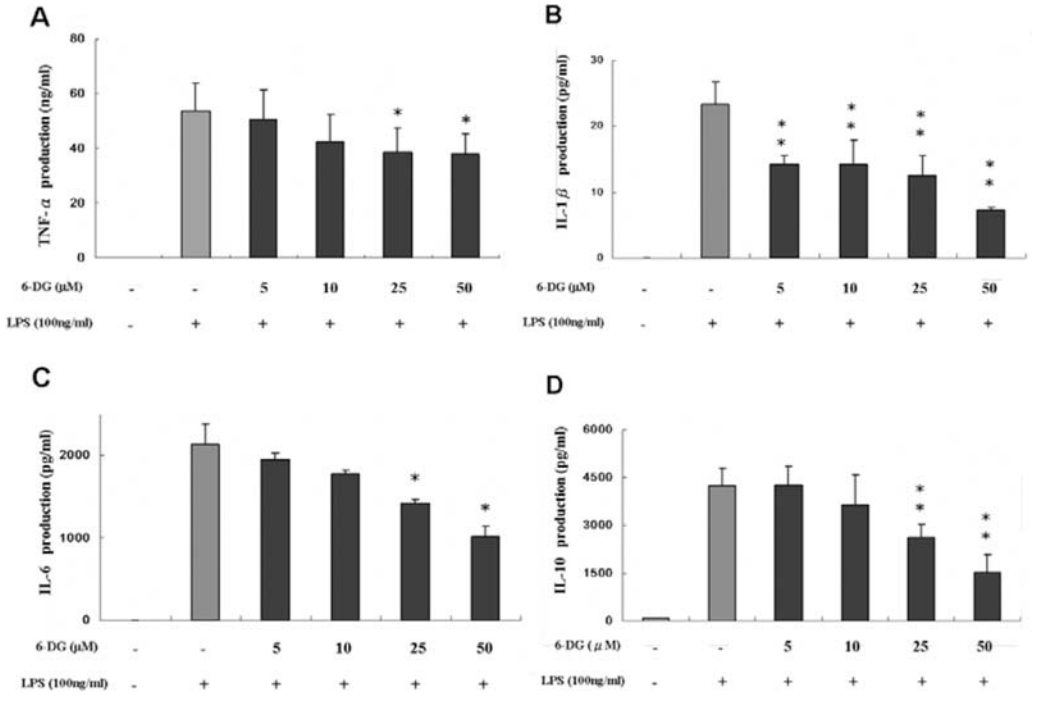


**Figure 5.** Effects of 6-DG on LPS-induced IL-1$\beta$, IL-6, IL-10, and TNF-$\alpha$ productions. Cells were pretreated with 6-DG for 30 min in various concentrations (5, 10, 25, and 50 $\mu$M) before stimulation with LPS (100 ng/mL) for 24 h. The concentrations of IL-1$\beta$, IL-6, IL-10, and TNF-$\alpha$ were measured by using ELISA. Results show the mean ± SD of three experiments. (∗) $p < 0.05$ and (∗∗) $p < 0.001$ versus LPS treatment, by Student's $t$ test, $n = 3–5$.

similarly mutual phenomenon p-STAT1 upregulation and p-STAT3 downregulation in Figure 6A. We postulate that 6-DG inhibits the gene mediated by STAT3 possibly through elevating the p-STAT1/p-STAT3 ratio. Our STAT1 knock-


dx.doi.org/10.1021/jf501665v | J. Agric. Food Chem. 2014, 62, 9171–9179

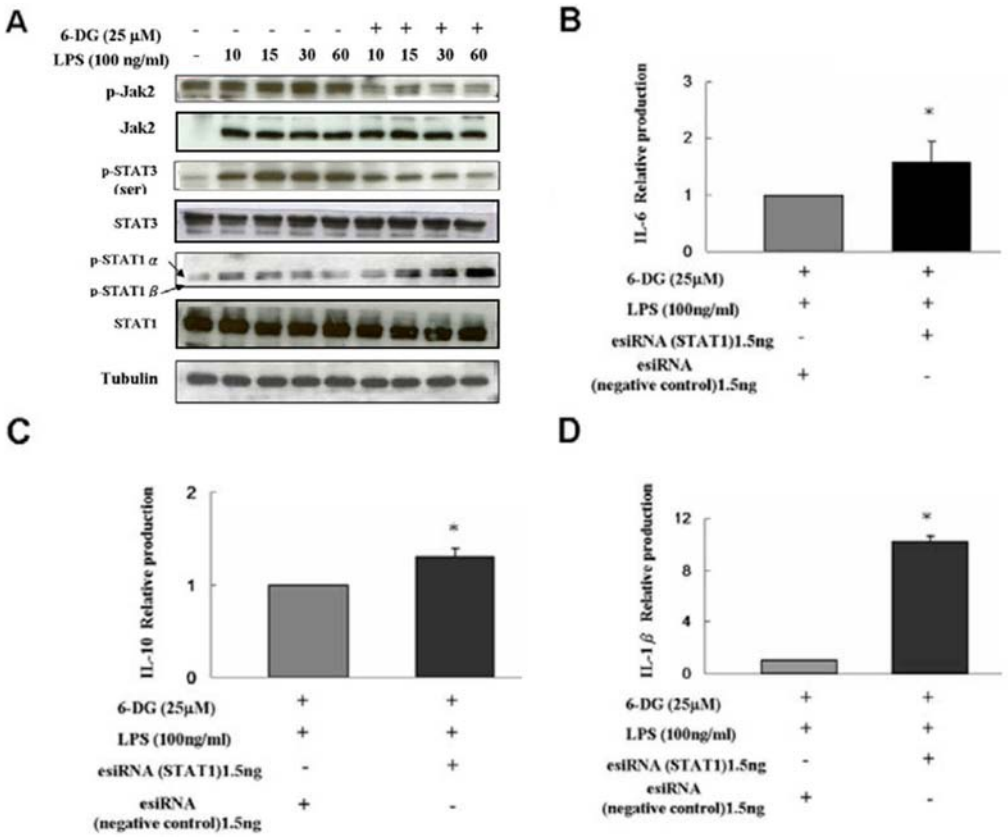


**Figure 6.** Effects of 6-DG on LPS-induced p-JAK2, p-STAT1, and p-STAT3 expression and effects of STAT1 knockdown on 6-DG inhibition of IL-1$\beta$, IL-6, and IL-10 productions induced by LPS. (A) Western blot analysis of phosphorylated and total amount of key proteins in the JAK/STAT pathway induced by LPS. Intensities of the bands for p-JAK2, p-STAT3, p-STAT1 were normalized to tubulin and relative to the control. There were no changes of these three total protein levels. (B–D) Cells were transfected with negative control or STAT1 esiRNA for 24 hand then pretreated with 6-DG for 30 min in various concentrations (5, 10, 25, and 50 $\mu$M) before stimulation with LPS (100 ng/mL) for 24 h. The concentrations of IL-1$\beta$, IL-6, and IL-10 were meausred by using ELISA. Results show the mean ± SD of three experiments. (*) $p < 0.05$ versus LPS treatment, by Student's $t$ test, $n = 3–5$.

down experiments confirmed this assumption, whereas the knockdown of STAT1 significantly reversed the 6-DG inhibition of LPS-induced cytokines (IL-6, IL-1$\beta$, and IL-10) (Figure 6B–D).

## DISCUSSION

Our study demonstrated 6-DG, one novel component of ginger, restrained several key inflammatory responses in RAW 264.7 macrophages induced by LPS and further investigated their potential molecular regulation mechanisms. 6-DG has the potent ability to inhibit the production of several major LPS-induced inflammatory mediators and cytokines, including NO, PGE2, IL-1$\beta$, IL-6, IL-10, and TNF-$\alpha$ induced by LPS via the regulation of several inflammation-related signal transduction pathways, including IKK-NF-$\kappa$B, p38, and JAK2/STAT1/STAT3.

The inflammation response is a complex reaction of the immune system regulated by many inflammatory mediators, such as NO, prostaglandins, and cytokines. An overproduction of iNOS-derived NO and COX-2-derived PGE2 can have cytotoxic effects in pathological processes, especially in inflammatory and autoimmune disorders.[29] These mediators play a regulatory role in a variety of physiological and pathological processes following an immune response and inflammation.[30] In addition, macrophages play a central role to mediate several immunopathological conditions and inducing overexpression of the pro-inflammatory mediators of the inflammatory process.[31] In the present study, we showed that the pretreatment of LPS-stimulated RAW 264.7 macrophages with 6-DG (5–50 $\mu$M) inhibited COX-2 and iNOS expression, thereby suppressing COX-2-derived PGE2 and iNOS-derived NO production (Figure 4). PGE2 has been proved able to up-regulate the levels of both IL-10 and IL-6 produced by activated murine macrophages.[32] Moreover, 6-DG suppressed LPS-induced TNF-$\alpha$ and IL-1$\beta$ production in RAW 264.7 macrophages. These results suggest that 6-DG exerts its anti-inflammatory effects via the suppression of inflammatory enzymes and mediators such as iNOS, COX-2, NO, PGE2, TNF-$\alpha$, and IL-1$\beta$ (Figures 4 and 5).

Recent studies showed that emphasis on attenuating inflammatory response may exacerbate the progressive development of immunosuppression.[3,33,34] MAPKs regulate inflammatory and immune responses,[35] and the MAPK signaling pathways are known to be involved in expressing iNOS and COX-2, as well as producing pro-inflammatory cytokines in LPS-induced macrophages.[36] The inhibition of p38 MAPK pathways is sufficient to block the induction of pro-inflammatory mediators by LPS.[37] One of the past studies suggested that p38 MAPK mediates the LPS-induced NF-$\kappa$B activation pathway through two different mechanisms that contributed to the phosphorylation of p65 NF-$\kappa$B.[24] NF-$\kappa$B activation regulates many gene encoding inflammatory


dx.doi.org/10.1021/jf501665v | J. Agric. Food Chem. 2014, 62, 9171–9179

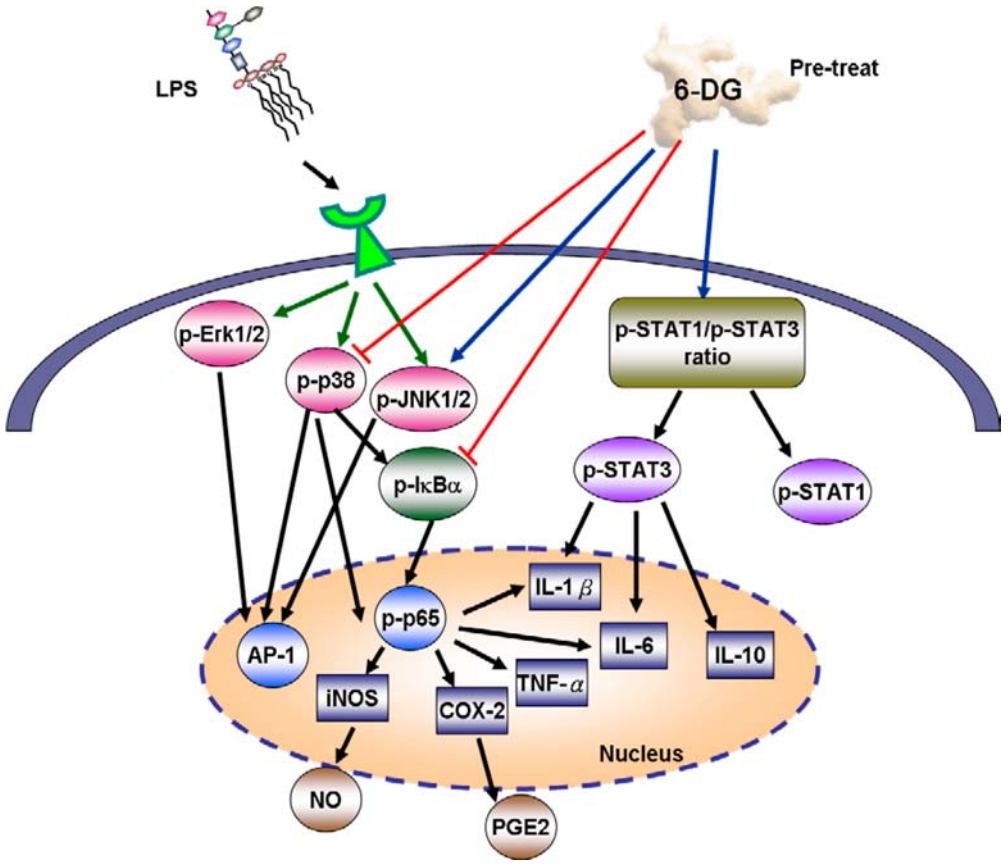


**Figure 7.** Schematic representation of suppression of LPS-induced production of NO, PGE2, IL-1$\beta$, IL-6, and TNF-$\alpha$ on 6-DG may be through the inhibition of p38 and I$\kappa$B$\alpha$ phosphorylation to prevent p-p65 NF$\kappa$B from entering the nucleus. Besides, 6-DG decreased LPS-induced IL-1$\beta$, IL-6, and IL-10 may be through elevating the p-STAT1/p-STAT3 ratio and down-regulating those genes (IL-1$\beta$, IL-6, and IL-10) mediated by STAT3.

mediators, and our results suggested that 6-DG may down-regulate both I$\kappa$B and p65 phosphorylation by attenuating the phosphorylation of p38 (Figure 3) expression and further decreases the expression of iNOS, COX-2, IL-1$\beta$, IL-6, TNF-$\alpha$ (Figures 4 and 5).

Another important pathway in inflammatory mediator production is Janus-kinase/signal transducers and the activators of transcription (Jak/STAT) pathway.[38] Prompt activation of JAK2, STAT1, and STAT3 was demonstrated after LPS stimulation. STAT1-mediated production will regulate pro-inflammatory mediators, such as COX-2[39] and iNOS.[40] Another previous study indicated that STAT3 activation is also critical for IL-1$\beta$,[41] IL-6,[42] and IL-10[43] production. A recent study indicated the regulatory mechanism of iNOS gene expression via cooperation of ISGF3 (a complex containing STAT1, STAT2, and IRF9 subunits) and NF-$\kappa$B.[44] The DNA binding for STAT3 in the promoter of acute-phase proteins was found to compete with NF-$\kappa$B.[45] Our data showed that 6-DG could inhibit the expression of p-p65 NF-$\kappa$B, but increase the expression of STAT1, and we presume that 6-DG decreases the expression of iNOS through the disruption of ISGF3 and NF-$\kappa$B cooperation (Figure 6A). Past research revealed that the overexpression of STAT1 suppresses the COX-2 promoter activity in insulin-secreting RINm5F cells.[46] Our data indicated 6-DG increased p-STAT1 (Figure 6A), but suppressed COX-2 (Figure 4), which might link to this regulation mechanism. STAT1 and STAT3 have similar structures and were found to not only act as functional antagonists but also work to mutually inhibit one another.[26] A previous study revealed STAT1 levels and activity elevated in the absence of STAT3.[28] The balance of pSTAT1 and pSTAT3, which was investigated in cancer immunity, played a pivotal role in regulation of cancer immune responses.[47,48] The higher pSTAT1/pSTAT3 ratio in tumor cells or in immune cells is related to the longer survival time of cancer patients.[47,49−51] However, this balance has not been studied in the regulation of IL-1$\beta$, IL-10, or IL-6 induced by LPS. On the basis of our Western blotting results, the expression of p-STAT increased and p-STAT3 was reduced (Figure 6A). We postulated that 6-DG may decrease LPS-induced IL-1$\beta$, IL-6, and IL-10 through elevating the p-STAT1/p-STAT3 ratio and down-regulating the genes (IL-1$\beta$, IL-6, and IL-10) mediated by STAT3. Furthermore, we have verified this assumption by using STAT1 esiRNA (Figure 6).

JNKs have been implicated in apoptotic response of cells exposed to pro-inflammatory cytokines.[52,53] We have previously shown that blocking the 6-DG-induced activation of JNK by chemical inhibitor could prevent Bax up-regulation and caspase-9 activity.[20] In this paper, our data suggested that 6-DG-induced JNK activation may contribute to 6-DG-induced mitochondrial apoptotic pathways.

In summary, we demonstrated that 6-DG decreased LPS-induced production of iNOS, COX-2, IL-1$\beta$, IL-6, and TNF-$\alpha$, which may be through the inhibition of p38 and I$\kappa$B$\alpha$ phosphorylation to prevent p-p65 NF$\kappa$B from translocating into the nucleus. Furthermore, 6-DG decreased LPS-induced IL-1$\beta$, IL-6, and IL-10 perhaps also through elevating the p-STAT1/p-STAT3 ratio and down-regulating the IL-1$\beta$, IL-6, and IL-10, mediated by STAT3 (Figure 7). The inhibition of


dx.doi.org/10.1021/jf501665v | J. Agric. Food Chem. 2014, 62, 9171−9179

p38 MAPK has been proposed as a mechanism by which the 5-hydroxytryptamine receptor type 3 (5-HT3) antagonist tropisetron could manifest its anti-inflammatory effects.[53] 6-DG is a potent antioxidant with 5-HT3 inhibitor.[20] Our experimental results indicate that 6-DG showed potential for the development of novel therapeutic targets for patients with sepsis in the future.

## AUTHOR INFORMATION


### Corresponding Authors

*(Y.-H.C.) Mail: Division of Infectious Diseases, Department of Internal Medicine, Kaohsiung Medical University Hospital, No. 100 Tzyou 1st Road, Kaohsiung 807, Taiwan. Phone: 886-7-3121101-5677. Fax: 886-7-3228547. E-mail: infchen@gmail.com

*(C.-Y.C.) Mail: Department of Medical Laboratory Science and Biotechnology, School of Medical and Health Sciences, Fooyin University, 151 Ching-Hsueh Road, Ta-Liao District, Kaohsiung 831, Taiwan. Phone: 886-7-7811151, ext. 6200. Fax: 886-7-7834548. E-mail: xx377@fy.edu.tw.

### Author Contributions

S.-H.H. and C.-H.L. contributed equally to this work.



### Funding

This work was financially supported by grants from the Taiwan National Science Council (NSC96-2314-B-037-018-MY3) and the Kaohsiung Medical University Hospital (KMUH-100-0R12).

### Notes

The authors declare no competing financial interest.


## REFERENCES


(1) Lin, C. Y.; Chen, T. C.; Lu, P. L.; Chen, H. J.; Bojang, K. S.; Chen, Y. H. Lower initial central venous pressure in septic patients from long-term care facilities than those from the community. *J. Microbiol. Immunol. Infect.* **2013**, DOI: 10.1016/j.jmii.2013.04.006.

(2) Hotchkiss, R. S.; Coopersmith, C. M.; McDunn, J. E.; Ferguson, T. A. The sepsis seesaw: tilting toward immunosuppression. *Nat. Med.* **2009**, *15*, 496−497.

(3) Hotchkiss, R. S.; Karl, I. E. The pathophysiology and treatment of sepsis. *N. Engl. J. Med.* **2003**, *348*, 138−150.

(4) Fischer, S. R.; Deyo, D. J.; Bone, H. G.; McGuire, R.; Traber, L. D.; Traber, D. L. Nitric oxide synthase inhibition restores hypoxic pulmonary vasoconstriction in sepsis. *Am. J. Respir. Crit. Care Med.* **1997**, *156*, 833−839.

(5) Smith, W. L.; Dewitt, D. L. Prostaglandin endoperoxide H synthases-1 and -2. *Adv. Immunol.* **1996**, *62*, 167−215.

(6) Lingnau, W.; McGuire, R.; Dehring, D. J.; Traber, L. D.; Linares, H. A.; Nelson, S. H.; Kilbourn, R. G.; Traber, D. L. Changes in regional hemodynamics after nitric oxide inhibition during ovine bacteremia. *Am. J. Physiol.* **1996**, *270*, R207−R216.

(7) Meade, E. A.; Smith, W. L.; DeWitt, D. L. Differential inhibition of prostaglandin endoperoxide synthase (cyclooxygenase) isozymes by aspirin and other non-steroidal anti-inflammatory drugs. *J. Biol. Chem.* **1993**, *268*, 6610−6614.

(8) Yan, J. J.; Jung, J. S.; Lee, J. E.; Lee, J.; Huh, S. O.; Kim, H. S.; Jung, K. C.; Cho, J. Y.; Nam, J. S.; Suh, H. W.; Kim, Y. H.; Song, D. K. Therapeutic effects of lysophosphatidylcholine in experimental sepsis. *Nat. Med.* **2004**, *10*, 161−167.

(9) Guha, M.; Mackman, N. LPS induction of gene expression in human monocytes. *Cell Signal.* **2001**, *13*, 85−94.

(10) Xie, Q. W.; Cho, H.; Kashiwabara, Y.; Baum, M.; Weidner, J. R.; Elliston, K.; Mumford, R.; Nathan, C. Carboxyl terminus of inducible nitric oxide synthase. Contribution to NADPH binding and enzymatic activity. *J. Biol. Chem.* **1994**, *269*, 28500−28505.

(11) Nakao, S.; Ogata, Y.; Shimizu-Sasaki, E.; Yamazaki, M.; Furuyama, S.; Sugiya, H. Activation of NFκB is necessary for IL-1β-induced cyclooxygenase-2 (COX-2) expression in human gingival fibroblasts. *Mol. Cell. Biochem.* **2000**, *209*, 113−118.

(12) Shalit, I.; Halperin, D.; Haite, D.; Levitov, A.; Romano, J.; Osherov, N.; Fabian, I. Anti-inflammatory effects of moxifloxacin on IL-8, IL-1β and TNF-α secretion and NFκB and MAP-kinase activation in human monocytes stimulated with *Aspergillus fumigatus*. *J. Antimicrob. Chemother.* **2006**, *57*, 230−235.

(13) Libermann, T. A.; Baltimore, D. Activation of interleukin-6 gene expression through the NF-κB transcription factor. *Mol. Cell. Biol.* **1990**, *10*, 2327−2334.

(14) Grzanna, R.; Lindmark, L.; Frondoza, C. G. Ginger − an herbal medicinal product with broad anti-inflammatory actions. *J. Med. Food* **2005**, *8*, 125−132.

(15) Wang, H. M.; Chen, C. Y.; Chen, H. A.; Huang, W. C.; Lin, W. R.; Chen, T. C.; Lin, C. Y.; Chien, H. J.; Lu, P. L.; Lin, C. M.; Chen, Y. H. *Zingiber officinale* (ginger) compounds have tetracycline-resistance modifying effects against clinical extensively drug-resistant *Acinetobacter baumannii*. *Phytother. Res.* **2010**, *24*, 1825−1830.

(16) Surh, Y. J. Anti-tumor promoting potential of selected spice ingredients with antioxidative and anti-inflammatory activities: a short review. *Food Chem. Toxicol.* **2002**, *40*, 1091−1097.

(17) Eguchi, A.; Murakami, A.; Ohigashi, H. Novel bioassay system for evaluating anti-oxidative activities of food items: use of basolateral media from differentiated Caco-2 cells. *Free Radical Res.* **2005**, *39*, 1367−1375.

(18) Aktan, F.; Henness, S.; Tran, V. H.; Duke, C. C.; Roufogalis, B. D.; Ammit, A. J. Gingerol metabolite and a synthetic analogue Capsarol inhibit macrophage NF-κB-mediated iNOS gene expression and enzyme activity. *Planta Med.* **2006**, *72*, 727−734.

(19) Chen, C. Y.; Chiu, C. C.; Wu, C. P.; Chou, Y. T.; Wang, H. M. Enhancements of skin cell proliferations and migrations via 6-dehydrogingerdione. *J. Agric. Food Chem.* **2013**, *61*, 1349−1356.

(20) Hsu, Y. L.; Chen, C. Y.; Hou, M. F.; Tsai, E. M.; Jong, Y. J.; Hung, C. H.; Kuo, P. L. 6-Dehydrogingerdione, an active constituent of dietary ginger, induces cell cycle arrest and apoptosis through reactive oxygen species/c-Jun N-terminal kinase pathways in human breast cancer cells. *Mol. Nutr. Food Res.* **2010**, *54*, 1307−1317.

(21) Grivennikov, S. I.; Greten, F. R.; Karin, M. Immunity, inflammation, and cancer. *Cell* **2010**, *140*, 883−899.

(22) Kiuchi, F.; Shibuya, M.; Sankawa, U. Inhibitors of prostaglandin biosynthesis from ginger. *Chem. Pharm. Bull. (Tokyo)* **1982**, *30*, 754−757.

(23) Ma, J.; Jin, X.; Yang, L.; Liu, Z. L. Diarylheptanoids from the rhizomes of *Zingiber officinale*. *Phytochemistry* **2004**, *65*, 1137−1143.

(24) Chen, Y. H.; Layne, M. D.; Chung, S. W.; Ejima, K.; Baron, R. M.; Yet, S. F.; Perrella, M. A. Elk-3 is a transcriptional repressor of nitric-oxide synthase 2. *J. Biol. Chem.* **2003**, *278*, 39572−39577.

(25) Kim, H. J.; Lee, H. S.; Chong, Y. H.; Kang, J. L. p38 Mitogen-activated protein kinase up-regulates LPS-induced NF-κB activation in the development of lung injury and RAW 264.7 macrophages. *Toxicology* **2006**, *225*, 36−47.

(26) Liu, H.; Yao, Y. M.; Yu, Y.; Dong, N.; Yin, H. N.; Sheng, Z. Y. Role of Janus kinase/signal transducer and activator of transcription pathway in regulation of expression and inflammation-promoting activity of high mobility group box protein 1 in rat peritoneal macrophages. *Shock* **2007**, *27*, 55−60.

(27) Hong, F.; Jaruga, B.; Kim, W. H.; Radaeva, S.; El-Assal, O. N.; Tian, Z.; Nguyen, V. A.; Gao, B. Opposing roles of STAT1 and STAT3 in T cell-mediated hepatitis: regulation by SOCS. *J. Clin. Invest.* **2002**, *110*, 1503−1513.

(28) Chapman, R. S.; Lourenco, P. C.; Tonner, E.; Flint, D. J.; Selbert, S.; Takeda, K.; Akira, S.; Clarke, A. R.; Watson, C. J. Suppression of epithelial apoptosis and delayed mammary gland involution in mice with a conditional knockout of Stat3. *Genes Dev.* **1999**, *13*, 2604−2616.

(29) Palmer, R. M.; Ashton, D. S.; Moncada, S. Vascular endothelial cells synthesize nitric oxide from L-arginine. *Nature* **1988**, *333*, 664−666.
(30) Griswold, D. E.; Adams, J. L. Constitutive cyclooxygenase (COX-1) and inducible cyclooxygenase (COX-2): rationale for selective inhibition and progress to date. *Med. Res. Rev.* **1996**, *16*, 181−206.
(31) Lin, H. W.; Chang, T. J.; Yang, D. J.; Chen, Y. C.; Wang, M.; Chang, Y. Y. Regulation of virus-induced inflammatory response by β-carotene in RAW 264.7 cells. *Food Chem.* **2012**, *134*, 2169−2175.
(32) Williams, J. A.; Pontzer, C. H.; Shacter, E. Regulation of macrophage interleukin-6 (IL-6) and IL-10 expression by prostaglandin E2: the role of p38 mitogen-activated protein kinase. *J. Interferon Cytokine Res.* **2000**, *20*, 291−298.
(33) Osuchowski, M. F.; Welch, K.; Siddiqui, J.; Remick, D. G. Circulating cytokine/inhibitor profiles reshape the understanding of the SIRS/CARS continuum in sepsis and predict mortality. *J. Immunol.* **2006**, *177*, 1967−1974.
(34) Adib-Conquy, M.; Cavaillon, J. M. Compensatory anti-inflammatory response syndrome. *Thromb. Haemost.* **2009**, *101*, 36−47.
(35) Ajizian, S. J.; English, B. K.; Meals, E. A. Specific inhibitors of p38 and extracellular signal-regulated kinase mitogen-activated protein kinase pathways block inducible nitric oxide synthase and tumor necrosis factor accumulation in murine macrophages stimulated with lipopolysaccharide and interferon-γ. *J. Infect. Dis.* **1999**, *179*, 939−944.
(36) Uto, T.; Fujii, M.; Hou, D. X. 6-(Methylsulfinyl)hexyl isothiocyanate suppresses inducible nitric oxide synthase expression through the inhibition of Janus kinase 2-mediated JNK pathway in lipopolysaccharide-activated murine macrophages. *Biochem. Pharmacol.* **2005**, *70*, 1211−1221.
(37) Yoon, W. J.; Lee, N. H.; Hyun, C. G. Limonene suppresses lipopolysaccharide-induced production of nitric oxide, prostaglandin E2, and pro-inflammatory cytokines in RAW 264.7 macrophages. *J. Oleo Sci.* **2010**, *59*, 415−421.
(38) Osna, N.; Elliott, K.; Chaika, O.; Patterson, E.; Lewis, R. E.; Khan, M. M. Histamine utilizes JAK-STAT pathway in regulating cytokine production. *Int. Immunol.* **2001**, *1*, 759−762.
(39) Regis, G.; Pensa, S.; Boselli, D.; Novelli, F.; Poli, V. Ups and downs: the STAT1:STAT3 seesaw of Interferon and gp130 receptor signalling. *Semin. Cell. Dev. Biol.* **2008**, *19*, 351−359.
(40) Samardzic, T.; Jankovic, V.; Stosic-Grujicic, S.; Trajkovic, V. STAT1 is required for iNOS activation, but not IL-6 production in murine fibroblasts. *Cytokine* **2001**, *13*, 179−182.
(41) Darnell, J. E., Jr. STATs and gene regulation. *Science* **1997**, *277*, 1630−1635.
(42) Shakhov, A. N.; Collart, M. A.; Vassalli, P.; Nedospasov, S. A.; Jongeneel, C. V. κB-type enhancers are involved in lipopolysaccharide-mediated transcriptional activation of the tumor necrosis factor α gene in primary macrophages. *J. Exp. Med.* **1990**, *171*, 35−47.
(43) Staples, K. J.; Smallie, T.; Williams, L. M.; Foey, A.; Burke, B.; Foxwell, B. M.; Ziegler-Heitbrock, L. IL-10 induces IL-10 in primary human monocyte-derived macrophages via the transcription factor Stat3. *J. Immunol.* **2007**, *178*, 4779−4785.
(44) Farlik, M.; Reutterer, B.; Schindler, C.; Greten, F.; Vogl, C.; Muller, M.; Decker, T. Nonconventional initiation complex assembly by STAT and NF-κB transcription factors regulates nitric oxide synthase expression. *Immunity* **2010**, *33*, 25−34.
(45) Zhang, Z.; Fuller, G. M. The competitive binding of STAT3 and NF-κB on an overlapping DNA binding site. *Biochem. Biophys. Res. Commun.* **1997**, *237*, 90−94.
(46) Zhang, X.; Zhang, J.; Yang, X.; Han, X. Several transcription factors regulate COX-2 gene expression in pancreatic β-cells. *Mol. Biol. Rep.* **2007**, *34*, 199−206.
(47) Yu, H.; Kortylewski, M.; Pardoll, D. Crosstalk between cancer and immune cells: role of STAT3 in the tumour microenvironment. *Nat. Rev. Immunol.* **2007**, *7*, 41−51.
(48) Adamkova, L.; Souckova, K.; Kovarik, J. Transcription protein STAT1: biology and relation to cancer. *Folia Biol.* **2007**, *53*, 1−6.
(49) Dunn, G. P.; Ikeda, H.; Bruce, A. T.; Koebel, C.; Uppaluri, R.; Bui, J.; Chan, R.; Diamond, M.; White, J. M.; Sheehan, K. C.; Schreiber, R. D. Interferon-γ and cancer immunoediting. *Immunol. Res.* **2005**, *32*, 231−245.
(50) Wang, W.; Edington, H. D.; Rao, U. N.; Jukic, D. M.; Wang, H.; Shipe-Spotloe, J. M.; Kirkwood, J. M. STAT3 as a biomarker of progression in atypical nevi of patients with melanoma: dose-response effects of systemic IFNα therapy. *J. Invest. Dermatol.* **2008**, *128*, 1997−2002.
(51) Wang, W.; Edington, H. D.; Rao, U. N.; Jukic, D. M.; Land, S. R.; Ferrone, S.; Kirkwood, J. M. Modulation of signal transducers and activators of transcription 1 and 3 signaling in melanoma by high-dose IFNα2b. *Clin. Cancer Res.* **2007**, *13*, 1523−1531.
(52) Zu, K.; Hawthorn, L.; Ip, C. Up-regulation of c-Jun-NH2-kinase pathway contributes to the induction of mitochondria-mediated apoptosis by α-tocopheryl succinate in human prostate cancer cells. *Mol. Cancer Ther.* **2005**, *4*, 43−50.
(53) Stratz, C.; Bhatia, H. S.; Akundi, R. S.; Nührenberg, T.; Trenk, D.; Muñoz, E.; Fiebich, B. L. The anti-inflammatory effects of the 5-$HT_3$ receptor antagonist tropisetron are mediated by the inhibition of p38 MAPK activation in primary human monocytes. *Int. Immunopharmacol.* **2012**, *13*, 398−402.

nism assumed in our previous work[18] contradicts the studies of Faria et al.[15] and Brazinha et al..[16] To clearly identify the limiting step of the oxygen transport through the cork stopper, a further study is required. This work presents the effect of oxygen pressure on diffusion coefficient to determine the underlying transport mechanism, Fick or Knudsen.

To answer this question, measurements of oxygen transfer through the cork stopper have been performed for different pressure gradients. Data are analyzed to determine permeabilities, and effective diffusion coefficients, interpreted by means of activation theory.

## THEORY

**Gas Transport.** Let us consider the diffusion of a gas through a semi-infinite wafer of solid when a pressure gradient of gas between the two sides of the wafer is imposed.

The permeability $P$ is defined by the general relationship

$$P = \frac{-J}{\nabla p} \approx \frac{-Je}{\Delta p} \tag{1}$$

where $J$ is the mass flow of gas diffusing through the membrane of thickness $e$, $\nabla_p$ the pressure gradient, $\Delta_p$ the difference in pressure between the two sides of the membrane, and $p$ the pressure. If one side of the wafer is maintained under vacuum while the other side is in contact with a gas under pressure $p$, $\Delta p = -p$.

In steady state, the mass flow $J$ can be calculated by doing a mass balance on the gas phase from the decrease in pressure as a function of time, using the equation

$$J = -\frac{VM}{RTS}\frac{\mathrm{d}p}{\mathrm{d}t} \tag{2}$$

where $V$ is the gas volume on one side on the cork wafer, $M$ the molecular weight of gas, $R$ the gas constant, $T$ the temperature, $S$ the cork surface in contact with the gas, and $\mathrm{d}p/\mathrm{d}t$ the derivative of pressure with time $t$.[18]

This expression is the same whatever the transfer mechanism of gas through cork, Darcy's, Knudsen's, or Fickian regime (or even a mix of them).

Therefore, combining eqs 1 and 2 leads to the permeability expression as

$$P = -\left(e\frac{VM}{RST}\right)\left(\frac{\mathrm{d}\ln p}{\mathrm{d}t}\right) \tag{3}$$

Integration of eq 3 leads to the relationship

$$\ln\left(\frac{p_0}{p}\right) = kt \tag{4}$$

with $p_0$ the initial pressure and $k$ the rate constant, which can be easily determined from measurements of the pressure with time by plotting $\ln(p_0/p) = f(t)$. The permeability can then be calculated from $k$ with the equation

$$P = \left(e\frac{VM}{RST}\right)k \tag{5}$$

In the Knudsen regime, the permeability is independent of the pressure as shown by the following expression of permeability, referred to as $P_K$:

$$P_K = \frac{d}{3}\sqrt{\frac{8M}{\pi RT}} \tag{6}$$

$d$ is the pore diameter in which the gas diffuses.

However, if the diffusion process follows a Fickian regime, the permeability, referred to in that case as $P_F$, can be dependent on the pressure according to the pressure range investigated and the shape of the adsorption isotherm of the diffusive species:

$$P_F = \frac{D\Psi M}{RT} \tag{7}$$

with the concentration factor

$$\Psi = \frac{C_a}{C_g} = \frac{C_a RT}{p} \tag{8}$$

$C_a$ is the concentration of gas adsorbed by the solid, and $C_g$ is the gas concentration at equilibrium (oxygen in the present case). Both $C_a$ and $C_g$ are given by the sorption isotherm of gas on the solid. $D$ is the diffusion coefficient, which can be calculated from $k$ using eqs 5 and 7.

**Transition State Theory.** In transition state theory, diffusion is considered as an activated process.[21] Thus, the dependence of the diffusion coefficient on the temperature is defined by an Arrhenius-type equation

$$D = D_0\, \mathrm{e}^{-\Delta G^*/k_B T} \tag{9}$$

where $D_0$ is a pre-exponential factor and $\Delta G^*$ the activation free enthalpy.

The activation free enthalpy $\Delta G^*$ corresponds to the energy barrier that the diffusing molecule has to get over for moving from one site to another one. As the free enthalpy is related to the pressure by the relationship

$$\mathrm{d}G = V\,\mathrm{d}p - S\,\mathrm{d}T \tag{10}$$

at constant temperature the entropic term vanishes and the dependence of the activation free enthalpy on the pressure is

$$\left(\frac{\partial G^*}{\partial p}\right)_T = \Delta V^* \tag{11}$$

where $\Delta V^*$ is the activation molecular volume.

By combining eqs 9 and 11 we obtain the relationship between the diffusion coefficient and the pressure

$$D = D_0\, \mathrm{e}^{-\Delta V^* p/k_B T} \tag{12}$$

or in the linear form

$$\ln D = \ln D_0 - \frac{\Delta V^*}{k_B T}p \tag{13}$$

Activation volume can be either positive (which means a decrease of $D$ with increasing $p$) or negative (an increase of $D$ with increasing $p$).[22] $\Delta V^*$ is the molecular volume difference between the activated complex and the nonactivated state. It represents the free space needed by a molecule to move from one adsorption site to another. Molecular transport is due to a redistribution of free volume and not due to a thermal activation, according to the free volume theory. Molecules can move from one site to another only when the local free volume exceeds a certain critical volume.[23]

## MATERIALS AND METHODS

**Cork Stopper.** Raw natural cork stoppers, from *Quercus suber* L. oak trees in the Mora (Portugal) production area, were supplied by the


dx.doi.org/10.1021/jf501918n | J. Agric. Food Chem. 2014, 62, 9180−9185

company Bouchons Trescases S.A. (Boulou, France). Cork was of high quality (class 0). Stoppers were neither washed nor surface treated (with paraffin or silicone) prior to use. Two cork wafers were cut with a cutting machine, Mecatome T201, with resinoid cutoff wheels of 180 mm diameter and 0.5 mm thickness (Presi S.A., France). They were cut following the section perpendicular to the axial axis of the stopper, which corresponds to the surface in contact with wine in a bottle. Cork wafers display a diameter of 24 mm and a thickness of 3 mm. Wafers were then inserted in a metal ring seal and stuck at the periphery of each axial section with Araldite 2012 glue to avoid gas transfer at the cork/ring interface. In this experiment, the cork wafer is not compressed and offers an effective surface area for oxygen transfer of $4.52 \times 10^{-4}$ m$^2$.

**Sorption of Oxygen.** Sorption of oxygen by cork was studied by means of a manometric device constructed in-house. The sorption isotherm of oxygen was measured on cubic pieces (around 3 mm edge) of cork at 298 K for pressure ranging from 0.1 to 1000 hPa. The mass of the sample was 1.028 g. Prior to sorption, cork was dehydrated at room temperature under vacuum (0.1 hPa) for 2 days.

**Oxygen Transfer.** Transfer of oxygen through cork wafer is measured using a homemade manometric apparatus. The equipment and the procedure used to determine the permeability and then the diffusion coefficient have been described in detail in a previous work.[18] For the present experiments, the initial pressure of oxygen is fixed between 50 and 800 hPa, at one side of the cork wafer, whereas the other side is maintained under dynamic vacuum (0.1 hPa). In the case of a bottle of wine, the partial pressure of oxygen is 210 hPa outside, whereas it can be considered to be 0 inside (under the hypothesis that the oxygen immediately reacts with the liquid phase).

Temperature is kept constant at 298 (±1) K, and the pressure sensor accuracy is 0.1 hPa. Moreover, the errors in thickness ($e$), surface ($S$), and volume ($V$) are negligible compared to instrumental error, <0.5%. The maximum instrumental error is 1%, and model fit lower than 0.5%, which allow an error below 2% on permeability and diffusion coefficient measurements.

In a previous work[18] focusing on a large number of samples to extract a statistical distribution for oxygen transfer through cork, we found that effective oxygen diffusion coefficients through 3 mm cork wafers were spread over four decades in the range from $10^{-10}$ to $10^{-6}$ m$^2$ s$^{-1}$ with a maximum between $10^{-9}$ and $10^{-8}$ m$^2$ s$^{-1}$ (values were determined at $T$ = 298 K and for an initial oxygen pressure of $p_i$ = 220 hPa). This is however largely reduced when considering the extrapolation to a full cork stopper of 48 mm, with effective diffusion coefficient values ranging from $2 \times 10^{-10}$ to $10^{-8}$ m$^2$ s$^{-1}$, which corresponds to permeabilities between $5 \times 10^{-16}$ and $2 \times 10^{-14}$ kg m$^{-1}$ s$^{-1}$ Pa$^{-1}$. In the present work, two cork wafers from two different cork stoppers were chosen according to this distribution, as two representative samples around the mean value. They are referred to as cork wafer 1 and 2. Their diffusion coefficients were $1.34 \times 10^{-8}$ and $4.68 \times 10^{-9}$ m$^2$ s$^{-1}$, respectively (for initial pressure, $p_i$ = 220 hPa and $T$ = 298 K).

## RESULTS AND DISCUSSION

**Sorption Isotherm of Oxygen.** The sorption isotherm of oxygen on cork at 298 K is shown in Figure 1. It exhibits a type III shape of the IUPAC classification,[24] characteristic of the sorption on a nonporous or macroporous material with a weak adsorption affinity. These data are in very good agreement with those of Lequin et al.[18] obtained on cork powder from another harvest. The sorption isotherm is well fitted with the FHH model defined by the relationship

$$\frac{C^a}{C^a_m} = \left[K_{FHH} \ln\left(\frac{C^g_s}{C^g}\right)\right]^{-1/s} \quad (14)$$

where $C^a_m$ is the concentration of adsorbate in the "equivalent" monolayer, $C^g_s$ is the concentration of gas in equilibrium with its liquid phase at the sorption temperature, $K_{FHH}$ is an adjustable parameter taking into account the energy of sorption, and $s$ is related to the nature of gas−solid interaction. Usually, $s$ = 3. A deviation of $s$ from this value is attributed to energy or geometric heterogeneity effects. Values of the FHH parameters are given in Table 1. The low values of $K_{FHH}$ and $s$ compared to those found for water on polymers (0.7 and 2, respectively, for a poly(styrenesulfonic acid), sodium salt, for example, by Toribio et al.,[25]) show that the sorption process of oxygen on cork is highly heterogeneous and involves very weak gas−solid interactions.

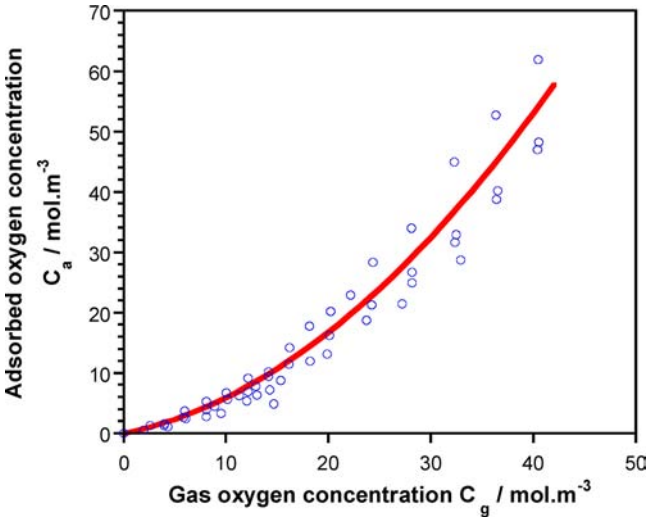


**Figure 1.** Adsorption isotherm of oxygen on cork at 298 K (—, FHH model; ○, experimental data;[18]).

**Table 1. Parameters of the FHH Model for the Sorption of Oxygen by Cork at 298 K**

| $C^a_m$ (mol m$^{-3}$) | $K_{FHH}$ | $C^g_s$ (mol m$^{-3}$) | $s$ |
|---|---|---|---|
| 7.5478 | 0.1373 | 17303 | 0.0948 |

**Fick or Knudsen Regime?** Figure 2 displays the permeability of oxygen through cork wafer as a function of the initial pressure of oxygen at constant temperature, 298 K.

For both cork samples, permeability is increasing with initial pressure following a linear trend. For sample 1, permeability values range between $1.5 \times 10^{-14}$ and $2.3 \times 10^{-14}$ kg m$^{-1}$ s$^{-1}$ Pa$^{-1}$. For sample 2, values vary between $6.3 \times 10^{-15}$ and $1.0 \times 10^{-14}$ kg m$^{-1}$ s$^{-1}$ Pa$^{-1}$ and are less dispersed.

As in the Knudsen regime the permeability is independent of the pressure (see eq 5), the fact that we observe an increase in the permeability with the initial oxygen pressure means that the limiting step of oxygen transport in cork is not the transfer of gas through lenticels or palsmodesmata as claimed by other authors.[15,16] Moreover, the permeability values are much too low to account for a gas transport in spaces as large as plasmodesmata (around 100 nm diameter). According to the Knudsen law, permeability can be calculated following the equation

$$P_K = \frac{d}{3}\sqrt{\frac{8M}{\pi RT}} \quad (6)$$

where $d$ is the pore diameter, $M$ the molar mass of $O_2$, $R$ the gas constant, and $T$ the temperature.

From the permeability range experimentally investigated, this would mean a pore diameter lying between $1.04 \times 10^{-4}$ and


dx.doi.org/10.1021/jf501918n | J. Agric. Food Chem. 2014, 62, 9180−9185

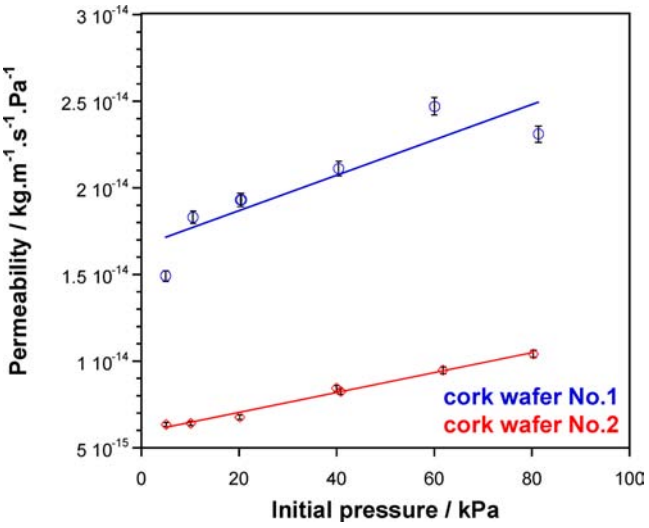


**Figure 2.** Dependence of the permeability of oxygen through 3 mm cork wafers on the initial oxygen pressure at 298 K (○, cork wafer 1; ◇, cork wafer 2; —, linear regression).

$3.80 \times 10^{-4}$ nm. These values are unrealistic. Cork is composed of empty cells (of characteristic dimension around 50 $\mu$m[26]), separated from each other by cell walls of 1 $\mu$m thickness, and of large pores called lenticels (which are macroscopic defects between 200 $\mu$m and 1 mm). Even plasmodesmata, if not obstructed, are pores of 100 nm diameter. It is also worthy of note that the mean free path, which is a function of pressure and temperature,[27] ranges between 130 and 2085 nm for oxygen pressures between 800 and 50 hPa, respectively, at 298 K. Therefore, considering the characteristic dimensions of voids in cork, the limiting step of the transfer cannot be governed by Darcy or Knudsen's mechanisms.

In addition, the probability that a molecule passes from one side to the opposite side of a cork wafer having a thickness of 3 mm by diffusing only in large channels such as lenticels or plasmodesmata is extremely low. When crossing the wafer, the oxygen molecule will inevitably encounter cork walls. Knudsen diffusion can occur in cork, but in any case it cannot be the limiting step. On the contrary, the dependence of the permeability on the pressure is well taken into account by the Fick law (eqs 7 and 8). These results reinforced what we still advanced in our previous paper.[18] The limiting step of oxygen transfer in cork is the diffusion between the polymeric chains of suberin, lignin, cellulose, and hemicellulose, which constitute the cork walls.

All stoppers have basically the same chemical composition and the same cell size. However, the heterogeneity lies in the distribution in size and number of lenticels. For 3 mm thickness samples this heterogeneity is thus probed through the determination of an effective diffusion coefficient. This largely reduces when increasing the length of the sample (from $10^{-10}$ to $10^{-6}$ m$^2$ s$^{-1}$ for a 3 mm sample down to $2 \times 10^{-10}$ to $10^{-8}$ m$^2$ s$^{-1}$ when extrapolated to a 48 mm stopper).[18] Nevertheless, for values of effective diffusion coefficients in the higher range of the distribution for 3 mm thickness sample, it tends to be out of the range for diffusion in solids, and obviously that could mean that another transport mechanism (Knudsen, Darcy) can occur. Very locally, at the millimeter scale, a faster transport mechanism (Knudsen, Darcy) may significantly contribute, but for a bigger system size, a full cork stopper of >12 times this size, these faster steps become completely hidden by the slower Fickian diffusion regime. This is the dominating mechanism at the scale of a full-length stopper.

**Activation Volume.** The effect of initial pressure on the diffusion coefficient is displayed in Figure 3, $D$ being

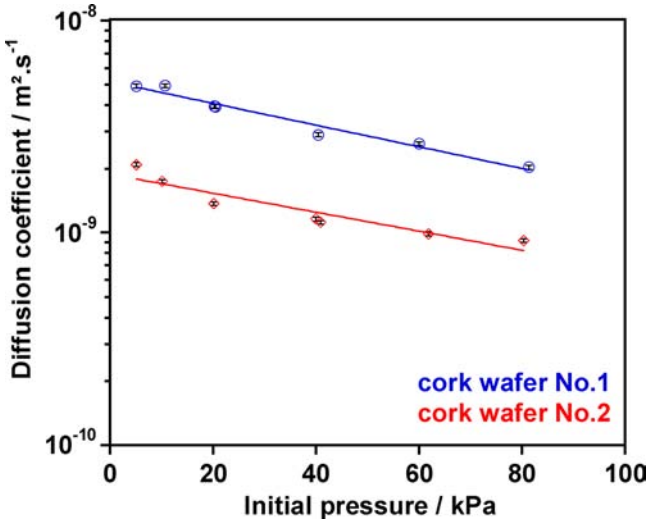


**Figure 3.** Effect of the initial oxygen pressure on the diffusion coefficient (○, cork wafer 1; ◇, cork wafer 2; —, exponential regression).

determined from eq 4. For both samples, the diffusion coefficient is not constant, but varies with pressure. Diffusion coefficients decrease from $4.93 \times 10^{-9}$ to $2.04 \times 10^{-9}$ m$^2$ s$^{-1}$ and from $2.09 \times 10^{-9}$ to $0.92 \times 10^{-9}$ m$^2$ s$^{-1}$ for the first and second cork wafers, respectively, for pressure increasing from 50 to 800 hPa. According to the semilog representation, this decrease is linear and the slopes are almost of the same order ($-1.18 \times 10^{-5}$ and $-1.00 \times 10^{-5}$ m$^2$ s$^{-1}$ Pa$^{-1}$ with coefficients of correlation of 0.98 and 0.94, respectively). By applying the transition state theory, the activation volume can be determined from the slope of the curves $\ln D = f(p)$ according to eq 13.

Surprisingly, the activation volumes are very high, 48 and 41 nm$^3$ per oxygen molecule. These activation volumes are of the same order as that found for an ideal gas at 298 K under 1 bar of pressure (41 nm$^3$).

There are many scientific papers related to the effect of pressure on the diffusion coefficient and activation volume in metals and crystals (Table 2) but not so much in natural polymer. As far as we know, there is no study reporting the dependence of diffusion coefficient on pressure in cork or other natural or synthetic polymeric materials having an alveolar structure.

Activation volumes in metals are very small, around $10^{-3}$ nm$^3$, which is around 45000 times smaller than in cork. Metals are dense and rigid, whereas cork has good elastic properties. Moreover, it is an alveolar solid containing >80% of empty space.[28] Such a high activation volume is closely related to this specific structure and the mechanism of diffusion of gas in this material. Therefore, it is worth noting that in the case of a heterogeneous material such as cork, $\Delta V^*$ must be considered as an apparent activation volume, $\Delta V^*_{app}$, because the diffusion coefficients are not the same inside the alveolus and the cell walls. Figure 4 represents a schematic view of the oxygen transfer through an alveolar structure such as cork. Such a system is composed of two environments (cork walls and


dx.doi.org/10.1021/jf501918n | J. Agric. Food Chem. 2014, 62, 9180−9185

**Table 2. Activation Volumes for Diffusion in Various Solids**

| solid | diffusant | $T$ (K) | pressure range (Pa) | activation volume $\Delta V^*$ (nm$^3$) | ref |
|---|---|---|---|---|---|
| cork | oxygen | 572 | $5 \times 10^3 < p < 80 \times 10^3$ | $45 \pm 4$ | this work |
| germanium | arsenic | 848 | $0.1 \times 10^9 < p < 4 \times 10^9$ | $-2.82 \times 10^{-3} \pm 2.32 \times 10^{-3}$ | 22 |
| amorphous $Co_{18}Zr_{19}$ | $^{57}$Co | 563 | $3 \times 10^9 < p < 8 \times 10^9$ | $(1 \pm 1.3) \times 10^{-4}$ | 29 |
| $(Fe_xMg_{1-x})SiO_4$ olivine | Ni | 1673 | $6 \times 10^9 < p < 12 \times 10^9$ | $9.0 \times 10^{-3} < \Delta V^* < 11.6 \times 10^{-3}$ | 30 |
| $(Fe_xMg_{1-x})SiO_4$ olivine | Mn | 1673 | $6 \times 10^9 < p < 12 \times 10^9$ | $(7.6 \pm 2.8) \times 10^{-3}$ | 30 |
| silicon | boron | 1083 | $10^9 < p < 5 \times 10^9$ | | 31 |

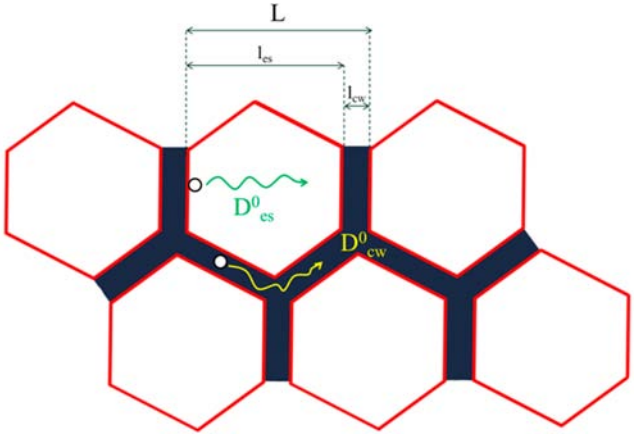


**Figure 4.** Schematic representation of oxygen diffusion through cork ($l_{es}$, cell length; $l_{cw}$, thickness of cell walls; $D^0_{es}$ and $D^0_{cw}$, diffusion coefficients of oxygen in empty cell and cell walls, respectively).

alveolus) in which the resistances of mass transfer are different. Lenticels and plasmodesmatas are not taken into account in this very simple model, but they can be considered as empty spaces.

Therefore, following ref 18, we can consider in this system two mass resistivities in series. As the mass resistivity is proportional to the length of the diffusing environment and to the inverse of the diffusion coefficient and using eq 12, the mean diffusion coefficient, $\bar{D}$, can be written as a harmonic average of local diffusion coefficients

$$\frac{L}{\bar{D}} = \frac{l_{cw}}{D_{cw}} + \frac{l_{es}}{D_{es}} = \frac{l_{cw}}{D^0_{cw}\, e^{-\Delta V^*_{cw} p/k_B T}} + \frac{l_{es}}{D^0_{ew}\, e^{-\Delta V^*_{ew} p/k_B T}} \quad (15)$$

where $l_{cw}$ and $l_{es}$ are respectively the thickness of the cell walls and the length of empty spaces, $L = l_{cw} + l_{es}$, $\bar{D}$ is the mean coefficient diffusion through cork, $D_{cw}$ and $\Delta V^*_{cw}$ are the diffusion coefficient and the activation volume in cell walls, and $D_{es}$ and $\Delta V^*_{es}$ are the same for empty spaces.

Therefore, the apparent activation volume is composed of two terms: one related to the activation in the empty space and one to the polymeric phase. However, it is not possible to experimentally determine $\Delta V^*_{cw}$ or $\Delta V^*_{es}$ as well as the respective diffusion coefficients.

As a whole, this work clearly shows that the limiting step of oxygen transport through cork is the diffusion in cell walls according to a Fickian mechanism. Even if Knudsen diffusion can occur, it will not govern the oxygen transport through cork. The apparent activation volume for oxygen diffusion in cork is $45 \pm 4$ nm$^3$. This value is very close to the molecular volume of the ideal gas (41 nm$^3$). This means that oxygen molecules do not reside only within the cell walls moving through the polymeric chains. In such a case, activation volume would be much lower. The large value of activation volume suggests that oxygen molecules also diffuse through a gas phase in large spaces such as lenticels, plasmodesmatas (if not obstructed), or, more probably, inside the empty cells (which have a volume around $5 \times 10^4$ $\mu$m$^3$) when moving from one site to another one. The limiting step of the transfer obviously remains the diffusion through the cell walls to cross cork. This better understanding of the diffusion mechanism of oxygen through cork is therefore interesting for applying the right model for prediction purposes and for saving time when doing permeation measurement on cork closures.

## AUTHOR INFORMATION


### Corresponding Author

*(J.-P.B.) Phone: +33 (0)3 80 39 59 29. E-mail: jean-pierre.bellat@u-bourgogne.fr.



### Funding

We gratefully acknowledge the Bureau Interprofessionnel des Vins de Bourgogne, the Comité Interprofessionnel du Vin de Champagne, and the Regional Council of Burgundy for their financial support.


### Notes

The authors declare no competing financial interest.

## ACKNOWLEDGMENTS


We gratefully acknowledge the Trescases Co. for providing cork stoppers.


## ABBREVIATIONS USED

$C_a$: adsorbed oxygen concentration, mol m$^{-3}$
$C_g$: gas oxygen concentration, mol m$^{-3}$
$D$: diffusion coefficient, m$^2$ s$^{-1}$
$D_0$: preexponential factor in the Arrhenius equation, m$^2$ s$^{-1}$
$\Delta G^*$: activation free enthalpy variation, J
$\Delta V^*$: activation volume, nm$^3$
$e$: thickness of membrane, m
$J$: mass flow, kg m$^{-2}$ s$^{-1}$
$l_{es}$: cell length, $\mu$m
$l_{cw}$: thickness of cell wall, $\mu$m
$k_B$: Boltzmann constant, m$^2$ kg s$^{-2}$ K$^{-1}$
$M$: molecular weight, g mol$^{-1}$
$P$: permeability, kg m$^{-1}$ Pa$^{-1}$ s$^{-1}$
$p$: pressure, hPa
$\nabla p$: pressure gradient, Pa m$^{-1}$
$R$: ideal gas constant, J mol$^{-1}$ K$^{-1}$
$S$: entropy, J K$^{-1}$
$T$: temperature, K
$\Psi$: partition coefficient of oxygen between gas and adsorbate calculated from oxygen adsorption isotherm

## REFERENCES


(1) Carvalho, F. J. In *L'Avenir du Liège dans le Monde*; Tlemcen, Oct 20, 2009; Amorim: Tlemcen, Algeria, 2009.

(2) Mano, J. F. The viscoelastic properties of cork. *J. Mater. Sci.* **2002**, *37*, 257−263.
(3) Anjos, O.; Pereira, H.; Rosa, M. E. Effect of quality, porosity and density on the compression properties of cork. *Wood Wood Prod.* **2008**, *66*, 295−301.
(4) *Charte des Bouchonniers Liègeurs*; Fédération Française du Liège: Gensac La Pallue, France, 2006; Vol. Vème édition.
(5) Karbowiak, T.; Gougeon, R. D.; Alinc, J.-B.; Brachais, L.; Debeaufort, F.; Voilley, A.; Chassagne, D. Wine oxidation and the role of cork. *Crit. Rev. Food Sci.* **2010**, *49*, 1−33.
(6) Lambri, M.; Silva, A.; De Faveri, D. M. Relationship between the inner cellulation of synthetic stoppers and the browning of a white over eighteen months of storage. *Ital. J. Food Sci.* **2012**, *24*, 149−158.
(7) Skouroumounis, G. K.; Kwiatkowski, M. J.; Francis, I. L.; Oakey, H.; Capone, D. L.; Duncan, B.; Sefton, M. A.; Waters, E. J. The impact of closure type and storage conditions on the composition, colour and flavour properties of a Riesling and a wooded Chardonnay wine during five years' storage. *Aust. J. Grape Wine Res.* **2005**, *11*, 369−377.
(8) Lee, D. H.; Kang, B. S.; Park, H. J. Effect of oxygen on volatile and sensory characteristics of cabernet sauvignon during secondary shelf life. *J. Agric. Food. Chem.* **2011**, *59*, 11657−11666.
(9) Silva, A.; Lambri, M.; De Faveri, M. D. Evaluation of the performances of synthetic and cork stoppers up to 24 months post-bottling. *Eur. Food Res. Technol.* **2003**, *216*, 529−534.
(10) Lopes, P.; Saucier, C.; Glories, Y. Nondestructive colorimetric method to determine the oxygen diffusion rate through closures used in wine making. *J. Agric. Food. Chem.* **2005**, *53*, 6967−6973.
(11) Brotto, L.; Battistutta, F.; Tat, L.; Comuzzo, P.; Zironi, R. Modified nondestructive colorimetric method to evaluate the variability of oxygen dffusion rate through wine bottle closures. *J. Agric. Food Chem.* **2010**, *58*, 3567−3572.
(12) Keenan, C. P.; Gozukara, M. Y.; Christie, G. B. Y.; Heyes, D. N. Oxygen permeability of macrocrystalline paraffin wax and relevance to wax coatings on natural corks used as wine bottle closures. *Aust. J. Grape Wine Res.* **1999**, *5*, 66−70.
(13) Vidal, J.-C.; Guillemat, B.; Chayvialle, C. Oxygen transmission rate of screwcaps by chemoluminescence and air/capsule/headspace/acidified water system. In *33rd World Congress of Wine 8th General Assembly of the OIV*, Tbilissi, Georgia; OIV: Paris, France, 2010.
(14) Bunner, D.; Landrieux, A.; Valade, M.; Langleron, E.; Tribaut-Sohier, I.; Moncomble, D.; Viaux, L.; Bourdelet Walter, L.; Chaperon, V.; Gouez, B. La mesure de l'oxygène dans les bouteilles par chimiluminescence. *Le Vigneron Champenois* **2010**, *131*, 84−101.
(15) Faria, D. P.; Fonseca, A. L.; Pereira, H.; Teodoro, O. M. N. D. Permeability of cork to gases. *J. Agric. Food Chem.* **2011**, *59*, 3590−3597.
(16) Brazinha, C.; Fonseca, A. P.; Pereira, H.; Teodoro, O.; Crespo, J. G. Gas transport through cork: modelling gas permeation based on the morphology of a natural polymer material. *J. Membr. Sci.* **2013**, *428*, 52−62.
(17) Rabiot, D.; Sanchez, J.; Aracil, J.-M. In *Study of the Oxygen Transfer Through Synthetic Corks for Wine Conservation*; Second European Congress of Chemical Engineering, Montpellier, France; 1999.
(18) Lequin, S.; Chassagne, D.; Karbowiak, T.; Simon, J. M.; Paulin, C.; Bellat, J. P. Diffusion of oxygen in cork. *J. Agric. Food Chem.* **2012**, *60*, 3348−3356.
(19) Cussler, E. L. *Diffusion: Mass Transfer in Fluid Systems*, 3rd ed.; Cambridge University Press: New York, 2009; p 626.
(20) Liger-Belair, G.; Villaume, S. Losses of dissolved $CO_2$ through the cork stopper during champagne aging: toward a multiparameter modeling. *J. Agric. Food Chem.* **2011**, *59*, 4051−4056.
(21) Ito, T.; Seta, J.; Urakawa, H. Effects of pressure and solvent on the diffusion of aromatic compounds through polymers. *Coilloid Polym. Sci.* **1987**, *265*, 557−573.
(22) Mitha, S.; Aziz, M. J.; Schiferl, D.; Poker, D. B. Activation volume for arsenic diffusion in germanium. *Appl. Phys. Lett.* **1996**, *69*, 922−924.
(23) Klopffer, M. H.; Flaconneche, B. Transport de molécules gazeuses dans les polymères: revue bibliographique. *Oil Gas Sci. Technol.* **2001**, *56*, 223−244.
(24) Sing, K. S. W.; Everett, D. H.; Haul, R. A. W.; Moscou, L.; Pierotti, R. A.; Rouquérol, J.; Siemieniewska, T. Reporting physisorption data for gas/solid systems. *Pure Appl. Chem.* **1985**, *57*, 603−619.
(25) Toribio, F.; Bellat, J. P.; Nguyen, P. H.; Dupont, M. Adsorption of water vapor by poly(styrenesulfonic acid), sodium salt: isothermal and isobaric adsorption equilibria. *J. Colloid Interface Sci.* **2004**, *280*, 315−321.
(26) Gibson, L. J.; Easterling, K. E.; Ashby, M. F. The structure and mechanics of cork. *Proc. R. Soc. London A* **1981**, *377*, 99−117.
(27) Karbowiak, T.; Gougeon, R. D.; Alinc, J. B.; Brachais, L.; Debeaufort, F.; Voilley, A.; Chassagne, D. Wine oxidation and the role of cork. *Crit. Rev. Food Sci.* **2010**, *50*, 20−52.
(28) Teti, A. J.; Rodriguez, D. E.; Federici, J. F.; Brisson, C. Non-destructive measurement of water diffusion in natural cork enclosures using terahertz spectroscopy and imaging. *J. Infrared, Millimeter, Tetrahertz Waves* **2011**, *32*, 513−527.
(29) Klugkist, P.; Ratzke, K.; Rehders, S.; Troche, P.; Faupel, F. Activation volume of $^{57}Co$ diffusion in amorphous $Co_{81}Zr_{19}$. *Phys. Rev. Lett.* **1998**, *80*, 3288−3291.
(30) Holzapfel, C.; Chakraborty, S.; Rubie, D. C.; Frost, D. J. Effect of pressure on Fe-Mg, Ni and Mn diffusion in $(Fe_xMg_{1-x})(2)SiO_4$ olivine. *Phys. Earth Planet. Inter.* **2007**, *162*, 186−198.
(31) Zhao, Y. C.; Aziz, M. J.; Gossmann, H. J.; Mitha, S.; Schiferl, D. Activation volume for boron diffusion in silicon and implications for strained films. *Appl. Phys. Lett.* **1999**, *74*, 31−33.

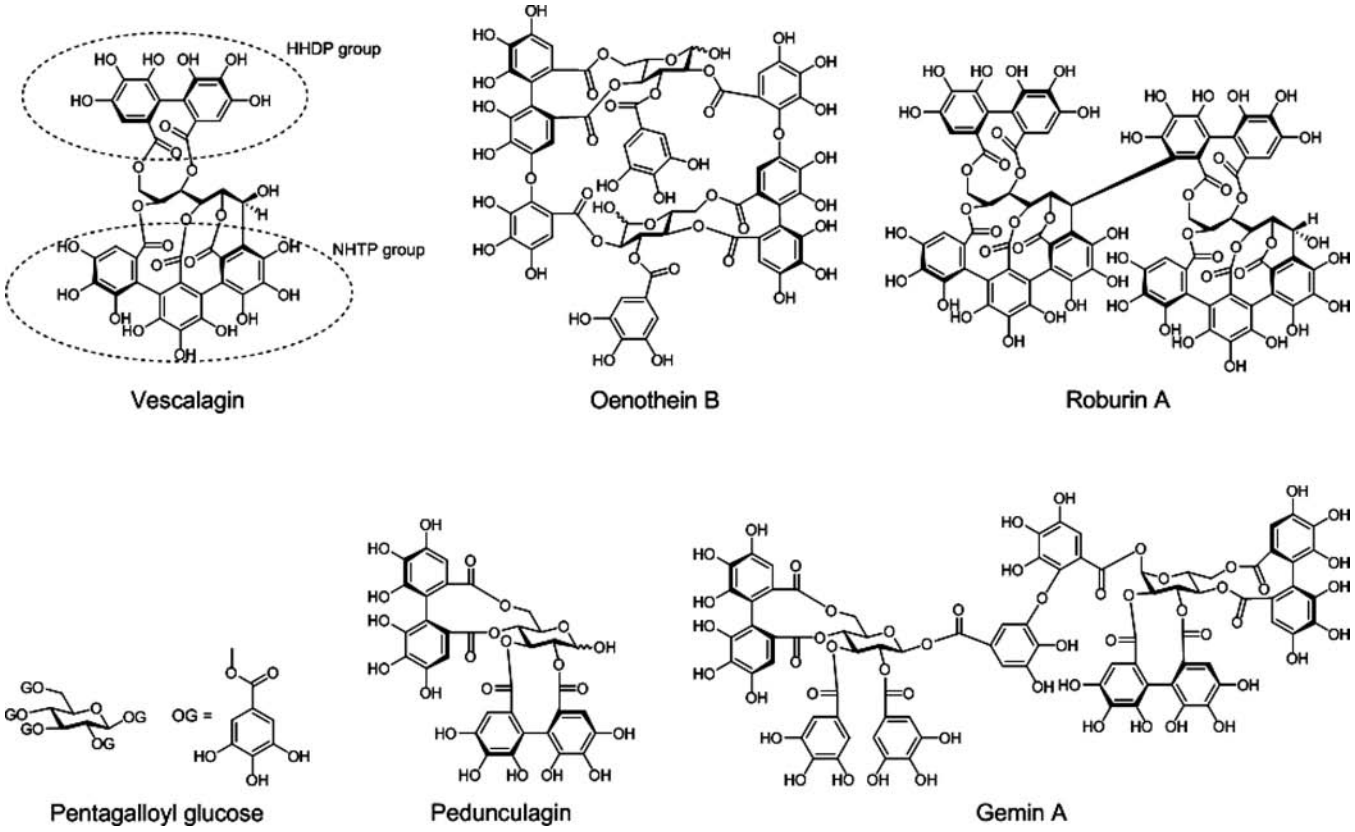


**Figure 1.** Structures of ellagitannins and pentagalloyl glucose.

$10^5$ $M^{-1}$, and for ETs interacting with the highly flexible gelatin these were ca. $10^6$ $M^{-1}$.[19]

ETs are unique among tannins as (i) they can be isolated as pure compounds (unlike most condensed tannins, which tend to be obtained as closely related mixtures), (ii) they possess a wide range of molecular flexibilities (in contrast to gallotannins or condensed tannins), and (iii) their water solubilities are inversely correlated to their protein precipitation capacities.[9] ETs, therefore, offer an opportunity for investigating the relative importance of molecular flexibility and size within a series of matched tannin compounds.

We chose two monomeric and three dimeric ETs that differ in molecular flexibility (i.e., their bond rotational flexibility) and water solubility. Vescalagin and its dimer, roburin A, represent ETs with NHTP groups that are linked to an acyclic glucose. They are consumed in wine that has been stored in oak barrels. Walnuts are a rich source of pedunculagin, which represents ETs with HHDP groups and a cyclic glucose. The dimers, oenothein B and gemin A, can be found in several European and Japanese herbal medicines[1,26] and differ in their molecular flexibilities. The water solubilities of these ETs decrease in the following order: vescalagin > pedunculagin ≈ roburin A > oenothein B > gemin A.[9]

The present study investigated the effects of flexibility and size on the thermodynamics of the ET−protein interaction using isothermal titration calorimetry and fluorescence spectroscopy to probe their interaction mechanisms and binding sites. We chose bovine serum albumin (BSA) as the protein-binding partner for two reasons. First, BSA is a widely used model for globular proteins such as Rubisco, which is a major dietary protein.[27,28] Recent studies have shown that the binding affinity in tannin−protein complexes was negatively correlated with digestibility.[29−31] Second, albumins are involved in transporting dietary polyphenols[32,33] and drugs to their molecular targets[34,35] and exhibit a large sequence homology, for example, 76% in the case of BSA and human serum albumin.[36] It is, therefore, important to understand how ellagitannins interact with globular proteins, as this may also affect protein−drug interactions in the digestive tract and in blood plasma.[35]

## MATERIALS AND METHODS

**Ellagitannins.** Two monomeric ellagitannins (pedunculagin and vescalagin) and three dimeric ellagitannins (oenothein B, roburin A, and gemin A) were extracted from plants and purified as described previously.[37]

**Isothermal Titration Calorimetry.** Titrations of BSA (purity ≥ 99%, essentially globulin free, 66 kDa; Sigma, Poole, Dorset, UK) with ellagitannins were performed using a NanoITC instrument (TA Instruments Ltd., Crawley, West Sussex, UK) as described previously[19,28] with few adaptations. All solutions were prepared in 50 mM citrate buffer at pH 6 and were degassed under vacuum prior to use. In a typical experiment, buffered BSA solution (20 $\mu$M) was placed in the 950 $\mu$L sample cell of the calorimeter, and buffered ellagitannin solution (3 mg $mL^{-1}$) was loaded into the injection syringe. Ellagitannin was titrated into the sample cell at 298 K as a sequence of 24 injections of 10 $\mu$L aliquots for monomeric ellagitannins (pedunculagin and vescalagin) and 48 injections of 10 $\mu$L aliquots for dimeric ellagitannins (oenothein B, roburin A, and gemin A). The time delay (to allow equilibration) between successive injections was 360 s. The contents of the sample cell were stirred throughout the experiment to ensure thorough mixing.

Raw data were obtained as plots of heat ($\mu$J) against injection number and featured a series of peaks for each injection. These raw data peaks were transformed using the instrument software to obtain a


dx.doi.org/10.1021/jf502174r | J. Agric. Food Chem. 2014, 62, 9186−9194

plot of observed enthalpy change per mole of injectant ($\Delta H_{obs}$, kJ mol$^{-1}$) against molar ratio (see ITC Data Analysis).

Control experiments included the titration of buffered ellagitannin solutions into buffer, buffer into BSA, and buffer into buffer; controls were repeated for each BSA concentration. Control experiments of buffer titrated into buffer or protein solutions both resulted in small and equal enthalpy changes for each successive injection of buffer and, therefore, were not further considered in the data analysis.[38] Experimental data were analyzed after subtraction of the tannin into buffer control data from the sample data. Ellagitannin molecules tend to self-associate into aggregates due to hydrophobic groups; therefore, when injected from the syringe into buffer the ellagitannin molecules undergo an endothermic process of deaggregation, analogous to surfactant demicellization.[39] The extent of deaggregation depends inversely on the concentration of ellagitannin already present in the sample cell; therefore, successive injections of ellagitannin into buffer lead to the observation of progressively lower endothermic enthalpy changes as has been illustrated in earlier work.[39] The data are shown after subtraction of the effects of ellagitannin deaggregation, which means that the assumption is made that ellagitannins dissociate prior to binding.

**Isothermal Titration Calorimetry Data Analysis.** Estimated binding parameters were obtained from ITC data using the Bindworks (version 3.1.13, Applied Thermodynamics, Hunt Valley, MD, USA) data analysis program. Data fits were obtained using a model for two independent sets of multiple binding sites. For this model, the analytical solution for the total heat measured ($Q$) is determined by the formula

$$Q = V[\mathrm{M}]\left\{\frac{n_1\Delta H_1 K_1[\mathrm{L}]}{1 + K_1[\mathrm{L}]} + \frac{n_2\Delta H_2 K_2[\mathrm{L}]}{1 + K_2[\mathrm{L}]}\right\} \quad (1)$$

where $n_1$ and $n_2$ are the molar ratios of interacting species, $\Delta H_1$ and $\Delta H_2$ are the enthalpies, and $K_1$ and $K_2$ are the equilibrium binding constants (syn. affinity constants) for each of the two sets of multiple binding sites.[40] The quality of fit was determined by calculation of $\chi^2$; the data fits were acceptable in each case because the $\chi^2$ values were less than the critical values for the appropriate degree of freedom.

**Tryptophan Fluorescence Quenching.** Fluorescence intensity was recorded using an FP-6200 spectrofluorometer (JASCO UK Ltd., Great Dunmow, Essex, UK) with selective excitation of tryptophan residues in BSA at 295 nm. The excitation and emission slits were 5 nm, and the emission spectrum was recorded between 300 and 500 nm. The measured fluorescence intensities are reported without correction for inner filter effects.[41]

Titration of BSA (5 $\mu$M, 2 mL) with ellagitannin (3 mg mL$^{-1}$, 500 $\mu$L) was carried out as a sequence of aliquots (10 $\mu$L up to volume of 100 $\mu$L, 20 $\mu$L up to a volume of 460 $\mu$L). For the calculation of quenching constants, the data were plotted as a Stern−Volmer plot of $F_0/F$ against [Q] and the quenching constant, $K_{SV}$, calculated by linear regression.[42] According to the Stern−Volmer equation

$$\frac{F_0}{F} = 1 + k_q\tau_0[\mathrm{Q}] = 1 + K_{SV}[\mathrm{Q}] \quad (2)$$

where $F_0$ and $F$ are the fluorescence intensities before and after the addition of the quencher, respectively, $k_q$ is the bimolecular quenching constant, $\tau_0$ is the lifetime of the fluorophore in the absence of quencher, [Q] is the concentration of the quencher (in this case tannin), and $K_{SV}$ is the Stern−Volmer quenching constant.

However, in the case of combined dynamic and static quenching, where the Stern−Volmer plot exhibits an upward curvature (concave toward the $y$-axis), an alternative equation[42]

$$\frac{F}{F_0} = 1 + K_{app}[\mathrm{Q}] \quad (3)$$

can be used for fitting, where

$$K_{app} = \left[\frac{F}{F_0} - 1\right]\frac{1}{[\mathrm{Q}]} = (K_D + K_S) + K_D K_S[\mathrm{Q}] \quad (4)$$

The actual plot of $K_{app}$ or $((F/F_. - 1)/Q)$ versus [Q] yields a straight line with an intercept of $K_D + K_S$ and a slope of $K_D K_S$.

**Molecular Modeling.** Molecular modeling was performed with MOE2011.10 (Chemical Computing Ltd., Montreal, Canada). Atomistic models of the respective tannins were built from chemical structures on an atom by atom basis using the Builder Module of MOE. All models were energy minimized to convergence (rms gradient of 0.05 kcal/mol) using the MMX94x force field by smart minimization (steepest descents, followed by conjugate gradient, and truncated Newton−Raphson methods). Physical parameters were calculated from these models using the QuasAR module in MOE. Parameters calculated were accessible surface area (ASA) and hydrophobic accessible surface area (ASA_H). Molecular flexibility was calculated by performing a conformational energy search about the torsion angles of each model using Lowmode Molecular Dynamics in the Conformational Analysis module of MOE. Results from conformational analysis were stored in databases of conformations for each tannin indexed by final energy.

## RESULTS AND DISCUSSION

This study investigated the interaction between BSA and five ellagitannin compounds using ITC and fluorescence spectroscopy. The molecular flexibility and surface areas of five ellagitannins and pentagalloyl glucose were modeled to improve our understanding of these interactions.

**Molecular Flexibility of Ellagitannins.** Molecular simulation was used to assess molecular flexibility in terms of numbers of low-energy conformations located and energy of these conformers (Table 1). Modeling experiments[43] demonstrated previously that the nonahydroxytriphenoyl (NHTP) group is much less flexible than the hexahydroxydiphenoyl (HHDP) group (Figure 1) and the low-energy conformers of the monomers clearly reflect the extent of these structural constraints: pentagalloyl glucose conformers ($n$ = 21) ranged from 110 to 116 kcal mol$^{-1}$ (no NHTP or HHDP groups), pedunculagin conformers ($n$ = 4) from 158 to 164 kcal mol$^{-1}$ (2 HHDP groups), and vescalagin conformers ($n$ = 18) from 229 to 236 kcal mol$^{-1}$ (1 NHTP, 1 HHDP group). The low-energy conformers of the dimers followed a similar trend: oenothein B conformers ($n$ = 2) had 278−280 kcal mol$^{-1}$ (2 HHDP groups), gemin A ($n$ = 1) had 323 kcal mol$^{-1}$ (3 HHDP groups), and roburin A conformers ($n$ = 4) had 406−412 kcal mol$^{-1}$ (2 NHTP, 2 HHDP groups).

**Table 1. Modeling of Minimized Energies and Associated Numbers of Conformers, Accessible Hydrophobic Surface Area (ASA_H), and Accessible Surface Area (ASA)**

| compound | mol wt (Da) | energy of conformers (kcal/mol) | no. of conformers | ASA_H (nm$^2$) | ASA (nm$^2$) |
|---|---|---|---|---|---|
| vescalagin | 935 | 229−236 | 18 | 253 | 914 |
| roburin A | 1843 | 406−412 | 4 | 407 | 1587 |
| pedunculagin | 769 | 158−164 | 4 | 293 | 867 |
| oenothein B | 1569 | 278−280 | 2 | 524 | 1485 |
| pentagalloyl glucose | 927 | 110−116 | 21 | 373 | 1041 |
| gemin A | 1841 | 323 | 1 | 574 | 1748 |

**Isothermal Titration Calorimetry of Ellagitannin−Bovine Serum Albumin Interactions and Data Fitting.** ITC experiments for ellagitannin titration into BSA were carried out for five ellagitannins (depicted in Figure 1). Figure 2 shows the ITC binding isotherms for the interaction with BSA of vescalagin and its dimer, roburin A, consisting of the

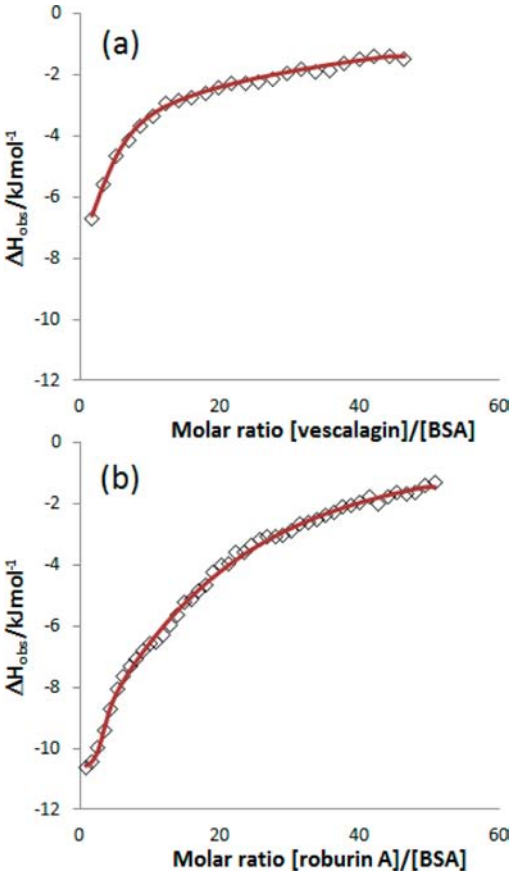


**Figure 2.** ITC binding isotherms for the interaction of bovine serum albumin with the monomer−dimer pair of (a) vescalagin and (b) roburin A. Data were fitted assuming a model for two independent binding sites, and values obtained from these fits are given in Table 2.

experimental data (as points) and the binding model that best fitted to each data set (as lines). For both ellagitannins, the binding interaction led to an exothermic response, which decreased in magnitude with successive titration injections and signifies a saturation of binding sites on BSA.

As found in previous studies,[24,39] small but significant exothermic peaks were observed at higher tannin/protein molar ratios at and beyond the point of apparent binding site saturation. This means that titration experiments did not reach zero enthalpy change, even after removal of effects from control experiments (e.g., tannin titration into buffer). Therefore, we have assumed that the interaction between ellagitannin and BSA has not reached completion at the higher ellagitannin/protein ratios measured. As a consequence, upon fitting the data to a binding model, this long tail of exothermic peaks prevents the use of a model based on a single set of multiple binding sites (one-site model), and, therefore, all data were fitted to a two independent binding site model. A previous study of the interaction between pentagalloyl glucose with BSA or Rubisco described the selection of the two independent binding site model in more detail.[28]

Figure 3 shows the ITC binding isotherms for pedunculagin and the related dimers oenothein B and gemin A. As observed for the vescalagin and roburin A isotherms, the binding isotherm for the dimers shows a clear two-phase shape to the isotherm that signifies two or more binding sites are involved in the interaction. For the oenothein B and gemin A ellagitannins, the titration experiments were extended by increasing the number of titration injections to observe the interaction at higher molar ratios (see Materials and Methods for more details). The thermodynamic binding parameters for the ellagitannin−BSA interaction were obtained from a two-site model and are shown in Table 2, which also includes data from our previous study on pentagalloyl glucose binding to BSA for comparison.[28]

**Thermodynamic Parameters of Ellagitannin−BSA Interactions in Relation to Molecular Flexibility.** In these studies, the excellent fits of the ITC data have enabled us to probe the effects of different structural characteristics of the ellagitannins on their interaction with BSA. The results will be discussed in terms of monomer−dimer pairs and molecular flexibilities. The weakness of the second binding site allows, however, for some uncertainties in exact values for these fits, but does confirm our previous observations, which included related ellagitannins and suggested that these were able to bind (adsorb) nonselectively.[24,28,39]

The ellagitannin monomers, pedunculagin and vescalagin, show equivalent strengths of interaction ($K_1$ = 4.2 and 5.2 × $10^4$ $M^{-1}$), and so do the roburin A and oenothein B dimers ($K_1$ = 2.3 and 6.5 × $10^5$ $M^{-1}$) (Table 2). In contrast, the $K_1$ affinity constants of pentagalloyl glucose and gemin A were 1 order of magnitude larger than for the other monomers and dimers ($K_1$ = 1.8 × $10^5$ and 1.8 × $10^6$ $M^{-1}$, respectively). This coincides with the fact, as pointed out above, that both have low conformational energies and are flexible molecules. Taken together, gemin A has several features, that is, single bonds and "free" galloyl groups, which may allow selective binding to specific amino acids on the protein surface. These findings are in line with two other studies that reported weaker binding by vescalagin[44] and by its isomer, castalagin,[29] to BSA compared to pentagalloyl glucose. It appears that pentagalloyl glucose and gemin A have optimal structures for BSA binding within the group of tannins studied here.

For both binding sites the interaction in terms of the affinity constants, $K_1$ and $K_2$, is approximately 1 order of magnitude different between monomers and dimers (Table 2). For each of the comparable ellagitannin monomer−dimer pairs, the dimer was shown to bind more strongly than the monomer. It can also be seen that $K_2$ is 1 order of magnitude weaker than $K_1$. This weaker second binding site is likely to correspond to nonspecific adsorption of tannins that may lead to coating of the protein surface[28,45] and eventual precipitation of the tannin−protein complex in some systems. The binding isotherms in Figures 2 and 3 for the dimers show a greater exothermic response than for the corresponding monomers, for example, roburin A versus vescalagin ($\Delta H_1$ = −15.3 vs −7.5 kJ $mol^{-1}$), oenothein B versus pedunculagin ($\Delta H_1$ = −21.6 vs −10.9 kJ $mol^{-1}$), and gemin A versus pentagalloyl glucose ($\Delta H_1$ = −47.4 vs −29 kJ $mol^{-1}$) (Table 2).

A closer look at the monomer series and the dimer series (each having tannins with similar molecular weights) suggests that the strength of binding is inversely related to the minimized energies and increases with a greater potential for rotational flexibility as follows (Table 1). The low-energy conformers and binding constants, $K_1$, of the monomers are 229−236 kcal/mol and 5.2 × $10^4$ $M^{-1}$ for vescalagin, 158−164 and 4.2 × $10^4$ for pedunculagin, and 110−116 and 1.8 × $10^5$ for pentagalloyl glucose, respectively. For the dimer series the corresponding values are 406−412 kcal/mol and 2.3 × $10^5$ $M^{-1}$ for roburin A, 278−280 and 6.5 × $10^5$ for oenothein B, 323 and 1.8 × $10^6$ for gemin A.


dx.doi.org/10.1021/jf502174r | J. Agric. Food Chem. 2014, 62, 9186−9194

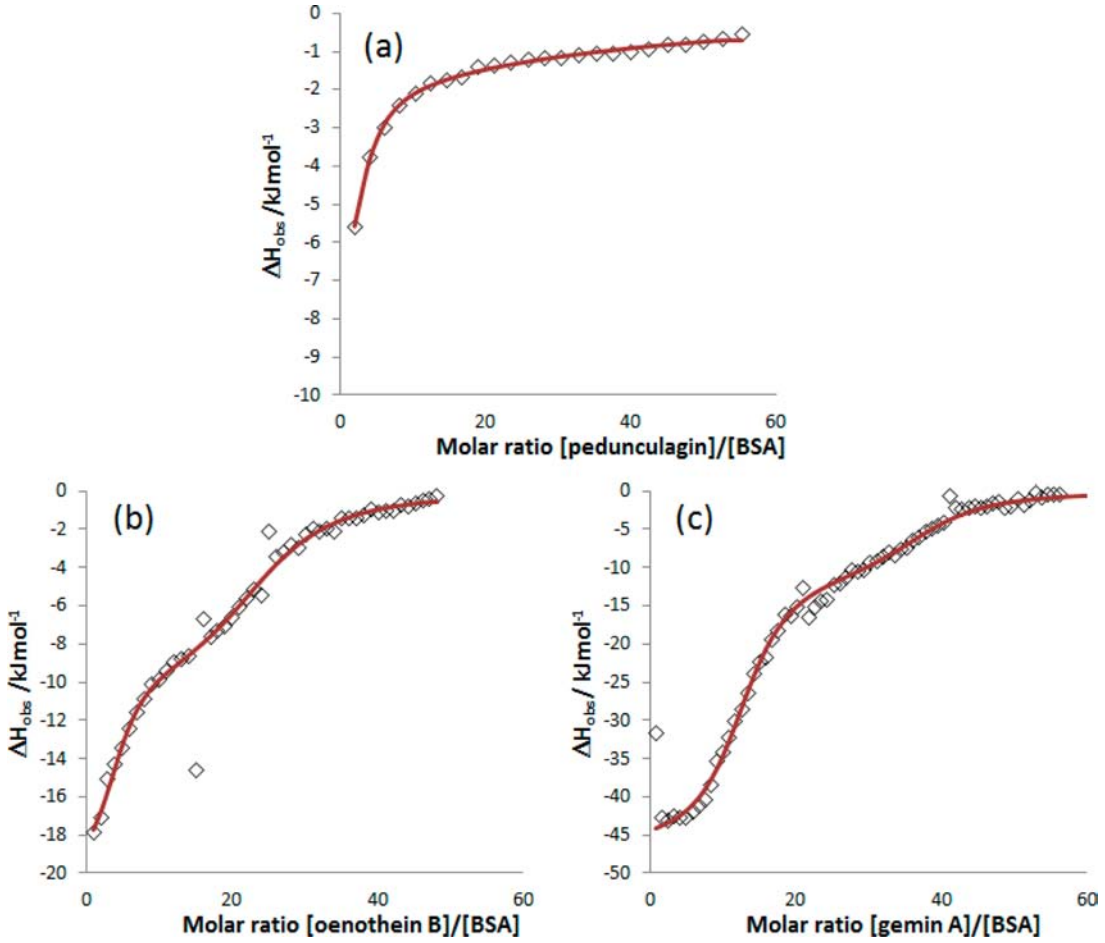


**Figure 3.** ITC binding isotherms for the interaction of bovine serum albumin with the monomer−dimer pairs of (a) pedunculagin, (b) oenothein B, and (c) gemin A. Data were fitted assuming a model for two independent binding sites, and values obtained from these fits are given in Table 2.

**Table 2. Estimated Thermodynamic Binding Parameters for the Interaction between Five Ellagitannins and Pentagalloyl Glucose[b] with Bovine Serum Albumin at pH 6[a]**

| | vescalagin | roburin A | pedunculagin | oenothein B | pentagalloyl glucose[b] | gemin A |
|---|---|---|---|---|---|---|
| $n_1$ | 2.5 ± 0.5[c] | 1.9 | 2.1 | 4.1 | 26 | 13 |
| $K_1$ ($M^{-1}$) | 5.2 (±2.3) × $10^4$ | 2.3 × $10^5$ | 4.2 × $10^4$ | 6.5 × $10^5$ | 1.8 × $10^5$ | 1.8 × $10^6$ |
| $\Delta H_1$ (kJ $mol^{-1}$) | −7.5 ± 1.0 | −15.3 | −10.9 | −20.6 | −29 | −47.4 |
| $\Delta S_1$ (J $mol^{-1}$ $K^{-1}$) | 65.1 | 33.2 | 51.9 | 42.2 | 3.3 | −39.3 |
| $n_2$ | 30 ± 4 | 16 | 30 | 20 | 26 | 25 |
| $K_2$ ($M^{-1}$) | 1.1 (±0.07) × $10^3$ | 1.8 × $10^4$ | 1.1 × $10^3$ | 3.3 × $10^4$ | 8 × $10^2$ | 6.3 × $10^4$ |
| $\Delta H_2$ (kJ $mol^{-1}$) | −6.7 ± 1.3 | −8.17 | −5.1 | −10.3 | −29 | −11.4 |
| $\Delta S_2$ (J $mol^{-1}$ $K^{-1}$) | 35.7 | 54.0 | 41.1 | 51.9 | −41.7 | 53.6 |
| $\chi^2$ | 0.65 ± 0.16 | 0.87 | 1.99 | 8.07 | | 3.29 |

[a] $\Delta H_1$ and $\Delta H_2$ are the enthalpies, and $K_1$ and $K_2$ are the equilibrium binding constants for two binding sites. [b] Data are included for comparison (Dobreva et al.[28]). [c] ± standard deviation, $n$ = 3.

The number of strong (type 1) binding sites increases for ellagitannins with more flexibility and "free" galloyl groups from $n_1$ = 1.9 for roburin A to $n_1$ = 4.1 for oenothein B and $n_1$ = 13 for gemin A. The binding parameters for two of the monomer−dimer pairs, that is, the vescalagin−roburin A and pedunculagin−oenothein B pairs, show similarities in the stoichiometry of the interaction. For the vescalagin−roburin A pair the stronger binding site $n_1$ is 2.5 for the monomer and 1.9 for the dimer, and for the second weaker binding site $n_2$ is 30 for the monomer and 16 for the dimer. For the pedunculagin−oenothein B pair $n_1$ is 2.1 for the monomer and 4.1 for the dimer, and $n_2$ is 30 for the monomer and 20 for the dimer. However, for the most flexible monomer−dimer pair, which will be able to better support H-bonding, the stoichiometric values were much higher for the stronger binding site: $n_1$ was 26 for pentagalloyl glucose and 13 for gemin A. The difference reflects the fact that gemin A is twice the molecular size of pentagalloyl glucose. We reported previously that the sum of $n_1$ and $n_2$ indicated that 52 pentagalloyl glucose molecules are bound to BSA, and this suggested surface coating as the BSA surface can theoretically accommodate 40−120 pentagalloyl glucose molecules.[28] Similarly, the sum of $n_1$ and $n_2$ for gemin A indicated that 38 gemin A dimers were bound (which equates to 76 "monomers") and matches with the calculated surface


dx.doi.org/10.1021/jf502174r | J. Agric. Food Chem. 2014, 62, 9186−9194

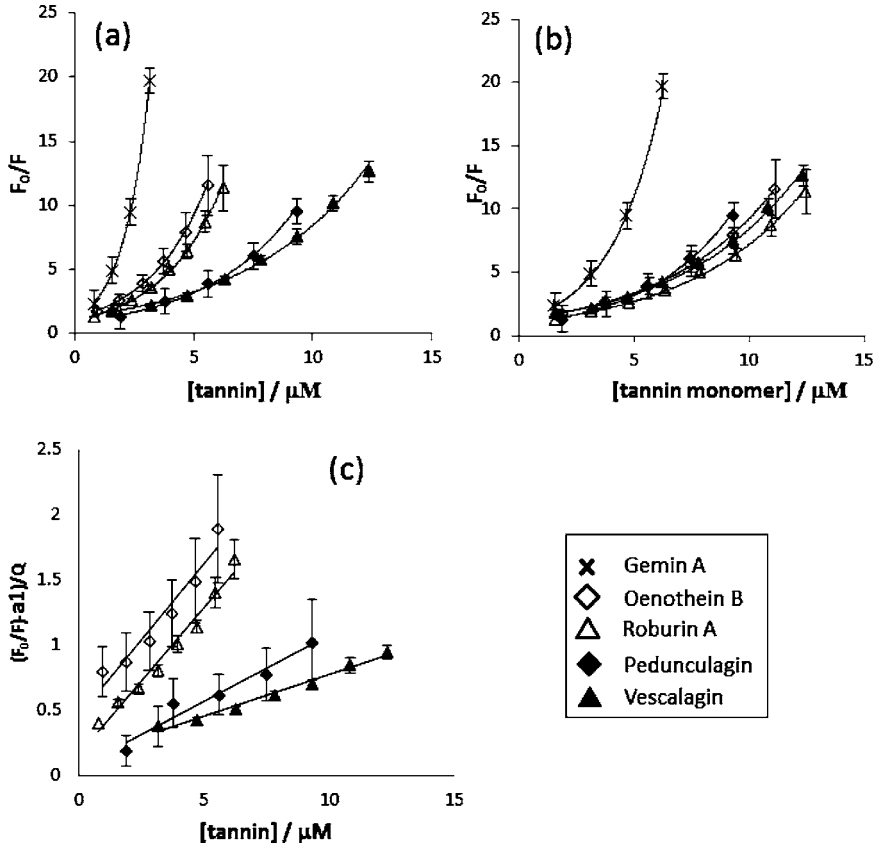


**Figure 4.** Fluorescence quenching of tryptophans in BSA by vescalagin, roburin A, pedunculagin, oenothein B, and gemin A plotted as (a) the ratio of initial fluorescence intensity to total fluorescence intensity versus ellagitannin concentration, (b) the ratio of initial fluorescence intensity to total fluorescence intensity versus ellagitannin monomer concentration, and (c) a modified Stern–Volmer plot to reflect contributions from both static and dynamic quenching (data are shown for vescalagin, roburin A, pedunculagin, and oenothein B only).

area. It also suggests that gemin A due to its flexibility is capable of coating the whole BSA protein just like pentagalloyl glucose.[28] Comparable stoichiometries were found for commercial preparations of the flexible taratannins when a molecular weight of 1500 was assumed: that is, 48:1 for the taratannin/BSA ratio.[39]

It is, however, of note that this molecular size effect was not observed to the same extent for the other pairs as monomers and dimers had similar $n_1$ values (2–4) and similar sums of $n_1 + n_2$ (i.e., 33 for vescalagin/18 for roburin A and 32 for pedunculagin/24 for oenothein B). This indicates that the less flexible structures and especially roburin A were less able to stretch out on the BSA surface.

Many more binding constants are available for flavonoids and condensed tannins than for ellagitannins. Nevertheless, pure flavonoid compounds tend to have affinities comparable to those of the ellagitannins investigated here. $K_a$ constants with BSA of $10^2$–$10^5$ $M^{-1}$ were reported for monomeric and polymeric flavanols[19,31] and of $10^4$–$10^5$ $M^{-1}$ for flavones and flavonols.[46−49] Examples of polyphenol complexes with human serum albumin include epigallocatechin gallate and diosmetin interactions that exhibited comparable Stern–Volmer affinity constants of ~$10^5$ $M^{-1}$ from fluorescence data.[50,51]

The findings also match results from previous studies, in which less pure tannins had been used, and confirm that the tannin components of those fractions did indeed dominate the interaction observed.[19,24,39] The present study used a two-site binding model and found $K_1$ of $10^4$–$10^5$ and $K_2$ of $10^3$–$10^4$ $M^{-1}$ for the monomers in BSA complexes. In comparison, data obtained with a single-site model gave $K$ values of ~$10^3$ $M^{-1}$ for chestnut– and myrabolan–BSA complexes.[24]

Quideau et al.[5] reported that most polyphenols, including ellagitannins, when bound at protein surfaces, exhibited affinity constants that were rarely above the micromolar range, that is, $K_a$ of ≤$10^6$ $M^{-1}$. However, Xiao et al.[52] also reported much larger constants of up to $10^8$ $M^{-1}$ for some flavanoid and flavonoid–human serum albumin complexes. Not surprisingly, some receptor and enzyme targets had particularly high selectivities with affinity constants at the subnanomolar scale and varied between ellagitannins even if these were of similar molecular weights.[5,53]

The data in Table 2 showed positive entropies at both types of binding sites for all but one ellagitannin, that is, gemin A. Positive $\Delta S_1$ values ranged from 33 to 65 and $\Delta S_2$ values from 36 to 54 J $mol^{-1}$ $K^{-1}$ and are indicative of a dominance of hydrophobic interactions.[19,50,54] Gemin A was the only ellagitannin giving a negative entropy, −39 J $mol^{-1}$ $K^{-1}$. For comparison purposes, we have included here also the entropies for pentagalloyl glucose, which show that the highly flexible pentagalloyl glucose and gemin A had noticeably lower entropies at the stronger binding site than the other ellagitannins and were, therefore, apparently better able to form hydrogen bonds.[54] The positive entropies for all ellagitannins at the second binding site are consistent with hydrophobic stacking on the BSA surface, although some uncertainty exists with these values as the affinities were very low for some tannins ($K_2$ = $10^3$ $M^{-1}$). The literature contains examples of both hydrogen bonding and hydrophobic


dx.doi.org/10.1021/jf502174r | J. Agric. Food Chem. 2014, 62, 9186–9194

Table 3. Estimated Quenching Parameters for the Interaction of Ellagitannins with Bovine Serum Albumin ($n$ = 3)

| fluorescence parameter | vescalagin | roburin A | pedunculagin | oenothein B | gemin A |
|---|---|---|---|---|---|
| $K_{SV}$ ($M^{-1}$) | 0.42 (±0.07) × $10^5$ | 1.03 (±0.07) × $10^5$ | 0.53 (±0.1) × $10^5$ | 1.44 (±0.28) × $10^5$ | 3.13 (±0.06) × $10^5$ |
| bathochromic (red) shift of $\lambda_{max}$ (nm) | 8.7 ± 0.4 | 8.7 ± 0.4 | 4.7 ± 0.9 | 4.0 ± 1.0 | 10.3 ± 0.4 |

interactions in tannin−protein complexes.[16,19,22,50,55] Taken together, the present study also suggests that both types of bonding interactions occur in these ellagitannin−BSA complexes, and slight structural differences appear to dictate which of these will dominate.

**Quenching of the BSA Tryptophan Fluorescence by Ellagitannins.** To complement the ITC measurements, ellagitannin binding to BSA was also investigated by fluorescence spectroscopy. These experiments measure the quenching of the intrinsic tryptophan fluorescence of BSA[32] after binding with each of the tannins. Two tryptophan residues are found near the BSA surface, one is within its hydrophobic binding pocket (Trp 212) and the other within the surface region of the protein (Trp 134).[49] Figure 4a shows Stern−Volmer plots that describe tryptophan quenching as a function of tannin concentration. In these plots $F_0/F$ increases as fluorescence intensity decreases in the presence of quencher ($F$) relative to the native fluorescence in the absence of quencher ($F_0$). The data suggest that the rate of decrease in fluorescence with respect to quencher concentration depends on the molecular size and flexibility of the tannin. The data in Figure 4a revealed that four of the tannins fall into either monomer or dimer groups: the monomers, vescalagin and pedunculagin, exhibit similar quenching behaviors, and the dimers, roburin A and oenothein B, also behave similarly to one another. The dimers were more efficient quenchers than the monomers, requiring approximately half the molar tannin concentration to produce equivalent levels of quenching. Indeed, if the quenching data are normalized, as in Figure 4b where Stern−Volmer plots are given as a function of "tannin monomer" concentration, thus removing the effects of molecular weight, it can be seen that related monomer−dimer pairs overlay, which demonstrates similar quenching efficiency per monomer unit. In contrast to these four tannins, the most flexible dimer, gemin A, is a much more efficient quencher at much lower concentrations. Pentagalloyl glucose is also a more efficient quencher, $K_{SV} \sim 2 \times 10^6$ $M^{-1}$,[28] than vescalagin and pedunculagin, but pentagalloyl glucose and gemin A are not a true monomer−dimer pair and thus do not overlay exactly.

The purpose of the Stern−Volmer plot of fluorescence quenching data is to generate a linearized data set that allows assessment of the ability of tannins to quench the BSA tryptophan residues. The slope of the straight line of best fit is termed the Stern−Volmer quenching constant ($K_{SV}$). From the data shown in Figure 4a, $K_{SV}$ values of $10^4$−$10^5$ $M^{-1}$ have been calculated from a straight-line plot through the linear region at low tannin concentrations (Table 3) and are comparable with $K_{SV}$ values of $10^4$ $M^{-1}$ for tea, coffee, and cocoa extracts[31] and with 6.85 × $10^4$ $M^{-1}$ for quenching of human serum albumin by epigallocatechin gallate (EGCg).[50] These fluorescence data complement the ITC data by providing additional support for the findings outlined above. The trend in terms of the quenching constants, $K_{SV}$, matches that seen from ITC measurements of the affinity constants, $K_1$, with a linear correlation ($R^2$ = 0.988) between $K_{SV}$ and the binding affinity constant, $K_1$ (Tables 2 and 3).

However, it should be noted that each of the Stern−Volmer plots is nonlinear and curves toward the $y$-axis with higher tannin concentration. This is not unusual in Stern−Volmer plots and provides information on the type of quenching. An upward slope suggests a combination of both static and dynamic quenching in these ellagitannin−BSA systems.[42] Static quenching is associated with a strong coupling (e.g., formation of a ground-state complex) between interacting molecules, whereas dynamic quenching is associated with weak coupling (e.g., through-space interactions or collisions).[42] To further confirm that the curvature was indeed due to combined static and dynamic quenching, a modified form of the Stern−Volmer equation was used (see Materials and Methods) that is second order with respect to [Q], and this gave as predicted a linear plot (Figure 4c).

**Polarity of the Tryptophan Environment.** Fluorescence spectra can also yield information on another parameter, that is, the position of the emission peak maximum ($\lambda_{em}$), which can reflect the polarity of the tryptophan environment.[50] The presence of ellagitannins led to a bathochromic or red shift in $\lambda_{em}$ (Table 3), suggesting that the tryptophan environment became more polar upon interaction with ellagitannins. The observed red shift may suggest a change to the protein's tertiary structure and thus account for the associated increase in the polarity of the tryptophan environment.[28] However, it is difficult to conclude this solely on the basis of the data reported here. A shift to a more polar environment could suggest unfolding of the protein and thus greater solvent exposure or more H-bonding between BSA and the tannins. However, Li et al.[30] reported a slight blue shift upon binding of tannic acid (i.e., a mixture of gallotannins containing either a central glucose or quinic acid) to ferritin, whereas Dobreva et al.[28] measured a red shift of 5 nm when pure pentagalloyl glucose bound with BSA. The magnitude of the red shift appears to be linked to tannin structure as related monomer−dimer pairs showed some similarities: vescalagin and roburin A generated a 8−9 nm shift and pedunculagin and oenothein B a 4−5 nm shift, but gemin A caused the greatest shift in $\lambda_{em}$ of 10.3 nm. A similarly large red shift of 12 nm was observed for Trp during EGCg binding to human serum albumin.[50] Other experiments will be needed to establish the precise reasons for the observed differences in red shifts.

In conclusion, our ITC data suggest that there are two types of binding sites for ellagitannin binding to BSA. A stronger binding site may well be more selective and dependent on tannin flexibility and the presence of free galloyl groups. Indeed, our previous study suggested a link between the number of aromatic residues on the surface of a globular protein, Rubisco, and pentagalloyl glucose binding.[28] This could explain the relationship between $K_1$ and the hydrophobic accessible surface area, ASA_H (Figure 5), that is, $K_1 = 0.2125e^{0.0114ASA_H}$ ($R^2$ = 0.965), and points to the fact that hydrophobic interactions are an important driver for affinity during BSA−ellagitannin complex formation as supported by positive entropies for five of the six ellagitannins studied here.

A second weaker binding site was required to fit our data to allow for the binding interactions observed at high tannin/

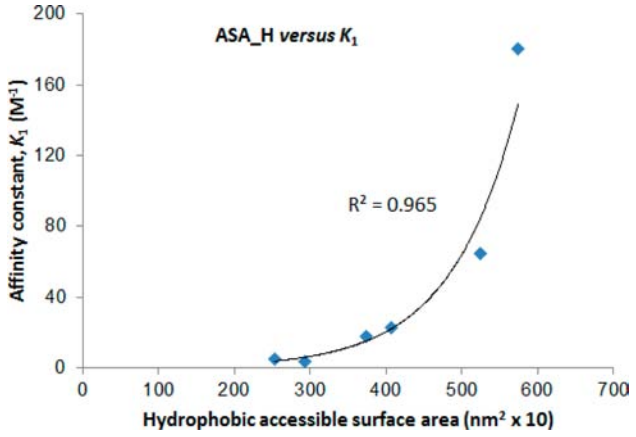


**Figure 5.** Relationship between the affinity constant, $K_1$, and the modeled accessible hydrophobic surface area (ASA_H).

protein molar ratios. This second binding site was associated with high values of $n_2$ for all tannins and suggests nonselective adsorption of tannin to the protein surface. Such findings suggest tannin binding to BSA is concentration dependent, where specific binding might dominate at low concentrations and nonselective adsorption at higher concentrations of tannin.[16] These studies have shown that ellagitannin binding to BSA increases in strength and affinity for the larger tannins (dimers) compared to their monomer forms. Bond rotational flexibility of the tannin also plays a role by increasing the strength of interaction and number of stronger (possibly hydrogen bonding) binding sites on the protein surface.

## AUTHOR INFORMATION


### Corresponding Authors

*(R.J.G.) Phone: +44-118-378-8446. Fax: +44-118-378-6562. E-mail: rebecca.green@reading.ac.uk.

*(I.M.-H.) Phone: +44-118-378-6619. Fax: +44-118-935-2421. E-mail: i.mueller-harvey@reading.ac.uk.



### Funding

This study was supported by the EU Marie Curie Research Training Network "HealthyHay" (Contract MRTN-CT-2006-035805) and Academy of Finland (Grant 258992 to J.-P.S.).


### Notes

The authors declare no competing financial interest.

## ACKNOWLEDGMENTS


Kristiina Lehtonen is acknowledged for help with ellagitannin purification.


## ABBREVIATIONS USED

BSA, bovine serum albumin; ET, ellagitannin; GT, gallotannin; HHDP, hexahydroxydiphenoyl; ITC, isothermal titration calorimetry; NHTP, nonahydroxytriphenoyl

## REFERENCES


(1) Okuda, T.; Ito, H. Tannins of constant structure in medicinal and food plants – hydrolysable tannins and polyphenols related to tannins. *Molecules* **2011**, *16*, 2191–2217.

(2) Vrhovsek, U.; Guella, G.; Gasperotti, M.; Pojer, E.; Zancato, M.; Mattivi, F. Clarifying the identity of the main ellagitannins in the fruit of the strawberry, *Fragaria vesca* and *Fragaria ananassa* Duch. *J. Agric. Food Chem.* **2012**, *60*, 2507–2516.

(3) Larrosa, M.; Garcia-Conesa, M. T.; Espin, J. C.; Tomas-Barberan, F. A. Ellagitannins, ellagic acid and vascular health. *Mol. Aspects Med.* **2010**, *31*, 513–539.

(4) Quideau, S.; Genot, E.; Saltel, F.; Douat-Casassus, C.; Delannoy Lopez, D. M. C-glucosidic ellagitannin compounds for use for altering the supramolecular arrangement of actin and for the treatment of osteoporosis, cancer, bacterial infection and viral infection. Int. Patent Appl. WO 2012/113835 A1 (PCT/EP2012/053017), 2012.

(5) Quideau, S.; Deffieux, D.; Douat-Casassus, C.; Pouységu, L. Plant polyphenols: chemical properties, biological activities, and synthesis. *Angew. Chem., Int. Ed.* **2011**, *50*, 5099–5104.

(6) Scalbert, A.; Andres-Lacueva, C.; Arita, M.; Kroon, P.; Manach, C.; Urpi-Sarda, M.; Wishart, D. Databases on food phytochemicals and their health-promoting effects. *J. Agric. Food Chem.* **2011**, *59*, 4331–4348.

(7) Rothwell, J. A.; Urpi-Sarda, M.; Boto-Ordonez, M.; Knox, C.; Llorach, R.; Eisner, R.; Cruz, J.; Neveu, V.; Wishart, D.; Manach, C.; Andres-Lacueva, C.; Scalbert, A. Phenol-Explorer 2.0: a major update of the Phenol-Explorer database integrating data on polyphenol metabolism and pharmacokinetics in humans and experimental animals. *Database* **2012**, DOI: 10.1093/database/bas031.

(8) Fotschki, B.; Milala, J.; Jurgonski, A.; Karlińska, E.; Zdunczyk, Z.; Juskiewicz, J. Strawberry ellagitannins the positive effects of dietary fructooligosaccharides in rat cecum. *J. Agric. Food Chem.* **2012**, *62*, 5871–5880.

(9) Salminen, J. P.; Karonen, M.; Sinkkonen, J. Chemical ecology of tannins: recent developments in tannin chemistry reveal new structures and structure-activity patterns. *Chem.–Eur. J.* **2011**, *17*, 2806–2816.

(10) Quideau, S.; Douat-Casassus, C.; Delannoy López, D. M.; Di Primo, C.; Chassain, S.; Jacquet, R.; Saltel, F.; Genot, E. Binding of filamentous actin and winding into fibrillar aggregates by the polyphenolic C-glucosidic ellgitannin vescalagin. *Angew. Chem., Int. Ed.* **2011**, *50*, 5099–5104.

(11) Okuda, T. Systematics and health effects of chemically distinct tannins in medicinal plants. *Phytochemistry* **2005**, *66*, 2012–2031.

(12) Kashiwada, Y.; Nonaka, G.-I.; Nishioka, I.; Lee, K. J.-H.; Bori, I.; Fukushima, Y.; Bastow, K. F.; Lee, K.-H. Tannins as potent inhibitors of DNA topoisomerase-II *in vitro*. *J. Pharm. Sci.* **1993**, *82*, 487–492.

(13) Quideau, S.; Jourdes, M.; Saucier, C.; Glories, Y.; Pardon, P.; Baudry, C. DNA topoisomerase inhibitor acutissimin A and other flavano-ellagitannins in red wine. *Angew. Chem., Int. Ed.* **2003**, *42*, 6012–6014.

(14) Auzanneau, C.; Montaudon, D.; Jacquet, R.; Puyo, S.; Pouységu, L.; Deffieux, D.; Elkaoukabi-Chaibi, A.; De Giorgi, F.; Ichas, F.; Quideau, S.; Pourquier, P. The polyphenolic ellagitannin vescalagin acts as a preferential catalytic inhibitor of the $\alpha$ isoform of human DNA topoisomerase II. *Mol. Pharmacol.* **2012**, *82*, 124–141.

(15) Kiss, A. K.; Granica, S.; Stolarczyk, M.; Melzig, M. F. Epigenetic modulation of mechanisms involved in inflammation: influence of selected polyphenolic substances on histone acetylation state. *Food Chem.* **2012**, *131*, 1015–1020.

(16) Cala, O.; Dufourc, E. J.; Fouquet, E.; Manigand, C.; Laguerre, M.; Pianet, I. The colloidal state of tannins impacts the nature of their interaction with proteins: the case of salivary proline-rich protein/procyanidins binding. *Langmuir* **2012**, *28*, 17410–17418.

(17) Fraga, C. G.; Galleano, M.; Verstraeten, S. V.; Oteiza, P. I. Basic biochemical mechanisms behind the health benefits of polyphenols. *Mol. Aspects Med.* **2010**, *31*, 435–445.

(18) Bacon, J. R.; Rhodes, M. J. C. Binding affinity of hydrolyzable tannins to parotid saliva and to proline-rich proteins derived from it. *J. Agric. Food Chem.* **2000**, *48*, 838–843.

(19) Frazier, R. A.; Deaville, E. R.; Green, R. J.; Willoughby, I.; Stringano, E.; Plant, J.; Mueller-Harvey, I. Interactions of tea tannins and condensed tannins with proteins. *J. Pharm. Biomed. Anal.* **2010**, *51*, 490–495.

(20) Canon, F.; Ballivian, R.; Chirot, F.; Antoine, R.; Sarni-Manchado, P.; Lemoine, J.; Dugourd, P. Folding of a salivary

intrinsically disordered protein upon binding to tannins. *J. Am. Chem. Soc.* **2011**, *133*, 7847−7852.
(21) Delannoy, D.; Deffieux, D.; Di Primo, C.; Quideau, S. Study in real time of polyphenol-protein interactions by surface plasmon resonance. *Polyphenols Commun.* **2012**, *1*, 59−60.
(22) Simon, C.; Barathieu, K.; Laguerre, M.; Schmitter, J.-M.; Fouquet, E.; Pianet, I.; Dufourc, E. J. Three-dimensional structure and dynamics of wine tannin-saliva protein complexes. A multitechnique approach. *Biochemistry* **2003**, *42*, 10385−10395.
(23) Hagerman, A. E. Chapter 3. Fifty years of polyphenol-protein complexes. In *Recent Advances in Polyphenol Research*; Cheynier, V., Sarni-Manchado, P., Quideau, S., Eds.; Wiley: Oxford, UK, 2012; Vol. 3, pp 71−97.
(24) Deaville, E. R.; Green, R. J.; Mueller-Harvey, I.; Willoughby, I.; Frazier, R. A. Hydrolysable tannin structures influence relative binding strengths to globular or random coil proteins. *J. Agric. Food Chem.* **2007**, *55*, 4554−4561.
(25) Hagerman, A. E.; Butler, L. G. The specificity of proanthocyanidin-protein interactions. *J. Biol. Chem.* **1981**, *256*, 4494−4497.
(26) Bazylko, A.; Kiss, K. K.; Kowalski, J. High-performance thin-layer chromatography method for quantitative determination of oenothein B and quercetin glucuronide in aqueous extract of *Epilobii angustifolii* herba. *J. Chromatogr., A* **2007**, *1173*, 146−150.
(27) Giner-Chavez, B.-I.; Van Soest, P. J.; Robertson, J. B.; Lascano, C.; Pell, A. N. Comparison of the precipitation of alfalfa leaf protein and bovine serum albumin by tannins in the radial diffusion method. *J. Sci. Food Agric.* **1997**, *74*, 513−523.
(28) Dobreva, M. A.; Frazier, R. A.; Mueller-Harvey, I.; Clifton, L. A.; Gea, A.; Green, R. J. Binding of pentagalloyl glucose to two globular proteins occurs via multiple surface sites. *Biomacromolecules* **2011**, *12*, 710−715.
(29) Hofmann, T.; Glabasnia, A.; Schwarz, B.; Wisman, K. N.; Gangwer, K. A.; Hagerman, A. E. Protein binding and astringent taste of a polymeric procyanidin, 1,2,3,4,6-penta-*O*-galloyl-$\beta$-D-glucopyranose, castalagin, and grandinin. *J. Agric. Food Chem.* **2006**, *54*, 9503−9509.
(30) Li, M.; Jia, X.; Yang, J.; Deng, J.; Zhao, G. Effect of tannic acid on properties of soybean (*Glycine max*) seed ferritin: a model for interaction between naturally-occurring components in foodstuffs. *Food Chem.* **2012**, *133*, 410−415.
(31) Stojadinovic, M.; Radosavljevic, J.; Ognjenovic, J.; Vesic, J.; Prodic, I.; Stanic-Vucinic, D.; Cirkovic Velickovic, T. Binding affinity between dietary polyphenols and $\beta$-lactoglobulin negatively correlates with the protein susceptibility to digestion and total antioxidant activity of complexes formed. *Food Chem.* **2013**, *136*, 1263−1271.
(32) Dufour, C.; Dangles, O. Flavonoid-serum albumin complexation: determination of binding constants and binding sites by fluorescence spectroscopy. *Biochim. Biophys. Acta* **2005**, *1721*, 164−173.
(33) Skrt, M.; Benedik, E.; Podlipnik, C.; Ulrih, N. P. Interactions of different polyphenols with bovine serum albumin using fluorescence quenching and molecular docking. *Food Chem.* **2012**, *135*, 2418−2424.
(34) Li, M.; Hagerman, A. E. Interactions between plasma proteins and naturally occurring polyphenols. *Curr. Drug Metab.* **2013**, *14*, 432−445.
(35) Zhang, Y.; Shi, S.; Chen, X.; Zhang, W.; Huang, K.; Peng, M. Investigation on the interaction between Ilaprazole and bovine serum albumin without or with different C-ring flavonoids from the viewpoint of food-drug interference. *J. Agric. Food Chem.* **2011**, *59*, 8499−8506.
(36) Huang, B. X.; Kim, H.-H.; Dass, C. Probing three-dimensional structure of bovine serum albumin by chemical cross-linking and mass spectrometry. *J. Am. Soc. Mass Spectrom.* **2004**, *15*, 1237−1247.
(37) Moilanen, J.; Salminen, J.-P. Ecologically neglected tannins and their biologically relevant activity: chemical structures of plant ellagitannins reveal their in vitro oxidative activity at high pH. *Chemoecology* **2008**, *18*, 73−83.
(38) O'Brien, R.; Ladbury, J. E.; Chowdhry, B. Z. Isothermal titration calorimetry of biomolecules. In *Protein−Ligand Interactions: Hydrodynamics and Calorimetry*; Harding, S. E., Chowdhry, B. Z., Eds.; Oxford University Press: Oxford, UK, 2001; pp 263−286.
(39) Frazier, R. A.; Papadopoulou, A.; Mueller-Harvey, I.; Kissoon, D.; Green, R. J. Probing protein-tannin interactions by isothermal titration microcalorimetry. *J. Agric. Food Chem.* **2003**, *51*, 5189−5195.
(40) Freire, E.; Mayorga, O. L.; Straume, M. Isothermal titration calorimetry. *Anal. Chem.* **1990**, *62*, A950−A959.
(41) Chi, Z.; Liu, R.; Zhang, H. Noncovalent interaction of oxytetracycline with the enzyme trypsin. *Biomacromolecules* **2010**, *11*, 2454−2459.
(42) Lakowicz, J. R. *Principles of Fluorescence Spectroscopy*, 2nd ed.; Kluwer Academic/Plenum Publishers: New York, 1999; p 698.
(43) Vivas, N.; Laguerre, M.; Pianet de Boissel, I.; Vivas de Gaulejac, N.; Nonier, M.-F. Conformational interpretation of vescalagin and castalagin physicochemical properties. *J. Agric. Food Chem.* **2004**, *52*, 2073−2078.
(44) McManus, J. P.; Davis, K. G.; Beart, J. E.; Gaffney, S. H.; Lilley, T. H.; Haslam, E. Polyphenol interactions. Part I. Introduction: some observations on the reversible complexation of polyphenols with proteins and polysaccharides. *J. Chem. Soc., Perkin Trans. 2* **1985**, 1429−1438.
(45) Charlton, A. J.; Baxter, N. J.; Khan, M. L.; Moir, A. J. G.; Haslam, E.; Davies, A. P.; Williamson, M. P. Polyphenol/peptide binding and precipitation. *J. Agric. Food Chem.* **2002**, *50*, 1593−1601.
(46) Mishra, B.; Barik, A.; Priyadarsini, K. I.; Mohan, H. Fluorescence spectroscopy studies on binding of a flavanoid antioxidant quercetin to serum albumins. *J. Chem. Sci.* **2005**, *117*, 641−647.
(47) Tian, J.; Liu, J.; Tina, X.; Hu, Z.; Chen, X. G. Study of the interaction of kaempferol with bovine serum albumin. *J. Mol. Struct.* **2004**, *691*, 197−202.
(48) Tian, J.; Liu, J.; Hu, Z.; Chen, X. G. Interaction of wogonin with bovine serum albumin. *Bioorg. Med. Chem.* **2005**, *13*, 4124−4129.
(49) Lorrain, B.; Dangles, O.; Genot, C.; Dufour, C. Chemical modeling of heme-induced lipid oxidation in gastric conditions and inhibition by dietary polyphenols. *J. Agric. Food Chem.* **2010**, *58*, 676−683.
(50) Maiti, T. K.; Gosh, K. S.; Dasgupta, S. Interaction of (−)-epigallocatchin-3-gallate with human serum albumin: fluorescence, Fourier transform infrared, circular dichroism, and docking studies. *Protein Struct. Funct. Genet.* **2006**, *64*, 355−362.
(51) Zhang, G.; Wang, L.; Pan, J. Probing the binding of the flavonoid diosmetin to human serum albumin by multispectroscopic techniques. *J. Agric. Food Chem.* **2012**, *60*, 2721−2729.
(52) Xiao, J.; Zhao, Y.; Wang, H.; Yuan, Y.; Yang, F.; Zhang, C.; Yamamoto, K. Noncovalent interaction of dietary polyphenols with common human plasma proteins. *J. Agric. Food Chem.* **2011**, *59*, 10747−10754.
(53) Zhu, M. J.; Phillipson, J. D.; Greengrass, P. M.; Bowery, N. E.; Cai, Y. Plant polyphenols: biologically active molecules or non-selective binders to protein? *Phytochemistry* **1997**, *44*, 441−447.
(54) Chandler, D. Interfaces and the driving force of hydrophobic assembly. *Nature* **2005**, *437*, 640−647.
(55) Butler, L. G.; Riedl, D. J.; Lebryk, D. G.; Blytt, H. J. Interaction of proteins with sorghum tannin: mechanisms, specificity and significance. *J. Am. Oil Chem. Soc.* **1984**, *61*, 916−920.

the goals of this work were the validation of appropriate methodologies for monitoring of total chromium and Cr(VI) in different lager beers to understand the variability between lager beer styles packaged in glass or cans and estimation of the contribution of beer to daily dietary intake of total Cr and Cr(VI).

## MATERIALS AND METHODS

**Reagents and Materials.** Hydrogen peroxide, nitric acid, hydrochloric acid, sodium hydroxide, ammonium nitrate, alizarin, sodium acetate, and acetic acid were of Suprapure grade and purchased from Merck (Rahway, NJ). Total Cr standards were prepared daily from a 1000 $\mu$g mL$^{-1}$ solution of Cr(III) nitrate (Spectrosol, BDH) in $HNO_3$ [0.2% (v/v)]. An aqueous stock solution of Cr(VI) at 1000 $\mu$g mL$^{-1}$ was prepared by dissolving 0.2829 g of potassium dichromate (Riedel-de-Haen) in 100 mL of doubly deionized water. Diluted standard solutions were prepared daily from these stock solutions. The chemical modifiers were a 1 g L$^{-1}$ $Mg(NO_3)_2$ solution and a mixture of 2 g L$^{-1}$ $Mg(NO_3)_2$ and a 3 g L$^{-1}$ $Pd(NO_3)_2$ solution, Suprapure grade from Merck, prepared in 15% (v/v) $HNO_3$. Chromabond $NH_2$, 3 mL, 500 mg columns (Macherey-Nagel, Düre, Germany) were used to selectively separate Cr(VI) both in standards and in beer samples before tis quantification.

A rigorous decontamination to eliminate possible contamination due to detergents was performed for all materials (Teflon vessels, test tubes, pipets, micropipet tips, and micro vessels). For this purpose, all materials were immersed for 24 h in freshly prepared 15% (v/v) $HNO_3$. Subsequently, they were rinsed thoroughly with doubly deionized water and dried in a dust-free environment before being used. The gloves used were of powder-free material.

**Instrumentation.** Chromium quantifications were conducted in a PerkinElmer HGA-850 furnace installed in a model Analyst 300 spectrometer with Zeeman background correction, equipped with an AS-800 autosampler. Then, measurements were performed using PerkinElmer HGA tubes with an integrated platform. Water purification systems were a Seralpur PRO 90 CN system and a Seradest LFM 20 system. All analytical weights were determined with a Mettler Toledo (Greifensee, Switzerland) AB265-S balance. The samples were homogenized in a GFL 3006 oscillating agitator and centrifuged in a 5810R Eppendorf. The pH-meter was a WTW pH 330/SET-2, Best NR 100 788 instrument.

**Samples.** Seventy beer samples from 38 brands were analyzed, including 56 bottled beers and 14 canned beers. Sampling included Portuguese and imported beers, one or two samples of each brand packed at different dates that were randomly acquired in local supermarkets in Porto, Portugal. All the samples had at least 3−6 months prior to their expiration dated and were lager type beers of different styles: pale lager (B1−B17; $n$ = 24), low-alcohol (B18−B26; $n$ = 13), fruit beer (B27 and B28; $n$ = 3), Dunkel (B29−B31; $n$ = 5), Schwarzbier (B32; $n$ = 2), premium lager (B33; $n$ = 2), amber (B34 and B35; $n$ = 3), and Heller Bock (B36−B38; $n$ = 4). Canned beers were all pale lager and were from the same brands as bottled beers; these samples were named C1−C8 ($n$ = 14). The major ingredients of the beer samples were sorghum, wheat, malt, barley, roasted barley, hops, and water. The percentage of alcohol by volume in the samples ranged from 0.3 to 6.4%; the mean pH value was 4.12, ranging between 3.90 and 4.24. The samples were stored at 4 °C until they were analyzed. All beer samples were degassed by centrifugation at 5000$g$ and 4 °C for 15 min and were analyzed twice for total Cr and Cr(VI), and some of them were also used to validate the analytical procedure.

**Pretreatment Procedure for Total Chromium Quantification.** Sample digestion and mineralization were conducted according to the procedure described by Soares et at.[13] Five milliliters of each beer sample was accurately measured and transferred to Teflon containers and supplemented with 0.4 mL of $H_2O_2$ and 2.0 mL of $HNO_3$ at room temperature for 3 h, and the Teflon containers covered with their caps overnight were heated in a thermostatically controlled stove at 105 °C. After the samples had cooled to room temperature, 1 mL of HCl was added, and the closed Teflon containers were heated again for 17 h at 105 °C to completely dissolve the samples. The cooled containers were opened, and the digests were transferred to decontaminated tubes and diluted to 5 mL with doubly deionized water. Blank reagent samples were processed in parallel with via digestion of the beer sample and subjected to the same procedure.

**Pretreatment Procedure for Chromium(VI) Quantification.** For selective extraction of Cr(VI), a procedure previously adopted by our group to other matrices[12,13] was adapted and validated for beer analyses. Briefly, 10 mL of beer was mixed with 1.5 mL of 3% sodium acetate and 750 $\mu$L of 0.001% alizarin until a final pH of 5.5 was achieved, which was selected according to the instructions of the Chromabond $NH_2$, 500 mg column. Each sample was agitated for 2 min for complete homogenization and transferred into previously conditioned columns. The conditioning was conducted with 2 mL of 1 N $HNO_3$ followed by 2 mL of doubly deionized water. Selective retention of Cr(VI) in the column was quantitatively achieved by passing the supernatant through the column. Afterward, it was dried under vacuum, and the Cr(VI) was eluted with 2 mL of 2 N $HNO_3$. Finally, Cr(VI) was measured in the eluate using the same instrumental conditions applied for total chromium. Cr(VI) standard solutions and blank reagents were submitted daily to pretreatment procedures similar to that applied for the beer samples.

**Analytical Conditions.** Both total Cr and Cr(VI) were quantified by graphite-furnace atomic absorption spectroscopy (GFAAS). The spectrometer settings and furnace programs used with pyrolytic graphite-coated tubes were as follows: drying temperature, 100−130 °C (10 s for ramp time and 20 s for hold time); ashing temperature, 1200 °C (20 s for ramp time and 20 s for hold time); atomization temperature, 2400 °C (30 s for ramp time and 30 s for hold time); chemical modifier, 3 g L$^{-1}$ $Pd(NO_3)_2$ and 2 g L$^{-1}$ $Mg(NO_3)_2$; Zeeman background correction; HGA tubes with an integrated platform; gas stop flow, atomization step. All data were taken at 353.7 nm. The slit width was 0.7 nm, and argon was used as the purge gas, with an internal flow rate of 300 mL min$^{-1}$. Readings on the spectrometer were taken by using the peak area mode (integrated absorbance) both for total chromium and for hexavalent chromium. The autosampler was programmed to pipet sequentially the modifier (10 $\mu$L) followed by the standard solution/acid digest/acid eluate mixture (20 $\mu$L) and to dispense them together onto the platform.

**Validation of Methods.** The analytical methods were evaluated according to linearity, precision, limit of detection (LOD), limit of quantification (LOQ), accuracy, and matrix effects. Standard solutions of both total Cr and Cr(VI) were prepared daily at the working concentrations for the determination of linearity. The calibration curve of total Cr and Cr(VI), plotted as concentration versus absorbance, was statistically evaluated using the straight line by the least-squares method of linear regression. For the evaluation of instrumental precision, 20 measurements of absorbance signals were taken using the same standard solution, while for evaluation of the analytical method, precision absorbance signals were determined 20 times in the same beer sample. Precision is presented as the ratio of the standard deviation to the mean [coefficient of variation (CV%)]. The limit of detection was calculated by the equation LOD = $3sm^{-1}$; the limit of quantification was calculated by the equation LOQ = $10sm^{-1}$ (where $s$ is the standard deviation of the measurements of the blank and $m$ is the slope in the calibration curve). Because Certified Reference Materials for Cr and Cr(VI) in a beer matrix are not available on the market, the method of addition of standards was applied for the evaluation of accuracy. Four different concentrations (1.0, 2.5, 5.0, and 10.0 $\mu$g L$^{-1}$) of standard solutions of Cr(VI) were added to different aliquots of the same beer sample (six replicates for each concentration) and subjected to the extraction procedure. After determination of the initial concentration of Cr(VI) in the unspiked beer samples and the final concentrations in the spiked beer samples, the respective Cr(VI) recoveries and coefficient of variation were calculated.

**Statistical Analysis.** Nonparametric comparison tests (Kruskal−Wallis test and Mann−Whitney U-test) with a statistical significance

Table 1. Analytical Features of the Quantification of Total Cr and Cr(VI) in Beer Samples

| | linearity ($\mu$g L$^{-1}$) | precision (CV%) | | limit of detection ($\mu$g L$^{-1}$) | limit of quantification ($\mu$g L$^{-1}$) |
|---|---|---|---|---|---|
| | | instrumental procedure | analytical procedure | | |
| total Cr | 0.26−20.0 | 1.5 | 10.7 | 0.26 | 0.87 |
| Cr(VI) | 0.68−15.0 | 2.5 | 5.9 | 0.68 | 1.61 |

set at $p < 0.05$ were conducted with SPSS version 17 (SPSS Inc., Chicago, IL).

## RESULTS AND DISCUSSION

**Validation of Methods.** Linearity ranged between 0.26 and 20.0 and between 0.68 and 15.0 $\mu$g L$^{-1}$ for total Cr and Cr(VI), respectively, as presented in Table 1. The precision, evaluated for instrumental and analytical procedures, was ≤10.7% for total chromium and Cr(VI). The LODs were 0.26 and 0.68 $\mu$g L$^{-1}$ for total Cr and Cr(VI), respectively. The LOQs were 0.87 and 1.61 $\mu$g L$^{-1}$ for total Cr and Cr(VI), respectively. These figures highlight that the method is precise and sensitive, allowing the quantification of low levels of total Cr and Cr(VI).

Recovery experiments were performed to evaluate the accuracy and specificity of the digestion and extraction methods. The total Cr and Cr(VI) concentrations obtained by the standard method of additions presented very small deviations from the expected values, between 1.6 and 3.3%, corresponding to mean recoveries of ≥93.3% (Table 2). These results highlight the absence of matrix interference and suggest that the wet acid digestion procedure in a closed vessel, including digestion with $H_2O_2$ and $HNO_3$ and subsequent mineralization with HCl and $HNO_3$, was effective for the simplification of the beer sample matrix to obtain the necessary dissolution of total chromium for GFAAS determination. In addition, the Chromabond $NH_2$, 500 mg column adopted for the extraction of Cr(VI) allowed the selective separation of this species from the beer matrix as verified by the results obtained during the validation procedure. Thus, the techniques applied for Cr total and Cr(VI) in beer samples were accurate and precise.

**Application of the Validated Methods to the Determination of Total Cr and Cr(VI) in Lager Beers.** The validated methods were applied to the analyses of chromium in 70 beer samples. Table 3 presents the concentrations of total chromium and Cr(VI) in bottled and canned beers. The concentrations of total chromium in the different samples of bottled beers ranged from lower than the LOQ (<0.87 $\mu$g L$^{-1}$) to 16.4 $\mu$g L$^{-1}$. The content of total Cr in canned beers ranged from lower than the LOQ (<0.87 $\mu$g L$^{-1}$) to 2.79 $\mu$g L$^{-1}$. Comparison between the chromium content of pale lager canned beers and the same brands of bottled beers showed that canned beers presented significantly lower total Cr contents ($p = 0.045$; $n = 38$). According to Farri et al.[6] who studied the occurrence of chromium in raw materials and its fate in the brewing process, the raw materials such as malt and rice are the major contributors of chromium to beer; however, a significant increase in the level of chromium was observed after the bottling process because of a transfer of chromium from the glass, caps, or steed used in the bottling machine. Kovács et al.[18] compared the composition of eight brands of beer from Hungary, Slovakia, and Czech Republic stored in cans and glass and observed similar total Cr contents ranging between 0.6 and 13.6 $\mu$g L$^{-1}$; however, they did not find significant differences in the Cr content of canned and glass bottled beers. Other previous studies analyzed the total Cr content of beer in 74 brands of Belgian and imported beers. The content ranged between 0.2 and 46 $\mu$g L$^{-1}$;[19] beers consumed in Spain contained 3.94−30.1 $\mu$g L$^{-1}$.[20] Higher contents of total Cr are described in beers from Venezuela and Nigeria, ranging between 10 and 104 $\mu$g L$^{-1}$ and between 100 and 400 $\mu$g L$^{-1}$, respectively,[16,21] and in beers from Brazil with a mean of total chromium content of 66 $\mu$g L$^{-1}$.[15]

Table 2. Statistical Results (means ± standard deviation) for the Recoveries of Total Chromium and Cr(VI) Obtained by the Standard Method of Additions to the Beer Sample Matrix ($n = 6$, for each added concentration)

| $C_1$ ($\mu$g L$^{-1}$)[a] | $C_2$ ($\mu$g L$^{-1}$)[b] | $C_3$ ($\mu$g L$^{-1}$)[c,d] | % recovery[d] |
|---|---|---|---|
| | | Total Cr | |
| 1.50 | 2.5 ($n = 6$) | 3.7 ± 0.08 | 93.3 ± 2.07 |
| | | (3.7−3.9) | (91.0−96.0) |
| | | CV% = 2.2 | CV% = 2.2 |
| | 5.0 ($n = 6$) | 6.3 ± 0.10 | 96.0 ± 1.55 |
| | | (6.1−6.4) | (94.0−98.0) |
| | | CV% = 2.2 | CV% = 1.6 |
| | 10.0 ($n = 6$) | 10.8 ± 0.20 | 93.8 ± 1.83 |
| | | (10.5−11.0) | (91.0−96.0) |
| | | CV% = 1.9 | CV% = 2.0 |
| | 20.0 ($n = 6$) | 20.3 ± 0.52 | 94.0 ± 2.10 |
| | | (19.5−21.0) | (91.0−97.0) |
| | | CV% = 2.6 | CV% = 2.2 |
| | | Cr(VI) | |
| 1.35 | 1.0 ($n = 6$) | 2.2 ± 0.06 | 95.3 ± 2.50 |
| | | (2.1−2.3) | (91.0−98.0) |
| | | CV% = 2.6 | CV% = 2.6 |
| | 2.5 ($n = 6$) | 3.6 ± 0.11 | 94.7 ± 2.88 |
| | | (3.5−3.8) | (90.0−98.0) |
| | | CV% = 3.0 | CV% = 3.0 |
| | 5.0 ($n = 6$) | 6.0 ± 0.17 | 94.7 ± 2.58 |
| | | (5.8−6.2) | (91.0−97.0) |
| | | CV% = 2.8 | CV% = 2.7 |
| | 10.0 ($n = 6$) | 10.6 ± 0.44 | 94.7 ± 3.14 |
| | | (10.0−11.2) | (90.0−99.0) |
| | | CV% = 4.1 | CV% = 3.3 |

[a] $C_1$ is the initial concentration of total chromium and Cr(VI) in a beer sample matrix. [b] $C_2$ is the concentration of standard total chromium and Cr(VI) solution added to beer sample matrix prior to the application of the overall procedure. [c] $C_3$ is the final concentration of total chromium and Cr(VI) found in the spiked beer sample matrix. [d] Maximal and minimal values measured in spiked beer samples are in parentheses.

The Cr(VI) content of pale lager beers ranged from below the LOQ (<1.61 $\mu$g L$^{-1}$) to 9.9 $\mu$g L$^{-1}$, whereas in low-alcohol beers, Cr(VI) varied from below the LOQ (<1.61 $\mu$g L$^{-1}$) to 13 $\mu$g L$^{-1}$. The Cr(VI) content in fruit beer, Dunkel, Schwarzbier, premium lager, amber lager, Heller Bock, and canned beers was below the LOQ (<1.61 $\mu$g L$^{-1}$) in all analyzed samples.

Mean contents expressed as micrograms per liter of total and hexavalent chromium, maximal and minimal values, and the Cr(VI)/total chromium ratio in bottled and canned beer samples grouped according to beer style are summarized in

Table 3. Total Cr and Cr(VI) Contents of Different Types of Lager Beers Packaged in Glass (coded as B) or Cans (coded as C)[a]

| code | beer style | alcohol (%) | origin | total Cr ($\mu$g L$^{-1}$) | Cr(VI) ($\mu$g L$^{-1}$) |
|---|---|---|---|---|---|
| B1(1) | pale lager | 5.1 | Portugal | <LOQ | <LOQ |
| B1(2) | pale lager | 5.1 | Portugal | <LOQ | <LOQ |
| B2(1) | pale lager | 5.2 | Portugal | 2.79 | <LOQ |
| B2(2) | pale lager | 5.2 | Portugal | 3.06 | <LOQ |
| B3(1) | pale lager | 5 | Portugal | 1.39 | <LOQ |
| B3(2) | pale lager | 5 | Portugal | <LOQ | <LOQ |
| B4(1) | pale lager | 5.1 | Portugal | 1.82 | <LOQ |
| B4(2) | pale lager | 5.1 | Portugal | 2.23 | <LOQ |
| B5(1) | pale lager | 4.6 | Mexico | 2.00 | <LOQ |
| B6(1) | pale lager | 5 | Portugal | 3.49 | <LOQ |
| B6(2) | pale lager | 5 | Portugal | 7.11 | 4.30 |
| B7(1) | pale lager | 5 | Portugal | 3.62 | 2.52 |
| B8(1) | pale lager | 5 | Portugal | 1.67 | <LOQ |
| B8(2) | pale lager | 5 | Portugal | 2.52 | <LOQ |
| B9(1) | pale lager | 5 | Portugal | 2.23 | <LOQ |
| B10(1) | pale lager | 5 | Portugal | <LOQ | <LOQ |
| B11(1) | pale lager | 5 | Portugal | 1.82 | <LOQ |
| B12(1) | pale lager | 4.7 | The Netherlands | 16.3 | 9.90 |
| B13(1) | pale lager | 5.1 | Portugal | 1.67 | <LOQ |
| B14(1) | pale lager | 4.8 | Denmark | 7.24 | 5.76 |
| B15(1) | pale lager | 5.1 | Portugal | 1.53 | <LOQ |
| B16(1) | pale lager | 5.1 | Portugal | 7.38 | 5.04 |
| B17(1) | pale lager | 5 | Czech Republic | 2.79 | <LOQ |
| B17(2) | pale lager | 5 | Czech Republic | 3.21 | <LOQ |
| B18(1) | low-alcohol | 0.3 | Portugal | 2.00 | <LOQ |
| B18(2) | low-alcohol | 0.3 | Portugal | 7.11 | <LOQ |
| B19(1) | low-alcohol | 0.3 | Portugal | 16.4 | 13.0 |
| B20(1) | low-alcohol | 0.5 | Portugal | <LOQ | <LOQ |
| B20(2) | low-alcohol | 0.5 | Portugal | 2.09 | <LOQ |
| B21(1) | low-alcohol | 0.3 | Portugal | 6.83 | 4.0 |
| B22(1) | low-alcohol | 0.5 | Portugal | 2.23 | <LOQ |
| B22(2) | low-alcohol | 0.5 | Portugal | 2.65 | <LOQ |
| B23(1) | low-alcohol | 0.5 | Portugal | 5.85 | 4.32 |
| B24(1) | low-alcohol | 0.3 | Portugal | 1.67 | <LOQ |
| B24(2) | low-alcohol | 0.3 | Portugal | 2.23 | <LOQ |
| B25(1) | low-alcohol | 0.3 | Portugal | 5.71 | 5.16 |
| B26(1) | low-alcohol | 0.3 | Portugal | 1.39 | <LOQ |
| B27(1) | fruit beer | 4 | Portugal | 2.51 | <LOQ |
| B27(2) | fruit beer | 4 | Portugal | 2.36 | <LOQ |
| B28(1) | fruit beer | 4 | Portugal | 1.53 | <LOQ |
| B29(1) | Dunkel/Tmavý | 5 | Portugal | 3.35 | <LOQ |
| B29(2) | Dunkel/Tmavý | 5 | Portugal | 2.79 | <LOQ |
| B30(1) | Dunkel/Tmavý | 5 | Portugal | 2.23 | <LOQ |
| B31(1) | Dunkel/Tmavý | 6.2 | Portugal | 1.39 | <LOQ |
| B31(2) | Dunkel/Tmavý | 6.2 | Portugal | <LOQ | <LOQ |
| B32(1) | Schwarzbier | 4.3 | Portugal | <LOQ | <LOQ |
| B32(2) | Schwarzbier | 4.3 | Portugal | 2.52 | <LOQ |
| B33(2) | premium lager | 4.8 | Germany | 1.96 | <LOQ |
| B33(1) | premium lager | 4.8 | Germany | 1.95 | <LOQ |
| B34(1) | amber lager/Vienna | 4.2 | Portugal | 1.67 | <LOQ |
| B34(2) | amber lager/Vienna | 4.2 | Portugal | 3.06 | <LOQ |
| B35(1) | amber lager/Vienna | 4.2 | Portugal | <LOQ | <LOQ |
| B36(1) | Heller Bock | 6.4 | Portugal | 2.23 | <LOQ |
| B36(2) | Heller Bock | 6.4 | Portugal | 3.49 | <LOQ |
| B37(1) | Heller Bock | 6.4 | Portugal | 1.96 | <LOQ |
| B38(1) | Heller Bock | 5 | The Netherlands | 1.82 | <LOQ |
| C1(1) | pale lager | 5.2 | Portugal | 1.39 | <LOQ |
| C1(2) | pale lager | 5.2 | Portugal | 1.67 | <LOQ |
| C2(1) | pale lager | 5.2 | Portugal | 1.59 | <LOQ |
| C3(1) | pale lager | 5 | Portugal | <LOQ | <LOQ |

Table 3. continued

| code | beer style | alcohol (%) | origin | total Cr ($\mu$g L$^{-1}$) | Cr(VI) ($\mu$g L$^{-1}$) |
|---|---|---|---|---|---|
| C3(2) | pale lager | 5 | Portugal | 2.09 | <LOQ |
| C4(1) | pale lager | 5.1 | Portugal | <LOQ | <LOQ |
| C5(1) | pale lager | 5 | Portugal | 1.53 | <LOQ |
| C5(2) | pale lager | 5 | Portugal | 2.02 | <LOQ |
| C6(1) | pale lager | 5 | Denmark | 1.67 | <LOQ |
| C6(2) | pale lager | 5 | Denmark | 2.79 | <LOQ |
| C7(1) | pale lager | 4.7 | The Netherlands | <LOQ | <LOQ |
| C7(2) | pale lager | 4.7 | The Netherlands | 1.82 | <LOQ |
| C8(1) | pale lager | 4.7 | The Netherlands | <LOQ | <LOQ |
| C8(2) | pale lager | 4.7 | The Netherlands | <LOQ | <LOQ |

[a]Mean values of duplicate assays.

Table 4. Total Cr and Cr(VI) in Bottled and Canned Beers as a Function of Fermentation Style[a]

| | | | total chromium ($\mu$g L$^{-1}$) | | | Cr(VI) ($\mu$g L$^{-1}$) | | |
|---|---|---|---|---|---|---|---|---|
| beer samples | beer style | $n$ | mean ± standard deviation | min−max | median | mean ± standard deviation | min−max | Cr(VI)/total Cr ratio |
| B1−B17 | pale lager | 24 | 3.27 ± 3.52 | <LOQ−16.3 | 2.23 | 0.94 ± 2.42 | <LOQ−9.9 | 0.29 |
| B18−B26 | low-alcohol | 14 | 4.32 ± 4.29 | <LOQ−16.4 | 2.23 | 2.51 ± 3.57 | <LOQ−13.0 | 0.58 |
| B27 and B28 | fruit beer | 3 | 2.13 ± 0.53 | 1.53−2.51 | 2.36 | <LOQ | <LOQ | − |
| B29−B31 | Dunkel/Tmavý | 5 | 2.00 ± 1.21 | <LOQ−3.35 | 2.23 | <LOQ | <LOQ | − |
| B32 | Schwarzbier | 2 | 1.39 ± 1.78 | <LOQ−2.52 | 1.39 | <LOQ | <LOQ | − |
| B33 | premium lager | 2 | 1.96 ± 0.01 | 1.95−1.96 | 1.96 | <LOQ | <LOQ | − |
| B34 and B35 | amber lager | 3 | 1.66 ± 1.40 | <LOQ−3.06 | 1.67 | <LOQ | <LOQ | − |
| B36−B38 | Heller Bock | 4 | 2.38 ± 0.76 | 1.82−3.49 | 2.10 | <LOQ | <LOQ | − |
| C1−C8 | canned pale lager | 14 | 1.13 ± 1.10 | <LOQ−2.92 | 1.46 | <LOQ | <LOQ | − |

[a]For calculations, when the total chromium and Cr(VI) values were lower than the LOQ, the value of the detection limit was taken.

Table 4. For mean calculations, when the total Cr or Cr(VI) values were lower than the LOQ (<0.87 and <1.61 $\mu$g L$^{-1}$, respectively), it was assumed as the LOD value (0.26 and 0.68 $\mu$g L$^{-1}$, respectively). In the different beer styles, the mean content of total Cr ranged between 1.13 $\mu$g L$^{-1}$ in canned pale lager and 4.32 $\mu$g L$^{-1}$ in low-alcohol beer, whereas the mean content of Cr(VI) was <2.51 $\mu$g L$^{-1}$. In these samples, the ratio of Cr(VI) to total Cr was 0.29 in lager beer and 0.58 in low-alcohol beer. Other beer styles presented Cr(VI) contents lower than LOQ values; thus, the ratio could not be evaluated. Comparable ratios were observed in previously studied foods, namely, milk (0.21−0.44),[12] bread (0.12),[14] or tea (0.12−0.24).[7] Although Cr(VI) is a genotoxic species well absorbed through the gastrointestinal tract, risks from these levels in beer are not foreseen, although efforts should be made to keep Cr content in beer as low as possible, because the two samples that presented higher levels of total Cr (~16.4 $\mu$g L$^{-1}$) also presented higher levels of Cr(VI), namely, 13.0 and 9.9 $\mu$g L$^{-1}$.

**Estimated Daily Intake of Total Cr and Cr(VI) Based on the Consumption of Beer.** To determine the daily estimated intake of total Cr and Cr(VI) from beer, a daily intake of 500 mL was considered. This was selected because most people do not consume beer on a daily basis, but when they consume beer, the intake is ~500 mL. Thus, the estimated intake of total Cr in beer ranged between 0.57 and 2.16 $\mu$g/day taking into consideration the mean total Cr contents found in canned and bottled beers, respectively. Estimation of Cr(VI) intake could be performed for only pale lager (0.47 $\mu$g/day) and low-alcohol beers (1.26 $\mu$g/day).

The Food and Nutrition Board of the U.S. National Academy of Sciences recommends that the chromium dietary intake for adults be set at 25 and 35 $\mu$g/day for women and men, respectively.[22] Considering these guidelines, it can be assumed from our study that beer ingestion can contribute approximately with 2.28−8.64% of the recommended daily intake of chromium for women and 1.62−6.17% for men.

## AUTHOR INFORMATION


### Corresponding Author

*E-mail: isabel.ferreira@ff.up.pt. Telephone: +351220428642. Fax: +351226093390.



### Funding

E.V. thanks FCT for Grant SFRH/BD/81845/2011. This work has been supported by Project PP-IJUP2011-332 from Universidade do Porto and European Union (FEDER funds through COMPETE) and National Funds (FCT, Fundação para a Ciência e Tecnologia) through Project Pest-C/EQB/LA0006/2013. The work also received financial support from the European Union (FEDER funds) under the framework of QREN through Project NORTE-07-0124-FEDER-000069. To all financing sources the authors are greatly indebted.

### Notes

The authors declare no competing financial interest.


## REFERENCES


(1) Nelson, M. *The Barbarian's Beverage: A History of Beer in Ancient Europe*; Routledge: Abingdon, U.K., 2005.

(2) Ferreira, I. M. P. L. V. O.; Pinho, O.; Vieira, E.; Tavarela, J. G. Brewer's *Saccharomyces* yeast biomass: Characteristics and potential applications. *Trends Food Sci. Technol.* **2010**, *21*, 77−84.

(3) *Beer statistics 2012 edition*, 1st ed.; Lichota, J., Ed.; The Brewers of Europe: Brussels, 2012.

(4) Bamforth, C. W. Nutritional aspects of beer: A review. *Nutr. Res. (N.Y., NY, U.S.)* **2002**, *22*, 227−237.

(5) Alcázar, A.; Pablos, F.; Jesús Martín, M.; Gustavo González, A. Multivariate characterisation of beers according to their mineral content. *Talanta* **2002**, *57*, 45−52.
(6) Farri, R.; Gimino, M. J.; Lagarda, M. J. The occurrence of chromium in raw materials and its fate in the brewing process. *J. Inst. Brew.* **1987**, *93*, 394−395.
(7) Mandiwana, K. L.; Panichev, N.; Panicheva, S. Determination of chromium(VI) in black, green and herbal teas. *Food Chem.* **2011**, *129*, 1839−1843.
(8) Environmental Protection Agency Toxicological Review of Hexavalent Chromium (CAS Registry No. 18540-29-9); Environmental Protection Agency: Washington, DC, 1998.
(9) *Chromium, Nickel and Welding*; IARC Monographs on the Evaluation of Carcinogenic Risks to Humans; International Agency for Research on Cancer: Lyon, 1990; Vol. *49*.
(10) Unceta, N.; Séby, F.; Malherbe, J.; Donard, O. F. Chromium speciation in solid matrices and regulation: A review. *Anal. Bioanal. Chem.* **2010**, *397*, 1097−1111.
(11) Pohl, P. Determination and fractionation of metals in beer: A review. *Food Addit. Contam.* **2008**, *25*, 693−703.
(12) Lameiras, J.; Soares, M. E.; Bastos, M. L.; Ferreira, M. Quantification of total chromium and hexavalent chromium in UHT milk by ETAAS. *Analyst* **1998**, *123*, 2091−2095.
(13) Soares, M. E.; Bastos, M. L.; Ferreira, M. Selective Determination of Chromium(VI) in Powdered Milk Infant Formulas by Electrothermal Atomization Atomic Absorption Spectrometry after Ion Exchange. *J. AOAC Int.* **2000**, *83*, 220−223.
(14) Soares, M. E.; Vieira, E.; Bastos, M. L. Chromium Speciation Analysis in Bread Samples. *J. Agric. Food Chem.* **2010**, *58*, 1366−1370.
(15) Matsushige, I.; Oliveira, E. Determination of trace elements in Brazilian beers by ICP-AES. *Food Chem.* **1993**, *47*, 205−207.
(16) Marcano, E.; Gómez, C.; Benzo, Z.; Laine, J. Estudio preliminar sobre la determinatión de elementos traza en cervezas venezoelanas por ICP-OES. *Quim. Nova* **2010**, *33*, 653−655.
(17) EFSA Panel on Contaminants in the Food Chain (CONTAM). Scientific Opinion on the risks to public health related to the presence of chromium in food and drinking water. *EFSA J.* **2014**, *12* (3), 3595.
(18) Kovács, R.; Béni, A.; Karosi, R.; Sógor, C.; Posta, J. Investigation of chromium content in foodstuffs and nutrition supplements by GFAAS and determination of changing Cr(III) to Cr(VI) during baking and toasting bread. *Food Chem.* **2007**, *105*, 1209−1213.
(19) Robberecht, H.; Van Schoor, O.; Deelstra, H. Selenium and Chromium Content of European Beers as Determined by AAS. *J. Food Sci.* **1984**, *49*, 300−301.
(20) Lendinez, E.; Lopez, M. C.; Cabrera, C.; Lorenzo, M. L. Determination of chromium in wine and other alcoholic beverages consumed in Spain by electrothermal atomic absorption spectrometry. *J. AOAC Int.* **1998**, *81*, 1043−1047.
(21) Iwegbue, C. M. A. Composition and Daily Intakes of Some Trace Metals from Canned Beers in Nigeria. *J. Inst. Brew.* **2010**, *116*, 312−315.
(22) *Dietary Reference Intakes: Vitamin A, Vitamin K, Arsenic, Boron, Chromium, Copper, Iodine, Iron, Manganese, Molybdenum, Nickel, Silicon, Vanadium and Zinc*; National Academy Press: Washington, DC, 2001; pp 620 (Appendix C, Table C 14).

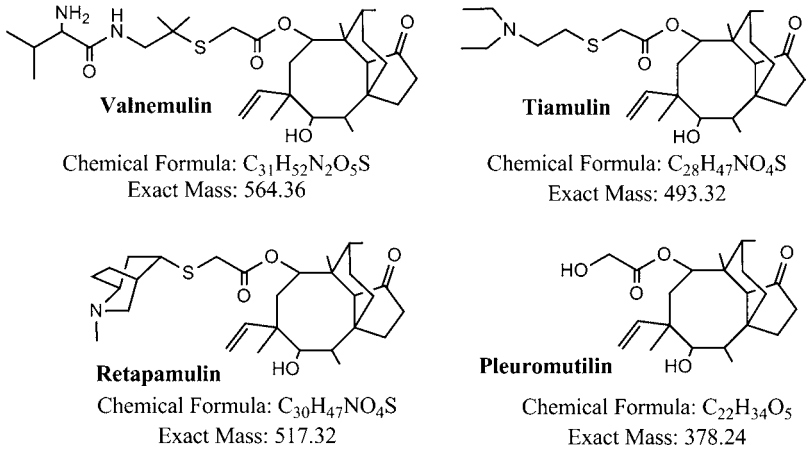


**Figure 1.** Chemical structures of valnemulin, tiamulin, retapamulin, and pleuromutilin.

be 8$\alpha$-hydroxytiamulin, 2$\beta$-hydroxytiamulin, and *N*-deethyltiamulin by using LC-MS, $^1$H NMR, and $^{13}$C NMR.[17]

In the past decades, due to the significant effect on the prevention and treatment of livestock diseases, antimicrobial agents have been widely used in clinical veterinary. Unfortunately, the accumulation of drug residues and metabolites in eggs, meat, and milk has led to potential hazards for humans.[18−20] Thus, the investigation of the metabolism of antimicrobial agents in food animals becomes very necessary. Valnemulin is one of the antimicrobial agents in animal husbandry. However, the literature on the metabolic research of valnemulin in animals is limited. Therefore, the aim of the present study is to investigate in detail the in vivo and in intro metabolism of valnemulin in different species and to provide the metabolic differences among different species. Valnemulin was separately incubated with rat, chicken, swine, goat, and cow liver microsomes, and the incubation mixtures were then analyzed using a sensitive UPLC-Q/TOF-MS method. In addition, the metabolites of valnemulin in in vivo rats, chickens, and swines were also investigated. As a result, many metabolites were identified, and the proposed metabolic pathways of valnemulin are presented in this paper. This work will contribute to comprehensively clarifying the differences among in vitro systems of different species and will give useful data for the explanation of the residues of valnemulin among different species and, moreover, will further facilitate food safety evaluation of valnemulin.

## MATERIALS AND METHODS

**Chemicals.** The valnemulin standards were obtained from the Council of Europe's European Pharmacopoeia. S-oxidized valnemulin (metabolite V6) was synthesized at the College of Science, China Agricultural University (Beijing, China). Acetonitrile and formic acid (HPLC grade) were purchased from Fisher Chemical Co. (USA). Water was purified using a Milli-Q system (Millipore, USA). $\beta$-Nicotinamide adenine dinucleotide phosphates (NADPH) was purchased from Roche Chemical Co. (Beijing, China). All other chemicals and reagents were of the highest analytical grade available.

**Animals.** Twelve Wistar rats (weight 200−250 g, six males and six females) were purchased from Vital River Laboratory Animal Technology Co. Ltd. (Beijing, China). Twelve Avian chickens (weight 1.0−1.2 kg, six males and six females) were purchased from Beijing Huadu Co. Ltd. (Beijing, China). Twelve Changbai swines (weight 20−25 kg, six males and six females), eight goats (weight 20−25 kg, four males and four females), and four cows (weight 150−250 kg, two males and two females) were purchased from Zhoukou Village Nursery (Beijing, China). All animals, after acclimatizing for 1 week in an animal room with standardized temperature (25−28 °C), humidity (50−60%), and 12 h light/dark cycle conditions before the experiment, were fed different commercial standard diets and given water ad libitum. All care and handling of animals was performed with approval of the Institutional Authority for Laboratory Animal Care.

**Preparation of Liver Microsomes.** Following a 12 h fast, animals (three male and three female rats, chickens, and swines; two male and two female goats; and one male and one female cow) were exsanguinated. Hepatic microsomes were prepared as a procedure reported in previous studies.[21] The livers were rapidly removed and washed several times with ice-cold 0.1 mol/L PBS (pH 7.4) and 0.05 mol/L Tris-HCl buffer (pH 7.4) to wash away residual blood, gently blotted, and weighed. The pooled livers were minced and immediately homogenized with 3 volumes of ice-cold 0.05 mol/L Tris-HCl buffer (pH 7.4) containing 1 mmol/L EDTA and 0.25 M sucrose using a glass homogenizer. The liver S9 fraction was obtained by centrifuging the homogenate at 10000*g* for 20 min at 4 °C, and then the supernatant was collected and centrifuged at 100000*g* for 60 min at 4 °C. The microsomal pellets were suspended in 0.05 mol/L Tris-HCl buffer, and the protein content of the microsomes was estimated according to the method of Lowry et al. using crystalline bovine serum albumin as standard.[22] To evaluate the activities of CYP enzymes in liver microsomes prepared in this work, the carbon monoxide (CO) difference spectrum and the metabolism of probe drug coumarin were applied. The liver microsomes of rat, chicken, swine, goat, and cow were incubated with coumarin, and then the metabolites of coumarin were analyzed by UPLC-Q/TOF-MS. The results showed that the maximum absorption wavelength of microsomes was 450 nm, but not 420 nm, which was consistent with the results of Pearce et al.[23] The CO difference spectrum of CYP in rat, chicken, pig, goat, and cow liver microsomes is shown in the Supporting Information (Figure 9). In addition, coumarin could be metabolized to 7-hydroxycoumarin in liver microsomes, indicating the systems had the activities of drug metabolism enzymes.

**Incubation of Valnemulin with Liver Microsomes.** Valnemulin was separately incubated with liver microsomes of rats, chickens, swines, goats, and cows under the same conditions. The incubation mixture, in 0.05 M Tris-HCl buffer (pH 7.4), consisted of 2 mg protein/mL liver microsomes, 100 mM valnemulin, and 1 mM NADPH with the total volume of 500 mL. After 2 h of incubation at 37 °C in a metabolic shaker, the reaction was terminated by adding 500 $\mu$L of ice-cold acetonitrile. After volution and centrifugation at 12000 rpm at 4 °C for 15 min, the supernatant was filtered through a 0.22 $\mu$m microbore cellulose membrane into an autosampler vial and analyzed by UPLC-Q/TOF-MS for identification of metabolites. Parallel controls include the absence of NADPH and incubation without valnemulin, respectively. All experiments were conducted in triplicate.

**Preparation of in Vivo Samples.** After a 12 h fast and free access to water, animals (three male and three female rats, chickens, and

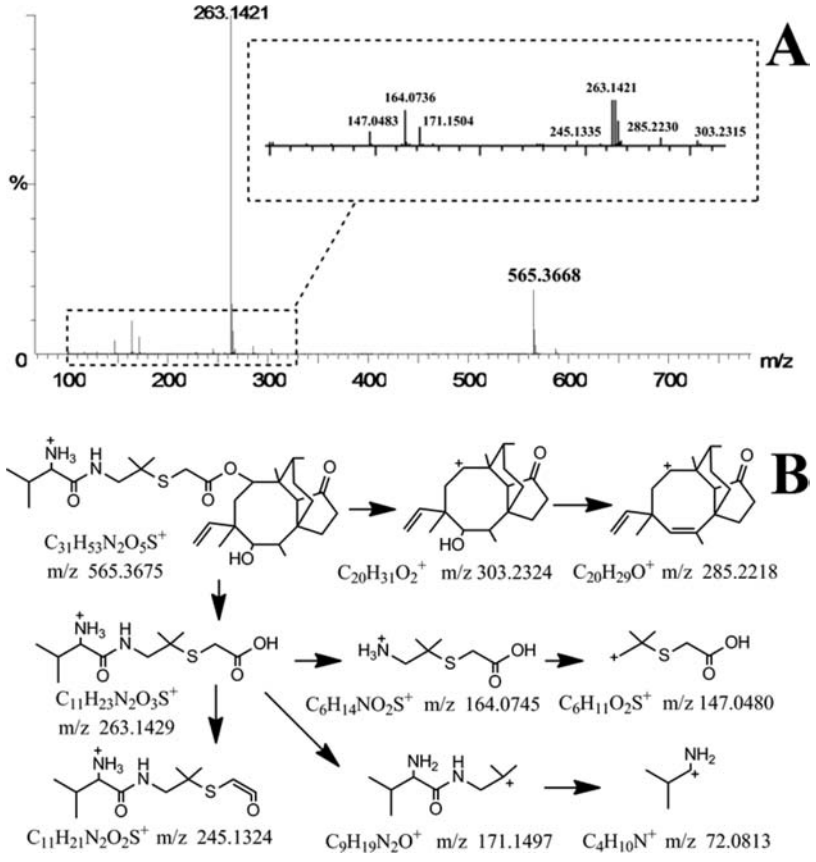


**Figure 2.** Accurate MS/MS spectra (A) and proposed fragmentation pathways (B) of valnemulin.

**Table 1. Elemental Composition, Measured and Calculated Masses, Double-Bond Equivalents (DBE), and Corresponding Mass Errors of Valnemulin and Its Fragment Ions**

| elemental composition | measured mass (Da) | calculated mass (Da) | DBE | mass errors (mDa) | corresponding mass errors (ppm) |
|---|---|---|---|---|---|
| $C_{31}H_{53}N_2O_5S^+$ | 565.3668 | 565.3675 | 6.5 | −0.7 | −1.2 |
| $C_{20}H_{31}O_2^+$ | 303.2315 | 303.2324 | 5.5 | −0.9 | −3.0 |
| $C_{20}H_{29}O^+$ | 285.2230 | 285.2218 | 6.5 | 1.2 | 4.6 |
| $C_{11}H_{23}N_2O_3S^+$ | 263.1421 | 263.1429 | 1.5 | −0.8 | −3.0 |
| $C_{11}H_{21}N_2O_2S^+$ | 245.1335 | 245.1324 | 2.5 | 1.1 | 4.5 |
| $C_9H_{19}N_2O^+$ | 171.1504 | 171.1497 | 1.5 | 0.7 | 4.1 |
| $C_6H_{14}NO_2S^+$ | 164.0736 | 164.0745 | 0.5 | −0.9 | −5.5 |
| $C_6H_{11}O_2S^+$ | 147.0483 | 147.0480 | 1.5 | 0.3 | 2.0 |
| $C_4H_{10}N^+$ | 72.0807 | 72.0813 | 0.5 | −0.5 | −6.9 |

swines) were administered a single dose of valnemulin (100 mg/kg, dissolved in water) by oral gavage. The urine and feces samples were individually collected prior to the experiment and during 0−24, 24−48, and 48−72 h postdose. All of the samples were frozen at −20 °C until analysis. Each fecal sample was well homogenized before weighing. Ten milliliters of ethyl acetate was added to 2 g of feces, and then the mixture was vortexed for 5 min and centrifuged at 9000*g* at 4 °C for 10 min. The organic layer was transferred into a new polypropylene tube, and the extraction of the feces was repeated following the same procedure. The resulting supernatants were pooled and evaporated to dryness with a gentle nitrogen flow at 45 °C. The residue was redissolved in 1.0 mL of acetonitrile/water (15:85, v/v), and then the resulting solution was loaded onto a preconditioned activated Oasis HLB cartridge (3 mL, 60 mg); the cartridge should be activated with 3 mL of methanol and then preconditioned with 3 mL of water. Furthermore, the cartridge was washed with 6 mL of water, and then the metabolites were eluted with 3 mL of methanol. The eluate was evaporated to dryness under nitrogen at 45 °C, and the residues were eventually reconstituted in 1.0 mL of acetonitrile/water (15:85, v/v). The redissolved solution was centrifuged at 12000*g* at 4 °C for 15 min. Finally, the supernatant was filtered through a 0.22 $\mu$m microbore cellulose membrane into an autosampler vial and analyzed by UPLC-Q/TOF-MS for the identification of metabolites. As to the urine samples, 10 mL of urine from rats and pigs was loaded onto a preconditioned activated Oasis HLB cartridge (3 mL, 60 mg). Afterward, the rest of the steps were performed as described for feces samples.

**Instrumental Conditions.** Identification of valnemulin metabolites was conducted using an ACQUITY UPLC system (Waters Co., USA) coupled with a hybrid Q/TOF-MS SYNAPT HDMS (Waters, UK). Chromatographic separation of valnemulin metabolites was performed on the ACQUITY ultraperformance liquid chromatography system with ambient temperature, using an Acquity BEH RP18 column (50 mm × 2.1 mm i.d., 1.7 $\mu$m particle size) (Waters, USA). The mobile phase of 0.1% formic acid in water (solvent A) and 0.1% formic acid in acetonitrile (solvent B) was pumped at a flow rate of 0.3 mL/min. The gradient elution program was as follows: 0−3.0 min, 5−15% solvent B; 3.0−16.0 min, 15−40% solvent B; 16.0−18.0 min, 40−


dx.doi.org/10.1021/jf5012402 | J. Agric. Food Chem. 2014, 62, 9201−9210

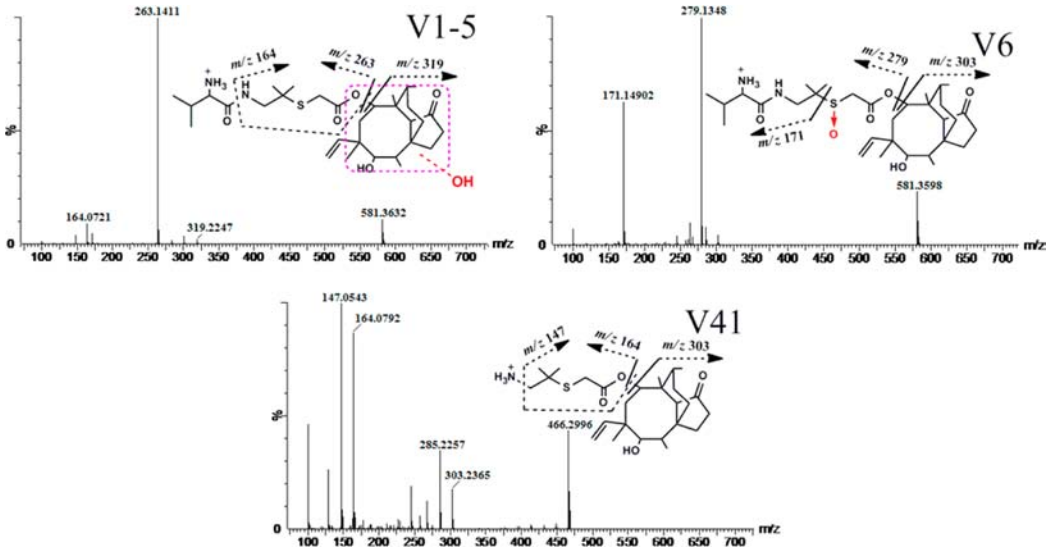


**Figure 3.** MS/MS spectra of the metabolites of valnemulin detected in in vitro rats, chickens, swines, goats, and cows.

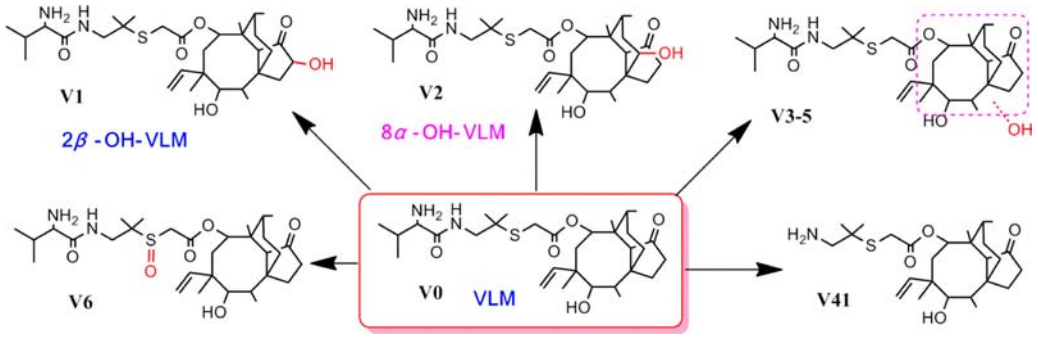


**Figure 4.** Metabolic pathways of valnemulin in rat, chicken, swine, goat, and cow liver microsomes.

70% solvent B; 18.0−19.0 min, 70−100% solvent B; 19.0−20 min, 100% solvent B; 20.0−21.0 min, 100− 5% solvent B; 21.0−22.0 min, 5% solvent B. The injection volume was 10 μL.

Mass spectrometric analysis was operated using a hybrid Q/TOF-MS SYNAPT HDMS (Waters, UK). Typical source conditions for maximum intensity of precursor ions were as follows: capillary voltage, 3.0 kV; source temperature, 120 °C; desolvation temperature, 300 °C; cone gas ($N_2$) flow rate, 10 L/h; desolvation gas ($N_2$) flow rate, 600 L/h. The argon pressure in the collision cell was $3.5 \times 10^{-3}$ mbar. For parent drug and metabolites, ESI source was operated in the positive ionization mode. Data were acquired from 100 to 700 Da and centroid during acquisition using an internal reference comprising a 1 ng/μL solution of leucine enkephalin infused at 50 μL/min, generating a reference ion at $m/z$ 556.2771 in ESI positive ionization mode. Low-energy data were acquired at a collision energy of 5 eV and high-energy data using a ramped collision energy of 10−45 eV.

**Data Processing.** Data processing was carried out using Metabolynx$^{XS}$ software (version 4.1), which could automatically identify metabolites by comparing the samples with the controls. A threshold of 5 mDa was set as a limit to filter the processed data for calculation of possible elemental composition. The mass window was 0.05 Da for both expected and unexpected mass chromatograms, and the absolute area was 50. The intensity threshold of spectrum condition was 10%. The availability of accurate masses and elemental composition data on precursor and all fragment ions in each MS/MS spectrum greatly enhanced confidence in the ion structure assignments.

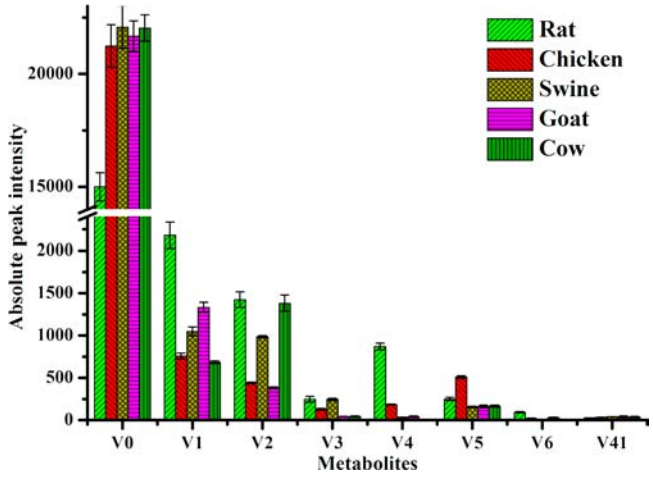


**Figure 5.** Peak areas of extraction ion chromatograms on valnemulin metabolites detected in rat, chicken, swine, goat, and cow liver microsomes.

## RESULTS AND DICUSSION

**Structural Assignment of Product Ions of Valnemulin.** Because it is critical to figure out the fragmentation pathways of valnemulin, UPLC-Q/TOF-MS was applied initially to analyze the protonated valnemulin. The product ion mass spectrum of valnemulin is shown in Figure 2A, which was used not only as a


dx.doi.org/10.1021/jf5012402 | J. Agric. Food Chem. 2014, 62, 9201−9210

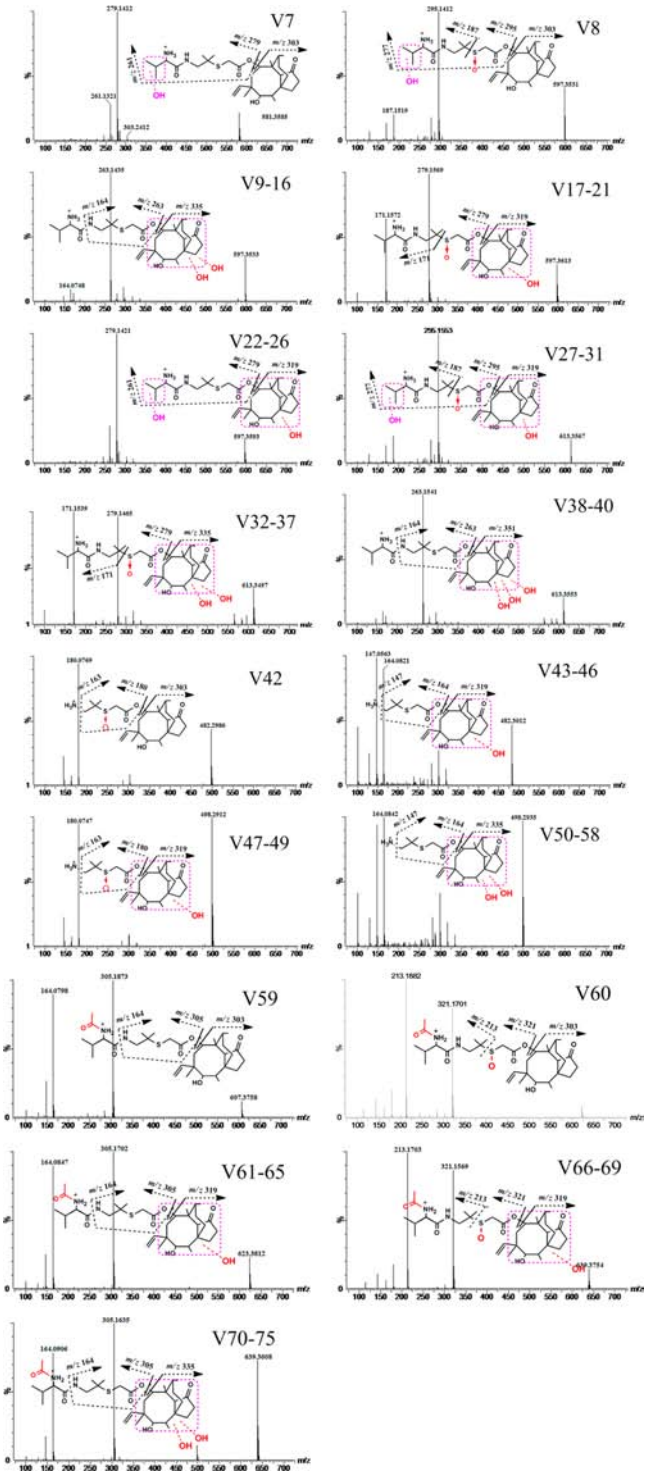


**Figure 6.** MS/MS spectra of the metabolites of valnemulin detected in in vitro rats, chickens, and swines.

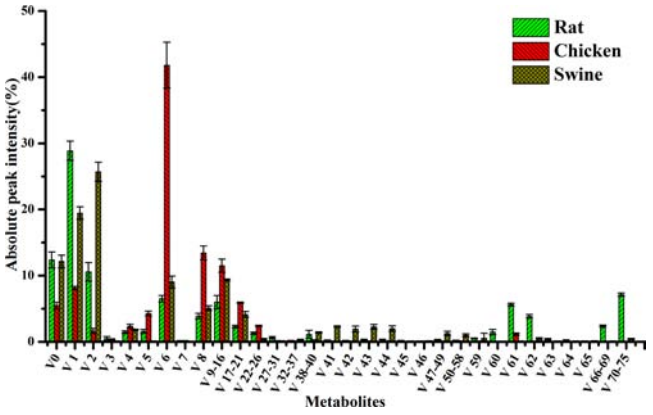


**Figure 7.** Peak areas of extraction ion chromatograms on valnemulin metabolites detected in in vivo rats, chickens, and swines.

reference to aid in the interpretation of product ions of the metabolites but also to examine the high resolution and mass accuracy of the instrument. With the help of formula predictor software, the formulas, the observed and calculated masses, and the mass errors of protonated valnemulin and its fragment ions are listed in Table 1. Relatively good accuracy was obtained with values between the measured and calculated masses ranging from −0.9 to 1.1 mDa (from −6.9 to 4.6 ppm), which powerfully enhanced the reliability for the structures of product ions.

As shown in Figure 2A, the main fragment ion at $m/z$ 263.1421 corresponded to cleavage of the ester bond from the protonated valnemulin. Meanwhile, $m/z$ 303.2315 can also be generated with cleavage of the ester bond. Subsequently, $m/z$ 285.2230 was generated with the loss of $H_2O$ from $m/z$ 303.2315. In addition, $m/z$ 263.1421 generates $m/z$ 164.0736 by losing $C_5H_9O$, which accorded with cleavage of the acidamide bond. Afterward, $m/z$ 147.0483 was generated by the loss of $NH_3$ from the $m/z$ 164.0736. In addition, $m/z$ 171.1504 can be generated by cleaving the bond of S−C in the absence of $C_2H_4O_2S$. According to the results above, the fragmentation pathways of valnemulin are proposed in Figure 2B.

**Identification of Valnemulin Metabolites in Swine Liver Microsomes.** To rapidly characterize the metabolism of valnemulin, incubation of swine liver microsomes with valnemulin and NADPH was initially carried out. The samples and the controls were first analyzed by UPLC-Q/TOF-MS. Subsequently, Metabolynx$^{XS}$ data-processing software utilizing MDF (mass defect filtering) technique was used to identify metabolite ions. As a result, seven potential metabolites were listed by the software. In addition, the accurate extracted ion chromatograms (EIC) (the window was 0.05 Da) of the potential metabolites V1−V6 ($m/z$ 581.3624) and V41 ($m/z$ 466.2991) are shown in the Supporting Information (Figure 10). To elucidate the molecular structure of the potential metabolites, the MS/MS experiments were conducted. Furthermore, the accurate MS/MS spectra of these metabolites are indicated in Figure 3. With the assistance of chromatographic behaviors, accurate mass measurements, and basic rules of drug metabolism, the chemical structures of metabolites were elucidated or clarified.

**Metabolites V1−V5.** Metabolites V1−V5 showed the same $[M + H]^+$ ions at $m/z$ 581.3620 ($[C_{31}H_{53}N_2O_6S]^+$), which was 16 Da higher than the protonated valnemulin at $m/z$ 565.3675, suggesting that they were isomers of mono-oxidized metabolites of valnemulin. Their difference was the position of hydroxylation. Fragment ions from MS/MS spectra of V1−V5 were $m/z$ 263, 171, 164, and 147, which were identical to valnemulin, implying that the side chains of these metabolites were not oxidized. Moreover, the fragment ions at $m/z$ 319 and 301 of V1−V5 were 16 Da higher than the ions at $m/z$ 303 and 285 of valnemulin, respectively, further suggesting that the


dx.doi.org/10.1021/jf5012402 | J. Agric. Food Chem. 2014, 62, 9201−9210

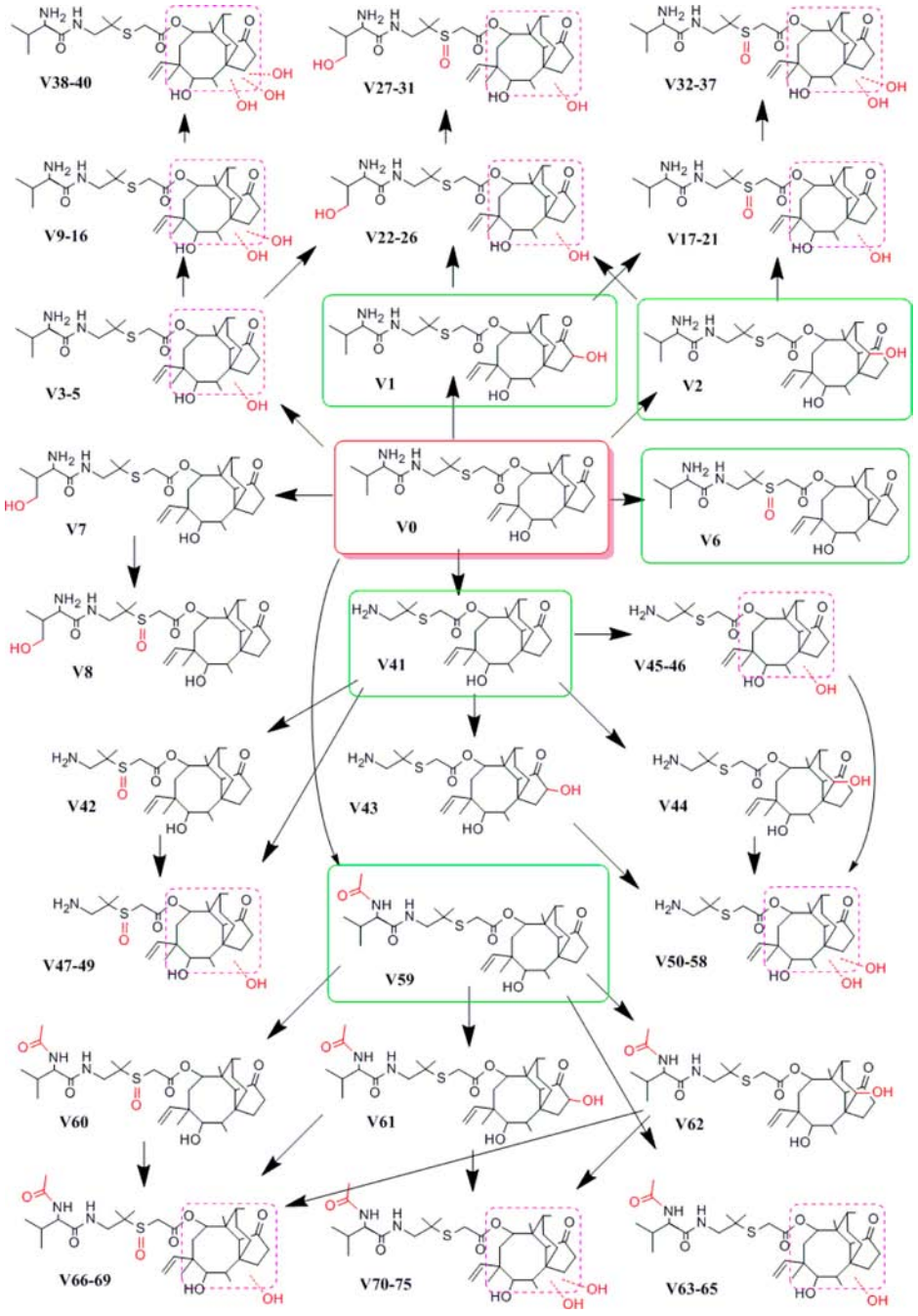


**Figure 8.** Metabolic pathways of valnemulin in in vivo rats, chickens, and swines.

hydroxylation takes place in the mutilin part (the ring system) of valnemulin. Owing to the complex structure of valnemulin with many similar moieties, it would be extremely difficult to unambiguously identify the exact position of hydroxylation in the mutilin part solely using mass spectrometry. NMR analysis would be ideal for such compounds, but it may be difficult to generate sufficient amounts of metabolites. However, earlier studies have shown that the derivates of pleuromutilin were often metabolized by hydroxylation on the 1$\beta$-, 2$\beta$-, and 8$\alpha$-positions. Therefore, it is probable that valnemulin and tiamulin can also be hydroxylated on these positions, which was confirmed by later research conducted by Lykkeberg et al.[17] After incubation of tiamulin with the liver microsomes of pigs, two hydroxylated metabolites were detected as 8$\alpha$-hydroxytiamulin and 2$\beta$-hydroxytiamulin by using LC-MS, $^{1}$H NMR, and $^{13}$C NMR.[17] In the present research, more than five metabolites hydroxylated in the mutilin part (V1−V5) were found, and two (V1 and V2) had larger amount output. On the basis of the analysis, metabolites V1 and V2 were probably 2$\beta$-hydroxyvalnemulin and 8$\alpha$-hydroxyvalnemulin, respectively. As to the trace metabolites V3−V5, it was hardly possible to identify the exact position of hydroxylation in the mutilin part.

**Metabolite V6.** The $[M + H]^+$ ion of metabolite V6 ($m/z$ 581.3627, $C_{31}H_{53}N_2O_6S^+$) was 16 Da higher than the protonated valnemulin. The main product ion at $m/z$ 279 was also 16 Da higher than the ion at $m/z$ 263 of valnemulin, implying that the side chain of V6 was alternatively hydroxylated or oxidized at the sulfur. The key fragment ion at $m/z$ 171 (loss of $C_2H_4O_3S$ from $m/z$ 279) of V6 further suggests that the side chain was oxidized at the sulfur to form *S*-


dx.doi.org/10.1021/jf5012402 | J. Agric. Food Chem. 2014, 62, 9201−9210

oxides. In addition, V6 showed the same retention time and fragment ions on the MS/MS spectrum as the synthesized S-oxidized valnemulin. Consequently, metabolite V6 was identified as S-oxidized valnemulin.

**Metabolite V41.** Metabolite V41 was eluted at 8.85 min with the $[M + H]^+$ ion at $m/z$ 466.2995 ($C_{26}H_{44}NO_5S^+$), which was 99 Da less than the protonated valnemulin at $m/z$ 565.3675, implying that the amido bond of the side chain was hydrolyzed. In addition, the major fragment ion at $m/z$ 164 from metabolite V41, corresponding to cleavage of the ester bond, was also 99 Da less than the main fragment ion at $m/z$ 263 of valnemulin, further suggesting that the amido bond was hydrolyzed.

**Metabolism of Valnemulin in Rat, Chicken, Swine, Goat, and Cow Liver Microsomes.** Considering that metabolic enzymes and metabolic rates were different among various species, the quantitative and qualitative evaluation of metabolites of valnemulin may present some distinctions. Therefore, it was essential and urgent to investigate the metabolism of valnemulin in rats, chickens, swines, goats, and cows, which will be very helpful for its application in pharmacology and clinical use in veterinary practice. Figure 9 (Supporting Information) shows the accurate EICs of valnemulin metabolites formed in liver microsomes of rats, chickens, goats, and cows. The results reveal the same number of valnemulin metabolites for incubation with liver microsomes of different species. Except that metabolite V4 was not detected in cow liver microsomes, seven metabolites (V1−V6 and V41) in swine liver microsmoes were also observed in the other four species. On the basis of these results, the possible metabolic pathways of valnemulin in liver microsomes were hydroxylation, S-oxidation, and hydrolysis, which are proposed in Figure 4.

However, as to the amount of metabolites, there were some differences in the five species. To better analyze the species differences in the metabolism of valnemulin, a semiquantitative analysis was conducted in in vitro systems using the peak areas of extracted ion chromatograms (the window was 0.05 Da) about metabolites; the results are summarized in Figure 5. The results indicated that the ability to metabolize valnemulin in rat liver microsomes was higher than that of the other four species, because the residual level of the unchanged valnemulin in rats was the lowest and there were many metabolites with larger production detected in rats. As to the other four animals, their abilities to metabolize valnemulin were roughly equivalent. The present results also suggest that hydroxylation in the mutilin part was the main metabolic pathway because abundant 2$\beta$-hydroxyvalnemulin (V1) and 8$\alpha$-hydroxyvalnemulin (V2) were produced during the incubation. Moreover, quantitative species differences in the metabolism of valnemulin among the five species were observed. For metabolite V1, the rank order of metabolism ability was rat > goat > pig > chicken > cow and that for metabolite V2, rat > cow > pig > chicken > goat. In addition, the amount of metabolite V1 produced in the liver microsomes of rats, chickens, swines, and goats was greater than that of V2, whereas in cow the amount of metabolite V1 was less than that of V2. Additionally, rat and chicken liver microsomes produced considerable yields of metabolites V4 and V5. The marked quantitative differences in the formation of valnemulin metabolites among the various animal species were perhaps in relation to the levels of the involved enzymes in the liver. As to the S-oxidized (V6) and hydrolyzed metabolites (V41), they were minor products in liver microsomes of the five species. In the absence of the NADPH, only two metabolites (V1 and V2) were detected with minor production in liver microsomes. The amount of metabolites V1 and V2 in the presence of the NADPH was 50-fold higher than that in the absence of the NADPH. These results indicate that NADPH-cytochrome P450 oxidase may be involved in hydroxylation in the mutilin part because NADPH was absolutely essential for this reaction.

**Metabolite Profiles of Valnemulin in in Vivo Rat, Chicken, and Swine.** Seven metabolites were detected and characterized in liver microsomes of different species. To investigate the correlation of in vitro findings with in vivo metabolism, animals (rats, chickens, and pigs) were orally dosed with valnemulin, and urine and feces were collected at different times (0−24 and 24−48 h). Then, these biological samples and the control samples after pretreatment were injected into the UPLC-Q/TOF-MS for analysis. In addition to the unchanged valnemulin, totald of 75, 61, and 74 metabolites of rats, chickens, and pigs were identified, respectively. Among the identified metabolites, 7 known metabolites have been confirmed in the in vitro research, and 68 new metabolites were found in vivo. In addition, the accurate extracted ion chromatograms (EIC) of valnemulin metabolites detected in vivo are shown in the Supporting Information (Figure 11). We assume that they were valnemulin metabolites because comparison of the samples with the control samples as well as the agreement between the accurate mass measurement in MS spectra and predicted formula calculation within 10 ppm. The predicted elemental compositions, exact masses, and mass errors of the metabolites are indicated in the Supporting Information (Table 2). The exact and measured masses agree to within <5 ppm, providing support for the proposed elemental compositions of the metabolites.

**Identification of Valnemulin Metabolites in Rats, Chickens, and Pigs after Oral Administration.** The metabolites were proposed by the Metabolynx$^{XS}$ software, and then the structures were confirmed using the MS/MS mode. As shown in Table 2 (Supporting Information), there were totally 75 metabolites of valnemulin discovered in rats, chickens, and swines, and the majority are being reported for the first time. In addition, the MS/MS spectra of the detected metabolites are shown in Figure 6. Using Q-TOF, the accurate masses for the protonated molecular ions of the metabolites and their product ions in MS and MSMS were obtained, respectively. The measured accurate masses, mass errors, fragment ions, and retention times for these proposed metabolites are presented in Table 2. In all cases, the structures of metabolites and their fragment ions were rapidly and reliably characterized on the basis of the determined elemental composition and accurate MS/MS spectra. Previously, seven metabolites (V1−V6 and V41) have been confirmed in liver microsomes, whereas the other metabolites detected in vivo need further identification.

**Metabolite V7.** The $[M + H]^+$ ion of metabolite V7 ($m/z$ 581.3627, $C_{31}H_{53}N_2O_6S^+$) was 16 Da higher than that of the protonated valnemulin. The main product ion at $m/z$ 279 was also 16 Da higher than the ion at $m/z$ 263 of valnemulin, implying that the side chain of V7 was hydroxylated. Furthermore, the ions at $m/z$ 164 and 147 of metabolite V7 were identical to those of valnemulin, suggesting that the position of hydroxylation should be located at the terminus of the side chain.

**Metabolites V8−V26.** The protonated molecule ions of metabolites V8−V26 were at *m/z* 597.3569 ($C_{31}H_{53}N_2O_7S^+$), which were 16 Da higher than the metabolites V1−V7 at *m/z* 581.3620, implying that they were further hydroxylated or oxidized products of metabolites V1−V7. The fragment ion at *m/z* 295 from metabolite V8 was 16 Da higher than the ion at *m/z* 279 of metabolites V6 and V7, implying that the side chain of V8 was not only hydroxylated but also oxidized at the sulfur in the side chain. Furthermore, the ion at *m/z* 187, generated by cleaving the S−C bond, was 16 Da higher than the ion at *m/z* 171 of metabolite V6, further proving the above point. Similar characteristic product ions were shown in the eight metabolites V9−V16 with different retention times, suggesting that they were the isomers. Fragment ions at *m/z* 263, 171, 164, and 147 from metabolites V9−V16 were identical to those of valnemulin, implying that their side chains were not hydroxylated. In addition, the fragment ions at *m/z* 335 and 317 of metabolites V9−V16 were 16 Da higher than the ions at *m/z* 319 and 301 of metabolites V1−V5, respectively, further implying that there was a couple of hydroxylated sites in the mutilin part of metabolites V9−V16.

Compared with metabolite V6, similar ions at *m/z* 279 and 171 were also detected in metabolites V17−V21, suggesting that oxidization at the sulfur occurs in the side chain. As to the fragment ions at *m/z* 279, 261, and 243 of metabolite V7, they were also available in metabolites V22−V26, implying that their side chains were hydroxylated. In addition, the ions at *m/z* 319 and 301 of metabolites V17−V21 and V22−V26 were identical to those of metabolites V1−V5. This indicated that the hydroxylation also occurs in the mutilin part of these metabolites.

**Metabolites V27−V40.** Mass spectra of metabolites V27−V40 showed the same $[M + H]^+$ ions at *m/z* 613.3530 ($C_{31}H_{53}N_2O_8S^+$), and their product ions were similar to those of V8−V26 except for a 16 Da (an oxygen atom) mass value shift, suggesting that they were further hydroxylated or oxidized on the basis of metabolites V8−V26. The fragment ion at *m/z* 295 from metabolites V27−V31, which is identical to metabolite that of V8, hints that they were further hydroxylated on the mutilin part on the basis of metabolite V8. As to the fragment ion at *m/z* 279 of metabolites V32−V37, it was identical to metabolites that of V17−V26, indicating that their side chains were hydroxylated or oxidized and they were also hydroxylated in the mutilin part on the basis of metabolites V17−V26. In addition, compared with metabolites V9−V16, the similar ions at *m/z* 263, 171, 164, and 147 were also detected in metabolites V38−V40, suggesting that the hydroxylation was in the mutilin part on the basis of metabolites V9−V16.

**Metabolites V42−V46.** Metabolites V42−V46 (*m/z* 482.2940, $C_{26}H_{44}NO_6S^+$) were 16 Da higher than the metabolite V41, suggesting that they were hydroxylated or oxidized at the sulfur to form *S*-oxides on the basis of metabolite V41. Fragment ion at *m/z* 180 of metabolite V42 was 16 Da higher than ion *m/z* 164 of metabolite V41, implying that the side chain of metabolite V42 was oxidized at the sulfur. Compared with metabolite V41, the major fragment ions at *m/z* 164, 147, 129, and 101 were also detected in metabolites V43−V46. Furthermore, the fragment ions at *m/z* 319, 301, and 283 of metabolites V43−V46, which were 16 Da higher than the ions at *m/z* 303, 285, and 267 of metabolite V41, further suggest that the mutilin part of metabolites V43−V46 was hydroxylated.

**Metabolites V47−V58.** Metabolites V47−V58 (*m/z* 498.2875 $C_{26}H_{44}NO_7S^+$) were detected during 3.11−6.03 min, and their product ions were similar to those of V42−V46 except for a 16 Da (an oxygen atom) mass value shift, suggesting that they were further hydroxylated. The fragment ions at *m/z* 180 and 162 from metabolites V47−V49, which were identical to metabolite V42, hinted that they were hydroxylated on the mutilin part on the basis of metabolite V42. Compared with metabolites V43−V46, the major fragment ions at *m/z* 164, 147, 129, and 101 were also detected in metabolites V50−V58, whereas other fragment ions at *m/z* 335, 317, and 299 of metabolites V50−V58 were 16 Da higher than the ions at *m/z* 319, 301, and 283 of metabolites V43−V46. On the basis of the analysis, it was concluded that metabolites V50−V58 were further hydroxylated on the mutilin part of metabolites V43−V46.

**Metabolite V59.** Metabolite V59 showed the $[M + H]^+$ ion at *m/z* 607.3775 ($C_{33}H_{55}N_2O_6S^+$), which was 42 Da higher than that of the protonated valnemulin, implying that it was acetylated. The main fragment ion at *m/z* 305 of metabolite V59, which corresponded to cleavage of the ester bond, was 42 Da higher than the fragment ion *m/z* 263 from valnemulin. Furthermore, the fragment at *m/z* 164, generated by cleavage of the amido bond from the ion at *m/z* 305, further suggests that the acetylization occurs on the amido side chain.

**Metabolites V60−V65.** Metabolites V60−V65 (*m/z* 623.3721, $C_{33}H_{55}N_2O_7S^+$) were 16 Da higher than metabolite V59. In addition, the fragment ion at *m/z* 321 from metabolite V60 was also 16 Da higher than the ion *m/z* 305 of metabolite V59, indicating that it was not only acetylated on the side chain but also oxidized at the sulfur. Fragment ions at *m/z* 305, 164, and 147 from metabolites V61−V65 were identical to the those of metabolite V59, implying that the side chain was not hydroxylated. Therefore, the mutilin part of metabolites V61−V65 should be hydroxylated. For metabolites V1−V4, it was hardly possible to know their exact position of hydroxylation in the mutilin part.

**Metabolites V66−V75.** Metabolites V66−V75 were detected during 7.56−10.98 min with the same $[M + H]^+$ ion at *m/z* 639.3684, which was 16 Da higher than those of metabolites V60−V65. Compared with metabolite V60, the major fragment ions at *m/z* 321 and 213 were also detected in metabolites V66−V69, implying that the mutilin part was hydroxylated on the basis of metabolite V60. Likewise, fragment ions at *m/z* 305, 164, and 147 of metabolites V70−V75 were identical to those of metabolites V61−V65, implying that the mutilin part was further hydroxylated on the basis of metabolites V61−V65.

**Comparison of Metabolism of Valnemulin in Rats, Chickens, and Swines.** Table 2 lists the metabolites of valnemulin detected in rats, chickens, and swines. There were 72 and 62 metabolites detected in the urine of rats and swines, respectively, whereas in the feces 71 and 72 metabolies were detected, suggesting that valnemulin undergoes extensive metabolism. Because the urine and feces are excreted together in chickens, it was difficult to naturally separate them. Thus, the excreta (mixture of feces and urine) of chicken were analyzed together, and totally 61 metabolites were detected. To find the major metabolites of valnemulin in the animals, the area of the every peak corresponding to the metabolites of valnemulin was surveyed. Owing to the different ionizations based on ESI resource in mass spectrometry, the peak areas can only be used to roughly quantify the metabolites. The majority of

metabolites of valnemulin were eliminated in 0−24 h, but there were a few metabolites detected in 24−48 h in three animals. Therefore, the excreta of three animals in the 0−24 h were used to roughly quantify the metabolites. The result is summarized in Figure 7, which shows that there were no major qualitative matabolites in the biotransformation of valnemulin between rats and pigs. Both main metabolites were 2$\beta$-hydroxyvalnemulin (V1) and 8$\alpha$-hydroxyvalnemulin (V2), which was consistent with the in vitro results. However, the metabolite V6, *S*-oxides, was the major metabolite in chickens and accounts for approximately 42.1% of total metabolites' peak area, which was very different from the in vitro results. This was because there were larger numbers of metabolic enzymes involved in valnemulin metabolism in vivo than in the liver microsomes. In addition, gastrointestinal microflora also participated in the metabolism of valnemulin, whereas, in vitro, the number of enzymes involved in drug metabolism was very limited in the liver microsomes. The above facts resulted in metabolic differences of valnemulin between in vivo and in vitro chickens. As to the metabolic differences of valnemulin among different species, it may be that metabolic enzymes in chickens were different from rats and pigs.[24,25] In addition, Figure 7 also reveals that the hydrolysis capabilities in three species were swines > rats > chickens, whereas they were chickens ≫ swines > rats for oxidation on the sulfur and rats > swines > chickens for acetylization.

**Metabolic Pathways of Valnemulin in Rats, Chickens, and Swines.** According to the summary report from EMEA, valnemulin was extensively metabolized to more than 22 different metabolites when rats were orally dosed with $^{3}$H-labeled valnemulin.[9,10] After pigs were given oral doses of 25 mg/kg bw valnemulin, twice a day, for 7.5 days, 11 metabolites were detected in bile, and 6 of these were also found in the liver.[9] Those studies indicate that valnemulin was extensively metabolized in various animals. Although $^{3}$H-labeled valnemulin was used, unfortunately, it did not succeed in the identification of exact molecular structures of the detected metabolites. In addition, the main metabolites of valnemulin were not indicated yet. The EMEA report shows that all of these metabolites retain the intact valnemulin skeleton and were oxidized either in the side chain or in the pleuromutilin ring. In this study, metabolism of valnemulin in rats, chickens, and swines was investigated using UPLC-Q/TOF-MS technology, and more than 75 metabolites were detected. The results showed that the main metabolic pathways of valnemulin were hydroxylation in the mutilin part and the side chain, oxidization on the sulfur of the side chain to form *S*-oxides, hydrolysis of the amido bond, and acetylization in the amido of the side chain. Numerous hydroxylated metabolites of valnemulin were detected. In addition, many metabolites (V9−40) having the mutilin part double or triple oxidized were first detected in the present research. This suggests that the pleuromutilin ring tends to be further oxidized on the basis of metabolites V1−V5. Metabolite V6, in which the sulfur of the side chain was oxidized to form *S*-oxides, was also found in three species, which have been reported by EMEA.[9] In addition, the metabolites of hydrolysis (V41−V58), acetylization (V59−V75), and hydroxylation (V7) in the side chain were also found first in this study. On the basis of the metabolites identified, the proposed metabolic pathways of valnemulin in rats, chickens, and pigs are shown in Figure 8.

In summary, UPLC-Q/TOF-MS was used to investigate the metabolic fate of valnemulin in in vitro rats, chickens, pigs, goats, and cows and in in vivo rats, chickens, and pigs. As a result, 7 and 75 metabolites of valnemulin were detected in vitro and in vivo, respectively, and most of them are reported for the first time. The results showed that the metabolic pathways of valnemulin were hydroxylation in the mutilin part (the ring system) and the side chain, and the former was the major metabolic route. In addition, the results also revealed that the metabolic pathways and the main metabolites of valnemulin in three species are different. All in all, the proposed metabolic pathways of valnemulin in rats, chickens, pigs, goats, and cows will give useful data for the explanation of the residue of valnemulin among different species and, moreover, will further facilitate food safety evaluation of valnemulin.

## ■ ASSOCIATED CONTENT

### Ⓢ Supporting Information

Figures 9−11 and Table 2. This material is available free of charge via the Internet at http://pubs.acs.org.

## ■ AUTHOR INFORMATION


### Corresponding Author

*(X.C.) Phone: +86-10-6273-1201. Fax: +86-10-6273-1032. E-mail: cxy@cau.edu.cn.

### Author Contributions

‖S.Y. and W.S. contributed equally to this work.



### Funding

This work was supported by Chinese Universities Scientific Fund (No. 2014JD001) and the National Natural Science Foundation of China (No. U1301214 and 31372475). D.H. is supported by the National Institute of Environmental Health Sciences (P42ES013661).


### Notes

The authors declare no competing financial interest.

## ■ ACKNOWLEDGMENTS


We acknowledge Haixia Wu, Ying Wang, Yanshen Li, Linxia Li, Kaili Liu, and Lu Zhang for their timely help.


## ■ REFERENCES


(1) Long, K. S.; Poehlsgaard, J.; Hansen, L. H.; Hobbie, S. N.; Bottger, E. C.; Vester, B. Single 23S rRNA mutations at the ribosomal peptidyl transferase centre confer resistance to valnemulin and other antibiotics in Mycobacterium smegmatis by perturbation of the drug binding pocket. *Mol. Microbiol.* **2009**, *71*, 1218−1227.

(2) Long, K. S.; Hansen, L. H.; Jakobsen, L.; Vester, B. Interaction of pleuromutilin derivatives with the ribosomal peptidyl transferase center. *Antimicrob. Agents Chemother.* **2006**, *50*, 1458−1462.

(3) Poulsen, S. M.; Karlsson, M.; Johansson, L. B.; Vester, B. The pleuromutilin drugs tiamulin and valnemulin bind to the RNA at the peptidyl transferase centre on the ribosome. *Mol. Microbiol.* **2001**, *41*, 1091−1099.

(4) Wattanaphansak, S.; Singer, R. S.; Gebhart, C. J. In vitro antimicrobial activity against 10 North American and European *Lawsonia intracellularis* isolates. *Vet. Microbiol.* **2009**, *134*, 305−310.

(5) Stipkovits, L.; Miller, D.; Glavits, R.; Fodor, L.; Burch, D. Treatment of pigs experimentally infected with *Mycoplasma hyopneumoniae*, *Pasteurella multocida*, and *Actinobacillus pleuropneumoniae* with various antibiotics. *Can. J. Vet. Res.* **2001**, *65*, 213−222.

(6) Stipkovits, L.; Ripley, P. H.; Varga, J.; Palfi, V. Use of valnemulin in the control of *Mycoplasma bovis* infection under field conditions. *Vet. Rec.* **2001**, *148*, 399−402.

(7) Bashiruddin, J. B.; De Santis, P.; Varga, E.; Stipkovits, L. Confirmation of the presence of *Mycoplasma bovis* in Hungarian cattle

with pneumonia resembling pleuropneumonia. *Vet. Rec.* **2001**, *148*, 743−746.
(8) Stipkovits, L.; Ripley, P. H.; Tenk, M.; Glavits, R.; Molnar, T.; Fodor, L. The efficacy of valnemulin (Econor) in the control of disease caused by experimental infection of calves with *Mycoplasma bovis*. *Res. Vet. Sci.* **2005**, *78*, 207−215.
(9) EMEA. Committee for Veterinary Medicinal Products Valnemulin. 1998; pp 339−398.
(10) (CVMP), The European Agency for the Evaluation of Medicinal Products. Scientific discussion, 2002; CVMP/031/99.
(11) Heilmann, C.; Jensen, L.; Jensen, J. S.; Lundstrom, K.; Windsor, D.; Windsor, H.; Webster, D. Treatment of resistant mycoplasma infection in immunocompromised patients with a new pleuromutilin antibiotic. *J. Infect.* **2001**, *43*, 234−238.
(12) Sun, J.; Yuan, L.; Zhu, L.; He, L.; Luo, X.; Wang, R.; Liu, Y. Pharmacokinetics and bioavailability of valnemulin in Muscovy ducks (*Cairina moschata*). *Br. Poult. Sci.* **2012**, *53*, 374−378.
(13) Wang, R.; Yuan, L. G.; He, L. M.; Zhu, L. X.; Luo, X. Y.; Zhang, C. Y.; Yu, J. J.; Fang, B. H.; Liu, Y. H. Pharmacokinetics and bioavailability of valnemulin in broiler chickens. *J. Vet. Pharmacol. Ther.* **2011**, *34*, 247−251.
(14) Yuan, L. G.; Luo, X. Y.; Zhu, L. X.; Wang, R.; Liu, Y. H. A physiologically based pharmacokinetic model for valnemulin in rats and extrapolation to pigs. *J. Vet. Pharmacol. Ther.* **2011**, *34*, 224−231.
(15) Huang, Q.; Li, J.; Xia, L.; Xia, X.; Duan, P.; Shen, J.; Ding, S. Residue depletion of valnemulin in swine tissues after oral administration. *Anal. Chim. Acta* **2010**, *664*, 62−67.
(16) Berner, H.; Vyplel, H.; Schulz, G.; Stuchlik, P. Inversion of configuration of the methylgroup at carbon 6 in the tricyclic skeleton of the diterpene pleuromutilin (chemistry of pleuromutilins, IX). *Monatsh. Chem.* **1983**, *114*, 1125−1136.
(17) Lykkeberg, A. K.; Cornett, C.; Halling-Sorensen, B.; Hansen, S. H. Isolation and structural elucidation of tiamulin metabolites formed in liver microsomes of pigs. *J. Pharm. Biomed.* **2006**, *42*, 223−231.
(18) Wang, X.; Liu, Y.; Su, Y.; Yang, J.; Bian, K.; Wang, Z.; He, L. M. High-throughput screening and confirmation of 22 banned veterinary drugs in feedstuffs using LC-MS/MS and high-resolution Orbitrap mass spectrometry. *J. Agric. Food Chem.* **2014**, *62*, 516−527.
(19) Fussell, R. J.; Garcia Lopez, M.; Mortimer, D. N.; Wright, S.; Sehnalova, M.; Sinclair, C. J.; Fernandes, A.; Sharman, M. Investigation into the occurrence in food of veterinary medicines, pharmaceuticals, and chemicals used in personal care products. *J. Agric. Food Chem.* **2014**, *62*, 3651−3659.
(20) Kim, M.; Cho, B. H.; Lim, C. M.; Kim, D. G.; Yune, S. Y.; Shin, J. Y.; Bong, Y. H.; Kang, J.; Kim, M. A.; Son, S. W. Chemical residues and contaminants in foods of animal origin in Korea during the past decade. *J. Agric. Food Chem.* **2013**, *61*, 2293−2298.
(21) Yang, S.; Li, Y.; Cao, X.; Hu, D.; Wang, Z.; Wang, Y.; Shen, J.; Zhang, S. Metabolic pathways of T-2 toxin in in vivo and in vitro systems of Wistar rats. *J. Agric. Food Chem.* **2013**, *61*, 9734−9743.
(22) Lowry, O. H.; Rosebrough, N. J.; Farr, A. L.; Randall, R. J. Protein measurement with the Folin phenol reagent. *J. Biol. Chem.* **1951**, *193*, 265−275.
(23) Pearce, R. E.; McIntyre, C. J.; Madan, A.; Sanzgiri, U.; Draper, A. J.; Bullock, P. L.; Cook, D. C.; Burton, L. A.; Latham, J.; Nevins, C.; Parkinson, A. Effects of freezing, thawing, and storing human liver microsomes on cytochrome P450 activity. *Arch. Biochem. Biophys.* **1996**, *331*, 145−169.
(24) Liu, Z. Y.; Chen, D. M.; Huang, L. L.; Tao, Y. F.; Yao, M.; Yuan, Z. H. In vitro biotransformation and investigation of metabolic enzymes possibly responsible for the metabolism of bisdesoxyolaquindox in the liver fractions of rats, chicken, and pigs. *Toxicology* **2011**, *279*, 155−166.
(25) Yuan, Y.; Zhou, X.; Yang, J.; Li, M.; Qiu, X. T-2 toxin is hydroxylated by chicken CYP3A37. *Food Chem. Toxicol.* **2013**, *62*, 622−627.

natural antioxidants for protection against ROS-induced health disorders.

In the ocean, the extreme environment, such as low light intensities and high oxygen concentrations, leads to the formation of free radicals and other ROS in cells. Therefore, for self-protection against serious oxidative damages, marine algae could produce potent antioxidants.[17] In fact, marine algae have been considered as a rich source of natural antioxidants due to the presence of various secondary metabolites with antioxidant effect.[18] Especially, the antioxidant activities of some protein hydrolysates or peptides from marine algae have been investigated. The protease extracts from brown seaweeds *Scytosiphon lomentaria* and *Ishige okamurae* displayed high scavenging activities.[19,20] A pepsin-hydrolyzed peptide (VECYGPNRPQF) from *Chlorella vulgaris* protein waste was reported to have potent antioxidant activity against various free radicals; especially, it exhibited gastrointestinal enzyme resistance, but no cytotoxicity was observed in human lung fibroblasts cell lines (WI-38).[21] Enzymatic hydrolysates from a benthic diatom *Navicula incerta* exhibited free radical scavenging effects on 2,2-diphenyl-1-picrylhydrazyl (DPPH), hydroxyl, and superoxide radicals.[22] In another study,[23] they purified two antioxidative peptides from the papain hydrolysate of *Navicula incerta*: NIPP-1 (PGWNQWFL) and NIPP-2 (VEVLPPAEL). Interestingly, NIPP-1 and NIPP-2 also displayed inhibition of ethanol-induced cytotoxicity in HepG2/CYP2E1 cells. Using different proteases (pepsin, papain, trypsin, and $\alpha$-chymotrypsin), protein hydrolysates were produced from the marine *Chlorella ellipsoidea*, and an antioxidant peptide LNGDVW (702.2 Da) was identified, which showed potent free radical (peroxyl, DPPH, and hydroxyl radicals) scavenging activities.[24]

However, these antioxidant activities of marine algae-derived peptides (Table 1) are based on in vitro assay; it is unknown if the in vitro antioxidant activities are consistent with their in vivo activities. On the one hand, many in vitro assays frequently use chemically generated radicals that do not occur in vivo, although in vitro assay is valuable. Therefore, it may be more reasonable to use biologically relevant radicals that occur in vivo.[25] For example, oxygen radical absorbance capacity (ORAC) is such an assay.[26] In this assay, a nonfluorescent product is formed by interaction between a fluorescent probe and the peroxyl radicals from the decomposition of 2,20-azobis-2-methyl-propanimidamide dihydrochloride (AAPH), and the antioxidant capacity is determined by changes in the fluorescent product formed over time. The ORAC assay has been applied to analyze the antioxidant capacity of nearly 300 fruits and vegetables by the U.S. Department of Agriculture.[27] Thus, in vivo antioxidant activities can be evaluated by plasma ORAC, malondialdehyde (MDA; a marker of lipid peroxidation), and antioxidant enzymes (glutathione peroxidase (GPX), superoxide dismutase (SOD), and catalase (CAT)), as well as thiobarbituric acid reactive substances (TBARS) in organs (heart, liver, and kidney).[28,29] On the other hand, the in vivo environment is much more complicated than the in vitro environment. Upon in vivo ingestion of a protein hydrolysate or a peptide, its availability is influenced by various factors such as the rate of gastric transit, intestinal motility, luminal hydrolysis, and mucosal absorption. At least, peptides must pass through the gastrointestinal tract to reach their target site intact. In addition, in human blood, there are a large number of serum peptidases, which can further hydrolyze bioactive peptides and reduce their activity. Therefore, it is very

**Table 1. Marine Algae-Derived Antioxidant Peptides**

| peptide name or sequence | source | enzyme | $IC_{50}$ | in vitro/in vivo | mechanism of action | ref |
|---|---|---|---|---|---|---|
| protease extracts | *Scytosiphon lomentaria* | multienzyme complex | <125 $\mu$g/mL | in vitro | hydroxyl, alkyl and DPPH radical | 19 |
| enzymatic digests | *Ishige okamurae* | multienzyme complex | <25 $\mu$g/mL | in vitro | hydrogen peroxide | 20 |
| VECYGPNRPQF | *Chlorella vulgaris* | | 9.8–58 $\mu$M | in vitro | hydroxyl radical, superoxide radical, peroxyl radical, DPPH radical and ABTS radicals | 21 |
| enzymatic hydrolysates | *Navicula incerta* | alcalase, Pronase-E, $\alpha$-chymotrypsin, Neutrase, papain, pepsin, and trypsin | 102–196 $\mu$g/mL | in vitro | hydroxyl, superoxide, DPPH | 22 |
| PGWNQWFL, VEVLPPAEL | *Navicula incerta* | alcalase, $\alpha$-chymotrypsin, Neutrase, papain, pepsin, Pronase-E, and trypsin | | in vitro (HepG2/CYP2E1 cells) | free radicals/antihepatotoxicity | 23 |
| LNGDVW | *Chlorella ellipsoidea* | papain, trypsin, pepsin, and $\alpha$-chymotrypsin | 0.02–1.42 mM | in vitro | peroxyl, DPPH and hydroxyl radicals | 24 |


dx.doi.org/10.1021/jf502420h | J. Agric. Food Chem. 2014, 62, 9211–9222

**Table 2. Marine Algae-Derived Anticancer Peptides**

| peptide name or sequence | source | enzyme | $IC_{50}$ | in vitro/in vivo | mechanism of action | ref |
|---|---|---|---|---|---|---|
| VECYGPNRPQF | *Chlorella vulgaris* | pepsin | 70 μg/mL | in vitro (gastric cancer AGS cells) | antiproliferation and post-G1 cell cycle arrest | 34 |
| polypeptide CPAP | *Chlorella pyrenoidosa* | papain, trypsin, and alcalase | 426 μg/mL | in vitro (HepG2 cells) | apoptosis | 35 |
| polypeptide Y2 | *Spirulina platensis* | trypsin, alcalase, pepsin, and papain | 61 μg/mL | in vitro (MCF-7 and HepG-2 cells) | | 36 |

necessary to conduct simultaneous evaluation of the in vitro and in vivo antioxidant capacity. Unfortunately, to date, no studies have evaluated the antioxidant efficacy of marine algae-derived peptides using animal models, except for a few papers related to extracts or compounds or whole algae, such as the in vivo antioxidant activity of carotenoids from *Dunaliella salina*, a green microalga;[30] the antioxidant effect of alcoholic extract from the marine alga *Chlorella vulgaris* against naphthalene-induced oxidative stress in the albino rats;[31] and the antioxidant activity of whole *Spirulina* in rats.[32]

**Anticancer Biopeptides.** Cancer is a continually increasing threat for human health. Radiotherapy and chemotherapy are the main approaches to fighting cancers, despite the presence of side effects and development of resistance. Marine algae-derived peptides have been shown to possess cytotoxic effects on human cancer cells (Table 2).[33] For example, from *Chlorella vulgaris* protein waste Sheih et al.[34] isolated a undecapeptide with the sequence VECYGPNRPQF, which exhibited strong dose-dependent antiproliferation ($IC_{50}$ value = 70.7 ± 1.2 μg/mL) and induced a post-G1 cell cycle arrest in gastric cancer AGS cells and no cytotoxicity in normal lung fibroblast WI-38 cells in vitro. Using low-temperature high-pressure extraction, enzymatic hydrolysis, ion exchange, and gel filtration chromatography, Wang and Zhang[35] isolated a polypeptide CPAP from *Chlorella pyrenoidosa*, which had inhibitory activity on human liver cancer HepG2 cells with an $IC_{50}$ value of 426 μg/mL. Phase contrast microscopy showed that HepG2 cells exhibited the characteristics of apoptosis, including cell membrane shrinkage, fragmentation of nuclear chromatin, and formation of black apoptotic bodies, in a high-dose group (0.3−0.5 mg/mL), suggesting the presence of CPAP-induced apoptosis and necrotic death in HepG2 cells. In addition, the micro- and nanoencapsulation of CPAP demonstrated the resistance of CPAP to gastrointestinal enzymatic degradation. Similarly, an antitumor polypeptide Y2 was obtained from the trypsin digest of *Spirulina platensis* proteins.[36] The polypeptide Y2 exhibited cytotoxicity toward MCF-7 and HepG2 cells with an $IC_{50}$ value of ∼61 μg/mL, suggesting that the activity of Y2 is 7-fold stronger than that of CPAP.

These results reveal that the use of peptides from marine algae has potential for the prevention and treatment of cancer, but their mechanisms of action (Figure 2) need to be extensively elucidated. Generally, marine anticancer peptides kill cancer cells by different mechanisms, including apoptosis induction, tubulin−microtubule imbalance, and angiogenesis inhibition.[37] Apoptosis, as a form of programmed cell death, occurs primarily through two well-characterized pathways initiated by caspase activation in cells: one is the extrinsic death receptor pathway, and another is the intrinsic mitochondrial pathway.[38] Many peptides originated from marine animals were reported to adopt a strategy of triggering apoptotic processes,[39] which should be useful for demonstrating the detailed mechanism of action of marine algae-derived peptides.

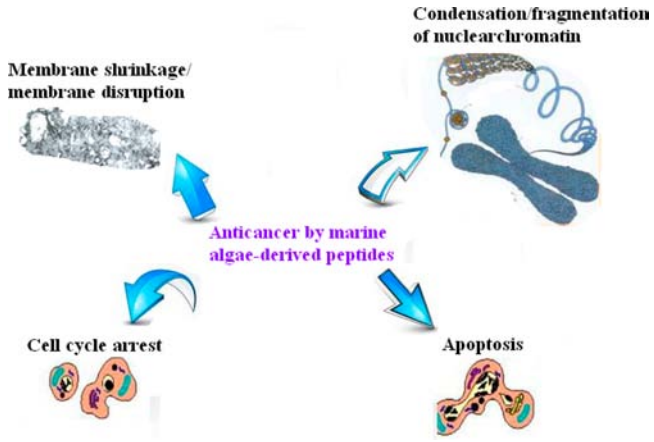


**Figure 2.** Anticancer mechanisms of marine algae-derived bioactive peptides. Apoptosis and cell cycle arrest could be involved.

**Antihypertensive Biopeptides.** Hypertension is recognized as a key target for controlling cardiovascular disease-related mortality.[40] There has been continuing interest in the search for bioactive peptides with antihypertensive bioactive peptides from marine algae (Table 3).[12] From *Undaria pinnatifida*, Suetsuna et al.[41] characterized 10 kinds of dipeptides; among them, four peptides (YH, KY, FY, and IY) significantly decreased the blood pressure in spontaneously hypertensive rats. Cha et al.[42] reported that five different enzymatic digests from a brown seaweed *Ecklonia cava* exhibited potent angiotensin-converting enzyme (ACE) inhibitory effects with $IC_{50}$ values of 2.33−3.56 μg/mL. Sheih et al.[43] observed that a purified undecapeptide (VECYGPNRPQF) from *Chlorella vulgaris* possessed ACE inhibitory activity ($IC_{50}$ = 29.6 μM). Similarly, a potent ACE inhibitory peptide (VEGY) from *Chlorella ellipsoidea* was discovered to have ACE inhibitory activity ($IC_{50}$ value = 128.4 μM).[44] In addition, the oral administration of purified peptide can significantly decrease systolic blood pressure in spontaneously hypertensive rats. Recently, from cultured marine microalga *Nannochloropsis oculata*, Samarakoon et al.[45] purified two novel peptides, GMNNLTP and LEQ; their $IC_{50}$ values of ACE inhibitory activity were 123 and 173 μM, respectively. However, in contrast, up to now, few rennin inhibitory peptides from marine algae have been reported. The first example is IRLIIVLMPILMA isolated from the macroalga *Palmaria palmata*, which inhibited renin activities by 58.97% at a concentration of 1 mg/mL.[46]

The renin−angiotensin system (RAS) and kinin−arginine−nitric oxide system pathways are the key targets for controlling blood pressure.[47] The enzyme rennin, after its release from the kidney, cleaves the inactive peptide angiotensinogen secreted from the liver and converts it into angiotensin-I. Subsequently,


dx.doi.org/10.1021/jf502420h | J. Agric. Food Chem. 2014, 62, 9211−9222

**Table 3. Marine Algae-Derived Antihypertension Peptides**

| peptide name or sequence | source | enzyme | $IC_{50}$ | in vitro/in vivo | mechanism of action | ref |
|---|---|---|---|---|---|---|
| YH, KY, FY, IY | *Undaria pinnatifida* | no enzyme used | 2.7−43.7 μmol/L | in vitro and in vivo (rats) | ACE inhibition | 41 |
| enzymatic digests | *Ecklonia cava* | Kojizyme, Flavourzyme, Neutrase, Alcalase, and Protamex | 2.33−3.56 μg/mL | in vitro | ACE inhibition | 42 |
| VECYGPNRPQF | *Chlorella vulgaris* | pepsin | 29.6 μM | in vitro | ACE inhibition | 43 |
| VEGY | *Chlorella ellipsoidea* | Protamex, Kojizyme, Neutrase, Flavourzyme, Alcalase, trypsin, α-chymotrypsin, pepsin, and papain | 128.4 μM | in vitro and in vivo (rats) | ACE inhibition | 44 |
| GMNNLTP, LEQ | *Nannochloropsis oculata* | pepsin, trypsin, α-chymotrypsin, and papain | 123−173 μM | in vitro | ACE inhibition | 45 |
| IRLIIVLMPILMA | *Palmaria palmata* | papain | 3.3 mM | in vitro | renin inhibition | 46 |

ACE converts angiotensin-I into angiotensin-II and inactivates the vasodilator bradykinin, leading to a rise in blood pressure. Thus, there are two ways to control blood pressure by modulating RAS; one is direct inhibition of angiotensin-I generation from angiotensinogen by rennin, and another is blockage of conversion from angiotensin-I to angiotensin-II by ACE. Therefore, rennin and ACE inhibitory factors are considered as the way to treat hypertension. On the other hand, the kinin−nitric oxide system works in concert with the RAS systems to regulate blood pressure. Bradykinin activates $Ca^{2+}$/calmodulin-dependent endothelial nitric oxide synthase (eNOS), which catalyzes the conversion of arginine to nitric oxide (NO) and citrulline, leading to a drop in blood pressure. Studies confirmed that eNOS knockout and NO deficiency can lead to clinical hypertension.[48,49] Therefore, the arginine-rich peptides can also be considered as a strategy for hypertension therapy.[50] As mentioned above, the acting mechanisms of marine algae-derived peptides are related to ACE and rennin inhibitions, and the eNOS/NO pathway is temporarily not involved (Figure 3).

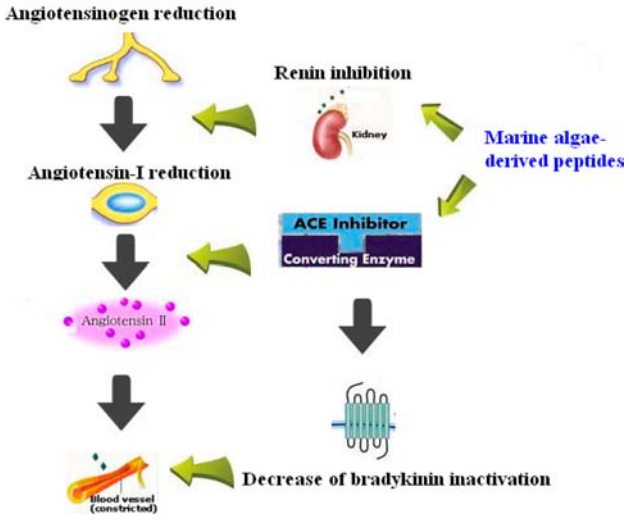


**Figure 3.** Antihypertension mechanisms of marine algae-derived bioactive peptides. ACE and rennin inhibitions are involved.

**Antiatherosclerotic Biopeptides.** Atherogenesis is a process by which plaques are gradually formed by fatty materials, which can lead to high blood pressure and cardiovascular disease as a result of compromised arteries. A recent study[51] showed that a *Chlorella* undecapeptide, with the amino sequence VECYGPNRPQF, significantly suppressed the levels of E-selectin, intercellular cell adhesion molecule-1 (ICAM-1), vascular cell adhesion molecule-1 (VCAM-1), monocyte chemoattractant protein (MCP-1), and endothelin-1 (ET-1) gene expression. On the other hand, the vascular inflammatory role of platelet activating factor acetylhydrolase (PAF-AH) is considered a promising therapeutic target for the prevention of atherosclerosis. Several oligopeptides were isolated and characterized from the red macroalga *Palmaria palmata*.[52] Among them, NIGK showed PAF-AH inhibition with an $IC_{50}$ value of 2.32 mM, suggesting a valid drug template for PAF-AH inhibitors. Furthermore, Vo and Kim[53] purified two bioactive peptides P1 (LDAVNR) and P2 (MMLD) from the gastric enzymatic hydrolysate of *Spirulina maxima*. P1 and P2 inhibited the production of adhesion molecules including P-selectin and E-selectin by down-regulating early growth response factor 1 (Egr-1) expression via histamine receptor and PKCδ-dependent MAPKs activation pathway. Additionally, P1 and P2 were shown to have anti-inflammatory activity by reducing ROS production and inhibiting histamine release and IL-8 expression.[54]

In the early stage of atherogenesis, the activation of endothelial cells leads to the production of IL-6 and MCP-1. IL-6 is a pro-atherogenic cytokine, and MCP-1 is implicated in the development of atherosclerosis by recruiting monocytes into the subendothelial cell layer.[55,56] ICAM-1, VCAM-1, MCP-1, and ET-1 are believed to have important roles in the etiology of atherosclerotic vascular disease.[57,58] Reduction of these molecules' expression has been demonstrated to be an effective approach to blocking the development of atherosclerosis.[59]On the other hand, inflammatory processes in endothelial cells are crucial events to initiate and promote early stage atherosclerotic lesions.[60] ROS is a common product of inflammatory processes; H1 receptor and platelet activating factor acetylhydrolase play a central role in the induction and maintenance of inflammatory reaction.[61] Moreover, Egr-1 is the target of some inflammatory genes including cytokines, chemokines, adhesion molecules, etc.[62] Thus, ROS, H1 receptor, and Egr-1 are also considered as key targets for atherosclerosis treatment. The above data suggest that the antiatherosclerosis effects of marine algae-derived peptides (Table 4) could be associated with adhesion molecule reduction, platelet activating factor acetylhydrolase inhibition, and anti-inflammation (Figure 4).

**Immunomodulatory Biopeptides.** In undernourished Balb/c mice, Morris et al.[63] reported that oral administration of protein hydrolysate from *Chlorella vulgaris* activates both innate and specific immune responses, including markedly increasing the lymphocyte pool, production of T cell-dependent antibody responses, and reconstitution of delayed-type

**Table 4. Marine Algae-Derived Antiatherosclerosis Peptides**

| peptide name or sequence | source | enzyme | $IC_{50}$ | in vitro/in vivo | mechanism of action | ref |
|---|---|---|---|---|---|---|
| VECYGPNRPQF | *Chlorella* sp. | pepsin, Flavourzyme, Alcalase, and Papain | | in vitro (endothelial cells Svec4-10 and macrophage RAW 264.7 cells) | inhibition of vascular adhesion molecules (E-selectin, ICAM, VCAM, MCP-1 and ET-1) gene expression | 51 |
| NIGK | *Palmaria palmata* | papain | 2.32 mM | in vitro | platelet activating factor acetylhydrolase (PAG-AH) inhibition | 52 |
| LDAVNR, MMLDF | *Spirulina maxima* | trypsin, α-chymotrypsin, and pepsin | | in vitro (EA hy926 cells and U937 cells) | adhesion inhibition/anti-inflammatory (inhibition of IL-6, IL-8, MCP-1, P-selectin, ROS, and Egr-1) | 53, 54 |

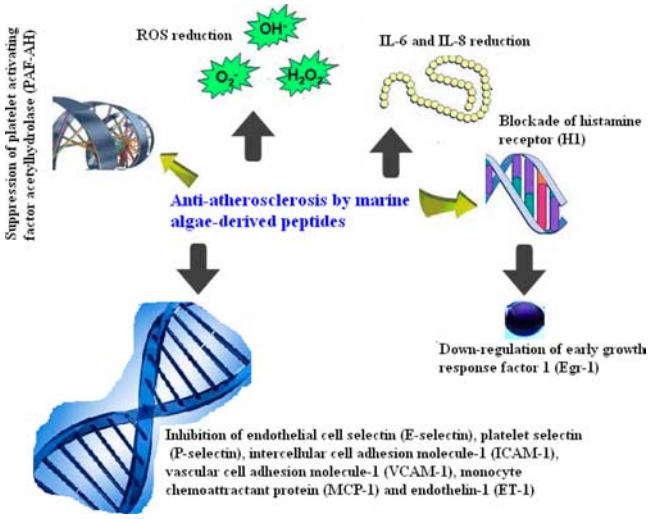


**Figure 4.** Antiatherogenesis mechanisms of marine algae-derived bioactive peptides, which could be associated with adhesion molecules reduction, platelet activating factor acetylhydrolase inhibition, and anti-inflammation.

hypersensitivity (DTH) responses. In another study,[64] *Ecklonia cava* hydrolysate was shown to have the immune-stimulating effect on murine splenocytes in vitro. Additionally, in ICR mice treated with *E. cava* hydrolysate, the proliferation of splenocytes was dramatically enhanced; the numbers of CD4+ T cells, CD8+ T cells, and CD45R/B220+ B cells were markedly increased; TNF-α and IFN-γ were down-regulated, and IL-4 and IL-10 were up-regulated. Cian et al.[65] found that enzymatic hydrolysates from a phycobiliprotein byproduct of *Porphyra columbina* exhibited immunosuppressive effects on rat splenocytes by enhancing IL-10 production and inhibiting the production of TNF-α and IFN-γ.

As an anti-inflammatory cytokine, IL-10 is expressed by spleen macrophages and regulatory T lymphocytes (Tregs). It is capable of inhibiting synthesis of pro-inflammatory cytokines such as IFN-γ, IL-2, IL-3, and TNF-α. IL-10 also can block NF-κB activity and enhances B cell survival, proliferation, and antibody production. IL-4 is a cytokine that induces differentiation of naive helper T cells (Th0 cells) to Th2 cells. It can stimulate B-cell and T-cell proliferation and decreases the production of IFN-γ, IL-12, Th1 cells, macrophages, and dendritic cells. CD4+T cells are an essential part of the human immune system, which primarily function in sending signals to other types of immune cells, including CD8 killer cells. The above observations suggest that the immunomodulatory mechanism of marine algae-derived proteins or peptides (Table 5) is primarily involved in cytokine regulation and T cell and B cell proliferation pathways (Figure 5).

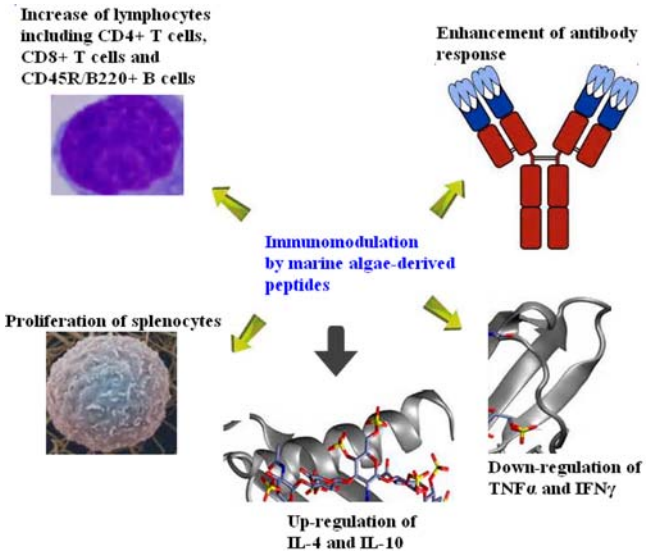


**Figure 5.** Immunomodulation mechanisms of marine algae-derived bioactive peptides, which are primarily involved in cytokine regulation and T cell and B cell proliferation pathways.

**Other Biopeptides.** Solar ultraviolet (UV) irradiation damages human skin and induces premature aging. UV irradiation leads to activation of transcription factor activator protein-1 (AP-1), increases matrix metalloproteinases (MMPs) expression, and causes collagen degradation.[66] Cysteine-rich 61 (CYR61) is an extracellular matrix-associated signaling

**Table 5. Marine Algae-Derived Immunomodulatory Peptides**

| peptide name or sequence | source | enzyme | $IC_{50}$ | in vitro/ in vivo | mechanism of action | ref |
|---|---|---|---|---|---|---|
| protein hydrolysates | *Chlorella vulgaris* | pancreatin | | in vivo (mice) | stimulation of both humoral and cell-mediated immune functions (T-dependent antibody response and the reconstitution of delayed-type hypersensitivity response) | 63 |
| protein hydrolysates | *Ecklonia cava* | Kojizyme | | in vivo (mice) | increases in lymphocytes, monocytes, and granulocytes; down-regulation of TNF-α and IFN-γ, up-regulation of IL-4 and IL-10 | 64 |
| protein hydrolysates | *Porphyra columbina* | trypsin, alcalase | 2.1−5.6 g/L | in vivo (rats) | cytokine modulations (inhibition of TNF-α and IFN-γ, increase of IL-10) | 65 |


dx.doi.org/10.1021/jf502420h | J. Agric. Food Chem. 2014, 62, 9211−9222

**Table 6. Marine Algae-Derived Anti-UV Radiation and Antiosteoporosis Peptides**

| peptide name or sequence | source | enzyme | $IC_{50}$ | in vitro/in vivo | mechanism of action | ref |
|---|---|---|---|---|---|---|
| Chlorella derived peptide | *Chlorella* sp. | no enzyme used | | in vitro (skin fibroblast 966SK) | inhibition of MMP-1, AP-1, CYR61, and MCP-1 | 68, 69 |
| MPDW | *Nannochloropsis oculata* | Alcalase, Neutrase, Flavourzyme, trypsin, and Protamex | | in vitro (human osteosarcoma (MG-63) and murine mesenchymal stem cell (D1)) | increases in ALP, osteocalcin, collagen type I, BMP-2, BMP2/4; phosphorylation of MAPK/Smad pathways | 76 |

molecule; it not only inhibits procollagen synthesis by decreasing transforming growth factor (TGF)-b receptor II (TbRII) but also up-regulates MMP-1 by activating AP-1.[67] Studies indicated that *Chlorella*-derived peptide (CDP) reduced UV-induced MMP-1 and CYR61 mRNA expression and MCP-1 production, restored UV-suppressed procollagen, and inhibited UV-induced c-fos and c-jun expressions.[68,69] These results (Table 6) suggest that the protective effect of CDP on UV radiation-induced damage in the skin is associated with the ameliorative effects of CDP on the expressions of AP-1, CYR61, and MCP-1 (Figure 6).

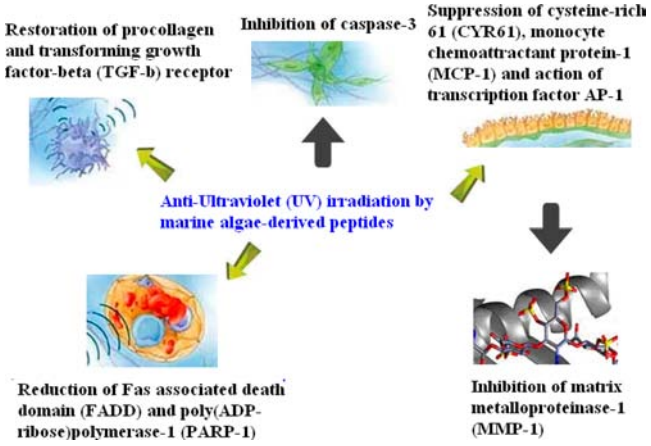


**Figure 6.** Anti-ultraviolet irradiation mechanisms of marine algae-derived bioactive peptides, which is related to the reduction in the expressions of AP-1, CYR61, and MCP-1.

Osteoporosis is a systemic skeletal disease and has become an important public health problem.[70] There are various signaling pathways involved in osteoblast differentiation, including mitogen-activated protein kinases (MAPKs), Smad, and nuclear factor kappa-light-chain-enhancer of activated B cells (NF-κB).[71−73] During osteoblast differentiation, many osteomarkers (alkaline phosphatase (ALP), collagen type I, and osteocalcin) are highly expressed, and the MAPK signaling cascades (ERK (p-ERK), p-p38, and p-JNK) are activated.[74] Smad 1, Smad5, and Smad8 become phosphorylated by interacting with activated bone morphogenetic proteins (BMPs) receptors and form a complex with Smad 4 to regulate the transcription of various target genes.[75] Nguyena et al.[76] purified an osteoblast-differentiatory peptide MPDW from biodiesel byproducts of microalgae *Nannochloropsis oculata*. The purified peptide was found to facilitate osteoblast differentiation by increasing the expression of several osteoblast phenotype markers, including osteocalcin, collagen type I, alkaline phosphatase (ALP), BMP-2, BMP2/4, and bone mineralization in both human osteoblastic cells (MG-63) and murine mesenchymal stem cells (D1). Moreover, the peptide increased phosphorylation of MAP kinases (p-ERK, p-JNK, p-p38) and Smads (p-Smad1/5/8) expression. This suggests potential application of algae-derived peptide (Table 6) in bone health, and its mechanism of action is shown in Figure 7.

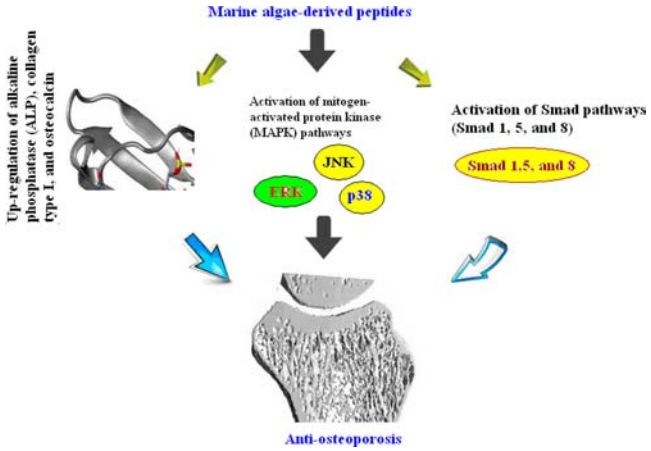


**Figure 7.** Antiosteoporosis mechanisms of marine algae-derived bioactive peptides, which are associated with the up-regulation of osteocalcin, collagen type I, alkaline phosphatase (ALP), and bone morphogenetic proteins (BMP)-2 and BMP2/4 and the increased phosphorylation of MAP kinases (p-ERK, p-JNK, p-p38) and Smads (p-Smad1/5/8).

## FUTURE CHALLENGES

**In Silico Proteolysis and Quantitative Structure−Activity Relationship Studies.** The traditional hydrolysis−purification−characterization protocol for bioactive peptide discovery is labor-intensive and costly. In addition, this strategy might exclude minor but potent peptides in the hydrolysate.[77] An emerging approach in the production of bioactive peptide is the use of an in silico approach, which generally involves the selection of appropriate protein/enzyme combinations by database search, generation of peptides of interests following in silico hydrolysis, quantitative structure−activity relationship (QSAR) model prediction, and synthesis and bioassay of satisfactory peptides. Among them, the in silico hydrolysis is able to select a suitable enzyme for the hydrolysis of a given protein, using some programs such as BIOPEP, POPS, NeuroPred, and PeptideCutter.[78] QSAR modeling provides a method to find mathematical expressions for describing the relationship between peptide structure and bioactivity, which may be useful for estimating the activity of any related peptides and for predicting structures with high activity. To date, information about the structural characteristics associated with specific bioactivity is limited, although some information is available, such as all of the most potent ACE-inhibitory peptides contain at least one proline residue,[79] and the very


dx.doi.org/10.1021/jf502420h | J. Agric. Food Chem. 2014, 62, 9211−9222

potent antimicrobial peptides have been known to be cationic with hydrophobic amino acid residues.[80]

On the basis of the QSAR modeling of antioxidative peptides for scavenging radicals in three databases, namely, Trolox equivalent antioxidant capacity (TEAC), oxygen radical absorption capacity (ORAC), and superoxide radical (SOR), a relationship between the physicochemical properties of the C-/N-terminal region and antioxidant potency was established.[81] Specifically, the C-terminal is more important than the N-terminal; the contribution of amino acids to antioxidant activity is ordered as C2 > C1 for TEAC, C3 > C4 > C1 for ORAC, and C4 > C1 > N1 for SOR. Bulky hydrophobic amino acids at the C-terminal are related to the antioxidant activity of peptides in the three free radical systems. Several publications explore the potential of in silico methods for the screening of bioactive peptides. For example, by in silico digestion of egg white protein and QSAR analysis of more than 20000 peptides generated from 75 in silico hydrolysates, Majumder and Wu[82] found that thermolysin−pepsin digestion of ovotransferrin was the best condition, and three novel antihypertensive peptides were identified. Sargadia et al.[83] identified six novel peptides with ACE-inhibitory activity ($IC_{50}$ values = 4−32 $\mu$M) from 231 peptides of milk proteins, using matrix-assisted laser desorption/ionization tandem time-of-flight (MALDI-TOF-TOF) mass spectrometry and QSAR modeling on ACE-inhibitory peptides with an amino acid length larger >5.

**In Vivo Fate of Bioactive Peptides.** Due to the susceptibility of peptides to protease degradation, the fate of bioactive peptides during gastrointestinal transit is a major problem. In fact, the antihypertensive peptide $\beta$-LG f(142−148) obtained from $\beta$-lactoglobulin could not be detected in the sera of human volunteers following its oral ingestion; that is, the peptide is not sufficiently stable to gastrointestinal and serum proteases.[84] To enhance the stability of peptides, one solution is chemical modification of peptides and the incorporation of unnatural amino acids (including D-amino acids). For example, at the carboxyl terminal end of a peptide, the presence of a proline residue has been shown to increase the peptide's resistance to degradation by digestive enzymes.[85] Shen et al.[86] developed a new chemical method of peptide synthesis to generate cyclic peptides by incorporating unnatural amino acids into a peptide chain, hence increasing stability. Another solution is encapsulation of peptides with polymers or particles such as dendrimers, liposomes, and polyectrolyte microspheres. For example, Wang and Zhang[35] investigated the micro- and nanoencapsulation of a *Chlorella pyrenoidosa* antitumor polypeptide (CPAP) by complex coacervation and ionotropic gelation. The in vitro release tests showed that CPAP was well preserved against gastric enzymatic degradation after micro/nanoencapsulation, and the slowly controlled release in the intestine could be potentially achieved. On the other hand, due to the existence of intestinal bacterial communities, it is necessary to consider whether or not potential toxic metabolites could be generated by fermentation of gut microbiota on bioactive peptides.[87] For example, the increased protein fermentation and decreased carbohydrate fermentation by gut microbiota was shown to cause a significant decrease in fecal cancer protective metabolites (e.g., butyrate) and the greatest formation of hazardous metabolites such as *N*-nitroso compounds, which is probably detrimental to colonic health.[88]

## NOVEL TECHNOLOGIES IN BIOACTIVE PEPTIDES STUDIES AND PRODUCTION

**Enzyme-Assisted Extraction Technology.** To obtain bioactive peptides from marine algae, the first step is to effectively extract proteins. Marine algae cell walls are made of sulfated and branched polysaccharides.[89] It is essential to break down cell walls for extracting marine algal proteins. Enzyme-assisted extraction (EAE) has received more attention than its counterparts; it is a highly sophisticated technique and can also be applied for large-scale operations.[3,90] EAE is an ecofriendly, nontoxic, high-bioactivity, and relatively low-cost technology. The commonly used food grade enzymes include cellulase, $\alpha$-amylase, and pepsin.[91] Compared to extracts obtained using conventional extraction methods, enzyme-assisted extracts have higher antioxidant activity.[92] Similarly, enzyme proteolysis was found to enhance extraction of ACE inhibitory and antioxidant peptides from *Porphyra columbina* residual cake.[93]

**Subcritical Water Extraction (SWE) Technology.** Besides EAE, another novel technology for algae protein extraction is SWE. It is reported that subcritical water hydrolysis is a feasible technique for high-yield protein and amino acid production from animal and vegetable materials.[94] Using subcritical water conditions (100−220 °C) for 30 min, high yields of peptides and amino acids (about 219 and 8.0 mg/g of dry bran, respectively) were produced from deoiled rice bran; importantly, the product obtained at 200 °C after 30 min of hydrolysis exhibited high antioxidant activity.[95] On the basis of SWE of microalga *Haematococcus pluvialis* at different temperatures (50−200 °C), antioxidant and antimicrobial compounds were obtained.[96] Employing flash hydrolysis (a few seconds of residence time and subcritical water conditions),[97] >60% of the total nitrogen content (dry basis) in microalgae *Scenedesmus* sp. was extracted within 10 s of residence time above 240 °C. The NMR spectra indicated that the extracted protein is present mainly as water-soluble peptides and free amino acids.

**Other Technologies.** In peptide preparation, a major challenge is how to conduct large-scale production of bioactive peptides. It is known that chemical synthesis is relatively expensive and not suitable for large-scale production.[80] In this respect, biotechnological methods may provide opportunities for manufacturing large amounts of bioactive peptides. Enzymatic hydrolysis under the condition of immobilized enzymes can avoid the generation of secondary metabolites by enzymatic autolysis and can be recycled. Enzymatic hydrolysis in continuous enzyme membrane reactor system allows faster reactions, higher yields, cleaner products, and lower operating costs, which are advantageous in industrial-scale production.[1,79,98] These methods have been applied to the production of some plant-derived bioactive peptides.[99−101] In addition, bioactive peptides can be produced by in situ microbial fermentation of parent proteins. Usually, lactic acid bacteria and bifidobacteria are widely used for the production of bioactive peptides,[102] for example, production of antibacterial peptide nisin by *Lactococcus lactis* and *Saccharomyces cerevisiae*[103] and antioxidant peptide production from bovine casein using *Bifidobacterium longum*.[104] Of course, other bacteria are also possible, such as the productions of antimicrobial peptides and ACE inhibitory peptide by *Streptococcus thermophilus*[105]

The second major challenge is how to realize the isolation of individual peptides with higher bioactivity from the hydrolysate,[106] because protein hydrolysates consist of complex

peptide mixtures with similar molecular weights. The most frequently used technologies include chromatography and pressure-driven filtration processes.[107,108] However, some drawbacks, such as the high cost of chromatographic technology and membrane fouling formation for pressure-driven processes, limit their wide application.[2] Recently, a patented electrodialysis with ultrafiltration membranes (EDUF) was developed to replace traditional separation methods for peptide recovery.[109] The driving force of EDUF is the electric field; hence, there is no significant fouling formation at the membrane interface due to the absence of pressure.[110] EDUF technology has been applied to the isolation of peptides from various hydrolysates.[111−114]

The third challenge is to understand the mechanisms of action of bioactive peptides. Fluorescence lifetime imaging (FLIM) technique is able to distinguish interacting and noninteracting fractions and to resolve changes in the binding, conformation, and composition of biologically relevant compounds in live cells.[115] Therefore, FLIM has become an inevitable technique for spatially resolving cellular processes and physical interactions of cellular components in real time.[116] Thus, it offers the opportunity to understand the mechanism of action for increasingly generated bioactive peptides, such as the interaction mechanisms of antimicrobial peptide (melittin) with live bacterial cells.[117] However, FLIM is unable to determine the detailed molecular changes in such an interaction process. In this respect, omics technologies (transcriptomics, proteomics, and metabolomics) could make contributions. For instance, proteomics is a promising technology in understanding mechanism of action for bioactive peptides. By two-dimensional electrophoresis (2DE) coupled to mass spectrometry, Huang and Chen[118] profiled proteome changes in antibacterial peptide epinecidin-1-treated zebrafish. A possible protein−protein interacting network regulated by epinecidin-1 was constructed, suggesting a potential role of epinecindin-1 in cytoskeletal assembly and organization to promote resistance to bacterial infection.

Currently, these novel methods are rarely applied to the production and study of marine algae peptides, but should be promising. Specifically, EAE and SWE technologies are first employed to extract proteins from marine algal biomass. On the one hand, the extracted proteins are subject to fermentation by probiotics such as lactic acid bacteria and bifidobacteria for peptide production. On the other hand, the extracted proteins are enzymatically hydrolyzed under the condition of immobilized enzymes or in a continuous enzyme membrane reactor system. Then, EDUF technology is employed to simultaneously isolate bioactive peptides from the complex peptides mixture. Finally, the mechanisms of action of bioactive peptides are investigated by FLIM and omics such as proteomics techniques (Figure 8).

In conclusion, bioactive peptides generated by enzymatic hydrolysis of algae protein or algae processing waste exhibit diverse biofunctionalities, which are promising in applications of functional foods, pharmaceuticals, and cosmeceuticals. However, there are still many challenges before bioactive peptides can be translated into practical use for human nutrition and health. In silico proteolysis and QSAR modeling can accelerate the discovery of bioactive peptides. Innovative technologies need to be developed for transferring laboratory-scale preparations to industrial-scale production. Extensive research is highly required to explore metabolic products of bioactive peptides during gastrointestinal digestion and to elucidate the detailed mechanisms of action in vivo. It is envisaged that the bioactive peptides market will become a self-standing industry in the next few decades. Hence, some regulations and standards that govern the production, utilization, and marketing of bioactive peptides should be set.

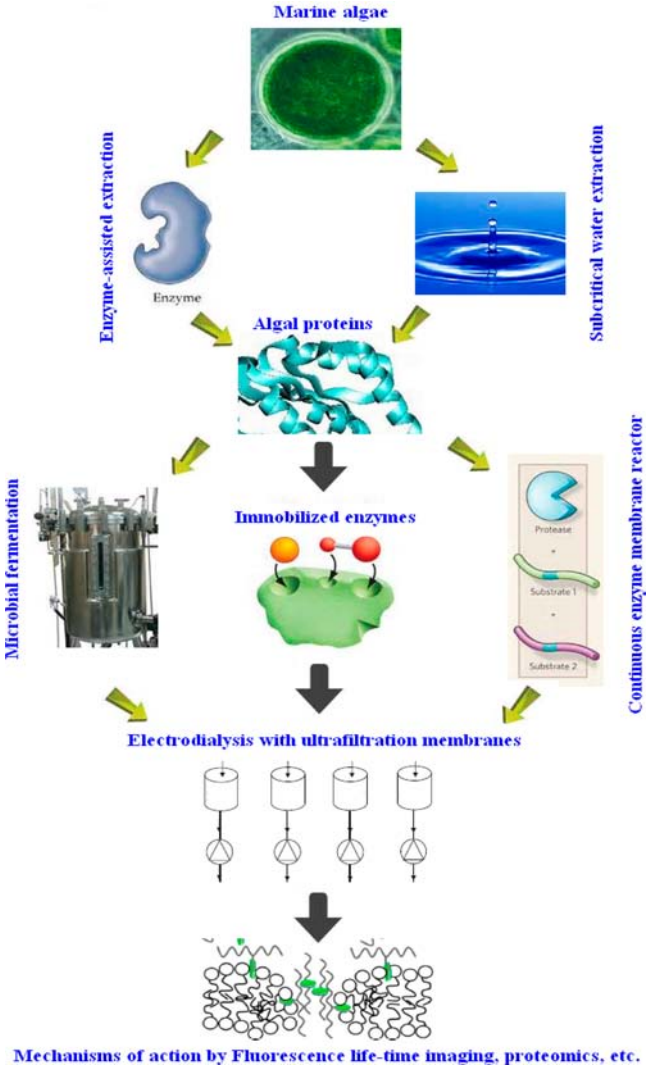


**Figure 8.** Proposed applications of novel technologies to produce and study marine algae-derived bioactive peptides.

## AUTHOR INFORMATION

### Corresponding Author

*(X.Z.) Mail: College of Light Industry and Food Sciences, South China University of Technology, 381 Wushan Road, Guangzhou 510640, China. Phone/fax: 86 20 87113848. E-mail: snow_dance@sina.com.

### Funding

This study was supported by an Ocean and Fisheries Development Project (A201301B04) from the Administration of Ocean and Fisheries of Guangdong Province and a National High-Tech Research and Development Project (863 Program) (2014AA022004). This study was supported by Key Laboratory of Enhanced Heat Transfer and Energy Conservation of the Ministry of Education, South China University of Technology, Guangzhou, China.

## Notes

The authors declare no competing financial interest.

## REFERENCES


(1) Korhonen, H.; Pihlanto, A. Bioactive peptides: production and functionality. *Int. Dairy J.* **2006**, *16* (9), 945−960.

(2) Chabeaud, A.; Vandanjon, L.; Bourseau, P.; Jaouen, P.; Guérard, F. Fractionation by ultrafiltration of a saithe protein hydrolysate (*Pollachius virens*): effect of material and molecular weight cut-off on the membrane performances. *J. Food Eng.* **2009**, *91*, 408−414.

(3) Samarakoon, K.; Jeon, Y. J. Bio-functionalities of proteins derived from marine algae − a review. *Food Res. Int.* **2012**, *48*, 948−960.

(4) Cheung, R. C.; Wong, J. H.; Pan, W. L.; Chan, Y. S.; Yin, C. M.; Dan, X. L.; Wang, H. X.; Fang, E. F.; Lam, S. K.; Ngai, P. H.; Xia, L. X.; Liu, F.; Ye, X. Y.; Zhang, G. Q.; Liu, Q. H.; Sha, O.; Lin, P.; Ki, C.; Bekhit, A. A.; Bekhit, A.-D.; Wan, D. C.; Ye, X. J.; Xia, J.; Ng, T. B. Antifungal and antiviral products of marine organisms. *Appl. Microbiol. Biotechnol.* **2014**, *98* (8), 3475−3494.

(5) Glaser, K. B.; Mayer, A. M. A renaissance in marine pharmacology: from preclinical curiosity to clinical reality. *Biochem. Pharmacol.* **2009**, *78* (5), 440−448.

(6) Hughes, C. C.; Fenical, W. Antibacterials from the sea. *Chem. Eur. J.* **2010**, *16* (42), 12512−12525.

(7) Mayer, A. M.; Gustafson, K. R. Marine pharmacology in 2005−2006: antitumour and cytotoxic compounds. *Eur. J. Cancer* **2008**, *44* (16), 2357−2387.

(8) Mayer, A. M.; Rodríguez, A. D.; Taglialatela-Scafati, O.; Fusetani, N. Marine pharmacology in 2009−2011: marine compounds with antibacterial, antidiabetic, antifungal, anti-inflammatory, antiprotozoal, antituberculosis, and antiviral activities; affecting the immune and nervous systems, and other miscellaneous mechanisms of action. *Mar. Drugs* **2013**, *11*, 2510−2573.

(9) Wijesekara, I.; Kim, S. K. Angiotensin-I-converting enzyme (ACE) inhibitors from marine resources: prospects in the pharmaceutical industry. *Mar. Drugs* **2010**, *8* (4), 1080−1093.

(10) Ibanez, E.; Cifuentes, A. Benefits of using algae as natural sources of functional ingredients. *J. Sci. Food Agric* **2013**, *93*, 703−709.

(11) Kim, S. K.; Kang, K. H. Medicinal effects of peptides from marine microalgae. *Adv. Food Nutr. Res.* **2011**, *64*, 313−323.

(12) Kim, S. K.; Wijesekara, I. Development and biological activities of marine-derived bioactive peptides: a review. *J. Funct Foods* **2010**, *2*, 1−9.

(13) Kim, J. A.; Kim, S. K. Bioactive peptides from marine sources as potential anti-inflammatory therapeutics. *Curr. Protein Pept. Sci.* **2013**, *14* (3), 177−182.

(14) Butterfield, D. A.; Castenga, A.; Pocernich, C. B.; Drake, J.; Scapagnini, G.; Calabrese, V. Nutritional approaches to combat oxidative stress in Alzheimer's disease. *J. Nutr. Biochem.* **2002**, *13*, 444−461.

(15) Valko, M.; Leibfritz, D.; Mancol, J.; Cronin, M. T. D.; Mazur, M.; Telser, J. Free radicals and antioxidants in normal physiological functions and human disease. *Int. J. Biochem. Cell Biol.* **2007**, *39*, 44−84.

(16) Lindenschmidt, R. C.; Trika, A. F.; Guard, M. E.; Witschi, H. P. The effect of dietary butylated hydroxyl toluene on liver and colon tumor development in mice. *Toxicology* **1986**, *38*, 151−160.

(17) Guedes, A. C.; Amaro, H. M.; Malcata, X. F. Microalgae as source of high added-value compounds — a brief review of recent work. *Biotechnol. Prog.* **2011**, *27*, 597−613.

(18) Ngo, D. H.; Wijesekara, I.; Vo, T. S.; Ta, Q. V.; Kim, S. K. Marine food-derived functional ingredients as potential antioxidants in the food industry: an overview. *Food Res. Int.* **2011**, *44*, 523−529.

(19) Ahn, C. B.; Jeon, Y. J.; Kang, D. S.; Shin, T. S.; Jung, B. M. Free radical scavenging activity of enzymatic extracts from a brown seaweed Scytosiphon lomentaria by electron spin resonance spectrometry. *Food Res. Int.* **2004**, *37*, 253−258.

(20) Heo, S. J.; Jeon, Y. J. Radical scavenging capacity and cytoprotective effect of enzymatic digests of Ishige okumurae. *J. Appl. Phycol.* **2008**, *20*, 1087−1095.

(21) Sheih, I. C.; Wu, T. K.; Fang, T. J. Antioxidant properties of a new antioxidative peptide from algae protein hydrolysate in different oxidation systems. *Bioresour. Technol.* **2009**, *100*, 3419−3425.

(22) Kang, K. H.; Qian, Z. J.; Ryu, B.; Kim, S. K. Characterization of growth and protein contents from microalgae *Navicula incerta* with the investigation of antioxidant activity of enzymatic hydrolysates. *Food Sci. Biotechnol.* **2011**, *20* (1), 183−191.

(23) Kang, K. H.; Qian, Z. J.; Ryu, B.; Karadeniz, F.; Kim, D.; Kim, S. K. Antioxidant peptides from protein hydrolysate of microalgae *Navicula incerta* and their protective effects in HepG2/CYP2E1 cells induced by ethanol. *Phytother. Res.* **2012**, *26* (10), 1555−1563.

(24) Ko, S. C.; Kim, D.; Jeon, Y. J. Protective effect of a novel antioxidative peptide purified from a marine *Chlorella ellipsoidea* protein against free radical-induced oxidative stress. *Food Chem. Toxicol.* **2012**, *50* (7), 2294−2302.

(25) Power, O.; Jakeman, P.; FitzGerald, R. J. Antioxidative peptides: enzymatic production, *in vitro* and *in vivo* antioxidant activity and potential applications of milk-derived antioxidative peptides. *Amino Acids* **2013**, *44* (3), 797−820.

(26) Ou, B.; Hampsch-Woodill, M.; Prior, R. Development and validation of an improved oxygen radical absorbance capacity assay using fluorescein as the fluorescent probe. *J. Agric. Food Chem.* **2001**, *49* (10), 4619−4626.

(27) Haytowitz, D.; Bhagwat, S. *USDA Database for the Oxygen Radical Absorbance Capacity (ORAC) of Selected Foods*, release 2; U.S. Department of Agriculture: Washington, DC, USA, 2010.

(28) Manso, M. A.; Miguel, M.; Even, J.; Hernández, R.; Aleixandre, A.; López Fandiñõ, R. Effect of the long-term intake of an egg white hydrolysate on the oxidative status and blood lipid profile of spontaneously hypertensive rats. *Food Chem.* **2008**, *109* (2), 361−367.

(29) Wang, D.; Wang, L.; Zhu, F.; Zhu, J.; Chen, X. D.; Zou, L.; Saito, M.; Li, L. *In vitro* and *in vivo* studies on the antioxidant activities of the aqueous extracts of Douchi (a traditional Chinese salt-fermented soybean food). *Food Chem.* **2008**, *107* (4), 1421−1428.

(30) Chidambara Murthy, K. N.; Vanitha, A.; Rajesha, J.; Mahadeva Swamy, M.; Sowmya, P. R.; Ravishankar, G. A. *In vivo* antioxidant activity of carotenoids from *Dunaliella salina* − a green microalga. *Life Sci.* **2005**, *76* (12), 1381−1390.

(31) Vijayavel, K.; Anbuselvam, C.; Balasubramanian, M. P. Antioxidant effect of the marine algae *Chlorella vulgaris* against naphthalene-induced oxidative stress in the albino rats. *Mol. Cell. Biochem.* **2007**, *303* (1−2), 39−44.

(32) Gad, A. S.; Khadrawy, Y. A.; El-Nekeety, A. A.; Mohamed, S. R.; Hassan, N. S.; Abdel-Wahhab, M. A. Antioxidant activity and hepatoprotective effects of whey protein and *Spirulina* in rats. *Nutrition* **2011**, *27* (5), 582−589.

(33) Kang, K. H.; Kim, S. K. Beneficial effect of peptides from microalgae on anticancer. *Curr. Protein Pept. Sci.* **2013**, *14* (3), 212−217.

(34) Sheih, I. C.; Fang, T. J.; Wu, T. K.; Lin, P. H. Anticancer and antioxidant activities of the peptide fraction from algae protein in waste. *J. Agric. Food Chem.* **2010**, *58*, 1202−1207.

(35) Wang, X.; Zhang, X. Separation, antitumor activities, and encapsulation of polypeptide from *Chlorella pyrenoidosa*. *Biotechnol. Prog.* **2013**, *29* (3), 681−687.

(36) Zhang, B.; Zhang, X. Separation and nanoencapsulation of antitumor polypeptide from *Spirulina platensis*. *Biotechnol. Prog.* **2013**, *29*, 1230−1238.

(37) Zheng, L. H.; Wang, Y. J.; Sheng, J.; Wang, F.; Zheng, Y.; Lin, X. K.; Sun, M. Antitumor peptides from marine organisms. *Mar. Drugs* **2011**, *9* (10), 1840−1859.

(38) Gupta, S.; Kass, G. E.; Szegezdi, E.; Joseph, B. The mitochondrial death pathway: a promising therapeutic target in diseases. *J. Cell. Mol. Med.* **2009**, *13*, 1004−1033.

(39) Zheng, L.; Lin, X.; Wu, N.; Liu, M.; Zheng, Y.; Sheng, J.; Ji, X.; Sun, M. Targeting cellular apoptotic pathway with peptides from marine organisms. *Biochim. Biophys. Acta* **2013**, *1836* (1), 42−48.

(40) Verdecchia, P.; Angeli, F.; Mazzotta, G.; Gentile, G.; Reboldi, G. The rennin angiotensin system in the development of cardiovascular

disease: role of aliskiren in risk reduction. *Vasc. Health Risk Manage.* **2008**, *4*, 971−981.
(41) Suetsuna, K.; Maekawa, K.; Chen, J. R. Antihypertensive effects of *Undaria pinnatifida* (wakame) peptide on blood pressure in spontaneously hypertensive rats. *J. Nutr Biochem.* **2004**, *15*, 267−272.
(42) Cha, S. H.; Ahn, G. N.; Heo, S. J.; Kim, K. N.; Lee, K. W.; Song, C. B.; et al. Screening of extracts from marine green and brown algae in Jeju for potential marine angiotensin-I converting enzyme (ACE) inhibitory activity. *J. Korean Soc. Food Sci. Nutr.* **2006**, *35*, 307−314.
(43) Sheih, I. C.; Fang, T. J.; Wu, T. K. Isolation and characterization of a novel angiotensin-I converting enzyme (ACE) inhibitory peptide from the algae protein waste. *Food Chem.* **2009**, *115*, 279−284.
(44) Ko, S. K.; Nalae, K.; Kim, E. A.; Kang, M. C.; Lee, S. H.; Kang, S. M.; et al. A novel angiotensin I-converting enzyme (ACE) inhibitory peptide from a marine *Chlorella ellipsoidea* and its antihypertensive effect in spontaneously hypertensive rats. *Process Biochem.* **2012**, *45*, 2005−2011.
(45) Samarakoon, K. W.; et al. Purification and identification of novel angiotensin-I converting enzyme (ACE) inhibitory peptides from cultured marine microalgae (*Nannochloropsis oculata*) protein hydrolysate. *J. Appl. Phycol* **2013**, *25*, 1595−1606.
(46) Fitzgerald, C.; Mora-Soler, L.; Gallagher, E.; O'Connor, P.; Prieto, J.; Soler-Vila, A.; Hayes, M. Isolation and characterization of bioactive pro-peptides with *in vitro* renin inhibitory activities from the macroalga *Palmaria palmata*. *J. Agric. Food Chem.* **2012**, *60* (30), 7421−7427.
(47) Chen, Z. Y.; Peng, C.; Jiao, R.; Wong, Y. M.; Yang, N.; Huang, Y. Anti-hypertensive nutraceuticals and functional foods. *J. Agric. Food Chem.* **2009**, *57* (11), 4485−4499.
(48) Huang, P. L.; Huang, Z. H.; Mashimo, H.; Bloch, K. D.; Moskowitz, M. A.; Bevan, J. A.; Fishman, M. C. Hypertension in mice lacking the gene for endothelia metric oxide synthase. *Nature* **1995**, *377*, 239−242.
(49) Thomas, G. D.; Zhang, W.; Victor, R. G. Nitric oxide deficiency as a cause of clinical hypertension. *JAMA−J. Am. Med. Assoc.* **2008**, *285*, 2055−2057.
(50) Udenigwe, C. C.; Mohan, A. Mechanisms of food protein-derived antihypertensive peptides other than ACE inhibition. *J. Funct. Foods* **2014**, *8*, 45−52.
(51) Shih, M. F.; Chen, L. C.; Cherng, J. Y. Chlorella 11-peptide inhibits the production of macrophage-induced adhesion molecules and reduces endothelin-1 expression and endothelial permeability. *Mar. Drugs* **2013**, *11* (10), 3861−3874.
(52) Fitzgerald, C.; Gallagher, E.; O'Connor, P.; Prieto, J.; Mora-Soler, L.; Grealy, M.; Hayes, M. Development of a seaweed derived platelet activating factor acetylhydrolase (PAF-AH) inhibitory hydrolysate, synthesis of inhibitory peptides and assessment of their toxicity using the zebrafish larvae assay. *Peptides* **2013**, *50*, 119−124.
(53) Vo, T. S.; Kim, S. K. Down-regulation of histamine-induced endothelial cell activation as potential anti-atherosclerotic activity of peptides from *Spirulina maxima*. *Eur. J. Pharm. Sci.* **2013**, *50* (2), 198−207.
(54) Vo, T. S.; Ryu, B. M.; Kim, S. K. Purification of novel anti-inflammatory peptides from enzymatic hydrolysate of the edible microalgal *Spirulina maxima*. *J. Funct. Foods* **2013**, *5*, 1336−1346.
(55) Huber, S. A.; Sakkinen, P.; Conze, D.; Hardin, N.; Tracy, R. Interleukin-6 exacerbates early atherosclerosis in mice. *Arterioscler. Thromb. Vasc. Biol.* **1999**, *19*, 2364−2367.
(56) Takaishi, H.; Taniguchi, T.; Takahashi, A.; Ishikawa, Y.; Yokoyama, M. High glucose accelerates MCP-1 production via p38 MAPK in vascular endothelial cells. *Biochem. Biophys. Res. Commun.* **2003**, *305*, 22−28.
(57) Little, P. J.; Ivey, M. E.; Osman, N. Endothelin-1 actions on vascular smooth muscle cell functions as a target for the prevention of atherosclerosis. *Curr. Vasc. Pharmacol.* **2008**, *6*, 195−203.
(58) Sheikine, Y.; Hansson, G. K. Chemokines and atherosclerosis. *Ann. Med.* **2004**, *36*, 98−118.
(59) Winkles, J. A.; Alberts, G. F.; Brogi, E.; Libby, P. Endothelin-1 and endothelin receptor mRNA expression in normal and atherosclerotic human arteries. *Biochem. Biophys. Res. Commun.* **1993**, *191*, 1081−1088.
(60) Ross, R. Atherosclerosis − an inflammatory disease. *N. Engl. J. Med.* **1999**, *340*, 115−126.
(61) Rozenberg, I.; Sluka, S. H.; Rohrer, L.; Hofmann, J.; Becher, B.; Akhmedov, A.; Soliz, J.; Mocharla, P.; Borén, J.; Johansen, P.; Steffel, J.; Watanabe, T.; Lüscher, T. F.; Tanner, F. C. Histamine H1 receptor promotes atherosclerotic lesion formation by increasing vascular permeability for low-density lipoproteins. *Arterioscler. Thromb. Vasc. Biol.* **2010**, *30*, 923−930.
(62) Blaschke, F.; Bruemmer, D.; Law, R. E. Egr-1 is a major vascular pathogenic transcription factor in atherosclerosis and restenosis. *Rev. Endocr. Metab. Disord.* **2004**, *5*, 249−254.
(63) Morris, H. J.; Carrillo, O.; Almarales, A.; Berm'udez, R. C.; Lebeque, Y.; Fontaine, R.; et al. Immunostimulant activity of an enzymatic protein hydrolysate from green microalga *Chlorella vulgaris* on undernourished mice. *Enzyme Microb. Technol.* **2007**, *40*, 456−460.
(64) Ahn, G.; Hwang, I.; Park, E. J.; Kim, J. H.; Jeon, Y. J.; Lee, J. H.; et al. Immunomodulatory effects of an enzymatic extracts from *Ecklonia cava* on murine splenocytes. *Mar. Biotechnol.* **2008**, *10*, 278−289.
(65) Cian, R. E.; Martínez-Augustin, O.; Drago, S. R. Bioactive properties of peptides obtained by enzymatic hydrolysis from protein byproducts of *Porphyra columbina*. *Food Res. Int.* **2012**, *49*, 364−372.
(66) Watanabe, H.; Shimizu, T.; Nishihira, J.; Abe, R.; Nakayama, T.; Taniguchi, M.; Sabe, H.; Ishibashi, T.; Shimizu, H. Ultraviolet A-induced production of matrix metalloproteinase-1 is mediated by macrophage migration inhibitory factor (MIF) in human dermal fibroblasts. *J. Biol. Chem.* **2004**, *279*, 1676−1683.
(67) Quan, T.; He, T.; Kang, S.; Voorhees, J. J.; Fisher, G. J. Elevated cysteine-rich 61 mediates aberrant collagen homeostasis in chronologically aged and photoaged human skin. *Am. J. Pathol.* **2006**, *169*, 482−490.
(68) Chen, C. L.; Liou, S. F.; Chen, S. J.; Shih, M. F. Protective effects of *Chlorella*-derived peptide on UVB-induced production of MMP-1 and degradation of procollagen genes in human skin fibroblasts. *Regul. Toxicol. Pharmacol.* **2011**, *60* (1), 112−119.
(69) Shih, M. F.; Cherng, J. Y. Potential protective effect of fresh grown unicellular green algae component (resilient factor) against PMA- and UVB-induced MMP1 expression in skin fibroblasts. *Eur. J. Dermatol.* **2008**, *18* (3), 303−307.
(70) Fazzalari, N. L. Bone remodeling: a review of the bone microenvironment perspective for fragility fracture (osteoporosis) of the hip. *Semin. Cell Dev. Biol.* **2008**, *19*, 467−472.
(71) Cao, X.; Chen, D. The BMP signaling and *in vivo* bone formation. *Gene* **2005**, *357*, 1−8.
(72) Ge, C.; Xiao, G.; Jiang, D.; Franceschi, R. T. Critical role of the extracellular signal regulated kinase-MAPK pathway in osteoblast differentiation and skeletal development. *J. Cell Biol.* **2007**, *176*, 709−718.
(73) Novack, D. V. Role of NF-κB in the skeleton. *Cell Res.* **2011**, *21*, 169−182.
(74) Rey, A.; Manen, D.; Rizzoli, R.; Ferrari, S. L.; Caverzasio, J. Evidences for a role of p38 MAP kinase in the stimulation of alkaline phosphatase and matrix mineralization induced by parathyroid hormone in osteoblastic cells. *Bone* **2007**, *41*, 59−67.
(75) Miyazono, K.; Maeda, S.; Imamura, T. BMP receptor signaling: transcriptional targets, regulation of signals, and signaling cross-talk. *Cytokine Growth Factor Rev.* **2005**, *16*, 251−263.
(76) Nguyena, M. H. T.; Qian, Z. J.; Nguyen, V. T.; Choic, I. W.; Heo, S. J.; Ohd, C. H.; Kang, D. H.; Kime, G. H.; Jung, W. K. Tetrameric peptide purified from hydrolysates of biodiesel byproducts of *Nannochloropsis oculata* induces osteoblastic differentiation through MAPK and Smad pathway on MG-63 and D1 cells. *Process Biochem.* **2013**, *48*, 1387−1394.
(77) Martínez-Maqueda, D.; Miralles, B.; Recio, I.; Hernandez-Ledesma, B. Antihypertensive peptides from food proteins: a review. *Food Funct.* **2012**, *3*, 350−361.

(78) Carrasco-Castilla, J.; Hernandez-Alvarez, A. J.; Jimenez-Martınez, C.; Gutierrez-Lopez, G. F.; Davila-Ortiz, G. Use of proteomics and peptidomics methods in food bioactive peptide science and engineering. *Food Eng. Rev.* **2012**, *4*, 224−243.
(79) Agyei, D.; Danquah, K. Industrial-scale manufacturing of pharmaceutical-grade bioactive peptides. *Biotechnol. Adv.* **2011**, *29*, 272−277.
(80) Hancock, R. E. W.; Sahl, H.-G. Antimicrobial and host-defense peptides as new anti-infective therapeutic strategies. *Nat. Biotechnol.* **2006**, *24* (12), 1551−1557.
(81) Li, Y. W.; Li, B. Characterization of structure-antioxidant activity relationship of peptides in free radical systems using QSAR models: key sequence positions and their amino acid properties. *J. Theor. Biol.* **2013**, *318*, 29−43.
(82) Majumder, K.; Wu, J. A new approach for identification of novel antihypertensive peptides from egg proteins by QSAR and bioinformatics. *Food Res. Int.* **2010**, *43* (5), 1371−1378.
(83) Sagardia, I.; Iloro, I.; Elortza, F.; Bald, C. Quantitative structure-activity relationship based screening of bioactive peptides identified in ripened cheese. *Int. Dairy J.* **2013**, *33*, 184−190.
(84) Walsh, D. J.; Bernard, H.; Murray, B. A.; MacDonald, J.; Pentzien, A. K.; Wright, G. A.; et al. *In vitro* generation and stability of the lactokinin β-lactoglobulin fragment (142−148). *J. Dairy Sci.* **2004**, *87* (11), 3845−3857.
(85) Yamamoto, N.; Ejiri, M.; Mizuno, S. Biogenic peptides and their potential use. *Curr. Pharm. Des.* **2003**, *9* (16), 1345−1355.
(86) Shen, B.; Makley, D. M.; Johnston, J. N. Umpolung reactivity in amide and peptide synthesis. *Nature* **2010**, *465* (7301), 1027−1032.
(87) Xu, X. F.; He, S. J.; Zhang, X. W. New food safety concerns associated with gut microbiota. *Trends Food Sci. Technol.* **2013**, *34*, 62−66.
(88) Russell, W. R.; Gratz, S. W.; Duncan, S. H.; Holtrop, G.; Ince, J.; Scobbie, L.; Duncan, G.; Johnstone, A. M.; Lobley, G. E.; Wallace, R. J.; Duthie, G. G.; Flint, H. J. High-protein, reduced carbohydrate weight-loss diets promote metabolite profiles likely to be detrimental to colonic health. *Am. J. Clin. Nutr.* **2011**, *93* (5), 1062−1072.
(89) Doi, R. H.; Kosugi, A. Cellulosomes: plant-cell-wall-degrading enzyme complexes. *Nat. Rev. Microbiol.* **2004**, *2*, 541−551.
(90) Heo, S. J.; Park, E. J.; Lee, K. W.; Jeon, Y. J. Antioxidant activities of enzymatic extracts from brown seaweeds. *Bioresour. Technol.* **2005**, *96*, 1613−1623.
(91) Wijesinghe, W. A.; Jeon, Y. J. Enzyme-assistant extraction (EAE) of bioactive components: a useful approach for recovery of industrially important metabolites from seaweeds: a review. *Fitoterapia* **2012**, *83*, 6−12.
(92) Park, P. J.; Shahidi, F.; Jeon, Y. J. Antioxidant activities of enzymatic extracts from an edible seaweed Sargassum horneri using ESR spectrometry. *J. Food Lipids* **2004**, *11*, 15−27.
(93) Cian, R. E.; Alaiz, M.; Vioque, J.; Drago, S. R. Enzyme proteolysis enhanced extraction of ACE inhibitory and antioxidant compounds (peptides and polyphenols) from *Porphyra columbina* residual cake. *J. Appl. Phycol.* **2013**, *25*, 1197−1206.
(94) Klingler, D.; Berg, J.; Vogel, H. Hydrothermal reactions of alanine and glycine insub- and supercritical water. *J. Supercrit. Fluids* **2007**, *43*, 112−119.
(95) Sereewatthanawut, I.; Prapintip, S.; Watchiraruji, K.; Goto, M.; Sasaki, M.; Shotipruk, A. Extraction of protein and amino acids from deoiled rice bran by subcritical water hydrolysis. *Bioresour. Technol.* **2008**, *99* (3), 555−561.
(96) Möller, M.; Nilges, P.; Harnisch, F.; Schroder, U. Subcritical water as reaction environment: fundamentals of hydrothermal biomass transformation. *ChemSusChem* **2011**, *4*, 566−579.
(97) Garcia-Moscoso, J. L.; Obeid, W.; Kumar, S.; Hatcher, P. G. Flash hydrolysis of microalgae (*Scenedesmus* sp.) for protein extractionand production of biofuels intermediates. *J. Supercrit. Fluids* **2013**, *82*, 183−190.
(98) Rios, G. M.; Belleville, M. P.; Paolucci, D.; Sanchez, J. Progress in enzymatic membrane reactors − a review. *J. Membr. Sci.* **2004**, *242*, 189−196.
(99) Pedroche, J.; Just, M. M.; Lqari, H.; Megias, C.; Giron- Calle, J.; Alaiz, M. Obtaining of *Brassica carinata* protein hydrolysates enriched in bioactive peptides using immobilized digestive proteases. *Food Res. Int.* **2007**, *40* (7), 931−938.
(100) Cui, J.; Kong, X.; Hua, Y.; Zhou, H.; Liu, K. Continuous hydrolysis of modified wheat gluten in an enzymatic membrane reactor. *J. Sci. Food Agric* **2011**, *91*, 2799−2805.
(101) Kapel, R.; Chabeau, A.; Lesage, J.; Riviere, G.; Ravallec-Ple, R.; Lecouturier, D.; Wartelle, M.; Guillochon, D.; Dhulster, P. Production, in continuous enzymatic membrane reactor, of an anti-hypertensive hydrolysate from an industrial alfalfa white protein concentrate exhibiting ACE inhibitory and opioid activities. *Food Chem.* **2006**, *98* (1), 120−126.
(102) Hayes, M.; Stanton, C.; Fitzgerald, G. F.; Ross, R. P. Putting microbes to work: dairy fermentation, cell factories and bioactive peptides. Part II: Bioactive peptide functions. *Biotechnol. J.* **2007**, *2* (4), 435−49.
(103) Liu, C.; Hu, B.; Liu, Y.; Chen, S. Stimulation of nisin production from whey by a mixed culture of *Lactococcus lactis* and *Saccharomyces cerevisiae*. *Appl. Biochem. Biotechnol.* **2006**, *131* (1−3), 751−761.
(104) Chang, O. K.; Seol, K. H.; Jeong, S. G.; Oh, M. H.; Park, B. Y.; Perrin, C.; Ham, J. S. Casein hydrolysis by *Bifidobacterium longum* KACC91563 and antioxidant activities of peptides derived therefrom. *J. Dairy Sci.* **2013**, *96* (9), 5544−5555.
(105) Renye, J. R.; Somkuti, G. A. Cloning of milk-derived bioactive peptides in *Streptococcus thermophilus*. *Biotechnol. Lett.* **2007**, *30* (4), 723−730.
(106) Poulin, J. F.; Amiot, J.; Bazinet, L. Simultaneous separation of acid and basic bioactive peptides by electrodialysis with ultrafiltration membrane. *J. Biotechnol.* **2006**, *123*, 314−328.
(107) Butylina, S.; Luque, S.; Nyström, M. Fractionation of whey-derived peptides using a combination of ultrafiltration and nano-filtration. *J. Membr. Sci.* **2006**, *280*, 418−426.
(108) Hsu, K. C. Purification of antioxidative peptides prepared from enzymatic hydrolysates of tuna dark muscle by-product. *Food Chem.* **2010**, *122*, 42−48.
(109) Bazinet, L.; Amiot, J.; Poulin, J.-F.; Labbé, D.; Tremblay, D. Process and system for separation of organic charged compounds. WO 2005082495A1, 2012.
(110) Firdaous, L.; Dhulster, P.; Amiot, J.; Gaudreau, A.; Lecouturier, D.; Kapel, R.; et al. Concentration and selective separation of bioactive peptides from an alfalfa white protein hydrolysate by electrodialysis with ultrafiltration membranes. *J. Membr. Sci.* **2009**, *329*, 60−67.
(111) Firdaous, L.; Dhulster, P.; Amiot, J.; Doyen, A.; Lutin, F.; Vézina, L.-P.; et al. Investigation of the large-scale bioseparation of an antihypertensive peptide from alfalfa white protein hydrolysate by an electromembrane process. *J. Membr. Sci.* **2010**, *355*, 175−181.
(112) Doyen, A.; Beaulieu, L.; Saucier, L.; Pouliot, Y.; Bazinet, L. Demonstration of *in vitro* anticancer properties of peptide fractions from a snow crab by-products hydrolysate after separation by electrodialysis with ultrafiltration membranes. *Sep. Purif. Technol.* **2011**, *78*, 321−329.
(113) Doyen, A.; Husson, E.; Bazinet, L. Use of an electrodialytic reactor for the simultaneous β-lactoglobulin enzymatic hydrolysis and fractionation of generated bioactive peptides. *Food Chem.* **2013**, *136*, 1193−1202.
(114) Doyen, A.; Udenigwe, C. C.; Mitchell, P. L.; Marette, A.; Aluko, R. E.; Bazinet, L. Anti-diabetic and antihypertensive activities of two flaxseed protein hydrolysate fractions revealed following their simultaneous separation by electrodialysis with ultrafiltration membranes. *Food Chem.* **2014**, *145*, 66−76.
(115) Becker, W. Fluorescence lifetime imaging − techniques and applications. *J. Microsc.* **2012**, *247* (2), 119−136.
(116) Ebrecht, R.; Don Paul, C.; Wouters, F. S. Fluorescence lifetime imaging microscopy in the medical sciences. *Protoplasma* **2014**,*251* (2), 293−295.
(117) Gee, M. L.; Burton, M.; Grevis-James, A.; Hossain, M. A.; McArthur, S.; Palombo, E. A.; Wade, J. D.; Clayton, A. H. Imaging the

action of antimicrobial peptides on living bacterial cells. *Sci. Rep.* **2013**, *3*, 1557.

(118) Huang, T. C.; Chen, J. Y. Proteomic and functional analysis of zebrafish after administration of antimicrobial peptide epinecidin-1. *Fish Shellfish Immunol.* **2013**, *34* (2), 593−598.

Table 1. Preventive Effect of Salts in the Control of Potato Soft Rot Caused by *P. atrosepticum* and *P. carotovorum* subsp. *carotovorum*

| | disease inhibition (%)[a] | |
|---|---|---|
| salt | *P. atrosepticum* | *P. carotovorum* subsp. *carotovorum* |
| aluminum dihydroxy acetate | 10.3 ef[b] | 9.6 g |
| aluminum chloride | 70.1 a | 66.0 b |
| aluminum lactate | 49.8 bc | 33.7 de |
| ammonium acetate | 18.8 de | 29.0 e |
| ammonium chloride | 11.0 ef | 11.6 fg |
| ammonium hydrogen phosphate | 11.3 ef | 0.0 i |
| calcium chloride | 18.8 de | 25.7 e |
| potassium chloride | 3.8 f | 1.4 i |
| potassium sorbate | 27.4 cd | 39.0 cd |
| sodium acetate | 14.5 de | 5.7 hi |
| sodium benzoate | 33.8 c | 41.3 c |
| sodium bicarbonate | 10.9 ef | 7.9 h |
| sodium carbonate | 10.3 ef | 6.5 h |
| sodium chloride | 1.0 f | 0.0 i |
| sodium formate | 6.7 ef | 0.0 i |
| sodium lactate | 10.3 ef | 0.0 i |
| sodium metabisulfite | 57.3 b | 71.9 a |
| sodium hydrogen phosphate | 11.0 ef | 0.0 i |
| sodium propionate | 27.4 cd | 28.4 e |
| sodium tartrate dibasic | 11.0 ef | 3.8 i |
| trisodium phosphate | 15.2 de | 14.9 f |

[a]Disease inhibition was calculated as follows: {[disease severity (control tubers) − disease severity (salt-treated tubers)]/disease severity (control tubers)} × 100. [b]Values of the same column followed by the same letter are not significantly different ($p < 0.05$) according to Fisher's protected LSD.

acids are highly saturated in bacteria,[27] lipid peroxidation by these salts in *Pectobacterium* sp. is unlikely to occur.

Previous work[28] showed an inverse sigmoidal relationship between the inhibitory effect of salts on the *in vitro* growth of *Pectobacterium* sp. and the water-ionizing capacity or p*K*′ (apparent acidity or basicity constant) of salt anions or cations primarily and lipophilicity of the salts, suggesting that these two parameters in combination may contribute to the antimicrobial action of the salts in the salt−microbe interactions. However, it is not known whether the observed *in vitro* antimicrobial action of the salts would persist *in vivo* in potato tubers. If it did, it raises the question whether those physicochemical characteristics of the salts could also provide a basis in the ternary salt−potato tissue−microbe interactions for the control of soft rot in potato tubers.

Thus, the objective of this work was to evaluate the inhibitory activity of several organic and inorganic salts against soft rot in potato tuber and to examine the general physicochemical basis of the inhibitory activity of salts on soft rot development when applied as preventive or curative treatments.

## MATERIALS AND METHODS

Strains of *P. carotovorum* subsp. *carotovorum* (ECC 1367) and *P. atrosepticum* (ECA 709) were provided by the Laboratoire de Diagnostic en Phytoprotection (MAPAQ, Quebec City, Quebec, Canada). The bacteria were maintained on nutrient agar (NA, Difco Laboratories, Detroit, MI) slants under mineral oil at 4 °C and served as stock cultures.

A total of 21 salts were used in these experiments (Table 1). All salts were purchased from Sigma Chemical Co. (St. Louis, MO), except for ammonium acetate, sodium chloride, and sodium bicarbonate (BDH, Inc., Toronto, Ontario, Canada) and aluminum lactate (Aldrich Chemical, Milwaukee, WI).

**Effect of Salts on Soft Rot Development.** Potato tubers (cv. Norland) were purchased from Propur, Inc. (St. Ambroise, Quebec, Canada) and stored at 4 °C until use. Selected tubers were washed with tap water, surface-sterilized by dipping in 0.525% sodium hypochlorite solution (10 min), rinsed by dipping twice in sterile distilled water for at least 10 min, and dried in ambient air. Four wounds (depth, 1 cm; diameter, 0.5 cm) were performed on each tuber from the apical to the basal ends,[29] using a pipet tip.

**Preventive Application of Salts.** Wounded tubers were immersed for 10 min in the different salt solutions (0.2 M) and dried in ambient air. Control tubers were immersed in sterile distilled water. Each wound was then inoculated with 20 μL of a suspension [$1 \times 10^7$ colony-forming units (CFU)/mL] of either *P. atrosepticum* or *P. carotovorum* subsp. *carotovorum*. Suspensions were prepared from 24 h old cultures grown in 20% tryptic soy broth (Difco). Tubers were subsequently incubated (24 °C) individually in a plastic chamber containing a wet sterile paper towel for 3 days. The disease severity was then assessed by measuring the largest diameter of each rotting lesion,[30] and the results were expressed in percentage of disease reduction compared to the control treatment (sterile distilled water; 1.3−2.2 cm lesion diameter). For each tuber, lesion diameter was a mean of the four inoculation sites. A completely randomized experimental design with three replicates was used, and the experiment was repeated twice.

**Curative Application of Salts.** Each wound was inoculated with 20 μL of one of the bacterial suspensions ($1 \times 10^7$ CFU/mL). After a 12 h incubation period at 24 °C, infected tubers were immersed (10 min) in the different salt solutions (0.2 M) or in distilled water (control). Tubers were then incubated (24 °C) individually in a plastic chamber containing a wet sterile paper towel for 3 days, and the disease severity was evaluated as previously described. A completely randomized experimental design with three replicates was used, and the experiment was repeated twice.

**Effect of Salt Treatments on Tissue pH.** The diffusion of salts in the tuber tissue was evaluated by monitoring the consequent modification of tissue pH for two acidic salts (aluminum chloride and sodium metabisulfite), two alkaline salts (trisodium phosphate and

Table 2. Curative Effect of Salts in the Control of Potato Soft Rot Caused by *P. atrosepticum* and *P. carotovorum* subsp. *carotovorum*

| | disease inhibition (%)[a] | |
|---|---|---|
| salt | *P. atrosepticum* | *P. carotovorum* subsp. *carotovorum* |
| aluminum dihydroxy acetate | 28.0 bc[b] | 7.6 cd |
| aluminum chloride | 41.3 a | 57.6 a |
| aluminum lactate | 30.7 bc | 29.6 b |
| ammonium acetate | 20.0 cd | 6.8 cd |
| ammonium chloride | 10.0 e | 0.0 e |
| ammonium hydrogen phosphate | 14.0 e | 22.4 bc |
| calcium chloride | 21.3 cd | 0.0 e |
| potassium chloride | 11.0 e | 3.6 de |
| potassium sorbate | 18.7 de | 13.6 c |
| sodium acetate | 18.7 de | 3.0 de |
| sodium benzoate | 33.3 b | 33.5 b |
| sodium bicarbonate | 14.0 e | 0.0 e |
| sodium carbonate | 16.0 de | 0.0 e |
| sodium chloride | 16.0 de | 3.8 de |
| sodium formate | 15.3 de | 0.0 e |
| sodium lactate | 16.7 de | 7.9 cd |
| sodium metabisulfite | 42.0 a | 52.8 a |
| sodium hydrogen phosphate | 17.0 de | 0.0 e |
| sodium propionate | 16.0 de | 0.0 e |
| sodium tartrate dibasic | 17.0 de | 0.0 e |
| trisodium phosphate | 15.0 de | 4.2 de |

[a]Disease inhibition was calculated as follows: {[disease severity (control tubers) − disease severity (salt-treated tubers)]/disease severity (control tubers)} × 100. [b]Values of the same column followed by the same letter are not significantly different ($p < 0.05$) according to Fisher's protected LSD.

sodium carbonate), and one lipophilic salt (sodium benzoate). Duplicate tuber slabs (1 cm wide × 3 cm long × 2 cm high) were dipped in 0.2 M of the salt solution and incubated at room temperature for up to 3 h. The slabs were removed from the salt solution at intervals and rinsed thoroughly using deionized water. Three consecutive 1 mm thick slivers (1 mm × 2 cm × 3 cm) were sliced from one end of the potato slab with a sharp knife. The slices were crushed using a garlic press (Atlantic Promotions, Inc., Longueuil, QC, Canada) and suspended in 30 mL of deionized water, and the pH of the slurry was measured. The experiment was repeated 3 times.

**Minimum Inhibitory Concentration (MIC) of Salts *in Vitro*.** The effect of the concentration of selected salts on the bacterial growth was evaluated. *P. carotovorum* subsp. *carotovorum* bacteria was grown in 250 mL flasks containing 50 mL of 20% tryptic soy broth (TSB, Difco) amended with 0−10 mM aluminum chloride, aluminum lactate, sodium metabisulfite, trisodium phosphate, or sodium carbonate or with 0−100 mM sodium benzoate, potassium sorbate, or sodium propionate by incubating at 24 °C with agitation (150 rpm, Lab-Line Instruments, Inc., Melrose Park, IL) for 24 h. The pH of the medium was not adjusted, and it varied with the type of salt. The flasks were inoculated with 100 μL of bacterial suspension ($1 \times 10^7$ CFU/mL). The bacterial growth was determined by turbidimetry at 600 nm on an ultraviolet/visible (UV/vis) spectrophotometer (Ultrospec 2000, Pharmacia Biotech, Ltd., Cambridge, U.K.), using appropriate blanks (non-inoculated media amended with salt). Results were expressed as the percentage of growth inhibition compared to the control (growth medium not amended with salt). A completely randomized experimental design with three replicates was used, with the experimental unit being a flask. The MIC of the salts was determined from the inhibition salt concentration plots.

**Statistical Analyses.** Analyses of variance were carried out with the GLM procedure of SAS (SAS Institute, Cary, NC). Treatment means were compared using Fisher's protected least significant difference (LSD) when the analysis of variation (ANOVA) indicated significant differences ($p < 0.005$).

## RESULTS AND DISCUSSION

The preventive inhibitory effect of the 21 salts against soft rot development in potato tuber is presented in Table 1. Disease lesion in the control tubers was 1.3−2.2 cm in diameter. Significant reduction of disease caused by *P. atrosepticum* and *P. carotovorum* subsp. *carotovorum* was obtained by the application of aluminum chloride (70.1 and 66.0%, respectively) and sodium metabisulfite (57.3 and 71.9%, respectively) and to a lesser extent by the application of sodium benzoate (33.8 and 41.3%, respectively), aluminum lactate (49.8 and 33.7%, respectively), and potassium sorbate (27.4 and 39.0%, respectively). Calcium chloride, ammonium acetate, and sodium propionate showed only a modest disease reduction. The other salts exhibited either negligible or no effect on disease development. When salts were applied as curative treatment, the highest inhibition of the disease caused by *P. atrosepticum* and *P. carotovorum* subsp. *carotovorum* was obtained with aluminum chloride (41.3 and 57.6%, respectively), sodium metabisulfite (42.0 and 52.8%, respectively), and sodium benzoate (33.3 and 33.5%, respectively) (Table 2). The other salts allowed for a disease reduction ranging from 10.0 to 30.7% on *P. atrosepticum* and from 0 to 29.0% on *P. carotovorum* subsp. *carotovorum*.

The dipping treatment of aluminum chloride, sodium metabisulfite, aluminum lactate, and sodium benzoate markedly decreased soft rot severity in infected tubers for both preventive and curative applications, whereas the *in vitro* test showed that a number of salts (aluminum dihydroxy acetate, aluminum chloride, aluminum lactate, ammonium acetate, potassium sorbate, sodium bicarbonate, sodium carbonate, sodium benzoate, sodium propionate, sodium metabisulfite, and trisodium phosphate) were effective against the causal agents of this disease.[28] We observed earlier that the inhibitory effect

of salts *in vitro* related primarily to the water ionization capacity of their ions, which is indicated by the acidity constant ($pK_a$) or basicity constant ($pK_b$) of the ions (the lower the $pK_a$ or $pK_b$ value of the ion, the greater its capacity to ionize water and alter the surrounding pH).[28] A greater ionization capacity of water was associated with a higher inhibitory effect *in vitro*. For higher salt concentrations (>0.1 M), apparent acidity or basicity constants ($pK'_a$ or $pK'_b$) of the ions are more appropriate, and hence, the $pK_a$ or $pK_b$ values were corrected for ionic strength of the salt solutions.[28]

Figure 1 shows that disease inhibition by the preventive application of salts relates inversely to the $pK_a'$ value of the cations (with common chloride anion) and that of the acidic bisulfite anion and the $pK_b'$ values of anions (with common sodium or potassium cation). It is seen clearly that some of the ions, bisulfite, aluminum, benzoate, sorbate, propionate, and calcium, are effective and exhibit a disease inhibition of more than 20%, whereas the other ions (acetate, bicarbonate, carbonate, chloride, formate, lactate, phosphate, potassium, sodium, and tartrate) show little effect. Although the inhibitory activities were attenuated overall for all of the salts tested in the presence of plant tissue compared to the *in vitro* activities, the decrease in the activity was drastic for salts, such as sodium phosphate, sodium carbonate, and sodium bicarbonate. In addition, both the effective and non-effective ions showed an apparent inverse linear relationship to the $pK'$ values of the ions in the presence of tissue, in contrast to the general inverse sigmoidal inhibitory pattern observed in *in vitro* inhibition,[28] suggesting that water ionization capacity of the ions should still play a role in their inhibitory activity in the tissue (Figure 1).

Disease inhibition by the curative application of salts in relation to the $pK'$ values of the ions is shown in Figure 2. While most ions exhibited no effect, three of the ions, $Al^{3+}$,

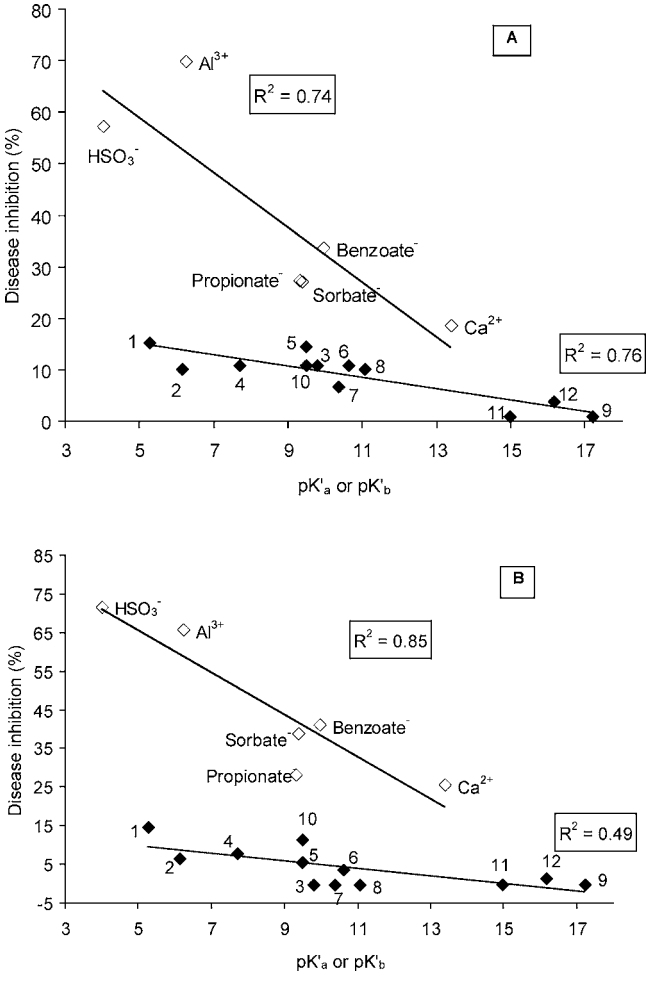


**Figure 1.** Relationship between inhibition of soft rot caused by (A) *P. atrosepticum* and (B) *P. carotovorum* subsp. *carotovorum* by preventive application of salts and apparent acidity ($pK'_a$) or basicity ($pK'_b$) constants of the salt ions: (1) $PO_4^{3-}$, (2) $CO_3^{2-}$, (3) $HPO_4^{2-}$, (4) $HCO_3^-$, (5) acetate$^-$, (6) tartrate$^{2-}$, (7) formate$^-$, (8) lactate$^-$, (9) $Cl^-$, (10) $NH_4^+$, (11) $Na^+$, and (12) $K^+$. Cations: common anion, chloride. Anions: common cation, sodium, except for sorbate, potassium.

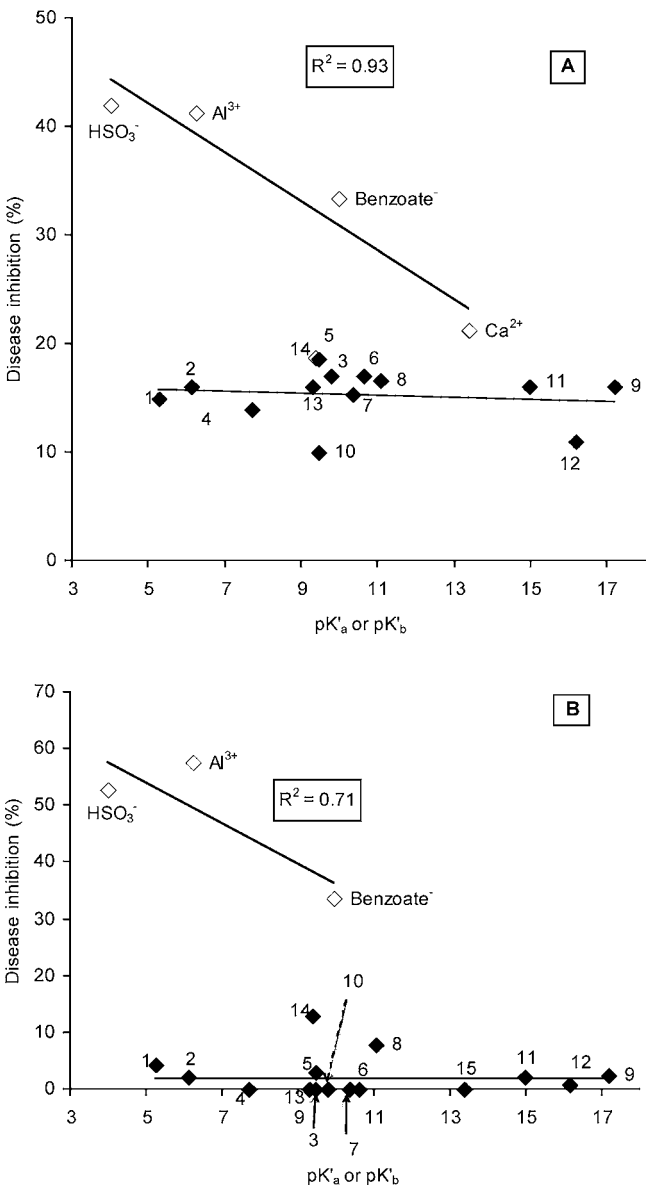


**Figure 2.** Relationship between inhibition of soft rot caused by (A) *P. atrosepticum* and (B) *P. carotovorum* subsp. *carotovorum* by curative application of salts and apparent acidity ($pK'_a$) or basicity ($pK'_b$) constants of the salt ions: (1) $PO_4^{3-}$, (2) $CO_3^{2-}$, (3) $HPO_4^{2-}$, (4) $HCO_3^-$, (5) acetate$^-$, (6) tartrate$^2$, (7) formate$^-$, (8) lactate$^-$, (9) $Cl^-$, (10) $NH_4^+$, (11) $Na^+$, (12) $K^+$, (13) propionate$^-$, (14) sorbate$^-$, and (15) $Ca^{2+}$. Cations: common anion, chloride. Anions: common cation, sodium, except for sorbate, potassium.


dx.doi.org/10.1021/jf5017863 | J. Agric. Food Chem. 2014, 62, 9223−9231

$HSO_3^-$, and benzoate, showed some inhibitory effect, suggesting that these ions may possess certain unique characteristics. The relationship between disease inhibition and the ion p$K'$ combined with the 1-octanol/water partition coefficient (p$K'$ − log $P_{o/w}$) generally followed the same pattern, with a slight improvement in the correlation coefficient for the effective salt group (Figures 3 and 4). Despite the

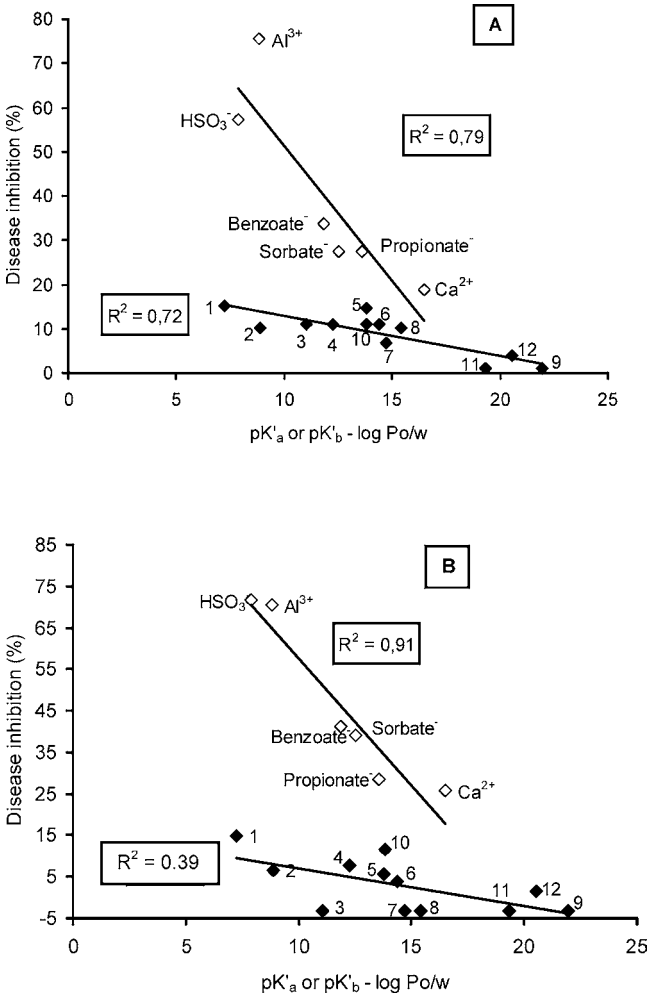


**Figure 3.** Relationship between inhibition of soft rot caused by (A) *P. atrosepticum* and (B) *P. carotovorum* subsp. *carotovorum* by preventive application of salts and the addition parameter p$K'_a$ or p$K'_b$ − log $P_{o/w}$, which combines apparent acidity (p$K'_a$) or basicity (p$K'_b$) constants of the salt ions and their octanol/water partition coefficient ($P_{o/w}$): (1) $PO_4^{3-}$, (2) $CO_3^{2-}$, (3) $HPO_4^{2-}$, (4) $HCO_3^-$, (5) acetate$^-$, (6) tartrate$^{2-}$, (7) formate$^-$, (8) lactate$^-$, (9) $Cl^-$, (10) $NH_4^+$, (11) $Na^+$, and (12) $K^+$. Cations: common anion, chloride. Anions: common cation, sodium, except for sorbate, potassium.

attenuated inhibitory effect of salts in the preventive and more so in the curative treatments, the water ionization capacity of the ions appears to play a role in the disease inhibition of the salts.

Figure 5 shows the time course of the migration of selected salts in the tuber tissue as implied by the changes in tissue pH, where the pH of the tissue dipped in water was 6.4. The pH of tissue dipped in the salt solutions reached a steady state in 2 h at 1 mm depth (Figure 5A) but not at the depths of 2 mm (Figure 5B) or 3 mm (Figure 5C). At the depth of 1 mm, the tissue pH was 11.2, 8.6, 6.2, 5.0, and 4.6 for trisodium

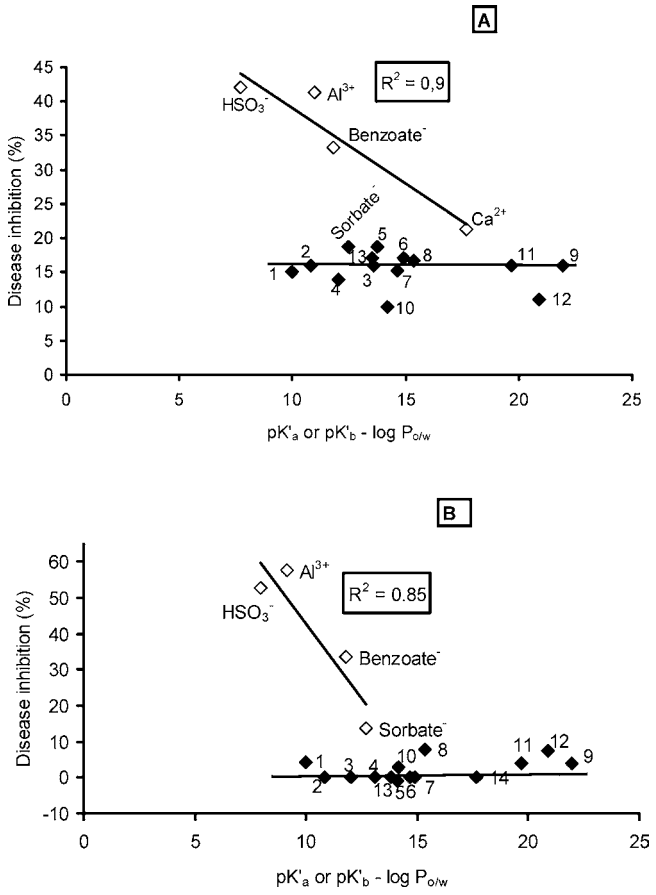


**Figure 4.** Relationship between inhibition of soft rot caused by (A) *P. atrosepticum* and (B) *P. carotovorum* subsp. *carotovorum* by curative application of salts and the addition parameter p$K'_a$ or p$K'_b$ − log $P_{o/w}$, which combines apparent acidity (p$K'_a$) or basicity (p$K'_b$) constants of the salt ions and their octanol/water partition coefficient ($P_{o/w}$): (1) $PO_4^{3-}$, (2) $CO_3^{2-}$, (3) $HPO_4^{2-}$, (4) $HCO_3^-$, (5) acetate$^-$, (6) tartrate$^2$, (7) formate$^-$, (8) lactate$^-$, (9) $Cl^-$, (10) $NH_4^+$, (11) $Na^+$, (12) $K^+$, (13) propionate$^-$, and (14) $Ca^{2+}$. Cations: common anion, chloride. Anions: common cation, sodium, except for sorbate, potassium.

phosphate, sodium carbonate, sodium benzoate, sodium metabisulfite, and aluminum chloride, respectively, after 2 h of dipping. There was little modification of tissue pH with sodium benzoate (pH 6.3). Whereas both trisodium phosphate and sodium carbonate increased the alkalinity of the tissue, both sodium metabisulfite and aluminum chloride acidified the tissue. At 2 mm depth, there was little change in tissue pH with sodium benzoate and aluminum chloride after 2 h of dipping, but changes in tissue pH were observed for trisodium phosphate (7.7), sodium metabisulfite (5.7), and to a small extent, sodium carbonate (6.7) (Figure 5B). At the depth of 3 mm, small changes in tissue pH were registered after 2 h of dipping only for trisodium phosphate (6.8) and sodium metabisulfite (6.2) (Figure 5C). The penetration of aluminum, a polyvalent cation, appeared to be restricted to the depth of 1 mm, presumably because of its binding to fixed negative charges in the cell wall.[31]

Among the salts, the *in vitro* MIC value of aluminum salts, metabisulfite, trisodium phosphate, sodium carbonate, and sodium propionate was ≤10 mM, whereas it was 100 mM for sodium benzoate and potassium sorbate. In effect, the inhibitory effect of salts *in vitro* did not bear a clear relationship


dx.doi.org/10.1021/jf5017863 | J. Agric. Food Chem. 2014, 62, 9223−9231

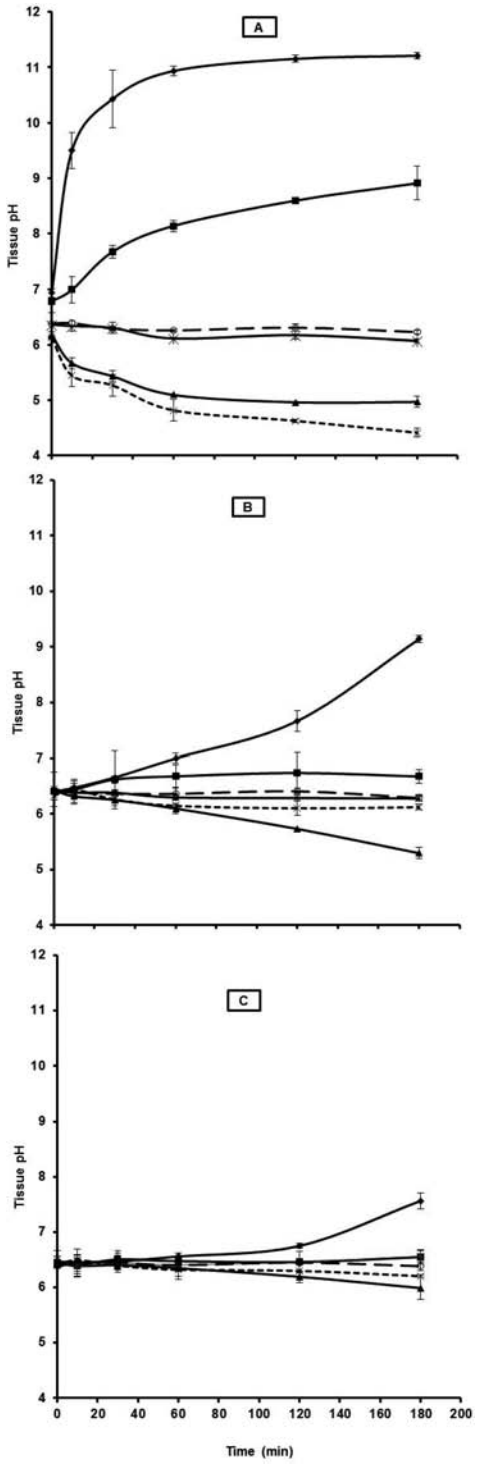


**Figure 5.** Kinetics of the migration of selected salts in the tuber tissue as indicated by changes in tissue pH. (A) pH change in the millimeter thick tissue, 1 mm from one end of the potato slab; (B) pH change in the millimeter thick tissue, 2 mm from the same end of the potato slab; and (C) pH change in the millimeter thick tissue, 3 mm from the same end of the potato slab, dipped in salt solutions for up to 3 h: (◆) trisodium phosphate, (■) sodium carbonate, (○) control, (∗) sodium benzoate, (▲) sodium metabisulfite, and (×) aluminum chloride. Vertical bars represent standard deviation.

to their activities in the presence of plant tissue. While trisodium phosphate and sodium carbonate (*in vitro* MIC, ≤10 mM) exhibited little activity *in vivo*, sodium benzoate and potassium sorbate (*in vitro* MIC, 100 mM) still maintained moderate activities *in vivo*. Overall, the acidic salts, such as aluminum chloride and sodium metabisulfite, and preservative salts, such as sodium benzoate, potassium sorbate, and propionate, still exhibited some significant effect, while alkaline salts, such as trisodium phosphate, sodium carbonate, and bicarbonate, showed little activity in the presence of the tissue compared to their *in vitro* activity. In addition, the inhibitory activity of all of the salts was attenuated to different degrees when applied as preventive treatment and, more so, when applied as curative treatment in potato tuber compared to their *in vitro* activity.

Several factors intrinsic to potato tubers, such as buffering capacity, or intrinsic to salts, such as water ionization, pH, and ion migration capacity, and salt−plant tissue interactions may be involved in the salt−plant−bacteria interactions, leading to the reduced activity of salts overall, and the near total loss of the activity of alkaline salts. As a result of salt−plant tissue interactions, the ions may undergo speciation, where the resulting ions may be less active against the bacteria. It is also possible that some of the salts that retain moderate activity even in the curative application may possess some unique properties that may have to do with the interaction with the plant tissue or their mobility in the tissue.

The buffering capacity of the tuber tissue could dissipate extreme pH conditions, and in the case of multiprotic salts (e.g., phosphates and carbonates), this could lead to their equilibrium favoring the formation of less effective ionic species, thereby dampening their inhibitory capacity in the plant tissue. In fact, the pH of the tuber tissue treated (10 min dipping, 1 mm from the wound surface) with trisodium phosphate (0.2 M solution at pH 12.5) was 10.1, where the predominant species, $HPO_4^{2-}$, is less inhibitory on the *Pectobacterium* bacteria than $PO_4^{3-}$ present in the salt solution.[28] Likewise, the pH of the tissue treated with sodium carbonate (solution pH of 11.1, predominant inhibitory species $CO_3^{2-}$) was 8.4, where $HCO_3^-$ predominates, which was shown *in vitro* to be slower than $CO_3^{2-}$ in killing those bacteria.[28] Although the buffering role of the tissue was evident when treated with aluminum chloride, sodium metabisulfite, or the organic acid salts, they still showed inhibitory activity in the tuber. For example, the pH of the treated tissue (10 min dipping, 1 mm from the wound surface) with sodium metabisulfite was 5.6 compared to the solution pH of 4.5, and that of aluminum chloride was 4.9 compared to the solution pH of 2.5.

A plausible argument can be made that salt−plant tissue interactions play a central role, leading to the attenuated inhibitory activity of salts in potato tuber by reducing the availability of the inhibitory ions for salt−bacteria interactions. The salt−plant interactions may involve alkalinization of plant cell walls and speciation of ions into less or more effective species by Donnan equilibrium[32] (ionic equilibrium of charged solutes in the presence of charged membranes or macromolecules such as the cell wall pectin) and electroneutrality, complexation of ions and their reduced migration into the tissue, and the partitioning of diffusible species, generated as a result of the salt−plant interactions, between the plant cells and the bacterial cells, leading to their reduced availability at the infection site.

The cell walls behave like a polyanion, owing to the presence of polygalacturonic acids, that sets up Donnan potential (electrostatic potential), resulting in the attraction of cations, including protons, and the repulsion of anions.[33−35] This cell


dx.doi.org/10.1021/jf5017863 | J. Agric. Food Chem. 2014, 62, 9223−9231

wall potential generates a proton gradient across the cell walls, which results in a difference of pH between the inside and outside of the walls[34] accompanied by hydrolysis of water. Entry of cations into the cell walls is driven by both chemical potential (higher concentration outside) and electrochemical potential (charges) across the cell walls. Thus, when a salt is present outside the cell walls, its cations would preferentially enter the cell walls, with its anions being excluded by the negative charges of the cell wall (Donnan exclusion), while the protons outflow would re-establish electroneutrality, thus rendering the cell walls more alkaline. However, in the presence of highly acidic salts, such as aluminum chloride (solution pH of 2.5), protons would also enter the cell walls with the cations ($Na^+$ and $Al^{3+}$) and the cell walls would become more acidic. In addition, water ionization by aluminum ions can generate protons and cause more acidification of the cell walls; otherwise, the cell walls would largely remain alkaline, arising from the Donnan effect, with $Na^+$ and $K^+$ cations, which possess low water ionization capacity.

The acidification of cell walls can also affect the activity of the bacterial macerating enzymes, such as the pectate lyases (optimum pH of 8.3−8.5), the cellulases and proteases (optimum pH of 7.0), and the polygalacturonase lyase (optimum pH of 8.5−9.5), which are secreted by the *Pectobacterium* bacteria.[36,37] When a neutral salt (NaCl, KCl, etc.) is present outside, the cell walls would be mainly loaded with the cation ($K^+$ or $Na^+$), to which the cell walls are also more permeable than $Cl^-$. Because the latter anion has low antimicrobial effect against the *Pectobacterium* bacteria, its presence outside the cell walls may have little effect on the pathogens.

The presence of aluminum and calcium salts would result in the cell walls being loaded by these multivalent cations, which can also complex with polygalacturonide residues, reinforcing the cell walls against pathogen attack. Thus, the tissue acidification and additional strengthening of the cell walls by complexation of multivalent aluminum species [$Al^{3+}$ and $Al(OH)^{2+}$] by pectins could contribute to the control of soft rot by the aluminum salts, such as $AlCl_3$. However, aluminum dihydroxy acetate exhibited disease inhibition to a lesser extent, probably because this salt solution contains mainly the monovalent $Al(OH)_2^+$ species, which has low cell wall complexing ability. The migration of aluminum ions into the plant tissue and the consequent water ionization (pH change) therein may have been limited to the depth of 1 mm (Figure 5A), in part, because of the complexation of aluminum ions to the pectic materials.[38] Nevertheless, the complexation of aluminum ions would also reduce their availability against the bacteria to a certain degree. Cell wall complexation of $Ca^{2+}$ ($CaCl_2$) and its strengthening could also explain the partial inhibitory effect of $CaCl_2$ on soft rot compared to either NaCl or KCl.

Although sodium metabisulfite is an acidic salt like aluminum chloride, it yields bisulfite anions which would be excluded by the negative charges of the cell wall (Donnan exclusion). However, proton efflux from the plant cell walls because of the Donnan effect may lead to the protonation of $HSO_3^-$ and $SO_3^{2-}$ species and the generation of molecular $SO_2$, which can diffuse freely through the plant cell walls and tissue. Thus, the presence of sulfite species can be expected deeper into the tissue, as seen by the tissue pH change profile (panels A and B of Figure 5). With respect to the organic acid salts (sodium benzoate, potassium sorbate, or sodium propionate) outside the cell walls, proton efflux could be expected to increase the concentrations of the non-dissociated and more effective antibacterial species, such as benzoic, sorbic, and propionic acids (by protonation) outside the cell, resulting in the inhibition of bacterial growth and the consequent tissue degradation to some extent.

In the presence of highly alkaline salts, such as trisodium phosphate (solution pH of 12.5) and sodium carbonate (solution pH of 11.1), which were effective in the *in vitro* inhibition of *P. atrosepticum* and *P. carotovorum* subsp. *carotovorum*, the electronegative status of the cell walls would limit the migration (Donnan exclusion) of the alkaline species ($HPO_4^{2-}$ or $PO_4^{3-}$ and $HCO_3^-$ or $CO_3^{2-}$) in the cell walls, which will be rather loaded with the sodium cation. In addition, protons would flow out from the cell walls to re-establish electroneutrality and pH gradient. Thus, not only would there be a lack of cell walls strengthening, but also the effective antibacterial alkaline species (e.g., $PO_4^{3-}$) will lose their inhibitory capacity because of gradual protonation into less inhibitory species, such as $HPO_4^{2-}$ and $H_2PO_4^-$. In addition, the efflux of protons from the cell walls would render them alkaline. Generation of less inhibitory species could therefore explain why these salts were ineffective in controlling soft rot in infected tubers, while they were highly effective inhibitors of bacterial growth *in vitro*. In contrast to alkaline anions, Donnan exclusion of bisulfite anions results in a different outcome as mentioned above, leading to the observed persistent inhibitory activity of sodium metabisulfite in the presence of plant tissue.

Disease inhibition upon preventive salt application was greater than in the curative treatment, indicating that a higher concentration of the salt ions is present at the wound site for salt−pathogen interactions. Presumably, the tissue had a head start in the tissue−pathogen interactions during the preventive treatment through its interactions with the salts as well as the tissue responses to wound stress. In contrast, the pathogen has the head start and advantage in invading the plant tissue in the curative application of salts. In curative salt application, $Al^{3+}$, $HSO_3^-$, and benzoate$^-$ maintained some activity in relation to their p$K'$ values, but the relationship to p$K'$ failed for those salts that exhibited less than 20% disease inhibition in the preventive treatment (Figure 2). Once the pathogen is well-established in the tissue, it becomes too late to ward off the infection for most of the ions that do not possess any special properties than simple modification of the surrounding pH (acid−base equilibria). The exceptions were the three ions, $Al^{3+}$, $HSO_3^-$, and benzoate$^-$, attributable to their inward diffusion into the tissue as ions or their speciated forms. Effectively, the generation of aqueous molecular $SO_2$ species from sodium metabisulfite, which can diffuse through the cell walls and membranes, may clarify the curative activity of this salt. Aluminum ions do not appear to penetrate far into the tissue (panels B and C of Figure 5), presumably because of complexation by pectins of the cell walls and their presence as complex hydrated ions in an aqueous medium. However, the migration of this ion into the cell walls of the exterior layers of the tissue is still appreciable (Figure 5A), attributable to its high electrochemical potential (electrostatic charge of +3). Because of the efflux of protons from the cell walls, benzoate, sorbate, and propionate ions can all be protonated into their corresponding non-dissociated acid forms, which are cell-wall-permeable and more potent bacterial growth inhibitors than their conjugated bases. In addition, benzoate and sorbate possess a conjugated double bond system that confers to them

a higher degree of hydrophobicity[28] and, consequently, a faster migration potential across the cell walls and a higher disease inhibition than propionate. The migration capacity across the cell walls of aliphatic sorbic acid (or propionic acid) can also be expected to be lesser than the aromatic benzoic acid and, hence, appears to be far less effective than benzoic acid in disease inhibition in the situation, where the pathogen has had a head start.

Finally, stimulation of defense mechanisms against diseases by certain salts has been shown in several plants. Jeandet et al.[20] observed that aluminum chloride stimulated the accumulation of phytoalexins (resveratrol) in grapevine leaves. The elicitation of callose synthesis by both aluminum and calcium has also been reported in several plants.[37] However, it is not known whether defense mechanisms are triggered in potato tuber in response to salts, such as aluminum chloride or sodium metabisulfite. It is conceivable that defense reaction may also be triggered in potato tubers, because the inhibitory effect of these salts is stronger in preventive application than in curative treatment, and this aspect deserves further investigation.

In conclusion, the results of this study support that aluminum chloride, sodium metabisulfite, and sodium benzoate have potential in controlling effectively soft rot development in potato tubers. This study also provides a general basis for the understanding of specific salt−tissue interactions and for salt selection to control plant diseases. The capacity of salt constituent ions to ionize water molecules appears to relate, in part, to their disease inhibition capacity for some ions, such as aluminum, bisulfite, and organic acid ions. The lack of activity of alkaline salts, such as trisodium phosphate and sodium carbonate, *in vivo* appears to be due to cell wall alkalinization by the Donnan effect and the speciation of their anions into less effective ions. The persistent, albeit reduced, *in vivo* activity of aluminum bisulfite, and organic acid salts may be attributed to their specific properties, in addition to the Donnan effect. The acidification of cell walls and complexation of ions by cell wall polymers (aluminum ions), the generation of highly diffusible molecular $SO_2$ (sodium metabisulfite), and generation of a more active and permeable acid form (sodium benzoate) may play a role in the persistent inhibitory activity of these salts in potato tuber, notwithstanding the induction of any biochemical defense mechanisms in the tissue in response to those salts, if any. The possible reduced aluminum ion penetration into the tissue by complexation and partitioning of the diffusible species, molecular $SO_2$ and acid form of benzoate, between the plant cells and the bacterial cells, leading to their reduced availability at the infection site, and the attenuated activity of these salts in the tissue. Further work would be required with respect to the formulation of salts exhibiting synergy and enhancement of disease inhibition in the tubers and the evaluation of potential health and environmental risks associated with salt applications before envisioning industrial application of these salts.

## AUTHOR INFORMATION

### Corresponding Author

*Telephone: 418-656-2839. Fax: 418-656-3353. E-mail: joseph.arul@fsaa.ulaval.ca.

### Funding

This study was supported by Conseil de Recherche en Agriculture, Pêche et Alimentation du Québec (CORPAQ), Cultures H. Dolbec, Inc., and Propur, Inc.

### Notes

The authors declare no competing financial interest.

## REFERENCES

(1) Sharga, B. M.; Lyon, G. D. *Bacillus subtilis* BS 107 as an antagonist of potato blackleg and soft rot bacteria. *Can. J. Microbiol.* **1998**, *44*, 777−783.

(2) Stevenson, W. R.; Loria, R.; Franc, G. D.; Weingartner, D. P. *Compendium of Potato Diseases*, 2nd ed.; The American Phytopathological Society: St. Paul, MN, 2001; pp 106.

(3) Howard, R. J.; Garland, J. A.; Seaman, W. L. *Diseases and Pests of Vegetable Crops in Canada: An Illustrated Compendium*; The Canadian Phytopathological Society and Entomological Society of Canada: Ottawa, Ontario, Canada, 1994; pp 554.

(4) Czajkowski, R.; Perombelon, M. C. M.; van Veen, J. A.; van der Wolf, J. M. Control of blackleg and tuber soft rot of potato caused by *Pectobacterium* and *Dickeya* species: A review. *Pathology* **2011**, *60*, 999−1013.

(5) Gardan, L.; Gouy, C.; Christen, R.; Samson, R. Elevation of three subspecies of *Pectobacterium carotovorum* to species level: *Pectobacterium atrosepticum* sp. nov., *Pectobacterium betavasculorum* sp. nov. and *Pectobacterium wasabiae* sp. nov. *Int. J. Syst. Evol. Microbiol.* **2003**, *53*, 381−391.

(6) Hauben, L.; Moore, E. R. B.; Vauterin, L.; Steenackers, M.; Mergaert, J.; Verdonck, L.; Swings, J. Phylogenetic position of phytopathogens within the *Enterobacteriaceae*. *Syst. Appl. Microbiol.* **1998**, *21*, 384−397.

(7) Mills, A. A. S.; Platt, H. W.; Hurta, R. A. R. Sensitivity of *Erwinia* spp. to salt compounds in vitro and their effect on the development of soft rot in potato tubers in storage. *Postharvest Biol. Technol.* **2006**, *41*, 208−214.

(8) Horst, R. K.; Kawamoto, S. O.; Porter, L. L. Effect of sodium bicarbonate and oils on the control of powdery mildew and black spot of roses. *Plant Dis.* **1992**, *76*, 247−251.

(9) Ziv, O.; Zitter, T. A. Effects of bicarbonates and film-forming polymers on cucurbit foliar diseases. *Plant Dis.* **1992**, *76*, 513−517.

(10) Aharoni, Y.; Fallik, E.; Copel, A.; Gil, M.; Grinberg, S.; Klein, J. D. Sodium bicarbonate reduces postharvest decay development on melons. *Postharvest Biol. Technol.* **1997**, *10*, 201−206.

(11) Fallik, E.; Grinberg, S.; Ziv, O. Potassium bicarbonate reduces postharvest decay development on bell pepper fruits. *J. Hortic. Sci.* **1997**, *72*, 35−41.

(12) Smilanick, J. L.; Margosan, D. A.; Mlikota, F.; Usall, J.; Michael, I. F. Control of citrus green mold by carbonate and bicarbonate salts and the influence of commercial postharvest practices on their efficacy. *Plant Dis.* **1999**, *83*, 139−145.

(13) Olivier, C.; MacNeil, C. R.; Loria, R. Application of organic and inorganic salts to field grown potato tubers can suppress silver scurf during potato storage. *Plant Dis.* **1999**, *83*, 814−818.

(14) Olivier, C.; Halseth, D. E.; Mizubuti, E. S. G.; Loria, R. Postharvest application of organic and inorganic salts for suppression of silver scurf on potato tubers. *Plant Dis.* **1998**, *82*, 213−217.

(15) Hervieux, V.; Yaganza, E. S.; Arul, J.; Tweddell, R. J. Effect of organic and inorganic salts on the development of *Helminthosporium solani*, the causal agent of potato silver scurf. *Plant Dis.* **2002**, *86*, 1014−1018.

(16) Punja, Z. K.; Gaye, M. M. Influence of postharvest handling practices and dip treatments on development of black root rot on fresh market carrots. *Plant Dis.* **1993**, *77*, 989−995.

(17) Mecteau, M. R.; Arul, J.; Tweddell, R. J. Effect of different salts on the development of *Fusarium solani* var. *coeruleum*, a causal agent of potato dry rot. *Phytoprotection* **2008**, *89*, 1−6.

(18) Mecteau, M. R.; Arul, J.; Tweddell, R. J. Effect of organic and inorganic salts on the growth and development of *Fusarium sambucinum*, a causal agent of potato dry rot. *Mycol. Res.* **2002**, *106*, 688−696.

(19) Yaganza, E. S.; Arul, J.; Tweddell, R. J. Postharvest application of organic and inorganic salts for the control of potato tuber soft rot. *Phytopathology* **2001**, *91*, S198.

(20) Jeandet, P.; Adrian, M.; Breuil, A. C.; Debord, S.; Sbaghi, M.; Joubert, J. M.; Weston, L. A.; Harmon, R.; Bessis, R. Chemical induction of phytoalexin synthesis in grapevines: Application to the control of grey mould in the vineyard. *Acta Hortic.* **2000**, *528*, 591−596.
(21) Sholberg, P. L. Fumigation of fruits with short-chain organic acids to reduce the potential of postharvest decay. *Plant Dis.* **1998**, *82*, 689−693.
(22) Sholberg, P. L.; Gaunce, A. P. Fumigation of fruits with acetic acid prevent postharvest decay. *HortScience* **1995**, *30*, 1271−1275.
(23) Sholberg, P. L.; Reynolds, A. G.; Gaunce, A. P. Fumigation of table grapes with acetic acid to prevent postharvest decay. *Plant Dis.* **1996**, *80*, 1425−1428.
(24) Yaganza, E. S.; Rioux, D.; Simard, M.; Arul, J.; Tweddell, R. J. Ultrastructural alterations of *Erwinia carotovora* subsp. *atroseptica* caused by treatment with aluminum chloride and sodium metabisulfite. *Appl. Environ. Microbiol.* **2004**, *70*, 6800−6808.
(25) Avis, T. J.; Rioux, D.; Simard, M.; Michaud, M.; Tweddell, R. J. Ultrastructural alterations in *Fusarium sambucinum* and *Heterobasidion annosum* treated with aluminum chloride and sodium metabisulfite. *Phytopathology* **2009**, *99*, 167−175.
(26) Avis, T. J.; Michaud, M.; Tweddell, R. J. Role of lipid composition and lipid peroxidation in the sensitivity of fungal plant pathogens to aluminum chloride and sodium metabisulfite. *Appl. Environ. Microbiol.* **2007**, *73*, 2820−2824.
(27) Welch, D. F. Applications of cellular fatty acid analysis. *Clin. Microbiol. Rev.* **1991**, *4*, 422−438.
(28) Yaganza, E. S.; Tweddell, R. J.; Arul, J. Inhibitory effects of organic and inorganic salts on the growth of *Pectobacterium carotovorum* subsp. *carotovorum* and *Pectobacterium atrosepticum*: Physico-chemical basis. *Appl. Environ. Microbiol.* **2009**, *75*, 1465−1469.
(29) Rousselle-Bourgeois, F.; Priou, S. Screening tuber-bearing *Solanum* spp. for resistance to soft rot caused by *Erwinia carotovora* ssp. *atroseptica* (van Hall) Dye. *Potato Res.* **1995**, *38*, 111−118.
(30) Ranganna, B.; Kushalappa, A. C.; Raghavan, G. S. V. Ultraviolet irradiance to control dry rot and soft rot of potato in storage. *Can. J. Plant Pathol.* **1997**, *19*, 30−35.
(31) Rengel, Z. Uptake of aluminium by plant cells. *New Phytol.* **1996**, *134*, 389−406.
(32) Bergethon, P. R.; Simons, E. R. *Biophysical Chemistry: Molecules to Membranes*; Springer-Verlag: New York, 1990; pp 285−288.
(33) Crasnier, M.; Moustacas, A. M.; Ricard, J. Electrostatic effects and calcium ion concentration as modulators of acid phosphatase bound to plant cell walls. *Eur. J. Biochem.* **1985**, *151*, 187−190.
(34) Noat, G.; Crasnier, M.; Ricard, J. Ionic control of acid phosphatase activity in plant cell walls. *Plant Cell Environ.* **1980**, *3*, 225−229.
(35) Ricard, J.; Noat, G.; Crasnier, M.; Job, D. Ionic control of immobilized enzymes. Kinetics of acid phosphatase bound to plant cell walls. *Biochem. J.* **1981**, *195*, 357−367.
(36) Barras, F.; van Gijsgem, F.; Chatterjee, A. K. Extracellular enzymes and pathogenesis of soft rot *Erwinia*. *Annu. Rev. Phytopathol.* **1994**, *32*, 201−234.
(37) Nasuno, S.; Starr, M. P. Polygalacturonase of *Erwinia carotovora*. *J. Biol. Chem.* **1966**, *241*, 5298−5306.
(38) Rengel, Z. Role of calcium in aluminum toxicity. *New Phytol.* **1992**, *121*, 499−513.

and different Sr sources. Furthermore, the compilation of $^{87}Sr/^{86}Sr$ data in soil and water covering all of South Korea offers a baseline for provenance studies by constraining $^{87}Sr/^{86}Sr$ in Sr sources on a national scale.

## MATERIALS AND METHODS

**Sampling Strategy and Study Area.** Soil, water (streamwater and groundwater), and plant (hot pepper and rice) samples were collected from September to October 2010 from every region in South Korea to obtain a representative nationwide sampling. Geologically, South Korea represents a remnant of the denudation of deformed Precambrian metamorphic basement rocks and sedimentary successions, as well as granitic intrusions and volcanics, concealing a long history of basin formation and crustal deformation.[13] The climate of Korea is temperate, with four distinct seasons and average monthly temperatures ranging from −1.1 °C in January to +24.9 °C in August (1971−2000). On the basis of the same 30 year period, the average annual precipitation is approximately 1302 mm, about 65% of which occurs from June to September.[14]

*Soil.* A total of 137 soil samples were collected at a depth of 5−10 cm, using high-density polyethylene (HDPE) measuring scoops to avoid any effects of fertilizers and plant litter, and stored in individual storage bags. All samples were air-dried, passed through a 2 mm mesh sieve, and then crushed in a shatter box equipped with a tungsten carbide grinding container. The exchangeable, carbonate, and silicate fractions were isolated using a sequential leaching and digestion procedure as follows.[12] Approximately 1.0 g of sample was reacted to isolate the exchangeable fraction with 10 mL of 1 M ammonium acetate ($NH_4OAc$) diluted using concentrated ultrapure $NH_4OAc$ (Fisher Scientific, Loughborough, UK) for 6 h. The mixture was centrifuged, and the supernatant was passed through a 0.45 $\mu$m polypropylene syringe filter, dried, and redissolved in 5% $HNO_3$ diluted using concentrated, ultrapure $HNO_3$ (reagent grade). The residue was reacted with 10 mL of 4 M acetic acid (HOAc) diluted using concentrated ultrapure HOAc (Fisher Scientific) for 6 h to isolate the carbonate fraction. The mixture was centrifuged, and the supernatant was passed through a 0.45 $\mu$m polypropylene syringe filter, dried, and dissolved in 5% $HNO_3$. The residue was dried, and a 0.1 g subsample was completely digested in a 5:3 mixture of HF (reagent grade) and $HNO_3$. The sample was dried, refluxed several times in 6.0 M HCl (reagent grade) to remove fluorides, and redissolved in 5% $HNO_3$.

*Water.* A total of 191 water (134 streamwater and 57 groundwater) samples were collected from the nearest location used for soil and plant sampling to avoid anthropogenic contamination. Water samples were passed through 0.45 $\mu$m filters, collected in I-CHEM low-density polyethylene (LDPE) bottles, and acidified to pH <2 using concentrated ultrapure $HNO_3$.

*Plants.* A total of 77 plant (31 hot pepper and 46 rice) samples were collected in plastic storage bags, cleaned several times by Milli-Q water to remove fine particles, dried at 75 °C for 24 h, and stored in a vacuum oven until analysis. Samples were crushed in a shatter box equipped with a tungsten carbide grinding container and homogenized. About 0.7 g of sample was sequentially reacted with ultrapure concentrated $HNO_3$ and a 4:1 (v/v) mixture of ultrapure concentrated $HNO_3$ and $HClO_4$ (reagent grade) for complete digestion. The sample was dried and redissolved in 5% $HNO_3$.

*Elemental and Isotope Analyses.* Strontium concentrations were measured using an X7 ICP-MS (Thermo Scientific, Bremen, Germany) at the Korea Basic Science Institute (KBSI). The following standard reference materials were also prepared and measured to verify the sample preparation and analytical quality of the instruments: SRMs 1570a and 1573a for hot pepper and rice; SRMs BCR-2 and MAG-1 for soil; and CRM NRC SLRS-5 for water. The average uncertainty associated with the whole procedure of all standard reference materials was ±6% ($n$ = 17).

For strontium isotope analysis, samples were first dried in Teflon vessels and redissolved in 8 M $HNO_3$. Strontium was then separated from matrix elements using Eichrom Sr resin (Eichrom Industries, Darien, IL, USA).[15] Strontium isotope ratios ($^{87}Sr/^{86}Sr$) were measured using a Neptune MC-ICP-MS (Thermo Scientific) at KBSI. $^{87}Sr/^{86}Sr$ ratios were normalized to $^{86}Sr/^{88}Sr$ = 0.1194,[9] and replicate analyses of NBS987 (U.S. National Bureau of Standards) gave $^{87}Sr/^{86}Sr$ = 0.710247 ± 0.000008 (2$\sigma$, $n$ = 24) with a background value of <0.1 ng.

**Statistical Analysis.** Nonparametric statistics were used to describe the $^{87}Sr/^{86}Sr$ distribution and to compare $^{87}Sr/^{86}Sr$ between samples. The structure of the data was visualized using kernel density estimation, which is a nonparametric method of estimating the probability density function of a random variable.[16] Differences in $^{87}Sr/^{86}Sr$ between samples were examined by applying a two-tailed Mann−Whitney $U$ test using freeware PAST software instead of the $t$ test due to important differences in sample sizes and some heterogeneity in variances.[17] A probability level of 5% was established to reject the null hypothesis of no difference between the ranks of two samples. The probability was given by the exact $p$ value when $n_1 + n_2 \leq 30$, based on all possible ground assignments.

The spatial $^{87}Sr/^{86}Sr$ patterns of samples were generated using ArcGIS 9.3 software (ESRI, Redlands, CA, USA). Spatial interpolation was performed using inverse distance weight (IDW), which assigns values to unknown points on the basis of a weighted average of the values at the known points.

## RESULTS AND DISCUSSION

**Soil.** Sr concentrations were variable within each fraction, ranging from 0.78 to 566 mg/kg (Table 1). Exchangeable and carbonate fractions had similar Sr concentrations, with averages of 8.22 ± 4.4 and 5.12 ± 5.01 mg/kg, respectively, accounting for 4 and 3% of the total Sr in soil, respectively. The silicate fraction had a much higher Sr concentration (171 ± 101 mg/kg), accounting for 93% of the total Sr in soil. These results

**Table 1. Sr Concentrations and $^{87}Sr/^{86}Sr$ Ratios of the Samples**

| sample ($n^a$) | Sr (mg/kg) | $^{87}Sr/^{86}Sr$ |
|---|---|---|
| rock (124) | | |
| maximum | 2830 | 0.76090 |
| minimum | 2.00 | 0.70485 |
| average | 273 ± 364 | 0.71566 ± 0.01063 |
| soil (137) | | |
| *exchangeable fraction* | | |
| maximum | 26.6 | 0.76283 |
| minimum | 1.43 | 0.70646 |
| average | 8.22 ± 4.40 | 0.71719 ± 0.00662 |
| *carbonate fraction* | | |
| maximum | 38.8 | 0.74561 |
| minimum | 0.78 | 0.70787 |
| average | 5.12 ± 5.01 | 0.71697 ± 0.00749 |
| *silicate fraction* | | |
| maximum | 566 | 0.76470 |
| minimum | 41 | 0.70821 |
| average | 171 ± 101 | 0.72315 ± 0.01156 |
| water (191) | | |
| maximum | 648[b] | 0.75753 |
| minimum | 1.30[b] | 0.70698 |
| average | 33.6 ± 50.6[b] | 0.71881 ± 0.00987 |
| plants (77) | | |
| maximum | 7.99 | 0.73909 |
| minimum | 0.08 | 0.70803 |
| average | 0.99 ± 1.34 | 0.71712 ± 0.00618 |

[a] $n$ = number of samples analyzed. [b] $\mu$g/L; error represents standard deviation (1$\sigma$).


dx.doi.org/10.1021/jf503498r | J. Agric. Food Chem. 2014, 62, 9232−9238

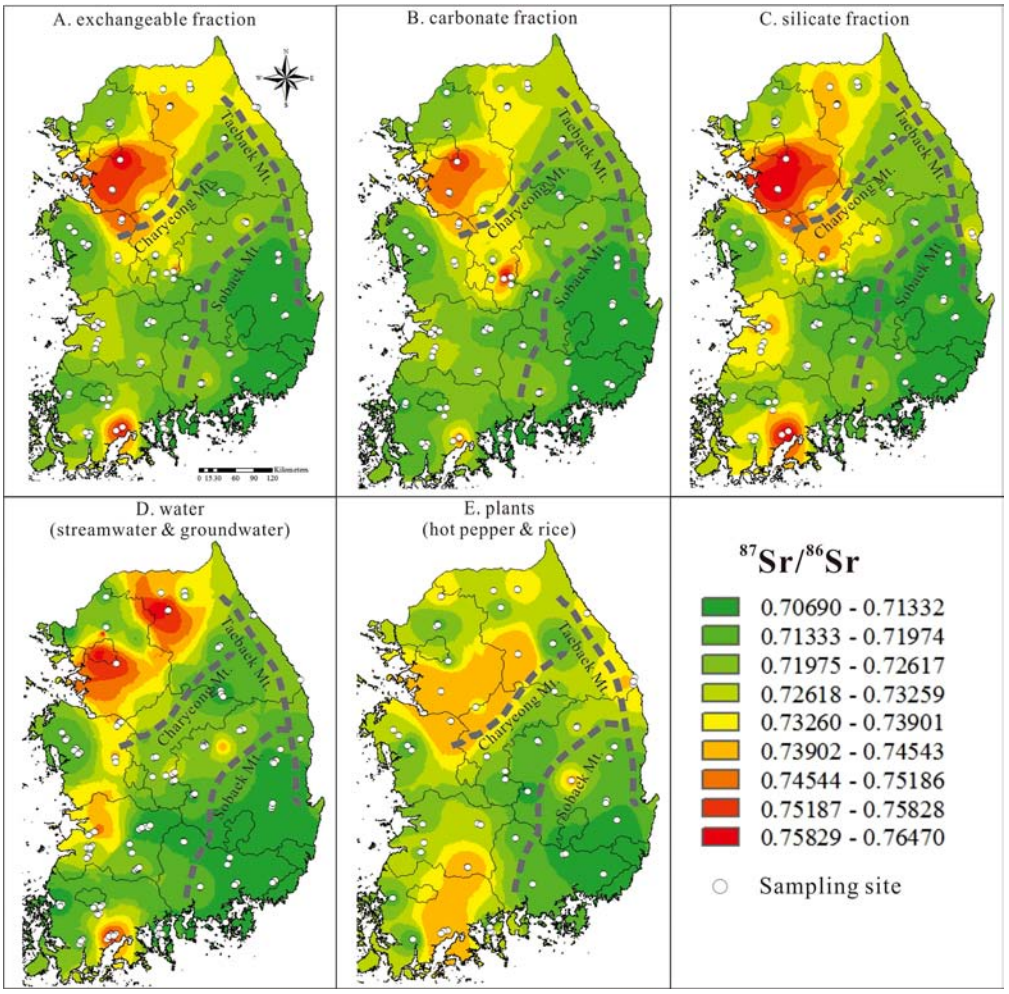


**Figure 1.** Maps showing the spatial $^{87}Sr/^{86}Sr$ distribution of (A–C) each soil fraction, (D) water, and (E) plants. Open circles display the sampling site.

indicate either that soil Sr is mostly incorporated into soil minerals protected from subsequent leaching or that the major part of Sr within a soil exists as structural Sr as a component of primary minerals. Although the exchangeable and carbonate Sr pools account for only 7% of the total Sr in soil, they are easily released into the soil solution, allowing the plant to take up Sr from the soil solution. On the other hand, the silicate Sr pool is available to the plant slowly over time because it is resistant to the weathering process. Therefore, it might be more feasible that plants will reflect Sr from bioavailable (exchangeable and/or carbonate) fractions rather than the silicate fraction.

The mean $^{87}Sr/^{86}Sr$ ratio spanned a wide range, from 0.71697 ± 0.00749 in the carbonate fraction to 0.72315 ± 0.01156 in the silicate fraction, indicating that the $^{87}Sr/^{86}Sr$ ratios are highly variable and on the whole broadly overlapping (Table 1). However, when observed in greater detail, the exchangeable fractions have slightly higher $^{87}Sr/^{86}Sr$ ratios than those measured in the carbonate fractions in all regions except one (Chungbuk), consistent with the fact that carbonates have low $^{87}Sr/^{86}Sr$ due to their low Rb content.[18] The silicate fractions have the highest radiogenic $^{87}Sr/^{86}Sr$ ratios (Table 1). These results indicate that Sr in the exchangeable and carbonate fractions is potentially different from that of the silicate fraction due to atmospheric deposition, cycling of Sr by plants, and weathering effects.[6] However, the effect of atmospheric deposition could be negligible because $^{87}Sr/^{86}Sr$ ratios of both fractions are different from those of either sea salt aerosol ($^{87}Sr/^{86}Sr$ = 0.70917)[19] or Asian dust ($^{87}Sr/^{86}Sr$ = 0.721).[19] On the basis of the Sr concentrations and $^{87}Sr/^{86}Sr$ ratios of each soil fraction, mass balance calculations showed that soils have similar $^{87}Sr/^{86}Sr$ ratios to the silicate fractions, suggesting that Sr in the bulk soil itself cannot elucidate the first-order relationship between soil and plant. With the fact that there is unlikely to be significant isotopic fractionation during plant uptake due to the small mass difference between Sr isotopes, it is reasonable to assume that plants have $^{87}Sr/^{86}Sr$ ratios different from those of the bulk soils because the exchangeable and carbonate fractions are vulnerable to weathering, whereas the silicate fraction is highly resistant to weathering.

Because little information about $^{87}Sr/^{86}Sr$ ratios of bedrocks in South Korea is available and is limited to typical areas, we were unable to obtain such data for the entire country.[20−41] Nevertheless, we compiled all reported data and compared those data with soil $^{87}Sr/^{86}Sr$ ratios to examine the relationship between them. The bedrock $^{87}Sr/^{86}Sr$ ratios are also variable, ranging from 0.70485 to 0.76090. In general, regions with Precambrian metamorphic and Mesozoic granitic rocks show much higher radiogenic $^{87}Sr/^{86}Sr$, whereas regions with carbonate and volcanic rocks yield the lowest $^{87}Sr/^{86}Sr$ values.[20−41] Differences in $^{87}Sr/^{86}Sr$ ratios were found between rock and soil, indicating either that Sr in soil is potentially


dx.doi.org/10.1021/jf503498r | J. Agric. Food Chem. 2014, 62, 9232−9238

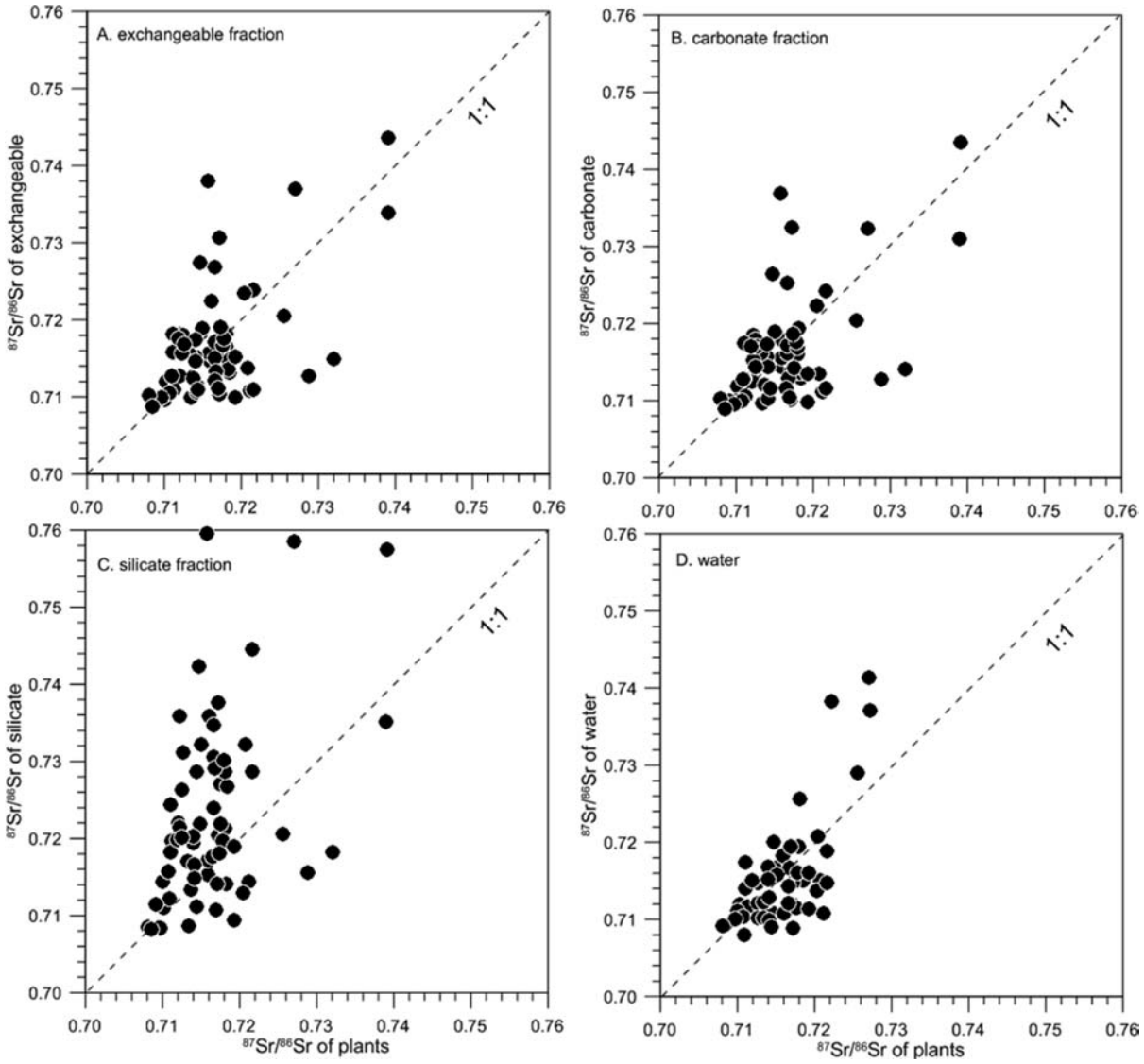


**Figure 2.** Plots of $^{87}Sr/^{86}Sr$ ratios of (A–C) each soil fraction and (D) water versus plants.

different from that of bedrock due to atmospheric deposition, cycling of Sr by plants, and weathering effects[6] or that reported bedrock $^{87}Sr/^{86}Sr$ ratios were insufficient to cover the whole country. Nevertheless, $^{87}Sr/^{86}Sr$ ratios between rock and soil collected at similar regions are consistent, indicating that soil inherits Sr and its isotopic composition from minerals in the bedrock even if there is a disturbance, such as cycling of Sr by plants.

**Water.** Sr concentrations and $^{87}Sr/^{86}Sr$ ratios in water come mainly from mineral dissolution with a minor contribution from atmospheric deposition and anthropogenic input.[42−44] However, a previous study[45] reported that the influences of atmospheric deposition and anthropogenic input on Sr concentrations and $^{87}Sr/^{86}Sr$ ratios in water are negligible in South Korea, and therefore rock/mineral dissolution can be considered the dominant Sr source in water. Sr concentrations in water were highly variable, ranging from 1.3 to 648 $\mu$g/L with an average of 33.6 ± 50.6 $\mu$g/L, and $^{87}Sr/^{86}Sr$ ratios ranged from 0.70698 to 0.75753, with an average of 0.71881 ± 0.00987. Although the range of $^{87}Sr/^{86}Sr$ ratios of water is similar to those of other samples, the mean value is consistent with those of the exchangeable and carbonate fractions rather than the silicate fraction, indicating that Sr in the exchangeable and carbonate fractions vulnerable to weathering is easily released into water, whereas Sr in the silicate fraction highly resistant to weathering is retained. Furthermore, there is a clear correspondence between soil fractions and water, whereas the correlation between water and bedrock is not exhibited clearly because reported $^{87}Sr/^{86}Sr$ data are limited to typical regions that do not represent the entire country (Figure 1). Nonetheless, it might be inferred that Sr released from minerals in the bedrock percolates through soil pore water and into the water, such as streamwater and groundwater, and thus water should reflect the $^{87}Sr/^{86}Sr$ ratio of soil fractions and/or bedrock.

**Plants.** The elemental and isotopic compositions of agricultural products are known to reflect the local geochemistry of the soil and water, but can also be influenced by agricultural practices.[5,6,46] In this context, Sr isotopic compositions are important because $^{87}Sr/^{86}Sr$ ratios are fractionated neither by low temperature nor by biogenic processes,[9,10] and therefore $^{87}Sr/^{86}Sr$ ratios of agricultural products reflect the sources of Sr available during their formation.[7] Sr concentrations ranged from 0.08 to 7.99 mg/


dx.doi.org/10.1021/jf503498r | J. Agric. Food Chem. 2014, 62, 9232−9238

kg, with an average of 0.99 ± 1.34 mg/kg, and $^{87}Sr/^{86}Sr$ ratios varied from 0.70803 to 0.73909, with an average of 0.71712 ± 0.00618, which are within the range of rock, each soil fraction, and water. These values indicate that agricultural products, in particular those relating to hot pepper and rice, reflect the combined local geochemistry of the environment in which they grow, as shown in the spatial interpolation in Figure 1. Although it is difficult to determine quantitatively which Sr source exerts dominant control over $^{87}Sr/^{86}Sr$ in agricultural products, the $^{87}Sr/^{86}Sr$ ratios appeared at first glance to be controlled much more by the exchangeable and carbonate fractions of soil and water than by bedrock and the silicate fraction of soil (Figure 2). Furthermore, it is interesting to note that agricultural products do not display radiogenic $^{87}Sr/^{86}Sr$ ratios comparable with other samples in the same region (Figure 1). As discussed above, because the influences of atmospheric deposition and anthropogenic input can be negligible, this is possibly due to cycling of Sr by plants because preferential assimilation of the light isotope ($^{86}Sr$) by plants can produce lower $^{87}Sr/^{86}Sr$ ratios. However, more detailed investigations are required to confirm this hypothesis.

**Relationships among the Isotopic Compositions of Soil, Bedrock, Water, and Plants.** Kernel density plots of $^{87}Sr/^{86}Sr$ ratios in rock, each soil fraction, water, and plants reveal the distribution mode for each sample, demonstrating that all samples possess one major mode lying between 0.70 and 0.73 and a few minor modes with higher $^{87}Sr/^{86}Sr$ values (Figure 3A). It is interesting to note that all soil fractions have higher $^{87}Sr/^{86}Sr$ ratios than bedrock, indicating that radiogenic, mafic, and bedrock-forming minerals, such as biotite and hornblende, are more easily weathered than felsic minerals, thus releasing their Sr easily into the soil, resulting in higher radiogenic $^{87}Sr/^{86}Sr$ values in soil than in bedrock. Although more bedrock $^{87}Sr/^{86}Sr$ data in South Korea are needed to support this result, our finding suggests that the assumption that the $^{87}Sr/^{86}Sr$ ratios of bedrock and soil should be the same should be considered carefully in investigations of the provenance and geographical origin. Hence, $^{87}Sr/^{86}Sr$ ratios can be used as tracers only if they are well understood and interpreted in the light of local geological, hydrological, and pedological assessment. Likewise, each soil fraction showed a different distribution mode; there was little difference between exchangeable and carbonate fractions but clear differences between these two fractions and the silicate fraction. This indicates that more radiogenic Sr exists in the silicate fraction, which is resistant to weathering. The distribution mode of plants was indistinguishable from the exchangeable and carbonate fractions, indicating that plants preferentially take up Sr from these fractions rather than from the silicate fraction. Water also showed distributions similar to that of plants, indicating that water also affects the $^{87}Sr/^{86}Sr$ ratio of plants. Our results indicate that among different Sr sources, the exchangeable and carbonate fractions in soil and water together influence the plant $^{87}Sr/^{86}Sr$ ratio, in agreement with previous studies.[17,47]

Statistical probability can specify which Sr source more reliably predicts the $^{87}Sr/^{86}Sr$ ratio of agricultural products. The two-tailed Mann−Whitney *U* test showed that water and the exchangeable fraction of soil had the highest probabilities, 90 and 89%, respectively, followed by the carbonate fraction (53%), but the silicate fraction and bedrock had zero probability (Figure 3B). Therefore, it can be inferred that bioavailable Sr mainly reflects water and the exchangeable fraction of soil. To the best of our knowledge, this is the first study showing that agricultural products best correspond to both water and the exchangeable fraction of soil in terms of their various potential Sr sources. Further investigations with other agricultural products are necessary to confirm our results.

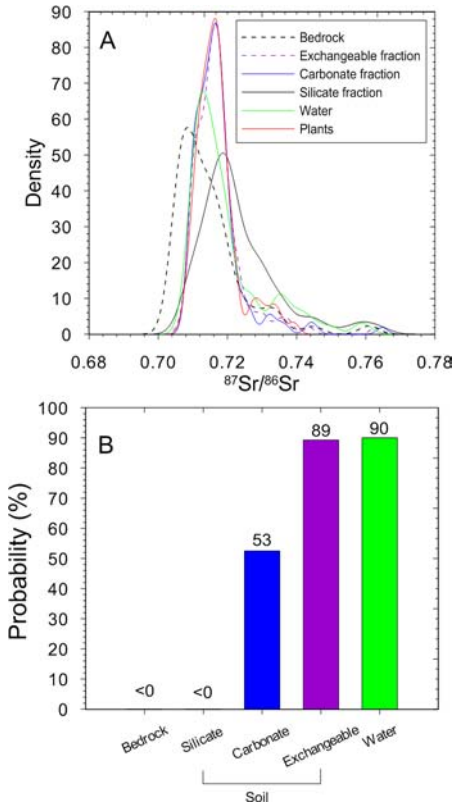


**Figure 3.** (A) Kernel density plots of $^{87}Sr/^{86}Sr$ ratios for all samples and (B) probability histogram of matching $^{87}Sr/^{86}Sr$ in plants and the $^{87}Sr/^{86}Sr$ of other samples.

## ■ ASSOCIATED CONTENT

### Supporting Information

Further details on the sampling sites and the reported $^{87}Sr/^{86}Sr$ ratios of bedrock (Figures S1 and S2, respectively); analytical results obtained for standard reference materials (Table S1); and further details on $^{87}Sr/^{86}Sr$ ratios of samples in each region (Table S2). This material is available free of charge via the Internet at http://pubs.acs.org.

## ■ AUTHOR INFORMATION

### Corresponding Author

*(K.-S.L.) Phone: +82-42-865-3410. E-mail: kslee@kbsi.re.kr.

### Funding

This work was supported by a national agenda program (NAP) of the Korea Research Council of Fundamental Science and Technology and partly by a KBSI grant (C34701).

### Notes

The authors declare no competing financial interest.

## ■ ACKNOWLEDGMENTS

We thank W. J. Shin and S. W. Lee for their support in collecting samples.

## REFERENCES


(1) Ariyama, K.; Shinozaki, M.; Kawasaki, A. Determination of the geographic origin of rice by chemometrics with strontium and lead isotope ratios and multielement concentrations. *J. Agric. Food Chem.* **2012**, *60*, 1628−1634.

(2) Marchionni, S.; Braschi, E.; Tommasini, S.; Bollati, A.; Cifelli, F.; Mulinacci, N.; Mattei, M.; Conticelli, S. High-precision $^{87}Sr/^{86}Sr$ analyses in wines and their use as a geological fingerprint for tracing geographic provenance. *J. Agric. Food Chem.* **2013**, *61*, 6822−6831.

(3) Rodrigues, C.; Brunner, M.; Steiman, S.; Bowen, G. J.; Nogueira, J. M.; Gautz, L.; Prohaska, T.; Máguas, C. Isotopes as tracers of the Hawaiian coffee-producing regions. *J. Agric. Food Chem.* **2011**, *59*, 10239−10246.

(4) Kawasaki, A.; Oda, H.; Hirata, T. Determination of strontium isotope ratio of brown rice for estimating its provenance. *Soil Sci. Plant Nutr.* **2002**, *48*, 635−640.

(5) Rummel, S.; Hoelzl, S.; Horn, P.; Rossmann, A.; Schlicht, C. The combination of stable isotope abundance ratios of H, C, N and S with $^{87}Sr/^{86}Sr$ for geographical origin assignment of orange juices. *Food Chem.* **2010**, *118*, 890−900.

(6) West, J. B.; Hurley, J. M.; Dudás, F. Ö.; Ehleringer, J. R. The stable isotope ratios of marijuana. II. Strontium isotopes relate to geographic origin. *J. Forensic Sci.* **2009**, *54*, 1261−1269.

(7) Baroni, M. V.; Podio, N. S.; Badini, R. G.; Inga, M.; Ostera, H. A.; Cagnoni, M.; Gallegos, E.; Gautier, E.; Peral-García, P.; Hoogewerff, J.; Wunderlin, D. A. How much do soil and water contribute to the composition of meat? A case study: meat from three areas of Argentina. *J. Agric. Food Chem.* **2011**, *59*, 11117−11128.

(8) Podio, N. S.; Baroni, M. V.; Badini, R. G.; Inga, M.; Ostera, H. A.; Cagnoni, M.; Gautier, E. A.; García, P. P.; Hoogewerff, J.; Wunderlin, D. A. Elemental and isotopic fingerprint of Argentinean wheat. Matching soil, water, and crop composition to differentiate provenance. *J. Agric. Food Chem.* **2013**, *61*, 3763−3773.

(9) Faure, G. *Principles of Isotope Geology*; Wiley: New York, 1986; Vol. 589.

(10) Stewart, B. W.; Capo, R. C.; Chadwick, O. A. Quantitative strontium isotope models for weathering, pedogenesis and biogeochemical cycling. *Geoderma* **1998**, *28*, 173−195.

(11) Dasch, E. J. Strontium isotopes in weathering profiles, deep-sea sediments, and sedimentary rocks. *Geochim. Cosmochim. Acta* **1969**, *33*, 1521−1552.

(12) Jacobson, A. D.; Blum, J. D.; Chamberlain, C. P.; Poage, M. A.; Sloan, V. F. Ca/Sr and Sr isotope systematics of a Himalayan glacial chronosequence: carbonate versus silicate weathering rates as a function of landscape surface age. *Geochim. Cosmochim. Acta* **2002**, *66*, 13−27.

(13) Chough, S.; Kwon, S.-T.; Ree, J.-H.; Choi, D. Tectonic and sedimentary evolution of the Korean peninsula: a review and new view. *Earth−Sci. Rev.* **2000**, *52*, 175−235.

(14) Korea Meteorological Adminstration, www.kma.go.kr/weather/climate/average_30year.jsp (accessed April 2014).

(15) Swoboda, S.; Brunner, M.; Boulyga, S.; Galler, P.; Horacek, M.; Prohaska, T. Identification of Marchfeld asparagus using Sr isotope ratio measurements by MC-ICP-MS. *Anal. Bioanal. Chem.* **2008**, *390*, 487−494.

(16) RSC, AMC Technical Brief 4, representing data distributions with kernel density estimates; Royal Society of Chemistry: London, UK, 2006; www.rsc.org/amc (accessed April 2014).

(17) Maurer, A.-F.; Galer, S. J.; Knipper, C.; Beierlein, L.; Nunn, E. V.; Peters, D.; Tütken, T.; Alt, K. W.; Schöne, B. R. Bioavailable $^{87}Sr/^{86}Sr$ in different environmental samples − effects of anthropogenic contamination and implications for isoscapes in past migration studies. *Sci. Total Environ.* **2012**, *433*, 216−229.

(18) Capo, R. C.; Stewart, B. W.; Chadwick, O. A. Strontium isotopes as tracers of ecosystem processes: theory and methods. *Geoderma* **1998**, *82*, 197−225.

(19) Chadwick, O. A.; Derry, L. A.; Bern, C. R.; Vitousek, P. M. Changing sources of strontium to soils and ecosystems across the Hawaiian Islands. *Chem. Geol.* **2009**, *267*, 64−76.

(20) Cheong, C.-S.; Chang, H.-W. Tectono-magmatism, -metamorphism, and -mineralization of the central Ogcheon belt, Korea (I): Sr, Nd and Pb isotopic systematics and geochemistry of granitic rocks in the Boeun area. *J. Geol. Soc. Korea* **1996**, *32*, 91−116 (in Korean with English abstract).

(21) Cheong, C.-S.; Chwae, U.; Kim, J. W.; Lee, S.-H.; Jeong, G. Y.; Im, C. B.; Chang, C.-J.; Chang, H. W. Rb-Sr dating of the wangsan fault, southeastern Korea. *J. Geol. Soc. Korea* **2003**, *39*, 403−412.

(22) Jeong, G. Y.; Cheong, C.-S.; Lee, B. H. Rb-Sr isotopic ages of biotite in the weathering profile of granodiorite, Yecheon. *J. Miner. Soc. Korea* **2005**, *18*, 53−59 (in Korean with English abstract).

(23) Kim, C.-S.; Kim, G.-S. Petrogenesis of the early tertiary A-type Namsan alkali granite in the Kyongsang Basin, Korea. *Geosci. J.* **1997**, *1*, 99−107.

(24) Kim, G.-S.; Kim, J.-Y.; Jung, K.-K.; Hwang, J.-Y.; Lee, J.-D. Rb-Sr Whole rock geochronology of the granitic rocks in the Kyeongju-Gampo area, Kyeongsangbugdo, Korea. *J. Korea Earth Sci. Soc.* **1995**, *16*, 272−279 (in Korean with English abstract).

(25) Kim, J. Y.; Joo, S. H.; Jo, D. R. Rb/Sr Age of Leucogranitic rocks in the Samcheog Area. *J. Korean Inst. Mining Geol.* **1984**, *17*, 231−236 (in Korean with English abstract).

(26) Kwon, S.-T.; Cheong, C.-S.; Sagong, H. Rb-Sr isotopic study of the Hwacheon granite in northern Gyeonggi massif, Korea: a case of spurious Rb-Sr whole rock age. *Geosci. J.* **2006**, *10*, 137−143.

(27) Kwon, S.-T.; Jin, M.-S.; Choo, S.-H. Origin of the Jechon granite: a review of the Sr isotope data. *J. Petrol. Soc. Korea* **1992**, *1*, 132−137 (in Korean with English abstract).

(28) Kwon, S.-T.; Lan, C.-Y.; Lee, T. Rb-Sr and Sm-Nd isotopic study of the Seoul granitic batholith in middle Korea. *Geosci. J.* **1999**, *3*, 107−114.

(29) Kwon, S.-T.; Lee, H.-Y.; Lam, C.-Y.; Lee, B.-S.; Suh, K.-S.; Do, S. J. Preliminary Sr-Nd isotopic study of lower Paleozoic carbonate rocks and conodonts, Korea. *J. Geol. Soc. Korea* **1991**, *27*, 587−596 (in Korean with English abstract).

(30) Lee, J. I.; Jwa, Y.-J.; Park, C.-H.; Lee, M. J.; Moutte, J.; Kagami, H. Sr and Nd isotopic compositions of late Paleozoic Youngju and Andong granites in the northeastern Yeongnam Massif, Korea. *Geochem. J.* **1999**, *33*, 153−166.

(31) Lee, J. I.; Kagami, H.; Nagao, K. Rb-Sr and K-Ar age determinations of the granitic rocks in the southern part of the Kyeongsang basin, Korea: implication for cooling history and evolution of granitic magmatism during late Cretaceous. *Geochem. J.* **1995**, *29*, 363−376.

(32) Lee, S.-G.; Kim, T.-G.; Lee, J.-S.; Song, Y.-H. Rb-Sr isotope geochemistry in Seokmodo granitoids and hot spring, Gangwha: An application of Sr isotope for clarifying the source of hot spring. *J. Petrol. Soc. Korea* **2006**, *15*, 61−71 (in Korean with English abstract).

(33) Lee, S.-G.; Lee, T. J.; Shin, H. J. Rb-Sr age and its geochemical implication of granitoid cores from deep borehole at Pohang area, Korea. *J. Geol. Soc. Korea* **2008**, *44*, 409−423 (in Korean with English abstract).

(34) Lee, S.-G.; Shin, S.-C.; Kim, K.-H.; Lee, T.; Koh, H.; Song, Y.-S. Petrogenesis of three Cretaceous granites in the Okcheon metamorphic belt, South Korea: geochemical and Nd−Sr−Pb isotopic constraints. *Gondwana Res.* **2010**, *17*, 87−101.

(35) Park, C. Y.; Yoon, J. H.; Park, Y. S. Studies of Rb-Sr isotope and rock geochemistry of igneous rocks in the Suncheon-Kwangyang area. *J. Korean Soc. Miner. Energy Resour. Eng.* **1993**, *30*, 53−65 (in Korean with English abstract).

(36) Park, K.-H.; Cheong, C.-S. $^{87}Sr/^{86}Sr$ ratios and ages of the Ogcheon metasedimentary rocks. *J. Geol. Soc. Korea* **1998**, *34*, 81−93 (in Korean with English astract).

(37) Park, Y.-S.; Kim, Y.-J.; Kwon, S.-T.; Park, J.-B. Rb-Sr isotopic study on igneous rocks from the Geochang-Koryong area. *J. Korean Earth Sci. Soc.* **1993**, *14*, 32−43 (in Korean with English abstract).

(38) Sagong, H.; Kwon, S.-T.; Han, R.; Ree, J.-H. Cretaceous thermal event around the Gongsuwon thrust in the northeastern Okcheon belt: evidence from Rb-Sr geochronology of Paleozoic sedimentary rocks. *Geosci. J.* **2006**, *10*, 59−66.
(39) Shin, S.; Jin, M. *Radiometric Age Maps of Volcanic, Plutonic and Metamorphic Rocks and Ore Deposits in the Korean Peninsula*; KIGAM: Daejeon City, Korea, 1995; KR-95 (B)-7, pp 22−43.
(40) Yi, J.-M.; Kim Kyu, H.; Tsuyoshi, T.; Iwao, K. REE and Sr isotopic compositions of earbonate pebbles in the phyllitic rocks of the Hwanggangni Formation, Okcheon zone. *J. Geol. Soc. Korea* **2000**, *36*, 257−278.
(41) Yun, S. H. Strontium isotope composition and petrochemistry of the Cretaceous Chaeyaksan volcanics, Northern Yucheon volcanic field, South Korea. *J. Geol. Soc. Korea.* **1998**, 161−171 (in Korean with English abstract).
(42) Drouet, T.; Herbauts, J.; Gruber, W.; Demaiffe, D. Strontium isotope composition as a tracer of calcium sources in two forest ecosystems in Belgium. *Geoderma* **2005**, *126*, 203−223.
(43) Kanayama, S.; Yabuki, S.; Yanagisawa, F.; Motoyama, R. The chemical and strontium isotope composition of atmospheric aerosols over Japan: the contribution of long-range-transported Asian dust (Kosa). *Atmos. Environ.* **2002**, *36*, 5159−5175.
(44) Nakano, T.; Tanaka, T.; Tsujimura, M.; Matsutani, J. Strontium isotopes in soil-plant-atmosphere continuum (SPAC). In *Tracers in Hydrology*; IAHS: Wallingford, UK, 1993; No. 215, pp 73−78
(45) Ryu, J.-S.; Lee, K.-S.; Chang, H.-W. Hydrogeochemical and isotopic investigations of the Han River basin, South Korea. *J. Hydrol.* **2007**, *345*, 50−60.
(46) Degryse, P.; Shortland, A.; De Muynck, D.; Van Heghe, L.; Scott, R.; Neyt, B.; Vanhaecke, F. Considerations on the provenance determination of plant ash glasses using strontium isotopes. *J. Archaeol. Sci.* **2010**, *37*, 3129−3135.
(47) Hartman, G.; Richards, M. Mapping and defining sources of variability in bioavailable strontium isotope ratios in the Eastern Mediterranean. *Geochim. Cosmochim. Acta* **2014**, *126*, 250−264.

Turkish raki. Long known as a carminative and expectorant, the essential oil of aniseed exhibits antibacterial and antioxidant properties.[34,35] The odor of aniseed is long-known to be elicited by *trans*-anethole, **1** (Figure 1), the major component of its

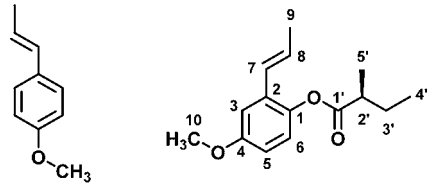


**Figure 1.** Chemical structures of *trans*-anethole (**1**) and *trans*-pseudoisoeugenyl 2-methylbutyrate (**2**).

essential oil.[36,37] By means of aroma extract dilution analysis and identification and quantitation of most intense odorants, followed by calculation of odor activity values, *trans*-anethole was confirmed to be the character impact compound responsible for the unique aniseed scent.[38] However, systematic study on the oro-sensory activities of aniseed components have not been performed.

Originally invented for the generation of compound libraries for high-throughput screening programs,[39−41] we here report for the first time the application of preparative HPLC-SPE-HPLC combined with a modified TDA for taste compound discovery using a sweet and licorice-like bitter-tasting aniseed extract as an example.

## MATERIALS AND METHODS

**Chemicals.** The following compounds were obtained commercially: formic acid, trifluoroacetic acid (Merck, Darmstadt, Germany), anethole, estragole (Sigma-Aldrich, Steinheim, Germany). Deuterated solvents were obtained from Euriso-Top (Gif-Sur-Yvette, France). Solvents were of HPLC grade (J. T. Baker, Deventer, The Netherlands) except for *n*-hexane and ethyl acetate (p.A.) (Merck), which were distilled prior to use. Water for HPLC analysis and extractions was obtained from a Milli-Q Advantage A10 high-purity water system (Millipore, Molsheim, France). For sensory analysis, 3 or 5% ethanol (>99.9%) (Merck) was added to Evian bottled water (Danone Waters Deutschland, Frankfurt, Germany). Aniseed was purchased from a local market (Bio Lebensmittel Zander, Mühlheim, Germany).

**Sequential Solvent Extraction.** After freezing with liquid nitrogen, aniseed was comminuted to a fine powder in an A11 basic batch mill (IKA Werke, Staufen, Germany). An aliquot (240 g) of the ground material was suspended in *n*-hexane (2.5 L) and ultrasonicated for 4 h at room temperature with vigorous stirring. After filtration through a 18.5 cm Schleicher & Schuell filter, the organic solvent was separated from the filtrate under vacuum (40 °C) to afford the solvent extractables. The residue was sequentially extracted with ethyl acetate (2.5 L), followed by methanol (2.5 L) and methanol/water (30:70, v/v; 2.5 L) using the same protocol to afford the *n*-hexane extractables (fraction I, yield = 14%), the ethyl acetate extractables (fraction II, yield = 5%), the methanol extractables (fraction III, yield = 17%), and the methanol/water extractables (fraction IV, yield = 21%); the latter two fractions were separated from solvent under vacuum and, then, freeze-dried twice.

For further separation of fraction I, an aliquot (25 g) was mixed with methanol/water (94:6, v/v; 500 mL) and, after 2 h, the bottom layer separated and again extracted with methanol/water (94:6, v/v; 500 mL). The supernatants were combined and kept at −20 °C until further use. After centrifugation (7000 rpm, 20 min, 0 °C), the liquid layer was separated from solvent under vacuum at 40 °C to afford the sensory active subfraction I-I.

**Dry-Injection and 2D-HPLC Separation of Subfraction I-I.** An aliquot (1.5 g) of fraction I-I was dissolved in methanol (50 mL), membrane filtered, mixed with Polygoprep 300-50 C4 silica (7 g) (Macherey-Nagel, Düren, Germany) and, after sonication for 20 min, the mixture was separated from solvent under vacuum, thus yielding a free-flowing powder. The stainless steel injection column (20 × 60 mm) was assembled, leaving one side open, and 1 g of blank C4 silica material (1.0 g) was added. After leveling the surface of the stationary phase, the adsorbed fraction I-I was funneled onto the top of the stationary phase, the surface was leveled, the remaining volume of the injection column was filled with blank C4 silica material, the column end fitting was attached, and, then, the injection column was connected to the Sepbox 2D-2000 2D-HPLC system (Sepiatec, Berlin, Germany). Using 0.1% formic acid and 0.02% trifluoroacetic acid in water as solvent A and 0.1% formic acid in acetonitrile as solvent B, the effluent of the injection column was continuously pumped onto a 150 × 32 mm i.d., 12 μm, VP150/32 Nucleoprep 100-12 C4-end-capped column (Macherey-Nagel) at a flow rate of 40 mL/min. Chromatography was performed with the following gradient: 0 min, 20% B; 6 min, 60% B; 16 min, 100% B; 20 min, 100% B; 21 min, 20% B; 27 min, 20% B. Concomitant with the separation, a flow gradient was run with water, which was mixed with the C4 column effluent using the following flow rates: 0 min, 0 mL/min; 1 min, 50 mL/min; 12 min, 25 mL/min; 16 min, 20 mL/min; 21 min, 20 mL/min; 24 min, 1 mL/min. The effluent was collected in 16 subfractions, namely I-I/1−I-I/16, which were trapped onto VP30/32 Nucleoprep 100-12 C4-end-capped SPE columns preconditioned with water (3 min, 40 mL/min) prior to the separation.

Each subfraction was further separated on a 250 × 21.2 mm, 5 μm, Luna Phenyl-Hexyl column (Phenomenex, Aschaffenburg, Germany) using the following gradient of water (solvent A), methanol (solvent B), and acetonitrile (solvent C) at a flow rate of 20 mL/min: fraction I-I/1, 0 min, A/B/C (83:17:0), 29 min, A/B/C (57:43:0), 30 min, A/B/C (0:100:0), 34 min, A/B/C (0:100:0); fraction I-I/2, 0 min, 38% B, 29 min, 58% B, 30 min, 100% B, 34 min, 100% B; fraction I-I/3, 0 min, A/B/C (56:44:0), 29 min, A/B/C (37:63:0), 30 min, A/B/C (0:100:0), 34 min, A/B/C (0:100:0); fraction I-I/4, 0 min, A/B/C (48:52:0), 29 min, A/B/C (23:67:0), 30 min, A/B/C (0:100:0), 34 min, A/B/C (0:100:0); fraction I-I/5, 0 min, A/B/C (32:68:0), 29 min, A/B/C (28:72:0), 30 min, A/B/C (0:100:0), 34 min, A/B/C (0:100:0); fraction I-I/6, 0 min, A/B/C (31:69:0), 29 min, A/B/C (20:80:0), 30 min, A/B/C (0:100:0), 34 min, A/B/C (0:100:0); fraction I-I/7, 0 min, A/B/C (22:78:0), 29 min, A/B/C (13:87:0), 30 min, A/B/C (0:100:0), 34 min, A/B/C (0:100:0); fraction I-I/8, 0 min, A/B/C (22:78:0), 29 min, A/B/C (9:91:0), 30 min, A/B/C (0:100:0), 34 min, A/B/C (0:100:0); fraction I-I/9, 0 min, A/B/C (21:79:0), 29 min, A/B/C (9:91:0), 30 min, A/B/C (0:100:0), 34 min, A/B/C (0:100:0); fraction I-I/10, 0 min, A/B/C (22:88:0), 29 min, A/B/C (7:93:0), 30 min, A/B/C (0:100:0), 34 min, A/B/C (0:100:0); fraction I-I/11, 0 min, A/B/C (7:93:0), 29 min, A/B/C (5:95:0), 30 min, A/B/C (0:100:0), 34 min, A/B/C (0:100:0); fraction I-I/12, 0 min, A/B/C (3:97:0), 16 min, A/B/C (3:97:0), 17 min, A/B/C (0:100:0), 29 min, A/B/C (0:93:7), 30 min, A/B/C (0:50:50), 34 min, A/B/C (0:50:50); fraction I-I/13, 0 min, A/B/C (3:97:0), 16 min, A/B/C (3:97:0), 17 min, A/B/C (0:100:0), 29 min, A/B/C (0:93:7), 30 min, A/B/C (50:50:0), 34 min, A/B/C (0:50:50); fraction I-I/14, 0 min, A/B/C (0:98:2), 29 min, A/B/C (0:89:11), 30 min, A/B/C (0:50:50), 34 min, A/B/C (0:50:50); fraction I-I/15, 0 min, A/B/C (0:98:2), 29 min, A/B/C (0:80:20), 30 min, A/B/C (0:50:50), 34 min, A/B/C (0:50:50); fraction I-I/16, 0 min, A/B/C (0:100:0), 29 min, A/B/C (0:34:66), 30 min, A/B/C (0:10:90), 34 min, A/B/C (0:10:90). Column equilibration for each separation was 11 min at the initial gradient conditions. Each subfraction, I-I/1−I-I/16, was separated into 16 additional subfractions; for example, fraction I-I/1 was cut into subfractions I-I/1-1−I-I/1-16.

**Identification of Key Taste-Active Compounds in 2D-HPLC Subfractions.** Aliquots of the first-dimension fractions I-I/1−I-I/16 were reconstituted by combining portions (10 mL) from each of the 16 subfractions collected in the second dimension. The reconstituted

fractions I-I/1−I-I/16 were diluted 1:1 with water and extracted with *n*-hexane (200 mL), and the organic layer was separated from solvent under vacuum at 40 °C and, then, used for sensory analysis. As reconstituted fractions I-I/8 and I-I/9 were judged with the highest sensory impact for sweetness and bitterness, aliquots of each individual of their second-dimension subfractions, namely, I-I/8-1−I-I/8-16 and I-I/9-1−I-I/9-16, were diluted 1:1 with water, extracted with *n*-hexane (50 mL), and, after solvent removal under vacuum (40 °C), the organic residues were kept at −20 °C until further used for sensory analysis. Fraction I-I/8-4, judged with the highest sensory impact, was identified as *trans*-anethole, **1**, by comparing chromatographic (retention time) and spectroscopic data (UV−vis, 1D/2D-NMR) with those of a commercially available reference material. Dried fraction I-I/9-5, judged with high sensory impact, was identified as *trans*-pseudoisoeugenyl 2-methylbutyrate, **2**, by means of LC-TOF-MS and 1D/2D-NMR experiments.

*trans-Anethole,* ***1***, Figure 1: UV−vis (water/methanol), $\lambda_{max}$= 260, 212 nm. NMR data were identical to those of the commercial reference.

*trans-Pseudoisoeugenol-2-methylbutyrate,* **2**, Figure 1: UV−vis (water/acetonitrile), $\lambda_{max}$ = 220, 248, 300 nm; UPLC-TOF-MS, *m/z* 249.1488 (measured), *m/z* 249.1491 (calculated for $[C_{15}H_{20}O_3 + H]^+$); $^1$H NMR (400 MHz, $CDCl_3$, COSY), $\delta$ 6.99 (d, *J* = 3.0 Hz, 1H, [H−C(3)]), 6.88 (d, *J* = 8.8 Hz, 1H, [H−C(6)]), 6.75 (dd, *J* = 8.8, 3.0 Hz, 1H, [H−C(5)]), 6.36 (dd, *J* = 15.8, 1.6 Hz, 1H, [H−C(7)]), 6.20 (dq, *J* = 15.8, 6.5 Hz, 1H, [H−C(8)]), 3.80 (s, 3H, [H−C(10)]), 2.65 (q, *J* = 7.0 Hz, 1H, [H−C(2′)]), 1.92−1.78 (m, 4H, [H−C(3′) and H−C(9)]), 1.63 (ddd, *J* = 13.7, 7.4, 6.4 Hz, 1H, [H−C(3′)]), 1.32 (d, *J* = 7.0 Hz, 3H, [H−C(5′)]), 1.03 (t, *J* = 7.4 Hz, 3H, [H−C(4′)]); $^{13}$C NMR (400 MHz, $CDCl_3$, HSQC, HMBC), $\delta$ 175.39 (C, [C(1′)]), 157.27 (C, [C(4)]), 141.35 (C, [C(1)]), 131.30 (C, [C(2)]), 128.42 (CH, [C(7)]), 124.49 (CH, [C(8)]), 123.14 (CH, [C(6)]), 113.25 (CH, [C(5)]), 110.98 (CH, [C(3)]), 55.56 (CH3, [C(10)]), 41.23 (CH, [C(2′)]), 29.51, (CH2, [C(3′)]), 18.79 (CH3, [C(9)]), 16.78 (CH3, [C(5′)]), 11.68. (CH3, [C(4′)]).

**Sensory Analyses.** *Training of the Sensory Panel.* Seven female and six male panelists (25−36 years in age), who had given informed consent to participate in the sensory tests of the present investigation and had no history of known taste disorders, participated in this study. Each panelist took place in a weekly training session for at least two years to get familiarized with the taste language and methodologies used. Aqueous solutions (2.0 mL; pH 5.9) of the following reference compounds were used for sensory training: sucrose (50 mmol/L) for sweet taste, L-lactic acid (20 mmol/L) for sour taste, NaCl (20 mmol/L) for salty taste, caffeine (1 mmol/L) for bitter taste, monosodium L-glutamate (3 mmol/L) for umami taste, and (+)-catechin (1 mmol/L) for astringency. Sensory analyses were performed by means of the sip-and-spit method in an air-conditioned room at 22−25 °C in three independent sessions. Aimed at preventing cross-model interactions with odorants, nose clips were used by the assessors.

*Taste Profile Analysis.* Aliquots of fractions I−IV were dissolved in ethanol and made up in water to a maximum content of 5% ethanol. The trained sensory panelists were then asked to judge the intensity of the sweet, sour, umami, salty, bitter, and astringent orosensation on a linear scale from 0 (not detectable) up to 5 (very intense).

*Taste Dilution Analysis (TDA).* Aliquots of the HPLC fractions were dissolved in "natural" ratios in 10.0 mL of bottled water containing 3% ethanol and sequentially diluted 1:1 with bottled water containing 3% ethanol. The serial dilutions of each of these fractions were then presented in order of increasing concentration to the trained sensory panel, which was asked to evaluate each dilution step by means of a two-alternative forced-choice test. As previously reported, the dilution at which a taste difference between the diluted extract and the blank (control) could just be detected was defined as the taste dilution (TD) factor.[2] The TD factors for each HPLC fraction evaluated by 10 different assessors in three different sessions were averaged. The TD factors between individuals and separate sessions did not differ by more than plus/minus one dilution step.

**Two-Dimensional High-Performance Liquid Chromatography System.** Preparative 2D-HPLC fractionation of fraction I-I was performed on a Sepbox 2D-2000 HPLC apparatus consisting of a Smartline UV Detector 2500 with a 4061 flow cell (Knaur, Berlin, Germany), a Sedex LT-ELSD detector model 80 (Sedere, Alfortville, France), and two 1800 pumps, one of which was equipped with an A4099-1 ternary low-pressure gradient unit (Knaur), a semipreparative two-channel degasser (Knaur), and a MIKA 3000 mixing chamber (Portman Instruments, Biel-Benken, Switzerland) and was connected to act on the first- and second-dimension flowpath (Figure 2). A self-made mixing chamber consisting of a 20 × 60 mm stainless steel column filled with glass beads (2 mm i.d.) was connected to the first-dimension flowpath (Figure 2). Valve manifolds and fraction collector were custom-made (Sepiatec GmbH, Berlin Germany). Chromatography of the first dimension was conducted using a preparative C4, 150 × 32 mm i.d., 12 μm, Nucleodur column (Macherey-Nagel), equipped with a 2 μm semipreparative frit (IDEX Health and Science, Oak Harbor, WA, USA) and operated at a flow rate of 40.0 mL/min. SPE trapping was facilitated by 16 C4 Nucleoprep VP 30/32 columns (Macherey-Nagel). Chromatography of the second dimension was conducted using a 250 × 21.2 mm i.d., 5 μm, Luna Phenyl-Hexyl column (Phenomenex) with a guard column of the same type at 20 mL/min. For both dimensions, the eluent split ratio was 1:20 (ELSD/UV). Data were acquired using Sepbox Control V2.0.0 software (Sepiatec GmbH, Berlin, Germany), and data analysis was conducted using Sepbox Reporter V2.0.0.3 software.

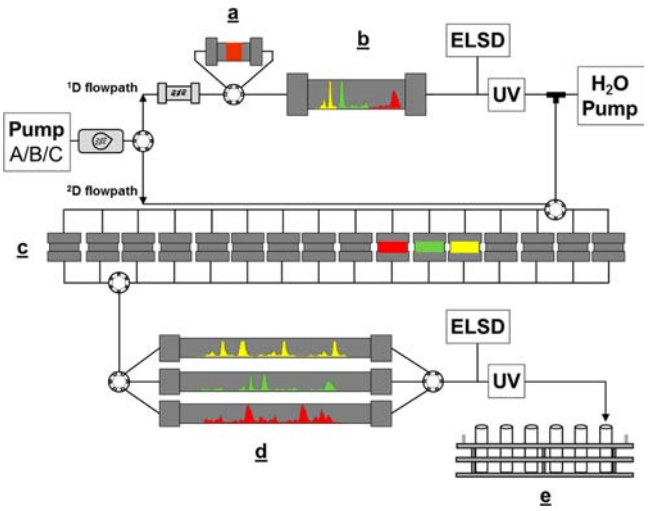


**Figure 2.** Scheme depicting the principle of operation of the preparative 2D-HPLC system. The sample is introduced using the injection column (a) and subsequently separated on the $^1$D column (b); fractions are then collected on SPE columns (c), and trapped fractions are further separated on the $^2$D column (d).

Analytical chromatography of fractions I-I/8-4 and I-I/9-5 was performed on a HPLC apparatus (Jasco, Groß-Umstadt, Germany) consisting of a DG-2080-53 degasser, an LG-2080-02S ternary gradient unit, a PU-2080 Plus pump, an AS-2055 Plus autosampler, an MD-2010 Plus detector with a 6824-H101A cell, and a Sedex LT-ELSD detector model 90 (Sedere). Chromatography was done using an analytical 250 × 4.6 mm i.d., 5 μm, HyperClone ODS 120 column (Phenomenex) operated with a flow rate of 1.0 mL/min. Data acquisition was done by means of Chrompass 1.9.302 (Jasco).

**UPLC/Time-of-Flight Mass Spectrometry (UPLC/TOF-MS).** High-resolution mass spectra were recorded on a SYNAPT G2S HDMS mass spectrometer (Waters UK Ltd., Manchester, UK) operated in the positive electrospray ionization and high-resolution modus. Sample aliquots (1 μL) in methanol were introduced into the instrument via an Acquity UPLC core system (Waters). The UPLC-TOF-MS system was equipped with a BEH Phenyl, 150 × 2.1 mm i.d., 1.7 μm, column (Waters) equipped with a guard column of the same type and operating at a flow rate of 0.3 mL/min and a temperature of 45 °C. The following gradient was used for chromatography: starting

with a mixture (40:60, v/v) of acetonitrile and aqueous formic acid (0.1% HCOOH), the acetonitrile content was increased to 100% within 3 min and kept at this level for 1 min. All data were lock mass corrected on the pentapeptide leucine enkephalin (Tyr-Gly-Gly-Phe-Leu, $m/z$ 556.2771, $[M + H]^+$) in a solution (2 ng/ $\mu$L) of acetonitrile/0.1% formic acid (1:1, v/v). Data acquisition and interpretation were performed by using MassLynx software version 4.1 (Waters) and the tools "isotope model" and "elemental composition".

**Nuclear Magnetic Resonance Spectroscopy (NMR).** 1D-NMR ($^1$H, $^{13}$C) and 2D-NMR experiments (COSY, HSQC, and HMBC) were acquired on a 400 MHz DRX spectrometer (Bruker, Rheinstetten, Germany). Experiments were carried out using the pulse sequences taken from the Bruker software library. Chemical shifts were referenced to TMS. Data processing and interpretation were performed using Topspin version 2.1 (Bruker) and MestRe-Nova version 7.0.2-10008 software (Mestrelab Research, La Coruna, Spain). Samples were analyzed in $CDCl_3$.

## RESULTS AND DISCUSSION

To introduce a fully automated, preparative HPLC-SPE-HPLC combined with a modified TDA for taste compound discovery in foods, a sweet and licorice-like tasting aniseed extract was used as an example. Prior to chromatographic separation, first, aniseed fruits were sequentially extracted with solvents of descending hydrophobicity to achieve a crude separation of sensory active components according to their polarity.

**Sequential Solvent Extraction and Taste Profile Analysis.** Ground aniseed fruits were sequentially extracted with *n*-hexane, ethyl acetate, methanol, and methanol/water (30:70, v/v) to afford fractions I–IV after removal of the solvent under vacuum. Aliquots of fractions I–IV were taken up in water containing 3% aqueous ethanol and were, then, sensorially evaluated by means of taste profile analysis using a linear five-point scale. Sweetness and bitterness were rated with the highest scores of 1.5 and 1.0 in fraction I, whereas fraction III showed the highest impact for astringency judged with a score of 1.2 (Table 1). To preseparate taste-active molecules from triglycerides in the *n*-hexane fraction, an aliquot of fraction I was further separated by extraction with methanol/water (94:6, v/v). The polar extract was separated from solvent under vacuum to afford subfraction I-I showing an increased intensity of sweetness (2.2) and bitterness (1.8) when compared to crude fraction I (Table 1). Therefore, subfraction I-I was used for automated HPLC-SPE-HPLC separation.

**Table 1. Taste Profiles of Fractions Isolated from Dried Aniseed Fruits**

| | fraction[a] | | | | |
|---|---|---|---|---|---|
| taste quality | I | II | III | IV | I-I |
| sweet | 1.5 | 0.8 | 0.4 | 0.3 | 2.2 |
| bitter | 1.0 | 0.8 | 0.5 | 0.5 | 1.8 |
| astringent | 1.1 | 1.2 | 1.2 | 1.1 | 1.4 |

[a]Fractions isolated from aniseed were sensorially evaluated in 5% aqueous ethanolic solution on a five-point scale from 0 (not detectable) to 5 (intensely perceived) (SD ±0.2).

**Setup of the HPLC-SPE-HPLC System.** To perform fully automated and comprehensive, offline two-dimensional separations,[42] a Sepbox 2D-2000 was used combining a first-dimension separation with SPE and a series of second-dimension separations (HPLC-SPE-HPLC). The 2D-HPLC instrument comprises two high-pressure pumps, a ternary pump delivering the solvent gradient (A/B/C pump) (Figure 2), and a second pump diluting the effluent of the first dimension with water ($H_2O$ pump) (Figure 2). Flowpath switching was accomplished via electrically actuated Rheodyne valves.

Because extract solubility is not a limiting factor and higher sample loads can be achieved, subfraction I-I was applied onto the column by means of dry-injection. To achieve this, RP4 carrier material was loaded with fraction I-I adsorbed and then placed on top of a layer of blank RP4 material into the injection column (a) (Figure 2) with one endfitting attached. Thereafter, another layer of blank RP4 material was added on top of the sample powder to support the distribution of the mobile phase stream entering the injection column during chromatography.

For chromatography, the mobile phase was delivered by the A/B/C gradient pump and the flow directed through the injection column to elute analytes from the injection column according to their polarity and to subsequently introduce them onto the first-dimension separation column filled with RP4 material (b) (Figure 2). The effluent of the main column was then split (1/20, v/v) between an evaporative light scattering detector (ELSD) and a UV–vis detector for comprehensive recording of eluting analytes. After running through the UV–vis detector, the effluent was diluted with water delivered from the water pump using a T-connector to decrease the acetonitrile content and the solubility of the analytes in the solvent (Figure 2). The effluent, cut into 16 subfractions (I-I/1–I-I/16), was pumped through RP4-end-capped SPE columns to subsequently trap the analytes according to their polarity (c) (Figure 2), whereas the mobile phase was sent to waste. The first dimension concludes with a flushing step of the main separation column, at which time no trap columns were placed in the flow path. To perform chromatography in the second dimension, the individual SPE columns loaded with the analytes of the fractions I-I/1–I-I/16 served as injection columns. One SPE column after the other was placed in the gradient flow path, and analytes are eluted from the trap column onto a second-dimension separation column filled with Phenyl-Hexyl stationary phase (d) (Figure 2). Using a ternary gradient of water, methanol, and acetonitrile, a total of 256 fractions was collected (e), corresponding to 16 fractions collected in the first dimension, each further separated into 16 subfractions, respectively.

**Identification and Sensory Analysis of Key Taste Compounds.** To effectively trace the compounds imparting the sweet and bitter taste in the 256 subfractions collected by means of 2D-HPLC, aliquots of the second-dimension subfractions corresponding to the same first dimension fractions were recombined to obtain the reconstituted first-dimension fractions I-I/1–I-I/16, and, after dilution with water, the hydrophobic taste compounds were extracted with hexane, the solvent was separated under vacuum, and the residues were taken up in 3% aqueous ethanol and used for taste dilution analysis.[2] To achieve this, the dissolved fractions were stepwise diluted 1:1 with 3% aqueous ethanol and then presented to the trained panelists, who were asked to determine their taste dilution (TD) factors by means of a two-alternative forced-choice procedure. Sweetness and bitterness of reconstituted fractions I-I/8 and I-I/9 were judged with the highest TD factors of 32 and 4, respectively (Figure 3). To trace the key taste molecules, a taste dilution analysis was applied onto aliquots of the corresponding second-dimension subfractions I-I/8-1–I-I/8-9 and I-I/9-1–I-I/9-9, thus showing subfraction I-

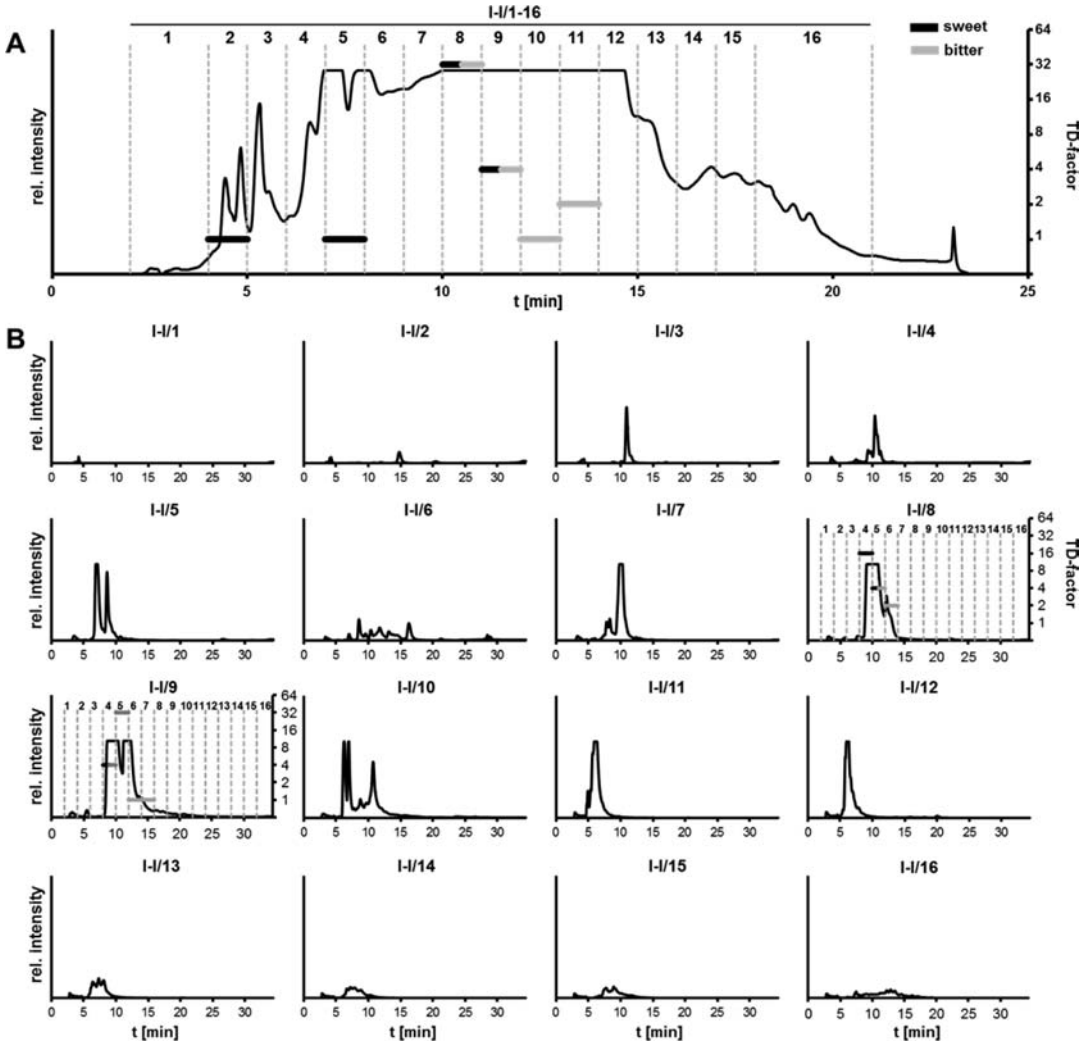


**Figure 3.** (A) First-dimension separation and taste dilution analysis of fraction I-I isolated from dried aniseed fruits and the corresponding second-dimension separations (B) with taste dilution analyses of the high-impact subfractions I-I/8 and I-I/9.

I/8-4 with the highest TD factor of 16 for licorice-like sweetness and I-I/9-5 with the highest TD factor of 32 for bitter taste, respectively.

Comparison of UV−vis, LC-MS, and 1D/2D-NMR data of the licorice-like sweet-tasting key compound in fraction I-I/8-4 with those found for a commercial reference compound led to the identification of *trans*-anethole (**1**), known to contribute to the typical flavor and sweetish taste of aniseed.[36,37,43,44]

UPLC-TOF-MS(ESI$^+$) analysis of the bitter-tasting key fraction I-I/9-5 revealed $m/z$ 249.1492 as the pseudomolecular ion ($[M + H]^+$), thus suggesting an elemental composition of $C_{15}H_{20}O_3$ for compound **2**. The $^1$H NMR spectrum of compound **2** showed the aromatic protons H−C(3), H−C(5), and H−C(6) in the chemical shift range between 6.75 and 6.99 ppm with the typical coupling pattern of a 3-fold substituted benzene ring, as well as two *trans*-configured olefinic protons (H−C(7), H−C(8)), resonating at 6.20 and 6.37 ppm with a coupling constant of 15.8 Hz. The remaining 15 aliphatic protons were assigned to the methoxy moiety H−C(10), resonating at 3.8 ppm, the methyl group of the propenyl substituent H−C(9), the terminal methyl protons of the 2-methyl butyrate side chain H−C(4′), the methylene group H−C(3′), the methine proton H−C(2′), and the methylene group H−C(5′) of the methyl branch of the 2-methyl butyrate side chain. Unequivocal assignment of all protons and carbon atoms could be successfully achieved by means of 2D-NMR spectroscopy. For example, the position of the substitutents in the aromatic ring could be assigned by means of an HMBC experiment, which showed a $^3J$ coupling of the methoxy protons H−C(10) to the quarternary carbon C(4) as well as $^2J$ and $^3J$ couplings between the carbon C(2) and H−C(7) at 6.37 ppm and H−C(8) at 6.20 ppm of the *trans*-propenyl substituent. The aliphatic side chain could be assigned by the $^{2,3}J$ C,H correlations of the carbonyl carbon resonating at 175.4 ppm with the protons H−C(2′), H−C(3′) and H−C(5′), respectively (Figure 4). With all spectroscopic data taken into consideration, the structure of bitter compound **2** was determined to be *trans*-pseudoisoeugenol 2-methyl butyrate. Figure 1 shows the (*S*)-enantiomer, which Karl et al.[49] described as the naturally occurring enantiomer. Although this compound has been reported earlier,[45−49] to the best of our knowledge, its bitter activity has not been previously reported in the literature.

To determine the recognition threshold concentration for the sweet taste of *trans*-anethole (**1**) and the bitter taste of pseudoisoeugenol 2-methyl butyrate (**2**), aqueous solutions containing 3% ethanol were evaluated by means of the two-alternative forced-choice test in linear ascending concentra-


dx.doi.org/10.1021/jf502896n | J. Agric. Food Chem. 2014, 62, 9239−9245

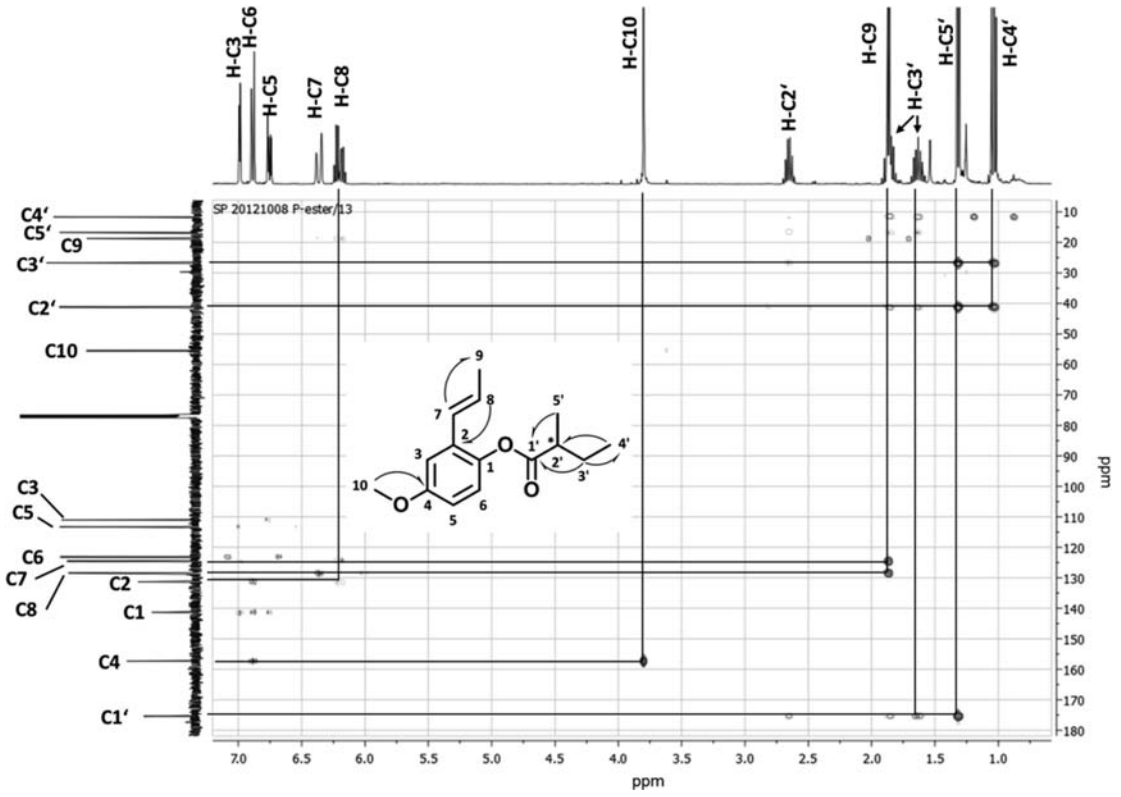


**Figure 4.** Excerpt of the HMBC spectrum (400 MHz, $CDCl_3$) of *trans*-pseudoisoeugenyl 2-methyl butyrate (**2**).

tions. Anethole was found to have a sweet taste recognition threshold of 70 μmol/L, whereas pseudoisoeugenol 2-methyl butyrate (**2**) showed a bitter recognition threshold of 68 μmol/L.

This is the first report on preparative, two-dimensional HPLC combined with sensory analysis in taste compound analysis. Compared to the traditional iterative fractionation of food extracts by sequential application of separation techniques and sensory analysis (e.g., MPLC → solvent separation → sensory evaluation → HPLC → solvent removal → sensory evaluation, etc.), the fully automated 2D-HPLC offers the possibility to comprehensively separate complex extracts into hundreds of subfractions and to reduce the fractionation time from about 1 week to <1day. Using a smart sensory strategy to locate high-impact fractions, e.g., by evaluating first-dimension fractions by reconstituting them from second-dimension subfractions, followed by straightforward application of the taste dilution analysis on the individual second-dimension subfractions seems to be a promising strategy to speed the discovery of the key players imparting the attractive taste of foods. Application of this technique to more complex food extracts and biofermentations, respectively, is currently in progress to fully evaluate the potential of this 2D-HPLC-Sensomics approach also when combined to cell-based taste receptor assays.

## AUTHOR INFORMATION

### Corresponding Author

*(T.H.) Phone: +49-8161/71-2902. Fax: +49-8161/71-2949. E-Mail: thomas.hofmann@tum.de.

### Notes

The authors declare no competing financial interest.

## REFERENCES

(1) Dunkel, A.; Steinhaus, M.; Kotthoff, M.; Nowak, B.; Krautwurst, D.; Schieberle, P.; Hofmann, T. Nature's chemical signatures in human olfaction: a foodborne perspective for future biotechnology. *Angew. Chem., Int. Ed.* **2014**, *53* (28), 7124−7143.

(2) Frank, O.; Ottinger, H.; Hofmann, T. Characterization of an intense bitter-tasting 1*H*,4*H*-quinolizinium-7-olate by application of the taste dilution analysis, a novel bioassay for the screening and identification of taste-active compounds in foods. *J. Agric. Food Chem.* **2001**, *49*, 231−238.

(3) Scharbert, S.; Holzmann, N.; Hofmann, T. Identification of the astringent taste compounds in black tea infusions by combining instrumental analysis and human bioresponse. *J. Agric. Food Chem.* **2004**, *52*, 3498−3508.

(4) Scharbert, S.; Hofmann, T. Molecular definition of black tea taste by means of quantitative studies, taste reconstitution, and omission experiments. *J. Agric. Food Chem.* **2005**, *53*, 5377−5384.

(5) Stark, T.; Hofmann, T. Isolation, structure determination, synthesis, and sensory activity of *N*-phenylpropenoyl-L-amino acids from cocoa (*Theobroma cacao*). *J. Agric. Food Chem.* **2005**, *53*, 5419−5428.

(6) Stark, T.; Bareuther, S.; Hofmann, T. Sensory-guided decomposition of roasted cocoa nibs (*Theobroma cacao*) and structure determination of taste-active polyphenols. *J. Agric. Food Chem.* **2005**, *53*, 5407−5418.

(7) Frank, O.; Zehentbauer, G.; Hofmann, T. Bioresponse-guided decomposition of roast coffee beverage and identification of key bitter taste compounds. *Eur. Food Res. Technol.* **2006**, *222*, 492−508.

(8) Frank, O.; Blumberg, S.; Kunert, Ch.; Zehentbauer, G.; Hofmann, T. Structure determination and sensory analysis of bitter-tasting 4-vinylcatechol oligomers and their identification in roasted coffee by means of LC-MS/MS. *J. Agric. Food Chem.* **2007**, *55*, 1945−1954.

(9) Glabasnia, A.; Hofmann, T. Identification and sensory evaluation of dehydro- and deoxy-ellagitannins formed upon toasting of oak wood (*Quercus alba* L.). *J. Agric. Food Chem.* **2007**, *55*, 4109−4118.

(10) Schwarz, B.; Hofmann, T. Sensory-guided decomposition of red currant juice (*Ribes rubrum*) and structure determination of key astringent compounds. *J. Agric. Food Chem.* **2007**, *55*, 1394−1404.
(11) Hufnagel, J. C.; Hofmann, T. Orosensory-directed identification of astringent mouthfeel and bitter-tasting compounds in red wine. *J. Agric. Food Chem.* **2008**, *56*, 1376−1386.
(12) Toelstede, S.; Hofmann, T. Sensomics mapping and identification of the key bitter metabolites in Gouda cheese. *J. Agric. Food Chem.* **2008**, *56*, 2795−2804.
(13) Intelmann, D.; Kummerlöwe, G.; Haseleu, G.; Desmer, N.; Schulze, K.; Fröhlich, R.; Frank, O.; Luy, B.; Hofmann, T. Structures of storage-induced transformation products of the beer's bitter principles, revealed by sophisticated NMR spectroscopic and LC-MS techniques. *Chem.−Eur. J.* **2009**, *15*, 13047−13058.
(14) Haseleu, G.; Intelmann, I.; Hofmann, T. Structure determination and sensory evaluation of novel bitter compounds formed from β-acids of hops (*Humulus lupulus* L.) upon wort boiling. *Food Chem.* **2009**, *116*, 71−81.
(15) Dawid, C.; Henze, A.; Frank, O.; Glabasnia, A.; Rupp, M.; Büning, K.; Orlikowski, D.; Bader, M.; Hofmann, T. Structural and sensory characterization of key pungent and tingling compounds from black pepper (*Piper nigrum* L.). *J. Agric. Food Chem.* **2012**, *60*, 2884−2895.
(16) Dawid, C.; Hofmann, T. Identification of sensory-active phytochemicals in asparagus (*Asparagus officinalis* L.). *J. Agric. Food Chem.* **2012**, *60*, 11877−11888.
(17) Toelstede, S.; Dunkel, A.; Hofmann, T. A series of kokumi peptides impart the long-lasting mouthfulness of matured Gouda cheese. *J. Agric. Food Chem.* **2009**, *57*, 1140−1448.
(18) Dunkel, A.; Köster, J.; Hofmann, T. Molecular and sensory characterization of γ-glutamyl peptides as key contributors to the kokumi taste of edible beans (*Phaseolus vulgaris* L.). *J. Agric. Food Chem.* **2007**, *55*, 6712−6719.
(19) Sonntag, T.; Kunert, C.; Dunkel, A.; Hofmann, T. Sensory-guided identification of *N*-(1-methyl-4-oxoimidazolidin-2-ylidene)-α-amino acids as contributors to the thick-sour taste and mouth-drying orosensation of stewed beef juice. *J. Agric. Food Chem.* **2010**, *58*, 6341−6350.
(20) Rotzoll, N.; Dunkel, A.; Hofmann, T. Activity-guided identification of (*S*)-malic acid 1-*O*-D-glucopyranoside (morelid) and gamma-aminobutyric acid as contributors to umami taste and mouth-drying oral sensation of morel mushrooms (*Morchella deliciosa* Fr.). *J. Agric. Food Chem.* **2005**, *53* (10), 4149−4156.
(21) Festring, D.; Hofmann, T. Discovery of $N^2$-(1-carboxyethyl)-guanosine 5′-monophosphate as an umami-enhancing Maillard-modified nucleotide in yeast extracts. *J. Agric. Food Chem.* **2010**, *58*, 10614−10622.
(22) Festring, D.; Hofmann, T. Systematic studies on the chemical structure and umami enhancing activity of Maillard-modified guanosine 5′-monophosphates. *J. Agric. Food Chem.* **2011**, *59*, 665−676.
(23) Hillmann, H.; Mattes, J.; Brockhoff, A.; Dunkel, A.; Meyerhof, W.; Hofmann, T. Sensomics analysis of taste compounds in balsamic vinegar and discovery of 5-acetoxymethyl-2-furaldehyde as a novel sweet taste modulator. *J. Agric. Food Chem.* **2012**, *60* (40), 9974−9990.
(24) Herrero, M.; Ibáñez, E.; Cifuentes, A.; Bernal, J. Multidimensional chromatography in food analysis. *J. Chromatogr., A* **2009**, *1216* (43), 7110−7129.
(25) Tranchida, P. Q.; Dugo, P.; Dugo, G.; Mondello, L. Comprehensive two-dimensional chromatography in food analysis. *J. Chromatogr., A* **2004**, *1054* (1−2), 3−16.
(26) Zhang, X.; Fang, A.; Riley, C. P.; Wang, M.; Regnier, F. E.; Buck, C. Multi-dimensional liquid chromatography in proteomics − a review. *Anal. Chim. Acta* **2010**, *664* (2), 101−113.
(27) Guiochon, G.; Marchetti, N.; Mriziq, K.; Shalliker, R. A. Implementations of two-dimensional liquid chromatography. *J. Chromatogr., A* **2008**, *1189* (1−2), 109−168.
(28) Evans, C. R.; Jorgenson, J. W. Multidimensional LC-LC and LC-CE for high-resolution separations of biological molecules. *Anal. Bioanal. Chem.* **2004**, *378*, 1952−1961.
(29) Guiochon, G. Preparative liquid chromatography. *J. Chromatogr., A* **2002**, *965*, 129−161.
(30) Yamamoto, E.; Niijima, J.; Asakawa, N. Selective determination of potential impurities in an active pharmaceutical ingredient using HPLC-SPE-HPLC. *J. Pharm. Biomed. Anal.* **2013**, *84*, 41−47.
(31) Acharya, A. N.; Saraswat, D.; Kaushik, M. P. Antimalarial activity of *Gomphostemma crinitum* leaf extracts. *Med. Chem. Res.* **2008**, *17*, 530−540.
(32) Bhandari, M.; Bhandari, A.; Bhandari, A. Sepbox technique in natural products. *J. Young Pharm.* **2011**, *3* (3), 226−231.
(33) Wong, V.; Shalliker, R. A. Isolation of the active constituents in natural materials by 'heart-cutting' isocratic reversed-phase two-dimensional liquid chromatography. *J. Chromatogr., A* **2004**, *1036*, 15−24.
(34) Özgiven, M. Aniseed. In *Handbook of Herbs and Spices*; Peter, K. V., Ed.; CRC Press: Boca Raton, FL, USA, 2001; pp 39−51.
(35) Gülçın, I.; Oktay, M.; Kıreçcı, E.; Küfrevıoğlu, Ö. I. Screening of antioxidant and antimicrobial activities of anise (*Pimpinella anisum* L.) seed extracts. *Food Chem.* **2003**, *83* (3), 371−382.
(36) Embong, M. B.; Hadziyev, D.; Molnar, S. Essential oils from spices grown in Alberta. Anise oil (*Pimpinella anisum*). *Can. J. Plant Sci.* **1977**, *57*, 681−688.
(37) Melchior, H.; Kastner, H. *Gewürze*; Verlag Paul Parey: Berlin, Germany, 1974; pp 83−88.
(38) Zeller, A.; Rychlik, M. Impact of estragole and other odorants on the flavour of anise and tarragon. *Flavour Fragrance J.* **2007**, *22*, 105−113.
(39) Lawrence, R. N. Rediscovering natural product biodiversity. *Drug Discovery Today* **1999**, *4* (10), 449−451.
(40) Houssen, W. E.; Jaspars, M. Isolation of marine natural products. In *Methods in Biotechnology, Vol. 20, Natural Products Isolation*, 2nd ed.; Sarker, S. D., Latif, Z., Gray, A. I., Eds.; Humana Press: Totowa, NJ, USA, 2006; pp 353−390.
(41) Bugni, T. S.; Harper, M. K.; McCulloch, M. W. B.; Whitson, E. L. Advances in instrumentation, automation, dereplication and prefractionation. In *Natural Product Chemistry for Drug Discovery*; RSC Biomolecular Sciences 18; Buss, A. D., Butler, M. S., Eds.; Royal Society of Chemistry: Cambridge, UK, 2010; pp 279.
(42) Schoenmakers, P. J.; Marriott, P.; Beens, J. Nomenclature and conventions in comprehensive multidimensional chromatography. *LC-GC Eur.* **2003**, *16*, 335−339 (the additional slash sign was suggested to distinguish between off-line (LC/×/LC) and online (LC×LC) comprehensive multidimensional liquid chromatography by the first author in his presentation at Analytica 2014 in Munich, Germany).
(43) Hussain, R. A.; Poveda, L. J.; Pezzuto, J. M.; Soejarto, D. D.; Kinghorn, A. D. Sweetening agents of plant origin: phenylpropanoid consituents of seven sweet-tasting plants. *Econ. Bot.* **1990**, *44* (2), 174−182.
(44) Kinghorn, A. D.; Soejarto, D. D. Discovery of terpenoid and phenolic sweeteners from plants. *Pure Appl. Chem.* **2002**, *74* (7), 1169−1179.
(45) Kubeczka, K. H.; von Massow, F.; Formacek, V.; Smith, M. A. A new type of phenylpropane from the essential fruit oil of *Pimpinella anisum* L. *Z. Naturforsch. B* **1976**, *31*, 283−284.
(46) Carter, G. T.; Schnoes, H. K.; Lichtenstein, E. P. 4-Methoxy-2-(*trans*-l-propenyl)phenyl (+)-2-methylbutanoate from anise plants. *Phytochemistry* **1976**, *16* (5), 615−616.
(47) Kleiman, R.; Plattner, R. D.; Weisleder, D. Antigermination activity of phenylpropenoids from the genus *Pimpinella*. *J. Nat. Prod.* **1988**, *51*, 249−251.
(48) Reichling, J.; Galati, E. M. Chemical constituents of the genus *Pimpinella*. In *Illicium, Pimpinella and Foeniculum*; Jodral, M. M., Ed.; CRC Press: Boca Raton, FL, USA, 2004.
(49) Karl, V.; Schumacher, K.; Mosandl, A. Enantiomeric 2-methylbutanoates: sensory evaluation and chirospecific analysis. *Flavour Fragrance J.* **1992**, *7*, 283−288.

sample is affected by the penetration depth of the IR waves. Therefore, NIR spectroscopy is very useful in exploring bulk materials with little or no sample preparation. The difference in the penetration depths between the NIR and MIR regions influences the precision of developed multivariate analytical models as the NIR region can penetrate several millimeters into the sample, whereas the penetration power of the MIR region is measured in micrometers.[9−11]

Various studies have investigated the potential of NIR and MIR spectroscopies to determine melamine adulteration in infant formula powder,[12] in dairy milk,[13] and in soybean meal.[14] The effectiveness of FT-IR spectroscopy and hyperspectral imaging has already been evaluated for the detection of adulteration in black pepper powder.[15] In addition, FT-IR spectroscopy in combination with a partial least-squares (PLS) model has also proved competent to detect melamine adulteration in dairy milk.[16] The use of FT-Raman and FT-IR spectroscopies was investigated in the characterization of irradiated starch, meaning a starch irradiated at 3, 5, or 10 kGy using a Gammacell 220 $Co^{60}$ gamma irradiator.[17] This research group developed a regression model with the spectroscopic data and observed that NIR performed better than MIR in terms of predicting chemical parameters (e.g., reducing sugars, ethanol, total phenolics, and flavonoids) involved in the fermentation process.

Our study sought to quantitatively detect starch in onion powder using FT-NIR and FT-IR spectroscopic techniques. Spectral analysis of 18 concentrations of starch in onion powder samples, ranging from 0 to 35%, was conducted. On the basis of the results, different adulterant concentrations were identified and categorized by developing a multivariate analytical method. The ultimate objective of this study was to predict and classify the added starch concentration in onion powder using FT-NIR and FT-IR spectroscopic techniques.

## MATERIALS AND METHODS

**Sample and Adulterant.** Onion powder and cornstarch (purities of 100 and 95%, respectively) were obtained from a local market in Korea. Cornstarch was used as the adulterant in the onion powder because of its cheap price, lack of significant effects on human health, and similar physical property. The samples were stored at room temperature until use.

**Sample Preparation.** The moisture content of the samples was equilibrated by drying in an oven at 74 °C for 2 h prior to mixing because spectroscopic measurement is highly sensitive to moisture content. The given temperature was chosen to dry the sample effectively without interfering with the chemical integrity of the samples.[15] Both the dried sample and adulterant material weights were measured with an electronic balance (model AR2130, Ohaus Corp., Parasippany, NJ, USA). Then, the cornstarch was mixed with the onion powder to final concentrations (w/w) of 1, 2, 3, 4, 5, 6, 7, 8, 9, 10, 12, 15, 18, 20, 25, 30, and 35%. Each combination was manually mixed and then transferred to a snap-cap vial. Further mixing was accomplished by placing the filled vials onto a high-speed shaker (Vortex-Genie 2, Scientific Industries, Inc., model G560, Bohemia, NY, USA) to reduce the variation in particle size. Ten samples of each of the pure and adulterated powders were used, and sample quantities were approximately 50 mg for the FT-NIR and 30 mg for the FT-IR studies.

**FT-NIR Spectra Collection.** NIR reflectance spectra of the pure and adulterated onion powder samples were obtained using an FT-NIR spectrometer (Antaris II FT-NIR analyzer, Thermo Scientific Co., Waltham, MA, USA) equipped with an InGaAs detector. The sample holder was furnished with an accessory that contained a central hole (20 mm thick × 20 mm diameter) to maintain a uniform shape and thickness for the sample over the irradiated surface during spectra collection. A reference scan was conducted with a golden slit before scanning each sample. The instrument measured the diffuse reflectance, and a total of 32 successive scans from each sample were collected over the wavelength range between 4000 and 10000 $cm^{-1}$ (1000−2500 nm) at 4 $cm^{-1}$ intervals. Averaged spectra were used for analysis.

**FT-IR Spectra Collection.** FT-IR measurements were performed in the mid-infrared region (4000−650 $cm^{-1}$) using a Nicolet 6700 (Thermo Scientific Co.) FT-IR spectrophotometer, configured with an attenuated total reflectance (ATR) sampling technique, deuterated triglycine sulfate (DTGS) detector, and KBr beam splitter controlled by OMNIC software. Samples to be analyzed were placed on a diamond crystal sampling plate and clamped with a pointed tip. A background scan was obtained before every sample scan with an empty sample plate. In addition, the ATR crystals and pointed tip were cleaned to remove any interference from the preceding sample. A total of 32 successive scans from each sample were collected at 4 $cm^{-1}$ intervals, and averaged spectra of each sample were used for analysis.

**Spectral Data Analysis.** The spectroscopic (NIR and mid-IR) detectors receive light from the sample in the form of diffuse reflectance after absorption, specular reflectance, and scattered light. Only the diffuse reflectance contains chemical information, whereas the latter two carry no useful information as there is no large variation in particle size between starch and onion powder (based on the result from Cilas 1090 particle size analyzer). The collected spectra might be affected by systemic noise due to light scattering, variation in particle size, and instrumental drift. Thus, to determine an accurate chemical composition from spectroscopic measurements, the raw spectra must be corrected at different levels by applying preprocessing methods.[18] In this study, both FT-NIR and FT-IR spectral data were treated with five preprocessing methods: three data normalization methods (minimum, maximum, and range), standard normal variate transformation (SNV), and multiple-scatter correlation (MSC). The original FT-NIR spectra of all the samples and the original spectra preprocessed by the SNV method are depicted in Figure 1, panels a and b, respectively. The raw FT-IR spectra for each sample and SNV-preprocessed spectra are shown in Figure 2, panels a and b, respectively.

For the data analysis, principal component analysis (PCA) was carried out on the SNV- and MSC-processed spectra from both FT-NIR and FT-IR. PCA can readily be applied to spectroscopic data to perceive the nature and scattering level of the data. The first principal component (PC1) describes the maximum of variation or spread in the samples. A second principal component (PC2), orthogonal to the first (i.e., completely uncorrelated), describes the maximum of the variation not described by the first eigenvector, and so on. With this procedure, the most important features of the data set can be seen in a low-dimensionality plot.[19] A multivariate calibration model of a partial least-squares regression (PLSR) was then developed using all of the preprocessed spectral data to predict the extent of adulteration in the pure onion and adulterated onion powder samples. PLSR is particularly suited when the matrix of predictors has more variables than observations, such as from spectral data. PLSR has been used in food authentication studies based in spectroscopic data.[11] Multivariate analysis was performed using MATLAB software version 7.0.4 (The Mathworks, Natick, MA, USA).

The whole data set (180 samples) was split into two sets: a calibration set consisting of 126 samples (7 samples from each group) and a prediction set consisting of 54 samples (3 samples from each group). The PLSR models were built with the calibration set using a full cross-validation method (leave-one-out), removing one observation at one time from the sample sets until all samples have been removed once. This is the method generally used in developing the PLSR model for detecting a specific material with a spectral data set.[20]

## RESULT AND DISCUSSION

**Interpretation of Spectral Analyses.** The FT-NIR original spectra of the pure and adulterated onion powder and the SNV-preprocessed spectra (Figure 1) reveal differences

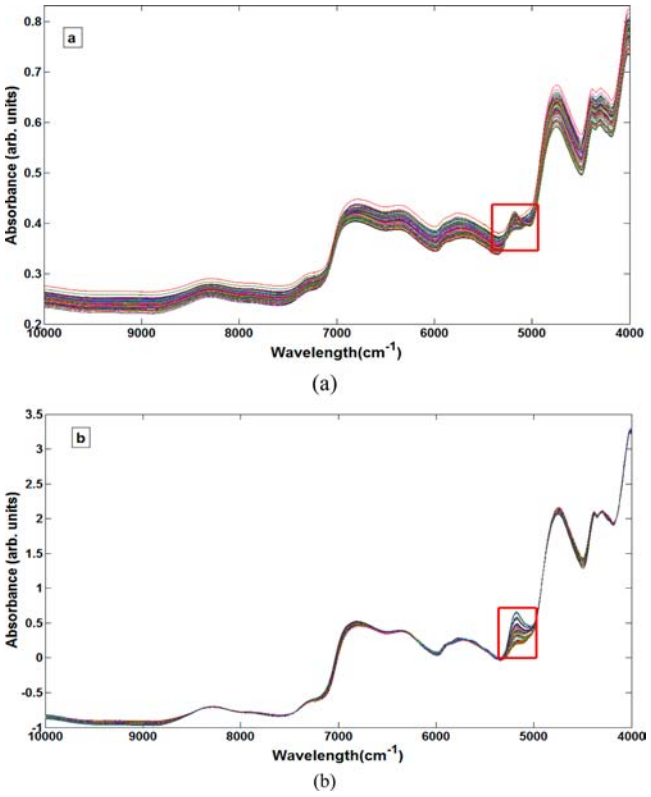


**Figure 1.** (a) Original FT-NIR spectra of pure onion and starch onion mixtures at different concentrations and (b) SNV-preprocessed original spectra.

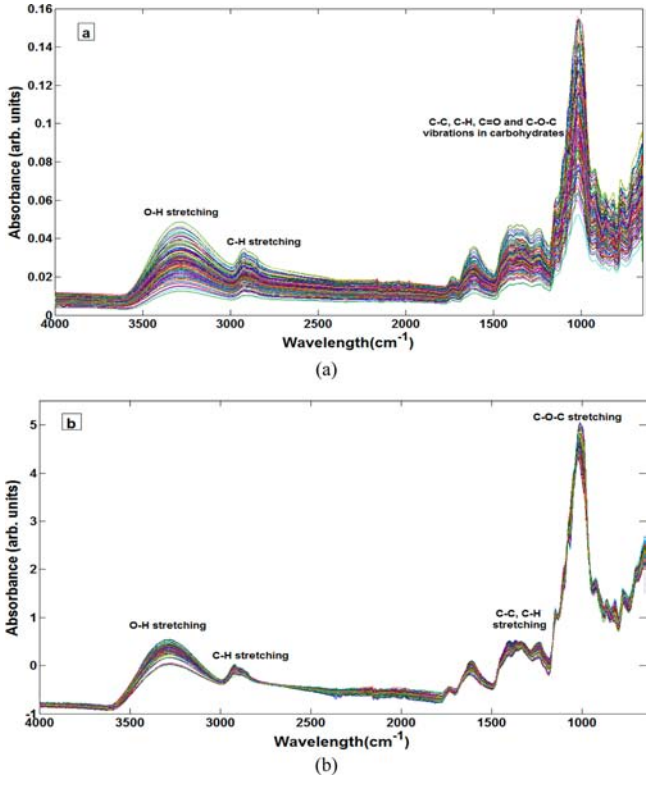


**Figure 2.** (a) Original FT-IR spectra of pure onion and starch onion mixtures at different concentrations and (b) the same spectra after SNV-preprocessing.

in the absorption intensities between 1920 and 1980 nm (marked) and can easily be identified. The absorption bands in this region correspond to the O−H stretch and O−H band combination and the H−O−H deformation combination, which represent the starch content.[21] Starch is a semicrystalline polymer composed of two polysaccharides, amylose and amylopectin. Amylose is a mostly linear chain consisting of up to 3000 glucose molecules interconnected primarily by $\alpha$-1,4-glycoside linkages.[13] The spectral fluctuations from 1400 to 1600 nm correspond to the first overtone of the hydroxyl group. The precise position of these bands is very sensitive to hydrogen bonding in the starch molecule.[22]

The regression coefficient plot (Figure 3) of the PLS model for the FT-NIR data indicates some meaningful bands that are

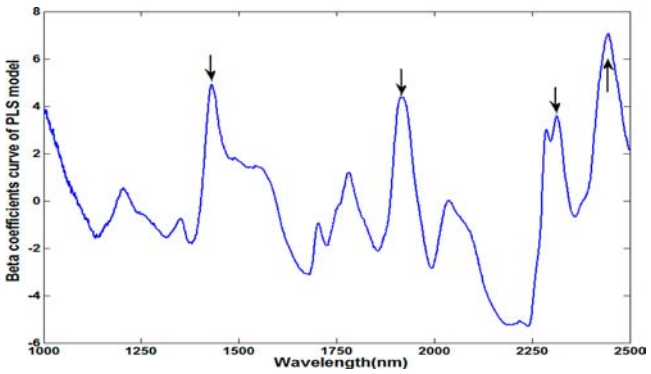


**Figure 3.** $\beta$ coefficient derived from the PLSR for the FT-NIR spectral data. Arrows indicate the characteristic wavelengths of starch.

attributable to the starch. The absorption band around 1420 nm corresponded to a combination of O−H first overtone. Another absorption band at 1920 nm related to CONH, which referred to an amide linkage. The absorption bands at 2312 and 2455 nm corresponded to C−H stretching and deformation vibrations, which represent starch content. Figure 4 shows the results of the PCA for the SNV-pretreated FT-NIR spectral data.

A data grouping was observed from the scatter plot of the PC scores (Figure 4a), but the data for samples adulterated at low concentration appear to overlap more. This confirmed our assumption that the different spectral attributes among the samples were associated with the concentration of the starch in the onion powder. Furthermore, we assessed the potential of PCA to distinguish among the low starch concentration samples (1−10%), but the data were overly scattered and overlapping (data not shown). The first three PC loadings account for nearly 99% of the total variance in the samples. PC loadings are correlation coefficients between the PC scores and the original variables, which measure the importance of each variable in accounting for the variability in the PC. It is possible to interpret the first few PCs in terms of overall effect of a contrast between groups of variables based on the structures of PC loadings. The PC loading plot (Figure 4b) shows the highest loading for PC1 and PC3 at ∼1960 nm, related to the starch. PC1 and PC2 show other important bands between 1435 and 1450 nm, corresponding to the first O−H stretching overtone, also assigned to the starch.

Typically, the MIR region can be divided into two distinct groups: The region of the spectrum below 1500 $cm^{-1}$ is called the fingerprint region.[23] Peaks in this region are very difficult to assign to specific molecular vibrations because each different


dx.doi.org/10.1021/jf500574m | J. Agric. Food Chem. 2014, 62, 9246−9251

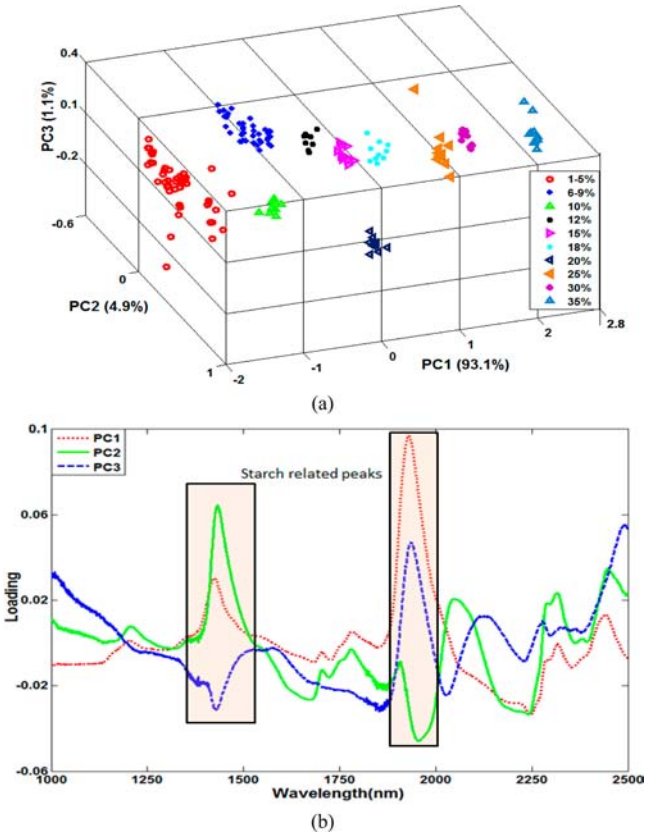


**Figure 4.** (a) Principal component score plot for the first three PCs for discrimination among different adulteration concentrations in onion powder and (b) the first three principal component loadings.

compound produces a different and unique absorption pattern in this part of the spectrum.[16] The MIR region from 4000−1500 $cm^{-1}$ is known as the functional group region. Most of the relevant information that is used to interpret the MIR spectrum usually obtains from the functional group region.[24] The most notable differences in the FT-IR spectra in this study can be categorized into three main regions, which interpret the significance of key bands (Figure 2). The first region was the fingerprint region (650−1500 $cm^{-1}$), which provided more complex spectra and fairly indistinguishable individual bands than the region at higher wavenumbers. The peaks in the region 1045−1087 $cm^{-1}$ are due to C—C bond vibrations related to the carbohydrate; those at 1170−1250 $cm^{-1}$ correspond to absorption bands for C—H, C═O, and C—C vibrations;[25] and the triplet bands for the C—O—C stretching absorption are found at 1147 and 1010 $cm^{-1}$.[26] The vibrations originate from the C—O—C bonds related to the $\alpha$-1,4-glycoside linkages, as these bonds are common in carbohydrates. The C−H stretching region, found between 2850 and 3000 $cm^{-1}$, includes a distinct band at 2920 $cm^{-1}$.[26] Finally, the higher wavenumber region (3000−3500 $cm^{-1}$) indicates the O—H stretching vibration bands. These peaks could be a result of moisture uptake in the samples during spectral analysis. The $\beta$ coefficient (Figure 5), which indicates the spectral differences among the samples, shows some important bands representative of the carbohydrates (starch) that contribute to the quantitative classification of the onion powder and adulterated samples.

PCA was executed on both the MSC- and SNV-preprocessed FT-IR spectral data to extract relevant information. However,

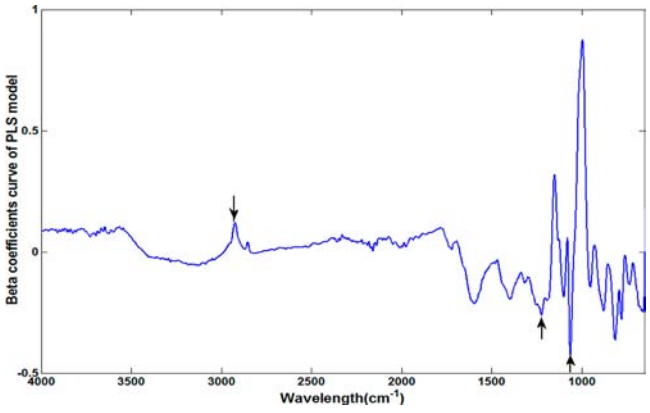


**Figure 5.** $\beta$ coefficient derived from the PLSR for the FT-IR spectral data. Arrows indicate the characteristic wavelengths of starch.

the data might be classified according to moisture content or particle size, rather than their chemical composition characteristics, because the IR data patterns are determined by not only absorption characteristics but also scattering characteristics. These spectral variations were removed by oven drying all of the samples and pretreating the spectra with MSC- and SNV-preprocessing methods. Neither the MSC- nor the SNV-preprocessed FT-IR data were able to quantify the level of adulteration by means of data clustering using PCA. The data were scattered over a vast range, and no distinct separations among the data groups were found from the PCA score plot (data not shown). PCA is a popular primary technique for data clustering. It is not, however, optimized for class separability. The loading plots of the first three PCs are depicted in Figure 6.

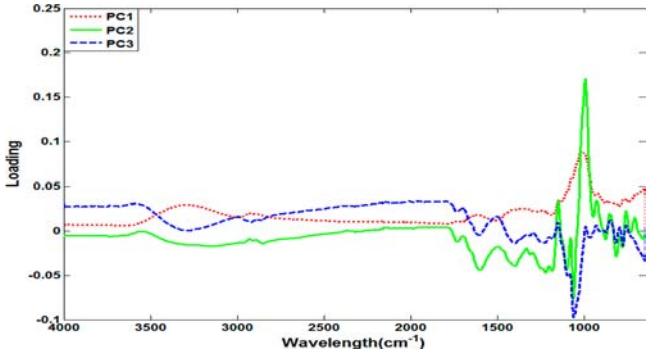


**Figure 6.** First three principal component loadings for starch-adulterated onion powder discrimination.

The PC1 loading accounts for 96.1% of the total sample variance, producing a pattern similar to the raw FT-IR spectra (Figure 2a). The loadings of PC1 and PC2 show the highest intensity at ∼980 $cm^{-1}$. Sankaran et al. also found a similar peak for starch in the spectral range of 950−1000 $cm^{-1}$.[27] In addition, Danwille observed a sharp peak at 975 $cm^{-1}$ arising from an $-OCH_3$ bond vibration related to cellulose.[15]

**Partial Least-Squares Regression Analysis.** A PLSR model was used to predict the added starch concentration in onion powder. The samples were categorized on the basis of the adulterant concentration, and a PLSR model was developed using the preprocessed spectra of samples from both FT-NIR and FT-IR spectroscopy. The highest correlation coefficient value, $R_p^2$, of 0.98 with a standard error of prediction (SEP) of 1.18% was observed by using the SNV-preprocessed FT-NIR


dx.doi.org/10.1021/jf500574m | J. Agric. Food Chem. 2014, 62, 9246−9251

spectra. The optimal number of factors used in the PLS models was automatically selected on the basis of the lowest value of predicted root-mean-square error (RMSE) in the cross-validation process. The PLSR results are listed in Table 1 for the FT-IR spectral data.

**Table 1. Ability of PLS To Predict Concentration of Added Starch in Onion Powder for SNV-Preprocessed FT-IR Spectra**

| | calibration | | validation | | prediction | | |
|---|---|---|---|---|---|---|---|
| spectral region ($cm^{-1}$) | $R_c^{2a}$ | SEC[b] (%) | $R_v^{2c}$ | SEV[d] (%) | $R_p^{2e}$ | SEP[f] (%) | factors |
| 650−4000 | 0.93 | 2.52 | 0.92 | 2.65 | 0.90 | 3.12 | 3 |
| 650−1500 | 0.93 | 2.58 | 0.92 | 2.70 | 0.89 | 3.24 | 3 |
| 1500−4000 | 0.92 | 2.65 | 0.90 | 3.04 | 0.84 | 4.04 | 4 |

[a]Calibration $R^2$. [b]SEC, standard error of calibration. [c]Validation $R^2$. [d]SEV, standard error of validation. [e]Prediction $R^2$. [f]SEP, standard error of prediction, respectively.

The PLSR result obtained for the FT-NIR data shows a strong relatioship ($R_p^2$ = 0.98) between the actual and predicted concentration values. The result suggests that four principal components were enough to extract 99% of the relevant information used to detect starch adulteration in onion powder.

On the basis of the pattern of the FT-IR spectra, the prediction efficiency of the PLSR model was evaluated using the SNV-preprocessed spectra of the full spectral region, as well as two different selected regions (i.e., the fingerprint region (650−1500 $cm^{-1}$) and the functional group region (1500−4000 $cm^{-1}$)). The highest correlation coefficients of prediction ($R_p^2$), 0.90 and 0.89, were obtained for the full spectral and fingerprint regions, respectively. In addition, these two spectral regions showed nearly the same $R_c^2$ and $R_v^2$ values, with a small difference in SEC and SEV (Table 1). The prediction by PLSR of the functional group region was acceptable ($R_p^2$ = 0.84) but lower than those of the first two groups.

Jawaid et al. and Sherman have suggested that the functional group region is better for classification and prediction than the fingerprint region, because most of the information used to interpret the MIR spectrum is usually obtained from the former, whereas the fingerprint region is normally complex with many frequently overlapped bands.[16,28] In our study, the fingerprint region gave better results than the functional group region with respect to the quantative prediction of starch adulteration in the onion powder samples. Moreover, Filippov also discribed the use of the fingerprint region of MIR for the identification of carbohydrates.[29] For more information readers should refer to ref 29 and references cited therein.

From the PLSR and PCA results, the FT-NIR spectral data were better able to quantitatively predict the extent of starch adulteration in onion powder samples than the FT-IR spectral data. It should be noted that limited amounts of sample are irradiated by MIR radiation during the FT-IR analysis. Additionally, the penetration of MIR radiation is usually less than that of the NIR. These reasons could be responsible for the low classification rate for the quantitative discrimination of adulteration using FT-IR spectroscopy. It is known that onions contain calcium, proteins, water-soluble carbohydrates (e.g., glucose, fructose, and sucrose), and other chemical components.[30] The concentration of added starch in the onion powder proportionally influences the concentration of these chemical compounds on a percentage basis. These chemical compounds have different absorption intensities at specific wavelengths in both the NIR and MIR regions. In our study, in addition to the starch concentration, these intrinsic chemical compounds might be responsible for distinct classifications.

In summary, two different vibrational spectroscopic techniques were investigated to quantitatively detect cornstarch contamination in onion powder. The potential of these techniques was evaluated by adding starch at various concentrations (1−35 wt %) into onion powder and by properly mixing the samples. Both FT-NIR and FT-IR spectroscopic methods demonstrated good potential; however, FT-NIR spectroscopy in combination with PLSR afforded a higher prediction accuracy ($R_p^2$ = 0.98) than FT-IR spectroscopy ($R_p^2$ = 0.90). SNV preprocessing, which has been useful in other quantitative applications, improved the accuracies overall. These techniques would seem to be promising for the effective, chemical-free, and rapid detection of product adulteration, as they require no sophisticated laboratory or well-trained personnel to perform the analysis. In addition, for quality control measurements, both FT-NIR and FT-IR spectroscopic techniques are fast and offer a solution for authenticity analysis of agricultural and food products. Further studies could be performed to establish qualitative methods for the detection of adulteration in spices.

## AUTHOR INFORMATION


### Corresponding Author

*(B.-K.C.) Phone: +82-42-821-6715. Fax: +82-42-823-6246. E-mail: chobk@cnu.ac.kr.



### Funding

This research was supported by the High Value-added Food Technology Development Program, Ministry of Agriculture, Food and Rural Affairs (MAFRA), Republic of Korea.


### Notes

The authors declare no competing financial interest.

## ABBREVIATIONS USED

FT-NIR, Fourier transform near-infrared; FT-IR, Fourier transform infrared; MIR, mid-infrared; PLSR, partial least-squares regression; PCA, principal component analysis; SEP, standard error of prediction; InGaAs, indium gallium arsenide; KBr, potassium bromide; ATR, attenuated total reflectance; DTGS, deuterated triglycine sulfate; SNV, standard normal variate transformation; MSC, multiple scatter correlation; PC, principal component; RMSE, root-mean-square error; $R^2$, correlation coefficient; $R_c^2$, $R_v^2$, $R_p^2$, correlation coefficient of calibration, validation, and prediction, respectively; SEC, standard error of calibration; SEV, standard error of validation; SEP, standard error of prediction

## REFERENCES


(1) Bhattacharjee, P.; Singhal, R. S.; Achyut, S. G. Supercritical carbon dioxide extraction for identification of adulteration of black pepper with papaya seeds. *J. Sci. Food Agric.* **2003**, *83*, 783−786.

(2) Lakshmi, V. Food adulteration. *Int. J. Sci. Invention Today* **2012**, *1* (2), 106−113.

(3) Everstine, K. *Economically Motivated Adulteration, Implication for Food Protection and Alternate Approaches to Detection*. Ph.D. thesis, Faculty of the Graduate School of the University of Minnesota, Minneapolis, MN, USA, 2013.

(4) ASTA (American Spice Trade Association). Spice adulteration − White paper, www.astaspice.org/files/public/SpiceAdulteration.pdf.

(5) Shaw, P. C.; Ngan, F. N.; But, P. P. H.; Wang, J. *Molecular Marker in Chinese Medicinal Materials*; World Scientific Publishing: Hackensack, NJ, USA, 2002; Chapter 1, pp 1−5.
(6) Lohumi, S.; Mo, C.; Kang, J. S.; Hong, S. J.; Cho, B. K. Nondestructive evaluation for the viability of watermelon (*Citrullus lanatus*) seeds using Fourier transform near infrared spectroscopy. *J. Biosyst. Eng.* **2013**, *38* (4), 312−317.
(7) Osborne, B. G.; Fearn, T.; Hindle, P. T. *Practical NIR Spectroscopy with Applications in Food and Beverage Analysis*, 2nd ed.; Longman Scientific and Technical: Singapore, 1993.
(8) Wen-Sun, D. *Infrared Spectroscopy for Food Quality and Control*, 1st ed.; Academic Press: San Diego, CA, USA, 2009.
(9) Bras, L. P.; Bernardino, S. A.; Lopes, J. A.; Menezes, J. C. Multiblock PLS as an approach to compare and combine NIR and MIR spectra in calibrations of soybean flour. *Chemom. Intell. Lab. Syst.* **2004**, *75* (2005), 91−99.
(10) Lammertyn, J.; Peirs, A.; Baerdemaeker, J. D.; Nicolai, B. Light penetration properties of NIR radiation in fruit with respect to non-destructive quality assessment. *Postharvest Biol. Technol.* **1999**, *18* (2000), 121−132.
(11) Domagala, W. U. *The Use of the Spectrometric Technique FTIR-ATR To Examine the Polymers Surface*; InTech: Rijeka, Croatia, 2012; Chapter 3, pp 85−104 (http://creativecommons.org/licenses/by/3.0).
(12) Mauer, L. J.; Chernyshova, A. A.; Hiatt, A.; Deering, A.; Davis, R. Melamine detection in infant formula powder using near- and mid-infrared spectroscopy. *J. Agric. Food Chem.* **2009**, *57*, 3974−3980.
(13) Balabin, R. M.; Smirnov, S. V. Melamine detection by mid and near-infrared spectroscopy: a quick and sensitive method for dairy products analysis including liquid milk, infant formula, and milk powder. *Talanta* **2011**, *15;85* (1), 562−568.
(14) Haughey, S. A.; Graham, S. F.; Concouet, E.; Elliott, C. T. The application of near-infrared spectroscopy (NIRS) to detect melamine adulteration of soya bean meal. *Food Chem.* **2012**, *136*, 1557−1561.
(15) Danwille, J. F. S. Detection and quantification of spice adulteration by near infrared hyperspectral imaging. Master of Science in food science (Master thesis), Stellenbosch University, Matieland, Stellenbosch, South Africa, 2011.
(16) Jawaid, S.; Talpur, F. N.; Sherazi, S. T. H.; Nizamani, S. M.; Khaskheli, A. A. Rapid detection of melamine adulteration in dairy milk by SB-ATR−Fourier transform infrared spectroscopy. *Food Chem.* **2013**, *141*, 3066−3071.
(17) Ramazan, K.; Irudyaraj, J.; Seetharaman, K. Characterization of irradiated starches by using FT-Raman and FTIR spectroscopy. *J. Agric. Food Chem.* **2002**, *50* (14), 3912−3918.
(18) Norris, K.; Williams, P. Optimization of mathematical treatment of raw near-infrared signal in the measurement of protein in hard red spring wheat. I. Influence of particle size. *Cereal Chem.* **1983**, *61*, 158−165.
(19) Benar, P.; Adilson, R. Principal component analysis of the hydroxymethylation of sugarcane lignin. *J. Wood Chem. Technol.* **1999**, *19* (1 & 2), 151−165.
(20) Kandpal, L. M.; Lee, H.; Kim, M. S.; Mo, C.; Cho, B. K. Hyperspectral reflectance imaging technique for visualization of moisture distribution in cooked chicken breast. *Sensor* **2013**, *13*, 13289−13300.
(21) Aenugu, H. P. R.; Kumar, D. S.; Parthiban, N.; Ghose, S. S.; Banji, D. Near infrared spectroscopy − an overview. *Int. J. ChemTeCh Res.* **2011**, *3* (2), 825−836.
(22) Noah, L.; Robert, P.; Millar, S.; Champ, M. Near-infrared spectroscopy as applied to starch analysis of digestive contents. *J. Agric. Food Chem.* **1997**, *45*, 2593−2597.
(23) Griffiths, P. R.; de Haseth, J. A. *Fourier Transform Infrared Spectroscopy*, 2nd ed.; Wiley: Hoboken, NJ, USA, 2007.
(24) Hsu, C. P. S. *Handbook of Instrumental Techniques for Analytical Chemistry*; Separation Sciences Research and Product Development; Mallinckrodt: Prentice Hall: Upper Saddle River, NJ, USA, 1997; Chapter 15, pp 247−282.
(25) Fagan, C. C.; Donnell, O. *Application of Mid-infrared Spectroscopy to Food Processing System in Nondestructive Testing of Food Quality*; Irudayaraj, J., Reh, C., Eds.; Wiley: Hoboken, NJ, USA, 2008; pp 119−142.
(26) Razali, M. A. A.; Sanusi, N.; Ismail, H.; Othman, N.; Ariffin, A. Application of response surface methodology (RSM) for optimization of cassava starch grafted polyDADMAC synthesis for cationic properties. *Starch J.* **2012**, *64*, 935−943.
(27) Sankaran, S.; Ehshani, R.; Etxeberria, E. Mid-infrared spectroscopy for the detection of Huanglongbing (greeening) in citrus leaves. *Talanta* **2010**, *83*, 574−581.
(28) Sherman, C. P. Infrared spectroscopy. *Handbook of Instrumental Techniques for Analytical Chemistry*; Separation Sciences Research and Product Development; Prentice Hall: Upper Saddle River, NJ, USA, 1997; Chapter 15, pp 247−282.
(29) Filippov, M. P. Practical infrared spectroscopy of pectic substances. *Food Hydrocolloids* **1992**, *6* (1), 115−142.
(30) Wall, D.; Mishra, M.; Corgan, J. N. Dehydrate onion bulb weight and water-soluble carbohydrates before and after maturity. *J. Am. Soc. Hortic. Sci.* **1999**, *124* (6), 581−586.

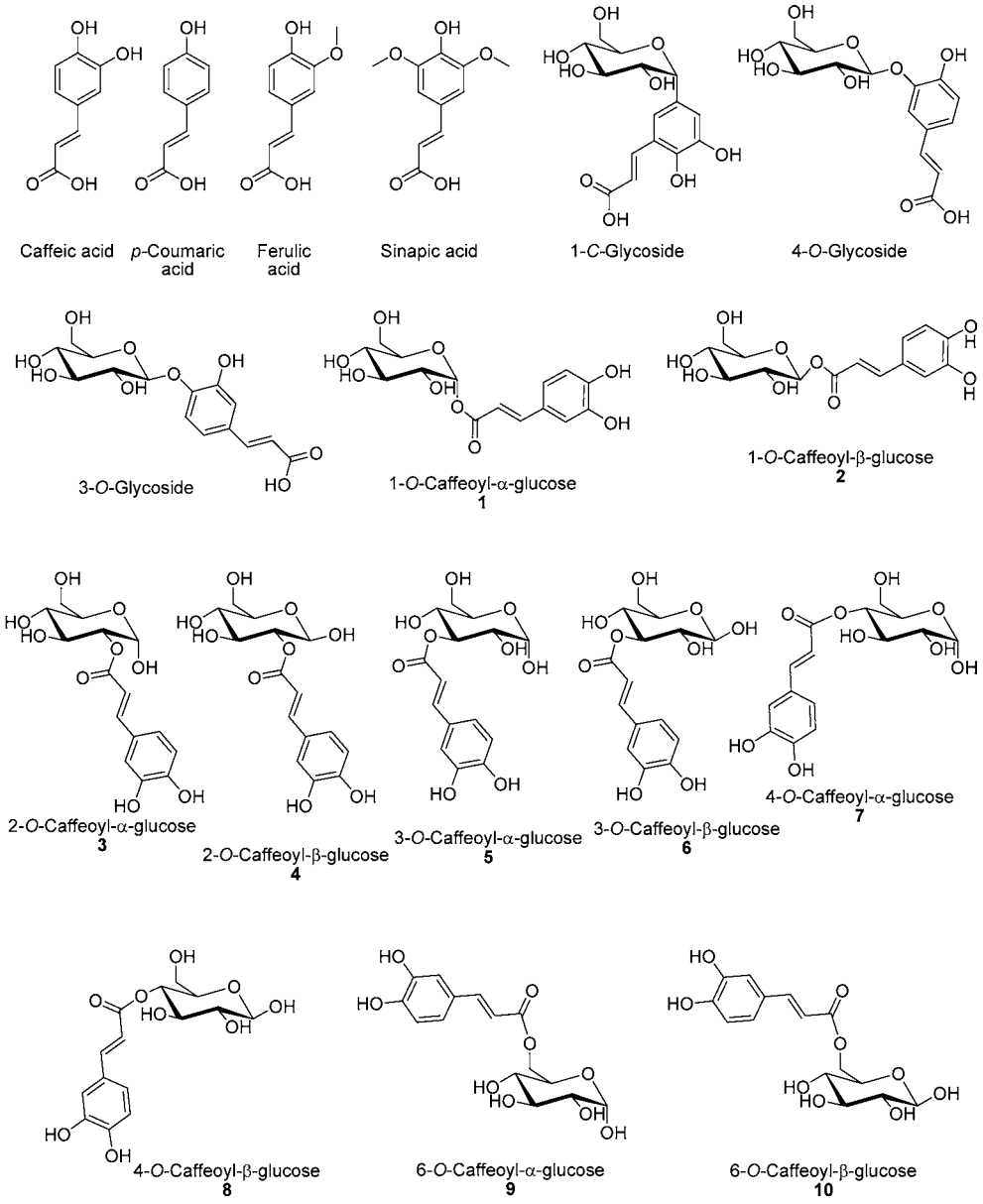


**Figure 1.** Selected structures of typical hydroxycinnamic acids present in the human diet and hydroxycinnamic acid carbohydrate conjugates.

showed that ferulic acid moieties bound to the 5-position of arabinose in arabinoglycans readily dimerized through a photochemical mechanism leading to cyclobutane dimers,[27,28] and, more importantly, they dimerized through radical coupling mechanisms[29] with dehydrodiferulates as reaction products, displaying a surprisingly rich structural chemistry. Caffeoylglucoses were also proposed as biosynthetic intermediates in the syntheses of other caffeoyl derivatives, including chlorogenic acids.

In our own experience, we have observed multiple isomers of caffeoylglucose over the past decade in at least one-half of all of the plant extracts analyzed. Following from many reports on caffeoylglucoses and other hydroxycinnamate conjugates to sugars, addressing and solving the structural assignment problem in this class of compounds constitutes an urgent problem. Only if an unambiguous analytical tool for structure elucidation becomes available with authentic reference materials available will we be able to fully assess the occurrence, dietary burden, and biological effects of this widespread but unexplored class of secondary plant metabolites.

Unambiguous structure elucidation of regioisomeric chlorogenic acids has become possible through the application of tandem $MS^n$ methods. This method has the advantage that chlorogenic acids do not need to be isolated but can be identified and their structure elucidated directly from analytical LC-tandem-MS runs, even if present as minor components or as chromatographically close eluting compounds. For example, we observed that all four regioisomeric mono caffeoylquinic acids and later all six regioisomeric dicaffeoylquinic acids showed dramatically different tandem mass spectra in the negative ion mode, using an ion trap mass spectrometer.[30,31] Because of the diagnostic differences in the tandem MS fragment spectra, a consistent and predictive structure diagnostic hierarchical key for chlorogenic acids structure elucidation has been established, which allows reliable determination of chlorogenic acids regiochemistry even for minor component chlorogenic acids from tandem MS data exclusively. The basis of these differences in fragment MS spectra was rationalized in terms of different hydrogen-bonding arrays found in gas-phase ions of regioisomeric

chlorogenic acids. In this study, we investigated methods for the chromatographic resolution and mass spectrometric characterization of all 10 isomers of caffeoylglucose present in yerba maté leaves (*Ilex paraguariensis*).

## MATERIALS AND METHODS

All of the chemicals were purchased from Sigma-Aldrich, Carl-Roth, and Iris Biotech (Bremen, Germany). Green dried maté leaves (of Argentinian origin) and kiwi fruit (of Italian origin) were purchased from a supermarket in Bremen, Germany.

**Methanolic Extract of Yerba Maté.** Yerba maté leaves (5 g) were ground to a fine powder and extracted with 70% aqueous methanol (100 mL) using ultrasonication for 30 min. This extract was filtered through a Whatman no. 1 filter paper. The methanol and the water were removed in vacuo, and the residue was stored at −20 °C until required, thawed at room temperature, dissolved in methanol (50 mg/10 mL), filtered through a membrane filter, and then used for LC−MS.

**LC−MS$^n$.** The LC equipment (1100 Series, Agilent, Karlsruhe, Germany) comprised a binary pump, an auto sampler with a 100 μL loop, and a DAD detector with a light-pipe flow cell, recording at 320 nm and scanning from 200 to 600 nm. This was interfaced with an ion-trap mass spectrometer fitted with an ESI source (HCT-Ultra, Bruker Daltonics, Bremen, Germany) operating in full scan, auto MS$^n$ mode to obtain fragment ion $m/z$ values. As necessary, MS$^2$, MS$^3$, and MS$^4$ fragment-targeted experiments were performed to focus only on compounds producing a pseudomolecular ion at $m/z$ 341. Tandem mass spectra were acquired in the auto-MS$^n$ mode (smart fragmentation) using a ramping of the collision energy. Maximum fragmentation amplitude was set to 1 V, starting at 30% and ending at 200%. The MS operating conditions (negative ion mode) had been optimized using 3-caffeoylglucoses (**5** and **6**) and 6-caffeoylglucoses (**9** and **10**) with a capillary temperature of 365 °C, a drying gas flow rate of 10 L/min, and a nebulizer pressure of 10 psi. High-resolution LC−MS was carried out using the same HPLC equipped with a high-resolution mass spectrometer (MicrOTOF Focus, Bruker Daltonics, Bremen, Germany) fitted with an ESI source, and internal calibration was achieved with 10 mL of a 0.1 M sodium formate solution injected through a six-port valve prior to each chromatographic run. Calibration was carried out using the enhanced quadratic mode, and the mass error was below 5 ppm.

**HPLC.** Separation was achieved on a 250 × 3 mm i.d. column containing 5 μm C18 amide, with a 5 mm × 3 mm inner-diameter guard column (Varian, Darmstadt, Germany). Solvent A was water/formic acid (1000:0.005 v/v), and solvent B was methanol. Solvents were delivered at a total flow rate of 500 μL/min. In the first HPLC method, the gradient profile was from 10% B to 70% B linearly in 60 min followed by 10 min isocratic and a return to 10% B at 90 min and finally 10 min isocratic to re-equilibrate. In the second HPLC method, 10% B was used isocratically for 80 min.

**NMR.** $^1$H and $^{13}$C NMR spectra were recorded on a JEOL-ECX 400 spectrometer operating at 400 MHz for $^1$H NMR and 100 MHz for $^{13}$C NMR at room temperature in $CDCl_3$, acetone-$d_6$, or methanol-$d_4$ using a 5 mm probe. The chemical shifts ($\delta$) are reported in ppm and were referenced to the residual solvent peak. The coupling constants ($J$) are quoted in hertz.

**Synthesis.** All synthetic procedures and spectroscopic data for intermediates, reference compounds, equilibration of anomers, and synthesis of mixtures of isomers are given below, employing strategies similar to those published before.[32,33]

**Synthesis of 3-*O*-Caffeoylglucoses (5 and 6).** To a solution of 1,2:5,6-di-*O*-isopropylidene-α-D-glucofuranose (1.00 g, 3.84 mmol) and 4-dimethylaminopyridine (200 mg, 1.63 mmol) in $CH_2Cl_2$ (50 mL) were added triethylamine (10 mL, 71.70 mmol) and 3,4-di-*O*-allylcaffeoyl chloride (1.58 g, 5.70 mmol)[32] at room temperature. The reaction mixture was refluxed for 24 h, cooled to room temperature, and acidified (pH ≈ 3) with 2 M HCl. The layers were separated, and the aqueous phase was extracted with $CH_2Cl_2$ (3 × 50 mL). The combined organic layers were dried over sodium sulfate, filtered, and the solvent was removed in vacuo. The crude product was purified by column chromatography on silica gel (ethyl acetate−petroleum ether, 30−50%) to give 3-*O*-(3,4-di-*O*-allyl)caffeoyl-1,2:5,6-di-*O*-isopropylidene-α-D-glucofuranose (75%) (Figure 2).

$\delta_H$ ($CDCl_3$): 7.61 (1H, d, *J* 16.0, $C_{Ar}$−C*H*), 7.11 (1H, dd, *J* 8.2, 1.9, $C_{Ar}H$), 7.09 (1H, d, *J* 1.7, $C_{Ar}H$), 6.87 (1H, d, *J* 8.2, $C_{Ar}H$), 6.24 (1H, d, *J* 15.5, $C_{Ar}$−CH=C*H*), 6.06 (2H, m, $CH_2$=C*H*), 5.90 (1H, d, *J* 3.6, *H*-3), 5.39 (2H, d, *J* 16.9, C*H*H=CH), 5.37 (1H, d, *J* 2.3, *H*-1), 5.31 (2H, d, *J* 9.6, CH*H*=CH), 4.64 (4H, m, $C_{Ar}$−OC$H_2$), 4.56 (1H, d, *J* 3.7, *H*-2), 4.28 (2H, m, *H*-6a, *H*-6b), 4.07 (2H, m, *H*-4, *H*-5), 1.53 (3H, s, OC$H_3$), 1.41 (3H, s, OC$H_3$), 1.30 (6H, s, OC$H_3$). $\delta_C$ ($CDCl_3$): 165.8 (−COOC), 151.1 ($C_{Ar}$−$OCH_2$), 148.6 ($C_{Ar}$−$OCH_2$), 146.0 ($C_{Ar}$−CH), 133.0 ($CH_2$=CH), 132.8 ($CH_2$=CH), 127.2 ($C_{Ar}$−CH), 123.1 ($C_{Ar}$), 118.1 ($CH_2$=CH), 114.7 (CH−COO), 113.4 ($C_{Ar}$), 112.7 ($C_{Ar}$), 112.3 ($H_3C$−O−*C*−O−$CH_3$), 109.4 ($H_3C$−O−C−O−$CH_3$), 105.1 (*C*-3), 83.5 (*C*-1), 79.8 (*C*-6), 75.9 (*C*-2), 72.7 (*C*-4), 70.0 ($C_{Ar}$−$OCH_2$), 69.7 ($C_{Ar}$−$OCH_2$), 67.2 (*C*-5), 26.9 ($OCH_3$), 26.8 ($OCH_3$), 26.2 ($OCH_3$), 25.3 ($OCH_3$).

To a solution of 3-*O*-(3,4-di-*O*-allyl)caffeoyl-1,2:5,6-di-*O*-isopropylidene-α-D-glucofuranose (1.00 g, 2.05 mmol) and *p*-toluenesulfonic acid (50 mg) in methanol−water (9:1, 50 mL) was added 10% Pd/C (300 mg) at room temperature. The reaction mixture was refluxed for 48 h, cooled to room temperature, filtered, and methanol was removed in vacuo. The aqueous reaction mixture was extracted with ethyl acetate (3 × 50 mL). The combined organic layers were dried over sodium sulfate, filtered, and the solvent was removed in vacuo. The crude product was purified by column chromatography on silica gel (ethyl acetate-petroleum ether, 50−95%) to give a mixture of 3-*O*-caffeoyl-1,2:5,6-di-*O*-isopropylidene-α-D-glucofuranose, 3-*O*-caffeoyl-1,2-*O*-isopropylidene-α-D-glucofuranose, and 3-*O*-caffeoyl-5,6-*O*-isopropylidene-α-D-glucofuranose (Figure 2).

The resulting mixture of the esters (500 mg) was dissolved in a mixture of 20 mL of trifluoroacetic acid and water (8:2) at room temperature and stirred for 1 h. The solvents were removed in vacuo to obtain the resulting esters 3-*O*-caffeoylglucoses (**5** and **6**) in quantitative yield (Figure 2).

$\delta_H$ (methanol-$d_3$): 7.51 (1H, d, *J* 16.0, $C_{Ar}$−C*H*), 7.03 (1H, s, $C_{Ar}$−*H*), 6.92 (1H, d, *J* 8.2, $C_{Ar}$−*H*), 6.77 (1H, d, *J* 8.2, $C_{Ar}$−*H*), 6.32 (1H, *J* 16.0, $C_{Ar}$−CH=*CH*), 5.31 (1H, t, *J* 9.6, α-gluc *H*-3), 5.15 (1H, *J* 3.2, α-gluc *H*-3), 5.02 (1H, t, *J* 9.6, β-gluc *H*-3), 4.59 (1H, t, *J* 7.8, β-gluc *H*-1), 3.60−3.90 (2H, m, gluc *H*-6a, gluc *H*-6b), 3.24−3.57 (3H, m, gluc *H*-2, gluc *H*-4, gluc *H*-5). $\delta_C$ (methanol-$d_3$): 168.1 (COOR), 148.1 ($C_{Ar}$), 145.6 ($C_{Ar}$-CH), 145.5 ($C_{Ar}$), 126.5 ($C_{Ar}$), 121.5 ($C_{Ar}$), 115.0 ($CH_2$=CH), 114.1 (CH−COO), 114.0 ($CH_2$=*C*H), 96.8 (β-gluc *C*-1), 92.6 (α-gluc *C*-1), 77.7 (β-gluc *C*-3), 76.5 (α-gluc *C*-3), 75.7 (β-gluc *C*-2), 75.5 (β-gluc *C*-5), 73.4 (α-gluc *C*-2), 71.5 (α-gluc *C*-5), 70.9 (α-gluc *C*-4), 68.6 (β-gluc *C*-4), 61.4 (β-gluc *C*-6), 61.1 (α-gluc *C*-6).

**Synthesis of 6-*O*-Caffeoylglucoses (9 and 10).** To a solution of 1,2-*O*-isopropylidene-α-D-glucofuranose (1.00 g, 4.54 mmol) and 4-dimethylaminopyridine (200 mg, 1.63 mmol) in $CH_2Cl_2$ (50 mL) were added pyridine (5 mL, 62 mmol) and 3,4-di-*O*-allylcaffeoyl chloride (1.58 g, 5.70 mmol)[32] at room temperature. The reaction mixture was stirred for 24 h at room temperature and acidified (pH ≈ 3) with 2 M HCl. The layers were separated, and the aqueous phase was extracted with $CH_2Cl_2$ (3 × 50 mL). The combined organic layers were dried over sodium sulfate, filtered, and the solvent was removed in vacuo. The crude product was purified by column chromatography on silica gel (ethyl acetate−petroleum ether, 30−50%) to give 6-*O*-(3,4-di-*O*-allyl)caffeoyl-1,2-*O*-isopropylidene-α-D-glucofuranose (80%) (Figure 2).

$\delta_H$ (acetone-$d_6$): 7.62 (1H, d, *J* 15.6, $C_{Ar}$−C*H*), 7.32 (1H, dd, *J* 1.8, $C_{Ar}H$), 7.17 (1H, dd, *J* 8.7, 2.3 $C_{Ar}H$), 6.99 (1H, d, *J* 8.2, $C_{Ar}H$), 6.41 (1H, d, *J* 16.0, $C_{Ar}$−CH=C*H*), 6.08 (2H, m, $CH_2$=C*H*), 5.85 (1H, d, *J* 3.6, *H*-3), 5.43 (2H, m, C*H*HCH), 5.23 (2H, m, CH*H*=CH), 4.65 (4H, m, $C_{Ar}$−OC$H_2$), 4.49 (1H, d, *J* 3.7, *H*-2), 4.31 (2H, m, *H*-6a, *H*-6b), 4.12 (2H, m, *H*-4, *H*-5), 1.39 (3H, s, OC$H_3$), 1.24 (3H, s, OC$H_3$). $\delta_C$ (acetone-$d_6$): 166.6 (−COOC), 150.9 ($C_{Ar}$−$OCH_2$), 148.9 ($C_{Ar}$−$OCH_2$), 144.5 ($C_{Ar}$−CH), 133.9 ($CH_2$=CH), 133.5 ($CH_2$=CH), 127.7 ($C_{Ar}$−CH), 122.9 ($C_{Ar}$), 116.9 ($CH_2$=CH), 116.5

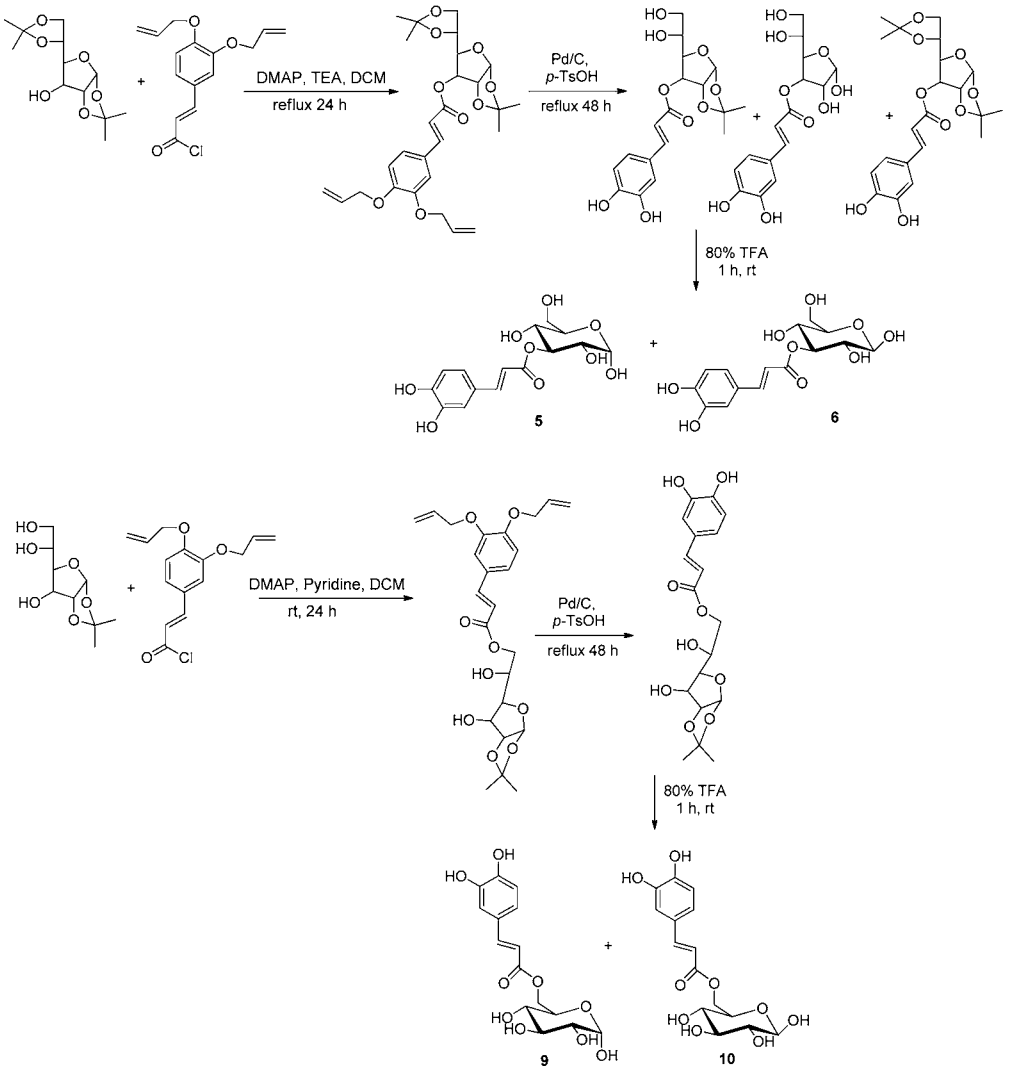


**Figure 2.** Synthesis pathway of 3-caffeoylglucoses (**5** and **6**) and 6-caffeoylglucoses (**9** and **10**).

(CH−COO), 115.7 ($C_{Ar}$), 113.7 ($C_{Ar}$), 112.6 ($H_3C-O-C-O-CH_3$), 111.2 ($H_3C-O-C-O-CH_3$), 105.0 (*C*-3), 85.3 (*C*-6), 80.4 (*C*-1), 74.4 (*C*-2), 69.4 (*C*-4), 69.2 ($C_{Ar}-OCH_2$), 67.1 ($C_{Ar}-OCH_2$), 66.8 (*C*-5), 26.4 ($OCH_3$), 25.6 ($OCH_3$).

To a solution of 6-*O*-(3,4-di-*O*-allyl)caffeoyl-1,2-*O*-isopropylidene-*α*-D-glucofuranose (1.00 g, 2.23 mmol) and *p*-TsOH (50 mg) in methanol−water (9:1, 50 mL) was added 10% Pd/C (350 mg) at room temperature. The reaction mixture was heated at 70 °C for 48 h, cooled to room temperature, filtered, and methanol was removed in vacuo. The aqueous reaction mixture was extracted with ethyl acetate (3 × 50 mL). The combined organic layers were dried over sodium sulfate, filtered, and the solvent was removed in vacuo. The crude product was purified by column chromatography on silica gel (ethyl acetate−petroleum ether, 50−95%) to give 6-*O*-caffeoyl-1,2-*O*-isopropylidene-*α*-D-glucofuranose (62%). The resulting ester 6-*O*-caffeoyl-1,2-*O*-isopropylidene-*α*-D-glucofuranose (400 mg, 1.10 mmol) was dissolved in a mixture of 20 mL of trifluoroacetic acid and water (8:2) at room temperature and stirred for 1 h. The solvents were removed in vacuo to obtain the resulting esters 6-*O*-caffeoylglucoses (**9** and **10**) in quantitative yield (Figure 2).

$\delta_H$ (methanol-$d_3$): 7.54 (1H, d, *J* 16.0, $C_{Ar}-CH$), 7.02 (1H, d, *J* 2.2, $C_{Ar}-H$), 6.92 (1H, dd, *J* 8.2, 1.4, $C_{Ar}-H$), 6.75 (1H, d, *J* 8.2, $C_{Ar}-H$), 6.25 (1H, *J* 16.5, $C_{Ar}-CH=CH$), 5.10 (1H, d, *J* 3.7, gluc *H*-1), 4.45 (1H, m, gluc *H*-6a), 4.30 (1H, m, gluc *H*-6b), 4.05 (1H, m, gluc *H*-4), 3.28−3.37 (2H, m, gluc *H*-2, gluc *H*-5). $\delta_C$ (methanol-$d_3$): 167.9 (COOC), 148.3 ($C_{Ar}$), 145.8 ($C_{Ar}-CH$), 145.5 ($C_{Ar}$), 126.4 ($C_{Ar}$), 123.6 ($C_{Ar}$), 121.6 ($C_{Ar}$), 115.2 ($CH_2=CH$), 113.7 (CH−COO), 113.6 ($CH_2=CH$), 96.8 (*β*-gluc *C*-1), 92.6 (*α*-gluc *C*-1), 76.7 (*β*-gluc *C*-3), 74.9 (*β*-gluc *C*-2), 74.1 (*β*-gluc *C*-5), 73.5 (*α*-gluc *C*-3), 72.2 (*α*-gluc *C*-2), 71.6 (*α*-gluc *C*-5), 70.4 (*α*-gluc *C*-4), 69.6 (*β*-gluc *C*-4), 63.6 (*β*-gluc *C*-6), 63.5 (*α*-gluc *C*-6).

**Synthesis of Stereo- and Regioisomeric Mixture of Caffeoylglucoses (1−6).** To a solution of 4,6-*O*-benzylidene-D-glucopyranose (268 mg, 1.00 mmol) and 4-dimethylaminopyridine (50 mg, 0.04 mmol) in $CH_2Cl_2$ (20 mL) were added pyridine (3 mL) and 3,4-di-*O*-acetylcaffeoyl chloride (387 mg, 1.38 mmol) at room temperature. The reaction mixture was stirred for 10 h and acidified with 1 M HCl (pH ≈ 3). The layers were separated, and the aqueous phase was re-extracted with ethyl acetate (2 × 20 mL). The combined organic layers were dried over $Na_2SO_4$ and filtered, and the solvents were dried in vacuo. The resulting esters were dissolved in a mixture of 20 mL of trifluoroacetic acid and water (7:3) at room temperature and stirred for 30 min. The solvents were removed in vacuo, and the resulting yellowish product was analyzed by HPLC−MS and shown to contain a mixture of caffeoylglucoses **1**−**6** (Figure 3).

**Synthesis of Stereo- and Regioisomeric Mixture of Caffeoylglucoses (1−10).** To a solution of D-glucose (180 mg, 1.00 mmol) and 4-dimethylaminopyridine (50 mg, 0.04 mmol) in $CH_2Cl_2$ (20 mL) were added pyridine (3 mL) and 3,4-di-*O*-acetylcaffeoyl chloride (387 mg, 1.38 mmol) at room temperature. The reaction mixture was stirred for 10 h and acidified with 1 M HCl (pH ≈ 3). The layers were separated, and the aqueous phase was re-extracted with ethyl acetate (2 × 20 mL). The combined organic layers were dried over $Na_2SO_4$ and filtered, and the solvents were dried in vacuo. The resulting


dx.doi.org/10.1021/jf501210s | J. Agric. Food Chem. 2014, 62, 9252−9265

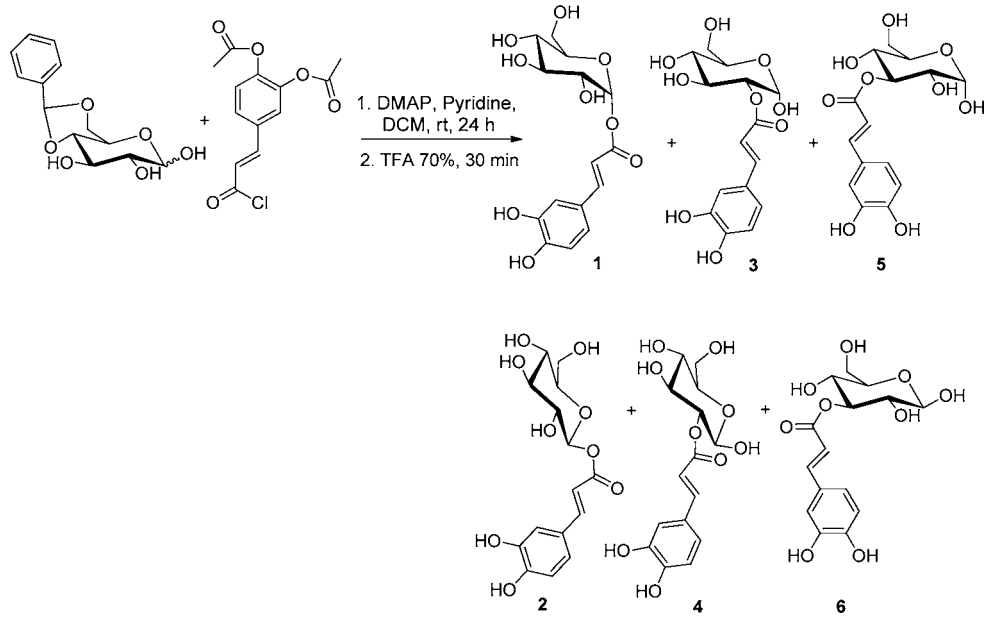


**Figure 3.** Synthesis pathway of 1-caffeoylglucoses, 2-caffeoylglucoses, and 3-caffeoylglucoses (**1**−**6**).

esters were dissolved in a mixture of 20 mL of trifluoroacetic acid and water (7:3) at room temperature and stirred for 30 min. The solvents were removed in vacuo, and the resulting yellowish product was analyzed by HPLC−MS and shown to contain a mixture of caffeoylglucoses **1**−**10** (Figure 4).

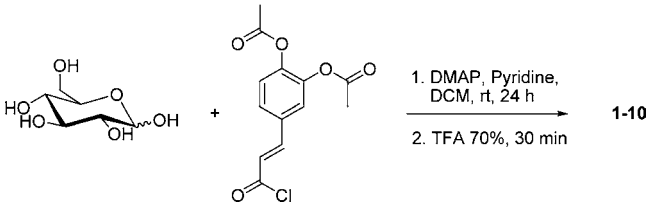


**Figure 4.** Synthesis pathway of regio- and stereoisomers of caffeoylglucose (**1**−**10**).

**Synthesis of 3-*O*-(3,4-Dimethoxy)cinnamoylglucoses (13 and 14).** To a solution of 1,2:5,6-di-*O*-isopropylidene-*α*-D-glucofuranose (1.00 g, 3.84 mmol) and 4-dimethylaminopyridine (200 mg, 1.63 mmol) in $CH_2Cl_2$ (50 mL) were added triethylamine (10 mL, 71.70 mmol) and 3,4-dimethoxycinnamoyl chloride (1.29 g, 5.70 mmol) at room temperature. The reaction mixture was refluxed for 24 h, cooled to room temperature, and acidified (pH ≈ 3) with 2 M HCl. The layers were separated, and the aqueous phase was extracted with $CH_2Cl_2$ (3 × 50 mL). The combined organic layers were dried over sodium sulfate, filtered, and the solvent was removed in vacuo. The crude product was purified by column chromatography on silica gel (ethyl acetate−petroleum ether, 30−40%) to give 3-*O*-(3,4-dimethoxy)cinnamoyl-1,2:5,6-di-*O*-isopropylidene-*α*-D-glucofuranose (80%).

$\delta_H$ ($CDCl_3$): 7.63 (1H, d, *J* 16.0, $C_{Ar}$−C*H*), 7.09 (1H, dd, *J* 9.0, 1.8 $C_{Ar}H$), 7.02 (1H, d, *J* 1.8, $C_{Ar}H$), 6.85 (1H, d, *J* 8.2, $C_{Ar}H$), 6.28 (1H, d, *J* 16.0, $C_{Ar}$−CHC*H*), 5.90 (1H, d, *J* 3.6, *H*-3), 5.37 (1H, d, *J* 2.7, *H*-1), 4.55 (1H, d, *J* 3.7, *H*-2), 4.28 (2H, m, *H*-6a, *H*-6b), 4.07 (2H, m, *H*-4, *H*-5), 3.90 (6H, s, $C_{Ar}$-O$CH_3$), 1.52 (3H, s, O$CH_3$), 1.40 (3H, s, O$CH_3$), 1.29 (6H, s, O$CH_3$). $\delta_C$ ($CDCl_3$): 165.8 (−COOC), 151.5 ($C_{Ar}$−$OCH_2$), 149.3 ($C_{Ar}$−$OCH_2$), 146.0 ($C_{Ar}$−CH), 127.1 ($C_{Ar}$−CH), 123.1 ($C_{Ar}$), 114.7 (CH−COO), 112.4 ($C_{Ar}$), 111.1 ($C_{Ar}$), 109.6 ($H_3C$−O−*C*−O−$CH_3$), 109.3 ($H_3C$−O−*C*−O−$CH_3$), 105.1 (*C*-3), 83.5 (*C*-1), 79.8 (*C*-6), 76.0 (*C*-2), 72.6 (*C*-4), 67.1 (*C*-5), 56.1 ($C_{Ar}$−O$CH_3$), 56.0 ($C_{Ar}$−O$CH_3$), 26.9 (O$CH_3$), 26.8 (O$CH_3$), 26.4 (O$CH_3$), 25.6 (O$CH_3$).

The resulting mixture of the esters (500 mg) was dissolved in a mixture of 20 mL of trifluoroacetic acid and water (8:2) at room temperature and stirred for 1 h. The solvents were removed in vacuo to obtain the resulting esters 3-*O*-(3,4-dimethoxy)cinnamoylglucoses (**13** and **14**) in quantitative yield.

$\delta_H$ (methanol-$d_3$): 7.65 (1H, d, *J* 16.0, $C_{Ar}$−C*H*), 7.19 (1H, s, $C_{Ar}$−*H*), 7.15 (1H, d, *J* 8.2, $C_{Ar}$−*H*), 6.95 (1H, d, *J* 8.2, $C_{Ar}$−*H*), 6.45 (1H, *J* 16.0, $C_{Ar}$−C*H*═*CH*), 5.32 (1H, t, *J* 9.6, *α*-gluc *H*-3), 5.15 (1H, *J* 3.2, *α*-gluc *H*-1), 5.02 (1H, t, *J* 9.6, *β*-gluc *H*-3), 4.59 (1H, d, *J* 7.8, *β*-gluc *H*-1), 3.65−3.90 (2H, m, gluc *H*-6a, gluc *H*-6b), 3.24−3.57 (3H, m, gluc *H*-2, gluc *H*-4, gluc *H*-5).

$\delta_C$ (methanol-$d_3$): 167.8, 167.6 (COOR); 151.4, 151.3 ($C_{Ar}$); 145.0 ($C_{Ar}$−CH); 148.1, 144.9 ($C_{Ar}$); 127.6, 127.5 ($C_{Ar}$); 122.6, 122.5 ($C_{Ar}$); 115.6 ($CH_2$═CH); 115.5 (CH−COO); 114.0 ($CH_2$═CH); 111.29, 110.16 ($C_{Ar}$−$OCH_3$); 96.9 (*β*-gluc *C*-1); 92.6 (*α*-gluc *C*-1); 77.8 (*β*-gluc *C*-3); 76.5 (*α*-gluc *C*-3); 75.8 (*β*-gluc *C*-2); 75.5 (*β*-gluc *C*-5); 73.4 (*α*-gluc *C*-2); 71.6 (*α*-gluc *C*-5); 70.9 (*α*-gluc *C*-4); 68.6 (*β*-gluc *C*-4); 61.3 (*β*-gluc *C*-6); 61.1 (*α*-gluc *C*-6).

**Synthesis of 6-*O*-(3,4-Dimethoxy)cinnamoylglucoses (15 and 16).** To a solution of 1,2-*O*-isopropylidene-*α*-D-glucofuranose (1.00 g, 4.54 mmol) and 4-dimethylaminopyridine (200 mg, 1.63 mmol) in $CH_2Cl_2$ (50 mL) were added pyridine (5 mL, 62 mmol) and 3,4-dimethoxycinnamoyl chloride (1.29 g, 5.7 mmol) at room temperature. The reaction mixture was stirred for 24 h at room temperature and acidified (pH ≈ 3) with 2 M HCl. The layers were separated, and the aqueous phase was extracted with $CH_2Cl_2$ (3 × 50 mL). The combined organic layers were dried over sodium sulfate, filtered, and the solvent was removed in vacuo. The crude product was purified by column chromatography on silica gel (ethyl acetate−petroleum ether, 30−40%) to give 6-*O*-(3,4-di-*O*-allyl)caffeoyl-1,2-*O*-isopropylidene-*α*-D-glucofuranose (75%).

$\delta_H$ (acetone-$d_6$): 7.68 (1H, d, *J* 16.0, $C_{Ar}$−C*H*), 7.32 (1H, dd, *J* 8.2, 1.8, $C_{Ar}H$), 7.17 (1H, d, *J* 1.8, $C_{Ar}H$), 6.86 (1H, d, *J* 8.2, $C_{Ar}H$), 6.33 (1H, d, *J* 16.0, $C_{Ar}$−CHC*H*), 5.97 (1H, d, *J* 3.6, *H*-3), 4.54 (1H, d, *J* 3.6, *H*-2), 4.31−4.40 (2H, m, *H*-6a, *H*-6b), 4.12 (2H, m, *H*-4, *H*-5), 3.90 (6H, s, $C_{Ar}$−O$CH_3$), 1.48 (3H, s, O$CH_3$), 1.31 (3H, s, O$CH_3$). $\delta_C$ (acetone-$d_6$): 168.2 (−COOC), 151.6 ($C_{Ar}$−$OCH_2$), 149.2 ($C_{Ar}$−$OCH_2$), 146.3 ($C_{Ar}$−CH), 127.2 ($C_{Ar}$−CH), 122.9 ($C_{Ar}$), 114.9 ($CH_2$═CH), 114.8 (CH−COO), 111.9 ($C_{Ar}$), 111.2 ($C_{Ar}$), 111.1 ($H_3C$−O−*C*−O−$CH_3$), 109.6 ($H_3C$−O−*C*−O−$CH_3$), 105.2 (*C*-3), 85.2 (*C*-6), 79.6 (*C*-1), 75.6 (*C*-2), 69.8 (*C*-4), 66.5 (*C*-5), 55.8 ($C_{Ar}$−$OCH_3$), 55.9 ($C_{Ar}$−$OCH_3$), 26.9 (O$CH_3$), 26.2 (O$CH_3$).

The resulting ester 6-*O*-(3,4-dimethoxy)cinnamoyl-1,2-*O*-isopropylidene-*α*-D-glucofuranose (400 mg) was dissolved in a mixture of 20 mL of

trifluoroacetic acid and water (8:2) at room temperature and stirred for 1 h. The solvents were removed in vacuo to obtain the resulting esters 6-*O*-(3,4-dimethoxy)cinnamoylglucoses (**15** and **16**) in quantitative yield.

$\delta_H$ (methanol-$d_3$): 7.55, 7.54 (1H, d, *J* 16.0, $C_{Ar}$–C*H*); 7.33 (1H, s, $C_{Ar}$–*H*); 7.20 (1H, d, *J* 8.2, $C_{Ar}$–*H*); 6.94 (1H, d, *J* 8.2, $C_{Ar}$–*H*); 6.55, 6.54 (1H, *J* 16.5, $C_{Ar}$–C*H*═C*H*); 4.88, 4.28 (1H, d, *J* 3.7, gluc *H*-1$\alpha$, 7.6, gluc *H*-1$\beta$); 4.37, 4.38 (1H, m, gluc *H*-6a); 4.10, 4.15 (1H, m, gluc *H*-6b); 3.77 (3H, s, $OCH_3$); 3.75 (3H, s, $OCH_3$); 3.41, 3.35 (1H, m, gluc *H*-4); 3.1 (2H, m, gluc *H*-2, *H*-3), 2.9 (1H, t, *J* 8.2, gluc *H*-5).

$\delta_C$ (methanol-$d_3$): 167.9 (COOC), 151.5 ($C_{Ar}$), 149.5 ($C_{Ar}$–CH), 145.5 ($C_{Ar}$), 127.4 ($C_{Ar}$), 123.6 ($C_{Ar}$), 115.9 ($CH_2$═CH), 112.0 (CH–COO), 110.8 ($CH_2$═CH), 97.4 ($\beta$-gluc *C*-1), 92.9 ($\alpha$-gluc *C*-1), 76.9 ($\beta$-gluc *C*-3), 75.2 ($\beta$-gluc *C*-2), 74.1 ($\beta$-gluc *C*-5), 73.4 ($\alpha$-gluc *C*-3), 72.7 ($\alpha$-gluc *C*-2), 71.1 ($\alpha$-gluc *C*-5), 70.6 ($\alpha$-gluc *C*-4), 69.7 ($\beta$-gluc *C*-4), 64.5 ($\beta$-gluc *C*-6), 64.4 ($\alpha$-gluc *C*-6), 56.2 ($OCH_3$), 56.1 ($OCH_3$).

**Synthesis of 2-*O*-(3,4-Dimethoxy)cinnamoylglucoses (17 and 18).** To a solution of 4,6-*O*-benzylidene-D-glucopyranose (268 mg, 1.00 mmol) and 4-dimethylaminopyridine (50 mg, 0.04 mmol) in $CH_2Cl_2$ (20 mL) were added pyridine (3 mL) and 3,4-dimethoxycinnamoyl chloride (312 mg, 1.38 mmol) at room temperature. The reaction mixture was stirred for 24 h and acidified with 1 M HCl (pH ≈ 3). The layers were separated, and the aqueous phase was re-extracted with ethyl acetate (2 × 20 mL). The combined organic layers were dried over $Na_2SO_4$ and filtered, and the solvents were dried in vacuo. The crude product was purified by column chromatography on silica gel (ethyl acetate–petroleum ether, 30–40%) to give 2-*O*-(3,4-dimethoxy)cinnamoyl-4,6-*O*-benzylidene-D-glucopyranose (25%). 2-*O*-(3,4-Dimethoxy)cinnamoyl-4,6-*O*-benzylidene-D-glucopyranose (100 mg) was dissolved in a mixture of 20 mL of trifluoroacetic acid and water (7:3) at room temperature and stirred for 30 min. The solvents were removed in vacuo, and the resulting yellowish product was analyzed by HPLC–MS and shown to contain a mixture of 2-*O*-(3,4-dimethoxy)cinnamoylglucoses **17** and **18**.

$\delta_H$ (methanol-$d_3$): 7.68, 7.64 (1H, d, *J* 16.0, $C_{Ar}$–C*H*); 7.19 (1H, s, $C_{Ar}$–*H*); 7.15 (1H, m, *J* 8.2, $C_{Ar}$–*H*); 6.95 (1H, d, *J* 8.2, $C_{Ar}$–*H*); 6.45, 6.42 (1H, *J* 16.0, $C_{Ar}$–C*H*═C*H*); 5.30 (1H, t, *J* 9.6, gluc *H*-2); 4.73 (1H, *J* 3.2, $\alpha$-gluc *H*-1); 4.65 (1H, m, *H*-3); 3.84 (6H, $C_{Ar}$–OCH3); 3.70–3.80 (2H, m, gluc *H*-6a, gluc *H*-6b); 3.56 (1H, m, gluc *H*-4); 3.30–3.40 (1H, m, gluc *H*-5).

$\delta_C$ (methanol-$d_3$): 167.2, 166.8 (COOR); 151.6, 151.5 ($C_{Ar}$); 145.0 ($C_{Ar}$–CH); 145.3 ($C_{Ar}$), 145.1 ($C_{Ar}$); 127.6, 127.4 ($C_{Ar}$); 122.7, 122.6 ($C_{Ar}$); 115.3 ($CH_2$═CH); 115.3 (CH–COO); 114.9 ($CH_2$═CH); 111.4, 110.2 ($C_{Ar}$-$OCH_3$); 95.4 ($\beta$-gluc *C*-1); 90.2 ($\alpha$-gluc *C*-1); 77.1 ($\beta$-gluc *C*-3); 75.4 ($\alpha$-gluc *C*-3); 75.0 ($\beta$-gluc *C*-2); 74.1 ($\beta$-gluc *C*-5); 71.7 ($\alpha$-gluc *C*-2); 70.9 ($\alpha$-gluc *C*-5); 70.7 ($\alpha$-gluc *C*-4); 70.4 ($\beta$-gluc *C*-4); 61.4 ($\beta$-gluc *C*-6); 61.3 ($\alpha$-gluc *C*-6).

**Synthesis of Stereo- and Regioisomeric Mixture of 3,4-Dimethoxycinnamoylglucoses (13–20).** To a solution of 4,6-*O*-benzylidene-D-glucopyranose (268 mg, 1.00 mmol) and 4-dimethylaminopyridine (50 mg, 0.04 mmol) in $CH_2Cl_2$ (20 mL) were added pyridine (3 mL) and 3,4-dimethoxycinnamoyl chloride (312 mg, 1.38 mmol) at room temperature. The reaction mixture was stirred for 24 h and acidified with 1 M HCl (pH ≈ 3). The layers were separated, and the aqueous phase was re-extracted with ethyl acetate (2 × 20 mL). The combined organic layers were dried over $Na_2SO_4$ and filtered, and the solvents were dried in vacuo. The resulting esters were dissolved in a mixture of 20 mL of trifluoroacetic acid and water (7:3) at room temperature and stirred for 30 min. The solvents were removed in vacuo, and the resulting yellowish product was analyzed by HPLC–MS and shown to contain a mixture of 3,4-dimethoxycinnamoylglucoses **13–20**.

## RESULTS AND DISCUSSION

The aqueous infusion of yerba maté was reported to be particularly rich in caffeoylglucoses[6,14] and therefore served as a model system for our investigations. In a typical extracted ion chromatogram (EIC) of an aqueous methanolic yerba maté extract, using a reversed phase LC–MS method, we observed 10 peaks with a *m*/*z* value of 341.0867 ± 0.005 (M–H, $C_{15}H_{17}O_9$) and $MS^2$ consistent with a caffeoyl ester of glucose. To assign the regio- and stereochemistry of the caffeoylglucoses, we first required authentic reference substances, both of individual compounds and of a mixture of possibly all 10 isomeric compounds, **1–10**, and an LC-method capable of resolving all 10 isomers.

A mixture comprising of all 10 isomeric caffeoylglucoses was obtained by reacting acetyl protected caffeoyl chloride with D-glucose, followed by trifluoroacetic acid mediated deprotection of the acetyl groups (Figure 4). For the analysis of the mixture, we optimized two complementary chromatographic methods. In the first method, baseline separation of seven isomers could be achieved. The remaining three isomers coeluted. In the second method, we achieved resolution of all 10 isomers, however, for four chromatographic peaks not to a baseline separation level. Therefore, the first method is suitable for the quantitation of 7 of the 10 isomeric compounds, whereas the second method is suitable for compound identification and structure assignment. Typical extracted ion chromatograms are shown in Figure 5.

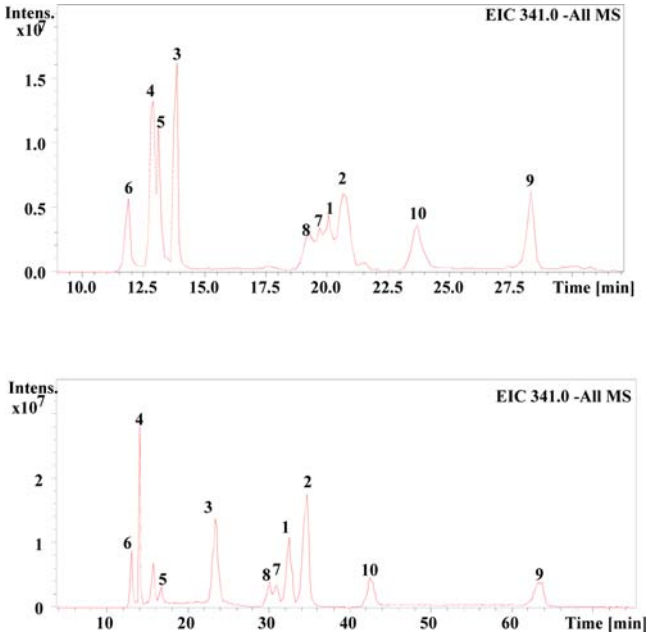


**Figure 5.** Extracted ion chromatograms (EICs) of regio- and stereoisomers of caffeoylglucose (**1–10**) at *m*/*z* 341 obtained by two different chromatographic methods.

Following the synthesis of a mixture of all 10 isomeric caffeoylglucoses, we embarked on a series of selective syntheses of caffeoylglucose regioisomers and dimethoxycinnamoylglucose isomers. In the first case, we employed diallylcaffeoyl chloride as the caffeic acid building block, while in the latter case we employed dimethoxycinnamoyl chloride. Using a selection of appropriately protected glucose derivatives, we could obtain 6-caffeoylglucoses (**9** and **10**),[32,33] 6-dimethoxycinnamoylglucoses (**15** and **16**), 3-caffeoylglucoses (**5** and **6**), 3- dimethoxycinnamoylglucoses (**13** and **14**), and 2-dimethoxycinnamoylglucoses (**17** and **18**), each as mixtures of $\alpha/\beta$ anomers (Figures 2 and 3). All of the compounds were characterized by NMR spectroscopy with 2-D NMR experiments clearly confirming the position of the caffeoyl and dimethoxycinnamoyl ester. A $\beta$-stereochemistry was assigned on the basis of the characteristic $^3J_{HCCH}$ coupling constant between the anomeric hydrogen at the hydrogen at C-2 of glucose, with $\alpha$-caffeoylglucoses showing values between


dx.doi.org/10.1021/jf501210s | J. Agric. Food Chem. 2014, 62, 9252–9265

3 and 4 Hz and β-caffeoylglucoses values between 7 and 8 Hz.[33] On standing in methanol-$d_3$, the mixtures of both 3-caffeoylglucoses and 6-caffeoylglucoses equilibrated, to yield after 1 day exclusively the β-anomers. We explain this observation by dipole moment considerations. The β-anomer of glucose is reported to have a larger dipole moment if compared to the α-isomer and is thus favored in polar solvents, overriding the anomeric effect. Despite all attempts, we failed to obtain 1-caffeoylglucoses and 4-caffeoylglucoses in purified form.

Access to the pure β-anomers of 3-caffeoylglucose and 6-caffeoylglucose allowed us to demonstrate that the α-anomer with smaller dipole moment eluted later from a reversed phase packing than the β-anomer with larger dipole moment. It seems reasonable to expect this effect to apply also to the other regioisomers unless there is a tendency for the β-anomer to form an internal hydrogen bond.

It was similarly possible to synthesize a mixture of all 10 dimethoxycinnamoylglucose esters. Fortunately, it was possible to synthesize specifically 2-dimethoxycinnamoylglucose, 3-dimethoxycinnamoylglucose, 4-dimethoxycinnamoylglucose, and 6-dimethoxycinnamoylglucose (as pairs of anomers), and this allowed the two 1-dimethoxycinnamoylglucose anomers to be identified by default. The order of elution of 3-caffeoylglucose and 6-caffeoylglucose corresponded to the order of elution of 3-dimethoxycinnamoylglucose and 6-dimethoxycinnamoylglucose, and we have tentatively concluded that the elution order of the dimethoxycinnamoylglucose regioisomers can be used to predict the elution order of the caffeoylglucose regioisomers.

To assign the 1-caffeoylglucoses (**1** and **2**), 1-dimethoxycinnamoylglucoses (**19** and **20**), 4-caffeoylglucoses (**7** and **8**), and 4-dimethoxycinnamoylglucoses (**21** and **22**), we obtained two further synthetic mixtures from 4,6-benzylidene protected glucose. On reaction with diallylcaffeoyl chloride followed by Pd-mediated deallylation, a mixture of six isomers was obtained. We assumed that the mixture exclusively contained the anomeric pairs of 1-caffeoylglucose/1-dimethoxycinnamoylglucose, 2-caffeoylglucose/2-dimethoxycinnamoylglucose, and 3-caffeoylglucose/3-dimethoxycinnamoylglucose. Both 2-dimethoxycinnamoylglucoses and 3-dimethoxycinnamoylglucoses were previously obtained by selective synthesis and could thus be readily identified on the basis of their retention times and unique tandem MS data. The remaining pair of isomers obtained in this unselective synthesis must therefore be the two anomers of 1-dimethoxycinnamoylglucose. In the initial chromatogram showing all 10 isomeric compounds, eight have now been identified, from which follows automatically that the regiochemistry of the two remaining isomers must be assigned as the two anomers of 4-caffeoylglucose with the β-anomer eluting earlier than the α-anomer (Figure 5).

**Tandem Mass Spectrometry and Compound Assignment.** In chlorogenic acids chemistry, all four regioisomers of monocaffeoylquinic acids can be readily identified on the basis of their unique tandem mass spectra.[31] The differences in observed fragment ions were rationalized by taking into account different hydrogen-bonding motifs in the gas-phase ions, activating groups for fragmentation depending on their relative stereochemistry.

To rationalize the fragmentation behavior of caffeoylglucoses, we propose to transfer the same approach successfully employed in chlorogenic acids chemistry, assuming different hydrogen-bonding motifs of gas-phase anions, depending on compound stereo- and regiochemistry. In the following discussion, we report on the fragmentation patterns of all 10 compounds **1**−**10** grouped according to their similarity in fragmentation behavior (Figure 6 and Table 1). Fragment ion elemental composition was determined using high resolution $MS^2$ experiments shown in Table 2. The discussion on fragmentation mechanisms always assumes that in the gas phase, anions of caffeoylglucoses exist in their cyclic pyranose form. This is not self-evident because under basic conditions, such as those employed in anion chromatography, hexoses with a $pK_a$ value between 12 and 13 are deprotonated in basic media at the anomeric hydroxyl group followed by rapid ring opening to shift the chemical equilibrium toward the open-chain aldehyde. The latter, however, would result in destruction of the anomeric stereogenic center and consequently in identical fragment spectra for both α/β anomers, which was not consistently observed here with $MS^2$ spectra of both anomers sometimes showing significant and always showing subtle differences, nor in any other tandem MS studies on carbohydrate derivatives carried out, and justifies the assumption made above.

**Fragmentation of 6-Caffeoylglucoses (9 and 10).** The two anomers (**9** and **10**) of 6-caffeoylglucose showed very similar fragment spectra in $MS^2$. The base peak in $MS^2$ could be observed at $m/z$ 281 ($C_{13}H_{13}O_7$, **D**) corresponding to a neutral loss of $C_2H_4O_2$ through a ring fission fragmentation (Figures 6, 7 and Tables 1, 2). Further fragment ions at $m/z$ 251 ($M - H^+ -$ caffeic acid, $C_{12}H_{11}O_6$, **B**), $m/z$ 221 ($C_{11}H_9O_5$, **C**), both obtained through ring fission fragmentation, $m/z$ 179 ($C_9H_7O_4$, caffeic acid anion **A**) and $m/z$ 323 ($M - H^+ - H_2O$, $C_{15}H_{15}O_8$, **E**) were observed with suggested structures of fragment ions shown in Figure 8 (Tables 1 and 2).

**Fragmentation of 2-Caffeoylglucoses (3 and 4).** The two anomers (**3** and **4**) of 2-caffeoylglucose showed very similar fragment spectra in $MS^2$. Anomers were assigned on the basis of their elution order with the more polar β-2-caffeoylglucose **4** eluting earlier. The $MS^2$ base peak at $m/z$ 203 was assigned as fragment ion **G** $[C_{11}H_7O_4]^-$ with a quinone methide ketene acetal structure (Figure 8 and Tables 1, 2).

The formation of **G** could be rationalized by assuming an inversion of the 2-caffeoylglucose derivative to its inverted chair conformation. In this inverted chair conformation, the caffeoyl moiety and the OH group at C-3 are in an *anti*-1,2 diaxial orientation, whereas the 3-OH and 6-OH are in a *syn*-1,3 diaxial position (Figure 8). Hence, the 6-OH is able to activate the 3-OH via hydrogen bonding as a leaving group with the 2-caffeoyl substituent acting as an intramolecular nucleophile in a 1,2 acyl-migration step, reminiscent of the Königs−Knorr reaction. This sequence of events results in bicyclic quinone acetal intermediate **F** seen as a weak $MS^2$ fragment at $m/z$ 323 $[M - H^+ - H_2O]^-$ or $[C_{15}H_{15}O_8]^-$ (Figure 8). Intermediate **F** undergoes subsequently a ring fission fragmentation to yield fragment ion **G** at $m/z$ 203. All intermediates and the proposed electron flow are shown in Figure 8.

**Fragmentation of 3-Caffeoylglucoses (5 and 6).** The two anomers (**5** and **6**) of 3-caffeoylglucose showed essentially identical fragment spectra in $MS^2$. The base peak of both anomers was $m/z$ 323 $[M - H^+ - H_2O]^-$ **E**/**F** accompanied by fragment ion signals at $m/z$ 203 $[M - H^+ - C_4H_8O_4]^-$ $[C_{11}H_7O_4]^-$ **G** and further minor fragments at $m/z$ 233 **H** and 179 **A** (Figures 6, 9 and Tables 1, 2). We assigned the $MS^2$ base peak as a quinone methide ketene acetal structure **F**.

There were significant differences between the anomers at $MS^3$, with the fragment ion at $m/z$ 219 exceeding 50% intensity in α-3-caffeoylglucose **5** but less than 10% in β-3-caffeoylglucose **6**, indicating that its precursor ion at $m/z$

323 must have retained the anomeric structure in the gas phase and therefore fragmentation occurs from a cyclic structure, most likely the pyranose form.

**Fragmentation of 4-Caffeoylglucoses (7 and 8).** The two anomers (7 and 8) of 4-caffeoylglucose showed very similar fragment spectra in $MS^2$; however, the difference was sufficiently large to allow discrimination through the intensity of the fragment ion at $m/z$ 233, being over 75% for $\alpha$-4-caffeoylglucose **7** and below 75% for $\beta$-4-caffeoylglucose **8** (Figure 6 and Table 1). The base peak for both anomers could be observed at $m/z$

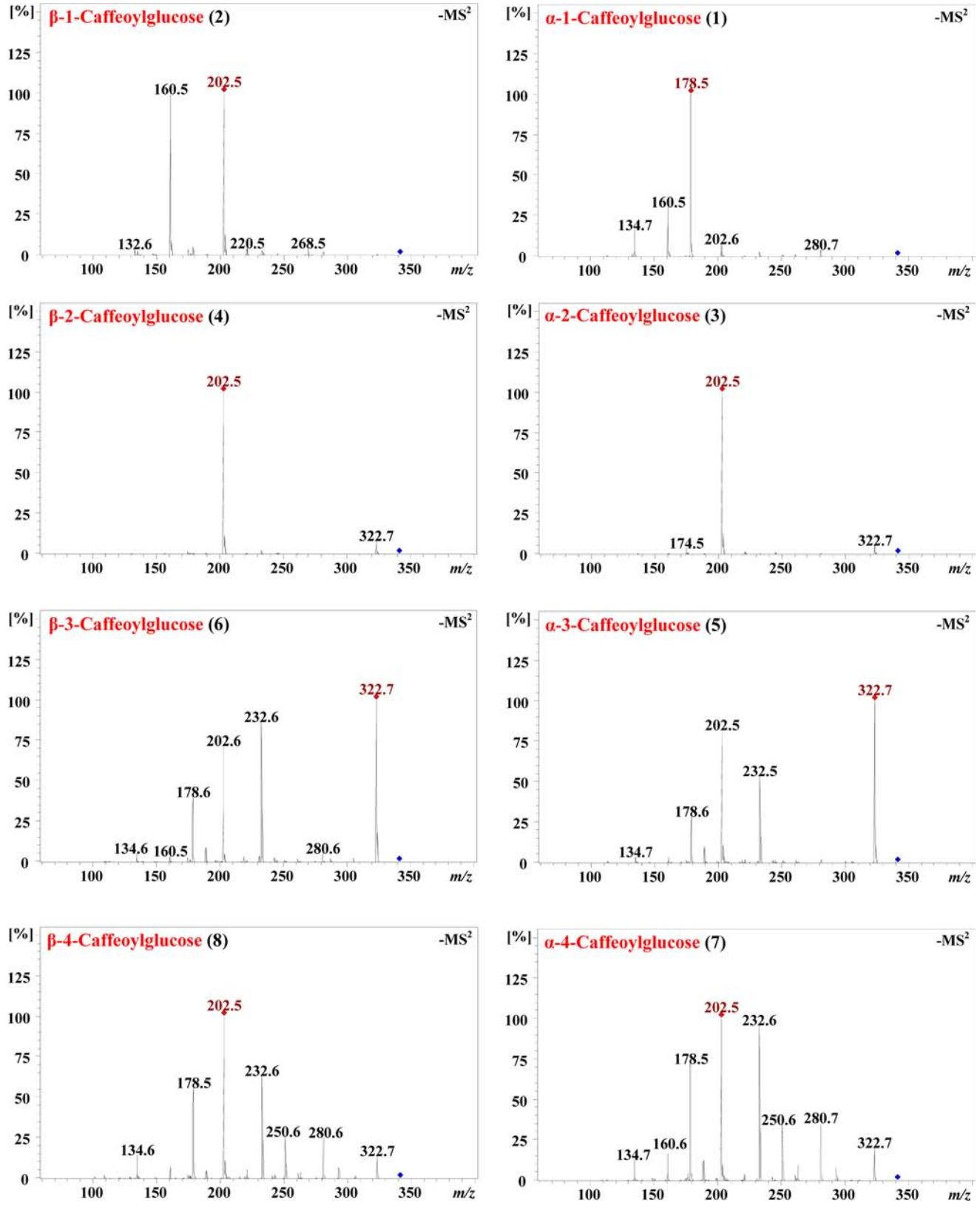


**Figure 6.** continued


dx.doi.org/10.1021/jf501210s | J. Agric. Food Chem. 2014, 62, 9252−9265

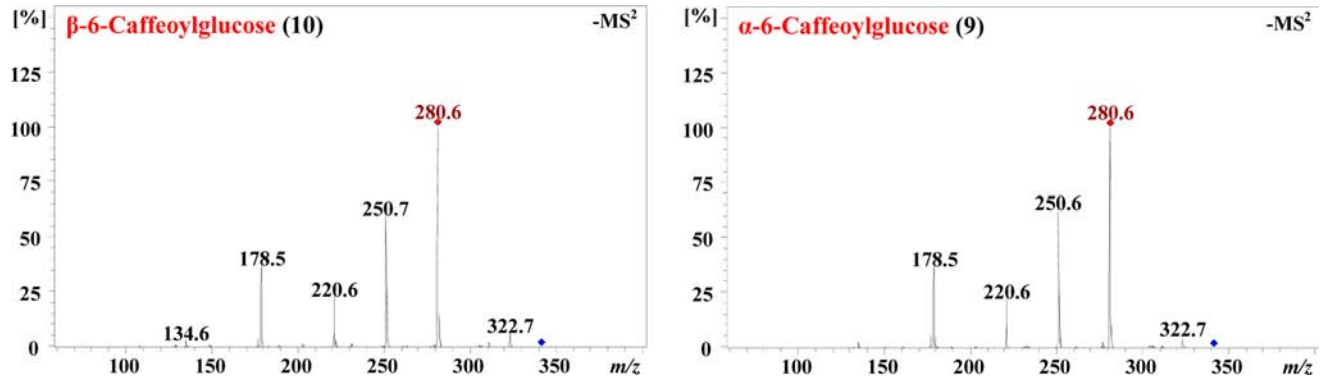


**Figure 6.** $MS^2$ spectra of caffeoylglucoses **1**−**10** at $m/z$ 341 in negative ion mode.

**Table 1. $MS^3$ Data of Caffeoylglucoses 1−10 in Negative Ion Mode**

| | | | $MS^2$ | | | | | | | | | | | | | |
|---|---|---|---|---|---|---|---|---|---|---|---|---|---|---|---|---|
| | | $MS^1$ | base peak | | | | | secondary peak | | | | | | | | |
| no. | caffeoylglucose | parent ion | $m/z$ | $m/z$ | int | $m/z$ | int | $m/z$ | int | $m/z$ | int | $m/z$ | int | $m/z$ | int | $m/z$ | int |
| **1** | α-1-caffeoylglucose | 340.8 | 178.5 | 280.6 | 5 | 202.6 | 8 | 160.5 | 31 | 134.6 | 16 | | | | | | |
| **2** | β-1-caffeoylglucose | 340.8 | 202.5 | 268.5 | 5 | 220.6 | 5 | 178.5 | 5 | 160.5 | 99 | | | | | | |
| **3** | α-2-caffeoylglucose | 340.8 | 202.5 | 322.7 | 6 | | | | | | | | | | | | |
| **4** | β-2-caffeoylglucose | 340.8 | 202.5 | 322.7 | 8 | | | | | | | | | | | | |
| **5** | α-3-caffeoylglucose | 340.8 | 322.7 | | | 232.5 | 54 | 202.5 | 72 | 188.8 | 4 | 178.6 | 29 | 134.7 | 5 | | |
| **6** | β-3-caffeoylglucose | 340.8 | 322.7 | 280.6 | 6 | 232.6 | 87 | 202.6 | 72 | 188.6 | 9 | 178.6 | 40 | 134.6 | 6 | | |
| **7** | α-4-caffeoylglucose | 340.8 | 202.5 | 322.7 | 21 | 280.7 | 36 | 250.6 | 35 | 232.6 | 96 | 178.5 | 72 | 160.6 | 17 | 134.7 | 13 |
| **8** | β-4-caffeoylglucose | 340.7 | 202.5 | 322.8 | 14 | 280.6 | 25 | 250.6 | 26 | 232.6 | 63 | 178.5 | 56 | 160.6 | 7 | 134.6 | 15 |
| **9** | α-6-caffeoylglucose | 340.8 | 280.6 | 322.7 | 5 | 250.6 | 63 | 220.6 | 23 | 178.6 | 38 | | | | | | |
| **10** | β-6-caffeoylglucose | 340.8 | 280.6 | 322.6 | 7 | 250.7 | 60 | 220.6 | 24 | 178.6 | 38 | | | | | | |

| | | | $MS^3$ | | | | | | | | |
|---|---|---|---|---|---|---|---|---|---|---|---|
| | | $MS^1$ | base peak | | secondary peak | | | | | | |
| no. | caffeoylglucose | parent ion | $m/z$ | $m/z$ | int | $m/z$ | int | $m/z$ | int | $m/z$ | int |
| **1** | α-1-caffeoylglucose | 340.8 | 134.6 | | | | | | | | |
| **2** | β-1-caffeoylglucose | 340.8 | 174.6 | | | | | | | | |
| **3** | α-2-caffeoylglucose | 340.8 | 174.6 | | | | | | | | |
| **4** | β-2-caffeoylglucose | 340.8 | 174.6 | | | | | | | | |
| **5** | α-3-caffeoylglucose | 340.8 | 232.6 | 260.6 | 9 | 242.6 | 7 | 218.6 | 56 | 188.6 | 13 |
| **6** | β-3-caffeoylglucose | 340.8 | 232.6 | 260.6 | 8 | 242.6 | 6 | 218.6 | 7 | 188.6 | 13 |
| **7** | α-4-caffeoylglucose | 340.8 | 174.5 | | | | | | | | |
| **8** | β-4-caffeoylglucose | 340.7 | 174.5 | | | | | | | | |
| **9** | α-6-caffeoylglucose | 340.8 | 178.5 | 220.5 | 35 | 134.6 | 13 | | | | |
| **10** | β-6-caffeoylglucose | 340.8 | 178.5 | 220.6 | 32 | 134.6 | 7 | | | | |

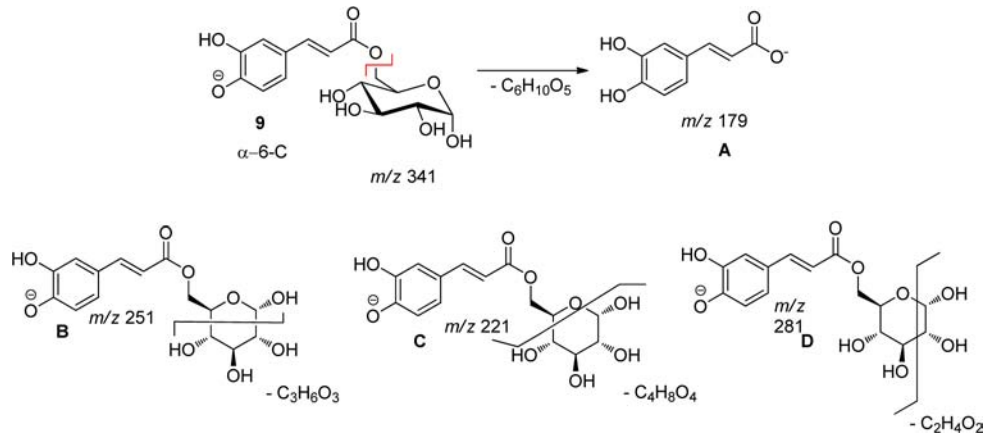


**Figure 7.** Fragmentation mechanism and pathway of 6-caffeoylglucoses (**9** and **10**).


dx.doi.org/10.1021/jf501210s | J. Agric. Food Chem. 2014, 62, 9252−9265

**Table 2. High-Resolution $MS^2$ Data of Synthetic Caffeoylglucoses (1−10) in Negative Ion Mode**

| no. | caffeoylglucose | $MS^2$ fragment ions |
|---|---|---|
| 1 | α-1-caffeoylglucose | 281.0644 ($C_{13}H_{13}O_7$), 203.0344 ($C_{11}H_7O_4$), 179.0340 ($C_9H_7O_4$), 161.0239 ($C_9H_5O_3$), 135.0450 ($C_8H_7O_2$) |
| 2 | β-1-caffeoylglucose | 269.0650 ($C_{12}H_{13}O_7$), 221.0448 ($C_{11}H_9O_5$), 203.0345 ($C_{11}H_7O_4$), 179.0345 ($C_9H_7O_4$), 161.0239 ($C_9H_5O_3$) |
| 3 | α-2-caffeoylglucose | 323.0756 ($C_{15}H_{15}O_8$), 233.0436 ($C_{12}H_9O_5$), 203.0332 ($C_{11}H_7O_4$), 179.0337 ($C_9H_7O_4$), 135.0445 ($C_8H_7O_2$) |
| 4 | β-2-caffeoylglucose | 281.0654 ($C_{13}H_{13}O_7$), 233.0436 ($C_{12}H_9O_5$), 203.0338 ($C_{11}H_7O_4$), 179.0336 ($C_9H_7O_4$), 135.0444 ($C_8H_7O_2$) |
| 5 | α-3-caffeoylglucose | 281.0652 ($C_{13}H_{13}O_7$), 233.0438 ($C_{12}H_9O_5$), 203.0337 ($C_{11}H_7O_4$), 179.0338 ($C_9H_7O_4$), 135.0449 ($C_8H_7O_2$) |
| 6 | β-3-caffeoylglucose | 323.0759 ($C_{15}H_{15}O_8$), 233.0437 ($C_{12}H_9O_5$), 203.0331 ($C_{11}H_7O_4$), 179.0339 ($C_9H_7O_4$), 135.0448 ($C_8H_7O_2$) |
| 7 | α-4-caffeoylglucose | 323.0760 ($C_{15}H_{15}O_8$), 281.0599 ($C_{13}H_{13}O_7$), 251.0495 ($C_{12}H_{11}O_6$), 233.0436 ($C_{12}H_9O_5$), 203.0335 ($C_{11}H_7O_4$), 179.0337 ($C_9H_7O_4$), 161.0238 ($C_9H_5O_3$), 135.0445 ($C_8H_7O_2$) |
| 8 | β-4-caffeoylglucose | 323.0764 ($C_{15}H_{15}O_8$), 281.0597 ($C_{13}H_{13}O_7$), 251.0496 ($C_{12}H_{11}O_6$), 233.0435 ($C_{12}H_9O_5$), 203.0332 ($C_{11}H_7O_4$), 179.0335 ($C_9H_7O_4$), 161.0239 ($C_9H_5O_3$), 135.0442 ($C_8H_7O_2$) |
| 9 | α-6-caffeoylglucose | 323.0765 ($C_{15}H_{15}O_8$), 281.0594 ($C_{13}H_{13}O_7$), 251.0499 ($C_{12}H_{11}O_6$), 221.0402 ($C_{11}H_9O_5$), 179.0305 ($C_9H_7O_4$) |
| 10 | β-6-caffeoylglucose | 323.0760 ($C_{15}H_{15}O_8$), 281.0590 ($C_{13}H_{13}O_7$), 251.0493 ($C_{12}H_{11}O_6$), 221.0399 ($C_{11}H_9O_5$), 179.0303 ($C_9H_7O_4$) |

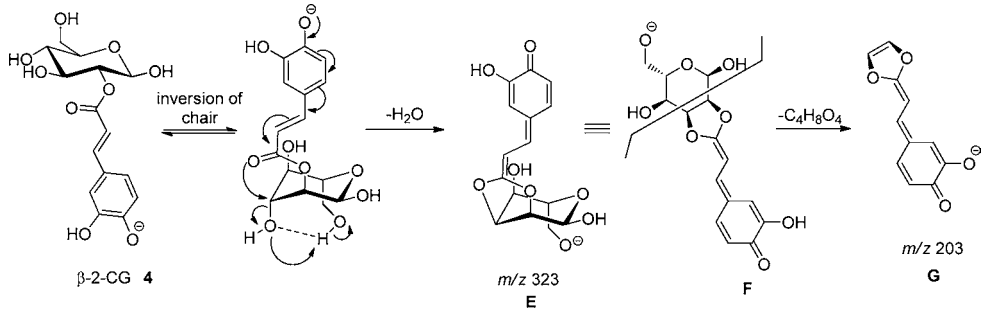


**Figure 8.** Fragmentation mechanism and pathway of 2-caffeoylglucoses (**3** and **4**).

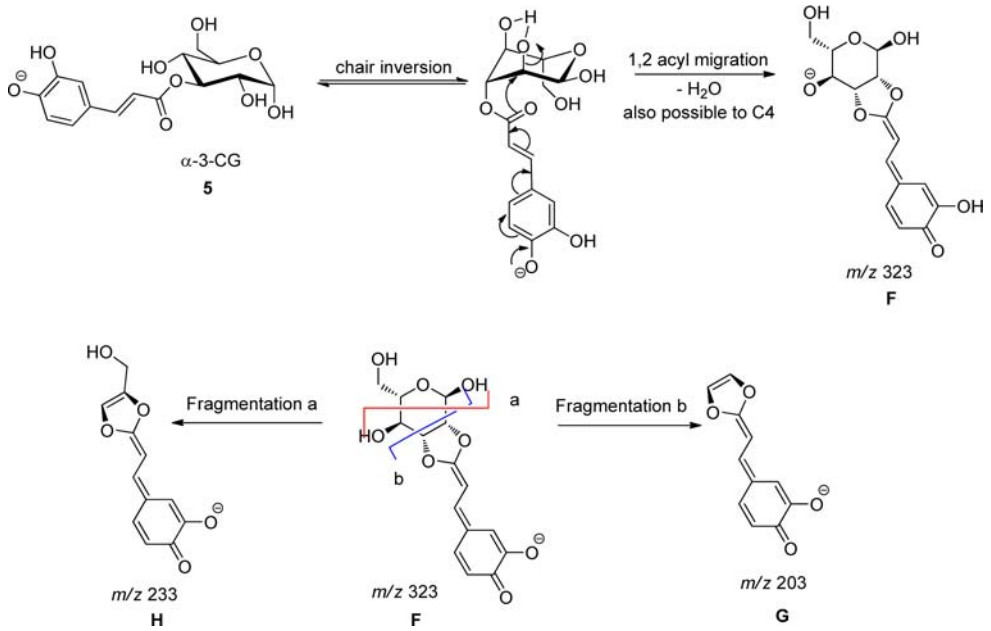


**Figure 9.** Fragmentation mechanism and pathway of 3-caffeoylglucoses (**5** and **6**).

203 and was assigned again to the quinone methide ketene acetal structure **G**, but in contrast to the fragment spectra of 2-caffeoylglucoses (**3** and **4**) and 3-caffeoylglucoses (**5** and **6**), a much larger number of fragments could be observed, at *m*/*z* 233 **H**, 135 **I**, 179 **A**, 251 **B**, 281 **D**, and 323 **E**/**F** (Figure 10 and Tables 1, 2).

We assigned the fragments at *m*/*z* 233 **H**, 179 **A**, and 323 **E**/**F** as previously. The fragments at *m*/*z* 251 **B** and 281 **D** were assigned as fragments resulting from a ring fission. It is interesting to note that 4-caffeoylglucoses showed these types of fragments, which could not be observed for 2-caffeoylglucoses (**3** and **4**) and 3-caffeoylglucoses (**5** and **6**). It appears that the loss of water by a 1,2 acyl participation mechanism is less favored for the 4-caffeoylglucoses (**7** and **8**), allowing ring fission fragmentation to compete with initial dehydration, in comparison to the 3-caffeoylglucoses (**5** and **6**) and 2-caffeoylglucoses (**3** and **4**).

Multiple reaction monitoring $MS^3$ experiments demonstrated that for 2-caffeoylglucose, 3-caffeoylglucose, and 4-caffeoylglucose, the $MS^2$ ion of *m*/*z* 323 fragmented identically, and this quinone methide ketene acetal **F** cannot be the precursor of the minor fragments that discriminate between the 3-caffeoylglucose and 4-caffeoylglucose anomers.


dx.doi.org/10.1021/jf501210s | J. Agric. Food Chem. 2014, 62, 9252−9265

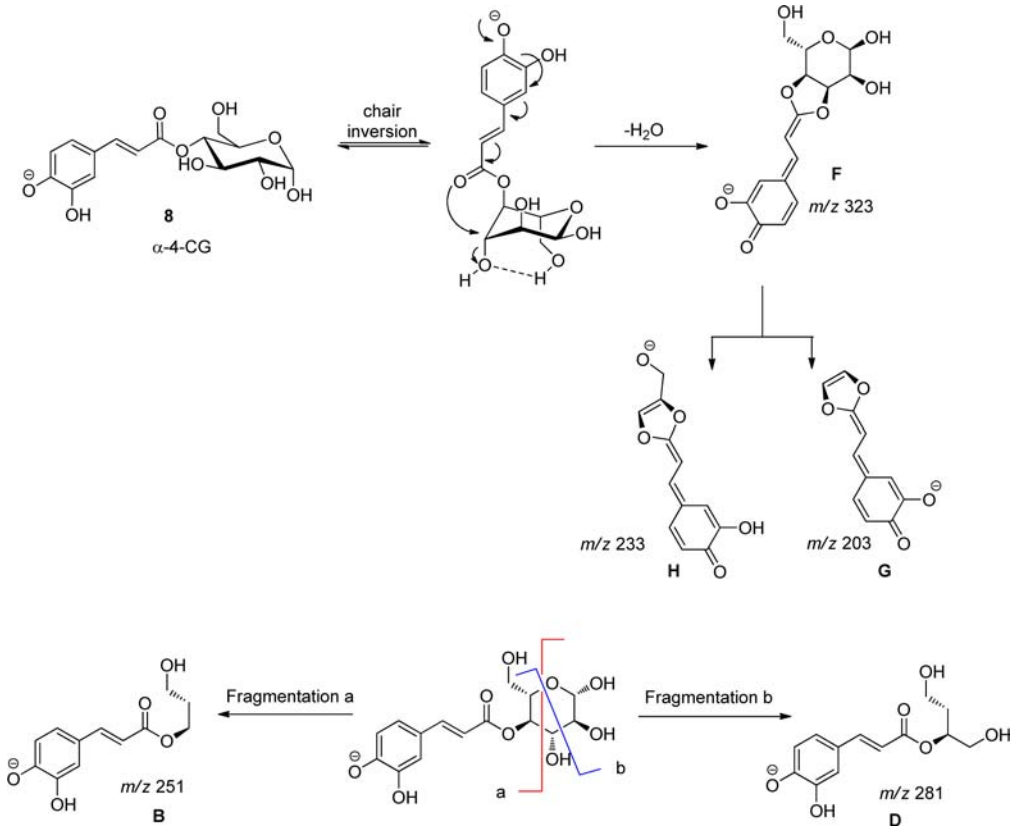


**Figure 10.** Fragmentation mechanism and pathway of 4-caffeoylglucoses (**7** and **8**).

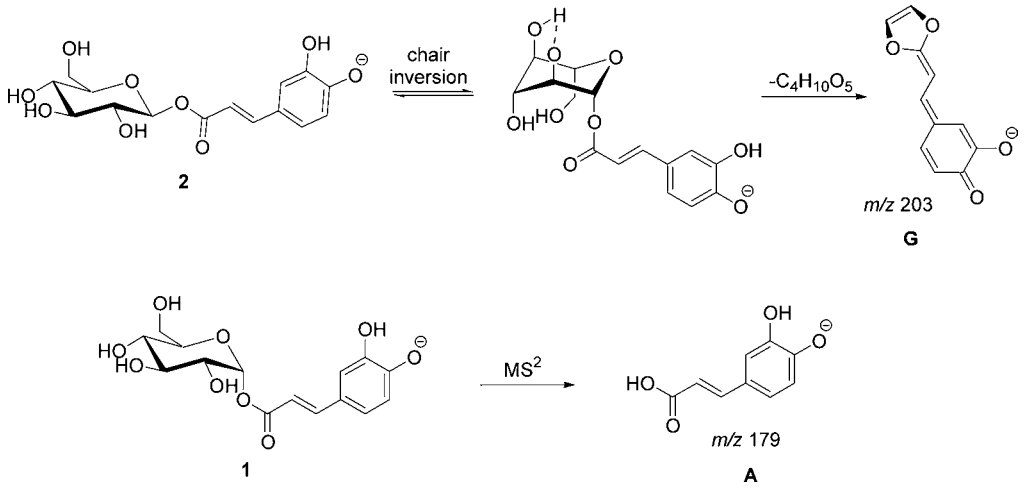


**Figure 11.** Fragmentation mechanism and pathway of 1-caffeoylglucoses (**1** and **2**).

**Fragmentation of 1-Caffeoylglucoses (1 and 2).** The two anomers (**1** and **2**) of 1-caffeoylglucose showed significantly different fragment spectra in $MS^2$ that could be rationalized mechanistically as set out in Figure 11. Our data showed that the earlier-eluting anomer gave a base peak at $m/z$ 179 corresponding to a neutral loss of glucose and a fragment **A** corresponding to caffeic acid anion. The later-eluting anomer gave an $MS^2$ base peak at $m/z$ 203 corresponding to the ketene acetal **J** (Figure 11). Following our previous arguments, the formation of ketene acetal fragment ion **J** is only possible for the $\beta$-1-caffeoylglucose **2** stereochemistry. The loss of the caffeic acid moiety should be facile in the $\alpha$-1-caffeoylglucose **1**, due to the anomeric effect.

The assignment of $\alpha$- and $\beta$-anomers was relatively straightforward for all four cases (except for 1-caffeoylglucoses **1** and **2**) where pure compounds were obtained by synthesis; isomerization furnished the more stable $\beta$-anomers in aqueous solvent, which could also be identified on the basis of their retention times. However, none of these arguments hold for 1-caffeoylglucose. $\beta$-1-Caffeoylglucose **2** was isolated by the group of Winterhalter,[13] and its structure was established by $^1$H NMR spectroscopy; however, no tandem MS data on this compound were reported by this group. Other groups have reported tandem MS data on 1-caffeoylglucoses (**1** and **2**), but assignment appeared to be random, and the two isomers obtained in the current study have been assigned previously


dx.doi.org/10.1021/jf501210s | J. Agric. Food Chem. 2014, 62, 9252−9265

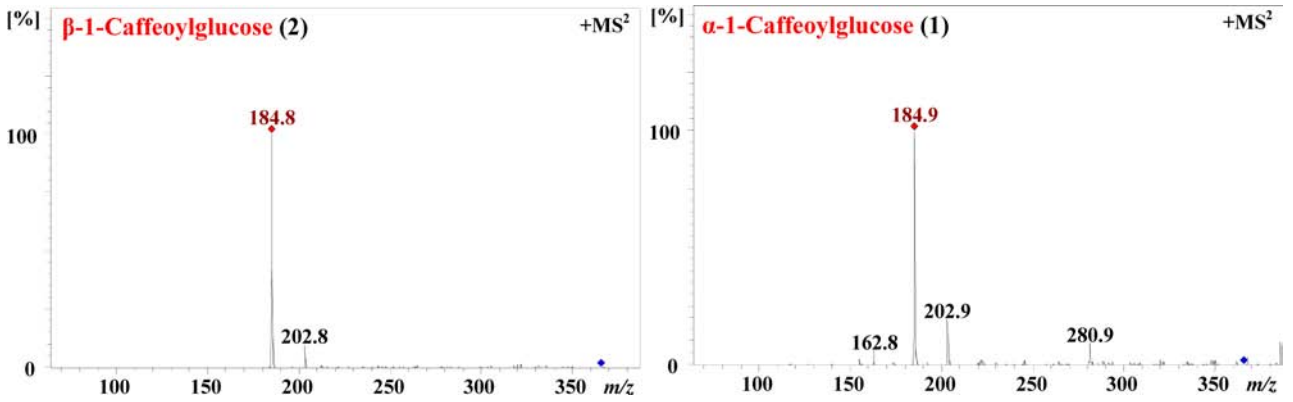


**Figure 12.** $MS^2$ spectra of 1-caffeoylglucoses (**1** and **2**) at $m/z$ 365 in positive ion mode.

in a nonconsistent way. The unambigious assignment of the two anomers of 1-caffeoylglucose must therefore be left open at this point.

**Positive Ion Mode Tandem Mass Spectra.** In the positive ion mode, all caffeoylglucoses can be observed as their sodiated ion at $m/z$ 347 $[M + Na^+]$ ($C_{15}H_{17}O_9Na$). All $MS^2$ spectra display fragment ions at $m/z$ 203 ($C_6H_{12}O_6 + Na^+$) and 185 ($C_9H_6O_3 + Na^+$) corresponding to sodiated glucose and the sodiated caffeoyl ions, respectively. As representative examples, the $MS^2$ spectra for 1-caffeoylglucoses (**1** and **2**) are shown in Figure 12. All positive mode $MS^2$ spectra of all further caffeoylglucose isomers are shown in the Supporting Information. As for the negative ion mode spectra, all five different regiochemistries can be distinguished on the basis of the different $MS^2$ spectra. However, it appears that in the positive ion mode the fragmentation is more difficult for all caffeoylglucoses with the exception of 1-caffeoylglucoses (**1** and **2**), which yield in the fragment spectra a rather large number of fragment ions with low intensities. For this reason, we refrain from a rigorous interpretation of the spectra at the current state.

**Tandem Mass Spectra of *O*-Caffeoyl Glycosides (Caffeic Acid-3-*O*-*β*-glucose 11 and Caffeic Acid-4-*O*-*β*-glucose 12).** To compare the data of the caffeoylglucose esters with those of isomeric *O*-caffeoyl-glycosides **11** and **12**, we recorded tandem MS spectra from an aqueous methanolic extract of kiwi fruit, which was reported to contain those exclusively (Figure 13).[8] The $MS^2$ spectra in negative ion mode showed in contrast to the esters a base peak at $m/z$ 179 [caffeic acid $- H^+$] and only one secondary peak at $m/z$ 135 [caffeic acid $- CO_2 - H^+$]. *O*-Caffeoyl glycosides do not show secondary peaks at $m/z$ 323, 281, 251, 221, 203, and 161 if compared to the esters. Compounds **11** and **12** produced identical MS spectra, and it was not possible to distinguish between them. However, in this particular case, we assigned the first eluting isomer as caffeic acid-3-*O*-*β*-glucose **11**, and the later eluting isomer as caffeic acid-4-*O*-*β*-glucose **12**. It is interesting to note that caffeic acid glycosides lose the glycone part in $MS^2$ spectra (negative ion mode), which is similar to other known phenolic glycosides, flavonoid glycosides, and chlorogenic acid glycosides.

**Hierarchical Key for Caffeoylglucose Isomers Assignment.** From the data shown, we present a hierarchical key or work flow for the analysis and assignment of all isomers of caffeoylglucoses.

All compounds that show in an LC–MS analysis a parent ion in the negative ion mode at $m/z$ 341.0867 $[M - H^+]$ and 365.0840 in the positive ion mode $[M + Na^+]$ with an additional absorption at 320 nm in the UV spectrum should be considered as caffeoylglucose derivatives. For assignment of the regiochemistry in the negative mode, the following key applies:

| | | |
|---|---|---|
| (1) | parent ion at $m/z$ 341 and base peak at $m/z$ 281 in $MS^2$ | 6-caffeoylglucoses (**9** and **10**) |
| (2) | parent ion at $m/z$ 341 and base peak at $m/z$ 323 in $MS^2$ | 3-caffeoylglucoses (**5** and **6**) |
| (2a) | $MS^2$ fragment at $m/z$ 232 >75% and $MS^3$ fragment at $m/z$ 219 <10% | *β*-3-caffeoylglucose (**6**) |
| (2b) | $MS^2$ fragment at $m/z$ 233 <75% and $MS^3$ fragment at $m/z$ 219 >50% | *α*-3-caffeoylglucose (**5**) |
| (3) | parent ion at $m/z$ 341 and base peak at $m/z$ 179 in $MS^2$ | *α*-1-caffeoylglucose (**1**) |
| (4) | parent ion at $m/z$ 341 and base peak at $m/z$ 203 in $MS^2$ accompanied by fragment ion at $m/z$ 161 (1-caffeoylglucose pending final sterochemical assignment) | *β*-1-caffeoylglucose (**2**) |
| (5) | parent ion at $m/z$ 341 and base peak at $m/z$ 203 in $MS^2$ with little further fragments | 2-caffeoylglucoses (**3** and **4**) |
| (6) | parent ion at $m/z$ 341 and base peak at $m/z$ 202.5 in $MS^2$ accompanied by fragment ion at $m/z$ 232.6 | 4-caffeoylglucoses (**7** and **8**) |
| (7) | assignment of *α* and *β* stereo chemistry is based on relative retention time with *β*-anomers eluting earlier on reversed phase if compared to *α*-anomers (exception 1-caffeoylglucoses) | |

**Assignment of Caffeoylglucoses from Yerba Maté.** A total of 10 peaks were detected in the extracted ion chromatograms, which produced a pseudomolecular ion at $m/z$ 341.0867 ± 0.005. These isomeric compounds were assigned as the 10 regio- and stereoisomeric caffeoylglucoses (**1**–**10**) after comparing their retention times, high resolution, and tandem MS data with the authentic caffeoylglucoses standards as outlined above. The two anomers of 6-caffeoylglucose dominate the extract. Similar to chlorogenic acid chemistry, this dietary plant produces a mixture of all possible stereoisomers of a given class of natural products.


dx.doi.org/10.1021/jf501210s | J. Agric. Food Chem. 2014, 62, 9252–9265

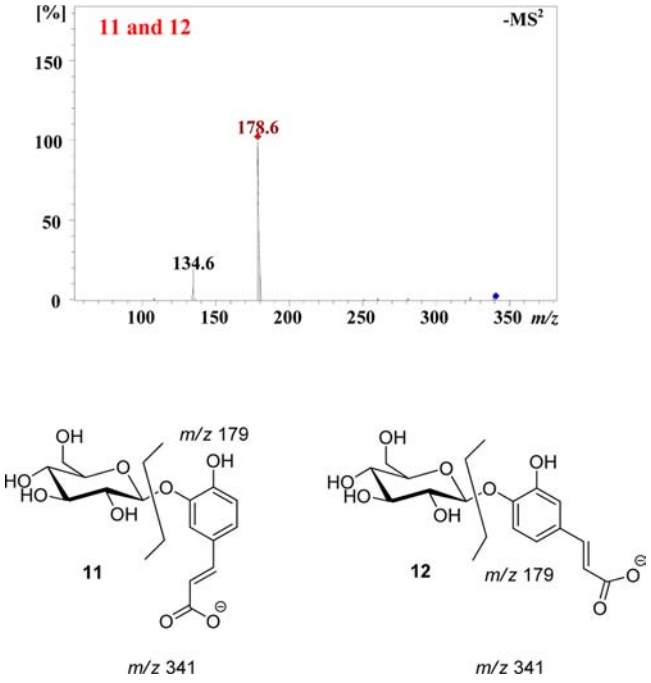


**Figure 13.** $MS^2$ spectra of caffeic acid-3-*O*-$\beta$-glucose **11** and caffeic acid-4-*O*-$\beta$-glucose **12** at *m*/*z* 341 in negative ion mode.

## ■ ASSOCIATED CONTENT

### Supporting Information

Figures of additional $MS^2$ spectra, $^1H$ NMR spectra, and table of HRMS data. This material is available free of charge via the Internet at http://pubs.acs.org.

## ■ AUTHOR INFORMATION

### Corresponding Author

*Tel.: 49 421 200 3120. Fax: 49 421 200 3229. E-mail: n.kuhnert@jacobs-university.de.

### Funding

This work was supported by Jacobs University Bremen, Germany.

### Notes

The authors declare no competing financial interest.

## ■ ACKNOWLEDGMENTS

Helpful comments and discussions with Prof. M. Clifford and excellent technical support from Anja Müller are acknowledged.

## ■ REFERENCES

(1) Clifford, M. N.; Marks, S.; Knight, S.; Kuhnert, N. Characterization by LC-$MS^n$ of four new classes of *p*-coumaric acid-containing diacyl chlorogenic acids in green coffee beans. *J. Agric. Food Chem.* **2006**, *54*, 4095−4101.

(2) Clifford, M. N.; Wu, W. G.; Kuhnert, N. The chlorogenic acids of *Hemerocallis*. *Food Chem.* **2006**, *95*, 574−578.

(3) Maruta, Y.; Kawabata, J.; Niki, R. Antioxidative caffeoylquinic acid-derivatives in the roots of burdock (*Arctium lappa* L). *J. Agric. Food Chem.* **1995**, *43*, 2592−2595.

(4) Greenaway, W.; Wollenweber, E.; Scaysbrook, T.; Whatley, F. R. Novel isoferulate esters identified by gas chromatography-mass spectrometry in bud exudate of *Populus nigra*. *J. Chromatogr., A* **1988**, *448*, 284−290.

(5) Jaiswal, R.; Kuhnert, N. Hierarchical scheme for liquid chromatography/multi-stage spectrometric identification of 3,4,5-triacyl chlorogenic acids in green Robusta coffee beans. *Rapid Commun. Mass Spectrom.* **2010**, *24*, 2283−2294.

(6) Jaiswal, R.; Sovdat, T.; Vivan, F.; Kuhnert, N. Profiling and characterization by LC-$MS^n$ of the chlorogenic acids and hydroxycinnamoylshikimate esters in maté (*Ilex paraguariensis*). *J. Agric. Food Chem.* **2010**, *58*, 5471−5484.

(7) Jaiswal, R.; Patras, M. A.; Eravuchira, P. J.; Kuhnert, N. Profile and characterization of the chlorogenic acids in green Robusta coffee beans by LC-$MS^n$: Identification of seven new classes of compounds. *J. Agric. Food Chem.* **2010**, *58*, 8722−8737.

(8) Fiorentino, A.; D'Abrosca, B.; Pacifico, S.; Mastellone, C.; Scognamiglio, M.; Monaco, P. Identification and assessment of antioxidant capacity of phytochemicals from kiwi fruits. *J. Agric. Food Chem.* **2009**, *57*, 4148−4155.

(9) Pizzolatti, M. G.; Brighente, I. M. C.; Bortoluzzi, A. J.; Schripsema, J.; Verdi, L. G.; Cyathenosin, A. a spiropyranosyl derivative of protocatechuic acid from *Cyathea phalerata*. *Phytochemistry* **2007**, *68*, 1327−1330.

(10) Bringmann, G.; Guenther, C.; Jumbam, D. N. Isolation of 4-O-beta-D-glucopyranosylcaffeic acid and gallic acid from *Cyathea dregei* Kunze (Cyatheaceae). *Pharm. Pharmacol. Lett.* **1999**, *9*, 41−43.

(11) Braham, H.; Mighri, Z.; Ben Jannet, H.; Matthew, S.; Abreu, P. M. Antioxidant phenolic glycosides from *Moricandia arvensis*. *J. Nat. Prod.* **2005**, *68*, 517−522.

(12) Yang, L.; Nakamura, N.; Hattori, M.; Wang, Z.; Bligh, S. W. A.; Xu, L. High-performance liquid chromatography-diode array detection/electrospray ionization mass spectrometry for the simultaneous analysis of cis-, trans- and dihydro-2-glucosyloxycinnamic acid derivatives from Dendrobium medicinal plants. *Rapid Commun. Mass Spectrom.* **2007**, *21*, 1833−1840.

(13) Du, Q.; Xu, Y.; Li, L.; Zhao, Y.; Jerz, G.; Winterhalter, P. Antioxidant constituents in the fruits of *Luffa cylindrica* (L.) Roem. *J. Agric. Food Chem.* **2006**, *54*, 4186−4190.

(14) Bastos, D. H. M.; Saldanha, L. A.; Catharino, R. R.; Sawaya, A. C. H. F.; Cunha, I. B. S.; Carvalho, P. O.; Eberlin, M. N. Phenolic antioxidants identifled by ESI-MS from yerba mate (*Ilex paraguariensis*) and green tea (*Camelia sinensis*) extracts. *Molecules* **2007**, *12*, 423−432.

(15) Jiang, Z. H.; Hirose, Y.; Iwata, H.; Sakamoto, S.; Tanaka, T.; Kouno, I. Caffeoyl, coumaroyl, galloyl, and hexahydroxydiphenoyl glucoses from *Balanophora japonica*. *Chem. Pharm. Bull.* **2001**, *49*, 887−892.

(16) Clifford, M. N.; Wu, W. G.; Kirkpatrick, J.; Kuhnert, N. Profiling the chlorogenic acids and other caffeic acid derivatives of herbal chrysanthemum by LC-MSn. *J. Agric. Food Chem.* **2007**, *55*, 929−936.

(17) Zhu, T. F.; Huang, K. Y.; Deng, X. M.; Zhang, Y.; Xiang, H.; Gao, H. Y.; Wang, D. C. Three new caffeoyl glycosides from the roots of *Picrorhiza scrophulariiflora*. *Molecules* **2008**, *13*, 729−735.

(18) Norbaek, R.; Aaboer, D. B. F.; Bleeg, I. S.; Christensen, B. T.; Kondo, T.; Brandt, K. Flavone C-glycoside, phenolic acid, and nitrogen contents in leaves of barley subject to organic fertilization treatments. *J. Agric. Food Chem.* **2003**, *51*, 809−813.

(19) Romani, A.; Vignolini, P.; Galardi, C. R.; Mulinacci, N.; Benedettelli, S.; Heimler, D. Germplasm characterization of Zolfino landraces (*Phaseolus vulgaris* L.) by flavonoid content. *J. Agric. Food Chem.* **2004**, *52*, 3838−3842.

(20) Ahluwalia, B.; Fry, S. C. Barley endosperm cell walls contain a feruloylated arabinoxylan and a non-feruloylated $\beta$-glucan. *J. Cereal Sci.* **1986**, *4*, 287−295.

(21) Chen, J. H.; Ho, C. T. Antioxidant activities of caffeic acid and its related hydroxycinnamic acid compounds. *J. Agric. Food Chem.* **1997**, *45*, 2374−2378.

(22) Levigne, S.; Ralet, M. C.; Quemener, B.; Thibault, J. F. Isolation of diferulic bridges ester-linked to arabinan in sugar beet cell walls. *Carbohydr. Res.* **2004**, *339*, 2315−2319.

(23) Renger, A.; Steinhart, H. Ferulic acid dehydrodimers as structural elements in cereal dietary fibre. *Eur. Food Res. Technol.* **2000**, *211*, 422−428.

(24) Winter, M.; Herrmann, K. Esters and glucosides of hydroxycinnamic acids in vegetables. *J. Agric. Food Chem.* **1986**, *34*, 616−620.
(25) Ohashi, H.; Yamamoto, E.; Lewis, N. G.; Towers, G. H. N. 5-Hydroxyferulic acid in *Zea mays* and *Hordeum vulgare* cell-walls. *Phytochemistry* **1987**, *26*, 1915−1916.
(26) Mathew, S.; Abraham, T. E. Ferulic acid: An antioxidant found naturally in plant cell walls and feruloyl esterases involved in its release and their applications. *Crit. Rev. Biotechnol.* **2004**, *24*, 59−83.
(27) Allerdings, E.; Ralph, J.; Schatz, P. F.; Gniechwitz, D.; Steinhart, H.; Bunzel, M. Isolation and structural identification of diarabinosyl 8-*O*-4-dehydrodiferulate from maize bran insoluble fibre. *Phytochemistry* **2005**, *66*, 113−124.
(28) Hartley, R. D.; Morrison, W. H.; Himmelsbach, D. S.; Borneman, W. S. Cross-linking of cell-wall phenolic arabinoxylans in Gramineous plants. *Phytochemistry* **1990**, *29*, 3705−3709.
(29) Ralph, J.; Quideau, S.; Grabber, J. H.; Hatfield, R. D. Identification and synthesis of new ferulic acid dehydrodimers present in grass cell-walls. *J. Chem. Soc., Perkin Trans. 1* **1994**, 3485−3498.
(30) Clifford, M. N.; Knight, S.; Kuhnert, N. Discriminating between the six isomers of dicaffeoylquinic acid by LC-MS$^n$. *J. Agric. Food Chem.* **2005**, *53*, 3821−3832.
(31) Clifford, M. N.; Johnston, K. L.; Knight, S.; Kuhnert, N. Hierarchical scheme for LC-MS$^n$ identification of chlorogenic acids. *J. Agric. Food Chem.* **2003**, *51*, 2900−2911.
(32) Jaiswal, R.; Dickman, M. H.; Kuhnert, N. First diastereoselective synthesis of methyl caffeoyl- and feruloyl-*muco*-quinates. *Org. Biomol. Chem.* **2012**, *10*, 5266−5277.
(33) Alakolanga, A. G. A. W.; Siriwardene, A. M. D. A.; Kumar, N. S.; Jayasinghe, L.; Jaiswal, R.; Kuhnert, N. LC-MSn identification and characterization of the phenolic compounds from the fruits of *Flacourtia indica* (Burm. F.) Merr. and *Flacourtia inermis* Roxb. *Food Res. Int.* **2014**, *62*, 388−396.

## MATERIALS AND METHODS

**Materials and Reagents.** Xanthine (X0625-5G), xanthine oxidase (XO, X4875-10U), nitroblue tetrazolium chloride (NBT, N6876-5G), and allopurinol (A8003-5G) were purchased from Sigma-Aldrich (St. Louis, MO, USA). Potassium phosphate monobasic ($KH_2PO_4$), potassium phosphate dibasic ($K_2HPO_4{\cdot}3H_2O$), ethylenediaminetetraacetic acid disodium salt (EDTA), sodium hydroxide (NaOH), dimethyl sulfoxide (DMSO), acetone, acetonitrile, ethanol, isopropanol, tetrahydrofuran, and hydrochloric acid (HCl) were purchased from Sinopharm Chemical Reagent Co., Ltd. (Shanghai, China). Ultrapure water was prepared by an Advantage A10 water purifier (Milli-Q Academic, Molsheim, France). All other chemicals were of analytical grade and used without further purification.

Rosmarinic acid, resveratrol, and rutin (purity > 98%) were obtained from Shanghai R&D Center for Standardization of Chinese Medicines (Shanghai, China). The individual food extracts of rosemary (whole plant, 2012030), ginger (rhizoma, 2012021), and green tea (leaves, 2012020) were purchased from Sichuan Tongtai Plant Chemical Industry Co., Ltd. (Shifang, Sichuan Province, China). The lotus extract (leaves, 20120620) was purchased from Shanghai Moochun Biological Technology Co., Ltd. (Shanghai, China).

A 0.2 M stock phosphate buffer solution (PBS, pH 8.0) was prepared by mixing equal volumes of 0.2 M $KH_2PO_4$ and 0.2 M $K_2HPO_4{\cdot}3H_2O$ solutions. A 1.0 mM EDTA stock solution was prepared in ultrapure water.

Stock solutions of the pure antioxidants were prepared in DMSO at concentrations of 6.0 mM, and the stock solutions of the food extracts were prepared in a mixture of DMSO/ultrapure water (1:1, v/v). A series of working solutions were made by appropriate stepwise dilutions of the above stock solutions with 0.2 M PBS buffer (pH 8.0). A fresh substrate solution containing 4 mM xanthine and 4 mM NBT was prepared in 0.05 M PBS (pH 8.0) just before use. A 0.04 U/mL XO solution (250 mL) was prepared by dilution of the 10 U XO stock solution with a mixture solution of 1 mM EDTA (125 mL) and 0.1 M PBS (pH 8.0, 125 mL). The enzyme activity of XO was determined by a reference method[31] before preparation.

**Conventional Colorimetric Assay.** The conventional colorimetric $O_2^{\bullet-}$ scavenging capacity assay was carried out according to a previously described laboratory protocol.[32] Briefly, an aliquot of 100 $\mu$L of different concentrations of tested antioxidants was added to a 1 mL substrate solution containing 0.4 mM xanthine and 0.24 mM NBT. After the addition of 1 mL of XO solution (50 mU/mL), the reaction mixture was incubated in a water bath at 37 °C for 20 min. The reaction was then terminated by the addition of 1 mL of 0.6 M HCl, and the absorbance ($A$) of each reaction mixture at 560 nm was measured against a blank without XO using a microplate spectrophotometer (Power Wave, Bio-Tek, Winooski, VT, USA). The $O_2^{\bullet-}$ scavenging capacity for each reaction was calculated as

$$O_2^{\bullet-}\text{scavening capacity \%} = [1 - (A_s - A_{s\text{-}b})/(A_c - A_{c\text{-}b})] \times 100\% \quad (1)$$

where $A_s$, $A_{s\text{-}b}$, $A_c$, and $A_{c\text{-}b}$ represent the absorbances of samples, sample control (without addition of XO), control (without addition of tested antioxidants), and vehicle control (without addition of tested antioxidants and XO), respectively, at 560 nm after 20 min of reaction. The $EC_{50}$ value is the concentration of an antioxidant capable of quenching 50% of the radicals in the reaction mixture under the assay condition. Triplicate reactions were carried out for each level of every individual sample.

**High-Throughput $O_2^{\bullet-}$ Scavenging Assay.** The high-throughput $O_2^{\bullet-}$ scavenging assay was carried out using a 96-well microplate spectrophotometer (Power Wave, Bio-Tek). The 96-well plate was covered with a lid to prevent solvent evaporation during reaction. Six or eight different concentrations were used for each antioxidant extract and antioxidant compound in the study. The antioxidant sample solution (6.67 $\mu$L) and 193.33 $\mu$L of substrate solution (including 6.43 $\mu$L of 4 mM xanthine, 12.86 $\mu$L of 4 mM NBT, and 174.04 $\mu$L of 0.05 M PBS) were added to each well. Then 20 $\mu$L of 0.04 U/mL XO solution was added to start the reaction. After gentle shaking for 10 s, the reaction mixture was incubated in a water bath at 37 °C for 20 min. Finally, 20 $\mu$L of 0.6 M HCl was added to terminate the reaction, followed by shaking for another 10 s. The absorbance at 560 nm was measured. The total volume for each reaction mixture in each well was 240 $\mu$L. A blank test without XO and a control test without antioxidants were also conducted. Allopurinol was used as a positive control for the assay. The level of $O_2^{\bullet-}$ scavenging capacity for each reaction was also calculated as formula 1. The $EC_{50}$ values were calculated under the assay condition. Triplicate reactions were carried out for each level of every individual sample.

## RESULTS AND DISCUSSION

**Selection of the Detection Wavelength for the X/XO Reaction.** The X/XO enzymatic system is based on XO oxidation of xanthine giving $O_2^{\bullet-}$, which subsequently reacts with NBT to yield a purple formazan. The formation of formazan is generally detected by absorbance at 560 nm. However, several wavelengths such as 560 nm,[32] 510 nm,[33] and 595 nm[34] have also been reported for the detection of formazan production. This divergence prompted us to investigate a suitable wavelength for this reaction system. Theoretically, the individual components involved in the reaction mixture including xanthine, NBT, and XO might interfere with the formazan absorbance. As shown in Supporting Information Figure SI1A, all of the components except formazan (the reaction product) in the reaction system showed no absorption maximum between 500 and 800 nm. The absorbance of formazan from 550 to 650 nm reached a platform, among which 560 nm turned out to be stable. Therefore, 560 nm was chosen as the detection wavelength, consistent with that used in most of the X/XO literature.

NBT is a classical biochemical reagent for the detection of $O_2^{\bullet-}$. During the reaction process, ditetrazolium ($NBT^{2+}$) is attacked by $O_2^{\bullet-}$, along with one electron being transferred to turn $NBT^{2+}$ into tetrazolinyl radical ($NBT^{\bullet+}$). In the following step, one more electron transfer turns $NBT^{\bullet+}$ into monoformazan (MF).[35] It should be noted, therefore, that the excess of NBT or $O_2^{\bullet-}$ might theoretically lead to the production of only MF or diformazan (DF). The difference in molecular structures of MF and DF may result in the different maximum absorption wavelengths of these two substances. Thus, the different molar ratios of xanthine to NBT (1:1, 1:2, and 1:3) in the X/XO reaction mixture were scanned over 450−800 nm (Supporting Information Figure SI1B). The results showed that the effect of different molar ratios of xanthine to NBT was small and of marginal importance to the maximum wavelength of formazan. As the absorption behaviors of the molar ratios (1:2 and 1:3) of xanthine to NBT acted similarly, a 1:2 ratio of xanthine to NBT was chosen.

**Effect of Temperatures on the X/XO Reaction.** Several reaction temperatures such as 25 °C[20] and 37 °C[32] have been used for this X/XO enzymatic reaction system. To better understand the effect of temperature on the $O_2^{\bullet-}$ formation, different reaction temperatures including 25, 31, 37, 43, and 49 °C on this X/XO enzymatic system were tested. As a result, the absorbance values increased when the temperature was increased from 25 to 37 °C (Supporting Information Figure SI2A), and slight decreases were observed with a temperature of >37 °C. The results indicated that the extent of the reaction reached the maximum at 37 °C. Therefore, 37 °C was selected as the reaction temperature in further experiments, which is consistent with that of $O_2^{\bullet-}$ physiologically generated.


dx.doi.org/10.1021/jf502160d | J. Agric. Food Chem. 2014, 62, 9266−9272

**Effect of pH on the X/XO Reaction.** The effect of the PBS buffer with different pH values (6.0, 6.5, 7.0, 7.5, 8.0, 8.5, and 9.0) on the X/XO enzymatic system was studied. As shown in Supporting Information Figure SI2B, the absorbance values increased with the increase of the pH values from 6.0 to 8.0, whereas absorbance values decreased from pH 8.0 to 9.0. A possible explanation is that the conformation of XO might be affected by the pH of the buffers.[22] Therefore, a pH of 8.0 was selected in this study.

**Effects of Enzyme and Substrate Concentrations on the X/XO Reaction.** The rate of an enzyme-catalyzed reaction depends on concentrations of enzymes and substrates.[22] The effect of XO concentrations on the formazan formation was studied. At eight concentrations of XO over a 8-fold range (10−80 mU/mL), the enzyme was incubated with 4 mM substrate solution and DMSO (without antioxidants) at 37 °C for 20 min. The absorbance values gradually increased with increasing XO concentrations from 10 to 40 mU/mL, whereas there was no significant change of the absorbance values in XO concentrations up to 40 mU/mL (Supporting Information Figure SI2C). These data suggested that the optimal XO concentration in this reaction was 40 mU/mL.

Similarly, several substrate concentrations (2.0, 2.5, 3.0, 3.5, 4.0, 4.5, 5.0, and 5.5 mM) with a constant molar ratio to NBT (1:2) were studied. Supporting Information Figure SI2D shows the effect of substrate concentrations on the rate of the reaction. For a given enzyme concentration (40 mU/mL), the absorbance values showed a rapid and marked increase with substrate concentrations from 2.0 to 4.0 mM and a subsequent slow increase up to 5.5 mM, which is consistent with the Michaelis−Menten kinetics theory.[36] Therefore, the optimal substrate concentration in this reaction system was 4.0 mM.

**Effect of Reaction Time on the X/XO Reaction.** Several reaction times such as 5 min,[37] 20 min,[32] and 30 min[38] have been applied for this enzymatic reaction system. For the consideration of stability, the reaction time required to reach the steady state for this enzymatic system was studied. The change in absorbance was measured for 44 min at 2 min interval, without the addition of terminators. As shown in Supporting Information Figure SI3, the absorbance values increased rapidly within 20 min, and reached a plateau from 20 to 44 min. The result indicated that the reaction mixture can be considered to reach the "steady state" at 20 min or anytime after that. Thus, a reaction time of 20 min was used.

**Effect of Different Sample Dissolving Solvents on the X/XO Reaction.** Enzymatic reactions can be conducted not only in water but also in organic solvents.[39] This suggests the feasible use of organic cosolvents for the hydrophilic and lipophilic antioxidant samples tested in the enzymatic assay. Therefore, several organic solvents including DMSO, acetone, acetonitrile, isopropanol, and tetrahydrofuran, as well as water, were selected to investigate the solvent effect on the reaction system. With a fixed ratio of solvent volume to the reaction mixture (1:30), none of these organic solvents had shown a significant effect on absorbance values compared with water (Figure 1), indicating the potential use of these solvents as sample dissolving solvents. This is especially important and useful for samples with lower solubility in water.

In addition, three other different ratios of solvent volume to the reaction mixture (1:10, 1:20, and 1:40, v/v) were investigated and compared with the ratio of 1:30. As shown in Figure 1, no significant absorbance changes were observed among the 1:20, 1:30, and 1:40 ratios of solvent volume to

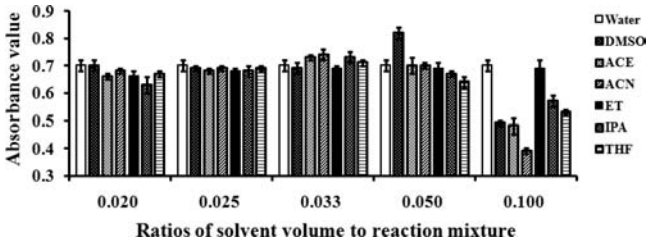


**Figure 1.** Effects of dissolving solvents and ratios of solvent volume to the reaction mixture on the xanthine/xanthine oxidase reaction. The reaction mixture contained 6.67 μL of different solvents, 193.33 μL of substrate solution (6.43 μL of 4 mM xanthine, 12.86 μL of 4 mM NBT, and 174.04 μL of 0.05 M PBS), and 20 μL of 40 mU/mL xanthine oxidase. The absorbance at 560 nm was determined for each reaction mixture after 20 min of reaction terminated by the addition of 20 μL of 0.6 M HCl. Four different volume ratios (1:10, 1:20, 1:30, and 1:40, v/v) were tested. ACE, ACN, ET, IPA, and THF represented acetone, acetonitrile, ethanol, isopropanol, and tetrahydrofuran, respectively. Data are means of triplicate measurements. Vertical bars represent the standard deviations.

reaction mixture, regardless of the nature of dissolving solvents. However, in a 1:10 ratio, all of the solvents except water and ethanol resulted in obvious decreases of the absorbance values (Figure 1). Therefore, the organic solvent effect should not be ignored in a relatively high ratio (1:10) of solvent volume to the reaction mixture (except water and ethanol). In consideration of its extensive use as a dissolving solvent in screening tests, DMSO with a 1:30 ratio of volume to the reaction mixture was used in this study.

**Effect of Different Terminators on the X/XO Reaction.** Significant pH changes can affect enzyme activity, which might be an effective way to terminate an enzymatic reaction. HCl, a commonly used acid terminator in the X/XO reaction,[40] was compared with NaOH, an alkaline terminator of other enzymes.[41] As shown in Figure 2A, the absorbance values increased with increasing concentrations of NaOH solutions (0.1−0.9 M), together with the production of green substances instead of the expected purple formazan. Thus, NaOH is not suitable to terminate the reaction due to the formation of side products with absorption at 560 nm.

In contrast to NaOH, a gradual decrease of the absorbance values was observed with the increase of HCl concentrations from 0.1 to 0.5 M (Figure 2B). Further increase of the HCl concentration to 1.0 M did not result in a further decrease in the absorbance values. Importantly, unlike with 0.1−0.4 M HCl solutions, the generation of the expected purple formazan cannot be observed with 0.5−1.0 M HCl, suggesting that the reaction could be totally terminated by 0.5−1.0 M HCl solutions. To further confirm the efficiency of the HCl terminator, the absorbances of the reaction mixtures at 10, 20, 40, and 60 min were determined after 10 min of reaction being terminated by 0.5−1.0 M HCl solutions. As shown in Figure 2C, no obvious increase of absorbance values was observed after the addition of 0.5−1.0 M HCl solutions at each time point, whereas that of the negative control (without addition of HCl solutions) increased rapidly from 10 to 20 min, indicating the great termination efficiency of HCl. Hence, a 0.6 M HCl solution beyond the inflection point was chosen as the optimal terminator.

Surface-active agents (SAAs) are also reported to terminate the enzymatic reactions, because SAAs could neutralize the surface charges of enzyme molecules, resulting in the

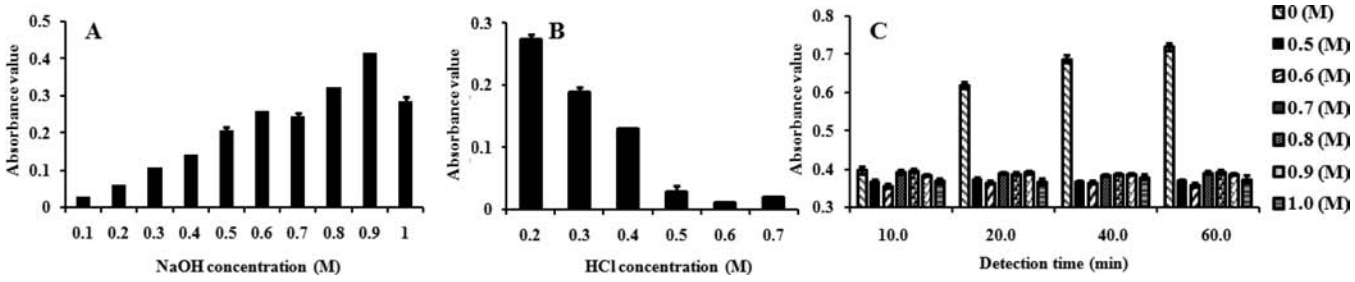


**Figure 2.** Effects of different terminators and HCl concentrations on the xanthine/xanthine oxidase reaction (A, NaOH; B, HCl; C, 0.5−1.0 M HCl). The reaction mixture contained 6.67 μL OF DMSO, 193.33 μL of substrate solution (6.43 μL of 4 mM xanthine, 12.86 μL of 4 mM NBT, and 174.04 μL of 0.05 M PBS), and 20 μL of 40 mU/mL xanthine oxidase. The absorbance at 560 nm was determined for each reaction mixture ternminated by 20 μL of 0.1−1.0 M NaOH (A) or 20 μL of 0.2−0.7 M HCl (B) after 20 min of reaction. For the termination efficiency of HCl, 20 μL of 0 M and 0.5−1.0 M HCl solutions was added to the xanthine/xanthine oxidase reactions, followed by determination of the absorbance at 10, 20, 40, and 60 min (C). Data are means of triplicate measurements. Vertical bars represent the standard deviations.

**Table 1. Linear Relationship between Antioxidant Concentrations and Percent $O_2^{\bullet-}$ Inhibition Obtained by the High-Throughput $O_2^{\bullet-}$ Scavenging Assay[a]**

| sample | slope | intercept | $r^2$ | linearity range | $n$[b] |
|---|---|---|---|---|---|
| allopurinol | 2954.4 | 41.619 | 0.9766 | 2.93−14.66 μM | 7 |
| rosmarinic acid | 932.94 | 23.971 | 0.9808 | 2.93−14.66 μM | 8 |
| resveratrol | 482.91 | −10.518 | 0.9911 | 58.65−131.97 μM | 8 |
| rutin | 275.58 | 13.265 | 0.9895 | 73.31−146.63 μM | 8 |
| rosemary | 399.36 | 7.1703 | 0.9844 | 18.33−146.63 μg/mL | 6 |
| ginger | 138.36 | −4.9684 | 0.9957 | 36.66−586.51 μg/mL | 6 |
| lotus | 126.24 | −5.9565 | 0.9789 | 73.31−586.51 μg/mL | 6 |
| green tea | 55.051 | 6.5041 | 0.9513 | 293.26−1173.02 μg/mL | 6 |

[a]The xanthine/xanthine oxidase reaction system included 193.33 μL of substrate solution (6.43 μL of 4 mM xanthine, 12.86 μL of 4 mM NBT, and 174.04 μL of 0.05 M PBS), 6.67 μL of antioxidant sample solution, and 20 μL of 40 mU/mL xanthine oxidase solution. The absorbance of each well was determined at 560 nm after 20 min of reaction terminated by the addition of 20 μL of 0.6 M HCl. [b]Number of concentrations tested for each antioxidant.

sedimentation of enzyme molecules.[42] As sodium dodecyl sulfonate (SDS) was previously used as a terminator for enzymatic sysytems,[32] its ability as a terminator was also studied. After the X/XO reaction for 20 min, 20 μL of 69 mM SDS was added to the reaction mixture without the addition of the other terminators. As a result, the sedimentation of enzyme molecules was indeed observed. However, the purple formazan was unexpectedly adsorbed by the sediments (data not shown), which in turn interfered with the analysis. Therefore, SDS was not a suitable termination agent for this reaction.

**Validation of the Proposed Assay.** The linear relationship between $O_2^{\bullet-}$ scavenging capacity and antioxidant concentrations was established using pure antioxidants and food extracts at different concentrations. Table 1 lists the linear calibration curves with their correlation coefficients $r^2$ and linear ranges of four pure antioxidants including allopurinol, rosmarinic acid, resveratrol, and rutin, along with four selected functional food extracts including rosemary, ginger, lotus, and green tea. As a result, all calibration curves showed good linear regression ($r^2 > 0.9513$) within test ranges.

The intraday and interday precisions of the assay were determined by analyzing three runs of allopurinol (0.07, 0.10, and 0.30 mM) in hexaplicate in one day and on three consecutive days, respectively. As shown in Table 2, the RSD values of the absorbance values were 4.05 and 5.05% (0.07 mM), 1.87 and 5.62% (0.10 mM), and 1.13 and 2.13% (0.30 mM), respectively, in the intraday and interday precision tests.

The accuracy of the proposed assay was assessed by quality control studies. Quality control samples were prepared in DMSO by adding known amounts of pure rosmarinic acid, resveratrol, and rutin to the reaction mixture. The accuracy was determined by analyzing three runs of the three individual standards at three different concentrations (rosmarinic acid, 0.0176, 0.0264, and 0.0411 μM; resveratrol, 0.0953, 0.11, and 0.1393 μM; and rutin, 0.0953, 0.1246, and 0.1393 μM) in triplicate. The accuracy data (expressed as percent of recovery)

**Table 2. Precision of the High-Throughput $O_2^{\bullet-}$ Scavenging Assay[a]**

| | intraday | | interday | |
|---|---|---|---|---|
| allopurinol (mM) | mean ± SD | RSD% | mean ± SD | RSD% |
| 0.07 | 0.25 ± 0.00 | 4.05 | 0.25 ± 0.00 | 5.05 |
| | 0.24 ± 0.00 | | 0.24 ± 0.00 | |
| | 0.25 ± 0.00 | | 0.24 ± 0.00 | |
| 0.10 | 0.32 ± 0.01 | 1.87 | 0.36 ± 0.01 | 5.62 |
| | 0.31 ± 0.01 | | 0.32 ± 0.01 | |
| | 0.32 ± 0.01 | | 0.34 ± 0.01 | |
| 0.30 | 0.45 ± 0.01 | 1.13 | 0.45 ± 0.01 | 2.13 |
| | 0.44 ± 0.01 | | 0.44 ± 0.01 | |
| | 0.45 ± 0.01 | | 0.45 ± 0.01 | |

[a]The xanthine/xanthine oxidase reaction mixture contained 193.33 μL of substrate solution (6.43 μL of 4 mM xanthine, 12.86 μL of 4 mM NBT, and 174.04 μL of 0.05 M PBS), 20 μL of 40 mU/mL xanthine oxidase, and 6.67 μL of allopurinol (0.07, 0.10, and 0.30 mM). The absorbance of each well was determined at 560 nm after 20 min of reaction terminated by the addition of 20 μL of 0.6 M HCl. Values are expressed as means ± SD ($n$ = 3).


dx.doi.org/10.1021/jf502160d | J. Agric. Food Chem. 2014, 62, 9266−9272

**Table 3. Accuracy of Quality Control (QC) Samples**[a]

| | QC1 ($\mu$M) | QC2 ($\mu$M) | QC3 ($\mu$M) | mean recovery (%) |
|---|---|---|---|---|
| rosmarinic acid | 0.0176 | 0.0264 | 0.0411 | |
| mean ($\mu$M) | 0.0169 | 0.0275 | 0.0356 | |
| recovery (%) | 96.02 ± 7.63 | 104.17 ± 3.38 | 86.62 ± 3.78 | 95.64 |
| RSD (%) | 7.95 | 3.24 | 4.36 | |
| resveratrol | 0.0953 | 0.1100 | 0.1393 | |
| mean ($\mu$M) | 0.0866 | 0.1162 | 0.1334 | |
| recovery (%) | 90.87 ± 1.92 | 105.64 ± 1.66 | 95.76 ± 1.33 | 97.42 |
| RSD (%) | 2.11 | 1.57 | 1.39 | |
| rutin | 0.0953 | 0.1246 | 0.1393 | |
| mean ($\mu$M) | 0.0837 | 0.1332 | 0.1316 | |
| recovery (%) | 87.83 ± 2.56 | 106.90 ± 2.51 | 94.47 ± 1.70 | 96.40 |
| RSD (%) | 2.92 | 2.35 | 1.80 | |

[a]The xanthine/xanthine oxidase reaction mixture contained 193.33 $\mu$L substrate solution (6.43 $\mu$L of 4 mM xanthine, 12.86 $\mu$L of 4 mM NBT, and 174.04 $\mu$L of 0.05 M PBS), 20 $\mu$L of 40 mU/mL xanthine oxidase, and 6.67 $\mu$L antioxidants. Three pure antioxidants (rosmarinic acid, resveratrol, and rutin) at three different concentration levels were used for this accuracy study. The absorbance of each well was determined at 560 nm after 20 min of reaction terminated by addition of 20 $\mu$L of 0.6 M HCl. Values were expressed as means of triplicate measurements. RSD, relative standard deviation. Quality control (QC) samples including rosmarinic acid, resveratrol, and rutin at three different concentration levels (QC1, QC2, and QC3) were used for this accuracy test.

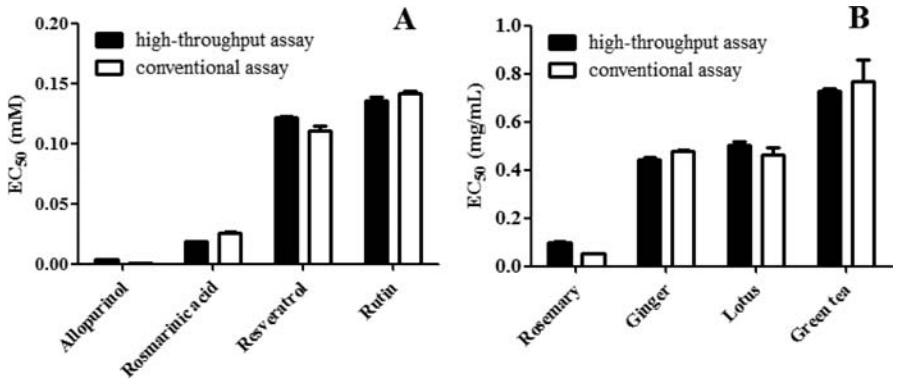


**Figure 3.** $EC_{50}$ values of four selected pure antioxidant compounds (A) and four food extracts (B) determined by the high-throughput and the conventional colorimetric methods. The xanthine/xanthine oxidase (X/XO) reaction system of the conventional colorimetric method contained 1 mL of a mixture of 0.4 mM xanthine and 0.24 mM NBT, 1 mL of 50 mU/mL xanthine oxidase solution, and 0.1 mL of tested samples. The X/XO reaction mixture of the high-throughput method contained 193.33 $\mu$L of substrate solution (6.43 $\mu$L of 4 mM xanthine, 12.86 $\mu$L of 4 mM NBT, and 174.04 $\mu$L of 0.05 M PBS), and 20 $\mu$L of 40 mU/mL xanthine oxidase. The absorbance at 560 nm was measured after 20 min of reaction terminated by 1 mL of 0.6 M HCl for the conventional colorimetric method and by 20 $\mu$L of 0.6 M HCl for the high-throughput assay. Data are means of triplicate measurements. Vertical bars represent the standard deviations.

from the calibration standard are listed in Table 3. The recovery values ranged from 86.62 to 104.17% for rosmarinic acid, from 90.87 to 105.64% for resveratrol, and from 87.83 to 106.90% for rutin, suggesting the acceptable accuracy of the assay.

The stability of the proposed assay was determined with blank (DMSO) and three different concentrations of allopurinol (0.07, 0.10, and 0.30 mM), respectively (Supporting Information Table SI1). After termination, the absorbances at 560 nm at different time periods (0, 10, and 30 min; 1, 2, 6, 12, and 24 h) were monitored. The RSD values of the absorbance values were all <6.19% (blank, 4.70%; allopurinol, 2.62, 3.93, and 6.19% for 0.07, 0.10, and 0.30 mM, respectively), indicating the acceptable stability of the assay.

**Determination of $O_2^{\bullet-}$ Scavenging Capacities for Pure Antioxidants and Food Extracts Using the High-Throughput Method.** Several known antioxidants including allopurinol, rosmarinic acid, resveratrol, and rutin were selected to evaluate their $O_2^{\bullet-}$ scavenging capacity by this high-throughput assay. The $EC_{50}$ value is the concentration of a selected antioxidant necessary to quench 50% $O_2^{\bullet-}$ radicals in the X/XO enzymatic system. A stronger antioxidant has a smaller $EC_{50}$ value. The $EC_{50}$ values of the four pure antioxidants are shown in Figure 3A. Their $O_2^{\bullet-}$ scavenging capacities were in the order allopurinol > rosmarinic acid > resveratrol > rutin determined at 20 min after the reaction was initiated. Our results were in accordance with the literature.[43] Similarly, four well-known antioxidant foods including rosemary, ginger, lotus, and green tea were also estimated for their $O_2^{\bullet-}$ scavenging capacities. The antioxidant activities of the four food extracts can be ranked in descending order of $EC_{50}$ values as follows: rosemary, ginger, lotus, and green tea (Figure 3B). The strongest antioxidant activity of rosemary might be ascribed to the presence of high levels of phenolic compounds (approximately 0.22% fresh weight, among which rosmarinic acid was 32.8 mg/100 g fresh weight).[44]

To validate the efficiency of the newly developed high-throughput 96-well microplate spectrophotometric assay, a comparison between the present method and the conventional colorimetric assay was conducted using a group of pure antioxidants and food extracts mentioned above, in terms of their $EC_{50}$ values. As shown in Figure 3A, the results obtained by the two methods were optimistically correlated to each other ($r$ = 0.991) for the pure antioxidants. As for the case of food extracts, the antioxidant activities were ranked in decreasing order rosemary > lotus > ginger > green tea, consistent with that of the conventional method (Figure 3B). The correlation coefficient was 0.994 between these two methods, indicating the feasibility of the present method.

It is worth noting that the consumption of the enzyme (0.8 mU) was much lower than that of the conventional colorimetric method (50 mU), which makes the current procedure less expensive.

In summary, a high-throughput $O_2^{\bullet-}$ scavenging capacity assay based on the X/XO enzymatic system was developed and validated. The method is easy to perform and time-saving, with a small amount of reagents and antioxidants consumed, and has acceptable precision, accuracy, and stability. The antioxidant data of the newly developed method are highly correlated with those of the conventional method. The high-throughput 96-well plate method can be used as an alternative method for screening and investigating potential antioxidant substances.

## ■ ASSOCIATED CONTENT

### Supporting Information

Stability data, figures of wavelength selection, effects of temperature, pH value, xanthine oxidase concentration, substrate concentration, and reaction time on the xanthine/xanthine oxidase reaction. This material is available free of charge via the Internet at http://pubs.acs.org.

## ■ AUTHOR INFORMATION


### Corresponding Authors

*(T.W.) Phone: +86-21-51322513. E-mail: laurawu2000@163.com Mail: 1200 Cailun Road, Institute of Chinese Materia Medica, Shanghai University of Traditional Chinese Medicine, Shanghai 201203, China.

*(Z.C.) Phone: +86-21-51980157. E-mail: chengzhh@fudan.edu.cn. Mail: 826 Zhangheng Road, Department of Pharmacognosy, School of Pharmacy, Fudan University, Shanghai 201203, China.

### Author Contributions

‖H.T. and J.Z. contributed equally to this work.



### Funding

This study was supported by an Innovation Research Team grant from the Shanghai Municipal Education Commission, a Program for New Century Excellent Talents in University from the Ministry of Education of China (NCET-10-0943), a grant from the National Natural Science Foundation of China (81102775), and an Outstanding Academic Leader Plan (XBR2011057) from Shanghai Municipal Health Bureau.


### Notes

The authors declare no competing financial interest.

## ■ REFERENCES


(1) Muramatsu, H.; Kogawa, K.; Tanaka, M.; Okumura, K.; Nishihori, Y.; Koike, K.; Kuga, T.; Niitsu, Y. Superoxide dismutase in SAS human tongue carcinoma cell line is a factor defining invasiveness and cell motility. *Cancer Res.* **1995**, *55*, 6210−6214.

(2) Cai, H.; Harrison, D. G. Endothelial dysfunction in cardiovascular diseases: the role of oxidant stress. *Circ. Res.* **2000**, *87*, 840−844.

(3) Wolff, S. P. Diabetes mellitus and free radicals, transition metals and oxidative stress in the aetiology of diabetes mellitus and complications. *Br. Med. Bull.* **1993**, *49*, 642−652.

(4) Sakurai, K.; Osaka, T.; Yamasaki, K. Rebamipide reduces recurrence of experimental gastric ulcers: role of free radicals and neutrophils. *Dig. Dis. Sci.* **2005**, *50*, S90−S96.

(5) Floyd, R. A. Antioxidants, oxidative stress, and degenerative neurological disorders. *Exp. Biol. Med.* **1999**, *222*, 236−245.

(6) Kokoszka, J. E.; Coskun, P.; Esposito, L. A.; Wallace, D. C. Increased mitochondrial oxidative stress in the Sod2 (±) mouse results in the age-related decline of mitochondrial function culminating in increased apoptosis. *Proc. Natl. Acad. Sci. U.S.A.* **2001**, *98*, 2278−2283.

(7) Bagchi, R. N.; Bond, A. M.; Scholz, F.; Stösser, R. Characterization of the ESR spectrum of the superoxide anion in the liquid phase. *J. Am. Chem. Soc.* **1989**, *111*, 8270−8271.

(8) Mitsuta, K.; Mizuta, Y.; Kohno, M.; Hiramatsu, M.; Mori, A. The application of ESR spin-trapping technique to the evaluation of SOD-like activity of biological substances. *Bull. Chem. Soc. Jpn.* **1990**, *63*, 187−191.

(9) Noda, Y.; Anzai, K.; Mori, A.; Kohno, M.; Shinmei, M.; Packer, L. Hydroxyl and superoxide anion radical scavenging activities of natural source antioxidants using the computerized JES-FR30 ESR spectrometer system. *IUBMB Life* **1997**, *42*, 35−44.

(10) Sekine, T.; Masumizu, T.; Maitani, Y.; Nagai, T. Evaluation of superoxide anion radical scavenging activity of shikonin by electron spin resonance. *Int. J. Pharm.* **1998**, *174*, 133−139.

(11) Yamaguchi, F.; Yoshimura, Y.; Nakazawa, H.; Ariga, T. Free radical scavenging activity of grape seed extract and antioxidants by electron spin resonance spectrometry in an $H_2O_2$/NaOH/DMSO system. *J. Agric. Food Chem.* **1999**, *47*, 2544−2548.

(12) Zhang, H.; Joseph, J.; Vasquez-Vivar, J.; Karoui, H.; Nsanzumuhire, C.; Martásek, P.; Tordo, P.; Kalyanaraman, B. Detection of superoxide anion using an isotopically labeled nitrone spin trap: potential biological applications. *FEBS Lett.* **2000**, *473*, 58−62.

(13) Zhao, H.; Joseph, J.; Zhang, H.; Karoui, H.; Kalyanaraman, B. Synthesis and biochemical applications of a solid cyclic nitrone spin trap: a relatively superior trap for detecting superoxide anions and glutathiyl radicals. *Free Radical Biol. Med.* **2001**, *31*, 599−606.

(14) Unno, T.; Yayabe, F.; Hayakawa, T.; Tsuge, H. Electron spin resonance spectroscopic evaluation of scavenging activity of tea catechins on superoxide radicals generated by a phenazine methosulfate and NADH system. *Food Chem.* **2002**, *76*, 259−265.

(15) Toyo'oka, T.; Kashiwazaki, T.; Kato, M. On-line screening methods for antioxidants scavenging superoxide anion radical and hydrogen peroxide by liquid chromatography with indirect chemiluminescence detection. *Talanta* **2003**, *60*, 467−475.

(16) Fink, B.; Laude, K.; McCann, L.; Doughan, A.; Harrison, D. G.; Dikalov, S. Detection of intracellular superoxide formation in endothelial cells and intact tissues using dihydroethidium and an HPLC-based assay. *Am. J. Physiol. Cell Physiol.* **2004**, *287*, 895−902.

(17) Sun, C.; Fu, J.; Chen, J.; Jiang, L.; Pan, Y. On-line HPLC method for screening of antioxidants against superoxide anion radical from complex mixtures. *J. Sep. Sci.* **2010**, *33*, 1018−1023.

(18) Liu, S.; Xing, J.; Zheng, Z.; Song, F.; Liu, Z.; Liu, S. Ultrahigh performance liquid chromatography-triple quadrupole mass spectrometry inhibitors fishing assay: a novel method for simultaneously screening of xanthine oxidase inhibitor and superoxide anion scavenger in a single analysis. *Anal. Chim. Acta* **2012**, *715*, 64−70.

(19) Ramallo, I. A.; Zacchino, S. A.; Furlan, R. L. A rapid TLC autographic method for the detection of xanthine oxidase inhibitors and superoxide scavengers. *Phytochem. Anal.* **2006**, *17*, 15−19.

(20) Fridovich, I. Quantitative aspects of the production of superoxide anion radical by milk xanthine oxidase. *J. Biol. Chem.* **1970**, *245*, 4053−4057.

(21) Sun, Y. I.; Oberley, L. W.; Li, Y. A simple method for clinical assay of superoxide dismutase. *Clin. Chem.* **1988**, *34*, 497−500.
(22) Ukeda, H.; Maeda, S.; Ishii, T.; Sawamura, M. Spectrophotometric assay for superoxide dismutase based on tetrazolium salt 3′-{1[(phenylamino)-carbonyl]-3,4- tetrazolium}-bis(4-methoxy-6-nitro)benzenesulfonic acid hydrate reduction by xanthine-xanthine oxidase. *Anal. Biochem.* **1997**, *251*, 206−209.
(23) Ukeda, H.; Kawana, D.; Maeda, S.; Sawamura, M. Spectrophotometric assay for superoxide dismutase based on the reduction of highly water-soluble tetrazolium salts by xanthine-xanthine oxidase. *Biosci., Biotechnol., Biochem.* **1999**, *63*, 485−488.
(24) Magnani, L.; Gaydou, E. M.; Hubaud, J. C. Spectrophotometric measurement of antioxidant properties of flavones and flavonols against superoxide anion. *Anal. Chim. Acta* **2000**, *411*, 209−216.
(25) Ukeda, H.; Shimamura, T.; Tsubouchi, M.; Harada, Y.; Nakai, Y.; Sawamura, M. Spectrophotometric assay of superoxide anion formed in Maillard reaction based on highly water-soluble tetrazolium salt. *Anal. Sci.* **2002**, *18*, 1151−1154.
(26) Hyland, K.; Voisin, E.; Banoun, H.; Auclair, C. Superoxide dismutase assay using alkaline dimethylsulfoxide as superoxide anion-generating system. *Anal. Biochem.* **1983**, *135*, 280−287.
(27) Nishikimi, M.; Appaji Rao, N.; Yagi, K. The occurrence of superoxide anion in the reaction of reduced phenazine methosulfate and molecular oxygen. *Biochem. Biophs. Res. Commun.* **1972**, *46*, 849−854.
(28) Valentão, P.; Fernandes, E.; Carvalho, F.; Andrade, P. B.; Seabra, R. M.; Bastos, M. L. Antioxidant activity of *Centaurium erythraea* infusion evidenced by its superoxide radical scavenging and xanthine oxidase inhibitory activity. *J. Agric. Food Chem.* **2001**, *49*, 3476−3479.
(29) Zhao, B. L.; Li, X. J.; He, R. G.; Cheng, S. J.; Xin, W. J. Scavenging effect of extracts of green tea and natural antioxidants on active oxygen radicals. *Cell Biophys.* **1989**, *14*, 175−185.
(30) Ito, A.; Krinsky, N. I.; Cunningham, M. L.; Peak, M. J. Comparison of the inactivation of *Bacillus subtilis* transforming DNA by the potassium superoxide and xanthine-xanthine oxidase systems for generating superoxide. *Free Radical Biol. Med.* **1987**, *3*, 111−118.
(31) Bergmeyer, H. U.; Gawehn, K.; Grassl, M. *Methods of Enzymatic Analysis*; Academic Press: New York, 1974; Vol. 2, pp 521−522.
(32) Lu, Y.; Foo, L. Y. Antioxidant and radical scavenging activities of polyphenols from apple pomace. *Food Chem.* **2000**, *68*, 81−85.
(33) Aitken, R. J.; Buckingham, D.; Harkiss, D. Use of a xanthine oxidase free radical generating system to investigate the cytotoxic effects of reactive oxygen species on human spermatozoa. *J. Reprod. Fertil.* **1993**, *97*, 441−450.
(34) Ries, W. L.; Key, L. L., Jr.; Rodriguiz, R. M. Nitroblue tetrazolium reduction and bone resorption by osteoclasts *in vitro* inhibited by a manganese-based superoxide dismutase mimic. *J. Bone Miner. Res.* **1992**, *7*, 931−939.
(35) Bielski, B. H. J.; Shiue, G. G.; Bajuk, S. Reduction of nitro blue tetrazolium by $CO_2^-$ and $O_2^-$ radicals. *J. Phys. Chem.* **1980**, *84*, 830−833.
(36) Bassingthwaighte, J. B.; Chinn, T. M. Reexamining Michaelis-Menten enzyme kinetics for xanthine oxidase. *Adv. Physiol. Educ.* **2013**, *37*, 37−48.
(37) Furuno, K.; Akasako, T.; Sugihara, N. The contribution of the pyrogallol moiety to the superoxide radical scavenging activity of flavonoids. *Biol. Pharm. Bull.* **2002**, *25*, 19−23.
(38) Lavelli, V.; Hippeli, S.; Peri, C.; Elstner, E. F. Evaluation of radical scavenging activity of fresh and air-dried tomatoes by three model reactions. *J. Agric. Food Chem.* **1999**, *47*, 3826−3831.
(39) Klibanov, A. M. Improving enzymes by using them in organic solvents. *Nature* **2001**, *409*, 241−246.
(40) Jothy, S. L.; Zuraini, Z.; Sasidharan, S. Phytochemicals screening, DPPH free radical scavenging and xanthine oxidase inhibitory activities of *Cassia fistula* seeds extract. *J. Med. Plant Res.* **2011**, *5*, 1941−1947.
(41) Robins, S. P. An enzyme-linked immunoassay for the collagen cross-link pyridinoline. *Biochem. J.* **1982**, *207*, 617−620.
(42) Loo, R. R.; Dales, N.; Andrews, P. C. Surfactant effects on protein structure examined by electrospray ionization mass spectrometry. *Protein Sci.* **1994**, *3*, 1975−1983.
(43) Masuoka, N.; Isobe, T.; Kubo, I. Antioxidants from *Rabdosia japonica*. *Phytother. Res.* **2006**, *20*, 206−213.
(44) Zheng, W.; Wang, S. Y. Antioxidant activity and phenolic compounds in selected herbs. *J. Agric. Food Chem.* **2001**, *49*, 5165−5170.

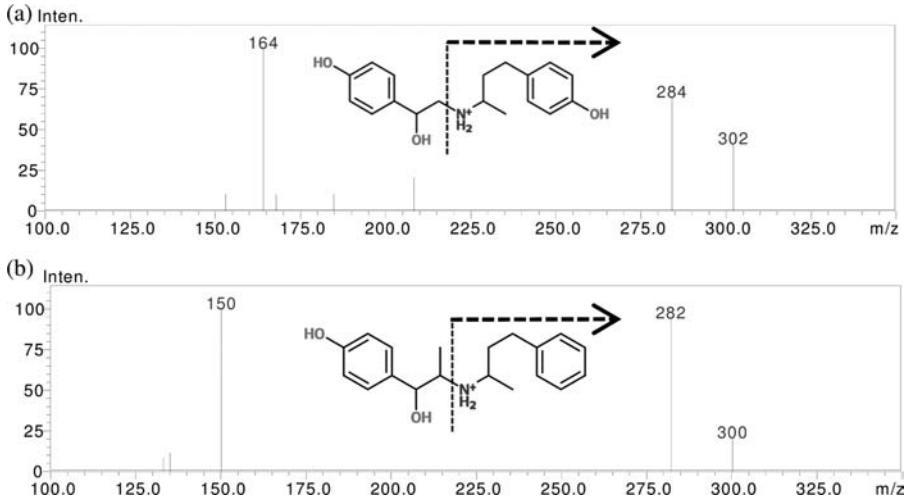


**Figure 1.** Structures and product ion mass spectra of (a) ractopamine ($m/z$ 302.10) and (b) nylidrin ($m/z$ 300.15) in electrospray positive-ion mode.

paraffin film as internal standard (30 ng/mL). All stock solutions were stored in darkness at −20 °C.

**Experimental Animals and Drug Administration.** *Experimental Animals.* Male Sprague−Dawley rats (230 ± 20 g) were purchased from the National Yang-Ming University Animal Center, Taipei, Taiwan. Rats were housed with a 12 h light/dark cycle. Laboratory rodent diet 5001 (PMI Feeds, Richmond, IN, USA) and water were provided freely at all times. The animal experimental protocol was approved by the Institutional Animal Care and Use Committee of National Yang-Ming University (IACUC no. 1011216) and was consistent with the guidelines of the National Research Council, USA.[12]

*Intravenous Administration of Ractopamine.* Rats were anesthetized with a mixture of urethane (1 g/kg) and $\alpha$-chloralose (0.1 g/kg) by intraperitoneal injection. Fur at the surgical site was shaved, and the skin was disinfected with 70% ethanol. The right jugular vein and the left femoral vein were catheterized with polyethylene tubing for blood sampling and drug administration, respectively.

After surgery, ractopamine was administered in normal saline at 1 or 10 mg/kg, intravenously (iv) ($n$ = 6 for each group). A 300 $\mu$L blood sample was collected from the jugular vein at 0, 15, 30, 45, 60, 90, 120, 180, 240, and 360 min after drug administration. Blood samples were placed in heparin-rinsed eppendorf vials and centrifuged at 6000$g$ for 10 min at 4 °C to obtain plasma. Plasma was stored at −20 °C until analysis.

If the concentration of ractopamine was above 50 ng/mL, the plasma sample was diluted with blank plasma, 5-fold (1 mg/kg, iv) or 50-fold (10 mg/kg, iv).

*Oral Administration of Ractopamine.* Pentobarbital sodium (50 mg/kg) was used to anesthetize the rats via intraperitoneal administration. Surgical sites were shaved and cleaned with 70% ethanol. The right jugular vein was catheterized with polyethylene tubing for blood sampling. The catheter was guided under the skin to the dorsal neck region and fixed.[13] After surgery, the rats were allowed to recover in a clean cage for at least 24 h before drug administration.

After the stabilization period, ractopamine in water (10 mg/kg, per os (po)) was administered to the rats ($n$ = 6). A 300 $\mu$L blood sample was collected from the jugular vein at 0, 5, 15, 30, 45, 60, 90, 120, 180, 240, and 360 min after drug administration. Blood samples were centrifuged at 6000$g$ for 10 min at 4 °C to obtain plasma. Plasma was stored at −20 °C until analysis.

*Organ Distribution.* Forty-five minutes after ractopamine administration (1 mg/kg, iv), blood samples were collected via cardiac puncture, and the rat was sacrificed by decapitation. The brain, liver, heart, spleen, lung, kidney, and gracilis muscle were collected and weighed. These organ samples were stored at −20 °C until analysis.

**Sample Preparation.** *Blood Samples.* Plasma samples (100 $\mu$L) were mixed with 10 $\mu$L of internal standard (nylidrin hydrochloride 30 ng/mL in acetonitrile) and 200 $\mu$L acetonitrile for protein precipitation. The mixture was centrifuged at 16000$g$ for 10 min at 4 °C. The supernatant was evaporated to dryness at 40 °C in a centrifuge evaporator. The dried residue was reconstituted in 100 $\mu$L of 0.1% formic acid/methanol (60:40, v/v) and filtered through a 0.22 $\mu$m filter. An aliquot (5 $\mu$L) of the filtrate was analyzed using HPLC-MS/MS.

*Organ Samples.* Organ samples were homogenized in 50% aqueous acetonitrile (1:5, w/v), and the homogenate was centrifuged at 16000$g$ for 15 min at 4 °C. The supernatant was collected and stored at −20 °C until analysis.

Organ sample preparation was as described under Blood Samples. In brief, the organ sample (100 $\mu$L) was mixed with 10 $\mu$L of internal standard, followed by 200 $\mu$L of acetonitrile for protein precipitation. Samples were then subjected to centrifugation, evaporation, reconstitution, and filtration. Finally, 5 $\mu$L of filtrate was introduced into the HPLC-MS/MS system for analysis.

If the concentration of ractopamine exceeded the upper limit of the linearity range (50 ng/mL), these organ homogenate samples were diluted with blank organ homogenate.

**HPLC-MS/MS.** The HPLC-MS/MS system consisted of an LCMS-8030 triple-quadrupole mass spectrometer (Shimadzu, Kyoto, Japan) equipped with an electrospray ionization interface, coupled to a Shimadzu LC-20AD HPLC system (Shimadzu). The HPLC system was equipped with two pumps, a system controller, an autosampler, a column oven, and an online degasser.

Chromatographic separation was carried out at 35 °C on an Acquity BEH $C_{18}$ column (100 × 2.1 mm, 1.7 $\mu$m) with an in-line filter (Phenomenex AF0-8497, 0.5 $\mu$m depth × 0.004 i.d.). Isocratic elution was used for separation. The mobile phase was 0.1% formic acid/methanol (60:40, v/v). The flow rate was 0.2 mL/min, and the injection volume was 5 $\mu$L. The temperature of the autosampler was 8 °C.

Before analysis, a standard solution of ractopamine (100 ng/mL) was injected into the tandem mass spectrometer. The precursor ion of ractopamine was found in full-scan positive-ion mode. The mass-to-charge ratio ($m/z$) of the precursor ion was 302. The product ion $m/z$ 164 was selected for quantification (Figure 1).

The mass transition of nylidrin was determined using the same procedure. The transition $m/z$ 300 → 150 was chosen for nylidrin (Figure 1).

The optimized parameters for the mass spectrometer were as follows: nebulizing gas (nitrogen) flow, 3.0 L/min; drying gas (nitrogen) flow, 15 L/min; collision gas (argon) pressure, 230 kPa;


dx.doi.org/10.1021/jf5026168 | J. Agric. Food Chem. 2014, 62, 9273−9278

dissolution line temperature, 250 °C; and heat block temperature, 400 °C.

**Method Validation.** *Linearity, Accuracy, and Precision.* The method validation confirms that the method used for the quantification of analyte in a biological sample is reliable and reproducible.[14] Calibration standards were prepared from stock solution of ractopamine and then added to blank plasma or homogenate to spike samples with concentrations of 0.5, 1, 5, 10, and 50 ng/mL. These spiked samples were processed as described under Sample Preparation. The calibration curve was constructed from the ratio of the peak areas of ractopamine and the internal standard (nylidrin) to the nominal concentration of ractopamine. The correlation coefficient ($r^2$) of all calibration curves was at least 0.995.

Six replications of the calibration curve were performed on the same day (intraday) and over six consecutive days (interday) to evaluate precision and accuracy. Accuracy describes the proximity of mean results (observed concentration, $C_{obs}$) of this method to the true concentration (nominal concentration, $C_{nom}$). Accuracy can be calculated as bias (%) = $[(C_{obs} - C_{nom})/C_{nom}] \times 100$. Precision means the closeness of each individual result to the others. Precision, quantified as relative standard deviation (RSD), was calculated as follows: RSD (%) = [standard deviation (SD)/$C_{obs}$] × 100.

The bias and coefficient of variation were kept within ±15%, except for the lower limit of quantification (LLOQ), which was not permitted to exceed ±20%.

*Matrix Effect and Recovery Evaluation.* The matrix effects and recovery were calculated using three sets of samples. Ractopamine was evaluated at 0.5, 5, and 50 ng/mL, and nylidrin was evaluated at 3 ng/mL. The three sets were as follows.

Set 1: For standard solutions of ractopamine, the ractopamine stock solution was diluted to 0.5, 5, or 50 ng/mL with 0.1% formic acid/methanol (60:40, v/v).

Set 2: Blank plasma or organ homogenate (100 μL) was processed as described under Sample Preparation and reconstituted to obtain blank matrix. Blank matrix (90 μL) was added to 10 μL of standard solution, giving postextraction spiked ractopamine samples at three different concentrations.

Set 3: Standard solution (10 μL) and blank plasma or organ homogenate (90 μL) were mixed and subjected to sample preparation and reconstitution. Then a pre-extraction spiked ractopamine sample was acquired and injected into the HPLC-MS/MS system.

The matrix effect is given as the ratio of mean peak area for the postextraction spiked samples (set 2) to that of the standard solution samples (set 1). Recovery was quantified as the ratio of mean peak area of the pre-extraction spiked samples (set 3) to that of the postextraction spiked samples (set 2).

*Stability.* The stability of ractopamine was evaluated by the following methods, as recommended by the FDA: 1, freeze and thaw; 2, short term; 3, long term; 4, postpreparative; and 5, stock solution.[14] Samples for freeze and thaw stability were stored at −20 °C for 24 h and thawed at room temperature. This freeze and thaw cycle was repeated a total of three times. The samples were analyzed after the third cycle. Short-term stability was measured by maintaining the samples at room temperature for 4 h and then analyzing them. Long-term stability was assessed by storing the samples at −20 °C for 30 days. The samples for postpreparative stability testing were processed as described under Sample Preparation. These samples were then maintained in an autosampler at 8 °C for 8 h. The stock solution stability was evaluated by keeping the stock solution at room temperature for 6 h.

Concentrations of 0.5, 5, and 50 ng/mL were used to measure the stability of ractopamine in plasma or organ homogenate. The stock solution for stability evaluation was prepared in the mobile phase before analysis. Stability was calculated using the relative error between the freshly prepared and stored samples. Sample stability was limited to within ±15%.

**Pharmacokinetic Analysis.** Pharmacokinetic parameters were calculated using WinNonlin Standard Edition 1.0 (Pharsight Corp., Mountain View, CA, USA) with compartmental and noncompartmental models for the intravenous and oral groups, respectively. Akaike's information criterion (AIC) was used to choose the pharmacokinetic models (one- or two-compartment).[15] The lowest AIC value indicated the best way to describe the pharmacokinetic data. The results are expressed as the mean ± standard deviation. The criterion of statistical significance was Student's $t$ test, with $p < 0.05$.

## RESULTS

**HPLC-MS/MS.** In positive-ion mode, the multiple reaction monitoring (MRM) transitions were $m/z$ 302 → 164 for ractopamine and $m/z$ 300 → 150 for nylidrin (internal standard). The fragmentation pathway of $m/z$ 302 → 164 was consistent with previous results for ractopamine.[16]

The second step was optimizing chromatographic separation. Peak shape, run time, and sensitivity were influenced by the composition of the mobile phase. To reduce tailing, 0.1% formic acid was selected as the aqueous phase. Different mobile phase ratios were examined: 0.1% formic acid/methanol (10:90, 60:40, and 90:10, v/v).

The experimental results revealed that 0.1% formic acid/methanol (60:40, v/v) gave the sharpest peak and the best run time. Thus, 0.1% formic acid/methanol (60:40, v/v) was chosen for the remaining experiments. Under these conditions, the retention time of ractopamine was 2.0 min and that of nylidrin was 5.5 min.

The similar structures of ractopamine and nylidrin justified the use of this internal standard. The similar fragmentation patterns and the structural similarity between ractopamine and nylidrin may ensure the specificity of this analytical method.[17] Thus, nylidrin was an ideal choice as internal standard.

Typical chromatograms are shown in Figures S1−S4 in the Supporting Information for blank plasma, liver, heart, spleen, lung, kidney, brain, and muscle homogenates; blank plasma or organ homogenates spiked with ractopamine; and finally samples collected from experimental animals after ractopamine administration (1 mg/kg, iv). There was no significant endogenous interference under optimized HPLC-MS/MS conditions (panels a and d of Figures S1−S4). These results show acceptable selectivity for the determination of ractopamine in the biological samples. Furthermore, carry-over effects were not observed in any experiment.

**Sample Preparation.** A pilot experiment was undertaken to determine the most appropriate sample preparation method. Liquid−liquid extraction and protein precipitation by methanol or acetonitrile were examined. Liquid−liquid extraction gave the lowest recovery of ractopamine in rat plasma, approximately 30%. The extraction recoveries via methanol and acetonitrile protein precipitation were 75 and 85%, respectively. The low recovery by liquid−liquid extraction may be due to the high polarity of ractopamine; thus, this method is not suitable.[18] Protein precipitation by acetonitrile was selected as the sample preparation method in this experiment. In the full study, the extraction recovery of ractopamine in rat plasma via acetonitrile protein precipitation was 86.7 ± 2.8% (Supporting Information Table S2, $n = 3$).

Unfortunately, the chromatographic peak obtained using acetonitrile protein precipitation was split, which made integration difficult. This problem was resolved by evaporating the supernatant after protein precipitation. After supernatant evaporation, the chromatographic peak was narrow and sharp.

**Method Validation.** *Linearity, Accuracy, And Precision.* To evaluate linearity, a calibration curve was derived from the peak area ratios of ractopamine and the internal standard, nylidrin. The linear range for ractopamine in rat plasma and


dx.doi.org/10.1021/jf5026168 | J. Agric. Food Chem. 2014, 62, 9273−9278

organ homogenates was 0.5−50 ng/mL; all correlation coefficients ($r^2$) were >0.999.

The limit of detection (LOD) for ractopamine was 0.01 ng/mL, with a signal-to-noise ratio of 3. The lower limit of quantification (LLOQ) in plasma and organ homogenate was 0.5 ng/mL.

Intraday and interday assays were used to evaluate accuracy (as % bias) and precision (as % RSD) for ractopamine (Supporting Information Table S1, $n$ = 6). All bias and RSD values were below 15%, except for the LLOQ (0.5 ng/mL). At this concentration, 20% is the maximum acceptable value.[14] These method validation results indicate that this analytical method is reproducible.

*Matrix Effect and Recovery.* The mean matrix effects for ractopamine in plasma, liver, heart, spleen, lung, kidney, brain, and muscle homogenates were 81.2 ± 4.2, 97.5 ± 2.3, 123.3 ± 2.6, 120.8 ± 3.7, 112.6 ± 2.9, 59.5 ± 2.6, 135.0 ± 4.5, and 113.1 ± 1.5%, respectively (Supporting Information Table S2, $n$ = 3). Compared with the standard solution (set 1) and postextraction spiked solution (set 2), it was very easy to determine ion suppression or enhancement in the plasma and organ samples. Thus, the matrix effect of ractopamine should not be ignored in these experiments.

Extraction recovery is defined as the difference between preextraction (set 3) and postextraction spiked (set 2) samples. The mean extraction recoveries for ractopamine varied from 86.7 ± 2.8 to 98.0 ± 0.6% (Supporting Information Table S2, $n$ = 3).

Significant matrix effects were observed in rat plasma and organ homogenates. However, within a given matrix, the matrix effects and recoveries were independent of concentration within the linear range. To examine the matrix effect and recovery in the whole experiment, samples collected from animals were diluted to within the linear range using blank plasma or organ homogenate. In addition, all experimental samples were diluted to the same linear range (0.5−50 ng/mL). The matrix effect and recovery, correlated with concentration, were not significantly different.

The average matrix effects and recoveries of nylidrin in rat plasma and organ homogenates ranged from 98.6 ± 1.3 to 106.9 ± 0.8 and from 80.8 ± 0.3 to 97.1 ± 0.2, respectively (Supporting Information Table S2, $n$ = 3). On the basis of these results, nylidrin had a small matrix effect and extraction loss after sample preparation. Thus, nylidrin is a suitable internal standard for this study.

*Stability.* Following FDA guidelines, five stability evaluation experiments (freeze−thaw cycle, long-term, short-term, postpreparative, and stock solution) were designed to simulate different conditions: sample collection, storage, preparation, or other handling conditions. Stability was quantified as the relative error in concentration between freshly prepared and stored samples. Stability in the freeze−thaw, short-term, long-term, postpreparative, and stock solution analyses were all within ±15% (Supporting Information Table S3, $n$ = 3). These results indicate that ractopamine was stable during all of these experimental processes.

**Pharmacokinetics of Ractopamine.** To investigate the pharmacokinetics and oral bioavailability of ractopamine, it was administered orally (10 mg/kg, po) and intravenously (1 and 10 mg/kg, iv) (Figure 2, $n$ = 6 for each group). Plasma samples were collected and analyzed by the validated method. To describe the pharmacokinetic profile precisely, it is important to select a proper compartmental model (one- or two-compartment models). Akaike's information criterion (AIC) provides a suitable criterion for the selection of compartmental models.[15] A smaller AIC value means the model has a better fit to the concentration−time curve calculated using WinNonlin. In this experiment, the average AIC values for the one-compartment model (ractopamine 1 and 10 mg/kg, iv) were −86.82 and −23.36, respectively. The mean AIC values of the two-compartment model were −98.27 and −41.16, respectively. The two-compartment model thus describes the pharmacokinetics of ractopamine better (Table 1).

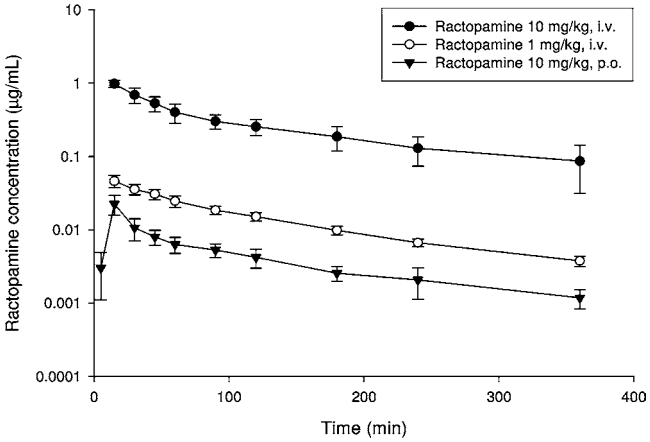


**Figure 2.** Concentration versus time profile of ractopamine in rat plasma (10 and 1 mg/kg, iv, and 10 mg/kg, po) Data are expressed as the mean ± SD ($n$ = 6).

**Table 1. Pharmacokinetic Data for Plasma Ractopamine in Rats**[a]

| pharmacokinetic parameter | ractopamine 1 mg/kg, iv | ractopamine 10 mg/kg, iv | ractopamine 10 mg/kg, po |
|---|---|---|---|
| AIC of one compartment | −86.82 ± 4.40 | −23.36 ± 2.93 | |
| AIC of two compartments | −98.27 ± 6.53 | −41.16 ± 6.92 | |
| AUC (min mg/mL) | 5.85 ± 0.70 | 123.92 ± 40.23[b] | 1.75 ± 0.24 |
| AUC/dose | 5.85 ± 0.70 | 12.39 ± 4.02[b] | |
| $t_{1/2,\alpha}$ (min) | 21 ± 7.4 | 18 ± 8.0 | |
| $t_{1/2,\beta}$ (min) | 118 ± 25 | 165 ± 49 | 113 ± 23 |
| $T_{max}$ (min) | | | 15 |
| $C_0$ (μg/mL) | 0.062 ± 0.015 | 1.65 ± 0.33[b] | |
| Cl (mL/min/kg) | 173 ± 22 | 87.4 ± 25.2[b] | 5800 ± 735 |
| MRT (min) | 146 ± 25 | 185 ± 65 | 148 ± 30 |
| $V_{ss}$ (L/kg) | 25.4 ± 5.7 | 14.9 ± 2.0[b] | 945 ± 196 |
| $F$ (%) | | | 2.99 ± 0.40 |

[a]Abbreviations: AIC, Akaike's information criterion; AUC, area under the concentration−time curve; $t_{1/2,\alpha}$, distribution half-life; $t_{1/2,\beta}$, elimination half-life; $T_{max}$, time of peak plasma level; $C_0$, initial drug concentration; Cl, clearance; MRT, mean residence time; $V_{ss}$, apparent volume of distribution at steady state; $F$, bioavailability. Data are expressed as the mean ± SD ($n$ = 6). [b]$p < 0.05$ compared with 1 mg/kg, iv.

The equation for the two-compartment model is $C_p = A\ e^{-\alpha t} + B\ e^{-\beta t}$. This reflects the sum of two different processes in the body: distribution and elimination, presented as $A\ e^{-\alpha t}$ and $B\ e^{-\beta t}$, respectively. The parameters $\alpha$ and $\beta$ are the distribution and elimination constants, respectively. The $A$ and $B$ values are the intercepts of the distribution and elimination phases.


dx.doi.org/10.1021/jf5026168 | J. Agric. Food Chem. 2014, 62, 9273−9278

Additional pharmacokinetic parameters are as follows. Distribution and elimination half-lives are referred to as $t_{1/2,\alpha}$ and $t_{1/2,\beta}$, respectively. AUC, the area under the concentration−time curve, is related to the extent of drug absorption. $C_0$, the initial drug concentration, is calculated by extrapolation using the pharmacokinetic equation. Cl, clearance, is an indicator of drug elimination. MRT, mean residence time, could be considered the average period of residence of individual molecules of the drug in the body. $V_{ss}$ is the apparent volume of distribution at steady state, derived from concentration and total amount. According to the pharmacokinetic parameters calculated using WinNonlin, intravenous ractopamine administration at 1 and 10 mg/kg gave the two-compartment models $C_p = 0.033\ e^{-0.037t} + 0.029\ e^{-0.006t}$ and $C_p = 1.258\ e^{-0.047t} + 0.392\ e^{-0.005t}$, respectively. The average elimination half-lives ($t_{1/2,\beta}$) for the two doses of ractopamine were 118 and 165 min, respectively (Table 1, $n = 6$ for each group).

The noncompartmental model was selected to describe the pharmacokinetic profile after oral administration of ractopamine (10 mg/kg, po) (Table 1, $n = 6$). The pharmacokinetic parameter $T_{max}$ indicates the time of peak plasma level. Bioavailability ($F$) was used to describe systemic availability: $F\ (\%) = 100 \times (AUC_{oral}/dose_{oral})/(AUC_{iv}/dose_{iv})$. $T_{max}$ was 15 min, indicating that ractopamine is rapidly absorbed in rats. Bioavailability was derived from the AUC after intravenous (1 mg/kg) and oral administration (10 mg/kg). The oral bioavailability of ractopamine ($F = 100 \times (1.75/10)/5.85$) was around 2.99%.

**Organ Distribution of Ractopamine.** To investigate the tissue distribution of ractopamine, tissues and organs were collected 45 min after administration (1 mg/kg, iv). The ractopamine levels in liver, heart, spleen, lung, kidney, brain, and muscle tissue were 307.85 ± 54.82, 391.11 ± 22.81, 675.77 ± 49.54, 1058.41 ± 78.44, 1211.17 ± 89.25, 24.35 ± 1.85, and 294.81 ± 28.00 ng/g, respectively (Figure 3, $n = 6$). Plasma samples for the organ distribution experiment were collected by cardiac puncture. Plasma ractopamine was 25.09 ± 3.51 ng/mL.

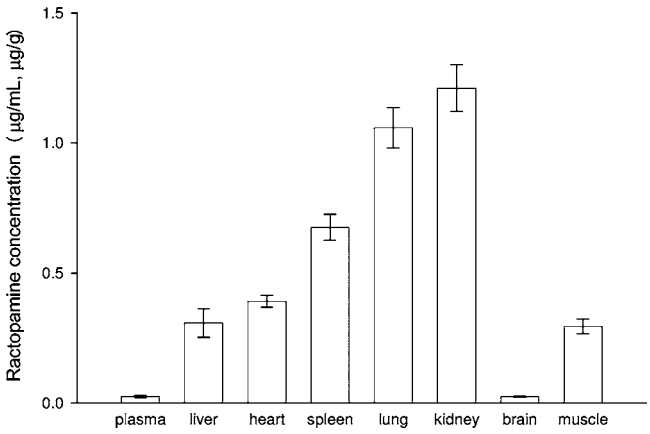


**Figure 3.** Plasma, liver, heart, spleen, lung, kidney, brain, and muscle levels of ractopamine after administration (1 mg/kg, iv). Data are expressed as the mean ± SD ($n = 6$). Concentrations in plasma and organs are micrograms per milliliter and micrograms per gram, respectively.

## DISCUSSION

**Nonlinear Pharmacokinetics of Ractopamine.** Significant differences were found ($p$ value < 0.05) in the pharmacokinetic parameters of the two intravenous doses: AUC/dose (5.85 ± 0.70 vs 12.39 ± 4.02), clearance (173.20 ± 21.75 vs 87.39 ± 25.21), and $V_{ss}$ (25402 ± 5734 vs 14879 ± 1971). That these pharmacokinetic parameters varied with dose may imply nonlinear pharmacokinetics after intravenous ractopamine administration at between 1 and 10 mg/kg.[19] From these results, we hypothesize that excess ractopamine may accumulate due to organ saturation and retarded elimination in the kidney.

**Oral Bioavailability of Ractopamine.** The oral bioavailability of ractopamine was derived from the AUC for intravenous and oral administration. Due to nonlinear pharmacokinetics at high doses, the AUC data for intravenous ractopamine (10 mg/kg) were not utilized. In this experiment, the oral bioavailability of ractopamine was 2.99%.

Oral bioavailability can be evaluated by comparing the amount of parent drug in the collected urine with the total amount administered. Smith and Paulson found, via urine collection, that the oral bioavailability of ractopamine in rats was 2%.[9] Although in our experiment the bioavailability of ractopamine was determined via plasma collection, the result is consistent with the previous study. However, due to the different methods of evaluation, the experimental results may differ. In addition, oral bioavailability has been studied in turkeys and swine, and the results were 8 and 4−16%, respectively.[8,20] Thus, bioavailability may vary between species.

**Ractopamine Accumulation in Rat Organs.** On the basis of the above pharmacokinetic results, a time point of 45 min was selected because that was close to the intersection of the first and second compartments.

The organ distribution results suggest that ractopamine is extensively distributed into tissues 45 min after intravenous administration. The lowest concentration was found in the brain, suggesting that the distribution of ractopamine, with its high polarity, may be restricted by the blood−brain barrier. The highest level was observed in the kidney, which may indicate that the kidney is the primary organ of elimination for this drug in rats. This is consistent with the hypothesis given under Nonlinear Pharmacokinetics of Ractopamine. The nonlinear pharmacokinetics of ractopamine in high doses may be due to nonlinear elimination in the kidney.

In a previous study, Smith and Paulson reported that after oral administration of ractopamine (9.9 mg/kg), approximately 59% of the drug was eliminated in bile. Thus, they suggested that bile excretion is the most important elimination pathway for ractopamine in rats.[9] Our findings differ. This inconsistency may be explained by the first-pass effect. If the rats were given ractopamine orally, most of the drug would be eliminated via bile and would not enter the circulation. Intravenous administration of ractopamine, however, avoids the first-pass effect. Thus, most of the drug may be eliminated by the kidney. This may also explain the low oral bioavailability of ractopamine in rats: most of it may be excreted in bile.

## ASSOCIATED CONTENT

### Supporting Information

Method validation results and typical HPLC-MS/MS chromatograms. This material is available free of charge via the Internet at http://pubs.acs.org.

## AUTHOR INFORMATION


### Corresponding Author

*(T.-H.T.) Mail: Institute of Traditional Medicine, School of Medicine, National Yang-Ming University, 155 Li-Nong Street, Section 2, Taipei 112, Taiwan. Fax: (886-2) 2822 5044. Phone: (886-2) 2826 7115. E-mail: thtsai@ym.edu.tw.



### Funding

This work was supported in part by research grants from the National Science Council Taiwan (NSC102-2113-M-010-001-MY3) and by TCH 103-02 and TCH 10301-62-021 from Taipei City Hospital, Taiwan.


### Notes

The authors declare no competing financial interest.

## REFERENCES


(1) Emery, P. W.; Rothwell, N. J.; Stock, M. J.; Winter, P. D. Chronic effects of $\beta$2-adrenergic agonists on body composition and protein synthesis in the rat. *Biosci. Rep.* **1984**, *4*, 83−91.

(2) Baker, P. K.; Dalrymple, R. H.; Ingle, D. L.; Ricks, C. A. Use of a $\beta$-adrenergic agonist to alter muscle and fat deposition in lambs. *J. Anim. Sci.* **1984**, *59*, 1256−1261.

(3) Ricks, C. A.; Dalrymple, R. H.; Baker, P. K.; Ingle, D. L. Use of a $\beta$-agonist to alter fat and muscle deposition in steers. *J. Anim. Sci.* **1984**, *59*, 1247−1255.

(4) Peterla, T. A.; Scanes, C. G. Effect of $\beta$-adrenergic agonists on lipolysis and lipogenesis by porcine adipose tissue in vitro. *J. Anim. Sci.* **1990**, *68*, 1024−1029.

(5) Hausman, D. B.; Martin, R. J.; Veenhuizen, E. L.; Anderson, D. B. Effect of ractopamine on insulin sensitivity and response of isolated rat adipocytes. *J. Anim. Sci.* **1989**, *67*, 1455−1464.

(6) Smith, D. J. The pharmacokinetics, metabolism, and tissue residues of $\beta$-adrenergic agonists in livestock. *J. Anim. Sci.* **1998**, *76*, 173−194.

(7) ESFA (European Food Safety Authority).. Scientific Opinion of the Panel on Additives and Products or Substances used in Animal Feed (FEEDAP) on a request from the European Commission on the safety evaluation of ractopamine. *EFSA J.* **2009**, *1041*, 1−52.

(8) Smith, D. J.; Feil, V. J.; Huwe, J. K.; Paulson, G. D. Metabolism and disposition of ractopamine hydrochloride by turkey poults. *Drug Metab. Dispos.* **1993**, *21*, 624−633.

(9) Smith, D. J.; Paulson, G. D. Growth characteristics of rats receiving ractopamine hydrochloride and the metabolic disposition of ractopamine hydrochloride after oral or intraperitoneal administration. *J. Anim. Sci.* **1994**, *72*, 404−414.

(10) Churchwell, M. I.; Holder, C. L.; Little, D.; Preece, S.; Smith, D. J.; Doerge, D. R. Liquid chromatography/electrospray tandem mass spectrometric analysis of incurred ractopamine residues in livestock tissues. *Rapid Commun. Mass Spectrom.* **2002**, *16*, 1261−1265.

(11) Chang, J. C.; Lee, W. C.; Wu, Y. T.; Tsai, T. H. Distribution of blood-muscle for clenbuterol in rat using microdialysis. *Int. J. Pharm.* **2009**, *372*, 91−96.

(12) National Research Council (USA). Committee on Guidelines for the Use of Animals in Neuroscience and Behavioral Research. *Guidelines for the Care and Use of Mammals in Neuroscience and Behavioral Research*; National Academies (US) Press: Washington, DC, USA, 2003.

(13) Thrivikraman, K. V.; Huot, R. L.; Plotsky, P. M. Jugular vein catheterization for repeated blood sampling in the unrestrained conscious rat. *Brain Res. Protoc.* **2002**, *10*, 84−94.

(14) U.S. FDA. *Guidance for Industry, Bioanalytical Method Validation*; U.S. Department of Health and Human Services, Food and Drug Administration Center for Drug Evaluation and Research (CDER): Washington, DC, USA, 2001.

(15) Yamaoka, K.; Nakagawa, T.; Uno, T. Application of Akaike's information criterion (AIC) in the evaluation of linear pharmacokinetic equations. *J. Pharmacokinetics Biopharm.* **1978**, *6*, 165−175.

(16) Thevis, M.; Opfermann, G.; Schanzer, W. Liquid chromatography/electrospray ionization tandem mass spectrometric screening and confirmation methods for $\beta$2-agonists in human or equine urine. *J. Mass Spectrom.* **2003**, *38*, 1197−1206.

(17) Antignac, J. P.; Marchand, P.; Le Bizec, B.; Andre, F. Identification of ractopamine residues in tissue and urine samples at ultra-trace level using liquid chromatography-positive electrospray tandem mass spectrometry. *J. Chromatogr., B, Anal. Technol. Biomed. Life Sci.* **2002**, *774*, 59−66.

(18) McDowall, R. D. Sample preparation for biomedical analysis. *J. Chromatogr.* **1989**, *492*, 3−58.

(19) Mehvar, R. Principles of nonlinear pharmacokinetics. *Am. J. Pharm. Educ.* **2001**, *65*, 178−184.

(20) Dalidowicz, J. E.; Thomson, T. D.; Babbitt, G. E. Ractopamine hydrochloride, a phenethanolamine repartitioning agent. In *Xenobiotics and Food-Producing Animals*; Hutson, D. H., Hawkins, D. R., Paulson, G. D., Struble, C. B., Eds.; American Chemical Society: Washington, DC, USA, 1992; Vol. 503, pp 234−243.

were obtained from Fluka (Buchs, Switzerland), whereas harmane, indoleacrylic acid (IAA), CHCA, 1,5-DAN, and harmine were obtained from Wako and DHB was purchased from TCI MARK (Tokyo, Japan). Strictinin was purchased from Nagara Science Co., Ltd. (Gifu, Japan). An indium tin oxide (ITO)-coated slide glass was obtained from Sigma-Aldrich.

**Animals.** Male 7-week-old BALB/C mice were purchased from Kyudo Co., Ltd. (Saga, Japan), housed in a temperature- and humidity-controlled room, and fed a commercial diet and water ad libitum. This experiment was carried out according to the guidelines for animal experiments at the Faculty of Agriculture, Kyushu University. The study protocol was approved (no. A26-090-0) by the Animal Care and Use Committee of Kyushu University, Fukuoka, Japan.

**Detection of Strictinin on a Stainless Steel MALDI Sample Plate.** Strictinin was dissolved in distilled water at 5 mM stock concentration and stored at −20 °C until use. The stock solution was diluted with 100% methanol, acetone, or acetonitrile to 100 μM to prepare the analyte solutions. Nine matrix candidate chemicals were initially examined as matrices for the detection of strictinin with MALDI-TOF-MS (AXIMA Performance; Shimadzu, Kyoto, Japan). Ten microliters of 100 μM strictinin was added to an equal volume of each matrix solution (10 mg/mL in 100% methanol, acetone, or acetonitrile). Aliquots (1 μL) of strictinin−matrix mixtures were spotted onto a 384-well stainless steel MALDI sample plate (50 pmol strictinin/well, on-plate, $n = 5$) and analyzed in both the negative and positive ionization modes. The experiment was performed under conditions in which the detection voltage of the base peaks was between 700 and 800 mV. This instrument was equipped with a 337 nm $N_2$ laser. Each sample spot was analyzed for 242 shots, and all spectrometric data were processed and analyzed using Shimadzu Biotech Lachlan software. Among the nine chemicals tested, we selected three matrix candidates (1,5-DAN, harmane, and ferulic acid) that could ionize strictinin. Next, the best condition for ionizing strictinin using 1,5-DAN (10 mg/mL in 80% acetone), harmane, and ferulic acid (10 mg/mL in 80% acetonitrile) was evaluated on the same MALDI sample plate.

**MALDI-MSI of Strictinin Spotted on Mouse Kidney Sections.** Sections (8 μm thick) of normal mouse kidney were prepared with a cryostat and then thaw mounted onto an ITO-coated glass slide. Strictinin (5 mM) was diluted with 80% acetone or 80% acetonitrile to prepare a series of solutions (5, 25, 50, 100, 250, and 500 μM). Diluted strictinin solution and a blank (0.2 μL) was spotted onto the mouse kidney sections. The final amounts of strictinin at each spot were 0, 1, 5, 10, 20, 50, or 100 pmol. Samples were allowed to dry for 5 min at room temperature before the matrix spray coating step. The matrix solution was prepared by dissolving 1,5-DAN in 80% acetone (10 mg/mL), harmane, or ferulic acid in 80% acetonitrile (10 mg/mL), respectively, and was sprayed in a draft hood using an airbrush (Testor, Rockford, IL, USA) at room temperature (22 °C, 50% humidity). In the MSI experiment, MALDI-TOF-MS (AXIMA Performance) was used. Data were acquired in the negative ionization mode with 50 μm spatial resolution (10 laser shots/data point), and signals between $m/z$ 100 and 1000 were collected. Acquired MSI data were normalized with the total ion count using SIMedit software (Shimadzu), and obtained data were further processed with the freely available BioMap software (Novartis, Basel, Switzerland). The signal intensity of each imaging datum is represented as the normalized intensity.

**Strictinin Treatment of Mouse and Tissue Sample Collection.** After 12 h of fasting, mice were given a single dose of strictinin (1000 mg/kg body weight, intragastric (ig)) as an aqueous solution with sterile saline containing 1% dimethyl sulfoxide (DMSO) and then sacrificed 1 h after administration. Mouse kidneys were collected and washed with an ice-cold 0.9% NaCl solution. Kidney samples were embedded in Tissue-Tek O.C.T. compounds (Sakura Finetechnical Co., Ltd., Tokyo, Japan) and stored at −80 °C until analysis by MALDI-MSI and LC-MS.

**LC-MS/MS Analysis of Strictinin in Mouse Kidney Samples.** Kidney samples were prepared and analyzed by Lambert's methods with modification.[19] Kidneys were homogenized in 4 volumes of ice-cold PBS (containing 2% ascorbic acid) using a mechanical TOMY MS mash homogenizer (TOMY, Tokyo, Japan) and extracted with ethyl acetate. The ethyl acetate fractions were pooled and dried under $N_2$ gas. Samples were reconstituted in 10% aqueous acetonitrile. All tissue extracts were subjected to electrospray ionization (ESI)-LC-MS analysis using an LCMS-IT-TOF instrument (Shimadzu). The column used was a 250 mm × 4.6 mm i.d., 5 μm, Luna C18 (2) 100 Å column (Phenomenex, Torrance, CA, USA). The oven temperature was 40 °C. The mobile phase was a binary gradient of solvent A ($H_2O$ containing 0.1% formic acid) and solvent B (methanol). Solvent B was increased from 5 to 60% over 2 min and then increased from 60 to 100% at 14 min. The mobile phase flow rate was 0.1 mL/min. Tissue homogenate extracts were resolved with sample buffer, 10% acetonitrile with 10 μM 4-hydroxybenzophenone, as an internal standard. Samples were filtered through a 0.2 μm polytetrafluoroethylene filter, and 20 μL was injected. The MS instrument was operated using an ESI source in the negative ionization mode with survey scans acquired from $m/z$ 100 to 800.

**MALDI-MSI of Strictinin in Kidney Sections from Mice Orally Administered Strictinin.** Strictinin-dosed mouse kidneys were sectioned (8 μm thick) with a cryostat and then thaw mounted onto an ITO-coated glass slide. As a positive control, 250 μM strictinin (0.2 μL) was directly spotted onto the tissue sections. Then, 1,5-DAN matrix solution (10 mg/mL in 80% acetone) was sprayed onto the kidney sections. Imaging data were acquired in the negative ionization mode with 50 μm spatial resolution (10 laser shots/data point) by MALDI-TOF-MS (AXIMA Performance), and signals between $m/z$ 100 and 1000 were collected. The signal intensity of each imaging datum in the figure is represented as the normalized intensity.

MSI analysis of orally dosed strictinin within kidney sections was also performed using an iMScope atmospheric pressure-MALDI-quadrupole ion trap (QIT)-TOF-MS (Shimadzu) equipped with a 355 nm Nd:YAG laser.[20,21] MSI analysis was performed in the negative ionization mode within a mass range of $m/z$ 600−900 for strictinin,

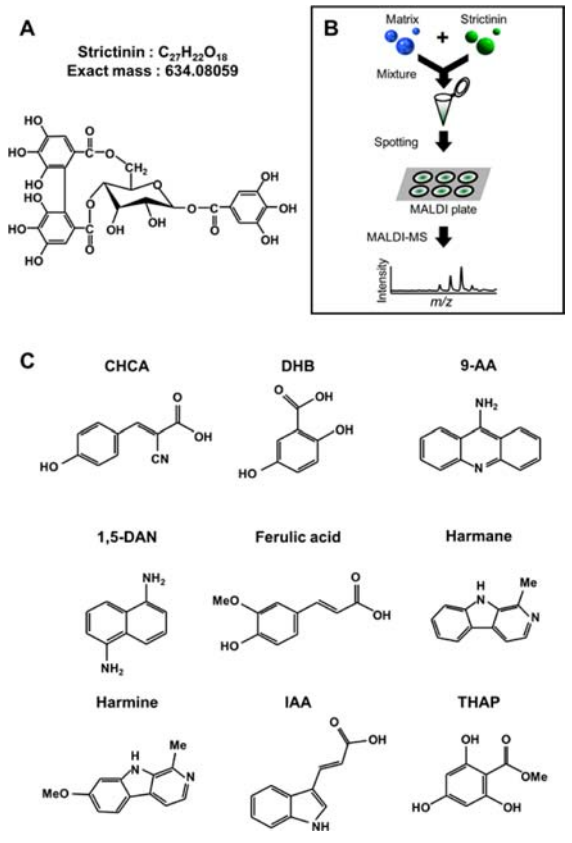


**Figure 1.** (A) Chemical structure of a bioactive ellagitannin, strictinin; (B) schematic representation of matrix screening on a stainless steel MALDI sample plate by MALDI-MS; (C) chemical structures of matrices used in this study.

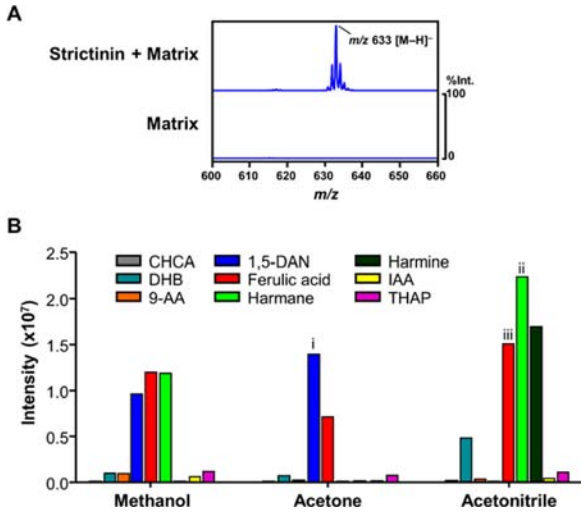


**Figure 2.** Evaluation of optimum conditions for detection of strictinin by MALDI-MS: (A) mass observation for strictinin−matrix mixture or matrix at $m/z$ 633 $[M - H]^-$ on a stainless steel MALDI sample plate (data represent the relative signal intensity when the intensity of the strongest intensity peak was 100%); (B) comparison of three representative solvents (100% methanol, 100% acetone, and 100% acetonitrile) for detection of strictinin ($m/z$ 633) in nine matrix candidates on a stainless steel MALDI sample plate (bar graphs represent the signal intensity at $m/z$ 633 in the negative ionization mode; data are the mean of three independent experiments ($n$ = 5 in each experiment)).

with a spatial resolution of 50 $\mu$m. The laser was irradiated at 50 shots/spectrum at a frequency of 1000 Hz, and the power was set to 80% using the Mass Microscope operation software.

## RESULTS AND DISCUSSION

**Determination of the Optimum Conditions for Ionization of Strictinin on a MALDI Sample Plate.** In MALDI-MS, matrix preparation including selection of the matrix and solvent is a critical step to effectively ionize the analyte because the detection of analyte is completely dependent on these conditions.[22] Because little is known about what matrices can ionize strictinin (Figure 1A), we first attempted to find the optimum conditions for detecting strictinin by selecting several determinants such as matrices, solvents, and ionization modes on the basis of peak detection conditions that achieve the maximum signal-to-noise (S/N) (Figure 1B).

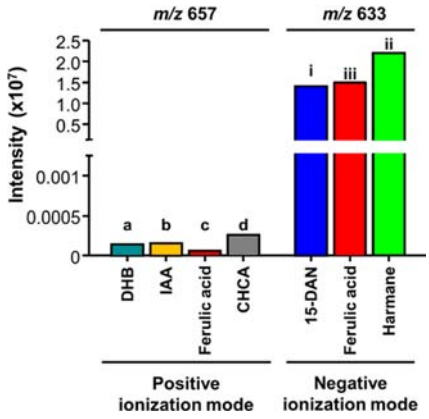


**Figure 4.** Comparison of ionization mode for detection of strictinin. Bar graphs represent the signal intensity at $m/z$ 657 $[M + Na]^+$ (positive ionization mode from Figure 3) or $m/z$ 633 $[M - H]^-$ (negative ionization mode from Figure 2B). Data are the mean of three independent experiments ($n$ = 5 in each experiment).

In this study, nine chemical compounds (Figure 1C) were investigated; some of these are generally used in the analysis of low-molecular-weight biomolecules (i.e., DHB,[23] CHCA,[24] and 9-AA[25−27]), and others are used in the identification and characterization of polyphenols (THAP,[28−30] IAA,[31,32] and ferulic acid[33]). Additionally, 1,5-DAN[34,35] and $\beta$-carbolines[36,37] (i.e., harmane and harmine) are known to be excellent matrices for high-mass proteins or lipids.

First, to detect the peak of strictinin, a matrix solution in 100% methanol was mixed with an equal volume of a strictinin solution in 100% methanol. The mixture of strictinin and matrix was spotted onto a stainless steel MALDI sample plate and analyzed by MALDI-TOF-MS in the negative ionization mode. The deprotonated ion peak at $m/z$ 633, corresponding to strictinin $[M - H]^-$, was detected using 1,5-DAN as a matrix without any background peaks (Figure 2A). Matrix−analyte interactions are important in the ionization/desorption process during MALDI-MS analysis, and they can potentially be modulated by solvent-mediated alternations in matrix−analyte pairing.[38] Next, we analyzed the best matrix and solvent to ionize strictinin among nine different chemical compounds dissolved in 100% methanol, acetone, or acetonitrile, respectively. As shown in Figure 2B, under conditions using the negative ionization mode and 100% methanol solvent, three matrices (1,5-DAN, ferulic acid, and harmane) showed higher sensitivity

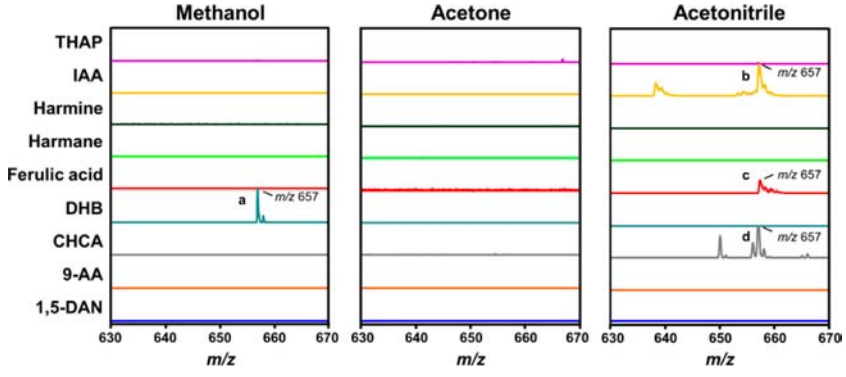


**Figure 3.** Mass spectra of each matrix or solvent on a stainless steel MALDI sample plate by MALDI-MS in the positive ionization mode. MS spectra of strictinin according to three different solvents (100% methanol, 100% acetone, and 100% acetonitrile) at $m/z$ 657 $[M + Na]^+$ in the positive ionization mode. Data represent the relative signal intensity when the intensity of the strongest intensity peak was 100%.


dx.doi.org/10.1021/jf503143g | J. Agric. Food Chem. 2014, 62, 9279−9285

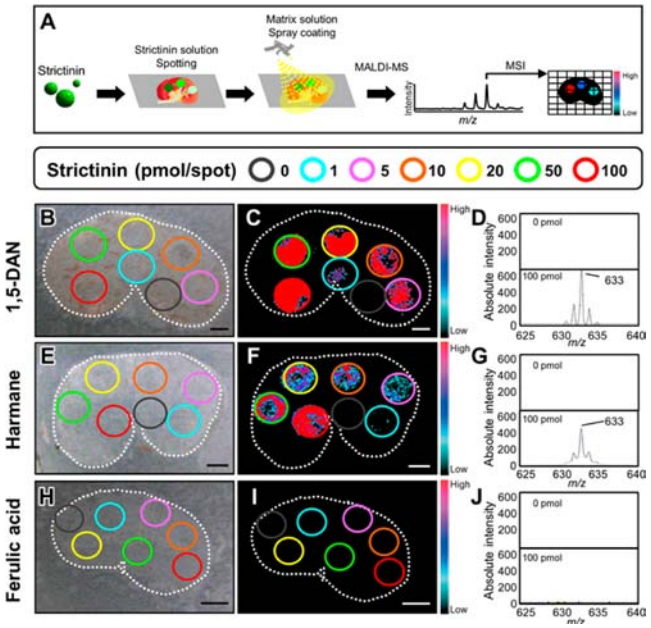


**Figure 5.** MALDI-MS imaging of strictinin spotted on mouse kidney sections: (A) schematic representation of matrix screening by MALDI-MSI; (B–J) MALDI-MSI of strictinin spotted on mouse kidney sections performed using three candidate matrices: (B, E, H) pptical microscopy images; (C, F, I) MALDI-MS images at $m/z$ 633 (scale bar = 1.0 mm); (D, G, J) mass observations of $m/z$ 633 obtained in the 0 and 100 pmol/spot in panels C, F, and I.

at $m/z$ 633 compared with DHB, CHCA, and 9-AA, which are the most effective major matrices for ionizing small molecules.[39,40] Although the peak intensities of CHCA, 9-AA, IAA, and THAP were not altered by different types of solvents, drastic changes in the detection ability were observed for DHB, 1,5-DAN, ferulic acid, harmane, and harmine (Figure 2B). However, when using the positive ionization mode, the protonated ion peak of strictinin $[M + H]^+$ at $m/z$ 635 was not detected with any combinations of matrices and solvents (Figure 3). Although the sodium adduct ion peak of strictinin $[M + Na]^+$ at $m/z$ 657 was observed in DHB, IAA, ferulic acid, or CHCA (Figure 3), they showed very poor intensity compared with peaks detected by the highly performing matrices (1,5-DAN, ferulic acid, and harmane) in the negative ionization mode (Figure 4). Thus, the negative ionization mode was preferable for ionizing strictinin as compared with the positive ionization mode.

Taken together, we found that an ellagitannin, strictinin, could be detected using 1,5-DAN, harmane, or ferulic acid as a preferable matrix in the negative ionization mode by MALDI-MS. Subsequent experiments were performed using these three matrices in the negative ionization mode.

**Determination of the Optimum Matrix for Visualizing Strictinin by MALDI-MSI.** Because ion suppressive effects are predominantly caused by competing endogenous species in tissues,[40] we determined which matrix candidates when dissolved in their corresponding optimum solvent (harmane or ferulic acid in acetonitrile or 1,5-DAN in acetone) could effectively ionize and visualize strictinin directly spotted onto sections of the representative tissue, kidney. Because strictinin solution dissolved in 100% solvent was diffused on kidney sections, the matrix and strictinin solution was prepared in 80% solvent, which could detect the strictinin spotted onto the MALDI sample plate (Supporting Information Figure S1). After strictinin solution had been spotted onto mouse kidney

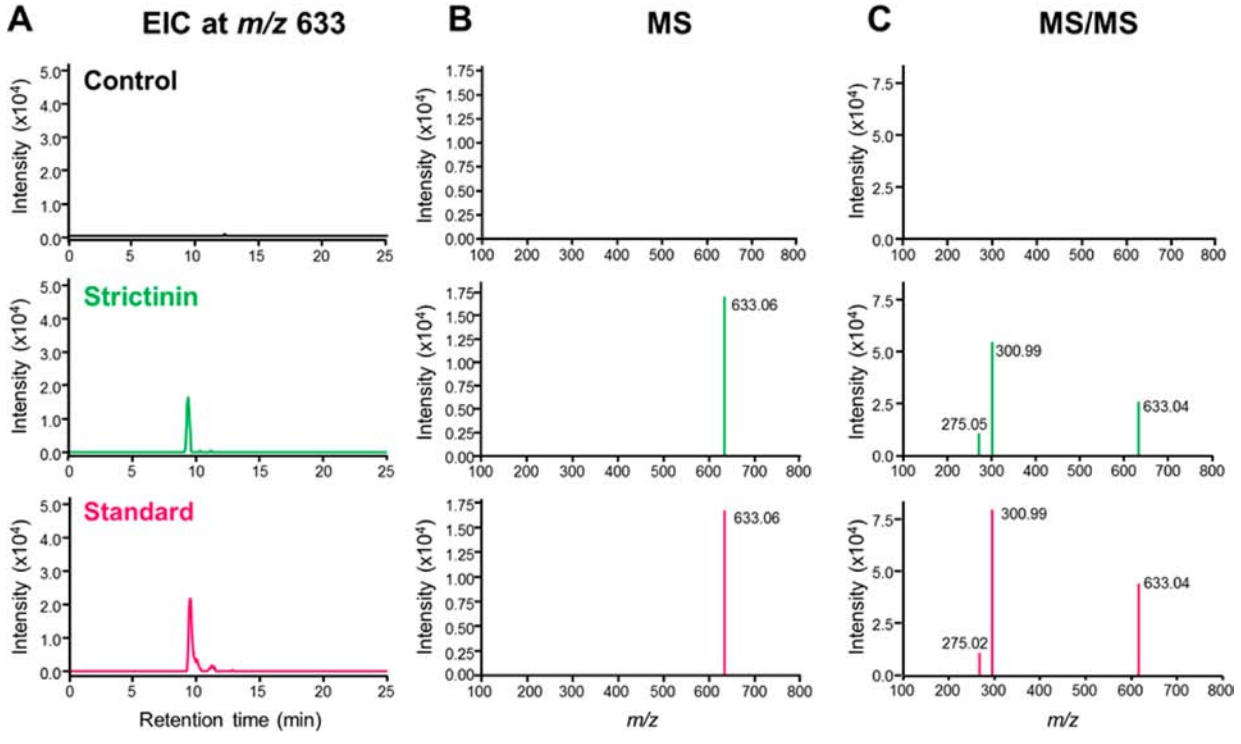


**Figure 6.** LC-MS-based identification of strictinin in mouse kidney after oral administration: (A) extracted ion chromatogram (EIC) at $m/z$ 633 of the strictinin standard (positive control) and kidney extracts in control and strictinin groups in the negative ionization mode; (B, C) mass spectra and tandem MS/MS spectra of strictinin at $m/z$ 633. Strictinin extracted from mouse kidney was determined by LC-MS analysis. MS data from kidney are shown.


dx.doi.org/10.1021/jf503143g | J. Agric. Food Chem. 2014, 62, 9279–9285

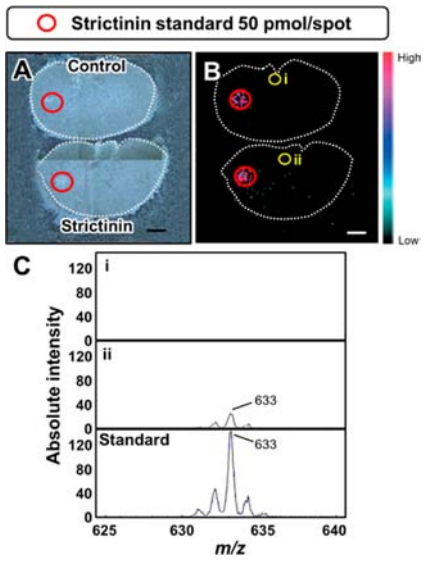


**Figure 7.** MALDI-MSI of orally administered strictinin in mouse kidney sections: (A) optical microscopy image; (B) MALDI-MS image at $m/z$ 633 (scale bar = 1.0 mm); (C) MS observation of $m/z$ 633 obtained in the region of interest (i and ii indicated in panel B).

cryosections, solutions of the three matrix candidates were applied by a spray coating method (Figure 5A). The ion image and peak of $m/z$ 633 $[M - H]^-$ were obtained using 1,5-DAN (Figure 5B–D) or harmane (Figure 5E–G). The best detection sensitivity was observed for 1,5-DAN at the level of 1 pmol/spot (Figure 5C). Although signal intensities were a little weaker than those with 1,5-DAN, harmane also could visualize the strictinin spot from 5 pmol/spot (Figure 5F). When ferulic acid was used as a matrix, no signal was observed (Figure 5H–J). Among the three matrix candidates, ferulic acid was most susceptible to the ion suppression on the kidney sections. These results suggest that 1,5-DAN is the best matrix for visualizing strictinin directly spotted onto intact tissue with high sensitivity in the negative ionization mode.

**In Vivo Administered Strictinin Can Be Visualized by 1,5-DAN-Based MALDI-MSI within Mouse Kidney Sections.** We next applied this label-free imaging technique, 1,5-DAN-based MALDI-MSI, to visualize orally administered strictinin within mouse kidney, a representative tissue capable of accumulating polyphenolic compounds[41,42] as well as being frequently used for MSI analysis.[43] Before the MALDI-MSI experiment, we evaluated whether strictinin can be observed by LC-MS analysis in the kidney 1 h after oral administration (Figure 6). An ion peak at $m/z$ 633.06, corresponding to the deprotonated ion of strictinin $[M - H]^-$, was observed in the strictinin-administered mouse kidney extract but not in the control (Figure 6A,B). Moreover, product ion peaks at $m/z$ 275.02 and 300.99 were detected by MS/MS of $m/z$ 633.06 (Figure 6C), which were identical to the standard peaks. These data suggested that strictinin was absorbed and localized in the kidney 1 h after oral dosing. Therefore, we next performed MALDI-MSI using kidney sections.

After strictinin (50 pmol) had been spotted onto kidney section as a positive control, 1,5-DAN was applied by the spray coating method and then subjected to MALDI-MS (Figure 7). The strictinin standard spot (red circle) was visualized, but the clear ion image of $m/z$ 633 was not obtained in strictinin-administered kidney sections (Figure 7A,B), although the ion peak of $m/z$ 633 was detected (Figure 7C). To obtain clear images of strictinin, we next used another type of MALDI-MS instrument, iMScope,[20,21,44] which is a MALDI-QIT-TOF-MS instrument with a higher performance level compared with the conventional MALDI-TOF-MS instrument (AXIMA Performance) used herein. MSI analysis was performed using the same matrix and the same series of sections tested in Figure 7. An ion image and peak of $m/z$ 633.067 was obtained only in the strictinin-dosed kidney sections (Figure 8). Tandem MS/MS analysis also showed that this peak was certainly strictinin (Supporting Information Figure S2). Interestingly, this label-free imaging technique revealed that the localization patterns of strictinin were different in kidney compartments (pelvis, medulla, and cortex) (Figure 8D). In particular, the highest abundance of strictinin was observed in the pelvis, in the funnel-like dilated proximal part of the ureter in the kidney. This result implies that absorbed strictinin may be immediately excreted from the body 1 h after oral administration.

Previously, MALDI-MS using the major matrix DHB was performed for determining the composition of ellagitannins in plant extract,[45] but this matrix did not allow us to sensitively detect one of ellagitannins, strictinin, at a concentration of <50 pmol (Figure 2B). In contrast, 1,5-DAN selected from matrix screening was able to visualize the in situ distribution of the strictinin in kidney sections after oral dosing, although the bioavailability of ellagitannins is very low.[46,47]

It is known that ellagitannins are quite stable in the stomach and undergo a massive metabolic transformation in the gut to ellagic acid and urolithins, and these gut metabolites play an

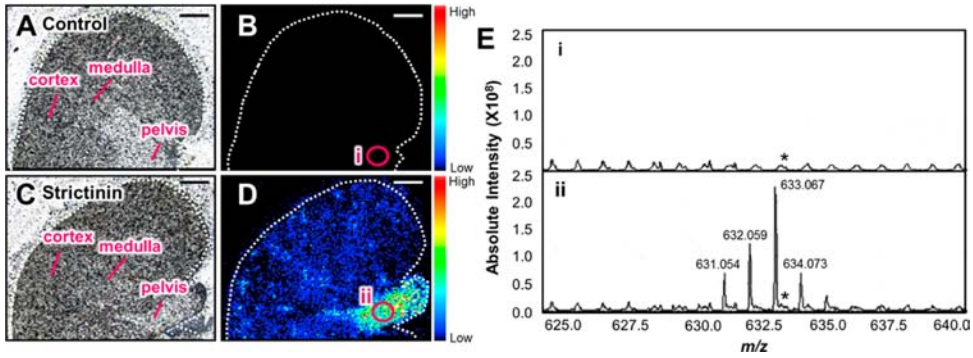


**Figure 8.** In situ visualization of orally administered strictinin using a MALDI-QIT-TOF-MS instrument, iMScope: (A, C) optical microscopy images; (B, D) MALDI-MS images at $m/z$ 633 (scale bar = 1.0 mm); (E) MS observation of $m/z$ 633 obtained in the region of interest (i and ii indicated in panels B and D; asterisk shows background peaks).


dx.doi.org/10.1021/jf503143g | J. Agric. Food Chem. 2014, 62, 9279–9285

important role in the biological activities of ellagitannins.[48,49] In vivo bioactivity of an orally dosed strictinin has been reported,[5] but there was no information on the amount of the intact strictinin within tissues and plasma. In contrast, the present study showed, for the first time, the existence of the intact strictinin within kidney 1 h after oral dosing. Visualization of the intact form in tissue other than the gastrointestinal tract may contribute to elucidation of the in vivo mechanism for action of strictinin. In this study, a gut metabolite, ellagic acid, was observed in kidney extracts, but not visualized by 1,5-DAN-MALDI-MS imaging (Supporting Information Figure 3S). Further improvement of detection sensitivity, including matrix selection and development, is required for comprehensive understanding of the in vivo action of strictinin.

In the future, our proposed in situ label-free imaging technique may contribute to localization analysis and understanding of the mechanism of action of ellagitannins.

## ■ ASSOCIATED CONTENT

### Supporting Information

Figures S1, S2, and S3. This material is available free of charge via the Internet at http://pubs.acs.org.

## ■ AUTHOR INFORMATION


### Corresponding Author

*(H.T.) Phone: +81-92-642-3008. Fax: +81-92-642-3008. E-mail: tatibana@agr.kyushu-u.ac.jp.



### Funding

This work was supported by the MEXT Funding-Project for Developing Innovation Systems-Creation of Innovation Centers for Advanced Interdisciplinary Research Areas Program in Japan. This work was also supported in part by JSPS KAKENHI Grants 22228002 and 26660115, grants for project research (Development of fundamental technology for analysis and evaluation of functional agricultural products and functional foods), Grants for the Urakami Foundation for Food and Food Culture Promotion, and a Grant-in-Aid for JSPS Fellows (25″2691).


### Notes

The authors declare no competing financial interest.

## ■ ABBREVIATIONS USED

MALDI-MSI, matrix-assisted laser desorption/ionization−mass spectrometry imaging; 1,5-DAN, 1,5-diaminonaphthalene; DHB, 2,5-dihydroxybenzoic acid; CHCA, α-cyano-4-hydroxycinnamic acid; EGCG, (−)-epigallocatechin-3-*O*-gallate; 9-AA, 9-aminoacridine; THAP, 2,4,6-trihyroxyacetophenone; IAA, indoleacrylic acid; ITO, indium tin oxide; TOF, time-of-flight; DMSO, dimethyl sulfoxide; QIT, quadrupole ion trap; ESI, electrospray ionization; S/N, signal-to-noise

## ■ REFERENCES


(1) Quideau, S.; Feldman, S. Ellagitannin chemistry. *Chem. Rev.* **1996**, *86*, 475−503.

(2) Yang, C.; Li, F.; Zhang, X.; Wang, L.; Zhou, Z.; Wang, M. Phenolic antioxidants from *Rosa soulieana* flowers. *Nat. Prod. Res.* **2013**, *27*, 2055−2058.

(3) Saha, R. K.; Takahashi, T.; Kurebayashi, Y.; Fukushima, K.; Minami, A.; Knbara, N.; Ichitani, M.; Sagesaka, Y. M.; Suzuki, T. Antiviral effect of strictinin on influenza virus replication. *Antiviral Res.* **2010**, *88*, 10−18.

(4) Patel, D.; Prasad, S.; Kumar, R.; Hemalatha, S. An overview on antidiabetic medicinal plants having insulin mimetic property. *Asian Pac. J. Trop. Biomed.* **2012**, *2*, 320−330.

(5) Tachibana, H.; Kubo, T.; Miyase, T.; Tanino, S.; Yoshimoto, M.; Sano, M.; Maeda-Yamamoto, M.; Yamada, K. Identification of an inhibitor for interleukin 4-induced epsilon germline transcription and antigen-specific IgE production in vivo. *Biochem. Biophys. Res. Commun.* **2001**, *280*, 53−60.

(6) Kim, Y. H.; Ninomiya, Y.; Yamashita, S.; Kumazoe, M.; Huang, Y.; Nakahara, K.; Won, Y. S.; Murata, M.; Fujimura, Y.; Yamada, K.; Tachibana, H. IL-4 receptor α in non-lipid rafts is the target molecule of strictinin in inhibiting STAT6 activation. *Biochem. Biophys. Res. Commun.* **2014**, *450*, 824−830.

(7) Monobe, M.; Ema, K.; Kato, F.; Maeda-Yamamoto, M. Immunostimulating activity of a crude polysaccharide derived from green tea (*Camellia sinensis*) extract. *J. Agric. Food Chem.* **2008**, *56*, 1423−1427.

(8) Hoffmann, T.; Friedlhuber, R.; Steinhauser, C.; Tittel, I.; Skowranek, K.; Schwab, W.; Fischer, T. C. Histochemical screening, metabolite profiling and expression analysis reveal Rosaceae roots as the site of flavan-3-ol biosynthesis. *Plant Biol.* **2012**, *14*, 33−40.

(9) Fricker, M. D.; Lee, J. A.; Bebber, D. P.; Tlalka, M.; Hynes, J.; Darrah, P. R.; Watkinson, S. C.; Boddy, L. Imaging complex nutrient dynamics in mycelial networks. *J. Microsc.* **2008**, *231*, 317−331.

(10) Suganuma, M.; Okabe, S.; Oniyama, M.; Tada, Y.; Ito, H.; Fujiki, H. Wide distribution of [3*H*](−)-epigallocatechin gallate, a cancer preventive tea polyphenol, in mouse tissue. *Carcinogenesis* **1998**, *19*, 1771−1776.

(11) Gester, S.; Wuest, F.; Pawelke, B.; Bergmann, R.; Pietzsch, J. Synthesis and biodistribution of an $^{18}$F-labelled resveratrol derivative for small animal positron emission tomography. *Amino Acids* **2005**, *29*, 415−428.

(12) Stoekli, M.; Chaurand, P.; Hallahan, D. E.; Caprioli, R. M. Imaging mass spectrometry: a new technology for the analysis of protein expression in mammalian tissues. *Nat. Med.* **2001**, *7*, 493−496.

(13) Shimma, S.; Sugiura, Y.; Hayasaka, T.; Zaima, N.; Setou, M. Mass imaging and identification of biomolecules with MALDI-QIT-TOF-based system. *Anal. Chem.* **2008**, *80*, 878−885.

(14) Khatib-Shahidi, S.; Andersson, M.; Herman, J. L.; Gillespie, T. A.; Caprioli, R. M. Direct molecular analysis of whole-body animal tissue sections by imaging MALDI-mass-spectrometry. *Anal. Chem.* **2006**, *78*, 6448−6456.

(15) Meriaux, C.; Franck, J.; Wisztorski, M.; Salzet, M.; Fournier, I. Liquid ionic matrixes for MALDI mass spectrometry imaging of lipids. *J. Proteomics* **2010**, *73*, 1204−1218.

(16) Snel, M. F.; Fuller, M. High-spatial resolution matrix-assisted laser desorption ionization imaging analysis of glucosylceramide in spleen sections from a mouse model of Gaucher disease. *Anal. Chem.* **2010**, *82*, 3664−3670.

(17) Lemaire, R.; Tabet, J. C.; Ducoroy, P.; Hendra, J. B.; Salzet, M.; Fournier, I. Solid ionic matrixes for direct tissue analysis and MALDI imaging. *Anal. Chem.* **2006**, *78*, 809−819.

(18) Kim, Y. H.; Fujimura, Y.; Hagihara, T.; Sasaki, M.; Yukihira, D.; Nagao, T.; Miura, D.; Yamaguchi, S.; Saito, K.; Tanaka, H.; Wariishi, H.; Yamada, K.; Tachibana, H. *In situ* label-free imaging for visualizing the biotransformation of a bioactive polyphenol. *Sci. Rep.* **2013**, *3*, No. 2805.

(19) Lambert, J. D.; Sang, S. M.; Yang, C. S. Biotransformation of green tea polyphenols and the biological activities of those metabolites. *Mol. Pharmaceutics* **2007**, *4*, 819−825.

(20) Harada, T.; Yuba-Kubo, A.; Sugiura, Y.; Zaima, N.; Hayasaka, T.; Goto-Inoue, N.; Wakui, M.; Suematsu, M.; Takeshita, K.; Ogawa, K.; Yoshida, Y.; Setou, M. Visualization of volatile substances in different organelles with an atmospheric-pressure mass microscope. *Anal. Chem.* **2009**, *81*, 9153−9157.

(21) Takizawa, Y.; Mizuta, K.; Hayasaka, T.; Nakanishi, H.; Okamura, J.; Mineta, H.; Setou, M. Specific localization of five phosphatidylcholine species in the cochlea by mass microscopy. *Audiol. Neurootul.* **2011**, *16*, 315−322.

(22) Schwartz, S. A.; Reyzer, M. L.; Caprioli, R. M. Direct tissue analysis using matrix-assisted laser desorption/ionization mass spectrometry: practical aspects of sample preparation. *J. Mass Spectrom.* **2003**, *38*, 699−708.
(23) Angel, P. M.; Spraggins, J. M.; Baldwin, H. S.; Caprioli, R. Enhanced sensitivity for high spatial resolution lipid analysis by negative ion mode matrix assisted laser desorption ionization imaging mass spectrometry. *Anal. Chem.* **2012**, *84*, 1557−1564.
(24) Trimpin, S.; Herath, T. N.; Inutan, E. D.; Wager-Miller, J.; Kowalski, P.; Claude, E.; Walker, J. M.; Mackie, K. Automated solvent-free matrix deposition for tissue imaging by mass spectrometry. *Anal. Chem.* **2010**, *82*, 359−367.
(25) Yukihira, D.; Miura, D.; Saito, K.; Takahashi, K.; Wariishi, H. MALDI-MS-based high-throughput metabolite analysis for intracellular metabolic dynamics. *Anal. Chem.* **2010**, *82*, 4278−4282.
(26) Miura, D.; Fujimura, Y.; Tachibana, H.; Wariishi, H. Highly sensitive matrix-assisted laser desorption ionization-mass spectrometry for high-throughput metabolic profiling. *Anal. Chem.* **2010**, *82*, 498−504.
(27) Miura, D.; Fujimura, Y.; Yamato, M.; Hyodo, F.; Utsumi, H.; Tachibana, H.; Wariishi, H. Ultrahighly sensitive in situ metabolomic imaging for visualizing spatiotemporal metabolic behaviors. *Anal. Chem.* **2010**, *82*, 9789−9796.
(28) Frison, S.; Sporns, P. Identification and quantification of flavonol glycosides in almond seedcoats using MALDI-TOF MS. *J. Agric. Food Chem.* **2002**, *50*, 2782−2787.
(29) Grant, D. C.; Helleur, R. J. Rapid screening of anthocyanins in berry samples by surfactant-mediated matrix-assisted laser desorption/ionization time-of-flight mass spectrometry. *Rapid Commun. Mass Spectrom.* **2008**, *22*, 156−164.
(30) Carpentieri, A.; Marino, G.; Amoresano, A. Rapid fingerprinting of red wines by MALDI mass spectrometry. *Anal. Bioanal. Chem.* **2007**, *389*, 969−982.
(31) Krueger, C. G.; Dopke, N. C.; Treichel, P. M.; Folts, J.; Reed, J. D. Matrix-assisted laser desorption/ionization time-of-flight mass spectrometry of polygalloyl polyflavon-3-ols in grape seed extract. *J. Agric. Food Chem.* **2000**, *48*, 1663−1667.
(32) Behrens, A.; Maie, N.; Knicker, H.; Kogel-Knabner, I. MALDI-TOF mass spectrometry and PSD fragmentation as means for the analysis of condensed tannins in plant leaves and needles. *Phytochemistry* **2003**, *62*, 1159−1170.
(33) Marczak, L.; Kachlicki, P.; Koźniewski, P.; Skirycz, A.; Krajewski, P.; Stobiecki, M. Matrix-assisted laser desorption/ionization time-of-flight mass spectrometry monitoring of anthocyanins in extracts from *Arabidopsis thaliana* leaves. *Rapid Commun. Mass Spectrom.* **2008**, *22*, 3949−3956.
(34) Molin, L.; Seraglia, R.; Dani, F. R.; Moneti, G.; Traldi, P. The double nature of 1,5-diaminonaphthalene as matrix-assisted laser desorption/ionization matrix: some experimental evidence of the protonation and reduction mechanisms. *Rapid Commun. Mass Spectrom.* **2011**, *25*, 3091−3096.
(35) Thomas, A.; Charbonneau, J. L.; Fournaise, E.; Chaurand, P. Sublimation of new matrix candidates for high spatial resolution imaging mass spectrometry of lipid: enhanced information in both positive and negative polarities after 1,5-diaminonaphthalene deposition. *Anal. Chem.* **2012**, *84*, 2048−2054.
(36) Nonami, H.; Tanaka, K.; Fukuyama, Y.; Erra-Balsells, R. $\beta$-Carboline alkaloids as matrices for UV-matrix-assisted laser desorption/ionization time-of-flight mass spectrometry in positive and negative ion modes: analysis of proteins of high molecular mass, and of cyclic and acyclic oligosaccharides. *Rapid Commun. Mass Spectrom.* **1998**, *12*, 285−296.
(37) Nonami, H.; Wu, F.; Thummel, R. P.; Fukuyama, Y.; Yamaoka, H.; Erra-Balsells, R. Evaluation of pyridoindoles, pyridylindoles and pyridylpyridoindoles as matrices for ultraviolet matrix-assisted laser desorption/ionization time-of-flight mass spectrometry. *Rapid Commun. Mass Spectrom.* **2001**, *15*, 2354−2373.
(38) Sun, G.; Yang, K.; Zhao, Z.; Guan, S.; Han, X.; Gross, R. W. Matrix-assisted laser desorption/Ionization-time of flight mass spectrometric analysis of cellular glycerophospholipids enabled by multiplexed solvent dependent analyte-matrix interaction. *Anal. Chem.* **2008**, *80*, 7576−7585.
(39) Miura, D.; Fujimura, Y.; Yamato, M.; Hyodo, F.; Utsumi, H.; Tachibana, H.; Wariishi, H. Ultrahighly sensitive in situ metabolomics imaging for visualizing spatiotemporal metabolic behaviors. *Anal. Chem.* **2010**, *82*, 9789−9796.
(40) Prideaux, B.; Stoeckli, M. Mass spectrometry imaging for drug distribution studies. *J. Proteomics* **2012**, *75*, 4999−5013.
(41) Chen, L.; Lee, M. J.; Li, H.; Yang, C. S. Absorption, distribution, elimination of tea polyphenols in rats. *Drug Metab. Dispos.* **1997**, *25*, 1045−1050.
(42) Lin, S. P.; Chu, P. M.; Tsai, S. Y.; Wu, M. H.; Hou, Y. C. Pharmacokinetics and tissue distribution of resveratrol, emodin and their metabolites after intake of *Polygonum cuspidatum* in rats. *J. Ethnopharmacol.* **2012**, *144*, 671−676.
(43) Watrous, J. D.; Alexandrov, T.; Dorrestein, P. C. The evolving field of imaging mass spectrometry and its impact on future biological research. *J. Mass Spectrom.* **2011**, *46*, 209−222.
(44) Yasunoga, M.; Furuta, M.; Ogata, K.; Koga, Y.; Yamamoto, Y.; Takigahira, M.; Matsumura, Y. The significance of microscopic mass spectrometry with high resolution in the visualization of drug distribution. *Sci. Rep.* **2013**, *3*, 3050.
(45) Hager, T. J.; Howard, L. R.; Liyanage, R.; Lay, J. O.; Prior, R. L. Ellagitannin composition of blackberry as determined by HPLC-ESI-MS and MALDI-TOF-MS. *J. Agric. Food Chem.* **2008**, *56*, 661−669.
(46) González-Barrio, R.; Borges, G.; Mullen, W.; Crozier, A. Bioavailability of anthocyanins and ellagitannins following consumption of raspberries by healthy humans and subjects with an ileostomy. *J. Agric. Food Chem.* **2010**, *58*, 3933−3939.
(47) Seeram, N. P.; Lee, R.; Heber, D. Bioavailability of ellagic acid in human plasma after consumption of ellagitannins from pomegranate (*Punica granatum* L.) juice. *Clin. Chim. Acta* **2004**, *348*, 63−68.
(48) Giménez-Bastida, J. A.; Larrosa, M.; González-Sarrías, A.; Tomás-Barberán, F.; Espín, J. C.; García-Conesa, M. T. Intestinal ellagitannin metabolites ameliorate cytokine-induced inflammation and associated molecular markers in human colon fibroblasts. *J. Agric. Food Chem.* **2012**, *60*, 8866−8876.
(49) Garcia-Muñoz, C.; Vaillant, F. Metabolic fate of ellagitannins: implications for health, and research perspectives for innovative functional foods. *Crit. Rev. Food Sci. Nutr.* **2014**, *54*, 1584−1598.

antioxidant activity of PC, we determined ROS and AA levels in SMP30/GNL KO mouse tissues after long-term oral ingestion of PC.

## MATERIALS AND METHODS

**Chemicals.** Ethylenediaminetetraacetic acid (EDTA) was purchased from Dojindo Laboratories (Kumamoto, Japan). Tris(2-carboxyethyl)-phosphine hydrochloride was purchased from Tokyo Chemical Industry Co., Ltd. (Tokyo, Japan). 5-(and 6)-carboxy-2′,7′-dichlorodihydrofluorescein diacetate (carboxy-$H_2$DCFDA) was purchased from Life Technologies Corp. (Carlsbad, CA, USA). Protease inhibitor cocktail (cOmplete, EDTA-free) was purchased from Roche Diagnostics GmbH (Mannheim, Germany). BCA protein assay reagent was purchased from Thermo Fisher Scientific Inc. (Waltham, MA, USA). L-Ascorbic acid used in the HPLC analysis and other reagents and chemicals were purchased from Wako Pure Chemical Industries, Ltd. (Osaka, Japan).

**Preparation of PC and PC Diet.** White potato (*S. tuberosum* cv. Toyoshiro) tubers of similar size and appearance were obtained for an experimental field in Hokkaido, Japan, in September 2010 and stored for several days. The unpeeled potatoes were washed with tap water and air-dried on filter paper. PC were prepared as the commercial product "Olivee" and were manufactured by CALBEE, Inc. (Tokyo, Japan). Briefly, peeled potatoes were sliced and immersed in tap water and then fried in olive oil for several minutes. After frying, the PC were finely ground and passed through a 1.5 mm sieve. To avoid AA degradation, the crushed PC were stored at −80 °C in a nitrogen gas-filled pouch with an aluminum vapor-deposited film. The stored-crushed PC were thawed before use and mixed with the AA-free powder CL-2 (CLEA Japan, Inc., Tokyo, Japan) to produce a final 20% (w/w) and 10% PC content. Diet compositions (moisture, crude protein, crude fat, crude fiber, crude ash, and nitrogen-free extract) of 20% PC CL-2, 10% PC CL-2, and CL-2 were analyzed at the Laboratories for Food and Environmental Science (Tokyo, Japan) and are shown in Table 1.

**Table 1. Nutritional Composition of PC Diets (in 100 Grams)**

| nutritional component | 20% PC CL-2 | 10% PC CL-2 | CL-2 |
|---|---|---|---|
| moisture (g) | 6.6 | 7.1 | 7.6 |
| crude protein (g) | 20.7 | 22.6 | 24.4 |
| crude fat (g) | 9.0 | 7.5 | 6.0 |
| crude fiber (g) | 3.3 | 3.4 | 3.6 |
| crude ash (g) | 7.9 | 8.4 | 8.9 |
| nitrogen-free extract (g) | 52.5 | 51.0 | 49.5 |
| calorie (kcal) | 387 | 376 | 364 |
| ascorbic acid (mg) | 13.6 | 6.0 | nd[a] |
| dehydroascorbic acid (mg) | 0.5 | 0.6 | nd |

[a]nd, not detectable.

**Assays of Oxygen Radical Absorbance Capacity (ORAC).** ORAC for hydrophilic and lipophilic antioxidants was measured using a previously described method.[16]

**Animals.** SMP30/GNL KO mice were established and maintained as described previously.[8] SMP30/GNL KO and C57BL/6N (wild type, WT) male mice were fed a commercial autoclaved chow diet (CRF-1, Oriental Yeast Co., Ltd., Tokyo, Japan) and had free access to water containing 1.5 g/L AA (DSM Nutrition Japan, Tokyo, Japan) and 10 μM EDTA until weaning. After weaning at the age of 4 weeks, all mice were used for the following two experiments. (1) All mice were fed CL-2 and divided into four groups: SMP30/GNL KO and WT mice given water with or without AA, that is, AA(−) KO, AA(+) KO, AA(−) WT, and AA(+) WT, whereas AA(+) mice had free access to water containing 1.5 g/L AA and 10 μM EDTA. AA(−) mice had free access to AA-free water containing 10 μM EDTA. (2) SMP30/GNL KO mice were divided into four groups that were given either 20% PC powder in CL-2 and AA-free water containing 10 μM EDTA, 10% PC powder in CL-2 and AA-free water containing 10 μM EDTA, powder CL-2 and AA-free water containing 10 μM EDTA, and powder CL-2 and water containing 1.5 g/L AA and 10 μM EDTA, that is, 20% PC, 10% PC, AA(−), and AA(+). Five mice were used in each group for these experiments. Mice were maintained on a 12 h light/dark cycle in a controlled environment. All experimental procedures using laboratory animals were approved by the Animal Care and Use Committee of the Tokyo Metropolitan Institute of Gerontology (permit no. 12016).

**Collection of Blood and Tissue Samples.** Mice were sacrificed, and each blood sample was drawn into an EDTA-containing syringe from the inferior vena cava. Plasma was obtained by centrifugation at 1700*g* for 15 min at 4 °C. Mice were then systemically perfused with ice-cold phosphate-buffered saline through the left ventricle to wash out any remaining blood cells. The tissues of interest were then collected. All samples were stored at −80 °C until use.

**Determination of AA and DHA.** Amounts of AA and dehydroascorbic acid (DHA), an oxidized form of AA, were determined by high-performance liquid chromatography using an Atlantis dC18 5 μm column (4.6 × 150 mm; Nihon Waters K.K., Tokyo, Japan) as described previously.[17] For determination of plasma AA, plasma was mixed with equal amounts of 10% metaphosphoric acid (MPA) and 1 mM EDTA and centrifuged at 21000*g* for 15 min at 4 °C. For analysis of AA content in PC, 20% PC powder diet, and 10% PC powder diet, 0.4 g samples were homogenized with 14 volumes of cold 5.4% MPA and 1 mM EDTA using a high-speed homogenizer (POLYTRON, Kinematica AG, Switzerland) and subsequently centrifuged at 21000*g* for 15 min at 4 °C. For AA determination in the brain, eyeball, heart, lung, testis, stomach, small intestine, large intestine, pancreas, kidney, liver, skin, and epididymal fat, tissues were homogenized with 14 volumes of cold 5.4% MPA and 1 mM EDTA using a Teflon homogenizer (model TH-M, Takashima, Tokyo, Japan). The soleus and plantaris muscles were homogenized with 14 volumes of cold 5.4% MPA and 1 mM EDTA using a Handy homogenizer (Moji-mojikun, Nippon Genetics Co., Ltd., Tokyo, Japan). Homogenates were then centrifuged at 21000*g* for 10 min at 4 °C. To reduce DHA to AA for determination of AA plus DHA, 90 μL of supernatant was incubated with 10 μL of 350 mM tris(2-carboxyethyl)phosphine hydrochloride for 2 h at 4 °C. The mobile phase was 50 mM phosphate buffer (pH 2.8), 0.2 g/L EDTA, and 2% methanol at a flow rate of 1.3 mL/min, and electrical signals were recorded using an electrochemical detector equipped with a glassy carbon electrode at +0.6 V. The value of DHA was determined by subtracting AA from AA plus DHA.

**Determination of ROS.** ROS were measured using carboxy-$H_2$DCFDA as described previously.[18,19] Carboxy-$H_2$DCFDA was de-esterified from diacetate by intracellular esterases and then oxidized to fluorescent 5-(and-6)-carboxy-2′,7′-dichlorofluorescein by various ROS such as hydroxyl radical, peroxynitrite anion, carbonate, nitrogen dioxide, peroxyl radical, and hydrogen peroxide according to the manufacturer's handbook and Wardman et al.[20] Briefly, tissues were homogenized with 14 volumes of cold homogenization buffer consisting of 50 mM sodium phosphate buffer (pH 7.4), 0.5 mM phenylmethanesulfonyl fluoride, 1 mM EDTA, and protease inhibitor cocktail using a Teflon homogenizer, and the homogenate was centrifuged at 900*g* for 15 min at 4 °C. One hundred microliters of 50 μM carboxy-$H_2$DCFDA, 25 μL of supernatants containing 15 μg total protein, and 75 μL of homogenization buffer were mixed to yield a 200 μL total reaction volume. Changes in fluorescence intensity were measured every 5 min for 60 min at 37 °C using a SPECTRAmax Gemini (Life Technologies Corp.) with excitation and emission wavelengths set at 485 and 530 nm, respectively. ROS in tissue homogenates were calculated using the values from 30 to 60 min and expressed as "counts/min/mg protein". The protein concentration was determined by BCA protein assay using bovine serum albumin as a standard.

**Statistical Analysis.** The values are expressed as means ± standard error of the mean (SEM). Statistical analysis was performed using Turkey's honestly significant difference test for multiple comparisons in body weight, AA plus DHA, and ROS among all groups, and in ORAC among all diets. All statistical analyses were performed using KaleidaGraph software (Synergy Software Inc., Reading, PA, USA). Statistically significant differences were defined as $p < 0.05$.

## RESULTS

**Body Weight of SMP30/GNL KO Mice during AA Depletion.** Compared to AA(+) KO mice, the body weights of AA(−) KO mice were reduced by 12 and 48% at 7 and 14 weeks, respectively, after weaning ($p < 0.05$ and $p < 0.001$, respectively) (Table S1 in the Supporting Information). Meanwhile, there were no significant differences in body weight among AA(+) KO, AA(−) WT, and AA(+) WT mice at 7 and 14 weeks. AA(−) KO mice at 7 weeks showed marginal initial manifestations of AA deficiency (e.g., bleeding from the knee junctions), and they had developed appreciable symptoms of scurvy (rachitic rosary and an abnormal gait) by 14 weeks.

**Depletion of AA and DHA Levels in SMP30/GNL KO Mice Fed an AA-free Diet and Water.** We first determined the AA and DHA levels in tissues and plasma from AA(−) KO mice during AA depletion. Seven weeks after weaning that occurred at 4 weeks, AA plus DHA concentrations in the brain, heart, lung, testis, soleus muscle, plantaris muscle, stomach, small intestine, large intestine, pancreas, kidney, liver, and plasma of AA(−) KO mice were 2.6, 3.4, 4.1, 8.5, 2.0, 3.6, 4.1, 3.1, 3.9, 3.5, 1.0, 2.0, and 0% that of AA(+) KO mice, respectively (Figure 1). There were no significant differences in AA plus DHA concentrations in tissues and plasma from AA(+) KO and AA(−) WT mice. The AA plus DHA concentrations in the lung, stomach, and liver were significantly (17, 20, and 29%, respectively) higher in AA(+) WT mice than those of AA(−) WT mice (Figure 1C,G,L). DHA per AA plus DHA levels in the brain, heart, lung, testis, soleus muscle, plantaris muscle, stomach, small intestine, large intestine, pancreas, kidney, liver, and plasma of AA(+) KO, AA(−) WT, and AA(+) WT mice were 1.6−4.9, 19.1−24.3, 6.4−20.2, 0−0.5, 25.2−29.6, 11.7−12.0, 4.3−7.8, 4.6−5.0, 1.0−2.2, 4.8−5.2, 5.6−9.0, 0−0.5, and 15.0−18.4%, respectively.

As shown in Figure S1 (Supporting Information), the AA plus DHA levels were lower in AA(−) KO mice at 14 weeks compared to 7 weeks. AA plus DHA concentrations in the brain, heart, lung, testis, soleus muscle, plantaris muscle, stomach, small intestine, large intestine, pancreas, kidney, liver, and plasma of AA(−) KO mice were 1.5, 2.2, 3.0, 5.6, 3.9, 2.0, 1.9, 1.9, 2.5, 2.1, 1.4, 0.9, and 0% that of AA(+) KO mice, respectively. AA plus DHA concentrations in these tissues and plasma did not differ significantly between AA(+) KO and AA(−) WT mice. The values in the testis and stomach of AA(+) WT mice were significantly (9 and 25%, respectively) higher than those of AA(−) WT mice. The DHA per AA plus DHA in the brain, heart, lung, testis, soleus muscle, plantaris muscle, stomach, small intestine, large intestine, pancreas, kidney, liver, and plasma of AA(+) KO, AA(−) WT, and AA(+) WT mice were 1.0−1.8, 19.6−27.5, 17.8−22.3, 0−0.1, 23.4−30.9, 20.7−22.0, 4.9−6.7, 3.4−8.0, 0−2.3, 4.5−7.2, 2.8−16.4, 0−0.7, and 15.6−38.9%, respectively.

**Increased ROS Levels in SMP30/GNL KO Mice Fed an AA-free Diet and Water.** To establish an evaluation method of the antioxidant activity of various foods using SMP30/GNL KO mice, we next investigated ROS levels in tissues from AA(−) KO mice using a simple method for ROS detection.[18] ROS levels in the brain, heart, lung, testis, soleus muscle, plantaris muscle, stomach, small intestine, and large intestine of AA(−) KO mice at 7 weeks were significantly (27, 39, 29, 32, 81, 28, 43, 42, and 64%, respectively) higher than those of AA(+) KO mice (Figure 2A−I). In the pancreas and kidney, ROS levels in AA(−) KO mice were 17 and 31% higher, respectively, than those of AA(+) KO mice, although the difference did not reach significant levels ($p = 0.09$ and 0.08, respectively) (Figure 2J,K). There were no significant differences in ROS levels in these tissues among AA(+) KO, AA(−) WT, and AA(+) WT mice. Interestingly, ROS levels in the liver of AA(+) KO mice were significantly (19%) higher than that of AA(−) WT mice. The ROS levels for AA(−) KO mice were 13% higher in the liver compared to AA(+) KO mice, although there were no significant differences ($p = 0.07$) (Figure 2L).

Likewise, at 14 weeks AA(−) KO mice showed increased ROS levels in tissues. ROS levels in the brain, heart, lung, testis, soleus muscle, plantaris muscle, stomach, small intestine, large intestine, pancreas, and kidney of AA(−) KO mice were significantly (74, 108, 117, 72, 95, 48, 29, 45, 35, 31, and 26%, respectively) higher compared with those of AA(+) KO mice (Figure S2A−K in the Supporting Information). No significant differences were observed in tissue ROS levels among AA(+) KO, AA(−) WT, and AA(+) WT mice. In livers, the ROS levels of AA(−) KO and AA(+) KO mice were 22 and 19%, respectively, higher than that of AA(−) WT mice, although the difference did not reach significant levels ($p = 0.14$ and 0.24, respectively) (Figure S2L in the Supporting Information).

**Nutritional Composition and ORAC of PC Diets.** For feeding PC to SMP30/GNL KO mice, we prepared PC diets by mixing the AA-free powder diet CL-2 and crushed PC to yield a final PC content of 10 or 20%. The AA content of the PC used in this study was 78.0 ± 1.6 mg/100 g, whereas DHA was under the detection limit. The nutritional composition of the PC diets was determined as listed in Table 1. Whereas moisture, crude protein, crude fiber, and crude ash were lower in the 20 and 10% PC diets compared with CL-2, crude fat, nitrogen-free extract, AA, and DHA, and calorie amounts of the 20 and 10% PC diets were higher than those of CL-2. Furthermore, we determined the radical scavenging ability of the PC diet and PC using the well-established ORAC method. The ORAC values of the 20 and 10% PC diets were significantly higher compared with PC, whereas the values were significantly (25 and 17%, respectively) lower than that of CL-2 (Figure S3 in the Supporting Information).

**Body Weight Change, Food Intake, and Water Intake of SMP30/GNL KO Mice Fed PC Diets.** To investigate the effect of the PC diet on growth, we compared SMP30/GNL KO mice fed a 20% PC diet and AA-free water, a 10% PC diet and AA-free water, an AA-free diet and water, or an AA-free diet and 1.5 g/L AA water after weaning at 4 weeks of age. Each group gained equal amounts of weight compared to the initial body weights (Figure 3A). Food and water intakes throughout the experimental period were 3.5 ± 0.1 g/day/mouse and 3.7 ± 0.1 mL/day/mouse in the 20% PC group, although there were no significant differences among all four groups (Figure 3B,C).

**Increase in AA and DHA Levels in SMP30/GNL KO Mice Fed PC Diets.** Because whether AA and DHA in PC diets were absorbed in intestines and transported into tissues was unclear, we determined the AA and DHA levels in tissues and plasma from SMP30/GNL KO mice fed PC diets (Figure 4). The AA plus DHA levels of the brain, heart, lung, testis, soleus muscle, plantaris muscle, stomach, small intestine, large intestine, eyeball, epididymal fat, skin, pancreas, kidney, liver, and plasma of the 10% PC group were 28, 34, 35, 36, 36, 32, 29, 24, 29, 51, 31, 25, 27, 18, 19, and 14%, respectively, those of the AA(+) group, which were significantly higher than those of the AA(−) group, although the differences in epididymal fat, liver, and plasma did not reach significant levels ($p = 0.830$, 0.222, and 0.179, respectively). The DHA per AA plus DHA levels in the brain, heart, lung, testis, soleus muscle, plantaris muscle, stomach, small

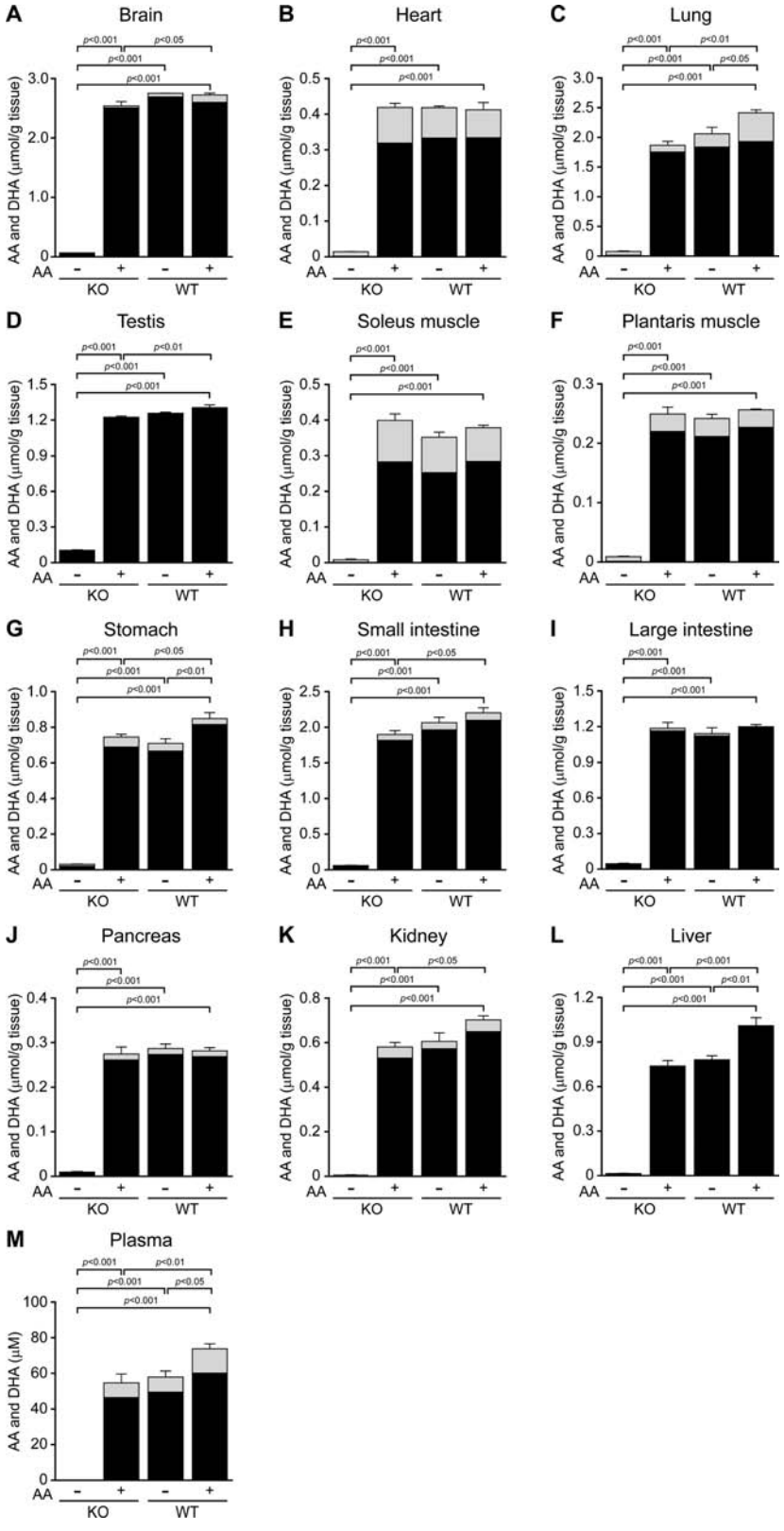


**Figure 1.** Ascorbic acid (AA) and dehydroascorbic acid (DHA) levels in SMP30/GNL KO mice fed an AA-free diet and water for 7 weeks: AA (black bars) and DHA (gray bars) concentrations in (A) brain, (B) heart, (C) lung, (D) testis, (E) soleus muscle, (F) plantaris muscle, (G) stomach, (H) small intestine, (I) large intestine, (J) pancreas, (K) kidney, (L) liver, and (M) plasma of AA(−) KO, AA(+) KO, AA(−) WT, and AA(+) WT mice. SMP30/GNL KO and WT mice were given water with or without AA for 7 weeks after weaning at 4 weeks of age. Values are given as means ± SEM (AA plus DHA) of five animals.

intestine, large intestine, eyeball, epididymal fat, skin, pancreas, kidney, liver, and plasma of the 10% PC group were 0, 25.6, 25.4, 3.1, 38.0, 15.6, 4.4, 0.2, 0, 17.6, 18.2, 16.9, 5.5, 17.7, 0.3, and 26.2%, respectively. The AA plus DHA levels in the brain, heart,


dx.doi.org/10.1021/jf502587j | J. Agric. Food Chem. 2014, 62, 9286−9295

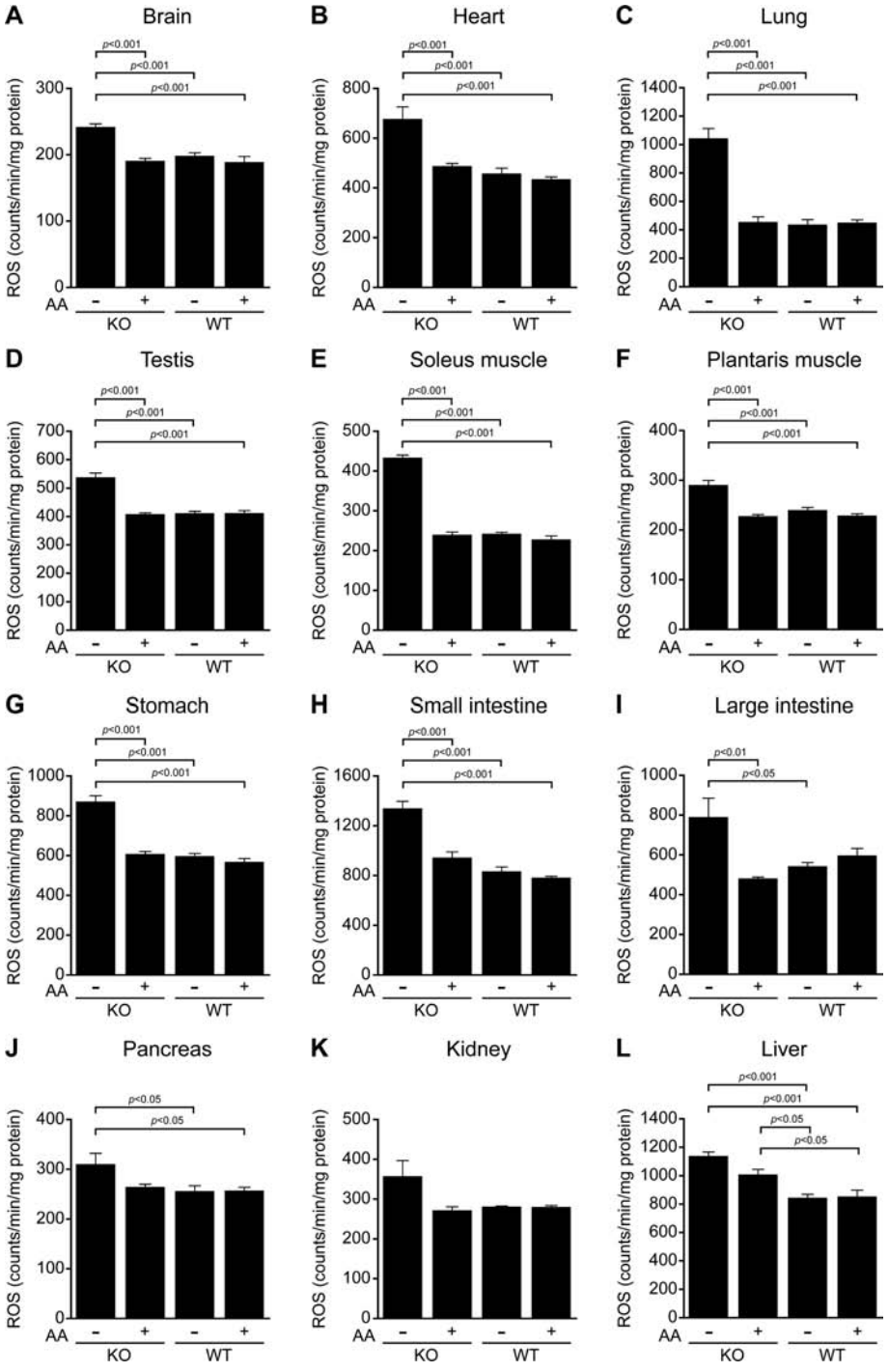


**Figure 2.** Reactive oxygen species (ROS) levels in SMP30/GNL KO mice fed an ascorbic acid (AA)-free diet and water for 7 weeks in (A) brain, (B) heart, (C) lung, (D) testis, (E) soleus muscle, (F) plantaris muscle, (G) stomach, (H) small intestine, (I) large intestine, (J) pancreas, (K) kidney, and (L) liver of AA(−) KO, AA(+) KO, AA(−) WT, and AA(+) WT mice. SMP30/GNL KO and WT mice were given water with or without AA for 7 weeks after weaning at 4 weeks of age. Values are given as means ± SEM of five animals.

lung, testis, soleus muscle, plantaris muscle, stomach, small intestine, large intestine, eyeball, epididymal fat, skin, pancreas, kidney, liver, and plasma of the 20% PC group were 97, 99, 83, 81, 99, 99, 86, 86, 87, 105, 100, 85, 91, 80, 89, and 89% of those of the AA(+) group, which were significantly higher than those of the AA(−) group. There were no significant differences in the AA plus DHA levels between the 20% PC and AA(+) groups except in the testis, small intestine, and kidney. The DHA per AA plus DHA in the brain, heart, lung, testis, soleus muscle, plantaris muscle, stomach, small intestine, large intestine, eyeball, epididymal fat, skin, pancreas, kidney, liver, and plasma of the 20% PC group were 0, 14.9, 7.2, 2.2, 20.2, 12.1, 1.9, 2.2, 0.1, 12.9, 3.9, 12.0, 4.8, 8.0, 1.7, and 25.2%, respectively.

**Decrease in ROS Levels of SMP30/GNL KO Mice Fed PC Diets.** To evaluate the antioxidant activity of PC in mice, we next determined ROS levels of tissues in SMP30/GNL KO mice fed a PC diet (Figure 5). Compared with the AA(−) group, ROS levels in the brain, heart, testis, soleus muscle, plantaris muscle,


dx.doi.org/10.1021/jf502587j | J. Agric. Food Chem. 2014, 62, 9286−9295

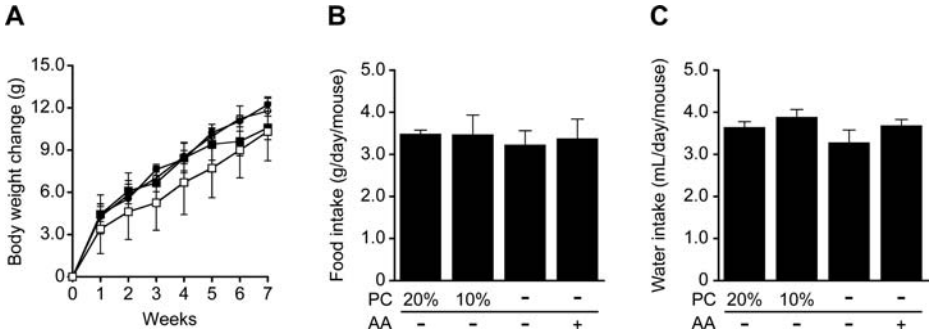


**Figure 3.** Body weight change, food intake, and water intake of SMP30/GNL KO mice fed a potato chip (PC) diet for 7 weeks: (A) body weight change of 20% PC (solid circles), 10% PC (open circles), AA(−) (solid squares), and AA(+) (open squares) groups from SMP30/GNL KO mice, that is, mice fed a 20% PC diet and AA-free water, a 10% PC diet and AA-free water, an AA-free diet and water, and an AA-free diet and 1.5 g/L AA water, respectively, for 7 weeks after weaning at 4 weeks of age (values are given as means ± SEM of five animals); (B) food intake and (C) water intake of each group (values are given as means ± SEM through the experimental period).

small intestine, and large intestine were significantly (40, 34, 18, 41, 29, 17, and 23%, respectively) lower in the 10% PC group, but the difference in tissues from the large intestine did not reach a significant level ($p = 0.08$). In the lung, stomach, eyeball, and epididymal fat, no significant differences were observed in ROS levels between the 10% PC and AA(−) groups. For the 20% PC group, ROS levels in the brain, heart, lung, testis, soleus muscle, plantaris muscle, stomach, small intestine, large intestine, eyeball, and epididymal fat were significantly (63, 46, 40, 27, 53, 54, 20, 33, 27, 33, and 42%, respectively) lower than those of the AA(−) group, and there were no significant differences between the 20% PC and AA(+) groups. Skin tissue showed a similar pattern, although it did not show significant differences. There were no differences among all four groups in tissue from the pancreas, kidney, and liver.

## DISCUSSION

In this study, we showed that AA depletion increases ROS levels in various tissues of SMP30/GNL-KO mice. Furthermore, we demonstrated that the dietary intake of PC increases total AA (AA plus DHA) levels and reduces ROS levels in tissues from SMP30/GNL KO mice. Our data suggest that SMP30/GNL KO mice are a promising model for evaluating the antioxidant activity of foods.

Here the ratio of DHA to total AA differed among tissues from AA(−) WT mice and was comparatively lower in the brain, testis, large intestine, and liver but higher in tissues from the heart, lung, soleus muscle, and plantaris muscle as well as in plasma (Figure 1 and Figure S1 in the Supporting Information). These results are consistent with our previous study.[17] DHA is transported into cells or generated from AA by a two-electron oxidation, but is rapidly and continuously reduced by dehydroascorbate reductase (DHAR) via a glutathione-dependent mechanism catalyzed by glutaredoxin, protein disulfide isomerase, and omega class glutathione transferase or by nicotinamide adenine dinucleotide phosphate (NADPH)-dependent mechanisms including reduction catalyzed by 3-$\alpha$-hydroxysteroid dehydrogenase.[3] DHAR activity was previously reported to be relatively higher in liver, adrenals, jejunum, ileum, colon, and testis, but lower in kidney, lung, thyroid, heart, and skeletal muscle.[21] Thus, our results suggest that the ratio of DHA to total AA might depend on DHAR activity in addition to ROS oxidation in tissues.

The superoxide anion radical is generated by the mitochondrial electron transport chain and in the enzymatic reaction that is catalyzed by NADPH oxidase. The reactivity and toxicity of the superoxide anion radical are reduced by the activity of superoxide dismutase (SOD), which catalyzes superoxide anion radical dismutation to hydrogen peroxide.[22] Hydrogen peroxide is relatively stable and thus can act as a signal molecule. Although glutathione peroxidase (GPX) and catalase convert hydrogen peroxide to water and oxygen, the Fenton reaction with excess hydrogen peroxide and $Fe^{2+}$ promote the production of the hydroxyl radical, which is extremely reactive and toxic. Peroxynitrite is generated from the reaction of the superoxide anion radical and nitric oxide produced by nitric oxide synthase and then converts into the hydroxyl radical and nitrogen dioxide radical. Accurate measurement of ROS in living tissues and animals is difficult because ROS are highly reactive and therefore have an extremely short life span. In our previous study, we used a real-time imaging system with lucigenin as a chemiluminescent probe to detect the superoxide anion radical,[9] although this approach is applicable only in the brain. Thus, for simple detection of ROS in a variety of tissues, we used tissue homogenates and fluorescein carboxy-$H_2$DCFDA to react with various ROS. Although the type of ROS generated during incubation of tissue homogenates was unclear, it is likely that superoxide anion radicals are generated first, and subsequently a series of ROS is produced. Therefore, this assay would be suitable for evaluating the antioxidant activity of foods that contain a wide variety of antioxidants.

AA can scavenge a broad spectrum of free radicals such as superoxide anion radical, hydroxyl radical, nitrogen dioxide radical, and carbonate.[22] A noteworthy finding of the present study is that compared to AA(+) KO mice, AA(−) KO mice exhibited much higher ROS levels in the brain, heart, lung, testis, soleus muscle, plantaris muscle, stomach, small intestine, large intestine, pancreas, and kidney (although not in the liver) with various levels for each tissue (Figure 2 and Figure S2 in the Supporting Information). Many previous studies have evaluated animal models that lack the capacity to synthesize AA. Harrison et al. reported that $F_4$-neuroprostanes, a brain-specific marker of lipid peroxidation, and malondialdehyde were elevated in the cortex and cerebellum of mice lacking Gulo that received low levels of AA.[23,24] AA-deficient Osteogenic Disorder Shionogi (ODS) rats were reported to exhibit increased lipid hydroperoxide levels in the brain, elevated thiobarbituric acid reactive substances (TBARS), and GPX activity in the heart and decreased amounts of glutathione in the plasma and liver.[25] TBARS levels were also increased in the plasma and liver of ODS rats, and lipid peroxide concentrations in plasma LDL and liver


dx.doi.org/10.1021/jf502587j | J. Agric. Food Chem. 2014, 62, 9286−9295

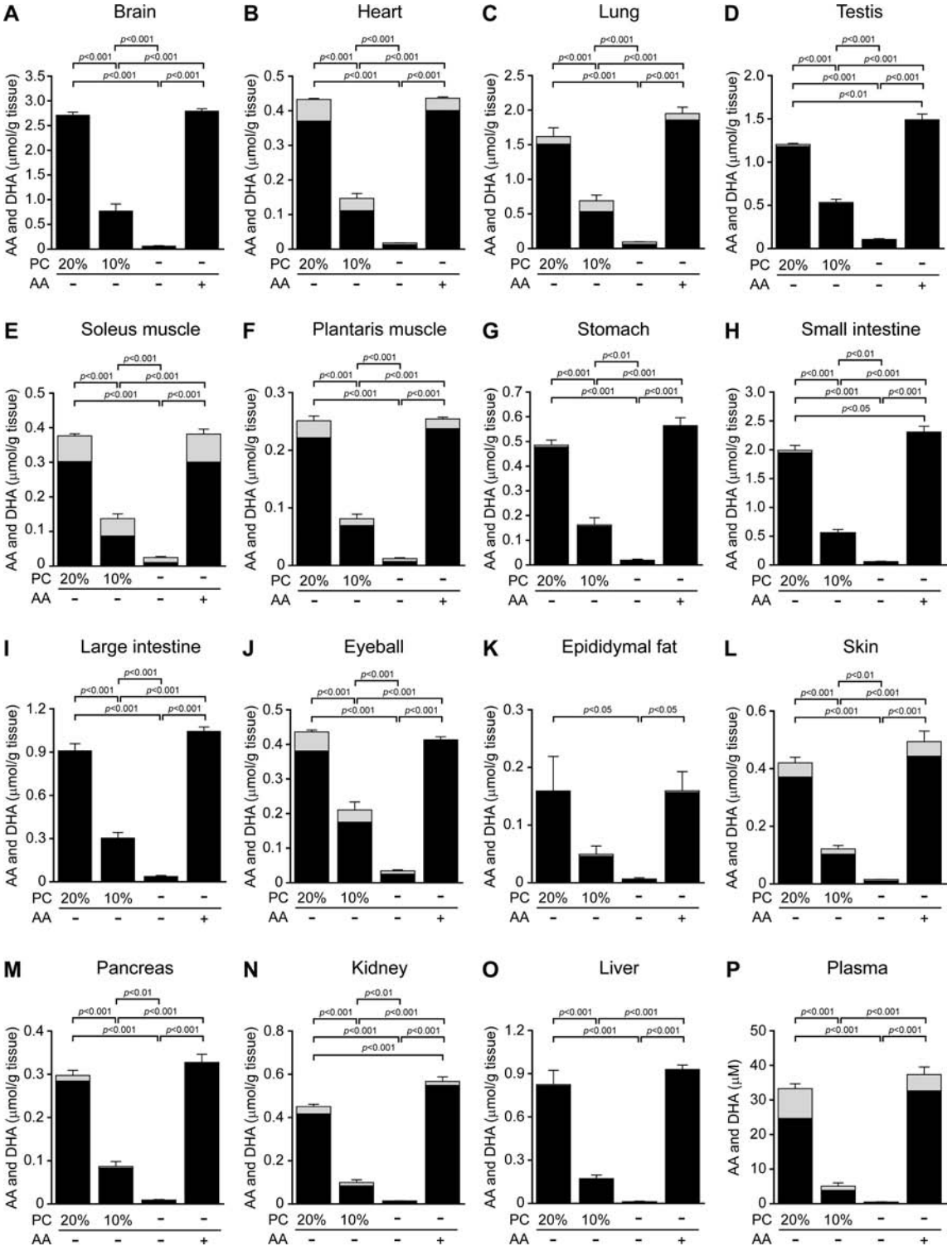


**Figure 4.** Ascorbic acid (AA) and dehydroascorbic acid (DHA) levels in SMP30/GNL KO mice fed potato chip (PC) diets for 7 weeks: AA (black bars) and DHA (gray bars) concentrations in (A) brain, (B) heart, (C) lung, (D) testis, (E) soleus muscle, (F) plantaris muscle, (G) stomach, (H) small intestine, (I) large intestine, (J) eyeball, (K) epididymal fat, (L) skin, (M) pancreas, (N) kidney, (O) liver, and (P) plasma of 20% PC, 10% PC, AA(−), and AA(+) groups from SMP30/GNL KO mice, that is, mice fed a 20% PC diet and AA-free water, a 10% PC diet and AA-free water, an AA-free diet and water, and an AA-free diet and 1.5 g/L AA water, respectively, for 7 weeks after weaning at 4 weeks of age. Values are given as means ± SEM (AA plus DHA) of five animals.

were elevated in animals fed an AA-free diet.[26] Lykkesfeldt et al. reported that guinea pigs 3 weeks after weaning showed decreases in tocopherols and glutathione as well as decreased SOD activity and an increase in protein oxidation in the liver. They also observed an increase in lipid and DNA oxidation but a decrease in protein oxidation in the brain.[27] On the other hand, the sodium-dependent vitamin C transporter (SVCT) 2 transgenic mouse showed that despite having increased AA levels


dx.doi.org/10.1021/jf502587j | J. Agric. Food Chem. 2014, 62, 9286−9295

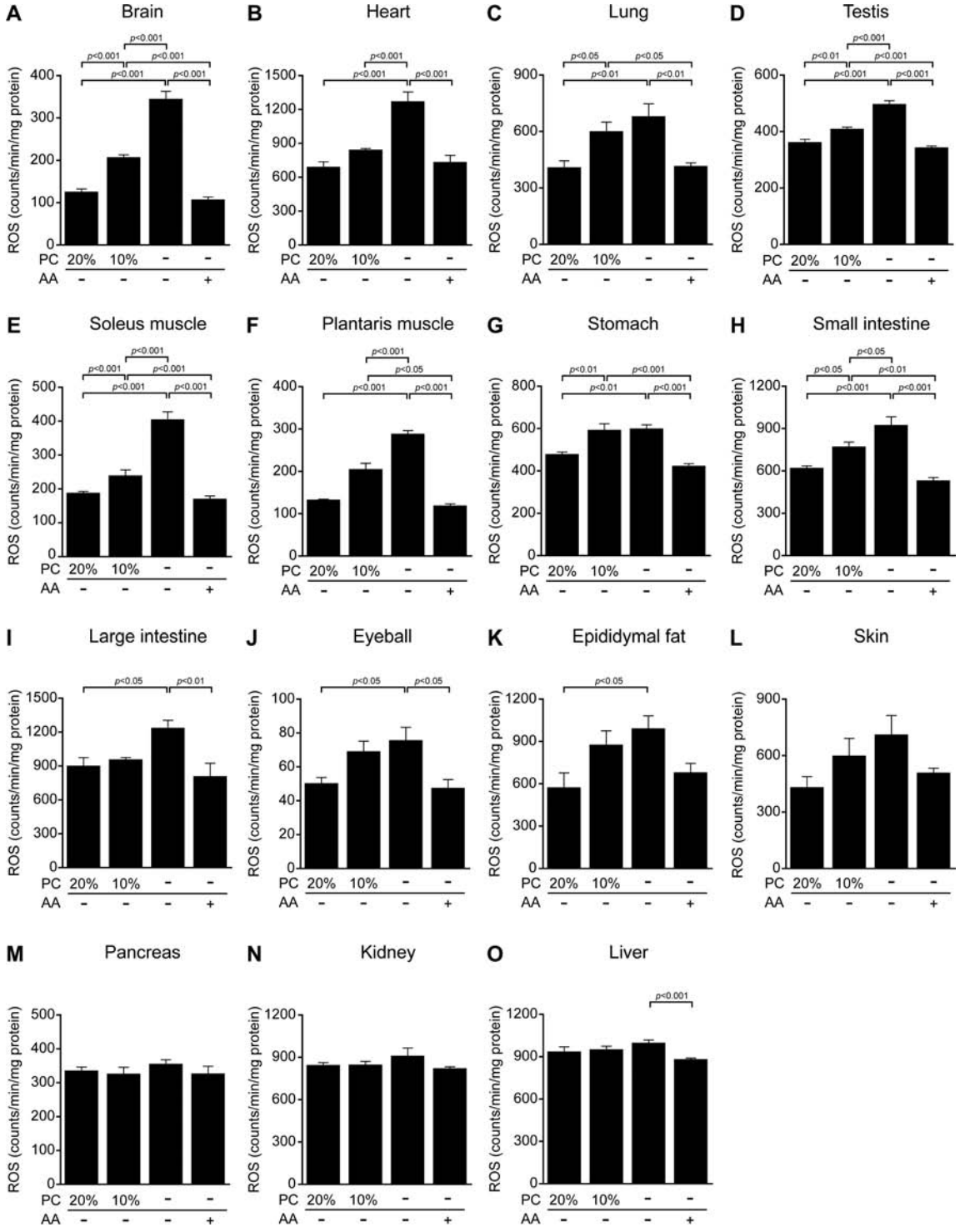


**Figure 5.** Reactive oxygen species (ROS) levels in SMP30/GNL KO mice fed potato chip (PC) diets for 7 weeks: ROS in (A) brain, (B) heart, (C) lung, (D) testis, (E) soleus muscle, (F) plantaris muscle, (G) stomach, (H) small intestine, (I) large intestine, (J) eyeball, (K) epididymal fat, (L) skin, (M) pancreas, (N) kidney, and (O) liver of 20% PC, 10% PC, AA(−), and AA(+) groups from SMP30/GNL KO mice, tht is, mice fed a 20% PC diet and AA-free water, a 10% PC diet and an AA-free water, an AA-free diet and water, and an AA-free diet and 1.5 g/L AA water, respectively, for 7 weeks after weaning at 4 weeks of age. Values are given as means ± SEM of five animals. AA, ascorbic acid.

in the cortex, spleen, kidney, heart, and lung, TBARS levels were not altered.[28] We previously reported that AA-depleted SMP30/GNL KO mice showed an increase in superoxide anion radical levels, although SOD activity was not altered in the brain.[9] In lung tissue of AA-depleted SMP30/GNL KO mice there were increased ROS and TBARS levels, but no alteration of GPX activity was observed.[10] Taken together, an AA deficiency is likely to have a different influence on ROS metabolism and oxidative stress in tissues. Because we do not presently have an explanation for the observed increase in ROS in AA-depleted SMP30/GNL KO mice, further work will be required to elucidate the molecular mechanisms involved in regulating oxidative stress markers such


dx.doi.org/10.1021/jf502587j | J. Agric. Food Chem. 2014, 62, 9286−9295

as lipid peroxidation, protein oxidation, and DNA oxidation, as well as the activity of antioxidants and antioxidative enzyme levels that could be responsible for this increase in ROS.

To our knowledge, no paper describes the bioavailability of AA from PC in animal tissues. Our data showed that the total AA levels in tissues such as the brain, heart, lung, soleus muscle, plantaris muscle, stomach large intestine, eyeball, epididymal fat, skin, pancreas, liver, and plasma of the 20% PC diet group were similar to those of the AA(+) KO group, whereas levels differed in the testis, small intestine, and kidney (Figure 4). The AA contents of 20 and 10% PC diets used in this experiment were 13.6 and 6.0 mg/100 g, respectively. The average AA intake in the 20 and 10% PC groups of SMP30/GNL KO mice was calculated using the food intake values for each 3.5 g/day/mouse to be 0.47 and 0.21 mg/day/mouse, respectively. Because AA(+) KO mice consumed 3.7 mL/day/mouse of 1.5 g/L AA water and thus AA intake was calculated to be 5.5 mg/day/mouse, the AA intakes of the 20 and 10% PC groups were only 8.6 and 3.7%, respectively, of AA(+) KO. SVCTs have high affinity and specificity and are capable of generating a steep AA concentration gradient. Despite small amounts of oral AA intake, the total tissue AA can therefore be maintained at a subsaturating concentration in the 20% PC groups. In contrast, the total tissue AA concentration showed tissue specificity in the 10% PC groups. SVCT1 having a low affinity for AA is known to be abundantly expressed in the liver and kidney,[29] which might be the reason why the ratio of total AA levels in the 10% PC group compared to AA(+) KO mice was lower in the kidney and liver (<20%).

An additional notable finding is that animals fed the 20% PC diet had completely reduced ROS levels that were similar to the AA(+) group in the brain, heart, lung, testis, soleus muscle, plantaris muscle, stomach, small intestine, large intestine, eyeball, and epididymal fat tissues (Figure 5). However, testing the ROS-suppressing effect of PC in the pancreas, kidney, and liver could not be performed, because there were no marked differences in ROS levels in these tissues between the AA(−) KO and AA(+) KO groups at 7 weeks. In the 10% PC group, ROS levels were decreased in the brain, heart, testis, soleus muscle, plantaris muscle, and small intestine, and large intestine tissues, but were unchanged in the lung, stomach, eyeball, and epididymal fat tissues. This tissue specificity may be attributed to the balance between ROS generation and antioxidant system that includes AA and other antioxidants. Many studies have shown that, other than AA, potato tubers contain antioxidants such as carotenoids and a wide variety of polyphenols such as chlorogenic acid, caffeic acid, gallic acid, protocatechuic acid, and quercetin and, therefore, exhibit significant antioxidant activity as measured by in vitro radical scavenging assays such as the ORAC.[30−32] Kaspar et al. also reported that consumption of pigmented potatoes containing high concentrations of antioxidants decreased plasma DNA oxidative damage and inflammation associated with IL-6 production in healthy adult human males.[33] Although there are no reports concerning the antioxidant activity of PC in animal tissues, these insights suggest that antioxidant nutrients included in PC also exhibit antioxidant activity in mouse tissues.

In contrast to the results of the present animal experiment, the ORAC values were significantly lower in the 20 and 10% PC diet compared to CL-2 (Figure S3 in the Supporting Information), suggesting that the ORAC value does not necessarily represent the antioxidant activity in the animal. Thus, an antioxidant activity assay using SMP30/GNL KO mice could be superior in that it reflects the bioavailability of dietary antioxidants in its targeted tissue.

Further studies will be required to define the exact molecular mechanism of the increase in ROS in AA-depleted SMP30/GNL KO mice and the antioxidant activity of PC in an animal model. However, our results suggest that PC intake increases total AA and enhances ROS scavenging activity in tissues of SMP30/GNL KO mice and that SMP30/GNL KO mice are a promising model for evaluating the antioxidant activity of various foods.

## ■ ASSOCIATED CONTENT

### Supporting Information

Body weight of SMP30/GNL KO and WT mice (Table S1), AA and DHA levels (Figure S1) and ROS levels (Figure S2) in SMP30/GNL KO mice fed an AA-free diet and water for 14 weeks, and the ORAC values of 20% PC CL-2, 10% PC CL-2, CL-2, and PC (Figure S3). This material is available free of charge via the Internet at http://pubs.acs.org.

## ■ AUTHOR INFORMATION

### Corresponding Author

*(Y.K.) Phone: +81-47-472-1677. Fax: +81-47-472-7696. E-mail: yoshitaka.kondo@sci.toho-u.ac.jp. Present address: Division of Molecular Medicine, Department of Biomolecular Science, Faculty of Science, Toho University, 2-2-1 Miyama, Funabashi, Chiba 274-8510, Japan.

### Notes

The authors declare no competing financial interest.

## ■ ABBREVIATIONS USED

AA, L-ascorbic acid; carboxy-$H_2$DCFDA, 5-(and-6)-carboxy-2′,7′-dichlorodihydrofluorescein diacetate; DHA, dehydroascorbic acid; DHAR, dehydroascorbate reductase; EDTA, ethylenediaminetetraacetic acid; GNL, gluconolactonase; GPX, glutathione peroxidase; Gulo, L-gulono-γ-lactone oxidase; KO, knockout; MPA, metaphosphoric acid; NADPH, nicotinamide adenine dinucleotide phosphate; ODS, osteogenic disorder Shionogi; ORAC, oxygen radical absorbance capacity; PC, potato chips; ROS, reactive oxygen species; SEM, standard error of the mean; SOD, superoxide dismutase; SVCT, sodium-dependent vitamin C transporter; TBARS, thiobarbituric acid reactive substances; WT, wild type

## ■ REFERENCES

(1) Murphy, M. P. How mitochondria produce reactive oxygen species. *Biochem. J.* **2009**, *417*, 1−13.

(2) Valko, M.; Leibfritz, D.; Moncol, J.; Cronin, M. T.; Mazur, M.; Telser, J. Free radicals and antioxidants in normal physiological functions and human disease. *Int. J. Biochem. Cell Biol.* **2007**, *39*, 44−84.

(3) Linster, C. L.; Van Schaftingen, E. Vitamin C. Biosynthesis, recycling and degradation in mammals. *FEBS J.* **2007**, *274*, 1−22.

(4) Pohanka, M.; Pejchal, J.; Snopkova, S.; Havlickova, K.; Karasova, J. Z.; Bostik, P.; Pikula, J. Ascorbic acid: an old player with a broad impact on body physiology including oxidative stress suppression and immunomodulation: a review. *Mini Rev. Med. Chem.* **2012**, *12*, 35−43.

(5) Ishigami, A.; Maruyama, N. Significance of SMP30 in gerontology. *Geriatr. Gerontol. Int.* **2007**, *7*, 316−325.

(6) Aizawa, S.; Senda, M.; Harada, A.; Maruyama, N.; Ishida, T.; Aigaki, T.; Ishigami, A.; Senda, T. Structural basis of the γ-lactone-ring formation in ascorbic acid biosynthesis by the senescence marker protein-30/gluconolactonase. *PLoS One* **2013**, *8*, No. e53706.

(7) Kondo, Y.; Inai, Y.; Sato, Y.; Handa, S.; Kubo, S.; Shimokado, K.; Goto, S.; Nishikimi, M.; Maruyama, N.; Ishigami, A. Senescence marker protein 30 functions as gluconolactonase in L-ascorbic acid biosynthesis, and its knockout mice are prone to scurvy. *Proc. Natl. Acad. Sci. U.S.A.* **2006**, *103*, 5723−5728.

(8) Ishigami, A.; Fujita, T.; Handa, S.; Shirasawa, T.; Koseki, H.; Kitamura, T.; Enomoto, N.; Sato, N.; Shimosawa, T.; Maruyama, N. Senescence marker protein-30 knockout mouse liver is highly susceptible to tumor necrosis factor-$\alpha$- and Fas-mediated apoptosis. *Am. J. Pathol.* **2002**, *161*, 1273−1281.
(9) Kondo, Y.; Sasaki, T.; Sato, Y.; Amano, A.; Aizawa, S.; Iwama, M.; Handa, S.; Shimada, N.; Fukuda, M.; Akita, M.; Lee, J.; Jeong, K. S.; Maruyama, N.; Ishigami, A. Vitamin C depletion increases superoxide generation in brains of SMP30/GNL knockout mice. *Biochem. Biophys. Res. Commun.* **2008**, *377*, 291−296.
(10) Koike, K.; Kondo, Y.; Sekiya, M.; Sato, Y.; Tobino, K.; Iwakami, S. I.; Goto, S.; Takahashi, K.; Maruyama, N.; Seyama, K.; Ishigami, A. Complete lack of vitamin C intake generates pulmonary emphysema in senescence marker protein-30 knockout mice. *Am. J. Physiol. Lung Cell Mol. Physiol.* **2010**, *298*, L784−L792.
(11) Camire, M. E.; Kubow, S.; Donnelly, D. J. Potatoes and human health. *Crit. Rev. Food Sci. Nutr.* **2009**, *49*, 823−840.
(12) Hamouz, K.; Lachman, J.; Pazderu, K.; Hejtmankova, K.; Cimr, J.; Musilova, J.; Pivec, V.; Orsak, M.; Svobodova, A. Effect of cultivar, location and method of cultivation on the content of chlorogenic acid in potatoes with different flesh colour. *Plant Soil Environ.* **2013**, *59*, 465−471.
(13) Lachman, J.; Hamouz, K.; Sulc, M.; Orsak, M.; Pivec, V.; Hejtmankova, A.; Dvorak, P.; Cepl, J. Cultivar differences of total anthocyanins and anthocyanidins in red and purple-fleshed potatoes and their relation to antioxidant activity. *Food Chem.* **2009**, *114*, 836−843.
(14) Miyoshi, T.; Ishihara, K.; Nakamura, K.; Koga, H. Antioxidative compounds in potato chips. *J. Cook. Sci. Jpn.* **2006**, *39*, 277−282.
(15) Kondo, Y.; Higashi, C.; Iwama, M.; Ishihara, K.; Handa, S.; Mugita, H.; Maruyama, N.; Koga, H.; Ishigami, A. Bioavailability of vitamin C from mashed potatoes and potato chips after oral administration in healthy Japanese men. *Br. J. Nutr.* **2012**, *107*, 885−892.
(16) Prior, R. L.; Hoang, H.; Gu, L.; Wu, X.; Bacchiocca, M.; Howard, L.; Hampsch-Woodill, M.; Huang, D.; Ou, B.; Jacob, R. Assays for hydrophilic and lipophilic antioxidant capacity (oxygen radical absorbance capacity ($ORAC_{FL}$)) of plasma and other biological and food samples. *J. Agric. Food Chem.* **2003**, *51*, 3273−3279.
(17) Sato, Y.; Uchiki, T.; Iwama, M.; Kishimoto, Y.; Takahashi, R.; Ishigami, A. Determination of dehydroascorbic acid in mouse tissues and plasma by using tris(2-carboxyethyl)phosphine hydrochloride as reductant in metaphosphoric acid/ethylenediaminetetraacetic acid solution. *Biol. Pharm. Bull.* **2010**, *33*, 364−369.
(18) Jung, K. J.; Lee, E. K.; Yu, B. P.; Chung, H. Y. Significance of protein tyrosine kinase/protein tyrosine phosphatase balance in the regulation of NF-$\kappa$B signaling in the inflammatory process and aging. *Free Radical Biol. Med.* **2009**, *47*, 983−991.
(19) Son, T. G.; Zou, Y.; Jung, K. J.; Yu, B. P.; Ishigami, A.; Maruyama, N.; Lee, J. SMP30 deficiency causes increased oxidative stress in brain. *Mech. Ageing Dev.* **2006**, *127*, 451−457.
(20) Wardman, P. Fluorescent and luminescent probes for measurement of oxidative and nitrosative species in cells and tissues: progress, pitfalls, and prospects. *Free Radical Biol. Med.* **2007**, *43*, 995−1022.
(21) Paolicchi, A.; Pezzini, A.; Saviozzi, M.; Piaggi, S.; Andreuccetti, M.; Chieli, E.; Malvaldi, G.; Casini, A. F. Localization of a GSH-dependent dehydroascorbate reductase in rat tissues and subcellular fractions. *Arch. Biochem. Biophys.* **1996**, *333*, 489−495.
(22) Winterbourn, C. C. Reconciling the chemistry and biology of reactive oxygen species. *Nat. Chem. Biol.* **2008**, *4*, 278−286.
(23) Harrison, F. E.; Green, R. J.; Dawes, S. M.; May, J. M. Vitamin C distribution and retention in the mouse brain. *Brain Res.* **2010**, *1348*, 181−186.
(24) Harrison, F. E.; Yu, S. S.; Van Den Bossche, K. L.; Li, L.; May, J. M.; McDonald, M. P. Elevated oxidative stress and sensorimotor deficits but normal cognition in mice that cannot synthesize ascorbic acid. *J. Neurochem.* **2008**, *106*, 1198−1208.
(25) Tokumaru, S.; Takeshita, S.; Nakata, R.; Tsukamoto, I.; Kojo, S. Change in the level of vitamin C and lipid peroxidation in tissues of the inherently scorbutic rat during ascorbate deficiency. *J. Agric. Food Chem.* **1996**, *44*, 2748−2753.
(26) Kimura, H.; Yamada, Y.; Morita, Y.; Ikeda, H.; Matsuo, T. Dietary ascorbic acid depresses plasma and low density lipoprotein lipid peroxidation in genetically scorbutic rats. *J. Nutr.* **1992**, *122*, 1904−1909.
(27) Lykkesfeldt, J.; Trueba, G. P.; Poulsen, H. E.; Christen, S. Vitamin C deficiency in weanling guinea pigs: differential expression of oxidative stress and DNA repair in liver and brain. *Br. J. Nutr.* **2007**, *98*, 1116−1119.
(28) Harrison, F. E.; Best, J. L.; Meredith, M. E.; Gamlin, C. R.; Borza, D. B.; May, J. M. Increased expression of SVCT2 in a new mouse model raises ascorbic acid in tissues and protects against paraquat-induced oxidative damage in lung. *PLoS One* **2012**, *7*, No. e35623.
(29) Macias, R. I.; Hierro, C.; de Juan, S. C.; Jimenez, F.; Gonzalez-San Martin, F.; Marin, J. J. Hepatic expression of sodium-dependent vitamin C transporters: ontogeny, subtissular distribution and effect of chronic liver diseases. *Br. J. Nutr.* **2011**, *106*, 1814−1825.
(30) Kulen, O.; Stushnoff, C.; Holm, D. G. Effect of cold storage on total phenolics content, antioxidant activity and vitamin C level of selected potato clones. *J. Sci. Food Agric.* **2013**, *93*, 2437−2444.
(31) Stushnoff, C.; Holm, D.; Thompson, M. D.; Jiang, W.; Thompson, H. J.; Joyce, N. I.; Wilson, P. Antioxidant properties of cultivars and selections from the Colorado potato breeding program. *Am. J. Potato Res.* **2008**, *85*, 267−276.
(32) Andre, C. M.; Ghislain, M.; Bertin, P.; Oufir, M.; Herrera Mdel, M. d. R.; Hoffmann, L.; Hausman, J. F.; Larondelle, Y.; Evers, D. Andean potato cultivars (*Solanum tuberosum* L.) as a source of antioxidant and mineral micronutrients. *J. Agric. Food Chem.* **2007**, *55*, 366−378.
(33) Kaspar, K. L.; Park, J. S.; Brown, C. R.; Mathison, B. D.; Navarre, D. A.; Chew, B. P. Pigmented potato consumption alters oxidative stress and inflammatory damage in men. *J. Nutr.* **2011**, *141*, 108−111.

tumor growth and antiatherosclerotic and antimicrobial activities.[15] *Ganoderma atrum* is a member of the most representative medical mushrooms of *Ganodermataceae*. The polysaccharide is the major bioactive substance in *G. atrum*.[16] For our unremitting pursuit of novel agents with antitumor activities, we reorganized and qualified the structure of PSG-1, which is a polysaccharide of *G. atrum*. The purity of PSG-1 is more than 99.8%. The polysaccharide is composed of glucose, mannose, galactose, and galacturonic acid with molar ratio of 4.91:1:1.28:0.71.[17] Furthermore, PSG-1 comprises a backbone of 1,3-linked and 1,6-linked $\beta$-Glcp residues substituted at O-3 and O-6 positions as the branch points.[18,19] Our previous studies suggested that PSG-1 had potent antioxidant activity, even stronger than that of *Ganoderma lucidium*.[17,20] PSG-1 was also shown to induce apoptosis in S180 xenografts in vivo.[21] Recently, we verified that PSG-1 possessed potent antitumor activity by inducing apoptosis via mitochondrial pathways and enhanced the antitumor effect via improving immune system functions through the TLR4-mediated NF-$\kappa$B and MAPK signaling pathway.[22,23]

Although PSG-1 has been crowned as one of the most active antineoplastic agents in the past decades, the exact molecular mechanisms that integrate these events have remained largely unclear. Therefore, research and development of PSG-1 as a novel agent with antitumor activity are of great importance. This study was designed to evaluate and characterize the antitumor activity and potential molecular mechanism of PSG-1 in CT26-bearing mice. The data have verified the excellent antitumor effect of PSG-1 in the CT26-bearing mice model, in which enhanced tumor growth inhibition accompanied by increased apoptosis as compared with control group was verified. We further demonstrated that such action may be associated with induction of apoptosis via the cAMP/PKA signaling pathway and downregulation of the PKC pathway, as well as improving the host immune system. These findings would pave the way for novel therapeutic approaches to treat CRC patients and open up new possibilities for the cancer control.

## MATERALS AND METHODS

**Materials.** PSG-1 was extracted and purified following our previously published method.[18] RPMI 1640 and fetal bovine serum (FBS) were purchased from Hyclone (Logan, UT). Penicillin and streptomycin were purchased from Life Technologies, Inc. (Gaithersburg, MD). Antibodies for PKA and PKC were purchased from Abcam (Cambridge, MA). Anti-$\beta$-actin, goat anti-rabbit IgG-conjugated horseradish peroxidase (HRP) and goat anti-mouse IgG-conjugated HRP were purchased from ZSGB-Bio (Beijing, China). 5-Fluorouracil was purchased from Sigma-Aldrich (St. Louis, MO). PKA, PKC, cAMP, and cGMP assay kits were obtained from IBL (Hamburg, Germany). IL-1$\beta$ and TNF-$\alpha$ ELISA kits were purchased from SenXiong Biotechnology (Shanghai, China). Cell culture products were obtained from Life Technologies (Paisley, Scotland).

**Cell Line and Animals.** CT26 WT mouse colon cell line was purchased from Type Culture Collection of Chinese Academy of Sciences, Shanghai, China. BALB/c mice (female, 4−6-weeks old, weighted 20.0 ± 2.0 g) were purchased from Beijing HFK Biotechnology Co. [Beijing, China; quality certificate number SCXK (jing) 2009-0004]. The animals were maintained in accordance with the Guide for the Care and Use of Laboratory Animals (NRC 2011), and all procedures were approved by Nanchang University Animal Ethnics Committee.

**Cell Viability Assay.** The effect of PSG-1 on the viability of CT26 cells was determined by MTT assay. CT26 cells were seeded in a flat-bottomed 96-well plate ($2.0 \times 10^4$ cells/mL) and treated with PSG-1 (20−320 $\mu$g/mL). Controls were exposed to culture medium without PSG-1. After incubation for 48 h, 20 $\mu$L of MTT solution (5 mg/mL) was added to each well, and the cells were incubated at 37 °C for 4 h. Crystalline formazan was dissolved in 150 $\mu$L of dimethyl suroxide (DMSO), and the absorbance at 490 nm was measured immediately on a microplate reader (Thermo, Shanghai, China).

**Animal Experiments.** The mice were injected hypodermically with $1 \times 10^7$ cells/mL of CT26 in 0.2 mL at the right hind groin. The xenograft tumor-bearing mice were divided randomly into five groups (eight mice in each group). The mice were treated with PSG-1 via gastric tube at doses of 50, 100, and 200 mg/kg body weight (BW) for 2 weeks. The negative control group was treated with 0.9% saline, and the positive control received 5-Fu (20 mg/kg BW). At the end of the experiments, mice were weighed and sacrificed by cervical dislocation, and then the solid tumors, thymus, and spleen were harvested. Thymus and spleen indexes were expressed as the thymus and spleen weight relative to body weight. The rate of inhibition (IR) was calculated according to the following formula:

$$\begin{aligned} \mathrm{IR} = {} & (\text{the average tumor weight of the treated group}) \\ & - (\text{the average tumor weight of the control group}) \\ & / (\text{the average tumor weight of the control group}) \times 100\% \end{aligned}$$

Blood samples obtained from retrobulbar venous plexus of each group of mice were centrifuged (12 000 rpm) for 10 min at 4 °C to separate serum and blood cells. The serum was stored at −80 °C for determination of cytokines (IL-2, IFN-$\gamma$, and TNF-$\alpha$). The serum cytokine levels were determined using ELISA kits (R&D Systems, Minneapolis, MN).

**Preparation of Murine CT26 Cells in the Tumor of CT26-Bearing Mice.** The tumor was isolated using sterile tissue dissection techniques from tumor-bearing mice and transferred to PBS. The tumor tissues were subsequently minced. The cell suspensions were filtered through a Steriflip unit. Then the cells were washed twice in PBS and further purified using gradient centrifugation. After centrifugation, the cells were resuspended in RPMI 1640 medium with 10% FBS ($2 \times 10^6$/mL).

**Analysis of Cell Apoptosis.** To define the apoptosis of tumor cells, CT26 cells were strained with Annexin V-FITC/PI detection kit (KeyGen, Nanjing, China) according to the manufacturer's instructions. Briefly, the CT26 cells from tumor-bearing mice were harvested and resuspended in 500 $\mu$L of binding buffer containing the Annexin V-FITC and PI fluorescence dyes at 37 °C for 15 min in the dark. The strained cells were washed twice with PBS and resuspended. The fluorescence was detected by FACSCalibur (Becton Dickinson) in the FL1-H and FL2-H channels.

**Determination of cAMP and cGMP Concentrations.** The intracellular cAMP and cGMP levels were determined by using the cAMP and cGMP ELISA kits (Enzo Life Sciences). First, the CT26 cells ($2 \times 10^5$ cells/mL) were prepared as described above and then resuspended in lysis reagent provided in the kit, followed by centrifugation at 12 000$g$ for 30 min at 4 °C. The supernatant was immediately collected and quantified by the cAMP or cGMP kit. Each sample and standard value was derived from triplicate measurements.

**Measurement of DAG and Adenylyl Cyclase (AC) Contents.** The DAG and AC contents were determined by using the DAG and AC ELISA kits (Antibodies-Online, Atlanta, GA). A total of $10^6$ CT26 cells from tumor-bearing mice were washed with PBS and harvested by centrifugation. The cells were lysed by the lysis reagent provided in the kit. The supernatant was collected and used for the determination of intracellular DAG and AC contents.

**PKA and PKC Activity Assays.** The CT26 cells from mice model were harvested as described above. The activities of intracellular PKC and PKA were determined by PKC and PKA kits (Enzo Life Sciences International), respectively. In brief, CT26 cells were scraped into $Ca^{2+}$-free PBS supplemented with 2.5 mM of EDTA or EGTA and then pelleted by a brief centrifugation. Cells were lysed in an ice-cold homogenization buffer and then centrifuged at 15 000$g$ for 30 min at 4 °C. The cell samples were added to the appropriate wells. The reaction was then stopped with acid-stop solution, and the absorbance was measured at 450 nm in a microplate reader (Thermo, Shanghai, China).

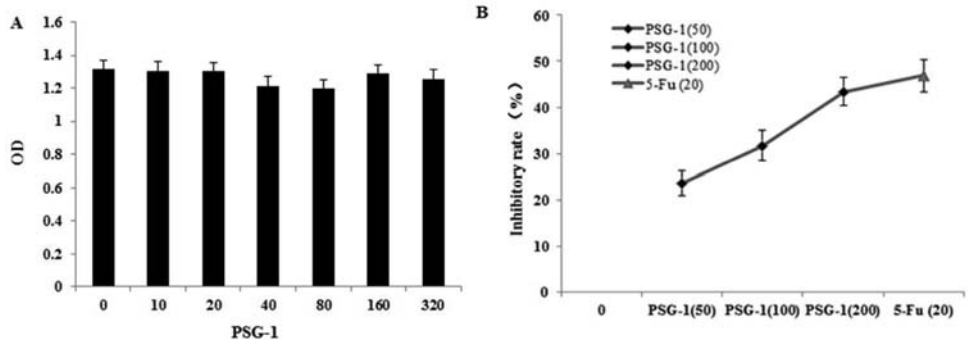


**Figure 1.** (A) Effect of PSG-1 on the proliferation of CT26 cells. CT26 cells were seeded into 96-well culture plates and treated with the indicated concentrations of PSG-1 for 48 h. Proliferation of CT26 was evaluated using the MTT method. (B) Antitumor effect of PSG-1 on the proliferation of tumor cells in CT26-bearing mice.

**Western Blot Analysis.** Total protein (15 $\mu$g) from CT26 cells was separated by SDS−PAGE and was transferred to nitrocellulose membranes. The membranes were blocked with Tris-buffered saline containing 5% fat-free dried milk for 2 h at room temperature and further incubated 16 h at 4 °C with anti-PKA or anti-PKC antibodies (Cell Signaling Technology, Danvers, MA). After washing three times with TBS-0.05% Tween 20, reactive bands were incubated with horseradish peroxidase-conjugated secondary antibody for 1 h at room temperature. The membranes were washed again, and the immunoreactive protein was visualized using enhanced chemiluminescent reagent (Beytin, Nanjing, China). The experiments were performed in triplicate, and representative results are shown.

**Neutral Red Phagocytosis Assay of Peritoneal Macrophages.** Macrophages were obtained from tumor-bearing mice peritoneal exudate cells (PECs). PECs were washed with PBS and resuspended in RPMI-1640 medium. Then PECs were seeded in a 96-well plate ($2 \times 10^5$ cells per well) and incubated at 37 °C, 5% $CO_2$ for 4 h in a humidified atmosphere to allow peritoneal macrophages to adhere. The supernatants were discarded, 100 $\mu$L 0.075% neutral red was added, and the mixture incubated for another 1 h. Cells were washed with PBS three times and incubated with cell lysis buffer (1 M acetic acid: ethanol = 1:1) overnight. The result was recorded with a microplate reader, using a test wavelength of 540 nm.

**Determination of Proliferation of Lymphocyte of CT26-Bearing Mice.** CT26-bearing mice were killed, and the spleens collected under aseptic condition were chopped into small pieces and filtered over a fine steel mesh. Lymphocytes were resuspended in lysis buffer to remove erythrocytes and then resuspended in 10% FBS RPMI-1640 ($2 \times 10^6$ cells per well) medium. The cells were planted into 96-well plates with or without ConA 1 mg/L or LPS 5 mg/L and incubated for 48 h. Cell proliferation was measured on the basis of the MTT method.

**Statistical Analysis.** All data were expressed as means ± SEM of at least three experiments. ANOVA was used to assess the statistical significance of the differences. Differences with $P$ values <0.05 were considered statistically significant.

## RESULTS

**PSG-1 Could Not Inhibit the Proliferation of CT26 Cells.** In order to examine whether PSG-1 possessed an antiproliferation effect on CT26 cells, we evaluated the proliferation of CT26 cells exposed to PSG-1. CT26 cells growing in 96-well plate were maintained in medium containing increasing concentrations of PSG-1 for 48 h. As seen in Figure 1A, PSG-1 at concentration 10−320 $\mu$g/mL showed little impact on the growth of CT26 cells and did not present any sign of toxicity in CT26 cells.

**Antitumor Effect of PSG-1 in CT26-Bearing Mice.** As shown in Figure 1B, the mice treated with PSG-1 had a marked reduction in the tumor volume when compared to the control group. The tumor inhibition of mice in the PSG-1 group was quite effective, and the inhibition rate was 44.68% at 200 mg/kg. It was also found that there was no significant difference between high dose PSG-1 (200 mg/kg) and 5-Fu treated group.

**Apoptosis in CT26-Bearing Mice.** Flow cytometry assays showed marked changes in cell profiles after treatment with 50, 100, and 200 mg/kg PSG-1. The apoptotic rates ranged from 1.68% to 41.04%; the 200 mg/kg PSG-1 group was the highest among them, indicating that administration of PSG-1 induced apoptosis (Figure 2A−E).

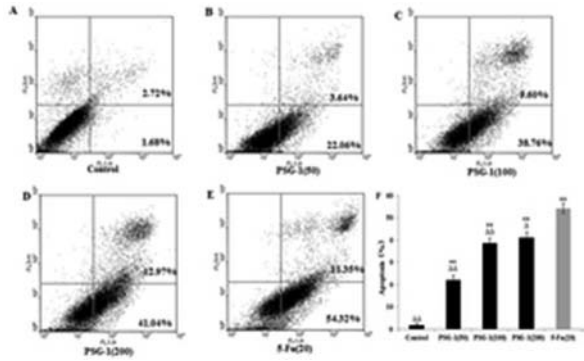

**Figure 2.** (A−E) Annexin V-FITC/PI double-staining assay of CT26 cells from the tumor-bearing mice. (F) Bar graph representing the percentage of CT26 cell apoptosis. Each value represents the mean of three experiments. $^{**}P < 0.01$ vs control group, $^{\Delta}P < 0.05$, $^{\Delta\Delta}P < 0.01$ vs 5-Fu group.

**Distinct Changes of Intracellular cAMP and cGMP Concentrations in Tumor.** Previous studies have indicated that the cAMP signaling pathway and cGMP mediator are known to be of paramount importance in PSG-1-induced apoptosis of S180 cells. To investigate the correlation between intracellular cAMP and cGMP levels and the percentage of apoptosis, we measured, for the first time, the intracellular cAMP and cGMP contents in CT26 cells from tumor-bearing mice treated with different doses of PSG-1. Significant improvement in the intracellular cAMP concentration was observed. In contrast, the intracellular cGMP level was decreased in the CT26 cells.

**Effect of PSG-1 Treatment on AC and DAG Contents.** Since the intracellular cAMP level is mainly regulated by the AC isoform, the activity of the AC system might be related to the alteration of cAMP levels triggered by PSG-1. DAG is a physiological activator of PKC. The production of DAG in the

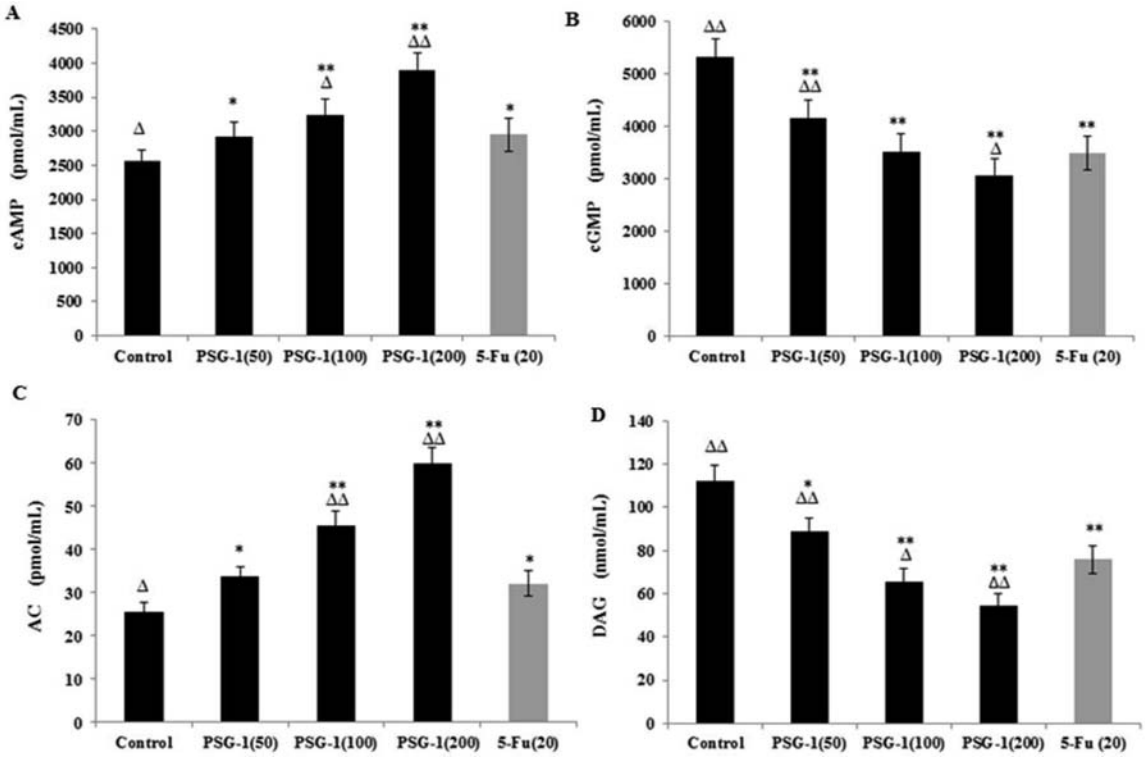


**Figure 3.** Effect of PSG-1 on intracellular (A) cAMP, (B) cGMP, (C) AC, and (D) DAG production in the tumor. The production was measured according to ELISA kit instructions. Bar graphs show mean ± SEM of three independent experiments performed. *$P$ < 0.05, **$P$ < 0.01 vs control group; $^{\Delta}P$ < 0.05, $^{\Delta\Delta}P$ < 0.01 vs 5-Fu group.

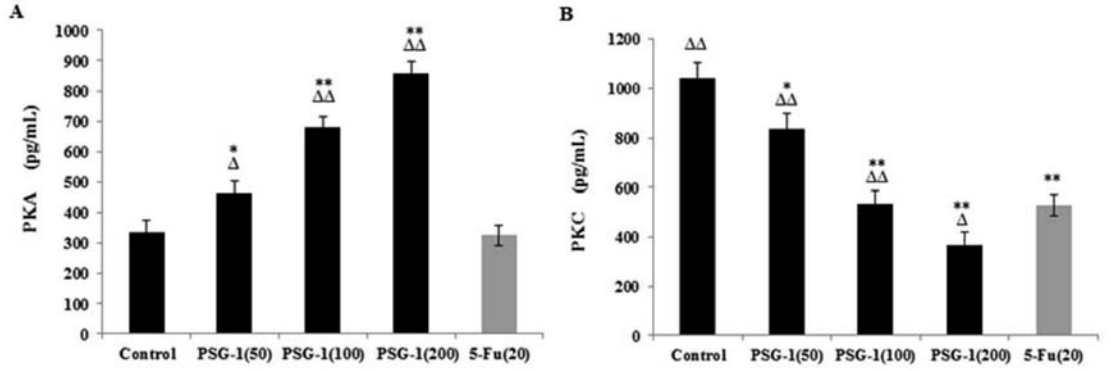


**Figure 4.** Effect of PSG-1 on the levels of (A) PKA and (B) PKC in tumor cells from tumor-bearing mice. *$P$ < 0.05, **$P$ < 0.01 vs control group; $^{\Delta}P$ < 0.05, $^{\Delta\Delta}P$ < 0.01 vs 5-Fu group.

membrane facilitates translocation of PKC from the cytosol to the plasma membrane. We thus determined the levels of intracellular AC and DAG. As shown in Figure 3C,D, a great change in the activity of AC was observed. The AC activity was enhanced along with the increase of the dose. However, the level of DAG was dramatically downregulated in the PSG-1 groups.

**Effect of PSG-1 on PKA and PKC in Tumor during PSG-1-Induced Apoptosis.** PKA, the cAMP-dependent kinase, is a central component of the signal transduction pathway. The activation of PKA is one of the primary elements in the cAMP signal transduction downstream cascade. As the crucial step toward understanding the mechanism of PSG-1-induced apoptosis, we thus measured intracellular PKA activity in the CT26 cells from tumor-bearing mice. It was found that in parallel to the significant increase of cAMP level, the activity of PKA was increased by PSG-1 treatment (Figure 4A), implying the importance of the cAMP-PKA pathway in PSG-1-induced apoptosis of CT26 cells.

PKC is transiently activated by DAG. It has been reported that PKA and PKC are critical signaling mediators in regulation of cell apoptosis. In the present study, we found that the intracellular PKC activity of the PSG-1-treated group was decreased significantly (Figure 4B).

To further confirm this potential role of PKA and PKC, we conducted Western blot experiments to examine the expression of PKA and PKC proteins. As shown in Figure 5, PSG-1 caused a marked increase in the expression of PKA protein. In contrast, the PKC level was decreased in the PSG-1-treated groups as compared to the control group.

**Immune Function of PSG-1 in CT26-Bearing Mice.** As shown in Table 1, compared with the control group, the thymus


dx.doi.org/10.1021/jf503250d | J. Agric. Food Chem. 2014, 62, 9296−9304

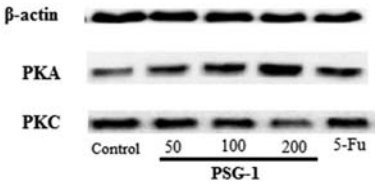


**Figure 5.** Expressions of PKA and PKC in tumor-bearing mice by Western blot. Total cellular proteins were separated by SDS−PAGE and analyzed by Western blot with specific antibodies.

and spleen indexes of tumor-bearing mice treated with 5-Fu at the dose of 20 mg/kg BW decreased significantly. Treatment with PSG-1 at different doses produced a marked and dose-dependent increase in both spleen and thymus indexes ($P < 0.05$), especially in the groups with high and middle doses. This finding suggested that PSG-1 enhanced the immunization of tumor-bearing mice.

**Effect of PSG-1 on Serum Cytokine Levels in CT26-Bearing Mice.** To further detect the immunomodulating effect of PSG-1, the levels of cytokines in serum from tumor-bearing mice were investigated. The treatment of PSG-1 markedly upregulated the levels of IL-2, TNF-$\alpha$, and IFN-$\gamma$ in serum when compared with control group ($P < 0.05$, Table 2). However, the levels of IL-2, TNF-$\alpha$, and IFN-$\gamma$ were slightly decreased by 5-Fu treatment during the experimental period, suggesting its immunosuppression effect in tumor-bearing animals. Therefore, PSG-1 is beneficial to the immune system in tumor-bearing mice.

**Effect of PSG-1 on Spleen Lymphocyte Proliferation in CT26-Bearing Mice.** To elucidate the mechanism of immunoregulatory activity of PSG-1, the effect on spleen lymphocyte proliferation was examined. Compared with the control group, proliferation of spleen lymphocyte induced by Con A and LPS was increased significantly in PSG-1-treated CT26-bearing mice. In contrast, 5-Fu administration decreased proliferation of spleen lymphocytes markedly in CT26-bearing mice (Table 3).

**Effect of PSG-1 on Peritoneal Macrophages Phagocytosis in CT26-Bearing Mice.** To verify the effect of PSG-1 on the activation of immune cells, we estimated the phagocytosis of macrophages from each group. As shown in Table 3, PSG-1 (50, 100, and 200 mg/kg) augmented the percentage of phagocytosis of NR by peritoneal macrophages in CT26-bearing mice, compared with the control group. We speculated PSG-1 restored impaired peritoneal macrophages phagocytosis.

## DISCUSSION

The health benefits of mushroom nutraceuticals have been widely reported.[24] Many studies support that *Cordyceps sinensis*, shiitake mushroom, and ganoderma have various biological

**Table 1. Effects of PSG-1 on Spleen Index and Thymus Index in CT26-Bearing Mice**[a]

| group | dose (mg/kg) | tumor weight (g) | thymus index (mg/g) | spleen index (mg/g) |
|---|---|---|---|---|
| CT26 control | | 1.32 ± 0.34$^{\Delta\Delta}$ | 1.67 ± 0.12$^{\Delta}$ | 5.54 ± 1.01$^{\Delta\Delta}$ |
| 5-Fu | 20 | 0.34 ± 0.10** | 1.01 ± 0.10* | 3..28 ± 0.85** |
| PSG-1 | 50 | 0.86 ± 0.37*$^{\Delta\Delta}$ | 1.84 ± 0.34$^{\Delta\Delta}$ | 6.57 ± 1.14*$^{\Delta\Delta}$ |
| | 100 | 0.58 ± 0.33**$^{\Delta}$ | 2.32 ± 0.25**$^{\Delta\Delta}$ | 7.24 ± 1.06**$^{\Delta\Delta}$ |
| | 200 | 0.46 ± 0.31** | 3.16 ± 0.36**$^{\Delta\Delta}$ | 8.53 ± 1.23**$^{\Delta\Delta}$ |

[a]Values are mean ± SEM of eight mice. Statistical significance is indicated as follows: *significantly different from CT26 control group at $P < 0.05$; **significantly different from CT26 control group at $P < 0.01$; $^{\Delta}$significantly different from 5-Fu group at $P < 0.05$; $^{\Delta\Delta}$significantly different from 5-Fu group at $P < 0.01$.

**Table 2. Effects of PSG-1 on Production of Serum Cytokines in CT26-Bearing Mice**[a]

| group | dose (mg/kg) | TNF-$\alpha$ (pg/mL) | IFN-$\gamma$ (pg/mL) | IL-2 (pg/mL) |
|---|---|---|---|---|
| CT26 control | | 1432.09 ± 84.67$^{\Delta}$ | 210.11 ± 13.12$^{\Delta}$ | 154.68 ± 14.01$^{\Delta\Delta}$ |
| 5-Fu | 20 | 1034.78 ± 82.10* | 161.01 ± 13.10* | 108.44 ± 12.34** |
| PSG-1 | 50 | 1832.86 ± 83.37*$^{\Delta\Delta}$ | 254.56 ± 24.67$^{\Delta\Delta}$ | 187.15 ± 13.43*$^{\Delta\Delta}$ |
| | 100 | 2109.58 ± 90.33**$^{\Delta\Delta}$ | 342.45 ± 25.56**$^{\Delta\Delta}$ | 204.21 ± 14.45**$^{\Delta\Delta}$ |
| | 200 | 3411.46 ± 89.31**$^{\Delta\Delta}$ | 536.76 ± 25.68**$^{\Delta\Delta}$ | 253.24 ± 15.18**$^{\Delta\Delta}$ |

[a]Values are mean ± SEM of eight mice. Statistical significance is indicated as follows: *significantly different from CT26 control group at $P < 0.05$; **significantly different from CT26 control group at $P < 0.01$; $^{\Delta}$significantly different from 5-Fu group at $P < 0.05$; $^{\Delta\Delta}$significantly different from 5-Fu group at $P < 0.01$.

**Table 3. Effect of PSG-1 on the Immune Function of the CT26-Bearing Mice**[a]

| | | | proliferation ratio (%) | |
|---|---|---|---|---|
| group | dose (mg/kg) | phagocytosis ratio (%) | Con A (1 mg/L) | LPS (5 mg/L) |
| normal | | 100 | 100 | 100 |
| CT26 control | | 74.03 ± 4.25$^{\Delta\Delta}$ | 78.04 ± 4.34$^{\Delta}$ | 80.26 ± 6.92$^{\Delta}$ |
| 5-Fu | 20 | 45.33 ± 5.21** | 61.67 ± 3.53* | 67.92 ± 4.64* |
| PSG-1 | 50 | 133.25 ± 8.78**$^{\Delta\Delta}$ | 93.68 ± 4.72*$^{\Delta\Delta}$ | 96.21 ± 5.73*$^{\Delta\Delta}$ |
| | 100 | 151.44 ± 10.65**$^{\Delta\Delta}$ | 114.22 ± 8.81**$^{\Delta\Delta}$ | 136.56 ± 6.78**$^{\Delta\Delta}$ |
| | 200 | 182.42 ± 17.93**$^{\Delta\Delta}$ | 132.31 ± 6.38**$^{\Delta\Delta}$ | 149.33 ± 5.87**$^{\Delta\Delta}$ |

[a]Values are mean ± SEM of eight mice. Statistical significance is indicated as follows: *significantly different from CT26 control group at $P < 0.05$; **significantly different from CT26 control group at $P < 0.01$; $^{\Delta}$significantly different from 5-Fu group at $P < 0.05$; $^{\Delta\Delta}$significantly different from 5-Fu group at $P < 0.01$.


dx.doi.org/10.1021/jf503250d | J. Agric. Food Chem. 2014, 62, 9296−9304

activities and pharmacological function.[25,26] Polysaccharides are major contributors to most of the biological activities. Lentinan shows effective antitumor and immunopotentiating activity.[27] Polysaccharides from *Cordyceps gunnii* showed significant antitumor activities against HeLa and HepG2 in vitro.[28] The efficacy of ganoderma as an anticancer and tonic agent has been recognized for thousands of years. The proposed anticancer activity of ganoderma has prompted its use by cancer patients. Wang et al. have reported the effects of the polysaccharide from *G. lucidum* on cancer.[29] Sharing the same genus, *G. atrum* also has similar potent antitumor effects. Our previous studies have found that PSG-1 possessed potent antitumor activity by inducing apoptosis of tumor cells related to activation of host immune response in S180-bearing mice.[22] Many researchers have suggested that PSG-1 might inhibit other types of cancer and be mainly mediated by the specific apoptotic pathway and the host immunological mechanism. So we focused on investigating the molecular mechanism of CT26 tumor growth repression by PSG-1.

In the present study, we first investigated the antitumor activity of PSG-1 in vitro. Unexpectedly, PSG-1-treated CT26 cells did not show any differences in cell viability compared to untreated cells. The above results suggest that PSG-1 did not exert any direct cytotoxic effect on the CT26 cells. However, oral administration of PSG-1 (50, 100, and 200 mg/kg) markedly inhibited the tumor growth in the CT26-bearing mice, indicating that PSG-1 has potent antitumor activity in vivo. Therefore, we can assume that administration of PSG-1 might activate some signaling pathways and the host immune response, preventing tumor growth.

Tumor development and growth are considered a result of the high proliferative capacity of tumor cells. It was reported that apoptosis and its related signaling pathways contributed to the high rate of cell loss in malignant tumors and, moreover, could be a defense against tumor progression.[30] Apoptosis is the process of cell death occurring in various multicellular organisms, and it is well-known to induce characteristic changes of cell morphology, such as membrance blebbing, cell shrinkage, chromatin condensation, and chromosomal DNA fragmentation.[31] It is now well-established that anticancer agents induce apoptosis and that disruption of apoptotic programs can promote tumor initiation, progression, and treatment resistance.[32] Thus, to understand the association between PSG-1 and apoptosis, we assessed its apoptosis-inducing effect on tumor cells in CT26-bearing mice. The results indicated that PSG-1 induced tumor apoptosis in a concentration-dependent manner.

The cAMP/PKA signal transduction is regarded as one of the best-understood biochemical pathways. The rate of cAMP production and degradation is sensitive to a wide range of extracellular and intracellular signals, such that cAMP can directly regulate a variety of cell functions, from metabolism to ion channel activation, cell growth and differentiation, gene expression, and apoptosis.[33] The cAMP/PKA pathway in cancer is started with AC activation, which leads to the formation of cAMP. PKA is activated by the newly minted cAMP and causes reversible phosphorylation of protein substrates that regulate a number of cellular processes.[34] Excessive PKA activity in yeast could trigger mitochondria-dependent apoptosis via a distinct signaling mechanism.[35] Chen et al. reported that upregulation of the cAMP/PKA pathway decreased proliferation, induced differentiation, and led to apoptosis in malignant gliomas.[36] This is consistent with the report of Hanson that the growth of neuroblastoma cells is inhibited by an increase in cAMP.[37] Similar results were obtained in this study. We found that cAMP level was dramatically increased by PSG-1 in a dose-dependent manner. Furthermore, the concentrations of subsequent PKA and upstream AC were found to be upregulated. To provide further evidence, we used a Western blot to analyze the PKA protein expression and found that the expression of PKA protein was markedly increased in a dose-dependent pattern in PSG-1-treated groups. Meanwhile, the important meditator of apoptosis cGMP content was also inhibited. Therefore, we speculated that PSG-1-induced apoptosis may be associated with the cGMP level. These results suggest that upregulation of the cAMP/PKA pathway and cGMP may be involved in the CT26 tumor cell apoptosis and the elicit antitumor effect.

PKC is a family of serine/threonine kinases that is involved in the transduction of signals for cell proliferation and differentiation.[38] The important role of PKC in processes relevant to neoplastic transformation, carcinogenesis, and tumor cell invasion renders it a potentially suitable target for anticancer therapy.[39] Early studies suggested a role for PKC isozymes in tumor promotion. A direct correlation between the ability of individual phorbol esters to promote tumors and activation of PKC has been demonstrated.[40] Increased levels of PKC have been associated with malignant transformation in a number of cell lines, including breast, lung, and gastric carcinomas.[41−43] In colon cancer, PKC $\beta$ II appears to be overexpressed early in the colon carcinogenic process.[44] A decrease in the content of PKC $\alpha$ by antisense or phorbol ester led to apoptosis in many different cell types, such as glioma cells, endothelial cells, and promyelocytic U937 cells.[45−47] Dean et al. have reported that the antisense PKC $\alpha$ oligonucleotides inhibited tumor growth in nude mice bearing implanted human glioblastomas and human bladder, lung, and colon carcinomas.[48] In addition, PKC $\delta$ has been implicated in apoptotic response and cytochrome *c* release.[49,50] Hence, inhibition of PKC may have an impact on the invasive and metastatic potential of malignant cells, resulting in tumor cell apoptosis. In the present study, the results showed that the PKC level was decreased in PSG-1-treated mice. Likewise, an apparent decline in PKC protein expression was also presented by Western blot. It is well-known that when cells are stimulated, PKC is transiently activated by DAG, which is produced in the membrane during the signal-induced turnover of inositol phospholipids.[40] On the basis of the preceding results, we examined the effects of PSG-1 administration on DAG concentration. Our study showed that DAG was consistently downregulated. These results suggest that suppression of the PKC pathway may be implicated in PSG-1-induced apoptosis and the elicit antitumor effect.

The host immune function is another key factor for cancer treatment and recovery. Clinical verification is being obtained that the maximal potential of anticancer treatments is based on exploiting the host's own antitumor defense mechanism.[51] Immunostimulation is a crucial strategy to improve the body's defense mechanism. The antitumor immune response can be divided into specific and nonspecific immunity. The thymus and spleen are two important immune organs. The thymus and spleen indexes were important indexes for nonspecific immunity. The present result showed that the thymus and spleen indexes were markedly increased in CT26-bearing mice treated with PSG-1 compared with the control group. Phagocytes, including neutrophils, monocytes, and macrophages, play essential and important roles in nonspecific immune responses.[52] The phagocytic function of macrophages represents the final and most indispensable step of the immunological defense system.

Activated macrophages are considered to be one of the important components of the host defense against tumor growth, and phagocytosis plays an essential role in building and consolidating immunological defense systems of humans and animals against malignancies.[53] On the other hand, the specific immune response includes humoral immunity and cellular immunity. The humoral defense via antibody response is regulated by B cells and other immune cells involved in antibody production and immunization. Cell-mediated immune defense was mediated specifically by T cells, including nature killer cells. These cells are able to kill autologous cells infected with tumor cells and pathogens. In this study, we found that PSG-1 increased macrophage phagocytosis and spleen lymphocyte proliferation in the CT26-bearing mice, while the positive control 5-Fu with high tumor inhibitory rate had an immunosuppressive effect. These results suggested that PSG-1 could enhance specific and nonspecific immunity in CT26-bearing mice. That is to say, PSG-1 has potent tumor therapeutic activity by improving the immune system.

Cytokines are low molecular weight biologically active proteins and peptides that are involved in the generation and control of immunological responses. Many polysaccharides could modulate and stimulate cytokines production.[54] They can bind to specific cell surface receptors directly and affect cell proliferation, differentiation, and function. Released to the blood, they act on like hormones and affect different tissues and organs, often distant from the original tumor. Cytokines have an effect on immune processes, including antitumor defense and acute phase reaction. They regulate both cellular and humoral responses.[55] IL-2 is synthesized when antigen and mitogen are stimulated by T-cells. It is the most crucial cytokine in adjusting the activation, proliferation, and differentiation of lymphocytes. IL-2 could augment cytotoxicites of T cells and NK cells and in vivo generation of lymphokine-activated killer cells, which exhibit high cytolytic activities against autologous tumor cells. So IL-2 plays an important role in the antitumor immune adjustment. Tumor necrosis factor (TNF-$\alpha$) is a cytokine possessing antitumor and immunomodulatory properties. TNF-$\alpha$ was reported to increase the immunogenicity of tumor cells due to the enhanced expression of MHC antigens and thus to intensify the antitumor immune response.[56] Hence, TNF-$\alpha$ has been recognized as an important host defense cytokine that affects tumor cells. In addition, IFN-$\gamma$ has a variety of function, e.g., inhibition of viral replication, antiproliferation effect in tumor cells, and activation of immune cells.[57] It plays important roles in depressing tumor cell growth and inducing apoptosis of tumor cells.[58] In this study, the serum concentrations of TNF-$\alpha$, IFN-$\gamma$, and IL-2 apparently increased in PSG-1-treated groups. They are potential endogenous products in mediating the effect of PSG-1 on the immune system in vivo. The increase may also explain the antitumor properties of PSG-1. Hence, the host antitumor immune responses are associated with the antitumor mechanism of PSG-1.

In summary, our study has demonstrated that PSG-1 inhibited the tumor growth and ameliorated the immune response in tumor-bearing mice. Further studies showed that its mechanism of action might be implicated in initiating apoptosis. Our results showed that PSG-1 induced the apoptosis of CT26 tumor cells; stimulated AC, PKA, and cAMP production; and reduced the PKC and DAG levels in CT26 cells from tumor-bearing mice. Additionally, the administration of PSG-1 notably elevated the spleen and thymus indexes and increased macrophage phagocytosis and spleen lymphocyte proliferation. The serum concentrations of TNF-$\alpha$, IFN-$\gamma$, and IL-2 were also markedly increased. Hence, we speculate that the antitumor mechanism of PSG-1 may be related to the induction of CT26 cell apoptosis throughthe cAMP-PKA signaling pathway and downregulation of the PKC signal pathway, as well as the activation of the immune response of the host. Therefore, PSG-1 may be considered as an efficacious adjacent immunopotentiating therapy in the treatment of tumors. Further clinical trials are required to confirm the effectiveness of this novel polysaccharide. It may provide new threads of hope for cancer treatment.

## AUTHOR INFORMATION

### Corresponding Author

*Tel and Fax: +86-791-88304452. E-mail: spnie@ncu.edu.cn.

### Funding

The financial support for this study by Key Program of National Natural Science Foundation of China (No. 31130041), National Natural Science Foundation of China (31071532), National Key Technology R & D Program of China (2012BAD33B06), the Program for New Century Excellent Talents in University (NCET-12-0749), the Project of Science and Technology of Jiangxi Provincial Education Department (KJLD13004), and Research Project of State Key Laboratory of Food Science and Technology (SKLF-ZZA-201301) is gratefully acknowledged.

### Notes

The authors declare no competing financial interest.

## ABBREVIATIONS USED

AC, adenylate cyclase; BSA, bovine serum albumin; BW, body weight; colorectal carcinoma, CRC; Con A, concanavalin A; cyclic AMP, cAMP; cyclic GMP, cGMP; DAG, diacylglycerol; horseradish peroxidase, HRP; PBS, phosphate-buffered saline; peritoneal exudate cells, PECs; PKA, protein kinase A; PKC, protein kinase C; PSG-1, *G. atrum* polysaccharide; TBS, Tris-buffered saline.

## REFERENCES

(1) Horton, K. M.; Abrams, R. A.; Fishman, E. K. Spiral CT of colon cancer: Imaging features and role in management. *Radiographics* **2000**, *20*, 419−430.

(2) Drake, C. G.; Antonarakis, E. S. Update: Immunological strategies for prostate cancer. *Curr. Urol. Rep.* **2010**, *11*, 202−207.

(3) Hsu, Y. L.; Kuo, P. L.; Liu, C. F.; Lin, C. C. Acacetin-induced cell cycle arrest and apoptosis in human non-small cell lung cancer A549 cells. *Cancer Lett.* **2004**, *212*, 53−60.

(4) Hengartner, M. O. The biochemistry of apoptosis. *Nature* **2000**, *407*, 770−776.

(5) Hanahan, D.; Weinberg, R. A. The hallmarks of cancer. *Cell* **2000**, *100*, 57−70.

(6) Hunter, T. Oncoprotein networks. *Cell* **1997**, *88*, 333−346.

(7) Muhl, H.; Nitsch, D.; Sandau, K.; Brune, B.; Varga, Z.; Pfeilschifter, J. Apoptosis is triggered by the cyclic AMP signalling pathway in renal mesangial cells. *FEBS Lett.* **1996**, *382*, 271−275.

(8) Loweth, A. C.; Williams, G. T.; Scarpello, J. H.; Morgan, N. G. Evidence for the involvement of cGMP and protein kinase G in nitric oxide-induced apoptosis in the pancreatic B-cell line, HIT-T15. *FEBS Lett.* **1997**, *400*, 285−288.

(9) Hayashi, S.; Morishita, R.; Matsushita, H.; Nakagami, H.; Taniyama, Y.; Nakamura, T.; Aoki, M.; Yamamoto, K.; Higaki, J.; Ogihara, T. Cyclic AMP inhibited proliferation of human aortic vascular smooth muscle cells, accompanied by induction of p53 and p21. *Hypertension* **2000**, *35*, 237−43.

(10) Kizaki, H.; Suzuki, K.; Tadakuma, T.; Ishimura, Y. Adenosine receptor-mediated accumulation of cyclic AMP-induced T-lymphocyte death through internucleosomal DNA cleavage. *J. Biol. Chem.* **1990**, *265*, 5280−5284.
(11) Lerner, A.; Kim, D. H.; Lee, R. The cAMP signaling pathway as a therapeutic target in lymphoid malignancies. *Leuk. Lymphoma* **2000**, *37*, 39−51.
(12) Cross, T. G.; Scheel-Toellner, D.; Henriquez, N. V.; Deacon, E.; Salmon, M.; Lord, J. M. Serine/threonine protein kinases and apoptosis. *Exp. Cell Res.* **2000**, *256*, 34−41.
(13) Montminy, M. Transcriptional regulation by cyclic AMP. *Annu. Rev. Biochem.* **1997**, *66*, 807−822.
(14) Izawa, M.; Teramachi, K. Down-regulation of protein kinase C activity by sorbitol rapidly induces apoptosis in human gastric cancer cell lines. *Apoptosis* **2001**, *6*, 353−358.
(15) Chen, Y.; Xie, M.; Gong, X. Microwave-assisted extraction used for the isolation of total triterpenoid saponins from *Ganoderma atrum*. *J. Food Eng.* **2007**, *81*, 162−170.
(16) Paterson, R. R. Ganoderma—A therapeutic fungal biofactory. *Phytochemistry* **2006**, *67*, 1985−2001.
(17) Chen, Y.; Xie, M.; Nie, S.; Li, C.; Wang, Y. Purification, composition analysis and antioxidant activity of a polysaccharide from the fruiting bodies of *Ganoderma atrum*. *Food Chem.* **2008**, *107*, 231−241.
(18) Chen, Y.; Xie, M. Y.; Wang, Y. X.; Nie, S. P.; Li, C. Analysis of the monosaccharide composition of purified polysaccharides in *Ganoderma atrum* by capillary gas chromatography. *Phytochem. Anal.* **2009**, *20*, 503−510.
(19) Zhang, H.; Li, W.; Nie, S.; Chen, Y.; Wang, Y.; Xie, M. Structural characterisation of a novel bioactive polysaccharide from *Ganoderma atrum*. *Carbohyd. Polym.* **2012**, *88*, 1047−1054.
(20) Gong, X. F.; Xie, M. Y.; Chen, Y. Comparison of the antioxidative effects of extracts from *Ganoderma atrum* and *Ganoderma lucidum*. *Food Science* **2006**, *27*, 44−47.
(21) Li, W. J.; Nie, S. P.; Chen, Y.; Xie, M. Y.; He, M.; Yu, Q.; Yan, Y. *Ganoderma atrum* polysaccharide protects cardiomyocytes against anoxia/reoxygenation-induced oxidative stress by mitochondrial pathway. *J. Cell. Biochem.* **2010**, *110*, 191−200.
(22) Li, W. J.; Chen, Y.; Nie, S. P.; Xie, M. Y.; He, M.; Zhang, S. S.; Zhu, K. X. *Ganoderma atrum* polysaccharide induces anti-tumor activity via the mitochondrial apoptotic pathway related to activation of host immune response. *J. Cell. Biochem.* **2011**, *112*, 860−871.
(23) Zhang, S.; Nie, S.; Huang, D.; Huang, J.; Wang, Y.; Xie, M. Polysaccharide from *Ganoderma atrum* evokes antitumor activity via toll-like receptor 4-mediated NF-kappaB and mitogen-activated protein kinase signaling pathways. *J. Agric. Food Chem.* **2013**, *61*, 3676−3682.
(24) Smith, J. E.; Rowan, N. J.; Tan, K. K. Functional food science and the medicinal mushrooms. *Int. J. Med. Mushrooms.* **2000**, *2*, 277−285.
(25) Nie, S.; Cui, S. W.; Xie, M.; Phillips, A. O.; Phillips, G. O. Bioactive polysaccharides from *Cordyceps sinensis*: Isolation, structure features and bioactivities. *Bioactive Carbohydr. Dietary Fibre* **2013**, *1*, 38−52.
(26) Rahman, T.; Choudhury, M. B. K. *Shiitake* mushroom: A tool of medicine. *Bangladesh J. Med. Biochem.* **2013**, *5*, 24−32.
(27) Ren, L.; Perera, C.; Hemar, Y. Antitumor activity of mushroom polysaccharides: A review. *Food Funct.* **2012**, *3*, 1118−1130.
(28) Yang, S.; Jin, L.; Ren, X.; Lu, J.; Meng, Q. Optimization of fermentation process of *Cordyceps militaris* and antitumor activities of polysaccharides in vitro. *J. Food Drug Anal.* **2014**, 1−9.
(29) Wang, P.; Zhu, X.; Lin, Z. Antitumor and immunomodulatory effects of polysaccharides from broken-spore of *Ganoderma lucidum*. *Front. Pharmacol.* **2012**, *3*, 135.
(30) Lowe, S. W.; Lin, A. W. Apoptosis in cancer. *Carcinogenesis* **2000**, *21*, 485−495.
(31) Doonan, F.; Cotter, T. G. Morphological assessment of apoptosis. *Methods* **2008**, *44*, 200−204.
(32) Schmitt, C. A.; Lowe, S. W. Apoptosis and therapy. *J. Pathol.* **1999**, *187*, 127−137.
(33) Chin, K. V.; Yang, W. L.; Ravatn, R.; Kita, T.; Reitman, E.; Vettori, D.; Cvijic, M. E.; Shin, M.; Iacono, L. Reinventing the wheel of cyclic AMP. *Ann. N.Y. Acad. Sci.* **2002**, *968*, 49−64.
(34) Leadsham, J. E.; Gourlay, C. W. cAMP/PKA signaling balances respiratory activity with mitochondria dependent apoptosis via transcriptional regulation. *BMC Cell Biol.* **2010**, *11*, 92.
(35) Leadsham, J. E.; Miller, K.; Ayscough, K. R.; Colombo, S.; Martegani, E.; Sudbery, P.; Gourlay, C. W. Whi2p links nutritional sensing to actin-dependent Ras-cAMP-PKA regulation and apoptosis in yeast. *J. Cell Sci.* **2009**, *122*, 706−715.
(36) Chen, T. C.; Hinton, D. R.; Zidovetzki, R.; Hofman, F. M. Up-regulation of the cAMP/PKA pathway inhibits proliferation, induces differentiation, and leads to apoptosis in malignant gliomas. *Lab. Invest.* **1998**, *78*, 165−174.
(37) Hanson, A. J.; Nahreini, P.; Andreatta, C.; Yan, X.; Prasad, K. N. Role of the adenosine 3′,5′-cyclic monophosphate (cAMP) in enhancing the efficacy of siRNA-mediated gene silencing in neuroblastoma cells. *Oncogene* **2005**, *24*, 4149−4154.
(38) Caponigro, F.; French, R. C.; Kaye, S. B. Protein kinase C: A worthwhile target for anticancer drugs? *Anti-Cancer Drug.* **1997**, *8*, 26−33.
(39) Mackay, H. J.; Twelves, C. J. Protein kinase C: A target for anticancer drugs? *Endocr.-Relat. Cancer* **2003**, *10*, 389−396.
(40) Nishizuka, Y. The role of protein kinase C in cell surface signal transduction and tumour promotion. *Nature* **1984**, *308*, 693−698.
(41) O'Brian, C. A.; Vogel, V. G.; Singletary, S. E.; Ward, N. E. Elevated protein kinase C expression in human breast tumor biopsies relative to normal breast tissue. *Cancer Res.* **1989**, *49*, 3215−3217.
(42) Takenaga, K.; Takahashi, K. Effects of 12-*O*-tetradecanoylphorbol-13-acetate on adhesiveness and lung-colonizing ability of Lewis lung carcinoma cells. *Cancer Res.* **1986**, *46*, 375−380.
(43) Schwartz, G. K.; Jiang, J.; Kelsen, D.; Albino, A. P. Protein kinase C: A novel target for inhibiting gastric cancer cell invasion. *J. Natl. Cancer Inst.* **1993**, *85*, 402−407.
(44) Gökmen-Polar, Y.; Murray, N. R.; Velasco, M. A.; Gatalica, Z.; Fields, A. P. Elevated protein kinase C betaII is an early promotive event in colon carcinogenesis. *Cancer Res.* **2001**, *61*, 1375−1381.
(45) Whelan, R. D.; Parker, P. J. Loss of protein kinase C function induces an apoptotic response. *Oncogene* **1998**, *16*, 1939−1944.
(46) Dooley, N. P.; Baltuch, G. H.; Groome, N.; Villemure, J.; Yong, V. W. Apoptosis is induced in glioma cells by antisense oligonucleotides to protein kinase C $\alpha$ and is enhanced by cycloheximide. *Neuroreport* **1998**, *9*, 1727−1733.
(47) Haimovitz-Friedman, A.; Balaban, N.; McLoughlin, M.; Ehleiter, D.; Michaeli, J.; Vlodavsky, I.; Fuks, Z. Protein kinase C mediates basic fibroblast growth factor protection of endothelial cells against radiation-induced apoptosis. *Cancer Res.* **1994**, *54*, 2591−2597.
(48) Dean, N.; McKay, R.; Miraglia, L.; Howard, R.; Cooper, S.; Giddings, J.; Nicklin, P.; Meister, L.; Ziel, R.; Geiger, T. Inhibition of growth of human tumor cell lines in nude mice by an antisense oligonucleotide inhibitor of protein kinase C-alpha expression. *Cancer Res.* **1996**, *56*, 3499−3507.
(49) Fujii, T.; Garcia-Bermejo, M. A. L.; Bernab, J. L.; Caamano, J.; Ohba, M.; Kuroki, T.; Li, L.; Yuspa, S. H.; Kazanietz, M. G. Involvement of protein kinase C delta (PKC delta) in phorbol ester-induced apoptosis in LNCaP prostate cancer cells. Lack of proteolytic cleavage of PKC delta. *J. Biol. Chem.* **2000**, *275*, 7574−7582.
(50) Majumder, P. K.; Pandey, P.; Sun, X.; Cheng, K.; Datta, R.; Saxena, S.; Kharbanda, S.; Kufe, D. Mitochondrial translocation of protein kinase C delta in phorbol ester-induced cytochrome *c* release and apoptosis. *J. Biol. Chem.* **2000**, *275*, 21793−21796.
(51) Ehrke, M. J. Immunomodulation in cancer therapeutics. *Int. Immunopharmacol.* **2003**, *3*, 1105−1119.
(52) Chen, X.; Jin, J.; Tang, J.; Wang, Z.; Wang, J.; Jin, L.; Lu, J. Extraction, purification, characterization and hypoglycemic activity of a polysaccharide isolated from the root of *Ophiopogon japonicus*. *Carbohyd. Polym.* **2011**, *83*, 749−754.

(53) Blander, J. M.; Medzhitov, R. Regulation of phagosome maturation by signals from toll-like receptors. *Science* **2004**, *304*, 1014−1018.
(54) Chen, X.; Nie, W.; Fan, S.; Zhang, J.; Wang, Y.; Lu, J.; Jin, L. A polysaccharide from *Sargassum fusiforme* protects against immunosuppression in cyclophosphamide-treated mice. *Carbohyd. Polym.* **2012**, *90*, 1114−1119.
(55) Terlikowski, S. J. Local immunotherapy with rhTNF-alpha mutein induces strong antitumor activity without overt toxicity—A review. *Toxicology* **2002**, *174*, 143−152.
(56) Kim, G.; Choi, G.; Lee, S.; Park, Y. Acidic polysaccharide isolated from *Phellinus linteus* enhances through the up-regulation of nitric oxide and tumor necrosis factor-alpha from peritoneal macrophages. *J. Ethnopharmacol.* **2004**, *95*, 69−76.
(57) Farrar, M. A.; Schreiber, R. D. The molecular cell biology of interferon-gamma and its receptor. *Annu. Rev. Immunol.* **1993**, *11*, 571−611.
(58) Spanaus, K. S.; Schlapbach, R.; Fontana, A. TNF-alpha and IFN-gamma render microglia sensitive to Fas ligand-induced apoptosis by induction of Fas expression and down-regulation of Bcl-2 and Bcl-xL. *Eur. J. Immunol.* **1998**, *28*, 4398−4408.

Table 1. Antibody Titer Detected with ELISA ($n$ = 3)

| | dilution | | | | | |
|---|---|---|---|---|---|---|
| | 5000 | 10 000 | 15 000 | 20 000 | 40 000 | CK |
| OD (450 nm) | 0.8389 ± 0.0069[a] | 0.6189 ± 0.0076[a] | 0.4528 ± 0.0008[a] | 0.3568 ± 0.0017[a] | 0.2444 ± 0.0059[a] | 0.1811 ± 0.0058 |

[a] $p$-value < 0.01 on Duncan's multiple range test.

## MATERIALS AND METHODS

**Standards and Reagents.** Recombinant Acc-royalisin (RAcc-royalisn) as standard peptide was expressed in *Eschericha coli* strain BL21 (DE3) containing RAcc-royalisin expression vector, pGEM-4T-2-Acc-royalisin, purified, and freeze-dried according to the method previously described.[12] Bovine serum albumin (BSA), goat antirabbit IgG-linked horseradish peroxidase (IgG/HRP), and diaminobenzidine (DAB) were purchased from Boster Biological Technology, Ltd. (Wuhan, China). Bradford kit was purchased from Najing Jiancheng Bioengineering Institute (Nangjing, China).

**Insects and Bacteria.** The Asian honeybee, *A. cerana cerana*, and the Western honeybee, *A. mellifera*, *Musca domestica*, *Tenebrio molitor*, *Barley pest*, were maintained at the Zhejiang University campus. Fresh royal jelly reserved under −80 °C was provided by Hnagzhou Biyutain Heath Food Corp., Ltd. (Hangzhou, China). Bacterium, *E. coli* CGMCC1.1139, preserved by our laboratory was incubated in sterile Luria−Bertani medium (10 g of polypepton, 5 g of yeast extract, 10 g of NaCl, and deionized water to 1000 mL, pH 7.0) at 37 °C for 12−15 h.

**Infection of Bacteria.** About 100 Western honeybee workers and 100 Asian honeybee workers at age of 3−5 days in summer were collected from their hives and maintained in a cage, respectively. Each worker was inoculated 2 μL of *E. coli* with a concentration of 50 cfu/g at intersegmental membrane with light $CO_2$ before workers were set into the cage. Workers fed with 10% honeybee solution were collected at 24 and 48 h post infection. The uninfected workers were used as a control (0 h).

**Preparation of the Hemolymphe.** The hemolymphe (insect blood) from 5 workers, which were cut head, was collected into 1.5 mL eppendorfs with a capillary. A small amount of phenylthiocarbamide was added in the hemolymphe to prevent oxidation. The hemolymphe was centrifuged under 10 000 rpm for 10 min, and the supernatant was reserved at −20 °C for detection. Three replications for each test were used. The hemolymphe of other insects was extracted with a protocol similar to that described above. The protein content in hemolymphe from different insect species was measured with a Bradford assay.[13]

Polyclonal antibody against recombinant Acc-royalisin (anti-RAcc-royalisin antibody) was previously obtained by immunization of male New Zealand white rabbits with a recombinant Acc-royalisin expressed in *E. coli* in our laboratory according to the method previously described[14] and stored at −80 °C. RAcc-royalisin antibody was purified with antigen affinity column filled in CNBr-activated Sepharose 4B conjucated to RAcc-royalisin. The column was washed with 10 volume PBS. The rabbit serum was filled with 0.45 through a Millex-GV 0.45 u filter, loaded to the column, and then washed with PBS. The purified antibody eluted with antibody elution buffer [7.5% (w/v) of glycine, pH 2.7] was collected, then dialyzed with deionized water ($ddH_2O$).

**Binding Activity of RAcc-Royalisin.** The binding activity (titer) of RAcc-royalisin antibody to react with RAcc-royalisin was tested by an indirect ELISA as described[15] with a Microplate spectrophotometer system, Multiskan MK3 (Thermo Scientific, U.S.). The diluted rabbit antiserum (1:5000−1:40 000), in a volume of 100 mL, was added to wells of microtitration plates coated with RAcc-royalisin for ELISA as later described. BSA was used as the control antigen. The lowest dilution of RAcc-royalisin antibody possessing significant difference of OD value with control is considered its binding activity. The specificity of the antibody was measured by comparison on binding activity of RAcc-royalisin antibody to react with different insect extracts with the same protein content by an indirect ELISA.

**Determination of Royalisin Content in Hemolymphe by ELISA.** Microtitration plates were coated overnight at 4 °C with 100 μL/well carbonate buffer solution (CBS: $Na_2CO_3$ 1.59 g, $NaHCO_3$ 2.93 g, pH 9.6) from 0 to 10 μg/mL (0, 2.3, 5.6, 11.3, 22.5, 55.0,110.0, 220.0, 330.0, 440.0, 550,0, 660.0, 770.0, 880.0, 990.0, 110.0, 1210, and 1320 ng/mL) of RAcc-royalisin, and then blocked with 1% dried milk in phosphate buffer saline (PBS; 137 mM NaCl, 2.7 mM KCl, 100 mM $Na_2HPO_4$, 2 mM $KH_2PO_4$, pH 7.4). Subsequently, 100 μL of anti-RAcc-royalisin antibody diluted with 0.1% dried milk in PBS was added and incubated in the coated wells for 1.5 h at 37 °C. The binding of anti-RAcc-royalisin antibody with antigen was visualized by using 100 mL of an antirabbit IgG conjugated to peroxidase for 1 h at 37 °C. The color reaction was initiated by adding 100 mL/well of TMB. The reaction was stopped after 15 min by adding 2 M $H_2SO_4$ to the wells. Optical density (OD) was measured at 450 nm with an ELISA plate reader. A calibration curve of RAcc-royalisin was generated on the basis of measurement of quantification limits.

The OD value of royalisin in hemolymphe of honeybee worker samples was determined by ELISA using anti-RAcc-royalisin antibody. The royalisin content of every well was performed through a calibration curve with its OD value. The royalisin content of hemolymphe (RCH) was used to quantify the antibacterial activity, respectively. Each assay was repeated with at least three independent replicates.

**Data Processing and Statistics.** For the ELISA, fitting curves were performed with Microsoft Office Exile 2007. The statistics analysis was carried out with the statistical software SPSS 16.0 (SPSS, Inc., Chicago, IL). One-way ANOVA with Duncan's post hoc tests was adopted to determine if there were any significant differences among treatment groups. The mean and standard deviation (SD) values are reported, and $p$-value <0.05 is considered statistically significant.

## RESULTS

**Binding Activity Assay of Anti-RAcc-royalisin Antibody in Antiserum to RAcc-Royalisin.** Table 1 presents the results for the binding activities of anti-RAcc-royalisin antibody in the antisera obtained from the immunized rabbits with antigen RAcc-royalisin. The OD valves of anti-RAcc-royalisin antibody at 40 000 dilution (0.2444) were higher than that of BSA (0.1811) ($p$ < 0.01). Therefore, 40 000 was considered as the binding activity of anti-RAcc-royalisin antibody.

Moreover, it was shown from Table 2 that the OD values of hemolymphe extracts from honeybee workers in both the Asian honeybee and the Western honeybee reacting to anti-RAcc-royalisin antibody were significantly higher than those of other insect extracts from *M. domestica*, *T. molitor*, *B. pest*, and royal jelly ($p$ < 0.00001), which suggests that the antibody possesses high binding activity and specificity to hemolymphe of honeybees.

**Standardization of ELISA.** First, a calibration curve of RAcc-royalisin in a broad concentration range from 2.3 to 1320 ng/mL was prepared in a 96-well plate in PBS, corresponding to the RAcc-royalisin content of diluted PBS. For exclusion of unspecific reactions, a control analysis was performed, without antigen (RAcc-royalisin). For routine determination of RAcc-royalisin in RJ antibody, the primary calibration curve (Figure 1A) in a concentration range from 2.3 to 1320 ng/mL of RAcc-royalisin in PBS was generated, and showed the quantification limits ranging from 55.0 to 1100.0 ng/mL. The formal calibration curve, $y = 0.001x + 0.108$, then was generated in a concentration range from 0 to 880 ng/mL of RAcc-royalisin in PBS, and showed a good correlation index of $R^2 = 0.995$ (Figure 1B).

Table 2. Specificity Test of RAcc-Royalisin Antibody Reacting to Different Insect Extracts with ELISA ($n$ = 3)

| | samples (500 μg/mL) | | | | | | |
|---|---|---|---|---|---|---|---|
| | *A. cerana* | *A. mellifera* | royal jelly | *M. domestica* | *T. molitor* | *B. pest* | CK |
| OD (450 nm)[a] | 0.2633 ± 0.0116 a | 0.2387 ± 0.0031 a | 0.1903 ± 0.0426 b | 0.1753 ± 0.0086 bc | 0.1740 ± 0.0079 bc | 0.1513 ± 0.0075 bc | 0.1093 ± 0.0032 c |

[a]The $p$-value <0.00001 on Duncan's multiple range test. Means denoted with the same letter (a−c) do not significantly differ from each other.

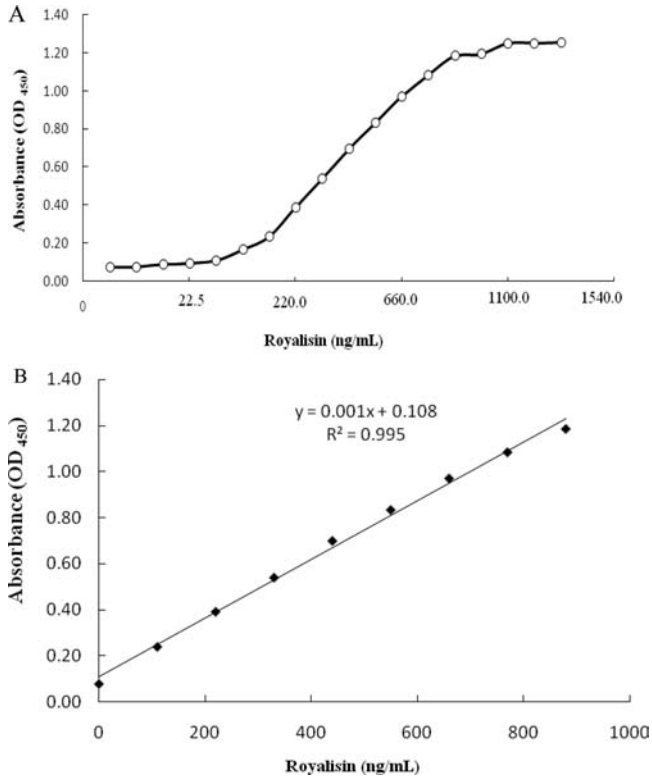


**Figure 1.** Calibration curve of royalisin in PBS. (A) The primary calibration curve from 2.3 to 1320 ng/mL of RAcc-royalisin in PBS solution. (B) The calibration curve from 0 to 880 ng/mL of royalisin in PBS solution was used for royalisin determination in 1.0% dilution of honeybee hemocytes samples. Curves were prepared using triplicates for each standard concentration.

**Quantification of Royalisin in the Hemolymphe of Honeybee Workers by Fast ELISA.** Ten microliters of hemolymphe of the Western honeybee and the Asian honeybee was diluted in 990 μL of PBS. 100 μL/well of the solution was distributed into 96-well microtitration plate. The obtained OD values detected by ELISA with anti-RAcc-royalisin antibody and the royalisin amount of every well were performed through a calibration curve with its OD values. It was shown from Figure 2 that the RCH of Asian honeybees collected before infection

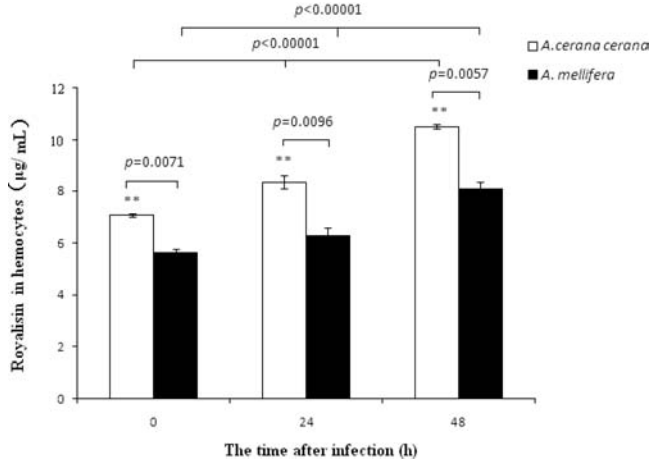


**Figure 2.** Comparison of RCH between *A. cerana cerana* and *A. mellifera* before and post infection.


dx.doi.org/10.1021/jf501637g | J. Agric. Food Chem. 2014, 62, 9305−9309

(7.06 ± 0.07 μg/mL) was significantly higher than that of the Western honeybee (5.64 ± 0.16 μg/mL, $p < 0.01$), which revealed that the innate immunity in the former is higher than that in the latter.

Moreover, it was shown that the RCH values of both the Asian honeybees and the Western honeybee were increased greatly post infection (Figure 2, $p < 0.01$). Relative to the sample before infection, the RCH of the Asian honeybees at 24 h (8.36 ± 0.25 μg/mL) and 48 h (10.49 ± 0.08 μg/mL) post infection increased 18.39 ± 4.60% and 48.55 ± 2.64%, respectively (Figure 3).

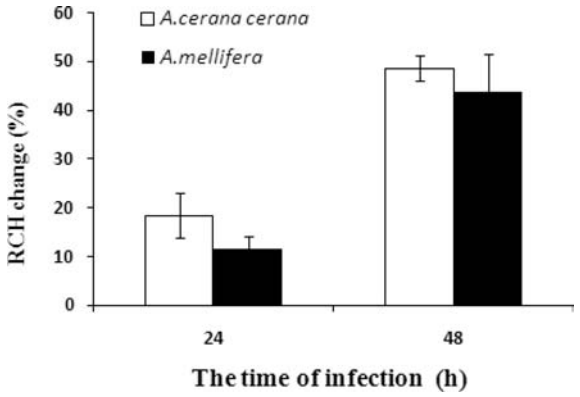


**Figure 3.** RCH change of *A. cerana cerana* and *A. mellifera* post infection (24 and 48 h) relative to non infection (0 h).

Relative to the sample before infection, the RCH of the Western honeybees at 24 h (6.29 ± 0.31 μg/mL) and 48 h (8.09 ± 0.23 μg/mL) post infection increased 11.56 ± 2.66% and 43.66 ± 7.84%, respectively (Figure 3). Meanwhile, the RCH post infection at 24 and 48 h in Asian honeybee were higher than those in the Western honeybee by 32.90% and 29.66%, respectively, which suggested that the Asian honeybees have a higher immune response against bacteria as compared to the Western honeybee.

## DISCUSSION

In the present work, the simple method for fast detection of immunity against pathogen bacteria in the Asian honeybee and the Western honeybee was developed on the basis of ELISA determination with anti-RAcc-royalisin antibody. The binding activity of anti-RAcc-royalisin antibody reached 40 000 dilution. The standard curve with the purified recombinant Acc-royalisin expressed in *E. coli* as standard was prepared. ELISA results on RCH of the Asian honeybee and the Western honeybee under infection and non infection of *E. coli* demonstrated that the former possesses higher innate immunity and immune response against pathogens than the latter.

Honeybees face a number of pathogens from bacteria, viruses, fungi, and parasites. When honeybees are infected by pathogens, four antimicrobial peptide families are synthesized, representing a broad spectrum of antimicrobial activity in the hemolymphe. All of these are cationic peptides identified as apidaecins, abaecin, hymenoptaecin, and defensin (defensin 1 or royalisin, and defensin 2).[6,16] It has been found that royalisin possesses bactericidal and fungicidal activity against bacterial pathogens and fungi such as *Botrytis cinerea*[3] and *Alternaria brassicae*,[17] food-borne bacteria;[11,12] hence, this peptide is a potential target for application of beekeeping and human therapeutics.[17] Evidence demonstrated that more cDNA sequences of royalisin in the hemocytes were found in the Asian honeybee than in the Western honeybee.[6] Honeybee brood food, RJ, containing royalisin is able to inhibit in vitro growth of the pathogen causing AFB. The royalisin mRNA levels of RJ in nurse worker header were used to evaluate the potential defense function of different colonies.[5] The immunoblot procedure employing antibodies generated against the recombinant peptide was developed.[5] Obtained data demonstrated that royalisin is constitutively expressed into RJ in colonies, and indicated that its levels in RJ are determined by genetic factors regulating transcription and/or translation/posttranslation processes in nurses.[5] Therefore, breeding novel honeybee lines expressing higher amounts of royalisin into RJ was suggested.[5]

Mite *V. destructor* is currently the most serious threat to beekeeping of the Western honeybee around the world.[18] This mite not only weakens honeybees by feeding hemolymphe but also serves as a vector and inducer of viral infections, causing severe damage to bee populations worldwide.[19] Furthermore, the mite has been attributed, in part, to the recent widespread Colony Collapse Disorder (CCD) as a disease vector.[20,21] However, colonies of the Asian honeybee (the original host of mite *Varroa*) suffer less damage from this parasite than the Western honeybee despite the presence of the mite in the hives.[7] Antibacterial peptides were observed in a humoral immune response of bees parasitized by mite *Varroa*, such as abaecin and defensin including royalisin, known to be immune-responsive.[2] Honeybees appear also to mount a cellular immune response at wound sites caused by mite *Varroa*.[23] Therefore, the detection of the difference of royalisin level between honeybee species and different colonies of the same honeybee species will be applied to evaluate the resistant characters against mite *Varroa*.

Hemolymphe is well-suited for studying insect immunity as it contains antimicrobial factors produced largely by the fat body and, to a lesser extent, hemocytes.[24] Several methods to detect the immune response of honeybee hemolymph have been employed. The levels of the immune factors prophenoloxidase, lysozyme, and the antimicrobial peptide hymenoptaecin were found to be increased from the analysis of mass spectrometry-based proteomics techniques on the hemolymph proteins of the Western honeybee against *P. larvae*.[24] Genes of the Western honeybees related to the infection of mite *Varroa* or to differences in bee tolerance were identified by microarrays.[25] Gene expression on honeybee immunity in responses to microbial pathogens was investigated by a quantitative-PCR array.[26] The expression of seven immune-related genes in the honeybee head after infection with *E. coli* was determined by qRT-PCR.[27] The consistency of gene expression changes for a subset of differentially expressed genes from the honeybee larvae samples at both 48 and 72 h post infection of *P. larvae* was measured by using qRT-PCR. It was found that for antimicrobial peptides, apidaecin was responsive at both time-points studied, whereas hymenoptaecin had the greatest increase in expression by RNA-seq analysis.[28] However, ELISA to determine the immune response of the hemolymph with antibody against antimicrobial peptides, including royalisin, remains to be developed.

ELISA as a fast and lower-cost diagnostic tool in medicine, toxicology, as well as a quality-control check in various industries has been widely applied around the world.[15] It is anticipated that, in the near future, such an ELISA method using recombinant royalisin as antigen and anti-RAcc-royalisin antibody for measuring RCH will be developed as a useful tool for both determining immunity against pathogens or disease resistance of

honeybee colonies in beekeeping, and as an anticorrosion property of RJ in commerce.

## AUTHOR INFORMATION


### Corresponding Author

*Tel./fax: +86-571-88982167. E-mail: shenlirong@zju.edu.cn.



### Funding

This work was supported by grants from the Applied Research of Public Beneficial Technology of Zhejiang (no. 2011C22039), Projects of Scientific and Technical Development of Hangzhou (no. 20110232B52), Fuli Institute of Food Science, Zhejiang University (no. KY201404), and The National Natural Science Foundation of China (no. 31271848).


### Notes

The authors declare no competing financial interest.

## ACKNOWLEDGMENTS


We thank Dr. Huo-Qing Zheng, College of Animal Science, Zhejiang University, for providing living honeybees, and Dr. Liang Liu, Department of Statistics, The University of Georgia, for his help with statistical analysis and manuscript revision.


## ABBREVIATIONS USED

RJ, royal jelly; MRJPs, major royal proteins; ELISA, enzyme-linked immunosorbent assay; AFB, American foulbrood; RCH, royalisin content in hemolymphe; RAcc-royalisn, recombinant royalisin from *Apis cerana ceran*; HRP, horseradish peroxidase; goat antirabbit IgG/HRP, goat antirabbit IgG-linked horseradish peroxidase; BSA, bovine serum albumin; DAB, diaminobenzidine; CBS, carbonate buffer solution; PBS, phosphate-buffered saline; OD, the optical density or absorbance; BSA, bovine serum albumin; standard deviation, SD

## REFERENCES


(1) Fujiwara, S.; Imai, J.; Fujiwara, M.; Yaeshima, T.; Kawashima, T.; Kobayashi, K. A potent antibacterial protein in royal jelly. *J. Biol. Chem.* **1990**, *265*, 11333−11337.

(2) Klaudiny, J.; Albert, S.; Bachanova, K.; Kopernicky, J.; Simuth, J. Two structurally different defensin genes, one of them encoding a novel defensin isoform, are expressed in honeybee *Apis mellifera*. *Insect Biochem. Mol. Biol.* **2005**, *35*, 11−22.

(3) Bilicova, K.; Wu, G.; Simuth, J. Isolation of a peptide fraction from honeybee royal jelly as a potential antifoulbrood factor. *Apidologie* **2001**, *32*, 275−283.

(4) Bachanova, K.; Klaudiny, J.; Kopernicky, J.; Simuth, J. Identification of honeybee peptide active against *Paenibacillus larvae larvae* through bacterial growth- inhibition assay on polyacrylamide gel. *Apidologie* **2002**, *33*, 259−269.

(5) Klaudiny, J.; Bachanová, K.; Kohútová, K.; Dzúrová, M.; Kopernický, J.; Majtán, J. Expression of larval jelly antimicrobial peptide defensin 1 in *Apis mellifera* colonies. *Biologia* **2012**, *67*, 200−211.

(6) Xu, P.; Shi, M.; Chen, X. X. Antimicrobial peptide evolution in the Asiatic honey bee *Apis cerana*. *PLoS One* **2009**, *4*, e4239.

(7) Peng, Y. S.; Fang, Y. Z.; Xu, S. Y.; Ge, L. S. The resistance mechanism of the Asian honey bee, *Apis cerana* Fabr. to an ectoparasitic mite, *Varroa jacobsoni* Oudemans. *J. Invertebr. Pathol.* **1987**, *49*, 54−60.

(8) Zhang, Y.; Liu, X.; Zhang, W.; Han, R. Differential gene expression of the honey bees *Apis mellifera* and *A. cerana* induced by *Varroa destructor* infection. *J. Insect Physiol.* **2010**, *56*, 1207−1218.

(9) Guzman-Novoa, E.; Emsen, B.; Unger, P.; Espinosa-Montad, L. G.; Petukhov, T. Genotypic variability and relationships between mite infestation levels, mite damage, grooming intensity, and removal of Varroa destructor mites in selected strains of worker honey bees (*Apis mellifera* L.). *J. Invertebr. Pathol.* **2012**, *110*, 314−320.

(10) Chaimanee, V.; Pettis, J. S.; Chen, Y.; Evans, J. D.; Khongphinitbunjong, K.; Chantawannakula, P. Susceptibility of four different honey bee species to *Nosema ceranae*. *Vet. Parasitol.* **2013**, *193*, 260−265.

(11) Shen, L. R.; Ding, M. H.; Zhang, L. W.; Jin, F.; Zhang, W. G.; Li, D. Expression of acc-royalisin gene from royal jelly of Chinese honeybee in *Escherichia coli* and its antibacterial activity. *J. Agric. Food Chem.* **2010**, *58*, 2266−2273.

(12) Shen, L. R.; Liu, D. D.; Li, M. L.; Jin, F.; Din, M. H.; Parnell, L. D.; Lai, C. Q. Mechanism of action of recombinant Acc-Royalisin from royal jelly of Asian honeybee against Gram-positive bacteria. *PloS One* **2012**, *7*, e47194.

(13) Bradford, M. M. A rapid and sensitive method for the quantitation of microgram quantities of protein utilizing the principle of protein-dye binding. *Anal. Biochem.* **1976**, *72*, 248−254.

(14) Ding, M. H.; Jin, F.; Shen, L. R.; Chen, Z. X. Expression of Acc-royalisin from royal jelly of *Apis cerana cerana* in *Escherichia coli* and preparation of its polyclonal antibody. *J. Zhejiang Univ., Agric. Life Sci.* **2010**, *36*, 609−614.

(15) Lequin, R. M. Enzyme immunoassay (EIA)/enzyme-linked immunosorbent assay (ELISA). *Clin. Chem.* **2005**, *51*, 2415−2418.

(16) Casteels-Josson, K.; Zhang, W.; Capaci, T.; Casteelsl, P.; Temp, P. Acute transcriptional response of the honeybee peptide-antibiotics gene repertoire and required post-translational conversion of the precursor structures. *J. Biol. Chem.* **1994**, *269*, 28569−28575.

(17) Tseng, J. M.; Huang, J. R.; Huang, H. C.; Tzen, T. C.; Chou, W. M.; Peng, C. C. Facilitative production of an antimicrobial peptide royalisin and its antibody via an artificial oil-body system. *Biotechnol. Prog.* **2011**, *27*, 153−161.

(18) De Jong, D.; Morse, R. A.; Eickwort, G. C. Mite pests of honey bees. *Annu. Rev. Entomol.* **1982**, *27*, 229−252.

(19) Ball, B. V. Host-parasite-pathogen interactions. *Int. Bee Res. Assoc.* **1994**, *218*, 5−11.

(20) van Englesdorp, D.; Hayes, J.; Underwood, R. M.; Pettis, J. A survey of honey bee colony losses in the US, fall 2007 to spring 2008. *PLoS One* **2007**, *3*, 4071.

(21) Anderson, D.; East, I. J.; Cox-Foster, D.; Conlan, S.; Holmes, E. C.; Palacios, G. The latest buzz about colony collapse disorder. *Science* **2008**, *319*, 724−725.

(22) Gregory, P. G.; Evans, J. D.; Rinderer, T.; Guzman, L. Conditional immune-gene suppression of honeybees parasitized by *Varroa* mites. *J. Insect Sci.* **2005**, *5*, 7.

(23) Kanbar, G.; Engels, W. Ultrastructure and bacterial infection of wounds in honey bee (*Apis mellifera*) pupae punctured by *Varroa* mites. *Parasitol. Res.* **2003**, *90*, 349−354.

(24) Chan, Q. W. T.; Melathopoulos, A. P.; Pernal, S. F.; Foster, L. J. The innate immune and systemic response in honey bees to a bacterial pathogen Paenibacillus larvae. *BMC Genomics* **2009**, *10*, 387 DOI: 10.1186/1471-2164-10-387.

(25) Navajas, M.; Migeon, A.; Alaux, C.; Martin-Magniette, M. L.; Robinson, G. E.; Evans, J. D. Differential gene expression of the honey bee *Apis mellifera* associated with *Varroa destructor* infection. *BMC Genomics* **2008**, *9*, 301.

(26) Evans, J. D. Beepath: an ordered quantitative-PCR array for exploring honey bee immunity and disease. *J. Invertebr. Pathol.* **2006**, *93*, 135−139.

(27) Scharlakena, B.; Graafa, D. C.; Goossensb, K.; Peelmanb, L. J.; Jacobsa, F. J. Differential gene expression in the honeybee head after a bacterial challenge. *Dev. Comp. Immunol.* **2008**, *32*, 883−889.

(28) Cornman, R. S.; Lopez, D.; Evans, J. D. Transcriptional response of honey bee larvae infected with the bacterial pathogen *Paenibacillus larvae*. *PLoS One* **2013**, *8*, e65424.

Table 1. Two Malting Processes (I and II) of Dan'er Barley

| malting parameters | | process A | process B |
|---|---|---|---|
| steeping | temperature (°C) | 17 | 16 |
| | ex-steeping moisture (%) | 43 | 45 |
| germination | time (h) | 108 ± 3 | 120 ± 2 |
| | temperature (°C) | 17, 18 on the last day | 16, 17 on the last day |
| | moisture (%) | 46 | 47 |
| kilning | program | 45−55 °C, 3 h (5 °C/h); 60 °C, 4 h; 65 °C, 5 h; 68 °C, 1 h; 70 °C, 1 h; 77 °C, 1 h; 85 °C, 3 h | 35−50 °C, 5 h; 55 °C, 1 h; 60 °C, 5 h; 65 °C, 6 h; 70 °C, 1 h; 77 °C, 1 h; 85 °C, 3 h |
| equipment | | Saladin Box (150 t) | Tower (300 t) |

The release and synthesis of hydrolytic enzymes initiate starch, protein, and cell wall polysaccharide degradation. When germination has proceeded to an optimal state, it is stopped by kilning to avoid excess sugar and amino acid consumption. The kilning uses two levels of temperature, mild settings (~50−60 °C) to dry the seed and higher curing temperatures (~80−85 °C) to develop the color and aroma of the malt. After the completion of the malting process, the enzyme potential of the malt is established.

Dan'er is one of the most widely grown malt barley cultivars in China, especially along the Yangtze River. Its primary agronomic advantage is salt resistance for growing in Jiangsu province of China. However, the Dan'er malt quality traits are still not considered to be as good as those from the high-quality imported barley cultivars Metacalfe (Canada) or Gairdner (Australia). Besides the genetic deficiencies in the potential malt quality of Dan'er, the process used to produce malt may also limit its potential malting quality.[11] Chinese maltsters typically use two malting processes for Dan'er cultivar that produce malts with distinctly different malt qualities. Therefore, in this investigation we have applied comparative proteomics with 2D-DIGE (two-dimensional fluorescence difference in gel electrophoresis) to highlight the differences between malts made from the Dan'er barley cultivar grown under identical environmental conditions and to study the effect of malting process schedule on malt quality. These insights were considered to provide clues for optimizing the malting process for Dan'er.

## MATERIALS AND METHODS

**Commercial Malt Samples.** The malt samples were collected from two commercial malt companies in China. The barley cultivar of Dan'er was grown in Jiangsu province in China in 2011. The harvested barleys were then malted at industrial scale (150/300 t) under two different processes, process I and process II (Table 1), which were frequently used by commercial malt companies during the same year. Malt samples (malt I from malting process I and malt II under malting condition II) were stored in sterilized sample sacks at −20 °C in our laboratory after receipt.

**Determination of Malt Quality Traits and Macromolecule Contents.** The malt quality traits and macromolecule contents were determined as previously described.[8] In particular, the filtration volume of initial turbid wort for 30 min was defined as separation rate. The European Brewery Convention (EBC) Congress mash was carried out for malt quality parameters determination by EBC official analytical methods.[14] The contents of arabinoxylan (AX), β-glucan, starch, and polyphenol were determined according to the Douglas method,[15] Congo-red method,[16] iodine value,[17] and Folin−Ciocalteu colorimetry,[18] respectively. High-molecular-weight protein (HWP) representing the difference value between protein contents in the congress wort and that in the filtrate was precipitated with tannin[19] and then measured.

**Proteomic Analysis with 2D-DIGE.** Low-salt-soluble proteins of triplicates for each malt sample were extracted as described,[10] with 5 mM Tris-HCl (pH 7.5) buffer containing 1 mM $CaCl_2$. Protein concentrations were determined using the 2D-Quant kit (GE Healthcare, Pittsburgh, PA, USA).

The extracted protein samples were labeled with *N*-hydroxysuccinimidyl-ester dyes Cy2, Cy3, and Cy5 (GE Healthcare)[20] and separated by 2DE as described previously.[11] The differentially labeled coresolved proteome maps within each gel were imaged separately with dye-specific excitation and emission wavelengths using a Typhoon TRIO scanner (GE Healthcare). The gel images were analyzed using the software Decyder 7.0 (GE Healthcare). Spot positions in gels were defined with the Differential In-Gel Analysis (DIA) module, and their fluorescent intensity values were standardized by forming the ratio of Cy3 or Cy5 over the Cy2 signal of the internal standard. The DIA data sets for all gels of one sample were then collectively analyzed using the Biological Variation Analysis (BVA) module, which allowed for the matching of protein spot patterns across gels and statistical analysis of matched spots. Statistical significance was assigned using Student's *t* test based on log abundances of the standardized proteins (log standard abundance). Principal component analysis (PCA) was performed using the Extended Data Analysis (EDA) DeCyder module (GE Healthcare).

Preparative gels were run in parallel with 2D-DIGE gels and stained with Collidal Coomassie Blue G250 and scanned by Image Master LabScan (GE Healthcare).[10] Eight hundred micrograms of proteins extracted from each malt sample was loaded. Spots of interest assigned by DIGE analysis were located on the preparative 2D gels, then excised and subjected to in-gel trypsin digestion and an Ultraflex MALDI-TOF/TOF mass spectrometer (Bruker-Daltonics, Billerica, MA, USA) analysis as described previously.[11] An in-house Mascot server (http://www.matrixscience.com) was used for database search, and scores calculated by the Mowse scoring algorithm in MASCOT ($p < 0.05$) were considered as positive identifications.

**Activity of Amylase and Limit Dextrinase in Crude Extracts.** Crude enzyme was extracted from each malt for amylase and limit dextrinase activity assay. In detail, 2 g of malt was milled and then mixed with 20 mL of distilled water. Samples were vortexed for 3 min every 15 min during the 1 h crude enzyme extraction procedure, after which the extraction mixture was filtered.

Amylase activity was determined as described previously.[21] The reaction mixture comprised 1 mL of diluted crude enzyme and 1 mL of 1% (w/v) soluble starch solution in 0.05 M citrate buffer (pH 5.0). Reaction was carried out at 40 °C for 10 min and then quenched by adding 2 mL of DNS in the reaction tube. The control tube was added with dinitrosalicylic acid (DNS) prior to incubation at 40 °C. The reducing sugars liberated were estimated by DNS method[22] at 540 nm. One unit of amylase activity was defined as the release of 1 mg of reducing sugar as maltose per minute under the defined assay conditions. For α-amylase activity detection, the crude enzyme was incubated at 70 °C to inactivate β-amylase before mixing with the substrate. The activity of β-amylase was calculated by subtracting the activity of α-amylase from total amylase activity. Limit dextrinase


dx.doi.org/10.1021/jf5030483 | J. Agric. Food Chem. 2014, 62, 9310−9316

activity was determined with the same method as for amylase except that 0.5% (w/v) pullulan was used as substrate instead of 1% soluble starch. One unit of limit dextrinase activity was defined as the release of 1 mg of glucose reducing sugar equivalents per minute.

## RESULTS AND DISCUSSION

**Malt Quality Differences between Malts Produced by Different Malting Processes.** During malting, a series of biochemical changes of the grain occur, with perhaps the most important being the synthesis of hydrolytic enzymes. The enzymes synthesized hydrolyze grain storage materials such as starch and proteins so that the malt produced is in a suitable state for efficient brewing. There are three primary hydrolytic processes, namely, starch degradation, cell wall breakdown, and protein hydrolysis. It is therefore essentially differences in the malt quality traits linked to these hydrolytic processes that are directly determined by the different steps of the malting procedure.

Malt quality was measured by using the congress mash procedure and the wort produced by it for analysis by standard EBC analytical methods.[14] The results are shown in Table 2.

**Table 2. Comparison of Malt Quality Parameters and Macromolecule Contents in Congress Wort**

| malt parameter | malt I | malt II |
|---|---|---|
| moisture content (%) | 4.53 ± 0.06 | 4.60 ± 0.01 |
| total protein (g/100, dry) | 13.1 ± 0.2 | 13.0 ± 0.2 |
| wort separation rate (mL/30 min) | 140.0 ± 2.0[a] | 195.0 ± 2.5[a] |
| saccharification time (min) | 12.0 ± 0.5[a] | 11.0 ± 0.5[a] |
| iodine value | 0.03 ± 0.00[a] | 0.09 ± 0.00[a] |
| extract (%, dry) | 76.9 ± 0.1[a] | 78.5 ± 0.1[a] |
| diastatic power (°WK) | 244 ± 3[a] | 251 ± 6[a] |
| KI (%) | 44.5 ± 0.5 | 45.0 ± 0.4 |
| **wort** | | |
| viscosity (8.6%) (m Pa) | 1.65 ± 0.01[a] | 1.60 ± 0.00[a] |
| turbidity (EBC) | 6.74 ± 0.02[a] | 5.53 ± 0.03[a] |
| color (EBC) | 4.39 ± 0.05 | 4.65 ± 0.04 |
| free amino acid nitrogen (mg/100 mL, dry) | 168 ± 2.7 | 165 ± 2.1 |
| β-glucan content (mg/L) | 241.0 ± 4.8[a] | 211.1 ± 5.1[a] |
| AX content (mg/L) | 1009.5 ± 4.8[a] | 1134.5 ± 8.2[a] |
| HWP content (mg/L) | 245.4 ± 1.9[a] | 251.2 ± 3.1[a] |
| polyphenol content (mg GAE/L) | 618.3 ± 3.9[a] | 623.5 ± 2.6[a] |

[a]Parameters with more significant differences between the two malts ($p < 0.05$).

The quality data showed that malt II exhibited superior malt quality compared to malt I, especially for DP and filterability. In addition, malt II required a shorter saccharification time, whereas the DP of malt II was higher. Comparison of the wort filtration volume of malt I was three-fourths that of malt II after the first 30 min after recirculation. Other studies have also shown that measuring the amount of wort filtered after mashing was indicative of potential malt lautering performance.[23,24] The wort turbidity and viscosity of malt I were slightly higher than those of malt II.

Comparison of wort macromolecule contents found that more β-glucan but less AX was present in the congress wort of malt I compared to malt II (Table 2). AX and β-glucan are well-known to reduce the mash separation rate.[25] Besides lipids and fatty acids, turbid worts contain more HWP or protein−polyphenol complexes, which cause an intensified precipitation of colloids and a lower bitter substance yield during wort boiling.[26] There was little difference in the wort HWP and polyphenol contents between malts I and II.

**Proteome Comparison between the Two Malts from Different Malting Processes.** Low-salt-soluble protein fractions containing most of the metabolic proteins were prepared from malts I and II simultaneously and resulted in high-quality 2D separation (Figure 1a,b). On average, for three replicate gels, approximately 430 protein spots were detected in each gel. In selecting candidates for further analysis, very faint spots and poorly resolved spots were eliminated, leaving 370 well-focused spots for quantitative analysis. Validated spots were matched and normalized against the internal standard. By quantitative analysis, 30 spots presented >1.5-fold change in protein abundance with Student's $t$ test $p$ values of <0.05 (as indicated in Figure 1c) between the two malts. Among the differentially abundant proteins, 19 were in higher expression levels in malt II, with the remainder being more abundant in malt I.

Thirty spots were efficiently excised from the preparative gels and submitted for MALDI-TOF/TOF identification (Table 3). For most of the proteins identified, there was generally good agreement between the experimental and theoretical molecular masses and p$I$, except for some discrepancies due to post-translational modifications that presumably occur during the malting process.

**Comparison of Cell Wall Polysaccharides Hydrolyzed in Malts Produced by the Two Malting Processes.** Efficient hydrolysis of cell wall polysaccharides is essential for good quality traits of the final malt, because it is one of the first steps in gaining access to endosperm cell components realized during the malting process. Insufficient degradation will result in filterability and viscosity problems, leading to increasing production time and cost. Therefore, understanding of the key elements in cell wall degradation is important for a malting process optimization. Compared with malt I, the β-D-glucan exohydrolase ExoI and arabinoxylan arabinofuranohydrolase isoenzyme AXAH-I were more abundant in malt II. β-Glucan and arabinoxylan are the two major components of the barley cell wall.[27] During cell wall breakdown, β-glucan can be degraded to glucose directly by β-D-glucan exohydrolase or in two steps with the enzymes β-gluconanase, β-glucosidase, and β-D-glucan exohydrolase.[28] Arabinoxylan in the barley cell wall consists of a D-xylanopyranosyl unit backbone and L-arabinofuranose branches.[1] AXAH-I has been proved to act as a bifunctional α-arabinofuranose/β-D-xylosidase enzyme, thus playing an important role in arabionxylan hydrolysis.[29]

**Comparison of Starch Hydrolase Differences between Malts Produced by the Two Malting Processes.** The conversion of starch to sugars during malting is catalyzed by the enzymes α-amylase, β-amylase, limit dextrinase, and α-glucosidase,[30] which are collectively known as the DP enzymes of malt. The hydrolysis of starch is achieved by the coordinated cleavage of the α-1,4 linkages that are hydrolyzed by α-amylase, the α-1,6 linkages that are hydroylzed by limit dextrinase, and the maltose from the end of dextrins by β-amylase, to contribute yeast fermentable sugars to the wort used for beer production.[31] Limit dextrinase was thought to be a limiting factor in the conversion of starch to sugars during malting,[32] and it has been proved that with β-amylase, α-amylase will hydrolyze starch much more rapidly.[33] β-Amylase was regarded as the major contributor to DP generation.[34] More recent studies have demonstrated that the amount and balance of all three DP enzymes are related to the extent of starch hydrolysis

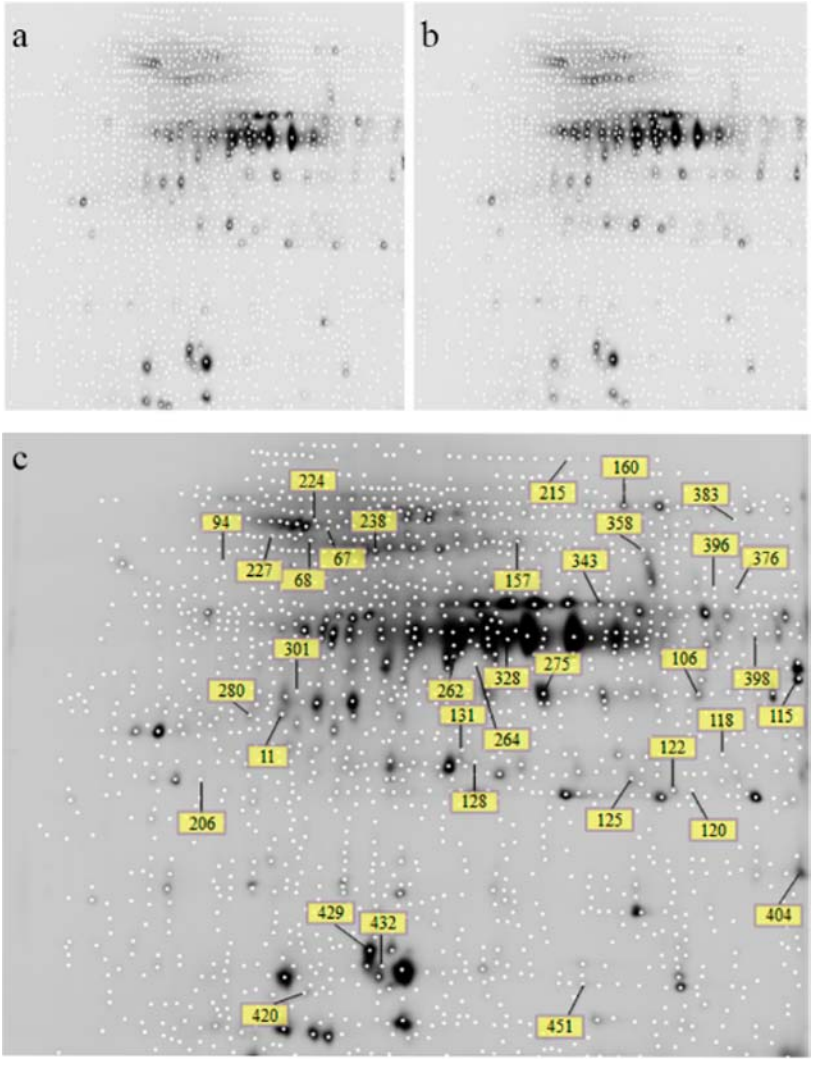


**Figure 1.** Representative 2DE gels of Dan'er malt I (a) and malt II (b) producing by different malting processes. Spots with significant difference between them are indicated by arrows and numbered in the preparative gel (c).

during mashing.[35] Compared between gels of the two malts, no differential spots were identified for limit dextrinase. However, malt extracts did show different limit dextrinase activities between the malts (Table 4). Both $\alpha$-amylase I and $\beta$-amylase exhibited more abundance in malt II than in malt I. However, amylase activity assay showed that the malt II extract exhibited higher total amylase and $\beta$-amylase activity but lower $\alpha$-amylase (as shown in Table 4). It was therefore concluded that the lower DP of malt I was the result of lower $\beta$-amylase despite the higher activity of limit dextrinase and $\alpha$-amylase.

**Comparison of Pathogenesis-Related Proteins (PRs) between Malts Produced by the Two Malting Processes.** Several PRs were found to be differentially expressed between the two malts. PRs are involved in protecting germinating cereal seeds against pathogenic microorganisms and pests. In addition, they have considerable quality importance for the brewing of beer, such as protein and starch degradation during malting and mashing, yeast fermentation during brewing, foam formation, and beer colloidal stability.[36]

PRs of barley and malt can affect the hydrolysis of the barley seed storage proteins, during the malting and mashing process, into peptides and amino acids that can be utilized by brewer's yeasts.[37] Malt contains four classes of endoproteinases.[37] The cysteine proteinases and metalloproteinase were found to hydrolyze barley storage proteins (hordeins) in vitro.[38,39] The serine proteinases were suggested to be present in malt to hydrolyze specific peptide bonds of a few specific proteins. The aspartic endoproteinase digests some of the components of a trypsin/amylase inhibitor protein mixture.[37] Besides endoproteinases, barley also contains a range of low-molecular-weight proteins that inhibit the activities of many of these endoproteinases.[6,37] High levels of inhibitors have been suggested to compromise the production of optimal levels of soluble proteins and amino acids, thereby potentially affecting yeast fermentation performance.[6] Between gels of the two malts, no differential spot was identified as endoproteinase. However, the ns-LTP1 and the storage protein B3-hordein in malt I exhibited greater abundance. The ns-LTP1 has been found to act as a cysteine protease inhibitor, potentially leading to reduced hordein hydrolysis in malt I compared with that in malt II. In addition, the B-hordein combined with D-hordein can form gel protein that slows the mash separation rate.[40] Except for ns-LTPs, members of the trypsin/amylase inhibitor protein family are able to inhibit serine proteinases.[41] The greater abundance of the trypsin/amylase inhibitor PUP38 in


dx.doi.org/10.1021/jf5030483 | J. Agric. Food Chem. 2014, 62, 9310−9316

**Table 3. Different Identified Proteins between Dan'er Malts I and II**

| spot ID | protein description | accession no. | theor MW (kDa)/p*I* | Mascot score | av ratio (log II/I)[a] |
|---|---|---|---|---|---|
| | **Cell Wall Polysaccharides Hydrolyze Enzymes** | | | | |
| 224 | arabinoxylan arabinofuranohydrolase isoenzyme AXAH-I | gil13398412 | 72.5/5.05 | 150 | 3.55 |
| 68 | arabinoxylan arabinofuranohydrolase isoenzyme AXAH-I | gil13398412 | 72.5/5.05 | 412 | 2.84 |
| 383 | β-D-glucan exohydrolase iosenzyme ExoI | gil4566505 | 65.4/6.25 | 302 | 3.06 |
| 160 | β-D-xylosidase | gil18025342 | 84.4/6.36 | 305 | 3.01 |
| **Starch Hydrolases** | | | | | |
| 94 | β-amylase | gil113786 | 59.9/5.58 | 74 | 5.8 |
| 343 | α-amylase I | gil166979 | 47.6/5.74 | 294 | 2.35 |
| | **Pathogenesis-Related Proteins** | | | | |
| 429 | trypsin/amylase inhibitor (pUP38) | gil225103 | 12.4/4.64 | 122 | −3.72 |
| 451 | LTP1 | gil19039 | 41.6/8.89 | 58 | −2.71 |
| 128 | peroxidase BP1 (POD) | gil167081 | 39.2/7.57 | 119 | −1.87 |
| 115 | peroxidase BP1 (POD) | gil167081 | 39.2/7.57 | 134 | −3.25 |
| 262 | serpin Z7 (BPZ7) | gil75282567 | 42.8/5.45 | 166 | −4.07 |
| 404 | 26 kDa endochitinase I precursor | gil2506281 | 34.3/8.58 | 114 | 2.32 |
| | **Metabolic Proteins** | | | | |
| 125 | glutamine amidotransferases class-II (predicted) | gil326489985 | 26.7/5.51 | 145 | 1.97 |
| 157 | multifunctional aminopeptidase A | gil326519046 | 56.2/5.57 | 366 | 1.52 |
| 264 | methylthioribose-1-phosphate isomerase (predicted) | gil326503502 | 38.7/5.56 | 85 | 1.85 |
| 215 | aconitate hydratase (predicted) | gil326495130 | 107.5/6.79 | 121 | 1.82 |
| 116 | glucose and ribitol dehydrogenase | gil7431022 | 31.9/6.54 | 270 | 1.73 |
| 275 | malate dehydrogenases (predicted) | gil326490940 | 35.9/5.62 | 675 | 1.67 |
| 396 | triacylglycerol lipase (predicted) | gil326512028 | 47.2/6.38 | 255 | −1.56 |
| 11 | predicated enolase | gil326490934 | 48.6/5.39 | 503 | −2.59 |
| | **Oxidation−Reduction Proteins** | | | | |
| 122 | thioredoxin peroxidase | gil1710077 | 24.1/6.31 | 132 | 2.8 |
| 227 | protein disulfide isomerases (predicted) | gil326532720 | 56.6/4.98 | 200 | 2.57 |
| 120 | iron/manganese superoxide dismutases (predicted) | gil326507668 | 24.8/7.89 | 386 | 1.94 |
| 358 | glutathione reductase (predicted) | gil326527845 | 53.3/6.07 | 239 | 1.76 |
| | **Others** | | | | |
| 398 | B3-hordein | gil123459 | 30.6/7.74 | 45 | −3.27 |
| 206 | hypothetical protein | gil2266664 | 24.9/4.80 | 191 | 2.61 |
| 280 | aminoimidazole ribonucleotide synthetase (predicted) | gil326511741 | 40.5/5.50 | 197 | 2.52 |
| 131 | hypothetical protein | gil326502266 | 26.4/5.51 | 283 | −1.93 |
| 238 | UDP-glucose pyrophosphorylase | gil6136111 | 51.8/5.20 | 223 | −2.39 |
| 301 | predicated universal stress protein | gil326494752 | 18.3/5.69 | 142 | −2.43 |
| 118 | predicted proteasome subunit α type-6-like | gil326495678 | 27.5/6.33 | 342 | −2.44 |

[a]Average ratio of log standard abundance of spots in malt II/malt I.

**Table 4. Activities of Amylase and Limit Dextrinase in Crude Extract from Two Malts**

| activity (U/g malt) | malt I | malt II |
|---|---|---|
| total amylase | 4404.76 ± 15.87 | 4505.95 ± 27.46 |
| α-amylase | 1028.27 ± 16.86[a] | 446.43.0 ± 13.89[a] |
| β-amylase | 3376.488 ± 2.0[a] | 4059.52 ± 13.57[a] |
| limit dextrinase | 54.57 ± 0.50[a] | 34.22 ± 0.50[a] |

[a]$p < 0.05$.

malt I indicated that it could be an important factor that negatively affects malt I quality traits.

In malt I, serpin Z7 that has been recognized as probable haze-active protein and pro-oxidant[42,43] was in greater abundance than in malt II and thus may reduce the colloidal and flavor stability of beer made from malt II. Serpin Z7 has also been suggested to be involved in foam stability.[36,44] Moreover, a higher content of peroxidase BP1, a negative effector of filterability,[11] in malt I was found. Peroxidases are heat stable and highly active enzymes involved in the oxidative polymerization of phenolic substrates that can result in increased wort color and turbidity.

**Comparison of Other Proteins between Malts Produced by the Two Malting Processes.** There are some other proteins with differential expression levels between the two malts, such as proteins involved metabolism, oxidation, and reduction. Enzymes responsible for aminopeptide and glucose metabolism were all more abundant in malt II, whereas enolase and triacylglycerol lipase for lipid metabolism showed higher contents in malt I. The more predicted aminopeptidase in malt II may improve its protein hydrolysis. At the same time, some enzymes involved in glucose metabolism, such as glucose and ribitol dehydrogenase, predicted aconitate hydratase and malate dehydrogenase, were with more abundance in malt II, which was proposed to be induced by the more complete hydrolysis of starch. Most of barley endosperm and embryo proteins undergo reduction during germination. Thereafter, the proteins became increasingly oxidized, concordant with their continued degradation. The proteins involved in oxidation and reduction were also more abundant in malt II, indicating the better hydrolysis of proteins. The more complete the hydrolysis

of proteins and starch, the better the filterability and stronger DP of the malt.

In conclusion, the present work has analyzed the effects of malting process, beyond the genetic background of barley cultivar, on malting quality traits. The proteomes of malt produced from the same cultivar by the two different malting processes I and II were also compared. The results showed that with malting condition II, the malt quality was superior to that of malt I in most aspects, such as macromolecular contents, turbidity, viscosity, DP, saccharification time, and especially mash filterability. This was attributed to the differentially expressed proteins involved in cell wall polysaccharide hydrolysis, and starch hydrolysis, PRs, and proteins involved in metabolism, oxidation, and reduction processes. The results are expected to indicate opportunities to modify the malting process to improve Dan'er malt quality for beer brewing.

## AUTHOR INFORMATION


### Corresponding Author

*(J.L.) E-mail: jlu@jiangnan.edu.cn. Phone: +86 510 8591 8191. Fax: +86 510 8591 8191.

### Author Contributions

‖X.L. and Z.J. contributed equally to this study.



### Funding

This research was supported by the Major State Basic Research Development Program of China (973 Program, 2012CB720802 and 2013CB733602), the National High Technology Research and Development Program of China (863 Program, 2013AA102109), the National Natural Science Foundation of China (31171736), the Key Program of National Natural Science Foundation of China (31130043), the Fundamental Research Funds for the Central Universities (JUDCF10047, JUSRP1015, and JUSRP51302A), the Key Technologies R&D Program of Jiangsu Province of China (BE2012397), and the Program of Introducing Talents of Discipline to Universities (111 Project, 111-2-06).


### Notes

The authors declare no competing financial interest.

## ACKNOWLEDGMENTS

We thank Dr. Evan Evans for critically reviewing the manuscript and English assistance.

## REFERENCES


(1) Jamar, C.; du Jardin, P.; Fauconnier, M. L. Cell wall polysaccharides hydrolysis of malting barley (*Hordeum vulgare* L.): a review. *Biotechnol. Agron. Soc.* **2011**, *15*, 301−313.

(2) Gupta, M.; Abu-Ghannam, N.; Gallaghar, E. Barley for brewing: characteristic changes during malting, brewing and applications of its by-products. *Compr. Rev. Food Sci. Food Saf.* **2010**, *9*, 318−328.

(3) Evans, D. E.; Li, C.; Eglinton, J. K. The properties and genetics of barley malt starch degrading enzymes. In *Genetics and Improvement of Barley Malting Quality*; Springer Verlag: New York, 2009.

(4) Buttimer, E. T.; Briggs, D. E. Mechanisms of the release of bound $\beta$-amylase. *J. Inst. Brew.* **2000**, *106*, 83−94.

(5) Buttimer, E. T.; Briggs, D. E. Characterization of solubilized forms of bound $\beta$-amylase released by various agents. *J. Inst. Brew.* **2000**, *106*, 71−82.

(6) Jones, B. L. The endogenous endoprotease inhibitors of barley and malt and their roles in malting and brewing. *J. Cereal Sci.* **2005**, *42*, 271−280.

(7) Echart-Almeida, C.; Cavalli-Molina, S. Hordein polypeptide patterns in relation to malting quality in Brazilian barley varieties. *Pesqui. Agropecu. Bras.* **2001**, *36*, 211−217.

(8) Chandra, G. S.; Proudlove, M. O.; Baxter, E. D. The structure of barley endosperm − an important determinant of malt modification. *J. Sci. Food Agric.* **1999**, *79*, 37−46.

(9) Holopainen, U. R. M.; Wilhelmson, A.; Salmenkallio-Marttila, M.; Peltonen-Sainio, P.; Rajala, A.; Reinikainen, P.; Kotavta, E.; Simolin, H.; Home, S. Endosperm structure affects the malting quality of barley (*Hordeum vulgare* L.). *J. Agric. Food Chem.* **2005**, *53*, 7279−7287.

(10) Jin, Z.; Mu, Y. W.; Sun, J. Y.; Li, X. M.; Gao, X. L.; Lu, J. Proteome analysis of metabolic proteins (pI 4−7) in barley (*Hordeum vulgare*) malts and initial application in malt quality discrimination. *J. Agric. Food Chem.* **2013**, *61*, 402−409.

(11) Jin, Z.; Li, X. M.; Gao, F.; Sun, J. Y.; Mu, Y. W.; Lu, J. Proteomic analysis of differences in barley (*Hardeum vulgare*) malts with distinct filterability by DIGE. *J. Proteomics* **2013**, *93*, 93−106.

(12) Appleford, N. E. J.; Lenton, J. R. Hormonal regulation of $\alpha$-amylase gene expression in germinating wheat (*Triticum aestivum*) grains. *Physiol. Plant.* **1997**, *100*, 534−542.

(13) Skadsen, R. W. Physiological and molecular genetic mechanisms regulating hydrolytic enzyme gene expression in cereal grains. *Physiol. Plant.* **1998**, *104*, 486−502.

(14) Malt. In *Analytica−European Brewery Convention*; Fachverlag Hans Carl: Nürnberg, Germany, 2006.

(15) Douglas, S. G. A rapid method for the determination of pentosans in wheat four. *Food Chem.* **1981**, *7*, 139−145.

(16) Naoyuki, I.; Masaru, O.; Masaharu, K.; Noriko, K. Improvement of the Congo Red method, a rapid $\beta$-glucan quantification method for the breeding of high quality malting barley. *Bull. Tochigi Prefectural Agric. Exp. Stn.* **1998**, *47*, 57−64.

(17) Wu, W. L.; Li, Z. Assay of iodine value in wort. *J. Beer Sci. Technol.* **2008**, *4*, 45−46.

(18) Zhao, H. F.; Fan, W.; Dong, J. J.; Lu, J.; Chen, J.; Shan, L. J.; Lin, Y.; Kong, W. B. Evaluation of antioxidant activities and total phenolic contents of typical malting barley varieties. *Food Chem.* **2008**, *107*, 296−304.

(19) Hough, J. S.; Briggs, D. E.; Stevens, R.; Young, T. W. Hopped wort and beer. In *Malting and Brewing Science*; Chapman and Hall/Aspen Publishers: New York, 1999; Vol. 2, 460 pp.

(20) Croes, E.; Gebruers, K.; Carpentier, S.; Swennen, R.; Robben, J.; Laukens, K.; Witters, E.; Delcour, J. A.; Courtin, C. M. A quantitative portrait of three xylanase inhibiting protein families in different wheat cultivars using 2D-DIGE and multivariate statistical tools. *J. Proteomics* **2009**, *72*, 484−500.

(21) Ramakrishna, S. V.; Suseela, T.; Ghildiyal, N. P.; Jaleel, S. A.; Prema, P.; Lonsane, B. K.; Ahmed, S. Y. Recovery of amyloglucosidase from mouldy bran. *Indian J. Sci. Technol.* **1982**, *20*, 476−480.

(22) Bandani, A. R.; Balvasi, A. Comparison of alpha-amylase activity in larval stages of flour beetles, *Tribolium confusum* (Coleoptera: Tenebionidae). *Commun. Agric. Appl. Biol. Sci.* **2006**, *71*, 537−541.

(23) Evans, D. E.; Goldsmith, M.; Dambergs, R.; Nischwitz, R. A comprehensive revaluation of small-scale congress mash protocol parameters for determining extract and fermentability. *J. Am. Soc. Brew. Chem.* **2011**, *69*, 13−27.

(24) Evans, D. E.; Redd, K.; Harysamow, S.; Elvig, N.; Metz, N.; Koutoulis, A. The influence of malt quality on malt brewing and barley quality on barley brewing with Ondea Pro, compared by small-scale analysis. *J. Am. Soc. Brew. Chem.* **2014**, *72*, 192−207.

(25) Vietor, R. J.; Voragen, A. G. J.; Angelino, S. A. G. F. Composition of nonstarch polysaccharides in wort and spent grain from brewing trials with malt from a good malting quality barley and a feed barley. *J. Inst. Brew.* **1993**, *99*, 243−248.

(26) Kuhbeck, F.; Back, W.; Krottenthaler, M. Influence of lauter turbidity on wort composition, fermentation performance and beer quality in large-scale trials. *J. Inst. Brew.* **2006**, *112*, 222−231.

(27) Lazaridou, A.; Chornick, T.; Biliaderis, C. G.; Lzydorczyk, M. S. Composition and molecular structure of polysaccharides released from barley endosperm cell walls by sequential extraction with water, malt enzymes, and alkali. *J. Cereal Sci.* **2008**, *48*, 304−318.

(28) Fincher, G. B. Molecular and cellular biology associated with endosperm mobilization in germinating cereal grains. *Annu. Rev. Plant Physiol. Plant Mol. Biol.* **1989**, *40*, 305−346.
(29) Lee, R. C.; Hrmova, M.; Burton, R. A.; Lahnstein, J.; Fincher, G. B. Bifunctional family 3 glycoside hydrolases from barley with α-L-arabinofuranosidase and β-D-xylosidase activity. Characterization, primary structures, and COOH-terminal processing. *J. Biol. Chem.* **2003**, *278*, 5377−5387.
(30) Manners, D. J. Some aspects of the metabolism of starch. *Cereal Foods World* **1985**, *30*, 722−727.
(31) MacGregor, A. W.; Bazin, S. L.; Macri, L. J.; Babb, J. V. Modelling the contribution of α-amylase, β-amylase and limit dextrinase to starch degradation during mashing. *J. Cereal Sci.* **1999**, *29*, 161−169.
(32) Sissons, M.; Taylor, M.; Proudlove, M. Barley malt limit dextrinase − its extraction, heat-stability, and activity during malting and mashing. *J. Am. Soc. Brew. Chem.* **1995**, *53*, 104−110.
(33) Maeda, I.; Nikuni, Z.; Taniguchi, H.; Nakamura, M. Purification of a debranching enzyme (R-enzyme) from malted barley, and the role of the enzyme in the digestion of starch granules during the germination of barley seeds. *Carbohydr. Res.* **1978**, *61*, 309−320.
(34) Gibson, T. S.; Solah, V.; Holmes, M. R. G.; Taylor, H. R. Diastatic power in malted barley − contributions of malt parameters to its development and the potential of barley-grain β-amylase to predict malt diastatic power. *J. Inst. Brew.* **1995**, *101*, 277−280.
(35) Evans, D. E.; Collins, H.; Eglinton, J.; Wilhelmson, A. Assessing the impact of the level of diastatic power enzymes and their thermostability on the hydrolysis of starch during wort production to predict malt fermentability. *J. Am. Soc. Brew. Chem.* **2005**, *63*, 185−198.
(36) Stanislava, G. Review: The role of barley seed pathogenesis-related proteins (PRs) in beer production. *J. Inst. Brew.* **2010**, *116*, 111−124.
(37) Jones, B. L. Endoproteases of barley and malt. *J. Cereal Sci.* **2005**, *42*, 139−156.
(38) Poulle, M.; Jones, B. L. A proteinase from germinated barley. I: Purfication and some physical properties. *Plant Physiol.* **1988**, *88*, 1454−1460.
(39) Fontanini, D.; Jones, B. L. A study of metallopeptidase isozymes from malted barley (*Hordeum vulgare* cv. Morex). *J. Agric. Food Chem.* **2001**, *49*, 4903−4911.
(40) Wallace, W.; Lance, R. C. M. The protein reserves of the barley grain and their degradation during malting and brewing. *J. Inst. Brew.* **1988**, *96*, 379−386.
(41) Jones, B. L.; Fontanini, D. Trypsin/α-amylase inhibitors inactivate the endogenous barley/malt serine endoproteinase SEP-1. *J. Agric. Food Chem.* **2003**, *51*, 5803−5814.
(42) Iimure, T.; Nankaku, N.; Watanabe-Sugimoto, M.; Hirota, N.; Zhou, T. S.; Kihara, M.; Hayashi, K.; Ito, K.; Sato, K. Identification of novel haze-active beer proteins by proteome analysis. *J. Cereal Sci.* **2009**, *49*, 141−147.
(43) Wu, M. J.; Rogers, P. J.; Clarke, F. M. 125th Anniversary Review: The role of proteins in beer redox stability. *J. Inst. Brew.* **2012**, *118*, 1−11.
(44) Perrocheau, L.; Rogniaux, H.; Boivin, P.; Marion, D. Probing heat-stable water-soluble proteins from barley to malt and beer. *Proteomics* **2005**, *5*, 2849−2858.

UV−vis absorption spectra is discussed in the present paper. This method requires only a mathematical treatment of the measured oil absorption spectrum avoiding any chemical manipulation of the sample. Within this approach, the spectra of EVOOs are analyzed in terms of the molar absorption spectra of four main pigments dissolved in purified triolein, namely, lutein (a xanthophyll), $\beta$-carotene (a carotenoid), pheophytin-a and pheophytin-b (two chlorophylls derivatives). The choice of this set of "main pigments", suggested by experimental analytical data, is discussed, as well as the use of triolein as the best solvent. Several examples of the application of this method to real experimental cases are reported, underlining its possible uses for the assessment of quality, freshness, and aging effects in EVOOs.

## MATERIALS AND METHODS

**Oil Samples.** The oil samples from Spain (Coprovir, Poniente de Granada, Fuentes de Dios, Loja) were a gift from San Isidro Deifontes S.C.A. (Granada), and they are of the same vintage year. The Italian oils (mixed cultivar of different origin) were provided by Salov S.p.A. (Massarosa, Lucca), and they were from the 2012 and 2013 harvests. Tuscan oils of Frantoio cultivar were provided from Carapelli Firenze S.p.A, and the harvest year is indicated case by case. The rest of oils used in the present study were purchased directly in the supermarket, and they are of the same vintage year (2012). For each measurement reported in this work, a minimum of three replicates were performed. All oil samples were maintained in dark conditions, in 25 mL dark glass bottles, at a temperature between 1 and 5 °C.

**Solvents and Purification Methods.** Methanol, *n*-hexane, and acetone were Carlo Erba HPLC solvents (Milan, Italy).

$\beta$-Carotene (>97% purity) and triolein were purchased by Fluka (Milan, Italy). $\beta$-Carotene was used as such, while triolein was purified by washing cycles with pure MeOH and freezing/partial crystallization of the mixture at $T < -20$ °C, followed by a phase separation, until the measured absorbance of triolein was equal to that of the previous washing cycle (minimum four cycles).[24]

Lutein and zeaxanthin were obtained through HPLC semipreparative isolation/purification of methanol extracts of maize flour. The mobile phase was methanol. The column was a Waters Spherisorb S5-ODS2 10 × 250 mm RP-C18, the flux was 2.4 mL/min at $T$ = 25 °C, and the spectrophotometric detector was at 450 nm. Retention times (Rt) were 15 and 16 min, respectively, for lutein and zeaxanthin.

Pheophytin-a and pheophytin-b were obtained through HPLC semipreparative isolation, by Waters Spherisorb S5-ODS2 10 × 250 mm RP-C18 column, detector at 415 nm, of acetone extracts of leaves of *Acer Negundo L. (Aceraceae)* acidified with 1 N HCl, after complete pheophytinization of chorophylls present in these extracts. Pheophytinization was controlled through UV spectrophotometry by observing the sharp diminution of absorbance at 434 nm, where the maximum of chlorophyll-a is located, and the corresponding increase at 410 nm near the absorbance maximum of pheophytin-a (65% of spectral change in 12 min). Retention times were Rt (pheo-b) = 25.9 min; Rt (pheo-a) = 32.5 min; flux 4.5 mL/min; $T$ = 45 °C; mobile phase: methanol.

**Instruments.** Absorbance spectra were measured with a Jasco V-550 spectrophotometer using quartz cells with 0.1−1 cm optical path length in order to measure absorbances smaller than 2 absorbance units.

A HPLC Jasco 880-Pu pump equipped with a Shimadzu SP-10A spectrophotometric detector was used isocratically for analytic and semipreparative experiments.

**Spectrophotometric Measurements.** Before absorbance measurements, the oil samples were centrifuged for 30 min at 5000 rpm in order to minimize the light absorption due to suspended materials. The absorbances used in the present analyses of EVOOs spectra are referred to 1 cm optical path. Clearly, in the actual absorbance measurements, cells whose optical path was compatible with the requirement of precise measurements, in particular to avoid any sensible stray light effect, were used. Spectroscopic parameters included spectral bandwidth = 1 nm and measurement step $\delta\lambda$ = 1 nm.

**Extinction Coefficients of the Pigments.** Because of the lack of relevant literature, the molar extinction spectra of lutein, pheophytin-a, and pheophytin-b in triolein (see Figure 1) were obtained through the

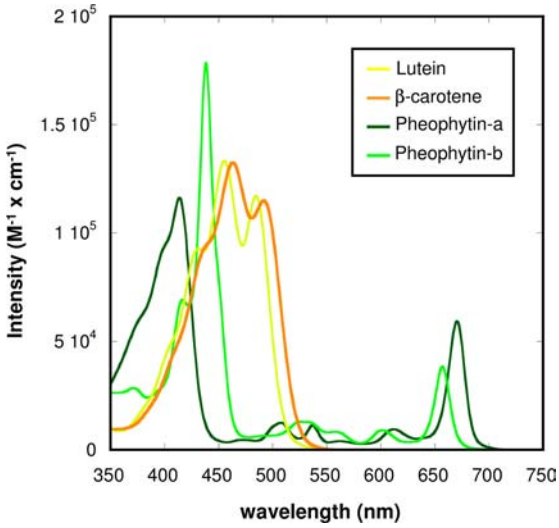


**Figure 1.** UV−vis molar extinction spectra of lutein, $\beta$-carotene, pheophytin-a, and pheophytin-b dissolved in purified triolein.

experimental procedure hereafter described. The methanol solutions of purified pigments from semipreparative HPLC were about $2 \times 10^{-5}$ M of pure pigments in volumes of 5−10 mL, i.e., sub-milligram masses of pigments. Their absorbance in methanol was measured, and the concentration of the pure analytes was calculated by using the values of their extinction coefficients found in the literature.[25−27] The volatile solvent in a precise volume (1 mL) of methanol solution was finally evaporated and a measured volume (1 mL) of purified triolein was added to the dry pigment.

For $\beta$-carotene a weighted mass (4.26 mg) was dissolved in a measured volume (25 mL) of *n*-hexane to obtain a relatively concentrated solution. A measured aliquot (40 $\mu$L) was conveniently diluted in 2 mL of solvent and its absorbance was measured. The molar extinction of $\beta$-carotene in hexane found in the literature was used to calculate its concentration. The volatile solvent was evaporated, and a measured volume of pure triolein was added. In this case, it was also possible to verify that the procedure was correct. In fact, the initial mass of $\beta$-carotene and the used volumes of solutions and solvents were measured, and the difference between the concentrations found by the two procedures is less than 2%.

The spectra were measured in pure triolein, since this *quasi*-transparent solvent is the most appropriate to represent the interactions of the olive oil matrix with the pigments. The spectra obtained was neatly different from the spectra in the more usual solvents (methanol, ethanol, acetone, diethyl ether, or hexane) reported in the literature.[28,29]

A sample of HPLC-pure zeaxanthin, a xanthophyll isomer of lutein, very common in nature, was also prepared. In two parallel experiments, known amounts of lutein and zeaxanthin were added to samples of a Tuscan EVOO. The measured increase of absorbance of the oil due to the added lutein, or zeaxanthin, was identical to the absorbance of an equal quantity of lutein, or zeaxanthin, dissolved in a volume of triolein equal to that of the EVOO used in the experiment. The two major peaks in the absorption spectrum of zeaxanthin in triolein were 4 and 7 nm red-shifted with respect to the corresponding lutein spectrum. The zeaxanthin spectrum peaks, in addition, seem to be less resolved than those of lutein. The above findings demonstrate the good choice of triolein as a solvent: no particular interactions of xanthophylls with the components of EVOOs different from triolein, should be present. Differences in the shapes and shifts of the order of

5−10 nm are expected for the absorption spectra of the other carotenoids present in EVOOs in concentration usually much smaller than lutein and β-carotene.

With a procedure similar to that used for lutein, triolein has been proven to well represent the *medium* in which pheophytin-a and pheophytin-b are present in olive oils.

**Mathematical Treatment of UV−vis Absorption Spectra.** In this section, the mathematical treatment of the EVOO absorption spectrum adopted in order to extract the concentration of the aforementioned four main pigments is reported.

As shown in Figure 1 and summarized in Table 1, while the two pheophytins spectra show sensible differences in their shapes and

**Table 1. Maxima in the UV-vis Absorption Spectra of Oil Pigments in Triolein**

| solvent: triolein | lutein | β-carotene | pheophytin-a | pheophytin-b |
|---|---|---|---|---|
| $\lambda_{max}$ (nm) | 486, 455, 432 | 490, 462 | 670, 414 | 657, 437 |
| $\varepsilon$ ($\lambda_{max}$) $M^{-1}$ $cm^{-1}$ | 11800, 133500, 95600 | 115200, 132500 | 59500, 116200 | 38500, 178500 |

absorption intensities, lutein and β-carotene show spectra similar in shape and intensity. In fact, the spectrum β-carotene is red-shifted and has a lower resolution of the peaks with respect to the xanthophyll one. However, there is no doubt about the linear independence of the four spectra, i.e., not one of them can be expressed as a linear combination of the other three spectra.

The UV−vis absorption spectrum of any EVOO can be conveniently described by four orthogonal functions (eigenvectors) by using a treatment similar to that adopted by Hennessey and Johnson[30] to calculate the contributions of various proteins basic structures (α-helix, β-sheet., etc.) to the measured circular dichroism (CD) spectra of proteins in solution.

First, the symmetric 4 × 4 overlap matrix, **S**, of the four molar extinction spectra $\varepsilon_i(\lambda)$ of the four pigments in triolein, is obtained. The elements $S_{i,j}$ are defined as

$$S_{i,j} = \int \varepsilon_i(\lambda)\varepsilon_j(\lambda)\, d\lambda \quad (1)$$

the integration being performed from 390 to 720 nm, the spectral range where light absorbance in EVOOs can be ascribed to the chosen pigments.

Then, four eigenvectors and the correspondent four eigenvalues are obtained by diagonalization of the **S** matrix.

The eigenvectors, $\Phi_j(\lambda)$, with $j$ = 1, 2, 3, and 4, are linear combinations of the four molar extinction coefficient of pigments, $\varepsilon_r(\lambda)$ according to eq 2, and they are reported in Figure 2.

$$\Phi_j(\lambda) = \Sigma_r P_r^j \varepsilon_r(\lambda) \quad (2)$$

where $P_r^j$, a fixed parameter, is the contribution to the eigenvector $\Phi_j(\lambda)$ of the molar extinction spectrum of pigment $r$. It must be observed that the diagonalization of the **S** matrix is possible only when the four spectra are linearly independent, as it is in this case.

The eigenvalues, $\alpha_i$ ($\times 10^{-12}$), are 0.022298, 0.202191, 0.403061, and 2.337122 $M^{-2}$ $cm^{-2}$ in correspondence to the eigenvectors $\Phi_j(\lambda)$. Only the eigenvector corresponding to the highest eigenvalue is positive in all the spectral range, while the other curves also have negative values in a number of spectral intervals separated by crossing points with the λ-axis. These progressively increase from 0 up to 7 (0, 2, 6, 7 with decreasing eigenvalues).

If the absorbance of an EVOO in the 390−720 nm range is due to the four pigments only, it can be expressed *exactly* as a linear combination of the above four functions $\Phi_j(\lambda)$. In any case, it is simple to calculate (eq 3) the four coefficients $\gamma_j$ of the linear combination that best represents the oil spectrum in terms of the spectra of the reference pigments:

$$\gamma_j = \int \Phi_i(\lambda)\mathrm{ABS}(\lambda)\, d\lambda/\alpha_j \quad (3)$$

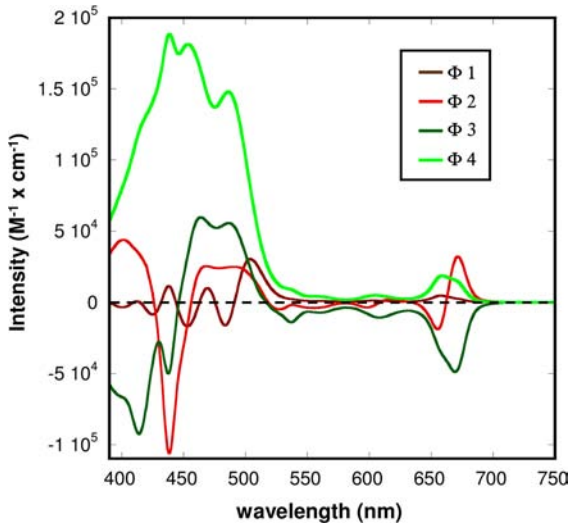


**Figure 2.** Eigenvector $\Phi_j(\lambda)$ calculated by the procedure described in the text.

where ABS $(\lambda)$ is the measured absorbance of the oil and $\alpha_j$ is the eigenvalue corresponding to $\Phi_j(\lambda)$.

Finally, the molar concentration of the pigment $r$, $C_r$, in the oil is determined through eq 4:

$$C_r = \sum_j \gamma_j P_r^j \quad j = 1, \ldots, 4 \quad (4)$$

With the values of the molar concentrations $C_{r=1,4}$ of the pigments, it is possible to calculate (eq 5) the absorption spectrum $\mathrm{ABS}_{calc}$ $(\lambda)$ of the EVOO, to be compared with the experimental one, ABS$(\lambda)$.

$$\mathrm{ABS}_{calc}(\lambda) = \sum_r C_r \varepsilon_r(\lambda) \quad (5)$$

From the discrepancies between these spectra, it is possible to evaluate the quality of the concentration values $C_{r=1,4}$ extracted from the experimental absorption spectrum, as well as the goodness of the procedure.

**Spectral and Data Analysis.** The measured spectra were mathematically treated by using properly adapted Excel sheets. The diagonalization of the matrix **S** was performed by using a package of MatLab 6. The evaluation of relevant statistic parameters was also performed by using Excel software.

**Validation of the Method.** In order to validate the method, the error due to both the experimental procedure and the mathematical treatment was evaluated. For the experimental contribution to the error, all UV−vis spectra were acquired by using rectangular quartz cuvettes with different path lengths of 0.1, 0.2, 0.5, and 1 cm and two cuvettes with the same path length of 0.1 cm, but with different geometry and shape were used: five spectra were acquired for each oil. After normalization for the path length, the five experimental spectra were scaled in order to have the absorbance values at $\lambda$ > 720 nm equal to zero. These five scaled spectra were used to calculate the average spectrum and the standard deviation, for each oil sample. From the statistical point of view, the method has been applied to more than 80 oils from Tuscany and Apulia,[31] and the average value of the standard deviation, $\sigma^{exp}$, calculated for each pigment, is reported in Table 2. It should be noticed, that the experimental error also contains a systematic error, which is not easy to evaluate, related to the intrinsic differences among the different cuvettes. In fact, by decreasing the path length, the effect of the stray light decreases, and it is not constant within the observed spectral window. However, the values reported in Table 2 can be taken as representative for the general case.

The analysis of the UV−vis spectra by using the mathematical approach presented above introduces an error, too. This error can be evaluated through the residues (see the Supporting Information for details). Moreover, the goodness of the mathematical treatment was


dx.doi.org/10.1021/jf503818k | J. Agric. Food Chem. 2014, 62, 9317−9325

Table 2. Values of Standard Deviation of Concentration (M) for Investigated Pigments Due to Experimental ($\sigma^{exp}$) and Deconvolution ($\sigma^{calc}$) Contributions[a]

| | triolein [M] | β-carotene [M] | pheophytin-b [M] | pheophytin-a [M] | lutein [M] |
|---|---|---|---|---|---|
| $\sigma^{exp}$ | 0.3 | $3 \times 10^{-7}$ | $5 \times 10^{-8}$ | $1 \times 10^{-7}$ | $2 \times 10^{-8}$ |
| $\sigma^{calc}$ | 0.3 | $5 \times 10^{-7}$ | $1 \times 10^{-7}$ | $3 \times 10^{-7}$ | $2 \times 10^{-7}$ |
| LOD | | $1 \times 10^{-06} \pm 6 \times 10^{-7}$ | $7 \times 10^{-08} \pm 3 \times 10^{-8}$ | $1 \times 10^{-07} \pm 6 \times 10^{-8}$ | $8 \times 10^{-07} \pm 2 \times 10^{-8}$ |
| LOQ | | $1 \times 10^{-06} \pm 6 \times 10^{-7}$ | $7 \times 10^{-08} \pm 3 \times 10^{-8}$ | $1 \times 10^{-07} \pm 6 \times 10^{-8}$ | $1 \times 10^{-13} \pm 6 \times 10^{-8}$ |

[a]LOD and LOQ values calculated as reported in the text.

verified by the "R-square" test, which estimates the correlation between the experimental values and the values predicted by the deconvolution procedure:

$$R\text{-square} = 1 - \frac{\sum_{i=1}^{n}(y_i - f_i)^2}{\sum_{i=1}^{n}(y_i - \bar{y})^2} \quad (6)$$

where $f_i$ is the value predicted by the fitting, $\bar{y}$ is the mean of the observed data, and $y_i$ is the observed data value. In particular, two tests were done by choosing two EVOOs representative of two opposite situations: a good and a bad fit, due, for example, to the turbidity of the oil, as reported in the Supporting Information.

The values of $R$ are 0.85 for the bad case and 0.96 for the good one. The range 0.85 ÷ 0.96 can be taken as representative for all other intermediate cases.

The standard deviation due to the deconvolution procedure, $\sigma^{calc}$, reported in Table 2, can be determined according to the following equation:

$$\sigma^{calc} = \sqrt{\frac{\sum_{i=1}^{n}(x_i - \bar{x})^2}{n-1}} \quad (7)$$

where $x_i$ is the pigment concentration obtained after fitting process for each path lengths cuvette, $\bar{x}$ is the mean value of the pigment concentration, and $n$ is the number of the values considered. In this case, it is equal to five (number of cuvettes used). It can be noted that triolein concentration is visibly higher than the other values, because it represents the matrix of the oil without any pigment.

A sample of refined olive oil was used for the measurement of the limit of detection (LOD) and limit of quantitation (LOQ). According to IUPAC definition, LOD and LOQ are mathematically defined equal to 3 and 10 times, respectively, the standard deviation of the results for a series of replicates (five in our case) used to determine a reliable limit of detection. The respective values of LOD and LOQ are reported in Table 2.

## RESULTS AND DISCUSSION

**Discussion about the Mathematic Treatment.** In this work on the extraction of pigment information, four pigments were chosen. In principle, other pigments could be added to these four ones, provided that their molar spectra are linearly independent from each other and from the previous ones. The maximum number of basis spectra is actually defined by the dimensionality of the functional space of the absorption spectra of all extra virgin olive oils. Physical restrictions have to be taken into account. For example, the precision of the absorbance measurements both of the oil samples and of the reference spectra, ca. 1%, has to be considered. Two spectra differing only within the experimental error cannot be considered linearly independent, and pigment concentrations identical, within the experimental error, have to result using the above treatment of their absorption spectra, i.e., by using eqs 3−5, in the previous section.

Two independent spectra cannot be proportional to each other and they must be different in their shape. As shown in Figure 1, even if the differences in the shape of the molar extinction of lutein and β-carotene are much smaller than that of any other couple of reference pigments, they are sufficient to represent EVOOs carotenoids. From a quantitative point of view, the difference in shape between spectra can be evaluated by the values of the overlaps of normalized extinction spectra (see the Supporting Information).

In this work, the minimum number of pigments, normally present in EVOOs, whose absorption spectra are significantly different from each other, was chosen in order to obtain calculated absorption spectra nearest to the measured ones. The possible presence of other pigments not included among the above reference components has to be addressed as well. If the outsider pigment has a spectrum equal to any of the reference components, its contribution to the absorbance of the oil is simply added up to the absorbance of this component, through eq 3, thereby increasing its calculated concentration, through eq 4. This situation actually occurs for some isomers of lutein, for lutein esters,[17,18] and for some pheophytins.[32] It must be noticed that, while there are large differences in the CD spectra of pheophytin stereoisomers, differences in their absorption spectra are undetectable.[30] When the spectrum of the outsider component pertains to the functional space of two of the basic four pigments, its contribution to the whole spectrum is included in the calculated amounts of these two pigments. This case is here briefly described.

A known amount of zeaxanthin, i.e., a carotenoid isomer of lutein that, as far we know, has never been detected in EVOOs, was added to a multicultivar Italian EVOO. The absorption spectra of the EVOO before (curve a) and after the addition (curve b) are reported in Figure 3A. The spectrum (curve c) is the difference between spectra (b) and (a) and represents the measured increase of the absorbance of the EVOO due to the added zeaxanthin. The spectra (a), (b), and (c) were analyzed by means of the mathematical method described above, and the calculated spectra are shown in dashed lines. The spectrum calculated from experimental (c) overlaps perfectly with the difference between the two absorption spectra (a) and (b), even if zeaxanthin is a carotenoid not likely to be found in EVOOs. Moreover, Figure 3B shows the contributions to absorbance proceeding from the two reference pigments lutein and β-carotene. It is evident the prevalent contribution of β-carotene to the absorbance of this "oil", as expected from the spectral characteristics of zeaxanthin. An increase of the calculated concentrations of lutein and of β-carotene corresponds to the increased absorbance of the oil caused by the added zeaxanthin. These concentration increments are a mathematical consequence of the linear dependence of the zeaxanthin spectrum on the spectra of lutein and β-carotene.

From these findings several considerations can be drawn:

(1) The presence of a carotenoid (here zeaxanthin) different from lutein and β-carotene leads to concentrations different from their analytical (e.g., determined by HPLC) values.

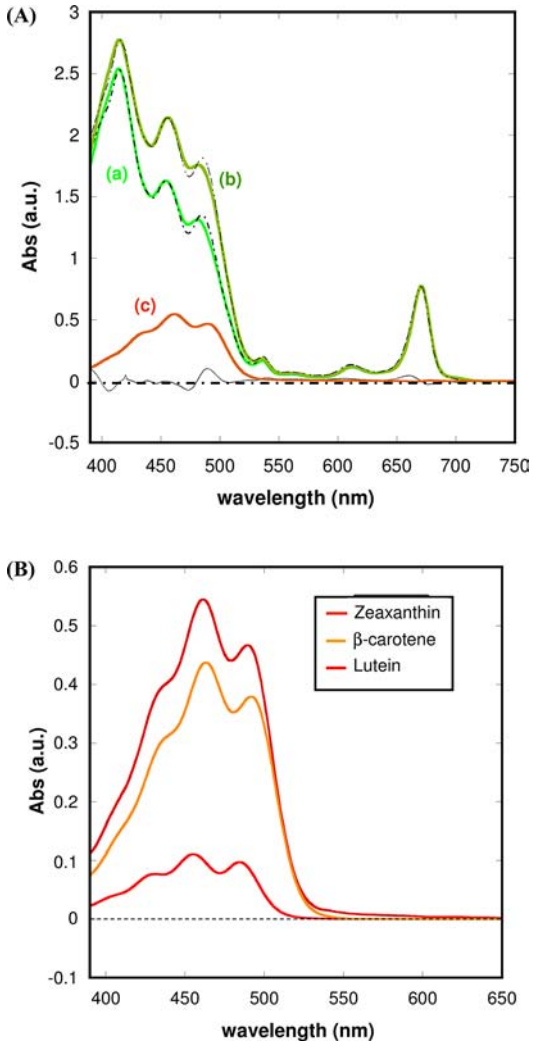


**Figure 3.** (A) UV−vis absorption spectra of an EVOO (a) and of the same one with the addition of a certain amount of zeaxanthin (b) with the respective calculated spectra (dashed lines) and residues (black line). The spectrum of the added zeaxanthin (c) is also reported. (B) Contributions of lutein and $\beta$-carotene to the same EVOO sample due the addition of zeaxantin.

(2) The introduction of zeaxanthin as a third carotenoid in the set of reference spectra would result in the impossibility to diagonalize the overlap matrix **S** (eq 1), given the evident linear dependence of its spectrum on those of lutein and $\beta$-carotene in the 390−720 nm spectral region.

Hence, this example demonstrates that it is impossible to extract specific and quantitative information about all carotenoids from the oil absorption spectrum, even when they are present in non-negligible concentrations.

Even if at least 15 carotenoids were found in extracts of different oils,[13,15,17,18,22,33] a much smaller number of carotenoids, two or three, is sufficient to describe their functional space. This is supported by two general observations: (1) the spectral range of their absorption spectra is limited to the 390−550 nm range; (2) most of them are typically shaped in a very similar way in this spectral range. For this reason, lutein and $\beta$-carotene have been chosen, since they are probably the most significant from both the analytical and the nutraceutical point of view.

**Addition of a Nonpigment Substance Spectrum to the Reference Spectra.** In our approach, a fifth spectrum vector has been added in order to reproduce the absorption in the 390−720 nm spectral region of an EVOO deprived of any pigment. In fact, other substances are present in oils, partially due to the degradation processes of the original components, including the same pigments. This absorption curve is well reproduced by the shape of the absorption spectrum of aged triolein or of refined olive oil. This absorption has an absorbance close to zero in the visible and gradually increases moving toward the near-UV spectral region. The absorption of an aged sample of triolein, reported in Figure 4 together with

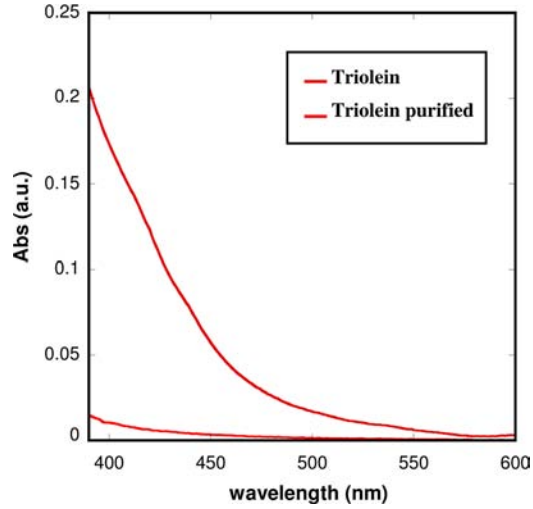


**Figure 4.** UV−vis absorption spectrum of purified (red) and "raw" commercial triolein (brown) curves.

the spectrum of purified triolein, is clearly due to impurities, whose concentration increases with the triolein aging: this absorption is used as that equivalent to an unspecified one-molar substance. It is interesting to observe that its shape is similar to the residual absorbance of EVOOs after complete photodestruction of the pigments.[19] Since the shape of this function is quite different from the absorbance of the pigments, it cannot be represented by the eigenvectors of the true pigment-space. Moreover, the presence of this function is especially interesting for studies of EVOO aging, as described in the following paragraph.

**Several Applications of the Method to EVOO Samples.** In Figure 5, the measured absorption spectra of four one-year-old EVOOs from Granada (Spain) are reported. Notable differences of their absorbance both in shape and in intensity can be observed. The calculated spectra (eq 5) and the difference between the calculated and the measured absorbances are reported as well. The experimental absorbance has been reproduced with remarkable precision by the absorptions of the four +1 light absorbers described: differences of ca. 1% are found only at the 485 nm maximum. The experimental spectra in Figure 5 present well resolved peaks. In correspondence to the differences of absorbance spectra, the four EVOOs have significant differences in pigment composition, as reported in Table 3.

However, not all the EVOOs are reproduced with the above quasi-absolute precision. In Figures 6A,B the spectra of two Italian EVOOs are represented. They show, respectively, medium and intense differences between experimental and


dx.doi.org/10.1021/jf503818k | J. Agric. Food Chem. 2014, 62, 9317−9325

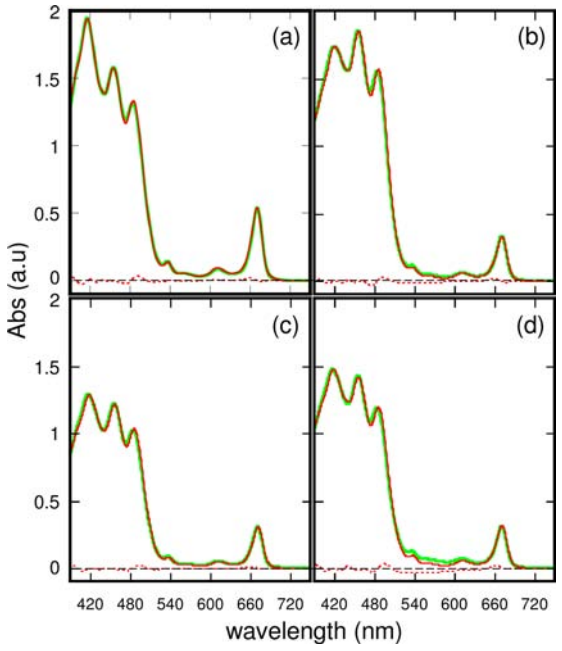


**Figure 5.** UV−vis absorption spectra of four Andalusian EVOOs (a, Coprovir; b, Poniente de Granada; c, Fuentes de Dios; d, Loja). Experimental spectrum (green), calculated one (red), and the residue curve (dashed red curve) are shown in each case.

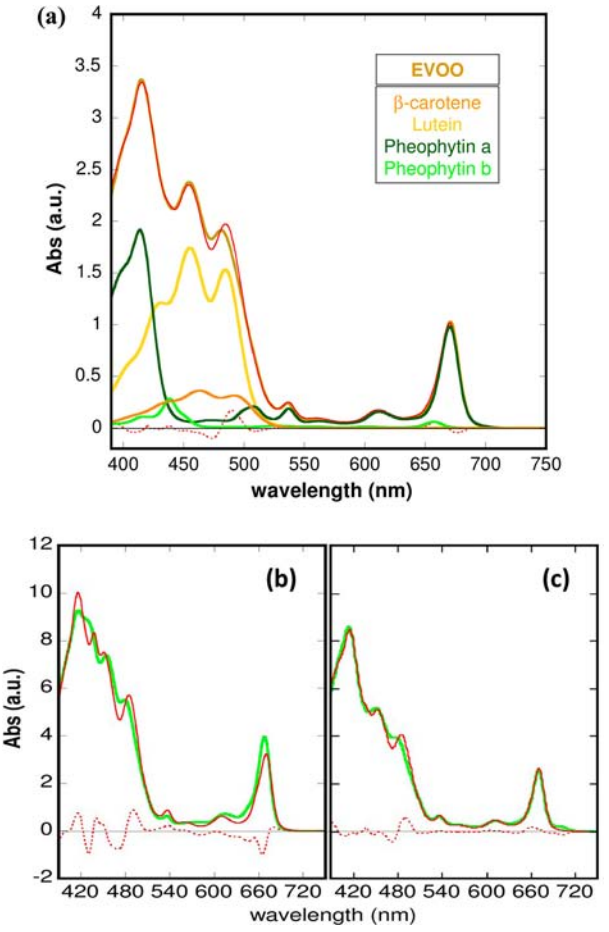


**Figure 6.** (a) Typical UV−vis absorption spectrum of a Tuscan EVOO produced from "Frantoio" olive cultivar. The concentration of the four pigments obtained from spectrum analysis is also reported (see Table 3). (b) UV−vis absorption of a young Tuscan EVOO (experimental and fitted spectra, with relative residues), (c) the same EVOO after three years at ∼3 °C in the darkness. See data about calculated concentration of pigments in Table 3.

calculated absorbance. In Table 3 the correspondent concentration of the pigments, calculated by means of eqs 3 and 4, is reported.

The spectrum in Figure 6A is typical of many Italian EVOOs. In the example (a one-year old monovarietal oil from fruits of "Frantoio" cultivar), the disagreement between calculated and experimental spectra is appreciable in a single spectral zone, i.e., in the 465−495 nm range (on the average 5.3%), where the calculated absorption is much more resolved than the experimental one. This disagreement regards part of the carotenoid spectral region, for which only lutein and $\beta$-carotene spectra define the spectroscopic functional space, as previously discussed. In Figure 6A, the contribution of these two pigments to the spectrum of "Frantoio" EVOO is also reported: the maxima of both pigments, at 484 and 491 nm, respectively, in the disagreement zone, are red-shifted with respect to the actual maximum (481 nm) of the oil. Thus, there is no possibility to obtain a maximum at 481 nm by combining the extinctions of lutein and $\beta$-carotene with positive coefficients. On the other hand, they are the only pigments, among the four mathematically present, appreciably absorbing light in the 480 nm region.

In a recent work on Italian EVOOs from different cultivars,[26] it has been shown that, on the average, lutein is present in these oils as 39% by weight of the sum of the weights of the other 12 xanthophylls HPLC-determined. In "Frantoio" oils lutein represents the 61%, i.e., the maximum content in the oils there investigated. Thus, minor carotenoids, such as neoxanthin, violaxanthin, luteoxanthin, antheraxanthin, mutatoxanthin etc., are present in concentrations well over the values reported for many Spanish EVOOs[17,34] in which the above minor xanthophylls are present in neatly lower percentage, and lutein is present from 61 up to 93.1% of total xanthophylls. The above data suggest that the contribute of minor xanthophylls to oil absorbance in the Italian EVOOs of Figures 3 and 6(a) is higher than in the Spanish EVOOs of Figure 5. As a consequence, the functional space of lutein and carotene spectra cannot represent the spectral contributions of some of these "minor" pigments. This is reflected by some inaccuracy in

**Table 3. Molar Concentration (mol/L) of the Four Pigments of the Four Andalusian EVOOs (Figure 5), of a Typical Tuscan "Frantoio" EVOO (Figure 6a), a Young Tuscan EVOO (2008 Harvest; Spectra Recorded in 2009) (Figure 6b) and the Aged Corresponding Tuscan EVOO (the Same Sample, but Spectra Recorded in 2013) (Figure 6c)**

| EVOO samples | Coprovir | Poniente de Granada | Fuentes de Dios | Loja | Typical Tuscan "Frantoio" | Young Tuscan | Aged Tuscan |
|---|---|---|---|---|---|---|---|
| pheophytin-a | $8.74 \times 10^{-06}$ | $5.00 \times 10^{-06}$ | $4.96 \times 10^{-06}$ | $5.13 \times 10^{-06}$ | $1.65 \times 10^{-05}$ | $5.20 \times 10^{-05}$ | $4.23 \times 10^{-05}$ |
| pheophytin-b | $9.43 \times 10^{-07}$ | $6.65 \times 10^{-07}$ | $4.42 \times 10^{-07}$ | $7.34 \times 10^{-07}$ | $1.58 \times 10^{-06}$ | $2.00 \times 10^{-05}$ | $6.10 \times 10^{-06}$ |
| lutein | $8.46 \times 10^{-06}$ | $7.16 \times 10^{-06}$ | $6.65 \times 10^{-06}$ | $1.00 \times 10^{-05}$ | $1.31 \times 10^{-05}$ | $4.60 \times 10^{-05}$ | $3.05 \times 10^{-05}$ |
| $\beta$-carotene | $2.35 \times 10^{-06}$ | $2.56 \times 10^{-06}$ | $1.82 \times 10^{-06}$ | $2.83 \times 10^{-06}$ | $2.73 \times 10^{-06}$ | $3.01 \times 10^{-07}$ | $6.95 \times 10^{-07}$ |


dx.doi.org/10.1021/jf503818k | J. Agric. Food Chem. 2014, 62, 9317−9325

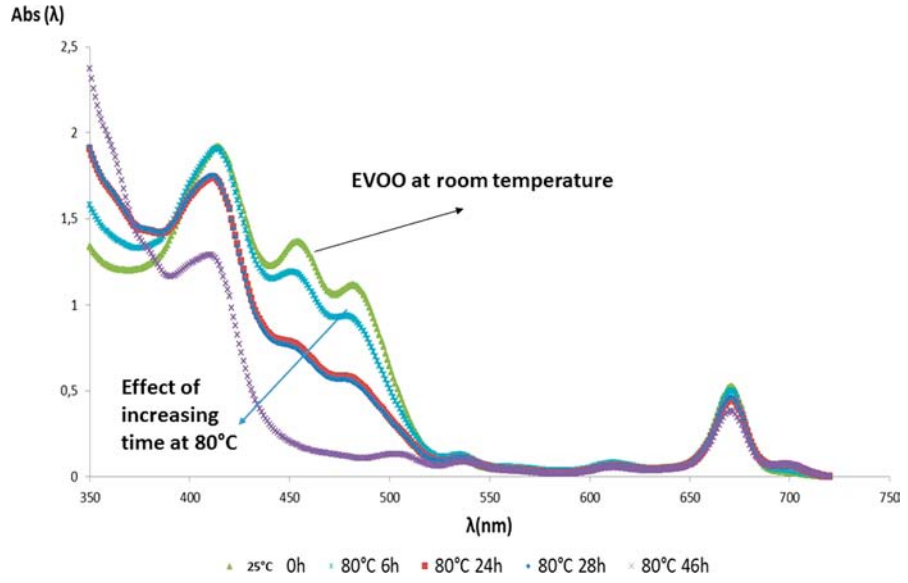


**Figure 7.** Series of UV−vis spectra of an EVOO sample at room temperature (green curve) and after several hours at 80 °C (see labels).

the calculated vs measured absorption spectra just in the 480 nm band.

Another interesting example is reported in Figure 6(a): in this case, the method fails in reproducing the intense experimental absorption spectrum of a young (less than two months) EVOO from southern Tuscany. In fact, there are two spectral intervals, centered at 430 and 665 nm, where the calculated absorption is about 1 absorbance unit lower than the measured one, in exact correspondence with the absorption peaks of chlorophyll-a in extra-virgin oils, as determined by addition of chlorophyll-a to triolein and to an EVOO. The same oil of Figure 6(b), after aging almost three years at ca. 4 °C in dark conditions and complete spontaneous pheophytinization, showed a changed absorption spectrum as shown in Figure 6(c), where the usual trend of calculated vs measured spectrum is observed. In Table 3, the calculated pigment concentrations are reported. In order to fit the spectrum of this particular oil before pheophytinization, it would be necessary to add in our treatment other pigments, i.e., chlorophylls. Since chlorophylls are present usually only in freshly extracted oils,[21,26] the number of pigments was limited to the four previously described. It is clear that the functional spectral space of chlorophylls pigments is complete only for oils in which pheophytinization processes are finished and pyropheophytinization processes are marginal.

In addition to the successful reproduction of the absorption spectra of nonfreshly extracted EVOOs, the method has been tested by measuring the spectra of some EVOO samples obtained by mixing, in defined proportions, two EVOOs with different spectra and pigments composition. The resulting composition in pigments reproduced the proportion of the constituent oils and their pigment compositions with an average error of 1.1 ± 0.6%.

**Use of the Method to Check Eventual Thermal Treatments.** An experiment was done in order to reproduce a case of bad storage. A sample of olive oil was forced to a controlled thermal degradation, to induce pigments degradation. Chlorophyll content generally reduces up to 80% during the oil extraction process, using only mechanical and physical processes for extraction. These processes result in a considerably reduced chlorophyll level in the oil compared to the olive fruit itself. Pyropheophytins are also produced by subsequent degradations of chlorophyll pigments, and the presence of pyropheophytins is an indication of probable heating or aging effects. In fact, chlorophyll converts to pheophytin and ultimately to pyropheophytins. The proportion of pyropheophytin-a to the total pheophytins is useful in discriminating fresh oil from oil which has been in long-term storage or which has been heated in the refining process.[35−37] Freshly extracted virgin olive oils do not contain pyropheophytins. However, they are generated during storage in different amounts depending on the conditions of exposition of oil. This reaction is boosted by heat treatments during refining processes, especially during deodorizing. This leads to the possibility of using these degradation products of chlorophyll as a marker for quality and traceability of virgin olive oils. For instance, in this way, it can be determined if an olive oil, labeled as virgin, was properly stored or, in contrast, if the virgin olive oil was cut with refined oils. For all investigations, it is essential to consider the exact harvesting date. Generally, the typical analysis according to ISO 29841:2009 is a chromatographic analysis. In this paragraph, we would like just to put the attention on the large spectral changes affecting the UV−vis spectra of EVOOs, when the temperature of storage increases. In Figure 7, a case of thermal degradation at 80 °C, after a different heating time, is shown. The curves obtained after heating at $T$ = 80 °C and after 6, 24, 28, and 46 h show a gradual change. It is possible to see that after few hours from the warming the oil spectrum changes in its shape and relative intensity. After more than 24 h, the changes are drastic. This method could indeed reveal the presence of oil undergone to a refined treatment or simply subjected to a bad storage condition for example during its transport, and further extentions of our method to include other pigments or to study different cases of thermal or illumination effects are expected to provide a useful, fast, and simple tool to check the quality of olive oils.

In this work, a mathematical treatment of UV−vis absorption spectra of olive oil is developed to extract quantitative information about four among the most important pigments in extra-virgin olive oils, namely, $\beta$-carotene, lutein, pheophytin-a, and pheophytin-b. To explain the reliability and applicability


dx.doi.org/10.1021/jf503818k | J. Agric. Food Chem. 2014, 62, 9317−9325

of this fast and not destructive method, several examples, underlining positive aspects and limits, have been reported.

The original aim of this research was to extract from the absorption spectrum (390−720 nm) of extra virgin olive oils the most complete information about the concentration of the *pigments* of interest. Our experiments show that reliable data on the concentration of the *chromophores* corresponding to these pigments can be extracted. For this reason, a direct comparison with data found by other techniques, such as HPLC, is not appropriate, as shown through an example in the Supporting Information. For instance, because of the typical presence in many EVOOs of fat acids-esterified lutein,[21] the concentration of lutein found by this spectral analysis is slightly higher than that determined by HPLC, since the absorption spectra of this xanthophyll and that of its known esterified-forms coincide within experimental errors. In parallel, the obtained UV-concentration of pheophytin-a represents the sum of the concentrations of pheophytin-a and its epimers, since the molar extinction spectra of these coincide almost exactly with the pheophytin-a one. This is also shown in the Supporting Information. The intrinsic differences between the HPLC method and that proposed in this work confirm that a direct comparison between them is not appropriate. However, as shown by the examples reported in this work, the data obtained from the analysis of UV−vis spectra, analytically oriented to the chromophores, preserve analytical interest for systems where the four pigments, chosen as mathematical spectral references, are dominant, as seems to be the case for most of the EVOOs analyzed so far.

Moreover, among the possible applications of this fast method, its successful applicability to put in evidence eventual thermal degradation or not-appropriate storage conditions of EVOOs is discussed. Despite its not strictly quantitative use, this method appears very useful for a fast screening of EVOOs.

## ■ ASSOCIATED CONTENT

### Supporting Information

Values of overlapped matrix for the four pigments used to perform the mathematical treatment. A detailed description of the validation of the method. A detailed comment about the comparison between data calculated from the method proposed and from HPLC analysis, with an example of HPLC determination of pigments quantity for an EVOO sample. This material is available free of charge via the Internet at http://pubs.acs.org.

## ■ AUTHOR INFORMATION

### Corresponding Authors

*(V.D.) E-mail: valentina.domenici@unipi.it.

*(M.Z.) E-mail: maurizio.zandomeneghi@gmail.com.

### Notes

The authors declare no competing financial interest.

## ■ REFERENCES

(1) Torrecilla, J. S.; Rojo, E.; Dominguez, J. C.; Rodriguez, F. A novel method to quantify the adulteration of extra virgin olive oil with low-grade olive oils by UV-Vis. *J. Agric. Food Chem.* **2010**, *58*, 1679−1684.

(2) Casale, M.; Oliveri, P.; Casolino, C.; Sinelli, N.; Zunin, P.; Armanino, C.; Forina, M.; Lanteri, S. Characterisation of PDO olive oil Chianti Classico by non-selective (UV−visible, NIR and MIR spectroscopy) and selective (fatty acid composition) analytical techniques. *Anal. Chim. Acta* **2012**, *712*, 56−63.

(3) Bengana, M.; Bakhouche, A.; Lozano-Sanchez, J.; Amir, Y.; Youyou, A.; Segura-Carretero, A.; Fernandez-Gutierrez, A. Influence of olive ripeness on chemical properties and phenolic composition of Chemlal extra-virgin olive oil. *Food Res. Int.* **2013**, *54*, 1868−1875.

(4) Ranalli, F.; Ranalli, A.; Contento, S.; Casanovas, M.; Antonucci, M.; Di Simone, G. Bioactives and nutraceutical phytochemicals naturally occurring in virgin olive oil. The case study of the Nocellara del Belice Italian olive cultivar. *Nat. Prod. Res.* **2013**, *27*, 1686−1690.

(5) El Riachy, M.; Priego-Capote, F.; Leon, L.; Rallo, L.; de Castro, M. D. L. Hydrophilic antioxidants of virgin olive oil. Part 1: Hydrophilic phenols: A key factor for virgin olive oil quality. *Eur. J. Lipid Sci. Technol.* **2011**, *113*, 678−691.

(6) Bakhouche, A.; Lozano-Sanchez, J.; Beltran-Debon, R.; Joven, J.; Segura-Carretero, A.; Fernandez-Gutierrez, A. Phenolic characterization and geographical classification of commercial Arbequina extra-virgin olive oils produced in southern Catalonia. *Food Res. Int.* **2013**, *50*, 401−408.

(7) Gandul-Rojas, B.; Minguez-Mosquera, M. I. Chlorophyll and Carotenoid Composition in Virgin Olive Oils from Various Spanish Olive Varieties. *J. Sci. Food Agric.* **1996**, *72*, 31−39.

(8) Pizarro, C.; Rodriguez-Tecedor, S.; Perez-del-Notario, N.; Esteban-Diez, I.; Gonzalez-Saiz, J. M. Classification of Spanish extra virgin olive oils by data fusion of visible spectroscopic fingerprints and chemical descriptors. *Food Chem.* **2013**, *138*, 915−922.

(9) Fuentes, E.; Báez, M. E.; Bravo, M.; Cid, C.; Labra, F. Determination of Total Phenolic Content in Olive Oil Samples by UV−visible Spectrometry and Multivariate Calibration. *Food Anal. Methods* **2012**, *5*, 1311−1319.

(10) Torrecilla, J. S.; Rojo, E.; Domínguez, J. C.; Rodríguez, F. Linear and non linear chemometric models to quantify the adulteration of extra virgin olive oil. *Talanta* **2010**, *83*, 404−409.

(11) Bendini, A.; Cerretani, L.; Vecchi, S.; Carrasco-Pancorbo, A.; Lercker, G. Protective effects of extra virgin olive oil phenolics on oxidative stability in the presence or absence of copper ions. *J. Agric. Food Chem.* **2006**, *54*, 4880−7.

(12) Rahmani, M.; Saari-Csallany, A. Chlorophyll and $\beta$-carotene pigments in moroccan virgin olive oils measured by high-performance liquid chromatography. *J. Am. Oil Chem. Soc.* **1991**, *68*, 672−674.

(13) Rahmani, M.; Saari Csallany, A. Role of Minor Constituents in the Photooxidation of Virgin Olive Oil. *J. Am. Oil Chem. Soc.* **1998**, *75*, 837−843.

(14) Feltl, L.; Pacáková, V.; Stulík, K.; Volk, K. Reliability of Carotenoid Analyses: A Review. *Curr. Anal. Chem.* **2005**, *1*, 93−102.

(15) Minguez-Mosquera, M. I.; Gandul-Rojas, B.; Gallardo-Guerrero, M. L. Rapid Method of Quantification of Chlorophylls and Carotenoids in Virgin Olive Oil by High-Performance Liquid Chromatography. *J. Agric. Food Chem.* **1992**, *40*, 60−63.

(16) Pineau, B.; Gérard-Hirne, C.; Douce, R.; Joyard, J. Identification of the Main Species of Tetrapyrrolic Pigments in Envelope Membranes from Spinach Chloroplasts. *Plant Physiol.* **1993**, *102*, 821−828.

(17) Mínguez-Mosquera, M.; Gandul-Rojas, B.; Garrido-Fernández, J. Pigments Present in Virgin Olive Oil. *J. Am. Oil Chem. Soc.* **1990**, *67*, 192−196.

(18) Dupuy, N.; Le Dreau, Y.; Ollivier, D.; Artaud, J.; Pinatel, C.; Kister, J. Origin of French Virgin Olive Oil Registered Designation of Origins Predicted by Chemometric Analysis of Synchronous Excitation-Emission Fluorescence Spectra. *J. Agric. Food Chem.* **2005**, *53*, 9361−9368.

(19) Ayuso, J.; Haro, M. R.; Escolar, D. Simulation of the Visible Spectra for Edible Virgin Olive Oils: Potential Uses. *Appl. Spectrosc.* **2004**, *58*, 474−480.

(20) Psomiadou, E.; Tsimidou, M. Simultaneous HPLC Determination of Tocopherols, Carotenoids, and Chlorophylls for Monitoring Their Effect on Virgin Olive Oil Oxidation. *J. Agric. Food Chem.* **1998**, *46*, 5132−5138.

(21) Giuffrida, D.; Salvo, F.; Salvo, A.; La Pera, L.; Dugo, G. Pigments composition in monovarietal virgin olive oils from various sicilian olive varieties. *Food Chem.* **2007**, *101*, 833−837.

(22) Criado, M. N.; Morellò, J. R.; Motilva, M. J.; Romero, M. P. Effect of Growing Area on Pigment and Phenolic Fractions of Virgin Olive Oils in the Arbequina Variety in Spain. *J. Am. Oil Chem. Soc.* **2004**, *81*, 633.
(23) Criado, M. N.; Romero, M. P.; Casanovas, M.; Motilva, M. J. Pigment profile and colour of monovarietal virgin olive oils from Arbequina cultivar obtained during two consecutive crop seasons. *Food Chem.* **2008**, *110*, 873−880.
(24) Lebo, J. A.; Almeida, F. V.; Cranor, W. L.; Petty, J. D.; Huckins, J. N.; Rastall, A.; Alvarez, D. A.; Mogensen, B. B.; Johnson, B. T. Purification of triolein for use in semipermeable membrane devices. *Chemosphere* **2004**, *54*, 1217−1224.
(25) Tsao, R.; Yang, R. Lutein in selected Canadian crops and agri-food processing by-products and purification by high-speed counter-current chromatography. *J. Chromatogr., A* **2006**, *1112*, 202−208.
(26) Cortes, C.; Esteve, M. J.; Frigola, A.; Torregrosa, F. Identification and quantification of carotenoids including geometrical isomers in fruit and vegetable juices by liquid chromatography with ultraviolet-diode array detection. *J. Agric. Food Chem.* **2004**, *52*, 2203−2212.
(27) Hasni, Z.; Yaacob, J. S.; Yusoff, A. I. M.; Taha, R. M.; Yahya, R.; Ahmed, A. B. A.; Ramesh, K. Effect of different solvents extraction on recovery of pigments in Xylocarpus granatum, endangered medicinal plant. *Mater. Res. Innov.* **2011**, *15*, 141−143.
(28) Maia, L.; Casal, S.; Oliveira, M. B. P. P. Validation of a micromethod for quantification of lutein and beta-carotene in olive oil. *J. Liq. Chromat. Rel. Technol.* **2008**, *31*, 733−742.
(29) Seppanen, C. M.; Rahmani, M.; Csallany, A. S. Simultaneous determination of chlorophylls, pheophytins, beta-carotene, tocopherols, and tocotienols in olive and soybean oils by high-performance liquid chromatography. *J. Food Sci.* **2003**, *68*, 1644−1647.
(30) Hennessey, J. P.; Curtis Johnson, W. Information Content in the Circular Dichroism of Proteins. *Biochemistry* **1981**, *20*, 1085−1094.
(31) Ancora, D. Master Thesis in Chemistry, University of Pisa, 2014.
(32) Watanabe, T.; Hongu, A.; Honda, K.; Nakazato, M.; Konno, M.; Saitoh, S. Preparation of chlorophylls and pheophytins by isocratic liquid chromatography. *Anal. Chem.* **1984**, *56*, 251−256.
(33) Giuffrida, D.; Salvo, F.; Salvo, A.; Cossignani, L.; Dugo, G. Pigments profile in monovarietal virgin olive oils from various Italian olive varieties. *Food Chem.* **2011**, *124*, 1119−1123.
(34) Guerrero, L. G.; Gandul-Rojas, B.; Roca, M.; Minguez-Mosquera, I. Effect of Storage on the Original Pigment Profile of Spanish Virgin Olive Oil. *J. Am. Oil Chem. Soc.* **2005**, *82*, 33−39.
(35) Boskou, D.; Blekas, G.; Tsimidou, M. Phenolic compounds in olive oil and olives. *Curr. Top. Nutraceutical Res.* **2005**, *3*, 125−136.
(36) Boskou, G.; Salta, F. N.; Chrysostomou, S.; Chiou, A.; Andikopoulos, K. Antioxidant capacity and phenolic profile of table olives from the Greek market. *Food Chem.* **2006**, *94*, 558−564.
(37) Dag, A.; Kerem, Z.; Yogev, N.; Zipori, I.; Lavee, C.; Ben-Davida, E. Influence of time of harvest and maturity index on olive oil yield and quality. *Sci. Hortic.* **2011**, *170*, 358−366.

accumulation make it difficult to study rheology in fermenting dough, our approach here focused on the direct addition of ethanol to the dough recipe to assess its potential impact on dough behavior. To study the ethanol-induced changes in dough mixing behavior and rheology, Mixograph, Farinograph, dough spread test, Kieffer rig, and Alveograph dough extensibility tests were used. Ethanol solvent retention capacity and gluten agglomeration experiments with chromatographic analyses of the gluten fractions were performed to gain further insight in the molecular mechanism at the basis of the observed changes in dough properties. They allowed assessment of the impact of ethanol on gluten properties as main determinant of dough rheology. Together, the results of these tests indicate that the ethanol is indeed a yeast metabolite that strongly influences the rheology of fermenting dough.

## MATERIALS AND METHODS

**Materials.** A low protein content flour (flour A, commercial biscuit flour) from Ceres Soufflet (Brussels, Belgium) and a medium protein content flour (Kolibri, flour B, bread making flour) from Meneba (Rotterdam, The Netherlands), both free of additives, were used for dough making. For flour A, two batches were used due to exhaustion of the first batch. Commercial wheat gluten [moisture content, 5.62%; crude protein content (N × 5.7), 83.2% on dry matter basis (dm)] was from Tereos Syral (Aalst, Belgium). All chemicals, solvents, and reagents used in the experiments were of analytical grade and from Sigma-Aldrich unless specified otherwise. Water used in the experiments was deionized unless specified otherwise.

**Flour Characterization.** Flour moisture and protein content were measured in triplicate according to AACC International Approved Methods 44-19.01[18] and a Dumas combustion method,[19] adapted for an automated Dumas protein analysis system (EAS, VarioMax N/CN, Elt, Gouda, The Netherlands), respectively. The moisture contents of flour A (batch 1), A (batch 2), and B were 13.1, 13.9, and 14.3% respectively. The protein contents (N × 5.7) of flour A (batch 1), A (batch 2), and B were 10.5, 8.9, and 11.5% on dm basis, respectively. Flour A (batch 1) was used for all experiments except for gluten agglomeration and sequential extraction analyses, where flour A (batch 2) was used. Optimal mixing time and water absorption were determined with a Mixograph (National Manufacturing, Lincoln, NE, USA) and a Farinograph (Brabender, Duisburg, Germany) based on AACC International Approved Methods 54-40.02 and 54-21.01, respectively.[18]

**Farinograph Analyses.** Farinograph analysis was performed on a Farinograph E with a 10 g mixing bowl (Brabender, Duisburg, Germany) at a constant temperature of 30 °C. The farinogram, representing the evolution of dough consistency as a function of mixing time, was obtained according to AACC International Approved Methods 54-21.01.[18] Flour (10.0 g, 14.0% moisture basis) was mixed for 20 min with the amount of deionized water (% v/w) that leads to a maximal average consistency of 500 Brabender units (BU), i.e., the Farinograph water absorption. It was 5.3 and 5.6 mL for flours A and B, respectively. To study the effect of ethanol on dough formation in the Farinograph, the water in the procedure was substituted with aqueous ethanol solutions of the correct molarity to reach ethanol concentrations of 0, 20, 40, 60, and 80 mmol per 100 g of flour in the dough.

**Mixograph Analyses.** Mixograph (National Manufacturing, Lincoln, NE, USA) analyses were performed on a 10 g scale according to the procedure of Finney and Shogren.[20] Flour (10.0 g, 14.0% moisture basis) was mixed with the optimum amount of water for 8 min at 25 °C in a Mixograph bowl. To study the effect of ethanol on dough formation in the Mixograph, the water in the procedure was substituted with aqueous ethanol solutions of the correct molarity to reach ethanol concentrations of 0, 20, 40, 60, and 80 mmol per 100 g of flour in the dough recipe. The resulting mixograms were analyzed to obtain three parameters. Dough development time (DDT, min) is the time at which the developing dough reaches its maximum consistency. Dough strength (DS, cm) is defined as the maximum height of the curve center, i.e., at the dough development time. The mixing tolerance index (MTI, %) is defined as the ratio of the difference between peak dough resistance and dough resistance at 3 min after the peak to peak dough resistance. The experiments were performed in duplicate.

**Dough Spread Test.** Dough spread behavior was studied by adapting the method described by Hoseney et al.[2] Dough was prepared with a 10 g scale pin bowl mixer (National Manufacturing). Flour (10.0 g, 14.0% moisture basis) was mixed with the optimum amount of water for 210 and 230 s for flours A and B, respectively. To test the effect of ethanol on dough properties, the water in the procedure was substituted with aqueous ethanol solutions of the correct molarity to reach ethanol concentrations of 0, 20, 40, 60, and 80 mmol per 100 g of flour. Mixed dough was transferred to a lightly greased bowl and was rested for 0, 60, 120, or 180 min in the fermentation cabinet with 90% relative humidity at 30 °C. Then the spread measurement was performed. Height ($H$) and orthogonal widths ($W_1$ and $W_2$) were measured immediately after rounding and after a time span of 60 min in which flow could take place. The $W/H$ and $\Delta(W/H)$ (measure for dough spread during proofing) were calculated according to the following formula, described previously by Decamps et al.:[21]

$$\Delta(W/H) = \text{average}(W/H)_{X+60\text{min}} - \text{average}(W/H)_{X\text{min}},$$

with $X$ representing the resting time before rounding the dough. All spread tests were performed in duplicate.

**Kieffer Rig Uniaxial Dough Extensibility Test.** For uniaxial dough extensibility measurements, dough was prepared in a 10 g scale pin bowl mixer and extension tests were performed using the Kieffer rig dough extensibility fixture (Stable Micro Systems Ltd., Surrey, U.K.) mounted on an Instron 3342 single column testing system (Norwood, MA, USA) with a 50 N load cell as described previously by Jayaram et al.[21] To study the effect of ethanol on dough properties, a part of the water was replaced with an aqueous ethanol solution of correct molarity resulting in dough containing 0, 20, 40, 60, and 80 mmol of ethanol per 100 g of flour. For each concentration of ethanol, three different doughs were made. From each dough, 6 to 8 dough strands were used for analysis. For the results, the average of the values obtained for the three separate doughs was considered and the respective standard deviation calculated. The parameters derived from the resulting load−displacement curve are maximum extensibility (mm), maximum force for extension (N), and the total force needed for breakage (mJ), i.e., the area under the load−displacement curve.[22,23]

**Alveograph Biaxial Dough Extensibility Analysis.** Alveograph parameters were determined according to AACC International Approved Methods 54-30.02[18] using a Chopin Alveograph (Chopin, Villeneuve-La-Garenne, France). Both flour samples used were mixed with the optimum amount of water for 6 min in the built-in mixer of the Alveograph. To study the effect of ethanol on dough properties, the water in the procedure was substituted with aqueous ethanol solutions of the correct molarity to reach ethanol concentrations of 0, 20, 40, 60, and 80 mmol per 100 g of flour in the dough recipe. Each Alveograph curve was analyzed for four factors: $P$, the maximum pressure needed to blow the dough bubble, represents dough elasticity ($mmH_2O$); $L$, the average abscissa at the bubble rupture, is a measure of dough extensibility (mm); $W$, the energy needed to make the bubble up to the point of rupture, expresses deformation energy ($10^{-4}$ J), and $P/L$ is the Alveograph ratio. The test was performed in duplicate, and five dough pieces were formed and measured for each replicate.

**Solvent Retention Capacity Test.** Flours A and B, commercially available gluten, gliadin enriched fractions, and glutenin enriched fractions were used to study the swelling behavior of protein in ethanol−water mixtures. A gliadin and a glutenin enriched fraction were prepared from this commercial wheat gluten. Gluten (20.0 g) was first extracted with 250 mL of 70% ethanol. Hereto, the gluten−ethanol suspension was homogenized and subsequently shaken for 1 h at 150 rpm. After centrifugation (10 min; 10000$g$), the supernatant

was separated from the residue. The ethanol was removed by evaporation at 30 °C under reduced pressure. After removal of the ethanol the samples were freeze-dried to remove the water. This fraction will be referred to as the gliadin enriched fraction. The residue remaining after the first extraction was extracted another two times with 60% ethanol to remove all remaining gliadins, and the supernatants were discarded. The insoluble residue after the third extraction was extensively washed with deionized water to remove starch. Hereto, the insoluble residue was kneaded under a flow of deionized water at room temperature. The sample was freeze-dried after washing. This fraction will be referred to as the glutenin enriched fraction. After freeze-drying, both fractions were ground with a laboratory mill (IKA, Staufen, Germany) and sieved (250 $\mu$m). The moisture content of these samples was determined before performing the SRC test.

The solvent retention capacity (SRC) tests of flour with aqueous solutions with different ethanol concentration (0, 5, and 10%), based on the concentration of ethanol in fermenting dough, was conducted according to AACC International Approved Methods 56-11.02[18] with some minor modifications. Flour samples (5.000 g) were weighed in 50 mL centrifuge tubes (height, 115 mm; internal diameter, 27 mm) with a conical bottom. Commercial gluten and gliadin and glutenin enriched fractions (1.000 g) were weighed in 10 mL centrifuge tubes. Then, 25.0 mL of water or respective water/ethanol solution for flour samples or 5.0 mL of water/ethanol solution for gluten and gliadin and glutenin enriched fractions was added, and the mixtures were shaken vigorously for 5 s to suspend the material. Thereafter, the samples were horizontally shaken for 20 min at room temperature at 150 strokes per minute (spm) to allow the samples to solvate and swell. Samples were centrifuged (15 min, 1000*g*, room temperature). Supernatant was decanted from the tubes, and the pellet was drained for 15 min and weighed. The SRC values were calculated as follows:[24]

$$\mathrm{SRC}\ (\%) = \left[\frac{\text{wet pellets (g)}}{\text{flour (g)}} - 1\right] \times \left[\frac{86}{100 - \text{flour moisture (\%)}}\right] \times 100$$

All SRC analyses were performed in triplicate.

**Gluten Agglomeration Analysis.** Gluten agglomeration was analyzed using a dough batter gluten starch separation procedure as described by Frederix et al.[25] Wheat flour (250.0 g, 14% moisture basis) was mixed with water (based on Farinograph water absorption) in a KitchenAid mixer (K5SS/KPM5, St. Joseph, MI, USA) equipped with a dough hook for 4 min. For ethanol containing dough, water was replaced with aqueous ethanol solution in the dough recipe resulting in dough containing 0 (control), 9, 17, 44, and 87 mmol of ethanol per 100 g of flour. The dough was then allowed to rest for 8 min. Additional tap water (250 mL) was added to the dough, and the resulting suspension was stirred using a flat beater for 25 min. After extra tap water (1000 mL) was added, the suspension was stirred for an additional 35 min. The suspension was poured over a set of vibrating sieves with decreasing pore size (400, 250, and 125 $\mu$m). The gluten retained on the different sieves was washed by pouring water (1000 mL) over the vibrating sieves. Gluten fractions were recovered from the three sieves, lyophilized, and ground to pass a 250 $\mu$m sieve. Protein content of the lyophilized gluten fractions was determined with the Dumas combustion method (AOAC, 1995, VarioMax N/CN).

The parameters derived from these experiments are gluten yield ($GY_x$), i.e., total mass (g dm) retained on the sieve with a pore diameter of $x$ $\mu$m per 100 g dm flour, total gluten yield ($GY_{tot}$), i.e., total mass (g) dm retained on the three consecutive sieves per 100 g dm flour, gluten protein recovery ($GPR_x$), i.e., the total amount of protein agglomerated on the sieve with a pore diameter of $x$ $\mu$m (g dm) per 100 g dm flour proteins, total gluten protein recovery ($GPR_{tot}$), i.e., the total amount dm protein agglomerated on the three consecutive sieves per 100 g of dm flour proteins, and gluten protein agglomeration index (GPAI), i.e., the percentage of proteins recovered on the 400 $\mu$m sieve compared to the protein recovery on the three consecutive sieves. These experiments were performed in triplicate.

**Protein Fractionation and Compositional Analysis.** Albumin−globulin and gliadin and glutenin fractions were obtained by an Osborne type sequential protein fractionation.[26] Samples containing 100.0 mg dm protein were extracted (10 min, 150 spm, room temperature) twice with 6 mL of 0.05 M disodium hydrogen phosphate−sodium dihydrogen phosphate (pH 7.6) containing 0.4 M sodium chloride (for the albumin and globulin fraction) and three times (10 min, 150 spm, room temperature) with 3.0 mL of 60.0% (v/v) ethanol (for the gliadin fraction). After each extraction, suspensions were centrifuged (10 min, 10000*g*, 20 °C) (J2-21, Beckman Coulter, Pasadena, CA, USA). The residual nonextracted protein fraction was considered to be the glutenin fraction. The protein levels of the three fractions were determined and expressed on a flour protein basis. Each sample was analyzed at least in duplicate. After filtration (Millex-HP 0.45 $\mu$m, poly(ether sulfone), Millipore, Carrigtwohill, Ireland), the gliadin and glutenin extracts were loaded (80 $\mu$L) on a Nucleosil 300-5 C8 column (Macherey-Nagel, Düren, Germany) and separated by reverse phase high-performance liquid chromatography (RP-HPLC) with a LC-2010HT system (Shimadzu, Kyoto, Japan). Elution was carried out with water containing 0.1% (v/v) trifluoroacetic acid (A) and acetonitrile containing 0.1% trifluoroacetic acid (v/v) (B) with a flow rate of 1 mL/min. Proteins were eluted with a linear gradient from 24% B to 56% B in 50 min and detected at 214 nm. $\alpha$-Gliadin, $\gamma$-gliadin, and $\omega$-gliadin were distinguished based on absorbance minima between specific peaks as outlined by Wieser.[27]

**Size Exclusion Chromatography.** Flour A samples containing 1.0 mg of protein were extracted using 1 mL of disodium hydrogen phosphate−sodium dihydrogen phosphate buffer (0.05 M; pH 6.8) containing 2% sodium dodecyl sulfate (SDS) for 1 h at room temperature. Samples were then centrifuged (10 min, 10000*g*, 20 °C) and filtered (Millex-HP 0.45 $\mu$m) before they were analyzed by size exclusion high-performance liquid chromatography (SE-HPLC) on a LC-2010 system (Shimadzu, Kyoto, Japan) with automatic injection. The column used was a Biosep-SEC S4000 (Phenomenex, Torrance, CA, USA). The used eluent was acetonitrile/water (1:1, v/v) containing 0.05% (v/v) trifluoroacetic acid. The flow rate was 1.0 mL/min at a temperature of 30 °C. The eluted proteins were detected at 214 nm.

**Sequential Ethanol Extraction of Flour.** 100.0 mg protein equivalent of flour A sample was sequentially extracted (10 min, 150 spm, room temperature) with 3.0 mL each of an aqueous 2%, 5%, 10%, 30%, and 60% (v/v) ethanol solution three times individually. After each extraction, suspensions were centrifuged (10 min, 10000*g*, 20 °C) (J2-21, Beckman Coulter, Pasadena, CA, USA). The residual nonextracted protein fraction was considered to be the glutenin fraction. Each sample was analyzed at least in duplicate. After filtration (Millex-HP 0.45 $\mu$m), the gliadin was loaded (80 $\mu$L) on a Nucleosil 300-5 C8 column and separated by RP-HPLC as explained above (Protein Fractionation and Compositional Analysis).

**Statistical Analysis.** Statistical analysis of the results was performed using SAS software 9.2 (SAS Institute, Inc., Cary, NC). For Mixograph, uniaxial and biaxial dough extensibility tests, and gluten agglomeration test, a one-way analysis of variation (ANOVA) was performed separately for each flour to study the effect of ethanol concentration. For dough spread test, a two-way ANOVA was performed to study the effect of resting time and ethanol concentration on each flour separately. A Tukey multiple comparison procedure was used with a 5% family significance level.

## RESULTS

**Effect of Ethanol on Dough Mixing Properties.** For the Farinograph and Mixograph dough mixing analyses, ethanol concentrations in the recipe (0, 20, 40, 60, and 80 mmol of ethanol per 100 g of flour) were chosen to be in the same range as the ethanol concentrations that accumulated during a 3 h dough fermentation, i.e., up to 60 mmol of ethanol per 100 g of flour.[11] Flour A is a biscuit grade flour, which means the flour

has a low protein content. Flour B is a bread making grade flour, which coincides with a higher protein level and better gluten quality. Mixogram data of flours A and B (Table 1) in the absence of ethanol showed slightly higher dough development time for flour B than flour A and similar dough stabilities, while a lower mixing tolerance index for flour B than flour A was observed. These results show that flour B was indeed a stronger flour than flour A, in accordance with the supplier's specifications.[28] With the addition of ethanol, there was no change in dough development time and dough strength for both flours A and B (Table 1). However, mixing tolerance index for flour A increased by 2.6-fold, and there were no significant changes in mixing tolerance index for flour B. The Farinograph water absorption, Farinograph dough development time, arrival time, and departure time were largely unaffected (results not shown).

**Table 1. Mixograph Parameters for Flours A and B with Ethanol in Concentrations of 0, 20, 40, 60, and 80 mmol per 100 g of Flour**[a]

| ethanol (mmol/100 g of flour) | DDT (min) | DS (cm) | MTI (%) |
|---|---|---|---|
| | Flour A | | |
| 0 | 2.8 ± 0.4 a | 4.4 ± 0.1 a | 9.1 ± 0.1 c |
| 20 | 2.7 ± 0.1 a | 4.4 ± 0.1 a | 8.0 ± 1.5 c |
| 40 | 2.9 ± 0.1 a | 4.3 ± 0.1 a | 17.6 ± 1.4 b |
| 60 | 2.9 ± 0.2 a | 4.2 ± 0.1 a | 23.8 ± 0.1 a |
| 80 | 3.0 ± 0.1 a | 4.1 ± 0.2 a | 21.9 ± 2.7 ab |
| | Flour B | | |
| 0 | 3.5 ± 0.1 a | 4.3 ± 0.1 a | 3.5 ± 1.6 a |
| 20 | 3.6 ± 0.1 a | 4.4 ± 0.1 a | 5.7 ± 1.4 a |
| 40 | 3.3 ± 0.2 a | 4.2 ± 0.1 a | 2.4 ± 0.1 a |
| 60 | 3.6 ± 0.1 a | 4.2 ± 0.1 a | 4.8 ± 0.1 a |
| 80 | 3.6 ± 0.1 a | 4.2 ± 0.1 a | 4.8 ± 0.1 a |

[a]DDT, dough development time; DS, dough strength; MTI, mixing tolerance index. Mean values ± standard deviation; for each flour type, values followed by the same letter in the same column are not significantly different ($p < 0.05$).

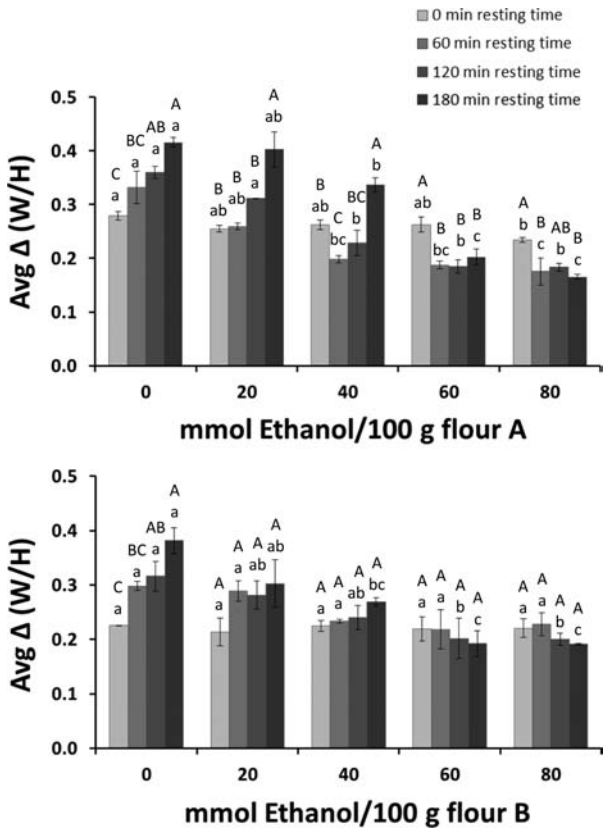


**Figure 1.** Effect of ethanol in concentrations of 0, 20, 40, 60, and 80 mmol per 100 g of flour on the dough spread behavior of flours A and B using the dough spread test. Average Δ [width ($W$)/height ($H$)] values (average $W/H_{X+60\text{min}}$ − average $W/H_{X\text{min}}$ with $X$ representing the resting time before rounding the dough) of spread of dough as a function of ethanol concentration for different resting times. The experiments were performed in duplicate. For each flour, bars with the same capital letter across the same ethanol concentration and bars with the same small letter across the same resting time are not significantly different from each other ($p < 0.05$).

**Effect of Ethanol on Dough Spread.** Dough spread tests allow easy and uncomplicated assessment of the flow behavior of dough. The procedure used in this study was adapted from that of Hoseney et al.[2] to simulate dough fermentation times. Figure 1 shows that the $\Delta(W/H)$ values of control dough gradually increased with resting time, going from 0.28 (0 min resting) to 0.42 (180 min resting) for flour A and from 0.22 (0 min) to 0.38 (180 min) for flour B. These results indicate that longer resting times prior to the actual spread measurement lead to a significant ($p < 0.05$) increase in dough spread. While at low ethanol concentrations a similar effect was observed, at higher ethanol concentrations the $\Delta(W/H)$ values decreased with resting time. For 80 mmol of ethanol per 100 g of flour, the $\Delta(W/H)$ value drops from 0.23 (0 min) to 0.16 (180 min) for flour A ($p < 0.05$) and from 0.22 to 0.18 for flour B. Dough hence shows less spread as a function of resting time with higher ethanol levels.

**Effect of Ethanol on Dough Extensibility.** To investigate the effect of ethanol on dough extension, both uniaxial Kieffer rig (Figure 2) and biaxial Alveograph dough extensibility tests (Figure 3) were performed. Ethanol was used in dough recipe by replacing the same volume of water. Flour A control dough showed more extensibility than flour B control dough in both the tests. In the uniaxial dough extensibility test, the maximum force needed for dough breakage was higher for flour B, which clearly indicates that flour A is weaker than flour B. Upon incorporation of increasing levels of ethanol, the maximum extensibility (Figure 2C) and the total force for dough breakage (Figure 2E) decreased significantly for both flours A and B. Flour A maximum extensibility, for example, decreased from 57.6 ± 1.9 mm (0 mmol of ethanol/100 g of flour) to 33.7 ± 0.7 mm (80 mmol of ethanol/100 g of flour), while the total work required for breakage decreased from 7.2 ± 0.4 mJ (0 mmol of ethanol/100 g of flour) to 4.1 ± 0.8 mJ (80 mmol of ethanol/100 g of flour). For both flour types (Figures 2A and 2B), the more extensible dough changed into a stiffer dough upon adding ethanol (Figure 2D).

For both flours, we observed up to about 40% reduction in maximum dough extensibility and 24% increase in maximum force required for extension with 80 mmol of ethanol per 100 g of flour. Addition of 80 mmol of ethanol per 100 g of flour on top of the water, instead of partially replacing water, resulted in similar results with a maximum dough extension decrease down to 41 ± 1.0 mm. The force needed to break the dough strand was then 3.8 ± 0.6 mJ, and the maximum force required for dough extension was 0.14 ± 0.01 N.


dx.doi.org/10.1021/jf502547a | J. Agric. Food Chem. 2014, 62, 9326−9335

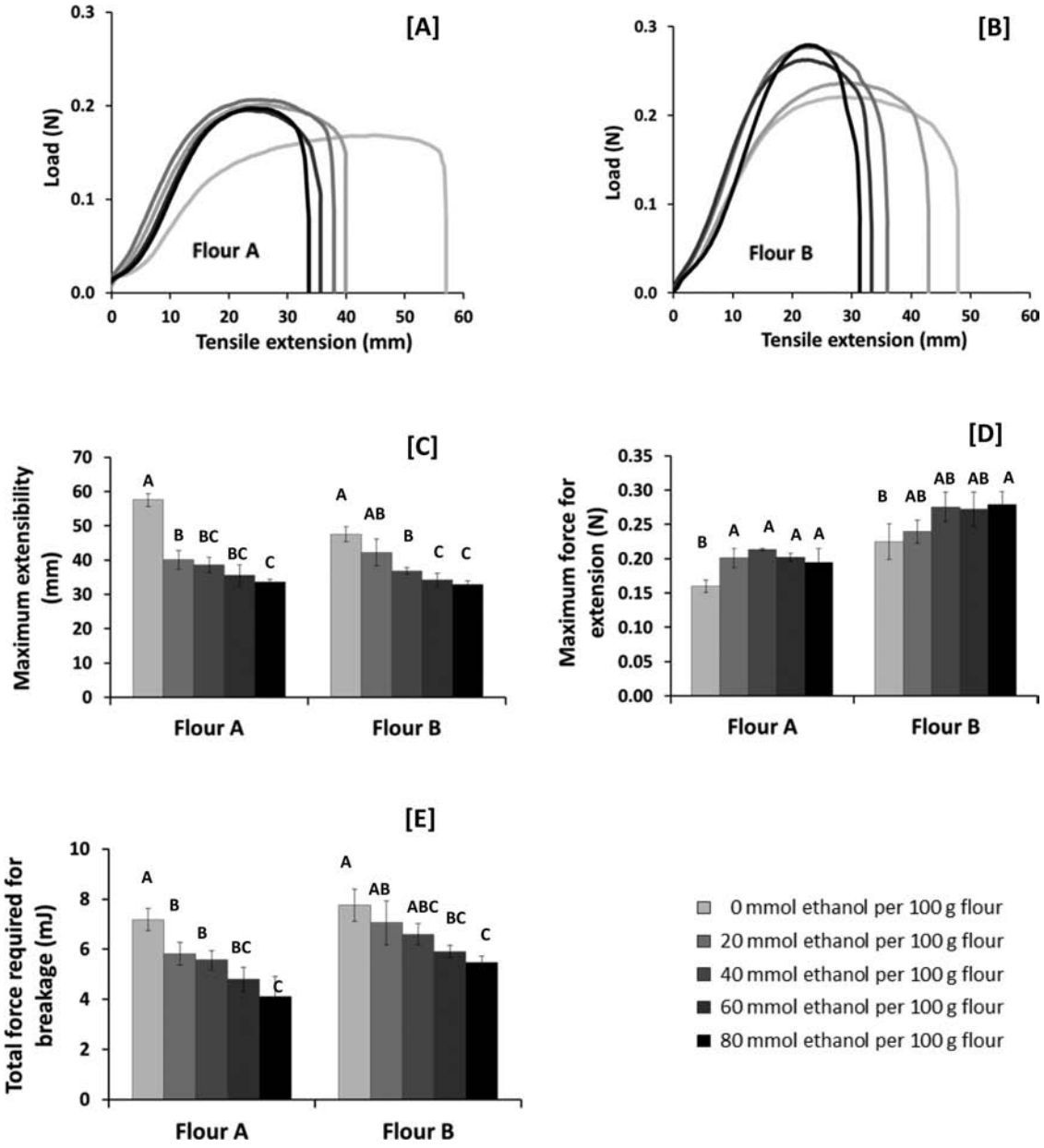


**Figure 2.** Effect of ethanol in concentrations of 0, 20, 40, 60, and 80 mmol per 100 g of flour on uniaxial dough extensibility of flours A and B using the Kieffer dough extensibility rig. Representative load−displacement curves are given for flour A (A) and flour B (B). The following analysis parameters are shown: maximum extensibility (C), maximum force for dough extension (D), and total force required for dough breakage (E). For each flour, bars with the same letter across the same ethanol concentration are not significantly different from each other ($p < 0.05$).

Biaxial dough extensibility results for ethanol (Figure 3) were in line with uniaxial dough extensibility results. For both flours, there was a significant increase in $P$ value, the parameter representing dough strength (Figure 3D), and a mostly linear decrease in the $L$ value, the parameter representing dough extensibility (Figure 3C). Ethanol (80 mmol/100 g of flour) in flours A and B gave up to a 31 and 20% increase in $P$ value, respectively, compared to the control dough. Biaxial measurement gave more insights on the dough tenacity as noticed in $P$ value. It shows that the maximum pressure needed for bubble rupture increased with the increase in ethanol inclusion. Conversely, the $L$ value decreased significantly with up to 64 and 63% for 80 mmol of ethanol per 100 g of flour for flours A and B, respectively. This is similar to the uniaxial test, showing the decreased dough extensibility. The Alveograph $P/L$ ratio, indicating the balance between dough strength and extensibility (Figure 3F), increased 3.8- and 3.1-fold with 80 mmol of ethanol per 100 g of flour for flours A and B, respectively. For flour A, the deformation energy ($W$) (Figure 3E) decreased from $(157 \pm 4) \times 10^{-4}$ J (0 mmol of ethanol/100 g of flour) to $(112 \pm 13) \times 10^{-4}$ J (80 mmol of ethanol/100 g of flour), whereas, for flour B, the decrease was from $(193 \pm 6) \times 10^{-4}$ J (0 mmol of ethanol/100 g of flour) to $(97 \pm 16) \times 10^{-4}$ J (80 mmol of ethanol/100 g of flour). Together, these Alveograph parameters provided insight into the effect of ethanol on dough properties. These experiments support the effect of ethanol on dough rheology, besides the possible effect of a loss of plasticizer caused by the use of less water in the dough recipe.

**Effect of Ethanol on Gluten Swelling.** To assess the molecular origin of the changes in dough rheology in the


dx.doi.org/10.1021/jf502547a | J. Agric. Food Chem. 2014, 62, 9326−9335

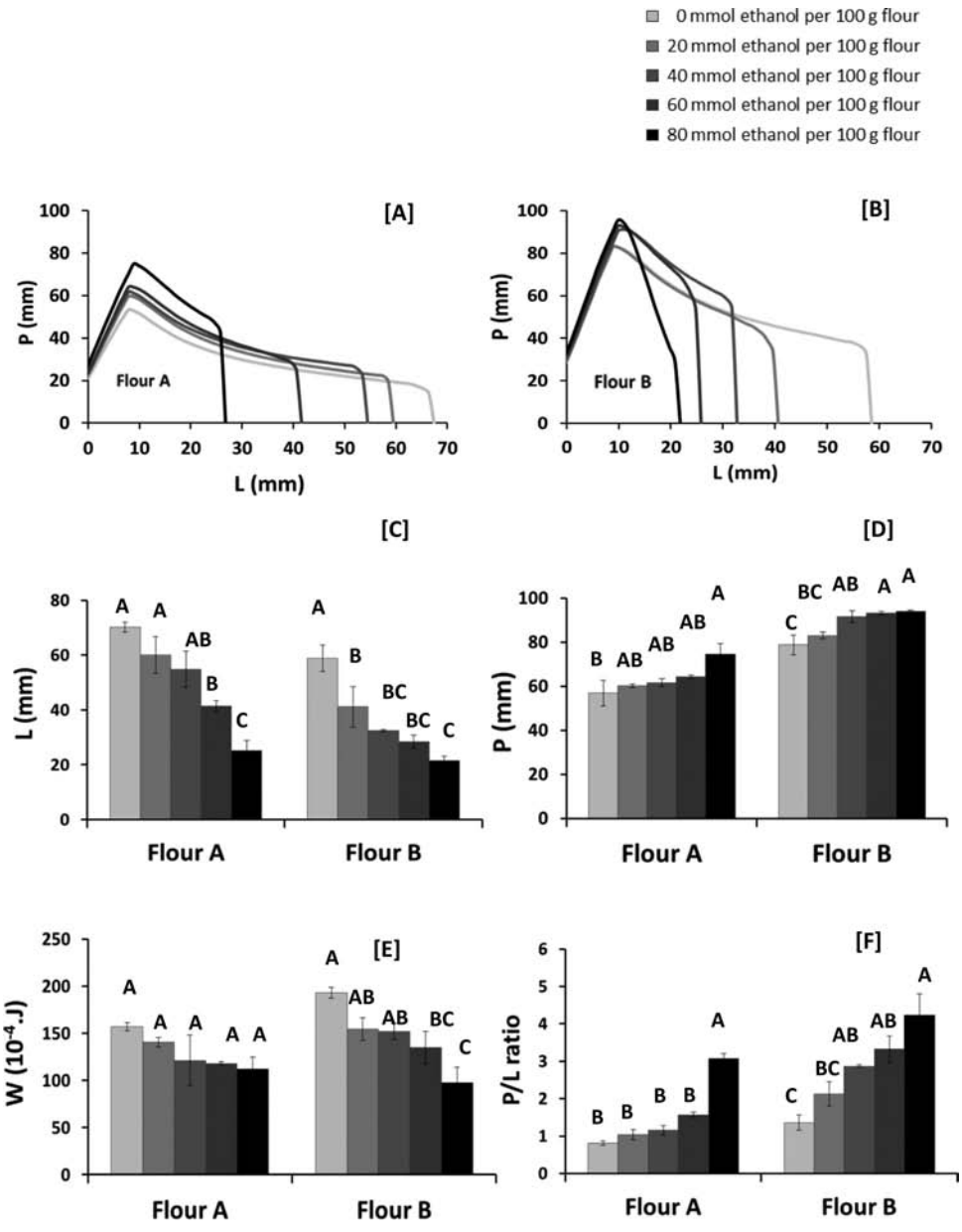


**Figure 3.** Effect of ethanol in concentrations of 0, 20, 40, 60, and 80 mmol per 100 g of flour on biaxial dough extensibility of flours A and B using the Alveograph. Representative Alveograph curves are given for flour A (A) and flour B (B). The following analysis parameters are shown: extensibility ($L$, mm) (C), maximum pressure ($P$, mm) (D), deformation energy ($W$, $10^{-4}$ J) (E), and the Alveograph $P/L$ ratio (F). For each flour, bars with the same letter across the same ethanol concentration are not significantly different from each other ($p < 0.05$).

presence of ethanol, flour and gluten swelling behavior was studied in aqueous ethanol solvents (0, 5, and 10%, v/v) using the SRC test. In the SRC methodology, the swelling behavior of flour polymer networks in a solvent and, hence, their ability to retain that solvent are quantified.[29] The results (data not shown) indicate that the polymer networks in flour showed no significant swelling with the ethanol concentrations used here. In order to test directly on gluten, commercial gluten material and the extracted gliadin- and glutenin-enriched fractions were used. No noticeable change in SRC was observed (data not shown).

**Effect of Ethanol on Gluten Agglomeration.** Gluten–starch separation experiments were performed using a dough batter method (Figure 4). Different ethanol concentrations were used in the dough recipe, but for the subsequent batter stages, only tap water was used. Nevertheless, gluten yields (GY) (Figure 4A) and protein recoveries (GPR) (Figure 4B) increased with increasing ethanol concentrations in the dough recipe of flour A. The pronounced impact of ethanol on flour A made its GY and GPR emulate those of strong flour (flour B results not shown). The largest increase in GPR upon inclusion of ethanol during the dough preparation was observed on the 125 $\mu$m sieve. The gluten protein agglomeration index (GPAI) (Figure 4C) dropped from 56.7 ± 2.0 to 46.9 ± 0.2% for 87 mmol of ethanol per 100 g of flour.

Because the effects of ethanol were mainly observed when using flour A, the protein composition of the fractions obtained on the different sieves was further determined for the latter flour (Figure 5). Although the albumin/globulin content on different sieve fractions remained almost same (results not shown), differences were observed in the gliadin fractions. Figure 5A–C shows the composition of gliadin proteins on the


dx.doi.org/10.1021/jf502547a | J. Agric. Food Chem. 2014, 62, 9326–9335

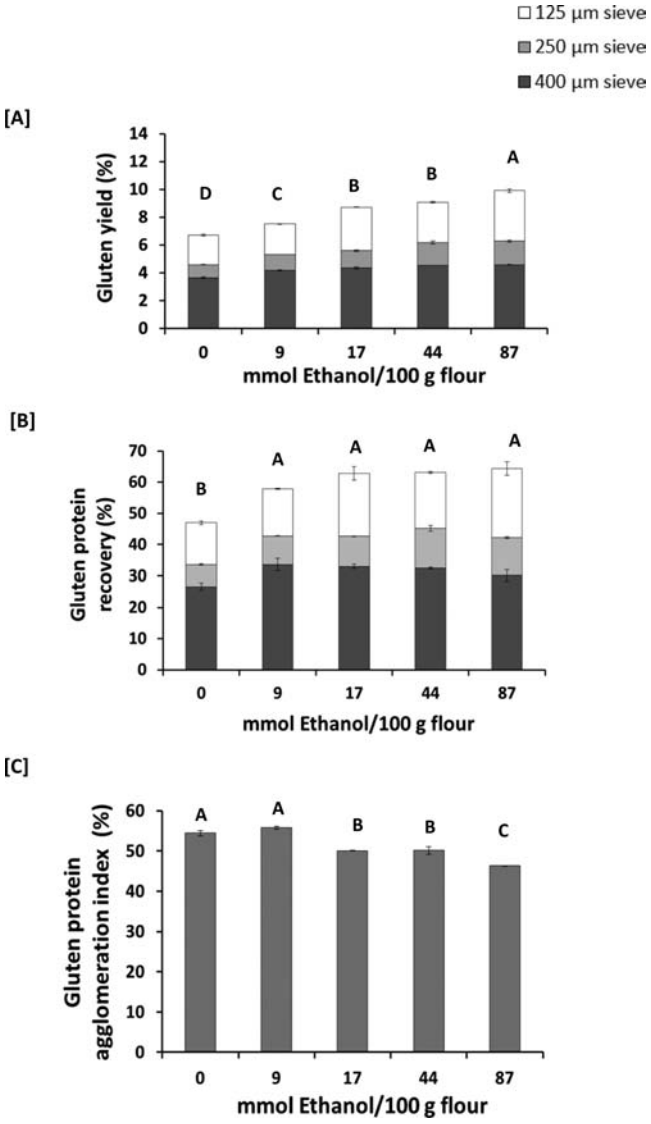


**Figure 4.** Effect of ethanol in concentrations of 0, 9, 17, 44, and 87 mmol per 100 g of flour on gluten agglomeration of flour A using a dough batter method. Gluten yield (A), gluten protein recovery on the different sieves (B), and gluten protein agglomeration index (C) for flour A are shown. For each sample, total bars with the same letter are not significantly different from each other ($p < 0.05$).

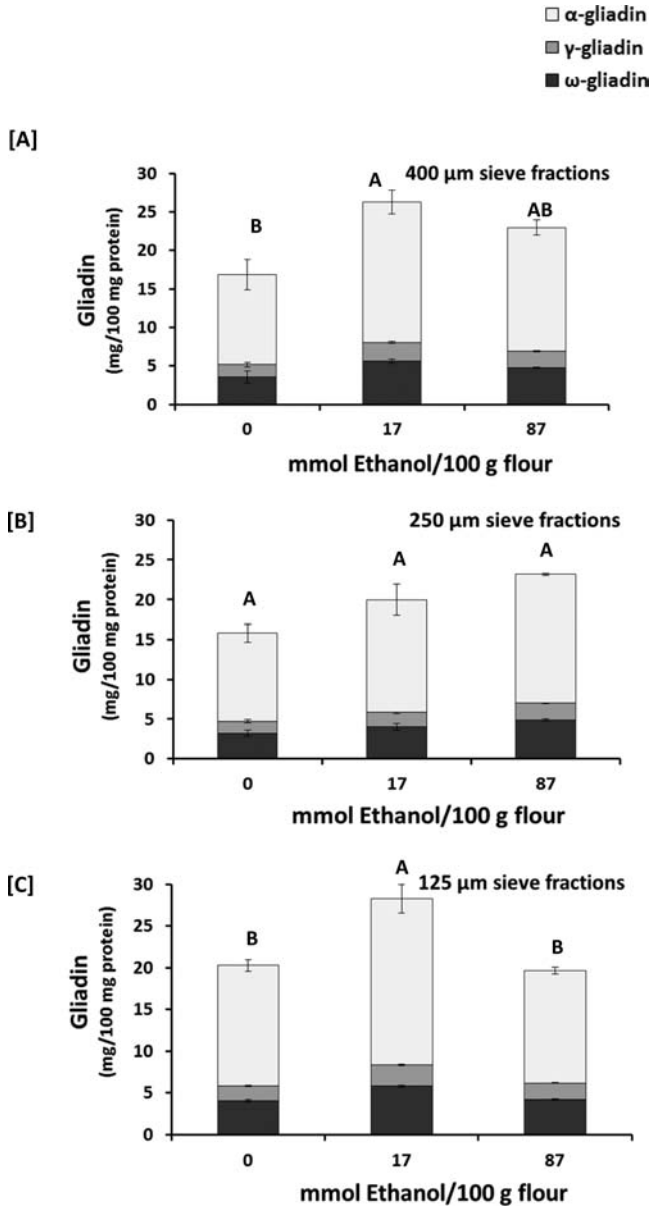


**Figure 5.** Composition of gliadins in gluten fractions obtained from gluten agglomeration experiment for flour A in concentrations of 0, 17, and 87 mmol of ethanol per 100 g of flour and determined using reversed-phase high-performance liquid chromatography (RP-HPLC). The composition of gliadin in the gluten fractions retained on the 400 $\mu$m (A), 250 $\mu$m (B), and 125 $\mu$m (C) sieves. For each sample, total bars with the same letter are not significantly different from each other ($p < 0.05$).

different sieves analyzed in more detail using RP-HPLC. Low ethanol concentrations added to dough from flour A led to significantly higher levels of gliadin retained on the three sieves. There was a noticeable increase in retention of all three gliadin types, but specially, $\alpha$-gliadin concentration increased from 11.6 $\pm$ 1.9 to 18.2 $\pm$ 1.5 mg/100 mg of protein on a 400 $\mu$m sieve, 11.0 $\pm$ 1.1 to 14.1 $\pm$ 1.9 mg/100 mg of protein on a 250 $\mu$m sieve and 14.4 $\pm$ 0.1 to 19.9 $\pm$ 1.7 mg/100 mg of protein on a 125 $\mu$m sieve.

**Sequential Extraction of Flour with Increasing Ethanol Concentration.** To further investigate the effect of ethanol on dough and gluten behavior, flour A was sequentially extracted with 2, 5, 10, 30, and 60% ethanol in water solutions. Prior to the ethanol extraction, the flour sample was pre-extracted with sodium phosphate buffer (0.05 M, pH 7.6) to remove albumins and globulins. Figure 6 shows the RP-HPLC profiles of the gliadin fractions. Addition of ethanol to water improved the solvent quality for gliadin, since increasing ethanol concentrations were able to increasingly dissolve the protein fractions defined as gliadins (Figure 6). The impact of low ethanol concentrations as used in this study became apparent by a selective dissolution of the more hydrophilic $\omega$-gliadins (Figure 6).

## DISCUSSION

During dough fermentation, a yeasted dough undergoes significant rheological changes. These changes could be mediated by one or more metabolites produced by yeast during the fermentation process. Surprisingly, research in this field has mainly been limited to studying effects of dough acidification by the progressive buildup of $CO_2$, acetic acid, or


dx.doi.org/10.1021/jf502547a | J. Agric. Food Chem. 2014, 62, 9326−9335

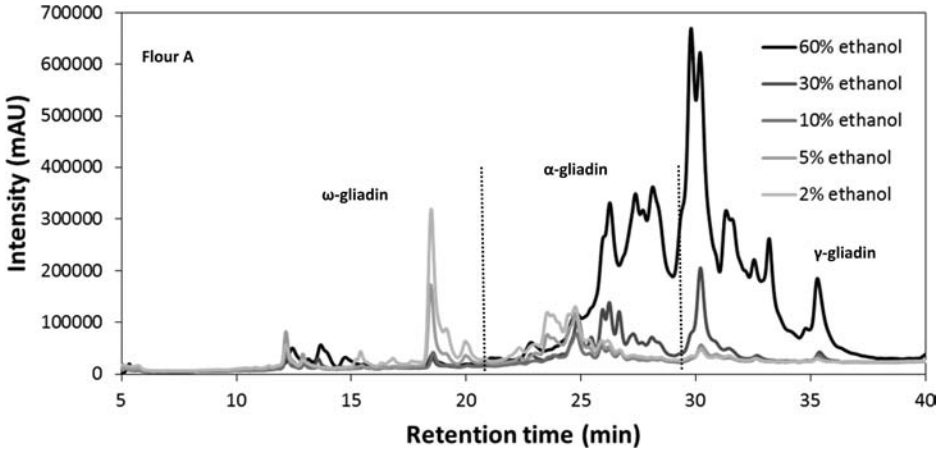


**Figure 6.** Reversed-phase high-performance liquid chromatography (RP-HPLC) profiles of flour A sample sequentially extracted with 2%, 5%, 10%, 30%, and 60% ethanol.

lactic acid[4] and of $H_2O_2$.[10] Recently, Jayaram et al.[8] showed that addition of succinic acid to the dough in the levels produced by the yeast during dough fermentation significantly decreases dough extensibility. With regard to $H_2O_2$, a recent study by Rezaei et al.[11] showed that yeast does not excrete $H_2O_2$ to the dough during fermentation, in contrast to an earlier report stating that $H_2O_2$ produced by yeast during dough fermentation is responsible for the oxidative-like effect of yeast on dough rheology.[10]

The impact of accumulating ethanol, produced in yeast's fermentative metabolism, has not been studied. The research here hence focused on the potential role that ethanol in a concentration range from 0 to 80 mmol per 100 g of flour has on mixing properties, dough spread behavior, and dough extensibility. Its effect on the gluten proteins was studied in more detail. Because the dynamic process of ethanol buildup during fermentation is very hard to implement in sound experiments, our approach comprehended the introduction of ethanol in the dough recipe at the levels at which it is produced in fermenting dough.[11]

As observed in Table 1, the dough development time and dough strength were unaffected with the inclusion of ethanol in both flours A and B. This indicates that the dough retained its stability throughout the mixing process. However, there was a slight increase in mixing tolerance index in flour A suggesting that the dough may turn softer. This was not the case in flour B as the mixing tolerance index remained the same here. Mixograph results indicate that ethanol has a positive effect on dough mixing characteristics as further supported by dough spread test and dough extensibility test results. In dough spread tests (Figure 1), the flow behavior of the dough changed in the presence of ethanol. Instead of having more spread with increasing resting time prior to the spread measurement, as seen for the control, the higher levels of ethanol led to reduced dough spread. The observed increase in $\Delta(W/H)$ values of control dough could possibly be explained in part by the presence of endogenous or kernel associated enzymes such as peptidases present in flour. When considering a constant resting time in the spread test, an increase in ethanol concentration resulted in a decrease in $\Delta(W/H)$. This reduction in spreadability of the dough was more pronounced in flour A, a weak flour, than flour B, a strong flour. While an increase in resting time of the control dough resulted in a higher dough spreadability, increasing levels of ethanol caused increasingly less pronounced changes in the $\Delta(W/H)$ with resting time. This observation could be explained by the ethanol counteracting the action of flour peptidases. This indicates that ethanol turns the dough stiffer. This observation is in line with the more elaborate analysis of dough behavior using the uniaxial Kieffer rig and biaxial Alveograph dough extensibility tests. In both procedures reduced extensibility and an increased maximum force needed to extend the dough were demonstrated as a function of ethanol concentration. This coincided with a decrease in the energy required for deformation until rupture.

To assess the contribution of gluten to these effects, several additional experiments were performed. On the one hand, the SRC of both flours A and B was similar in water and two ethanol−water solvents. Gluten agglomeration analysis for flour A, on the other hand, showed strongly increased gluten yield and gluten protein recovery with increasing ethanol concentration in the dough recipe using a lab scale gluten−starch separation procedure. These increases were mostly due to increases in the yield of smaller aggregates. Using ethanol as a washing liquid has previously been described to improve gluten yield.[30] However, small quantities of ethanol were used here, only in the dough formation and not in the batter formation.

Different hypotheses can be put forward to explain the effect of low levels of ethanol on dough properties. One of the explanations could be the evaporation of ethanol during resting, fermentation, or handling of dough. The dough is left with less solvent, and a stiffer dough results. The Kieffer rig results obtained with dough to which ethanol was added on top of the regular amount of water, instead of a replacement for part of the water, seems to disprove this hypothesis, as results were very similar in both instances.

As a second hypothesis, a change in gluten properties due to the presence of ethanol seems to better explain the observed results. It can be postulated that ethanol, possibly even in low levels in an aqueous environment, creates a different environment for proteins to interact and develop a network in. Aqueous ethanol can be assumed to be a better solvent for gluten proteins than water, in line with the use of ethanol containing solvents for extraction of gliadins and reduced glutenin subunits. In a good solvent, the protein network can be expected to swell and become more expanded,[31] but also have reduced cohesiveness due to a decrease in number or strength of intermolecular secondary structures. This could lead to an


dx.doi.org/10.1021/jf502547a | J. Agric. Food Chem. 2014, 62, 9326−9335

increased gluten yield but, at the same time, a less well-aggregated gluten network. This hypothesis seems to be supported by most results obtained in this study. Spread test, Kieffer rig, and Alveograph results show increased resistance to deformation and reduced extensibility of dough in the presence of ethanol. Gluten agglomeration analysis showed an increase in gluten yield, mostly due to an increase in gluten material on the smaller sieves (250 and 125 $\mu$m) for flour A. Sequential extraction with increasing levels of ethanol showed extraction and hence solubilization of specific gliadin fractions already at low ethanol concentrations, illustrating the better solvent quality of aqueous ethanol versus water alone. Next to the early work of Osborne,[26] the more recent studies of Robertson and co-workers also seem to corroborate this hypothesis. Using ethanol as a washing liquid in gluten starch separation, they observed an improved gluten yield.[30] Also rapid swelling of gluten and a concomitant volume increase was seen upon the use of aqueous ethanol with ethanol concentration up to 50% (v/v).[31,32] In our experiments, this swelling of the gluten matrix was not observed.

With regard to the gliadins, it is not clear what the consequences could be of their improved solvation or partial solubilization, such as observed for $\omega$- and $\alpha$-gliadins in the conditions tested. Their partial solubilization may reduce the plastic and/or viscous properties they confer on gluten. The outcome of this could be a more elastic but stiffer network, which coincides with the results of the flow and extensibility measurements. How the phenomenon of improved solvation or partial solubilization of gliadins has to be unified with the observation of somewhat increased relative levels of gliadins in the small gluten aggregates obtained in the gluten agglomeration test is not clear. Ethanol can be expected to have an effect not only on the chemical interactions but also on the physical interactions through network swelling and expansion.

Based on the results obtained in this manuscript, it is tempting to speculate that the rheological properties of weak flour can be partly brought to the level of good flour by partially changing the solvent and, hence, changing solvent protein interactions. Here, this change seemed to lead to better interactions but resulted in stiffer dough showing resistance to extension upon analysis. For bread making, dough strengthening is often desirable, but dough that is too strong or stiff will also not rise sufficiently.

In conclusion, it was demonstrated in this study that ethanol, at the levels at which it is formed during dough fermentation, has a significant impact on dough properties. Similar to organic acids produced by the yeast during dough fermentation, low levels of ethanol decrease dough extensibility and make dough more stiff and tenacious, albeit through a different mechanism of action than acid metabolites.[8] The results indicate that ethanol might have a more pronounced effect on weak flours than on strong flours. Aqueous ethanol enhances gluten agglomerate yield by acting as a better solvent than pure water, allowing small gluten aggregates to swell more extensively. Taking into account that ethanol, together with $CO_2$, is by far the most produced component by yeast in fermenting dough, it can be suggested that ethanol accumulation is one of the elements responsible for the changes observed in dough rheology upon fermentation. However, in view of the approach used in these experiments, i.e., using yeastless dough to which ethanol is added at the start of mixing, more research in fermenting dough itself is needed to corroborate these findings. Indeed, the difference in impact of providing a bolus amount of ethanol at the start of mixing versus gradual accumulation in dough during fermentation needs to be investigated.

## AUTHOR INFORMATION

### Corresponding Author

*Tel: + 3216321917. Fax: + 3216321997. E-mail: christophe.courtin@biw.kuleuven.be.

### Funding

We acknowledge the financial support from the Erasmus Mundus External Cooperation Window Lot 15 India program under European Commission for V.B.J. and the Research Fund KU Leuven for the postdoctoral fellowship of S.C. This research was conducted in the framework of research projects G.0544.10N (FWO, Brussels, Belgium) and IDO/12/011 (KU Leuven) and is part of the Methusalem program "Food for the Future" at the KU Leuven. Research in the lab of K.J.V. is supported by ERC, HFSP, VIB, EMBO YIP program, KU Leuven, FWO, IWT and the AB InBev Baillet-Latour foundation.

### Notes

The authors declare no competing financial interest.

## ACKNOWLEDGMENTS

Dr. Bert Lagrain and Dr. Emmie Dornez are thanked for helpful discussions.

## ABBREVIATIONS USED

GY, gluten yield; GPR, gluten protein recovery; GPAI, gluten protein agglomeration index; *L*, dough extensibility; *P*, dough elasticity; RP-HPLC, reversed-phase high-performance liquid chromatography; SE-HPLC, size exclusion high-performance liquid chromatography; SDS, sodium dodecyl sulfate; SRC, solvent retention capacity; *W*, dough deformation energy

## REFERENCES

(1) Delcour, J. A.; Hoseney, R. C. In *Principles of cereal science and technology*; AACC International: St. Paul, MN, USA, 2010; Vol. 3, pp 87−96.

(2) Hoseney, R. C.; Hsu, K. H.; Junge, R. C. Simple spread test to measure the rheological properties of fermenting dough. *Cereal Chem.* **1979**, *56*, 141−143.

(3) Nagao, S.; Endo, S.; Tanaka, K. Effect of fermentation on the Do-Corder and bread-making properties of a dough. *Cereal Chem.* **1981**, *58*, 388−391.

(4) Galal, A. M.; Varrianomarston, E.; Johnson, J. A. Rheological dough properties as affected by organic acids and salt. *Cereal Chem.* **1978**, *55*, 683−691.

(5) Wehrle, K.; Grau, H.; Arendt, E. K. Effects of lactic acid, acetic acid, and table salt on fundamental rheological properties of wheat dough. *Cereal Chem.* **1997**, *74*, 739−744.

(6) Clarke, C. I.; Schober, T. J.; Dockery, P.; O'Sullivan, K.; Arendt, E. K. Wheat sourdough fermentation: Effects of time and acidification on fundamental rheological properties. *Cereal Chem.* **2004**, *81*, 409−417.

(7) Jayaram, V. B.; Cuyvers, S.; Lagrain, B.; Verstrepen, K. J.; Delcour, J. A.; Courtin, C. M. Mapping of *Saccharomyces cerevisiae* metabolites in fermenting wheat straight-dough reveals succinic acid as pH-determining factor. *Food Chem.* **2013**, *136*, 301−308.

(8) Jayaram, V. B.; Cuyvers, S.; Verstrepen, K. J.; Delcour, J. A.; Courtin, C. M. Succinic acid in levels produced by yeast (*Saccharomyces cerevisiae*) during fermentation strongly impacts wheat bread dough properties. *Food Chem.* **2014**, *151*, 421−428.

(9) Rezaei, M. N.; Dornez, E.; Jacobs, P.; Parsi, A.; Verstrepen, K. J.; Courtin, C. M. Harvesting yeast (*Saccharomyces cerevisiae*) at different

physiological phases significantly affects its functionality in bread dough fermentation. *Food Microbiol.* **2014**, *39*, 108−115.
(10) Liao, Y. E.; Miller, R. A.; Hoseney, R. C. Role of hydrogen peroxide produced by Baker's yeast on dough rheology. *Cereal Chem.* **1998**, *75*, 612−616.
(11) Rezaei, M. N.; Dornez, E.; Verstrepen, K. J.; Courtin, C. M. Critical assessment of the formation of hydrogen peroxide in dough by fermenting yeast cells. *Food Chem.* **2015**, *168*, 183−189.
(12) Cooper, E. J.; Reed, G. Yeast fermentation-Effects of temperature, pH, ethanol, sugars, salt, and osmotic pressure. *Baker's Dig.* **1968**, 22−29.
(13) Robertson, G. H.; Cao, T. K.; Ong, I. Interactions between wheat gluten, water, and ethanol contribution to separability during ethanol washing. *Cereal Foods World* **1998**, *43*, 523.
(14) Robertson, G. H.; Cao, T. Mixograph responses of gluten and gluten-fortified flour for gluten produced by cold-ethanol or water displacement of starch from wheat flour. *Cereal Chem.* **2002**, *79*, 737−740.
(15) Robertson, G. H.; Hurkman, W. J.; Cao, T. K.; Gregorski, K. S.; Tanaka, C.; Glenn, G. M.; Orts, W. J. Wheat flour exposed to ethanol yields dough with unexpected properties. *Cereal Chem.* **2011**, *88*, 509−517.
(16) Rao, R. K.; Arnold, L. Alcoholic extraction of vegetable oils. Part IV. Solubilities of vegetable oils in aqueous 2-propanol. *J. Am. Oil Chem. Soc.* **1957**, *34*, 401−404.
(17) Krochta, J. M.; Look, K. T.; Hudson, J. S.; Pavlath, A. E. Extraction with ethanol as an energy-saving alternative to conventional drying of corn starch. *J. Food Sci.* **1981**, *46*, 1054−1058.
(18) AACC. *Approved methods of the AACC*, 11th ed.; AACC: St. Paul, MN, USA, 2010; Methods 44-19.01, 54-21.01, 54-30.02, 54-40.02 and 56-11.02.
(19) AOAC. *Official methods of analysis*; AOAC: Washington, DC, USA, 1995; Method 993.13.
(20) Finney, K. F.; Shogren, M. A ten gram Mixograph for determining and predicting functional properties of wheat flours. *Baker's Dig.* **1972**, *46*, 77.
(21) Decamps, K.; Joye, I. J.; Courtin, C. M.; Delcour, J. A. Glucose and pyranose oxidase improve bread dough stability. *J. Cereal Sci.* **2012**, *55*, 380−384.
(22) Nash, D.; Lanning, S. P.; Fox, P.; Martin, J. M.; Blake, N. K.; Souza, E.; Graybosch, R. A.; Giroux, M. J.; Talbert, L. E. Relationship of dough extensibility to dough strength in a spring wheat cross. *Cereal Chem.* **2006**, *83*, 255−258.
(23) Kieffer, R.; Wieser, H.; Henderson, M. H.; Graveland, A. Correlations of the breadmaking performance of wheat flour with rheological measurements on a micro-scale. *J. Cereal Sci.* **1998**, *27*, 53−60.
(24) Haynes, L.; Bettge, A.; Slade, L. Soft wheat and flour products methods review: Solvent retention capacity equation correction. *Cereal Foods World* **2009**, *54*, 174−175.
(25) Frederix, S. A.; Courtin, C. M.; Delcour, J. A. Influence of process parameters on yield and composition of gluten fractions obtained in a laboratory scale dough batter procedure. *J. Cereal Sci.* **2004**, *39*, 29−36.
(26) Osborne, T. B. *The proteins of the wheat kernel*; Carnegie Institute of Washington, Press of Judd & Detweiler, Inc.: Washington, DC, 1907; Vol. *84*.
(27) Wieser, H. Investigations on the extractability of gluten proteins from wheat bread in comparison with flour. *Z. Lebensm.-Unters. Forsch.* **1998**, *207*, 128−132.
(28) Walker, C. E.; Hazelton, J. L.; Shogren, M. D. *The Mixograph handbook*, 1st ed.; National Manufacturing Co.: Lincoln, NE, 1998.
(29) Slade, L.; Levine, H. Structure-function relationships of cookie and cracker ingredients. In *The science of cookie and cracker production*; Faridi, H., Ed.; Chapman & Hall: New York, USA, 1994; pp 23−141.
(30) Robertson, G. H.; Cao, T.; Orts, I. Wheat proteins extracted from flour and batter with aqueous ethanol at subambient temperatures. *Cereal Chem.* **2007**, *84*, 497−501.
(31) Robertson, G. H.; Cao, T. Substitution of concentrated ethanol for water in the laboratory washing fractionation of protein and starch from hydrated wheat flour. *Cereal Chem.* **1998**, *75*, 508−513.
(32) Robertson, G. H.; Cao, T. K.; Ong, I. Wheat gluten swelling and partial solubility with potential impact on starch-from-gluten separation by ethanol washing. *Cereal Chem.* **1999**, *76*, 843−845.

**Table 1. Description of Calibration Set and Validation Set of Tea Samples**

| fermentation degrees | categories | calibration set | | | | | validation set | geographical origins |
|---|---|---|---|---|---|---|---|---|
| | | classes | | | | total | | |
| unfermented | green tea | steamed green tea | roasted green tea | baked green tea | sun-dried green tea | 164 | 10 | Zhejiang, Jiangsu and Fujian, China; |
| | | 30 | 69 | 50 | 15 | | | |
| partially fermented | white tea | Baihaoyinzhen | Baimudan | Gongmei | Shoumei | 50 | 10 | Fujian, China |
| | | 10 | 20 | 10 | 10 | | | |
| semifermented | oolong tea | faint-scent oolong | familiar scent oolong | | baking type oolong | 198 | 10 | Fujian and Guangdong, China; Taiwan |
| | | 60 | 75 | | 63 | | | |
| fully fermented | black tea | Lapsang Souchong | Gongfu black tea | | broken black tea | 51 | 10 | Fujian, Guangdong, Yunnan and Anhui, China |
| | | 15 | 21 | | 15 | | | |
| total | 522 | | | | | 463 | 40 | 19 (Japan, Sri Lanka) |

developed. Therefore, it is necessary to develop accurate and stable methods to distinguish different levels of fermented teas.

Flavor, frequently described as taste and aroma, is the most significant element for tea evaluation. Scientists are highly concerned about the relationship of flavor and biochemical nature. Tea is abundant in chemical components that differ in both content and their component ratio, which not only causes the multiple dimensions of tea quality but also brings some difficulties to the qualitative analysis of tea, especially when tea chemical information far exceeds the taster's subjective analysis. Thus, it is crucial to take advantage of quantitative indicators to identify the tea. More recently, the tea field has made its greatest progress in characterizing the nature of tea at the level of chemistry. Unremitting efforts have been made to research the key components of various teas on the basis of biochemistry and physical characteristics by instrumental techniques. So far, to analyze the characteristic constituents and identify the categories or geographical origins of teas, researchers have been using spectrophotometry,[6] high-performance liquid chromatography (HPLC),[7,8] gas chromatography−mass spectrometry (GC-MS),[9,10] inductively coupled plasma mass spectrometry (ICP-MS),[11] surface desorption chemical ionization mass spectrometry (DAPCI-MS),[12] total luminescence spectroscopy (TLS),[13] near-infrared spectroscopy (FT-NIRS),[14] electronic nose and electronic tongue,[15,16] and machine vision technique.[17,18] Among the various analytical tools, HPLC is widely used by the main exporting and importing countries for the purpose of identifying chemical compositions, providing high accuracy and sensitivity. As widely mentioned, the biochemical characteristics of tea should be attributable to the patterns composed of taste; however, such a method has not been applied systematically for the classification of tea categories. Therefore, we paid close attention to key components such as polyphenols and caffeine, which may be the first consideration for setting a discrimination standard.[19]

"Fermentation" in tea science is typically defined as the oxidation of polyphenols. Increased attention in potential health functions of flavonoid-rich tea has prompted the use of HPLC analysis and pattern recognition to optimize the method of qualitative and quantitative flavonoid analysis. There is certain progress in terms of Wuyi Rock tea distinction, accumulation, and identification of nonvolatile compounds of the tea by the application of HPLC.[20−23] As an effective chemometrics method, stepwise linear discriminant analysis (S-LDA) is incomparable to others in terms of discrimination for its good statistical learning theory and highly efficient discriminant functions,[24] which exclusively selected fewer useful variables by neglecting influences of other variables. Hence, this study applied HPLC analysis in combination with S-LDA to categorize the different fermented teas.

Conducting stable and accurate classification of different kinds of tea in the current tea market is an important issue as well as the essential component of the international standard system. For the above reasons, the proposal of tea chemical classification has passed at the 24th International Conference of International Organization for Standardization (ISO), along with the setup of working groups. Therefore, we aimed to develop an accurate and efficient method based on HPLC to discriminate teas by potential nonvolatile compounds. The study was based on the fact that the biochemical composition varies significantly among different degrees of fermented teas. In our study, numerous representational samples covering four main tea categories in accordance with different fermentation degrees were collected. Polyphenols and caffeine were taken as the distinct variables to establish internationally recognized models of teas, providing reference for the establishment of chemical classification, which would help international tea trade and consumers.

## MATERIALS AND METHODS

**Tea Samples.** A total of 522 tea samples were collected according to fermentation degree, as described in Table 1. Among these samples, 482 tea samples, as the calibration set, were produced in 2010 and 2011, which were collected and purchased from reliable sources in China (463 samples, Table S1 in the Supporting Information) and other countries (19 samples, Table S2 in the Supporting Information).


dx.doi.org/10.1021/jf5025483 | J. Agric. Food Chem. 2014, 62, 9336−9344

Another 40 samples, as the validation set, were produced in 2012 (Table S3 in the Supporting Information). Teas with different degrees of fermentation were sorted from different grades and producing regions and analyzed by HPLC and spectrophotometry for categories discriminate investigation. All samples were kept in ziplock bags and stored in a refrigerator at 4 °C until determined.

**HPLC and Spectrophotometry Analysis.** All of the determinations were assayed in triplicate according to International Standards, which have been applied to provide robust validated analytical tools in cases of international transactions and disputes. The determination of total polyphenols and catechins was performed according to the procedure described by previously reported ISO 14502.[23,25]

*Chemicals.* The following chemicals and solvents were used: Methanol (≥99.5%), Folin−Ciocalteu phenol reagent, sodium carbonate (≥99.8%), gallic acid (≥98.5%), ethylenediaminetetraacetic acid disodium salt, dehydrate (EDTA, ≥99.0%), and L-ascorbic acid (≥99.7%) were purchased from Sinopharm (Beijing, China). (+)-Catechin (C, ≥99%), (−)-epicatechin (EC, ≥98%), (−)-epigallocatechin (EGC, ≥95%), (−)-epigallocatechin gallate (EGCG, ≥95%), and (−)-epicatechin gallate (ECG, ≥98%) were obtained from Sigma-Aldrich (St. Louis, MO, USA.). Caffeine (Aladdin, Shanghai, China), acetonitrile (HPLC grade, ≥99.9%, Lichrosolv, Germany), and acetic acid (HPLC grade, ≥99.7%) were obtained from Fisher Scientific.

*Determination of Dry Matter Content.* The dry matter content was assayed according to the protocol described by ISO 1572 and ISO 1573. Processed tea leaves were milled into a dried fine powder by using a grinding mill and then passed through a sieve of aperture size 500 μm. A sample of 5 ± 0.001 g of tea was weighed to place in a preweighed aluminum dish and dried in a drying oven (DHG-9140A, Lantian, Hangzhou, China) at 103 ± 2 °C for 6 h and weighed until two successive weighings did not exceed 0.005 g. The dry matter content of the samples was calculated from the weight differences.

*Preparation of Extracts.* Samples weighing 0.2 ± 0.001 g were placed in extraction tubes (10 mL). Five milliliters of preheated 70% water/methanol extraction mixture was filled into each tube individually and incubated in the water bath for 10 min at 70 °C (DK-S22 Electric Water Bath, Jing Hong, Shanghai, China) and vortexed for 5 and 10 min, respectively. The extraction tubes were removed from the water bath, allowed to cool to room temperature, and centrifuged for 10 min at 3500 rpm using a centrifuge (Lu Xiang Yi, Shanghai, China). The supernatant was carefully decanted into graduated tubes. The extraction steps were repeated as described above. The extracts were combined and made up to 10 mL with cold methanol/water extraction mixture.

*Analysis of Total Polyphenols (TPs).* The total polyphenol content was determined spectrophotometrically according to International Standard ISO 14502-1:2005, using Folin−Ciocalteu's reagent. Using a pipet, 1 mL of sample extract was pipetted into a 100 mL volumetric flask and filled to the mark with distilled water. One milliliter of the diluted sample was transferred into each tube, mixed with 5 mL of diluted Folin−Ciocalteu phenol reagent, allowed to stand for 3−8 min, and then mixed with 4 mL of 7.5% sodium carbonate solution for 1 h before spectrometric analysis. Distilled water was used as blank, whereas the gallic acid standards were used for quantification. A best-fit linear calibration graph was constructed from the mass of anhydrous gallic acid. The total polyphenols content of tea was detected by using a Shimadzu UV-260 spectrophotometer with a maximum absorption of 765 nm.

*Analysis of Catechins and Caffeine Content.* Catechins and caffeine analyses were conducted according to ISO 14502-2:2005 protocol. One milliliter of the sample extract was made up to 5 mL with stabilizing solution (10% v/v acetonitrile, 500 μg/mL EDTA, and ascorbic acid). The mixture was filtered through a 0.45 μm Millipore filter and put into vials, and it can maintain stability for 24 h when stored at 4 °C. Catechins and caffeine analysis were assayed by using a Dionex UltiMate 3000 HPLC on a phenyl bonded column, using gradient elution with a thermostatically controlled column compartment and an ultraviolet detector set at 278 nm. Elution was performed according to the following system: flow rate, 1 mL/min; temperature, 35 ± 0.5 °C; injection volume, 10 μL; A = 9% acetonitrile (volume fraction), 2% acetic acid (volume fraction) with 20 μg/mL EDTA, B = 80% acetonitrile (volume fraction), 2% acetic acid (volume fraction) with 20 μg/mL EDTA. Binary gradient conditions were as follows: The 100% mobile phase A lasted for 10 min, followed by a linear gradient to 68% mobile phase A and to 32% mobile phase B for 15 min, and was retained at this composition for 10 min. The system was reset to 100% mobile phase A and allowed to remain stable before the next injection.

The five most abundant catechins from the extract, catechin (C), epicatechin (EC), epigallocatechin (EGC), epigallocatechin gallate (EGCG), and epicatechingallate (ECG), were assayed. Catechin and caffeine quantifications were performed using a caffeine calibration curve. For the quantification of the individual catechins, external catechin standards of defined purity and moisture content were used as a standard in conjunction with relative response factors (RRFs), calculated on a dry matter basis. The qualitative analysis of catechin monomer was performed by comparison of their peak areas and retention time on the basis of authentic compounds that were obtained from Sigma. Caffeine content was quantified as follows in accordance with ISO 14502-2:2005.

$$\%\ \text{caffeine} = \frac{(A_{\text{sample}} - A_{\text{intercept}}) \times F_{\text{std}} \times V_{\text{sample}} \times d \times 100}{S_{\text{caffeine}} \times m_{\text{sample}} \times 10000 \times w_{\text{DM,sample}}}$$

where $A_{\text{sample}}$ = peak area of the individual component in the test sample, $A_{\text{intercept}}$ = peak area at the point the caffeine calibration line intercepts the $y$-axis, $S_{\text{caffeine}}$ = caffeine calibration line slope, $V$ = sample extraction volume, $d$ = dilution factor, $m_{\text{sample}}$ = mass in grams of test sample, and $w_{\text{DM,sample}}$ = dry matter content of test sample.

As a percentage by mass on a sample dry matter basis, the total catechin content of tea was calculated by the summation of individual catechins. Nongalloylated catechins and galloylated catechins were calculated as follows:

$$\%\ \text{total catechins} = (\%\ \text{EGC}) + (\%\ \text{C}) + (\%\ \text{EC}) + (\%\ \text{EGCG}) + (\%\ \text{ECG})$$

$$\%\ \text{nongalloylated catechins} = (\%\ \text{EGC}) + (\%\ \text{C}) + (\%\ \text{EC})$$

$$\%\ \text{galloylated catechins} = (\%\ \text{EGCG}) + (\%\ \text{ECG})$$

**Data Analysis.** The instrumental data were constructed by several pattern recognition methods, such as principal component analysis (PCA) and stepwise linear discriminant analysis (S-LDA). PCA was performed by SIMCA (version 13.0.2), which was processed for the sake of having a better visualization of differences among the various objects by projecting them into the space of the first significant components. One-way ANOVA and S-LDA were processed by the SPSS statistical package (version 17.0 for Windows). The ANOVA analysis was used for calibration set (463 samples) covering four kinds of tea samples to identify statistical separation among the means. Experimental results were performed as means ± standard deviation (SD) by SigmaPlot (version 10.0). S-LDA was carried out to extract best discriminant variable separating tea categories, which enters or removes variables by analyzing their effects on the discrimination of the groups based on the Wilks' lambda criterion. In our study, EGC, C, EC, nongalloylated catechins (N-GC), EGCG, ECG, galloylated catechins (G-C), total catechins (TC), caffeine (CAF), and total polyphenols (TP) were assayed; considering the differences in processing, we also calculated the ratios of TC and TP, N-GC and G-C, N-GC and TC, G-C and TC, EGCG and TC, and EGC and TC.[26] For the discriminant four-class problem, we constructed three discriminant functions (DFs) by a linear combination of the extracted features. The $F$ values to enter and to remove were set at 3.84 and 2.71, respectively. The approach yielded four equations that matched each tea category. For the discrimination of oolong and other teas, the values were set at 2.6 and 1.6, respectively. All 16 variables were used in the above analysis. For the classification of different fermentation degrees of oolong tea, the values were set at 1.0 and 0.5, respectively, and the first 10 variables without the ratios were utilized. The

**Table 2. Polyphenols and Caffeine Content and ANOVA Analysis of Tea Categories[a]**

| | | content (%) of calibration set | | | | |
|---|---|---|---|---|---|---|
| no. | compound | GT ($n$ = 164) | WT ($n$ = 50) | OT ($n$ = 198) | BT ($n$ = 51) | $F$ value, significance * |
| 1 | EGC | 1.87 ± 0.50 a | 0.88 ± 0.28 b | 2.14 ± 0.90 c | 0.15 ± 0.30 d | 145.66 * |
| 2 | C | 0.04 ± 0.05 a | 0 ± 0.01 b | 0.08 ± 0.05 c | 0.07 ± 0.05 ac | 23.16 * |
| 3 | EC | 0.40 ± 0.11 a | 0.25 ± 0.13 b | 0.68 ± 0.27 c | 0.27 ± 0.32 b | 94.24 * |
| 4 | EGCG | 6.83 ± 1.61 a | 5.02 ± 1.64 b | 5.07 ± 1.79 b | 0.37 ± 0.40 c | 214.83 * |
| 5 | ECG | 1.47 ± 0.41 a | 1.76 ± 0.55 b | 1.13 ± 0.27 c | 0.41 ± 0.50 d | 119.94 * |
| 6 | N-GC | 2.32 ± 0.56 a | 1.14 ± 0.36 b | 2.90 ± 1.14 c | 0.50 ± 0.66 d | 137.96 * |
| 7 | G-C | 8.30 ± 1.87 a | 6.79 ± 2.12 b | 6.20 ± 2.01 b | 0.79 ± 0.86 c | 209.57* |
| 8 | TC | 10.63 ± 2.30 a | 7.93 ± 2.34 b | 9.10 ± 2.54 c | 1.28 ± 1.34 d | 213.78 * |
| 9 | CAF | 2.39 ± 0.49 a | 4.06 ± 0.51 b | 2.52 ± 0.58 ac | 2.87 ± 0.95 c | 109.88 * |
| 10 | TP | 14.94 ± 2.04 a | 16.03 ± 2.92 ab | 16.76 ± 3.11 bc | 11.73 ± 3.76 d | 45.67 * |

[a]Values are shown as means ± standard deviation, analyzed by one-way ANOVA, utilizing the Dunnett T3 test. Values that do not share a common letter within the same row are significantly different ($P$ < 0.05) from each other.

classification criterion of the equations was as follows: each equation is evaluated by substituting the biochemical data, for which the highest outcome can be regarded as the tea category. In our study, original classification, cross-validation (with the characteristic of "leaving-one-out"), and external validation were used to test the performance of models based on the feature variables.

## RESULTS AND DISCUSSION

**Theoretical Basis of Tea Classification.** As listed in Table 2 and shown in Figure 1, it is remarkable that several compounds were found to have statistically significant differences in tea categories. Almost all of the measured compounds had significant differences ($P$ < 0.05) of relative abundance with respect to categories. The highest compounds of green tea compared to other teas were EGCG, galloylated catechins, and total catechins as the steaming process preserves the greatest degree of polyphenols, resulting in the bitter and astringent taste, although caffeine was the lowest of all teas. With regard to white tea, ECG and caffeine showed the highest contents because the processes include neither pan-frying nor rolling. Because drying temperature and cell damage rates of white tea are lower than those of other teas, the sublimation of caffeine of white tea is much less than that of other teas. On the contrary, white tea showed the lowest content of C and EC; in addition, it also had lower EGCG, non-galloylated catechins, and TC compared to oolong and green teas.[27] For oolong tea, total content and constituents of nongalloylated catechins and total polyphenols were the maximum compared to other teas, but total content and constituents of galloylated catechins were significantly lower than in green tea. It is possible that galloylated catechins are the dominant autoxidation compounds in the oxidation process of oolong tea. The results showed that green tea contained higher ECG and EGCG, but lower EGC, than oolong tea,[1] but when compared to white tea it had lower ECG and higher EGC and EGCG. Except C, EC, and caffeine, other compounds of black tea were at the lowest level compared with other teas. Most polyphenols of black tea are dramatically decreased during enzymatic oxidation, involving polyphenol oxidase. Prevailing biochemistry of teas was mainly consistent with previous results.[26] Therefore, the significant

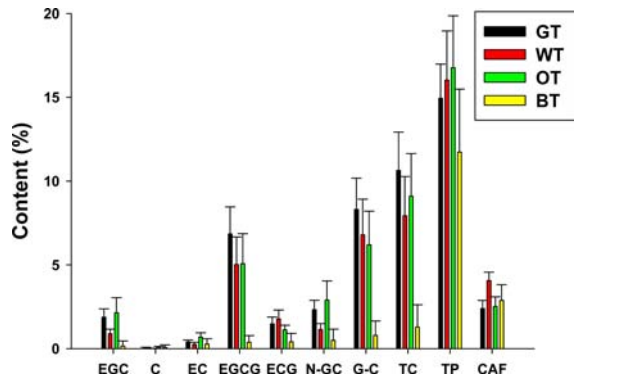


**Figure 1.** Differences of polyphenols and caffeine contents.

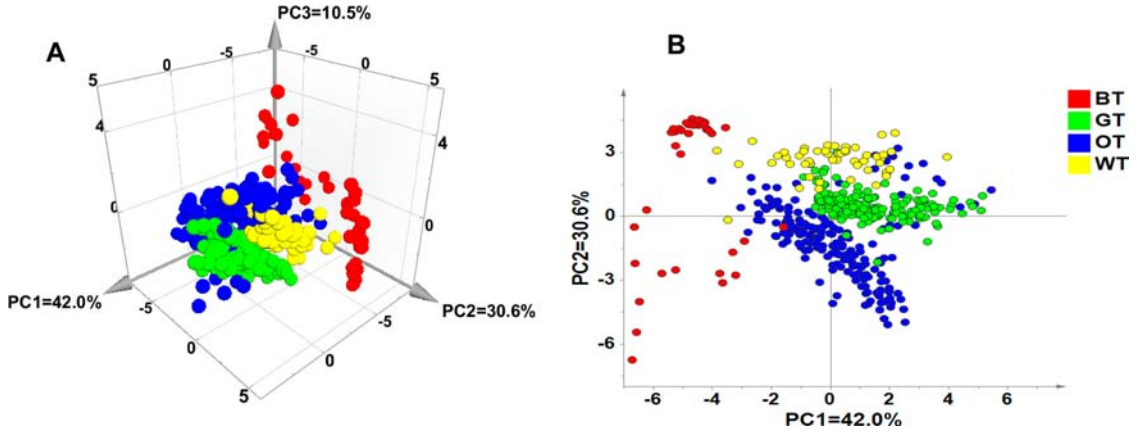


**Figure 2.** Scatter plots of (A) the three first principal components and (B) the two first principal components.


dx.doi.org/10.1021/jf5025483 | J. Agric. Food Chem. 2014, 62, 9336−9344

differences of chemical compounds of tea might provide the fundamental condition of tea classification and were preferred for further analysis using PCA and S-LDA.

**Tea Classification with PCA.** The 463 samples were divided into four groups ranked according to their fermentation degrees. PCA calculations using a reduced number of variables were performed to have a better recognition of the sample information. It is useful for data visualization because a multiplex data set can be effectively observed when it is reduced to a lesser dimensionality. Three significant components were obtained when PCA was performed using the calibration set, jointly accumulating 83.1% of the total variance. Figure 2A shows the PCA 3D score plot with the first, second, and third components explaining 42.0, 30.6, and 10.5% of the total variance, respectively. All 463 samples are projected as small balls of different colors depending on their categories in the plot.

Although there was no clear separation between the objects, some trends can be observed. As is shown in Figure 2A, clear separations of green tea (green balls) and black tea (red balls) samples can be detected, indicating that the degrees of fermentation were quite different from each other. The different producing methods may contribute to the distinctive chemical profile of green tea and black tea, besides their appearance differences. Normally, green tea is characterized by its nonfermentation by steaming process, whereas black tea is fully fermented by the fermentation process, which may explain their distinctive chemical profiles. Separation of white tea (yellow balls) and oolong tea (blue balls) samples was indistinct, indicating that their chemical profiles are much more similar in contrast to those of green tea and black tea. Although all 16 variables gave meaningful information to the classified differences in some degree, some might virtually detract from the simultaneous discrimination of the four tea categories. The results of separating fermented tea from nonfermented tea on the basis of the two first components were negative when some variables were concentrated by the procedure (Figure 2B). Therefore, a more effective feature selection and extraction procedure is desired.

**Tea Classification with S-LDA.** To extract the most discriminating features for the simultaneous discrimination of the four tea categories, S-LDA was performed with the whole variables. Twelve variables apart from EGCG, EGC, N-GC, and the ratio of G-C and TC were selected by Wilks' lambda criterion, whereas the three discrimination functions were constructed, describing 67.5% (DF1), 21.6% (DF2), and 10.9% (DF3) of the total variance, respectively, as shown in Table3. Furthermore, the absolute correlation and contribution of each variable were associated with discriminant function for reflecting its discriminant capacity. The feature variables contributing the most between green tea and oolong tea basically had significant differences, apart from the caffeine that was not of remarkable content, whereas EC was not significant between white tea and black tea (Table 2).

Figure 3 shows the biplot and 3D score plot of canonical discriminant functions, with corresponding tea categories that have been satisfactorily separated. All samples are projected as different shapes and colors depending on their categories in the plot. Green tea and oolong tea have a very distinct separation in the biplot of DF2 and DF3 (Figure 3A), whereas white tea and black tea have a very distinct separation in the biplot of DF1 and DF2 (Figure 3B). Figure 3C shows that green tea and white tea can be effectively classified by DF1 and DF3.

**Table 3. Prediction Results of S-LDA of Tea Categories Using the Original Cases and Cross-Validation and Corresponding Discriminant Functions and Chemical Compounds**

| | prediction of calibration set | | |
|---|---|---|---|
| tea category | original cases (%) | cross-validated (%) | discriminant functions and chemical compounds |
| green | 98.2 (161/164) | 97.6 (160/164) | DF2 and DF3: EC, EGC/TC, ECG, N-GC/TC, C, N-GC/G-C, CAF, TP |
| oolong | 96.5 (191/198) | 94.9 (188/198) | |
| white | 100.0 (50/50) | 98.0 (49/50) | DF1 and DF2: TC/TP, TC, G-C, EGCG/TC, EC, EGC/TC, ECG, N-GC/TC, C, N-GC/G-C |
| black | 100.0 (51/51) | 94.1 (48/51) | |
| total | 97.8 | 96.1 | |

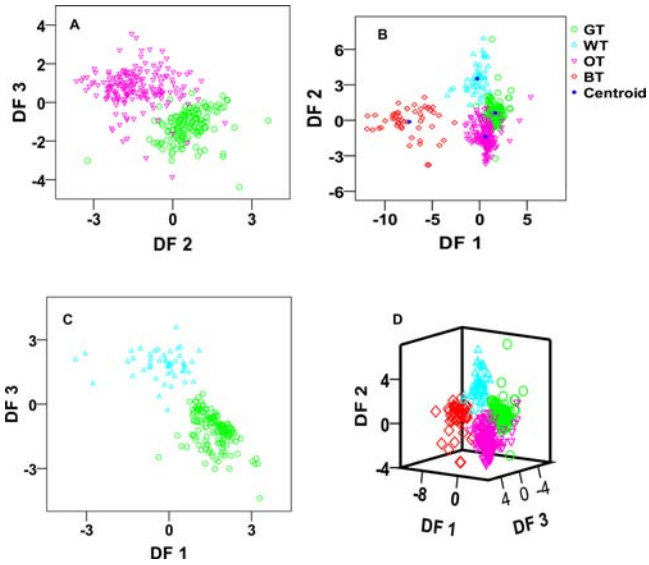


**Figure 3.** Scatter plots of (A) DF2 and DF3, (B) DF1 and DF2, (C) DF1 and DF3, and (D) 3D score of DF1, DF2, and DF3.

Meanwhile, Figure 3D shows the S-LDA 3D score plot with the first, second, and third functions explaining 100% of the total system variance, showing the three significant functions can maximally separate all samples. In summary, four categories can be well separated by using the three DFs extracted.

**Oolong and Other Tea Classification with S-LDA.** For the sake of establishing the International Standard of oolong tea, we also conducted the discrimination of oolong and other teas. Oolong tea usually has a higher unit price than green and black teas in the international tea market for its complex processing steps and limited supply.[1] Hence, it is important to distinguish oolong from other teas. There were 198 samples of oolong tea and 265 samples of other teas (total 463 samples), which were performed by S-LDA, yielding one DF derived from the canonical discriminant fuction (Table S4 in the Supporting Information) and two equations derived from classification function coefficients (Table S5 in the Supporting Information) with the best capacity of their discrimination. Most samples could be successfully differentiated according to their chemical markers. When DF1 yields a positive value, the tea is classified as oolong tea (group centroids, 1.574) and when negative, other teas (group centroids, −1.176).


dx.doi.org/10.1021/jf5025483 | J. Agric. Food Chem. 2014, 62, 9336−9344

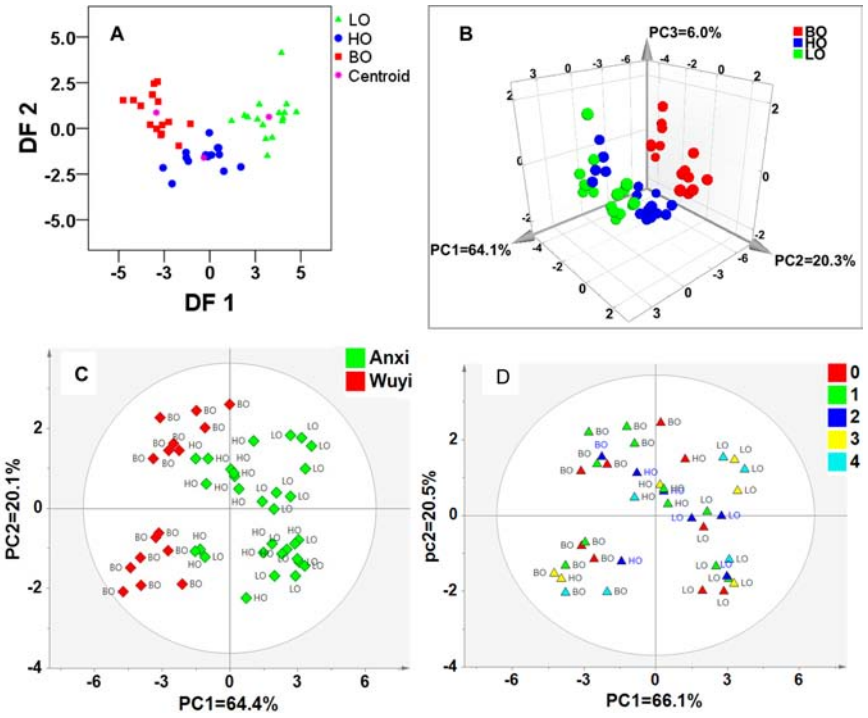


**Figure 4.** Scatter plots of (A) 48 samples elaborated by DF1 and DF2, (B) 48 samples of the three first principal components, (C) 47 samples from different producing regions (Anxi and Wuyi Mountain) of the two first principal components, and (D) 39 samples collected from high to low grades (special grade, levels 1, 2, 3, and 4) of the two first principal components.

$$\begin{aligned}\text{DF1} = {} & 5.406 \times \text{EC} - 1.616 \times \text{ECG} - 0.553 \times \text{N-GC} \\ & - 0.124 \times \text{TC} + 0.255 \times \text{TP} \\ & - 0.014 \times (\text{N-GC/G-C}) + 0.028 \times (\text{N-GC/TC}) \\ & + 0.035 \times \text{EGCG/TC} + 0.082 \times \text{EGC/TC} \\ & - 5.926\end{aligned}$$

An unknown sample also can be predicted by the following equations. After the feature compounds are detected, we bring the data into the two equations, the result of which is higher and could be regarded as the tea category. This method is more convenient and visualized than DF1.

$$\begin{aligned}\text{Equ (oolong)} = {} & 12.246 \times \text{EC} + 19.699 \times \text{ECG} \\ & + 16.712 \times \text{N-GC} - 10.745 \times \text{TC} \\ & + 3.716 \times \text{TP} + 0.114 \times (\text{N-GC/G-C}) \\ & + 1.127 \times (\text{N-GC/TC}) \\ & + 2.549 \times \text{EGCG/TC} \\ & - 0.315 \times \text{EGC/TC} - 110.037\end{aligned}$$

$$\begin{aligned}\text{Equ (others)} = {} & -2.621 \times \text{EC} + 24.144 \times \text{ECG} \\ & + 18.232 \times \text{N-GC} - 10.404 \times \text{TC} \\ & + 3.015 \times \text{TP} + 0.152 \times (\text{N-GC/G-C}) \\ & + 1.050 \times (\text{N-GC/TC}) \\ & + 2.452 \times \text{EGCG/TC} \\ & - 0.542 \times \text{EGC/TC} - 93.193\end{aligned}$$

**Fermentation Degree Classification of Oolong Tea with S-LDA.** For the purpose of further testing the applicability of chemical compounds coupled with S-LDA in different fermentation degrees of tea, this study conducted S-LDA of different fermentation degrees of oolong tea. It is important for us to know whether polyphenols and caffeine are suitable for the same tea category with different fermentation degrees. According to the processing procedure, oolong tea can mainly be divided into three typical kinds with the lightest, intermediate, and highest degree of fermentation, respectively. In this study, 48 observations (Table S6 in the Supporting Information) of 3 classes were selected from 198 samples of oolong tea: faint-scent Tieguanyin (LO, lightest fermentation degree) and familiar-scent Tieguanyin (HO, intermediate fermentation degree) derived from Anxi and baking type oolong (BO, highest fermentation degree) derived from Wuyi Mountain in Fujian province. These samples were collected at distinct grades so as to confirm the applied effect of chemistry on tea classification. Figure 4A shows different fermentation degrees of oolong tea have been well-separated by the biplot of canonical discriminant functions. As expected, a clear separation of the three kinds of oolong tea was achieved with the DF1 (84.4%) and DF2 (15.6%) representing 100% of the total variance, with a 100% correct rate. PCA of the three kinds of oolong tea were also separated dramatically (Figure 4B).

Although separations of the different fermentation degrees of oolong tea obtained by S-LDA and PCA are very encouraging results, we also want to ascertain how other features, such as producing region and quality, may affect the fermentation separations. In our study, PCA was put forward on 47 observations (Table S7 in the Supporting Information) of the above kinds of oolong tea derived from the two producing regions (Anxi and Wuyi Mountain, Fujian province). A clear separation according to fermentation degree was achieved, although producing areas were also considered (Figure 4C). To evaluate the effect of quality on fermentation discrimination, a


dx.doi.org/10.1021/jf5025483 | J. Agric. Food Chem. 2014, 62, 9336−9344

second PCA was put forward on 39 observations (Table S8 in the Supporting Information) of different kinds of oolong teas collected at distinct grades (special grade and levels 1, 2, 3, and 4). As expected, fermentation degrees still played a crucial role in sample clustering compared to quality grades, as shown in Figure 4D. Taking all of the results of PCA into consideration, it is possible to confirm that the processing technology clearly dominates over the other features (such as producing areas and quality) contained in the nonvolatile compounds of tea. On the basis of the results obtained in our work, fermentation discrimination by potential composition demonstrated that it is also applicative for different fermentation degrees of oolong tea.

It was previously reported that taste reconstruction experiments were conducted to identify the key nonvolatile compounds in ready-to-drink green teas using HPLC, and regression models were developed to assess the intensities of bitterness and astringency.[22] Our study confirmed that the HPLC method was also feasible for fermentation discrimination of various teas, even though the different fermentation degrees of the same tea category were of similar appearance and producing area. Moreover, our study provides an objective method based on chemical compounds for detecting fermentation degrees of teas.

**External Authentication of the Models of Teas.** To test the merits of the model, we also conducted two strategies of validation. Foremost, the discriminant ability of the model carried out by S-LDA was tested using the original cases and cross-validation procedure, as shown in Table 3. The external validation was carried out as the secondary validation strategy, as shown in Table S3 in the Supporting Information. It is a useful method that takes the accurate classification of the validation set as the outstanding criterion to evaluate the established tea models.

By the original cases program, the majority of samples (the correctly classified rate was 97.8%) of the four categories were correctly predicted. The results showed that there were few samples overlapping between green and oolong teas. There were three samples of green tea wrongly identified as oolong tea, whereas seven samples of oolong tea were misclassified as green tea (shown in Figure 3A). The major misclassified samples of oolong were of low grade. On the other hand, by the cross-validation procedure, the discriminant results were similar to the original cased program (the correctly classified rate was 96.1%). Furthermore, by the results of absolute correlation of each variable related to any discriminant function, which was not shown (in the SPSS processed results of S-LDA), it is possible to be the marker for each category. For instance, green tea and oolong tea were separated effectively by DF2 and DF3 (Figure 3A), indicating chemical compounds with the largest absolute correlation, with these two discriminant functions, contributing most to the distinction of the two kinds of teas.

In the classification of oolong and other teas, 93.4% samples of oolong tea and 95.5% samples of other teas were classified correctly using DF1. The results showed that four samples of green tea, seven samples of black tea, and one sample of white tea were wrongly discriminated as oolong tea. Thirteen samples of oolong tea were misclassified as other teas. The results indicated that it became more difficult to classify oolong tea from other teas when two-class discrimination was conducted. It is supposed that the feature information on each tea category was lost by their combination to be a class.

In our study, 10 samples of each category produced in 2012 were collected from the dominant market to perform the external validation. Both the discrimination of the four kinds of tea categories and the discrimination of separating oolong tea from other teas were ideal. In external validation of the four different teas, two samples of oolong tea were discriminated wrongly; one wrongly identified sample was oolong crude tea, and the other one was oolong dust tea. The two kinds of tea are of poor quality, resulting in their having lower levels of biochemical compounds than other oolong teas. Besides, there were each samples of green tea and white tea wrongly classified. In external validation of oolong and other teas, one sample of oolong and two samples of other teas were identified incorrectly.

**Comparison of S-LDA and PCA.** By S-LDA compared to PCA, sufficient information for the simultaneous discrimination of the four tea categories was provided, without nearly indistinctive separation, and a simple and effective discriminant model can be constructed on the basis of the reduced variable. In other words, it is possible that the chemicals or biochemicals can be extracted from the complex data when S-LDA was processed, which is most effective in sorting tea categories by different degrees of fermentation. Even so, PCA is still a useful tool for preliminary data analysis and effective visualization of the sample structure.[24]

**Comparison of Green and Black Tea from Other Countries.** To study whether this method can apply to international teas, we collected 10 samples of green tea from Japan and 9 samples of black tea from Sri Lanka and then conducted the two-class discrimination. Utilizing the same 16 variables, we carried out the S-LDA procedure; as expected, all 19 samples were classified correctly with the introduction of three variables. The variables were EGCG, TP, and the ratio of EGCG and TC. In addition, when these samples were added into the external validation to test the models of the four kinds of teas constructed by 463 samples, all 19 samples were discriminated correctly. This is a milestone for future research in chemical classification.

In conclusion, a novel approach to accurately identify analytical markers for discriminating fermentatin degrees of tea was provided, based on potential chemical compounds analyzed by HPLC and spectrophotometry. Moreover, this study discovered that significant differences in chemical compounds may remarkably discriminate tea categories and their fermentation degrees, even if the teas are similar in appearance and taste, which can only be correctly distinguished by experienced tea tasters. The feature of chemical compounds caused by processing also seems dominate over other features (such as producing region and quality). Feature extraction and selection achieved by S-LDA could successfully construct robust models for tea discrimination and fermentation degree. In the future, greater international samples should be collected to improve the applicability of the models. Other standardized methods for catechin oxidation polymers, such as theaflavins or thearubigins, might become available and useful to discriminate the tea categories.[19] Additional data will also contribute to establish more robust classification models of teas.

## ■ ASSOCIATED CONTENT

### Ⓢ Supporting Information

Calibration set of four kinds of teas discriminant (Table S1), calibration set of the discriminant of green tea and black tea (Table S2), validation set of four kinds of teas discriminant

(Table S3), canonical discriminant function coefficients (Table S4), classification function coefficients (Table S5), calibration set of different fermentation degrees of oolong tea (Table S6), 47 samples of different fermentation degrees of oolong collected from different producing areas (Table S7) and 39 samples of oolong collected from high to low grades (Table S8). This material is available free of charge via the Internet at http://pubs.acs.org.

## AUTHOR INFORMATION

### Corresponding Author

*(W.-J.S.) Phone: + 86 591 86392857; Fax: + 86 591 86392736;. E-mail: swj8103@126.com.

### Funding

This study was kindly supported by grants from the Specialized Research Fund for the Doctoral Program of Higher Education (SRFDP) (20133515110006) and the Public Welfare Industry Research Project (201410225-4) undertook by General Administration of Quality Supervision, Inspection and Quarantine of the People's Republic of China.

### Notes

The authors declare no competing financial interest.

## ACKNOWLEDGMENTS

We are grateful to Jin-lei Li, Abrar Muhammad (Department of Plant Protection, Fujian Agriculture and Forestry University, Fujian, China), Kai-jin Kuang (Cross-Strait Nature Reserve Research Center, Fujian Agriculture and Forestry University), and Mubasher Hussain (Institute of Applied Ecology, Fujian Agriculture and Forestry University) for their technical advice. We acknowledge Tie Guan Yin Group, Ba Ma Tea Co., Wuyi Star Tea Co., Fujian Tea Import and Export Co., Yan Shang Tea Co., Lapsang Tea Industry, Fujian Yuan Thai Tea Industry, Many Tasty Tea Co., Pin Pin Xiang Tea Co., Fujian Tian Hao Tea Co., Zhenghe Rui Ming Tea Co., and Guangdong Grand Tea Co. (China) for their assistance with sample collection.

## ABBREVIATIONS USED

C, catechin; EC, epicatechin; EGC, epigallocatechin; EGCG, epigallocatechin gallate; ECG, epicatechin gallate; N-GC, nongalloylated catechins; GC, galloylated catechins; TC, total catechins; TP, total polyphenols; CAF, caffeine; ISO 14502-1:2005, determination of substances characteristic of green and black tea − part 1: content of total polyphenols in tea − colorimetric method using Folin−Ciocalteu reagent; ISO 14502-2:2005, determination of substances characteristic of green and black tea − part 2: content of catechins in green tea − method using high-performance liquid chromatography; ISO 1572, tea preparation of ground sample of known dry matter content; ISO 1573, tea determination of loss in mass at 103 °C; DF, discriminant function; LO, faint-scent Tieguanyin; HO, familiar scent Tieguanyin; BO, baking type oolong

## REFERENCES

(1) Wang, L. F.; Lee, J. Y.; Chung, J. O.; Baik, J. H.; So, S.; Park, S. K. Discrimination of teas with different degrees of fermentation by SPME-GC analysis of the characteristic volatile flavour compounds. *Food Chem.* **2008**, *109* (1), 196−206.

(2) Wu, D.; Yang, H. Q.; Chen, X. J.; He, Y.; Li, X. L. Application of image texture for the sorting of tea categories using multi-spectral imaging technique and support vector machine. *J. Food Eng.* **2008**, *88* (4), 474−483.

(3) Söhle, J.; Knott, A.; Holtzmann, U.; Siegner, R.; Grönniger, E.; Schepky, A.; Gallinat, S.; Wenck, H.; Stäb, F.; Winnefeld, M. White tea extract induces lipolytic activity and inhibits adipogenesis in human subcutaneous (pre)-adipocytes. *Nutr. Metab. (London)* **2009**, *6*, 20.

(4) López, V.; Calvo, M. I. White tea (*Camellia sinensis* Kuntze) exerts neuroprotection against hydrogen peroxide-induced toxicity in PC12 cells. *Plant Foods Hum. Nutr. (N.Y.)* **2011**, *66* (1), 22−26.

(5) Koutelidakis, A. E.; Argyri, K.; Serafini, M.; Proestos, C.; Komaitis, M.; Pecorari, M.; Kapsokefalou, M. Green tea, white tea, and *Pelargonium purpureum* increase the antioxidant capacity of plasma and some organs in mice. *Nutrition* **2009**, *25* (4), 453−458.

(6) Valera, P.; Pablos, F.; González, A. G. Classification of tea samples by their chemical composition using discriminant analysis. *Talanta* **1996**, *43* (4), 415−419.

(7) Wang, L. Y.; Wei, K.; Cheng, H.; He, W.; Li, X. H.; Gong, W. Y. Geographical tracing of Xihu Longjing tea using high performance liquid chromatography. *Food Chem.* **2014**, *146*, 98−103.

(8) Jayasekera, S.; Kaur, L.; Molan, A. L.; Garg, M. L.; Moughan, P. J. Effects of season and plantation on phenolic content of unfermented and fermented Sri Lankan tea. *Food Chem.* **2014**, *152*, 546−551.

(9) Gong, J. S.; Tang, C.; Peng, C. X. Characterization of the chemical differences between solvent extracts from Pu-erh tea and Dian Hong black tea by CP-Py-GC/MS. *J. Anal. Appl. Pyrolysis* **2012**, *95*, 189−197.

(10) Katsuno, T.; Kasuga, H.; Kusano, Y.; Yaguchi, Y.; Tomomura, M.; Cui, J.; Yang, Z.; Baldermann, S.; Nakamura, Y.; Ohnishi, T.; Mase, N.; Watanabe, N. Characterisation of odorant compounds and their biochemical formation in green tea with a low temperature storage process. *Food Chem.* **2014**, *148*, 388−395.

(11) Szymczycha-Madeja, A.; Welna, M.; Pohl, P. Elemental analysis of teas and their infusions by spectrometric methods. *TrAC, Trends Anal. Chem.* **2012**, *35*, 165−181.

(12) Chen, H.; Liang, H.; Ding, J.; Lai, J.; Huan, Y.; Qiao, X. Rapid differentiation of tea products by surface desorption atmospheric pressure chemical ionization mass spectrometry. *J. Agric. Food Chem.* **2007**, *55* (25), 10093−10100.

(13) Nitin Seetohul, L.; Islam, M.; O'Hare, W. T.; Ali, Z. Discrimination of teas based on total luminescence spectroscopy and pattern recognition. *J. Sci. Food Agric.* **2006**, *86* (13), 2092−2098.

(14) Ren, G. X.; Wang, S. P.; Ning, J. M.; Xu, R. R.; Wang, Y. X.; Xing, Z. Q.; Wan, X. C.; Zhang, Z. Z. Quantitative analysis and geographical traceability of black tea using Fourier transform near-infrared spectroscopy (FT-NIRS). *Food Res. Int.* **2013**, *53* (2), 822−826.

(15) Hayashi, N.; Ujihara, T.; Chen, R. G.; Irie, K.; Ikezaki, H. Objective evaluation methods for the bitter and astringent taste intensities of black and oolong teas by a taste sensor. *Food Res. Int.* **2013**, *53* (2), 816−821.

(16) Huo, D.; Wu, Y.; Yang, M.; Fa, H.; Luo, X.; Hou, C. Discrimination of Chinese green tea according to varieties and grade levels using artificial nose and tongue based on colorimetric sensor arrays. *Food Chem.* **2014**, *145*, 639−645.

(17) Li, X. L.; Nie, P. C.; Qiu, Z. J.; He, Y. Using wavelet transform and multi-class least square support vector machine in multi-spectral imaging classification of Chinese famous tea. *Expert Syst. Appl.* **2011**, *38* (9), 11149−11159.

(18) Laddi, A.; Prakash, N. R.; Sharma, S.; Mondal, H. S.; Kumar, A.; Kapur, P. Significant physical attributes affecting quality of Indian black (CTC) tea. *J. Food Eng.* **2012**, *113* (1), 69−78.

(19) Obuchowicz, J.; Engelhardt, U. H.; Donnelly, K. Flavanol database for green and black teas utilising ISO 14502-1 and ISO 14502-2 as analytical tools. *J. Food Compos. Anal.* **2011**, *24*, 411−417.

(20) Wang, L. Y.; Chen, H.; Zhou, J.; hE, X. Y. Discriminant classification of Wuyi Yan tea based on multiple chemical fingerprint (in Chinese). *J. Tea Sci.* **2010**, *30*, 83−88.

(21) Zielinski, A. A. F.; Haminiuk, C. W. I.; Alberti, A.; Nogueira, A.; Demiate, I. M.; Granato, D. A comparative study of the phenolic compounds and the in vitro antioxidant activity of different Brazilian

teas using multivariate statistical techniques. *Food Res. Int.* **2014**, *60*, 246−254.
(22) Yu, P. G.; Yeo, A. S. L.; Low, M. Y.; Zhou, W. B. Identifying key non-volatile compounds in ready-to-drink green tea and their impact on taste profile. *Food Chem.* **2014**, *155*, 9−16.
(23) Kerio, L. C.; Wachira, F. N.; Wanyoko, J. K.; Rotich, M. K. Total polyphenols, catechin profiles and antioxidant activity of tea products from purple leaf coloured tea cultivars. *Food Chem.* **2013**, *136* (3−4), 1405−1413.
(24) Lin, J.; Zhang, P.; Pan, Z.; Xu, H.; Luo, Y.; Wang, X. Discrimination of oolong tea (*Camellia sinensis*) varieties based on feature extraction and selection from aromatic profiles analysed by HS-SPME/GC-MS. *Food Chem.* **2013**, *141* (1), 259−265.
(25) Wei, K.; Wang, L. Y.; Zhou, J.; He, W.; Zeng, J. M.; Jiang, Y. W.; Cheng, H. Comparison of catechins and purine alkaloids in albino and normal green tea cultivars (*Camellia sinensis* L.) by HPLC. *Food Chem.* **2012**, *130* (3), 720−724.
(26) Stodt, U. W.; Blauth, N.; Niemann, S.; Stark, J.; Pawar, V.; Jayaraman, S.; Koek, J.; Engelhardt, U. H. Investigation of processes in black tea manufacture through model fermentation (oxidation) experiments. *J. Agric. Food Chem.* **2014**, *62* (31), 7454−7461.
(27) Wang, Y. F.; Liu, Y. Y.; Huo, J. L.; Zhao, T. T.; Ren, J.; Wei, X. L. Effect of different drying methods on chemical composition and bioactivity of tea polysaccharides. *Int. J. Biol. Macromol.* **2013**, *62*, 714−719.

such that it becomes difficult to assess the role of conformational changes induced by enzymatic cross-linking.

An alternative to mTG-catalyzed protein cross-linking is oxidative cross-linking of endogenous or exogenous phenolic compounds, such as tyrosine residues, caffeic acid, or ferulic acid, that can be used to cross-link to either protein or polysaccharides (e.g., arabinoxylan) using various oxidative enzymes.[28−30] While tyrosine is the most reactive residue for enzymatic oxidation, oxidative enzymes are capable of reacting with phenylalanine, tryptophan, and cysteine and, thus, results in a range of different types of chemical bonds (tyrosine−tyrosine, lysine−tyrosine, cysteine−tyrosine).[31−33] In addition to phenylalanine, tryptophan, and cysteine, laccase has also been found to oxidize histidine, arginine, and methionine.[34] The functional and technological impacts of oxidative enzymes as an alternative mTG are still under investigation. Whereas promising results of enhanced functionality have already been reported for various oxidative enzymes,[35−38] little is known about conformational changes of globular proteins induced by oxidative enzymatic cross-linking so far.

Previously, we have investigated the development of protein nanostructures during enzymatic cross-linking of apo-$\alpha$-lactalbumin by horseradish peroxidase (HRP).[39,40] The apo-form or calcium-free form of $\alpha$-lactalbumin has a "molten globule" structure, making the protein quite accessible to enzymatic cross-linking, and thus allows for studying the enzymatic cross-linking of $\alpha$-lactalbumin without using heat treatment or denaturants.[41] Heijnis et al.[42] have shown that horseradish peroxidase induces the initial step of cross-linking between Tyr18 and Tyr50 in the apo-form. We have found that nanostructures evolve in a two-stage process: (1) In an initial phase, with rapid conversion of tyrosines, monomers are cross-linked to form oligomers. (2) Upon prolonged cross-linking, protein nanoparticles are formed via cross-linking of the oligomers. In this last phase, the conversion rate of the remaining tyrosines is much slower than that in the first phase. The final protein nanoparticles have a very open structure, are very heterogeneous in size and architecture, and exhibit a size-mass scaling of $R_H = M^a$, with an exponent $a \approx 0.4$, where $R_H$ is the hydrodynamic radius and $M$ is the molar mass. The internal protein density of the protein nanoparticles is approximately a few percent (w/v) for particles with a molar mass $M$ of $10^6$ Da and a hydrodynamic radius $R_H$ of 30 nm.[39,40]

In order to link the impact of cross-linking on food functionality across all length scales, we here investigate conformational changes in apo-$\alpha$-LA upon HRP-catalyzed cross-linking. We consider both conformational changes in the initial phase of cross-linking and the changes that occur upon prolonged cross-linking, and we find significant differences between these two cases. As we will show, these differences correlate with changes in the surface hydrophobicity that we also quantify, thus linking structure to the techno-functionality of cross-linked apo-$\alpha$-LA also at molecular length scales.

## MATERIALS AND METHODS

**Materials.** A commercial preparation of calcium-free $\alpha$-lactalbumin (here simply referred to as apo-$\alpha$-LA) was supplied by Davisco Foods International Inc. (Le Sueur, MN). The protein preparation is reported to consist of 85% apo-form ($Ca^{2+}$-depleted) and 15% holo-form ($Ca^{2+}$-saturated). For all experiments in this study, the same protein source and batch were used. Horseradish peroxidase (HRP) type VI-A (P6782) and 2,2′-azino-bis(3-ethylbenzothiazoline-6-sulfonic acid) (ABTS) were also supplied by Sigma-Aldrich. All other chemicals used were of analytical grade.

**Enzyme Activity.** In order to determine HRP activity, an ABTS assay was performed according to the published procedure.[40] The activity of the enzyme preparation as given by the manufacturer is ∼1000 units/mg). This is in agreement with our own determinations, for which we find a variation of enzyme activity from batch to batch of less than about 15%.

**Sample Preparation.** Stock solutions of apo-$\alpha$-LA (12 mg/mL) and HRP (15 mg/mL) were separately prepared by dissolving protein and enzyme powder in 0.1 M ammonium acetate buffer ($NH_4Ac$) at 25 °C, respectively. After centrifugation (3 h, 45 000*g*, 25 °C) of the protein solution, the pH was adjusted to 6.8 using 0.1 mM HCl. Finally, the protein concentration was determined using UV spectroscopy assuming an absorbance $A_{280}$ = 20.1 for a 1% (w/v) solution of $\alpha$-lactalbumin.[43] The concentration of HRP solutions was also determined using UV spectroscopy, assuming a molar extinction coefficient of $\varepsilon_{403}$ = 102 $mM^{-1}$ $cm^{-1}$.[44] To prepare hydrogen peroxide ($H_2O_2$) stock solutions, an aqueous solution of 30% (w/w) of $H_2O_2$ was diluted into deionized water to a concentration of 0.05 M. Before use, the precise concentration of the $H_2O_2$ stock solution was determined using UV spectroscopy, assuming a molar extinction coefficient of $\varepsilon_{240}$ = 43.6 $M^{-1}$ $cm^{-1}$.[45]

**Reactions.** *Reaction 1.* Conditions for the reaction leading to "partially" cross-linked apo-$\alpha$-LA, were similar to those published before.[39,40] The concentration of apo-$\alpha$-LA in the reaction mixture was 10 mg/mL (or 0.7 mM). The apo-$\alpha$-LA solution was incubated in a 50 mL water-jacketed glass vessel under continuously stirring at 37 °C in 0.1 M $NH_4Ac$ at pH 6.8 for 1 h. Next, HRP stock solution was added into protein solution (i.e., a final concentration of the enzyme of 0.5 mg/mL in the reaction mixture). Finally, small amounts (2 $\mu$L per mL of reaction mixture) of 50 mM $H_2O_2$ were added periodically into the reaction mixture, every 10 min. $H_2O_2$ addition was done using a computer-controlled Schott Geräte TA01 titration system. Every addition corresponded to a change in the $H_2O_2$ concentration of $\Delta[H_2O_2]$ = 0.1 mM. The total reaction consisted of 15 additions of $H_2O_2$ into the reaction mixture. The final reaction product was cooled down at room temperature and stored at 4 °C. Analysis on the mixture was performed the following day, without any further purification and filtration.

*Reaction 2.* Conditions for the reaction leading to "fully" cross-linked apo-$\alpha$-LA were identical to the conditions for reaction 1, except that 80 additions of $H_2O_2$ were used, in a 250 mL water-jacketed glass vessel.

**Freeze-Drying and Dialysis.** For long-term preservation of reaction mixture 2, after the enzymatic reaction, which was performed at 37 °C, it was first cooled down to 25 °C. Then, the reaction mixture was mixed with 1 M sucrose in a volume ratio of 1:1. Finally, the reaction mixture was freeze-dried at −80 °C. The resulting powder was stored at −80 °C. We have shown before that this procedure does not affect the particle properties when the freeze-dried powder is redissolved.[39] For sample preparation, the powder was redissolved and dialyzed in 10 mM sodium phosphate buffer using a 300 kDa cellulose ester membrane (Spectra/Por CE dialysis) to remove the sucrose and low molecular weight reaction products. The concentration of dialyzed protein nanoparticles was determined using UV spectroscopy, assuming an absorbance $A_{280}$ = 20.1 for a 1% (w/v) solution of fully cross-linked apo-$\alpha$-LA nanoparticles. Dialyzed samples (fully cross-linked apo-$\alpha$-LA nanoparticles, $M_w \geq 10^6$ Da) from the same batch were used for all experiments.

**Instrumental Analysis.** *Size Exclusion Chromatography (SEC) and Fractionation.* Reaction products were analyzed and fractionated by size exclusion chromatography (SEC) using a Superose 6 column (separation range reported for globular proteins between $5 \times 10^3$ and $5 \times 10^6$ Da; exclusion limit $4 \times 10^7$ Da) connected to an AKTA purifier system (GE Healthcare). A volume of 100 $\mu$L of reaction product was injected into the column and eluted with 10 mM sodium phosphate buffer (pH 7.0) at a flow rate of 0.5 mL/min. The UV absorbance of the eluate was monitored at wavelengths of 280 and 318 nm. For fractionation of reaction mixture 1, SEC fractions were

collected into 10 mL tubes at 1 mL intervals, with a collection volume of 0.5 mL for each fractionation step. Protein particles (F), oligomers (from P1 to P7), and un-cross-linked native apo-$\alpha$-LA were collected on the basis of retention volume: F, 7.5 mL ($M_w$ > 2000 kDa); P7, 9 mL, and P6, 10 mL (2000 kDa > $M_w$ > 660 kDa); P5, 11 mL (660 kDa > $M_w$ > 440 kDa); P4, 12 mL, P3, 13 mL, and P2 14 mL (440 kDa > $M_w$ > 66.5 kDa); P1, 15 mL (66.5 kDa > $M_w$ > 18.4 kDa); and $\alpha$-LA, 16.6 mL ($M_w$ = 14 kDa). For further analysis, SEC fractions were concentrated by a factor of 10 in volume using centrifugal filter devices (3 kDa cutoff). Concentrations of concentrated fractions were determined using UV spectroscopy, assuming an absorbance $A_{280}$ = 20.1 for a 1% (w/v) solution of $\alpha$-LA.[40] Finally, concentrations were adjusted to the required values by dilution with buffer.

**Structural Analysis.** *Secondary Structure Analysis.* Far-UV CD spectra (190−260 nm) were acquired using a JASCO J-715 spectropolarimeter (Tokyo, Japan) equipped with a PTC-348WI Peltier temperature-control system. Quartz cuvettes (Starna, Hainault, UK) with 1 mm cell length were used as a sample container. The concentration of all samples was 0.12 mg/mL. CD spectra of samples and blanks were recorded by averaging 20 scans. CD spectra of samples were corrected by subtracting spectra of blanks (10 mM sodium phosphate buffer). From the far-UV spectra, contents of secondary structure ($\alpha$-helix, $\beta$-strands, $\beta$-turns, and random coil) were estimated using the ridge regression algorithm CONTINLL as implemented by the Dichroweb server.[46−48]

*Tertiary Structure Analysis.* Near-UV CD spectra (250−350 nm) of nanoparticle solutions (1 mg/mL) were recorded in 3 mL quartz cuvettes (path length 1 cm) (Starna, Hainault, UK) at 25 °C for reaction 2. CD spectra of samples and blanks were determined by averaging 20 scans. CD spectra of samples were corrected by subtracting spectra of the blanks (10 mM sodium phosphate buffer).

*Secondary Structure of Extensively Heat-Denatured $\alpha$-LA.* Extensively heat-denatured apo-$\alpha$-LA was used for structural comparison with enzymatically cross-linked protein. In order to prepare the denatured protein,[49] apo-$\alpha$-LA (1 mg/mL or 0.07 mM) was dissolved into 10 mM sodium phosphate buffer at pH 7.0 at 25 °C containing 2-mercaptoethanol (2-ME) (1 mM) (Sigma, M6250). In order to allow for complete protein denaturation, the protein solution was heated for 24 h at 90 °C. Next, the sample was quickly cooled down using running tap water and diluted to final concentrations of 0.12 mg/mL for far-UV CD spectroscopy (performed as described above).

*Determination of Hydrodynamic Radius ($R_H$) and Zeta ($\zeta$) Potential.* Dynamic light scattering (DLS) and electrophoretic light scattering (ELS) experiments were done on dialyzed reaction products using a Malvern Nanosizer ZS (Malvern) equipped with an argon ion laser emitting vertically polarized light with a wavelength of 633 nm. For DLS measurements, the scattering angle was 173°. For ELS measurements, the scattering angle was 12.8°. Average hydrodynamic radii $R_H$ and $\zeta$-potential reported are the major peak from the peak analysis as performed by the Malvern DTS software (version 6.20). For DLS, protein samples were measured in a low-volume quartz batch cuvette (ZEN2112). For $\zeta$-potential measurements, a disposable capillary cell (DTS1070) was used. For both measurements, the concentration of sample is 1 mg/mL.

*Fluorescence Spectroscopy.* Fluorescence spectra of apo-$\alpha$-LA and partially and fully cross-linked apo-$\alpha$-LA nanoparticles were obtained using a PerkinElmer LS 50 B spectrofluorimeter at 25 °C. In all experiments, a quartz cuvette with a 1 cm excitation path length was used. For partially and fully cross-linked apo-$\alpha$-LA, samples were diluted to final concentrations of 0.12 mg/mL in 10 mM sodium phosphate buffer at pH 7.0 at 25 °C. In order to monitor fluorescence from cross-linked tyrosines, in particular dityrosines, an excitation wavelength of 315 nm was used. Emission was monitored for wavelengths between 330 and 550 nm. Excitation and emission slits were set at 5 nm.

In order to compare with the spectrum of free dityrosine, we synthesized dityrosine using HRP-catalyzed cross-linking of L-tyrosine. First, 0.72 mg of L-tyrosine was dissolved in 20 mL of 10 mM sodium phosphate buffer at pH 8.0 and transferred into 2 mL Eppendorf tubes. In order to ensure complete dissolution, L-tyrosine solutions were heated at 95 °C for 15 min in a thermal incubator (Thermomixer comfort, Eppendorf, Harmburg, Germany). A HRP stock solution was prepared by dissolving 1.77 mg of horseradish peroxidase (HRP) in 0.2 mL of 10 mM sodium phosphate buffer at pH 8.0. Next, protein and enzyme solutions were mixed at a molar ratio of protein to enzyme of 1000. The enzymatic reaction was performed by the periodic addition of $H_2O_2$ (2 $\mu$L of 0.03% into 2 mL) every 210 s at 37 °C for 2 h. For fluorescence measurements, the reaction mixture (containing L-tyrosine and dityrosine) was diluted to a final concentration of 0.12 mg/mL (based on the initial concentration of L-tyrosine) with 10 mM sodium phosphate buffer, pH 7.0.

*Surface Hydrophobicity.* The anionic fluorescent probe ANSA was used to measure the exposed surface hydrophobicity of proteins and protein particles.[50] First, an ANSA stock solution (2.4 mM) was prepared in 10 mM sodium phosphate buffer at pH 7.0 at 25 °C. The ANSA solution was stored at 4 °C overnight to ensure complete dissolution. Protein samples were diluted to a final concentration of 0.12 mg/mL using 10 mM sodium phosphate buffer at pH 7.0. Aliquots of ANSA stock solution (10 $\mu$L) were titrated into protein solutions (0.12 mg/mL, 1 mL). Between each addition, fluorescence emission spectra were recorded at wavelengths between 400 and 650 nm. The excitation wavelength was 385 nm and the scan rate 120 nm/min. Excitation and emission slits were set at 5 nm. The system was thermostated at 20 °C. The relative exposed hydrophobicity of each sample was expressed as the difference between the minimum and maximum area of an integrated titration curve between 400 and 600 nm after blank subtraction.

## RESULTS AND DISCUSSION

**Partially and Fully Cross-Linked $\alpha$-Lactalbumin.** We refer to the apo-$\alpha$-LA oligomers that are formed in the initial phase of the cross-linking process as "partially cross-linked" proteins (reaction 1: 150 min of reaction time or 15 additions of $H_2O_2$ in 10 min intervals). The larger hierarchical apo-$\alpha$-LA particles that formed at later stages of the cross-linking reaction are referred to as "fully cross-linked" protein (reaction 2: 800 min of reaction time or 80 additions of $H_2O_2$ in 10 min intervals). Conformational changes as compared to apo-$\alpha$-LA are studied separately for the two cases, such that we can also elucidate possible structural transitions in going from oligomers to larger protein particles. In addition, in the early stages, the reaction mixture contains a mix of monomers and a range of oligomers[40] that possibly differ strongly in the extent of conformational change. Therefore, for partially cross-linked proteins (P), we focus on a fixed, short reaction time of 2.5 h, separate the reaction mixture using size exclusion chromatography (fractions P1−P7 from reaction 1), and study conformational changes as compared to apo-$\alpha$-LA for all of the fractions. Figure 1A shows the size exclusion chromatogram (SEC) and indicates the retention volumes corresponding to the different SEC fractions (apo-$\alpha$-LA + P1−P7). Cross-linked tyrosines (i.e., dityrosines) exhibit a strong absorption at 318 nm; hence, Figure 1A also shows the ratio $A_{318}/A_{280}$ which is a qualitative measure for the conversion of tyrosines into cross-linked reaction products, mainly dityrosines. As can be seen in Figure 1A, the conversion of tyrosines increases with oligomer size for the different fractions, whereas apo-$\alpha$-LA fraction shows no signal at 318 nm, as expected. For fully cross-linked protein (F; from reaction 2), we dialyze the reaction product (using a 300 kDa cutoff membrane) to remove oligomers and any remaining monomers from the final reaction mixture. The fully cross-linked protein elutes in the void of the column (see Figure 1B).

**Changes in Secondary and Tertiary Structure upon Enzymatic Cross-Linking.** Changes in secondary structure

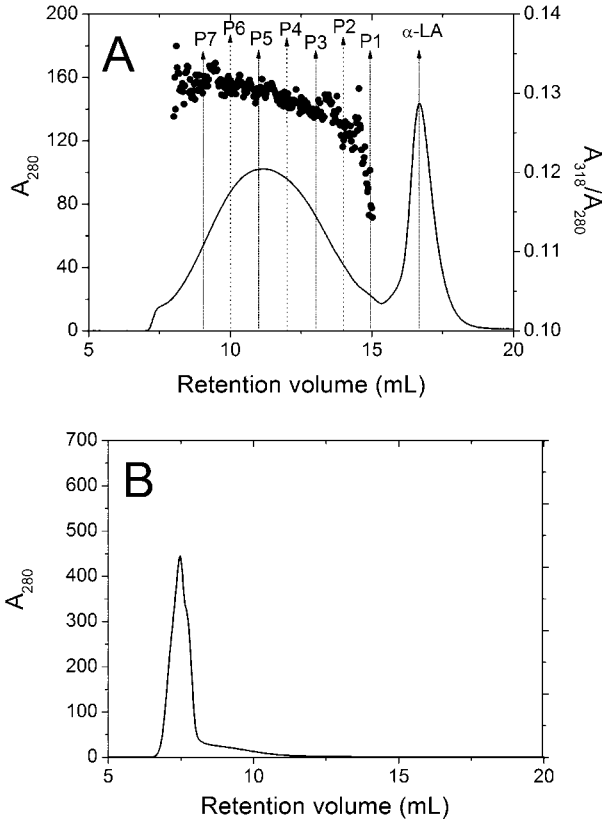


**Figure 1.** (A) SEC chromatograms of HRP-cross-linked apo-$\alpha$-LA. Solid line: UV absorption at 280 nm ($A_{280}$) versus retention volume for partially cross-linked apo-$\alpha$-LA. Retention volumes of SEC fractions from P1 to P7 used in further studies and monomeric protein (apo-$\alpha$-LA) are indicated by arrows (dotted lines). Spheres indicate the ratio $A_{318}/A_{280}$ (a measure for tyrosine conversion) versus retention volume. (B) UV absorption at 280 nm ($A_{280}$) versus retention volume for dialyzed fully cross-linked apo-$\alpha$-LA nanoparticles using 300 kDa cutoff membrane (F). The fully cross-linked nanoparticles elute in the void of the column.

upon enzymatic cross-linking for partially (P1−P7) and fully cross-linked protein (F) were quantified using CD spectroscopy. Far-UV CD spectra are shown in Figure 2 and compared with that of apo-$\alpha$-LA. The latter exhibits a typical spectrum of $\alpha$-helix-rich proteins, with two dips at 208 and 222 nm. For partially cross-linked $\alpha$-LA fraction P1, the ellipticity changes significantly as compared to the native apo-$\alpha$-LA. For the fractions P2−P7 with a higher molar mass and a larger extent of cross-linking (as determined by their $A_{318}/A_{280}$ ratio), there are no further major changes in the ellipticity with fraction number (Figure 2, inset). The spectrum of fully cross-linked $\alpha$-LA (F) is again distinctly different from that of the fractions P1−P7, with a pronounced dip at 208 nm (Figure 2). Hence, it appears that it is the earliest cross-linking event that leads to the formation of the smallest oligomers P1 and P2, which induce the biggest changes in protein conformation. Also it appears that there are significant changes in conformation when going from partially to fully cross-linked protein.

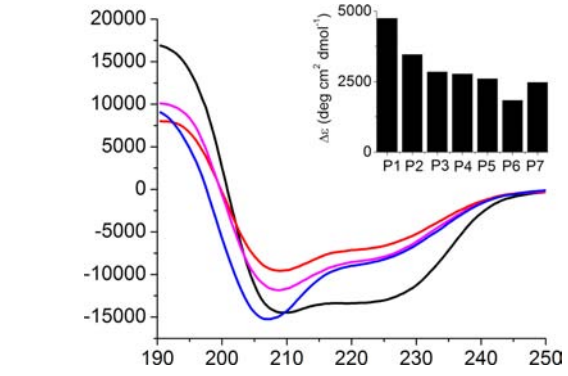


**Figure 2.** Far-UV CD spectra of apo-$\alpha$-LA and cross-linked apo-$\alpha$-LA: black, native apo-$\alpha$-LA; blue, fully cross-linked protein nanoparticles (F). The inset shows the evolution of ellipticity at 208 nm [$\Delta\varepsilon = \varepsilon_1$ (ellipticity of SEC fractions) − $\varepsilon_2$ (ellipticity of native $\alpha$-LA)] for SEC fractions of partially cross-linked protein oligomers, from P1 (red) to P7 (magenta). The solvent is 10 mM sodium phosphate buffer, pH 7.0 at 25 °C. The protein concentration of all samples is 0.12 mg/mL.

From the spectra, we have deduced approximate contents of secondary structure elements ($\alpha$-helix, $\beta$-strands, $\beta$-turns, and random coil) using the ridge regression algorithm CONTINLL as implemented by the Dichroweb server.[46−48] The estimated percentages of secondary structure elements obtained from this analysis are reported in Table 1. A plot of the percentage of $\alpha$-helix versus the fraction number is shown in Figure 3.

**Table 1. Percentages of Secondary Structure Elements for Native Apo-$\alpha$-LA (N, native form) and Partially Cross-Linked (fractions P1−P7) and Fully Cross-Linked Apo-$\alpha$-LA (F) As Deduced from the CD Spectra of Figure 2**

| sample | $\alpha$-helix | $\beta$-sheet | $\beta$-turns | random coil |
|---|---|---|---|---|
| N | 38.5 | 18.1 | 19.3 | 24.1 |
| P1 | 23.8 | 24.8 | 21.3 | 30.1 |
| P2 | 23.9 | 23.9 | 21.3 | 30.8 |
| P3 | 26.4 | 23 | 20.8 | 29.6 |
| P4 | 26.8 | 22.8 | 20.8 | 29.5 |
| P5 | 26.9 | 21.4 | 21.1 | 30.6 |
| P6 | 29.3 | 19.1 | 21.7 | 29.9 |
| P7 | 27.5 | 21.8 | 20.7 | 29.9 |
| F | 31.2 | 17.2 | 21.8 | 29.8 |

Somewhat surprisingly, the analysis of the far-UV CD spectra shows that the highest loss of $\alpha$-helical content as compared to native apo-$\alpha$-LA is observed for the partially cross-linked fractions P1 and P2, which have the lowest extent of tyrosine conversion, whereas the fully cross-linked $\alpha$-LA (F) exhibits the

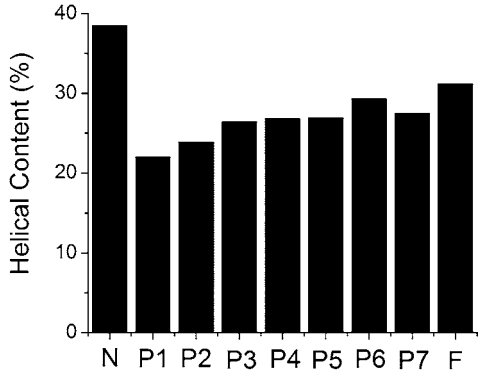


**Figure 3.** Total percentage of $\alpha$-helix as deduced from CD spectroscopy for native apo-$\alpha$-LA (N), SEC fractions of partially cross-linked apo-$\alpha$-LA (P1−P7), and fully cross-linked apo-$\alpha$-LA nanoparticles (F).


dx.doi.org/10.1021/jf502664q | J. Agric. Food Chem. 2014, 62, 9345−9352

lowest loss of $\alpha$-helical content as compared to native apo-$\alpha$-LA (Figure 3). This confirms that the first few tyrosines that are converted lead to the largest loss of $\alpha$-helicity, with further conversion leading to a partial recovery of $\alpha$-helicity.

We have also compared the impact of HRP-induced cross-linking on protein conformation (as deduced from CD spectroscopy) with that of extensively heat-denatured apo-$\alpha$-LA (i.e., heated for 24 h at 90 °C in 10 mM sodium phosphate buffer at pH 7 in the presence of 1 mM 2-ME). The far-UV CD spectrum of extensively heat-denatured apo-$\alpha$-LA (D) is shown in Figure 4 and compared with those of native apo-$\alpha$-LA and fully cross-linked apo-$\alpha$-LA (F).

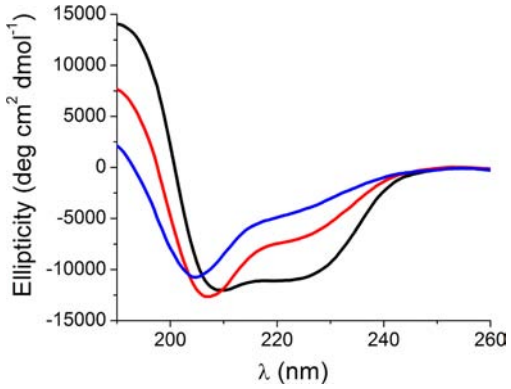


**Figure 4.** Far-UV CD spectra of native apo-$\alpha$-LA (black), fully cross-linked apo-$\alpha$-LA (red), and extensively heat-denatured apo-$\alpha$-LA (blue, 90 °C for 24 h in the presence of 1 mM 2-ME). Solution conditions for CD measurements were 10 mM sodium phosphate buffer at pH 7.0 at 25 °C.

As expected, conformational changes as compared to native apo-$\alpha$-LA are largest for heat-denatured $\alpha$-LA. From the far-UV CD spectra in Figure 4, it appears that the secondary structure of fully cross-linked apo-$\alpha$-LA is intermediate between that of native and extensively heat-denatured apo-$\alpha$-LA. This analysis is confirmed by a more quantitative interpretation of the CD spectra in terms of approximate contents of secondary structure elements. Results for native (N), heat-denatured (D), and fully cross-linked (F) $\alpha$-LA are given in Table.2. Our findings indicate that fully cross-linked apo-$\alpha$-LA has significantly higher secondary structure than fully denatured apo-$\alpha$-LA.

**Table 2. Percentages of $\alpha$-Helix, $\beta$-Strands, $\beta$-Turns, and Random Coil for Native Apo-$\alpha$-LA (N), Fully Cross-Linked Apo-$\alpha$-LA (F), and Extensively Heat-Denatured Apo-$\alpha$-LA (D), Estimated from the CD Spectra of Figure 4**

| sample | $\alpha$-helix | $\beta$-strands | $\beta$-turns | random coil |
|---|---|---|---|---|
| N | 38.5 | 18.1 | 19.3 | 24.1 |
| F | 31.2 | 17.2 | 21.8 | 29.8 |
| D | 20.5 | 23.3 | 24.2 | 32 |

With regards to the tertiary structure, earlier investigations have shown that in the "molten globule" structure of calcium-free apo-$\alpha$-LA, much of the tertiary structure is already lost, as compared to holo-$\alpha$-LA.[51] As is shown in Figure 5, apo-$\alpha$-LA nevertheless retains the characteristic features of the near-UV CD spectrum of holo-$\alpha$-LA, but with lower intensity. Note that complete removal of all $Ca^{2+}$ from the apo-$\alpha$-LA preparation that we have used does not change the near-UV CD spectrum,

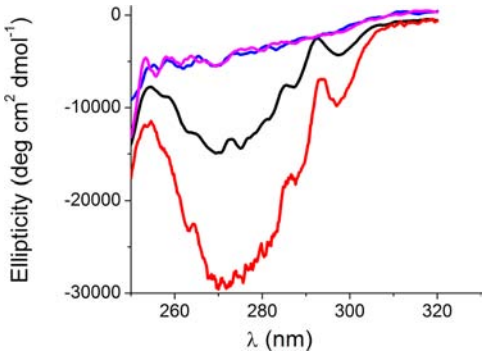


**Figure 5.** Near-UV spectra of apo-$\alpha$-LA (0.07 mM) (black), apo-$\alpha$-LA (0.07 mM) in the presence of $Ca^{2+}$ (1 mM) (red), fully cross-linked apo-$\alpha$-LA (0.05 mM) (blue), and fully cross-linked apo-$\alpha$-LA (0.05 mM) in the presence of $Ca^{2+}$ (1 mM) (magenta).

such that the remaining near-UV CD signature that we observe for our apo-$\alpha$-LA preparation is not due to the small fraction of holo-$\alpha$-LA that is also present (Supporting Information, Figure S1). In contrast, we find that the near-UV CD spectrum of partially and fully cross-linked $\alpha$-LA has lost all characteristic features and is nearly flat (Supporting Information, Figure S2B). It is worth mentioning that even an excess amount of $H_2O_2$ does not influence the secondary and tertiary structure of apo-$\alpha$-LA by itself, indicating that conformational changes that we observe are indeed due to enzymatic cross-linking (Supporting Information, Figure S3). Finally, whereas for native $\alpha$-LA the change from apo to holo (by the addition or removal of $Ca^{2+}$) is reversible, we find that the near-UV CD spectra of fully cross-linked apo-$\alpha$-LA are not affected by the addition of $Ca^{2+}$ (Figure 5), indicating irreversible loss of tertiary structure upon HRP-catalyzed cross-linking.

**Dityrosine Fluorescence upon Enzymatic Cross-Linking.** In order to study the changes around the local environment of dityrosine, we recorded fluorescence emission spectra, using an excitation wavelength of 315 nm. At this wavelength, it may be expected that mainly dityrosines are excited[52] and that excitation of tryptophan is negligible. First, in order to obtain a reference spectrum, we synthesized dityrosine by HRP-catalyzed cross-linking of tyrosine (see Materials and Methods). A comparison of fluorescence spectra [dityrosine reference, native apo-$\alpha$-LA, partially cross-linked fractions P1−P7 and fully cross-linked apo-$\alpha$-LA (F)] is shown in Figure 6. As expected, native apo-$\alpha$-LA does not exhibit any dityrosine fluorescence emission. Fluorescence intensity first increases and then saturates with increasing fraction number of the partially cross-linked $\alpha$-LA (P1−P7). The fluorescence intensity of fully cross-linked protein (F) is much lower. Also, in going from partially cross-linked (P1−P7) to fully cross-linked protein (F), the peak position shifts to the red spectrum by about 11 nm, ending up very close to the peak position of free dityrosine (Figure 6).

Most likely the increase and saturation of the fluorescence with increasing fraction number (from P1−P7) reflects the increase and then saturation of the number of dityrosines per molecule (and possibly trityrosines etc.) (Figure 6, the inset). This is consistent with a modest increase in dityrosine density (corresponding to $A_{318}/A_{280}$) from P2 to P7 (Figure 1A). On the other hand, the strong decrease of the fluorescence intensity for the fully cross-linked $\alpha$-LA (F) most likely is due to quenching, which must be caused by a local structural


dx.doi.org/10.1021/jf502664q | J. Agric. Food Chem. 2014, 62, 9345−9352

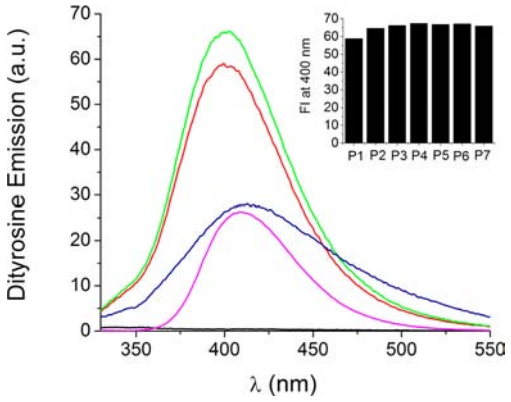


**Figure 6.** Dityrosine fluorescence emission spectra of native apo-$\alpha$-LA, partially and fully cross-linked apo-$\alpha$-LA, and dityrosine reference, at an excitation wavelength of 315 nm: black, native apo-$\alpha$-LA (N); blue, dialyzed fully cross-linked apo-$\alpha$-LA; magenta, dityrosine reference. The inset shows the dityrosine fluorescence intensity at 400 nm for SEC fractions of partially cross-linked apo-$\alpha$-LA from P1 (red) to P7 (green).

rearrangement around the dityrosines. This process might arise from the change in inter- and intramolecular interaction of dityrosine with solvent and neighboring amino acid residues. Finally, the shift of the peak position toward the direction of free dityrosines suggests that the dityrosines are becoming more exposed to the solvent when going from partially to fully cross-linked protein.

**Correlation of Changes in Conformation with Changes in Surface Hydrophobicity.** Changes in protein structure often correlate with changes in food functionality. Here we consider surface hydrophobicity as an underlying parameter that impacts properties such as emulsifying and foaming capacity and protein aggregation. In order to get a qualitative measure of the exposed surface hydrophobicity of apo-$\alpha$-LA and cross-linked protein, we use the ANSA fluorescent probe, which shows a strong enhancement of fluorescence when binding to hydrophobic surfaces.[50] The evolution of surface hydrophobicity of $\alpha$-LA upon enzymatic cross-linking is shown in Figure 7. Partial cross-linking rapidly induces a significant increase in hydrophobicity, which then saturates with increasing fraction number (P1−P7). Remarkably, full cross-linking leads to a decrease in surface hydrophobicity as compared with partially cross-linked protein

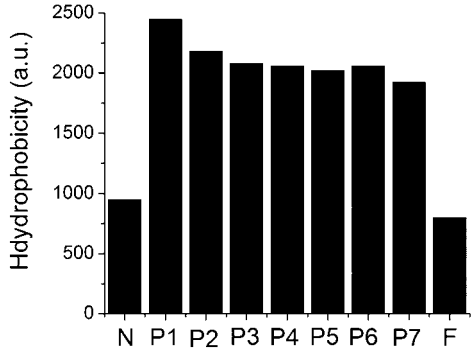


**Figure 7.** Surface hydrophobicity (arbitrary units) of native (N), partially cross-linked (P1−P7), and fully cross-linked apo-$\alpha$-LA (F) as determined using the fluorescent probe ANSA. Solution conditions: 10 mM sodium phosphate buffer at pH 7.0 at 25 °C.

(P1−P7), with final values that are (within the margin of error) similar to that of native apo-$\alpha$-LA.

The remarkable changes in local structure upon going from native apo-$\alpha$-LA to the smallest cross-linked oligomers (P1) with the lowest number of dityrosines (lowest ratio $A_{318}/A_{280}$) most probably relate to the initial steps of the cross-linking reaction. Heijnis et al. have shown that the initial step of cross-linking most likely involves a reaction between Tyr18 and Tyr50.[42] Our results show that apparently this first reaction already leads to a relatively large conformational change. The difference in dityrosine fluorescence and surface hydrophobicity for partially and fully cross-linked $\alpha$-LA might be a consequence of conformational changes induced by the additional cross-linking reactions involving the other tyrosine residues (Tyr36 and Tyr103) that occur at a later stage.

The objective of this study was to determine the conformational transition in apo-$\alpha$-LA in going from native apo-$\alpha$-LA, to oligomers, and then to larger protein particles upon HRP-catalyzed cross-linking. Our results show that, surprisingly, the surface hydrophobicity of apo-$\alpha$-LA first increases upon partially cross-linking and then decreases upon fully cross-linking. Differences between partially and fully cross-linked proteins that are consistent with this result are also found for the local environment of the dityrosines (as probed using fluorescence) and for the secondary structure (as probed using CD).

The impact of nonenzymatic oxidation of tyrosine on the conformations and surface hydrophobicity of globular proteins has also been investigated.[53−57] For example, Kanwar and Balasubramanian[55] reported that cross-linking of a range of globular proteins (calmodulin, bovine pancreatic ribonuclease A, and bovine eye lens $\gamma$-B-crystallin) had no major effect on the secondary and tertiary structure of the proteins. It has also been reported[56] that dimers of $\gamma$-B-crystallin, formed by chemical dityrosine cross-linking, have a significantly lower solubility than monomers. In contrast, we have found that fully cross-linked apo-$\alpha$-LA is highly soluble at neutral pH. In another study, Dalsgaard et al.[57] found that photo-oxidation of globular whey proteins resulted in a different level of structural changes. In general, secondary structure content (i.e., $\alpha$-helix for $\alpha$-lactalbumin and $\beta$-sheet for $\beta$-lactoglobulin, as measured by CD spectroscopy) of globular whey proteins decreased over time upon photo-oxidation, while random coil structure increased. Tryptophan fluorescence emission also indicated 10% and 3% unfolding in tertiary structures of $\alpha$-lactalbumin and $\beta$-lactoglobulin, respectively, after photo-oxidation. In contrast, we find that the loss in tertiary structure is already complete after a small number of additions of $H_2O_2$ (Supporting Information, Figure S2B).

With respect to the mTG-induced cross-linking of the globular whey proteins $\alpha$-LA and $\beta$-lactoglobulin (BLG), it has been found that $\alpha$-LA, and in particular apo-$\alpha$-LA, is a much better substrate for mTG than BLG,[24,25] such that in WPI, in fact, it may be expected that most of the cross-linking occurs for the $\alpha$-lac fraction in WPI. For whey protein isolate (WPI), only minor changes in tertiary structure have been reported upon cross-linking with mTG, and then only for very long reaction times. Also, it has been found that incubation with mTG does not lead to dramatic changes in secondary structure for WPI.[24,25] However, the changes in the apparent hydrophobicity have been reported for mTG-catalyzed cross-linking of whey proteins. Surface hydrophobicity of WPI gradually decreased upon increasing cross-linking degree. A decrease of the


dx.doi.org/10.1021/jf502664q | J. Agric. Food Chem. 2014, 62, 9345−9352

apparent hydrophobicity of WPI after TG-catalyzed cross-linking (as detected using the fluorescent dye ANSA) was attributed to occlusion of hydrophobic cavities in protein.[25] At the same time, however, it was reported that the reduction of net positive charge due to cross-linking of lysyl residues led to aggregation of TG-cross-linked WPI particles at acidic pH. In contrast, we find that the surface hydrophobicity of $\alpha$-LA particles first increases with the first cross-linking, but after full cross-linking, the surface hydrophobicity has decreased again to a value that is nearly the same of that of native $\alpha$-LA. In contrast to TG-catalyzed cross-linking, where the cross-linking led to changes in the surface charge that impacted colloidal stability, we have found that the $\zeta$-potential of $\alpha$-LA increases from −12.4 mV to −29.6 mV upon full cross-linking at neutral pH in 10 mM sodium phosphate buffer (please see the Supporting Information, Figure S4).

Taken together, we find that HRP-catalyzed cross-linking leads to physical properties of cross-linked protein that can be beneficial in beverages and for food structuring, in particular, the highly hydrophilic nature and high $\zeta$-potential of the particles, as well as the fact that a significant fraction of secondary structure is retained. As we have observed in the rheology of dispersions of these hydrophilic particles, the cross-linked apo-$\alpha$-LA particles are interesting novel protein-based thickeners, with a completely reversible yield-stress and shear thinning behavior that is highly unusual for globular protein systems (data not shown). Moreover, the tunability of the hydrophilicity/hydrophobicity may also have an impact on the interaction of the cross-linked $\alpha$-LA with other molecules and, thus, on their functionality as carrier molecules in delivery applications. For example, it is known that $\alpha$-LA specifically interacts with oleic acid, which has been exploited for applications in medicine.[58]

In combination with our earlier work on the structure of cross-linked $\alpha$-LA at larger length scales,[39,40] by zooming in on the structural impact of enzymatic cross-linking at nanometer length scales, we now have a complete overview of the impact of HRP-catalyzed cross-linking of apo-$\alpha$-LA across a range of length scales. Indeed, only by linking changes at nanometer length scales to the architecture and physical properties of cross-linked protein at larger length scales will we be able to rationally use enzymatic cross-linking to modulate food structure.

## ■ ASSOCIATED CONTENT

### Supporting Information

Figure S1: Near-UV CD spectra of apo and holo-$\alpha$-LA. Figure S2: The change in near- and far-UV CD spectra of the reaction mixtures as a function of added $H_2O_2$. Figure S3: The change in protein conformation of native apo-$\alpha$-LA as a function of added $H_2O_2$. Figure S4: $\zeta$-potential distribution of native apo-$\alpha$-LA and dialyzed HRP-cross-linked apo-$\alpha$-LA. This material is available free of charge via the Internet at http://pubs.acs.org.

## ■ AUTHOR INFORMATION

### Corresponding Author

*Phone: +31317482277. E-mail: yunus.saricay@wur.nl.

### Funding

This work is part of the Industrial Partnership Programme (IPP) Bio(-Related) Materials of the Stichting voor Fundamenteel Onderzoek der Materie (FOM), which is financially supported by the Nederlandse Organisatie voor Wetenschappelijk Onderzoek (NWO). The IPP BRM is cofinanced by the Top Institute Food and Nutrition and the Dutch Polymer Institute.

### Notes

The authors declare no competing financial interest.

## ■ REFERENCES

(1) Jones, O. G.; McClements, D. J. Functional biopolymer particles: Design, fabrication, and applications. *Compr. Rev. Food Sci. Food Saf.* **2010**, *9*, 374−397.

(2) Panyam, D.; Kilara, A. Enhancing the functionality of food proteins by enzymatic modification. *Trends Food Sci. Technol.* **1996**, *7*, 120−125.

(3) Foegeding, E. A.; Davis, J. P. Food protein functionality: A comprehensive approach. *Food Hydrocolloids* **2011**, *25*, 1853−1864.

(4) Kluger, R.; Alagic, A. Chemical cross-linking and protein−protein interactions—A review with illustrative protocols. *Bioorg. Chem.* **2004**, *32*, 451−472.

(5) Considine, T.; Patel, H. A.; Anema, S. G.; Singh, H.; Creamer, L. K. Interactions of milk proteins during heat and high hydrostatic pressure treatments—A review. *Innov. Food Sci. Emerg. Technol.* **2007**, *8*, 1−23.

(6) Fass, D. Disulfide bonding in protein biophysics. *Annu. Rev. Biophys.* **2012**, *41*, 63−79.

(7) Shimada, K.; Cheftel, J. C. Sulfhydryl-group disulfide bond interchange reactions during heat-induced gelation of whey-protein isolate. *J. Agric. Food Chem.* **1989**, *37*, 161−168.

(8) Liu, X. M.; Powers, J. R.; Swanson, B. G.; Hill, H. H.; Clark, S. Modification of whey protein concentrate hydrophobicity by high hydrostatic pressure. *Innov. Food Sci. Emerg. Technol.* **2005**, *6*, 310−317.

(9) Nicolai, T.; Britten, M.; Schmitt, C. $\beta$-Lactoglobulin and WPI aggregates: Formation, structure and applications. *Food Hydrocolloids* **2011**, *25*, 1945−1962.

(10) Alting, A. C.; Hamer, R. J.; de Kruif, C. G.; Paques, M.; Visschers, R. W. Number of thiol groups rather than the size of the aggregates determines the hardness of cold set whey protein gels. *Food Hydrocolloids* **2003**, *17*, 469−479.

(11) Huebner, F. R.; Bietz, J. A.; Wall, J. S. Disulfide bonds: Key to wheat protein functionality. *Adv. Exp. Med. Biol.* **1977**, *86A*, 67−88.

(12) Okumura, K.; Miyake, Y.; Taguchi, H.; Shimabayashi, Y. Formation of stable protein foam by intermolecular disulfide cross-linkages in thiolated $\alpha_{s1}$-casein as a model. *J. Agric. Food Chem.* **1990**, *38*, 1303−1306.

(13) Foegeding, E. A.; Davis, J. P.; Doucet, D.; McGuffey, M. K. Advances in modifying and understanding whey protein functionality. *Trends Food Sci. Technol.* **2002**, *13*, 151−159.

(14) Schmitt, C.; Moitzi, C.; Bovay, C.; Rouvet, M.; Bovetto, L.; Donato, L.; Leser, M. E.; Schurtenberger, P.; Stradner, A. Internal structure and colloidal behaviour of covalent whey protein microgels obtained by heat treatment. *Soft Matter* **2010**, *6*, 4876−4884.

(15) Miller, A. G.; Meade, S. J.; Gerrard, J. A. New insights into protein crosslinking via the maillard reaction: Structural requirements, the effect on enzyme function, and predicted efficacy of crosslinking inhibitors as anti-ageing therapeutics. *Bioorg. Med. Chem.* **2003**, *11*, 843−852.

(16) Oliver, C. M.; Melton, L. D.; Stanley, R. A. Creating proteins with novel functionality via the Maillard reaction: A review. *Crit. Rev. Food Sci. Nutr.* **2006**, *46*, 337−350.

(17) Liu, J.; Ru, Q.; Ding, Y. Glycation a promising method for food protein modification: Physicochemical properties and structure, a review. *Food Res. Int.* **2012**, *49*, 170−183.

(18) De Goes-Favoni, S. P.; Bueno, F. R. Microbial transglutaminase: General characteristics and performance in food processing technology. *Food Biotechnol.* **2014**, *28*, 1−24.

(19) Partanen, R.; Forssell, P.; Mackie, A.; Blomberg, E. Interfacial cross-linking of $\beta$-casein changes the structure of the adsorbed layer. *Food Hydrocolloids* **2013**, *32*, 271−277.

(20) Truong, V. D.; Clare, D. A.; Catignani, G. L.; Swaisgood, H. E. Cross-linking and rheological changes of whey proteins treated with microbial transglutaminase. *J. Agric. Food Chem.* **2004**, *52*, 1170−1176.
(21) Ozrenk, E. The use of transglutaminase in dairy products. *Int. J. Dairy Technol.* **2006**, *59*, 1−7.
(22) Jaros, D.; Partschefeld, C.; Henle, T.; Rohm, H. Transglutaminase in dairy products: Chemistry, physics, applications. *J. Texture Stud.* **2006**, *37*, 113−155.
(23) Nieuwenhuizen, W. F.; Dekker, H. L.; Gröneveld, T.; de Koster, C. G.; de Jong, G. A. H. Transglutaminase-mediated modification of glutamine and lysine residues in native bovine $\beta$-lactoglobulin. *Biotechnol. Bioeng.* **2004**, *85*, 248−258.
(24) Eissa, A. S.; Puhl, C.; Kadla, J. F.; Khan, S. A. Enzymatic cross-linking of $\beta$-lactoglobulin: Conformational properties using FTIR spectroscopy. *Biomacromolecules* **2006**, *7*, 1707−1713.
(25) Agyare, K. K.; Damodaran, S. pH-stability and thermal properties of microbial transglutaminase-treated whey protein isolate. *J. Agric. Food Chem.* **2010**, *58*, 1946−1953.
(26) Faergemand, M.; Otte, J.; Qvist, K. B. Enzymatic cross-linking of whey proteins by a $Ca^{2+}$-independent microbial transglutaminase from *Streptomyces lydicus*. *Food Hydrocolloids* **1997**, *11*, 19−25.
(27) Burke, M. D.; Ha, S. Y.; Pysz, M. A.; Khan, S. A. Rheology of protein gels synthesized through a combined enzymatic and heat treatment method. *Int. J. Biol. Macromol.* **2002**, *31*, 37−44.
(28) Buchert, J.; Cura, D. E.; Ma, H.; Gasparetti, C.; Monogioudi, E.; Faccio, G.; Mattinen, M.; Boer, H.; Partanen, R.; Selinheimo, E.; Lantto, R.; Kruus, K. Crosslinking food proteins for improved functionality. *Annu. Rev. Food Sci. Technol.* **2010**, *1*, 113−38.
(29) Thalmann, C. R.; Lotzbeyer, T. Enzymatic cross-linking of proteins with tyrosinase. *Eur. Food Res. Technol.* **2002**, *214*, 276−281.
(30) Faergemand, M.; Otte, J.; Qvist, K. B. Cross-linking of whey proteins by enzymatic oxidation. *J. Agric. Food Chem.* **1998**, *46*, 1326−1333.
(31) Heck, T.; Faccio, G.; Richter, M.; Thony-Meyer, L. Enzyme-catalyzed protein crosslinking. *Appl. Microbiol. Biotechnol.* **2013**, *97*, 461−475.
(32) Mattinen, M. L.; Hellman, M.; Permi, P.; Autio, K.; Kalkkinen, N.; Buchert, J. Effect of protein structure on laccase-catalyzed protein oligomerization. *J. Agric. Food Chem.* **2006**, *54*, 8883−8890.
(33) Elliott, K. A. Oxidations catalysed by horseradish- and milk-peroxidases. *Biochem. J.* **1932**, *26*, 1281−1290.
(34) Steffensen, C. L.; Andersen, M. L.; Degn, P. E.; Nielsen, J. H. Cross-Linking proteins by laccase-catalyzed oxidation: Importance relative to other modifications. *J. Agric. Food Chem.* **2008**, *56*, 12002−12010.
(35) Lantto, R.; Puolanne, E.; Katina, K.; Niemisto, M.; Buchert, J.; Autio, K. Effect of laccase and transglutaminase on the textural and water-binding properties of cooked chicken breast meat gels. *Eur. Food Res. Technol.* **2007**, *225*, 75−83.
(36) Lantto, R.; Puolanne, E.; Kalkkinen, N.; Buchert, J.; Autio, K. Enzyme-aided modification of chicken-breast myofibril proteins: Effect of laccase and transglutaminase on gelation and thermal stability. *J. Agric. Food Chem.* **2005**, *53*, 9231−9237.
(37) Ma, H.; Forssell, P.; Partanen, R.; Buchert, J.; Boer, H. Improving laccase catalyzed cross-linking of whey protein isolate and their application as emulsifiers. *J. Agric. Food Chem.* **2011**, *59*, 1406−1414.
(38) Cura, D. E.; Lantto, R.; Lille, M.; Andberg, M.; Kruus, K.; Buchert, J. Laccase-aided protein modification: Effects on the structural properties of acidified sodium caseinate gels. *Int. Dairy J.* **2009**, *19*, 737−745.
(39) Dhayal, S. K.; Gruppen, H.; de Vries, R.; Wierenga, P. A. Controlled formation of protein nanoparticles by enzymatic cross-linking of $\alpha$-lactalbumin with horseradish peroxidase. *Food Hydrocolloids* **2014**, *36*, 53−59.
(40) Saricay, Y.; Wierenga, P.; de Vries, R. Nanostructure development during peroxidase catalysed cross-linking of $\alpha$-lactalbumin. *Food Hydrocolloids* **2013**, *33*, 280−288.
(41) Heijnis, W. H.; Wierenga, P. A.; van Berkel, W. J. H.; Gruppen, H. Directing the oligomer size distribution of peroxidase-mediated cross-linked bovine $\alpha$-lactalbumin. *J. Agric. Food Chem.* **2010**, *58*, 5692−5697.
(42) Heijnis, W. H.; Dekker, H. L.; de Koning, L. J.; Wierenga, P. A.; Westphal, A. H.; de Koster, C. G.; Gruppen, H.; van Berkel, W. J. H. Identification of the peroxidase-generated intermolecular dityrosine cross-link in bovine $\alpha$-lactalbumin. *J. Agric. Food Chem.* **2011**, *59*, 444−449.
(43) Kronman, M. J.; Andreotti, R. E. Inter- and intramolecular interactions of $\alpha$-lactalbumin. I. Apparent heterogeneity at acid pH. *Biochemistry* **1964**, *3*, 1145−1151.
(44) Ohlsson, P. I.; Paul, K. G. Molar absorptivity of horseradish-peroxidase. *Acta Chem. Scand. B* **1976**, *30*, 373−375.
(45) Noble, R. W.; Gibson, Q. H. Reaction of ferrous horseradish peroxidase with hydrogen peroxide. *J. Biol. Chem.* **1970**, *245*, 2409−2413.
(46) Provencher, S. W.; Glockner, J. Estimation of globular protein secondary structure from circular-dichroism. *Biochemistry* **1981**, *20*, 33−37.
(47) Whitmore, L.; Wallace, B. A. Dichroweb, an online server for protein secondary structure analyses from circular dichroism spectroscopic data. *Nucleic Acids Res.* **2004**, *32*, W668−W673.
(48) Whitmore, L.; Wallace, B. A. Protein secondary structure analyses from circular dichroism spectroscopy: Methods and reference databases. *Biopolymers* **2008**, *89*, 392−400.
(49) Chang, J. Y.; Li, L. The structure of denatured $\alpha$-lactalbumin elucidated by the technique of disulfide scrambling—Fractionation of conformational isomers of $\alpha$-lactalbumin. *J. Biol. Chem.* **2001**, *276*, 9705−9712.
(50) Wierenga, P. A.; Meinders, M. B. J.; Egmond, M. R.; Voragen, F.; de Jongh, H. H. J. Protein exposed hydrophobicity reduces the kinetic barrier for adsorption of ovalbumin to the air−water interface. *Langmuir* **2003**, *19*, 8964−8970.
(51) Yutani, K.; Ogasahara, K.; Kuwajima, K. Absence of the thermal transition in apo-$\alpha$-lactalbumin in the molten globule state: A study by differential scanning microcalorimetry. *J. Mol. Biol.* **1992**, *228*, 347−350.
(52) Harms, G.; Pauls, S.; Hedstrom, J.; Johnson, C. Fluorescence and rotational dynamics of dityrosine. *J. Fluoresc.* **1997**, *7*, 283−292.
(53) Davies, K. J. A.; Delsignore, M. E. Protein damage and degradation by oxygen radicals. 3. Modification of secondary and tertiary structure. *J. Biol. Chem.* **1987**, *262*, 9908−9913.
(54) Davies, K. J. A.; Lin, S. W.; Pacifici, R. E. Protein damage and degradation by oxygen radicals. 4. Degradation of denatured protein. *J. Biol. Chem.* **1987**, *262*, 9914−9920.
(55) Kanwar, R.; Balasubramanian, D. Structural studies on some dityrosine-cross-linked globular proteins: Stability is weakened, but activity is not abolished. *Biochemistry* **2000**, *39*, 14976−14983.
(56) Kanwar, R.; Balasubramanian, D. Structure and stability of the dityrosine-linked dimer of $\gamma$B-crystallin. *Exp. Eye Res.* **1999**, *68*, 773−784.
(57) Dalsgaard, T. K.; Otzen, D.; Nielsen, J. H.; Larsen, L. B. Changes in structures of milk proteins upon photo-oxidation. *J. Agric. Food Chem.* **2007**, *55*, 10968−10976.
(58) Svensson, M.; Fast, J.; Mossberg, A. K.; Duringer, C.; Gustafsson, L.; Hallgren, O.; Brooks, C. L.; Berliner, L.; Linse, S.; Svanborg, C. $\alpha$-Lactalbumin unfolding is not sufficient to cause apoptosis, but is required for the conversion to HAMLET (human $\alpha$-lactalbumin made lethal to tumor cells). *Protein Sci.* **2003**, *12*, 2794−2804.

maize,[24,25] and rice.[9,26] Although some progress has been made in defining PL synthesis and metabolism in plants,[27] our understanding of the PL synthesis pathway is limited to knowledge of several genes in *Arabidopsis*,[28] with single nucleotide polymorphisms identified in seed-expressed phospholipase D, an important enzyme in PL biosynthesis.[29,30] There are few reports of the extent of genotypic diversity in specific PLs in rice grain due to the limited capacity of existing extraction and quantification assays.[3,26]

Rice grain lipids are influenced by both genetic and environmental factors.[31] During rice grain ripening, linoleic and linolenic acid content appear to decrease with increasing growing temperature, whereas the myristic, palmitic, and oleic acid content rise, although there is negligible seasonal and cultivar variation of these LPL precursors.[32] Sowing date and field location also appear to play a greater role in accounting for variation in rice LPL levels than genetic factors.[33] Although these studies suggest genotype and environment have a significant influence on rice PL components and accumulation, data that reveal the extent of genotype × environment (G × E) interaction on rice LPLs are still lacking.

The objective of this study was to quantify the variation in LPLs among 20 diverse rice accessions originating from a wide geographical distribution over two growing seasons. The results will contribute to our understanding of the factors that may contribute to selecting and managing rice grain LPL composition, either through breeding or agronomic manipulation.

## MATERIALS AND METHODS

**Plant Materials.** The 20 rice accessions (Table1) from the OryzaSNP project (http://www.oryzasnp.org/) were used in this study and represent a wide range of geographical origin and genetic diversity.[34] All were nonwaxy cultivars with apparent amylose content ranging from 11 to 26%.[35] These cultivars were grown in the field over two consecutive seasons (2010−2011 and 2011−2012) in a randomized block design with two replications in the same field in Lingshui, Hainan province, China (18.48°N).[35,36] Sowing was in early December and harvest in April. Associated metrological data (mean temperature, sunshine duration, and precipitation) were reported previously.[35] Grain was stored at 4 °C prior to milling to white rice using a Satake rice machine (Satake Corp., Japan) and grinding to flour in a Cyclone sample mill (UDY, Fort Collins, CO, USA) in the laboratory. When some accessions were of insufficient sample weights for analysis, mixed samples from two replications in the same year were used in this study.

**Chemicals.** All solvents and reagents were of HPLC grade. Four LPL standard samples, 1-palmitoyl-2-hydroxy-*sn*-glycero-3-phosphocholine (LPC16:0), 1-oleoyl-2-hydroxy-*sn*-glycero-3-phosphocholine (LPC18:1), 1-palmitoyl-2-hydroxy-*sn*-glycero-3-phosphoethanolamine (LPE16:0), and 1-oleoyl-2-hydroxy-*sn*-glycero-3-phosphoethanolamine (LPE18:1), were purchased from Avanti Polar Lipids Inc. (Alabaster, AL, USA).

**Starch Phospholipid Extraction.** A rapid single-step LPL extraction method[26] was used. Briefly, LPLs were extracted directly from triplicate milled rice flour samples with 75% *n*-propanol (v/v, 8 mL/0.16 g sample) at 100 °C in Pyrex culture tubes (capped) for 2 h. The weight of the capped culture tube before and after extraction was measured to ensure an accurate extraction solvent/sample ratio (m/m) was used for subsequent calculations of LPL content. A 1 mL aliquot of the extract was used for quantitative HPLC-MS analysis of LPLs.

**Determination of LPLs by HPLC-MS.** Quantitative analysis of LPLs was carried out with three technical replications according to the method of Liu et al.[26] using an Agilent HPLC-MS series 1290 (Agilent Technologies, Palo Alto, CA, USA) equipped with a vacuum degasser, binary pump, autoinjector, and an Agilent quadrupole mass detector (MSD, 6120). An Agilent Eclipse Plus C18 RRHD column with 1.8 μm, 50 × 2.1 mm internal diameter, was used to separate PLs.

The linear gradient elution program consisted of a mobile phase of acetonitrile with 0.005% TFA and water with 0.005% TFA. The solvent gradient was programmed from 10 to 99% acetonitrile in 10 min at a flow rate of 0.3 mL/min and held at 99% acetonitrile for 1.5 min. An electrospray ionization (ESI) source was used for MSD; the MS parameters were as follows: drying nitrogen gas flow, 12.0 L/min; nebulizer pressure, 35 psig; SIM mode same as our previous study;[26] fragmentor, 150; capillary voltage, 3000 V (positive); drying gas temperature, 350 °C; vaporizer temperature, 350 °C. Control of the HPLC-MS system was by Agilent ChemStation software. An external standard was applied, and each sample was measured in triplicate.

**Statistical Analysis.** Data analyses were conducted using SAS program version 9 (SAS Institute Inc., Cary, NC, USA). Analysis of variance (ANOVA) was used with the general linear model procedure (Proc glm). PROC means was performed for means of genotypes and environments, followed by Duncan's multiple-comparison tests ($P < 0.05$). Correlation between phenotypes was calculated with PROC CORR, and principal component analysis was conducted with PRINCOMP. Hierarchical cluster analysis was computed using Ward's method in SPSS version 19.0.

## RESULTS

Of the 20 rice genotypes studied, eight represented the *japonica* subspecies, eight the *indica* subspecies, and four belonged to the *aus* group. A total of 10 individual LPLs were identified in the classes of lysophosphatidylcholine (LPC14:0, LPC16:0, LPC18:1, LPC18:2, LPC18:3) and lysophosphatidylethanolamine (LPE14:0, LPE16:0, LPE18:1, LPE18:2, LPE18:3).

**Rice Lysophosphatidylcholine.** The effects of genotype by season (year) interaction for rice LPC components LPC14:0, LPC16:0, LPC18:1, LPC18:2, LPC18:3, and total LPC (TLPC) (where TLPC = LPC14:0 + LPC16:0 + LPC18:1 + LPC18:2 + LPC18:3) were significant ($P < 0.001$) (Table 2). In particular, genotypic variance of LPC14:0, LPC16:0, LPC18:1, LPC18:2, LPC18:3, and TLPC accounted for 79.9, 59.5, 93.2, 61.6, 83.2, and 59.5% of the total variance, respectively, whereas year accounted for 18.1, 33.9, 3.7, 36.6, 14.0, and 38.9% of the total variance, respectively. Genotype × season interaction also affected rice LPCs ($P < 0.001$), although they accounted for only 1.8−6.6% of the total variance (Table 2).

Extensive variation in LPC composition was observed among the 20 rice accessions (Table 1). The main LPC components were LPC16:0 and LPC18:2, which accounted for 54.7−64.7 and 19.5−31.0% of total LPCs, respectively. Minor components included LPC18:1, LPC14:0, and LPC18:3, which represented 5.6−14.8, 4.6−11.1, and 0.3−1.1% of total LPCs, respectively (Table 1; Figure 1).

Mean individual LPC content was similar across the two seasons, ranging from 406.2 to 436.0 μg/g for LPC14:0, from 3752.0 to 3918.6 μg/g for LPC16:0, from 562.8 to 576.2 μg/g for LPC18:1, from 1464.2 to 1581.5 μg/g for LPC18:2, and from 37.0 to 39.9 μg/g for LPC18:3 (Table 1; Figure 1). Significant difference between the two years ($P < 0.001$) was observed only for mean TLPC of the 20 accessions (Table 1). Among the three groups of rice accessions, the mean LPC18:1 content across two years in the *japonica* rice group was higher than those in *indica* and *aus* rice groups (Table 3).

**Rice Lysophosphatidylethanolamine.** Although genotype, season, and genotype × season interactions were significant (ANOVA; $P < 0.001$) for LPE14:0, LPE16:0, LPE18:1, LPE18:2, LPE18:3, and total LPE (TLPE) (where TLPE = LPE14:0 + LPE16:0 + LPE18:1 + LPE18:2 + LPE18:3) ($P < 0.001$; Table 2),

**Table 1. Mean of Rice Lysophospholipids of Different Genotypes at Different Years[a]**

| genotype | variety | group | LPC14:0 | LPC16:0 | LPC18:1 | LPC18:2 | LPC18:3 | TLPC | LPE14:0 | LPE16:0 | LPE18:1 | LPE18:2 | LPE18:3 | TLPE | TLPL |
|---|---|---|---|---|---|---|---|---|---|---|---|---|---|---|---|
| G01 | Azucena | *japonica* | 411.0 d | 3846.5 fg | 894.5 a | 1621.6 d | 33.4 e | 6807.0 de | 60.8 de | 1041.6 b | 128.5 a | 462.6 b | 6.8 fg | 1700.3 b | 8507.4 cd |
| G02 | Dom Sufid | *japonica* | 532.3 c | 4270.9 cde | 893.8 a | 1828.1 c | 66.5 a | 7591.6 ab | 77.7 b | 1139.8 a | 134.0 a | 444.4 c | 13.7 b | 1809.5 a | 9401.1 a |
| G03 | Dular | *aus* | 331.5 fg | 4697.8 a | 427.2 h | 2182.3 a | 46.5 d | 7685.2 a | 41.3 j | 971.3 cd | 54.2 k | 396.5 e | 7.0 f | 1470.3 ef | 9155.5 ab |
| G04 | FR13A | *aus* | 496.3 c | 4431.6 bcd | 465.3 g | 1437.9 fg | 23.0 h | 6854.1 de | 61.7 cde | 977.6 c | 63.2 ghi | 361.7 fg | 3.0 kl | 1467.2 ef | 8321.3 de |
| G05 | IR64-21 | *indica* | 504.1 c | 3758.0 gh | 398.2 hi | 1584.1 de | 58.2 b | 6302.7 fg | 61.6 cde | 890.1 efg | 56.0 jk | 386.3 e | 12.4 c | 1406.4 fg | 7709.0 fgh |
| G06 | LTH | *japonica* | 530.3 c | 3760.9 gh | 500.4 efg | 1464.3 f | 28.0 fg | 6284.0 fg | 72.6 b | 974.2 cd | 67.6 efgh | 378.9 ef | 3.6 jk | 1496.9 de | 7780.9 fg |
| G07 | M202 | *japonica* | 371.0 e | 3279.9 kl | 600.0 d | 1335.6 gh | 29.9 efg | 5616.4 ij | 41.9 j | 749.8 i | 70.7 ef | 311.5 h | 4.3 ij | 1178.1 hi | 6794.5 jk |
| G08 | Minghui63 | *indica* | 238.5 j | 3009.7 m | 537.1 e | 923.4 j | 18.4 i | 4727.1 l | 27.9 m | 625.7 j | 58.6 ijk | 170.6 k | ~0 n | 882.8 j | 5609.8 m |
| G09 | Moroberekan | *japonica* | 256.0 ij | 3572.4 hij | 496.7 fg | 1243.8 h | 32.4 ef | 5601.4 ij | 34.3 kl | 895.1 efg | 72.7 e | 356.3 g | 6.1 fg | 1364.4 g | 6965.8 ij |
| G10 | N22 | *aus* | 604.9 b | 4541.9 ab | 593.8 d | 1949.7 b | 27.7 g | 7718.0 a | 67.3 c | 941.2 cde | 65.6 fgh | 379.4 ef | 2.3 lm | 1455.7 ef | 9173.7 ab |
| G11 | Nipponbare | *japonica* | 430.8 d | 3909.3 fg | 680.6 c | 1503.1 ef | 34.4 e | 6558.1 ef | 52.4 gh | 861.3 fgh | 82.3 d | 353.6 g | 6.2 fg | 1355.8 g | 7913.9 efg |
| G12 | Pokkali | *indica* | 300.6 gh | 3345.6 jkl | 473.8 fg | 1115.7 i | 27.0 gh | 5262.7 jk | 43.3 ij | 820.3 h | 71.5 ef | 284.1 i | 3.6 jk | 1222.7 h | 6485.3 kl |
| G13 | Sadu-Cho | *indica* | 442.5 d | 4452.7 abc | 492.5 fg | 1808.2 c | 43.6 d | 7239.5 bc | 59.7 ef | 1123.9 a | 63.8 ghi | 421.2 d | 8.5 e | 1677.1 b | 8916.5 bc |
| G14 | SHZ-2 | *indica* | 305.7 gh | 3195.8 lm | 468.4 fg | 1813.6 c | 64.0 a | 5847.4 gi | 38.3 jk | 841.5 gh | 69.1 efg | 481.6 a | 15.7 a | 1446.1 ef | 7293.5 hi |
| G15 | Swarna | *indica* | 279.6 hi | 3500.5 ijk | 506.7 ef | 1248.8 h | 31.3 efg | 5566.8 ij | 32.3 lm | 733.1 i | 66.8 efgh | 293.8 i | 5.0 hi | 1130.7 i | 6697.5 jkl |
| G16 | Tainung67 | *japonica* | 294.1 h | 3190.6 lm | 755.2 b | 836.6 j | 17.8 i | 5094.3 k | 39.9 j | 812.1 h | 116.3 b | 250.3 j | 1.8 m | 1220.4 h | 6314.7 l |
| G17 | Zhenshan97B | *indica* | 353.0 ef | 4189.3 de | 415.9 h | 1608.0 de | 33.0 e | 6599.0 ef | 48.1 hi | 915.9 def | 56.4 jk | 395.2 e | 5.9 gh | 1421.5 efg | 8020.5 ef |
| G18 | Aswina | *indica* | 811.2 a | 4083.6 ef | 576.7 d | 1737.7 c | 53.6 c | 7262.8 bc | 102.4 a | 940.2 cde | 80.6 d | 415.1 d | 9.6 d | 1547.9 cd | 8810.6 bc |
| G19 | Cypress | *japonica* | 512.3 c | 3934.9 fg | 746.5 b | 1761.3 c | 67.8 a | 7022.8 cd | 65.8 cd | 985.3 c | 92.4 c | 438.8 c | 15.1 a | 1597.4 c | 8620.2 cd |
| G20 | Rayada | *aus* | 416.6 d | 3734.1 ghi | 466.8 fg | 1452.7 f | 33.1 e | 6103.3 gh | 55.3 gh | 939.0 cde | 62.2 hij | 353.8 g | 5.8 gh | 1416.1 fg | 7519.5 gh |
| year | | | | | | | | | | | | | | | |
| 2011 | | | 436.0 a | 3918.6 a | 576.2 a | 1581.5 a | 39.9 a | 6552.2 a | 56.4 a | 921.8 a | 77.1 a | 372.1 a | 7.0 a | 1433.5 a | 7985.6 a |
| 2012 | | | 406.2 a | 3752.0 a | 562.8 a | 1464.2 a | 37.0 a | 6222.2 b | 52.0 a | 896.2 a | 76.2 a | 361.4 a | 6.6 a | 1393.2 a | 7615.5 a |

[a]Different letters in the same column represent significance at the 0.05 level. Units: $\mu$g/g.



dx.doi.org/10.1021/jf503213p | J. Agric. Food Chem. 2014, 62, 9353−9361

Table 2. Mean Square Values of Analysis of Variance (ANOVA) for Rice Lysophospholipids[a]

| source | df | LPC14:0 | LPC16:0 | LPC18:1 | LPC18:2 | LPC18:3 | TLPC | LPE14:0 | LPE16:0 | LPE18:1 | LPE18:2 | LPE18:3 | TLPE | TLPL |
|---|---|---|---|---|---|---|---|---|---|---|---|---|---|---|
| genotype (G) | 19 | 117337.2 | 1462034.7 | 134367.4 | 694767.3 | 1483.0 | 4812061.5 | 1960.3 | 94686.5 | 3317.3 | 34425.3 | 118.5 | 275660.8 | 6966212.0 |
| year (E) | 1 | 26602.5 | 832716.8 | 5352.0 | 412755.2 | 249.7 | 3265383.2 | 569.4 | 19668.5 | 24.8 | 3447.6 | 6.2 | 48622.0 | 4110997.0 |
| G × E | 19 | 2884.6 | 1619892 | 4466.2 | 19860.7 | 49.7 | 317542.1 | 69.3 | 5756.7 | 130.6 | 792.2 | 2.8 | 12118.0 | 413046.9 |

[a] All mean square values were significant at the $P < 0.001$ level.

they were mainly affected by genotype, accounting for 75.4−95.5%, and season, accounting for 0.7−21.9% of the total variance. Genotype × season interactions accounted for only 2.1−4.8% of the total variance (Table 2).

The main LPE components were LPE16:0 and LPE18:2, accounting for 58.2−70.9 and 19.3−33.3% of total LPEs, respectively (Table 1 and Figure 1). LPE16:0 content ranged from 625.7 μg/g in genotype G08 to 1139.8 μg/g in G02. LPE18:2 varied from 170.6 μg/g in G08 to 481.6 μg/g in G14 (range = 311.0 μg/g). The mean LPE16:0 and LPE18:2 values were relatively stable over the two years, being 921.8 and 372.1 μg/g in 2011 versus 896.2 and 361.4 μg/g in 2012, suggesting environment had little effect on LPE16:0 and LPE18:2 contents (Table 2). TLPE varied from 882.8 μg/g in G08 to 1809.5 μg/g in G02 among the 20 different accessions (Table 1). There was little variation in mean TLPE between years, suggesting environmental influence on TLPE was minor (Table 2). The *japonica* rice group had higher mean LPE18:1 content than those in the *indica* and *aus* rice groups (Table 3).

**Rice Total Lysophospholipids (TLPL).** TLPL (where TLPL = TLPC + TLPE) content varied extensively among the 20 genotypes (ANOVA; $P < 0.001$) such that genotype accounted for 60.6% of the total variation (Table 2). Environment and genotype × environment interaction accounted for 35.8 and 3.6% of the total variance of TLPL, respectively, representing a small but significant effect ($P < 0.001$).

The lowest TLPL content was found in *indica* cultivar Minghui63 (G08, 5609.8 μg/g), whereas the highest was found in *japonica* cultivar Dom Sufid (G02, 9401.1 μg/g) (Table 1; Figure 2). Mean TLPL levels were similar between years, 7985.6 μg/g in 2011 and 7615.5 μg/g in 2012, reflecting the relatively stable response to environmental effects (Table 2).

**Correlation Analysis of Lysophospholipids.** LPL composition between years was significantly correlated ($P < 0.01$), suggesting rice LPLs were little affected by environment (Table 4). The lowest correlation coefficient between years was 0.810 for LPC16:0 ($P < 0.01$), whereas the highest was 0.967 for LPC14:0 ($P < 0.01$).

Correlations between LPL composition were all positive ($P < 0.01$). TLPL was correlated with its major components, that is, LPC16:0, LPC18:2, LPE16:0, LPE18:2 ($r > 0.723$, $P < 0.01$) (Table 4; Figure 1B,D,G,I). Additionally, the correlation between LPC and LPE components with the same fatty acid composition, for example, LPC14:0 and LPE14:0, LPC16:0 and LPE16:0, and so on, were higher than those between different fatty acid compositions.

**Cluster Analysis of Lysophospholipids.** Hierarchical cluster analysis of the 20 rice genotypes was based on individual LPLs. Two groups separated at a relative distance of 13 were identified, whereas there were three groups at a distance of approximately 11 (Figure 3). Genotypes G07, G08, G09, G12, G15, and G16 formed the first group, G01, G02, and G19 formed the second group, and the remaining genotypes formed the third group. Principal component analysis suggested that the first three components accounted for 51.8, 19.8, and 14.8% of the total variance, respectively. The three groups of 20 accessions were also clearly defined by the first two principal components (Figure 4). The mean LPL components were lowest in group 1, except for LPC18:1 and LPE18:1, and highest in group 2, whereas those of group 3 were intermediate to groups 1 and 2 (Table 5).

## DISCUSSION

Rice grain PLs are of significance for storage, consumption, processing, and eating quality[3] and, as with starch properties, may be

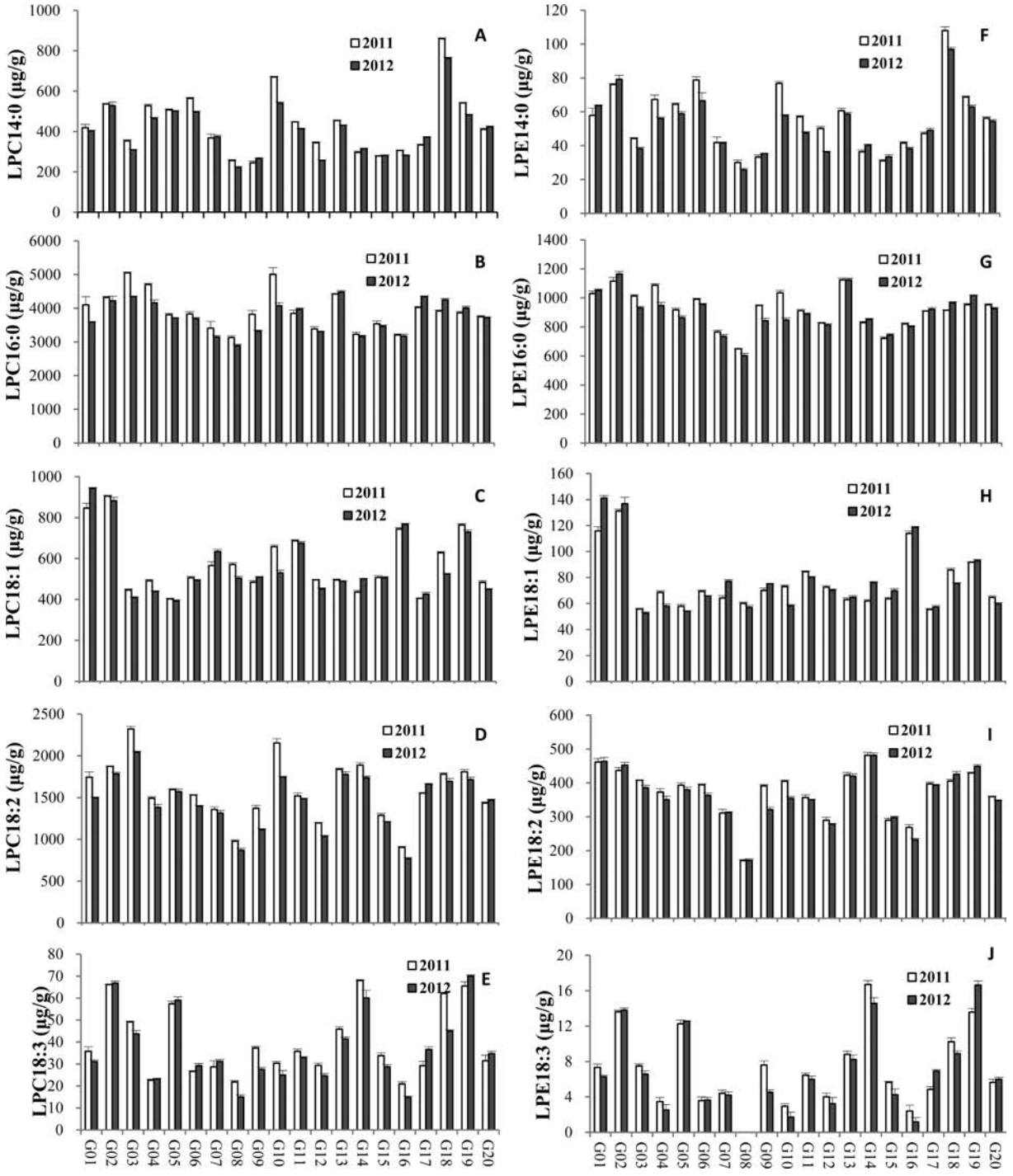


**Figure 1.** Individual rice LPL component content in two years: (A) LPC14:0 content; (B) LPC16:0 content; (C) LPC18:1 content; (D) LPC18:2 content; (E) LPC18:3 content; (F) LPE14:0 content; (G) LPE16:0 content; (H) LPE18:1 content; (I) LPE18:2 content; (J) LPE18:3 content. See Table 1 for rice accession information.

**Table 3. Mean of Lysophospholipids among Different Rice Subspecies[a]**

| group | LPC14:0 | LPC16:0 | LPC18:1 | LPC18:2 | LPC18:3 | TLPC | LPE14:0 | LPE16:0 | LPE18:1 | LPE18:2 | LPE18:3 | TLPE | TLPL |
|---|---|---|---|---|---|---|---|---|---|---|---|---|---|
| *aus* | 462.3 a | 4351.4 a | 488.3 b | 1755.7 a | 32.6 a | 7090.2 a | 56.4 a | 957.3 a | 61.3 b | 372.9 a | 4.5 a | 1452.3 a | 8542.5 a |
| *indica* | 404.4 a | 3691.9 a | 483.7 b | 1479.9 a | 41.1 a | 6101.0 a | 51.7 a | 861.3 a | 65.4 b | 356.0 a | 7.6 a | 1341.9 a | 7442.8 a |
| *japonica* | 417.2 a | 3720.7 a | 696.0 a | 1449.3 a | 38.8 a | 6322.0 a | 55.7 a | 932.4 a | 95.6 a | 374.6 a | 7.2 a | 1465.4 a | 7787.3 a |

[a]Different letters in the same column represent significance at the 0.05 level. See Table 1 for rice accession information. Units: μg/g.

affected by both genotype and environment.[37] In the past decade, several reports of quantitative PL analysis by HPLC coupled with ESI-MS, silica column, or thin layer chromatography have been published.[25,38−40] Although these methods have demonstrated LPLs differ between rice accessions, the influence of environment was not investigated.[41,42] In the present study, the


dx.doi.org/10.1021/jf503213p | J. Agric. Food Chem. 2014, 62, 9353−9361

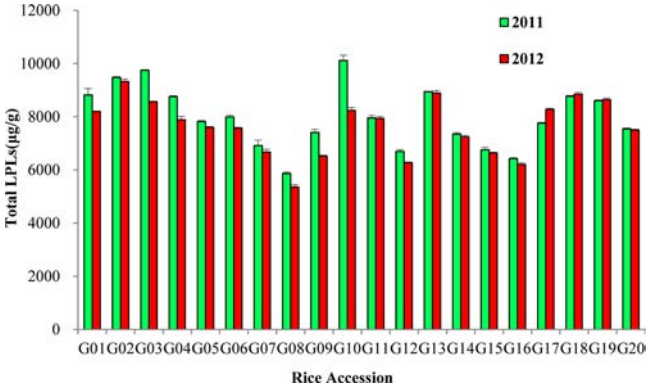


**Figure 2.** Total LPL content of 20 rice accession in two years. See Table 1 for rice accession information.

TLPL content varied from 5609.8 to 9401.1 μg/g in the 20 nonwaxy rice genotypes, which is similar to results from rice planted in the Philippines and Portugal, where TLPL concentration ranged from 5520 to 8310 μg/g in 12 nonwaxy rice cultivars.[41] LPC accounted for 80.0−84.3% of TLPLs, whereas LPE accounted for only 15.7−20.0%. We identified the main components of LPLs as including LPC16:0 43.7−54.0% (Figure 1B), LPC18:2 12.4−24% (Figure 1D), LPE16:0 10.2−13.0% (Figure 1G), and LPE18:2 4.6−12.4% (Figure 1C) in agreement with Majumder et al.[42] and Liu et al.[26] These four LPLs accounted for the TLPL content of Dom Sufid (G02) representing the highest among the genotypes in both years, and was consistently 1.68 times higher than Minghui63 (G08), the lowest in both years. This suggests a difference primarily attributable to genetic factors. Further investigation of the genetic control of LPLs may contribute to breeding superior rice varieties for human consumption or industrial use.

Although genetic factors accounted for the primary component of LPL variation, environmental factors may also affect grain lipid accumulation and concentration.[9,34,43] For example, cold can stimulate synthesis of unsaturated lipids during rice grain filling,[5,42] and the concentration of PL18:2 in rice planted in cold environments was higher than that in mild and tropical environments (37.2−40.0% compared to 30.3−33.1%). In contrast, the PL18:1 was lower in cold conditions than in warm conditions.[11] LPL content in nonwaxy rice cultivars accounted for 48−67% of starch lipids depending on growing location (Asia or Europe), highlighting the role of environment in controlling LPL content in rice.[41] In the present study, genotype, environment, and genotype × environment interaction effects on rice LPLs were significant at $P < 0.001$ (ANOVA) (Table 2). For individual LPC and LPE, genotype accounted for 57.3−95.5%, environment (season) for 0.7−38.9%, and genotype × environment interaction for 1.8−6.6% of the total variation. Thus, genotype appears to be the major factor determining the difference in rice individual LPL concentration in this study. Year of cultivation was a minor but significant factor influencing LPC18:2, LPC16:0, TLPC, and TLPL composition and variation. The extent and timing of how environmental factors such as temperature during grain filling, soil type, and water availability affect LPL content in rice need to be further investigated.

A previous study of brown rice found negative correlations between myristic (C14:0) and linoleic (C18:2), between C14:0 and linolenic (C18:3), between palmitic (C16:0) and oleic (C18:1), between C16:0 and C18:2, between C18:1 and C18:2, and between C18:1 and C18:3 acids, whereas positive correlations existed between C14:0 and C16:0 and between C18:2

**Table 4. Correlation Analysis of Rice Lysophospholipids between Years[a]**

| correlation | LPC14:0 | LPC16:0 | LPC18:1 | LPC18:2 | LPC18:3 | TLPC | LPE14:0 | LPE16:0 | LPE18:1 | LPE18:2 | LPE18:3 | TLPE | TLPL |
|---|---|---|---|---|---|---|---|---|---|---|---|---|---|
| LPC14:0 | **0.967**** | 0.417 | 0.273 | 0.485* | 0.435 | 0.614** | 0.957** | 0.520* | 0.248 | 0.502* | 0.333 | 0.616** | 0.600** |
| LPC16:0 | 0.584** | **0.810**** | 0.052 | 0.684** | 0.327 | 0.816** | 0.613** | 0.768** | 0.045 | 0.567** | 0.247 | 0.736** | 0.823** |
| LPC18:1 | 0.075 | −0.085 | **0.938**** | −0.007 | 0.148 | 0.104 | 0.121 | 0.154 | 0.911** | 0.163 | 0.180 | 0.260 | 0.138 |
| LPC18:2 | 0.481* | 0.683** | −0.011 | **0.947**** | 0.662** | 0.819** | 0.468* | 0.632** | −0.064 | 0.806** | 0.608** | 0.720** | 0.827** |
| LPC18:3 | 0.307 | 0.147 | 0.135 | 0.592 | **0.935**** | 0.840 | 0.332 | 0.330 | 0.161 | 0.669** | 0.931** | 0.504* | 0.420 |
| TLPC | 0.670** | 0.759** | 0.238 | 0.823** | 0.544 | **0.883**** | 0.689** | 0.779** | 0.206 | 0.739** | 0.470* | 0.831** | 0.899** |
| LPE14:0 | 0.893** | 0.375 | 0.401 | 0.464* | 0.489 | 0.591** | **0.940**** | 0.601** | 0.435 | 0.578** | 0.411 | 0.712** | 0.630** |
| LPE16:0 | 0.482* | 0.557** | 0.365 | 0.597** | 0.498 | 0.674** | 0.597** | **0.878**** | 0.461* | 0.774** | 0.521* | 0.923** | 0.738** |
| LPE18:1 | 0.018 | −0.136 | 0.860** | −0.042 | 0.208 | 0.043 | 0.101 | 0.178 | **0.942**** | 0.217 | 0.265 | 0.297 | 0.093 |
| LPE18:2 | 0.440 | 0.421 | 0.176 | 0.776** | 0.743** | 0.631** | 0.482* | 0.638** | 0.226 | **0.957**** | 0.794** | 0.812** | 0.683** |
| LPE18:3 | 0.245 | 0.042 | 0.146 | 0.513* | 0.927** | 0.287 | 0.280 | 0.286 | 0.192 | 0.678** | **0.958**** | 0.790* | 0.334 |
| TLPE | 0.506* | 0.483* | 0.404 | 0.655** | 0.625** | 0.664** | 0.601** | 0.802** | 0.490* | 0.863** | 0.658** | **0.914**** | 0.730** |
| TLPL | 0.456** | 0.723** | 0.281 | 0.813** | 0.578** | 0.863** | 0.691** | 0.808** | 0.273 | 0.789** | 0.525* | 0.875** | **0.890**** |

[a]* and ** indicate significance at $P < 0.05$ and 0.01 levels, respectively. 2011, above diagonal; 2012, below diagonal; and 2011 and 2012, in diagonal.


dx.doi.org/10.1021/jf503213p | J. Agric. Food Chem. 2014, 62, 9353−9361

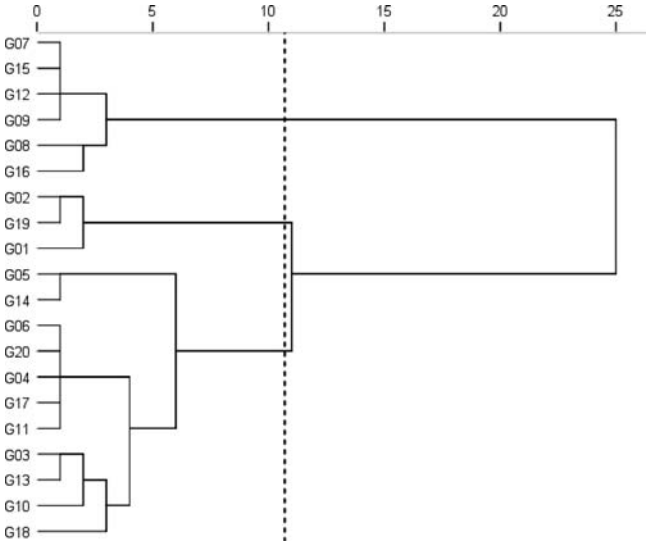


**Figure 3.** Hierarchical cluster analysis dendrogram (Ward's method) based on individual LPL content of 20 accessions. The vertical dashed line indicated all 20 accessions could be divided into 3 groups at a relative distance of 11. See Table 1 for rice accession information.

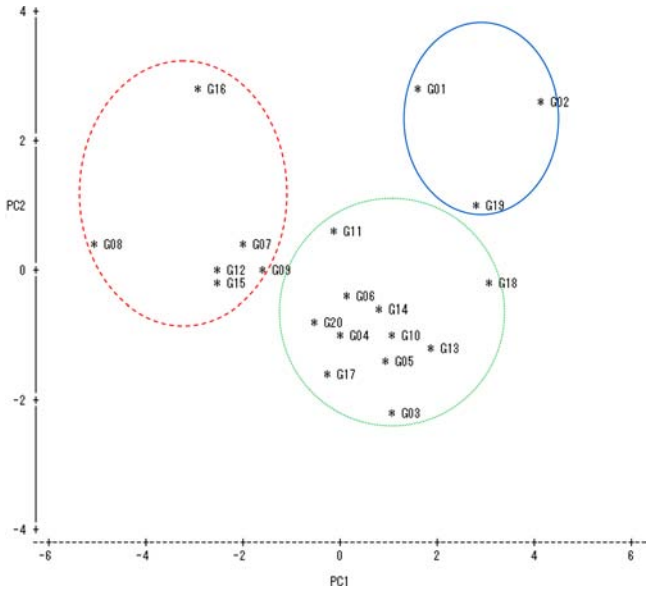


**Figure 4.** Principal component analysis for the genotypes based on their individual LPL content. PC1 and PC2 accounted for 73.9% of total variation, and a plot of PC1 and PC2 separates all 20 genotypes into 3 groups. See Table 1 for rice accession information.

and C18:3.[34] Several different relationships were discovered in this study. LPC16:0 was correlated with LPC18:2, TLPC, TLPE, and TLPL ($P < 0.01$), which may be caused by the abundance of LPC16:0 and its dominant role in synthesis and metabolism. The high correlations between LPC18:1 and LPE18:1 and between LPC18:2 and LPE18:2 as well as between LPC18:3 and LPE18:3 ($P < 0.01$) support the results of an earlier study,[9] suggesting there might be a relationship between unsaturated LPLs in rice. Positive correlations between LPC14:0 and LPE14:0, between LPC16:0 and LPE16:0, and between TLPC and TLPE are also observed in this study.

The results from the correlation analysis may provide insight into the putative biosynthesis pathways of LPLs in rice grain. PLs may be synthesized via three pathways in plants, the cytidinediphosphate-diacylglycerol pathway, the 1,2-diacylglycerol pathway, and the headgroup through exchange reactions with other PLs pathway.[44] As the main starch lipids, LPLs are probably the hydrolysis products of diacylphospholipid transferred from amyloplast membrane[3,45] or catalyzed by phospholipase $A_2$ from PLs.[46] The fatty acid composition (C14:0, C16:0, C18:1, C18:2, and C18:3) accounted for a similar percentage in LPC and LPE among different rice accessions (Table 1). If the LPLs were synthesized from PL, fatty acid distributions (C14:0, C16:0, C18:1, C18:2, and C18:3) in PLs were possibly in certain percentage, too. Previous study indicated that the fatty acids distributions were very similar to each other between PC and PE in rice endosperm[26] and bran.[7,40] These results may imply that each fatty acid composition reacted with choline or ethanolamine at an equal percentage to produce PC and PE, respectively. This possible relationship may provide a useful interpretation of detailed LPL biosynthesis and regulation in metabolism, although the biosynthetic pathway of LPL synthesis in grain endosperm is unclear, particularly the integration of headgroup and fatty acids.

Cluster analysis and principal component analysis demonstrated the 20 rice genotypes could be divided into 3 groups according to LPL composition (Figures 3 and 4; Table 5). Variation in LPL composition among the three groups may reflect their genetic relatedness because rice LPL concentration is primarily dependent on genotype.[3,5,9,41] Further genetic analyses such as quantitative trait locus (QTL) mapping and genome wide associations studies (GWAS) are warranted to identify the genes responsible for controlling LPLs in rice grain.

In summary, broad ranges of LPL composition and content were identified among the 20 rice genotypes over two years, and these differences arose primarily due to genotype differences with environment (season) and genotype × environment interaction effects playing a minor role. Correlation analysis between LPL components provided insight into the possible LPL biosynthesis pathway in plants. Further genetic studies are needed to characterize the genes or QTLs underlying LPLs in milled rice.

**Table 5. Mean Rice Lysophospholipid Content in Three Groups[a]**

| group[b] | LPC14:0 | LPC16:0 | LPC18:1 | LPC18:2 | LPC18:3 | TLPC | LPE14:0 | LPE16:0 | LPE18:1 | LPE18:2 | LPE18:3 | TLPE | TLPL |
|---|---|---|---|---|---|---|---|---|---|---|---|---|---|
| 1 | 290.0 b | 3316.5 b | 561.6 b | 1117.3 b | 26.1 b | 5311.5 b | 36.6 b | 772.7 c | 76.1 b | 277.8 b | 3.5 b | 1166.5 c | 6477.9 b |
| 2 | 485.2 a | 4017.4 a | 844.9 a | 1737.0 a | 55.9 a | 7140.5 a | 68.1 a | 1055.6 a | 118.3 a | 448.6 a | 11.9 a | 1702.4 a | 8842.9 a |
| 3 | 475.2 a | 4068.6 a | 498.7 b | 1685.6 a | 40.5 ab | 6768.6 a | 60.1 a | 943.3 b | 65.5 b | 393.0 a | 7.3 ab | 1469.2 b | 8237.7 a |

[a]Different letters in the same column represent significance at the 0.05 level. Units: μg/g. [b]Group 1 consists of M202 (G07), Minghui63 (G08), Moroberekan (G09), Pokkali (G12), Swarna (G15), and Tainung (G16). Group 2 consists of Azucena (G01), Dom Sufid (G02), and Cypress (G19). Group 3 consists of the remaining genotypes.


dx.doi.org/10.1021/jf503213p | J. Agric. Food Chem. 2014, 62, 9353−9361

## AUTHOR INFORMATION


### Corresponding Author

*(J.B.) Phone: +86-571-86971932. Fax: +86-571-86971421. E-mail: jsbao@zju.edu.cn.


### Notes

The authors declare no competing financial interest.

## ABBREVIATIONS USED

ALC, amylose lipids complex
ANOVA, analysis of variance
HPLC-MS, high-performance liquid chromatographic-mass spectrometric
LPC 14:0, 1-myristoyl-2-hydroxy-*sn*-glycero-3-phosphocholine (MHPC)
LPC16:0, 1-palmitoyl-2-hydroxy-*sn*-glycero-3-phosphocholine (PHPC)
LPC18:1, 1-oleoyl-2-hydroxy-*sn*-glycero-3-phosphocholine (OHPC)
LPC18:2, 1-linoleoyl-2-hydroxy-*sn*-glycero-3-phosphocholine (LHPC)
LPC18:3, 1-linolenoyl-2-hydroxy-*sn*-glycero-3-phosphocholine (LnHPC)
LPE14:0, 1-myristoyl-2-hydroxy-*sn*-glycero-3-phosphoethanolamine (MHPE)
LPE16:0, 1-palmitoyl-2-hydroxy-*sn*-glycero-3-phosphoethanolamine (PHPE)
LPE18:1, 1-oleoyl-2-hydroxy-*sn*-glycero-3-phosphoethanolamine (OHPE)
LPE18:2, 1-linoleoyl-2-hydroxy-*sn*-glycero-3-phosphoethanolamine (LHPE)
LPE18:3, 1-linolenoyl-2-hydroxy-*sn*-glycero-3-phosphoethanolamine (LnHPE)
LPC, lysophosphatidylcholine
LPE, lysophosphatidylethanolamine
LPLs, lysophospholipids
PLs, phospholipids

## REFERENCES


(1) Bao, J. S. Toward understanding the genetic and molecular bases of the eating and cooking qualities of rice. *Cereal Foods World* **2012**, *57*, 148−156.

(2) Zhou, Z.; Robards, K.; Helliwell, S.; Blanchard, C. Composition and functional properties of rice. *Int. J. Food Sci. Technol.* **2002**, *37*, 849−868.

(3) Liu, L.; Waters, D. L. E.; Rose, T. J.; Bao, J. S.; King, G. J. Phospholipids in rice: Significance in grain quality and health benefits: a review. *Food Chem.* **2013**, *139*, 1133−1145.

(4) Piggott, J. R.; Morrison, W. R.; Clyne, J. Changes in lipids and in sensory attributes on storage of rice milled to different degrees. *Int. J. Food Sci. Technol.* **1991**, *26*, 615−628.

(5) Choi, S.-K.; Takahashi, E.; Inatsu, O.; Mano, Y.; Ohnishi, M. Component fatty acids of acidic glycerophospholipids in rice grains: universal order of unsaturation index in each lipid among varieties. *J. Oleo Sci.* **2005**, *54*, 369−373.

(6) Cohn, J. S.; Wat, E.; Kamili, A.; Tandy, S. Dietary phospholipids, hepatic lipid metabolism and cardiovascular disease. *Curr. Opin. Lipidol.* **2008**, *19*, 257−262.

(7) Yoshida, H.; Tanigawa, T.; Yoshida, N.; Kuriyama, I.; Tomiyama, Y.; Mizushina, Y. Lipid components, fatty acid distributions of triacylglycerols and phospholipids in rice brans. *Food Chem.* **2011**, *129*, 479−484.

(8) Juliano, B. O. Lipids in rice and rice processing. In *Lipids in Cereal Technology*; Barnes, P. J., Ed.; Academic Press: London, UK, 1983; pp 305−330.

(9) Mano, Y.; Kawaminami, K.; Kojima, M.; Ohnishi, M.; Ito, S. Comparative composition of brown rice lipids (lipid fractions) of indica and japonica rices. *Biosci., Biotechnol., Biochem.* **1999**, *63*, 619−626.

(10) Putseys, J. A.; Lamberts, L.; Delcour, J. A. Amylose-inclusion complexes: formation, identity and physico-chemical properties. *J. Cereal Sci.* **2010**, *51*, 238−247.

(11) Kugimiya, M.; Donovan, J. W.; Wong, R. Y. Phase-transitions of amylose-lipid complexes in starches − a calorimetric study. *Stärke* **1980**, *32*, 265−270.

(12) Morrison, W. R.; Law, R. V.; Snape, C. E. Evidence for inclusion complexes of lipids with v-amylose in maize, rice and oat starches. *J. Cereal Sci.* **1993**, *18*, 107−109.

(13) Gelders, G. G.; Goesaert, H.; Delcour, J. A. Amylose−lipid complexes as controlled lipid release agents during starch gelatinization and pasting. *J. Agric. Food Chem.* **2006**, *54*, 1493−1499.

(14) Morrison, W. R. Starch lipids and how they relate to starch granule structure and functionality. *Cereal Foods World* **1995**, *40*, 437−446.

(15) Ahmadi-Abhari, S.; Woortman, A. J. J.; Oudhuis, A. A. C. M.; Hamer, R. J.; Loos, K. The influence of amylose-LPC complex formation on the susceptibility of wheat starch to amylase. *Carbohydr. Polym.* **2013**, *97*, 436−440.

(16) Cui, R.; Oates, C. G. The effect of amylose-lipid complex formation on enzyme susceptibility of sago starch. *Food Chem.* **1999**, *65*, 417−425.

(17) Ahmadi-Abhari, S.; Woortman, A. J. J.; Hamer, R. J.; Oudhuis, A. A. C. M.; Loos, K. Influence of lysophosphatidylcholine on the gelation of diluted wheat starch suspensions. *Carbohydr. Polym.* **2013**, *93*, 224−231.

(18) Kaur, K.; Singh, N. Amylose-lipid complex formation during cooking of rice flour. *Food Chem.* **2000**, *71*, 511−517.

(19) Larsson, K. Inhibition of starch gelatinization by amylose-lipid complex-formation. *Starch/Staerke* **1980**, *32*, 125−126.

(20) Lopez, C. A.; de Vries, A. H.; Marrink, S. J. Amylose folding under the influence of lipids. *Carbohydr. Res.* **2012**, *364*, 1−7.

(21) Debet, M. R.; Gidley, M. J. Three classes of starch granule swelling: influence of surface proteins and lipids. *Carbohydr. Polym.* **2006**, *64*, 452−465.

(22) O'Neill, C. M.; Morgan, C.; Hattori, C.; Brennan, M.; Rosas, U.; Tschoep, H.; Deng, P. X.; Baker, D.; Wells, R.; Bancroft, I. Towards the genetic architecture of seed lipid biosynthesis and accumulation in *Arabidopsis thaliana*. *Heredity* **2012**, *108*, 115−123.

(23) Montealegre, C.; Verardo, V.; Gomez-Caravaca, A. M.; Garcia-Ruiz, C.; Marina, M. L.; Caboni, M. F. Molecular characterization of phospholipids by high-performance liquid chromatography combined with an evaporative light scattering detector, high-performance liquid chromatography combined with mass spectrometry, and gas chromatography combined with a flame ionization detector in different oat varieties. *J. Agric. Food Chem.* **2012**, *60*, 10963−10969.

(24) Li, H.; Peng, Z. Y.; Yang, X. H.; Wang, W. D.; Fu, J. J.; Wang, J. H.; Han, Y. J.; Chai, Y. C.; Guo, T. T.; Yang, N.; Liu, J.; Warburton, M. L.; Cheng, Y. B.; Hao, X. M.; Zhang, P.; Zhao, J. Y.; Liu, Y. J.; Wang, G. Y.; Li, J. S.; Yan, J. B. Genome-wide association study dissects the genetic architecture of oil biosynthesis in maize kernels. *Nat. Genet.* **2013**, *45*, 43−50.

(25) Riedelsheimer, C.; Brotman, Y.; Meret, M.; Melchinger, A. E.; Willmitzer, L. The maize leaf lipidome shows multilevel genetic control and high predictive value for agronomic traits. *Sci. Rep.* **2013**, *3*, 1−7.

(26) Liu, L.; Tong, C.; Bao, J. S.; Waters, D. L. E.; Rose, T. J.; King, G. J. Determination of starch lysophospholipids in rice using liquid chromatography mass spectrometry (LCMS). *J. Agric. Food Chem.***2014**, *62*, 6600−6607.

(27) Bessoule, J. J.; Moreau, P. Phospholipid synthesis and dynamics in plant cells. In *Lipid Metabolism and Membrane Biogenesis*; Daum, G., Ed.; Springer: Berlin, Germany, 2004; Vol. 6, pp 89−124.

(28) Eastmond, P. J.; Quettier, A. L.; Kroon, J. T. M.; Craddock, C.; Adams, N.; Slabas, A. R. Phosphatidic acid phosphohydrolase 1 and 2 regulate phospholipid synthesis at the endoplasmic reticulum in arabidopsis. *Plant Cell* **2010**, *22*, 2796−2811.

(29) Suzuki, Y. Isolation and characterization of a rice (*Oryza sativa* L.) mutant deficient in seed phospholipase D, an enzyme involved in the degradation of oil-body membranes. *Crop Sci.* **2011**, *51*, 567−573.
(30) Suzuki, Y.; Takeuchi, Y.; Shirasawa, K. Identification of a seed phospholipase D null allele in rice (*Oryza sativa* L.) and development of SNP markers for phospholipase D deficiency. *Crop Sci.* **2011**, *51*, 2113−2118.
(31) Nakamura, T.; Ohnishi, M.; Kojima, M.; Mano, Y.; Inazu, O.; Ito, S. Comparative analyses of fatty acid compositions in rice grain glycerolipids among three cultivars with different chilling susceptibilities. *Biosci., Biotechnol., Biochem.* **1995**, *59*, 2309−2311.
(32) Kitta, K.; Ebihara, M.; Iizuka, T.; Yoshikawa, R.; Isshiki, K.; Kawamoto, S. Variations in lipid content and fatty acid composition of major non-glutinous rice cultivars in Japan. *J. Food Compos. Anal.* **2005**, *18*, 269−278.
(33) Chang, Y.; Zhao, C.; Zhu, Z.; Wu, Z.; Zhou, J.; Zhao, Y.; Lu, X.; Xu, G. Metabolic profiling based on LC/MS to evaluate unintended effects of transgenic rice with cry1Ac and sck genes. *Plant Mol. Biol.* **2012**, *78*, 477−487.
(34) McNally, K. L.; Childs, K. L.; Bohnert, R.; Davidson, R. M.; Zhao, K.; Ulat, V. J.; Zeller, G.; Clark, R. M.; Hoen, D. R.; Bureau, T. E.; Stokowski, R.; Ballinger, D. G.; Frazer, K. A.; Cox, D. R.; Padhukasahasram, B.; Bustamante, C. D.; Weigel, D.; Mackill, D. J.; Bruskiewich, R. M.; Ratsch, G.; Buell, C. R.; Leung, H.; Leach, J. E. Genomewide SNP variation reveals relationships among landraces and modern varieties of rice. *Proc. Natl. Acad. Sci. U.S.A.* **2009**, *106*, 12273−12278.
(35) Tong, C.; Chen, Y. L.; Tang, F. F.; Xu, F. F.; Huang, Y.; Chen, H.; Bao, J. S. Genetic diversity of amylose content and RVA pasting parameters in 20 rice accessions grown in Hainan, China. *Food Chem.* **2014**, *161*, 239−245.
(36) Xu, F. F.; Tang, F. F.; Shao, Y. F.; Chen, Y. L.; Tong, C.; Bao, J. S. Genotype × environment interactions for agronomic traits of rice revealed by association mapping. *Rice Sci.* **2014**, *21*, 133−141.
(37) Bao, J. S.; Kong, X. L.; Xie, J. K.; Xu, L. J. Analysis of genotypic and environmental effects on rice starch. 1. Apparent amylose content, pasting viscosity, and gel texture. *J. Agric. Food Chem.* **2004**, *52*, 6010−6016.
(38) Pulfer, M.; Murphy, R. C. Electrospray mass spectrometry of phospholipids. *Mass Spectrom. Rev.* **2003**, *22*, 332−364.
(39) Ho, Y. P.; Huang, P. C.; Deng, K. H. Metal ion complexes in the structural analysis of phospholipids by electrospray ionization tandem mass spectrometry. *Rapid Commun. Mass Spectrom.* **2003**, *17*, 114−121.
(40) Yoshida, H.; Tanigawa, T.; Kuriyama, I.; Yoshida, N.; Tomiyama, Y.; Mizushina, Y. Variation in fatty acid distribution of different acyl lipids in rice (*Oryza sativa* L.) brans. *Nutrients* **2011**, *3*, 505−514.
(41) Azudin, M. N.; Morrison, W. R. Non-starch lipids and starch lipids in milled rice. *J. Cereal Sci.* **1986**, *4*, 23−31.
(42) Majumder, M. K.; Seshu, D. V.; Shenoy, V. V. Implication of fatty-acids and seed dormancy in a new screening-procedure for cold tolerance in rice. *Crop Sci.* **1989**, *29*, 1298−1304.
(43) Morrison, W. R.; Azudin, M. N. Variation in the amylose and lipid contents and some physical properties of rice starches. *J. Cereal Sci.* **1987**, *5*, 35−44.
(44) Kinney, A. J. Phospholipid head groups. In *Lipid Metabolism in Plants*; Moore, T. S. J., Ed.; CRC Press: Boca Raton, FL, USA, 1993; pp 259−284.
(45) Morrison, W. R. Lipids in cereal starches: a review. *J. Cereal Sci.* **1988**, *8*, 1−15.
(46) D'Arrigo, P.; Servi, S. Synthesis of lysophospholipids. *Molecules* **2010**, *15*, 1354−1377.

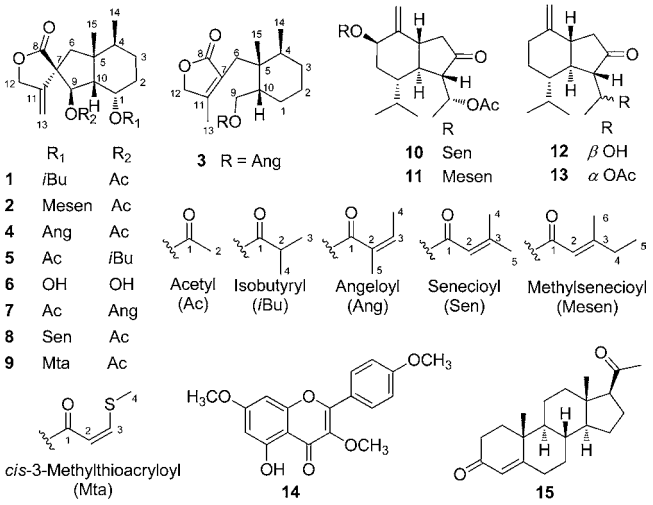


**Figure 1.** Structures of compounds **1**−**15** from *P. tatewakianus*.

used for column chromatography (200−300 mesh, Qingdao Marine Chemical Group Co. Ltd., China). Chemical reagents for isolation were of analytical grade and purchased from Tianjin Chemical Reagent Company, China. Biological reagents were from Sigma Company. The murine microglial BV-2 cell line was from Shanghai Institutes for Biological Sciences, Chinese Academy of Sciences (China).

**Plant Material.** The leaves of *P. tatewakianus* were collected in July 2013 from Changbai Mountain area, Jilin province, China. A voucher specimen (No. 20130716) was identified by Dr. Yuanqiang Guo (College of Pharmacy, Nankai University, China) and deposited at the laboratory of the Research Department of Natural Medicine, College of Pharmacy, Nankai University, China.

**Extraction and Isolation.** The air-dried leaves of *P. tatewakianus* (7.9 kg) were powdered and extracted with MeOH (3 × 48 L) under reflux. The organic solvent was evaporated to obtain a crude extract (910 g). The crude extract was suspended in $H_2O$ (0.9 L) and partitioned with EtOAc (3 × 0.9 L). The EtOAc soluble part (277 g) was subjected to a silica gel column chromatography (⌀ 9 × 70 cm), using a gradient of acetone in petroleum ether (1%−30%), to give seven fractions ($F_1$−$F_7$) based on TLC analyses. $F_1$ was fractionated by middle pressure liquid chromatography (MPLC) over octadecylsilyl (ODS) eluting with a step gradient from 75% to 95% MeOH in $H_2O$ to give three subfractions ($F_{1-1}$−$F_{1-3}$). $F_{1-3}$ was further purified by preparative HPLC (YMC-pack ODS-AM, 250 × 20 mm, 84% MeOH in $H_2O$) to produce compounds **1** ($t_R$ = 19 min, 11.3 mg), **2** ($t_R$ = 26 min, 12.4 mg), **5** ($t_R$ = 17 min, 15.6 mg), **10** ($t_R$ = 31 min, 11.6 mg), **11** ($t_R$ = 36 min, 12.1 mg), **12** ($t_R$ = 24 min, 13.2 mg), and **13** ($t_R$ = 29 min, 43.7 mg). By the above HPLC system, the purification of $F_{1-1}$ (75% MeOH in $H_2O$) afforded compounds **4** ($t_R$ = 34 min, 25.5 mg) and **7** ($t_R$ = 31 min, 24.4 mg). Fraction $F_3$ was subjected to the same MPLC (65−90% MeOH in $H_2O$)

**Table 1. NMR Data of Compounds 1−4 ($\delta$ ppm in $CDCl_3$ and $J$ in Hz)[a]**

| | | 1 | | 2 | | 3 | | 4 |
|---|---|---|---|---|---|---|---|---|
| position | | $^{13}C$ | $^1H$ | $^{13}C$ | $^1H$ | $^{13}C$ | $^1H$ | $^{13}C$ |
| 1 | | 70.4 | $\beta$ 5.06 dt (11.8, 4.8) | 69.4 | $\beta$ 5.10 dt (11.6, 4.8) | 25.6 | $\alpha$ 1.70 m | 70.3 |
| | | | | | | | $\beta$ 1.75 m | |
| 2 | | 26.4 | $\alpha$ 1.84 m | 26.8 | $\alpha$ 1.81 m | 20.1 | $\alpha$ 1.45 m | 26.7 |
| | | | $\beta$ 1.70 m | | $\beta$ 1.70 m | | $\beta$ 1.60 m | |
| 3 | | 29.5 | $\alpha$ 1.67 m | 29.5 | $\alpha$ 1.68 m | 29.0 | $\alpha$ 2.20 m | 29.4 |
| | | | $\beta$ 1.36 m | | $\beta$ 1.37 m | | $\beta$ 1.33 m | |
| 4 | | 35.3 | $\alpha$ 1.59 m | 35.3 | $\alpha$ 1.58 m | 35.0 | $\alpha$ 1.55 m | 35.1 |
| 5 | | 43.3 | | 43.2 | | 40.0 | | 43.2 |
| 6 | | 45.8 | 2.23 d (14.3) | 45.7 | 2.24 d (14.3) | 27.2 | 2.75 d (13.6) | 45.6 |
| | | | 1.95 d (14.3) | | 1.96 d (14.3) | | 2.09 d (13.6) | |
| 7 | | 54.8 | | 54.8 | | 125.7 | | 54.9 |
| 8 | | 177.8 | | 177.6 | | 175.6 | | 177.4 |
| 9 | | 80.8 | $\alpha$ 5.80 d (11.2) | 80.8 | $\alpha$ 5.77 d (11.2) | 65.5 | 4.44 dd (10.8, 3.7) | 80.7 |
| | | | | | | | 4.03 dd (10.8, 8.9) | |
| 10 | | 51.9 | $\beta$ 2.67 dd (11.2, 4.8) | 51.6 | $\beta$ 2.74 dd (11.2, 4.8) | 41.0 | $\beta$ 1.86 m | 51.4 |
| 11 | | 147.6 | | 147.7 | | 159.0 | | 147.6 |
| 12 | | 70.6 | 4.71 d (13.0) | 70.6 | 4.70 d (13.2) | 72.5 | 4.67 d (17.2) | 70.5 |
| | | | 4.61 d (13.0) | | 4.66 d (13.2) | | 4.62 d (17.2) | |
| 13 | | 108.4 | 5.22 s | 108.2 | 5.21 s | 13.8 | 2.04 s | 108.3 |
| | | | 5.18 s | | 5.18 s | | | |
| 14 | | 15.5 | 0.90 d (6.7) | 15.5 | 0.91 d (6.6) | 14.9 | 0.90 d (7.2) | 15.5 |
| 15 | | 19.6 | 1.10 s | 19.6 | 1.12 s | 24.6 | 0.94 s | 19.5 |
| OR-1 | 1 | 176.3 | | 165.7 | | | | 167.2 |
| | 2 | 34.0 | 2.33 set (7.1) | 114.1 | 5.44 s | | | 128.1 |
| | 3 | 18.7 | 1.11 d (7.1) | 162.1 | | | | 136.7 |
| | 4 | 19.1 | 1.09 d (7.1) | 33.6 | 2.12 q (7.4) | | | 15.5 |
| | 5 | | | 11.7 | 1.03 t (7.4) | | | 20.3 |
| | 6 | | | 18.8 | 2.14 s | | | |
| OR-9 | 1 | 169.8 | | 169.9 | | 168.3 | | 169.9 |
| | 2 | 21.2 | 2.06 s | 21.1 | 2.03 s | 128.0 | | 20.9 |
| | 3 | | | | | 137.8 | 6.06 qq (7.2, 1.5) | |
| | 4 | | | | | 15.8 | 2.00 dq (7.2, 1.5) | |
| | 5 | | | | | 20.7 | 1.90 quint (1.5) | |

[a]The assignments of NMR data are based on $^1H$, $^{13}C$, DEPT, $^1H$−$^1H$ COSY, HMQC, and HMBC NMR experiments.


dx.doi.org/10.1021/jf5034224 | J. Agric. Food Chem. 2014, 62, 9362−9367

to obtain four subfractions $F_{3-1}$–$F_{3-4}$, and the following purification of $F_{3-2}$ by the same HPLC system (94% MeOH in $H_2O$) yielded compound **3** ($t_R$ = 29 min, 4.5 mg), **8** ($t_R$ = 17 min, 14.7 mg), **9** ($t_R$ = 19 min, 17.1 mg), and **15** ($t_R$ = 26 min, 5.4 mg). Compounds **6** ($t_R$ = 26 min, 14.7 mg) and **14** ($t_R$ = 22 min, 15.4 mg) were isolated from $F_{5-3}$ (87% MeOH in $H_2O$), which was obtained from $F_5$ by the above MPLC.

**Tatewakipene A (1).** Colorless oil; $[\alpha]_D^{27}$: −75.7 (*c* 0.3, $CH_2Cl_2$); CD ($CH_3CN$): 201 ($\Delta\varepsilon$ −29.30) nm; IR (KBr) $\nu_{max}$ 2964, 2933, 1780, 1733, 1635, 1265, 1154, and 1045 $cm^{-1}$; $^{13}C$ NMR (100 MHz, $CDCl_3$) and $^1H$ NMR (400 MHz, $CDCl_3$) data, see Table 1; ESIMS *m*/*z* 401 $[M + Na]^+$; HR-ESIMS *m*/*z* 401.1935 $[M + Na]^+$, calcd. for $C_{21}H_{30}NaO_6$, 401.1940.

**Tatewakipene B (2).** Colorless oil; $[\alpha]_D^{27}$: −129.6 (*c* 0.2, $CH_2Cl_2$); IR (KBr) $\nu_{max}$ 2964, 2926, 1780, 1747, 1696, 1650, 1233, 1145, and 1046 $cm^{-1}$; $^{13}C$ NMR (100 MHz, $CDCl_3$) and $^1H$ NMR (400 MHz, $CDCl_3$) data, see Table 1; ESIMS *m*/*z* 427 $[M + Na]^+$; HR-ESIMS *m*/*z* 427.2095 $[M + Na]^+$, calcd. for $C_{23}H_{32}NaO_6$, 427.2097.

**Tatewakipene C (3).** Colorless oil; $[\alpha]_D^{27}$: +10.9 (*c* 0.1, $CH_2Cl_2$); CD ($CH_3CN$): 205 ($\Delta\varepsilon$ −0.73), 227 ($\Delta\varepsilon$ +2.84) nm; IR (KBr) $\nu_{max}$ 2925, 2857, 1750, 1637, and 1276 $cm^{-1}$; $^{13}C$ NMR (100 MHz, $CDCl_3$) and $^1H$ NMR (400 MHz, $CDCl_3$) data, see Table 1; ESIMS *m*/*z* 357 $[M + Na]^+$; HR-ESIMS *m*/*z* 357.2032 $[M + Na]^+$, calcd. for $C_{20}H_{30}NaO_4$, 357.2042.

**Computation.** For those compounds needed to determine the absolute configurations, their calculated ECD spectra were performed using TDDFT method as follows. A preliminary conformational search was carried out in Conflex 6.7 using MMFF94 force field.[8] Conformers within 6 kcal/mol were saved and further optimized on B3LYP/6-31+G(d,p) level in the Gaussian 09 package.[9] The stable conformers with populations greater than 1% were submitted to ECD calculation by the TDDFT [B3LYP/6-31+G(d,p)] method with CPCM model in acetonitrile, and the calculated ECD spectra of different conformers were simulated with a half bandwidth of 0.3 eV. The final ECD curve were generated according to the Boltzmann distribution of each conformer.

**Bioassay for NO Production.** Murine microglial BV-2 cells were cultured at 37 °C in DMEM supplemented with 10% (v/v) inactivated fetal bovine serum and 100 U/mL penicillin/streptomycin under a water-saturated atmosphere of 95% air and 5% $CO_2$. The cells were seeded in 96-well culture plates ($5 \times 10^4$ cells/well) and allowed to adhere for 24 h at 37 °C. The cells were incubated for 20 h with or without 0.15 $\mu$g/mL of LPS (Sigma Chemical Co., St. Louis, MO) in the absence or presence of the test compounds. 2-Methyl-2-thiopseudourea, sulfate (SMT) was used as a positive control. As a parameter of NO synthesis, the nitrite concentration was measured by the Griess reaction using the supernatant of the BV-2 cells. Briefly, 50 $\mu$L of the cell culture supernatant was reacted with 50 $\mu$L of Griess reagent [1:1 mixture of 0.1% *N*-(1-naphtyl)ethylenediamine in $H_2O$ and 1% sulfanilamide in 5% phosphoric acid] in a 96-well plate, and the absorbance was read with a microplate reader (Thermo Fisher Scientific Inc. America) at 550 nm. The experiment was performed three times, and the $IC_{50}$ values for the inhibition of NO production were determined on the basis of linear or nonlinear regression analysis of the concentration–response data curves.

## RESULTS AND DISCUSSION

Compound **1** was obtained as a colorless oil. Its HR-ESIMS provided the molecular formula, $C_{21}H_{30}O_6$, through the presence of a peak at *m*/*z* 401.1935 $[M + Na]^+$ (calcd. for $C_{21}H_{30}NaO_6$, 401.1940). The molecular formula indicated seven unsaturation degrees for **1**. The $^1H$ NMR spectrum of **1** exhibited five methyl signals [$\delta_H$ 0.90 (3H, d, *J* = 6.7 Hz, $H_3$-14), 1.10 (3H, s, $H_3$-15), 2.06 (3H, s, $COCH_3$-9), and 1.11 and 1.09 (each 3H, d, *J* = 7.1 Hz, $COCH(CH_3)_2$-1)] (Table 1), two olefinic protons of a terminal double bond [$\delta_H$ 5.22 and 5.18 (each 1H, s, $H_2$-13)], a set of oxygenated methylene protons [$\delta_H$ 4.61 and 4.71 (each 1H, d, *J* = 13.0 Hz, $H_2$-12)], and two oxygenated methine protons [$\delta_H$ 5.06 (1H, dt, *J* = 11.8, 4.8 Hz, H-1) and 5.80 (1H, d, *J* = 11.2 Hz, H-9)]. The $^{13}C$ NMR spectrum of **1** showed 21 carbon resonances. From the $^1H$ and $^{13}C$ NMR spectra, one acetyl group and one isobutyryl group were evident from the above methyl signals and corresponding carbon resonances ($\delta_C$ 169.8 and 21.2 and 176.3, 34.0, 18.7, and 19.1). Apart from the above six signals for two acyl groups, there are additional 15 resonances exhibited for the parent skeleton in the $^{13}C$ NMR spectrum, which comprised two methyls [$\delta_C$ 15.5 (C-14) and 19.6 (C-15)], five methylenes [$\delta_C$ 26.4 (C-2), 29.5 (C-3), 45.8 (C-6), 70.6 (C-12), and 108.4 (C-13)], four methines [$\delta_C$ 70.4 (C-1), 35.3 (C-4), 80.8 (C-9), and 51.9 (C-10)], and four quaternary carbons [$\delta_C$ 43.3 (C-5), 54.8 (C-7), 177.8 (C-8), and 147.6 (C-11)] based on the DEPT and HMQC spectra. The above spectroscopic features and the 15 skeletal carbons displayed in the $^{13}C$ NMR spectrum suggested that compound **1** should be a sesquiterpene with two acyloxy groups (one acetoxy and one isobutyryloxy group).[10−16] On comparing the chemical shifts from C-1 to C-15 of compound **1** with those of bakkenolide sesquiterpenes reported in the literature,[14−16] the presence of the same parent skeleton of bakkenolide-type was obvious. The following experiments and interpretation of HMQC and HMBC spectra corroborated the above deductions, which verified that compound **1** was a bakkenolide-type sesquiterpene with two acyloxy groups. The positions of the acyloxy groups were determined via interpretation of the HMBC data. The HMBC correlation of the proton signal at $\delta_H$ 5.06 (H-1) with the carbonyl signal at $\delta_C$ 176.3 (CO of the isobutyryloxy group), indicated the presence of the isobutyryloxy group at C-1. Similarly, the long-range coupling of the proton signal at $\delta_H$ 5.80 (H-9) with the carbonyl carbon signal at $\delta_C$ 169.8 demonstrated that the acetoxy group was located at C-9. By further analyzing the HMQC, HMBC, and $^1H$–$^1H$ COSY spectra (Figure 2), all the proton and carbon signals were assigned unambiguously, which resulted in the establishment of the planar structure for **1**.

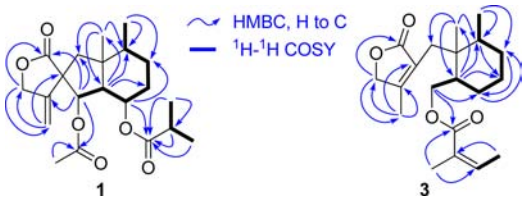


**Figure 2.** Selected HMBC and $^1H$–$^1H$ COSY correlations of compounds **1** and **3**.

The relative configuration of compound **1** was established based on the NOESY spectrum and Chem3D modeling (Figure 3). NOESY correlations observed for H-10/$H_3$-15, $H_3$-15/$H_3$-

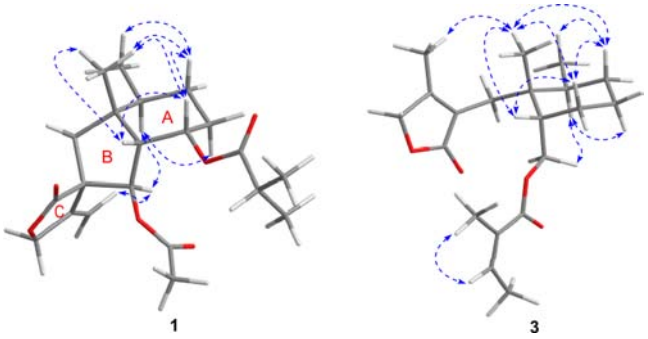


**Figure 3.** Key NOESY correlations of compounds **1** and **3**.


dx.doi.org/10.1021/jf5034224 | J. Agric. Food Chem. 2014, 62, 9362−9367

14, H-1/H-10, H-9/H-4, H-4/H-2$\alpha$, and H-9/H-13a, but not for H-9/$H_3$-15, H-9/H-1, and H-4/$H_3$-15, and the Chem3D modeling suggested a conformation for compound **1** as depicted in Figure 3, where the six-membered ring A and the five-membered ring B were *cis*-fused and existed in a chair and envelope conformation, and the lactone ring C was perpendicular to the five-membered ring B. The conformations of the three rings and the NOESY correlations required that the C-15 methyl group was $\beta$-axially oriented, the C-14 methyl group and the proton H-10 were $\beta$-equatorially oriented, the C-1 isobutyryloxy group was $\alpha$-equatorially oriented, and the C-9 acetoxy group was in a $\beta$-position. Thus, the relative configuration of **1** was assigned as shown in Figure 3. The absolute configuration of **1** was tentatively established by comparison of its experimental CD spectrum with those calculated by the TDDFT method. The optimized geometries were obtained by systematic conformational search with the MMFF94 force field and further optimized on B3LYP/6-31+G(d,p) level by Gaussian 09 package.[8,9] Then the ECD spectra were calculated at the CAM-B3LYP/SVP level with CPCM model in acetonitrile. The calculated ECD spectrum of **1**a (Figure 4) matches the experimental result very well. Thus,

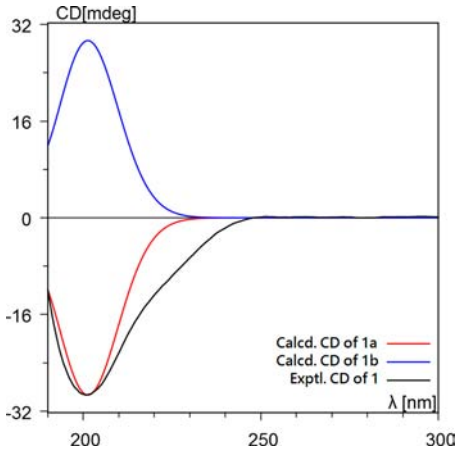


**Figure 4.** Calculated ECD spectra of **1**a (1*S*, 4*S*, 5*R*, 7*R*, 9*R*, 10*R*)- and **1**b (1*R*, 4*R*, 5*S*, 7*S*, 9*S*, 10*S*)-isomers and the experimental ECD spectrum of **1** in acetonitrile.

the absolute configuration of **1** was determined as 1*S*, 4*S*, 5*R*, 7*R*, 9*R*, 10*R*. The structure of **1** was therefore characterized and named tatewakipene A.

Compound **2**, a colorless oil, possessed a molecular formula of $C_{23}H_{32}O_6$ as determined from the HR-ESIMS (427.2095 [M + Na]$^+$, calcd. for $C_{23}H_{32}NaO_6$, 427.2097). From the $^1$H NMR spectrum of **2**, four methyl groups, six olefinic protons, and two oxygenated methine protons were displayed (Table 1). The $^{13}$C NMR spectrum of **2** showed 23 carbon resonances. From the $^1$H and $^{13}$C NMR spectra, one acetoxy was apparent from the methyl singlet and the corresponding carbon signals. In addition, one methylsenecioyloxy group was also deduced and defined from the observation of the following carbon signals ($\delta_C$ 165.7, 114.1, 162.1, 33.6, 11.7, and 18.8) and the corresponding proton signals (Table 1) based on the reported sesquiteprnes with acyloxy groups from the genus *Patesites* in the literature.[14−17] Apart from the above 7 resonances for the substituent groups, the remaining 15 carbon resonances displayed in the $^{13}$C NMR spectrum constitute a bakkenolide-type sesquiterpene skeleton, which was the same as that of compound **1**.[17] In order to confirm the above deductions and achieve the assignments of the proton and carbon signals, the following HMQC and HMBC experiments were performed. By interpretation of the 2D NMR spectra, the same bakkenolide-type sesquiterpene skeleton as that in **1** was defined, and the acyloxy groups, especially the methylsenecioyloxy group, were validated. The HMBC correlations of the proton signals at $\delta_H$ 5.10 (H-1) and 5.77 (H-9) with the carbonyl carbons at $\delta_C$ 165.7 and 169.9, respectively, demonstrated that the methylsenecioyloxy group was attached at C-1, and the acetoxy group was at C-9. Further analyses of the HMQC, HMBC, and $^1$H−$^1$H COSY spectroscopic data led to the assignments of all the proton and carbon signals. Thus, the planar structure with a bakkenolide-type sesquiterpene skeleton for **2** was disclosed. The same relative configuration was inferred for compounds **2** and **1** on the basis of comparison of their NOESY spectra. Compounds **2** and **1** had the same parent skeleton and there were no additional chiral carbons in compound **2**, so, from the biosynthetic point of view, the absolute configuration of compound **2** was also defined as 1*S*, 4*S*, 5*R*, 7*R*, 9*R*, 10*R*, which was also supported by the identical laeotropic optical rotation of two compounds. Therefore, the structure of compound **2** was characterized and named tatewakipene B.

Compound **3** possessed a molecular formula $C_{20}H_{30}O_4$ as determined by the HR-ESIMS ($m/z$ 357.2032 [M + Na]$^+$ calcd. for $C_{20}H_{30}NaO_4$, 357.2042), which implied six unsaturation degrees. The $^1$H NMR spectrum of compound **3** exhibited five methyl signals [$\delta_H$ 2.04 (3H, s, $H_3$-13), 0.90 (3H, d, $J$ = 7.2 Hz, $H_3$-14), 0.94 (3H, s, $H_3$-15), 2.00 (3H, dq, $J$ = 7.2, 1.5 Hz, COCH($CH_3$)=CH($CH_3$)-9), and 1.90 (3H, quint, $J$ = 1.5 Hz, COCH($CH_3$)=CH($CH_3$)-9], one olefinic proton [$\delta_H$ 6.06 (1H, qq, $J$ = 7.2, 1.5 Hz, COCH($CH_3$)=C*H*($CH_3$)-9)], and two sets of oxygenated methylene protons [$\delta_H$ 4.44 (1H, dd, $J$ = 10.8, 3.7 Hz, H-9a) and 4.03 (1H, dd, $J$ = 10.8, 8.9 Hz, H-9b), and 4.62 and 4.67 (each 1H, d, $J$ = 17.2, $H_2$-12)] (Table 1). The $^{13}$C NMR spectrum of **3** showed 20 carbon resonances. From the $^1$H and $^{13}$C NMR spectra, one angeloyl group in compound **3** was deduced from the above characteristic protons and the corresponding carbons ($\delta_C$ 168.3, 128.0, 137.8, 15.8, and 20.7). Apart from the five carbon signals for the angeloyl group, there were 15 residual resonances displayed in the $^{13}$C NMR spectrum, which were classified into three methyls [$\delta_C$ 13.8 (C-13), 14.9 (C-14), and 24.6 (C-15)], six methylenes [$\delta_C$ 25.6 (C-1), 20.1 (C-2), 29.0 (C-3), 27.2 (C-6), 65.5 (C-9), and 72.5 (C-12)], two methines [$\delta_C$ 35.0 (C-4) and 41.0 (C-10)], and four quaternary carbons [$\delta_C$ 40.0 (C-5), 125.7 (C-7), 175.6 (C-8), and 159.0 (C-11)] based on the DEPT and HMQC spectra. According to the unsaturation degrees, the aforementioned spectroscopic features, and the sesquiterpenes isolated from the genus *Petaistes*,[11−17] compound **3** might be a bicyclic sesquiterpene with an angeloyloxy group. In order to confirm the above assumption and elucidate the structure, the following HMBC and $^1$H−$^1$H COSY experiments were performed. By interpretation of the HMBC spectrum, one ring, the $\alpha,\beta$-saturated $\gamma$-lactone ring, was validated based on the long-range correlations of $H_2$-12 to C-7, C-8, C-11, and C-13, and $H_3$-13 to C-7, C-11, and C-12. The other ring was also deduced and defined from the HMBC correlations of H-10 to C-1, C-2, C-4, and C-5, $H_3$-14 to C-3, C-4, and C-5, and $H_3$-15 to C-4, C-5, and C-10. The above two rings, one $\alpha,\beta$-saturated $\gamma$-lactone ring and one six-membered ring, were connected through the methylene unit of C-6, which was demonstrated by the long-range couplings of the methylene protons at $\delta_H$ 2.75 and 2.09 (each 1H, d, $J$ = 13.6 Hz, $H_2$-6) to the carbons of two rings at $\delta_C$ 35.0 (C-4), 40.0 (C-5), 41.0 (C-10), 125.7 (C-7), 175.6 (C-8), and 159.0 (C-11). Accordingly, the


dx.doi.org/10.1021/jf5034224 | *J. Agric. Food Chem.* 2014, 62, 9362−9367

three methyl carbons at $\delta_C$ 13.8, 14.9, and 24.6 and the remaining oxygenated methylene carbon at $\delta_C$ 65.5 were assigned to C-13, C-14, C-15, and C-9, respectively, based on the HMBC correlations of the methyl and methylene protons to the corresponding carbons of the two rings. The skeleton of bicyclic sesquiterpene for **3** was therefore elucidated, which possessed an unusual skeleton of 7,9-seco-bakkenolide. After defining the 7,9-seco-bakkenolide skeleton, the HMBC correlations of the methylene protons $H_2$-9 to the carbonyl carbon at $\delta_C$ 168.3 indicated that the angeloyloxy group was attached at C-9. By further analyzing the HMQC, HMBC, and $^1H-^1H$ COSY spectra (Figure 2), all the proton and carbon signals were assigned unambiguously. Thus, the planar structure of 7,9-seco-bakkenolide sesquiterpene for compound **3** was established.

The relative configuration of compound **3** was established based on the NOESY spectrum. NOESY correlations observed for H-10/$H_3$-15, $H_3$-15/$H_3$-14, H-1$\beta$/H-10, H-9a/H-4, H-4/H-2$\alpha$, H-3$\beta$/$H_3$-15, H-3$\beta$/$H_3$-14, and H-1$\beta$/H-3$\beta$ (Figure 3), but not for H-9a(b)/$H_3$-15, and the Chem3D modeling revealed that the six-membered ring had the same conformation as those in compounds **1** and **2**, where the H-10 proton was $\beta$-equatorially oriented, the C-14 methyl group was in a $\beta$-position with an equatorial orientation, and the C-15 methyl group was in a $\beta$-position with an axial orientation. Thus, the relative configuration of **3** was assigned as depicted in Figure 3. After the relative configuration was determined, the absolute configuration of **3**, a new sesquiterpene with an unusual carbon skeleton, was also considered to elucidate. As in the case of compound **1**, the calculated CD spectra were performed using time-dependent density functional theory (TDDFT) method, and the experimental CD spectrum was recorded (Figure 5). By comparison of its experimental and calculated CD spectra, the absolute configuration of **3** was established as 4*S*, 5*R*, 10*S*. Thus, compound **3** was characterized as a new sesquiterpnene with an unusual carbon skeleton and named tatewakipene C.

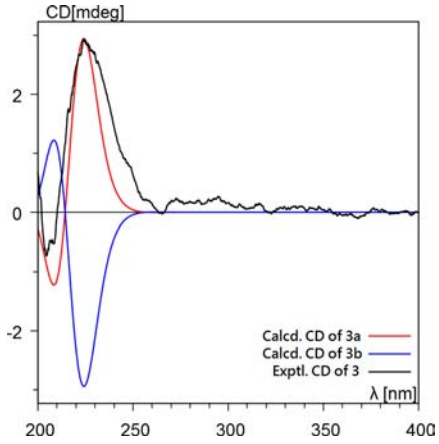


**Figure 5.** Calculated ECD spectra of **3**a (4*S*, 5*R*, 10*S*)- and **3**b (4*R*, 5*S*, 10*R*)-isomers and the experimental ECD spectrum of **3** in acetonitrile.

Based on the spectroscopic analyses and the comparison with the literature, the known compounds were identified as bakkenolide B (**4**),[18] japonipene A (**5**),[17] bakkenolide III (**6**),[14] valerilactone A (**7**),[18] petatewalide A (**8**),[3] bakkenolide D (**9**),[19] 14-acetoxy-7$\beta$-senecioyloxy-notonipetranone (**10**),[20] tussilagone (**11**),[21] [1*S*-[1$\alpha$(*R**), 3a$\beta$, 7$\alpha$, 7a$\alpha$] ]-octahydro-1-(1-hydroxyethyl)-4-methylene-7-(1-methylethyl)-2*H*-inden-2-one (**12**),[22] petasipaline B (**13**),[23] 5-hydroxy-3,7,4′-trimethoxy-flavone (**14**),[24] and pregn-4-ene-3,20-dione (**15**).[25]

Studies on the role of NO in the process of inflammation have demonstrated that reagents with NO inhibitory activities may be useful for the development of anti-inflammatory agents.[7] In order to search and obtain the bioactive substances inhibiting NO production as candidates of anti-inflammatory agents, these compounds isolated from *P. tatewakianus* were evaluated for their inhibitory effects on LPS-induced NO production in murine microglial BV-2 cells by the Griess reaction.[26] 2-Methyl-2-thiopseudourea sulfate (SMT) was used as a positive control ($IC_{50}$ 3.6 $\mu$M). All the evaluated isolates exhibited inhibitory effects on LPS-induced NO production and the inhibitory effects are shown in Table 2. Compounds **10**, **12**, and **14** inhibited LPS-induced NO production dose-dependently with $IC_{50}$ values of 38.7, 47.0, and 45.8 $\mu$M, respectively. Compounds **4**, **8**, **9**, **11**, **13**, and **15** showed moderate inhibitory effects and compounds **1**, **2**, and **5**−**7** showed weak activities ($IC_{50}$ values >100 $\mu$M). Compound **3** was not investigated for the NO inhibitory effects because of inadequate amount. Among these bioactive compounds, eight compounds (**1**, **2**, and **4**−**9**) had the same parent skeleton, and the analysis of the preliminary structure activity relationship (SAR) inhibiting NO production revealed that the presence of the C-1 *cis*-methylthioacryloyloxy group seems to increase NO inhibitory effects markedly. MTT assay indicated that all the assayed compounds had no significant cytotoxicity to the BV-2 cells at their effective concentrations for the inhibition of NO production (data not shown).

**Table 2. IC50 Values of Compounds 1, 2, and 4−15 Inhibiting NO Production in BV-2 Cells**

| compound | $IC_{50}$ ($\mu$M) | compound | $IC_{50}$ ($\mu$M) |
|---|---|---|---|
| **1** | >100 | **10** | 38.7 ± 3.1 |
| **2** | >100 | **11** | 64.4 ± 3.1 |
| **4** | 65.8 ± 2.5 | **12** | 47.0 ± 2.0 |
| **5** | >100 | **13** | 62.4 ± 3.2 |
| **6** | >100 | **14** | 45.8 ± 3.6 |
| **7** | >100 | **15** | 52.0 ± 1.5 |
| **8** | 84.1 ± 2.5 | SMT[a] | 3.6 ± 0.2 |
| **9** | 55.1 ± 4.1 | | |

[a]SMT (2-methyl-2-thiopseudourea, sulfate) was used as a positive control. Data are presented based on three experiments. Compound **3** was not assayed for the inhibitory effects because of inadequate amount.

In summary, 3 new sesquiterpenes (**1**−**3**), including one with an unusual carbon skeleton (**3**), and 12 known compounds (**4**−**15**) were successfully isolated from the leaves of *P. tatewakianus*. Their structures were elucidated on the basis of the spectroscopic data analyses and the TDDFT CD calculations. Biological studies disclosed that all of the evaluated isolates exhibited inhibitory effects on LPS-induced NO production and compound **10** exerted the most inhibition against LPS-induced NO production in BV-2 cells. The results of our chemical investigation, including two new bakkenolide sesquiterpenes (**1** and **2**), one new sesquiterpene with an unusual carbon skeleton (**3**), and the first report of compounds **5**−**7** and **10**−**15** from this species, further revealed the chemical composition of *P. tatewakianus* as an edible plant, and the biological studies implied that *P. tatewakianus*, containing bioactive substances with the inhibitory activities of NO production, may be potentially beneficial to human health.


dx.doi.org/10.1021/jf5034224 | J. Agric. Food Chem. 2014, 62, 9362−9367

## ■ ASSOCIATED CONTENT

### Supporting Information

1D and 2D NMR and HR-ESIMS spectra of compounds **1**−**3**. This material is available free of charge via the Internet at http://pubs.acs.org.

## ■ AUTHOR INFORMATION


### Corresponding Authors

*Tel./fax: +86-22-23502595. E-mail address: xujing611@nankai.edu.cn

*Tel./fax: +86-22-23502595. E-mail address: victgyq@nankai.edu.cn.



### Funding

This work was supported by the National Natural Science Foundation of China (No. 21372125).


### Notes

The authors declare no competing financial interest.

## ■ REFERENCES


(1) Editorial Committee of Flora of China, Chinese Academy of Sciences. *Flora of China*; Science Press: Beijing, China, 1999; Vol. *77* (1), pp 95−96.

(2) Sun, Z. L.; Gao, G. L.; Luo, J. Y.; Zhang, X. L.; Zhang, M.; Feng, J. A new neuroprotective bakkenolide from the rhizome of *Peatasites tatewakianus*. *Fitoterapia* **2011**, *82*, 401−404.

(3) Dong, X. W.; Li, R. J.; Gao, X.; Row, K. H. Bakkenolides from *Petasites tatewakianus*. *Fitoterapia* **2010**, *81*, 153−156.

(4) Xie, W. D.; Miao, Y. L.; Lai, P. X.; Row, K. H. Sesquiterpenoids from *Petasites tatewakianus*. *Chem. Nat. Compd.* **2011**, *47*, 850−851.

(5) Xu, J.; Jin, D. Q.; Liu, C.; Xie, C.; Guo, Y.; Fang, L. Isolation, characterization, and NO inhibitory activities of sesquiterpenes from *Blumea balsamifera*. *J. Agric. Food Chem.* **2012**, *60*, 8051−8058.

(6) Chen, H.; Xie, C.; Wang, H.; Jin, D. Q.; Li, S.; Wang, M.; Ren, Q.; Xu, J.; Ohizumi, Y.; Guo, Y. Sesquiterpenes inhibiting the microglial activation from *Laurus nobilis*. *J. Agric. Food. Chem.* **2014**, *62*, 4784−4788.

(7) Calixto, J. B.; Otuki, M. F.; Santos, A. R. Anti-inflammatory compounds of plant origin. Part I. Action on arachidonic acid pathway, nitric oxide, and nuclear factor kappa B (NF-kappa B). *Planta Med.* **2003**, *69*, 973−983.

(8) Conflex software, version 6.7; Conflex Corp., Tokyo, Japan, 2010.

(9) Frisch, M. J.; et al.*Gaussian 09*, revision B. 01; Gaussian Inc.: Pittsburgh, PA, 2010.

(10) Cui, H. S.; Kim, M. R.; Sok, D. E. Protection by petaslignolide A, a major neuroprotective compound in the butanol extract of *Petasites japonicus* leaves, against oxidative damage in the brains of mice challenged with kainic acid. *J. Agric. Food Chem.* **2005**, *53*, 8526−8532.

(11) Yaoita, Y.; Kikuchi, M. Seco-eremophilane derivatives from rhizomes of *Petasites japonicus*. *Phytochemistry* **1996**, *42*, 751−755.

(12) Tori, M.; Kawahara, M.; Sono, M. Eremophilane-type sesquiterpenes from fresh rhizomes of *Petasites japonicus*. *Phytochemistry* **1998**, *47*, 401−409.

(13) Bodensieck, A.; Kunert, O.; Haslinger, E.; Bauer, R. New eremophilane sesquiterpenes from a rhizome extract of *Petasites hybridus*. *Helv. Chim. Acta* **2007**, *90*, 183−195.

(14) Wu, T. S.; Kao, M. S.; Wu, P. L.; Lin, F. W.; Shi, L. S.; Liou, M. J.; Li, C. Y. The bakkenolides from the root of *Petasites formosanus* and their cytotoxicity. *Chem. Pharm. Bull.* **1999**, *47*, 375−382.

(15) Wu, T. S.; Kao, M. S.; Wu, P. L.; Lin, F. W.; Shi, L. S.; Teng, C. M. Antiplatelet principles from the root of *Petasites formosanus*. *Phytochemistry* **1999**, *52*, 901−905.

(16) Wang, Y. L.; Li, R. P.; Guo, M. L.; Zhang, G.; Zhang, N.; Ma, Y. L. Bakkenolides from *Petasites tricholobus* and their neuroprotective effects related to antioxidant activities. *Planta Med.* **2009**, *75*, 230−235.

(17) Wang, S.; Jin, D. Q.; Xie, C.; Wang, H.; Wang, M.; Xu, J.; Guo, Y. Isolation, characterization, and neuroprotective activities of sesquiterpenes from *Petasites japonicus*. *Food Chem.* **2013**, *141*, 2075−2082.

(18) Xu, J.; Yang, B.; Guo, Y.; Jin, D. Q.; Guo, P.; Liu, C.; Hou, W.; Zhang, T.; Gui, L.; Sun, Z. Neuroprotective bakkenolides from the roots of *Valeriana jatamansi*. *Fitoterapia* **2011**, *82*, 849−853.

(19) Abe, N.; Onoda, R.; Shirahata, K.; Kato, T.; Woods, M. C.; Kitahara, Y.; Ro, K.; Kurihara, T. Structures of bakkenolides- B, - C, and - D as determined by the use of a nuclear Overhauser effect. *Tetrahedron Lett.* **1968**, *16*, 1993−1997.

(20) Kikuchi, M.; Suzuki, N. Studies on the constituents of *Tussilago farfara* L. II. Structures of new sesquiterpenoids isolated from the flower buds. *Chem. Pharm. Bull.* **1992**, *40*, 2753−2755.

(21) Park, H. R.; Yoo, M. Y.; Seo, J. H.; Kim, N. Y.; Kang, J. Y.; Cui, L.; Lee, C. H.; Lee, H. S. Sesquiterpenoids isolated from the flower buds of *Tussilago farfara* L. inhibit diacylglycerol acyltransferase. *J. Agric. Food Chem.* **2008**, *56*, 10493−10497.

(22) Pedro, J. N.; J. Roberto, V.; Mirna, R. G.; Luisa, U. R.; Juan, D. H. Minor oplopanes from *Senecio mexicanus*. *Phytochemistry* **1989**, *28*, 2397−2401.

(23) Koji, H. Oplopane sesquiterpenes from *Petasites palmatus*. *Phytochemistry* **1989**, *28*, 3373−3376.

(24) Tong, X.; Cheng, Y. Chemical constituents from *Acorus tatarinowii*. *Tianran Chanwu Yanjiu Yu Kaifa* **2011**, *23*, 404−409.

(25) Qi, S.; Su, G.; Zhang, S. Pregnane steroids in Gorgonian *Subergorgia suberosa* from the South China Sea. *Tianran Chanwu Yanjiu Yu Kaifa* **2008**, *20*, 1−4.

(26) Schmidt, H. H. H. W.; Kelm, M. Determination of nitrite and nitrate by the Griess reaction. In *Methods in Nitric Oxide Research*; Feelisch, M., Stamler, J. S., Eds.; John Wiley and Sons: West Sussex, U.K., 1996; pp 491−497.

Studies in animal subjects have demonstrated that phenolics are bioavailable and exert a protective role against oxidative stress and free radical damages. Oxidative damage triggered by free radicals can cause structural and functional alterations of cell macromolecules, leading to molecular mechanisms instrumental in human chronic diseases. Epidemiological studies have suggested that phenolic compounds such as flavonoids, phenolic acids, anthocyanins, and carotenoid compounds including quercetin, kaempferol, myricetin, *p*-coumaric acid, gallic acid, and ellagic acid can act as antioxidants and/or cancer-inhibiting compounds and thus may be involved in the prevention of degenerative diseases such as epithelial (but not hormone-related) cancers and cardiovascular diseases, type II diabetes, thrombotic stroke, obesity, and neurodegenerative diseases associated with aging and infections.[7] Although phenolic compounds have long been studied for their antioxidant properties, which are now well-characterized in vitro, recent studies have stressed that the mechanisms of biological actions of phenolics extend beyond their antioxidant properties. It is now believed that phenolics may exert their beneficial action through modulation of gene expression and the activity of a wide range of enzymes and cell receptors; however, the health effects of dietary phenolics depend on the amounts consumed, their chemical structure, and bioavailability.[8] Although polyphenols are ubiquitous in Rosaceous plants, their content, distribution, bioavailability, and identity vary depending on genetics, fruit location, plant structure, preharvest and postharvest factors, and climatic conditions. In this review, we will discuss the common phenolic compounds (and briefly summarize the newly emergent exploration into *nonextractable* phenolics) identified in representative Rosaceae crops in five subgroups, their health benefits, and pre- and postharvest factors as well as climatic conditions that affect their amounts and concentrations. Finally, we will discuss their bioavailabilty and profer suggestions on possible methods for biofortification to increase consumer appeal and enhance fruit consumption.

## ■ ECONOMIC AND HEALTH BENEFITS OF ROSACEOUS FRUIT AND NUT CROPS

Rosaceae is the 19th largest plant family, comprising >90 genera with >3000 distinct species and having a cosmopolitan distribution, being found just about everywhere except Antarctica. Four subfamilies are distinguished on the basis of fruit type including the Maloideae (apples, loquat, quince, and pear), the Prunoideae (*Prunus* being the largest genus of Rosaceae with cherries, plums, peaches, apricots, and almonds among the representative fruit), the Rosoideae (roses, strawberries, blackberries, and raspberries), and the Spiraeoideae. Rosaceous crops (some examples previously mentioned) contribute to human health and well-being and provide an economic foundation for many rural communities in North America.[1,2]

Included in the Rosaceae family is a huge variety of edible fruit and nut crops as well as highly valued ornamental trees and shrubs. Consumers prefer a wide range of choice in their purchases of produce or processed foods, and the Rosaceae provides it with colorful and flavorful health-promoting fruits and nuts. A huge variety of textures and flavors can be found in fruits from this family, which can be purchased fresh or processed.[1] In addition to the gustatory variety provided by these crops, Rosaceous fruits provide a major source of dietary phytochemicals (flavonoids and other phenolic compounds) purported to promote health by mitigating oxidative stress and inflammation, which can ultimately lead to chronic disease. Some well-known antioxidants and/or cancer-inhibiting compounds that have been identified in the Rosaceae are ascorbic acid, quercetin, kaempferol, myricetin, *p*-coumaric acid, gallic acid, and ellagic acid.

Ellagic acid present in Rosaceae members such as strawberry, red raspberry, cloudberry, apple, pears, and other Rosaceous fruits has been shown to affect cell proliferation and apoptosis in human pancreatic adenocarcinoma cell lines, suggesting a potential anticancer role.[9] Following the examination of 728 men aged 65−84 years in the Zutphen Elderly Study,[10] dietary Rosaceous catechins were shown to have a significant effect in the reduction of epithelial cancer. The same study showed that tea, which contributed 87% of the total catechin intake, has a lesser effect in decreasing epithelial lung cancer when compared to apple, which contributed only about 8% of the catechin consumption. Furthermore, the intake of Rosaceous fruits also reduces the risk of cardiovascular disease. For example, the role of anthocyanins in cardiovascular disease includes protecting lipids from oxidant damage, thereby aiding in the prevention of cardiovascular vessel plaque formation, providing anti-inflammatory action, induction of nitric oxide formation leading to vascular dilation, etc. Prior et al.[11] reported that the consumption of 280 g of cherries (the equivalent of ∼28 'Bing' sweet cherry fruits) caused a statistically significant increase in plasma lipophilic antioxidant capacity that was approximately 7 times greater compared to the control.

Tabak et al.[12] have demonstrated a beneficial relationship between consumption of catechin from solid fruit (apple/pear) and general pulmonary health. The study, consisting of >13000 adults in The Netherlands, observed a positive correlation between the consumption of solid fruit (especially apple and pear) and an increase in pulmonary function/decrease in symptoms of COPD. A separate study of approximately 2500 middle-aged men (age 45−59 years) suggested a strong positive correlation between apple consumption and lung function as measured by forced expiratory volume in 1 s ($FEV_1$).[13] Following adjustment for confounding influences such as smoking, body mass index, social class, and exercise, the consumption of fresh apple remained positively correlated with lung function, whereas the consumption of citrus fruit and/or fruit juices did not. Greater $FEV_1$ of 138 mL was recorded for those who consumed five or more apples per week when compared to those who did not consume apple.

Conceição de Oliveira et al.[14] reported that a high intake of quercetin, a major component of Rosaceous fruits, was associated with a decreased risk of type II diabetes. In addition, intake of myricetin, common in Rosaceous fruits such as strawberry, may also decrease the risk of type II diabetes. Although evidence is limited on the protective role of cherry in diabetes, a few researchers have reported the role of cherry anthocyanins in reducing insulin resistance and glucose intolerance.[15] Sweet cherry has a relatively low glycemic index of 22 compared to other fruits such as grapes, which scored 46. This lower glycemic index makes sweet cherry a potentially better fruit-based snack food for people with diabetes.

Cyanidins and malvidin, which are very abundant in sweet cherry and other Rosaceous fruits, have been shown to inhibit the cyclooxygenase (COX) enzymes responsible for inflammatory response. Thomson and Kubota[16] suggested that flavonoids and proanthocyanidin compounds, which are

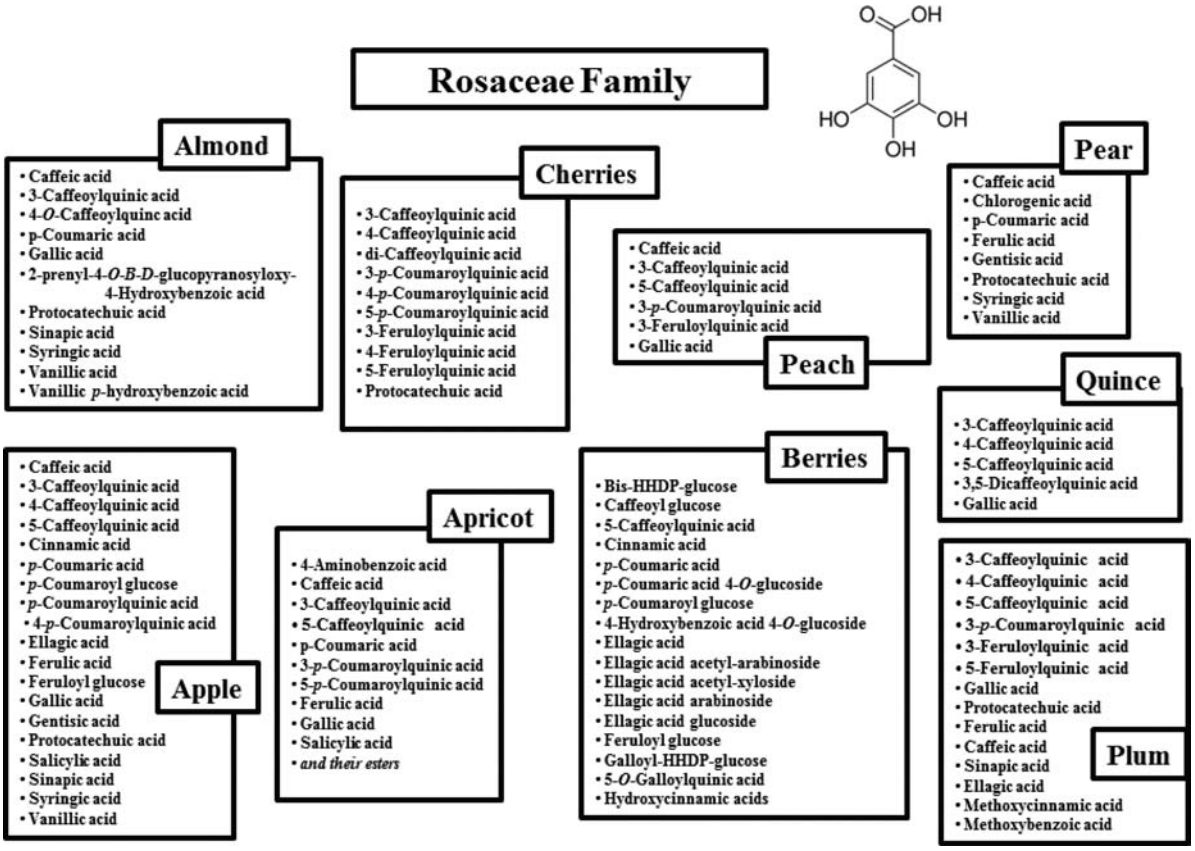


**Figure 1.** Phenolic acids.

common in Rosaceous plants, in particular, cherries, might reduce oxidative stress and amyloid production, thereby reducing the risk of Alzheimer's disease. Rosaceous fruits contain a large number of antioxidants (free radical neutralizers) that purportedly help prevent arthritis and brain dysfunctions. The accumulation of uric acid (the primary cause of gouty arthritis) and other toxic substances in the body is one of the ill effects of un-neutralized free radicals. Consumption of Rosaceous produce, extremely abundant in antioxidants, can effectively help alleviate such health hazards. Memory decline and loss of limb control are common in older individuals due to aging of the brain and the nervous system, facilitated, at least in part, by the action of free radicals present in the system. Dietary phenolics provide an additional mechanism of neutralizing the effect of these oxidants, thereby serving to protect the system.

A recent study[17] with mice implanted with aggressive breast cancer cells, MDA-MB-435, demonstrated an inhibition of a marker gene in the lungs after a few weeks of being fed peach extracts containing a mixture of phenolic compounds. This mixture of phenolic compounds was believed to be responsible for the tumor growth inhibition and metastasis in mice. The authors suggested that the dose necessary to see these effects in mice will be equivalent to the consumption of two to three peaches per day by humans.

## ■ PHENOLIC COMPOUNDS IN ROSACEAE FRUITS AND NUTS

The five major phenolic compounds including pheolic acids, flavanols, flavanols, anthocyanins, and dihydrochalcones will be discussed within each Rosaceous crop as follows.

**Apple (*Malus* × *domestica* Borkh.).** Apple is a good source of phytochemicals including phenolic acids, anthocyanins, flavan-3-ols, and flavonols.[6] No wonder the saying "an apple a day keeps the doctor away"! Major apple phenolic acids include 3-, 4-, and 5-caffeoylquinic acid (CQA) (neochlorogenic, cryptochlorogenic, and chlorogenic acids, respectively) and 3-coumarylquinic acid with chlorogenic acid as the main phenolic acid in apple juice. Minor phenolic acids identified and characterized are presented in Figure 1.[5,6,18−20] The concentration of phenolic acids varies depending on cultivar, with cider varieties in general having a higher phenolic acid concentration than dessert apples.[18]

The major flavonols are quercetin glycosides (arabinose, galactose, glucose, rhamnose, and rutinose) and kaempferol and are found mainly in the peel (Figure 2).[18,21,22] As with phenolic acids, apple cider varieties have a higher concentration of flavonols than dessert apples.[18] For example, the average quercetin glycoside content in the peel and pulp of a dessert apple is 0.5 mg/100 g, while cider apple peel and pulp contain 5.7 mg/100 g of quercetin glycoside (see http/phenol-explorer.eu/reports/39).

Flavan-3-ol compounds, also called flavanols, exist in both the monomer form (catechins) and the polymer form (proanthocyanidins) in apple. Many such compounds exist in apple (see Figure 2),[23,24] and apple is a rich source of (−)-epicatechin, (+)-catechin, and procyanidin (a proanthocyanidin) dimer B2.[24] The concentration of flavanols varies from one variety to the other, with cider apples having a comparatively high content of procyanidins, which are particularly responsible for their astringency and bitterness. Procyanidins are found in the whole apple fruit, and their levels


dx.doi.org/10.1021/jf501574q | J. Agric. Food Chem. 2014, 62, 9369−9386

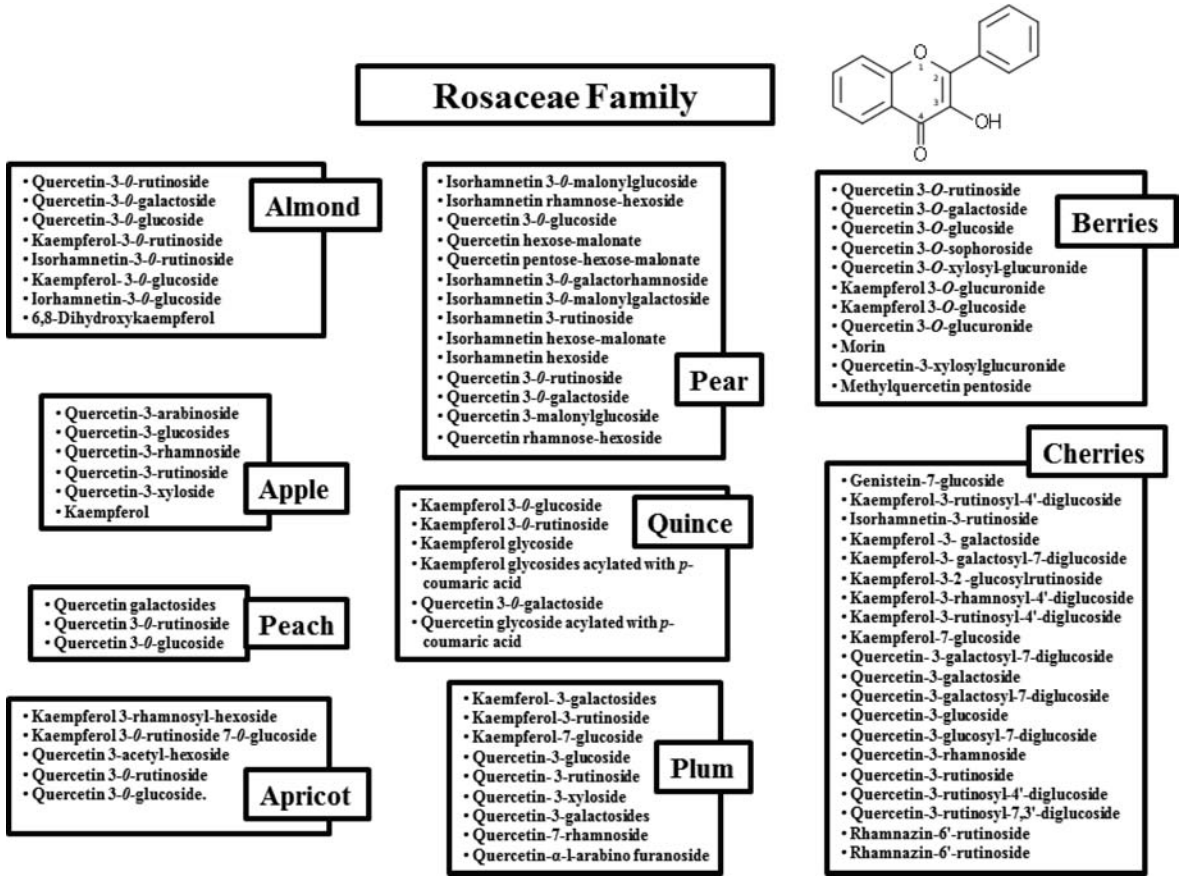


**Figure 2.** Flavanols.

gradually increase from 1232 mg/kg in the seeds to 4964 mg/kg in the epidermal tissue of the fruit.[25,26] The concentration of flavan-3-ols in apple is often affected by preparation methods. For example, only about 3% of the catechins are recovered in the juice, whereas a majority is retained in the pomace.[27] Pure juice of dessert apple contains ∼7.8 mg/100 mL (−)-epicatechin, whereas pure juice of cider apple contains ∼9.0 mg/100 mL (−)-epicatechin.

Some apple cultivars do not produce high anthocyanins in their skin except under high sunlight. Examples include 'Granny Smith' and 'Golden Delicious'. The main anthocyanins are cyanin derivatives such as cyanidin 3-galactoside (cy3-gal), cyanidin 3-glucoside (cy3-glu), cyanidin 3-arabinoside (cy3-ara), and cyanidin 3-xyloside (cy3-xyl) (Figure 4). Cyanidin 3-galactoside (cy3-gal) is the major pigment accounting for 80% of the total anthocyanins in apple.[28−30]

Studies including those of Spanos et al.[31,32] and Tomás-Barberán et al.[33] have shown that dihydrochalcone derivatives such as phloridzin (phloretin 2-*O*-D-glucoside) and phloretin 2-*O*-(6-D-xylosyl)-D-glucoside are major constituents of apple. However, phloretin xylogalactoside and phloretin xyloglucoside are much lower in concentration. Vrhovsek et al.[34] reported 2−6% of dihydrochalcones, whereas Lee et al.[35] found 5.59 mg/100 g phloretin glycosides in apple fruit. Phloridzin is highly concentrated in the seeds, representing 98% of seed flavonoids.[36] Awad et al.[37] reported 10 times more phloridzin in seeds than in skin and 100 times more than in the flesh. Gosch et al.[38] observed >90% phloridzin in the soluble phenolic compounds extracted from apple leaves. The high concentration of dihyrochalcones in apple makes apple unique among the Rosaceae as very low amounts (or none, as in pear) are found in other Rosaceous fruit.

**Sweet Cherry (*Prunus avium* L.) and Tart Cherry (*Prunus cerasus* L.).** Although sweet cherry and sour cherry have small fruit in comparison to other *Prunus* species including peach, nectarine, apricot, plum, etc., they contain a relatively high amount of phytochemicals. Phenolic acids in cherries have been characterized by different authors and summarized by Macheix and Fleuriet[39] and are listed in Figure 1. Sweet cherry contains about 70−80% hydroxycinnamic acid esters[40] with neochlorogenic acid (3-CQA) and 3′-*p*-coumaroylquinic acid being predominant. The ratio of neochlorogenic acid to 3′-*p*-coumaroylquinic acid differs among cherry cultivars as well. For example, 'Bing', a midseason variety, contains 60% neochlorogenic acid and 40% 3′-*p*-coumaroylquinic acid, whereas 'Burlat' (a founder variety for many modern early cultivars) contains 16.5% neochlorogenic acid and 75% 3′-*p*-coumaroylquinic acid.[41]

Flavonols, particularly quercetins and kaempferols, are found in high concentrations in cherry (Figure 2). Both sweet cherry and sour cherry contain a high number and concentration of flavonols when compared to other Rosaceous fruits, with the majority consisting of glycosylated quercetins and kaempferols (see Figure 2).[42,43] Both sour and sweet cherry share many of the same flavonols with differences mainly attributable to the sugar moiety of the derivative, for example, kaempferol-3-rhamnosyl-4′-diglucoside as opposed to kaempferol-3-rutinosyl-4′-diglucoside and quercetin-3-galactosyl-7-diglucoside as opposed to quercetin-3-rutinosyl-7,3′-diglucoside, etc. (see Figure 2).[40,44]


dx.doi.org/10.1021/jf501574q | J. Agric. Food Chem. 2014, 62, 9369−9386

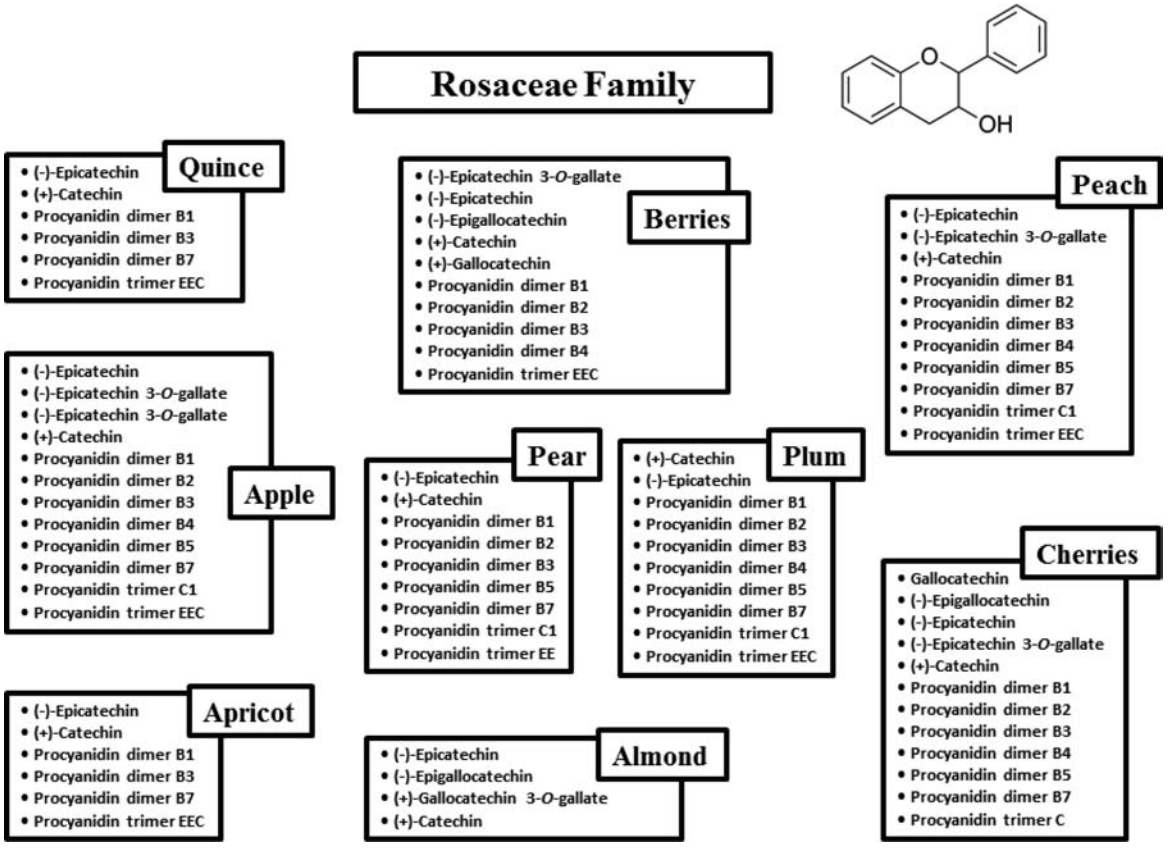


**Figure 3.** Flavan-3-ols.

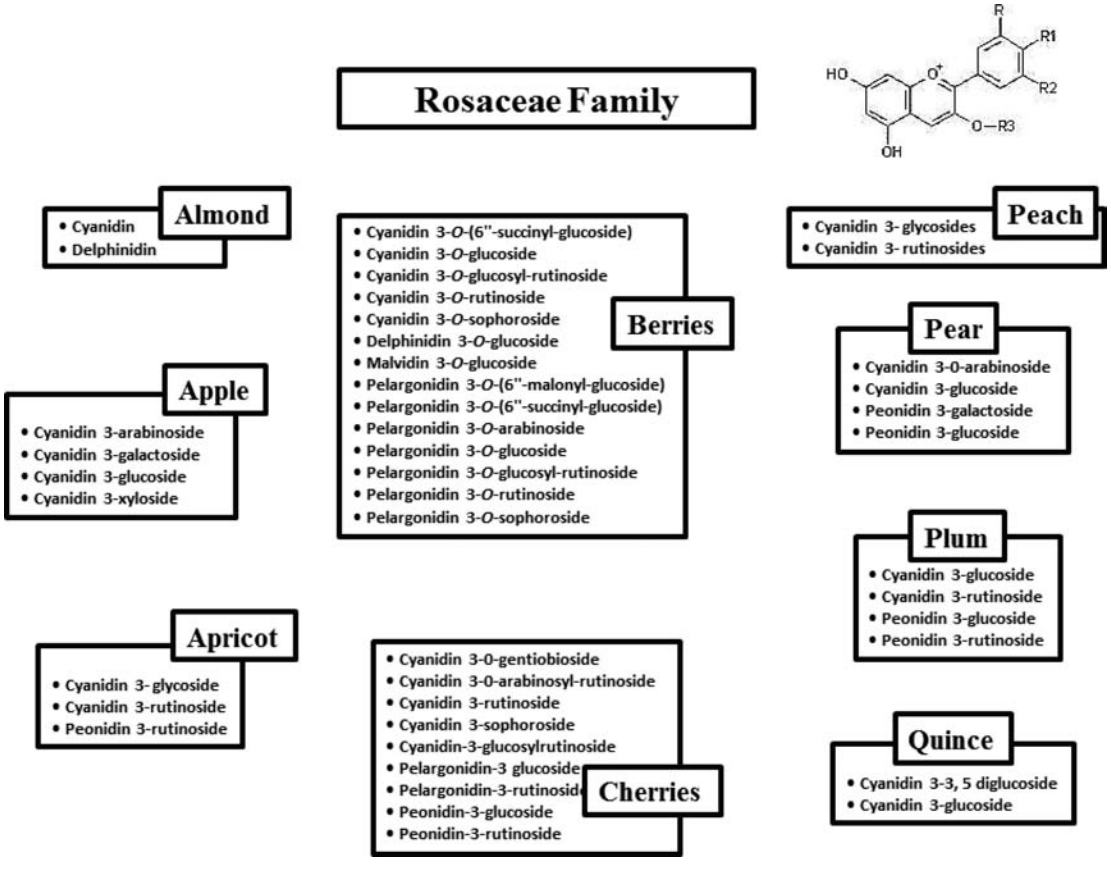


**Figure 4.** Anthocyanins.


dx.doi.org/10.1021/jf501574q | J. Agric. Food Chem. 2014, 62, 9369−9386

Sweet cherry and sour cherry contain flavanols including catechins, epicatechins, gallocatechin, and epigallocatechin (Figure 3).[39] The 2013 USDA Database for the flavonoid content of selected food reports that catechin and epicatechin values of raw sweet cherries are 4.4 and 5.0 mg/100 g, respectively, which is higher than in pear, quince, raspberry, or strawberry.[45,46] These results are corroborated in an independent study by Henning and Herrmann,[47] who reported an epicatechin content of 4.8 mg/100 g in sour cherry.

Different authors have identified and characterized major anthocyanin pigments in sweet and sour cherries. The eight anthocyanins identified are listed in Figure 4 and consist mainly of the glucosides and rutinosides of cyanidin, pelargonidin, and peonidin.[40] Cyanidin-3-rutinoside is the main anthocyanin in sweet cherry, representing 84% of the total anthocyanins, with cyanidin-3-glucoside making up most of the remainder. However, a different anthocyanin profile exists in sour cherry. Sour cherry contains all of the anthocyanidins found in sweet cherry except pelargonidin-3-rutinoside, in addition to the following cyanidins unique to sour cherry: cyanidin 3-*O*-glucosyl-rutinoside, cyanidin 3-*O*-sophoroside, cyanidin 3-*O*-arabinosyl-rutinoside, and cyanidin 3-*O*-gentiobioside.[48,49] Cyanidin-3-arabinosylrutinoside has been detected only in 'Balaton' sour cherry.[50] The predominant anthocyanin in sour cherry is cyanidin-3-*O*-glucosyl-rutinoside, which represents 80% of the total anthocyanins[40] Generally, the skin contains higher anthocyanins than the pit and flesh. Gao and Mazza[42] reported that 'Bing' was the only sweet cherry containing anthocyanins in the skin, flesh, and pit, with the pit having higher concentrations. However, skin pigmentation may not in most cases qualify as a determinant of anthocyanin concentration. For example, 'Bing' has pigmentation in the flesh, whereas other cherries such as 'Royal Ann' (sweet cherry) and 'Montmorency' (sour cherry) do not.[40] Cyanidin-3-rutinoside is the major anthocyanin in the skin and flesh (about 79 and 56%, respectively), whereas 'Bing's pit contains mainly cyanidin-3-glucoside (about 51%). Anthocyanins are absent in the flesh of 'Montmorency', 'Royal Ann', and 'Rainier' cherries. The distribution of cyanidin-3-sophoroside (unique to sour cherries) differs from that of other anthocyanins in that it is present in a higher proportion in 'Montmorency' pit than in the skin.

**Plum (*Prunnnus domestica* L.).** Both dried and fresh plums are rich sources of nutritive and bioactive compounds among which is phenolic acid. However, dried plum (prune) from prune-making varieties has higher amounts of phenolic acids than fresh plum due to concentration during the drying process despite partial degradation. Generally, plum varieties contain high quantities of hydroxycinnamic acids, especially neochlorogenic acid, with hydroxycinnamates (caffeoylquinic acids) constituting 86% of the total phenolic acids in plum.[50] Identified and characterized phenolic acids in plum and prune are listed in Figure 1.

Sultana and Anwar[51] detected 564.8 mg/kg total flavonols in plum, whereas Justesen et al.[52] reported 1.5 mg/100 g quercetin, 564.1 mg/kg myricetin, and 0.7 mg/kg kaempferol. The flavonol glycosides found in plum include 3-glucosides, 3-galactosides, 3-rutinosides, and 3-arabinoside-7-rhamnosides of quercetin and kaempferol.[39] Quercetin-3-rutinoside appears to be the major quercetin, constituting about 2% of all phenolics in plum.[47] The major and minor contributors to flavonol content in plum can be found in Figure 2.

The main flavan-3-ols in plum are catechins, procyanidin B1, procyanidin B2, procyanidin B3, epicatechin, and procyanidin B4 (Figure 3).[53] The same authors also reported the availability of A-type dimers and trimers in smaller concentrations. According to Donovan et al.,[54] plum is rich in proanthocyanidins, contributing about 70% of the total polyphenols in plum. Fresh plum contains flavan-3-ols in the range of 20−40 mg/kg.[55] The edible portion of plum has an average of 3.35 mg/100 g catechin and 2.84 mg/100 g epicatechin.[56] The peeled plum contains flavan-3-ols in the range of 662−1837 mg/kg (as catechin equivalent).[56] The concentration of catechins increases with fruit development and decreases when the fruit reaches maturity.[57]

Anthocyanins include cyanidin 3-*O*-rutinoside, cyanidin 3-*O*-glucoside, and peonidin 3-*O*-rutinoside (Figure 4). Anthocyanins have not been detected in prune and prune juice.[54] The total anthocyanin content ranges from 18 to 125 mg/100 g in fresh weight.[54,58,59] Cyanidin-3-rutinoside is predominant in plum (14.1−33.0 mg/100 g), whereas cyanidin-3-glucoside and peonidin-3-rutinoside are minor, ranging between 1.9 and 13.5 mg/100 g and between 1.1−1.2 mg/100 g, respectively.[59]

**Apricot (*Prunus armeniaca* L.).** Apricot contains a significant amount of phenolic acids that contribute to its nutritive value. The major phenolic acids are 3-CQA and 5-CQA, with 5-CQA being more dominant.[60] Sochor et al.[61] also confirmed that 5-CQA is the principal phenolic acid. See Figure 1 for identified phenolic acids in apricot. Processed and unprocessed apricots share similar qualitative phenolic acid profiles, although lower quantities are found in the processed products.

The flavonols occur mostly as glucosides and rutinosides of quercetin and kaemferol, with quercetin 3-rutinoside being the most identified in various cultivars (Figure 2).[39] The total flavonol level in apricot was estimated at 784.8 ± 32.6 mg/kg dry weight, whereas the concentrations of myricetin, quercetin, and kaempferol were 406.9 ± 16.3, 322.1 ± 6.4, and 5.8 ± 0.2 mg/kg dry matter, respectively.[51]

Flavan-3-ol is one of the major phenolic compounds in apricot, with (+)-catechin and (−)-epicatechin being the most important flavan-3-ols.[56] The concentrations of (−)-epicatechin in the fruit and jam are 4.6 and 0.5 mg/100 g, respectively, whereas (+)-catechin concentrations are 3.9 mg/100 g in the fruit and 0.4 mg/100 g in the jam.[36] The fruit also contains procyanidin B1, procyanidin B2, and procyanidin B3 (Figure 3).[61,62] Processed and unprocessed apricots share similar qualitative profiles, although lower quantities are found in the processed products.

The study of anthocyanins in apricot seems relatively rare, because the orange color of the unblushed side of the fruit is conferred by carotenoids. However, a study by Bureau et al.[63] looked at anthocyanin concentrations during ripening in two red apricot accessions. In addition to the presence of cyanidin-3-*O*-rutinoside (representing 75% of the total anthocyanins detected), these authors also found cyanidin-3-*O*-glucoside and peonidin-3-*O*-rutinoside at concentrations of approximately 12% each. Their study was the first to identify peonidin-3-*O*-rutinoside in apricot fruit. Figure 4 lists anthocyanins found in some apricot varieties.

**Peach and Nectarine (*Prunus persica* L.).** Peach and nectarine are similar in appearance and color, although they differ by a single gene for skin texture. They possess similar qualitative and quantitative phenolic acid profiles. Phenolic acids include chlorogenic acid, neochlorogenic acid, gallic acid,

and caffeic acid (Figure 1). The major phenolic acid is 5-CQA, which is about 15.6 mg/100 g in peach peel and cortex, 5.3 mg/100 g in peach cortex, 6.1 mg/100 g in nectarine peel and cortex, and 8.2 mg/100 g in nectarine cortex.[36] Peach and nectarine also contain a good amount of 3-CQA (8.8 mg/100 g in peach peel and cortex, 4.1 mg/100 g in peach cortex, 4.0 mg/100 g in nectarine peel and cortex, and 5.1 mg/100 g in nectarine cortex).[36] Lee et al.[64] reported that the concentrations of 5-CQA, 3-CQA, and caffeic acid decreased significantly in various peach cultivars sampled during the ripening process in New York state in 1987 and 1988, from a high at green immature stage (mid-July) to a level approximately 25% that value at harvest (mid-September).

Major flavonols include quercetin glucosides and galactosides (Figure 2). Chang et al.[65] observed malvidin 3,5-*O*-diglucoside (malvin), quercetin 3-*O*-rutinoside (rutin), and quercetin 3-*O*-glucoside (isoquercetin). These authors also reported that rutin and isoquercetin were the primary flavonols found in peach, particularly in the peels rather than in the flesh.

Peach and nectarine share similar flavan-3-ol profiles including catechins, epicatechin, procyanidin B1, and procyanidin B2 (Figure 3).[53]

The main anthocyanins in peach are cyanidin-3-glucoside and cyanidin-3-rutinoside, with the former being the most predominant (Figure 4).[66] Peach cultivars with dark red colored flesh have higher anthocyanin contents than those with white or yellow flesh.[67] The anthocyanin content ranges from 6.0 to 37 mg/100 g.

**Pear: European Pear (*Pyrus communis* L.) and Asian Pear (*P. pyrifolia* Nakai.).** Pear has a phenolic acid profile similar to that of apple, the major difference being (in pear) the presence of arbutin (a hydroquinone glucoside) and the lack of phloretin derivatives.[32] In fact, the presence of arbutin can be exploited as a chemical marker for pear in cases when suppliers might be tempted to cut apple juice with less expensive cider pear juice.[68] Identified and characterized pear phenolics are summarized in Figure 1.[69] Amiot et al.[46] reported that chlorogenic acid was the major hydroxycinnamic ester, whereas Spanos and Wrolstad[32] found chlorogenic acid to predominate with caffeic acid making a respectable second-place appearance.

Pear contains several quercetins and isorhamnetins including their glycosides.[69] See Figure 2 for a summary of the major and minor flavonol constituents of pear.

Studies have shown that pear contains 96% flavan-3-ol. Galvis Sánchez et al.[69] reported flavanols, particularly procyanidins, in the peel and not in the flesh.[46] Catechin, epicatechin, epigallocatechin, gallate, and proanthocyanidins have also been reported in pear (Figure 3).[70,71] Amiot et al.[46] reported concentrations of 0.6−8.7 and 0−0.5 mg/100 g for epicatechin and catechin, respectively, whereas Risch et al.[72] reported concentrations of 5−60 mg/kg for epicatechin and 0−10 mg/kg for catechin.

The major procyanidins in 'Bartlett' are B1 and B2.[32] Red pear skin contains cyanidins and peonidins (Figure 4).[71,73,74] Cyanidin-3-galactoside is the main anthocyanin in red pear with a relative percentage of 63% ,whereas the second main anthocyanin is peonidin 3-galactoside.[73] Galvis Sánchez et al.[69] reported that the peels of 'Red D'Anjou' and 'Forelle' contain 12.0 and 1.2 mg/100 g anthocyanins, respectively. The study also confirmed cyanidin 3-*O*-galactoside as the main pigment.

**Quince (*Cydonia oblonga* Miller).** Studies have shown that quince is a natural source of phenolic acids (Figure 1).[71,74,75] Quince fruit is very firm, acidic, and astringent and not well suited to raw consumption in the human diet. In Portugal a major use of the fruit is in the production of jams and jellies.[76] Six phenolic compounds can be found in quince pulps including 3-*O*-, 4-*O*-, and 5-*O*-CQAs, 3,5-*O*-diCQA, and two glycosylated quercetins. Quince peel contains the same six phenolic compounds as the pulp (but at a much higher concentration) plus seven flavonol derivatives, which, if detected in a jam product, can be used as an indicator of adulteration with unpeeled fruit.[77]

The concentration of phenolic acids in quince foodstuffs varies depending on the final product. According to the observations of Silva et al.,[77] 3-CQA can be found in quince pulp at a concentration of about 3.7 mg/100 g, but approximately 62% of this is lost in jam-making with an additional loss of 27% in jelly-making. Cryptochlorogenic acid (4-CQA; concentration in pulp is ∼0.5 mg/100 g) fares a little better, with no significant loss from fruit to jam and a 60% loss from fruit to jelly. The fate of 5-CQA (∼8.6 mg/100 g in pulp) is similar to that of 3-CQA. With respect to 3,5-diCQA (0.6 mg/100 g in pulp), only about 34% is lost from fruit to jam.[36,77]

According to Silva et al.[76,77] and Andrade et al.,[71] quince contains glycosides of quercetin and kaempferol and quercetin and kaempferol glycosides acylated with *p*-coumaric acid (Figure 2). Quince peel contains five phenolic compounds in common with the pulp, and, in addition, kaempferol 3-glucoside, kaempferol 3-rutinoside, and several partially identified compounds including kaempferol glycosides, quercetin glycosides acylated with *p*-coumaric acid, and kaempferol glycosides also acylated with *p*-coumaric acid. Higher concentrations of quercetin-3-*O*-rutinoside are found in the peel than in the pulp.[77]

Nine flavan-3-ols, mainly (−)-epicatechin, procyanidin B2, three procyanidin dimers and trimers, and one tetramer, have been identified and characterized (Figure 3).[78] Flavan-3-ols constitute between about 78 and 94% of the total polyphenolic compounds in quince.[79]

Unlike apple, cherry, and pear, quince is low in anthocyanins. However, Markh[79] reported two anthocyanins in red quince, including cyanidin-3-glucoside and cyanidin-3,5-diglucosides (Figure 4).

**Almond (*Prunus dulcis* Mill. syn. *Prunus amygdalus*).** The phenolic acid content of almond has been associated with astringent taste, discoloration, and inhibition of enzyme activity and antioxidant activities.[81] Various investigators have isolated and characterized phenolic acids in almond.[80−82] Most of these studies noted that the phenolic acid content occurs in the form of soluble esters and free phenolic acids.[81] It was observed that the total amount of free phenolic acid is ∼16.3 μg/g in the skin, whereas the total amounts of esterified phenolic acid in the skin, shell, and whole seed extract were ∼279.6, 167.1, and 40 μg/g, respectively. These phenolic acids are summarized in Figure 1[80,81] and are mainly benzoic acid or cinnamic acid derivatives. Glycosides of protocatechuic acid and vanillic *p*-hydroxybenzoic acid are common in the skins.[82] The seed contains mainly rutinose- and glucose-glycosides of kaempferol and isorhamnetin, whereas the skin and kernel largely contain quercetin-3-*O*-galactoside, kaempferol glycosides (as in seed), and isorhamnetin glycosylated with galactose instead of glucose.[82,83] The hulls also contain chlorogenic acid and its isomers such as cryptochlorogenic acid (4-CQA) and neochlorogenic acid (5-CQA).[84]

Glycosides of quercetin, kaempferol, and isorhamnetin have been identified in almond by several researchers, and their consolidated findings can be viewed in Figure 2.[85,86] According to Milbury et al.,[85] the predominant flavonoid across eight varieties tested in their examination of California almonds is isorhamnetin (as the 3-*O*-rutinoside or 3-*O*-glucoside), representing about 70% of the total, followed by catechin, kaempferol-3-*O*-rutinoside, epicatechin, quercetin-3-*O*-galactoside, and isorhamnetin-3-*O*-galactoside. The seed contains the majority of kaempferol- and isorhamnetin-3-*O*-rutinosides and glucosides, whereas the skin and kernel contain quercetin- and isorhamnetin- 3-*O*-galactoside in addition to the conjugates found in the seed.[86]

Information on anthocyanin content of almond is limited, but at least one report has suggested the presence of cyanidin and delphinidin (Figure 4).[86]

**Raspberry and Strawberry (*Rubus* spp. and *Fragaria* Species).** Raspberries and strawberries contain significant amounts of phenolic acids (Figure 1). Ellagic acid and its conjugates such as ellagic acid arabinoside, ellagic acid acetyl-xyloside, and ellagic acid acetyl-arabinoside are the most predominant phenolic acids in red raspberry.[87−89] However, this is quite different in strawberry, where the major phenolic acids are *p*-hydroxybenzoic acid and *p*-coumaric acid.[90] Berries also contain ellagitannins with the highest content in red raspberry and strawberry.[91,92] The ellagitanins found in raspberry include sanguiin H6, lambertianin C, and sanguiin H10.[36] Recent studies[93] reported two other compounds, bis-hexahydroxydiphenoyl-glucose (bis-HHDP-glucose) and galloyl-HHDP-glucose, in four cultivars including 'Jewel', 'Mira', 'Kent', and 'St. Pierre'. The author observed higher concentrations of bis-HHDP-glucose in 'Mira' than in other cultivars, whereas no significant differences were observed in galloyl-HHDP-glucose among cultivars.

Flavonols such as quercetin and kaempferol, including their glycosides, have been reported.[87,90] Mullen et al.,[87] in particular, reported the presence of various quercetins and kaempferols in raspberry (Figure 2). These studies also indicated that quercetin-3-glucuronide was the major flavonol in red raspberry juice. The flavonol profile of strawberry is similar to the exception of the predominance of kaempferol and the presence of myricetin in strawberry. Mahmood et al.[90] also reported that kaempferol was the dominant flavonol in strawberry followed by myricetin and quercetin.

There is limited information on raspberry and strawberry flavanols. However, Määttä-Riihinen et al.[92] and Gu et al.[94] reported that strawberry and raspberry proanthocyanidins occur in the form of procyanidins and propelargonidins. Flavanols isolated and characterized in both strawberry and raspberry include catechins, epicatechin, procyanidin B1, and procyanidin B2 (Figure 3). Lesser amounts of proanthocyanidins are found in strawberry compared to raspberry and other berries. De Pascual-Teresa et al.[95] and Pallauf et al.[96] have reported that the values of raspberry and strawberry flavanols ranged from 2 to 48 mg/100 g FW and from 10 to 29 mg/100 g FW, respectively.

The berries of Rosaceae, in particular strawberry and raspberry, are among the lowest in anthocyanin content compared to berries such as chokecherries, gooseberries, and blueberries. The anthocyanins in strawberry and raspberry are principally the glycosides of cyanidin and pelargonidin (Figure 4).[97,98] The anthocyanins in raspberry are glycosylated with glucose, galactose, arabinose, or rutinose and, to a lesser extent, sophorose. Cyanidin derivatives (sophorosides) are the major anthocyanins in red raspberry. The main anthocyanin in black raspberry is cyanidin 3-(6′-*p*-coumaroyl)-glucoside.[99] Pelargonidins in the form of pelargonidin 3-*O*-glucoside and pelargonidin 3-*O*-(6′-succinyl-glucoside) are also found in strawberry. Borges et al.[98] identified variously glycosylated cyanidins and pelargonidins, along with delphinidin and malvidin, in raspberry (see Figure 4). Cyanidin-3-*O*-sophoroside was characterized as the major anthocyanin in raspberry, at 42% of the total.

The anthocyanin profile in strawberry is quite different from that in raspberry, as the majority of strawberry anthocyanins are pelargonidins, with pelargonidin-3-glucoside representing 71% of the total.[97]

Although dihydrochalcone is more common in apple, Hilt et al.[100] reported the presence of phloridzin in strawberry.

## NONEXTRACTABLE POLYPHENOLS (NEPP) IN THE ROSACEAE

Arranz et al.[101−103] showed that apple and other Rosaceae crops including peach, nectarine, pear, and quince contain many NEPP. NEPP are a group of phenolic compounds that cannot be extracted using organic solvents or conventional analytical procedures but require acid hydrolysis of the corresponding residues to release the compounds from the food matrix. NEPP are mostly hydrolyzable tannins, high molecular weight proanthocyanidins, and phenolic acids closely associated with dietary fiber and protein occurring in the food matrix.[101,104,105]

Nonextractable phenolic acids are insoluble or associated with cell wall polysaccharides and can include (depending on the food type) caffeic acid, *p*-coumaric acid, ferulic acid, *o*-, *m*-, and *p*-hydroxybenzoic acid, sinapic acid, salicylic acid, syringic acid, and vanillic acid.[105] Although NEPP are not detectable using conventional procedures, studies have reported their existence in fruits and plant-based foods including the Rosaceae.[102,104] NEPP as dietary polyphenols are not released for digestion in the intestines by mastication, stomach pH,and enzymatic activity;rather, they pass intact into the colon for possible fermentation by colonic microflora.[104] Arranz et al.[102] reported a huge gap in the content of NEPP and extractable polyphenols (EPP) in the Rosaceae (Table 1). The study showed EPP content of ∼18.8−28 mg/100 g in methanol/acetone/water extracts of fresh apple, peach,and nectarine in comparison to NEPP of ∼112−126 mg/100 g of acidic hydrolysates of the extraction residue from the fruit, indicating that >80% of total phenolic compounds are left behind with conventional extraction techniques. As a specific example, apple gallic acid content was determined at ∼2.9 mg/100 g NEPP and ∼0.53 mg/100 g EPP, such that almost 85% of the total of this particular phenolic acid required acid hydrolysis for chemical conversion to the analyte detected as gallic acid. The NEPP determined in the study were mainly hydroxybenzoic and hydroxycinnamic acids. Although NEPP are often disregarded in nutritional studies, they do contribute to the antioxidant activity of polyphenols through a surface reaction in the small intestine. As observed in different animal models, NEPP have been shown to increase antioxidant and antiproliferative capacities, reduce intestinal tumorigenesis,and modify gene expression.[104,105]

**Table 1. Extractable Phenols (EPP) and Nonextractable Polyphenols (NEPP) in Representative Rosaceae Crops**

| crop | compound | NEPP content (mg/100 g fw) | EPP content (mg/100 g fw) | ref |
|---|---|---|---|---|
| apple | gallic acid | 2.9 ± 0.8 | 0.5 ± 0.2 | 102 |
| | *p*-hydroxybenzoic acid | 19.3 ± 3.2 | *a* | 102 |
| | protocatechuic acid | 1.3 ± 0.3 | *a* | 102 |
| | ellagic acid | 0.2 ± 0.3 | *a* | 102 |
| | catechin | 5.4 ± 2.7 | 0.2 ± 0.0 | 102 |
| | gallocatechin | 2.8 ± 1.5 | 0.5 ± 0.1 | 102 |
| | vanillic acid | 0.3 ± 0.3 | *a* | 102 |
| | ferulic acid | 48.9 ± 4.5 | *a* | 102 |
| apple pomace | hydrolyzable proanthocyanidins | 18.0−20.0 | *a* | 104 |
| | hydrolyzable phenolics | 78.0 | *a* | 104 |
| | hydrolyzable proanthocyanidins | 37.0−43.0 | *a* | 104 |
| peach | gallic acid | 1.0 ± 0.2 | *a* | 102 |
| | *p*-hydroxybezoic acid | 13.5 ± 1.3 | *a* | 102 |
| | protocatechins | 1.2 ± 0.4 | *a* | 102 |
| | catechins | 2.5 ± 0.4 | 5.7 ± 0.5 | 102 |
| | gallocatechins | 0.6 ± 0.4 | 1.1 ± 0.2 | 102 |
| | epicatechins | 0.1 ± 0.0 | *a* | 102 |
| | vanilic acid | 0.1 ± 0.0 | *a* | 102 |
| | ferulic acid | 33.8 ± 3.5 | *a* | 102 |
| nectarine | gallic acid | 1.9 ± 0.1 | *a* | 102 |
| | *p*-hydroxybezoic acid | 14.4 ± 0.8 | *a* | 102 |
| | protocatechins | 1.4 ± 0.2 | *a* | 102 |
| | ellagic acid | 0.1 ± 0.0 | *a* | 102 |
| | catechins | 4.9 ± 0.2 | 0.7 ± 0.4 | 102 |
| | gallocatechins | 1.6 ± 0.4 | 1.0 ± 0.2 | 102 |
| | epicatechins | 0.1 ± 0.0 | 1.7 ± 0.0 | 102 |
| | ferulic acid | 40.8 ± 1.9 | *a* | 102 |
| | caffeic acid | 0.9 ± 1.0 | *a* | 102 |
| quince | hydrolyzable proanthocyanidins | 48.0 | *a* | 104 |
| Chinese quince | catechin | 0.5 (%) | *a* | 103 |
| | epicatechins | 2.1 (%) | *a* | 103 |
| pear | catechins | 0.1 (%) | *a* | 103 |
| | epicatechins | 0.6 (%) | *a* | 103 |

[a]Data not available.

## INFLUENCE OF STORAGE AND PROCESSING ON PHENOLICS

**Apple (*Malus* × *domestica* Mill.).** Van der Sluis et al.[21] reported that the content of some flavonols such as quercetin glycosides, phloridzin,and anthocyanins in 'Jonagold', 'Golden Delicious', 'Red Delicious', 'Elstar', and 'Cox's Orange Pippin' were not affected by 52 weeks of storage in controlled atmospheric conditions. The study also found that the concentration of chlorogenic acid and total catechins decreased slightly in 'Jonagold', whereas the total catechin concentration decreased slightly in 'Golden Delicious' but the chlorogenic acid concentrations remained stable. Furthermore, after 25 weeks of cold storage, there was no decrease in chlorogenic acid in any of the varieties, whereas catechins decreased slightly in 'Golden Delicious', 'Elstar', and 'Cox's Orange Pippin'. The effects of storage on apple peel phenolics by Golding et al.[106] confirmed that storage at 0 °C in air for up to 9 months has little effect on peel phenolic content. In further corroboration of the stability of apple peel phenolic content, Lattanzio et al.[107] studied the collective action of phenolic compounds for fungicidal properties in cold-stored (2 °C) 'Golden Delicious' apples and found no significant decrease in phenolic concentration after 200 days.[108]

Tokusoglu[108] reported variations in dihydrochalcone content among different apple varieties after processing into juice. In a review of studies conducted on polyphenolic content of whole apple compared to freshly prepared and commercially prepared juices, he reported a higher content and concentration of hydroxycinnamic acids, procyanidins, and anthocyanins in whole apple followed by (in decreasing range of concentrations) fresh juice (cider apples), fresh juice (dessert apples), "clear" commercial juice, and "cloudy" commercial juice. Anthocyanins were found in red apple peel but were not detected in the fresh or commercial juices tested. Chlorogenic acid, *p*-coumaroylquinic acid, procyanidins B2, procyanidins C1, (−) epicatechin, and (+) epicatechin were found in whole apple but not in apple juice. In a review of apple components and their relationship to human health, Hyson[109] cites work reporting a wide range of total polyphenolic contents in whole apple, fresh juice, and commercial juice. Depending on the variety and growing conditions, total polyphenolic content ranged from 5230 to 27240 mg/kg in freeze-dried whole apple representing 67 cultivars, from 154 to 970 mg/L in fresh juice (with greater values typically representing juice prepared from cider apples), and from 110 to 459 mg/L in commercial juices (with higher values found in "cloudy" versus "clear" juice preparations).[109]

**Sweet Cherry and Tart Cherry (*P. avium* L. and *P. cerasus* L.).** Processed and stored cherries are available year-round as frozen, whole canned, juice concentrate, etc. During their investigation into the changes in anthocyanins and polyphenolics during canning and canned storage of cherries, Chaovanalikit and Wrolstad[40] determined that approximately half of the anthocyanins and phenolic acids leach from the fruit into the syrup with minimal total loss. The proportions of cyanidin and pelargonidin rutinosides slightly decreased, whereas cyanidin and pelargonidin glucosides increased, perhaps due to partial hydrolysis of rutinose to glucose. The same investigator also determined that hydroxycinnamates and epicatechins were affected by storage and temperature, decreasing significantly after 5 months of storage at both 2 and 22 °C. The degradation of epicatechins was found to increase significantly at 22 °C. Flavonol glycosides were more stable, with a slight increase at 22 °C. Additionally, the anthocyanin and phenolic compositions of fresh frozen 'Bing' fruit stored at −23 and −70 °C for 3 and 6 months, respectively, were compared. A 67% loss of total anthocyanins was observed after 3 months of storage at −23 °C and an 88% loss after 6 months. At the much lower temperature of −70 °C, only 11 and 12% losses were observed after 3 and 6 months, respectively.[40] In corroboration, Polesello and Bonzini[110] observed 34−74% anthocyanin loss in sweet cherry after 4 months of storage at −20 °C.


dx.doi.org/10.1021/jf501574q | J. Agric. Food Chem. 2014, 62, 9369−9386

**Apricot (*P. armeniaca* L.).** The influence of drying parameters on the phenolic compounds in two apricot cultivars, Pelese and Cafona, using air temperatures of 55 and 75 °C was investigated by Madrau et al.[111] Relative to fresh fruit, total phenolic concentration experienced an across-the-board decrease. However, the study reported significantly greater decrease in chlorogenic acid, neochlorogenic acid, and catechin at 55 °C than at 75 °C, which was attributed to attenuation of polyphenol oxidase enzymatic activity at the higher temperature. Epicatechin and quercetin 3-*O*-glucoside incurred greater losses at the higher temperature than at the lower temperature. Processed and unprocessed apricots share similar qualitative profiles, but lower quantities of phenolic compounds were found in the processed products.

**Plum (*P. domestica* L.).** Bioactive compounds in plum are degraded during drying, and this affects anthocyanins in particular. The polyphenolic contents are degraded by half in commercial prune compared to fresh plum.[54] Hydroxycinnamic acids, (+)-catechin, and quercetin-3-*O*-rutinoside were slowly degraded as a function of drying time.[112] Piga et al.[113] reported the disappearance of anthocyanins in prune during the first month of storage. These authors also observed, in both fresh and dried fruits, that changes in catechins, hydroxycinnamic acids, anthocyanins, and flavonols were affected by both processing parameters and cultivar. Drying destroyed the anthocyanin compounds, and there was a significant decrease in the flavonols generally.

**Quince (*C. oblonga* Miller).** There are limited studies on the effect of storage and cultural practices on bioactive compounds in quince. However, homemade jellies showed lower concentrations of different phenolic compounds than commercial jams, with the exception of procyanidins.[114] Arbutin was identified in commercial but not in the homemade quince jam, suggesting adulteration of commercial jam with pear.

**Strawberry (*Fragaria* spp.).** In a study conducted by Amaro et al.,[115] the effects of cultivar choice and storage conditions were investigated as they relate to the fate of anthocyanins in strawberry jams. Homemade jam from two cultivars, stored at room temperature with and without exposure to light, was analyzed for total anthocyanin content and antioxidant activity. Anthocyanin content and stability are critical for an attractive red color as well as antioxidant capacity. Although the two cultivars chosen for this study had radically different anthocyanin profiles, the total anthocyanin contents of each jam were similar immediately after preparation. However, after 15 days of storage 'Camarosa' jam maintained its anthocyanin content at approximately the 90% level, whereas that of 'American 13' dropped by about 67%. After 60 days, approximately 50% of 'Camarosa' anthocyanins were quantified, whereas only about 14% of the 'American 13' anthocyanins were still detected. For both cultivars, jam stored in the dark fared just slightly better than jam stored with exposure to light.

**Raspberry (*Rubus* spp.).** Zafrilla et al.[116] conducted a study on the effect of processing and storage on the ellagic acid/derivatives and flavonoid content of raspberry jam. Ellagic acid glycosides and flavonol glycosides were found to be little affected by thermal processing; however, the content of free ellagic acid increased 2.5-fold after processing. Although a decrease in total flavonoids was observed, evaluation of individual phenolics in the processed jam during 6 months of dark storage at 20 °C showed that ellagic acid continued to increase during the first month of storage up to 45 mg/kg and then decreased slightly during the remaining storage period to a steady concentration of 20−25 mg/kg. The authors note this increase in free ellagic acid could be due to its chemical release from ellagitannins or through increased extractability afforded during processing. Quercetin glucoside content decreased significantly during the first 3 months from ∼66 to ∼40 mg/kg of fresh weight, then became stable during the rest of the storage period.[116] Häkkinen et al.[117] investigated the influence of processing and storage on flavonol content of various berries and found that quercetin was well preserved in frozen red raspberries during 9 months of storage at −20 °C, whereas myricetin and kaempferol were more susceptible to losses during storage.

**Peach (*P. persica* L.).** Asami et al.[118] investigated the impact of cold storage on total phenolics (TP). Peach stored at 4 °C for a period of 14 days was measured for TP levels in peeled and unpeeled fruits on days 0, 7, and 14. The study showed that cold storage for 14 days resulted in no loss of TP activity in either the peeled or unpeeled fruit compared to fresh peach. However, a small increase ($p < 0.05$) in TP levels was observed on day 14 in peeled fruit and on days 7 and 14 in unpeeled fruit. Peach stored in a climate-controlled temperature at 30 °C for a period of 48 h with total phenolics measured at 0, 12, 24 and 48 h showed that storage for 24 h at 30 °C resulted in a 69% increase in TP in peeled fruit and a 36% increase in unpeeled fruit. The study showed that the levels of TP began to decline after 24 h, with total phenolics being 50% higher than initial levels in peeled fruit and 28% higher in unpeeled fruit at 48 h. This apparent counterintuitive discrepancy is probably a result of activation of phenylalanine ammonia-lyase (PAL) in response to the stress of peeling; enzymes would be more active above room temperature such that PAL-catalyzed phenolic synthesis would cause levels in peeled fruit to be higher than in unpeeled fruit. The comparison of procyanidin oligomer profile in frozen peach and in processed peach at 104.4 °C for 10 min showed a profound reduction in procyanidins in canned peach relative to frozen peach. The flavonoid profile in canned freestone cultivars differed from that in clingstone types, as freestone cultivars contained higher levels of leucoanthocyanins than clingstone cultivars.[118]

**Almond (*P. dulcis* L. syn. *P. amygdalus*).** The polyphenolic content of almond is affected by roasting, pasteurization, and storage.[119] Pasteurization did not significantly change the flavonoids and phenolic acids, whereas roasted almonds had 26% less total phenolics and 34% less flavonoids than raw almonds. Storing almond at 4 and 23 °C for 15 months resulted in gradual increases in phenolic acid by up to 2%. At 4 °C during 15 months of storage, polyphenols increased up to 18-fold for *p*-hydroxybenzoic acid, whereas other phenolic acids increased up to 45-fold.[120] The total contents of phenolic compounds were higher in the roasted samples than in blanched almonds (freeze-dried). Roasting is the most suitable type of industrial processing of almond to obtain almond skin extracts with the greatest antioxidant capacity.[120]

## EFFECT OF FRUIT DEVELOPMENT STAGE AND ENVIRONMENTAL CONDITIONS ON PHENOLICS

Developmental stage and environmental factors such as nutrient availability, temperature, and (most particularly) light influence the synthesis of polyphenols.[121] Treutter[122] reported that sunlight induces many enzymes involved in flavonoid

synthesis. The effect of environmental factors on quercetin glycosides, phloridzin, catechins, and chlorogenic acid concentrations in 'Jonagold' and 'Elstar' apples has been shown to be the highest early in the season, decreasing to a steady level during maturation and ripening.[123] The same investigators reported anthocyanins decreasing midseason but rising rapidly just prior to maturation and quercetin glycosides being greater in fruit grown in the outer canopy. Awad et al.[37] also found that sun-exposed fruits (in 'Jonagold' and 'Elstar') had greater levels of anthocyanins and quercetin glycosides compared to shaded fruits, suggesting that exposure to sunlight affects production of these compounds. Although sunlight has no effect on phloridzin, catechin, and chlorogenic acid, Treutter[122] reported that many apple cultivars produced anthocyanins as red pigments when exposed to sun light. 'Fuji' apple grown in orchards where the ground was covered with light-reflecting films showed an increase in red pigmentation from 11 to 38%, which corresponds to an increase in anthocyanin concentrations in the peel from 0.18 to 0.37 mg/g fresh weight.[123] The same study also observed that the accumulation of anthocyanins and the concentration of flavonols in apple skin depended on the position of fruit on the tree.

Plant nutrition also contributes to the content and distribution of phenolic compounds in apple varieties. Awad amd de Jager[124] found that nitrogen fertilization was associated with a decrease in anthocyanins, catechins, and total flavonoids in apple. The same author associated an increase in anthocyanins and total flavonoids of 'Elstar' apple to calcium fertilization. According to Wang and Lin,[125] strawberry accumulates the highest phenolic amounts when grown under compost substrate and full-strength fertilizer (NPK, 20/20/20). These authors observed that the distribution and content of phenolic compounds such as anthocyanins, flavonols, hydroxycinamic acids, and ellagic acid significantly changed following fertilizer application.

Chemicals that enhance ripening can affect phytochemical biosynthesis. An example is the use of ethephon to increase anthocyanin production without increase in other flavonoid compounds and chlorogenic acid in 'Jonagold' apple.[126] Gibberellins, in particular, $GA_3$, and (*S*)-*trans*-2-amino-4-(2-aminoethoxy)-3-butenoic acid hydrochloride (ABG-3168) significantly decreased anthocyanin contents. However, application of other chemicals such as alar, cycocel (CCC), Prohexadione-Ca, $Ga_{4+7,}$ seniphos, shikimic acid, plantacur-E, and galactose was observed to have no effect on these phytochemicals.

Yearly weather changes can also affect thepolyphenol content of apple. Significantly higher concentrations of phenolic compounds in apple cultivars planted in 2006 and 2007 were observed by Mainla et al.[127] The study showed that 2007 plantings had higher contents of phenolic compounds due to longer sunlight hours, less precipitation, and a higher temperature in August 2007 compared to August 2006. The authors suggested that better light conditions in 2007 before harvest might have caused the higher polyphenol concentration in the apple peel.

Another factor that affects phytochemicals in apple as well as in other Rosaceous fruits is rootstock. According to a study in Estonia by Mainla et al.,[127] apples grown on vegetative rootstocks had significantly higher concentrations of polyphenols than those grown as seedlings. This is probably because rootstocks significantly influence the uptake of mineral elements from the soil. Other studies have also shown that the content of macronutrients in the leaves varies depending on rootstock.[128] Less vigorous rootstocks have a weaker root system and are therefore usually more susceptible to weather conditions.

Various studies have elucidated the effect of maturity and developmental stage on accumulation of phenolic compounds. Mahmood et al.[90] and Pineli et al.[129] reported that the total phenolic content (TPC) as well as the total flavonoid content (TFC) of strawberry and mulberry cultivars increases as fruit ripens. These studies observed that as fruit maturity progressed, TPC and TFC of strawberry fruit increased from ∼8.5 to ∼53.3%. The amount of individual phenolic acids and flavonoids in relation to different maturity stages varies. Major phenolic acids found in strawberry at maturity were *p*-hydroxybenzoic acid and *p*-coumaric acid. From unripened to fully ripened stage, concentrations in strawberry cultivars ranged from 21.4 to 65.4 mg/100 g DW *p*-hydroxybenzoic acid, followed by *p*-coumaric acid (17.3−47.5 mg/100 g DW), gallic acid (6.8−24.6 mg/100 g DW), ferulic acid (7.6−24.1 mg/100 g DW), chlorogenic acid (11.5−18.2 mg/100 g DW), and vanillic acid (2.8−16.1 mg/100 g DW).[90] In Wang et al.'s[130] look at the influence of maturity on fruit quality and phenolic content in red raspberry, anthocyanins were found to prevail in ripe fruit, whereas ellagic acid and quercetin-3-glucuronide were the most abundant in green fruit. Anthocyanins increased during fruit ripening, whereas other polyphenols decreased significantly during fruit ripening.

The effect of low night temperatures on anthocyanin accumulation in grape berries has been studied by Mori et al.[131] The authors found that berries grown under low night temperature conditions accumulated up to 5.5 mg anthocyanins/g fresh weight, whereas, those grown during warm nights accumulated 4 mg/g fresh weight. Treutter[132] reported a higher accumulation of phenolic compounds in strawberry with higher day/night temperatures up to 30/22 °C than lower temperatures. The least accumulation of phenolic compounds was obtained at temperatures of 18/22 °C. Of the five phenolic compounds studied, pelargonidin glycosides consistently showed the highest concentration with increasing temperatures up to 30/22 °C, whereas kaempferol glycosides had the lowest concentration.

The effect of light intensity on color enhancement and higher anthocyanin content has been reported in raspberry.[130,133] Wang et al.[130] showed that red raspberry harvested before full maturity continued to synthesize pigments during storage under favorable conditions, with no significant differences in color or total anthocyanins after 4 days. Light intensity does not affect the total phenolics in 50 and 80% mature fruit, but can affect immature berries (5 and 20% maturities).

Temperature, light intensity, and fruit maturity affect the content and stability of phytochemicals in sweet cherry. Different growing temperatures (i.e., day/night) affect total phenolic and anthocyanin contents.[134] High-temperature growing conditions (25/30 °C) significantly enhance anthocyanin and total phenolic content.[135] Total phenolic compounds decreased during the early stages of development, but later skin color development started with the accumulation of anthocyanins.[136] Also, rootstock affects the content and distribution of phytochemicals.[137] For example, 'Lapins' on 'PiKu 1' and 'Weiroot 13' produced significantly higher phenolic acid and flavonols. This could be attributed to the adjustment of the metabolism genetically between rootstock and scion varieties, which causes higher amounts of metabolic

Table 2. Pharmacokinetic Data from Bioavailability Studies[a]

| | $T_{max}$[b] (h) | | $C_{max}$[c] (mol/L) | | urinary excretion (% of intake) | | elimination half-life (h) | |
|---|---|---|---|---|---|---|---|---|
| phenolic compound | mean | range | mean | range | mean | range | mean | range |
| quercetin glucosides | 1.1 ± 0.3 | 0.5−2.9 | 1.5 ± 0.5 | 0.5−3.8 | 2.5 ± 1.2 | 0.3−6.4 | 17.9 ± 2.2 | 10.9−28.0 |
| rutin | 6.5 ± 0.7 | 4.3−9.3 | 0.2 ± 0.1 | 0.1−0.5 | 0.7 ± 0.3 | 0.1−1.0 | 19.9 ± 8.1 | 11.8−28.1 |
| (epi)catechin | 1.8 ± 0.1 | 0.5−2.5 | 0.4 ± 0.1 | 0.1−1.1 | 18.5 ± 5.7 | 2.1−55.0 | 2.5 ± 0.4 | 1.1−4.1 |
| gallic acid | 1.6 ± 0.2 | 1.3−1.5 | 4.0 ± 0.6 | 2.6−4.7 | 37.7 ± 1.0 | 36.4−9.6 | 1.3 ± 0.1 | 1.1−1.5 |
| chlorogenic acid | 1.0 | *d* | 0.3 ± 0.0 | *d* | 0.3 ± 0.0 | *d* | *d* | *d* |
| caffeic acid | 1.4 ± 0.6 | 0.7−2.0 | 1.0 ± 0.3 | 0.5−1.3 | 10.7 ± 0.0 | *d* | *d* | *d* |
| ferulic acid | 2.0 ± 0.0 | *d* | 0.0 | | 27.6−17.6 | 3.1−61.7 | *d* | *d* |
| anthocyanins | 1.5 ± 0.4 | 0.7−4.0 | 0.0 ± 0.0 | 0.0−0.2 | 0.4−0.3 | 0.0−5.1 | *d* | *d* |
| proantho-cyanidin dimers | 2.0 ± 0.0 | *d* | 0.0 ± 0.0 | 0.0−0.0 | *d* | *d* | *d* | *d* |

[a]Data adapted from ref 148. [b]All data were converted to correspond to a supply of 50 mg of aglycone equivalent. [c]$T_{max}$, time to reach $C_{max}$. [d]Data not available.

stress. Furthermore, trees of different vigors may produce sweet cherry fruits with different phenolic acid and flavonol contents.[138]

Murray et al.[139] have linked plum color development to an increase in anthocyanin accumulation. Shading of plum fruit may reduce light intensity and will likely result in poor color development. Tomás-Barberán and Espin[140] reported that ultraviolet radiation is an indicator of anthocyanin accumulation because PAL, chalcone synthase, and dihydroflavinol reductase enzymes involved in phenylpropanoid metabolism are induced by UV radiation. Temperature differences between day and night affect anthocyanin accumulation in plums, and plums grown on soil covered with natural meadow (organic fertilizer) have higher total phenolics than conventional plums (without organic fertilizer)[141,142] Although Bourn and Prescott[143] suggested further studies to fully understand the influence of inorganic and organic fertilizers on the nutritional value of crops, Winter and Davis[144] disagreed that organically grown products are not nutritionally superior to those obtained by conventional agricultural techniques. Further studies are needed to confirm either of these arguments.

The studies of Kan and Bostan[145] on the phenolic content of organically and conventionally grown apricot have shown that apricot cultivars grown organically have higher (+)-catechin levels than those grown conventionally. A >30% decrease in epicatechin levels has been recorded in conventionally grown apricot, whereas higher ferrulic acid levels have been observed in organically grown apricot. Furthermore, the quality of soil and fertilizer level have pronounced effects on phenolic content. Hegedüs et al.[146] reported that the content of total phenolics varied during fruit ripening in two apricot genotypes, 'Gonci magyarkajszi' and 'Preventa'. The study showed that there is an increase in color during ripening from green to yellow and orange due to significant phenolic accumulation in unripe to fully ripe fruit.

## BIOAVAILABILITY AND METABOLISM OF PHENOLICS

Bioavailable substances are those delivered from the digestive system to the circulatory system for further distribution into designated tissues and are therefore biologically available for biochemical functions. Phenolics, like other micronutrients, are ingested, digested, and then transported across the gastrointestinal epithelium into circulatory vessels. Bioavailability also refers to the *extent* to which a drug or other substance enters a specific tissue or organ or to the *dose proportion* reaching systemic circulation intact (systemic availability) by alternate routes of administration to the intravenous system. Researchers have tried to establish that some phytochemicals can be linked to chronic diseases.[11,147] An important question worth asking is if these phytochemicals are in a bioavailable form as processed or fresh fruit. Studies have shown that anthocyanins are less bioavailable than flavonoids.[148] Poor anthocyanin absorption and efficiency in the system have been reported by Manach et al.[148] $C_{max}$ is reached between 75 min and 4 h after ingestion of an anthocyanin-containing meal in the plasma and at 2.5 h in urine excretion (Table 2). Most studies indicate a relatively low rate of urinary excretion of anthocyanins at 0.004−0.1% of the quantity ingested (Table 2), although Felgines et al.[149] reported 5% excretion after red wine or strawberry consumption.

Flavonoids occur as either glycosides or aglycones, with glycosides being the most common form in plants and foods.[150] Flavonoids are absorbed and metabolized in the small intestine to form methylated, glucuronidated, or sulfated metabolites in urine.[148] Flavanols (such as proanthocyanidins and tea catechins) and anthocyanins are poorly absorbed and therefore have low bioavailability, whereas isoflavones (a category to which phytoestrogens belong) are the most bioavailable.[151] Many different phytochemicals are found in members of the Rosaceae; thus, their concentrations and bioavailability are important in evaluating the effect on human health. The degree to which phenolic compounds are bioavailable depends on factors such as cell wall digestibility of the food source, chemical structure of the compound, how the food source was processed, and the individual efficiency of the human gastrointestinal system.

Determination of phenolic bioavailability is done via in vitro and in vivo approaches. DuPont et al.[152] conducted a human study on apple phytochemical bioavailability from alcoholic apple cider. The study found that quercetin is not efficiently absorbed in humans because it was not identified in the volunteers' plasma after administration. Rather, low levels of 3′-methylquercetin and 4′-methylquercetin were seen within 60 min after drinking 1.1 L of apple cider. In their investigation into the bioavailability of quercetin from various foods, Hollman et al.[153] reported that glucosides of quercetin are more efficiently and more rapidly absorbed than quercetin or quercetin rutinoside, and the specific sugar moiety has a predominant effect on absorption profile and plasma levels of quercetin. Catechin, epicatechin, and phloridzin were not identified in the plasma. Bioavailability of quercetin from apple, as well as from pure quercetin rutinoside, was 30% of that from onion, with plasma levels peaking after 0.7 h for onion, 2.5 h for apple, and 9 h for the pure rutinoside. It should be noted that

onions contain only quercetin glucosides, apples contain variously glycosylated quercetins, and tea contains mostly quercetin rutinoside. A separate study by Boyer and Liu[154] used Caco-2 colon cancer cells to ascertain the bioavailability of quercetin and quercetin-3-glycoside from apple peel extracts and onion extracts. No free quercetin was found in apple peel extracts, and no free quercetin accumulation was seen in the Caco-2 cells following incubation. However, low amounts of quercetin-3-glucoside were absorbed by the cells (4%). The absorption of quercetin into the cells from onion extract was much greater, most likely due to the fact that onions contain free quercetin (already available for assimilation into cells), and more quercetin glucosides, which are easily converted to the free form. Apples contain quercetin conjugates that are not easily hydrolyzed by lactase phloridzin hydrolase incubation and, so, most likely are not readily absorbed into the small intestine.

The studies of Fazzari et al.[155] on polyphenol bioaccessibility of cherry at different degrees of maturity indicated that immature cherry had high *percentages* of bioavailable phenolic compounds but lower overall *concentrations*. Higher concentrations of the readily absorbed forms of phenolic compounds in mature and overmature fruit made the actual bioavailable amounts of these compounds higher than in immature fruit. In a study to assess the bioavailability of phenolic compounds from five cultivars of frozen sweet cherry, fruit was digested to simulate either gastric or small intestine digestion and then dialyzed to determine serum-available and colon-available fractions. After pepsin digestion (stomach), the percentage recovery of the total phenolics increased, whereas the percentage anthocyanins did not change. With pancreatic digestion, the total phenolic available in the serum was about 26−30 and about 77−101% in the colon. The anthocyanin content in the serum was about 15−21 and 52−67% in colon.[155]

Azzini et al.[156] studied the bioavailability of fresh strawberry (FS) and stored strawberry (SS) in human subjects. In the study, 13 healthy volunteers consumed 300 g each of FS and SS on two separate occasions. The study found that quercetin and anthocyanins were not found in the plasma, whereas coumaric acid, 4-hydroxybenzoic acid, pelargonidin-3-glucoside (Pel-glc), protocatechuic acid, and cyanidin-3-glucoside were detected in the plasma over a period of 8 h after ingestion of either FS or SS. Pelargonidin conjugates and pelargonidin aglycone peaked in the urine within 2 h of strawberry consumption, and after 24 h, the amount excreted was approximately 0.9% of the Pel-glc dose ingested. These results suggested that the content of phenolics in strawberry might influence the bioavailability of individual compounds. In raspberry, McDougall et al.[157] studied polyphenol bioavailability as influenced by different food matrices. The study showed that bioavailability patterns varied when raspberry was codigested with commonly combined foodstuff such as bread, breakfast cereal, ice cream, and cooked minced beef. Co-digestion with ice cream and cereal seemed to decrease phenolic bioavailability, bread had no effect, and minced beef caused an increase in phenolic availability. Anthocyanin bioavailability was either unaffected or increased by co-digestion with foodstuff, suggesting that food matrices may protect them from degradation during digestion.

Torabian et al.[158] demonstrated that bioavailability of polyphenols was linked with associated reduction in plasma lipid peroxidation and increased antioxidant capacity following consumption of almond. The study reported significant increase in plasma total phenolic content 30 min after the consumption of 91 g of almond (blended in water), whereas no changes were observed following an isocaloric control meal.

Numerous advances in the assessment of polyphenol bioavailability using both in vitro and in vivo approaches have been made, but there is room for more studies to enable consumers to benefit from the abundant polyphenolic compounds in Rosaceous fruits.

## BIOFORTIFICATION OF PHENOLICS IN THE ROSACEAE

Nutritionists, food scientists, and consumers have become increasingly interested in dietary polyphenols due to their role in human health and nutrition. A huge body of research now exists that supports the role of polyphenols in the prevention of degenerative diseases, including cancers, cardiovascular, and neurodegenerative disorders.[8−11,159] Thus, improving the composition as well as the concentration of phenolic compounds in foods originating from plants would be a great benefit to human health through dietary intervention. Plant geneticists have attempted to improve phytochemical levels through traditional breeding or through bioengineering of PAL, leading to secondary metabolite accumulation. To the best of our knowledge, there is limited systematic or concerted effort in the Rosaceae to increase or decrease the concentrations of particular bioactive compounds or a group of compounds related to human health. Although there are various approaches for biofortification, breeding would appear to provide a more systematic and sustainable enrichment. We believe that initial studies on genetic improvement will perhaps focus on understanding the heritability of these compounds such as has been done in strawberry[160] and blueberry.[161] Although other methods such as genetic modification may seem plausible, they still have a major issue with public acceptance. At this stage, the technology could at best be used in the laboratory for testing gene function. Another potential approach is the exploitation of biotic and abiotic stress factors, including optimization of growth conditions such as light, temperature, and soil fertility, for actualization of genetic potential of a particular cultivar or genotype. Although it is possible to increase the content of these compounds by manipulating the physiology of plants using different agronomic treatments, it is important to consider their effects on other quality parameters including yield and organoleptic properties such as color, bitterness, astringency, and texture. To achieve this goal through breeding, gene technologies that are increasingly being used to accelerate breeding progress and increase efficiency would be essential. The use of metabolomic approaches in the identification of quantitative trait loci (QTL) is a promising novel area. For example, metabolite analysis coupled with QTL mapping will offer an unprecedented opportunity to investigate and map hundreds of metabolic features simultaneously. These analyses will yield knowledge of the inheritance of complex economic traits such as polyphenols and their health-promoting compounds in relation to specific metabolites. Mapping key metabolites to molecular markers will give a detailed understanding of the genetic basis of these traits to facilitate incorporation into elite cultivars through marker-assisted breeding.


dx.doi.org/10.1021/jf501574q | J. Agric. Food Chem. 2014, 62, 9369−9386

## AUTHOR INFORMATION


### Corresponding Author

*(N.O.) Phone: (509) 786-9271. Fax: (509) 786-9370. E-mail: noraguzie@wsu.edu.



### Funding

We acknowledge financial support from Ebonyi State University and the Federal Government of Nigeria through the TETFund Program, which enabled O.O. to visit Washington State University to undertake this study.


### Notes

The authors declare no competing financial interest.

## ACKNOWLEDGMENTS


We thank Scott Mattinson for useful discussions and the anonymous reviewers for critical reveiews that significantly improved the quality of the manuscript.


## REFERENCES


(1) Shulaev, V.; Korban, S. S.; Sosinski, B.; Abott, A. G.; Aldwinkle, H. S.; Folta, K. M.; Iezzoni, A. M.; Main, D.; Arus, P.; Dandekar, A. M.; Lewers, K.; Brown, S. K.; Davis, T. M.; Gardiner, S. E.; Potter, D.; Veilleux, R. E. Multiple models for Rosaceae genomics. *Plant Physiol.* **2008**, *147*, 985−1003.

(2) Hummer, K. E.; Janick, J. Rosaceae: taxonomy, economic importance, genomics. In *Genetics and Genomics of Rosaceae*; Springer: Berlin, Germany, 2009; pp 1−17.

(3) Jakobek, L.; Seruga, M.; Medvidovic-Kosanovic, M.; Novak, I. Anthocyanin content and antioxidant activity of various red fruit juices. *Dtsch. Lebensm.-Rundsch.* **2007**, *103*, 58−64.

(4) Volz, R. K.; McGhie, T. K. Genetic variability in apple fruit polyphenol composition in *Malus* × *domestica* and *Malus sieversii* germplasm grown in New Zealand. *J. Agric. Food Chem.* **2011**, *59*, 11509−11521.

(5) Soares, M. C.; Ribeiro, E.; Kuskoski, E. M.; Gonzaga, L. V.; Lima, A.; Mancini Filho, J. Composition of phenolic acids content in apple (*Malus* sp) pomace. *Semina: Cienc. Agrar.. Londrina* **2008**, *29*, 339−348.

(6) Mattila, P.; Hellström, J.; Törrönen, R. Phenolic acids in berries, fruits, and beverages. *J. Agric. Food Chem.* **2006**, *54*, 7193−7199.

(7) Arts, I. C.; Hollman, P. C. Polyphenols and disease risk in epidemiologic studies. *Am. J. Clin. Nutr.* **2005**, *81*, 317S−325S.

(8) Karakaya, S. Bioavailability of phenolic compounds. *Crit. Rev. Food Sci. Nutr.* **2004**, *44*, 453−464.

(9) Edderkaoui, M.; Odinokova, I.; Ohno, I.; Gukovsky, I.; Go, V. L.; Pandol, S.; Gukovskaya, A. S. Ellagic acid induces apoptosis through inhibition of nuclear factor kB in pancreatic cancer cells. *World J. Gastroenterol.* **2008**, *14*, 3672−3680.

(10) Arts, I. C.; Hollman, P. C.; Bueno de Mesquita, H. B.; Feskens, E. J.; Kromhout, D. Dietary catechins and epithelial cancer incidence: the Zutphen Elderly Study. *Int. J. Cancer* **2001**, *92*, 298−302.

(11) Prior, R. L.; Gu, L.; Wu, X.; Jacob, R. A.; Sotoudeh, G.; Kader, A. A.; Cook, R. A. Plasma antioxidant capacity changes following a meal as a measure of the ability of a food to alter in vivo antioxidant status. *J. Am. Coll. Nutr.* **2007**, *26*, 170−181.

(12) Tabak, C.; Arts, I. C.; Smit, H. A.; Heederik, D.; Kromhout, D. Chronic obstructive pulmonary disease and intake of catechins, flavonols, and flavones: the MORGEN Study. *Am. J. Respir. Crit. Care Med.* **2001**, *164*, 61−64.

(13) Butland, B. K.; Fehily, A. M.; Elwood, P. C. Diet, lung function, and lung function decline in a cohort of 2512 middle aged men. *Thorax* **2000**, *55*, 102−108.

(14) Conceição de Oliveira, M.; Sichieri, R.; Sanchez Moura, A. Weight loss associated with a daily intake of three apples or three pears among overweight women. *Nutrition* **2003**, *19*, 253−256.

(15) Seymour, E.; Lewis, S. K.; Urcuyo-Llanes, D. E.; Tanone, I. I.; Kirakosyan, A.; Kaufman, P. B.; Bolling, S. F. Regular tart cherry intake alters abdominal adiposity, adipose gene transcription, and inflammation in obesity-prone rats fed a high fat diet. *J. Med. Food* **2009**, *12*, 935−942.

(16) Thomson, C.; Kubota, C. *Health Benefits of Cherries*, National Cherry Growers and Industries Foundation, 2009; http://www.nationalcherries.com/health.html.

(17) Noratto, G.; Porter, W.; Byrne, D.; Cisneros-Zevallos, L. Polyphenolics from peach (*Prunus persica* var. Rich Lady) inhibot tumor growth and metastasis of MDA-MB-435 breast cancer cells *in vivo*. *J. Nutr. Biochem.* **2014**, DOI: 10.1016/j.jnutbio.2014.03.001.

(18) Sanoner, P.; Guyot, S.; Marnet, N.; Molle, D.; Drilleau, J.-F. Polyphenol profiles of French cider apple (*Malus domestica*) varieties. *J. Agric. Food Chem.* **1999**, *47*, 4847−4853.

(19) Karaman, Ş.; Tütem, E.; Sözgen Başkan, K.; Apak, R. Comparison of total antioxidant capacity and phenolic composition of some apple juices with combined HPLC−CUPRAC assay. *Food Chem.* **2010**, *120*, 1201−1209.

(20) Wu, J.; Gao, H.; Zhao, L.; Liao, X.; Chen, F.; Wang, Z.; Hu, X. Chemical compositional characterization of some apple cultivars. *Food Chem.* **2007**, *103*, 88−93.

(21) van der Sluis, A. A.; Dekker, M.; de Jager, A.; Jongen, W. M. Activity and concentration of polyphenolic antioxidants in apple: effect of cultivar, harvest year, and storage conditions. *J. Agric. Food Chem.* **2001**, *49*, 3606−3613.

(22) Dick, A. J.; Redden, P. R.; DeMarco, A. C.; Lidster, P. D.; Grindley, T. B. Flavonoid glycosides of Spartan apple peel. *J. Agric. Food Chem.* **1987**, *35*, 529−531.

(23) Guyot, S.; Marnet, N.; Sanoner, P.; Drilleau, J. F. Variability of the polyphenolic composition of cider apple (*Malus domestica*) fruits and juices. *J. Agric. Food Chem.* **2003**, *51*, 6240−6247.

(24) Guyot, S.; Le Bourvellec, C.; Marnet, N.; Drilleau, J. Procyanidins are the most abundant polyphenols in dessert apples at maturity. *LWT−Food Sci. Technol.* **2002**, *35*, 289−291.

(25) Chen, C.-S.; Zhang, D.; Wang, Y.-Q.; Li, P.-M.; Ma, F.-W. Effects of fruit bagging on the contents of phenolic compounds in the peel and flesh of 'Golden Delicious', 'Red Delicious', and 'Royal Gala' apples. *Sci. Hortic.* **2012**, *142*, 68−73.

(26) Guyot, S.; Marnet, N.; Laraba, D.; Sanoner, P.; Drilleau, J. F. Reversed-phase HPLC following thiolysis for quantitative estimation and characterization of the four main classes of phenolic compounds in different tissue zones of a French cider apple (*Malus domestica* var. Kermerrien) variety. *J. Agric. Food Chem.* **1998**, *46*, 1698−1705.

(27) Price, K.; Prosser, T.; Richetin, A.; Rhodes, M. A comparison of the flavonol content and composition in dessert, cooking and cider-making apples; distribution within the fruit and effect of juicing. *Food Chem.* **1999**, *66*, 489−494.

(28) Wojdyło, A.; Oszmiański, J.; Laskowski, P. Polyphenolic compounds and antioxidant activity of new and old apple varieties. *J. Agric. Food Chem.* **2008**, *56*, 6520−6530.

(29) Ubi, B. E. The genetics of anthocyanin reddening in apple fruit skin. *J. Food Agric. Environ.* **2004**, *2*, 163−165.

(30) Ubi, B. E.; Honda, C.; Bessho, H.; Kondo, S.; Wada, M.; Kobayashi, S.; Moriguchi, T. Expression analysis of anthocyanin biosynthetic genes in apple skin: effect of UV-B and temperature. *Am. J. Plant Sci.* **2006**, *170*, 571−578.

(31) Spanos, G. A.; Wrolstad, R. E.; Heatherbell, D. A. Influence of processing and storage on the phenolic composition of apple juice. *J. Agric. Food Chem.* **1990**, *38*, 1572−1579.

(32) Spanos, G. A.; Wrolstad, R. E. Phenolics of apple, pear, and white grape juices and their changes with processing and storage. A review. *J. Agric. Food Chem.* **1992**, *40*, 1478−1487.

(33) Tomas-Barberan, F.; Garcia-Viguera, C.; Nieto, J.; Ferreres, F.; Tomás-Lorente, F. Dihydrochalcones from apple juices and jams. *Food Chem.* **1993**, *46*, 33−36.

(34) Vrhovsek, U.; Rigo, A.; Tonon, D.; Mattivi, F. Quantitation of polyphenols in different apple varieties. *J. Agric. Food Chem.* **2004**, *52*, 6532−6538.

(35) Lee, K. W.; Kim, Y. J.; Kim, D.-O.; Lee, H. J.; Lee, C. Y. Major phenolics in apple and their contribution to the total antioxidant capacity. *J. Agric. Food Chem.* **2003**, *51*, 6516−6520.
(36) Neveu, V.; Perez-Jiménez, J.; Vos, F.; Crespy, V.; du Chaffaut, L.; Mennen, L.; Knox, C.; Eisner, R.; Cruz, J.; Wishart, D.; Scalbert, A. Phenol-Explorer: an online comprehensive database on polyphenol contents in foods. *Database* **2010**, DOI: 10.1093/database/bap024.
(37) Awad, M. A.; de Jager, A.; van Westing, L. M. Flavonoid and chlorogenic acid levels in apple fruit: characterisation of variation. *Sci. Hortic.* **2000**, *83*, 249−263.
(38) Gosch, C.; Halbwirth, H.; Kuhn, J.; Miosic, S.; Stich, K. Biosynthesis of phloridzin in apple (*Malus domestica* Borkh.). *Am. J. Plant Sci.* **2009**, *176*, 223−231.
(39) Macheix, J. J.; Fleuriet, A. *Fruit Phenolics*; CRC Press: Boca Raton, FL, USA, 1990.
(40) Chaovanalikit, A.; Wrolstad, R. Total anthocyanins and total phenolics of fresh and processed cherries and their antioxidant properties. *J. Food Sci.* **2004**, *69*, FCT67−FCT72.
(41) Mozetic, B.; Trebse, P.; Hribar, J. Determination and quantitation of anthocyanins and hydroxycinnamic acids in different cultivars of sweet cherries (*Prunus avium* L.) from Nova Gorica region (Slovenia). *Food Technol. Biotechnol.* **2002**, *40*, 207−212.
(42) Gao, L.; Mazza, G. Characterization, quantitation, and distribution of anthocyanins and colorless phenolics in sweet cherries. *J. Agric. Food Chem.* **1995**, *43*, 343−346.
(43) Eichner, K. Antioxidative effect of Maillard reaction intermediates. In *Autoxidation in Food and Biological Systems*; Springer: Berlin, Germany, 1980; pp 367−385.
(44) Wang, H.; Nair, M. G.; Strasburg, G. M.; Booren, A. M.; Gray, J. I. Antioxidant polyphenols from tart cherries (*Prunus cerasus*). *J. Agric. Food Chem.* **1999**, *47*, 840−844.
(45) Bhagwat, S. Haytowitz, D. B.; Holden, J. M. USDA Database for the Flavonoid Content of Selected Foods, 2013; 155.
(46) Amiot, M. J.; Tacchini, M.; Aubert, S. Y.; Oleszek, W. Influence of cultivar, maturity stage, and storage conditions on phenolic composition and enzymic browning of pear fruits. *J. Agric. Food Chem.* **1995**, *43*, 1132−1137.
(47) Henning, W.; Herrmann, K. Flavonol glycosides of plums (*Prunus domestica* and *Prunus salicina*). Phenolics of fruits. Part 12. *Z. Lebensm. Unters. Forsch.* **1980**, *171*, 111−118.
(48) Dekazos, E. D. Anthocyanin pigments in red tart cherries. *J. Food Sci.* **1970**, *35*, 237−241.
(49) Chandra, A.; Nair, M. G.; Iezzoni, A. Evaluation and characterization of the anthocyanin pigments in tart cherries (*Prunus cerasus* L.). *J. Agric. Food Chem.* **1992**, *40*, 967−969.
(50) Stacewicz-Sapuntzakis, M.; Bowen, P. E.; Hussain, E. A.; Damayanti-Wood, B. I.; Farnsworth, N. R. Chemical composition and potential health effects of prunes: a functional food? *Crit. Rev. Food Sci. Nutr.* **2001**, *41*, 251−286.
(51) Sultana, B.; Anwar, F. Flavonols (kaempeferol, quercetin, myricetin) contents of selected fruits, vegetables and medicinal plants. *Food Chem.* **2008**, *108*, 879−884.
(52) Justesen, U.; Knuthsen, P.; Leth, T. Quantitative analysis of flavonols, flavones, and flavanones in fruits, vegetables and beverages by high-performance liquid chromatography with photo-diode array and mass spectrometric detection. *J. Chromatogr., A* **1998**, *799*, 101−110.
(53) Tomás-Barberán, F. A.; Gil, M. I.; Cremin, P.; Waterhouse, A. L.; Hess-Pierce, B.; Kader, A. A. HPLC-DAD-ESIMS analysis of phenolic compounds in nectarines, peaches, and plums. *J. Agric. Food Chem.* **2001**, *49*, 4748−4760.
(54) Donovan, J. L.; Meyer, A. S.; Waterhouse, A. L. Phenolic composition and antioxidant activity of prunes and prune juice (*Prunus domestica*). *J. Agric. Food Chem.* **1998**, *46*, 1247−1252.
(55) Mosel, H.; Herrmann, K. Phenolics of fruits. 4. Phenolics of blackberries and raspberries and their changes during development and ripeness of fruits. *Z. Lebensm. Unters. Forsch.* **1974**, *154*, 324−327.
(56) Arts, I. C.; van de Putte, B.; Hollman, P. C. Catechin contents of foods commonly consumed in The Netherlands. 1. Fruits, vegetables, staple foods, and processed foods. *J. Agric. Food Chem.* **2000**, *48*, 1746−1751.
(57) Stöhr, H.; Mosel, H.; Herrmann, K. The phenolics of fruits. VII. The phenolics of cherries and plums and the changes in catechins and hydroxycinnamic acid derivatives during the development of fruits. *Z. Lebensm. Unters. Forsch.* **1975**, *159*, 85−91.
(58) Cevallos-Casals, B. A.; Byrne, D.; Okie, W. R.; Cisneros-Zevallos, L. Selecting new peach and plum genotypes rich in phenolic compounds and enhanced functional properties. *Food Chem.* **2006**, *96*, 273−280.
(59) Kim, D.-O.; Jeong, S. W.; Lee, C. Y. Antioxidant capacity of phenolic phytochemicals from various cultivars of plums. *Food Chem.* **2003**, *81*, 321−326.
(60) Radi, M.; Mahrouz, M.; Jaouad, A.; Tacchini, M.; Aubert, S.; Hugues, M.; Amiot, M. Phenolic composition, browning susceptibility, and carotenoid content of several apricot cultivars at maturity. *HortScience* **1997**, *32*, 1087−1091.
(61) Sochor, J.; Zitka, O.; Skutkova, H.; Pavlik, D.; Babula, P.; Krska, B.; Horna, A.; Adam, V.; Provaznik, I.; Kizek, R. Content of phenolic compounds and antioxidant capacity in fruits of apricot genotypes. *Molecule* **2010**, *15*, 6285−6305.
(62) Dragovic-Uzelac, V.; Levaj, B.; Mrkic, V.; Bursac, D.; Boras, M. The content of polyphenols and carotenoids in three apricot cultivars depending on stage of maturity and geographical region. *Food Chem.* **2007**, *102*, 966−975.
(63) Bureau, S.; Renard, C. M. G. C.; Reich, M.; Ginies, C.; Audergon, J.-M. Change in anthocyanin concentrations in red apricot fruits during ripening. *LWT−Food Sci. Technol.* **2009**, *42*, 372−377.
(64) Lee, C. Y.; Kagan, V.; Jaworski, A. W.; Brown, S. K. Enzymic browning in relation to phenolic compounds and polyphenoloxidase activity among various peach cultivars. *J. Agric. Food Chem.* **1990**, *38*, 99−101.
(65) Chang, S.; Tan, C.; Frankel, E. N.; Barrett, D. M. Low-density lipoprotein antioxidant activity of phenolic compounds and polyphenol oxidase activity in selected clingstone peach cultivars. *J. Agric. Food Chem.* **2000**, *48*, 147−151.
(66) Hsia, C. L.; Luh, B.; Chichester, C. Anthocyanin in freestone peaches. *J. Food Sci.* **1965**, *30*, 5−12.
(67) Vizzotto, M.; Cisneros-Zevallos, L.; Byrne, D. H.; Ramming, D. W.; Okie, W. Large variation found in the phytochemical and antioxidant activity of peach and plum germplasm. *J. Am. Soc. Hortic. Sci.* **2007**, *132*, 334−340.
(68) Thavarajah, P. Adulteration of apple with pear juice: emphasis on major carbohydrates, proline and arbutin. *J. Agric. Food Chem.* **2006**, *54*, 4861−4867.
(69) Galvis Sánchez, A. C.; Gil-Izquierdo, A.; Gil, M. I. Comparative study of six pear cultivars in terms of their phenolic and vitamin C contents and antioxidant capacity. *J. Sci. Food Agric.* **2003**, *83*, 995−1003.
(70) Oleszek, W.; Amiot, M. J.; Aubert, S. Y. Identification of some phenolics in pear fruit. *J. Agric. Food Chem.* **1994**, *42*, 1261−1265.
(71) Andrade, P.; Carvalho, A.; Seabra, R.; Ferreira, M. A previous study of phenolic profiles of quince, pear, and apple purees by HPLC diode array detection for the evaluation of quince puree genuineness. *J. Agric. Food Chem.* **1998**, *46*, 968−972.
(72) Risch, B. H.; Hermann, K. Die Gehalte an Hydroxyzimtsaure-Verbindungen und Catechinen in Kern- und Steinobst. *Z. Lebensm. Unters. Forsch.* **1988**, *186*, 225−230.
(73) Francis, F. Anthocyanins in pears. *Hortic. Sci.* **1970**, *5*, 42.
(74) Redelinghuys, H.; Koeppen, B.; De Swardt, G. Anthocyanins of a South African red sport of *Pyrus communis* L. cv. Williams Bon Chretien. *Agrochemophysica* **1973**, *5*, 21−24.
(75) Silva, B. M.; Andrade, P. B.; Valentão, P.; Ferreres, F.; Seabra, R. M.; Ferreira, M. A. Quince (*Cydonia oblonga* Miller) fruit (pulp, peel, and seed) and jam: antioxidant activity. *J. Agric. Food Chem.* **2004**, *52*, 4705−4712.
(76) Silva, B.; Valentão, P.; Seabra, R.; Andrade, P. Quince (*Cydonia oblonga* Miller): an interesting dietary source of bioactive compounds. *Food Chem. Res. Dev.* **2008**, 243−266.

(77) Silva, B. M.; Andrade, P. B.; Ferreres, F.; Domingues, A. L.; Seabra, R. M.; Ferreira, M. A. Phenolic profile of quince fruit (*Cydonia oblonga* Miller) (pulp and peel). *J. Agric. Food Chem.* **2002**, *50*, 4615−4618.
(78) Wojdyło, A.; Oszmiański, J.; Bielicki, P. Polyphenolic composition, antioxidant activity, and polyphenol oxidase (PPO) activity of quince (*Cydonia oblonga* Miller) varieties. *J. Agric. Food Chem.* **2013**, *61*, 2762−2772.
(79) Markh, A. T., Kozenko, S. I., Biochemical characteristics of quince fruits. *Prikl. Biokhim. Mikrobiol.* **1964**, 380−387.
(80) Senter, S.; Horvat, R.; Forbus, W. Comparative GLC-MS. Analysis of phenolic acids of selected tree nuts. *J. Food Sci.* **1983**, *48*, 798−799.
(81) Wijeratne, S. S.; Abou-Zaid, M. M.; Shahidi, F. Antioxidant polyphenols in almond and its co-products. *J. Agric. Food Chem.* **2006**, *54*, 312−318.
(82) Sang, S.; Lapsley, K.; Rosen, R. T.; Ho, C.-T. New prenylated benzoic acid and other constituents from almond hulls (*Prunus amygdalus* Batsch). *J. Agric. Food Chem.* **2002**, *50*, 607−609.
(83) Amarowicz, R.; Troszńska, A.; Shahidi, F. Antioxidant activity of almond seed extract and its fractions. *J. Food Lipids* **2005**, *12*, 344−358.
(84) Takeoka, G. R.; Dao, L. T. Antioxidant constituents of almond [*Prunus dulcis* (Mill.) DA Webb] hulls. *J. Agric. Food Chem.* **2003**, *51*, 496−501.
(85) Milbury, P. E.; Chen, C.-Y.; Dolnikowski, G. G.; Blumberg, J. B. Determination of flavonoids and phenolics and their distribution in almonds. *J. Agric. Food Chem.* **2006**, *54*, 5027−5033.
(86) Frison-Norrie, S.; Sporns, P. Identification and quantification of flavonol glycosides in almond seedcoats using MALDI-TOF MS. *J. Agric. Food Chem.* **2002**, *50*, 2782−2787.
(87) Mullen, W.; McGinn, J.; Lean, M. E.; MacLean, M. R.; Gardner, P.; Duthie, G. G.; Yokota, T.; Crozier, A. Ellagitannins, flavonoids, and other phenolics in red raspberries and their contribution to antioxidant capacity and vasorelaxation properties. *J. Agric. Food Chem.* **2002**, *50*, 5191−5196.
(88) Amarowicz, R.; Pegg, R. B. Content of proanthocyanidins in selected plant extracts as determined via *n*-butanol/HCl hydrolysis and a colorimetric assay or by HPLC − a short report. *Polym. J. Food Nutr. Sci.* **2006**, *15*, 319.
(89) Zadernowski, R.; Naczk, M.; Nesterowicz, J. Phenolic acid profiles in some small berries. *J. Agric. Food Chem.* **2005**, *53*, 2118−2124.
(90) Mahmood, T.; Anwar, F.; Abbas, M.; Saari, N. Effect of maturity on phenolics (phenolic acids and flavonoids) profile of strawberry cultivars and mulberry species from Pakistan. *Int. J. Mol. Sci.* **2012**, *13*, 4591−4607.
(91) Clifford, M. N.; Scalbert, A. Ellagitannins − nature, occurrence and dietary burden. *J. Sci. Food Agric.* **2000**, *80*, 1118−1125.
(92) Määttä-Riihinen, K. R.; Kamal-Eldin, A.; Törrönen, A. R. Identification and quantification of phenolic compounds in berries of *Fragaria* and *Rubus* species (family Rosaceae). *J. Agric. Food Chem.* **2004**, *52*, 6178−6187.
(93) Misran, A. *Evaluation of Post Harvest Technologies for Improving Strawberry Fruit Quality*. Ph.D. thesis, Department of Plant Agriculture, University of Guelph, Ontario, Canada, 2013.
(94) Gu, L.; Kelm, M. A.; Hammerstone, J. F.; Beecher, G.; Holden, J.; Haytowitz, D.; Gebhardt, S.; Prior, R. L. Concentrations of proanthocyanidins in common foods and estimations of normal consumption. *J. Nutr.* **2004**, *134*, 613−617.
(95) de Pascual-Teresa, S.; Santos-Buelga, C.; Rivas-Gonzalo, J. C. Quantitative analysis of flavan-3-ols in Spanish foodstuffs and beverages. *J. Agric. Food Chem.* **2000**, *48*, 5331−5337.
(96) Pallauf, K.; Rivas-Gonzalo, J.; Del Castillo, M.; Cano, M.; de Pascual-Teresa, S. Characterization of the antioxidant composition of strawberry tree (*Arbutus unedo* L.) fruits. *J. Food Compos. Anal.* **2008**, *21*, 273−281.
(97) Donno, D.; Cavanna, M.; Beccaro, G. L.; Mellano, G. M.; Marinoni, D. T.; Cerutti, A. K.; Bounous, G. Currants and strawberries as bioactive compounds source: determination of antioxidant profile with HPLC-DAD/MS system. *J. Appl. Bot. Food Qual.* **2013**, *86*, 1−10.
(98) Borges, G.; Degeneve, A.; Mullen, W.; Crozier, A. Identification of flavonoid and phenolic antioxidants in black currants, blueberries, raspberries, red currants, and cranberries. *J. Agric. Food Chem.* **2009**, *58*, 3901−3909.
(99) Wada, L.; Ou, B. Antioxidant activity and phenolic content of Oregon caneberries. *J. Agric. Food Chem.* **2002**, *50*, 3495−3500.
(100) Hilt, P.; Schieber, A.; Yildirim, C.; Arnold, G.; Klaiber, I.; Conrad, J.; Beifuss, U.; Carle, R. Detection of phloridzin in strawberries (*Fragaria* × *ananassa* Duch.) by HPLC-PDA-MS/MS and NMR spectroscopy. *J. Agric. Food Chem.* **2003**, *51*, 2896−2899.
(101) Arranz, S.; Silván, J. M.; Saura-Calixto, F. Nonextractable polyphenols, usually ignored, are the major part of dietary polyphenols: a study on the Spanish diet. *Mol. Nutr. Food Res.* **2010**, *54*, 1646−1658.
(102) Arranz, S.; Saura-Calixto, F.; Shaha, S.; Kroon, P. A. High contents of nonextractable polyphenols in fruits suggest that polyphenol contents of plant foods have been underestimated. *J. Agric. Food Chem.* **2009**, *57*, 7298−7303.
(103) Hamauzu, Y.; Mizuno, Y. Non-extractable procyanidins and lignin are important factors in the bile acid binding and radical scavenging properties of cell wall material in some fruits. *Plant Foods Hum. Nutr.* **2011**, *66*, 70−77.
(104) Pérez-Jiménez, J.; Díaz-Rubio, M. E.; Saura-Calixto, F. Non-extractable polyphenols, a major dietary antioxidant: occurrence, metabolic fate and health effects. *Nutr. Res. Rev.* **2013**, *26*, 118−129.
(105) Perez-Jimenez, J.; Torres, J. L. Analysis of nonextractable phenolic compounds in foods: the current state of the art. *J. Agric. Food Chem.* **2011**, *59*, 12713−12724.
(106) Golding, J. B.; McGlasson, W. B.; Wyllie, S. G.; Leach, D. N. Fate of apple peel phenolics during cool storage. *J. Agric. Food Chem.* **2001**, *49*, 2283−2289.
(107) Lattanzio, V.; Di Venere, D.; Linsalata, V.; Bertolini, P.; Ippolito, A.; Salerno, M. Low temperature metabolism of apple phenolics and quiescence of *Phlyctaena vagabunda*. *J. Agric. Food Chem.* **2001**, *49*, 5817−5821.
(108) Tokusoglu, Ö. Bioactive phytochemicals in pome fruits. In *Fruit and Cereal Bioactives: Sources, Chemistry, and Applications*; Tokusoglu, Ö., Ed.; CRC Press: Boca Raton, FL, USA, 2011; pp 107−114.
(109) Hyson, D. A. A comprehensive review of apples and apple components and their relationship to human health. *Adv. Nutr.* **2011**, *2*, 408−420.
(110) Polesello, A.; Bonzini, C. Observations on pigments of sweet cherries and on pigment stability during frozen storage. I. Anthocyanin composition. *Confructa* **1977**, *22*, 170−175.
(111) Madrau, M. A.; Piscopo, A.; Sanguinetti, A. M.; Del Caro, A.; Poiana, M.; Romeo, F. V.; Piga, A. Effect of drying temperature on polyphenolic content and antioxidant activity of apricots. *Eur. Food Res. Technol.* **2009**, *228*, 441−448.
(112) Raynal, J.; Moutounet, M.; Souquet, J. M. Intervention of phenolic compounds in plum technology. 1. Changes during drying. *J. Agric. Food Chem.* **1989**, *37*, 1046−1050.
(113) Piga, A.; Del Caro, A.; Corda, G. From plums to prunes: influence of drying parameters on polyphenols and antioxidant activity. *J. Agric. Food Chem.* **2003**, *51*, 3675−3681.
(114) Silva, B.; Andrade, P.; Mendes, G.; Valentao, P.; Seabra, R.; Ferreira, M. Analysis of phenolic compounds in the evaluation of commercial quince jam authenticity. *J. Agric. Food Chem.* **2000**, *48*, 2853−2857.
(115) Amaro, L.; Soares, M.; Pinho, C.; Almeida, I.; Ferreira, I.; Pinho, O. Influence of cultivar and storage conditions in anthocyanin content and radical-scavenging activity of strawberry jams. *World Acad. Sci. Eng. Technol.* **2012**, *69*, 118−121.
(116) Zafrilla, P.; Ferreres, F.; Tomás-Barberán, F. A. Effect of processing and storage on the antioxidant ellagic acid derivatives and flavonoids of red raspberry (*Rubus idaeus*) jams. *J. Agric. Food Chem.* **2001**, *49*, 3651−3655.

(117) Häkkinen, S. H.; Kärenlampi, S. O.; Mykkänen, H. M.; Törrönen, A. R. Influence of domestic processing and storage on flavonol contents in berries. *J. Agric. Food Chem.* **2000**, *48*, 2960−2965.
(118) Asami, D. K.; Hong, Y. J.; Barrett, D. M.; Mitchell, A. E. Processing-induced changes in total phenolics and procyanidins in clingstone peaches. *J. Sci. Food Agric.* **2003**, *83*, 56−63.
(119) Bolling, B. W.; Blumberg, J. B.; Oliver Chen, C.-Y. The influence of roasting, pasteurisation, and storage on the polyphenol content and antioxidant capacity of California almond skins. *Food Chem.* **2010**, *123*, 1040−1047.
(120) Garrido, I.; Monagas, M.; Gómez-Cordovés, C.; Bartolomé, B. Polyphenols and antioxidant properties of almond skins: influence of industrial processing. *J. Food Sci. Nutr.* **2008**, *73*, 106−115.
(121) Saure, M. C. External control of anthocyanin formation in apple. *Sci. Hortic.* **1990**, *42*, 181−218.
(122) Treutter, D. Biosynthesis of phenolic compounds and its regulation in apple. *J. Plant Growth Regul.* **2001**, *34*, 71−89.
(123) Awad, M. A.; de Jager, A.; van der Plas, L. H.; van der Krol, A. R. Flavonoid and chlorogenic acid changes in skin of 'Elstar' and 'Jonagold' apples during development and ripening. *Sci. Hortic.* **2001**, *90*, 69−83.
(124) Awad, M. A.; de Jager, A. Relationships between fruit nutrients and concentrations of flavonoids and chlorogenic acid in 'Elstar' apple skin. *Sci. Hortic.* **2002**, *92*, 265−276.
(125) Wang, S. Y.; Lin, H.-S. Compost as a soil supplement increases the level of antioxidant compounds and oxygen radical absorbance capacity in strawberries. *J. Agric. Food Chem.* **2003**, *51*, 6844−6850.
(126) Awad, M. A.; de Jager, A. Formation of flavonoids, especially anthocyanin and chlorogenic acid in 'Jonagold' apple skin: influences of growth regulators and fruit maturity. *Sci. Hortic.* **2002**, *93*, 257−266.
(127) Mainla, L.; Moor, U.; Karp, K.; Püssa, T. The effect of genotype and rootstock on polyphenol composition of selected apple cultivars in Estonia. *Zemdirbystes Agric.* **2011**, *98*, 63−70.
(128) Poniedziałek, W.; Nosal, K.; Porebski, S.; Baszczyk, J. Melrose, Gloster and Jonagold apple cultivars. *Folia Hortic.* **1993**, *5*, 99−108.
(129) Pineli, L. d. L. d. O.; Moretti, C. L.; dos Santos, M. S.; Campos, A. B.; Brasileiro, A. V.; Córdova, A. C.; Chiarello, M. D. Antioxidants and other chemical and physical characteristics of two strawberry cultivars at different ripeness stages. *J. Food Compos. Anal.* **2011**, *24*, 11−16.
(130) Wang, S. Y.; Chen, C.-T.; Wang, C. Y. The influence of light and maturity on fruit quality and flavonoid content of red raspberries. *Food Chem.* **2009**, *112*, 676−684.
(131) Mori, K.; Sugaya, S.; Gemma, H. Decreased anthocyanin biosynthesis in grape berries grown under elevated night temperature condition. *Sci. Hortic.* **2005**, *105*, 319−330.
(132) Treutter, D. Managing phenol contents in crop plants by phytochemical farming and breeding − visions and constraints. *Int. J. Mol. Sci.* **2010**, *11*, 807−857.
(133) Hall, I.; Stark, R. Anthocyanin production in cranberry leaves and fruit, related to cool temperatures at a low light intensity. *Hortic. Res.*. **1972**, *1972*.
(134) Ferretti, G.; Bacchetti, T.; Belleggia, A.; Neri, D. Cherry antioxidants: from farm to table. *Molecules* **2010**, *15*, 6993−7005.
(135) Wang, S. Effect of pre-harvest conditions on antioxidant capacity in fruits. *Acta Hortic.* **2006**, *712*, 299−305.
(136) Usenik, V.; Fabčič, J.; Štampar, F. Sugars, organic acids, phenolic composition and antioxidant activity of sweet cherry (*Prunus avium* L.). *Food Chem.* **2008**, *107*, 185−192.
(137) Jakobek, L.; Šeruga, M.; Voća, S.; Šindrak, Z.; Dobričević, N. Flavonol and phenolic acid composition of sweet cherries (cv. Lapins) produced on six different vegetative rootstocks. *Sci. Hortic.* **2009**, *123*, 23−28.
(138) Usenik, V.; Štampar, F.; Fajt, N. Seasonal changes in polyphenols of 'Lapins' sweet cherry grafted on different rootstocks. *IV International Cherry Symposium 667*; ISHS: Leuven, Belgium, 2001; pp 239−246.
(139) Murray, X. J.; Holcroft, D. M.; Cook, N. C.; Wand, S. J. Postharvest quality of 'Laetitia' and 'Songold' (*Prunus salicina* Lindell.) plums as affected by preharvest shading treatments. *Postharvest Biol. Technol.* **2005**, *37*, 81−92.
(140) Tomás-Barberán, F. A.; Espin, J. C. Phenolic compounds and related enzymes as determinants of quality in fruits and vegetables. *J. Sci. Food Agric.* **2001**, *81*, 853−876.
(141) Lombardi-Boccia, G.; Lucarini, M.; Lanzi, S.; Aguzzi, A.; Cappelloni, M. Nutrients and antioxidant molecules in yellow plums (*Prunus domestica* L.) from conventional and organic productions: a comparative study. *J. Agric. Food Chem.* **2004**, *52*, 90−94.
(142) Tsuji, M.; Harakawa, M.; Komiyama, Y. Inhibition of increase of pulp color and phenylalanine ammonia-lyase activity in plum [*Prunus salicina*] fruit at high temperature (30 °C). *J. Jpn. Soc. Food Sci. Technol.* **1983**, *30*, 688−692.
(143) Bourn, D.; Prescott, J. A comparison of the nutritional value, sensory qualities, and food safety of organically and conventionally produced foods. *Crit. Rev. Food Sci. Nutr.* **2002**, *42*, 1−34.
(144) Winter, C. K.; Davis, S. F. Organic foods. *J. Food Sci.* **2006**, *71*, R117−R124.
(145) Kan, T.; Bostan, S. Z. Changes of contents of polyphenols and vitamin A of organic and conventional fresh and dried apricot cultivars (*Prunus armeniaca* L.). *World J. Agric. Sci.* **2010**, *6*, 120−126.
(146) Hegedüs, A.; Pfeiffer, P.; Papp, N.; Abrankó, L.; Blázovics, A.; Pedryc, A.; Stefanovits-Bányai, É. Accumulation of antioxidants in apricot fruit through ripening: characterization of a genotype with enhanced functional properties. *Biol. Res.* **2011**, *44*, 339−344.
(147) Machlin, L. J.; Bendich, A. Free radical tissue damage: protective role of antioxidant nutrients. *FASEB J.* **1987**, *1*, 441−445.
(148) Manach, C.; Williamson, G.; Morand, C.; Scalbert, A.; Rémésy, C. Bioavailability and bioefficacy of polyphenols in humans. I. Review of 97 bioavailability studies. *Am. J. Clin. Nutr.* **2005**, *81*, 230S−242S.
(149) Felgines, C.; Talavéra, S.; Gonthier, M.-P.; Texier, O.; Scalbert, A.; Lamaison, J.-L.; Rémésy, C. Strawberry anthocyanins are recovered in urine as glucuro-and sulfoconjugates in humans. *J. Nutr.* **2003**, *133*, 1296−1301.
(150) Bakker, J.; Timberlake, C. F. The distribution of anthocyanins in grape skin extracts of port wine cultivars as determined by high performance liquid chromatography. *J. Sci. Food Agric.* **1985**, *36*, 1315−1324.
(151) Aura, A.-M.; Martin-Lopez, P.; O'Leary, K. A.; Williamson, G.; Oksman-Caldentey, K.-M.; Poutanen, K.; Santos-Buelga, C. In vitro metabolism of anthocyanins by human gut microflora. *Eur. J. Nutr.* **2005**, *44*, 133−142.
(152) DuPont, M. S.; Bennett, R. N.; Mellon, F. A.; Williamson, G. Polyphenols from alcoholic apple cider are absorbed, metabolized and excreted by humans. *J. Nutr.* **2002**, *132*, 172−175.
(153) Hollman, P. C.; van Trijp, J. M.; Buysman, M. N.; Mengelers, M. J.; de Vries, J. H.; Katan, M. B. Relative bioavailability of the antioxidant flavonoid quercetin from various foods in man. *FEBS Lett.* **1997**, *418*, 152−156.
(154) Boyer, J.; Liu, R. H. Apple phytochemicals and their health benefits. *Nutr J.* **2004**, *3*, 12.
(155) Fazzari, M.; Fukumoto, L.; Mazza, G.; Livrea, M. A.; Tesoriere, L.; Marco, L. D. In vitro bioavailability of phenolic compounds from five cultivars of frozen sweet cherries (*Prunus avium* L.). *J. Agric. Food Chem.* **2008**, *56*, 3561−3568.
(156) Azzini, E.; Vitaglione, P.; Intorre, F.; Napolitano, A.; Durazzo, A.; Foddai, M. S.; Fumagalli, A.; Catasta, G.; Rossi, L.; Venneria, E. Bioavailability of strawberry antioxidants in human subjects. *Br. J. Nutr.* **2010**, *104*, 1165−1173.
(157) McDougall, G. J.; Dobson, P.; Smith, P.; Blake, A.; Stewart, D. Assessing potential bioavailability of raspberry anthocyanins using an in vitro digestion system. *J. Agric. Food Chem.* **2005**, *53*, 5896−5904.
(158) Torabian, S.; Haddad, E.; Rajaram, S.; Banta, J.; Sabate, J. Acute effect of nut consumption on plasma total polyphenols, antioxidant capacity and lipid peroxidation. *J. Hum. Nutr. Diet.* **2009**, *22*, 64−71.
(159) Harris, G.; Gupta, A.; Nines, R.; Kresty, L.; Habib, S.; Frankel, W.; LaPerle, K.; Gallaher, D.; Schwartz, S.; Stoner, G. Effects of lyophilized black raspberries on azoxymethane-induced colon cancer

and 8-hydroxy-2′-deoxyguanosine levels in the Fischer 344 rat. *Nutr. Cancer* **2001**, *40*, 125−133.
(160) Connor, A. M.; Stephens, M. J.; Hall, H. K.; Alspach, P. A. Variation and heritabilities of antioxidant activity and total phenolic content estimated from a red raspberry factorial experiment. *J. Am. Soc. Hortic. Sci.* **2005**, *130*, 403−411.
(161) Connor, A. M.; Luby, J. J.; Tong, C. B.; Finn, C. E.; Hancock, J. F. Genotypic and environmental variation in antioxidant activity, total phenolic content, and anthocyanin content among blueberry cultivars. *J. Am. Soc. Hortic. Sci.* **2002**, *127*, 89−97.

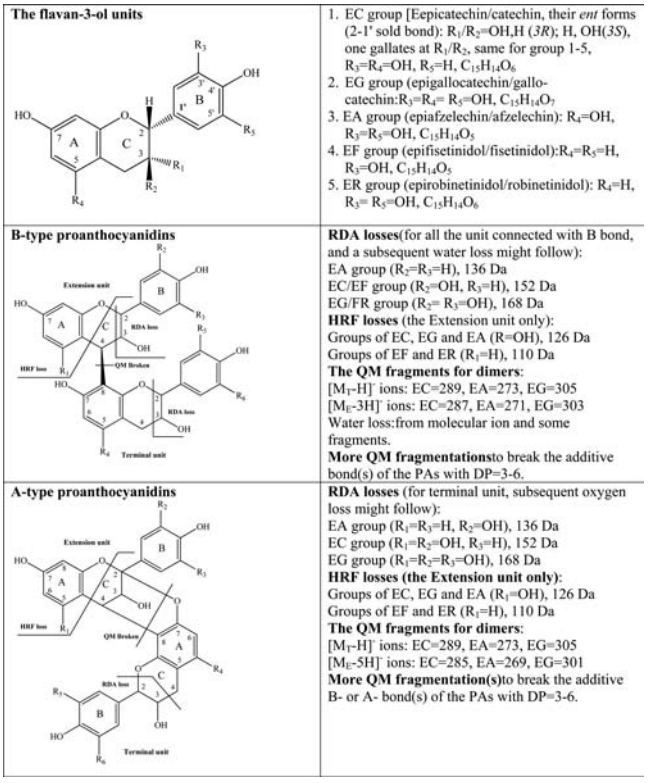


**Figure 1.** Structures of flavan-3-ol units and common fragmentation patterns for proanthocyanidins.

mixtures has also been used for quantification of PAs.[1−4,6,10−12] However, direct quantification of the different PAs comprising each oligomeric class is still problematic due to the difficulty of separation and the lack of standards.[1−4]

As a part of a project to systematically identify and quantify food phenolic compounds, a standardized HPLC-PDA-ESI/MS method was developed for the identification and quantification of food polyphenols, including some PAs.[24] Quantification was based on UV absorbance and molar relative response factors (MRRFs).[25] This method has been upgraded and now uses ultrahigh-performance liquid chromatography−photodiode array detection−high-resolution mass spectrometry operated in the tandem mode (UHPLC-PDA-ESI/HRMS$^n$).[26] In the current study, this method was employed to identify nearly 300 oligomeric PAs in selected plants (fruit pericarps of litchi and mangosteen), extracts (from grape seed and cranberry), and food samples (jujube, Fuji apple, and chocolate) and to quantify PAs in grape seed extract. The main PAs in each of the oligomeric classes were quantified.

## MATERIALS AND METHODS

**Chemicals.** Formic acid, HPLC grade methanol, and acetonitrile were purchased from VWR International, Inc. (Clarksburg, MD, USA). HPLC grade water was prepared from distilled water using a Milli-Q system (Millipore Laboratory, Bedford, MA, USA).

**Standards.** (+)-Catechin, (−)-epicatechin, (−)-gallocatechin-3-*O*-gallate, (−)-epigallocatechin-3-*O*-gallate, procyanidin $B_1$, procyanidin $B_2$, procyanidin $C_1$, and procyanidin $A_2$ were obtained from Chromadex, Inc. (Irvine, CA, USA). The standards were vacuum-dried using a vacuum drying box (National Appliance Co., Portland, OR, USA) at 110 °C until a constant weight was reached (about 24 h). These dried standards were used to determine the MRRF that were used for calibration.[25]

**Plant Materials and Extraction.** Fresh fruits of jujube (*Ziziphus jujuba* Mill), Fuji apple (*Malus domestica* Borkh cv. Fuji), litchi (*Litchi chinensis* Sonn.), and mangosteen (*Garcinia mangostana* Linn.) were purchased from local food stores. Dark chocolate was purchased from a local Trader Joes store in Maryland, USA. The extracts of grape seed and cranberry were kindly supplied by Triarco Industries, Inc. (Paterson, NJ, USA). The fruit pericarps of litchi and mangosteen and the skins of fresh jujubes and apples were lyophilized, and the dried materials were powdered.[24−26]

Each of the powdered fruit samples (250 mg) was extracted with 5.000 mL of a methanol/water (60:40, v/v) solvent using sonication for 60 min at room temperature. The slurry mixture was centrifuged at 2500 rpm for 15 min. The supernatant (4.000 mL) was taken from the tube and filtered through a 17 mm (0.45 μm) PVDF syringe filter (VWR Scientific, Seattle, WA, USA) for injections.[24−26] A second extraction using acetone/methanol/water (2:2:1, v/v/v, 4.000 mL) was treated in the same way to check the extraction efficiency of the general extraction method. The result showed that >95% of the mass for each main compound was extracted from the plant material by the first extraction.

Powdered chocolate samples (2000 mg) were extracted with 40 mL of the same aqueous methanol and treated as described above, and the supernatant was taken to dryness under vacuum at 40 °C. The approximately 30 mg of the residue was dissolved in water (1 mL) and passed through Sep-PakVac RC (500 mg) $C_{18}$ cartridge (Waters Corp., Milford, MA, USA). After washing with water (5 mL), the PAs were eluted with methanol (5 mL) and again taken to dryness under vacuum. The residue was dissolved in 1.000 mL of the methanol/water solvent and filtered for injection.

The grape seed (10.80 mg) and cranberry (10.20 mg) extracts were dissolved in the same aqueous methanol (1.0 mL) and filtered. Triplicate injections (1 μL) of each solution were used to determine the average concentration and the relative standard deviation for each of the PAs in the extract. Dried catechin was used as the external calibration standard; 4 mg was placed in a 10 mL volumetric flask, dissolved in the methanol/water (60:40, v/v) solvent, and brought to volume. This stock solution was diluted 1:4 and 1:16. The stock and each dilution were injected onto the column three times and used to construct a calibration curve.

**UHPLC-PDA-ESI/HRMS$^n$ Conditions.** The UHPLC-HRMS system used consisted of an LTQ Orbitrap XL mass spectrometer with an Accela 1250 binary pump, a PAL HTC Accela TMO autosampler, a PDA detector (ThermoScientific, San Jose, CA, USA), and a G1316A column compartment (Agilent, Palo Alto, CA, USA). The separation was carried out on a U-HPLC column (200 mm × 2.1 mm i.d., 1.9 μm, Hypersil Gold AQ RP-$C_{18}$) (Thermo- Scientific) with an HPLC/UHPLC precolumn filter (UltraShield Analytical Scientific Instruments, Richmond, CA, USA) at a flow rate of 0.3 mL/min. The mobile phase consisted of a combination of A (0.1% formic acid in water, v/v) and B (0.1% formic acid in acetonitrile, v/v). The linear gradient was from 4 to 20% B (v/v) at 40 min, to 35% B at 60 min, and to 100% B at 61 min and held at 100% B to 65 min. The PDA recorded spectra from 200 to 700 nm and provided real-time monitoring at 280 and 330 nm.[26]

The HRMS was operated in the negative ionization mode using the following conditions: sheath gas at 70 (arbitrary units), aux and sweep gas at 15 (arbitrary units), spray voltage at 4.8 kV, capillary temperature at 300 °C, capillary voltage at 15 V, and tube lens at 70 V. The mass range was from $m/z$ 50 to 2000 with a resolution of 15000, FTMS AGC target at 2e5, FT-MS/MS AGC target at 1e5, isolation width of 1.5 amu, and maximum ion injection time of 500 ms. The most intense ion was selected for the data-dependent scan to provide $MS^2$ to $MS^5$ product ions with a normalized collision energy at 35%.[26] The selective ion monitoring (SIM) mode was used to select the molecular ions of the isomers from each of the PA groups in grape seed extract for their quantification.

Table 1. Computed High-Resolution Mass, Molecular Weight, Molecular Ions, and Composition of Common Oligomeric PAs[a]

| DP | proanthocyanidin | HRMW (Da) | HR $[M - H]^-$ ($m/z$) | HR $[M - 2H]^{2-}$ ($m/z$) | HR $[M - 3H]^{3-}$ ($m/z$) | C | H | O | EA/EF | EG | galloyl | A-bond |
|---|---|---|---|---|---|---|---|---|---|---|---|---|
| dimers | B-type propelargonidin | 546.1518 | 545.1440 | | | 30 | 26 | 10 | 2 | 0 | 0 | 0 |
| | B-type proanthocyanidin | 560.1311 | 559.1233 | | | 30 | 24 | 11 | 1 | 0 | 0 | 1 |
| | B-type proanthocyanidin | 562.1467 | 561.1389 | | | 30 | 26 | 11 | 1 | 0 | 0 | 0 |
| | B-type procyanidin | 578.1416 | 577.1338 | | | 30 | 26 | 12 | 1 | 1 | 0 | 0 |
| | A-type procyanidin | 576.1260 | 575.1182 | | | 30 | 24 | 12 | 0 | 0 | 0 | 1 |
| | **B-type procyanidin** | **578.1416** | **577.1338** | | | **30** | **26** | **12** | **0** | **0** | **0** | **0** |
| | galloylated procyanidin | 730.1524 | 729.1446 | | | 37 | 30 | 16 | 0 | 0 | 1 | 0 |
| | galloylated procyanidin | 882.1632 | 881.1554 | | | 44 | 34 | 20 | 0 | 0 | 2 | 0 |
| | B-type proanthocyanidin | 592.1209 | 591.1131 | | | 30 | 24 | 13 | 0 | 1 | 0 | 1 |
| | B-type proanthocyanidin | 594.1365 | 593.1287 | | | 30 | 26 | 13 | 0 | 1 | 0 | 0 |
| | B-type prodelphinidin | 610.1314 | 609.1236 | | | 30 | 26 | 14 | 0 | 2 | 0 | 0 |
| | galloylated proanthocyanidin | 746.1473 | 745.1395 | | | 37 | 30 | 17 | 0 | 1 | 1 | 0 |
| | galloylated prodelphinidin | 914.1530 | 913.1452 | | | 44 | 34 | 22 | 0 | 2 | 2 | 0 |
| trimers | B-type propelargonidin | 818.2199 | 817.2121 | | | 45 | 38 | 15 | 3 | 0 | 0 | 0 |
| | A-type proanthocyanidin | 832.1992 | 831.1914 | | | 45 | 36 | 16 | 2 | 0 | 0 | 1 |
| | B-type proanthocyanidin | 834.2148 | 833.2070 | | | 45 | 38 | 16 | 2 | 0 | 0 | 0 |
| | A-type proanthocyanidin | 848.1941 | 847.1863 | | | 45 | 36 | 17 | 1 | 0 | 0 | 1 |
| | B-type proanthocyanidin | 850.2097 | 849.2019 | | | 45 | 38 | 17 | 1 | 0 | 0 | 0 |
| | galloylated proanthocyanidin | 986.2256 | 985.2178 | | | 52 | 42 | 20 | 2 | 0 | 1 | 0 |
| | A-type procyanidin | 862.1734 | 861.1656 | | | 45 | 34 | 18 | 0 | 0 | 0 | 2 |
| | A-type procyanidin | 864.1890 | 863.1812 | | | 45 | 36 | 18 | 0 | 0 | 0 | 1 |
| | **B-type procyanidin** | **866.2046** | **865.1968** | | | **45** | **38** | **18** | **0** | **0** | **0** | **0** |
| | galloylated procyanidin | 1018.2154 | 1017.2076 | | | 52 | 42 | 22 | 0 | 0 | 1 | 0 |
| | galloylated procyanidin | 1170.2262 | 1169.2184 | | | 59 | 46 | 26 | 0 | 0 | 2 | 0 |
| | B-type proanthocyanidin | 882.1995 | 881.1917 | | | 45 | 38 | 19 | 0 | 1 | 0 | 0 |
| | B-type proanthocyanidin | 898.1944 | 897.1866 | | | 45 | 38 | 20 | 0 | 2 | 0 | 0 |
| | B-type prodelphinidin | 914.1893 | 913.1815 | | | 45 | 38 | 21 | 0 | 3 | 0 | 0 |
| | galloylated prodelphinidin | 1034.2103 | 1033.2025 | | | 52 | 42 | 23 | 0 | 1 | 1 | 0 |
| tetramers | A-type proanthocyanidin | 1120.2622 | 1119.2544 | | | 60 | 48 | 22 | 2 | 0 | 0 | 1 |
| | B-type proanthocyanidin | 1122.2778 | 1121.2700 | | | 60 | 50 | 22 | 2 | 0 | 0 | 0 |
| | A-type proanthocyanidin | 1136.2571 | 1135.2493 | | | 60 | 48 | 23 | 1 | 0 | 0 | 1 |
| | B-type proanthocyanidin | 1138.2727 | 1137.2649 | | | 60 | 50 | 23 | 1 | 0 | 0 | 0 |
| | A-type procyanidin | 1148.2208 | 1147.2130 | | | 60 | 44 | 24 | 0 | 0 | 0 | 3 |
| | A-type procyanidin | 1150.2364 | 1149.2286 | | | 60 | 46 | 24 | 0 | 0 | 0 | 2 |
| | A-type procyanidin | 1152.2520 | 1151.2442 | | | 60 | 48 | 24 | 0 | 0 | 0 | 1 |
| | **B-type procyanidin** | **1154.2676** | **1153.2598** | | | **60** | **50** | **24** | **0** | **0** | **0** | **0** |
| | galloylated procyanidin | 1306.2784 | 1305.2706 | | | 67 | 54 | 28 | 0 | 0 | 1 | 0 |
| | galloylated procyanidin | 1458.2892 | 1457.2814 | | | 74 | 58 | 32 | 0 | 0 | 2 | 0 |
| | A-type proanthocyanidin | 1168.2469 | 1167.2391 | | | 60 | 48 | 25 | 0 | 1 | 0 | 1 |
| | B-type proanthocyanidin | 1170.2625 | 1169.2547 | | | 60 | 50 | 25 | 0 | 1 | 0 | 0 |
| pentamers | A-type proanthocyanidin | 1392.3303 | 1391.3225 | 695.1574 | | 75 | 60 | 27 | 3 | 0 | 0 | 1 |
| | B-type proanthocyanidin | 1410.3408 | 1409.3330 | 704.1626 | | 75 | 62 | 28 | 2 | 0 | 0 | 0 |
| | A-type proanthocyanidin | 1424.3201 | 1423.3123 | 711.1523 | | 75 | 60 | 29 | 1 | 0 | 0 | 1 |
| | B-type proanthocyanidin | 1426.3357 | 1425.3279 | 712.1601 | | 75 | 62 | 29 | 1 | 0 | 0 | 0 |
| | A-type procyanidin | 1436.2838 | 1435.2760 | 717.1341 | | 75 | 56 | 30 | 0 | 0 | 0 | 3 |
| | A-type procyanidin | 1438.2994 | 1437.2916 | 718.1419 | | 75 | 58 | 30 | 0 | 0 | 0 | 2 |
| | A-type procyanidin | 1440.3150 | 1439.3072 | 719.1497 | | 75 | 60 | 30 | 0 | 0 | 0 | 1 |
| | **B-type procyanidin** | **1442.3306** | **1441.3228** | **720.1575** | | **75** | **62** | **30** | **0** | **0** | **0** | **0** |
| | galloylated procyanidin | 1594.3414 | 1593.3336 | 796.1629 | | 82 | 66 | 34 | 0 | 0 | 1 | 0 |
| | B-type proanthocyanidin | 1458.3255 | 1457.3177 | 728.1550 | | 75 | 62 | 31 | 0 | 1 | 0 | 0 |
| hexamers | B-type proanthocyanidin | 1682.4089 | 1681.4011 | 840.1967 | | 90 | 74 | 33 | 3 | 0 | 0 | 0 |
| | A-type proanthocyanidin | 1696.3882 | 1695.3804 | 847.1863 | | 90 | 72 | 34 | 2 | 0 | 0 | 1 |


dx.doi.org/10.1021/jf501011y | J. Agric. Food Chem. 2014, 62, 9387−9400

Table 1. continued

| DP | proanthocyanidin | HRMW (Da) | HR $[M - H]^-$ ($m/z$) | HR $[M - 2H]^{2-}$ ($m/z$) | HR $[M - 3H]^{3-}$ ($m/z$) | C | H | O | EA/EF | EG | galloyl | A-bond |
|---|---|---|---|---|---|---|---|---|---|---|---|---|
| | B-type proanthocyanidin | 1698.4038 | 1697.3960 | 848.1941 | | 90 | 74 | 34 | 2 | 0 | 0 | 0 |
| | A-type proanthocyanidin | 1710.3675 | 1709.3597 | 854.1760 | | 90 | 70 | 35 | 1 | 0 | 0 | 2 |
| | A-type proanthocyanidin | 1712.3831 | 1711.3753 | 855.1838 | | 90 | 72 | 35 | 1 | 0 | 0 | 1 |
| | B-type proanthocyanidin | 1714.3987 | 1713.3909 | 856.1916 | 570.4584 | 90 | 74 | 35 | 1 | 0 | 0 | 0 |
| | A-type procyanidin | 1724.3468 | 1723.3390 | 861.1656 | 573.7745 | 90 | 68 | 36 | 0 | 0 | 0 | 3 |
| | A-type procyanidin | 1726.3624 | 1725.3546 | 862.1734 | 574.4463 | 90 | 70 | 36 | 0 | 0 | 0 | 2 |
| | A-type procyanidin | 1728.3780 | 1727.3702 | 863.1812 | 575.1182 | 90 | 72 | 36 | 0 | 0 | 0 | 1 |
| | **B-type procyanidin** | **1730.3936** | **1729.3858** | **864.1890** | **575.7901** | **90** | **74** | **36** | **0** | **0** | **0** | **0** |
| | galloylated procyanidin | 1882.4044 | 1881.3966 | 940.1944 | 626.4603 | 97 | 78 | 40 | 0 | 0 | 1 | 0 |
| | B-type proanthocyanidin | 1746.3885 | 1745.3807 | 872.1865 | 581.1217 | 90 | 74 | 37 | 0 | 1 | 0 | 0 |
| | galloylated proanthocyanidin | 1898.3993 | 1897.3915 | 948.1919 | 631.7920 | 97 | 78 | 41 | 0 | 1 | 1 | 0 |
| heptamers | A-type proanthocyanidin | 1980.4200 | 1979.4122 | 989.2022 | 659.1322 | 105 | 80 | 40 | 2 | 0 | 0 | 3 |
| | A-type proanthocyanidin | 1996.4149 | 1995.4071 | 997.1997 | 664.4638 | 105 | 80 | 41 | 1 | 0 | 0 | 3 |
| | B-type proanthocyanidin | 2002.4617 | 2001.4539 | 1000.2231 | 666.4794 | 105 | 86 | 41 | 1 | 0 | 0 | 0 |
| | A-type procyanidin | 2012.4098 | 2011.4020 | 1005.1971 | 669.7955 | 105 | 80 | 42 | 0 | 0 | 0 | 3 |
| | A-type procyanidin | 2014.4254 | 2013.4176 | 1006.2049 | 670.4673 | 105 | 82 | 42 | 0 | 0 | 0 | 2 |
| | A-type procyanidin | 2016.4410 | 2015.4332 | 1007.2127 | 671.1392 | 105 | 84 | 42 | 0 | 0 | 0 | 1 |
| | **B-type procyanidin** | **2018.4566** | **2017.4488** | **1008.2205** | **671.8111** | **105** | **86** | **42** | **0** | **0** | **0** | **0** |
| | galloylared procyanidin | 2170.4674 | 2169.4596 | 1084.2259 | 722.4813 | 112 | 90 | 46 | 0 | 0 | 1 | 0 |
| | A-type proanthocyanidin | 2032.4359 | 2031.4281 | 1015.2102 | 676.4708 | 105 | 84 | 43 | 0 | 1 | 0 | 1 |
| | B-type proanthocyanidin | 2034.4515 | 2033.4437 | 1016.2180 | 677.1427 | 105 | 86 | 43 | 0 | 1 | 0 | 0 |
| octamers | B-type proanthocyanidin | 2274.5298 | 2273.5220 | 1136.2571 | 757.1688 | 120 | 98 | 46 | 2 | 0 | 0 | 0 |
| | B-type proanthocyanidin | 2290.5247 | 2289.5169 | 1144.2546 | 762.5004 | 120 | 98 | 47 | 1 | 0 | 0 | 0 |
| | A-type procynidin | 2302.4884 | 2301.4806 | 1150.2364 | 766.4883 | 120 | 94 | 48 | 0 | 0 | 0 | 2 |
| | A-type procynidin | 2304.5040 | 2303.4962 | 1151.2442 | 767.1602 | 120 | 96 | 48 | 0 | 0 | 0 | 1 |
| | **B-type procynidin** | **2306.5196** | **2305.5118** | **1152.2520** | **767.8321** | **120** | **98** | **48** | **0** | **0** | **0** | **0** |
| | galloylated procyanidin | 2454.4992 | 2453.4914 | 1226.2418 | 817.1586 | 127 | 98 | 52 | 0 | 0 | 1 | 2 |
| | B-type proanthocyanidin | 2322.5145 | 2321.5067 | 1160.2495 | 773.1637 | 120 | 98 | 49 | 0 | 1 | 0 | 0 |
| nonamers | B-type proanthocyanidin | 2562.5928 | 2561.5850 | 1280.2886 | 853.1898 | 135 | 110 | 52 | 2 | 0 | 0 | 0 |
| | B-type proanthocyanidin | 2578.5877 | 2577.5799 | 1288.2861 | 858.5214 | 135 | 110 | 53 | 1 | 0 | 0 | 0 |
| | A-type procyanidin | 2592.5670 | 2591.5592 | 1295.2757 | 863.1812 | 135 | 108 | 54 | 0 | 0 | 0 | 1 |
| | **B-type procyanidin** | **2594.5826** | **2593.5748** | **1296.2835** | **863.8531** | **135** | **110** | **54** | **0** | **0** | **0** | **0** |
| | galloylated procyanidin | 2742.5622 | 2741.5544 | 1370.2733 | 913.1796 | 142 | 110 | 58 | 0 | 0 | 1 | 2 |
| | B-type proanthocyanidin | 2610.5775 | 2609.5697 | 1304.2810 | 869.1847 | 135 | 110 | 55 | 0 | 1 | 0 | 0 |
| decamers | B-type proanthocyanidin | 2850.6558 | 2849.6480 | 1424.3201 | 949.2108 | 150 | 122 | 58 | 2 | 0 | 0 | 0 |
| | B-type proanthocyanidin | 2866.6507 | 2865.6429 | 1432.3176 | 954.5424 | 150 | 122 | 59 | 1 | 0 | 0 | 0 |
| | A-type procyanidin | 2878.6144 | 2877.6066 | 1438.2994 | 958.5303 | 150 | 118 | 60 | 0 | 0 | 0 | 2 |
| | **B-type procyanidin** | **2882.6456** | **2881.6378** | **1440.3150** | **959.8741** | **150** | **122** | **60** | **0** | **0** | **0** | **0** |
| | galloylated procyanidin | **3030.6252** | **3029.6174** | 1514.3048 | 1009.2006 | 157 | 122 | 64 | 0 | 0 | 1 | 2 |
| | B-type proanthocyanidin | 2898.6405 | 2897.6327 | 1448.3125 | 965.2057 | 150 | 122 | 61 | 0 | 1 | 0 | 0 |
| | galloylated proanthocyanidin | **3050.6513** | **3049.6435** | 1524.3179 | 1015.8760 | 157 | 126 | 65 | 0 | 1 | 1 | 0 |

[a]Composition is used for the numbers of the atoms of carbon, hydrogen, and oxygen of the molecular formula and the numbers of the flavan-3-ol units, A-type bonds, and galloyls. Abbreviations: DP, degree of polymerization; G, galloyl; EC, EA, EG, epicatechin, epiafzelechin, and epigallocatechin, respectively; C, H, O, carbon, hydrogen, and oxygen.

## RESULTS AND DISCUSSION

**Exact Masses and Molecular Formula for Proanthocyanidins.** Chemically, each flavan-3-ol unit of a PA has two stereogenic (or chiral) centers (Figure 1), which can result in four (or $2^2$) stereoisomers, that is, (2*R*,3*S*)-catechin or (+)-C, (2*R*,3*R*)-epicatechin or (+)-EC, (2*S*,3*R*)-catechin, or (−)-C, and (2*S*,3*S*)-epicatechin or (−)-EC. In this paper, EC will be used to represent all four isomers in the text, tables, and figures. Similarly, the abbreviations for epiafzelechin (EA), epigallocatechin (EG), epifisetinidol (EF), and robinetinidol (ER) will be used to represent their isomers in PAs. In this paper, the PAs formed with only EA, EC, or EG units are called propelargonidin, procyanidin, or prodelpeinidin, whereas those formed from two different units are called proanthocyanidins.

The B-type PA dimers have two flavan-3-ol units (i.e., four chiral centers) and an additional asymmetric center at C4.


dx.doi.org/10.1021/jf501011y | J. Agric. Food Chem. 2014, 62, 9387−9400

**Table 2. Proanthocyanidins Found in Seven Samples**

| DP | proanthocyanidin | plant source[a] | HR [M − H]$^-$ ($m/z$) | mol formula | major MS$^2$ ions ($m/z$)(%) |
|---|---|---|---|---|---|
| monomer | epiazfelechin | L, C | 273.0761 | $C_{15}H_{13}O_5$ | 167(100) |
| | catechin | ALL | 289.0710 | $C_{15}H_{13}O_6$ | 245(100), 205(35), 179(12) |
| | epicatechin | ALL | 289.0714 | $C_{15}H_{13}O_6$ | 245(100), 205(33), 179(11) |
| | epigallocatechin | standard | 305.0665 | $C_{13}H_{13}O_7$ | 305(100), 221(19), 219(29), 179(20) |
| | epicatechin-3-gallate | G | 441.0827 | $C_{22}H_{17}O_{10}$ | 331(16), 289(100), 271(9), 169(20) |
| | catechin-3-gallate | G, M | 441.0827 | $C_{22}H_{17}O_{10}$ | 331(19), 289(100), 271(10), 193(6), 169(21) |
| | gallocatechin-3-gallate | standard | 457.0775 | $C_{22}H_{17}O_{11}$ | 331(67), 305(36), 287(10), 193(10), 169(100) |
| | epigallocatechin-3-gallate | M | 457.0779 | $C_{22}H_{17}O_{10}$ | 331(53), 305(38), 287(9), 269(7), 193(9), 169(100) |
| dimer | EA→EC(1) | M(2) | 561.1393 | $C_{30}H_{25}O_{11}$ | 543(34), 435(50), 425(19), 407(19), 289(100), 271(13), 245(7) |
| | EC→EA(1) | M(1) | 561.1380 | $C_{30}H_{25}O_{11}$ | 543(9)435(100), 409(64), 391(7), 299(44), 287(50), 273(57), 161(8) |
| | EF→EC(1) | G(2) | 561.1382 | $C_{30}H_{25}O_{11}$ | 451(40), 435(89), 423(100), 409(49), 325(17), 289(13), 271(26) |
| | EF→EC(2) | G(3) | 561.1383 | $C_{30}H_{25}O_{11}$ | 451(100), 435(78), 423(91), 409(56), 397(17), 299(25), 289(15), 271(48) |
| | EF→EC(3) | G(5) | 561.1389 | $C_{30}H_{25}O_{11}$ | 451(42), 435(100), 423(100), 409(39), 325(13), 289(15), 271(21) |
| | EC→A→EC(1) | A(2) | 575.1190 | $C_{30}H_{23}O_{12}$ | 539(23), 449(82), 423(100), 411(13), 407(19), 289(26), 285(18) |
| | EC→A→EC(2) | C(11), D(1), L(8), M(5) | 575.1181 | $C_{30}H_{23}O_{12}$ | 557(15), 539(30), 453(20), 452(16), 449(100), 447(20), 423(30), 407(20), 289(26), 287(16), 285(27) |
| | EC→A→EC(3) | C(1) | 575.1179 | $C_{30}H_{23}O_{12}$ | 449(27), 413(13), 395(88), 377(100), 333(21) |
| | EC→A→EC(4) | C(1) | 575.1202 | $C_{30}H_{23}O_{12}$ | 535(22), 509(47), 391(29), 347(100), 329(84), 285(22) |
| | EC→EC(1) | B(1), B(2), G(10), M(3), A(3) | 577.1345 | $C_{30}H_{25}O_{12}$ | 559(17), 451(37), 425(100), 407(53), 299(8), 289(26), 287(8) |
| | EC→EC(2) | G(3) | 577.1335 | $C_{30}H_{25}O_{12}$ | 559(57), 467(20), 451(100), 425(86), 407(59), 289(65) |
| | EC→EC(3) | D(1), M(1) | 577.1340 | $C_{30}H_{25}O_{12}$ | 559(75), 533(46), 451(29), 439(67), 425(75), 407(20), 393(100), 289(29), 269(35) |
| | EC→EC(4) | D(1), G(1), M(1) | 577.1335 | $C_{30}H_{25}O_{12}$ | 559(100), 533(31), 451(21), 439(34), 425(32), 407(18), 393(35) |
| | EC→EG(1) | G(1) | 593.1279 | $C_{30}H_{25}O_{13}$ | 575(13), 525(6), 467(24), 441(100), 427(6), 423(12), 305(16) |
| | (EC→EC)g(1) | G(5) | 729.1434 | $C_{37}H_{29}O_{16}$ | 603(14), 577(100), 559(46), 451(13), 425(20), 407(50) |
| | (EC→EC)g(2) | G(2) | 729.1435 | $C_{37}H_{29}O_{16}$ | 711(23), 603(45), 577(99), 559(88), 451(46), 441(42), 407(100), 289(19) |
| | (EC→EC)g(3) | G(1) | 729.1437 | $C_{37}H_{29}O_{16}$ | 711(35), 619(29), 603(100), 577(80), 559(51), 451(31), 441(29), 433(18), 407(28), 289(15), 245(17) |
| | (EC→EC)2g | G(2) | 881.1541 | $C_{44}H_{33}O_{20}$ | 729(100), 711(26), 559(20), 407(23) |
| trimer | EA→EA→EC(1) | M(1) | 833.2083 | $C_{45}H_{37}O_{16}$ | 816(23), 707(81), 561(91), 543(100), 435(23), 289(35) |
| | EA→A→EC→EC (1) | M(1), L(1) | 847.1853 | $C_{45}H_{37}O_{17}$ | 711(30), 693(12), 557(34), 435(37), 411(100), 289(13) |
| | EA→EC→EC(1) | M(5) | 849.2026 | $C_{45}H_{37}O_{17}$ | 723(31), 697(31), 577(100), 571(15), 559(51), 451(17), 425(28), 407(23),289(9), 287(15) |
| | EA→EC→EC(2) | G (4) | 849.2014 | $C_{45}H_{37}O_{17}$ | 831(94), 723(69), 697(26), 679(79), 561(100) |
| | EA→EC→EC(3) | M (2) | 849.2017 | $C_{45}H_{37}O_{17}$ | 831(45), 723(68), 697(16), 679(70), 561(38), 559(100), 433(36), 407(50), 289(19) |
| | EA→EC→EC(4) | M (2) | 849.2204 | $C_{45}H_{37}O_{17}$ | 723(100), 697(37), 679(49), 577(51), 571(39), 561(39), 451(43), 425(24), 407(37), 289(32) |
| | EA→EC→EC(5) | G(2) | 849.2010 | $C_{45}H_{37}O_{17}$ | 831(16), 723(30), 697(100), 679(71), 561(14), 545(12) |
| | EA→EC—EC(6) | G(2) | 849.2018 | $C_{45}H_{37}O_{17}$ | 831(100), 723(61), 679(35), 561(41) |
| | EF→EC→EC(7) | G(2) | 849.2010 | $C_{45}H_{37}O_{17}$ | 739(21), 697(100), 679(59), 559(67), 545(26), 527(16), 451(12), 407(11), 397(17), 289(13) |
| | EC→EC→A→EC (1) | L(3), M(6), C(1) | 863.1814 | $C_{45}H_{35}O_{18}$ | 737(72), 711(62), 693(42), 591(69), 575(100), 573(58), 449(34), 439(32), 289(89), 287(67) |
| | EC→EC→A→EC (2) | M(2) | 863.1823 | $C_{45}H_{35}O_{18}$ | 845(13), 737(19), 711(100), 693(41), 575(94), 573(15), 451(23), 411(17) |
| | EC→A→EC→EC (1) | C(2) | 863.1804 | $C_{45}H_{35}O_{18}$ | 737(8), 711(100), 693(8), 575(9), 573(41), 559(7), 531(10), 451(47), 411(43), 299(6), 289(19), 285(7) |
| | EC-(4$\beta$-8)-EC-(4$\beta$-8)-EC(2) | C(1), A(4) | 865.1971 | $C_{45}H_{37}O_{18}$ | 847(18), 749(48), 695(100), 577(68), 575(31), 425(27), 407(30) |
| | EC-(4$\beta$-8)-EC-(4$\beta$-8)-EC(2) | M(12), G(10), J(7), D(3), L(2) | 865.1971 | $C_{45}H_{37}O_{18}$ | 847(18), 749(48), 695(100), 577(68), 575(31), 425(27), 407(30) |
| | EC→EC→EC(3) | M(4), G(1), A(2), D (2) | 865.1961 | $C_{45}H_{37}O_{18}$ | 847(40), 779(51), 739(56), 713(57), 695(68), 577(89), 575(100), 449(22), 407(35), 289(27), 287(24) |
| | EC→EC→EC(4) | M(1) | 865.1939 | $C_{45}H_{37}O_{18}$ | 801(41), 789(49), 779(100), 720(70), 695(51), 577(74), 575(55) |
| | EC→EC→EC(5) | J(2), D(2) | 865.1955 | $C_{45}H_{37}O_{18}$ | 847(38), 739(100), 713(58), 695(87), 577(64), 575(35), 451(37), 449(26), 407(30), 287(29) |

**Table 2. continued**

| DP | proanthocyanidin | plant source[a] | HR [M − H]$^-$ ($m/z$) | mol formula | major MS$^2$ ions ($m/z$)(%) |
|---|---|---|---|---|---|
| | (EC→EC→EC)g(1) | G(4) | 1017.2069 | $C_{52}H_{41}O_{22}$ | 999(31), 891(47), 865(40), 847(57), 739(19), 729(100), 727(23), 695(28), 677(32), 575(20) |
| | (EC→EC→EC)g(2) | G(1) | 1017.2054 | $C_{52}H_{41}O_{22}$ | 999(100), 891(48), 865(50), 847(62), 729(40), 695(39), 677(25) |
| | (EC→EC→EC)g(3) | G(2) | 1017.2054 | $C_{52}H_{41}O_{22}$ | 999(19), 891(54), 865(33), 847(100), 729(83) |
| | (EC→EC→EC)g(4) | G(3) | 1017.2056 | $C_{52}H_{41}O_{22}$ | 999(20), 891(24), 865(100), 847(53), 727(24), 695(24) |
| | (EC→EC→EC)→2g (1) | G(1) | 1169.2184 | $C_{59}H_{45}O_{26}$ | not recorded |
| tetramer | EC→EA→A→EC →EC(1) | L(1) | 1135.2472 | $C_{60}H_{47}O_{23}$ | 983(36), 965(22), 847(100), 845(30), 829(11), 693(26), 557(22), 411(15) |
| | EA→EC→EC→EC (1) | M(3) | 1137.2649 | $C_{60}H_{49}O_{23}$ | 1119(42), 1011(59), 865(100), 847(51), 739(26), 577(46), 559(33), 407(26) |
| | EA→EC→EC→EC (2) | M(3) | 1137.2666 | $C_{60}H_{49}O_{23}$ | 1119(42), 1011(67), 985(35), 967(85), 849(87), 847(100), 723(36), 575(32), 561(32) |
| | HA→EC→HC→EC (3) | M(1) | 1137.2651 | $C_{60}H_{49}O_{23}$ | 1119(32), 1011(56), 985(41), 967(62), 849(74), 847(88), 577(100), 559(58), 407(50) |
| | EC→A→EC→E-C→A→EC(1) | L(2), C(1) | 1149.2268 | $C_{60}H_{45}O_{24}$ | 997(58), 997(19), 979(34), 845(43), 737(22), 575(100), 573(85), 411(85) |
| | EC→A→EC→E-C→A→EC(2) | L(1) | 1149.2285 | $C_{60}H_{45}O_{24}$ | 1131(20), 997(75), 979(35), 845(24), 737(17), 575(80), 573(75), 411(100) |
| | EC→EC→A→E-C→EC(1) | L(3) | 1151.2423 | $C_{60}H_{47}O_{24}$ | 1133(14), 1025(41), 999(45), 981(87), 863(100), 861(45), 711(32), 573(41), 411(34) |
| | EC→A→EC→E-C→EC(2) | L(2), C(1) | 1151.2419 | $C_{60}H_{47}O_{24}$ | 1005(32), 999(48),981(48), 861(100), 739(68), 573(58), 611(61), 407(35) |
| | EC→A→EC→E-C→EC(3) | L(1) | 1151.2419 | $C_{60}H_{47}O_{24}$ | 1133(32), 999(81), 981(70), 863(43), 861(84), 739(100), 699(38), 577(72), 573(49), 411(39), 407(43) |
| | EC→A→EC→E-C→EC(3) | L(1) | 1151.2421 | $C_{60}H_{47}O_{24}$ | 1133(45), 999(100), 981(48), 863(35), 861(90), 739(83), 587(39), 577(45), 573(59), 411(87), 407(38) |
| | EC→EC→E-C→A→EC(4) | L(1) | 1151.2416 | $C_{60}H_{4}9O_{24}$ | 999(78), 981(100), 863(86), 861(76), 739(70), 709(35), 577(38), 573(57), 531(38), 451(30),411(38) |
| | EC→EC→EC→. A→EC(5) | L(1) | 1151.2419 | $C_{60}H_{47}O_{24}$ | 1133(33), 1067(12), 1025(49), 999(21), 981(100), 863(57), 739(12), 737(15), 711(30), 575(48) |
| | EC→EC→EC→EC (1) | J(12), G(3), M(3), A (1), D(2) | 1153.2571 | $C_{60}H_{49}O_{24}$ | 1135(54), 1027(74), 1002(42), 983(100), 907(21), 865(63), 863(62), 739(35), 695(32), 577(40), 407(21) |
| | EC→EC→EC→EC (2) | D(2), J(2), M(2), G (2) | 1153.2565 | $C_{60}H_{49}O_{24}$ | 1135(55), 1027(52), 1027(23), 1001(59), 983(96), 865(100), 863(48) , 695(21), 577(46), 575(54) |
| | EC→EC→EC→EC (3) | J(2) | 1153.2582 | $C_{60}H_{49}O_{24}$ | 1135(53), 1027(41), 1001(100), 984(71), 865(79), 863(94), 847(26), 739(50), 701(35), 577(44), 575(65) |
| | EC→EC→EC→EC (4) | J(2) | 1153.2577 | $C_{60}H_{49}O_{24}$ | 1135(55), 1027(64), 1001(50), 983(77), 907(41), 865(50), 863(100), 701(32), 577(55), 575(73), 407(27) |
| | EC→EC→EC→EC (5) | J(1) | 1153.2577 | $C_{60}H_{49}O_{24}$ | 1135(89), 1027(78), 1001(56), 983(44), 907(44), 865(44), 863(44), 739(67), 701(67), 577(33), 575(100) |
| | EC→EC→EC→EC (6) | J(2), A(1), D(1) | 1153.2590 | $C_{60}H_{49}O_{24}$ | 1135(48),1027(100), 1001(30), 983(83), 965(16), 908(36), 865(52), 739(55), 695(26), 575(31) |
| | EC→EC→EC→EC (7) | A(1) | 1153.2590 | $C_{60}H_{49}O_{24}$ | 1135(100), 1028(72), 983(50), 865(50), 739(39), 737(33) |
| pentamer | EC→EC→EC→E-C→A→EC(1) | L(2) | 1439.3058 | $C_{75}H_{59}O_{30}$ | 1421(50), 1313(50), 1295(50), 1149(90), 1007(50), 863(100), 861(50) |
| | EC→EC→EC→E-C→EC(2) | L(1) | 1439.3058 | $C_{75}H_{59}O_{30}$ | 1421(67), 1287(100), 1151(67), 1113(33), 863(100), 753(100), 711(67), 637(33), 411(33) |
| | EC→EC→EC→E-C→EC(3) | L(1) | 1439.3058 | $C_{75}H_{59}O_{30}$ | 1379(100), 1353(75), 1313(75), 1269(50), 1131(50), 1111(50), 863(75), 857(50), 751 (25) |
| | EC→EC→EC→E-C→EC(4) | L(1) | 1439.3058 | $C_{75}H_{59}O_{30}$ | 1421(100), 1089(33), 1013(67), 997(33), 863(67), 711(33), 589(33), 587(67), 575(33), 531(67) |
| | EC→EC→EC→E-C→A→EC(5) | L(1) | 1439.3058 | $C_{75}H_{59}O_{30}$ | 1421(33), 1395(33), 1285(33), 981(100), 863(50), 665 (50), 445(33) |
| | EC→EC→EC→E-C→A→EC(6) | L(2) | 1439.3058 | $C_{75}H_{59}O_{30}$ | 1314(17), 1269(100), 1149(17), 1117(33), 863(67), 817(17), 737(17) , 709(17), 575(17), 453(33) |
| | EC→EC→EC→E-C→EC(7) | L(1) | 1439.3058 | $C_{75}H_{59}O_{30}$ | 1441(14), 1421(43), 1269(100), 1151(14), 1107(14), 957(14), 955(29), 863(43), 829(14), 573(14), 531(14) |
| | EC→EC→A→E-C→EC→EC(S) | L(1) | 1439.3058 | $C_{75}H_{59}O_{30}$ | 1371(50), 1269(50), 1143(50), 987(50), 861(50), 711(100), 671(50), 585(50), 575(50), 573(90), 411(50) |
| | EC→EC→EC→E-C→EC(1) | M(1) | 1441.3229 | $C_{75}H_{61}O_{30}$ | 1421(100), 1315(64), 1271(67), 1153(74), 1153(33), 1151(48), 1027(38), 865(86), 863(43),739(36), 575(36) |

[a]Abbreviations: A, apple; C, cranberry extract; D, dark chocolate; G, grape seed extract; J, jujube; L, litchi; M, mangosteen; AL, all tested plants (the number of similar peaks in the sample is listed in parentheses); $B_1$, $B_2$, $A_2$, and $C_1$, procyanidin B-type dimers $B_1$, $B_2$, A-type dimers $A_2$, and trimer $C_1$;

**Table 2. continued**

DP, degree of polymerization; g, galloyl; EC, EA, EG, and EF, epicatechin, epiafzelechin, epigallocatechin, and epifisetinidol, respectively. The signal $unit_1 \rightarrow unit_2$ or $unit_1 \rightarrow A \rightarrow unit_2$ expresses the units bonded by B-type (4,8- or 4,6-) bond or A-type (plus additional $C_2-O-C_7-$ or $C_2-O-C_5-$) bond, respectively.

Thus, it is possible for them to be connected in two ways, through a $C_4-C_8$ or $C_4-C_6$ linkage, providing 64 (i.e., $2^6$) possible isomers.[1−4,10−23] The formation of B-type trimers and tetramers leads to an exponential increase in the possible number of isomers, which makes the separation and quantification of such complex PA isomers an enormous challenge.[1−4]

UHPLC columns (with 1.9 $\mu$m or smaller particles) provide much better separation of the PA isomers than HPLC columns.[1,20−23] In addition, the molecular ions detected by HRMS provide high-resolution molecular weight (HRMW) and exact molecular formula (MF). The HRMW, MF, and singly and multiply charged ions for different PAs are related to the DP, the flavan-3-ols (EC, EA, EF, EG, and ER) in the oligomer, the number of galloyls, and the number of type A bonds as described in the equations

$$\begin{aligned} \mathrm{HRMW} = {} & 12.0000 \times (15n + 7c) + 1.0078 \\ & \times (12n + 2 + 4c - 2d) + 15.9949 \\ & \times (6n + 4b - a + b) \end{aligned} \quad (1)$$

$$\mathrm{MF} = C_{15n+7c}H_{12n+2+4c-2d}O_{6n-a+b+4c} \quad (2)$$

$$\begin{aligned} [\mathrm{M} - \mathrm{H}]^- = {} & 12.0000 \times (15n + 7c) + 1.0078 \\ & \times (12n + 1 + 4c - 2d) + 15.9949 \\ & \times (6n + 4c - a + b) \end{aligned} \quad (3)$$

$$[\mathrm{M} - 2\mathrm{H}]^{2-} = (\mathrm{HRMW} - 2 \times 1.0078)/2 \quad (4)$$

$$[\mathrm{M} - 3\mathrm{H}]^{3-} = (\mathrm{HRMW} - 3 \times 1.0078)/3 \quad (5)$$

where $n$ = degree of polymerization, $a$ = number of ECs that were replaced by EAs or EFs (as regioisomers), $b$ = number of ECs replaced by EGs, $c$ = number of galloyls, and $d$ = number of A-type bonds; 12.0000, 1.0078, and 15.9949 are the accurate masses of carbon, hydrogen, and oxygen, and 15, 12, and 6, and 7, 4, and 4 are the numbers of carbon, hydrogen, and oxygen atoms for each EC (or its regioisomer ER) and galloyl unit, respectively. The equations can be easily modified to accommodate the PAs that contain acyl, glycosyl, or phloroglucinol adducts.[1,19]

Low-resolution ions are usually expressed to two decimal places in most cases and can be obtained directly from the high-resolution $[M - H]^-$ values. Formulas have been described for computing the PA molecular ion metal adduct values (in low resolution) from MALDI-TOF-MS, but the PA mass values can be obtained only after the mass of the metal has been subtracted.[11−13,20] Thus, eqs 1−5, for PA mass, are easier to use.

Table 1 presents the HRMW and deprotonated molecule ($[M - H]^-$) ($m/z$) for most of the PAs (DP = 2−10) detected in common foods in this laboratory and described in the literature.[1,4] For each oligomer, the nongalloylated B-type procyanidins (in bold) have the simplest formulas ($a = b = c = d = 0$), indicating that the PAs have no EC units replaced by EA, EF, or EG and do not contain any galloyls and A-type bonds. To be as systematic as possible, for each oligomer class, the related propelargonidins and proanthocyanidin-containing EA units are listed above the procyanidins, whereas the related prodelphinidins containing EG units are listed below the procyanidins. Similarly, all of the A-type PAs for each oligomer are listed above the B-type PAs and the galloylated PAs are listed below.

The data in Table 1, calculated from eqs 1−5, were found to agree well with experimentally determined $[M - H]^-$ values with an error of <3 ppm in most cases. Consequently, Table 1 can be used to provide the PA structure based on experimental high-resolution $[M - H]^-$ values. For example, trace ions recorded in grape seed extract were easily identified as galloylated procyanidin tetramers (1305.2698, error < 3 ppm), pentamers (1441.3250), hexamers (1729.3898), and their gallates (1593.3354 and 1881.4033). Thus, a detailed analysis of plant PAs can be achieved easily without using purified PA or PA-enriched samples.

The data in Table 1 permit a detailed PA oligomeric profile of a sample to be obtained from a single chromatogram using HRMS. Although identification of specific PAs based on the recorded HR $[M - H]^-$ values is putative, they are all correctly identified as PAs. It should be noted that nominal MS (typically masses to two decimal places) cannot positively identify them as PAs. The data in Table 1 also provide the opportunity to fully identify interesting or minor PAs (i.e., to specify the flavan-3-ol units and their connectivity) by selecting specific ions for fragmentation as described below.

**Identification of Proanthocyanidins in Foods.** The UHPLC-PDA-ESI-HRMS$^n$ profiling method provides retention time, UV, $[M - H]^-$, and $MS^{2-5}$ product ions for the PAs. Consideration of the product ions, especially $MS^2$ ions, permits easy putative identification of PAs. Table 2 lists 247 proanthocyanidins in 90 isomeric groups from 7 food materials, their plant sources, single-parent ions, formulas, and diagnostic and main $MS^2$ productions. The number of the isomers identified in each sample is in parentheses following the plant name. Approximately 130 of the PAs were detected in the grape seed and mangosteen extracts, and the rest were detected in the other five samples (Fuji apples, cranberry extract, dark chocolate, jujube, and litchi). Many of the PAs were detected in these plants for the first time.

It was noted that catechin and epicatechin showed the same product ions and very similar ratios at $MS^2$ [245 (100%), 205 (35%), and 179 (11−12%)], $MS^3$ [227 (28−30%), 203 (100), and 187 (20−25%)], and even at $MS^4$ [185, (20−37%), 175 (100%), 161 (28−42%)]. Similarly, dimeric procyanidins $B_1$ (EC-4$\beta$-8-C) and $B_2$ (EC-4$\beta$-8-EC) have very similar $MS^2$ [451 (27−37%), 425 (100%), 407 (41−47%), 289 (17−26%), and 287 (7−8%)], $MS^3$ [407 (100%) and 273 (6−8%)], $MS^4$ [285 (100%), 283 (36−43%), 389 (29−36%), 297 (27−37%), and 255 (17−27%)] and $MS^5$ [257 (100%) and 213 (4−7%)] fragments.

These data indicate that the slight differences in the relative ratio among the fragments might be caused by the stereochemistry of the monomers. However, there are insufficient data to predict the effect of the linkages and the positions of the PA flavan-3-ol units on product ion formation and relative abundance. At present, LC-MS$^n$ methods are not able to

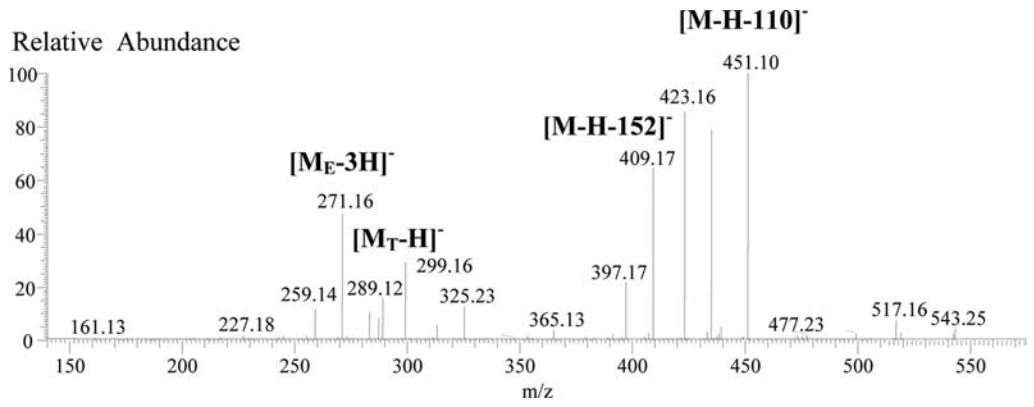


**Figure 2.** $MS^2$ spectrum of the EF−EC dimer with retention time at 26.98 min.

discriminate between the regioisomeric forms of the PAs or the related stereoisomeric forms.

As shown in Figure 1, the most important $MS^2$ fragments of B- and A-type PA dimers are formed by quinone methide (QM) fission, that is, breaking of the interflavan bond between the monomers to form $[M_T - H]^-$ and $[M_E - 3H]^-$ ions for B-type PAs and $[M_E - 5H]^-$ ions for A-type PAs, where E = extension unit and T = terminal unit. Other typical PA fragments were formed by retro-Diels−Alder (RDA) fission (loss of the whole B-ring with $C_2$−$C_3$ part of the C-ring, i.e., loss of 152, 136, and 168 Da for EC, EA, and EG, respectively) and by heterocyclic ring fission (HRF) of the extension unit (loss of the A-ring, i.e., loss of 126 Da for EC, EA, or EG and loss of 110 Da for EF or ER). Product ions formed by the loss of water (−18 Da), O (−16 Da), CO (−28 Da), HC≡CH (−26 Da), HC≡COH (−42 Da), and HC≡CH—CO (−54 Da) were also observed.[4,13,14,19−23,27] For PAs with DP ≥ 3, further fragmentation can occur from repeated QM breaks of interflavan bonds connecting the flavan-3-ols of the extension units. These product ions were also frequently used to identify the PAs. Information obtained from the analysis of thiolytic degradation products of the PAs from similar plants has proven useful for the identification of PAs.[1,4,13,14,19−23,27−30]

In this study, 247 PAs were identified in 7 tested materials (Table 2) using only the most intense ions among the coeluted ions (each peak) as the target ions. However, the identified PAs can be enhanced by selecting more target ions, such as the second and third most intense ions of each peak. The PAs are denoted as combinations of EC, EA, EG, and EF, and A-type bonds are designated by placing an "-A-" between the flavan-3-ols. Although there are numerous isomers in each oligomeric class, only one isomer was selected to represent all of the remaining isomers (each having the same $MS^2$ base and main fragments). There was no correlation between the PAs found in the different samples. Positive identification was achieved for only some of the PAs in Table 2 based on direct comparison to reference PAs (procyanidins $B_1$, $B_2$, $C_1$, $A_2$) or PAs positively identified in other studies.[1,4]

Procyanidins with DP = 2−5 have been previously reported in common foods.[4,19−23,27] Consequently, special attention was paid to PAs containing different flavan-3-ol units or A-type bonds because these features lead to more regioisomers. For example, 13 PA dimers ($[M - H]^-$ at 561.1388) contained two different flavan-3-ols. One of the three detected in mangosteen had $MS^2$ fragments at $m/z$ 435 (−126 Da, HRF from EA or EC), 409 (−152 Da, RDA from EA or EC), 287 ($[M_E - 3H]^-$), and 273 ($[M_T - H]^-$), suggesting it to be EC-EA, a PA dimer containing an EA unit as the terminal unit. The other two in mangosteen had $MS^2$ fragments at $m/z$ 289 ($[M_T - H]^-$, 100%), 435 (−126 Da), 425 (−136 Da), 407 [−(136 + 18) Da), and 271 ($[M_E - 3H]^-$), corresponding to EA-EC, the isomers containing EA as extension unit (Figure 1).

Another 10 interesting dimers were detected in grape seed extract. Three had $MS^2$ fragments at $m/z$ 451 (HRF loss of 110 Da, $C_6H_6O_2$ for the deoxy-A-ring of EF or ER, 100%), 423 [−(110 +28), 91−98%], 409 (−152 Da, RDA loss, 29−60%), 289 ($[M_T - H]^-$, 12−18%), and 271($[M_E - 3H]^-$, 20−48%) (Figure 2). Five had the same $MS^2$ fragments but with different intensities; one at $m/z$ 423 (100%), 451 (around 50%), 409 (28−64%), 289, and 271. The remaining two had $MS^2$ fragments at $m/z$ 435 (100) and 451 (40−50%). These fragments suggested that all might be proanthocyanidin dimeric isomers (EF-EC). To date, the PAs containing an EF unit have only been reported to exist in plant woods, such as quebracho (*Schinopsis balansae* var. *chaqueno*) wood, but rarely in common foods, such as grapes.[1,28−31]

A PA dimer ($[M - H]^-$ at 593.1279 Da) detected in grape seed extract had mass fragments at $m/z$ 441 (−152, RDA) and 305 ($[M_T - H]^-$), suggesting it was an EC-EG isomer. A PA trimer containing two EAs ($[M - H]^-$ at $m/z$ 833.2083) was found in mangosteen with $MS^2$ fragments at $m/z$ 543 (100%, $[M_E - 3H]^-$), 707, and 289 ($[M_T - H]^-$) and $MS^3$ fragments at $m/z$ 271 (100%, the second $[M_E - 3H]^-$), 417, and 407, indicating that two EA units were formed the extension units and that the EC was the terminal unit. Two PA trimers found in mangostenn and litchi with $[M - H]^-$ of 847.1860 Da had one A-type bond, $MS^2$ fragments at $m/z$ 557, 411, and 289, and a $MS^3$ base fragment at $m/z$ 285. This suggested that EA was the extension unit with the A-type bond connected to one of the two ECs and that the remaining EC was the terminal unit.

Nineteen PA trimers (9 in mangosteen and 10 in grape seed extract) had $[M - H]^-$ fragments at 849.2030 Da indicating EA or its constitutional isomer EF. Of these, 5 had $MS^2$ fragments at 577 (−272 Da, 100%) and 559 (−290 Da around 40−50%), 1 had $MS^2$ fragments at $m/z$ 561 (−288 Da), and the others had $MS^2$ fragments at 559 (−290 Da), 723 (−126 Da), 697 (−152 Da), and 831 (−18 Da). All of these PAs might be EA-EC-EC isomers. The two detected in grape seed extract (expressed as EF-EC-EF in the last line for this oligomeric class) had a $MS^2$ fragment at $m/z$ 739 (−110 Da, ∼20%) and might have EF instead of EA as the extension unit.

Fourteen procyanidin trimers ($[M - H]^-$ at 863.1800 Da) contained one A-type bond. Ten of them (6 from mangosteen, 3 from litchi, and 1 from cranberry) had $MS^2$ fragments at $m/z$


dx.doi.org/10.1021/jf501011y | J. Agric. Food Chem. 2014, 62, 9387−9400

**Table 3. Doubly and Triply Charged Proanthocyanidins Found in Mangosteen and Litchi**

| proanthocyanidin | HRMS (Da) | HR $[M - 2H]^{2-}$ ($m/z$) | $^{12}C$ isotope ($m/z$) | $^{13}C$ isotope ($m/z$) | plant source[a] (no. of PAs) |
|---|---|---|---|---|---|
| A-type procyanidin pentamers with two A-bonds | 1438.2994 | 718.1419 | 718.1417 | 718.6428 | L(2) |
| A-type procyanidin pentamers with one A-bond | 1440.3150 | 719.1497 | 719.1494 | 719.6509 | M(1), L(1) |
| B-type procyanidin pentamers | 1442.3306 | 720.1575 | 720.1566 | 720.6591 | M(5) |
| B-type proanthocyanidin hexamers with two EA units | 1698.4038 | 848.1941 | 848.1951 | 848.6995 | M(2) |
| B-type proanthocyanidin hexamers with one EA unit | 1714.3987 | 856.1916 | 856.1921 | 856.6930 | M(6) |
| A-type procyanidin hexamers with two A-bond | 1726.3624 | 862.1734 | 862.1740 | 862.6748 | L(2) |
| B-type procyanidin hexamers | 1730.3936 | 864.1890 | 864.1893 | 864.6890 | M(3) |
| B-type proanthocyanidin heptamers with one EA units | 2002.4617 | 1000.2231 | 1000.2235 | 1000.7247 | M(1) |
| A-type procyanidin heptamers with two A-bond | 2014.4254 | 1006.2049 | 1006.0000 | 1006.7057 | L(1) |
| A-type procyanidin heptamers with one A-bond | 2016.4410 | 1007.2127 | 1007.2120 | 1007.7230 | M(1), L(1) |
| B-type procyanidin heptamers | 2018.4566 | 1008.2205 | 1008.2223 | 1008.7228 | M(6) |
| B-type proanthocyanidin octamers with two EA units | 2274.5298 | 1136.2571 | 1136.2540 | 1136.7643 | M(2) |
| B-type procynidin octamers | 2306.5196 | 1152.2520 | 1152.2527 | 1152.7537 | M(7) |
| B-type proanthocyanidin nonamers with one EA unit | 2578.5877 | 1288.2861 | 1288.2840 | 1288.7855 | M(1) |
| B-type procyanidin nonamers | 2594.5826 | 1296.2835 | 1296.2828 | 1296.7859 | M(1) |
| B-type proanthocyanidin decamers with two EA units | 2850.6558 | 1424.3201 | 1424.3212 | 1424.8262 | M(1) |
| B-type proanthocyanidin decaamers | 2866.6507 | 1432.3176 | 1432.3185 | 1432.8220 | M(1) |
| A-type procyanidin decamers with two A-bond | 2878.6144 | 1438.2994 | 1438.2985 | 1438.7967 | M(1) |
| B-type procyanidin decamers | 2882.6456 | 1440.3150 | 1440.3169 | 1440.8147 | M(1) |
| | HR $[M - 3H]^{3-}$ $m/z$ | | $^{12}C$ isotope $m/z$ | $^{13}C$ isotope $m/z$ | |
| B-type procyanidn decamers | 959.8741 | | 959.8727 | 960.2103 | M(4) |

[a]Abbreviations: L, litchi; M, mangosteen (number of similar peaks in the sample is listed in parentheses). The value was taken from one of the PA and close to those of the remaining ones.

575 (−288 Da, 21−100%), 711 (42−100%), and 289 (20−89%), indicating they were EC-EC-A-EC isomers. Others (two from litchi and two from cranberry) had $MS^2$ fragments at $m/z$ 573 (−290 Da, 35−62%), 411 (43−100%), and 711 (91−100%) to suggest they were EC-A-EC-EC isomers.

One A-type PA tetramer in litchi ($[M - H]^-$ at 1135.2472) contained one EA and one A-type bond and had $MS^2$ fragments at $m/z$ 847 (−288 Da, 100%), 983 (−152 Da, 36%), 845 (−290 Da, −30%), 693 [−(152 + 290) Da, 26%], and 557 [−(288 + 290) Da, 22%]. This suggested it might be an EC-EA-A-EC-EC or EC-EC-A-EA-EC isomer.

Seven PA tetramers in mangosteen ($[M - H]^-$ at 1137.2450) contained one EA. Three had $MS^2$ fragments at $m/z$ 865 (−272 Da, 100%), 847 (−290 Da, 30%), and 577 [−(288 + 272) Da, 46%]. Another three had $MS^2$ fragments at $m/z$ 847 (−290 Da, 100%) and 575 [−(288 + 274 or 290 + 272) Da]. The remaining tetramer had $MS^2$ fragments at $m/z$ 1011, 985, 967, 849 (−288 Da), 847, and 577 [−(290 + 274) Da]. These fragments indicated EA was a part of the extension unit with two ECs and might be the final extension unit.

Four procyanidin tetramers (three from Litchi and one from cranberry) with $[M - H]^-$ at 1149.2280 had two A-type bonds and $MS^2$ fragment at $m/z$ 575 (80−100%) {−(288 + 286) Da for $[M_T - H]^-$} and 573 (75−85%) {−(2 +286 × 2) Da for $[M_E - 3H]^-$}, indicating that the A-type bonds were between the first and second and between the third and fourth flavan-3-ols. Ten procyanidin tetramers (9 from Litchi and 1 from cranberry) with $[M - H]^-$ at 1151.2415 had one A-type bond. Three (group 1) had $MS^2$ fragments at $m/z$ 863 (100%) (−288 Da for $[M_E - 3H]^-$) and 573 (41%) indicating the A-type bond was between the second and third flavan-3-ols. Five (groups 2−4) had $MS^2$ fragments at $m/z$ 861 (84−100%) (−290 Da for $[M_T - H]^-$) and 573 (49−59%) {−(2 +286 × 2) Da for $[M_E - 3H]^-$} indicating an A-type bond between the first and second flavan-3-ols. Two (groups 4 and 5) had $MS^2$ fragments at $m/z$ 863 (57−86%), 575 (48%) {−(288 + 286) Da for $[M_T - H]^-$ }, or 577 (38%) and 573 (57%) indicating an A-type bond between the third and fourth flavan-3-ols.[14,19] Similarly, the PA pentamers in eight groups (1−8) have one A-type bond, and the PAs of the first six groups (1−6) showed main fragment at $m/z$ 863 (50−100%), indicating the A-type bond between the fourth and fifth flavan-3-ols. The PS of the last group (8) showed the main fragment at $m/z$ 861 (50%), indicating the A-type bond between second and third flavan-3-ols, whereas the remaining one in group 7 showed fragments at $m/z$ 863 and 573 to suggest that this compound might have its A-type bond between the third and fourth flavan-3-ols.[14]

Ten galloylated dimers and 11 trimers were detected in grape seed extract. The existence of a galloyl connected to a PA with DP ≥ 2 provides the possibility of forming regioisomers; for example, EC-ECg and ECg-EC and EC-EC-ECg, EC-ECg-EC, and ECg- EC-EC. Unfortunately, the ECg position cannot be deduced from the mass fragments because gallate was very easy to lose. Thus, they were expressed as (EC-EC)g or (EC-EC-EC)g, respectively.

Jujube fruit was analyzed because PAs (DP = 2, 3, 5, and 7) consisting of both EA and EG have been isolated from jujube leaves and bark.[32] These PAs have the same molecular weight and formula as those of their related procyanidins, but can be easily distinguished from the procyanidins by the noticeable difference in their fragments. For example, the dimers of EA and EG will have QM (271 and 305 Da for EA-EG or 303 and 273 Da for EG-EA) and RDA fragments formed by the loss of 136 Da from EA and 168 Da from EG, whereas the related procyanidin dimers should have QM (289 and 287 Da) and RDA fragments formed by the loss of 152 Da. A careful check confirmed that all 30 of the detected PAs in jujube consisted of EC units only.

**Identification of Highly Polymerized PAs Based on the Doubly and Triply Charged Molecular Ions.** Negative


dx.doi.org/10.1021/jf501011y | J. Agric. Food Chem. 2014, 62, 9387−9400

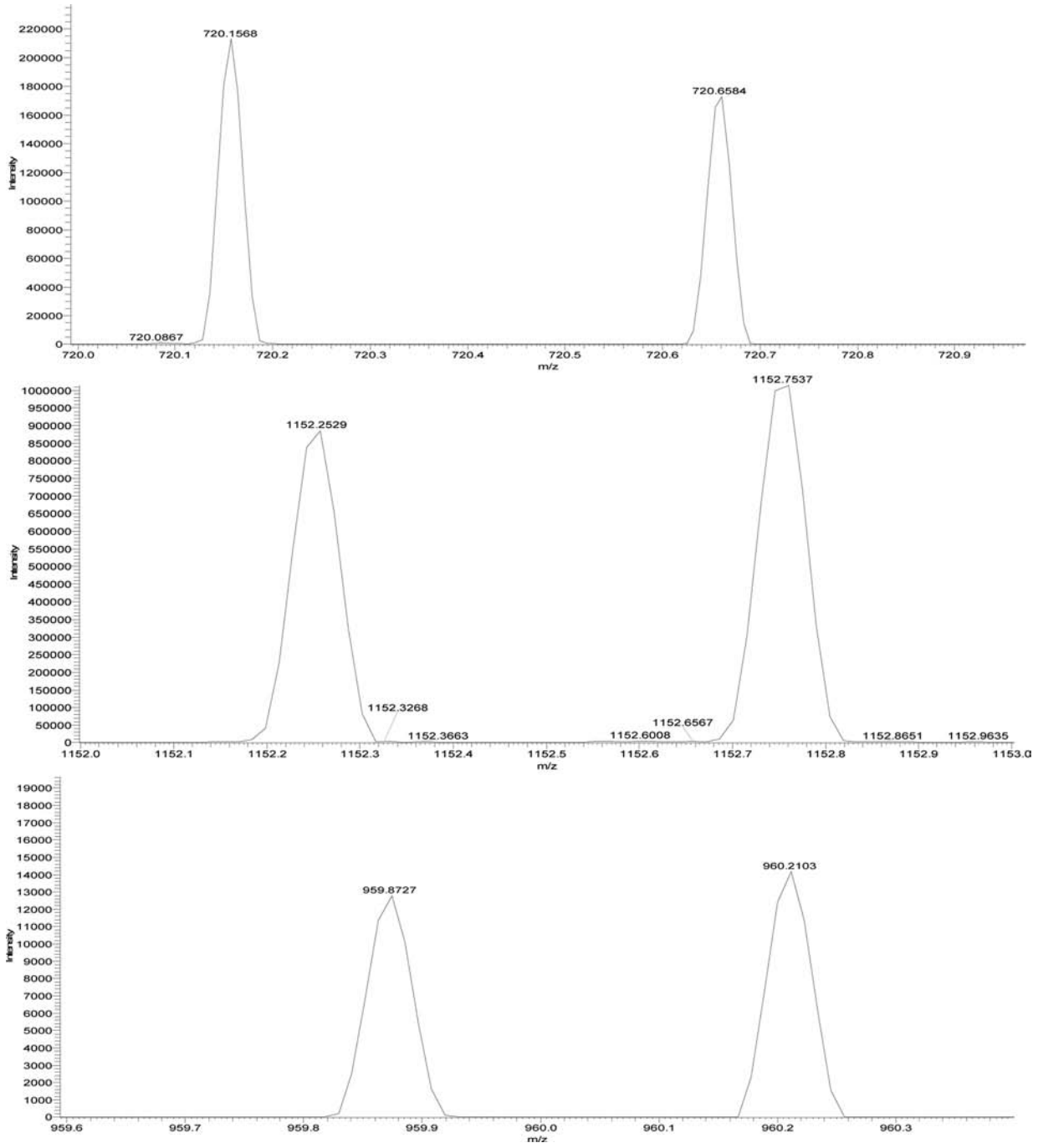


**Figure 3.** Accurate $^{12}C$ and $^{13}C$ isotope ion peaks for $[M - 2H]^{2-}$ of $m/z$ 720 and 1152 and for $[M - 3H]^{3-}$ of $m/z$ 960.

ionization of many highly polymerized PAs (DP ≥ 5) produces multiply (mainly doubly and triply) charged molecular ions. To date, several dozen multiply charged molecular ions have been reported and used to identify PAs with DP = 7−25.[1,4,13−19] With nominal resolution MS, these ions were recognized as doubly or triply charged molecules on the basis of the distance between the $^{12}C$ and $^{13}C$ isotope ions. As the charge increases from 1 to 2 to 3, the distance between the isotopes will decrease from 1 to 0.5 to 0.33 amu.[17,18] It was noted that the ion masses for PA isotopes were always slightly different.[1,4,13−20] This was attributed to the differences in the relative abundances of the $^{12}C$ and $^{13}C$ isotopes.

Table 1 contains the accurate $[M - 2H]^{2-}$ and $[M - 3H]^{3-}$ values for PAs with DP = 5−10, which matched the $[M - 2H]^{2-}$ or $[M - 3H]^{3-}$ of around 50 proanthocyanidins detected in mangosteen and litchi extracts (Table 3). The $^{12}C$ and $^{13}C$ isotope ions of each proanthocyanidin were easily found by examining the distance between the two isotopic ion peaks. For example, in mangosteen the main $[M - 2H]^{2-}$ ions were found at $m/z$ 720.1566, 856.1928, 864.1863, 1000.2235, 1008.7217, and 1152.7537 (Figure 3; Tables 1 and 3). The first four values were taken from the $^{12}C$ isotope ion and perfectly matched (error < 3 ppm) the listed $[M - 2H]^{2-}$ data in Table 1 for the B-type procyanidin pentamer and hexamer, the B-type propelargonidin hexamer containing one EA unit, and the B-type propelargonidin heptamer containing two EAs. The values of the $^{13}C$ isotope were $m/z$ 0.500 more than that from $^{12}C$ isotope (Table 3). However, the last two values, $m/z$ 1008.7217


dx.doi.org/10.1021/jf501011y | J. Agric. Food Chem. 2014, 62, 9387−9400

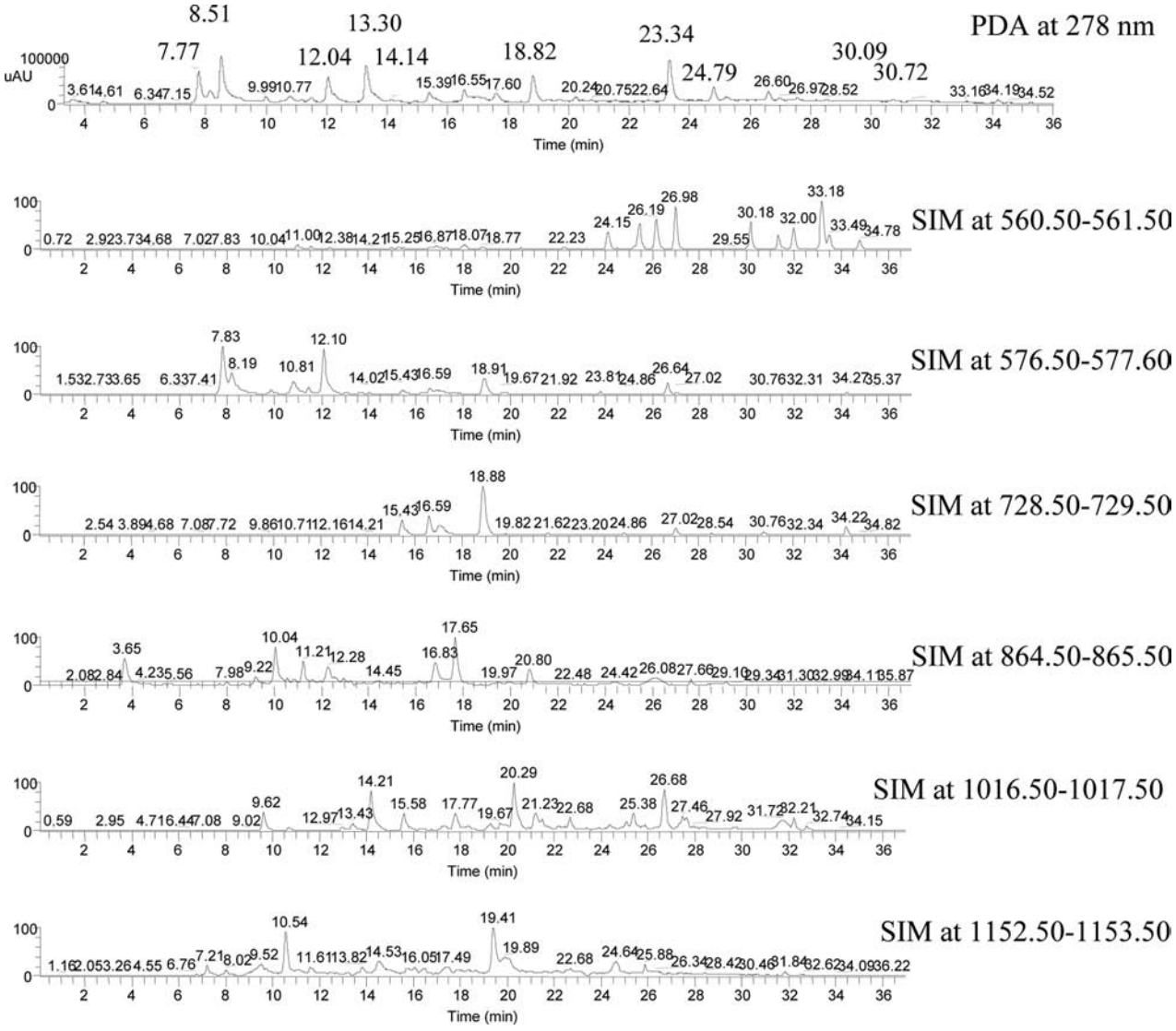


**Figure 4.** PDA (at 278 nm) and SIM chromatograms of grape seed extract.

and 1152.7537, were taken from the $^{13}C$ isotope ions of B-type procyanidin heptamer and octamer, respectively, so these masses were larger than the listed $[M - 2H]^{2-}$ values for the $^{12}C$ isotope ion by 0.50 amu.

Checking the distance between isotopes led to the detection of several minor PA ions in the TIC chromatogram of mangosteen extract. For example, the ions at $m/z$ 1296.2828, 1007.2120, 1136.2540, and 1288.2840 were close matches to the listed values for doubly charged B-type procyanidin octamers, A-type procyanidin heptamers with one A bond, B-type propelargonidin octamers with two EA, and B-type propelargonidin nonamers with one EA (Tables 1 and 3), respectively.

Similarly, checking for $^{12}C$ and $^{13}C$ isotopes with a 0.33 amu distance led to the discovery of several $[M - 3H]^{3-}$ ions. However, only one of them (in mangosteen) was for a PA with a DP $\leq$ 10. As shown in Table 3 and Figure 3, the HRMS values for this PA for the $^{12}C$ and $^{13}C$ isotope ions were 959.8727 and 960.2103 (Figure 3), respectively. To date, only five multiply changed ions have been reported in the pericarps of mangosteen.[12] This is the first report to use the high-resolution isotope ion values for accurate identification of multiply charged PAs based on the use of $^{12}C$ and $^{13}C$ isotope ions.

**Quantification of Proanthocyanidin Oligomers.** The extraction efficiency of the standardized method for PAs in plant materials was determined by a follow-up extraction using acetone/methanol/water (2:2:1, v/v/v), a solvent frequently used for PA extraction in other studies.[2−4,21,22] No additional material was found in the follow-up extractions as determined by the lack of detectable peaks. This indicated that the general extraction method was suitable for the quantification of PAs in jujube, Fuji apple, litchi, and mangosteen.

The UV absorbance of phenolic compounds is widely used for the quantification of PAs.[2−4,7,19,20,22] The MRRF of flavan-3-ol (catechin and epicatechin) monomers, dimeric procyanidin $B_1$, $B_2$, and $A_2$, and trimeric procyanidin $C_1$ at 274−280 nm were found to be proportional to the DP number in our previous study.[25] This established that, in molar units, the response of the monomers was additive. The MRRF values for catechin, gallocatechin, and gallic acid were determined to be 1.00, 0.31, and 2.8.[25] Thus, the MRRF for EC-EC is 2.0, that for EC-EC-A-EC is 3.0, and that for EC-EC-ECg is 4.8. There were no commercial standards for afzelechin or fisetinodol, so an


dx.doi.org/10.1021/jf501011y | J. Agric. Food Chem. 2014, 62, 9387−9400

**Table 4. Retention Time, Molecular Weight, MRRF Value, and Concentration for the Main PAs in Grape Seed Extract**

| compound (or code) (min) | $t_R$ (UV) (min) | $t_R$(SIM) (min) | $MW_x$ | MRRF | content (%, w/w on dry basis), av ± SD |
|---|---|---|---|---|---|
| catechin | 8.51 | | 290 | 1.0 | 6.55 ± 0.26 |
| epicatechin | 13.30 | | 290 | 1.0 | 7.58 ± 0.30 |
| epicatechin-gallate | 23.34 | | 442 | 3.8 | 2.34 ± 0.09 |
| catechin-gallate | | 25.25 | 442 | 3.8 | 0.16 ± 0.01 |
| **monomer concentration** | | | | | **16.63 ± 0.67** |
| | | | | | |
| proanthocyanins | | | | | |
| EF-EC-5 | 30.09 | 30.18 | 562 | 2.0 | 0.07 ± 0 |
| EF-EC-1 | | 24.15 | 562 | 2.0 | 0.05 ± 0 |
| EF-EC-2 | | 25.05 | 562 | 2.0 | 0.08 ± 0 |
| EF-EC-3 | | 2619 | 562 | 2.0 | 0.08 ± 0 |
| EF-EC-4 | | 26.98 | 562 | 2.0 | 0.11 ± 0 |
| EF-EC-6 | | 31.34 | 562 | 2.0 | 0.03 ± 0 |
| EF-EC-7 | | 32.00 | 562 | 2.0 | 0.05 ± 0 |
| EF-EC-8 | | 33.18 | 562 | 2.0 | 0.11 ± 0 |
| EF-EC-9 | | 33.46 | 562 | 2 0 | 0 05 ± 0 |
| EF-EC-10 | | 34.78 | 562 | 2.0 | 0.03 ± 0 |
| EC-EC-1 | 7.76 | 7.83 | 578 | 2.0 | 2.53 ± 0.10 |
| EC-EC-2 | | 8 19 | 578 | 2.0 | 1.88 ± 0.08 |
| EC-EC-3 | | 9.86 | 578 | 2.0 | 0.22 ± 0.01 |
| EC-EC-4 | | 10.81 | 578 | 2.0 | 0.87 ± 0.03 |
| EC-EC-S | | 11.46 | 578 | 2 0 | 0.19 ± 0.01 |
| EC-EC-6 | | 12.10 | 578 | 2.0 | 2.41 ± 0.10 |
| EC-EC-7 | | 16.59 | 578 | 2.0 | 1.60 ± 0.06 |
| EC-EC-S | | 18.91 | 578 | 2.0 | 1.07 ± 0.04 |
| EC-EC-9 | | 26.64 | 578 | 2.0 | 1.18 ± 0.05 |
| EC-EG | | 6.41 | 594 | 2.0 | 0.01 ± 0 |
| (EC-EC)g-4 | 18.83 | 18.88 | 730 | 4.8 | 1.61 ± 0.06 |
| (EC-EC)g-1 | | 15.43 | 730 | 4.8 | 0.53 ± 0.02 |
| (EC-EQg-2 | | 16.59 | 730 | 4.8 | 1.13 ± 0 |
| (EC-EC)g-3 | | 17.40 | 730 | 4.8 | 0.54 ± 0.02 |
| (EC-EC)g-5 | | 27.04 | 730 | 4.8 | 0.23 ± 0.01 |
| (EC-EC)g-6 | | 34.23 | 730 | 4.8 | 0.21 ± 0.01 |
| $(EC\text{-}EC)_2$g-1 | 24.79 | 24.86 | 882 | 7.6 | 0.57 ± 0 |
| **dimer concentration** | | | | | **17.44 ± 0.70** |
| | | | | | |
| EA-EC-EC-7 | 30.72 | 30.76 | 850 | 3.0 | 0.04 ± 0 |
| EF-EC-EC-1 | | 18.55 | 850 | 3.0 | 0.03 ± 07 |
| EA-EC-EC-2 | | 19.67 | 850 | 3.0 | 0.04 ± 0 |
| EF-EC-EC-3 | | 22.80 | 850 | 3.0 | 0.03 ± 0 |
| EA-EC-EC-4 | | 23.67 | 850 | 3.0 | 0.04 ± 0 |
| EA-EC-EC-5 | | 28.04 | 850 | 3.0 | 0.03 ± 0 |
| EA-EC-EC-6 | | 30.03 | 850 | 3.0 | 0.02 ± 0 |
| EC-EC-EC-4 | 12.04 | 12.28 | 866 | 3.0 | 2.25 ± 0.09 |
| EC-EC-EC-1 | | 3.65 | 866 | 3 0 | 1.95 ± 0.08 |
| EC-EC-EC-2 | | 10.04 | 866 | 3.0 | 1.92 ± 0.08 |
| EC-EC-EC-3 | | 11.21 | 866 | 3.0 | 0.78 ± 0.03 |
| EC-EC-EC-5 | | 16.83 | 866 | 3.0 | 1.35 ± 0.05 |
| EC-EC-EC-6 | | 17.65 | 866 | 3.0 | 2.34 ± 0.09 |
| EC-EC-EC-7 | | 20.76 | 866 | 3.0 | 0.89 ± 0.04 |
| EC-EC-EC-8 | | 26.08 | 866 | 3.0 | 1.73 ± 0.07 |
| (EC-EC-EC)g-2 | 14.14 | 14.21 | 1018 | 5.8 | 0.14 ± 0.01 |
| (EC-EC-EC)g-1 | | 9.62 | 1018 | 5.8 | 0 06 ± 0 |
| (EC-EC-EC)g-3 | | 13.43 | 1018 | 5.8 | 0.06 ± 0 |
| (EC-EC-EC)g-4 | | 20.29 | 1018 | 5.8 | 0.16 ± 0.01 |
| (EC-EC-EC)g-5 | | 25.38 | 1018 | 5 8 | 0.07 ± 0 |
| (EC-EC-EC)g-6 | | 26.68 | 1018 | 5.8 | 0.12 ± 0 |
| (EC-EC-EC)g-7 | | 27.46 | 1018 | 5.8 | 0.08 ± 0 |
| (EC-EC-EC)g-8 | | 32.21 | 1018 | 5 8 | 0.10 ± 0 |
| $(EC\text{-}EC\text{-}EC)_2$g-1 | | 28.23 | 1170 | 8.6 | trace |
| **trimer concentration** | | | | | **14.24 ± 0.57** |


dx.doi.org/10.1021/jf501011y | J. Agric. Food Chem. 2014, 62, 9387−9400

**Table 4. continued**

| compound (or code) (min) | $t_R$ (UV) (min) | $t_R$(SIM) (min) | $MW_x$ | MRRF | content (%, w/w on dry basis), av ± SD |
|---|---|---|---|---|---|
| EC-EC-EC-EC-5 | 19.34 | 19.40 | 1154 | 4.0 | 0.23 ± 0.01 |
| EC-EC-EC-EC-1 | | 9.62 | 1154 | 4.0 | 0.06 ± 0 |
| EC-EC-EC-EC-2 | | 10.63 | 1154 | 4.0 | 0.09 ± 0 |
| EC-EC-EC -EC-3 | | 14.81 | 1154 | 4.0 | 0.06 ± 0 |
| EC-EC-EC-EC-4 | | 17.31 | 1154 | 4.0 | 0.03 ± 0 |
| EC-EC-EC-EC-6 | | 24.64 | 1154 | 4.0 | 0 04 ± 0 |
| EC-EC-EC-EC-7 | | 25.88 | 1154 | 4.0 | 0.03 ± 0 |
| **tetramer concentration** | | | | | **0.47 ± 0.20** |
| **total catechin and PA concentration** | | | | | **48.79 ± 1.95** |

MRRF value of 1.00 was assigned to each. The additivity of the molar absorption coefficient makes it possible to quantify most of the PAs using (+)-catechin as a standard with the MRRF values listed above.

Unfortunately, even with UHPLC, only a few PAs were well separated and could be quantified on the basis of their UV peak area. Most PAs, when viewed with UV or TIC, had peaks that overlapped (coeluted) with other PAs. Selected ion monitoring (SIM) and multiple reaction monitoring (MRM) are the only methods that allow deconvolution of the overlapping peaks, that is, isolation of the ions of interest.[33,34] Consequently, concentrations had to be computed on the basis of ion counts obtained from SIM or MRM as reported in previous studies[19,22] The few well-separated absorbance peaks were used to equate the peak area in absorbance to integrated counts of specific ions. In other words, MRRF values based on absorbance were converted to MRRF values based on integrated ion counts. This approach allowed catechin and the MRRF values reported above to be used for computing PA concentrations.

Use of MRRFs based on ion counts assumes constant ionization efficiency for all PAs. Unlike absorbance, the ion count of a PA isomer can be expected to be dependent on its structural ionization sensitivity and the mobile phase. The SIM peak intensity might change with the solvent ratio at different retention times, the isomer concentration, and the presence of coeluting PAs (Figure 4). Tests performed with flavan-3-ol monomers and procyanidins $B_1$ and $B_2$ showed the variation in ionization efficiency to be <±10%. Further testing with PAs with DP = 3−5, A-type bond, or galloyls is needed but must wait on the availability of suitable standards.

The PA concentrations in dry weight percent (%) and milligrams per 100 g of dry plant material were calculated using the formulas

$$C\ (\%, w/w) = [100A_x \times MW_x \times V_s \times M_s \times W_s] / [A_s \times MW_s \times W_x \times V_x \times MRRF] \quad (6)$$

$$C\ (mg/100\ g) = [1000A_x \times MW_x \times W_s \times V_s] / [A_s \times MW_S \times V_x \times W_x \times MRRF] \quad (7)$$

where $A_x$, $MW_x$, $W_x$, and $V_x$ and $A_s$, $MW_s$, $W_s$, and $V_s$ are the peak area, molecular weight, sample weight, and volume of the extract for the sample and standard, respectively.

As shown in Table 4 for grape seed extract, at least one PA in each of the oligomers was found to have a well-separated peak (no coeluting compounds) that could be used to equate absorbance with ion counts from SIM. The concentrations of monomers, dimers, trimers, and tetramers as percent dry weight were 16.63 ± 0.67, 17.44 ± 0.70, 14.24 ± 0.57, and 0.47 ± 0.20%, respectively. The concentration for PAs with DP > 4 was negligible. The total concentration of PAs was 48.79 ± 1.95%.

Highly accurate masses can be computed for PAs on the basis of the degree of polymerization, the specific flavan-3-ol components, the number of A-type bonds, and the number of galloyls. PAs can be identified by comparing experimentally obtained high-accuracy masses to the computed masses. Identifications can be further confirmed by the analysis of fragments from tandem MS. Conversion of MRRF values from UV absorbance to ion counts with SIM was used for the quantification of individual PAs. Thus, this standardized UHPLC-PDA-ESI/HRMS$^n$ profiling method was able to offer identification and quantification of oligomeric PAs in plant-derived foods.

## AUTHOR INFORMATION


### Corresponding Author

*(L.-Z.L.) Phone: (301)-504-9136. Fax: (301)-504-8314. E-mail: Longze.lin@are.usda.gov.



### Funding

This research is supported by the Agricultural Research Service of the U.S. Department of Agriculture and an Interagency Agreement with the Office of Dietary Supplements of the National Institutes of Health.


### Notes

The authors declare no competing financial interest.

## REFERENCES


(1) Hümmer, W.; Schreier, P. Analysis of proanthocyanidins. *Mol. Nutr. Food Res.* **2008**, *52*, 1381−1398.

(2) Hellström, J. K.; Mattila, P. H. HPLC determination of extractable and unextractable proanthocyanidins in plant materials. *J. Agric. Food Chem.* **2008**, *56*, 7617−7624.

(3) Hellström, J. K.; Törrönen, A. R.; Mattila, P. H. Proanthocyanidins in common food products of plant origin. *J. Agric. Food Chem.* **2009**, *57*, 7899−7906.

(4) Gu, L.; Kelm, M. A.; Hammerstone, J. F.; Beecher, G.; Holden, J.; Haytowitz, D.; Gebhardt, S.; Prior, R. L. Screening of foods containing proanthocyanidins and their structural characterization using LC-MS/MS and thiolytic degradation. *J. Agric. Food Chem.* **2003**, *51*, 7513−7521.

(5) Aron, P. M.; Kennedy, J. A. Flavan-3-ols: nature, occurrence and biological activity. *Mol. Nutr. Food Res.* **2008**, *52*, 79−104.

(6) Prior, R. L.; Gu, L. Occurrence and biological significance of proanthocyanidins in the American diet. *Phytochemistry* **2005**, *66*, 2264−2280.

(7) Monagas, M.; Quintanilla-López, J. E.; Gómez-Cordovés, C.; Bartolomé, B.; Lebrón-Aguilar, R. MALDI-TOF MS analysis of plant proanthocyanidins. *J. Pharm. Biomed. Anal.* **2010**, *51*, 358−372.

(8) Es-Safi, N. E.; Guyot, S.; Ducrot, P. H. NMR, ESI/MS, and MALDI-TOF/MS analysis of pear juice polymeric proanthocyanidins with potent free radical scavenging activity. *J. Agric. Food Chem.* **2006**, *54*, 6969−6977.
(9) Zhou, H.-C.; Lin, Y.-M.; Li, Y.-Y.; Li, M.; Wei, S.-D.; Chai, W.-M.; Tam, F.-Y. Antioxidant properties of polymeric proanthocyanidins from fruit stones and pericarps of *Litchi chinensis* Sonn. *Food Res. Int.* **2011**, *44*, 613−620.
(10) Chai, W.-M.; Shi, Y.; Feng, H.-L.; Qiu, L.; Zhou, H.-C.; Deng, Z.-W.; Yan, C.-L.; Chen, Q.-S. NMR, HPLC-ESI-MS, and MALDI-TOF MS analysis of condensed tannins from *Delonix regia* (Bojer ex Hook.) Raf. and their bioactivities. *J. Agric. Food Chem.* **2012**, *60*, 5013−5022.
(11) Fu, C.; Loo, A. E.; Chia, F. P.; Huang, D. Oligomeric proanthocyanidins from mangosteen pericarps. *J. Agric. Food Chem.* **2007**, *55*, 7689−7694.
(12) Zhou, H.-C.; Lin, Y.-M.; Wei, S.-D.; Tam, F.-Y. Structural diversity and antioxidant activity of condensed tannins fractionated from mangosteen pericarp. *Food Chem.* **2011**, *129*, 1710−1720.
(13) Mouls, L.; Mazauric, J.-P.; Sommerer, N.; Fulcrand, H.; Mazerolles, G. Comprehensive study of condensed tannins by ESI mass spectrometry: average degree of polymerisation and polymer distribution determination from mass spectra. *Anal. Bioanal. Chem.* **2011**, *400*, 613−623.
(14) Gu, L.; Kelm, M. A.; Hammerstone, J. F.; Zhang, Z.; Beecher, G.; Holden, J.; Haytowitz, D.; Prior, R. L. Liquid chromatographic/electrospray ionization mass spectrometric studies of proanthocyanidins in foods. *J. Mass Spectrom.* **2003**, *38*, 1272−1280.
(15) Hayasaka, Y.; Waters, E. J.; Cheynier, V.; Herderich, M. J.; Vidal, S. Characterization of proanthocyanidins in grape seeds using electrospray mass spectrometry. *Rapid Commun. Mass Spectrom.* **2003**, *17*, 9−16.
(16) Roux, E. L.; Doco, T.; Sarni-Manchado, P.; Lozano, Y.; Cheynier, V. A-type proanthocyanidins from pericarp of *Litchi chinensis*. *Phytochemistry* **1998**, *48*, 1251−1258.
(17) Wollgast, J.; Pallaroni, L.; Agazzi, M.-E.; Anklam, E. Analysis of procyanidins in chocolate by reversed-phase highperformance liquid chromatography with electrospray ionization mass spectrometric and tandem mass spectrometric detection. *J. Chromatogr. A* **2001**, *926*, 211−220.
(18) Núñez, V.; Gómez-Cordovés, C.; Bartolomé, B.; Hong, Y.-J.; Mitchell, A. E. Non-galloylated and galloylated proanthocyanidin oligomers in grape seeds from *Vitus vinifera* L. cv. Graciano, Tempranillo and Cabernet Sauvignon. *J. Sci. Food Agric.* **2006**, *86*, 915−921.
(19) Sarnosk, P. J.; Johnson, J. V.; Reed, K. V.; Tanko, J. M.; O'Keefe, S. F. Separation and characterisation of proanthocyanidins in Virginia type peanut skins by LC−MS. *Food Chem.* **2012**, *131*, 927−939.
(20) Appeldoorn, M. M.; Vincken, J. P.; Sanders, M.; Hollman, P. C. H.; Gruppen, H. Combined normal-phase and reversed-phase liquid chromatography/ESI-MS as a tool to determine the molecular diversity of A-type procyanidins in peanut skins. *J. Agric. Food Chem.* **2009**, *57*, 6007−6013.
(21) Cooper, K. A.; Campos-Giménez, E.; Jiménez Alvarez, D.; Nagy, K.; Donovan, J. L.; Williamson, G. Rapid reversed phase ultra-performance liquid chromatography analysis of the major cocoa polyphenols and inter-relationships of their concentrations in chocolate. *J. Agric. Food Chem.* **2007**, *55*, 2841−2847.
(22) Li, S.; Xiao, J.; Chen, L.; Hu, C.; Chen, P.; Xie, B.; Sun, Z. Identification of A-series oligomeric procyanidins from pericarp of *Litchi chinensis* by FT-ICR-MS and LC-MS. *Food Chem.* **2012**, *135*, 31−38.
(23) Hokkanen, J.; Mattila, S.; Jaakola, L.; Pirttilä, A. M.; Tolonen, A. Identification of phenolic compounds from lingonberry (*Vaccinium vitis-idaea* L.), bilberry (*Vaccinium myrtillus* L.) and hybrid bilberry (*Vaccinium* × *intermedium* Ruthe L.) leaves. *J. Agric. Food Chem.* **2009**, *57*, 9437−9447.
(24) Lin, L.-Z.; Harnly, J. M. A screening method for the identification of glycosylated flavonoids and other phenolic compounds using a standard analytical approach for all plant materials. *J. Agric. Food Chem.* **2007**, *55*, 1084−1096.
(25) Lin, L.-Z.; Harnly, J. M. Quantitation of flavanols, proanthocyanidins, isoflavones, flavananes, dihydroxychalcones, stilbens and benzoic acid derivatives using UV absorbance after identification by LC-MS. *J. Agric. Food Chem.* **2012**, *60*, 5832−5840.
(26) Lin, L.-Z.; Sun, J.; Chen, P.; Harnly, J. M. U-HPLC-PDA-EIS/HRMS/MS$^n$ analysis of anthocyanins, flavonol glycosides and hydroxycinnamic acid derivatives in red mustard green (*Brassica juncea* Coss variety). *J. Agric. Food Chem.* **2011**, *59*, 12059−12072.
(27) Li, H.-J.; Deinzer, M. L. The mass spectral analysis of isolated hops A-type proanthocyanidins by electrospray ionization tandem mass spectrometry. *J. Mass Spectrom.* **2008**, *43*, 1353−1363.
(28) Monagas, M.; Gómez-Cordovés, C.; Bartolomé, B.; Laureano, O.; Ricardo da Silva, J. M. Monomeric, oligomeric, and polymeric flavan-ol composition of wines and grapes from *Vitis vinifera* L. cv. Graciano, Tempranillo, and Cabernet Sauvignon. *J. Agric. Food Chem.* **2003**, *51*, 6475−6481.
(29) Escribano-Bailón, M. T.; Guitiérrez-Fernández, Y.; Rivas-Gonzalo, J. C.; Santos-Buelga, C. Characterization of procyanidins of *Vitis vinifera* variety Tinta del Pais grape seeds. *J. Agric. Food Chem.* **1992**, *40*, 1794−1799.
(30) Ricardo da Silva, J. M.; Rigaud, J.; Cheynier, V.; Cheminat, A.; Moutounet, M. Procyanidin dimers and trimers from grape seeds. *Phytochemistry* **1991**, *30*, 1259−1264.
(31) Ricardo da Silva, J. M.; Rosec, J.-Ph.; Bourzeix, M.; Mourgues, J.; Moutounet, M. Dimer and trimer procyanidins in Carignan and Mourvèdre grapes and red wines. *Vitis* **1992**, *31*, 55−63.
(32) Malik, A.; Kuliev, Z. A.; Akhmedov, Y. A.; Vdovin, A. D.; Abdullaev, N. D. Proanthocyanidins of *Ziziphus jujuba*. *Chem. Nat. Compd.* **1997**, *33*, 165−173.
(33) Prasain, J. K.; Wang, C. C.; Barnes, S. Mass spectrometric methods for the determination of flavonoids in biological samples. *Free Radical Biol. Med.* **2004**, *37*, 1324−1350.
(34) Redeuil, K.; Bertholet, R.; Kussmann, M.; Steiling, H.; Rezzi, S.; Nagy, K. Quantification of flavan-3-ols and phenolic acids in milk-based food products by reversed-phase liquid chromatography−tandem mass spectrometry. *J. Chromatogr. A* **2009**, *1216*, 8362−8370.

Several methods are available to detect EVOO adulteration with HO, targeting different chemical markers such as free fatty acids,[4,18,19] triacylglycerols,[20,21] sterols,[22] volatile organic compounds (VOC)[23] and, in particular, filbertone,[24] a ketone absent in olive oils. Filbertone determination is generally performed by liquid or gas chromatography (L-GC) coupled to mass spectrometry.[25] However, this marker becomes useless in the case of adulteration of EVOO with refined HO, because it undergoes a partial or full degradation during the refining process.[26] Recently, a method based on hydrophilic interaction chromatography (HILIC) microsolid phase extraction ($\mu$SPE) coupled to matrix assisted laser desorption ionization (MALDI) time-of-flight (ToF) mass spectrometry (MS) for the detection of the polar components in hazelnut and olive oil has been developed.[27] Consecutive analysis by tandem mass spectrometry allowed the identification of lysophosphatidylcholines as HO markers. More recently, phospholipids were confirmed[28] to be promising markers of EVOO adulteration with HO by a MALDI-MS approach involving an ionic liquid[29,30] (tributylamine-CHCA) as matrix.

However, existing literature dealing with the direct determination of HO residual proteins in EVOO, in order to get an immediate evaluation of the allergenic potential, is poor, and the attention is mainly focused toward intact proteins rather than peptides. Furthermore, MALDI-MS has never been applied on this topic—regardless, this technique has widely demonstrated its great potential on similar analytical problems[31,32] due to its rapidity and sensitivity.

A recent study[17] developed a biosensor immunoassay for residues of hazelnut proteins in olive oil, whereas Arlorio et al.[5] set up a simulation of olive oil adulterated with hazelnut oils to identify possible risks for allergic consumers, demonstrating the presence of hazelnut proteins in solvent-extracted hazelnut oil.

Further approaches, based on DNA and immunoassays analysis, are also available in the literature, and they now include an array of platforms. The fundamental principle of this approach is that the amount of DNA remaining in processed foods is sufficient for analytical purposes to obtain traceability, to detect the presence of both genetically modified organisms and allergens.[33−37]

Some of these methods are routinely used by industry and administration agencies even if they lack accuracy and robustness, especially in the case of processed foods.[38,39]

In this work, we tested different approaches for the extraction of residual proteins from various hazelnut oils. The resulting extracts were in-solution digested and analyzed by MALDI-MS. The most efficient extraction protocol was based on cold-acetone protein precipitation. The whole procedure is rapid and simple and facilitated the detection of hazelnut marker peptides in both HO and EVOO adulterated with HO.

## MATERIALS AND METHODS

**Reagents.** Acetone, water, chloroform ($CHCl_3$), acetonitrile (ACN), and methanol (MeOH) were LC-MS grade; hexane and *tert*-butyl methyl ether were HPLC grade. Trichloroacetic acid (TCA), trifluoroacetic acid (TFA), Trizma hydrochloride (Tris-HCl), sodium chloride (NaCl), all the reagents for the tryptic digestion (dithiothreitol (DTT), iodoacetamide, ammonium bicarbonate ($NH_4HCO_3$), urea, porcine trypsin), ACTH 18−39 fragment, angiotensin I, and renin were obtained from Sigma-Aldrich (St. Louis, MO). $C_{18}$Zip Tips were from Millipore (Billerica, MA). Tris-Glycine buffer, Laemmli buffer, 4−15% Mini-PROTEAN TGX precast gels, molecular weight marker "Precision Plus Protein Standards Dual Color", Mini-PROTEAN II electrophoresis cell, were acquired from Bio-Rad Laboratories (Hemel Hempstead, Hertfordshire, U.K.). $\alpha$-Cyano-4-chlorocinnamic acid (CClCA), obtained as a synthetic product, was recrystallized four times before use.

**Samples.** Different hazelnut oils were analyzed: two Italian (Monferrato, Piedmont), cold-pressed, from roasted and raw hazelnuts, respectively; one German, cold-pressed, from roasted hazelnuts; one Turkish, refined, from raw hazelnuts; one Greek, refined, from raw hazelnuts (the last two were seized by Italian Customs agencies). Commercial (five brands) and raw Italian extra-virgin olive oils (homemade by various Apulia cultivars) were analyzed. EVOO was intentionally adulterated by cold-pressed HO at different percentages (50/50 and 80/20, w/w). Each experiment was performed in triplicate.

**Protein Extraction Methods from Oils.** Experimental protocols available in the literature were applied with slight modifications.

**Cold Acetone Precipitation.**[10] To 5 g of pure hazelnut oil and pure olive oil, 12.5 mL of cold acetone (4 °C) was added, the mixture was shaken vigorously, kept for 1 h at 4 °C, and shaken every 10 min; then it was centrifuged at 4200*g* for 1 h, and the precipitate was washed twice with 1 mL of cold acetone. The pellet obtained from extraction was dried at 40 °C for 5 min in a vacuum concentrator.

**Hexane/Acetone Precipitation.**[10] To 5 g of pure hazelnut oil or pure olive oil, 12.5 mL of cold hexane/acetone (1:1, v/v) was added, the mixture was shaken vigorously, kept for 1 h at 4 °C, and shaken every 10 min; then it was centrifuged at 4200*g* for 1 h, and the precipitate was washed twice with 1 mL of cold hexane/acetone. The pellet obtained from extraction was dried at 40 °C for 5 min in a vacuum concentrator.

**Diethyl Ether/Trichloroacetic Acid Precipitation.**[5] Ten milliliters of *tert*-butyl methyl ether was added to 10 g of pure hazelnut oil and pure olive oil, and the mixtures were maintained at 18 °C for 30 min. Then, 10 mL of 20% w/v trichloroacetic acid (4 °C) was added, the mixture was transferred to a separating funnel, and the extraction was repeated three times. The three aqueous phases were collected and washed twice with 10 mL of *tert*-butyl methyl ether to remove lipids. The aqueous fractions were partially concentrated and centrifuged at 28 000*g* for 20 min at 4 °C. The supernatant was discarded; the pellet was washed twice with 1 mL of acetone and finally dried.

**Ammonium Hydrogen Carbonate.**[40] Hazelnut oil (7.5 mL) was extracted with 3.5 mL of ammonium hydrogen carbonate (0.2 M, pH 7.8) on a shaker for 2 h at room temperature. The mixture was centrifuged at 11 180*g* for 20 min at 4 °C, and the aqueous layer was dried in a vacuum concentrator.

**TBS Extraction.**[41] Tris-buffered saline (TBS) was prepared with 40 mM Tris-HCl and 300 mM NaCl. In particular, to 2 g of hazelnut oil, 5 mL of TBS was added. Extraction was done at 60 °C for 20 min under shaking. The extract was centrifuged at 4200*g* for 20 min, defatted by extracting twice with *n*-hexane, and dried under a nitrogen stream.

**Bligh−Dyer Extraction.**[42] $CHCl_3$/MeOH (1:2, 1.87 mL) was added to 0.5 mL of hazelnut oil or olive oil followed by vigorous vortex-mixing. Then, 0.62 mL of $CHCl_3$ was added, and the solution was vortexed again. Afterward, 0.62 mL of $H_2O$ was added, and the solution was vortexed again. Finally, the solution was centrifuged for 5 min at 4200*g*, and the

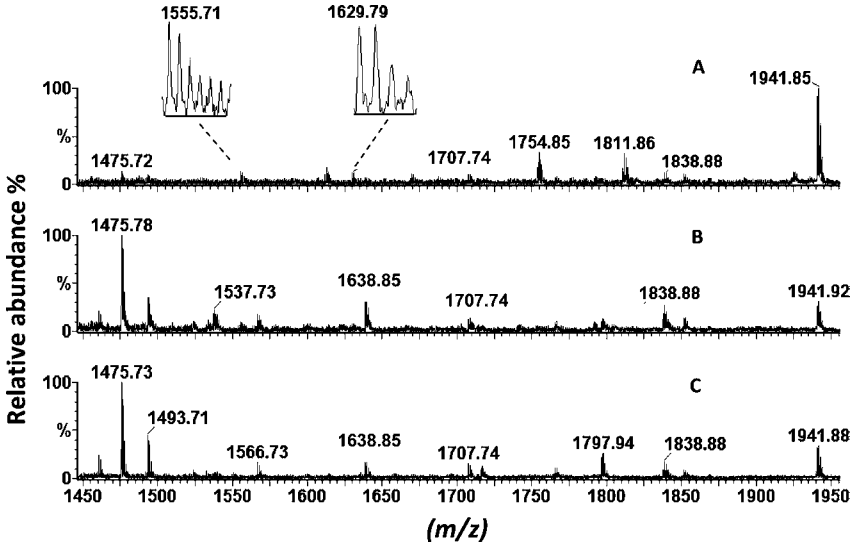


**Figure 1.** MALDI mass spectra relevant to the in-solution tryptic digests of hazelnut oil extracts obtained using Bligh−Dyer (A), diethyl ether/trichloroacetic acid (B), and hexane/acetone (C) protocols, respectively. The two peaks shown in figure (A), at *m/z* 1555.71 (RAESEGFEWVAFK) and 1629.79 (ALPDDVLANAFQISR), were attributed to Cor a 9.

aqueous upper layer, containing the proteins, was collected, divided in several aliquots, and dried under a stream of nitrogen. This aqueous extract was used for the following analysis steps.

**In-Solution Tryptic Digestion.** The pellets obtained from the different extraction methods were digested in solution following a reported protocol.[32] Dried pellets were resuspended in 40 $\mu$L of 400 mM $NH_4HCO_3$ in 8 M urea. Five microliters of DTT (50 mM) was added, and the mixture was incubated for 40 min at 60 °C and chilled at room temperature. Next, 5 $\mu$L of iodoacetamide (150 mM) was added, followed by an incubation in the dark at room temperature for 45 min. water (120 $\mu$L) and 20 pmol of porcine trypsin were added, and the solution was incubated overnight at 37 °C. The digestion was stopped with 10% TFA. The tryptic digests were mixed 1:1 (v/v) with the matrix $\alpha$-cyano-4-chloro-cinnamic acid (5 mg/mL), and then 1 $\mu$L of the sample/matrix solution was spotted, dried, washed at least once on target, and analyzed by MALDI-TOF-MS. In some cases, due to the low concentration of hazelnut derived peptides in the samples, a procedure of desalting and preconcentration using $C_{18}$Zip Tips was employed.

**SDS-PAGE.** As a reference, a roasted hazelnut protein extract was separated on SDS-PAGE gel. The extract for SDS-PAGE was prepared according to Sheoran et al.[43] with slight modifications. To 0.03 g of hazelnut powder, 1 mL of Tris-HCl buffer (50 mM) was added, and the mixture was kept at 4 °C for 30 min and then centrifuged at 16 000*g* for 20 min at 4 °C. The supernatant was collected, the pellet re-extracted, and the supernatants pooled. The proteins were precipitated with 5 vols (v/v) of 100% acetone and incubated at −20 °C for 2 h. After centrifugation at 4000*g* for 40 min, the pellet was washed twice with acetone, dried for 5 min at 40 °C, and suspended in Laemmli buffer (1:1, v/v). Then, 1 $\mu$L of DTT 50 mM was added and the samples were reduced at 90 °C for 5 min. Twenty microliters were loaded onto the gel, and electrophoresis was carried out at two different voltages—50 V to compact the proteins in the stacking gel and 80 V until the end of the run.

**In-Gel Digestion of Hazelnut Proteins.** The protein bands were cut and digested by porcine trypsin using a specific protocol. At first, the bands were cut in small pieces that were covered with 200 $\mu$L of 200 mM $NH_4HCO_3$ in 40% of ACN, and the samples were incubated at 37 °C for 30 min in a thermo shaker. The step was repeated until the gel pieces were decolorized. The gel fragments were dried in a speed vacuum for 15 min. Porcine trypsin (0.05 $\mu$g/$\mu$L) and 50 $\mu$L of 40 mM $NH_4HCO_3$ in 9% ACN were added, and the samples were incubated at 37 °C overnight. After the incubation, the liquid fraction, containing peptides, was collected and acidified with TFA before MALDI analysis.

**MALDI-ToF-MS.** MALDI-ToF-MS analyses were performed on a Micromass M@LDI - LR time-of-flight mass spectrometer (Waters MS Technologies, Manchester, U.K.) equipped with a nitrogen UV laser (337 nm wavelength), reflectron optics, and a fast dual microchannel plate (MCP) detector.

Positive ion spectra were acquired in reflectron mode. The following voltages were applied: pulse, 2610 V; source, 15 000 V; reflectron, 2000 V; MCP 1900 V. The laser firing rate was 5 Hz, and, unless otherwise specified, 50 laser shots were used for each well. The 50 resulting spectra were averaged, background subtracted, and smoothed by a Savitzky−Golay algorithm.

For peptide analysis, the explored mass range was 800−4000 *m/z*, and mass calibration was performed using a peptide mixture composed of angiotensin I, ACTH 18−39, and renin substrate tetradecapeptide porcine.

**Database Search.** For the attribution of hazelnut tryptic peptides, FindPept was employed as a main tool (www.expasy.org). The set parameters were the following: cysteines treated with iodoacetamide as a fixed modification and oxidation of methionines as a variable modification for in-solution digestion and in-gel digestion. A mass tolerance of 0.1 Da was set. Another useful tool was PeptideMass (http://web.expasy.org/peptide_mass/), accepting up to three missed cleavages.

ClustalO software was used for alignment study and the sequences of hazelnut, and avena 11S globulins, in FASTA format, were provided as an input.

## RESULTS AND DISCUSSION

**Methodology Development on Pure Hazelnut Oil.** At first, different protein extraction approaches were tested on

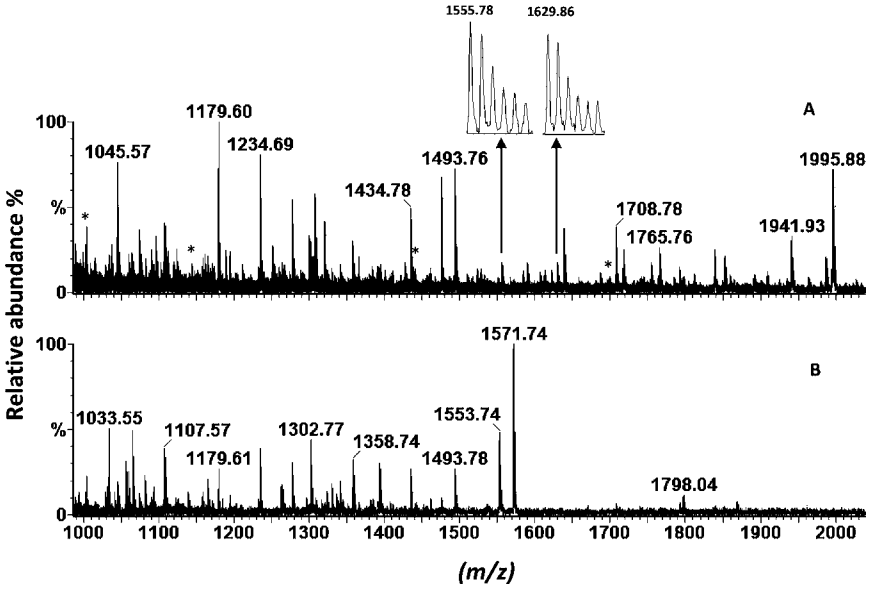


**Figure 2.** MALDI mass spectra (range 1000 to 2000 $m/z$) relevant to the in-solution tryptic digests of hazelnut oil extracts obtained using TBS (A) and ammonium hydrogen carbonate (B) protocols, respectively. In figure (A), the isotopic profiles of the peaks at $m/z$ 1555.78 and 1629.86 from Cor a 9 were magnified, and peptides from the same protein at $m/z$ 1002.53, 1144.54, 1440.76, and 1698.82 were marked with an asterisk.

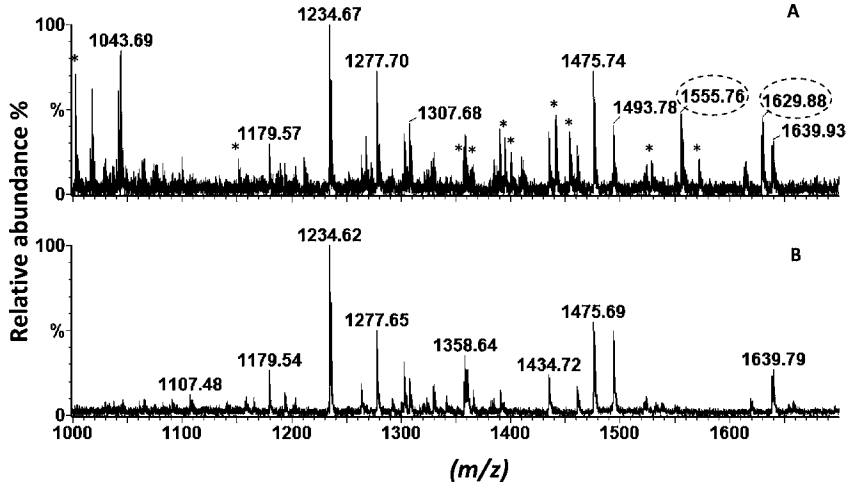


**Figure 3.** MALDI mass spectra (range shown 1000 to 1700 $m/z$) relevant to the in-solution tryptic digests of (A) an Italian cold-pressed hazelnut oil extract and (B) an extra-virgin olive oil extract, obtained using the cold acetone protocol. In 3(A), the two main peptides of Cor a 9 (at $m/z$ 1555.76 and 1629.88) were encircled. The peptides at $m/z$ 990.52, 1151.57, 1356.71, 1394.70, 1399.71, 1440.81, and 1571.84 from Cor a 9, 1528.67 from Cor a 1, 1363.73 from Cor a 11 and 1453.89 most likely from Cor a 14, were marked with an asterisk.

various raw hazelnut oil samples; it is worth noting that a very low quantity of oil (5−10 g) was used if compared to the usually employed amount (100 g).[5,10,40,41] After the extraction, all samples were in-solution digested and analyzed by MALDI-MS. Eventually, the best method was selected on the basis of the simplicity, rapidity, and reproducibility of the procedure and according to the number of detected hazelnut peptides. Because of the sample complexity and the high number of existing allergen isoforms, their identification was achieved by using a combination of literature data[5,8,44−46] and two different informatics tools, that is, the classic peptide mass fingerprint and FindPept (in the latter, proteins are individually compared with a reference list of hazelnut proteins).

Figure 1 reports the MALDI mass spectra relevant to the in-solution tryptic digests of hazelnut oil extracts obtained using Bligh−Dyer (A), diethyl ether/trichloroacetic acid (B), and hexane/acetone (C) protocols, respectively. Only two peptides at $m/z$ 1555.71 and 1629.79, originating from the hazelnut protein ***Cor a 9***, were observed in the MALDI spectrum relevant to the Bligh−Dyer extract (Figure 1A), although no peptides arising from hazelnut proteins were detected by using the other two extraction procedures (diethyl ether/TCA and hexane/acetone). Here, due to the very low protein content in the oil extracts, the level of background proteins introduced during sample preparation (in the form of dust or contaminated chemicals) might mask the presence of the target proteins; indeed, the spectra of Figure 1B,C were dominated by intense signals attributable to human keratins (for instance, the $m/z$ ions 1475.78, 1707.74, and 1638.85).

Then, protein extraction was carried out by using different buffers; the first method was based on the use of ammonium hydrogen carbonate, successfully applied by Rigby et al.[40] in the extraction of proteins from soybean oil, whereas the second protocol was based on the use of TBS as reported by Poms et


dx.doi.org/10.1021/jf504007d | J. Agric. Food Chem. 2014, 62, 9401−9409

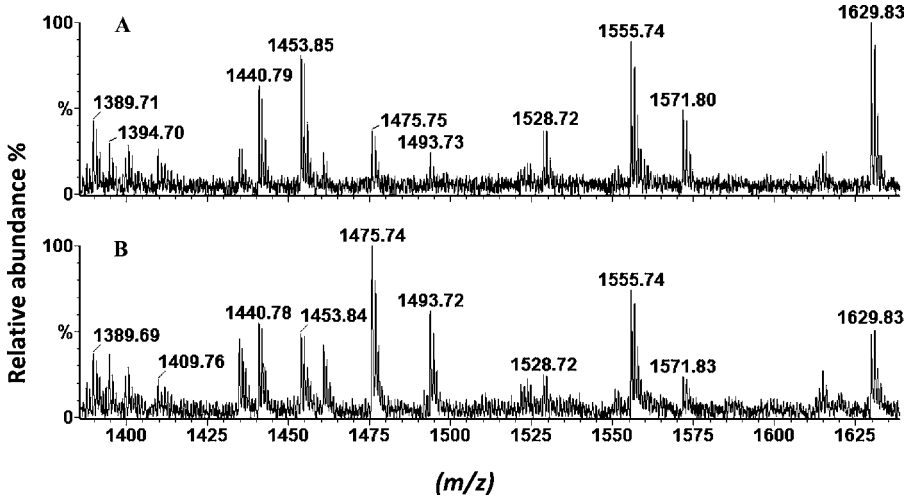


**Figure 4.** Representative $m/z$ range of the MALDI spectra relevant to the in-solution tryptic digests of EVOO extracts adulterated with 50% (A) and 20% (B) of HO obtained from roasted hazelnuts.

**Table 1. List of Hazelnut Peptides Identified in HO by Using Different Protein Extraction Methods**

| protein extraction method | number and related $m/z$ ratios of identified hazelnut peptides |
|---|---|
| Bligh−Dyer | 2:1555.71, 1629.77 |
| diethyl ether/TCA | - |
| hexane/acetone | - |
| TBS | 8:990.51, 1002.53, 1144.54, 1440.76, 1555.75, 1629.83, 1695.84, 1698.82 |
| ammonium hydrogen carbonate | - |
| cold acetone (100% hazelnut oil) | 13:990.52, 1002.52, 1151.57, 1356.71, 1363.73, 1394.70, 1399.71, 1440.81, 1453.89, 1528.67, 1555.76, 1571.84, 1629.88, 1934.87 |
| cold acetone (50% hazelnut oil) | 11:1002.52, 1356.71, 1363.73,1394.70, 1399.71, 1440.79, 1453.85, 1528.72,1555.74, 1571.80, 1629.83, 2643.44 |
| cold acetone (20% hazelnut oil) | 11:1002.52, 1151.57, 1356.71, 1363.73, 1394.70, 1399.71, 1440.78, 1453.84,1528.72, 1555.74, 1571.83, 1698.76 |

al.[41] in the case of peanut proteins. Figure 2 shows the MALDI spectra (range 1000 to 2000 $m/z$) relevant to the in-solution tryptic digests of hazelnut oil extracts obtained using TBS (A) and ammonium hydrogen carbonate (B) protocols, respectively. The inset in Figure 2A reports the close-up image of two ***Cor a 9*** peptides ($m/z$ 1555.75 and 1629.83), whereas the other peptides of the same protein at $m/z$ 1002.53, 1144.54, 1440.76, 1698.82 have been marked with an asterisk. On the contrary, by using ammonium hydrogen carbonate as extraction buffer (Figure 2B), no hazelnut peptides were detected.

After replicating the procedure on other oils, it was possible to confirm that the most recurrent hazelnut peptides were at $m/z$ 1555.75, 1629.83, 1002.53, 1440.76, 1698.82.

Finally, protein precipitation was carried out by using the cold acetone protocol described by Martin-Hernandez et al.[10] The MALDI spectrum (range shown 1000 to 1700 $m/z$) relevant to the in-solution tryptic digest of an Italian cold-pressed hazelnut oil extract is reported in Figure 3A. Despite the intense signals arising from human keratins ($m/z$ ions 1234.67, 1277.70, and 1475.74), typical hazelnut peptides at $m/z$ values 1555.76, 1629.88, 990.52, 1151.57, 1356.71, 1394.70, 1399.71, 1440.81, 1571.84 (*Cor a 9*), 1528.67 (*Cor a 1*), 1363.73 (*Cor a 11*), and 1453.89 (most likely *Cor a 14*), were detected (marked with an asterisk). Of course, the peptide at $m/z$ 1528.67 attributed to Cor a 1 arises[7] from the isoform Cor a 1.0401−1.0404.

When replicating the whole strategy on other oils, the number of recognized peptides was between 10 and 15, even if the stable markers found in all the replicates were at $m/z$ 1002.53, 1151.57, 1356.71, 1394.70, 1440.76, 1555.75, 1629.83, and 1698.82.

The same procedure was then applied to extra virgin olive oil samples; the relevant MALDI spectrum is shown in Figure 3B. As expected, no peptides arising from hazelnut proteins were detected. Moreover, even peptides attributable to EVOO proteins were not observed probably due to their very low concentration (10−50 $\mu$g/100 g).[47] It was noted that the pellets obtained after cold-acetone protein precipitation of the EVOO samples investigated were not observable. On the contrary, in the case of hazelnut oil samples, visible pellets were obtained; their estimated protein concentration, determined by the Bradford method,[48] was in the range 20−100 $\mu$g/mL.

The cold acetone protocol proved to be the most efficient method for protein extraction and detection and was used for further experiments.

**Methodology Application on Adulterated Samples.** The cold acetone protocol was applied to the analysis of EVOO samples adulterated by cold-pressed hazelnut oil (50/50 and 80/20, w/w). Figure 4 shows the MALDI spectra relevant to the in-solution tryptic digests of EVOO extracts adulterated with 50% (A) and 20% (B) of HO obtained from roasted hazelnuts; only the most informative $m/z$ range was reported. The detected $m/z$ ions belong to ***Cor a 9*** ($m/z$ 1394.70, 1440.79, 1555.74, 1571.80, 1629.83), ***Cor a 1*** (1528.72 $m/z$), and ***Cor a 14*** (1453.85 $m/z$); Table 1 depicts the most significant hazelnut peptides showed in the spectra of Figure 4 (three replicates of the whole procedure were performed). It is worth noting that, among the various peptides detected in this work, the one at 1440.81 $m/z$ (INTVNSNTLPVLR) was recently included[46] in a list of the most stable peptide markers for hazelnut detection in processed food, because it does not contain amino acids susceptible to oxidation.


dx.doi.org/10.1021/jf504007d | J. Agric. Food Chem. 2014, 62, 9401−9409

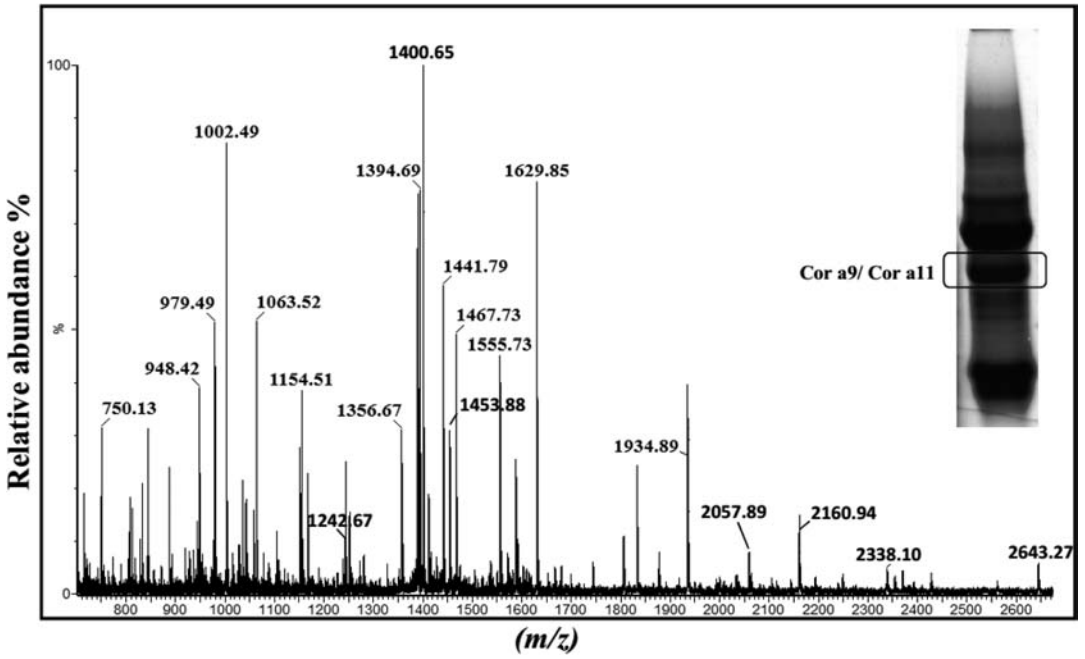


**Figure 5.** SDS-PAGE of a hazelnut kernels protein extract (inset) and MALDI mass spectrum relevant to the in-gel digestion of the band at 55 kDa.

The procedure was subsequently applied to different kinds of hazelnut oils of different origin (see experimental section), obtained from raw and roasted hazelnuts. Similar results were obtained for all samples, even if, as already reported,[17] the amount of extracted protein was always higher in the case of raw hazelnut oils.

As clearly stated in the introduction, the objective of the present work was the detection of hidden hazelnut allergens in EVOO samples. In general, the lowest dose of allergens that provokes a reaction is called LOAEL or lowest observed adverse effect level. Recent clinical studies[49,50] reported that the most sensitive patients had a LOAEL eliciting objective signs after the ingestion of only 1 mg of hazelnut protein, whereas the dosage eliciting reaction in a 10% of the food-allergic population is 133.8 mg. The present approach permitted the assessment of a total protein concentration in the range 20−100 $\mu$g per mL of hazelnut oil; then, 1 mL of EVOO adulterated with 20% of HO would contain a total protein concentration between 4 and 20 $\mu$g. It means that this method was able to reach detection limits well below the LOAEL value.

Thus, the present strategy allowed fast detection of a very low hazelnut protein content in complex matrices as edible oils by recurring to a simple acetone precipitation and in solution tryptic digestion.

**SDS PAGE for Confirming Hazelnut Proteins Attribution.** A more conventional approach, based on SDS-PAGE followed by in gel tryptic digestion, was then applied to a hazelnut kernels protein extract, with the aim to create a small reference database. All the bands obtained (see gel in the inset of Figure 5) were eventually analyzed by MALDI-MS. It should be noted that a univocal identification of these proteins is difficult to achieve, in particular by using a monodimensional gel, due to the presence of different isoforms, multiple glycoforms, and post-translational protease-cleaved subunits.[51] In fact, some peptides attributable to Cor a 9 and Cor a 11 were detected in all the processed bands at different molecular weights. Considering that hazelnut proteins are present as high molecular weight complexes (300−450 kDa) of minor subunits linked by noncovalent disulfide bridges, these weak bonds can be broken during the extraction processes, thus originating lower molecular weight units.

For instance, in the MALDI spectrum shown in Figure 5, relevant to the in gel digestion of the band at 55 kDa, the most intense peak was attributed to Cor a 9 even if some Cor a 11 peptides were also present. The complete attribution of the main peaks observed in the spectrum of Figure 5 is reported in Table 2. Other significant $m/z$ ions (750.13, 1154.51, 1242.67, 1400.65, 1453.88, 1467.73, 2057.89, and 2160.94) were not attributable with any known identification tool. Only the $m/z$ ions 1400.65 and 1453.88 were identified as the alkaline and immunogenic subunit of a new hazelnut allergen, an isoform of Cor a 9, recently identified by Nitride et al.[8]

Furthermore, by using FindPept and ClustalO (UniProt), it was possible to propose an attribution for the $m/z$ ion 1242.67 by homology with similar proteins. Indeed, from the in-silico digestion of the Avena globulin 11S (*Avena sativa*), a peptide at 1242.66 $m/z$ is generated. Then, aligning the sequences of *Avena sativa* globulin 11S (Q38780) and *Corylus avellana* 11S globulin-like protein (Q8W1C2), a similarity of 70% between the peptide QEARNLKNNR from *Avena s.* and the peptide EEARRLKYNR from *Corylus a.* was found suggesting an attribution as possible protein variants (Figure 6). Of course, de novo sequencing is needed to confirm this hypothesis and suggest possible protein variants.

In the present study, a cold-acetone protein precipitation followed by in-solution tryptic digestion and MALDI-MS analysis was applied for the first time for the direct determination of hidden hazelnut oil proteins in extra virgin olive oil.

The method, applied on oils of different geographical origin, showed to be reproducible and independent from oil processing and cultivars. In fact, contrary to usual markers (fatty acids, triacylglycerols, volatile compounds, and tocopherols) that are affected by the environmental conditions of plant growth, proteins, being more stable and species-specific, could

**Table 2. Probable Attributions of the Peptides Observed in the MALDI Mass Spectrum Relevant to the Tryptic Digest of a SDS-PAGE Band (55 kDa) from a Hazelnut Protein Extract**

| *m/z* | position | sequence | protein |
|---|---|---|---|
| 935.41 | 507−515 | SESEGRAEA | Cor a 9 |
| 976.49 | 505−512 | RRSESEGR | Cor a 9 |
| 979.49 | 333−340 | E**N**ICTRSR[a] | Cor a 9 |
| 1002.49 | 364−371 | WLQLSAER | Cor a 9 |
| 1027.50 | 139−146 | SEQDRHQK | Cor a 9 |
| 1027.50 | 43−51 | LNALEPTNR | Cor a 9 |
| 1063.52 | 301−308 | ESE**Q**ERER[a] | Cor a 9 |
| 1077.49 | 395−403 | GNIVNEFER | Cor a 11 |
| 1089.53 | 5−13 | EDPELKKCK | Cor a 11 |
| 1151.53 | 341−350 | ADIYTEQVGR | Cor a 9 |
| 1220.55 | 258−268 | $GSM_{ox}AGPYYNSR$ | Cor a 11 |
| 1226.54 | 270−279 | RRNIVKVEGR | Cor a 9 |
| 1279.65 | 486−495 | YNRQETTLVR | Cor a 9 |
| 1327.62 | 1−11 | MLPKEDPELKK | Cor a 11 |
| 1356.67 | 446−458 | TNDNAQISPLAGR | Cor a 9 |
| 1394.69 | 339−350 | SRADIYTEQVGR | Cor a 9 |
| 1400.65 | | HDGQNLFDWLR | Cor a 9 isoallergen |
| 1416.75 | 94−105 | ESFNVEHGDIIR | Cor a 11 |
| 1440.81 | 351−363 | INTVNSNTLPVLR | Cor a 9 |
| 1453.88 | | ITSLNSLNLPILR | Cor a 9 isoallergen |
| 1555.73 | 433−445 | RAESEGFEWVAFK | Cor a 9 |
| 1577.75 | 216−228 | REQLEKVFGEQSK | Cor a 11 |
| 1587.72 | 364−376 | WLQLSAERGDLQR | Cor a 9 |
| 1609.84 | 486−498 | YNRQETTLVRSSR | Cor a 9 |
| 1629.85 | 464−478 | ALPDDVLANAFQISR | Cor a 9 |
| 1698.75 | 195−208 | HFYLAGNPDDEHQR | Cor a 9 |
| 1805.93 | 75−89 | TEEGRVQVLENFTKR | Cor a 11 |
| 1832.83 | 288−300 | SRQEWERQERQER | Cor a 9 |
| 1876.90 | 73−88 | VKTEEGRVVLENFTK | Cor a 11 |
| 1934.89 | 401−417 | VQVVDDNGNTVFDDELR | Cor a 9 |
| 2338.10 | 377−396 | EGLYVPHWNLNAHSVVYAIR | Cor a 9 |
| 2643.27 | 80−102 | TIEPNGLLLPQYSNAPELIYIER | Cor a 9 |
| 2943.3 | 128−154 | ILQPVSAPGHFEAFYGAGGEDPESFYR | Cor a 11 |

[a]Underlined amino acids in bold are probably deamidated.

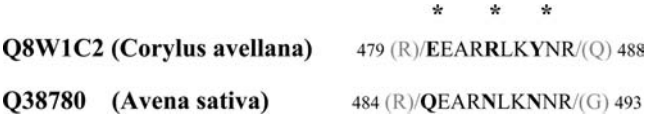


**Figure 6.** Alignment of the peptide at 479-488 from Cor a 9 with the peptide at *m/z* 1242.66 of 11S globulin from *Avena sativa*. The differences in the amino acid sequences are shown in bold with an asterisk and suggest possible protein variants.

be used for identifying each vegetable oil used for EVOO adulteration.

Stable hazelnut peptide markers in HO were detected at *m/z* 1002.52, 1356.71, 1394.70, 1399.71, 1440.81, 1555.76, 1571.84, 1629.83 from Cor a 9, at *m/z* 1453.85 from Cor a 9 isoform, at *m/z* 1363.73 from Cor a 11, and at *m/z* 1528.67 from Cor a 1. The peptides found in hazelnut oils can potentially be analytical targets for the determination of hazelnut traces in other processed foods.

## AUTHOR INFORMATION

### Corresponding Author

*E-mail: cosimadamiana.calvano@uniba.it. Fax: +39-080-5442026. Tel: +39-080-5443589

### Notes

The authors declare no competing financial interest.

## REFERENCES

(1) Foods—Food and Drug Administration. http://www.fda.gov/Food/default.htm (Released on August 2014).

(2) European Commission. http://ec.europa.eu/energy/oil/index_en.htm (Released on August 2014).

(3) Savage, G. P.; McNeil, D. L.; Dutta, P. C. Lipid composition and oxidative stability of oils in hazelnuts (*Corylus avellana L.*) grown in New Zealand. *J. Am. Oil Chem. Soc.* **1997**, *74*, 755−759.

(4) Vichi, S.; Pizzale, L.; Toffano, E.; Bortolomeazzi, R.; Conte, L. Detection of hazelnut oil in virgin olive oil by assessment of free sterols and triacylglycerols. *J. AOAC Int.* **2001**, *84*, 1534−1541.

(5) Arlorio, M.; Coisson, J. D.; Bordiga, M.; Travaglia, F.; Garino, C.; Zuidmeer, L.; Van Ree, R.; Giuffrida, M. G.; Conti, A.; Martelli, A. Olive oil adulterated with hazelnut oils: simulation to identify possible risks to allergic consumers. *Food Addit. Contam., Part A* **2010**, *27*, 11−18.

(6) Rigby, N. M.; Marsh, J.; Sancho, A. I.; Wellner, K.; Akkerdaas, J.; van Ree, R.; Knulst, A.; Montserrat, F. R.; Brettlova, V.; Schilte, P. P.; Summer, C.; Pumphrey, R.; Shewry, P. R.; Mills, E. N. The purificationand characterisation of allergenic hazelnut seed proteins. *Mol. Nutr. Food Res.* **2008**, *52*, S251−S261.

(7) Zuidmeer, L.; Garino, C.; Marsh, J.; Lovegrove, A.; Morati, M.; Versteeg, S.; Schilte, P.; Shewry, P.; Arlorio, M.; van Ree, R. Isolation,

cloning and confirmation as an allergen of the 2S albumin from hazelnut. *Allergy* **2009**, *64*, 235−242.
(8) Nitride, C.; Mamone, G.; Picariello, G.; Mills, C.; Nocerino, R.; Berni Canani, R.; Ferranti, P. Proteomic and immunological characterization of a new food allergen from hazelnut (*Corylus avellana*). *J. Proteomics* **2013**, *86*, 16−26.
(9) Luttkopf, D.; Muller, U.; Skov, P. S.; Ballmer-Weber, B. K.; Wuthrich, B.; SkamstrupHansen, K.; Poulsen, L. K.; Kastner, M.; Haustein, D.; Vieths, S. Comparison of four variants of a major allergen in hazelnut (*Corylus avellana*) Cor a 1.04 with the major hazel pollen allergen Cor a 1.01. *Mol. Immunol.* **2002**, *38*, 515−525.
(10) Martin-Hernandez, C.; Benet, S.; Obert, L. Determination of Proteins in Refined and Nonrefined Oils. *J. Agric. Food Chem.* **2008**, *56*, 4348−4351.
(11) Crevel, R. W. R.; Kerkhoff, M. A. T.; Koning, M. M. G. Allergenicity of refined vegetable oils. *Food Chem. Toxicol.* **2000**, *38*, 385−393.
(12) Olszewski, A.; Pons, L.; Moutete, F.; Aimone-Gastin, I.; Kanny, G.; Moneret-Vautrin, D. A.; Gueant, J. L. Isolation and characterization of proteic allergens in refined peanut oil. *Clin. Exp. Allergy* **1998**, *28*, 850−859.
(13) Teuber, S. S.; Brown, R. L.; Haapanen, L. A. Allergenicity of gourmet nut oils processed by different methods. *J. Allergy Clin. Immunol.* **1997**, *99*, 502−507.
(14) Moneret-Vautrin, D. A.; Rance, F.; Kanny, G.; Olszewski, A.; Guéant, J. L.; Dutau, G.; Guérin, L. Food allergy to peanuts in France—evaluation of 142 observations. *Clin. Exp. Allergy* **1998**, *28*, 1113−1119.
(15) Moneret-Vautrin, D. A. Food allergy: present problems and perspectives. In *Advances in Allergology and Clinical Immunology: The Proceedings of the Plenary Sessions and Afternoon Symposia of the Xvth European Congress of Alle*; Godard, P., Bousquet, J., Michel, F.B., Eds.; Parthenon Publishing Group Ltd.: U.K., 1992; pp 473−483.
(16) Moneret-Vautrin, D. A.; Hatahet, R.; Kanny, G.; Ait-Djafer, Z. Allergenic peanut oil in milk formulas. *Lancet* **1991**, *338*, 1149−1152.
(17) Bremer, M. G. E. G.; Smits, N. G. E.; Haasnoot, W. Biosensor immunoassay for traces of hazelnut protein in olive oil. *Anal. Bioanal. Chem.* **2009**, *395*, 119−126.
(18) Ayorinde, F. O.; Garvin, K.; Saeed, K. Determination of the fatty acid composition of saponified vegetable oils using matrix-assisted laser desorption/ionization time-of-flight mass spectrometry. *Rapid Commun. Mass Spectrom.* **2000**, *14*, 608−615.
(19) Park, K. H.; Kim, H. J. Analysis of fatty acids by graphite plate laser desorption/ionization time-of-flight mass spectrometry. *Rapid Commun. Mass Spectrom.* **2001**, *15*, 1494−1499.
(20) Jakab, A.; Nagy, K.; Heberger, K.; Vekey, K.; Forgacs, E. Differentiation of vegetable oils by mass spectrometry combined with statistical analysis. *Rapid Commun. Mass Spectrom.* **2002**, *16*, 2291−2297.
(21) Cozzolino, R.; De Giulio, B. Application of ESI and MALDI-TOF MS for triacylglycerols analysis in edible oils. *Eur. J. Lipid Sci. Technol.* **2011**, *113*, 160−167.
(22) Cercaci, L.; Rodriguez-Estrada, M. T.; Lercker, G. Analysis of the oxidation products of cis- and trans-octadecenoate methyl esters by capillary gas chromatography-ion-trap mass spectrometry. I. Epoxide and dimeric compounds. *J. Chromatogr. A* **2003**, *985*, 211−220.
(23) Bail, S.; Stuebiger, G.; Unterweger, H.; Buchbauer, G.; Krist, S. Characterization of volatile compounds and triacylglycerol profiles of nut oils using SPME-GC-MS and MALDI-TOF-MS. *Eur. J. Lipid Sci. Technol.* **2009**, *111*, 170−182.
(24) Pavon, J. L. P.; del Nogal Sanchez, M.; Fernandez Laespada, E. M.; Cordero, B. M. Determination of filbertone in spiked olive oil samples using headspace-programmed temperature vaporization−gas chromatography−mass spectrometry. *Anal. Bioanal. Chem.* **2009**, *394*, 1463−1470.
(25) Flores, G.; del Castillo, M. L. R.; Herraiz, M.; Blanch, G. P. Study of the adulteration of olive oil with hazelnut oil by on-line coupled high-performance liquid chromatographic and gas chromatographic analysis of filbertone. *Food Chem.* **2006**, *97*, 742−749.
(26) Cert, A.; Moreda, W.; Pérez-Camino, M. C. Chromatographic analysis of minor constituents in vegetable oils. *J. Chromatogr. A* **2000**, *881*, 131−148.
(27) Calvano, C. D.; Aresta, A.; Zambonin, C. G. Detection of hazelnut oil in extra-virgin olive oil by analysis of polar components by micro-solid phase extraction based on hydrophilic liquid chromatography and MALDI-ToF mass spectrometry. *J. Mass Spectrom.* **2010**, *45*, 981−988.
(28) Koidis, A.; Boskou, D. The contents of proteins and phospholipids in cloudy (veiled) virgin olive oils. *Eur. J. Lipid Sci. Technol.* **2006**, *108*, 323−328.
(29) Calò, V.; Nacci, A.; Monopoli, A. Pd-benzothiazol-2-ylidene complex in ionic liquids: Efficient catalyst for carbon-carbon coupling reactions. *J. Organomet. Chem.* **2005**, *690*, 5458−5466.
(30) Calvano, C. D.; De Ceglie, C.; D'Accolti, L.; Zambonin, C. G. MALDI-TOF mass spectrometry detection of extra-virgin olive oil adulteration with hazelnut oil by analysis of phospholipids using an ionic liquid as matrix and extraction solvent. *Food Chem.* **2012**, *134*, 1192−1198.
(31) Cozzolino, R.; Passalacqua, S.; Salemi, S.; Garozzo, D. Identification of adulteration in water buffalo mozzarella and in ewe cheese by using whey proteins as biomarkers and matrix-assisted laser desorption/ionization mass spectrometry. *J. Mass Spectrom.* **2002**, *37*, 985−991.
(32) Calvano, C. D.; Monopoli, A.; Loizzo, P.; Faccia, M.; Zambonin, C. G. Proteomic Approach Based on MALDI-TOF MS To Detect Powdered Milk in Fresh Cow's Milk. *J. Agric. Food Chem.* **2013**, *61*, 1609−1617.
(33) Cucu, T.; Platteau, C.; Taverniers, I.; Devreese, B.; De Loose, M.; De Meulenaer, B. ELISA detection of hazelnut proteins: effect of protein glycation in the presence or absence of wheat proteins. *Food Addit. Contam., Part A* **2011**, *28*, 1−10.
(34) Breton, C.; Claux, D.; Metton, I.; Skorski, G.; Bervillé, A. Comparative study of methods for DNA preparation from olive oil samples to identify cultivar SSR alleles in commercial oil samples: possible forensic applications. *J. Agric. Food Chem.* **2004**, *52*, 531−537.
(35) Busconi, M.; Foroni, C.; Corradi, M.; Bongiorni, C.; Cattapan, F.; Fogher, C. DNA extraction from olive oil and its use in the identification of the production cultivar. *Food Chem.* **2003**, *83*, 127−134.
(36) Pafundo, S.; Gullì, M.; Marmiroli, N. Multiplex real-time PCR using SYBR® GreenER for detection of DNA allergens in food. *Anal. Bioanal. Chem.* **2010**, *396*, 1831−1839.
(37) Agrimonti, C.; Vietina, M.; Pafundo, S.; Marmiroli, N. The use of food genomics to ensure the traceability of olive oil. *Trends Food Sci. Techn.* **2011**, *22*, 237−244.
(38) Downs, M. L.; Taylor, S. L. Effects of thermal processing on the enzyme-linked immunosorbent assay (ELISA) detection of milk residues in a model food matrix. *J. Agric. Food Chem.* **2010**, *58*, 10085−10091.
(39) Scaravelli, E.; Brohee, M.; Marchelli, R.; van Hengel, A. J. The effect of heat treatment on the detection of peanut allergens as determined by ELISA and real-time PCR. *Anal. Bioanal. Chem.* **2009**, *395*, 127−137.
(40) Rigby, N. M.; Sancho, A. I.; Salt, L. J.; Foxall, R.; Taylor, S.; Raczynski, A.; Cochrane, S. A.; Crevel, R. W.; Mills, E. N. Quantification and partial characterization of the residual protein in fully and partially refined commercial soybean oils. *J. Agric. Food Chem.* **2011**, *59*, 1752−1759.
(41) Poms, R. E.; Capelletti, C.; Anklam, E. Effect of roasting history and buffer composition on peanut protein extraction efficiency. *Mol. Nutr. Food Res.* **2004**, *48*, 459−464.
(42) Bligh, E. G.; Dyer, W. J. A rapid method of total lipid extraction and purification. *Can. J. Biochem. Physiol.* **1959**, *37*, 911−917.
(43) Sheoran, I. S.; Ross, A. R. S.; Olson, D. J. H.; Sawhney, V. K. Compatibility of plant protein extraction methods with mass spectrometry for proteome analysis. *Plant Sci.* **2009**, *176*, 99−104.
(44) Lauer, I.; Foetisch, K.; Kolarich, D.; Ballmer-Weber, B. K.; Conti, A.; Altmann, F.; Vieths, S.; Scheurer, S. Hazelnut (*Corylus*

*avellana*) vicilin Cor a 11: molecular characterization of a glycoprotein and its allergenic activity. *Biochem. J.* **2004**, *383*, 327−334.
(45) Ansari, P.; Stoppacher, N.; Baumgartner, S. Marker peptide selection for the determination of hazelnut by LC-MS/MS and occurrence in other nuts. *Anal. Bioanal. Chem.* **2012**, *402* (8), 2607−2615.
(46) Cucu, T.; De Meulenaer, B.; Devreese, B. MALDI-based identification of stable hazelnut protein derived tryptic marker peptides. *Food Addit. Contam., Part A* **2012**, *29*, 1821−1831.
(47) Hidalgo, F. J.; Alaiz, M.; Zamora, R. Determination of peptides and proteins in fats and oils. *Anal. Chem.* **2001**, *73*, 698−702.
(48) Bradford, M. M. A rapid and sensitive method for the quantitation of microgram quantities of protein utilizing the principle of protein-dye binding. *Anal. Biochem.* **1976**, *72*, 248−54.
(49) Eller, E.; Hansen, T. K.; Bindslev-Jensen, C. Clinical thresholds to egg, hazelnut, milk and peanut: results from a single-center study using standardized challenges. *Ann. Allergy Asthma Immunol.* **2012**, *108*, 332−336.
(50) Allen, K. J.; Remington, B. C.; Baumert, J. L.; Crevel, R. W. R.; Houben, G. F.; Brooke-Taylor, S.; Kruizinga, A. G.; Taylor, S. L. Allergen reference doses for precautionary labeling (VITAL 2.0): Clinical implications. *J. Allergy Clin. Immunol.* **2014**, *133*, 156−164.
(51) Guo, F.; Kothary, M. H.; Wang, Y.; Yu, X.; Howard, A. J.; Fu, T. J.; Zhang, Y. Z. Purification and crystallization of Cor a 9, a major hazelnut allergen. *Acta Crystallogr., Sect. F: Struct. Biol. Cryst. Commun.* **2009**, *65*, 42−46.

comparison to ESI, APCI is a less soft ionization technique that generates more fragment ions relative to the parent ion. Furthermore, the quadrupole time-of-flight (Q-TOF) analyzer is a suitable tool for screening for known and unknown SGs, whereas triple quadrupole (QqQ) is advisible only for monitoring targeted SGs.[13] Previously, Wewer et al. reported quantification of SGs by nanospray direct infusion by Q-TOF MS/MS experiments.[14] However, no chromatographic separation was conducted in that study prior to MS analysis, which makes the differentiation between isomers impossible. Rocio et al.[15] used HPLC-TOF-MS, and Van Gerpen et al.[16] used MALDI-TOF-MS for identification of SGs; however, MS-based quantification was not performed. With regard to chromatographic techniques, ultraperformance liquid chromatography (UPLC) is the newest state-of-the-art technology providing higher resolution, optimized signal-to-noise ratio, and shorter run times as compared to HPLC. To the best of our knowledge, no UPLC methods for SGs have been published so far.

In this study, the highly efficient separation af single, intact SG species by RP-UPLC was combined with detection by a Q-TOF analyzer, which led to high mass accuracy. The UPLC-Q-TOF-MS method was developed, optimized, and validated to enable rapid, mass accurate, and highly sensitive SG detection as the sodiated adduct of the molecular ion. Furthermore, the applicability of the validated method was demonstrated for selected foods (oat bran and whole wheat) with various SG amounts and profiles and including consideration of the matrix effect.

## MATERIALS AND METHODS

**Reagents.** Acetone, acetic acid, ammonium acetate, formic acid of LC-MS grade, and cholesterol $\beta$-D-glucoside (≥97% purity) were purchased from Sigma-Aldrich (Buchs, Switzerland). LC-MS grade acetonitrile, isopropanol, methanol, and water were from Biosolve (Dieuze, France). The commercial mixture of steryl glycosides (>98% purity) used as reference substances was from Matreya Inc. (Pleasant Gap, PA, USA) containing approximately 56% sitosteryl glucoside, 25% campesteryl glucoside, 18% stigmasteryl glucoside, and 1% $\Delta^5$-avenasteryl glucoside. HPLC grade hexane and isopropanol used for sample extraction were from Fluka (Buchs, Switzerland).

**Instrumentation and Chromatographic Conditions.** The UPLC system was a Waters Acquity UPLC System equipped with an Acquity UPLC BEH C18 column (50 mm × 2.1 mm, i.d., 1.7 $\mu$m). The MS system (Synapt G2) was composed of an electrospray ionization source and a Q-TOF analyzer (Waters Corp., Milford, MA, USA).

*Selection of the Mobile Phase and Additive.* The mobile phases for method development in positive mode consisted of acetonitrile, methanol, or a mixture of 50% acetonitrile and 50% isopropanol combined with water to which either 0.1% (v/v) acetic acid or formic acid was added, leading to suitable acidic conditions for positive mode (see Table 2). Less acidic conditions obtained by a buffered solution with 0.1% (v/v) acetic acid and 1 mM ammonium acetate solved in water and acetonitrile on the other hand allowed measurements in both positive- and negative-ion modes. Another advantage of the buffered system is an increased solubility of ammonium acetate in acetonitrile.[17] The resolution and sensitivity were assessed by extracted ion chromatograms (EIC) of sodiated ions of the two isomers stigmasteryl glucoside and $\Delta^5$-avenasteryl glucoside, with equal masses ($m/z$ 597.4131 as $[M + Na]^+$), that occur in the SG standard (Figure 2). For better comparability, the same ESI parameters and mobile phase gradient were used for all measurements in positive mode.

For the optimization of the UPLC mobile phase composition, 5 $\mu$L of the SG standard with a concentration of 9 $\mu$M (calculated on the basis of the mass of sitosteryl glucoside) dissolved in the same solvent as the organic mobile phase was injected in partial loop mode. All measurements for method development were carried out with the same UPLC gradient from 30% water + additive (A) and 70% organic solvent + additive (B) to 100% B in 3 min, followed by isocratic condition of 100% B for 2 min (total run time = 5 min). Column temperature was maintained at 40 °C with a flow rate of 0.3 mL/min. Each run was followed by re-equilibration period of 3 min with a mobile phase composition of 30% A and 70% B.

*UPLC Gradient Used for Food Analysis.* For a more precise injection volume, 10 $\mu$L of the sample was injected in full loop mode. The analysis was performed using the following gradient elution: 50% water + 0.1% (v/v) formic acid (A) and 50% methanol + 0.1% (v/v) formic acid (B) for 1 min changing to 87.5% B during 2 min. During the next 2 min, B was increased to 90% and finally during the next 2 min to 100%, which was kept for 3 min. The total run time was 10 min. The flow rate was 0.3 mL/min and the column temperature, 40 °C. Each run was followed by a re-equilibration period of 3 min with 50% B.

**MS Conditions.** *Optimization of Ionization Parameters by Direct Infusion and in Combination with LC.* For optimization of the ionization parameters a standard mixture of SG (3 $\mu$M, concentration calculated on the basis of the mass of sitosteryl glucoside) was injected by direct infusion into the MS using ESI. For ESI positive-ion mode the voltages of capillary, sample cone, and extraction cone were set at 3000, 60, and 4 V, respectively. The desolvation gas flow rate was 900 L/h at 550 °C. Source temperature was 130 °C. Cone gas flow was 10 L/h. For ESI negative-ion mode the voltages of capillary, sample cone, and extraction cone were set at 2000, 30, and 4.5 V, respectively. The desolvation gas flow rate was 950 L/h at 500 °C. Source temperature was 130 °C. Cone gas flow was 20 L/h.

APCI was performed using ESCI multi-mode ionization source. This mode switched between ESI and APCI at a high speed and, thus, made it possible to measure both ionization modes within the same chromatographic run. The ionization parameters were adopted from ESI with the addition of a corona current of 5 $\mu$A. Nitrogen served as desolvation gas and as cone gas for both ESI and APCI measurements.

Full scan mass spectra were acquired from $m/z$ 50 to 1200 at a scan rate of 0.5 s. EIC of sodium adducts and $[M - H + Hac]^-$ were used for method evaluation (Table 1). Peaks were identified on the basis of the mass-to-charge ratio ($m/z$) of the compounds and comparison of the relative retention time to cholesteryl glucoside. Each chromatographic peak was integrated using Mass-Lynx 4.1 software (Waters) without smoothing. Data evaluation was conducted with a mass range window of 0.02 Da (equivalent to approximately 33 ppm for sodiated SG adducts).

**Table 1. Mass-to-Charge Ratio $m/z$ of Targeted SGs as $[M + Na]^+$ in Positive and as $[M - H + Hac]^-$ in Negative Scan Mode**

| compound | $[M + Na]^+$ | $[M - H + Hac]^-$ |
|---|---|---|
| cholesteryl glucoside | 571.3975 | 607.4210 |
| campesteryl glucoside | 585.4131 | 621.4366 |
| $\Delta^5$-avenasteryl glucoside | 597.4131 | 633.4366 |
| $\Delta^7$-avenasteryl glucoside | 597.4131 | 633.4366 |
| stigmasteryl glucoside | 597.4131 | 633.4366 |
| sitosteryl glucoside | 599.4288 | 635.4523 |

*ESI Conditions Used for SG Analysis in Foods.* The final optimized conditions used for the validation and analysis of samples were all carried out in positive ionization mode. The voltages of capillary, sample cone, and extraction cone were set at 3000, 60, and 4.5 V, respectively. The desolvation gas flow rate was 850 L/h at 520 °C. The source temperature was 130 °C. Cone gas flow was 20 L/h. Full scan mass spectra were acquired from $m/z$ 350 to 1200 at a scan rate of 0.5 s.

**Internal Standard Preparation and Method Validation.** A stock solution of the internal standard cholesterol glucoside was prepared at a concentration of 4.8 $\mu$g/mL in methanol. The seven-


dx.doi.org/10.1021/jf501509m | J. Agric. Food Chem. 2014, 62, 9410−9419

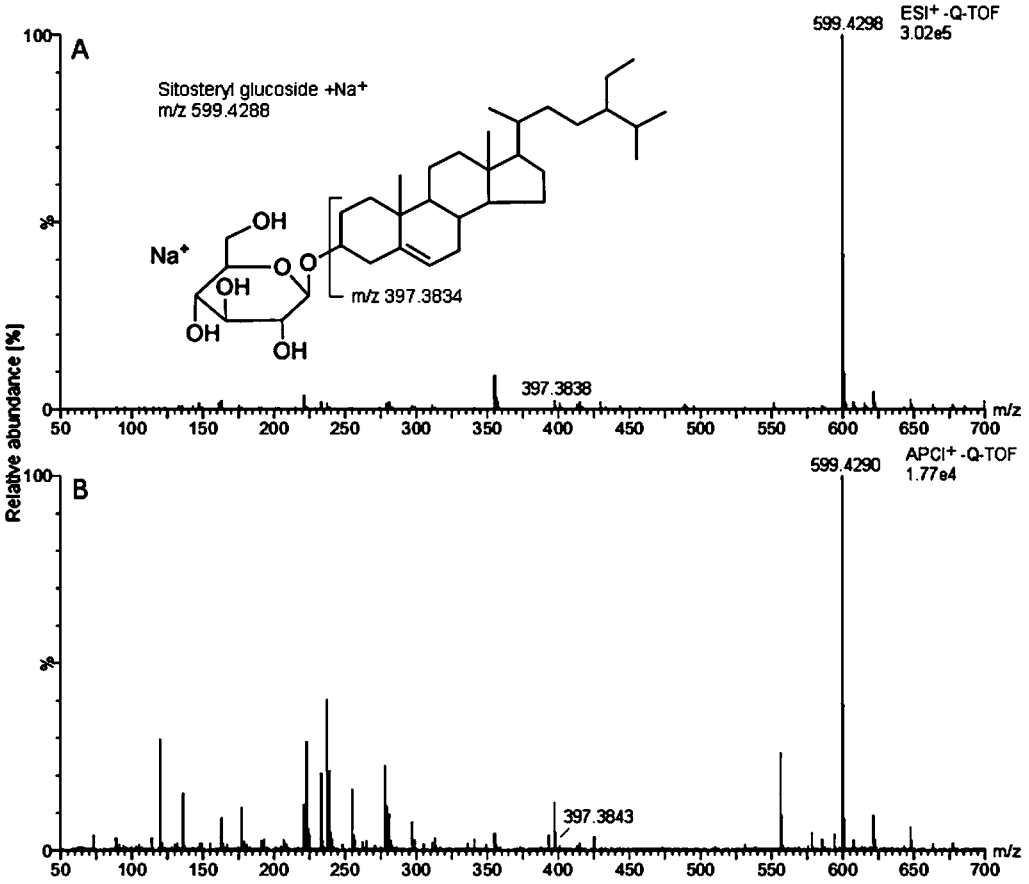


**Figure 1.** ESI (A) and APCI (B) mass spectra of sitosteryl glucoside ($[M + Na]^+ = m/z$ 599.4288, $[\text{aglycone} + H - H_2O]^+ = m/z$ 397.3834) in SG standard solution measured in one UPLC-MS analysis run using ESCI multi-mode ionization and MeOH/water gradient + 0.1% (v/v) formic acid acquired in positive scan mode.

point calibration curve of cholesteryl glucoside in 100% methanol was determined at the following levels: 14.4, 43.2, 72.0, 108.0, 144.0, 180.0, and 216.0 ng/mL, each measured in triplicate with an injection volume of 10 $\mu$L. The calibration curve was weighted by $1/x$, and the point of origin was excluded from the equation. To determine the interday and intraday variabilities, five repetitive analyses of quality control samples containing 54 and 90 ng/mL cholesteryl glucoside were performed on three different days. The limit of detection (LOD) and the limit of quantification (LOQ) were defined as 3 and 10 times the noise signal in the region of cholesteryl glucoside in the chromatogram, respectively. The determination of the LOD and LOQ was based on a calibration curve with lower cholesteryl glucoside levels (0.72, 1.44, 2.88, 5.76, and 14.40 ng/mL) all run in triplicate. For quantification of the SGs in food samples the lowest point of the calibration curve (14.4 ng/mL) was used as the LOQ.

**Sample Preparation for the Analysis of Steryl Glycosides Extracted from Foods.** Whole wheat flour was bought from a local grocery store, and oat bran (Oatwell 28%) was obtained from DSM Nutritional Products Ltd. (Kaiseraugst, Switzerland). For sample preparation the method described by Nyström et al. was used with small adaptions.[2] First, accelerated solvent extractor (ASE) was performed to extract the lipids. Afterward, 5 and 10 mL of the internal standard stock solution of 4.8 $\mu$g/mL were added to the wheat and oat extract, respectively. Next the extracts were evaporated to dryness and redissolved in a hexane/isopropanol mixture at a ratio of 95:5. To separate SGs from other sterols and neutral lipids, a fractionation by solid phase extraction (SPE) was performed with hexane and isopropanol. After evaporation under a gentle nitrogen stream at 50 °C of the SG fraction, the residue was dissolved in methanol.

**Determination of Matrix Effect Profile by Postcolumn Infusion.** First, the impact of the matrix effect on different SG species was evaluated by postcolumn infusion according to the method of Stahnke et al. with small adaptions.[18] In short, the matrix effect was defined as the alteration of the signal intensity of the target analyte (postcolumn infusion) caused by injected food compounds compared to an injected reference sample. Therefore, SGs extracted from oat and wheat as well as a reference sample (pure methanol) were measured in triplicates with the final UPLC-Q-TOF-MS method while a SG solution (2.4 $\mu$g/mL cholesteryl glucoside and 2.8 $\mu$g/mL SG standard solution with 8.2 ng/mL sodium acetate and 0.1% (v/v) formic acid) was continuously postcolumn infused. As the food samples naturally contained SG, they were additionally measured without postcolumn infusion, and the signal intensities were subtracted from the detected signal intensities of the infused SGs. The calculation of the matrix effect profile of particular sample matrices including smoothing of the data ($f = 0.6$) was performed according to the method of Stahnke et al.[18]

Second, the matrix profile of the wheat and oat samples was evaluated by postcolumn infusion using cholesterol glucoside as monitor substance. The infused solution was composed of 2.4 $\mu$g/mL cholesteryl glucoside in methanol, 8.2 ng/mL sodium acetate, and 0.1% (v/v) formic acid. The matrix effect profile of wheat was determined for 1 g per 500 mL and per 25 mL, whereas oat was measured at the concentrations of 1 g per 1000 mL and per 100 mL.

The four most common SGs (sitosteryl, campesteryl, stigmasteryl, and $\Delta^5$-avenasteryl glucoside) and $\Delta^7$-avenasteryl glucoside were identified on the basis of the relative retention times to cholesteryl glucoside and their $m/z$ (extracted ion chromatograms of $[M + Na]^+$). The SG contents of oat bran and whole wheat were quantified on the basis of the internal standard including matrix effect compensation at the retention time of each analyte of interest. Because the peak width had to be included, the mean of the 11 data points around the retention time of each analyte was used for the calculation.

Data acquisition and processing was performed using Mass-Lynx and Quan-Lynx software with automatic Savitzky−Golay smoothing (smoothing parameters were iterations = 1 and width = 2). A mass range window of 0.02 Da was used with a scan time of 0.5 s. For the matrix effect evaluation and application on food samples, all data points were considered, whereas for graphical illustration only one-fourth of the data were used.

**Statistical Analysis.** All experiments were carried out in triplicates. Results were presented as mean values ± standard deviation. For data analysis SPSS 20.0 statistical software was used. One-way ANOVA, together with Tukey's test, was performed using a confidence interval of 95%.

## RESULTS AND DISCUSSION

To optimize the methodology for the analysis of SG using UPLC-MS, we evaluated a range of conditions and their effects on the separation and ionization efficacy of the SG species. First, the ESI and APCI parameters were modified to reach the highest signal intensity of intact SG, using sitosteryl glucoside, campesteryl glucoside, and the three isomers stigmasteryl, $\Delta^5$-avenasteryl, and $\Delta^7$-avenasteryl glucoside as the target analytes. Second, the mobile phase and the additive were selected for UPLC separation, and the whole method was optimized, validated, and used to analyze SG contents and profiles in foods.

**Optimization of Ionization Parameters To Detect the Intact Steryl Glycosides.** We observed that the ESI parameters, assessed by direct infusion of the SG standard solution, had a significant impact on ionization efficiency, as shown by the varying intensities of the targeted ion species. Before optimization, SG ion species with the highest intensity were the aglycone ions $[\text{aglycone} + H - H_2O]^+$, the sodiated adducts $[M + Na]^+$, and the potassiated adducts $[M + K]^+$, as well as $[2\ M + Na]^+$ (in decreasing order of intensity), when experiments were performed with lower sample cone voltage (40 V), lower desolvation temperature (200 °C), and lower source temperature (100 °C) than the final optimized ionization parameters. A high intensity of the molecular ion of SG was targeted; however, $[M + H]^+$ was not formed in high abundance under any conditions tested. Thus, the ionization conditions were optimized to obtain the highest abundance of sodiated ion species $[M + Na]^+$. Formation of $[M + Na]^+$ in SG analysis was also reported by Yamauchi et al.[12] when using positive mode APCI analyzing bell pepper samples and by Van Gerpen et al.[16] measuring purified biodiesel residue with MALDI in positive mode. The advantage of adducts is their stability toward high ionization voltage, whereas nonadduct ion species are less stable and, thus, eliminated at high energy input. This makes quantitative analysis more reliable and increases reproducibility. In this study, high formation of sodiated SG adducts $[M + Na]^+$ was accomplished by increasing the cone voltage to 60 V, and the respective aglycone $[\text{aglycone} + H - H_2O]^+$ was detected only at a small intensity (Figure 1A). This was a major improvement compared to previous reports of APCI and nanospray ionization methods for SG, which have mainly enabled the detection of the aglycone ions, but not the respective molecular ions.[8,12,19] Although Strobl[20] demonstrated an improved signal for SG molecular ions with APCI using a QqQ analyzer, a high percentage of aglycone still occurred. The advantage of measuring the intact SG is the possibility of identifying the type of sugar attached, given the fact that both hexoses and pentoses have been identified in SGs.[21] Furthermore, SGs exist not only as monoglycosides but also as other oligoglycosides as reported, for instance, in rice and adzuki beans.[21−23]

In this study, we were able to show that different SG species have the same ionization behavior, which allows evaluation of only one ion species while enabling calculation of SG content. The $[\text{aglycone} + H - H_2O]^+$ signal was between 0.5 and 6% compared to the $[M + Na]^+$ signal for the different investigated SGs (sitosteryl, campesteryl, stigmasteryl, $\Delta^5$-avenasteryl, cholesteryl, and $\Delta^7$-avenasteryl glucoside). This led to the conclusion that different SG species demonstrate the same ionization behavior under the conditions applied.

The most abundant ion species of SGs and their respective $m/z$, in positive and negative mode, are listed in Table 1. $[M + Na]^+$ was the predominant ion species observed in positive mode. Earlier studies, by Schrick et al.[11] using ESI and by Wewer et al.[14] using nanospray, have reported the formation of $NH_4^+$ adducts. They both used direct infusion without chromatographic separation and enhanced the $[M + NH_4]^+$ formation by adding ammonium acetate to the sample. In the present study, $[M - H + Hac]^-$ was the most abundant ion species in negative mode.

**Comparison of APCI to ESI for the Analysis of Steryl Glycosides.** The usage of APCI for the analysis of SGs was shown to be inferior when compared to ESI. With APCI (Figure 1B), 10 times lower intensity of $[M + Na]^+$ and more fragment ions were obtained than with ESI (Figure 1A). APCI was used by Rudell et al.,[19] Yamauchi et al.,[12] and Rozenberg et al.,[8] who all detected the aglycone ion as the predominant ion species. In our study, APCI was harsher and caused more fragmentation, whereas ESI was shown to be milder. Therefore, ESI was the method of choice for the analysis of intact SG and led to higher intensity of targeted species and, thus, provided higher sensitivity.

Furthermore, a major benefit of the Q-TOF MS system used in this study was the high mass accuracy. In ESI and APCI modes, the mass accuracies of the sodiated SG were 1.7 and 0.3 ppm, respectively, and 1.0 and 2.3 ppm, respectively, for the aglycone ion (Figure 1). The mass accuracy of the method on average was 1.3 ppm (equivalent to approximately 0.76 mDa) for SG detection. Thus, our method was shown to be highly reliable for the identification of SGs based on their elemental composition.

**Effect of Mobile Phase and Additive of Sodiated Steryl Glycoside Ion Separation.** To compare the effects of different mobile phases and additives on sensitivity and resolution, a solution of purified SG standard mixture was used. In addition to the four SGs declared by the distributor, another SG with $m/z$ 597 was detected. This peak was tentatively identified as $\Delta^7$-avenasteryl glucoside, on the basis of the observations of Breinhölder et al.[9] on relative retention time (RRT) order of the SGs used in this study, also using a C18 column. Additionally, the retention time of cholesteryl glucoside was identified on the basis of the standard compound. Thus, the order of elution using the UPLC BEH C18 column was $\Delta^7$-avenasteryl glucoside (RRT = 0.99), cholesteryl glucoside (RRT = 1.00), $\Delta^5$-avenasteryl glucoside (RRT = 1.00), campesteryl glucoside (RRT = 1.03), stigmasteryl glucoside (RRT = 1.03), and sitosteryl glucoside (RRT = 1.06). All SGs were separated, except for stigmasteryl and campesteryl glucosides, $\Delta^5$-avenasteryl, and cholesteryl glucosides, which coeluted, but which could still be distinguished by their $m/z$ values.

**Table 2. Mobile Phases and Additives Evaluated for UPLC-QTOF-ESI-MS Analysis[a]**

| | ion mode | mobile phase A | mobile phase B | additive added to phases A + B[b] | area of peak c[c] | peak c/noise[c] | resolution[c] (b:c) |
|---|---|---|---|---|---|---|---|
| A | positive | $H_2O$ | IPA/ACN[d] | 0.1% FA | 973 ± 43a | 106 ± 35c | 2.5 ± 0.1e |
| B | positive | $H_2O$ | ACN | 0.1% FA | 1645 ± 116a | 286 ± 143c | 4.6 ± 0.3f |
| C | positive | $H_2O$ | MeOH | 0.1% FA | 20126 ± 2328b | 1880 ± 696d | 0.7 ± 0.1g |
| D | positive | $H_2O$ | ACN | 0.1% AcOH + 1 mM $NH_4Ac$ | 566 ± 16a | 163 ± 48c | 5.3 ± 0.1h |
| E | positive | $H_2O$ | IPA/ACN[d] | 0.1% AcOH | 1752 ± 166a | 177 ± 50c | 2.3 ± 0.1e |
| F | positive | $H_2O$ | ACN | 0.1% AcOH | 312 ± 79a | 45 ± 9c | 3.8 ± 0.1i |
| G | positive | $H_2O$ | MeOH | 0.1% AcOH | 22682 ± 5525b | 1856 ± 965d | 0.8 ± 0.0g |
| H | negative | $H_2O$ | ACN | 0.1% AcOH + 1 mM $NH_4Ac$ | 581 ± 22a | 302 ± 38c | 4.3 ± 0.4fi |

[a]Calculation of peak area and signal-to-noise ratio based on stigmasteryl glucoside (peak c) and resolution between $\Delta^5$-avenasteryl glucoside (peak b) and stigmasteryl glucoside (peak c). Different letters within peak area, signal-to-noise ratio, and resolution denote a sigificant difference. [b]$NH_4Ac$, ammonium acetate; FA, formic acid; % (v/v). [c]Mean values ± standard deviation ($n$ = 3). [d]50% IPA/50% ACN.

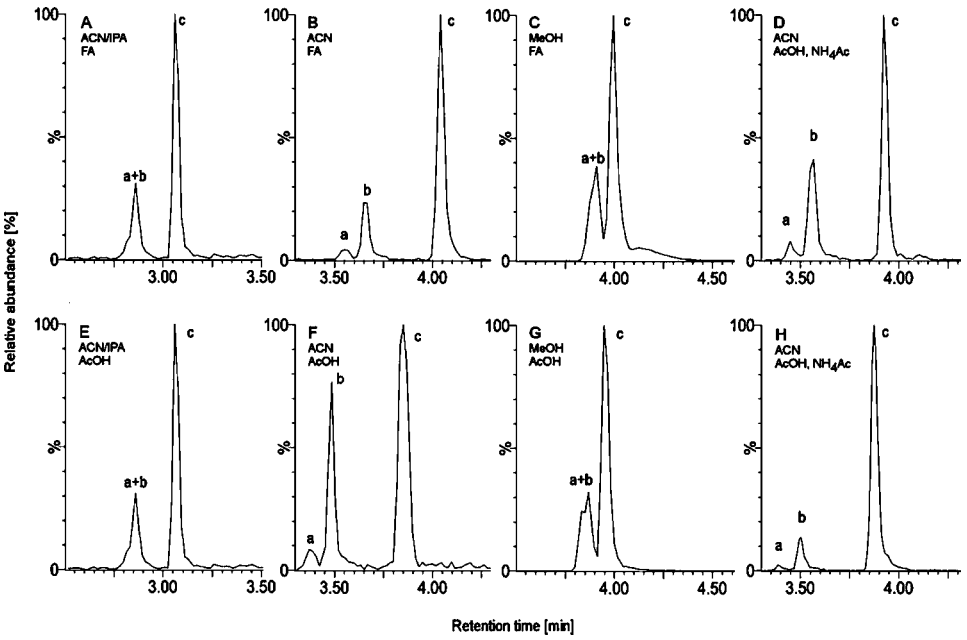


**Figure 2.** Extracted ion chromatograms (EIC) of $m/z$ 597.4131 (A–G) as $[M + Na]^+$ in ESI positive mode and $m/z$ 633.4366 (H) as $[M - H + Hac]^-$ in negative mode using different mobile phase compositions. Details of mobile phase compositions A–H are described in Table 2. The SG standard solution used contained three isomeric SGs: (a) $\Delta^7$-avenasteryl glucoside; (b) $\Delta^5$-avenasteryl glucoside; (c) stigmasteryl glucoside. No smoothing applied. ACN, acetonitrile; FA, formic acid; IPA, isopropanol; MeOH, methanol.

The separation and sensitivity of SGs were highly affected by the composition of the mobile phase (Table 2; Figure 2). The shortest retention time for stigmasteryl glucoside (3.07 min) was obtained with and isopropanol/acetonitrile mixture as the organic mobile phase at a flow rate of 0.3 mL/min. This mixture has a high eluting strength, whereas SGs were more retained with methanol. Selection of the mobile phase, and in the case of acetonitrile in positive mode, choice of the additive, had a significant influence on the resolution. The highest resolutions of 4.3–5.3 between the two isomers stigmasteryl glucoside and $\Delta^5$-avenasteryl glucoside were achieved using an acetonitrile/water gradient. $\Delta^5$-Avenasteryl glucoside and stigmasteryl glucoside were baseline separated, and a third peak, tentatively identified as $\Delta^7$-avenasteryl glucoside, eluted prior to $\Delta^5$-avenasteryl glucoside. Moreover, with the buffered system of acetic acid and ammonium acetate, an improvement in resolution and peak shape was observed as compared to those from formic acid or acetic acid. These improvements of the buffered system have been previously reported for HPLC-ESI-MS measurements of peptides.[17]

$[M - H + Hac]^-$ was the most abundant ion species in negative mode in this study (Table 1). Analysis of SGs in negative mode did not lead to any improvement when compared to the methods that showed best results with regard to resolution and sensitivity.

The sensitivity obtained using a methanol/water gradient was superior to that of the other systems tested. The area of the stigmasteryl glucoside peak in methanol/water systems was >10 times higher and the peak-to-noise ratio >6 times higher than with other eluents. These high values imply that detection and quantification of lower concentrations of SG are possible with methanol-based eluents. The improvement of LOD of the analytes with methanol has been previously reported for LC-ESI measurements of peptides.[24] In that study, the signal-to-noise ratio with methanol was 2.2–6.9 times higher than with acetonitrile. We detected an even greater increase, specifically 6.6–41.2 times higher with methanol compared to acetonitrile. Due to this advantage, methanol was chosen as the organic mobile phase component. Water and methanol were also used as mobile phases in other studies for SG analysis using HPLC combined with UV, ELSD, or MS detection.[8,12,16,25] The

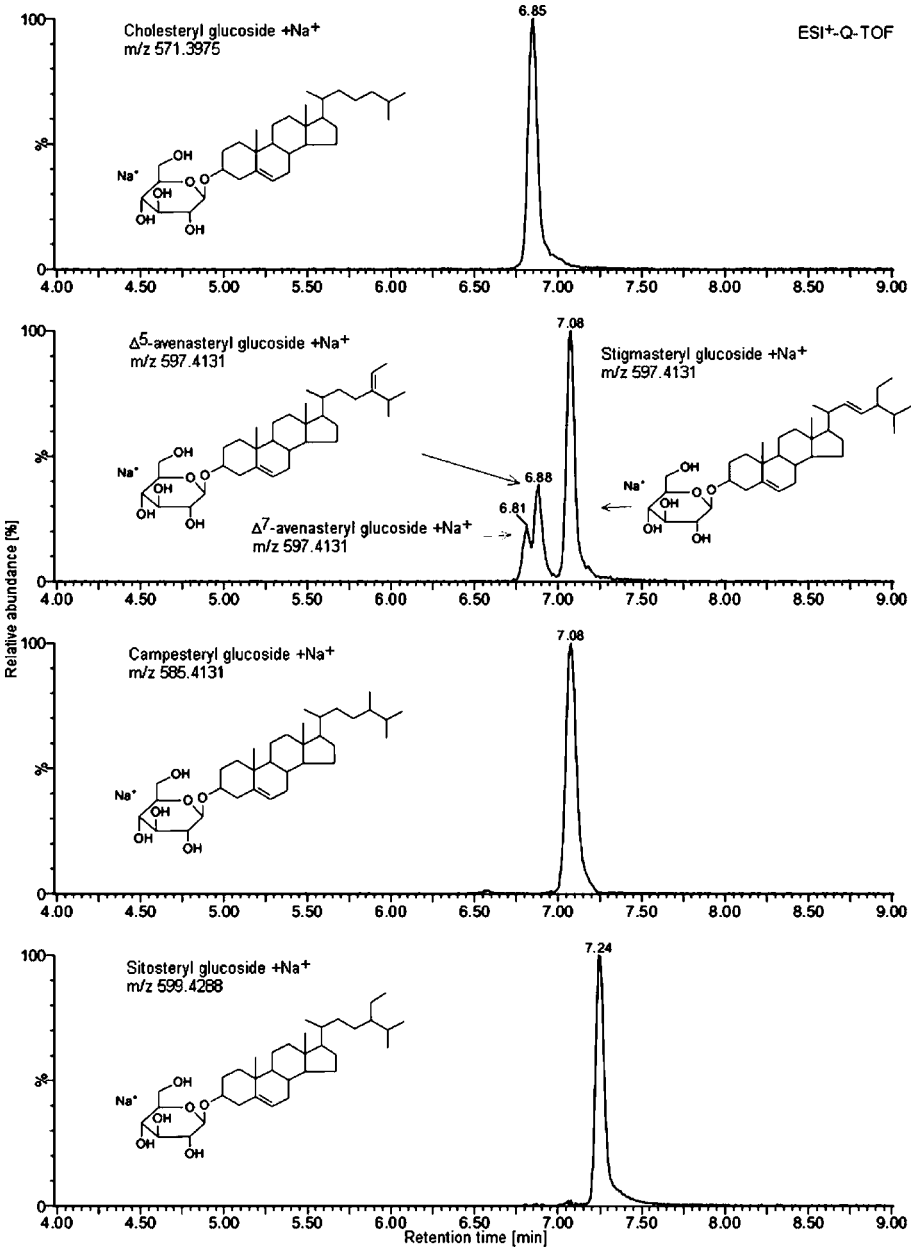


**Figure 3.** UPLC separation of targeted compounds as $[M + Na]^+$ obtained by measuring SG standard solution (sitosteryl glucoside, campesteryl glucoside, stigmasteryl glucoside, $\Delta^5$-avenasteryl glucoside, and $\Delta^7$-avenasteryl glucoside) and cholesteryl glucoside detected by Q-TOF-MS in positive ESI mode, obtained with optimized method (MeOH/water gradient + 0.1% (v/v) formic acid, BEH C18 column, total run time = 10 min). Savitzky−Golay smoothing was applied (iteration = 1 and width = 2).

addition of formic acid and acetic acid did not lead to significantly different results, and of these two, formic acid was chosen for further experiments.

**UPLC-Q-TOF-MS Method Optimization and Validation.** Peaks were assigned with respect to the $m/z$ of the compounds and the relative retention times to cholesteryl glucoside. Extracted ion chromatograms for the five SGs occurring in the SG standard mixture obtained under final UPLC-Q-TOF-MS conditions are shown in Figure 3. With adjusted gradient and run time, the resolution between $\Delta^5$-avenasteryl glucoside and stigmasteryl glucoside increased from 0.7 to 1.4. This provided suitable resolution for quantification using peak area, although the peaks were not baseline separated. Furthermore, the asymmetric factor $A_s$ (10% height) was improved from 3.1 to 2.0, and the tailing factor $T_f$ (5% height) was improved from 3.9 to 1.7 by method optimization. The major benefit of this UPLC method is that efficient separation was obtained with only 10 min runs, thus being far more rapid than conventional HPLC methods, which require 30 min per run.[8,19]

The calibration curve ranging from 14.4 to 216 ng/mL showed linear behavior with a correlation coefficient $R^2$ >0.993. The LOD and LOQ were 1 and 3 ng/mL, respectively. These values improved on earlier results, by >500-fold, where the LOD achieved by GC-FID or by HPLC-ELSD was in the lower micrograms per milliliter range.[25−28] However, it should be mentioned that the LOD was determined using methanol solutions without any sample matrix. The LOQ determined in this study was even lower than the LOQ of 27.4 ng/mL achieved by Q-TOF MS/MS.[14]


dx.doi.org/10.1021/jf501509m | J. Agric. Food Chem. 2014, 62, 9410−9419

**Table 3. Intra- and Interday Accuracy and Precision of Quantification Using Optimized UPLC-ESI-Q-TOF-MS Method Based on Pure Cholesteryl Glucoside ($m/z$ 571.3975) Solution**

| intraday variation ($n$ = 5) | | | | interday variation (3 days, $n$ = 15) | | | |
|---|---|---|---|---|---|---|---|
| QC[a] (ng/mL) | mean[b] ($\mu$g/mL) | RSD (%) | accuracy (%) | QC[a] (ng/mL) | mean[b] ($\mu$g/mL) | RSD (%) | accuracy (%) |
| 54 | 56.94 | 2.74 | 105.4 | 54 | 56.68 | 4.51 | 105.0 |
| 90 | 88.66 | 2.75 | 98.5 | 90 | 91.06 | 3.33 | 101.2 |

[a]Targeted concentration of quality control sample (QC). [b]Mean observed concentration.

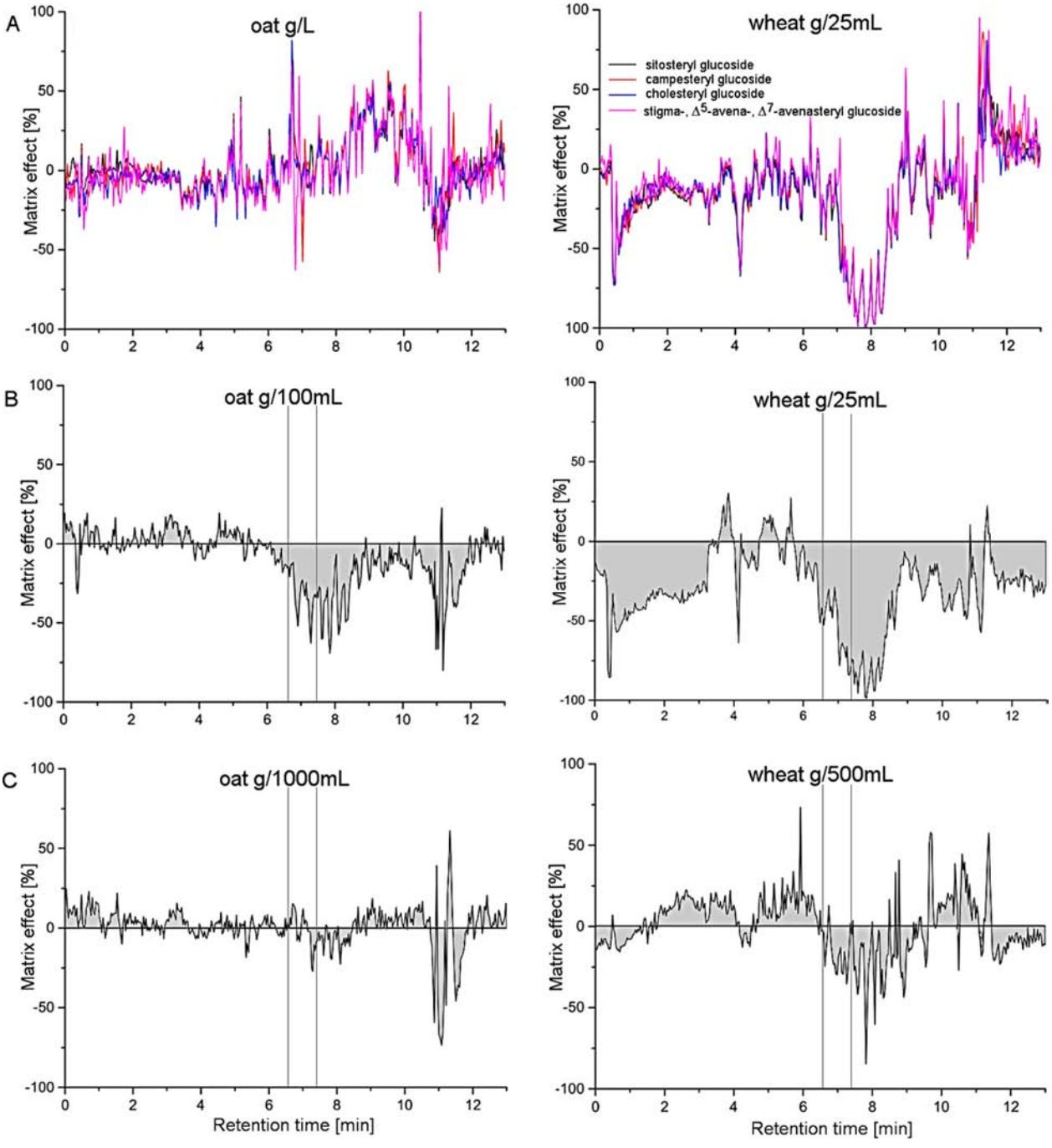


**Figure 4.** Postcolumn infusion matrix effect profile of sitosteryl glucoside, campesteryl glucoside, cholesteryl glucoside, and the isomers stigmasteryl glucoside, $\Delta^5$-avenasteryl glucoside, and $\Delta^7$-avenasteryl glucoside of SG extracts from whole wheat and oat bran (A); matrix effect profile of more (B) and less (C) concentrated wheat and oat SG extracts obtained by postcolumn infusion of cholesteryl glucoside. The bigger the gray area, the more pronounced the matrix effect at a given retention time (positive values, enhancement; negative values, suppression). SGs elute between 6.6 and 7.4 min (demonstrated with gray lines).


dx.doi.org/10.1021/jf501509m | J. Agric. Food Chem. 2014, 62, 9410−9419

**Table 4. Total SG Content, Percentage SG Composition, and IS Recovery of More and Less Concentrated Wheat and Oat Bran SG Extracts with and without Inclusion of Matrix Effect Compensation**

| | wheat | | oat | |
|---|---|---|---|---|
| | − matrix effect[a] | + matrix effect[a] | − matrix effect[a] | + matrix effect[a] |
| total SGs (μg/g DM) | 164.9* ± 1.8 | 184.4* ± 3.2 | 310.9 ± 17.4 | 330.7 ± 8.9 |
| sitosteryl glucoside (%) | 74.2* ± 0.1 | 75.5* ± 0.1 | 52.7* ± 0.9 | 59.0* ± 0.8 |
| campesteryl glucoside (%) | 16.7* ± 0.4 | 15.3* ± 0.4 | 10.3* ± 0.3 | 7.5* ± 0.3 |
| stigmasteryl glucoside (%) | 2.1* ± 0.2 | 3.3* ± 0.3 | 2.1* ± 0.3 | 1.6* ± 0.2 |
| $\Delta^5$-avenasteryl glucoside (%) | 5.5* ± 0.2 | 4.6* ± 0.1 | 31.0* ± 0.4 | 28.8* ± 0.4 |
| $\Delta^7$-avenasteryl glucoside (%) | 1.5 ± 0.2 | 1.2 ± 0.1 | 3.9* ± 0.3 | 3.1* ± 0.2 |
| recovery less concentrated[b] (%) | 93.3* ± 2.8 | 110.7* ± 3.2 | 96.7 ± 13.1 | 102.8 ± 13.8 |
| recovery more concentrated[c] (%) | 36.8* ± 1.6 | 67.1* ± 2.9 | 56.6* ± 1.8 | 105.6* ± 5.8 |

[a]Mean values ± standard deviation ($n$ = 3). *, statistically significant difference between with and without ME compensation. [b]Per g/500 mL (wheat) and g/1000 mL (oat). [c]Per g/25 mL (wheat) and g/100 mL (oat).

The accuracy and precision of the method were determined by an intra- and interday variation test of two QC samples containing 54 and 90 ng/mL of cholesteryl glucoside. The accuracies of the detected concentrations were always >94%, and the highest standard deviations were 4.51% for interday and 2.75% for intraday measurements (Table 3). Therefore, good reproducibility and high accuracy of the investigated method were demonstrated.

**Quantification of Steryl Glycosides Extracted from Food Samples.** In a final step, the optimized and validated method was applied to analyze SG in whole wheat and oat bran samples. Although glycosylated cholesterol can occur in plant samples,[10,23,29] cholesteryl glucoside was selected as internal standard (IS) because it is essentially the only single SG commercially available as pure standard. To demonstrate the applicability of the IS for food samples with different SG profiles, containing high or low SG concentrations and containing cholesteryl glucoside or not, food samples of whole wheat and oat bran were selected. Wheat was found to contain low SG concentrations, and cholesteryl glucoside was detected only in traces. Oat bran contained a high concentration of SGs and cholesteryl glucoside in significant amounts, and therefore sample spiking was performed.

When the SG content in extracts of wheat and oat bran was analyzed, the recovery of the IS was only between 36 and 97% due to ion suppression produced by coeluting matrix compounds. This matrix effect is a well-known limitation of MS methods. Usually this effect can be reduced or eliminated by improved extraction and sample cleanup or by chromatographic separation of the investigated analytes from the food matrix compounds.[30] However, the matrix effect is time-dependent and therefore varies for different SGs. Due to a lack of pure standards, the reduction of the ion suppression cannot be evaluated for individual SG. Hence, another strategy, including matrix effect quantification and application to data as a correction, was chosen. Therefore, the matrix effects of our samples were assessed by permanent postcolumn infusion of cholesteryl glucoside and of the SG standard based on the method by Stahnke et al.[18] In this way, the matrix effect profile was detected throughout the whole run time and the re-equilibration period. The various SG species were similarly suppressed or enhanced, allowing the usage of a single monitoring substance representing other SGs (Figure 4A). Even though the postcolumn infused SG standard consists of SGs at different concentrations, they showed similar signal inhibitions. Thus, the matrix effect was independent of the abundance of the individual SGs in the sample (Figure 4A).

For wheat and oat bran, two different dilutions were selected for quantification of the SG content, and two different matrix effect profiles were produced, as the profile is highly dependent on the matrix concentration.[31] Therefore, cholesteryl glucoside, used as monitor substance, was infused postcolumn to the more concentrated (Figure 4B) and less concentrated (Figure 4C) oat and wheat samples. As expected, the more diluted samples showed less ion suppression, with inhibition between 3 and 25% around SG elution from the column, whereas in the less diluted samples the signal suppression was between 30 and 68%. The two different food samples generated different matrix effect profiles as a result of their different matrix compositions. Furthermore, it was also observed that some background matrix compounds were still eluting during the re-equilibration period, as ion suppression continued to occur between 10 and 13 min (Figure 4).

The SG composition and the IS recovery in wheat and oat samples were calculated with and without matrix effect correction (Table 4). By including compensation for the matrix effect, the IS recovery rates of the concentrated extracts experiencing higher matrix effect were increased from 36.8 and 56.6 to 67.1 and 105.6% in wheat and oat bran, respectively. Thus, ion suppression could be compensated, and inclusion of the matrix effect was highly necessary for concentrated samples. Furthermore, time dependence of the matrix effect was observed. The ionization of the early eluting $\Delta^7$-avenasteryl glucoside was inhibited by 39%, whereas the later eluting stigmasteryl glucoside signal was reduced 68% by the matrix in the concentrated wheat sample. Due to the variation of suppression of the different SGs, the SG composition changed significantly by inclusion of matrix effect correction. Furthermore, applying compensation for the matrix effect increased the total SGs quantified in wheat by about 12% from 164.9 to 184.4 μg/g DM.

With consideration of the matrix effect, the total SG content in whole wheat was 184.4 μg/g DM and was composed of 75.5, 15.3, 4.6, 3.3, and 1.2% of sitosteryl, campesteryl, $\Delta^5$-avenasteryl, stigmasteryl, and $\Delta^7$-avenasteryl glucosides, respectively. Compared to the results of our earlier study, the proportions of different sterols were similar, but in the current study more than double the amount of total SGs was detected.[2] Sugawara et al. detected 54 μg/g total SGs in wheat by HPLC-ELSD, which is only a third of what we measured.[26] These differences may, however, be due to analytical variability because Ruibal-Mendieta et al. measured steryl glycosides (SG + ASG) in winter wheat at a similar concentration to this study by HPLC-MS.[32]

The total SG content of oat bran under consideration of the matrix effect was 330.7 μg/g DM, demonstrating that the oat bran analyzed is a better source for SGs than whole wheat. Oat bran SGs consisted of 59.0, 7.5, 28.8, 1.6, and 3.1% of sitosteryl, campesteryl, $\Delta^5$-avenasteryl, stigmasteryl, and $\Delta^7$-avenasteryl glucosides, respectively. Kesselmeier et al. measured SGs in oat seed samples by HPLC-UV.[10] They found that sitosteryl glycoside and $\Delta^5$-avenasteryl glycoside are the two most abundant glycosylated sterols (in SG + ASG). These two accounted for 82% of the total SG content, which is in great accordance with our result (sitosteryl and $\Delta^5$-avenasteryl glucoside contributing 81% of the total SG content in oat). A mild analysis method, like the one developed in this study, is important for the analysis of oat SGs because $\Delta^5$-avenasteryl glycoside is a labile SG that is easily degraded or isomerized by the acidic hydrolysis included in several GC procedures.

To conclude, we developed a rapid, highly sensitive, and accurate UPLC-ESI-MS method for the detection of molecular ions of SGs as sodiated adducts. The possibility to separate SGs on the basis of different polarities, in combination with high sensitivity and mass accurate detection, makes this method a powerful tool for full screening of SG profiles in foods and other biological samples, even those with low SG content. Furthermore, we demonstrated that evaluation of the matrix effect is extremely important for accurate quantification of SGs in complex food samples.

## AUTHOR INFORMATION


### Corresponding Author

*(L.N.) Phone: +41 44 632 91 65. E-mail: laura.nystroem@hest.ethz.ch.

### Author Contributions

‖S.R.O. and L.H.M contributed equally to this work.



### Funding

This study was funded by the Swiss National Science Foundation (SNSF) and ETH Zurich.

### Notes

The authors declare no competing financial interest.


## ABBREVIATIONS USED

ASG, acylated steryl glycosides; APCI, atmospheric pressure chemical ionization; DM, dry matter; ESCI, electrospray chemical ionization; ESI, electrospray ionization; FS, free sterols; Q-TOF, quadrupole time-of-flight; SE, steryl esters; SG, steryl glycosides; UPLC, ultraperformance liquid chromatography

## REFERENCES


(1) Grille, S.; Zaslawski, A.; Thiele, S.; Plat, J.; Warnecke, D. The functions of steryl glycosides come to those who wait: recent advances in plants, fungi, bacteria and animals. *Prog. Lipid Res.* **2010**, *49*, 262−288.

(2) Nyström, L.; Schär, A.; Lampi, A. M. Steryl glycosides and acylated steryl glycosides in plant foods reflect unique sterol patterns. *Eur. J. Lipid Sci. Technol.* **2012**, *114*, 656−669.

(3) Pegel, K. H. The importance of sitosterol and sitosterolin in human and animal nutrition. *S. Afr. J. Sci.* **1997**, *93*, 263−268.

(4) Bouic, P. J. D.; Etsebeth, S.; Liebenberg, R. W.; Albrecht, C. F.; Pegel, K.; VanJaarsveld, P. P. *β*-Sitosterol and *β*-sitosterol glucoside stimulate human peripheral blood lymphocyte proliferation: Implications for their use as an immunomodulatory vitamin combination. *Int. J. Immunopharmacol.* **1996**, *18*, 693−700.

(5) Lin, X. B.; Ma, L.; Racette, S. B.; Spearie, C. L. A.; Ostlund, R. E. Phytosterol glycosides reduce cholesterol absorption in humans. *Am. J. Physiol.: Gastrointest. Liver Physiol.* **2009**, *296*, G931−G935.

(6) Nyström, L. Analysis methods of phytosterols. In *Analysis of Antioxidant-Rich Phytochemicals*; Wiley-Blackwell: Hoboken, NJ, USA, 2012; pp 313−351.

(7) Kamal-Eldin, A.; Määttä, K.; Toivo, J.; Lampi, A. M.; Piironen, V. Acid-catalyzed isomerization of fucosterol and Δ(5)-avenasterol. *Lipids* **1998**, *33*, 1073−1077.

(8) Rozenberg, R.; Ruibal-Mendieta, N. L.; Petitjean, G.; Cani, P.; Delacroix, D. L.; Delzenne, N. M.; Meurens, M.; Quetin-Leclercq, J.; Habib-Jiwan, J. L. Phytosterol analysis and characterization in spelt (*Triticum aestivum* ssp *spelta* L.) and wheat (*T. aestivum* L.) lipids by LC/APCI-MS. *J. Cereal Sci.* **2003**, *38*, 189−197.

(9) Breinhölder, P.; Mosca, L.; Lindner, W. Concept of sequential analysis of free and conjugated phytosterols in different plant matrices. *J. Chromatogr., B* **2002**, *777*, 67−82.

(10) Kesselmeier, J.; Eichenberger, W.; Urban, B. High performance liquid chromatography of molecular species from free sterols and sterylglycosides isolated from oat leaves and seeds. *Plant Cell Physiol.* **1985**, *26*, 463−471.

(11) Schrick, K.; Shiva, S.; Arpin, J. C.; Delimont, N.; Isaac, G.; Tamura, P.; Welti, R. Steryl glucoside and acyl steryl glucoside analysis of arabidopsis seeds by electrospray ionization tandem mass spectrometry. *Lipids* **2012**, *47*, 185−193.

(12) Yamauchi, R.; Aizawa, K.; Inakuma, T.; Kato, K. Analysis of molecular species of glycolipids in fruit pastes of red bell pepper (*Capsicum annuum* L.) by high-performance liquid chromatography-mass spectrometry. *J. Agric. Food Chem.* **2001**, *49*, 622−627.

(13) Hernandez, F.; Pozo, O. J.; Sancho, J. V.; Lopez, F. J.; Marin, J. M.; Ibanez, M. Strategies for quantification and confirmation of multi-class polar pesticides and transformation products in water by LC-$MS^2$ using triple quadrupole and hybrid quadrupole time-of-flight analyzers. *TrAC, Trends Anal. Chem.* **2005**, *24*, 596−612.

(14) Wewer, V.; Dombrink, I.; vom Dorp, K.; Dormann, P. Quantification of sterol lipids in plants by quadrupole time-of-flight mass spectrometry. *J. Lipid Res.* **2011**, *52*, 1039−1054.

(15) Chavez-Santoscoy, R. A.; Tovar, A. R.; Serna-Saldivar, S. O.; Torres, N.; Gutierrez-Uribe, J. A. Conjugated and free sterols from black bean (*Phaseolus vulgaris* L.) seed coats as cholesterol micelle disruptors and their effect on lipid metabolism and cholesterol transport in rat primary hepatocytes. *Genes Nutr.* **2014**, *9*, DOI: 10.1007/s12263-013-0367-1.

(16) Van Gerpen, J.; He, B. B.; Duff, K. *Measurement and Control Strategies for Sterol Glucosides to Improve Biodiesel Quality − Year 2*; University of Idaho, National Institute for Advanced Transportation Technology: Moscow, ID, USA, 2011

(17) Leitner, A.; Emmert, J.; Boerner, K.; Lindner, W. Influence of solvent additive composition on chromatographic separation and sodium adduct formation of peptides in HPLC-ESI MS. *Chromatographia* **2007**, *65*, 649−653.

(18) Stahnke, H.; Reemtsma, T.; Alder, L. Compensation of matrix effects by postcolumn infusion of a monitor substance in multiresidue analysis with LC-MS/MS. *Anal. Chem.* **2009**, *81*, 2185−2192.

(19) Rudell, D. R.; Buchanan, D. A.; Leisso, R. S.; Whitaker, B. D.; Mattheis, J. P.; Zhu, Y. M.; Varanasi, V. Ripening, storage temperature, ethylene action, and oxidative stress alter apple peel phytosterol metabolism. *Phytochemistry* **2011**, *72*, 1328−1340.

(20) Strobl, M. *Δ-7-Sterole und Δ-7-Sterolglykoside aus Samen von Cucurbita pepo L.: Isolierung und Strukturaufklärung.* Dissertation, Faculty of Chemistry and Pharmacy, LMU, München, Germany, 2004.

(21) Kovganko, N. V.; Kashkan, Z. N. Sterol glycosides and acylglycosides. *Chem. Nat. Compd.* **1999**, *35*, 479−497.

(22) Fujino, Y.; Ohnishi, M. Isolation and structure of diglycosylsterols and triglycosylsterols in rice bran. *Biochim. Biophys. Acta* **1979**, *574*, 94−102.

(23) Kojima, M.; Ohnishi, M.; Ito, S.; Fujino, Y. Characterization of acylmonoglycosylsterol, monoglycosylsterol, diglycosylsterol, triglyco-

sylsterol and tetraglycosylsterol and saponin in adzuki bean (Vigna, Angularis) seeds. *Lipids* **1989**, *24*, 849−853.
(24) Giorgianni, F.; Cappiello, A.; Baranova-Giorgianni, S.; Palma, P.; Trufelli, H.; Desiderio, D. M. LC-MS/MS analysis of peptides with methanol as organic modifier: improved limits of detection. *Anal. Chem.* **2004**, *76*, 7028−7038.
(25) Moreau, R. A.; Scott, K. M.; Haas, M. J. The identification and quantification of steryl glucosides in precipitates from commercial biodiesel. *J. Am. Oil Chem. Soc.* **2008**, *85*, 761−770.
(26) Sugawara, T.; Miyazawa, T. Separation and determination of glycolipids from edible plant sources by high-performance liquid chromatography and evaporative light-scattering detection. *Lipids* **1999**, *34*, 1231−1237.
(27) Gomez-Coca, R. B.; Perez-Camino, M. D.; Moreda, W. Specific procedure for analysing steryl glucosides in olive oil. *Eur. J. Lipid Sci. Technol.* **2012**, *114*, 1417−1426.
(28) White, J. M.; Shah, P.; Sanford, S.; Valverde, M.; Meier, G. *Evaluation of Low Concentrations of Steryl Glucosides in Biodiesel by Gas Chromatography*, http://www.regfuel.com (22.10.2013).
(29) Duperon, R.; Thiersault, M.; Duperon, P. High-level of glycosylated sterols in species of *Solanum* and sterol changes during the development of the tomato. *Phytochemistry* **1984**, *23*, 743−746.
(30) Chambers, E.; Wagrowski-Diehl, D. M.; Lu, Z. L.; Mazzeo, J. R. Systematic and comprehensive strategy for reducing matrix effects in LC/MS/MS analyses. *J. Chromatogr., B* **2007**, *852*, 22−34.
(31) Stahnke, H.; Kittlaus, S.; Kempe, G.; Alder, L. Reduction of matrix effects in liquid chromatography-electrospray ionization-mass spectrometry by dilution of the sample extracts: how much dilution is needed? *Anal. Chem.* **2012**, *84*, 1474−1482.
(32) Ruibal-Mendieta, N. L.; Rozenberg, R.; Delacroix, D. L.; Petitjean, G.; Dekeyser, A.; Baccelli, C.; Marques, C.; Delzenne, N. M.; Meurens, M.; Habib-Jiwan, J. L.; Quetin-Leclercq, J. Spelt (*Triticum spelta* L.) and winter wheat (*Triticum aestivum* L.) wholemeals have similar sterol profiles, as determined by quantitative liquid chromatography and mass spectrometry analysis. *J. Agric. Food Chem.* **2004**, *52*, 4802−4807.

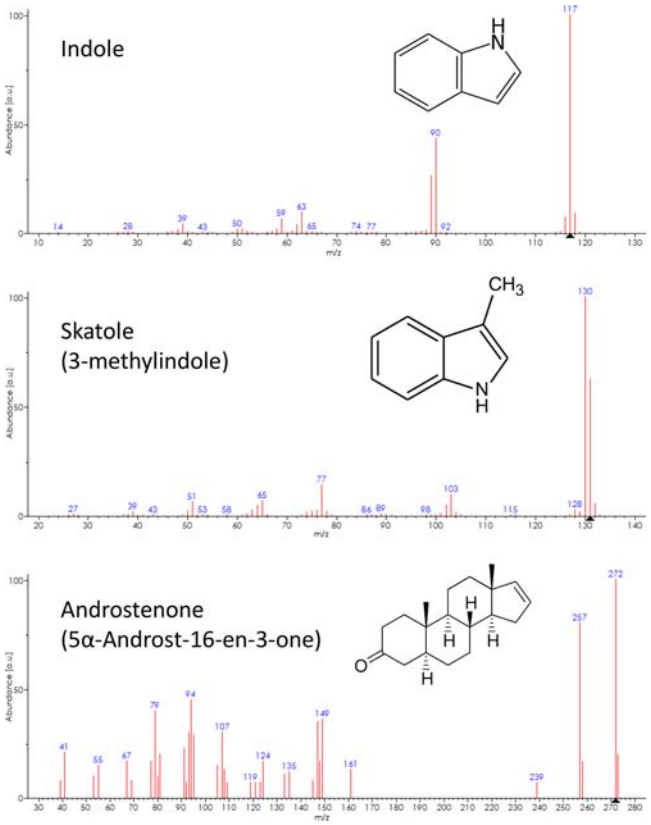


**Figure 1.** Electron ionization (EI) mass spectra at 70 eV for each of the three structures of (a) indole, (b) skatole, and (c) androstenone. (Mass spectral data were taken from the NIST 11 Mass Spectral Database, Gaithersburg, MD, USA.)

is homogenized (by mechanical means or by melting) and thoroughly mixed with methanol.

More recently, Fischer et al.[29] have reported a novel combination of internal labeled standards and headspace sampling and have achieved a LOQ of 0.7 ng/g for indole, 3.1 ng/g for skatole, and 64 ng/g for androstenone using gas chromatography, which makes their combined work very attractive for reference analysis of fat samples. In this method approximately 14 min is spent on manual sample preparation, approximately 60 min is spent on headspace sampling, and 35 min is spent on the GC run (times stated per sample).

The ideal abattoir situation is an absolute quantification of the relevant boar-taint compounds at the full processing speed of the carcasses. In modern abattoirs, this will require sampling as fast as 3 s per carcass and the measurement result and decision preferably in less than 20 min. However, if discrete risk levels can be accepted, the detection method does not need to produce results with high quantitative accuracy. A method that can discriminate carcasses in a low-, medium-, or high-risk group will be adequate if the method is quick, reliable, and applicable to the minimally equipped and staffed laboratories often found in slaughterhouses. Such a method calls for a very high degree of automation and, preferably, with no human involvement in the sample processing at all.

While the method described here is not an online method, it facilitates the use of high-throughput at-line GC-MS analysis in an industrial setting by simplifying the sample preprocessing and the chromatographic requirements. This method presumes that the industrial users in everyday evaluation of production carcasses do not need very high absolute accuracy, but that high accuracy can be compromised for faster analysis. This work exploits how far the envelope of chromatographic parameters can be pushed, and how crude the sample preparation can be performed while retaining reliable results for industrial boar-taint detection. The method developed is based on the use of dynamic headspace sampling (DHS) via thermal adsorption/desorption and gas chromatography−mass spectrometry directly on pure fat samples for the prediction of the risk for the meat to emit boar taint at human detectable levels.

## MATERIALS AND METHODS

The method development was made primarily through two experiments described as follows:

(I) Construction of a response calibration curve for each of the three compounds indole, skatole, and androstenone in order to map the response of the detector system to the actual masses of analytes presented to the system. This experiment is also used to define the basic chromatographic behavior of the three compounds and how the chromatography can be accelerated.

(II) Method validation on a set of samples from slaughter boars which are measured both with the new method and by a reference measurement obtained by liquid chromatography.[27] The method is evaluated by its ability to quantify and discriminate tainted samples.

**Experiment I: Direct Injection of Standards.** Methanolic standard solutions for each of the three compounds skatole, indole, and androstenone (all Sigma-Aldrich, Munich, Germany) were prepared in the laboratory. The analytes were weighed, placed into 20 mL vials, and capped (after a nitrogen fill to avoid oxidation), followed by addition of methanol (Sigma-Aldrich) to reach 1.0 and 0.1 μg of analyte/(μL of solution). The concentrations were used to prepare a series of sorbent tubes (Markes International Ltd., Llantrisant, U.K.), each loaded with 200 mg of Tenax TA (Sigma-Aldrich) in different concentrations as outlined in Table 1, by injection on a standard solution loading rig (Markes), in a $N_2$ (ALPHAGAZ 2, Air Liquide, Taastrup, Denmark) flow of 50 mL/min allowing for analyte adsorption in 5 min postinjection at 20 °C. Separate syringes (Sigma-Aldrich Hamilton GASTIGHT syringes, 10 and 25 μL) were kept for each of the six standard vials to avoid cross-contamination. The syringe needles were cleaned with methanol after each septum

**Table 1. Analyte Levels in Sorbent Tubes**

| | analyte added (ng) | |
|---|---|---|
| tube no. | skatole and indole | androstenone |
| 1 | 4.9 | 4.9 |
| 2 | 10.0 | 10.0 |
| 3 | 21.0 | 21.0 |
| 4 | 40 | 40 |
| 5 | 60 | 60 |
| 6 | 79 | 79 |
| 7 | 110 | 110 |
| 8 | 210 | 210 |
| 9 | 300 | 300 |
| 10 | 400 | 400 |
| 11 | 490 | 490 |
| 12 | 600 | 600 |
| 13 | 700 | 700 |
| 14 | 790 | 790 |
| 15 | 950 | 950 |
| 16 | 1500 | 1500 |
| 17 | 2000 | 2000 |
| 18 | [a] | 5000 |
| 19 | [a] | 10000 |

[a]No analyte added.


dx.doi.org/10.1021/jf5022785 | J. Agric. Food Chem. 2014, 62, 9420−9427

penetration. Following standard injection the tubes were sealed using brass storage caps and PFTE (poly-tetrafluoroethylene) ferrules (Markes), and kept refrigerated at 5 °C until analysis. The tubes were prepared in duplicates, one series at a time over two separate days. The instrument response for duplicates was averaged for further analysis. Standard deviation for the instrument response of the duplicates is provided in Table 3.

A second set of tubes was manufactured similarly, each prepared with 0.5 μg of indole, 0.5 μg of skatole, and 1.0 μg of androstenone. These tubes were used to identify retention times and chromatographic properties for various temperature and flow profiles (not shown).

**Experiment II: Analysis of the Natural Fat Matrix.** Tainted fat (backfat) samples were made available from an experiment conducted by The Danish Pig Research Center (Copenhagen, Denmark),[14] including reference values determined by LC-MS.[27] The samples were cut from the carcass loin neck region and individually vacuum packed and labeled. The collection of samples has been stored at −18 °C until its use in this experiment. A total of 25 samples were selected from this experiment so that the LC-MS reference values of each of the boar-taint compounds spans the minimum to maximum levels observed. The 25 samples and their analyte levels are listed in Table 2.

**Table 2. Analyte Concentrations for Selected Natural Fat Samples Used in Experiment II**

| | indole (ng/g) | skatole (ng/g) | androstenone (ng/g) |
|---|---|---|---|
| min | 28 | 37 | 344 |
| max | 543 | 1415 | 12348 |
| mean | 161.1 | 508.8 | 4946.6 |

For each sample approximately 2 g were removed from the cut and placed into a 10 mL headspace vial, which was weighed before and after fat addition. Samples were processed as coarsely as possible—from the cut-out piece of tissue, skin and meat were removed and an approximately 2 g piece of the remaining fat was cut and added to the vial. The headspace vial was filled with $N_2$ before capping with an airtight septa using a manual crimp tool. After preparation, the samples were labeled and stored at 5 °C until analysis (total storage time < 3 days). The cut, fill, purge, and crimp procedure was in average of less than 45 s.

**Instrumentation.** All experiments have been conducted on an Agilent 6890 gas chromatograph and Agilent 5973N mass spectrometer (Agilent, Hannover, Germany) with electronic ionization source. Data were collected in Agilent MSD Chemstation version E.01.01.335. A Markes International UNITY thermal desorber (Markes) was connected to the GC EPC inlet pneumatic module via the EPC carrier feed gas and EPC septum purge connections to enable GC control of a constant column flow. To supply the UNITY through the EPC pneumatic controls, the EPC inlet was configured with the heater set to off, in splitless mode, without split venting. Based on findings in refs 5 and 28 a Phenomenex Zebron ZB-5MSi low-polarity capillary was selected with dimensions 30 m × 0.25 mm o.d. × 0.25 μm i.d. The column was connected to the thermal desorber through a Phenomenex Zebron Z-Guard guard column (5 m × 0.25 mm o.d.), acting as a transfer line, and merged with the capillary column in the oven using a glass union secured with a high-temperature polyamide resin. The unity desorber was fitted with a Tenax cold trap (Markes). In experiment I, the sorbent tubes were loaded manually in the oven of the UNITY desorber. For experiment II, dynamic headspace sampling was achieved through a Markes International U-inlet direct sampling accessory replacing the sorbent tube in the UNITY flow line. The U-inlet accessory was modified to have sharp tips for easy insertion in the sample vials through the vial septa. The exhaust line was intentionally kept 2 cm longer than the intake line in order to avoid excessive looping of the exhaust gas when inserted into the sample vial. Furthermore, the U-inlet accessory was complemented with approximately 10 mm loosely packed fine glass wool acting as a filter to avoid excessive amounts of the fat matrix to enter the heated valve of the UNITY. Heating of the vials was achieved by using a CTC-PAL heated agitator. Hydrogen was supplied to the equipment using an in-laboratory hydrogen generator (PEAK Scientific, Inchinnan, Scotland, U.K.).

**Analytical Procedure.** A compromise between speed and chromatographic resolution was investigated in several separate experiments, where flow rates, temperatures, trap breakthrough volumes, and run times were tested (not shown here) in order to optimize recovery of the three analytes from the biological samples and to reduce the total analysis time. For all tests, evaluations were made on how the chromatographic method was able to return reproducible and quantifiable peaks for the three compounds. As shown in Figure 1, indole and skatole, with mass weights 117 and 131 g $mol^{-1}$, respectively, have relatively simple mass spectra, in that they show a low degree of fragmentation, and only target ions with $m/z$ 117 and (for skatole the more abundant) $m/z$ 130 were necessary to include obtaining a proper quantification. Androstenone, however, has two significant mass targets of $m/z$ 257 and 272. It was found that androstenone could be efficiently quantified by accounting for $m/z$ 257 alone (see Results and Discussion). Emphasis was given to identify proper temperatures where all three analytes become volatile enough for transport in the flow system and on the other hand not break apart into smaller components. In addition, the amount of vaporized fat present in the headspace of the sample vials for experiment II should be as low as possible, requiring that the equilibration and sample temperature of the sample vials should be kept as low as possible as well.

These experiments led to the following final analytical configuration: a constant column flow of 1.4 mL/min, with an oven program of 130 °C for 1 min, 30 °C/min to 250 °C, held for 1 min, which

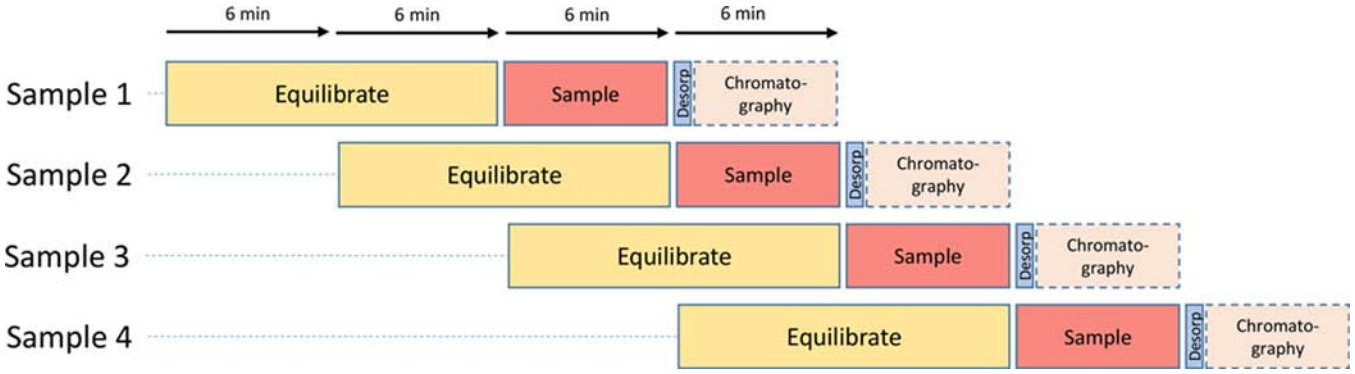


**Figure 2.** Sequence diagram of the analytical procedure. If sequenced by a multipurpose sampler robot, the analytical procedure can be arranged into a front-to-back sample mode of the GC-MS. If each step is kept in multiples of 6 min, the shown sample configuration could be achieved: a result delivered every 6 min, with a 24 min processing time for delivery of the first result.

combined gives a total analysis time of 6 min. The end temperature of 250 °C is relatively low (the ZB5-MSi column used has a maximum temperature of 350 °C), but was found sufficient for keeping the column clean between runs (experiment conducted but not shown), and advantageous for keeping the GC oven cool-down time postrun to a minimum. This 6 min chromatographic run time was subsequently imposed on the sample preparation steps; i.e., the fat sample processing should have equilibration and sample times in multiples of 6 min. The final measurement setup used is shown in Figure 2, where the processing sequence of the first four samples is shown. Each sample is set to equilibration of the sample/headspace concentration for 12 min, followed by a 6 min headspace purge. When the purge is complete, the 6 min chromatographic run is started. A multipurpose sample robot attached to the GC-MS equipment could be programmed to execute this sequence and, accordingly, allow the method to produce a chromatogram every 6 min.

The transfer line between the GC and the UNITY desorber and the desorber heated valve were kept at 220 °C throughout all experiments. The sorbent tube oven was operated at 250 °C during desorption/sampling. The UNITY cold trap was kept at −10 °C during primary desorption/sampling, elevated to 300 °C at the maximum heating rate (>40 °C/s) during cold trap fire, and held high for 45 s. The cold trap and sample tube was purged of atmospheric air at 0.5 min prior to desorption with carrier gas. Although previous experiments have established that the stated temperatures and times do not leave any analyte in the system to be observed as carryover between samples, empty tubes were run at regular intervals to test for carryover (data now shown).

In experiment I, an inlet split of 2:1 was achieved by enabling a split flow of 50 mL/min against a desorption flow of 50 mL/min, and was further split by enabling the split flow during trap desorption, resulting in an outlet split of 37.5:1. Hence, in total, the sample was split 75:1 and transferred to the column.

In experiment II, a vial purge flow of 20 mL/min was used to sample the vial headspace for 6 min at 150 °C. Prior to headspace sampling, the vial headspace was equilibrated in 12 min at 150 °C, while being shaked at 250 rpm for 30 s and then having a 10 s pause (and rotation direction reversal). During desorption, a split flow of 100 mL/min was enabled, resulting in a sample split of 72.4:1 (transferred to the column).

The MS temperatures were set to 230 °C for the ion source, 280 °C for the foreline and 150 °C as the quadropole temperature. The MS was operated in scan mode (scan range, 50−300 $m/z$). For quantification of the analyte concentration from the chromatograms, abundances of the target ions with $m/z$ 117 ± 0.5 for indole, $m/z$ 130 ± 0.5 for skatole, and $m/z$ 257 ± 0.5 for androstenone were accumulated for all MS samples in retention time windows of 1.5−3.5 min for indole and skatole and 4.5−5.5 min for androstenone. MS target ion samples with abundances less than 5000 au were rejected as noise and were not included in the accumulation. All processing of the chromatograms was performed in Matlab R2013b using a script developed for the purpose (a source code listing for the script can be obtained from the authors). MS data were loaded into Matlab through a CDF data export from Chemstation. The accumulated abundance results are corrected with the sample split ratios (as listed previously) and averaged for two separate series of sorbent tubes.

**Calibration of Response Regressions.** When chromatograms and $m/z$ abundances were accumulated for all target ions for all analyte levels, a calibration was made to allow for prediction of analyte mass from the instrument response. Assuming linearity between the analyte mass and measured accumulated peak abundance, the relationship between a concentration mass, $m_a$, and its corresponding accumulated instrument target ion response area, $r_a$, can be formalized as shown in

$$m_a = \beta r_a + \beta_o \quad (1)$$

where the regression coefficient $\beta$ is used to project the instrument response onto the analyte mass with an offset $\beta_o$. A regression vector $\mathbf{b} = [\beta_o \beta]$ can be determined in a least-squares sense[30] as in

$$\mathbf{b} = (\mathbf{R}^T\mathbf{R})^{-1}\mathbf{R}^T\mathbf{m}_a \quad (2)$$

from vectors of the $n$ known analyte masses $\mathbf{m}_a = [m_{a_1}\ m_{a_2}\ m_{a_3}\ \ldots\ m_{a_n}]$ and corresponding accumulated target ion instrument responses $\mathbf{r}_a = [r_{a_1}\ r_{a_2}\ r_{a_3}\ \ldots\ r_{a_n}]$. The matrix $R$ in eq 2 is the column-wise collation of and numerical ones *and* $\mathbf{r}_a$ (eq 3).

$$\mathbf{R} = [\mathbf{1}\mathbf{r}_a] \quad (3)$$

Having determined $\mathbf{b}$, a prediction $\mathbf{p}_a = [p_{a_1}\ p_{a_2}\ p_{a_3}\ \ldots\ p_{a_n}]$ (eq 4) of the known analyte masses $\mathbf{m}_a$ is used to summarize the prediction accuracy into a RMSE (root-mean-square error)[31] estimate (5).

$$\mathbf{p}_a = \beta \mathbf{r}_a + \beta_o \quad (4)$$

$$\mathrm{RMSE} = \sqrt{n^{-1}\sum_{i=0}^{n}(p_{a_i} - m_{a_i})^2} \quad (5)$$

## RESULTS AND DISCUSSION

**Experiment I: Direct Injection of Standards.** An example total ion chromatogram of a sorbent tube run is shown in Figure 3A. Three peaks, corresponding to the analytes, are observed at retention times 1.8, 2.1, and 5.0 min for indole, skatole, and androstenone, respectively. Despite the fact that the sorbent tube in Figure 3A is loaded with the same mass of each compound, large differences in peak areas are observed between the two indoles and the androstenone. However, the areas of the two indoles are comparable for the different runs. Figure 3B shows a plot of the relationship between the sorbent tube loading mass and the accumulated response area for the selected ions (detailed correlations of the relationships are listed in Table 3 for different decade ranges of the concentration masses). No response was recorded for indole and skatole of masses less than or equal to 10 ng and for

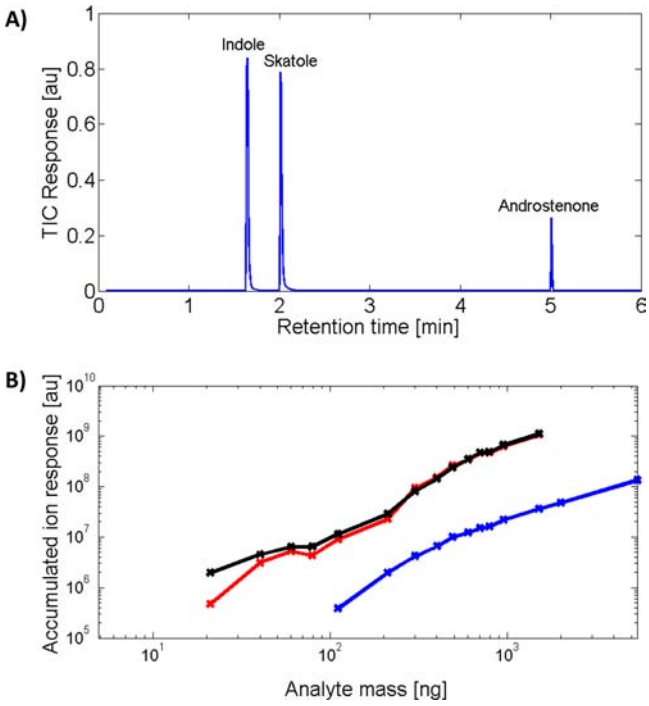


**Figure 3.** (A) Chromatogram showing the three analytes. (B) Prediction of analyte mass from instrument response using least-squares fit model. Black curve, skatole ($m/z$ = 130) with $R^2$ = 0.96; red curve, indole ($m/z$ = 117) with $R^2$ = 0.98; blue curve, androstenone ($m/z$ = 257) with $R^2$ = 1.00.


dx.doi.org/10.1021/jf5022785 | J. Agric. Food Chem. 2014, 62, 9420−9427

**Table 3. Instrument Response for Various Analyte Ranges of Directly Introduced Standards and Associated Calibration Performance for the Same Analyte Ranges**

| | instrument response | | | | calibration performance | | | | | |
|---|---|---|---|---|---|---|---|---|---|---|
| | | $R^2$ | | | $R^2$ | | | RMSE (ng) | | |
| response range (ng) | std dev (%)[a] | indole | skatole | androstenone | indole | skatole | androstenone | indole | skatole | androstenone |
| 1−10 | <2 | 0.837 | 0.94 | | 0.74 | 0.86 | | 61.7 | 70.6 | |
| 10−100 | <1 | 0.994 | 0.99 | 0.99 | 0.98 | 0.98 | 0.99 | 48.9 | 56.1 | 19.1 |
| 100−1000 | <0.8 | | | 0.99 | | | 0.99 | | | 35.8 |

[a]Standard deviation is expressed for all three analytes per range and is expressed as percentage of the mean of the duplicate.

androstenone levels equal to or less than 79 ng. The detection limit of the method (i.e., the minimum masses distinguishable from background) was estimated to 21 ng for the indoles and 110 ng for androstenone.

As can be observed from Figure 3B, some nonlinearity is present in the relationship of the indoles for the low mass abundances of masses less than 90 ng. In contrast, no nonlinearity was observed for the androstenone quantification to analyte abundance relationship. Moreover, Figure 3B shows that the quantification areas of the indoles are highly similar in the high range of analyte concentrations but deviate slightly in the lower part of the concentration range. The androstenone area was a factor of 10−15 lower for the same analyte concentrations.

Statistics of the calibration performed in this experiment is given in Table 3. It is noticeable that the model provides a poorer fit for the 1−10 ng response range than for the 10−100 ng range for the indoles, which indicates that the system's LOQ is near the 1−10 ng range.

**Experiment II: Analysis of the Natural Fat Matrix.** A total ion chromatogram of a natural fat sample is shown in Figure 4. The fgure includes excerpts of assignments of the most abundant peaks (see also Table 4). The compounds observed are mainly a mix of intact free fatty acids (octadecanoic acid, caprylic acid, decanoic acid, palmitic acid, and others not annotated) and the aliphatic tails of fatty acids broken into varying sizes from the thermal transfer of the fat (heptane, nonanal, dodecane, undecane, and heptadecane). In addition, the presence of aldehydes (nonanal) is a typical product of fat oxidation, here occurring during the sampling procedure. Some volatile aroma compounds, including furan and (*E*,*E*)-2,4-nonadienal, also appear in the chromatogram, and these types of compounds may contribute to an altered perception of the odor profile of the fat when heated. Especially the short fatty acid caprylic acid (C8:0), reported to have an odor profile labeled "pungent, sour and rancid",[32] can potentially provide this effect. These observations were not pursued further in this work. The relatively broad peaks of indole and skatole indicate that either other compounds may be coeluting with the two analytes or that the chromatographic procedure used is not optimal for the two analytes. However, as the calibration method uses a single quantification ion (or by MS single ion monitoring (SIM) scanning) accumulated over a retention time gap, reliable quantifications can be made from the chromatogram. The peak area of androstenone in Figure 4 is visibly disproportional to other peaks representing compounds more abundant in the sample (fatty acids and so on) and is the combined effect of column polarity, the sampling method, and the difference in vaporization points for the various compounds.

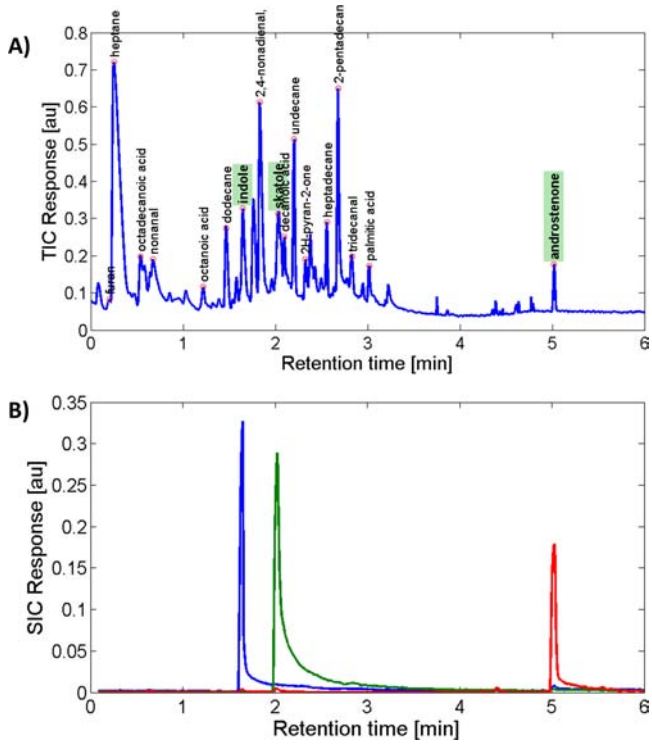


**Figure 4.** (A) Total ion chromatogram of a fat sample with annotated compounds (excerpt of full list). (B) Single ion chromatograms of the three analytes. Blue curve, indole ($m/z$ = 117 ± 0.5); green curve, skatole ($m/z$ = 130 ± 0.5); red curve, androstenone ($m/z$ = 257 ± 0.5).

In order to validate the ion and the retention-time-window selection, blank samples were run on fat determined with the LC method to have no noticeable boar-taint compounds (not shown). No instrument response could be accumulated on these samples, showing that the selected ions and window does target the three analytes.

The calibrations obtained in experiment I were used to predict analyte concentration levels from the chromatographic response, and to study how the analytes in the fat matrix are released compared to the directly injected standards. As the analyte concentrations in the biological samples previously have been determined using a high-performance LC (HPLC) reference method,[14] the relationship between the predicted and known levels can be expressed as in Figure 5A for the three analytes. Overall, the curves show a strong linear trend, and the minor deviations of the curves can be explained by variations in the biological sample material or by method sensitivity to (unrecorded) variations in the sampling procedure. The absolute level of the predicted masses in the fat matrix is lower than for the directly introduced standards, which indicate


dx.doi.org/10.1021/jf5022785 | J. Agric. Food Chem. 2014, 62, 9420−9427

**Table 4. Excerpts of the List of Compounds Tentatively Identified in Fat Chromatogram Using the NIST 11 Database[a]**

| retention time (min) | compound name |
|---|---|
| 0.20 | furan |
| 0.25 | heptane |
| 0.54 | octadecanoic acid |
| 0.68 | nonanal |
| 1.22 | octanoic acid |
| 1.47 | dodecane |
| 1.65 | indole |
| 1.83 | (*E*,*E*)-2,4-nonadienal |
| 2.03 | skatole |
| 2.10 | decanoic acid |
| 2.20 | undecane |
| 2.33 | 2*H*-pyran-2-one |
| 2.56 | heptadecane |
| 2.68 | 2-pentadecanone |
| 2.83 | tridecanal |
| 3.02 | palmitic acid |
| 5.02 | androstenone |

[a]Only compounds with high accuracy are shown.

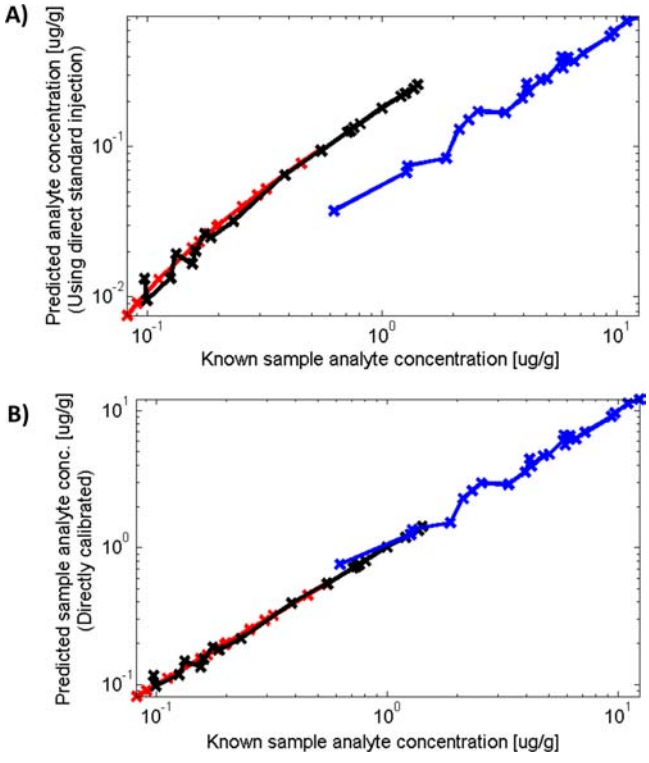


**Figure 5.** (A) Prediction of analyte concentration from instrument response using calibration obtained from the direct introduction of standards. Red curve, indole, $R^2$ = 1.00; black curve, skatole, $R^2$ = 0.99; blue curve, androstenone, $R^2$ = 0.98. (B) Prediction of known analyte concentration directly from instrument response to biological samples. Red curve, indole; black curve, skatole; blue curve, androstenone.

that the total analyte mass stored in the fat matrix was not released into the headspace during equilibration or sampling but rather is a function of temperature and time. However, the strong linear relationship observed shows that the released amount of analyte is quantifiable and reflects the known amount present in the sample.

In the recorded chromatograms no response (LOD) was recorded for fat samples with indole concentrations lower than 82 ng/g (backfat concentration), skatole concentrations lower than 97 ng/g, and androstenone concentrations lower than 623 ng/g. These levels are higher than for the directly introduced standards (experiment I), which may be explained by the fact that a lower concentration of analyte exists in the headspace of the fat samples and accordingly the actual mass concentration reaching the column is lower.

Finally, a direct calibration approach was examined in which the known analyte concentrations are predicted directly from the chromatographic response to the biological samples. The obtained calibration is shown in Figure 5B, and the corresponding statistics are listed in Table 5. This calibration yields on average prediction errors (LOQ) of RMSE = 96 ng/g for indole, 94 ng/g for skatole, and 331.3 ng/g for androstenone.

**Perspective.** *Boar-Taint Risk Assessment.* While the method presented here does not provide for the high prediction accuracy in absolute terms compared to existing laboratory reference methods (the produced results are one order of magnitude lower in precision than the used LC reference method), it does allow for discrete classifications. Based on the human olfactory response levels, a classification flowchart (decision tree) for a sample predicted to have analyte concentrations of $p_i$, $p_s$, and $p_a$, and quantification errors of $e_i$, $e_s$, and $e_a$, for indole, skatole, and androstenone, respectively, is proposed in Figure 6. The flowchart classifies the sample into three groups—a high-risk, intermediate-risk, or low-risk group. The high-risk group is selected if the predicted amount plus the quantification error is higher than thresholds $i_h$, $s_h$, or $a_h$. If this is not the case, the intermediate group is selected for indole and skatole if a prediction is found higher than the quantification error—as analyte definitely *is* present. In order to accommodate for the wider range of androstenone detection levels, an intermediate class is defined if the quantified mass plus its quantification error is higher than a threshold $a_l$. If none of the preceding conditions are fulfilled, the sample is categorized as being low risk. The decision tree may be extended with more nodes (checks and thresholds), if necessary, and the threshold limits should be determined so that they apply to a particular product or general abattoir screening procedure. This use of a decision tree provides possibilities for different actions to concentration levels of different compounds. If the thresholds $i_h$ and $i_s$ are set to the agreed-upon response level of 0.1 $\mu$g of analyte/(g of fat), the sample will be marked high-risk if this occurs—independent of the androstenone level. The androstenone level has two thresholds, a high, $a_h$, and low, $a_l$, in order to take into account the different perception levels as previously described. The decision tree also takes into account that the indole and androstenone levels are uncorrelated in real samples. The method can be used in highly automated setups, using already commercially available equipment. Several samples can be queued for processing with the method, yielding a result every 6 min, where the maximum time from measurement to result delivery limits the queue length. Considering a practical queue length, the method is suitable for verification of premium products for small abattoirs or for overnight batch verification in an abattoir laboratory setting.

*Calibration.* Because the method relies on calibration on known standard samples, the calibration should be maintained frequently to reflect changes in the desorber system (cold trap performance), chromatographic performance (column degra-


dx.doi.org/10.1021/jf5022785 | J. Agric. Food Chem. 2014, 62, 9420−9427

**Table 5. Prediction Performance for Various Analyte Concentrations, Natural Samples**

| | $R^2$ | | | RMSE (ng/g) | | |
|---|---|---|---|---|---|---|
| response range (ng/g)[a] | indole | skatole | androstenone | indole | skatole | androstenone |
| 10−100 | 1.00[b] | 1.00[b] | | 61.7[b] | 54[b] | |
| 100−1,000 | 0.94 | 0.93 | [c] | 96 | 94 | 133.3[c] |
| 1,000−10,000 | | 0.98 | 0.98 | | 86 | 331.3 |
| 10,000−100,000 | | | 1.00[b] | | | 246.9[b] |

[a]Samples included in statistics. For indole: 10−100 ng/g, 2 samples; 100−1000 ng/g, 11 samples. For skatole: 10−100 ng/g, 2 samples; 100−1000 ng/g, 11 samples; 1000−10000 ng/g, 4 samples (all below 2000ng). For androstenone: 100−1000 ng/g, 1 sample; 1000−10,000 ng/g, 21 samples; 10,000−100,000 ng/g, 2 samples (both below 12,000 ng). [b]Only two samples included. [c]Only one sample included.

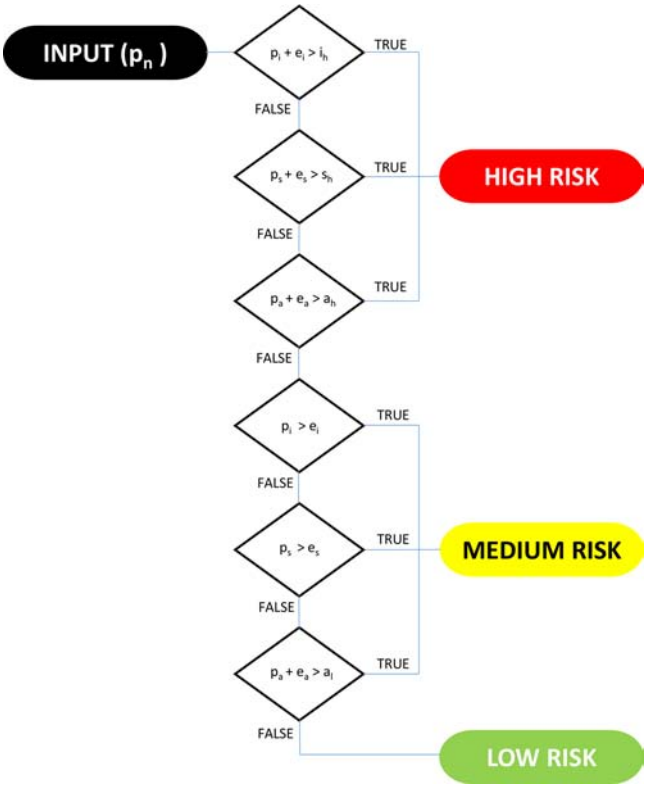


**Figure 6.** Proposed structure to perform classification of fat sample taint risk. Symbols: $p_i$, predicted indole mass; $e_i$, indole mass prediction error; $i_h$, indole high-risk detection threshold mass level; $p_s$, predicted skatole mass; $e_s$, skatole mass prediction error; $s_h$, skatole high-risk detection threshold mass level; $p_a$, predicted androstenone mass; $e_a$, androstenone mass prediction error; $a_h$, androstenone high-risk detection threshold mass level; $a_i$, androstenone intermediate-risk detection threshold mass level.

dation), and mass spectrometer tune changes. For this purpose, laboratory-produced samples of fat spiked with analytes—a high and low concentration—should be measured at daily intervals and the calibration adjusted accordingly (not shown). If a linear relationship between analyte concentration level and instrument response is assumed, a simple bias/slope correction of the instrument response would be sufficient to correct for changes in the chromatographic system. It is suggested that these steps are collected in a software system that maintains the classification and calibration algorithms, so that calibration can be made automatically on the spiked standard samples measured and analyzed in-sequence of the real samples. To avoid degradation of the system performance, it is recommended that a standard sample is run at regular intervals, for instance every 20 samples, with a suitable check against relevant acceptance criteria for the method.

*Comments on the Method and Suggestion for Further Work.* The GC-MS data presented in this work have been obtained using a mass spectrometer in scan mode in order to retain information on other components present in the released gas stream. It is possible and advisible to use the targeted SIM which will increase scan speed and provide a higher accuracy. For the quantification of androstenone, reliable calibration results were obtained by including only the $m/z$ 257 ion instead of separately accumulating instrument response for both $m/z$ 257 and $m/z$ 272. However, it is recommended that both ions are used for quantification. For the purpose of method development, a 30 m column with i.d. 250 $\mu$m was used for the GC results presented here. Since the complexity of the compounds coeluting with the analytes of interest is now known, a shorter column may be used to further reduce run time, just as the film thickness could be reconsidered. However, given the back-to-back nature of the method, an increase in overall analysis speed can only be gained if the desorption and equilibrate phases of the methods are reduced as well.

This work only examines quantification of androstenone to prove the principle of operation. Other similar steroids, also described to have boar-taint odor profiles, should also be examined. Moreover, the material available limited the number of samples for some analyte ranges (Table 5) wherefore a more complete range should be examined before implementation of the method.

## AUTHOR INFORMATION

### Corresponding Author

*E-mail: kms@food.ku.dk. Phone: +45 35 33 29 53.

### Funding

The work presented here has been partially financed by the Danish National Advanced Foundation (Holbergsgade 14 3, DK-1057 Copenhagen, Denmark) and has been made in cooperation with Carometec A/S, Transformervej 9, DK-2860 Søborg, Denmark.

### Notes

The authors declare no competing financial interest.

## ACKNOWLEDGMENTS

We thank Chief Research Scientist Hanne Maribo (Danish Centre for Pig Research, Axelborg, Axeltorv 3, DK-1609 Copenhagen, Denmark, http://www.pigresearchcentre.dk/) for providing the biological sample material and reference values.

## REFERENCES


(1) Claus, R.; Weiler, U.; Herzog, A. Physiological aspects of androstenone and skatole formation in the boar—A review with experimental data. *Meat Sci.* **1994**, *38*, 289−305.

(2) Brooks, R. I.; Pearson, A. M. Odor thresholds of the c19-delta-16-steroids responsible for boar odor in pork. *Meat Sci.* **1989**, *25*, 11−19.

(3) INRA. *Report on the practice of castration*; French National Institute for Agricultural Research, Paris, France. http://w3.rennes.inra.fr/pigcas/Public%20reports/D2%204%20Report%20practice.pdf, 2009. Accessed May 2014.

(4) Leidig, M. S.; Hertrampf, B.; Failing, K.; Schumann, A.; Reiner, G. Pain and discomfort in male piglets during surgical castration with and without local anaesthesia as determined by vocalisation and defence behaviour. *Appl. Anim. Behav. Sci.* **2009**, *116*, 174−178.

(5) Boeker, P.; Haas, T.; Schulze-Lammers, P.; Tholen, E. Measurement of 'boar taint' with trace gas measurement technology via gas phase. *Zuchtungskunde* **2012**, *84*, 439−458.

(6) Vold, E. Fleishproduktionseigenschaften bei Ebern und Kastraten. IV. Organoleptische und gaschromatografische Untersuchungen Wassedampfflüchtiger Stooffe des Rückenspeckes von Ebern. *Meldinger Nordandbruckhoegskole* **1970**, 1−25.

(7) Walstra, P. M. H. *Onderzoek geslachtgeur van mannelijke mestvarkens*; Researchgroep Vlees en Vleesvare. T.N.O.: Zeist, The Netherlands, **1970**; pp 1−30.

(8) Patterson, R. Salpha-androst-16-ene-3−1- compound responsible for taint in boar fat. *J. Sci. Food Agric.* **1968**, *19*, 31−38.

(9) Font-i-Furnols, M. Consumer studies on sensory acceptability of boar taint: A review. *Meat Sci.* **2012**, *92*, 319−329.

(10) Bonneau, M. Use of entire males for pig meat in the European Union. *Meat Sci.* **1998**, *49*, S257−S272.

(11) Wysocki, C. J.; Dorries, K. M.; Beauchamp, G. K. Ability to perceive androstenone can be acquired by ostensibly anosmic people. *Proc. Natl. Acad. Sci. U. S. A.* **1989**, *86*, 7976−7978.

(12) Babol, J.; Squires, E. J. Quality of meat from entire male pigs. *Food Res. Int.* **1995**, *28*, 201−212.

(13) Aluwe, M.; Tuyttens, F. A. M.; Bekaert, K. M.; De Smet, S.; De Brabander, D. L.; Millet, S. Evaluation of various boar taint detection methods. *Animal* **2012**, *6*, 1868−1877.

(14) Maribo, H. Screening of organic boars. *Videncenter for svineproduktion*, Publication No. 955; Danish Agriculture & Food Council Pig Research Center: Copenhagen, Denmark, 2012.

(15) Mörlein, D. Boar taint: The sensory perspective—Olfactory perception, consumer acceptance and trained sensory panel evaluation of boar taint. *Zuchtungskunde* **2012**, *84*, 427−438.

(16) Meier-Dinkel, L.; Sharifi, A. R.; Tholen, E.; Frieden, L.; Bücking, M.; Wicke, M.; Mörlein, D. Sensory evaluation of boar loins: Trained assessors' olfactory acuity affects the perception of boar taint compounds. *Meat Sci.* **2013**, *94*, 19−26.

(17) Mörlein, D.; Meier-Dinkel, L.; Moritz, J.; Sharifi, A. R.; Knorr, C. Learning to smell: Repeated exposure increases sensitivity to androstenone, a major component of boar taint. *Meat Sci.* **2013**, *94*, 425−431.

(18) Lunde, K.; Skuterud, E.; Egelandsdal, B.; Furnols, M. F. I.; Nute, G. R.; Bejerholm, C.; Nilsen, A.; Stenstrom, Y. H.; Hersleth, M. The importance of the recruitment method for androstenone sensitivity with respect to accurate sensory evaluation of androstenone tainted meat. *Food Qual. Prefer.* **2010**, *21*, 648−654.

(19) Lunde, K.; Skuterud, E.; Hersleth, M.; Egelandsdal, B. Norwegian consumers' acceptability of boar tainted meat with different levels of androstenone or skatole as related to their androstenone sensitivity. *Meat Sci.* **2010**, *86*, 706−711.

(20) Sørensen, K. M.; Petersen, H.; Engelsen, S. B. An On-Line Near-Infrared (NIR) Transmission Method for Determining Depth Profiles of Fatty Acid Composition and Iodine Value in Porcine Adipose Fat Tissue. *Appl. Spectrosc.* **2012**, *66*, 218−226.

(21) van den Berg, F.; Lyndgaard, C. B.; Sørensen, K. M.; Engelsen, S. B. Process Analytical Technology in the food industry. *Trends Food Sci. Technol.* **2013**, *31*, 27−35.

(22) Mathur, P. K.; ten Napel, J.; Bloemhof, S.; Heres, L.; Knol, E. F.; Mulder, H. A. A human nose scoring system for boar taint and its relationship with androstenone and skatole. *Meat Sci.* **2012**, *91*, 414−422.

(23) Bekaert, K. M.; Aluwe, M.; Vanhaecke, L.; Heres, L.; Duchateau, L.; Vandendriessche, F.; Tuyttens, F. A. M. Evaluation of different heating methods for the detection of boar taint by means of the human nose. *Meat Sci.* **2013**, *94*, 125−132.

(24) Mörlein, D.; Trautmann, J.; Meier-Dinkel, L. Boar Taint in Male Pigs Procedure for the Selection of Test-Persons. *Fleischwirtschaft* **2013**, *93*, 105−110.

(25) Haugen, J. E.; Brunius, C.; Zamaratskaia, G. Review of analytical methods to measure boar taint compounds in porcine adipose tissue: The need for harmonised methods. *Meat Sci.* **2012**, *90*, 9−19.

(26) Bekaert, K. M.; Vanden Bussche, J.; Francois, S.; Tuyttens, F. A. M.; De Brabander, H. F.; Vandendriessche, F.; Vanhaecke, L. A validated ultra-high performance liquid chromatography coupled to high resolution mass spectrometry analysis for the simultaneous quantification of the three known boar taint compounds. *J. Chromatogr. A* **2012**, *1239*, 49−55.

(27) Hansenmoller, J. Rapid high-performance liquid-chromatographic method for simultaneous determination of androstenone, skatole and indole in back fat from pigs. *Biomed. Chrom.* **1994**, *661*, 219−230.

(28) Fischer, J.; Elsinghorst, P. W.; Bucking, M.; Tholen, E.; Petersen, B.; Wust, M. Development of a Candidate Reference Method for the Simultaneous Quantitation of the Boar Taint Compounds Androstenone, 3 alpha-Androstenol, 3 beta-Androstenol, Skatole, and Indole in Pig Fat by Means of Stable Isotope Dilution Analysis-Headspace Solid-Phase Microextraction-Gas Chromatography/Mass Spectrometry. *Anal. Chem.* **2011**, *83*, 6785−6791.

(29) Fischer, J.; Haas, T.; Leppert, J.; Schulze Lammers, P.; Horner, G.; Wust, M.; Boeker, P. Fast and solvent-free quantitation of boar taint odorants in pig fat by stable isotope dilution analysis-dynamic headspace-thermal desorption-gas chromatography/time-of-flight mass spectrometry. *Food Chem.* **2014**, *158*, 345−350.

(30) Næs, T.; Martens, H. Multivariate calibration—2. Chemometric methods. *TrAC, Trends Anal. Chem.* **1984**, *3*, 266−271.

(31) Næs, T.; Isaksson, T. SEP or RMSEP, which is best? *NIR news* **1991**, *2* (4), 16.

(32) Guler, Z. Quantification of free fatty acids and flavor characteristics of Kasar cheeses. *J. Food Lipids* **2005**, *12*, 209−221.

Table 1. Self-Made Samples As Described in Materials and Methods[a]

| sample | type | processing type | species | declaration | state at purchase | source |
|---|---|---|---|---|---|---|
| S_1 | frikadeller | frying | beef | roast from the hip | raw - chilled | supermarket Münster |
| S_2 | meatballs | cooking | | | | |
| S_3 | meatloaf | baking | | | | |
| S_4 | frikadeller | frying | pork | roast from the topside | raw - chilled | supermarket Münster |
| S_5 | meatballs | cooking | | | | |
| S_6 | meatloaf | baking | | | | |
| S_7 | frikadeller | frying | horse | roast | raw - chilled | farmer's market Münster |
| S_8 | meatballs | cooking | | | | |
| S_9 | meatloaf | baking | | | | |

[a]All samples were screened with the described method.

using species-specific marker peptides.[17] Based on this method, we present here an optimized approach for the detection of specific horse meat and pork marker peptides in different processed food samples.

## MATERIALS AND METHODS

**Chemicals.** LC-MS grade methanol (MeOH) and acetonitrile (ACN) were purchased from Sigma-Aldrich. Formic acid (FA) was purchased from Grüssing (Filsum, Germany). Water ($H_2O$) was prepared on a Milli-Q Gradient A10 system by Millipore (Schwalbach, Germany) and used for all buffers and other solutions including HPLC eluents.

**Commercially Available Samples.** All samples were purchased from German or Dutch supermarkets, butcher shops and farmer's markets, and directly stored at −20 °C in Corning (Amsterdam, Netherlands) 50-mL plastic centrifuge tubes. For self-made samples, pure beef, pork, and horse meat were bought as whole pieces to avoid contamination. Sample details are given in Table 1 for in-house prepared samples and in Supporting Information (SI) Table 1 for commercially available samples.

**Preparation of In-House Processed Samples.** The meat was cut into slices and minced using an electric meat grinder. The minced meat was formed to meat loafs, and frikadeller, a common European product similar to a fried hamburger patty, or meatballs. The meat loaf was placed in a porcelain tray and heated in a conventional kitchen oven to 200 °C until a core temperature of 100 °C was reached. Frikadeller were fried in a Teflon-coated pan until a brown crust typical for this dish was formed. The meatball was cooked in gently boiling water until a core temperature of 100 °C was reached.

For all in-house processed meat products no ingredients other than meat were used.

Products were cooled to room temperature and were precrushed in a freezing bag. The precrushed pieces were frozen in liquid nitrogen until the liquid nitrogen stopped boiling. Frozen pieces were ground at 8000 rpm for about 5 min in a Fritsch Pulverisette 14 rotor mill (Idar-Oberstein, Germany) with a 2-mm sieve. The powdered samples were stored at −20 °C in 50-mL plastic centrifuge tubes.

**Preparation of Sample Mixtures.** Samples containing more than one meat species were either prepared by weighing different amounts of ground pork or horse meat in ground beef followed by extraction of the mixture or by mixing desalted peptide solutions of relevant species (for details see Results and Discussion).

Powdered samples that contained at least 1.0 mg of pork or horse meat as contamination were prepared directly by weighing the different meat species directly in a 50-mL Corning tube on an analytical scale and were further prepared as described under sections "Extraction", "Digest", and "Desalting".

Samples that contained below 1.0 mg pork or horse meat (absolute amounts) were prepared by mixing desalted peptide solutions of respective species. In this case, pure beef (matrix) or either pork or horse meat (contamination) were processed as described below. A defined amount of the resulting, desalted pure beef peptide solution was spiked with either pure, desalted pork or horse meat peptide solution.

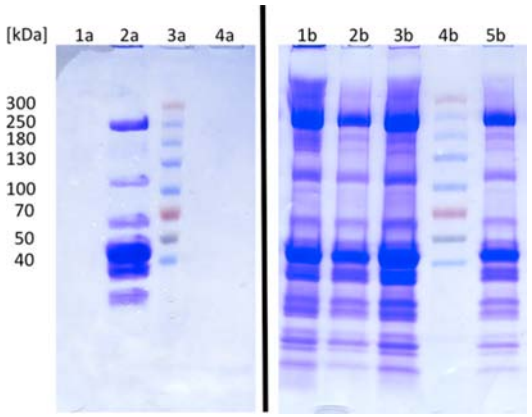


**Figure 1.** SDS-PAGE Gel showing the previously used extraction method (0.3 M KCl, 0.15 M $KH_2PO_4$, and 0.15 M $K_2HPO_4$) for meat samples (left gel, lanes marked #a) and the newly developed extraction method (6 M urea, 1 M thiourea, and 50 mM Tris-HCl) for processed samples (right gel, lanes marked #b). Loading scheme (in brackets volume of sample extract); all samples were made from pure pork; 1a: meatball (8 μL); 2a: raw (8 μL); 3a: marker; 4a: frikadeller (4 μL); 1b: raw (4 μL); 2b: meatball (2 μL); 3b: meatball (4 μL); 4b: marker; 5b: frikadeller (2 μL).

**Preparation of Commercial Processed Samples.** Salamis, sausages, meatballs, canned meat, and Frikandeln (Dutch convenience product similar to sausages) were diced to approximately 2 cm length with a kitchen knife.

Pasta sauce was removed from products by washing them with water on a lab sieve. The residue consisting of small meat and vegetable pieces was homogenized using an Ultra Turrax T-25 basic (ika, Staufen, Germany) with a 10 N dispersing element.

In the case of frozen lasagna and chilled pasta, Bolognese noodles and sauce were removed and the residual samples were also homogenized.

**Extraction.** Approximately 1 g of sample material was weighed in 50-mL plastic centrifuge tube, and 10 mL of extraction buffer (6 M urea, 1 M thiourea, and 50 mM TRIS-HCl (all Carl Roth, Karlsruhe, Germany) adjusted to pH 8) were added. For samples with a low overall meat content in the sample, this amount was slightly increased to approximately 1.4 g.

All samples were vortexed for 20 s and extracted using an Ultra Turrax T-25 (ika, Staufen, Germany) with a 10 N dispersing element. Samples with a higher content of connective tissue, e.g. salami, were dispersed for 30 s at 9500 rpm, followed by 40 s at 13 500 rpm and finally 40 s at 20 500 rpm. For all other sample types, the last step at 20 500 rpm was omitted. Finally, all samples were vortexed again for 20 s.

Following extraction, samples were centrifuged for 60 min at 4 °C at 12 000*g*. A 100-μL aliquot of the supernatant was transferred into a 1.5-mL Eppendorf reaction tube (Hamburg, Germany)

**Sodium Dodecyl Sulfate Polyacrylamide Gel Electrophoresis.** Precast 4−20% gradient gels (Mini-Protean TGX, Bio-Rad, München, Germany) were used to asses extraction efficiency. Running


dx.doi.org/10.1021/jf503468t | J. Agric. Food Chem. 2014, 62, 9428−9435

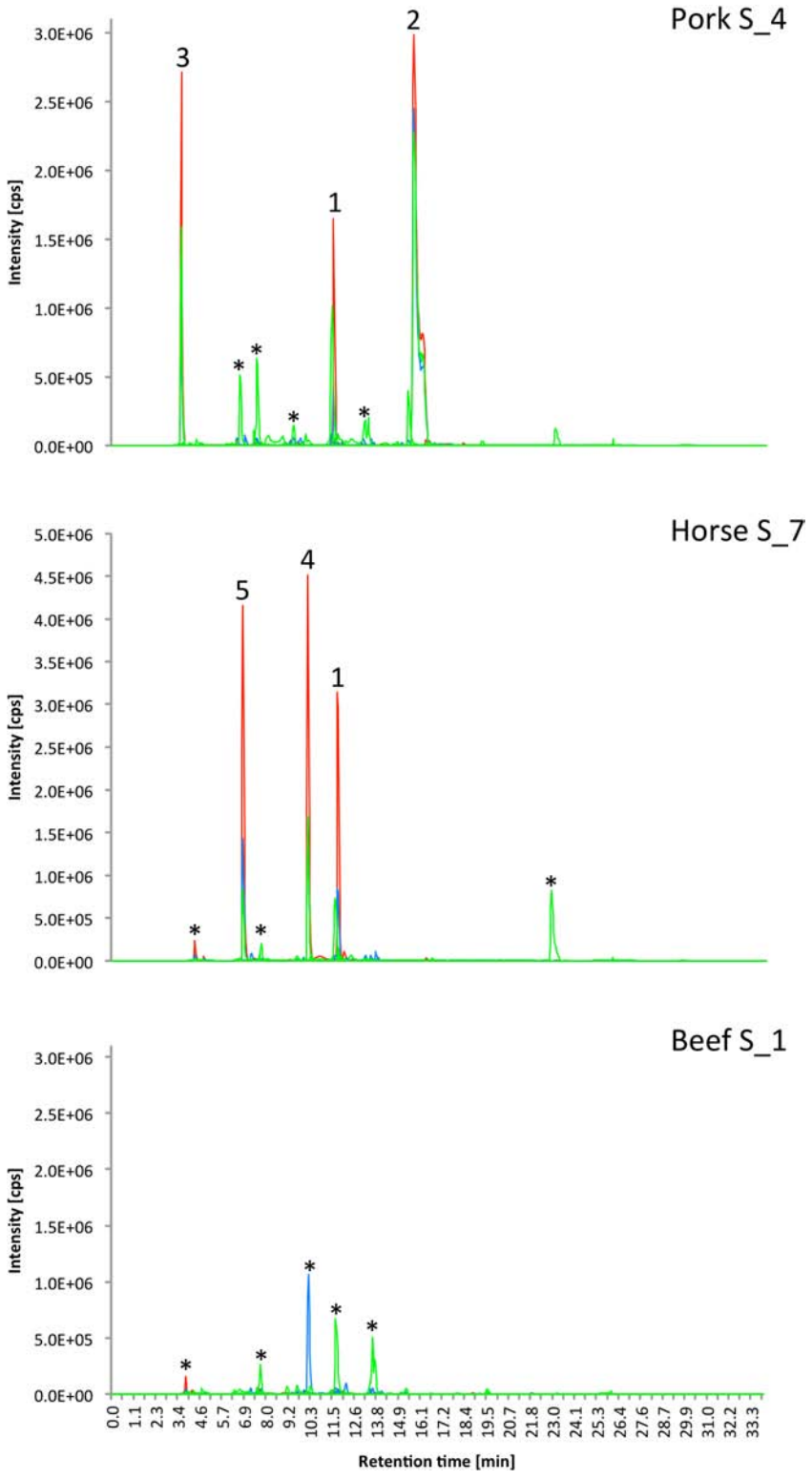


**Figure 2.** HPLC-MS/MS chromatograms of frikadeller samples made from pure pork, beef, or horse meat. To reduce complexity, only the three most intense MRM traces are shown for every peptide. The most intense transition is given in red, 2nd most intense is in blue, and 3rd most intense is in green. Unspecific signals are marked with asterisk. Markers are numbered according to Table 2 (for MS and HPLC parameters see SI Table 2).

buffer and sample buffer were prepared according to Lämmli.[18] SDS, Glycin, and TRIS-HCl were purchased from Roth in Bufferan quality. The protein molecular weight standard used was the Spectra Multicolor High Range Protein Ladder (Thermo Fisher Scientific, Rockford, IL, USA)

Briefly, samples were diluted with water and sample buffer, denatured at 95 °C for 5 min. Following sample application, SDS-gels were focused for 20 min at 100 V and then run at 140 V until the bromophenol blue front reached the end of the gel. Gels were fixed and stained using Coomassie brilliant blue dye for 25 min and destained. Gel pictures were taken on a standard flatbed scanner for personal computers.

**Digest.** An aliquot of the extract of the processed meat samples was subjected to tryptic digest following a standard protocol.[14] For each


dx.doi.org/10.1021/jf503468t | J. Agric. Food Chem. 2014, 62, 9428−9435

**Table 2. Characteristic Marker Peptides for Horse and Pork[a]**

| marker | species | name | uniprot accession | sequence | AA position |
|---|---|---|---|---|---|
| 1 | pig/horse | troponin T/uncharacterized protein | Q75NG7/F6 × 010 | YDIINLR | 239−245/185−191 |
| 2 | pig | myosin-4 | Q9TV62 | TLAFLFAER | 619−627 |
| 3 | pig | myosin-1 and -4 | Q9TV61/Q9TV62 | SALAHAVQSSR | 1331−1341/1329−1339 |
| 4 | horse | myosin-2 | Q8MJV1 | EFEIGNLQSK | 1086−1095 |
| 5 | horse | myosin-1 | Q8MJV0 | LVNDLTGQR | 1272−1280 |

[a]Markers 1, 2, and 4 are the most sensitive and are displayed in the subsequent figures. AA position: Position of the biomarker peptide in the sequence of the identified protein.

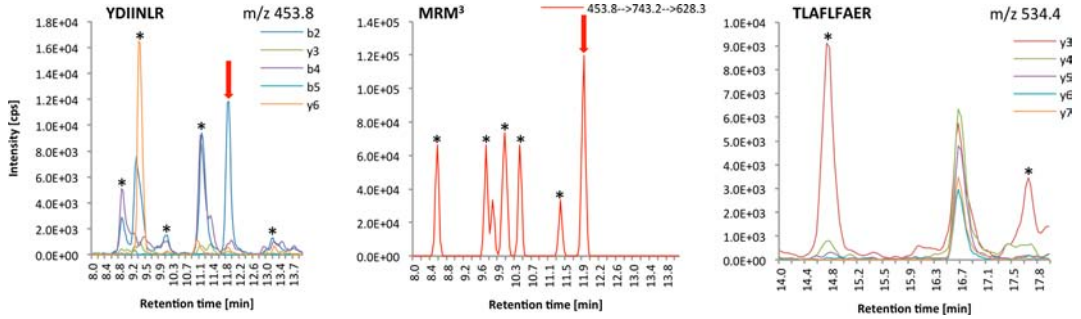


**Figure 3.** HPLC-MS/MS and MRM$^3$ chromatograms of a beef frikadeller spiked with 0.51% of pork frikadeller (mixed peptide solutions). Shown are the horse/pork-specific marker 1 (YDIINLR) and the pork-specific marker 2 (TLAFLFAER). For marker 1, four MRM transitions are detectable, but the s/n for y6 is only 3. However, the MRM$^3$ signal was detectable, showing a huge improvement for the sensitivity. For marker 2, all MRM transitions, but with a low overall intensity defining the LOD for this marker, were detectable. Unspecific signals have been marked with asterisks.

sample, an aliquot of 100 μL containing about 1.5 mg of protein was reduced, alkylated, diluted 1:10 with $H_2O$, and supplemented with 20 μg of Promega Sequencing grade modified trypsin (Promega, Mannheim). To allow complete digest, samples were incubated in a thermo shaker at 37 °C under slow shaking for at least 12 h.

**Desalting.** Digested samples were diluted 1:2 with $H_2O$ and desalted using Phenomenex (Aschaffenburg, Germany) Strata-X 33u polymeric reversed phase cartridges filled with 30 mg/mL RP material. Cartridges were washed and activated using 1 mL of MeOH followed by equilibration with 1 mL of 1% FA according to the manual. The samples were loaded onto the cartridge and washed with 1 mL of 5% MeOH/1% FA. Finally, peptides were eluted with 1 mL of ACN/$H_2O$ (90/10, 0.1% FA) and the eluate was collected in Eppendorf reaction tubes prefilled with 6 μL of dimethyl sulfoxide (DMSO) purchased from Roth (Karlsruhe, Germany).

**Preparation for HPLC.** After desalting, the solvent was removed under vacuum at 39 °C using an S-Concentrator BA-VC-300H purchased from H. Saur Laborbedarf (Reutlingen, Germany). DMSO is not removed during this procedure, which prevents peptides from sticking to the vessel surface and enhances peptide recovery. The samples were redissolved in ACN/$H_2O$ (3/97; 0.1% FA) and analyzed.

**MS/MS.** All samples were analyzed using a QTrap 5500 LC-MS/MS system (AB SCIEX, Darmstadt, Germany) with a VWR Hitachi HPLC (Pump L-2160U; autosampler L-2200U and column oven L-2300) and a Phenomenex Kinetex 2.6 u C18 100 Å (100 × 2.10 mm) column (Phenomenex, Aschaffenburg, Germany). A Turbo V ESI source was used. For details on HPLC gradient, source, and MS parameters see SI Table 2.

Data were evaluated using Analyst Software Version 1.5.2.

To survey retention time stability and relative intensity of MRM transitions, control samples of respective species were routinely analyzed accordingly.

A more detailed and basic description of the MS experiments is given directly after SI Table 2.

## RESULTS AND DISCUSSION

One of the most critical steps for the analysis of processed samples in targeted proteomics is efficient sample extraction. In our previous publication, we applied mild extraction conditions to reduce complexity of the extracted proteome and to focus on the readily soluble and highly abundant proteins of the myofibrillar and sarcoplasmic fraction in raw sample material.[17] Although target proteins in raw meat are soluble in low molar salt buffers (0.3 M KCl, 0.15 M $KH_2PO_4$, and 0.15 M $K_2HPO_4$)(Figure 1, lane 2a), heat treatment such as frying or boiling strongly reduced solubility for different meat products and led to lack of solubility of target proteins (Figure 1, lanes 1a and 4a). To overcome this problem, 11 different buffer compositions in combination with different extraction protocols such as vigorous shaking, vortexing, or the use of Ultra Turrax were assessed concerning efficiency of extraction and comparability with downstream sample preparation (data not shown) and best results were observed with 6 M urea, 1 M thiourea, and 50 mM Tris-HCl (see Materials and Methods for details). This extraction buffer gives excellent results for raw and for different processed samples as can be seen from the right gel in Figure 1 (lanes 1b−5b). In addition, the extraction time was strongly reduced to only approximately 2 min and a simple 10-fold dilution of the extract is sufficient to reduce urea and thiourea concentrations to allow tryptic digest.

It has, however, to be kept in mind that sample complexity is increased after processing and harsher extraction. We therefore assessed specificity and sensitivity of biomarker peptides under the modified conditions using pure, in-house processed beef, pork, and horse meat. Figure 2 and Table 2 give an overview of the five previously described[17] most important pork and horse meat biomarker peptides, demonstrating excellent specificity of the modified method. As expected, the specific horse and pork markers were not detectable in the beef sample. Though unspecific single MRM transitions occur, the specific marker peptides are only observed in the according samples and show retention time match, as well as matching MRM signal ratios and the full spectrum of MRM transitions. (See SI Table 3 for MRM Transitions and MS conditions). Similar results were observed for all in-house processed sample types (data not

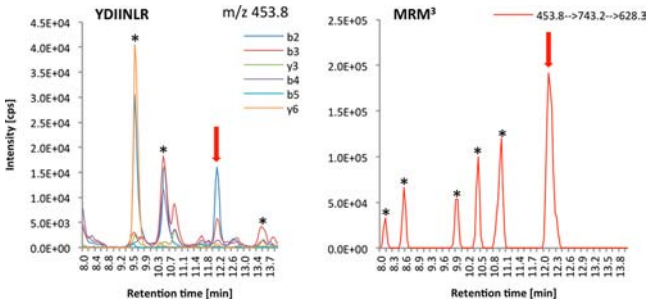


**Figure 4.** HPLC-MS/MS and MRM$^3$ chromatograms of a beef meatball spiked with 0.25% of horse meat ball (mixed peptide solutions). Shown is the most sensitive marker, the horse/pork-specific marker 1 (YDIINLR) and its corresponding MRM$^3$ experiment. Compared to Figure 3 it is obvious that the meatball matrix is less complex resulting in better overall intensities at lower concentration. Unspecific signals have been marked with asterisks.

shown), indicating that heat processing in general does not interfere with critical steps of our method (extraction, tryptic digest, MS analysis).

We next analyzed the sensitivity of the modified method using in-house processed samples containing trace amounts of pork and horse meat, respectively. At present, no official thresholds levels are in place for undeclared meat species. We therefore used the threshold level of 0.9% for genetically modified organisms (GMO) issued in Regulation (EC) 1830/2003 of the European Union[19] as orientation for "technically unavoidable" contaminations and the minimal performance level of our method.

Figure 3 shows results for a fried frikadeller containing 0.51% pork in beef. Marker 1 (YDIINLR) is still detectable with four MRM transitions. In addition, MRM$^3$ experiments provide a significant improvement of the signal-to-noise ratio and further improve specificity. In addition, all 5 MRM transitions for marker 2 (TLAFLFAER) were detected, demonstrating the specific detection of pork in this sample. However, we noted the increase in unspecific signals (as marked by asterisk) in MRM and MRM$^3$ experiments for highly processed samples. Fried meat products had a deep brown surface due to pronounced Maillard reaction and respective peptide solutions showed a yellow to brown color indicative for complex modification of the protein matrix.

As expected, for milder processing techniques such as boiling sensitivity was increased compared to fried samples. Figure 4 shows the results for boiled meatballs at a concentration of 0.24% horse in beef matrix. This concentration was achieved by mixing peptide solution of pure horse and beef samples. At this concentration, only marker 1 (YDIINLR) was detectable in MRM and MRM$^3$ experiments. Again, four MRM transitions were detectable and MRM$^3$ improved s/n and specificity (Figure 4). Similarly, for respective samples containing 0.24% of pork, we identified marker 1 as most sensitive marker but not the other pork-specific peptides (data not shown).

**Measurement of Commercially Available Processed Samples.** We next assessed the applicability of the detection method on a broad range of commercially available processed products obtained from supermarkets and a local farmers market (see SI Table 1 for details). All samples were prepared and analyzed with the described method.

Figure 5 shows the results for frikadeller (sample C_12 in SI Table 1) that was labeled to contain only pork meat. All MRM transitions from all specific peptides (see SI Table 3 for details) expected for pork were found in this sample and none of the marker peptide markers for horse, demonstrating excellent specificity for this processed sample.

An example of a more complex food matrix is given in Figure 6 (sauce Bolognese, sample C_11, see details in SI Table 1). The total meat content of the sample was declared with 3% pork and 7% beef. Detection of YDIINLR and TLAFLFAER (markers 1 and 2) confirmed the pork meat content of the product. As expected, no horse-specific markers (EFEIGNLQSK and LVNDLTGQR) were detected in this product (Figure 6). An overview of the results of the 23 different commercial samples

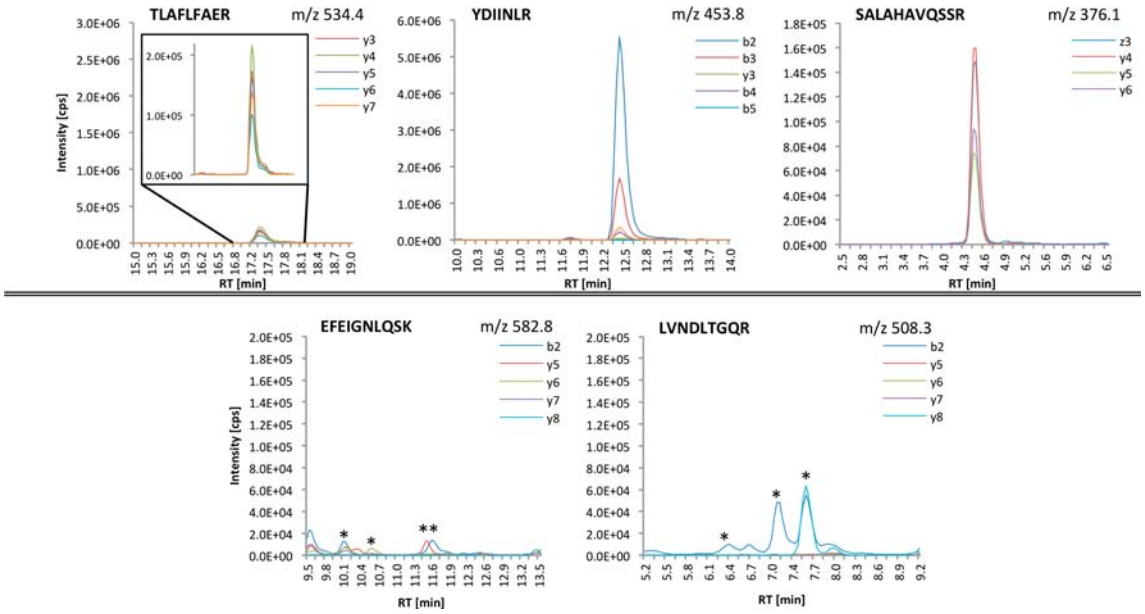


**Figure 5.** HPLC-MS/MS chromatograms of a commercial frikadeller (C_12) declared as pure pork. Shown are the horse/pork-specific marker 1 (YDIINLR), the pork-specific markers 2 (TLAFLFAER) and 3 (SALAHAVQSSR), and the horse-specific markers 4 (EFEIGNLQSK) and 5 (LVNDLTGQR). It is obvious that the sample C_12 contains pork and no horse was detected. Unspecific signals have been marked with asterisks.


dx.doi.org/10.1021/jf503468t | J. Agric. Food Chem. 2014, 62, 9428−9435

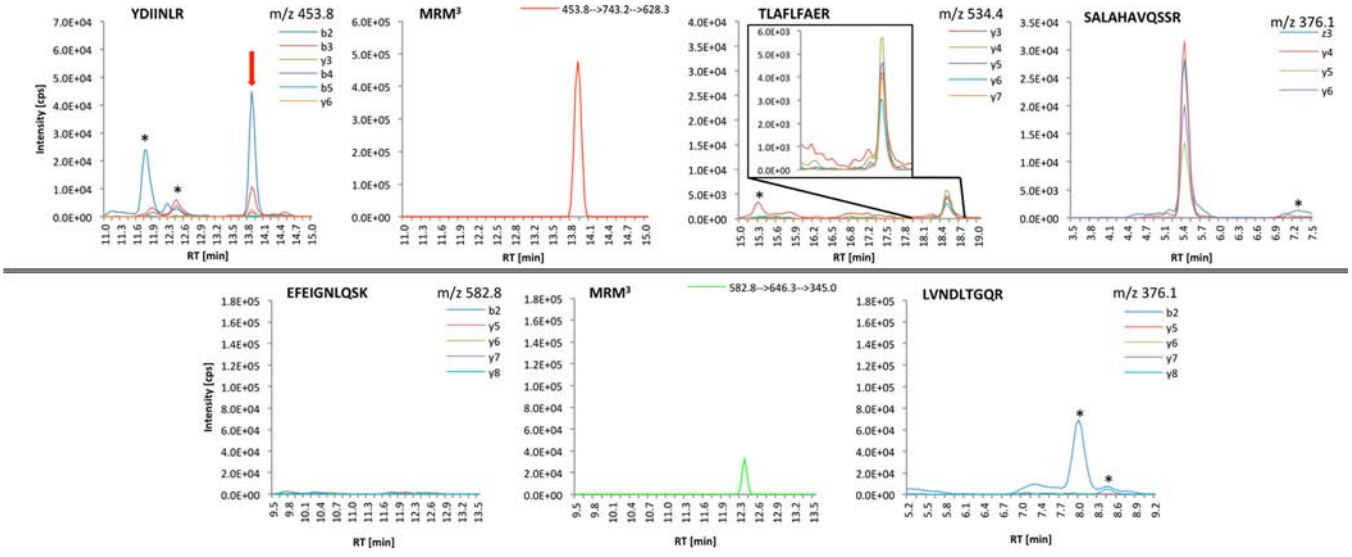


**Figure 6.** HPLC-MS/MS and MRM$^3$ chromatograms of a sauce Bolognese (C_11) declared as a mixture of beef and pork. Shown are the horse/pork-specific marker 1 (YDIINLR) with its corresponding MRM$^3$ experiment, the pork-specific markers 2 (TLAFLFAER) and 3 (SALAHAVQSSR), and the horse-specific markers 4 (EFEIGNLQSK) with its corresponding MRM$^3$ experiment and 5 (LVNDLTGQR). Unspecific signals have been marked with asterisks.

**Table 3. Screening Results of Commercial Samples**[a]

| | | | pork | | pork/horse | | horse | | | |
|---|---|---|---|---|---|---|---|---|---|---|
| sample | declaration | species declared | SALAHAVQSSR | TLAFLFAER | YDIINLR | MRM$^3$ | EFEIGNLQSK | MRM$^3$ | LVNDLTGQR | declaration confirmed |
| C_1 | corned beef A | beef | n.d. | n.d. | match | match | match | match | match | no |
| C_2 | corned beef B | beef | n.d. | n.d. | n.d. | n.d. | n.d. | n.d. | n.d. | yes |
| C_3 | corned beef C | beef | n.d. | n.d. | n.d. | n.d. | n.d. | n.d. | n.d. | yes |
| C_4 | mini salami A | beef and pork | match | match | match | match | n.d. | n.d. | n.d. | yes |
| C_5 | pork in jus | pork | match | match | match | match | n.d. | n.d. | n.d. | yes |
| C_6 | salami A | beef | n.d. | n.d. | n.d. | n.d. | n.d. | n.d. | n.d. | yes |
| C_7 | salami B | deer and pork | match | match | match | match | n.d. | n.d. | n.d. | yes |
| C_8 | salami C | pork and wild boar | match | match | match | match | n.d. | n.d. | n.d. | yes |
| C_9 | mini salami B | pork | match | match | match | match | n.d. | n.d. | n.d. | yes |
| C_10 | Bolognese sauce A | beef and pork | match | match | match | match | n.d. | n.d. | n.d. | yes |
| C_11 | Bolognese sauce B | beef and pork | match | match | match | match | n.d. | n.d. | n.d. | yes |
| C_12 | frikadeller | pork | match | match | match | match | n.d. | n.d. | n.d. | yes |
| C_13 | hamburger patty | beef | n.d. | n.d. | n.d. | n.d. | n.d. | n.d. | n.d. | yes |
| C_14 | spaghetti Bolognese (sauce and noodles) | beef and pork | match | match | match | match | n.d. | n.d. | n.d. | yes |
| C_15 | lasagnese Bolognese | beef and pork | match | match | match | match | n.d. | n.d. | n.d. | yes |
| C_16 | meatball in sauce | beef and pork | match | match | match | match | n.d. | n.d. | n.d. | yes |
| C_17 | mini salami C | horse | n.d. | n.d. | match | match | match | match | match | yes |
| C_18 | frikandeln A | pork | match | match | match | match | n.d. | | n.d. | yes |
| C_19 | frikandeln B | pork and chicken | match | match | match | match | n.d. | n.d. | n.d. | yes |
| C_20 | frikandeln C | pork and chicken | match | match | match | match | n.d. | n.d. | n.d. | yes |
| C_21 | frikandel D | pork and chicken | n.d. | 3 MRM | match | match | n.d. | n.d. | n.d. | (yes) |
| C_22 | frankfurter sausage | horse | n.d. | n.d. | match | match | match | match | match | yes |
| C_23 | salami D | horse | n.d. | n.d. | match | match | match | match | match | yes |

[a]Match = MRM transitions were detectable at expected retention time with good intensities; n.d. = no MRM transitions were detectable.

analyzed in this study is given in Table 3 (sample details found in SI Table 1). Results of species identification and labeling was consistent for all analyzed samples except one corned beef sample (C_1, see Table 3). This sample was labeled to contain only beef material, but we detected horse-specific peptide markers using MRM and MRM$^3$ experiments, indicating unlabeled amounts of horse meat in this sample (Figure 7, upper chromatograms). We confirmed this result by the analysis


dx.doi.org/10.1021/jf503468t | J. Agric. Food Chem. 2014, 62, 9428−9435

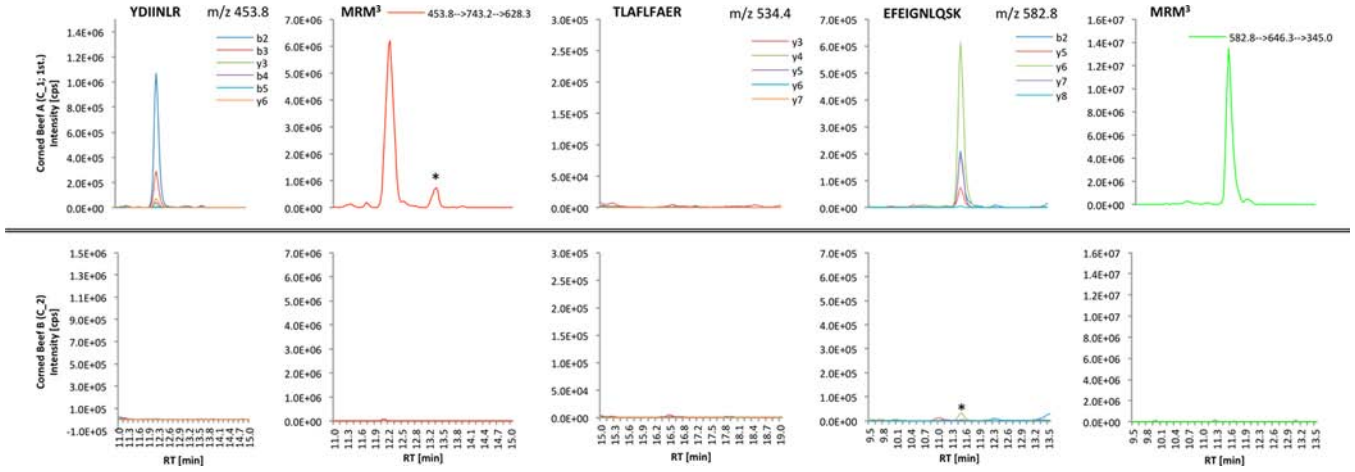


**Figure 7.** HPLC-MS/MS and MRM³ chromatograms of corned beef (C_1) declared as a pure beef. Shown are the horse/pork-specific marker 1 (YDIINLR) with its corresponding MRM³ experiment, the pork-specific marker 2 (TLAFLFAER), and the horse-specific marker 4 (EFEIGNLQSK) with its corresponding MRM³ experiment. It is obvious that sample C_1 contains horse meat because marker 1 and marker 4 both with corresponding MRM³ experiments were detectable. In sample C_2 (lower chromatograms), as declared, no horse or pork was detectable. Unspecific signals have been marked with asterisks.

of a biological replicate and analyzed two additional corned beef samples to rule out matrix effects of this sample material. As an example, results for corned beef sample C_2 are given in Figure 7 (lower chromatogram). Neither pork nor horse meat marker peptides were detectable, indicating that this sample contained only beef meat and that detection of horse in sample C_1 was not due to unspecific matrix effects (Figure 7). This was further underlined by use of droplet digital PCR to confirm the detection of horse meat in sample C_1 with a second analytical technique.

Taken together, we present in this study an optimized method for the specific detection of horse and pork meat in processed and highly processed food samples. Using MRM and the novel MRM³ detection of specific marker peptides, we were able to detect down to 0.24% horse or pork in a beef meat matrix. When necessary, a further reduction of sensitivity (approximately factor 3−4) can be achieved by the application of microLC systems instead of high flow LC as shown previously.[18] We were able to demonstrate that the identified marker peptides are sufficiently stable to resist thermal processing of different types of meat products and thus allow specific and sensitive detection also in processed food. The optimization of protein extraction had major impact on method performance, as demonstrated by the systematic evaluation of different extraction protocols. Optimal results were achieved by use of high molar urea and thiourea buffer systems. In addition, streamlining of extraction and sample preparation allowed us to drastically reduce extraction time to 20 s up to 2 min, depending on sample type. It is one of the huge advantages of this method that no special proteomics infrastructure such as 2D-PAGE or offgel-fractionation is necessary for prefractionation of samples and that separation and detection is performed on conventional C18 RP-columns and triple quadrupole instumentation. The protocol can therefore easily be implemented in routine analysis of laboratories without specific proteomics knowledge.

## ■ ASSOCIATED CONTENT

### Ⓢ Supporting Information

Additional tables and experimental details as noted in the text. This material is available free of charge via the Internet at http://pubs.acs.org.

## ■ AUTHOR INFORMATION


### Corresponding Author

*Tel.: +49 251 8333391. Fax: +49 251 8333396. E-mail: humpf@wwu.de.


### Notes

The authors declare no competing financial interest.

## ■ ACKNOWLEDGMENTS

We thank AB Sciex (Darmstadt, Germany) for supplying us with a QTRAP 5500 mass spectrometer, Merck/VWR (Darmstadt, Germany) for supplying us with a Merck-Hitachi/VWR LaChromeUltra HPLC system, and Dr. Andreas Finger (Wessling Laboratory, Münster, Germany) for the droplet digital PCR analysis of sample C_1.

## ■ REFERENCES

(1) Depreux, F. F. S.; Okamura, C. S.; Swartz, D. R.; Grant, A. L.; Brandstetter, A. M.; Gerrard, D. E. Quantification of myosin heavy chain isoform in porcine muscle using an enzyme-linked immunosorbent assay. *Meat Sci.* **2000**, *56*, 261−269.

(2) Patterson, R. L. S.; Jones, S. J. Review of current techniques for the verification of the species origin of meat. *Analyst* **1990**, *115*, 501.

(3) Chen, F.-C.; Hsieh, Y. H. P. Detection of pork in heat-processed meat products by monoclonal antibody-based ELISA. *J. AOAC Int.* **2000**, *83*, 79−85.

(4) O'Mahony, P. J. Finding horse meat in beef products–a global problem. *QJM* **2013**, *106*, 595−597.

(5) Soares, S.; Amaral, J. S.; Mafra, I.; Oliveira, M. B. Quantitative detection of poultry meat adulteration with pork by a duplex PCR assay. *Meat Sci.* **2010**, *85*, 531−536.

(6) Arslan, A.; Ilhak, O. I.; Calicioglu, M. Effect of method of cooking on identification of heat processed beef using polymerase chain reaction (PCR) technique. *Meat Sci.* **2006**, *72*, 326−330.

(7) Matsunaga, T.; Chikuni, K.; Tanabe, R.; Muroya, S.; Shibata, K.; Yamada, J.; Shimura, Y. A quick and simple method for the identification of meat species and meat products by PCR assay. *Meat Sci.* **1999**, *51*, 143−148.

(8) Abdel-Fattah, F.; Gaede, W. Influences on the sensitivity of real-time PCR for the detection of bovine DNA in heat-sterilised feedstuffs. *Arch. Anim. Nutr.* **2011**, *65*, 175−185.

(9) Musto, M.; Faraone, D.; Cellini, F.; Musto, E. Changes of DNA quality and meat physicochemical properties in bovine supraspinatus

muscle during microwave heating. *J. Sci. Food Agric.* **2014**, *94*, 785−791.
(10) Sakalar, E.; Abasiyanik, M. F.; Bektik, E.; Tayyrov, A. Effect of heat processing on DNA quantification of meat species. *J. Food Sci.* **2012**, *77*, N40−4.
(11) Ulca, P.; Balta, H.; Cagin, I.; Senyuva, H. Z. Meat species identification and Halal authentication using PCR analysis of raw and cooked traditional Turkish foods. *Meat Sci.* **2013**, *94*, 280−284.
(12) Köppel, R.; Eugster, A.; Ruf, J.; Rentsch, J. Quantification of meat proportions by measuring DNA contents in raw and boiled sausages using matrix-adapted calibrators and multiplex real-time PCR. *J. AOAC Int.* **2012**, *95*, 494−499.
(13) Buckley, M.; Melton, N. D.; Montgomery, J. Proteomics analysis of ancient food vessel stitching reveals >4000-year-old milk protein. *Rapid Commun. Mass Spectrom.* **2013**, *27*, 531−538.
(14) Montowska, M.; Pospiech, E. Species-specific expression of various proteins in meat tissue: Proteomic analysis of raw and cooked meat and meat products made from beef, pork and selected poultry species. *Food Chem.* **2013**, *136*, 1461−1469.
(15) Mazzeo, M. F.; De Giulio, B.; Guerriero, G.; Ciarcia, G.; Malorni, A.; Russo, G. L.; Siciliano, R. A. Fish authentication by MALDI-TOF mass spectrometry. *J. Agric. Food Chem.* **2008**, *56*, 11071−11076.
(16) Hollung, K.; Grove, H.; Faergestad, E. M.; Sidhu, M. S.; Berg, P. Comparison of muscle proteome profiles in pure breeds of Norwegian Landrace and Duroc at three different ages. *Meat Sci.* **2009**, *81*, 487−492.
(17) von Bargen, C.; Dojahn, J.; Waidelich, D.; Humpf, H. U.; Brockmeyer, J. New sensitive high-performance liquid chromatography-tandem mass spectrometry method for the detection of horse and pork in Halal beef. *J. Agric. Food Chem.* **2013**, *61*, 11986−11994.
(18) Laemmli, U. K. Cleavage of structural proteins during the assembly of the head of bacteriophage T4. *Nature* **1970**, *227*, 680−685.
(19) European Union.. Regulation (EC) No 1830/2003 of the European Parliament and of the Council of 22 September 2003 concerning the traceability and labelling of genetically modified organisms and the traceability of food and feed products produced from genetically modified organisms and amending Directive 2001/18/EC. *Off. J. Eur. Union* **2003**, *268*, 24−28.

tea germplasms.[1,6,7] However, there are no comprehensive investigations about the catechin content of Chinese tea germplasms. Variations of the total catechins (TC) content of 119 accessions have been reported by the CNGTR.[7] However, the catechin compositions of Chinese tea germplasms were not clarified. To understand tea germplasms better and to use them effectively for breeding and production, the present study had the following main objectives: (1) to clarify the variation and profile of major catechins in tea germplasms of China, (2) to investigate the variability in catechin content of tea varieties and, (3) to understand the diversity of catechins of tea germplasms from main tea-producing regions of China.

## MATERIALS AND METHODS

**Materials.** A total of 403 accessions of representative tea germplasms were sampled for analysis. Having been introduced as cuttings or seedlings from 15 tea-growing provinces in China, they are currently preserved as genetic resources in the CNGTR (120°10′ E, 30°18′ N, 50 m in altitude) at Hangzhou, China, and are maintained through similar horticultural practices. Their geographic origins are shown in Figure 1. Among them, 320 accessions were *C. sinensis* var. *sinensis* (*sinensis* variety), 21 were *C. sinensis* var. *assamica* (*assamica* variety), 30 were *C. sinensis* var. *pubilimba* Chang (*pubilimba* variety), 8 were *C. taliensis* (W. W. Smith) Melchior, 4 were *C. crassicolumna* Chang, 3 were *C. tachangensis* F. C. Zhang, 1 was *C. gymnogyna* Chang, and 16 were uncategorized germplasms. All belong to the section *Thea* (L.) Dyer genus *Camellia* L. To analyze the main catechin components, 20−60 g of one bud and two leaves young shoots of the first flush in spring were harvested from individual plant of 403 accessions of tea germplasms in 2010 and 2011. All samples were immediately fixed with air at 120 °C for 5 min to deactivate polyphenol oxidase and then dried at 70 °C by a 1.1 kW drying machine (Zhejiang Chunjiang Tea Machinery Co., Hangzhou, China). The dried samples were stored in polyethylene bags and then kept frozen (−20 °C) until analysis. At the time of analysis, the frozen samples were ground and sifted through a 0.5 mm screen. Samples were analyzed in triplicate and results were averaged. Analysis of tea germplasms was performed over the course of two years. Because the difference in catechin content between two years was not significant ($P \geq 0.05$) (data not shown), data analysis utilized the mean catechin content of each tea accession in 2010 and 2011.

**Figure 1.** Sampling size and distribution of tea germplasms in China. Abbreviations represent different provinces. AH: Anhui, CQ: Chongqing, FJ: Fujian, GD: Guangdong, GX: Guangxi, GZ: Guizhou, HeN: Henan, HuB: Hubei, HuN: Hunan, JS: Jiangsu, JX: Jiangxi, SC: Sichuan, TW: Taiwan, YN: Yunnan, and ZJ: Zhejiang. A total of 403 accessions of tea germplasms were obtained.

**Chemicals and Standards.** The standard substances EGCG (97% purity), ECG (98% purity), EGC (95% purity), EC (98% purity), GC (98% purity), C (98% purity), and (−)-gallocatechin gallate (GCG) (98% purity) were bought from Sigma-Aldrich Chemicals Co. (St. Louis, MO, U.S.A.). Other chemicals were obtained from Huadong Medicine Co., Ltd. (Hangzhou, China).

**Sample Preparation and HPLC Conditions.** The isolation and detection of tea catechins, by high performance liquid chromatography (HPLC), was performed according to the International Standards Organization (ISO) ISO 14502-2-2005(E) procedure[25] with minor modifications. The powdered tea sample (0.2 g) was extracted by intermittent shaking with 5 mL of 70% (v/v) methanol at 70 °C, and the mixture was centrifuged at 1400*g* for 10 min. The supernatant was decanted into a 10 mL volumetric flask, and the extraction steps were repeated until a final volume of 10 mL was reached. The extracts were filtered through a 0.45 μm Millipore filter into autosampler vials. The sample injection volume was 10 μL. Tea extracts were analyzed for catechins. A Waters e2695 series HPLC system (Waters Co., Milford, MA, U.S.A.) with a reversed-phase C12 column (4 μm, 250 mm × 4.6 mm, Phenomenex) and a C12 guard column was utilized for analysis. The columns were maintained at 30 °C. The mobile phases were 0.5% (v/v) formic acid in double-distilled water (eluent A) and acetonitrile (eluent B). The flow rate was 1 mL/min. The gradient program was as follows: 0−16 min, linear gradient from 6.5% to 16% B; 16−20 min, linear gradient to 25% B; 20−25 min, 25% B; 25−26 min, linear gradient to 6.5% B; 26−30 min, 6.5% B. Corresponding changes in A were made. The eluate was monitored at 280 nm. Chromatographic peaks were identified by UV spectra using diode array detector, and retention times were compared with those of reference compounds. Figure 2 shows chromatograms of the standards and of a typical tea sample. Quantification was carried out by using the external standard method, and standard curves were constructed by linear regression analyses. The regression equations, linear ranges, and correlation coefficients of seven standards are summarized in Supporting Information Table S1. Recovery experiments were repeated three times. The samples were spiked with known amounts of the standards during the extraction. Mean values for the recoveries of EGCG, ECG, EGC, EC, GC, C, and GCG were 97.5% ± 2.6%, 96.9% ± 2.2%, 98.8% ± 4.1%, 97.3% ± 2.6%, 95.2% ± 6.5%, 96.4% ± 3.3%, and 93.1% ±

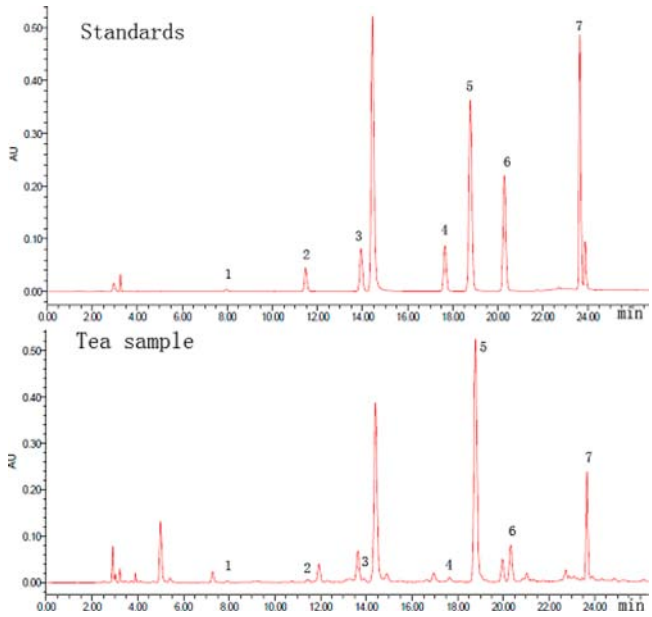


**Figure 2.** Chromatograms of standards and of a typical tea sample. 1, (+)-gallocatechin (GC); 2, (−)-epigallocatechin (EGC); 3, (+)-catechin (C); 4, (−)-epicatechin (EC); 5, (−)-epigallocatechin gallate (EGCG); 6, (−)-gallocatechin gallate (GCG); and 7, (−)-epicatechin gallate (ECG).


dx.doi.org/10.1021/jf5024559 | J. Agric. Food Chem. 2014, 62, 9436−9441

Table 1. Variation and Distribution of Catechins in Chinese Tea Germplasms ($n$ = 403)[a]

| catechin | min (mg/g) | max (mg/g) | median (mg/g) | mean ± SD (mg/g) | CV (%) | kurtosis | skewness | $H'$ |
|---|---|---|---|---|---|---|---|---|
| GC | 1.4 | 22.7 | 2.7 | 3.6 ± 3.0 | 81.9 | 13.3 | 3.4 | 1.32 |
| EGC | 2.1 | 39.4 | 15.6 | 16.1 ± 5.6 | 35.0 | 0.9 | 0.6 | 2.03 |
| C | 0.3 | 30.9 | 2.0 | 2.3 ± 2.0 | 87.9 | 135.9 | 10.4 | 1.31 |
| EC | 2.0 | 54.0 | 7.6 | 8.2 ± 3.7 | 45.7 | 56.7 | 5.3 | 1.86 |
| EGCG | 13.0 | 137.5 | 94.3 | 94.1 ± 14.6 | 15.6 | 3.3 | −0.5 | 2.05 |
| GCG | 0.1 | 77.6 | 0.5 | 1.5 ± 4.7 | 323.6 | 169.4 | 11.3 | 1.36 |
| ECG | 3.2 | 72.8 | 27.6 | 28.9 ± 7.8 | 27.1 | 5.3 | 1.6 | 1.85 |
| TC | 56.6 | 231.9 | 153.3 | 154.5 ± 18.1 | 11.7 | 2.13 | 0.03 | 2.05 |

[a]The catechin content of each accession was the mean of two years. C, (+)-catechin; EC, (−)-epicatechin; ECG, (−)-epicatechin gallate; EGC, (−)-epigallocatechin; EGCG, (−)-epigallocatechin gallate; GC, (+)-gallocatechin; GCG, (−)-gallocatechin gallate; TC, total catechins; min, minimum value; max, maximum value; SD, standard deviation; CV, coefficient of variation; and $H'$, diversity index.

1.9%, respectively. The TC content was calculated as the sum of the above seven individual catechins.

**Statistical Analysis.** The results were analyzed by using SPSS 13.0 (SPSS Inc., Chicago, U.S.A.) statistical software. Differences among means were evaluated using Tukey's test. Factor analysis was performed using the method of principal component extraction to derive the factor matrix. The structure of the original factor matrix was simplified using Varimax rotation. A scatter plot of the first two factors was prepared to bring out their distribution in the factor space represented by these two factors.[26] The overall entry mean ($X$) and standard deviation ($\sigma$) for the parameters examined in this study were used to subdivide the accession values ($x_i$) into ten frequency classes ranging from class 1 (if $x_i < X - 2\sigma$) to 10 (if $x_i > X + 2\sigma$), with class interval of $0.5\sigma$.[27] The diversity of each parameter was estimated by using the Shannon−Weave index ($H'$),[28] expressed as $H' = -\Sigma\, P_i \ln P_i$, where $P_i$ is the proportion of the total number of entries in the $i$th class.

## RESULTS

**Variation in Catechin Content among Different Germplasms.** The variation and distribution for catechins contents of the 403 accessions are summarized in Table 1. Wide variation and diversity of the Chinese tea germplasms were observed. The average TC content was 154.5 ± 18.1 mg/g, varying from 56.6 to 231.9 mg/g, and that of the 396 accessions ranged from 120.0 to 200.0 mg/g (Tables 1 and 2). EGCG was the most abundant catechin (60.9%), its amount averaging 94.1 ± 14.6 mg/g; ECG, EGC, EC, GC, C, and GCG were next in abundance.

Table 2. Variation in Total Catechin Content among Tea Germplasms in China

| catechins (mg/g) | accessions | percent (%) |
|---|---|---|
| <120 | 4 | 1.0 |
| 120.1−140.0 | 80 | 19.9 |
| 140.1−160.0 | 178 | 44.2 |
| 160.1−180.0 | 106 | 26.3 |
| 180.1−200.0 | 32 | 7.9 |
| >200.1 | 3 | 0.7 |
| total | 403 | 100 |

Levels of TC, EGCG, ECG, EC, and EGC in the 403 accessions had a normal distribution and their $H'$ values were high (>1.85) (Table 1). In contrast, minor components such as GC, C, and GCG did not have a normal distribution and their $H'$ values were lower, although their coefficient of variation (CV) was higher. Through this study, several valuable transnormal tea germplasms were found in the 403 accessions, including one low-TC (<60 mg/g) and three high-TC (>200.0 mg/g) accessions.

**Variations in Catechin Content among the Three Varieties of *C. sinensis*.** Average values of the TC content of *sinensis*, *assamica*, and *pubilimba* varieties of *C. sinensis* (L.) O. Kuntze were 152.9 ± 16.2 mg/g, 162.8 ± 22.3 mg/g, and 165.1 ± 21.3 mg/g, respectively (Table 3). The TC content of the *assamica* and *pubilimba* varieties was significantly higher than that of the *sinensis* variety. Data in Table 3 clearly illustrate that there were statistically significant differences ($P < 0.05$) in the catechin content among the three varieties. The *assamica* variety had the highest levels of ECG and EC and the lowest levels of EGCG and GCG, whereas the *pubilimba* variety had the highest levels of EGCG, GC, C, and GCG and the lowest levels of EGC and EC. In particular, the GCG content of the *pubilimba* variety was 6−9 times higher than that of the other two varieties (Table 3). The CI value of the *assamica* variety was significantly higher ($P < 0.05$) than those of the *pubilimba* and *sinensis* varieties. The CI value of more than half of the accessions for the *assamica* variety was higher than 0.45.

Table 3. Catechin Profile of Three Varieties of *C. sinensis*[a]

| | var. *sinensis* ($n$ = 320) | var. *assamica* ($n$ = 21) | var. *pubilimba* ($n$ = 30) |
|---|---|---|---|
| GC | 3.2 ± 2.3b | 3.4 ± 1.5b | 7.7 ± 4.9a |
| EGC | 16.6 ± 5.6a | 17.0 ± 5.5a | 12.4 ± 5.4b |
| C | 2.0 ± 0.7c | 2.7 ± 1.1b | 3.3 ± 1.3a |
| EC | 7.9 ± 2.3b | 10.6 ± 3.9a | 6.3 ± 3.9c |
| EGCG | 94.6 ± 12.6ab | 90.7 ± 18.0b | 99.5 ± 15.4a |
| GCG | 0.9 ± 2.2b | 0.6 ± 1.1b | 5.7 ± 5.3a |
| ECG | 28.0 ± 6.7b | 37.8 ± 10.2a | 29.9 ± 9.3b |
| TC | 152.9 ± 16.2b | 162.8 ± 22.3a | 165.1 ± 21.3a |
| CI | 0.35 ± 0.16b | 0.50 ± 0.16a | 0.36 ± 0.17b |

C, (+)-catechin; EC, (−)-epicatechin; ECG, (−)-epicatechin gallate; EGC, (−)-epigallocatechin; EGCG, (−)-epigallocatechin gallate; GC, (+)-gallocatechin; GCG, (−)-gallocatechin gallate; TC, total catechins; CI, catechin index. All units except those for CI are in mg/g. [a]Values are mean ± SD. Means within each line that are followed by the same letter are not different at $P \geq 0.05$, based on Tukey's honestly different significance test.

On the basis of the 9 catechin patterns of 371 tea accessions of *C. sinensis*, factor analysis was performed. The percentage variances explained by the first three factors are given in Table 4. These three factors together accounted for 81.9% of the total variance. GC, C, and GCG largely influenced the first factor, ECG, and CI dominated the second factor, while the third factor was largely associated with EGCG and TC. Spatial

Table 4. Factor Analysis of 371 Accessions of *C. sinensis*[a]

| variable | factor 1 | factor 2 | factor 3 |
|---|---|---|---|
| GC | 0.88 | −0.10 | 0.09 |
| EGC | −0.42 | 0.09 | 0.68 |
| C | 0.85 | 0.26 | −0.01 |
| EC | −0.33 | 0.75 | 0.35 |
| EGCG | 0.05 | −0.35 | 0.83 |
| ECG | 0.11 | 0.90 | 0.06 |
| GCG | 0.85 | −0.15 | −0.07 |
| TC | 0.23 | 0.23 | 0.93 |
| CI | 0.03 | 0.94 | −0.31 |
| Eigenalue | 2.59 | 2.54 | 2.25 |
| cumulative (%) | 28.73 | 56.97 | 81.93 |

[a]C, (+)-catechin; EC, (−)-epicatechin; ECG, (−)-epicatechin gallate; EGC, (−)-epigallocatechin; EGCG, (−)-epigallocatechin gallate; GC, (+)-gallocatechin; GCG, (−)-gallocatechin gallate; TC, total catechins; and CI, catechin index.

distribution of 371 tea accessions of *C. sinensis* in relation to first two factors is presented in Figure 3. Most of the accessions from the *sinensis*, *assamica*, and *pubilimba* varieties were in groups I, II, and III, respectively.

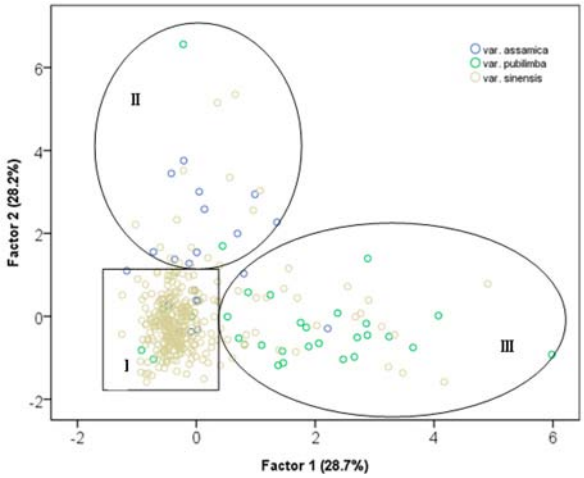


**Figure 3.** Spatial distribution of 371 accessions of *C. sinensis* in relation to the first two factors.

**Variation in Catechin Content of Germplasms from Different Geographical Origins.** The levels of main catechin constituents in the germplasms collected from various provinces were significantly different ($P < 0.05$, Table 5). Catechin levels were affected by the geographical origin of the tea plant. Germplasms from Henan province had the highest mean TC content (167.0 ± 14.6 mg/g), and those from Jiangsu had the lowest (141.6 ± 10.6 mg/g) (Table 5). The TC content of samples tended to decline from the southern to the northern provinces, with the exception of Henan. Henan had the highest average EGC and EGCG content, and the lowest mean ECG content. The highest mean ECG and combined EC and C contents were observed in germplasms from Yunnan. The CI value of genetic resources from Yunnan was significantly higher ($P < 0.05$) than that of the others (Table 5).

To survey the differentiation level of catechins among germplasms from the different provinces, 10 provinces with large number of accessions were selected for statistical analysis and comparison (Figure 4). Because of the differences in sample sizes, the calculation was based on a random selection of 18 accessions from each province. This selection was repeated three times for comparison. Samples from Yunnan province showed the highest differentiation level ($H' = 1.89$, CV = 15.6%), and those from Guangxi province had next highest level ($H' = 1.87$, CV = 13.5%). Those from Zhejiang and Fujian provinces had the lowest $H'$ (1.39) and CV (7.5%), respectively. These results indicate that tea germplasms from the southern provinces had higher differentiation levels of TC.

## DISCUSSION

There were significant differences in the composition of catechins among the three varieties of *C. sinensis*. The CI value, a measure of the difference in catechin composition, has been proven to be affected by the genetic background.[22−24] The CI value of the *assamica* variety was significantly higher ($P < 0.05$) than those of the *pubilimba* and *sinensis* varieties. C and GC are mainly derived from leucocyanidin through a reaction catalyzed by leucoanthocyanidin reductase (LAR) instead of anthocyanidin reductase, as in the case of EC, ECG, EGC, or EGCG.[29,30] The higher GC and C content of the *pubilimba* variety might be attributed to changes in the LAR activity. Factor analysis result based on the catechins as phenetic markers shows that it is basically consistent with morphological classifications, and catechins can be utilized for quantitative data to determine the characteristics of tea plant.

Catechins are converted from nonesterified to esterified derivatives during flavan-3-ol biosynthesis.[31] Catechol or dihydroxy derivatives of catechins such as EC and C are found mostly in primitive tea plants.[31,32] The present study showed that Yunnan germplasms had the highest sum of EC and C contents, suggesting that these are more primitive than those from the other provinces. The genetic diversity decreased from the central region (Yunnan and Guangxi provinces) toward the northern and eastern regions, as revealed by expressed sequence tags based on simple sequence repeat (EST-SSR) markers.[1] Among the 10 provinces investigated, those from the southwestern provinces Yunnan and Guangxi had the highest differentiation level of TC, whereas those from Fujian and Zhejiang had the lowest differentiation level. Results for TC differentiation level show a similar tendency for the genetic diversity.

Depending on the type of processing, which mainly differ in the oxidization degree of the catechins, tea is generally divided into green, white, oolong, black, yellow, and dark varieties. Each tea variety has a unique character, taste, and chemical profile.[33] Different tea cultivars are suitable for different types of tea, and catechins are important factors for the quality of tea.[16−19] This study provides comprehensive information on the catechin content of Chinese tea germplasms, as well as useful guidance for tea manufacturing. Germplasms with high catechin content have been used as commercial raw materials for extracting functional components. Their extraction ratio is higher than that of conventional materials.[7] The TC content increased by ~40 mg/g or 26% from spring to autumn (data not shown). Therefore, autumn tea leaves might be of greater potential use in the extraction of natural catechins. Among the genetic resources of tea with varied catechin contents, germplasms with high catechin content are useful as breeding materials for black and green tea.[34] For black tea, the target individuals might be selected from progenies resulting from crosses between accessions with high catechin content and cultivars of *assamica*


dx.doi.org/10.1021/jf5024559 | J. Agric. Food Chem. 2014, 62, 9436−9441

Table 5. Catechin Profiles of Tea Germplasms from Different Geographical Regions[a,b]

| regions | EGC | EC + C | EGCG | ECG | TC | CI |
|---|---|---|---|---|---|---|
| Anhui ($n$ = 12) | 16.6 ± 5.5ab | 8.5 ± 2.0b | 92.9 ± 10.3bc | 25.7 ± 4.6b | 146.5 ± 14.4bc | 0.33 ± 0.07b |
| Chongqing ($n$ = 21) | 16.3 ± 4.8ab | 12.5 ± 10.0ab | 94.3 ± 8.1bc | 27.2 ± 4.2b | 156.2 ± 15.9abc | 0.38 ± 0.13ab |
| Fujian ($n$ = 32) | 17.4 ± 3.7ab | 9.8 ± 1.4ab | 95.1 ± 12.0abc | 27.4 ± 5.3b | 153.0 ± 13.8abc | 0.34 ± 0.08b |
| Guangdong($n$ = 33) | 12.7 ± 4.8b | 10.7 ± 6.9ab | 98.1 ± 20.2ab | 30.0 ± 8.9ab | 161.9 ± 15.8ab | 0.40 ± 0.26ab |
| Guangxi ($n$ = 38) | 13.6 ± 7.4b | 10.1 ± 4.1ab | 94.8 ± 16.4abc | 29.0 ± 9.9b | 161.2 ± 22.3ab | 0.37 ± 0.20b |
| Guizhou ($n$ = 27) | 17.8 ± 6.4ab | 11.5 ± 2.7ab | 93.5 ± 12.1bc | 30.2 ± 6.0ab | 156.0 ± 14.9abc | 0.39 ± 0.11ab |
| Henan ($n$ = 8) | 20.9 ± 5.4a | 9.8 ± 1.2ab | 109.9 ± 12.3a | 22.9 ± 3.6b | 167.0 ± 14.6a | 0.26 ± 0.04b |
| Hubei ($n$ = 30) | 16.0 ± 4.8ab | 8.5 ± 1.7b | 96.1 ± 12.2abc | 27.1 ± 4.0b | 151.2 ± 15.3abc | 0.33 ± 0.07b |
| Hunan ($n$ = 10) | 15.8 ± 5.1ab | 9.4 ± 2.8b | 98.1 ± 11.2abc | 26.7 ± 4.9b | 154.8 ± 16.1abc | 0.33 ± 0.06b |
| Jiangsu ($n$ = 16) | 15.4 ± 3.5ab | 9.9 ± 1.8ab | 84.2 ± 7.3c | 29.2 ± 5.3ab | 141.6 ± 10.6c | 0.40 ± 0.07ab |
| Jiangxi ($n$ = 18) | 15.4 ± 7.4ab | 9.4 ± 3.9b | 100.1 ± 10.4ab | 26.9 ± 5.3b | 155.4 ± 15.5abc | 0.33 ± 0.08b |
| Sichuan ($n$ = 45) | 17.7 ± 5.7ab | 10.2 ± 2.0ab | 96.5 ± 10.5abc | 27.4 ± 3.7b | 154.9 ± 15.3abc | 0.34 ± 0.05b |
| Yunnan ($n$ = 46) | 16.8 ± 5.6ab | 13.8 ± 5.2a | 89.7 ± 21.7bc | 36.8 ± 12.8a | 160.6 ± 25.6ab | 0.53 ± 0.24a |
| Zhejiang ($n$ = 66) | 15.8 ± 4.8ab | 9.7 ± 2.1ab | 90.4 ± 12.5bc | 27.6 ± 6.1b | 146.9 ± 15.3bc | 0.36 ± 0.08b |

[a]Values are mean ± SD. Means within each column that are followed by the same letter are not different at $P \geq 0.05$, based on Tukey's honestly different significance test. [b]C, (+)-catechin; EC, (−)-epicatechin; ECG, (−)-epicatechin gallate; EGC, (−)-epigallocatechin; EGCG, (−)-epigallocatechin gallate; TC, total catechins; CI, catechin index. All units except those for CI are in mg/g.

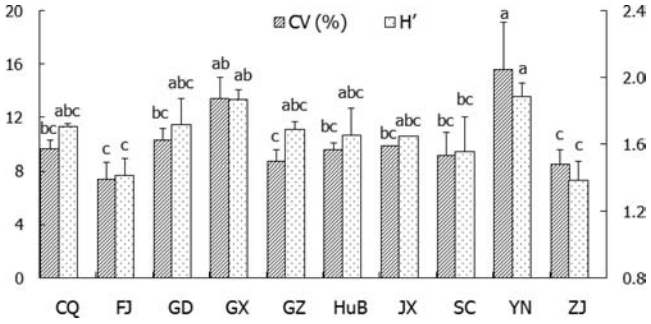


**Figure 4.** Coefficient of variation (CV) and diversity indices ($H'$) of the total catechin (TC) content of tea germplasms from different provinces. Abbreviations represent different provinces. CQ: Chongqing, FJ: Fujian, GD: Guangdong, GX: Guangxi, GZ: Guizhou, HuB: Hubei, JX: Jiangxi, SC: Sichuan, YN: Yunnan, and ZJ: Zhejiang. Identical letters above columns denote the absence of significant difference ($P > 0.05$) based on Tukey's honestly different significance test.

variety. However, crosses between accessions with high catechin content and *sinensis* variety are usually more desirable for breeding green tea.

## ■ ASSOCIATED CONTENT

### Ⓢ Supporting Information

Table S1. Regression equations, linear ranges, and correlation coefficients of seven standards. This material is available free of charge via the Internet at http://pubs.acs.org. .

## ■ AUTHOR INFORMATION


### Corresponding Author

*Phone: +86 571 8665 2835; fax: +86 571 8665 0417; e-mail: liangchen@mail.tricaas.com.

### Author Contributions

†These authors contributed equally to this work.



### Funding

This work was partially supported by the Earmarked Fund for China Agriculture Research System (CARS-23), the National Science Foundation of China (Nos. 30901159, 31170624, and 31100504), and the Natural Science Foundation of Zhejiang Province (No. LY13C160005).


### Notes

The authors declare no competing financial interest.

## ■ ACKNOWLEDGMENTS


The authors thank Professor Dr. Zeno Apostolides of the University of Pretoria, South Africa and anonymous reviewers for their valuable suggestions and critical peer review.


## ■ ABBREVIATIONS USED

C, (+)-catechin; CI, catechin index; EC, (−)-epicatechin; ECG, (−)-epicatechin gallate; EGC, (−)-epigallocatechin; EGCG, (−)-epigallocatechin gallate; CV, coefficient of variation; FA, factor analysis; GC, (+)-gallocatechin; GCG, (−)-gallocatechin gallate; TC, total catechins

## ■ REFERENCES


(1) Yao, M. Z.; Ma, C. L.; Qiao, T. T.; Jin, J. Q.; Chen, L. Diversity distribution and population structure of tea germplasms in China revealed by EST-SSR markers. *Tree Genet. Genomes* **2012**, *8*, 205−220.

(2) Chang, H. T. *Thea*—a section of beveragial tea trees of the genus. *Camellia. Acta Sci. Natur. Univ. Sunyatseni* **1984**, *20*, 87−99.

(3) Yu, F. L. Discussion on the originating place and the originating center of tea plant. *J. Tea Sci.* **1986**, *6*, 1−8.

(4) Ming, T. L. A revision of *Camellia* sect. *Thea. Acta Bot. Yunnanica* **1992**, *14*, 115−132.

(5) Chen, L.; Yu, F. L.; Tong, Q. Q. Discussions on phylogenetic classification and evolution of sect. *Thea. J. Tea Sci.* **2000**, *20*, 89−94.

(6) Chen, L.; Yu, F. L.; Yang, Y. J. *Germplasm and Genetic Inprovement of Tea Plant*; Chinese Agricultural Science and Technology Press: Beijing, China, 2006; pp 33−35.

(7) Chen, L.; Zhou, Z. X. Variations of main quality components of tea genetic resources [*Camellia sinensis* (L.) O. Kuntze] preserved in the China National Germplasm Tea Repository. *Plant Food Hum. Nutr.* **2005**, *60*, 31−35.

(8) Balentine, D. A.; Wiseman, S. A.; Bouwens, L. C. The chemistry of tea flavonoids. *Crit. Rev. Food Sci. Nutr.* **1997**, *37*, 693−704.

(9) Gramza, A.; Korczak, J. Tea constituents (*Camellia sinensis* L.) as antioxidants in lipid systems. *Trends Food Sci. Technol.* **2005**, *16*, 351−358.

(10) Negishi, H.; Xu, J. W.; Ikeda, K. Black and green tea polyphenols attenuate blood pressure increases in stroke-prone spontaneously hypertensive rats. *J. Nutr.* **2004**, *134*, 38−42.

(11) Chung, F. L.; Schwartz, J.; Herzog, C. R. Tea and cancer prevention: studies in animals and humans. *J. Nutr.* **2003**, *133*, 3268−3274.
(12) Higdon, J. V.; Frei, B. Tea catechins and polyphenols: health effects, metabolism, and antioxidant functions. *Crit. Rev. Food Sci. Nutr.* **2003**, *43*, 89−143.
(13) Yang, Y. Y.; Deng, Y.; Lu, B. M.; Liu, Y. X.; Li, j.; Bao, J. K. Green tea catechins: A fresh flavor to anticancer therapy. *Apoptosis* **2014**, *19*, 1−18.
(14) Leung, L. K.; Su, Y.; Chen, R.; Zhang, Z. S.; Huang, Y.; Chen, Z. Y. Theaflavins in black tea and catechins in green tea are equally effective antioxidants. *J. Nutr.* **2001**, *131*, 2248−2251.
(15) Chen, Z.; Zhu, Q. Y.; Tsang, D.; Huang, Y. Degradation of green tea catechins in tea drinks. *J. Agric. Food Chem.* **2001**, *49*, 477−482.
(16) Yuan, Y. C.; Cheng, C. K. The relation between the components of tea catechins and the quality of green tea. *Acta Hortic. Sinica* **1964**, *3*, 287−300.
(17) Obanda, M.; Owuor, P. O.; Taylor, S. J. Flavanol composition and caffeine content of green leaf as quality potential indicators of Kenyan black teas. *J. Sci. Food Agr.* **1997**, *74*, 209−215.
(18) Wright, L. P.; Mphangwe, N. I. K.; Nyirenda, H. E.; Apostolides, Z. Analysis of caffeine and flavan-3-ol composition in the fresh leaf of *Camellia sinensis* for predicting the quality of the black tea produced in Central and Southern Africa. *J. Sci. Food Agr.* **2000**, *80*, 1823−1830.
(19) Owuor, P. O.; Obanda, M. The use of green tea (*Camellia sinensis*) leaf flavan-3-ol composition in predicting plain black tea quality potential. *Food Chem.* **2007**, *100*, 873−884.
(20) Yao, L. H.; Caffin, N.; D'Arcy, B.; Jiang, Y. M.; Shi, J.; Singanusong, R.; Liu, X.; Datta, N.; Kakuda, Y.; Xu, Y. Seasonal variations of phenolic compounds in Australia-grown tea (*Camellia sinensis*). *J. Agr. Food Chem.* **2005**, *53*, 6477−6483.
(21) Gerats, A. M.; Martin, C. Flavonoid synthesis in *Petuniahybrida*: genetics and molecular biology of flower colour. In *Phenolic Metabolism in Plant*; Stafford, H. A., Ibrahim, R. K., Eds; Plenum Press: New York, 1992; pp 167−175.
(22) Magoma, G. N.; Wachira, F. N.; Obanda, M.; Imbuga, M.; Agong, S. G. The use of catechins as biochemical markers in diversity studies of tea (*Camellia sinensis*). *Genet. Resour. Crop Ev.* **2000**, *47*, 107−114.
(23) Saravanan, M.; Maria John, K. M.; Raj Kumar, R.; Pius, P. K.; Sasikumar, R. Genetic diversity of UPASI tea clones (*Camellia sinensis* (L.) O. Kuntze) on the basis of total catechins and their fractions. *Phytochemistry* **2005**, *66*, 561−565.
(24) Gulati, A.; Rajkumar, S.; Karthigeyan, S.; Suda, R. K.; Vijayanb, D.; Thomasb, J.; Rajkumar, R.; Das, S. C.; Tamuly, P.; Hazarika, M.; Ahuja, P. S. Catechin and catechin fractions as biochemical markers to study the diversity of Indian tea (*Camellia sinensis* (L.) O. Kuntze) germplasm. *Chem. Biodivers.* **2009**, *6*, 1042−1052.
(25) ISO 14502-2-2005E. Determination of substances characteristic of green and black tea (Part 2: Contents of catechins in green tea: Method using high performance liquid chromatography), 2006.
(26) Nair, N. V.; Balakrishnan, R.; Sreenivasan, T. V. Variability for quantitative traits in exotic hybrid germplasm of sugarcane. *Genet. Resour. Crop Evol.* **1998**, *45*, 459−464.
(27) Li, Y.; Wu, S. Z.; Cao, Y. S.; Zhang, X. Z. A phenotypic diversity analysis of foxtail millet (*Setaria italica* (L.) P. Beauv.) landraces of Chinese origin. *Genet. Resour. Crop Evol.* **1996**, *43*, 377−384.
(28) Jain, S. K.; Qualset, C. O.; Bhatt, G. M.; Wu, K. K. Geographical patterns of phenotypic diversity in a world collection of durum wheats. *Crop Sci.* **1975**, *15*, 700−704.
(29) Punyasiri, P. A. N.; Abeysinghe, I. S. B.; Kumar, V.; Treutter, D.; Duy, D.; Gosch, C.; Martens, S.; Forkmann, G.; Fischer, T. C. Flavonoid biosynthesis in the tea plant *Camellia sinensis*: Properties of enzymes of the prominent epicatechin and catechin pathways. *Arch. Biochem. Biophys.* **2004**, *431*, 22−30.
(30) Ashihara, H.; Deng, W. W.; Mullen, W.; Crozier, A. Distribution and biosynthesis of flavan-3-ols in *Camellia sinensis* seedlings and expression of genes encoding biosynthetic enzymes. *Phytochemistry* **2010**, *71*, 559−566.
(31) Wan, X. C. *Biochemistry of Tea*, 3rd ed.; Chinese Agriculture Publisher: Beijing, China, 2003; pp 107−109.
(32) Li, J. H.; Atsushi, N.; Shimizu, K.; Sakata, Y.; Liang, M. Z.; Zhou, H. J.; Hashimoto, F. Chemosystematics of tea trees based on tea leaf polyphenols as phenetic markers. *Phytochemistry* **2010**, *71*, 1342−1349.
(33) Wu, C. Y.; Xu, H. R.; Héritier, J.; Andlauer, W. Determination of catechins and flavonol glycosides in Chinese tea varieties. *Food Chem.* **2012**, *132*, 144−149.
(34) Takeda, Y. Differences in caffeine and tannin contents between tea [*Camellia sinensis*] cultivars, and application to tea breeding. *JARQ* **1994**, *28*, 117−123.

possess fewer hydroxyl groups on the B ring.[17] Although the detailed molecular mechanisms underlying the inhibitory effects of flavonoids remain unclear, these results suggest that differences in hydroxyl groups contained within the flavonoid structure may influence the formation of hydrogen bonds between A$\beta$ and its hydroxyl arms, and is possibly the key determinant of antiamyloidogenic activity.[17]

Many of the currently investigated small-molecule inhibitors act as general antiamyloid agents, which affect a range of amyloidogenic proteins.[18−20] Although the property of non-specificity is typically not desirable for drug design, it can offer the possibility of broad-spectrum therapeutics, but only provided there is no effects on functional human fibrous proteins such as those that constitute the cytoskeletal system. Currently myricetin has been demonstrated as exhibiting antiamyloidogenic activity against A$\beta$, $\alpha$-synuclein, IAPP.[17,21,22] We sought to assess further the general nature of inhibitory activity by investigating whether myricetin could inhibit fibril formation *in vitro* of hen egg white lysozyme. HEWL has two domains, $\alpha$ and $\beta$, and each consists of four $\alpha$-helices and an antiparallel $\beta$-sheet. Its structure is highly homologous to human lysozyme, which is responsible for the formation of systemic amyloidosis.[23]

In this study, thioflavin T (ThT) fluorescence assays and transmission electron microscopy (TEM) were used to detect and assess the inhibitory activity of myricetin upon fibril formation by HEWL. Additionally, the interaction between myricetin and the monomeric form of HEWL was investigated using a combination of anilinonaphthalene-8-sulfonic (ANS) and intrinsic fluorescence assays coupled with *in silico* simulations.

## MATERIALS AND METHODS

**Proteins and Reagents.** HEWL was purchased from Solarbio (Beijing, China). ThT, ANS, myricetin, and quercetin were purchased from Sigma-Aldrich (St. Louis, MO, USA).

**HEWL Sample Preparation.** A stock solution of myricetin (50 mM) was prepared in dimethyl sulfoxide (DMSO). HEWL sample solutions were prepared by dissolving 1 mg of HEWL powder in 1 mL of 50 mM glycine−hydrochloric acid buffer (pH 2.0) with or without an aliquot of myricetin solution. The final concentration of DMSO in HEWL sample solution is 0.2%, of which we confirmed that 0.2% DMSO had no obvious effect on fibrillar structure and ThT fluorescence. Incubation was carried out with constant agitation at 140 rpm at 65 °C during the course of aggregation.

**Thioflavin T Fluorescence Assay.** Phosphate buffer (50 mM $Na_2HPO_4$, 50 mM $NaH_2PO_4$, pH 7.0) was used to dissolve ThT to a stock concentration of 1 mM. Aliquots of HEWL samples taken at different times were diluted with phosphate buffer (pH 7.0), followed by the addition of an aliquot (30 $\mu$L stock solution) of ThT stock solution. ThT fluorescence measurement was conducted by exciting the sample at 440 nm and recording the emission intensity at 485 nm over 120 s. The measurement was carried out using a Cary Eclipse fluorescence spectrophotometer (Varian, Palo Alto, CA, USA).

**Intrinsic Fluorescence Assay.** Steady state intrinsic fluorescence spectrum was measured with a Cary Eclipse fluorescence spectrophotometer (Varian) using a quartz cuvette with a path length of 1 cm. HEWL samples (30 $\mu$L) with or without myricetin were diluted to a final volume of 3 mL and then subjected to analysis. The sample was excited at 280 nm, and the spectrum was recorded between 300 and 500 nm.

**ANS Fluorescence Assay.** A stock solution of ANS (0.4 mM) was prepared by dissolving ANS in phosphate-buffered saline (PBS; pH 7.0). The ANS stock solution was stored at 4 °C. Aliquots of HEWL solution with or without myricetin taken at different times were mixed with an aliquot of ANS solution, followed by the addition of PBS (pH7.0) to a final of volume of 3 mL. After incubation in the dark for 30 min at room temperature, the samples were subjected to fluorescence assay using a Cary Eclipse fluorescence spectrophotometer (Varian). The samples were excited at 380 nm, and fluorescence was recorded between 400 and 600 nm. Both the ANS fluorescence intensity and the average emission wavelength were recorded to account for the changes in intensity and spectrum. We confirmed that myricetin had no obvious effects on ThT, ANS, and intrinsic fluorescence.

**Transmission Electron Microscopy.** HEWL samples with and without myricetin were diluted 5-fold, and 10 $\mu$L of each sample was dispensed onto a coated copper-mesh grid. The grid was negatively stained with 1% (w/v) phosphotungstic acid and then observed with a Hitachi H-7650 transmission electron microscope with an accelerating voltage of 80 kV.

**Molecular Dynamic Simulations and Docking Studies.** All molecular dynamics (MD) simulations were carried out using the GROMACS 4.0.7 software package.[24] The crystal structure of HEWL (PDB entry 1GXV) was downloaded from the Protein Data Bank (PDB).[25] The GROMOS96 43a1[26] force field was adopted in all simulations in this study. The monomer model was solvated in a water box containing 10,124 simple point-charge water molecules[27] and neutralized by adding eight $Cl^-$ counterions. The linear constraint solver method[27] was used to constrain the bond length, allowing for integration time steps of 2 fs throughout the whole simulation. Electrostatic interactions were calculated with the particle-mesh Ewald algorithm.[28] A cutoff of 9 Å was used for all calculations. The solvated and neutralized systems were then energy-minimized for 20,000 steps to remove bad contacts. Then the side chains and solvent were allowed to move unrestrained for 40 ps, with the backbone atoms of the structure fixed. To investigate the structural fluctuation of HEWL under amyloid fibril forming conditions, MD simulations at 338 K and pH 2.0 were carried out. For the control, a physiological condition of 310 K and pH 7.0 was used. After equilibration, two independent simulations were carried out for 20 ns.

Docking studies were performed using Autodock 4.2.5.1. The 3D structure of myricetin was obtained from TCM Database@Taiwan.[29] Prior to autodocking the HEWL molecule and myricetin were prepared using AutoDockTools 1.5.4, including addition of polar hydrogen atoms and setting the charges of HEWL residues using Kollman charges and adding Gasteiger charges to myricetin.

The docking grids were carried out with a default spacing value of 0.375 Å and a grid volume of 60 × 60 × 60 points covering the entire surface of HEWL. The protein molecule was set to be rigid while the ligand molecule was considered to be flexible. In the docking simulation, a Lamarckian geneti algorithm was used to generate 50 binding models, each of which was individually selected as the lowest binding energy (calculated using the Autodock scoring function) among a maximum of 2,500,000 evaluations. These 50 complexes were clustered according to their root-mean-square deviation (RMSD) values and binding energies in order to distinguish the preferred binding model.

**Statistical Analysis.** All experiments were performed at least three times, and all data are presented as means ± standard deviations (SDs). Comparisons between groups were tested by one-way ANOVA analysis. Statistical significances of data were considered at the $P < 0.05$ level.

## RESULTS

**Analysis of HEWL Fibril Formation Using ThT Fluorescence.** HEWL is a model protein for amyloid research as it is known to readily form fibrils under conditions of low pH and elevated temperature, when coupled with mechanical agitation.[30] By monitoring the kinetics of HEWL fibril formation by fluorescence spectroscopy, we found that the relative fluorescence of HEWL increased with extended incubation times (Figure 2A), which is in agreement with previous studies.[31] The consistent increase in ThT fluorescence intensity observed when HEWL was incubated alone, demonstrates that formation of amyloid fibrils proceeded rapidly and without a lag phase (Figure 2A). The inhibitory effect exerted on the formation of HEWL fibril by the addition of myricetin (100 $\mu$M) into the assay resulted in a strong inhibition of HEWL fibril formation (Figure

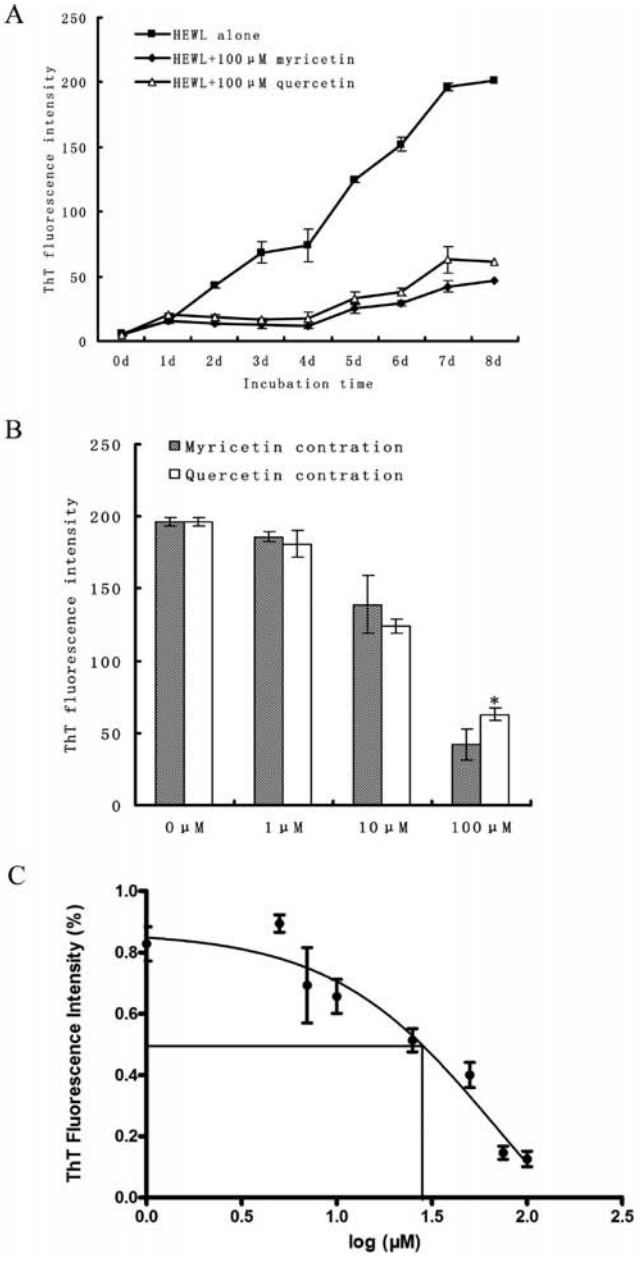


**Figure 2.** Effects of myricetin and quercetin on amyloid formation by HEWL: (A) the kinetics of HEWL fibril formation in the absence (filled squares) or the presence of myricetin (filled diamonds) or quercetin (filled upward triangles) as monitored by ThT fluorescence; (B) dose-dependent inhibitory capacity of myricetin and quercetin on amyloid formation by HEWL 7 days after incubation; (C) dose–response curve plotting the plateau value of the ThT fluorescence intensity of the HEWL sample against myricetin concentration.

2A). Compared to quercetin-containing HEWL samples (the positive control group), myricetin showed a reproducible moderately stronger inhibition.

To determine an effective concentration range of myricetin for inhibiting HEWL fibril formation, varying aliquots of myricetin were mixed with HEWL to final concentrations of 1, 10, and 100 $\mu$M; at these concentrations we did not observe significant toxic effects of myricetin on cell survival (data not shown) and the ThT fluorescence intensity measured (Figure 2B). Myricetin (and quercitin control) was observed to exhibit a dose-dependent effect on HEWL fibril formation (Figure 2B). Although fibril inhibition was observed up to a concentration of 10 $\mu$M, major inhibitory effects were only observed at a concentration of 100 $\mu$M, indicating effective fibril inhibition occurs between these two concentrations. Importantly, at 100 $\mu$M the inhibitory effect of myricetin on HEWL fibril formation was significantly stronger ($p$-value = 0.037626 < 0.05) than that previously obtained with quercetin (Figure 2B), the positive control.

By calculating the percentage of protection from the ThT curve of HEWL alone and fitting a logarithmic concentration–response curve, myricetin inhibited HWEL fibril formation with a median effective concentration (IC50 value) of 28.2 $\mu$M (Figure 2C).

**Assessing Structural Changes during HEWL Fibril Formation.** ANS is a fluorescencent dye that has high affinity for the hydrophobic surfaces of proteins. Upon binding to the hydrophobic regions of a protein surface, the intensity of the light emission is increased, with the emission maximum showing a blue shift.[32] This technique allows changes in the hydrophobic core and the stability of a whole protein to be monitored during the course of aggregation. As shown in Figure 3A, a significant

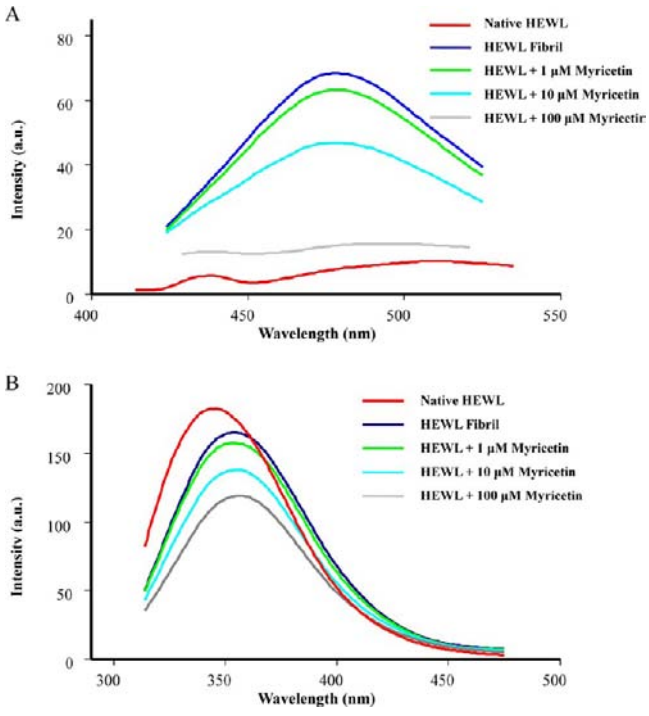


**Figure 3.** (A) ANS fluorescence emission spectra of HEWL fibril incubated with (pink) or without (red) myrecetin after incubation for 7 days. (B) Intrinsic fluorescence emission spectra of HEWL fibril in the absence (red) and presence (purple) of myricetin after incubation for 7 days.

blue shift from 515 to 473 nm and increase in intensity of ANS fluorescence, compared to native HEWL, is caused by HEWL fibril formation. The addition of 100 $\mu$M restores HEWL fibril ANS intensity to levels comparable with the native protein.

Variation in the microenvironment of tryptophan residues and monitoring the intrinsic fluorescence of a protein allow assessment of structural characteristics.[33] To further probe the effect of myricetin on the conformation of HEWL, the intrinsic fluorescence of HEWL in the absence or presence of myricetin was measured. A decreased intensity in intrinsic fluorescence of


dx.doi.org/10.1021/jf5025449 | J. Agric. Food Chem. 2014, 62, 9442–9449

HEWL fibril group with a shift from 344 to 355 nm was observed compared to the native HEWL group (Figure 3B). This indicated that tryptophan in HEWL became more accessible to solvent during the process of fibril formation, resulting in the quenching of fluorescence by water.[34,35] However, the presence of myricetin significantly reduced the fluorescence intensity during fibril formation (Figure 3B). The quenching of intrinsic fluorescence may possibly result from the interactions between aromatic residues of myricetin and the aromatic residues of target proteins.[36,37]

**Physical Analysis of HEWL Fibril formation.** Direct information on the formation of fibril by HEWL as well as by the antifibrillogenic activity of myricetin was obtained using TEM. The morphology of HEWL fibers and/or aggregates in the absence or presence of myricetin is shown in Figure 4A–G. In the absence of myricetin or quercetin, HEWL displayed straight and regular premature or mature amyloid fibril structures with typical diameters ranging from 2 to 20 nm and several micrometers in length (Figure 4A,E). The presence of quercetin (Figure 4B) clearly resulted in reduced amounts of HEWL fibrils. In contrast, the presence of myricetin resulted in formation of amorphous aggregates, with virtually no HEWL fibrils being observed (Figure 4C). This result provides further evidence that myricetin exhibits a stronger inhibition against fibril formation by HEWL compared to quercetin. To elucidate the physical nature of myricetin fibril inhibition, by using TEM we also examined HEWL fibril formation and myricetin inhibition with prolonged incubation time and found 25 $\mu$M myricetin (close to IC50 value) incubated with HEWL resulted in a reduced amount of amyloid fibril after 12 days incubation (Figure 4G). In contrast, the presence of 100 $\mu$M myricetin resulted in formation of amorphous aggregates, with virtually no HEWL fibrils being observed (Figure 4D). Taken together, we concluded that the physical nature of fibril inhibition is determined by the concentration of myricetin. We also confirmed that the TEM images of myricetin at 100 $\mu$M show only the deposition of the compound alone and no fibril structure was found (Figure 4H).

**Computational Analysis of HEWL Fibril Formation.** Based on the spectrometric and electron microscopy data, it can be inferred that myricetin inhibition of amyloid fibrils formation of HEWL mainly occurs at a very early stage in the process. To better understand the process of amyloid fibril formation by HEWL as well as the interaction of myricetin with lysozyme at the atomic level, we carried out MD simulations (see Materials and Methods).

Figure 5A compares the degree of conformational changes that occur in HEWL under two different MD simulation conditions, one favoring amyloid fibril formation (338 K and pH 2.0) and the other under normal cellular physiological parameters (310 K and pH 7.0). The backbone RMSD trajectory in fibril-forming condition (represented by the red trace) has a higher value, indicating a less stable state than that in physiological conditions (black trace). The root-mean-square fluctuation (RMSF) of each residue (Figure 5B) revealed a major contribution of the $\beta$-domain (residues from 36 to 87) toward the instability of HEWL under fibril-forming conditions. This is consistent with the dramatic changes of $\beta$-sheet content in the $\beta$-domain observed during the 20 ns MD simulation, particularly the major difference in stability observed after 15 ns compared to changes seen under physiological conditions (Figure 5C). In contrast, the $\alpha$-domain maintained much of the native conformation with the content of $\alpha$-helix being constant (data not shown). From the superposition of the final conformational state following the 20 ns MD simulation, the clear disruption in the $\beta$-domain could be directly observed (Figure 5D).

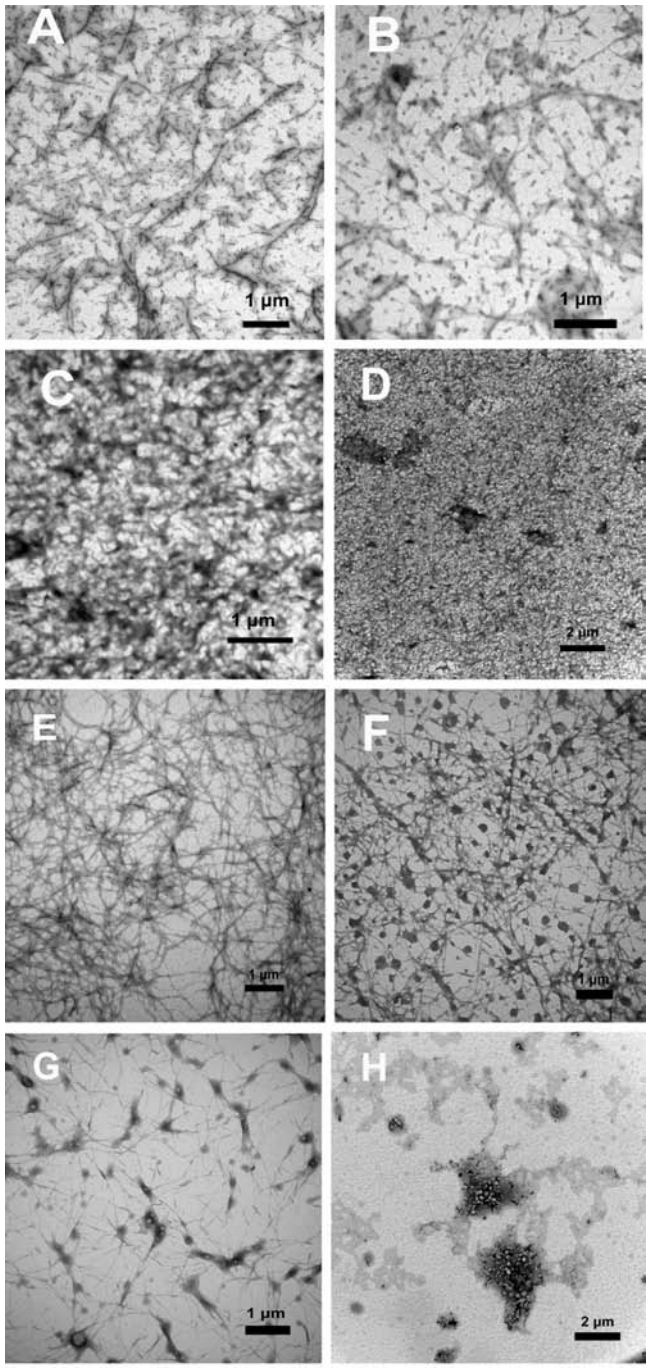


**Figure 4.** Transmission electron microscopic images of HEWL fibrils formed in the absence or presence of myricetin or quercetin, after incubation at 65 °C and pH 2.0 for 7 days or 12 days: (A) HEWL fibril after incubation for 7 days; (B) HEWL fibril in the presence of 100 $\mu$M quercetin; (C) images of HEWL in the presence of 100 $\mu$M myricetin after incubation for 7 days; (D) images of HEWL in the presence of 100 $\mu$M myricetin after incubation for 12 days; (E) HEWL fibril after incubation for 12 days; (F) images of HEWL in the presence of 10 $\mu$M myricetin after incubation for 12 days; (G) images of HEWL in the presence of 25 $\mu$M myricetin after incubation for 12 days; (H) images of 100 $\mu$M myricetin after incubation for 12 days. Scale bars represent 1 and 2 $\mu$m.

To investigate how myricetin may affect the conformation of HEWL, we carried out docking simulations between these two


dx.doi.org/10.1021/jf5025449 | J. Agric. Food Chem. 2014, 62, 9442–9449

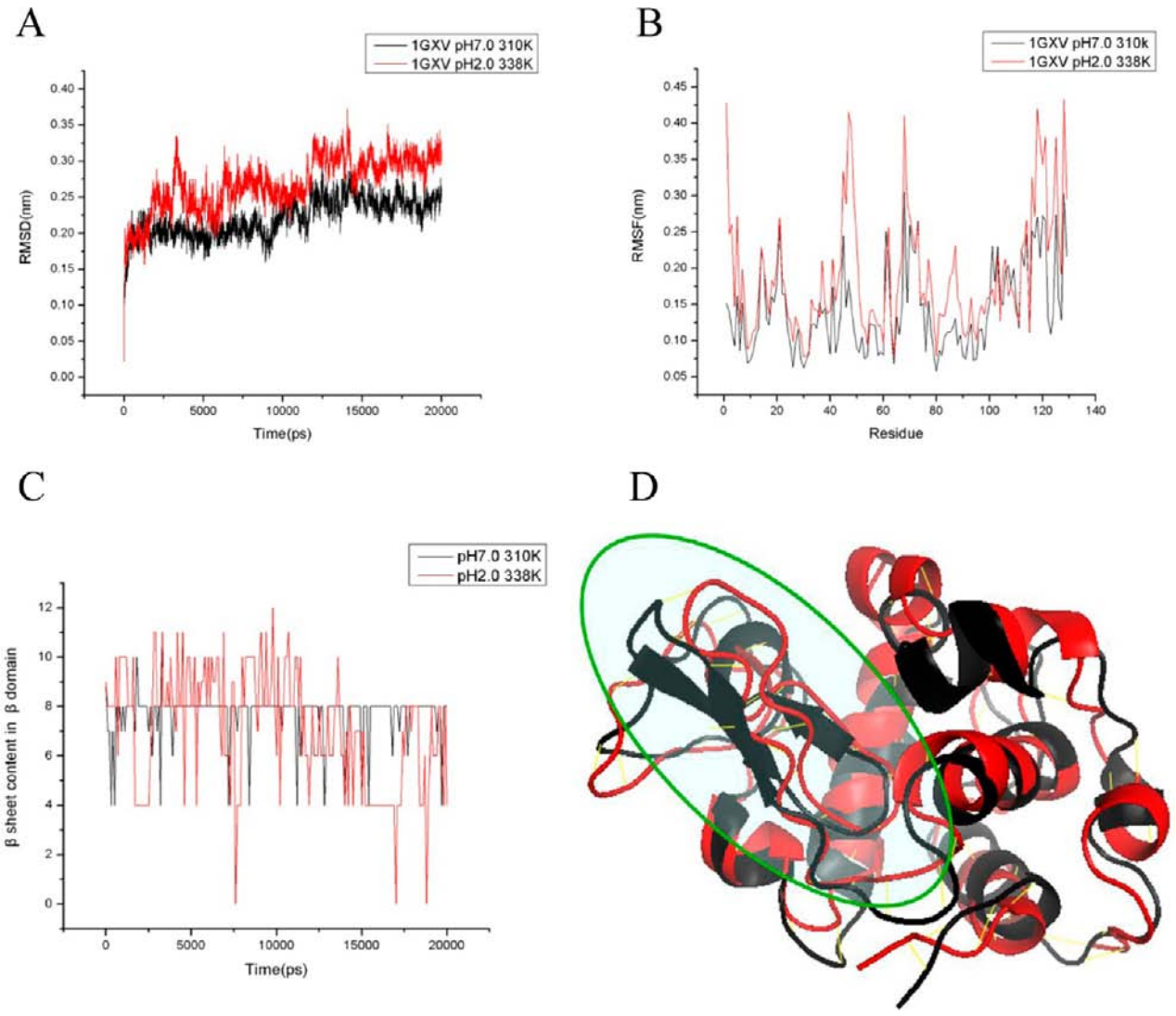


**Figure 5.** (A) RMSD of the C$\alpha$-positions during the 20 ns simulations. (B) RMSF trajectory per residue during the period of MD simulations. (C) Fluctuation of $\beta$-sheet content in $\beta$-domain through the 20 ns MD simulation. (D) Superposition of the final state of the 20 ns MD simulation at physiological condition (black) and amyloid fibril forming condition (red).

molecules. According to the docking results, myricetin was located in an area between the $\alpha$-domain and the $\beta$-domain (Figure 6A). The predicted binding site for myricetin on HEWL was clustered around many residues, such as Asn44, Asn46, Asp52, Asn59 and Glu35, Ala107, Val109, and Trp62 and Trp63. The interactions between myricetin and these residues were through van der Waals interactions and hydrogen bonding. Of particular note are the interactions with residues Trp62 and Trp63 in the $\beta$-domain, which could explain the quenching of intrinsic fluorescence (Figure 6B).

## DISCUSSION

Amyloid diseases are either sporadic or familial in their nature. Usually, in the sporadic forms of the diseases the aggregated peptides/proteins display wild-type sequences, while in rarer early onset familial forms of the diseases the aggregation results from genetic mutations that exhibit a greater propensity for aggregation.[38] A major risk factor for most sporadic amyloid diseases is aging.[39] In older people, the age-related decline in cellular proteostasis includes the unfolded protein response, the ubiquitin proteasome system, autophagy, and the encapsulation of damaged proteins in aggresomes, all of which lead to the accumulation of protein aggregates.[40−43] Progression of the aging process means that most kinds of amyloid diseases occur undetected in their early stages. However, an increasing number of research investigations suggest that the intake of diets containing natural small molecules with inhibitory activities toward amyloid fibril formation may help to prevent such diseases or at least delay early onset.[44−46]

Myricetin is a cell-permeable flavanoid often used in inflammatory, diabetes, and cancer studies, since it has a variety of pharmacological properties such as antioxidant activity and an ability to reduce blood sugar levels.[47,48] High-throughput screens for small molecules exhibiting antiamyloidogenic activity demonstrated that myricetin could prevent amyloid fibril formation of A$\beta$, $\alpha$-synuclein, and IAPP. To further develop and characterize myricetin as a potential antiamyloid therapeutic agent, we assessed the ability of this small molecule to inhibit amyloid fibril formation by the model protein HEWL.

The inhibitory effect exerted by myricetin on HEWL fibril formation, as assessed by ThT fluorescence, was greater than the well-characterized polyphenol quercetin (Figure 2A). However,


dx.doi.org/10.1021/jf5025449 | J. Agric. Food Chem. 2014, 62, 9442−9449

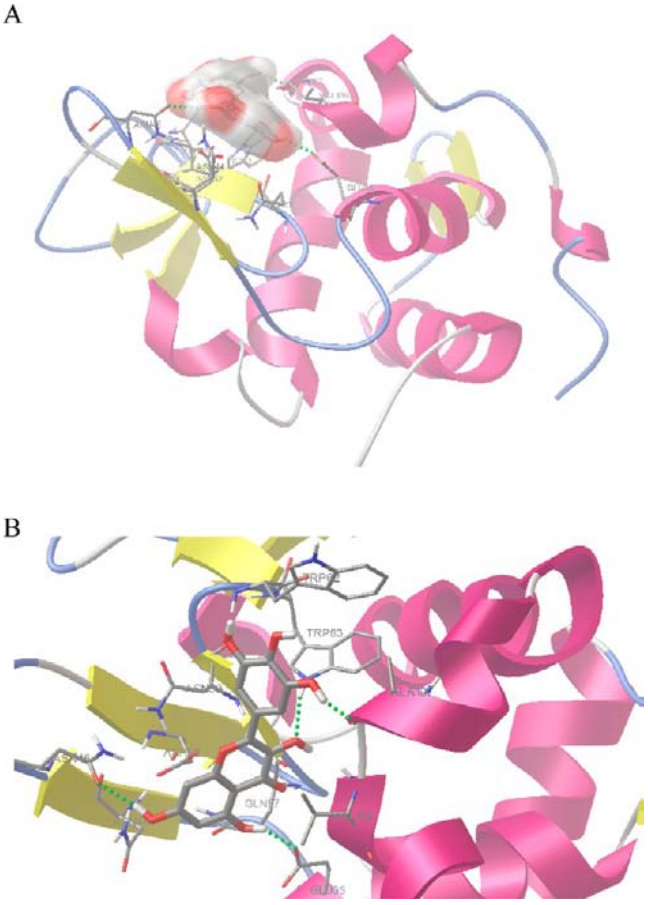


**Figure 6.** (A) Panoramic view showing the mode of binding between myricetin and HEWL. (B) Close-up view of the complex showing the binding between myricetin and HEWL, with hydrogen bonding marked as a green dotted line.

since ThT fluorescence induction can be biased by the presence of exogenous compounds,[49] we also assessed the physical nature of myricetin fibril inhibition using TEM. Incubation of myricetin with HEWL resulted in the formation of amorphous aggregates, with little or no fibrils being observed (Figure 4C,D). This was in contrast to incubation of HEWL in the presence of quercetin, which resulted in a reduction of amyloid fibril formation, but no formation of amorphous aggregates (Figure 4B). The results from the TEM analysis therefore are in agreement with the ThT assay and clearly demonstrate that myricetin inhibits HEWL fibril formation more effectively than quercetin. While these experiments reveal the inhibitory potential of myricetin against amyloid fibrils, they do not provide any information regarding the potential molecular mechanisms underlying this activity. In an attempt to gain insight into the molecular nature of fibril inhibition we turned to well-developed computational approaches.

Previous studies demonstrated that amyloidogenic variants of human lysozyme such as I56T and D67H, undergo transient and local cooperative unfolding in the $\beta$-domain region of the protein, a process that occurs at the early stage of amyloid fibril formation and under physiologically relevant conditions (pH and temperature).[50,51] Furthermore, the local unfolding of $\beta$-domain is considered to be the main trigger for fibril formation. Consistent with previous studies, we observed a similar phenomenon during MD simulations carried out using wild-type HEWL; that is, the localized unfolding of $\beta$-domain appeared to be the key event in inducing fibril formation (Figure 5A–D).

According to Sugimoto and colleagues,[52] a peptide located in the $\beta$-domain of HEWL referred to as K peptide (consisting of residues 54–62 GILQINSRW) was found to act as a core for aggregation and subsequent amyloid fibril formation. Likewise, Lara et al. recently found the shorter peptide sequence ILQINS to be highly amyloidogenic at room temperature.[53] This region of the protein is partially embedded inside the HEWL structure as a pocket in the junction connecting the $\alpha$-domain and the $\beta$-domain. Combined with results from previous studies, our findings in this work indicated that the stability of this region in the $\beta$-domain directly determines the aggregation fate of the entire protein, dictating whether it proceeds to form amorphous aggregates or amyloid fibril. Further understanding of the early events in conformation changes that occur in HEWL unfolding will not only allow a better understanding of the process of HEWL fibril formation but may also enable development of effective ways to inhibit amyloid fibril formation by reducing the ability of HEWL to form locally unfolded intermediates.

Computational approaches to studying how molecules interact are well-established.[54,55] Applying computational docking studies allowed the exploration of the mechanism of myricetin-induced inhibition of HEWL fibril formation. The smaller blue shift and reduced fluorescence intensity observed by ANS fluorescence assay, an indicator of a less hydrophobic core exposed to solvent, suggested that myricetin could stabilize the whole conformation of HEWL even though it was subjected to fibril-forming conditions (Figure 4A). The docking study revealed that the HEWL binding site for myricetin is located in the region that partly includes the K peptide located between the $\alpha$-domain and the $\beta$-domain (Figure 6A), the key region associated with amyloid fibril formation. A plausible explanation for the inhibitory action of myricetin is a reduction of locally unfolded intermediates, which in turn will reduce the propensity for amyloid fibril formation. In this binding mode, myricetin may be acting as an adhesive via hydrogen bonding and van der Waals interaction to glue the aggregation-prone region of the $\beta$-domain with the otherwise stable $\alpha$-domain, consequently resulting in a reduced population of transiently $\beta$-domain unfolded intermediates. Thus, no formation of amyloid fibril would occur under this condition. However, further biophysical experimentation is required to fully address the mechanism of fibril inhibition.

Support for the authenticity of the binding site for myricetin, derived from the docking study, is supported by the experimental data from the intrinsic fluorescence assay. Results from the intrinsic fluorescence assay showed that the interaction between the aromatic residues of myricetin and HEWL could account for the quenching of intrinsic fluorescence (Figure 3B). The normalized fluorescence changes versus the different incubation time appeared almost the same for the emission spectra obtained from excitation at 280 and 295 nm (data not shown), indicating that the quenching of fluorescence can be attributed to Trp residues. Taken together with the fact that Trp62 is one of the two dominant emitters (the other is Trp108),[56] the binding site which is located close to Trp62, identified by the docking study, is very likely to be the real scenario. This is consistent with previous investigations in which certain small molecules with inhibitory activity toward HEWL fibril formation, such as EGCG, EUK-8, and EUK-134 (two kinds of salen–manganese complexes) were also suggested to bind to Trp62 and Trp63 in docking studies.[10,57,58] Taken together, our findings provided a plausible rationale by which fibril formation by HEWL could be


dx.doi.org/10.1021/jf5025449 | J. Agric. Food Chem. 2014, 62, 9442–9449

inhibited by small molecules by targeting the aggregation-prone regions in monomers of this amyloidogenic protein.

Human lysozyme is a bacteriolytic enzyme. According to the Phillips mechanism,[59] the amino acid side chains glutamic acid 35 (Glu35) and aspartate 52 (Asp52) have been found to be critical to the activity of this enzyme. Our docking study predicted that the binding site for myricetin on HEWL was clustered around many residues, such as Asn44, Asn46, Asp52, Asn59 and Glu35, Ala107, Val109, and Trp62 and Trp63. Thus, it is possible that myricetin docking with lysozyme could inhibit its physiological functions to some extent; however, detailed inhibitory studies need to be carried out to determine at what concentration of myricetin is safe and efficient for dietary flavonol consumption or as a drug candidate. It is important to note that fibrillar tangles as well as amorphous aggregates can be cytotoxic;[60,61] also, a recent study on HEWL amorphous aggregates has demonstrated that Cu(II) directs formation of toxic amorphous aggregates resulting in inhibition of HEWL fibrillation under alkaline-salt-mediated conditions.[62] The potential cytotoxicity of amorphous aggregates of HEWL needs to be assessed in detail to fully appreciate the potential of myricetin as a drug candidate.

## AUTHOR INFORMATION


### Corresponding Authors

*(J.H.) E-mail: jwhe@lnu.edu.cn.
*(Y.S.) E-mail: ysong@lnu.edu.cn.
*(G.W.J.) E-mail: gary.jones@nuim.ie.



### Funding

This publication has emanated from research conducted with the financial support of Science Foundation Ireland under the International Strategic Cooperation Award Grant No. SFI/13/ISCA/2845. This work was supported by grants from the Joint Specialized Research Fund for the Doctoral Program of Higher Education and partially sponsored by the Fund of Science and Technology project (No. F12-277-1-59) from Shenyang Science and Technology Bureau.


### Notes

The authors declare no competing financial interest.

## REFERENCES


(1) Sipe, J. D.; Benson, M. D.; Buxbaum, J. N.; Ikeda, S.; Merlini, G.; Saraiva, M. J.; Westermark, P. Amyloid fibril protein nomenclature: 2012 recommendations from the Nomenclature Committee of the International Society of Amyloidosis. *Amyloid* **2012**, *19* (4), 167−70.

(2) Pepys, M. B.; Hawkins, P. N.; Booth, D. R.; Vigushin, D. M.; Tennent, G. A.; Soutar, A. K.; Totty, N.; Nguyen, O.; Blake, C. C.; Terry, C. J.; et al. Human lysozyme gene mutations cause hereditary systemic amyloidosis. *Nature* **1993**, *362* (6420), 553−7.

(3) Valleix, S.; Drunat, S.; Philit, J. B.; Adoue, D.; Piette, J. C.; Droz, D.; MacGregor, B.; Canet, D.; Delpech, M.; Grateau, G. Hereditary renal amyloidosis caused by a new variant lysozyme W64R in a French family. *Kidney Int.* **2002**, *61* (3), 907−12.

(4) Yazaki, M.; Farrell, S. A.; Benson, M. D. A novel lysozyme mutation Phe57Ile associated with hereditary renal amyloidosis. *Kidney Int.* **2003**, *63* (5), 1652−7.

(5) Rocken, C.; Becker, K.; Fandrich, M.; Schroeckh, V.; Stix, B.; Rath, T.; Kahne, T.; Dierkes, J.; Roessner, A.; Albert, F. W. ALys amyloidosis caused by compound heterozygosity in exon 2 (Thr70Asn) and exon 4 (Trp112Arg) of the lysozyme gene. *Human Mutat.* **2006**, *27* (1), 119−20.

(6) Palmer, A. M. Neuroprotective therapeutics for Alzheimer's disease: Progress and prospects. *Trends Pharmacol. Sci.* **2011**, *32* (3), 141−7.

(7) Cohen, F. E.; Kelly, J. W. Therapeutic approaches to protein-misfolding diseases. *Nature* **2003**, *426* (6968), 905−9.

(8) Gazit, E. Mechanisms of amyloid fibril self-assembly and inhibition. Model short peptides as a key research tool. *FEBS J.* **2005**, *272* (23), 5971−8.

(9) Porat, Y.; Abramowitz, A.; Gazit, E. Inhibition of amyloid fibril formation by polyphenols: Structural similarity and aromatic interactions as a common inhibition mechanism. *Chem. Biol. Drug Des.* **2006**, *67* (1), 27−37.

(10) Ghosh, S.; Pandey, N. K.; Dasgupta, S. (−)-Epicatechin gallate prevents alkali-salt mediated fibrillogenesis of hen egg white lysozyme. *Int. J. Biol. Macromol.* **2013**, *54*, 90−8.

(11) Wang, S. S.; Liu, K. N.; Lee, W. H. Effect of curcumin on the amyloid fibrillogenesis of hen egg-white lysozyme. *Biophys. Chem.* **2009**, *144* (1−2), 78−87.

(12) Vuong, Q. V.; Siposova, K.; Nguyen, T. T.; Antosova, A.; Balogova, L.; Drajna, L.; Imrich, J.; Li, M. S.; Gazova, Z. Binding of glyco-acridine derivatives to lysozyme leads to inhibition of amyloid fibrillization. *Biomacromolecules* **2013**, *14* (4), 1035−43.

(13) Gazova, Z.; Bellova, A.; Daxnerova, Z.; Imrich, J.; Kristian, P.; Tomascikova, J.; Bagelova, J.; Fedunova, D.; Antalik, M. Acridine derivatives inhibit lysozyme aggregation. *Eur. Biophys. J.* **2008**, *37* (7), 1261−70.

(14) Antosova, A.; Chelli, B.; Bystrenova, E.; Siposova, K.; Valle, F.; Imrich, J.; Vilkova, M.; Kristian, P.; Biscarini, F.; Gazova, Z. Structure-activity relationship of acridine derivatives to amyloid aggregation of lysozyme. *Biochim. Biophys. Acta* **2011**, *1810* (4), 465−74.

(15) Wu, J. W.; Liu, K. N.; How, S. C.; Chen, W. A.; Lai, C. M.; Liu, H. S.; Hu, C. J.; Wang, S. S. Carnosine's effect on amyloid fibril formation and induced cytotoxicity of lysozyme. *PLoS One* **2013**, *8* (12), e81982.

(16) Stefani, M.; Rigacci, S. Protein folding and aggregation into amyloid: The interference by natural phenolic compounds. *Int. J. Mol. Sci.* **2013**, *14* (6), 12411−57.

(17) Akaishi, T.; Morimoto, T.; Shibao, M.; Watanabe, S.; Sakai-Kato, K.; Utsunomiya-Tate, N.; Abe, K. Structural requirements for the flavonoid fisetin in inhibiting fibril formation of amyloid beta protein. *Neurosci. Lett.* **2008**, *444* (3), 280−5.

(18) McKoy, A. F.; Chen, J.; Schupbach, T.; Hecht, M. H. A novel inhibitor of amyloid beta (Abeta) peptide aggregation: from high throughput screening to efficacy in an animal model of Alzheimer disease. *J. Biol. Chem.* **2012**, *287* (46), 38992−9000.

(19) Ehrnhoefer, D. E.; Bieschke, J.; Boeddrich, A.; Herbst, M.; Masino, L.; Lurz, R.; Engemann, S.; Pastore, A.; Wanker, E. E. EGCG redirects amyloidogenic polypeptides into unstructured, off-pathway oligomers. *Nat. Struct. Mol. Biol.* **2008**, *15* (6), 558−66.

(20) Bulic, B.; Pickhardt, M.; Schmidt, B.; Mandelkow, E. M.; Waldmann, H.; Mandelkow, E. Development of tau aggregation inhibitors for Alzheimer's disease. *Angew. Chem.* **2009**, *48* (10), 1740−52.

(21) Ono, K.; Yamada, M. Antioxidant compounds have potent anti-fibrillogenic and fibril-destabilizing effects for alpha-synuclein fibrils in vitro. *J. Neurochem.* **2006**, *97* (1), 105−15.

(22) Zelus, C.; Fox, A.; Calciano, A.; Faridian, B. S.; Nogaj, L. A.; Moffet, D. A. Myricetin Inhibits Islet Amyloid Polypeptide (IAPP) Aggregation and Rescues Living Mammalian Cells from IAPP Toxicity. *Open Biochem. J.* **2012**, *6*, 66−70.

(23) Frare, E.; Polverino De Laureto, P.; Zurdo, J.; Dobson, C. M.; Fontana, A. A highly amyloidogenic region of hen lysozyme. *J. Mol. Biol.* **2004**, *340* (5), 1153−65.

(24) Hess, B.; Kutzner, C.; Van Der Spoel, D.; Lindahl, E. GROMACS 4: Algorithms for highly efficient, load-balanced, and scalable molecular simulation. *J. Chem. Theory Comput.* **2008**, *4*, 435−447.

(25) Refaee, M.; Tezuka, T.; Akasaka, K.; Williamson, M. P. Pressure-dependent changes in the solution structure of hen egg-white lysozyme. *J. Mol. Biol.* **2003**, *327* (4), 857−65.

(26) Scott, W. R. P.; Hünenberger, P. H.; Tironi, I. G.; Mark, A. E.; Billeter, S. R.; Fennen, J.; Torda, A. E.; Huber, T.; Krüger, P.; van Gunsteren, W. F. The GROMOS biomolecular simulation program package. *J. Phys. Chem. A* **1999**, *103*, 3596−607.

(27) Berendsen, H. J. C.; Postma, J. P. M.; van Gunsteren, W. F.; Hermans, J. Interaction models for water in relation to protein hydration. *Intermol. Forces* **1981**, *11* (Suppl. 1), 331−8.
(28) Essmann, U.; Perera, L.; Berkowitz, M. L.; Darden, T.; Lee, H. J.; Pedersen, L. G. A smooth particle mesh Ewald potential. *J. Chem. Phys.* **1995**, *103*, 8577−92.
(29) Chen, C. Y. TCM Database@Taiwan: The world's largest traditional Chinese medicine database for drug screening in silico. *PLoS One* **2011**, *6* (1), No. e15939.
(30) Swaminathan, R.; Ravi, V. K.; Kumar, S.; Kumar, M. V.; Chandra, N. Lysozyme: A model protein for amyloid research. *Adv. Protein Chem. Struct Biol.* **2011**, *84*, 63−111.
(31) LeVine, H., 3rd Thioflavine T interaction with synthetic Alzheimer's disease beta-amyloid peptides: Detection of amyloid aggregation in solution. *Protein Sci.* **1993**, *2* (3), 404−10.
(32) Semisotnov, G. V.; Rodionova, N. A.; Razgulyaev, O. I.; Uversky, V. N.; Gripas, A. F.; Gilmanshin, R. I. Study of the ″molten globule″ intermediate state in protein folding by a hydrophobic fluorescent probe. *Biopolymers* **1991**, *31* (1), 119−28.
(33) Cowgill, R. W. Fluorescence and the Structure of Proteins. Ii. Fluorescence of Peptides Containing Tryptophan or Tyrosine. *Biochim. Biophys. Acta* **1963**, *75*, 272−3.
(34) Di Stasio, E.; Bizzarri, P.; Misiti, F.; Pavoni, E.; Brancaccio, A. A fast and accurate procedure to collect and analyze unfolding fluorescence signal: The case of dystroglycan domains. *Biophys. Chem.* **2004**, *107* (2), 197−211.
(35) Duy, C.; Fitter, J. How aggregation and conformational scrambling of unfolded states govern fluorescence emission spectra. *Biophys. J.* **2006**, *90* (10), 3704−11.
(36) Suryaprakash, P.; Kumar, R. P.; Prakash, V. Thermodynamics of interaction of caffeic acid and quinic acid with multisubunit proteins. *Int. J. Biol. Macromol.* **2000**, *27* (3), 219−28.
(37) Rawel, H. M.; Czajka, D.; Rohn, S.; Kroll, J. Interactions of different phenolic acids and flavonoids with soy proteins. *Int. J. Biol. Macromol.* **2002**, *30* (3−4), 137−50.
(38) Gama Sosa, M. A.; De Gasperi, R.; Elder, G. A. Modeling human neurodegenerative diseases in transgenic systems. *Hum. Genet.* **2012**, *131* (4), 535−63.
(39) Kikis, E. A.; Gidalevitz, T.; Morimoto, R. I. Protein homeostasis in models of aging and age-related conformational disease. *Adv. Exp. Med. Biol.* **2010**, *694*, 138−59.
(40) Cuanalo-Contreras, K.; Mukherjee, A.; Soto, C. Role of Protein Misfolding and Proteostasis Deficiency in Protein Misfolding Diseases and Aging. *Int. J. Cell Biol.* **2013**, *2013*, No. 638083.
(41) Demontis, F.; Perrimon, N. FOXO/4E-BP signaling in Drosophila muscles regulates organism-wide proteostasis during aging. *Cell* **2010**, *143* (5), 813−25.
(42) Ben-Zvi, A.; Miller, E. A.; Morimoto, R. I. Collapse of proteostasis represents an early molecular event in Caenorhabditis elegans aging. *Proc. Natl. Acad. Sci. U. S. A.* **2009**, *106* (35), 14914−9.
(43) Cohen, E.; Paulsson, J. F.; Blinder, P.; Burstyn-Cohen, T.; Du, D.; Estepa, G.; Adame, A.; Pham, H. M.; Holzenberger, M.; Kelly, J. W.; Masliah, E.; Dillin, A. Reduced IGF-1 signaling delays age-associated proteotoxicity in mice. *Cell* **2009**, *139* (6), 1157−69.
(44) Truelsen, T.; Thudium, D.; Gronbaek, M.; Copenhagen City Heart Study.. Amount and type of alcohol and risk of dementia: The Copenhagen City Heart Study. *Neurology* **2002**, *59* (9), 1313−9.
(45) Ono, K.; Li, L.; Takamura, Y.; Yoshiike, Y.; Zhu, L.; Han, F.; Mao, X.; Ikeda, T.; Takasaki, J.; Nishijo, H.; Takashima, A.; Teplow, D. B.; Zagorski, M. G.; Yamada, M. Phenolic compounds prevent amyloid beta-protein oligomerization and synaptic dysfunction by site-specific binding. *J. Biol. Chem.* **2012**, *287* (18), 14631−43.
(46) Smid, S. D.; Maag, J. L.; Musgrave, I. F. Dietary polyphenol-derived protection against neurotoxic beta-amyloid protein: From molecular to clinical. *Food Funct.* **2012**, *3* (12), 1242−50.
(47) Cazarolli, L. H.; Zanatta, L.; Alberton, E. H.; Figueiredo, M. S.; Folador, P.; Damazio, R. G.; Pizzolatti, M. G.; Silva, F. R. Flavonoids: Cellular and molecular mechanism of action in glucose homeostasis. *Mini-Rev. Med. Chem.* **2008**, *8* (10), 1032−8.
(48) Narayana, K. R.; Reddy, M. S.; Chaluvadi, M. R.; Krishna, D. R. Bioflavonoids classification, pharmacological, biochemical effects and therapeutic potential. *Indian J. Pharmacol.* **2001**, *33* (1), 2−16.
(49) Hudson, S. A.; Ecroyd, H.; Kee, T. W.; Carver, J. A. The thioflavin T fluorescence assay for amyloid fibril detection can be biased by the presence of exogenous compounds. *FEBS J.* **2009**, *276* (20), 5960−72.
(50) Canet, D.; Last, A. M.; Tito, P.; Sunde, M.; Spencer, A.; Archer, D. B.; Redfield, C.; Robinson, C. V.; Dobson, C. M. Local cooperativity in the unfolding of an amyloidogenic variant of human lysozyme. *Nat. Struct. Biol.* **2002**, *9* (4), 308−15.
(51) Dumoulin, M.; Canet, D.; Last, A. M.; Pardon, E.; Archer, D. B.; Muyldermans, S.; Wyns, L.; Matagne, A.; Robinson, C. V.; Redfield, C.; Dobson, C. M. Reduced global cooperativity is a common feature underlying the amyloidogenicity of pathogenic lysozyme mutations. *J. Mol. Biol.* **2005**, *346* (3), 773−88.
(52) Tokunaga, Y.; Sakakibara, Y.; Kamada, Y.; Watanabe, K.; Sugimoto, Y. Analysis of core region from egg white lysozyme forming amyloid fibrils. *Int. J. Biol. Sci.* **2013**, *9* (2), 219−27.
(53) Lara, C.; Reynolds, N. P.; Berryman, J. T.; Xu, A.; Zhang, A.; Mezzenga, R. ILQINS hexapeptide, identified in lysozyme left-handed helical ribbons and nanotubes, forms right-handed helical ribbons and crystals. *J. Am. Chem. Soc.* **2014**, *136* (12), 4732−9.
(54) Leach, A. R.; Shoichet, B. K.; Peishoff, C. E. Prediction of protein-ligand interactions. Docking and scoring: successes and gaps. *J. Med. Chem.* **2006**, *49* (20), 5851−5.
(55) Kann, M. G. Protein interactions and disease: Computational approaches to uncover the etiology of diseases. *Briefings Bioinf.* **2007**, *8* (5), 333−46.
(56) Imoto, T.; Forster, L. S.; Rupley, J. A.; Tanaka, F. Fluorescence of lysozyme: emissions from tryptophan residues 62 and 108 and energy migration. *Proc. Natl. Acad. Sci. U. S. A.* **1972**, *69* (5), 1151−5.
(57) Bahramikia, S.; Yazdanparast, R. Anti-amyloidogenic and fibril-destabilizing effects of two manganese-salen derivatives against hen egg-white lysozyme aggregation. *Int. J. Biol. Macromol.* **2012**, *50* (1), 187−97.
(58) Kalyan, S. G.; Bijaya, K. S.; Swagata, D. Spectrophotometric studies on the interaction between (−)-epigallocatechin-3-gallate and lysozyme. *Chem. Phys. Lett.* **2008**, *452*, 193−7.
(59) Phillips, D. C. The three-dimensional structure of an enzyme molecule. *Sci. Am.* **1966**, *215* (5), 78−90.
(60) Bucciantini, M.; Giannoni, E.; Chiti, F.; Baroni, F.; Formigli, L.; Zurdo, J.; Taddei, N.; Ramponi, G.; Dobson, C. M.; Stefani, M. Inherent toxicity of aggregates implies a common mechanism for protein misfolding diseases. *Nature* **2002**, *416* (6880), 507−11.
(61) Lorenzo, A.; Yankner, B. A. Beta-amyloid neurotoxicity requires fibril formation and is inhibited by congo red. *Proc. Natl. Acad. Sci. U. S. A.* **1994**, *91* (25), 12243−7.
(62) Ghosh, S.; Pandey, N. K.; Banerjee, P.; Chaudhury, K.; Nagy, N. V.; Dasgupta, S. Copper(II) directs formation of toxic amorphous aggregates resulting in inhibition of hen egg white lysozyme fibrillation under alkaline salt-mediated conditions. *J. Biomol. Struct. Dyn.* **2014**, 1−17.

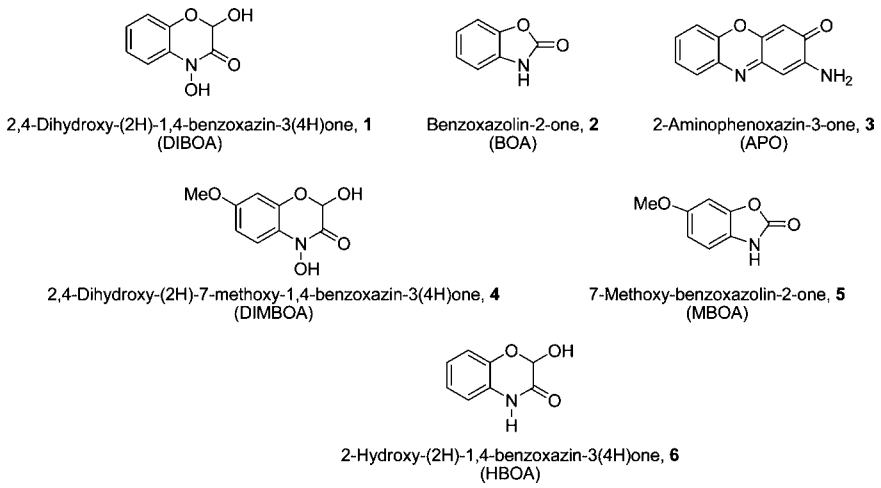


**Figure 1.** Structures of the compounds under discussion.

or their degradation products, as characterized inside the target plant. All of the analyses were conducted in a single bioassay involving a coculture of both species in order to ensure direct and mutual interactions between the donor and target plant. The dynamic character of the different determinations performed adds the value of a real-time description of the various processes that are involved in the allelopathic phenomenon.

The study focused on the interaction of rye (*Secale cereale* L.), as a strategic crop, with one of its most common weeds (wild oat, *Avena fatua* L.). This interaction is mediated by benzoxazinone allelochemicals, and we propose a relevant role for the degradation products on the basis of the experimental results.[9] *S. cereale* is well-known as a producer of 2,4-dihydroxy-(2*H*)$^{-1}$,4-benzoxazin-3(4*H*)one (DIBOA, **1**) (Figure 1). Extensive research has been performed on the phytotoxic effects of this compound and its degradation products benzoxazolin-2-one (BOA, **2**) and 2-aminophenoxazin-3-one (APO, **3**),[10,11] as well as the fate of allelochemicals[12,13] and the physiological aspects of the mode of action.[14−16] (2*H*)-1,4-Benzoxazin-3(4*H*)-ones have been isolated from Poaceae, Acanthaceae, Ranunculaceae and Scrophulariceae plants. Indeed, degradation in different systems, such as aqueous solutions,[7,11,17] microbial biotransformation,[18] or crop soils,[7,11,19,20] has been widely studied along with the dynamics of these systems. In addition, these compounds have shown a wide spectrum of biological activities,[21−24] as have some of their degradation products[25,26] and a wide variety of synthetic analogs.[27] Compounds such as 2,4-dihydroxy-(2*H*)-1,4-benzoxazin-3(4*H*)-one (DIBOA, **1**) and its 7-methoxy analog (DIMBOA, **4**) have been described as chemicals with relevant roles in chemical ecology for the last 50 years.[9] The levels of DIBOA (**1**), BOA (**2**), and APO (**3**) were monitored in *S. cereale*, culture medium, and *A. fatua*, and the results were correlated with the phytotoxic effects observed.

## MATERIALS AND METHODS

**Statistical Analysis.** Data for the lengths of root and shoot were statistically analyzed using Welch's test, with significance fixed at 0.01 and 0.05. The results are represented in bar charts as percentages from the control. Thus, zero represents the control, positive values represent stimulation of the studied parameter, and negative values represent inhibition. The fresh weights of seedlings were determined in triplicate, and the mean and standard deviation were calculated. A similar procedure was followed for endogenous (root and shoot content) and exogenous (exudate content) contents of the different metabolites. The quantitation of DIBOA (**1**), BOA (**2**), and APO (**3**) was carried out in quintuplicate using calibration curves and outlying values were discarded (values out of the range of the spiked value ±20%).

**Bioassays.** *S. cereale-A. fatua Pregermination.* The seeds used for the coculture experiment were surface-sterilized by soaking for 30 min in calcium hypochlorite 75 g/L (Merck, Darmstadt, Germany) with traces of Tween 20 (Sigma-Aldrich, St. Louis, MO, U.S.A.) followed by rinsing with sterilized deionized water. The sterilized seeds were placed in Petri dishes (8.5 mm diameter) containing a semisolid culture medium from Sigma-Aldrich (Agar-agar 7 g/L, Hoagland No. 2 basal salt mixture, pH 5.7). Petri dishes were placed in a growth chamber Celsius 2000 (Memmert, Duesseldorf, Germany) for a 16 h photoperiod at 25 °C, 70% relative humidity, with cold white light (standard illuminant D65; 6500 K). The activities were assessed under sterile conditions.

*S. cereale-A. fatua Coculture.* The bioassay substrate was designed by considering two criteria: an accurate simulation of the field interaction conditions and ease of monitoring the exuded chemicals. Glass perlite (3 mm diameter, 200 g) was placed in a glass flask (2.5 L) and culture solution (Hoagland No. 2 basal salt mixture, pH 5.7, 300 mL) was added. Glass perlite was chosen due to its negligible interference on the analysis by adsorption or absorption of the test solution and also because it minimizes the sample conditioning operations required prior to analysis. In this respect, a simple filtration was sufficient, and this avoided the need for extraction processes with organic solvents. Minimization of the absorption or adsorption of chemicals also enhances their bioavailability. Seedlings of *A. fatua* (3 d old) and *S. cereale* (6 d old) were placed inside the flasks, and they were allowed to grow for 6 d. The number of *A. fatua* seedlings was fixed at 4 and the number of *S. cereale* seedlings was set up according to the following donor/target plant ratios: 1:1, 2:1, 3:1, 7:1, 10:1, and 20:1. These donor/target proportions were optimized for maximum effect by performing bioassays under identical culture conditions. *A. fatua* and *S. cereale* monocultures, prepared under analogous conditions, were used as controls for phytotoxicity and DIBOA (**1**) production measurements.

*Phytotoxicity Parameters.* Phytotoxicity on *A. fatua* was measured by comparing its root length, shoot length, and shoot fresh weight after exposure to *S. cereale* seedlings under the experimental conditions described above. In addition, potential effects of *A. fatua* on *S. cereale* were studied and described in terms of root length, shoot fresh weight, and DIBOA (**1**) content.

**Analytical Method.** DIBOA (**1**), BOA (**2**), and APO (**3**) levels in culture solution were recorded using the previously described HPLC-DAD method.[28] Quantitation was performed using a method with an external standard. BOA (**2**) was purchased from Fluka Chemika Co.


dx.doi.org/10.1021/jf503840d | J. Agric. Food Chem. 2014, 62, 9450−9457

(Sigma-Aldrich, St. Louis, MO, U.S.A.). DIBOA (**1**) and APO (**3**) standards were obtained by the previously described methodology.[29] Compounds were identified by comparison of retention times and UV/vis spectra at two wavelengths, namely 253 and 264 nm (95% confidence), using external and internal standards. A single analysis therefore provided a description of the chemical situation of the whole system at a given time, and subsequent repetition of the analysis provided a complete description of the chemical evolution in terms of production and exudation by the donor plants (*S. cereale*), assimilation by the target plant (*A. fatua*) and degradation or retention by the environment.

**DIBOA Detection and Quantitation in *A. fatua*.** These experiments were performed on a Inova 600 NMR spectrometer (Varian, Palo Alto, CA, U.S.A.) equipped with an interchangeable triple-resonance microflux probe (Varian $^{1}H[^{13}C/^{15}N]$ 3 mm pulsed-field gradients PFG, 60 $\mu$L active volume) and connected to a Varian HPLC-UV/MS system (Varian 1200L quadrupole mass spectrometer, Varian HPLC-UV system). The UV/vis outlet was connected to the NMR equipment by means of a Rheodyne sampling unit. Stop-flow experiments were performed by using a Valco stop-flow valve. This valve was controlled by the LC-NMR software, considering the UV/vis and NMR detector delay. Liquid chromatography was carried out using an analytical column 150 mm × 4.6 mm i.d., 5 $\mu$m Gemini 110A RP-18 (Phenomenex, Torrance, CA, U.S.A.) with a guard column SecurityGuard Cartridges Gemini RP-18 (Phenomenex, Torrance, CA, U.S.A.) under reverse phase and isocratic conditions with a mixture of MeOH (1% TFA):$H_2O$ (1% TFA) (7:3). Gradient separation was performed using (A) MeOH;1% TFA and (B) $H_2O$;1% TFA with the following elution pattern: $t_0$ = 30% B; $t$ = 40 min, 100% B. The system was operated at room temperature and the eluent flow was set to 0.8 mL/min. $^{1}H$ NMR spectra were recorded under on-flow and stop-flow conditions for standard solutions and *A. fatua* tissue extracts, respectively. Solvent suppression was performed by using the WET2 method. Thirty-two NMR accumulations were used for standards and 256 for samples. The spectral width was set to 10 000 Hz in all experiments. WETG-COSY spectra were acquired using 48 accumulations, 128 and 2 K increments with a 10 000 Hz spectral width in both dimensions and a 1 s relaxation time. $CD_3OD$ was used as the solvent and the residual MeOH peak ($\delta$ 3.30 ppm) was used as a reference. A 10 $\mu$L injection of an equimolecular mixture of DIMBOA (**4**), DIBOA (**1**), BOA (**2**), and MBOA (**5**) (standard solution) was carried out. *A. fatua* methanol extracts were used for allelochemical detection and these were injected at a concentration of 3 mg/mL.

## RESULTS AND DISCUSSION

**Experimental Design.** The overall objective of this study was to characterize completely the allelopathic pathway with living plants and real exudates. To achieve this aim, we developed an experimental design that balances two factors: to model the real phenomenon under laboratory conditions and to mimic the real situation as closely as possible. The design allowed us to record the following information: the release of allelochemicals into the culture substrate in bioactive concentrations, monitorization of the degradation phenomena, identification of the final products, detection of the uptake of the "bioactive cocktail" by the target plant, and, finally, a beneficial or detrimental effect described using appropriate parameters. The experimental design was optimized by fixing the following elements: allelochemicals, donor plant, target plant, and substrate.

**Donor Plant Selection.** Wheat, rye, and maize have shown allelopathic effects, and they produce benzoxazinones. Farmers have taken advantage of these properties by employing them for crop rotation and by using their residues to treat the soil.[30] The activities of some mulches have also been tested. The effects of soil-incorporated wheat on the germination of 12 different weed species have been studied.[31] These allelochemicals have two desirable features for the present study: first, it is possible to measure accurately their concentrations in the donor plant, target plant, and the environment in which they grow; second, their degradation products are known and can be measured simultaneously with the initially released allelochemicals. Fortunately, a great deal of research has been focused on the bioactivity and biodegradability of these compounds and this has led to one of the most in-depth studies published to date.[27]

A key point in the selection of the donor plant is the stability of the allelochemicals present. Thus, the persistence of DIBOA (**1**) in soil and other environments is much higher than that of DIMBOA (**4**). The half-life of DIBOA (**1**) is 62 h in soil, 48 h in water and 12 h in bioassay media,[7] whereas the corresponding values for DIMBOA (**4**) are 31 min, 18 and 8 h, respectively.[11] Wheat and rye both produce DIMBOA (**4**) and DIBOA is also produced in the case of wheat. A higher level of activity was found in *S. cereale* and the major benzohydroxamic acid produced for this species is the more stable DIBOA (**1**).[32] These facts led us to select *S. cereale* as the donor plant.

**Target Plant Selection.** It has been reported that the following plant species, among others, are sensitive to DIBOA (**1**): *Lepidium sativum*, *Eruca sativa*, *Lactuca sativa*, *Sinapis alba*, *Vicia hirsute*, *Spinacia oleracea*, *Raphanus sativus*, *Brassica rapa* var. *oleifera*, *Lolium rigidum*, *Brassica rapa* var. *esculenta*, *Avena fatua*, and *Echinochloa crus-galli*. Exploratory bioassays were performed in order to select the target species and *Avena fatua* was found to be the optimal model for several reasons: this weed has rapid growth and biomass development (which facilitates extraction and analysis) and it has been used for phytotoxicity tests under field conditions for *Secale cereale* and *Triticum aestivum*. Finally, this species interacts in the field with Gramineae crops and is classified as one of the most problematic weed species.

**Influence of Seedling Density on the Experimental Design.** Phytotoxicity data recorded on *A. fatua* for the different *S. cereale* seedling densities are shown in Figure 2.

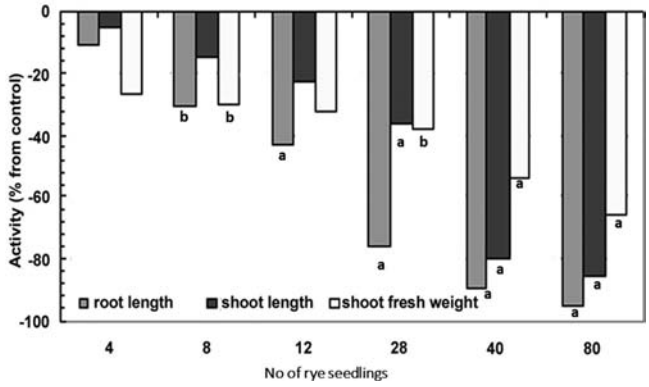


**Figure 2.** Phytotoxic activity on *A. fatua* seedlings in coculture bioassay with *S. cereale*.

Dose–response effects could be observed and mathematically treated (Figure 3). The presence of 14 *S. cereale* seedlings caused 50% inhibition of root length, whereas 35 seedlings were needed to cause the same level of toxicity when measured on shoot length. The growth parameters and the DIBOA (**1**) levels were evaluated for the donor plant, as some interaction caused by the organism chosen as the target could also take place. In

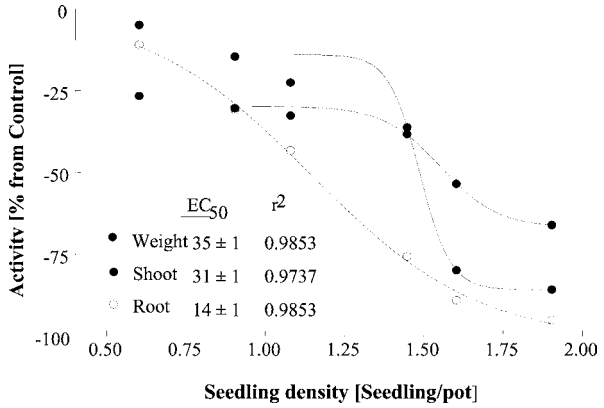


**Figure 3.** Dose–response curves for *A. fatua* growth vs *S. cereale* ratios.

control samples, the number of seedlings of the target species was replaced by the same number of rye seedlings.

The effects on weight, length, and the accumulation of DIBOA (**1**) for *S. cereale* in coculture with *A. fatua* are shown in Figure 4. In general, growth inhibition was very low, with the highest effect at around 12%. As can be observed, at lower donor seedling densities the growth parameters were inhibited to a greater extent. This trend is consistent with a detrimental effect caused on the donor plant. In addition, endogenous DIBOA (**1**) production decreased when the proportion of the target plant was decreased. This result is consistent with production of the defense metabolite being triggered by the presence of the target organism. The mutual character of the allelopathic interaction was therefore clearly displayed, and the plants chosen as donor and target played their expected roles under the selected experimental conditions.

The study of the chemical interference between two species continued with the detection of the allelochemicals in the donor plant exudates. Chromatograms were obtained for exudates at three ratios of donating seedlings in the coculture and the amounts of DIBOA (**1**), BOA (**2**), and APO (**3**) were also determined. In general, the levels of DIBOA (**1**) are similar to those obtained without target species although they do tend to be slightly lower in the latter case. A progressive increase in the amounts of DIBOA (**1**) in the media was observed on increasing the density of donating seedlings. This trend was less marked in the cases of BOA (**2**) and APO (**3**). In terms of concentration units, defined by the volume of initial nutrient solution, the highest concentration of DIBOA (**1**) in the system was 0.3 mM. Under these experimental conditions, the exudation, absorption, changes in solution volume, and degradation generated a phytotoxic concentration gradient that affected the target organism rather than a fixed concentration. These conditions are much more similar to an environmental allelopathic interaction than those used in most dose–response bioassays, in which there is a fixed concentration of a potentially active substance.

Once we had dynamically determined the donor plant exudation potential, degradation phenomena led to changes in the composition of the culture solution. In addition to the chemicals identified, DIMBOA (**4**) and the lactam HBOA (**6**) were detected (Figure 5). The presence of DIMBOA (**4**) in

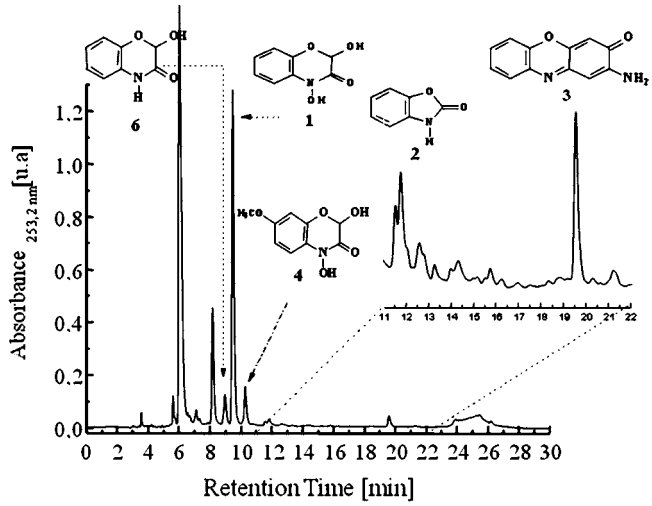


**Figure 5.** Chromatographic profile of the growth medium in coculture of *S. cereale* and *A. fatua*. Conditions: 300 seedlings, 12 d of growth from germination.

roots of rye and its exudates has been discussed. The production of this compound by seedlings seems to be dependent upon genetic and environmental factors as well as the bioassay design. In addition, secondary metabolites, and particularly the production of benzoxazinones in crops, have been characterized as highly accession-dependent, as indicated

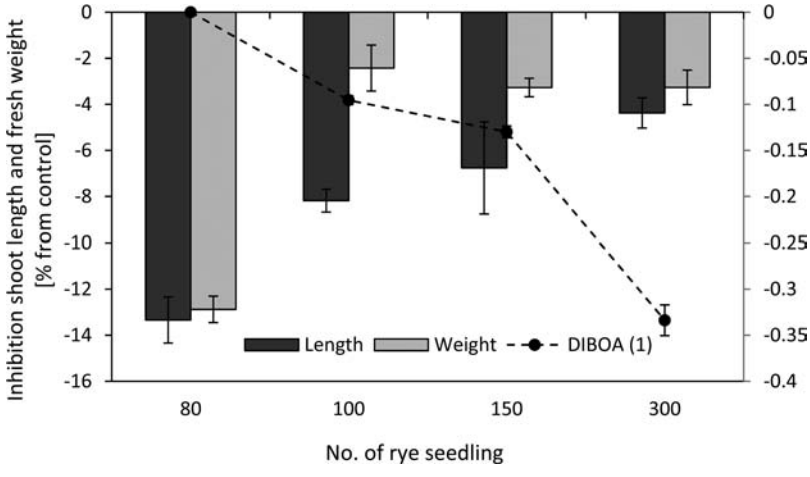


**Figure 4.** Effects on growth and accumulation of DIBOA (**1**) in the *S. cereale* bioassay.


dx.doi.org/10.1021/jf503840d | *J. Agric. Food Chem.* 2014, 62, 9450–9457

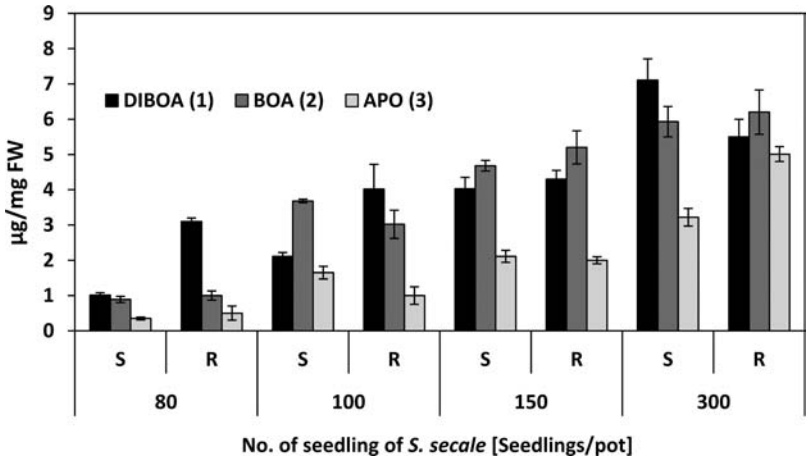


**Figure 6.** Levels of DIBOA (**1**), BOA (**2**), and APO (**3**) in shoot and root of *A. fatua* for different densities of *S. cereale*.

by a particular study on benzoxazinones from wheat.[33] Thus, in this case the phytotoxic effects on the target plant must correspond partly to the action of DIBOA (**1**), DIMBOA (**4**), and HBOA (**6**). Nevertheless, qualitatively it is evident that the DIBOA (**1**) concentration in the exudates was much higher than those of DIMBOA (**4**) and HBOA (**6**). Moreover, the phytotoxicity of DIBOA (**1**) to *A. fatua* was found to be much higher than that found for the other two benzoxazinones.[34] Therefore, DIBOA (**1**) and related compounds should be the most relevant molecules in considering phytotoxic effects and, consequently, the analysis was focused on these compounds.

DIBOA (**1**) and its degradation products BOA (**2**) and APO (**3**), present in the culture medium were studied inside the target plant tissue. The results of this study provided information on the contribution of each chemical to the observed phytotoxicity and confirmed their previously suspected[35] contribution to the interaction phenomena mediated by chemicals.

**Time Dependence.** As mentioned above, the concentrations of allelochemicals in the culture medium depended on the exudation rate, changes in the solution volume during the bioassay, and degradation of the primary products released by the donor plant. Thus, the degradation processes affected the amount of allelochemical by diminishing its concentration, whereas the consumption of nutritient solution caused an increase in the concentration in the system. These findings are not unique to this particular bioassay. In nature, it has been estimated that the concentrations of compounds are also in a gradient, with maximum and minimum values defined by the dynamics of the exudation phenomenon and the transformation processes.[36,37] This phenomenon was also studied in some detail by considering culture solution consumption for a density of 50 seedlings during 12 d of growth. It was found that a volume of 10 mL was sufficient for regular plant development. In the present bioassay, 60 mL of culture solution was used. This approach allowed us to infer that 10 mL of solution must still remain at the end of the bioassay with 300 seedlings (12 d).

**Unambiguous Identification.** The identification criteria in the analysis of DIBOA (**1**) in the nutrient solution were based on the commonly used chromatographic methodologies: retention time, addition of standard to the sample, recording of the ultraviolet spectrum, and comparison with pure standards. The unambiguous determination of the compound in target plant extracts was ensured by combining liquid chromatography with UV/vis spectrophotometry, mass spectrometry, and nuclear magnetic resonance spectroscopy. A full analytical system based on these techniques was designed and this provided the UV/vis spectrum, mass spectrum, and $^{1}$H NMR and $^{1}$H—$^{1}$H 2D WET-gCOSY NMR spectra. All of the techniques were standardized and optimized for the analysis of mixtures prepared from pure standards of DIBOA (**1**), BOA (**2**), and MBOA (**5**). The spectra (UV/vis, NMR, and MS) obtained from the sample were identical to those of the extracts, thus confirming the presence of the allelochemicals generated by the donor plant in the tissue of the target species and verifying the absorption of potentially allelopathic compounds from one species to another in the vicinity.

Once the structures of the compounds had been confirmed as DIBOA (**1**), BOA (**2**), and APO (**3**), their concentrations were determined by HPLC-DAD. An increase in the level of the detected compound in the target plant was observed when the population of donor species was increased. It should be pointed out that the amounts of DIBOA (**1**), BOA (**2**), and APO (**3**) in roots were similar to those in shoots, except for the lowest density, in which DIBOA (**1**) root levels were higher (Figure 6). Absorption through the root is a process that is governed by several factors, both biotic and abiotic. These factors include concentration in the medium. The metabolic effects caused by the compounds taken up can modify the absorption capacity, which would then vary with time. This phenomenon is related to the capacity for translocation of the chemicals from roots to shoots and the ability to metabolize and detoxify them.

With regard to the molecules to be taken up, their physical properties play a fundamental role in their absorption by roots. The molecular weights and functional groups of these compounds modify their solubilities and are among the determining factors. DIBOA (**1**), BOA (**2**), and APO (**3**) have different solubilities and their different structures also influence the molecular interactions, transport within the plant, and the final access to their molecular target sites of action for phytotoxicity. In the present case, APO (**3**) is absorbed the least and DIBOA (**1**) the most. This fact can be positively correlated with their concentrations in the test environment. However, considering that APO (**3**) has the lowest solubility in water of the compounds in question, it is not surprising that it has a lower concentration in the target plant.

**Phytotoxic Effect on the Target Plant.** Once the presence of the allelochemicals in the target plant had been

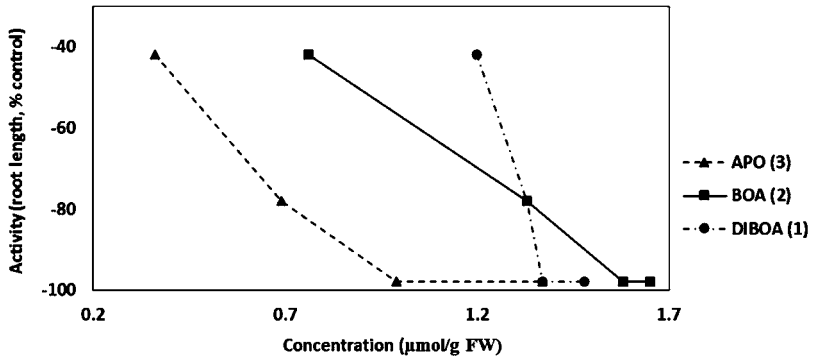


**Figure 7.** Levels of DIBOA (**1**), BOA (**2**), and APO (**3**) in *A. fatua* (μmol/PFW) roots and activity on the root growth parameters.

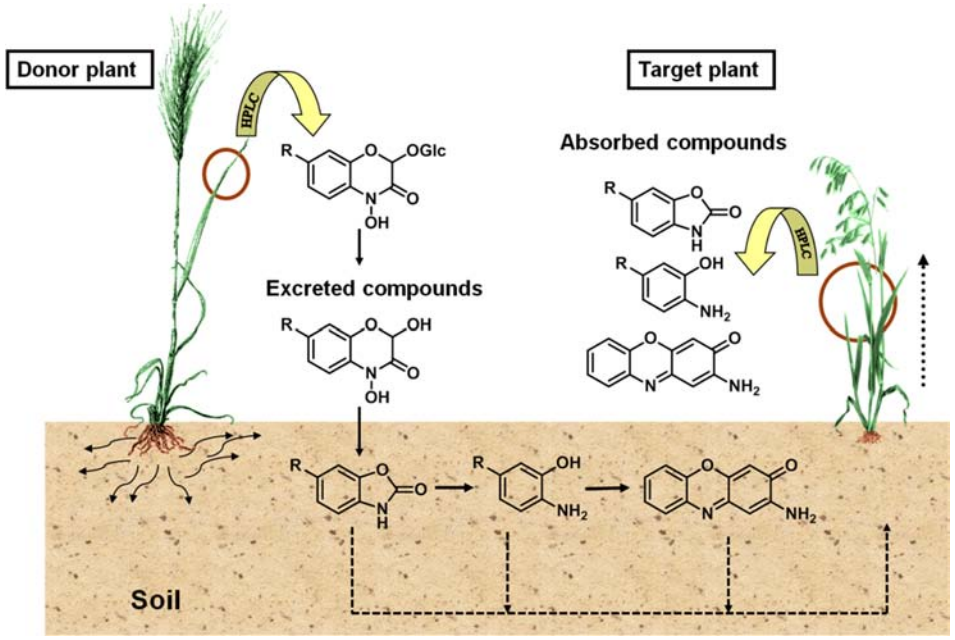


**Figure 8.** Proposed representation for the allelopathic pathway in the coculture of *S. cereale* and *A. fatua*.

confirmed, the dependence on the donor plant density from which they originate had to be described along with their bioactivity. A greater phytotoxic effect was observed as the amounts of allelochemicals found in the target plant tissue increased (Figure 7). The concentration of each chemical inside the plant, along with the resulting phytotoxic effect, followed a typical dose−response relationship. This correlation was observed for the three analyzed compounds DIBOA (**1**), BOA (**2**), and APO (**3**). All of the compounds were found in shoots and roots, albeit at different concentrations. Under these conditions, the higher concentration of DIBOA (**1**) could indicate that this is the compound that contributes most to the observed effects. Nevertheless, the higher phytotoxicity of APO (**3**) on *A. fatua*[29] implies that this compound would require a lower concentration to achieve the same effect. This result clearly establishes these chemicals as the agents responsible for the phytotoxic effects observed.

In summary, this is the first allelopathy study in which the mediators of the allelopathic phenomenon have been detected in all plant species under investigation and also in the environment in which they were grown (Figure 8). Since this experiment was conducted with living plants and real exudates, the system could capture multicompound interactions that influence the bioavailability of allelochemicals, effects that are otherwise obscured in allelopathy research.[38]

The results provide valuable information for the study of the allelopathic phenomenon and shed light on the role of benzoxazinones and their related chemicals in Gramineae crop-weed interactions. The production, transformation, and degradation processes that occur concomitantly have been fully characterized for the biocommunication process between *S. cereale* and *A. fatua*. Although the process reported here is a specific example of allelopathy, the results allowed us to show the complexity of this phenomenon, especially in terms of the dynamic nature of exudation, uptake, and degradation processes. The route of the allelochemicals from donor to target plant was fully characterized and the role of benzoxazinones and their degradation products on the interaction was confirmed. We suggest that exudation and uptake dynamics, together with degradation products, are factors that must be considered in studies aimed at the characterization of allelopathic phenomena.

The dynamics of the processes involved in allelopathy are extremely complex and gaining knowledge and understanding requires an in-depth investigation. For example, all experimental variables are time-dependent, from allelochemical structures to concentrations. Allelochemicals should be released


dx.doi.org/10.1021/jf503840d | J. Agric. Food Chem. 2014, 62, 9450−9457

to the environment and, as a consequence, data on their concentrations within the donor plant are not sufficient to characterize the process. Additionally, degradation products could be more active than the released compound and allelochemicals should also be incorporated into the target plant. This dynamic situation cannot be elucidated by simply recording macroscopic growth effects and analysis of the target plant is also required.

The experimental design described here eliminates the need to consider the soil system as a variable. However, with a view to the possible application of this approach in a field situation, one should consider the role of sorption in the soil and the resulting modification of the bioavailability of components in complex allelochemical mixtures.[39] Consideration of the experimental results in a field community and at the ecosystem level is crucial in understanding the ecological role of allelochemicals in plant interference.[40]

## ■ ASSOCIATED CONTENT

### Supporting Information

Chromatographic data of the studies. This material is available free of charge via the Internet at http://pubs.acs.org.

## ■ AUTHOR INFORMATION


### Corresponding Author

*Phone: +34 956.012.770; fax: +34 956.016.193; e-mail: famacias@uca.es.



### Funding

This research was supported by the Ministerio de Economía y competitividad (MINECO) (Project AGL2013-42238-R) and Consejería de Economía Innovación y Ciencia, Junta de Andalucía (Project AGR-5822-2011).


### Notes

The authors declare no competing financial interest.

## ■ REFERENCES


(1) Macias, F. A.; Molinillo, J. M. G.; Varela, R. M.; Galindo, J. C. G. Allelopathy—A natural alternative for weed control. *Pest Manage. Sci.* **2007**, *63*, 327−348.

(2) Sinkkonen, A. Ecological Relationships and Allelopathy. In *Allelopathy: A Physiological Process with Ecological Implications*; Reigosa, M. J., Pedrol, N., González, L., Eds.; Springer: Heidelberg, 2006; pp 373−393.

(3) Bertin, C.; Weston, L. A.; Huang, T.; Jander, G.; Owens, T.; Meinwald, J.; Schroeder, F. C. Grass roots chemistry: meta-tyrosine, an herbicidal nonprotein amino acid. *Proc. Natl. Acad. Sci. U.S.A.* **2007**, *104*, 16964−16969.

(4) Wilson, D. S. Biological communitties as funtionally organized units. *Ecology* **1997**, *78*, 2018−2024.

(5) Reigosa, M. J.; Sanchez-Moreiras, A.; Gonzalez, L. Ecophysiological approach in allelopathy. *Crit. Rev. Plant Sci.* **1999**, *18*, 577−608.

(6) Macías, F. A.; Marin, D.; Oliveros-Bastidas, A.; Simonet, A. M.; Molinillo, J. M. G., Ecological Relevance of the Degradation Processes of Allelochemicals. In *Allelopathy: New Concepts & Methodology*; Fujii, Y., Hiradate, S., Eds.; Science Publishers Inc.: Enfield, 2007; pp 91−107.

(7) Macias, F. A.; Oliveros-Bastidas, A.; Marin, D.; Castellano, D.; Simonet, A. M.; Molinillo, J. M. G. Degradation studies on benzoxazinoids. Soil degradation dynamics of 2,4-dihydroxy-7-methoxy-(2h)-1,4-benzoxazin-3(4h)-one (DIMBOA) and its degradation products, phytotoxic allelochemicals from gramineae. *J. Agric. Food Chem.* **2004**, *52*, 6402−6413.

(8) Williamson, G. B.; Obee, E. M.; Weidenhamer, J. D. Inhibition of *Schizachyrium scoparium* (Poaceae) by the allelochemical hydrocinnamic acid. *J. Chem. Ecol.* **1992**, *18*, 2095−2105.

(9) Macias, F. A.; Marin, D.; Oliveros-Bastidas, A.; Molinillo, J. M. G. Rediscovering the bioactivity and ecological role of 1,4-benzoxazinones. *Nat. Prod. Rep.* **2009**, *26*, 478−489.

(10) Oliveros-Bastidas, A. d. J.; Macias, F. A.; Marin, D.; Carrera-Fernandez, C. A.; Molinillo, J. M. G. Decomposition of 2,4-dihydroxy-2H-1,4-benzoxazin-3(4H)-one (DIBOA), an allelochemical of grasses. Consequences for measurements of biological activity. *Quim. Bras.* **2009**, *3*, 53−60.

(11) Macias, F. A.; Oliveros-Bastidas, A.; Marin, D.; Castellano, D.; Simonet, A. M.; Molinillo, J. M. G. Degradation studies on benzoxazinoids. Soil degradation dynamics of (2*R*)-2-O-*β*-D-glucopyranosyl-4-hydroxy-(2*H*)- 1,4-benzoxazin-3(4*H*)-one (DIBOA-Glc) and its degradation products, phytotoxic allelochemicals from Gramineae. *J. Agric. Food Chem.* **2005**, *53*, 554−561.

(12) Adhikari, K. B.; Laursen, B. B.; Gregersen, P. L.; Schnoor, H. J.; Witten, M.; Poulsen, L. K.; Jensen, B. M.; Fomsgaard, I. S. Absorption and metabolic fate of bioactive dietary benzoxazinoids in humans. *Mol. Nutr. Food Res.* **2013**, *57*, 1847−1858.

(13) Adhikari, K. B.; Laursen, B. B.; Lærke, H. N.; Fomsgaard, I. S. Bioactive benzoxazinoids in rye bread are absorbed and metabolized in pigs. *J. Agric. Food Chem.* **2012**, *60*, 2497−2506.

(14) Burgos, N. R.; Talbert, R. E.; Kim, K. S.; Kuk, Y. I. Growth inhibition and root ultrastructure of cucumber seedlings exposed to allelochemicals from rye (*Secale cereale*). *J. Chem. Ecol.* **2004**, *30*, 671−689.

(15) Hussain, M. I.; Reigosa, M. J. Allelochemical stress inhibits growth, leaf water relations, PSII photochemistry, non-photochemical fluorescence quenching, and heat energy dissipation in three C3 perennial species. *J. Exp. Bot.* **2011**, *62*, 4533−4545.

(16) Kato-Noguchi, H. Effects of four benzoxazinoids on gibberellin-induced *α*-amylase activity in barley seeds. *J. Plant Physiol.* **2008**, *165*, 1889−1894.

(17) Woodward, M. D.; Corcuera, L. J.; Helgeson, J. P.; Upper, C. D. Decomposition of 2,4-dihydroxy-7-methoxy-(2*H*)-1,4-benzoxazin-3(4*H*)-one in aqueous solutions. *Plant Physiol.* **1978**, *61*, 796−802.

(18) Fomsgaard, I. S.; Mortensen, A. G.; Carlsen, S. C. K. Microbial transformation products of benzoxazolinone and benzoxazinone allelochemicals: A review. *Chemosphere* **2004**, *54*, 1025−1038.

(19) Gagliardo, R. W.; Chilton, W. S. Soil transformation of 2(3*H*)-benzoxazolone of rye into phytotoxic 2-amino-3*H*-phenoxazin-3-one. *J. Chem. Ecol.* **1992**, *18*, 1683−1691.

(20) Kumar, P.; Gagliardo, R.; Chilton, W. Soil transformation of wheat and corn metabolites MBOA and $DIM_2BOA$ into aminophenoxazinones. *J. Chem. Ecol.* **1993**, *19*, 2453−2461.

(21) Honkanen, E.; Virtanen, A. I. Synthesis of some 1,4-benzoxazine derivatives and their antimicrobial activity. *Acta Chem. Scand.* **1960**, *14*, 1214−1217.

(22) Escobar, C.; Sicker, D.; Niemeyer, H. Evaluation of dimboa analogs as antifeedants and antibiotics towards the aphid *Sitobion avenae* in artificial diets. *J. Chem. Ecol.* **1999**, *25*, 1543−1554.

(23) Schulz, M.; Friebe, A.; Kueck, P.; Seipel, M.; Schnabl, H. Allelopathic effects of living quack grass (*Agropyron repens* L.). Identification of inhibitory allelochemicals exuded from rhizome borne roots. *Angew. Bot.* **1994**, *68*, 195−200.

(24) Wolf, R. B.; Spencer, G. F.; Plattner, R. D. Benzoxazolinone, 2,4-dihydroxy-1,4-benzoxazin-3-one, and its glucoside from *Acanthus mollis* seeds inhibit velvetleaf germination and growth. *J. Nat. Prod.* **1985**, *48*, 59−63.

(25) Bravo, H. R.; Lazo, W. Antialgal and antifungal activity of natural hydroxamic acids and related compounds. *J. Agric. Food Chem.* **1996**, *44*, 1569−1571.

(26) Sahi, S. V.; Chilton, M. D.; Chilton, W. S. Corn metabolites affect growth and virulence of *Agrobacterium tumefaciens*. *Proc. Natl. Acad. Sci. U.S.A.* **1990**, *87*, 3879−3883.

(27) Macias, F. A.; Marin, D.; Oliveros-Bastidas, A.; Castellano, D.; Simonet, A. M.; Molinillo, J. M. G. Structure-activity relationships (SAR) studies of benzoxazinones, their degradation products and analogues. phytotoxicity on standard target species (STS). *J. Agric. Food Chem.* **2005**, *53*, 538−548.

(28) Eljarrat, E.; Guillamon, M.; Seuma, J.; Mogensen, B. B.; Fomsgaard, I. S.; Olivero-Bastidas, A.; Macias, F. A.; Stochmal, A.; Oleszek, W.; Shakaliene, O.; Barcelo, D. First European interlaboratory study of the analysis of benzoxazinone derivatives in plants by liquid chromatography. *J. Chromatogr. A* **2004**, *1047*, 69−76.
(29) Macias, F. A.; Marin, D.; Oliveros-Bastidas, A.; Chinchilla, D.; Simonet, A. M.; Molinillo, J. M. G. Isolation and synthesis of allelochemicals from gramineae: benzoxazinones and related compounds. *J. Agric. Food Chem.* **2006**, *54*, 991−1000.
(30) Schulz, M.; Marocco, A.; Tabaglio, V.; Macias, F. A.; Molinillo, J. M. G. Benzoxazinoids in rye allelopathy—From discovery to application in sustainable weed control and organic farming. *J. Chem. Ecol.* **2013**, *39*, 154−174.
(31) Mathiassen, S. K.; Kudsk, P.; Mogensen, B. B. Herbicidal effects of soil-incorporated wheat. *J. Agric. Food Chem.* **2006**, *54*, 1058−1063.
(32) Olivero-Bastidas, A. *Allelopathic studies from Gramineae. Benzoxazinones as allelochemicals*. PhD dissertation, University of Cádiz, Spain, 2006.
(33) Wu, H.; Haig, T.; Pratley, J.; Lemerle, D.; An, M. Allelochemicals in wheat (*Triticum aestivum* L.): production and exudation of 2,4-dihydroxy-7-methoxy-1,4-benzoxazin-3-one. *J. Chem. Ecol.* **2001**, *27*, 1691−1700.
(34) Macias, F. A.; Chinchilla, N.; Varela, R. M.; Oliveros-Bastidas, A.; Marin, D.; Molinillo, J. M. G. Structure-activity relationship studies of benzoxazinones and related compounds. Phytotoxicity on *Echinochloa crus-galli* (L.) P. Beauv. *J. Agric. Food Chem.* **2005**, *53*, 4373−4380.
(35) Bais, H. P.; Walker, T. S.; Stermitz, F. R.; Hufbauer, R. A.; Vivanco, J. M. Enantiomeric-dependent phytotoxic and antimicrobial activity of (±)-catechin. A rhizosecreted racemic mixture from spotted knapweed. *Plant Physiol.* **2002**, *128*, 1173−1179.
(36) Kobayashi, K. Factors affecting phytotoxic activity of allelochemicals in soil. *Weed Biol. Manage.* **2004**, *4*, 1−7.
(37) An, M.; Liu, D. L.; Johnson, I. R.; Lovett, J. V. Mathematical modelling of allelopathy: II. The dynamics of allelochemicals from living plants in the environment. *Ecol. Model.* **2003**, *161*, 53−66.
(38) Tharayil, N.; Bhowmik, P. C.; Xing, B. Bioavailability of allelochemicals as affected by companion compounds in soil matrices. *J. Agric. Food Chem.* **2008**, *56*, 3706−3713.
(39) Tharayil, N.; Bhowmik, P. C.; Xing, B. Preferential sorption of phenolic phytotoxins to soil: implications for altering the availability of allelochemicals. *J. Agric. Food Chem.* **2006**, *54*, 3033−3040.
(40) Inderjit; Callaway, R. M. Experimental designs for the study of allelopathy. *Plant Soil* **2003**, *256*, 1−11.

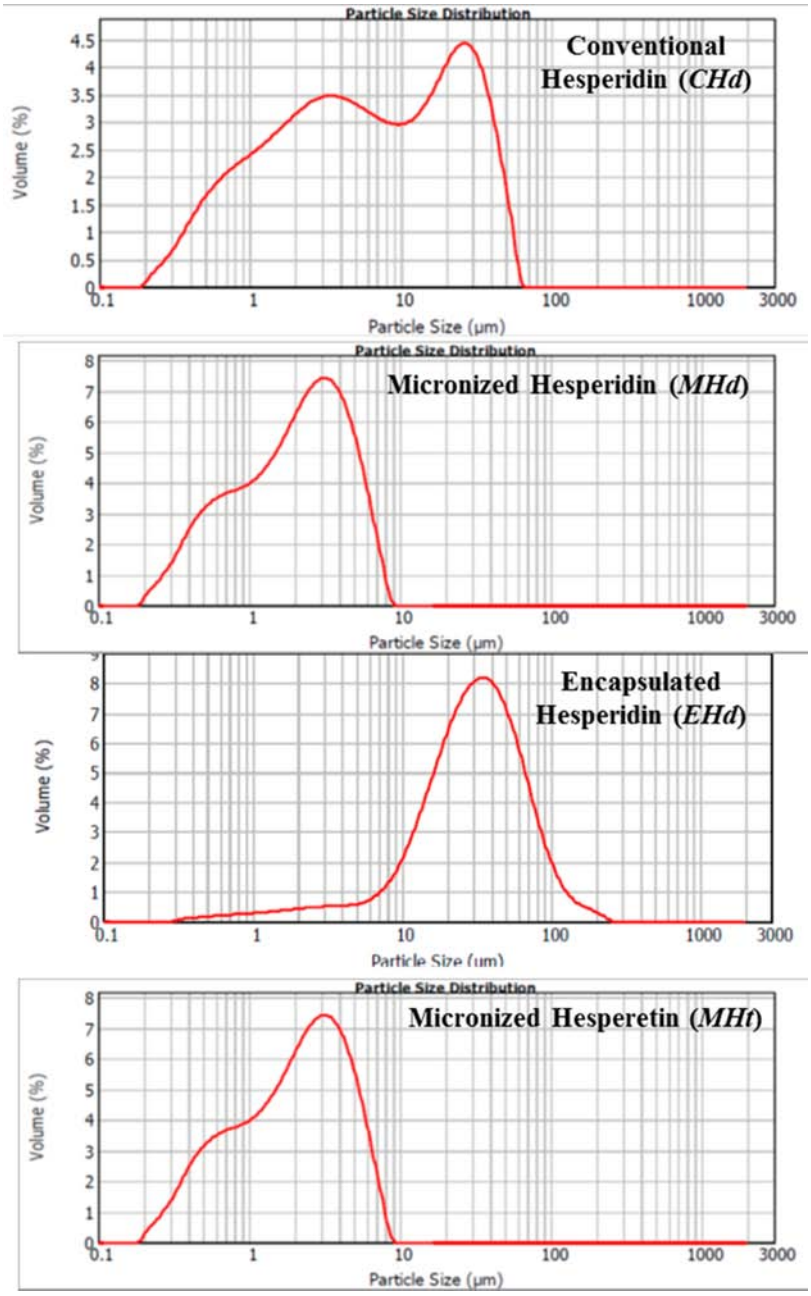


**Figure 1.** Representative particle size distribution of the four treatments after encapsulation and micronization processes.

Arabic as solubilizing agent. It has a $d(0.9)$ particle size of 74.2 $\mu$m. Conventional hesperidin (CHd), the standard hesperidin that has not been subjected to treatments to enhance its solubility, served as a control. It has a $d(0.9)$ particle size of 32.8 $\mu$m. Micronized hesperidin (MHd) is conventional hesperidin that has been micronized to a $d(0.9)$ particle size of 5.1 $\mu$m. Micronized hesperetin (MHt) is the aglycone that has been micronized to a $d(0.9)$ particle size of 5.1 $\mu$m.

**Sampling Procedure. Quantitative Analysis of Flavanones in the Beverages.** Flavanone formulations were UHPLC analyzed on a 1260-DAD single-quadrupole (Agilent 6100 series). Ten milligrams of each sample was weighed and dissolved in 1 mL of water. Samples were vortexed for 5 min and centrifuged using an Eppendorf centrifuge at 10000 rpm (Eppendorf 5804R, Hamburg, Germany). The supernatant was filtered through a 0.45 $\mu$M PVDF Millex filter (Millipore, Tokyo, Japan) and directly analyzed. The pellet was dissolved in 2 mL of dimethyl sulfoxide/methanol (50:50) by vortexing and then filtered through a 0.45 $\mu$M Nylon Millex filter (Millipore, Tokyo, Japan). One hundred microliters of dissolved pellet were diluted with 1900 $\mu$L of methanol and finally HPLC analyzed.

A Poroshell 120 C18 column (100 × 3.0 mm i.d., 2.7 $\mu$m) from Agilent (Palo Alto, CA, USA) was used at room temperature, and the injected volume was 5 $\mu$L. Gradient elution was carried out using water/formic acid (99:1, v/v) and acetonitrile at a constant flow rate of 0.5 mL/min. The gradient started with the following proportions (v/v) of acetonitrile [$t$ (min), % acetonitrile]: 0, 1; 10, 40; 12, 90; and 15, 1. Quantification was achieved using an external standard of hesperidin, and it was performed using UV detection set at 290 nm.

**Design of the Human Intervention Study.** This was a crossover study with 18 healthy volunteers (10 males and 8 females) between 25 and 50 years old. Volunteers were healthy, nonsmokers, non-vegetarians, without a history of gastrointestinal disease, and apparently without any hematological alterations, cardiovascular disease, or chronic diseases and had not been following body-weight-loss diets. Before the intervention study begun, the participants were informed of the background, objectives, methodology,


dx.doi.org/10.1021/jf502933v | J. Agric. Food Chem. 2014, 62, 9458−9462

**Table 1. Conventional Hesperidin (CHd), Micronized Hesperidin (MHd), Encapsulated Hesperidin (EHd), and Micronized Hesperetin (MHt) Excretion after the Intake of Encapsulated and Micronized Flavanone Beverages and Stratification of Volunteers by Their Excretion Capabilities (High, Medium, and Low Excretors)**

| hesperetin content | | treatments | | | |
|---|---|---|---|---|---|
| | | CHd | MHd | EHd | MHt |
| ingested dose (mg) in 200 mL of juice | | 89.1 | 89.1 | 89.1 | 89.1 |
| all excretors[a] | excreted equivalents (mg) | 2.0 (±0.3)B | 4.3 (±0.8)A | 4.8 (±0.7)A | 5.2 (±0.6)A |
| | total excreted equivalents 24 h (%) | 2.2 (±0.3)B | 4.8 (±0.9)A | 5.4 (±0.8)A | 5.9 (±0.7)A |
| high excretors[b] | excreted equivalents (mg) | 3.6 (±0.5)Ba | 9.1 (±2.3)Aa | 9.3 (±0.7)Aa | 7.4 (±1.0)Aa |
| | total excreted equivalents 24 h (%) | 4.0 (±0.6)Ba | 10.2 (±2.6)Aa | 10.4 (±0.8)Aa | 8.3 (±1.1)Aa |
| medium excretors[c] | excreted equivalents (mg) | 2.2 (±0.2)Bb | 5.5 (±0.4)Ab | 5.5 (±0.3)Ab | 4.8 (±1.0)Ab |
| | total excreted equivalents 24 h (%) | 2.4 (±0.2)Bb | 6.2 (±0.5)Ab | 6.2 (±0.4)Ab | 5.4 (±1.1)Ab |
| low excretors[d] | excreted equivalents (mg) | 1.2 (±0.2)Cc | 1.6 (±0.3)Cc | 2.7 (±0.2)Bc | 4.3 (±0.6)Ac |
| | total excreted equivalents 24 h (%) | 1.4 (±0.2)Cc | 1.8 (±0.4)Cc | 3.0 (±0.3)Bc | 4.8 (±0.7)Ab |

[a]Mean values ($n$ = 18) ± standard errors. Means followed by the same capital letter within a row are not significantly different according to Duncan's test ($p < 0.05$). Means followed by the same lower case letter within a column are not significantly different according to Duncan's test ($p < 0.05$). [b]$n$ = 4. [c]$n$ = 7. [d]$n$ = 7.

advantages, and risks of the experiment, as well as the benefits and results that were expected to come out of the study. Participants were required to sign informed consent to be enrolled in the study. The volunteers avoided any intake of both citrus- and tomato-derived foods prior to and during the experiment, starting 7 days before the first day and including the wash-out periods between the intakes. In the same way they had restricted the consumption of fruits and plant-derived food products such as chocolate, tea, beer, wine, and fruit juices. The intake of these products was forbidden starting the day before every assay. Meals were not strictly controlled, but during the whole study, the volunteers wrote down in a notebook any food intake. Thus, breakfast, lunch, and dinner were checked. In addition, the protocol of the study was approved by the UCAM (Universidad Católica S. Antonio de Murcia) Ethics Committee before the start of the study.

The ingested flavanone dose was calculated as hesperetin equivalents for all of the flavanone beverages assayed in order to supply similar amounts as those given with the intake of 200 mL of fresh orange juice. A hesperetin equivalent of 90 mg added to 200 mL of a colored and non-flavanone-containing beverage was ingested on the same day of the week and at the same time over the 4 weeks of the study (Table 1).

As has been widely described in the literature, the interindividual variation observed was high, and therefore the percentages of excretion among volunteers were rather different. Therefore, volunteers were stratified into three categories, high (flavanone excretion values >10% of the ingested flavanones), medium (excretion values between 5 and 10%), and low excretors (excretion values <5%).[6] The percentage of flavanone excretion in individual volunteers is usually very stable, and therefore their respective classifications as high, medium, or low excretors are regularly maintained.[6]

**Sampling Procedure of Urine Samples. Analysis of Flavanone Metabolites by UPLC-QqQ.** Urine samples were processed following a previously developed protocol.[6] Optimization of both mass spectometer parameters and metabolite calibration curves has been previously reported.[6] Flavanone glucuronides and sulfates were previously synthesized by Villapharma (Murcia, Spain), and quantification in urine samples was completed using an UPLC-QqQ method.[6]

The limit of detection (LOD) was determined as the concentration of analytes with a signal-to-noise ratio of at least 3, and the limit of quantification (LOQ) was the lowest standard with a signal-to-noise ratio of at least 10. LOQs were 80 nM for hesperetin, 50 and 80 nM for hesperetin 7- and 3′-glucuronides, respectively, and finally 40 and 50 nM for hesperetin 7- and 3′-sulfates, respectively. LODs were 30 nM for hesperetin, 20 and 30 nM for hesperetin 7- and 3′-glucuronides respectively, and finally 15 and 20 nM for hesperetin 7- and 3′-sulfates, respectively.

The intraday repeatability of the UPLC-QqQ method was assessed from 10 consecutive chromatographic runs using a standard solution with 2.5 $\mu$M of every standard in MeOH/0.1% (v/v) formic acid. The interday repeatability of the method was assessed by analyzing the same standard solution for two consecutive days. The relative standard deviation (RSD) for peak area was in the range of 0.5−4.7% in the intraday test and 1.3−3.5% in the case of the interday test.

**Statistical Analysis.** Analysis of variance (ANOVA) was carried out, and means were separated by Duncan's test ($p < 0.05$%).

## RESULTS

**Assessment of the Effect of Encapsulation and Micronization on Flavanone Absorption.** The analysis of the urine samples after the intake of hesperidin beverages shows that, as a general rule, among the different hesperetin phase II metabolites found, either hesperetin 7-sulfate or hesperetin 7-glucuronide was the most abundant (depending on each individual). Their isomers in the 3′-position, however, were found in smaller concentrations (between 2 and 5 times). Hesperetin sulfoglucuronide was also present in smaller amounts, and hesperetin diglucuronide was a minor metabolite. These results are consistent with those found in studies of flavanone pharmacokinetics after orange juice intake.[12,13]

Hesperidin encapsulation (EHd) and micronization (MHd) led to a significant impact on hesperetin bioavailability because it was clearly increased, between 2 and 3 times, compared with that of conventional hesperidin (CHd) (Figure 2). This increase was also observed when the equivalent dose of micronized hesperetin (MHt) was supplied. However, no clear differences were observed between the three different treatments (encapsulation, micronization, and hydrolysis to render hesperetin) (Table 1; Figure 2). The total excretion percentage expressed as hesperetin equivalents ranged between 2.2 and 5.9% for CHd and MHt, respectively (Table 1).

The percentage of hesperetin equivalents excreted after the intake of encapsulated hesperidin (EHd) (5.4%) was 11% higher than the excretion value recently reported after the intake of an ultrahomogenized orange juice with a $d(0.5)$


dx.doi.org/10.1021/jf502933v | J. Agric. Food Chem. 2014, 62, 9458−9462

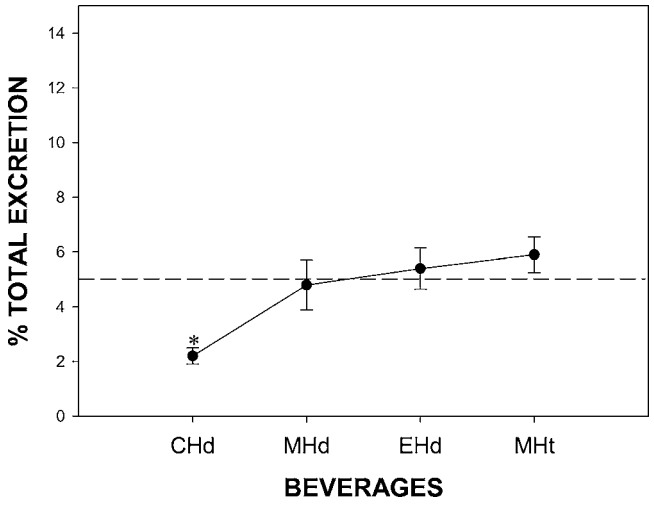


**Figure 2.** Urinary excretion of hesperetin after the intake of encapsulated and micronized hesperdin beverages in all volunteers ($n$ = 18): conventional hesperidin (CHd), micronized hesperidin (MHd), encapsulated hesperidin (EHd), and micronized hesperetin (MHt). Error bars are standard errors. Values are percentage of the total hesperetin intake excreted in urine. (*) $p < 0.05$ significantly different according to Duncan's test.

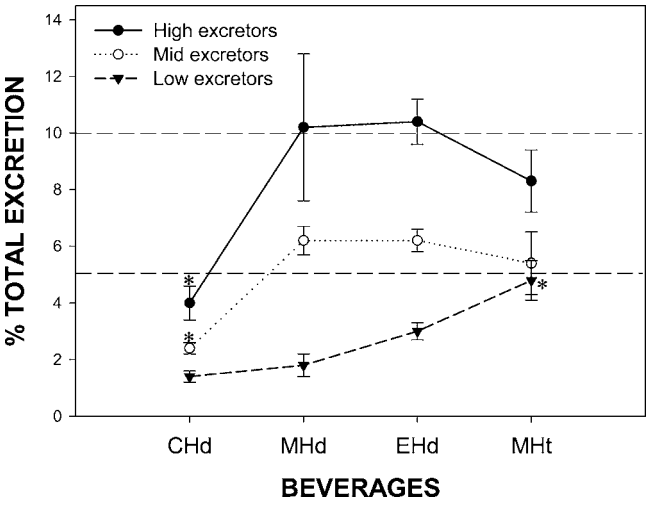


**Figure 3.** Urinary excretion of hesperetin after the intake of encapsulated and micronized hesperidin beverages in volunteers stratified as high ($n$ = 4), medium ($n$ = 7), and low ($n$ = 7) excretors: conventional hesperidin (CHd), micronized hesperidin (MHd), encapsulated hesperidin (EHd), and micronized hesperetin (MHt). Error bars are standard errors. Values are percentage of the total hesperetin intake excreted in urine. (*) $p < 0.05$ significantly different according to Duncan's test.

particle size of 61.6 $\mu$m for the same volunteers used in this study.[6]

However, in absolute terms the micronized aglycone (MHt) was the most bioavailable flavanone, reaching therefore the highest excretion values, deserving a particular comment. Its absorption at the small intestine level explains the marked increment of urinary excretion in volunteers with low excretion capabilities, because the rhamnosidases from gut microbiota are no longer determinant factors for absorption. Furthermore, among the 18 volunteers, there were 14 medium and low excretors in which the supply of the micronized aglycone (MHt) improved the final excretion value of hesperetin compared with that observed after the intake of micronized hesperidin (MHd).

**Stratification of Volunteers.** When volunteers were stratified into high, medium, and low excretors, the results showed additional evidence from that observed when all volunteers were considered together (Table 1; Figure 3). Thus, with a focus on high excretors (subjects with the appropriate microbiota to hydrolyze efficiently hesperidin to hesperetin),[14] percentages of excretion of both encapsulated (EHd) and micronized (MHd) hesperidin were clearly increased, reaching values above 10% of the total hesperetin equivalents intake due to the efficient metabolic activity of colon gut microbiota rhamnosidase activity. However, the micronized aglycone (MHt) reached a lower excretion in high excretors, although with no significant differences with hesperidin (Table 1; Figure 3). Different polymorphisms in intestinal transporters could also be involved in the absorption of flavanones and might explain the significantly higher excretion percentage reached by high excretors with respect to medium and low excretors after supply of the micronized hesperetin (MHt) beverage (Figure 3).

In the case of medium excretors, encapsulated (EHd) and micronized (MHd) hesperidin reached similar hesperetin excretion values, and those were slightly higher than those observed after the intake of the micronized aglycone (MHt) (Table 1). This higher bioavailability of micronized hesperidin than of micronized hesperetin could be explained by the higher solubility of hesperidin versus hesperetin in the gut environment (from 3.5- to 7-fold higher for hesperidin) as previously reported.[15,16]

Opposite to high and medium excretors, the bioavailability of micronized hesperetin (MHt) in low excretors was significantly higher (38 and 63%) than that of encapsulated hesperidin (EHd) and micronized hesperidin (MHd), respectively (Table 1). This clearly shows that low excretors do not have the proper gut microbiota to hydrolyze rutinosides (the appropriate rhamnosidases), and therefore a significant increase in bioavailability is observed when hesperetin is ingested.

As a summary, high excretors showed an efficient biovailability of orange flavanones as they harbor gut microbiota with rhamnosidase activity, as well as proper absorption and phase II metabolism as revealed by the highest excretion values even after the intake of conventional (nontreated) orange flavanone beverages. Thus, although conventional hesperidin was the less bioavailable form, high excretors were able to maximize conventional hesperidin metabolism and absorption with values up to 40 and 65% higher than those observed in medium and low excretors, respectively (Table 1).

No gender differences were observed in this study, in agreement with previous trials on flavanone excretion after orange beverages intake.[6]

To increase flavanone biovailability in low excretors, two strategies can be envisaged: (i) to fortify orange juice with micronized hesperetin or (ii) to encapsulate hesperidin, which enhanced flavanone excretion up to 3% of the intake, which is a value similar to that observed after the intake of fresh orange juice by the same volunteers in a previous study.[6]

## AUTHOR INFORMATION

### Corresponding Author

*(F.A.T.-B.) E-mail: fatomas@cebas.csic.es. Phone: +34-968396334. Fax: +34-968396213.

## Notes

The authors declare no competing financial interest.

## REFERENCES


(1) Rizza, S.; Muniyappa, R.; Iantorno, M.; Kim, J.; Chen, H.; Pullikotil, P.; Senese, N.; Tesauro, M.; Lauro, D.; Cardillo, C.; Quon, M. J. Citrus polyphenol hesperidin stimulates production of nitric oxide in endothelial cells while improving endothelial function and reducing inflammatory markers in patients with metabolic syndrome. *J. Clin. Endocrinol. Metab.* **2011**, *96*, E782−E792.

(2) Milenkovic, D.; Deval, C.; Dubray, C.; Mazur, A.; Morand, C. Hesperidin displays relevant role in the nutrigenomic effect of orange juice on blood leukocytes in human volunteers: a randomized controlled cross-over study. *PLoS One* **2011**, *6* (11), e26669.

(3) Morand, C.; Dubray, C.; Milenkovic, D.; Lioger, D.; Martin, J. F.; Scalbert, A.; Mazur, A. Hesperidin contributes to the vascular protective effects of orange juice: a randomized crossover study in healthy volunteers. *Am. J. Clin. Nutr.* **2011**, *93*, 73−80.

(4) Chanet, A.; Milenkovic, D.; Deval, C.; et al. Naringin, the major grapefruit flavonoid, specifically affects atherosclerosis development in diet-induced hypercholesterolemia in mice. *J. Nutr. Biochem.* **2012**, *23*, 469−477.

(5) Chanet, A.; Milenkovic, D.; Manach, C.; Mazur, A.; Morand, C. Citrus flavanones: what is their role in cardiovascular protection? *J. Agric. Food Chem.* **2012**, *60*, 8809−8822.

(6) Tomás-Navarro, M.; Vallejo, F.; Sentandreu, E.; Navarro, J. L.; Tomás-Barberán, F. A. Volunteer stratification is more relevant than technological treatment in orange juice bioavailability. *J. Agric. Food Chem.* **2014**, *62*, 24−27.

(7) Ma, Q.; Sun, H.; Che, E.; Zheng, X.; Jiang, T.; Sun, C.; Wang, S. Uniform nano-sized valsartan for dissolution and bioavailability enhancement: influence of particle size and crystalline state. *Int. J. Pharm.* **2013**, *441*, 75−81.

(8) Da Silva, F.; Rodrigues da Fonseca, C.; Matias de Alencar, S.; Thomazini, M.; Balieiro, J. C.; Pittia, P.; Favaro-Trindade, C. S. Assessment of production efficiency, physicochemical properties and storage stability of spray-dried propolis, a natural food additive, using gum Arabic and OSA starch-based carrier systems. *Food Bioprod. Process.* **2013**, *91*, 28−36.

(9) Tommasini, S.; Calabró, M. L.; Stancanelli, R.; Donato, P.; Costa, C.; Catania, S.; Villari, V.; Ficarra, P.; Ficarra, R. The inclusion complexes of hesperetin and its 7-rhamnoglucoside with (2-hydroxypropyl)-$\beta$-cyclodextrin. *J. Pharm. Biomed. Anal.* **2005**, *39*, 572−580.

(10) Yen, F.; Wu, T.; Lin, L.; Cham, T.; Lin, C. Naringenin-loaded nanoparticles improve the physicochemical properties and the hepatoprotective effects of naringenin in orally-administered rats with $CCl_4$-induced acute liver failure. *Pharm. Res.* **2009**, *26*, 893−901.

(11) Uchiyama, H.; Tozuka, Y.; Imono, M.; Takeuchi, H. Improvement of dissolution and absorption properties of poorly water-soluble drug by preparing spray-dried powders with $\alpha$-glucosyl hesperidin. *Int. J. Pharm.* **2010**, *392*, 101−106.

(12) Mullen, W.; Archeveque, M. A.; Edwards, C. A.; Matsumoto, H.; Crozier, A. Bioavailability and metabolism of orange juice flavanones in humans: impact of a full-fat yogurt. *J. Agric. Food Chem.* **2008**, *56*, 11157−11164.

(13) Vallejo, F.; Larrosa, M.; Escudero, E.; Zafrilla, M. P.; Cerdá, B.; Boza, J.; García-Conesa, M. T.; Espin, J. C.; Tomás-Barberán, F. A. Concentration and solubility of flavanones in orange b everages affect their bioavailability in humans. *J. Agric. Food Chem.* **2010**, *58*, 6516−6524.

(14) Tomás-Barberán, F. A.; Mine, Y. A key to understanding the effects of food bioactives in health. Gut microbiota. *J. Agric. Food Chem.* **2013**, *61*, 9755−9757.

(15) Liu, L.; Chen, J. Solubility of hesperetin in various solvents from (288.2 to 323.2) K. *J. Chem. Eng. Data* **2008**, *53*, 1649−1650.

(16) Mauludin, R.; Müller, R. H. Physicochemical properties of hesperidin nanocrystal. *Int. J. Pharm. Pharm. Sci.* **2013**, *5*, 954−960.

stirred with water (1000 mL) and then centrifuged (6000 rpm) for 10 min to remove the sediment. The supernatant was then lyophilized (at −80 °C for 12 h) to obtain the MWEs and stored at −20 °C.

**High-Performance Liquid Chromatography (HPLC).** Using a Hewlett-Packard Vectra 436/33N system and a diode array detector, the components of the MWEs were determined by HPLC analysis[28] employing a 5 μm RP-18 column (4.6 × 150 mm inner diameter). After filtering through a 0.22 μm filter disk, the MWEs (25 mg/mL) were injected into the column. Two systems of mobile phase (A, 2% acetic acid/water; B, 0.5% acetic acid in water/acetonitrile) were used. The peak purity was confirmed with chromatography at 280 nm and ultraviolet (UV) spectra. The total phenolic compound content was measured according to the Folin−Ciocalteu method. The samples (20 μL/1.6 mL of water) were added in 100 μL of Folin−Ciocalteu reagent (Sigma, St. Louis, MO) and 300 μL of sodium carbonate (20%), then mixed, and incubated at 40 °C for 40 min. Absorption at 725 nm was measured.

**Animals and Diet.** A total of 30 male New Zealand white rabbits weighing 2000−2500 g (Animal Center of Chung Shan Medical University) were used in this study. They were individually housed in metal cages under the standard laboratory conditions (22 ± 2 °C, 55 ± 5% relative humidity, and 12 h light/12 h dark cycle) with free access to food and water. According to a suitable pharmacological dose of MWE for humans in a daily diet, five groups ($n = 6$) of animals were described as follows: group I, standard chow; group II, standard chow with 1% MWEs in the daily diet; group III, high-cholesterol diet (HCD) (containing 95.7% standard Purina chow (Purina Mills, Inc., Gray Summit, MO), 3% lard oil, and 1.3% cholesterol) for 10 weeks; and groups IV and V, HCD with 0.5 and 1.0% MWEs, respectively, in the daily diet. During the experimental period, all of the animals were handled according to the guidelines of the Institutional Animal Care and Use Committee of Chung Shan Medical University. After 10 weeks, the rabbits were sacrificed by exsanguination after deep anesthesia with pentobarbital (30 mg/kg intravenous) via the marginal ear vein. Serum was stored at −80 °C prior to serum lipid analysis and measurement of serum values. The aortic arch and thoracic aortas were carefully removed to protect the endothelial lining, collected, and freed of adhering soft tissue.

**Evaluation of Atherosclerotic Lesions.** Sudan IV is a fat-soluble dye often used for staining triglycerides, lipids, and lipoproteins present in cells and tissues. Aortic arches were rapidly dissected and stained with Sudan IV and then kept at −80 °C or in 10% neutral-buffer formalin. The sections of the aortic arch were stained with hematoxylin and eosin or α-smooth muscle actin antibodies (Santa Cruz Biotechnology, Inc., Dallas, TX) by immunohistochemistry.

**Cell Cultures.** Thea rat A7r5 thoracic aorta smooth muscle cells, obtained from American Type Culture Collection (ATCC, CRL-1444, Manassas, VA), were maintained in Dulbecco's modified Eagle's medium supplemented with 10% fetal bovine serum (FBS), 1% glutamine, 1% penicillin−streptomycin, and 1.5 g/L sodium bicarbonate (all from Gibco/BRL, Gaithersburg, MD) at 37 °C in a humidified atmosphere of 5% $CO_2$. The medium was changed every 2 or 3 days, and the cells were subcultured when confluence was achieved.

**Wound Healing.** The $1 \times 10^6$/mL A7r5 cells were cultured in 6-well plates for 48 h. A line was drawn on the underside of the well with a yellow P200 pipet tip. These lines served as fiducial marks for the wound areas to be analyzed. The non-adhering cells were washed out with phosphate-buffered saline (PBS), and the remaining cells were treated with MWEs (0.05−1.0 mg/mL). Under a 40× lens, images of the linear wounds were taken in nine fields per well at 0, 12, 24, 36, 48, 60, 72, 84, and 96 h. The migrated cells were counted per well, and the counts were averaged.[29]

**MMP Gelatin Zymography.** The levels of MMP-2 and MMP-9 released in the cultured medium were assayed by gelatin zymography as described previously.[30] MWE-treated A7r5 cells were plated onto 6-well culture plates ($5 \times 10^5$/well) and incubated with 1 mL of 0.5% FBS in Dulbecco's modified Eagle's medium for 24 h. The culture medium was prepared with a 5× loading buffer containing 0.01% sodium dodecyl sulfate (SDS) without β-mercaptoenthanol and subjected to electrophoresis with 8% SDS polyacrylamide gels containing 0.1% gelatin. Following electrophoresis, the gels were washed twice with 2.5% Triton X-100 on a gyrating shaker for 30 min at room temperature to remove SDS. The gels were then incubated in 50 mL of reaction buffer (40 mM Tris-HCl, 10 mM $CaCl_2$, and 0.01% $NaN_3$) at 37 °C overnight on a rotary shaker, stained with Coomassie Brilliant Blue R-250, and destained with methanol/acetic acid/water (50:75:87.5, v/v/v). Gelatinolytic activities were detected as horizontal white bands on a blue background.

**Western Blot Analysis.** Analysis of TIMP-2, VEGF, FAK, integrin-$\beta_3$, c-Raf, Src, Ras, PI3K, Akt, Cdc42, RhoA, RhoB, Rac1, p-FAK, IκB, and NF-κB (all from Santa Cruz Biotechnology, Dallas, TX), PI3K (Becton-Dickinson, San Jose, CA), and p-Akt and β-actin (Sigma, St. Louis, MO) was performed using western blot analysis.[31]. After the indicated treatment with MWEs (0−2.0 mg/mL) for 48 h, the cells were lysed and equal amounts of cell lysates (50 μg of protein) were separated by electrophoresis on 8−12% SDS polyacrylamide gels and transferred to nitrocellulose membranes (Millipore, Bedford, MA). The membranes were incubated with Tris-buffered saline containing 1% (w/v) nonfat milk and 0.1% (v/v) Tween-20 for 1 h to block non-specific binding, washed with Tween-20 for 30 min, incubated with the appropriate primary antibody for 2 h, incubated with horseradish-peroxidase-conjugated second antibody (Sigma, St. Louis, MO) for 1 h, developed using enhanced chemiluminescence (ECL, Millipore, Bedford, MA), and analyzed by densitometry using AlphaImager Series 2200 software. The results were representative of at least three independent experiments.

**Immunoprecipitation Assay.** Approximately 0.5 mg of the lysate protein was immunoprecipitated[32] using monoclonal anti-integrin-$\beta_3$ (Santa Cruz Biotechnology, Dallas, TX) antibodies. Immune complexes were harvested with protein-A-conjugated sepharose beads. After centrifugation at 2500 rpm, the eluates were analyzed by immunoblotting against FAK, Src, Ras, and PI3K antibodies.

**Electrophoretic Mobility Shift Assay of NF-κB.** An electrophoretic mobility shift assay[33] was performed using a Lightshift kit from Promega. A total of 10 μg of nuclear protein was mixed with the binding reaction buffer containing 10 mM Tris, 50 mM KCl, 1 mM dithiothreitol (DTT), 5 mM $MgCl_2$, 2 μg poly(dI·dC), and 2 pmol of oligonucleotide probe and incubated for 20 min at room temperature. Specific binding was confirmed using a 200-fold excess of unlabeled probe as a specific competitor. Protein−DNA complexes were separated by 6% non-denaturing acrylamide gel electrophoresis and then transferred to positively charged nylon membranes and cross-linked in a Stratagene cross-linker. Gel shifts were visualized with streptavidin−horseradish peroxidase, followed by chemiluminescent detection.

**Visualization of the F-Actin Cytoskeleton.** A7r5 cells ($5 \times 10^4$ cells/well) were treated with 0.1−1.0 mg/mL MWEs for 48 h, then fixed in 4.6% formaldehyde in PBS for 10 min, and permeabilized in 0.2% Triton X-100/PBS for 5 min. The cells were stained with phalloidin−fluorescein isothiocyanate (FITC, A12379, Invitrogen, Grand Island, NY) to visualize polymerized F-actin microfilaments under a Nikon upright fluorescence microscope (100× objective)[34] (red color). Then, they were extensively washed with PBS, briefly counterstained with 1 mg/mL 4′,6-diamidino-2-phenylindole (DAPI) to visualize the nuclei, and photographed (blue color).

**Reverse Transcription Polymerase Chain Reaction (RT-PCR) Analysis.** Total RNA was isolated from cells using a RNA Isolation Kit (Ultraspec, Biotecx, Houston, TX) according to the instructions of the manufacturer and quantified spectrophotometrically. For reverse transcription, total RNA (4 μg) was used as templates in the raction buffer containing oligo dT primer and 4 units/μL RTase (MMLV) in an Applied Biosystems GeneAmp PCR system 2700 at 42 °C for 60 min and then at 99 °C for 5 min to inactivate the RT. PCR master mix containing 1 mM deoxyguanosine triphosphate, 1 mM deoxyadenosine triphosphate, 1 mM deoxycytidine triphosphate, 1 mM deoxythymidine triphosphate, Dyna PCR buffer II, 2 units/μL AmpliTaq DNA polymerase, and the following primers was added at a 0.5 μM concentration: murine MMP, upstream primer (5′-ACACCCAG-TACTCATTCCCTG-3′) and downstream primer (5′-GTCCTGAC-CAAGGATATAGCC-3′); VEGF, upstream primer (5′-TGCACC-CACGACAGAAGGGGA-3′) and downstream primer (5′-

TCACCGCCTTGGCTTGTCACA-3′); GADPH, upstream primer (5′-ACCACAGTCCATGCCATCAC-3′) and downstream primer (5′-TCCACCACCCTGTTGCTGTA-3′). The complementary DNAs (cDNAs) in the samples were amplified for 30 cycles as follows: 1 min at 94 °C as an initial step, followed by 30 thermal cycles of 60 s at an annealing temperature and 2 min at 72 °C, and finally 20 min at 72 °C. The RT-PCR products were analyzed by agarose gel electrophoresis, and the intensity of the bands corresponding to MMP-2, VEGF, and GADPH were measured using Fujifilm Image Gauge software (version 3.1, Fujifilm Co., Ltd., Tokyo, Japan).[35]

**Statistical Analysis.** Data were shown as the means (standard deviation) of three independent experiments. Statistical comparisons were evaluated by one-way analysis of variance (ANOVA). A $p$ value of less than 0.05 was considered to be statistically significant.

## RESULTS

**Polyphenolic Compounds of MWEs.** The main polyphenolic constituents of MWEs have been identified as gallic acid (0.31%), protocatechuic acid (2.92%), catechin (0.54%), epigallocatechin gallate (2.68%), caffeic acid (1.10%), epicatechin (1.21%), $p$-coumaric acid (0.35%), rutin (3.22%), ferulic acid (0.27%), gossypin (0.26%), hesperetin (0.34%), resveratrol (0.35%), quercetin (0.50%), naringenin (0.52%), and hydroxyflavin (0.58%) (Table 1). The other constituents include protein (1.77%), fat (4.40%), polysaccharide (24.83%), and unknown components without standards (data not shown).

**Table 1**

| HPLC assay | | MWEs (%) | retention time (RT) (min) |
|---|---|---|---|
| polyphenolic compound | gallic acid | 0.31 ± 0.05 | 7.85 |
| | protocatechuic acid | 2.92 ± 0.45 | 15.17 |
| | catechin | 0.54 ± 0.03 | 23.49 |
| | epigallocatechin gallate | 2.68 ± 0.20 | 23.95 |
| | caffeic acid | 1.10 ± 0.24 | 26.08 |
| | epicatechin | 1.21 ± 0.17 | 27.27 |
| | $p$-coumaric acid | 0.35 ± 0.04 | 31.57 |
| | rutin | 3.22 ± 1.01 | 33.44 |
| | ferulic acid | 0.27 ± 0.01 | 34.00 |
| | gossypin | 0.26 ± 0.02 | 41.72 |
| | hesperetin | 0.34 ± 0.10 | 42.85 |
| | resveratrol | 0.35 ± 0.23 | 45.17 |
| | quercetin | 0.50 ± 0.07 | 51.83 |
| | naringenin | 0.52 ± 0.17 | 56.28 |
| | hydroxyflavin | 0.58 ± 0.12 | 57.44 |
| | total | 15.13 ± 0.93 | |

**MWEs Inhibited Proliferation of VSMCs and the Expression of SMA, Ras, and MMP-2 in Neointima.** Histological analysis was performed on a representative atherosclerotic lesion from a HCD-fed rabbit after treatment with 0.5−1% MWEs for 10 weeks. As shown in Figure 1, hematoxylin and eosin staining showed that the MWEs dose-dependently inhibited HCD-fed-induced intimal hyperplasia of vessel walls. After immunohistochemical staining, the expressions of SMA, Ras, and MMP-2 in the VSMCs were also found to be dose-dependently inhibited after MWE treatment.

**MWEs Effectively Inhibited VSMC (A7r5 Cell) Migration.** Monolayers of growth-arrested A7r5 cells treated with or without different concentrations of MWEs (0.1−1.0 mg/mL) were scraped, and the number of cells in the denuded zone (i.e., wound) were analyzed at the indicated times (0−96 h) under light microscopy and Boyden chamber assay. Both panels A and B of Figure 2 show that MWEs could effectively dose-dependently inhibit migration of the VSMCs.

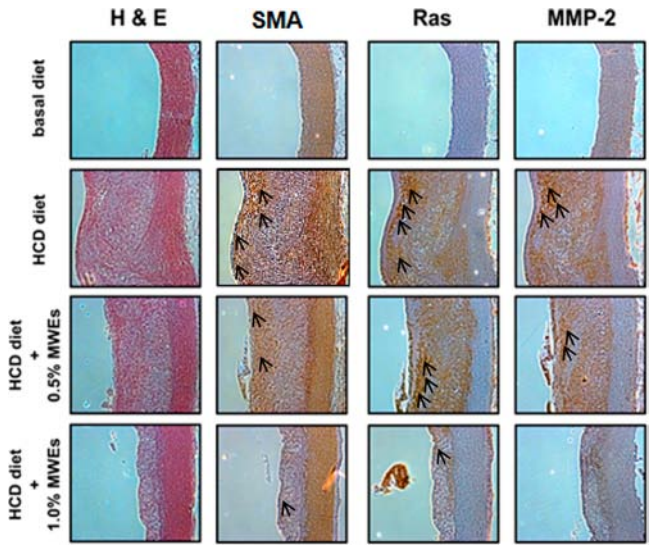


**Figure 1.** Histological analysis of a representative atherosclerotic lesion from HCD-fed rabbits treated for 10 weeks with 0.5 and 1% MWEs. The same group of slices were from the same area of the artery and stained with different antibodies. Primary antibodies were detected with $\alpha$-actin, Ras, and MMP-2. Semi-quantitative computer-assisted image analysis of the atherosclerotic lesion was performed on six randomly selected 400× magnified images of slides from individual animals.

**MWEs Inhibited MMP Activity and VEGF Secretion of the A7r5 Cells.** A7r5 cells were treated with or without MWEs for 0−48 h. The 0.5% FBS starvation medium of the A7r5 cells was changed after treatment with MWEs, and gelatin zymography was then performed to analyze the activities of MMP-9 and MMP-2. Figure 3A shows that more MMP-2 was secreted by the A7r5 cells than MMP-9. After treatment with MWEs, the activities of MMP-2 and MMP-9 decreased time-dependently. In time-dependent assays, A7r5 cells were treated with 1.0 mg/mL MWEs at the indicated times. Cell lysates (50 $\mu$g) were prepared and subjected to western blot analysis. Proteins were detected by TIMP-2 and VEGF antibodies, and albumin and $\beta$-actin were used for equal loading. The activity of TIMP-2 was time-dependently increased after MWE treatment (Figure 3B), and the activity of VEGF was time-dependently decreased (Figure 3C).

**MWEs Inhibited the Activities of FAK and Akt in A7r5 Cells.** Cultured cells were treated with MWEs (0.5−2 mg/mL) for 48 h. A7r5 cells were treated with MWEs (1.0 mg/mL) for 0−48 h, and cell lysates (50 $\mu$g) were prepared and subjected to western blot analysis. Proteins were detected by phospho-FAK, integrin-$\beta_3$, PI3K, Akt, and GSK3$\beta$ antibodies, and $\beta$-actin was used for equal loading. As shown in panels A and B of Figure 4, the activities of FAK-p, PI3K, Akt-p, GSK3$\beta$-p, and c-Raf were dose- and time-dependently decreased by MWE treatment. Total cell lysates were then immunoprecipitated with anti-integrin-$\beta_3$ antibodies, and the precipitated complexes were examined by immunoblotting with anti-FAK, Src, Ras, and PI3K antibodies. MWE treatment dose-dependently decreased the activities of Src, Ras, and PI3K (Figure 4C).

**MWEs Inhibited the Activity of NF-κB in A7r5 Cells.** A7r5 cells were treated with MWEs (0−1.5 mg/mL) for 48 h, and cultured cells were treated with MWEs (1.0 mg/mL) for 0−48 h. Cell lysates (50 $\mu$g) were prepared and subjected to western


dx.doi.org/10.1021/jf502942r | J. Agric. Food Chem. 2014, 62, 9463−9471

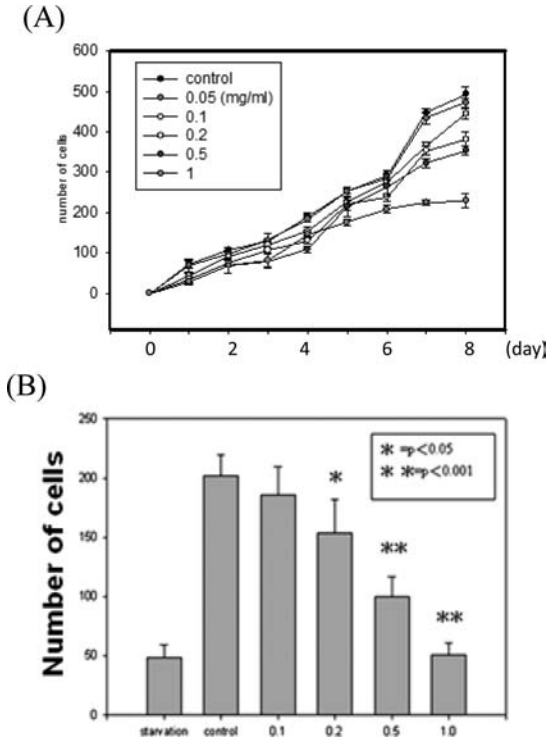


**Figure 2.** Effect of MWEs on the migration of A7r5 cells. Monolayers of growth-arrested A7r5 cells treated with or without different concentrations of MWEs (0.1−1.0 mg/mL) were scraped, and the number of cells in the denuded zone (i.e., wound) was analyzed at the indicated times (0−96 h) under (A) light microscopy and (B) Boyden chamber assay. Quantitative assessment of the mean number of cells at the indicated times in the denuded zone represents the average of three independent experiments ± standard deviation.

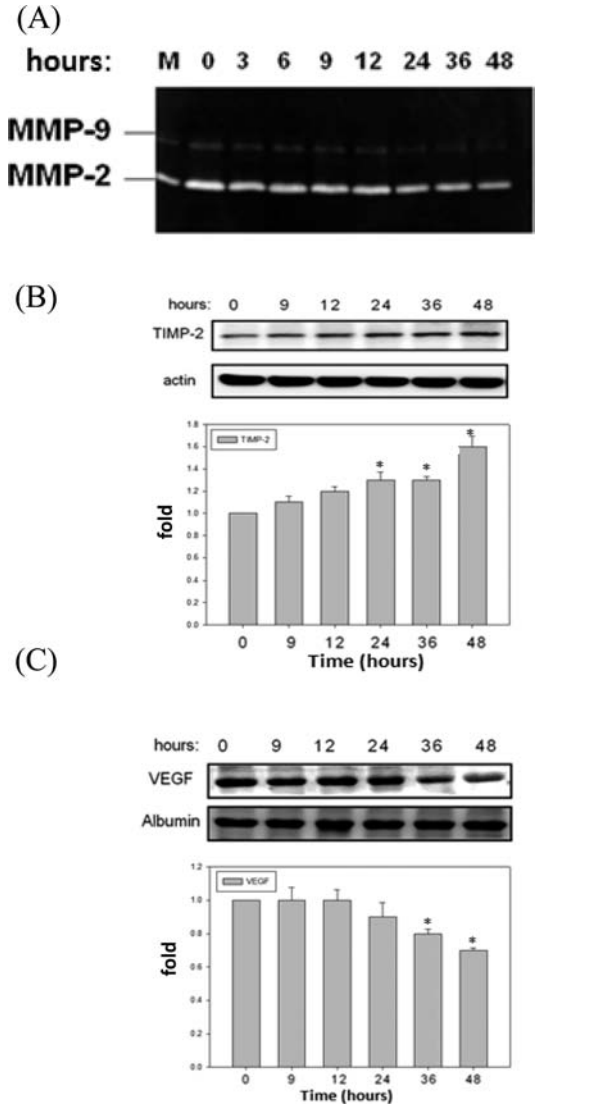


**Figure 3.** Effects of MWEs on MMP activity and VEGF secretion of A7r5 cells. A7r5 cells were treated with or without MWEs for 0−48 h. The 0.5% FBS starvation medium of the A7r5 cells was changed after treatment with MWEs, and (A) gelatin zymography was then performed to analyze the activities of MMP-9 and MMP-2 as described in the Materials and Methods. In time-dependent assays, A7r5 cells were treated with 1.0 mg/mL MWEs at the indicated times. Cell lysates (50 $\mu$g) were prepared and subjected to western blot analysis. Proteins were detected by (B) TIMP-2 and (C) VEGF antibodies. Albumin and $\beta$-actin were used for equal loading. The results from three separate experiments were similar.

blot analysis. As shown in panels A and B of Figure 5, MWE treatment dose- and time-dependently decreased the activity of NF-$\kappa$B and increased the activity of I$\kappa$B. The cell lysates were then immunoprecipitated with anti-NF-$\kappa$B and immunoblotted with anti-I$\kappa$B. $\beta$-actin was used for equal loading. MWE treatment dose-dependently increased the combination of I$\kappa$B and NF-$\kappa$B (Figure 5C). Thereafter, the A7r5 cells were treated with or without MWEs for 12 h, and then nuclear extracts were prepared. C23 was used as a nuclear control. NF-$\kappa$B DNA binding activity was analyzed by an electrophoretic mobility shift assay. MWE treatment dose-dependently inhibited the activity of NF-$\kappa$B in nuclei (Figure 5D). Finally, total RNA was extracted. Expressions of MMP-2 and VEGF mRNA were analyzed by RT-PCR with GAPDH as the loading control. Figure 5E shows that the mRNA expressions of MMP-2 and VEGF were dose-dependently decreased by MWE treatment.

**MWEs Inhibited the Expressions of Small G Proteins and Cytoskeletal F-Actin in A7r5 cells.** A7r5 cells were treated with MWEs (0−2 mg/mL) for 48 h. The A7r5 cells were then treated with MWEs (1.0 mg/mL) for 0−48 h. Cell lysates (50 $\mu$g) were prepared and subjected to western blot analysis. Proteins were detected by specific antibodies (Cdc42, Ras, RhoA, and Rac1), and $\beta$-actin was used for equal loading. As shown in panels A and B of Figure 6, MWE treatment dose- and time-dependently decreased the expressions of Ras, RhoA, cdc42, and Rac-1 and increased the activity of RhoB. Finally, cultured cells were treated with different concentrations of MWEs or without MWEs for 48 h. The cells were fixed and labeled for F-actin with phalloidin−TRITC (red) and for nucleic acid with DAPI (blue). Immunofluorescence microcopy of phalloidin (F-actin)- and DAPI (nuclei)-stained A7r5 cells revealed a marked increase in phalloidin staining in the control group (medium with FBS) compared to the starvation group (medium without FBS) (Figure 6C). After MWE treatment in the control group, the phalloidin staining decreased significantly again and was similar to that of the starvation group. Taken together, these results demonstrate that MWEs are a positive regulator of actin organization.

## DISCUSSION

*Nelumbo nucifera* leaf extracts, which contain a large amount of phenolic acids and flavonoids, including gallic acid, rutin,


dx.doi.org/10.1021/jf502942r | J. Agric. Food Chem. 2014, 62, 9463−9471

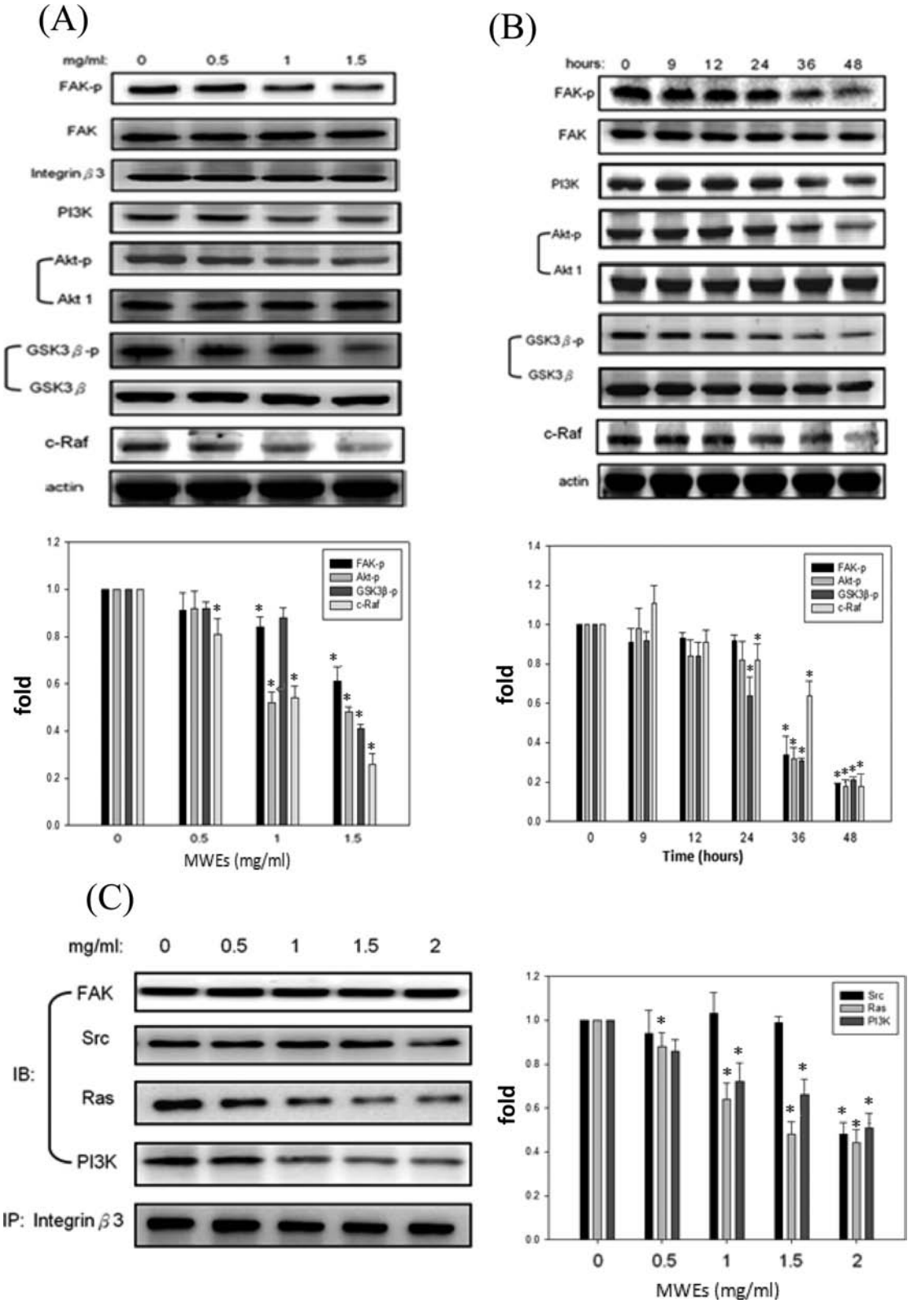


**Figure 4.** Effect of MWEs on the activities of FAK and Akt in A7r5 cells. (A) Cultured cells were treated with MWEs (0.5−2 mg/mL) for 48 h. (B) A7r5 cells were treated with MWEs (1.0 mg/mL) for 0−48 h. Cell lysates (50 $\mu$g) were prepared and subjected to western blot analysis. (C) Proteins were detected by phospho-FAK, integrin-$\beta_3$, PI3K, Akt, and GSK3$\beta$ antibodies. $\beta$-actin was used for equal loading. Total cell lysates were immunoprecipitated with anti-integrin-$\beta_3$ antibodies, and the precipitated complexes were examined by immunoblotting with anti-FAK, Src, Ras, and PI3K antibodies. The results from representative experiments were normalized to immunoprecipitated integrin-$\beta_3$ expression. The results from three separate experiments were similar.


dx.doi.org/10.1021/jf502942r | J. Agric. Food Chem. 2014, 62, 9463−9471

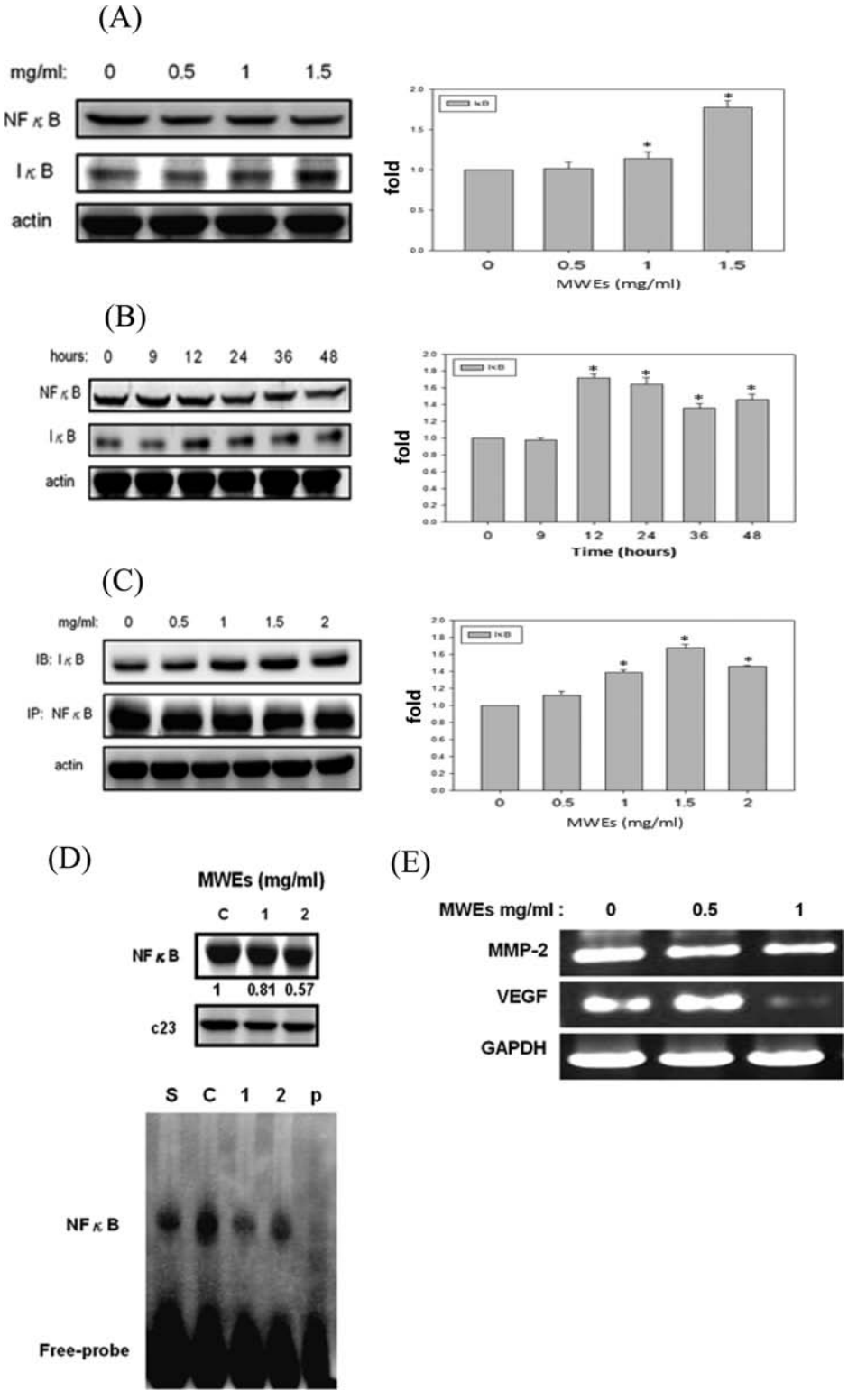


**Figure 5.** Effect of MWEs on the activity of NF-κB in A7r5 cells. (A) A7r5 cells were treated with MWEs (0−1.5 mg/mL) for 48 h. (B) Cultured cells were treated with MWEs (1.0 mg/mL) for 0−48 h. Cell lysates (50 μg) were prepared and subjected to western blot analysis. (C) Cell lysates were also immunoprecipitated with anti-NF-κB and then immunoblotted with anti-IκB. β-actin was used for equal loading. (D) A7r5 cells were treated with or without MWEs for 12 h, and then nuclear extracts were prepared. C23 was used as the nuclear control. NF-κB DNA binding activity was analyzed by an electrophoretic mobility shift assay as described in the Materials and Methods. "S" represented starvation, and "P" represented nuclear extracts incubated with unlabeled oligonucleotides (free probe), to confirm the specificity of binding. (E) Total RNA was extracted. Expressions of MMP-2 and VEGF mRNA were analyzed by RT-PCR. GAPDH served as the loading control. The results from three separate experiments were similar.

quercetin, catechin, epicatechin, and epigallocatechin gallate, have been reported to inhibit neointimal hyperplasia through modulation of smooth muscle cell proliferation and migration.[36] A previous study showed that red wine polyphenolic compounds


dx.doi.org/10.1021/jf502942r | J. Agric. Food Chem. 2014, 62, 9463−9471

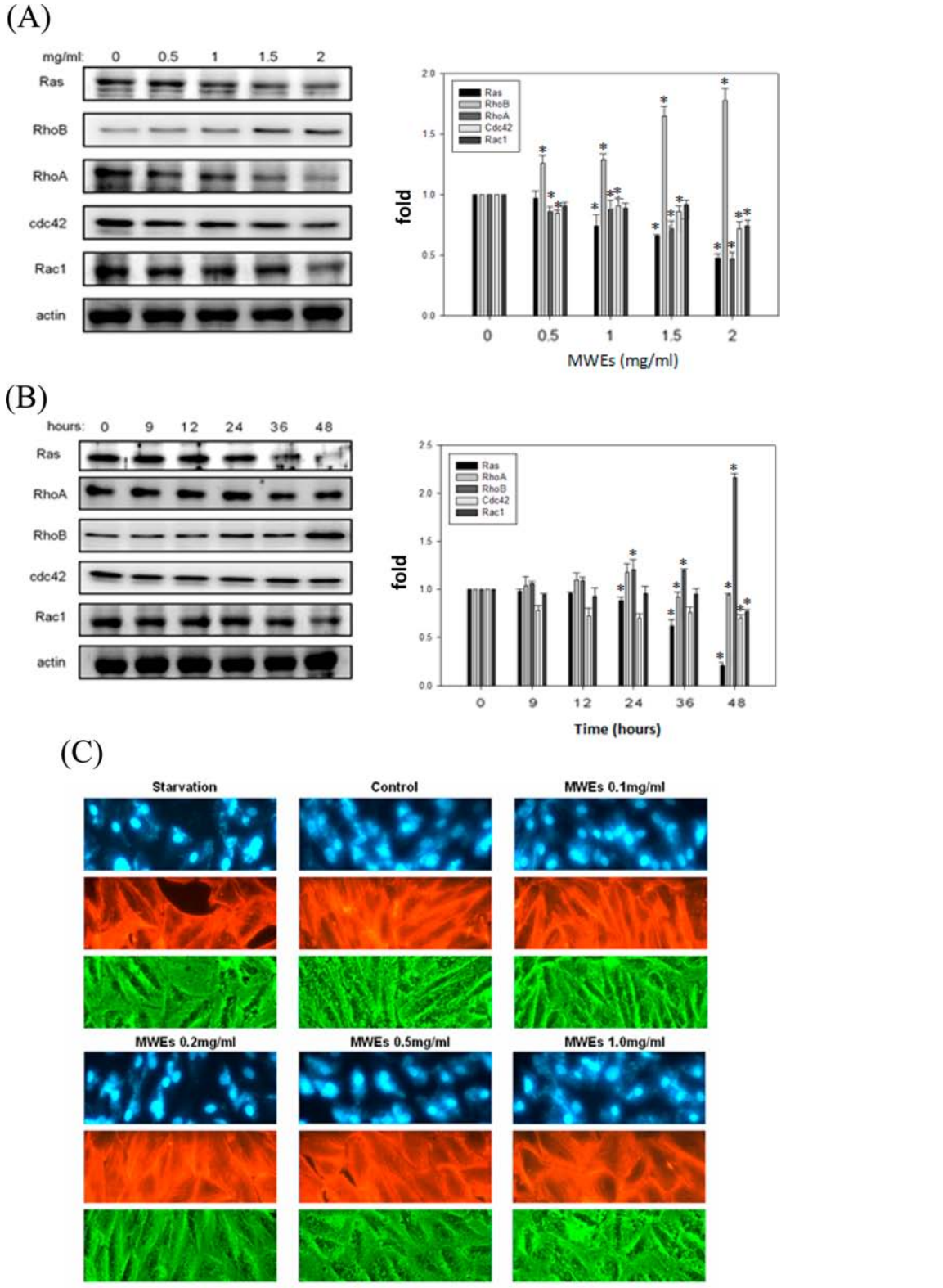


**Figure 6.** Effect of MWEs on the expressions of small G proteins and cytoskeletal F-actin in A7r5 cells. (A) A7r5 cells were treated with MWEs (0−2 mg/mL) for 48 h. (B) A7r5 cells were treated with MWEs (1.0 mg/mL) for 0−48 h. Cell lysates (50 $\mu$g) were prepared and subjected to western blot analysis. Proteins were detected by specific antibodies (Cdc42, Ras, RhoA, and Rac1). $\beta$-actin was used for equal loading. (C) Cultured cells were treated with different concentrations of MWEs or without MWEs for 48 h. The cells were fixed and labeled for F-actin with phalloidin−TRITC (red) and for nucleic acid with DAPI (blue).

and green tea polyphenols are able to inhibit the proliferation and migration of VSMCs and the expressions of VEGF and MMP-2.[37] Gallic acid has been reported to have a hypolipidemic effect on high-fat-diet-fed mice, and the antioxidative properties of protocatechuic acid has been reported to contribute to its suppression of platelet-derived growth factor (PDGF)-induced


dx.doi.org/10.1021/jf502942r | J. Agric. Food Chem. 2014, 62, 9463−9471

migration and proliferation in VSMCs.[38] Catechins have been reported to be able to suppress VSMC proliferation and migration via the inhibition of $\beta$PDGF receptors.[39] Quercetin, catechin, epicatechin, and epigallocatechin gallate have also been reported to inhibit the activity of xanthine oxidase, thereby reducing oxidative stress on vascular walls.[40] Quercetin has also been reported to inhibit the proliferation and migration of VSMCs by suppressing the phosphorylation of mitogen-activated protein kinase.[41] In addition, quercetin 3-*O*-$\beta$-D-glucuronide has been shown to inhibit PDGF-induced migration of rat aortic smooth muscle cells by suppression of PDGF-induced c-Jun N-terminal kinase (JNK) and Akt activations.[42] MWEs are also rich in phenolic acids and flavonoids, including gallic acid, caffeic acid, protocatechuic acid, catechin, epigallocatechin gallate, epicatechin, rutin, quercetin, and naringenin. As we know, protein, fat, and polysaccharide were not reported to have an antiatherosclerotic effect before. Therefore, the inhibitory effect of MWEs on VSMC migration may be attributed to the polyphenol compounds in MWEs.

We found that 0.5−1.0% MWEs effectively reduced HCD-fed-induced intimal hyperplasia in rabbits (Figure 1), which is consistent with the results of our previous study.[26] This further suggests that 2.5−5.0 g/day of MWEs may be enough to prevent atherosclerosis in humans. In the present *in vivo* and *in vitro* studies, we found that MWEs effectively inhibited migration of A7r5 VSMCs (Figure 2), which is important to prevent neointima formation in atherosclerosis. It is known that MMP and VEGF are vital regulators of VSMC migration and angiogenesis, and our results showed that MWEs could time-dependently decrease the activities of MMP-2, MMP-9, and VEGF (Figure 3). On the other hand, the activity of TIMP-2 (a MMP inhibitor) was time-dependently increased after MWE treatment. These results indicate that MWEs can effectively inhibit the activities of MMP-2, MMP-9, and VEGF and thereby inhibit VSMC migration and angiogenesis. Previous reports have shown that PI3K can induce the activation of Akt, thus mediate the phosphorylation of GSK3$\beta$, and inhibit its activity, thereby preventing migration. The FAK/Src complex plays a role in integrin signaling and actin cytoskeleton rearrangement. In addition, Ras-related small GTPases of the Rho family are involved in the regulation of the actin cytoskeleton, and Raf is an important downstream effector of Ras. Our results showed that the activities of FAK-p, PI3K, Akt-p, GSK3$\beta$-p, Src Ras, c-Raf, and integrin-$\beta_3$ were all decreased after MWE treatment (Figure 4), which suggests that MWEs can inhibit VSMC migration via inhibition of the FAK, PI3K/Akt, and Ras pathways. Previous studies have reported that NF-$\kappa$B may regulate angiogenesis via MMP induction and that I$\kappa$B is an inhibitor of NF-$\kappa$B. Our results showed that MWEs dose- and time-dependently decreased the activity of NF-$\kappa$B and increased the activity of I$\kappa$B (Figure 5). In addition, the combination of I$\kappa$B and NF-$\kappa$B was increased after MWE treatment. MWEs also dose-dependently inhibited the activity of NF-$\kappa$B in nuclei. These results indicate that MWEs inhibit VSMC migration via the NF-$\kappa$B pathway. Previous reports have also shown that NF-$\kappa$B is activated by RhoA, Rac1, and cdc42 and inhibited by RhoB. Rho and Rho kinase can also mediate VSMC migration, and RhoA has been reported to regulate the actin cytoskeleton. Our results showed that the activities of Ras and Ras-related small GTPases, including RhoA, cdc42, and Rac, were all significantly decreased after MWE treatment (Figure 6); however, the activity of RhoB was increased after MWE treatment. These results indicate that MWEs can inhibit VSMC migration via Ras and Ras-related small GPTase pathways. We also found that MWEs were a positive regulator of actin organization. In conclusion, MWEs inhibit VSMC migration via reducing the interactions between the integrin-$\beta_3$ and FAK complex and downregulating GSK3$\beta$ and NF-$\kappa$B signaling.

## AUTHOR INFORMATION


### Corresponding Authors

*Telephone: 886-4-24730022, ext. 11671. Fax: 886-4-23248110. E-mail: cs1670@csmu.edu.tw.

*Telephone: 886-4-24730022, ext. 11670. Fax: 886-4-23248167. E-mail: wcj@csmu.edu.tw.



### Funding

This study was supported by a grant from the Ministry of Science and Technology (NSC99-2320-B-040-013-MY3), Taiwan.


### Notes

The authors declare no competing financial interest.

## ABBREVIATIONS USED

FAK, focal adhesion kinase; GSK3$\beta$, glycogen synthase kinase 3$\beta$; HCD, high-cholesterol diet; MMP, matrix metalloproteinase; MWE, mulberry water extract; NF-$\kappa$B, nuclear factor $\kappa$B; RT-PCR, reverse transcription polymerase chain reaction; TIMP, tissue inhibitor of metalloproteinase; VEGF, vascular endothelial growth factor; VSMC, vascular smooth muscle cell

## REFERENCES


(1) Chan, K. C.; Wu, C. H.; Huang, C. N.; Lan, K. P.; Chang, W. C.; Wang, C. J. Simvastatin inhibits glucose-stimulated vascular smooth muscle cell migration involving increased expression of RhoB and a block of Ras/Akt signal. *Cardiovasc. Ther.* **2012**, *30*, 75−84.

(2) Ma, H.; Calderon, T. M.; Kessel, T.; Ashton, A. W.; Berman, J. W. Mechanisms of hepatocyte growth factor-mediated vascular smooth muscle cell migration. *Circ. Res.* **2003**, *93*, 1066−1073.

(3) Bond, M.; Fabunmi, R. P.; Baker, A. H.; Newby, A. C. Synergistic upregulation of metalloproteinase-9 by growth factors and inflammatory cytokines: An absolute requirement for transcription factor NF-$\kappa$B. *FEBS Lett.* **1998**, *435*, 29−34.

(4) Goncharova, E. A.; Ammit, A. J.; Irani, C.; Carroll, R. G.; Eszterhas, A. J.; Panettieri, R. A.; Krymskaya, V. P. PI3K is required for proliferation and migration of human pulmonary vascular smooth muscle cells. *Am. J. Physiol.: Lung Cell. Mol. Physiol.* **2002**, *283*, L354−L363.

(5) Khwaja, A. Apoptosis: Akt is more than just a bad kinase. *Nature* **1999**, *401*, 33−34.

(6) Gui, B.; Hua, F.; Chen, J.; Xu, Z.; Sun, H.; Qian, Y. Protective effects of pretreatment with oleanolic acid in rats in the acute phase of hepatic ischemia-reperfusion injury: Role of the PI3K/Akt pathway. *Mediators Inflammation* **2014**, *2014*, 451826.

(7) Hazeki, K.; Nigorikawa, K.; Hazeki, O. Metabolism and functions of phosphoinositides. *Biol. Pharm. Bull.* **2007**, *30*, 1617−1623.

(8) Turner, C. E.; Brown, M. C. Cell motility: ARNO and ARF6 at the cutting edge. *Curr. Biol.* **2001**, *11*, R875−R877.

(9) Koivisto, L.; Alavian, K.; Häkkinen, L.; Pelech, S.; McCulloch, C. A.; Larjava, H. Glycogen synthase kinase-3 regulates formation of long lamellipodia in human keratinocytes. *J. Cell Sci.* **2003**, *116*, 3749−3760.

(10) Kobayashi, T.; Hino, S. i.; Oue, N.; Asahara, T.; Zollo, M.; Yasui, W.; Kikuchi, A. Glycogen synthase kinase 3 and h-prune regulate cell migration by modulating focal adhesions. *Mol. Cell. Biol.* **2006**, *26*, 898−911.

(11) Rubenstein, P. A. The functional importance of multiple actin isoforms. *BioEssays* **1990**, *12*, 309−315.

(12) Cary, L.; Han, D.; Guan, J. Integrin-mediated signal transduction pathways. *Histol. Histopathol.* **1999**, *14*, 1001−1009.

(13) Cary, L. A.; Chang, J. F.; Guan, J. L. Stimulation of cell migration by overexpression of focal adhesion kinase and its association with Src and Fyn. *J. Cell Sci.* **1996**, *109*, 1787−1794.

(14) Zheng, Y.; Lu, Z. Paradoxical roles of FAK in tumor cell migration and metastasis. *Cell Cycle* **2009**, *8*, 3474−3479.
(15) Vojtek, A. B.; Der, C. J. Increasing complexity of the Ras signaling pathway. *J. Biol. Chem.* **1998**, *273*, 19925−19928.
(16) Kundra, V.; Anand-Apte, B.; Feig, L. A.; Zetter, B. R. The chemotactic response to PDGF-BB: Evidence of a role for Ras. *J. Cell Biol.* **1995**, *130*, 725−731.
(17) Seasholtz, T. M.; Majumdar, M.; Kaplan, D. D.; Brown, J. H. Rho and Rho kinase mediate thrombin-stimulated vascular smooth muscle cell DNA synthesis and migration. *Circ. Res.* **1999**, *84*, 1186−1193.
(18) Takai, Y.; Sasaki, T.; Tanaka, K.; Nakanishi, H. Rho as a regulator of the cytoskeleton. *Trends Biochem. Sci.* **1995**, *20*, 227−231.
(19) Van Aelst, L.; D'Souza-Schorey, C. Rho GTPases and signaling networks. *Genes Dev.* **1997**, *11*, 2295−2322.
(20) Perona, R.; Montaner, S.; Saniger, L.; Sanchez-Perez, I.; Bravo, R.; Lacal, J. C. Activation of the nuclear factor-κB by Rho, CDC42, and Rac-1 proteins. *Genes Dev.* **1997**, *11*, 463−475.
(21) Fritz, G.; Kaina, B. Ras-related GTPase RhoB represses NF-κB signaling. *J. Biol. Chem.* **2001**, *276*, 3115−3122.
(22) Baeuerle, P. A.; Baltimore, D. IκB: A specific inhibitor of the NF-κB transcription factor. *Science* **1988**, *242*, 540−546.
(23) Goldman, S.; Shalev, E. MMPS and TIMPS in ovarian physiology and pathophysiology. *Front. Biosci.* **2004**, *9*, 2.
(24) Valente, P.; Fassina, G.; Melchiori, A.; Masiello, L.; Cilli, M.; Vacca, A.; Onisto, M.; Santi, L.; Stetler-Stevenson, W. G.; Albini, A. TIMP-2 over-expression reduces invasion and angiogenesis and protects B16F10 melanoma cells from apoptosis. *Int. J. Cancer* **1998**, *75*, 246−253.
(25) Ferrara, N.; Gerber, H. P.; LeCouter, J. The biology of VEGF and its receptors. *Nat. Med.* **2003**, *9*, 669−676.
(26) Chan, K. C.; Ho, H. H.; Lin, M. C.; Wu, C. H.; Huang, C. N.; Chang, W. C.; Wang, C. J. Mulberry water extracts inhibit rabbit atherosclerosis through stimulation of vascular smooth muscle cell apoptosis via activating p53 and regulating both intrinsic and extrinsic pathways. *J. Agric. Food Chem.* **2014**, *62*, 5092−5101.
(27) Chen, C. C.; Liu, L. K.; Hsu, J. D.; Huang, H. P.; Yang, M. Y.; Wang, C. J. Mulberry extract inhibits the development of atherosclerosis in cholesterol-fed rabbits. *Food Chem.* **2005**, *91*, 601−607.
(28) Matuszewski, B.; Constanzer, M.; Chavez-Eng, C. Strategies for the assessment of matrix effect in quantitative bioanalytical methods based on HPLC−MS/MS. *Anal. Chem.* **2003**, *75*, 3019−3030.
(29) Darby, I.; Skalli, O.; Gabbiani, G. α-smooth muscle actin is transiently expressed by myofibroblasts during experimental wound healing. *Lab. Invest.* **1990**, *63*, 21−29.
(30) Wysocki, A. B.; Staiano-Coico, L.; Grinneill, F. Wound fluid from chronic leg ulcers contains elevated levels of metalloproteinases MMP-2 and MMP-9. *J. Invest. Dermatol.* **1993**, *101*, 64−68.
(31) Lee, D. C.; Stenland, C. J.; Hartwell, R. C.; Ford, E. K.; Cai, K.; Miller, J. L.; Gilligan, K. J.; Rubenstein, R.; Fournel, M.; Petteway, S. R., Jr. Monitoring plasma processing steps with a sensitive western blot assay for the detection of the prion protein. *J. Virol. Methods* **2000**, *84*, 77−89.
(32) ONG, H.; Chen, J.; Chataway, T.; Brereton, H.; Zhang, L.; Downs, T.; Tsiokas, L.; Barritt, G. Specific detection of the endogenous transient receptor potential (TRP)-1 protein in liver and airway smooth muscle cells using immunoprecipitation and western-blot analysis. *Biochem. J.* **2002**, *364*, 641−648.
(33) Hellman, L. M.; Fried, M. G. Electrophoretic mobility shift assay (EMSA) for detecting protein−nucleic acid interactions. *Nat. Protoc.* **2007**, *2*, 1849−1861.
(34) Hall, A. Rho GTPases and the actin cytoskeleton. *Science* **1998**, *279*, 509−514.
(35) Pfaffl, M. W. A new mathematical model for relative quantification in real-time RT-PCR. *Nucleic Acids Res.* **2001**, *29*, No. e45.
(36) Karki, R.; Jeon, E. R.; Kim, D. W. Nelumbo nucifera leaf extract inhibits neointimal hyperplasia through modulation of smooth muscle cell proliferation and migration. *Nutrition* **2013**, *29*, 268−275.
(37) Oak, M. H.; El Bedoui, J.; Schini-Kerth, V. B. Antiangiogenic properties of natural polyphenols from red wine and green tea. *J. Nutr. Biochem.* **2005**, *16*, 1−8.
(38) Moon, C. Y.; Ku, C. R.; Cho, Y. H.; Lee, E. J. Protocatechuic aldehyde inhibits migration and proliferation of vascular smooth muscle cells and intravascular thrombosis. *Biochem. Biophys. Res. Commun.* **2012**, *423*, 116−121.
(39) Rosenkranz, S.; Knirel, D.; Dietrich, H.; Flesch, M.; Erdmann, E.; Böhm, M. Inhibition of the PDGF receptor by red wine flavonoids provides a molecular explanation for the "French paradox". *FASEB J.* **2002**, *16*, 1958−1960.
(40) Chan, K. C.; Ho, H. H.; Peng, C. H.; Lan, K. P.; Lin, M. C.; Chen, H. M.; Wang, C. J. Polyphenol-rich extract from mulberry leaf inhibits vascular smooth muscle cell proliferation involving upregulation of p53 and inhibition of cyclin-dependent kinase. *J. Agric. Food Chem.* **2010**, *58*, 2536−2542.
(41) Alcocer, F.; Whitley, D.; Salazar-Gonzalez, J. F.; Jordan, W. D.; Sellers, M. T.; Eckhoff, D. E.; Suzuki, K.; MacRae, C.; Bland, K. I. Quercetin inhibits human vascular smooth muscle cell proliferation and migration. *Surgery* **2002**, *131*, 198−204.
(42) Ishizawa, K.; Izawa-Ishizawa, Y.; Ohnishi, S.; Motobayashi, Y.; Kawazoe, K.; Hamano, S.; Tsuchiya, K.; Tomita, S.; Minakuchi, K.; Tamaki, T. Quercetin glucuronide inhibits cell migration and proliferation by platelet-derived growth factor in vascular smooth muscle cells. *J. Pharmacol. Sci.* **2009**, *109*, 257−264.

>97%), chlorogenic acid (purity >95%), nordihydroguaiaretic acid (purity >97%), syringic acid (purity >95%), dihydrocaffeic acid (purity >98%), and tyrosinase (from mushroom) were obtained from Sigma-Aldrich (St. Louis, MO). Vanillic acid (purity >96%) was purchased from Wako Pure Chemicals (Osaka, Japan). Kaempferol (purity >97%), taxifolin (purity >96%), and 5,5′-dithiobis(2-nitrobenzoic acid) were obtained from Funakoshi (Tokyo, Japan). All organic solvents (extra pure grade or HPLC grade) were obtained from Nacalai Tesque. Distilled water produced by a water-distilling instrument (SA-2100E, EYELA, Tokyo, Japan) was used for all experiments. NMR spectra were obtained from an ECS-400 spectrometer (JEOL, Tokyo, Japan) using the manufacturer's pulse sequences. High-resolution mass spectrometric data were obtained using a XEVO QtofMS spectrometer (Waters Japan, Tokyo, Japan) in negative ESI mode. A PU-2089 low-pressure gradient system (JASCO, Tokyo, Japan) equipped with an MD-2018 photodiode array detector (PDA) was employed for analytical HPLC. PDA data were analyzed using ChromNAV ver. 1.8 (JASCO). An LC-6AD system (Shimadzu, Kyoto, Japan) equipped with a UV-970 detector (JASCO) was used for preparative HPLC.

**Preparation of MetMb.** The MetMb solution was prepared from a stock solution of $MbO_2$, which was prepared using a method reported previously.[8] Potassium hexacyanoferrate(III) (2 mg) was added to a solution of $MbO_2$ (120 μmol/L) in a phosphate buffer (50 mmol/L, pH 7.4, 3 mL) at 23 °C. After gentle stirring for 0.5 min, the solution was desalted three times at 14 000*g* for 6 min, at 4 °C, with an Amicon Ultra-0.5, Ultracel-10 ultrafiltration membrane (Merck Millipore, Cork, Ireland) using phosphate buffer. The final residual solution (≈0.5 mL) was diluted with buffer, yielding 120 μmol/L of the MetMb solution (3 mL). The purity and concentration of the MetMb solution were confirmed using a UVmini 1240 UV/vis spectrometer (Shimadzu).[12]

**Measurement of MetMb Reduction to $MbO_2$.** Briefly, 50 mmol/L of phosphate buffer (pH 7.4, 100 μL), 120 μmol/L of MetMb (150 μL, in the same buffer), test samples (polyphenols) dissolved in DMSO (18 or 9 mmol/L, 10 μL), and cysteine dissolved in water (4.5 or 2.3 mmol/L, 40 μL) were subsequently added to a 96-well microplate. The microplate was then incubated at 37 °C in a Multiskan GO microplate reader (Thermo Fisher Scientific, Yokohama, Japan) for 2 h, and absorbance was measured at 500 and 582 nm. The $MbO_2$ and MetMb concentrations in the wells were calculated using the following equation[8] $MbO_2$ (μmol/L) = $89.7A_{582} - 32.9A_{500}$, where $A_{500}$ and $A_{582}$ refer to absorbance at 500 and 582 nm, respectively. The reductive conversion efficiency from MetMb to $MbO_2$ was expressed as a percentage by calculating the $MbO_2$ concentration relative to the initial concentration (60 μmol/L) of MetMb.

**HPLC and LC−MS Analyses of Caffeic Acid during MetMb Reduction.** For caffeic acid analysis, 10 μL of caffeic acid in DMSO (18 mmol/L), 40 μL of cysteine in water (4.5 mmol/L), and 120 μL of MetMb buffer solution were added to 150 μL of a phosphate buffer (50 mmol/L, pH 7.4) in a microplate well. After shaking the plate, it was incubated at 37 °C in a Multiskan GO microplate reader. At 1 h intervals, an aliquot (5 μL) was removed from the above-mentioned reaction, and the reaction products were analyzed under the following conditions: column, a 250 mm × 4.6 mm i.d., 5 μm, Cosmosil $5C_{18}$-AR-II (Nacalai Tesque); flow rate, 1.0 mL/min; solvent A, 1% acetic acid in water; solvent B, acetonitrile; gradient conditions: linear gradient of 5−100% solvent B (40 min); detection, absorbance at 280 nm. The concentrations of the caffeic acid and its derivative in the reaction mixture were measured by an external standard method and calculated using calibration curves, which were made from the peak areas of several concentrations of authentic samples. The MS data for each product were obtained by performing LC−MS. An additional aliquot (5 μL) was also withdrawn after 2 h for analyzing the compounds of peaks 1 and 2, and the analyses were carried out under the following conditions: column, a 250 mm × 4.6 mm i.d., 5 μm, Cosmosil $5C_{18}$-AR-II (Nacalai Tesque); flow rate, 0.5 mL/min; solvent A, 1% acetic acid in ultrapure water (Wako Pure Chemicals), solvent B, acetonitrile (LC−MS grade) (Merck, Darmstadt, Germany); gradient conditions, linear gradient of 5−100% solvent B (80 min). MS conditions: mode, negative ESI; capillary voltage, 2.4 kV; cone voltage, 40 V; source temperature, 150 °C; desolvation temperature, 500 °C; cone gas flow rate, 50 L/h; desolvation gas flow rate, 1000 L/h, $MS^E$ low collision energy, 6 V; $MS^E$ high collision energy, 20−30 V. The elemental composition of each peak compound was calculated from the high-resolution MS data of the deprotonated molecular ion by using MassLynx software v. 4.1 (Waters).

**Quantitative Analysis of Cysteine and Cystine during MetMb Reduction.** Quantitation of cysteine in the reaction was carried out by using a modified Ellman's method.[13,14] Briefly, at 1 h intervals, an aliquot (20 μL) was withdrawn from the above-mentioned reaction mixture. To the aliquot were subsequently added 30 μL of phosphate buffer (50 mmol/L, pH 7.4), 200 μL of distilled water, and 50 μL of 5,5′-dithiobis(2-nitrobenzoic acid) (0.4 mmol/L). After stirring for 5 min at 23 °C, 10 μL of the solution was withdrawn and the generated 5-hydrosulfuryl-2-nitrobenzoic acid was analyzed via HPLC under the following conditions: column, a 150 mm × 3.0 mm i.d., 3 μm, Cosmosil $3C_{18}$-EB (Nacalai Tesque); flow rate, 0.3 mL/min; solvent A, 0.1% phosphoric acid in water; solvent B, acetonitrile; gradient conditions, linear gradient of 0−100% of solvent B (30 min), detection at 330 min, with a retention time of 10.5 min. The quantitation of the cysteine in the incubating solution was performed using a calibration curve obtained by analyzing the reaction using known concentrations of cysteine.

The quantitation of cystine was carried out by using the method of Mizuta and Sakai[15] with a slight modification.[16] Briefly, 2 or 3 h after the start of incubation, an additional aliquot (20 μL) was withdrawn from the reaction mixture, and 10 μL of benzoyl chloride (8 mmol/L in $CH_3CN$) and 10 μL of triethylamine (8 mmol/L in $CH_3CN$) were added to the aliquot at 0 °C with stirring. After keeping the mixture for 1 h at 0 °C, 10 μL of the reaction mixture was analyzed by HPLC under the following conditions: column, a 250 mm × 4.6 mm i.d., 5 μm, Cosmosil $5C_{18}$-AR-II (Nacalai Tesque); flow rate, 0.5 mL/min; solvent A, 0.1% trifluoroacetic acid in water; solvent B, acetonitrile; gradient conditions, linear gradient of 10−100% of solvent B (50 min); detection, absorbance at 254 nm. The concentration of cystine was determined using a calibration curve, which was derived from the analytical data of authentic cystine.

**Preparation of Cysteinylcaffeic Acids.** 2′- and 5′-*S*-cysteinylcaffeic acids were synthesized enzymatically. Tyrosinase (2 mg) was added to a mixture of caffeic acid (50 mg) and cysteine (68 mg) in 10 mL of a phosphate buffer (50 mmol/L, pH 6.8). After keeping the mixture for 0.5 h at 23 °C, the mixture was concentrated to ≈10 mL in vacuo. The solution was then purified by a preparative HPLC as follows: column, a 250 × 20 mm i.d., 5 μm, Cosmosil $5C_{18}$-AR-II; solvent, $CH_3OH$−1% acetic acid in $H_2O$ (15:85, v/v); flow rate, 8.0 mL/min; detection, 280 nm. 5′-*S*-Cysteinylcaffeic acid (**5**) (7 mg) and 2′-*S*-cysteinylcaffeic acid (**4**) (38 mg) showing peaks at the retention times of 33 and 48 min, respectively, were collected.

*5′-S-Cysteinylcaffeic Acid.* HR-ESIMS (*m*/*z*) $[M - H]^-$ calcd for $C_{12}H_{12}NO_6S$ 298.0385, found 298.0374; $^1H$ NMR (DMSO-$d_6$) δ 8.30 (1H, brs), 7.25 (1H, d, *J* = 15.6 Hz), 6.95 (1H, d, *J* = 1.6 Hz), 6.83 (1H, d, *J* = 1.6 Hz), 5.88 (1H, d, *J* = 15.6 Hz), 2.95 (1H, dd, *J* = 14.8 and 4.0 Hz), 2.90−2.75 (2H, m).

*2′-S-Cysteinylcaffeic Acid.* HR-ESIMS (*m*/*z*) $[M - H]^-$ calcd for $C_{12}H_{12}NO_6S$ 298.0385, found 298.0397; $^1H$ NMR (DMSO-$d_6$) δ 8.17 (1H, d, *J* = 15.8 Hz), 7.18 (1H, d, *J* = 8.2 Hz), 6.76 (1H, d, *J* = 8.2 Hz), 6.25 (1H, d, *J* = 15.8 Hz), 2.95 (1H, t, *J* = 7.8 Hz), 2.77 (2H, d, *J* = 7.8 Hz).

**Statistical Analysis.** Data obtained from the experiments in triplicate are presented as mean ± standard deviation (SD). The differences between means were evaluated using the Student's *t*-test. Statistical significance was considered at $p < 0.05$.

## RESULTS AND DISCUSSION

**MetMb Reduction by Polyphenols in the Presence of Cysteine.** In the previous investigation, the effect of various kinds of polyphenols and the related phytophenols on MetMb reduction was examined (Figure 1). Most of the polyphenols

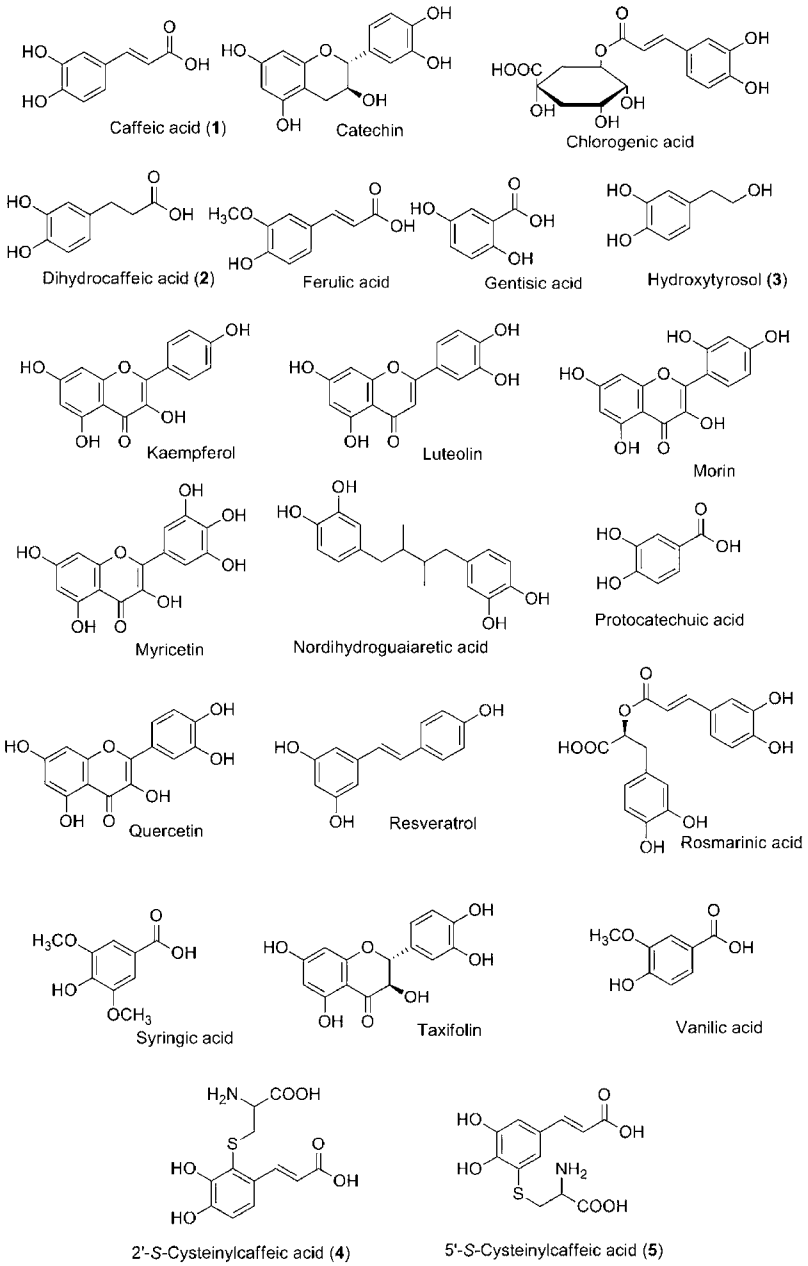


**Figure 1.** Chemical structures of the polyphenols and related phenols investigated for MetMb reduction in the presence of cysteine and two synthesized cysteinylcaffeic acids.

did not show sufficient reducing activity for MetMb, as compared to ascorbic acid. Although cysteine shows no reducing activity toward MetMb, it was expected that cysteine would facilitate the polyphenol-mediated MetMb reduction. Figure 2 shows the results of MetMb reduction in air and the polyphenol-mediated $MbO_2$ formation (concentrations of polyphenols 600 or 300 $\mu$mol/L) in the presence or absence of cysteine (600 or 300 $\mu$mol/L). The data are expressed as a percentage of the ratio of $MbO_2$ produced in air to the total amount of myoglobins (MetMb + $MbO_2$), which was calculated on the basis of the previously reported equation.[8] The figure shows that the reducing activity of most polyphenols was remarkably enhanced by the presence of cysteine, whereas the activity of cysteine itself was extremely weak. In particular, the activity of caffeic acid (**1**), dihydrocaffeic acid (**2**), and hydroxytyrosol (**3**) increased significantly in the presence of cysteine. Caffeic acid, dihydrocaffeic acid, and hydroxytyrosol are powerful antioxidants[17−19] and also have a strong reducing ability.[20,21] Both activities are dependent on their catechol substructures. The catechol structure is readily oxidized to orthoquinone, which may interact with $MbO_2$ to stimulate its oxidation to MetMb. When cysteine is present, the nucleophilic thiol group reacts with quinone to afford more stable polyphenolic derivatives as a result. Further investigation for elucidating the mechanism was carried out using the highly potent caffeic acid.

**Concentration Effect of Caffeic Acid and Cysteine on the Reduction of MetMb.** Two concentration levels, 600 or 300 $\mu$mol/L, of polyphenols and cysteine for carrying out the experiment on MetMb reduction were employed, according to the method reported in a previous study.[8] These above-mentioned concentrations of polyphenols and cysteine are


dx.doi.org/10.1021/jf5039508 | J. Agric. Food Chem. 2014, 62, 9472−9478

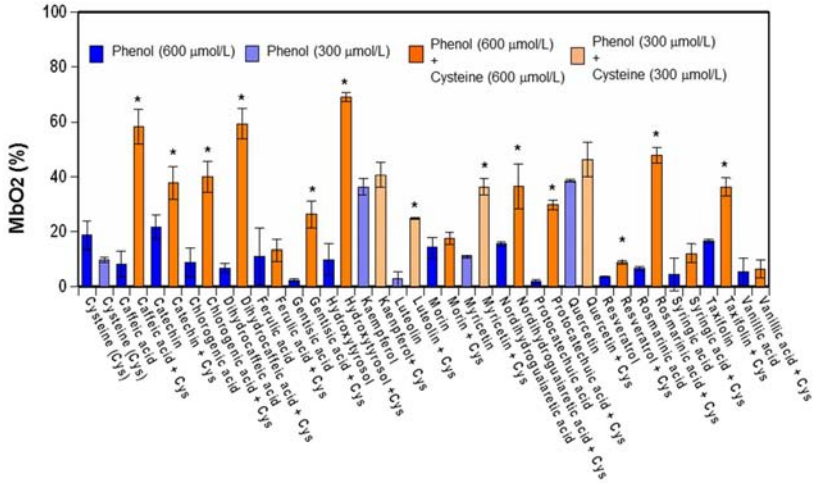


**Figure 2.** Effects of phenols (600 or 300 $\mu$mol/L) on MetMb reduction in the presence of cysteine (600 or 300 $\mu$mol/L). Results are expressed as mean ± standard deviation (SD) ($n$ = 3) and * signifies significantly different data against data from the corresponding experiment in the absence of cysteine ($t$-test, $p < 0.05$).

much higher than the concentration of MetMb (60 $\mu$mol/L). Therefore, we initially examined the concentration effects of not only caffeic acid but also cysteine on the MetMb-reducing reaction, using a microplate method. The obtained matrix data are shown in Figure 3. Pure caffeic acid and cysteine

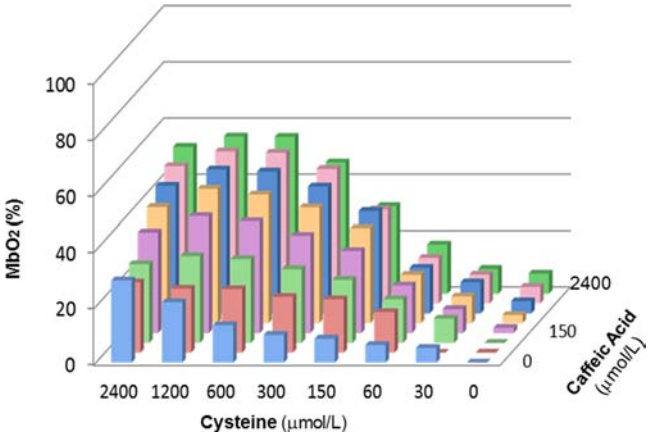


**Figure 3.** Matrix data of the various concentrations of caffeic acid and cysteine used for MetMb reduction. Reducing activity of MetMb is expressed as a percent of the formed $MbO_2$, from the MetMb in the air. All data were presented as mean values of two independent experiments.

independently showed a concentration-dependent activity up to 2400 $\mu$mol/L, but these activities were not very significant. On the other hand, the mixtures of caffeic acid and cysteine showed a remarkable reducing activity. The optimal concentrations of caffeic acid and cysteine were between 600 and 2400 $\mu$mol/L for caffeic acid and 600 $\mu$mol/L for cysteine, 2 h after the reaction commenced. In general, higher concentrations of active compounds are expected to result in an increased efficiency. However, in this case, higher concentrations of cysteine did not show the expected linear concentration-dependent effect. Tang et al.[22] have reported that glutathione, a biothiol related to cysteine, accelerated the oxidation of $MbO_2$ to MetMb at pH 7.2 and 37 °C. This could be the reason why a higher concentration of cysteine (>600 $\mu$mol/L) prevented $MbO_2$ formation.

**HPLC Analysis of MetMb Reduction in the Presence of Caffeic Acid and Cysteine and Identification of the Reaction Products.** We carried out the HPLC analysis of the MetMb-reducing reaction of caffeic acid (600 $\mu$mol/L) in the presence of cysteine (600 $\mu$mol/L). In the HPLC profile, 2 h after the initiation of reaction (Figure 4), two noticeable

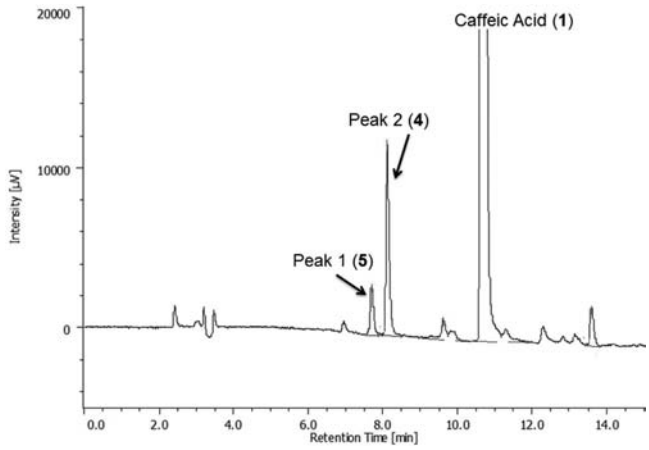


**Figure 4.** HPLC analytical profile for the reaction products from caffeic acid in the presence of cysteine, during the reducing reaction of MetMb at 2 h.

product peaks were observed at the retention times of 7.6 and 8.1 min, respectively, in addition to a large peak corresponding to caffeic acid (10.7 min). To obtain the structure information corresponding to these two peak compounds, they were subjected to MS analysis using LC−TOFMS. High-resolution MS data for peak 1 ($m/z$ 298.0384 $[M - H]^-$) and peak 2 ($m/z$ 298.0400 $[M - H]^-$) indicated that the molecular formula of both peak compounds was $C_{12}H_{13}NO_6S$. From the molecular formula, peaks 1 and 2 were thought to be the isomeric coupling products of an equimolar amount of caffeic acid and cysteine. In our previous study,[10] the radical oxidation of caffeic ester in the presence of a cysteine derivative afforded 2′-*S*-substituted caffeic ester as the main product, which was produced by the addition of cysteinyl thiol to a quinone derivative of the caffeic ester. Therefore, we prepared a similar


dx.doi.org/10.1021/jf5039508 | J. Agric. Food Chem. 2014, 62, 9472−9478

quinone derivative of caffeic acid and then added cysteine to the quinone. A quinone of caffeic acid was synthesized with the help of tyrosinase oxidation, and cysteine was then reacted to obtain the two products, whose structures were fully determined as 2′-*S*-cysteinylcaffeic acid (a major product) and 5′-*S*-cysteinylcaffeic acid (a minor product) by performing MS and NMR. These synthetically obtained cysteinylcaffeic acids were identical to the peak compounds by comparison of the retention times of the HPLC and MS data. Therefore, the structures of the compounds giving peaks 1 and 2 were determined to be 5′-*S*-cysteinylcaffeic acid (**5**) and 2′-*S*-cysteinylcaffeic acid (**4**), respectively. (Figure 1)

**Time Course Analysis of Caffeic Acid and Cysteine and the Oxidation Products during MetMb Reduction.** The time-course analytical results of the formation of two cysteinylcaffeic acids (2′-*S*-cysteinylcaffeic acid and 5′-*S*-cysteinylcaffeic acid) and the decrease of caffeic acid and cysteine in the MetMb-reducing solution are summarized in Figure 5A–C. Figure 5C shows that both the coupling products

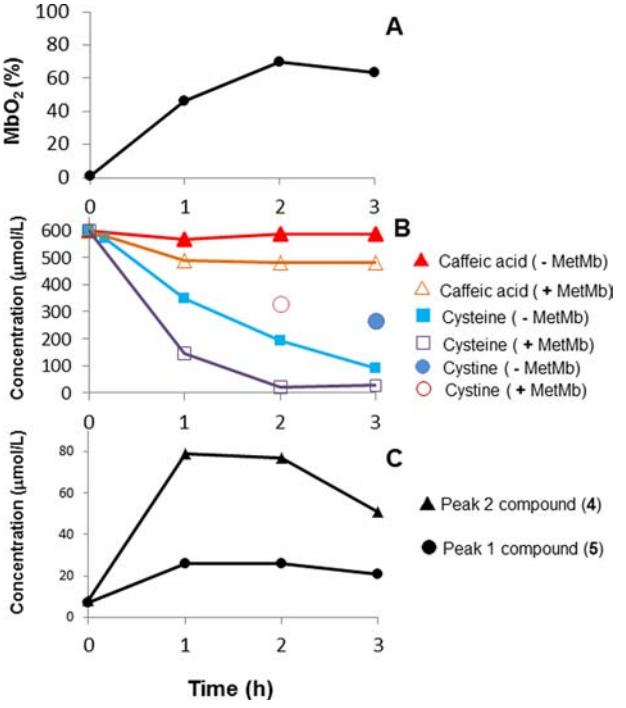


**Figure 5.** Time-course analytical data for $MbO_2$ (A); caffeic acid, cysteine, and cystine (2 or 3 h data only) (B); and reaction products (C) in the reducing reaction of MetMb. All the analytical experiments were performed in duplicate, and the data are expressed in terms of the corresponding mean values.

(2′-*S*-cysteinylcaffeic acid and 5′-*S*-cysteinylcaffeic acid) increased during the first 2 h. During this period, $MbO_2$ was continuously accumulated from the reduction of MetMb, as shown in Figure 5A. The amount of caffeic acid was partially decreased at 2 h, as shown in Figure 5B. Figure 5B also shows that cysteine decreased drastically during this time period. This decreased cysteine was oxidatively converted to cystine owing to the corresponding cystine concentration measured in the 2 h reaction. During the MetMb-reducing reaction, cysteine was completely oxidized. However, Romero et al.[23] reported that the reducing activity of cysteine toward MetMb was negligible. It should be noted that cysteine was unstable under the alkaline aerobic conditions. Therefore, we measured reaction rate of the same concentration of cysteine and caffeic acid without MetMb, and the corresponding results are shown in Figure 5B. Figure 5B shows that the reaction rate of cysteine in the absence of MetMb was lower than that in the presence of MetMb. Moreover, caffeic acid did not decrease during the same time period. These results indicated that MetMb primarily oxidized caffeic acid and then produced two cysteinylcaffeic acids from a subsequent coupling reaction of the remaining cysteine and the oxidized caffeic acid (quinone of caffeic acid). In our previous study,[3] high concentrations of caffeic acid were found to promote the oxidation of $MbO_2$ to MetMb. This $MbO_2$ oxidation may be attributed to interaction between $MbO_2$ and the electrophilically oxidized polyphenols such as caffeic quinone.[24,25] When cysteine was present in the solution, the caffeic quinone that was derived by the oxidation of caffeic acid quickly reacted with the cysteine to form cysteinylcaffeic acids. The cysteinylcaffeic acids might not stimulate $MbO_2$ oxidation because of the absence of any reactive quinone structures.

**Effect of Cysteinylcaffeic Acid on the Redox States of Mb.** During the reduction of MetMb, caffeic acid was oxidized to a corresponding quinone derivative. However, the coexisting cysteine quenched the quinone to produce cysteinylcaffeic acids. Next, we examined the redox activities of the cysteinylcaffeic acids on Mb. Cysteinylcaffeic acids were synthesized with tyrosinase oxidation, and the major product obtained (2′-*S*-cysteinylcaffeic acid) was used for this assessment. The MetMb-reducing activity and $MbO_2$-oxidizing activity of 2′-*S*-cysteinylcaffeic acid were measured. The corresponding results are shown in parts A and B of Figure 6, respectively. Figure 6A shows that 2′-*S*-cysteinylcaffeic acid

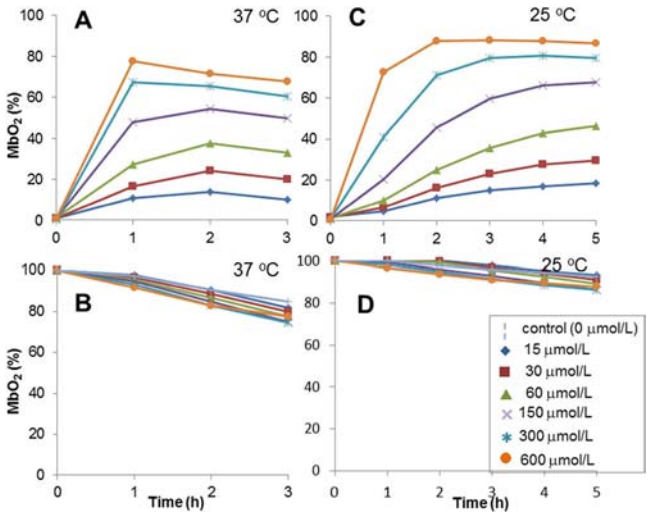


**Figure 6.** Concentration effect of 2′-*S*-cysteinylcaffeic acid on MetMb reduction (A and C) and $MbO_2$ oxidation (B and D) at 37 and 25 °C, respectively. Redox values of MetMb and $MbO_2$ were expressed as the $MbO_2$ percent of Mbs in the reaction. All the analytical experiments were performed in duplicate, and the data are expressed as mean values.

exhibited a potent MetMb-reducing activity in a concentration-dependent manner, but the same concentrations of 2′-*S*-cysteinylcaffeic acid did not show any oxidation activity of $MbO_2$ as compared to the control experiment, as shown in Figure 6B. These results were also observed clearly at lower temperature conditions corresponding to 25 °C as an ambient temperature (Figure 6C,D). At that temperature, $MbO_2$ was


dx.doi.org/10.1021/jf5039508 | *J. Agric. Food Chem.* 2014, 62, 9472–9478

stable until 5 h, and 2′-*S*-cysteinylcaffeic acid did not affect the stability of $MbO_2$ during this time period (Figure 6D). However, 2′-*S*-cysteinylcaffeic acid had a slower but more effective reducing activity for the conversion of MetMb to $MbO_2$, as shown in Figure 6C. It is known that sulfur substitutions in polyphenols alter their redox properties.[10,26] Substituted cysteinyl sulfur can modulate the pro-oxidant activity of caffeic acid and make it nonreactive toward $MbO_2$, while still retaining the powerful reducing activity of the caffeic acid. One of the objectives of the current study[3,8] was the development of a polyphenol-based technology for the preservation of fresh meat color. The cysteine-modified polyphenols may thus provide a novel alternative for the prevention of changes of meat color.

From the results obtained in this study, some highly antioxidative polyphenols produced bright red $MbO_2$ in the presence of cysteine by reducing brown MetMb at pH 7.4. The mechanism is thought to be a combination of the potent reducing activity of polyphenols and the preventive effect of cysteine on the expression of the pro-oxidant property of polyphenols by nucleophilic addition of cysteinyl thiol to oxidized polyphenols, as illustrated in Figure 7. Cysteinylcaffeic acid, a thiol-substituted polyphenol, exhibited no oxidation-stimulating property toward $MbO_2$ after the reduction of MetMb. These results show that the polyphenols were indeed useful in retaining the bright red color of $MbO_2$, with support from biothiols such as cysteine. The bright red color of meat is very important in the food industry. These findings in this investigation should contribute not only to meat science but also to the chemistry of meat products.

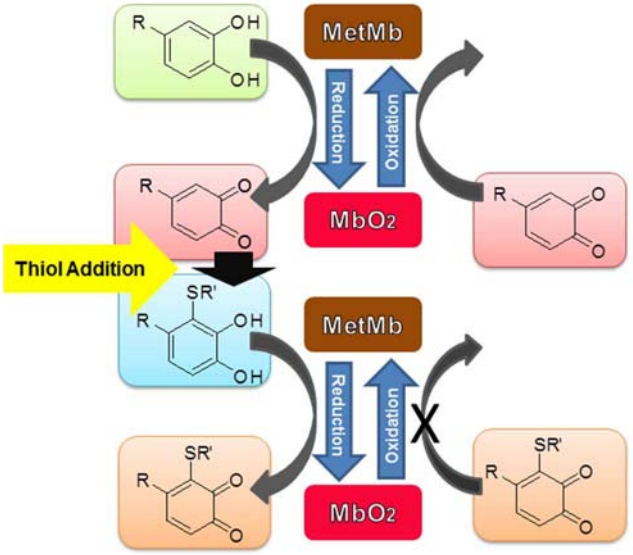


**Figure 7.** Proposed mechanism for redox change between MetMb and $MbO_2$ by polyphenols in the presence of thiols.

## AUTHOR INFORMATION

### Corresponding Author

*Fax: +81-88-656-7244. E-mail: masuda.ias@tokushima-u.ac.jp.

### Funding

Financial support from The Ito Foundation (Meguro, Tokyo, Japan) is gratefully acknowledged.

### Notes

The authors declare no competing financial interest.

## REFERENCES

(1) Issanchu, S. Consumer expectations and perceptions of meat and meat product quality. *Meat Sci.* **1999**, *43*, S5−19.
(2) Mancini, R. A.; Hunt, M. C. Current research in meat color. *Meat Sci.* **2005**, *71*, 100−121.
(3) Masuda, T.; Inai, M.; Miura, Y.; Masuda, A.; Yamauchi, S. Effect of polyphenols on oxymyoglobin oxidation: Prooxidant activity of polyphenols in vitro and inhibition by amino acid. *J. Agric. Food Chem.* **2013**, *61*, 1097−1104.
(4) Bekhit, A. E. D.; Faustman, C. Metmyoglobin reducing activity. *Meat Sci.* **2005**, *71*, 407−439.
(5) Tukahara, K.; Yamamoto, Y. Kinetic studies on the reduction of metmyoglobin by ascorbic acid. *J. Biochem.* **1983**, *93*, 15−22.
(6) Lien, E. J.; Ren, S.; Bui, H.-H.; Wang, R. Quantitative structure−activity relationships analysis of phenolic antioxidants. *Free Radical Biol. Med.* **1999**, *26*, 285−294.
(7) Pietta, P.-G. Flavonoids as antioxidants. *J. Nat. Prod.* **2000**, *63*, 1035−1042.
(8) Inai, M.; Miura, Y.; Honda, S.; Masuda, A.; Masuda, T. Metmyoglobin reduction by polyphenols and mechanism of the conversion of metmyoglobin to oxymyoglobin by quercetin. *J. Agric. Food Chem.* **2014**, *62*, 893−901.
(9) Khalife, H. K.; Lupidi, G. Reduction of hypervalent states of myoglobin and hemoglobin to their ferrous forms by thymoquinone: The role of GSH, NADH and NADPH. *Biochim. Biophys. Acta* **2008**, *1780*, 627−637.
(10) Fujimoto, A.; Inai, M.; Masuda, T. Chemical evidence for the synergistic effect of a cysteinyl thiol on the antioxidant activity of caffeic and dihydrocaffeic esters. *Food Chem.* **2013**, *138*, 1483−1492.
(11) Masuda, T.; Miura, Y.; Inai, M.; Masuda, A. Enhancing effect of a cysteinyl thiol on the antioxidant activity of flavonoids and identification of antioxidative thiol-adducts of myricetin. *Biosci. Biotechnol. Biochem.* **2013**, *77*, 1753−1758.
(12) Bowen, W. J. The absorption spectra and extinction coefficients of myoglobin. *J. Biol. Chem.* **1949**, *179*, 235−245.
(13) Ellman, G. L. Tissue sulfhydryl groups. *Arch. Biochem. Biophys.* **1959**, *82*, 70−77.
(14) Sedlak, J.; Lindsay, R. H. Estimation of total, protein-bound, and nonprotein sulfhydryl groups in tissue with Ellman's reagent. *Anal. Biochem.* **1968**, *25*, 192−205.
(15) Mizuta, H.; Sakai, J. High performance liquid chromatographic determination of cysteine esters. *Jpn. Soc. Anal. Chem.* **1978**, *27*, 744−748.
(16) Miura, Y.; Honda, S.; Masuda, A.; Masuda, T. Antioxidant activities of cysteine derivatives against lipid oxidation in anhydrous media. *Biosci. Biotechnol. Biochem.* **2014**, *78*, 1452−1455.
(17) Gülçin, İ. Antioxidant activity of caffeic acid (3,4-dihydroxycinnamic acid). *Toxicology* **2006**, *217*, 213−220.
(18) Silva, F. A. M.; Borges, F.; Guimarães, C.; Lima, J. L. F. C.; Matos, C.; Reis, S. Phenolic acids and derivatives: Studies on the relationship among structure, radical scavenging activity, and physicochemical parameters. *J. Agric. Food Chem.* **2000**, *48*, 2122−2126.
(19) Papadopiulos, G.; Boskou, D. Antioxidant effect of natural phenols on olive oil. *J. Am. Oil Chem. Soc.* **1991**, *68*, 669−671.
(20) Nenadis, N.; Boyle, S.; Bakalbassis, E. G.; Tsimidou, M. An experimental approach to structure−activity relationships of caffeic and dihydrocaffeic acids and related monophenols. *J. Am. Oil Chem. Soc.* **2003**, *80*, 451−458.
(21) Carrasco-Pancorbo, A.; Cerretani, L.; Bendini, A.; Segura-Carretero, A.; Del Carlo, M.; Gallina-Toschi, T.; Lercker, G.; Compagnone, D.; Fernándes-Gutiérrez, A. Evaluation of the antioxidant capacity of individual phenolic compounds in virgin olive oil. *J. Agric. Food Chem.* **2005**, *53*, 8918−8925.
(22) Tang, J.; Faustman, C.; Lee, S.; Hoagland, T. A. Effect of glutathione on oxymyoglobin oxidation. *J. Agric. Food Chem.* **2003**, *51*, 1691−1695.
(23) Romero, F. J.; Ordonez, I.; Arduini, A.; Cadenas, E. The reactivity of thiols and disulfides with different redox states of

myoglobin. Redox and addition reaction and formation of thiyl radical intermediates. *J. Biol. Chem.* **1992**, *267*, 1680−1688.
(24) Alderton, A. L.; Faustman, C.; Liebler, D. C.; Hill, D. W. Induction of redox instability of bovine myoglobin by addition with 4-hydroxy-2-nonenal. *Biochemistry* **2003**, *42*, 4398−4405.
(25) Hurrell, R. F.; Finot, P. A. Protein−polyphenol reactions 1. Nutritional and metabolic consequences of the reaction between oxidized caffeic acid and the lysine residue of casein. *Br. J. Nutr.* **1982**, *47*, 191−211.
(26) Malmström, J.; Jonsson, M.; Cotreave, I. A.; Hammarström, L.; Sjödin, M. The antioxidant profile of 2,3-dihydrobenzo[*b*]furan-5-ol and its 1-thio, 1-seleno, amd 1-telluro analogues. *J. Am. Chem. Soc.* **2001**, *123*, 3434−3440.

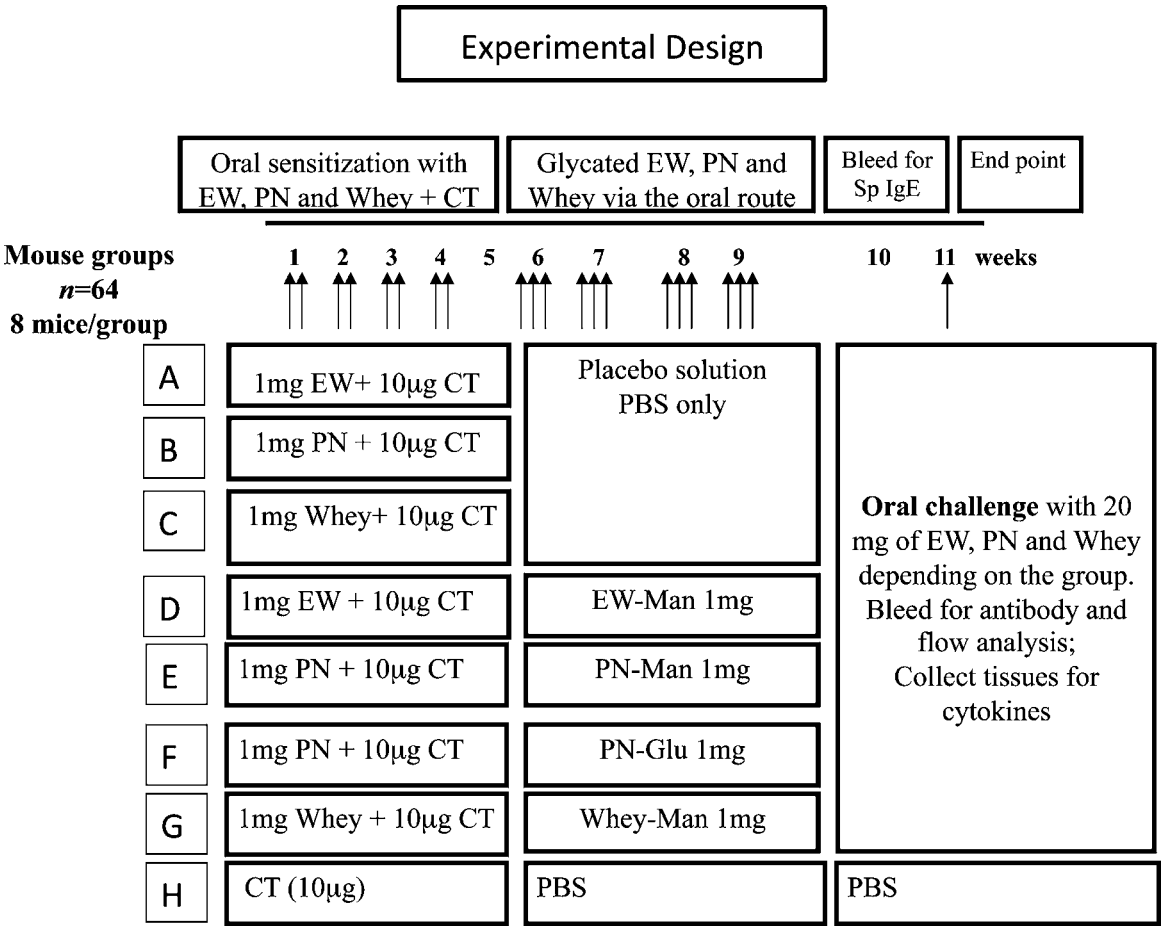


**Figure 1.** Experimental design. Mice were sensitized with 1 mg of egg white (EW), peanut (PN), and whey proteins and 10 $\mu$g of cholera toxin (CT) for 4 weeks, twice a week, followed by a 4 week treatment with mannosylated EW, PN, and whey proteins. The glucosylated PN group was used as a positive test group, and the negative control group received PBS. Clinical signs of allergy were recorded post oral challenge (0−30 min), and all mice were euthuanized for collection of blood and spleen. Both blood and spleen were pooled within groups such that $n$ = 4.

earlier research that mannosylation of OVA did have a potential impact on DCs and antigen recognition and uptake and in reducing allergenicity in vivo in mice. With this background we proposed to study different mannosylated glycoforms of major food allergens such as egg white (EW), peanut (PN), and whey proteins on tolerance induction in vivo in mice. It would be of interest to know under "the glycation allergen concept" if mannosylation influences different allergens in a similar fashion as observed with OVA with regard to reducing allergy or otherwise.

## MATERIALS AND METHODS

**Chemicals.** Carbohydrates such as D-mannose and D-glucose were obtained from Sigma (Oakville, ON, Canada). All antibodies used in the experiments were purchased from BD Biosciences (Pharmingen, San Diego, CA, USA), Sigma (Sigma-Aldrich, Oakville, ON, Canada), or eBioscience (eBiosciences, San Diego, CA, USA).

**Glycation of Common Allergens.** Egg white, PN, and whey proteins were all in-house-extracted and partially purified according to methods previously described.[15−17] Maillard reaction or glycation was performed as described in a previously established method with slight modifications.[11] In brief, mannose (Sigma-Aldrich, St. Louis, MO, USA) was added to the three proteins at a ratio of 1:1 (w/w protein/mannose), mixed into a solution, freeze-dried, and incubated at 55 °C for 3 days (72 h) at 65% relative humidity using saturated potassium iodide solution in a laboratory incubator. Native proteins were treated in a similar manner without mannose and regarded as the native, nonmodified form. All samples were dialyzed (5 kDa cutoff, Millipore, Bedford, MA, USA) with PBS to get rid of the nonconjugated saccharides. As an additional test group, PN proteins were glycated with glucose to be used as a positive control, on the basis of our earlier results that OVA conjugated to glucose did not alleviate allergic signs in mice.[11]

**Determination of Molar Binding Ratios.** Total carbohydrate (CHO) content was determined by the phenol/sulfuric acid colorimetric method at 490 nm with D-mannose as standard.[18] Protein concentration was measured using the standard bicinchoninic acid method.[19] Due to complex total proteins used, conjugation binding ratios for binding of CHO to total protein were calculated on the basis of the concentration using the following formula: concentration of CHO/concentration of total protein.

**SDS-PAGE.** Glycation was also confirmed with running the conjugated samples on sodium dodecyl sulfate−polyacrylamide gel electrophoresis (SDS-PAGE) gel. Each of the samples was mixed with 2× sample loading buffer and incubated for 10 min at 65 °C prior to SDS-PAGE on a 12% polyacrylamide separating gel with a 5% stacking gel. Electrophoresis was performed at a constant current of 30 mA using a mini Protean apparatus (Bio-Rad). The gel was placed into Coomassie Blue stain solution for 1 h postelectrophoresis and then destained in distilled water for 1 h and photographed.

**Mice and Sensitization.** All animal use protocols were based on Canadian Council for Animal Care guidelines and approved by the University of Guelph Animal Care Committee (eAUP No-1567). Briefly, 64 female Balb/c mice were randomly divided into eight groups ($n$ = 8/group). Mice were orally sensitized with 1 mg of EW, PN, and whey proteins adjuvanated with 10 $\mu$g of cholera toxin (CT;

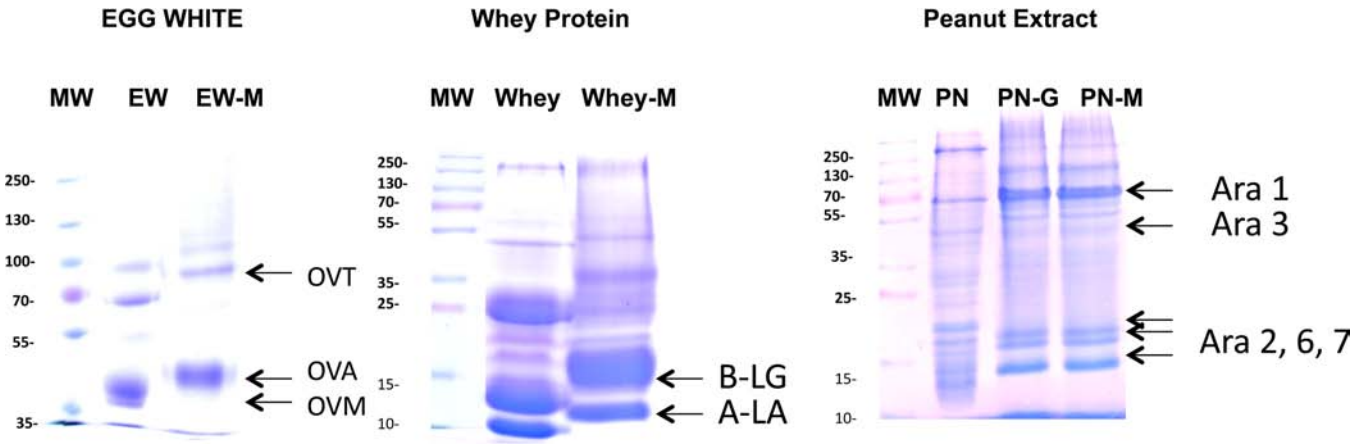


**Figure 2.** Coomassie staining of SDS-PAGE patterns of native and glycated allergens. EW represents egg white, and EW-M represents mannosylated EW. PN represents peanut proteins, PN-M represents mannosylated PN, and PN-G represents glucosylated PN. Whey-M represents mannosylated whey. MW in all panels represents molecular weight markers (kDa).

List Biologicals, Campbell, CA, USA) for 4 weeks (twice a week) as presented in Figure 1. Mice were further treated with mannosylated and glucosylated antigens (1 mg) for 4 weeks (three times/week). At week 11 mice were orally challenged with 20 mg of each antigen and monitored for clinical signs of allergy as described earlier.[11] Clinical scores were assigned in a blind fashion by three experienced observers. Total scores for each animal were obtained by adding scores for each individual sign. Blood was collected for measurement of histamine, antibody activity, and flow cytometry, and all samples were centrifuged for 20 min at 2000*g* and kept at 4 °C to obtain sera. All samples were stored at 20 °C until further analysis. Spleens were collected for measuring cytokines.

**Measurement of Serum Histamine and Mouse Mast Cell Protease.** Concentration of serum histamine post oral challenge was determined using an enzyme immunoassay kit (Labor Diagnostika Nord, Nordhon, Germany) according to the manufacturer's instructions. The mouse mast cell protease enzyme (MMCP) concentration was determined by ELISA as recommended by the manufacturer (eBioscience).

**Measurement of Allergen-Specific IgG, IgE, IgG1, and IgG2a.** Serum allergen-specific IgE, IgG1, and IgG2a were detected by an indirect sandwich-type enzyme-linked immunosorbent assay (ELISA) using standard protocols as described earlier.[11,15−17] In brief, 96-well microtiter plates (Costar, Corning Inc., NY, USA) were coated with 100 μL of EW, PN, and whey antigens (50 μg/mL in 50 mM carbonate buffer; $NaHCO_3/Na_2CO_3$, pH 9.6) for 24 h at 4 °C. Rabbit anti-mouse IgG conjugated to alkaline phosphatase was used for the detection of IgG, and rat monoclonal anti-mouse IgE was used for IgE followed by streptavidin−HRP conjugate. For IgG1 and IgG2 rat monoclonal anti-mouse IgG1 and IgG2a were used followed by streptavidin−HRP conjugate. In brief, plates were washed and blocked with 2% bovine serum albumin/phosphate-buffered saline (PBS) at 37 °C for 1 h. Serum samples (diluted 1:10 for IgE measurement, 1:100 for IgG, IgG1, or IgG2a) in PBS containing 0.05% Tween 20 (PBS/Tween) were added and incubated for 2 h at room temperature in duplicates. Plates were again washed, and the bound antibodies were detected by adding respective detection antibodies at room temperature for 1 h. Specific binding activity was detected by the addition of 100 μL/well of 3,3′,5,5′-tetramethylbenzidine substrate (Sigma). The reaction was terminated with 2 N $H_2SO_4$ after 30 min, and absorbance at 415 nm was measured by a microtiter reader (Bio-Rad 550, Hercules, CA, USA). The data were expressed as percentage of positive control in optical density units. Percentage of positive control activity = (mean test OD/mean positive control serum OD) × 100.

**Determination of Specific IgA in Mouse Fecal Pellets.** Antigen-specific IgA was measured in mouse fecal pellets collected freshly on a weekly basis at weeks 9, 10, and 11 and was processed as described earlier.[11] Indirect ELISA procedure for measuring specific IgA was followed as described earlier[11] except for the coating antigens replaced with EW, PN, and whey (10 μg/100 μL/well of antigens).

**Quantification of Specific Cytokines in Splenocytes.** Post oral challenge, mice from each group were euthanized, and individual spleens were aseptically removed and minced. After erythrocyte lysis, spleen cells were resuspended in complete medium (RPMI 1640 containing 10% fetal bovine serum, 2 mM L-glutamine, 25 mM Hepes, 100 IU/mL penicillin, 100 mg/mL streptomycin). Spleen lymphocytes from individual mice were used in further analysis of cytokine measurements. Splenocyte suspensions at a concentration of $2.5 \times 10^6$ cells/well were daily stimulated with 50 μg/well of EW, PN, and whey antigens, respectively, for 72 h, whereas splenocytes from the mice treated with CT were added with 50 μL of saline as controls (unstimulated). The plates were covered and incubated at 37 °C in a 5% $CO_2$ incubator with 95% humidity, and after 72 h, the aliquots were stored at −80 °C until further use. Concentrations of cytokines IFN-γ, IL-4, IL-10, IL-12, and TGF-β were determined using commercially available ELISA kits according to the manufacturer's instructions as described earlier.[11]

**Flow Cytometry.** Flow cytometry was done using whole blood collected postchallenge from individual mice and pooled in duplicates ($n$ = 4/group). Staining protocols were carried out as recommended by the manufacturer (BD Bioscience, San Jose, CA, USA). Samples were stained with 100 μL of FITC-conjugated anti-mouse CD25 antibody (558642; BD Bioscience) and phycoerythrin (PE)-conjugated anti-mouse Foxp3 (clone FJKS-16; eBioscience) measured via a fluorescence activated cell sorter (FACScan Flow cytometer; BD Bioscience). After forward-scatter versus side-scatter gating, fluorescence channels were analyzed and thresholds were set on isotype controls. Analysis was done using FCS Express 4 Plus software, and results were presented as percentage of double-stained $CD25^+$ $Foxp3^+$ cells.

**Statistical Analyses.** All data were analyzed using GraphPad Prism software version 5.0 (GraphPad Software, San Diego, CA, USA). All data were expressed as means ± SEM and subjected to ANOVA analyses followed by post hoc multiple comparison using Tukey's test. Comparison of all the end point differences with a level of $p < 0.05$ was considered significant.

## RESULTS

**SDS-PAGE.** Modifications of proteins due to the Maillard reaction in the presence or absence of CHO were observed as evidenced by the electrophoretic pattern. Figure 2 presents the SDS-PAGE pattern of the common allergens (EW, PN, and whey) before Maillard reaction (native, nonmodified protein) and after heating with allergen in the presence of mannose. All proteins heated in the presence of CHO appeared to be more

stable and were detected with a molecular weight slightly higher than that of the native protein, indicating occurrence of glycosylation. Moreover, slight aggregate formation was observed with PN and whey proteins, which was manifested by its presence at the boundary of the resolving and stacking gel. Nonglycated fractions were not visible, confirming negligible amounts of intact proteins in the glycated fractions. The binding ratios of the glycated fractions are given in Table 1.

**Table 1. Binding Ratio of the Conjugates**

| glycated protein | CHO concn/protein concn ratio (w/w) |
|---|---|
| EW-M | 3.85 |
| PN-M | 6.67 |
| PN-G | 6.67 |
| whey-M | 8.00 |

**Attenuation of Allergic Phenotype.** Both clinical signs and clinical scores were less severe and frequent in the mannosylated EW group (Figure 3A; $p < 0.05$). Histamine concentration was significantly reduced in the mannosylated EW group (Figure 3B; $p < 0.05$), and MMCP concentration (Figure 3C; $p < 0.05$) was significantly reduced in both mannosylated EW and PN groups. All other groups did not differ significantly ($p > 0.05$).

**Immunoglobulin Isotype-Related Antibody Activity.** Specific IgG, IgG1, and IgE isotypes were significantly different in the mannosylated EW group (Figure 4; $p < 0.05$). Specific IgG2 did not differ between groups ($p > 0.05$). Also, specific IgA as observed with glucosylated and mannosylated PN groups was less as compared to the native PN ($p < 0.05$) group. Specific IgA did not differ for the EW and whey groups ($p > 0.05$).

**Cytokine Concentration.** Concentrations of type-1 cytokines IL-12 and IFN-$\gamma$, type-2 cytokine IL-4, regulatory cytokines IL-10 and TGF-$\beta$, and pro-inflammatory cytokine IL-17A were measured. There was a significant decrease (Figure 5; $p < 0.05$) in IL-4 and a significant increase (Figure 5; $p < 0.05$) with IL-10 cytokines measured with the mannosylated EW group. Other groups did not differ significantly for the measured cytokines ($p > 0.05$).

**Proportion of T-Regulatory Cells.** The proportion of blood T-regs was measured, and there was a significant increase in the percentage of $CD25^+$ $Foxp3^+$ cells as measured in the mannosylated EW group (Figure 6; $p < 0.05$). All other groups treated otherwise did not differ significantly ($p > 0.05$). A representative image for each treatment group is shown in Figure 6.

## DISCUSSION

Structural changes of proteins that evolve due to conjugation of proteins with reducing sugars through the Maillard reaction are an effective way of improving the functionality of the protein, and this also seems to be a promising method for masking food protein allergenicity. We have for the first time, to the best of our knowledge, established that mannosylated EW plays a

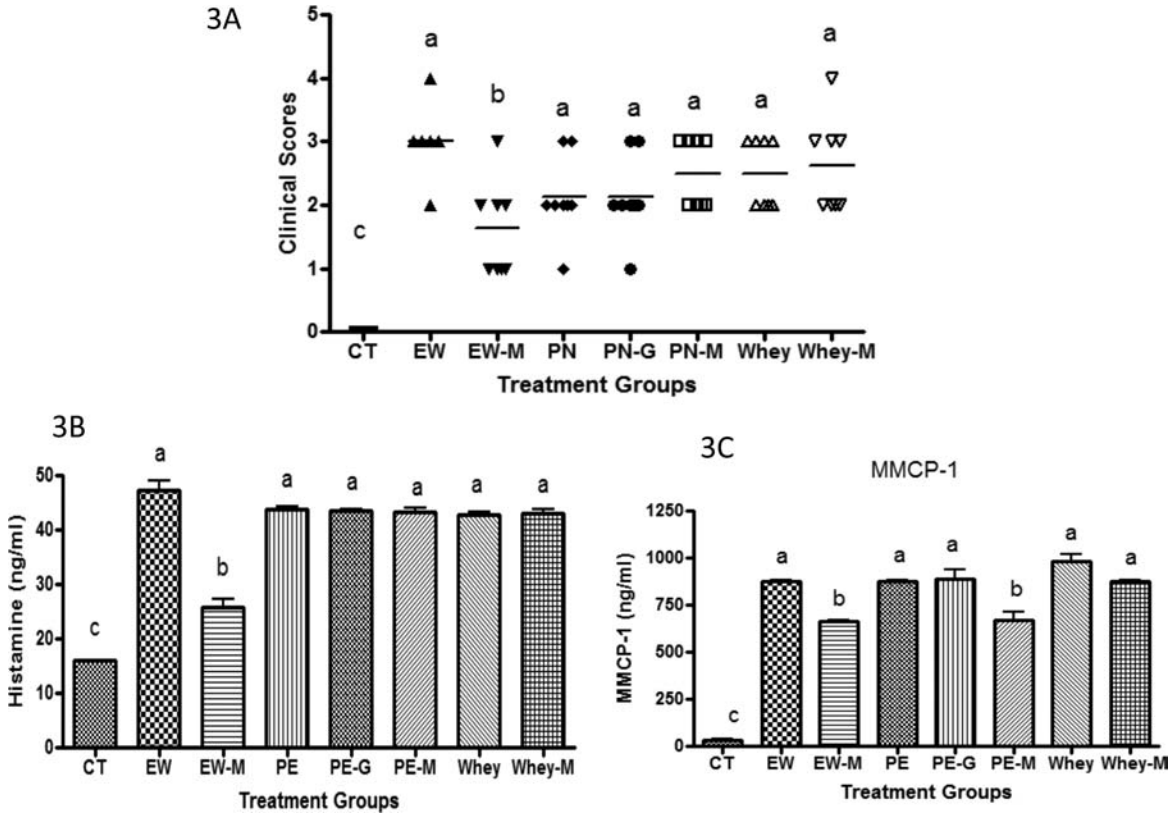


**Figure 3.** (A) Clinical scores for individual mice. Total clinical scores for each mouse post oral challenge on week 11 were calculated. Average scores were assigned by three independent observers in a blind fashion. Treatment groups differed significantly ($p \leq 0.05$; GraphPad Instat) in frequency of mice expressing allergic signs. (B) Serum histamine concentration. Data for serum histamine concentration are presented as mean ± standard deviation ($n = 4$ pooled sera). (C) Mouse mast cell protease (MMCP) concentration. Data for MMCP concentration are presented as mean ± SD. Different letters indicate statistically significant differences ($p < 0.05$) between groups of mice.

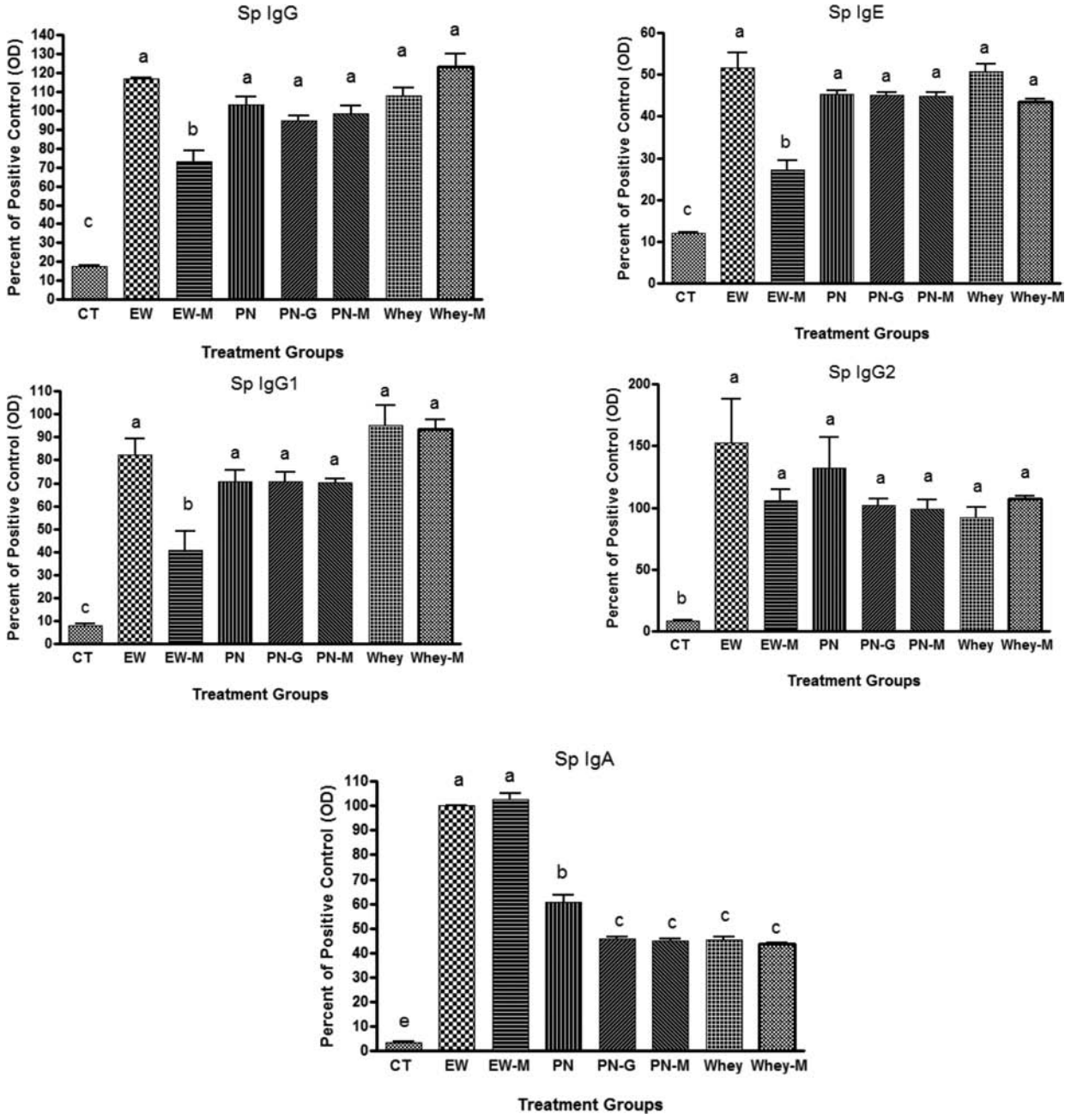


**Figure 4.** Antigen-specific IgG, IgE, IgG1, IgG2, and IgA-related antibody activity. Antigen-specific serum antibody activity was measured by ELISA in triplicates for each sample. Rabbit anti-mouse IgG conjugated to alkaline phosphatase was used for the detection of IgG, and rat monoclonal anti-mouse IgE was used for IgE followed by streptavidin−HRP conjugate. For IgG1 and IgG2 rat monoclonal anti-mouse IgG1 and IgG2a were used followed by streptavidin−HRP conjugate. IgA was detected from pooled fecal samples collected during weeks 9−11 using biotinylated rat monoclonal anti-mouse IgA antibody followed by avidin−HRP conjugate. Data are presented as percentage of positive control (sera from mice that had high Ovm-specific IgG) activity, calculated as [optical density (OD) of test serum]/(OD of positive control serum − OD of negative control) × 100%. Significance was taken at $p \leq 0.05$. Different letters indicate statistically significant differences.

critical role in attenuating the development of allergic sensitization. Mice were significantly protected against most of the aspects of allergic inflammatory response for the biomarkers tested. There was a significant difference in the IR phenotype measured with the mannosylated EW group, such that the mice had reduced clinical scores, histamine, and MMCP. Mice also had less specific IgG and IgE as compared to the EW group. Cytokine profiles revealed that the mannosylated EW group had less IL-4 and more IL-10. The proportion of T-regs differed significantly from those of the native EW group. It may be postulated that structural changes to mannosylated EW may have affected the stability and uptake of the protein, thereby altering its digestability and absorption, and this may have resulted in reduction of its allergenic potential.

Mannosylated PN and whey did not attenuate allergic signs, indicating that these proteins do not functionally interact to augment inhibition of the effector phase of the allergic inflammatory response and did not appear to be important determinants of modulating the outcomes of allergic signs. It


dx.doi.org/10.1021/jf503109r | J. Agric. Food Chem. 2014, 62, 9479−9487

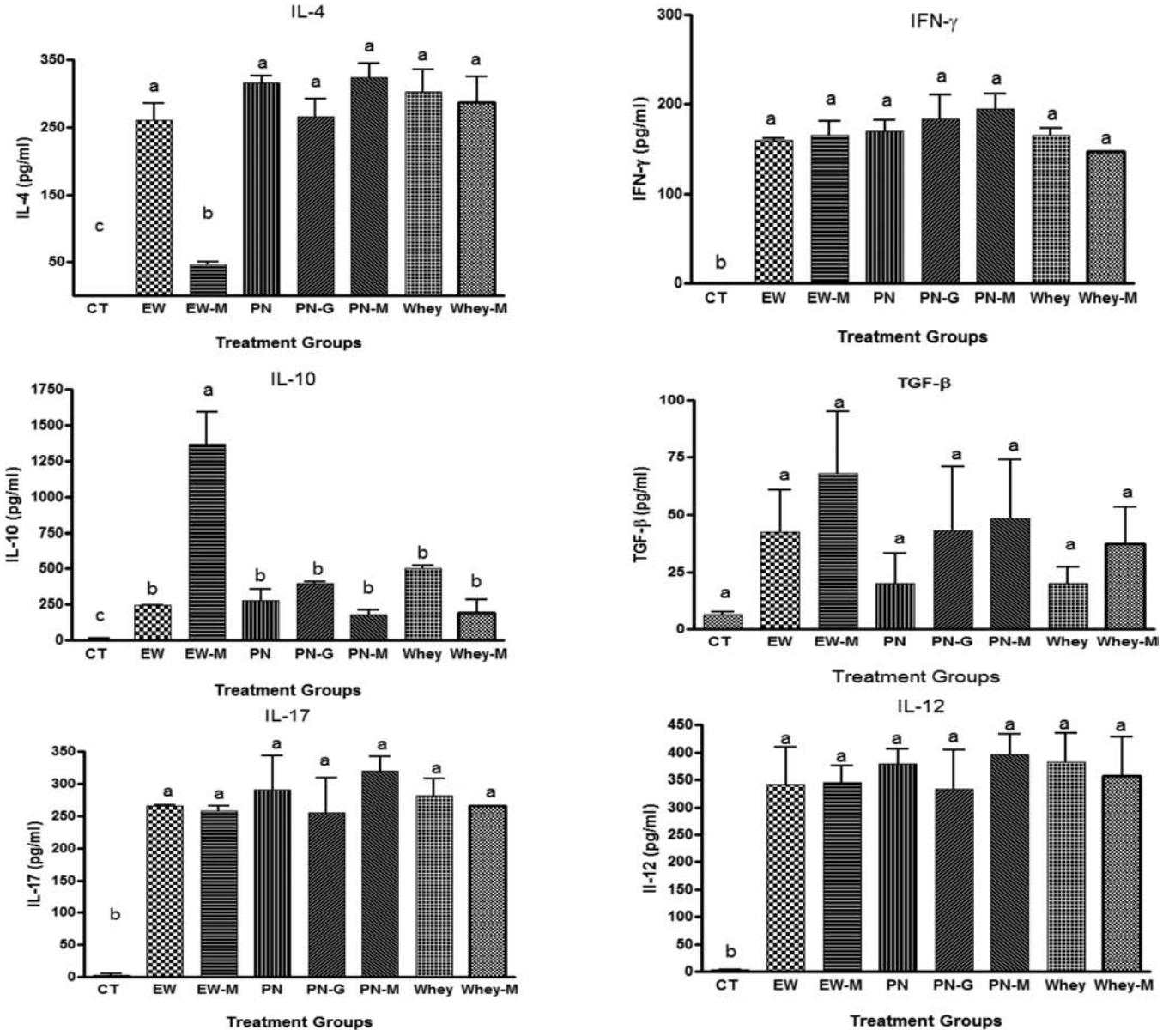


**Figure 5.** Cytokine concentration. Spleens were collected from each mouse and pooled within groups ($n$ = 4), and splenocytes were isolated and cultured at $2.5 \times 10^6$ cells/mL concentration of cells in triplicate wells as unstimulated (control) or stimulated with 50 $\mu$g/well each antigen for 72 h. The cytokine concentration of cell culture supernatants for IL-4, IFN-$\gamma$, IL-12, IL-10, TGF-$\beta$, and IL-17 was determined by ELISA. Different letters indicate significant difference between groups for each cytokine. Significance was taken at $p \leq 0.05$.

was earlier demonstrated that extracts from roasted PN were shown to bind higher IgE levels than extracts from raw PN,[20] and other studies have supported a role of advanced glycated products in enhancing IgE binding.[21] This is in good agreement with the study conducted here that both glucosylated and mannosylated PN did not alleviate clinical signs of allergy in Balb/c mice. Most of the biomarkers tested for allergy did not differ significantly as compared to the native PN antigen group, except for reduced MMCP concentration as observed in the mannosylated PN group. MMCPs under normal/unprovoked conditions are sequestered within the MC granule, and degranulation of MC leads to the massive release of fully active MC proteases.[22] An inhibitory allergic effect may result from reduced concentration of MMCP; however, in this case, although protein mediator releasing capacity was low with MMCP, it is unclear what contibuted to overall allergic signs of the mannosylated PN group, so this hypothesis requires further studies.

Effects of heat treatment on whey protein isolate (WPI) were reported earlier by Bu et al.,[23] and they showed that the antigenicity of WPI increased with increasing temperature from 50 to 90 °C. However, antigenicity remarkably decreased above 90 °C. This was similar to the observation in this study that whey protein incubated at 55 °C for 3 days did not decrease allergenicity in vivo. It may be possible that Maillard reaction may have led to the exposure of allergenic whey protein epitopes of the native molecule due to the unfolding of conformational structure. New epitopes may have emerged as a result of the conjugation process and led to the exposure of the hydrophobic region. On the other hand, effects of Maillard reaction of WPI with glucose were investigated earlier using response surface methodology, and the results demonstrated that the conjugation of WPI with glucose effectively reduced


dx.doi.org/10.1021/jf503109r | J. Agric. Food Chem. 2014, 62, 9479−9487

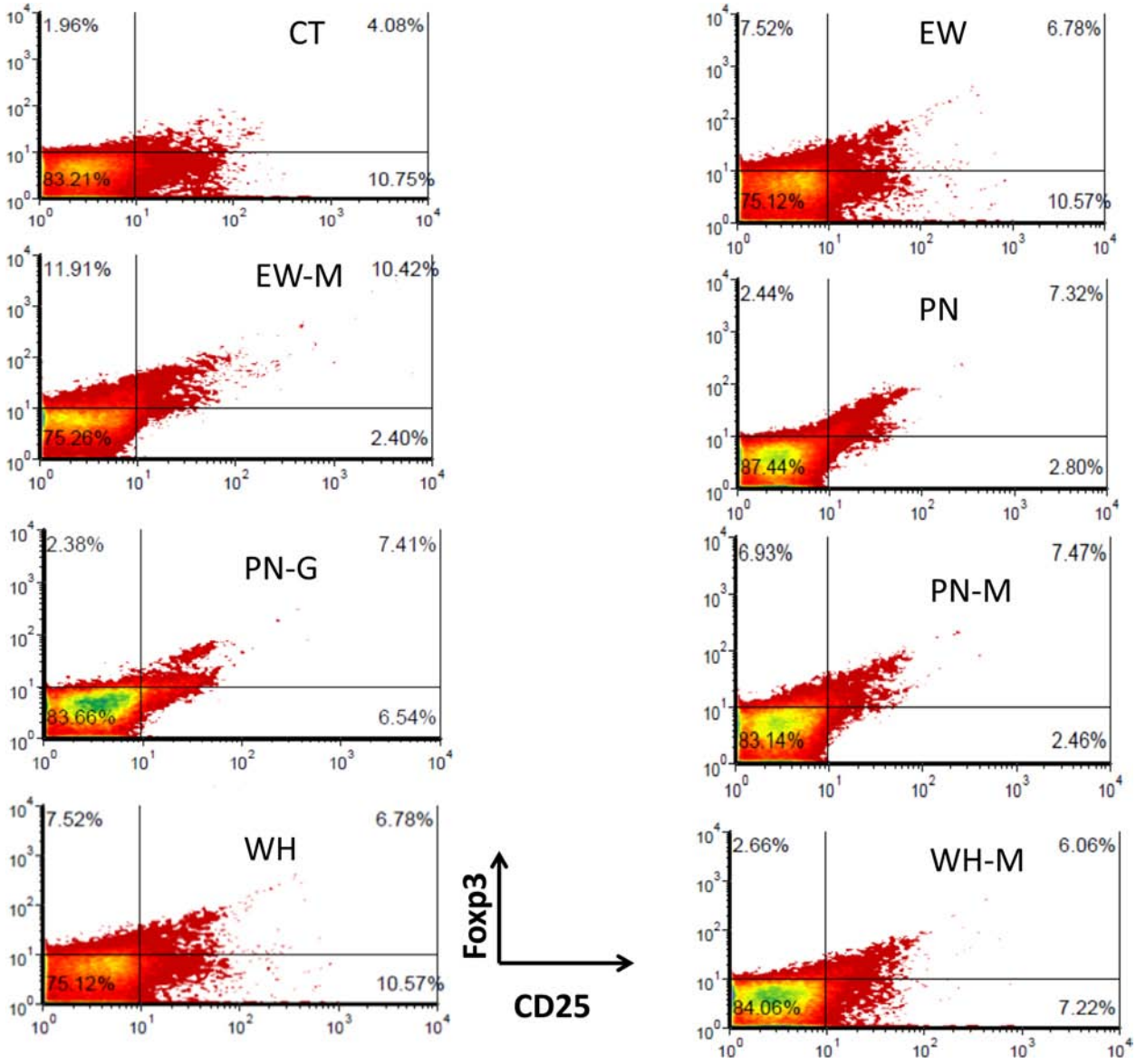


**Figure 6.** Flow cytometry. Percentage of $CD25^+$ $Foxp3^+$ cells was determined by FACS from whole blood of mice collected post oral challenge. A representative image of $CD25^+$ $Foxp3^+$ cells for each group and respective percentage of cells for each quadarant are shown.

the antigenicity.[24] It was also shown earlier that that the antigenicity of $\beta$-lactoglobulin and bovine serum albumin, major allergens in WPI, were significantly reduced by glycation with maltopentaose (MP) or glycation and phosphorylation, respectively.[25,26]

Several studies have earlier demonstrated that antigen mannosylation or mannosylated Ag delivery systems, such as mannosylated liposomes, could enhance not only MHC class II- but also MHC class I-restricted Ag presentation and T cell stimulation by targeting mannose receptors on Ag-presenting cells.[27,28] It was also shown that oligomannose-coated liposome ameliorates allergic signs in OVA-sensitized allergic mice.[29] In this study, the Maillard reaction induced changes in mannosylated EW allergic functionality. We speculate that the loss of secondary structure may have led to the destruction of conformational epitopes and thus to a decreased IgE binding capacity, and this may have had an effect on EW allergenicity. Also, mannosylation may have reduced the digestibility and absorption of the EW allergen in mouse. It was earlier reported that glycation of EW with MP reduced antiovomucoid and anti-OVA antibody response, and glycation and phosphorylation of EW by dry-heating overall improved the functional properties of EW protein.[30] We had demonstrated earlier via mannosylation of OVA that a change in secondary structure and processing via dendridic cell uptake and T cell activation led to alleviated allergic signs in mice.[11] However, circular dichroism for measuring secondary structure of EW, PN, and whey was not performed here due to the complex nature of the proteins. It was earlier shown that the transfer of $CD25^+$ T regs suppresses Th2-dependent reactions to allergens in vivo by an IL-10-mediated pathway and is thus able to reduce airway hyper-reactivity in a mouse model.[31] It is also known that the skew from type-2 allergic response to T reg predominance and influence of T reg-derived IL-10 response are known to strongly suppress allergen-specific IgE production.[32] Work done here confirms this and supports the concept that T reg-derived IL-10 may have used a similar molecular pathway to suppress allergen-specific IgG, IgG1, and IgE with mannosy-


dx.doi.org/10.1021/jf503109r | J. Agric. Food Chem. 2014, 62, 9479−9487

lated EW. Also, Aoki et al. have earlier confirmed that attachments of mannose to Cry j 1 allergen increased the colocalization of antigen with immune cells, such as dendritic cells, which have a mannose receptor, and it is expected that Cry j 1−mannnose conjugate is presented to antigen-presenting cells, such as dendritic cells, by mediation of a mannose receptor, leading to sequent antigen presenting to regulatory T cells.[33] This may be one of the possible mechanisms occurring here for increased frequency of T reg cells in the EW-M group.

Overall, this study reveals that mannosylated EW effectively suppressed orally induced allergic IR in mice. Several pieces of mechanistic evidence as derived from this study suggest that mannosylated EW modifies numerous surrogate clinical markers of allergy and validates a practical approach to cure egg allergy. Nevertheless, it also concludes that this approach does not seem to apply to any given allergen such as PN or whey. These results could have important implications for therapeutic use and potentially be targeted as a valid strategy for the effective treatment of egg allergy.

## AUTHOR INFORMATION

### Corresponding Author

*(Y.M.) Phone: (519) 824-4120, ext. 52901. Fax: (519) 824-6631. E-mail: ymine@uoguelph.ca.

### Notes

The authors declare no competing financial interest.

## REFERENCES

(1) Sicherer, S. H.; Sampson, H. A. Food allergy. *J. Allergy Clin Immunol.* **2006**, *117*, S470−S475.

(2) Wood, R. A. The natural history of food allergy. *Pediatrics* **2003**, *111*, 1631−1637.

(3) Escudero, C.; Quirce, S.; Fernández-Nieto, M.; Miguel, J.; Cuesta, J.; Sastre, J. Egg white proteins as inhalant allergens associated with baker's asthma. *Allergy* **2003**, *58*, c616−c620.

(4) Clark, A. T.; Islam, S.; King, Y. Successful oral tolerance induction in severe peanut allergy. *Allergy* **2009**, *64*, 1218−1220.

(5) Mondoulet, L.; Paty, E.; Drumare, M. F.; Ah-Leung, S.; Scheinmann, P.; Willemot, R. M.; Wal, J. M.; Bernard, H. Influence of thermal processing on the allergenicity of peanut proteins. *J. Agric. Food Chem.* **2005**, *53*, 4547−4553.

(6) Vissers, Y. M.; Blanc, F.; Skov, P. S.; Johnson, P. E.; Rigby, N. M.; Przybylski-Nicaise, L.; Bernard, H.; Wal, J. M.; Ballmer-Weber, B.; Zuidmeer-Jongejan, L.; Szépfalusi, Z.; Ruinemans-Koerts, J.; Jansen, A. P.; Savelkoul, H. F.; Wichers, H. J.; Mackie, A. R.; Mills, C. E.; Adel-Patient, K. Effect of heating and glycation on the allergenicity of 2S albumins (Ara h 2/6) from peanut. *PLoS One* **2011**, *6*, No. e23998.

(7) Taheri-Kafrani, A.; Gaudin, J.; Rabesona, H.; Nioi, C.; Agarwal, D.; Drouet, M.; Chobert, J. M.; Bordbar, A. K.; Haertle, T. Effects of heating and glycation of $\beta$-lactoglobulin on its recognition by IgE of sera from cow milk allergy patients. *J. Agric. Food Chem.* **2009**, *57*, 4974−4982.

(8) Hilmenyuk, T.; Bellinghausen, I.; Heydenreich, B. Effects of glycation of the model food allergen ovalbumin on antigen uptake and presentation by human dendritic cells. *Immunology* **2010**, *129*, 437−445.

(9) Ilchmann, A.; Burgdorf, S.; Scheurer, S.; Waibler, Z.; Nagai, R.; Wellner, A.; Yamamoto, Y.; Yamamoto, H.; Henle, T.; Kurts, C.; Kalinke, U.; Vieths, S.; Toda, M. Glycation of a food allergen by the Maillard reaction enhances its T-cell immunogenicity: role of macrophage scavenger receptor class A type I and II. *J. Allergy Clin. Immunol.* **2010**, *125*, 175−183.

(10) Heilmann, M.; Wellner, A.; Gadermaier, G.; Ilchmann, A.; Briza, P.; Krause, M.; Nagai, R.; Burgdorf, S.; Scheurer, S.; Vieths, S.; Henle, T.; Toda, M. Ovalbumin modified with pyrraline, a Maillard reaction product, shows enhanced T-cell immunogenicity. *J. Biol. Chem.* **2014**, *289*, 7919−7928.

(11) Rupa, P.; Nakamura, S.; Katayama, S.; Mine, Y. Effects of ovalbumin glycoconjugates on alleviation of orally induced egg allergy in mice via dendritic-cell maturation and T-cell activation. *Mol. Nutr. Food Res.* **2013**, *58*, 405−417.

(12) Gazi, U.; Martinez-Pomares, L. Influence of the mannose receptor in host immune responses. *Immunobiology* **2009**, *214*, 554−561.

(13) Royer, P. J.; Emara, M.; Yang, C.; Al-Ghouleh, A.; Tighe, P.; Jones, N.; Sewell, H. F.; Shakib, F.; Martinez-Pomares, L.; Ghaemmaghami, A. M. The mannose receptor mediates the uptake of diverse native allergens by dendritic cells and determines allergen-induced T cell polarization through modulation of IDO activity. *J. Immunol.* **2010**, *185*, 1522−1531.

(14) Al-Ghouleh, A.; Johal, R.; Sharquie, I. K.; Emara, M.; Harrington, H.; Shakib, F.; Ghaemmaghami, A. M. The glycosylation pattern of common allergens: the recognition and uptake of Der p 1 by epithelial and dendritic cells is carbohydrate dependent. *PLoS One* **2012**, *7*, No. e33929.

(15) Jiménez-Saiz, R.; Rupa, P.; Mine, Y. Immunomodulatory effects of heated ovomucoid-depleted egg white in a BALB/c mouse model of egg allergy. *J. Agric. Food Chem.* **2011**, *59*, 13195−13202.

(16) Rupa, P.; Hamilton, K.; Cirinna, M.; Wilkie, B. N. Porcine IgE in the context of experimental food allergy: purification and isotype-specific antibodies. *Vet. Immunol. Immunopathol.* **2008**, *125*, 303−314.

(17) Li, E. W. Y.; Mine, Y. Comparison of chromatographic profile of glycomacropeptide from cheese whey isolated using different methods. *J. Dairy. Sci.* **2004**, *87*, 174−177.

(18) Dubois, M.; Gilles, K. A.; Hamilton, J. K.; Rebers, P. A.; Smith, F. Colorimetric method for determination of sugars and related substances. *J. Anal. Chem.* **1956**, *28*, 350−356.

(19) Smith, P. K.; Krohn, R. I.; Hermanson, G. T.; Mallia, A. K.; Gartner, F. H.; Provenzano, M. D.; Fujimoto, E. K.; Goeke, N. M.; Olson, B. J.; Klenk, D. C. Measurement of protein using bicinchoninic acid. *Anal. Biochem.* **1985**, *150*, 76−85.

(20) Maleki, S. J.; Chung, S. Y.; Champagne, E. T.; Raufman, J. P. The effects of roasting on the allergenic properties of peanut proteins. *J. Allergy Clin. Immunol.* **2000**, *106*, 763−768.

(21) Nesbit, J. B.; Hurlburt, B. K.; Schein, C. H.; Cheng, H. P.; Wei, H.; Maleki, S. J. Ara h 1 structure is retained after roasting and is important for enhanced binding to IgE. *Mol. Nutr. Food Res.* **2012**, *56*, 1739−1747.

(22) Pejler, G.; Rönnberg, E.; Waern, I.; Wernersson, S. Mast cell proteases: multifaceted regulators of inflammatory disease. *Blood* **2010**, *115*, 4981−4990.

(23) Bu, G. H.; Luo, Y. K.; Zheng, Z.; Zheng, H. Effect of heat treatment on the antigenicity of bovine $\alpha$-lactalbumin and $\beta$-lactoglobulin in whey protein isolate. *Food Agric. Immunol.* **2009**, *20*, 195−206.

(24) Bu, G. H.; Lu, J.; Zheng, Z.; Luo, Y. K. Influence of Maillard reaction conditions on the antigenicity of bovine $\alpha$-lactalbumin using response surface methodology. *J. Sci. Food Agric* **2009**, *89*, 2428−2434.

(25) Enomoto, H.; Li, C. P.; Morizane, K.; Ibrahim, H. R.; Sugimoto, Y.; Ohki, S.; Ohtomo, H.; Aoki, T. Glycation and phosphorylation of $\beta$-lactoglobulin by dry-heating: effect on protein structure and some properties. *J. Agric. Food Chem.* **2007**, *55*, 2392−2398.

(26) Enomoto, H.; Li, C. P.; Morizane, K.; Ibrahim, H. R.; Sugimoto, Y.; Ohki, S.; Ohtomo, H.; Aoki, T. Improvement of functional properties of bovine serum albumin through phosphorylation by dry-heating in the presence of pyrophosphate. *J. Food Sci.* **2008**, *73*, 84−91.

(27) Sheng, K. C.; Kalkanidis, M.; Pouniotis, D. S.; Esparon, S.; Tang, C. K.; Apostolopoulos, V.; Pietersz, G. A. Delivery of antigen using a novel mannosylated dendrimer potentiates immunogenicity in vitro and in vivo. *Eur. J. Immunol.* **2008**, *38*, 424−436.

(28) Zhou, X.; Liu, B.; Yu, X.; Zha, X.; Zhang, X.; Wang, X.; Jin, Y.; Wu, Y.; Chen, Y.; Shan, Y.; Chen, Y.; Liu, J.; Kong, W.; Shen, J. Controlled release of PEI/ DNA complexes from mannose-bearing chitosan microspheres as a potent delivery system to enhance immune

response to HBV DNA vaccine. *J. Controlled Release* **2007**, *121*, 200−207.
(29) Kawakita, A.; Shirasaki, H.; Yasutomi, M.; Tokuriki, S.; Mayumi, M.; Naiki, H.; Ohshima, Y. Immunotherapy with oligomannose-coated liposomes ameliorates allergic symptoms in a murine food allergy model. *Allergy* **2012**, *67*, 371−379.
(30) Enomoto, H.; Nagae, S.; Hayashi, Y.; Li, C. P.; Ibrahim, H. R.; Sugimoto, Y.; Aoki, T. Improvement of functional properties of egg white protein through glycation and phosphorylation by dry-heating. *Asian−Aust. J. Anim. Sci.* **2009**, *22*, 591−597.
(31) Kearley, J.; Barker, J. E.; Robinson, D. S.; Lloyd, C. M. Resolution of airway inflammation and hyperreactivity after *in vivo* transfer of $CD4^+$ $CD25^+$ regulatory T cells is interleukin 10 dependent. *J. Exp. Med.* **2005**, *202*, 1539−1547.
(32) Meiler, F.; Klunker, S.; Zimmermann, M.; Akdis, C. A.; Akdis, M. Distinct regulation of IgE, IgG4 and IgA by T regulatory cells and Toll-like receptors. *Allergy* **2008**, *63*, 1455−1463.
(33) Aoki, R.; Saito, A.; Azakami, H.; Kato, A. Effects of various saccharides on the masking of epitope sites and uptake in the gut of cedar allergen Cry j 1-saccharide conjugates by a naturally occurring Maillard reaction. *J. Agric. Food Chem.* **2010**, *58*, 7986−7990.

handling of fish was licensed by the Government of the Hong Kong Special Administrative Region and endorsed by the Animal Experimentation Ethics Committee of The Chinese University of Hong Kong.

SU5416 (1,3-dihydro-3-[(3,5-dimethyl-1*H*-pyrrol-2-yl)methylene]-2*H*-indol-2-one), a selective vascular endothelial growth factor (VEGF) receptor-2 inhibitor, was from Sigma.

**Cell Culture.** Human umbilical vein endothelial cells, HUVEC-C (CRL-1730, ATCC) at early passages (passages 8−15) were cultured in Dulbecco's modified Eagle's medium/Ham's nutrient mixture F12 (1:1) (DMEM/F12) (Gibco, catalog no. 12400-024) supplemented with 10% fetal bovine serum (Gibco, Gaithersburg, MD, USA), 0.1 mg/mL heparin (Sigma, catalog no. H3393), 0.03 mg/mL endothelial cell growth supplement (ECGS) (Sigma, catalog no. E2759), and 1% penicillin−streptomycin. Cells were incubated at 37 °C under 5% $CO_2$.

**Sample Preparation.** Samples of sclerotium were lyophilized before they were pulverized into powders to pass through a screen with a 0.5 mm sieve using a cyclotech mill (Tecator, Höganäs, Sweden). The milled powders (400 g) were extracted with 4 L of 60% ethanol three times at room temperature for 24 h, and the extract was centrifuged and filtered through no. 2 filter paper (Whatman International Ltd., Maidstone, Kent, UK), and concentrated in a rotary evaporator (Rotavapor R-200; Buchi, Postfach, Swizerland).

**Folin−Ciocalteu Assay.** The total phenolic content of EE was determined by using the Folin−Ciocalteu method with some modifications.[17] One milliliter of EE solution (1 mg/mL) was mixed with Folin−Ciocalteu reagent (1 mL). After 3 min of incubation at room temperature, 1 mL of saturated $Na_2CO_3$ (35% aqueous solution) was added to the mixture and adjusted to 10 mL with distilled water. The mixture was kept in the dark for 90 min, followed by the absorbance being read at 725 nm. Gallic acid was used to prepare the standard curve (0.01−0.4 mM). The total phenolic content of EE was expressed as gallic acid equivalents (GAE) as the amount of gallic acid (mg) per gram of extract.

**DPPH Radical Scavenging Assay.** The DPPH radical scavenging activity of EE was assayed according to the method described previously[18] with some modifications. Various concentrations (0.05−2 mg/mL) of EE or negative control (60% ethanol) (0.5 mL) were mixed with 1.0 mL of 0.1 mM DPPH radical solution. The mixture was vortex-mixed and left to stand for 30 min in the dark, the reduction of DPPH radical was determined by measuring the absorbance at 520 nm. *tert*-Butylhydroquinone (TBHQ) (1.5 g/mL) was used as standard.

The DPPH radical scavenging activity (%) was calculated by using the following equation:

$$\text{scavenging activity (\%)} = [1 - (\text{Abs}_{520\text{nm, sample}}/\text{Abs}_{520\text{nm, control}})] \times 100$$

The $IC_{50}$ value (mg/mL) refers to the effective concentration to scavenge the DPPH radicals by 50%.

**$ABTS^+$ Radical Scavenging Assay.** The $ABTS^+$ scavenging potency of EE was assayed according to the method described previously[19] with some modifications. Five milliliters of 7 mM ABTS was mixed with 88 μL of 140 mM potassium persulfate and kept for 12−16 h at room temperature in the dark to allow the completion of radical generation. The reagent was diluted with 95% ethanol to give an absorbance of 0.70 ± 0.05 at 734 nm. Then 1 mL of ABTS solution was mixed thoroughly with 10 μL of EE solution of different concentrations, and the absorbance was recorded at 734 nm at 6 min after the initial mixing, using the ethanol as blank. Trolox, with a concentration range of 0.5−2 mM, was prepared as a standard. The percentage scavenging effect was calculated as

$$\text{scavenging rate (\%)} = [1 - (\text{Abs}_{734\text{nm, sample}}/\text{Abs}_{734\text{nm, control}})] \times 100$$

The antioxidant activity of sample was expressed as Trolox equivalent antioxidant capacity (TEAC), which represented the concentration (mM) of Trolox, having the same activity as 1 mg of sample.

**Hydrogen Peroxide Scavenging Assay.** The scavenging activity of hydrogen peroxide was measured using a commercial kit (PeroXOquant Quantitative Peroxide Assay Kits, Pierce, catalog no. 23280) according to the manufacturer's instruction. Working reagent was prepared by mixing reagent A (25 mM ammonium ferrous(II) sulfate, 2.5 M $H_2SO_4$) with reagent B (100 mM sorbitol, 125 M xylenol orange in water) (1:100, v/v). EE at various concentrations (0.02−2 mg/mL) was mixed with 0.1 mM $H_2O_2$ (Wako, catalog no. 080-01206) for 15 min before assay, whereas standard was prepared by diluting 30% $H_2O_2$ to various concentrations (0−1000 μM) with water. An aliquot (20 μL) of sample or standard and 200 μL of working reagent were added into a 96-well plate. The plate was then incubated at room temperature for 20 min for the reaction. The absorbance was read at 595 nm. The concentration of $H_2O_2$ present in the sample was determined by interpolating from the sample absorbance value using the standard curve. The hydrogen peroxide scavenging activity (%) was calculated by using the following equation:

$$\text{scavenging activity (\%)} = \{1 - ([H_2O_2]_{\text{in sample}}/[H_2O_2]_{\text{in control}})\} \times 100$$

**HPLC-UV-ESI/MS Analyses.** Thirteen phenolic compound standards including flavonoids (quercetin) and phenolic acids (ellagic acid, sinapic acid, gallic acid, protocatechuic acid, chlorogenic acid, caffeic acid, syringic acid, cinnamic acid, ferulic acid, folic acid, salicylic acid, and coumaric acid) were purchased from Sigma-Aldrich (St. Louis, MO, USA). The standard stock solutions (30.3, 100, and 1000 μM) were made with the appropriate HPLC grade solvents. All standard calibration curves showed high degrees of linearity ($R^2$> 0.99) (data not shown). Sample compounds were identified on the basis of the retention times, UV spectrum, and MS spectrum of standard compounds and were quantified by comparing their peak areas with those of standard curves.

The FT-ICR MS analysis was performed using the Apex Ultra 7.0 Hybride Qh-FTMS (Bruker Daltonics Inc., USA) equipped with an Apollo II ion source and Dionex Ultimate 3000 2D Nanoflow LC system (Bruker Daltonics Inc., USA).

EE was redissolved in 60% aqueous methanol (HPLC grade) (J. T. Baker, Phillipsburg, NJ, USA) and filtered through a 0.45 μm nylon membrane filter (TITAN, Rockwood, TN, USA). A 3 μL filtrate was loaded on the HPLC and FT-MS system. Separation was achieved on an analytical (2.1 × 150 mm) C18 column (5 μm) (XBridge, Waters, Dublin, Ireland). The system was connected to two solvents used as mobile phases: Solvent A was 0.1% formic acid in Milli-Q water, and solvent B was 100% acetonitrile (Scharlau, catalog no. AC03402500). Table 1 shows the elution profile. The flow rate was 0.3 mL/min, and the temperature of the column was kept at 30 °C.

**Table 1. Elution Profile Used in the HPLC and LC-MS Analyses**

| time (min) | % formic acid (%) | 100% acetonitrile (%) |
|---|---|---|
| 0 | 95 | 5 |
| 40 | 70 | 30 |
| 45 | 50 | 50 |
| 65 | 30 | 70 |
| 70 | 30 | 70 |
| 71 | 95 | 5 |

**MTT Assay.** The MTT (3-(4,5-dimethylthiazol-2-yl)-2,5-diphenyltetrazolium bromide) assay was used to evaluate the cytotoxicity of EE on normal cell growth. In brief, cells were seeded in a 0.1% gelatin-coated 96-well plate at 2 × $10^4$ cells/well overnight. After incubation with various concentrations of EE solution for 24 h, 20 μL of 5 mg/mL MTT in phosphate-buffered saline (PBS) was added, and incubation was continued for another 4 h at 37 °C. The culture


dx.doi.org/10.1021/jf5031604 | J. Agric. Food Chem. 2014, 62, 9488−9498

**Table 2. Primers Used in Real-Time qPCR**

| gene | accession no. | primer sequence | expected size (bp) |
|---|---|---|---|
| VEGFR | NM_002253.2 | 5′-GGAACCTCACTATCCGCAGAGT-3′<br>5′-CCAAGTTCGTCTTTTCCTGGGC-3′ | 132 |
| Tie2 | NM_000459.3 | 5′-GTTCTGTCTCCCTGACCCCTAT-3′<br>5′-TAAGCTTACAATCTGGCCCGTA-3′ | 107 |
| Ang-2 | NM_001147.2 | 5′-AGATTTTGGACCAGACCAGTGA-3′<br>5′-GGATGATGTGCTTGTCTTCCAT-3′ | 139 |
| MMP-2 | NM_004530.4 | 5′-AGCGAGTGGATGCCGCCTTTAA-3′<br>5′-CATTCCAGGCATCTGCGATGAG-3′ | 138 |
| bFGF | NM_002006.4 | 5′-AGCGGCTGTACTGCAAAAACGG-3′<br>5′-CCTTTGATAGACACAACTCCTCTC-3′ | 138 |
| $\beta$-actin | NM_001101.3 | 5′-CACCATTGGCAATGAGCGGTTC-3′<br>5′-AGGTCTTTGCGGATGTCCACGT-3′ | 135 |

medium was removed, and DMSO (100 $\mu$L/well) was added. Then, after complete dissolution, absorbance was detected at 570 nm.

$$\text{cell viability expressed as \% of control vehicle} = (\text{Abs}_{570\text{nm, sample}}/\text{Abs}_{570\text{nm, control vehicle}}) \times 100\%$$

**Lactate Dehydrogenase (LDH) Toxicity Assay.** The LDH release assay was performed using a cytotoxicity detection kit plus (LDH) (Cayman) according to the manufacturer's instructions. In brief, HUVECs were seeded in a 96-well plate at a density of $2 \times 10^5$ cells/well. After incubation with various concentrations of EE solution for 24 h, cell supernatants were collected and analyzed. The absorbance of formazan formed was read at 490 nm.

**Wound-Healing Assay.** The wound-healing method was performed according to protocols reported previously[20] with some modifications. In brief, cells were seeded in a 24-well plate at a density of $3 \times 10^5$ cells/well overnight. After two washings with PBS, the cells were then scraped away horizontally in each well using a sterilized P100 pipet tip. After two washings with PBS, the cells were treated with 300 $\mu$L of various concentrations of EE (cotreated with 20 ng/mL VEGF) or 20 ng/mL VEGF only (serving as vehicle control) for 24 h. Three random views along the line were selected and photographed using an inverted microscope (Nikon ECLIPSE TS-100F) at 0 h. After 24 h, another set of images were taken by using the same method.

Image analysis for determining the extent of migration was performed by ImageJ software (NIH, Bethesda, MD, USA). The percentage of wound size after 24 h was calculated using the following equation (wound size was expressed as % of wound area when it was made):

$$\text{wound area (\%)} = [\text{wound area } (t = 24\text{ h})/\text{wound area } (t = 0\text{ h})] \times 100$$

**Transwell Culture Insert Assay.** Cell invasion properties was carried out in a modified Boyden chamber (Transwell, Corning, NY, USA) with a poly(ethylene terephthalate) filter inserted coated with a Matrigel matrix in 24-well plates containing 8 mm pores. In brief, $1 \times 10^4$ cells suspended in 100 $\mu$L of starved medium were seeded on the upper chamber followed by filling the lower chamber with 600 $\mu$L of medium with or without EE under VEGF-induced migration. After 6 h of incubation, the nonmigrated cells on the upper side of the membrane were carefully removed by cotton swab. The migrated cells on the bottom side of the membrane were fixed with methanol for 20 min and then stained with 0.1% crystal violet for 10 min. Four randomly selected fields under 10× magnification of each well were scored for migrated cells. The quantification of the invaded cells was made by submerging the chambers in 1% SDS and measuring the absorbance of the solution at 570 nm. The mean of triplicate assays for each experimental condition was calculated, and values were normalized to the untreated cells.

$$\text{invasiveness expressed as \% of control vehicle} = (\text{Abs}_{570\text{nm, sample}}/\text{Abs}_{570\text{nm, control}}) \times 100$$

**Endothelial Tube Formation Assay.** The tube formation assay was performed according to previous protocols[21] with some modifications. Cells ($1 \times 10^4$ cells/well) were seeded on a layer of Matrigel (BD Biosciences, catalog no. 354234) and exposed to various concentrations of EE with 20 ng/mL VEGF in starved medium or with starved medium only (served as vehicle control) .

After incubation for 6 h in 37 °C, images of three randomly selected fields were captured using the inverted microscope.

**Measurement of Reactive Oxygen Species.** The 2′,7′-dichlorofluorescein diacetate (DCFH-DA, Sigma) assay was used to determine the scavenging activity of ROS in HUVECs following the exposure to EE as previously described.[22] After exposure to different concentrations of EE with 20 ng/mL VEGF in starved medium or with starved medium only (serving as vehicle control) for 24 h, endothelial cells (ECs) were then incubated in DCFH-DA (0.5 $\mu$g/mL) at 37 °C for 30 min. Cells were washed with PBS three times to remove DCFH-DA that had not entered into cells. The fluorescence was measured immediately by a fluorescent plate reader ($\lambda_{ex}$ = 485 nm, $\lambda_{em}$ = 535 nm).

**RT-PCR Study for mRNA Expression.** Total RNA was isolated by using an SV Total RNA Isolation System according the manufacturer's protocol (Z3100, Promega, Madison, WI, USA) followed by reverse transcription (cDNA synthesis). Real-time qPCR was performed on the ABI7500 real-time PCR detection system in a volume of 20 $\mu$L containing 10 $\mu$L of SYBR Premix Ex *Taq*II (2×), 0.4 $\mu$L of ROX reference Dye II (50×), 2 $\mu$L of cDNA, 6 $\mu$L of $dH_2O$, and 0.8 $\mu$L of each 10 $\mu$M primer. The primers of all tested genes are listed in Table 2. The reaction mixture was subjected to denaturation at 95 °C for 2 min followed by 40 cycles of denaturation at 95 °C for 5 s, annealing at 60 °C for 15 s, and elongation at 72 °C for 35 s. A melt-curve analysis was performed at the end of the reaction consisting of 40 cycles. The relative expression levels of the mRNAs of the target genes were normalized using the $\beta$-actin internal standard.

**Quantitative Endogenous Alkaline Phosphatase Assay on Zebrafish Embryo.** During zebrafish development, the stage between 48 and 72 h past fertilization (hpf) has the highest angiogenic activity,[23] and a quantitative endogenous alkaline phosphatase (EAP) assay was performed as previouly described.[24] In brief, embryos (24

hpf) was arrayed in a 96-well plate (one embryo per well) and incubated with 100 μL of embryo water per well containing various concentrations of EE, whereas only 100 μL of embryo water without samples was set as control. After further incubation at 28.5 °C for 48 h, the medium in each well was removed, and embryos were treated with 70% ethanol (100 μL) at room temperature for 15 min and then with 100% ethanol (100 μL) at −20 °C for 30 min for dehydration purposes. The embryos were washed three times with 1× diethanolamine buffer (Pierce, Rockford, IL, USA). Then, 100 μL of staining solution was added to each well. After staining, 50 μL of the 2 M NaOH was added to stop the reaction. The optical density was determined at the wavelength of 405 nm. SU5416, a known effective inhibitory compound on angiogenesis, was chosen to conduct the parallel experiments.[24]

Vessel growth was presented as percentage formation of vessels in optical density compared to control:

$$\%\text{vessel formation} = (OD_{405nm,\ sample,\ day\ 3} - OD_{405nm,\ sample,\ day\ 1}) / (OD_{405nm,\ control,\ day\ 3} - OD_{405nm,\ control,\ day\ 1}) \times 100$$

**Microscopic Imaging.** The embryos from the Tg (fli1a: EGFP) y1 zebrafish line were used to further evaluate the antiangiogenic effect of EE. The enhanced green fluorescent protein-expressing ECs of the subintestinal vessel plexus (SIVs) were observed and recorded at 72 hpf using an Olympus IX71S8F-2 inverted microscope (Olympus, Tokyo, Japan).

**Statistical Analysis.** All experiments were performed at least three times. All data are presented as means ± SEM, and all statistics were performed using GraphPad Prism 5.0 software. Differences between means were determined by one-way analysis of variance (ANOVA) or Student's *t* test. Differences were considered to be statistically significant at $p < 0.05$.

## RESULTS

**Amount of Total Phenolics in EE and HPLC-UV-ESI/MS Analysis.** The total phenolic content (TAC) was measured and expressed in terms of gallic acid equivalents (GAE; mg/g of GAE). The amount of total phenolics in EE from sclerotium of *PTR* was 420 ± 0.33 μg/mg extract, indicating that EE contained a substantial amount of phenolic compounds.

At least five phenolic acids (including protocatechuic, chlorogenic, syringic, ferulic, and folic acid) were positively identified and quantified in EE by HPLC-UV-ESI/MS on the basis of their chromatographic characteristics and absorption spectra with reference to standard compounds (Figure 1) and confirmed by mass analysis. The results are summarized in Table 3.

**Antioxidant Activity of EE.** Three methods were utilized to analyze the antioxidant activity of EE. The results on DPPH free radical scavenging activity of EE are shown in Figure 2A. EE inhibited DPPH radicals in a dose-dependent manner with an $IC_{50}$ at about 1 mg/mL. Furthermore, EE also had demonstrated both $ABTS^+$ radical scavenging activity (13.54 ± 2.51% at 5 mg/mL) (Figure 2B) and hydrogen peroxide scavenging activity (30.82 ± 4.28% at 5 mg/mL).

The above results suggested that EE demonstrated scavenging activity toward DPPH radical, $ABTS^+$ radical, and hydrogen peroxide, which might be related to its high phenolic content.

**Cytotoxicity Evaluation of EE on HUVECs.** MTT results showed that EE did not significantly affect the viability of the HUVECs when they were cultured in normal cell culture medium (DMEM/F12 supplemented with 10% FBS) at a concentration below 200 μg/mL (Figure 3A). The MTT

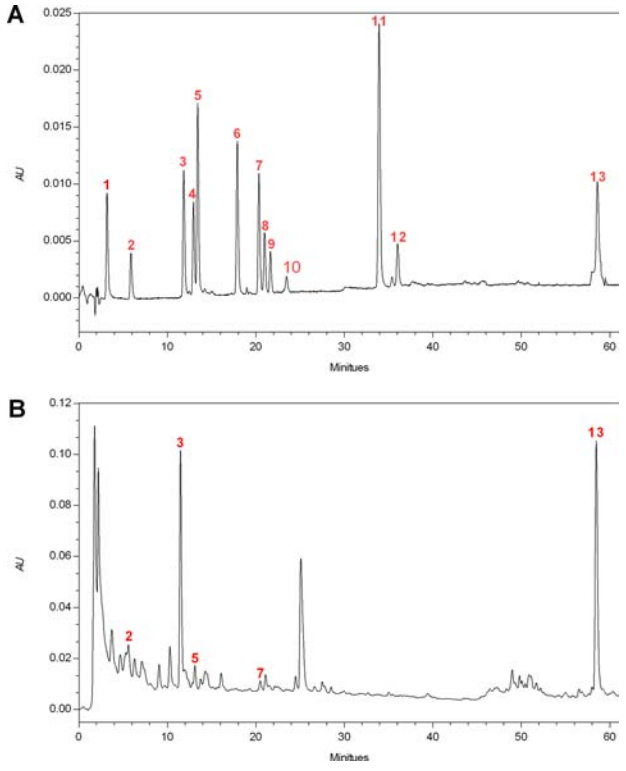


**Figure 1.** Chromatogram of phenolic compound analysis by HPLC: (A) standard mixture of 13 phenolic compounds (peaks: 1, gallic acid; 2, protocatechuic acid; 3, chlorogenic acid; 4, caffeic acid; 5, syringic acid; 6, coumaric acid; 7, ferulic acid; 8, sinapic acid; 9, ellagic acid; 10, salicylic acid; 11, cinnamic acid; 12, quercetin; 13, folic acid); (B) phenolic prolile of 60% ethanol extract from sclerotium of *PTR*.

results were further confirmed by the LDH release assay (Figure 3B). Therefore, a concentration range of EE from 3.125 to 200 μg/mL was chosen for the following cell culture experiments.

**Effects of EE on VEGF-Induced HUVEC Migration.** To find out the effects of EE on HUVEC migration, the scratch wound healing assay was performed. After scratching the monolayer HUVEC cells using a scraping tool, a denuded area was produced with the same width (red arrow shown in Figure 4A,a). Because activated motile ECs could move randomly in the direction of the angiogenic factors across a horizontal surface, the size of the wound could indicate the extent of wound closure and, therefore, the rate of cell migration.

Figure 4 illustrates the wound size of the monolayer HUVEC cells in different treatment groups after 24 h. The inhibitory effect on wound healing was increased in a dose-dependent manner after 24 h of treatment of EE. At the highest concentration of 200 μg/mL (Figure 4A,f), the percentage of wound size at 24 h was 40.90 ± 2.59%, which was significantly larger than that of the control (2.88 ± 1.76%, $p < 0.001$) (Figure 4A,c).

It was noted that quantification of the wound healing test was only arbitrary, and there were difficulties to ensure the consistency of identical growth conditions of confluence and the scraped area between control and different treatment groups.[25] Therefore, an alternative type of 2-D migration assay, the transwell culture insert method, was also performed to further confirm the inhibitory effect of VEGF-induced HUVECs migration by EE.


dx.doi.org/10.1021/jf5031604 | J. Agric. Food Chem. 2014, 62, 9488−9498

**Table 3. Identification of Phenolic Compounds in EE**

| peak | RT | UV spectrum | detected ionization form | observed mass (Da) | identified known phenolics | proportion in dry extract (%) |
|---|---|---|---|---|---|---|
| 2 | 5.583 | 259.4, 293.7 | $[2M + K]^+$ | 347.00773 | protocatechuic acid | 0.11 |
| 3 | 11.484 | 217, 240.5, 324.6 | $[M + Na]^+$ | 377.08874 | chlorogenic acid | 0.218 |
| 5 | 13.117 | 217, 274.8 | $[3M + K]^+$ | 633.12038 | syringic acid | 0.004 |
| 7 | 20.517 | 217, 234.6, 322.2 | $[2M + K]^+$ | 427.0789 | ferulic acid | 0.016 |
| 13 | 58.468 | 239.3 | $[M + H]^+$ | 442.14923 | folic acid | 0.012 |

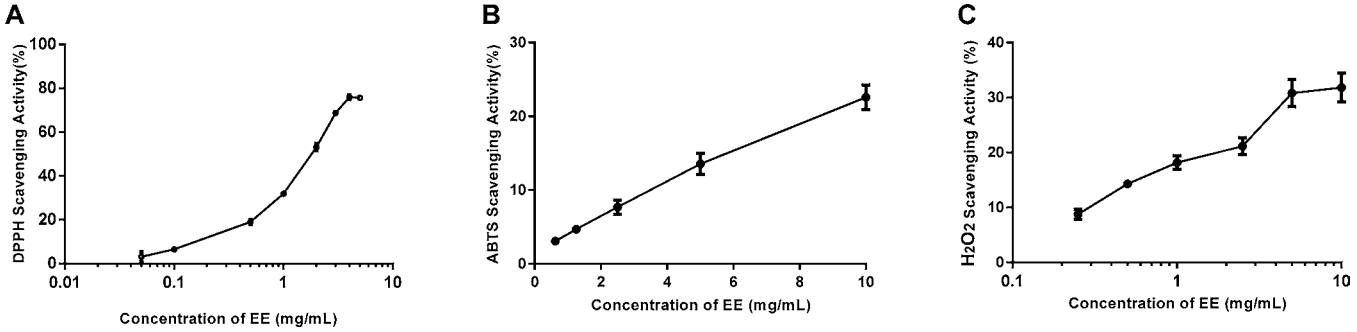


**Figure 2.** Scavenging activity of 60% ethanol extract from sclerotium of *PTR* (mean ± SD $n = 3$) on DPPH (A), $ABTS^+$ (B), and $H_2O_2$ (C) radicals.

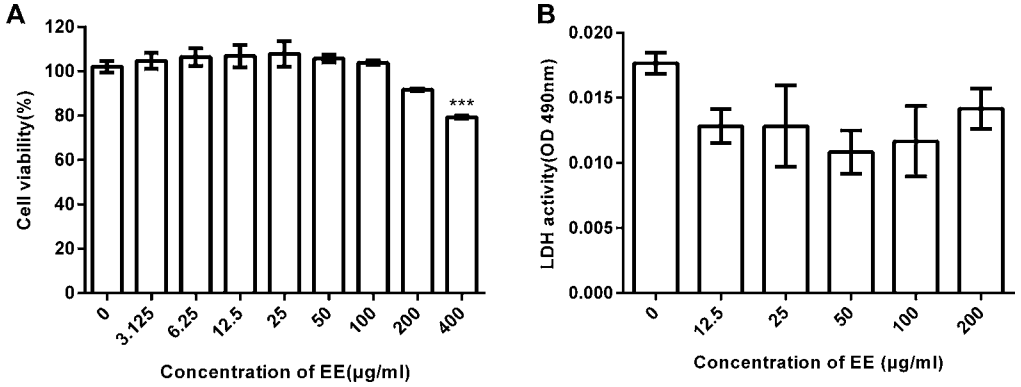


**Figure 3.** Cell viability (mean ± SD $n = 6$) after treatment with 60% ethanol extract from sclerotium of *PTR* by MTT assay (A) and LDH release activity (B) from HUVECs after treatment with 60% ethanol extract from sclerotium of *PTR*. Statistical significance was assessed by one-way ANOVA (Student's *t* test). (**) $p < 0.01$ compared with the control group.

As marked by red arrows in Figure 5, the stimulation of VEGF (20 ng/mL) could strongly promote cell migration. In contrast, co-incubation with VEGFR2 inhibitor SU5416 (4 μM) could strongly inhibit HUVEC migration by 15.02 ± 2.23%. Similarly, with the addition of various concentrations of EE, this VEGF-induced cell migration was suppressed significantly in a dose-dependent way (Figure 5C−E). When the concentration of EE reached 25 μg/mL, the number of cells migrating from the upper to the lower chamber was similar to that of the positive control (SU5416, 4 μM) (Figure 5F). These values were significantly lower ($p < 0.001$) than that of the control, indicating EE could effectively inhibit VEGF-induced HUVEC migration.

**EE Inhibit VEGF-Induced HUVEC Tube Formation.** Under normal culture conditions, ECs cultured on a Matrigel matrix could form tube-like structures within 6 h (Figure 6A), which could be further promoted by VEGF treatment (Figure 6B).

However, when treated with EE at various concentrations (6.25−200 μg/mL), this formation of a mesh of tubes on Matrigel could be inhibited dose-dependently (Figure 6C−F). The tube formation pattern of HUVECs treated with 25 μg/mL (Figure 6E) of EE was similar to that in the control group (Figure 6A), whereas those treated with 200 μg/mL (Figure 6F) mostly remained dotted on the Matrigel without extensive network of tube formation.

**Effects of EE on Intracellular ROS Level in HUVECs.** ROS derived from NADPH oxidase, which is the major source of ROS in ECs,[26] could enhance VEGFR2 autophosphorylation by inactivating protein tyrosine phosphatases (PTPs) and subsequently mediates related gene expression or signal pathways activities, such as the MMP family, angiopoetin family, Tie, PI3-kinase/Akt, and ERK1/2, and leads to the angiogenic responses including EC proliferation and migration.[27,28] We also detected the ROS levels by the DCFH-DA assay. The results indicated that VEGF (20 ng/mL) induced an 80% increase in ROS formation in untreated HUVECs after 24 h of exposure as compared to the control (Figure 7). Such an increase was alleviated after exposure to EE at a concentration of 3.125−50 μg/mL. However, when the concentration of EE was ≥100 μg/mL, the ROS level was similar to that of the control (Figure 7). This could be due to the possible activation of cell apoptosis, causing an up-regulation of the ROS level.[29]

**EE Suppress Angiogenesis-Related Gene Expression in HUVECs.** To investigate how EE could attenuate the progression of angiogenesis, the expression of the genes


dx.doi.org/10.1021/jf5031604 | J. Agric. Food Chem. 2014, 62, 9488−9498

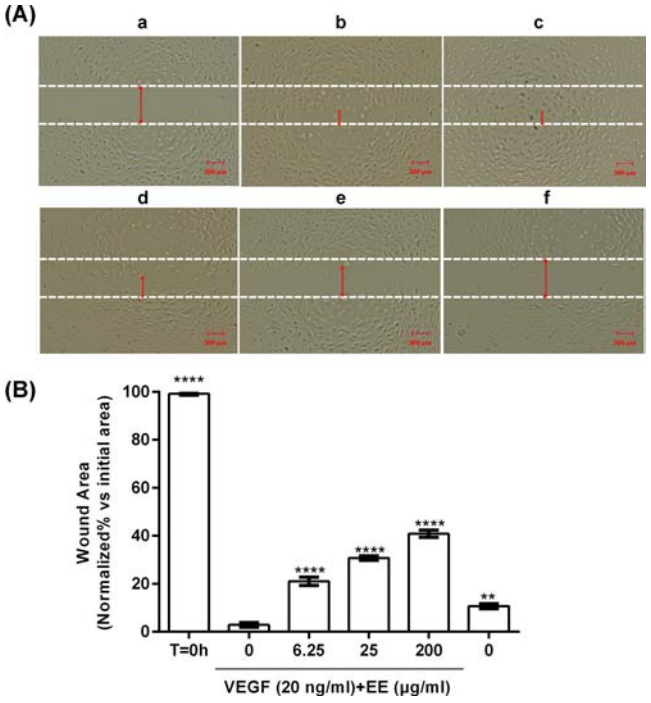


**Figure 4.** Inhibition of VEGF-induced HUVECs migration by 60% ethanol extract from sclerotium of *PTR* in wound healing assay: (A,a) microscopic image of wound size at 0 h; (A,b) without VEGF at 24 h; (A,c) with VEGF at 24 h; (A,d–f) with VEGF and 6.25, 25, and 200 $\mu$g/mL of 60% ethanol extract from sclerotium of *PTR* at 24 h (length between arrowheads indicates wound length); (B) graph of healing effect in percent wound area of EE (mean ± SEM $n = 6$) on VEGF-induced HUVECs motility (statistical significance was assessed by one-way ANOVA (Student's $t$ test); (**) $p < 0.01$; (****) $p < 0.001$ compared with VEGF-stimulated group).

involved in this process was evaluated. It was found that EE significantly decreased VEGF-induced FGF, ANG-Tie, and MMP gene expression as well as VEGFR at the mRNA level (Figure 8) in HUVECs treated with EE in a dose-dependent manner. These results indicated that the VEGF–VEGFR signal pathway was inhibited in the presence of EE in HUEVCs, which provides a critical link between the bioactive compounds in EE and VEGF-mediated activation of angiogenesis. Taken together, these results suggested that EE could regulate the angiogenesis-related signal transduction pathway and suppress the expression of angiogenesis regulation genes.

**EE Inhibits Vessel Formation in Zebrafish Embryos.** The above observations were also further examined in a zebrafish model. Quantitative EAP assay was used to measure the formation of blood vessels in the animal. It showed that incubation with 50 $\mu$g/mL EE significantly inhibited vessel formation at around 21.84 ± 0.24% in wild-type zebrafish embryos, which was similar to the positive control SU5416 at 4 $\mu$M (Figure 9).

Further experiments were conducted using transgenic zebrafish embryos [Tg (fli1a: EGFP)y1], which provides higher resolution and more definitive results. The Tg (fli1a:EGFP)y1 zebrafish contains the enhanced green fluorescent proteins (EGFP) cDNA under control of the fli1 promoter, which is expressed in all ECs of the vasculature.[30] Therefore, the ECs of the vasculature in the SIVs could be observed more clearly at 72 hpf through a fluorescent microscope on the basis of their EGFP.

The microscopic imaging results clearly showed that the control group (Figure 10A,B) treated with 0.1% DMSO had normal vessel formation, the SIVs developed normally as a smooth basket-like structure with approximately 5–6 arcades (Figure 10A,B), whereas in the transgenic zebrafish treated with 100 $\mu$g/mL EE, the development of SIVs was clearly inhibited (highlighted in arrows) (Figure 10C,D).

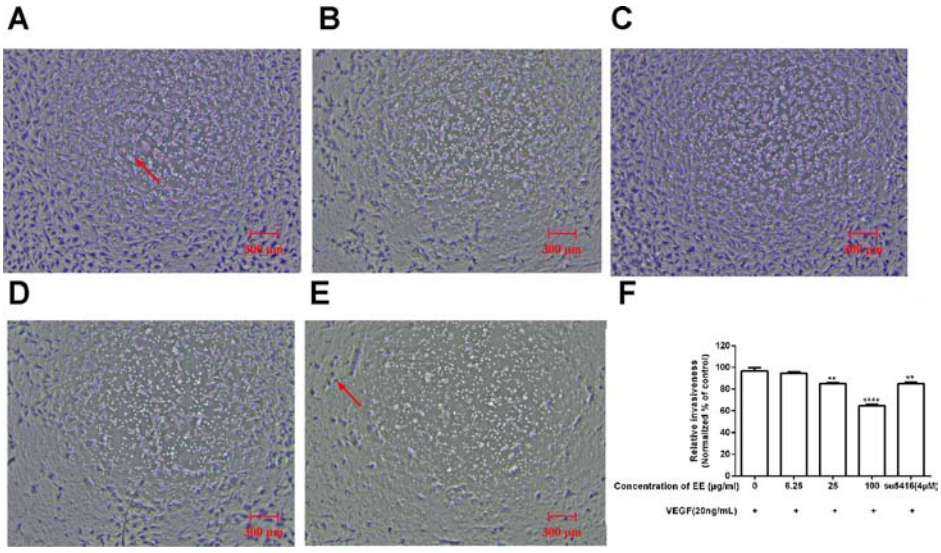


**Figure 5.** Effect of 60% ethanol extract from sclerotium of *PTR* on VEGF-induced HUVEC migration measured by transwell culture insert method: (A) microscopic image of HUVEC migration induced with 20 ng/mL VEGF; (B) with 20 ng/mL VEGF and SU5416 (4 $\mu$M); (C–E) with 20 ng/mL VEGF and 6.25, 25, and 100 $\mu$g/mL 60% ethanol extract from sclerotium of *PTR*; (F) graph shows percent invasion of 60% ethanol extract from sclerotium of *PTR* (mean ± SEM $n = 6$) on VEGF-induced HUVECs migration. Red arrows represent the migrated cells from the upper chamber to the lower chamber. Statistical significance was assessed by one-way ANOVA (Student's $t$ test). (**) $p < 0.01$ and (***) $p < 0.001$ compared with VEGF-stimulated group.


dx.doi.org/10.1021/jf5031604 | J. Agric. Food Chem. 2014, 62, 9488–9498

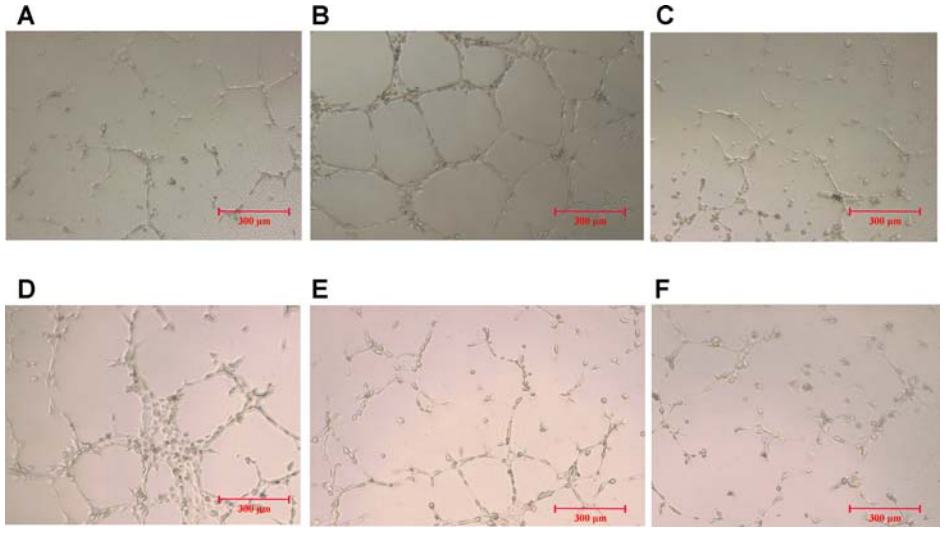


**Figure 6.** Inhibition of VEGF-induced HUVEC tubule formation by 60% ethanol extract from sclerotium of *PTR* after 6 h of incubation: (A) microscopic image of inducement without VEGF; (B) with 20 ng/mL VEGF; (C) with 20 ng/mL VEGF and SU5416 (4 $\mu$M); (D−F) with 20 ng/mL VEGF and 6.25, 25, and 200 $\mu$g/mL 60% ethanol extract from sclerotium of *PTR*.

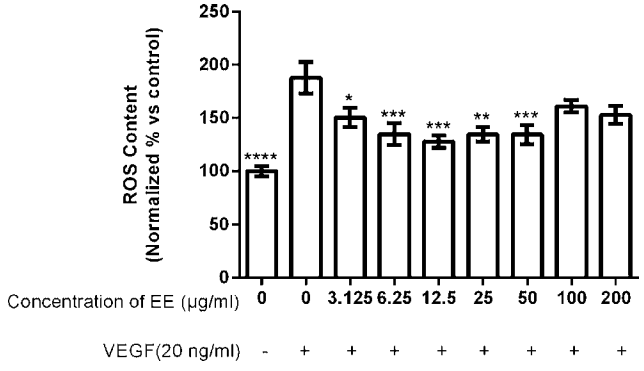


**Figure 7.** Scavenging activity of 60% ethanol extract from sclerotium of *PTR* on VEGF-induced ROS production in HUVECs. Serum-starved HUVECs were incubated with 60% ethanol extract from sclerotium of *PTR* (0−200 $\mu$g/mL) in the presence or not of VEGF (20 ng/mL) for 24 h. Statistical significance was assessed by one-way ANOVA (Student's *t* test). (**) $p < 0.01$ and (***) $p < 0.001$ compared with VEGF-stimulated group.

## DISCUSSION

*PTR* has been reported for its high nutritive value and use as a functional food,[31] although the present study is the first to report the antioxidant and antiangiogenic activities of extract from the sclerotium of *PTR*. In this study, the 60% ethanol extract of *PTR* enriched with phenolic compounds had demonstrated strong antioxidant activity and inhibition of the VEGF-induced HUVECs angiogenesis in vitro and in vivo. Three different antioxidant assays confirmed that EE could significantly scavenge free radicals (DPPH, $ABTS^{+}$, and hydrogen peroxide), implying its powerful antioxidant activity. Phenolic compounds from plants have been reckoned as the main source of antioxidants, which have beneficial implications for cancer treatments.[32,33,34] It has also been suggested that the antioxidant activities of mushrooms are contributed by their phenolic compounds.[35,36] Several studies suggested a strong correlation between the total phenolic content in mushrooms and their antioxidant activity.[19] In the present study, the HPLC-UV-ESI/MS analysis confirmed the presence of phenolic compounds in EE, of which five known phenolic acids had been identified and quantified. Not surprisingly, these identified phenolic compounds had also been reported in other mushroom species, including protocatechuic acid in *Lepista nuda* and *Ramaria botrytis*[37] and chlorogenic acid in *Flammulina Velutipes* and *Pleurotus ostreatus*.[38] It was also noted that there were other phenolics or nonphenolic compounds present in EE, which could also act as antioxidants and need to be further studied.

Several research studies have investigated the effects of polyphenolic compounds on VEGF expression and angiogenesis process. Oak et al.[39] reported that the red wine polyphenolic compounds (RWPCs) with their antioxidant properties could significantly inhibit the $PDGF_{AB}$-induced expression of VEGF, which was associated with the prevention of the ROS formation. In addition, epigallocatechin-3-gallate (EGCG) has also been shown to inhibit the expression of subunits of NADPH oxidase, which plays a pivotal role in producing superoxide in endothelial cells, namely, $p47^{phox}$ induced by angiotensin II (Ang II) in human umbilical vein endothelial cells.[40] Meanwhile, EGCG could also decrease VEGF production in head and breast carcinoma cells by inhibiting epidermal growth factor receptor-related pathways of signal transduction.[41] Meanwhile, as one of the main compounds identified in EE, folic acid has been shown to inhibit EC proliferation through activating the cSrc/ERK 2/NF-$\kappa$B/p53 pathway mediated by folic acid receptor;[42] besides, it was also found to inhibit EC migration through inhibiting RhoA activity mediated by activating the folic acid receptor/cSrc/p190RhoGAP-signaling pathway.[43] Considering the strong link between antioxidant and antiangiogenesis reported previously,[28,44] the antiangiogenic effects of EE on HUVECs were evaluated. In the present study, our findings demonstrated that VEGF-induced HUVEC migration, tube formation, and intracellular ROS level were significantly reduced after EE treatment. However, in the presence of VEGF, EE seemed to be less effective in its antiangiogenic effect when applied at a high concentration (100 $\mu$g/mL) and could even up-regulate the ROS level. This might be explained by the possible triggering of cell apoptosis due to the high concentration of phenolics. Previous studies demonstrated that high concen-


dx.doi.org/10.1021/jf5031604 | J. Agric. Food Chem. 2014, 62, 9488−9498

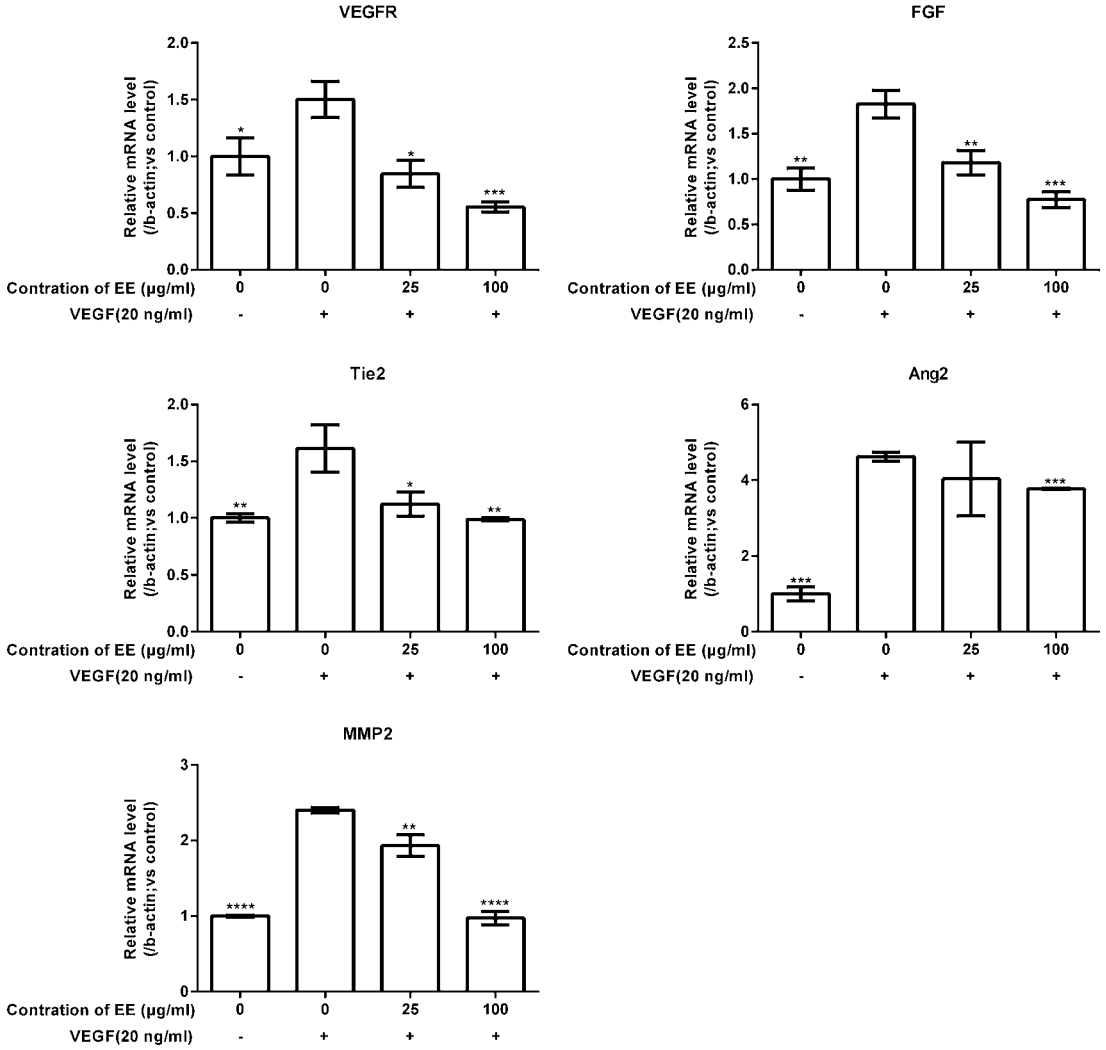


**Figure 8.** Effect of 60% ethanol extract from sclerotium of *PTR* on mRNA levels (mean ± SEM $n = 3$) of related intracellular genes (VEGFR, FGF, ANG2, Tie2, and MMP2) determined by RT-PCR. Total RNAs and cDNAs were prepared from HUVECs that had been treated with increasing concentrations of 60% ethanol extract from sclerotium of *PTR* for 7 h. Statistical significance was assessed by one-way ANOVA (Student's *t* test). (**) $p < 0.01$ and (***) $p < 0.001$ compared with VEGF-stimulated group.

tration of an apple extract rich in polyphenols increased the formation of ROS in HT-29 cells.[45] On the basis of these results, it is possible that the antiangiogenic effect observed in EE might be partly due to its phenolic compounds and is mediated by its antioxidant effect.

Angiogenesis is a process regulated by complex enzymatic and signal transduction pathway. Among the known mediators networks, VEGFA-VEGFR and angiopoietin (angpt)-Tie are two most widely studied signaling pathways involved in angiogenesis;[46−48] VEGF is the best characterized angiogenic cytokine and the most important angiogenic factor in sustaining tumor growth[49] by inducing proliferation, migration, and tubule formation of ECs.[50−52] There is much evidence suggesting that overexpression of VEGF in most hematologic malignancies is responsible for increased angiogenesis found in the malignancies.[53] Furthermore, VEGF stimulation could increase ROS production via activation of Rac1-dependent NADPH oxidase in HUVECs[54,55] and subsequently evoke the redox signaling pathway leading to angiogenic responses such as EC proliferation and migration. Many researchers[56,57] have shown that ROS are involved in VEGF-induced VEGFR2 autophosphorylation in ECs. In this research, we found EE from *PTR* could significantly decrease VEGF-induced ROS up-regulation, which was presumed to be mediated by its antioxidant activity and contribute to its antiangiogenic activity through ROS scavenging. Another important stimulator of angiogenesis is the fibroblast growth factors (FGF), first identified in 1975[58] and subsequently demonstrated to play an important role in modulating the angiogenesis process.[59] VEGF receptor signals for the effects in ECs include migration, proliferation, cell survival, and expression of downstream genes. MMP2 is also an important enzyme that degrades components of the extracellular matrix to allow the progression of angiogenesis to occur.[60] These major molecules participating in angiogenesis including VEGFR, FGF, and MMP2 were thus investigated after the HUVECs treated with EE. Indeed, mRNA expression of these angiogenic biomarkers was down-regulated by EE in a dose-dependent manner (Figure 8), suggesting a stronger effect of EE on migration and tube formation of HUVEC can be reflected in a decreased level of these angiogenic biomarkers. Besides, two other endothelial cell-specific surface receptors (Tie-1 and Tie-2) with tyrosine kinase activity are known so far and are found to hold unique functions in vascular biology as revealed by gene knockout experiments.[61] Tie-2 is present on


dx.doi.org/10.1021/jf5031604 | J. Agric. Food Chem. 2014, 62, 9488−9498

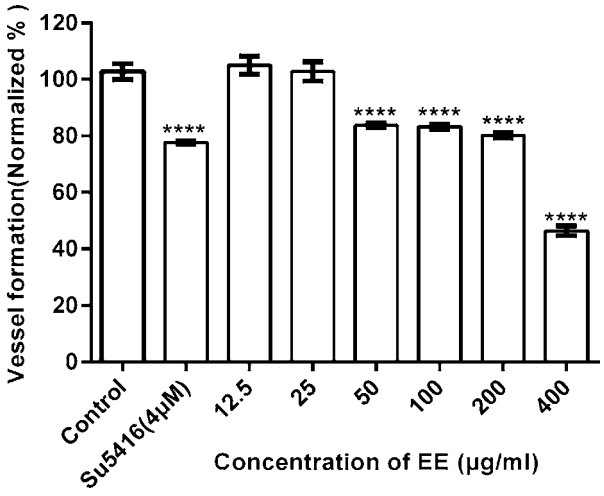


**Figure 9.** Antiangiogenic activities of 60% ethanol extract from sclerotium of *PTR* (mean ± SEM $n = 3$) in zebrafish through EAP assay. Effects were assessed by measuring the vessel formation of samples as compared to the control using the quantitative EAP assay. Statistical significance was assessed by one-way ANOVA (Student's $t$ test). (****) $p < 0.001$ compared to control.

ECs in human glioblastoma tissues,[62] suggesting a connection to tumor angiogenesis. Its activation has been related to EC migration.[63] Our results showed that EE inhibited HUVEC migration, which might be due to its down-regulation effect on Tie2 expression (Figure 8). Besides, angiopoietin-2 (Ang2) exhibits broad expression in the remodeling vasculature of human tumors but has very limited expression in normal tissues, making it an attractive candidate target for antiangiogenic cancer therapy.[64] Our results also revealed that Ang2 gene expression was decreased after treatment with EE (Figure 8).

It has been well recognized that all successful tumors must undergo neovascularization (angiogenesis) to acquire adequate nutrients and oxygen for continuous growth.[65] To further ascertain the effect of EE on inhibiting angiogenesis, studies were then conducted in the zebrafish, which has been successfully used previously as the model system for evaluating antiangiogenic agents.[66] Many researchers[67−69] have shown that embryonic, young, and growing zebrafish are ideal animal models to observe blood vessel formation. The zebrafish vasculature system is highly characteristic in the developing zebrafish embryo. The small molecules added directly to the fish culture media could diffuse into the embryo and induce observable angiogenesis effect.[70] Besides, the blood vessel formation through angiogenic sprouting requires the same proteins that are necessary for blood vessel growth in mammals.[71] Here, our results clearly demonstrated that EE exposure altered the development of SIVs in zebrafish. More importantly, EE exposure did not induce apoptosis in zebrafish, which was in agreement with the toxicity assay in normal cells. This paper further demonstrated that the zebrafish model is a very promising platform not only for screening antiangiogenic compounds but also for delineating the drug action mechanism when incorporated with the use of powerful genetic tools and other molecular techniques.

In conclusion, to our knowledge, this is the first study reporting the profile of phenolic compounds and the antioxidant and antiangiogenic activities of ethanol extract (EE) isolated from the sclerotium of *PTR*. The antiangiogenic effect of EE was demonstrated by the inhibition of EC migration and tube formation. The mechanism underlying this inhibitory effect might be due to a decrease in both the ROS production and the mRNA expression of angiogenic biomarkers (such as VEGF, FGF, MMP2, Tie2, and Ang2). These antiangiogenic effects of EE were also clearly observed in the zebrafish model.

Therefore, our findings strongly suggest that the phenolics-enriched extract obtained from the sclerotium of *PTR* might be a potential target for further investigation of its antiangiogenic effect in cancer treatment. Mushroom phenolic antioxidants might be potential anticancer agents to target tumor angiogenesis, tumor development, and metastasis.

## AUTHOR INFORMATION

### Corresponding Author

*(P.C.K.C.) E-mail: petercheung@cuhk.edu.hk.

### Author Contributions

Conceived and designed the experiments: P.C.K.C., S.L., T.L., L.C. Performed the experiments: S.L. Analyzed the data: S.L, P.C.K.C. Contributed reagents/materials/analysis tools: S.L., H.K., C.B.L., P.C.K.C. Wrote the paper: S.L., P.C.K.C.

### Notes

The authors declare no competing financial interest.

**Figure 10.** Lateral view of Tg (fli 1a: EGFP) y1 zebrafish embryos at 72 hpf: (A, B) control (live fluorescence microscopy highlights EGFP expressing subintestinal vessel plexus (SIVs), which appears as a smooth basket-like structure with five to six arcades); (C, D) treatment with 100 μg/mL (60% ethanol extract from sclerotium of *PTR*) (development of SIVs was inhibited after treatment). The arrow represents the regression of the SIVs. Treatments were done in triplicate. Sample size $n = 30$. The data represented were pooled from the experiments.

## ■ ABBREVIATIONS USED

EAP, endogenous alkaline phosphatase assay; ECs, endothelial cell; EE, ethanol extract of sclerotium from *Pleurotus tuber-regium*; GAE, gallic acid equivalents; Hpf, hour past fertilization; HUVEC, human umbilical vein endothelial cells; LDH, lactate dehydrogenase; *PTR*, *Pleurotus tuber-regium*; SIVs, subintestinal vessel plexus; TBHQ, *tert*-butylhydroquinone

## ■ REFERENCES


(1) Willetts, H. J. The survival of fungal sclerotia under adverse environmental conditions. *Biol. Rev.* **1971**, *46*, 387−407.

(2) Isikhuemhen, O.; Nerud, F.; Vilgalys, R. Cultivation studies on wild and hybrid strains of *Pleurotus tuberregium* (Fr.) Sing. on wheat straw substrate. *World J. Microbiol. Biotechnol.* **2000**, *16*, 431−435.

(3) Okhuoya, J. A.; Etugo, J. E. Studies of the cultivation of *Pleurotus tuberregium* (FR) sing. An edible mushroom. *Bioresour. Technol.* **1993**, *44*, 1−3.

(4) Carmeliet, P. VEGF as a key mediator of angiogenesis in cancer. *Oncology* **2005**, *69* (Suppl. 3), 4−10.

(5) Scappaticci, F. A. Mechanisms and future directions for angiogenesis-based cancer therapies. *J. Clin. Oncol.* **2002**, *20*, 3906−3927.

(6) Panyathep, A.; Chewonarin, T.; Taneyhill, K.; Surh, Y.-J.; Vinitketkumnuen, U. Effects of dried longan seed (*Euphoria longana* Lam.) extract on VEGF secretion and expression in colon cancer cells and angiogenesis in human umbilical vein endothelial cells. *J. Funct. Foods* **2013**, *5*, 1088−1096.

(7) Lin, M. T.; Yen, M. L.; Lin, C. Y.; Kuo, M. L. Inhibition of vascular endothelial growth factor-induced angiogenesis by resveratrol through interruption of Src-dependent vascular endothelial cadherin tyrosine phosphorylation. *Mol. Pharmacol.* **2003**, *64*, 1029−1036.

(8) Kubo, M.; Li, T. S.; Suzuki, R.; Ohshima, M.; Qin, S. L.; Hamano, K. Short-term pretreatment with low-dose hydrogen peroxide enhances the efficacy of bone marrow cells for therapeutic angiogenesis. *Am. J. Physiol. Heart Circ. Physiol.* **2007**, *292*, H2582−H2588.

(9) Jung, Y. D.; Kim, M. S.; Shin, B. A.; Chay, K. O.; Ahn, B. W.; Liu, W.; Bucana, C. D.; Gallick, G. E.; Ellis, L. M. EGCG, a major component of green tea, inhibits tumour growth by inhibiting VEGF induction in human colon carcinoma cells. *Br. J. Cancer* **2001**, *84*, 844−850.

(10) Reuter, S.; Gupta, S. C.; Chaturvedi, M. M.; Aggarwal, B. B. Oxidative stress, inflammation, and cancer: how are they linked? *Free Radical Biol. Med.* **2010**, *49*, 1603−1616.

(11) Singh, R. P.; Agarwal, R. Tumor angiogenesis: a potential target in cancer control by phytochemicals. *Curr. Cancer Drug Targets* **2003**, *3*, 205−217.

(12) Muslim, N.; Nassar, Z.; Aisha, A.; Shafaei, A.; Idris, N.; Majid, A.; Ismail, Z. Antiangiogenesis and antioxidant activity of ethanol extracts of *Pithecellobium jiringa*. *BMC Complement. Altern. Med.* **2012**, *12*, 210.

(13) Fassina, G.; Venè, R.; Morini, M.; Minghelli, S.; Benelli, R.; Noonan, D. M.; Albini, A. Mechanisms of inhibition of tumor angiogenesis and vascular tumor growth by epigallocatechin-3-gallate. *Clin. Cancer. Res.* **2004**, *10*, 4865−4873.

(14) Shahidi, F.; Janitha, P. K.; Wanasundara, P. D. Phenolic antioxidants. *Crit. Rev. Food Sci. Nutr.* **1992**, *32*, 67−103.

(15) Ferreira, I. C. F. R.; Baptista, P.; Vilas-Boas, M.; Barros, L. Free-radical scavenging capacity and reducing power of wild edible mushrooms from northeast Portugal: individual cap and stipe activity. *Food Chem.* **2007**, *100*, 1511−1516.

(16) Sharangi, A. B. Medicinal and therapeutic potentialities of tea (*Camellia sinensis* L.) − a review. *Food Res. Int.* **2009**, *42*, 529−535.

(17) Singleton, V. L.; Rossi, J. A. Colorimetry of total phenolics with phosphomolybdic-phosphotungstic acid reagents. *Am. J. Enol. Vitic.* **1965**, *16*, 144−158.

(18) Chu, Y.-H.; Chang, C.-L.; Hsu, H.-F. Flavonoid content of several vegetables and their antioxidant activity. *J. Sci. Food Agric.* **2000**, *80*, 561−566.

(19) Thaipong, K.; Boonprakob, U.; Crosby, K.; Cisneros-Zevallos, L.; Byrne, D. H. Comparison of ABTS, DPPH, FRAP, and ORAC assays for estimating antioxidant activity from guava fruit extracts. *J. Food Compos. Anal.* **2006**, *19*, 669−675.

(20) Sato, Y.; Rifkin, D. B. Autocrine activities of basic fibroblast growth factor: regulation of endothelial cell movement, plasminogen activator synthesis, and DNA synthesis. *J. Cell Biol.* **1988**, *107*, 1199−1205.

(21) Lee, O.-H.; Kim, Y.-M.; Lee, Y. M.; Moon, E.-J.; Lee, D.-J.; Kim, J.-H.; Kim, K.-W.; Kwon, Y.-G. Sphingosine 1-phosphate induces angiogenesis: its angiogenic action and signaling mechanism in human umbilical vein endothelial cells. *Biochem. Biophys. Res. Commun.* **1999**, *264*, 743−750.

(22) Latchoumycandane, C.; Chitra, K. C.; Mathur, P. P. 2,3,7,8-Tetrachlorodibenzo-*p*-dioxin (TCDD) induces oxidative stress in the epididymis and epididymal sperm of adult rats. *Arch. Toxicol.* **2003**, *77*, 280−284.

(23) He, Z.-H.; Gilli, C.; Yue, G. G.-L.; Lau, C. B.-S.; Greger, H.; Brecker, L.; Ge, W.; But, P. P.-H. Anti-angiogenic effects and mechanisms of zerumin A from *Alpinia caerulea*. *Food Chem.* **2012**, *132*, 201−208.

(24) Yu, X.; Tong, Y.; Han, X.-Q.; Kwok, H.-F.; Yue, G. G.-L.; Lau, C. B.-S.; Ge, W. Anti-angiogenic activity of herba epimedii on zebrafish embryos in vivo and HUVECs in vitro. *Phytother. Res.* **2013**, *27*, 1368−1375.

(25) Auerbach, R. Vascular endothelial cell differentiation: organ-specificity and selective affinities as the basis for developing anti-cancer strategies. *Int. J. Radiat. Biol.* **1991**, *60*, 1−10.

(26) Ahn, H. Y.; Kim, C. H.; Ha, T. S. Epigallocatechin-3-gallate regulates NADPH oxidase expression in human umbilical vein endothelial cells. *Korean J. Physiol. Pharmacol.* **2010**, *14*, 325−329.

(27) Colavitti, R.; Pani, G.; Bedogni, B.; Anzevino, R.; Borrello, S.; Waltenberger, J.; Galeotti, T. Reactive oxygen species as downstream mediators of angiogenic signaling by vascular endothelial growth factor receptor-2/KDR. *J. Biol. Chem.* **2002**, *277*, 3101−3108.

(28) Oak, M. H.; El Bedoui, J.; Schini-Kerth, V. B. Antiangiogenic properties of natural polyphenols from red wine and green tea. *J. Nutr. Biochem.* **2005**, *16*, 1−8.

(29) Wang, J.; Yi, J. Cancer cell killing via ROS: to increase or decrease, that is the question. *Cancer Biol. Ther.* **2008**, *7*, 1875−1884.

(30) Lawson, N. D.; Weinstein, B. M. In vivo imaging of embryonic vascular development using transgenic zebrafish. *Dev. Biol.* **2002**, *248*, 307−318.

(31) Wu, G.-H.; Hu, T.; Li, Z.-Y.; Huang, Z.-L.; Jiang, J.-G. In vitro antioxidant activities of the polysaccharides from *Pleurotus tuber-regium* (Fr.) Sing. *Food Chem.* **2014**, *148*, 351−356.

(32) Peterson, G.; Barnes, S. Genistein inhibition of the growth of human breast cancer cells: independence from estrogen receptors and the multi-drug resistance gene. *Biochem. Biophys. Res. Commun.* **1991**, *179*, 661−667.

(33) Rodrigues, S.; Calhelha, R. C.; Barreira, J. C. M.; Dueñas, M.; Carvalho, A. M.; Abreu, R. M. V.; Santos-Buelga, C.; Ferreira, I. C. F. R. Crataegus monogyna buds and fruits phenolic extracts: growth inhibitory activity on human tumor cell lines and chemical characterization by HPLC−DAD−ESI/MS. *Food Res. Int.* **2012**, *49*, 516−523.

(34) Nakachi, K.; Matsuyama, S.; Miyake, S.; Suganuma, M.; Imai, K. Preventive effects of drinking green tea on cancer and cardiovascular disease: epidemiological evidence for multiple targeting prevention. *BioFactors* **2000**, *13*, 49−54.

(35) Patthamakanokporn, O.; Puwastien, P.; Nitithamyong, A.; Sirichakwal, P. P. Changes of antioxidant activity and total phenolic compounds during storage of selected fruits. *J. Food Compos. Anal* **2008**, *21*, 241−248.

(36) Barros, L.; Ferreira, M.-J.; Queirós, B.; Ferreira, I. C. F. R.; Baptista, P. Total phenols, ascorbic acid, $\beta$-carotene and lycopene in Portuguese wild edible mushrooms and their antioxidant activities. *Food Chem.* **2007**, *103*, 413−419.

(37) Barros, L.; Dueñas, M.; Ferreira, I. C. F. R.; Baptista, P.; Santos-Buelga, C. Phenolic acids determination by HPLC−DAD−ESI/MS in sixteen different Portuguese wild mushrooms species. *Food Chem. Toxicol.* **2009**, *47*, 1076−1079.
(38) Kim, M.-Y.; Seguin, P.; Ahn, J.-K.; Kim, J.-J.; Chun, S.-C.; Kim, E.-H.; Seo, S.-H.; Kang, E.-Y.; Kim, S.-L.; Park, Y.-J.; Ro, H.-M.; Chung, I.-M. Phenolic compound concentration and antioxidant activities of edible and medicinal mushrooms from Korea. *J. Agric. Food Chem.* **2008**, *56*, 7265−7270.
(39) Oak, M.-H.; Chataigneau, M.; Keravis, T.; Chataigneau, T.; Beretz, A.; Andriantsitohaina, R.; Stoclet, J.-C.; Chang, S.-J.; Schini-Kerth, V. B. Red wine polyphenolic compounds inhibit vascular endothelial growth factor expression in vascular smooth muscle cells by preventing the activation of the p38 mitogen-activated protein kinase pathway. *Arterioscler. Thromb. Vasc. Biol.* **2003**, *23*, 1001−1007.
(40) Ahn, H. Y.; Kim, C. H.; Ha, T.-S. Epigallocatechin-3-gallate regulates NADPH oxidase expression in human umbilical vein endothelial cells. *Korean J. Physiol. Pharmacol.* **2010**, *14*, 325−329.
(41) Du, G.-J.; Zhang, Z.; Wen, X.-D.; Yu, C.; Calway, T.; Yuan, C.-S.; Wang, C.-Z. Epigallocatechin gallate (EGCG) is the most effective cancer chemopreventive polyphenol in green tea. *Nutrients* **2012**, *4*, 1679−1691.
(42) Lin, S. Y.; Lee, W. R.; Su, Y. F.; Hsu, S. P.; Lin, H. C.; Ho, P. Y.; Hou, T. C.; Chou, Y. P.; Kuo, C. T.; Lee, W. S. Folic acid inhibits endothelial cell proliferation through activating the cSrc/ERK 2/NF-κB/p53 pathway mediated by folic acid receptor. *Angiogenesis* **2012**, *15*, 671−683.
(43) Hou, T. C.; Lin, J. J.; Wen, H. C.; Chen, L. C.; Hsu, S. P.; Lee, W. S. Folic acid inhibits endothelial cell migration through inhibiting the RhoA activity mediated by activating the folic acid receptor/cSrc/p190RhoGAP-signaling pathway. *Biochem. Pharmacol.* **2013**, *85*, 376−384.
(44) Chen, Y.; Tseng, S.-H. Pro- and anti-angiogenesis effects of resveratrol. *In Vivo* **2007**, *21*, 365−370.
(45) Bellion, P.; Olk, M.; Will, F.; Dietrich, H.; Baum, M.; Eisenbrand, G.; Janzowski, C. Formation of hydrogen peroxide in cell culture media by apple polyphenols and its effect on antioxidant biomarkers in the colon cell line HT-29. *Mol. Nutr. Food Res.* **2009**, *53*, 1226−1236.
(46) Thomas, M.; Augustin, H. The role of the angiopoietins in vascular morphogenesis. *Angiogenesis* **2009**, *12*, 125−137.
(47) Ellis, L. M.; Hicklin, D. J. VEGF-targeted therapy: mechanisms of anti-tumour activity. *Nat. Rev. Cancer* **2008**, *8*, 579−591.
(48) Thurston, G. Role of angiopoietins and Tie receptor tyrosine kinases in angiogenesis and lymphangiogenesis. *Cell Tissue Res.* **2003**, *314*, 61−68.
(49) Goto, F.; Goto, K.; Weindel, K.; Folkman, J. Synergistic effects of vascular endothelial growth factor and basic fibroblast growth factor on the proliferation and cord formation of bovine capillary endothelial cells within collagen gels. *Lab Invest.* **1993**, *69*, 508−517.
(50) Waltenberger, J.; Claesson-Welsh, L.; Siegbahn, A.; Shibuya, M.; Heldin, C. H. Different signal transduction properties of KDR and Flt1, two receptors for vascular endothelial growth factor. *J. Biol. Chem.* **1994**, *269*, 26988−26995.
(51) Cai, J.; Jiang, W. G.; Ahmed, A.; Boulton, M. Vascular endothelial growth factor-induced endothelial cell proliferation is regulated by interaction between VEGFR-2, SH-PTP1 and eNOS. *Microvasc. Res.* **2006**, *71*, 20−31.
(52) Belloni, D.; Scabini, S.; Foglieni, C.; Veschini, L.; Giazzon, A.; Colombo, B.; Fulgenzi, A.; Helle, K. B.; Ferrero, M. E.; Corti, A.; Ferrero, E. The vasostatin-I fragment of chromogranin A inhibits VEGF-induced endothelial cell proliferation and migration. *FASEB J.* **2007**, *21*, 3052−3062.
(53) Dong, X.; Han, Z. C.; Yang, R. Angiogenesis and antiangiogenic therapy in hematologic malignancies. *Crit. Rev. Oncol./Hematol.* **2007**, *62*, 105−118.
(54) Ushio-Fukai, M.; Tang, Y.; Fukai, T.; Dikalov, S. I.; Ma, Y.; Fujimoto, M.; Quinn, M. T.; Pagano, P. J.; Johnson, C.; Alexander, R. W. Novel role of gp91phox-containing NAD(P)H oxidase in vascular endothelial growth factor-induced signaling and angiogenesis. *Circ. Res.* **2002**, *91*, 1160−1167.
(55) Yamaoka-Tojo, M.; Ushio-Fukai, M.; Hilenski, L.; Dikalov, S. I.; Chen, Y. E.; Tojo, T.; Fukai, T.; Fujimoto, M.; Patrushev, N. A.; Wang, N.; Kontos, C. D.; Bloom, G. S.; Alexander, R. W. IQGAP1, a novel vascular endothelial growth factor receptor binding protein, is involved in reactive oxygen species-dependent endothelial migration and proliferation. *Circ. Res.* **2004**, *95*, 276−283.
(56) Ikeda, S.; Ushio-Fukai, M.; Zuo, L.; Tojo, T.; Dikalov, S.; Patrushev, N. A.; Alexander, R. W. Novel role of ARF6 in vascular endothelial growth factor-induced signaling and angiogenesis. *Circ. Res.* **2005**, *96*, 467−475.
(57) Colavitti, R.; Pani, G.; Bedogni, B.; Anzevino, R.; Borrello, S.; Waltenberger, J.; Galeotti, T. Reactive oxygen species as downstream mediators of angiogenic signaling by vascular endothelial growth factor receptor-2/KDR. *J. Biol. Chem.* **2002**, *277*, 3101−3108.
(58) Gospodarowicz, D. Purification of a fibroblast growth factor from bovine pituitary. *J. Biol. Chem.* **1975**, *250*, 2515−2520.
(59) Hagedorn, M.; Bikfalvi, A. Target molecules for anti-angiogenic therapy: from basic research to clinical trials. *Crit. Rev. Oncol./Hematol.* **2000**, *34*, 89−110.
(60) Cárdenas, C.; Quesada, A. R.; Medina, M. A. Anti-angiogenic and anti-inflammatory properties of kahweol, a coffee diterpene. *PLoS One* **2011**, *6*, No. e23407.
(61) Sato, T. N.; Tozawa, Y.; Deutsch, U.; Wolburg-Buchholz, K.; Fujiwara, Y.; Gendron-Maguire, M.; Gridley, T.; Wolburg, H.; Risau, W.; Qin, Y. Distinct roles of the receptor tyrosine kinases Tie-1 and Tie-2 in blood vessel formation. *Nature* **1995**, *376*, 70−74.
(62) Stratmann, A.; Risau, W.; Plate, K. H. Cell type-specific expression of angiopoietin-1 and angiopoietin-2 suggests a role in glioblastoma angiogenesis. *Am. J. Pathol.* **1998**, *153*, 1459−1466.
(63) Fiedler, P. C.; Talley, L. D. Hydrography of the eastern tropical Pacific: a review. *Prog. Oceanogr.* **2006**, *69*, 143−180.
(64) Oliner, J.; Min, H.; Leal, J.; Yu, D.; Rao, S.; You, E.; Tang, X.; Kim, H.; Meyer, S.; Han, S. J.; Hawkins, N.; Rosenfeld, R.; Davy, E.; Graham, K.; Jacobsen, F.; Stevenson, S.; Ho, J.; Chen, Q.; Hartmann, T.; Michaels, M.; Kelley, M.; Li, L.; Sitney, K.; Martin, F.; Sun, J.-R.; Zhang, N.; Lu, J.; Estrada, J.; Kumar, R.; Coxon, A.; Kaufman, S.; Pretorius, J.; Scully, S.; Cattley, R.; Payton, M.; Coats, S.; Nguyen, L.; Desilva, B.; Ndifor, A.; Hayward, I.; Radinsky, R.; Boone, T.; Kendall, R. Suppression of angiogenesis and tumor growth by selective inhibition of angiopoietin-2. *Cancer Cell* **2004**, *6*, 507−516.
(65) Folkman, J. Tumor angiogenesis: therapeutic implications. *N. Engl. J. Med.* **1971**, *285*, 1182−1186.
(66) Paramasivam, A.; Kalaimangai, M.; Sambantham, S.; Anandan, B.; Jayaraman, G. Anti-angiogenic activity of thymoquinone by the down-regulation of VEGF using zebrafish (*Danio rerio*) model. *Biomed. Prev. Nutr.* **2012**, *2*, 169−173.
(67) Liu, C.-L.; Kwok, H.-F.; Cheng, L.; Ko, C.-H.; Wong, C.-W.; Ho, T. W. F.; Leung, P.-C.; Fung, K.-P.; Lau, C. B.-S. Molecular mechanisms of angiogenesis effect of active sub-fraction from root of *Rehmannia glutinosa* by zebrafish sprout angiogenesis-guided fractionation. *J. Ethnopharmacol.* **2014**, *151*, 565−575.
(68) Tran, T. C.; Sneed, B.; Haider, J.; Blavo, D.; White, A.; Aiyejorun, T.; Baranowski, T. C.; Rubinstein, A. L.; Doan, T. N.; Dingledine, R.; Sandberg, E. M. Automated, quantitative screening assay for antiangiogenic compounds using transgenic zebrafish. *Cancer Res.* **2007**, *67*, 11386−11392.
(69) He, M.-F.; Liu, L.; Ge, W.; Shaw, P.-C.; Jiang, R.; Wu, L.-W.; But, P. P.-H. Antiangiogenic activity of *Tripterygium wilfordii* and its terpenoids. *J. Ethnopharmacol.* **2009**, *121*, 61−68.
(70) Serbedzija, G.; Flynn, E.; Willett, C. Zebrafish angiogenesis: a new model for drug screening. *Angiogenesis* **1999**, *3*, 353−359.
(71) Bansode, R. R.; Ahmedna, M.; Svoboda, K. R.; Losso, J. N. Coupling in vitro and in vivo paradigm reveals a dose dependent inhibition of angiogenesis followed by initiation of autophagy by C6-ceramide. *Int. J. Biol. Sci.* **2011**, *7*, 629−644.

and does not exist as free GSH in plasma, but was deposited into red cells or liver for future uses.

The objective of this work was to examine whether intact glutathione (GSH) can be transported across the intestinal epithelium and to characterize its uptake, as well as to determine the fate of orally administered GSH in animal models.

## MATERIALS AND METHODS

**Materials.** GSH was kindly provided by Kohjin Life Science Ltd., Tokyo, Japan. $^{13}$C-GSH was synthesized by a conventional liquid-phase method via $^{13}$C-GSSG using the disulfide bond as a thiol-protecting group. L-Cystine containing 1,1′-$^{13}$C isotopes (L-cystine-1,1′-$^{13}C_2$, Sigma-Aldrich, St. Louis, MO, USA) was converted into the corresponding *N*,*N*′-*tert*-butyloxycarbonyl (Boc) protected $^{13}$C-cystine using di-*tert*-butyl dicarbonate. The crude $^{13}$C-GSH was purified using reversed-phase HPLC on a Nakalai Tesque C18 column (COSMOSIL 5C18-AR-II, 20 × 250 mm). The final product was characterized by reversed-phase HPLC using a TSKgel ODS-100S (3.0 × 150 mm; Tosoh, Tokyo, Japan) and electrospray ionization time-of-flight mass spectrometry (ESI-TOFMS) with a Hitachi NanoFrontier LC-MS system (Tokyo, Japan). MS (ESI) *m*/*z*: 308.99 $[M + H]^+$ (calcd 309.09) (data not shown).

**In Vitro Transport of GSH across Human Intestinal Epithelial Cell Monolayers.** In vitro transport experiments were performed using Caco-2 or HT-29 human intestinal epithelial cells (ATCC). Caco-2 or HT-29 cell monolayers were grown in Costar transwell inserts (1.0 cm$^2$, 0.4 μm pore size) (Corning, Cambridge, MA, USA) in Eagle's minimal essential medium (MEM) (Invitrogen, Burlington, ON, Canada) containing 2 mM L-glutamine, 1 mM sodium pyruvate (Invitrogen), 0.1 mM nonessential amino acids (Invitrogen), 50 U/mL penicillin−streptomycin (Invitrogen), and 20% FBS (HyClone) (Fisher Scientific, Ottawa, ON, Canada). The cells were seeded at a density of 0.6 × 10$^5$ cells/cm$^2$, and the culture medium was changed every second day until confluent monolayers with transepithelial electrical resistance (TEER) values >500 Ω·cm$^2$ were obtained. TEER values were measured using a Millicell-ERS Volt-Ohm Meter (Millipore, Bedford, MA, USA). Cell monolayers were rinsed with Hanks' balanced salt solution (HBSS) adjusted to pH 7.4 with 10 mM HEPES, and the same buffer was added to both apical and basolateral chambers. After equilibration in buffer for 30 min, GSH (1 mM) was added to the apical chamber. Cells were incubated at 37 °C, and aliquots were removed from the basolateral chamber at the indicated time points. Apparent permeability coefficients ($P_{app}$) were calculated using the formula

$$P_{app} = V_R/A \times C_0 \, dC/dt$$

where $V_R$ is the volume in the basolateral chamber, $A$ is the filter surface area, $C_0$ is the initial GSH concentration in the apical chamber, and $dC/dt$ is the slope of the curve of basolateral GSH concentration versus time. To examine the effect of pH on GSH uptake, 1 mM GSH was prepared in HBSS buffer adjusted to pH 6.0 with 10 mmol/L MES and was added to the apical chamber.

To examine if GSH could be transported intact, Caco-2 cells were first incubated with 0.25 mM Acivicin (AT-125; Santa Cruz Biotechnology, Santa Cruz, CA, USA) for 30 min and/or 0.5 mM buthionine sulfoximine (BSO) (Sigma-Aldrich), to inhibit GSH degradation and synthesis, respectively. Probenecid (PB) (Sigma-Aldrich) (1 mM), a known organic anion transport inhibitor and inhibitor of GSH transport, was added 30 min before the addition of GSH.

**Cell Viability Assay.** Viability of the treated cells was measured using the WST-1 Cell Proliferation Reagent (Roche Applied Sciences, Laval, Quebec, Canada) according to the manufacturer's instructions. Briefly, 20 μL of WST-1 was added to the basolateral chamber, and cells were incubated for 1−2 h. Absorbances were read at 450 nm and converted to percent viability relative to untreated control cells.

**Ex Vivo Transport of GSH across Rat Intestinal Epithelial Tissue.** Sections of small intestine were removed from 8-week-old male Sprague−Dawley rats (SPF/VAF Crj:SD; Charles River Japan., Kanagawa, Japan) and mounted into an Ussing chamber for transport. Krebs−Ringer bicarbonate (KRB) buffer, adjusted to pH 6.0 and 7.4, was added to apical and basolateral chambers, respectively. After equilibration for 30 min, 10 mM GSH was added to the apical chamber, and transport was allowed to proceed for 60 min. After the 60 min incubation, the intestinal tissue membrane was removed and frozen using powdered dry ice. The frozen tissue was cryosectioned by a cryostat (Leica) with 12 μm thickness to prepare cross sections of intestinal wall and thaw-mounted to an indium−tin oxide (ITO)-coated glass slide followed by drying under $N_2$ gas for analysis by mass spectrometry.[17]

**In Vivo Supplementation with $^{13}$C-GSH in Mice.** Six 8-week-old female BALB/c mice (16−20 g) (Charles River Laboratories Inc., Montreal, Quebec, Canada) were group housed on a 12 h light−dark cycle and allowed unrestricted access to standard mouse chow and water. All animal studies were approved by the University of Guelph Animal Care Committee and carried out in accordance with the Canadian Council on Animal Care Guide to the Care and Use of Experimental Animals. Balb/c mice were administered $^{13}$C-GSH (10 mg/mouse) by oral gavage. Control mice received vehicle alone. The dose of 10 mg $^{13}$C-GSH per mouse was determined on the basis of in vitro assay and actual human subject trial in the past. Mice (5 mice/group) were euthanized at the time points indicated, and blood and liver samples were collected. Liver samples were flash-frozen (−80 °C) for further analysis. Blood samples were immediately flushed with $N_2$ gas under heparin-treated clinical tube (Fisher Sci) and centrifuged at 4 °C (3500*g* for 10 min). The red blood cells (RBCs) were treated by lysate buffer (Sigma-Aldrich) and subjected to further analysis. The plasma and RBC samples were immediately subjected to GSH and GSSH measurement. A reference GSH was used to confirm that GSH was not converted to GSSG during these sample pretreatments (data not shown).

**Enzymatic Detection of Transported GSH.** GSH was quantified in the Caco-2 cells and HT-29 basolateral chamber using an enzymatic assay for the detection of GSH/GSSG, according to the manufacturer's instructions (Oxford Biomedical Research, Rochester Hills, MI, USA). Briefly, a GSH/GSSG assay was designed to measure total, reduced, and oxidized glutathione using an Ellman's reagent (DTNB) and glutathione reductase (GR). This method can be used to measure oxidized (GSSG) by using a specific protocol, which first scavenges all GSH with 1-methyl-2-vinylpyridinium triflate. GSH concentrations were calculated from a GSSG standard curve, and results are expressed as micromolar total GSH ($GSH_t$) in the basolateral solution. The total GSH, reduced GSH, and GSSG in mouse plasma, red cells, and liver were quantified using the same protocol.

**Detection of GSH and $^{12}$C-GSH by Mass Spectrometry.** To confirm transport of intact GSH across Caco-2 monolayers, basolateral solutions were analyzed by LC/TOF-MS for the presence of GSH or GSH degradation products. Samples were derivatized using ThioGlo3 reagent (Covalent Associates, Inc., Corvallis, OR, USA) by incubating 20 μL of basolateral solution with 20 μL of 0.2 mM reagent and incubating for 1 h at room temperature. LC-MS was carried out using a Cosmosil 5$C_{18}$-MS-II column (i.d. 2.0 mm × 150 mm, Nacalai Tesque, Kyoto, Japan) with a linear gradient of 0−100% methanol containing 0.1% formic acid at a flow rate of 0.2 mL/min. MS conditions were as follows: mode, negative-low, expert mode; nebulizer, 1.6 bar; dry gas, 8.0 L/min; mass range, 100−1000; hexapole RF, 200 Vpp; dry temperature, 200 °C.

Detection of $^{12}$C-GSH transported by rat small intestine was carried out using matrix-assisted laser desorption/ionization time-of-flight imaging mass spectrometry (MALDI-IMS) as described by Hong et al. with modifications.[17] Briefly, the matrix reagent and ionization enhancer (20 mg/mL 2,4,6-trihydroxyacetophenone (THAP) with 10 mM diammonium citrate) were dissolved in 50% ACN/0.1% TFA and uniformly sprayed using an ImagePrep automatic matrix sprayer (Bruker-Daltonics, Tokyo, Japan). MALDI-MS imaging was preformed using autoflex III equipped with smart beam (Bruker-Daltonics) with the following analytical parameters: mode, positive; ion source 1, 20.00 kV; ion source 2, 18.80 kV; lens, 7.50 kV; pulsed ion extraction, 0 ns; mass range, 120−1000 Da; laser frequency, 200.0 Hz; number of shots, 500 shots/spot; spatial resolution (spot distance), 50 μm; laser attenuator, 1 minimum; laser power, 100%.

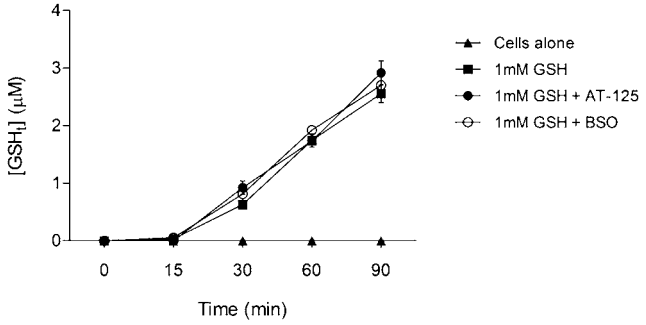


**Figure 1.** Time-dependent transport of 1 mM GSH across Caco-2 cell monolayers in the presence or absence of 0.25 mM AT-125 or 0.5 mM buthionine sulfoximine (BSO).

**Table 1. Apparent Permeability Coefficients (*Papp*) for the Transport of 1 mM GSH across Caco-2 Cell Monolayers in the Presence or Absence of 0.25 mM AT-125 or 0.5 mM Buthionine Sulfoximine (BSO)**

| treatment | $P_{app} \times 10^{-6}$ (cm/s) |
|---|---|
| 1 mM GSH | 1.28 ± 0.11[a] |
| 1 mM GSH + AT-125 | 1.23 ± 0.35[a] |
| 1 mM GSH + BSO | 1.20 ± 0.15[a] |

[a]Similar letters following entries indicate no statistically significant difference.

**Determination of $^{13}$C-GSH and $^{13}$C-GSSG by Liquid Chromatography–Tandem Mass Spectrometry (LC-MS/MS).** The concentrations of $^{13}$C-GSH and $^{13}$C-GSSG in the blood, red cells, and liver samples were determined with a slight modification of a previously reported $^{13}$C-stable isotope labeled dipeptide detection method.[18] Sample preparation followed the method described by Nakashima et al.[18] To prevent oxidation of GSH, all samples were flushed by $N_2$ gas at 4 °C. The derivates of GSH were prepared by the same method described above using ThioGlo3 reagent. A chromatographic separation was performed on a Biosuite C18 PA-A column (Waters, Milford, MA, USA), and a mobile phase of $CH_3CN$-water containing 0.1 FA) and a flow rate (0.20–0.30 mL/min) were applied. LC-MS/MS was performed as described above. Three separate replicates of $^{13}$C-GSH with different concentrations between 0.1 and 5.0 ng/mL were conducted for obtaining the calibration curve. We detected about 7% of endogenous $^{13}$C-GSH against $^{12}$C-GSH in vehicle mouse tissue samples (data not shown); therefore, we determined the actual exogenous $^{13}$C-GSH by subtracting the endogenous one. The $^{13}$C-GSSG and reduced $^{13}$C-GSH were quantified on the basis of a combination of the LC-MS/MS and an enzymatic assay.

**Statistical Analysis.** Data are expressed as means ± SEM. Statistical analyses were performed with GraphPad Prism version 5.0 (GraphPad, San Diego, CA, USA) using one-way ANOVA followed by Tukey's multiple-comparison test. Student's *t* test was used when comparisons between only two groups were carried out. Differences were considered significant when $p < 0.05$.

## RESULTS AND DISCUSSION

Several mechanisms may be involved in the uptake and utilization of luminal GSH by brush-border membrane enzymes in the intestine, including (1) cleavage of GSH into cysteinyl glycine, γ-glutamyl amino acids, or its constituent amino acids (Glu, Cys, Gly) by γ-glutamyltransferase, followed by their transport and intracellular GSH synthesis; and (2) transport of intact GSH directly by specific transporters.[19] GSH transport systems have been identified in the membranes of various tissues and organs, including renal cells, pulmonary alveolar

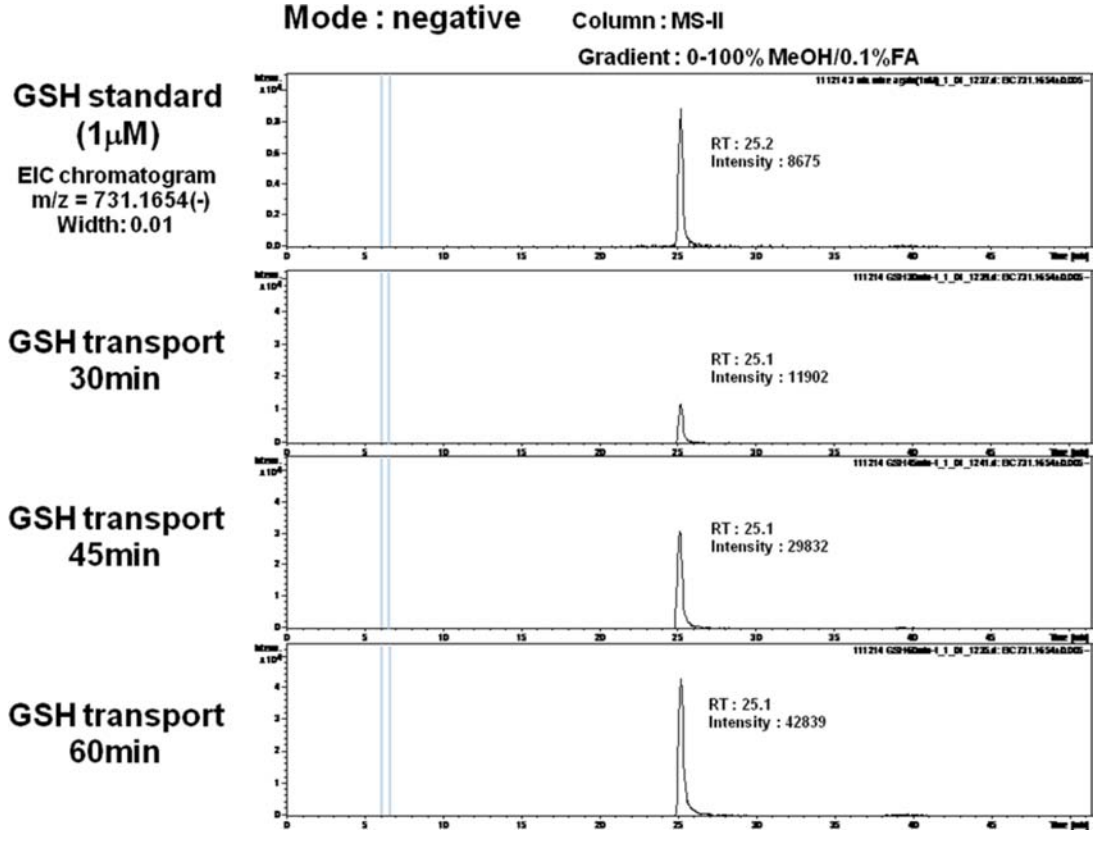


**Figure 2.** LC-MS analysis of transported GSH over 60 min. Transported samples were compared to a known GSH standard (top panel).


dx.doi.org/10.1021/jf503257w | J. Agric. Food Chem. 2014, 62, 9499–9506

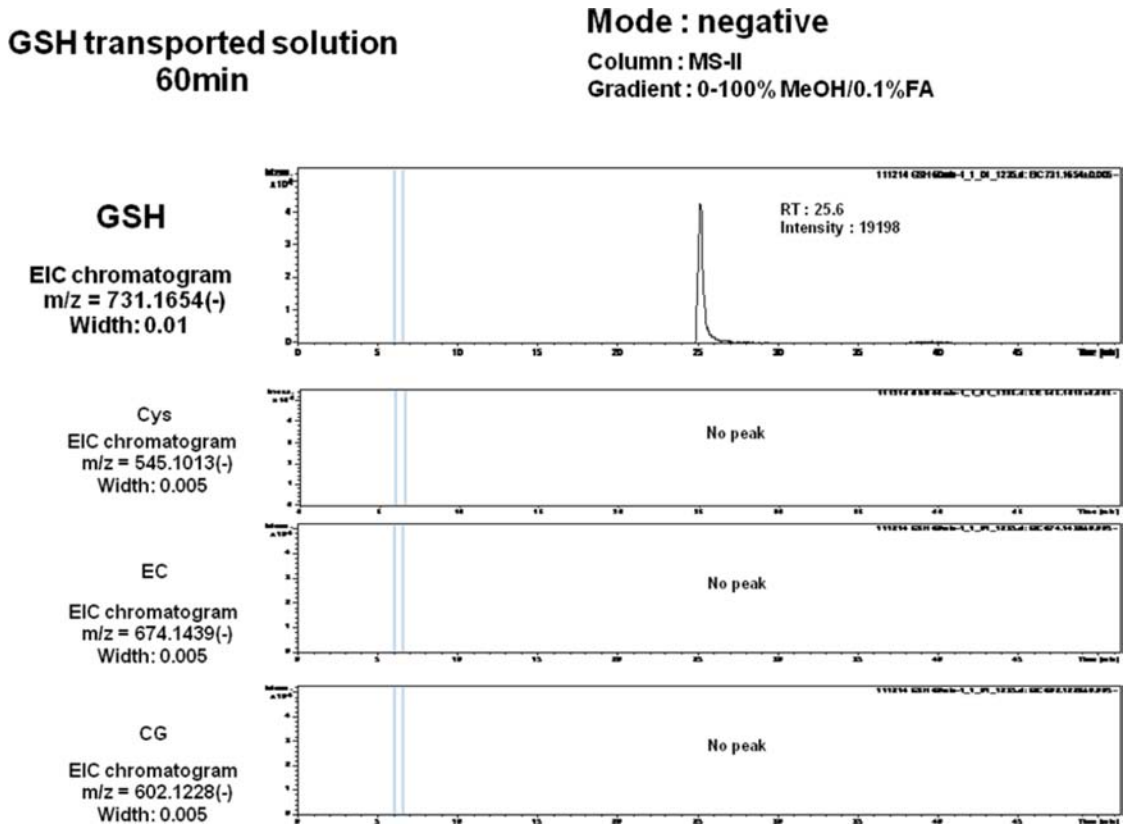


**Figure 3.** LC-MS analysis of transported GSH (top panel), showing absence of GSH degradation products.

cells, retinal pigment epithelial cells, brain endothelial cells, but less is known about its transport across the intestinal epithelium. Several studies examining GSH uptake in the intestine have been carried out using different animal species and techniques including pig and rabbit intestinal brush-border membrane vesicles (BBMV),[5,11,20,21] vascularly perfused rat small intestine,[8] and rat intestinal epithelial cells.[22] However, little is known regarding GSH transport across intestinal epithelial cells. Here, the transport of intact GSH across human intestinal epithelial cells was examined in vitro using Caco-2 cell monolayers. GSH was detected in the basolateral transport chamber of the cell monolayers using a GSH/GSSG enzyme assay and the structure of intact GSH confirmed by mass spectrometry (LC-MS).

Caco-2 cell monolayers were treated with exogenous GSH (1 mM), and the amount of GSH present in the basolateral transport chamber of Caco-2 cell monolayers was measured at different time points using a GSH/GSSG enzyme assay. To confirm that the GSH detected in the basolateral chamber was not as a result of GSH degradation by brush-border membrane enzymes and subsequent resynthesis within the cells, cells were treated with Acivicin (AT-125) and/or buthionine sulfoximine (BSO). AT-125 can prevent GSH degradation by irreversibly inhibiting $\gamma$-glutamyltransferase, and BSO can prevent GSH synthesis through inhibition of $\gamma$-glutamylcysteine synthetase. To test whether intact GSH is transported across Caco-2 cell monolayers, cells were pretreated with AT-125 or BSO, and GSH concentration in the basolateral chamber was measured as a function of time during incubation with 1 mM exogenous GSH.

Transported GSH was measured at various time points (Figure 1), and the apparent permeability coefficients, $P_{app}$, were calculated. There was no significant difference between the concentration of GSH detected in the presence or absence of the inhibitors AT-125 or BSO, indicating that the GSH present in the basolateral chamber was likely due to the uptake/transport of intact GSH across the Caco-2 monolayers, and not GSH resynthesis. No GSH was detected from untreated control cells (cells alone). Likewise, there was no difference in the permeability ($P_{app}$) of GSH in the presence or absence of either inhibitor (Table 1). Cell viability did not appear to be affected by the treatments (data not shown). Analysis by LC-MS confirmed that the detected sample was indeed intact

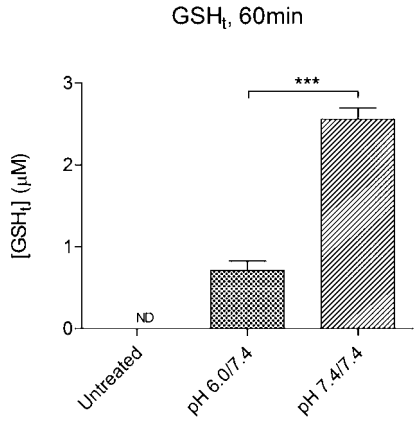


**Figure 4.** pH-dependent uptake of 1 mM GSH across Caco-2 cell monolayers in the presence of 0.25 mM AT-125 after 60 min at pH 6.0/7.4 indicates an apical pH of 6.0 and a basolateral pH of 7.4. pH 7.4/7.4 indicates apical and basolateral pH values of 7.4. ND, none detected. (***) $P < 0.001$. Untreated denotes 60 min of incubation in the absence of GSH at pH 7.4.

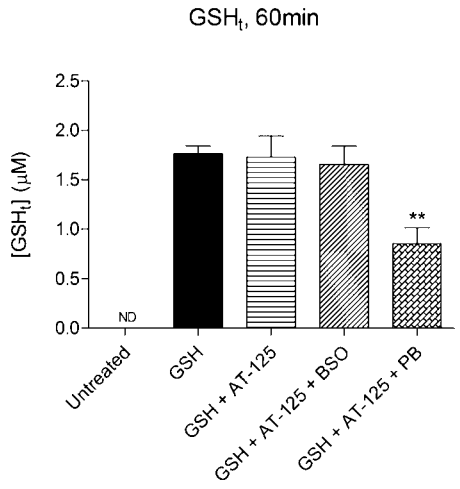


**Figure 5.** Uptake of 1 mM GSH across Caco-2 cell monolayers in the presence or absence of 0.25 mM AT-125 and 0.5 mM buthionine sulfoximine (BSO) or 1 mM Probenecid (PB) after 60 min. ND, none detected. (**) $P < 0.01$ relative to GSH, GSH + AT-125, and GSH + AT-125 + BSO. Untreated denotes 60 min of incubation in the absence of GSH at pH 7.4.

GSH by comparison to a known GSH standard (Figure 2). Moreover, no products of GSH degradation (e.g., cysteine, cysteinyl-glycine) were observed in the transported samples (Figure 3). These results indicated that intact GSH can cross intestinal epithelial cells without degradation, in contrast to previous reports.[14−16] Previously, it was speculated that intestinal epithelial cells also have the same mechanistic transport of GSH with other tissues of renal cells, pulmonary alveolar cells, retinal pigment epithelial cells, and brain endothelial cells,[19] whereas no-one has reported clearly with direct evidence until the current work. This is the first study to demonstrate direct uptake of GSH using human intestinal epithelial cells.

To examine whether GSH uptake is pH dependent or not, we carried out a proton-dependent study using different pH gradients at apical and basolateral sides (both apical and basolateral pH values of 7.4 or an apical pH of 6.0 and a basolateral pH of 7.4, typical of proton-dependent transporters such as the di/tripeptide transporter PepT1). The amount of GSH detected in the basolateral solution was significantly higher when an apical pH of 7.4 was used when compared to an apical pH of 6.0 (Figure 4), suggesting that GSH uptake is not proton-dependent. These results are in line with previous reports that uptake of GSH into brush-border membrane vesicles was not proton-driven and occurred optimally around pH 7.5.[21] To further characterize GSH uptake across the Caco-2 monolayers, transport was carried out in the presence of the inhibitor Probenecid (PB), a known organic anion transport inhibitor and inhibitor of GSH transport in basolateral membrane vesicles.[23] The amount of GSH detected in the basolateral solution of PB-treated cells was significantly reduced when compared to all other samples (Figure 5), suggesting transport of intact GSH.

It was notable when we used HT-29 cell monolayer, which does not express the human PepT1 transporter with the same conditions. We observed similar results (data not shown) and

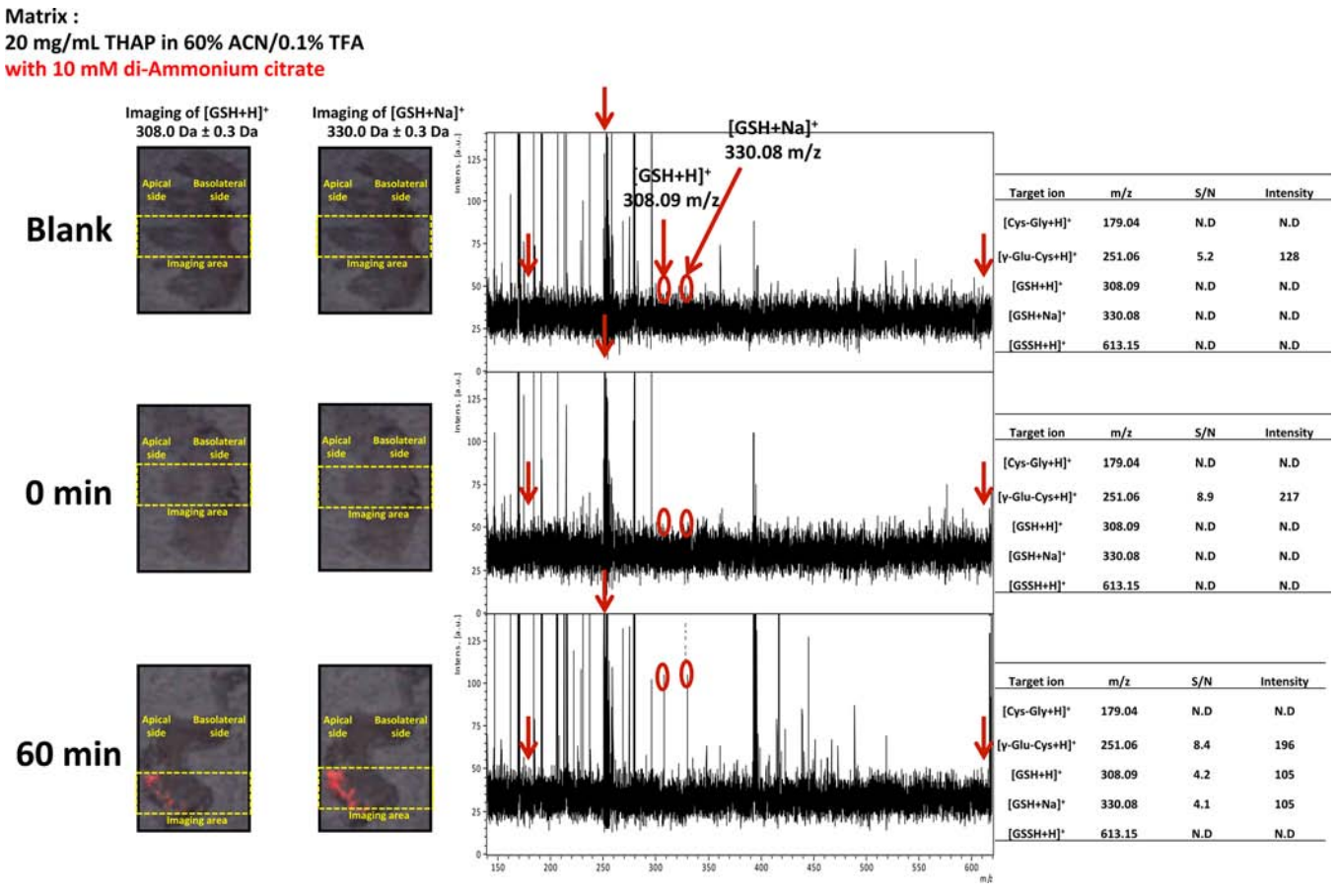


**Figure 6.** MALDI-MS imaging and spectra of transported GSH using rat intestinal membrane.


dx.doi.org/10.1021/jf503257w | J. Agric. Food Chem. 2014, 62, 9499−9506

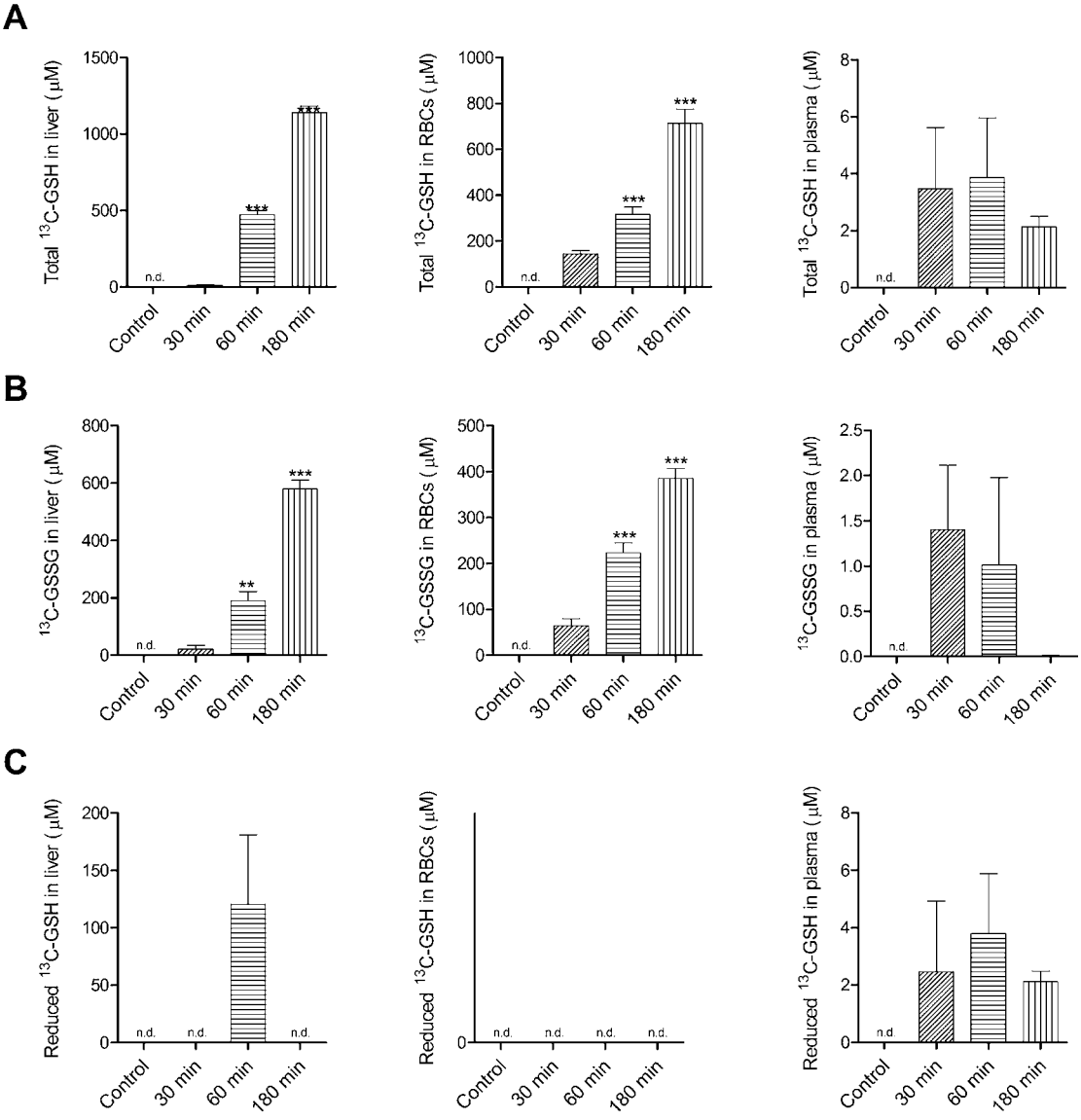


**Figure 7.** Measurement of (A) total $^{13}$C-GSH, (B) $^{13}$C-GSSG, and (C) reduced $^{13}$C-GSH in liver, red blood cells (RBCs), and plasma of mice orally administered 10 mg of $^{13}$C-GSH. n.d., none detected. (**) $P < 0.01$ and (***) $P < 0.001$ relative to vontrol.

could confirm that intact GSH is likely being taken up or transported across the HT-29 monolayers, and not GSH resynthesis. GSH transportation across human epithelial cells is not PepT1-mediated transport. The GSH-specific transport system in human small intestine epithelial cells was reported as a $Na^+$-independent transport system[24] or $Na^+$-coupled GSH transport.[25] However, its detailed transport mechanism is still not well understood. Further characterization of GSH transport may be required, including using the Caco-2 BB (C2BBe1) cell line or examining the effect of mono- and bivalent cations on GSH uptake, and using a more sensitive detection method to detect GSH uptake at earlier time points to gain a better understanding of uptake kinetics as from the literature it would appear that the initial uptake of GSH into cells is a rapid process.[20,21]

Rat intestinal epithelial tissues were treated with exogenous GSH, and transported $^{12}$C-GSH was visualized using MALDI-IMS, which has been similarly used to detect small transportable peptides in rat small intestine.[17] MALDI-MS imaging of GSH in the intestinal tissue sections showed clear localization of transported $^{12}$C-GSH as $[GSH + H]^+$ and $[GSH + Na]^+$ in the apical side of the intestinal wall after 60 min of incubation with 10 mM GSH (Figure 6). The presence of endogenous GSH in the intestinal tissue was not visualized in blank intestinal wall subjected to 60 min of incubation with KBR buffer without GSH. Neither endogenous nor transported GSSH (oxidized form of GSH), Cys-Gly, or γ-Glu-Cys was visualized in any of the intestinal samples tested (blank, 0 and 60 min GSH treated intestines). The absence of GSH on the apical surface of intestinal tissue after 0 min (actually ∼10 s of incubation) of incubation with GSH would strongly suggest that the visualized GSH after 60 min of transport showed localization of intact GSH inside the intestinal wall. To our knowledge, this is the first report of visualized intact GSH in the intestinal wall and demonstrates its presence in the tissues with intact form. Matrix-assisted laser desorption/ionization time-of-flight imaging mass spectrometry (MALDI-IMS) has been developed to visualize the target molecules in tissues, and this technique is a powerful tool for bioactive metablomics study. However, it was limited for only biological compounds with molecular weight of 1−50 kDa, and no small bioactive peptides (<500 Da) were visualized. Recently,


dx.doi.org/10.1021/jf503257w | J. Agric. Food Chem. 2014, 62, 9499−9506

there has been much attention to the study of small di/tripeptides metabolomics, and we reported a new technique of small peptide MALDI-IMS.[17] The current MALDI-IMS visualization of GSH in intestinal wall can provide new insights of intestinal absorption behavior of bioactive small compounds as foods and drugs and omics analysis of small metabolites in various tissues.

To determine the fate of orally ingested GSH, mice were supplemented with $^{13}$C-GSH (10 mg/mouse), and total $^{13}$C-GSH, $^{13}$C-GSSG, and reduced $^{13}$C-GSH in liver, RBCs, and plasma were quantified. Total $^{13}$C-GSH in liver and RBCs was significantly elevated 60 min after ingestion when compared to control mice, but no change in plasma total GSH was observed (Figure 7A). Interestingly, we found that ingested $^{13}$C-GSH was rapidly converted to GSSG and accumulated in RBCs and liver, but was not present in plasma (Figure 7B). Reduced $^{13}$C-GSH was low or negligible in all samples tested (Figure 7C), suggesting that $^{13}$C-GSH was predominantly deposited in the form of GSSG in the red cells and liver tissues after ingestion of GSH. Previously, it has been reported that dietary GSH does not increase serum GSH level after ingestion and its bioavailability is low, but increases only liver cysteine originating from the breakdown of ingested GSH in the gut.[14−16] This is in line with orally ingested GSH not altering plasma total, GSSG, and reduced GSH level from the current work as reported previously. However, the previous study overlooked analyzing GSH or GSSG level from red cells and liver. In this study, we found mostly orally ingested GSH was immediately converted into GSSG and deposited into red cells and predominantly carried into liver tissues. We speculate some of the ingested $^{13}$C-GSH could be degraded during the circulation of intact GSH into γ-glutamyl amino acid, cysteine, and glycine or γ-glutamyl cysteine by endogenous enzymes. However, the current LC-MS/MS technique could not detect notable degradation of ingested GSH. This must be further clarified in the future by developing a more sensitive method. Our recent small-scale work on human subjects indicated that there was no significant change of plasma GSH after ingestion of GSH. However, the GSH contents in the protein-bound fraction of plasma significantly ($P < 0.01$) increased from 15 to 120 min after GSH supplementation.[26] This is a very unique biological system because reduced GSH has a free thiol group (−SH) in cysteine, and an excess presence of reduced GSH in the plasma or tissues might have some harmful effects for the body due to the potential risk of reactive oxygen species (ROS) generation. If ingested GSH is deposited in circulating red cells or liver tissue as a GSSG form, it could be safer and used for detoxification in the body or liver.

GSH is the major intracellular nonprotein thiol compound and plays a major role in the protection of cells and tissue structures.[12] GSH allows the detoxification of free radicals and oxygen-reactive species involved in such diseases as atherosclerosis, rheumatoid arthritis, adult respiratory distress syndrome, or reoxygenation injury; consequently, its concentration decreases in such diseases.[27] Hepatic GSH concentrations have been observed in alcoholic[2829] and nonalcoholic[30,31] liver diseases. Plasma GSHt concentrations also decrease in such diseases. Therefore, supplemental ingested GSH can benefit the treatment of these diseases and increase liver GSH concentration for detoxification. The ingested GSH has potent nutraceutical benefits for human health to improve oxidative stress and defense in humans. These data indicated that there are several unknown pathways for GSH deposit in the circulating system and transfer into the liver. Further studies will unveil the exact mechanisms of orally administered GSH transport pathway and biological roles in the body.

## AUTHOR INFORMATION


### Corresponding Author

*(Y.M.) Phone: (519) 824-4120. Fax: (519) 824-6631. E mail: ymine@uoguelph.ca.



### Funding

This work was supported in part by AFM Canada (Guelph, ON, Canada). Kohjin Life Science provided GSH and partial financial support for this work. However, they were not involved in any data analysis or manuscript preparation.


### Notes

The authors declare no competing financial interest.

## ACKNOWLEDGMENTS

We thank Annette Morrison, Maka Natsvlishvili, and Jackie Rombeek for their assistance with the animal studies.

## REFERENCES


(1) Franco, R.; Schoneveld, O. J.; Pappa, A.; Panaviotidis, M. I. The central role of glutathione in the pathophysiology of human diseases. *Arch. Physiol. Biochem.* **2007**, *113*, 234−258.

(2) Townsend, D. M.; Tew, K. D.; Tapiero, H. The importance of glutathione in human disease. *Biomed. Pharmacother.* **2003**, *57*, 145−155.

(3) Wu, G.; Fan, Y.-Z.; Yang, S.; Lupton, J. R.; Turner, N. D. Glutathione metabolism and its implications for health. *J. Nutr.* **2004**, *134*, 489−492.

(4) Paolicchi, A.; Dominici, S.; Pieri, L.; Maellaro, E.; Pompella, A. Glutathione catabolism as a signaling mechanism. *Biochem. Pharmacol.* **2002**, *64*, 1027−1035.

(5) Linder, M.; De Burlet, G.; Sudaka, P. Transport of glutathione by intestinal brush border membrane vesicles. *Biochem. Biophys. Res. Commun.* **1984**, *123*, 929−936.

(6) Lash, J. H. Measurement of glutathione transport. In *Current Protocols in Toxicology*; Wiley: Hoboken, NJ, USA, 1999; pp 6.3.1−6.3.14.

(7) Bachhawat, A. K.; Thakur, A.; Kaur, J.; Zulkifli, M. Glutathione transporters. *Biochim. Biophys. Acta* **2013**, *1830*, 3154−3164.

(8) Hagen, T. M.; Jones, D. P. Transepithelical transport of glutathione in vascularly perfused small intestine of rat. *Am. J. Physiol.* **1987**, *252*, G607−G613.

(9) Vina, J. C.; Perez, T.; Furukawa, M.; Palacin, M.; Vina, J. R. Effect of oral glutathione on hepatic glutathione levels in rats and mice. *Br. J. Nutr.* **1989**, *62*, 683−691.

(10) Hagen, T. M.; Wierzbicka, A. H.; Sillau, B. B.; Bowman, B. B.; Jones, P. Bioavailability of dietary glutathione-effect on plasma concentration. *Am. J. Physiol.* **1990**, *259*, G524−G529.

(11) Vincenzini, M. T.; Favilli, F.; Iantomasi, T. Intestinal glutathione transport system: possible detxication role. *Biochim. Biophys. Acta* **1991**, *1073*, 571−579.

(12) Meister, A.; Anderson, M. E. Glutathione. *Annu. Rev. Biochem.* **1983**, *52*, 711−760.

(13) Meister, A. Glutathione deficiency produced by inhibition of its synthesis, and its reversal; applications in research and therapy. *Pharmacol. Ther.* **1991**, *51*, 155−194.

(14) Witschi, A.; Reddy, S.; Stofer, B.; Lauterburg, B. H. The systemic availability of oral glutathione. *Eur. J. Clin. Pharmacol.* **1992**, *43*, 667−669.

(15) Allen, J.; Bradley, R. D. Effects of oral glutathione supplementation on systemic oxidative stress biomarkers in human volunteers. *J. Altern. Complement. Med.* **2011**, *17*, 827−833.

(16) Grattagliano, I.; Wieland, P.; Schranz, C.; Lauterburg, B. H. Effect of oral glutathione monoethyl ester and glutathione on circulating and hepatic sulfhydryls in the rat. *Pharmacol. Toxicol.* **1994**, *75*, 343−347.

(17) Hong, S.-M.; Tanaka, M.; Yoshii, S.; Mine, Y.; Matsui, T. Enhanced visualization of small peptides absorbed in rat small intestine

by phytic-acid-aided matrix-assisted laser desorption/ionization-imaging mass spectrometry. *Anal. Chem.* **2013**, *85*, 10033−10039.
(18) Nakashima, E. M. N.; Kudo, A.; Iwaihara, Y.; Tanaka, M.; Matsumoto, K.; Matsui, M. Application of $^{13}$C-stable isotope labeling liquid chromatography-multiple reaction monitoring-tandem mass spectrometry method for determining intact absorption of bioactive dipeptides in rats. *Anal. Biochem.* **2011**, *414*, 109−116.
(19) Vincenzini, M. T.; Favilli, F.; Iantomasi, T. Intestinal uptake and transmembrane transport systems of intact GSH; characteristics and possible biological role. *Biochim. Biophys. Acta* **1992**, *1113*, 13−23.
(20) Vincenzini, M. T.; Favilli, F.; Iantomasi, T. Glutathione-mediated transport across intestinal brush-border membranes. *Biochim. Biophys. Acta* **1988**, *942*, 107−114.
(21) Vincenzini, M. T.; Iantomasi, T.; Favilli, F. Glutathione transport across intestinal brush-border membranes: effects of ions, pH, $\Delta\psi$, and inhibitors. *Biochim. Biophys. Acta* **1989**, *987*, 29−37.
(22) Lash, L. H.; Hagen, T. M.; Jones, D. P. Exogenous glutathione protects intestinal epithelial cells from oxidative injury. *Proc. Natl. Acad. Sci. U.S.A.* **1986**, *83*, 4641−4645.
(23) Hagen, T. M.; Aw, T. Y.; Jones, D. P. Glutathione uptake and protection against oxidative injury in isolated kidney cells. *Kidney Int.* **1988**, *34*, 74−81.
(24) Iantomasi, T. Glutathione transport system in human intestinal epithelial tract. *Biochim. Biophys. Acta* **1997**, *1330*, 274−283.
(25) Gukasyan, H. J.; Lee, V. H. L.; Simityan, H.; Kim, K.-J.; Kannan, R. Thermodynamic stoichiometry of $Na^+$-coupled glutathione transport. *Can. J. Physiol. Pharmacol.* **2006**, *84*, 1223−1227.
(26) Park, E. Y.; Shimura, N.; Sauchi, Y.; Wada, S.; Aoi, W.; Higashi, A.; Nakamura, Y.; Sato, K. Increase in the protein-bound form of glutathione in human blood after glutathione supplementation. *J. Agric. Food Chem.* **2014**, *62*, 6183−6189.
(27) Uhlig, S.; Wendel, A. The physiological consequences of glutathione variations. *Life Sci.* **1992**, *51*, 1083−1094.
(28) Beutler, E.; Moroose, R.; Kramer, L.; Gelbart, T.; Forman, L. $\gamma$-Glutamylcysteine synthetase deficiency and hemolytic anemia. *Blood* **1990**, *75*, 271−273.
(29) Lauterburg, B. H.; Veley, M. E. Glutathione deficiency in alcoholics: risk factor for paracetamol hepatotoxicity. *Gut* **1988**, *29*, 1153−1157.
(30) Shaw, S.; Kenneth, P. R.; Lieber, C. S. Depressed hepatic glutathione and increased diene conjugates in alcoholic liver disease. *Dig. Dis. Sci.* **1993**, *28*, 585−589.
(31) Summer, K. H.; Eisenburg, J. Low content of hepatic reduced glutathione in patients with Wilson's disease. *Biochem. Med.* **1985**, *34*, 107−111.

without any side effects. The antiobesity effects of Oolong tea polyphenols may be produced by interacting with and inhibiting α-amylase, then reducing the carbohydrate digestibility.[25−27] However, the potential mechanisms of Oolong tea polyphenols in preventing obesity are complicated. Therefore, there is practical significance for development of α-amylase inhibitors through understanding the inhibitory effects and potential mechanisms of Oolong tea polyphenols, EGCG, and EGCG3″Me against α-amylase.

In this study, Oolong tea polyphenols, EGCG and EGCG3″Me were prepared from Oolong tea and their inhibitory effects against α-amylase were investigated. Furthermore, ultraviolet (UV) absorption spectroscopy and fluorescence emission spectroscopy were applied to analyze the nature of binding interaction of α-amylase with Oolong tea polyphenols, EGCG and EGCG3″Me.

## MATERIALS AND METHODS

**Materials.** Oolong tea was purchased from a local market in Guangdong province of China. Toyopearl HW-40S and polyamide resins for column chromatography were purchased from Tosoh Corp. (Tokyo, Japan) and Qingdao Ocean Chemical Co., Ltd. (Qingdao, China), respectively. Standards of EGCG, ECG, EGC, and EC were purchased from Funakoshi Co., Ltd. (Tokyo, Japan), and standards of EGCG3″Me, (−)-catechin gallate (CG) and (−)-gallocatechin gallate (GCG) were prepared according to our reported method.[28] 3,5-Dinitrosalicylic acid (DNS) and porcine pancreatic α-amylase were purchased from Sigma Chemical Co., Ltd. (St. Louis, MO, U.S.A.). Folin-Ciocalteu reagent was purchased from Kayon Biological Technology Co., Ltd. (Shanghai, China). All solvents used for chromatographic purposes were grade of high performance liquid chromatography (HPLC).

**Preparation of Oolong Tea Polyphenols, EGCG and EGCG3″Me.** The preparation of Oolong tea polyphenols, EGCG and EGCG3″Me was performed according to the reported methods[7,28,29] with some modifications. Briefly, 100.0 g of Oolong tea was extracted with distilled water (1600 mL) at 96 °C for 40 min. The extract was centrifuged at 4500*g* for 15 min, and the resulting insoluble residue was treated again as described above. The supernatants were combined, concentrated and dissolved with deinoized water. The resulting solution was filtered through 0.45 μm microfiltration membrane and applied to a polyamide resin column (30 × 1.6 $cm^2$). The column was first washed with 2 times bed volume (BV) of distilled water, and then was eluted with 4 times BV of ethanol solution (80%, v/v). The elution of ethanol solution was collected, concentrated and freeze-dried by a Freeze-Dry System (Labconco, Kansas City, MO, U.S.A.), affording Oolong tea polyphenols.

Part of the Oolong tea polyphenols was dissolved with distilled water and loaded onto a Toyopearl HW-40S column (30 × 1.6 $cm^2$). The column was eluted with 80% ethanol solution at a flow rate of 2.5 mL/min, and the elution was autocollected (10 mL/tube). The eluted fractions were analyzed by HPLC with diode array detector (HPLC-DAD), and the fractions containing EGCG and EGCG3″Me were collected, concentrated, and freeze-dried, affording EGCG and EGCG3″Me, respectively. The structures of resulting EGCG and EGCG3″Me were characterized by HPLC, electrospray ionization time-of-flight mass spectrometry (ESI-TOF-MS) and $^1$H nuclear magnetic resonance (NMR) spectrometry.

**Determination of Contents of Oolong Tea Polyphenols, EGCG, and EGCG3″Me.** The total polyphenols content in sample of Oolong tea polyphenols was determined by the Folin-Ciocalteu method according to the reported procedure.[30] The contents of EC, ECG, CG, GCG, EGCG, and EGCG3″Me were determined according to the reported method[28] by using an Agilent 1100 series HPLC-DAD system (Agilent Technologies Inc., St. Clara, CA, U.S.A.). The separation was achieved on a TSKgel ODS-100Z column (4.6 × 150 $mm^2$, 5 μm; Tosoh Corp., Tokyo, Japan) with a gradient mobile phase consisted of formic acid solution (A, pH 2.5) and methanol (B) at a flow rate of 1.0 mL/min. The linear gradient was as follows: mobile phase A from 82% to 40% in 15 min. The injection volume was 20 μL. The temperature of column oven was set at 40 °C. The wavelength of detector was set at 280 nm.

**Assay of α-Amylase Inhibition.** The determination of α-amylase inhibition was carried out according to the reported method[26,31] with slight modifications. First, α-amylase was dissolved in phosphate buffer saline (PBS, 0.02 mol/L, pH 6.8) at a concentration of 0.1 mg/mL. Various concentrations of Oolong tea polyphenols, EGCG, and EGCG3″Me solutions (0.25 mL) were mixed with α-amylase solution (0.25 mL) and incubated at 37 °C for 5 min. Then the reaction was initiated by adding 0.5 mL 1.0% (w/v) starch substrate solution to the incubation medium. After incubation at 37 °C for 3 min, the reaction was stopped by adding 0.5 mL DNS reagent (1% DNS, 0.2% phenol, 0.05% $Na_2SO_3$, and 1% NaOH in aqueous solution) to the reaction mixture and boiling at 100 °C for 8 min. After cooling to room temperature, the absorbance (Abs) at 540 nm was recorded by a spectrophotometer. The inhibition percentage was calculated by the following equation:

$$\text{inhibition rate } (\%) = [(\text{Abs}_1 - \text{Abs}_2)/\text{Abs}_1] \times 100$$

where $Abs_1$ and $Abs_2$ represent Abs at 540 nm without and with inhibitor, respectively. The half inhibitory concentration ($IC_{50}$) was calculated from inhibition curve.

**Determination of Inhibition Types and $V_{max}$ and $K_m$ Values.** The inhibition types of Oolong tea polyphenols, EGCG, and EGCG3″Me against α-amylase and values of maximum reaction velocity ($V_{max}$) and Michaelis constant ($K_m$) were determined by using the Lineweavere-Burk plots from the relevant Michaelis−Menten equations according the reported method.[32] The substrate solutions at concentrations of 6.0, 8.0, 10.0, 12.0, 14.0, and 16.0 mg/mL were reacted with α-amylase with or without inhibitor, respectively. The concentrations of α-amylase and inhibitor were 0.06 and 0.4 mg/mL, respectively, while distilled water was used as a control. The $V_{max}$ and $K_m$ values were obtained from the least-squares regression lines of the double reciprocal plots of the tested sample (inhibitor) concentration versus the reciprocal of reaction rate.

**UV Absorption Spectroscopy.** The general procedure to probe the interaction relationship between α-amylase and polyphenols by UV absorption spectroscopy was to mix the sample and enzyme solutions, incubate for 3−5 min and then determine the absorption spectrum in the range of 200−300 nm with a UV-2600 spectrophotometer (Shimadzu Corp., Kyoto, Japan). The concentration of α-amylase was 1.0 mg/mL, and the concentrations of Oolong tea polyphenols, EGCG and EGCG3″Me varied from 0.06 to 1.00 mg/mL. The control treatment was carried out without inhibitor.

**Fluorescence Emission Spectroscopy.** Fluorescence spectra were recorded with a Spectra Max Gemini XS spectrofluorometer (Molecular Devices, Sunnyvale, CA, U.S.A.) according to the reported method[33] with some modifications. Briefly, 3D fluorescence spectrum of α-amylase (0.1 mg/mL) was scanned under 20 °C and pH 6.9, the excitation wavelength ($\lambda_{ex}$) and emission wavelength ($\lambda_{em}$) were determined, respectively. Under the same conditions, the solutions of different concentrations of Oolong tea polyphenols, EGCG and EGCG3″Me were added into α-amylase solution and reacted for 3 min, respectively, then the relative fluorescence intensities were determined at excitation wavelength of 340 nm and emission wavelength of 280 nm.

**Statistical Analysis.** The results obtained were analyzed by SPSS version 16.0 (SPSS Inc.; Chicago, IL, U.S.A.). Any significant difference was determined by one-way analysis of variance (ANOVA) followed by the Tukey test for multiple comparisons at $P < 0.05$ level.

## RESULTS AND DISCUSSION

The water extract of Oolong tea was first separated by polyamide column chromatography to afford Oolong tea polyphenols that the total polyphenols content was 83.92%. As shown in Figure 2B, the main components in Oolong tea

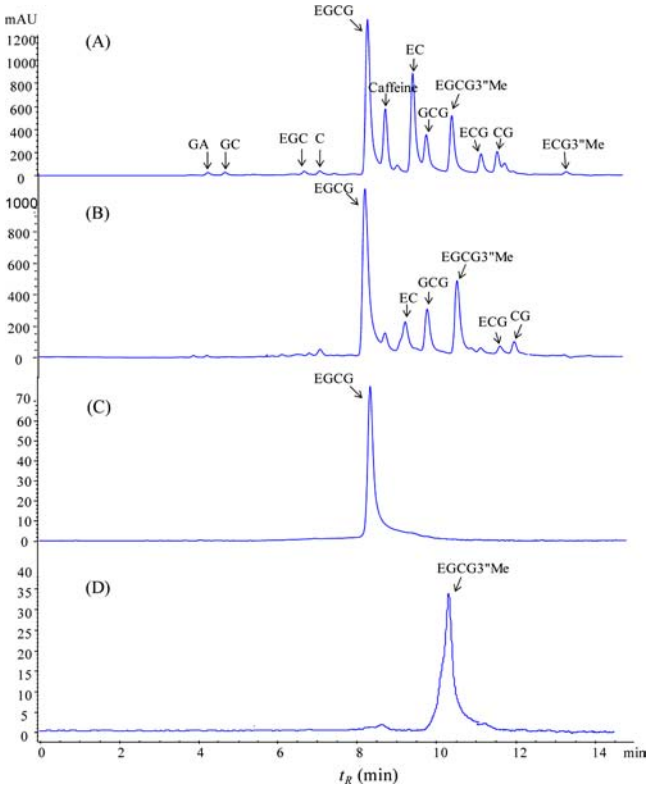


**Figure 2.** HPLC chromatograms of Oolong tea extract (A), Oolong tea polyphenols (B), purified EGCG (C), and purified EGCG3″Me (D).

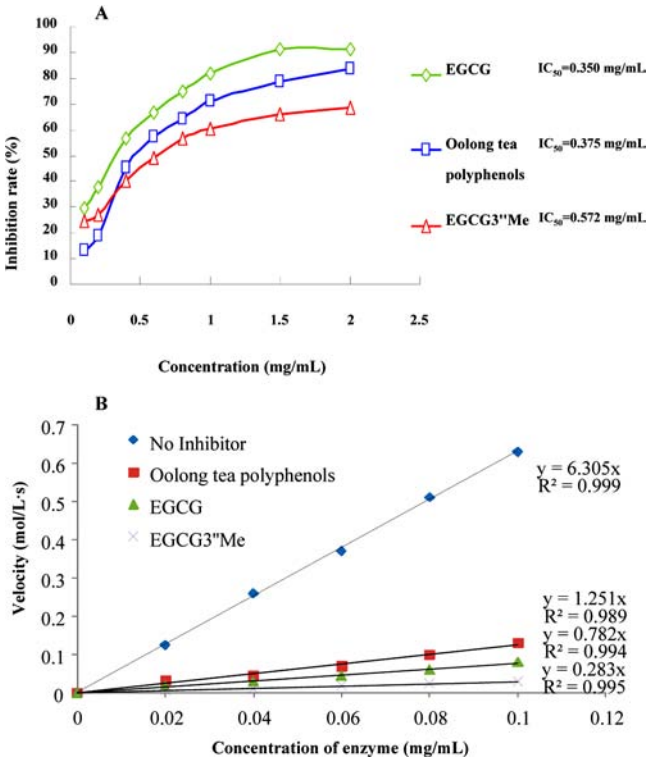


**Figure 3.** Inhibitory effects (A) and inhibition types (B) of Oolong tea polyphenols, EGCG, and EGCG3″Me on α-amylase.

polyphenols were EGCG (27.58 ± 1.73%), EGCG3″Me (14.30 ± 0.32%), GCG (9.28 ± 0.18%), EC (7.83 ± 0.11%), ECG (4.21 ± 0.29%), and CG (3.72 ± 0.17%). Notably, EGCG and EGCG3″Me occupied about 42% of the total polyphenols. The resulting Oolong tea polyphenols were separated by column chromatography of Toyopearl HW-40S, affording high purity of EGCG (98.00%, Figure 2C) and EGCG3″Me (96.68%, Figure 2D). By comparison with reported data,[16,34,35] their chemical structures were confirmed to be EGCG and EGCG3″Me by HPLC, ESI-TOF-MS, and $^1$H NMR.

**Inhibition of Oolong Tea Polyphenols, EGCG, and EGCG3″Me on α-Amylase.** The inhibitory effects of Oolong tea polyphenols, EGCG and EGCG3″Me against α-amylase were investigated. As shown in Figure 3A, the $IC_{50}$ values of Oolong tea polyphenols, EGCG and EGCG3″Me were 0.375, 0.350, and 0.572 mg/mL, respectively. EGCG exhibited relative lower $IC_{50}$ value, indicating its relative higher inhibitory potency in comparison with Oolong tea polyphenols and EGCG3″Me. It is consistent with reported results that the inhibitory effects of C, EC, EGC, and EGCG on α-amylase are in the following order: EGCG > EC > EGC > C.[27,36] The results also suggested that EGCG should be one of the main inhibitory compounds against α-amylase in Oolong tea polyphenols. However, EGCG3″Me showed the highest $IC_{50}$ value, indicating its relative weaker inhibitory effect on α-amylase. The inhibitory difference between EGCG and EGCG3″Me might be due to the difference in their structures. It has been reported that polyphenols interacted with α-amylase primarily through noncovalent interactions, such as hydrophobic interaction and hydrogen bonding between the hydroxyl groups of polyphenols and the catalytic residues of binding site in α-amylase, forming the polyphenols−enzyme complex.[27,37] Thus, the substitution of 3-OH in D ring of EGCG (Figure 1) by methoxy group might be the possible reason for relative weaker inhibitory effect of EGCG3″Me on α-amylase.[25,38] However, it has been reported that the methylation of polyphenols could greatly improve the transport through biological membranes and increase the oral bioavailability.[39,40] Thus, the in vivo inhibitory effect of EGCG3″Me is worthy of further study due to its relative higher bioavailabilty in vivo than EGCG.[41]

To explore the inhibition types of Oolong tea polyphenols, EGCG and EGCG3″Me against α-amylase, the kinetic reactions of α-amylase were investigated with different concentrations of α-amylase. As shown in Figure 3B, it was found that the lines obtained from the Lineweaver−Burk plots were all passed through the origin point (0, 0) of the coordinates, indicating that the inhibition types of Oolong tea polyphenols, EGCG, and EGCG3″Me against α-amylase were all reversible inhibition. To further investigate the inhibitory characteristics, Lineweaver−Burk double reciprocal plots were performed. As shown in Figure 4, the Lineweaver−Burk plots for Oolong tea polyphenols and EGCG showed the same intersection on *Y*-axis, indicating that the inhibition on α-amylase by Oolong tea polyphenols and EGCG were competitive. In contrast, EGCG3″Me had an intersection on *X*-axis, suggesting that EGCG3″Me inhibited α-amylase in a noncompetitive fashion. The difference of inhibition types of EGCG and EGCG3″Me, being worthy of further study, might also be due to the structural difference between EGCG and EGCG3″Me. Furthermore, kinetic inhibition parameters on α-amylase were calculated according to Lineweaver−Burk plots, and the results are shown in Table 1. In the presence of EGCG3″Me, $V_{max}$ value for α-amylase decreased, while the value of $K_m$ remained unchanged. In contrast, $K_m$ value for α-


dx.doi.org/10.1021/jf5032907 | J. Agric. Food Chem. 2014, 62, 9507−9514

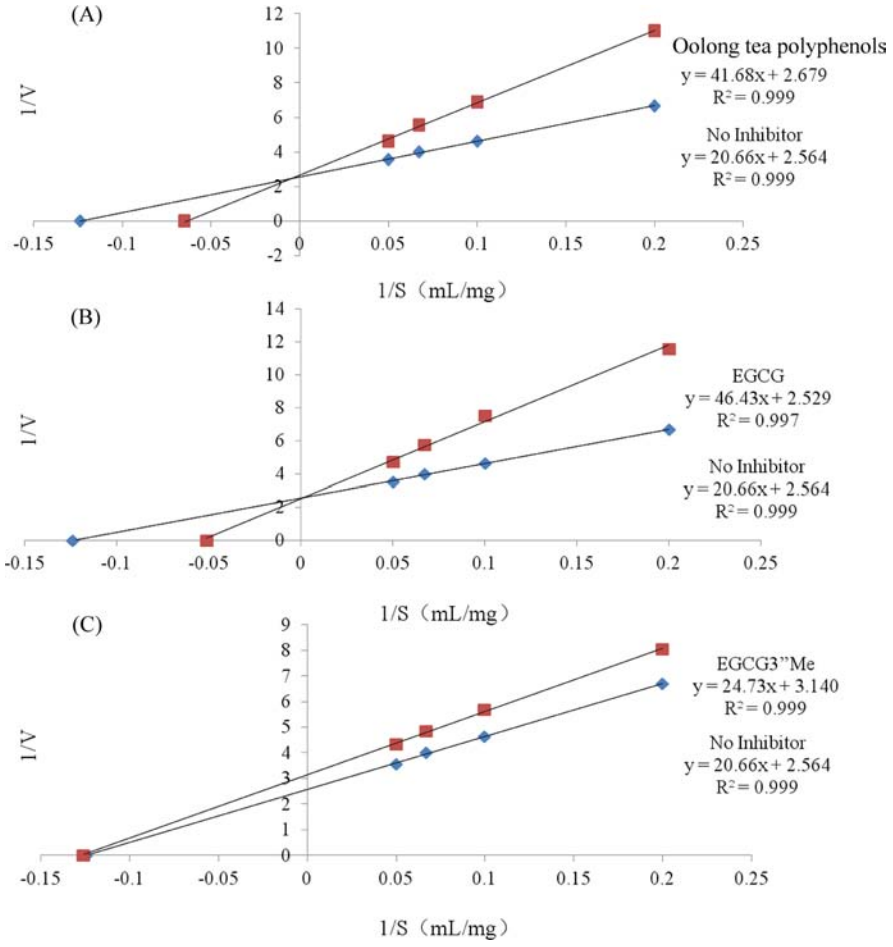


**Figure 4.** Lineweaver–Burk plots of the reaction of α-amylase in the presence of Oolong tea polyphenols (A), EGCG (B), and EGCG3″Me (C).

**Table 1. Kinetic Results of Inhibition against α-amylase by Oolong tea Polyphenols, EGCG, and EGCG3″Me**

| | $K_m$ (mg/mL) | $V_{max}$ (mg/mL·min) | inhibition type |
|---|---|---|---|
| no inhibitior | 8.06[a] | 0.39[a] | |
| Oolong tea polyphenols | 15.38[b] | 0.38[a] | competitive inhibition |
| EGCG | 18.51[c] | 0.39[a] | competitive inhibition |
| EGCG3″Me | 7.94[a] | 0.32[b] | noncompetitive inhibition |

amylase increased while $V_{max}$ value remained unchanged in the presence of Oolong tea polyphenols or EGCG. Such results are consistent with their inhibitory characteristics.

**Changes of α-Amylase UV Spectra Induced by Oolong Tea Polyphenols, EGCG or EGCG3″Me.** α-Amylase has an absorption peak at 270 nm due to the presence of tryptophan (Trp) and tyrosine (Tyr) aromatic heterocyclic residues, thus, the change of microenvironment of the aromatic amino acid residues would cause the change of α-amylase absorption wavelength. As shown in Figure 5, changes in UV spectra of α-amylase were observed after the addition of Oolong tea polyphenols, EGCG, and EGCG3″Me. With the increase of sample concentration, a red-shift for α-amylase was found, but there was no significant difference among the samples. It has been reported that the main mechanism of polyphenols-enzyme binding was considered to be noncovalent interactions, including hydrogen bond and hydrophobic association.[42−44] Interaction of polyphenols and α-amylase was conducive to intermolecular and intramolecular agglomeration effects of enzyme, which made the residues of Trp and Tyr within the aromatic heterocyclic and hydrophobic groups surrounded by α-amylase exposed, led to the microenvironmental change of the aromatic amino acid residues in the spatial structure and caused the conformational change of protein. However, the composition and quantity of the polar groups in the enzyme protein may affect the formation and stability of hydrogen bonds between polyphenols and α-amylase.[27,37] Thus, with the increase of sample concentration, the protein (enzyme) peptide bond extension phenomenon occurred, hydrophobic interaction enhanced slightly, and then absorption peak and red-shift amplitude increased correspondingly.

**Quenching of α-Amylase Fluorescence Spectra by Oolong Tea Polyphenols, EGCG, or EGCG3″Me.** Fluorescence quenching measures the decrease of the quantum yield of fluorescence from a fluorophore induced by a variety of molecular interactions with a quencher molecule. It is a useful approach to investigate intermolecular interactions. In the present study, therefore, the interaction between polyphenols and α-amylase was investigated from the changes of the fluorescence emission spectra of α-amylase in the absence and presence of polyphenols. From 3D fluorescence spectrum of α-amylase (Figure 6A), it was found that α-amylase had two absorption peaks at excitation wavelength of 340 nm, whereas Oolong tea polyphenols did not show any interference (Figure


dx.doi.org/10.1021/jf5032907 | J. Agric. Food Chem. 2014, 62, 9507−9514

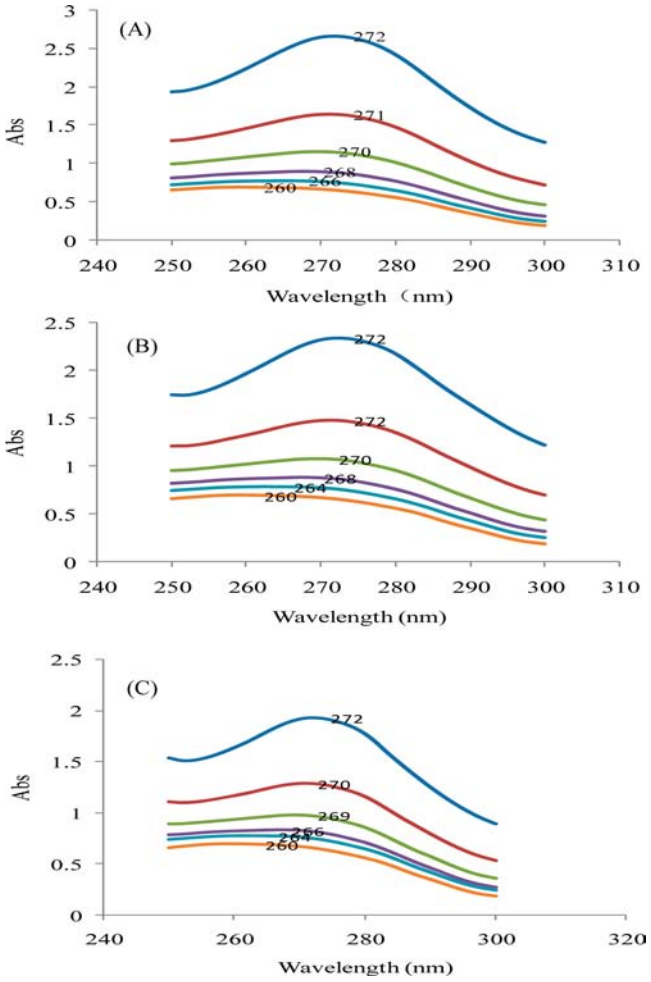


**Figure 5.** UV absorption spectra of $\alpha$-amylase in the presence of different concentrations of Oolong tea polyphenols (A), EGCG (B), and EGCG3″Me (C). From top down, 1.00, 0.500, 0.25, 0.13, 0.06, and 0.00 mg/mL for sample concentration.

6B). With the addition of Oolong tea polyphenols, EGCG, or EGCG3″Me, the fluorescence emission intensity of $\alpha$-amylase decreased (Figure 6C−H), indicating that Oolong tea polyphenols, EGCG, and EGCG3″Me could quench the intrinsic fluorescence of $\alpha$-amylase. The reason might be due to the fact that polyphenols bind to $\alpha$-amylase, which leads to the unfolding of $\alpha$-amylase fluorescent amino acid residues and causes quenching of the inherent fluorescence property. The observed spectral changes of $\alpha$-amylase reflected direct or indirect interactions of polyphenols with the hydrophobic and hydrophilic regions located in the vicinity of Trp and Tyr and induced conformational changes of $\alpha$-amylase. As Brayer et al.[5] reported, inhibitors may directly contact with the side chains of Asp197, Glu233, and Asp300 of $\alpha$-amylase. Computational ligand docking indicates that the inhibitory activity of EGCG on $\alpha$-amylase depends on hydrogen bonds between the hydroxyl groups of EGCG and the catalytic residues of the binding site and formation of a conjugated $\pi$-system that stabilizes the interaction with active site.[37,45,46]

As shown in Figure 6C−H, Oolong tea polyphenols, EGCG, and EGCG3″Me exhibited different quenching effects on $\alpha$-amylase. The absorption characteristics of Oolong tea polyphenols and EGCG with $\alpha$-amylase was roughly the same, but it was significantly different from that of EGCG3″Me. The difference in quenching effects between EGCG and EGCG3″Me might be due to the difference of their structures: hydroxyl group for EGCG and methoxy group for EGCG3″Me at C-3 of D ring (Figure 1). The interaction between polyphenol and $\alpha$-amylase was reported to depend on the structures of polyphenols and $\alpha$-amylase.[27,37] Some researchers also explored the structure−activity relationship of inhibitors with $\alpha$-amylase and possible mechanisms by molecular docking and other measurements, such as the binding of flavonols, flavones, and EGCG with human salivary $\alpha$-amylase.[6,38,47] On the basis of the present results and some previous reports, thus, we conclude that Oolong tea polyphenols, EGCG, and EGCG3″Me may act as antiobesity factor, in terms of their inhibitory effects on $\alpha$-amylase, due to the cooperative effects of hydrophobic association and hydrogen bond formation between polyphenols and $\alpha$-amylase.

The relationship between fluorescence quenching intensity and concentration of quencher can be described by following Stern−Volmer equation.[46,48]

$$F_0/F = 1 + k_q\tau_0[Q] = 1 + K_{sv}[Q]$$

$F_0$ and $F$ are the fluorescence intensities in the absence and presence of quencher, respectively. $k_q$ is the bimolecular quenching constant, $\tau_0$ is the native lifetime of the fluorophore, and $[Q]$ is the concentration of quencher. $K_{sv}$, the Stern−Volmer quenching constant, is given by $k_q\tau_0$. A linear Stern−Volmer plot is generally indicative of a single class of fluorophore in a protein, all equally accessible to the quencher. Here, the following modified Stern−Volmer equation was applied to analyze the fluorescence quenching.

$$\frac{F_0}{F_0 - F} = \frac{1}{fK[Q]} + \frac{1}{f}$$

where $f$ is the fraction of fluorophore accessible to the quencher and $K$ is the modified Stern−Volmer quenching constant which is very close to the binding constant. The plot of $F_0/(F_0 - F)$ versus $1/[Q]$ yields $1/f$ as the intercept and $1/fK$ as the slope. Thus, from the intercept and slope, the $f$ and $K$ can be obtained. The fluorescence quenching parameters are list in Table 2. On the basis of the fluorescence quenching parameters ($K_{sv}$ and $K_q$), we could verified that Oolong tea polyphenols and EGCG had almost the same binding ability on $\alpha$-amylase, which further proved that EGCG was one of the main inhibitory ingredients in Oolong tea polyphenols against $\alpha$-amylase as mentioned above. Besides, the lower $K$ value for EGCG3″Me indicated a lower affinity interaction between $\alpha$-amylase and EGCG3″Me compared to EGCG. EGCG-$\alpha$-amylase complex was reflected to have more exposure of Trp residues and unfolding of protein structure than EGCG3″Me-$\alpha$-amylase. It has been reported that the binding constants for the larger polyphenol-protein complexes are larger than those of smaller polyphenol−protein adducts, which can be due to the presence of more hydroxyl groups associated with the polyphenols.[49] Due to the tightening of protein structure through intramolecular interactions such as hydrogen bonds, polyphenol−$\alpha$-amylase complexes might induce Trp residues in a more hydrophobic environment. We could speculate that, therefore, hydroxyl but not the methoxy group in polyphenols played the main role in the binding process.

Fluorescence quenching can be dynamic (resulting from collisional encounters between fluorophore ($\alpha$-amylase) and quencher) or static (resulting from formation of a ground state


dx.doi.org/10.1021/jf5032907 | J. Agric. Food Chem. 2014, 62, 9507−9514

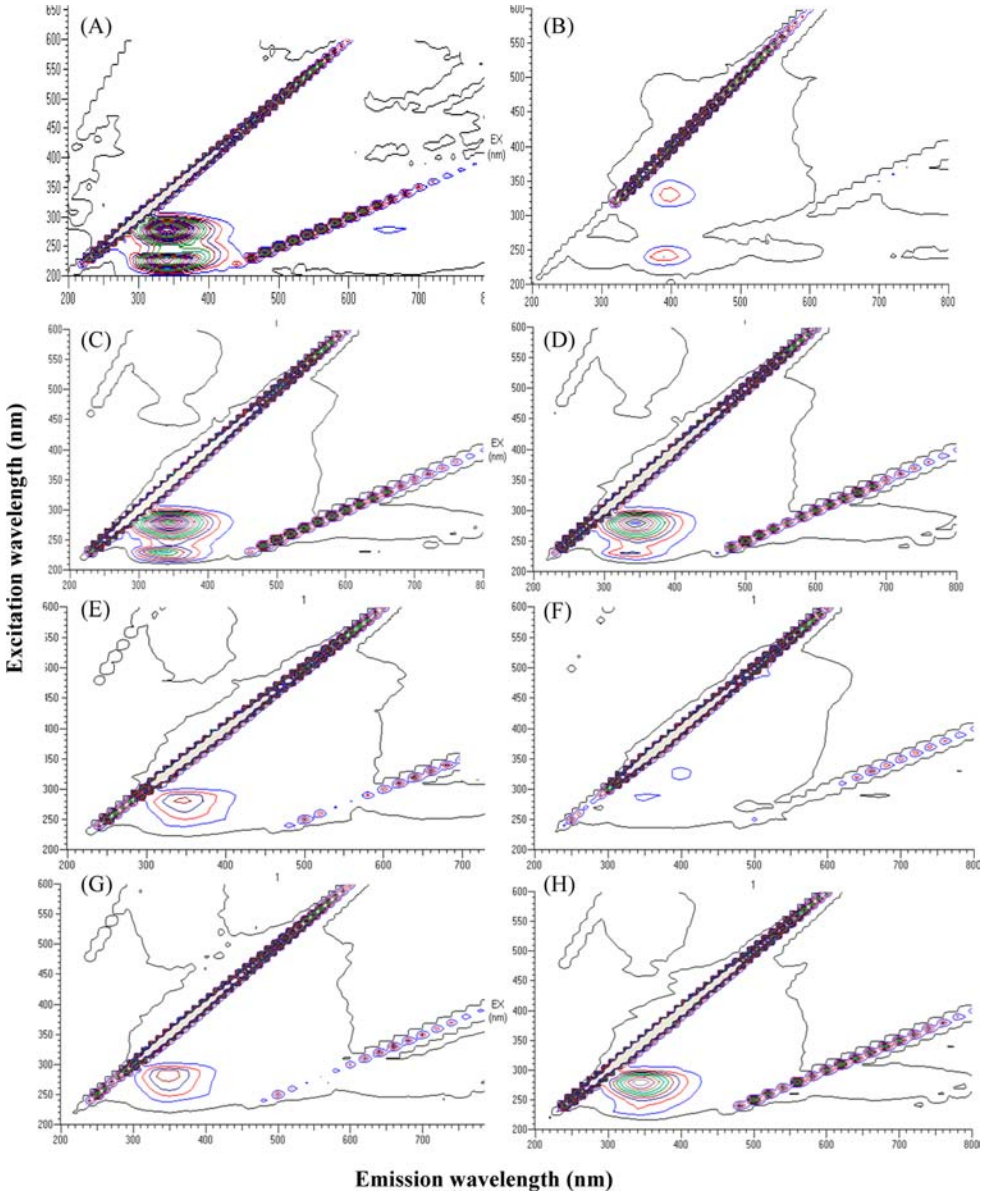


**Figure 6.** 3D Fluorescence spectra of $\alpha$-amylase (A) and Oolong tea polyphenols (B) and fluorescence quenching effects on $\alpha$-amylase by Oolong tea polyphenols (C, D, E, and F at concentrations of 10, 40, 100, and 200 $\mu$g/mL, respectively), EGCG (G, 100 $\mu$g/mL), and EGCG3″Me (H, 100 $\mu$g/mL).

**Table 2. Fluorescence Quenching Parameters for the Interactions of Oolong Tea Polyphenols, EGCG, and EGCG3″Me with $\alpha$-Amylase**

| | $K_{sv}$ (L·g$^{-1}$) | $K_q$ ( × 10$^{12}$ L·g$^{-1}$·s$^{-1}$) | $K$ (L·g$^{-1}$) |
|---|---|---|---|
| Oolong tea polyphenols | 53177.0[a] | 5.318[a] | 23684.1[a] |
| EGCG | 53174.4[a] | 5.317[a] | 39272.0[b] |
| EGCG3″Me | 61542.0[b] | 6.154[b] | 33746.0[b] |

between fluorophore and quencher).[50] Dynamic quenching is related to diffusion, and the rising of the temperature will increase the diffusion coefficient, thus increase the bimolecular quenching constant. Conversely, if it is static quenching, the temperature rise will improve the stability of the complexes, quenching constant will diminish.[51] As shown in Figure 7, the quenching constant slope increased slightly with the increase of temperature. Hence, the fluorescence quenching of Oolong tea polyphenols, EGCG, and EGCG3″Me on $\alpha$-amylase was determined to be dynamic one.

In conclusion, the inhibitory effects on $\alpha$-amylase of Oolong tea polyphenols, EGCG, and EGCG3″Me, prepared from Chinese Oolong tea, were investigated in the present study. EGCG appeared to be one of the main compounds in Oolong tea polyphenols for the inhibitory effects against $\alpha$-amylase. The differences of inhibitory effect and inhibition type between EGCG and EGCG3″Me might be due to substitution of the hydroxyl group in EGCG by methoxy group. In addition, it is speculated that Oolong tea polyphenols, EGCG, and EGCG3″Me exhibited their inhibitory effects against $\alpha$-amylase through the cooperative effects of hydrophobic association and hydrogen bond formation between polyphenols and $\alpha$-amylase. Further works on inhibitory effect in vivo and possible action mechanisms of EGCG3″Me are in progress.


dx.doi.org/10.1021/jf5032907 | J. Agric. Food Chem. 2014, 62, 9507−9514

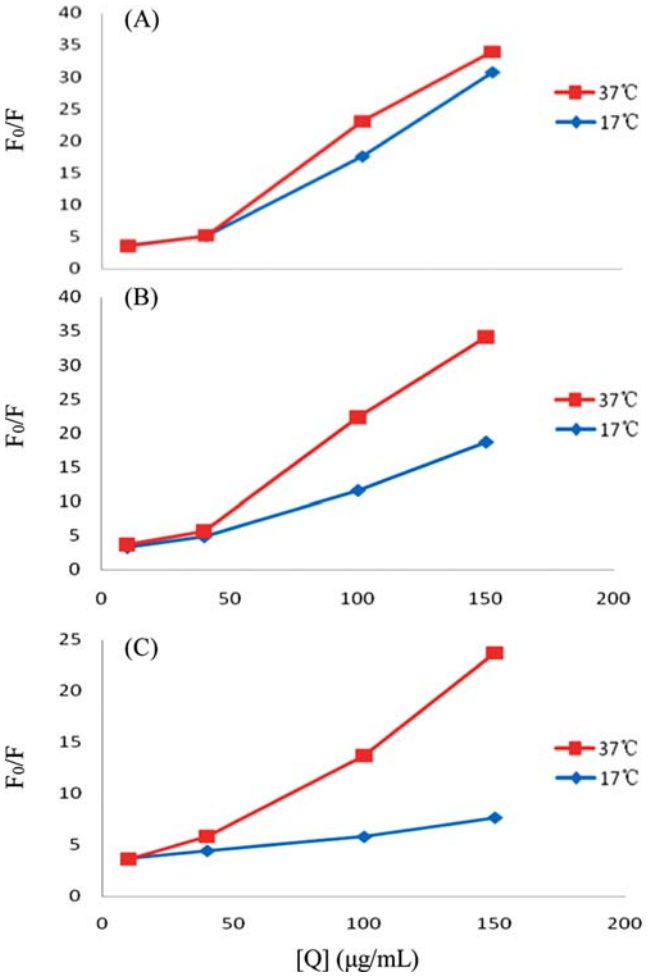


**Figure 7.** Stem−Volmer diagrams of Oolong tea polyphenols (A), EGCG (B), and EGCG3″Me (C).

## AUTHOR INFORMATION


### Corresponding Author

*Fax: +86 25 84396791; e-mail: zengxx@njau.edu.cn.


### Notes

The authors declare no competing financial interest.

## ACKNOWLEDGMENTS

This work was supported by a project funded by National Natural Science Foundation of China (31360076), a grant-in-aid from Key Technology R&D Program of Jiangsu Province under (BE2013313), and a grant-in-aid from a Project Funded by the Priority Academic Program Development of Jiangsu Higher Education Institutions (PAPD).

## REFERENCES


(1) WHO. Obesity and overweight. Fact sheet N°311, 2011. Available from <http://www.who.int/mediacentre/factsheets/fs311/en/>.

(2) Puhl, R. M.; Heuer, C. A. The stigma of obesity: a review and update. *Obesity* **2009**, *17*, 941−964.

(3) Shen, J.; Goyal, A.; Sperling, L. The emerging epidemic of obesity, diabetes, and the metabolic syndrome in China. *Cardiol. Res. Pract.* **2012**, article ID 178675 (doi:10.1155/2012/178675).

(4) Ferguson, R. D.; Gallagher, E. J.; Scheinman, E. J.; Damouni, R.; LeRoith, D. The epidemiology and molecular mechanisms linking obesity, diabetes, and cancer. *Vitam. Horm.* **2013**, *93*, 51−98.

(5) Brayer, G. D.; Sidhu, D.; Maurus, R.; Rydberg, E. H.; Braun, C.; Wang, Y.; Nguyen, N. T.; Overall, C. M.; Withers, S. G. Subsite Mapping of the human pancreatic α-amylase active site through structural, kinetic, and mutagenesis techniques. *Biochem.* **2000**, *39*, 4778−4791.

(6) Robyt, J. F.; French, D. The action pattern of porcine pancreatic α-amylase in relationship to the substrate binding site of the enzyme. *J. Biol. Chem.* **1970**, *245*, 3917−3927.

(7) Zhang, X.; Zhu, X. L.; Sun, Y. K.; Hu, B.; Sun, Y.; Jabbar, S.; Zeng, X. Fermentation in vitro of EGCG, GCG and EGCG3″Me isolated from Oolong tea by human intestinal microbiota. *Food Res. Int.* **2013**, *54*, 1589−1595.

(8) Siddiqui, I. A.; Afaq, F.; Adhami, V. M.; Ahmad, N.; Mukhtar, H. Antioxidants of the beverage tea in promotion of human health. *Antioxid. Redox Signaling* **2004**, *6*, 571−582.

(9) Kuroda, Y.; Hara, Y. Antimutagenic and anticarcinogenic activity of tea polyphenols. *Mutat. Res.* **1999**, *436*, 69−97.

(10) Yang, C. S.; Wang, Z. Y. Tea and cancer. *J. Natl. Cancer Inst.* **1993**, *85*, 1038−1049.

(11) Yang, T. T. C.; Koo, M. W. L. Hypocholesterolemic effects of Chinese tea. *Pharmacol. Res.* **1997**, *35*, 505−512.

(12) Yang, T. T. C.; Koo, M. W. L. Chinese green tea lowers cholesterol level through an increase in fecal excretion. *Life Sci.* **2000**, *66*, 411−423.

(13) Bolling, B. W.; Chen, C. Y. O.; Blumberg, J. B. Tea and health, preventive and therapeutic usefulness in the elderly? *Curr. Opin. Clin. Nutr. Metab. Care* **2009**, *12*, 42−48.

(14) Grove, K. A.; Sae-Tan, S.; Kennett, M. J.; Lambert, J. D. (−)-Epigallocatechin-3-gallate inhibits pancreatic lipase and reduces body Weight gain in high fat-fed obese mice. *Obesity* **2012**, *20*, 2311−2313.

(15) Nagle, D. G.; Ferreira, D.; Zhou, Y. D. Epigallocatechin-3-gallate (EGCG): Chemical and biomedical perspectives. *Phytochemistry* **2006**, *67*, 1849−1855.

(16) Sano, M.; Suzuki, M.; Miyase, T.; Yoshino, K.; Maeda-Yamamoto, M. Novel anti-allergic catechin derivatives isolated from Oolong tea. *J. Agric. Food Chem.* **1999**, *47*, 1906−1910.

(17) Suzuki, M.; Yoshino, K.; Maeda-Yamamoto, M.; Miyase, T.; Sano, M. Inhibitory effects of tea catechins and *O*-methylated derivatives of (−)-epigallocatechin-3-*O*-gallate on mouse type IV allergy. *J. Agric. Food Chem.* **2000**, *48*, 5649−5653.

(18) Kagaya, N.; Hara, Y.; Saijo, R.; Kamiyoshi, A.; Tagawa, Y. I.; Kawase, M.; Yagi, K. Novel function of rare catechin, epigallocatechin-3-(3″-*O*-methyl) gallate, against cold injury in primary rat hepatocytes. *J. Biosci. Bioeng.* **2003**, *96*, 559−563.

(19) Kurita, I.; Maeda-Yamamoto, M.; Tachibana, H.; Kamei, M. Antihypertensive effect of Benifuuki tea containing *O*-methylated EGCG. *J. Agric. Food Chem.* **2010**, *58*, 1903−1908.

(20) Cai, S. X.; Zhong, Y.; Li, Y. H.; Huang, J. A.; Zhang, J.; Luo, G. A.; Liu, Z. H. Blockade of the formation of insoluble ubiquitinated protein aggregates by EGCG3″Me in the alloxan-induced diabetic kidney. *PLoS One* **2013**, *8*, e75687 DOI: 10.1371/journal.-pone.0075687.

(21) Kagaya, N.; Tagawa, Y.; Nagashima, H.; Saijo, R.; Kawase, M.; Yagi, K. Suppression of cytotoxin-induced cell death in isolated hepatocytes by tea catechins. *Eur. J. Pharmacol.* **2002**, *450*, 231−236.

(22) Rumpler, W.; Seale, J.; Clevidence, B.; Judd, J.; Wiley, E.; Yamamoto, S.; Komatsu, T.; Sawaki, T.; Ishikura, Y.; Hosoda, K. Oolong tea increases metabolic rate and fat oxidation in men. *J. Nutr.* **2001**, *131*, 2848−2852.

(23) Hsu, T. F.; Kusumoto, A.; Abe, K.; Hosoda, K.; Kiso, Y.; Wang, M. F.; Yamamoto, S. Polyphenol-enriched oolong tea increases fecal lipid excretion. *Eur. J. Clin. Nutr.* **2006**, *60*, 1330−1336.

(24) He, R. R.; Chen, L.; Lin, B. H.; Yokichi, M.; Yao, X. S.; Hiroshi, K. Beneficial effects of Oolong tea consumption on diet-induced overweight and obese subjects. *Chin. J. Integr. Med.* **2009**, *15*, 34−41.

(25) Xiao, J.; Ni, X.; Kai, G.; Chen, X. A review on structure-activity relationship of dietary polyphenols inhibiting α-amylase. *Crit. Rev. Food Sci. Nutr.* **2013**, *53*, 497−506.

(26) Hara, Y.; Honda, M. The inhibition of α-amylase by tea polyphenols. *Agric. Biol. Chem.* **1990**, *54*, 1939−1945.
(27) Miao, M.; Jiang, H.; Jiang, B.; Li, Y. G.; Cui, S. W.; Zhang, T. Structure elucidation of catechins for modulation of starch digestion. *LWT-Food Sci. Technol.* **2014**, *57*, 188−193.
(28) Hu, B.; Wang, L.; Zhou, B.; Zhang, Xin.; Sun, Y.; Ye, H.; Zhao, L. Y.; Hu, Q. H.; Wang, G. X.; Zeng, X. Efficient procedure for isolating methylated catechins from green tea and effective simultaneous analysis of ten catechins, three purine alkaloids, and gallic acid in tea by high-performance liquid chromatography with diode array detection. *J. Chromatogr. A* **2009**, *1216*, 3223−3231.
(29) Zhang, X.; Lei, S. C.; Jabbar, S.; Hu, B.; Sun, Y.; Zeng, X. Simultaneous separation and purification of tea bioactives from summer green tea by column chromatography. *J. Chem. Soc. Pak.* **2013**, *35*, 1258−1267.
(30) Liu, L. X.; Sun, Y.; Laura, T.; Liang, X. F.; Ye, H.; Zeng, X. Determination of polyphenolic content and antioxidant activity of kudingcha made from *Ilex kudingcha* C.J. Tseng. *Food Chem.* **2009**, *112*, 35−41.
(31) Kandra, L.; Zajácz, Á.; Remenyik, J.; Gyémánt, G. Kinetic investigation of a new inhibitor for human salivary α-amylase. *Biochem. Biophys. Res. Commun.* **2005**, *334*, 824−828.
(32) You, Q.; Chen, F.; Wang, X.; Jiang, Y. M.; Lin, S. Y. Anti-diabetic activities of phenolic compounds in muscadine against alpha-glucosidase and pancreatic lipase. *LWT-Food Sci. Technol.* **2012**, *46*, 164−168.
(33) Sheng, L. Q.; Run, X. Y.; Xu, H. J. Spectral studies of nicotine and bovine serum albumin. *Spectrosc. Spectral Anal.* **2007**, *27*, 306−308.
(34) Davis, A. L.; Cai, Y.; Davies, A. P.; Lewis, J. R. $^{1}$H and $^{13}$C NMR assignments of some green tea polyphenols. *Magn. Reson. Chem.* **1996**, *34*, 887−890.
(35) Saijo, R. Isolation and chemical structures of two new catechins from fresh tea leaf. *Agric. Biol. Chem.* **1982**, *46*, 1969−1970.
(36) Tadera, K.; Minami, Y.; Takamatsu, K.; Matsuoka, T. Inhibition of α-glucosidase and α-amylase by flavonoids. *J. Nutr. Sci. Vitaminol.* **2006**, *52*, 149−153.
(37) Bandyopadhyay, P.; Ghosh, A. K.; Ghosh, C. Recent developments on polyphenol-protein interactions: effects on tea and coffee taste, antioxidant properties and the digestive system. *Food Funct.* **2012**, *3*, 592−605.
(38) Piparo, E. L.; Scheib, H.; Frei, N.; Williamson, G.; Grigorov, M.; Chou, C. J. Flavonoids for controlling starch digestion: structural requirements for inhibiting human α-amylase. *J. Med. Chem.* **2008**, *51*, 3555−3561.
(39) Wen, X.; Walle, T. Methylated flavonoids have greatly improved intestinal absorption and metabolic stability. *Drug Metab. Dispos.* **2006**, *34*, 1786−1792.
(40) Walle, T. Methylation of dietary flavones increases their metabolic stability and chemopreventive effects. *Int. J. Mol. Sci.* **2009**, *10*, 5002−5019.
(41) Oritani, Y.; Setoguchi, Y.; Ito, R.; Maruki-Uchida, H.; Ichiyanagi, T.; Ito, T. Comparison of (−)-epigallocatechin-3-*O*-gallate (EGCG) and *O*-methyl EGCG bioavailability in rats. *Biol. Pharm. Bull.* **2013**, *36*, 1577−1582.
(42) He, Q.; Shi, B.; Yao, K. Interactions of gallotannins with proteins, amino acids, phospholipids and sugars. *Food Chem.* **2006**, *95*, 250−254.
(43) Xiao, J.; Kai, G.; Ni, X.; Yang, F.; Chen, X. Interaction of natural polyphenols with α-amylase *in vitro*: molecular property-affinity on relationship aspect. *Mol. BioSyst.* **2011**, *7*, 1883−1890.
(44) Siebert, K. J.; Troukhanova, N. V.; Lynn, P. Y. Nature of polyphenol-protein interactions. *J. Agri. Food Chem.* **1996**, *44*, 80−85.
(45) Machius, M.; Vértesy, L.; Huber, R.; Wiegand, G. Carbohydrate and protein-based inhibitors of porcine pancreatic α-amylase: Structure analysis and comparison of their binding characteristics. *J. Mol. Biol.* **1996**, *260*, 409−421.
(46) Liang, L.; Tajmir-Riahi, H. A.; Subirade, M. Interaction of β-lactoglobulin with resveratrol and its biological implications. *Biomacromolecules* **2008**, *9*, 50−56.
(47) Lee, J. Y.; Jeong, K. W.; Kim, Y. Epigallocatechin 3-gallate binds to human salivary α-amylase with complex hydrogen bonding interactions. *Bull. Korean Chem. Soc.* **2011**, *32*, 2222−2226.
(48) Lakowicz, J. R. *Principles of Fluorescence Spectroscopy*, 3rd ed.; Springer: New York, 2006.
(49) Kanakis, C. D.; Hasni, I.; Bourassa, P.; Tarantilis, P. A.; Polissiou, M. G.; Tajmir-Riahi, H. A. Milk β-lactoglobulin complexes with tea polyphenols. *Food Chem.* **2011**, *127*, 1046−1055.
(50) Soares, S.; Mateus, N.; De Freitas, V. Interaction of different polyphenols with bovine serum albumin (BSA) and human salivary alpha-amylase (HSA) by fluorescence quenching. *J. Agric. Food Chem.* **2007**, *55*, 6726−6735.
(51) Yang, J.; Jing, Z. H.; Jie, J. J.; Guo, P. Fluorescence spectroscopy study on the interaction between Gossypol and bovine serum albumin. *J. Mol. Struct.* **2009**, *920*, 227−230.

containing 1:1:1 methanol, acetone, and ethanol. The mixture was stirred for 30 min and filtered through cheesecloth, and the remaining solids were re-extracted twice under the same conditions. Following a final filtration through no. 4 Whatman filter paper, the solvents were evaporated under reduced pressure at 45 °C, and the concentrate was brought up to 15 mL in water acidified with 0.01% HCl. Insoluble solids were removed by centrifugation prior to filtration through a Whatman 0.45 $\mu$m PTFE membrane for HLPC-MS characterization.

Additional isolation and concentration were deemed necessary to characterize minor compounds in mango pulp and were accomplished by extracting 1 kg of fruit as previously described.[9] Phytochemicals were partitioned from 10 g $C_{18}$ Sep Pak cartridges. Columns were preconditioned with 10 column volumes of methanol followed by 10 column volumes of water. Extracts were loaded onto the column and eluted with 100% methanol. $C_{18}$ nonretained compounds were further extracted by liquid−liquid partition with 2 volumes of ethyl acetate with a solvent to sample ratio of 1:1. The solvent fractions were pooled for evaporation and likewise dissolution in 0.01% HCl water.

**Characterization and Quantitation of Phytochemicals with HPLC-MS.** Polyphenolics were characterized and quantified using a Thermo Finnigan LCQ Deca XP Max $MS^n$ ion trap mass spectrometer equipped with an ESI source. Separations were in reversed phase using a Finnigan Surveyor HPLC coupled to a Surveyor PDA detector, and gradient separations were performed using a Dionex Acclaim (Bannockburn, IL, USA) $C_{18}$ column (250 × 4.6 mm, 5 $\mu$m) at room temperature. Injections were made into the column by use of a 25 $\mu$L sample loop. Mobile phase A was 0.1% formic acid in water, and mobile phase B was 0.1% formic acid in methanol run at 0.4 mL/min. A gradient was run of 0% phase B for 3 min and changed to 21% phase B in 20 min, from 21 to 35% phase B in 30 min, from 35 to 49% phase B in 50 min, and from 49 to 70% phase B in 70 min before returning to initial conditions. The electrospray interface worked in negative ionization mode. Source and capillary temperatures were set at 300 °C, source voltage was 3.50 kV, capillary voltage was set at −42 V, and collision energy for MS/MS analysis was set at 35 eV. The instrument operated with sheath gas and auxiliary gas ($N_2$) flow rates set at 40 and 5 units/min, respectively. In addition to chromatographic separations, the mango concentrate was infused to capture $MS^n$ fragmentation patterns of poorly ionized compounds using instrument tuning specific to gallic acid, methyl gallate, and pentagalloylglucose.

All compounds were quantified at 280 nm with their corresponding aglycones. If an aglycone standard was lacking, concentrations were measured with the use of gallic acid as a standard. As the majority of the compounds were tentatively identified and lacked standards, results of this study represent a relative concentration of polyphenols in 'Keitt' mango pulp.

**Commercial Enzyme Hydrolysis.** Cell wall active enzymes were applied to a 'Keitt' mango puree at a uniform rate of 0.05% v/w to simulate an average commercial application rate of the enzyme and to evaluate their effects on mango chemistry. Enzymes included Validase TRL (Val), a mixed-function enzyme with predominantly cellulase activity (6800 U/g) with side activities as a pectinase and hemicellulase; Crystalzyme 200XL (Cz), an enzyme with predominantly pectinase activity (200,000 depectinizing units/g); and Rapidase AR 2000 (Rap), a pectinase with approximately 25% $\beta$-glucosidase side activity (>4000 U/g). Enzyme and mango puree mixtures were incubated at 50 °C for up to 4 h under a blanket of nitrogen. Following incubation, an aliquot of the fruit pulp was placed in boiling water for 3 min to inactivate the enzyme and immediately cooled on ice. Prior to analysis, both control and enzyme-treated pulps were centrifuged at 2000*g* to separate solids from the supernatant, which was further filtered through a 0.45 $\mu$m PTFE filter and quantified under the same conditions as the characterized mango.

**Statistics.** Semiquantifications were evaluated in triplicate in independent reaction vessels. Data for commercial enzyme application represent the mean of triplicate analyses using ANOVA (analysis of variance) followed by each pair Student's *t* test using the JMP statistics software package, which provided corresponding probability ($p < 0.05$) values to indicate significant differences between treatments.

## RESULTS AND DISCUSSION

**Phytochemicals in 'Keitt' Mango.** The phytochemical composition in mango pulp, mostly phenolic acids, is poorly characterized in the literature. Like most fruits, mango chemistry and resultant bioactivity can differ on the basis of variety and postharvest handling,[15,16] yet all varieties with reported phytochemical characterizations have identified GA and derivatives of GA in the form of hydrolyzable gallotannins. In addition to derivates of GA, mango pulp contains a variety of low molecular weight compounds that are present in relatively low concentrations, yet these compounds may be critical for understanding the benefits of mango consumption. For the first time, tentative identification and semiquantification of many polyphenols and apocarotenoids were accomplished in 'Keitt' mango pulp using UV spectroscopic evaluations, mass fragmentation patterns, comparison to other reports of compound identity, and resultant changes following hydrolysis. (Figures 1−3; Table 1).

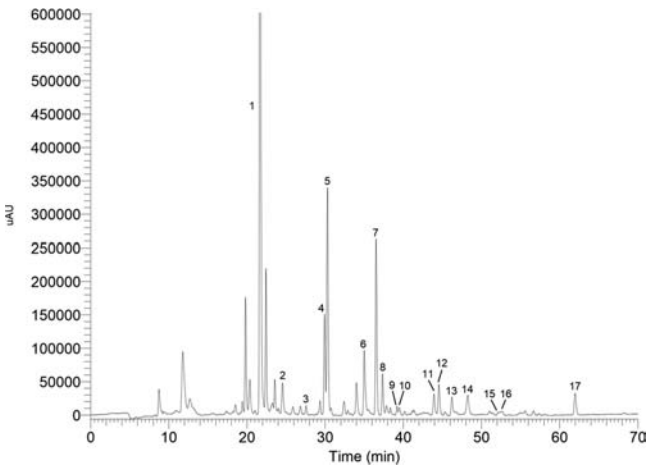


**Figure 1.** HPLC chromatogram of compounds present in mango (*Mangifera indica* L. cv. 'Keitt') pulp at 280 nm. Peak assignments are shown in Table 1.

**Hydroxybenzoic Acids.** Peaks 1 and 4 were tentatively identified as isomers of mono galloyl glucoside (MGG) as each compound showed a parent ion of $m/z$ 331.2 and a secondary ion fragment with a loss of 162 Da (Da) indicating the loss of a glucosyl to the base aglycone GA. Compound **1** additionally had a $m/z$ 271.1 fragment consistent with the loss of a 60 Da unit from the dissociation of a C6 sugar that resisted fragmentation in relation to compound **4** that exhibited characteristic losses of 162 and 206 Da [M − H − 162 − 44] from losses of both glucose and carboxylic acid. Therefore, these fragmentation patterns indicated that the glucose moiety of compound **1** was linked to an ester bond via the carboxylic acid of GA and that the glucose moiety of compound **4** was ether linked to a hydroxyl group of GA (Figure 2). Additional confirmation of these linkages was confirmed by alkali hydrolysis, which has been shown to preferentially hydrolyze ester bonds after brief exposure.[17] Within 5 min of exposure to pH 10 conditions, the complete hydrolysis of compound **1** to GA was observed, whereas compound **4** remained unchanged after 15 min. The ester-linked MGG accounted for 50% of the quantified phytochemicals at 37.7 mg/kg compared to only 3.82 mg/kg for the ether-linked species. The type of linkage between GA and glucose may be important for human


dx.doi.org/10.1021/jf5031554 | J. Agric. Food Chem. 2014, 62, 9515−9521

**Table 1. Tentative Characterization and Semiquantification of Compounds Present in *Mangifera indica* L. cv. 'Keitt' Pulp**

| peak | RT (min) | compound | $\lambda_{max}$ (nm) | $[M - H]^-$ ($m/z$) | MS/MS ($m/z$)[a] | concn[b] (mg/kg) |
|---|---|---|---|---|---|---|
| 1 | 21.67 | ester[c]-monogalloyl glucoside | 278 | 331.2 | 271.1, 169.2, 211.2, 125.3 | 37.67 ± 0.56 |
| 2 | 24.55 | gallic acid | 271 | 169.2 | 125.3 | 1.74 ± 0.10 |
| 3 | 27.55 | galloyl diglucoside | 274 | 493.1 | 313.22 | 0.45 ± 0.01 |
| 4 | 29.93 | ether[c]-mono galloyl glucoside | 254, 298 | 331.2 | 169.2, 125.4 | 3.82 ± 0.13 |
| 5 | 30.3 | *p*-hydroxybenzoic acid glycoside | 256 | 299.1 | 239, 179, 137, 209 | 18.49 ± 0.72 |
| 6 | 35.00 | coumaric glycoside | 295 | 324.8 | 163.2 | 1.61 ± 0.05 |
| 7 | 36.52 | dihydrophaseic acid glucoside | 265 | 443.5 | 237.0, 219.1, 281.1, 425.3 | 2.60 ± 0.04 |
| 8 | 37.35 | ferulic acid hexoside | 290, 314 | 355.0 | 193.2, 149.3 | 0.91 ± 0.02 |
| 9 | 41.17 | sinapic acid hexoside-pentoside | 251, 283, 328 | 517.1 | 385.1, 205.3, 223.3 | 0.13 ± 0.01 |
| 10 | 41.42 | sinapic acid hexoside | 247, 327 | 385.1 | 223.0, 153.2, 205.3, 161.0 | 0.164 ± 0.01 |
| 11 | 43.93 | dihydrophaseic acid glucoside | 267 | 443.4 | 263.1, 219.1, 143.2 | 0.47 ± 0.03 |
| 12 | 44.55 | hydroxy-dimethyl decadiene-dioic acid glucopyranosyl ester[d] | 275 | 403.2 | 241.0, 343.0, 197.2 | 1.78 ± 0.09 |
| 13 | 46.22 | hydroxy-dimethyl decadiene-dioic acid glucopyranosyl ester[d] | 274 | 403.2 | 241.1, 343.1, 197.1 | 1.25 ± 0.13 |
| 14 | 48.23 | abscisic acid glucoside | 273 | 425.0 | 263.0, 219.2, 189.1 | 0.57 ± 0.02 |
| 15 | 52.02 | eriodictyol-*O*-dihexoside[d] | 277 | 611.4 | 449.2, 287.2, 389.1 | tr[e] |
| 16 | 52.62 | eriodictyol-*O*-hexoside[d] | 278 | 449.3 | 287.2, 389.1, 269.2, 227.1 | tr |
| 17 | 61.98 | abscisic acid | 265 | 263.2 | 219.2, 153.2, 151.2 | 0.55 ± 0.04 |

[a]Ordered by predominance of ion in spectrum. [b]Values represent the means and standard errors from three replicates. [c]Designates type of glycosidic linkage. [d]Tentative identification based on spectral characteristics and similarities of ESI-MS$^n$ fragmentation. [e]tr, trace.

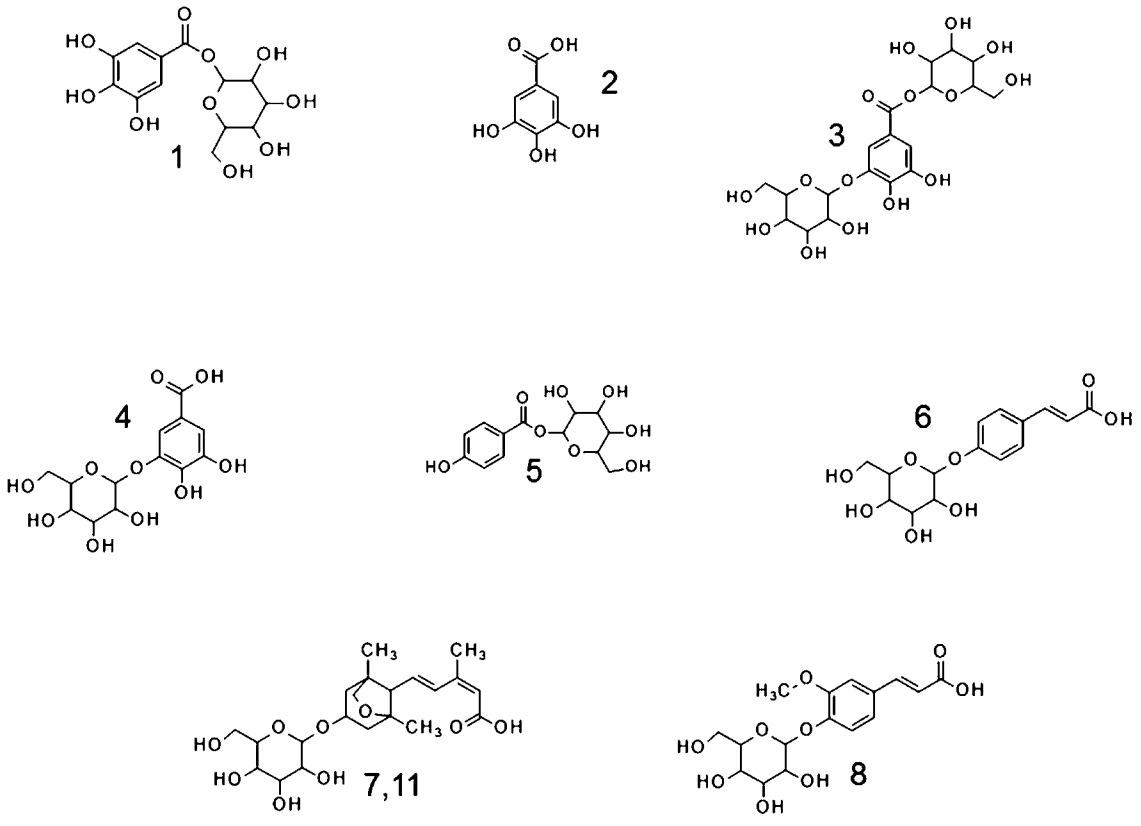


**Figure 2.** Tentative chemical structures for compounds **1**–**8** and **11**.

bioavailability because the ester linkage is more susceptible to hydrolysis in the high-pH environment of the human intestine,[18] whereas the ether bonds would require the action of $\beta$-glucosidase.[19]

Compound **2** was identified as free GA on the basis of comparison to a standard. Compound **2** had a $\lambda_{max}$ of 271 nm, a $m/z$ of 169.2, and the subsequent loss of $CO_2$ under MS/MS conditions to yield pyrogallol at $m/z$ 125.3. Compound **3** was also a GA derivative with a pseudomolecular ion of $m/z$ 493.4 with secondary ionization showing fragments of $m/z$ 313.2 [M − H − 180] and 169.2 [M − H − 324] corresponding to the loss of two glucose moieties from galloyl diglucoside, a compound previously reported in longan seed.[20] Compound **5** was characterized as a hydroxybenzoic acid glycoside (HBG) at $m/z$ 299.1 with a six-carbon sugar esterified to its carboxylic acid similar to ester-linked MGG. Secondary ionization produced fragments ($m/z$ 239, 209, and 179) typical of an acid-resistant glycosidic bond corresponding to the ring fission


dx.doi.org/10.1021/jf5031554 | J. Agric. Food Chem. 2014, 62, 9515–9521

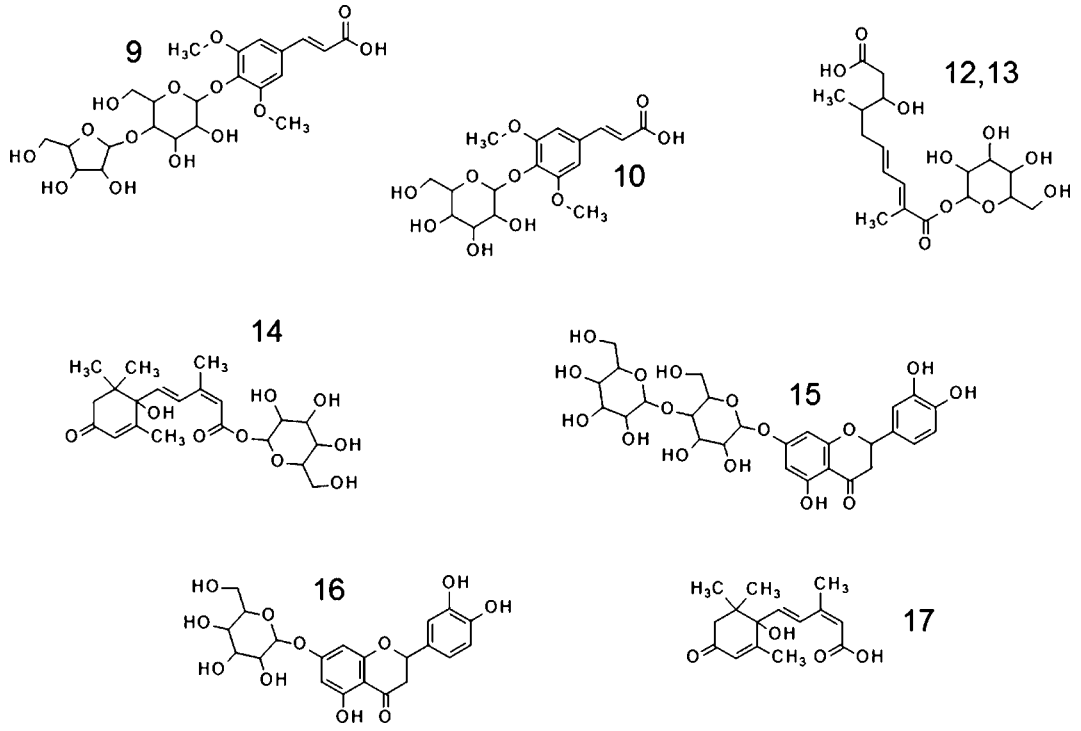


**Figure 3.** Tentative chemical structures for compounds **9**, **10**, and **12**−**17**.

of glucose that produced 60, 90, and 120 Da neutral fragments as previously reported for C-linked glycosides.[21] The corresponding aglycone at $m/z$ 137 corresponded to a *p*-hydroxybenzoic acid on the basis of its characteristic UV spectral bands at 256 and 299 nm as compared to a standard of *p*-hydroxybenzoic acid used for quantification.

**Cinnamic Acids.** Compounds **6** and **8**−**10** were characterized as cinnamic acid derivatives on the basis of their typical diode array absorbance patterns between 300 and 320 nm. These compounds were present in relatively low concentrations (<1.6 mg/kg) and were a strong indication that metabolic equilibrium is greatly shifted toward hydroxybenzoic acid production in mango pulp. Specifically, compound **6** was characterized as a coumaric acid glycoside with a pseudomolecular ion of $m/z$ 324.8 and a corresponding fragment of $m/z$ 163.2 indicating the loss of a C6 sugar moiety resulting in free coumaric acid. Compound **8** was characterized as a ferulic acid hexoside, $m/z$ 355.0 with a ferulic acid ion detected in $MS^2$, with an $m/z$ of 193.2 as well as the decarboxylated ferulate ion at $m/z$ 149 [M − H − 162 − 44]. Compounds **9** and **10** (Figure 3) were both identified as glycosylated sinapic acids. Compound **9** presented three UV spectral bands at 251, 283, and 328 nm and had a parent mass of $m/z$ 517.1. In the $MS^2$ scan event, fragments of $m/z$ 385.1 [M − H − 132] corresponded to the loss of a pentoside; $m/z$ 205.3 [M − H − 132 − 162 − 18] corresponded to the loss of a pentoside, a hexoside, and water; and $m/z$ 223.3 [M − H − 132 − 162] corresponded to sinapic acid. A similar sinapic acid pentoside−hexoside compound was previously reported in both eucalyptus and jocote fruits.[22] Compound **10** at $m/z$ 385.1 similarly produced fragments of $m/z$ 223.0 [M − H − 162] and 205.3 [M − H − 180], and the compound was identified as a sinapic acid hexoside. The cinnamic acids in 'Keitt' mango pulp were all glycosylated species, inconsistent with previous studies for which only aglycones were reported using HPLC-PDA.[6,7,10,23]

**Flavonoids.** Flavonoids such as quercetin and kaempferol have been previously reported in mango peel, seed kernel, and leaves[3,23] but are not commonly found in mango pulp and were not identified in 'Keitt' mango pulp in this study. However, the flavonoids eriodictyol-*O*-dihexoside and eriodictyol-*O*-hexoside (compounds **15** and **16**) were found in trace amounts and tentatively identified on the basis of the observed parent masses at $m/z$ 611.4 and 449.3, respectively. Identification was based on fragmentation patterns similar to those reported in tomato juice.[24]

**Apocarotenoids.** Mango pulp is known to be a rich source of C40 carotenoids[25] that contribute to the color and physical attractiveness of the fruit. Through oxidative cleavage of carotenoids, apocarotenoids are produced, which are utilized by plants to form various volatile compounds and are a source of important plant hormones.[26] 'Keitt' mango pulp contained six identifiable water-soluble apocarotenoids and many more related compounds hypothesized to exist in the fruit that are not characterized herein. Compounds **7**, **11**, **14**, and **17** all shared similar UV spectral properties ($\lambda_{max}$ 265 nm) and similar MS fragmentation patterns indicating structural similarities. Compound **14** was identified as an abscisic acid (ABA) glycoside with $m/z$ 425.0 that ionized under MS/MS to give a fragment of $m/z$ 263.0. The fragment of $m/z$ 263.0 when further ionized produced a fragment of $m/z$ 219.2. This pattern was also observed in the ionization of compound **17**, ABA, with a $m/z$ at 263.2 and MS/MS fragment of $m/z$ 219.2 confirming the structure of compound **14**. ABA is a known phytohormone responsible in part for mango ripening along with ethylene,[27,28] but derivatives of ABA have not been reported in the phytochemical composition of mango pulp. Additionally, compounds **7** and **11** both produced pseudomolecular ions of $m/z$ 443.5, the former with fragments of $m/z$ 237.0 [M − H − 162 − 44], $m/z$ 219.1 [M − H − 162 − 44 − 18], and $m/z$ 425.3 [M − H − 18], and were tentatively identified as dihydrophaseic acid (DPA) glycosides.[29] DPA is a known


dx.doi.org/10.1021/jf5031554 | J. Agric. Food Chem. 2014, 62, 9515−9521

product of endogenous abscisic acid metabolism[30] and serves a role in the regulation of ABA.[31] Lastly, compounds **12** and **13** were characterized as isomers each with a molecular ion of $m/z$ 403.2 that was tentatively identified as $^{12}$C dicarboxylic acid derivatives. The fragments $m/z$ 241.0 [M − H − 162], $m/z$ 343.0 [M − H − 60], and $m/z$ 197.2 [M − H − 162 − 44] were identical to those reported for the compound (2*E*,4*E*)-8-hydroxy-2,7-dimethyl-2,4-decadiene-1,10-dioic acid 6-*O*-$\beta$-D glucopyranosyl ester previously identified in walnuts.[32] The presence of a $^{12}$C dicarboxylic acid derivative would be expected in plants known to synthesize oxygenated carotenoids and is derived from a similar biosynthetic pathway as ABA with violaxanthin serving as the precursor molecule.[33,34] Violaxanthin is the predominate carotenoid in ripe mango pulp with *all-trans*-violaxanthin alone compromising almost 50% of pulp carotenoids by weight in some varieties.[35]

**Gallotannins.** Tannins are historically difficult to resolve by reversed phase chromatography, and numerous reports have attempted to elucidate and quantify gallotannins with varied results due to the coelution of the polymers and extensive band broadening.[36,37] The concentration of gallotannins in mango pulp differs extensively among varieties, with concentrations in 'Keitt' reported to range from 500 to 1000 mg/kg.[6] In this study, gallotannins were present in 'Keitt' mango pulp in relatively low concentrations and were not found during routine quantification, likely due to interactions with native proteins during sample preparation and poor chromatographic resolution. However, more concentrated extracts revealed gallotannin polymers ranging from 4 to 12 galloyl groups as both single- and double-charged ions in the total ion current from 42 to 70 min.

**Commercial Cell Wall Active Enzymes.** The activity of commercial cell wall degrading enzymes Val, Cz, and Rap was investigated for their role in modifying the phenolic acid composition of 'Keitt' mango pulp, specifically, the potential for these enzymes to possess side activities such as $\beta$-glucosidase that could have a major impact on the resultant chemistry and potential bioactive properties of processed mango. The changes in concentration observed for GA, ester-linked MGG, ether-linked MGG, and HBG after 4 h of enzyme incubation at 50 °C are reported in Figure 4. Among the enzymes, a complete loss of the ether-linked MGG was observed after incubation with Rap and Val, suggesting a strong $\beta$-glucosidase side activity, and served as additional support for the type of glycosidic linkage present for compound **4**. The hydrolysis of ether-linked MGG could be a good predictor for the capacity of hydrolysis to occur in vivo by cytosolic $\beta$-glucosidases,[38] which would internally produce aglycones, which are known to be better absorbed in the small intestine compared to their glycosylated counterparts.[39,40]

Cz was shown to have significant ester glucosidase side activity with 66 and 75% losses of ester-linked MGG and HBG observed, respectively. This further confirmed the ester glycosidic linkage observed for compounds **1** and **5** because the use of Rap and Val caused no significant reduction in ester-linked MGG, signifying that the glucose moiety was not ether linked. The hydrolysis of both ester and ether MGG led to overall changes in the free GA concentration and increased GA from 10.36 to 11.71, 18.38, and 29.76 mg/L for Rap, Val, and Cz, respectively. The use of Cz significantly increased the amount of free GA compared to the control ($p < 0.001$) and created a processed pulp that was higher in GA than MGG. The in vitro hydrolysis of ester-linked MGG could be useful for aiding absorption of its aglycone GA if hydrolysis is limited in the small intestine.

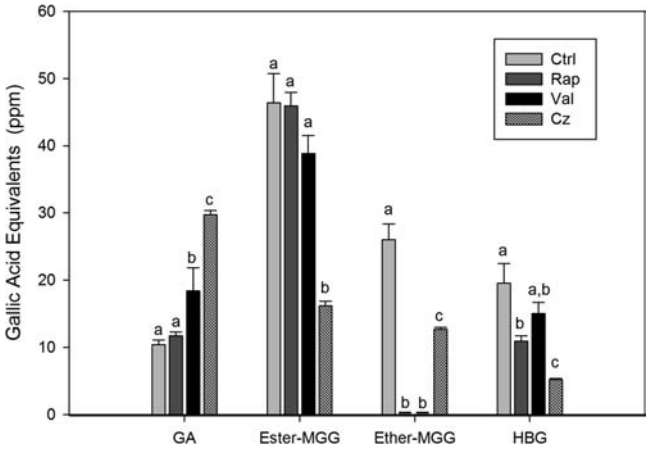


**Figure 4.** Quantity of free gallic acid (GA), ester-linked mono galloyl glucoside (Ester-MGG), ether-linked mono galloyl glucoside (Ether-MGG), and hydroxybenzoic acid glycoside (HBG) in mango pulp after enzymatic incubation of 0.05% Rapidase AR 2000 (Rap), Validase TRL (Val), and Crystalzyme 200XL (Cz) at 50 °C for 4 h. Different letters within groupings of the same compound are significantly different ($p < 0.05$).

Benefits of mango consumption have been attributed to its phytochemical composition, which largely includes polyphenols. The presence of glycosides on a polyphenol has been shown to affect in vivo stability and absorption. In general, deglycosylated polyphenols have higher absorption rates, but are more prone to degradation at physiological pH compared to their glycosylated counterparts.[41] Therefore, consumption of a fruit product that contains an altered phytochemical composition due to glycoside hydrolysis could potentially have different in vivo properties compared to an equivalent consumption of the whole fruit. Additional studies are needed before a conclusion can be reached regarding the in vivo differences of consuming a polyphenol glycoside or its respective aglycone. Therefore, phytochemical characterization both before and after any processes is crucial to understanding any potential health benefits due to the different mechanisms of absorption and metabolism with various phytochemical chemistries. This study found that the use of any of the tested enzyme preparations would significantly affect the phenolic acid composition of a 'Keitt' mango product compared to the unprocessed fruit and could potentially alter the bioactivity compared to that of the whole fruit.

For the first time, a detailed characterization and semi-quantification of phenolic acids and other minor phytochemicals was accomplished for 'Keitt' mango pulp, leading to the identification of five hydroxybenzoic acids, four cinnamic acids, two flavonoids, and six apocarotenoids in the pulp extract. The phenolic acid composition of the pulp was affected by the side activity of cell wall degrading enzymes. Addition of Cz reduced the amount of ester-linked MGG by 66%, indicating strong esterase side activity, and both Rap and Val showed $\beta$-glucosidase activity by the complete hydrolysis of ether-linked MGG. Phytochemical composition is critical in understanding the bioefficacy of any fruit or vegetable, and any changes are sure to affect the health-promoting properties.

## AUTHOR INFORMATION


### Corresponding Author

*(S.T.T.) Phone: (979) 862-4056. Fax: (979) 458-3704. E-mail: stalcott@tamu.edu.



### Funding

The authors would like to thank the National Mango Board, Orlando, Florida for research support.


### Notes

The authors declare no competing financial interest.

## REFERENCES


(1) Iyer, C. In *Recent Advances in Varietal Improvement in Mango*, III International Mango Symposium; ISHS: Leuven, Belgium, 1981; Vol. 291, pp 109−132.

(2) Tharanathan, R.; Yashoda, H.; Prabha, T. Mango (*Mangifera indica* L.), "the king of fruits" − an overview. *Food Rev. Int.* **2006**, *22*, 95−123.

(3) Barreto, J. C.; Trevisan, M. T.; Hull, W. E.; Erben, G.; de Brito, E. S.; Pfundstein, B.; Würtele, G.; Spiegelhalder, B.; Owen, R. W. Characterization and quantitation of polyphenolic compounds in bark, kernel, leaves, and peel of mango (*Mangifera indica* L.). *J. Agric. Food Chem.* **2008**, *56*, 5599−5610.

(4) Sairam, K.; Hemalatha, S.; Kumar, A.; Srinivasan, T.; Ganesh, J.; Shankar, M.; Venkataraman, S. Evaluation of anti-diarrhoeal activity in seed extracts of (*Mangifera indica.*). *J. Ethnopharmacol.* **2003**, *84*, 11−15.

(5) Singh, Y. N. Traditional medicine in Fiji: some herbal folk cures used by Fiji Indians. *J. Ethnopharmacol.* **1986**, *15*, 57−88.

(6) Manthey, J. A.; Perkins-Veazie, P. Influences of harvest date and location on the levels of $\beta$-carotene, ascorbic acid, total phenols, the in vitro antioxidant capacity, and phenolic profiles of five commercial varieties of mango (*Mangifera indica* L.). *J. Agric. Food Chem.* **2009**, *57*, 10825−10830.

(7) Kim, Y.; Lounds-Singleton, A. J.; Talcott, S. T. Antioxidant phytochemical and quality changes associated with hot water immersion treatment of mangoes (*Mangifera indica* L.). *Food Chem.* **2009**, *115*, 989−993.

(8) Ribeiro, S.; Barbosa, L.; Queiroz, J.; Knödler, M.; Schieber, A. Phenolic compounds and antioxidant capacity of Brazilian mango *Mangifera indica* L. varieties. *Food Chem.* **2008**, *110*, 620−626.

(9) Noratto, G. D.; Bertoldi, M. C.; Krenek, K.; Talcott, S. T.; Stringheta, P. C.; Mertens-Talcott, S. U. Anticarcinogenic effects of polyphenolics from mango (*Mangifera indica*) varieties. *J. Agric. Food Chem.* **2010**, *58*, 4104−4112.

(10) Percival, S. S.; Talcott, S. T.; Chin, S. T.; Mallak, A. C.; Lounds-Singleton, A.; Pettit-Moore, J. Neoplastic transformation of BALB/3T3 cells and cell cycle of HL-60 cells are inhibited by mango (*Mangifera indica* L.) juice and mango juice extracts. *J. Nutr.* **2006**, *136*, 1300−1304.

(11) FAOSTAT Trade Information, http://faostat.fao.org/ (accessed Dec 16, 2013).

(12) Buchert, J.; Koponen, J. M.; Suutarinen, M.; Mustranta, A.; Lille, M.; Törrönen, R.; Poutanen, K. Effect of enzyme-aided pressing on anthocyanin yield and profiles in bilberry and blackcurrant juices. *J. Sci. Food Agric.* **2005**, *85*, 2548−2556.

(13) Wightman, J. D.; Wrolstad, R. E. Anthocyanin analysis as a measure of glycosidase activity in enzymes for juice processing. *J. Food Sci.* **1995**, *60*, 862−867.

(14) Talcott, S. T.; Moore, J. P.; Lounds-Singleton, A. J.; Percival, S. S. Ripening associated phytochemical changes in mangos (*Mangifera indica*) following thermal quarantine and low-temperature storage. *J. Food Sci.* **2005**, *70*, C337−C341.

(15) Sturm, K.; Koron, D.; Stampar, F. The composition of fruit of different strawberry varieties depending on maturity stage. *Food Chem.* **2003**, *83*, 417−422.

(16) Berardini, N.; Fezer, R.; Conrad, J.; Beifuss, U.; Carle, R.; Schieber, A. Screening of mango *Mangifera indica* L. cultivars for their contents of flavonol *O*- and xanthone *C*-glycosides, anthocyanins, and pectin. *J. Agric. Food Chem.* **2005**, *53*, 1563−1570.

(17) Komprda, T.; Štohandlová, M.; Foltýn, J.; Pozdíšek, J.; Míka, V. Content of *p*-coumaric and ferulic acid in forbs with potential grazing utilization. *Arch. Tierernaehr.* **1999**, *52*, 95−105.

(18) Hagerman, A. E. Hydrolyzable tannin structural chemistry. *Tannin Handbook*, 2002; pp 1−5, http://www.users.muohio.edu/hagermae/.

(19) Brown, J. E.; Khodr, H.; Hider, R. C.; Rice-Evans, C. A. Structural dependence of flavonoid interactions with $Cu^{2+}$ ions: implications for their antioxidant properties. *Biochem. J.* **1998**, *330*, 1173−1178.

(20) Soong, Y. Y.; Barlow, P. J. Isolation and structure elucidation of phenolic compounds from longan (*Dimocarpus longan* Lour.) seed by high-performance liquid chromatography−electrospray ionization mass spectrometry. *J. Chromatogr.* **2005**, *1085*, 270−277.

(21) Cuyckens, F.; Claeys, M. Mass spectrometry in the structural analysis of flavonoids. *J. Mass Spectrom.* **2004**, *39*, 1−15.

(22) Boulekbache-Makhlouf, L.; Meudec, E.; Chibane, M.; Mazauric, J.-P.; Slimani, S.; Henry, M.; Cheynier, V.; Madani, K. Analysis by high-performance liquid chromatography diode array detection mass spectrometry of phenolic compounds in fruit of *Eucalyptus globulus* cultivated in Algeria. *J. Agric. Food Chem.* **2010**, *58*, 12615−12624.

(23) Schieber, A.; Ullrich, W.; Carle, R. Characterization of polyphenols in mango puree concentrate by HPLC with diode array and mass spectrometric detection. *Innovative Food Sci. Emerging Technol.* **2000**, *1*, 161−166.

(24) Vallverdú-Queralt, A.; Jáuregui, O.; Di Lecce, G.; Andrés-Lacueva, C.; Lamuela-Raventós, R. M. Screening of the polyphenol content of tomato-based products through accurate-mass spectrometry (HPLC-ESI-QTOF). *Food Chem.* **2011**, *129*, 877−883.

(25) Mercadante, A. Z.; Rodriguez-Amaya, D. B.; Britton, G. HPLC and mass spectrometric analysis of carotenoids from mango. *J. Agric. Food Chem.* **1997**, *45*, 120−123.

(26) Auldridge, M. E.; McCarty, D. R.; Klee, H. J. Plant carotenoid cleavage oxygenases and their apocarotenoid products. *Curr. Opin. Plant Biol.* **2006**, *9*, 315−321.

(27) Parikh, H.; Nair, G.; Modi, V. Some structural changes during ripening of mangoes (*Mangifera indica* var. Alphonso) by abscisic acid treatment. *Ann. Bot.* **1990**, *65*, 121−127.

(28) Zaharah, S. S.; Singh, Z.; Symons, G. M.; Reid, J. B. Role of brassinosteroids, ethylene, abscisic acid, and indole-3-acetic acid in mango fruit ripening. *J. Plant Growth Regul.* **2012**, *31*, 363−372.

(29) del Refugio Ramos, M.; Jerz, G.; Villanueva, S.; López-Dellamary, F.; Waibel, R.; Winterhalter, P. Two glucosylated abscisic acid derivates from avocado seeds (*Persea americana* Mill. Lauraceae cv. Hass). *Phytochemistry* **2004**, *65*, 955−962.

(30) Zeevaart, J. A. D.; Milborrow, B. V. Metabolism of abscisic acid and the occurrence of epi-dihydrophaseic acid in *Phaseolus vulgaris*. *Phytochemistry* **1976**, *15*, 493−500.

(31) Kondo, S.; Sungcome, K.; Setha, S.; Hirai, N. ABA catabolism during development and storage in mangoes: influence of jasmonates. *J. Hortic. Sci. Biotechnol.* **2004**, *6*, 891−896.

(32) Gómez-Caravaca, A. M.; Verardo, V.; Segura-Carretero, A.; Caboni, M. F.; Fernández-Gutiérrez, A. Development of a rapid method to determine phenolic and other polar compounds in walnut by capillary electrophoresis−electrospray ionization time-of-flight mass spectrometry. *J. Chromatogr.* **2008**, *1209*, 238−245.

(33) Ito, H.; Okuda, T.; Fukuda, T.; Hatano, T.; Yoshida, T. Two novel dicarboxylic acid derivatives and a new dimeric hydrolyzable tannin from walnuts. *J. Agric. Food Chem.* **2007**, *55*, 672−679.

(34) Zeevaart, J. A.; Heath, T. G.; Gage, D. A. Evidence for a universal pathway of abscisic acid biosynthesis in higher plants from $^{18}O$ incorporation patterns. *Plant Physiol.* **1989**, *91*, 1594−1601.

(35) Mercadante, A. Z.; Rodriguez-Amaya, D. B. Effects of ripening, cultivar differences, and processing on the carotenoid composition of mango. *J. Agric. Food Chem.* **1998**, *46*, 128−130.

(36) Mueller-Harvey, I. Analysis of hydrolysable tannins. *Anim. Feed Sci. Technol.* **2001**, *91*, 3−20.

(37) Berardini, N.; Carle, R.; Schieber, A. Characterization of gallotannins and benzophenone derivatives from mango (*Mangifera indica* L. cv. 'Tommy Atkins') peels, pulp and kernels by high-performance liquid chromatography/electrospray ionization mass spectrometry. *Rapid Commun. Mass Spectrom.* **2004**, *18*, 2208−2216.
(38) Németh, K.; Plumb, G. W.; Berrin, J.-G.; Juge, N.; Jacob, R.; Naim, H. Y.; Williamson, G.; Swallow, D. M.; Kroon, P. A. Deglycosylation by small intestinal epithelial cell $\beta$-glucosidases is a critical step in the absorption and metabolism of dietary flavonoid glycosides in humans. *Eur. J. Nutr.* **2003**, *42*, 29−42.
(39) Knaup, B.; Kahle, K.; Erk, T.; Valotis, A.; Scheppach, W.; Schreier, P.; Richling, E. Human intestinal hydrolysis of phenol glycosides−a study with quercetin and *p*-nitrophenol glycosides using ileostomy fluid. *Mol. Nutr. Food Res.* **2007**, *11*, 1423−1429.
(40) Manach, C.; Scalbert, A.; Morand, C.; Rémésy, C.; Jiménez, L. Polyphenols: food sources and bioavailability. *Am. J. Clin. Nutr.* **2004**, *79*, 727−747.
(41) Boyer, J.; Brown, D.; Liu, R. In vitro digestion and lactase treatment influence uptake of quercetin and quercetin glucoside by the Caco-2 cell monolayer. *Nutr. J.* **2005**, *4*, 1.

**Table 1. Characteristics of Belgian Special Beer Samples**

| type | beer | alcohol (%) | original extract (g extract/100 g wort) | characteristics |
|---|---|---|---|---|
| blond | BL1 | 8.5 | 16.3 | Pilsen malt, unfiltered, bottle refermentation |
| | BL2 | 7.5 | 14.9 | Pilsen malt, organic beer (organic version of BL1), unfiltered, bottle refermentation |
| | BL3 | 6.3 | 14.4 | Pilsen malt,[a] POF(+) yeast, centrifuged, flash pasteurization |
| | BL4 | 7.5 | 16.8 | Pilsen malt,[a] POF(+) yeast, unfiltered, bottle refermentation, flash pasteurization |
| dry-hopped Trappist | TR1 | 6.2 | 13.3 | caramel malt,[a] POF(+) yeast, *Brettanomyces* for secondary fermentation and bottle refermentation, dry hopping, unfiltered |
| amber | AM1 | 12.0 | 20.8 | caramel malt, filtered |
| | AM2 | 4.5 | 10.93 | caramel malt,[a] POF(+) yeast, filtered |
| | AM3 | 5.4 | 12.77 | caramel malt, filtered |
| brown | BR1 | 8.0 | 19.8 | torrefied malt (7%),[a] POF(+) yeast, light filtration, bottle refermentation |
| | BR2 | 6.5 | 15.58 | torrefied malt,[a] POF(+) yeast |
| | BR3 | 5.2 | 12.71 | torrefied malt (12%), bottle refermentation |
| white Belgian | W1 | 4.9 | 11.8 | Pilsen malt and wheat, spices (orange peels, coriander),[a] POF(+) yeast, centrifuged |

[a]The POF(+) yeast descriptor is given only for yeasts that have been previously investigated in our laboratory for the PAD1 phenotype.[32]

**Malt Samples.** Five commercial barley malts (*Hordeum vulgare* L.) were provided by the Malterie du Château (Beloeil, Belgium): Pilsen malt (5 EBC), caramel malts (Cara 50 °EBC and coffee 500 °EBC; final kilning temperature = 125 and 180 °C, respectively), and torrefied malts (chocolate 900 °EBC and black 1500 °EBC; final roasting temperature = 225 °C).

**Chemicals.** Methanol (99.9%) and dichloromethane (99.9%, redistilled twice prior to use) were purchased from Romil (Prosan, Belgium). Ultrapure water (Milli-Q water purification system, Millipore, Bedford, MA, USA) was used. 2-Methoxy-4-vinylphenol (4-vinylguaiacol, 98%), dodecane (external standard for vanillin glucoside extraction, 99.9%), decane (external standard for phenol extraction, 99.9%), naphthol (internal standard for phenol extraction, 99.5%), guaiacol (98%), 4-methylguaiacol (97%), 4-ethylguaiacol (98%), 4-vinylphenol (solution 10% in propylene glycol), 4-ethylphenol (98%), 4-hydroxy-3-methoxy-$\alpha$-methylbenzyl alcohol (apocynol, 97%), diethyl ether (99,9%), octyl-$\beta$-D-glucopyranoside (internal standard for vanillin glucoside extraction, >98%), and $\beta$-glucosidase from almond were obtained from Sigma-Aldrich (Bornem, Belgium). *p*-Cresol (4-methylphenol, 99%) came from Acros Organics (Geel, Belgium). Vanillin (99%), sodium sulfate (99%), sodium chloride (99.5%), chloroform (99%), and potassium hydroxide (85%) were from Merck (Darmstadt, Germany). Hydrochloric acid (37%) was purchased from Fisher Scientific (Leicestershire, UK). Amberlite XAD-2 resin (Supelco, Bellefonte, PA, USA) (with a pore size of 9 nm and a specific area of 330 $m^2/g$) was sequentially washed with methanol and diethyl ether (each for 4 h) in a Soxhlet and stored in methanol at 4 °C.

**Wort Production.** Laboratory congress worts were produced in an LB 8 electronic normal-version mashing unit (Lochner, Germany) according to European Brewery Convention procedures (EBC Analytica 1998, method 4.5.1). Fifty grams of finely ground malt was added to 200 mL of water at 46 °C. The temperature was kept at 45 °C under constant stirring for 30 min. The caramel malts (Cara 50 and coffee 500) and torrefied malts (chocolate 900 and black 1500) were used with Pilsen malt at the ratio of 50:50 w/w (quantitations given for 100% specialty malt). The temperature was raised to 70 °C at 1 °C/min, then 100 mL of water was added, and the temperature was kept for 1 h at 70 °C with constant stirring before the mixture was cooled to room temperature and the weight to 450 g with water. After paper filtration (MN 614 × 32 cm diameter; Macherey-Nagel GmbH), the wort samples were stored at −32 °C until extraction.

**Samples Aging.** All beers were stored in a dark room at 20 °C before analysis.

**Phenol-Specific Liquid−Liquid Extraction Procedure.** All extractions were carried out in duplicate, according to a procedure derived from Callemien.[25] First, 50 mL of beer, 100 $\mu$L of IST (50 mg/L naphthol; 100 $\mu$g/L in beer), 1 mL of 37% hydrochloric acid, and 6.45 g of sodium chloride were mixed. After complete salt dissolution, 150 mL of chloroform/methanol (3:1, v/v) was added and the mixture stirred for 10 min at 1500 rpm. The lower organic phase was retained, whereas the aqueous phase was extracted a second time in the same manner. The collected 300 mL of organic phase was then shaken with 50 mL of 10% potassium hydroxide solution for 10 min at 1500 rpm. The upper aqueous phase (pH 13) was recovered and the lower organic phase extracted once again. The pH of the aqueous phase was then adjusted to pH 9.0 with hydrochloric acid and extracted twice with 25 mL of dichloromethane after stirring for 10 min at 1500 rpm. The combined organic phase was dried with anhydrous sodium sulfate, and 0.1 mL of EST (50 mg/L decane) was added to the extract before concentration to 0.5 mL in a Danish-Kuderna apparatus at 45 °C (total concentration factor = 100). The final extracts were stored at −81 °C and analyzed by GC-FID, GC-MS (Figure 1), and GC-O.

**Vanillin Glucoside Enzymatic Extraction Procedure.** First, 150 mL of BR1, 500 $\mu$L of IST (1 g/L octyl-glucopyranoside; 3.3 mg/L in beer), and 6 g of Amberlite XAD-2 resin thoroughly rinsed with Milli-Q water (approximately 400 mL) were poured into a 250 mL Schott flask. Samples were shaken in a dark room for 2 h and then poured into a glass column for separation. Aqueous eluate from the XAD-2 resin was drained, and 50 mL of water and 25 mL of diethyl ether were consecutively poured for washing. Glucosides were finally eluted with 25 mL of methanol. The extract was evaporated to dryness and resuspended in 25 mL of acetate buffer (pH 5). Enzymatically treated samples and controls were incubated at 35 °C for 2 h, with or without $\beta$-glucosidase (14 mg). Both were extracted three times with 15 mL of diethyl ether (10 min, 1000 rpm). The combined organic phase was dried with anhydrous sodium sulfate, and 0.5 mL of EST (20 mg/L dodecane) was added to the extract before concentration to 0.5 mL in a Danish-Kuderna apparatus at 39 °C. The final extracts were stored at −81 °C and semiquantitatively analyzed by GC-MS (just using the area ratio to the IST and the IST concentration; relative recovery factors and molar response coefficients fixed at 1).

**Gas Chromatography Hyphenated to Mass Spectrometry (GC-MS).** Electronic impact (EI) mass spectra were recorded at 70 eV on a ThermoFinnigan Trace MS mass spectrometer connected to a ThermoFinnigan Trace GC 2000 gas chromatograph equipped with a splitless injector (250 °C; opened 0.8 min after injection of 1 $\mu$L) and an apolar CP-Sil 5 CB MS capillary column (50 m × 0.32 mm i.d., 1.2

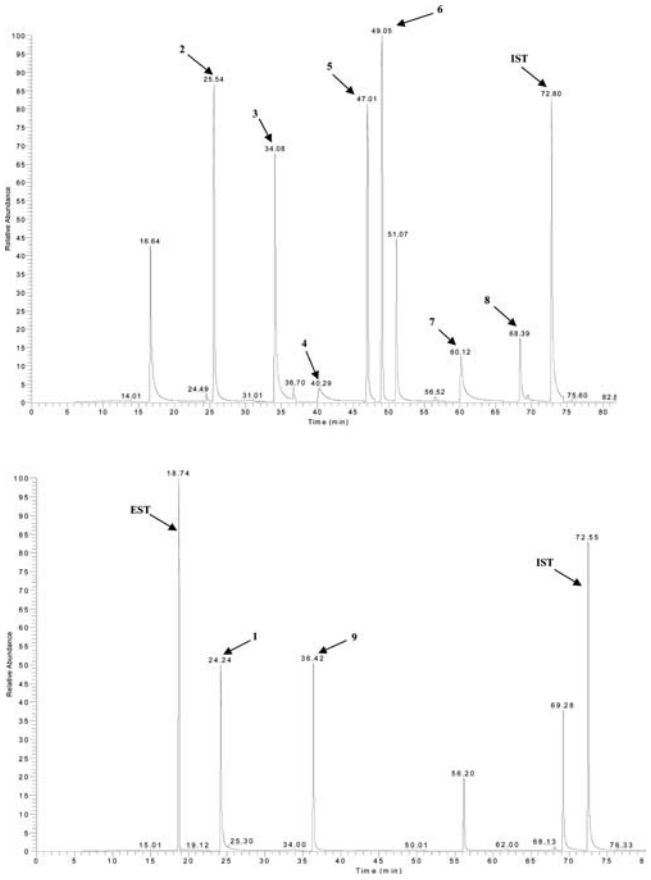


**Figure 1.** GC-MS-SIM chromatograms of our nine phenols spiked (20 mg/L) into a beer extract.

$\mu$m film thickness). The carrier gas was helium, and the pressure was set at 100 kPa. The oven temperature was raised from 36 to 85 °C at 20 °C/min, then to 145 °C at 1 °C/min, and finally to 250 °C at 3 °C/min. For all compounds, the single ion monitoring (SIM) mode was applied (selected $m/z$ given in Table 2). As depicted in Figure 1, two separate SIM programs were used to analyze our nine phenols. Xcalibur software was used for spectral recording throughout the chromatographic separation. The mass spectra obtained were compared to those of commercial standards and to the NIST library.[26] Quantification of phenols was done by standard addition to beer or to wort.

**Gas Chromatography−Olfactometry (GC-O).** Beer extracts (1 $\mu$L) were analyzed on a Chrompack CP9001 gas chromatograph equipped with a splitless injector maintained at 250 °C and opened 0.5 min postinjection. The carrier gas was nitrogen at a flow rate of 1 mL/min. Compounds were analyzed with a wall-coated open tubular (WCOT) apolar CP-Sil 5 CB capillary column (50 m × 0.32 mm i.d., 1.2 $\mu$m film thickness). The oven temperature was programmed to rise from 36 to 85 °C at 20 °C/min, then to 145 °C at 1 °C/min, and finally to 250 °C at 3 °C/min. This temperature was maintained for 30 min. To assess the olfactory potential of the extract, the column was connected to a GC-O port (Chrompack) maintained at 250 °C. The effluent was diluted with a large volume of air (20 mL/min) prehumidified with an aqueous copper(II) sulfate solution. The extracts of three beers (BL1, TR1, and BR1) were analyzed by aroma extract dilution analysis (AEDA)[27] to estimate the relative impact of each odorant. According to the AEDA method, the extracts were diluted stepwise with dichloromethane (1 + 2 by volume). The flavor dilution (FD) factor is defined as the highest dilution at which the compound can still be detected (FD = $3^n$, where $n$ + 1 is the number of dilutions applied to the extract until there was no detection by GC-O).

**Statistical Analyses.** Analyses were carried out in duplicate, and Student−Newman−Keuls tests were performed with SAS software version 9.2 (SAS Institute, Inc., Cary, NC, USA) to compare the means. Values sharing no common letter are significantly different ($p$ < 0.05).

**Table 2. Phenolic Concentrations ($\mu$g/L) in Fresh Belgian Special Beers Determined by GC-MS[a]**

| N° | RI CP-Sil5 | Substance | Structure | Odor (GCO) | Threshold in beer (µg/l) | Selected $m/z$ | BL1 | BL2 | BL3 | BL4 | TR1 | AM1 | AM2 | AM3 | BR1 | BR2 | BR3 | W1 |
|---|---|---|---|---|---|---|---|---|---|---|---|---|---|---|---|---|---|---|
| 1 | 1046 | 4-Methylphenol | 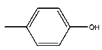 | Burned, dentist | 20 | 108/107 | $0.3^{c}$ (1) | $0.3^{c}$ | $0.2^{c}$ | $0.4^{c}$ | $0.5^{c}$ (1) | $0.6^{c}$ | $0.25^{c}$ | $0.2^{c}$ | $1.6^{b}$ (9) | $1.1^{b}$ | $3.8^{a}$ | ud$^{c}$ |
| 2 | 1063 | Guaiacol | | Roasted, coffee | 70 | 124/109 | $1.1^{d}$ (27) | $1.3^{d}$ | $0.8^{d}$ | $1.5^{d}$ | $0.87^{d}$ (9) | $0.6^{d}$ | $0.9^{d}$ | $0.4^{d}$ | $7.62^{b}$ (27) | $3.5^{c}$ | $9.7^{a}$ | $1.2^{d}$ |
| 3 | 1140 | 4-Ethylphenol | 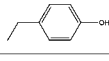 | Cresol | 150 | 122/107 | $2.2^{b}$ (9) | $0.8^{b}$ | $0.7^{b}$ | $2.8^{b}$ | $1601^{a}$ (27) | $2.5^{b}$ | ud$^{b}$ | ud$^{b}$ | $6.6^{b}$ (27) | ud$^{b}$ | ud$^{b}$ | $0.3^{b}$ |
| 4 | 1191 | 4-Vinylphenol | 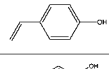 | Phenolic | 170 | 120/105 | $470.1^{b,c}$ (3) | $485.1^{b,c}$ | $0.2^{d}$ | $30.9^{d}$ | $0.2^{d}$ (0) | $16.4^{d}$ | $330.9^{b,c}$ | $8.2^{d}$ | $166.7^{d}$ (3) | $570.3^{a}$ | $173.9^{c,d}$ | $504.8^{a,b}$ |
| 5 | 1257 | 4-Ethylguaiacol | 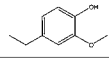 | Clove | 130 | 152/137 | $0.7^{b}$ (1) | $0.6^{b}$ | $0.3^{b}$ | $0.7^{b}$ | $1603^{a}$ (243) | $0.5^{b}$ | $1.6^{b}$ | $0.2^{b}$ | $12.6^{b}$ (9) | $0.7^{b}$ | $23.9^{b}$ | $0.1^{b}$ |
| 6 | 1289 | 4-Vinylguaiacol | 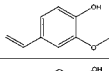 | Clove | 125 | 150/135 | $1197.4^{b}$ (729) | $1724.6^{a}$ | $35^{c}$ | $115.6^{c}$ | $0.5^{e}$ (3) | $52.2^{c}$ | $375.8^{c,d,e}$ | $18.7^{c}$ | $374.4^{c,d}$ (243) | $700.6^{b,c}$ | $205.9^{d,e}$ | $603.2^{b,c,d}$ |
| 7 | 1365 | Vanillin | 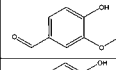 | Vanilla | 50 | 152/151 | $66.1^{b}$ (9) | $113.8^{a}$ | $6.7^{b}$ | $9^{b}$ | $6.9^{b}$ (3) | $4.5^{b}$ | $27.4^{b}$ | $2.3^{b}$ | $25.9^{b}$ (9) | $38.1^{b}$ | $21.7^{b}$ | $19.6^{b}$ |
| 8 | 1451 | Apocynol | 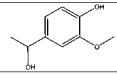 | Vanilla | 50 | 153/93 | $1.5^{a}$ (3) | $2.9^{a}$ | $2.2^{a}$ | $2^{a}$ | $2^{a}$ (1) | $1.6^{a}$ | $0.5^{a}$ | $0.4^{a}$ | $1.7^{a}$ (1) | $3.3^{a}$ | $2.4^{a}$ | $1.4^{a}$ |
| 9 | 1180 | 4-Methylguaiacol | 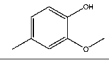 | Burnt | 20 | - | undetected | | | | | | | | | | | |

[a]Assays in duplicate. GC-O AEDA analyses of phenol-specific extracts of three beers (BL1, TR1, and BR1) (FD in parentheses = $3^n$ with $n$ + 1 = number of dilutions of the extract before no detection − precision: $n$ ±1 or a factor 3 between FD values).


dx.doi.org/10.1021/jf5015654 | J. Agric. Food Chem. 2014, 62, 9522−9528

## RESULTS AND DISCUSSION

**Volatile Phenols in Fresh Belgian Special Beers.** Specific phenolic extraction enabled us to quantify eight volatile phenols (**1**−**8**) in fresh beers (Table 2). Identification was confirmed by mass spectrometry (coincidence of the main $m/z$ values with those of commercial references and entries in the NIST library), capillary column (CP-Sil 5 CB MS) retention indices, and odors. All of the phenols were perceived at the sniffing port in the three beers investigated by AEDA, with descriptors such as burned, dentist, roasted, coffee, clove, vanilla, and smoked. Analytical results revealed different phenolic profiles according to the style of beer.

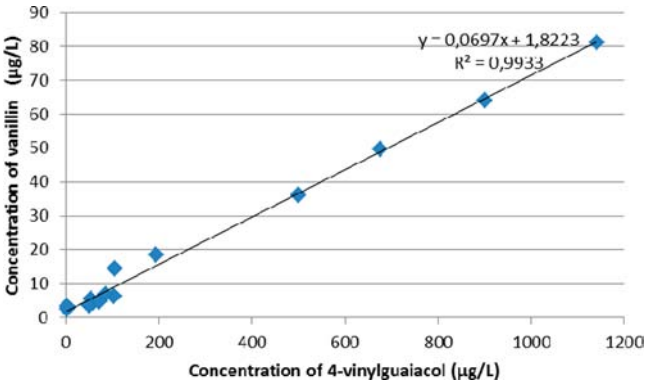


**Figure 2.** Correlation between the 4-vinylguaiacol and vanillin concentrations ($\mu$g/L) in fresh beers.

*4-Vinylphenol, 4-Vinylguaiacol, Vanillin, and Apocynol.* As shown in Table 2, the level of 4-vinylguaiacol and its analogues was not linked to the style of beer but rather to the yeast strain used (POF+ phenotype confirmed in Table 1 when data available). For instance, the blond BL1 and its organic version, BL2 (fermented with the same yeast), as well as W1 (a traditional Belgian white beer) proved to contain large amounts of all ferulic and coumaric acid-derived phenols. Up to 504.8 $\mu$g/L 4-vinylphenol, 1724.6 $\mu$g/L 4-vinylguaiacol, and 113.8 $\mu$g/L vanillin were evidenced, to be compared with the odor thresholds determined as 170, 125, and 50 $\mu$g/L, respectively. Among the amber beers investigated, AM2 reached 330.9 $\mu$g/L 4-vinylphenol, 375.8 $\mu$g/L 4-vinylguaiacol, and 27.4 $\mu$g/L vanillin, whereas AM3 gave rise to very low levels (8.2, 18.7, and 2.3 $\mu$g/L, respectively). One brown beer (BR2) was also characterized by high concentrations of 4-vinylphenol and 4-vinylguaiacol (570.3 and 700.6 $\mu$g/L, respectively). A nice correlation was observed between the 4-vinylguaiacol and vanillin concentrations in the different beers, suggesting that vanillin could arise through 4-vinylguaiacol oxidation (Figure 2). Apocynol, which results from the addition of a water molecule on 4-vinylguaiacol, was detected only as traces in all

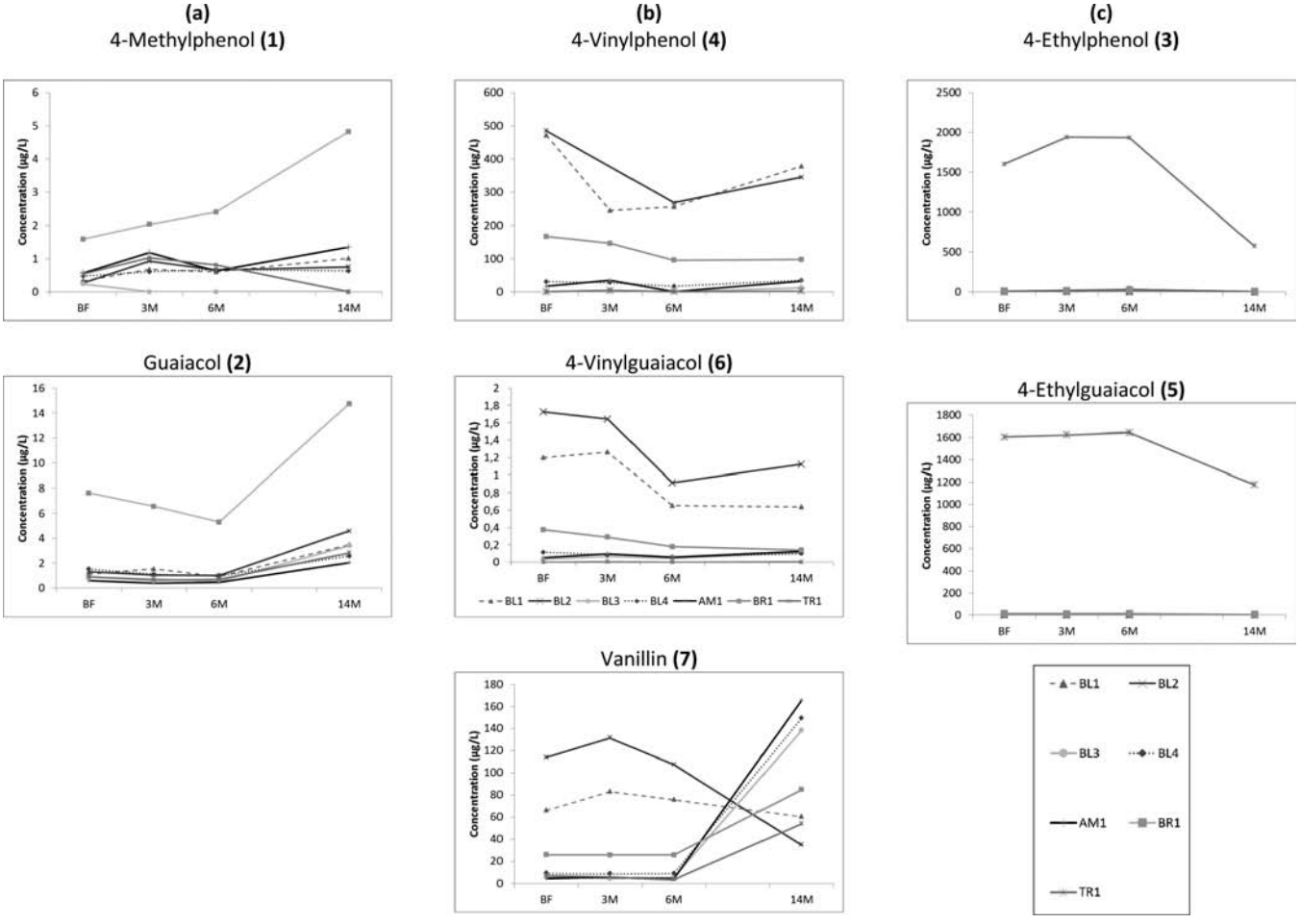


**Figure 3.** Fate of (a) 4-methylphenol and guaiacol, (b) 4-vinylphenol, 4-vinylguaiacol, and vanillin, and (c) 4-ethylphenol and 4-ethylguaiacol ($\mu$g/L) during beer aging.


dx.doi.org/10.1021/jf5015654 | J. Agric. Food Chem. 2014, 62, 9522−9528

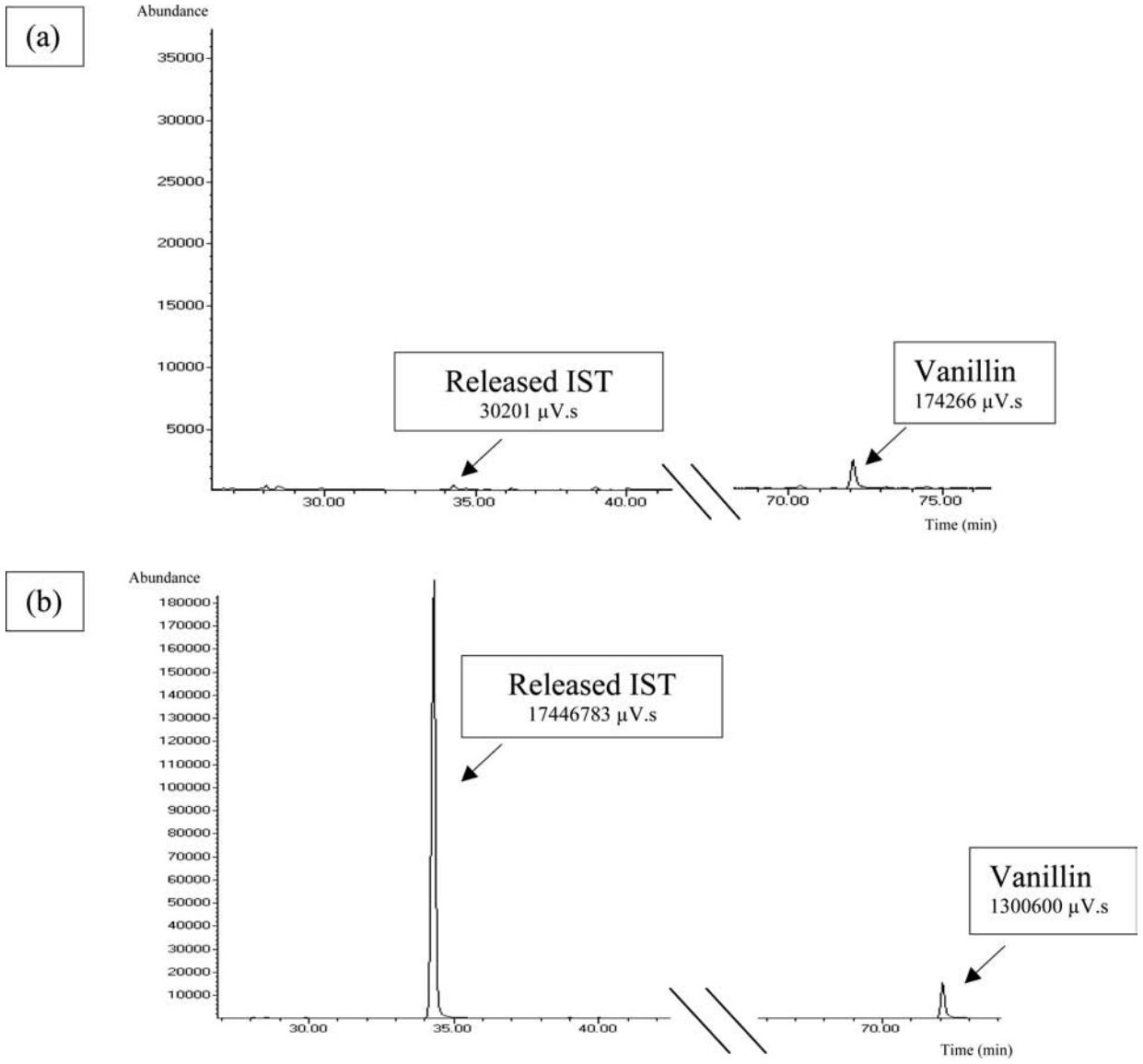


**Figure 4.** GC-MS-SIM chromatograms of (a) fresh BR1 untreated and (b) fresh BR1 treated with $\beta$-glucosidase.

beers. 4-Vinylguaiacol and vanillin were detected at the highest concentrations in BL2, for which organic malts were used. Very recently, Melotte et al.[28] found organic malts to contain higher amounts of ferulic acid (not true for cinnamic acid and its decarboxylated analogue, vinylphenol).

*4-Ethylphenol and 4-Ethylguaiacol.* Only TR1 showed high levels of 4-ethylphenol (1601 $\mu$g/L) and 4-ethylguaiacol (1603 $\mu$g/L) (Table 2). After hydroxycinnamic acid decarboxylation to vinylphenols (use of POF(+) yeasts for primary fermentation), the vinylphenol reductase activity of *Brettanomyces* yeasts (added only for secondary fermentation and bottle refermentation) allowed biotransformation of 4-vinylguaiacol and 4-vinylphenol. The residual 4-vinylguaiacol concentration was 0.5 $\mu$g/L in TR-1 and above 18 in all 11 other beers. The key role of *Brettanomyces* for reducing 4-vinylguaiacol into 4-vinylphenol was recently confirmed by Collin et al.,[29] who found only traces of 4-ethylguaiacol in TR1 before secondary fermentation ($\leq$2 $\mu$g/L). It steadily increases, in the presence of *Brettanomyces*, during the second part of maturation and through bottle refermentation, according to the pitching rate.

*Guaiacol and 4-Methylphenol.* The brown beers BR1, BR2, and BR3 contained the highest amounts of guaiacol (3.5−9.7 versus 0.4−0.9 $\mu$g/L in amber beers) and 4-methylphenol (1.1−3.8 versus 0.2−0.6 $\mu$g/L). Chocolate malts were used for all three of these beers, characterized by typical roasted and chocolate odors.[30,31]

**Volatile Phenols in Aged Belgian Special Beers.** The fate of phenols was monitored in seven beers for 14 months.

Guaiacol, described above as particularly relevant in fresh brown special beers made with chocolate malts, showed a significant concentration rise in all beers after 6 months (reaching 14 $\mu$g/L in BR1 after 14 months, Figure 3a). To a lesser extent, this was also the case of 4-methylphenol, which reached 4.9 $\mu$g/L in brown beer BR1 after 14 months. With their respective individual odor thresholds of 70 and 20 $\mu$g/L, guaiacol and 4-methylphenol could affect the organoleptic properties of aged dark beers. Acid hydrolysis of glycosides is suspected to gradually release these two compounds.

In contrast, 4-vinylphenol and 4-vinylguaiacol proved to be degraded over the first 6 months of storage (Figure 3b), particularly in BL1 and BL2. Oxidation of the double bond to


dx.doi.org/10.1021/jf5015654 | J. Agric. Food Chem. 2014, 62, 9522−9528

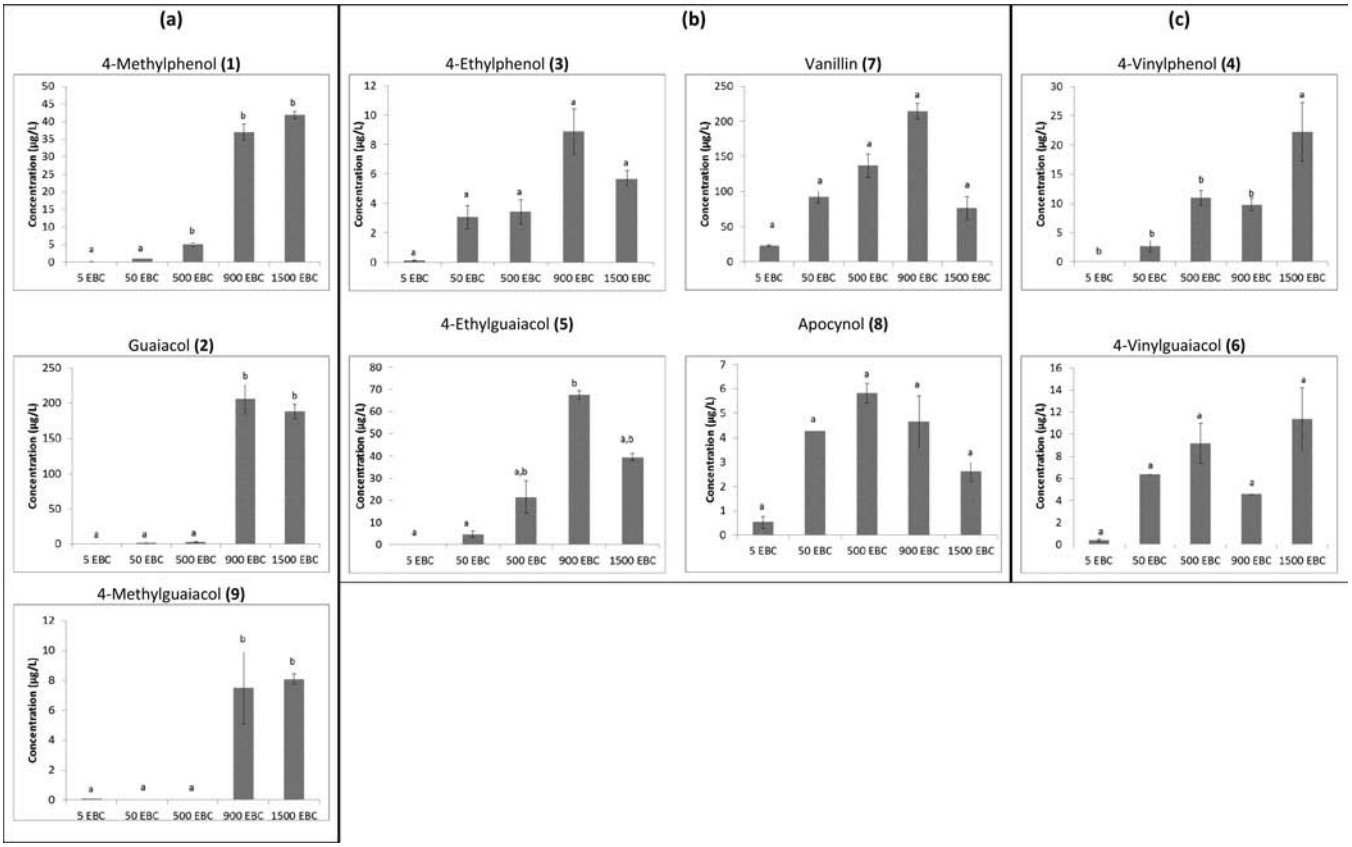


**Figure 5.** Concentrations ($\mu$g/L) of (a) 4-methylphenol, guaiacol, and 4-methylguaiacol; (b) 4-ethylphenol, 4-ethylguaiacol, vanillin, and apocynol; and (c) 4-vinylphenol and 4-vinylguaiacol in EBC laboratory worts, according to the color. Values sharing no common letter are significantly different ($p < 0.05$).

aldehyde might partly explain this evolution, as suggested in five beers by the strong increase in vanillin concentration between 6 and 14 months (Figure 3b). Yet vanillin degradation was observed in sample BL2, characterized by higher levels of both 4-vinylguaiacol and vanillin before aging. Hence, hydrolysis of glycosides most probably also partly contributes to the strong increase in vanillin concentration in BL3, BL4, AM1, BR1, and TR1 (up to 180 $\mu$g/L). From a sensory standpoint, these five beers reached the vanillin threshold value only after aging, whereas in BL2 the level of this active constituent of fresh beer fell below its threshold value during storage. BL1 was the only sample in which aldehyde oxidation was nearly balanced by 4-vinylguaiacol oxidation and/or glycoside hydrolysis.

To roughly assess if malt or hop vanillin glucosides could survive through the brewing process to be further hydrolyzed in beer (lower pH than wort), an enzymatic assay was applied on a fresh beer (BR1). As depicted in Figure 4, a $\beta$-glucosidase treatment applied on the XAD-2 glucoside extract did release 0.2 mg/L IST equivalent of vanillin. Complementary analyses will be needed to correlate the accurate concentrations of vanillin glucoside in each beer to the amount of free vanillin released through aging. The assay could be also optimized to quantify traces of other suspected glucosides (e.g., guaiacol and 4-methylphenol).

The hydrogenated derivatives 4-ethylphenol and 4-ethylguaiacol found in TR1 were also degraded between 6 and 14 months of aging (Figure 3c). Due to the presence of *Brettanomyces* yeasts in this Trappist bottled beer, 4-ethylphenol was, however, still synthesized during the first 3 months of storage (vinylphenol bioreduction).

**Volatile Phenols in EBC Laboratory Worts Produced with Five Different Malts.** The origin of guaiacol and 4-methylphenol in dark beers was investigated by analyzing worts produced with five differently colored malts (color ranging from 5 to 1500 °EBC; laboratory worts brewed with 50% special malts; values given for 100%). As depicted in Figure 5a, our results confirmed that high levels of 4-methylphenol (37−42 $\mu$g/L) and guaiacol (188−205 $\mu$g/L) are specific to the use of torrefied malts ($\leq$5 $\mu$g/L 4-methylphenol and $\leq$3 $\mu$g/L guaiacol for all other worts). The high temperatures applied during roasting (>250 °C) most probably allow thermal degradation of either free hydroxycinnamic acids or lignins. Also to be mentioned is the presence of 7−8 $\mu$g/L 4-methylguaiacol in both worts made with roasted malts only. Taking into account that <10% of torrefied malts are usually used by brewers for special beers, the concentration of this compound was logically too low to be detected in the above-described commercial beers (compound **9** in Table 2). The other phenols are not necessarily found in higher amounts in congress worts made with torrefied malts. Figure 5b shows a similar pattern for four phenols (4-ethylphenol, 4-ethylguaiacol, vanillin, and apocynol): a very low level in pale malt, a maximum concentration in malts of intermediate color, and again a lower level in 1500 °EBC malt. In the case of 4-vinylguaiacol, caramel and torrefied malts can bring similar concentrations (e.g., 500 and 900 °EBC in Figure 5c). For 4-vinylphenol, only the black malt shows a significantly higher concentration.

In conclusion, because guaiacol and 4-methylphenol were always found under 3 $\mu$g/L in EBC laboratory worts made with


dx.doi.org/10.1021/jf5015654 | J. Agric. Food Chem. 2014, 62, 9522−9528

caramel malt or pale malts, we suggest that these compounds, especially guaiacol, might be used as markers of torrefied malts.

## AUTHOR INFORMATION


### Corresponding Author

*(S.C.) E-mail: sonia.collin@uclouvain.be. Fax: +32-10-47 21 78.


### Notes

The authors declare no competing financial interest.

## ACKNOWLEDGMENTS

We thank the CONSALIM project members (Région Wallonne, Belgium) for their kind collaboration.

## ABBREVIATIONS USED

EBC, European Brewery Convention; GC-MS, gas chromatography−mass spectrometry; GC-O, gas chromatography−olfactometric detection; AEDA, aroma extract dilution analysis; FD, dilution factor; NIST, National Institute of Standards and Technology; *m/z*, mass-to-charge ratio; POF, phenolic off-flavor

## REFERENCES


(1) Schieberle, P. Primary odorants of pale lager beer. *Z. Lebensm.-Unters. -Forsch.* **1991**, *193*, 558−565.

(2) Wackerbauer, K.; Kramer, P.; Siepert, J. Phenolic aromatic substances in beer. Phenolic carboxylic acid and phenols in the raw material and beer preparation. *Brauwelt* **1982**, *122*, 618−620, 622, 624, 626.

(3) Achilli, G.; Cellerino, G. P.; Gamache, P. H.; Deril, G. V. M. Identification and determination of phenolic constituents in natural beverages and plant-extracts by means of a coulometric electrode array system. *J. Chromatogr.* **1993**, *632*, 111−117.

(4) McMurrough, I.; Madigan, D.; Donnelly, D.; Hurley, J.; Doyle, A. M.; Hennigan, G.; Mcnulty, N.; Smyth, M. R. Control of ferulic acid and 4-vinyl guaiacol in brewing. *J. Inst. Brew.* **1996**, *102*, 327−332.

(5) Vanbeneden, N.; Delvaux, F.; Delvaux, F. R. Determination of hydroxycinnamic acids and volatile phenols in wort and beer by isocratic high-performance liquid chromatography using electrochemical detection. *J. Chromatogr.* **2006**, *1136*, 237−242.

(6) Coghe, S.; Benoot, K.; Delvaux, F.; Vanderhaegen, B.; Delvaux, F. R. Ferulic acid release and 4-vinylguaiacol formation during brewing and fermentation: indications for feruloyl esterase activity in *Saccharomyces cerevisiae*. *J. Agric. Food Chem.* **2004**, *52*, 602−608.

(7) Fiddler, W.; Parker, W. E.; Wasserman, A. E.; Doerr, R. C. Thermal decomposition of ferulic acid. *J. Agric. Food Chem.* **1967**, *15*, 757−761.

(8) Clausen, M.; Lamb, C. J.; Megnet, R.; Doerner, P. W. Pad1 encodes phenylacrylic acid decarboxylase which confers resistance to cinnamic acid in *Saccharomyces cerevisiae*. *Gene* **1994**, *142*, 107−112.

(9) Meaden, P. G.; Taylor, N. R. Cloning of a yeast gene which causes phenolic off-flavors in beer. *J. Inst. Brew.* **1991**, *97*, 353−357.

(10) Van Beek, S.; Priest, F. G. Decarboxylation of substituted cinnamic acids by lactic acid bacteria isolated during malt whisky fermentation. *Appl. Environ. Microbiol.* **2000**, *66*, 5322−5328.

(11) Vanbeneden, N.; Gils, F.; Delvaux, F.; Delvaux, F. R. Formation of 4-vinyl and 4-ethyl derivatives from hydroxycinnamic acids: Occurrence of volatile phenolic flavour compounds in beer and distribution of Pad1-activity among brewing yeasts. *Food Chem.* **2008**, *107*, 221−230.

(12) Wackerbauer, K.; Kossa, T.; Tressl, R. Phenol formation by yeasts. *Monatsschr. Brauerei.* **1978**, *31*, 52−55.

(13) Meilgaard, M. C. Flavor chemistry of beer − part II: Flavor and threshold of 239 aroma volatiles. *MBAA Technol. Q.* **1975**, *12*, 151−168.

(14) Derdelinckx, G.; Neven, H.; Arnott, P.; Demeyer, I.; Delvaux, F. Belgian special beers: refermented beers, white and wheat beers, amber and dark beers, spiced and hoppy beers. *Cerevisia* **1995**, *21*, 67−73.

(15) Kieninger, H.; Narziss, L.; Liedaner, H.; Hecht, S. Changes of quality-determining compounds in the preparation of Bavarian wheat beers. *Monatsschr. Brauwiss.* **1984**, *37*, 9−18, 55.

(16) Wackerbauer, K.; Kramer, P. Bavarian wheat beer - an alternative. Production and composition. *Brauwelt* **1982**, *122*, 758−760, 762.

(17) Verachtert, H.; Iserentant, D. Properties of Belgian acid beers and their microflora − part I: the production of Gueuze and related refreshing acid beers. *Cerevisia* **1995**, *20*, 37−41.

(18) Chatonnet, P.; Dubourdieu, D.; Boidron, J. N.; Pons, M. The origin of ethylphenols in wines. *J. Sci. Food Agric.* **1992**, *60*, 165−178.

(19) Moll, M. *Beers & Coolers: Definition, Production, And Composition*; Collection Sciences of Techniques Agro-alimentaires, Apria; TEC&DOC Lavoisier: Paris, France, 1991.

(20) Briggs, D. E.; Boulton, C. A.; Brookes, P. A.; Stevens, R. *Brewing Science and Practice*; Woodhead Publishing: Cambridge, UK, 2009.

(21) Hérent, M.-F.; Collin, S. Pyrazine and thiazole structural properties and their influence on the recovery of such derivatives in aroma extraction procedures. *J. Agric. Food Chem.* **1998**, *46*, 1975−1980.

(22) Maillard, M. N.; Berset, C. Evolution of antioxidant activity during kilning: role of insoluble bound phenolic acids of barley and malt. *J. Agric. Food Chem.* **1995**, *43*, 1789−1793.

(23) Vandecan, S. M. G.; De Schutter, D. P.; Saison, D.; Delvaux, F. R. Alkylpyrazines in dark specialty malts. *Agric. Appl. Biol. Sci.* **2007**, *72*, 307−311.

(24) Sterckx, F. L.; Saison, D.; Delvaux, F. R. Wood aging of beer − part II. Influence of wood aging parameters on monophenols concentration. *J. Am. Soc. Brew. Chem.* **2012**, *70*, 62−69.

(25) Callemien, D.; Collin, S. Structure, organoleptic properties, quantification methods, and stability of phenolic compounds in beer. A review. *Food Rev. Int.* **2010**, *26*, 1−84.

(26) Scholtes, C.; Nizet, S.; Collin, S. Occurrence of sotolon, abhexon and theaspirane-derived molecules in Gueuze beers. Chemical similarities with 'yellow wines'. *J. Inst. Brew.* **2012**, *118*, 223−225.

(27) Ullrich, F.; Grosch, W. Identification of the most intensive volatile flavour compounds formed during autoxidation of linoleic acid. *Z. Lebensm.-Unters. -Forsch.* **1987**, *184*, 277−282.

(28) Mélotte, L.; Nizet, S.; Bodart, E.; Collin, S. Impact of organic practices on organoleptic properties of beer. In *32nd Congress European Brewery Convention*, Hamburg, Germany, May 10−14, 2009.

(29) Collin, S.; Nizet, S.; Gros, J. Le houblonnage à cru des bières spéciales belges est bien plus qu'une simple dissolution des composés aromatiques du houblon. *Cerevisia* **2012**, *36*, 119−124.

(30) *Test-achat, Bières belges*; Dereume: Drogenbos, Belgium, 2011; pp 206−210.

(31) Tressl, R.; Renner, R.; Apetz, M. Volatile phenolic components in beer, smoked beer and sherry. *Z. Lebensm.-Unters. -Forsch.* **1976**, *162*, 115−122.

(32) Perpète, Ph.; Van Cutsem, P.; Boutte, Ch.; Corbisier, A. M.; Collin, S. Amplified fragment-length polymorphism, a new method for the analysis of brewers yeast DNA polymorphism. *J. Am. Soc. Brew. Chem.* **2001**, *59*, 195−200.

enzymes extracted from apple are suspected to have activity in reducing higher alcohols of alcoholic drinks in acid condition. In this study, we prepared crude enzymes from five different apple varieties and optimized the conditions of Fuji sodium alginate-immobilized enzyme powder (SA-IEP), then applied this new product to treat three Chinese liquors in which ethanol content was from 45 to 56% (v/v). The results are hoped to demonstrate an enzymatic method to reduce higher alcohols in high ethanol content liquors.

## MATERIALS AND METHODS

**Apples and Chemicals.** Fresh apple fruits of five different cultivars (*Malus domestica* Borkh. cv. Fuji, Gala, Golden Delicious, Red Star, and Jonagold) were bought from the local market of Yangling city, Shaanxi province, China. Three liquors with different ethanol contents (45% Xifeng, 50% Taibai, and 56% Erguotou) were bought from the local supermarket and used to test the effect of apple enzymes on reducing higher alcohols in these products.

Acetone, 50% glutaraldehyde, citric acid, sodium citrate, and anhydrous calcium chloride were purchased from Bodi Chemical Ltd. (Tianjin, China). Ammonium sulfate was bought from Zonghengxing Industrial and Trading Co., Ltd., Chemical Reagent Branch (Tianjin, China). MD25 dialysis tubing was purchased from Sigma (St. Louis, MO, USA). Chitosan was obtained from Wolsen Biotechnology Co., Ltd. (Xi'an, China). Sodium alginate of food grade was obtained from Ming Yue Seaweed Group Co., Ltd. (Qingdao, China). All of these chemicals were of analytical grade.

**Preparation of Crude Enzymes.** Crude enzymes were prepared using a previously developed method described by Zhu et al.[27] In brief, apple peels (about 4 mm thick) were prepared as dry, fluffy, and white powders containing crude enzymes after removal of pigments and other ester-soluble impurities with cold acetone (−30 °C). A sample of 1 g of the prepared crude enzyme powder was extracted into 25 mL of citrate buffer (0.1 mol/L, pH 4.0) after extraction for 30 min at 4 °C with continuously gentle agitation. The liquid phase containing crude enzymes was obtained after a centrifugation at 4000 rpm and 4 °C for 30 min in an ALC PK121R refrigerated benchtop centrifuge (ALC International S.r.l., Cologno Honzese, Italy). The obtained supernatant was used as crude enzyme solution. Protein content in the prepared enzyme powder (EP) and enzyme solution (ES) was estimated using the method developed by Bradford.[28]

**Preparation of Immobilized Enzymes.** The prepared EP and ES were immobilized using the methods reported by Yen and Wang.[29,30] In brief, sodium alginate solution was prepared by dissolving 0.4 g of sodium alginate in 10 mL of distilled water, and then 0.125 g of EP or 2.5 mL of ES was added, in which protein contents were equal. After thorough mixing, the mixture was dropped into 10 mL of 20 g/kg $CaCl_2$ solution at a speed of 20 drops per minute using an injector to form beads containing enzymes. The enzyme beads were kept at 4 °C for 2 h to enhance the mechanical stability and then washed three times with distilled water, 20 mL per time. The obtained immobilized EP and ES were designated SA-IEP and SA-IES, respectively.

Chitosan was also used to prepare immobilized enzymes according to the method described by Jin et al.[31] Briefly, 0.565 g of chitosan polymer was dissolved in 3.75 mL of a 500 mL/L glutaraldehyde solution and then kept statically for 3 h to activate chitosan. After that, the treated chitosan powder was collected and thoroughly rinsed with sterilized water 10 times to remove the surplus glutaraldehyde and then mixed with 2.5 mL of ES for 1 h to get immobilized enzymes. The obtained powder was chitosan-immobilized enzyme solution and designated CTS-IES in the following text.

For the treatments as control, EP and SA-IEP were replaced with equivalent inactive EP and SA-immobilized inactive EP, respectively. ES, SA-IES, and CTS-IES were replaced with equivalent citrate buffer (0.1 mol/L, pH 4.0), SA, and chitosan-immobilized citrate buffer (0.1 mol/L, pH 4.0), respectively. Inactive EP was obtained by heating EP in boiling water for 1 h.

**Effect of Enzymes on Higher Alcohol Content in Taibai Liquor.** All prepared enzymes were preheated at 37 °C for 30 min. For all enzymes prepared from the five different apple varieties, samples of 0.125 g of EP, 2.5 mL of ES, SA-IEP prepared from 0.125 g of EP, SA-IES prepared from 2.5 mL of ES and, CTS-IES prepared from 2.5 mL of ES were added into 20 mL of Taibai liquor (50% ethanol by volume). The treatment was carried out at 37 °C for 1 h according to the method reported by Zhu et al.[32] The corresponding inactive enzyme preparations were used at the same time as control. All treatments were carried out in triplicate.

**Optimization of the Conditions for Preparing Immobilized Fuji Enzyme Powder Using SA.** The single-factor design was used to investigate the influence of enzyme dosage, sodium alginate concentration, calcium chloride concentration, and immobilizing time on higher alcohol degradation.

In enzyme dosage effect tests, 10 mL of a 40 g/L sodium alginate solution was mixed with Fuji EP at different dosages of 0.1, 0.3, 0.5, and 0.8 g, dropped into 10 mL of a 20 g/L $CaCl_2$ solution, and kept at 4 °C for 2 h to get the immobilized enzymes.

In sodium alginate concentration effect tests, sodium alginate solutions with different concentrations (25, 30, 35, 40, and 45 g/L) were separately mixed with 0.3 g of Fuji EP, dropped into 10 mL of a 20 g/L $CaCl_2$ solution, and kept at 4 °C for 2 h to get the immobilized enzymes.

In $CaCl_2$ solution concentration effect tests, 40 g/L sodium alginate solution was mixed with 0.3 g of Fuji EP and then dropped into 10 mL of a $CaCl_2$ solution with different concentrations (15, 20, 25, 30, and 35 g/L) and kept at 4 °C for 2 h to get the immobilized enzymes.

In immobilizing time effect tests, 40 g/L sodium alginate solution was mixed with 0.3 g of Fuji enzyme powder, dropped into 10 mL of a 20 g/L $CaCl_2$ solution, and then kept 4 °C for different times (1.25, 2, 2.75, 3.5, and 4.25 h) to get immobilized enzymes.

All of the obtained SA-IEPs were used to treat Taibai liquor (50% ethanol by volume) as described above, and their activities in degrading higher alcohols were measured using gas chromatography (GC) analysis.

Response surface methodology was also used to test the comprehensive effect of different factors on the higher alcohol degradation by SA-IEP, and Box−Behnken central composite design was used to design the experiments. Enzyme dosage, sodium alginate concentration, and $CaCl_2$ concentration were selected as independent variables, and their levels and codes are listed in Table 1. Immobilized time (2 h) and temperature (4 °C) were set as the fixed conditions. Design expert 8.0.5 software (Stat-Ease, Inc., Minneapolis, MN, USA) was used to perform the experimental design and data analysis.

**Table 1. Factors and Their Levels of the Parameters Used in Box−Behnken Design**

| | factors | | |
|---|---|---|---|
| level | sodium alginate A (g/L) | calcium chloride B (g/L) | enzyme powder C (g) |
| −1 | 35 | 15 | 0.2 |
| 0 | 40 | 20 | 0.3 |
| 1 | 45 | 25 | 0.4 |

**Effect of the Optimized SA-IEP Made from Fuji on Higher Alcohols of Different Liquors.** Xifeng (45% ethanol v/v), Taibai (50% ethanol v/v), and Erguotou (56% ethanol v/v) were used here. To evaluate the effect of the optimized SA-IEP made from Fuji on liquor flavor, 20 mL of all liquors was sampled after treatment with SA-IEP for 1 h and gas chromatography−mass spectrometry analysis (GC-MS). The liquors without any treatment were used as control. All treatments were carried out in triplicate.

**Activity of the Optimized SA-IEP Made from Fuji in Continuous Treatments.** The optimized SA-IEP was continuously used to treat Taibai liquor (containing 50% ethanol) eight times, 20 mL per time. For each time, the treatment was carried out at 37 °C for 1 h using preheated SA-IEP containing 0.3 g of enzyme powder. After each treatment, SA-IEP was collected by filtration, and 20 mL of new liquor was added again. This operation was repeated until a total of

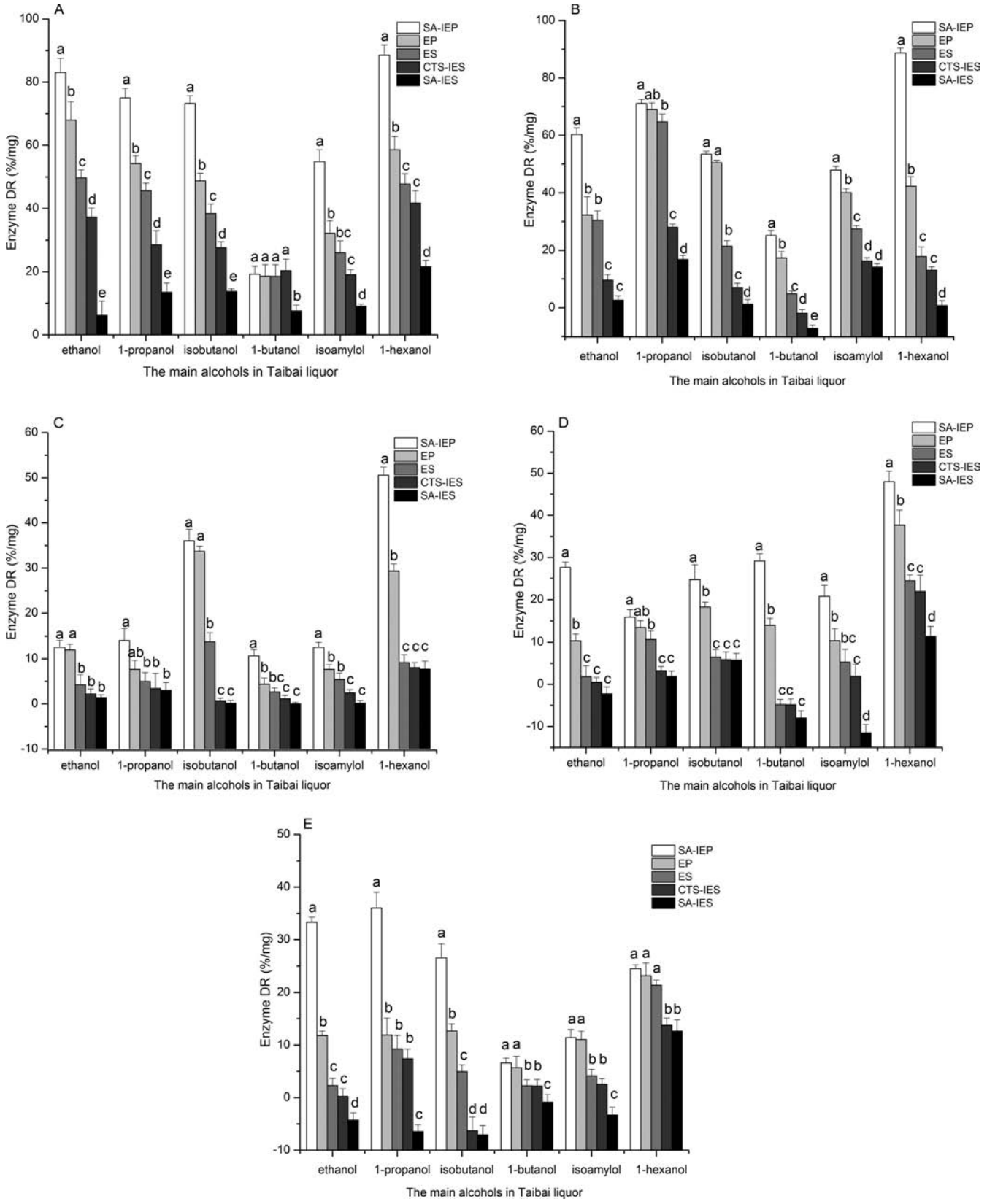


**Figure 1.** Degradation rates of different alcohols in Taibai liquor (50% ethanol v/v) using crude enzyme preparations made from Fuji (A), Golden Delicious (B), Jonagold (C), Red Star (D), and Gala (E). SA-IEP, sodium alginate-immobilized enzyme powder; SA-IES, sodium alginate-immobilized enzyme solution; CTS-IES, chitosan-immobilized enzyme solution; EP, enzyme powder; ES, enzyme solution. The bars show standard deviation of triplicate. Different letters in the same group indicate significant difference at the $P < 0.05$ level, according to ANOVA and Tukey's difference test.


dx.doi.org/10.1021/jf5018862 | J. Agric. Food Chem. 2014, 62, 9529−9538

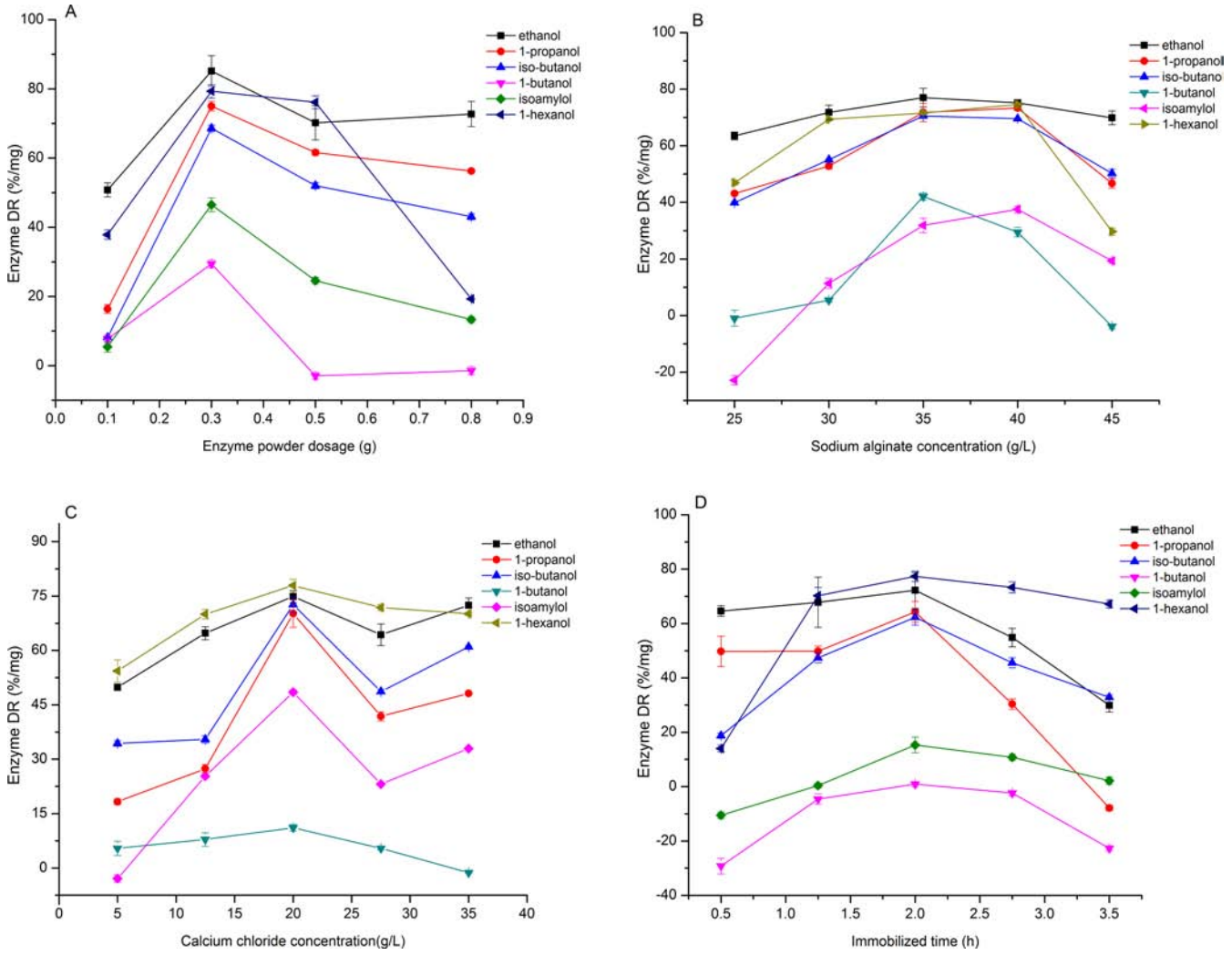


**Figure 2.** Degradation rates of different alcohols in Taibai liquor (50% ethanol v/v) using Fuji SA-IEP prepared under different levels of enzyme powder (A), sodium alginate concentration (B), calcium chloride concentration (C), and immobilization time (D). Bars show standard deviation of triplicate.

160 mL of liquor was treated. Measurement of the residue higher alcohols in the liquor was carried out by GC after each treatment.

**Measurement of Higher Alcohol Degradation Rate.** After each treatment, 3 mL of treated liquor was injected into an 8 mL GC vial together with 60 $\mu$L of internal standard (5% 4-methyl-2-pentanol/acetone g/v) and sealed immediately for measurement. The measurement was carried out in a gas chromatograph (GC-17A/FID, Shimadzu, Japan) combined with a SupelcoWax 10 capillary column (30 m × 0.32 mm i.d. × 0.25 $\mu$m film thickness; Bellefonte, PA, USA). Nitrogen was used as carrier gas with a linear flow rate of 30 mL/min. The column temperature was programmed as follows: 55 °C for 3 min, increasing to 200 °C at a rate of 5 °C/min, held at 200 °C for 3 min. Before determination, all samples were kept at 60 °C for 30 min in a water bath and subsequently injected to the GC system at a sample volume of 300 $\mu$L.

Volatile profiles of the liquors with and without treatment of Fuji SA-IEP were also tested using headspace solid phase microextraction coupled to gas chromatography spectrometry (HS-SPME-GC-MS) in a gas chromatograph−mass spectrometer equipped with a capillary column DB-WAX (3 m × 0.25 mm i.d. × 0.25 $\mu$m film thickness; Agilent, USA). Before measurement, the samples were kept at 60 °C for 30 min to release the volatiles from the liquid phase to the headspace. In measurements, 8 mL of the liquor sample was mixed together with 2.5 g of NaCl and 40 $\mu$L of an 8.00 mg/L 2-octanol solution (used as internal standard) and then was put into a 20 mL SPME vial. The SPME procedure and chromatographic conditions were the same as those detailed by Rodríguez Bencomo et al.[33] The flow rate of carrier gas (He) was 1 mL/min. The oven temperature program was set from 40 °C (2.5 min) to 200 °C (5 min) at an increasing rate of 5 °C/min. Data acquisition was made in different segments with electronic impact mode. The transfer line was kept at 230 °C and fed into an electron ionization (EI) source with an emission current of 100 $\mu$A. The masses in the range of $m/z$ 34−350 were tested. The volatile compounds were identified by comparing their mass spectra and retention indices with standards and from NIST 2002.

Measurement of 3 mL of untreated liquors was also carried out as control. Each assay was performed in duplicate.

The enzyme degradation rate (DR) of each higher alcohol by per milligram of crude enzyme was calculated according to eqs 1, 2, and 3:

$$\text{DR of treated sample (\%)} = \left(1 - \frac{T_1 \times S_0}{T_0 \times S_1}\right) \times 100 \quad (1)$$

$$\text{DR of control (\%)} = \left(1 - \frac{C_1 \times S_0}{C_0 \times S_1}\right) \times 100 \quad (2)$$


dx.doi.org/10.1021/jf5018862 | J. Agric. Food Chem. 2014, 62, 9529−9538

Table 2. Runs and Results of the Box−Behnken Design

| run[a] | sodium alginate (g/L) | calcium chloride (g/L) | enzyme powder (g) | degradation rate (%) | | | | | |
|---|---|---|---|---|---|---|---|---|---|
| | | | | ethanol | 1-propanol | isobutanol | 1-butanol | isoamylol | 1-hexanol |
| 1 | 1 | −1 | 0 | 75.48 | 66.94 | 67.68 | −6.11 | 28.16 | 74.98 |
| 2 | 0 | 0 | 0 | 82.74 | 74.67 | 73.26 | 19.24 | 54.87 | 88.53 |
| 3 | −1 | 1 | 0 | 77.64 | 74.28 | 70.21 | 0.62 | 36.40 | 80.38 |
| 4 | 1 | 1 | 0 | 81.68 | 71.64 | 72.63 | 10.41 | 42.99 | 87.49 |
| 5 | 0 | 1 | 1 | 74.33 | 65.69 | 64.68 | −5.25 | 26.56 | 74.09 |
| 6 | 0 | 0 | 0 | 84.51 | 78.69 | 72.28 | 18.93 | 51.46 | 89.80 |
| 7 | −1 | 0 | −1 | 79.81 | 70.48 | 71.64 | 1.98 | 41.26 | 82.82 |
| 8 | 1 | 0 | 1 | 74.14 | 62.33 | 62.75 | −13.67 | 24.17 | 59.39 |
| 9 | 1 | 0 | −1 | 77.94 | 70.47 | 70.21 | 2.62 | 39.67 | 81.37 |
| 10 | −1 | −1 | 0 | 80.58 | 70.66 | 71.82 | 5.79 | 41.72 | 83.33 |
| 11 | 0 | 0 | 0 | 81.98 | 71.57 | 74.24 | 19.53 | 58.28 | 87.27 |
| 12 | −1 | 0 | 1 | 74.13 | 67.61 | 63.49 | −9.04 | 25.29 | 70.83 |
| 13 | 0 | −1 | 1 | 66.78 | 47.45 | 58.19 | −16.3 | 4.07 | 49.53 |
| 14 | 0 | −1 | −1 | 77.33 | 67.51 | 69.74 | 0.42 | 35.52 | 78.67 |
| 15 | 0 | 1 | −1 | 76.04 | 66.34 | 68.88 | 0.46 | 30.68 | 76.27 |

[a]Fifteen runs were carried out, including 12 factorial experiments and 3 central experiments to estimate error.

$$\text{enzyme DR (\%/mg)} = \text{DR of treated sample} - \text{DR of control} = \left(\frac{C_1 \times S_0}{C_0 \times S_1} - \frac{T_1 \times S_0}{T_0 \times S_1}\right) \times 100/M \quad (3)$$

$M$ is the protein concentration of the used enzyme, $S_1$ is the relative area of alcohol in the original liquor, $S_0$ is the relative area of internal standard in the original liquor, $T_1$ is the relative area of alcohol in the treated liquor, $T_0$ is the relative area of internal standard in the treated liquor, $C_1$ is the relative area of alcohol in the control, and $C_0$ is the relative area of internal standard in the control.

**Statistical Analysis.** The statistical analyses were performed using the Statistic Package for Social Sciences (SPSS version 13.0, IBM, Armonk, NY, USA) for Windows and Design expert 8.0.5 software (Stat-Ease, Inc., Minneapolis, MN, USA).

## RESULTS

**Degradation of Higher Alcohols by the Enzymes Prepared from Different Apple Varieties.** Figure 1 shows enzyme preparations made from five apple varieties had degrading activity toward ethanol and the tested higher alcohols, such as 1-propanol, isobutanol, 1-butanol, isoamylol, and 1-hexanol, in Taibai liquor (containing 50% ethanol). However, the degradation rate (DR) of the tested alcohols varied greatly depending on the apple varieties used, alcohols tested, and enzyme preparations. Generally, DR of SA-IEP was the highest for all apple varieties and all tested alcohols, followed by EP, ES, CTS-IES, and SA-IES in decreasing order at different degrees of significance. This demonstrated that enzyme powder was more efficient than enzyme solution in degrading alcohols, indicating that enzymes prepared in solid phase had higher activity than those in liquid phase in liquors. High DR of EP and immobilized EP might also be due to the absorption effect of solid materials in the enzyme preparations. In most cases, CTS-IES and SA-IES resulted in lower DR values than ES, manifesting the operation of immobilization lowered the enzyme activities, which is more serious when SA was used.

Figure 1A shows SA-IEP prepared from Fuji had DR values >80% for ethanol and 1-hexanol, >70% for 1-propanol and isobutanol, around 52% for isoamylol, and only 20% for 1-butanol, indicating high efficiency of Fuji SA-IEP in degrading most alcohols. SA-IEP prepared from Golden Delicious had DR values >80% for 1-hexanol and DR values <30% for 1-butanol, indicating better substrate specificity. However, the DR value of ethanol was still up to 60% when Golden Delicious SA-IEP was used (Figure 1B). Jonagold SA-IEP showed good substrate specificity for different alcohols with DR >50% for 1-hexanol, around 35% for isobutanol, but only 15% for ethanol (Figure 1C). SA-IEP made from Red Star had DR values about 28% for ethanol, 48% for 1-hexanol, and 15−28% for other higher alcohols (Figure 1D). SA-IEP made from Gala had DR values 33% for ethanol, 35% for 1-propanol, and <30% for other higher alcohols, showing low degrading efficiency and uncompetitive substrate specificity to ethanol and higher alcohols (Figure 1E).

Comparatively, Fuji enzymes were the most efficient in reducing ethanol and higher alcohols. So they had potential application in getting rid of drunken symptoms caused by alcoholic drinks. Jonagold enzymes were more suitable to selectively reduce higher alcohols in liquors with slight reduction of ethanol content. Therefore, they had potential in selectively reducing higher alcohols in liquors. For practical purposes, however, the application of the latter enzyme would be difficult to deploy into the processing of liquor-making in China. Thus, we would focus on Fuji enzymes in this study and designed the experiments as follows.

**Optimization of Conditions for Preparing SA-Immobilized Enzymes.** To optimize the conditions for preparing immobilized Fuji enzymes, the single-factor design and response surface methodology were used. Figure 2 shows the DR values of different Fuji SA-IEPs obtained at different conditions designed by the single-factor experiment. All tested factors showed significant effect on the activity of SA-IEP in reducing alcohols in Taibai liquor (50% ethanol v/v), following a similar trend that first increased and then decreased for all tested alcohols (Figure 2). Comparatively, the highest DR values of both ethanol and most higher alcohols were obtained at conditions of 0.3 g enzyme dosage (Figure 2A), 35−40 g/L sodium alginate concentration (Figure 2B), 20 g/L $CaCl_2$ concentration (Figure 2C), and 2 h immobilization time (Figure 2D). Therefore, these levels were selected as the central point in the surface response design. Results of the DRs of


dx.doi.org/10.1021/jf5018862 | J. Agric. Food Chem. 2014, 62, 9529−9538

**Table 3. Analysis of ANOVA for the Obtained Regression Models for DRs of different higher alcohols**

| | DR of ethanol | | | | | DR of 1-propanol | | | | | DR of isobutanol | | | | |
|---|---|---|---|---|---|---|---|---|---|---|---|---|---|---|---|
| source | sum of squares | df | mean square | *F* value | *P* value prob > *F* | sum of squares | df | mean square | *F* value | *P* value prob > *F* | sum of squares | df | mean square | *F* value | *P* value prob > *F* |
| model | 274.48 | 7 | 39.21 | 33.89 | <0.0001[a] | 647.46 | 6 | 107.91 | 15.03 | 0.0006[a] | 290.22 | 7 | 41.46 | 78.59 | <0.0001[a] |
| *A*, sodium alginate | 1.07 | 1 | 1.07 | 0.92 | 0.3691 | 16.97 | 1 | 16.97 | 2.36 | 0.1629 | 1.89 | 1 | 1.89 | 3.59 | 0.1002 |
| *B*, calcium chloride | 11.33 | 1 | 11.33 | 9.79 | 0.0166 | 80.58 | 1 | 80.58 | 11.22 | 0.0101 | 10.06 | 1 | 10.06 | 19.06 | 0.0033 |
| *C*, enzyme powder | 59.08 | 1 | 59.08 | 51.06 | 0.0002 | 125.77 | 1 | 125.77 | 17.51 | 0.0031 | 122.93 | 1 | 122.93 | 233.02 | <0.0001 |
| *AB* | 20.88 | 1 | 20.88 | 18.05 | 0.0038 | — | — | — | — | — | 10.76 | 1 | 10.76 | 20.39 | 0.0027 |
| *BC* | 19.54 | 1 | 19.54 | 16.89 | 0.0045 | 94.19 | 1 | 94.19 | 13.11 | 0.0068 | 13.51 | 1 | 13.51 | 25.6 | 0.0015 |
| $B^2$ | 45.67 | 1 | 45.67 | 39.47 | 0.0004 | 96.91 | 1 | 96.91 | 13.49 | 0.0063 | 16.74 | 1 | 16.74 | 31.73 | 0.0008 |
| $C^2$ | 126.96 | 1 | 126.96 | 109.73 | <0.0001 | 253.76 | 1 | 253.76 | 35.33 | 0.0003 | 120.07 | 1 | 120.07 | 227.59 | <0.0001 |
| residual | 8.1 | 7 | 1.16 | | | 57.45 | 8 | 7.18 | | | 3.69 | 7 | 0.53 | | |
| lack of fit | 4.73 | 5 | 0.95 | 0.56 | 0.7395 | 31.97 | 6 | 5.33 | 0.42 | 0.8278 | 1.77 | 5 | 0.35 | 0.37 | 0.8405 |
| pure error | 3.37 | 2 | 1.69 | | | 25.49 | 2 | 12.74 | | | 1.92 | 2 | 0.96 | | |
| cor total | 282.58 | 14 | | | | 704.91 | 14 | | | | 293.91 | 14 | | | |

| | DR of 1-butanol | | | | | DR of isoamylol | | | | | DR of 1-hexanol | | | | |
|---|---|---|---|---|---|---|---|---|---|---|---|---|---|---|---|
| source | sum of squares | df | mean square | *F* value | *P* value prob > *F* | sum of squares | df | mean square | *F* value | *P* value prob > *F* | sum of squares | df | mean square | *F* value | *P* value prob > *F* |
| model | 1800.43 | 9 | 200.05 | 277.3 | <0.0001[a] | 2631.61 | 8 | 328.95 | 54.88 | <0.0001[a] | 1654.78 | 7 | 236.4 | 22.27 | 0.0003[a] |
| *A*, sodium alginate | 4.65 | 1 | 4.65 | 6.45 | 0.0519 | 11.71 | 1 | 11.71 | 1.95 | 0.2116 | 24.96 | 1 | 24.96 | 2.35 | 0.169 |
| *B*, calcium chloride | 62.94 | 1 | 62.94 | 87.25 | 0.0002 | 92.21 | 1 | 92.21 | 15.38 | 0.0078 | 125.77 | 1 | 125.77 | 11.85 | 0.0108 |
| *C*, enzyme powder | 309.26 | 1 | 309.26 | 428.68 | <0.0001 | 561.8 | 1 | 561.8 | 93.73 | <0.0001 | 532.85 | 1 | 532.85 | 50.21 | 0.0002 |
| *AB* | 117.61 | 1 | 117.61 | 163.03 | <0.0001 | 101.51 | 1 | 101.51 | 16.93 | 0.0062 | 59.75 | 1 | 59.75 | 5.63 | 0.0494 |
| *AC* | 6.94 | 1 | 6.94 | 9.62 | 0.0268 | | | | | | | | | | |
| *BC* | 30.31 | 1 | 30.31 | 42.01 | 0.0013 | 186.73 | 1 | 186.73 | 31.15 | 0.0014 | 181.71 | 1 | 181.71 | 17.12 | 0.0044 |
| $A^2$ | 233.83 | 1 | 233.83 | 324.12 | <0.0001 | 77.49 | 1 | 77.49 | 12.93 | 0.0114 | | | | | |
| $B^2$ | 272.95 | 1 | 272.95 | 378.35 | <0.0001 | 621.24 | 1 | 621.24 | 103.65 | <0.0001 | 106.67 | 1 | 106.67 | 10.05 | 0.0157 |
| $C^2$ | 922.09 | 1 | 922.09 | 1278.15 | <0.0001 | 1155.62 | 1 | 1155.62 | 192.8 | <0.0001 | 657.17 | 1 | 657.17 | 61.92 | 0.0001 |
| residual | 3.61 | 5 | 0.72 | | | 35.96 | 6 | 5.99 | | | 74.29 | 7 | 10.61 | | |
| lack of fit | 3.43 | 3 | 1.14 | 12.69 | 0.0739 | 12.71 | 4 | 3.18 | 0.27 | 0.8752 | 71.09 | 5 | 14.22 | 8.88 | 0.1042 |
| pure error | 0.18 | 2 | 0.09 | | | 23.26 | 2 | 11.63 | | | 3.2 | 2 | 1.6 | | |
| cor totel | 1804.04 | 14 | | | | 2667.57 | 14 | | | | 1729.07 | 14 | | | |

[a]The model is significant at the $P < 0.01$ level.



dx.doi.org/10.1021/jf5018862 | J. Agric. Food Chem. 2014, 62, 9529−9538

different alcohols obtained in the surface response design are shown in Table 2.

After multiple regression analyses and optimization, five equations were obtained between DR values of different alcohols and coded condition factors (sodium alginate concentration, $CaCl_2$ concentration, enzyme dosage). They were as follows:

$$\mathrm{DR\ (ethanol)} = 82.66 - 0.36A + 1.19B - 2.72C + 2.28AB + 2.21BC - 3.51B^2 - 5.85C^2$$

$$\mathrm{DR\ (1\text{-}propanol)} = 75.55 - 1.46A + 3.17B - 3.97C + 4.85BC - 5.11B^2 - 8.27C^2$$

$$\mathrm{DR\ (isobutanol)} = 72.94 - 0.49A + 1.12B - 3.92C + 1.64AB + 1.84BC - 2.12B^2 - 5.69C^2$$

$$\mathrm{DR\ (1\text{-}butanol)} = 19.23 - 0.76A + 2.81B - 6.22C + 5.42AB - 1.32AC + 2.75BC - 7.96A^2 - 8.60B^2 - 15.80C^2$$

$$\mathrm{DR\ (isoamylol)} = 54.87 - 1.21A + 3.40B - 8.38C + 5.04AB + 6.83BC - 4.58A^2 - 12.97B^2 - 17.69C^2$$

$$\mathrm{DR\ (1\text{-}hexanol)} = 87.60 - 1.77A + 3.96B - 8.16C + 3.87AB + 6.74BC - 5.36B^2 - 13.30C^2$$

$A$ is sodium alginate concentration, $B$ is $CaCl_2$ concentration, $C$ is enzyme dosage, and DR is the degradation rate of alcohols.

One-way ANOVA (Table 3) shows the obtained equations were extremely significant ($P < 0.01$). The lack of fit $F$ value and the associated $P$ value of each obtained model were >0.05, which indicated that the lack of fit was not significant and the model fitted the data well. Sodium alginate ($A$) had no significant influence on all results. Enzyme dosage ($C$), quadratic term of $CaCl_2$ concentration ($B^2$), enzyme dosage item ($C^2$), and the interaction of $CaCl_2$ and enzyme dosage ($BC$) had significant influence on all results. Except for 1-propanol, the interaction between sodium alginate concentration and calcium chloride ($AB$) had significant influence on DRs of other higher alcohols as well. The quadratic term of sodium alginate ($A^2$) had a remarkable effect on the degradation of 1-butanol and isoamylol.

By solving the equations, the best condition for preparing Fuji SA-IEP with highest DRs for all alcohols was obtained at enzyme dosage 0.3 g, sodium alginate concentration 40 g/L, $CaC1_2$ concentration 20 g/L, and immobilization time 2 h. Under these optimal conditions for preparing SA-IEP, DR of each alcohol was predicted to be 82.66, 75.55, 72.94, 19.23, 54.87, and 87.60% for ethanol, 1-propanol, isobutanol, 1-butanol, isoamylol, and 1-hexanol, respectively. The difference between the theoretical value and the practical value was <1%.

**Application of Fuji SA-IEP in Different Liquors.** In all tested liquors, Fuji SA-IEP showed significant degradation of ethanol and higher alcohols and generated some new substrates, such as ethyl hexanoate and ethyl heptanoate (Table 4). Interestingly, we found other esters (i.e., ethyl acetate, ethyl butyrate, ethyl valerate), aldehydes, and acids were degraded by Fuji SA-IEP or could not be detected, which demonstrated ethyl hexanoate and ethyl heptanoate might be the products of alcohol degradation in terms of the law of conservation. Furthermore, the conclusion of our laboratory's previous study further proved some apple enzymes had the same ability with alcohol dehydrogenase. In this way, the enzyme possibly had catalyzed the synthesis of esters with alcohols and acids. In all liquors, DR of 1-hexanol was the highest (>84%) among the degraded higher alcohols. In Erguotou (56% ethanol v/v), DRs of 1-propanol, isobutanol, isoamylol, and hexanol reached >80%, illustrating high efficiency of Fuji SA-IEP in reducing multiple higher alcohols. It was also found that, except for 1-butanol, DRs of ethanol and other higher alcohols increased with the ethanol content in liquors from Xifeng (45% ethanol v/v) to Erguotou (56% ethanol v/v). This might be due to higher alcohol contents increased with the ethanol content in liquors. Thus, Fuji SA-IEP was very effective in reducing higher alcohols in high ethanol content liquors. This is acceptable in practice.

**Table 4. Degradation Rates of Higher Alcohols in Three Liquors Treated with Fuji SA-IEP**

| | degradation rate (%) | | |
|---|---|---|---|
| compound | Xifeng (45% ethanol) | Taibai (50% ethanol) | Erguotou (56% ethanol) |
| ethanol | 68.06 | 80.29 | 82.02 |
| 1-propanol | 43.30 | 67.67 | 80.89 |
| isobutanol | 37.29 | 70.01 | 82.29 |
| 1-butanol | 31.42 | 10.59 | 27.71 |
| isoamylol | 55.37 | 75.69 | 80.33 |
| hexanol | 84.33 | 88.59 | 88.24 |
| ethyl hexanoate | 47.54 | 69.83 | −62.65 |
| heptanoate | −70.35 | −11.40 | 29.97 |

**Activity of Fuji SA-IEP in Continuous Treatments.** When SA-IEP prepared from Fuji was continuously used to treat Taibai liquor (50% ethanol), DRs of all alcohols generally decreased with the increase of liquor volume (Figure 3). This

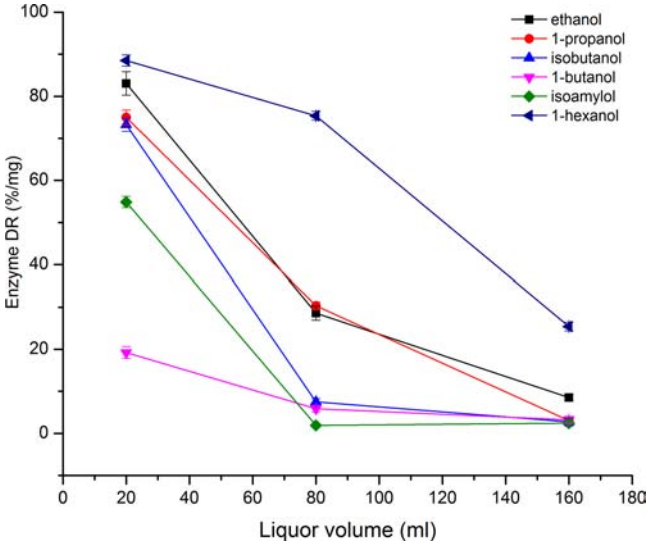


**Figure 3.** Degradation rates of different alcohols in Taibai liquor (50% ethanol v/v) during continuous treatment with Fuji SA-IEP. Bars show standard deviation of triplicate.


dx.doi.org/10.1021/jf5018862 | J. Agric. Food Chem. 2014, 62, 9529−9538

might be caused by the decrease of enzyme activity or the release of enzyme from the immobilizing material to liquid phase during the separation of SA-IEP from treated liquor. The decrease of 1-hexanol DR was comparatively much lower than that of other alcohols, illustrating 1-hexanol degrading enzymes were more stable than other alcohol-degrading enzymes. When 100 mL of liquor was treated with 0.3 g of enzyme, DR of 1-hexanol was still >70%, whereas DRs of other alcohols were <30%. When liquor volume increased to >100 mL, DR of 1-hexanol also decreased greatly. Therefore, the reasonable liquor to enzyme ratio should be 100 mL to 0.3 g of enzyme in batch treatment to produce acceptable higher alcohol degrading efficiency. To sum up, Fuji SA-IEP showed good stability in continuous treatments and it would be a novel and prospective way to reduce higher alcohols and improve flavors of alcoholic products.

## DISCUSSION

Enzyme preparations used in the study were all made of apple peels. SA-IEP and EP obtained in the study had high efficiency in degrading alcohols in liquors, implying the potential of apple pomace in improving liquor quality. SA-IEP and EP were made from apple peel that is the main constituent in apple pomace. Apple pomace is the waste of fresh apple processing, and its disposal is a major environmental problem. Many efforts have been made to process apple pomace into value-added products, such as solid state fermentation, extraction, and so on.[34,35] In the study, apple peels were extracted and prepared as solution and powder containing fiber. The latter showed higher efficiency in degrading alcohols. Therefore, it is possible to use apple pomace in Chinese liquor-making, which is carried out in solid state fermentation. In addition, enzyme preparations made from apple peels also showed significant degradation of higher alcohols in market liquors that have been separated from solid material by distillation. It is applicable and reasonable to use these enzyme preparations during or after the period of aging to enhance liquor quality, because the treatment and separation would be easily done when immobilized enzymes were used. However, it should be mentioned that the obtained results could not be used directly because they did not indicate the influence of apple ripeness and growing place on the treatment efficiency. Furthermore, ethanol was also degraded by the enzyme preparations in the study, indicating purification might be needed to increase substrate specificity of the obtained apple enzymes. In any case, the study provided useful information and proposed a new way to reduce higher alcohols in liquor and application of apple peel in this processing.

The enzyme preparations made in the study were more efficient than previously reported enzymes in higher alcohol degradation. Some enzymes have been previously used to treat alcoholic drinks. Kłosowski et al.[36] used pullulanase and proteolytic enzymes to reduce higher alcohols in maize wine during the fermentation, but the DRs were only 8.29 and 43.64%, respectively. Armada et al.[37] found that when maceration enzyme, clarificant enzyme, and the mixture of enzymes were separately added into Albariño wines, maceration enzyme reduced methanol and isobutanol, clarificant enzyme reduced 1-propanol, and the mixture of enzymes reduced 1-butanol. In this paper, all crude enzymes prepared from the five different apple varieties showed significant degradation of most alcohols, including ethanol and higher alcohols. In our previous studies, the enzyme that has activity on degrading 1-hexanol was identified as NADH-dependent hexanol-degrading enzyme.[27] It was different from all of the previously reported enzymes used in alcoholic drinks. More important, most enzymes prepared in this study had DRs of >60% to one or more higher alcohols.

The influence of the adsorption effect caused by immobilizing materials was excluded in the study by using enzyme degradation rate, which excluded the blank control that represented the used immobilizing materials without enzymes. For all apple varieties, SA-IEP and EP had higher efficiency than CTS-IES, SA-IES, and ES in most cases, indicating the carriers keeping solid state of the enzyme preparation might contribute to the enhancement of enzyme activities.[38] However, in some instances, immobilization would cause a decrease of enzyme activity, for example, the activities of CTS-IES and SA-IES were lower than that of ES. The Ehrlich mechanism indicated that the overall formation of higher alcohols was extremely complex.[39]

The obtained results showed the overall activity of crude enzymes extracted from apples. The enzymes that exactly contributed to the degradation of the alcohols might be different from each other. 1-Hexanol was comparatively easier to be degraded by most enzyme preparations extracted from four apple varieties, except of Gala. According to the results reported by Zhu et al.,[27] the hexanol-degrading enzyme extracted from Fuji also had activity to 1-propanol, isobutanol, and isoamylol, but not toward methanol and ethanol. However, the crude enzymes extracted from Fuji had significant degradation of ethanol as well, indicating the enzyme contributing to the degradation of ethanol was different from the reported hexanol-degrading enzyme. Alcohol dehydrogenase (ADH) has been reported to play an important role in alcohol degradation.[40] ADH and aldehyde dehydrogenase (ALDH) are responsible for the metabolism of alcohol to aldehyde and finally oxidizing to acid, in which NAD or NADP are indispensable.[41,42] The obtained GC-MS results showed that Fuji SA-IEP generated ethyl hexanoate in liquor (Xifeng and Taibai, 45 and 50% ethanol v/v) and heptanoate in liquor (Erguotou, 56% ethanol v/v), consistent with the characteristics of ADH. However, further study is still needed to identify the enzymes in apples that contribute to the degradation of each alcohol and confirm their corresponding substrates by purification and optimization of the conditions of GC-MS. After treatment, we invited an expert from the College of Enology of our school to evaluate the quality of the liquors. Her conclusion was that there was less pungent smell of alcohols in the liquor treated by Fuji SA-IEP and it tasted good. Later, we will expand the reaction system and carry on the normal sensory evaluation.

## AUTHOR INFORMATION

### Corresponding Author

*(J.S.) Phone: +86 29 88460541. Fax: +86 29 88460541. E-mail: sjlshi2004@nwpu.edu.cn.

### Funding

We appreciate financial support from the Ministry of Agriculture of the People's Republic of China through Project CAR-30 and 201003021.

### Notes

The authors declare no competing financial interest.

## ABBREVIATIONS USED

SA-IEP, sodium alginate-immobilized enzyme powder; SA-IES, sodium alginate-immobilized enzyme solution; CTS-IES, chitosan-immobilized enzyme solution; EP, enzyme powder; ES, enzyme solution; DR, degradation rate

## REFERENCES


(1) Longo, E.; Velazquez, J.; Sieiro, C.; Cansado, J.; Calo, P.; Villa, T. Production of higher alcohols, ethyl acetate, acetaldehyde and other compounds by 14 *Saccharomyces cerevisiae* wine strains isolated from the same region (Salnés, NW Spain). *World J. Microbiol. Biotechnol.* **1992**, *8*, 539−541.

(2) Fan, W.; Qian, M. C. Identification of aroma compounds in Chinese 'Yanghe Daqu' liquor by normal phase chromatography fractionation followed by gas chromatography/olfactometry. *Flavour Fragrance J.* **2006**, *21*, 333−342.

(3) Zhang, W.-X.; Wu, Z.-Y.; Zhang, Q.-S.; Wang, R.; Li, H. Combination of newly developed high quality Fuqu with traditional Daqu for Luzhou-flavor liquor brewing. *World J. Microbiol. Biotechnol.* **2009**, *25*, 1721−1726.

(4) Yang, D.; Luo, X.; Wang, X. Characteristics of traditional Chinese *shanlan* wine fermentation. *J. Biosci. Bioeng.* **2013**, *117*, 203−207.

(5) Lachenmeier, D. W.; Haupt, S.; Schulz, K. Defining maximum levels of higher alcohols in alcoholic beverages and surrogate alcohol products. *Regul. Toxicol. Pharmacol.* **2008**, *50*, 313−321.

(6) Schlottmann, U. *SIDS Initial Assessment Report for SIAM 20*; OECD: Paris, France, 2005.

(7) Bai, J.; Baldwin, E. A.; Imahori, Y.; Kostenyuk, I.; Burns, J.; Brecht, J. K. Chilling and heating may regulate C6 volatile aroma production by different mechanisms in tomato (*Solanum lycopersicum*) fruit. *Postharvest Biol. Technol.* **2011**, *60*, 111−120.

(8) Reddy, L.; Reddy, O. Effect of enzymatic maceration on synthesis of higher alcohols during mango wine fermentation. *J. Food Qual.* **2009**, *32*, 34−47.

(9) Rapp, A.; Mandery, H. Wine aroma. *Experientia* **1986**, *42*, 873−884.

(10) Carrau, F.; Medina, K.; Fariña, L.; Boido, E.; Dellacassa, E. Effect of *Saccharomyces cerevisiae* inoculum size on wine fermentation aroma compounds and its relation with assimilable nitrogen content. *Int. J. Food Microbiol.* **2010**, *143*, 81−85.

(11) Molina, A. M.; Guadalupe, V.; Varela, C.; Swiegers, J. H.; Pretorius, I. S.; Agosin, E. Differential synthesis of fermentative aroma compounds of two related commercial wine yeast strains. *Food Chem.* **2009**, *117*, 189−195.

(12) Carrascosa, A. V.; Bartolome, B.; Robredo, S.; Leon, A.; Cebollero, E.; Juega, M.; Nunez, Y.; Martinez, M.; Martinez-Rodriguez, A. J. Influence of locally-selected yeast on the chemical and sensorial properties of Albariño white wines. *LWT−Food Sci. Technol.* **2012**, *46*, 319−325.

(13) Arellano, M.; Pelayo, C.; Ramírez, J.; Rodriguez, I. Characterization of kinetic parameters and the formation of volatile compounds during the tequila fermentation by wild yeasts isolated from agave juice. *J. Ind. Microbiol. Biotechnol.* **2008**, *35*, 835−841.

(14) Varela, C.; Kutyna, D.; Solomon, M. R.; Black, C.; Borneman, A.; Henschke, P.; Pretorius, I. S.; Chambers, P. J. Evaluation of gene modification strategies for the development of low-alcohol-wine yeasts. *Appl. Environ. Microbiol.* **2012**, *78*, 6068−6077.

(15) Yamamoto, H.; Mizutani, M.; Yamada, K.; Iwaizono, H.; Takayama, K.; Hino, M.; Kudo, T.; Ohta, H.; Kida, K.; Morimura, S. Characteristics of aromatic compound production using new shochu yeast MF062 isolated from shochu mash. *J. Inst. Brew.* **2013**, *118*, 406−411.

(16) González-Álvarez, M.; Noguerol-Pato, R.; González-Barreiro, C.; Cancho-Grande, B.; Simal-Gándara, J. Sensory quality control of young vs. aged sweet wines obtained by the techniques of both postharvest natural grape dehydration and fortification with spirits during vinification. *Food Anal. Methods* **2013**, *6*, 289−300.

(17) Varela, C.; Torrea, D.; Schmidt, S. A.; Ancin-Azpilicueta, C.; Henschke, P. A. Effect of oxygen and lipid supplementation on the volatile composition of chemically defined medium and Chardonnay wine fermented with *Saccharomyces cerevisiae*. *Food Chem.* **2012**, *135*, 2863−71.

(18) Coetzee, C.; Lisjak, K.; Nicolau, L.; Kilmartin, P.; du Toit, W. J. Oxygen and sulfur dioxide additions to Sauvignon blanc must: effect on must and wine composition. *Flavour Fragrance J.* **2013**, *28*, 155−167.

(19) Rous, C.; Snow, R.; Kunkee, R. Reduction of higher alcohols by fermentation with a leucine-auxotrophic mutant of wine yeast. *J. Inst. Brew.* **1983**, *89*, 274−278.

(20) Barbosa, C.; Mendes-Faia, A.; Mendes-Ferreira, A. The nitrogen source impacts major volatile compounds released by *Saccharomyces cerevisiae* during alcoholic fermentation. *Int. J. Food Microbiol.* **2012**, *160*, 87−93.

(21) Rapp, A.; Versini, G. Influence of nitrogen compounds in grapes on aroma compounds of wines. *Wein−Wiss* **1996**, *51*, 193−203.

(22) Carrau, F. M.; Medina, K.; Farina, L.; Boido, E.; Henschke, P. A.; Dellacassa, E. Production of fermentation aroma compounds by *Saccharomyces cerevisiae* wine yeasts: effects of yeast assimilable nitrogen on two model strains. *FEMS Yeast Res.* **2008**, *8*, 1196−1207.

(23) Vilanova, M.; Ugliano, M.; Varela, C.; Siebert, T.; Pretorius, I. S.; Henschke, P. A. Assimilable nitrogen utilisation and production of volatile and non-volatile compounds in chemically defined medium by *Saccharomyces cerevisiae* wine yeasts. *Appl. Microbiol. Biotechnol.* **2007**, *77*, 145−157.

(24) Vilanova, M.; Siebert, T. E.; Varela, C.; Pretorius, I. S.; Henschke, P. A. Effect of ammonium nitrogen supplementation of grape juice on wine volatiles and non-volatiles composition of the aromatic grape variety Albariño. *Food Chem.* **2012**, *133*, 124−131.

(25) Gutierrez, L. Effect of some vitamins and micronutrient deficiencies on the production of higher alcohols by *Saccharomyces cerevisiae*. *Sci. Agric.* **1993**, *50*, 484−489.

(26) Hsieh, C. W.; Huang, Y. H.; Lai, C. H.; Ho, W. J.; Ko, W. C. Develop a novel method for removing fusel alcohols from rice spirits using nanofiltration. *J. Food Sci.* **2010**, *75*, N25−N29.

(27) Zhu, J.; Shi, J. L.; Pan, Z. L. Purification and characterization of a hexanol-degrading enzyme extracted from apple. *J. Agric. Food Chem.* **2012**, *60*, 3246−3252.

(28) Bradford, M. M. A rapid and sensitive method for the quantitation of microgram quantities of protein utilizing the principle of protein-dye binding. *Anal. Biochem.* **1976**, *72*, 248−254.

(29) Yen, H.; Lee, Y. Production of lactic acid from raw sweet potato powders by *Rhizopus oryzae* immobilized in sodium alginate capsules. *Appl. Biochem. Biotechnol.* **2010**, *162*, 607−615.

(30) Wang, B. E.; Hu, Y. Y. Comparison of four supports for adsorption of reactive dyes by immobilized *Aspergillus fumigatus* beads. *J. Environ. Sci.−China* **2007**, *19*, 451−457.

(31) Jin, Z.; Su, Y.; Duan, Y. A novel method for polyaniline synthesis with the immobilized horseradish peroxidase enzyme. *Synth. Met.* **2001**, *122*, 237−242.

(32) Zhu, J.; Shi, J. L.; Liu, Y. L. Extraction and characteristics of hexanol-converting enzyme in apple. *J. Chinese Inst. Food Sci. Technol.* **2010**, *4*, 017.

(33) Rodríguez Bencomo, J. J.; Muñoz González, C.; Andújar Ortiz, I.; Martín Álvarez, P. J.; Moreno Arribas, M. V.; Pozo Bayón, M. Á. Assessment of the effect of the non-volatile wine matrix on the volatility of typical wine aroma compounds by headspace solid phase microextraction/gas chromatography analysis. *J. Sci. Food Agric.* **2011**, *91*, 2484−2494.

(34) Attri, D.; Joshi, V. Optimization of apple pomace based medium and fermentation conditions for pigment production by *Chromobacter* sp. *J. Food Sci. Technol.* **2006**, *43*, 484−487.

(35) Kumar, A.; Chauhan, G. S. Extraction and characterization of pectin from apple pomace and its evaluation as lipase (steapsin) inhibitor. *Carbohydr. Polym.* **2010**, *82*, 454−459.

(36) Kłosowski, G.; Mikulski, D.; Czupryński, B.; Kotarska, K. Characterisation of fermentation of high-gravity maize mashes with the

application of pullulanase, proteolytic enzymes and enzymes degrading non-starch polysaccharides. *J. Biosci. Bioeng.* **2010**, *109*, 466−471.
(37) Armada, L.; Fernández, E.; Falqué, E. Influence of several enzymatic treatments on aromatic composition of white wines. *LWT−Food Sci. Technol.* **2010**, *43*, 1517−1525.
(38) Rodrigues, R. C.; Ortiz, C.; Berenguer Murcia, Á.; Torres, R.; Fernández-Lafuente, R. Modifying enzyme activity and selectivity by immobilization. *Chem. Soc. Rev.* **2013**, *42*, 6290−6307.
(39) Ikeda, R.; Webb, A.; Kepner, R. Wine constituents, comparative analysis of fusel oils from Thompson Seedless, Emperor, and Muscat of Alexandria wines. *J. Agric. Food Chem.* **1956**, *4*, 355−363.
(40) Defilippi, B. G.; Dandekar, A. M.; Kader, A. A. Relationship of ethylene biosynthesis to volatile production, related enzymes, and precursor availability in apple peel and flesh tissues. *J. Agric. Food Chem.* **2005**, *53*, 3133−3141.
(41) Yin, S. J.; Liao, C. S.; Lee, Y. C.; Wu, C. W.; Jao, S. W. Genetic polymorphism and activities of human colon alcohol and aldehyde dehydrogenases: no gender and age differences. *Alcohol.: Clin. Exp. Res.* **1994**, *18*, 1256−1260.
(42) Koutsompogeras, P.; Kyriacou, A.; Zabetakis, I. Characterizing NAD-dependent alcohol dehydrogenase enzymes of *Methylobacterium extorquens* and strawberry (*Fragaria*× *ananassa* cv. Elsanta). *J. Agric. Food Chem.* **2006**, *54*, 235−242.

Table 1. Mean (Standard Deviation) Total Tocopherols in Base Product and UHPH-Treated Almond Beverage Samples[a]

| | α-tocopherol (mg/L) | γ-tocopherol (mg/L) | δ-tocopherol (mg/L) | total[b] (mg/L) |
|---|---|---|---|---|
| base product | 46.60 (2.44) | 1.47 (0.30) | 2.56 (0.31) | 50.63 (3.74) |
| 200 MPa, 55 °C $T_{in}$ | 7.92 (0.48) | 1.58 (0.25) | <LOD[c] | 9.51 (0.52)a |
| 200 MPa, 65 °C $T_{in}$ | 7.06 (0.19) | 0.99 (0.06) | <LOD | 8.05 (0.22)a |
| 200 MPa, 75 °C $T_{in}$ | 4.14 (0.23) | <LOD | <LOD | 4.14 (0.23)b |
| 300 MPa, 55 °C $T_{in}$ | 7.14 (0.55) | 1.47 (0.18) | <LOD | 8.61 (0.65)a |
| 300 MPa, 65 °C $T_{in}$ | 5.98 (0.77) | <LOD | <LOD | 5.98 (0.77)c |
| 300 MPa, 75 °C $T_{in}$ | 3.15 (0.12) | <LOD | <LOD | 3.15 (0.12)d |

[a]Three productions of all almond beverages were performed. Analyses were made by triplicate. [b]Letters indicate the existence of statistically significant differences ($p < 0.05$) in the total tocopherol contents between the different UHPH treatments applied. [c]<LOD, below the limit of detection (0.02 mg/L).

(Frigomat, Milan, Italy) for 20 min with recirculation in a colloidal mill (E. Bachiller B. S.A, Barcelona, Spain). The pulp was separated by filtration using a 0.10 mm steel sieve to collect the almond beverage base product (BP) for further processing by UHPH. One hundred milliliters of BP had the following composition: 1.08 ± 0.10 g of protein; 2.04 ± 0.10 g of fat; 1.29 ± 0.08 g of carbohydrates; 4.53 ± 0.11 g of dry matter; 0.12 ± 0.02 g of ash; and a mean pH value of 7.20 ± 0.03.

To study the effect of the UHPH in almond beverage, six different treatments from each production were conducted. Then, BP was treated at 200 MPa with 55, 65, or 75 °C inlet temperature ($T_{in}$) and at 300 MPa with 55, 65, or 75 °C $T_{in}$.

During the pressurization operation, almond beverage experienced an adiabatic heating in the high pressure (HP) valve during approximately 0.7 s. Then, the temperature at the exit of the HP valve was 103.5 ± 0.9, 109.7 ± 3.9, and 114.3 ± 7.2 °C in the case of samples treated at 200 MPa with 55, 65, or 75 °C $T_{in}$ and 124.3 ± 7.5, 127.7 ± 9.7, and 129.3 ± 12.6 °C in the case of samples treated at 300 MPa with 55, 65, or 75 °C $T_{in}$, respectively. The temperature after cooling the liquid was between 28 and 31 °C for all treatments. Samples of BP and UHPH-treated almond beverages were stored in amber sterile bottles at −30 °C until analysis.

**Methods.** *Tocopherol Determination.* Sample preparation was carried out following the method described by Alves et al.,[16] slightly modified. Briefly, samples were lyophilized with a freeze-dryer (Telstar, Terrassa, Spain). Then, almond beverage powder (0.2 g) was dissolved in 1.25 mL of deionized water and spiked with 20 μL of α-tocopherol acetate (1000 mg/L) as internal standard, 0.125 mL of ascorbic acid (100 mg/L) as an antioxidant for prevention of tocopherol oxidation during the extraction procedure, and 2.5 mL of methanol. After mixing, extraction was performed three times with 1.5 mL of *n*-hexane/ethyl acetate (90:10). The organic phases collected were combined and taken to dryness under a nitrogen stream. The residue was resuspended in 750 μL of dichloromethane/methanol (2:1) for chromatographic analysis. All operations were performed in the absence of light and using amber glassware.

Determination of α-, γ-, and δ-tocopherol (Sigma S.A., St. Louis, MO, USA) was performed by ultra-high-performance liquid chromatography with fluorescence detection (UPLC) (Waters Acquity System, Milford, MA, USA) with a diode array detector (Waters 2996) following the method described by Moltó-Puigmartí et al.[17] Analysis was made by triplicate.

*Polyamines Determination.* An aliquot of 5−10 g of sample was mixed with 10 mL of 0.6 M perchloric acid in a magnetic stirring plate (JP Selecta, Barcelona, Spain) for 20 min to precipitate the proteins. Thereafter, the mixture was centrifuged at 5600*g* at 4 °C for 20 min. The liquid was filtered and adjusted to a final volume of 25 mL with 0.6 M perchloric acid. Polyamines, spermidine (SPM), and spermine (SPD) (Sigma S.A.) were determined by a UPLC system (Waters Acquity System) following the method described by Latorre-Moratalla et al.[18] Analyses were made by triplicate.

*Phytosterol Determination.* Samples were lyophilized with a freeze-dryer (Telstar). Then, fat was extracted from almond beverage powder three times with 10 mL of a chloroform/methanol mixture (2:1 v/v) with 5% acetic acid. The extracts were combined and evaporated to dryness under vacuum at room temperature with a rotary evaporator. Phytosterols were determined from 100 mg of the extracted fat according to the European Pharmacopoeia (01/2008:20423).[19] An aliquot of 20 μL of 5-α-colestane (1000 mg/L) (Sigma S.A.) as internal standard and 30 mL of 2 M alcoholic potassium hydroxide were added to the extracted fat and heated on a water bath for 1 h. Once cooled to a temperature below 25 °C, the unsaponifiable matter was extracted three times with 30 mL of hexane. The extracts were combined and evaporated to dryness under vacuum at room temperature with a rotary vapor. Derivatization of phytosterols was carried out with 150 μL of bis(trimethylsilyl)-trifluoroacetamide for 30 min at 150 °C. Then, the mixture was evaporated to dryness under a nitrogen stream, and the residue was resuspended in 400 μL of hexane prior to chromatographic determination.

Campesterol, stigmasterol, stigmastanol, fucosterol, $\Delta^5$-avenasterol, and β-sitosterol (Sigma S.A.) were determined by gas chromatography using a Thermo Trace GC Ultra system (Thermo Scientific, Waltham, MA, USA) equipped with a BD-5 MS column (30 m × 0.25 mm i.d. × 0.25 μm film thickness) operating with helium as carrier gas, coupled to a Thermo ITQ 900 mass spectrometer (MS). The GC injector was operated in a pulsed splitless mode. The volume of injection was l μL. Injector temperature was 270 °C, and the GC oven was programmed to hold at 70 °C for 0.5 min; the temperature was then raised at 20 °C/min to 210 °C, which was held for 0.5 min, and then temperature was again raised at 3 °C/min to 300 °C, which was held for 10 min. The MS was operated in electron impact at 70 eV with the ion source at 200 °C, scanning from $m/z$ 50 to 550 at 3 scans per second. Analyses were made by triplicate.

**Statistical Analysis.** Nonparametrical statistics Kruskal−Wallis analysis was performed because the data did not meet the assumptions of homoscedasticity and normality. The least significant difference test was employed to determine differences between means at a 5% significance level. Results were analyzed using the Statistical Software Package for Windows PASW Statistic 20.0 (SPSS, Chicago, IL, USA).

## RESULTS AND DISCUSSION

**UHPH Effect on the Tocopherols of Almond Beverage.** There are no previous studies on how the UHPH treatment affects the contents and profile of tocopherols in almond beverages. In contrast, in soy milk, a decrease in the total tocopherols was reported upon UHPH treatment at the same combinations of pressure and temperature as in the current work.[14] Total tocopherols were affected in UHPH-treated almond beverages (Table 1). Losses in the tocopherol contents were from 80 to 95% of the BP depending on the intensity of the UHPH treatments. α-Tocopherol was the predominant chemical form that represented >90% of the total tocopherols determined in BP, followed by δ-tocopherol and, to a lesser extent, γ-tocopherol (Table 1). These results are in accordance with the tocopherol distribution in almonds, in which α-tocopherol is the main tocopherol.[20] In comparison

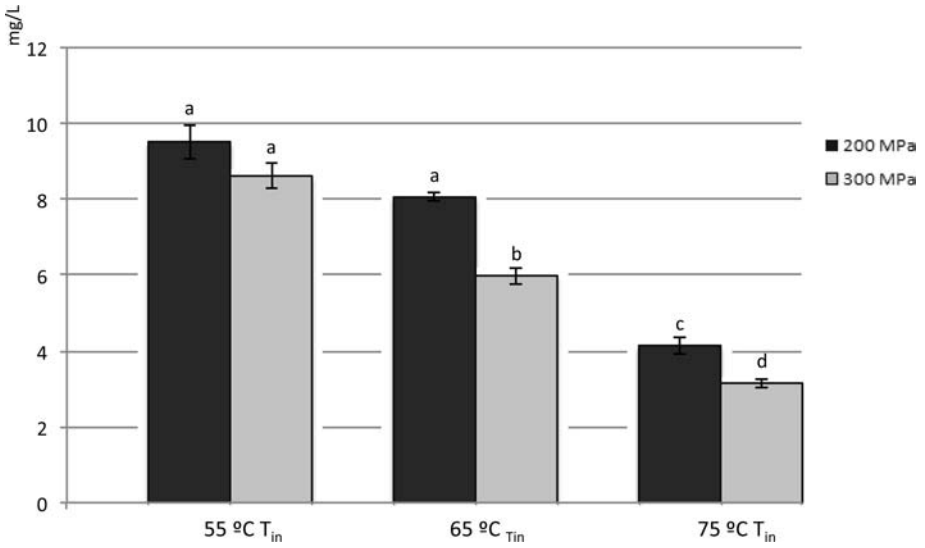


**Figure 1.** Total tocopherols (mg/L) in UHPH-treated almond beverage samples. Three productions of all almond beverages were performed. Analyses were made by triplicate. Letters indicate the existence of statistically significant differences ($p < 0.05$) in the total tocopherol contents.

**Table 2. Mean (Standard Deviation) $\beta$-Sitosterol, Avenasterol, Campesterol, Stigmasterol, and Stigmastanol Contents in Base Product and UHPH-Treated Almond Beverage Samples[a]**

| | phytosterol contents (mg/L) | | | | | | |
|---|---|---|---|---|---|---|---|
| | base product | 200 MPa, 55 °C $T_{in}$ | 200 MPa, 65 °C $T_{in}$ | 200 MPa, 75 °C $T_{in}$ | 300 MPa, 55 °C $T_{in}$ | 300 MPa, 65 °C $T_{in}$ | 300 MPa, 75 °C $T_{in}$ |
| $\beta$-sitosterol | 13.52 (0.66) | 15.13 (0.98) | 15.94 (1.41) | 16.37 (0.75) | 16.75 (0.61) | 18.00 (0.85) | 18.30 (0.88) |
| $\Delta^5$-avenasterol | 5.11 (0.31) | 5.77 (0.21) | 5.72 (0.44) | 6.79 (0.55) | 6.27 (0.41) | 7.90 (0.52) | 8.26 (0.41) |
| campesterol | 1.46 (0.04) | 2.31 (0.14) | 1.99 (0.25) | 1.71 (0.01) | 2.17 (0.55) | 1.05 (0.03) | 1.02 (0.05) |
| stigmaterol | 1.10 (0.05) | 1.52 (0.04) | 1.77 (0.11) | 1.33 (0.22) | 0.95 (0.03) | 1.24 (0.16) | 1.05 (0.02) |
| stigmastanol | 0.89 (0.04) | 1.23 (0.08) | 0.89 (0.06) | 1.05 (0.05) | 1.30 (0.05) | 0.78 (0.05) | 0.90 (0.04) |
| total[b] | 22.08 (1.34)a | 25.96 (1.32)b | 26.32 (1.48)b | 27.24 (0.78)b | 27.45 (1.04)bc | 28.97 (1.08)bc | 29.54 (1.17)c |

[a]Three productions of all almond beverages were performed. Analysis was made by triplicate. [b]Letters indicate the existence of statistically significant differences ($p < 0.05$) in the total phytosterol contents. Fucosterol was not detected.

with BP, only 10−20% of $\alpha$-tocopherol remained in all samples, whereas $\delta$-tocopherol was not found in any sample. On the contrary, 100% of the $\gamma$-tocopherol of BP sample was found in almond beverages treated at 200 MPa with 55 °C $T_{in}$ and at 300 MPa with 55 °C $T_{in}$, and 60% remained in the sample treated at 200 MPa with 65 °C $T_{in}$ (Table 1). Therefore, $\gamma$-tocopherol was the most resistant to the UHPH treatment at the mildest conditions of temperature. $\gamma$-Tocopherol is also more stable to heat than $\alpha$-tocopherol.[21]

These antioxidant compounds decreased as the temperature increased at the same pressure level, and they also decreased to a lesser extent as the pressure increased at the same temperature, suggesting that both temperature and pressure affected the tocopherol contents (Figure 1). In a previous work, tocopherols decreased by 20% in the soy milk treated at the mildest conditions of pressure and temperature of UHPH compared to untreated sample and by 50% in the soy milk treated at the strongest conditions.[14] In this work, tocopherols in almond beverages were less stable to UHPH treatments than those in soy milks. It is known that tocopherols are affected by conventional heat treatments, such as pasteurization or UHT.[22] Moreover, some authors reported no significant changes or even an increase in the total tocopherol content upon isostatic HP processing at low temperatures in different food matrices.[23,24] In the case of isostatic HP processing, pressure is uniformly and instantly applied throughout the liquid. Pressure induces some compression, but there is no shearing effect or biomolecule covalent bond compression in the food area. In the dynamic HP homogenization, also called UHPH, high pressure is applied for a few seconds in the pressure intensifier, generating intense mechanical forces through the HP valve. Besides, during UHPH treatments, samples through the HP valve gap are accompanied by short-life heating phenomena, that in the case of our samples represent temperatures from 103 to 129 °C (with a total jump in temperature by 17−21 °C per 100 MPa). Probably this temperature reached in the UHPH treatments could be responsible for the high tocopherol losses. Our results suggest that, to minimize tocopherol degradation in the almond beverages, the UHPH conditions should be as mild as possible. It is important to maintain the tocopherols in the almond beverages because of their recognized role as antioxidants.

**UHPH Effect on the Polyamines of Almond Beverage.** Polyamines have a recognized role as antioxidant compounds especially against the cellular oxidative stress.[25,26] As the capacity for the endogenous synthesis of SPD and SPM decreases with age, enhancing the intake of SPD and SPM appears to have a positive effect on health as people become older.[6] Thus, an increased intake of SPD and SPM is involved in decreasing the risk of cardiovascular diseases and age-


dx.doi.org/10.1021/jf503324f | J. Agric. Food Chem. 2014, 62, 9539−9543

associated pathologies.[27] There are no previous studies about the effect of UHPH treatment on the stability of the polyamines in almond beverages. However, polyamines were stable in all soy milks treated at the same UHPH conditions as in the current work.[14]

The polyamine SPD was found in all samples; meanwhile, SPM was not detected in any samples. The occurrence of SPD and SPM was expected because they are natural polyamines in plants and animal tissues. The SPD level is commonly higher than the SPM level in vegetable foods.[28] It has been reported that almonds contain 30 mg/kg SPD and 10 mg/kg SPM.[29] SPM was not detected, which can be ascribed to the low raw almond content used for the elaboration of the almond beverages. SPD mean contents were very low, 0.79 ± 0.04 mg/L. Consequently, because almond beverage is not a polyamine-rich food product, it is intriguing that the conditions of high pressure and temperature applied maintained the low amount of polyamines.

**UHPH Effect on the Phytosterols of Almond Beverage.** No studies have reported the effect of UHPH treatment on the phytosterols in almond beverages; however, an increase in the total phytosterol compounds was previously reported in soy milk treated by using the same UHPH conditions as in this work.[14] In almond beverages, total phytosterols were 22.08 ± 1.34 mg/L determined in BP, and they ranged from 25.96 ± 1.32 to 31.54 ± 1.69 mg/L in UHPH-treated almond beverages (Table 2). The total phytosterols determined in BP were significantly lower than UHPH-treated samples; therefore, the combination of pressure/temperature in the UHPH treatment applied resulted in an increase in the total phytosterols extractability in almond beverage. Among the UHPH-treated almond beverage samples, the highest extraction of phytosterols was found at 300 MPa, independent of the temperature conditions. Table 2 shows that total phytosterol content in samples treated at 300 MPa with 75 °C $T_{in}$ was statistically higher than those in samples treated at 200 MPa with 55, 65, and 75 °C $T_{in}$. Results indicate that the strongest conditions of UHPH favor the better extraction of phytosterols.

In all samples, the main phytosterol was $\beta$-sitosterol, which corresponded to >50% of total phytosterols, followed by $\Delta^5$-avenasterol, which represents almost 30% of the total. No data on the phytosterol composition in almond beverage were found in the literature. However, similar profiles were reported for phytosterol composition in almonds by Phillips et al.[30]

Phytosterols are integral lipid components of plant cell membranes. During the UHPH treatment several mechanical forces, shear stresses, turbulence, shocks, and cavitation phenomena occurring through the high-pressure valve could induce mechanical disruption and/or at least alteration of cell membranes.[31,32] The disruption of plant cell membrane by the UHPH treatment could release the phytosterols, which can explain the increase in total phytosterol content observed in the UHPH-treated samples.

Although phytosterols undergo oxidation, they are relatively stable in pure state and also when heated alone at temperatures ≤100 °C.[33] However, some degradation has been described under strong conditions of temperature and heating time.[34−36] Despite the temperatures reached during UHPH treatments being close to those that affect the phytosterols, the combination of pressure and short-time heating in the current work seemed not to affect phytosterol stability.

Phytosterols, which are structurally similar to cholesterol, play an important role in the control of cholesterol serum levels lowering total and LDL cholesterol.[8] Consequently, an adequate intake of these health-related compounds is strongly recommended to prevent cardiovascular diseases.

To summarize, UHPH treatment using the combination of the highest pressure and temperature would be optimum to increase the total phytosterols in almond beverage. On the contrary, UHPH treatment using the combination of the lowest pressure and temperature would be better to minimize tocopherol losses in almond beverage. UHPH treatments could be useful to increase the extractability of phytosterols from a vegetal matrix and, thereby, have a potential application in the food industry.

## AUTHOR INFORMATION


### Corresponding Author

*(M.C.V.-C.) Phone: +34 934033785. Fax: +34 934035931. E-mail: mcvidal@ub.edu.



### Funding

We thank the Direcció General de Recerca of the Generalitat de Catalunya (2014-1438 SGR) for their support and for a grant from the Ministerio de Educación y Ciencia (Spain) to Ph.D. student N.T.-F. This work was also supported by the Interministerial Commission for Science and Technology (CICYT) of the Ministerio de Educación y Ciencia (Spain) through Project AGL-2008-05430-C02-02.

### Notes

The authors declare no competing financial interest.


## ACKNOWLEDGMENTS


We thank the Centre Especial Planta de Tecnologia dels Aliments (CERPTA) for providing the almond beverage samples and especially Dr. Victoria Ferragut for her technological support.


## REFERENCES


(1) King, J. C.; Blumberg, J.; Ingwersen, L.; Jenab, M.; Tucker, K. Tree nuts and peanuts as components of a healthy diet. *J. Nutr.* **2008**, *138*, 1736S−1740S.

(2) Coates, A. M.; Howe, P. R. C. Edible nuts and metabolic health. *Curr. Opin. Lipidol.* **2007**, *18*, 25−30.

(3) Griel, A. E.; Kris-Etherton, P. M. Tree nuts and the lipid profile: a review of clinical studies. *Br. J. Nutr.* **2006**, *96*, S68−S78.

(4) Richardson, D. P.; Astrup, A.; Cocaul, A.; Ellis, P. The nutritional and health benefits of almonds: a healthy food choice. *Food Sci. Technol. Bull. Funct. Foods* **2009**, *6*, 41−50.

(5) Sabaté, J.; Haddad, E.; Tanzman, J. S.; Jambazian, P.; Rajaram, S. Serum lipid response to the graduated enrichment of a step I diet with almonds: a randomized feeding trial. *Am. J. Clin. Nutr.* **2003**, *77*, 1379−1384.

(6) Hunter, D. C.; Burritt, D. J. Chapter 12. Polyamines of plant origin − an important dietary consideration for human health. *Phytochemicals as Nutraceuticals − Global Approaches to Their Role in Nutrition and Health*, 1st ed.; Rao, V., Ed.; INTECH: Rijeka, Croatia, 2012.

(7) Brigelius-Flohe, R.; Traber, M. G. Vitamin E: function and metabolism. *FASEB J.* **1999**, *13*, 1145−1155.

(8) Marangoni, F.; Poli, A. Phytosterols and cardiovascular health. *Pharmacol. Res.* **2010**, *61*, 191−199.

(9) Desrumaux, A.; Marcand, J. Formation of sunflower oil emulsions stabilized by whey proteins with high-pressure homogenization (up to 350 MPa): effect of pressure on emulsion characteristics. *Int. J. Food Sci. Technol.* **2002**, *37*, 263−269.

(10) Floury, J.; Desrumaux, A.; Lardiéres, J. Effect of high-pressure homogenization on droplet size distribution and rheological properties

of model oil-in-water emulsions. *Innovative Food Sci. Emerging Technol.* **2000**, *1*, 127−34.
(11) Dumay, E.; Chevalier-Lucia, D.; Picart-Palmade, L.; Benzaria, A.; Gràcia-Julià, A.; Blayo, C. Technological aspects and potential applications of (ultra) high-pressure homogenisation. *Trends Food Sci. Technol.* **2013**, *31*, 13−26.
(12) Poliseli-Scopel, F. H.; Hernández-Herrero, M.; Guamis, B.; Ferragut, V. Comparison of ultra high pressure homogenization and conventional thermal treatments on the microbiological, physical and chemical quality of soymilk. *LWT − Food Sci. Technol.* **2012**, *64*, 42−48.
(13) Valencia-Flores, D. C.; Hernández-Herrero, M.; Guamis, B.; Ferragut, V. Comparing the effects of ultra-high-pressure homogenization and conventional thermal treatments on the microbiological, physical, and chemical quality of almond beverages. *J. Food Sci.* **2013**, *78*, E199−E205.
(14) Toro-Funes, N.; Bosch-Fusté, J.; Veciana-Nogués, M. T.; Vidal-Carou, M. C. Effect of ultra high pressure homogenization treatment on the bioactive compounds of soymilk. *Food Chem.* **2014**, *152*, 597−602.
(15) Barba, F. J.; Esteve, M. J.; Frígola, A. High pressure treatment effect on physicochemical and nutritional properties of fluid foods during storage: a review. *Compr. Rev. Food Sci. Food Saf.* **2012**, *11*, 307−322.
(16) Alves, R. T.; Casal, S.; Oliveira, P. P. Tocopherols in espresso coffee: analytical method development and validation. *Food Chem.* **2009**, *115*, 1549−1555.
(17) Moltó-Puigmartí, C.; Castellote, A. I.; López-Sabater, M. C. Ultra-high-pressure liquid chromatographic method for the analysis of tocopherols in human colostrum and milk. *J. Chromatogr., A* **2009**, *1216*, 4388−4394.
(18) Latorre-Moratalla, M. L.; Bosch-Fusté, J.; Lavizzari, T.; Bover-Cid, S.; Veciana-Nogués, M. T.; Vidal-Carou, M. C. Validation of an ultrahigh pressure liquid chromatographic method for the determination of biologically active amines in food. *J. Chromatogr., A* **2009**, *1216*, 7715−7720.
(19) *European Pharmacopoeia*, 8th ed.; Council of Europe: Strasbourg, France, 2008.
(20) Kodad, O.; Estopañán, G.; Juan, T.; Mamouni, A.; Socias i Company, R. Tocopherol concentration in almond oil: genetic variation and environmental effects under warm conditions. *J. Agric. Food Chem.* **2011**, *59*, 6137−6141.
(21) Seppanen, C. M.; Song, Q. The antioxidant functions of tocopherol and tocotrienol homologues in oils, fats, and food systems. *J. Am. Oil Chem. Soc.* **2010**, *87*, 469−481.
(22) Lešková, E.; Kubíková, J.; Kováčiková, E.; Košická, M.; Porubská, J.; Holčíková, K. Vitamin losses: retention during heat treatment and continual changes expressed by mathematical models. *J. Food Compos. Anal.* **2006**, *19*, 252−276.
(23) Barba, F. J.; Esteve, M. J.; Frijola, A. Impact of high-pressure processing on vitamin E ($\alpha$-, $\gamma$-, and $\delta$-tocopherol), vitamin D (cholecalciferol and ergocalciferol), and fatty acid profiles in liquid foods. *J. Agric. Food Chem.* **2012**, *60*, 3763−3768.
(24) Moltó-Puigmartí, C.; Permanyer, M.; Castellote, A. I.; López-Sabater, M. C. Effects of pasteurisation and high-pressure processing on vitamine C, tocopherols and fatty acids in mature human milk. *Food Chem.* **2011**, *124*, 697−702.
(25) Das, K. C.; Misra, H. P. Hydroxyl radical scavenging and singlet oxygen quenching properties of polyamines. *Mol. Cell. Biochem.* **2004**, *262*, 127−133.
(26) Toro-Funes, N.; Bosch-Fusté, J.; Veciana-Nogués, M. T.; Izquierdo-Pulido, M.; Vidal-Carou, M. C. In vitro antioxidant activity of dietary polyamines. *Food Res. Int.* **2013**, *51*, 141−147.
(27) Minois, N.; Carmona-Gutierrez, D.; Madeo, F. Polyamines in aging and disease. *Aging* **2011**, *3*, 716−732.
(28) Kalač, P.; Krausová, P. A review of dietary polyamines: formation, implications for growth and health and occurrence in foods. *Food Chem.* **2005**, *90*, 219−230.
(29) Cipolla, B. G.; Havouis, R.; Moulinoux, J. P. Polyamine contents in current foods: a basis for polyamine reduced diet and a study of its long term observance and tolerance in prostate carcinoma patients. *Amino Acids* **2007**, *33*, 202−212.
(30) Phillips, K. M.; Ruggio, D. M.; Ashraf-Khorassani, M. A. Phytosterol composition of nuts and seeds commonly consumed in the United States. *J. Agric. Food Chem.* **2005**, *53*, 9436−9445.
(31) Gogate, P. R.; Pandit, A. B. Application of cavitational reactors for cell disruption for recovery of intracellular enzymes. *J. Chem. Technol. Biotechnol.* **2008**, *83*, 1083−1093.
(32) Kleinig, A. R.; Middelberg, A. P. J. On the mechanism of microbial cell disruption in high-pressure homogenisation. *Chem. Eng. Sci.* **1998**, *53*, 891−898.
(33) Osada, K.; Kodama, T.; Yamada, K.; Sugano, M. Oxidation of cholesterol by heating. *J. Agric. Food Chem.* **1993**, *41*, 1198−1202.
(34) Rudzinska, M.; Przybylski, R.; Wąsowicz, E. Products formed during thermo-oxidative degradation of phytosterols. *J. Am. Oil Chem. Soc.* **2009**, *86*, 651−662.
(35) Przybylski, R.; Zambiazi, R.; Li, W. Kinetics of sterols changes during storage and frying of canola oils. In *Proceedings of the 10th International Rapeseeds Congress*, Canberra, Australia, 1999.
(36) Oehrl, Ll.; Hansen, A. P.; Rohrer, C. A.; Fenner, G. P.; Boyd, L. C. Oxidation of phytosterols in a test food system. *J. Am. Oil Chem. Soc.* **2001**, *78*, 1073−1078.

toward aroma compounds (2-methyl-butanal, methional, 2-pentanone, 2-heptanone, and nonanal) using solid phase microextraction combined with gas chromatography−mass spectrometry (SPME-GC/MS) analysis. In addition, the interactions between oxidized protein and aroma compounds were further investigated using fluorescence quenching studies to better understand the underlying binding mechanism.

## MATERIALS AND METHODS

**Materials.** Longissimus muscle from three pork carcasses (48 h post-mortem) was purchased from a local commercial abattoir (Zhongshan, China), and the pigs were slaughtered about 6 months of age following standard industrial procedures. Fat was trimmed away and muscle was cut into cubes, minced, vacuum packaged (ca. 100 g), and frozen at −80 °C until use (used within 1 week). The aroma compounds 2-methylbutanal and 3-(methylthio) propanal (methional) were purchased from Sigma−Aldrich (Steinheim, Germany). 2-Pentanone, 2-heptanone, and nonanal were obtained from Aladdin (Shanghai, China). Methanol used was of the highest commercial grade and obtained from Sinopharm Chemical Reagent Co. Ltd. (Shanghai, China). All other chemicals were of analytical reagent grade.

**Preparation of Myofibrillar Proteins.** Raw muscle was thawed at 4 °C and then used for the myofibrillar protein preparation according to the method of Park, Xiong, Alderton, and Ooizumi[22] with slight modifications. The pH of myofibrillar protein suspension at 0.1 M NaCl in the last wash was adjusted to 6.25 before centrifugation. The pellet was finally suspended in 20 mM sodium phosphate buffer (pH 6.0) containing 0.5 M NaCl, and the protein concentration was determined by the Biuret method using BSA as standard.

**Protein Oxidation.** Myofibrillar protein suspension (28 mg/mL containing 0.5 mg/mL $NaN_3$) was incubated at 37 °C for 3 h in 20 mM sodium phosphate buffer (pH 6.0) containing 0.5 M NaCl with a hydroxyl radical-generating system.[22,23] The hydroxyl radicals were produced by a 100 $\mu$M $FeCl_3$/100 $\mu$M ascorbic acid solution with $H_2O_2$ at various concentrations (0−25 mM). The same myofibrillar protein treated without incubation or $H_2O_2$ was chosen as the control. To prevent further oxidation, butylated hydroxyl toluene (BHT) (1 mM final concentration) was then added.

**Evaluation of Oxidative Changes.** *Carbonyls.* The content of carbonyls was determined by the reaction with 2,4 dinitrophenylhydrazine (DNPH) using a Varioskan Flash (Thermo Scientific 3001, Thermo Fisher Scientific Oy, Finland), as described by Oliver et al.[24] with some modifications. Briefly, 200 $\mu$L of 5 mg/mL protein suspension in 20 mM sodium phosphate buffer (pH 6.0) was mixed with 800 $\mu$L of 2 M HCl (control) or 10 mM DNPH in 2 M HCl and incubated at room temperature (25 °C) for 1 h. The DNPH-reacted samples after 10% trichloroacetic acid (TCA) precipitation were recovered by centrifugation at 8000*g* for 10 min and then washed three times with 1 mL of ethanol:ethyl acetate (1:1, v/v) to eliminate free DNPH. The final protein pellets were dissolved in 1.2 mL of 6 M guanidine HCl with 20 mM sodium phosphate buffer (pH 6.0) and were then centrifuged at 8000*g* for 10 min. Protein concentration in the supernatant was calculated at 280 nm in the HCl control using BSA in 6 M guanidine as standard. The carbonyl concentration was calculated using an absorption of 21.0 $mM^{-1}cm^{-1}$ at 370 nm against the HCl control for protein hydrazones.

*Protein Surface Hydrophobicity.* The hydrophobicity was determined using the hydrophobic chromophore bromophenol blue (BPB) method reported by Chelh et al.[25] with slight modifications. The 0.5 mL protein suspension (5 mg/mL in 20 mM sodium phosphate buffer at pH 6.0) was thoroughly mixed with 100 $\mu$L of 1 mg/mL BPB (in distilled water). The resulting samples were continually shaken at room temperature (25 °C) for 10 min and then centrifuged at 4000*g* for 15 min (4 °C). The absorbance of supernatant was measured at 595 nm against a phosphate buffer blank. The sample with the same treatment in the absence of protein was used as the control. The amount of bound BPB was calculated according to the following formula (eq 1) and expressed as an index of hydrophobicity.

$$\text{BPB bound } (\mu\text{g}) = 100\ \mu\text{g} \times (\text{A control} - \text{A sample})/\text{A control} \quad (1)$$

*Mean Particle Size of Oxidized Proteins.* The mean particle size and size distribution of oxidized proteins were measured by a Mastersizer 2000 (Malvern Instruments Co. Ltd., Worcestershire, U.K.) at 25 °C, as described by Sun et al.[18] The refractive index was taken as 1.57, and the absorption index was 0.001. The particle sizes measured are reported as the surface-weighted mean diameter $d_{3,2}$ ($d_{3,2} = \sum n_i d_i^3 / \sum n_i d_i^2$) and volume-weighted mean diameter $d_{4,3}$ ($d_{4,3} = \sum n_i d_i^4 / \sum n_i d_i^3$), where $n_i$ is the number of particles with diameter $d_i$.

*SDS−PAGE Analysis.* SDS−PAGE was performed according to the method of Flores.[26] Briefly, myofibrillar protein suspensions (5 mg/mL in 20 mM phosphate buffer at pH 6.0) were mixed with sample buffer with and without 5% $\beta$-mercaptoethanol ($\beta$ ME) at a ratio of 1:1. The ones with $\beta$ ME were incubated for 5 min at 100 °C before centrifugation (10000*g*, 10 min). Then, 14 $\mu$L of samples were loaded onto the polyacrylamide gel made of 12% running gel and 5% stacking gel and subjected to electrophoresis using a Mini-PROTEAN 3 Cell apparatus (Bio-Rad Laboratories, Hercules, CA).

*Microstructure.* The surface morphology of oxidized proteins were examined using field emission scanning electron microscopy (FE-SEM, model S4800, Hitachi, Japan) at an accelerator voltage of 10 kV. Before imaging, freeze-dried protein samples were mounted on a holder with double-sided adhesive tape and sputter-coated with gold (JEOL JFC-1200 fine coater, Japan).

**Protein−Aroma Binding Measurements.** *Preparation of Aroma Compounds Solution.* A stock solution containing each aroma compound was prepared in methanol. The aroma compounds were then simultaneously added to protein suspension (control or oxidized, 8 mg/mL in 20 mM phosphate buffer containing 0.5 M NaCl at pH 6.0), resulting in a final concentration of 1 ppm for 2-pentanone, 2-heptanone, and nonanal and 2 ppm for 2-methyl-butanal and 5 ppm for methional. Both the control and the oxidized protein samples at different levels were prepared in duplicate. The selection of the five aroma compounds was based on their presence in the headspace and the contribution to the flavor of typical Cantonese sausage as well as other dry-cured meat products.[2,27]

*Solid-Phase Microextraction (SPME) and Gas Chromatography−Mass Spectrometry (GC/MS) Analysis.* Eight milliliters of the mixture was placed in a 20 mL headspace vial and sealed with a PTFE-faced silicone septum (Supelco, Bellefonte, PA). The control vial contained exactly the same buffer just without protein. Control and protein vials were stored overnight (12 h) at 30 °C to allow equilibration.[9] The quantity of aroma compounds in the headspace of protein and control vial was determined using SPME and GC/MS analysis using conditions as described by Gianelli et al.[6] with slight modifications. A 75 $\mu$m carboxen/poly(dimethylsiloxane) (CAR/PDMS) fiber (Supelco, Bellefonte, PA) was exposed to the headspace for sampling the aroma compounds. After 30 min of adsorption, the aroma compounds were desorbed by inserting the fiber into the GC injection port of a gas chromatograph set at 220 °C for 5 min in splitless mode. The split valve was opened for 1 min after injection. The fiber was heated for 5 min in the injection port at 220 °C to avoid analyte carryover between the samples. Analysis of the aromas was performed using Trace GC/MS system equipped with an Ultra GC, a Trisplus automated sampler, and a TR-Wax column (30 m × 0.32 mm × 0.25 $\mu$m, J&W Scientific, Folsom, CA). Helium was used as the carrier gas with a linear velocity of 20.4 cm $s^{-1}$. The fiber was placed in the injector, and the GC oven temperature was started at 38 °C and held for 6 min; next, the temperature was increased to 105 °C at a rate of 6 °C $min^{-1}$, then raised to 220 °C at the rate of 15 °C $min^{-1}$, and held for 5 min. The detector temperature was set at 240 °C. The mass spectrometer was operated in electron impact (EI) mode. The ionization energy, detector voltage, scan range, and scan rate applied for the analysis were 70 eV, 350 V, $m/z$ 35−350, and 3.00 scans/s, respectively. Chromatograms and mass spectra were evaluated using Xcalibur version 2.0 (Thermo Finnigan, San Jose, CA). The results are


dx.doi.org/10.1021/jf502540p | J. Agric. Food Chem. 2014, 62, 9544−9552

expressed as a percentage of the free aroma compound found in the headspace without protein in the solution.

**Fluorescence Spectroscopy Measurements.** Protein intrinsic fluorescence was measured at a constant protein concentration (0.8 mg/mL) with various methional concentrations (0.05−0.5 ppm) in 20 mM phosphate buffer (pH 6.0) using a Varioskan Flash (Thermo Scientific 3001, Thermo Fisher Scientific Oy, Finland). Emission spectra were recorded from 300 to 400 nm at an excitation wavelength of 283 nm. Both the excitation and emission slit widths were set at 5 nm. The fluorescence spectra of the phosphate buffer were subtracted from the respective spectra of the samples. Fluorescence quenching is described according to the Stern−Volmer equation (eq 2):[28]

$$F_0/F = 1 + k_q\tau_0[Q] = 1 + K_{SV}[Q] \quad (2)$$

In this equation $F_0$ and $F$ are the fluorescence intensities in the absence and presence of a quencher, respectively, [Q] is the quencher concentration (mol/L), $K_{SV}$ is the Stern−Volmer quenching constant, $k_q$ is the bimolecular quenching rate constant, and $\tau_0$ is the lifetime of fluorescence in the absence of a quencher ($\sim 10^{-8}$ s). Hence, eq 1 was applied to determine $K_{SV}$ by linear regression of a plot of $F_0/F$ versus [Q].

**Statistical Analysis.** Statistical calculation was investigated using the statistical package SPSS 11.5 (SPSS Inc., Chicago, IL) for one-way ANOVA. Student−Newman−Keuls test was used for comparison of mean values among determinations using a level of significance of 5%. Triplicate preparations of myofibrillar proteins were carried out to confirm the accordance. Data were expressed as means ± standard deviations (SD) of triplicate determinations unless specifically mentioned.

## RESULTS AND DISCUSSION

**Oxidative Modifications of Myofibrillar Proteins.** *Carbonyls.* The carbonyl contents of the control and oxidized myofibrillar proteins are presented in Figure 1A. In this work, carbonyl content of the control protein was 1.66 nmol/mg protein, similar to those reported by Traore et al.[29] on raw *longissimus thoracis* muscle and Morzel et al.[23] on skeletal muscle myofibrillar proteins from pig *longissimus dorsi*. Compared to the control, carbonyl content of the incubated protein sample (0 mM) exhibited no significant difference ($p < 0.05$). Nevertheless, in the presence of oxidant, protein carbonyl content linearly increased ($R^2 = 0.998$) with the increasing $H_2O_2$ concentrations, and a maximum value of 14.03 nmol/mg protein was observed at 25 mM $H_2O_2$. This indicated that the formation carbonyl was weakly affected by the thermal process alone but was markedly exacerbated by the presence of $H_2O_2$, in agreement with previous studies.[19,22] In addition, considering the increase in carbonyl content during storage of meat for 10 days could be reached at approximately 2.5−10 mM oxidizing agent in our experiment,[19] the oxidative system used could be compared to real meat products to some extent.

*Protein Surface Hydrophobicity.* In view of its capacity to monitor subtle changes in chemical and physical states of protein, surface hydrophobicity could be a suitable parameter to estimate protein denaturation.[30] Figure 1B shows the surface hydrophobicity of the control and oxidized myofibrillar proteins. Compared to that of the control (44.74 μg bound BPB), the hydrophobicity of incubated protein sample (0 mM $H_2O_2$) was significantly increased ($p < 0.05$). This indicated that the thermal treatments could markedly increase the protein surface hydrophobicity, which could be related to the unfolding of actomyosin fibers, which begins at 35 °C.[31] For oxidized proteins, as can be seen, relatively low addition of $H_2O_2$ (0.5−1 mM) decreased the hydrophobicity level, while the further ($H_2O_2 \geq 2.5$ mM) significantly ($p < 0.05$) enhanced it. The

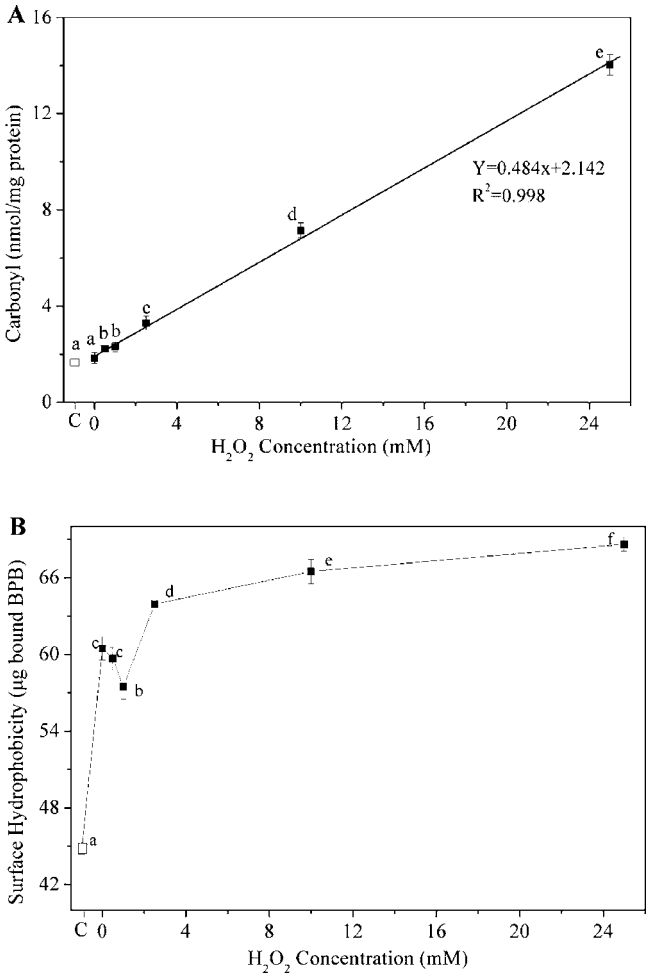


**Figure 1.** Physicochemical changes (A: carbonyl content; B: protein surface hydrophobicity) of the myofibrillar proteins upon oxidation by 100 μM $FeCl_3$/100 μM Ascorbic acid/0−25 mM $H_2O_2$. For the letters a−f, means ($n = 3$) without a common letter differ significantly ($p < 0.05$).

hydrophobicity for protein at 25 mM $H_2O_2$ was 68.61 μg, indicating an obvious increase by about 53% when compared with that of control (44.74 μg). Similar results have also been obtained stating that heating at temperatures close to the physiological temperature under slight oxidative stress might lead to protein refolding,[32,33] which could further lead to the decrease in hydrophobicity. However, with the further increase in $H_2O_2$ concentration (>2.5 mM), the hydrophobic amino acids, which are buried in protein inside, were exposed and thus enhanced protein surface hydrophobicity.[30,34] Moreover, the cleavage of certain peptide under oxidative attack might also contribute to the enhancement of surface hydrophobicity.[13]

*Mean Particle Size and Distribution.* The mean particle size ($d_{3,2}$ and $d_{4,3}$) and size distributions for the oxidized proteins were used to assess the aggregation behavior of protein during oxidation, as shown in Figure 2. It can be clearly seen that, compared to the control, the incubated protein sample (0 mM $H_2O_2$) exhibited a better size distribution, although no significant difference ($p > 0.05$) was observed in the mean particle size values ($d_{3,2}$ and $d_{4,3}$). Upon the presence of $H_2O_2$, it is noted that, compared to the control, the proteins showed markedly higher particle size values ($d_{3,2}$ and $d_{4,3}$) and the particle size distribution was monomodal and narrow. More-


dx.doi.org/10.1021/jf502540p | J. Agric. Food Chem. 2014, 62, 9544−9552

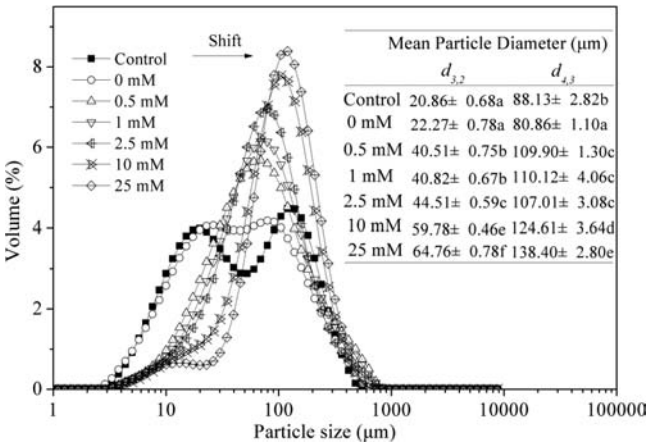


**Figure 2.** Particle size distributions of the myofibrillar proteins upon oxidation. Inset: Mean particle diameter ($d_{3,2}$ and $d_{4,3}$) of the control and oxidized proteins.

over, with the increasing addition of oxidants, an evident shift of the size distribution peak to the right was observed (Figure 2). These results should be attributed to the fact that the $H_2O_2$-induced protein oxidation might promote the intermolecular aggregation behaviors,[15] thus resulting in the change on the size distribution and the increase in particle size values ($d_{3,2}$ and $d_{4,3}$) of proteins. On the basis of the result of protein surface hydrophobicity (Figure 1B), we can thus conclude that the increase in surface hydrophobicity might favor the association between proteins mainly due to hydrophobic interactions and thereby the increase of intermolecular aggregation. In addition, it is interesting to note that, within the $H_2O_2$ concentration range from 0.5 to 2.5 mM, no marked changes on the values of $d_{4,3}$ and $d_{3,2}$ for the oxidized proteins were observed. However, with further increase in $H_2O_2$ concentrations (2.5−25 mM), the $d_{4,3}$ and $d_{3,2}$ values for proteins began to dramatically increase. These results should probably be related to the surface modification of myofibrillar protein under the $H_2O_2$-induced oxidative stresses and were in accordance with the sudden increase in protein surface hydrophobicity when the $H_2O_2$ added reached 2.5 mM (Figure 1B).

*SDS−PAGE.* The aggregation behavior of oxidized proteins was further studied by the SDS−PAGE analysis (Figure 3). As shown in Figure 3, oxidative modification significantly altered the electrophoretic pattern of myofibrillar protein. In the absence of $\beta$ ME, the exposure of myofibrillar protein to •OH caused a gradual disappearance of several subunits in a $H_2O_2$ dose-dependent manner (Figure 3A), among which changes in myosin were most remarkable, similar to those previous reports.[15,35] Herein, both myosin heavy chain (MHC) and heavy meromyosin−myosin heavy chain (HMM-MHC) began to reduce at 0.5 mM of $H_2O_2$ and almost completely vanished since $H_2O_2$ reached 1 mM. A similar, albeit less conspicuous, actin loss was also observed with increasing addition of $H_2O_2$ despite remaining faint even at high $H_2O_2$ concentrations. Simultaneously, upon oxidation, high molecular weight polymers, which barely entered the stacking gel, became accentuated (Figure 3A). These results indicated the occurrence of cross-linking under oxidation, which was consistent with the changes in particle size distributions as aforementioned (Figure 2), and myosin and actin were mainly involved. In addition, changes in troponin T (TnT) and tropomyosin (Tm) were also noticeable for their band intensity both declined upon oxidation and almost disappeared when the oxidant reached 1 mM. Nevertheless, they reappeared with further oxidation. The results implied that TnT and Tm were also involved in the formation of aggregates within the $H_2O_2$, ranging from 0 to1 mM, well explaining the corresponding significant ($p < 0.05$) decrease in protein surface hydrophobicity (Figure 1B). Nevertheless, further oxidation caused the reappearance of TnT and Tm, indicating that they were gradually no longer involved in the aggregates, which might be related with the degradation of protein backbone under •OH attack.[36] In the presence of $\beta$ ME, MHC, actin, TnT, and Tm were mostly recovered (Figure 3B), suggesting that these polymers were formed largely by disulfide bonds (S−S) or mainly through this mechanism. Nevertheless, samples treated with more than 2.5 mM of $H_2O_2$ exhibited rather diffused bands at the top of the resolving gel, and the band intensity increased along with $H_2O_2$ concentration. This suggested the presence of other covalent polymers containing no S−S bonds, such as Tyr−Tyr and active carbonyl−$NH_2$ interaction, as

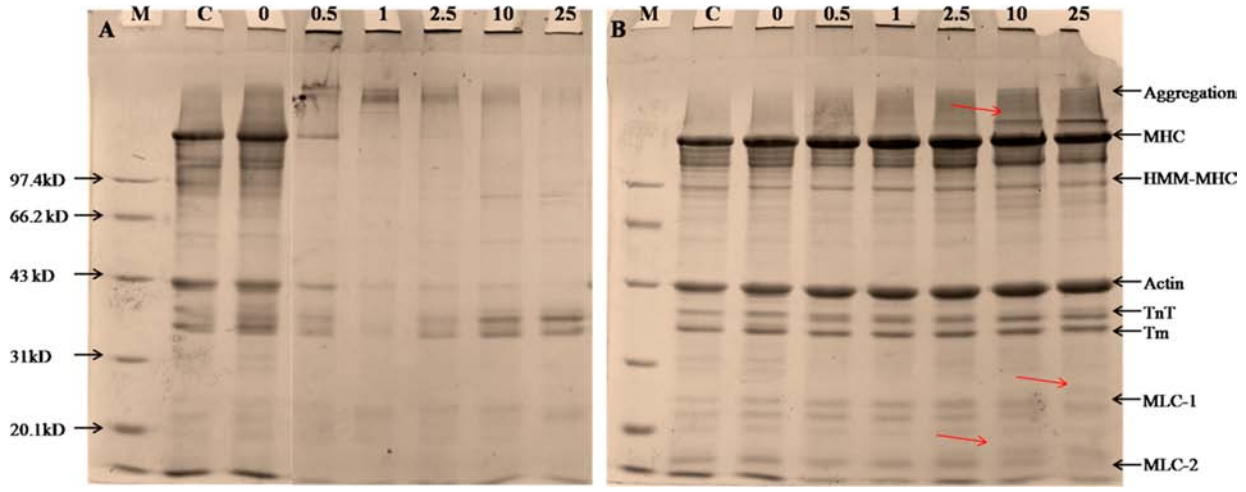


**Figure 3.** Representative SDS−PAGE patterns of the control and myofibrillar proteins oxidized by 100 $\mu$M $FeCl_3$/100 $\mu$M ascorbic acid/0−25 mM $H_2O_2$ (A) without and (B) with 5% $\beta$ ME. MHC, myosin heavy chain; HMM-MHC, heavy meromyosin−myosin heavy chain; TnT, troponin T; Tm, tropomyosin; MLC-1, myosin light chain-1; MLC-2, myosin light chain-2.


dx.doi.org/10.1021/jf502540p | J. Agric. Food Chem. 2014, 62, 9544−9552

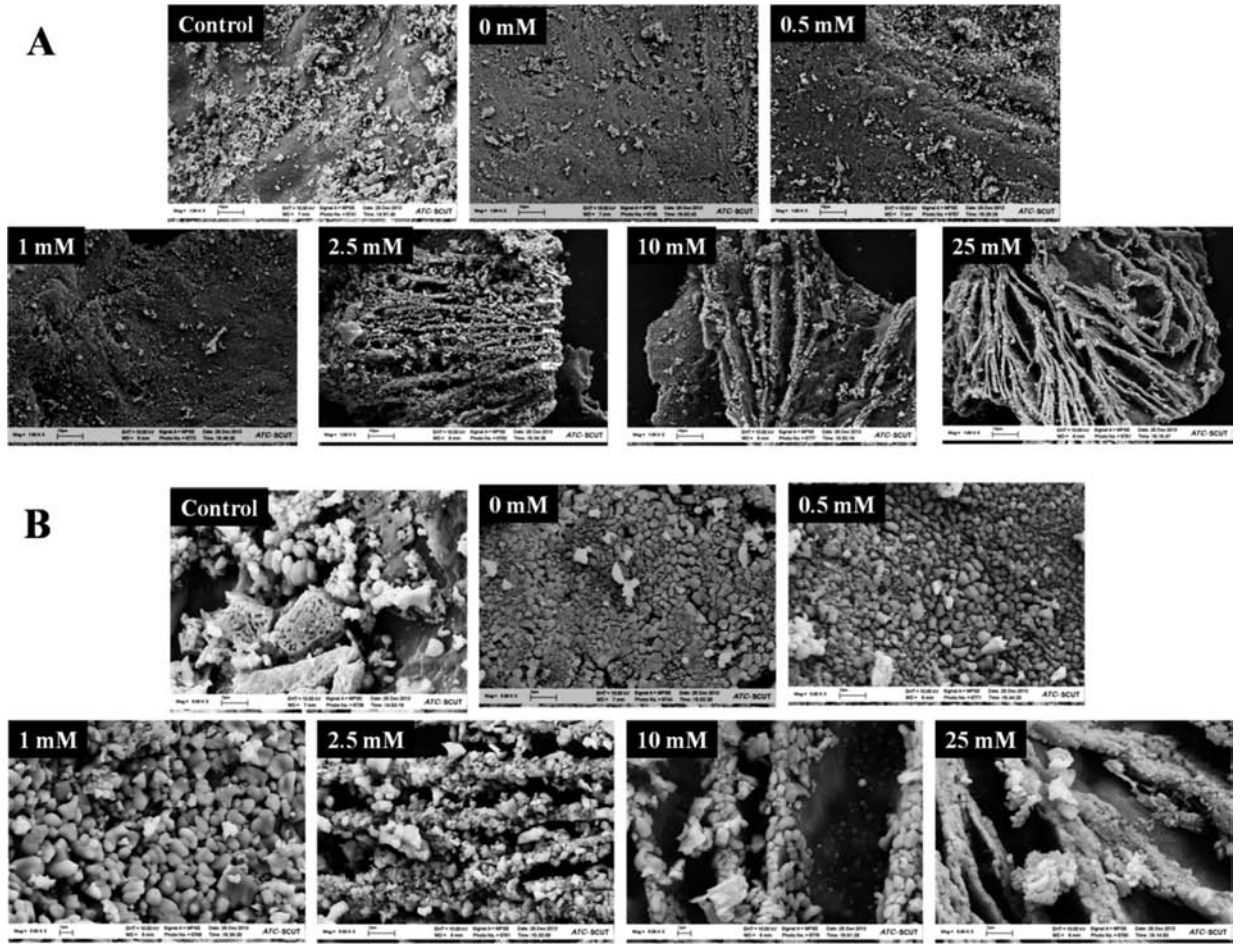


**Figure 4.** Scanning electron microscope micrographs at (A) ×1000 and (B) ×5000 magnification of the control and oxidized (100 $\mu$M $FeCl_3$/100 $\mu$M ascorbic acid/0−25 mM $H_2O_2$) myofibrillar proteins. Scale bars indicate (A) 10 $\mu$m and (B) 2 or 1 $\mu$m.

previously reported.[15,23] These covalent polymers, previously linked together by S−S (therefore too large to enter the stacking gel),[37] were present in those oxidized protein samples. In addition, new but hazy bands with molecular weight similar to MCL-1 and MCL-2 generated in samples treated with more than 2.5 mM of $H_2O_2$, suggesting the fragmentation or degradation of protein backbone under •OH attack, as has been previously reported by Berlett et al.,[36] which could contribute to the increase in protein surface hydrophobicity (Figure 1B).

*Microstructure.* The changes in the physicochemical properties of oxidized myofibrillar proteins were further investigated by the measurements of their morphologic properties. Microstructures of oxidized proteins under different $H_2O_2$ levels, in comparison with the control, are presented in Figure 4. For the control, protein appeared in an intactly dense and firm pattern with the heterogeneous surface (Figure 4, panels A and B). Compared to the control, the incubated protein sample (0 mM $H_2O_2$) showed a more flat surface with few visible pores (Figure 4A), which might be due to the unfolding and slight shrinkage of myofibrillar protein upon incubation.[38] Additionally, evenly distributed granular aggregates, which has been reported by Astruc et al.,[38] were also observed when further magnified (Figure 4B). For proteins with oxidants, at low $H_2O_2$ concentrations (0.5 and 1 mM), the surface microstructures of samples were not appreciably different despite the increasing roughness of overlapped surface (Figure 4A). Moreover, the increase in granular size of the aggregates (Figure 4B) well indicated the accelerated state of aggregation, in agreement with the results of surface hydrophobicity and mean particle size (Figures 1B and 2). When $H_2O_2$ concentrations were increased to higher levels (2.5−25 mM), it was noteworthy that an obvious morphological change was observed and this morphological transition occurred between 1 and 2.5 mM of oxidants. This trend was in accordance with changes in the data of protein surface hydrophobicity, mean particle size, and results revealed by SDS−PAGE (Figures 1B, 2, and 3). It was more likely that samples treated with 2.5 mM of oxidants, which underwent steric modifications, rendered the layered surface with discontinuous aggregates (Figure 4). The enlarged surface area thus resulted in the sudden increase in protein surface hydrophobicity (Figure 1B), which was also consistent with the results revealed by SDS−PAGE (Figure 3). When being further oxidized (10−25 mM $H_2O_2$), myofibrillar protein showed a surface with more wrinkles at a larger size (Figure 4). This suggested that higher levels of oxidation would further modify the protein surface properties and plausibly simultaneously involved protein reaggregation and degradation, as indicated by SDS−PAGE analysis (Figure 3).

**Binding of Aroma Compounds with Oxidized Myofibrillar Proteins.** On the basis of the characterization of oxidized proteins, we attempted to investigate the influence of structural changes of proteins on their binding ability with aroma compounds. Thus, the free percentages of each aroma


dx.doi.org/10.1021/jf502540p | J. Agric. Food Chem. 2014, 62, 9544−9552

compound in the headspace in the presence of myofibrillar protein at different oxidizing levels were determined, as shown in Figure 5. One hundred percent of free aroma compound

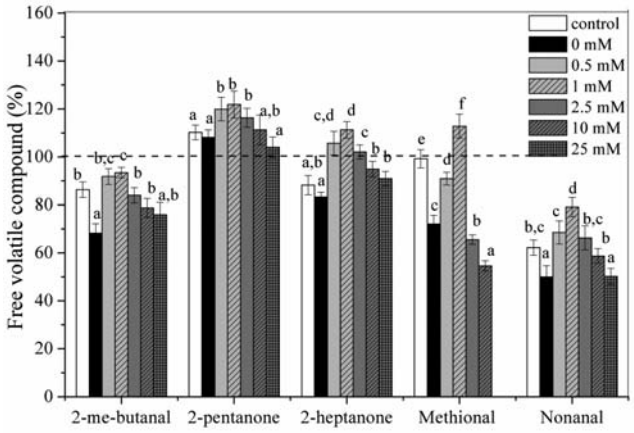


**Figure 5.** Effect of protein oxidation on the binding of aroma compounds. Results are expressed as percentage of free aroma compounds found in the headspace without protein in solution. Bars with different letters are significantly different ($p < 0.05$) among oxidation levels.

corresponds to the headspace concentration present in the control vial that does not contain protein.[10] As can be seen in Figure 5, the presence of the control protein produced a marked reduction of the percentages of free nonanal and a slight decrease of 2-methyl-butanal and 2-heptanone, suggesting that the control protein was able to bind those aroma compounds. In contrast, the increase in 2-pentanone implied its releasing behavior. These results were similar to that reported by Pérez-Juan et al.[2,10] Compared to the control, the incubated protein sample (0 mM $H_2O_2$) exhibited significantly lower percentages of 2-methyl-butanal, nonanal, and methional ($p < 0.05$), suggesting that thermal treatment could enhance the binding ability of protein toward them, which could be mainly attributed to the fact that the unfolding of actomyosin fibers after heating (37 °C) increased the sites available for hydrophobic binding.[10,31] For oxidized proteins, oxidation further affected the protein binding ability in a dose-dependent way. When the $H_2O_2$ added ranged from 0 to 1 mM, the percentages of all aroma compounds increased, indicating the decreased binding ability of protein. However, it was very interesting to note that, with the further increase in $H_2O_2$ concentration (>1 mM $H_2O_2$), an inverse effect on the percentages of aroma compounds was observed. As can be seen with increasing protein oxidation level, the percentages of all the selected aroma compounds decreased, implying the increased binding ability of protein toward them. Specifically, the percentages of free methional dramatically decreased with further oxidation (>1 mM $H_2O_2$) and even could not be detected when the highest concentration of $H_2O_2$ was added (25 mM).

As has been reported, the concentration of free aroma compounds in the gas phase largely depends on their interactions with protein, and changes in the protein conformation affect the interaction between aroma compounds and proteins due to the modification of the available protein binding sites.[3,39] As aforementioned, treatment with 0.5−1 mM of oxidants enhanced protein−protein interactions, mainly leading to the formation of protein aggregates and overlapped/reduced surface, as confirmed by SDS−PAGE and microstructure analysis (Figures 3 and 4). These changes (structural hindrance) impaired the affinity of the aroma compounds for the protein matrix by reducing the number of binding sites for the aroma compound[2] and thus decreased the binding ability of protein with all the selected aroma compounds (Figure 5). However, for protein treated with oxidants more than 2.5 mM, the binding ability of oxidized proteins toward the aroma compounds (especially for methional) increased (Figure 5). This could be explained by the remarkable increase in the protein surface hydrophobicity and modified protein surface properties (wrinkled surfaces) within the oxidant range (Figures 1B and 4), which might contribute to the interaction between protein and these compounds mainly driven by hydrophobic forces, thus enhancing the corresponding binding ability (Figure 5).

**Interactions between Oxidized Proteins and Methional.** Fluorescence spectroscopy is commonly used to study the binding between protein and small molecules, and fluorescence quenching refers to any process that decreases the fluorescence intensity of a sample.[40−42] A variety of mechanisms can cause quenching, such as excited state reaction, molecular rearrangement, energy transfer, ground state complex formation, and collision quenching.[40,43] Since myofibrillar proteins have tryptophan (Trp) residues that possess intrinsic fluorescence, the interaction mechanisms between myofibrillar proteins and aroma compounds could be further studied by the fluorescence quenching method. In the present work, we have demonstrated that oxidation-induced structural changes could markedly influence the protein binding ability with aroma compounds (Figure 5), especially for methional. Thus, methional was first selected as a model aroma compound, and the interaction between oxidized myofibrillar proteins and methional in the aqueous phase was subsequently investigated using fluorescence quenching studies (Figure 6). Figure 6A displays the example of fluorescence emission spectra of oxidized myofibrillar protein (25 mM $H_2O_2$) with various concentrations of methional. The fluorescence spectra of control and other oxidized protein (0−10 mM $H_2O_2$) samples in the presence of methional were also measured (data not shown). Evidently, the oxidized protein alone exhibited a strong fluorescence emission at 330 nm following an excitation at 283 nm. With the increasing of methional, a gradual attenuation of the fluorescence intensity of oxidized protein was observed (Figure 6A). Under the experimental conditions, methional revealed no fluorescence emission in the range of 300−400 nm, which did not affect protein intrinsic fluorescence. Thus, it could be concluded that there was interactions between oxidized myofibrillar protein (25 mM $H_2O_2$) and methional, in agreement with the results of protein binding ability with aroma compounds (Figure 5).

To further discern the influence of protein oxidation on fluorescence quenching mechanism, Stern−Volmer eq 2 was used for data analysis, and the corresponding results fitted from Stern−Volmer plots (Figure 6B) are summarized in Table 1. As shown in Table 1, the Stern−Volmer quenching constant $K_{SV}$ varied among the oxidized protein samples. Compared to the control, the $K_{SV}$ value of the incubated protein sample (0 mM $H_2O_2$) significantly ($p < 0.05$) increased, in agreement with its enhanced binding ability with methional (Figure 5), which might be related to the increased surface hydrophobicity (Figure 1B). For oxidized proteins, with the low addition of


dx.doi.org/10.1021/jf502540p | J. Agric. Food Chem. 2014, 62, 9544−9552

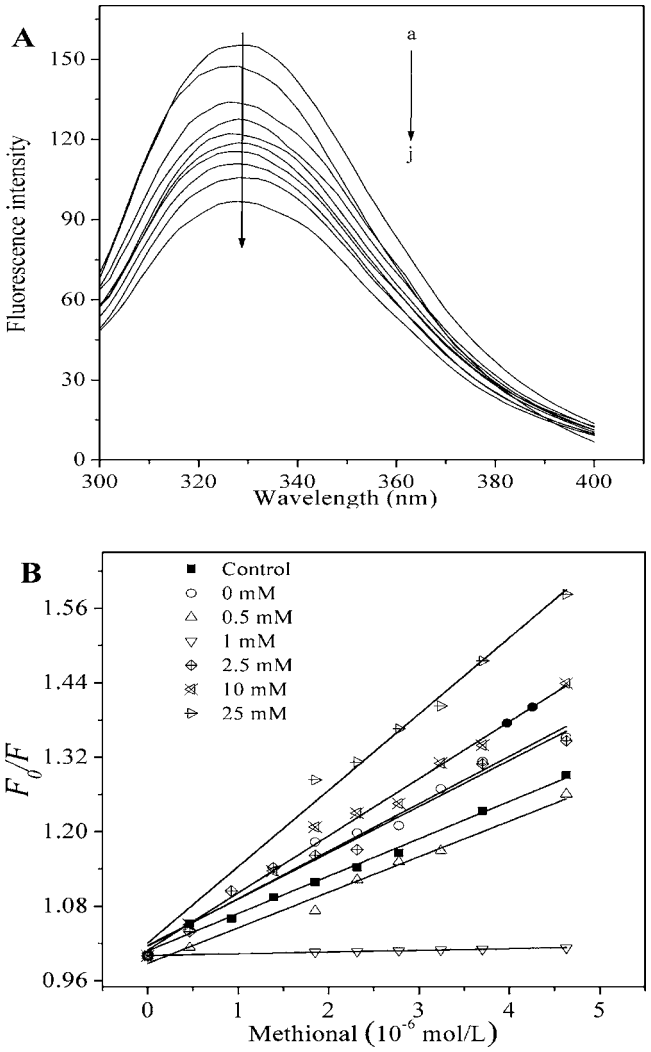


**Figure 6.** (A) Example of fluorescence emission spectra of oxidized myofibrillar protein (25 mM $H_2O_2$) with various amounts of methional in 20 mM phosphate buffer B containing 0.5 M NaCl at pH 6.0: (a) 0.8 mg/mL oxidized protein alone; (b–j) 0.8 mg/mL oxidized protein with 0.05, 0.1, 0.15, 0.2, 0.25, 0.30, 0.35, 0.40, and 0.50 ppm methional, respectively. (B) Stern–Volmer plots describing fluorescence quenching of the control and oxidized proteins at different levels in the presence of methional.

oxidants (0–1 mM $H_2O_2$), the values of $K_{SV}$ dramatically decreased. However, upon the further increase of oxidant concentration (2.5–25 mM $H_2O_2$), an obvious increase in the $K_{SV}$ values was observed when compared to that of the control. This result perfectly matched the general trends seen in the data of surface hydrophobicity (Figure 1B) and protein binding ability with aroma compounds (Figure 5), further implying the interesting influence of protein oxidation on the protein binding reaction with aroma compounds. Furthermore, all the values of $k_q$ calculated (Table 1) were much higher than the maximum value for diffusion-controlled quenching in water ($\sim 10^{10}$ $M^{-1}$ $s^{-1}$), signifying the possible quenching mechanism for control and oxidized protein fluorescence by methional is a static type.[28,40] These results indicated that the methional may bind with hydrophobic sites of protein, forming the protein–aroma compound complex. This is in agreement with previous studies, which have reported that hydrophobic binding of flavor

**Table 1. Stern–Volmer Quenching Constants for the Binding of Methional by Myofibrillar Proteins at Different Oxidation Levels**

| $H_2O_2$ | $K_{sv}$[a] ($\times 10^4$ $M^{-1}$) | $k_q$ ($\times 10^{12}$ $M^{-1}$ $s^{-1}$) | $R^2$ |
|---|---|---|---|
| control | 6.02 ± 0.19[c] | 6.02 ± 0.19[c] | 0.992 |
| 0 mM | 7.65 ± 0.53[d] | 7.65 ± 0.53[d] | 0.972 |
| 0.5 mM | 5.73 ± 0.30[c] | 5.73 ± 0.30[c] | 0.983 |
| 1 mM | 0.28 ± 0.01[b] | 0.28 ± 0.01[b] | 0.989 |
| 2.5 mM | 7.45 ± 0.45[d] | 7.45 ± 0.45[d] | 0.975 |
| 10 mM | 9.20 ± 0.34[e] | 9.20 ± 0.34[e] | 0.989 |
| 25 mM | 12.29 ± 0.56[f] | 12.29 ± 0.56[f] | 0.988 |

[a]The mean value of three independent experiments with standard deviation (SD). [b]Means in the same column with different superscript letters are significantly different ($p < 0.05$). [c]Means in the same column with different superscript letters are significantly different ($p < 0.05$). [d]Means in the same column with different superscript letters are significantly different ($p < 0.05$). [e]Means in the same column with different superscript letters are significantly different ($p < 0.05$). [f]Means in the same column with different superscript letters are significantly different ($p < 0.05$).

compounds by food proteins could lead to the formation protein–aroma compound complex.[42]

On the basis of the above analysis, we can conclude that the oxidative system applied could either increase or decrease the binding ability of aroma compounds with myofibrillar proteins, depending on the structural changes, especially the surface modifications of protein under oxidative stress. Specifically, treatment with low oxidant concentration (0.5–1 mM $H_2O_2$) mainly decreased protein surface hydrophobicity due to the formation of aggregates and the subsequent refolding of protein surface structure (Figures 1B, 3, and 4). This led to the reduction of the affinity of the aroma compounds for the protein matrix and thus the decreased binding ability with all aroma compounds selected (Figure 5). However, treatment with oxidant over 2.5 mM further aggregated the protein and at the same time remarkably modified protein surface properties (Figures 3 and 4), which dramatically enhanced protein surface hydrophobicity (Figure 1B). This resulted in the increased binding ability of protein with aroma compounds (especially for methional) (Figure 5) mainly driven by hydrophobic interaction, forming the protein–aroma compound complex, as evidenced by fluorescence quenching (Figure 6). In addition, considering the real meat system, the link between protein structure and flavor binding is not straightforward. However, in view of all these present results, it could be speculated that there is a clear correlation between protein structure modified by hydroxyl radical-induced oxidative system and its aroma binding ability.

In summary, this study clearly showed that the protein binding ability with aroma compounds was correlated with its structural changes, which was found to be strongly influenced by the hydroxyl radical-induced oxidative modifications. Incubation with low oxidant concentration (0.5–1 mM $H_2O_2$) mainly accelerated the aggregation and thus decreased protein surface hydrophobicity, reducing the binding ability with aroma compounds, while the presence of higher oxidant concentrations (>2.5 mM $H_2O_2$) would cause the protein reaggregation and partial degradation, and thus the subsequent modification of protein surface properties. The aggregated protein with wrinkled surfaces largely favored the binding with aroma compounds (especially for methional) mainly driven by hydrophobic interaction, forming the protein–aroma com-


dx.doi.org/10.1021/jf502540p | J. Agric. Food Chem. 2014, 62, 9544–9552

pound complex. These findings provided interesting correlation between protein structure and its aroma binding ability and are critical for the food industry to manufacture meat-flavored foods with myofibrillar protein that underwent oxidative stress.

## AUTHOR INFORMATION


### Corresponding Author

*E-mail: fewzhsun@scut.edu.cn. Tel/Fax: +86 20 22236089.



### Funding

This work was supported by the National Natural Science Foundation of China (Grant 31201387), the Natural Science Foundation of Guangdong Province (Grant S2012040007533), and the Doctoral Fund of Ministry of Education of China (Grant 20120172120017).


### Notes

The authors declare no competing financial interest.

## ACKNOWLEDGMENTS


The assistance provided by Dr. Zhi-Li Wan is gratefully acknowledged and appreciated.


## REFERENCES


(1) Robbins, K.; Jensen, J.; Ryan, K.; Homco-Ryan, C.; McKeith, F.; Brewer, M. Consumer attitudes towards beef and acceptability of enhanced beef. *Meat Sci.* **2003**, *65*, 721−729.

(2) Pérez-Juan, M.; Flores, M.; Toldrá, F. Model studies on the efficacy of protein homogenates from raw pork muscle and dry-cured ham in binding selected flavor compounds. *J. Agric. Food Chem.* **2006**, *54*, 4802−4808.

(3) Gianelli, M. P.; Flores, M.; Toldrá, F. Interactions of soluble peptides and proteins from skeletal muscle on the release of volatile compounds. *J. Agric. Food Chem.* **2003**, *51*, 6828−6834.

(4) Guichard, E. Interactions between flavor compounds and food ingredients and their influence on flavor perception. *Food Rev. Int.* **2002**, *18*, 49−70.

(5) Fischer, N.; Widder, S. How proteins influence food flavor: The chemistry of flavor interactions. *Food Technol.* **1997**, *51*, 68−70.

(6) Gianelli, M. P.; Flores, M.; Toldrá, F. Interaction of soluble peptides and proteins from skeletal muscle with volatile compounds in model systems as affected by curing agents. *J. Agric. Food Chem.* **2005**, *53*, 1670−1677.

(7) Landy, P.; Druaux, C.; Voilley, A. Retention of aroma compounds by proteins in aqueous solution. *Food Chem.* **1995**, *54*, 387−392.

(8) Relkin, P.; Fabre, M.; Guichard, E. Effect of fat nature and aroma compound hydrophobicity on flavor release from complex food emulsions. *J. Agric. Food Chem.* **2004**, *52*, 6257−6263.

(9) Damodaran, S.; Kinsella, J. E. Binding of carbonyls to fish actomyosin. *J. Agric. Food Chem.* **1983**, *31*, 856−859.

(10) Pérez-Juan, M.; Flores, M.; Toldrá, F. Binding of aroma compounds by isolated myofibrillar proteins: Effect of protein concentration and conformation. *Food Chem.* **2007**, *105*, 932−939.

(11) Lund, M. N.; Heinonen, M.; Baron, C. P.; Estevez, M. Protein oxidation in muscle foods: A review. *Mol. Nutr. Food. Res.* **2011**, *55*, 83−95.

(12) Zhang, W.; Xiao, S.; Ahn, D. U. Protein oxidation: Basic principles and implications for meat quality. *Crit. Rev. Food Sci. Nutr.* **2013**, *53*, 1191−1201.

(13) Davies, K. Protein damage and degradation by oxygen radicals. I. general aspects. *J. Biol. Chem.* **1987**, *262*, 9895−9901.

(14) Jongberg, S.; Skov, S. H.; Tørngren, M. A.; Skibsted, L. H.; Lund, M. N. Effect of white grape extract and modified atmosphere packaging on lipid and protein oxidation in chill stored beef patties. *Food Chem.* **2011**, *128*, 276−283.

(15) Xiong, Y. L.; Park, D.; Ooizumi, T. Variation in the cross-linking pattern of porcine myofibrillar protein exposed to three oxidative environments. *J. Agric. Food Chem.* **2008**, *57*, 153−159.

(16) Zhou, F.; Zhao, M.; Zhao, H.; Sun, W.; Cui, C. Effects of oxidative modification on gel properties of isolated porcine myofibrillar protein by peroxyl radicals. *Meat Sci.* **2014**, *96*, 1432−1439.

(17) Zhou, F.; Zhao, M.; Su, G.; Cui, C.; Sun, W. Gelation of salted myofibrillar protein under malonaldehyde-induced oxidative stress. *Food Hydrocolloids* **2014**, *40*, 153−162.

(18) Sun, W.; Zhou, F.; Sun, D.-W.; Zhao, M. Effect of oxidation on the emulsifying properties of myofibrillar proteins. *Food Bioprocess Technol.* **2013**, *6*, 1703−1712.

(19) Martinaud, A.; Mercier, Y.; Marinova, P.; Tassy, C.; Gatellier, P.; Renerre, M. Comparison of oxidative processes on myofibrillar proteins from beef during maturation and by different model oxidation systems. *J. Agric. Food Chem.* **1997**, *45*, 2481−2487.

(20) Utrera, M.; Armenteros, M.; Ventanas, S.; Solano, F.; Estévez, M. Pre-freezing raw hams affects quality traits in cooked hams: Potential influence of protein oxidation. *Meat Sci.* **2012**, *92*, 596−603.

(21) Huang, L.; Xiong, Y. L.; Kong, B.; Huang, X.; Li, J. Influence of storage temperature and duration on lipid and protein oxidation and flavour changes in frozen pork dumpling filler. *Meat Sci.* **2013**, *95*, 295−301.

(22) Park, D.; Xiong, Y. L.; Alderton, A. L.; Ooizumi, T. Biochemical changes in myofibrillar protein isolates exposed to three oxidizing systems. *J. Agric. Food Chem.* **2006**, *54*, 4445−4451.

(23) Morzel, M.; Gatellier, P.; Sayd, T.; Renerre, M.; Laville, E. Chemical oxidation decreases proteolytic susceptibility of skeletal muscle myofibrillar proteins. *Meat Sci.* **2006**, *73*, 536−543.

(24) Oliver, C. N.; Ahn, B.-W.; Moerman, E. J.; Goldstein, S.; Stadtman, E. R. Age-related changes in oxidized proteins. *J. Biol. Chem.* **1987**, *262*, 5488−5491.

(25) Chelh, I.; Gatellier, P.; Santé-Lhoutellier, V. Technical note: A simplified procedure for myofibril hydrophobicity determination. *Meat Sci.* **2006**, *74*, 681−683.

(26) Flores, M.; Barat, J. M.; Aristoy, M.; Peris, M. M.; Grau, R.; Toldrá, F. Accelerated processing of dry-cured ham. Part 2. Influence of brine thawing/salting operation on proteolysis and sensory acceptability. *Meat Sci.* **2006**, *72*, 766−772.

(27) Sun, W.; Zhao, Q.; Zhao, H.; Zhao, M.; Yang, B. Volatile compounds of Cantonese sausage released at different stages of processing and storage. *Food Chem.* **2010**, *121*, 319−325.

(28) Lakowicz, J. R. *Principles of fluorescence spectroscopy*. Springer: New York, 2009.

(29) Traore, S.; Aubry, L.; Gatellier, P.; Przybylski, W.; Jaworska, D.; Kajak-Siemaszko, K.; Santé-Lhoutellier, V. Effect of heat treatment on protein oxidation in pig meat. *Meat Sci.* **2012**, *91*, 14−21.

(30) Sante-Lhoutellier, V.; Aubry, L.; Gatellier, P. Effect of oxidation on in vitro digestibility of skeletal muscle myofibrillar proteins. *J. Agric. Food Chem.* **2007**, *55*, 5343−5348.

(31) Wasserman, A. E. Thermally produced flavor components in the aroma of meat and poultry. *J. Agric. Food Chem.* **1972**, *20*, 737−741.

(32) Promeyrat, A.; Daudin, J.; Gatellier, P. Kinetics of protein physicochemical changes induced by heating in meat using mimetic models: (1) Relative effects of heat and oxidants. *Food Chem.* **2013**, *138*, 581−589.

(33) Pulford, D.; Fraga Vazquez, S.; Frost, D.; Fraser-Smith, E.; Dobbie, P.; Rosenvold, K. The intracellular distribution of small heat shock proteins in post-mortem beef is determined by ultimate pH. *Meat Sci.* **2008**, *79*, 623−630.

(34) Grune, T.; Jung, T.; Merker, K.; Davies, K. J. Decreased proteolysis caused by protein aggregates, inclusion bodies, plaques, lipofuscin, ceroid, and 'aggresomes' during oxidative stress, aging, and disease. *Int. J. Biochem. Cell Biol.* **2004**, *36*, 2519−2530.

(35) Ooizumi, T.; Xiong, Y. L. Biochemical susceptibility of myosin in chicken myofibrils subjected to hydroxyl radical oxidizing systems. *J. Agric. Food Chem.* **2004**, *52*, 4303−4307.

(36) Berlett, B. S.; Stadtman, E. R. Protein oxidation in aging, disease, and oxidative stress. *J. Biol. Chem.* **1997**, *272*, 20313−20316.

(37) Li, C.; Xiong, Y. L.; Chen, J. Oxidation-induced unfolding facilitates myosin cross-linking in myofibrillar protein by microbial transglutaminase. *J. Agric. Food Chem.* **2012**, *60*, 8020−8027.
(38) Astruc, T.; Gatellier, P.; Labas, R.; Lhoutellier, V. S.; Marinova, P. Microstructural changes in *m. rectus abdominis* bovine muscle after heating. *Meat Sci.* **2010**, *85*, 743−751.
(39) Landy, P.; Courthaudon, J.-L.; Dubois, C.; Voilley, A. Effect of interface in model food emulsions on the volatility of aroma compounds. *J. Agric. Food Chem.* **1996**, *44*, 526−530.
(40) Zhang, Y.; Zhong, Q. X. Binding between bixin and whey protein at pH 7.4 studied by spectroscopy and isothermal titration calorimetry. *J. Agric. Food Chem.* **2012**, *60*, 1880−1886.
(41) Wan, Z. L.; Wang, J. M.; Wang, L. Y.; Yang, X. Q.; Yuan, Y. Enhanced physical and oxidative stabilities of soy protein-based emulsions by incorporation of a water-soluble stevioside−resveratrol complex. *J. Agric. Food Chem.* **2013**, *61*, 4433−4440.
(42) Liu, X.; Powers, J. R.; Swanson, B. G.; Hill, H. H.; Clark, S. High hydrostatic pressure affects flavor-binding properties of whey protein concentrate. *J. Food Sci.* **2005**, *70*, C581−C585.
(43) Wan, Z. L.; Wang, J. M.; Wang, L. Y.; Yuan, Y.; Yang, X. Q. Complexation of resveratrol with soy protein and its improvement on oxidative stability of corn oil/water emulsions. *Food Chem.* **2014**, *161*, 324−331.

distributed in cytoplasm when uptaken into Caco-2 cells. The above studies suggest that soy protein nanoparticles have some unique qualities. However, much more studies are needed to find a convenient way to produce stable soy protein nanoparticles, to elucidate the mechanism of particles formation, and to illustrate their inner structure.

In this investigation, we explored the possibility to produce stable soy protein nanogels by heating soy protein dispersion at the critical pH point where it had the lowest polydispersity index. The *z*-average hydrodynamic diameter, polydispersity index, $\zeta$-potential, turbidity, and morphology were evaluated to characterize the nanogels. Their resistance to pH and ionic strength change was also investigated. Influence of heat load (temperature and time) on the stability of soy protein particles would be discussed. A possible mechanism of the nanogels formation was proposed. Soy protein nanogels produced in this study would be useful functional ingredients to modify the optical or rheological properties of food products, or to encapsulate and deliver bioactive ingredients.

## MATERIALS AND METHODS

**Materials.** Defatted soy flakes were purchased from Yuwang Group (Shangdong, China). Soy protein (94.2% protein (Kjeldahl, N × 6.25), 4.5% moisture, and 1.3% ash) was prepared from defatted soy flakes by the method described in this Article. BCA (bicinchoninic acid) protein assay kit and dithiothreitol (DTT) were purchased from Dingguo (Beijing, China). 1-Anilinonaphthalene-8-sulfonic acid (ANS) was purchased from Sigma-Aldrich (St. Louis, MO). Iodoacetamide was purchased from Aladdin Reagent Co., Ltd. (Shanghai, China). All other chemicals were of analytical reagent grade and obtained in China.

**Soy Protein Preparation.** Defatted soy flakes powder was mixed with 15-fold (in weight) deionized water, and the mixture (pH 6.8) was adjusted to pH 7.5 with 2.0 M NaOH. After being stirred for 2 h, the resulting suspension was centrifuged at 8000*g* for 20 min at 4 °C to remove the insoluble material. The pH of the supernatant then was adjusted to pH 4.5 with 2.0 M HCl, and the precipitate was collected by centrifugation at 8000*g* for 10 min at 4 °C. The precipitate was then redissolved with 5-fold (in weight) deionized water, and the pH was adjusted to 7.0 with 2.0 M NaOH. The neutral soy protein solution was dialyzed against deionized water at 4 °C for 48 h and then freeze-dried and stored at 4 °C until use.

**Soy Protein Dispersion Preparation.** The soy protein dispersion was prepared by dispersing soy protein powder in deionized water (1.1%, w/v) and stirring at 25 °C for 2 h. The soy protein dispersion was left for 12 h at 4 °C to allow complete hydration. Afterward, the dispersion was centrifuged at 10 000*g* for 15 min to remove insoluble matter. The protein concentration was analyzed using BCA assay. The protein concentration then was adjusted to 1% (w/v).

**Creation of Soy Protein Nanogels.** The pH of soy protein dispersion was modified to 2.6−7.0 by stepwise addition of 2.0 M HCl. Samples were withdrawn at different pH values for size and polydispersity index analysis. For producing nanogels, soy protein dispersion was adjusted to the pH (5.9) where the dispersion had the lowest polydispersity index and poured into 100 mL glass vials (with a screw-top and solid cap) and heated in a water bath without stirring at 95 °C for 30 min. After the heat treatment, samples were immediately cooled in ice water to 4 °C. Correspondingly, soy protein dispersion (pH 5.9) without heat was used as control. For the study of the effects of holding temperature on the stability of particles, soy protein dispersion (pH 5.9) was heated at 50−95 °C for 30 min (room temperature was 25 °C). For the study of the effects of holding time on stability of particles, soy protein dispersion (pH 5.9) was heated at 95 °C for 0−60 min. Samples were withdrawn at different temperatures and times for further analysis. It should be noted that the reported heating time zero did not take into account the preheating time needed to reach the selected final temperature (it would take a maximum of 6 min to reach 95 °C in this experiment).

**pH Stability of Soy Protein Nanogels.** The effects of pH on the properties of the protein nanogels prepared by heating protein dispersion (pH 5.9) at 95 °C for 30 min were measured by modifying the pH of the dispersions from 2.6 to 7.0. Samples without heat were used as control. For samples withdrawn from different temperatures and times, pH was adjusted to 7.0. Characteristics of particles in different pH were further analyzed.

**Salt Stability of Soy Protein Nanogels.** The effects of salt addition on the stability of the protein nanogels prepared by heating protein dispersion (pH 5.9) at 95 °C for 30 min was measured by adjusting the NaCl concentration of the dispersion from 0−200 mM. Samples without heat were used as control. For the samples withdrawn from different temperatures and times, NaCl concentration of dispersions was adjusted to 150 mM.

**Sedimentation Stability.** The stability of the samples to sedimentation after pH and NaCl concentration adjustment was recorded by taking photographs using a digital camera after they had been stored at 4 °C for 24 h.

**Particle Size, Polydispersity, and Surface Charge Measurements.** Protein dispersion was diluted to 0.1% (w/v) for particle size, polydispersity, and surface charge measurements using a commercial dynamic light scattering and microelectrophoresis device (Nano-ZS, Malvern Instruments, Worcestershire, UK). The particle size was reported as the *z*-average hydrodynamic diameter ($D_h$), polydispersity was reported as polydispersity index (PDI), while the particle surface charge was reported as the $\zeta$-potential. The $D_h$, PDI, and $\zeta$-potential were analyzed by Dispersion Technology Software (DTS) version 4.20 supplied by the manufacturer (Malvern Instruments Ltd.). PDI were calculated by the cumulant analysis method of the autocorrelation function. The autocorrelation function ($G(t)$) was calculated from the fluctuation of the scattered intensity with time: $\ln(G(t)) = a + bt + ct^2$. $t$ is the time (s), and $a$, $b$, and $c$ are terms of polynomial fit calculated. The polydispersity index was calculated from the ratio $2c/b^2$.

**Turbidity Measurement.** The turbidity of soy protein dispersions was determined by measuring the absorbance of the dispersions without dilution at $\lambda$ 500 nm using a UV−vis spectrophotometer (Genesys 10s, Thermo Fisher, America).

**Microscopic Observations.** Transmission electron microscopy (TEM) was used with the negative staining method. Observations were made with JEM-2100F transmission electron microscope operating at 200 kV (JEOL, Japan). A drop of sample was deposited onto a Formvar-carbon-coated copper grid, and excess of product was removed after 5 min using filter paper. The grid was dried at room temperature for 5 min. Phosphotungstic acid (1%) was then added for 5 min, with excess being removed as before. Samples (pH 5.9) with or without heat and the corresponding samples with pH adjusted to pH 2.6 and 7.0 were observed.

**Electrophoresis.** Reducing sodium dodecyl sulfate-polyacrylamide gel electrophoresis (SDS-PAGE) was performed on a discontinuous buffered system, using 12% separating gel and 5% stacking gel according to our previous method with minor modification.[24] Soy protein dispersion (pH 5.9) after heating at 95 °C for 30 min was adjusted to pH 6.4, 7.0, and 8.0. Then samples with and without pH adjustment were ultracentrifuged at 156 000*g* for 30 min, which was supposed to separate the protein particles and soluble proteins.[25] The supernatant and the sample without ultracentrifugation (pH 5.9 after heat) (250 $\mu$L) were then mixed with 250 $\mu$L of 0.06 M Tris−HCl buffer (pH 6.8), containing 2% (w/v) SDS, 25% (v/v) glycerol, 0.1% (w/v) bromophenol blue, and 5% (v/v) 2-mercaptoethanol (2-ME). Molecular weight marker made from rabbit phosphorglase B (97.4 kDa), bovine serum albumin (66.2 kDa), rabbit actin (43 kDa), bovine carbonic anhydrase (31 kDa), human growth hormone (22 kDa), and hen egg white lysozyme (14.4 kDa) was used as reference.

**Particle Size of Nanogels in Various Solvents.** To unravel the interactive forces involved in the formation and maintenance of the nanogels structure, the *z*-average hydrodynamic diameter of the soy protein nanogels in the presence of 8.0 M urea, 1% SDS, and 30 mM DTT, alone or in combinations, was also determined according to the

method described above. To unravel if the disulfide bonds were accessible, nanogels were first dispersed in 30 mM DTT; second, it was added with iodoacetamide to remove the DTT;[26] and finally SDS was added (final concentration 1%). The corresponding particle size of this nanogel dispersion was then measured. All solvents were prepared with 20 mM pH 8.0 Tris-HCl buffer.

**Sulfhydryl (SH) Group Content.** SH group content before and after heat treatment of soy protein dispersion at pH 5.9 was measured using Ellman's reagent.[27]

**Surface Hydrophobicity Measurement.** Surface hydrophobicity before and after heat treatment of soy protein dispersion was evaluated using ANS as the fluorescent probe according to the method of Alizadeh-Pasdar and Li-Chan.[28] Protein dispersion was diluted with 10 mM pH 7.0 sodium phosphate buffer. Fluorescent intensity was measured via a F7000 fluorescence spectrophotometer (Hitachi Co., Japan).

**Intrinsic Fluorescence of Tryptophan.** Intrinsic fluorescence of the tryptophan before and after heat treatment of soy protein dispersion was measured on a F7000 fluorescence spectrophotometer. Protein concentration was diluted to 0.002% with 10 mM sodium phosphate buffer (pH 7.0). Excitation and emission slits were set at 5 nm. The excitation wavelength was 295 nm to excite tryptophan. The emission spectra were recorded from 300 to 400 nm with a scan speed of 240 nm/min. Each spectrum was the average of two scans and corrected for a protein-free sample.

**Statistical Analysis.** Statistical calculations were performed using the statistical package SPSS 11.5 (SPSS Inc., Chicago, IL) for one-way ANOVA. Least-squares difference was used for comparison of mean values among treatments and to identify significant differences ($p < 0.05$) among treatments.

## RESULTS AND DISCUSSION

**Characteristics of Protein Particles before Heat Treatment.** The initial pH of soy protein dispersion was 7.0. As shown in Figure 1, when the pH decreased, there was no significant increase of particle size above pH 6.2. With the further decreased pH, the surface charge on the protein particle was neutralized, reducing the electrostatic repulsion between particles, which would induce protein aggregation. Therefore, at pH 6.2, particle size significantly increased, indicating the large particle formation. The particle size then increased gradually with a sudden increase at pH 5.7. Correspondingly, the PDI decreased gradually from 0.52, with a sudden decrease at pH 6.2, reaching the lowest at pH 6.0, 5.9, and 5.8, with the value below 0.1. After that, PDI began to increase. Therefore, in the pH range of 5.8−6.0, aggregation would lead to a relatively monodisperse protein particle distribution. The particle size was relatively large and the corresponding dispersion was translucent, but the dispersion was stable and homogeneous, without precipitation. However, protein particles formed at pH 5.8−6.0 were unstable with pH change, taking the particles formed at pH 5.9 as an example. Similar particle size and PDI distribution were observed when pH increased from 5.9 to 7.0, indicating a relatively reversible process. The appearance of the dispersion gradually became transparent (Figure 3A). The soy protein dispersion was unstable in the pH range of 3.5−5.5 as secondary aggregation of protein particles happened and the particles precipitated (Figure 3A). Under pH 3.5, protein precipitates were dissociated and the solution became transparent again (Figure 3A), but PDI was larger than 0.25 (data are no shown), indicating the relative poly dispersiveness of the protein dispersion.

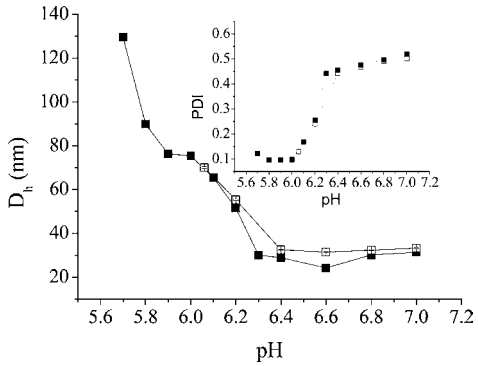


**Figure 1.** Effects of pH on the *z*-average hydrodynamic diameter and polydispersity index of soy protein dispersion before thermal treatment. pH was adjusted from 7.0 to 5.7 (■); from 5.9 to 7.0 (□).

**Characteristics of Protein Nanogels Made by Heat Treatment.** To make protein particles stable, thermal treatment was performed on soy protein dispersion of pH 5.9 under 95 °C for 30 min (the effects of changing the heating protocol are discussed later in this Article). This pH was supposed to make the largest production of stable particles within a narrow range of particle size as it had the lowest PDI. After heat treatment, the pH of the protein dispersion increased from 5.9 to 6.06, which might be the result of self-assembly of protein particle. The increase of pH after thermal treatment was also observed by Donato et al. when they heated dematerialized $\beta$-lactoglobulin solution at 70 and 85 °C under mild acidic pH conditions (pH 5.7−5.9).[8] The behavior of the heated soy protein particles was totally different from that without heat. In the pH range of 6.06−7.0, the particle size increased gradually with the increasing pH (Figure 2A). Surprisingly, the turbidity decreased with the increased particle size, while the PDI value was still very low and remained relatively constantly at about 0.1. This result excluded the possibility that the size changes were caused by the aggregation of the protein particle. Instead, the nanoparticles swelled with the increased pH, containing large amounts of water. It should be pointed out that swelling was the most important characteristic of nanogels.[4,5] Therefore, nanoparticles formed after heating in our study were deemed as nanogels. The appearance of the dispersion was still translucent in pH 7.0 (Figure 3B), indicating the irreversible change of protein particles after heating. In pH 5.9 and 5.8, the particle size, turbidity, and the PDI value increased, which was due to the aggregation of the protein particle. Precipitation of nanogels happened when the protein dispersion pH was in the range of 3.7−5.7 (Figure 3B), but these aggregates were redispersible when the dispersion pH was out of this range. In the pH 2.6−3.2, with the decreased pH, particle size at first decreased and then increased gradually (Figure 2B). The visual appearance of the dispersion was still translucent (Figure 3B). The PDI value decreased to 0.1 at pH 3.0 and remained constantly around 0.1 thereafter. Interestingly, in pH 2.6−3.0, the turbidity decreased with increased particle size. Therefore, nanogels were stable and would also swell in this pH range. The $\zeta$-potential was higher than that before heating when the pH increased from 6.06 to 7.0 (Figure 2C), indicating the redistribution of particle inner structure. The internal and external charge distribution of the aggregated proteins was optimized to promote the structuring of nanogels, resulting in more negatively charged residues exposing. The higher surface charge would contribute to the stability of the protein nanogels as the electrostatic repulsion between them was enhanced. In the pH range 2.6−3.2, the $\zeta$-potential was lower than that without heating. For the salt stability, precipitation occurred, when the ionic strength


dx.doi.org/10.1021/jf502572d | J. Agric. Food Chem. 2014, 62, 9553−9561

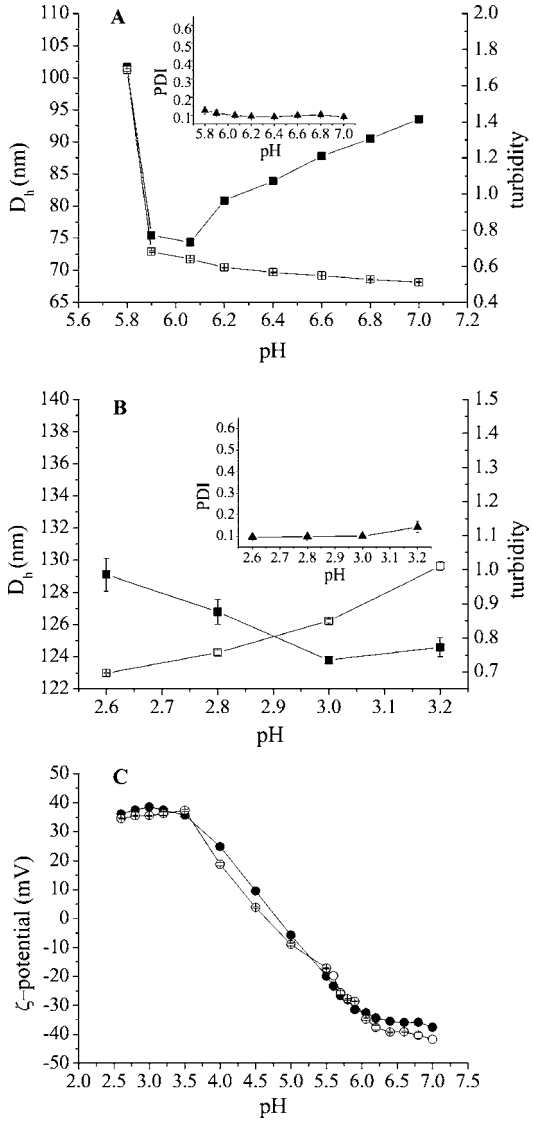


**Figure 2.** Effects of pH on the *z*-average hydrodynamic diameter (■), polydispersity index (▲), and turbidity (□) of soy protein dispersion after thermal treatment (A, pH 5.8−7.0; B, pH 2.6−3.2) and ζ-potential of particles (C) before (●) and after thermal treatment (○).

increased to 50 mM NaCl for protein dispersion (pH 5.9) without heat treatment (Figure 3C). After heat treatment, however, even the NaCl concentration increased to 200 mM, and no precipitation occurred (Figure 3D). When protein concentration increased from 1% to 5%, particle size and PDI would increase, but they still had pH and salt stability as well as swelling characteristics (see the Supporting Information).

To shed more light on the soy protein nanogels, the morphology of the soy protein particles was observed by TEM performed on selected samples. At pH 5.9 without heat, protein particles were mainly characterized by a spherical shape and exhibited a narrow range of apparent lengths (Figure 4B). When pH increased to 7.0 or decreased to 2.6, the number of spherical particles decreased, and some irregular particles were observed. They exhibited a wide range of apparent lengths. At pH 5.9 after heat, protein particles were still mainly characterized by a spherical shape and exhibited a narrow range of apparent lengths (Figure 4E). The spherical particles could still be found when pH increased to 7.0 or decreased to

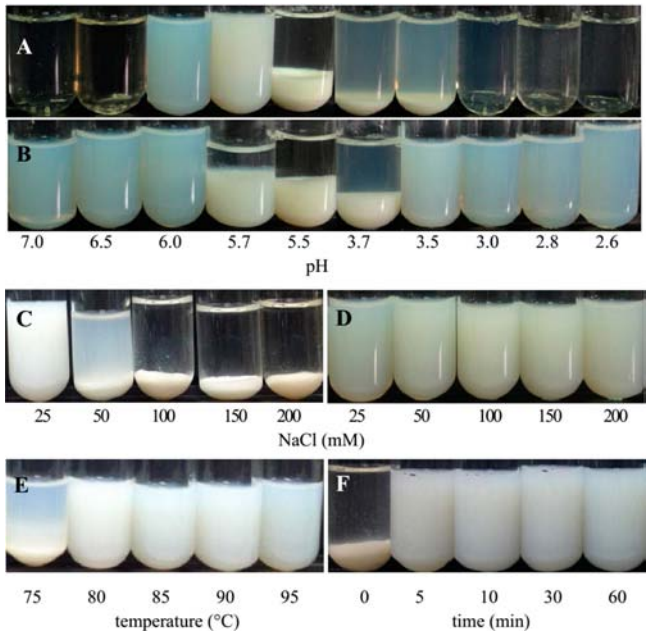


**Figure 3.** Influences of pH and NaCl concentration on the visual appearance of soy protein dispersion (pH 5.9) without (A,C) or with heating (B,D) at 95 °C for 30 min. Influence of holding temperature (for 30 min) on the salt stability (150 mM NaCl) of soy protein dispersion (E). Influence of holding time (under 95 °C) on the salt stability (150 mM NaCl) of soy protein dispersion (F).

2.6 and exhibited a narrow range of apparent lengths. Besides, the apparent lengths of protein particles were larger than that at pH 5.9, which might be the swelling of protein nanogels. These results were in accordance with particle size distribution characteristics at various pH values as described before. The observed particle size by TEM was different from the $D_h$, which might be due to the air-drying process and phosphotungstic acid addition.

All of the above observations led us to conclude that spherical soy protein nanogels with pH and salt stability as well as swelling characteristics were formed by heating soy protein dispersion (pH 5.9) under 95 °C for 30 min. Their stability was closely related to thermal treatment. Therefore, we further did some experiments on the influence of holding temperature and time on the stability of soy protein particles.

**Effect of Holding Temperature on the Protein Particle Stability.** As shown in Figure 5A, before the pH was adjusted to 7.0, there was a very little increase of particle size at 50 °C. Thereafter, particle size decreased gradually from 65 °C, reached the lowest at 80 and 85 °C, and subsequently increased at 90 °C. The turbidity observed almost a similar trend (Figure 5B). Around pH 6.0, the onset denaturation temperature in deionized water is about 85 °C of soy glycinin and 65 °C for β-conglicinin.[21] Therefore, the decrease of particle size was supposed to relate to the denaturation of soy β-conglicinin. The increase of particle size after 85 °C was supposed to relate to the denaturation of glicinin. PDI value was relatively constant around 0.1 (Figure 5C). The ζ-potential increased significantly after 60 °C (Figure 5D). Thus, higher temperature contributed to the exposing of negative charge residues. After the pH of the protein dispersion was adjusted to 7.0, both particle size and turbidity increased with the holding temperature. Before 70 °C, particle size was smaller and PDI value was significantly higher than that before pH adjustment, proving the dissociation of


dx.doi.org/10.1021/jf502572d | J. Agric. Food Chem. 2014, 62, 9553−9561

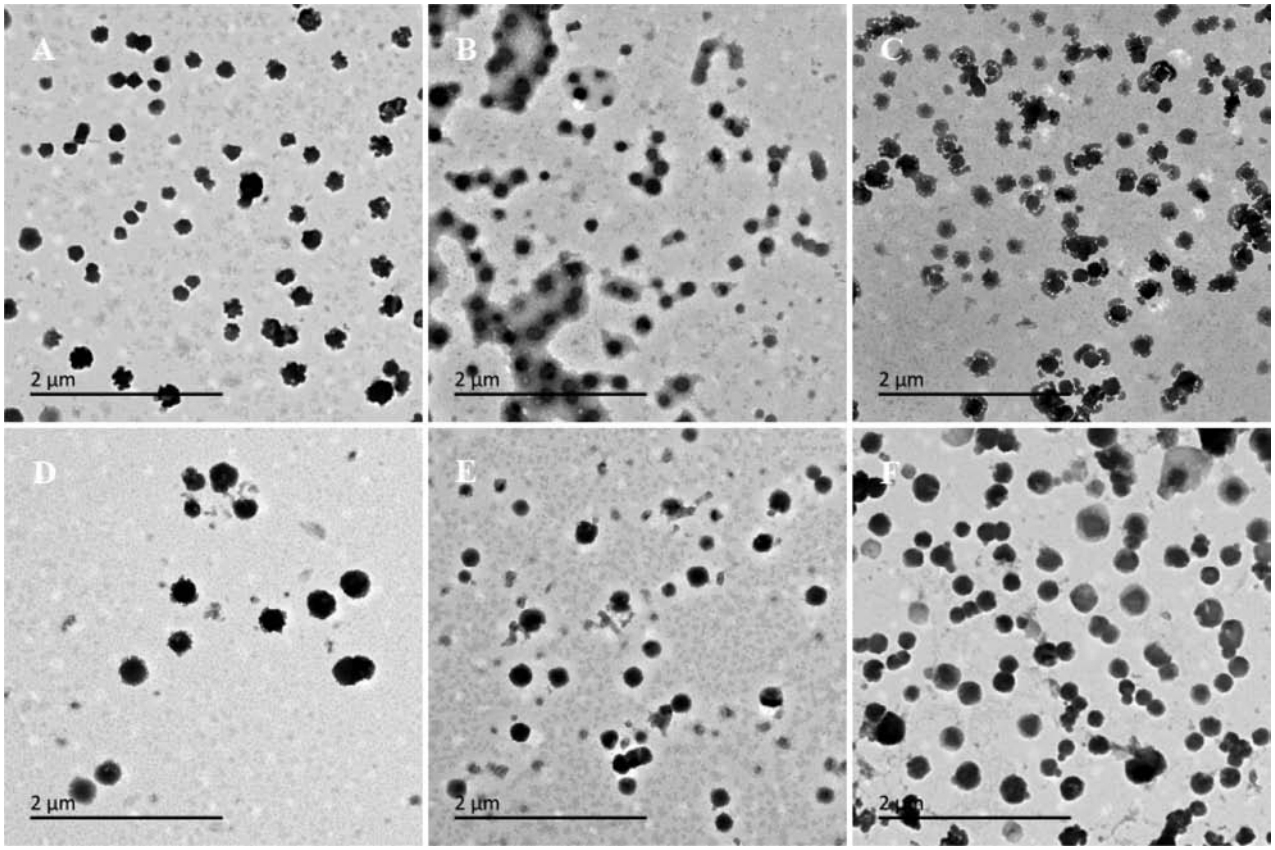


**Figure 4.** TEM negative-staining micrographs of soy protein dispersions (pH 5.9) without heat: pH adjusted to 2.6 (A), not adjusted (pH 5.9) (B), adjusted to 7.0 (C); and the corresponding heat treated dispersion with pH adjusted to pH 2.6 (D), not adjusted (pH 5.9) (E), and adjusted to 7.0 (F). The scale bar represents 2 $\mu$m.

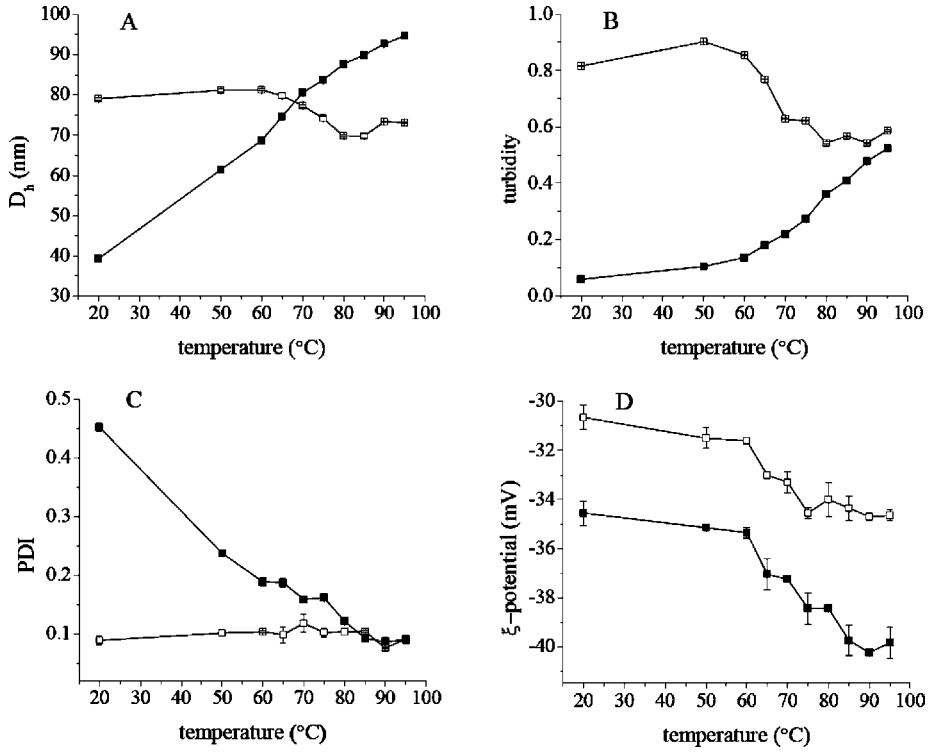


**Figure 5.** Effects of holding temperature (30 min) on the *z*-average hydrodynamic diameter (A), turbidity (B), polydispersity index (C), and $\zeta$-potential (D) of protein particles. Open squares (□) represent the protein dispersion at pH 5.9, while the solid squares (■) represent the protein dispersion with pH adjustment to 7.0.


dx.doi.org/10.1021/jf502572d | *J. Agric. Food Chem.* 2014, 62, 9553−9561

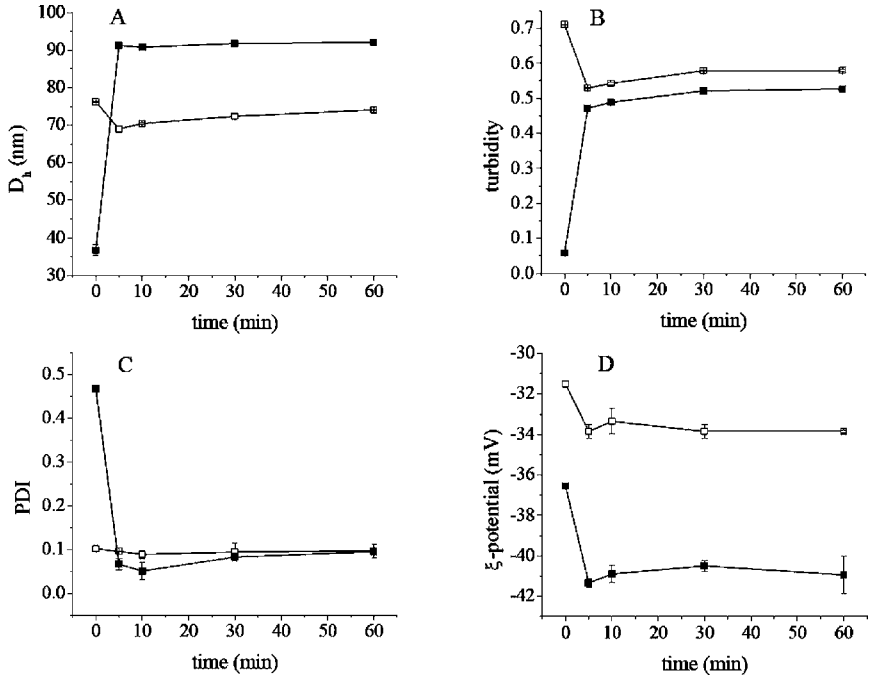


**Figure 6.** Effects of holding time at 95 °C on the *z*-average hydrodynamic diameter (A), turbidity (B), polydispersity index (C), and ζ-potential (D) of protein particles. Open squares (□) represent the protein dispersion at pH 5.9, while the solid squares (■) represent the protein dispersion with pH adjustment to 7.0.

particles. After 70 °C, protein particles gradually swelled as the particle size increased but turbidity decreased. Therefore, the denaturation of β-conglicinin might have induced the swelling of protein particles. Yet before 85 °C, the particle was unstable, as the PDI value increased after pH adjustment. The surface charges of all samples after pH adjustment were larger than those before and increased more noticeably for sample after heating above 80 °C. When the ionic strength of the protein dispersion was adjusted to 150 mM, the above 75 °C treated samples did not precipitate after 24 h (Figure 3E). The above observations indicated that the denaturing of soy glycinin was crucial for the formation of stable soy protein nanogels.

**Effect of Holding Time on the Protein Particle Stability.** As shown in Figure 6A, before the pH was adjusted to 7.0, particle size decreased significantly at 5 min, then increased mildly within the 60 min. It has been proved by many investigations that β-conglycinin could prevent thermal aggregation of glycinin.[29,30] This explained the limited increasing of particle size as the time increased. Correspondingly, turbidity decreased remarkably at 5 min, and then mildly increased as the time increased (Figure 6B). The PDI value was still constantly around 0.1 (Figure 6C). The ζ-potential increased significantly after heating for 5 min, and remained relatively constant thereafter (Figure 6D). When the pH was adjusted to 7.0, the particle size of samples without heat treatment decreased significantly, while that with heat treatment increased remarkably and remained relatively constant as the time increased. The turbidity of the control sample decreased significantly and became transparent, while that of the thermal treated sample decreased mildly. For dispersion without heat treatment, the PDI increased from 0.1 to 0.47 after pH adjustment, proving the dissociation of particles, while that of the thermal treated sample still remained at a constant value around 0.1. The ζ-potential of all samples increased after pH adjustment, while that of samples with heat treatment increased more significantly than the control. This indicated that after heat treatment, more negatively charged residues were exposed. All of the above observations indicated that nanogels began to form after 5 min under 95 °C. Besides, the increase of particle size, surface charge, and the decrease of turbidity after 5 min were relatively constant, indicating that when soy protein nanogels formed, their swelling capacity under a certain pH was constant regardless of heating time. When ionic strength increased to 150 mM NaCl, the protein dispersion without heat treatment precipitated; however, after heat treatment even for 5 min, no precipitation occurred (Figure 3F). The above observation proved that the stable nanogels formed within a very short time at 95 °C. Yet it should be pointed out that with the further increased time to 5 h, the stability of nanogels was disturbed and precipitation occurred.

**Structure Characteristics of Soy Protein Nanogels.** Before ultracentrifugation, reducing SDS-PAGE (Figure 7) observed all of the main subunits of soy protein (lane 5). However, after ultracentrifugation (lane 4), only small amounts of α′, α, acid polypeptides, and some lower molecular fraction were still remaining in the supernatant, indicating that all of the basic poly peptides, β subunits, and most of the α′/α subunits, acid polypeptides took part in the formation of nanogels. When pH increased (lanes 1−3), the content of α′, α, and acid polypeptides in the supernatant increased, indicating that these free α′, α, and acid polypeptides might locate on the surface of the nanogels. They might interact with the nanogels through electrostatic interaction so when the electrostatic repulsion force increased, some of them were "pealed" from the surface. This result was in accordance with Chen et al.[25] Besides, α′/α subunits have an extension region that has been proved to limit the aggregation of soy protein.[31] They located on the surface of the nanogels so that the size of the nanogels was relatively constant despite heating time as indicated formerly (Figure


dx.doi.org/10.1021/jf502572d | J. Agric. Food Chem. 2014, 62, 9553−9561

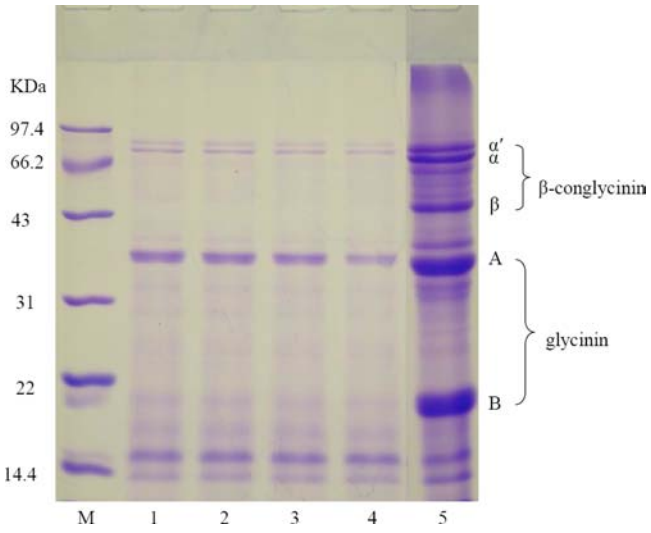


**Figure 7.** Electrophoretic patterns of soy protein nanogels and supernatant protein fraction of different pH nanogels dispersion after ultracentrifugation. Lane M: marker proteins. Lanes 1, 2, and 3 represent supernatant protein fraction in pH 8.0, 7.0, and 6.4 protein dispersions by adjusting the pH of initial nanogels dispersion (pH 6.06). Lane 4 represents the supernatant protein fraction in the initial soy nanogels dispersion. Lane 5 represents the protein electrophoretic pattern of the initial nanogels dispersion. Soy protein constituents: $\alpha'$, $\alpha$, and $\beta$ represent subunits for $\beta$-conglycinin; A and B represent the acidic and basic polypeptides for glycinin.

6A). When heated above 80 °C, both $\beta$-conglicinin and glicinin unfolded and dissociated into monomers (polypeptides).[32] The hydrophobic residues exposed and induced the aggregation. In soy protein, basic polypeptides are highly hydrophobic and would preferentially interact with $\beta$ subunits.[32] On the other hand, basic polypeptides have an isoelectric point around 8.0–8.5,[33] while other subunits ($\alpha'$, $\alpha$, $\beta$, and acid polypeptides) have isoelectric points around 4.0–5.5.[34] Therefore, in the pH range 6.06–7.0, basic polypeptides were positively charged and others were negatively charged. Combined with the increased surface charge after heating, it was reasonable to propose that the positively charged basic polypeptides together with $\beta$ subunits were buried and located in the core of the nanogels, forming the hydrophobic core, while highly negatively charged $\alpha'$, $\alpha$, and acid polypeptides were located on the surface of the nanogels as they were relatively more hydrophilic.[31,35] This kind of core–shell model has also been proposed by Ren et al. when they studied the protein particle formation mechanism in defatted soymilk.[36]

Association of monomers was mainly driven by hydrophobic interaction. After the hydrophobic aggregation, there were still some hydrophobic residues exposed that increased the surface hydrophobicity of nanogels (Table 1). The red shift of $\lambda_{max}$ for tryptophan residues further confirmed the exposure of hydrophobic residues to a more polar environment (Table 1), although it was not significantly different in value. The disulfide bonds between different subunits formed during the heating process as SH decreased significantly (Table 1). To further elucidate the definite inner force stabilizing the nanogels, nanogels were dispersed in various kinds of protein-perturbing solvents, and the particle size was measured. As shown in Figure 8, 30 mM DTT alone could not dissociate

**Table 1. Surface Hydrophobicity ($S_0$), $\lambda_{max}$ of Tryptophan Residues, and Sulfhydryl (SH) Content of Soy Protein (pH 5.9) before and after Heating[a]**

| samples | $S_0 \times 10^3$ | $\lambda_{max}$ (nm) | SH (nmol/mg) |
|---|---|---|---|
| pH 5.9 | 91.13 ± 1.22 a | 337.5 ± 0.14 a | 5.19 ± 0.18 a |
| heat–pH 5.9 | 167.82 ± 11.4 b | 338.7 ± 0.15 a | 3.25 ± 0.07 b |

[a]Values in the same column followed by different letters are of significant difference ($p < 0.05$).

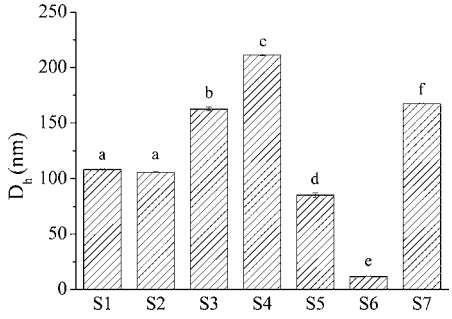


**Figure 8.** Effects of various protein-perturbing solvents on the *z*-average hydrodynamic diameter of nanogels. S1, 20 mM pH 8.0 Tris-HCl buffer; S2, 30 mM DTT; S3, 1% SDS; S4, 8.0 M urea; S5, urea +DTT; S6, SDS+DTT; S7, iodoacetamide was added into nanogels dispersion in S2 to remove the DTT first and then SDS was added. Different letters represent significant difference ($p < 0.05$).

the nanogels. In the 1% SDS and 8 M urea, the particle size increased significantly. This might be that the nanogels were unfolded by SDS and urea, which could disturb the hydrophobic interaction and hydrogen bonds, respectively. Yet they still could not dissociate the nanogels into smaller particles. However, when nanogels were dispersed in SDS and urea solution combined with DTT, the particle size decreased significantly, especially for that of SDS and DTT solution. These results indicated that the inner structure of nanogels had a disulfide bonds cross-linked "skeleton". These disulfide bonds play a crucial role in the stability of nanogels. They were inaccessible without the destroying of hydrophobic interaction as when DTT was removed by iodoacetamide, and addition of SDS could not dissociate the particles. Therefore, hydrophobic interaction was also very important in the formation of nanogels. As compared to hydrophobic interaction and disulfide bonds, hydrogen bonds seemed to play a relatively minor role in the stabilization of the nanogels structure. This kind of structure might be related to the pH and salt stability of the nanogels. According to the above discussion, the proposed model of the soy protein nanogels formation pathway was illustrated in Figure 9.

In conclusion, soy protein nanogels with a hydrophobic core and a hydrophilic shell have been made successfully by a simple

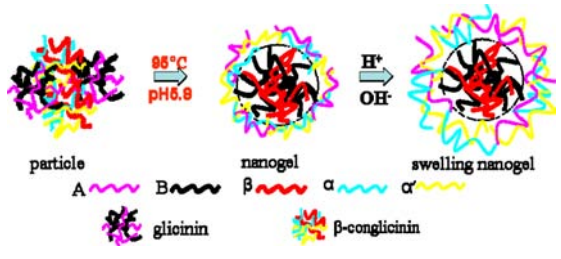


**Figure 9.** Diagrammatic depiction of soy protein nanogels formation.


dx.doi.org/10.1021/jf502572d | J. Agric. Food Chem. 2014, 62, 9553–9561

thermal process under a certain pH value. They are resistant to pH and ionic strength change. They will swell when the electrostatic repulsion force is large enough. Further work will be carried out to explore their inner structure with other technology as well as their functionality.

## ■ ASSOCIATED CONTENT

### Supporting Information

Figures 1S, 2S, and 3S showing the influence of protein concentration on the particle size, PDI, and salt stability of nanogels, respectively. This material is available free of charge via the Internet at http://pubs.acs.org.

## ■ AUTHOR INFORMATION


### Corresponding Author

*Tel./fax: +86 20 87113914. E-mail: femmzhao@scut.edu.cn.



### Funding

This work was supported by the National High Technology Research and Development Program of China (863 Program) (no. 2013AA102201), the National Natural Science Foundation of China (no. 31171783), and the Fundamental Research Funds for the Central Universities (2013ZB0017).


### Notes

The authors declare no competing financial interest.

## ■ REFERENCES


(1) Jones, O. G.; McClements, D. J. Functional biopolymer particles: design, fabrication, and applications. *Compr. Rev. Food Sci. Food Saf.* **2010**, *9*, 374−397.

(2) Jones, O. G.; McClements, D. J. Recent progress in biopolymer nanoparticle and microparticle formation by heat-treating electrostatic protein-polysaccharide complexes. *Adv. Colloid Interface Sci.* **2011**, *167*, 49−62.

(3) Nicolai, T.; Durand, D. Controlled food protein aggregation for new functionality. *Curr. Opin. Colloid Interface Sci.* **2013**, *18*, 249−256.

(4) Saunders, B. R.; Vincent, B. Microgel particles as model colloids: theory, properties and applications. *Adv. Colloid Interface Sci.* **1999**, *80*, 1−25.

(5) Zha, L.; Banik, B.; Alexis, F. Stimulus responsive nanogels for drug delivery. *Soft Matter* **2011**, *7*, 5908−5916.

(6) Hu, J.; Yu, S.; Yao, P. Stable amphoteric nanogels made of ovalbumin and ovotransferrin via self assembly. *Langmuir* **2007**, *23*, 6358−6364.

(7) Yu, S.; Yao, P.; Jiang, M.; Zhang, G. Nanogels prepared by self-assembly of oppositely charged globular proteins. *Biopolymers* **2006**, *83*, 148−158.

(8) Donato, L.; Schmitt, C.; Bovetto, L.; Rouvet, M. Mechanism of formation of stable heat-induced β-lactoglobulin microgels. *Int. Dairy J.* **2009**, *19*, 295−306.

(9) Schmitt, C.; Bovay, C.; Vuilliomenet, A. M.; Rouvet, M.; Bovetto, L.; Barbar, R.; Sanchez, C. Multiscale characterization of individualized β-lactoglobulin microgels formed upon heat treatment under narrow pH range conditions. *Langmuir* **2009**, *25*, 7899−7909.

(10) Phan-Xuan, T.; Durand, D.; Nicolai, T.; Donato, L.; Schmitt, C.; Bovetto, L. On the crucial importance of the pH for the formation and self-stabilization of protein microgels and strands. *Langmuir* **2011**, *27*, 15092−15101.

(11) Moitzi, C.; Donato, L.; Schmitt, C.; Bovetto, L.; Gillies, G.; Stradner, A. Structure of β-lactoglobulin microgels formed during heating as revealed by small-angle X-ray scattering and light scattering. *Food Hydrocolloids* **2011**, *25*, 1766−1774.

(12) Schmitt, C.; Bovay, C.; Vuilliomenet, A.-M.; Rouvet, M.; Bovetto, L. Influence of protein and mineral composition on the formation of whey protein heat-induced microgels. *Food Hydrocolloids* **2011**, *25*, 558−567.

(13) Schmitt, C.; Moitzi, C.; Bovay, C.; Rouvet, M.; Bovetto, L.; Donato, L.; Leser, M. E.; Schurtenberger, P.; Stradner, A. Internal structure and colloidal behaviour of covalent whey protein microgels obtained by heat treatment. *Soft Matter* **2010**, *6*, 4876−4884.

(14) Bengoechea, C.; Peinado, I.; McClements, D. J. Formation of protein nanoparticles by controlled heat treatment of lactoferrin: factors affecting particle characteristics. *Food Hydrocolloids* **2011**, *25*, 1354−1360.

(15) Pan, X.; Yu, S.; Yao, P.; Shao, Z. Self-assembly of β-casein and lysozyme. *J. Colloid Interface Sci.* **2007**, *316*, 405−412.

(16) Endres, J. G. *Soy Protein Products: Characteristics, Nutritional Aspects, and Utilization*; AOCS Press: Champaign, IL, 2001.

(17) Staswick, P. E.; Hermodson, M. A.; Nielsen, N. C. Identification of the acidic and basic subunit complexes of glycinin. *J. Biol. Chem.* **1981**, *256*, 8752−8755.

(18) Staswick, P. E.; Hermodson, M. A.; Nielsen, N. C. Identification of the cystines which link the acidic and basic components of the glycinin subunits. *J. Biol. Chem.* **1984**, *259*, 13431−13435.

(19) Thanh, V. H.; Shibasaki, K. Major proteins of soybean seeds. Reconstitution of β-conglycinin from its subunits. *J. Agric. Food Chem.* **1978**, *26*, 695−698.

(20) Thanh, V. H.; Shibasaki, K. Major proteins of soybean seeds. Subunit structure of β-conglycinin. *J. Agric. Food Chem.* **1978**, *26*, 692−695.

(21) Renkema, J. M. S.; Gruppen, H.; Van Vliet, T. Influence of pH and ionic strength on heat induced formation and rheological properties of soy protein gels in relation to denaturation and their protein compositions. *J. Agric. Food Chem.* **2002**, *50*, 6064−6071.

(22) Liu, F.; Tang, C. H. Soy protein nanoparticle aggregates as pickering stabilizers for oil-in-water emulsions. *J. Agric. Food Chem.* **2013**, *61*, 8888−8898.

(23) Zhang, J.; Liang, L.; Tian, Z.; Chen, L.; Subirade, M. Preparation and in vitro evaluation of calcium-induced soy protein isolate nanoparticles and their formation mechanism study. *Food Chem.* **2012**, *133*, 390−399.

(24) Chen, N.; Zhao, Q.; Sun, W.; Zhao, M. Effects of malondialdehyde modification on the in vitro digestibility of soy protein isolate. *J. Agric. Food Chem.* **2013**, *61*, 12139−12145.

(25) Chen, Y.; Ono, T. Protein particle and soluble protein structure in prepared soymilk. *Food Hydrocolloids* **2014**, *39*, 120−126.

(26) Hill, H. D.; Straka, J. G. Protein determination using bicinchoninic acid in the presence of sulfhydryl reagents. *Anal. Biochem.* **1988**, *170*, 203−208.

(27) Beveridge, T.; Toma, S. J.; Nakai, S. Determination of SH- and SS- groups in some food proteins using Ellman's reagent. *J. Food Sci.* **1974**, *39*, 49−51.

(28) Alizadeh-Pasdar, N.; Li-Chan, E. C. Y. Comparison of protein surface hydrophobicity measured at various pH values using three different fluorescent probes. *J. Agric. Food Chem.* **2000**, *48*, 328−334.

(29) Damodaran, S.; Kinsella, J. E. Effect of conglycinin on the thermal aggregation of glycinin. *J. Agric. Food Chem.* **1982**, *30*, 812−817.

(30) German, B.; Damodaran, S.; Kinsella, J. E. Thermal dissociation and association behavior of soy protiens. *J. Agric. Food Chem.* **1982**, *30*, 807−811.

(31) Nobuyuki, M.; Ryohei, S.; Yusuke, W.; Yasuki, M.; Hideyuki, G.; Eiko, O.; Shuko, N.; Shigeru, U. Structure-physicochemical function relationships of soybean β-conglycinin constituent subunits. *J. Agric. Food Chem.* **1999**, *47*, 5278−5284.

(32) Utsumi, S.; Damodaran, S.; Kinsella, J. E. Heat-induced interactions between soybean proteins: preferential association of 11S basic subunits and β subunits of 7S. *J. Agric. Food Chem.* **1984**, *32*, 1406−1412.

(33) Catsimpoolas, N. Isolation of glycinin subunits by isoelectric focusing in urea-mercaptoethanol. *FEBS Lett.* **1969**, *4*, 259−261.

(34) Thanh, V. H.; Shibasaki, K. Beta-conglycinin from soybean proteins. Isolation and immunological and physicochemical properties of the monomeric forms. *Biochim. Biophys. Acta, Protein Struct.* **1977**, *490*, 370−384.

(35) Chen, Y.; Ono, T. The mechanisms for Yuba formation and its stable lipid. *J. Agric. Food Chem.* **2010**, *58*, 6485−6489.
(36) Ren, C.; Tang, L.; Zhang, M.; Guo, S. Structural characterization of heat-induced protein particles in soy milk. *J. Agric. Food Chem.* **2009**, *57*, 1921−1926.

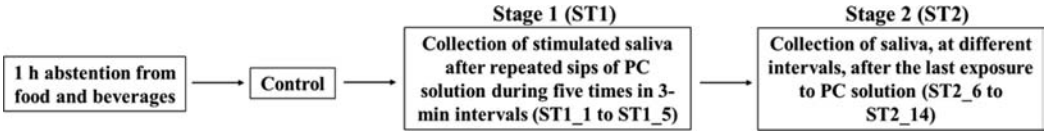


**Figure 1.** Illustration of the experimental approach used to study in vivo interaction between SP and PC.

over effect by a sensory study, evaluating the time−intensity curves for astringency of two red wines.

The central physiological mechanism underlying astringency caused by different foods remains a controversial subject.[30] The aim of this study is to provide new insights on the phenomenon of astringency perception. To evaluate the interaction of the different SP families, a repeated astringency model was developed in which it is possible to understand how the different families of SP interact in an in vivo assay with condensed tannins (procyanidins, PC). In addition, in vitro assays were also performed to investigate which SP families are more susceptible to form insoluble or soluble complexes, and the size of these complexes was evaluated by DLS measurements.

## MATERIALS AND METHODS

**Reagents.** All reagents used were of analytical grade or better. Acetonitrile (ACN) was purchased from Panreac Quimica; trifluoroacetic acid (TFA) and sodium acetate were purchased from Fluka Biochemica; commercial procyanidins (Vitisol) were purchased from Berkem, Plant Extraction; and ethanol was purchased from AGA, Álcool e Géneros Alimentares, SA.

**In Vivo Interaction between Procyanidins and Salivary Proteins.** Human saliva was collected from healthy and nonsmoking volunteers. The experiences were conducted with four subjects aged from 21 to 31 years. Each volunteer contributed to three independent samples ($n$ = 12). All participants were instructed to avoid food and beverages for at least 1 h before the sessions started. The recording procedure was explained in detail to the subjects who provided written consent prior to participation. The study was conducted according to the Declaration of Helsinki and was approved by the Ethics Committee of Medical School of University of Porto (EK84032011).

The PC solution (2.5 g $L^{-1}$) was prepared, and human saliva was collected from different subjects after repeated sips of this solution. The experimental procedure was divided into two stages: Stage 1 (ST1) comprises saliva collected during approximately 15 min with repeated sips of the PC solution at 3 min intervals. It was asked of the subjects to hold 5 mL of this solution in their mouth for 5 s, spit it out, and 3 min later the saliva was collected. This procedure was repeated five times (ST1_1−ST1_5).

On the other hand, stage 2 (ST2) comprises saliva collected at different intervals during 60 min (ST2_6−ST2_14) after the last exposure to PC solution (Figure 1). These intervals (min) and respective designation are indicated in Table 1. ST1_5 was used as reference, so for example ST2_6 refers to saliva collected 5 min after ST1_5, ST2_7 refers to saliva collected 10 min after ST1_5, and so on.

All samples of saliva were mixed with 10% TFA (final concentration 0.1%), centrifuged 5 min at 8000$g$, and the supernatant (acidic saliva, AS) was analyzed by high performance liquid chromatography (HPLC).

**In Vitro Interaction between Salivary Proteins and Procyanidins.** To reduce the variability connected to diurnal variations[31,32] and the influence of circadian rhythms,[33] a pool of saliva collected at 11 am on three different days was prepared. Saliva was collected from the same subjects that participated in the in vivo astringency analysis. The saliva pool was mixed with 10% TFA (final concentration 0.1%), centrifuged (8000$g$ for 5 min), and supernatant (AS) was separated from the precipitate and used for the following experiments.

**Table 1. Time Intervals (min) after the Last Exposure to PC Solution (ST1_5) and Respective Designation in ST2**

| interval (min) | designation |
|---|---|
| 5 | ST2_6 |
| 10 | ST2_7 |
| 20 | ST2_8 |
| 30 | ST2_9 |
| 40 | ST2_10 |
| 45 | ST2_11 |
| 50 | ST2_12 |
| 55 | ST2_13 |
| 60 | ST2_14 |

The AS sample was analyzed by HPLC before and after interaction with PC solution (2.5 g $L^{-1}$). The control condition was a mixture of AS (150 $\mu$L) and 0.1 M acetate buffer (pH 5.0, 12% ethanol) (50 $\mu$L) (final volume 200 $\mu$L).

For the experiments with PC, the necessary volume (50 $\mu$L) of PC solution (2.5 g $L^{-1}$) was added to AS (150 $\mu$L) to obtain the final volume 200 $\mu$L. After shaking, the mixture reacted at room temperature (20 °C) for 2 min and was then centrifuged (8000$g$, 5 min). One-half of the supernatant was directly injected into the HPLC, and the other half was filtered (cellulose acetate 0.22 $\mu$m) and only then injected into the HPLC.

The percentage of insoluble complexes was obtained by subtracting the area of the chromatographic peaks of each family obtained in the HPLC analysis of the nonfiltered solution from the respective area obtained in the control saliva (AS without tannin). The percentage of soluble complexes was calculated in the same way but by subtracting the data obtained in the HPLC analysis of the nonfiltered solution from the respective area obtained in the filtered solution.

**Salivary Flow Rate.** Salivary flow rates were measured at 11 am according to the procedure described by Gaviao et al.[34] During 5 min, subjects spat out the saliva passively accumulating in their mouth into a preweighed plastic container. The salivary flow rate was assessed by three repetitions and was expressed in mL $min^{-1}$.

**Dynamic Light Scattering (DLS) Measurements.** The size of procyanidin/salivary protein aggregates present in solution was measured by DLS, using the Zetasizer Nano ZS Malvern instrument. The same procedure described for protein−tannin interaction in this section was applied herein. Thus, to determine the size of the aggregates, one-half of the supernatant resulting from protein−procyanidins reaction was evaluated by DLS, and the other one-half was filtered (cellulose acetate 0.22 $\mu$m) and then also analyzed by DLS.

This technique measures the time-dependent fluctuations in the intensity of scattered light that occur because particles undergo Brownian motion. The analysis of these intensity fluctuations enables determination of the diffusion coefficients of particles, which are converted into a size distribution. The sample solution was illuminated by a 633 nm laser, and the intensity of light scattered at an angle of 173 was measured by an avalanche photodiode. This analysis provides information concerning particle size (obtained by average size parameter) and polydispersity. In general, $Z$ average size results were considered valid when the polydispersity of solutions was below 0.5. These experiments were performed in triplicate.

**HPLC Analysis.** The method used in the HPLC analysis was adapted from the method described by Soares et al.[11] Ninety microliters of each solution were injected on HPLC Lachrom system (Merck Hitachi, L-7100) equipped with a Vydac C8 column (Grace


dx.doi.org/10.1021/jf502721c | J. Agric. Food Chem. 2014, 62, 9562−9568

Davison Discovery Sciences); the column dimensions are 150 × 2.1 mm, and the particle diameter is 5 μm; detection was carried out at 214 nm, using a UV−vis detector (L-7420). The HPLC solvents were 0.2% aqueous TFA (eluent A) and 0.2% TFA in ACN/water 80/20 (v/v) (eluent B). The gradient applied was linear from 10% to 40% (eluent B) in 75 min, at a flow rate of 0.30 mL $min^{-1}$. After the program, the column was washed with 100% eluent B for 20 min to elute S-type cystatins and other late-eluting proteins. After being washed, the column was stabilized with the initial conditions.[11,35]

**Data and Statistical Analysis.** The mean values of chromatographic peaks and standard error of mean (SEM) were evaluated using analysis of variance (ANOVA), followed by the Bonferroni test. The mean values of salivary flow rates, the percentage of SP involved in the formation of (in)soluble complexes, and standard deviations were evaluated by statistical analysis using *t* test unparametric. Differences were considered to be statistically significant when *P* was at least <0.05, and in each case *P* is indicated in the respective figure. These statistical data were processed using GraphPad Prism version 5.0 for Windows. The correlations between different factors analyzed in this work were assessed by IBM SPSS Statistics version 21 for Windows.

## RESULTS AND DISCUSSION

This work intends to better understand the physiological mechanism underlying the phenomenon of astringency by an in vivo analysis, which could give important informations about the interaction between SP and PC. Factors such as the amount of SP, salivary flow rates, and size of the protein−tannin aggregates could be extremely important in the mechanism responsible for different perceptions of astringency and will hence be analyzed in this study.

**Salivary Proteins and Interaction with Procyanidins.** The initial acidic treatment of saliva with TFA is used to precipitate several high molecular weight SP (such as α-amylases, mucins, carbonic anhydrase, and lactoferrin) and to preserve sample protein composition because TFA partially inhibits intrinsic protease activity.[35] However, peptides and proteins like histatins, bPRPs and aPRPs, statherin, cystatins, and defensins are soluble in AS solution and may be directly analyzed by HPLC, as previously described.[11,35]

The HPLC chromatogram of AS solution detected at 214 nm can be divided into four SP regions: the first region comprises proteins that belong to bPRP and histatin classes (Figure 2). The second region comprises gPRPs, the next region corresponds entirely to aPRPs, and the last region contains phosphorylated and nonphosphorylated forms of statherin.[11]

As it was described in the literature, the intensity of astringency is supposed to increase upon successive sips of red wines.[27] Thus, it became important to investigate how the different families of SP may be affected along this continued astringent stimuli. The experimental approach described herein intends to mimic the phenomenon that occurs in the oral cavity during the ingestion of a product rich in polyphenols, such as the case of red wine. For this, a PC solution (2.5 g $L^{-1}$) was prepared, and it was asked to the subjects to sip this solution five times in 3 min intervals. After this stage, saliva continued to be collected to assess the recovering of the SP families. The HPLC profile of AS solution before and after in vivo interaction with PC solution is shown in Figure 2.

In Figure 2, ST1_1 and ST1_5 were used as examples, and the difference of areas of each peak between control and the other times represents the amount of protein that precipitated with tannins. The difference observed between the peaks of aPRPs and statherin relative to control and different times

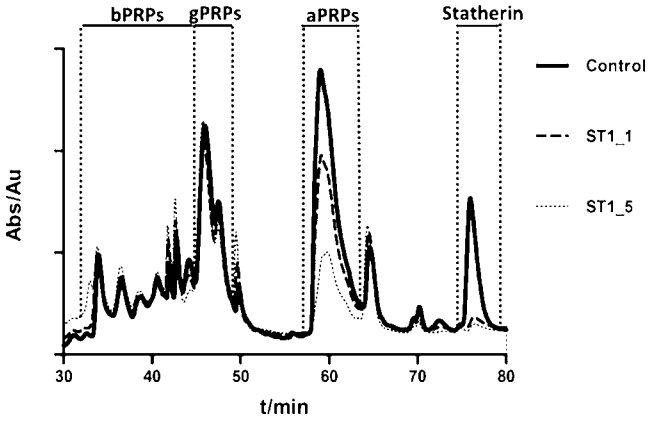


**Figure 2.** HPLC profile detected at 214 nm of the AS solution before (control saliva) and after (ST1_1 and ST1_5) in vivo interaction with PC solution (2.5 g $L^{-1}$). The dotted lines show the different families of SP studied in this work.

tends to be higher with the increase in number of repeated sips of PC solution (data not shown).

The variations in the chromatographic peaks of each SP family during ST1 are presented in Figure 3. The results are

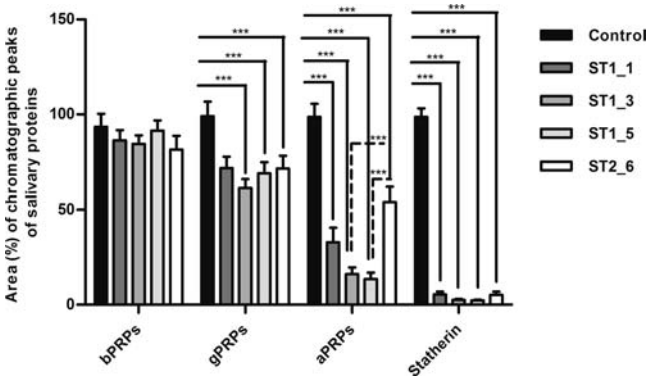


**Figure 3.** Influence of the interaction of SP with the PC solution during ST1, when saliva was collected during repeated sips of this solution (ST1_1−ST1_5). ST2_6 is presented for comparison. The results are expressed as percentage of the area of each protein relative to the control (100%), and each value represents the mean ± SEM ($n$ = 12). Only the significant statistical differences more important to this work are presented (***$p$ < 0.001).

expressed as percentage of the area of these proteins relative to the control saliva (without tannin). To simplify Figure 3, only the times with more relevant changes are presented.

The results displayed in Figure 3 show that the area of each different family of proteins is interestingly affected in a different way by the interaction with a PC solution (2.5 g $L^{-1}$). It was observed that repeated sips of the PC solution practically depleted aPRPs and statherin, and significantly reduced the amount of gPRPs. On the other hand, bPRPs were not significantly affected.

After the last sip of the PC solution, saliva continued to be collected during 60 min to assess the evolution of the SP families (Figure 4). The results are expressed as percentage of the area of these proteins relative to the control saliva (without tannin). To simplify Figure 4, only the times with more relevant changes are presented.


dx.doi.org/10.1021/jf502721c | J. Agric. Food Chem. 2014, 62, 9562−9568

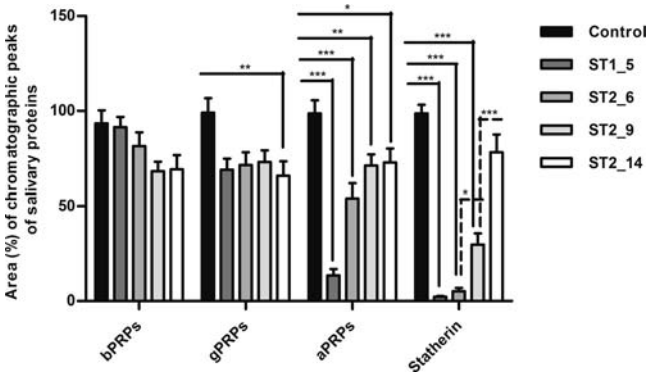


**Figure 4.** Saliva protein composition after the last exposure to PC solution (ST2). ST1_5 is presented for comparison. The results are expressed as percentage of the area of each protein relative to the control (100%), and each value represents the mean ± SEM ($n$ = 12). Only the significant statistical differences more important to this work are presented (*$p$ < 0.05; **$p$ < 0.01; ***$p$ < 0.001).

In the analysis performed at ST2, it was seen a significant recovering of the chromatographic peaks corresponding especially to aPRPs and statherin. On the other hand, the chromatographic peaks of bPRPs and gPRPs seem to slightly decrease or remain practically constant. However, the observed increase of the chromatographic peaks of different SP in ST2 was not sufficient to achieve the control levels during the period studied.

As previously referred, the different families of SP have distinct affinities toward tannins. So, it was expected that these proteins evolved differently over the time after the interaction with PC. Although the area of aPRPs and statherin decreased during astringent stimulus (ST1) and increased significantly during ST2, the same behavior was not observed for the other proteins. The gPRPs family seems to be the least affected, because its percentage remains practically constant during both ST1 and ST2. On the other hand, bPRPs' area seems to be constant during ST1 and to decrease, although nonsignificant, during ST2 (Figure 4). Therefore, the different behaviors of SP during and after the interaction with the PC solution can suggest that several SP families could be involved in different stages of the development of astringency.[36]

The main families affected by the interaction with PC solution were aPRPs and statherin, a common characteristic in all subjects studied. However, it was possible to verify the existence of individual differences, in the percentage of reduction of chromatographic peaks area of these proteins (data not shown).

SPs are stored in secretory granules, and they are released into the mouth gradually in unstimulated conditions. Therefore, saliva collected in these conditions can be considered representative of a basal composition because it results from secretion of preformed vesicles.[37] However, by an appropriate stimulus, such as the case of PC solution, the secretion may be accelerated, depleting statherin. Some works show that de novo synthesis and processing of a protein through the secretory apparatus requires approximately 30 min.[28,38] Considering that ST2_9 corresponds to 30 min after the last sip of PC solution, it is possible to verify a significant recovery of statherin at this time as compared to ST2_6.

Moreover, Castagnola and co-workers[39] verified that statherin was not affected by circadian rhythms, which strongly suggests that its route of secretion is different from that of other proteins, such as the case of histatins.

**In Vitro Reactivity of Salivary Proteins and Procyanidins.** The method for the study of protein−tannin interaction used in these experiments was selected on the basis of the work developed by Soares et al.[20,40] The aim of this part of the work was to verify the in vitro reactivity of PC and SP, respecting the individual characteristics of saliva protein profile. To reduce the variations referred to in the Materials and Methods, saliva pool was made of saliva collected 3 days from each subject. The control condition was prepared with AS and acetate buffer. The volume of 50 $\mu$L of PC solution (2.5 g $L^{-1}$) was added to AS and was allowed to react during 2 min. This reaction time was chosen to be close to what happens in the in vivo astringency analysis. After the reaction, the solution was centrifuged, which results in insoluble complexes. One-half of the supernatant was analyzed by HPLC (nonfiltered solution), and the other half was filtered and then was also analyzed by HPLC (filtered solution).

Figure 5 shows the difference of chromatographic peaks' area of several SP families before (AS without tannin) and after in vitro interaction with the PC solution (nonfiltered and filtered solution). From these results, it is possible to observe that aPRPs and statherin were the proteins that have a higher relative affinity toward PC complexation and precipitation, comparatively to other SP, such as gPRPs that have a medium relative affinity. It is important to note that aPRPs and statherin also formed soluble complexes with PC. On the other hand, these results seem to indicate that bPRPs, when present in a competitive assay, have a lower relative tannin affinity, because they practically did not complex with tannins. It is also possible to observe that filtration induced a decrease of some chromatographic peaks of SP, in particular for aPRPs and statherin, which could be explained by the retention of salivary protein/tannin soluble complexes by the filter.

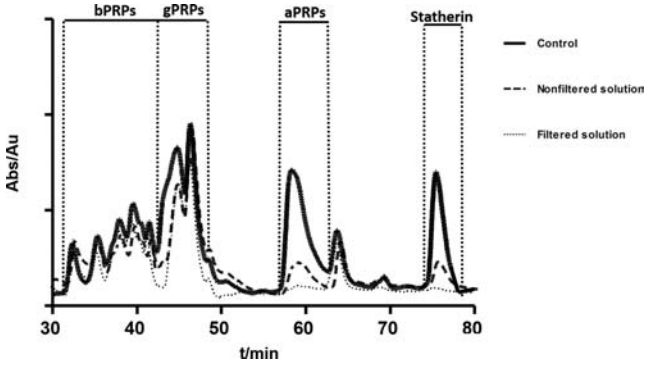


**Figure 5.** HPLC profiles detected at 214 nm of the AS solution before and after the addition of the PC solution (2.5 g $L^{-1}$). The graphics show the difference between chromatographic peaks before (control saliva) and after interaction with PC solution. These solutions were nonfiltered and filtered (0.22 $\mu$m) prior to HPLC analysis.

Differences between saliva protein profiles of subjects can influence the affinity of SP toward tannins and, consequently, the size of (in)soluble complexes formed. The differences between nonfiltered and filtered solutions were also detectable in the experiment size measurements by DLS. Indeed, the average size (nm) of complexes in nonfiltered and filtered solutions was 189.9 ± 9.1 and 83.3 ± 9.2, respectively. The


dx.doi.org/10.1021/jf502721c | J. Agric. Food Chem. 2014, 62, 9562−9568

Table 2. Percentage of SP and Standard Deviation (SD) Present in the Control and That Are Involved in the Formation of Complexes (Soluble and Insoluble) Formed by the Interaction with PC Solution (2.5 g $L^{-1}$)[a]

| | | subject | | | |
|---|---|---|---|---|---|
| | salivary protein (%) | A | B | C | D |
| control | bPRPs | 19.9 ± 6.0 | 24.0 ± 0.8 | 13.9 ± 2.1 | 25.3 ± 2.4 |
| | gPRPs | 35.4 ± 0.7 | 35.4 ± 0.9 | 28.6 ± 1.2 | 26.4 ± 0.1 |
| | aPRPs | 20.0 ± 6.2 | 24.2 ± 1.3 | 42.9 ± 1.7 | 36.9 ± 3.7 |
| | statherin | 24.8 ± 0.7 | 16.4 ± 0.5 | 14.6 ± 0.1 | 11.4 ± 1.5 |
| insoluble complexes | bPRPs | 0.0 ± 0.0 | 0.0 ± 0.0 | 0.0 ± 0.0 | 0.0 ± 0.0 |
| | gPRPs | 30.7 ± 4.8 | 11.4 ± 1.5 | 1.8 ± 3.0 | 24.7 ± 1.6 |
| | aPRPs | 19.2 ± 6.1 | 18.1 ± 5.8 | 37.2 ± 0.9 | 36.6 ± 0.8 |
| | statherin | 22.4 ± 3.0 | 12.5 ± 0.9 | 14.1 ± 1.2 | 10.1 ± 0.2 |
| soluble complexes | bPRPs | 0.0 ± 0.0 | 0.0 ± 0.0 | 0.0 ± 0.0 | 0.0 ± 0.0 |
| | gPRPs | 4.9 ± 0.5 | 3.7 ± 1.3 | 1.5 ± 4.7 | 1.5 ± 1.4 |
| | aPRPs | 0.3 ± 0.2 | 5.3 ± 4.6 | 5.1 ± 1.0 | 0.7 ± 0.9 |
| | statherin | 2.1 ± 0.5 | 3.5 ± 0.4 | 0.4 ± 1.2 | 0.4 ± 0.4 |
| salivary flow rate (mL $min^{-1}$) | | 0.33 ± 0.03 | 0.31 ± 0.02 | 0.64 ± 0.08 | 0.52 ± 0.13 |

[a]The values of salivary flow rates are also presented.

results indicate the existence of soluble salivary protein−tannin complexes that are retained by the filter (0.22 $\mu$m).

To highlight the differences between nonfiltered and filtered solutions, the percentages of proteins involved in the formation of complexes (soluble and insoluble) are presented in Table 2, considering four subjects ($n$ = 3).

Overall, these results show that the amount of SP involved in the formation of insoluble complexes is in general higher for aPRPs and statherin. On the other hand, bPRPs practically do not complex with PC. However, the behavior for gPRPs is not entirely similar between subjects. It was observed that the percentage of gPRPs involved in the formation of insoluble complexes can be higher than the percentage of the other SP. Interestingly, using the conditions of the present work, there is a little amount of SP involved in the formation of soluble complexes as compared to the amount in the insoluble ones, which can suggest that interaction between SP and tannins results possibly in precipitated aggregates.

Nevertheless, it is important to analyze the quantity of each SP in the control solution. Attending to the control values, the area of aPRPs and statherin together is the highest, and these are the major families responsible for insoluble complexes. In turn, the initial amount of gPRPs (control) is considerably higher, but in some cases, only a small percentage of these proteins is involved in complex formation. These facts are in agreement with the data previously referred to on the higher affinity of aPRPs and statherin to complex and to precipitate with tannins.

Salivary flow rate is also an important factor that should be taken into account in studies dealing with astringency because it can modulate the intensity of astringency induced by phenolic compounds.[29,41] The salivary flow rates of the different subjects are presented in Table 2. Interestingly, results suggest that subjects with higher salivary flow rate have higher amounts of aPRPs and statherin involved in the formation of insoluble complexes. Dinnella and colleagues[28,42] suggested that the subject group with high salivary flow rate perceives astringency at a significantly lower level than the low flow rate group, and the analysis of time−intensity curves showed a longer time of recovering from astringency for the latter group.

Comparing in vitro and in vivo interactions between SP and PC, the descending order of relative affinity is the same: aPRPs and statherin, then gPRPs, and finally bPRPs.

Indeed, aPRPs and statherin have been recently described to interact more strongly with condensed tannins than the other SP families. There are in the literature some recent studies that have used experimental conditions similar to those used in this work and corroborate the results obtained herein. Soares et al.[20] assessed the ability of two different structures of tannins (condensed and hydrolyzable) to precipitate the several SP. For this, saliva was collected from different subjects, a pool of whole saliva was made, and then tannins were added. They found that aPRPs and statherin were the SP more affected by the interaction with tannins.

Besides the central role of the tannin structure, results presented herein point to the importance of the protein structure for the protein−tannin interaction. PRPs are classified into different classes (acidic, basic, and glycosylated) on the basis of small and specific structural differences, in particular, richness in acidic or basic residues and the presence of sugar molecules in their structure.[43−45] The acidic character of aPRPs is confined roughly to the first 30 amino acids, due to the presence of many aspartic and glutamic acid residues. The presence of these acid residues may favor hydrogen-bond interactions, which probably explain the high affinity of aPRPs to tannins. The remaining part is basic and, similarly to bPRPs, shows repeated sequences of proline and glutamine often separated by glycine residues. Regarding the gPRPs, there is little information about the glycosylation pattern of these proteins. Pascal et al.[46] reported that gPRPs are in fact effective in binding tannins; however, these interactions do not necessarily result in precipitation.[47] Possibly, this happens because of the presence of the sugar moiety in their structure.[47] Nayak and Carpenter[48] showed that statherin is precipitated by polyphenols, tea polyphenols. Statherin is rich in tyrosine residues and is phosphorylated at Ser-2 and Ser-3. The presence of protic groups (phosphates) with acidic character may favor the hydrogen-bond interactions, which probably explain statherin's high affinity to tannins.[48]

The results present herein provide important insights concerning the influence of the different families of SP in the development of astringency. In fact, when all of the main families of SP are present in a competitive assay, like in the oral cavity, they demonstrate that tannins interact first with statherin and aPRPs, and then with gPRPs.

In summary, SP families have relative discriminatory functions in rating the perception of astringency depending on the type of astringent stimuli used. Repeated stimulations with PC may affect differently the several families of SP, suggesting that they could be involved in different stages of the development of astringency.

## AUTHOR INFORMATION


### Corresponding Author

*Tel.: +351 220402558. Fax: +351 220402659. E-mail: vfreitas@fc.up.pt.



### Funding

This work was supported by FEDER funds through COMPETE, POPH/FSE, QREN, and FCT (Fundação para a Ciência e Tecnologia) from Portugal by one postdoctoral fellowship and through project PEst-C/QUI/UI0081/2011.


### Notes

The authors declare no competing financial interest.

## ABBREVIATIONS USED

ACN, acetonitrile; aPRPs, acidic proline-rich proteins; AS, acidic saliva; bPRPs, basic proline-rich proteins; gPRPs, glycosylated proline-rich proteins; HPLC, high-performance liquid chromatography; PC, procyanidins; PRPs, proline-rich proteins; SP, salivary proteins; ST1, stage 1; ST2, stage 2; TFA, trifluoroacetic acid

## REFERENCES


(1) de Freitas, V.; Mateus, N. Protein/polyphenol interactions: Past and present contributions. Mechanisms of astringency perception. *Curr. Org. Chem.* **2012**, *16*, 724−746.

(2) Faria, A.; Calhau, C.; de Freitas, V.; Mateus, N. Procyanidins as antioxidants and tumor cell growth modulators. *J. Agric. Food Chem.* **2006**, *54*, 2392−2397.

(3) Perez-Vizcaino, F.; Duarte, J.; Andriantsitohaina, R. Endothelial function and cardiovascular disease: Effects of quercetin and wine polyphenols. *Free Radical Res.* **2006**, *40*, 1054−1065.

(4) Quideau, S.; Deffieux, D.; Douat-Casassus, C.; Pouysegu, L. Plant polyphenols: Chemical properties, biological activities, and synthesis. *Angew. Chem., Int. Ed.* **2011**, *50*, 586−621.

(5) Dangles, O. Antioxidant activity of plant phenols: Chemical mechanisms and biological significance. *Curr. Org. Chem.* **2012**, *16*, 692−714.

(6) Lee, C. B.; Lawless, H. T. Time-course of astringent sensations. *Chem. Senses* **1991**, *16*, 225−238.

(7) Bajec, M. R.; Pickering, G. J. Astringency: Mechanisms and perception. *Crit. Rev. Food Sci. Nutr.* **2008**, *48*, 858−875.

(8) Bate-Smith, E. C. Astringency in foods. *Food Chem.* **1954**, *23*, 124.

(9) Kallithraka, S.; Bakker, J.; Clifford, M. N. Evidence that salivary proteins are involved in astringency. *J. Sens. Stud.* **1998**, *13*, 29−43.

(10) Lu, Y.; Bennick, A. Interaction of tannin with human salivary proline-rich proteins. *Arch. Oral Biol.* **1998**, *43*, 717−728.

(11) Soares, S.; Vitorino, R.; Osorio, H.; Fernandes, A.; Venancio, A.; Mateus, N.; Amado, F.; de Freitas, V. Reactivity of human salivary proteins families toward food polyphenols. *J. Agric. Food Chem.* **2011**, *59*, 5535−5547.

(12) Smith, A. K.; June, H.; Noble, A. C. Effects of viscosity on the bitterness and astringency of grape seed tannin. *Food. Qual. Prefer.* **1996**, *7*, 161−166.

(13) Payne, C.; Bowyer, P. K.; Herderich, M.; Bastian, S. E. P. Interaction of astringent grape seed procyanidins with oral epithelial cells. *Food Chem.* **2009**, *115*, 551−557.

(14) de Wijk, R. A.; Prinz, J. F. The role of friction in perceived oral texture. *Food Qual. Prefer.* **2005**, *16*, 121−129.

(15) De Wijk, R. A.; Prinz, J. F. Mechanisms underlying the role of friction in oral texture. *J. Texture Stud.* **2006**, *37*, 413−427.

(16) Rossetti, D.; Bongaerts, J. H. H.; Wantling, E.; Stokes, J. R.; Williamson, A. M. Astringency of tea catechins: More than an oral lubrication tactile percept. *Food Hydrocolloids* **2009**, *23*, 1984−1992.

(17) Sarni-Manchado, P.; Cheynier, V.; Moutounet, M. Interactions of grape seed tannins with salivary proteins. *J. Agric. Food Chem.* **1999**, *47*, 42−47.

(18) Siebert, K. J.; Troukhanova, N. V.; Lynn, P. Y. Nature of polyphenol-protein interactions. *J. Agric. Food Chem.* **1996**, *44*, 80−85.

(19) de Freitas, V.; Mateus, N. Structural features of procyanidin interactions with salivary proteins. *J. Agric. Food Chem.* **2001**, *49*, 940−945.

(20) Soares, S.; Mateus, N.; de Freitas, V. Interaction of different classes of salivary proteins with food tannins. *Food Res. Int.* **2012**, *49*, 807−813.

(21) Charlton, A. J.; Baxter, N. J.; Khan, M. L.; Moir, A. J. G.; Haslam, E.; Davies, A. P.; Williamson, M. P. Polyphenol/peptide binding and precipitation. *J. Agric. Food Chem.* **2002**, *50*, 1593−1601.

(22) Humphrey, S. P.; Williamson, R. T. A review of saliva: Normal composition, flow, and function. *J. Prosthet. Dent.* **2001**, *85*, 162−169.

(23) Hay, D. I.; Carlson, E. R.; Schluckebier, S. K.; Moreno, E. C.; Schlesinger, D. H. Inhibition of calcium-phosphate precipitation by human salivary acidic proline-rich proteins - structure-activity-relationships. *Calcif. Tissue Int.* **1987**, *40*, 126−132.

(24) Schlesinger, D. H.; Hay, D. I.; Levine, M. J. Complete primary structure of statherin, a potent inhibitor of calcium-phosphate precipitation, from the saliva of the monkey, macaca-arctoides. *Int. J. Pept. Protein Res.* **1989**, *34*, 374−380.

(25) Shomers, J. P.; Tabak, L. A.; Levine, M. J.; Mandel, I. D.; Ellison, S. A. Characterization of cysteine-containing phosphoproteins from human submandibular-sublingual saliva. *J. Dent. Res.* **1982**, *61*, 764−767.

(26) Monteleone, E.; Condelli, N.; Dinnella, C.; Bertuccioli, M. Prediction of perceived astringency induced by phenolic compounds. *Food Qual. Prefer.* **2004**, *15*, 761−769.

(27) Lesschaeve, I.; Noble, A. C. Polyphenols: factors influencing their sensory properties and their effects on food and beverage preferences. *Am. J. Clin. Nutr.* **2005**, *81*, 330S−335S.

(28) Dinnella, C.; Recchia, A.; Fia, G.; Bertuccioli, M.; Monteleone, E. Saliva characteristics and individual sensitivity to phenolic astringent stimuli. *Chem. Senses* **2009**, *34*, 295−304.

(29) Horne, J.; Hayes, J.; Lawless, H. T. Turbidity as a measure of salivary protein reactions with astringent substances. *Chem. Senses* **2002**, *27*, 653−659.

(30) Lee, C. A.; Ismail, B.; Vickers, Z. M. The role of salivary proteins in the mechanism of astringency. *J. Food Sci.* **2012**, *77*, C381−C387.

(31) Quintana, M.; Palicki, O.; Lucchi, G.; Ducoroy, P.; Chambon, C.; Salles, C.; Morzel, M. Inter-individual variability of protein patterns in saliva of healthy adults. *J. Proteomics* **2009**, *72*, 822−830.

(32) Hardt, M.; Witkowska, H. E.; Webb, S.; Thomas, L. R.; Dixon, S. E.; Hall, S. C.; Fisher, S. J. Assessing the effects of diurnal variation on the composition of human parotid saliva: Quantitative analysis of native peptides using iTRAQ reagents. *Anal. Chem.* **2005**, *77*, 4947−4954.

(33) Ekström, J.; Khosravani, N.; Castagnola, M.; Messana, I. In *Dysphagia: Diagnosis and Treatment*; Ekberg, O., Ed.; Springer-Verlag: Berlin, Heidelberg, 2012; pp 19−47.

(34) Gaviao, M. B. D.; Engelen, L.; van der Bilt, A. Chewing behavior and salivary secretion. *Eur. J. Oral Sci.* **2004**, *112*, 19−24.

(35) Messana, I.; Cabras, T.; Inzitari, R.; Lupi, A.; Zuppi, C.; Olmi, C.; Fadda, M. B.; Cordaro, M.; Giardina, B.; Castagnola, M. Characterization of the human salivary basic proline-rich protein complex by a proteomic approach. *J. Proteome Res.* **2004**, *3*, 792−800.

(36) Soares, S.; Sousa, A.; Mateus, N.; de Freitas, V. Effect of condensed tannins addition on the astringency of red wines. *Chem. Senses* **2012**, *37*, 191−198.

(37) Messana, I.; Cabras, T.; Pisano, E.; Sanna, M. T.; Olianas, A.; Manconi, B.; Pellegrini, M.; Paludetti, G.; Scarano, E.; Fiorita, A.;

Agostino, S.; Contucci, A. M.; Calo, L.; Picciotti, P. M.; Manni, A.; Bennick, A.; Vitali, A.; Fanali, C.; Inzitari, R.; Castagnola, M. Trafficking and postsecretory events responsible for the formation of secreted human salivary peptides: A proteomics approach. *Mol. Cell. Proteomics* **2008**, *7*, 911−926.
(38) Becerra, L.; Soares, R. V.; Bruno, L. S.; Siqueira, C. C.; Oppenheim, F. G.; Offner, G. D.; Troxler, R. F. Patterns of secretion of mucins and non-mucin glycoproteins in human submandibular/sublingual secretion. *Arch. Oral Biol.* **2003**, *48*, 147−154.
(39) Castagnola, M.; Cabras, T.; Denotti, G.; Fadda, M. B.; Gambarini, G.; Lupi, A.; Manca, I.; Onnis, G.; Piras, V.; Soro, V.; Tambaro, S.; Messana, I. Circadian rhythms of histatin 1, histatin 3, histatin 5, statherin and uric acid in whole human saliva secretion. *Biol. Rhythm Res.* **2002**, *33*, 213−222.
(40) Soares, S.; Mateus, N.; de Freitas, V. Carbohydrates inhibit salivary proteins precipitation by condensed tannins. *J. Agric. Food Chem.* **2012**, *60*, 3966−3972.
(41) Condelli, N.; Dinnella, C.; Cerone, A.; Monteleone, E.; Bertuccioli, M. Prediction of perceived astringency induced by phenolic compounds II: Criteria for panel selection and preliminary application on wine samples. *Food Qual. Prefer.* **2006**, *17*, 96−107.
(42) Dinnella, C.; Recchia, A.; Vincenzi, S.; Tuorila, H.; Monteleone, E. Temporary modification of salivary protein profile and individual responses to repeated phenolic astringent stimuli. *Chem. Senses* **2010**, *35*, 75−85.
(43) Inzitari, R.; Cabras, T.; Onnis, G.; Olmi, C.; Mastinu, A.; Sanna, M. T.; Pellegrini, M. G.; Castagnola, M.; Messana, I. Different isoforms and post-translational modifications of human salivary acidic proline-rich proteins. *Proteomics* **2005**, *5*, 805−815.
(44) Messana, I.; Inzitari, R.; Fanali, C.; Cabras, T.; Castagnola, M. Facts and artifacts in proteomics of body fluids. What proteomics of saliva is telling us? *J. Sep. Sci.* **2008**, *31*, 1948−1963.
(45) Vitorino, R.; Alves, R.; Barros, A.; Caseiro, A.; Ferreira, R.; Lobo, M. C.; Bastos, A.; Duarte, J.; Carvalho, D.; Santos, L. L.; Amado, F. L. Finding new posttranslational modifications in salivary proline-rich proteins. *Proteomics* **2010**, *10*, 3732−3742.
(46) Pascal, C.; Poncet-Legrand, C.; Cabane, B.; Vernhet, A. Aggregation of a proline-rich protein induced by epigallocatechin gallate and condensed tannins: Effect of protein glycosylation. *J. Agric. Food Chem.* **2008**, *56*, 6724−6732.
(47) Sarni-Manchado, P.; Canals-Bosch, J. M.; Mazerolles, G.; Cheynier, V. Influence of the glycosylation of human salivary proline-rich proteins on their interactions with condensed tannins. *J. Agric. Food Chem.* **2008**, *56*, 9563−9569.
(48) Nayak, A.; Carpenter, G. H. A physiological model of tea-induced astringency. *Physiol. Behav.* **2008**, *95*, 290−294.

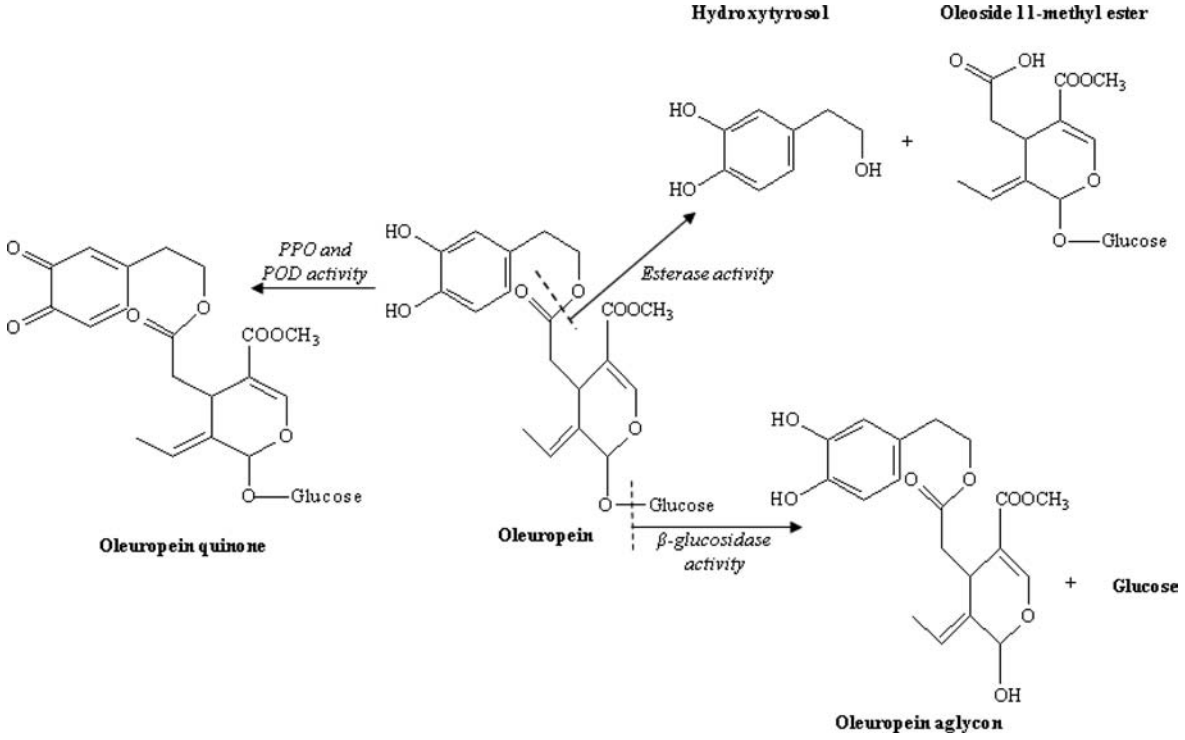


**Figure 1.** Oleuropein and products of its enzymatic transformations.

California-style. Twelve and six samples for each variety during the 2010/2011 and 2011/2012 seasons, respectively, were assessed. The fruits were processed on the same day without any storage period.

**Analysis of Phenolic Compounds.** The extraction of phenolic compounds from the olive pulp was based on the methodology proposed elsewhere.[19] Around 10 g of fresh olive pulp was mixed in an Ultra-Turrax homogenizer with 30 mL of dimethyl sulfoxide (DMSO). After 30 min of resting contact, the mixture was centrifuged at 6000*g* for 5 min (22 °C), and 0.25 mL of the supernatant was diluted with 0.5 mL of DMSO plus 0.25 mL of 0.2 mM syringic acid in DMSO (internal standard). The extraction of phenolic compounds from the fresh olive skin was made similarly to the olive pulp as described above, but this time the mixing ratio was 0.1 g of olive skin and 0.5 mL of DMSO.

Samples were filtered through a 0.22 $\mu$m pore size nylon filter, and an aliquot (20 $\mu$L) was injected into the chromatograph. The chromatographic system consisted of a Waters 717 plus autosampler, a Waters 600 E pump, a Waters column heater module, and a Waters 996 photodiode array detector operated with Empower software (Waters Inc.). A 25 cm × 4.6 mm i.d., 5 $\mu$m, Spherisorb ODS-2 (Waters Inc.) column, at a flow rate of 1 mL/min and a temperature of 35 °C, was used in all experiments. Separation was achieved by gradient elution using (A) water (pH 2.5 adjusted with 0.15% phosphoric acid) and (B) methanol. The initial composition was 90% A and 10% B. The concentration of B was increased to 30% over 10 min and was maintained for 20 min. Subsequently, B was raised to 40% over 10 min, maintained for 5 min, and then increased to 50%. Finally, B was increased to 60, 70, and 100% in 5 min periods. The initial conditions were reached in 10 min. Chromatograms were recorded at 280 nm.[15]

The evaluation of each compound was performed using a regression curve with the corresponding standard. Hydroxytyrosol, oleuropein, verbascoside, luteolin 7-glucoside, luteolin, rutin, and apigenin were purchased from Extrasynthese S.A. (Lyon Nord, Genay, France) and tyrosol, caffeic acid, and *p*-coumaric acid from Sigma Chemical Co. (St. Louis, MO, USA). Hydroxytyrosol-1-glucoside, caffeoyl ester of secologanoside, and comselogoside were quantified using the response factors of hydroxytyrosol, caffeic acid, and *p*-coumaric acid, respectively. Salidroside and ligustroside were quantified using the response factors of tyrosol. Hydroxytyrosol-4-glucoside was obtained using an HPLC preparative system.[20]

**Preparation of Acetone Powder.** Acetone powders were obtained from 50 g of olive pulp or skin homogenized with 100 mL of cold acetone (−30 °C) containing 2.5 g of polyethylene glycol.[6] The mixture was then vacuum-filtered in a Büchner funnel through paper, and the residue was re-extracted three times with 100 mL of cold acetone, obtaining a white solid that was dried overnight at room temperature to remove residual acetone. The acetone powder was stored at −40 °C until use.

**PPO and POD Activity.** A crude enzyme extract was obtained from the above acetone powder as described elsewhere.[11] Half a gram of acetone powder was suspended in 20 mL of 0.1 M sodium phosphate buffer, containing 1 M NaCl, and the pH was adjusted to 6.2 units with NaOH. The suspension was stirred at 4 °C for 30 min and then centrifuged at 15550*g* for 20 min at 4 °C. The pellet was discarded and the supernatant divided into two aliquots; one was used as the active crude enzyme extract, and the other was boiled for 30 min to get the denatured enzyme extract.

The PPO activity was determined spectrophotometrically using a Shimadzu UV−vis 1800 spectrophotometer as described elsewhere.[21] All measurements of PPO activity were carried out with 4-methylcatechol (Sigma Chemical Co.) as substrate by measuring the changes in absorbance at 410 nm at 25 °C for 10 min at intervals of 5 s. The incubation mixture contained 0.5 mL of crude enzyme preparation and 2.5 mL of 0.1 M sodium citrate buffer at pH 5 with 0.02 M substrate. The assay mixture with the denatured enzyme extract served as the control. One unit of enzyme activity was defined as the amount of the enzyme giving a change in absorbance of 0.05 unit (AU) per minute under the above-mentioned conditions. All assays were carried out in duplicate.

The POD activity was determined spectrophotometrically as described elsewhere.[22] All measurements of POD activity were carried out with guaiacol (Sigma Chemical Co.) as substrate by measuring the changes in absorbance at 470 nm at 25 °C for 10 min at intervals of 1 min. The assay mixture with the denatured enzyme extract served as the control. The incubation mixture contained 0.3 mL of crude enzyme extract and 2.7 mL of phosphate buffer at pH 6 containing 0.04 M substrate and 0.026 M hydrogen peroxide. The composition of


dx.doi.org/10.1021/jf5027982 | J. Agric. Food Chem. 2014, 62, 9569−9575

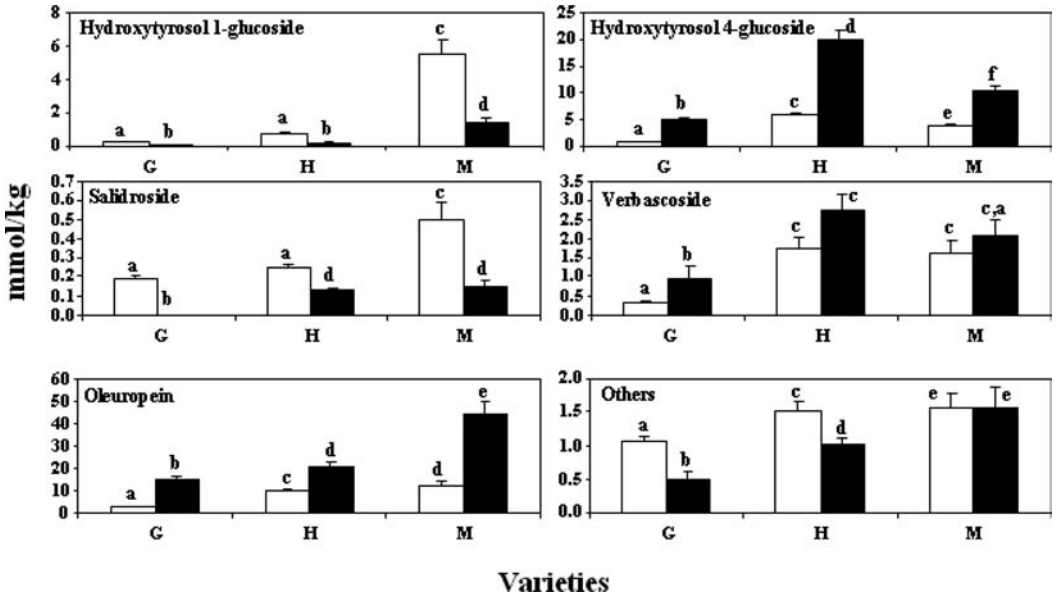


**Figure 2.** Concentration of phenolic composition (mmol/kg) in fruits of Gordal (G), Hojiblanca (H), and Manzanilla (M) varieties. The phenol compounds analyzed were hydroxytyrosol-1-glucoside, hydroxytyrosol-4-glucoside, salidroside, verbascoside, oleuropein, and the sum of tyrosol, luteolin-7-glucoside, rutin, caffeic and *p*-coumaric acid, caffeoyl ester of secologanoside, comselogoside, luteolin, apigenin, and ligustroside ("Others"). Bars indicate the standard error of 12 and 6 samples from the 2010/2011 (white bars) and 2011/2012 (black bars) seasons, respectively. Columns with the same letter are not significantly different by Duncan's multiple-range test at the 5% level for each phenol.

the phosphate buffer was 0.02 M sodium acid phosphate and 0.08 M sodium monobasic phosphate. Initially, the reaction buffer was incubated for 15 min at 30 °C, and the reaction was started by the addition of crude enzyme extract.

One unit of enzyme activity was defined as the amount of enzyme required to increase 0.001 unit (AU) per minute under the above-mentioned conditions. All reactions were carried out in duplicate.

**β-Glucosidase Activity.** A crude enzyme extract was obtained from the above-mentioned acetone powder. Acetone powder (0.14 g) was suspended in 10 mL of a 0.01 M sodium carbonate buffer, containing 0.005 M ethylenediaminotetraacetic acid (EDTA), 0.001 M phenylmethylsulfonyl fluoride (PMSF), and 1% of 2-mercaptoethanol. The pH was adjusted to 9.0 units with NaOH. The suspension was stirred at 4 °C for 1 h and then centrifuged at 15550*g* for 20 min at 4 °C. The pellet was discarded and the supernatant divided into two aliquots; one was used as the active crude enzyme extract, and the other was boiled for 30 min to obtain the denatured enzyme extract.

The β-glucosidase activity analysis was based on the methodology proposed elsewhere.[14] This activity was determined by monitoring the increase in absorbance at 405 nm for 30 min at intervals of 5 min related to the increasing amount of *p*-nitrophenol (p-NP) liberated from the synthetic glucoside *p*-nitrophenyl-β-D-glucopyranoside (p-NPG) (Sigma Chemical Co.). The reaction medium consisted of 100 μL of crude enzyme extract and 100 μL of 0.050 M sodium acetate buffer at pH 5.4 units containing 0.015 M p-NPG as substrate. The mixture was incubated for 30 min at 45 °C. Then, the reaction was stopped by adding 1 mL of 0.5 M sodium carbonate and the spectrophotometrical measurement started at 405 nm. The assay mixture with the denatured enzyme extract served as the control.

The evaluation was performed using a regression curve with p-NP in a range of 0−0.0003 M. One unit of enzyme activity was defined as the amount of enzyme required to produce 1 μmol of p-NP per minute. All reactions were carried out in duplicate.

**Esterase Activity.** A crude enzyme extract was obtained from the above-mentioned acetone powder. Acetone powder (0.25 g) was suspended in 10 mL of a 0.01 M sodium borate buffer, containing 0.005 M EDTA and 0.001 M PMSF. The pH was adjusted to 9.0 units with NaOH. The suspension was stirred at 4 °C for 1 h and then centrifuged at 15550*g* for 20 min at 4 °C. The pellet was discarded, and the supernatant was the enzyme extract.

The esterase activity was analyzed according to the methodology proposed elsewhere.[23] This activity was determined by continuously monitoring the increase in absorbance at 405 nm for 10 min at 40 °C related to the increasing amount of p-NP liberated from the synthetic *p*-nitrophenyl acetate (p-NPA) (Sigma Chemical Co.). The incubation mixture contained 50 μL of crude enzyme extract, 50 μL of 0.15 M p-NPA in ethanol as substrate, and 2.9 mL of a 0.0092 M Tris-HCl buffer at pH 7.5. The reaction was initiated by the addition of the enzyme extract. The assay mixture with 50 μL of extraction buffer served as the control.

The evaluation was performed using a regression curve with p-NP in a range of 0−0.00003 M. One unit of enzyme activity was defined as the amount of enzyme required to produce 1 μmol of p-NP per minute. All reactions were carried out in duplicate.

**Effect of pH.** The enzyme assays at different pH values were performed by measuring the activity of each enzyme using different buffer solutions under standard conditions. In the case of PPO and POD, 0.1 M sodium citrate and a 0.1 M sodium phosphate buffer in the pH range of 4−5 and 6−8 units were used, respectively. The effect of pH on olive β-glucosidase and esterase activity was assessed with a 0.05 M acetic acid−sodium acetate trihidrate solution, 0.05 M sodium phosphate, and a 0.0092 M Tris-HCl buffer in the pH range of 4−5, 6−7, and 7.5−8 units, respectively. In all cases, the pH was finally adjusted with suitable amounts of 1.0 M NaOH and 1.0 M HCl.

**Effect of Temperature.** The optimal temperature for PPO, POD, β-glucosidase, and esterase enzymes was determined by measuring the activity of each enzyme in the temperature range of 10−70 °C under standard conditions.

**Statistical Analysis.** Data were expressed as mean values ± error standard. Statistical software version 7.0 was used for data processing (Statistical for Windows, Tulsa, OK, USA). A comparison among mean variables was made by Duncan's multiple-range tests, and the differences were considered significant when $p < 0.05$.

## RESULTS AND DISCUSSION

**Polyphenolic Compounds.** Hojiblanca, Manzanilla, and Gordal are the main olive varieties employed by the Spanish table olive industry. The concentration of the phenolic composition in the fruit of these varieties for two seasons


dx.doi.org/10.1021/jf5027982 | J. Agric. Food Chem. 2014, 62, 9569−9575

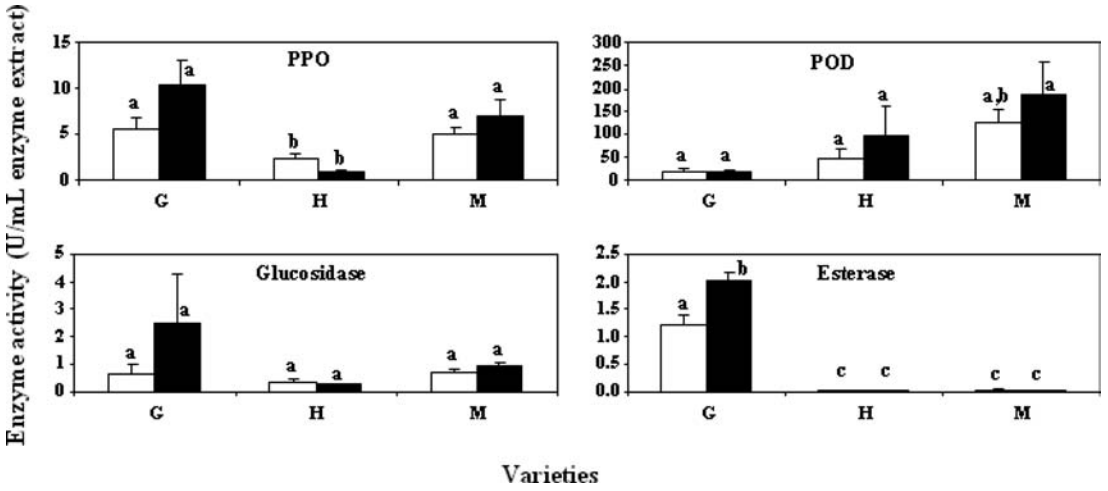


**Figure 3.** Enzymatic activity (U/mL enzyme extract) in fruits of Gordal (G), Hojiblanca (H), and Manzanilla (M) varieties. Bars indicate the standard error of 12 and 6 samples from the 2010/2011 (white bars) and 2011/2012 (black bars) seasons, respectively. Columns with the same letter are not significantly different by Duncan's multiple-range test at the 5% level for each enzyme.

and several orchards is shown in Figure 2. As was expected from previous works,[24−26] the main phenolic compound was oleuropein, followed by hydroxytyrosol 4-glucoside, hydroxytyrosol 1-glucoside, verbascoside, and salidroside, with minor concentrations of tyrosol, luteolin 7-glucoside, caffeic and *p*-coumaric acids, the ester of caffeic acid with secologanoside, comselogoside, luteolin, apigenin, and ligustroside. The hydroxytyrosol 4-glucoside concentration was particularly high in the Hojiblanca variety. This polyphenol increases its concentration in mature olives,[20] but all samples, including those of the Hojiblanca variety, were picked at the same maturity index. Salidroside was not detected in the samples of the Gordal variety as other authors have reported.[27]

In summary, the olives of the Manzanilla variety showed the highest concentration in total polyphenols, 25.4 ± 2.6 and 59.6 ± 6.7 mM, followed by the Hojiblanca variety, 19.7 ± 1.0 and 44.7 ± 1.5 mM, and the Gordal variety, 5.2 ± 0.3 and 21.6 ± 1.4 mM, for the 2010/2011 and 2011/2012 seasons, respectively. These differences among varieties were statistically significant according to Duncan's multiple-range test at the 5% level, and it must also be noted that big differences were found between seasons. A much higher concentration of polyphenols was found in olives from the 2011/2012 season than from the 2010/2011 season, except for hydroxytyrosol 1-glucoside and salidroside. These data are of great importance because of the lack of previous studies and the fact that research was carried out for only one season. In addition, the hydrolysis rate of oleuropein and its residual concentration in edible olives depends on the concentration of this substance in the raw material.

**Enzyme Activity.** Figure 3 shows the PPO activity in fruits of the Gordal, Hojiblanca, and Manzanilla varieties picked with a green-yellow color for two seasons and from several cooperatives.

The first finding that must be noted is the high variability found among the different samples analyzed within the same variety, especially those of the Gordal variety. The standard error of the mean PPO activity of Gordal was 1.28 and 2.61 U/mL enzyme extract for the two seasons studied, whereas these data were recorded as 0.63 and 0.06 U/mL enzyme extract for the Hojiblanca variety. This variability is common in nature, and it has been observed for Italian olive varieties[28] and many other fruits such as peaches.[29]

Regardless of the season, the Gordal variety showed a high PPO activity, followed by Manzanilla and Hojiblanca. In Spain, the Hojiblanca variety destined for table olives is mechanically harvested, whereas the other varieties (Manzanilla and Gordal), which are very prone to bruising, are picked by hand. Indeed, Jiménez-Jiménez et al.[30] found the Hojiblanca variety to have a lower susceptibility to bruising than the others, but no explanation for this phenomenon was reported. Both phenolic compounds and PPO participate in the appearance of bruising after harvesting but from the data reflected in Figures 2 and 3, it seems that the PPO activity could better explain the behavior of the Hojiblanca variety. The low PPO activity in this variety probably contributes to the slow formation of brown spots in harvested olives, whereas the high activity in Manzanilla and Gordal favors their appearance.

The phenolic composition and the PPO activity in both the pulp and the skin of the Manzanilla variety were also characterized (Table 1), which is the variety more prone to bruising. The concentration of the phenolic compounds, except verbascoside, was much higher in the skin than in the pulp but, in contrast, the PPO activity was much lower in the skin than in the pulp. These data are in agreement with those reported by

**Table 1. Enzyme Activity and Polyphenol Compounds in the Skin and Pulp of Manzanilla Olives**

| | skin | pulp |
|---|---|---|
| enzyme activity (U/mL enzyme extract) | | |
| PPO | 4.3 ± 0.1[a] | 19.5 ± 0.4 |
| polyphenol compounds (mmol/kg) | | |
| hydroxytyrosol 1-glucoside | 2.7 ± 0.1 | 0.6 ± 0.2 |
| hydroxytyrosol 4-glucoside | 3.8 ± 0.8 | 2.2 ± 0.7 |
| salidroside | 0.2 ± 0.1 | 0.2 ± 0.1 |
| verbascoside | 0.3 ± 0.1 | 2.4 ± 0.4 |
| oleuropein | 129.4 ± 18.4 | 45.9 ± 8.6 |
| others[b] | 6.8 ± 1.8 | 2.5 ± 0.2 |

[a]Each value is the mean ± standard deviation of three samples. [b]Sum of rutin, caffeoyl ester of secologanoside, comselogoside, and ligustroside.


dx.doi.org/10.1021/jf5027982 | J. Agric. Food Chem. 2014, 62, 9569−9575

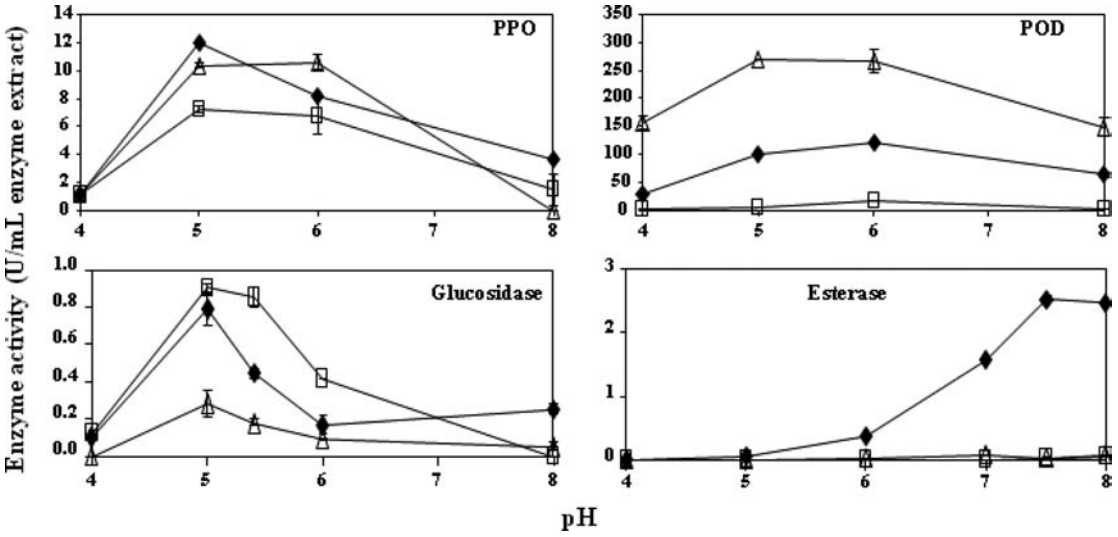


**Figure 4.** Effect of pH on enzymatic activity (U/mL enzyme extract) in the fruits of Gordal (◆), Hojiblanca (△), and Manzanilla (□) varieties. Bars indicate the standard deviation of two samples.

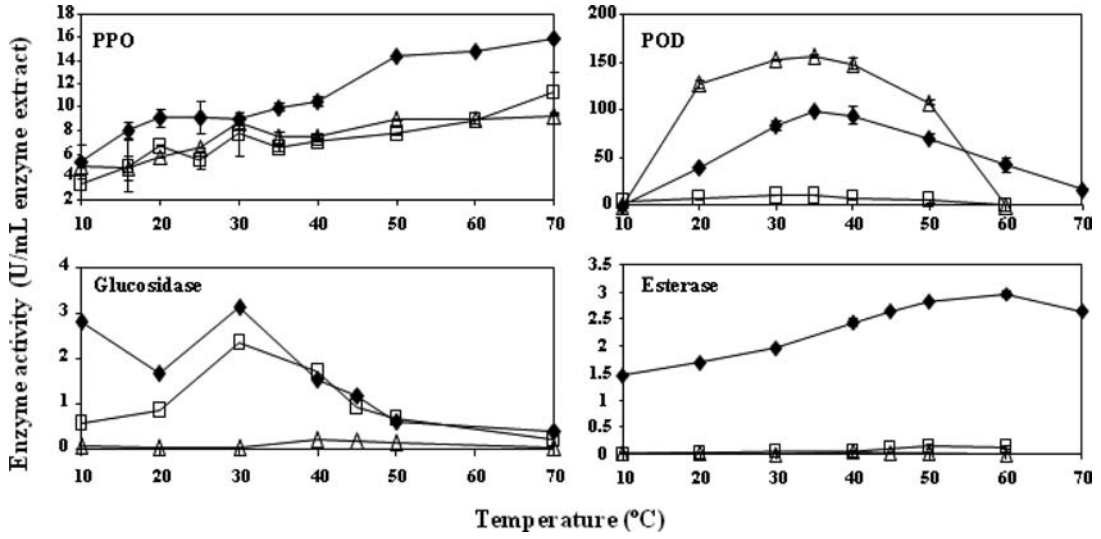


**Figure 5.** Effect of temperature on enzymatic activity (U/mL enzyme extract) in the fruits of Gordal (◆), Hojiblanca (△), and Manzanilla (□) varieties. Bars indicate the standard deviation of two samples.

Chang et al.,[29] who found that in five of nine peach varieties, the PPO activity was higher in the pulp than in the skin.

With regard to the peroxidase activity (Figure 3), the variability of results within a single variety was much higher than that of PPO activity. Particularly, 33% of Hojiblanca samples did not present POD activity for the two seasons studied. In contrast, 50% of Manzanilla samples had a very high POD activity, >170 U/mL enzyme extract, but 15% of the samples had <20 U/mL enzyme extract. The mean values reflect that the Manzanilla variety had the highest POD activity, followed by Hojiblanca and Gordal. The participation of POD in the browning of olives is unknown ,but some researchers have found a much higher concentration of this enzyme in the olive seed than in the rest of the fruit.[31,32] This has been associated with phenolic oxidation of the olive paste during the malaxation step of the olive oil extraction process.

In relation to the $\beta$-glucosidase activity, again a high variability among orchards was found within the same variety for the two seasons (Figure 3). The Gordal variety showed the highest activity, followed by the Manzanilla and Hojiblanca varieties. There are few data about endogenous $\beta$-glucosidase activity in olive varieties, and they were focused mainly on Spanish,[14,17] Tunisian,[18] and Italian[10] olive oil varieties. Furthermore, these studies were carried out with samples from one orchard, one season, and few varieties and did not find the great variability detected in this study.

The cleavage of the ester bond in the oleuropein molecule either chemically with the use of NaOH or enzymatically by esterases gives rise to nonbitter compounds (Figure 1). The activity of this enzyme for the three olive varieties and the two seasons studied is reflected in Figure 3. The two varieties with a high concentration in phenolic compounds and bitterness, Hojiblanca and Manzanilla, had very low esterase activity, whereas the sweet variety Gordal with low concentrations in phenolic compounds showed a very high activity of this enzyme, particularly during the second season. Similar behavior has been reported for the sweet Tunisian variety Dhokar; a low


dx.doi.org/10.1021/jf5027982 | J. Agric. Food Chem. 2014, 62, 9569−9575

concentration in oleuropein was correlated with a high β-glucosidase and esterase activity.[18]

**Influence of External Parameters: pH and Temperature.** The influence of pH on enzyme activity in the fruits of Gordal, Manzanilla, and Hojiblanca varieties is shown in Figure 4. Oxidase enzymes showed a maximum activity in a pH range between 5 and 6 units, which is in agreement with previous data reported for tPPO in Manzanilla olives.[33] However, there are many contradictory findings in the literature on the effect of pH on oxidase activities. Researchers have reported a maximum activity of PPO at pH 4.5[34] and 7.5[35] for the Turkish Domat variety. A maximum POD activity has also been reported at pH 7 and in the range of 4−6 units for Portuguese and Greek olive varieties, respectively.[36,37] These data agree with the result shown in Figure 4, where an optimal pH value of 6 units for POD activity is evident for all varieties.

It must be noted that these oxidase enzymes primarily act in olives during the postharvest period when the pH of the fruit is around 5.

The β-glucosidase activity was at its maximum at pH 5, which is in accordance with data reported by other researchers.[14,38] In contrast, the esterase activity decreased from pH 7 to 4, particularly for the Gordal variety. To our knowledge, there are no data available about the influence of pH on the olive esterase, but our findings mean that the low pH in olives during brining is not favorable for the action of this enzyme.

The effect of temperature on enzyme activity is reflected in Figure 5. It can be observed that the PPO activity increased with increasing temperature up to 70 °C for the three olive varieties studied, which is in contrast to previous data that indicated a maximum activity in the range of 30−50 °C.[34,39] We have no explanation for these results. It could be thought that some nonenzymatic reactions took place during the analyses at high temperature, but the PPO activity was calculated with the difference in absorbance originated from the enzyme extract and the denatured control. It must be noted that PPO stability is high at elevated temperature[35,39] and the analysis was carried out in a few minutes.

The POD presented maximum activity over a temperature range of 30−40 °C, which is in agreement with the range of 30−35 °C reported by other researchers.[36,37]

The β-glucosidase activity in the Gordal variety presented two maximum activity levels at temperatures of 10 and 30 °C, the former temperature was not expected, and the second is similar to previous data found for other olive varieties,[38] even for the Manzanilla variety. Moreover, Hojiblanca showed a maximum activity at 40−45 °C, which agrees with the results found for the Picual variey.[14]

With regard to the esterase activity, the behavior was similar in all varieties, reaching an optimal temperature at around 50−60 °C, particularly for the Gordal variety. This is a very high temperature and not common during the processing of Spanish table olives. Also, there is no information in the literature on the influence of temperature on olive esterase activity.

In conclusion, a great variability in the phenolic content and enzyme activity of olives harvested with the same degree of maturation but from different orchards was found. Variety and season also had a great influence on the contents of polyphenols and enzyme activity in olive fruits. The Manzanilla variety showed the highest concentration in phenolic compounds, followed by Hojiblanca and Gordal with the lowest. With respect to the enzyme activity, it is relevant to say that the lowest PPO activity was found in the Hojiblanca variety, which could explain why this variety is less prone to bruising than the others. Therefore, the results obtained in this study could contribute to the explanation of the great variability found in the quality of processed table olives. Besides, enzyme knowledge can help processors to optimize the elaboration methods of table olives due to the enzymatic transformation of the bitter substance oleuropein instead of the current alkaline hydrolysis.

## AUTHOR INFORMATION


### Corresponding Author

*(C.R.) Phone: +34 954690850. Fax: +34 954691262. E-mail: crb@cica.es.



### Funding

This work was supported by Project AGL 2009-07512 from the Spanish government and European Union (European Regional Development Funds). E.R. thanks MINECO for her FPI fellowship.


### Notes

The authors declare no competing financial interest.

## REFERENCES


(1) Brenes, M.; de Castro, A. Transformation of oleuropein and its hydrolysis products during Spanish-style green olive processing. *J. Sci. Food Agric.* **1998**, *77*, 353−358.

(2) Ben-Shalom, N.; Kahn, V.; Harel, E.; Mayer, A. M. Olive cathecol oxidase-changes during fruit development. *J. Sci. Food Agric.* **1977**, *28*, 545−550.

(3) Segovia-Bravo, K.; Jarén-Galán, M.; García-García, P.; Garrido-Fernández, A. Browning reactions in olives: mechanism and polyphenols involved. *Food Chem.* **2009**, *114*, 1380−1385.

(4) Sánchez, A. H.; Romero, C.; Ramírez, E.; Brenes, M. Storage of mechanically harvested Manzanilla olives under controlled atmospheres. *Postharvest Biol. Technol.* **2013**, *81*, 60−65.

(5) García, A.; Romero, C.; Medina, E.; García, P.; de Castro, A.; Brenes, M. Debittering of olives by polyphenol oxidation. *J. Agric. Food Chem.* **2008**, *56*, 11862−11867.

(6) Sciancalepore, V.; Longone, V. Polyphenol oxidase activity and browning in green olives. *J. Agric. Food Chem.* **1984**, *32*, 320−321.

(7) Goupy, P.; Fleuriet, A.; Amiot, M. J.; Macheix, J. J. Enzymatic browning, oleuropein content, and diphenol oxidase activity in olive cultivars (*Olea europaea* L.). *J. Agric. Food Chem.* **1991**, *39*, 92−95.

(8) Ortega-García, F.; Blanco, S.; Peinado, M. A.; Peragón, J. Polyphenol oxidase and its relationship with oleuropein concentration in fruits and leaves of olive (*Olea europaea*) cv. 'Picual' trees during fruit ripening. *Tree Physiol.* **2008**, *28*, 45−54.

(9) Ortega-García, F.; Peragón, J. Phenylalanine ammonia-lyase, polyphenol oxidase, and phenol concentration in fruits of *Olea europaea* L. cv. Picual, Verdial, Arbequina, and Frantoio during ripening. *J. Agric. Food Chem.* **2009**, *57*, 10331−10340.

(10) Briante, R.; Patumi, M.; Limongelli, S.; Febbraio, F.; Vaccaro, C.; Di Salle, A.; La Cara, F.; Nucci, R. Changes in phenolic and enzymatic activities content during fruit ripening in two Italian cultivars of *Olea europaea* L. *Plant Sci.* **2002**, *162*, 791−798.

(11) Hornero-Méndez, D.; Gallardo-Guerrero, L.; Jarén-Galán, M.; Mínguez-Mosquera, M. I. Differences in the activity of superoxide dismutase, polyphenol oxidase and Cu-Zn content in the fruits of Gordal and Manzanilla olive varieties. *Z. Naturforsch.* **2002**, *57*, 113−120.

(12) Medina, E.; Romero, C.; Brenes, M.; García, P.; de Castro, A.; García, A. Profile of anti-lactic acid bacteria compounds during the storage of olives which are not treated with alkali. *Eur. Food Res. Technol.* **2008**, *228*, 133−138.

(13) Servili, M.; Taticchi, A.; Esposto, S.; Urbani, S.; Selvaggini, R.; Montedoro, G. Influence of the decrease in oxygen during malaxation

of oliva paste on the composition of volátiles and phenolic compounds in virgin olive oil. *J. Agric. Food Chem.* **2008**, *56*, 10048−10055.
(14) Romero-Segura, C.; Sanz, C.; Pérez, A. G. Purification and characterization of an olive fruit β-glucosidase involved in the biosynthesis of virgin olive oil phenolics. *J. Agric. Food Chem.* **2009**, *57*, 7983−7988.
(15) Medina, E.; Brenes, M.; Romero, C.; García, A.; de Castro, A. Main antimicrobial compounds in table olives. *J. Agric. Food Chem.* **2007**, *55*, 9817−9823.
(16) Gutiérrez-Rosales, F.; Romero, M. P.; Casanovas, M.; Motilva, M. J.; Mínguez-Mosquera, M. I. Metabolites involved in oleuropein accumulation and degradation in fruits of *Olea europaea* L.: Hojiblanca and Arbequina varieties. *J. Agric. Food Chem.* **2010**, *58*, 12924−12933.
(17) Gutiérrez-Rosales, F.; Romero, M. P.; Casanovas, M.; Motilva, M. J.; Mínguez-Mosquera, M. I. β-Glucosidase involvement in the formation and transformation of oleuropein during the growth and development of olive fruits (*Olea europaea* L. cv. Arbequina) grown under different farming practices. *J. Agric. Food Chem.* **2012**, *60*, 4348−4358.
(18) Jemai, H.; Bouaziz, M.; Sayadi, S. Phenolic composition, sugar contents and antioxidant activity of Tunisian sweet olive cultivar with regard to fruit ripening. *J. Agric. Food Chem.* **2009**, *57*, 2961−2968.
(19) Kumral, A.; Korukluoglu, M.; Romero, C.; de Castro, A.; Ruiz-Barba, J. L.; Brenes, M. Phenolic inhibitors involved in the natural fermentation of Gemlik cultivar black olives. *Eur. Food Res. Technol.* **2013**, *236*, 101−107.
(20) Romero, C.; Brenes, M.; García, P.; Garrido, A. Hydroxytyrosol 4-β-D-glucoside, an important phenolic compound in olive fruits and derived products. *J. Agric. Food Chem.* **2002**, *50*, 3835−3839.
(21) Ramírez, E.; García-García, P.; de Castro, A.; Romero, C.; Brenes, M. Debittering of black dry-salted olives. *Eur. J. Lipid Sc. Technol.* **2013**, *115*, 1319−1324.
(22) Civello, P. M.; Martínez, G. A.; Chaves, A. R.; Añón, M. C. Peroxidase from strawberry fruit (*Fragaria ananassa* Duch.): partial purification and determination of some properties. *J. Agric. Food Chem.* **1995**, *43*, 2596−2601.
(23) Khoufi, S.; Hamza, M.; Sayadi, S. Enzymatic hydrolysis of olive wastewater for hydroxytyrosol enrichment. *Bioresour. Technol.* **2011**, *102*, 9050−9058.
(24) Brenes, M.; García, P.; Durán, M. C.; Garrido, A. Concentration of phenolic compounds change in storage brines of ripe olives. *J. Food Sci.* **1993**, *58*, 347−350.
(25) Bastoni, L.; Biando, A.; Piccioni, F.; Uccella, N. Biophenolic profile in olives by nuclear magnetic resonance. *Food Chem.* **2001**, *73*, 145−151.
(26) Medina, E.; Morales-Sillero, A.; Ramírez, E. M.; Rallo, P.; Brenes, M.; Romero, C. New genotypes of table olives: profile of bioactive compounds. *Int. J. Food Sci. Technol.* **2012**, *47*, 2334−2341.
(27) Medina, E.; García, A.; Romero, C.; de Castro, A.; Brenes, M. Study of the anti-lactic acid bacteria compounds in table olives. *Int. J. Food Sci. Technol.* **2009**, *44*, 1286−1291.
(28) De Stefano, G.; Sciancalepore, V. Polyphenol oxidases and peroxidases in 5 table olive cv. *Ind. Aliment.* **1993**, *32*, 731−733.
(29) Chang, S.; Tan, C.; Frankel, E. N.; Barrett, D. N. Low-density lipoprotein antioxidant activity of phenolic compounds and polyphenol oxidase activity in selected clingstone peach cultivars. *J. Agric. Food Chem.* **2000**, *48*, 147−151.
(30) Jiménez-Jiménez, F.; Castro-García, S.; Blanco-Roldán, G. L.; Ferguson, L.; Rosa, U.; Gil-Ribes, J. A. Table olive cultivar susceptibility to impact bruising. *Postharvest Biol. Technol.* **2013**, *86*, 100−106.
(31) Luaces, P.; Romero, C.; Gutiérrez, F.; Sanz, C.; Pérez, A. G. Contribution of olive seed to the phenolic profile and related quality parameters of virgin olive oil. *J. Sci. Food Agric.* **2007**, *87*, 2721−2727.
(32) García-Rodríguez, R.; Romero-Segura, C.; Sanz, C.; Sánchez-Ortiz, A.; Pérez, A. G. Role of polyphenol oxidase and peroxidase in shaping the phenolic profile of virgin olive oil. *Food Res. Int.* **2011**, *44*, 629−635.
(33) Segovia-Bravo, K.; Jarén-Galán, M.; García-García, P.; Garrido-Fernández, A. Characterization of polyphenol oxidase from the Manzanilla cultivar (*Olea europea pomiformis*) and prevention of browning reactions in bruised olive fruits. *J. Agric. Food Chem.* **2007**, *55*, 6515−6520.
(34) Ünal, M. Ü.; Taş, C.; Şener, A. Determination of biochemical properties of polyphenol oxidase from Domat olives. *GIDA* **2011**, *36*, 185−192.
(35) Gençer, N.; Sinan, S.; Arslan, O. Kinetic properties of polyphenol oxidase obtained from various olives (*Olea europa* L.). *Asian J. Chem.* **2012**, *24*, 2159−2161.
(36) Saraiva, J. A.; Nunes, C. S.; Coimbra, M. A. Purification and characterization of olive (*Olea europaea* L.) peroxidase − evidence for the occurrence of a pectin binding peroxidase. *Food Chem.* **2007**, *101*, 1571−1579.
(37) Tzika, E. D.; Sotiroudis, T. G.; Papadimitriou, V.; Xenakis, A. Partial purification and characterization of peroxidase from olives (*Olea europaea* cv. Koroneiki). *Eur. Food Res. Technol.* **2009**, *228*, 487−495.
(38) Kara, H. E.; Sinan, S.; Turan, Y. Purification of β-glucosidase from olive (*Olea europaea* L.) fruit tissue with specifically designed hydrophobic interaction chromatography and characterization of the purified enzymatic. *J. Chromatogr., B* **2011**, *879*, 1507−1512.
(39) Taticchi, A.; Esposto, S.; Veneziani, G.; Urbani, S.; Selvaggini, R.; Servili, M. The influence of the malaxation temperature on the activity of polyphenoloxidase and peroxidase and on the phenolic composition of virgin olive oil. *Food Chem.* **2013**, *136*, 975−983.

**Table 1. Juices Used in This Study**

| scientific name | common name | local name | status |
|---|---|---|---|
| | **Mature Flesh** | | |
| *Averrhoa bilimbi* | bilimbi | belimbing buluh | native |
| *Averrhoa carambola* cv. B10 | star fruit | belimbing segi | native |
| *Barringtonia racemosa* | hippo apple | putat | native |
| *Cynometra cauliflora* | nam nam | nam nam, katak puru | native and endemic |
| *Garcinia atroviridis* | Malabar tamarind | gelugor | native |
| *Myristica fragrans* | nutmeg | pala | native |
| *Phyllanthus acidus* | Indian gooseberry | cermai | native |
| *Psidium guajava* cv. GU8 | guava | jambu batu | introduced |
| *Sandoricum koetjape* | santol, kechapi | sentul | native |
| *Spondias pinnata* | wild mango, hog plum | kedondong, amra | native |
| *Syzygium malaccense* | Malay apple | jambu susu, jambu bol | native and endemic |
| *Syzygium samarangense* | wax apple | jambu semarang | native |
| *Zizyphus mauritiana* | Indian jujube | bidara | introduced |
| | **Ripe Flesh** | | |
| *Bouea macrophylla* | gandaria | kundang, remia | native and endemic |
| *Carica papaya* cv. Batu Arang | papaya | betik | introduced |
| *Citrullus lanatus* cv. New Dragon | watermelon | tembikai | introduced |
| *Citrus aurantifolia* | lime | limau nipis | native |
| *Citrus maxima* cv. PO52 | pommelo | limau bali | native |
| *Citrus microcarpa* | calamansi | limau kasturi | native |
| *Cucumis melo* cv. Inodorus | melon | honeydew | introduced |
| *Mangifera indica* cv. Malgoa | mango | mangga | native |
| *Manilkara zapota* cv. CM19 (mega) | sapodilla | ciku | introduced |
| *Musa acuminata* cv. Mas | banana | pisang | native |
| | **Ripe Aril** | | |
| *Annona muricata* | sour sop | durian belanda | introduced |
| *Annona squamosa* | sugar-apple, sweetsop | nona | introduced |
| *Artocarpus heterophyllus* cv. J33 (tekam yellow) | jackfruit | nangka | native |
| *Baccaurea montleyana* | rambai | rambai | native |
| *Baccaurea polyneura* | jentik | jentik | native and endemic |
| *Dimocarpus longan* cv. Edaw | longan | mata kucing | introduced |
| *Garcinia mangostana* | mangosteen | manggis | native |
| *Lansium domesticum* | dokong | dokong | native |
| *Nephelium lappaceum* cv. R191 (Anak sekolah) | rambutan | rambutan | native |
| *Nephelium ramboutan-ake* | pulasan | pulasan | native |
| *Salacca edulis* cv. Z6 (Raja) | snake fruit | salak | native |
| *Sandoricum koetjape* | santol, kechapi | sentul | native |
| | **Young Endosperm** | | |
| *Cocos nucifera* cv. Pandan wangi | coconut | kelapa | introduced |
| | **Ripe Peduncle** | | |
| *Ananas comosus* cv. Moris | pineapple | nenas | introduced |
| | **Stem** | | |
| *Apium graveolens* | celery | saleri | introduced |
| *Saccharum officinarum* | sugar cane | tebu | introduced |
| | **Root** | | |
| *Daucus carota* | carrot | lobak merah | introduced |

Elevation of blood sugar level (hyperglycemia) can be minimized to normal (euglycemia) by inhibiting the carbohydrate-digesting enzymes such as $\alpha$-glucosidase. $\alpha$-Glucosidase is known to catalyze the final step in the digestion of carbohydrate to absorbable monosaccharides. Thus, in this study the juices were also screened for their $\alpha$-glucosidase inhibitory activity to determine their antihyperglycemic effect. Due to the dose-limiting side effects of oral antihyperglycemic drugs, we hypothesized that consumption of the antioxidant-rich juices with $\alpha$-glucosidase inhibitory activity prior to a meal is a safer and appropriate alternative for the treatment of hyperglycemia.

On the basis of the published data from various comparative studies of phenolic-rich extracts from fruits, several tropical fruits were proven to be effective against $\alpha$-glucosidase, such as *Pouteria lucuma* (lucuma), a native Peruvian fruit;[14] *Campomanesia phaea* (cambuci) and *Eugenia dysenterica* (cagaita), which are native to Brazil;[15] *Eugenia uniflora* (pinanga), which is native to tropical America;[16] and *Aristotelia chilensis* (maqui), a Latin-American fruit.[17] However, all of these fruits are not found in Malaysia, and no earlier study on $\alpha$-glucosidase inhibitory activity of tropical juices had been reported.

To the best of our knowledge, there was only one comparative study that had determined the $\alpha$-glucosidase inhibitory activity of five juice samples from fruits and vegetables that are commonly consumed in Korea.[18] However, the highest percentage of inhibition, 30.4% (indicated by the juice from lotus root), was considered very low. Our literature search indicated that, to date, there have only been four reports on the $\alpha$-glucosidase inhibitory activity of 10 fruits selected for this study, which are 99.5% ethanol extracts of dried mature fleshes of *Phyllanthus acidus* (Indian gooseberry), *Spondias pinnata* (hog plum), *Zizyphus mauritiana* (Indian jujube), and *Manilkara zapota* (sapodilla) and *Artocarpus heterophyllus* (jackfruit);[19] 70% methanol extracts of lyophilized ripe fleshes of *Averrhoa carambola* (star fruit) and *Annona muricata* (sour sop);[15] aqueous extracts of fresh ripe fleshes of *Averrhoa carambola, Phyllanthus acidus, Spondias pinnata, Zizyphus mauritiana, Manilkara zapota, Annona squamosa* (sugar-apple), and *Dimocarpus longan* (longan);[20] and 70% methanol extract of lyophilized ripe flesh of *Carica papaya* (papaya).[17] Different extraction solvents and sample matrices were used in these studies.

The aims of the present study were to comparatively analyze the total phenolic contents and vitamin C as well as antioxidant and $\alpha$-glucosidase inhibitory activities of 40 fresh and pure juices from juicy and fleshy fruit parts, stems, and roots that are commonly consumed in Malaysia. The results were correlated with each other, and the unknown phenolic compounds in the juices with higher activities were identified.

## MATERIALS AND METHODS

**Plant Materials.** Table 1 shows a list of 40 juices that were used in this study. For several fruit crops, the information about the cultivars or clones used were also included in Table 1. The juicy parts at their


dx.doi.org/10.1021/jf502912t | J. Agric. Food Chem. 2014, 62, 9576−9585

Table 2. Yield of Juice from 20 g of Sample, pH Values, and Total Soluble Solids[a]

| scientific name | juice yield (%) | pH | total soluble solids (°Brix) |
|---|---|---|---|
| **Mature Flesh** | | | |
| *Averrhoa bilimbi* | 57.5 ± 2.50ef | 1.67 ± 0.67δ | 1.03 ± 0.01w |
| *Averrhoa carambola* | 64.17 ± 1.44bc | 3.68 ± 0.01r | 11.74 ± 0.14p |
| *Barringtonia racemosa* | 56.67 ± 2.89efg | 3.77 ± 0.02q | 7.14 ± 0.14u |
| *Cynometra cauliflora* | 50.01 ± 5.00hi | 2.75 ± 0.03z | 11.26 ± 0.14q |
| *Garcinia atroviridis* | 49.17 ± 1.44hi | 1.81 ± 0.01ε | 11.26 ± 0.14q |
| *Myristica fragrans* | 57.05 ± 0.87efg | 3.08 ± 0.02v | 7.88 ± 0.14t |
| *Phyllanthus acidus* | 60.04 ± 2.50cde | 2.80 ± 0.02y | 1.04 ± 0.01w |
| *Psidium guajava* | 51.67 ± 2.89hi | 4.15 ± 0.01o | 12.06 ± 0.14p |
| *Sandoricum koetjape* | 36.67 ± 1.44l | 3.06 ± 0.01v | 13.63 ± 0.14n |
| *Spondias pinnata* | 50.17 ± 1.26hi | 2.91 ± 0.04x | 1.01 ± 0.01w |
| *Syzygium malaccense* | 56.67 ± 5.20efg | 3.00 ± 0.02w | 1.01 ± 0.01w |
| *Syzygium samarangense* | 63.50 ± 3.61bcd | 3.16 ± 0.04u | 1.01 ± 0.01w |
| *Zizyphus mauritiana* | 62.50 ± 2.50bcd | 2.66 ± 0.01β | 7.99 ± 0.30t |
| **Ripe Flesh** | | | |
| *Bouea macrophylla* | 47.50 ± 2.50ij | 4.37 ± 0.01n | 3.25 ± 0.30v |
| *Carica papaya* | 47.50 ± 2.50ij | 5.09 ± 0.01i | 16.26 ± 0.13m |
| *Citrullus lanatus* | 71.67 ± 2.89a | 5.48 ± 0.01h | 12.77 ± 0.14° |
| *Citrus aurantifolia* | 35.83 ± 1.44l | 2.47 ± 0.01ᵋ | 10.06 ± 0.14s |
| *Citrus maxima* | 53.33 ± 2.89fgh | 3.38 ± 0.03s | 13.71 ± 0.14n |
| *Citrus microcarpa* | 19.67 ± 0.58n | 2.34 ± 0.01σ | 11.26 ± 0.14q |
| *Cucumis melo* | 53.33 ± 2.89fgh | 6.21 ± 0.01d | 7.72 ± 0.14t |
| *Mangifera indica* | 43.17 ± 2.75jk | 3.36 ± 0.01s | 28.83 ± 0.27d |
| *Manilkara zapota* | 48.33 ± 2.89hi | 5.53 ± 0.03g | 29.13 ± 0.27d |
| *Musa acuminata* | 6.33 ± 1.26p | 5.09 ± 0.01i | 13.71 ± 0.14n |
| **Ripe Aril** | | | |
| *Annona muricata* | 26.67 ± 2.89m | 3.36 ± 0.01s | 19.32 ± 0.28l |
| *Annona squamosa* | 14.50 ± 0.50° | 5.78 ± 0.01f | 30.66 ± 0.72b |
| **Ripe Aril** | | | |
| *Artocarpus heterophyllus* | 39.17 ± 1.44kl | 4.97 ± 0.01j | 22.52 ± 0.28i |
| *Baccaurea montleyana* | 67.00 ± 0.87b | 3.07 ± 0.01v | 29.76 ± 0.28c |
| *Baccaurea polyneura* | 74.17 ± 1.44a | 2.71 ± 0.01α | 32.83 ± 0.27a |
| *Dimocarpus longan* | 66.67 ± 2.87b | 6.87 ± 0.01a | 30.99 ± 0.27b |
| *Garcinia mangostana* | 50.00 ± 5.00hi | 2.92 ± 0.01x | 24.90 ± 0.28h |
| *Lansium domesticum* | 50.83 ± 1.44hi | 3.69 ± 0.01r | 27.89 ± 0.27f |
| *Nephelium lappaceum* | 59.17 ± 1.44de | 4.98 ± 0.01j | 27.89 ± 0.27f |
| *Nephelium ramboutan-ake* | 65.83 ± 1.44b | 4.64 ± 0.01l | 25.85 ± 0.27g |
| *Salacca edulis* | 42.50 ± 2.50k | 4.53 ± 0.01m | 29.13 ± 0.27d |
| *Sandoricum koetjape* | 11.67 ± 1.44o | 3.26 ± 0.01t | 28.36 ± 0.28e |
| **Young Endosperm** | | | |
| *Cocos nucifera* | 52.50 ± 2.50gh | 6.56 ± 0.02b | 10.86 ± 0.14qr |
| **Ripe Peduncle** | | | |
| *Ananas comosus* | 53.33 ± 2.89fgh | 3.86 ± 0.01p | 20.28 ± 0.28k |
| **Stem** | | | |
| *Apium graveolens* | 53.33 ± 2.89fgh | 5.96 ± 0.01e | 2.90 ± 0.15v |
| *Saccharum officinarum* | 63.33 ± 2.89bcd | 4.94 ± 0.01k | 21.08 ± 0.28j |
| **Root** | | | |
| *Daucus carota* | 43.33 ± 2.89jk | 6.46 ± 0.01c | 10.62 ± 0.14r |

[a]Values are means ± standard deviations of triplicate analyses. Results from different analyses were analyzed separately. Values per each analysis followed by different letters are significantly different ($p < 0.05$).

commercial maturity stages were harvested by skilled and knowledgeable farmers from various orchards in Penang, Malaysia. This is an important procedure to ensure the identity of the plants and the use of identical maturity stages for each sample. Only top-quality juicy parts (without bruise/injury) were selected for the experimental work. For each of the samples, at least three handpicked fruit parts, stems, or roots from three different trees were combined. To maintain the freshness of the sample, the interval between harvesting and extraction was specified to be <4 h. The skin, peel, husk, or rind and seed were then removed.

**Chemicals.** All chemicals and reagents used in this study were of analytical grade. Folin−Ciocalteu phenol reagent, metaphosphoric acid, 2,6-dichloroindophenol (DCIP), 1,1-diphenyl-2-picrylhydrazyl radical (DPPH), 2,4,6-tri(2-pyridyl)-*s*-triozine (TPTZ), ferric chloride hexahydrate, ferrous chloride hexahydrate, ferrozine, 6-hydroxy-2,5,7,8-tetramethylchroman-2-carboxylic acid (Trolox), myricetin, quercetin, kaempferol, dihydroquercetin, ascorbic, gallic acid, and ellagic acid were obtained from Sigma-Aldrich Chemicals (St. Louis, MO, USA). Sodium carbonate and sodium bicarbonate were purchased from Fluka (Buchs, Switzerland).

**Extraction.** For each sample, the fresh succulent part (200 g fresh weight) was washed with distilled water, and the water remaining at the external surface of the sample was dried out using blotting paper (Whatman 3MM Chr). The sample was later ground for 2 min using a grinder to yield a fine puree (40 mesh or 400 μm of particle size). The puree was equally divided into two groups. The puree from the first group (100 g) was then soaked in 500 mL of distilled water for 15 min at room temperature (27 ± 1 °C). The pure puree from the second group and the diluted puree (from the first group of puree) were then filtered using a clean muslin cloth and centrifuged using a Hittech EBA 20 centrifuge (Japan) at 704*g* for 15 min. The yields of the pure juices (%) were calculated. Concentration of the obtained diluted juice was referred to fresh sample weight resulting in 200 mg/mL (w/v). The pure juices and diluted juices were stored at 4 °C in the dark until further analysis. The interval between extraction process and experimental work was specified to be <1 h. For each sample, the extraction process was carried out in triplicate, using the juicy part from different trees each time.

**Total Soluble Solids (°Brix) and pH.** The total soluble solids and pH values of the pure juices were determined using a hand refractometer (Atago 2340 HSR-500, Japan) and a pH meter (Mettler Toledo 320, Columbus, OH, USA), respectively. Refractive indices were recorded and converted to degrees Brix using a conversion table. All of the measurements were performed at room temperature (27 ± 1 °C) in triplicate.

**Determination of Total Phenolic and Vitamin C Contents.** The total phenolic and vitamin C contents from the diluted juices (200 mg/mL) were quantified as described by Sulaiman and Ooi.[21] Diluted juices were used in both experiments to compare our results with the published data that mostly measured the contents of total phenolic and vitamin C in 1 g of fresh weight or dry weight of sample. The experiments were carried out in triplicate. Standard curves were plotted using gallic acid (0−1 mg/mL) and ascorbic acid (0−2.5 mg/mL). The total phenolic contents were expressed as micrograms of

gallic acid equivalent per gram of fresh weight of sample (μg GAE/g sample), and the contents of vitamin C were expressed as micrograms of ascorbic acid equivalent per gram fresh weight of sample (μg AAE/g sample).

**DPPH Free Radical Scavenging and Ferric Reducing Antioxidant Potential (FRAP) Assays.** The activities of the samples were separately analyzed using DPPH free radical scavenging and ferric reducing antioxidant potential (FRAP) assays according to the methods as described by Sulaiman and Ooi.[21] All tests were run in triplicate. Diluted juices (200 mg/mL) were used in both assays to compare the obtained results with the earlier findings that mostly quantified the contents of antioxidants in 1 g of fresh weight or dry weight of sample. Standard curves were obtained using different concentrations of ascorbic acid (0−0.5 mg/mL) for DPPH assay and Trolox (0−1 mg/mL) for FRAP assay. The absorbance of the diluted juice reaction was compared to that of the standard, and the results from the DPPH assay were expressed as micrograms of vitamin C equivalent antioxidant capacity per gram of fresh weight of sample (μg VCEAC/g sample). The results from the FRAP assay were expressed as micrograms of Trolox equivalent antioxidant capacity per gram of fresh weight of sample (μg TEAC/g sample).

**Metal Chelating Assay.** The metal chelating assay was performed according to the method as described by Sulaiman and Ooi.[21] The metal chelating percentage of pure juices was determined in this study. It was calculated as follows: % metal chelating = [(absorbance of negative control − absorbance of pure juice)/absorbance of negative control] × 100%. All experiments were performed in triplicate.

**α-Glucosidase Inhibitory Assay.** The α-glucosidase inhibitory activity was determined according to the method of Ooi et al.[22] The percentage of α-glucosidase inhibitory activity of pure juices was determined in this study. It was calculated as follows: % α-glucosidase inhibition = [(absorbance of negative control − absorbance of pure juice)/absorbance of negative control] × 100%. All measurements were done in triplicate.

**Ultraperformance Liquid Chromatography (UPLC) Analysis of Phenolic Compounds in *Barringtonia racemosa* and *Phyllanthus acidus*.** The fresh pure juices from *Barringtonia racemosa* and *Phyllanthus acidus* were filtered through a 0.2 μm syringe filter. The phenolic compounds in the juices were separated using an Acquity ultraperformance liquid chromatography (UPLC) system (Waters, Milford, MA, USA) equipped with a reverse-phase Acquity UPLC BEH $C_{18}$ column 1.7 μm (100 mm × 2.1 mm i.d.) and photodiode array detector. Different mobile phases and gradient modes were used to obtain the best separation for each juice. The fresh pure juices (5 mL) were also hydrolyzed according to the method of Harborne[23] with 10 mL of 2 M hydrochloric acid for 40 min in boiling water. Ethyl acetate was used for extracting the aglycones from the hydrolyzed juices. Each extract (5 mg/mL) was filtered through a 0.2 μm syringe filter.

The phenolic compounds in the hydrolyzed juice extracts were quantified using the UPLC system. The mobile phase consisted of solvent A (1% acetic acid) and solvent B (methanol/acetic acid/water, 18:1:1). Each extract was separated using a gradient mode that was initially set at an A/B ratio of 75:25 and then linearly increased to 50:50 at 1.3 min, 25:75 at 3.3 min, and 10:90 at 6 min. The detector was set at 280 nm for quantification of gallic acid and at 350 nm for ellagic acid, myricetin, quercetin, kaempferol, and dihydroquercetin, with a flow rate of 0.20 mL/min and an injection volume of 5.0 μL. Phenolic compounds in the extracts were identified and quantified by comparison of their retention times and UV spectra (detected by photodiode array detector) against the standards. A standard calibration curve of different concentrations (7.81−500 μg/mL) of each standard was plotted. The concentration of phenolic compounds in each extract was calculated using the regression equation of its peak area to peak area of a known concentration of standard from the calibration curve. The results were expressed as milligrams of phenolic compound per 100 g of extract (mg/100 g of extract).

**Statistical Analysis.** Data were analyzed using SPSS 16.0 for Windows (SPSS Inc., Chicago, IL, USA). Values were expressed as means ± standard deviations. Analysis of variance was determined by one-way ANOVA using GraphPadPrism (San Diego, CA, USA). A $p$ value of <0.05 was considered as statistically significant.

## RESULTS AND DISCUSSION

**Total Soluble Solids (°Brix) and pH.** As indicated in Table 2, the pure juice yields varied largely among the samples. *Baccaurea polyneura* achieved the highest yield (74.17 ± 1.44%), and *Musa acuminata* gave the lowest yield (6.33 ± 1.26%). The total soluble solids ranged from 1.01 ± 0.01 °Brix (in *Syzygium malaccense*, *Syzygium samarangense*, and *Spondias pinnata*) to 32.83 ± 0.27 °Brix (in *Baccaurea polyneura*). Meanwhile, the pH values ranged from 1.67 ± 0.67 (in *Averrhoa bilimbi*) to 6.87 ± 0.01 (in *Dimocarpus longan*).

**Total Phenolic Content (TPC).** From 40 juices, juice obtained from *Psidium guajava* exhibited the highest value of TPC (Table 3). Our findings are in agreement with many earlier comparative studies that had reported higher content of TPC in *Psidium guajava* than that of other fruits. However, the value obtained from this study was found to be lower than those quantified from 70% acetone extract,[5] methanol extract,[6] 50% ethanol extract,[7,24] and in acetone/water/acetic acid (70:29.5:0.5).[9] The high reported values of TPCs might be due to the efficiency of the solvent systems in extracting phenolic compounds from the fleshes. The juices of *Barringtonia racemosa*, *Averrhoa carambola*, *Myristica fragrans*, *Garcinia mangostana*, *Sandoricum koetjape* (mature flesh), and *Citrus maxima* ranked next with TPC values >600 μg GAE/g sample.

This is found to be the first TPC quantification for the above-listed fruit juices excluding *A. carambola* and *G. mangostana*. Fu et al.[24] measured lower TPC in the 50% ethanol extracts of these two fruits, whereas >1000 μg GAE/g sample was estimated from the ripe fleshes of *A. carambola*, extracted using 100% methanol,[5] 70% acetone,[6] and 50% ethanol.[7] Higher TPCs were also detected from *Citrus aurantifolia* and *Citrus microcarpa*. These two juices are often freshly consumed and added in various Southeast Asian foods such as tom-yum and curries. The phenolic compounds of *Citrus* are generally dominated by flavanone glycosides.[25] Flavanone glycosides such as hesperidin, neohesperidin, and hesperitin had been isolated from the juice of *Citrus aurantifolia*[26] and might also contribute to increase the content.

**Vitamin C Content.** Vitamin C contents ranged from 51.87 ± 0.74 μg AAE/g sample in *Cocos nucifera* to 590.31 ± 7.44 μg AAE/g sample in *Psidium guajava* (Table 3). Isabelle et al.[9] and Kubola et al.[12] respectively reported 714 and 780 μg AAE/g sample of vitamin C from *Psidium guajava*, whereas other studies mostly found >1000 μg AAE/g sample in this fruit.[5−7] The differences may result from the cultivars and methodologies used to extract and quantify vitamin C from the fresh sample matrices. The juices of *Spondias pinnata* and *Dimocarpus longan* were also found to contain >300 μg AAE/g sample, and the values were respectively higher than that of Kubola et al.[12] (90 μg AAE/g sample) and Mahattanatawee et al.[6] (140 μg AAE/g sample). Moreover, Isabelle et al.[9] reported 633.9 μg AAE/g sample from *Dimocarpus longan* and had identified *Psidium guajava* and *Dimocarpus longan* as fruits with high vitamin C contents. Contents ranging from 200 to 300 μg AAE/g sample were measured from the juices of *Citrus maxima*, *Garcinia atroviridis*, *Carica papaya*, *Citrus aurantifolia*, and *Citrus microcarpa*. Previous studies had reported higher vitamin C contents from the fleshes of *Carica papaya* cv. Exotica,[5] cv. Red Lady,[6] and cv. Solo.[7] Other aforementioned fruits are believed

**Table 3. Total Phenolic Content (TPC) and Vitamin C Content of the Juices[a]**

| scientific name | TPC ($\mu$g GAE/g sample) | vitamin C ($\mu$g AAE/g sample) |
|---|---|---|
| | **Mature Flesh** | |
| *Averrhoa bilimbi* | 251.83 ± 0.79p | 154.14 ± 6.44h |
| *Averrhoa carambola* | 699.67 ± 2.24c | 85.39 ± 3.72no |
| *Barringtonia racemosa* | 790.40 ± 0.23b | 108.16 ± 1.49k |
| *Cynometra cauliflora* | 52.59 ± 0.53$\sigma$ | 106.01 ± 3.24kl |
| *Garcinia atroviridis* | 117.28 ± 0.40y | 280.91 ± 7.44d |
| *Myristica fragrans* | 658.76 ± 4.04d | 139.10 ± 3.72i |
| *Phyllanthus acidus* | 204.75 ± 4.99s | 102.58 ± 6.44klm |
| *Psidium guajava* | 857.24 ± 12.65a | 590.31 ± 7.44a |
| *Sandoricum koetjape* | 617.04 ± 2.23f | 98.28 ± 3.72m |
| *Spondias pinnata* | 421.64 ± 0.32j | 396.93 ± 3.94b |
| *Syzygium malaccense* | 81.51 ± 0.06$\alpha$ | 100.43 ± 3.72lm |
| *Syzygium samarangense* | 374.83 ± 4.03m | 72.50 ± 3.72pqr |
| *Zizyphus mauritiana* | 396.96 ± 7.77k | 84.10 ± 2.68no |
| | **Ripe Flesh** | |
| *Bouea macrophylla* | 372.35 ± 1.43m | 156.29 ± 3.72h |
| *Carica papaya* | 377.43 ± 1.10m | 268.02 ± 7.44e |
| *Citrullus lanatus* | 104.97 ± 0.19z | 61.75 ± 3.72stu |
| *Citrus aurantifolia* | 463.08 ± 8.48h | 259.42 ± 7.44f |
| *Citrus maxima* | 606.50 ± 0.22g | 285.21 ± 7.44d |
| *Citrus microcarpa* | 453.47 ± 1.38i | 227.20 ± 3.72g |
| *Cucumis melo* | 162.72 ± 0.81v | 74.64 ± 3.72pq |
| *Mangifera indica* | 79.72 ± 2.77$\alpha$ | 121.06 ± 1.28j |
| *Manilkara zapota* | 255.88 ± 0.91p | 72.50 ± 3.72pqr |
| *Musa acuminata* | 120.37 ± 0.85y | 72.50 ± 3.72pqr |
| | **Ripe Aril** | |
| *Annona muricata* | 185.80 ± 0.59t | 104.72 ± 3.72klm |
| *Annona squamosa* | 134.35 ± 1.43x | 98.28 ± 3.72m |
| *Artocarpus heterophyllus* | 319.01 ± 1.02o | 72.50 ± 1.97pqr |
| *Baccaurea montleyana* | 149.49 ± 3.06w | 67.34 ± 0.744qrst |
| *Baccaurea polyneura* | 417.14 ± 3.41j | 149.85 ± 3.72h |
| *Dimocarpus longan* | 399.13 ± 5.15k | 380.61 ± 1.49c |
| *Garcinia mangostana* | 647.59 ± 9.52e | 66.91 ± 3.24rst |
| *Lansium domesticum* | 386.82 ± 5.53l | 87.54 ± 3.72n |
| *Nephelium lappaceum* | 223.75 ± 0.57r | 60.89 ± 0.74tu |
| *Nephelium ramboutan-ake* | 199.07 ± 2.18s | 65.62 ± 1.49rst |
| *Salacca edulis* | 175.99 ± 0.94u | 98.28 ± 3.72m |
| *Sandoricum koetjape* | 60.96 ± 1.44$\tau$ | 120.19 ± 1.97j |
| | **Young Endosperm** | |
| *Cocos nucifera* | 71.85 ± 7.84$\beta$ | 51.87 ± 0.74v |
| | **Ripe Peduncle** | |
| *Ananas comosus* | 359.28 ± 2.53n | 78.94 ± 3.72op |
| | **Stem** | |
| *Apium graveolens* | 200.99 ± 0.34s | 56.60 ± 0.74uv |
| *Saccharum officinarum* | 116.55 ± 0.30y | 79.80 ± 1.49op |
| | **Root** | |
| *Daucus carota* | 236.02 ± 0.57q | 63.04 ± 1.49stu |

[a]Values are means ± standard deviations of triplicate analyses. Results from different analyses were analyzed separately. Values per each analysis followed by different letters are significantly different ($p < 0.05$).

to be native to Southeast Asia, and this study apparently was the first comparative evaluation that revealed higher vitamin C contents of their juices.

**Antioxidant Activities.** The antioxidant activities of the juices were evaluated using DPPH free radical scavenging, ferric reducing power (FRAP), and metal chelating assays. DPPH and FRAP assays were used to measure the direct involvement of an extract as a primary antioxidant. As indicated in Table 4, the juice of *Phyllanthus acidus* was found to exhibit the greatest scavenging and reducing activities. This was followed by the juice of *Barringtonia racemosa*. To date, the phytochemical and antioxidant evaluations of these two species were mainly focused on the leaf extracts.[27,28] Only a pentacyclic triterpenoid, bartogenic acid, was isolated from *Barringtonia racemosa* fruit extract,[29] and 46 volatile compounds were identified from *Phyllanthus acidus* fruit.[30] In Malaysia, *Barringtonia racemosa* fruit is traditionally consumed to treat asthma, sore throat, and stomachache, and *Phyllanthus acidus* fruit is used as a diuretic.[2]

Interestingly, the juice of *Psidium guajava* demonstrated the third highest values of DPPH and FRAP. This fruit juice was found to have the richest in TPC and vitamin C contents (Table 3). The major contents of flavonols such as rutin and flavones such as luteolin in *Psidium guajava*[12] may also be responsible for the activities. Meanwhile, the juice of *Ziziphus mauritiana*, with a low content of vitamin C and moderate TPC, ranked fourth best in DPPH value. The activity might be contributed by *p*-hydroxybenzoic acid that was reported to be the most abundant phenolic compound in the fruit extract.[31] The juices of the ripe aril of *Salacca edulis* and the mature flesh of *Sandoricum koetjape* were found to rank in the top six for both activities. Shui and Leong[32] had identified chlorogenic acid, epicatechin, and proanthocyanidins as the major antioxidants in *Salacca edulis*. The antioxidant activities of *Sandoricum koetjape* could be associated with its high TPC. However, no phenolic compound was previously identified from its flesh. The only phytochemical that was isolated from the flesh is a triterpenoid, bryononic acid.[33]

Other juices that gave DPPH values of >280 $\mu$g VCEAC/g sample and FRAP values of >800 $\mu$g TEAC/g sample were obtained from *Spondias pinnata* and *Citrus maxima*. It is found that the activities of the juices were well-correlated with their TPCs and vitamin C contents (Table 3). The major contents of ferulic and syringic acids in the fruit of *Spondias pinnata*[12] and naringin (a flavanone glycoside) in the juice of *Citrus maxima*[25] might act synergistically or individually to enhance the antioxidant activities of the juices. Furthermore, the FRAP value >750 $\mu$g TEAC/g sample was also measured from the juice of *Manilkara zapota*. This could be due to the presence of several polyphenolics such as methyl 4-*O*-galloylchlorogenate, 4-*O*-galloylchlorogenic acid, methyl chlorogenate, dihydromyricetin, quercitrin, myricitrin, (+)-catechin, (−)-epicatechin, (+)-gallocatechin, and gallic acid in the fruit.[34]

The metal chelating assay assesses the indirect involvement of an extract as a secondary antioxidant by binding the ferrous (Fe(II)) ion that catalyzes oxidation and subsequently prevents the formation of the Fe(II)−ferrozine complex. The highest metal chelating activity was detected from the juice of *Syzygium samarangense*. This was followed by the juices of *Averrhoa bilimbi* and *Averrhoa carambola* with no significant difference. Lim et al.[7] reported lower activity (only 30%) of the 50% ethanol extract of *Averrhoa carambola* at 100 mg/mL. This might be due to higher contents of metal chelating compounds in the juice compared to the extract.

With the exception of the juices of *Averrhoa carambola* and *Barringtonia racemosa*, the juices with >50% of activity were found to contain low TPCs (Table 3). Thus, the results revealed the minor contribution of TPC to the chelating activity. Besides, the activity of polyphenols is related to the presence of an *o*-dihydroxy moiety in their chemical structures

**Table 4. Antioxidant Activities of the Juices[a]**

| scientific name | DPPH (μg VCEAC/g sample) | FRAP (μg TEAC/g sample) | metal chelating[b] (%) | α-glucosidase inhibition[b] (%) |
|---|---|---|---|---|
| | | **Mature Flesh** | | |
| *Averrhoa bilimbi* | 156.92 ± 0.58o | 192.66 ± 0.23s | 81.33 ± 0.17a | 0d |
| *Averrhoa carambola* | 111.88 ± 1.36uv | 154.55 ± 3.32u | 78.94 ± 0.42a | 0d |
| *Barringtonia racemosa* | 534.09 ± 1.41b | 2129.66 ± 2.04b | 56.56 ± 0.77d | 93.75 ± 0.14a |
| *Cynometra cauliflora* | 105.28 ± 0.41vw | 60.86 ± 1.18α | 63.61 ± 1.11c | 88.59 ± 0.34a |
| *Garcinia atroviridis* | 115.14 ± 1.15u | 168.27 ± 0.74t | 36.22 ± 1.67fg | 65.94 ± 0.32bc |
| *Myristica fragrans* | 242.54 ± 1.08i | 229.74 ± 0.85q | 28.61 ± 2.43hi | 86.98 ± 0.23ab |
| *Phyllanthus acidus* | 613.71 ± 2.59a | 2784.89 ± 3.93a | 18.67 ± 0.44k | 95.37 ± 0.15a |
| *Psidium guajava* | 517.95 ± 6.06c | 1924.34 ± 1.65c | 44.06 ± 2.80e | 0d |
| *Sandoricum koetjape* | 418.22 ± 5.17e | 933.39 ± 2.21e | 24.67 ± 0.44ij | 46.15 ± 5.22c |
| *Spondias pinnata* | 289.00 ± 3.25g | 866.82 ± 10.69f | 24.83 ± 0.17ij | 64.85 ± 3.24bc |
| *Syzygium malaccense* | 137.11 ± 2.07q | 189.94 ± 2.95s | 22.67 ± 0.29jk | 0d |
| *Syzygium samarangense* | 149.77 ± 2.61op | 625.18 ± 0.84j | 82.28 ± 0.10a | 79.44 ± 0.45ab |
| *Zizyphus mauritiana* | 460.58 ± 17.93d | 484.79 ± 4.68l | 22.11 ± 1.68jk | 0d |
| | | **Ripe Flesh** | | |
| *Bouea macrophylla* | 258.17 ± 4.25h | 133.31 ± 0.70w | 23.00 ± 0.25jk | 83.44 ± 0.10ab |
| *Carica papaya* | 202.78 ± 0.61l | 469.44 ± 1.05m | 7.89 ± 5.97l | 0d |
| *Citrullus lanatus* | 74.64 ± 0.70zα | 37.81 ± 0.39β | 32.89 ± 4.62gh | 0d |
| *Citrus aurantifolia* | 170.14 ± 5.32n | 347.61 ± 3.71n | 11.56 ± 0.42l | 0d |
| *Citrus maxima* | 397.68 ± 4.21f | 834.22 ± 7.28g | 0n | 0d |
| *Citrus microcarpa* | 185.83 ± 7.40m | 262.31 ± 1.40p | 38.39 ± 0.75f | 75.24 ± 0.71ab |
| *Cucumis melo* | 98.13 ± 1.18wxy | 123.44 ± 1.11x | 0n | 0d |
| *Mangifera indica* | 133.75 ± 9.61qr | 311.13 ± 2.66o | 25.33 ± 1.33ij | 0d |
| *Manilkara zapota* | 116.55 ± 0.74tu | 759.90 ± 17.34h | 0n | 0d |
| *Musa acuminata* | 123.47 ± 0.91st | 554.94 ± 4.55k | 40.22 ± 1.36ef | 0d |
| | | **Ripe Aril** | | |
| *Annona muricata* | 132.57 ± 1.67qr | 210.80 ± 3.18r | 0n | 0d |
| *Annona squamosa* | 145.57 ± 1.50p | 146.92 ± 0.09v | 24.56 ± 0.35ij | 0d |
| *Artocarpus heterophyllus* | 127.76 ± 1.35rs | 142.94 ± 1.16v | 0n | 0d |
| *Baccaurea montleyana* | 96.88 ± 0.34xy | 116.64 ± 0.67x | 10.78 ± 1.11l | 0d |
| *Baccaurea polyneura* | 233.21 ± 0.55j | 210.71 ± 3.24r | 23.89 ± 4.89ij | 0d |
| *Dimocarpus longan* | 61.37 ± 0.48β | 694.56 ± 4.76i | 0n | 0d |
| *Garcinia mangostana* | 225.70 ± 9.23k | 171.48 ± 0.79t | 71.83 ± 1.17b | 85.20 ± 0.59ab |
| *Lansium domesticum* | 111.27 ± 1.10uv | 120.27 ± 0.41x | 58.22 ± 5.51d | 0d |
| *Nephelium lappaceum* | 94.17 ± 1.60y | 96.85 ± 1.37y | 3.39 ± 1.92m | 0d |
| *Nephelium ramboutan-ake* | 49.19 ± 0.68δ | 73.06 ± 0.29z | 72.78 ± 1.13b | 0d |
| *Salacca edulis* | 421.56 ± 8.61e | 1556.79 ± 8.73d | 0n | 0d |
| *Sandoricum koetjape* | 116.20 ± 0.46tu | 97.01 ± 0.70y | 56.72 ± 1.18d | 0d |
| | | **Young Endosperm** | | |
| *Cocos nucifera* | 102.79 ± 4.64wx | 174.93 ± 0.82t | 28.56 ± 1.92hi | 0d |
| | | **Ripe Peduncle** | | |
| *Ananas comosus* | 105.55 ± 1.42vw | 172.45 ± 1.99t | 9.11 ± 4.52l | 0d |
| | | **Stem** | | |
| *Apium graveolens* | 78.00 ± 0.72z | 59.78 ± 0.11α | 21.33 ± 0.50jk | 0d |
| *Saccharum officinarum* | 124.37 ± 1.97s | 159.01 ± 0.65u | 71.00 ± 0.17b | 0d |
| | | **Root** | | |
| *Daucus carota* | 69.91 ± 0.67α | 76.14 ± 0.30z | 38.06 ± 3.78f | 0d |

[a]Values are means ± standard deviations of triplicate analyses. Results from different assays were analyzed separately. Values for each assay followed by different letters are significantly different ($p < 0.05$). [b]Resulted from assay using pure juices.

or those bearing catechol or galloyl groups.[35] Polyphenolics that were previously isolated from *Syzygium samarangense* fruit pulps such as reynoutrin, hyperin, myricitrin, quercitrin, quercetin, guaijaverin, gallic acid, and ellagic acid[36] and from *Averrhoa carambola*, which are chlorogenic, caffeic acids,[24] catechin, epicatechin, and gallic acid,[37] were found having these characteristics.

**α-Glucosidase Inhibitory Activity.** As indicated in Table 4, only 11 juices mostly obtained from the mature fleshes show positive results. The pH values of juices ranged from 1.81 ± 0.01 (in *Garcinia atroviridis*) to 4.37 ± 0.01 (in *Bouea macrophylla*). This indicated no effect of the juice pH on the assay system. The highest α-glucosidase inhibitory percentage (95.37 ± 0.15%) was measured from the juice of *Phyllanthus acidus*. The value was not significantly different from the juices of *Barringtonia racemosa*, *Cynometra cauliflora*, *Myristica fragrans*, *Garcinia mangostana*, *Bouea macrophylla*, *Syzygium samarangense*, and *Citrus microcarpa*. The α-glucosidase inhibitory activity of these fruit parts (excluding *Phyllanthus acidus*) was highlighted for the first time in this study. It is


dx.doi.org/10.1021/jf502912t | J. Agric. Food Chem. 2014, 62, 9576−9585

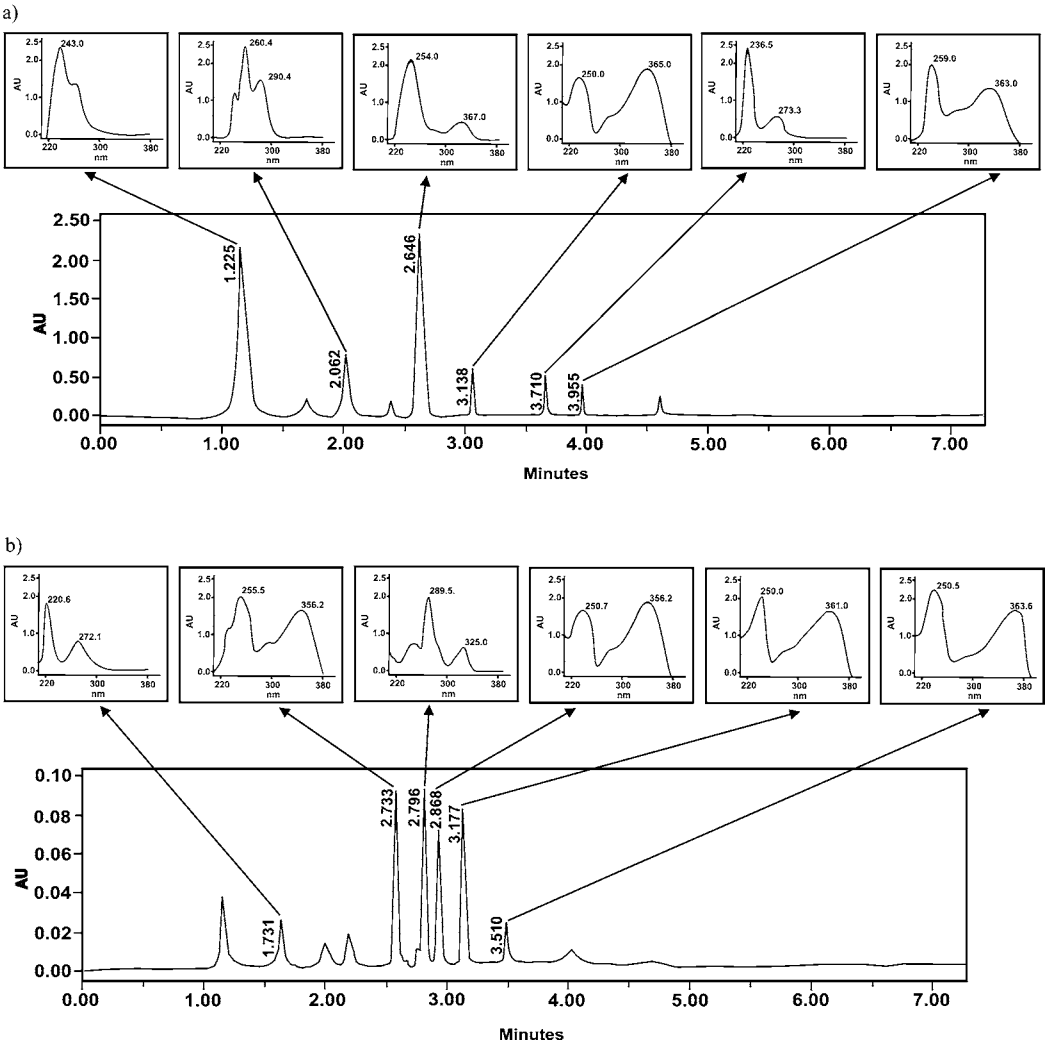


**Figure 1.** UPLC chromatograms (at 350 nm) of the juices of (a) *Barringtonia racemosa* and (b) *Phyllanthus acidus*. The UV spectra of several peaks generated by a photodiode array detector are indicated.

interesting to note that *Cynometra cauliflora* and *Bouea macrophylla* fruits that are endemic and native to Malaysia were also found to have higher activity. To date, no compound was identified from *Cynometra cauliflora* fruit, and only volatile components were identified from *Bouea macrophylla* fruit. The major volatile components of this fruit are (*E*)-*β*-ocimene (68.59%) and *α*-pinene (8.04%).[38] These compounds were also detected in the essential oil of black pepper (*Piper guineense*) seeds, which was reported to inhibit *α*-glucosidase.[39] A very low *α*-glucosidase inhibitory activity was determined from the extracts of *Phyllanthus acidus* in two earlier investigations.[19,20] This might be due to higher contents of *α*-glucosidase inhibitors in the juice compared to the extracts.

The activity of the juices of *Barringtonia racemosa*, *Myristica fragrans*, and *Garcinia mangostana* is in line with their high TPCs (>600 *μ*g GAE/g sample; Table 3). Bartogenic acid, which was also isolated in the fruit[29] and the seed of *Barringtonia racemosa*, was reported to possess *α*-glucosidase inhibitory activity.[40] Caffeic acid and catechin, which were found in the mature flesh of *Myristica fragrans*,[41] were identified as potent *α*-glucosidase inhibitors from the phenolic group.[42] The present study in fact is the first to determine the *α*-glucosidase inhibitory activity of the flesh of *Myristica fragrans* and the aril of *Garcinia mangostana*. Extracts from another two fruit parts of *Myristica fragrans*, which are the methanol extract of the mace (aril)[43] and the water extract of nutmeg (seed),[44] were previously reported to possess a moderate *α*-glucosidase inhibitory activity. Furthermore, three prenylated xanthones (*α*-mangostin, *γ*-mangostin, and gartanin) that were identified as *α*-glucosidase inhibitors were abundantly quantified from the ethanol extract of the seedcase of *Garcinia mangostana*.[45]

The major phenolic compound in the 80% methanol extract of the aril of *Garcinia mangostana* was *p*-hydroxybenzoic acid,[46] and in the juice of *Citrus microcarpa* was *p*-coumaric acid.[47] However, according to Kwon et al.,[42] these compounds have a low capacity to inhibit *α*-glucosidase. Therefore, the low contents of protocatechuic acid and vanillic acid that were also quantified from the extract of *Garcinia mangostana*[46] and caffeic acid in the juice of *Citrus microcarpa*[47] may be responsible for the activity.[42] On the basis of the comparative *α*-glucosidase inhibitory activity of various flavonoids, Tadera et al.[48] had suggested that unsaturated C-ring, hydroxylation on the C-ring at the 3-position, and an increase in the number of hydroxyl group on the B-ring might enhance the inhibitory activity. Therefore, quercetin, four quercetin glycosides (quercitrin, guaijaverin, reynoutrin, and hyperin), and a myricetin glycoside (myricitrin) that were previously isolated from *Syzygium samarangense* fruit pulps could be attributed with the activity.[36]

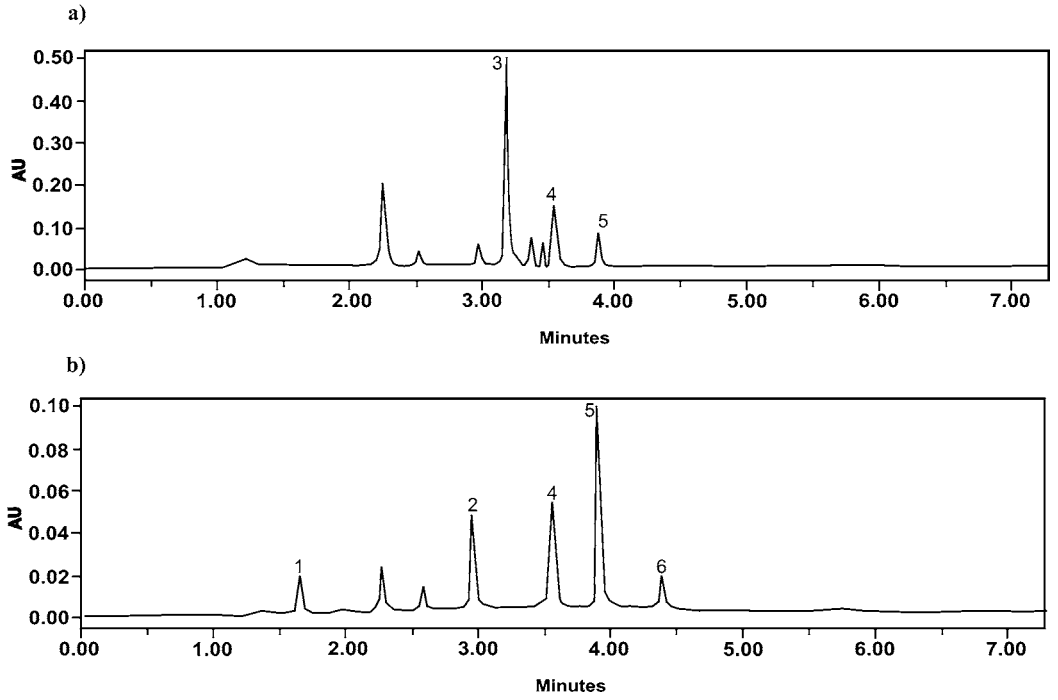


**Figure 2.** UPLC chromatograms (at 350 nm) of the hydrolyzed juice extracts of (a) *Barringtonia racemosa* and (b) *Phyllanthus acidus*. The identified compounds of the labeled peaks are shown in Table 5.

**Table 5. Content of Phenolic Compounds in Hydrolyzed Juice Extracts of *Barringtonia racemosa* and *Phyllanthus acidus* (Milligrams per 100 g of Extract)**

| peak | phenolic | retention time (min) | *B. racemosa* | *P. acidus* |
|---|---|---|---|---|
| 1 | gallic acid | 1.709 | | 230.69 ± 3.31 |
| 2 | dihydroquercetin (taxifolin) | 2.919 | | 103.33 ± 9.31 |
| 3 | ellagic acid | 3.217 | 1269.48 ± 33.82 | |
| 4 | myricetin | 3.661 | 265.57 ± 2.45 | 85.42 ± 6.51 |
| 5 | quercetin | 3.919 | 61.70 ± 1.97 | 142.68 ± 12.49 |
| 6 | kaempferol | 4.407 | | 4.54 ± 0.19 |

**Identification and Quantification of Phenolic Compounds in *Barringtonia racemosa* and *Phyllanthus acidus*.** The fruit juices of *Barringtonia racemosa* and *Phyllanthus acidus* have indicated the highest FRAP, DPPH, and $\alpha$-glucosidase inhibitory activities (Table 4). This is considered the first comparative evaluation to highlight the pronounced activities of these juices. We hypothesized that polyphenolics are the major contributors of the activities. However, no polyphenolics had been previously identified from these two fruits. Thus, polyphenolics were separated from the juices using UPLC, and different chromatograms were obtained when different mobile phases and gradient modes were used. Figure 1 shows one of the UPLC chromatograms that indicated a good separation of polyphenolics of the juices (detected at 350 nm) using solvent A (0.5% acetic acid) and solvent B (acetonitrile) as the mobile phase. The juices were separated using a gradient mode that was initially set at an A/B ratio of 80:20 and then linearly increased to 60:40 at 1 min, to 30:70 at 2 min, and to 10:90 at 4.5 min until 5.5 min. The UV spectrum of each separated peak was detected by the photodiode array detector. Only the peaks of gallic acid in *Phyllanthus acidus* chromatogram and ellagic acid in *Barringtonia racemosa* chromatogram (at retention times of 1.731 and 2.646 min, respectively) were positively identified by comparing the retention times and UV spectra of the peaks with the standards. The UV spectra of myricetin (a flavonol) were detected at the peaks with retention times of 2.868 and 3.138 min, and this indicated the presence of different glycosidic myricetins in *Phyllanthus acidus* and *Barringtonia racemosa* juices, respectively. The presence of three glycosidic quercetins (also a flavonol) was detected by the UV spectra of peaks at retention times of 2.733 and 3.510 min in the chromatogram of *Phyllanthus acidus* and 3.955 min in the *Barringtonia racemosa* chromatogram. The UV spectra of glycosidic dihydroquercetin (a flavanone) and kaempferol (a flavonol) were observed at peaks with retention times of 2.796 and 3.177 min, respectively, in the *Phyllanthus acidus* chromatogram.

Due to the diversity of unknown glycosidic flavonoids and/or bound phenolics found in these two fresh juices, we quantified the polyphenolics as aglycones, after hydrolysis. Moreover, glycosylation of flavonoids was reported to decrease the antioxidant[49] and $\alpha$-glucosidase inhibitory activities.[50] Figure 2 shows the UPLC chromatograms of the hydrolyzed juice extracts of *Barringtonia racemosa* and *Phyllanthus acidus* (at 350 nm) and six labeled peaks that were positively identified by comparison with standards.

The contents of these compounds in the extracts are summarized in Table 5. Ellagic acid (peak 3, Figure 2) was identified as the major compound in the hydrolyzed juice extract of *Barringtonia racemosa*. The hydrolyzed juice extract of


dx.doi.org/10.1021/jf502912t | J. Agric. Food Chem. 2014, 62, 9576−9585

*Phyllanthus acidus* was found to contain the highest content of gallic acid (peak 1, Figure 2). These compounds respectively bear catechol and galloyl groups that might be responsible for enhancing the antioxidant activity of the juices. However, these compounds were reported to possess low $\alpha$-glucosidase inhibitory activity.[42] Two flavonols, myricetin (peak 4, Figure 2) and quercetin (peak 5, Figure 2), were also quantified from these hydrolyzed juice extracts. The contents of these compounds in *Barringtonia racemosa* are respectively more than 3-fold higher and 2-fold lower than *Phyllanthus acidus*. These flavonols with structural configurations of 2−3 double bonds conjugated with the 4-oxo function and hydroxyl groups at the 3-, 5-, 7-, 3′-, and 4′-positions play a major role in enhancing the antioxidant[49] and $\alpha$-glucosidase inhibitory activities.[48]

As indicated in Table 5, a low content of kaempferol (a flavonol) and a moderate content of dihydroquercetin were also detected from the hydrolyzed juice extract of *Phyllanthus acidus*. With the exception of kaempferol, all of the quantified compounds have an *o*-dihydroxy moiety in their chemical structures. This may indicate the major contribution of the compounds to increase the activities of the juices.

Our results indicate that various tropical fruit juices serve as rich sources of antioxidants and $\alpha$-glucosidase inhibitors. The activities can be associated with the combined effect of polyphenolics in the juices or the structure−activity relationships of the major polyphenolics. The results obtained from this study were in line with several earlier comparative antioxidant studies that highlighted higher primary antioxidant activities of *Psidium guajava* fruit compared with other tropical fruits. However, the activities were found lower than those of *Phyllanthus acidus* and *Barringtonia racemosa*. These two medicinal fruits are native to Southeast Asia and were also found to have higher $\alpha$-glucosidase inhibitory activity. The new information obtained by this study would be useful for promoting their consumption and the development of functional foods.

## AUTHOR INFORMATION


### Corresponding Author

*(S.F.S.) Phone: +60-4-6534095. Fax: +60-4-6565125. E-mail: shaida@usm.my.



### Funding

We acknowledge financial support provided by the Universiti Sains Malaysia (Research University Grant 1001/PBIOLOGI/813049).


### Notes

The authors declare no competing financial interest.

## ACKNOWLEDGMENTS

We acknowledge the Universiti Sains Malaysia for providing laboratory facilities.

## REFERENCES


(1) Aman, R. *Buah-Buahan Malaysia*; Dewan Bahasa dan Pustaka: Kuala Lumpur, Malaysia, 2002.

(2) Chooi, O. H. *Buah: Khasiat Makanan & Ubatan*; Utusan Publication and Distributors: Kuala Lumpur, Malaysia, 2004.

(3) Díaz-García, M. C.; Obón, J. M.; Castellar, M. R.; Collado, J.; Alacid, M. Quantification by UHPLC of total individual polyphenols in fruit juices. *Food Chem.* **2013**, *138*, 938−949.

(4) Xiao, J.; Kai, G.; Yamamoto, K.; Chen, X. Advance in dietary polyphenols as $\alpha$-glucosidases inhibitors: a review on structure-activity relationship aspect. *Crit. Rev. Food Sci. Nutr.* **2013**, *53*, 818−836.

(5) Luximon-Ramma, A.; Bahorun, T.; Crozier, A. Antioxidant actions and phenolic and vitamin C contents of common Mauritian exotic fruits. *J. Sci. Food Agric.* **2003**, *83*, 496−502.

(6) Mahattanatawee, K.; Manthey, J. A.; Luzio, G.; Talcott, S. T.; Goodner, K.; Baldwin, E. A. Total antioxidant activity and fiber content of select Florida-grown tropical fruits. *J. Agric. Food Chem.* **2006**, *54*, 7355−7363.

(7) Lim, Y. Y.; Lim, T. T.; Tee, J. J. Antioxidant properties of several tropical fruits: a comparative study. *Food Chem.* **2007**, *103*, 1003−1008.

(8) Ikram, E. H. K.; Eng, K. H.; Jalil, A. M. M.; Ismail, A.; Idris, S.; Azlan, A.; Nazri, H. S. M.; Diton, N. A. M.; Mokhtar, R. A. M. Antioxidant capacity and total phenolic content of Malaysian underutilized fruits. *J. Food Compos. Anal.* **2009**, *22*, 388−393.

(9) Isabelle, M.; Lee, B. L.; Lim, M. T.; Koh, W.-P.; Huang, D.; Ong, C. N. Antioxidant activity and profiles of common fruits in Singapore. *Food Chem.* **2010**, *123*, 77−84.

(10) Rufino, M. d. S. M.; Alves, R. E.; Brito, E. S. d.; Pérez-Jiménez, J.; Saura-Calixto, F.; Mancini-Filho, J. Bioactive compounds and antioxidant capacities of 18 non-traditional tropical fruits from Brazil. *Food Chem.* **2010**, *121*, 996−1002.

(11) Contreras-Calderón, J.; Calderón-Jaimes, L.; Guerra-Hernández, E.; García-Villanova, B. Antioxidant capacity, phenolic content and vitamin C in pulp, peel and seed from 24 exotic fruits from Colombia. *Food Res. Int.* **2011**, *44*, 2047−2053.

(12) Kubola, J.; Siriamornpun, S.; Meeso, N. Phytochemicals, vitamin C and sugar content of Thai wild fruits. *Food Chem.* **2011**, *126*, 972−981.

(13) Tiwari, A. K.; Reddy, K. S.; Radhakrishnan, J.; Kumar, D. A.; Zehra, A.; Agawane, S. B.; Madhusudana, K. Influence of antioxidant rich fresh vegetable juices on starch induced postprandial hyperglycemia in rats. *Food Funct.* **2011**, *2*, 521−528.

(14) Pinto Mda, S.; Ranilla, L. G.; Apostolidis, E.; Lajolo, F. M.; Genovese, M. I.; Shetty, K. Evaluation of antihyperglycemia and antihypertension potential of native Peruvian fruits using *in vitro* models. *J. Med. Food* **2009**, *12*, 278−291.

(15) Goncalves, A.; Franco, M. L.; Genovese, M. I. Chemical composition and antioxidant/antidiabetic potential of Brazilian native fruits and commercial frozen pulps. *J. Agric. Food Chem.* **2010**, *58*, 4666−4674.

(16) Correia, R. T. P.; Borges, K. C.; Medeiros, M. F.; Genovese, M. I. Bioactive compounds and phenolic-linked fuctionality of powdered tropical fruit residues. *Food Sci. Technol. Int.* **2012**, *18*, 539−547.

(17) Girones-Vilaplana, A.; Baenas, N.; Villano, D.; Speisky, H.; Garcia-Viguera, C.; Moreno, D. A. Evaluation of Latin-American fruits rich in phytochemicals with biological effects. *J. Funct. Foods* **2014**, *7*, 599−608.

(18) Park, J.-H.; Kim, R.-Y.; Park, E. Antidiabetic activity of fruits and vegetables commonly consumed in Korea: inhibitory potential against $\alpha$-glucosidase and insulin-like action in vitro. *Food Sci. Biotechnol.* **2012**, *21*, 1187−1193.

(19) Hossain, S. J.; Tsujiyama, I.; Takasugi, M.; Islam, M. A.; Biswas, R. S.; Aoshima, H. Total phenolic content, antioxidative, anti-amylase, anti-glucosidase and antihistamine release activities of Bangladeshi fruits. *Food Sci. Technol. Res.* **2008**, *14*, 261−268.

(20) Das, S.; Das, S.; De, B. *In vitro* inhibition of key enzymes related to diabetes by aqueous extracts of some fruits of West Bengal, India. *Curr. Nutr. Food Sci.* **2012**, *8*, 19−24.

(21) Sulaiman, S. F.; Ooi, K. L. Polyphenolic and vitamin C contents and antioxidant activities of aqueous extracts from mature-green and ripe fruit fleshes of *Mangifera* sp. *J. Agric. Food Chem.* **2012**, *60*, 11832−11838.

(22) Ooi, K. L.; Muhammad, T. S. T.; Tan, M. L.; Sulaiman, S. F. Cytotoxic, apoptotic and anti-$\alpha$-glucosidase activities of 3,4-di-*O*-caffeoyl quinic acid, an antioxidant isolated from the polyphenolic-rich

extract of *Elephantopus mollis* Kunth. *J. Ethnopharmacol.* **2011**, *135*, 685−695.
(23) Harborne, J. B. *Phytochemical Methods: A Guide to Modern Techniques of Plant Analysis*, 3rd ed.; Chapman and Hall: London, UK, 1998.
(24) Fu, L.; Xu, B.-T.; Xu, X.-R.; Gan, R.-Y.; Zhang, Y.; Xia, E.-Q.; Li, H.-B. Antioxidant capacities and total phenolic contents of 62 fruits. *Food Chem.* **2011**, *129*, 345−350.
(25) Xu, G.; Liu, D.; Chen, J.; Ye, X.; Ma, Y.; Shi, J. Juice components and antioxidant capacity of citrus varieties cultivated in China. *Food Chem.* **2008**, *106*, 545−551.
(26) Patil, J. R.; Chidambara Murthy, K. N.; Jayaprakasha, G. K.; Chetti, M. B.; Patil, B. S. Bioactive compounds from Mexican lime (*Citrus aurantifolia*) juice induce apoptosis in human pancreatic cells. *J. Agric. Food Chem.* **2009**, *57*, 10933−10942.
(27) Leeya, Y.; Mulvany, M. J.; Queiroz, E. F.; Marston, A.; Hostettmann, K.; Jansakul, C. Hypotensive activity of an *n*-butanol extract and their purified compounds from leaves of *Phyllanthus acidus* (L.) Skeels in rats. *Eur. J. Pharmacol.* **2010**, *649*, 301−313.
(28) Kong, K. W.; Mat-Junit, S.; Ismail, A.; Aminudin, N.; Abdul-Aziz, A. Polyphenols in *Barringtonia racemosa* and their protection against oxidation of LDL, serum and haemoglobin. *Food Chem.* **2014**, *146*, 85−93.
(29) Patil, K. R.; Patil, C. R.; Jadhav, R. B.; Mahajan, V. K.; Patil, P. R.; Gaikwad, P. S. Anti-arthritic activity of bartogenic acid isolated from fruits of *Barringtonia racemosa* Roxb. (Lecythidaceae). *Evidence Based Complement. Alternat. Med.* **2011**, 785245, 7 pp.
(30) Quijano, C. E.; Linares, D.; Pino, J. A. Changes in volatile compounds of fermented cereza agria (*Phyllanthus acidus* (L.) Skeels) fruit. *Flavour Fragrance J.* **2007**, *22*, 392−394.
(31) Muchuweti, M.; Zenda, G.; Ndhlala, A. R.; Kasiyamhuru, A. Sugars, organic acid and phenolic compounds of *Ziziphus mauritiana* fruit. *Eur. Food Res. Technol.* **2005**, *221*, 570−574.
(32) Shui, G.; Leong, L. P. Screening and identification of antioxidants in biological samples using high-performance liquid chromatography-mass spectrometry and its application on *Salacca edulis* Reinw. *J. Agric. Food Chem.* **2005**, *53*, 880−886.
(33) Sim, K. M.; Lee, H. T. Triterpenoid and other constituents from *Sandoricum indicum*. *Phytochemistry* **1972**, *11*, 3341−3343.
(34) Ma, J.; Luo, X.-D.; Protiva, P.; Yang, H.; Ma, C.; Basile, M. J.; Weinstein, I. B.; Kennelly, E. J. Bioactive novel polyphenols from the fruit of *Manilkara zapota* (Sapodilla). *J. Nat. Prod.* **2003**, *66*, 983−986.
(35) Andjelković, M.; Camp, J. V.; Meulenaer, D. B.; Depaemelaere, G.; Socaciu, C.; Verloo, M.; Verhe, R. Iron-chelation properties of phenolic acids bearing catechol and galloyl groups. *Food Chem.* **2006**, *98*, 23−32.
(36) Simirgiotis, M. J.; Adachi, S.; To, S.; Yang, H.; Reynertson, K. A.; Basile, M. J.; Gil, R. R.; Weinstein, I. B.; Kennelly, E. J. Cytotoxic chalcones and antioxidants from the fruits of a *Syzygium samarangense* (Wax Jambu). *Food Chem.* **2008**, *107*, 813−819.
(37) Shui, G.; Leong, L. P. Analysis of polyphenolic antioxidants in star fruit using liquid chromatography and mass spectrometry. *J. Chromatogr., A* **2004**, *1022*, 67−75.
(38) Wong, C.; Loi, H. K. Volatile constituents of *Bouea macrophylla* Griff. fruit. *J. Essent. Oil Res.* **1996**, *8*, 99−100.
(39) Oboh, G.; Ademosun, A. O.; Odubanjo, O. V.; Akinbola, I. A. Antioxidative properties and inhibition of key enzymes relevant to type-2 diabetes and hypertension by essential oils from black pepper. *Adv. Pharmacol. Sci.* **2013**, 926047, 6 pp.
(40) Gowri, P. M.; Tiwari, A. K.; Ali, A. Z.; Rao, J. M. Inhibition of α-glucosidase and amylase by bartogenic acid isolated from *Barringtonia racemosa* Roxb. seeds. *Phytother. Res.* **2007**, *21*, 796−799.
(41) Shan, B.; Cai, Y. Z.; Sun, M.; Corke, H. Antioxidant capacity of 26 spice extracts and characterization of their phenolic constituents. *J. Agric. Food Chem.* **2005**, *53*, 7749−7759.
(42) Kwon, Y.-I.; Apostolidis, E.; Shetty, K. Inhibitory potential of wine and tea against α-amylase and α-glucosidase for management of hyperglycemia linked to type 2 diabetes. *J. Food Biochem.* **2008**, *32*, 15−31.
(43) Patil, S. B.; Ghadyale, V. A.; Taklikar, S. S.; Kulkarni, C. R.; Arvindekar, A. U. Insulin secretagogue, α-glucosidase and antioxidant activity of some selected spices in streptozotocin-induced diabetic rats. *Plant Food Hum. Nutr.* **2011**, *66*, 85−90.
(44) Nasu, R.; Miura, M.; Gomya, T. Effects of fruit, spices and herbs on α glucosidase activity and glycemic index. *Food Sci. Technol. Res.* **2005**, *11*, 77−81.
(45) Ryu, H. W.; Cho, J. K.; Curtis-Long, M. J.; Yuk, H. J.; Kim, Y. S.; Jung, S.; Kim, Y. S.; Lee, B. W.; Park, K. H. α-Glucosidase inhibition and antihyperglycemic activity of prenylated xanthones from *Garcinia manostana*. *Phytochemistry* **2011**, *72*, 2148−2154.
(46) Zadernowski, R.; Czaplicki, S.; Naczk, M. Phenolic acid profiles of mangosteen fruits (*Garcinia mangostana*). *Food Chem.* **2009**, *112*, 685−689.
(47) Cheong, M. W.; Zhu, D.; Sng, J.; Liu, S. Q.; Zhou, W.; Curran, P.; Yu, B. Characterisation of calamansi (*Citrus microcarpa*). Part II: Volatiles, physicochemical properties and non-volatiles in the juice. *Food Chem.* **2012**, *134*, 696−703.
(48) Tadera, K.; Minami, Y.; Takamatsu, K.; Matsuoka, T. Inhibition of α-glucosidase and α-amylase by flavonoids. *J. Nutr. Sci. Vitaminol.* **2006**, *52*, 149−153.
(49) Rice-Evans, C. A.; Miller, N. J.; Paganga, G. Structure-antioxidant activity relationships of flavonoids and phenolic acids. *Free Radical Biol. Med.* **1996**, *20*, 933−956.
(50) Li, Y. Q.; Zhou, F. C.; Gao, F.; Bian, J. S.; Shan, F. Comparative evaluation of quercetin, isoquercetin and rutin as inhibitors of α-glucosidase. *J. Agric. Food Chem.* **2009**, *57*, 11463−11468.

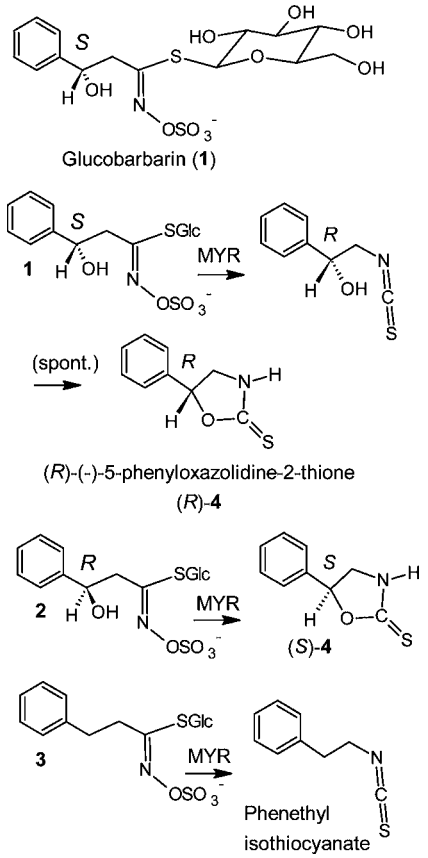


**Figure 1.** Structures of glucobarbarin, epiglucobarbarin, gluconasturtiin, and their natural 5-phenyloxazolidine-2-thione hydrolysis products after hydrolysis catalyzed by myrosinase (MYR), the endogenous glucosinolate-hydrolyzing enzyme in watercress. "Glc" in abbreviated structures indicates the β-D-glucopyranoside part of the structure as detailed in the uppermost full structure of glucobarbarin.

watercress is not only attractive for its taste and culinary value but may also be a health-promoting vegetable.

There are several reports of physiological effects of dietary watercress on markers of human disease.[13−15] Although the physiological effects of watercress may well be due to many phytochemicals, glucosinolates are likely an important class of constituents and are the focus of this paper. We are aware of five reports of the glucosinolate profile of watercress foliage, of which three are considered European material,[14,16,17] one is considered Japanese material,[18] and one is considered U.S. material.[19] In the reports of European material, it was found that **3** was dominant, whereas two indole glucosinolates, two long-chain methylsulfinylalkyl glucosinolates (7-methylsulfinylheptyl and 8-methylsulfinyloctyl glucosinolates), and the corresponding methylthioalkyl glucosinolates were less abundant constituents with some variation in the levels of the aliphatics.[14,16,17]

The reports on North American and Japanese material deviate from the reports on European material. Japanese material was reported to have a profile similar to that reported for European material, except for a quite prominent peak suggested to be **2** and a minor peak suggested to be **1** (common names were interchanged).[18] The reported evidence for **2** and **1** was the exact mass and comparison with published retention times in another laboratory. The calculated and observed $m/z$ values for both **2** and **1** differed by 3 Da.[18] In contrast, U.S. material was reported to contain 4-hydroxybenzylglucosinolate (sinalbin) and 3-butenylglucosinolate (gluconapin) in addition to the dominating **3** and less abundant indoles.[19] Both reports were inconclusive as definitive isomer distinction needs detailed comparison with authentic standards or exhaustive spectroscopic analysis.[1] In the case of **1** and **2**, seven isomers were known by 2014.[1,22,23] Moreover, a number of the isomers were found to exhibit very similar HPLC retention times.[1,23]

The reports of contrasting glucosinolate profiles in non-European watercress were interesting because structural types of glucosinolates and their hydrolysis products have complementary biological effects, such as different inductions of xenobiotic detoxification enzymes.[12] In particular, isothiocyanates with methylsulfinylalkyl and methylthioalkyl side chains exert promising bioactivities.[20] Furthermore, synergistic effects of different classes of hydrolysis products have been demonstrated.[21] In the case of U.K. watercress, the long-chain sulfinyl glucosinolates rather than dominant **3** were concluded to be mainly responsible for a phase II induction effect of the investigated watercress.[17]

The purpose of this work was to investigate glucosinolate profiles of watercress from a wide variety of sources, reflecting material typically used for human consumption around the world, to obtain a better basis for predicting and investigating nutritional and ecological effects of this vegetable. Due to the inconclusive nature of some previous reports of atypical profiles, we aimed at using isomer-specific methods including NMR and MS/MS analysis of HPLC peaks. During the investigation, after the discovery of a 2-hydroxylated glucosinolate and contrasting profiles in some U.S. material, it became relevant to identify the corresponding glucosinolate hydrolysis product and to check deviating material for the possibility of a deviating botanical identity.

## MATERIALS AND METHODS

**Chemicals.** 5-Phenyloxazolidine-2-thione and desulfated derivatives of the glucosinolates **1**, **2**, **3**, **11**, **12**, **13**, sinalbin, gluconapin, *p*-hydroxy-**2**, *p*-hydroxy-**3**, and *p*-methoxybenzylglucosinolate were obtained as previously described,[1,24,25] whereas standards of desulfated **7**, **9**, and **10** (isolated from *Rorippa* species and identified by NMR and MS) were from unpublished work. Sinigrin used as external standard was from Karl Roth, Karlsruhe, Germany.

**HPLC, MS, and NMR Equipment.** HPLC with UV detection was carried out using an LC-10AT pump with an SPD-M10AVP PDA detector (Shimadzu, Kyoto, Japan) at a flow rate of 1 mL/min. Two column stationary phases were used as specified, either "C18" (250 mm × 4.6 mm i.d., 5 μm, Luna C18 (2)) or "phenylhexyl" (250 mm × 4.6 mm i.d., 5 μm, Luna Phenylhexyl) (both Phenomenex, Torrance, CA, USA). The HPLC-MS instrument was an Agilent 1100 series LC (Agilent Technologies, Waldbronn, Germany) coupled to a Bruker HCT-Ultra ion trap mass spectrometer (Bruker Daltonics, Bremen, Germany) fitted with a Zorbax SB-C18 column (Agilent; 1.8 μm, 2.1 × 50 mm). The oven temperature was maintained at 35 °C. The mobile phases were (A) water with 0.1% (v/v) HCOOH and 50 μM NaCl and (B) acetonitrile with 0.1% (v/v) HCOOH. The NMR spectrometer was a Bruker Avance 400 instrument operated at 400.1 MHz, using $D_2O$ as solvent and dioxane ($\delta_H$ = 3.75 ppm) as internal standard.

**Plants.** Fresh commercial watercress for isolation of intact glucosinolates (July and November 2012), glucosinolate analysis (2004, 2005, 2012), and rooting followed by cytological investigation and glucosinolate analysis (November 2013) was obtained from food stores near Boston, Massachusetts (MA), USA. Fresh commercial watercress for rooting, hydroponics growth, glucosinolate analysis, and botanical identification by floral parts morphology was obtained in 2012 from a grocery store in Dayton, Ohio (OH), USA. In all cases of


dx.doi.org/10.1021/jf5032795 | J. Agric. Food Chem. 2014, 62, 9586−9596

commercial Ohio and Massachusetts watercress, the same producer (B&W Quality Growers, FL, USA) was indicated, but material was in no case obtained directly from this producer, so the origin is not absolutely certain. Wild Danish watercress for rooting followed by cytological investigation and glucosinolate analysis was from St. Vejleaa, Taastrup (55°40′ N, 12°19′ E). Fresh watercress for the autolysis experiment, indicated to be from Santa Clara Valley, California (CA), USA, was obtained in a food store (Safeway, Willits) and immediately transported to Denmark by plane, in accordance with relevant Danish legislation. After the autolysis experiment, remains were autoclaved.

Additional watercress was obtained for glucosinolate analysis with the aim of sampling as consumers around the world would typically acquire it: wild-collected, home-grown, or from a food store (fresh or in one case desiccated). Wild watercress was collected in nature in Massachusetts (near Lenox, 42°21′ N; 73°17′ W), Ohio (near Yellow Springs, 39°48′ N; 83°53′ W), and Denmark (Mors, 56° N, 8° E). Watercress seeds were obtained from three different Web-based seed suppliers: Chiltern Seeds (Ulverston, UK), Johnny's Select Seeds (Winslow, ME, USA), and Kitazawa Seed Co. (Oakland, CA, USA). Commercial fresh watercress was obtained in food stores. Chinese desiccated watercress was obtained in a Chinese shop in Copenhagen.

Watercress cultivated from seeds, U.S. food store material from Ohio, and U.S. wild material was grown in a hydroponics system: Tubs for hydroponic growth were filled to 200 L with distilled water. To each tub, 66 mL each of the fertilizer concentrates FloraGro (2−1−6), FloraBloom (0−5−4), and FloraMicro (5−0−1) (General Hydroponics) were added at the start of the planting and not replenished. The growth solution was under continuous aeration by an aquarium pump. Seeds or shoots were placed in glass wool suspended in holes punched in floating Styrofoam blocks, with roots hanging into the nutrient solution. Tubs were placed under fluorescent lights providing ∼75 μmol PAR/($m^2$ s) on a 16:8 light/dark cycle at 22 °C. This light intensity, comparable to reduced natural light intensity in forest streams, promoted abundant growth, flowering, and seed set and did not seem limiting in any way.

**Botanical Identification.** Wild-collected watercress was tentatively identified as *N. officinale* by the collector (either F.S.C, M.Ø. or D.C.) on the basis of general morphology and growth site. For wild U.S. material from 2012, material grown from seeds, commercial watercress obtained on the root in Denmark, and commercial watercress obtained from a grocery store in Ohio, and rooted, the identity was further confirmed by cultivation to flowering and seed set for inspection of key morphological characters. Voucher specimens have been deposited at the Wright State University Herbarium and at CP in the case of Danish material. For cytological analysis, two accessions were rooted in tap water, and numbers of chromocenters in root tip cells were counted as previously described.[26]

**Lyophilization/Drying and Transport to Analysis Laboratory.** Watercress foliage from Denmark (except wild collection), Spain, Portugal, and Massachusetts was lyophilized soon after acquisition (without previous freezing to avoid glucosinolate breakdown during freeze−thaw cycles) until completely crisp. Watercress foliage from Ohio and from growth in our hydroponics system was air-dried at ambient conditions in the laboratory and then placed in plastic bags with silica gel. Watercress foliage from California, Australia, and Argentina and the wild-collected sample from Denmark was dried domestically at ambient indoor conditions until crisp. Dried samples were shipped to the University of Copenhagen analysis laboratory by mail or plane travel. Upon arrival, all material was stored frozen (−20 °C) in closed plastic bags until extraction to prevent reabsorption of moisture. Variable drying conditions were due to lack of availability of freeze-drying at some origins and are discussed under Results and Discussion.

**Intact Glucosinolate Isolation and Identification.** U.S. food store watercress was lyophilized, and two batches (in total 1.42 g) were briefly and repeatedly extracted in boiling 70% aqeuous MeOH in a total of 70 mL. The extracts were filtered (paper), centrifuged (4000*g*), and applied to four 100 mg (dry wt) DEAE Sephadex A-25 anion exchange columns.[1] Each column with bound glucosinolates was washed with 2 mL of 70% aqueous MeOH, 6 mL of AcOH/EtOH/$H_2O$ (1:1:3) to elute weak acids (eluate intensely red), and 2 mL of $H_2O$. Bound glucosinolates were eluted with 10 × 1 mL of aqueous $K_2SO_4$ (saturated, ca. 0.5 M). Most $K_2SO_4$ in fractions was removed by the addition of 2 volumes of 96% EtOH, leaving the mix at −5 °C for 30 min, and centrifugation (4000*g*), discarding the pellet. EtOH was removed by evaporation of two-thirds of the volume under a gentle air stream, and remaining solvent was removed by freezing followed by lyophilization. To remove the remaining the $K_2SO_4$, glucosinolates in the yellowish residue were dissolved in 2 + 2 mL of pure MeOH for each batch, leaving insoluble $K_2SO_4$. The MeOH solution was removed from the insoluble crystals and placed under a gentle air stream for solvent evaporation. The residue was dissolved in a total of 1 mL of $H_2O$ (for the combined batches after testing each separately), and this solution was used for injection to the HPLC, injecting 150 μL six times. We used the analytical HPLC with the phenylhexyl analytical column described above, A = 0.1% aqueous $CF_3COOH$ and B = MeOH: isocratic A for 2 min, 48 min linear gradient to 60% B, 2 min linear gradient to 100% B, isocratic B for 5 min, 3 min linear gradient to 100% A, 7 min isocratic A. Fractions were collected manually (after the waste solvent line had been replaced with a short piece of HPLC tubing after the UV detector), guided by the PDA output followed in real time. To avoid hydrolysis of glucosinolates by $CF_3COOH$, collected fractions were neutralized with 1% (v/v) of a 3 M aqueous potassium acetate solution at the end of the collection day. Neutralized fractions were dried under a gentle air stream and then in vacuo overnight and dissolved in $D_2O$ for NMR analysis and subsequent HPLC-MS carried out as previously reported for intact glucosinolates,[1] except that MS detection was in positive mode (observing $[M - H + 2Na]^+$ adducts) for logistic reasons. Although positive mode detection of glucosinolates is rarely done, both glucosinolates and other anions such as carboxylic acids form positively charged disodium adducts with good ionization efficiency when the eluent is doped with NaCl as here (unpublished observation).

**Autolysis of Fresh Watercress.** The apex of individual branches, with about three small leaves and further primordia, was used. Fresh apex (one large or two small, combined wt 0.4−0.8 g) was either extracted immediately in boiling 70% aqueous MeOH for glucosinolate determination ($n$ = 4) or subjected to autolysis (homogenized in a mortar and incubated as macerated material with 3 mL of $H_2O$ ($n$ = 5) or without any liquid added ($n$ = 5)). After autolysis for 3−4 h, the macerate was either used for glucosinolate determination ($n$ = 2 + 2), using the same extract as for intact material, or subjected to determination of **4** ($n$ = 3 + 3). As a control for the effect of autolysis ($n$ = 2), freshly picked apex was boiled (1 min) before homogenization, then homogenized (including water from the initial boiling), and extracted for **4**. Macerates for determination of **4** were extracted twice with a total of 15 mL of boiling water (2 × 1 min). The extraction volume included any previously added water. Each extract was brought to 15.0 mL; 8.00 mL was taken, mixed with 2.00 mL of MeOH, and allowed to settle at −20 °C overnight. From settled extracts, 1.2 mL was taken and centrifuged at 4000*g*, and the supernatant was transferred to an HPLC vial.

Quantitative analysis for **4** was by HPLC-PDA set at 242 nm, bandwidth 8 nm (phenylhexyl column, injection volume = 100 μL, A = water, B = MeOH: isocratic A for 2 min, 48 min linear gradient to 70% B, 2 min linear gradient to 100% B, isocratic B for 5 min, 3 min linear gradient to 100% A, 7 min isocratic A). Glucosinolates in the studied material were quantitated by the desulfoglucosinolate method (see below). For HPLC-MS analysis of **4**, the gradient program was as follows: 0−0.5 min, isocratic 6% B; 0.5−12.5 min, linear gradient from 6 to 55% B; 12.5−13.1 min, linear gradient from 55 to 95% B; 13.1−15.5 min, isocratic 95% B; 15.6−20 min, isocratic 6% B. The flow rate was 0.2 mL/min but increased to 0.3 mL/min from 15.2 to 17.5 min. For extracted ion chromatograms (combined 202 + 180 + 146 + 120 Da), the width was set to ±0.5 Da.

**Glucosinolate Analysis.** Each accession was extracted at least in duplicate, using around 100 mg of dried foliage (or 0.3−1 g of fresh foliage) per extraction. Extraction, enzymatic desulfation, and HPLC-PDA was carried out as previously reported,[1] except that the C18

column was used. Peak overlap or coelution of either **3** and **13** or **3** and **10** occurred on two other reversed phase columns[1] tested. The elution order in HPLC-PDA, with typical $t_R$ in minutes, was **11** (17.0), **8** (17.7)*, **2** (19.8), **1** (21.5), **9** (23.8), **11** (26.6), **10** (30.3), **3** (31.6), **13** (32.54), **5** (39.7)*, **6** (46.9)*, **7** (53.1). Peaks labeled * were only tentatively identified on the basis of $MS^2$ but not compared with authentic standards. Quantitation was based on UV detection at 229 nm, relative to an external standard of sinigrin desulfated in parallel, using the following response factors: 0.95 for **1**, **2**, and **3**, 1.00 for aliphatic side chain glucosinolates, 0.29 for **11**, 0.28 for **12**, and 0.25 for **13**. Peak identification was based on UV spectra and comparison of $t_R$ with those of authentic desulfoglucosinolate references. HPLC-MS of one sample from each accession was also carried out to support the peak identification. The gradient program was as follows: 0−0.5 min, isocratic 2% B; 0.5−7.5 min, linear gradient from 2 to 40% B; 7.5−8.5 min, linear gradient from 40 to 90% B; 8.5−11.5, isocratic 90% B; 11.60−17 min, isocratic 2% B. The flow rate was 0.2 mL/min but increased to 0.3 mL/min from 11.2 to 13.5 min. The mass spectrometer was run in positive electrospray mode. The elution order was similar in the more condensed HPLC-MS gradient, except that **3** and **13** coeluted. Peak identity inferred from quantitative HPLC with UV detection was confirmed by observation of expected $m/z$ values for sodium adducts in HPLC-MS and inspection of $MS^2$ spectra. $MS^2$ spectra were acquired in automatic mode using SmartFrag with the instrument default settings (isolation width, 4 $m/z$; MS/MS fragmentation amplitude, 1 V; start amplitude, 30%; end amplitude, 200%; acquisition time, 40 ms).

**Statistical Evaluation.** Levels of phytochemicals were log-transformed to ensure variance homogeneity (tested and confirmed by $F$ test) and compared statistically using a two-tailed $t$ test. All procedures were carried out in Excel 2010.

## RESULTS AND DISCUSSION

**Identification of Epiglucobarbarin as a Major U.S. Watercress Glucosinolate by NMR and MS.** To unequivocally identify glucosinolates in watercress obtained in the Massachusetts area, we extracted two independent batches obtained in separate months and separate stores and analyzed the intact glucosinolate fraction by HPLC. As the same eight peaks were detected in both chromatograms, we pooled the fractions and isolated the glucosinolates by preparative HPLC (Figure 2). Three major peaks were identified by NMR and MS: an early-eluting peak was **2**, not previously documented from watercress, whereas the other two peaks proved to be well-established watercress constituents, **3** and 7-methylsulfinylheptylGSL (**9**) (Figure 2). The identification of **2** was unequivocal: not only did the mass, coupling pattern, and chemical shifts agree with the structure of **2**, but the NMR spectrum also closely matched the previously reported spectrum.[24] From this latter comparison it was evident that the *R*-epimer (**2**) was present, as the *S*-epimer (**1**) exhibits slightly different chemical shifts and coupling constants at the 1-, 2-, 1′-, and 6′-positions. The *S*-epimer **1** (Figure 2) was also identified at low levels on the basis of a very weak NMR spectrum[24] and UV and mass spectra, and four minor peaks (Figure 2) were tentatively identified as previously reported[17] watercress constituents by UV and mass spectra (results not shown).

**Formation of 5-Phenyloxazolidine-2-thione during Autolysis of U.S. Watercress.** After crushing fresh watercress from a U.S. food store to allow autolysis catalyzed by endogenous myrosinase, we found the oxazolidine-2-thione type product **4** at similar levels as the combined levels of **1** and **2** in control experiments without autolysis (Table 1). The identification of **4** was by retention time in two different HPLC systems and UV and mass spectra as compared with an

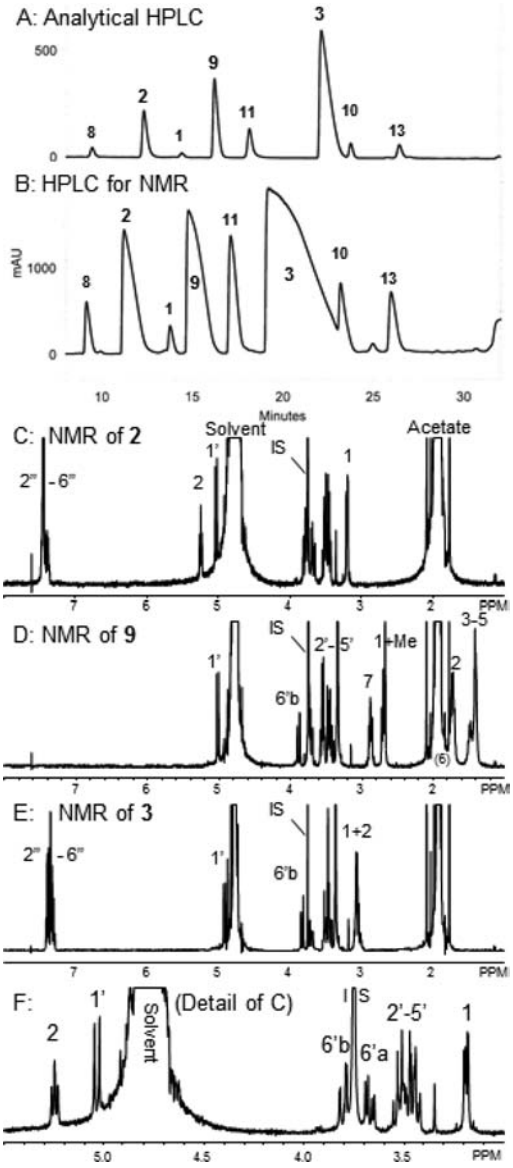


**Figure 2.** Analysis of the total glucosinolate preparation from U.S. food store watercress (Boston, MA) by HPLC followed by $^1$H NMR. HPLC was carried out in (A) analytical scale and (B) preparative scale using the same instrument, conditions, and glucosinolate preparation, but with different injection volumes (10 and 150 $\mu$L, respectively). (C−E) $^1$H NMR spectra of individual peaks after neutralization with acetate and solvent change to $D_2O$. (F) Detail of the NMR spectrum of **2** (=C).

authentic standard (Figures 3 and 4).[1] Four main ions were observed in HPLC-MS from **4**: 202, 180, 146, and 120 (corresponding to $[M + Na]^+$, $[M + H]^+$, $[M - H_2S + H]^+$, and $[M - CSO + H]^+$); this fragmentation and the UV maximum are both characteristic of the oxazolidine-2-thione moiety.[1,23] The products formed from **1** and **2**, (*R*)-**4** and (*S*)-**4**), constitute an enantiomeric pair (Figure 1), but the enantiomers are indistinguishable using achiral HPLC columns and were not distinguished in the analysis. The detected product, probably a mixture of enantiomers dominated by the product of **2**, is for this reason simply termed **4** without specification of enantiomer and compared with the sum of the epimeric precursors. Interestingly, levels of **4** were higher when water was immediately added to the macerated tissue than when the


dx.doi.org/10.1021/jf5032795 | J. Agric. Food Chem. 2014, 62, 9586−9596

**Table 1. Levels of Glucobarbarins (1 + 2) and 5-Phenyloxazolidine-2-thione (4) in Macerated Watercress Shoot Apex after Autolysis for about 3 h[a]**

| | 1 + 2 (μmol/g fresh wt) | | | 4 (μmol/g fresh wt) | | | |
|---|---|---|---|---|---|---|---|
| condition | mean | SD | $n^b$ | mean | SD | $n$ | signif |
| control | 3.6 | 0.2 | 4 | 0.5[c] | 0.02 | 2 | n/a |
| autolysis − water | 0.03 | 0.02 | 2 | 1.0 | 0.4 | 3 | ns |
| autolysis + water | 0.03 | 0.02 | 2 | 3.5 | 1.2 | 3 | **[d] |

[a]Mean levels of other major glucosinolates in the analyzed material (Santa Clara Valley, CA, USA) were as follows: **3**, 6.1; **9**, 3.9; **11**, 0.8; **6**, 0.6. The extent of hydrolysis was in all cases >98%. Statistical significance (signif) relates to levels of **4** and is relative to the control: **, $P < 0.01$; *, $P < 0.05$; ns, $P \geq 0.05$. [b]The number of replicates $n$ generally differs for glucosinolates and hydrolysis products because the values resulted from independent experiments and extractions. [c]Maximum estimate including minor coeluting flavonoid-like matrix component. [d]Level of significance relative to autolysis without water: *, the $F$ test for variance inhomogeneity after log transformation was insignificant but close to significance ($P = 0.10$). However, a $t$ test assuming variance inhomogeneity was still significant (*, $P = 0.010$).

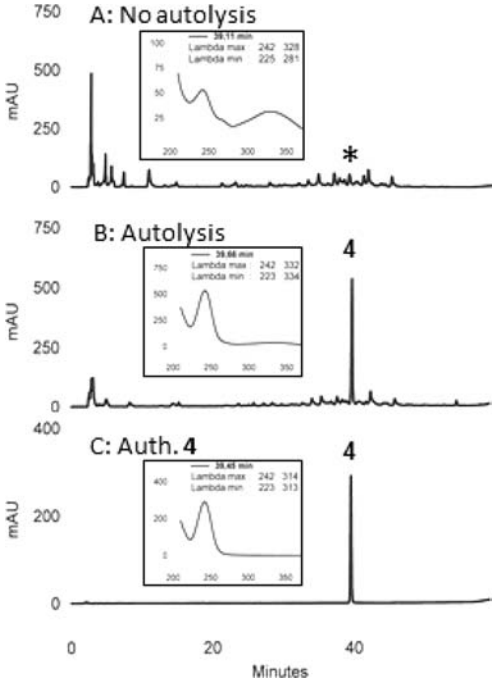


**Figure 3.** Identification and quantitation by HPLC with UV detection at 242 nm of 5-phenyloxazolidine-2-thione (**4**) in U.S. food store watercress either (A) extracted directly or (B) subjected to autolysis. The asterisk indicates a peak containing **4** and an unknown metabolite. (Insets) Photodiode array UV spectra at the peak apex of the **4** peak. (C) Chromatogram of authentic **4** (35 μM) analyzed in parallel.

autolysis happened in macerated tissue alone, even though glucosinolate hydrolysis was essentially complete at both conditions (Table 1).

An unexpected result of the autolysis experiment was the apparent detection of low levels of **4** in fresh watercress believed not to have been subject to autolysis (Table 1). Moderate interference from coeluting matrix components was likely in both HPLC-PDA and HPLC-MS, but the correct $\lambda_{max}$ and diagnostic MS fragments were observed (Figures 3 and 4D). Despite the modest background signals, we suggest that

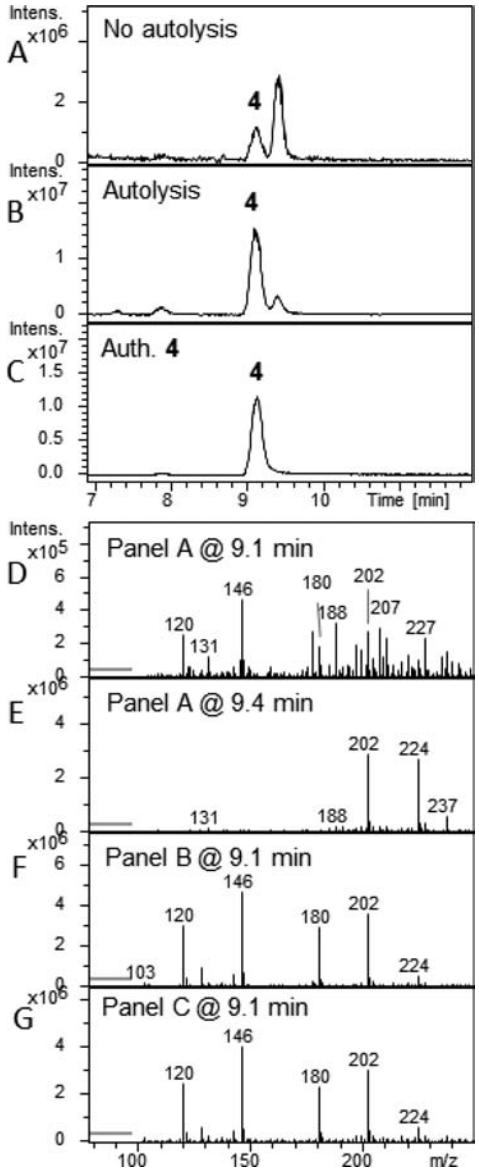


**Figure 4.** Identification by HPLC-MS of 5-phenyloxazolidine-2-thione (**4**) in U.S. food store watercress either (A) extracted directly or (B) subjected to autolysis with water. The trace is the combined extracted ion chromatogram of $m/z$ 202, 180, 146, and 120. (C) Chromatogram of authentic **4** (35 μM) analyzed in parallel. (D−G) Mass spectra of the POAT peak at 9.1 min or an unidentified peak at 9.4 min as indicated.

HPLC-PDA is reliable for quantitative determination of **4** *after* autolysis. Whether the minor level observed in control experiments was a natural constituent in intact tissue or due to slight incidental tissue damage is unknown. A baseline-separated peak in HPLC-MS ($t_R = 9.5$ min) shared the $m/z$ 202 ion, but in this case it was interpreted as $[M + H]^+$ (Figure 4E) and appeared to be unrelated to glucosinolate hydrolysis (Figure 4).

**Identification of Desulfated Glucosinolates by HPLC and MS/MS.** Separation of all watercress glucosinolates (Figures 1 and 5) after desulfation was accomplished in HPLC-PDA. To obtain additional certainty, analyses were complemented by HPLC-MS/MS. The initial peak identification was based on retention times, UV spectra, and $m/z$ values of $[M + Na]^+$ adducts in HPLC-MS. In an attempt to


dx.doi.org/10.1021/jf5032795 | J. Agric. Food Chem. 2014, 62, 9586−9596

**Aliphatic methylthioalkyl glucosinolates**

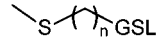


n=6: 6-MethylthiohexylGSL: **5**
n=7: 7-MethylthioheptylGSL: **6**
n=8: 8-MethylthiooctylGSL: **7**

**Aliphatic methylsulfinylalkyl glucosinolates**

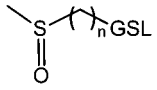


n=6: 6-MethylsulfinylhexylGSL: **8**
n=7: 7-MethylsulfinylheptylGSL: **9**
n=8: 8-MethylsulfinyloctylGSL: **10**

**Indole glucosinolates**

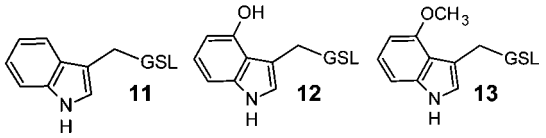


**Figure 5.** Structures, names, and abbreviations of aliphatic and indole glucosinolates detected in watercress. Three of them, **5**, **6**, and **8**, were only tentatively identified on the basis of $MS^2$, whereas the remaining were identified with certainty. "GSL" indicates the constant part of glucosinolates in structures and is an abbreviation of "glucosinolate" in names.

better distinguish isomers, we characterized the known peaks in $MS^2$ of sodium adducts. A universal fragment ion was $[M + Na - 162]^+$ representing an expectable loss of $C_6H_{10}O_5$ (fragment type c) (Figure 6). However, desulfo glucobarbarins and methylthio and methylsulfinylalkyl glucosinolates yielded specific fragmentations that could be rationalized from side-chain structures. Authentic references of both desulfo **1** and **2** showed a fragment at $m/z$ 364 indicating a characteristic loss of water (fragment type f). In addition, a fragment at $m/z$ 276 indicating the loss of benzaldehyde (fragment type e) was observed for both desulfo **1** and **2**. Interestingly, loss of water and benzaldehyde was not observed for available isomers of the desulfoglucobarbarins, desulfated *p*-hydroxy-**3** and *p*-methoxybenzylglucosinolate, whereas loss of water and hydroxybenzaldehyde was observed for desulfo *p*-hydroxy **2**.[23] Hence, loss of water and benzaldehyde provided a useful signature of **1** and **2** specifically reflecting the presence of the 2-hydroxy-2-phenyl substituents. Likewise, the $MS^2$ spectra of $Na^+$ adducts of the two methylsulfinylalkyl desulfoglucosinolates available as authentic references, **9** and **10**, were highly characteristic. Besides apparent loss of $[CH_4SO]$ resulting in $[M + Na - 64]$ fragments (type g), the characteristic feature of this homologous series was the *absence* of the usually observed desulfoGSL fragments at $m/z$ 185 and 219 (corresponding to $Na^+$ adducts of $C_6H_{10}O_5$ and thioglucose, fragment types a and b, respectively) and the *presence* of a major fragment ion corresponding to a $Na^+$ adduct of the aglucone after loss of thioglucose (loss of 196, fragment type h) (Figure 6). On the basis of similar $MS^2$ fragmentation and reasonable retention time and UV spectrum, the lower homologue **8** (not available as authentic desulfo reference) was tentatively identified in a variety of watercress samples. Methylthioalkyl desulfoglucosinolates exhibited a less intense $[M + Na - 196]^+$ fragment ion ($m/z$ 210 in the case of desulfo **6**), whereas the remaining tested desulfoGSLs did not produce this fragment type (type h) (Figure 6). Only one desulfoglucosinolate from this homologous series was available as authentic reference (desulfo **7**), but the two lower homologues (**5** and **6**) were tentatively identified

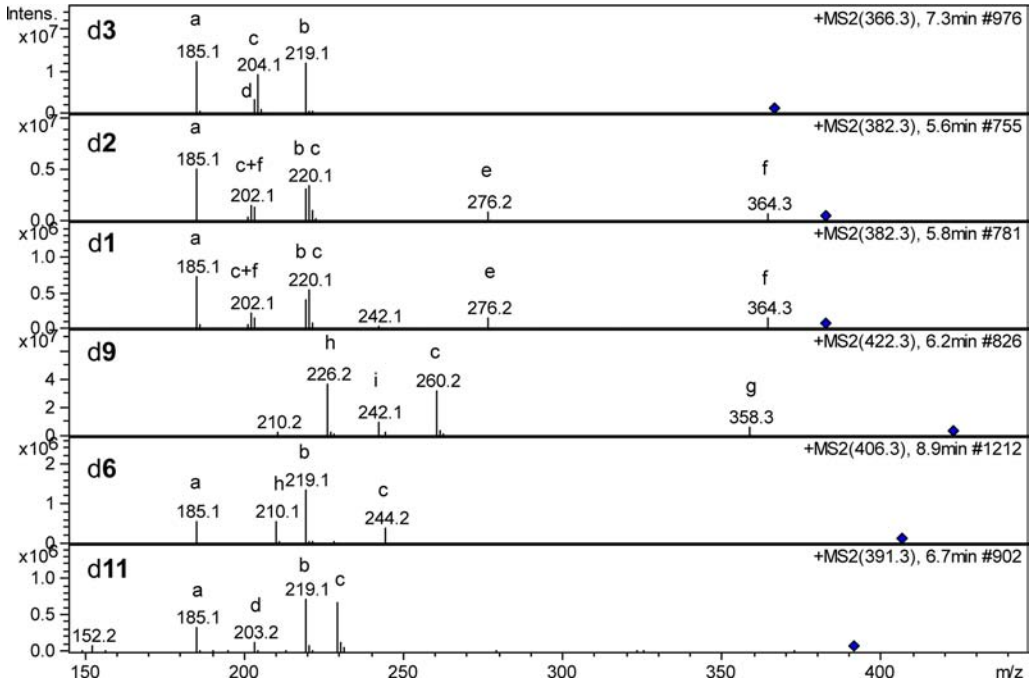


**Figure 6.** Fragments of sodium adducts of desulfated glucosinolates from U.S. food store watercress observed in $MS^2$ after HPLC separation. Types of fragments are indicated with letters as follows: a, $[C_6H_{10}O_5 + Na]^+$; b [thioGlc + Na]$^+$; c, loss of 162 $[M + Na - C_6H_{10}O_5]^+$; d, $[Glc + Na]^+$; e, loss of 106, benzaldehyde $[M + Na - C_7H_6O]^+$; f, loss of 18, water $[M + Na - H_2O]^+$; g, loss of 64, $CH_3(SO)H$ $[M + Na - CH_4SO]^+$; h, loss of 196 $[M + Na -$ thioGlc$]^+$; i, loss of 180 $[M + Na - Glc]^+$.


dx.doi.org/10.1021/jf5032795 | J. Agric. Food Chem. 2014, 62, 9586−9596

Table 2. Glucosinolate Levels[a] in Watercress of Different Origins[b]

| | glucosinolates (μmol/g dry wt) | | | | | | | | | | | | | |
|---|---|---|---|---|---|---|---|---|---|---|---|---|---|---|
| | benzenic | | | aliphatic methylthioalkyl | | | aliphatic methylsulfinylalkyl | | | indolic | | | | |
| accession | 1 | 2 | 3 | 5 | 6 | 7 | 8 | 9 | 10 | 11 | 12 | 13 | sum | n |
| **wild-collected** | | | | | | | | | | | | | | |
| Lenox, MA[c] | 0.02 | 0.34 | **20.64** | **0.06** | **1.02** | **0.16** | 0.44 | **6.02** | **1.30** | **0.54** | **0.27** | 0.05 | **30.79** | 3 |
| Lenox, MA (2005) | 0.02 | 0.45 | 14.86 | 0.01 | 0.04 | 0.00 | 0.31 | **4.91** | **0.85** | **0.64** | 0.00 | 0.00 | 22.09 | 1 |
| Yellow Springs, OH[c] | 0.01 | 0.06 | **34.34** | 0.01 | **0.40** | **0.17** | 0.09 | 2.91 | **1.91** | 0.26 | 0.01 | **0.37** | **40.52** | 4 |
| Mors, DK[c] | 0.02 | 0.05 | **41.10** | 0.00 | 0.00 | 0.00 | 0.12 | 2.38 | **1.08** | 0.39 | 0.00 | 0.16 | **45.30** | 2 |
| **home-grown from seeds or wild plants** | | | | | | | | | | | | | | |
| Johnny's Select Seeds[c] | 0.00 | 0.01 | **22.82** | 0.00 | 0.05 | 0.00 | 0.03 | 0.76 | 0.35 | 0.30 | 0.00 | 0.10 | 24.44 | 2 |
| Kitazawa Seeds[c] | 0.00 | 0.01 | 19.56 | 0.00 | 0.03 | 0.01 | 0.03 | 0.42 | 0.26 | 0.24 | 0.00 | 0.11 | 20.66 | 2 |
| Chiltern Seeds[c] | 0.00 | 0.01 | **24.42** | 0.01 | 0.11 | 0.02 | 0.03 | 0.74 | 0.35 | 0.41 | 0.00 | 0.14 | 26.23 | 2 |
| wild, MA[c] | 0.01 | 0.29 | 8.66 | 0.01 | 0.00 | 0.00 | **0.32** | **5.40** | **1.23** | 0.14 | 0.00 | 0.00 | 16.05 | 3 |
| **obtained fresh in shop** | | | | | | | | | | | | | | |
| Boston, MA | **0.52** | **6.27** | 16.41 | **0.03** | **0.36** | 0.04 | **1.47** | **11.81** | **1.42** | **0.78** | 0.00 | 0.17 | **39.25** | 2 |
| Boston, MA (2004/5) | **0.35** | **4.40** | 11.21 | 0.01 | **0.51** | 0.05 | **0.82** | **7.80** | 0.98 | **0.80** | 0.00 | 0.16 | 27.09 | 2 |
| Dayton, OH[c] | **0.25** | **3.92** | 7.99 | 0.01 | 0.01 | 0.01 | **0.49** | **5.31** | **0.63** | 0.51 | 0.00 | 0.06 | 19.19 | 3 |
| San Francisco, CA | **0.48** | **5.66** | 15.76 | **0.10** | **1.58** | **0.20** | **1.82** | **21.11** | **4.08** | **1.58** | **0.47** | 0.24 | **52.99** | 2 |
| Buenos Aires, AR | 0.00 | 0.03 | 13.67 | 0.00 | 0.01 | 0.00 | 0.02 | 0.10 | 0.31 | 0.50 | 0.05 | **0.68** | 15.36 | 4[d] |
| Melbourne, AU | 0.01 | 0.02 | 20.20 | 0.00 | 0.00 | 0.00 | 0.02 | 0.23 | 0.06 | 0.21 | 0.04 | **0.53** | 21.31 | 2 |
| Peralta, ES | 0.00 | 0.01 | **32.75** | 0.00 | 0.00 | 0.00 | 0.02 | 0.01 | 0.00 | **1.03** | 0.00 | **0.44** | **34.27** | 2 |
| Pamplona, ES | 0.00 | 0.01 | **25.04** | 0.00 | 0.00 | 0.00 | 0.00 | 0.00 | 0.00 | **0.96** | 0.00 | 0.10 | 26.11 | 2 |
| Odemira, PT | 0.00 | 0.04 | **27.47** | **0.07** | **1.68** | **0.94** | 0.04 | 0.97 | 0.54 | 0.46 | **0.13** | **1.14** | **33.41** | 2 |
| Copenhagen, DK (A)[c] | 0.00 | 0.03 | **21.23** | 0.00 | 0.11 | 0.05 | 0.03 | 0.65 | 0.32 | 0.13 | 0.00 | 0.16 | 22.72 | 2 |
| Copenhagen, DK (B) | 0.00 | 0.02 | 9.59 | 0.00 | 0.25 | **0.12** | 0.01 | 0.07 | 0.04 | 0.20 | 0.02 | **0.44** | 10.75 | 2 |
| **obtained dried in shop** | | | | | | | | | | | | | | |
| DK/CN | 0.03 | 0.52 | 1.12 | 0.03 | **0.39** | 0.04 | 0.12 | 1.45 | 0.21 | 0.08 | 0.01 | 0.20 | 4.16 | 2 |
| **seeds, not germinated** | | | | | | | | | | | | | | |
| Chiltern Seeds | 0.03 | 0.23 | 52.82 | 0.14 | 5.25 | 2.73 | 0.06 | 3.44 | 4.46 | 0.02 | 0.00 | 0.00 | 69.05 | 1 |

[a]Levels (in leaves) are shown in bold if they are numerically larger than the average of all freshly obtained leaves for that glucosinolate. Accessions were from 2012 or 2013 unless otherwise indicated. [b]MA, Massachusetts, USA; OH, Ohio, USA; DK, Denmark; CA, California, USA; AR, Argentina; AU, Australia; ES, Spain; PT, Portugal; CN, China. [c]Plants were confirmed as *Nasturtium officinale* by observation of two rows of seeds in siliques. [d]Mean of two similar accessions.

in a variety of watercress samples on the basis of similar $MS^2$ fragmentation, UV, and reasonable retention time.

In general, whether $Na^+$ associates with the glucone or aglucone moiety of desulfoglucosinolates upon fragmentation in the ion trap seems to depend on the nature of the side chain. The highly polar sulfinyl group seems to have higher affinity for $Na^+$ than the thioglucose residue, whereas affinities of the thioether and the thioglucose residue are roughly comparable. A terminal methylsulfinyl group can additionally be recognized by the loss of $[CH_4SO]$. Also, desulfoglucosinolates with a combined 2-hydroxy-2-phenyl substitution seem to be recognizable by the loss of water and a benzaldehyde in a reaction that is somewhat similar to a retro-aldol reaction.

**Diversity of Watercress as Available to Consumers.** We investigated whether consumers would likely obtain watercress containing glucobarbarins (**1** and **2**). Initial inspection of the distribution of high levels revealed an unexpected pattern: **2** was found at relatively high levels in all tested food store accessions from the United States, whereas only very low levels were found in accessions from Europe and in a few tested accessions from other continents (Table 2; Figure 7). The apparent grouping of the accessions was tested statistically in the relevant subset of data: material obtained fresh in food stores. The mean levels of **2** in four U.S. food store samples were significantly higher than the levels in the remaining eight food store samples ($P < 0.001$). Wild material from the United States was variable: watercress from

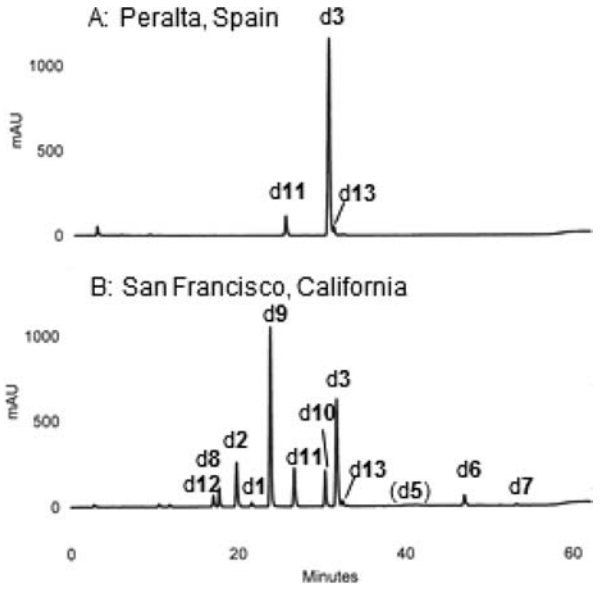


**Figure 7.** Contrasting glucosinolate chromatograms of a typical European accession of watercress from (A) Spain and (B) a typical U.S. food store watercress from California. Glucosinolates were enzymatically desulfated before analysis as indicated by "d" before glucosinolate numbers, and UV detection at 229 nm was employed.


dx.doi.org/10.1021/jf5032795 | J. Agric. Food Chem. 2014, 62, 9586−9596

Massachusetts showed moderate levels of **2**, whereas wild material from Ohio was very low in **2**. Plants grown from commercially obtained seeds were low in glucobarbarins irrespective of the supplier, whereas wild-collected plants grown in parallel retained approximately the same relative levels found in the wild-collected material. We considered whether the apparent trace peaks of **2** in European material and material grown from seeds could be confirmed with certainty by MS/MS. This was the case for seeds of a European type and for material from Denmark (wild), Argentina, and Portugal. Neither sinalbin nor gluconapin[19] was detected.

Interestingly, the four tested U.S. food store accessions were also remarkably high in methylthioalkyl and methylsulfinylalkyl glucosinolates, whereas the remaining eight food store accessions from Europe ($n$ = 5), Argentina ($n$ = 2), and Australia ($n$ = 1) were lower in these kinds of glucosinolates ($P$ < 0.001 for the sum of **5**−**10**). Indeed, 34−55% of the glucosinolate content of U.S. food store samples consisted of these aliphatic glucosinolates (Table 2; Figure 7). Wild material appeared to be more homogeneous for aliphatics, with intermediate levels, whereas material grown from seeds had rather low levels (Table 2). Considering total glucosinolate levels, there was no obvious association of high or low levels with specific origins, except for a tendency for higher total levels in wild-collected watercress compared to watercress grown at our particular artificial light conditions.

To obtain the widest possible temporal and geographical diversity of samples, we had to accept a range of drying methods and storage periods. Spontaneous air-drying was used for some samples, was used in classical qualitative natural product chemistry, and is reliable (N.A., unpublished results) for preparative purposes. However, it cannot be considered optimal for quantitative analysis because of the extended period in which physiological postharvest processes can occur. However, our use of spontaneous air-drying at some remote sampling sites and in the Wright State University laboratory was not a factor in the distinction of two chemotypes of watercress. Indeed, nearly the full range of **1**, **2** and aliphatics (**5**−**10**) was observed in samples from Wright State University, Dayton (Ohio), where spontaneous drying at ambient conditions was used for logistic reasons. This range was comparable with the combined results from Copenhagen, Peralta, and Boston, where lyophilization was used (Table 2). Storage conditions and time were likewise not factors for the distinction of two chemotypes. First, analytical results of our 2004−2005 samples were essentially the same initially and after storage until this investigation (results not shown). Furthermore, the 2012 sample had essentially the same glucosinolate content after storage for a year, although glucosinolate hydrolysis occurred rapidly after the addition of water to the stored sample, so uptake of water during storage was apparently insignificant. Hence, we do not consider even extended frozen storage in closed plastic bags a problem for glucosinolate stability, with the possible exception of the oxidation-sensitive **12**, which was not observed in old samples (Table 2). Indeed, a reliable glucosinolate profile of a 90-year-old herbarium specimen was recently reported with comparison with more recent material,[27] indicating long-term stability.

**Botanical Identity of Watercress Accessions.** Because of the observation of two distinct chemotypes of commercially available watercress, it was relevant to test by conclusive botanical identification whether the chemotypes reflected any of the established watercress taxa mentioned in the Introduction. The key morphological distinction between the two species of watercress discussed here, *N. officinale* and *N. microphyllum*, is based on mature siliques. All tested accessions were fertile and had seeds in two rows in siliques, including watercress foliage from the same grocery store in Dayton (Ohio) as used for glucosinolate analysis, wild-collected material from Ohio, Massachussets, and Denmark, material from a Danish food store, and all accessions grown from seed (Table 2). We concluded that all of these accessions belonged to *N. officinale* as opposed to *N. microphyllum*. The liberal seed set would suggest that the partially sterile hybrid *N.* × *sterile* was not represented.

Because of the unusual glucosinolate profile of the material from U.S. food stores, we also established chromosome numbers based on the number of chromocenters, defined as stainable regions in interphase nuclei that approximately reflect individual chromosomes.[28] The result was striking: whereas the number of chromocenters in Danish material was close to the established chromosome number of *N. officinale*, the U.S. food store material revealed approximately twice as many chromocenters (Figure 8), indicative of chromosome doubling. It was

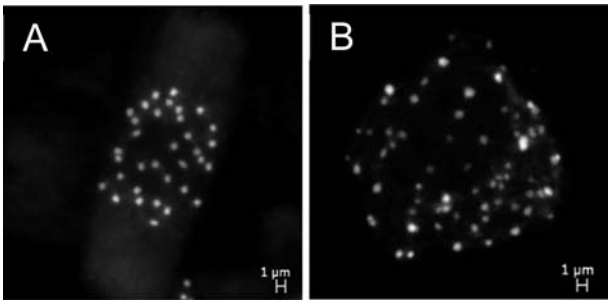


**Figure 8.** Cytological analysis (DAPI-stained interphases) of (A) wild Danish watercress with 34 chromocenters and (B) U.S. food store watercress (Boston, Massachusetts) with ca. 68 chromocenters.

confirmed by glucosinolate analysis that the U.S. food store material with double chromosome number was relatively high in **2** (4.3% of total) and aliphatic glucosinolates (38%), whereas the investigated wild Danish material was low in **2** (0.2%) and had moderate levels of aliphatic glucosinolates (21%).

**Watercress Is Polymorphic for Glucosinolate Profiles and Chromosome Numbers and Is a Dietary Source of 5-Phenyloxazolidine-2-thione.** Combining the morphological, cytological, and chemical evidence, we conclude that watercress, *N. officinale*, as available to consumers is polymorphic for glucosinolate profile and chromosome number. In the cases tested for both characters, they were correlated, but further research will be needed to test for a general association. Specifically, epiglucobarbarin (**2**) was a significant constituent of watercress from U.S. food stores and some wild accessions including chromosome-doubled material, in contrast to the remaining tested accessions mainly from Europe including diploid material. Furthermore, watercress from U.S. food stores exhibited a distinct profile of aliphatic glucosinolates, with considerable levels of long-chain methylsulfinylalkyl and methylthioalkyl glucosinolates in addition to the traditionally recognized glucosinolate in watercress, **3**. These aliphatic glucosinolates were previously known from watercress, with some variation also within European material.[14,16] In the following, we term the complex chemotype obtained in U.S. food stores "the U.S. food store type", whereas

the simpler chemotype dominated by **3** and obtained from a number of European sources is termed "the European type". Altered postharvest glucosinolate biosynthesis induced by storage conditions could in principle explain differences between freshly harvested and shelf-stored produce, but this was not what we observed. Rather, the two chemotypes were observed within both the wild-collected and commercially obtained watercress accessions and in commercial material cultivated and rooted for chromosome counts, suggesting that genetic factors were important for the observed chemical differences.

We have also confirmed the conversion product **4** from U.S. food store watercress. This is the first unequivocal demonstration of **1**, **2**. and **4** in a regular food crop. The formation of **4** suggests that this hydrolysis product will also be formed when watercress is chewed and possibly also by microbial breakdown in the colon.[11,12] The detection method for **4** (achiral HPLC) did not allow distinction of absolute configuration, but from the dominance of **2** in watercress the detected **4** can be inferred to consist mainly of (*S*)-**4** (Figure 1). The common name "barbarin" has been suggested for (*R*)-**4**[29] and may be preferable for daily use. The (*S*)-**4** formed from watercress should preferably be called (*S*)-barbarin in cases when precision is needed.

**Health Benefits and Hypothetical Risks of Watercress Glucosinolates.** There seems to be a consensus regarding phenethyl isothiocyanate (from **3**) and methylsulfinylalkyl and methylthioalkyl isothiocyanates as health-promoting.[12,16,20,21,30,31] Indeed, an increase in the consumption of glucosinolate-containing vegetables seems to be advantageous and is recommended by public health authorities such as the National Cancer Institute.[32−34]

However, the detection of **1** and **2** as well as their product **4** in some watercress needs separate scrutiny because **4** is a different type of hydrolysis product. We are aware of a single investigation of nutritional effects (in rats at quite high levels) of **1** and a hydrolysis product assumed to be (*R*)-**4**.[35] Significant detrimental effects of **1** and/or (*R*)-**4** were observed on the palatability of the feed and on weights of liver, kidney, suprarenal glands, testicles, and thyroid gland. The detrimental effect on thyroid weight is in accordance with the general disturbance of iodine metabolism in the thyroid gland by oxazolidine-2-thiones.[36] Facile conversion of these to mutagenic *N*-nitroso derivatives in the presence of nitrite at "stomach conditions" is also known.[37] A different effect is inhibition of tyrosinase enzymes by (*R*)-**4**.[38] This effect was not suggested to be toxic or antinutritional, but was suggested to be useful in preventing enzymatic browning of fruits and vegetables as well as in cosmetic and medical applications. It is not simple to predict whether the (*S*)-**4** formed in U.S. food store type of watercress would have the same effects as (*R*)-**4** formed from **1**, but it seems relevant to expect physiological effects.

It is relevant to consider the occurrence of a related oxazolidine-2-thione-forming glucosinolates in many cabbages: progoitrin, the precursor of goitrin ((*S*)-5-vinyloxazolidine-2-thione). This glucosinolate causes negative effects of rapeseed meal in animal fodder and also showed antinutritional effects on rats and formed nitrosamides under stomach conditions.[35−37] Nevertheless, we are not aware of any health risk of eating even considerable amounts of, for example, Chinese cabbage containing this glucosinolate at 2−5 μmol/g dry wt,[39] whereas the contribution to bitterness is well established as could also be the case for glucobarbarins.[40,41] This general acceptance of an oxazolidine-2-thione-forming glucosinolate should perhaps be extended to **1** and **2** unless future research shows otherwise.

**Origins, Potentials, and Ecological Risks of U.S. Food Store Watercress.** The difference between European and U.S. food store material suggests a non-European origin of U.S. food store watercress. As watercress is considered introduced in the United States, the ultimate origin must be overseas or by a recent evolutionary event such as hybridization or chromosome number mutation. A simple explanation of the apparent chromosome number difference would be artificial chromosome doubling.[42] However, hybridization or chromosome number mutation is by no means a prerequisite for glucosinolate variation.[23,43,44] The finding of wild material with significant levels of **2** and aliphatic glucosinolates at a natural habitat in United States in both 2005 and 2012 (Table 2) would suggest that the U.S. food store type of watercress occurs in nature to some extent and may have been naturalized for at least a decade. There is some evidence to suggest that the difference in glucosinolate profile between the two types could have ecological effects, and it is possible that variation in glucosinolate profiles may relate to variation in the prevalence of watercress in invaded habitats,[9,10,44−49] including possible conversion of **1**, **2**, **3**, and **4** to phytoalexins.[50,51]

A cultivar of broccoli with increased levels of another methylsulfinylalkyl glucosinolate, glucoraphanin, has been commercialized under the name "superbroccoli".[52] Perhaps a "super watercress" can be created or selected on the basis of the already available material, or the current U.S. material might in itself merit this designation. However, comparison of nutritional effects of watercress with different glucosinolate profiles is needed before one type of watercress can be recommended over another. Although we have discovered a new class of glucosinolates and glucosinolate products in watercress, associated with nutritional problems in animal feed at high doses[35] and possibly in insect resistance in a wild crucifer,[44] there is nothing in our results to suggest that current varieties constitute any nutritional risk at usual human intakes. However, the potentially different invasive properties of the U.S. food store variant with distinct glucosinolate profile and chromosome number should be considered before introduction of this high chromosome number chemotype for cultivation abroad.[9,10]

## AUTHOR INFORMATION

### Corresponding Author

*(N.A.) Phone: +45 35 33 37 23. E-mail nia@plen.ku.dk.

### Funding

This work was supported by the Torben and Alice Frimodts Fond (N.A.), the *Arabis* Fund (F.S.C.), and the Ohio Plant Biotechnology Consortium (D.C.).

### Notes

The authors declare no competing financial interest.

## ACKNOWLEDGMENTS

We thank four anonymous reviewers for helpful comments and suggestions and the following individuals for contributing watercress samples: Francisco R. Badenes-Peréz (ES, PT), Marta A. Carballo (AR), Deyang Xu (CN), Maya and Marie Louise Mileck (CA), Elizabeth Neilson (AU). We also thank Birgitte Rasmussen and Cecilie Ida Cetti Hansen for skillful

glucosinolate analysis, Samantha Davis for assistance with watercress cultivation, Karen R. Munk for chromosome preparation, and M. S. C. Pedras for sharing a paper in press.

## REFERENCES

(1) Agerbirk, N.; Olsen, C. E. Glucosinolate structures in evolution. *Phytochemistry* **2012**, *77*, 16−45.
(2) Kjær, A.; Gmelin, R. isoThiocyanates XXVIII. A new isothiocyanate glucoside (glucobarbarin) furnishing (−)-5-phenyl-2-oxazolidinethione upon enzymic hydrolysis. *Acta Chem. Scand.* **1957**, *11*, 906−907.
(3) Gmelin, R.; Kjær, A.; Schuster, A. Glucosinolates in seeds of *Sibara virginica* (L.) Rollins: two new glucosinolates. *Acta Chem. Scand.* **1970**, *24*, 3031−3037.
(4) Bleeker, W.; Huthmann, M.; Hurka, H. Evolution of hybrid taxa in *Nasturtium* R. Br. (Brassicaceae). *Folia Geobot.* **1999**, *34*, 421−433.
(5) Manton, I. The cytological history of watercress (*Nasturtium officinale* R. Br.). *Z. Indukt. Abstamm. Vererbungsl.* **1935**, *69*, 132−157.
(6) Howard, H. W.; Lyon, A. G. *Nasturtium officinale* R. Br. (*Rorippa nasturtium-aquaticum* (L.) Hayek). *J. Ecol.* **1952**, *40*, 228−245.
(7) Green, P. S. Watercress in the New World. *Rhodora* **1962**, *64*, 32−43.
(8) U.S. Department of Agriculture. *Nasturtium officinale*, http://plants.usda.gov/core/profile?symbol=NAOF (accessed Dec 9, 2013).
(9) Hurka, H.; Bleeker, W.; Neuffer, B. Evolutionary processes associated with biological invasions in the Brassicaceae. *Biol. Invasions* **2003**, *5*, 281−292.
(10) Schierenbeck, K. A.; Ellstrand, N. C. Hybridization and the evolution of invasiveness in plants and other organisms. *Biol. Invasions* **2009**, *11*, 1093−1105.
(11) Holst, B.; Williamson, G. A critical review of the bioavailability of glucosinolates and related compounds. *Nat. Prod. Rep.* **2004**, *21*, 425−447.
(12) Higdon, J. V.; Delage, B.; Williams, D. E.; Dashwood, R. H. Cruciferous vegetables and human cancer risk: epidemiological evidence and mechanistic basis. *Pharmacol. Res.* **2007**, *55*, 224−236.
(13) Hecht, S. S.; Chung, F.-L.; Richie, J. P.; Akerkar, S. A.; Borukhova, A.; Skowronski, L.; Carmella, S. G. Effects of watercress consumption on metabolism of a tobacco-specific lung carcinogen in smokers. *Cancer Epidemiol. Biomarkers Prev.* **1995**, *4*, 877−884.
(14) Gill, C. I. R.; Haldar, S.; Boyd, L. A.; Bennett, R.; Whiteford, J.; Butler, M.; Pearson, J. R.; Bradbury, I.; Rowland, I. R. Watercress supplementation in diet reduces lymphocyte DNA damage and alters blood antioxidant status in healthy adults. *Am. J. Clin. Nutr.* **2007**, *85*, 504−510.
(15) Casanova, N. A.; Carballo, M. A. Antigenotoxic activity of watercress extract in an in vitro mammalian system using comet assay. *Phytother. Res.* **2011**, *25*, 1743−1746.
(16) Aires, A.; Carvalho, R.; Rosa, E. A. S.; Saavedra, M. J. Phytochemical characterization and antioxidant properties of baby-leaf watercress produced under organic production system. *CyTA J. Food* **2013**, *11*, 343−351.
(17) Rose, P.; Faulkner, K.; Williamson, G.; Mithen, R. 7-Methylsulfinylheptyl and 8-methylsulfinyloctyl isothiocyanates from watercress are potent inducers of phase II enzymes. *Carcinogenesis* **2000**, *21*, 1983−1988.
(18) Suzuki, C.; Ohnishi-Kameyama, M.; Sasaki, K.; Murata, T.; Yoshida, M. Behaviour of glucosinolates in pickling cruciferous vegetables. *J. Agric. Food Chem.* **2006**, *54*, 9430−9436.
(19) Kopsell, D. A.; Barickmann, T. C.; Sams, C. E.; McElroy, J. S. Influence of nitrogen and sulfur on biomass production and carotenoid and glucosinolate concentrations in watercress (*Nasturtium officinale* R. Br.). *J. Agric. Food Chem.* **2007**, *55*, 10628−10634.
(20) Munday, R.; Munday, C. M. Induction of phase II detoxification enzymes in rats by plant-derived isothiocyanates: comparison of allyl isothiocyanate with sulforaphane and related compounds. *J. Agric. Food Chem.* **2004**, *52*, 1867−1871.
(21) Bonnesen, C.; Eggleston, I. M.; Hayes, J. D. Dietary indoles and isothiocyanates that are generated from cruciferous vegetables can both stimulate apoptosis and confer protection against DNA damage in human colon cell lines. *Cancer Res.* **2001**, *61*, 6120−6130.
(22) Fahey, J. W.; Zalcmann, A. T.; Tatalay, P. The chemical diversity and distribution of glucosinolates and isothiocyanates among plants. *Phytochemistry* **2001**, *56*, 5−51.
(23) Agerbirk, N.; Olsen, C. E.; Heimes, C.; Christensen, S.; Hauser, T. P.; Bak, S. Multiple hydroxyphenethyl glucosinolate isomers from a geographically structured glucosinolate polymorphism in the crucifer *Barbarea vulgaris*. *Phytochemistry* **2014**, DOI: 10.1016/j.phytochem.2014.09.003, accepted for publication.
(24) Agerbirk, N.; Olsen, C. E.; Nielsen, J. K. Seasonal variation in leaf glucosinolates and insect resistance in two types of *Barbarea vulgaris* ssp. *arcuata*. *Phytochemistry* **2001**, *58*, 91−100.
(25) Agerbirk, N.; Warwick, S.; Hansen, P. R.; Olsen, C. E. *Sinapis* phylogeny and evolution of glucosinolates and specific nitrile degrading enzymes. *Phytochemistry* **2008**, *69*, 2937−2949.
(26) Ørgaard, M.; Linde-Laursen, I. Cytogenetics of Danish species of *Barbarea* (Brassicaceae): chromocentres, chromosomes and rDNA sites. *Hereditas* **2007**, *144*, 159−170.
(27) Mithen, R.; Bennett, R.; Marquez, J. Glucosinolate biochemical diversity and innovation in the Brassicales. *Phytochemistry* **2010**, *71*, 2074−2086.
(28) Fransz, P.; Soppe, W.; Schubert, I. Heterochromatin in interphase nuclei of *Arabidopsis thaliana*. *Chromosome Res.* **2003**, *11*, 227−240.
(29) Kjær, A. Naturally derived isothiocyanates (mustard oils) and their parent glucosides. *Fortschr. Chem. Org. Naturst.* **1960**, *18*, 122−176.
(30) Barillari, J.; Canistro, D.; Paolini, M.; Ferroni, F.; Pedulli, G. F.; Iori, R.; Valgimigli, L. Direct antioxidant activity of purified glucoerucin, the dietary secondary metabolite contained in rocket (*Eruca sativa* Mill) seeds and sprouts. *J. Agric. Food Chem.* **2005**, *53*, 2475−2482.
(31) Armah, C. N.; Traka, M. H.; Dainty, J. R.; Defernez, M.; Janssens, A.; Leung, W.; Doleman, J. F.; Potter, J. F.; Mithen, R. F. A diet rich in high-glucoraphanin broccoli interacts with genotype to reduce discordance in plasma metabolite profiles by modulating mitochondrial function. *Am. J. Clin. Nutr.* **2013**, *98*, 712−722.
(32) Zhang, X.; Shu, X. O.; Xiang, Y. B.; Yang, G.; Li, H.; Gao, J.; Cai, H.; Gao, Y. T.; Zheng, W. Cruciferous vegetable consumption is associated with a reduced risk of total and cardiovascular disease mortality. *Am. J. Clin. Nutr.* **2011**, *94*, 240−246.
(33) Wu, Q. J.; Yang, Y.; Vogtmann, E.; Wang, J.; Han, L. H.; Li, H. L.; Xiang, Y. B. Cruciferous vegetables intake and the risk of coleorectal cancer: a meta-analysis of observational studies. *Ann. Oncol.* **2013**, *24*, 1079−1087.
(34) National Cancer Institute. Cruciferous vegetables and cancer prevention, www.cancer.gov/cancertopics/factsheet/diet/cruciferous-vegetables (accessed Nov 20, 2013).
(35) Bille, N.; Eggum, B. O.; Jacobsen, I.; Olsen, O.; Sørensen, H. Antinutritional and toxic effects in rats of individual glucosinolates (± myrosinases) added to a standard diet. *Z. Tierphysiol. Tierernaehr. Futtermitteilkd.* **1983**, *49*, 195−210.
(36) Vanderpas, J. Nutritional epidemiology and thyroid hormone metabolism. *Annu. Rev. Nutr.* **2006**, *26*, 293−322.
(37) Lüthy, J.; Garden, B.; Friederich, U.; Bachmann, M. Goitrin − a nitrosatable constituent of plant foodstuffs. *Experientia* **1984**, *40*, 452−453.
(38) Seo, B.; Yun, J.; Lee, S.; Kim, M.; Hwang, K.; Kim, J.; Min, K. R.; Kim, Y.; Moon, D. Barbarin as a new tyrosinase inhibitor from *Barbarea orthocerus*. *Planta Med.* **1999**, *65*, 683−686.
(39) Hong, E.; Kim, S.-J.; Kim, G.-H. Identification and quantitative determination of glucosinolates in seeds and edible parts of Korean Chinese cabbage. *Food Chem.* **2011**, *128*, 1115−1120.
(40) Fenwick, G. R.; Griffiths, N. M.; Heaney, R. K. Bitterness in Brussels sprouts (*Brassica oleracea* L. var. *gemmifera*): the role of

glucosinolates and their breakdown products. *J. Sci. Food Agric.* **1983**, *34*, 73−80.
(41) Badenes-Pérez, F. R. Simultaneous use of *Barbarea vulgaris* R. Br. (Brassicaceae) as a trap crop for insect pest management and a salad vegetable. *Acta Hortic.* **2013**, *979*, 737−742.
(42) Howard, H. W.; Manton, I. Autopolyploid and allopolyploid watercress with the description of a new species. *Ann. Bot.* **1946**, *37*, 1−13.
(43) Agerbirk, N.; Olsen, C. E.; Chew, F. S.; Ørgaard, M. Variable glucosinolate profiles of *Cardamine pratensis* (Brassicaceae) with equal chromosome numbers. *J. Agric. Food Chem.* **2010**, *58*, 4693−4700.
(44) van Leur, H.; Vet, L. E. M.; van der Putten, W. H.; van Dam, N. M. *Barbarea vulgaris* glucosinolate phenotypes differentially affect performance and preference of two different species of lepidopteran herbivores. *J. Chem. Ecol.* **2008**, *34*, 121−131.
(45) Buskov, S.; Serra, B.; Rosa, E.; Sørensen, H.; Sørensen, J. C. Effects of intact glucosinolates and products produced from glucosinolates in myrosinase-catalyzed hydrolysis on the potato cyst nematode (*Globodera rostochiensis* cv. Woll). *J. Agric. Food Chem.* **2002**, *50*, 690−695.
(46) Manici, L. M.; Lazzeri, L.; Palmieri, S. In vitro fungitoxic activity of some glucosinolates and their enzyme-derived products toward plant pathogenic fungi. *J. Agric. Food Chem.* **1997**, *45*, 2768−2773.
(47) Huang, X.; Renwick, J. A. A.; Sachdev-Gupta, K. Oviposition stimulants in *Barbarea vulgaris* for *Pieris rapae* and *P. napi oleraceae*: isolation, identification and differential activity. *J. Chem. Ecol.* **1994**, *20*, 423−438.
(48) Shapiro, A. M. The role of watercress (*Nasturtium officinale*) as a host of native and introduced pierid butterflies in California. *J. Res. Lepid.* **1975**, *14*, 158−168.
(49) Newman, R. M.; Kerfoot, W. C.; Hanscom, Z. Watercress allelochemical defends high-nitrogen foliage against consumption: effects on freshwater invertebrate herbivores. *Ecology* **1996**, *77*, 2312−2323.
(50) Agerbirk, N.; Olsen, C. E.; Poulsen, E.; Jacobsen, N.; Hansen, P. R. Complex metabolism of aromatic glucosinolates in *Pieris rapae* caterpillars involving nitrile formation, hydroxylation, demethylation, sulfation, and host plant dependent carboxylic acid formation. *Insect Biochem. Mol. Biol.* **2010**, *40*, 126−137.
(51) Pedras, M. S. C.; To, Q. H. The first non-indolyl cruciferous phytoalexins: nasturlexins and tridentatols, a striking convergent evolution of defenses in terrestrial plants and marine animals. *Phytochemistry* **2014**, DOI: 10.1016/j.phytochem.2014.07.024.
(52) Traka, M. H.; Saha, S.; Huseby, S.; Kopriva, S.; Walley, P. G.; Barker, G. C.; Moore, J.; Mero, G.; van den Bosch, F.; Constant, H.; Kelly, L.; Schepers, H.; Boddupalli, S.; Mithen, R. F. Genetic regulation of glucoraphanin accumulation in Beneforte((R)) broccoli. *New Phytol.* **2013**, *198*, 1085−1095.

Grain was harvested from three replicated field sites across Chile during the 2006−2007 season. Twelve different conventional maize hybrids were included to provide supplementary data on compositional variability due to field location and water treatment. All field sites utilized a strip-plot design with three replicates per site, with water treatment (well-watered or water-limited) as the whole plot factor and substance type as the subplot factor. Compositional analyses included measurement of proximates, fibers, total amino acids, fatty acids, minerals, vitamins, raffinose, phytic acid, *p*-coumaric acid, and ferulic acid.

## MATERIALS AND METHODS

**Maize Samples for Compositional Analysis.** The drought-tolerant maize MON 87460 (D1) provides a yield benefit when yield is limited by water availability.[1] D1 was produced by stable insertion of the coding sequence of cold shock protein B (CSPB) from *B. subtilis*. Conventional breeding techniques have now developed the combined-trait products D1 × NK603, D1 × MON 89034 × NK603, and D1 × MON 89034 × MON 88017. Each biotechnology-derived trait contributes specific benefits of drought tolerance (D1), herbicide tolerance (NK603), or insect resistance (MON 89034 and MON 88017) to the final product.

Seed of the drought-tolerant combined-trait products and a near-isogenic conventional control were planted in the winter of 2006 at three sites in major maize-producing regions of Chile. Seeds from four different commercial conventional hybrids were also included at each field site (for a total of 12 unique hybrids). Locations of the field sites were as follows: Colina, Region Metropolitana; Calera de Tango, Region Metropolitana; and Lumbreras, Region Metropolitana. All field sites utilized a strip-plot design with three replicates per site, with water treatment (well-watered or water-limited) as the whole plot and substance type as the subplot. The whole-plot factor was arranged as a randomized complete block design. The strip-plot factor consisted of the different maize varieties. The well-watered treatment was managed to provide optimal grain yield. The water-limited treatment was managed to impose a drought stress by withholding water during the late vegetative through early grain fill growth stages (i.e., approximately V10 through R2). The use of a split-plot design allowed comparisons of the drought-tolerant hybrids to the control under two separate irrigation regimens. Tissue was collected from all three blocks for each treatment; tissue from the different commercial references grown at each site was collected from a single block for each treatment. This resulted in a total of 90 test and control samples (5 substances × 3 biological replicates × 3 field sites × 2 water treatments) and 24 commercial reference samples (4 substances × 1 biological replicate × 3 field sites × 2 water treatments).

The genetic purity of the maize plants was maintained by bagging the tassels and ear shoots at anthesis and self-pollinating each plant by hand. Forage was collected at the late dough/early dent stage, and the grain was collected at normal kernel maturity (Supporting Information). After harvest, samples were shipped to Monsanto, St. Louis, MO, USA. The samples were ground to a fine powder in the presence of dry ice and maintained frozen at −20 °C until required for compositional analysis. The identity of forage and grain samples was based on sample handling records and Southern blot or polymerase chain reaction analyses of genomic DNA isolated from grain tissue.

**Compositional Analyses.** Components assessed in grain samples included proximates (protein, fat, ash, and moisture), carbohydrates by calculation, acid detergent fiber (ADF), neutral detergent fiber (NDF), total dietary fiber (TDF), total amino acid composition, fatty acid composition, minerals (calcium, copper, iron, magnesium, manganese, phosphorus, potassium, sodium, zinc), vitamins [vitamin B1 (thiamin), vitamin B2 (riboflavin), vitamin B6 (pyridoxine), vitamin E, niacin, folic acid], furfural, raffinose, phytic acid, *p*-coumaric acid, and ferulic acid. Components assessed in forage samples (Supporting Information) included proximate, carbohydrates by calculation, ADF, NDF, calcium, and phosphorus.

Compositional analyses were performed at Covance Laboratories, Inc. (Madison, WI, USA). Brief descriptions of the methods utilized for the analyses are described in refs 2−5. To control and minimize bias, the samples produced from the three field sites were analyzed in a randomized order.

**Statistical Analysis of Composition Data.** In all, 68 different grain components were measured. The following 16 analytes with >50% of the observations at or below the limits of quantitation (LOQ) of the assay were excluded from statistical analysis: sodium, furfural, caprylic acid, capric acid, lauric acid, myristic acid, myristoleic acid, pentadecanoic acid, pentadecenoic acid, palmitoleic acid, heptadecanoic acid, heptadecenoic acid, γ-linolenic acid, eicosadienoic acid, eicosatrienoic acid, and arachidonic acid. The LOQs for sodium, furfural, and fatty acids were 0.5 ppm, 100 ppm, and 0.004%, respectively. Except for moisture and fatty acids, all component values were converted from a fresh weight to a dry weight basis and into their respective units as presented in Tables 1−6 and Supplementary Table 1 (Supporting Information).

PRESS residuals were used to identify outliers. Extreme data points that were outside the ±6 studentized PRESS residual range were considered for exclusion, as outliers, from the final analyses. This resulted in a single copper value recorded for one of the commercial conventional reference hybrids grown at the Colina site being excluded.

Compositional components were statistically analyzed using a mixed-model analysis of variance from each of the three sites and from the combination of all sites. The combined-site analysis used the model

$$Y_{ijkl} = U + L_i + B(L)_{ij} + T_k + LT_{ik} + TB(L)_{ijk} + S_l + TS_{kl} + LS_{il} + LTS_{ikl} + e_{ijkl}$$

where $Y_{ijkl}$ = unique individual observation, $U$ = overall mean, $L_i$ = random location effect, $B(L)_{ij}$ = random block within location effect, $T_k$ = irrigation treatment effect, $LT_{ik}$ = random location by treatment interaction effect, $TB(L)_{ijk}$ = random treatment by block within location interaction effect, $S_l$ = substance effect, $TS_{kl}$ = treatment by substance interaction effect, $LS_{il}$ = random location by substance interaction effect, $LTS_{ikl}$ = random location by treatment by substance interaction effect, and $e_{ijkl}$ = residual error.

For each component analysis, mean comparison tests of each of the drought-tolerant hybrids to the conventional control within each water treatment were conducted.

SAS software was used to generate all summary statistics and perform all analyses (SAS Institute, 2002−2003). All statistical analyses were conducted by Certus International, Inc. (Chesterfield, MO, USA).

## MULTIVARIATE ANALYSIS

To assess the effect of each factor better, MB-PCA and ASCA were applied to the data. Both models are extensions of the classical PCA model and can separate variances caused by multiple factors and thus provide a better view of the effect of each factor of interest.

For MB-PCA, the original compositional data were repartitioned into a series of *blocks* according to the experiment design (i.e., blocking). Through such blocking, one particular factor would become baseline and no longer have an effect on the data, whereas the other factor(s) would become a *common trend* across all of the blocks and have their influence enhanced, assuming that the samples are properly matched and the effect of the factor(s) of interest is consistent across different blocks. This is clearly a useful approach to analyze a system with multiple and potentially interacting factors. A MB-PCA model comprises three main components, (1) super scores, (2) block scores, and (3) block loadings, where the common trend across all of the blocks is shown in the super scores, the individual patterns of the blocks are shown in the block scores, and the variable contributions to the pattern shown by the MB-PCA model can be found in the block loadings.

ASCA is another recently proposed model aimed at the analysis of data with multiple factors. In ASCA, the data matrix is decomposed into the sum of a series effect matrices and each effect matrix contains the level averages for each factor, which represents the effect of that particular factor. The variations that cannot be explained by the model are put into the residual matrix $\boldsymbol{\varepsilon}$. In this study there are three factors of interest, and thus the ASCA model is written as

$$\boldsymbol{X} = \boldsymbol{1} \times \boldsymbol{m}^{\boldsymbol{T}} + \boldsymbol{X}_{\mathrm{i}} + \boldsymbol{X}_{\mathrm{l}} + \boldsymbol{X}_{\mathrm{s}} + \boldsymbol{X}_{(\mathrm{il})} + \boldsymbol{X}_{(\mathrm{is})} + \boldsymbol{X}_{(\mathrm{ls})} + \boldsymbol{X}_{(\mathrm{ils})} + \boldsymbol{\varepsilon}$$

**Table 1. Proximate and Fiber Composition of Grain from D1 Maize Grown under Well-Watered and Water-Limited Conditions**

| component[a] | D1 mean[b] (range)[c] | D1 × NK603 mean[b] (range)[c] | D1 × MON 89034 × NK603 mean[b] (range)[c] | D1 × MON 89034 × MON 88017 mean[b] (range)[c] | control mean[b] (range)[c] | commercial hybrids (range)[c] |
|---|---|---|---|---|---|---|
| ash | 1.44 (1.35−1.53) | 1.41 (1.29−1.53) | 1.44 (1.30−1.64) | 1.38 (1.26−1.53) | 1.42 (1.26−1.60) | (1.14−1.47) |
| | 1.47 (1.24−1.75) | 1.49 (1.28−1.66) | 1.55 (1.32−1.70) | 1.55 (1.35−1.71) | 1.50 (1.39−1.63) | (1.27−1.63) |
| carbohydrates | 85.17 (82.98−87.63 | 85.45 (84.81−85.91) | 85.43 (84.86−85.89) | 85.68 (85.02−86.30) | 85.53 (84.91−86.31) | (83.60−86.65) |
| | 84.21 (82.64−85.64) | 84.08 (82.89−85.77) | 83.82 (83.05−84.72) | 84.11 (82.89−85.40) | 84.10 (82.95−85.98) | (82.10−85.17) |
| moisture | 12.09 (11.80−12.50) | 12.00 (11.70−12.40) | 11.88 (11.20−12.20) | 12.04 (11.80−12.40) | 12.09 (11.30−12.80) | (11.00−12.20) |
| | 12.10 (11.60−12.50) | 12.20 (11.20−13.40) | 12.06 (11.60−12.70) | 12.21 (10.90−13.00) | 11.98 (11.30−12.50) | (11.70−13.20) |
| protein | 9.50 (7.57−11.32) | 9.36 (8.81−9.83) | 9.33 (8.86−9.62) | 9.18 (8.56−9.77) | 9.32 (8.55−9.77) | (8.69−11.33) |
| | 10.30 (9.41−11.45) | 10.46 (9.00−11.53) | 10.57 (9.74−11.13) | 10.28 (9.18−11.41) | 10.44 (9.17−11.50) | (9.99−12.19) |
| fat | 3.89 (3.45−4.23) | 3.78 (3.60−4.06) | 3.79 (3.59−4.27) | 3.76 (3.49−4.03) | 3.72 (3.60−3.90) | (3.16−4.07) |
| | 4.02 (3.71−4.28) | 3.97 (3.83−4.08) | 4.05 (3.87−4.37) | 4.07 (3.77−4.22) | 3.96 (3.47−4.23) | (3.18−4.22) |
| ADF | 2.57 (2.08−3.18) | 2.71 (1.81−3.40) | 2.67 (1.89−3.65) | 2.53 (1.93−3.53) | 2.47 (1.41−4.41) | (1.95−3.76) |
| | 2.59 (1.85−3.58) | **3.05[d] (1.99−4.24)** | 2.40 (1.71−3.42) | **3.05[d] (2.02−4.21)** | 2.33 (1.83−3.05) | (1.83−3.39) |
| NDF | 8.66 (8.19−9.45) | 8.90 (7.87−9.43) | 8.91 (7.60−10.77) | 9.13 (7.88−10.67) | 8.60 (7.74−9.70) | (7.15−9.41) |
| | 8.87(7.33−11.31) | **9.35[d] (7.62−12.17)** | 8.83 (7.84−9.52) | 8.87 (7.39−10.85) | 8.22 (7.91−8.66) | (6.08−10.36) |
| TDF | 12.70 (11.59−16.00) | 13.54 (12.36−14.90) | 12.39 (11.49−14.27) | 12.85 (11.12−14.64) | 12.53 (11.20−13.98) | (10.24−13.51) |
| | 12.48 (10.78−14.43) | 13.10 (11.97−14.32) | 12.70 (11.73−14.20) | 13.18 (11.58−16.16) | 12.15 (11.06−13.70) | (10.57−14.56) |

[a]Percent dry weight of sample, except moisture. [b]Least-square means; upper values are for well-watered, lower values are for water-limited. [c]Range denotes the lowest and highest individual values across all sites. [d]Significantly different ($\alpha$ = 0.05) from control and are highlighted in bold font.



dx.doi.org/10.1021/jf5019609 | J. Agric. Food Chem. 2014, 62, 9597−9608

where $m^T$ is the mean vector of the full matrix; $1$ is a column vector of ones; $X_i$, $X_l$ and $X_s$ are the effect matrices of the three factors, namely, irrigation conditions, locations, and substances, respectively. $X_{(il)}$, $X_{(is)}$, $X_{(ls)}$, and $X_{(ils)}$ are the interaction matrices between these factors, respectively. PCA was performed on each effect matrix, respectively, to calculate loadings, and the score of each effect matrix was obtained by adding the residual matrix $\varepsilon$ back to the effect matrix and projected into the PC space via the corresponding loadings. For example, the score of the effect matrix of the irrigation condition $T_i$ factor is given as

$$X_i = (\Gamma_i) \times P_i^T$$

where $\Gamma_i$ and $P_i$ are the scores and loadings matrix obtained by PCA performed on $X_i$.

$$T_i = (X_i + \varepsilon) \times P_i$$

Unlike MB-PCA, ASCA is essentially a supervised technique; thus, an appropriate validation procedure is needed. In this paper, we employed a permutation test-based validation procedure proposed by Zwanenburg et al.[16] In the validation, the magnitude of the effect of the factor of interest is expressed as the sum of squares (SSQs) of $\Gamma$. A total number of $n$ permutations (in this study $n$ = 1000) are performed, and in each permutation the labels of the samples are randomly permutated, ASCA is performed on the data using the permuted label, and the SSQs of $\Gamma$ are recorded. All of the SSQs of $\Gamma$ form a null distribution, and the SSQ of $\Gamma$ calculated from the ASCA model using the known labels (i.e., the observed SSQ) is then compared with the null distribution. An empirical $p$ value can then derived by counting the number of permutations that obtained equal or higher SSQs than the observed SSQ.

Compositional data were autoscaled so that each variable had zero mean and unit standard deviation before being subjected to MB-PCA and ASCA. All of the multivariate analyses were conducted using in-house scripts written in MATLAB R2012a environment (Mathworks, Natick, MA, USA).

## RESULTS AND DISCUSSION

**Univariate Analysis.** Tables 1−6 show means and ranges of grain components combined across all sites (the combined-site analysis) for all maize hybrids and for both well-watered and water-limited treatments. Forage data are presented in Supplementary Table 1 (Supporting Information). Individual site data for the conventional control are presented in Supplementary Tables 2−8. Overall, the combined-site analysis of the grain data was characterized by extremely few significant differences ($\alpha$ = 0.05) between the drought-tolerant combined-trait products and the conventional control (and in all Tables the statistically relevant differences are highlighted in bold font). From a total of 416 comparisons (comparison of 4 test substances to the control at 2 different water treatments × 52 analytes) only 23 (5.53%) were significant ($\alpha$ = 0.05). These included only 9 comparisons from the well-watered treatments and 14 from the water-limited treatments. Clearly, given the paucity of observed differences, no meaningful trends were observed that would distinguish drought-tolerant hybrids from conventional control. This is described in more detail below.

**Proximate and Fiber Composition.** Levels of proximates and fiber were similar across all of the drought-tolerant hybrids and the conventional control under both water treatments (Table 1). No differences ($\alpha$ = 0.05) between mean values of proximates and fiber of the drought-tolerant hybrids and the conventional control grown under well-watered conditions were observed. Within the water-limited treatment, differences ($\alpha$ = 0.05) from the control ADF and NDF mean values were observed for D1 × NK603 and from control ADF mean values for D1 × MON 89034 × MON 88017. For D1 × NK603, the magnitudes of the differences in mean values for ADF and NDF were 0.72 and 1.13% dwt, respectively. For D1 × MON 89034 × MON 88017, the magnitude of the differences in mean values for ADF was 0.72% dwt. Given the known variability of grain fiber[2−5,7] this was not considered a meaningful difference. Our results, however, did suggest that, for all maize hybrids, the levels of proximate and fibers differed consistently between the two irrigation treatments. Mean values, when combined across all samples, for ash, protein, and fat were ∼5, ∼11, and ∼6% higher, respectively, under water-limited conditions relative to well-watered conditions in the combined-site analyses. Conversely, mean values for ADF (∼6.%), NDF (∼5%), and TDF (∼3%) were lower under water-limited conditions.

**Total Amino Acid Composition.** No differences ($\alpha$ = 0.05) in mean values of amino acids of the drought-tolerant hybrids and the conventional control grown under well-watered conditions were observed (Table 2). Under water-limited conditions, differences were observed for methionine in D1 × NK603 and D1 × MON 89034 × NK603 (see Table 2). The overall lack of differences is clearly related to the lack of differences in protein levels noted above.

**Fatty Acid Composition.** Under well-watered conditions, differences ($\alpha$ = 0.05) between the drought-tolerant combined-trait products were observed for palmitic acid, linoleic acid, and eicosenoic acid in D1 × NK603; for oleic acid and eicosenoic acid in D1 × MON 89034 × NK603; and for palmitic acid in D1 × MON 89034 × MON 88017 (Table 3). Under water-limited conditions, significant differences were observed for eicosenoic acid in D1, palmitic acid in D1 × NK603, and palmitic acid and linolenic acid in D1 × MON 89034 × MON 88017. All differences were characterized by small mean differences, and no trends in differences between the different D1 hybrids and the conventional control were observed. There is little in the scientific literature on the effect of water treatment or drought on fatty acid composition. The data presented in Table 3 also provide some of the first scientific information that fatty acid composition is not greatly affected by water limitation.

**Vitamin Composition.** Overall, levels of vitamins were similar across all of the drought-tolerant hybrids and the conventional control under both water treatments (Table 4). Under well-watered conditions, significant differences ($\alpha$ = 0.05) were observed for vitamin E in D1 × MON 89034 × NK603 and for thiamin (vitamin B1) and pyridoxine (vitamin B6) in D1 × MON 89034 × MON 88017. Under water-limited conditions, differences ($\alpha$ = 0.05) were observed for niacin and riboflavin (vitamin B2) in D1 × NK603; for vitamin E in D1 × MON 89034 × NK603; and for thiamin and vitamin E in D1 × MON 89034 × MON 88017.

To our knowledge, there is little literature on the effect of abiotic stress on grain levels of maize vitamins. In the combined-site analysis, mean values for most vitamins were higher under water-limited conditions relative to well-watered conditions. These included niacin, vitamin B2 (riboflavin), vitamin B1 (thiamin), and vitamin E, which were increased ∼11, ∼14, ∼4, and ∼10%, respectively, upon water restriction. In contrast to the above results, combined-site analysis revealed that mean values for vitamin B6 (pyridoxine) were lower (∼11%) under water-limited conditions relative to well-watered conditions.

**Antinutrient and Secondary Metabolite Composition.** No differences ($\alpha$ = 0.05) between the drought-tolerant combined-trait products and the control for phytic acid, raffinose, ferulic acid, and $p$-coumaric acid were observed (Table 5).

**Mineral Composition.** Overall, levels of minerals were similar across all of the drought-tolerant hybrids and the conventional control under both water treatments (Table 6). No differences

**Table 2. Amino Acid Composition of Grain from D1 Maize Grown under Well-Watered and Water-Limited Conditions**

| amino acid[a] | D1 mean[b] (range)[c] | D1 × NK603 mean[b] (Range)[c] | D1 × MON 89034 × NK603 mean[b] (range)[c] | D1 × MON 89034 × MON 88017 mean[b] (range)[c] | control mean[b] (range)[c] | commercial hybrids (range)[c] |
|---|---|---|---|---|---|---|
| alanine | 0.71 (0.63−0.86) | 0.69 (0.62−0.75) | 0.68 (0.63−0.71) | 0.68 (0.63−0.72) | 0.70 (0.63−0.76) | (0.66−0.89) |
| | 0.78 (0.67−0.85) | 0.79 (0.67−0.88) | 0.79 (0.74−0.83) | 0.77 (0.60−0.87) | 0.79 (0.68−0.89) | (0.77−0.96) |
| arginine | 0.39 (0.32−0.47) | 0.38 (0.33−0.42) | 0.39 (0.32−0.43) | 0.40 (0.35−0.43) | 0.38 (0.32−0.43) | (0.34−0.46) |
| | 0.43 (0.41−0.44) | 0.44 (0.37−0.50) | 0.43 (0.35−0.48) | 0.43 (0.37−0.49) | 0.42 (0.34−0.47) | (0.41−0.50) |
| aspartic acid | 0.61 (0.54−0.70) | 0.60 (0.53−0.63) | 0.59 (0.55−0.61) | 0.59 (0.55−0.61) | 0.60 (0.56−0.63) | (0.58−0.77) |
| | 0.65 (0.59−0.71) | 0.65 (0.58−0.72) | 0.65 (0.62−0.68) | 0.64 (0.52−0.73) | 0.65 (0.59−0.73) | (0.63−0.76) |
| cystine | 0.22 (0.20−0.23) | 0.22 (0.20−0.23) | 0.21 (0.21−0.22) | 0.21 (0.20−0.22) | 0.21 (0.20−0.22) | (0.20−0.24) |
| | 0.23 (0.22−0.25) | 0.24 (0.22−0.26) | 0.24 (0.21−0.25) | 0.23 (0.21−0.25) | 0.23 (0.20−0.24) | (0.20−0.26) |
| glutamic acid | 1.84 (1.63−2.21) | 1.78 (1.59−1.91) | 1.76 (1.62−1.82) | 1.75 (1.62−1.83) | 1.80 (1.62−1.97) | (1.64−2.26) |
| | 2.01 (1.74−2.21) | 2.05 (1.73−2.29) | 2.05 (1.92−2.15) | 1.99 (1.56−2.24) | 2.03 (1.71−2.29) | (1.94−2.44) |
| glycine | 0.35 (0.32−0.39) | 0.34 (0.31−0.35) | 0.34 (0.33−0.35) | 0.34 (0.33−0.35) | 0.34 (0.31−0.35) | (0.31−0.38) |
| | 0.36 (0.34−0.39) | 0.37 (0.33−0.40) | 0.37 (0.36−0.39) | 0.37 (0.30−0.40) | 0.36 (0.33−0.39) | (0.35−0.42) |
| histidine | 0.29 (0.26−0.34) | 0.28 (0.26−0.30) | 0.28 (0.27−0.29) | 0.28 (0.27−0.29) | 0.29 (0.26−0.30) | (0.24−0.30) |
| | 0.31 (0.28−0.32) | 0.31 (0.28−0.34) | 0.31 (0.30−0.33) | 0.31 (0.25−0.34) | 0.31 (0.27−0.34) | (0.27−0.33) |
| isoleucine | 0.33 (0.29−0.42) | 0.33 (0.29−0.35) | 0.32 (0.29−0.34) | 0.32 (0.30−0.35) | 0.33 (0.30−0.36) | (0.30−0.41) |
| | 0.37 (0.32−0.38) | 0.37 (0.32−0.41) | 0.37 (0.35−0.40) | 0.37 (0.28−0.43) | 0.37 (0.32−0.41) | (0.34−0.44) |
| leucine | 1.23 (1.08−1.52) | 1.18 (1.05−1.28) | 1.17 (1.07−1.22) | 1.16 (1.07−1.24) | 1.19 (1.08−1.30) | (1.06−1.53) |
| | 1.36 (1.16−1.47) | 1.37 (1.14−1.52) | 1.38 (1.26−1.47) | 1.33 (1.04−1.52) | 1.37 (1.13−1.56) | (1.29−1.65) |
| lysine | 0.28 (0.26−0.31) | 0.28 (0.25−0.29) | 0.27 (0.27−0.28) | 0.28 (0.27−0.29) | 0.28 (0.26−0.29) | (0.25−0.31) |
| | 0.29 (0.27−0.31) | 0.29 (0.27−0.31) | 0.29 (0.28−0.30) | 0.29 (0.24−0.32) | 0.29 (0.28−0.31) | (0.28−0.31) |
| methionine | 0.18 (0.16−0.21) | 0.18 (0.17−0.19) | 0.18 (0.17−0.19) | 0.18 (0.16−0.18) | 0.18 (0.16−0.19) | (0.18−0.23) |
| | 0.20 (0.18−0.22) | **0.21[d] (0.18−0.24)** | **0.21[d] (0.18−0.25)** | 0.20 (0.17−0.23) | 0.20 (0.16−0.22) | (0.19−0.30) |
| phenylalanine | 0.49 (0.43−0.60) | 0.47 (0.42−0.51) | 0.47 (0.43−0.49) | 0.46 (0.43−0.49) | 0.48 (0.43−0.52) | (0.44−0.60) |
| | 0.53 (0.46−0.58) | 0.54 (0.46−0.60) | 0.54 (0.51−0.57) | 0.53 (0.42−0.60) | 0.54 (0.45−0.61) | (0.51−0.63) |
| proline | 0.88 (0.77−1.07) | 0.87 (0.76−0.95) | 0.86 (0.78−0.90) | 0.86 (0.80−0.91) | 0.87 (0.82−0.95) | (0.72−0.99) |
| | 0.96 (0.85−1.04) | 0.97 (0.83−1.08) | 0.97 (0.88−1.06) | 0.95 (0.74−1.07) | 0.97 (0.84−1.11) | (0.78−1.03) |
| serine | 0.47 (0.43−0.54) | 0.45 (0.41−0.50) | 0.45 (0.42−0.47) | 0.44 (0.39−0.49) | 0.45 (0.40−0.50) | (0.43−0.55) |
| | 0.51 (0.45−0.58) | 0.52 (0.45−0.56) | 0.52 (0.50−0.54) | 0.49 (0.41−0.54) | 0.51 (0.43−0.59) | (0.48−0.60) |



dx.doi.org/10.1021/jf5019609 | J. Agric. Food Chem. 2014, 62, 9597−9608

**Table 2. continued**

| amino acid[a] | D1 mean[b] (range)[c] | D1 × NK603 mean[b] (Range)[c] | D1 × MON 89034 × NK603 mean[b] (range)[c] | D1 × MON 89034 × MON 88017 mean[b] (range)[c] | control mean[b] (range)[c] | commercial hybrids (range)[c] |
|---|---|---|---|---|---|---|
| threonine | 0.32 (0.28–0.37) | 0.32 (0.30–0.33) | 0.32 (0.30–0.34) | 0.31 (0.29–0.32) | 0.32 (0.29–0.33) | (0.30–0.37) |
| | 0.35 (0.32–0.39) | 0.35 (0.31–0.38) | 0.35 (0.34–0.37) | 0.34 (0.29–0.37) | 0.35 (0.31–0.39) | (0.33–0.39) |
| tryptophan | 0.051 (0.039–0.063) | 0.052 (0.045–0.058) | 0.047 (0.037–0.055) | 0.051 (0.046–0.058) | 0.051 (0.046–0.054) | (0.040–0.059) |
| | 0.053 (0.046–0.059) | 0.053 (0.046–0.060) | 0.055 (0.045–0.065) | 0.053 (0.045–0.060) | 0.052 (0.042–0.063) | (0.047–0.070) |
| tyrosine | 0.23 (0.12–0.35) | 0.23 (0.14–0.30) | 0.23 (0.12–0.30) | 0.25 (0.15–0.30) | 0.25 (0.13–0.32) | (0.14–0.32) |
| | 0.29 (0.18–0.33) | 0.30 (0.22–0.36) | 0.28 (0.14–0.37) | 0.28 (0.20–0.38) | 0.24 (0.12–0.35) | (0.25–0.41) |
| valine | 0.52 (0.42–0.56) | 0.46 (0.40–0.48) | 0.45 (0.41–0.46) | 0.45 (0.42–0.48) | 0.52 (0.41–0.49) | (0.41–0.54) |
| | 0.50 (0.44–0.51) | 0.51 (0.44–0.56) | 0.51 (0.48–0.55) | 0.50 (0.39–0.57) | 0.51 (0.45–0.55) | (0.47–0.58) |

[a]Percent dry weight of sample. [b]Least-square means; upper values are for well-watered, lower values are for water-limited. [c]Range denotes the lowest and highest individual values across all sites. [d]Significantly different ($\alpha$ = 0.05) from control and are highlighted in bold font.

($\alpha$ = 0.05) in mean values of minerals of the drought-tolerant hybrids and the conventional control grown under well-watered conditions were observed (see Table 6). Within the water-limited treatment differences were observed for potassium in D1 × MON 89034 × NK603.

Mean values for all tested minerals, with the exception of K, were higher (~8−15%) under water-limited conditions relative to well-watered conditions in the combined site analyses. There are few reports on the effect of limited water availability on mineral composition in maize grain. A three year study of tropical varieties subjected to preanthesis drought concluded that there was no significant impact of water restriction.[17] Restricting water availability after silking also showed no effect on the levels of measured minerals (P and K) despite a ~33% grain yield reduction.[18] The changes observed imply that water deficit affects mineral composition in grain only modestly, an observation consistent with results from other peer-reviewed studies.[17,18]

**Multivariate Analysis.** The original focus of the study was a comparison of grain composition of the D1 maize hybrids to a near-isogenic conventional comparator. Review of the data presented in Tables 1−6 and in the Supporting Information clearly suggested, however, that water treatment and location contributed more to compositional variation than genetic modification. We were therefore interested in reviewing multivariate options to present meaningful visualization and interpretation of different sources of variation. PCA is one of the most popular tools for exploratory analysis, but it is not always effective when an experiment comprises multiple influential factors such as are present in our study. We initially performed PCA on the full data matrix, and the results appeared to be a complex mixture of the effects of all three factors (substance, location, and water treatment), and no obvious pattern could be observed (data not shown). We therefore attempted to use two different PCA variants, MB-PCA and ASCA, to better discern the effects of each factor.

**MB-PCA.** To better assess the effect of each factor, we created a series of MB-PCA models by repartitioning (i.e. blocking) the data in different ways so that one particular factor became a background and the effect of the factor of interest became a common trend across all blocks. Blocking was performed as follows.

*(1) Three-Locations Blocking, with Each Block Containing Both Irrigation Conditions.* The scores plots from this MB-PCA model are shown in Figure 1. These clearly show that water treatment conditions had a significant influence on the data. On the super scores (Figure 1a), a clear separation between the well-watered condition (wet) and water-limited (dry) condition was seen across the first PC. The block scores (Figure 1b−d) showed similar patterns for all three locations. In addition, the loadings (Figure 2) of the three blocks were highly similar to each other, suggesting that water treatment had a similar impact on grain composition, regardless of location.

Consistent with results from the univariate analysis, no clear separation between the different substances was observed in the scores plots of this model. Two further MB-PCA models were computed, which also blocked according to locations but contained only samples from the same water treatment (either wet or dry, respectively); results of these two models again showed no sign of separation between different substances (data not shown).

*(2) Five-Substances Blocking Where the Data Were Repartitioned into Five Blocks, One for Each Substance.* We first incorporated samples from both water treatments into each block; the super scores plot of the MB-PCA model is given in

**Table 3. Fatty Acid Composition of Grain from D1 Maize Grown under Well-Watered and Water-Limited Conditions**

| fatty acid[a] | D1 mean[b] (range)[c] | D1 × NK603 mean[b] (range)[c] | D1 × MON 89034 × NK603 mean[b] (range)[c] | D1 × MON 89034 × MON 88017 mean[b] (range)[c] | control mean[b] (range)[c] | commercial hybrids (range)[c] |
|---|---|---|---|---|---|---|
| palmitic | 10.93 (10.63−11.60) | **10.19[d] (10.10−10.42)** | 11.03 (10.82−11.41) | **11.61[d] (11.32−11.75)** | 11.15 10.96−11.32) | (9.53−12.33) |
| | 11.06 (10.54−11.33) | 10.23 (9.91−10.54) | 10.94 (10.63−11.36) | **11.76[d] (11.16−13.85)** | 11.18 (10.75−11.45) | (9.84−12.33) |
| stearic | 1.80 (1.74−1.97) | 1.84 (1.75−1.96) | 1.82 (1.74−1.92) | 1.78 (1.72−1.84) | 1.78 (1.66−1.91) | (1.28−2.13) |
| | 1.86 (1.73−1.95) | 1.96 (1.82−2.19) | 1.87 (1.81−1.93) | 1.91 (1.75−2.17) | 1.86 (1.68−2.08) | (1.30−2.10) |
| oleic | 20.93 (20.29−21.28) | 20.68 (19.71−21.64) | **20.39[d] (19.34−20.98)** | 20.75 (19.81−21.58) | 21.01 (19.78−21.93) | (22.13−31.09) |
| | 20.99 (20.20−21.60) | 21.07 (20.10−22.90) | **20.37[d] (19.81−20.99)** | 20.93 (19.66−22.38) | 20.83 (19.59−21.98) | (20.78−29.13) |
| linoleic | 64.51 (63.92−65.27) | **65.46[d] (64.40−66.39)** | 64.92 (63.84−66.11) | 64.04 (63.05−65.03) | 64.21 (63.22−65.48) | (55.17−64.97) |
| | 64.29 (63.27−65.10) | 64.89 (62.85−65.96) | 65.00 (63.97−65.57) | 63.58 (59.81−65.35) | 64.30 (62.75−65.65) | (56.51−64.46) |
| linolenic | 1.18 (1.15−1.23) | 1.21 (1.17−1.24) | 1.21 (1.15−1.25) | 1.19 (1.16−1.22) | 1.21 (1.19−1.25) | (1.00−1.32) |
| | 1.19 (1.13−1.25) | 1.19 (1.14−1.22) | 1.19 (1.14−1.26) | **1.17[d] (1.03−1.23)** | 1.21 (1.12−1.26) | (1.03−1.38) |
| arachidic | 0.31 (0.0.29−0.34) | 0.31 (0.29−0.35) | 0.32 (0.30−0.35) | 0.32 (0.31−0.35) | 0.32 (0.29−0.34) | (0.29−0.42) |
| | 0.31 (0.30−0.34) | 0.32 (0.29−0.35) | 0.32 (0.30−0.34) | 0.32 (0.30−0.39) | 0.32 (0.30−0.33) | (0.30−0.41) |
| eicosenoic | 0.18 (0.17−0.20) | **0.18[d] (0.16−0.19)** | **0.18[d] (0.16−0.19)** | 0.19 (0.18−0.20) | 0.19 (0.17−0.20) | (0.20−0.31) |
| | **0.18[d] (0.16−0.19)** | 0.18 (0.17−0.19) | 0.18 (0.17−0.20) | 0.19 (0.17−0.22) | 0.18 (0.17−0.20) | (0.18−0.27) |
| behenic | 0.15 (0.062−0.26) | 0.12 (0.060−0.22) | 0.13 (0.056−0.24) | 0.12 (0.063−0.20) | 0.15 (0.063−0.17) | (0.061−0.33) |
| | 0.12 (0.058−0.20) | 0.16 (0.060−0.33) | 0.13 (0.061−0.17) | 0.14 (0.066−0.19) | 0.12 (0.059−0.15) | (0.062−0.18) |

[a]Expressed as % of total fatty acid. [b]Least-square means; upper values are for well-watered, lower values are for water-limited. [c]Range denotes the lowest and highest individual values across all sites. [d]Significantly different ($\alpha$ = 0.05) from control and are highlighted in bold font.



dx.doi.org/10.1021/jf5019609 | J. Agric. Food Chem. 2014, 62, 9597−9608

**Table 4. Vitamin Composition of Grain from D1 Maize Grown under Well-Watered and Water-Limited Conditions**

| vitamin[a] | D1 mean[b] (range)[c] | D1 × NK603 mean[b] (range)[c] | D1 × MON 89034 × NK603 mean[b] (range)[c] | D1 × MON 89034 × MON 88017 mean[b] (range)[c] | control mean[b] (range)[c] | commercial hybrids (range)[c] |
|---|---|---|---|---|---|---|
| folic acid | 0.26 (0.23−0.29) | 0.28 (0.23−0.33) | 0.28 (0.23−0.37) | 0.28 (0.23−0.35) | 0.27 (0.22−0.33) | (0.26−0.41) |
| | 0.29 (0.25−0.37) | 0.29 (0.25−0.39) | 0.29 (0.24−0.37) | 0.29 (0.22−0.34) | 0.28 (0.23−0.35) | (0.26−0.42) |
| niacin | 19.17 (16.42−21.50) | 21.05 (16.91−34.24) | 19.29 (17.23−21.29) | 20.06 (17.08−25.09) | 19.23 (17.42−21.17) | (14.92−26.80) |
| | 18.54 (16.23−25.00) | **17.79[d] (14.53−20.71)** | 21.17 (15.69−42.58) | 19.01 (17.06−22.18) | 21.73 (16.36−42.06) | (13.64−27.42) |
| riboflavin/vitamin B2 | 2.01 (1.61−2.54) | 2.03 (1.41−2.58) | 1.95 (1.42−2.29) | 1.96 (1.54−2.39) | 1.97 (1.46−2.63) | (1.62−2.62) |
| | 2.12 (1.43−2.89) | **1.93[d] (1.26−2.51)** | 2.09 (1.66−2.60) | 2.01 (1.78−2.37) | 2.29 (1.64−2.81) | (1.81−2.78) |
| thiamin/vitamin B1 | 2.86 (2.61−3.19) | 2.88 (2.72−3.06) | 2.85 (2.62−3.06) | **2.19[d] (1.93−2.85)** | 2.86 (2.74−3.06) | (2.94−4.78) |
| | 3.10 (2.84−3.42) | 3.14 (2.89−3.38) | 3.11 (2.71−4.01) | **2.23[d] (1.95−2.41)** | 2.98 (2.71−3.19) | (2.87−4.33) |
| pyridoxine/vitamin B6 | 6.32 (5.49−7.39) | 6.16 (5.16−6.79) | 6.18 (5.63−7.37) | **5.77[d] (4.67−7.75)** | 6.83 (6.17−7.37) | (4.01−6.70) |
| | 6.17 (5.43−6.57) | 6.06 (4.57−6.99) | 6.43 (5.23−7.56) | 6.41 (4.97−7.41) | 6.15 (4.97−8.27) | (5.30−8.22) |
| vitamin E | 11.90 (10.64−13.57) | 11.49 (9.90−12.80) | **12.24[d] (10.20−13.55)** | 12.08 (10.29−13.81) | 10.99 (9.30−12.78) | (2.83−11.69) |
| | 13.01 (12.16−14.24) | 12.78 (11.49−13.65) | **13.98[d] (13.15−16.49)** | **13.76[d] (10.82−15.17)** | 12.16 (10.15−13.64) | (2.84−15.53) |

[a]Expressed as mg/kg dry weight. [b]Least-square means; upper values are for well-watered, lower values are for water-limited. [c]Range denotes the lowest and highest individual values across all sites. [d]Significantly different ($\alpha$ = 0.05) from control and are highlighted in bold font.



**Table 5. Antinutrient and Secondary Metabolite Composition of Grain from D1 Maize Grown under Well-Watered and Water-Limited Conditions**

| component[a] | D1 mean[b] (range)[c] | D1 × NK603 mean[b] (range)[c] | D1 × MON 89034 × NK603 mean[b] (range)[c] | D1 × MON 89034 × MON 88017 mean[b] (range)[c] | control mean[b] (range)[c] | commercial hybrids (range)[c] |
|---|---|---|---|---|---|---|
| phytic acid (% dwt) | 0.76 (0.58−0.93) | 0.72 (0.63−0.84) [ | 0.76 (0.65−0.92) | 0.72 (0.56−0.89) | 0.76 (0.63−0.90) | (0.58−0.97) |
| | 0.79 (0.63−0.89) | 0.77 (0.67−0.85) | 0.82 (0.70−0.87) | 0.83 (0.68−0.99) | 0.77 (0.60−0.89) | (0.67−0.94) |
| raffinose (% dwt) | 0.11 (0.075−0.12) | 0.11 (0.079−0.14) | 0.11 (0.083−0.14) | 0.10 (0.075−0.15) | 0.12 (0.077−0.14) | (0.028−0.15) |
| | 0.11 (0.087−0.14) | 0.11 (0.067−0.14) | 0.13 (0.092−0.15) | 0.11 (0.080−0.14) | 0.12 (0.097−0.15) | (0.061−0.15) |
| ferulic acid ($\mu$g/g dwt) | 1849.20 (1265.68−2240.00) | 1703.66 (1059.02−2277.90) | 1946.83 (1585.50−2144.47) | 1936.39 (1175.80−2462.94) | 1753.19 (820.14−2128.15) | (1504.52−2224.72) |
| | 1923.79 (1208.67−2352.27) | 1872.80 (1244.29−2207.05) | 1975.89 (1628.70−2260.27) | 1863.51 (1089.87−2391.80) | 1852.11 (1088.34−2301.59) | (1011.40−2539.86) |
| *p*-coumaric acid ($\mu$g/g dwt) | 137.39 (68.64−188.64) | 136.43 (69.74−198.18) | 160.76 (116.65−187.71) | 151.90 (74.46−206.35) | 149.37 (64.03−204.06) | (84.79−239.33) |
| | 137.29 (85.52−168.18) | 140.00 (83.33−192.26) | 145.18 (110.14−188.21) | 138.93 (72.81−248.29) | 149.95 66.48−208.43) | (84.15−259.68) |

[a]Expressed as shown. [b]Least-square means; upper values are for well-watered, lower values are for water-limited. [c]Range denotes the lowest and highest individual values across all sites.

dx.doi.org/10.1021/jf5019609 | J. Agric. Food Chem. 2014, 62, 9597−9608

**Table 6. Mineral Composition of Grain from D1 Maize Grown under Well-Watered and Water-Limited Conditions**

| mineral[a] | D1 mean[b] (range)[c] | D1 × NK603 mean[b] (range)[c] | D1 × MON 89034 × NK603 mean[b] (range)[c] | D1 × MON 89034 × MON 88017 mean[b] (range)[c] | control mean[b] (range)[c] | commercial hybrids (range)[c] |
|---|---|---|---|---|---|---|
| calcium | 0.0047 (0.0035−0.0058) | 0.0044 (0.0036−0.0066) | 0.0044 (0.0034−0.0054) | 0.0049 (0.0033−0.0084) | 0.0045 (0.0036−0.0059) | (0.0032−0.0057) |
| | 0.0052 (0.0046−0.0065) | 0.0052 (0.0040−0.0063) | 0.0052 (0.0036−0.0065) | 0.0052 (0.0043−0.0065) | 0.0050 (0.0041−0.0063) | (0.0035−0.0070) |
| copper | 1.86 (1.58−2.17) | 2.22 (1.68−4.34) | 1.93 (1.61−2.25) | 1.93 (1.52−2.67) | 1.87 (1.47−2.81) | (1.29−4.16) |
| | 2.19 (1.88−2.49) | 2.64 (1.75−4.32) | 2.29 (2.01−2.51) | 2.61 (1.79−3.96) | 2.12 (1.87−2.30) | (1.39−2.76) |
| iron | 16.59 (14.53−20.30) | 17.20 (15.10−20.32) | 17.09 (15.49−19.68) | 16.08 (14.19−17.50) | 16.95 (15.22−19.95) | (14.37−19.48) |
| | 17.67 (16.38−19.27) | 18.41 (15.70−22.15) | 18.32 (16.33−21.00) | 17.61 (15.04−19.18) | 18.60 (16.12−22.21) | (15.90−24.66) |
| magnesium | **0.12[d] (0.10−0.14)** | 0.11 (0.10−0.12) | 0.11 (0.10−0.12) | 0.11 (0.10−0.12) | 0.11 (0.10−0.11) | (0.095−0.13) |
| | 0.13 (0.11−0.14) | 0.13 (0.12−0.15) | 0.13 (0.11−0.15) | 0.13 (0.11−0.14) | 0.13 (0.10−0.14) | (0.11−0.14) |
| manganese | 6.27 (5.25−7.08) | 5.75 (4.87−6.58) | 6.17 (5.62−7.29) | 6.02 (5.69−6.96) | 6.03 (4.64−7.58) | (4.55−9.02) |
| | 6.71 (5.28−8.66) | 6.08 (5.10−6.63) | 6.52 (5.35−7.37) | 6.34 (5.44−7.35) | 6.54 (5.25−7.76) | (4.78−9.35) |
| phosphorus | 0.32 (0.29−0.34) | 0.30 (0.26−0.33) | 0.30 (0.26−0.33) | 0.29 (0.26−0.32) | 0.30 (0.26−0.33) | (0.27−0.36) |
| | 0.32 (0.25−0.36) | 0.33 (0.29−0.36) | 0.33 (0.31−0.36) | 0.32 (0.29−0.35) | 0.33 (0.27−0.38) | (0.30−0.38) |
| potassium | 0.40 (0.37−0.41) | 0.40 (0.38−0.43) | 0.41 (0.39−0.44) | 0.41 (0.37−0.44) | 0.40 (0.36−0.45) | (0.32−0.42) |
| | 0.40 (0.37−0.43) | 0.40 (0.37−0.44) | **0.42[d] (0.39−0.45)** | 0.40 (0.37−0.43) | 0.40 (0.37−0.43) | (0.36−0.43) |
| zinc | 22.00 (19.20−25.09) | 21.85 (18.11−25.65) | 21.44 (18.51−24.37) | 21.16 (17.97−24.38) | 21.02 (18.36−25.34) | (18.12−29.69) |
| | 23.30 (18.36−26.77) | 24.81 (21.27−27.02) | 24.55 (21.43−26.36) | 23.63 (20.50−25.98) | 24.37 (21.29−27.79) | (18.25−30.44) |

[a]Percent dry weight of sample, except manganese and zinc which are expressed as mg/kg dry weight. [b]Least-square means; upper values are for well-watered, lower values are for water-limited. [c]Range denotes the lowest and highest individual values across all sites. [d]Significantly different ($\alpha$ = 0.05) from control and are highlighted in bold font.



dx.doi.org/10.1021/jf5019609 | J. Agric. Food Chem. 2014, 62, 9597−9608

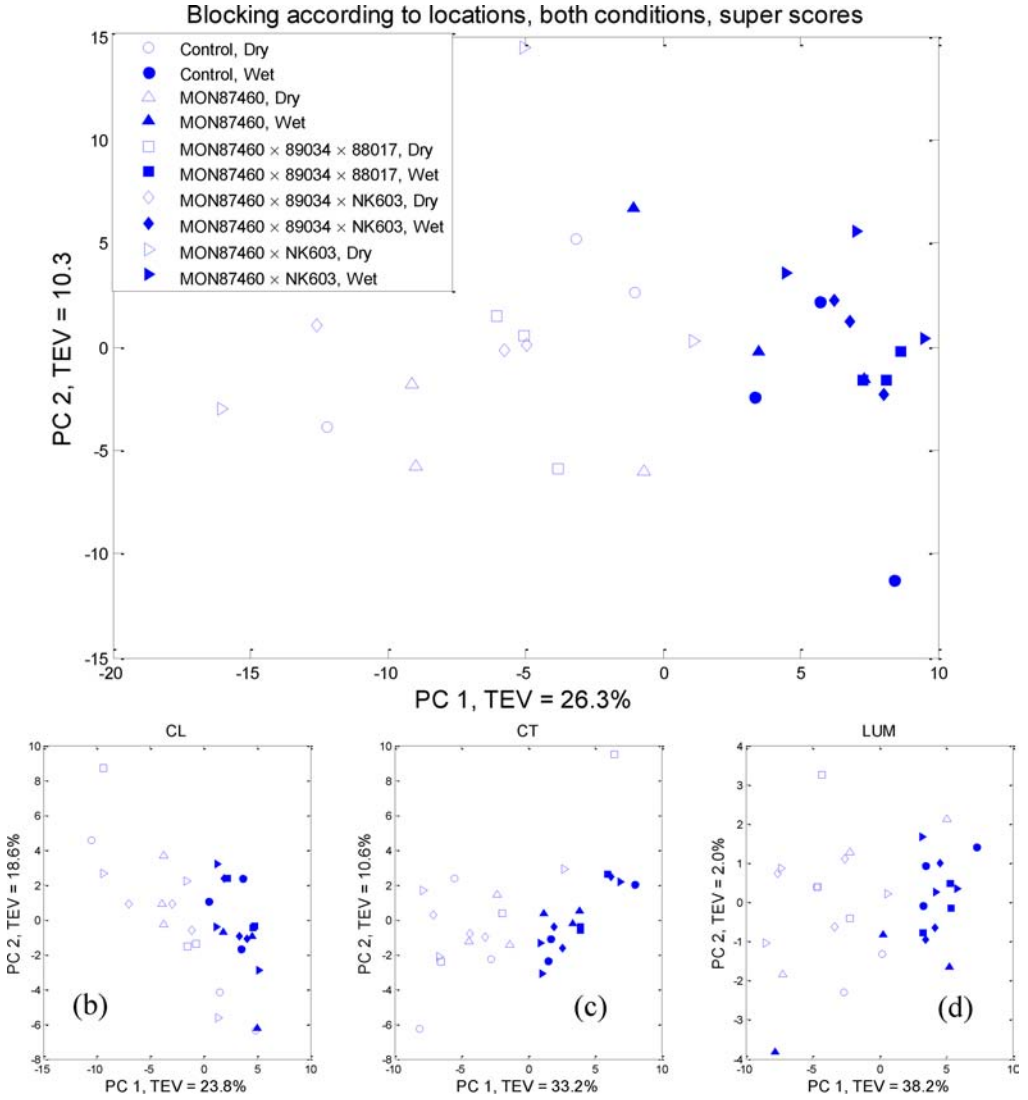


**Figure 1.** MB-PCA performed on the location blocking data set: (a) super scores plot; (b) block scores plot on the site CL block; (c) block scores plot on the site CT block; (d) block scores plot on the site LUM block. TEV, total explained variance.

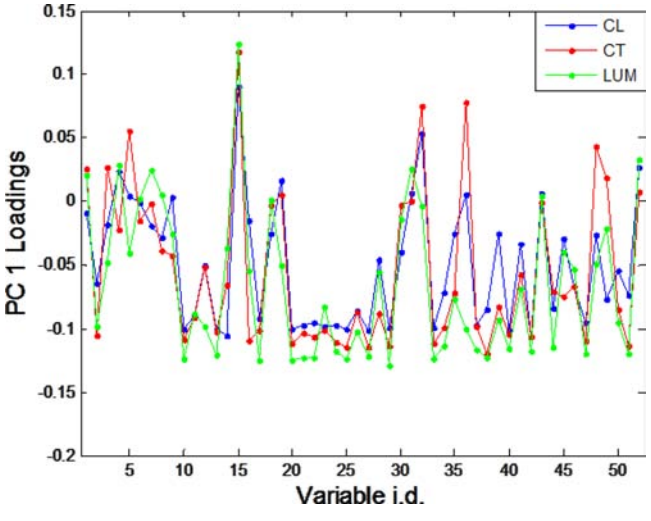


**Figure 2.** Loading plots from MB-PCA. The colors represent the different sites: (blue) site CL; (red), site CT; (green) site LUM. The list of variables (analytical components) is presented in Supporting Information.

Figure 3a. PC 1 clearly separated the two water treatments, and PC 2 separated (albeit with some overlap) the three sites along its axis. This suggested that water treatment had a stronger influence on composition compared to location differences. The super scores plot also showed that separation between the three different locations was better under well-watered conditions than under water-limited conditions. To confirm this, we built another two MB-PCA models using substances blocking, where each block contained only one water treatment, that is, wet or dry only. The super scores of the MB-PCA model based on well-watered samples (Figure 3b) indeed showed a much better separation than the MB-PCA model based on water-limited samples (Figure 3c).

**ASCA.** The MB-PCA models confirmed a lack of substance effect consistent with results from the univariate analysis. On the basis of different blocking strategies, the MB-PCA models further suggested that water treatment had the greatest impact on grain composition. Locations also had an effect, albeit weaker than that of water treatment. These location effects appeared to be greater under well-watered conditions than under water-limited conditions. We tested this observation by employing an ASCA model. The scores plots of the three submatrices of the ASCA model are given in Figure 4. It can be seen that separation


dx.doi.org/10.1021/jf5019609 | J. Agric. Food Chem. 2014, 62, 9597−9608

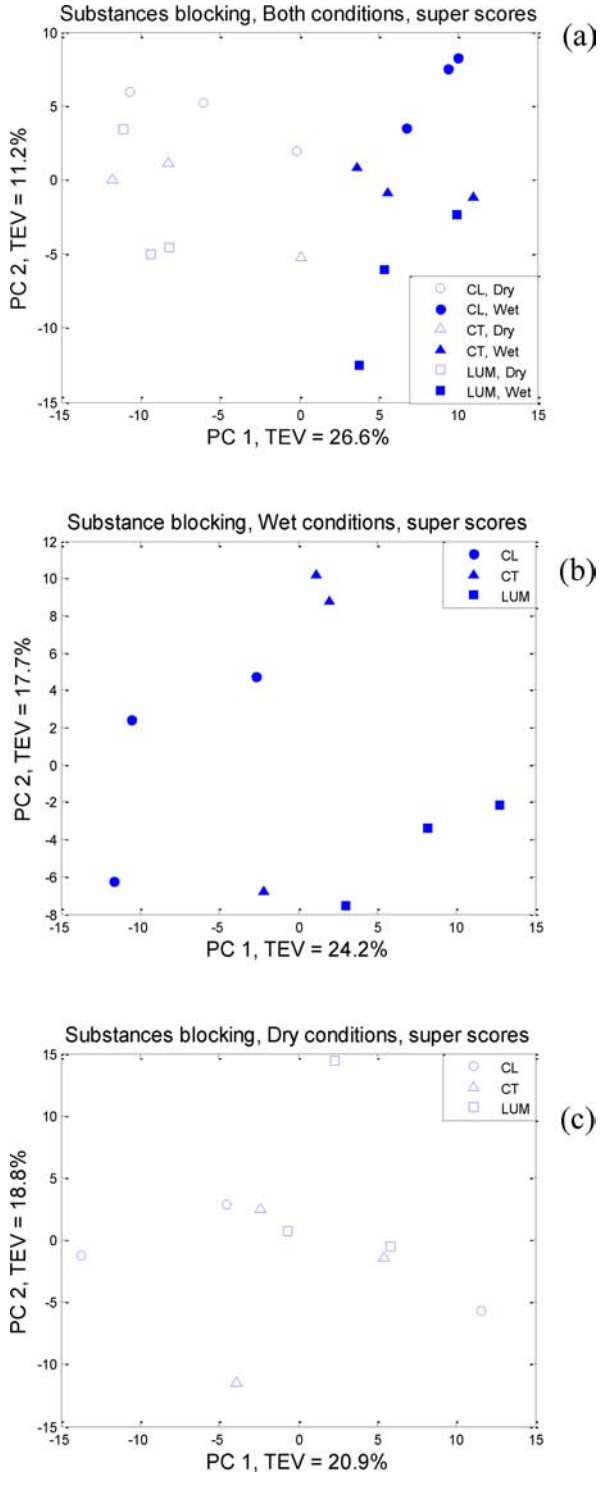


**Figure 3.** Super scores plots of the MB-PCA models based on substances blocking: (a) substances blocking with both conditions; (b) substances blocking with well-watered condition; (c) substances blocking with water-limited condition. TEV, total explained variance.

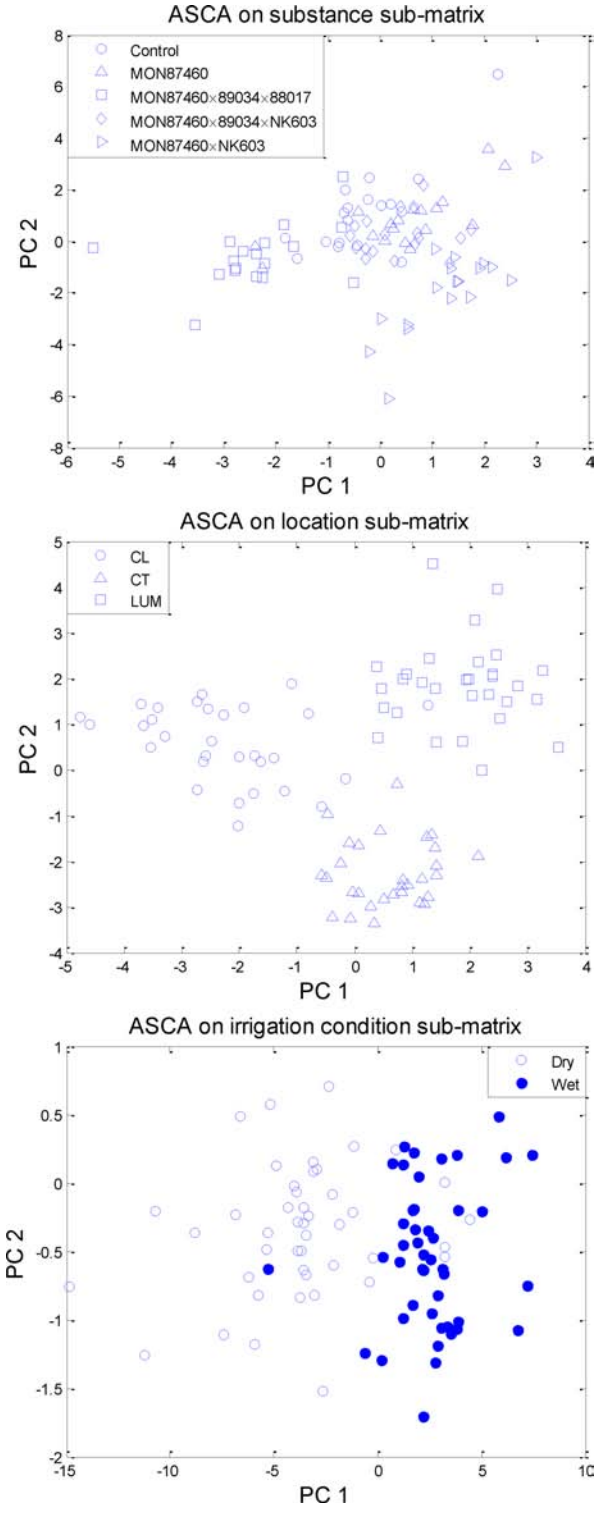


**Figure 4.** Scores plots of the three submatrices of the ASCA model.

between the five different substances was very weak indeed, and a nonsignificant $p$ value of 0.470 was obtained from the corresponding permutation test. By contrast, the scores plots obtained from the location submatrix and the water treatment submatrix showed clear separations between the classes. The $p$ value of the scores of the location submatrix was 0.002, and that of the water treatment matrix was also highly significant at <0.001 (i.e., not a single case of 1000 permutations had obtained higher SSQs than the observed one). The figures of the observed SSQs superimposed on the corresponding null distributions are given in Supplementary Figure S1 (Supporting Information). In summary, ASCA confirmed the results derived through MB-PCA that water treatment was the factor with the most significant impact on grain composition, followed by location, whereas there was significant substance effect.

**Conclusion.** The compositional equivalence of transgenic drought-tolerant maize hybrids to a near-isogenic conventional


dx.doi.org/10.1021/jf5019609 | J. Agric. Food Chem. 2014, 62, 9597−9608

comparator was demonstrated, and additional insights on the effect of drought on maize grain composition were offered. In this study, the effect of genetic modification was contrasted to other experimental factors: water treatment and location. Using the PCA variants MB-PCA and ASAC, it was demonstrated that water treatment had the greatest effect on composition followed by location; moreover, location effects were greater under well-watered conditions than under water-limited conditions. The multivariate options showed no significant differences between the drought-tolerant hybrids and the near-isogenic control, and both options corroborated results from the univariate analysis. This study represents the first application of MB-PCA and ASCA to crop compositional data. Results suggest these multivariate options are of value in unraveling coexisting multiple factors in a complex compositional study and thus present an opportunity to gain better views of each factor of interest whether these be germplasm, environment, management practices, or genetic modification.

## ■ ASSOCIATED CONTENT

### Supporting Information

Proximate, fiber, and mineral composition of forage (Supplementary Table 1) and individual site compositional data for the conventional control (Supplementary Tables 2−8) and Supplementary Figure S1. This material is available free of charge via the Internet at http://pubs.acs.org.

## ■ AUTHOR INFORMATION

### Corresponding Authors

*(R.G.) E-mail: roy.goodacre@manchester.ac.uk.

*(G.G.H.) E-mail: george.g.harrigan@monsanto.com.

### Funding

R.G. is grateful to the UK BBSRC for financial support of metabolomics.

### Notes

The authors declare no competing financial interest.

## ■ ACKNOWLEDGMENTS

We thank the Monsanto Field Agronomy group and the many field cooperators for conducting field trials, the Monsanto Product Characterization group for the molecular characterization of the test and control substances, and Monsanto's Sample Preparation Group for preparing maize samples for analysis.

## ■ REFERENCES

(1) Castiglioni, P.; Warner, D.; Bensen, R. J.; Anstrom, D. C.; Harrison, J.; Stoecker, M.; Abad, M.; Kumar, G.; Salvador, S.; D'Ordine, R.; Navarro, S.; Back, S.; Fernandes, M.; Targolli, J.; Dasgupta, S.; Bonin, C.; Luethy, M. H.; Heard, J. E. Bacterial RNA chaperones confer abiotic stress tolerance in plants and improved grain yield in maize under water-limited conditions. *Plant Physiol.* **2008**, *147*, 446−455.

(2) Harrigan, G.; Ridley, W. P.; Miller, K. D.; Sorbet, R.; Riordan, S. G.; Nemeth, M. A.; Reeves, W.; Pester, T. A. The forage and grain of MON 87460, a drought tolerant corn hybrid, are compositionally equivalent to that of conventional corn. *J. Agric. Food Chem.* **2009**, *57*, 9754−9763.

(3) Drury, S. M.; Reynolds, T. L.; Ridley, W. P.; Bogdanova, N.; Riordan, S.; Nemeth, M. A.; Sorbet, R.; Trujillo, W. A.; Breeze, M. L. Composition of forage and grain from second-generation insect-protected corn MON 89034 is equivalent to that of conventional corn (*Zea mays* L.). *J. Agric. Food Chem.* **2008**, *56*, 4623−4630.

(4) Ridley, W. P.; Sidhu, R. S.; Pyla, P. D.; Nemeth, M. A.; Breeze, M. L.; Astwood, J. D. Comparison of the nutritional profile of glyphosate-tolerant corn event NK603 with that of conventional corn (*Zea mays* L.). *J. Agric. Food Chem.* **2002**, *50*, 7235−7243.

(5) McCann, M. C.; Trujillo, W. A.; Riordan, S. G.; Sorbet, R.; Bogdanova, N. N.; Sidhu, R. S. Comparison of the forage and grain composition from insect-protected and glyphosate-tolerant MON 88017 corn to conventional corn (*Zea mays* L.). *J. Agric. Food Chem.* **2007**, *55*, 4034−4042.

(6) Zhou, J.; Harrigan, G. G.; Berman, K. H.; Webb, E. G.; Klusmeyer, T. H.; Nemeth, M. A. Stability of the compositional equivalence of grain from insect-protected corn and seed from herbicide-tolerant soybean over multiple seasons, locations and breeding germplasms. *J. Agric. Food Chem.* **2011**, *59*, 8822−8828.

(7) Harrigan, G. G.; Lundry, D.; Drury, S.; Ridley, W. P.; Riordan, S. G.; Nemeth, M. A. Natural variation in crop composition and the impact of biotechnology. *Nat. Biotechnol.* **2011**, *28*, 402−404.

(8) Herman, R. A.; Price, W. D. Unintended compositional changes in genetically modified (GM) crops: 20 years of research. *J. Agric. Food Chem.* **2013**, *61*, 11695−11701.

(9) Harrigan, G. G.; Harrison, J. M. Assessing compositional variability through graphical analysis and Bayesian statistical approaches; case studies on transgenic crops. *Biotechnol. Genet. Eng. Rev.* **2012**, *28*, 15−32.

(10) Harrison, J. M.; Breeze, M. L.; Harrigan, G. G. Introduction to Bayesian statistical approaches to compositional analyses of transgenic crops 1. Model validation and setting the stage. *Regul. Toxicol. Pharmacol.* **2012**, *60*, 381−388.

(11) Harrison, J. M.; Breeze, M. L.; Berman, K. H.; Harrigan, G. G. Bayesian statistical approaches to compositional analyses of transgenic crops. 2. Application and validation of informative prior distributions. *Regul. Toxicol. Pharmacol.* **2013**, *61*, 251−258.

(12) Harrison, J. M.; Culp, D.; Harrigan, G. G. Bayesian MCMC analyses for regulatory assessments of food composition. *Proceedings of Kansas State University Conference on Applied Statistics in Agriculture*, Manhattan, KS, USA, 2013; pp 73−87.

(13) Harrison, J. M.; Howard, D.; Malven, M.; Halls, S. C.; Culler, A. H.; Harrigan, G. G.; Wolfinger, R. D. Principal variance component analysis of crop composition data: a case study on herbicide-tolerant cotton. *J. Agric. Food Chem.* **2013**, *61*, 6412−6422.

(14) Harrigan, G. G.; Culler, A. H.; Culler, M.; Breeze, M. L.; Berman, K. H.; Halls, S. C.; Harrison, J. M. Investigation of biochemical diversity in a soybean lineage representing 35 years of breeding. *J. Agric. Food Chem.* **2013**, *61*, 10807−10815.

(15) Xu, Y.; Goodacre, R. Multiblock principal component analysis: an efficient tool for analyzing metabolomics data which contain two influential factors. *Metabolomics* **2012**, *8*, 37−51.

(16) Zwanenburg, G.; Hoefsloot, H. C. J.; Westerhuis, J. A.; Jansen, J. J.; Smilde, A. K. ANOVA-principal component analysis and ANOVA-simultaneous component analysis: a comparison. *J. Chemom.* **2011**, *25*, 561−567.

(17) Feil, B.; Moser, S. B.; Jampatong, S.; Stamp, P. Mineral composition of the grains of tropical maize varieties as affected by pre-anthesis drought and rate of nitrogen fertilization. *Crop Sci.* **2005**, *45*, 516−523.

(18) Harder, G. J.; Carlson, R. E.; Shaw, R. H. Yield, yield components, and nutrient content of corn grain as influenced by post-silking moisture stress. *Agron. J.* **1982**, *74*, 275−278.

fescues, dried, and ground as described below for ergovaline determination.

**Experimental Pastures.** A 0.75 ha plot was sown in September 2009 in Saint-Affrique (Aveyron, France) with an endophyte-infected tall fescue (*L. arundinaceum*, Kentucky 31 E+, infection rate of 94% measured on seedling) provided by RAGT 2n SAS (Rodez, France). Seeds (27 kg seeds/ha) were sown after conventional soil preparation (plowing and harrowing). Plant growth was monitored weekly according to the scale provided by the Biologische Bundesanstalt Bundessortenamt and Chemische Industrie (BBCH scale).[24] The plot was mowed each year at the fully ripe stage (stage 89 on the BBCH scale): June 18, 2010; June 10, 2011; June 19, 2012. In 2011, 120 units of nitrogen per hectare was added in the form of urea on the plot: 70 U/ha on March 9, 2011, and 50 U/ha on April 13, 2011. Rainfall events were recorded with a pluviometer at the Saint-Affrique site, and temperatures were taken daily at the Montlaur meteorological station located 9 km from Saint-Affrique. Effects of temperature were estimated by calculating cumulative degree-d from the beginning of February.[25,26]

**Plant Material.** The concentration of ergovaline in fescue cultivated in the experimental pastures was monitored from April 2010 to June 2012. During the growing season (spring), plants were sampled weekly, whereas outside this period (summer, fall, winter), plants were sampled once or twice a month. At each sampling date, the whole plants were cut just above the ground. From the heading stage (stage 51 on the BBCH scale) to the fully ripe stage (stage 89 on the BBCH scale) three other parts of the plant were collected: inflorescence (after the heading stage), leaves (stem and leaf blade), and base (stem and leaf sheath). On each occasion around 100 g of fresh material was harvested in five different representative areas of each plot. All of the samples were placed in a ventilated ULE 500 oven (Memmert, Schwabach, Germany) for 24 h at 60 °C. One hundred grams of oven-dried sample was then ground to 0.5 mm with a Cyclotech 1093 mill (Foss, Hogande, Sweden) and then stored at room temperature until analysis.

**Chemical Analysis of Ergovaline.** The ergovaline standard was kindly provided by G. E. Rottinghaus (College of Veterinary Medicine, University of Missouri, USA). All reagents and chemicals were of HPLC grade and were purchased from Sigma Chemical Co. (St. Louis, MO, USA). Ergovaline concentrations in the samples were determined by HPLC by fluorescence detection according to the method of Rottinghaus et al.[20] with slight modifications. Five grams of oven-dried milled grass was extracted with 100 mL of chloroform and 5 mL of 0.1 M sodium hydroxide for 2 h on an orbital shaker. Extracts were filtered on 1PS-Whatman phase separators and purified through a homemade column prepared as follows: 1 cm of Ergosil silica gel (Analtech Inc., Newark, DE, USA) was placed in a 5 mL empty SPE cartridge (Silicycle, Quebec, Canada) followed by a biological disk (Silicycle, Quebec, Canada) and 1 cm of sodium sulfate. Columns were preconditioned with 2 mL of dichloromethane, and 10 mL of the extract was then passed through the columns. The extract was eluted with 3 mL of methanol and dried under nitrogen. The dried extract was suspended in 500 $\mu$L of methanol, and 20 $\mu$L was injected in the HPLC system. Separation was achieved with acetonitrile (35%) in aqueous ammonium carbonate (200 mg/L, 65%) through a 150 × 4.6 mm, 5 $\mu$m, 120 Å Prontosil C18 column (Bischoff Chromatography, Leonberg, Germany). Ergovaline was detected by fluorescence with excitation and emission wavelengths of 250 and 420 nm, respectively. The retention time was 9.4 min. The percentage of recovery was 83 ± 4%. The limit of quantitation was 20 $\mu$g ergovaline/kg DM. Samples with ergovaline levels >500 $\mu$g/kg DM were diluted before new analysis.

**Statistical Analysis.** Statistical analysis was performed using R version 2.11.1 (R Foundation for Statistical Computing, Vienna, Austria). Distribution of ergovaline concentration in seeds was assessed by using the Shapiro test. The ergovaline levels in the plant were compared by year using one-way ANOVA. The slopes of ergovaline concentration in whole plant, base, leaves, and inflorescence plotted according to the stage of maturation were compared using ANCOVA. The effects of the year (factor 1) and cumulative temperature or cumulative rainfall (factor 2) on ergovaline concentration were evaluated using two-way ANOVA. The $P$ values obtained at each analysis are reported in results. Results were considered different with a $P$ value below 0.05.

## RESULTS AND DISCUSSION

Since the discovery of ergovaline and its vasoactive properties, most cases of fescue toxicosis have been linked to the presence of this toxin in the plant, and a range of toxic levels has been established. In cattle, threshold levels of approximately 300−400 $\mu$g ergovaline/kg DM have been proposed, higher concentrations of ergovaline in feed and cold temperatures being required to develop necrosis of the extremities.[5,10,27,28] Studies on endophyte-infected fescue in several countries demonstrated the presence of ergovaline at relatively high concentrations, which could explain the cases of toxicity observed in Australia, New Zealand, and the United States.[5,14,19,20] In Europe, although tall fescue is infected with *E. coenophiala*, only a few data are available on the ergovaline concentrations and its factors of variation. Ergovaline (Figure 1) concentrations in seeds and plants were monitored by

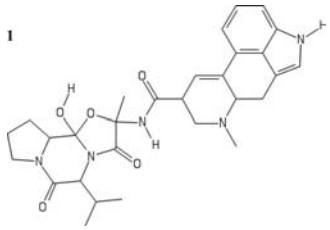

**Figure 1.** Structure of ergovaline.

fluorescence detection after separation by HPLC that permitted a limit of quantitation of 20 $\mu$g ergovaline/kg DM to be reached.[20]

**Ergovaline Concentrations in Wild Tall Fescue Seeds.** Ninety-nine plants of the 166 we collected (60%) were endophyte-infected according to the Phytoscreen immunoblot kit. The level of E+ in the populations collected ranged from 0 to 100%, depending on the point of collection. This rate of infection is consistent with that obtained in a study conducted in central France, where 65% infection was reported.[18] It is within the range of infection reported in Europe, 7% infection being observed in mainland Greece and 100% in Sardinia.[2,17] Figure 2 shows the concentrations of ergovaline in the seeds obtained after 1 year of growth outside without complementary water or fertilizer inputs. All of the endophyte-infected seeds analyzed had ergovaline concentrations higher than the limit of quantitation, the lowest and highest concentrations being 3.1 and 29.3 mg ergovaline/kg DM, respectively. The distribution of ergovaline in the seeds did not follow a normal distribution (Shapiro test, $P = 0.003$). The mean ± SD and the median were 14.8 ± 7.3 and 15.5 mg ergovaline/kg DM, respectively. The ergovaline concentration of the endophyte-infected fescue seeds of Kentucky 31 sown in the experimental pastures was 6.0 mg ergovaline/kg DM. This value is among the highest reported in 25 genotypes of Kentucky 31 tall fescue seeds with high endophyte infection; levels usually range from 1.1−4.8 to 2.0−8.0 mg ergovaline/kg DM, depending on the year of analysis and the country.[8,19] Therefore, 86% of the wild endophyte-infected fescue seeds collected in southern France had higher concentrations of ergovaline than the Kentucky 31 endophyte-infected fescue seeds.

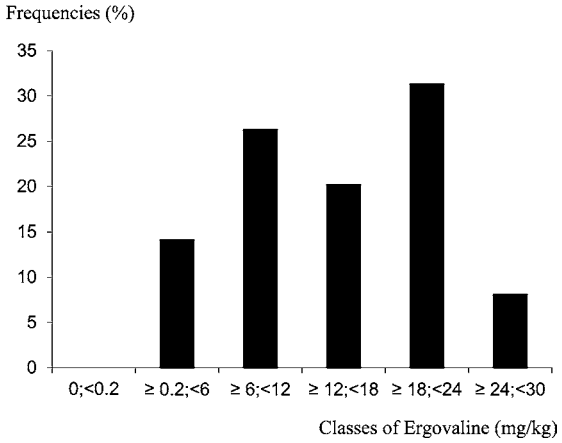


**Figure 2.** Repartition of the concentrations in ergovaline in endophyte-infected tall fescue seeds collected in southern France ($n$ = 99).

**Ergovaline Concentration in Plants.** Because ergovaline production in plants varies with biotic (endophyte strain) and abiotic factors, as well as with the part of the plant analyzed, seeds of endophyte-infected Kentucky 31 were sown in field conditions to monitor the ergovaline concentration in tall fescue under French agricultural conditions. The level of ergovaline in the plant has been reported to vary with the genotype of endophyte-infected tall fescue.[19,29,30] This cultivar was selected because no endophyte-infected tall fescue was commercialized in France and because data on ergovaline levels are available for comparison in other countries. Figure 3 shows the levels of ergovaline in the endophyte-infected tall fescue Kentucky 31 as a function of the sampling period. Each year, the ergovaline concentration increased from the heading stage

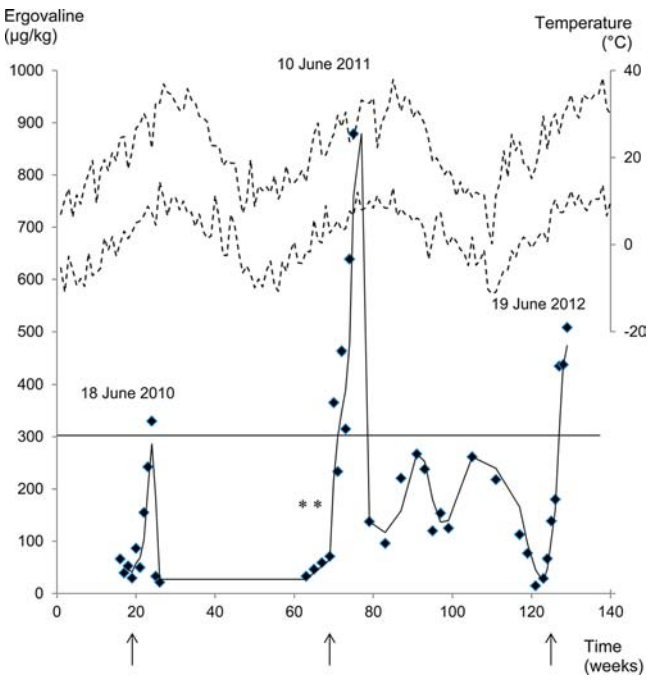


**Figure 3.** Ergovaline concentration in the whole endophyte-infected tall fescue Kentucky 31 plant sown in September 2009 in Saint-Affrique (Aveyron, France): (↑) beginning of heading; (*) fertilization; (—) toxic threshold level; (- - -) minimum and maximum temperatures. Week 1 is the first week in 2010.

(end of April) to reach its maximum level 6 weeks later, at the fully ripe stage. This result agrees with previous data obtained in field conditions and in studies demonstrating that ergovaline accumulates in the seed during its formation.[20,21] Although the maximum levels were always in June (June 18, 2010; June 10, 2011; and June 19, 2012) the concentrations of ergovaline in the plants varied considerably with the year: from 330 $\mu$g ergovaline/kg DM in 2010 to 879 $\mu$g ergovaline/kg DM in 2011. The greatest variations in ergovaline concentrations in the whole plant occurred after the beginning of heading (weeks 20, 70, and 124), when the inflorescences emerged (Figure 3). Before emergence of the inflorescence, mean ergovaline concentrations in the whole plants were 47, 52, and 58 $\mu$g/kg DM for the years 2010, 2011, and 2012, respectively. No significant difference was observed between years (ANOVA), and the mean concentration was 53 $\pm$ 27 $\mu$g ergovaline/kg DM. From emergence of the inflorescence to the fully ripe stage, the concentration of ergovaline in the whole plant was significantly lower in 2010 than in 2011 and 2012 (ANCOVA, $P$ = 0.045 and 0.049, respectively), whereas the difference between the years 2011 and 2012 was not significant. Two other ergovaline peaks were observed, one in September 2011 (weeks 91−93) and another in January 2012 (weeks 105−111). The fall peak corresponded to plant regrowth ("regain"), at the same time as an increase in ergovaline production in planta, and has been previously reported.[21] By contrast, the winter peak is probably linked to the accumulation of ergovaline in the plant that occurs during senescence. High ergovaline has already been reported in leaves in winter.[7] The presence of high levels of ergovaline in the whole plant in winter is of interest because fescue foot disease occurs in winter, even if other factors such as external temperature are involved in the severity of the lesions.[31] Of these three periods, the levels of ergovaline in whole plant were low, in agreement with data obtained in Kentucky 31 tall fescue in Columbia, MO, USA.[20]

Table 1 lists the concentrations of ergovaline measured in the base, leaves, and inflorescence from the heading stage to the fully ripe stage in 2011 and 2012. At the beginning of heading, weeks 69 and 123, the ergovaline concentrations were similar in base, leaves, and inflorescence, but slightly higher in inflorescences in 2011. From 70% of inflorescence emerged to fully ripe, weeks 70−75 and 124−129, the highest level of ergovaline was generally measured in the inflorescence, whereas the concentrations in the base and leaves were lower, except in weeks 70 and 72. Irrespective of the part of the plant analyzed, the ergovaline level obtained at the fully ripe stage did not appear to be correlated with the level at the heading stage. For example, the concentrations of ergovaline in the inflorescences ranged from 57 to 1861 $\mu$g/kg DM in 2012 and from 96 to 1406 $\mu$g/kg DM in 2011.

A comparison of the slope of ergovaline accumulation in the different parts of the plant showed that accumulation in the leaves varied with the year ($P$ = 0.031, ANCOVA), whereas differences in the inflorescence and the bases were not significant. Also, the kinetics of accumulation of ergovaline appeared to vary from year to year. When the inflorescences emerged, weeks 70−71 and 124−125 (Table 1), ergovaline concentrations were markedly higher in bases and leaves in 2011 than in 2012. Later, weeks 72−74 and 126−128, ergovaline concentrations in the bases increased in 2012 to reach values near those measured in 2011, whereas the ergovaline levels in leaves were usually lower in 2012 than in 2011. At the fully ripe stage, weeks 75 and 129 (Table 1), the


dx.doi.org/10.1021/jf503015m | J. Agric. Food Chem. 2014, 62, 9609−9614

Table 1. Ergovaline Concentrations in Endophyte-Infected Tall Fescue (Kentucky 31 E+) from Heading to Fully Ripe ($\mu$g/kg Dry Matter)[a]

| | | 2011 | | | | 2012 | | | |
|---|---|---|---|---|---|---|---|---|---|
| stage description | code | weeks | B | L | I | weeks | B | L | I |
| beginning of heading | 51 | 69 | 44 | 39 | 96 | 123 | 50 | 63 | 57 |
| 70% of inflorescence emerged | 57 | 70 | 305 | 142 | 516 | 124 | 59 | 45 | 166 |
| inflorescence fully emerged | 59 | 71 | 237 | 127 | 272 | 125 | 70 | 70 | 386 |
| beginning of flowering | 61 | 72 | 289 | 304 | 221 | 126 | 192 | 148 | 463 |
| end of flowering | 69 | 73 | 287 | 248 | 571 | 127 | 479 | 156 | 400 |
| late milk | 77 | 74 | 331 | 629 | 1308 | 128 | 302 | 143 | 537 |
| fully ripe | 89 | 75 | 535 | 408 | 1406 | 129 | 216 | 182 | 1861 |

[a]B, base; L, leaves; I, inflorescence.

concentration of ergovaline was around 2-fold higher in bases and leaves in 2011 than in 2012, whereas levels in inflorescences were higher in 2012 (1861 and 1406 $\mu$g ergovaline/kg DM in 2012 and 2011, respectively). Finally, these results showed that the speed and the level of accumulation of ergovaline in the bases and in the leaves were higher in 2011 than in 2012, whereas no difference was observed for the inflorescences.

**Factors of Variation.** The relatively wide range of ergovaline concentrations observed in this study depending on the year is in agreement with data obtained in other countries[19,20] and older reports of toxicosis in cattle.[32] The levels obtained at the fully ripe stage agree with the results of studies conducted in 1983 and 1984 in Watskinville, GA, USA, in which maximum mean ergovaline concentrations ranging from 275 to 464 $\mu$g/kg DM were reported depending on the year of analysis and the use of fertilizer.[21] Likewise, ergovaline concentrations measured in head seeds did not differ markedly from those reported in other studies. In the present study, ergovaline concentrations in inflorescences ranged from 1406 to 1861 $\mu$g/kg DM in 2011 and 2012, respectively, whereas they ranged from 1700 to 5000 $\mu$g/kg DM the 1988 and 1987 in a study conducted in Columbia, MO, USA.[20]

Fertilizer was added in 2011. The nitrogen input was within the usual recommendations for this kind of pasture.[33] After fertilization, a rapid increase in ergovaline was observed in the bases and leaves, and concentrations in these parts of the plant were around 2-fold higher in 2011 than in 2012 when no fertilizer was added. Although factors other than nitrogen inputs to the pasture could explain these differences, this result agrees with previous data demonstrating an increase in ergovaline concentrations in fertilized plants.[20] The levels reached in plants are difficult to compare between studies because ergot alkaloid contents vary with the dose and the kind of fertilizer used.[7,20] In the present study, fertilization appears to have had no effect on the level of ergovaline in the inflorescence. No difference in ergovaline content in the whole plant was observed between 2011 and 2012, suggesting that fertilization has only a weak effect on the final level of toxin in the forage, the degree of maturation of the plant being the most important factor in terms of risk of toxicosis. This result is in agreement with data obtained in Watskinville, GA, USA, where different effects of nitrogen fertilization on the level of ergovaline in the whole plant were observed depending on the year of the assay.[21] This result is also in agreement with data showing a lack of correlation between nitrogen and ergovaline concentration in straw.[19]

**Climatic Factors.** Correlations between ergovaline levels in the whole plant and climatic factors were performed to investigate putative risk factors during the three study years. Concentrations of ergovaline in the whole plant were plotted according to the cumulative degree-d observed each year from the beginning of February to the fully ripe stage (Figure 4A). When cumulative degree-d values were below 900 °C, the mean

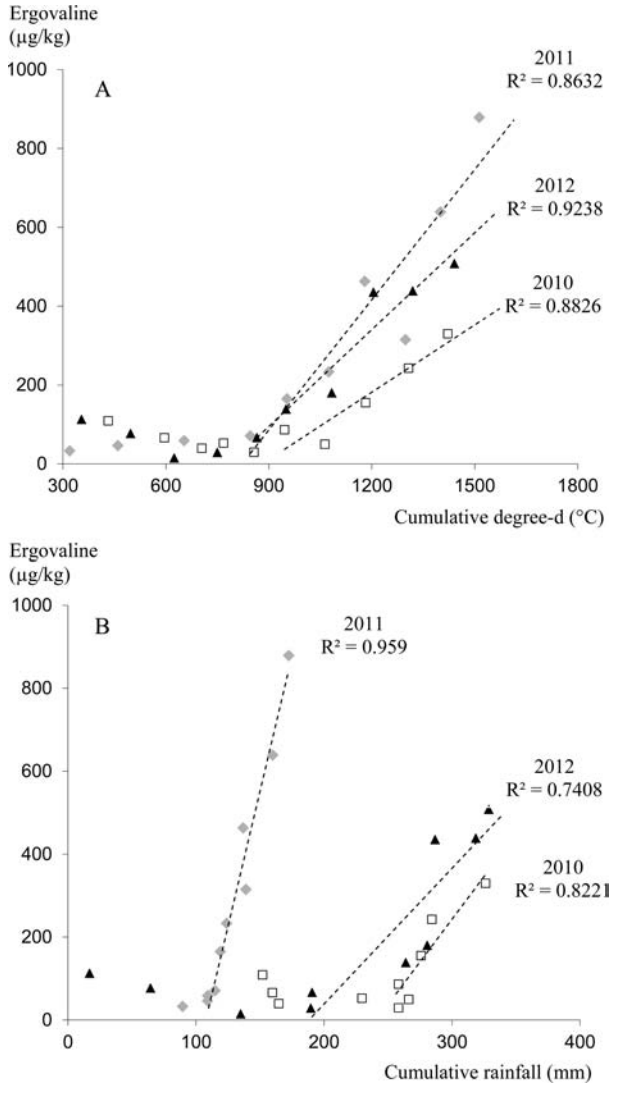


Figure 4. Concentrations of ergovaline in whole endophyte-infected tall fescue Kentucky 31 plants sown in September 2009 in Saint-Affrique (Aveyron, France) plotted according to cumulative degree-d (A) or cumulative rainfall (B) observed each year from the beginning of February to the fully ripe stage.


dx.doi.org/10.1021/jf503015m | J. Agric. Food Chem. 2014, 62, 9609−9614

ergovaline concentration in the whole plant was low and did not differ by year. When cumulative degree-d values were higher than 900 °C, a linear increase of ergovaline in the whole plant was observed, with very high $R^2$ in each study year. Analysis of the effect of year and temperature on the concentration of ergovaline in the whole plant (two-way ANOVA) revealed a strong effect of cumulative temperature ($P < 0.001$), whereas the effect of year was not significant. However, the day for which the cumulative degree-d of 900 °C was reached varied with the year: May 17, 2010; May 3, 2011; and May 19, 2012 (Figure 5). Interestingly, cumulative degree-

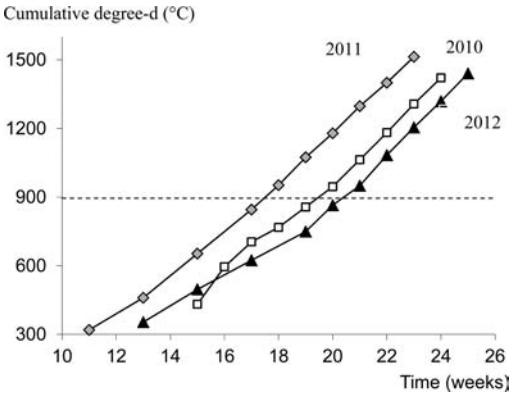


**Figure 5.** Cumulative degree-days according to the week of the year; (---) level required for having an increase of ergovaline concentration in plants.

d values of around 900 °C were required for the development of inflorescence of tall fescue.[25] The fully ripe stage was observed for a cumulative degree-d around 1500 °C (Figure 5). This stage was reached on June 18, 2010; June 10, 2011; and June 19, 2012. Subsequently, ergovaline increased with the increase in cumulative degree-d but with no significant difference between years. This result obtained in the field agrees with data obtained in controlled conditions demonstrating the lack of effect of high temperatures on total ergot contents in tall fescue.[34] Finally, this suggests that, during this assay, the correlation observed between ergovaline content in the whole plant and cumulative degree-d is due to an effect of temperature on plant growth.

Cumulative rainfall from the beginning of February to the fully ripe stage plotted against ergovaline concentrations in the whole plant showed major differences between years (Figure 4B). Concerning plant growth, a linear correlation between the concentration of ergovaline and cumulative rainfall was observed in each year. Comparison of rainfall in 2010 and 2012 revealed no significant difference whatever the period analyzed (from February to June or from the emergence of the inflorescence to the fully ripe stage). By contrast, the year 2011 was drier than either 2010 or 2012. However, analysis of the effect of year and cumulative rainfall on the ergovaline concentration in the whole plant (two-way ANOVA) failed to reveal a significant effect of cumulative rainfall ($P = 0.927$) or of the year of analysis ($P = 0.336$). Finally, the concentration of ergovaline in the whole plant was significantly lower in 2010 than in 2011 or 2012, whereas there was no difference in rainfall between 2010 and 2012, and 2011 was the driest year. Although it has been suggested that a limited supply of water could increase alkaloid production,[23] this result in the field agrees with data obtained under controlled conditions, demonstrating the lack of effect of water availability on total ergot contents in tall fescue.[34]

In conclusion, this study demonstrates for the first time that around 60% of wild tall fescue is infected with *Epichloe* in southern France and that most of the infected plants are able to produce very high ergovaline levels in seeds. Determination of ergovaline contents in Kentucky 31 tall fescue infected with *E. coenophiala* at different growth stages revealed that the levels in plant can be high and do not markedly differ from levels measured in other countries where fescue toxicosis has been reported. Analysis of the factors of variation of ergovaline concentrations revealed that the maturation of the plant is the main factor that needs to be taken into consideration when the risk of toxicity is estimated. Three peaks of concentration were identified: the end of spring, the beginning of fall, and mid-winter. Accurate estimation of the course of maturation of tall fescue is also recommended for better comparison of data between studies. Although fertilization increased the level of ergovaline in bases and leaves, only slight effects were observed in the whole plant. Cumulative temperature appears to affect the level of ergovaline via its effect on plant growth, whereas cumulative rainfall appears to have no effect on the level of ergovaline under the field conditions in the present study.

## AUTHOR INFORMATION

### Corresponding Author

*(P.G.) E-mail: p.guerre@envt.fr. Fax: +335 61 19 32 40. Phone: +335 61 19 32 17.

### Funding

This study was supported by the French government (Fond Unique Interministériel, Project 082906510) and the region Midi-Pyrénées within the framework of a project qualified by the French Competitiveness Cluster AGRIMIP-INNOVATION.

### Notes

The authors declare no competing financial interest.

## ACKNOWLEDGMENTS

We especially thank Hervé Gryta, Olivier Navaud (EDB, UMR 5174 CNRS-UPS-ENFA, Toulouse, France) and Laurent Hazard (UMR 1248 AGIR, INRA Toulouse, France) for collecting tall fescue samples in 2009 and Faouzi Lyazrhi (UP Biostatistique, INP, ENVT, Toulouse, France) for helpful discussion of the statistical analysis of the results.

## ABBREVIATIONS USED

RAGT, Rouergue Auvergne Gévaudan Tarnais; BBCH, Biologische Bundesanstalt Bundessortenamt and CHemische Industrie; DM, dry matter

## REFERENCES

(1) Christensen, M. J.; Leuchtmann, A.; Rowan, D. D.; Tapper, B. A. Taxonomy of *Acremonium* endophytes of tall fescue (*Festuca arundinacea*), meadow fescue (*F. pratensis*) and perennial ryegrass (*Lolium perenne*). *Mycol. Res.* **1993**, *97*, 1083−1092.

(2) Takach, J. E.; Mittal, S.; Swoboda, G. A.; Bright, S. K.; Trammell, M. A.; Hopkins, A. A.; Young, C. A. Genotypic and chemotypic diversity of *Neotyphodium* endophytes in tall fescue from Greece. *Appl. Environ. Microbiol.* **2012**, *78*, 5501−5510.

(3) Schardl, C. L.; Florea, S.; Pan, J.; Nagabhyru, P.; Bec, S.; Calie, P. J. The epichloae: alkaloid diversity and roles in symbiosis with grasses. *Curr. Opin. Plant Biol.* **2013**, *16*, 480−488.

(4) Kuldau, G.; Bacon, C. *Clavicipitaceous* endophytes: Their ability to enhance resistance of grasses to multiple stresses. *Biol. Control* **2008**, *46*, 57−71.
(5) Tor-Agbidye, J.; Blythe, L. L.; Craig, A. M. Correlation of endophyte toxins (ergovaline and lolitrem B) with clinical disease: fescue foot and perennial ryegrass staggers. *Vet. Hum. Toxicol.* **2001**, *43*, 140−146.
(6) Garner, G. B.; Rottinghaus, G. E.; Cornell, C. N.; Testereci, H. Chemistry of compounds associated with endophyte/grass interaction: ergovaline- and ergopeptine-related alkaloids. *Agric. Ecosyst. Environ.* **1993**, *44*, 65−80.
(7) Lyons, P. C.; Plattner, R. D.; Bacon, C. W. Occurrence of peptide and clavine ergot alkaloids in tall fescue grass. *Science* **1986**, *232*, 487−489.
(8) TePaske, M. R.; Powell, R. G.; Clement, S. L. Analyses of selected endophyte-infected grasses for the presence of loline-type and ergot-type alkaloids. *J. Agric. Food Chem.* **1993**, *41*, 2299−2303.
(9) Lane, G. A.; Christensen, M. J.; Miles, C. O. Coevolution of fungal endophytes with grasses: the significance of secondary metabolites. *Microb. Endophytes* **2000**, 341−388.
(10) Zbib, N.; Repussard, C.; Tardieu, D.; Guerre, P. Toxicité des mycotoxines produites par des champignons endophytes du genre *Neotyphodium*. *Rev. Med Vet.* **2014**, *165*, 116−135.
(11) Bouton, J. H.; Latch, G.; Hill, N. S.; Hoveland, C. S.; McCann, M. A.; Watson, R. H.; Parish, J. A.; Hawkins, L. L.; Thompson, F. N. Reinfection of tall fescue cultivars with non-ergot alkaloid-producing endophytes. *Agron. J.* **2002**, *94*, 567−574.
(12) Hopkins, A. A.; Young, C. A.; Panaccione, D. G.; Simpson, W. R.; Mittal, S.; Bouton, J. H. Agronomic performance and lamb health among several tall fescue novel endophyte combinations in the South-Central USA. *Crop Sci.* **2010**, *50*, 1552−1561.
(13) Schmidt, S. P.; Osborn, T. G. Effects of endophyte-infected tall fescue on animal performance. *Agric. Ecosyst. Environ.* **1993**, *44*, 233−262.
(14) Repussard, C.; Zbib, N.; Tardieu, D.; Guerre, P. Les champignons endophytes du genre *Neotyphodium* et leurs toxines: généralités et problématique française. *Rev. Med. Vet.* **2013**, *164*, 583−606.
(15) Bacon, C. W.; Siegel, M. R. Endophyte parasitism of tall fescue. *J. Prod. Agric.* **1988**, *1*, 45−55.
(16) Glenn, A. E.; Bacon, C. W.; Price, R.; Hanlin, R. T. Molecular phylogeny of *Acremonium* and its taxonomic implications. *Mycologia* **1996**, *88*, 369−383.
(17) Clement, S. L.; Elberson, L. R.; Youssef, N. N.; Davitt, C. M.; Doss, R. P. Incidence and diversity of fungal endophytes in tall fescue from Morocco, Tunisia, and Sardinia. *Crop Sci.* **2001**, *41*, 570−576.
(18) Guillaumin, J. J.; Frain, M.; Pichon, N.; Ravel, C. Survey of the fungal endophytes in wild grass species of the Auvergne region (central France). In *Proceedings of the Fourth International Neotyphodium/Grass Interactions Symposium*; Paul, V. H., Dapprich, P. D., Eds.; Fachbereich Agrarwirtschaft: Soest, Germany, 2001; pp 85−92.
(19) Welty, R. E.; Craig, A. M.; Azevedo, M. D. Variability of ergovaline in seeds and straw and endophyte infection in seeds among endophyte-infected genotypes of tall fescue. *Plant Dis.* **1994**, *78*, 845−849.
(20) Rottinghaus, G. E.; Garner, G. B.; Cornell, C. N.; Ellis, J. L. HPLC method for quantitating ergovaline in endophyte-infested tall fescue: seasonal variation of ergovaline levels in stems with leaf sheaths, leaf blades, and seed heads. *J. Agric. Food Chem.* **1991**, *39*, 112−115.
(21) Belesky, D. P.; Stuedemann, J. A.; Plattner, R. D.; Wilkinson, S. R. Ergopeptine alkaloids in grazed tall fescue. *Agron. J.* **1988**, *80*, 209−212.
(22) Arechavaleta, M.; Bacon, C. W.; Plattner, R. D.; Hoveland, C. S.; Radcliffe, D. E. Accumulation of ergopeptide alkaloids in symbiotic tall fescue grown under deficits of soil water and nitrogen fertilizer. *Appl. Environ. Microbiol.* **1992**, *58*, 857−861.
(23) Schardl, C. L.; Leuchtmann, A.; Spiering, M. J. Symbioses of grasses with seedborne fungal endophytes. *Annu. Rev. Plant Biol.* **2004**, *55*, 315−340.
(24) Hess, M.; Barralis, G.; Bleiholder, H.; Buhr, L.; Eggers, T. H.; Hack, H.; Stauss, R. Use of the extended BBCH scale-general for the descriptions of the growth stages of mono- and dicotyledonous weed species. *Weed Res.* **1997**, *37*, 433−441.
(25) Duru, M.; Cruz, P.; Martin, G.; Theau, J. P.; Charron-Moirez, M. H.; Desange, M.; Jouany, C.; Zerourou, A. Herb'sim: un modèle pour raisonner la production et l'utilisation de l'herbe. *Fourrages* **2010**, *201*, 37−46.
(26) Duru, M.; Cruz, P.; Theau, J. P. Un modèle générique de digestibilité des graminées des prairies semées et permanentes pour raisonner les pratiques agricoles. *Fourrages* **2008**, *193*, 79−102.
(27) Stamm, M. M.; DelCurto, T.; Horney, M. R.; Brandyberry, S. D.; Barton, R. K. Influence of alkaloid concentration of tall fescue straw on the nutrition, physiology, and subsequent performance of beef steers. *J. Anim. Sci.* **1994**, *72*, 1068−1075.
(28) Brown, K. R.; Anderson, G. A.; Son, K.; Rentfrow, G.; Bush, L. P.; Klotz, J. L.; Strickland, J. R.; Boling, J. A.; Matthews, J. C. Growing steers grazing high versus low endophyte (*Neotyphodium coenophialum*)-infected tall fescue have reduced serum enzymes, increased hepatic glucogenic enzymes, and reduced liver and carcass mass. *J. Anim. Sci.* **2009**, *87*, 748−760.
(29) Siegel, M. R.; Bush, L. P. Defensive chemicals in grass-fungal endophyte associations. In *Phytochemical Diversity and Redundancy in Ecological Interactions*, 1st ed.; Romeo, J. T., Saunders, J. A., Barbosa, P., Eds.; Springer: New York, 1996; Vol. 30, pp 81−119.
(30) Najafabadi, A. S.; Mofid, M. R.; Mohammadi, R.; Moghim, S. Quantification of ergovaline using HPLC and mass spectrometry in Iranian *Neotyphodium* infected tall fescue. *Res. Pharm. Sci.* **2010**, *5*, 135−143.
(31) Bacon, C. W. Toxic endophyte-infected tall fescue and range grasses: historic perspectives. *J. Anim. Sci.* **1995**, *73*, 861−870.
(32) Jacobson, D. R.; Carr, S. B.; Hatton, R. H.; Buckner, R. C.; Graden, A. P.; Dowden, D. R.; Miller, W. M. Growth, physiological responses, and evidence of toxicity in yearling dairy cattle grazing different grasses. *J. Dairy Sci.* **1970**, *53*, 575−587.
(33) Protin, P. V.; Corre-Hellou, G.; Naudin, C.; Trochard, R. Impact des pratiques de fertilisation sur la productivité des prairies et mélanges céréales − protéagineux et la qualité du fourrage. *Fourrages* **2009**, *198*, 115−130.
(34) Brosi, G. B.; McCulley, R. L.; Bush, L. P.; Nelson, J. A.; Classen, A. T.; Norby, R. J. Effects of multiple climate change factors on the tall fescue-fungal endophyte symbiosis: infection frequency and tissue chemistry. *New Phytol.* **2011**, *189*, 797−805.

condensation reaction, where the donor substrate is a monosaccharide, or as (2) kinetically controlled trans-glycosylation, where an activated donor, for example, a disaccharide or a *p*-nitrophenyl (*p*NP) monosaccharide, is employed. In reverse hydrolysis, the maximum yield is determined by the equilibrium, and reaction times are often extended. In contrast, trans-glycosylation makes it possible to "overshoot" the equilibrium to favor the glycosylated acceptor product if the substrate is more reactive than the product, and reaction times are generally shorter than in reverse hydrolysis.[7,17−19] In both cases, the synthetic reaction takes place in competition with hydrolysis of both substrate and product.

As first established by Koshland,[20] glycosidases can catalyze the hydrolysis of substrates or the synthesis of products with either retention or inversion of the anomeric configuration. The glycosidases in focus in this review, that is, $\beta$-galactosidases, belonging to glycosyl hydrolase (GH) families 1, 2, 35, and 42, sialidases, mainly belonging to GH family 33, and $\alpha$-L-fucosidases, mainly belonging to GH family 29, are all retaining glycosidases and employ the classical Koshland double-displacement mechanism. This double-displacement mechanism involves the formation of a covalent glycosyl-enzyme intermediate upon binding of the donor in the active site.[20,21] Figure 1 shows the reactions catalyzed by sialidases, $\beta$-galactosidases, and $\alpha$-L-fucosidases with formation of the glycosyl-enzyme intermediate and concomitant release of the aglycone from the active site, consistent with a ping-pong bibi mechanism, which reduces to an ordered unibi mechanism in the competing hydrolysis.[22] This mechanism has been observed for many glycosidases,[23−26] but evidence of an ordered bibi mechanism with formation of a ternary donor−acceptor−enzyme complex has also been reported for the retaining $\beta$-galactosidase from *Bacillus circulans* (EC 3.2.1.23; GH 42).[1] Recently, a hybrid of the two mechanisms with formation of the ternary complex prior to formation of the sialyl-enzyme intermediate has been suggested for the native trans-sialidase from *Trypanosoma cruzi* (EC 3.2.1.18; GH 33).[27] In the ping-pong bibi mechanism, the glycosyl-enzyme intermediate then undergoes nucleophilic attack, either by water, resulting in hydrolysis, or by another acceptor, resulting in trans-glycosylation (Figure 1). It has been hypothesized that increased stabilization of the covalent glycosyl-enzyme intermediate favors trans-glycosylation over hydrolysis.[28] The trans-glycosylation product is also a substrate for the glycosidase and can thus undergo subsequent hydrolysis (secondary hydrolysis) or function as a donor substrate (Figure 1), the rate being dependent on the regioselectivity in the product formation because not all regioisomers are equally good substrates.[29] The trans-glycosylation yield is therefore the result of a delicate balance between the rates of synthesis, donor hydrolysis, and product hydrolysis (Figure 1). At first glance, the three reactions in Figure 1 appear identical, but all three reactions have been included to emphasize the structural differences in the substrates and products related to each of the three enzyme classes.

The ratio between the trans-glycosylation rate ($r_S$) and the hydrolysis rate ($r_H$) thus describes how efficiently the glycosyl-enzyme intermediate gives the desired trans-glycosylation product (Figure 1). It follows that in order to maximize trans-glycosylation yields, the $r_S/r_H$ ratio must be maximized:[7,18,30]

$$\frac{r_S}{r_H} = S \times \frac{a_{\text{glycosyl acceptor}}}{a_w} = S_c \times \frac{[\text{glycosyl acceptor}]}{[\text{water}]} \quad (1)$$

Thus, the trans-glycosylation yield is influenced both by the activities (or concentrations) of the competing nucleophiles and by the selectivity factor $S$ (or $S_c$), which is dependent on enzyme source and also on choice of donor, acceptor, and reaction conditions.[7,18,30,31] Indeed, the glycosidases most suitable for synthetic reactions are the ones with a high $r_S/r_H$ ratio, especially because product hydrolysis occurs through the same glycosyl-enzyme intermediate.[18] However, much can also be gained from optimizing the reaction conditions, that is, choice of donor, acceptor, acceptor concentration, acceptor/donor ratio, $a_w$, and reaction time as discussed below.

## SELECTIVITY AND SPECIFICITY

The anomeric selectivity of glycosidases is absolute because it is determined by the reaction mechanism.[7] In contrast, glycosidases often show broad selectivity for the donor and particularly for the acceptor molecules as outlined in the following sections. Regioselectivity in the product formation varies from enzyme to enzyme, is dependent on donor and acceptor structures, and may also be adjusted by the use of cosolvents or protein engineering (as discussed below).

**Donor Specificity.** In trans-glycosylation, the glycosyl donor must carry a good anomeric leaving group. Disaccharides such as lactose are sufficiently activated, but nitrophenyl glycosides are also widely used.[32,33] The donor must be fast-reacting to keep reaction times short, thus allowing less time for product hydrolysis. Furthermore, a donor that binds tightly to the catalyst (low $K_m$) also minimizes product hydrolysis.[7] In several cases, aryl donor substrates have given up to 2.5 times higher yields than a di- or trisaccharide donor; this improved yield has been suggested to be due to the aryl aglycone being a better leaving group than the mono- or disaccharides.[14,19,34−36] This is beneficial for synthesis on a smaller scale, but for large-scale synthesis the price of both donors and acceptors becomes an important consideration. For instance, substances such as lactose and casein glycomacropeptide (to be discussed below) are interesting because they are abundantly available in industrial dairy streams. In comparison, nitrophenyl glycosides are expensive substrates and are not suitable for large-scale synthesis unless the resulting product is of extremely high value. Furthermore, the toxicity of the nitrophenol byproduct will be an issue in the approval of this process for use in food applications.

Sialidases (EC 3.2.1.18) specifically catalyze the release of terminal sialic acid (*N*-acetylneuraminic acid) residues $\alpha$-linked to glycoproteins, glycolipids, and polysaccharides, resulting in hydrolysis or trans-sialylation (Figure 1A). Typically, donor substrates such as *p*NP-$\alpha$-sialic acid (Sia-$\alpha$-*p*NP), 2′-(4-methylumbelliferyl)-$\alpha$-D-*N*-acetylneuraminic acid (Sia-$\alpha$-MU), 3′-sialyl-lactose, and dimers and polymers of $\alpha$(2,8)-linked sialic acid, as well as the fetal calf serum glycoprotein fetuin, have been used in trans-sialylation (Tables 1 and 2).[15,35,37−39] Recently, however, a much cheaper source of sialic acid has been introduced in the synthesis of biomimetic compounds, namely, casein glycomacropeptide (CGMP), which is the soluble glycosylated casein residue produced by chymosin action on $\kappa$-casein during cheese manufacture (Tables 1 and 2).[2,4,40−44] CGMP contains 5−11% (w/w) sialic acid depending on the source,[40,45,46] of which approximately half is $\alpha$(2,3)-linked to galactose and the other half is $\alpha$(2,6)-linked to *N*-acetyl-D-galactosamine (GalNAc).[47] The well-studied trans-sialidase from *T. cruzi* is specific for the $\alpha$(2,3)-linked sialyl residues only,[38,48] whereas sialidases from *Clostridium perfringens*, *Arthrobacter*

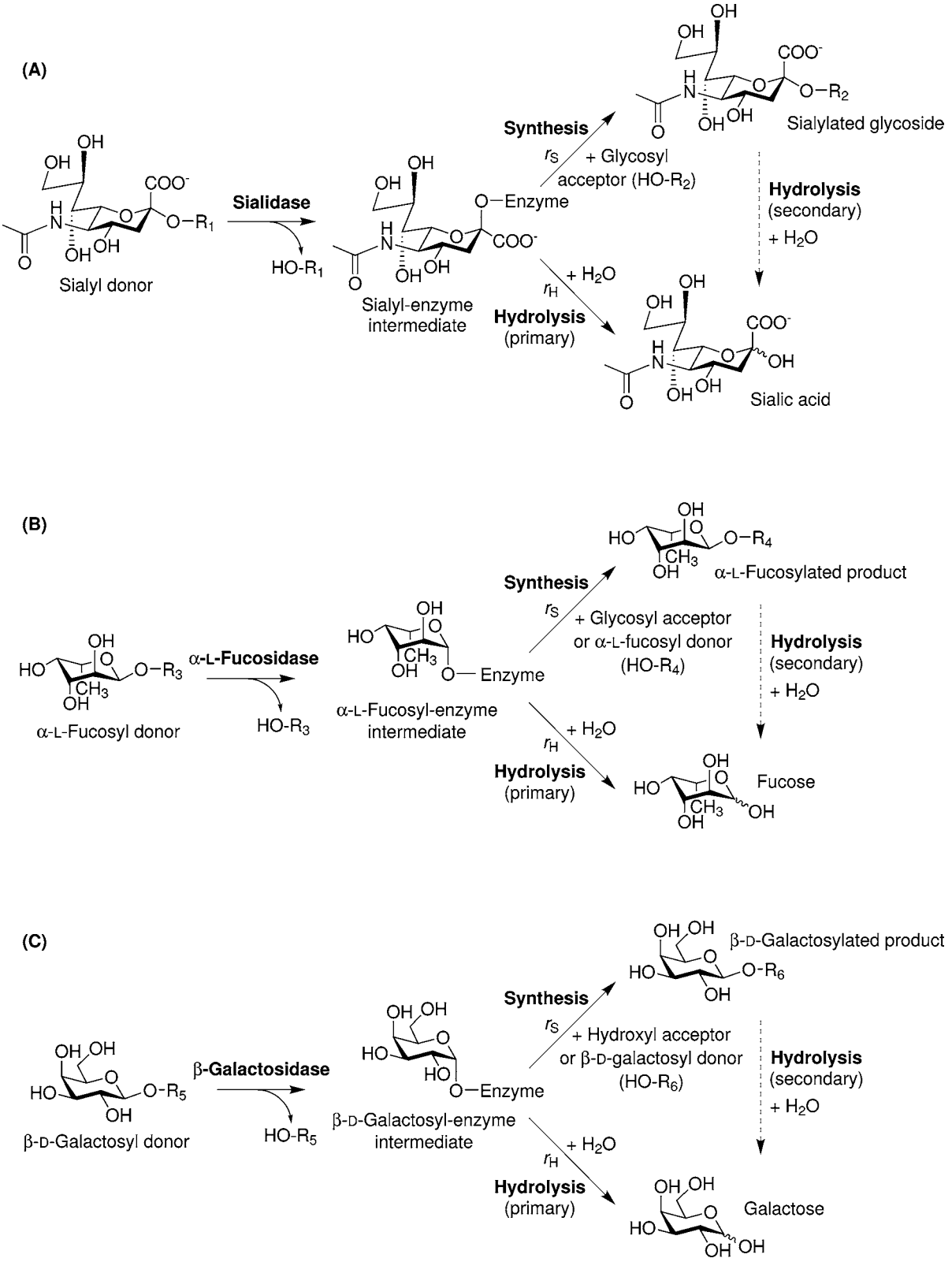


**Figure 1.** Scheme of competing reactions catalyzed by (A) sialidases, (B) α-L-fucosidases, and (C) β-galactosidases. For graphic simplicity, reaction schemes are shown according to the ping-pong bibi mechanism (see text). If the nucleophile attacking the glycosyl-enzyme intermediate is water, hydrolysis occurs. If another nucleophile attacks the intermediate, trans-glycosylation occurs. For β-galactosidases and some α-L-fucosidases, the donor substrate can also function as acceptor, resulting in donor self-condensation (see text). Regioselectivity in the product formation may vary (see text).

*ureafaciens*, *Vibrio cholerae* (all EC 3.2.1.18; GH 33), and Newcastle disease virus (EC 3.2.1.18; GH 83) can also utilize terminal sialyl residues α(2,8)-linked in sialic acid di- and polymers (Table 1).[35] So far, it is unclear whether α(2,6)-linked sialyl moieties on CGMP are utilized. Most sialidases accept aryl sialyl donors (Tables 1 and 2).[14,35]


dx.doi.org/10.1021/jf502619p | J. Agric. Food Chem. 2014, 62, 9615−9631

**Table 1. Donor, Acceptor, and Acceptor/Donor (A:D) Ratio of Trans-sialylations Catalyzed by Sialidases as well as the Linkages, Total Trans-sialylation Yield, and Regioselectivity Obtained[a]**

| sialidase | donor | acceptor | linkages formed in trans-sialylation[b] | A:D[c] | yield[d] (%) | regioselectivity[e] | ref |
|---|---|---|---|---|---|---|---|
| *Arthrobacter ureafaciens* | Sia-α(2,8)-Sia | Lac | α(2,6′) | 18[f] | nq | complete | 35 |
| | Sia-α-*p*NP | Lac | α(2,6′) | 5[f] | nq[f] | complete | 35 |
| | CGMP | Lac | nd | 44[g] | 5[g] | | 44 |
| *Bacteroides fragilis* | colominic acid | Lac | α(2,6′), α(2,3′) | | 0.3 | high (99%) | 115 |
| *Bifidobacterium infantis* | CGMP | Lac | nd | 44[g] | 1[g] | | 44 |
| *Clostridium perfringens* | Sia-α(2,8)-Sia | Lac | α(2,6′) | 18 | 7[h] | complete | 35 |
| | Sia-α(2,8)-Sia | LacNAc | α(2,6′) | 16[f] | nq | complete | 35 |
| | colominic acid | Lac | α(2,6′) | | 2[h] | complete | 35 |
| | Sia-α-*p*NP | Lac | α(2,6′), α(2,3′) | 5[f] | nq | medium (70%) | 35 |
| | Sia-α-*p*NP | Tn-antigen | α(2,6) | 7 | 10 | complete | 39 |
| | Sia-α-*p*NP | T-antigen | α(2,6′) | 7 | 4 | complete | 39 |
| | Sia-α-*p*NP | T-antigen precursor | α(2,6′) | 7 | 7 | complete | 39 |
| | Sia-α-*p*NP | 2-deoxy-Gal-β-O-Me | α(2,6) | 7 | 14 | complete | 39 |
| | Sia-α-*p*NP | 2-deoxy-Gal-α-O-Me | α(2,6) | 7 | 15 | complete | 39 |
| | Sia-α-*p*NP | Gal-β(1,4)-2-deoxy-Gal-α-O-Me | α(2,6′) | 7 | 5 | complete | 39 |
| | Sia-α-*p*NP | Gal-α-O-Me | α(2,6) | 7 | 10 | complete | 39 |
| | Sia-α-*p*NP | Gal-β-O-Me | α(2,6) | 7 | 10 | complete | 39 |
| Newcastle disease virus | Sia-α(2,8)-Sia | Lac | α(2,3′) | 18[f] | 5[h] | complete | 35 |
| | Sia-α(2,8)-Sia | LacNAc | α(2,3′) | 16[f] | nq | complete | 35 |
| | colominic acid | Lac | α(2,3′), α(2,6′) | | nq | medium (75%) | 35 |
| | Sia-α-*p*NP | Lac | α(2,3′), α(2,6′) | 5[f] | nq[f] | medium (76%) | 35 |
| | Sia-α-*p*NP | LacNAc | α(2,3′) | 4 | 10[f,h] | complete | 35 |
| | Sia-α-*p*NP | Tn-antigen | α(2,3) | 5 | 10 | complete | 39 |
| | Sia-α-*p*NP | T-antigen | α(2,3′) | 5 | 10 | complete | 39 |
| | Sia-α-*p*NP | T-antigen precursor | α(2,3′) | 5 | 11 | complete | 39 |
| | Sia-α-*p*NP | 2-deoxy-Gal-β-O-Me | α(2,3) | 5 | 14 | complete | 39 |
| | Sia-α-*p*NP | 2-deoxy-Gal-α-O-Me | α(2,3) | 5 | 14 | complete | 39 |
| | Sia-α-*p*NP | Gal-β(1,4)-2-deoxy-Gal-α-O-Me | α(2,3′) | 5 | 8 | complete | 39 |
| | Sia-α-*p*NP | Gal-α-O-Me | α(2,3) | 5 | 17 | complete | 39 |
| | Sia-α-*p*NP | Gal-β-O-Me | α(2,3) | 5 | 18 | complete | 39 |
| *Salmonella typhimurium* | Sia-α-*p*NP | Tn-antigen | α(2,3), α(2,6) | 5 | 15 | high (95%) | 39 |
| | Sia-α-*p*NP | T-antigen | α(2,3′), α(2,6′) | 5 | 11 | high (93%) | 39 |
| | Sia-α-*p*NP | T-antigen precursor | α(2,3′), α(2,6′) | 5 | 11 | medium (88%) | 39 |
| | Sia-α-*p*NP | 2-deoxy-Gal-β-O-Me | α(2,3) | 5 | 20 | complete | 39 |
| | Sia-α-*p*NP | 2-deoxy-Gal-α-O-Me | α(2,3), α(2,6) | 5 | 22 | high (92%) | 39 |
| | Sia-α-*p*NP | Gal-β(1,4)-2-deoxy-Gal-α-O-Me | α(2,3′), α(2,6′) | 5 | 10 | medium (86%) | 39 |
| | Sia-α-*p*NP | Gal-α-O-Me | α(2,3), α(2,6) | 5 | 16 | high (95%) | 39 |
| | Sia-α-*p*NP | Gal-β-O-Me | α(2,3) | 5 | 15 | complete | 39 |
| | Sia-α-*p*NP | Lewis$^X$ | α(2,3) | 13 | 9 | complete | 116 |
| | Sia-α-*p*NP | Lewis$^A$ | α(2,3) | 13 | 12 | complete | 116 |
| *Trypanosoma rangeli* mutant Tr6 | CGMP | Lac | α(2,3′) | 25 | 28 | complete | 40 |
| | CGMP | Lac | α(2,3′) | 25 | 37[i] | complete | 40 |
| | CGMP | Lac | α(2,3′) | 25 | 32[j] | complete | 41 |
| | CGMP | LNT | nd[k] | 25 | nq | | 4 |
| | CGMP | LNnT | nd[k] | 5 | nq | | 4 |
| | CGMP | LNFP V | nd[k] | 5 | nq | | 4 |
| | CGMP | LNFP I | nd[k] | 5 | nq | | 4 |
| immobilized Tr6 | CGMP | Lac | α(2,3′) | 25 | 40 | complete | 40 |
| *Trypanosoma rangeli* mutant Tr13 | CGMP | Lac | α(2,3′) | 44 | ≥31 | complete | 2 |
| | CGMP | lactulose | nd[k] | 44 | 23 | | 2 |
| | CGMP | melibiose | nd[k] | 44 | 12 | | 2 |


dx.doi.org/10.1021/jf502619p | J. Agric. Food Chem. 2014, 62, 9615−9631

**Table 1. continued**

| sialidase | donor | acceptor | linkages formed in trans-sialylation[b] | A:D[c] | yield[d] (%) | regioselectivity[e] | ref |
|---|---|---|---|---|---|---|---|
| | CGMP | maltose | nd[k] | 44 | 13 | | 2 |
| | CGMP | Fuc | nd[k] | 44 | 18 | | 2 |
| | CGMP | GOS | nd[k] | 44 | nq | | 2 |
| | CGMP | IMO | nd[k,l] | 44 | nq | | 2 |
| *Vibrio cholerae* | Sia-α(2,8)-Sia | Lac | α(2,6′) | 18[f] | nq | complete | 35 |
| | Sia-α-*p*NP | Lac | α(2,6′), α(2,3′) | 5[f] | nq[f] | high (90%) | 35 |
| | Sia-α-*p*NP | Gal-β-O-Me | α(2,6), α(2,3) | 4 | 1.8 | medium (62%) | 37 |
| | Sia-α-*p*NP | Gal-β-O-Me | α(2,6), α(2,3) | 7 | 9.5 | medium (85%) | 37 |
| | Sia-α-*p*NP | Gal-β-O-Me | α(2,6), α(2,3) | 15 | 5.4 | high (90%) | 37 |
| | Sia-α-*p*NP | Tn-antigen | α(2,6) | 7 | 16 | complete | 39 |
| | Sia-α-*p*NP | T-antigen | α(2,6′) | 7 | 12 | complete | 39 |
| | Sia-α-*p*NP | T-antigen precursor | α(2,6′) | 7 | 12 | complete | 39 |
| | Sia-α-*p*NP | 2-deoxy-Gal-β-O-Me | α(2,6) | 7 | 21 | complete | 39 |
| | Sia-α-*p*NP | 2-deoxy-Gal-α-O-Me | α(2,6) | 7 | 26 | complete | 39 |
| | Sia-α-*p*NP | Gal-β(1,4)-2-deoxy-Gal-α-O-Me | α(2,6′), α(2,3′) | 7 | 15 | high (90%) | 39 |
| | Sia-α-*p*NP | Gal-α-O-Me | α(2,6) | 7 | 18 | complete | 39 |
| | Sia-α-*p*NP | Gal-β-O-Me | α(2,6) | 7 | 16 | complete | 39 |
| immobilized *Vibrio cholerae* | Sia-α-*p*NP | Gal-β-O-Me | α(2,6), α(2,3) | 7 | 20 | medium (74%) | 37 |
| | Sia-α-*p*NP | Gal-β-O-Me | α(2,6), α(2,3) | 7 | 20[m] | medium (67%) | 37 |
| | Sia-α-*p*NP | Gal-α-O-Me | α(2,6), α(2,3) | 7 | 24 | medium (86%) | 37 |
| | Sia-α-*p*NP | Glc-β-O-Me | α(2,6), α(2,3) | 7 | 16 | medium (76%) | 37 |
| | Sia-α-*p*NP | Lac-β-O-Me | α(2,6′), α(2,3′) | 7 | 16 | medium (67%) | 37 |
| | Sia-α-*p*NP | LacNAc-β-O-Me | α(2,6′), α(2,3′) | 7 | 14 | medium (74%) | 37 |

[a]All of the microbial sialidases belong to GH 33, whereas the sialidase of viral origin (Newcastle disease virus) belongs to GH 83. Abbreviations: Sia, sialic acid (*N*-acetylneuraminic acid); Lac, β-D-lactose; nq, not quantified; Sia-α-*p*NP, *p*-nitrophenyl α-sialic acid (2-*O*-(*p*-nitrophenyl)-α-D-*N*-acetylneuraminic acid); CGMP, casein glycomacropeptide; nd, not determined; LacNAc, *N*-acetyl-D-lactosamine; LNT, lacto-*N*-tetraose; LNnT, lacto-*N*-neotetraose; LNFP V, lacto-*N*-fucopentaose V; LNFP I, lacto-*N*-fucopentaose I; Fuc, L-fucose; GOS, galacto-oligosaccharides; DP, degree of polymerization; IMO, isomalto-oligosaccharides; Gal-β-O-Me, methyl β-D-galactopyranoside; Gal-α-O-Me, methyl α-D-galactopyranoside; Glc-β-O-Me, methyl β-D-glucopyranoside; Lac-β-O-Me, methyl β-D-lactoside; LacNAc-β-O-Me, methyl β-D-*N*-acetyl-D-lactosaminide. [b]The linkage between the transferred sialyl group and the acceptor listed according to prevalence; only single sialylations have been observed. [c]The molar acceptor/donor ratio has been rounded to the nearest integer (for CGMP the A:D is based on the molar sialic acid content in the donor substrate). [d]Total molar trans-sialylation yield on donor (for CGMP the yield is based on the molar sialic acid content in the donor substrate). [e]Complete, no other linkage detected; high, ≥90% of the desired linkage; medium, ≥50% of the desired linkage; low, <50% of the desired linkage; the percentage of the most prevalent linkage (top of 'linkages formed in trans-sialylation' column) is given. [f]Thirty percent acetonitrile added. [g]Sialic acid content in CGMP is given as 4−7%, so an exact number cannot be given. [h]Mass yields estimated from the mass isolation yields and the information that approximately 65% of 3′-sialyl-lactose stayed on the column used for purification. [i]In membrane reactor. [j]Twenty-five percent *tert*-butanol added. [k]The sialyl linkage has not been determined, but this enzyme has been observed to form only α(2,3)-linkages and only single peaks were observed on LC-MS. [l]Note that glucose present in the IMO preparation is also sialylated. [m]Thirty percent DMSO added.

α-L-Fucosidases (EC 3.2.1.51) catalyze the release of terminal fucose residues α-linked to glycans, resulting in hydrolysis or trans-fucosylation (Figure 1B). Fucosidases, which are specific for a given α-linkage, may be classified as α-1,2-fucosidases (EC 3.2.1.63), α-1,3-fucosidases (EC 3.2.1.111), or α-1,6-fucosidases (EC 3.2.1.127). By far, the most trans-fucosylations have used *p*NP-α-L-fucopyranoside (Fuc-α-*p*NP) as fucosyl donor[5,13,29,49−51] (Table 3). In two cases, methyl α-L-fucopyranoside[52] and α-fucosyl fluoride[53] have also been used as donor substrates (Table 3). For large-scale trans-fucosylation there is a need for cheaper substrates.

β-Galactosidases (EC 3.2.1.23) catalyze the release of terminal β-galactosyl residues, resulting in hydrolysis or trans-galactosylation (Figure 1C). However, some β-galactosidases used for trans-galactosylation can also act as β-glucosidases (EC 3.2.1.21) catalyzing trans-glucosylation.[30] Lactose is widely used as a β-galactosyl donor in trans-galactosylation, not least because it is a cheap substrate. Lactose is especially used for production of GOS, where it also functions as acceptor. However, for synthesis of LacNAc or lacto-*N*-biose, *p*NP-β-galactopyranoside (Gal-β-*p*NP) and *o*-nitrophenyl-β-galactopyranoside (Gal-β-*o*NP) are also encountered as a donor substrates,[6,15,35,54,55] even though successful synthesis of these compounds can also be achieved when using lactose as donor, albeit with lower yields (Table 4).[19,36,56,57]

**Acceptor Specificity.** In general, β-galactosidases, sialidases, and α-L-fucosidases show broad acceptor specificity. β-Galactosidases can catalyze trans-galactosylation of various mono-, di-, and oligosaccharides (on terminal moieties as well as nonterminal ones) of both anomeric configurations, *N*-substituted saccharides (*N*-acetyl-D-glucosamine (GlcNAc) and GalNAc), and methyl and aryl glycosides, as well as primary and secondary alcohols and phenols,[31,36,54,58,59] thus emphasizing their widespread potential (Table 4).

The much studied trans-sialidase from *T. cruzi* is known to be specific for terminal β-galactosyl acceptors,[38,48] but can also catalyze sialylation of nonterminal moieties in GOS[42] and galactose dimers[60] (Table 2). Indeed, mainly β-galactosyl acceptors have been used for sialidases,[4,35,38,40,42,44,61] but some sialidases also catalyze sialyl transfer to α-galactosyl residues, α-glucosyl residues, monomers of glucose and fucose, and methyl

**Table 2. Donor, Acceptor, and Acceptor/Donor (A:D) Ratio of Trans-sialylations Catalyzed by the Well-Studied Trans-sialidase from *Trypanosoma cruzi* (GH 33) as well as the Products and Trans-sialylation Yield Obtained[a]**

| donor | acceptor | products | A:D[b] | yield[c] (%) | ref |
|---|---|---|---|---|---|
| CGMP | Lac | Sia-α(2,3′)-Lac | 5 | 32 | 42 |
| CGMP | LNT | Sia-α-LNT[d] | 5 | nq | 42 |
| CGMP | GOS | Sia-α-GOS (DP2-DP5)[d] | 5 | nq | 42 |
| | | bis(Sia)-α-GOS[d] | | | |
| fetuin | Lac | Sia-α(2,3′)-Lac | 3 | 76 | 61 |
| fetuin | LacNAc | Sia-α-LacNAc[d] | 1 | 47 | 61 |
| fetuin | lacto-*N*-biose | Sia-α-lacto-*N*-biose[d] | 1 | 45 | 61 |
| Sia-α(2,3′)-Lac | Lac-BSA | Sia-α-Lac-BSA[d] | 0.05 | 95 | 38 |
| Sia-α(2,3′)-Lac | LNT | Sia-α-LNT[d] | 0.5 | 66 | 38 |
| Sia-α(2,3′)-Lac | LacNAc | Sia-α(2,3′)-LacNAc | 1 | 23 | 14 |
| Sia-α(2,3′)-Lac | LacNAc | Sia-α-LacNAc[d] | 1 | 47 | 61 |
| Sia-α(2,3′)-Lac | lacto-*N*-biose | Sia-α-lacto-*N*-biose[d] | 1 | 45 | 61 |
| Sia-α(2,3′)-Lac | LNnT[e] | Sia-α-LNnT[d] | 1 | nq | 38 |
| Sia-α(2,3′)-Lac | allo-LacNAc | Sia-α-allo-LacNAc[d] | 1 | nq | 38 |
| Sia-α(2,3′)-Lac | LNFP V | Sia-α-LNFP V[d] | 1 | nq | 38 |
| Sia-α(2,3′)-Lac | GOS (DP3) | Sia-α-GOS (DP3)[d] | 1 | nq | 38 |
| Sia-α(2,3′)-Lac | Gal-β(1,4)-Man | Sia-α-Gal-β(1,4)-Man[d] | 1 | nq | 38 |
| Sia-α(2,3′)-Lac | Gal-β(1,3)-GalNAc | Sia-α-Gal-β(1,3)-GalNAc[d] | 1 | nq | 38 |
| Sia-α(2,3′)-Lac | Gal-β(1,6)-Gal | Sia-α-Gal-β(1,6)-Gal[d] | 1 | nq | 38 |
| Sia-α-MU | LacNAc | Sia-α(2,3′)-LacNAc | 1 | 60 | 14 |
| Sia-α-MU | LacNAc | Sia-α-LacNAc[d] | 1 | 67 | 61 |
| Sia-α-MU | lacto-*N*-biose | Sia-α(2,3′)-lacto-*N*-biose | 1 | 35 | 15 |
| Sia-α-*p*NP | Lac | Sia-α(2,3′)-Lac | 6[f] | 87 | 60 |
| Sia-α-*p*NP | LacNAc | Sia-α(2,3′)-LacNAc | 6 | 85 | 60 |
| Sia-α-*p*NP | Gal-α-O-Me | Sia-α(2,3)-Gal-α-O-Me | 11[f] | 54 | 60 |
| Sia-α-*p*NP | Gal-β-O-Me | Sia-α(2,3)-Gal-β-O-Me | 11[f] | 81 | 60 |
| Sia-α-*p*NP | Gal-α(1,6)-Gal-β-O-Me | Sia-α(2,3)-Gal-β(1,6)-Gal-β-O-Me | 6[f] | 89 | 60 |
| Sia-α-*p*NP | Gal-β(1,6)-Gal-β-O-Me | Sia-α(2,3)-Gal-β(1,6)-Gal-β-O-Me (44%) | 6[f] | 93 | 60 |
| | | Gal-β(1,6)-(Sia-α(2,3))-Gal-β-O-Me (44%) | | | |
| | | Sia-α(2,3)-Gal-β(1,6)-(Sia-α(2,3))-Gal-β-O-Me (5%) | | | |

[a]Trans-sialidase from *T. cruzi* specifically catalyzes the formation of α(2,3)-linkages, but not only at the reducing end.[42,60] The current table serves to emphasize the wide variety of donor and acceptors used. Abbreviations: CGMP, casein glycomacropeptide; Lac, β-D-lactose; Sia, sialic acid (*N*-acetylneuraminic acid); LNT, lacto-*N*-tetraose; GOS, galacto-oligosaccharides; DP, degree of polymerization; LacNAc, *N*-acetyl-D-lactosamine; Lac-BSA, β-D-lactose linked to bovine serum albumin; LNnT, lacto-*N*-neotetraose; allo-LacNAc, Gal-β(1,6)-GlcNAc; LNFP V, lacto-*N*-fucopentaose V; Gal, D-galactose; Man, D-mannose; GalNAc, *N*-acetyl-D-galactosamine; Sia-α-MU, 2′-(4-methylumbelliferyl)-α-D-*N*-acetylneuraminic acid; Sia-α-*p*NP, *p*-nitrophenyl α-sialic acid (2-*O*-(*p*-nitrophenyl)-α-D-*N*-acetylneuraminic acid); Gal-α-O-Me, methyl α-D-galactopyranoside; Gal-β-O-Me, methyl β-D-galactopyranoside; Gal-α(1,6)-Gal-β-O-Me, methyl β-D-galactopyranosyl α(1,6)-D-galactopyranoside; Gal-β(1,6)-Gal-β-O-Me, methyl β-D-galactopyranosyl β(1,6)-D-galactopyranoside. [b]The molar acceptor/donor ratio has been rounded to the nearest integer except when <1 (for CGMP and fetuin the A:D is based on the molar sialic acid content in the donor substrate). [c]Total molar trans-sialylation yield on donor (for CGMP and fetuin the yield is based on the molar sialic acid content in the donor substrate). [d]The sialyl linkage has not been determined, but this enzyme has been observed to form only α(2,3)-linkages. [e]Other acceptors were also tested at these conditions, but no product was observed. [f]An assumption based on the sparse description of the experimental procedure.

galactopyranoses of both anomeric configurations (Table 1).[2,37,39] Some studies have indicated that acceptor size affects the yield, with smaller acceptors being favored.[4,39]

It has been suggested that the presence of aromatic amino acid residues in the +2 acceptor binding site of the α-L-fucosidase from *Thermotoga maritima* (EC 3.2.1.51; GH 29) induces a preference for monosaccharide acceptors or, in particular, *p*NP-monosaccharide acceptors.[51] Indeed, (*N*-substituted) monosaccharides or their methyl, *p*NP, or allyl derivatives are most commonly used as acceptors in trans-fucosylation (Table 3).[5,29,49,50,53,62,63] An example of the use of lactose and LacNAc by α-L-fucosidase from *Alcaligenes* sp. does exist, but even here the presence of a methyl group at the reducing end increased the trans-fucosylation yields (Table 3).[13]

In several cases, the formed products may also function as acceptors for further trans-glycosylation (Tables 2, 3, and 4).[29,42,55,60,64−66] There is a tendency that the most prevalently formed product is also the one used as acceptor in the further trans-glycosylation.[29,65,66]

**Regioselectivity.** Although glycosidase-catalyzed synthesis is more regioselective than chemical synthesis, the regioselectivity varies from enzyme to enzyme, and not all enzymes are equally selective. Whereas some β-galactosidases show complete regioselectivity for *O*-3,[15,54,67] *O*-4,[35] or *O*-6,[19,59,64] others are more promiscuous in the trans-galactosylation (Table 4).[6,55,64] In fact, β-galactosidases from the same organism have shown different regioselectivities: The *B. circulans* ATCC 31382 strain is the source of the much-used commercial β-galactosidase preparation Biolacta, which contains one or more GH 42 β-galactosidases, which mainly catalyze the formation of β(1,4)-linkages and to a lesser extent β(1,6)-linkages.[36,57,65,68,69] In contrast, the GH 35 β-galactosidase purified from the same *B. circulans* strain appears to be primarily specific for β(1,3)-linkages in trans-galactosylation as well as in hydrolysis.[54,68]

**Table 3. Donor, Acceptor, and Acceptor/Donor (A:D) Ratio of α-L-Fucosidase-Catalyzed Reactions as well as the Products, Total Trans-fucosylation Yield, and Regioselectivity Obtained[a]**

| α-L-fucosidase | donor | acceptor | products[b] | A:D[c] | yield[d] (%) | regio-selectivity[e] | cosolvent | ref |
|---|---|---|---|---|---|---|---|---|
| *Alcaligenes* sp. | Fuc-α-*p*NP | LacNAc | Fuc-α(1,3′)-LacNAc | 25 | 54 | complete | | 13 |
| | Fuc-α-*p*NP | Lac | Fuc-α(1,3′)-Lac | 19 | 34 | complete | | 13 |
| | Fuc-α-*p*NP | LacNAc-β-O-Me | Fuc-α(1,3′)-LacNAc-β-O-Me | 25 | 67 | complete | | 13 |
| | Fuc-α-*p*NP | Lac-β-O-Me | Fuc-α(1,3′)-Lac-β-O-Me | 19 | 42 | complete | | 13 |
| | Fuc-α-*p*NP | Gal-β(1,3)-Glc-β-O-Me | Fuc-α(1,3′)-Gal-β(1,3)-Glc-β-O-Me | 19 | 67 | complete | | 13 |
| | Fuc-α-*p*NP | LacNAc-β-*p*NP | Fuc-α(1,2′)-LacNAc-β-*p*NP<br>Fuc-α(1,3′)-LacNAc-β-*p*NP | 2 | 38 | high (97%) | | 49 |
| | Fuc-α-*p*NP | Lac-β-*p*NP | Fuc-α(1,2′)-Lac-β-*p*NP<br>Fuc-α(1,3′)-Lac-β-*p*NP<br>Fuc-α(1,6′)-Lac-β-*p*NP | 3 | 38 | medium (89%) | | 49 |
| | Fuc-α-*p*NP | Glc-β-*p*NP | Fuc-α(1,3)-Glc-β-*p*NP<br>Fuc-α(1,4)-Glc-β-*p*NP | | 53 | medium (85%) | | 49 |
| | Fuc-α-*p*NP | GlcNAc-β-*p*NP | Fuc-α(1,3)-GlcNAc-β-*p*NP<br>Fuc-α(1,4)-GlcNac-β-*p*NP | | 13 | high (92%) | | 49 |
| Ampullaria | Fuc-α-*p*NP | Gal-β-O-Me | Fuc-α(1,6)-Gal-β-O-Me | 10 | 14 | complete | 25% DMSO | 62 |
| *Aspergillus niger* | Fuc-α-*p*NP | GlcNAc | Fuc-α(1,3)-GlcNAc | 5 | 24 | complete | | 63 |
| | Fuc-α-*p*NP | GlcNAc | Fuc-α(1,3)-GlcNAc | 6 | 58 | complete | 8.5% DMF | 62 |
| | Fuc-α-*p*NP | Glc | Fuc-α(1,3)-Glc | 8 | 61 | complete | 8.5% DMF | 62 |
| canine, recombinant[f] | Fuc-α-*p*NP | Fuc-α-O-Me | Fuc-α(1,3)-Fuc-O-Me<br>Fuc-α(1,2)-Fuc-O-Me | 3 | 13 | medium (55%) | no effect | 29 |
| | Fuc-α-*p*NP | Gal-β-O-Me | Fuc-α(1,6)-Gal-O-Me<br>Fuc-α(1,3)-Gal-O-Me<br>Fuc-α(1,3)-Gal-O-Me<br>trisaccharides<br>tetrasaccharides | 3 | 17 | low (45%) | no effect | 29 |
| | Fuc-α-*p*NP | Glc-β-O-Me | Fuc-α(1,2)-Glc-O-Me<br>Fuc-α(1,3)-Glc-O-Me<br>Fuc-α(1,6)-Glc-O-Me<br>trisaccharides | 3 | 3 | low (45%) | no effect | 29 |
| *Coryne-bacterium* sp. | Fuc-α-*p*NP | Gal-β-O-Me | Fuc-α(1,2)-Gal-β-O-Me | 10 | 25 | complete | 25% DMSO | 62 |
| | Fuc-α-*p*NP | Gal | Fuc-α(1,2)-Gal | 10 | 18 | complete | 24% DMSO | 62 |
| *Lactobacillus casei* AlfB | Fuc-α-*p*NP | GlcNAc | Fuc-α(1,3)-GlcNAc | 4 | 23 | complete | | 5 |
| *Lactobacillus casei* AlfC | Fuc-α-*p*NP | GlcNAc | Fuc-α(1,6)-GlcNAc | 4 | 56 | complete | | 5 |
| *Penicillium multicolor* | Fuc-α-*p*NP | Glc | Fuc-α(1,3)-Glc | 6 | 28 | complete | 10% DMF | 50 |
| | Fuc-α-*p*NP | GlcNAc | Fuc-α(1,3)-GlcNAc | 8 | 49 | complete | 20% DMSO | 50 |
| | Fuc-α-*p*NP | GlcNAc-α-O-Me | Fuc-α(1,3)-GlcNAc-α-O-Me | 5 | 29 | complete | | 53 |
| | Fuc-α-*p*NP | GlcNAc-α-O-All | Fuc-α(1,3)-GlcNAc-α-O-All | 5 | 34 | complete | | 53 |
| | Fuc-α-*p*NP | GlcNAc-β-O-All | Fuc-α(1,3)-GlcNAc-β-O-All | 5 | 25 | complete | | 53 |
| | Fuc-α-F | GlcNAc-α-O-Me | Fuc-α(1,3)-GlcNAc-α-O-Me | 5 | 13 | complete | | 53 |
| | Fuc-α-F | GlcNAc-α-O-All[g] | Fuc-α(1,3)-GlcNAc-α-O-All | 5 | 8 | complete | | 53 |
| | Fuc-α-F | GlcNAc | Fuc-α(1,3)-GlcNAc | 5 | 7 | complete | | 53 |
| | Fuc-α-F | Glc | Fuc-α(1,3)-Glc | 5 | 34 | complete | | 53 |
| porcine liver | Fuc-α-*p*NP | LacNAc | Fuc-α(1,2′)-LacNAc<br>Fuc-α(1,3′)-LacNAc<br>Fuc-α(1,6′)-LacNAc | 13 | 13 | low (40%) | 5.5% MeOH | 13 |
| *Thermotoga maritima* | Fuc-α-*p*NP | Fuc-α-*p*NP | Fuc-α(1,3)-Fuc-α-*p*NP<br>unidentified disaccharide<br>trisaccharide | | 27 | medium (63%) | | 51 |
| | Fuc-α-*p*NP | Gal-β-*p*NP | Fuc-α(1,2)-Gal-β-*p*NP<br>Fuc-α(1,6)-Gal-β-*p*NP<br>Fuc-α(1,3)-Fuc-α-*p*NP | 5 | 31 | medium (74%) | | 51 |


dx.doi.org/10.1021/jf502619p | J. Agric. Food Chem. 2014, 62, 9615−9631

**Table 3. continued**

| α-L-fucosidase | donor | acceptor | products[b] | A:D[c] | yield[d] (%) | regio-selectivity[e] | cosolvent | ref |
|---|---|---|---|---|---|---|---|---|
| | Fuc-α-*p*NP | Gal-β-*p*NP | Fuc-α(1,2)-Gal-β-*p*NP<br>Fuc-α(1,3)-Fuc-α-*p*NP<br>Fuc-α(1,6)-Gal-β-*p*NP | 2 | 29 | low (48%) | | 51 |
| | Fuc-α-*p*NP | Gal-β(1,3)-Glc-β-O-Ph | Fuc-α(1,3)-Fuc-α-*p*NP<br>Fuc-α(1,2)-Gal-β(1,3)-Glc-β-O-Ph<br>unidentified trisaccharide | 2 | 31 | medium (61%) | | 51 |
| | Fuc-α-*p*NP | Gal-β-*p*NP | Fuc-α(1,3)-Fuc-α-*p*NP<br>Fuc-α(1,2)-Gal-β-*p*NP<br>Fuc-α(1,6)-Gal-β-*p*NP | 1 | ≥17 | medium (≤60%) | | 51 |
| *Thermotoga maritima* mutant P25[h] | Fuc-α-*p*NP | Gal-β-*p*NP | Fuc-α(1,2)-Gal-β-*p*NP<br>Fuc-α(1,3)-Fuc-α-*p*NP | 1 | 67 | high (92%) | | 51 |
| *Thermus* sp. Y5 | Fuc-α-O-Me | GlcNAc | Fuc-α-GlcNAc (linkage nd) | 5 | 20 | | | 52 |
| | Fuc-α-O-Me | GalNAc | Fuc-α-GlcNAc (linkage nd) | 5 | 20 | | | 52 |
| | Fuc-α-*p*NP | MeOH | Fuc-α-O-Me | 371 | 40 | | | 52 |
| | Fuc-α-*p*NP | EtOH | ethyl α-L-fucoside | 257 | 35 | | | 52 |

[a]The use of co-solvent is indicated where relevant. The α-L-fucosidases used (all GH 29) are mainly of microbial origin, but a few of mammal or mollusk origin have also been used. Abbreviations: *p*NP-α-Fuc, *p*-nitrophenyl α-L-fucopyranosidse; LacNAc, *N*-acetyl-D-lactosamine; Lac, β-D-lactose; LacNAc-β-O-Me, methyl β-D-*N*-acetyl-D-lactosaminide; Lac-β-O-Me, methyl β-D-lactoside; Gal-β(1,3)-Glc-β-O-Me, methyl β-D-galactopyranosyl β(1,3)-D-glucopyranoside; *p*NP-β-LacNAc, *p*-nitrophenyl β-D-*N*-acetyl-D-lactosaminide; *p*NP-β-Lac, *p*-nitrophenyl β-D-lactoside; *p*NP-β-Glc, *p*-nitrophenyl β-D-glucoside; *p*NP-β-GlcNAc, *p*-nitrophenyl β-D-*N*-acetyl-D-glucosaminide; Gal-β-O-Me, methyl β-D-galactopyranoside; DMSO, dimethyl sulfoxide; GlcNAc, *N*-acetyl-D-glucosamine; DMF, dimethylformamide; Glc, D-glucose; Fuc-α-O-Me, methyl α-L-fucopyranoside; Glc-β-O-Me, methyl β-D-glucopyranoside; Gal, D-galactose; GlcNAc-α-O-Me, methyl α-D-*N*-acetyl-D-glucosaminide; GlcNAc-α-O-All, allyl α-D-*N*-acetyl-D-glucosaminide; GlcNAc-β-O-All, allyl β-D-*N*-acetyl-D-glucosaminide; Fuc-α-F, α-L-fucosyl fluoride; MeOH, methanol; *p*NP-β-Gal, *p*-nitrophenyl β-D-galactopyranoside; Gal-β(1,3)-Glc-β-O-Ph, phenyl β-D-galactopyranosyl β(1,3)-D-glucopyranoside; GalNAc, *N*-acetyl-D-galactosamine; nd, not determined; EtOH, ethanol. [b]Listed according to prevalence. [c]The molar acceptor/donor ratio has been rounded to the nearest integer. [d]Total molar trans-fucosylation yield on donor, including donor self-condensation. [e]Complete, no other linkage detected, high, ≥90% of the desired linkage; medium, ≥50% of the desired linkage; low, <50% of the desired linkage; the percentage of the most prevalent linkage (top of "products" column) is given. [f]Similar results were obtained with α-L-fucosidase from *Pecten maximus*, and more acceptors were included for both enzymes, but these are not included here because the yields were not quantified. [g]GlcNAc-β-O-All was also tested as acceptor, but the yield was 0%. [h]Many other mutants gave similar results, but this one has the best combination of high activity, high trans-fucosylation/hydrolysis ratio, and high yield of the desired product.

Most sialidases are specific for either *O*-3[2,4,39,48] or *O*-6[35,39] on the glycosyl acceptor, whereas a few have been reported to show fairly poor regioselectivity (Table 1).[35,37,39] Interestingly, α-L-fucosidases may be specific for *O*-2,[51,62] *O*-3,[5,53,63] or *O*-6,[5,62] but several α-L-fucosidases have shown poor regioselectivity in the trans-fucosylation (Table 3).[29,51,70] Poor regioselectivity may complicate product purification. An alternative method to avoid the presence of isomers in the reaction mixture is to use a promiscuous trans-glycosidase in combination with a glycosidase with specific hydrolytic activity to remove the undesired isomer(s).[57]

The regioselectivity is also dependent on the acceptor structure, that is, substitutions and anomeric configuration, and its interplay with the conformation of the active site. For instance, the anomeric configuration and the presence and/or position of an *N*-acetyl group has been shown to influence regioselectivity of both β-galactosidases and sialidases (Table 1).[35,37,39,59,71] The orientation of the secondary hydroxyl groups is similarly determining for regioselectivity of both β-galactosidases and α-L-fucosidases (Table 3).[29,51,71]

In a few cases, the donor substrate has also been found to influence regioselectivity.[35,36] For sialidases, the effect of each donor substrate on regioselectivity did, however, vary between enzymes (Table 1).[35]

The regioselectivity of β-galactosidases, which are the most studied of the enzyme classes covered by this review, may also be influenced by the acceptor/donor ratio and by the presence of cosolvents, as well as by temperature and pH (see below).

**Donor Self-Condensation.** Another selectivity issue, which may compromise the yield of the desired trans-glycosylation product, is the fact that β-galactosidases can also catalyze donor self-condensation because the galactosyl donor substrate also functions as acceptor (Figure 1C).[6,65,67] This is indeed the goal in GOS production, but not in the selective biocatalytic formation of, for example, LacNAc. Among the relatively few trans-fucosylations reported, only α-L-fucosidase from *T. maritima* has been reported to catalyze donor self-condensation.[51] However, the α-L-fucosidase from *Pecten maximus* and a recombinant canine α-L-fucosidase could easily utilize methyl α-L-fucose as acceptor substrate.[29] Donor self-condensation has not been observed for sialidases, most likely because the sialyl moiety is too unlike the "natural" acceptor substrates (see below), where the ring structure is much less heavily substituted (Figure 1A).

## ■ WATER ACTIVITY ($a_w$)

It follows from eq 1 that a decrease in $a_w$ will favor the desired trans-sialylation over hydrolysis. However, glycosidases require fairly high $a_w$ (≥0.9) for displaying activity compared to, for example, lipases.[72] In a study of β-galactosidase from *B. circulans* (GH 42), trans-galactosylation of GlcNAc in aqueous media with organic cosolvents was maximized at $a_w$ values between 0.92 and 0.99 with a mean of approximately 0.96.[55] The underlying mechanism proposed in several studies is that at low $a_w$ the glycosidase becomes less flexible, thus favoring the smaller water molecule as acceptor even if its activity is low.[30,55,73]

**Table 4. Donor and Acceptor/Donor (A:D) Ratio of Trans-galactosylation Reactions Catalyzed by β-Galactosidases as well as the Products, Total Trans-galactosylation Yield, and Regioselectivity Obtained When Using *N*-Acetyl-D-glucosamine (GlcNAc) as Acceptor[a]**

| β-galactosidase | donor | products[b] | A:D[c] | yield[d] (%) | regio-selectivity[e] | cosolvent/immobilization | ref |
|---|---|---|---|---|---|---|---|
| *Aspergillus oryzae* (GH 35) | Lac | unidentified OS<br>allo-LacNAc<br>LacNAc<br>lacto-*N*-biose | 1 | 36 | medium (84%)[f] | | 64 |
| *Bacillus circulans* (GH 35) | Gal-β-*p*NP | lacto-*N*-biose | 5 | 51 | complete | | 54 |
| | Gal-β-*p*NP | lacto-*N*-biose | 5 | 97 | complete[g] | 30% $[BMIm][PF_6]$[g] | 54 |
| | Gal-β-*p*NP | lacto-*N*-biose | 5 | 99 | complete | 22% *N*,*N*-dimethyl lactamide[h] | 75 |
| *Bacillus circulans* (GH 42) | Gal-β-*o*NP | LacNAc<br>allo-LacNAc<br>Gal-β-1,4-LacNAc<br>Gal-β-1,4-Gal-β-1,4-LacNAc<br>lacto-*N*-biose<br>Gal-β-1,6-LacNAc | 10[i] | 44 | medium (87%) | | 55 |
| | Gal-β-*o*NP | LacNAc<br>Gal-β-1,4-LacNAc<br>allo-LacNAc<br>Gal-β-1,4-Gal-β-1,4-LacNAc<br>lacto-*N*-biose<br>Gal-β-1,6-LacNAc | 20 | 81 | high (90%) | | 55 |
| | Gal-β-*o*NP | LacNAc<br>Gal-β-1,4-LacNAc<br>Gal-β-1,4-Gal-β-1,4-LacNAc<br>allo-LacNAc<br>Gal-β-1,6-LacNAc<br>lacto-*N*-biose | 1 | 47 | high (92%) | 10% 2-methyl-2-butanol[j] | 55 |
| | Gal-β-*o*NP | LacNAc[k] | 0.33[l] | 35[k] | nd | | 78 |
| | Gal-β-*o*NP | LacNAc[k] | 0.33 | 50[k] | nd | 20% cyclohexane[m] | 78 |
| | Gal-β-*p*NP | LacNAc<br>allo-LacNAc | 8 | 33 | high (91%) | | 69 |
| | Gal-β-*p*NP | LacNAc | 8 | 36 | complete | immobilized enzyme | 69 |
| | Lac | LacNAc<br>allo-LacNAc | 2 | 25 | high (90%) | | 57 |
| | Lac | LacNAc<br>allo-LacNAc<br>Gal-β-1,4-LacNAc<br>Gal-β-1,4-Gal-β-1,4-LacNAc<br>allo-Lac<br>GOS (DP3) | 1[n] | 46 | high (95%) | | 65 |
| | Lac | LacNAc[k] | 10 | 30[k] | nd | | 56 |
| | Lac | LacNAc[k] | 10 | 58[k] | nd | 30% $[MMIm][MeSO_4]$ | 56 |
| *Bifidobacterium bifidum* (GH 42)[o] | Lac | LacNAc<br>allo-LacNAc | 3 | 25 | medium (86%) | | 19 |
| | Lac | LacNAc<br>allo-LacNAc | 3 | 23 | high (95%) | 20% diglyme[p] | 19 |
| | Lac | LacNAc<br>allo-LacNAc | 3 | 18 | medium (83%) | 20% trimethyl phosphate[p] | 19 |
| | Lac | LacNAc<br>allo-LacNAc | 3 | 25 | high (92%) | 20% acetone[p] | 19 |
| | Gal-β-*p*NP | LacNAc<br>allo-LacNAc | 3 | 45 | high (92%) | 20% diglyme[p] | 19 |
| | Gal-β-*p*NP | LacNAc<br>allo-LacNAc | 3 | 37 | high (97%) | 20% trimethyl phosphate[p] | 19 |
| | Gal-β-*p*NP | LacNAc<br>allo-LacNAc | 3 | 35 | high (95%) | 20% acetone[p] | 19 |
| | Gal-β-F | LacNAc<br>allo-LacNAc | 3 | 23 | medium (84%) | 20% diglyme[p] | 19 |


dx.doi.org/10.1021/jf502619p | J. Agric. Food Chem. 2014, 62, 9615−9631

**Table 4. continued**

| β-galactosidase | donor | products[b] | A:D[c] | yield[d] (%) | regio-selectivity[e] | cosolvent/immobilization | ref |
|---|---|---|---|---|---|---|---|
| *Diplococcus (Streptococcus) pneumoniae* (GH 2) | Gal-β-*p*NP | LacNAc | 5 | 12 | complete | 14% DMSO | 35 |
| | Gal-β-*o*NP | LacNac | 3 | 31 | complete | 20% triethylene glycol | 84 |
| *Escherichia coli* (GH 2) | Lac | allo-LacNAc<br>unidentified OSs<br>lacto-*N*-biose | 1 | 32 | high (98%)[f] | | 64 |
| | Gal-β-*o*NP | allo-LacNAc | 2 | 23 | complete | | 84 |
| | Gal-β-*o*NP | allo-LacNAc | 4 | 28 | complete | | 84 |
| | Gal-β-*o*NP | allo-LacNAc | 8 | 30 | complete | | 84 |
| | Gal-β-*o*NP | allo-LacNAc | 12 | 26 | complete | | 84 |
| | Gal-β-*o*NP | allo-LacNAc | 16 | 22 | complete | | 84 |
| *Kluyveromyces lactis* (GH 2) | Lac | allo-LacNAc<br>LacNAc | 2 | 19 | medium (89%) | | 57 |
| *Sulfolobus solfataricus* (GH 1) | Lac | allo-LacNAc<br>unidentified OSs<br>LacNAc<br>lacto-*N*-biose | 1 | 48 | medium (73%)[f] | | 64 |
| *Thermus thermophilus* TTP0042 (GH 1) | Gal-β-*p*NP | Gal-β(1,3)-Gal-β-*p*NP<br>LacNAc<br>Gal-β(1,6)-Gal-β-*p*NP<br>allo-LacNAc | 5 | 97 | medium (56%) | | 6 |
| | Gal-β-*p*NP | LacNAc<br>allo-LacNAc<br>Gal-β(1,6)-Gal-β-*p*NP<br>Gal-β(1,3)-Gal-β-*p*NP | 5 | 95 | medium (83%) | 30% [OMIm][$PF_6$][q] | 6 |
| | Gal-β-*p*NP | LacNAc<br>allo-LacNAc<br>Gal-β(1,6)-Gal-β-*p*NP<br>Gal-β(1,3)-Gal-β-*p*NP | 5 | 100 | high (94%) | 49% 1,3-dibutoxy-2-methoxypropane[h] | 76 |
| *Xanthomonas manihotis* (GH 35) | Gal-β-*p*NP | lacto-*N*-biose | 10 | 55 | complete | | 15 |

[a]The use of cosolvent or enzyme immobilization is indicated where relevant. All β-galactosidases used are of microbial origin, but belong to several different GH families as indicated. Abbreviations: Lac, β-D-lactose; OS, oligosaccharide; LacNAc, *N*-acetyl-D-lactosamine; Gal-β-*p*NP, *p*-nitrophenyl β-D-galactopyranoside; [BMIm][$PF_6$], 1-butyl-3-methylimidazolium hexafluorophosphate; Gal-β-*o*NP, *o*-nitrophenyl β-D-galactopyranoside; Gal, D-galactose; GOS, galacto-oligosaccharides; DP, degree of polymerization; [MMIm][$MeSO_4$], 1,3-dimethylimidazolium methyl sulfate; Gal-β-F, β-galactosyl fluoride; DMSO, dimethyl sulfoxide; [OMIm][$PF_6$], 1-octyl-3-methylimidazolium hexafluorophosphate. [b]Listed according to prevalence. [c]The molar acceptor/donor ratio has been rounded to the nearest integer except when <1. [d]Total molar trans-galactosylation yield on donor. [e]Complete, no other linkage detected; high, ≥90% of the desired linkage; medium, ≥50% of the desired linkage; low, <50% of the desired linkage; the percentage of the most prevalent linkage (top of "products" column) is given. [f]Based on yield of identified disaccharides only. [g]Nine other ionic liquids were tested (30% v/v), but this one gave highest yields and no formation of allo-LacNAc, which was observed for the majority of the other ILs. [h]Fourteen other biosolvents were tested (2 M), but this one gave highest yields of the desired compound. [i]More acceptor/donor ratios (1−20) were tested at higher enzyme concentration, where the effect on trans-galactosylation yield was pronounced (1−57%). [j]Five other organic cosolvents (dimethyl sulfoxide, acetonitrile, pyridine, *tert*-butanol, and acetone) were also tested at the same conditions, giving similar results, but the highest yield was obtained with 2-methyl-2-butanol. [k]Only LacNAc yield was determined in this study, and the presence of no other compounds was reported or quantified. [l]More acceptor/donor ratios (0.1−10) were tested, but this one gave the highest yield. [m]Fourteen other organic solvents were tested, of which six (*n*-dibutyl ether, tetracloromethane, 2-butanone, methyl *tert*-butyl ether, ethyl acetate, and toluene) gave higher yields than obtained without cosolvent (but lower than that obtained with cyclohexane), whereas eight (1,4-dioxane, tetrahydrofuran, *n*-hexane, acetonitrile, acetone, *tert*-butanol, trichloromethane, and diglyme) gave lower yields. [n]More acceptor/donor ratios (0.33−2) were tested, but this one gave the highest yields. [o]β-Galactosidse from *Bifidobacterium bifidum* DSM 20456 (also ATCC 29521 and JCM 1255) is not listed in the CAZy database, but in its UniProt entry U2BYL7 GH family 42 is indicated. [p]Other cosolvent concentrations were tested, but yields were generally highest at 20%, and only this concentration is shown here to enable comparison between donors. [q]Three other ionic liquids were tested, but this one gave the highest yield of the desired compound.

Although this review focuses on solute acceptors, not least due to the valuable products they can become, glycosidases can equally well trans-glycosylate primary or secondary alcohol solvents and phenols.[7] Issues and recommendations relating to glycosidase-catalyzed formation of alkyl glycosides were thoroughly reviewed 15 years ago.[7] Major conclusions then included the fact that trans-glycosylation is to be preferred over reverse hydrolysis and that $a_w$ is determining for reaction yields (cf. eq 1). For alkyl glycoside formation where the alcohol is the main solvent, glycosidases that tolerate low $a_w$ conditions are needed, for example, hyperthermostable or immobilized glycosidases.[7,58] For solute acceptors, $a_w$ can only be lowered

according to eq 1 by using very high acceptor concentrations, which is often not favorable for valuable compounds, or by addition of cosolvents (see below).

## COSOLVENTS

It has been shown that the $r_S/r_H$ ratio (eq 1) and consequently the trans-glycosylation yield for glycosidases can be improved by the addition of cosolvents including organic solvents,[41,55,74] ionic liquids (ILs),[31,41,54,56] or glycerol-based biosolvents[75] (Tables 1 and 4). The cosolvents affect the $a_w$ of the reaction mixture[55] as well as the selectivity of the enzyme for the competing nucleophiles, that is, the desired acceptor and water, expressed as the selectivity factor $S$ (or $S_c$)[31] in eq 1. Some controversy exists regarding the mechanism by which the cosolvents alter the enzyme selectivity. Sandoval and co-workers[6,76] hypothesized that the improved trans-galactosylation yields obtained with $\beta$-galactosidase from *Thermus thermophilus* (EC 3.2.1.23; GH 1) when using ILs or biosolvents as cosolvents were linked to alterations in the enzyme's secondary and tertiary structure. It is believed that increased enzyme flexibility makes glycosidases favor the larger acceptor molecules over water.[55,76] In contrast, Lang et al.[31] showed that the effect of an IL cosolvent on enzyme selectivity was acceptor-dependent and hypothesized that the IL removed hydrogen-bonded water from strongly hydrated acceptors, thus improving the selectivity of the enzyme by modification of the acceptor hydration. In a study on $\beta$-galactosidase from *B. circulans* (GH 35) with IL cosolvents,[54] it was found that the addition of [BMIm][$PF_6$] (1-butyl-3-methylimidazolium hexafluorophosphate) to the aqueous medium decreased the distance between the reactive hydroxyl group on the acceptor and the nucleophilic Glu residue in the active site, thus increasing the reactivity with the glycosyl acceptor. In addition, the presence of [BMIm][$PF_6$] increased the binding energy between the enzyme and the substrate, particularly by increasing their electrostatic interaction.[54] Furthermore, the effect on enzyme selectivity, that is, the $r_S/r_H$ ratio, is also dependent on the cosolvent nature.[41,54,55,77,78]

When employing the GH family 42 $\beta$-galactosidase from *B. circulans* for the trans-galactosylation of GlcNAc with *o*NP-$\beta$-Gal, it was seen that total trans-galactosylation yields comparable to those obtained in aqueous medium at an acceptor/donor ratio of 10 could be obtained at an acceptor/donor ratio of 1 by the addition of 10−20% (v/v) organic solvent.[55] This may thus be a useful method to improve reaction yields with expensive acceptors.

For $\beta$-galactosidase-catalyzed reactions, cosolvents have been shown to significantly improve the regioselectivity and/or reduce the extent of donor self-condensation.[6,54,55,76] However, when using aryl saccharide donors, addition of a cosolvent that enhances donor solubility can improve trans-glycosylation yields, but a too high cosolvent concentration may lead to increased donor self-condensation.[78,79] Indeed, the amount of cosolvent must be carefully adjusted, not least to avoid extensive inactivation of the biocatalyst.[19,31,55,78]

The main disadvantage of using cosolvents is the fact that these should be removed from the final product, an issue that is rarely addressed in the studies mentioned above. Whereas some organic solvents can be removed by simple distillation, others form azeotropes with water and cannot be.[41] Sialylated products can be purified by anion exchange chromatography,[4] and it is likely that this can also be used for purification from azeotropic mixtures. Water-immiscible ILs may be removed by centrifugation,[6] whereas water-miscible ones can be removed from saccharide mixtures by a combination of filtration and electrodialysis.[80]

## ACCEPTOR CONCENTRATION AND ACCEPTOR/DONOR RATIO

It follows from eq 1 that an increase in acceptor concentration improves trans-glycosylation. For oligosaccharide synthesis, saccharide concentrations as high as 80% (w/w) have been used to effectively increase reaction yields.[81,82] At these high concentrations, $a_w$ is significantly lowered to as little as 0.6−0.7.[83] Michalak et al.[4] found significant improvement of the trans-sialylation yield from approximately 3% to >50% when increasing the lactose acceptor concentration from 1.3 to 4% (w/w). However, even 4% (w/w) lactose is unlikely to lower the $a_w$ from 1.0. Consequently, this improvement in trans-sialidase activity is more likely linked to the corresponding increase in acceptor/donor ratio from 14 to 25. An increase in acceptor/donor ratio from 1 to 10 also dramatically increased the yield of LacNAc from <1 to 43% in the trans-galactosylation of GlcNAc catalyzed by the GH 42 $\beta$-galactosidase from *B. circulans* when using *o*NP-$\beta$-Gal as donor.[55] Interestingly, another study of the same reaction with the same enzyme reported that whereas an increase in acceptor/donor ratio from 1 to 10 increased the LacNAc yield from 12 to 22%, a decrease to one-third increased the LacNAc yield further to 35%, albeit with a concomitant increase in donor self-condensation.[78] However, by far the majority of the available results supports the correlation between an increase in acceptor/donor ratio and an increase in trans-glycosylation yield for $\beta$-galactosidases, sialidases, and $\alpha$-L-fucosidases, at least to a certain extent (Tables 1, 3, and 4).[4,37,42,51,55,64,67,84] A high acceptor/donor ratio thus increases the probability of a nucleophilic attack from the desired acceptor on the formed glycosyl-enzyme intermediate, thus increasing trans-sialylation yields even if the competing nucleophile, water, is always present in large excess (usually at approximately 55.5 M). An increased acceptor/donor ratio may also improve the regioselectivity and decrease the extent of donor self-condensation.[37,51,55] However, whereas too low substrate concentrations, that is, of both donor and acceptor, promote hydrolysis, too high substrate concentrations may produce lower regioselectivity and promote the formation of higher oligosaccharides.[65,69,78] This is exploited in GOS production, but may compromise the yield of the desired compound in the production of specific human milk oligosaccharides.

In a more recent study with the GH family 42 $\beta$-galactosidase from *B. circulans*,[85] it was found that increasing the concentration of acceptor molecules not functioning as donor substrates had a positive effect on the $V_{max}$ through accelerating the liberation of the transferred $\beta$-galactosyl group from the active site. This acceptor acceleration was not observed with the addition of inert carbohydrates, nor was it caused by a decrease in $a_w$. Furthermore, a decrease in $K_m$ was also observed with increasing concentrations of both inert and acceptor carbohydrates; this increase in enzyme affinity was hypothesized to be caused by molecular crowding, where the enzymatic activity increases if the volume of the enzyme−substrate complex is smaller than the sum of the volume of the enzyme and the volume of the substrate ($V_{E+S} < V_E + V_S$). This molecular crowding effect was, however, much smaller than the effect of acceptor acceleration.[85] In essence, much seems to be gained from ensuring a high acceptor concentration as well as an adequately high acceptor/donor ratio in trans-glycosylation reactions.


dx.doi.org/10.1021/jf502619p | J. Agric. Food Chem. 2014, 62, 9615−9631

## REACTION TIME CONTROL

It follows from Figure 1 that in the kinetically controlled reaction, the maximum trans-glycosylation yield is reached when the rate of trans-glycosylation product formation equals the rate of trans-glycosylation product hydrolysis. From this point, the reaction will no longer be kinetically controlled, and it is important to stop the reaction before thermodynamic control takes over and the trans-glycosylation product undergoes hydrolysis.[18] Indeed, trans-glycosylation product yields often reach a maximum before decreasing due to product hydrolysis.[2,51,56,58] Consequently, it is of major importance to establish the optimal reaction time. Reaction time can be controlled simply by terminating the reaction with a change in pH or temperature or, more elegantly and efficiently, by employing enzyme immobilization/confinement or continuous product removal[40] (see below).

In a few cases, product hydrolysis at extended reaction times has been avoided because the product formed was not a substrate for the glycosidase. For instance, for α-L-fucosidases it has been been reported that α(1,6)-linked fucosyl residues are poor substrates for the hydrolytic activity, resulting in relatively high trans-fucosylation yields (Table 3).[5,29] Recently, a sialyl transferase from *Pasteurella multocida* (EC 2.4.99.1/EC 2.4.99.4; GT 80) was shown to also possess dual trans-sialidase activity, resulting in the formation of both 3′- and 6′-sialyl-lactose from lactose and CGMP.[43] 3′-Sialyl-lactose was formed more rapidly than 6′-sialyl-lactose, but whereas 3′-sialyl-lactose was subject to product hydrolysis during the enzyme catalysis, the 6′-sialyl-lactose was not, eventually resulting in higher yields of 6′-sialyl-lactose at extended reaction times.[43] Other special-case glycosidases have very low hydrolytic activity, for example, a mutant of the α-L-fucosidase from *T. maritima*[51] and the well-studied true trans-sialidase from *T. cruzi*.[38] Even so, also for these reactions the trans-glycosylation yield does reach a plateau, at which point the reaction may be stopped.

## TEMPERATURE AND PH

Generally, trans-glycosylation yields are optimized at low or moderate temperatures (25−40 °C).[4,42,43,65] Indeed, an increase in temperature can compromise reaction yields due to decreased regioselectivity.[57,65,86] For β-galactosidase from *B. circulans* (GH 42) it was found that both pH and temperature influenced the ratio between the LacNAc and allo-LacNAc (Gal-β(1,6)-GlcNAc) produced, favoring LacNAc at low pH and low temperature.[57,86] Similarly, it was found that for the trans-sialidase activity possessed by the sialyl transferase from *Pasteurella multocida*, the optimal pH for production of 3′-sialyl-lactose was different from the optimal pH for producing 6′-sialyl-lactose.[43]

## ENZYME DOSAGE

Data on the optimization of enzyme dosage in trans-glycosylation are scarce. However, it may be an important point to consider as it has been shown that a decrease in concentration of the GH 42 β-galactosidase from *B. circulans* dramatically improved the trans-galactosylation yields.[55] Probably, a high enzyme dosage accelerates primary and secondary hydrolyses, thus compromising trans-glycosylation yields. However, the results obtained may depend on the reaction time (see above), which was not optimized in the aforementioned study.[55] It deserves to be highlighted that an increase in enzyme concentration has also been found to reduce the regioselectivity of the GH 42 β-galactosidase from *B. circulans*.[57,65]

## CONTINUOUS PRODUCT REMOVAL

Another means of avoiding product hydrolysis is to continuously remove the product from the reaction mixture, known as continuous product removal or in situ product removal (ISPR). In β-galactosidase-catalyzed production of GOS from lactose, this has been achieved by adsorption of oligosaccharides to activated carbon, resulting in a yield improvement of 30%.[87] In a model reaction studying β-galactosidase-catalyzed self-condensation of Gal-β-*p*NP, the adsorption of *p*NP-β-galactobioside to a boronate resin gave a yield improvement of 10−15%, the major issue being the discrepancy between the optimal reaction pH and the optimal binding pH.[88] In the sialidase-catalyzed production of 3′-sialyl-lactose from lactose and CGMP, the large size of the limiting substate, that is, CGMP, has been exploited to facilitate continuous product removal in an enzymatic membrane reactor.[40] The use of a membrane reactor also allows for enzyme recycling. Indeed, the biocatalytic productivity of an engineered sialidase from *T. rangeli* was improved by >9-fold in an enzymatic membrane reactor (EMR) compared to the batch process.[40] In this process the acceptor also passed the membrane, but because the acceptor is not limiting (used in 25-fold excess), this did not affect reaction yields negatively. By nanofiltration it was possible to recycle the majority of the unreacted lactose.[89] However, when all substrates are similar in size to, or even smaller than, the product, for example, in the case of GOS production from lactose, the EMR cannot be used because the substrate will not be rejected if the product is not. Nevertheless, EMRs have been used for removal of monosaccharides to avoid β-galactosidase inhibition in GOS production.[90,91]

## ENZYME IMMOBILIZATION

For a mutant sialidase from *T. rangeli* it was observed that the trans-sialylation yield was improved when the enzyme was immobilized, mainly due to a reduction in secondary hydrolysis.[40] Increased trans-glycosylation yields upon immobilization have also been observed for a sialidase from *V. cholerae*[37] and the GH family 42 β-galactosidase from *B. circulans*,[69] but with mixed effects on regioselectivity. It has also been reported that β-galactosidase-catalyzed GOS production is improved by enzyme immobilization, not only due to increased enzyme stability but also as a result of an improved balance between trans-galactosylation and hydrolysis.[87,92] Possible explanations for such an improvement in enzyme selectivity upon immobilization have recently been reviewed.[93]

## PROTEIN ENGINEERING

As outlined above, the rate of hydrolysis is decisive for trans-glycosylation yields. Consequently, several studies have aimed at producing mutant enzymes with lowered hydrolytic activity and unchanged or improved trans-glycosylation activity. The protein engineering approaches include directed evolution of a *T. maritima* α-L-fucosidase[51] and a β-galactosidase from *T. thermophilus*[94] as well as site-directed mutagenesis, or rational design, of a sialidase from *T. rangeli*.[2,95]

For the β-galactosidase from *T. thermophilus* a single mutation (F401S) just in front of the donor binding site caused repositioning of the donor and a better fit of the acceptor, thus favoring an attack by the glycosyl acceptor rather than from water.[94] The trans-galactosylation yield was improved from 8 to 60% when using cellobiose as acceptor. In fact, this mutant gave higher yields than the corresponding glycosynthase (see below) but with cheaper substrates. However, whereas the

trans-galactosylation/hydrolysis ratio was improved 23 times, the trans-galactosylation activity was only approximately 10% that of the wild type.[94] Molecular modeling was subsequently used for another mutant (N282T) that efficiently catalyzed donor self-condensation. This rational approach allowed identification of a mutation (A221W) that prevents donor access to the acceptor binding site without affecting the binding of the preferred donor (GlcNAc-$\beta$-*p*NP).[96] Both N282 and F401 are conserved and located around the donor binding site, and it was recently substantiated that targeting conserved residues in this location might be a general approach for improving trans-glycosylation in enzymes belonging to GH family 1.[97]

For the $\alpha$-L-fucosidase from *T. maritima* the regioselective trans-fucosylation yield increased from 7 to 62% upon introduction of three mutations in the second amino acid shell around the active site via directed evolution.[51] These mutations resulted in a 32-fold increase in the trans-fucosylation/hydrolysis ratio, and the regioselectivity was moreover significantly improved, whereas the mutant maintained 57% of the total activity of the wild type enzyme. On the basis of molecular modeling, the second shell mutations were hypothesized to cause reorientation of amino acids in the active site, resulting in a better docking energy of the product in the binding site.[51]

Due to strong structural and sequence similarity (70% identity) between the *T. cruzi* trans-sialidase and a strict sialidase from the nonpathogenic *T. rangeli*, this was used as a model system to understand the molecular basis for the trans-sialidase activity.[95,98] The pathogenic origin of trans-sialidases may complicate the process of obtaining approval for use in food applications,[4] and this has led to interest in the use of *T. rangeli* sialidase mutants.[2,4] Introduction of five mutations in the *T. rangeli* sialidase ($TrSA_{5mut}$) that affected the acceptor binding site and the sialic acid binding pocket conferred a weak trans-sialidase activity, equivalent to 1% that of *T. cruzi*.[95] Either of two additional mutations increased trans-sialidase activity 10-fold, but also increased $k_{cat}/K_m$ of the hydrolysis of the desired product 3′-sialyl-lactose 1.8-fold.[95] Additional substitution of a seven-amino-acid loop located near the acceptor binding site reduced the hydrolytic activity 4 times without affecting the trans-sialidase activity. The mutation introduced a net charge change of +3 that was hypothesized to result in partial reversal of the water network in the active site, consequently impairing the nucleophilicity of the water.[2] Molecular dynamics and free energy computations have improved the understanding of the mechanism of the *T. cruzi* trans-sialidase.[99,100] A redesign of the *T. rangeli* mutant $TrSA_{5mut}$ by five additional mutations identified by free energy computations was recently suggested but not validated experimentally.[101]

It is clear that alteration of the acceptor binding site and repositioning of the acceptor making its nucleophilic attack more favorable as well as stabilization of the glycosyl-enzyme intermediate are keys to improving trans-glycosylation activity. Toward the development of generic strategies for improving trans-glycosylation in glycosidases, there is a need for improving the understanding of the structure−function relationship to which mutational and structural studies are key. As outlined above, approaches such as molecular modeling and free energy computations have been used in a few cases, but can at present mainly be considered tools for the generation of hypotheses. Thus, improvement of trans-glycosylation by protein engineering requires a significant research effort compared to the other strategies for improving trans-glycosylation yields mentioned above.

**Glycosynthases.** Glycosynthases represent another protein engineering route to avoid contaminating hydrolysis.[102] They are mutant glycosidases, most often retaining ones, where the nucleophilic Asp/Glu residue has been changed to a non-nucleophilic one, for example, Ala, Ser, or Gly. By doing so, the enzyme loses its hydrolytic activity, but also its ability to form a covalent intermediate with the donor substrate (cf. Figure 1). Using an activated donor, most often a glycosyl fluoride, in the configuration opposite to that of the natural substrate they can efficiently catalyze the transfer of the glycosyl group to an appropriate acceptor with high yields.[103,104] Glycosyl azides and aryl glycosides have also been suggested as useful donors, but the field is dominated by glycosyl fluorides, although these are often unstable (especially the $\beta$-glycosyl fluorides used for $\alpha$-glycosynthase catalysis) and hardly commercially available.[105,106] The acceptors mainly include nitrophenyl or methylumbelliferyl derivatives of mono- and disaccharides.[105,107]

An $\alpha$-L-fucosynthase derived from an inverting 1,2-$\alpha$-L-fucosidase from *Bifidobacterium bifidum* (EC 3.2.1.63; GH 95) catalyzed the synthesis of 2′-fucosyl-lactose from $\beta$-fucosyl fluoride and lactose, reaching a 2′-fucosyl-lactose yield of only 6%, mainly due to decomposition of the unstable $\beta$-fucosyl fluoride donor.[108] An $\alpha$-L-fucosynthase based on the retaining $\alpha$-L-fucosidase (EC 3.2.1.51; GH 29) from the hyperthermophilic archaeon *Sulfolobus solfataricus* catalyzed fucosylation using the more stable $\beta$-fucosyl azide as donor. Fucosylation of Gal-$\beta$-*p*NP generated various regioisomers in a total yield of 26%, whereas GlcNAc-$\beta$-*p*NP was selectively fucosylated on *O*-3 with an efficiency of 86%.[109]

Complete regioselectivity was observed for an $\alpha$-L-fucosynthase developed from a retaining 1,3−1,4-$\alpha$-L-fucosidase (EC 3.2.1.111; GH 29) from *B. bifidum*; the enzyme catalyzed the synthesis of valuable biomimetic tri- and tetrasaccharides, including the HMOs 3-fucosyl-lactose (13% yield) and lacto-*N*-fucopentaose II (41% yield) as well as blood group antigens $Lewis^A$ (47% yield) and $Lewis^X$ (55% yield), using $\beta$-fucosyl fluoride as donor.[110] No products were obtained with $\beta$-fucosyl azide as donor.[110]

Sialidases employ a nucleophilic Tyr instead of the more common Asp/Glu. Not being actual glycosynthases, mutations of this nucleophilic Tyr in *Micromonospora viridifaciens* sialidase (EC 3.2.1.18; GH 33) resulted in a number of mutants that retained hydrolytic activity with either retention or inversion of configuration.[111,112] Using phenyl $\beta$-D-sialic acid as a donor, the inverting mutant Y370G catalyzed production of sialyl-lactose with a yield of 13%, with >90% being the $\alpha(2,6)$-isomer and with no subsequent product hydrolysis.[113]

However, it follows that glycosynthase catalysis releases either hydrofluoric acid (HF) or hydrazoic acid ($HN_3$) as its byproduct. Although numerous methods for the removal of fluoride ions from aqueous solution exist,[114] this issue of removal has hardly been addressed by any of the otherwise thorough reviews (see, e.g., refs 103, 105, and 106) of glycosynthases and the use of glycosyl fluorides as substrates. More importantly, the requirement for chemical synthesis to introduce the fluoride or azide groups into the donor substrates significantly increases the cost, thereby lowering the large-scale potential.[106] In conclusion, glycosynthases represent a simple protein engineering route to improved trans-glycosylation, but their use is restricted by the requirement for specialized and, in the case of $\alpha$-glycosidases, unstable substrates.

## CONCLUSIONS

All trans-glycosylation yields given in this paper are molar yields based on the donor. The yields obtained in the literature range from negligible values to as much as 99% of the desired trans-glycosylation product. Generally, the highest yields have been obtained by one or more of the following strategies to improve trans-glycosylation yields: (1) high acceptor/donor ratio; (2) protein engineering; and/or (3) addition of cosolvents, at least for enzymes that tolerate nonconventional solvents (Tables 1−4). When optimizing trans-glycosylation processes, not only the pH−temperature optimum but also the optimal reaction time must be established to avoid undesirable product hydrolysis. Alternatively, continuous product removal can be employed. If combined with enzyme recycling in an EMR, biocatalytic productivity may also be significantly enhanced.

Regioselectivity in the trans-glycosylation is mainly a result of the choice of enzyme, but can also be influenced by acceptor and donor structures, the acceptor/donor ratio, and the presence of cosolvents, as well as by temperature and pH. Thus, all of these factors need to be considered in the design of a trans-glycosylation process, where regioselectivity is important.

For food applications it is important to consider both cost and biocompatibility of substrates and reaction routes. Thus, it is desirable to employ substrates from natural sources such as lactose and CGMP, even if higher yields may be obtained with aryl or fluoride donor substrates.

## AUTHOR INFORMATION

### Corresponding Author

*(A.S.M.) Phone: +45 4525 2909. E-mail: am@kt.dtu.dk.

### Notes

The authors declare no competing financial interest.

## REFERENCES

(1) Bridiau, N.; Maugard, T. A comparative study of the regioselectivity of the β-galactosidases from *Kluyveromyces lactis* and *Bacillus circulans* in the enzymatic synthesis of *N*-acetyl-lactosamine in aqueous media. *Biotechnol. Prog.* **2011**, *27*, 386−394.

(2) Jers, C.; Michalak, M.; Larsen, D. M.; Kepp, K. P.; Li, H.; Guo, Y.; Kirpekar, F.; Meyer, A. S.; Mikkelsen, J. D. Rational design of a new *Trypanosoma rangeli* trans-sialidase for efficient sialylation of glycans. *PLoS One* **2014**, *9*, No. e83902.

(3) Lu, L.; Xu, S.; Jin, L.; Zhang, D.; Li, Y.; Xiao, M. Synthesis of galactosyl sucralose by β-galactosidase from *Lactobacillus bulgaricus* L3. *Food Chem.* **2012**, *134*, 269−275.

(4) Michalak, M.; Larsen, D. M.; Jers, C.; Almeida, J. R. M.; Willer, M.; Li, H.; Kirpekar, F.; Kjærulff, L.; Gotfredsen, C. H.; Nordvang, R. T.; Meyer, A. S.; Mikkelsen, J. D. Biocatalytic production of 3′-sialyllactose by use of a modified sialidase with superior *trans*-sialidase activity. *Process Biochem.* **2014**, *49*, 265−270.

(5) Rodríguez-Díaz, J.; Carbajo, R. J.; Pineda-Lucena, A.; Monedero, V.; Yebra, M. J. Synthesis of fucosyl-*N*-acetylglucosamine disaccharides by transfucosylation using α-L-fucosidases from *Lactobacillus casei*. *Appl. Environ. Microbiol.* **2013**, *79*, 3847−3850.

(6) Sandoval, M.; Cortés, A.; Civera, C.; Treviño, J.; Ferreras, E.; Vaultier, M.; Berenguer, J.; Lozano, P.; Hernáiz, M. J. Efficient and selective enzymatic synthesis of *N*-acetyl-lactosamine in ionic liquid: a rational explanation. *RSC Adv.* **2012**, *2*, 6306−6314.

(7) van Rantwijk, F.; Woudenberg-van Oosterom, M.; Sheldon, R. A. Glycosidase-catalysed synthesis of alkyl glycosides. *J. Mol. Catal. B: Enzym.* **1999**, *6*, 511−532.

(8) Ichikawa, Y.; Wang, R.; Wong, C.-H. Regeneration of sugar nucleotide for enzymatic oligosaccharide synthesis. *Methods Enzymol.* **1994**, *247*, 107−127.

(9) Fierfort, N.; Samain, E. Genetic engineering of *Escherichia coli* for the economical production of sialylated oligosaccharides. *J. Biotechnol.* **2008**, *134*, 261−265.

(10) Drouillard, S.; Mine, T.; Kajiwara, H.; Yamamoto, T.; Samain, E. Efficient synthesis of 6′-sialyllactose, 6,6′-disialyllactose, and 6′-KDO-lactose by metabolically engineered *E. coli* expressing a multifunctional sialyltransferase from the *Photobacterium* sp. JT-ISH-224. *Carbohydr. Res.* **2010**, *345*, 1394−1399.

(11) Bode, L. Human milk oligosaccharides: every baby needs a sugar mama. *Glycobiology* **2012**, *22*, 1147−1162.

(12) Brocke, C.; Kunz, H. Synthesis of tumor-associated glycopeptides antigens. *Bioorg. Med. Chem.* **2002**, *10*, 3085−3112.

(13) Murata, T.; Morimoto, S.; Zeng, X.; Watanabe, S.; Usui, T. Enzymatic synthesis of α-L-fucosyl-*N*-acetyllactosamines and 3′-*O*-α-L-fucosyllactose utilizing α-L-fucosidases. *Carbohydr. Res.* **1999**, *320*, 192−199.

(14) Vetere, A.; Paoletti, S. Complete synthesis of 3′-sialyl-*N*-acetyllactosamine by regioselective transglycosylation. *FEBS Lett.* **1996**, *399*, 203−206.

(15) Vetere, A.; Miletich, M.; Bosco, M.; Paoletti, S. Regiospecific glycosidase-assisted synthesis of lacto-*N*-biose I (Galβ1-3GlcNAc) and 3′-sialyl-lacto-*N*-biose I (NeuAcα2-3Galβ1-3GlcNAc). *Eur. J. Biochem.* **2000**, *267*, 942−949.

(16) Gosling, A.; Stevens, G. W.; Barber, A. R.; Kentish, S. E.; Gras, S. L. Recent advances refining galactooligosaccharide production from lactose. *Food Chem.* **2010**, *121*, 307−318.

(17) Ichikawa, Y.; Look, G. C.; Wong, C.-H. Enzyme-catalyzed oligosaccharide synthesis. *Anal. Biochem.* **1992**, *202*, 215−238.

(18) Kasche, V. Mechanism and yields in enzyme catalysed equilibrium and kinetically controlled synthesis of β-lactam antibiotics, peptides and other condensation products. *Enzyme Microb. Technol.* **1986**, *8*, 4−16.

(19) Yoon, J. H.; Rhee, J. S. The efficient enzymatic synthesis of *N*-acetyllactosamine in an organic co-solvent. *Carbohydr. Res.* **2000**, *327*, 377−383.

(20) Koshland, D. Stereochemistry and the mechanism of enzymatic reactions. *Biol. Rev.* **1953**, *28*, 416−436.

(21) Rye, C. S.; Withers, S. G. Glycosidase mechanisms. *Curr. Opin. Chem. Biol.* **2000**, *4*, 573−580.

(22) Cleland, W. W. The kinetics of enzyme-catalyzed reactions with two or more substrates and products. I. Nomenclature and rate equations. *Biochim. Biophys. Acta* **1963**, *67*, 104−137.

(23) Cogoli, A.; Semenza, G. A probable oxocarbonium ion in the reaction mechanism of small intestinal sucrase and isomaltase. *J. Biol. Chem.* **1975**, *250*, 7802−7809.

(24) Peruffo, A. D. B.; Renosto, F.; Pallavicini, C. α-Glucosidase from grape berries: partial purification and characterization. *Planta* **1978**, *142*, 195−201.

(25) Suzuki, K.; Fukumura, T.; Shibasaki-Kitakawa, N.; Yonemoto, T. Kinetic model for synthesis of fructosyl-stevioside using suspended β-fructofuranosidase. *Biochem. Eng. J.* **2002**, *10*, 207−215.

(26) Damager, I.; Buchini, S.; Amaya, M. F.; Buschiazzo, A.; Alzari, P.; Frasch, A. C.; Watts, A.; Withers, S. G. Kinetic and mechanistic analysis of *Trypanosoma cruzi* trans-sialidase reveals a classical ping-pong mechanism with acid/base catalysis. *Biochemistry* **2008**, *47*, 3507−3512.

(27) Oliveira, I. A.; Gonçalves, A. S.; Neves, J. L.; von Itzstein, M.; Todeschini, A. R. Evidence of ternary complex formation in *Trypanosoma cruzi* trans-sialidase catalysis. *J. Biol. Chem.* **2014**, *289*, 423−436.

(28) Amaya, M. F.; Watts, A. G.; Damager, I.; Wehenkel, A.; Nguyen, T.; Buschiazzo, A.; Paris, G.; Frasch, A. C.; Withers, S. G.; Alzari, P. M. Structural insights into the catalytic mechanism of *Trypanosoma cruzi* trans-sialidase. *Structure* **2004**, *12*, 775−784.

(29) Berteau, O.; Bielicki, J.; Kilonda, A.; Machy, D.; Anson, D. S.; Kenne, L. α-L-Fucosidases: exoglycosidases with unusual trans-glycosylation properties. *Biochemistry* **2004**, *43*, 7881−7891.

(30) Hansson, T.; Andersson, M.; Wehtje, E.; Adlercreutz, P. Influence of water activity on the competition between β-glycosidase catalysed transglycosylation and hydrolysis in aqueous hexanol. *Enzyme Microb. Technol.* **2001**, *29*, 527−534.

(31) Lang, M.; Kamrat, T.; Nidetzky, B. Influence of ionic liquid cosolvent on transgalactosylation reactions catalyzed by thermostable β-glycosylhydrolase CelB from *Pyrococcus furiosus*. *Biotechnol. Bioeng.* **2006**, *95*, 1093−1100.
(32) Thiem, J. Applications of enzymes in synthetic carbohydrate chemistry. *FEMS Microbiol. Rev.* **1995**, *16*, 193−211.
(33) Trincone, A.; Giordano, A. Glycosyl hydrolases and glycosyltransferases in the synthesis of oligosaccharides. *Curr. Org. Chem.* **2006**, *10*, 1163−1193.
(34) Woudenberg-van Oosterom, M.; van Belle, H. J. A.; van Rantwijk, R.; Sheldon, R. A. Immobilised β-galactosidases and their use in galactoside synthesis. *J. Mol. Catal. A: Chem.* **1998**, *134*, 267−274.
(35) Ajisaka, K.; Fujimoto, H.; Isomura, M. Regioselective transglycosylation in the synthesis of oligosaccharides: comparison of β-galactosidases and sialidases of various origins. *Carbohydr. Res.* **1994**, *259*, 103−115.
(36) Farkas, E.; Schmidt, U.; Thiem, J.; Kowalczyk, J.; Kunz, M.; Vogel, M. Regioselective synthesis of galactosylated tri- and tetrasaccharides by use of β-galactosidase from *Bacillus circulans*. *Synthesis* **2003**, *5*, 699−706.
(37) Thiem, J.; Sauerbrei, B. Chemoenzymatic syntheses of sialyloligosaccharides with immobilized sialidase. *Angew. Chem., Int. Ed. Engl.* **1991**, *30*, 1503−1505.
(38) Scudder, P.; Doom, J. P.; Chuenkova, M.; Manger, I. D.; Pereira, M. E. A. Enzymatic characterization of β-D-galactoside α2,3-*trans*-sialidase from *Trypanosoma cruzi*. *J. Biol. Chem.* **1993**, *268*, 9886−9891.
(39) Schmidt, D.; Sauerbrei, B.; Thiem, J. Chemoenzymatic synthesis of sialyl oligosaccharides with sialidases employing transglycosylation methodology. *J. Org. Chem.* **2000**, *65*, 8518−8526.
(40) Zeuner, B.; Luo, J.; Nyffenegger, C.; Aumala, V.; Mikkelsen, J. D.; Meyer, A. S. Optimizing the biocatalytic productivity of an engineered sialidase from *Trypanosoma rangeli* for 3′-sialyllactose production. *Enzyme Microb. Technol.* **2014**, *55*, 85−93.
(41) Zeuner, B.; Riisager, A.; Mikkelsen, J. D.; Meyer, A. S. Improvement of *trans*-sialylation versus hydrolysis activity of an engineered sialidase from *Trypanosoma rangeli* by use of co-solvents. *Biotechnol. Lett.* **2014**, *36*, 1315−1320.
(42) Holck, J.; Larsen, D. M.; Michalak, M.; Li, H.; Kjærulff, L.; Kirpekar, F.; Gotfredsen, C. H.; Forssten, S.; Ouwehand, A. C.; Mikkelsen, J. D.; Meyer, A. S. Enzyme catalysed production of sialylated human milk oligosaccharides and galactooligosaccharides by *Trypanosoma cruzi* trans-sialidase. *New Biotechnol.* **2014**, *31*, 156−165.
(43) Guo, Y.; Jers, C.; Meyer, A. S.; Arnous, A.; Li, H.; Kirpekar, F.; Mikkelsen, J. D. A *Pasteurella multocida* sialyltransferase displaying dual trans-sialidase activities for production of 3′-sialyl and 6′-sialyl glycans. *J. Biotechnol.* **2014**, *170*, 60−67.
(44) Mcjarrow, P.; Garman, J.; Harvey, S.; Van Amelsfort, A.; Amelsfort, A. V. Dairy process and product. International Patent WO2003/049547 A2, 2003.
(45) Fernando, S. F.; Woonton, B. W. Quantitation of *N*-acetylneuraminic (sialic) acid in bovine glycomacropeptide (GMP). *J. Food Compos. Anal.* **2010**, *23*, 359−366.
(46) Neelima; Rao, P. S.; Sharma, R.; Rajput, Y. S. Direct estimation of sialic acid in milk and milk products by fluorimetry and its application in detection of sweet whey adulteration in milk. *J. Dairy Res.* **2012**, *79*, 495−501.
(47) Saito, T.; Itoh, T. Variations and distributions of O-glycosidically linked sugar chains in bovine κ-casein. *J. Dairy Sci.* **1992**, *75*, 1768−1774.
(48) Vandekerckhove, F.; Schenkman, S.; Pontes de Carvalho, L.; Tomlinson, S.; Kiso, M.; Yoshida, M.; Hasegawa, A.; Nussenzweig, V. Substrate specificity of the *Trypanosoma cruzi* trans-sialidase. *Glycobiology* **1992**, *2*, 541−548.
(49) Zeng, X.; Murata, T.; Usui, T. Glycosidase-catalyzed synthesis of fucosyl di- and trisaccharide derivatives using α-L-fucosidase from *Alcaligenes* sp. *J. Carbohydr. Chem.* **2003**, *22*, 309−316.
(50) Ajisaka, K.; Fujimoto, H.; Miyasato, M. An α-L-fucosidase from *Penicillium multicolor* as a candidate enzyme for the synthesis of α(1→3)-linked fucosyl oligosaccharides by transglycosylation. *Carbohydr. Res.* **1998**, *309*, 125−129.
(51) Osanjo, G.; Dion, M.; Drone, J.; Solleux, C.; Tran, V.; Rabiller, C.; Tellier, C. Directed evolution of the α-L-fucosidase from *Thermotoga maritima* into an α-L-transfucosidase. *Biochemistry* **2007**, *46*, 1022−1033.
(52) Eneyskaya, E. V.; Kulminskaya, A. A.; Kalkkinen, N.; Nifantiev, N. E.; Arbatskii, N. P.; Saenko, A. I.; Chepurnaya, O. V.; Arutyunyan, A. V.; Shabalin, K. A.; Neustroev, K. N. An α-L-fucosidase from *Thermus* sp. with unusually broad specificity. *Glycoconjugate J.* **2001**, *18*, 827−834.
(53) Farkas, E.; Thiem, J.; Ajisaka, K. Enzymatic synthesis of fucose-containing disaccharides employing the partially purified α-L-fucosidase from *Penicillium multicolor*. *Carbohydr. Res.* **2000**, *328*, 293−299.
(54) Bayón, C.; Cortés, Á.; Berenguer, J.; Hernáiz, M. J. Highly efficient enzymatic synthesis of Galβ-(1→3)-GalNAc and Galβ-(1→3)-GlcNAc in ionic liquids. *Tetrahedron* **2013**, *69*, 4973−4978.
(55) Bridiau, N.; Issaoui, N.; Maugard, T. The effects of organic solvents on the efficiency and regioselectivity of *N*-acetyl-lactosamine synthesis, using the β-galactosidase from *Bacillus circulans* in hydro-organic media. *Biotechnol. Prog.* **2010**, *26*, 1278−1289.
(56) Kaftzik, N.; Wasserscheid, P.; Kragl, U. Use of ionic liquids to increase the yield and enzyme stability in the β-galactosidase catalysed synthesis of *N*-acetyllactosamine. *Org. Process Res. Dev.* **2002**, *6*, 553−557.
(57) Sakai, K.; Katsumi, R.; Ohi, H.; Usui, T.; Ishido, Y. Enzymatic syntheses of *N*-acetyllactosamine and *N*-acetylallolactosamine by the use of β-D-galactosidases. *J. Carbohydr. Chem.* **1992**, *11*, 553−565.
(58) Hansson, T.; Adlercreutz, P. Enzymatic synthesis of hexyl glycosides from lactose at low water activity and high temperature using hyperthermostable β-glycosidases. *Biocatal. Biotransform.* **2002**, *20*, 167−178.
(59) Zeng, X.; Yoshino, R.; Murata, T.; Ajisaka, K.; Usui, T. Regioselective synthesis of *p*-nitrophenyl glycosides of β-D-galactopyranosyl-disaccharides by transglycosylation with β-D-galactosidases. *Carbohydr. Res.* **2000**, *325*, 120−131.
(60) Singh, S.; Scigelova, M.; Hallberg, M. L.; Howarth, O. W.; Schenkman, S.; Crout, D. H. G. Synthesis of sialyloligosaccharides using the *trans*-sialidase from *Trypanosoma cruzi*: novel branched and di-sialylated products from digalactoside acceptors. *Chem. Commun.* **2000**, 1013−1014.
(61) Lee, S.-G.; Shin, D.-H.; Kim, B.-G. Production of sialyloligosaccharides by *trans*-sialidase catalyzed reaction using fetuin as a sialic acid donor. *Enzyme Microb. Technol.* **2002**, *31*, 742−746.
(62) Ajisaka, K.; Shirakabe, M. Regioselective synthesis of α-L-fucosyl-containing disaccharides by use of α-L-fucosidases of various origins. *Carbohydr. Res.* **1992**, *224*, 291−299.
(63) Vetere, A.; Galateo, C.; Paoletti, S. All-aqueous, regiospecific tranglycosylation synthesis of 3-*O*-α-L-fucopyranosyl-2-acetamido-2-deoxy-D-glucopyranose, a building block for the synthesis of branched oligosaccharides. *Biochem. Biophys. Res. Commun.* **1997**, *234*, 358−361.
(64) Reuter, S.; Nygaard, A. R.; Zimmermann, W. β-Galactooligosaccharide synthesis with β-galactosidases from *Sulfolobus solfataricus*, *Aspergillus oryzae*, and *Escherichia coli*. *Enzyme Microb. Technol.* **1999**, *25*, 509−516.
(65) Li, W.; Sun, Y.; Ye, H.; Zeng, X. Synthesis of oligosaccharides with lactose and *N*-acetylglucosamine as substrates by using β-D-galactosidase from *Bacillus circulans*. *Eur. Food Res. Technol.* **2010**, *231*, 55−63.
(66) Bridiau, N.; Maugard, T. *Bacillus circulans* β-galactosidase catalyses the synthesis of *N*-acetyl-lactosamine in a hydro-organic medium via a steady-state ordered Bi Bi reaction mechanism. *J. Mol. Catal. B: Enzym.* **2012**, *77*, 24−31.
(67) Schröder, S.; Schmidt, U.; Thiem, J.; Kowalczyk, J.; Kunz, M.; Vogel, M. Synthesis of oligosaccharides as potential novel food components and upscaled enzymatic reaction employing the β-galactosidase from bovine testes. *Tetrahedron* **2004**, *60*, 2601−2608.
(68) Ito, Y.; Sasaki, T. Cloning and characterization of the gene encoding a novel β-galactosidase from *Bacillus circulans*. *Biosci., Biotechnol., Biochem.* **1997**, *61*, 1270−1276.

(69) Hernaiz, M. J.; Crout, D. H. G. A highly selective synthesis of *N*-acetyllactosamine catalyzed by immobilised β-galactosidase from *Bacillus circulans*. *J. Mol. Catal. B: Enzym.* **2000**, *10*, 403−408.
(70) Benešová, E.; Lipovová, P.; Dvořáková, H.; Králová, B. α-L-Fucosidase from *Paenibacillus thiaminolyticus*: its hydrolytic and transglycosylation abilities. *Glycobiology* **2013**, *23*, 1052−1065.
(71) Usui, T.; Morimoto, S.; Hayakawa, Y.; Kawaguchi, M.; Murata, T.; Matahira, Y.; Nishida, Y. Regioselectivity of β-D-galactosyl-disaccharide formation using the β-D-galactosidase from *Bacillus circulans*. *Carbohydr. Res.* **1996**, *285*, 29−39.
(72) Ma, L.; Persson, M.; Adlercreutz, P. Water activity dependence of lipase catalysis in organic media explains successful transesterification reactions. *Enzyme Microb. Technol.* **2002**, *31*, 1024−1029.
(73) Partridge, J.; Dennison, P. R.; Moore, B. D.; Halling, P. J. Activity and mobility of subtilisin in low water organic media: hydration is more important than solvent dielectric. *Biochim. Biophys. Acta* **1998**, *1386*, 79−89.
(74) Giacomini, C.; Irazoqui, G.; Gonzalez, P.; Batista-Viera, F.; Brena, B. M. Enzymatic synthesis of galactosyl-xylose by *Aspergillus oryzae* β-galactosidase. *J. Mol. Catal. B: Enzym.* **2002**, *19*−*20*, 159−165.
(75) Bayón, C.; Cortés, A.; Aires-Trapote, A.; Civera, C.; Hernáiz, M. J. Highly efficient and regioselective enzymatic synthesis of β-(1→3) galactosides in biosolvents. *RSC Adv.* **2013**, *3*, 12155−12163.
(76) Sandoval, M.; Civera, C.; Berenguer, J.; García-Blanco, F.; Hernáiz, M. J. Optimised *N*-acetyl-D-lactosamine synthesis using *Thermus thermophilus* β-galactosidase in bio-solvents. *Tetrahedron* **2013**, *69*, 1148−1152.
(77) Goldfeder, M.; Egozy, M.; Shuster Ben-Yosef, V.; Adir, N.; Fishman, A. Changes in tyrosinase specificity by ionic liquids and sodium dodecyl sulfate. *Appl. Microbiol. Biotechnol.* **2013**, *97*, 1953−1961.
(78) Franke, J.; Braun, K.; Kuhl, P. Enzymatic synthesis of *N*-acetyllactosamine in aqueous-organic reaction media. *Pharmazie* **2003**, *58*, 857−859.
(79) Svensson, S. C. T.; Thiem, J. Purification of α-L-fucosidase by *C*-glycosylic affinity chromatography, and the enzymic synthesis of α-L-fucosyl disaccharides. *Carbohydr. Res.* **1990**, *200*, 391−402.
(80) Abels, C.; Thimm, K.; Wulfhorst, H.; Spiess, A. C.; Wessling, M. Membrane-based recovery of glucose from enzymatic hydrolysis of ionic liquid pretreated cellulose. *Bioresour. Technol.* **2013**, *149*, 58−64.
(81) Roberts, H. R.; Pettinati, J. D. Oligosaccharide production, concentration effects in the enzymatic conversion of lactose to oligosaccharides. *J. Agric. Food Chem.* **1957**, *5*, 130−134.
(82) Rastall, R. A.; Rees, N. H.; Wait, R.; Adlard, M. W.; Bucke, C. α-Mannosidase-catalysed synthesis of novel manno-, lyxo-, and hetero-manno-oligosaccharides: a comparison of kinetically and thermodynamically mediated approaches. *Enzyme Microb. Technol.* **1992**, *14*, 53−57.
(83) Baeza, R.; Pérez, A.; Sánchez, V.; Zamora, M. C.; Chirife, J. Evaluation of Norrish's equation for correlating the water activity of highly concentrated solutions of sugars, polyols, and polyethylene glycols. *Food Bioprocess Technol.* **2010**, *3*, 87−92.
(84) Finch, P.; Yoon, J. H. The effects of organic solvents on the synthesis of galactose disaccharides using β-galactosidases. *Carbohydr. Res.* **1997**, *303*, 339−345.
(85) Warmerdam, A.; Wang, J.; Boom, R. M.; Janssen, A. E. M. Effects of carbohydrates on the *o*NPG converting activity of β-galactosidases. *J. Agric. Food Chem.* **2013**, *61*, 6458−6464.
(86) Vetere, A.; Paoletti, S. High-yield synthesis of *N*-acetyllactosamine by regioselective transglycosylation. *Biochem. Biophys. Res. Commun.* **1996**, *219*, 6−13.
(87) Boon, M. A.; van't Riet, V.; Janssen, A. E. M. Enzymatic synthesis of oligosaccharides: product removal during a kinetically controlled reaction. *Biotechnol. Bioeng.* **2000**, *70*, 411−420.
(88) Ahmed, F.; Stein, A.; Lye, G. J. In-situ product removal to enhance the yield of biocatalytic reactions with competing equilibria: α-glucosidase catalysed synthesis of disaccharides. *J. Chem. Technol. Biotechnol.* **2001**, *76*, 971−977.
(89) Luo, J.; Nordvang, R. T.; Morthensen, S. T.; Zeuner, B.; Meyer, A. S.; Mikkelsen, J. D.; Pinelo, M. An integrated membrane system for the biocatalytic production of 3′-sialyllactose from dairy by-products. *Bioresour. Technol.* **2014**, *166*, 9−16.
(90) Sen, D.; Sarkar, A.; Das, S.; Chowdhury, R.; Bhattacharjee, C. Batch hydrolysis and rotating disk membrane bioreactor for the production of galacto-oligosaccharides: a comparative study. *Ind. Eng. Chem. Res.* **2012**, *51*, 10671−10681.
(91) Nath, A.; Bhattacharjee, C.; Chowdhury, R. Synthesis and separation of galacto-oligosaccharides using membrane bioreactor. *Desalination* **2013**, *316*, 31−41.
(92) Sen, D.; Sarkar, A.; Gosling, A.; Gras, S. L.; Stevens, G. W.; Kentish, S. E.; Bhattacharya, P. K.; Barber, A. R.; Bhattacharjee, C. Feasibility study of enzyme immobilization on polymeric membrane: a case study with enzymatically galacto-oligosaccharides production from lactose. *J. Membr. Sci.* **2011**, *378*, 471−478.
(93) Rodrigues, R. C.; Ortiz, C.; Berenguer-Murcia, Á.; Torres, R.; Fernández-Lafuente, R. Modifying enzyme activity and selectivity by immobilization. *Chem. Soc. Rev.* **2013**, *42*, 6290−6307.
(94) Feng, H. Y.; Drone, J.; Hoffmann, L.; Tran, V.; Tellier, C.; Rabiller, C.; Dion, M. Converting a β-glycosidase into a β-transglycosidase by directed evolution. *J. Biol. Chem.* **2005**, *280*, 37088−37097.
(95) Paris, G.; Ratier, L.; Amaya, M. F.; Nguyen, T.; Alzari, P. M.; Frasch, A. C. C. A sialidase mutant displaying *trans*-sialidase activity. *J. Mol. Biol.* **2005**, *345*, 923−934.
(96) Tran, V.; Hoffmann, L.; Rabiller, C.; Tellier, C.; Dion, M. Rational design of a GH1 β-glycosidase to prevent self-condensation during the transglycosylation reaction. *Protein Eng., Des. Sel.* **2010**, *23*, 43−49.
(97) Teze, D.; Hendrickx, J.; Czjzek, M.; Ropartz, D.; Sanejouand, Y. H.; Tran, V.; Tellier, C.; Dion, M. Semi-rational approach for converting a GH1 β-glycosidase into a β-transglycosidase. *Protein Eng., Des. Sel.* **2014**, *27*, 13−19.
(98) Buschiazzo, A.; Tavares, G. A.; Campetella, O.; Spinelli, S.; Cremona, M. L.; Paris, G.; Amaya, M. F.; Frasch, A. C.; Alzari, P. M. Structural basis of sialyltransferase activity in trypanosomal sialidases. *EMBO J.* **2000**, *19*, 16−24.
(99) Mitchell, F. L.; Miles, S. M.; Neres, J.; Bichenkova, E. V.; Bryce, R. A. Tryptophan as a molecular shovel in the glycosyl transfer activity of *Trypanosoma cruzi* trans-sialidase. *Biophys. J.* **2010**, *98*, L38−L40.
(100) Pierdominici-Sottile, G.; Horenstein, N. A.; Roitberg, A. E. Free energy study of the catalytic mechanism of *Trypanosoma cruzi trans*-sialidase. From the Michaelis complex to the covalent intermediate. *Biochemistry* **2011**, *50*, 10150−10158.
(101) Pierdominici-Sottile, G.; Palma, J.; Roitberg, A. E. Free-energy computations identify the mutations required to confer trans-sialidase activity into *Trypanosoma rangeli* sialidase. *Proteins: Struct., Funct., Bioinf.* **2014**, *82*, 424−435.
(102) Mackenzie, L. F.; Wang, Q.; Warren, R. A. J.; Withers, S. G. Glycosynthases: mutant glycosidases for oligosaccharide synthesis. *J. Am. Chem. Soc.* **1998**, *120*, 5583−5584.
(103) Bojarová, P.; Křen, V. Glycosidases: a key to tailored carbohydrates. *Trends Biotechnol.* **2009**, *27*, 199−209.
(104) Shaikh, F. A.; Withers, S. G. Teaching old enzymes new tricks: engineering and evolution of glycosidases and glycosyl transferases for improved glycoside synthesis. *Biochem. Cell. Biol.* **2008**, *86*, 169−177.
(105) Cobucci-Ponzano, B.; Strazzulli, A.; Rossi, M.; Moracci, M. Glycosynthases in biocatalysis. *Adv. Synth. Catal.* **2011**, *353*, 2284−2300.
(106) Williams, S. J.; Withers, S. G. Glycosyl fluorides in enzymatic reactions. *Carbohydr. Res.* **2000**, *327*, 27−46.
(107) Perugino, G.; Trincone, A.; Rossi, M.; Moracci, M. Oligosaccharide synthesis by glycosynthases. *Trends Biotechnol.* **2004**, *22*, 31−37.
(108) Wada, J.; Honda, Y.; Nagae, M.; Kato, R.; Wakatsuki, S.; Katayama, T.; Taniguchi, H.; Kumagai, H.; Kitaoka, M.; Yamamoto, K. 1,2-α-L-Fucosynthase: a glycosynthase derived from an inverting α-glycosidase with an unusual reaction mechanism. *FEBS Lett.* **2008**, *582*, 3739−3743.

(109) Cobucci-Ponzano, B.; Conte, F.; Bedini, E.; Corsaro, M. M.; Parrilli, M.; Sulzenbacher, G.; Lipski, A.; Dal Piaz, F.; Lepore, L.; Rossi, M.; Moracci, M. $\beta$-Glycosyl azides as substrates for $\alpha$-glycosynthases: preparation of efficient $\alpha$-L-fucosynthases. *Chem. Biol.* **2009**, *16*, 1097−1108.
(110) Sakurama, H.; Fushinobu, S.; Hidaka, M.; Yoshida, E.; Honda, Y.; Ashida, H.; Kitaoka, M.; Kumagai, H.; Yamamoto, K.; Katayama, T. 1,3−1,4-$\alpha$-L-Fucosynthase that specifically introduces Lewis a/x antigens into type-1/2 chains. *J. Biol. Chem.* **2012**, *287*, 16709−16719.
(111) Watson, J. N.; Dookhun, V.; Borgford, T. J.; Bennet, A. J. Mutagenesis of the conserved active-site tyrosine changes a retaining sialidase into an inverting sialidase. *Biochemistry* **2003**, *42*, 12682−12690.
(112) Newstead, S.; Watson, J. N.; Knoll, T. L.; Bennet, A. J.; Taylor, G. Structure and mechanism of action of an inverting mutant sialidase. *Biochemistry* **2005**, *44*, 9117−9122.
(113) Watson, J. N.; Indurugalla, D.; Cheng, L. L.; Narine, A. A.; Bennet, A. J. The hydrolases and transferase activity of an inverting mutant sialidase using non-natural $\beta$-sialoside substrates. *Biochemistry* **2006**, *45*, 13264−13275.
(114) Mohapatra, M.; Anand, S.; Mishra, B. K.; Giles, D. E.; Singh, P. Review of fluoride removal from drinking water. *J. Environ. Manage.* **2009**, *91*, 67−77.
(115) Tanaka, H.; Ito, F.; Iwasaki, T. A system for sialic acid transfer by colominic acid and a sialidase that preferentially hydrolyzes sialyl $\alpha$-2,8 linkages. *Biosci., Biotechnol., Biochem.* **1995**, *59*, 638−643.
(116) Makimura, Y.; Ishida, H.; Kondo, A.; Hasegawa, A.; Kiso, M. Regioselective $\alpha(2\rightarrow3)$-sialylation of $Le^x$ and $Le^a$ by sialidase-catalyzed transglycosylation. *J. Carbohydr. Chem.* **1998**, *17*, 975−979.

>0.99. For method validation, intraday ($n$ = 5) and interday ($n$ = 5) accuracy and precision were determined by repeated analysis of three QC samples (10, 200, and 1000 ng/mL), and the resulting accuracy (as a percent difference from nominal values) and precision (as a percent relative standard deviation) did not exceed ±15% for all QC samples tested.

**Assay of β-D-glucosidase, α-L-rhamnosidase, and β-D-galactosidase Activities.** The enzyme activities were measured according to the previously reported method.[18]

**Statistical Analysis.** Data were presented as means ± standard deviation (SD). The statistical significance of the data was analyzed using Student's $t$ test. Differences at $p < 0.05$ were considered statistically significant.

## RESULTS AND DISCUSSION

In this study, we investigated the effects of the gut microbiota on the bioavailability of geniposide, a principal ingredient of *Gardenia* fruits, by using an antibiotics-treated rat model. We optimized the conditions for developing the antibiotics-treated rat model in our preliminary study; we examined the effects of several antibiotics and their combinations on the gut microbiota on the basis of their glycosidase activities (data not shown). Our results showed that an antibiotic mixture consisting of cefadroxil, oxytetracycline, and erythromycin showed the greatest inhibitory effect on metabolism by the gut microorganims and, thus, we used this mixture for treating the rats. Treatment with a mixture of these antibiotics significantly decreased the glycosidase activities of the intestinal microorganisms of the rat, including those of glucosidase, rhamnosidase, and galactosidase, and these effects lasted at least 2 days after the treatment (Figure 1).

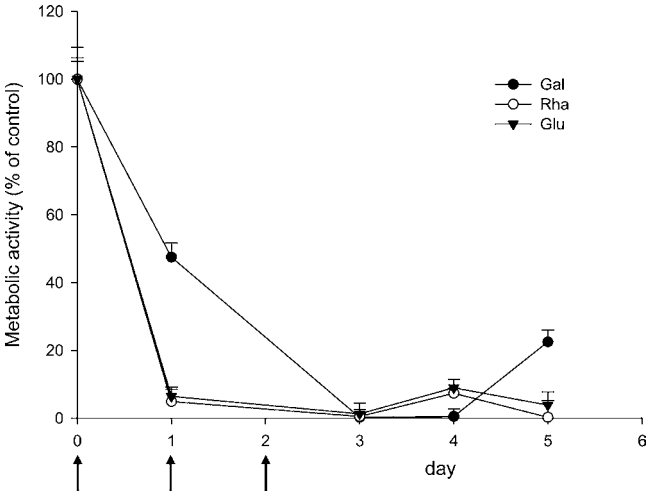


**Figure 1.** β-D-glucosidase (Glu), β-D-galactosidase (Gal), and α-L-rhamnosidase (Rha) activities in fecal samples of antibiotics-treated rats ($n$ = 3). Rats were orally administered cefadroxil (100 mg/kg), oxytetracyclin (300 mg/kg), and erythromycin (300 mg/kg) once per day for 3 days, and the fecal metabolic activities were measured for 5 days. Arrows indicate the administration of the antibiotic mixture. The control value represents the data measured before antibiotic treatment.

On the basis of the results of the intestinal metabolic activity profiles, we performed a pharmacokinetic analysis 2 days after the antibiotics treatment to rule out any possible pharmacokinetic interactions between the antibiotics and geniposide.

We administered GF to the rats to investigate the plasma pharmacokinetics of geniposide. GF is a standardized extract of *Gardenia* fruits, which contains geniposide as a principal ingredient (41.7%) and has trace amounts of genipin (<1.0%). Therefore, any possible effects caused by the biotransformation of GF-originated genipin can be excluded from the interpretation of the results of the pharmacokinetic data of geniposide.

After oral administration of GF to control and antibiotics-treated rats, geniposide level was determined in plasma and feces using LC-MS/MS. Representative LC-MS/MS chromatograms for geniposide are shown in Figure 2. The mean plasma concentration−time profiles of geniposide after oral administration of GF to control and antibiotics-treated rats are shown in Figure 3, and the pharmacokinetic parameters are summarized in Table 1. A marked difference was observed in the time to reach the maximum plasma concentration ($T_{max}$) and area under the curve (AUC) values between the control and antibiotics-treated groups (Table 1); the $T_{max}$ values were 1.69 and 3.13 h and the AUC values were 7.34 and 11.9 μg·h/mL, respectively, in the control and antibiotics-treated groups. A higher AUC value in the antibiotics-treated rats indicated that uptake of geniposide from the gastrointestinal tract increased by suppression of the enzyme activities of the intestinal microorganisms and subsequent increase in the concentration of unmetabolized geniposide.

**Table 1. Pharmacokinetic Parameters of Geniposide after Oral Administration in Control and Antibiotics-Treated Rats ($n$ = 4)**

| parameter | control | antibiotics-treated |
|---|---|---|
| $C_{max}$ | 0.91 ± 0.26 | 1.01 ± 0.04 |
| $T_{max}$ (h) | 1.69 ± 1.72 | 3.13 ± 2.39 |
| $T_{\lambda 1/2}$ (h) | 3.49 ± 1.13 | 3.28 ± 0.22 |
| AUC (μg·h/mL) | 7.34 ± 3.32 | 11.9 ± 2.1*[a] |

[a]*, $p < 0.05$, significant difference compared with control group.

The level of geniposide in the feces was determined to confirm that the biotransformation of geniposide to genipin was attenuated by treatment with antibiotics. The amounts of geniposide in the feces of the control and antibiotics-treated rats were 0.64 ± 0.96 and 15.6 ± 3.2 mg, respectively ($p < 0.01$). The significant increase in the level of fecal geniposide in the antibiotics-treated rats may be because of an increase in unabsorbed geniposide or an increase in the excretion of geniposide via the biliary route. However, in both circumstances, the increase can be attributed to an increase in the level of unmetabolized geniposide. The prolonged $T_{max}$ values in the antibiotics-treated rats could be understood in this context. Thus, the above factors may explain the prolonged $T_{max}$ values as well as the increased AUC values in antibiotics-treated rats.

Functional foods or medicinal plants have several different glycoside compounds as their bioactive ingredients. These glycoside compounds may be transformed to active, nonactive, or toxic metabolites by the intestinal bacterial glycosidase and, then, are absorbed from the gastrointestinal tract.[19] Therefore, alteration or differences in the profile and composition of the intestinal microbiota may lead to different metabolic capabilities of the gut microbiota and, consequently, result in different bioavailabilities of the bioactive ingredients. Thus, individual differences in the gut microbiota may cause different biological effects in individuals after consumption of functional foods. In addition, alterations in the intestinal microbiota induced by medication or pathological conditions may affect the biological activities of functional foods.

The role of gut microbiota in the metabolism of dietary compounds or phytochemicals and the resultant impacts on

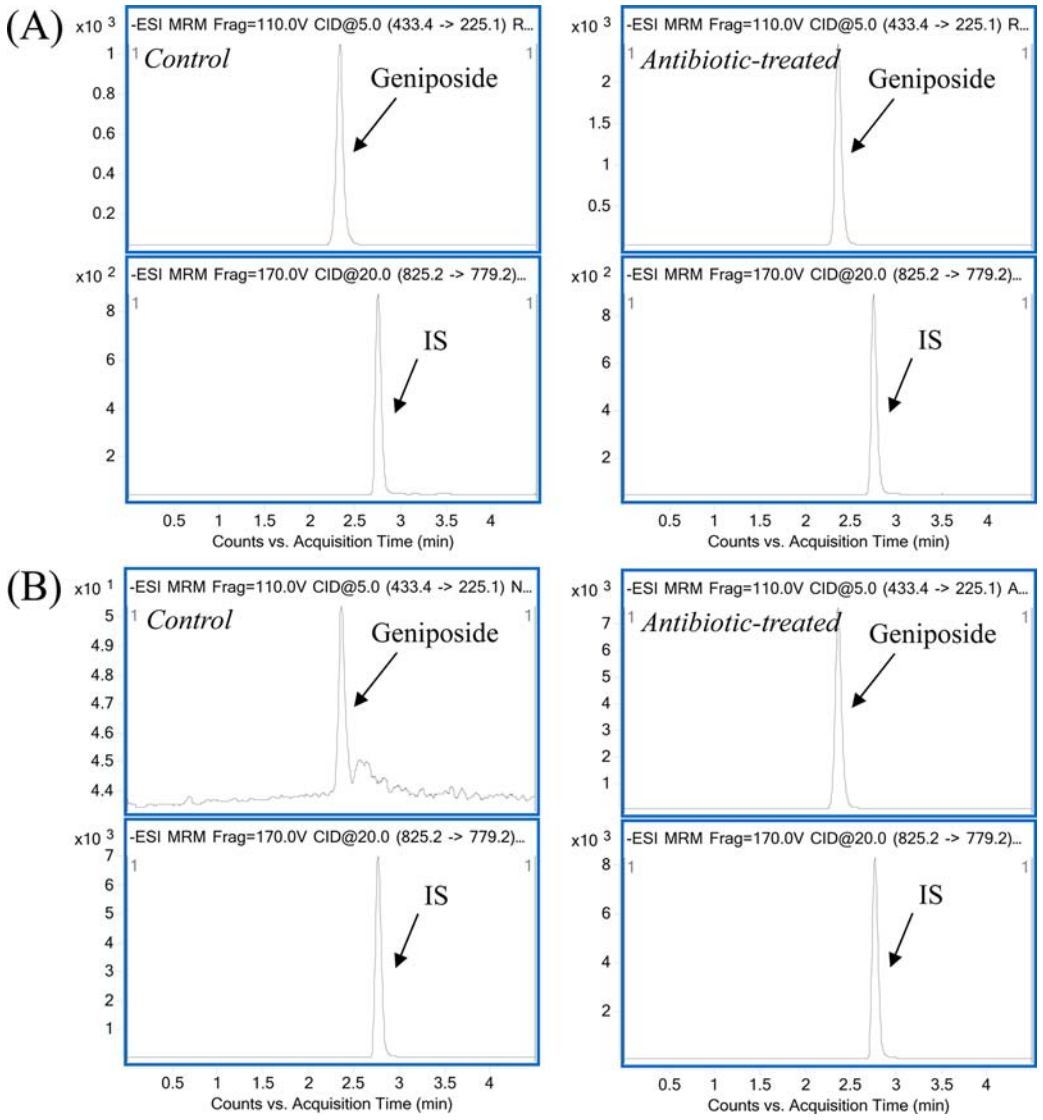


**Figure 2.** Representative LC-MS/MS chromatograms for geniposide in (A) plasma and (B) feces samples from control (left) and antibiotics-treated (right) rats. IS, internal standard (digoxin).

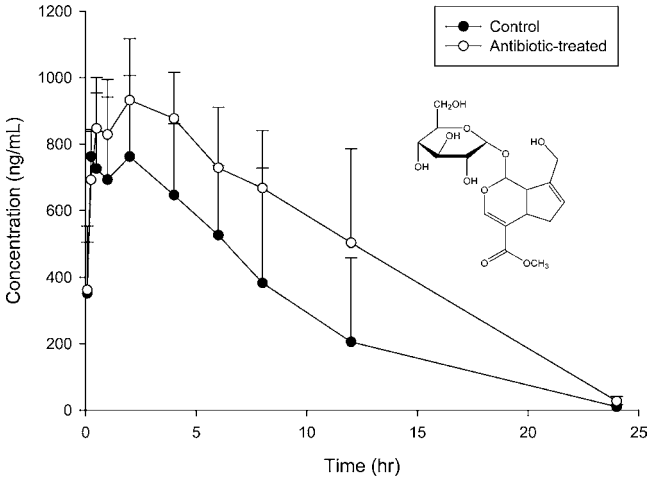


**Figure 3.** Mean plasma concentration−time profile of geniposide after oral administration of GF (equivalent to 250 mg/kg of geniposide) in control and antibiotics-treated rats ($n$ = 4).

bioactivity or toxicity have been extensively investigated.[20−24] Cycasin, a phytotoxin found in cycad trees, is hydrolyzed into the carcinogenic metabolite, methylazoxymethanol, by gut microbial enzymes and directly exerts its toxic effect.[25] Rutin, a citrus flavonoid glycoside found in many plants, also undergoes gut microbiota-mediated hydrolysis to yield its corresponding aglycone (quercetin) and phenolic metabolites, which may cause mutagenic effects.[26] Meanwhile, 2-methoxyestrone is converted to the active steroid form via demethylation, in which gut microbiota are believed to play an important role.[27] Microbial metabolism potentiates the clinical effects of baicalin by hydrolyzing it to generate its corresponding aglycone baicalein, which is readily absorbable and subject to reconjugation into baicalin.[28] Previously, we reported that the pharmacokinetics of hesperidin, a bioactive citrus flavonoid glycoside, was modulated by alteration of the metabolic activities of the intestinal microorganisms.[18]

In conclusion, our study showed that bioavailability of geniposide may depend on its metabolism by the gut microbiota. Thus, alterations in gut microbiota by external factors such as medications, pathological conditions, and food habits


dx.doi.org/10.1021/jf502557f | J. Agric. Food Chem. 2014, 62, 9632−9636

affect the bioavailability of geniposide. Geniposide possesses various biological activities; however, a recent study indicates that it may have toxic effects,[29] and a recent study has shown that human intestinal bacteria may affect the toxicity of geniposide through involvement in the biotransformation to genipin, its toxic metabolite.[30] Therefore, gut microbiota should be considered as a critical factor for understanding the clinical effects of geniposide.

**Ming Ji Jin**[†]
**In Sook Kim**[†]
**Dong-Hyun Kim***[,§]
**Hye Hyun Yoo***[,†]

[†]Institute of Pharmaceutical Science and Technology and College of Pharmacy, Hanyang University, Ansan, Gyeonggi-do, Korea
[§]Department of Pharmacy, College of Pharmacy, Kyung Hee University, Dongdaemun-gu, Seoul, Korea

## AUTHOR INFORMATION

### Corresponding Authors

*(H.H.Y.) Mail: College of Pharmacy, Hanyang University, 55 Hanyangdaehak-ro, Sangnok-gu, Ansan-si, Gyeonggi-do 426-791, Korea. Phone: +82-31-400-5804. Fax: +82-31-400-5958. E-mail: yoohh@hanyang.ac.kr.

*(D.-H.K.) Department of Life and Nanopharmaceutical Sciences and Department of Pharmacy, College of Pharmacy, Kyung Hee University, Dongdaemun-gu, Seoul 130-701, Korea. Phone: +82-2-961-0374. Fax: + 82-2-966-2297. E-mail: dhkim@khu.ac.kr.

### Notes

The authors declare no competing financial interest.

### Funding

This research was supported in part by a grant (09172KFDA996) from the Korea Food and Drug Administration and in part by the Basic Science Research Program through the National Research Foundation of Korea (NRF) funded by the Ministry (NRF-2014R1A1A1A05002840).

## REFERENCES

(1) Hsu, H.-Y.; Yang, J.-J.; Lin, S.-Y.; Lin, C.-C. Comparisons of geniposidic acid and geniposide on antitumor and radioprotection after sublethal irradiation. *Cancer Lett.* **1997**, *113*, 31−37.

(2) Koo, H.-J.; Lee, S.; Shin, K.-H.; Kim, B.-C.; Lim, C.-J.; Park, E.-H. Geniposide, an anti-angiogenic compound from the fruits of *Gardenia jasminoides*. *Planta Med.* **2004**, *70*, 467−469.

(3) Koo, H.-J.; Lim, K.-H.; Jung, H.-J.; Park, E.-H. Anti-inflammatory evaluation of gardenia extract, geniposide and genipin. *J. Ethnopharmacol.* **2006**, *103*, 496−500.

(4) Liaw, J.; Chao, Y.-C. Effect of in vitro and in vivo aerosolized treatment with geniposide on tracheal permeability in ovalbumin-induced guinea pigs. *Eur. J. Pharmacol.* **2001**, *433*, 115−121.

(5) Suzuki, Y.; Kondo, K.; Ikeda, Y.; Umemura, K. Antithrombotic effect of geniposide and genipin in the mouse thrombosis model. *Planta Med.* **2001**, *67*, 807−810.

(6) Chang, W.-L.; Wang, H.-Y.; Shi, L.-S.; Lai, J.-H.; Lin, H.-C. Immunosuppressive iridoids from the fruits of *Gardenia jasminoides*. *J. Nat. Prod.* **2005**, *68*, 1683−1685.

(7) Lee, P.; Lee, J.; Choi, S. Y.; Lee, S. E.; Lee, S.; Son, D. Geniposide from *Gardenia jasminoides* attenuates neuronal cell death in oxygen and glucose deprivation-exposed rat hippocampal slice culture. *Biol. Pharm. Bull.* **2006**, *29*, 174.

(8) Liu, J. H.; Yin, F.; Guo, L. X.; Deng, X. H.; Hu, Y. H. Neuroprotection of geniposide against hydrogen peroxide induced PC12 cells injury: involvement of PI3 kinase signal pathway. *Acta Pharmacol. Sin.* **2009**, *30*, 159−165.

(9) Wu, S. Y.; Wang, G. F.; Liu, Z. Q.; Rao, J. J.; Lü, L.; Xu, W.; Wu, S. G.; Zhang, J. J. Effect of geniposide, a hypoglycemic glucoside, on hepatic regulating enzymes in diabetic mice induced by a high-fat diet and streptozotocin. *Acta Pharmacol. Sin.* **2009**, *30*, 202−208.

(10) Kojima, K.; Shimada, T.; Nagareda, Y.; Watanabe, M.; Ishizaki, J.; Sai, Y.; Miyamoto, K.-i.; Aburada, M. Preventive effect of geniposide on metabolic disease status in spontaneously obese type 2 diabetic mice and free fatty acid-treated HepG2 cells. *Biol. Pharm. Bull.* **2011**, *34*, 1613−1618.

(11) Chen, Q. C.; Zhang, W. Y.; Kim, H.; Lee, I. S.; Ding, Y.; Youn, U. J.; Lee, S. M.; Na, M.; Min, B. S.; Bae, K. Effects of gardeniae fructus extract and geniposide on promoting ligament cell proliferation and collagen synthesis. *Phytother. Res.* **2010**, *24*, S1−S5.

(12) Hou, Y.; Tsai, S.-Y.; Lai, P.; Chen, Y.; Chao, P. Metabolism and pharmacokinetics of genipin and geniposide in rats. *Food Chem. Toxicol.* **2008**, *46*, 2764−2769.

(13) Ueno, K.; Takeda, Y.; Iwasaki, Y.; Yoshizaki, F. Simultaneous estimation of geniposide and genipin in mouse plasma using high-performance liquid chromatography. *Anal. Sci.* **2001**, *17*, 1237−1239.

(14) Wang, F.; Cao, J.; Hao, J.; Liu, K. Pharmacokinetics, bioavailability and tissue distribution of geniposide following intravenous and peroral administration to rats. *Biopharm. Drug Dispos.* **2013**, *35*, 97−103.

(15) Cheng, S.; Lin, L. C.; Lin, C. H.; Tsai, T. H. Comparative oral bioavailability of geniposide following oral administration of geniposide, *Gardenia jasminoides* Ellis fruits extracts and *Gardenia* herbal formulation in rats. *J. Pharm. Pharmacol.* **2014**, *66*, 705−712.

(16) Akao, T.; Kobashi, K.; Aburada, M. Enzymic studies on the animal and intestinal bacterial metabolism of geniposide. *Biol. Pharm. Bull.* **1994**, *17*, 1573−1576.

(17) Jin, M. J.; Kim, I. S.; Kim, D.-H.; Yoo, H. H. Liquid chromatography-tandem mass spectrometric determination of geniposide in rat plasma and its pharmacokinetic application. *Bull. Korean Chem. Soc.* **2013**, *34*, 2760−2764.

(18) Jin, M. J.; Kim, U.; Kim, I. S.; Kim, Y.; Kim, D.-H.; Han, S. B.; Kwon, O.-S.; Yoo, H. H. Effects of gut microflora on pharmacokinetics of hesperidin: a study on non-antibiotic and pseudo-germ-free rats. *J. Toxicol. Environ. Health Part A* **2010**, *73*, 1441−1450.

(19) Yim, J.-S.; Kim, Y.-S.; Moon, S.-K.; Cho, K.-H.; Bae, H.-S.; Kim, J.-J.; Park, E.-K.; Kim, D.-H. Metabolic activities of ginsenoside Rb1, baicalin, glycyrrhizin and geniposide to their bioactive compounds by human intestinal microflora. *Biol. Pharm. Bull.* **2004**, *27*, 1580−1583.

(20) Saad, R.; Rizkallah, M. R.; Aziz, R. K. Gut pharmacomicrobiomics: the tip of an iceberg of complex interactions between drugs and gut-associated microbes. *Gut Pathog.* **2012**, *4*, 16.

(21) Selma, M. V.; Espín, J. C.; Tomaś-Barberań, F. A. Interaction between phenolics and gut microbiota: role in human health. *J. Agric. Food Chem.* **2009**, *57*, 6485−6501.

(22) Tomás-Barberán, F. A.; Mine, Y. A key to understanding the effects of food bioactives in health, gut microbiota. *J. Agric. Food Chem.* **2013**, *61*, 9755−9757.

(23) Jeong, H. G.; Kang, M. J.; Kim, H. G.; Oh, D. G.; Kim, J. S.; Lee, S. K.; Jeong, T. C. Role of intestinal microflora in xenobiotic-induced toxicity. *Mol. Nutr. Food Res.* **2013**, *57*, 84−99.

(24) Kang, M. J.; Kim, H. G.; Kim, J. S.; Oh, D. G.; Um, Y. J.; Seo, C. S.; Han, J. W.; Cho, H. J.; Kim, G. H.; Jeong, T. C.; Jeong, H. G. The effect of gut microbiota on drug metabolism. *Expert Opin. Drug Metab. Toxicol.* **2013**, *9*, 1295−1308.

(25) Spatz, M.; Smith, D.; McDaniel, E.; Laqueur, G. Role of intestinal microorganisms in determining cycasin toxicity. *Exp. Biol. Med.* **1967**, *124*, 691−697.

(26) Rowland, I. R. Interactions of the gut microflora and the host in toxicology. *Toxicol. Pathol.* **1988**, *16*, 147−153.

(27) Axelson, M.; Sjövall, J. Formation of catechol estrogens by intestinal bacterial demethylation of 2-methoxyestrone. *Biochim. Biophys. Acta* **1983**, *751*, 162−165.

(28) Akao, T.; Kawabata, K.; Yanagisawa, E.; Ishihara, K.; Mizuhara, Y.; Wakui, Y.; Sakashita, Y.; Kobashi, K. Balicalin, the predominant flavone glucuronide of scutellariae radix, is absorbed from the rat gastrointestinal tract as the aglycone and restored to its original form. *J. Pharm. Pharmacol.* **2000**, *52*, 1563−1568.
(29) Ding, Y.; Zhang, T.; Tao, J. S.; Zhang, L. Y.; Shi, J. R.; Ji, G. Potential hepatotoxicity of geniposide, the major iridoid glycoside in dried ripe fruits of *Gardenia jasminoides* (Zhi-zi). *Nat. Prod. Res.* **2013**, *27*, 929−933.
(30) Kang, M. J.; Khanal, T.; Kim, H. G.; Lee, D. H.; Yeo, H. K.; Lee, Y. S.; Ahn, Y. T.; Kim, D. H.; Jeong, H. G.; Jeong, T. C. Role of metabolism by human intestinal microflora in geniposide-induced toxicity in HepG2 cells. *Arch. Pharm. Res.* **2012**, *35*, 733−738.

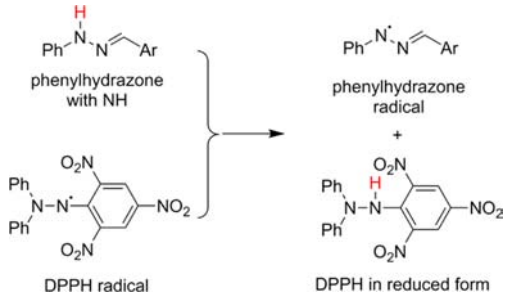


**Figure 1.** Reaction pattern of phenylhydrazones with DPPH radical proposed by predecessors,[28] in which the NH proton is necessary for the radical scavenging activity.

## METHODS

Materials and spectral data are presented in the Supporting Information.

**Synthesis and Purification.** The reaction route is outlined in Scheme 1. The previously reported protocol[29] has been adopted for preparing **2** and **3**. The authors changed "heating" to a milder "sun light at room temperature" condition in the bromination step. In the purification step, because of their similar polarities, single and double brominated substances along with nonbrominated compound **2** were collected together from a column using petroleum ether−EtOAc (2:1). Then, the mixture was oxidized by DMSO to give aldehyde **3** which was later purified by column (petroleum ether−EtOAc = 5:1). The preparations of **5a**−**5z** and **6a**−**6z** were performed according to the methods described by Harden et al.[30] and Belkheiri et al.,[25] respectively. The substituents introduced here include −Me, −OMe, −F, −Cl, −Br, $-NO_2$, $-CF_3$, $-OCF_3$, and −CN. Hydrazone crystals precipitated from methanol in the last step were filtered and washed gently with petroleum ether.

**Crystallographic Study.** The crystal of **6x** was obtained directly from mother methanol liquor without recrystallization. X-ray single-crystal diffraction data for compound **6x** were collected on a Bruker SMART AEPEX CCD diffractometer at 273(2) K using Mo K$\alpha$ radiation ($\lambda$ = 0.71073 Å) by the $\pi$ and $\omega$ scan mode. The program SAINT was used for integration of the diffraction profiles. The structure was solved by direct methods using the SHELXS program of the SHELXTL package and refined by full-matrix least-squares methods with SHELXL.[31] All non-hydrogen atoms of compound **6x** were refined with anisotropic thermal parameters. All hydrogen atoms were placed in geometrically idealized positions and constrained to ride on their parent atoms.

**Antifungal Activity Assay.** The antifungal activity was evaluated as reported protocols.[32,33] Preliminary determination of the inhibitory activity of compounds **6a**−**6z** against four plant-pathogenic fungi (*Rhizoctonia solani*, *Fusarium graminearum*, *Sclerotinia sclerotiorum*, and *Phytophthora capsici*) was conducted *in vitro* by using the mycelial growth test on PDA (Potato Dextrose Agar) medium. The compounds were dissolved in DMSO and then mixed with sterile molten PDA to obtain final concentrations of 10 $\mu g \cdot mL^{-1}$ (containing 4‰ DMSO). PDA with different compounds was poured into 90 mm Petri dishes (15 $mL \cdot dish^{-1}$), on which 5 mm mycelial disks of the four fungi were planted in the center. The disks were obtained from a pure PDA culture plate by punching at the edge of the actively growing mycelia colony. Three replicates were conducted for each treatment. The widely used commercial fungicides validamycin A and

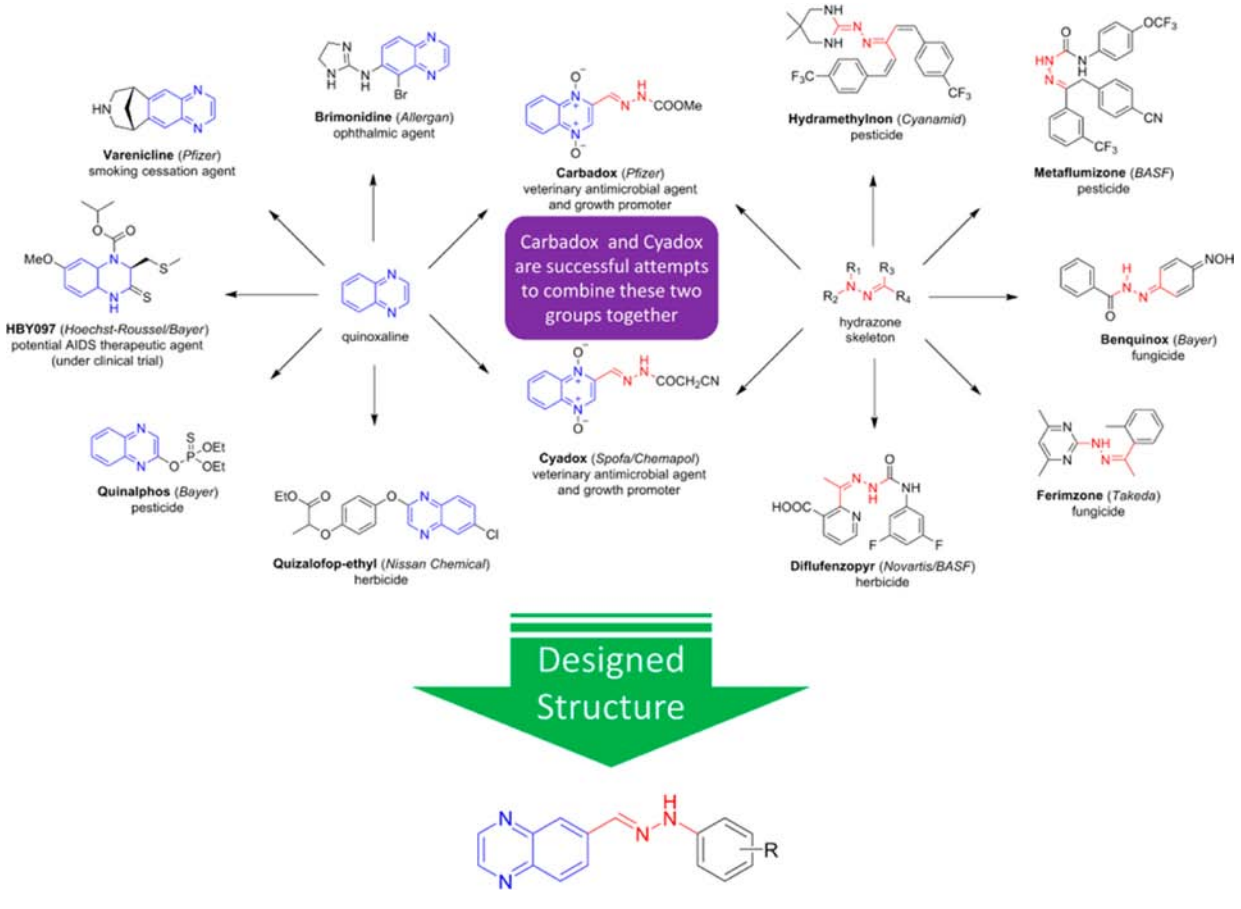


**Figure 2.** Design of the target structure: Above are examples of quinoxaline and hydrazone derivatives commercialized or under clinical trials as agrochemicals or pharmaceuticals. There are earlier successful attempts as Carbadox and Cyadox of combining the two groups together. Herein, we designed the structure below to discover novel biologically active candidates.


dx.doi.org/10.1021/jf504359p | J. Agric. Food Chem. 2014, 62, 9637−9643

**Scheme 1. Synthesis Route and Structures of the Phenylhydrazone Analogues**[a]

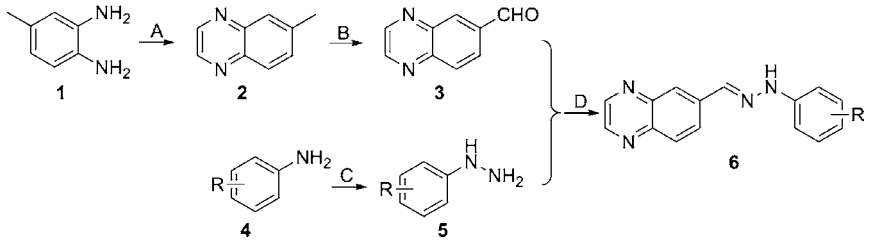


| | R= | | R= | | R= | | R= | | R= | | R= |
|---|---|---|---|---|---|---|---|---|---|---|---|
| **6a** | H | **6e** | 4-$OCH_3$ | **6i** | 2,4-F | **6n** | 2,5-Cl | **6r** | 2-Br | **6v** | 2-$CF_3$ |
| **6b** | 2-$CH_3$ | **6f** | 2-F | **6j** | 3-Cl-4-F | **6o** | 2,6-Cl | **6s** | 4-Br | **6w** | 3-$CF_3$ |
| **6c** | 3-$CH_3$ | **6g** | 3-F | **6k** | 2-Cl | **6p** | 3,4-Cl | **6t** | 4-$NO_2$ | **6x** | 4-$CF_3$ |
| **6d** | 4-$CH_3$ | **6h** | 4-F | **6l** | 3-Cl | **6q** | 2,4,6-Cl | **6u** | 2,4-$NO_2$ | **6y** | 4-$OCF_3$ |
| | | | | **6m** | 4-Cl | | | | | **6z** | 4-CN |

[a](A) oxalaldehyde (40% aqueous), $Na_2CO_3$, 100 °C, 2 h. (B) (i) NBS, benzoyl peroxide, $CCl_4$, sun light, r.t., 3−4 h; (ii) $NaHCO_3$, DMSO, 120 °C, 2 h. (C) (i) HCl, $NaNO_2$, 0 °C, 1 h; (ii) $SnCl_2$, 0 °C, 30 min, r.t., 1 h; (iii) NaOH (40%), pH 7. (D) MeOH, r.t.

**Table 1. Crystallographic Data of Compound 6x**

| compound | **6x** |
|---|---|
| chemical formula | $C_{16}H_{11}F_3N_4$ |
| formula weight | 316.29 |
| crystal system | monoclinic |
| space group | $P2_1/c$ |
| crystal color | light yellow |
| $a$ (Å) | 15.322(4) |
| $b$ (Å) | 8.462(2) |
| $c$ (Å) | 11.824(3) |
| $\alpha$ (deg) | 90.00 |
| $\beta$ (deg) | 106.013(9) |
| $\gamma$ (deg) | 90.00 |
| $V$ (Å) | 1473.5(7) |
| $Z$ | 4 |
| $D_{calc}$ (g·cm$^{-3}$) | 1.426 |
| $\theta$ range (deg) | 2.77−25.71 |
| $hkl$ range | $-16 \le h \le 18$; $-10 \le k \le 10$; $-14 \le l \le 14$ |
| $F$(0 0 0) | 648 |
| no. collected refl. | 13602 |
| no. ind. refl. ($R_{int}$) | 2806 (0.0584) |
| data/restraints/parameters | 2806/0/208 |
| absorption coefficient (mm$^{-1}$) | 0.115 |
| $R_1$; $wR_2$ [$I > 2\sigma(I)$] | 0.0822; 0.2189 |
| $R_1$; $wR_2$ (all data) | 0.1456; 0.2448 |
| GOOF | 0.956 |

carbendazim were co-tested as positive controls while mere DMSO (4‰ contained in PDA) as negative control. After a certain incubation period (1.5 d for *R. solani*, 3 d for *F. graminearum*, 2.5 d for *S. sclerotiorum*, and 4 d for *P. capsici*, according to their different mycelial growth rates) at 25 °C in the dark, mycelial growth diameters were measured. The inhibition percentages were calculated as $(B - A)/(B - 5) \times 100\%$, where $A$ is the mycelial diameter (mm) in Petri dishes with compounds and $B$ is the diameter (mm) of the negative control.

Furthermore, the fungicidal activity of these compounds against *R. solani* was assessed in the same method as above. According to the preliminary test, these compounds were dissolved in DMSO to obtain different final concentration grads. Mycelial growth diameters were measured, and the inhibition percentages relative to the control with 4‰ DMSO were calculated. The $EC_{50}$ values were calculated using linear-regression analysis.

**DPPH Radical Scavenging Assay (RSA).** The scavenging rate of DPPH radical was carried out by the improved protocol of previous literatures.[34,35] Briefly, in 96-well microliter plates, 100 μL of different concentrations (2.5, 5, 10, 20, 40, 80, and 160 μg·mL$^{-1}$ in EtOH) of compounds **6a−6z** were mixed with 100 μL of DPPH solution (0.2 mmol·L$^{-1}$ in EtOH) to be detected as $OD_{6a}$−$OD_{6z}$. 100 μL of different concentrations (as above) of these compounds were mixed with 100 μL of EtOH to be detected as $OD_{6a}'$−$OD_{6z}'$. 100 μL of DPPH was mixed with 100 μL of EtOH to be detected as $OD_{blank}$. 200 μL of EtOH was to be detected as $OD_E$. And 100 μL of different concentrations (as above) of Trolox (positive control) were mixed with 100 μL of DPPH solution to be detected as $OD_T$. The reaction mixtures were shaken vigorously and stored in the dark at 25 °C for 30 min, and the absorbance (OD) was measured at 517 nm using a SpectraMax M5 microplate reader. All of the assays were performed


dx.doi.org/10.1021/jf504359p | J. Agric. Food Chem. 2014, 62, 9637−9643

three times. The radical scavenging rate was measured as a decrease in the OD of DPPH and was calculated using the following equation:

$$\text{scavenging rate } \% = 100 \times [(OD_{blank} - OD_E) - (OD_{6(a-z)} - OD_{6(a-z)}')]/(OD_{blank} - OD_E)$$

The concentration of a certain compound necessary to decrease the initial DPPH concentration by 50% ($EC_{50}$ $\mu g \cdot mL^{-1}$) was determined by linear regression analysis of data obtained by plotting the scavenging rate % against the concentrations of that compound.

**Inhibition of Microsomal LPO.** Mouse liver microsomes used for the LPO studies were prepared adopting the method in the literature.[36] The adult male mice (8−12 weeks old) of Kunming strain (purchased from the Comparative Medicine Center of Yangzhou University) were used for the preparation of liver microsomes. The protein content of microsomes was measured using the method in the literature.[37] Briefly, microsomes (0.67 mg of protein/mL) were incubated at 37 °C for 60 min with test compounds at varying concentrations, 10 mM $FeSO_4$ and 0.1 mM ascorbic acid in 1.0 mL of potassium phosphate buffer solution (0.2 M, pH 7.4). Afterward, the reaction was stopped by 20% (w/v) trichloroacetic acid (1.0 mL) and 0.67% (w/v) 2-thiobarbituric acid (1.5 mL) in succession. Then, the solution was heated to 100 °C for 15 min. After centrifugation of precipitated protein, the absorbance (OD) of the color reaction of malondialdehyde (MDA)−TBA complex was detected at 535 nm by a SpectraMax M5 microplate reader. Trolox was the positive control. In the same way as DPPH-RSA, the inhibition rates and $EC_{50}$ ($\mu g \cdot mL^{-1}$) values were determined.

## RESULTS AND DISCUSSION

**Synthesis.** The synthetic procedure for the title compounds is illustrated in Scheme 1. The condensation of 4-methylbenzene-1,2-diamine (**1**) and oxalaldehyde gave 6-methylquinoxaline (**2**) in high yield (85%). Next, **2** was bromized by *N*-bromosuccinimide. This free radical reaction was initialized by benzoyl peroxide giving single and double brominated substances, which were later oxidized by DMSO under base conditions to give quinoxaline-6-carbaldehyde (**3**). The yield from **2** to **3** is 33%. In order to investigate how substituents on the phenyl ring influence the activities, 26 substituted anilines were treated to give the final products. The anilines **4(a−z)** were diazotized by $NaNO_2$ to give substituted benzenediazoniums, which were then reduced by $SnCl_2$ to give substituted phenylhydrazines **5(a−z)** in 60−80% yield. Finally, **3** and **5(a−z)** were condensed to form the —C═N—NH— bond, giving (*E*)-6-((2-phenylhydrazono)methyl)quinoxaline derivatives **6(a−z)** in 62−84% yield. $^1H$ NMR, $^{13}C$ NMR, and ESI-MS spectra and elemental analysis data of the achieved compounds given in the Supporting Information were in full accordance with their assigned structures.

**The Crystal Structure of Compound 6x.** The crystal data of compound **6x** are presented in Table 1, and Figure 3 gives a perspective view of **6x** with the atomic labeling system.[38] The result demonstrates the —C═N—NH— bond bears an (*E*) rather than (*Z*) conformation.

**Antifungal Activities *in Vitro*.** The preliminary determination of the inhibition rates of compounds **6a−6z** (10 $\mu g \cdot mL^{-1}$) against four plant-pathogenic fungi (*R. solani*, *F. graminearum*, *S. sclerotiorum*, and *P. capsici*) is shown in Table 2. The data suggest that all the compounds show great activities against *R. solani*, with only **6q** lower than 10% and the other 25 compounds higher than 50%. At the tested dose, five compounds inhibited *F. graminearum* with an inhibition rate higher than 50% and four compounds against *S. sclerotiorum*. In contrast, all the compounds inhibited the growth of *P. capsici*

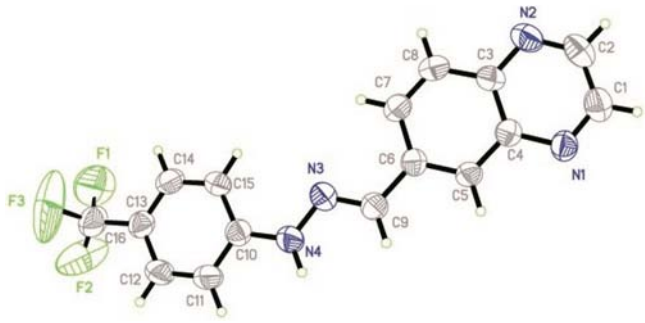


**Figure 3.** ORTEP view showing the atom-labeling scheme with thermal ellipsoids drawn at 30% probability for compound **6x**.

**Table 2. Inhibitory Percentage Test against the Mycelial Growth**[a]

| | inhibitory percentage of compounds in 10 $\mu g \cdot mL^{-1}$ (%) | | | |
|---|---|---|---|---|
| compound | *Rhizoctonia solani* | *Fusarium graminearum* | *Sclerotinia sclerotiorum* | *Phytophthora capsici* |
| **6a** | 78.34 | 64.02 | <10 | 29.81 |
| **6b** | 73.25 | 55.03 | <10 | 35.4 |
| **6c** | 79.62 | 67.2 | 55.17 | 44.72 |
| **6d** | 75.16 | 68.25 | 37.93 | 40.99 |
| **6e** | 81.04 | <10 | <10 | <10 |
| **6f** | 86.43 | 21.63 | <10 | 24.18 |
| **6g** | 81.57 | 27.15 | <10 | 25.27 |
| **6h** | 77.14 | 35.98 | 11.34 | 48.63 |
| **6i** | 77.71 | 47.62 | 37.07 | 45.34 |
| **6j** | 75.16 | 30.16 | <10 | 21.74 |
| **6k** | 67.52 | 18.52 | <10 | <10 |
| **6l** | 83.14 | 27.15 | 21.26 | 32.97 |
| **6m** | 58.57 | <10 | <10 | <10 |
| **6n** | 76.43 | 17.46 | <10 | <10 |
| **6o** | 89.17 | 47.09 | 74.14 | 22.98 |
| **6p** | 92.99 | 42.86 | 39.65 | 16.15 |
| **6q** | <10 | <10 | <10 | <10 |
| **6r** | 71.34 | 20.63 | <10 | <10 |
| **6s** | 64.33 | 30.16 | <10 | <10 |
| **6t** | 65.71 | 66.23 | <10 | 19.78 |
| **6u** | 42.67 | 11.11 | 28.45 | <10 |
| **6v** | 79.62 | 30.16 | 41.38 | <10 |
| **6w** | 89.17 | 39.68 | 67.24 | 25.47 |
| **6x** | 88.53 | 32.27 | 59.48 | 10.56 |
| **6y** | 78.34 | 28.04 | 42.24 | 15.53 |
| **6z** | 80.89 | 17.46 | <10 | <10 |

[a]Four plant-pathogenic fungi were employed with the concentration of compounds (**6a−6z**) being 10 $\mu g \cdot mL^{-1}$.

with an inhibition rate lower than 50%. It is obvious that these derivatives are exclusively efficient against *R. solani* mycelial growth *in vitro* but not potent enough against the other three candidates. Thus, *R. solani* was selected as the target for further research.

Afterward, different concentrations of compounds **6a−6z** were treated against *R. solani*. The $EC_{50}$ values were calculated using linear-regression analysis, with validamycin A and carbendazim as positive controls (Table 3). Except for **6q** and **6u**, all the other compounds show great inhibitory activities. Among these 24 compounds, **6a−6c**, **6e**, and **6o** are slightly weaker than validamycin A (5.07 $\mu g \cdot mL^{-1}$), while the other 19 compounds are more potent than validamycin A. Interestingly, 15 compounds are superior to carbendazim (1.42


dx.doi.org/10.1021/jf504359p | J. Agric. Food Chem. 2014, 62, 9637−9643

Table 3. $EC_{50}$ Values against *R. solani* Mycelial Growth *in Vitro* of Compounds 6a−6z[a]

| compound | $EC_{50}$ ± SD ($\mu g \cdot mL^{-1}$) | compound | $EC_{50}$ ± SD ($\mu g \cdot mL^{-1}$) |
|---|---|---|---|
| **6a** | 4.98 ± 0.42 | **6o** | 5.33 ± 0.03 |
| **6b** | 6.58 ± 0.55 | **6p** | 0.16 ± 0.01 |
| **6c** | 4.68 ± 0.50 | **6q** | |
| **6d** | 1.84 ± 0.20 | **6r** | 0.76 ± 0.04 |
| **6e** | 5.98 ± 0.57 | **6s** | 0.48 ± 0.03 |
| **6f** | 3.34 ± 0.22 | **6t** | 0.67 ± 0.05 |
| **6g** | 1.84 ± 0.21 | **6u** | |
| **6h** | 2.28 ± 0.23 | **6v** | 0.82 ± 0.08 |
| **6i** | 0.62 ± 0.04 | **6w** | 0.33 ± 0.02 |
| **6j** | 0.52 ± 0.04 | **6x** | 0.32 ± 0.01 |
| **6k** | 0.81 ± 0.03 | **6y** | 0.35 ± 0.01 |
| **6l** | 0.73 ± 0.05 | **6z** | 0.74 ± 0.02 |
| **6m** | 0.33 ± 0.01 | validamycin A | 5.07 ± 0.28 |
| **6n** | 0.67 ± 0.03 | carbendazim | 1.42 ± 0.14 |

[a]Values are the mean ± SD of three replicates.

$\mu g \cdot mL^{-1}$). The most promising compound **6p** is 10-fold more potent than the control carbendazim (0.16 vs 1.42 $\mu g \cdot mL^{-1}$). Structure and activity relationship (SAR) analysis indicates two general rules: (i) The electron-withdrawing groups are more favorable than the electron-donating counterparts. The electron-withdrawing compounds (**6f−6z**) as a whole are more potent than **6a** (nonsubstituted) and electron-donating compounds (**6b−6e**). Among the later, except **6d** (1.84) which is slightly stronger than **6a** (4.98), the other three **6b** (6.57), **6c** (4.68), and **6e** (5.98) share the same order of magnitude with **6a**. (ii) *meta* and *para* positions are more beneficial than *ortho* ones. Taking chloro substituents (**6k−6p**) into account, it is obvious that **6m** (*p*-Cl, 0.33) > **6l** (*m*-Cl, 0.73) > **6k** (*o*-Cl, 0.81) (">" means more potent). The di-*ortho* substituent **6o** (2,6-Cl, 5.33) shows the poorest activity, which is even weaker than **6a** (4.98). The 3,4-dichloro substituent **6p** (0.16) shows the strongest activity, which is much more superior than carbendazim (1.42 $\mu g \cdot mL^{-1}$). This rule can also be found in **6b−6d** (−Me), **6f−6i** (−F), **6r−6s** (−Br), and **6w−6x** ($-CF_3$) groups. In conclusion, *meta* and *para* substituents enhance the activity, whereas *ortho* ones debase.

**Antioxidant Activities *in Vitro*.** Two methods were applied to evaluate the antioxidant activities of the 26 compounds. The DPPH method was adopted to assess the radical scavenging activity (RSA), while the LPO method (*in vitro*) was employed to measure the inhibitory activity of microsomal lipid peroxide (LPO). Two series of data are exhibited in Table 4. In RSA, the most potent compound **6e** (7.60) is comparable with the positive control Trolox (5.90), indicating strong radical scavenging activity. As for LPO, besides **6u**, **6q**, and **6t**, the other 23 compounds show greater activities than Trolox (18.23). The most potent compound **6a** (0.96) displays an excellent LPO inhibitory activity with an $EC_{50}$ as low as 1/19 that of Trolox.

SAR analysis reveals some common rules for the two methods referring to antioxidant. The electron-donating groups (**6b−6e**) are generally more beneficial than the electron-withdrawing ones (**6f−6z**). The electron-withdrawing substituents, especially $-NO_2$, $-CF_3$, and −CN, are not favorable in both evaluation systems.

In conclusion, 26 novel phenylhydrazone derivatives linked to the quinoxaline nucleus (**6a−6z**) were synthesized. Antifungal and antioxidant evaluations indicated them to be potential fungicides and/or antioxidants.

Table 4. DPPH Radical Scavenging Activity (RSA) and LPO Assay *in Vitro* Data of Compounds 6a−6z[a]

| | DPPH-RSA | microsome LPO |
|---|---|---|
| compound | $EC_{50}$ ± SD ($\mu g \cdot mL^{-1}$) | $EC_{50}$ ± SD ($\mu g \cdot mL^{-1}$) |
| **6a** | 27.33 ± 1.58 | 0.96 ± 0.18 |
| **6b** | 14.61 ± 0.89 | 2.99 ± 0.22 |
| **6c** | 30.94 ± 1.76 | 1.85 ± 0.21 |
| **6d** | 11.04 ± 0.91 | 1.99 ± 0.16 |
| **6e** | 7.60 ± 0.72 | 3.19 ± 0.15 |
| **6f** | 53.85 ± 3.34 | 3.55 ± 0.34 |
| **6g** | 72.24 ± 5.12 | 3.57 ± 0.48 |
| **6h** | 27.78 ± 1.78 | 1.90 ± 0.29 |
| **6i** | 45.19 ± 2.11 | 6.04 ± 0.52 |
| **6j** | 36.11 ± 2.35 | 5.53 ± 0.42 |
| **6k** | 105.89 ± 8.86 | 3.69 ± 0.40 |
| **6l** | 64.40 ± 3.79 | 10.96 ± 0.72 |
| **6m** | 32.90 ± 1.95 | 2.59 ± 0.15 |
| **6n** | 63.81 ± 3.85 | 5.99 ± 0.33 |
| **6o** | 84.02 ± 6.26 | 4.35 ± 0.29 |
| **6p** | 41.56 ± 4.22 | 4.51 ± 0.28 |
| **6q** | 30.00 ± 2.36 | 89.60 ± 2.78 |
| **6r** | 103.55 ± 9.80 | 5.75 ± 0.37 |
| **6s** | 58.55 ± 3.88 | 7.67 ± 0.42 |
| **6t** | 101.09 ± 7.61 | 23.04 ± 1.07 |
| **6u** | | |
| **6v** | 170.41 ± 15.31 | 12.24 ± 0.77 |
| **6w** | 59.46 ± 4.05 | 14.32 ± 0.62 |
| **6x** | 55.51 ± 3.13 | 13.57 ± 0.58 |
| **6y** | 44.29 ± 2.90 | 3.30 ± 0.28 |
| **6z** | 63.80 ± 4.65 | 6.86 ± 0.47 |
| Trolox | 5.90 ± 0.44 | 18.23 ± 0.13 |

[a]Values are the mean ± SD of three replicates.

## ■ ASSOCIATED CONTENT

### Ⓢ Supporting Information

Materials and spectral data. This material is available free of charge via the Internet at http://pubs.acs.org.

## ■ AUTHOR INFORMATION

### Corresponding Author

*Phone: +86-25-84399753. Fax: +86-25-84399753. E-mail: yeyh@njau.edu.cn.

### Author Contributions

[⊥]M.Z. and Z.-C.D. contributed equally to this paper.

### Funding

This work was cosupported by National Basic Research Program of China (2010CB126100), Fundamental Research Funds for the Central Universities (KYZ201107), and Special Fund for Agro-scientific Research in the Public Interest (201303023).

### Notes

The authors declare no competing financial interest.

## REFERENCES

(1) Bai, Y. B.; Zhang, A. L.; Tang, J. J.; Gao, J. M. Synthesis and antifungal activity of 2-chloromethyl-1H-benzimidazole derivatives against phytopathogenic fungi *in vitro*. *J. Agric. Food Chem.* **2013**, *61*, 2789−2795.

(2) Schirra, M.; D'Aquino, S.; Cabras, P.; Angioni, A. Control of postharvest diseases of fruit by heat and fungicides: efficacy, residue levels, and residue persistence. A review. *J. Agric. Food Chem.* **2011**, *59*, 8531−8542.

(3) Savary, S.; Teng, P. S.; Willocquet, L.; Nutter, F. W., Jr. Quantification and modeling of crop losses: A review of purposes. *Annu. Rev. Phytopathol.* **2006**, *44*, 89−112.

(4) Zhang, Y. J.; Yu, J. J.; Zhang, Y. N.; Zhang, X.; Cheng, C. J.; Wang, J. X.; Hollomon, D. W.; Fan, P. S.; Zhou, M. G. Effect of carbendazim resistance on trichothecene production and aggressiveness of *Fusarium graminearum*. *Mol. Plant-Microbe Interact.* **2009**, *22*, 1143−1150.

(5) Seifi, A.; Visser, R. G. F.; Bai, Y. L. How to effectively deploy plant resistances to pests and pathogens in crop breeding. *Euphytica* **2013**, *190*, 321−334.

(6) Finkel, T.; Holbrook, N. J. Oxidants, oxidative stress and the biology of ageing. *Nature* **2000**, *408*, 239−247.

(7) Vukovic, N.; Sukdolak, S.; Solujic, S.; Niciforovic, N. Substituted imino and amino derivatives of 4-hydroxycoumarins as novel antioxidant, antibacterial and antifungal agents: Synthesis and *in vitro* assessments. *Food Chem.* **2010**, *120*, 1011−1018.

(8) Zhang, Y.; Fang, Y. L.; Liang, H.; Wang, H. S.; Hu, K.; Liu, X. X.; Yi, X. H.; Peng, Y. Synthesis and antioxidant activities of 2-oxo-quinoline-3-carbaldehyde Schiff-base derivatives. *Bioorg. Med. Chem. Lett.* **2013**, *23*, 107−111.

(9) Gonzalez, M.; Cerecetto, H. Quinoxaline derivatives: a patent review (2006-present). *Expert Opin. Ther. Pat.* **2012**, *22*, 1289−1302.

(10) Carta, A.; Piras, S.; Loriga, G.; Paglietti, G. Chemistry, biological properties and SAR analysis of quinoxalinones. *Mini-Rev. Med. Chem.* **2006**, *6*, 1179−1200.

(11) Ishikawa, H.; Sugiyama, T.; Yokoyama, A. Synthesis of 2,3-bis (halomethyl) quinoxaline derivatives and evaluation of their antibacterial and antifungal activities. *Chem. Pharm. Bull.* **2013**, *61*, 438−444.

(12) Tandon, V. K.; Yadav, D. B.; Maurya, H. K.; Chaturvedi, A. K.; Shukla, P. K. Design, synthesis, and biological evaluation of 1,2,3-trisubstituted-1,4-dihydrobenzog quinoxaline-5,10-diones and related compounds as antifungal and antibacterial agents. *Bioorg. Med. Chem.* **2006**, *14*, 6120−6126.

(13) Zheng, H.; Jiang, C.; Chiu, M. H.; Covey, J. M.; Chan, K. K. Chiral pharmacokinetics and inversion of enantiomers of a new quinoxaline topoisomerase II beta poison in the rat. *Drug Metab. Dispos.* **2002**, *30*, 344−348.

(14) Wilhelmsson, L. M.; Kingi, N.; Bergman, J. Interactions of antiviral indolo [2,3-b] quinoxaline derivatives with DNA. *J. Med. Chem.* **2008**, *51*, 7744−7750.

(15) Gerchakov, S.; Schultz, H. P. Quinoxalines. XIV. Potential anticancer agents. Quinoxaline amino acid and dipeptide derivatives related to quinoxaline antibiotics. *J. Med. Chem.* **1969**, *12*, 141−144.

(16) El Aissi, R.; Liu, J.; Besse, S.; Canitrot, D.; Chavignon, O.; Chezal, J. M.; Miot-Noirault, E.; Moreau, E. Synthesis and biological evaluation of new quinoxaline derivatives of ICF01012 as melanoma-targeting probes. *ACS Med. Chem. Lett.* **2014**, *5*, 468−473.

(17) Ancizu, S.; Moreno, E.; Solano, B.; Villar, R.; Burguete, A.; Torres, E.; Perez-Silanes, S.; Aldana, I.; Monge, A. New 3-methylquinoxaline-2-carboxamide 1,4-di-N-oxide derivatives as anti-*Mycobacterium tuberculosis* agents. *Bioorg. Med. Chem.* **2010**, *18*, 2713−2719.

(18) Rangisetty, J. B.; Gupta, C.; Prasad, A. L.; Srinivas, P.; Sridhar, N.; Parimoo, P.; Veeranjaneyulu, A. Synthesis of new arylaminoquinoxalines and their antimalarial activity in mice. *J. Pharm. Pharmacol.* **2001**, *53*, 1409−1413.

(19) Hassan, S. Y.; Khattab, S. N.; Bekhit, A. A.; Amer, A. Synthesis of 3-benzyl-2-substituted quinoxalines as novel monoamine oxidase A inhibitors. *Bioorg. Med. Chem. Lett.* **2006**, *16*, 1753−1756.

(20) Li, J.; Chen, J.; Zhang, L.; Wang, F.; Gui, C.; Qin, Y.; Xu, Q.; Liu, H.; Nan, F.; Shen, J.; Bai, D.; Chen, K.; Shen, X.; Jiang, H. One novel quinoxaline derivative as a potent human cyclophilin A inhibitor shows highly inhibitory activity against mouse spleen cell proliferation. *Bioorg. Med. Chem.* **2006**, *14*, 5527−5534.

(21) Padmini, K.; Preethi, P. J.; Divya, M.; Rohini, P.; Lohita, M.; Swetha, K.; Kaladar, P. A review on biological importance of hydrazones. *Int. J. Pharm. Res. Rev.* **2013**, *2*, 43−58.

(22) Dimmock, J. R.; Vashishtha, S. C.; Stables, J. P. Anticonvulsant properties of various acetylhydrazones, oxamoylhydrazones and semicarbazones derived from aromatic and unsaturated carbonyl compounds. *Eur. J. Med. Chem.* **2000**, *35*, 241−248.

(23) Grossmann, K.; Caspar, G.; Kwiatkowski, J.; Bowe, S. J. On the mechanism of selectivity of the corn herbicide BAS 662H: a combination of the novel auxin transport inhibitor diflufenzopyr and the auxin herbicide dicamba. *Pest Manage. Sci.* **2002**, *58*, 1002−1014.

(24) Bin, L.; Zhu, F. C.; Ying, H.; Wang, Y. H.; Fei, Y.; Fan, B. T.; Yao, J. H. Screening rules for leads of fungicides, herbicides, and insecticides. *J. Agric. Food Chem.* **2010**, *58*, 2673−2684.

(25) Belkheiri, N.; Bouguerne, B.; Bedos-Belval, F.; Duran, H.; Bemis, C.; Salvayre, R.; Negre-Salvayre, A.; Baltas, M. Synthesis and antioxidant activity evaluation of a syringic hydrazones family. *Eur. J. Med. Chem.* **2010**, *45*, 3019−3026.

(26) Kaugars, G.; Gemrich, E. G.; Rizzo, V. L. Miticidal activity of benzoyl chloride phenylhydrazones. *J. Agric. Food Chem.* **1973**, *21*, 647−650.

(27) Wiley, R. H.; Clevenger, R. L. Aldehyde hydrazone derivatives in cancer chemotherapy. *J. Med. Pharm. Chem.* **1962**, *5*, 1367−1371.

(28) Pleskushkina, E. I.; Nikolaevskii, A. N.; Filippenko, T. A. Antiradical and antioxidant activity of phenylhydrazones of aromatic aldehydes. *Russ. J. Appl. Chem.* **2001**, *74*, 792−795.

(29) Chen, L. J.; Wei, Y. Q.; Luo, Y. F.; Wu, X. H. Method for preparing AS-605240 and application thereof on preparing medicines for treating inflammatory diseases. Chinese Patent CN 101550135(A), 2009.

(30) Harden, F. A.; Quinn, R. J.; Scammells, P. J. Synthesis and adenosine receptor affinity of a series of pyrazolo [3,4-D] pyrimidine analogs of 1-methylisoguanosine. *J. Med. Chem.* **1991**, *34*, 2892−2898.

(31) Sheldrick, G. M. *SHELXTL-97: program for crystal structure solution and refinement*; University of Göttingen: Göttingen, Germany, 1997.

(32) Xiao, Y.; Li, H. X.; Li, C.; Wang, J. X.; Li, J.; Wang, M. H.; Ye, Y. H. Antifungal screening of endophytic fungi from *Ginkgo biloba* for discovery of potent anti-phytopathogenic fungicides. *FEMS Microbiol. Lett.* **2013**, *339*, 130−136.

(33) Li, X. H.; Ji, M. S.; Qi, Z. Q.; Li, X. W.; Shen, Y. X.; Gu, Z. M.; Zhang, Y.; Wei, S. H.; Wang, Y. Z.; Wang, D. Q. Synthesis of 2- amino-6- oxocyclohexenylsulfonamides and their activity against *Botrytis cinerea*. *Pest Manage. Sci.* **2011**, *67*, 986−992.

(34) Blois, M. S. Antioxidant determination by the use of a stable free radical. *Nature* **1958**, *181*, 1199−1200.

(35) Matute, A. I. R.; Cardelle-Cobas, A.; García-Bermejo, A. B.; Montilla, A.; Olano, A.; Corzo, N. Synthesis, characterization and functional properties of galactosylated derivatives of chitosan through amide formation. *Food Hydrocolloids* **2013**, *33*, 245−255.

(36) Gao, L. W.; Wang, J. W. Antioxidant potential and DNA damage protection activity of aqueous extract from *Amillaria mellea*. *J. Food Biochem.* **2012**, *36*, 139−148.
(37) Ma, L.; Xiao, Y.; Li, C.; Xie, Z. L.; Li, D. D.; Wang, Y. T.; Ma, H. T.; Zhu, H. L.; Wang, M. H.; Ye, Y. H. Synthesis and antioxidant activity of novel Mannich base of 1,3,4- oxadiazole derivatives possessing 1,4- benzodioxan. *Bioorg. Med. Chem.* **2013**, *21*, 6763−6770.
(38) CCDC-1001315 contains the supplementary crystallographic data for this paper. These data can be obtained free of charge from the Cambridge Crystallographic Data Centre via www.ccdc.cam.ac.uk/data_request/cif.

commercial enzymes Olivex, Novoferm 31, Celluclast, and Pectinex AR were kindly provided by Novozymes A/S (Madrid, Spain).

**Plant Material.** White asparagus byproducts were obtained from local producers (Seville, Spain) and were frozen with liquid nitrogen until further use.

**Extraction of Cell Wall Bound PODs.** The residue from the extraction of the soluble POD[9] was re-extracted as described below. The residue (500 g) was homogenized in a Janke & Kunkel Ultraturrax T-25 (IKA-Labortechnik, Staufen, Germany) at top speed for 3 min with 500 mL of 50 mM Tris-HCl buffer, pH 7.0, containing 1 g/L ascorbic acid and 1 M potassium chloride. Afterward, the solid residue was recovered by filtration through nylon. This procedure was repeated twice to maximize the extraction yield. The filtrates were pooled to get the ionic POD extract. The solid residue was washed three times with water prior to the extraction of the covalent peroxidases. Then it was resuspended in a 50 mM sodium acetate buffer, pH 5.0, with 5.0% (v/v) of a commercial enzymatic mixture, Olivex (Novozymes A/S) and subjected to agitation for 12 h at 25 °C followed by centrifugation at 21214*g* for 30 min. The supernatant was saved and aliquoted for further analysis.

**Assay for the POD Activity.** POD activity was determined with ABTS as the reducing substrate in a total volume of 0.2 mL. The assay mixture contained 20 $\mu$L of a 1 M acetate buffer with a pH of 5.0, 20 $\mu$L of 1 mM ABTS, and 20 $\mu$L of 0.3% $H_2O_2$ and variable amounts of $H_2O$ and enzyme preparations to reach the final assay volume. The oxidation of ABTS was followed by monitoring the increase in absorbance at 415 nm and using $\varepsilon_{415\ nm}$ = 31.1 $mM^{-1}$ $cm^{-1}$ for ABTS cation radical formation.[17] One unit of activity (UA) was defined as the amount of enzyme required to oxidize 1 $\mu$mol of ABTS per minute at pH 5.0 and 25 °C. A Bio-Rad iMark microplate reader was used for the spectroscopic measurements.

**Protein Determination.** Protein was quantified on the basis of the dye-binding method of Bradford using bovine serum albumin (BSA) as standard.[18]

**Isoelectric Focusing (IEF).** Preparative IEF was carried out using a Rotofor preparative IEF cell (Bio-Rad). The protein samples were dialyzed against deionized water overnight, supplemented with 2% (v/v) Biolytes (Bio-Rad) of 3.0−10.0 pH range, and then loaded into the Rotofor cell. The IEF, without prerunning, was done according to the manufacturer's instructions. The power supply was set at a constant power of 12 W. Once focusing was complete, the electrofocusing cell was fractionated into 20 aliquots ranging from acidic to basic isoelectric point (p*I*) proteins. POD activity and protein contents were determined for each aliquot.

**Gel Electrophoresis.** SDS-PAGE of the crude extract and purified fraction was performed on a 12% acrylamide minigel in a Bio-Rad protein II electrophoresis cell set at 150 V for 120 min according to the method of Laemmli.[19] Protein band detection was conducted by silver staining as previously described by Rabilloud.[20] Molecular weights of the bands were calculated using Labimage software v2.7.1 (Kapelan Bio-Imaging).

**Purification of Anionic POD.** The different samples were dialyzed against deionized water, centrifuged at 21214*g* for 2 h at 4 °C, and filtered prior to purification. The chromatography purification steps were carried out at room temperature.

**Affinity Chromatography.** The low p*I* fractions from the IEF showing POD activity were combined and loaded into a concanavalin A−Sepharose affinity column (Amersham Pharmacia Biotech, Uppsala, Sweden) pre-equilibrated with 20 mM Tris-HCl buffer at pH 7.0 containing 0.5 M NaCl at a flow rate of 0.3 mL/min. Unbound proteins were removed by repeated washings with concanavalin A loading buffer at 1.0 mL/min. Anionic PODs were eluted from the resin with two successive washes with 5 column volumes of loading buffer containing 0.5 M methyl-$\alpha$-D-glucopyranoside. The resin was left in contact with the buffer for 1 h for the first elution and overnight for the second elution. Afterward, the column was washed with 1.0 M methyl-$\alpha$-D-glucopyranoside to elute the proteins strongly bound to the column. Fractions of 6 mL were collected during all of the chromatography steps, and the POD activity and protein content were measured.

**Effect of pH on POD.** POD activity as a function of pH was established by incubating the purified POD in 1 M sodium acetate buffer (pH 3.0−5.0), 1 M sodium phosphate buffer (pH 5.0−7.0), and 0.05 M Tris-HCl buffer (pH 7.0−9.0). Analysis conditions were the same as those described for the POD activity assay.

**Determination of Optimum Temperature and Thermal Stability.** The optimal temperature and thermal stability of PODs were assayed using a water bath (Precis-Term P-Selecta) with the optimal pH at temperatures ranging from 15 to 80 °C for 10 min prior to substrate addition. After heating, the solutions were rapidly cooled in ice water, and the POD activity was immediately determined. The percent residual activity was plotted against different temperatures. Thermal stability was also tested at various temperatures in the range of 50−85 °C with exposure times ranging from 1 to 30 min.

**Kinetic Constants for ABTS and $H_2O_2$.** Kinetic parameters were calculated from Lineweaver−Burk plots for the two-substrate mechanisms followed by POD[15] using $H_2O_2$ and ABTS concentrations from 0.1 to 10 mM, respectively. Temperature and pH were kept constant in the optimum values determined previously. Taking into account the reciprocal of both sides of the Michaelis−Menten equation leads to the Lineweaver−Burk relationship

$$1/\nu_0 = K_a/A_0V_{max} + K_b/B_0V_{max} + 1/V_{max}$$

where $\nu_0$ is the initial reaction velocity, $V_{max}$ is the maximum reaction velocity, $K_a$ and $K_b$ are $K_m$ values, the Michaelis−Menten constant for substrate A ($H_2O_2$) and B (ABTS), respectively, and $A_0$ and $B_0$ are substrate A and B concentrations. The $\nu_0$ were determined as a function of both substrate concentrations. A plot of $1/\nu_0$ versus $1/B_0$ for varying values of $A_0$ will give a series of parallel lines, each of slope $K_b/V_{max}$. A plot of intercept versus $1/A_0$ will give a line of slope $K_a/V_{max}$ and intercept $1/V_{max}$. Hence, $K_a$, $K_b$, and $V_{max}$ may be determined.

**Removal of Phenolic Compounds.** We evaluated the catalytic activity of the purified PODs using different model compounds such as monoaromatic phenolic type 4-chlorophenol (4-CP), 2,4-dichlorophenol (2,4-DCP) as a model of the disubstituted substrate, and 2-(3,4-dihydroxyphenyl)ethanol [hydroxytyrosol (HT)], a polyphenol present in olive mill wastewater. The assays were performed in a reactor at room temperature. All substances were dissolved in 1 M acetate buffer at pH 4.0. The optimal ratio of AAP and $H_2O_2$ concentration for phenol removal was investigated using $H_2O_2$ concentrations between 1 and 20 mM. To study the influence of AAP, $H_2O_2$, and their combination on the removal of phenols, we followed different incubation conditions: (a) a control solution that consisted of 2 mM phenol, (b) 2 mM phenol and $H_2O_2$, (c) 2 mM phenol and CAP, and (d) 2 mM phenol, $H_2O_2$, and CAP. The course of the reaction was monitored by taking 1 mL of sample, and the concentration of the phenol was analyzed until the value was constant.

**Phenol Quantification.** The removal of each phenol was monitored by high-performance liquid chromatography (HPLC) and an ultraviolet detector. The aliquots were taken from model wastewaters at the indicated times. The reaction was stopped by the addition of 10 $\mu$L of 20% trichloroacetic acid (TCA). After centrifugation, 20 $\mu$L was injected into a MediterraneaSea C18 (Teknokroma), 5 $\mu$m, 25 × 0.6 mm reversed phase HPLC column. The initial mobile phase consisted of 70:30 (v/v) water/acetonitrile with 0.1% formic acid, which was brought to 0:100 (v/v) in a linear gradient lasting for 20 min, held for another 10 min, and then 5 min of 30% acetonitrile. Phenol concentrations were determined from a straight-line standard calibration obtained using known concentrations (standards) of each compound. The results are expressed as removal efficiency, which is defined as the percentage of phenols removed from the solution under the established experimental conditions.

**Statistical Analysis.** The mean ± SD of three replicates was calculated. All data were analyzed using multivariate analysis of variance (MANOVA) followed by the Fisher−LSD multicomparison test. The level of significance was $p < 0.05$.

## RESULTS AND DISCUSSION

**Extraction of Cell Wall Bound PODs.** It is known that a great part of the apoplastic PODs is associated with cell walls either by ionic interactions or by covalent bonds. In this study, we

have developed a sequential method to extract the different forms of peroxidases that were ionically and covalently bound to the cell wall of the asparagus tissues.

The wall-bound POD can partially be released by treatment with a high-molarity solution of NaCl or other salts. In our method, after the extraction of the soluble fraction,[9] the cell walls still contained a considerable amount of POD activity. We performed a washing procedure to determine if POD activities were loosely bound to the cell wall or entrapped inside the intracellular vesicles. The residue obtained after soluble POD extraction was suspended in the same buffer used but with added 1.0 M KCl. Then we followed the extraction procedure for ionic isoenzymes as described under Materials and Methods. The crude extract contained 0.89 UA POD/g fresh material. This value represents a small quantity of the ionically bound PODs (IBPs) compared to soluble PODs (5.31 UA/g fresh material).[9] The highly soluble to IBP ratio has also been reported for other plant foods, such as peaches (5:1),[21] mustard (2:1),[22] and artichoke hearts (6:1).[29]

After extraction with high ionic strength, the cell walls were used as substrate to test the further extractability of POD by the enzymatic method to get the covalently bound PODs (CBPs). Treatment of the cell walls for 12 h with 50 mM acetate buffer, pH 5.0, and various commercial enzymatic preparations with different hydrolytic activities was assayed (Table 1). The POD activity was measured after the enzymatic hydrolysis of the cell walls. As shown in Figure 1, Novoferm 31 extracted the same peroxidase amounts as those detected in the control. After the hydrolysis by Celluclast, the POD activity was higher than that detected in the control sample, but Celluclast did not efficiently extract the CBPs. The treatments of cell wall with Pectinex AR or Olivex resulted in the most efficient extractions. These enzymatic mixtures contain similar polygalacturonase and pectin esterase activities (Table 1), but Olivex possesses higher cellulase activity. To determine if the different efficiencies of these two commercial preparations were due to their different cellulase activities, a mixture of Pectinex AR plus Celluclast was also tested. A similar treatment on oat cell wall led to maximum recovery of CBPs.[23] However, in asparagus byproduct cell walls, the CBP released after the treatment with the combination enzymatic mixture was the same as that obtained with Olivex alone. On the other hand, it is noteworthy that Novoferm 31, despite possessing an enzymatic composition similar to those of Olivex and Pectinex AR, is not effective for the release of peroxidase tightly bound to the cell wall. This fact could be due to the inactivation of the enzymatic mixture or to the presence of some inhibitors. These findings suggest that the concerted action of polygalacturonase, pectin esterase, and cellulase is required to efficiently release CBPs. In fact, with this method we found that the cell walls from the asparagus byproduct possess a high CBP (4.11 UA/g fresh material). This value was similar to the previously reported cytoplasmatic POD (5.31 UA/g).[9] In total, the POD activity in the crude extract of asparagus byproducts was 10.31 UA/g fresh material. This value is higher than values reported for typical sources of peroxidase such as turnip extract (6.5 UA/g)[24] and broccoli (3.5 UA/g).[25] Ionic forms of POD represent <10% of the activity detected (0.89 UA/g); thereby, the CBP is a good source for peroxidase, whereas in other plants this fraction is considered too low to be assayed.[13]

**Table 1. Relation of Enzymatic Commercial Mixtures Used for Covalently Bound to the Cell Wall Peroxidase Extraction and Enzymatic Activity[a]**

| | Celluclast | Pectinex AR | Olivex | Novoferm 31 |
|---|---|---|---|---|
| polygalacturonase | 0.0 | 12.3 | 15.8 | 17.3 |
| pectin esterase | 0.3 | 3.6 | 3.3 | 2.3 |
| cellulase | 8.6 | 0.1 | 1.5 | 3.8 |
| glucosidase | 0.1 | 0 | 0 | 0 |

[a]Values corresponding to activity measured as $\mu$kat mL$^{-1}$.

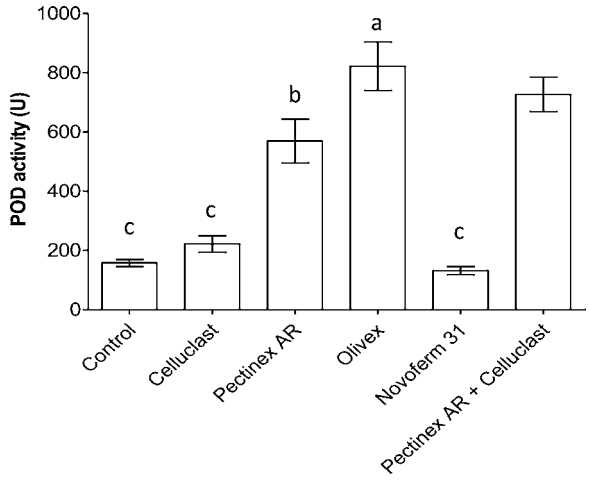


**Figure 1.** Covalently bound peroxidase activity released by different enzymatic mixtures.

**Isoelectric Focusing of Cell Wall Bound POD.** The distinct forms of the peroxidases from the cell walls were characterized by IEF in a pH range of 1−12. Different patterns of activity were obtained for the ionic and covalent fractions (Figure 2). IBP included a broad range of acid (p*I* ca. 4−5), neutral (p*I* ca. 6−7), and basic (p*I* ca. 8−12) isoforms (Figure 2A). A similar IEF profile has been described in flax fibers.[26] However, in green asparagus the IEF profile for ionic POD was similar to that of the soluble POD.[9] These isoenzymes are mainly neutral isoforms, and the activities of the isoenzymes with p*I* between 5 and 7 were weak.[27]

The IEF profiles obtained for CBP showed a group of anionic isoforms (p*I* ca. 5−6), whereas the extreme cationic isoforms present in the soluble and ionic fractions were absent or negligible in the covalent fraction (Figure 2B). A similar IEF pattern has been described for the covalent fraction of proteins from pea root.[28]

Consequently, although CBP is constituted mainly of anionic isoenzymes, the IBP showed a very broad isoenzymatic profile and is a mixture of cationic neutral and anionic isoforms.

**Purification of Anionic POD.** The POD activity in the crude IBP was lower (0.89 UA/g fresh material) than the activity measured in the CBP (4.11 UA/g fresh material), which was similar to the POD activity in the soluble fraction.[9] Previously, we had developed a method for the purification of cationic POD,[9] and here we present a new method to purify the anionic asparagus POD present in the cell wall of asparagus byproducts (AAP). The specific activity and purification factor for the CBP extract are shown in Table 2. The CBP was purified in two consecutives steps: isoelectric focusing and affinity chromatography on concanavalin A. The specific activity of the crude extract was low due to a high content of proteins from the commercial enzymatic mixture and the proteins extracted.

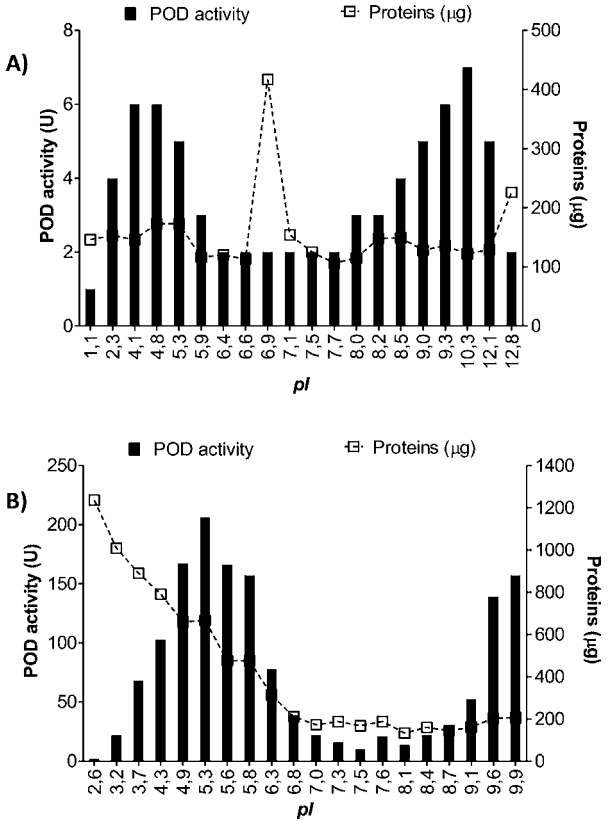


**Figure 2.** Isoelectric profile for ionically bound (A) and covalently bound (B) to cell wall POD from asparagus byproducts.

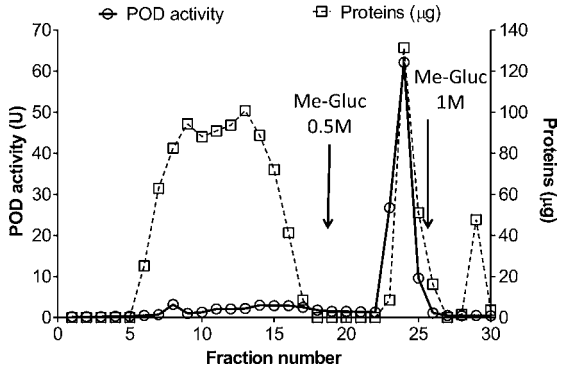


**Figure 3.** Typical elution profile for affinity chromatography of the anionic isoperoxidase fraction.

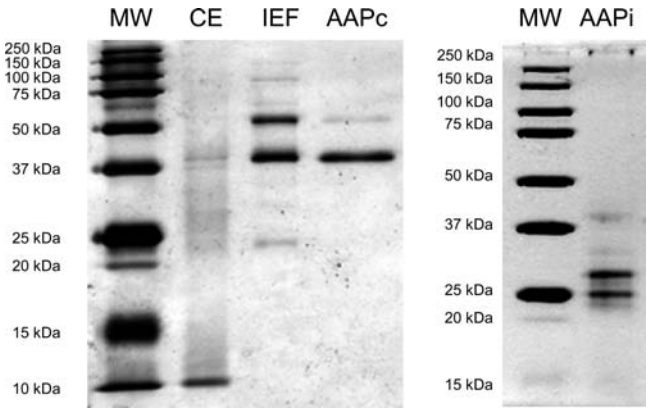


**Figure 4.** SDS-PAGE after 5 min of exposure to the developer ($Na_2CO_3$) of the crude extract, the A1 fraction, and the Con A-purified AAP. Molecular weights (MW) are for 250, 150, 100, 75, 50, 37, 25, 20, 15, and 10 kDa.

The IEF profile of the CBP showed several bands with p*I* values between 4.3 and 5.8 (Figure 2B). These fractions were pooled and separated from the basic isoenzymes, which improved the purity of the enzymes (21-fold, Table 2) and reduced the volume of the crude sample by 32% before the subsequent chromatography step. The pooled acidic fractions, representing 68% of the total activity of the crude extract, were dialyzed and transferred onto the concanavalin A−Sepharose column as described under Materials and Methods. Concanavalin A is a lectin that binds to the carbohydrate molecules containing α-D-mannopyranosyl, α-D-glucopyranosyl, and sterically analogous residues. Figure 3 indicates that POD activity was mainly distributed as a single peak separated from the protein fraction. This purification step allowed us to obtain pure anionic asparagus POD (AAP) with high specific activity from asparagus byproducts (Table 2). Overall, the enzyme was purified about 236 times and showed a high yield for recovery of the activity.

**Partial Characterization of AAP.** SDS electrophoresis was monitored through protein band analysis to determine the molecular weight of the proteins of the isolated fractions (Figure 4). After the IEF purification step, the ionic and covalent proteins showed different protein bands after SDS electrophoresis. The ionic fraction contained two main bands of 25 and 28 kDa and three other faint bands of 23, 32, and 40 kDa. Conversely, the IEF fraction contained two main bands of 40 and 53 kDa and four other faint bands of 20, 65, 90, and 130 kDa. These faint bands were not present after concanavalin A column purification, and the band of 53 kDa was greatly diminished, suggesting that most of the anionic proteins of this molecular weight lack glycosidic residues. Interestingly, small proteins seemed to be ionically bound to the cell walls, whereas medium and large proteins are mainly bound to the cell wall covalently. A previous study on artichokes also found that the molecular weight of POD isoforms in the ionic fraction was smaller than that of covalently bound proteins in the leaf and heart.[29] In pea root, a covalent POD of 70 kDa with nine isoenzymes was described.[28] A relationship between the size, the ionic strength of the POD, and the number of glycosylated residues of amino acids for cell wall anchoring may exist. As we have detailed by IEF, the p*I* of the ionically bound POD is lower than the covalently bound POD. Moreover, basic PODs from asparagus have a p*I* far from 7.0, and their molecular weights have been described to be 23, 27, and 43 kDa.[9]

**Table 2. Summary of the Purification of AAP from Asparagus Byproducts**

| purification step | total activity (UA) | total protein (mg) | specific activity (UA/mg) | recovery activity (%) | purification factor |
|---|---|---|---|---|---|
| crude extract | 491 ± 7 | 923 ± 8 | 0.53 | 100 ± 1 | 1 |
| IEF | 334 ± 9 | 30 ± 4 | 11.08 | 68 ± 4 | 21 |
| dialyzed extract | 323 ± 7 | 27 ± 5 | 11.96 | 66 ± 6 | 22 |
| Con-A | 75 ± 4 | 0.6 ± 0.03 | 125.0 | 25 ± 3 | 236 |


dx.doi.org/10.1021/jf502560k | J. Agric. Food Chem. 2014, 62, 9644−9650

**Optimal pH of AAP.** The optimal activity of AAP was tested against different pH values by using ABTS as substrate. To rule out any buffer effect on the peroxidase activity, we checked that at pH 5 with acetate buffer and with phosphate buffer the POD activity was the same and that this was also true at pH 7 with phosphate buffer and Tris buffer, respectively. AAP displayed a typical bell-shaped pH profile (Figure 5A), which exhibited

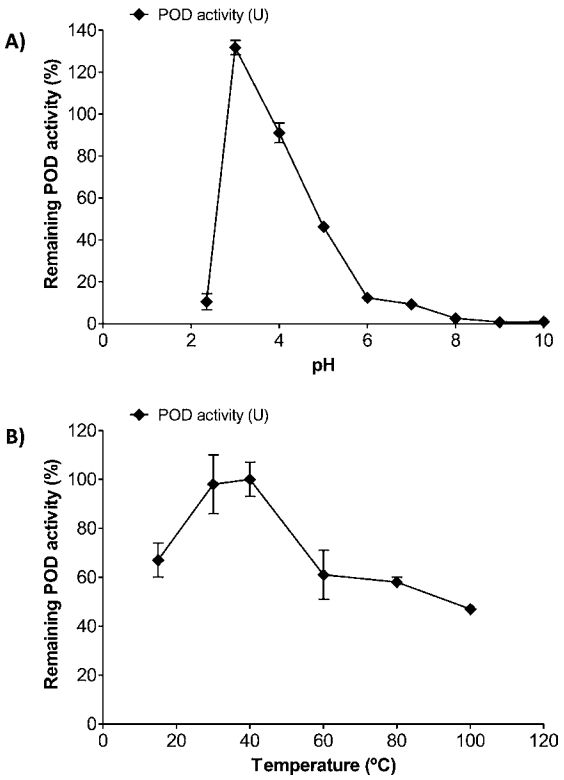


**Figure 5.** Optimal pH (A) and temperature (B) for the enzymatic activity of purified AAP using ABTS as substrate. Values are the means of triplicates ± SD.

stronger activity in a pH range of 3.0−5.0, with an optimal pH of 3.5. At pH 5.0 the AAP activity was around 50% of the maximum activity. In asparagus, the optimal pH for the activity of AAP was lower than those purified from other vegetable sources such as red cabbage (pH 4.0),[12] red algae (pH 5.0),[30] or sweet potato tubers (pH 4.5).[31]

**Thermal Stability of AAP.** The optimal temperature for AAP was between 35 and 40 °C (Figure 5B). These values agree with those obtained for the covalent POD of green asparagus.[27] The $T_m$ value for AAP was around 100 °C, which highlights the thermal stability of the enzyme compared to CAP.[9] To characterize the biocatalytic properties of the AAP, the percent remaining activity was plotted against time (Figure 6). The exposure of the AAP for 30 min at 60 °C did not decrease its activity, whereas the exposure of the AAP at 70 °C for 30 min reduced the POD activity by up to 50%. These results corresponded with the monophasic behavior described for green asparagus extracts treated between 50 and 60 °C.[32] Other authors reported that several POD forms had a higher thermal stability as no reduction in the POD activity was found below 80 °C.[32] From a technological point of view, this is an important outcome as treatment at high temperatures (80−90 °C) provoked a drastic loss in the AAP activity in 5 min. Similar to CAP,[9] Figure 6 shows that the remaining activity gradually

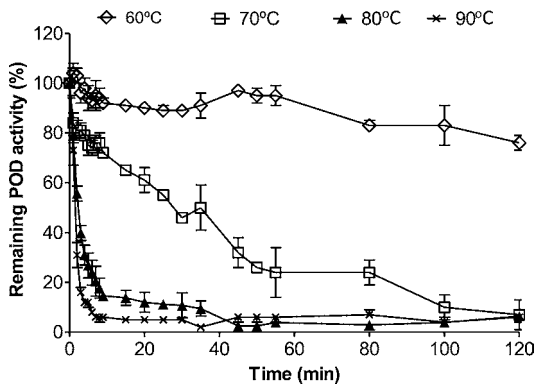


**Figure 6.** Thermal inactivation of purified AAP at 60, 70, 80, and 90 °C. Values are means of triplicates ± SD.

decreased as the temperature increased, yielding nonlinear curves. Our results agreed with those of Ganthavorn et al.,[33] who reported on partially purified raw POD extracts from green asparagus. Their data closely corresponded to a monophasic behavior at 50 and 60 °C and a biphasic behavior at 70 °C.

**Kinetic Constants for ABTS and $H_2O_2$.** The Michaelis−Menten equation is used to distinguish among the ordered, random, and ping-pong mechanisms and to obtain the $K_m$ values for both substrates (ABTS and $H_2O_2$). The purified AAP showed typical Michaelis−Menten kinetics for both ABTS and $H_2O_2$. The substrate saturation curve was obtained by interpolating the substrate concentrations against activity values. Michaelis−Menten constants ($K_m$) were determined from Lineweaver−Burk plots. The double-reciprocal plots of the AAP kinetics are shown in Figure 7A, where the parallel lines indicate that AAP follows a ping-pong mechanism. The calculated *y*-intercepts were plotted against $1/A_0$ and resulted in a straight line (Figure 7B), from which we achieved the $V_{max}$ = 0.695 mM ABTS $min^{-1}$. The $K_m$ value for $H_2O_2$ was found to be 0.53 mM. This value was lower than that reported for turnip POD (0.8 mM).[34] The ABTS $K_m$ value was 0.21 mM, which is 60 times lower than the value reported for red algae POD (13 mM)[30] or turnip POD (0.71 mM).[34] This indicated that AAP may be suitable for applications requiring a high sensitivity for ABTS.

**Phenolic Compound Removal by AAP.** We have previously characterized the activity of cationic POD from asparagus byproducts for removing phenolic compounds such as HT (which is found in olive oil wastewaters at high concentrations), 4-CP, and 2,4-DCP.[9] We now extend this knowledge to the AAP from the same source. The relationship between phenols removed as a function of hydrogen peroxide for 1 h in a stirred batch reaction is shown in Figure 8A. All of the experiments were carried out at the optimal pH and temperature for AAP (as shown in Figure 5). At 2 mM $H_2O_2$, 59% of the total HT was already removed, whereas only 14.6 and 4% were removed for 2,4-CP and 4-C, respectively. The optimal $H_2O_2$ concentration for HT and 2,4-CP removal was 4 mM, whereas for 4-CP 8 mM $H_2O_2$ was needed. Within 1 h, the preferred substrate for AAP was HT > 2,4-DCP > 4-CP. The results clearly show that the optimal relationship of AAP/$H_2O_2$ for the removal of 2,4 DCF and HT was 5 UA AAP $mL^{-1}$ $mmol^{-1}$ $H_2O_2$, whereas for 4-CP it was 10 UA AAP $mL^{-1}$ $mmol^{-1}$ $H_2O_2$. The incubation of AAP with phenolic compounds assayed without $H_2O_2$ did not produce a significant decrease in the concentration of the initial compounds (data not shown), suggesting that phenolic

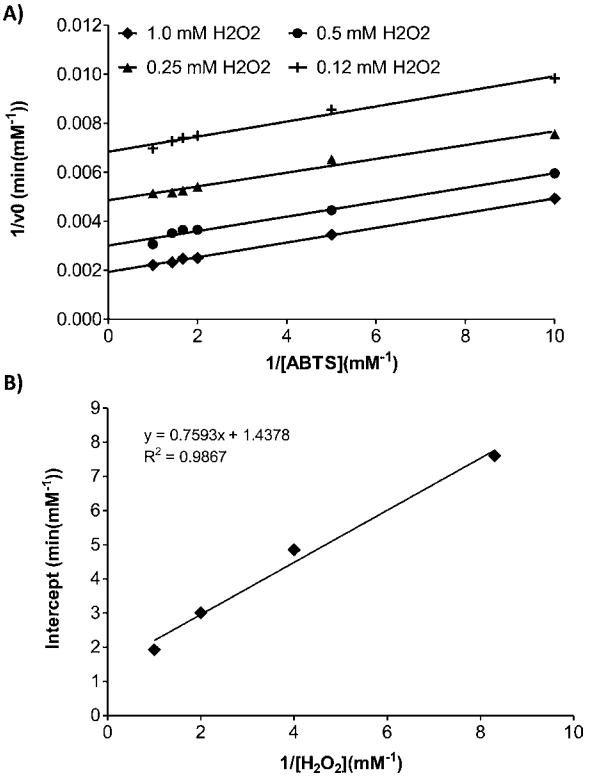


**Figure 7.** Kinetic behavior of the two substrate reactions for purified AAP: (A) plot of 1/[substrate] versus 1/velocity according to the Michaelis−Menten equation; (B) plot of the *y*-intercepts of the lines of panel A versus $1/[H_2O_2]$.

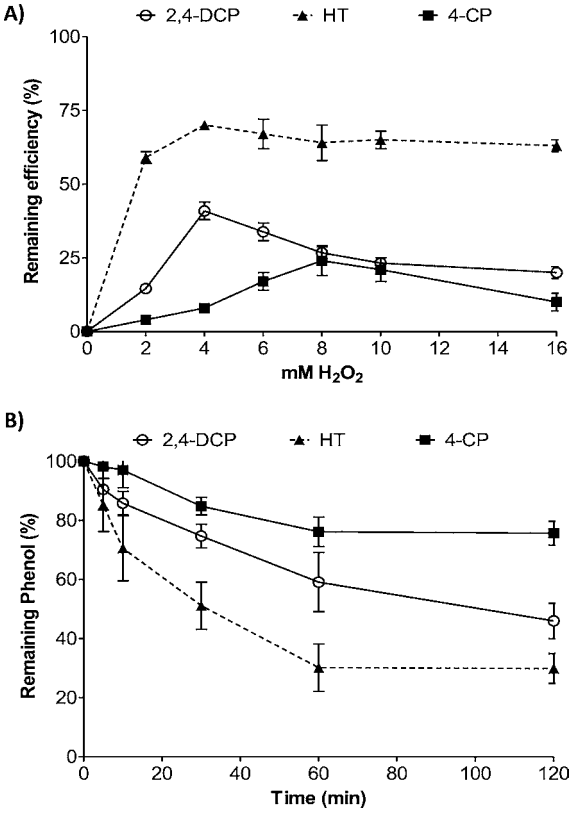


**Figure 8.** Phenols removed as a function of AAP and peroxide concentrations in batch treatment: (A) effect of $H_2O_2$ concentration on phenol reduction (conditions: 2 mM phenol, 20 UA $mL^{-1}$ CAP after 1 h); (B) course of the oxidation with time of 4-chlorophenol, 2,4-dichlorophenol, and hydroxytyrosol (2 mM each) at pH 4.0, 5 UA CAP $mL^{-1}$, and either 4 mM $H_2O_2$ (2,4-DCF and HT) or 8 mM $H_2O_2$ (4-CP).

oxidation is due to POD activity and not to other enzymatic activities that could be present in the extract.

Finally, we studied the time courses of the changes in the phenolic compound concentrations (Figure 8B). The rates of degradation of the three phenols assayed differed. AAP was most active against HT; >70% of the total HT disappeared within the first 1 h compared to 2,4-CP and 4-CP, which were removed at 42 and 25% of the initial concentration, respectively. In the same conditions CAP was able to remove only 25% of the HT.[9] Longer times of exposure of the HT and 4-CP to the AAP did not reduce the amount of phenol concentrations. However, AAP was still active after 2 h in the presence of 2,4-DCP, which was removed by up to 50% for its initial concentration (Figure 8B). Intriguingly, most of the PODs from vegetables are reported to be more active for monophenols such as 4-CP[35] than for orthophenols such as HT. Therefore, the botanical source of PODs plays an important role in the efficiency of bioremediation. Taking into account our previous studies,[9] it can be concluded that in the POD from asparagus byproducts, CAP isoforms have higher efficiency in removing chorophenols, whereas AAPs have higher efficiency in removing orthophenols such as HT. Extensive knowledge about the bioremediation of mono- and dichorophenols exists,[36] whereas little information can be found in relation to the removal of the phenols present in olive oil wastewater.

In conclusion, large differences were found between acidic and basic wall isoperoxidases in relation to their efficacy in the oxidation of the phenolic compounds assayed. Whereas CAP was found to be a good alternative for the removal of chlorinated compounds, the AAP is a better option for the removal of the main phenol present in olive mill wastewaters. Both isoenzymes might exert their activities in an acidic environment, and AAP showed a very high thermostability and resistance to inhibitor action. All of these features make AAP a valuable enzyme for the removal of highly polluted wastewater produced by the agro-food industries.

## AUTHOR INFORMATION

### Corresponding Author

*(R.G.-B.) Phone: +34 954611550. Fax: +34 954616790. E-mail: rguillen@cica.es.

### Funding

S.J.-C. and S.L. acknowledge financial support from the Spanish CSIC (JAE-doc Program), a contract cofunded by the ESF. S.V.-C. thank the Spanish CSIC for her contract (JAE Pre Program).

### Notes

The authors declare no competing financial interest.

## ABBREVIATIONS USED

*A*, activity; ABTS, 2,2′-azinobis(3-ethylbenzthiazoline-6-sulfonic acid); BSA, bovine serum albumin; AAP, anionic asparagus peroxidase; CAP, cationic asparagus peroxidase; CE, crude extract; CBP, covalently bound peroxidase; 4-CP, 4-chlorophenol; 2,4-DCP, 2,4-dichlorophenol; E, enzyme; HPLC, high-performance liquid chromatography; HT, hydroxytyrosol; IBP, ionically bound peroxidase; IEF, isoelectric focusing; p*I*, isoelectric point; POD(s), peroxidase(s); $T_m$, midpoint

inactivation temperature; TCA, trichloroacetic acid; Tris, 2-amino-2-hydroxymethylpropane-1,3-diol; UA, units of activity

## REFERENCES


(1) Botalova, O.; Schwarzbauer, J.; al Sandouk, N. Identification and chemical characterization of specific organic indicators in the effluents from chemical production sites. *Water Res.* **2011**, *45*, 3653−3664.

(2) Rajkumar, D.; Palanivelu, K. Electrochemical treatment of industrial wastewater. *J. Hazard. Mater.* **2004**, *113*, 123−129.

(3) Du, Y. X.; Fu, Q. S.; Li, Y.; Su, Y. L. Photodecomposition of 4-chlorophenol by reactive oxygen species in UV/air system. *J. Hazard. Mater.* **2011**, *186*, 491−496.

(4) Gholizadeh, A.; Kermani, M.; Gholami, M.; Farzadkia, M.; Yaghmaeian, K. Removal efficiency, adsorption kinetics and isotherms of phenolic compounds from aqueous solution using rice bran ash. *Asian J. Chem.* **2013**, *25*, 3871−3878.

(5) Maza-Marquez, P.; Martinez-Toledo, M. V.; Gonzalez-Lopez, J.; Rodelas, B.; Juarez-Jimenez, B.; Fenice, M. Biodegradation of olive washing wastewater pollutants by highly efficient phenol-degrading strains selected from adapted bacterial community. *Int. Biodeterior. Biodegrad.* **2013**, *82*, 192−198.

(6) Klibanov, A. M.; Morris, E. D. Horseradish peroxidase for the removal of carcinogenic aromatic amines from water. *Enzyme Microb. Technol.* **1981**, *3*, 119−122.

(7) Wagner, M.; Nicell, J. A. Detoxification of phenolic solutions with horseradish peroxidase and hydrogen peroxide. *Water Res.* **2002**, *36*, 4041−4052.

(8) Fuentes-Alventosa, J. M.; Jaramillo-Carmona, S.; Rodriguez-Gutierrez, G.; Guillen-Bejarano, R.; Jimenez-Araujo, A.; Fernandez-Bolanos, J.; Rodriguez-Arcos, R. Preparation of bioactive extracts from asparagus by-product. *Food Bioprod. Process.* **2013**, *91*, 74−82.

(9) Jaramillo-Carmona, S.; Lopez, S.; Vazquez-Castilla, S.; Rodriguez-Arcos, R.; Jimenez-Araujo, A.; Guillen-Bejarano, R. Asparagus by-products as a new source of peroxidases. *J. Agric. Food Chem.* **2013**, *61*, 6167−6174.

(10) Mader, M. Compartimentation of peroxidase isoenzymes in plant cells. In *Plant Peroxidases 1980−1990, Topics and Detailed Literature on Molecular Biochemical and Physiological Aspects*; Penel, C., Gaspar, T., Greppin, H., Eds.; University of Geneva: Switzerland, 1992.

(11) Sergio, L.; Cardinali, A.; De Paola, A.; Di Venere, D. Biochemical properties of soluble and bound peroxidase from artichoke heads and leaves. *Food Technol. Biotechnol.* **2009**, *47*, 32−38.

(12) Boeuf, G.; Bauw, G.; Legrand, B.; Rambour, S. Purification and characterization of a basic peroxidase from the medium of cell suspension cultures of chicory. *Plant Physiol. Biochem.* **2000**, *38*, 217−224.

(13) Monerri, C.; Guardiola, J. L. Peroxidase activity and isoenzymes profile in buds and leaves in relation to flowering in Satsuma mandarin (*Citrus unshiu*). *Sci. Hortic.* **2001**, *90*, 43−56.

(14) Martinez-Pastur, G.; Zappacosta, D.; Arena, M.; Curvetto, N. Changes in isoperoxidase patterns during the in vitro rooting of nothofagus Antarctica. *Bulg. J. Plant Physiol.* **2001**, *27*, 43−53.

(15) Lepeduš, H.; Cesar, V.; Krsnik-Raso, M. Guaiacol peroxidases in carrot (*Daucus carota* L.) root. *Food Technol. Biotechnol.* **2004**, *42*, 33−36.

(16) Hamed, R. R.; Maharem, T. M.; Fatah, M. M. A.; Ataya, F. S. Purification of peroxidase isoenzymes from turnip roots. *Phytochemistry* **1998**, *48*, 1291−1294.

(17) Fortea, M. I.; Pellicer, J. A.; Serrano-Martínez, A.; López-Miranda, S.; Lucas-Abellán, C.; Núñez-Delicado, E. Red cabbage (*Brassica oleracea*) as a new source of high-thermostable peroxidase. *J. Agric. Food Chem.* **2012**, *60*, 10641−10648.

(18) Bradford, M. M. A rapid and sensitive method for the quantitation of microgram quantities of protein utilizing the principle of protein-dye binding. *Anal. Biochem.* **1976**, *72*, 248−254.

(19) Laemmli, U. K. Cleavage of structural proteins during the assembly of the head of bacteriophage T4. *Nature* **1970**, *227*, 680−685.

(20) Rabilloud, T. Mechanisms of protein silver staining in polyacrylamide gels: a 10-year synthesis. *Electrophoresis* **1990**, *11*, 785−794.

(21) Neves, V. A. Ionically bound peroxidase from peach fruit. *Braz. Arch. Biol. Technol.* **2002**, *45*, 7−16.

(22) Saroop, S.; Chanda, S. V.; Singh, Y. D. Changes in soluble and ionically bound peroxidase activities during *Brassica juncea* seed development. *Bulg. J. Plant Physiol.* **2002**, *28*, 26−34.

(23) González, L. F.; Rojas, M.C.; Perez, F. J. Diferulate and lignin formation is related to biochemical differences of wall-bound peroxidases. *Phytochemistry* **1999**, *50*, 711−717.

(24) Duarte-Vázquez, M. A.; García-Almendárez, B.; Regalado, C.; Whitaker, J. R. Purification and partial characterization of three turnip (*Brassica napus* L. var *esculenta* D.C.) peroxidases. *J. Agric. Food Chem.* **2000**, *48*, 1574−1579.

(25) Duarte-Vázquez, M. A.; García-Padilla, S.; García-Almendárez, B. E.; Whitaker, J. R.; Regalado, C. Broccoli processing wastes as a source of peroxidase. *J. Agric. Food Chem.* **2007**, *55*, 10396−10404.

(26) McDougall, G. J. Changes in cell wall-associated peroxidases during the lignification of flax fibers. *Phytochemistry* **1992**, *31*, 3385−3389.

(27) Wang, Z.; Luh, B. S. Characterization of soluble and bound peroxidases in green asparagus. *J. Food Sci.* **1983**, *48*, 1412−1421.

(28) Kukavica, B. M.; Veljovic-Jovanovic, S. D.; Menckhoff, L.; Luthje, S. Cell wall-bound cationic and anionic class III isoperoxidases of pea root: biochemical characterization and function in root growth. *J. Exp. Bot.* **2012**, *63*, 4631−4645.

(29) Sergio, L.; Pieralice, M.; Di Venere, D.; Cardinali, A. Thermostability of soluble and bound peroxidases from artichoke and a mathematical model of its inactivation kinetics. *Food Technol. Biotechnol.* **2007**, *45*, 367−373.

(30) Fortea, M. I.; Lopez-Miranda, S.; Serrano-Martinez, A.; Hernandez-Sanchez, P.; Zafrilla, M. P.; Martinez-Cacha, A.; Nunez-Delicado, E. Kinetic characterisation and thermal inactivation study of red alga (*Mastocarpus stellatus*) peroxidase. *Food Chem.* **2011**, *127* (676), 1091−1096.

(31) Castillo-Leon, J.; Alpeeva, I. S.; Chubar, T. A.; Galaev, I. Y.; Csoregi, E.; Sakharov, I. Y. Purification and substrate specificity of peroxidase from sweet potato tubers. *Plant Sci.* **2002**, *163*, 1011−1019.

(32) Morales-Blancas, E. F.; Chandia, V. E.; Cisneros-Zevallos, L. Thermal inactivation kinetics of peroxidase and lipoxygenase from broccoli, green asparagus and carrots. *J. Food Sci.* **2002**, *67*, 146−154.

(33) Ganthavorn, C.; Nagel, C. W.; Powers, J. R. Thermal inactivation of asparagus lipoxygenase and peroxidase. *J. Food Sci.* **1991**, *56*, 47−49.

(34) Agostini, E.; Hernández-Ruiz, J.; Arnao, M. B.; Milrad, S. R.; Tigier, H. A.; Acosta, M. A peroxidase isoenzyme secreted by turnip (*Brassica napus*) hairy-root cultures: inactivation by hydrogen peroxide and application in diagnostic kits. *Biotechnol. Appl. Biochem.* **2002**, *35*, 1−7.

(35) Lopez-Molina, D.; Hiner, A. N. P.; Tudela, J.; Garcia-Canovas, F.; Rodriguez-Lopez, J. N. Enzymatic removal of phenols from aqueous solution by artichoke (*Cynara scolymus* L.) extracts. *Enzyme Microb. Technol.* **2003**, *33*, 738−742.

(36) Praveen, K.; Usha, K. Y.; Viswanath, B.; Reddy, B. R. Kinetic properties of manganese peroxidase from the mushroom stereum ostrea and its ability to decolorize dyes. *J. Microbiol. Biotechnol.* **2012**, *22*, 1540−1548.

In this work, we have carried out two sets of experiments involving PMG interaction with metals: (i) surface-enhanced Raman spectroscopy (SERS) experiments after PMG was deposited from an aqueous solution on different metallic surfaces and (ii) attenuated total reflectance Fourier transform infrared (ATR−FTIR) spectra experiments of PMG interacting with metallic ions in aqueous solution. We have used density functional theory (DFT) calculations to identify the vibrational bands, looking for fingerprints of the AMPA and PMG presence. Both experiments show evidence of an abiotic pathway of PMG degradation into AMPA.

## MATERIALS AND METHODS

**Raman Experiments.** SERS experiments were made *ex situ* using a Jobin-Yvon T64000 triple spectrometer operating in subtractive mode and equipped with a liquid-$N_2$-cooled charge-coupled device. The excitation was performed using the 647.1 nm line of an Ar−Kr laser. Typical acquisitions employed three integrations of 60 s using laser powers of 20−50 mW, concentrated on a 7 mm long and around 100 mm wide line focus. This was chosen to reduce the photon-induced degradation of the samples. Product formation because of reactions occurring at these excitation wavelengths were further ruled out by checking that the spectra remained constant in time.

Glyphosate and AMPA were purchased from Sigma-Aldrich (analytical standard quality). All other supplies used were of the best analytical grade commercially available.

SERS experiments were performed on sphere segment void (SSV) arrays, fabricated via an hexagonal close packed self-assembly of 600 nm radius polystyrene spheres, followed by an electrochemical Au deposition, as originally described by Bartlett and co-workers.[28,29]

Structured copper surfaces were prepared by underpotential deposition (UPD) on SSV gold arrays from a $5 \times 10^{-4}$ M $CuSO_4$ + 1 M $H_2SO_4$ aqueous solution in a conventional electrochemical cell. A voltammetry sweep from −0.6 to 0 V at 0.25 V $s^{-1}$ was performed with a Pt large area foil as the counter electrode and a Cu wire as the pseudo-reference electrode.

Ag nanoparticles (NPs) were deposited to further increase the Raman signal.[6,30,31] These nanoparticles (spheric, 20 nm mean size) were synthesized according to the Turkevich method.[32] Briefly, 100 mL of 1 mM $AgNO_3$ aqueous solution was stirred and heated until 90 °C and then reduced with 20 mg of sodium citrate. After the color change to yellow, the solution was cooled while stirring until room temperature. Always a fresh stash of Ag NPs was used for each experiment.

PMG and AMPA adsorption on SSV substrates was made following two different methods. (I) Drop casting: a 10 $\mu$L drop of 1 mg/mL PMG or AMPA aqueous solution with Milli-Q water (18.0 MΩ) was deposited on the SSV surface and dried with $N_2$ flux; immediately, the sample was dipped in a Ag nanoparticle solution overnight and then rinsed with Milli-Q water and dried with $N_2$ flux. (II) Dipping: SSV substrate was dipped in 1 mg/mL PMG aqueous solution overnight and then carefully rinsed with Milli-Q water and dried with $N_2$ flux; finally, 10 $\mu$L of Ag nanoparticles were drop-casted on top and dried with $N_2$ flux.

**ATR−FTIR Experiments.** The ATR−FTIR experiments were performed in the 500−4000 $cm^{-1}$ region in a Nicolet 8700 FTIR spectrometer (128 scans, resolution of 4 $cm^{-1}$) equipped with a DTGS detector and a Smart Orbit ATR accessory with a diamond crystal unit with a single reflection. A baseline correction was made for instrumental instabilities, and the background was subtracted. Data were evaluated using OMNIC, version 7.3, Thermo Electron Corporation software.

All chemical reagents were analytical-grade and used without any further purification. Water was purified in a Milli-Q system from Millipore, Inc. Glyphosate was provided by Sigma Co. Copper chloride dehydrated ($CuCl_2 \cdot 2H_2O$) and AMPA (99% pure) were from Aldrich Chemical.

Stock solutions of 1000 mg $L^{-1}$ of each reagent ($Cu^{II}$, AMPA, and PMG) were prepared. The stock solution of $Cu^{II}$ was prepared by dissolving $CuCl_2 \cdot 2H_2O$ in Milli-Q water. The reactant molar ratios of 2.7:1 $Cu^{II}$/PMG and 2.6:1 $Cu^{II}$/AMPA were obtained by adding the required aliquots of $Cu^{II}$ and PMG (or AMPA) stock solutions into a flask, reaching the final volume by the addition of the required volume of Milli-Q water.

The colorless solution of PMG (or AMPA) changed to light blue as soon as the light green solution of $CuCl_2$ was added. The complex solution was frozen and freeze-dried, and a bright green solid was obtained.

**DFT Calculations.** The DFT calculations were carried out within the slab-supercell approach by means of the Vienna *ab initio* simulation program (VASP).[33−35] The electron−ion interactions were described through the projector-augmented plane-wave (PAW) Perdew−Burke−Ernzerhof (PBE) pseudo-potentials. Exchange and correlation (XC) was described within the van der Waals density functional with optB86b as the exchange functional. We used an energy cutoff of 450 eV, and the Brillouin zone integration was performed within the Methfessel−Paxton technique,[36] with an electron smearing of 0.1 eV. The energies and forces were converged to $10^{-4}$ eV and $10^{-1}$ eV/nm. The Cu(111) and Cu(100) surfaces were represented by a $4 \times 4$ unit cell with five-layer slabs. AMPA was adsorbed only on one side of the slab, and during full geometry optimizations, we allowed for relaxation of the three topmost layer metal atoms and all of the atoms of the molecule.

## RESULTS AND DISCUSSION

We started by characterizing the vibration spectra of PMG[17] and AMPA[18] crystals using DFT calculations. Table 1 shows the theoretical frequencies for PMG and AMPA and the vibration mode identification. The crystals have non-equivalent molecules within the unit cell; consequently, the frequencies in Table 1 correspond to averages over sets of modes in similar vibration states.[37]

From the analysis of the DFT results, we identify the mode at 717 $cm^{-1}$ for AMPA and 761 $cm^{-1}$ for PMG (highlighted in blue in Table 1) as a P−C stretching vibration. This mode is separated from neighboring modes by more than 90 $cm^{-1}$, with the only exception of a mode appearing at 783 $cm^{-1}$ in the PMG crystal, which corresponds to a complex vibration [$\nu$(PC) + $\rho(CH_2)$ + $\rho(NH_2)$ + $\nu$(CCOO)]. This feature together with the fact that the AMPA P−C and PMG P−C are separated enough from each other makes these modes easily resolvable in vibrational spectra, therefore providing respective fingerprints for the AMPA and PMG presence.

To study the effect of the molecule surface adsorption on the vibrational spectra, we performed DFT calculations for AMPA on Cu(111) and Cu(100) surfaces (see Tables S2 and S3 of the Supporting Information). The calculated P−C mode frequencies shift down, relative to the crystal, 15 and 7 $cm^{-1}$ for Cu(111) and Cu(100) surfaces, respectively.

The Raman spectra obtained for the AMPA and PMG crystals are shown in panels A and B of Figure 1, respectively. Fits of the P−C peaks are shown in blue for PMG and green for AMPA.

We show in Figure 1C the SERS spectrum of PMG deposited from aqueous solutions on Cu_UPD/Au with Ag nanoparticles, using the drop-casting method. It presents a peak at the frequency previously assigned to the P−C mode of the PMG crystal, but unexpectedly, a second peak is also observed. This second peak is in a region free of PMG vibrations and at the frequency of the AMPA P−C mode, indicating the presence of AMPA in this sample. To the best of our knowledge, this

Table 1. DFT-Calculated Frequencies ($cm^{-1}$) and Vibration Modes for PMG and AMPA Crystals[a]

| PMG crystal | AMPA crystal | Vibration modes |
|---|---|---|
| | 460 | δ(HO-P=O)/δ(O=P=O) |
| 473 | | δ(PO3)+δ(NCCO) |
| 495 | | δ(HO-P=O)+ρ(PCN)+ δ(NCC)+δ(OH-C=O)+ ρ(CH2)* |
| 520 | | δ(HO-P=O)+δ(CNC)+ δ(OH-C=O)+ρ(CH2)* |
| | 529 | δ(P-C-N)+ω(HO-P=O) |
| 541 | | δ(HO-P=O)+ δ(PCN)+δ(C=C-OH) |
| | 558 | τ(NH3) |
| 559 | | δρ(PO3)+skel(NCCO2) |
| 629 | | ν(PC)+δ(NCC)+δ(COO) |
| | 717 | ν(PC) |
| 761 | | ν(PC) |
| 783 | | ν(PC)+ρ(CH2)+ρ(NH2)+ν(CCOO) |
| | 819 | ρ(CH2)+ν(P-OH) |
| 851 | | ν(CC) |
| 906 | | CNCC skeleton |
| | 908 | ν(HO-P) |
| 948 | | νs(PO3)+ν(PC) |
| 978 | | νs(PO3)+τ(CH2)+ ρ(NH2)+skel(CNCC) |
| | 983 | ν(OP) |
| | 1007 | ν(CN) |
| 999 | | CNCC skeleton |
| | 1032 | ν(PO3) |
| 1039 | | ν(CN)/CNCC skel+ νa(HO-P=O)/νa(POO) |
| 1059 | | CNC skeleton |
| | 1078 | δ(HNC)+νa(PO2)/ν(PO) |
| 1085 | | νa(PO3)+ν(NC) |
| | 1107 | νa(O=P=O)+δ(HCNH) |
| 1123 | | νa(P-OH) |
| | 1131 | ρ(NH3) |
| 1184 | | (CH2+NH2+CH2*)/HCNCH+ν(COH) |
| | 1166 | ν(P=O) |
| 1226 | | (CH2+NH2+CH2*)+ν(CN)+ν(COH) |
| 1242 | | ν(P-OH)+τ(CH2)+ ν(COH) +δ(CNC) |
| 1280 | | ν(PC)+ν(POH)+ω(CH2) |
| 1303 | | ω(CH2)+ωτ(CH2)*+ δ(COH)+ν(PC) |
| | 1311 | δ(HOP)+ν(PC)+δ(HCNH) |
| 1327 | | ωτ(CH2)*+δ(COH)+ δ(CNC)/ν(POH)+... |
| | 1339 | δ(HCNH)+δ(PCN) |
| 1406 | | δ(CH2)+ν(CCOH) |
| 1431 | | δ(CH2)+δ(POH) |
| | 1432 | δ(CH2) |
| 1452 | | ν(CC)+δ(CNH)/τ(NH2) |
| 1485 | | ω(NH2)+δ(POH) |
| | 1534 | δ(NH3) |
| 1567 | 1628 | δ(NH2) |
| | 1653 | δ(NH2) |
| 1705 | | ν(CO) |

[a]Mode notation: $\delta$ for bending, $\nu$ for stretching ($\nu_a$ and $\nu_s$ for asymmetric and symmetric stretching), $\omega$ for wagging, $\rho$ for rocking, $\tau$ for twisting, and "skel" for skeleton. In PMG, $CH_2$* refers to the methyl farthest away from the phosphonate group. For further details, see the captions of Tables S2−S3 of the Supporting Information.

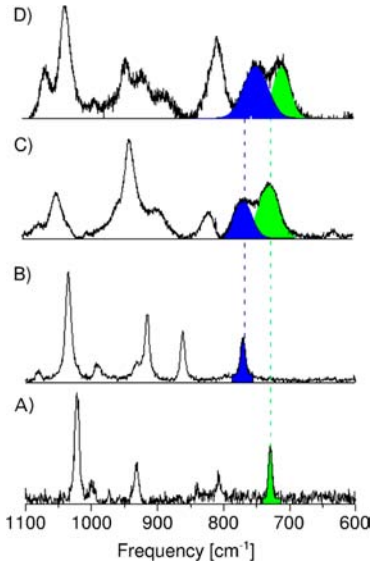


**Figure 1.** SERS spectra for (A) AMPA crystals, (B) PMG crystals, (C) PMG deposited on Cu_UPD/Au with Ag NPs using the drop-casting method, and (D) PMG deposited on Cu_UPD/Au with Ag NPs using the dipping method. The shadowed areas correspond to the P−C mode region for AMPA (green) and PMG (blue).

result provides the first evidence of an abiotic path for PMG degradation into AMPA.

Figure 1D shows the SERS spectrum of a sample prepared with the dipping method. It is noteworthy that, in this preparation, the samples are rinsed before the addition of Ag NPs, and thus, most of the molecules that are not adsorbed on the surface are removed from it.

The P−C peaks of AMPA and PMG are also present in Figure 1D, even though they are shifted to lower frequencies (shifts of 20 $cm^{-1}$ for AMPA and 22 $cm^{-1}$ for PMG). Based on the DFT results for AMPA/Cu, these experimentally observed shifts to lower frequencies indicate that both AMPA and PMG are predominantly adsorbed on the Cu surface.

From the analysis of Figure 1, we conclude that (i) for both sample preparation methods, an abiotic degradation process of PMG into AMPA has taken place, (ii) when the drop-casting method is used, the P−C mode of PMG and AMPA is not shifted relative to the PMG or AMPA crystal mode, indicating that most of the molecules are not bonded to the Cu surface, and (iii) in samples prepared with the dipping method, the resulting PMG and AMPA are mainly adsorbed on the surface.

An estimation of the percentage of PMG degraded into AMPA can be obtained by means of a fitting procedure of the P−C mode frequency region of panels C and D of Figure 1. The approximate amount of degradation is 56% in drop-casted samples and 50% in dipped samples. For a detailed description, see Figure S1 and Table S1 of the Supporting Information.

From further analysis, some additional information regarding the adsorbed molecule configuration can be extracted. By means of DFT calculations for crystals, the most intense peak in Figure 1C is identified with the stretching P−O mode (931 $cm^{-1}$) of both PMG and AMPA (see Table 1). In Figure 1D, this peak decreases, implying that the adsorbed molecules interact with the surface via the phosphonic group.

Complementary SERS spectra for drop-casting experiments of PMG deposited on Ag and Au with Ag NPs show that the degradation of PMG into AMPA is not specific to the


dx.doi.org/10.1021/jf502979d | J. Agric. Food Chem. 2014, 62, 9651−9656

interaction of PMG with a Cu surface but also occurs in the presence of other metallic substrates. The spectra obtained (see Figure S2 of the Supporting Information) are very similar to the spectra in Figure 1C; particularly, the P−C peaks of both molecules appear in all of the samples.

The interaction of PMG with metal atoms in solution is known to result in chelate formation.[20,21,24] This raises the question of whether the surface is itself needed for the degradation process or whether the interaction of PMG with isolated metal atoms can also degrade it into AMPA. To elucidate this point, we prepared a mixture of Cu and PMG in aqueous solution (hereafter referred to as PMG + Cu) using a molar ratio of 2.7:1 Cu/PMG and, after sample lyophilization, characterized it by ATR−FTIR experiments. We also measured the ATR−FTIR spectra for AMPA crystals, PMG crystals, and a 2.6:1 Cu/AMPA mixture in aqueous solution (hereafter AMPA + Cu), to use as references. Figure 2 shows the spectra obtained.

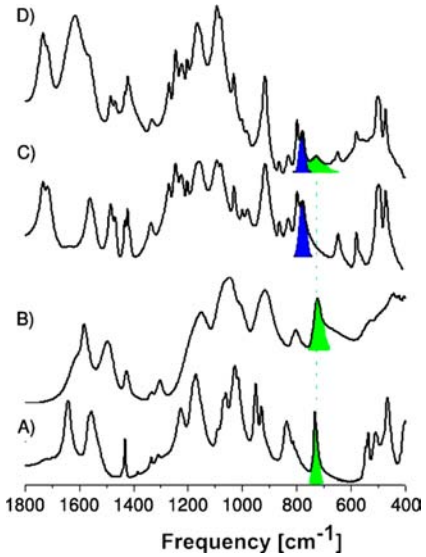


**Figure 2.** IR spectra of (A) pure AMPA crystals, (B) AMPA + Cu with a molar ratio of 2.6:1 Cu/AMPA, (C) pure PMG crystals, and (D) PMG + Cu with a molar ratio of 2.7:1 Cu/PMG. The shadowed areas correspond to the P−C mode region for AMPA (green) and PMG (blue).

The AMPA P−C peak can be clearly observed in the AMPA (Figure 2A) and AMPA + Cu (Figure 2B) spectra, although slightly shifted to lower frequencies in the latter. Likewise, the PMG P−C peak is present in PMG (Figure 2C) and PMG + Cu (Figure 2D) spectra. For both AMPA and PMG, the respective P−C peaks are distinct and appear at frequencies consistent with the Raman measurements. The PMG spectrum shows a wide gap between the P−C (at 777 $cm^{-1}$) and the skeleton (at 643 and 577 $cm^{-1}$) modes. However, in the PMG + Cu spectrum, there is a peak at the frequency of the AMPA P−C mode (729 $cm^{-1}$), indicating the presence of AMPA molecules and/or AMPA−Cu complexes in the sample.

It must be highlighted that the presence of AMPA in the spectra of PMG + Cu samples is also observed for lower Cu/PMG molar ratios. In fact, the AMPA P−C peak can be clearly identified in samples prepared with a 0.7:1 Cu/PMG molar ratio (see Figure S3 of the Supporting Information).

We find further evidence of PMG into AMPA degradation in the 1600−1700 $cm^{-1}$ region. Our calculations show three vibration modes in the AMPA amino group [$\delta(NH_2)$ at 1648 and 1588 $cm^{-1}$, and $\delta(NH_3)$ at 1525 $cm^{-1}$], in agreement with Raman data. Infrared (IR) peaks of AMPA at 1555 and 1641 $cm^{-1}$ correspond to two of these modes. PMG has a single $\delta(NH_2)$ mode at 1567 $cm^{-1}$ (Raman peak at 1568 $cm^{-1}$ and IR peak at 1560 $cm^{-1}$) and a $\nu(C{=}O)$ mode of the carboxylate group at 1705 $cm^{-1}$, associated with Raman and IR structures at 1715−1730 $cm^{-1}$. These two PMG peaks remain in place in the PMG + Cu IR spectrum, but an intense peak in between, at 1616 $cm^{-1}$, is also visible. In IR spectroscopic studies of PMG + metal complexes,[22,23] this peak is usually assigned to a $\nu_a(COO)$ mode and interpreted as the result of the interactions of the carboxylate group with Cu atoms. However, we observe that the $\nu(C{=}O)$ mode at 1715−1730 $cm^{-1}$ is not affected much by the presence of Cu atoms. We hence conclude that the 1616 $cm^{-1}$ peak is a combination of the PMG $\delta(NH_2)$ mode and the $\delta(NH_2)$ and $\delta(NH_3)$ modes coming from AMPA and AMPA + Cu.

Additionally, some information regarding AMPA and PMG reactivity to Cu atoms can be drawn from Figure 2. In the 900−1200 $cm^{-1}$ region, the main contribution to AMPA spectra comes from the phosphonate group.[24] Consequently, the changes observed when comparing the AMPA and AMPA + Cu spectra in that region are consistent with Cu atoms being bonded to this group. Also, the significant frequency shift in the $NH_2{-}NH_3$ region, around 1600 $cm^{-1}$, signals Cu−N interactions. These features are consistent with our AMPA/Cu adsorption analysis, where we find that the most stable configuration involves both Cu−O and Cu−N bonds.

Tables S2 and S3 of the Supporting Information show the calculated DFT frequencies and the complete band assignment of the SERS and IR spectra.

In conclusion, in this work, we have detected the presence of AMPA in SERS spectra of pure PMG deposited on several metal surfaces and in IR spectra after the PMG interaction with metallic ions in aqueous solution. Only an abiotic degradation process of PMG, where metal atoms play a central role, can explain the presence of AMPA in the experiments reported.

Previous experimental studies of glyphosate−metal complexes have not considered the PMG degradation pathway revealed in this work. Reported IR spectra do not include the frequency region around the P−C modes, or when they do, thus exposing the AMPA P−C peak[25] at approximately 730 $cm^{-1}$, the presence of AMPA is not taken into account in the analysis.[6,23,25,26] On the basis of the results presented here, it would be enriching to revisit this literature.

Precision in the dose of application of herbicide products is crucial not only to ensure efficient herbicide treatments but also to reduce the unwanted effects on the environment. Then, it is necessary to study the effectiveness of this abiotic degradation process in agriculture conditions.

Consequently, we expect our results will encourage further research to characterize quantitatively this new PMG into AMPA degradation process.

## ■ ASSOCIATED CONTENT

### Supporting Information

Fitting of the SERS spectra in the P−C frequency region (Figure S1), proportion of molecules according to type and configuration relative to the total number of molecules resulting from the fitting of Figure S1 (Table S1), SERS spectra of

glyphosate deposited on different metal surfaces using the drop-casting method (Figure S2), ATR−FTIR spectra of PMG + Cu samples with different molar ratios (Figure S3), and IR, SERS, and DFT frequencies and band assignments for PMG and AMPA (Tables S2 and S3). This material is available free of charge via the Internet at http://pubs.acs.org.

## AUTHOR INFORMATION

### Corresponding Author

*E-mail: mluz@cab.cnea.gov.ar.

### Funding

The authors acknowledge partial support from ANPCyT-Argentina (Projects PICT-2010-1962 and PICT-2008-1260), CONICET (Project PIP 0667), MinCyT-CNRS (LIFAN), Instituto de Nanociencia y Nanotecnología, CNEA, and Universidad Nacional de Cuyo (06/C390 and 06/C383).

### Notes

The authors declare no competing financial interest.

## ACKNOWLEDGMENTS

The authors thank G. Zampieri for a thorough reading of the manuscript.

## REFERENCES

(1) Nowack, B. Environmental chemistry of phosphonates. *Water Res.* **2003**, *37*, 2533−2546.

(2) Vereecken, H. Mobility and leaching of glyphosate: A review. *Pest Manage. Sci.* **2005**, *61*, 1139−1151.

(3) Borggaard, V.; Gimsing, A. L. Fate of glyphosate in soil and the possibility of leaching to ground and surface waters: A review. *Pest Manage. Sci.* **2008**, *64*, 441−456.

(4) Fenner, K.; Canonica, S.; Wackett, L. P.; Elsner, M. Evaluating pesticide degradation in the environment: Blind spots and emerging opportunities. *Science* **2013**, *341*, 752.

(5) Dieter, H. H. The relevance of "non-relevant metabolites" from plant protection products (PPPs) for drinking water: The German view. *Regul. Toxicol. Pharmacol.* **2010**, *56*, 121−125.

(6) Costa, J. C. S.; Ando, R. A.; Sant'Ana, A. C.; Corio, P. Surface-enhanced Raman spectroscopy studies of organophosphorous model molecules and pesticides. *Phys. Chem. Chem. Phys.* **2012**, *14*, 15645−11565.

(7) Khoury, G. A.; Gehris, T. C.; Tribe, L.; Torres Sánchez, R. M.; dos Santos Afonso, M. Glyphosate adsorption on montmorillonite: An experimental and theoretical study of surface complexes. *Appl. Clay Sci.* **2010**, *50*, 167−175.

(8) Laitinen, P.; Rämö, S.; Nikunen, U.; Jauhiainen, L.; Siimes, K.; Turtola, E. Glyphosate and phosphorus leaching and residues in boreal sandy soil. *Plant Soil* **2009**, *323*, 267−283.

(9) Rampazzo, N.; Rampazzo Todorovic, G.; Mentler, A.; Blum, W. E. H. Adsorption of glyphosate and aminomethylphosphonic acid in soils. *Int. Agrophys.* **2013**, *27*, 203−209.

(10) Ndjeri, M.; Pensel, A.; Peulon, S.; Haldys, V.; Desmazieres, B.; Chausse, A. Degradation of glyphosate and AMPA (amino methylphosphonic acid) solutions by thin films of birnessite electrodeposited: A new design of material for remediation processes? *Colloids Surf., A* **2013**, *435*, 154−169.

(11) Reddy, K. N.; Rimando, A. M.; Duke, S. O.; Nandula, V. K. Aminomethylphosphonic acid accumulation in plant species treated with glyphosate. *J. Agric. Food Chem.* **2008**, *56*, 2125−2130.

(12) Franz, J. E.; Mao, M. K.; Sikorski, J. A. Glyphosate: A unique global herbicide. *ACS Monogr.* **1997**, *189*, 653.

(13) Barrett, K. A.; McBride, M. B. Oxidative degradation of glyphosate and aminomethylphosphonate by manganese oxide. *Environ. Sci. Technol.* **2005**, *39*, 9223−9228.

(14) Reddy, K. N.; Rimando, A. M.; Duke, S. O. Amino-methylphosphonic acid, a metabolite of glyphosate, causes injury in glyphosate-treated, glyphosate-resistant. *J. Agric. Food Chem.* **2004**, *52*, 5139−5143.

(15) Duke, S. O. Glyphosate degradation in glyphosate-resistant and -susceptible crops and weeds. *J. Agric. Food Chem.* **2011**, *59*, 5835−5841.

(16) Dinga, W.; Reddya, K. N.; Zablotowicz, R. M.; Bellaloui, N.; Bruns, A. Physiological responses of glyphosate-resistant and glyphosate-sensitive soybean to aminomethylphosphonic acid, a metabolite of glyphosate. *Chemosphere* **2011**, *83*, 593−598.

(17) Knuuttila, P.; Knuuttila, H. The crystal and molecular structure of *N*-(phosphonomethyl)glycine (glyphosate). *Acta Chem. Scand., Ser. B* **1979**, *33*, 623.

(18) Benbrahim, N.; Rahmouni, A.; Ruiz-López, M. F. A theoretical study of medium effects on the structure of the glycine analogue aminomethylphosphonic acid. *Phys. Chem. Chem. Phys.* **2008**, *10*, 5624−5632.

(19) Piccolo, A.; Celano, G. Hydrogen-bonding interactions between the herbicide glyphosate and water-soluble humic substances. *Environ. Toxicol. Chem.* **1994**, *13*, 1737−1741.

(20) Popov, K.; Rönkkömäki, H.; Lajunen, L. H. J. Critical evaluation of stability constants of phosphonic acids. *Pure Appl. Chem.* **2001**, *73*, 1641.

(21) Barja, B. C.; Herszage, J.; dos Santos Afonso, M. Iron(III)−phosphonate complexes. *Polyhedron* **2001**, *20*, 1821−1830.

(22) Subramaniam, V.; Hoggard, P. Metal complex of glyphosate. *J. Agric. Food Chem.* **1988**, *36*, 1326−1329.

(23) Sheals, J.; Persson, P.; Hedman, B. IR and EXAFS spectroscopic studies of glyphosate protonation and copper(II) complexes of glyphosate in aqueous solution. *Inorg. Chem.* **2001**, *40*, 4302−4309.

(24) Barja, B. C.; Dos Santos Afonso, M. Aminomethylphosphonic acid and glyphosate adsorption onto goethite: A comparative study. *Environ. Sci. Technol.* **2005**, *39*, 585−592.

(25) Undabeytia, T.; Morillo, E.; Maqueda, C. FTIR study of glyphosate−copper complexes. *J. Agric. Food Chem.* **2002**, *50*, 1918−1921.

(26) Harris, W. R.; Sammons, R. D.; Grabiak, R. C.; Mehrsheikh, A. Computer simulation of the interactions of glyphosate with metal ions in phloem. *J. Agric. Food Chem.* **2012**, *60*, 6077−6087.

(27) Glyphosate technical fact sheets currently leave the possibility of stored PMG in copper vessels.

(28) Tognalli, N. G.; Fainstein, A.; Calvo, E. J.; Abdelsalam, M.; Bartlett, P. N. Incident wavelength resolved resonant SERS on Au sphere segment void (SSV) arrays. *J. Phys. Chem. C* **2012**, *116* (5), 3414−3420.

(29) Tognalli, N. G.; Cortés, E.; Hernandez-Nieves, A. D.; Carro, P.; Usaj, G.; Balseiro, C.; Vela, M. E.; Salvarezza, R. C.; Fainstein, A. From single to multiple Ag-layer modification of Au nanocavity substrates: A tunable probe of the chemical surface-enhanced Raman scattering mechanism. *ACS Nano* **2011**, *5* (7), 5433−5443.

(30) Fan, M.; Brolo, A. G. Silver nanoparticles self assembly as SERS substrates with near single molecule detection limit. *Phys. Chem. Chem. Phys.* **2009**, *11*, 7381−7389.

(31) Orendorff, C. J.; Gole, A.; Sau, T. K.; Murphy, C. J. Surface-enhanced Raman spectroscopy of self-assembled monolayers: Sandwich architecture and nanoparticle shape dependence. *Anal. Chem.* **2005**, *77*, 3261−3266.

(32) Turkevich, J.; Stevenson, P. C.; Hillier, J. A study of the nucleation and growth processes in the synthesis of colloidal gold. *Discuss. Faraday Soc.* **1951**, *11*, 55−75.

(33) Hafner, R. Ab-initio simulations of materials using VASP: Density-functional theory and beyond. *J. Comput. Chem.* **2008**, *29*, 2044−2078.

(34) Kresse, G.; Hafner, J. Ab initio molecular dynamics for liquid metals. *Phys. Rev. B: Condens. Matter Mater. Phys.* **1993**, *47*, 558−561.

(35) Kresse, G.; Hafner, J. Ab initio molecular-dynamics simulation of the liquid-metal−amorphous-semiconductor transition in germanium. *Phys. Rev. B: Condens. Matter Mater. Phys.* **1994**, *49*, 14251−14269.

(36) Methfessel, M.; Paxton, A. High-precision sampling for Brillouin-zone integration in metals. *Phys. Rev. B: Condens. Matter Mater. Phys.* **1989**, *40*, 3616−3621.

(37) Although in some cases, there were slight differences in either the atoms involved or the vibration mode of a given group. For those cases, the notation mode 1/mode 2 refers to averages over states, some of which include the "mode 1" vibration, while some include the other "mode 2" vibration.

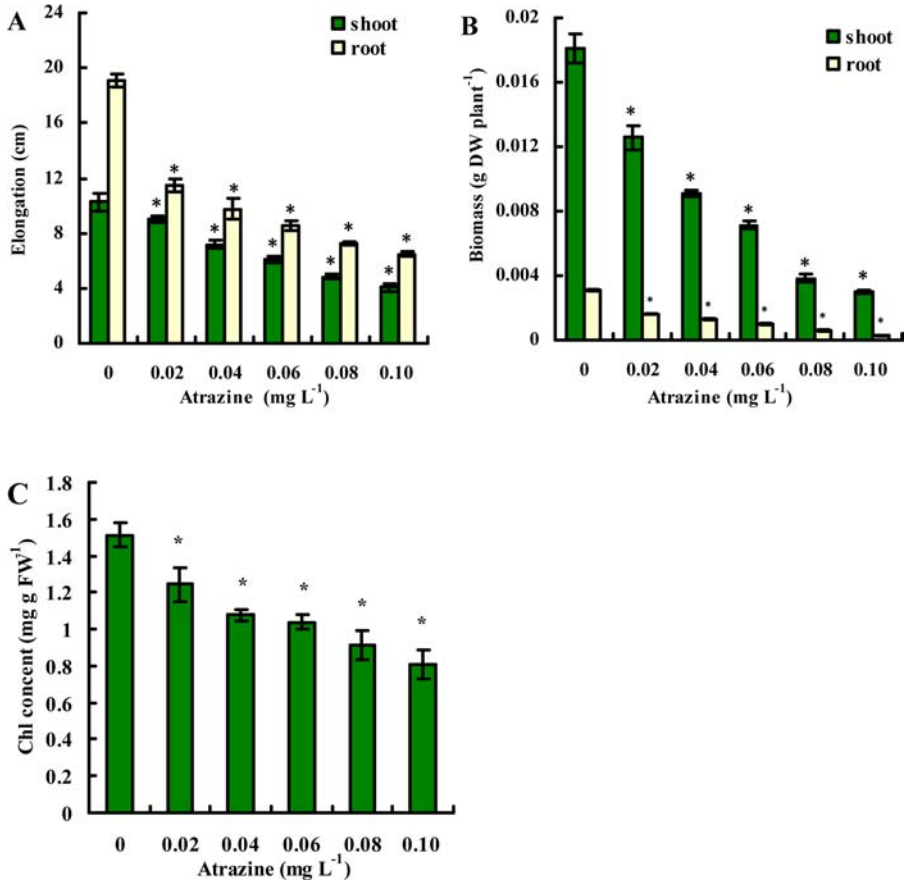


**Figure 1.** Effect of atrazine on the elongation (A), biomass (B), and the content of chlorophyll (C) of *Medicago sativa*. *Medicago sativa* seedlings were cultured in the 1/2 strength Hoagland nutrient solution containing atrazine at 0, 0.02, 0.04, 0.06, 0.08, and 0.10 mg $L^{-1}$ for 6 d. Values are the means ± SD ($n$ = 3). Asterisks indicate significant differences between the treatments and the control ($p < 0.05$). DW: dry weight. FW: fresh weight.

(1) to assess the ability of alfalfa to accumulate and degrade atrazine and (2) to investigate the possible atrazine catabolic pathway with detailed characterization of atrazine derivatives or atrazine-conjugated products in alfalfa.

## MATERIALS AND METHODS

**Materials and Treatments.** The herbicide atrazine was obtained from the Institute of Pesticide Science, Academy of Agricultural Sciences in Nanjing, China, with 99% purity. Alfalfa seeds (*Medicago sativa*, cv. Golden Empress) were surface-sterilized with 5% solution of sodium hypochlorite for 15 min, rinsed with distilled water, and placed on moist filter paper for germination. Germinating seeds were placed on a plastic net floating on distilled water in the dark at 25 °C for 2 d. Then, uniform seedlings were transferred to black polyvinyl chloride pots (1 L) that contained 1/2 strength Hoagland nutrient solution.[26] Culture solutions were renewed every 2 days. When the third true leaf was well developed, seedlings were treated with atrazine at 0, 0.02, 0.04, 0.06, 0.08, and 0.10 mg $L^{-1}$ for 6 d, respectively, in 1/2 strength nutrient solution. Treatment solutions were renewed every 2 d. Each pot contained 30 seedlings, which were grown in a growth chamber under the conditions of 14 h photoperiod, 200 $\mu$mol of photons $m^{-2}$ $s^{-1}$, and 25/20 °C (day/night). Each treatment was repeated thrice.

**Determination of Growth and Chlorophyll Content.** The elongation of shoots and roots of fresh individual plants was measured with a normal ruler. A forced-air oven was used for determination of biomass. Fresh shoots and roots were dried at 105 °C for 20 min, then oven-dried at 80 °C for 48 h, and weighed afterward.[26] Chlorophyll was assayed according to the method of extraction with 80% acetone[27] Fresh leaves (0.1 g) were extracted with 8 mL of 80% acetone (pH 7.8). After extracting solution was centrifuged at 5000$g$ for 10 min, the supernatant was collected, the chlorophyll content was assayed spectrophotometrically, and the content of chlorophyll was expressed as mg $g^{-1}$ fresh weight (FW).

**Analysis of Atrazine.** Alfalfa plants were cultured in 1/2 strength Hoagland nutrient solutions containing 0, 0.02, 0.04, 0.06, 0.08, and 0.10 mg $L^{-1}$ atrazine, respectively. Shoots and roots of plants were separately harvested after atrazine treatment. Fresh shoots or roots (3.0 g) were ground and dissolved in 15 mL of acetone−water (3:1, v:v) and ultrasonicated for 30 min. The homogenate was centrifuged at 4000$g$ for 7 min and filtrated. The above steps were repeated in triplicate. The filtrate was vaporized to remove acetone at 40 °C using a rotary vacuum evaporator. The residual water was partitioned in petroleum ether three times, each time with 10 mL of the solvent. The petroleum ether was concentrated to dryness at 40 °C. The residue was dissolved in 0.5 mL of methanol and diluted with 20 mL of water. The mixture was passed through an LC-18 solid-phase extraction (SPE) column. Eluates were discarded, and the column was washed with 2 mL of methanol−water (80:20, v:v). The washing solution was collected for analysis of high performance liquid chromatography (HPLC, Waters 515; Waters Technologies Co. Ltd., USA) with ultraviolet (UV) detector. The operating conditions of HPLC were as follows: wavelength, 225 nm; room temperature; Hypersil reversed-phase C18 column (Thermo, 250 mm × 4.6 mm i.d.); mobile phase, methanol:water (70:30, v:v); flow rate, 0.6 mL $min^{-1}$; injection volume, 20 $\mu$L. Atrazine in the plant-culture solution was also measured with the LC-$C_{18}$ SPE column as described above. The spiked recovery and determination limit of the above method are shown in Table S1 in the Suppporting Information.

**Assay of Enzyme Activities.** Fresh shoot (1 g) or root tissues (1.5 g) were homogenized in 6 mL of ice-cold sodium phosphate buffer (50 mM, pH 7.8) containing 1 mM EDTA and 1% (w/w) polyvinylpyrrolidone. The homogenate was centrifuged at 12000$g$ at 4 °C for 20 min. Glutathione $S$-transferase (GST, EC 2.5.1.18) activity


dx.doi.org/10.1021/jf503221c | J. Agric. Food Chem. 2014, 62, 9657−9668

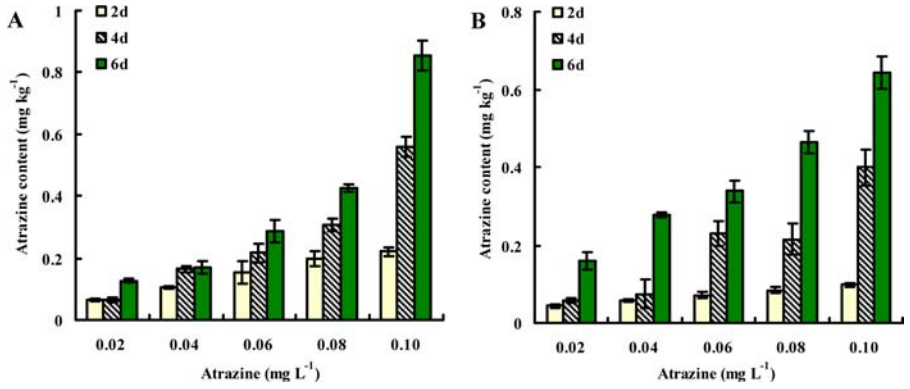


**Figure 2.** Accumulation of atrazine in shoots (A) and roots (B) of *Medicago sativa*. Alfalfa seedlings were cultured in the 1/2 strength Hoagland nutrient solution containing atrazine at 0, 0.02, 0.04, 0.06, 0.08, and 0.10 mg $L^{-1}$ for 2, 4, and 6 d, respectively. Values are the means ± SD ($n$ = 3).

was determined by the method of Song et al.[28] The reaction mixture consisted of 3 mL of 100 mM sodium phosphate buffer (pH 6.5) containing 1 mM GSH, 75 μL of 40 mM 1-chloro-2,4-dinitrobenzene (CDNB), and 100 μL of enzyme extract. The change in absorbance was recorded at 340 nm during 3 min.

Fresh shoots or roots (1 g) were ground and extracted with 1 mM EDTA, 50 mM NaCl, 1% (w/v) polyvinylpolypyrrolidone, and 50 mM Tris−HCl (pH 8.0). The homogenate was centrifuged at 10000*g* at 4 °C for 30 min. The supernatant was collected as crude extract for measurement of UDP-glycosyltransferases (GTs, EC 2.4.*x*.*y*).[9,29] The 250 μL of reaction mixture contained 100 μL of the enzymatic extraction, 0.04 mM *p*-nitrophenol, and 2 mM UDP-glucose. The reaction was carried out at 30 °C for 2 h, terminated by addition of 250 μL of methanol, and chilled to −20 °C for 0.5 h. The reduced rate of the *p*-nitrophenol concentration was assayed by HPLC. One unit of the GT activity was defined as the amount of enzyme activity needed to consume 1 mol of *p*-nitrophenol per minute. The protein concentration in enzyme extract was assayed by the method of dye-binding according to Bradford.[30]

**Analysis of Atrazine Metabolites and Conjugates in Alfalfa.** Fresh shoots or roots (7.0 g) were ground with liquid nitrogen. The process of extraction and purification was run with the same analytical method indicated above except petroleum ether extraction. The washing solution for the LC-18 column was collected for analysis. Metabolites and conjugates of atrazine in alfalfa were analyzed using ultrahigh performance liquid chromatography (UHPLC) (Thermo, USA) coupled to a linear ion trap−Orbitrap hybrid mass spectrometer (LTQ Orbitrap XL) equipped with a heated-electrospray ionization probe. Instrument control was through Tune 2.6.0 and Chromeleon programs. Separations were performed on a Hypersil gold C18 (100 mm × 2.10 mm, 3 μm particle size, Thermo Fisher Scientific). Mobile phase was composed of (A) water + 0.1% formic acid and (B) acetonitrile + 0.1% formic acid. A linear gradient program was performed in 36 min at a flow rate of 0.20 mL/min under the following conditions: 5% B for 1 min, 1−15 min from 5% to 35% B, 15−25 min from 35% to 95% B, 95% B for 5 min, 30−31 min from 95% to 5% B, and 5% B for 5 min. Column oven and autosampler temperature were set at 35 and 10 °C, respectively. The injection volume was 10 μL.

The mass spectrometer was operated in negative mode. HESI-source parameters were as follows: capillary temperature 300 °C, the source voltage 4 kV, and auxiliary gas 25. Accurate mass spectra were recorded from 100 to 800 *m*/*z*. For fragmentation study, a data dependent scan was performed by deploying collision-induced dissociation (CID). The product ions were generated by the LTQ ion trap at normalized collision energy of 35% and *q*-activation of 0.25 using an isolation width of 2 Da. The external mass calibration of the Orbitrap was performed once a week to ensure a working mass accuracy <5 ppm. Data analysis was handled by a computer equipped with Xcalibur software, version 2.1. Atrazine and its metabolism products were identified according to the corresponding spectral characteristics: accurate mass, mass spectra, and characteristic fragmentation.

**Statistical Analysis.** The biological study was performed independently three times. Each experiment was performed in triplicate. Results in figures and tables were the mean of three replicated treatments and expressed as mean ± standard deviation. Statistical analysis between the treatments and control was made by Student's *t* test methods ($p < 0.05$).

## RESULTS

**Effect of Atrazine on Growth.** The elongation and biomass of alfalfa shoots and roots were progressively reduced following the treatment with atrazine at 0−0.10 mg $L^{-1}$ for 6 d (Figure 1). Treatment with 0.10 mg $L^{-1}$ atrazine reduced the elongation of shoots and roots to 39.7% and 33.9% of the controls, respectively (Figure 1A). In comparison with elongation, the biomass appeared more sensitive to atrazine. Under the same condition, the biomass of shoots and roots was reduced to 16.6% and 8.5% of the controls, respectively (Figure 1B). The content of chlorophyll in alfalfa was significantly decreased after exposure to atrazine. At 0.04 mg $L^{-1}$, the chlorophyll content was decreased by 28.9% compared to the control (Figure 1C).

**Accumulation and Translocation of Atrazine in Alfalfa.** Both shoots and roots accumulated atrazine progressively with the concentrations over the time of exposure (Figure 2). A time-dependent change in atrazine accumulation was observed. Accumulation of atrazine in shoots and roots increased significantly for 4 and 6 d compared to 2 d. When plants were treated with atrazine at 0.10 mg $L^{-1}$ for 4 and 6 d, the contents of atrazine in shoots were 0.559 and 0.854 mg $kg^{-1}$, respectively (Figure 2A).

To investigate the uptake and translocation of atrazine in alfalfa, we calculated the bioconcentration factor (BCF), the ratio of atrazine concentration in plant to the nutrient solution, and the translocation factor (TF), the ratio of atrazine concentrations in shoots to roots. As shown in Table 1, BCFs of shoots decreased from 3.71 to 2.19 at 0.02−0.10 mg $L^{-1}$ of atrazine, and under the same condition, BCFs of roots decreased from 2.54 to 0.97. By contrast, the TF values progressively increased from 1.47 to 2.39 when plants were exposured to atrazine at 0.02−0.10 mg $L^{-1}$ (Table 1).

**Analysis of Atrazine Residues and Metabolites in Alfalfa.** The accurate mass data by high resolution MS was used to confirm elemental formula. The isotope (M + 2) was crucial for identifying the chlorine-containing transformation products of atrazine. The structures of metabolites were


dx.doi.org/10.1021/jf503221c | J. Agric. Food Chem. 2014, 62, 9657−9668

**Table 1. Bioconcentration Factors (BCFs) and Translocation Factors (TFs) for Atrazine in Shoot and Root of Alfalfa[a]**

| concn (mg $L^{-1}$) | BCF[b] | | TF[c] |
|---|---|---|---|
| | shoot | root | |
| 0.02 | 3.714 ± 0.225 a | 2.542 ± 0.258 a | 1.471 ± 0.178 b |
| 0.04 | 3.086 ± 0.162 b | 1.657 ± 0.073 b | 1.864 ± 0.117 a |
| 0.06 | 2.932 ± 0.751 b | 1.366 ± 0.142 c | 2.200 ± 0.812 a |
| 0.08 | 2.816 ± 0.378 b | 1.192 ± 0.115 c | 2.389 ± 0.492 a |
| 0.10 | 2.194 ± 0.112 b | 0.973 ± 0.042 d | 2.389 ± 0.161 a |

[a]Concentrations of atrazine were determined in shoot and root after alfalfa exposure to atrazine 0.02−0.10 mg $L^{-1}$ in nutrient solution for 2 d. Values are the means ± SD ($n$ = 3). The different letters indicate significant difference between treatments ($p$ < 0.05). [b]BCF: fresh weight ratio of atrazine in plant to the nutrient solution. [c]TF: ratio of shoot BCF to root BCF.

determined by analyzing collision-induced dissociation (CID) fragmentation patterns from $MS^2$ and $MS^3$ data. The external mass calibration of the Orbitrap was performed once a week to ensure a working mass accuracy of <5 ppm. The mass spectrometric data of atrazine along with its 10 metabolites of atrazine are summarized in Table 2.

Atrazine (ATZ) peaked at 19.19 min (Figure 3A). The $MS^2$ and $MS^3$ data of atrazine with fragment ions were $m/z$ 188, 174, 146, 138, 132, 104, 96, and 76 (Figure 4A and Table 2). Deisopropylated atrazine (DIA, metabolite #1) was one of the *N*-dealkylation products, peaking at 8.81 min with fragment ion of $m/z$ 146 (Figures 3B and 4B and Table 2). Hydroxyatrazine (HA, metabolite #2), which peaked at 9.20 min, was derived from atrazine by substitution of a hydroxyl group for the chlorine, while the loss of isopropenylacetylene and $H_2O$ resulted in formation of fragment ions of $m/z$ 156 and $m/z$ 180, respectively (Figure 4C and Table 2). Desethylated atrazine (DEA, metabolite #3), which peaked at 11.97 min with fragment ion of $m/z$ 146, was another *N*-dealkylation product (Figures 3B and 4D and Table 2).

Hydroxylation (+O) of atrazine detected at $m/z$ 232 included three isomers, and their retention times were 12.73, 13.28, and 14.22 min, respectively (Figure 3C). The first isomer, hydroxyisopropyl atrazine (HIA, metabolite #4), was confirmed by loss of $H_2O$ and isopropenyl to form $m/z$ 214 and $m/z$ 174, and the oxygenation on isopropyl to form $m/z$ 146 from precursor ion of $m/z$ 174 (Figure 4E and Table 2). The second isomer, which peaked at 13.28 min, was identified as *N*-hydroxy atrazine with the ion of $m/z$ 190 (NHA, metabolite #5), indicating that the oxygen was added to nitrogen atom on *N*-ethyl (Figure 4F and Table 2). The site of oxidation should occur on the ethyl side according to $m/z$ 188 in $MS^2$ (Figure 4G). Because hydroxylation of imine carbon allowed keto−enol type resonance, the loss of $COCH_2$ ($m/z$ 42) resulted in forming the fragment ion of $m/z$ 146 (Figure 4G and Table 2). Therefore, the structure of $m/z$ 230 at 13.73 min was assigned as hydroxy-dehydrogenated atrazine (HDHA, metabolite #6). The third isomer, hydroxyethyl atrazine (HEA, metabolite #7), was identified at 14.22 min ($m/z$ 232), due to the loss of $H_2O$, which resulted in the formation of $m/z$ 214. A further loss of vinyl, forming fragment ion of $m/z$ 188, confirmed that the oxygenation occurring on ethyl and oxygen was added to $\alpha$-carbon on *N*-ethyl of HEA (Figure 4H and Table 2).[31] Demethylated atrazine (DMA, metabolite #8), with a loss of $m/z$ 14, was identified according to the fragment ion of $m/z$ 174 (Figure 4I and Table 2), which occurred on isopropyl but not on ethyl, because the fragment ion of $m/z$ 160 or $m/z$ 188 was not found from $MS^2$ or $MS^3$ data.

For $m/z$ 214, which peaked at 20.28 min, the fragment ion of $m/z$ 172 from the loss of isopropenylacetylene indicated that the double bond occurred on the ethyl group (Figure 3C). The systematic −2 $m/z$ shift for some fragments retaining ethyl showed the double bond that was not on the isopropyl. The structure of metabolite #9 (dehydrogenated atrazine, DHA) did not cause any loss of ethyl moiety such as $m/z$ 146, indicating that imine was formed rather than terminal alkene (Figure 4J and Table 2). Methylated atrazine (MEA, metabolite #10) with a high response was detected with fragment ions of $m/z$ 188 and 146 (Figure 4K and Table 2). Taken together, this study demonstrated that metabolites #4−10 have been reported for the first time in plants.

**Identification of Atrazine Conjugates.** Seven atrazine-homoglutathione metabolites and two glucosylated-atrazine conjugates were identified by analyzing collision-induced dissociation (CID) fragmentation patterns from $MS^2$ and $MS^3$ data (Table 2 and Figure 5A−I). Polarity of nine atrazine conjugates was higher than that of atrazine, resulting in peaking earlier (Figure 3E−H).

Two isomeric glycosylation conjugates of atrazine, hydroxyisopropyl atrazine *O*-glucoside (HIA+Glc-$H_2O$, conjugate #1) and hydroxyethyl atrazine *O*-glucoside (HEA+Glc-$H_2O$, conjugate #2), were distinguished according to $MS^3$ data of $m/z$ 232 from the parent ion of $m/z$ 394. It was obvious that the classical loss of glucose at $m/z$ 162 took place, forming fragment ion of $m/z$ 232. Loss of $H_2O$ on glycosyl for $m/z$ 394 yielded the fragment ion of $m/z$ 376. The $MS^3$ data with fragment ions of $m/z$ 232, $m/z$ 214, and $m/z$ 174 indicated that the receptor was HIA (Figure 5A and Table 2). The parent ion of $m/z$ 394 at 11.64 min was assigned to HIA+Glc-$H_2O$ (conjugate #1), a sugar ring linked to HIA by the *O*-glycosidic bond. The other conjugate was formed by glycosylation and yielded a similar fragment ion. Based on the fragment ions of $m/z$ 232, $m/z$ 174, and $m/z$ 190, HEA was the reasonable receptor (Figure 5B and Table 2). So the parent ion of $m/z$ 394 at 11.75 min should point to HEA+Glc-$H_2O$ (conjugate #2), and a sugar ring was linked with HEA by the *O*-glycosidic bond.

As shown in Figure 5C, the $MS^3$ data with fragment ions of $m/z$ 214, $m/z$ 136, and $m/z$ 94 indicated that the compound was formed by conjugation of DHA and cysteine (Cys). The loss of $H_2O$ from the parent ion of $m/z$ 335 formed the fragment ion of $m/z$ 317. The skeleton rearrangement of hydroxyl formed the fragment ion of $m/z$ 292 after loss of carbonyl and amino, and yielded a fragment ion of $m/z$ 260 by loss of methanol (Figure 5C and Table 2). Thus, the parent ion of $m/z$ 335 at 11.85 min (Figure 3F) was confirmed as a cysteine conjugate for DHA (DHA+Cys, conjugate #3).

A major ATZ conjugate ($m/z$ 301) eluting at 12.02 min with stronger response than other conjugates was detected according to $MS^2$ and $MS^3$ (Figure 3G and Figure 5D). For $m/z$ 301, the loss of $NH_3$ produced the fragment ion of $m/z$ 284 in $MS^2$. The $MS^3$ data with the fragment ions of $m/z$ 214, $m/z$ 172, and $m/z$ 144 showed that a protonated thiol atrazine was generated (Figure 5D and Table 2). This conjugate was clearly identified as a cysteine conjugate by chlorine substitution for atrazine (ATZ-HCl+Cys, conjugate #4). A protonated molecule ($m/z$ was 501, $t_R$ =12.24 min) was created by conjugation (Figure 3H and Figure 5E). The loss of glutamic acid (Glu) for $m/z$ 501

**Table 2. Summary of All $MS^2$ and $MS^3$ Data for Metabolites of Atrazine in Alfalfa**

| no. | | chemical formula | $t_R$[a] | theor $m/z$, $[M + H]^+$ | exptl $m/z$, $[M + H]^+$ | delta (ppm) | location[b] | fragments | |
|---|---|---|---|---|---|---|---|---|---|
| | | | | | | | | $MS^2$[c] | $MS^3$[d] |
| | metabolite of atrazine | | | | | | | | |
| 1 | DIA | $C_5H_8ClN_5$ | 8.81 | 174.0541 | 174.0541 | −0.232 | shoot | 146, 138, **132**, 96, 79 | (132)[e] **104**, 90, 71 |
| 2 | HA | $C_8H_{15}N_5O$ | 9.20 | 198.1349 | 198.1350 | 0.269 | shoot; root | 180, **156**, 128, 114, 86 | (156) 128, 114, **86** |
| 3 | DEA | $C_6H_{10}ClN_5$ | 11.97 | 188.0697 | 188.0699 | 0.959 | shoot; root | **146** | (146) 128, 118, **110**, 104, 86, 79 |
| 4 | HIA[f] | $C_8H_{14}ClN_5O$ | 12.73 | 232.0960 | 232.0958 | −0.751 | shoot; root | **214**, 174, 154, 145 | (214) 186, 173, **136**, 132, 119, 96; (174) **146** |
| 5 | NHA[f] | $C_8H_{14}ClN_5O$ | 13.28 | 232.0960 | 232.0961 | 0.584 | shoot | **214**, 204, 198, 190, 179, 150, 141 | (214) **172** |
| 6 | HDHA[f] | $C_8H_{12}ClN_5O$ | 13.73 | 230.0803 | 230.0804 | 0.373 | shoot | 212, 202, **188**, 146 | (188) **146** |
| 7 | HEA[f] | $C_8H_{14}ClN_5O$ | 14.22 | 232.0960 | 232.0959 | −0.148 | shoot; root | **214**, 188 | (214) **172**; (188) 160, 146, 107 |
| 8 | DMA[f] | $C_7H_{12}ClN_5$ | 15.98 | 202.0855 | 202.0855 | 0.546 | shoot; root | 184, 174, 166, 132, **124**, 104, 96 | (174) **146**, 138, 132, 96, 79 |
| 9 | DHA[f] | $C_8H_{12}ClN_5$ | 20.28 | 214.0854 | 214.0855 | 0.282 | shoot; root | **172**, 158, 136, 88 | (172) 145, 130, **105**, 94, 79, 69 |
| 10 | MEA[f] | $C_9H_{16}ClN_5$ | 21.44 | 230.1167 | 230.1167 | 0.001 | shoot; root | **188**, 146 | (188) **146** |
| | ATZ | $C_8H_{14}ClN_5$ | 19.19 | 216.1010 | 216.1009 | −0.508 | shoot; root | 188, **174**, 146, 138 | (174) **146**, 138, 132, 104, 96, 79 |
| | conjugates of atrazine | | | | | | | | |
| 1 | HIA+Glc-$H_2O$[f] | $C_{14}H_{24}ClN_5O_6$ | 11.64 | 394.1488 | 394.1489 | 0.361 | shoot | 376, 320, 291, 273, 263, **232**, 214 | (232) **214**, 204, 196, 178, 174 |
| 2 | HEA +Glc-$H_2O$[f] | $C_{14}H_{24}ClN_5O_6$ | 11.75 | 394.1488 | 394.1487 | −0.349 | shoot | 376, 348, **232**, 174, 140 | (232) **214**, 196, 190, 176, 172, 154 |
| 3 | DHA +Cys | $C_{11}H_{19}ClN_6O_2S$ | 11.85 | 335.1051 | 335.1050 | −0.414 | shoot; root | 317, 292, 285, 273, 250, **214**, 180 | (214) **172**, 136, 105, 94 |
| 4 | ATZ-HCl +Cys | $C_{11}H_{20}N_6O_2S$ | 12.02 | 301.1441 | 301.1443 | 0.561 | shoot; root | 284, **214**, 155 | (214) **172**, 144, 130, 102 |
| 5 | ATZ-HCl +hGSH | $C_{19}H_{32}N_8O_6S$ | 12.24 | 501.2238 | 501.2236 | −0.455 | shoot; root | **372**, 288, 270, 214, 172, 159 | (214) 172, **155**, 130, 113 |
| 6 | ATZ-HCl +(Cys-$\beta$-Ala) | $C_{14}H_{25}N_7O_3S$ | 12.51 | 372.1812 | 372.1813 | 0.094 | shoot; root | 355, **214**, 172, 155 | (214) **172**, 144, 130, 102 |
| 7 | DHA +hGSH | $C_{19}H_{31}ClN_8O_6S$ | 12.95 | 535.1849 | 535.1849 | 0.158 | shoot; root | 517, 373, 348, **322**, 219, 193, 180 | |
| 8 | MEA-HCl +hGSH[f] | $C_{20}H_{34}N_8O_6S$ | 13.95 | 515.2395 | 515.2394 | −0.074 | shoot; root | 386, **228**, 186 | (228) **186**, 144 |
| 9 | MEA-HCl +Cys[f] | $C_{12}H_{22}N_6O_2S$ | 14.33 | 315.1598 | 315.1598 | 0.155 | shoot; root | 298, **228** | (228) **186**, 144 |

[a]Retention time. [b]Location: Distribution of metabolites of atrazine in plant. [c]$MS^2$ fragments: Base peak of $MS^2$ fragment ions are shown in bold. [d]$MS^3$ fragments: Base peak of $MS^3$ fragment ions are shown in bold. [e]Figure within the brackets: The precursor ions used to produce $MS^2$ and $MS^3$ fragment ions. [f]Compounds that have been reported for the first time.

formed the fragment ion of $m/z$ 372, and the loss of thiol atrazine generated the fragment ion of $m/z$ 288. The $MS^3$ data with $m/z$ 214 and $m/z$ 172 confirmed the existence of protonated thiol atrazine fragment (Figure 5E and Table 2). These data were consistent with the conjugation of ATZ and homoglutathione (hGSH) (ATZ-HCl+hGSH, conjugate #5). A peak ($t_R$ =12.51 min) at $m/z$ 372 was detected (Figure 3H and Figure 5F). The loss of $NH_3$ for $m/z$ 372 formed the fragment ion of $m/z$ 355. The $MS^3$ data contained $m/z$ 214, $m/z$ 172, and $m/z$ 144, indicating that the ATZ conjugate was transformed to protonated thiol atrazine by cracking. Therefore, the conjugate was identified as cysteinyl $\beta$-alanine conjugate by chlorine substitution for atrazine (ATZ-HCl +(Cys-$\beta$-Ala), conjugate #6). The loss of $H_2O$ and DEA from the parent ion of $m/z$ 535 at 12.95 min yielded fragment ions of $m/z$ 517 and $m/z$ 348, respectively (Figure 3E and Figure 5G), indicating that hGSH was not linked to nitrogen. The $m/z$ 322 and $m/z$ 193 were the characteristic ions for hGSH (Table 2). Based on the $MS^2$ spectrum, the structure of the conjugate was confirmed as homoglutathione conjugate for dehydrogenated atrazine (DHA+hGSH, conjugate #7). The conjugates peaking at 13.95 and 14.33 min were detected (Figure 3F). The fragment ion of $m/z$ 386 was the result of the loss of Glu, and the $MS^3$ data with fragment ions of $m/z$ 228, $m/z$ 186, and $m/z$ 144 provided the foundation for fragment-protonated thiol-MEA (Figure 5H and Table 2). Thus, conjugate #8 ($m/z$ 515) was identified as homoglutathione conjugate by chlorine substitution for methylated atrazine (MEA-HCl+hGSH). The loss of $NH_3$ from the parent ion of $m/z$ 315 formed the $m/z$ 298. Similarly, fragment ions of $m/z$ 228, $m/z$ 186, and $m/z$ 144 were evidence for the fragment protonated thiol-MEA (Figure 5I and Table 2). The parent ion of $m/z$ 315 was


dx.doi.org/10.1021/jf503221c | J. Agric. Food Chem. 2014, 62, 9657−9668

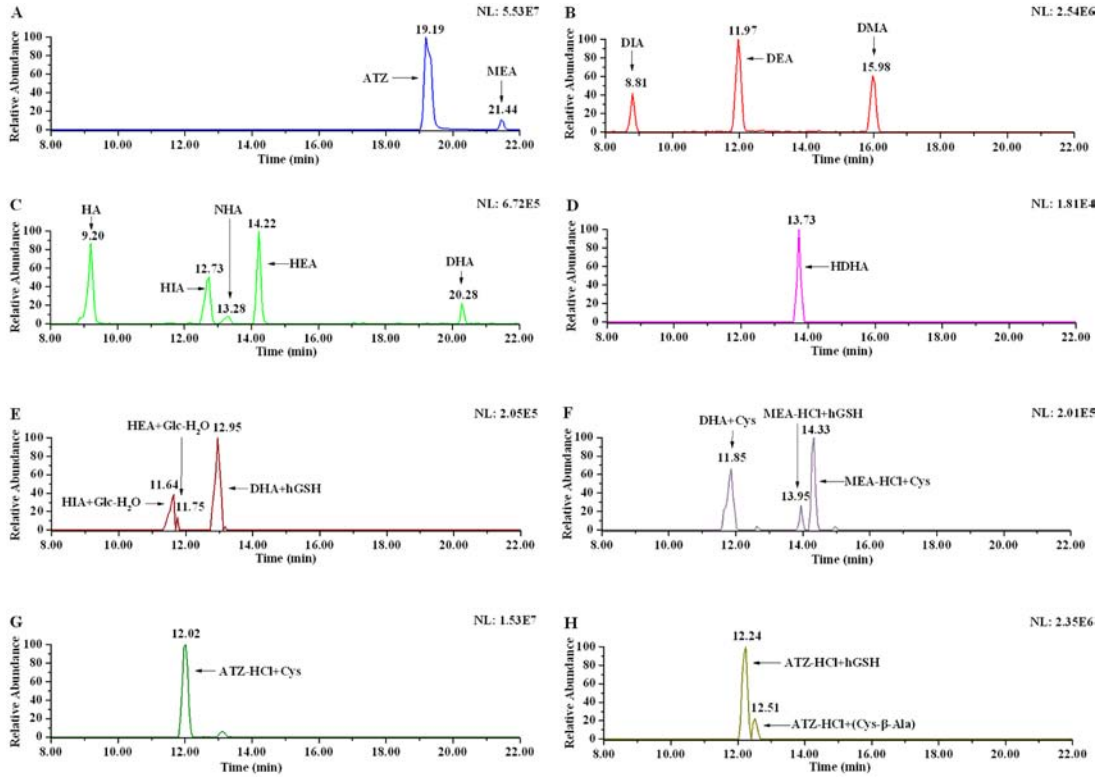


**Figure 3.** Extracted ion chromatograms of atrazine (ATZ) and its metabolites and conjugates in alfalfa from UHPLC LTQ Orbitrap XL analysis. (A) Extracted ion chromatogram of $m/z$ = 216.1009 (ATZ) and $m/z$ = 230.1167 (MEA) with strength of the maximum signal of $5.53 \times 10^7$. (B) Extracted ion chromatogram of $m/z$ = 174.0541 (DIA), $m/z$ = 188.0699 (DEA), and $m/z$ = 202.0855 (DMA) with strength of the maximum signal of $2.54 \times 10^6$. (C) Extracted ion chromatogram of $m/z$ = 198.1350 (HA), $m/z$ = 232.0958 (HIA), $m/z$ = 232.0961 (NHA), $m/z$ = 232.0959 (HEA), and $m/z$ = 214.0855 (DHA) with strength of the maximum signal of $6.72 \times 10^5$. (D) Extracted ion chromatogram of $m/z$ = 230.0804 (HDHA) with strength of the maximum signal of $1.81 \times 10^4$. (E) Extracted ion chromatogram of $m/z$ = 394.1489 (HIA+Glc-$H_2O$), $m/z$ = 394.1487 (HEA+Glc-$H_2O$), and $m/z$ = 535.1849 (DHA+hGSH) with strength of the maximum signal of $2.05 \times 10^5$. (F) Extracted ion chromatogram of $m/z$ = 335.1050 (DHA+Cys), $m/z$ = 515.2394 (MEA-HCl+hGSH), and $m/z$ = 315.1598 (MEA-HCl+Cys) with strength of the maximum signal of $2.01 \times 10^5$. (G) Extracted ion chromatogram of $m/z$ = 301.1443 (ATZ-HCl+Cys) with strength of the maximum signal of $1.53 \times 10^7$. (H) Extracted ion chromatogram of $m/z$ = 501.2236 (ATZ-HCl+hGSH) and $m/z$ = 372.1813 [ATZ-HCl+(Cys-$\beta$-Ala)] with strength of the maximum signal of $2.35 \times 10^6$.

identified as cysteine conjugate by chlorine substitution for the methylated atrazine (MEA-HCl+Cys, conjugate #9).

Most of the conjugates could be found in both shoot and root tissues, except HIA+Glc-$H_2O$ and HEA+Glc-$H_2O$, which were only detected in shoots (Table 2). ATZ-HCl+hGSH (conjugate #5) from sorghum was reported previously,[32] whereas HIA+Glc-$H_2O$ (conjugate #1), HEA+Glc-H2O (conjugate #2), ATZ-HCl+Cys (conjugate #4), MEA-HCl +hGSH (conjugate #8), and MEA-HCl+Cys (conjugate #9) have not been documented in plants. Meanwhile, there were few reports about conjugates DHA+Cys (conjugate #3), ATZ-HCl+(Cys-$\beta$-Ala) (conjugate #6), and DHA+hGSH (conjugate #7) transformed from atrazine in plants.

**Effect of Atrazine on Activities of Enzymes.** We further determined the activities of enzymes GST and GTs in plants. The activity of GTs in shoots was highest at 0.06 mg $L^{-1}$ atrazine compared to the control, while in roots the activity of GTs was mildly induced by atrazine from 0.04 to 0.08 mg $L^{-1}$ (Figure 6A). Similarly, the activity of GST was progressively increased in roots with atrazine at 0.02−0.08 mg $L^{-1}$ (Figure 6B). In shoots, the activity of GST was generally unchanged, and only at 0.02 mg $L^{-1}$ atrazine was the activity slightly increased.

## DISCUSSION

Plants (or crops) have developed sophisticated strategies to degrade a broad range of xenobiotics such as pesticides into detoxified products. Chemical modification of these pesticides is the first and most important step leading to the following cellular appartmentation and degradation. Although certain processes are known for the removal of pesticides in plants, the mechanisms underlying the processes remain to be elusive. The present study identified an array of atrazine derivatives including their glucosylated products in alfalfa using multiple analytical and biological approaches. A total of ten atrazine metabolites have been detected. Of these, metabolite #4 (HIA), metabolite #5 (NHA), metabolite #6 (HDHA), metabolite #7 (HEA), metabolite #8 (DMA), metabolite #9 (DHA), and metabolite #10 (MEA) have been characterized for the first time in this study (Table 2). Importantly, two glucosylated products, HIA+Glc-$H_2O$ and HEA+Glc-$H_2O$, along with two other hGSH- and Cys-conjugated products, MEA-HCl+hGSH and MEA-HCl+Cys, are also the new products identified in this study (Table 2). The atrazine degradation in the alfalfa plant may represent a mode in which atrazine is chemically transformed into a variety of other compounds. Also, its derivatives conjugated to thiol-containing amino acids and


dx.doi.org/10.1021/jf503221c | J. Agric. Food Chem. 2014, 62, 9657−9668

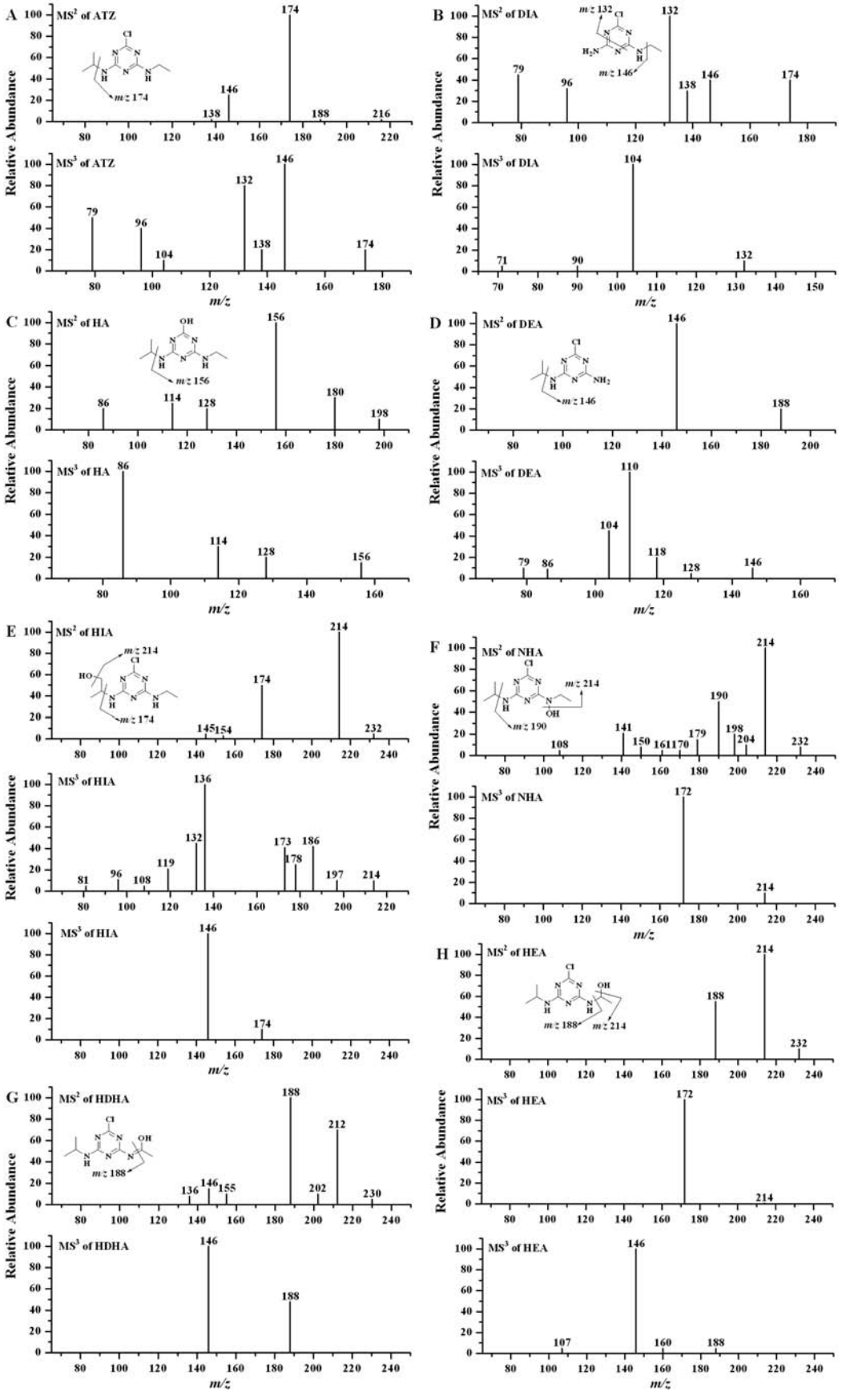


**Figure 4.** continued


dx.doi.org/10.1021/jf503221c | J. Agric. Food Chem. 2014, 62, 9657−9668

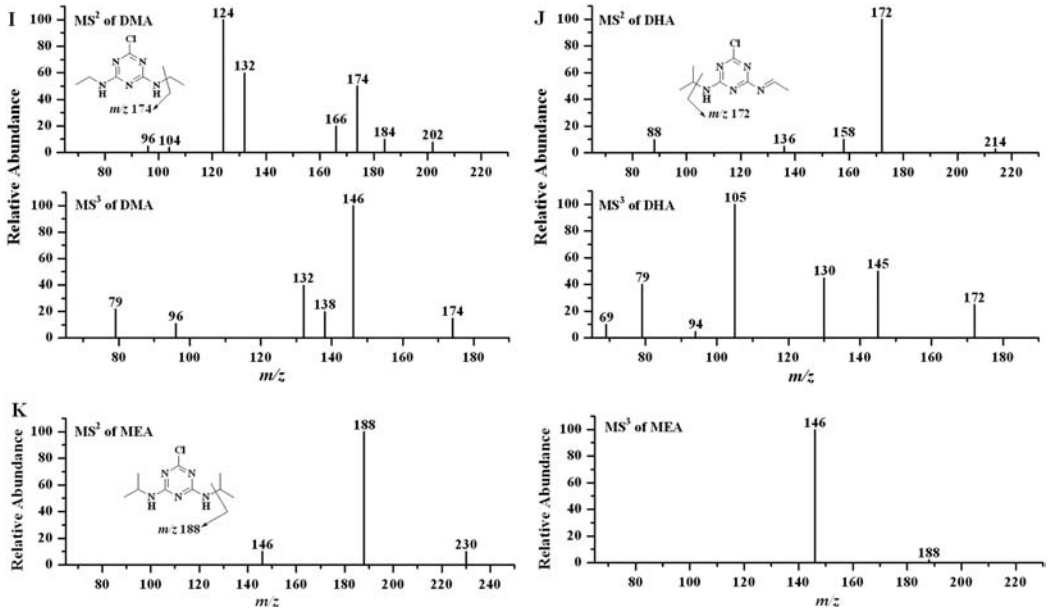


**Figure 4.** $MS^2$ and $MS^3$ spectra of atrazine (ATZ) and its metabolites in alfalfa from UHPLC LTQ Orbitrap XL analysis. (A) $MS^2$ and $MS^3$ data of ATZ with precursor ion $m/z$ = 174 for $MS^3$. (B) $MS^2$ and $MS^3$ data of DIA with precursor ion $m/z$ = 132 for $MS^3$. (C) $MS^2$ and $MS^3$ data of HA with precursor ion $m/z$ = 156 for $MS^3$. (D) $MS^2$ and $MS^3$ data of DEA with precursor ion $m/z$ = 146 for $MS^3$. (E) $MS^2$ and $MS^3$ data of HIA with precursor ion $m/z$ = 214 and $m/z$ = 174 for $MS^3$. (F) $MS^2$ and $MS^3$ data of NHA with precursor ion $m/z$ = 214 for $MS^3$. (G) $MS^2$ and $MS^3$ data of HDHA with precursor ion $m/z$ = 188 for $MS^3$. (H) $MS^2$ and $MS^3$ data of HEA with precursor ion $m/z$ = 214 and $m/z$ = 188 for $MS^3$. (I) $MS^2$ and $MS^3$ data of DMA with precursor ion $m/z$ = 174 for $MS^3$. (J) $MS^2$ and $MS^3$ data of DHA with precursor ion $m/z$ = 172 for $MS^3$. (K) $MS^2$ and $MS^3$ data of MEA with precursor ion $m/z$ = 188 for $MS^3$.

glutathione are possibly the major process for atrazine degradation.

It is generally considered that herbicides are detoxified through three phases in plants.[33] Phase I is the most important step, by which a herbicide can be activated through oxidoreduction and hydrolysis reaction; phase II in the process is through the conjugation of the activated herbicide with polar donor molecules, such as glutathione, sugars, and amino acids, and it is anticipated that glycosyltransferases and glutathione *S*-transferase are involved. Following conjugation, the conjugates are either compartmented into the vacuole or released into the apoplast region through phase III.

There were ten metabolites of atrazine through phase I reaction and nine conjugates through phase II reaction (Table 2). Metabolic pathways of atrazine are shown in Figure 7; phase I reaction products are DIA, HA, DEA, HIA, NHA, hydroxy-dehydrogenated atrazine (HDHA), HEA, DMA, dehydrogenated atrazine (DHA), and MEA. Atrazine and four phase I reaction products DHA, MEA, HIA, and HEA were brought in phase II reaction. HIA and HEA were reactants for glycosylation, being generated into HIA+Glc-$H_2O$ and HEA +Glc-$H_2O$ with $\beta$-D-glucose. Moreover, conjugation of DHA and MEA with hGSH or amino acids resulted in production of DHA+hGSH or DHA+Cys, respectively. The $\alpha$-carbon double bond formed on the ethyl group acts as an electrophilic Michael acceptor, which covalently binds to hGSH or cysteine (Cys) and is capable of forming DHA+hGSH or DHA+Cys. As both MEA and atrazine contain chlorine, the substitution reaction favorably occurred with sulfydryl of hGSH, dipeptide, or amino acids generating ATZ-HCl+hGSH, ATZ-HCl+(Cys-$\beta$-Ala), ATZ-HCl+Cys, MEA-HCl+hGSH, and MEA-HCl+Cys. In addition to binding directly with atrazine, DHA+Cys, ATZ-HCl+(Cys-$\beta$-Ala), ATZ-HCl+Cys, and MEA-HCl+Cys might be also formed by losing amino acids from the corresponding parent molecules (Figure 7).

The structure of methylated atrazine (MEA) is identical with another triazine herbicide called propazine. The action mechanism of propazine is similar to that of atrazine. This herbicide is used to control broadleaf weeds and annual grasses during the production of milo grain sorghum, with less toxicological effect on humans.[34] MEA is of low solubility in water due to the additional methyl group. In this study, MEA was detected in alfalfa plants. Nevertheless, it has been identified as conjugates with hGSH and cysteine in the form of MEA-HCl+hGSH and MEA-HCl+Cys, indicating that MEA is easy to interact with a thiol-containing group.

Glycosyltransferase (GT; EC 2.4.*x*.*y*)-dependent detoxification (phase II metabolism) is one of the important mechanisms to cope with absorbed toxic compounds.[35] GTs comprise a large group of enzymes that form glycosidic bonds through the transfer of sugars from activated donor molecules to acceptor molecules. The present study has detected two new glucosylated compounds (HIA+Glc-$H_2O$ and HEA+Glc-$H_2O$) for atrazine in alfalfa (Table 2). HIA+Glc-$H_2O$ and HEA+Glc-$H_2O$ were maximally detected at 11.53 and 11.64 min, which were earlier than other conjugates linked to hGSH or amino acids (Figure 3). This suggests that the polarity of glucosides is stronger than that of other conjugates. The two compounds belong to the *O*-glucosylation type. There were no other types such as *N*-glucosylated and *C*-glucosylated atrazine detected. This could be plant species specific. For example, the persistent pollutant 3,4-dichloroaniline with amino group could interact with *N*-glucosylation in *Arabidopsis thaliana*.[36] Also, Gandia-Herrero et al.[22] found that 2,4,6-trinitrotoluene was shown to undergo *C*-glucosylation on the carbon of benzene ring in *Arabidopsis*. Although both DEA and DIA are equipped with amino group, *N*-glucosylation was not identified in alfalfa. It


dx.doi.org/10.1021/jf503221c | J. Agric. Food Chem. 2014, 62, 9657−9668

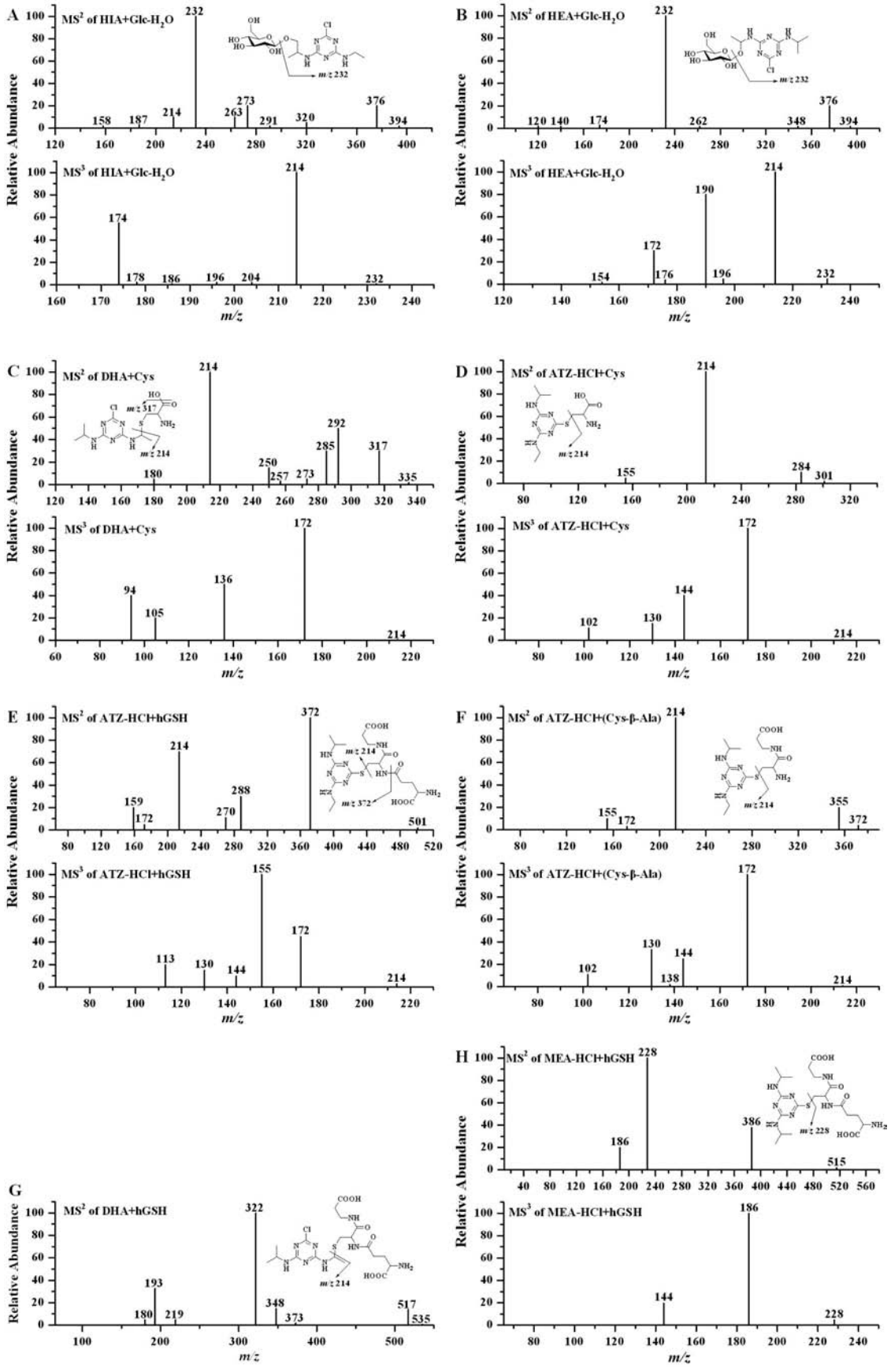


**Figure 5.** continued


dx.doi.org/10.1021/jf503221c | J. Agric. Food Chem. 2014, 62, 9657−9668

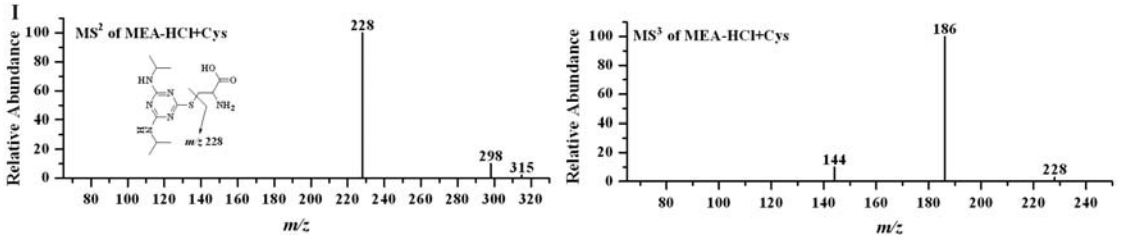


**Figure 5.** $MS^2$ and $MS^3$ spectra of conjugates of atrazine (ATZ) in alfalfa from UHPLC LTQ Orbitrap XL analysis. (A) $MS^2$ and $MS^3$ data of HIA +Glc-$H_2O$ with precursor ion $m/z$ = 232 for $MS^3$. (B) $MS^2$ and $MS^3$ data of HEA+Glc-$H_2O$ with precursor ion $m/z$ = 232 for $MS^3$. (C) $MS^2$ and $MS^3$ data of DHA+Cys with precursor ion $m/z$ = 214 for $MS^3$. (D) $MS^2$ and $MS^3$ data of ATZ-HCl+Cys with precursor ion $m/z$ = 214 for $MS^3$. (E) $MS^2$ and $MS^3$ data of ATZ-HCl+hGSH with precursor ion $m/z$ = 214 for $MS^3$. (F) $MS^2$ and $MS^3$ data of ATZ-HCl+(Cys-$\beta$-Ala) with precursor ion $m/z$ = 214 for $MS^3$. (G) $MS^2$ data of DHA+hGSH. (H) $MS^2$ and $MS^3$ data of MEA-HCl+hGSH with precursor ion $m/z$ = 228 for $MS^3$. (I) $MS^2$ and $MS^3$ data of MEA-HCl+Cys with precursor ion $m/z$ = 228 for $MS^3$.

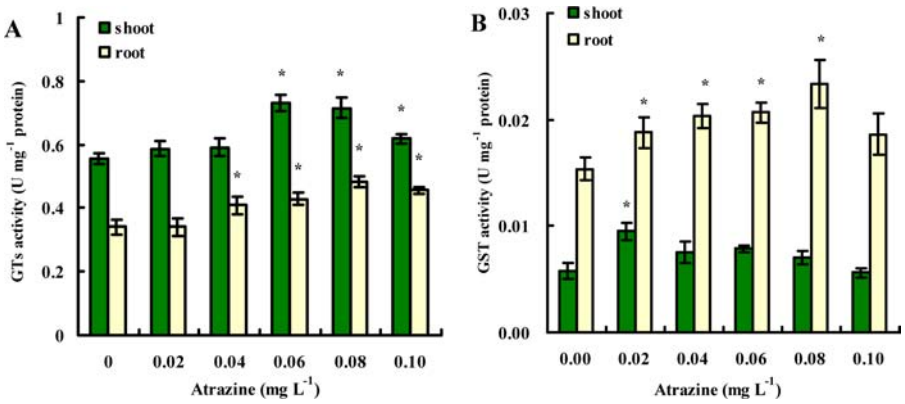


**Figure 6.** Effect of atrazine on the activity of GTs (A) and GST (B) in *Medicago sativa*. Seedlings were cultured in the 1/2 strength Hoagland nutrient solution containing atrazine at 0, 0.02, 0.04, 0.06, 0.08, and 0.10 mg $L^{-1}$ for 6 d. Values are the means ± SD ($n$ = 3). Asterisks indicate significant differences between the treatments and the control ($P < 0.05$).

may be that the concentration of conjugates was too low to be detected. Also, it cannot be ruled out that the alfalfa plants are not able to undergo *C*- or *N*-glucosylation dependent detoxification. Before glucosylation, hydroxyl was added to ethyl and isopropyl of atrazine, forming acceptors HEA and HIA, respectively, which were favorable for *O*-glucosylation. This mechanism is in agreement with the previous reports in which the detoxification of the model benzoxazolinone allelochemical (BOA) in *Arabidopsis* occurred predominantly through *O*-glucosylation of BOA-6-OH.[37] The process most likely requires sequential action of cytochrome P450 and UDP-glucosyltransferase activities. To confirm the involvement of atrazine glucosylation in alfalfa, the activity of GTs was assayed in the plant. The increased activity of GTs with atrazine in alfalfa roots and shoots was observed. The GTs in higher plants are thought to glycosylate many aglycons, and thereby the plant secondary metabolites, hormones, and xenobiotics regulate the development and detoxification of toxic compounds in plants.[10,38] The elevated activity of GTs suggests that the glycosylation-mediated pathway is involved in the detoxification of atrazine.

γGlu-Cys-Gly (glutathione; GSH), a thiol redox tripeptide, is a major water-soluble redox buffer and antioxidant in plants.[39] Its homologous molecule, γGlu-Cys-βAla (homoglutathione; hGSH), exists in legume and has similar functions in plants including transport and storage of sulfur, scavenging of ROS, and defense to toxicants.[40,41] *Medicago sativa* belongs to the Fabaceae family containing both GSH and hGSH.[42] But hGSH is the most abundant thiol compound in alfalfa leaves, stems, and roots.[40] In this study, the conjugates of atrazine with hGSH were detected in the forms of ATZ-HCl+hGSH, DHA+hGSH, and MEA-HCl+hGSH, suggesting that the sufficient generation of hGSH should be beneficial for binding and detoxifying atrazine. By high intensity LC-MS analysis, we also detected the Cys conjugate with a function similar to that of hGSH in alfalfa. According to Leustek et al.,[43] the conjugates with GSH are hydrolyzed to Cys conjugates by action of γ-glutamyl transpeptidases and Cys-Gly dipeptidases in succession. Thus, it is possible that DHA+hGSH, MEA-HCl+hGSH, and ATZ-HCl+hGSH could be hydrolyzed to produce the corresponding Cys conjugates in addition to being transformed by conjugation of Cys and xenobiotics directly (Figure 7).

Classically, GSTs catalyze the transfer of glutathione to a cosubstrate with a reactive electrophilic center to form *S*-glutathionylated product.[44] The function was confirmed in alfalfa with the distinction that atrazine was conjugated with hGSH. The GST enzyme was activated in plants, particularly in the root with atrazine. The result was in accordance with our previous reports with other plant species.[26,45] The GST conjugates are usually processed by phase III pathway, making the conjugates compartmentalize into vacuoles, release into apoplasts, or combine into the insoluble residues within cell wall.[33] Detoxification of atrazine in alfalfa plants is most likely to undergo the same pathways.

In conclusion, the present study demonstrated that alfalfa had a great ability to accumulate atrazine in tissues from its growing environments. As a recognizable symptom, elongation and biomass were reduced and the total chlorophyll accumulation was impaired with treatment of atrazine. The BCF of alfalfa shoots and roots showed a downtrend with the

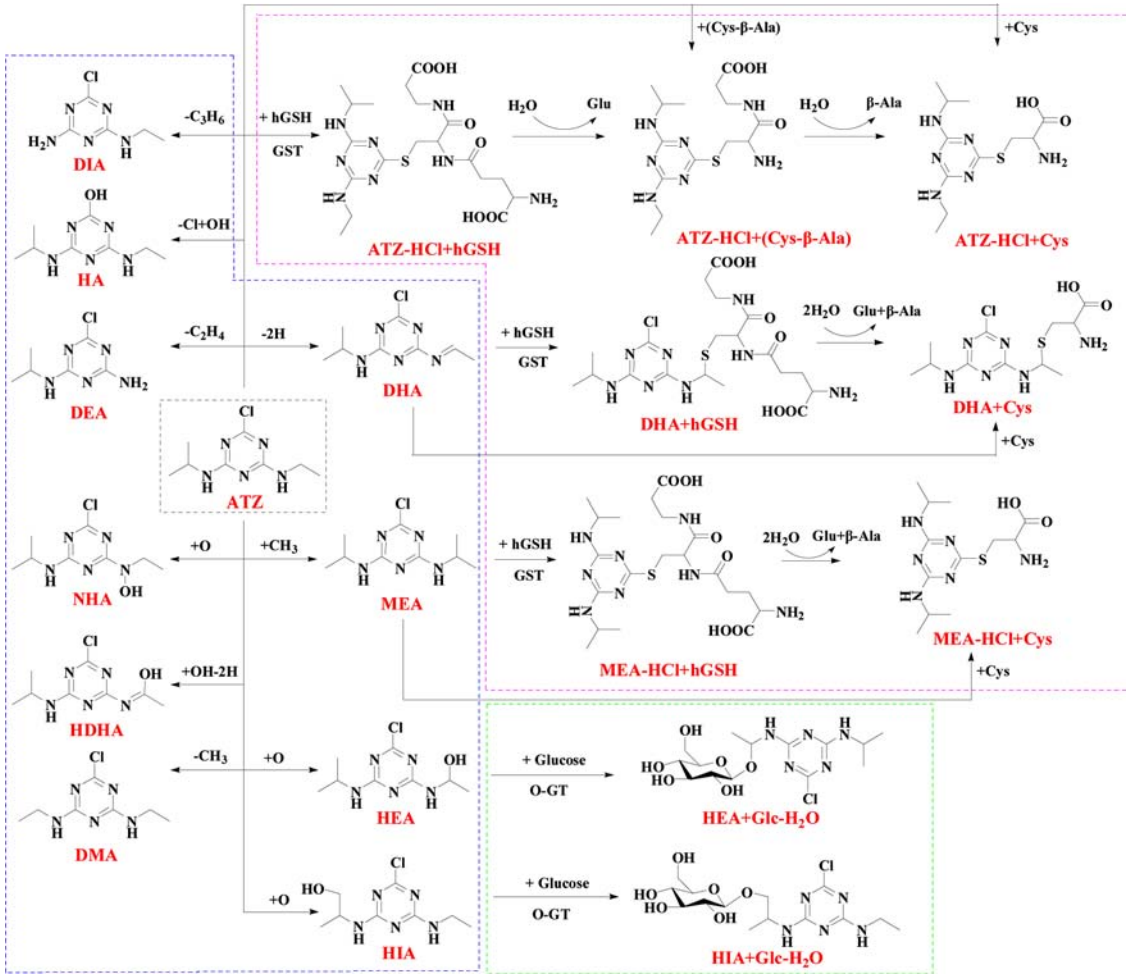


**Figure 7.** Proposed metabolic pathway of atrazine in *Medicago sativa*. The substance in the black dashed-line box is atrazine. The contents in the blue box are from phase I reaction metabolized from atrazine. The substances in the pink box are conjugates from phase II reaction conjugated with hGSH and amino acid of atrazine. The contents in the green box are from phase II reaction, i.e., glycosylation of atrazine.

increasing concentration of atrazine stress, whereas the TF values increased when the concentration of atrazine was elevated, suggesting that a translocation of atrazine occurred from roots to shoots. There were 10 metabolites of atrazine from phase I reaction and 9 conjugates from phase II reaction identified. Furthermore, the activity of GST and GTs was activated. These results indicate that the atrazine toxicity in alfalfa plants could be attenuated by conjugation with polar donor molecules, such as sugars, glutathione, and amino acids. The biochemical responses and metabolism pathway will serve as useful indicators for assessment of the herbicide contamination in agricultural environments.

## ■ ASSOCIATED CONTENT

### Supporting Information

Spiked recoveries of atrazine in nutrient solution, shoot, and root. This material is available free of charge via the Internet at http://pubs.acs.org.

## ■ AUTHOR INFORMATION

### Corresponding Author

*Weigang No.1, Chemistry Building, College of Sciences, Nanjing Agricultural University, Nanjing 210095, China. Tel: +86-25-84395207. E-mail: hongyang@njau.edu.cn.

### Funding

The authors acknowledge the financial support of the National Natural Science Foundation of China (No. 21377058) and the Special Fund for Agro-scientific Research in the Public Interest (No. 201203022) from the Ministry of Agriculture of China.

### Notes

The authors declare no competing financial interest.

## ■ REFERENCES

(1) Mandelbaum, R. T.; Allan, D. L.; Wackett, L. P. Isolation and characterization of a *Pseudomonas* sp. that mineralizes the *s*-triazine herbicide atrazine. *Appl. Environ. Microbiol.* **1995**, *61* (4), 1451.

(2) Hayes, T. B.; Collins, A.; Lee, M.; Mendoza, M.; Noriega, N.; Stuart, A. A.; Vonk, A. Hermaphroditic, demasculinized frogs after exposure to the herbicide atrazine at low ecologically relevant doses. *Proc. Natl. Acad. Sci. U.S.A.* **2002**, *99*, 5476−5480.

(3) Jablonowski, N. D.; Schäffer, A.; Burauel, P. Still present after all these years: persistence plus potential toxicity raise questions about the use of atrazine. *Environ. Sci. Pollut. Res.* **2011**, *18*, 328−331.

(4) Jablonowski, N. D.; Köppchen, S.; Hofmann, D.; Schäffer, A.; Burauel, P. Persistence of $^{14}$C-labeled atrazine and its residues in a field lysimeter soil after 22 years. *Environ. Pollut.* **2009**, *157*, 2126−2131.

(5) Su, Y. H.; Zhu, Y. G. Bioconcentration of atrazine and chlorophenols into roots and shoots of rice seedlings. *Environ. Pollut.* **2006**, *139*, 32−39.

(6) Sathiakumar, N.; MacLennan, P. A.; Mandel, J.; Delzell, E. A review of epidemiologic studies of triazine herbicides and cancer. *Crit. Rev. Toxicol.* **2011**, *41*, 1−34.
(7) Solomon, K.; Baker, D. B.; Richards, R. P.; Dixon, K. R.; Klaine, S. J.; Point, T. W. L.; Kendall, R. J.; Weisskopf, C. P.; Giddings, J. M.; Giesy, J. P.; Hall, L. W.; Williams, W. M. Ecological risk assessment of atrazine in north American surface waters. *Environ. Toxicol. Chem.* **1996**, *15* (1), 31−76.
(8) Knauert, S.; Singer, H.; Hollender, J.; Knauer, K. Phytotoxicity of atrazine, isoproturon, and diuron to submersed macrophytes in outdoor mesocosms. *Environ. Pollut.* **2010**, *158*, 167−174.
(9) Moore, M. T.; Kröger, R. Effect of three insecticides and two herbicides on rice (*Oryza sativa*) seedling germination and growth. *Arch. Environ. Contam. Toxicol.* **2010**, *59*, 574−581.
(10) Lu, Y. C.; Yang, S. N.; Zhang, J. J.; Zhang, J. J.; Tan, L. R.; Yang, H. A collection of glycosyltransferases from rice (*Oryza sativa*) exposed to atrazine. *Gene* **2013**, *531*, 243−252.
(11) Babakhani, B.; Khavari-Nejad, R. A.; Hassan-sajedi, R.; Fahimi, H.; Saadatmand, S. Biochemical responses of alfalfa (*Medicago sativa* L.) cultivars subjected to NaCl salinity stress. *Afr. J. Biotechnol.* **2011**, *10* (55), 11433−11441.
(12) Pini, F.; Frascella, A.; Santopolo, L.; Bazzicalupo, M.; Biondi, E. G.; Scotti, C.; Mengoni, A. Exploring the plant-associated bacterial communities in *Medicago sativa* L. *BMC Microbiol.* **2012**, *12*, 78.
(13) Cuadrado, V.; Merini, L.; Giulietti, A. M. Phytostimulation of atrazine degradation by alfalfa (*Medicago sativa*, L.) extracts and exudates. *J. Biotechnol.* **2010**, *150*, S251−S251.
(14) Hintz, R. L.; Harmoney, K. R.; Moore, K. J.; George, J. R.; Brummer, E. C. Establishment of switchgrass and big bluestem in corn with atrazine. *Agron. J.* **1998**, *90*, 591−596.
(15) Wang, L.; Samac, D. A.; Shapir, N.; Wackett, L. P.; Vance, C. P.; Olszewski, N. E.; Sadowsky, M. J. Biodegradation of atrazine in transgenic plants expressing a modified bacterial atrazine chlorohydrolase (*atzA*) gene. *Plant Biotechnol. J.* **2005**, *3*, 475−486.
(16) Hijano, N.; Monquero, P. A.; Munhoz, W. S.; Gusmão, M. R. Herbicide selectivity in alfalfa crops. *Planta Daninha* **2013**, *31*, 903−918.
(17) Cui, L. E.; Yang, H. Accumulation and residue of napropamide in alfalfa (*Medicago sativa*) and soil involved in toxic response. *J. Hazard. Mater.* **2011**, *190*, 81−86.
(18) Sui, Y.; Yang, H. Bioaccumulation and degradation of atrazine in several Chinese ryegrass genotypes. *Environ. Sci.: Processes Impacts* **2013**, *15*, 2338−2344.
(19) Peralta-Videa, J. R.; Gardea-Torresdey, J. L.; Gomez, E.; Tiemann, K. J.; Parsons, J. G.; de la Rosa, G.; Carrillo, G. Potential of alfalfa plant to phytoremediate individually contaminated montmorillonite-soils with cadmium(II), chromium(VI), copper (II), nickel(II), and zinc(II). *Bull. Environ. Contam. Toxicol.* **2002**, *69*, 74−81.
(20) Zhou, Z. S.; Wang, S. J.; Yang, Z. M. Biological detection and analysis of mercury toxicity to alfalfa (*Medicago sativa*) plants. *Chemosphere* **2008**, *70*, 1500−1509.
(21) Kawahigashi, H. Transgenic plants for phytoremediation of herbicides. *Cur. Opin. Biotechnol.* **2009**, *20*, 1−6.
(22) Gandia-Herrero, F.; Lorenz, A.; Larson, T.; Graham, I. A.; Bowles, D. J.; Rylott, E. L.; Bruce, N. C. Detoxification of the explosive 2, 4, 6-trinitrotoluene in Arabidopsis, discovery of bifunctional *O*- and *C*- glucosyltransferases. *Plant J.* **2008**, *56*, 963−974.
(23) Cameron, M. D.; Timofeevski, S.; Aust, S. D. 2000, Enzymology of *Phanerochaete chrysosporium* with respect to the degradation of recalcitrant compounds and xenobiotics. *Appl. Microbiol. Biotechnol.* **2000**, *54*, 751−758.
(24) Vogt, T.; Jones, P. Glycosyltransferases in plant natural product synthesis, characterization of a supergene family. *Trends Plant Sci.* **2000**, *5* (9), 380−386.
(25) Lim, A.; Reed-Bogan, A.; Harmon, B. J. Glycosylation profiling of a therapeutic recombinant monoclonal antibody with two N-linked glycosylation sites using liquid chromatography coupled to a hybrid quadrupole time-of-flight mass spectrometer. *Anal. Biochem.* **2008**, *375*, 163−172.
(26) Zhang, J. J.; Lu, Y. C.; Zhang, J. J.; Tan, L. R.; Yang, H. Accumulation and toxicological response of atrazine in rice crops. *Ecotoxicol. Environ. Saf.* **2014**, *102*, 105−112.
(27) Inskeep, W. P.; Bloom, P. R. Extinction coefficients of chlorophyll *a* and *b* in *N*,*N*-Dimethylformamide and 80% acetone1. *Plant Physiol.* **1985**, *77*, 483−485.
(28) Song, N. H.; Zhang, S.; Hong, M.; Yang, H. Impact of dissolved organic matter on bioavailability of chlorotoluronn to wheat. *Environ. Pollut.* **2010**, *158*, 906−912.
(29) Suzuki, T.; Kim, S. J.; Yamauchi, H.; Takigawa, S.; Honda, Y.; Mukasa, Y. Characterization of a flavonoid 3-*O*-glucosyltransferase and its activity during cotyledon growth in buckwheat (*Fagopyrum esculentum*). *Plant Sci.* **2005**, *169*, 943−948.
(30) Bradford, M. M. A rapid and sensitive method for the quantitation of microgram quantities of protein utilizing the principle of protein-dye binding. *Ann. Biochem.* **1976**, *72*, 248−259.
(31) Joo, H.; Choi, K.; Hodgson, E. Human metabolism of atrazine. *Pestic. Biochem. Phys.* **2010**, *98*, 73−79.
(32) Shimabukuro, R. H.; Frear, D. S.; Swanson, H. R.; Walsh, W. C. Glutathione conjugation an enzymatic basis for atrazine resistance in corn. *Plant Physiol.* **1971**, *47*, 10−14.
(33) Brazier−Hicks, M.; Edwards, R. Functional importance of the family 1 glucosyltransferase UGT72B1 in the metabolism of xenobiotics in *Arabidopsis thaliana*. *Plant J.* **2005**, *42*, 556−566.
(34) Gholivand, M. B.; Karimian, N.; Malekzadeh, G. Computational design and synthesis of a high selective molecularly imprinted polymer for voltammetric sensing of propazine in food samples. *Talanta* **2012**, *82*, 513−520.
(35) Su, Z. H.; Xu, Z. S.; Peng, R. H.; Tian, Y. S.; Zhao, W.; Han, H. J.; Yao, Q. H.; Wu, A. Z. Phytoremediation of trichlorophenol by phase II metabolism in transgenic Arabidopsis overexpressing a Populus glucosyltransfease. *Environ. Sci. Technol.* **2012**, *46*, 4016−4024.
(36) Loutre, C.; Dixon, D. P.; Brazier, M.; Slater, M.; Cole, D. J.; Edwards, R. Isolation of a glucosyltransferase from *Arabidopsis thaliana* active in the metabolism of the persistent pollutant 3,4-dichloroaniline. *Plant J.* **2003**, *34*, 485−493.
(37) Baerson, S. R.; Sánchez-Moreiras, A.; Pedrol−Bonjoch, N.; Schulz, M.; Kagan, I. A.; Agarwal, A. K.; Reigosa, M. J.; Duke, S. O. Detoxification and transcriptome response in arabidopsis seedlings exposed to the allelochemical Benzoxazolin-2(*3H*)-one. *J. Biol. Chem.* **2005**, *280*, 21867−21881.
(38) Ross, J.; Li, Y.; Lim, E.; Bowles, D. J. Higher plant glycosyltransferases. *Genome Biol.* **2001**, *2*, 3004.1−3004.6.
(39) Maughan, S.; Foyer, C. H. Engineering and genetic approaches to modulating the glutathione network in plants. *Physiol. Plant.* **2006**, *126*, 382−397.
(40) Matamoros, M. A.; Moran, J. F.; Iturbe-Ormaetxe, I.; Rubio, M. C.; Becana, M. Glutathione and homoglutathione synthesis in legume root nodules. *Plant Physiol.* **1999**, *121*, 879−888.
(41) Matamoros, M. A.; Dalton, D. A.; Clemente, M. R.; Rubio, M. C.; Ramos, J.; Becana, M. Biochemistry and molecular biology of antioxidants in the rhizobia-legume symbiosis. *Plant Physiol.* **2003**, *133*, 1−11.
(42) Pasternak, T.; Asard, H.; Potters, G.; Jansen, M. A. K. The thiol compounds glutathione and homoglutathione differentially affect cell development in alfalfa (*Medicago sativa* L.). *Plant Physiol. Biochem.* **2014**, *74*, 16−23.
(43) Leustek, T.; Matin, M. N.; Bick, J. A.; Davies, J. P. Pathways and regulation of sulfur metabolism revealed through molecular and genetic studies. *Plant Mol. Biol.* **2000**, *51*, 141−165.
(44) Dixon, D. P.; Lapthorn, A.; Edwards, R. Plant glutathione transferases. *Genome Biol. Rev.* **2002**, *3* (3), 3004.1−3004.10.
(45) Li, Y. Y.; Yang, H. Bioaccumulation and degradation of pentachloronitrobenzene in *Medicago sativa*. *J. Environ. Manage.* **2013**, *119*, 143−150.

humidity, light intensity of 340 $\mu$mol·m$^{-2}$·s$^{-1}$) and irrigated three times a week with distilled water (200−300 mL) to maintain saturation. Yoshida nutrient solution[11] was used to fertilize the plant as described in Supporting Information Table S1. Wheat green bug (*Schizaphis graminum*) appeared 65 days after transplanting (DAT), and plants were immediately sprayed with malathion (5 mg/L) (Ortho MAX Malathion). At harvest (94 DAT), spikes, flag leaves, and roots were collected and oven-dried at 80 °C for 5 days. Roots were cleaned thoroughly for 30 min in running tap water and rinsed for 5 min in distilled water. The grains were dehulled and stored at 4 °C until use. Samples for analysis were powdered and passed through mesh no. 40 (W. S. Tyler).

**Evaluation of Agronomic Traits and Yield Components.** Agronomic traits (plant height, chlorophyll content, number of tillers, peduncle length, and number of internodes) were assessed by five measurements from randomly selected plants in each pot. Plant height and chlorophyll content were measured at heading stage (30 DAT). Plant height was determined from soil surface to the flag leaf, while chlorophyll content was measured in the flag leaf by use of a SPAD chlorophyll meter (Spectrum Technologies, Aurora, IL). The number of spikes was counted when the spikes were fully exposed, while physiological maturity was recorded when the spike was completely dry. Shoot biomass from each pot was determined at harvest. For the yield components, the following parameters were measured for five random samples: spike length, number of spikes, number of spikelets/spike, number of grains/spike, gain yield/spike, 100-grain weight, and grain yield/pot. The five measurements from each pot for agronomic and yield components, except grain yield/pot, were averaged and used as one replicate measurement for statistical analyses.

**Cerium and Macro- and Micronutrient Concentrations in Wheat.** A microwave-accelerated reaction system (CEM Mars$_X$, Matthews, NC) was used to digest the samples in a mixture of plasma pure $HNO_3$ and $H_2O_2$ (1:4) and analyzed for elemental composition by inductively coupled plasma optical emission spectroscopy/mass spectrometry (ICP-OES/MS) (PerkinElmer, Waltham, MA) according to the method previously employed by Rico et al.[10] Blank, spikes, and standard reference material (NIST-SRF 1570a) were used to validate the digestion and analytical method.

**Amino Acid Profiling.** Amino acid analysis was performed following the method of Anjum et al.[12] Briefly, the powdered grains (50 mg) were mixed with 10 mL of 6 N HCL in a test tube, which was subsequently evacuated by nitrogen, sealed, and placed in an oven (110 °C) for 24 h. The hydrolysate was filtered and dried under vacuum (60 °C) before dissolving in 1 mL of phosphate buffer (pH 2.2). An aliquot (100 $\mu$L) was diluted 10 times with buffer, filtered in a 45 $\mu$m syringe filter, and analyzed on a Biochrom 20 amino acid analyzer.

**Fatty Acid Analysis.** Fatty acid content was estimated according to Asekova et al.[13] The powdered grains (500 mg) were placed in a 5 mL solution of chloroform/hexane/methanol (8:5:2 v/v/v) overnight. Derivatization was performed by mixing 100-$\mu$L extract with 75 $\mu$L of methylating reagent [0.25 M methanolic sodium methoxide/petroleum ether/ethyl ether (1:5:2 v/v/v)]. After 10 h, the solution was diluted to 1 mL with hexane. Fatty acid content was analyzed on an Agilent (Palo Alto, CA) Series 7890 capillary gas chromatograph fitted with a flame ionization detector with an AT-Silar capillary column (Alltech Associates, Derfield, IL). The temperatures of the oven, injector, and detector were set at 210, 250, and 230 °C, respectively. Standard fatty acid mixtures (Animal and Vegetable Oil Reference Mixture 6, AOACS) were used as calibration reference standards.

**Data Analysis.** The effect of $n$CeO$_2$ treatment on measured parameters was determined by the general linear model procedure in SAS statistical package, version 9.3 (SAS Institute, Cary, NC). Statistical significance between means was tested with Tukey's honestly significant difference test at $p \leq 0.05$.

## RESULTS AND DISCUSSION

**Cerium Accumulation in Wheat Tissues.** The accumulation of ENMs and their component metals in edible portions of plants is becoming a concern. Table 1 presents the Ce concentration in different wheat tissues. In the roots, control and $n$CeO$_2$-L yielded Ce concentration (1974 and 16 828 $\mu$g/kg, respectively) significantly lower than those in $n$CeO$_2$-M and $n$CeO$_2$-H (80 933 and 111 121 $\mu$g/kg, respectively). The Ce accumulations in $n$CeO$_2$-treated leaves and grains were in the range 430−442 and 155−263 $\mu$g/kg, respectively. However, these values did not reach statistical differences compared with values recorded in their respective controls (600 and 248 $\mu$g/kg, respectively). Similarly, the Ce concentration in the hull did not change significantly across treatments (412−450 $\mu$g/kg), strongly suggesting a lack of Ce translocation in wheat grains. Cornelis et al.[3] reported that $n$CeO$_2$ were stable in 16 different types of soil and found a dissolution rate of <3.1% at pH 4. Microscopy techniques have also shown that $n$CeO$_2$ accumulated largely in nanoparticulate form in food crops cultivated in soil and hydroponic suspension.[1] The current findings are in good agreement with previous reports in wheat showing that $n$CeO$_2$ adsorbed on the root surface[7] but are in stark contrast with the remarkable increases in Ce accumulation in rice grains, soybean pods, and tomato and cucumber fruits,[10,14−16] signifying the differences in root storage and above-ground tissues transport of Ce in plants.

**Table 1. Cerium Concentration in Different Tissues of Wheat Cultivated to Grain Production in $n$CeO$_2$-Amended Soil[a]**

| | Ce concn ($\mu$g/kg) | | | |
|---|---|---|---|---|
| soil[b] | root | leaves | hull | grains |
| 0 | 1974 ± 549 c | 600 ± 85 a | 435 ± 20 a | 248 ± 96 a |
| 125 | 16828 ± 332 c | 442 ± 19 a | 412 ± 9 a | 155 ± 45 a |
| 250 | 80934 ± 200 b | 431 ± 50 a | 450 ± 12 a | 186 ± 32 a |
| 500 | 111121 ± 650 a | 430 ± 64 a | 428 ± 7 a | 263 ± 44 a |

[a]Values are means ± SE ($n$ = 3). Same letters mean no statistical difference between treatments at Tukey's test ($p \leq 0.05$). [b]Control = 0 mg/kg; $n$CeO$_2$-L = 125 mg/kg; $n$CeO$_2$-M = 250 mg/kg; $n$CeO$_2$-H = 500 mg/kg.

**Modifications in Growth Characteristics.** The agronomic characteristics of $n$CeO$_2$-exposed wheat are presented in Table 2 and Figure 1. It is evident from Table 2 that $n$CeO$_2$ had no effect on the exposed peduncle length, number of tillers, number of internodes, and chlorophyll content. $n$CeO$_2$-H improved plant height and shoot biomass by up to 5.32% and 12.71%, respectively, compared to the rest of the treatments. Previous studies found that $n$CeO$_2$ had no impact on growth, gas exchange, and chlorophyll content of cucumber[17] but improved dry stem and leaf biomass in soybean[14] and slightly enhanced plant growth but not chlorophyll content in tomato.[15] On the contrary, $n$ZnO- or $n$TiO$_2$-exposed wheat had reduced biomass production.[6]

In addition, $n$CeO$_2$ treatment caused a 6-day delay in spike formation and physiological maturity in wheat compared to control (Figure 1; Supporting Information Tables S2 and S3). Wang et al.[15] found that $n$CeO$_2$ prolonged by 2 days the fruit ripening in tomato. Although the extended period of time for spike formation and physiological maturity could improve yield in wheat,[8] it may have significant impacts on seeding time since correct planting date is important for growth stages and

Table 2. Growth Characteristics of Wheat Cultivated to Grain Production in $n$CeO$_2$-Amended Soil[a]

| soil[b] | plant height (cm) | exposed peduncle length (cm) | no. of tillers | no. of internodes | chlorophyll content (SPAD units) | shoot biomass (g) |
|---|---|---|---|---|---|---|
| 0 | 43.6 ± 0.7 b | 10.4 ± 1.0 a | 6.7 ± 0.2 a | 4.5 ± 0.1 a | 38.7 ± 0.8 a | 18.1 ± 0.2 b |
| 125 | 45.1 ± 0.5 b | 10.3 ± 0.1 a | 5.9 ± 0.2 a | 4.7 ± 0.1 a | 40.6 ± 0.8 a | 18.5 ± 0.6 a |
| 250 | 45.4 ± 0.5 ab | 10.5 ± 0.1 a | 5.8 ± 0.3 a | 4.3 ± 0.2 a | 39.2 ± 0.8 a | 19.2 ± 0.1 ab |
| 500 | 47.5 ± 0.2 a | 11.1 ± 0.9 a | 6.5 ± 0.1 a | 4.5 ± 0.1 a | 39.3 ± 0.4 a | 20.4 ± 0.3 a |

[a]Values are means ± SE ($n$ = 3). Same letters mean no statistical difference between treatments at Tukey's test ($p \leq 0.05$). [b]Control = 0 mg/kg; $n$CeO$_2$-L = 125 mg/kg; $n$CeO$_2$-M = 250 mg/kg; $n$CeO$_2$-H = 500 mg/kg.

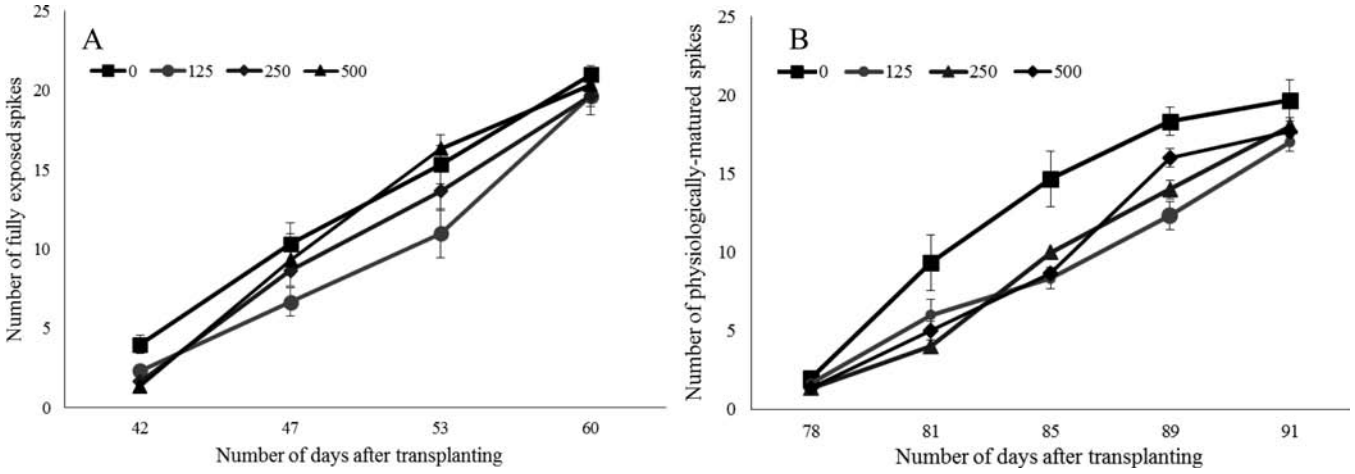


Figure 1. (A) Spike formation and (B) spike physiological maturity in wheat cultivated to grain production in $n$CeO$_2$-amended soil. 0, 125, 250, and 500 denote control, $n$CeO$_2$-L, $n$CeO$_2$-M, and $n$CeO$_2$-H, respectively. Each data point represents mean ± SE ($n$ = 3).

Table 3. Yield Parameters of Wheat Cultivated to Grain Production in $n$CeO$_2$-Amended Soil[a]

| soil[b] | spike length (cm) | no. of spikelets/spike | no. of grains/spike | grain yield/spike (mg) | 100-grain weight (g) | yield/pot (g) |
|---|---|---|---|---|---|---|
| 0 | 7.9 ± 0.2 a | 30.8 ± 0.8 c | 21.9 ± 0.5 b | 761.8 ± 9.3 ab | 2.65 ± 0.03 a | 9.3 ± 0.4 b |
| 125 | 7.7 ± 0.1 a | 36.1 ± 0.4 b | 25.3 ± 0.7 a | 663.8 ± 20.8 c | 2.63 ± 0.09 a | 10.2 ± 0.3 ab |
| 250 | 7.8 ± 0.2 a | 34.9 ± 1.1 bc | 21.6 ± 0.3 b | 738.9 ± 8.4 b | 2.71 ± 0.09 b | 10.5 ± 0.2 ab |
| 500 | 8.3 ± 0.1 a | 42.5 ± 1.5 a | 26.0 ± 0.8 a | 808.9 ± 8.2 a | 2.83 ± 0.04 a | 12.7 ± 0.4 a |

[a]Values are means ± SE ($n$ = 3). Same letters mean no statistical difference between treatments at Tukey's test ($p \leq 0.05$). [b]Control = 0 mg/kg; $n$CeO$_2$-L = 125 mg/kg; $n$CeO$_2$-M = 250 mg/kg; $n$CeO$_2$-H = 500 mg/kg.

phenological development to occur at appropriate environmental conditions.[18]

**Changes in Yield Parameters.** The impact of metal oxide ENMs on the crop yield is not yet well explored. Table 3 displays the influence of $n$CeO$_2$ on yield parameters of wheat. $n$CeO$_2$ altered all yield parameters, except for spike length and 100-grain weight. The number of spikelets per spike was highest (42.5) at $n$CeO$_2$-H and lowest (30.8) in control. However, the number of grains per spike in $n$CeO$_2$-L (25.3) and $n$CeO$_2$-H (26.0) were higher than that of the control (21.9) and $n$CeO$_2$-M (21.6). The grain yield per spike was significantly enhanced at $n$CeO$_2$-H (808.9 mg), but markedly reduced at $n$CeO$_2$-L (663.8 mg). In case of yield, only $n$CeO$_2$-H recorded a significantly higher yield per pot (12.7 g) compared to control (9.3 g). Current literature shows varying effects of $n$CeO$_2$ on the productivity of food crops; $n$CeO$_2$ had no impact on pod yield in soybean,[14] enhanced fruit production in tomato,[15] and reduced yield in cucumber.[17]

Wang et al.[15] found that longer vegetative stage enhanced fruit yield in $n$CeO$_2$-exposed tomato. Similarly, the superior yield at $n$CeO$_2$-H was consistent with the delayed spike formation and maturity as well as improved plant height, shoot biomass, number of grains and spikelets per spike, and grain yield per spike. It is interesting to note that the reduced yield in the control could be due to low number of grains, whereas at $n$CeO$_2$-L, the superior number of grains per spike and low grain weight did not result in improved yield.

**Mineral Accumulation.** Table 4 presents the elemental concentrations in roots, leaves, and grains of wheat. The $n$CeO$_2$ treatments did not modify the Ca, Zn, and Cu concentrations but altered the accumulations of K, P, S, Na, Fe, and Mn in roots; P, Mg, and Fe in leaves; and S and Mn in grains. In roots, K concentration markedly improved at $n$CeO$_2$-H (18 173 mg/kg) compared to the rest of the treatments (8081−12 658 mg/kg) while P accumulation significantly increased at $n$CeO$_2$-M (3686 mg/kg) relative to control and $n$CeO$_2$-L (2417 and 2903 mg/kg, respectively). S concentration was elevated at $n$CeO$_2$-M (2445 mg/kg) and $n$CeO$_2$-H (2772 mg/kg) in the roots but decreased at $n$CeO$_2$-L and $n$CeO$_2$-M (1621 mg/kg) in the grains compared to their respective controls (1667 and 1726 mg/kg, respectively). Mg accumulation in leaves was enhanced at $n$CeO$_2$-M (4559 mg/kg) relative to the control (3944 mg/kg).

The Na concentration in roots increased in all $n$CeO$_2$ treatments (3526−4121 mg/kg) relative to the control (2447 mg/kg), whereas Fe accumulation in all $n$CeO$_2$ treatments in roots (388−426 mg/kg) and $n$CeO$_2$-M and $n$CeO$_2$-H in leaves (97 and 101 mg/kg, respectively) decreased compared to their


dx.doi.org/10.1021/jf503526r | J. Agric. Food Chem. 2014, 62, 9669−9675

**Table 4. Elemental Concentrations in Different Tissues of Wheat Cultivated to Grain Production in $n$CeO$_2$-Amended Soil[a]**

| soil[b] | elemental concn (mg/kg) | | | | | | | | | |
|---|---|---|---|---|---|---|---|---|---|---|
| | K | P | Ca | Mg | S | Na | Fe | Mn | Zn | Cu |
| | | | | | Roots | | | | | |
| 0 | 8081 ± 191 c | 2417 ± 111 c | 4642 ± 805 a | 910 ± 86 a | 1667 ± 51 b | 2447 ± 72 c | 455 ± 86 a | 49 ± 5 b | 45 ± 4 a | 50.8 ± 4.3 a |
| 125 | 9600 ± 346 c | 2903 ± 250 bc | 3761 ± 672 a | 1079 ± 122 a | 2224 ± 182 ab | 3526 ± 125 b | 408 ± 75 b | 56 ± 7 ab | 56 ± 5 a | 78.6 ± 19.6 a |
| 250 | 12658 ± 319 b | 3686 ± 162 a | 4315 ± 296 a | 1184 ± 47 a | 2445 ± 76 a | 4103 ± 102 a | 388 ± 60 b | 57 ± 4 ab | 49 ± 3 a | 67.1 ± 3.1 a |
| 500 | 18173 ± 620 a | 3173 ± 28 ab | 4828 ± 305 a | 1257 ± 45 a | 2772 ± 177 a | 4121 ± 164 a | 426 ± 27 b | 72 ± 2 a | 53 ± 2 a | 60.3 ± 5.0 a |
| | | | | | Leaves | | | | | |
| 0 | 25181 ± 481 a | 2935 ± 162 ab | 6219 ± 205 a | 3944 ± 93 b | 2706 ± 122 a | 280 ± 12 a | 117 ± 2 a | 162 ± 15 a | 24 ± 3 a | 3.1 ± 0.4 a |
| 125 | 24783 ± 878 a | 2626 ± 173 b | 6301 ± 346 a | 4011 ± 81 ab | 2701 ± 115 a | 264 ± 29 a | 112 ± 5 ab | 136 ± 14 a | 32 ± 3 a | 2.8 ± 0.2 a |
| 250 | 23345 ± 665 a | 3076 ± 355 ab | 7360 ± 192 a | 4559 ± 7 a | 2501 ± 31 a | 248 ± 19 a | 97 ± 1 c | 129 ± 2 a | 24 ± 2 a | 3.1 ± 0.2 a |
| 500 | 22973 ± 482 a | 3684 ± 106 a | 6416 ± 332 a | 3956 ± 218 b | 2518 ± 123 a | 213 ± 9 a | 101 ± 2 bc | 159 ± 7 a | 24 ± 2 a | 2.9 ± 0.2 a |
| | | | | | Grains | | | | | |
| 0 | 5079 ± 94 a | 5262 ± 93 a | 387 ± 1 a | 1906 ± 30 a | 1726 ± 55 a | 18 ± 1 a | 50 ± 1 ab | 57 ± 1 a | 75 ± 2 a | 7.3 ± 0.2 a |
| 125 | 4787 ± 132 a | 5064 ± 137 a | 380 ± 6 a | 1803 ± 15 a | 1621 ± 34 b | 20 ± 1 a | 46 ± 3 b | 50 ± 1 ab | 75 ± 3 a | 7.3 ± 0.2 a |
| 250 | 4765 ± 28 a | 5250 ± 85 a | 378 ± 8 a | 1886 ± 35 a | 1621 ± 10 b | 22 ± 2 a | 53 ± 1 ab | 48 ± 2 b | 71 ± 1 a | 6.9 ± 0.2 a |
| 500 | 5295 ± 268 a | 5584 ± 220 a | 386 ± 7 a | 1824 ± 83 a | 1648 ± 33 ab | 22 ± 1 a | 60 ± 3 a | 52 ± 1 ab | 73 ± 1 a | 7.3 ± 0.2 a |

[a]Values are means ± SE ($n$ = 3). Same letters mean no statistical difference between treatments at Tukey's test ($p \leq 0.05$). [b]Control = 0 mg/kg; $n$CeO$_2$-L = 125 mg/kg; $n$CeO$_2$-M = 250 mg/kg; $n$CeO$_2$-H = 500 mg/kg.



dx.doi.org/10.1021/jf503526r | J. Agric. Food Chem. 2014, 62, 9669−9675

Table 5. Amino Acid Content in Wheat Grains Harvested from Wheat Cultivated in $n$CeO$_2$-Amended Soil[a,b]

| | amino acid content ($\mu$g/g) | | | |
|---|---|---|---|---|
| amino acid | control | $n$CeO$_2$-L | $n$CeO$_2$-M | $n$CeO$_2$-H |
| alanine | 17.10 ± 1.12 a | 18.31 ± 0.83 a | 15.16 ± 0.29 a | 15.54 ± 0.50 a |
| cysteine | 7.56 ± 0.20 a | 7.88 ± 0.19 a | 7.29 ± 0.14 a | 7.41 ± 0.23 a |
| glutamic acid | 148.97 ± 2.59 a | 158.53 ± 3.83 a | 139.28 ± 3.84 a | 154.45 ± 7.96 a |
| leucine | 32.61 ± 0.95 a | 36.42 ± 1.28 a | 32.76 ± 1.69 a | 33.84 ± 1.88 a |
| methionine | 5.51 ± 0.97 a | 6.12 ± 0.42 a | 5.65 ± 0.05 a | 5.92 ± 0.18 a |
| proline | 54.49 ± 2.15 a | 55.96 ± 1.55 a | 55.51 ± 2.44 a | 52.51 ± 2.23 a |
| arginine | 24.64 ± 0.42 b | 29.96 ± 1.39 a | 25.08 ± 0.68 b | 24.53 ± 1.02 b |
| aspartic acid | 23.29 ± 0.43 b | 26.77 ± 0.99 a | 22.46 ± 0.44 b | 22.67 ± 0.66 b |
| glycine | 19.13 ± 0.31 b | 21.83 ± 0.80 a | 18.39 ± 0.32 b | 18.68 ± 0.74 b |
| histidine | 11.76 ± 0.30 b | 13.67 ± 0.29 a | 12.74 ± 0.39 ab | 13.34 ± 0.04 a |
| isoleucine | 15.23 ± 0.39 ab | 17.02 ± 0.66 a | 14.24 ± 0.29 b | 14.64 ± 0.58 b |
| lysine | 13.24 ± 0.41 b | 15.33 ± 0.54 a | 12.88 ± 0.30 b | 13.89 ± 0.46 ab |
| phenylalanine | 22.87 ± 0.40 ab | 25.01 ± 0.71 a | 21.36 ± 0.49 b | 24.61 ± 0.52 a |
| serine | 22.92 ± 0.31 ab | 24.70 ± 0.77 a | 21.59 ± 0.49 b | 21.82 ± 0.97 ab |
| threonine | 14.66 ± 0.31 ab | 16.10 ± 0.51 a | 13.91 ± 0.27 b | 13.99 ± 0.45 b |
| tyrosine | 14.77 ± 0.21 ab | 16.52 ± 0.53 a | 14.24 ± 0.36 b | 15.15 ± 0.41 ab |
| valine | 21.95 ± 0.45 ab | 24.10 ± 0.83 a | 20.74 ± 0.32 b | 20.73 ± 0.84 b |
| amide-NH$_3$ | 24.05 ± 0.19 b | 26.50 ± 0.50 a | 26.30 ± 0.25 a | 25.36 ± 0.49 ab |
| total | 494.72 ± 11.38 a | 540.73 ± 15.61 a | 479.60 ± 9.34 a | 499.08 ± 18.46 a |

[a]Values are means ± SE ($n$ = 3). Same letters in each row mean no statistical difference between treatments at Tukey's test ($p \leq 0.05$). [b]Control = 0 mg/kg; $n$CeO$_2$-L = 125 mg/kg; $n$CeO$_2$-M = 250 mg/kg; $n$CeO$_2$-H = 500 mg/kg.

Table 6. Fatty Acid Content in Wheat Grains Harvested from Wheat Cultivated in $n$CeO$_2$-Amended Soil[a]

| | % relative fatty acid | | | | |
|---|---|---|---|---|---|
| soil[b] | palmitic (C16) | stearic (C18) | oleic (C18:1) | linoleic (C18:2) | linolenic (C18:3) |
| 0 | 18.70 ± 0.10 a | 1.98 ± 0.10 a | 14.85 ± 0.18 a | 59.65 ± 0.13 a | 4.63 ± 0.06 b |
| 125 | 18.46 ± 0.12 a | 1.88 ± 0.08 a | 15.64 ± 0.33 a | 58.98 ± 0.16 b | 4.82 ± 0.01 a |
| 250 | 18.70 ± 0.07 a | 1.84 ± 0.02 a | 15.02 ± 0.07 a | 59.71 ± 0.10 a | 4.54 ± 0.03 b |
| 500 | 18.60 ± 0.07 a | 1.85 ± 0.03 a | 14.67 ± 0.23 a | 59.96 ± 0.08 a | 4.66 ± 0.03 ab |

[a]Values are means ± SE ($n$ = 3). Same letters mean no statistical difference between treatments at Tukey's test ($p \leq 0.05$). [b]Control = 0 mg/kg; $n$CeO$_2$-L = 125 mg/kg; $n$CeO$_2$-M = 250 mg/kg; $n$CeO$_2$-H = 500 mg/kg.

controls (455 and 117 mg/kg, respectively). In contrast, Mn concentration in roots and grains did not differ between $n$CeO$_2$ treatments (56−72 and 48−52 mg/kg, respectively); however, $n$CeO$_2$-H yielded a superior amount of Mn (72 mg/kg) in roots compared to control (49 mg/kg), while $n$CeO$_2$-M had reduced Mn accumulation (48 mg/kg) in grains relative to control (57 mg/kg).

These findings suggest that $n$CeO$_2$ modulated the elemental accumulation in roots and leaves without detrimental impact on the nutritional content of grains. It is possible that the modulation in P storage was due to the association of Ce with $PO_4^{3-}$ as observed in $n$CeO$_2$-exposed soybean and cucumber.[1] The increase in S concentration was opposite to that recorded in $n$CeO$_2$-treated soybean, wherein S accumulation did not change in all tissues analyzed.[19] Likewise, $n$CeO$_2$ altered Na and Fe concentrations in wheat roots and leaves, which was not observed in previous studies in soybean.[19] Unfortunately, there is a lack of understanding in current literature regarding the aggregation, association, and mobility of elements in $n$CeO$_2$-amended soil that could help explain the changes in their accumulation in wheat. In grains, only S concentration at $n$CeO$_2$-L and $n$CeO$_2$-M and Mn concentration at $n$CeO$_2$-M had marked reductions compared to their respective controls. Previous reports also revealed that $n$CeO$_2$ altered S and Mn accumulations in rice grains[10] and cucumber fruit,[16] respectively, but not in soybean pods.[19] At this point it is difficult to determine the cause of the reduced accumulation of S and Mn in grains, but their decrease may have negative implications on food quality.

**Amino Acid Content in Grains.** The effects of $n$CeO$_2$ on amino acid (AA) content of wheat grains was examined and the data are displayed in Table 5. Results showed that $n$CeO$_2$ did not modify the contents of alanine, cysteine, leucine, methionine, proline, and glutamic acid. $n$CeO$_2$-L had generally elevated AA content, but statistical difference relative to the control was achieved only for aspartic acid, glycine, lysine, histidine, and arginine. The control, $n$CeO$_2$-M, and $n$CeO$_2$-H had similar levels of AA except for superior amounts at $n$CeO$_2$-H treatment compared to control and $n$CeO$_2$-M for histidine and phenylalanine, respectively. Among the essential AA, $n$CeO$_2$-L increased lysine and histidine content (15.33 and 13.67 $\mu$g/g, respectively) compared to control (13.24 and 11.76 $\mu$g/g, respectively). The amide-NH$_3$ was highest at $n$CeO$_2$-L and $n$CeO$_2$-M (26.50 and 26.30-$\mu$g/g, respectively) and lowest in the control (24.05 $\mu$g/g), whereas total AA contents did not change between treatments, although it had the tendency to increase at $n$CeO$_2$-L (540.73 $\mu$g/g) compared to the rest of the treatments (494.72−499.08 $\mu$g/g).

These findings revealed that $n$CeO$_2$ interfered with AA synthesis in wheat, with $n$CeO$_2$-L demonstrating the tendency to improve AA content in wheat grains. Currently, there is no other study regarding the effects of ENMs on AA or protein

synthesis in cereal grains, which makes interpretation of the present results difficult. However, studies exhibited that AA metabolism or protein content was modified in ENM-exposed wheat and rice[10,20] while various ENMs (*n*Ag, *n*S, $n$SiO$_2$, $n$TiO$_2$, and *n*ZnO) modified protein levels in different crops.[1]

**Relative Fatty Acid Abundance in Grains.** The influence of $n$CeO$_2$ on the relative fatty acid (FA) abundance in wheat grains was analyzed and presented in Table 6. The analysis revealed that $n$CeO$_2$ treatments did not alter the relative FA abundance of palmitic, oleic, and stearic acids. In contrast, $n$CeO$_2$-L caused a remarkable reduction in the relative FA content of linoleic acid by up to 1.63% relative to the rest of the treatments but afforded a marked increase in the relative FA content of linolenic acid by up to 6.17% relative to the rest of the treatments. These data revealed that $n$CeO$_2$ also disturbed FA synthesis and storage in wheat grains.

Similar to what was observed in the AA analysis, $n$CeO$_2$-L provoked significant changes on FA contents, indicating the impact of this treatment on the nutritional value of wheat grains. Previous studies have shown that $n$CeO$_2$ modified the FA content in rice grains[10] while *n*Au stimulated oil production in mustard seeds (*Brassica juncea*).[21] The modifications in AA and FA contents signify that $n$CeO$_2$ could have serious implications on the nutritional value of wheat grains.

**Pearson's Correlations.** Table 7 displays the correlations between measured parameters and Ce concentration in roots or grains. The data illustrate that, in roots, Ce concentration was positively correlated with K, S, and Na at $p \leq 0.01$ and with P, Mg, and Mn at $p \leq 0.05$. In grains, root Ce concentration was positively correlated with Fe at higher significance level (0.773 08, $p \leq 0.01$) than Na (0.680 55, $p \leq 0.05$). Likewise, root Ce concentration manifested stronger positive correlations ($p \leq 0.01$) with plant height, shoot biomass, number of spikelets, and yield per pot than with spike length ($p \leq 0.10$). Furthermore, the data displayed that root Ce concentration was negatively correlated with threonine, serine, alanine, and valine at greater significance level ($p \leq 0.05$) than in aspartic acid, glycine, and isoleucine ($p \leq 0.10$). Only linoleic acid displayed a positive correlation with root Ce concentration (0.63156, $p \leq 0.05$). The highly significant positive correlations between Ce and growth parameters are in agreement with the fertilizer effect of Ce. However, the improvement in growth and yield was accompanied by detrimental impacts on AA compositions of grains, especially since four essential amino acids were negatively affected. On the other hand, the positive correlation of Ce with P, S, Mg, Mn, and Na concentrations in roots could indicate important implications or associations of these elements with $n$CeO$_2$. Unfortunately, there is limited understanding of this aspect in current literature.

In grains, Ce concentration displayed positive correlation with Ca (0.59941, $p \leq 0.05$) similar to what was observed in $n$CeO$_2$-exposed rice grains[10] and $Ce^{3+}$-treated rice seedlings.[22] On the other hand, the negative correlations between Ce and chlorophyll content, threonine, isoleucine, and lysine suggest that Ce content could have significant impacts on essential amino acids in grains.

In summary, the study revealed that $n$CeO$_2$ improved the plant height, biomass, and grain yield and modified the amino acid and fatty acid contents despite the apparent lack of Ce transport and accumulation in above-ground tissues of wheat. The findings underscore the significance of examining the long-term impacts of ENMs on the productivity and quality of food crops.

**Table 7. Pearson's Correlations between Cerium Concentration in Roots or Grains and Measured Parameters in Wheat Cultivated in $n$CeO$_2$-Amended Soil**

| Correlations with Ce Concentration in Roots | | | |
|---|---|---|---|
| | *r* | *p* values | significance[a] |
| Elemental Concentration in Roots | | | |
| K | 0.94436 | <0.0001 | *** |
| P | 0.68376 | 0.0142 | ** |
| Mg | 0.70770 | 0.0100 | ** |
| Mn | 0.66793 | 0.0176 | ** |
| S | 0.86067 | 0.0003 | *** |
| Na | 0.84243 | 0.0006 | *** |
| Growth/Yield Components | | | |
| spike length | 0.50375 | 0.0950 | * |
| plant height | 0.81039 | 0.0014 | *** |
| shoot biomass | 0.86938 | 0.0002 | *** |
| no. of spikelets | 0.77962 | 0.0028 | *** |
| yield/pot | 0.76626 | 0.0037 | *** |
| Elemental Concentration in Grains | | | |
| Na | 0.68055 | 0.0149 | ** |
| Fe | 0.77308 | 0.0032 | *** |
| Nutritional Components in Grains | | | |
| aspartic acid | −0.52992 | 0.0764 | * |
| glycine | −0.50954 | 0.0906 | * |
| isoleucine | −0.54759 | 0.0653 | * |
| threonine | −0.60554 | 0.0369 | ** |
| serine | −0.60142 | 0.0386 | ** |
| alanine | −0.64724 | 0.0229 | ** |
| valine | −0.62534 | 0.0297 | ** |
| linoleic acid | 0.63156 | 0.0276 | ** |
| Correlations with Ce Concentration in Grains | | | |
| | *r* | *p* values | significance[a] |
| Elemental Concentration in Grains | | | |
| Ca | 0.59941 | 0.0394 | ** |
| Growth/Yield Components | | | |
| SPAD | −0.56499 | 0.0556 | * |
| Nutritional Components in Grains | | | |
| threonine | −0.50398 | 0.0948 | * |
| isoleucine | −0.50237 | 0.0960 | * |
| lysine | −0.51175 | 0.0890 | * |

[a]Significance at *$p \leq 0.10$, **$p \leq 0.05$, and ***$p \leq 0.01$.

## ■ ASSOCIATED CONTENT

### Ⓢ Supporting Information

Three tables listing details on fertilization, spike formation, and physiological maturity. This material is available free of charge via the Internet at http://pubs.acs.org.

## ■ AUTHOR INFORMATION


### Corresponding Author

*Tel 915-747-5359; fax 915-747-5748; e-mail jgardea@utep.edu.


### Notes

The authors declare no competing financial interest.

## ■ ACKNOWLEDGMENTS

This material is based upon work supported by the National Science Foundation and the Environmental Protection Agency under Cooperative Agreement DBI-0830117. Any opinions, findings, and conclusions or recommendations expressed in this material are those of the author(s) and do not necessarily

reflect the views of the National Science Foundation or the Environmental Protection Agency. This work has not been subjected to EPA review and no official endorsement should be inferred. We acknowledge the USDA grant number 2011-38422-30835, the NSF Grant #CHE-0840525, and the Toxicology Unit of the BBRC (NIH NCRR Grant No. 2G12MD007592). J. G.-T. acknowledges the Dudley family for the Endowed Research Professorship and the the Academy of Applied Science/U.S. Army REAP program at UTEP for Grant W11NF-10-2-0076, subgrant 13-7. We also acknowledge Dr. Brad Brown of the University of Idaho, who provided the wheat seeds.

## REFERENCES

(1) Gardea-Torresdey, J. L.; Rico, C. M.; White, J. C. Trophic transfer, transformation, and impact of engineered nanomaterials in terrestrial environments. *Environ. Sci. Technol.* **2014**, *48*, 2526−2540.

(2) Keller, A.; McFerran, S.; Lazareva, A.; Suh, S. Global life cycle releases of engineered nanomaterials. *J. Nanopart. Res.* **2013**, *15*, 1692−1709.

(3) Cornelis, G.; Ryan, B.; McLaughlin, M. J.; Kirby, J. K.; Beak, D.; Chittleborough, D. Solubility and batch retention of $CeO_2$ nanoparticles in soils. *Environ. Sci. Technol.* **2011**, *45*, 2777−2782.

(4) FAOSTAT. Food and Agriculture Organization of the United Nations. http://faostat.fao.org/site/339/default.aspx (accessed October 2013).

(5) Shewry, P. R. Wheat. *J. Exp. Bot.* **2009**, *60*, 1537−1553.

(6) Du, W. C.; Sun, Y. Y.; Ji, R.; Zhu, J. G.; Wu, J. C.; Guo, H. Y. $TiO_2$ and ZnO nanoparticles negatively affect wheat growth and soil enzyme activities in agricultural soil. *J. Environ. Monitor.* **2011**, *13*, 822−828.

(7) Schwabe, F.; Schulin, R.; Limbach, L. K.; Stark, W.; Burge, D.; Nowack, B. Influence of two types of organic matter on interaction of $CeO_2$ nanoparticles with plants in hydroponic culture. *Chemosphere* **2013**, *91*, 512−520.

(8) Li, P.; Chen, J.; Wu, P. Agronomic characteristics and grain yield of 30 spring wheat genotypes under drought stress and nonstress conditions. *Agron. J.* **2011**, *103*, 1619−1628.

(9) Keller, A. A.; Wang, H.; Zhou, D.; Lenihan, H. S.; Cherr, G.; Cardinale, B. J.; Miller, R.; Ji, Z. Stability and aggregation of metal oxide nanoparticles in natural aqueous media. *Environ. Sci. Technol.* **2010**, *344*, 1962−1967.

(10) Rico, C. M.; Morales, M. I.; Barrios, A. C.; McCreary, R.; Hong, J.; Lee, W. Y.; Nunez, J.; Peralta-Videa, J. R.; Gardea-Torresdey, J. L. Effect of cerium oxide nanoparticles on the quality of rice (*Oryza sativa* L.) grains. *J. Agric. Food Chem.* **2013**, *61*, 11278−11285.

(11) Yoshida, S.; Forno, D. A.; Cock, J. H.; Gomez, K. A. *Laboratory Manual for Physiological Studies of Rice*; International Rice Research Institute: Los Baños, Laguna, Philippines, 1976.

(12) Anjum, F. M.; Ahmad, I.; Butt, M. S.; Sheikh, M. A.; Pasha, I. Amino acid composition of spring wheats and losses of lysine during chapati baking. *J. Food Compos. Anal.* **2005**, *18*, 523−532.

(13) Asekova, S.; Chae, J. H.; Ha, B. K.; Dhakal, K. H.; Chung, G.; Shannon, J. G.; Lee, J. D. Stability of elevated $\alpha$-linolenic acid derived from wild soybean (*Glycine soja* Sieb. & Zucc.) across environments. *Euphytica* **2014**, *195*, 409−418.

(14) Priester, J. H.; Ge, Y.; Mielke, R. E.; Horst, A. M.; Cole Moritz, S.; Espinosa, K.; Gelb, J.; Walker, S. L.; Nisbet, R. M.; An, Y. J.; Schimel, J. P.; Palmer, R. G.; Hernandez-Viezcas, J. A.; Zhao, L.; Gardea-Torresdey, J. L.; Holden, P. A. Soybean susceptibility to manufactured nanomaterials: evidence for food quality and soil fertility interruption. *Proc. Natl. Acad. Sci. U.S.A.* **2012**, *109*, E2451−E2456.

(15) Wang, Q.; Ma, X. M.; Zhang, W.; Pei, H. C.; Chen, Y. S. The impact of cerium oxide nanoparticles on tomato (*Solanum lycopersicum* L.) and its implications for food safety. *Metallomics* **2012**, *4*, 1105−1112.

(16) Zhao, L.; Peralta-Videa, J. R.; Rico, C. M.; Hernandez-Viezcas, J. A.; Sun, Y.; Niu, G.; Servin, A.; Nunez, J. E.; Duarte-Gardea, M.; Gardea-Torresdey, J. L. $CeO_2$ and ZnO nanoparticles change the nutritional qualities of cucumber (*Cucumis sativus*). *J. Agric. Food Chem.* **2014**, *62*, 2752−2759.

(17) Zhao, L.; Sun, Y.; Hernandez-Viezcas, J. A.; Servin, A. D.; Hong, J.; Niu, G.; Peralta-Videa, J. R.; Duarte-Gardea, M.; Gardea-Torresdey, J. L. Influence of $CeO_2$ and ZnO nanoparticles on cucumber physiological markers and bioaccumulation of Ce and Zn: A life cycle study. *J. Agric. Food Chem.* **2013**, *61*, 11945−11951.

(18) He, Y.; Wang, H.; Qian, B.; McConkey, B.; DePauw, R. How early can the seeding dates of spring wheat be under current and future climate in Saskatchewan, Canada? *PLoS One* **2012**, *7*, No. e45153.

(19) Peralta-Videa, J. R.; Hernandez-Viezcas, J. A.; Zhao, L.; Corral Diaz, B.; Ge, Y.; Priester, J. H.; Holden, P. A.; Gardea-Torresdedy, J. L. Cerium oxide and zinc oxide nanoparticles alter the nutritional value of soil cultivated soybean plants. *Plant Physiol. Biochem.* **2014**, *80*, 128−135.

(20) Hu, X.; Zhou, Q. Novel hydrated graphene ribbon unexpectedly promotes aged seed germination and root differentiation. *Sci. Rep.* **2014**, *4*, 3782.

(21) Arora, S.; Sharma, P.; Kumar, S.; Nayan, R.; Khanna, P. K.; Zaidi, M. G. H. Gold-nanoparticle induced enhancement in growth and seed yield of *Brassica juncea*. *Plant Growth Regul.* **2012**, *66*, 303−310.

(22) Liu, D.; Wang, X.; Lin, Y.; Chen, Z.; Xu, H.; Wang, L. The effects of cerium on the growth and some antioxidant metabolisms in rice seedlings. *Environ. Sci. Pollut. Res.* **2012**, *19*, 3282−3291.

nonadienal in fish oil enriched milk.[6] The volatiles (*Z*)-4-heptenal and (*E*,*Z*)-2,6-nonadienal have been associated with fishy off-flavors in oxidized fish oil.[7] One study concluded that the volatile secondary oxidation products (*E*,*Z*)-2,6-nonadienal, 1-penten-3-one, (*Z*)-4-heptenal, and (*E*,*E*)-2,4-heptadienal, while individually not responsible for fishy malodors, were the cause of fishy malodors as a result of a combinatory effect.[1] They did not include 1,5-octadien-3-one in their sensory descriptive experiments even though it had been previously reported as a potent odorant in fish oil because it was not detected in their fish oil enriched milk having a strong fishy off-flavor.

Researchers studying fish oil enriched mayonnaise concluded that the following ketones probably contribute to fishy malodors: 1-penten-3-one, (*E*)-3-penten-2-one, 3-heptanone, (*Z*)-1,5-octadien-3-one, 1-nonen-3-one, 2-nonanone, (*E*,*Z*)-3,5-octadien-2-one, and (*E*,*E*)-3,5-octadien-2-one.[4] Furthermore, they surmise that (*Z*)-1,5-octadien-3-one is probably the most potent fishy odorant due its extremely low threshold value (0.00003 mg/kg in oil) and characteristic geranium-like odor.[2]

While the most potent odorants associated with DHA and EPA oxidation have been identified, demonstration of correlation between their presence and concentration levels with fishy malodor development is lacking. Assuming that the most potent odorants are the cause of fishy malodor could be erroneous. Few if any GC-O supportive studies have investigated odorant synergy effects as the cause of fishy malodors.

GC-O is traditionally used to identify individual odor-active GC fractions. Potential synergy effects cannot be evaluated when single compounds are evaluated over time. Many synergistic effects are known to occur between single compounds in complex food matrices.[8] Combinations of single substances can produce enhancing or masking interactive effects. For example, researchers investigating the aging of beer reported a change in sensory perception of components when evaluated singularly versus when evaluated in combination. Specifically, (*E*)-2-nonenal was evaluated by panelists as cardboard-like and (*E*,*Z*)-2,6-nonadienal was perceived as cucumber-like when the single chemicals were subjected to GC-O. However, the combined effect of the two compounds generated a sweet fruity flavor perception distinctly different from the single substances alone.[8] The researchers concluded that the new sensory perception of the combination appeared to be related to both the absolute and relative concentrations of the two compounds.

Numerous sample preparation analytical techniques prior to GC-O have been applied to the analysis of fishy off-flavors, including dynamic headspace with Tenax GR trapping,[4,9] simultaneous steam-distillation-solvent extraction (SDE using a Likens−Nickerson apparatus),[10] solid-phase microextraction (SPME) using a Carboxen/PDMS fiber,[11] and static headspace.[12] Headspace sorptive extraction (HSSE) with 2 cm PDMS Twisters was used in the present study.[13]

Naude and Rohwer developed a novel GC-O approach to studying odorant synergy effects. In their method, sorptive extraction of aroma volatiles is accomplished using multichannel open tubular silicone (polydimethylsiloxane [PDMS]) rubber traps (MCTs) for fraction collection of aroma compounds.[14] GC peaks from milk samples were collected on MCTs that were fitted into the GC FID (FID and flame gases were turned off) for fraction collection purposes. Selection of peaks to trap was made on a carefully timed basis after preanalyzing samples to determine significant odorants. The captured chemicals on the MCT were transferred to an off-line portable heating device (with a nitrogen flow of 20 mL/min and a temperature of 130 or 160 °C).The aroma of the thermally released compounds could then be evaluated by panelists. As aroma eluted from the MCT, it was sniffed by a team of six evaluators. Using this approach, researchers determined that a synergistic combination of 2-heptanone and 2-nonanone was responsible for a pungent cheese, sour milk-like aroma detected in UHT milk. Interestingly, when smelled individually, 2-heptanone has a fruity-floral-soapy aroma and 2-nonanone has a fruity-sweet aroma.

In the present study, an olfactometry detector was used as a fraction collector to trap various peaks in marine oil chromatograms. The nose cone of the olfactometry detector was replaced with a Gerstel PDMS foam absorption tube at various precise times during GC analysis. Combinations of GC peaks were trapped on PDMS tubes, desorbed in a Gerstel thermal extractor (off-line) at 160 °C, and sniffed by aroma evaluators to determine the combined synergistic perception of mixtures of aroma compounds present in marine oil contaminated with fishy malodors.

This study was conducted to (1) determine which chemicals cause fishy malodors and (2) provide an analytical methodology for studying odor synergy effects.

## MATERIALS AND METHODS

**Experimental Design.** This study was divided into several experiments. Algal oils with varying degrees of fishy malodor were tested by GC-MS. Sample preparation techniques investigated included purge-and-trap, SPME, and HSSE GC-MS. HSSE was selected as the primary analytical technique because it had the highest sensitivity and provided excellent replicate determinations.

In the next step, GC-O experiments were performed on samples with strong fishy malodors. When no single peak was found to contribute fishy malodors, synergy effects between two or more odorants were investigated. First, all sample analytes were trapped on a PDMS foam trap, desorbed simultaneously with the Gerstel Thermal Desorber, and sniffed by panelists. A strong fishy odor was detected by the panel of sniffers, suggesting that odorant synergy effects could be responsible for the fishy malodor. Attempts were made to isolate the odorants responsible for the fishy malodor by trapping odorants in various regions of the chromatogram and then evaluating odor characteristics of the trapped volatiles after simultaneous desorption in the Thermal Desorber. Using this process, only two chemicals—heptanal and (*E*,*Z*)-3,5-octadien-2-one—when present in the trapped volatiles were found essential for generating fishy malodor. To confirm that these two odorants were all that was necessary to generate fishy malodor, only these two chemicals were trapped and subjected to sniffing with the thermal extractor. Omission experiments were also conducted. In omission experiments all volatiles in the chromatogram except heptanal and (*E*,*Z*)-3,5-octadien-2-one were trapped and then desorbed in the Thermal Desorber to see if the fishy odor was present.

Experiments were then conducted to confirm the identity of these two chemicals and to check for the possibility of coelution of contaminating peaks. Identification of (*E*,*Z*)-3,5-octadien-2-one is based on retention index values using a DB-5 column and olfactometry odor characteristics compared to literature results, as well as mass spectra (EI and CI). Accurate mass measurements for the (*E*,*Z*)-3,5-octadien-2-one peak were made using a high resolution time-of-flight mass spectrometer (Leco Pegasus GC-HRT).

**Marine Oil Samples.** Fermentor grown microalgae samples were processed to extract the DHA-rich oil. The finished commercial product is a clear, amber-colored oil rich in DHA. Six algal oil samples were analyzed (two with no fishy malodor and four with fishy malodor). A commercial microencapsulated powder version of the

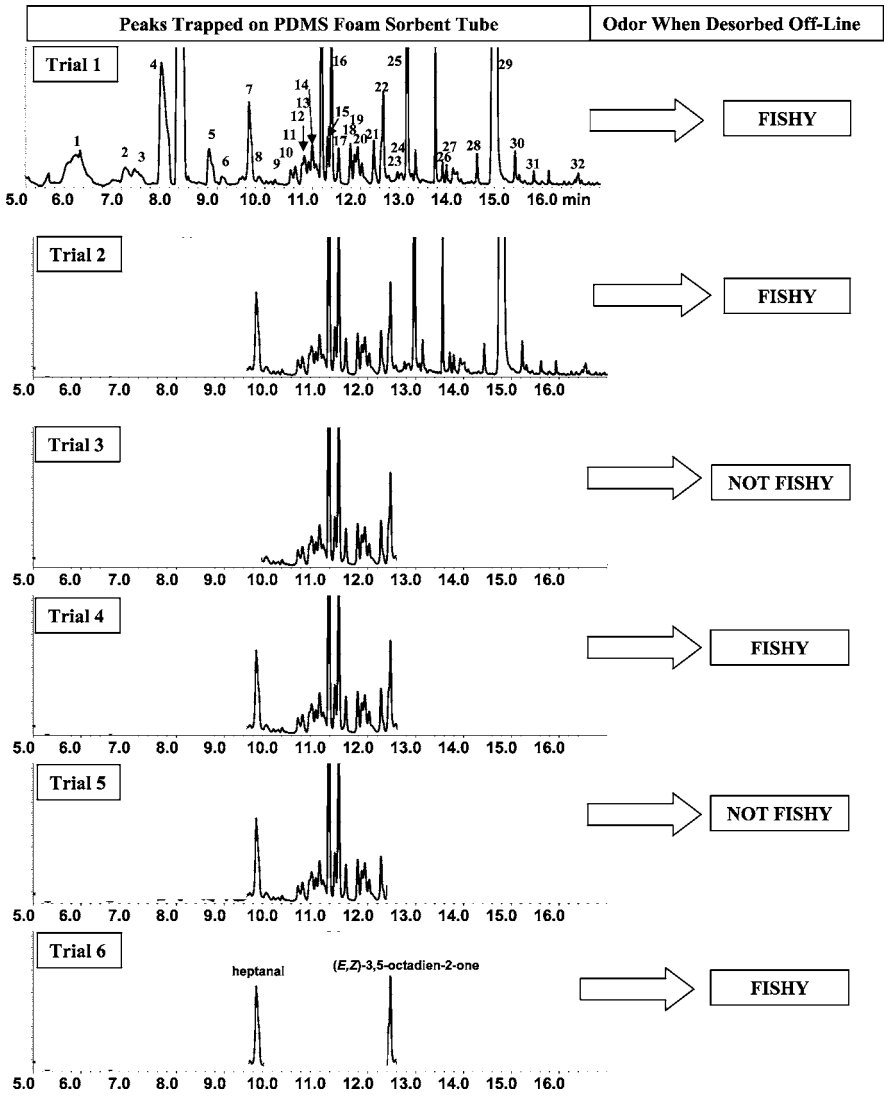


**Figure 1.** 2.00 g of marine oil extracted with 20 mm × df = 0.5 mm (47 $\mu$L) Twister stir bar (PDMS) in headspace for 2 h at 50 °C while stirring with Teflon-coated micro stir bar. The same sample was analyzed six times. Figure shows how peaks contributing to fishy malodor were isolated and identified. Off-line thermal desorption with a Gerstel thermal extractor was used for odor characterization. Peaks that are not numbered are background siloxane impurities in PDMS. Identity of numbered peaks and retention indices [in brackets] are as follows: (1) 1-penten-3-ol [682]; (2) 2-pentenal [750]; (3) 1-pentanol [767]; (4) hexanal [800]; (5) 2-hexenal [854]; (6) 1-hexanol [877]; (7) heptanal [901]; (8) 2,4-hexadienal [912]; (9) methylcyclohexane [933]; (10) 1,1-diethoxy-3-methylbutane [954]; (11) 2-heptenal [958]; (12) benzaldehyde [964] and 1-heptanol [967] coeluting; (13) 1-octen-3-one [970]; (14) 3,5,5,-trimethyl-1-hexene [975]; (15) (*E,Z*)-2,4-heptadienal [996]; (16) octanal [1004]; (17) (*E,E*)-2,4-heptadienal [1013]; (18) 2-ethyl-1-hexanol [1028]; (19) limonene [1030]; (20) eucalyptol [1032]; (21) 2-octenal [1063]; (22) 1-octanol [1074] and (*E,Z*)-3,5-octadien-2-one [1081] coeluting; (23) 2-nonanone [1090]; (24) (*E,E*)-3,5-octadien-2-one [1098]; (25) nonanal [1104]; (26) (*E,Z*)-2,6-nonadienal [1146]; (27) 2-nonenal [1150]; (28) decanal [1207]; (29) 2-ethylhexyl acrylate [1235]; (30) 2-decenal [1253]; (31) 2-undecanone [1291]; (32) 2-dodecenal [1469]. Reprinted with permission from ref 19. Copyright 2014 John Wiley & Sons Ltd.

DHA oil sample with a strong fishy malodor was also analyzed. The samples were sourced from a major supplier of DHA oils.

Algal oil is composed mainly of triglycerides. The composition is approximately 35−45% DHA and other triglycerides, including myristic acid (13−20%), palmitic acid (12−25%), oleic acid (10−25%), lauric acid (2−6%), and capric acid (1%). Heptanal, octanal, nonanal, decanal, 2-decenal, and 2-undecenal are formed from autoxidation of oleic acid, an *n*−9 monounsaturated fatty acid. The (*E,Z*)-3,5-octadien-2-one observed in the samples is derived from DHA oxidation.

**Chemicals.** Standards were obtained to assist in the identification of (*E,Z*)-3,5-octadien-2-one. A standard of (*E,E*)-3,5-octadien-2-one (CAS No. 30086-02-3) was purchased from Penta Manufacturing Company (Fairfield, NJ). A standard consisting of a mixture of (*E,E*)-3,5-octadien-2-one and (*E,Z*)-3,5-octadien-2-one (90% v/v and 10% v/v, respectively) was obtained as a gift from Allard Cossé, Crop Bioprotection Research Unit, USDA−ARS, Nat. Center for Agricultural Utilization Research (NCAUR), Peoria, IL. While this standard assisted in the identification of (*E,Z*)-3,5-octadien-2-one, it was not useful for conducting recombination/model system studies. Recombination studies, which involve spiking odorless control oils with odorant suspects, are frequently used for sensorial confirmation of which odorants are responsible for the odor of a product. Since (*E,Z*)-3,5-octadien-2-one was present in minor amounts compared to the major component of (*E,E*)-3,5-octadien-2-one, which has a strong geranium-like odor, the standard from Allard Cossé could not be used for recombination studies. A pure standard of (*E,Z*)-3,5-octadien-2-one was not commercially available.

**HSSE GC-MS Analysis.** Samples were analyzed by headspace sorptive extraction (HSSE) using the Gerstel Twister, length = 20 mm, df = 0.5 mm, 47 $\mu$L PDMS coating (Part No. 011444-001-00). Two grams of algal oil sample was placed in a 20 mL glass GC vial with a 10

Table 1. Olfactometry Results for Typical Algal Oil with Fishy Malodor[a]

| trial | region of chromatogram trapped (min) | odor characteristic | comment |
|---|---|---|---|
| T1 | 7.62−16.60 | fishy | fishy odorants trapped |
| T2 | 9.30−15.00 | fishy | fishy odorants trapped |
| T3 | 10.30−12.70 | not fishy | at least one contributor to fishy malodor excluded from trapping |
| T4 | 9.30−12.70 | fishy | heptanal suspected as contributor |
| T5 | 9.30−12.30 | not fishy | (*E*,*Z*)-3,5-octadien-2-one suspected as contributor |
| T6 | 9.30−9.75 and 12.35−12.50 | fishy | heptanal and (*E*,*Z*)-3,5-octadien-2-one confirmed contributors |
| T7 | 9.75−12.50 | not fishy | heptanal excluded; confirms heptanal as contributor |
| T8 | 9.30−12.35 | not fishy | (*E*,*Z*)-3,5-octadien-2-one excluded; confirms its contribution to fishy odor |

[a]Odor of combinations of chemicals evaluated off-line after trapping on PDMS foam followed by thermal desorption. Six evaluators used per test; all samples tested in triplicate.

mm Teflon coated micro stir bar. A paperclip was attached to the septum, and the Gerstel Twister was suspended from the paperclip in the headspace of the vial. The sample was heated to 50 °C. Extraction was continued for 2 h at 50 °C while the Teflon micro stir bar was stirred at 350 rpm; the Twister attached to the paperclip remained stationary. The Twister was then removed from the vial and subjected to thermal desorption using the Gerstel TDU. Samples were tested in triplicate.

Concentrations of the two oxidation products—heptanal and (*E*,*Z*)-3,5-octadien-2-one—were measured in samples using a method-of-additions HSSE technique. A nonfishy algal oil sample was spiked with varying levels of heptanal and (*E*,*Z*)-3,5-octadien-2-one to develop a standard calibration curve. Since a pure standard of (*E*,*Z*)-3,5-octadien-2-one was not available, the standard containing a mixture of 10% (v/v) (*E*,*Z*)-3,5-octadien-2-one and 90% (v/v) (*E*,*E*)-3,5-octadien-2-one was used for the calibration. Calibration curves were prepared by adding 0, 40, 100, 200, and 500 ppb heptanal ($R^2$ = 0.979) and 0, 4.8, 12, 23.9, and 60 ppb (*E*,*Z*)-3,5-octadien-2-one ($R^2$ = 0.969).

**Thermal Desorption Parameters.** The Gerstel cooled injection system (CIS), a programmed temperature vaporization (PTV) type inlet, was used in the solvent vent mode at 50 mL/min; cryofocusing was at −100 °C followed by heating at 12.0 °C/s to 280 °C and then holding at 280 °C for 3.00 min. The Gerstel cooled injection system (CIS) liner (Gerstel part number 012442-010-00) used was quartz wool. Gerstel TDU parameters were as follows: initial temperature was 30 °C, followed by heating at 60.0 °C/min to 280 °C and holding at 280 °C for 4.00 min.

**GC Parameters.** The column used was DB-5MS, 30 m × 0.25 mm × 0.25 μm (Agilent Technologies, catalog number 122-5532).The initial column temperature was 40 °C for 3 min, followed by heating at 10 °C/min to 270 °C for 3 min. Carrier gas flow was 1.0 mL/min through the column; the inlet was set to splitless mode. The flow was split 1:1 between the MS detector and the olfactometry detector. To check for possible coeluters, samples were reanalyzed on a Leco Pegasus HT GC-TOFMS instrument (sampling rate at 40 spectra/second) using the same method and GC conditions. The peak deconvolution capability of this instrument showed that 1-octanol tended to coelute on the front leading edge of the (*E*,*Z*)-3,5-octadien-2-one peak. Subsequent experiments showed that 1-octanol was not a contributor to the fishy odor. No other coelution of chemicals with heptanal or (*E*,*Z*)-3,5-octadien-2-one peaks was observed.

**Additional Dynamic Headspace Analyses.** Several samples were also analyzed by dynamic headspace GC-MS using either PDMS foam traps (Gerstel catalog number 013758-005-00) or Tenax TA traps (Gerstel catalog number 013741-005-00), both purchased from Gerstel. The PDMS foam traps, which can be heated up to 300 °C, were identical to those used to collect volatiles with the olfactometry detector (see Olfactometry Experiments). Two grams of algal oil and a Teflon stir bar (stirring at 350 rpm) were placed in a desorption tube with the sparging needle just above the surface of the oil. The dynamic headspace glassware was purchased from Scientific Instrument Services (Ringoes, NJ). The sample was heated to 50 °C for 20 min with a nitrogen purge gas flow rate of 50 mL/min. Results were not significantly different from HSSE results and are not reported here. The same TDU program as used for HSSE was used to desorb volatiles from the traps.

**Olfactometry Experiments.** All samples were subjected to GC-O experiments to assess odor quality and intensity of each individual peak. Four trained panelists, three females ages 24−35 years old and one male age 23, were used for GC-O experiments. The Gerstel ODP-3 was used at 160 °C. Panelists sniffed chromatogram effluents for the entire GC run time of the sample (29.0 min). Even though samples had a fishy malodor, none of the individual peaks shown in Figure 1 had a fishy smell. Studying synergistic olfactometry responses from combinations of odorants was more challenging. For example, the strategy used for collecting specific regions of the chromatogram is illustrated in Figure 1 and Table 1 (column titled "region of chromatogram trapped"). Initially (trial 1), all volatiles in the sample were trapped on a polydimethylsiloxane (PDMS) foam sorbent tube and desorbed off-line to characterize the odor of the entire sample. In trial 2, a wide swath of the chromatogram was trapped onto a PDMS tube. The PDMS foam trap is an open porous foam packing used for analyte trapping. PDMS strongly retains nonpolar analytes. The trap is then inserted into a Gerstel thermal extractor (off-line), which is preheated to 160 °C with a nitrogen flow gas at 50 mL/min. Evaluators (four) consecutively sniffed the effluent from the PDMS foam tube for 30 s after tube was placed in the thermal desorber to assess the overall odor impact (fishy or not fishy). If fishy aroma is not detected in the desorbed volatiles mixture but the algal oil sample has a fishy malodor, then the analytical method may not be trapping the analytes responsible for the fishy malodor and alternate sample preparation methods or traps should be considered. However, this was not the case. The "fishy" aroma was noted in all initial trials of complaint samples. The sample was reanalyzed (trial 3), but this time fewer chromatographic peaks were collected. If this sample fraction demonstrated a fishy aroma, then the sample was analyzed again with even fewer peaks collected. In this process, either the front or back end of the chromatogram was sequentially omitted from collection. This process continues until the sample sniffed at the thermal extractor shows no fishy odor, indicating that an important fishy odor contributor has not been captured. Monitoring the MS TIC trace on the computer screen during GC-MS analysis allows for accurate determination of times to attach and detach the PDMS tubes for trapping. To test the accuracy of the trapping technique to collect the desired peaks of interest, one PDMS tube was thermally desorbed after trapping only heptanal and (*E*,*Z*)-3,5-octadien-2-one and analyzed by GC-MS. Its chromatogram showed that the two major contributors to fishy malodor were indeed trapped with no significant background contamination from other peaks. When potential fishy odor causing candidates have been identified, only they are collected on the trap and desorbed off-line for aroma evaluation (trial 6). If the fishy odor is detected, these volatiles are confirmed as the cause of fishy odor development in the oil. Results are then confirmed in omission experiments: by reanalyzing the sample after all peaks are trapped except the ones suspected of causing the fishy odor.

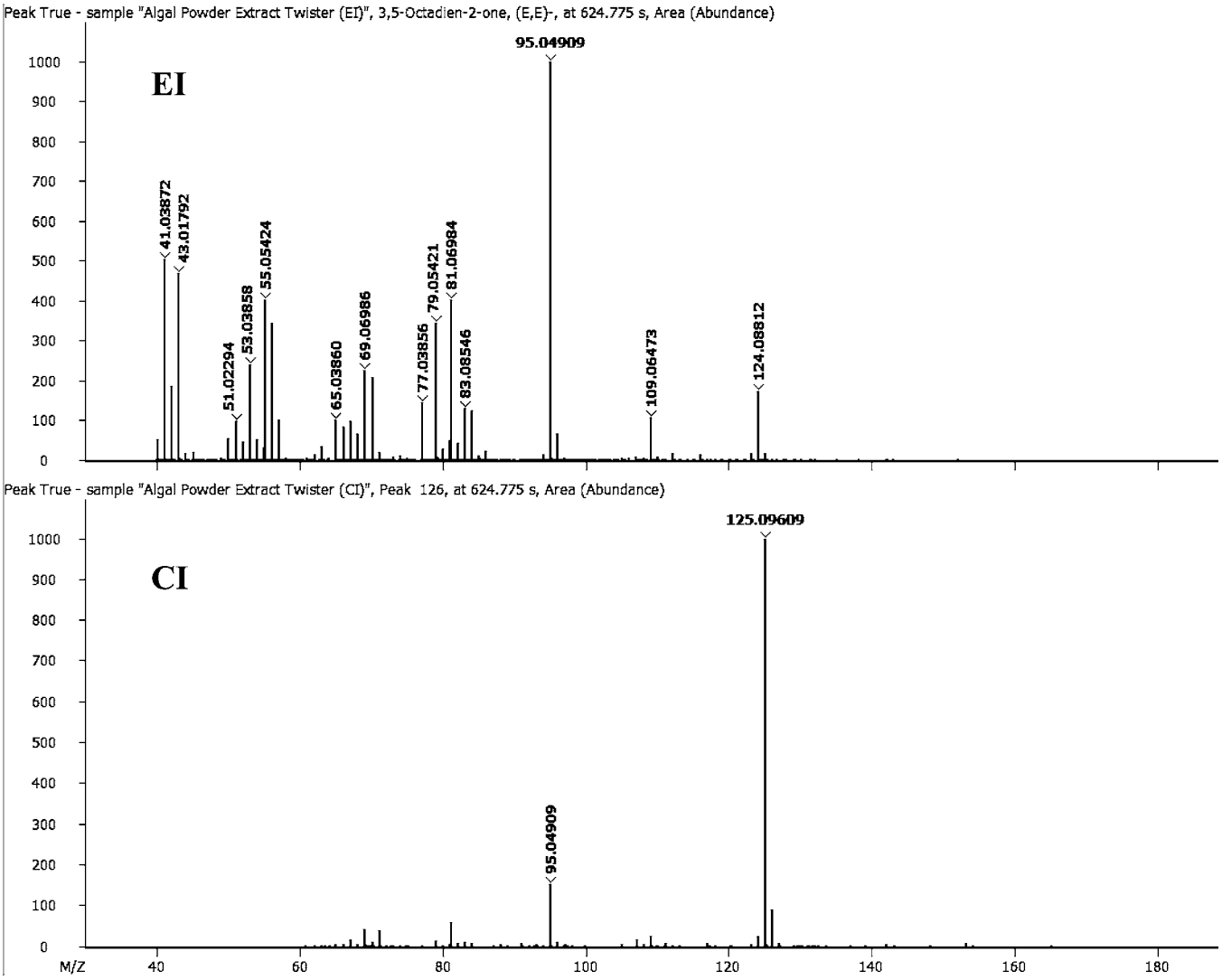


**EI results summary:**

| Name | Similarity | Expected Ion m/z | Observed Ion m/z | Formula | Mass Accuracy (ppm) |
|---|---|---|---|---|---|
| 3,5-Octadien-2-one, (E,E)- | 742 | 124.08827 | 124.08831 | C8H12O | 0.38 |

**CI results summary:**

| Species | Expected Ion m/z | Observed Ion m/z | Mass Accuracy (ppm) | Formula |
|---|---|---|---|---|
| H Gain | 125.09609 | 125.09609 | -0.007 | C8H12O |

**Figure 2.** EI and CI spectra for (*E*,*Z*)-3,5-octadien-2-one on Leco Pegasus GC-HRT.

## RESULTS AND DISCUSSION

A typical HSSE chromatogram of algal oil with a strong fishy aroma is shown in Figure 1 (trial 1). Approximately 32 significant odor-active peaks were detected. None of the chemicals in singularity imparts a fishy malodor to the sample, even though many have high odor activity values (OAVs), the ratio of the chemical concentration in the food to its threshold concentration in that food. No unusual chemicals were detected; most are expected lipid oxidation products that have been previously reported in algal oils. Recent research has shown that OAV measurements for predicting the perceived intensity of odorants and their contribution to their overall aroma are not good indicators of the actual sensory experience.[15]

As indicated in Figure 1 (trial 6) and Table 1, the combination of heptanal and (*E*,*Z*)-3,5-octadien-2-one when smelled together has been shown to cause fishy malodors. The results from olfactometry assessment show that the aromas of the individual oxidation products heptanal and (*E*,*Z*)-3,5-octadien-2-one are distinctly different from the aroma of the two compounds when evaluated in combination. With the off-line sniffing capability of the thermal extractor it is possible to use a team of several aroma evaluators for each sample that is thermally desorbed.

Using PDMS foam as the trapping medium is important because, like the MCTs used by Naude and Rohwer,[14] it has low in-line backpressure and does not cause peak shifting in


dx.doi.org/10.1021/jf502252q | J. Agric. Food Chem. 2014, 62, 9676−9682

chromatograms. Peak retention times when the PDMS trap is attached and when it is not attached are identical.

Identification of heptanal in samples is based on mass spectra (EI), rentention index (compared to pure heptanal standard using DB-5 column), and olfactometry odor characteristics compared to pure standard. Identification of (*E*,*Z*)-3,5-octadien-2-one is based on retention index values using a DB-5 column and olfactometry odor characteristics compared to literature results, as well as mass spectra (EI and CI). Accurate mass measurements for the (*E*,*Z*)-3,5-octadien-2-one peak were made using a high resolution time-of-flight mass spectrometer (Leco Pegasus GC-HRT). The EI spectrum for (*E*,*Z*)-3,5-octadien-2-one indicates the molecular ion at *m*/*z* 124.08831; the formula search indicated $C_8H_{12}O$ with a mass accuracy of 0.38 ppm. The CI spectrum for (*E*,*Z*)-3,5-octadien-2-one shows a strong protonated molecular ion at *m*/*z* 125.09609 that confirmed the molecular weight of the compound. The accurate mass measurement of the CI molecular ion also suggested $C_8H_{12}O$ with a mass accuracy of −0.007 ppm. Figure 2 shows accurate mass results and spectra. Instrument parameters for the Pegasus GC-HRT were as follows: mode, high resolution (*R* = 25,000); mass range, 40−400 *m*/*z* (EI), 60−510 *m*/*z* (CI); acquisition rate, 6 spectra/s; electron energy: −70 eV (EI), −140 eV (CI); and reagent gas for CI, 5% ammonia in methane at 0.8 mL/min.

Table 2 shows that concentrations of both heptanal and (*E*,*Z*)-3,5-octadien-2-one are higher in complaint fishy malodor samples compared to samples lacking the fishy aroma defect and tend to be highest in the most offensive sample (the DHA microencapsulated powder sample).

**Table 2. Concentrations of Heptanal and (*E*,*Z*)-3,5-Octadien-2-one in Algal Oil Samples with and without Fishy Malodor and DHA Powder with Strong Fishy Malodor[a]**

| sample description | heptanal (μg/kg) | (*E*,*Z*)-3,5-octadien-2-one (μg/kg) |
|---|---|---|
| oil #1a: not fishy | 1,715 | 6 |
| oil #2a: not fishy | 1,175 | 9 |
| oil #3a: medium fishy odor | 1,695 | 49 |
| oil #3b: medium fishy odor | 2,025 | 115 |
| oil #4a: medium fishy odor | 5,141 | 58 |
| oil #4b: strong fishy odor | 3,260 | 246 |
| DHA microencapsulated powder: strongest fishy odor | 10,226 | 3,127 |

[a]Samples analyzed by HSSE GC-MS. Method-of-additions calibration used.

Octanol, which tended to coelute on the front end of the (*E*,*Z*)-3,5-octadien-2-one peak with the chromatographic conditions used, was investigated as a potential contributor to fishy malodor; it did not make a significant impact on fishy malodor. (*E*,*E*)-3,5-Octadien-2-one and chemicals other than heptanal and (*E*,*Z*)-3,5-octadien-2-one did not contribute significantly to the fishy malodor.

Future studies will involve synthesizing (*E*,*Z*)-3,5-octadien-2-one in order to use it along with heptanal in recombination/model system studies to assess odor threshold levels required to generate fishy malodors in marine oils. Model system studies have been shown to be highly beneficial for studying combinations of odorants in food products.[16,17]

Synergy effects can impart unexpected and potent aroma changes to foods. For example, synergy can either enhance or diminish a food's perceived aroma. Even more remarkably, it can result in the emergence of a strikingly different sensory perception, completely unrelated to that of the individual compounds alone.

While GC-O experiments have resolved numerous flavor and off-flavor issues in the past, the limitations of methods that only assess odor contribution from individual components need to be reconsidered. Odorant behavior in mixtures demands more studying. Studying synergy effects in olfactometry experiments should be a significant future trend. GC-O experiments are useful for determining which aroma compounds most likely make a contribution to the odor of a food. However, these experiments should be supplemented with sensory work and olfactometric synergy studies.

When traditional GC-O experiments fail to detect the malodor present in the food sample, the researcher should attempt to determine if (1) the analytical sample preparation method is not collecting/trapping the offending odorant; (2) the offending odorant is being trapped efficiently but its concentration level is below the detection threshold of the analytical (MS) detector; (3) the offending odorant is being extracted from the sample but is thermally labile and is decomposing in the injector; or (4) the perceived malodor of the sample is due to odorant synergy effects related to smelling two or more odorants in combination.

An analytical technique for studying odorant synergy effects has been presented as well as an example of how it can be applied. Heptanal and (*E*,*Z*)-3,5-octadien-2-one appear to be significant contributors to fishy malodor in algal oils. It is possible that some additional higher boiling point compounds, not isolated in our methods, could contribute to fishy malodor as has been recently reported.[18] However, according to our present study, these higher molecular weight compounds do not appear to be as significant to fishy off-flavor as heptanal and (*E*,*Z*)-3,5-octadien-2-one, since simple headspace extractions by HSSE and SPME at relatively low temperature (50 °C) were shown to extract strong fishy odors from all samples. This article provides more details of the analytical methods and techniques used to identify odorants in our previous algal oil research.[19] Confirmation of the roles of heptanal and (*E*,*Z*)-3,5-octadien-2-one in causing fishy odors should be conducted using sensory paneling of odorless oil samples spiked with pure standards of these compounds.

## AUTHOR INFORMATION

### Corresponding Author

*E-mail: rtmarsili@gmail.com.

### Notes

The authors declare no competing financial interest.

## REFERENCES

(1) Venkateshwarlu, G.; Let, M. B.; Meyer, A. S.; Jocobsen, C. Modeling the sensory impact of defined combination of volatile lipid oxidation products on fishy and metallic off-flavors. *J. Agric. Food. Chem.* **2004**, *52*, 1635−1641.

(2) Venkateshwarlu, G.; Let, M. B.; Meyer, A. S.; Jacobsen, C. Chemical and olfactometric characterization of volatile flavor compounds in a fish oil enriched milk emulsion. *J. Agric. Food Chem.* **2004**, *52*, 311−317.

(3) Grosch, W. Low-MW products of hydroperoxide reactions. 1987. In *Autoxidation of Unsaturated Lipids*; Chan, H. W. S., Ed.; Academic Press: London, U.K., 1987; pp 95−139.

(4) Hartvigsen, K.; Lund, P.; Hansen, L. F.; Hølmer, G. Dynamic headspace gas chromatography/mass spectrometry characterization of

volatiles produced in fish oil enriched mayonnaise during storage. *J. Agric. Food Chem.* **2000**, *48*, 4858−4867.
(5) Jacobsen, C. Sensory impact of lipid oxidation in complex food systems. *Fett/Lipid* **1999**, *101*, 484−492.
(6) Let, M. B.; Jacobsen, C.; Frankel, E. N.; Meyer, A. S. Oxidative flavour deterioration of fish oil enriched milk. *Eur. J. Lipid Sci. Technol.* **2003**, *105*, 518−528.
(7) Karahadian, C.; Lindsay, R. C. Evaluation of compounds contributing characterizing fishy flavors in fish oils. *J. Am. Oil. Chem. Soc.* **1989**, *66*, 953−960.
(8) Hermann, M. B.; Klotzbucher, B.; Wurzbzcher, M. A new validation of relevant substances for the evaluation of beer aging depending on the employed boiling system. *J. Inst. Brewing* **2010**, *116* (1), 41−48.
(9) Refsgaard, H. H. F.; Haahr, A. M.; Jensen, B. Isolation and quantification of volatiles in fish by dynamic headspace sampling and mass spectrometry. *J. Agric. Food. Chem.* **1999**, *47*, 1114−1118.
(10) Le Guen, S.; Prost, C.; Demaimay, M. Critical comparison of three olfactometric methods for the identification of the most potent odorants in cooked mussels (*Mytilus edulis*). *J. Agric. Food Chem.* **2000**, *48*, 1307−1314.
(11) Shen, Z.; Mann, M. A.; Sanguansri, L.; Cheng, L. J. Oxidative stability of microencapsulated fish oil powders stabilized by blends of chitosan, modified starch, and glucose. *J. Agric. Food Chem.* **2010**, *58*, 4487−4493.
(12) Milo, C.; Grosch, W. Detection of odor defects in boiled cod and trout by gas chromatography-olfactometry of headspace samples. *J. Agric. Food Chem.* **1995**, *43*, 459−462.
(13) Marsili, R. Analysis of musty microbial metabolites by stir bar sorptive extraction. In *Flavor, Fragrance and Odor Analysis*, 2nd ed.; Marsili, R., Ed.; CRC Press: Boca Raton, FL, 2012; pp 63−91.
(14) Naude, Y.; Rohwer, E. R. The olfactometric analysis of milk volatiles using a novel gas-chromatography-based method: A case study in synergistic perception of aroma compounds. In *Flavor, Fragrance and Odor Analysis*, 2nd ed.; Marsili, R., Ed.; CRC Press: Boca Raton, FL, 2012; pp 93−110.
(15) Audouin, V.; Florence, B.; Vickers, Z. M.; Reineccius, G. A. Limitations in the use of odor activity values to determine important odorants in foods. In *Gas Chromatography-Olfactometry: The State of the Art*; Leland, J. V., Schieberle, P., Buettner, A., Acree, T. E., Eds.; American Chemical Society: Washington, DC, 2001; pp 156−171.
(16) Marsili, R.; Miller, N.; Kilmer, G. J.; Simmons, R.E. Identification and quantitation of the primary chemicals responsible for the characteristic malodor of beet sugar by purge and trap GC-MS-OD techniques. *J. Chromatogr. Sci.* **1994**, *32*, 165−171.
(17) Marsili, R. T.; Miller, N. Determination of major aroma impact compounds in fermented cucumbers by solid-phase microextraction-gas chromatography-mass spectrometry-olfactometry detection. *J. Chromatogr. Sci.* **2000**, *18*, 307−314.
(18) Hammer, M.; Schieberle, P. Model studies on the key aroma compounds formed by an oxidative degradation of omega-3 fatty acids initiated by either copper(II) Ions or lipoxygenase. *J. Agric. Food Chem.* **2013**, *61* (46), 10891−10900.
(19) Marsili, R. T.; Laskonis, C. The importance of odourant synergy effects in understanding malodour problems in DHA and EPA products. *Lipid Technology* **2014**, *26* (2), 31−34.

relatively expensive. Therefore, the development of effective extraction methods is critical for the quality control of NPTs while minimizing the environmental impact.

With the improvement of living conditions and economic development, the incidence of cardiovascular disease increases dramatically. There is therefore increased emphasis on prevention since the disease is the leading cause of death in many countries. Danshen (DS), also known as *Salvia miltiorrhiza* and derived from the dried root or rhizome of *Salvia miltiorrhiza* Bge, is one of the most popular traditional herbal medicines and has been widely used for the treatment of angina pectoris, myocardial infarction, dysmenorrhea, insomnia, and bacterial infections.[20] Danshen tea (DST), refined from *Salvia miltiorrhiza* and green tea, is a new type of health care product for the prevention and treatment of coronary heart disease and hyperlipidemia. Tanshinone capsules (TC) made from the extracts of *Salvia miltiorrhiza* are one of the most widely used plant preparations and have antibiotic and anti-inflammation functions. These DS products are now experiencing a particularly strong and rapid demand in China, Japan, the United States, and many European countries for treatment and prevention of cardiovascular and cerebrovascular system disorders. Numerous bioactive compounds, mainly including soluble phenolic acids and lipophilic tanshinones, have been isolated from *Salvia miltiorrhiza*. Among them, tanshinones, including dihydrotanshinone I, tanshinone I, cryptotanshinone, and tanshinone IIA, are gaining popularity because of their significant pharmacological activities such as dilating coronary artery, activating blood circulation, and preventing myocardial ischemia.[21−23] Therefore, extraction and quantitative determination of tanshinones are important for physiological and pharmacological studies.

In this study, a novel extraction technique, D-$\mu$-SPE, involving the use of MHM as the sorbent was evaluated for the extraction of semivolatile compounds (dihydrotanshinone I, tanshinone I, cryptotanshinone, and tanshinone IIA). The parameters affecting the extraction, such as mesoporous concentration, extraction time, sample agitation, and desorption solvents, were systematically studied and evaluated. The optimized microextraction methodology combined with ultra-high-performance liquid chromatography coupled with quadrupole time-of-flight tandem mass spectrometry (UHPLC-Q-TOF/MS) was then successfully applied to the determination of tanshinones in complex NPTs.

## MATERIALS AND METHODS

**Reagents and Materials.** HPLC grade hexane, ethanol, acetonitrile, acetone, and methanol were purchased from Sigma-Aldrich (St. Louis, MO). The dihydrotanshinone I, tanshinone I, cryptotanshinone, and tanshinone IIA standards were obtained from Winherb Medical Technology Co., Ltd. (Shanghai, China) (purity higher than 98%). The structures of these compounds are shown in Figure 1. Stock standard solutions for each of the analytes were prepared in methanol at a concentration of 0.5 $\mu$g/mL and were stored at 4 °C. The 0.45 $\mu$m disposable nylon filters were purchased from Anpel Scientific Instrument Co., Ltd. (Shanghai, China). Ultrapure water was produced using a Milli-Q (Millipore, Billerica, MA) water purification system. All tested samples, including DST, DS, and TC, were purchased from a local drugstore (Hangzhou, China). All other chemicals used were of analytical grade (Anpel Scientific Instrument Co., Ltd.) and were used as received without further purification.

**Apparatus.** The UHPLC instrument was an Agilent 1290 Series (Agilent Technologies, Santa Clara, CA), consisting of a binary pump, an autosampler, and a thermostated column compartment. Chromatographic separation was performed at a flow rate of 400 $\mu$L/min using

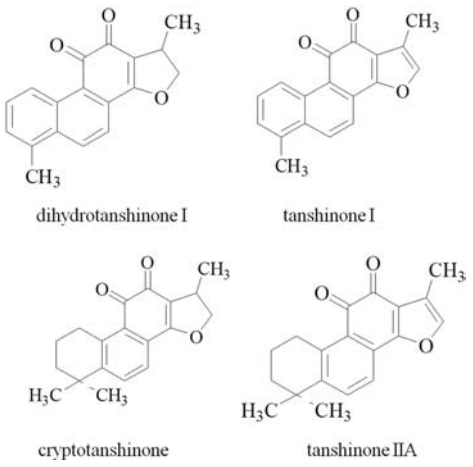


**Figure 1.** Chemical structures of the four tanshinones.

an Agilent Zorbax SB-$C_{18}$ column (1.8 $\mu$m, 2.1 mm i.d. × 50 mm) maintained at 30 °C. Mobile phases A and B were 0.1% formic acid in water and methanol, respectively, and were applied according to the following gradient: 0−1 min, 10−30% B; 1−2 min, 30−50% B; 2−6 min, 50−70% B; and 6−7 min, 70−100% B. The injection volume was 2 $\mu$L for the standards and sample extracts.

The UHPLC system was connected to an accurate mass Q-TOF instrument (Agilent Technologies, Santa Clara, CA) equipped with a Dual ESI ion source. Accurate product ion scan (MS/MS) spectra were acquired in the range of $m/z$ values from 100 to 1000 units, and compounds were ionized in positive ESI by applying a capillary voltage of 3500 V. The other experimental parameters were as follows: drying gas temperature, 350 °C; drying gas flow, 12 L/min; nebulizer, 45 psi; fragmentor, 175 V; skimmer voltage, 65 V; and octapole RFPeak, 750 V. Selective UHPLC−MS and UHPLC−MS/MS chromatograms were extracted with a mass window of 0.01 Da around the $[M + H]^+$ and the most intense product ion of each tanshinone, respectively. The Mass Hunter Workstation software (version B 05.00) was used to control the system and process the obtained data.

**Preparation of Mesoporous Hybrid Materials.** The MHM was obtained by following a previously optimized procedure.[24] Briefly, 1.0 g of [3-(trimethoxysilyl)propyl]-octadecyldimethylammonium chloride was mixed with 28.0 g of deionized water, 4.10 g of tetraethyl orthosilicate, and 0.60 g of 1,3,5-trimethylbenzene under vigorous stirring at room temperature for 15 min. Then, 3.0 g of (2.0 M) NaOH solution was added to the translucent mixture. The mixture was stirred for 2 h at 25 °C, transferred into a hydrothermal bomb, and treated at 110 °C for 24 h. Finally, the obtained precipitate was filtered, washed with 200 mL of ethanol and 50 mL of acetone, and then vacuum-dried at 60 °C overnight to obtain a fine powder.

**Sample Preparation.** A 0.3 g sample of the dried powder (DST, DS, or TC) was accurately weighed and extracted with 50 mL of hot water in an ultrasonic bath for 5 min. After cooling, the solution was centrifuged at 15 000 rpm for 5 min before being subjected to the D-$\mu$-SPE process.

**Extraction Procedures.** An accurately weighed 2 mg aliquot of pristine MHM, added in 10 mL of Milli-Q water, was ultrasonicated (100 W, 40 Hz) for 20 min. Subsequently, the mixture was agitated using a vortex for 2 min to facilitate the dispersion of the material. The experimental setup of the D-$\mu$-SPE extraction is illustrated in Figure 2. Briefly, 10 mL of the aqueous samples containing four tanshinones at a concentration within the quantification linear range was first placed in a 25 mL glass vial. After that, 1 mL of MHM dispersion at a final concentration of 0.02 g/L was quickly added to the vial, and the mixture was agitated at 3200 rpm for 2 min using an orbital shaker. Then, the MHM concentrated with the analytes was recovered by filtration on a 0.45 $\mu$m disposable nylon filter, which was previously cleaned with 3 mL of methanol and 3 mL of ultrapure water to remove any possible contamination. Finally, the analytes were desorbed by


dx.doi.org/10.1021/jf5029625 | J. Agric. Food Chem. 2014, 62, 9683−9689

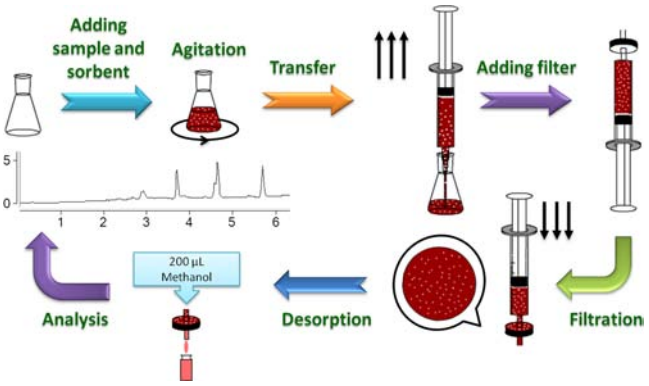


**Figure 2.** Schematic procedure of MHM D-$\mu$-SPE. For details, see text.

passing 200 $\mu$L of methanol through the nylon filter, and 2 $\mu$L was injected into the UHPLC-Q-TOF/MS for identification and quantification of the tanshinones.

**Validation Procedure.** The calibration samples were prepared using the described D-$\mu$-SPE procedure in the range from 0.25 to 100 ng/mL. Five concentrations of the four analytes' solution were extracted in triplicate, and then the calibration curves were constructed by plotting the mean peak areas versus the concentrations of target analytes. Intra- and interday variations, expressed by the relative standard deviations (RSD), were chosen to determine the precision of the proposed method. For intraday precision, the mixed standards solution was analyzed for six replicates on the same day, while, for interday precision, the solution was examined in duplicates for consecutive 3 days. The extraction solution containing 4 reference compounds was diluted to a series of appropriate concentrations, and an aliquot of the diluted solutions was injected into UHPLC-Q-TOF/MS for analysis. The limits of detection (LODs) and quantification (LOQs) under the optimal chromatographic conditions were calculated on the basis of peak areas at a signal-to-noise of 3 and 10, respectively. Recovery test was used to evaluate the accuracy of D-$\mu$-SPE method. The recoveries of four analytes were calculated by the following formula: recovery (%) = 100 × (amount found − original amount)/amount spiked. Table 1 shows the results of four analytes.

## RESULTS AND DISCUSSION

**Optimization of D-$\mu$-SPE Process.** The main parameters affecting the D-$\mu$-SPE process, namely, the mesoporous concentration, extraction time, sample agitation, and desorption solvents, were optimized to obtain optimum performance of the mesoporous D-$\mu$-SPE procedure. A 10 mL water sample containing 25 ng/mL of each tanshinone was used for the optimization experiments.

**Effect of the Mesoporous Concentration.** Previous studies have demonstrated the applicability of nanometric sorbent materials in D-$\mu$-SPE for the isolation and preconcentration of aromatic compounds from water samples, taking into account their higher surface areas.[14] In this study, the usefulness of MHM for the extraction of semivolatile compounds, such as tanshinones, was evaluated. The addition of MHM was expected to enhance the extraction efficiency of D-$\mu$-SPE because the material was different from that of the bulk counterparts due to the higher surface area and pore volume. Hence, the effect of adding MHM in microextraction, ranging from 0.01 to 0.04 (g/L) in the extraction phase, was studied. According to the obtained results (Figure 3), the peak areas of target analytes (25 ng/mL) were highest when 0.02 g/L MHM was used. The presence of MHM in sample solution resulted in an increase in the sensitivity of the analytes. This may be due to the increase in the interaction between the analytes and the sorbent surface following the addition of the appropriate sorbent material, thereby enhancing the mass transfer process. From the results shown in Figure 3, it is clear that the extraction efficiencies gradually decreased as the concentration of MHM increased from 0.02 to 0.04 (g/L). The possible reason for this observation was that the higher concentration of MHM increased the aggregation of the mesoporous material, which effectively reduced the surface available for analytes interaction. Finally, the proposed method permitted the use of a relatively small concentration of adsorbent (0.02 g/L) to ensure complete desorption of analytes from MHM by agitation, compared with other D-$\mu$-SPE (0.2 g/L) in the

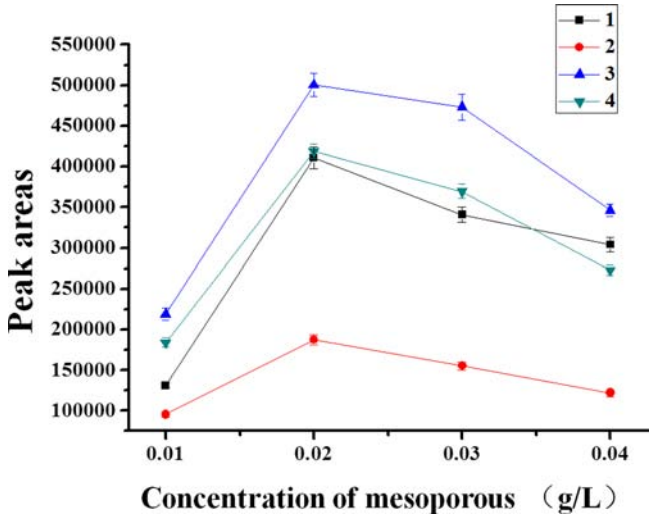


**Figure 3.** Effect of the MHM concentration (0.01−0.04 g/L) on the chromatographic peak areas of the selected tanshinones. Sample concentration: 25 ng/mL. Analytes: (1) dihydrotanshinone I, (2) tanshinone I, (3) cryptotanshinone, and (4) tanshinone IIA.

**Table 1. Linearity, Precision, and Limits of Detection (LODs) and Quantification (LOQs) of the Developed D-$\mu$-SPE Method**

| | | | | precision (RSD) | | | | | | |
|---|---|---|---|---|---|---|---|---|---|---|
| | | | | intraday ($n$ = 6) | | interday (3 days) | | LODs (pg) | | LOQs (pg) |
| analytes | regression eq | linear range (ng/mL) | $r^2$ | time | areas | time | areas | ultrasonic method[21] | proposed method | proposed method |
| dihydrotanshinone I | $y$ = 20 061$x$ + 9017 | 0.50−50.00 | 0.9990 | 0.14 | 2.60 | 0.44 | 4.17 | 10 | 0.026 | 0.083 |
| tanshinone I | $y$ = 9423$x$ + 2342 | 1.00−100.00 | 0.9991 | 0.16 | 2.23 | 0.91 | 5.51 | 22 | 0.046 | 0.153 |
| cryptotanshinone | $y$ = 63 401$x$ − 1911 | 0.25−25.00 | 0.9980 | 0.25 | 3.34 | 0.66 | 3.98 | 4 | 0.012 | 0.040 |
| tanshinone IIA | $y$ = 39 097$x$ − 8249 | 0.40−40.00 | 0.9995 | 0.13 | 2.51 | 0.78 | 6.11 | 8 | 0.022 | 0.070 |


dx.doi.org/10.1021/jf5029625 | J. Agric. Food Chem. 2014, 62, 9683−9689

literature.[14,15] Therefore, MHM at a concentration of 0.02 g/L was chosen for the following experiments.

**Effect of the Extraction Time.** Like SPME, D-$\mu$-SPE involves dynamic partitioning of analytes to the sorbent. The extraction efficiency depends on the mass transfer between the MHM and the sample solution. Because mass transfer was a time-dependent process, the effect of the extraction time was investigated in the range 1−32 min. The sample solution was continuously agitated at room temperature with an orbital shaker to facilitate the mass transfer process, and the agitation speed was fixed at 3200 rpm. The results are shown in Figure 4.

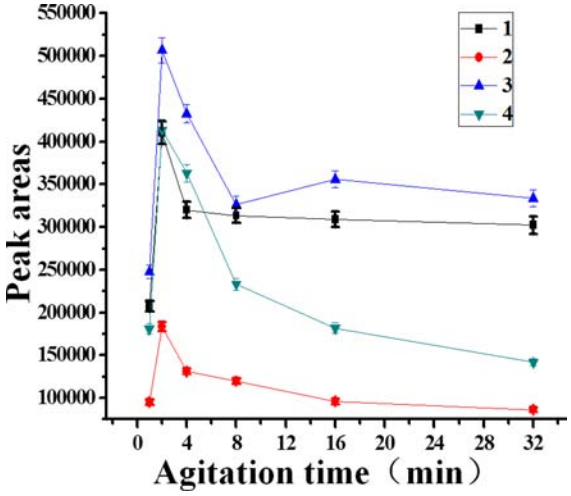


**Figure 4.** Effect of the agitation time (1, 2, 4, 8, 16, and 32 min) on the chromatographic peak areas of the selected tanshinones. Analytes: (1) dihydrotanshinone I, (2) tanshinone I, (3) cryptotanshinone, and (4) tanshinone IIA.

The highest extraction was achieved at 2 min, and after more than 2 min, a considerable decrease in the peak area response was observed for all of the target analytes. The results indicated that, at the given conditions, initial partitioning was rapid, followed by a protracted uptake; eventually, a steady state was reached at 16 min, except for dihydrotanshinone I. For dihydrotanshinone I, when the extraction time was increased from 4 to 32 min, the extraction profile remained flat, implying that the adsorption of the analyte was very efficient. Therefore, in this work, 2 min was chosen as the optimum extraction time.

**Form of Sample Agitation.** Sample agitation played an important role as an assisting factor in the D-$\mu$-SPE process and affected the mass transfer rates of the tested solutes.[15] Three alternatives for sample agitation (magnetic stirring, ultrasound and orbital shaking) were tested in the extraction step. Figure 5 compares the extraction performance of the three modes when samples spiked with 25 ng/mL tanshinones were extracted with 1 mL of mesoporous suspension with an extraction time of 2 min at room temperature (25 °C). The extraction efficiency of magnetic stirring was significantly lower than that of the other two methods, possibly because the MHM was lost as a result of its deposition on the magnetic bar, which reduced the extraction yield of the target analytes. Moreover, for the extraction yields of the four tanshinones, sonication was higher than magnetic stirring but lower than orbital shaking. The obtained results showed that the use of sonication significantly decreased the extraction affinity for the compounds of interest, leading to a low analytical response. Thus, the orbital shaker was chosen for the subsequent experiments because it provided

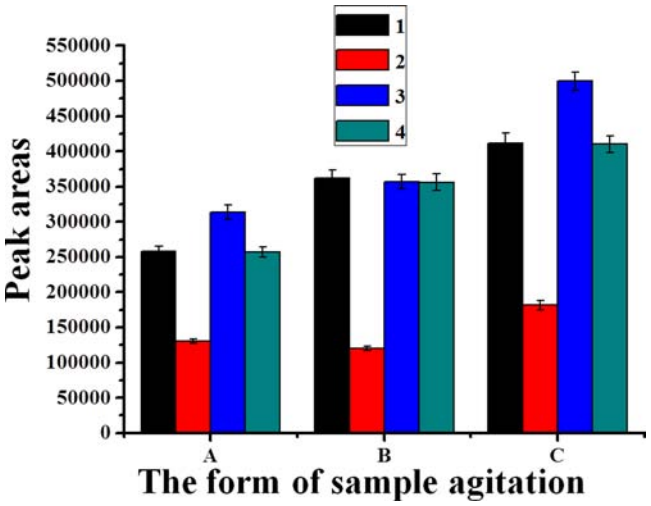


**Figure 5.** Effect of the form of sample agitation on the chromatographic peak areas of the selected tanshinones. (A) magnetic stirring, (B) ultrasound, and (C) orbital shaker. Analytes: (1) dihydrotanshinone I, (2) tanshinone I, (3) cryptotanshinone, and (4) tanshinone IIA.

a vigorous stirring of the analytes and extractant, favoring interactions of the MHM and sample.

**Effect of Desorption Solvents.** The tested tanshinones are relatively hydrophobic and are not easily eluted. Thus, a suitable organic solvent was needed for the desorption process to achieve optimum extraction performance.[25] For this purpose, five solvents, including hexane, ethanol, acetonitrile, acetone, and methanol, were investigated for their suitability as desorption solvents, with the volume fixed at 200 $\mu$L in all instances. Figure 6 shows the influence of the desorption

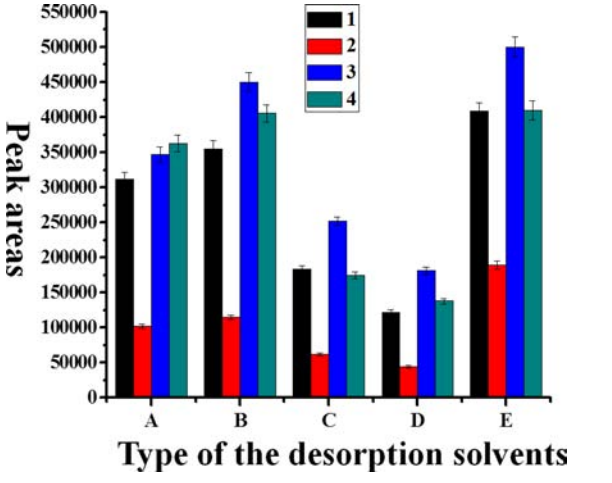


**Figure 6.** Effect of the desorption solvents on the chromatographic peak areas of the selected tanshinones: (A) hexane, (B) ethanol, (C) acetonitrile, (D) acetone, and (E) methanol. Analytes: (1) dihydrotanshinone I, (2) tanshinone I, (3) cryptotanshinone, and (4) tanshinone IIA.

capabilities of these solvents in D-$\mu$-SPE. For all of the tanshinones, methanol offered the highest desorption efficiency, whereas acetone showed the smallest peak areas under the same extraction and elution conditions. The results also indicated that the greater solubility of target compounds in desorption solvents resulted in higher elution performance in


dx.doi.org/10.1021/jf5029625 | J. Agric. Food Chem. 2014, 62, 9683−9689

terms of chromatographic peak areas from the MHM after extraction. Hence, methanol was selected as the optimal desorption solvent.

The suitable volume of methanol used for desorption was also determined to be between 100 and 400 μL. As seen from Figure 7, a small volume (100 μL) of desorption solvent gave

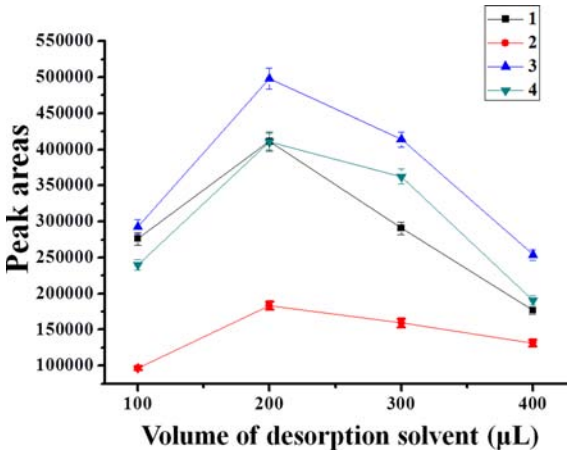


**Figure 7.** Effect of the volume of desorption solvent (100−400 μL) on the chromatographic peak areas of the selected tanshinones. Analytes: (1) dihydrotanshinone I, (2) tanshinone I, (3) cryptotanshinone, and (4) tanshinone IIA.

low peak areas with poor reproducibility. A volume of 200 μL of methanol was found to be sufficient to completely desorb the analytes from the filter containing functionalized mesoporous material. When the volume of methanol was increased from 200 to 400 μL, a considerable decrease in the peak areas for all of the analytes was observed. This phenomenon was due to the dilution of the analytes in the eluent with increasing volume of desorption solvent. To test the carryover effects, the extraction device was further eluted after the first desorption with the above conditions. No analytes remained on the filter in the second desorption using nylon filters with a 0.45 μm pore size. Consequently, 200 μL of methanol was chosen as the optimum volume.

**Analytical Figures of Merit.** The D-μ-SPE method was evaluated by characterizing its analytical performance in terms of linearity, precision, and limits of detection (LODs) at the optimized working conditions determined earlier (i.e., extractant phase, MHM; sample volume, 11 mL; agitation time, 2 min; desorption solvent, methanol). The obtained results are listed in Table 1. The linearity of the method was tested over a range 0.5−50, 1−100, 0.25−25, or 0.4−40 ng/mL, depending on target analytes. The calibration plots of each analyte prepared at five concentration levels were linear, with correlation coefficients ($r^2$) between 0.9980 and 0.9995. The precision of the method was evaluated by calculating the intraday and interday repeatabilities from four individual standards prepared at a concentration of 5 ng/mL. The results obtained are listed in Table 1 as the relative standard deviation (RSD); they ranged from 0.13% to 3.34% ($n$ = 6) for intraday precision and were lower than 6.11% for interday precision in 3 consecutive days. The LODs and LOQs for the tanshinones ranged from 0.012 to 0.046 pg and from 0.040 to 0.153 pg. This resulted in a 334- to 478-fold improvement in the LODs relative to the conventional method, illustrating the better sensitivity achieved by the proposed procedure.

**Application to Real Samples.** Under the indicated extraction and UHPLC-Q-TOF/MS conditions, the proposed D-μ-SPE method was applied to the identification and quantification of four tanshinones in real samples, such as DST, DS, and TC. The results are shown in Table 2. The target components in the samples were identified by matching their retention times and were confirmed by comparing the MS/MS spectra with those of the corresponding standards. Figure 8 shows the MS spectra of tanshinones in the positive ion mode. The accurate protonated molecule $[M + H]^+$ was selected as the precursor ion for CID fragmentation to produce MS/MS product ion spectra. The results showed that all compounds could be detected in all samples (Table 2). However, the contents of these four major compounds varied among three samples. The contents of four active compounds in the DST were much lower than those in the DS and TC. All of the real samples were spiked with the four hydrophobic standard solutions at different concentration levels to evaluate the analyte recovery and matrix effects. The recovery values were 89−102% for DS, 88−96% for TC, and 91−103% for DST, which indicated that the present method was effective for the determination of tanshinones in plant samples. Additionally, the developed D-μ-SPE showed a reduction in extraction time (12 min) when compared to a traditional ultrasonic method (80 min).[21]

In conclusion, an MHM-based D-μ-SPE technique, in conjunction with UHPLC-Q-TOF/MS, was developed in this report. After optimization of the experimental conditions affecting the D-μ-SPE procedure, the sorbent capacity of MHM was tested in plant samples from different sources (DST, DS, TC), yielding satisfactory results for the recovery values and in terms of linearity, precision, and LODs. Most importantly, this newly developed microextraction technique was easy to prepare in-house at a reasonable cost, and it was more precise compared to the conventional method. In general, this study demonstrated that the extraction technique was a fast, simple, and effective method for the preparation of complex samples while preventing coextraction of extraneous materials.

**Table 2. MS/MS Data and Concentrations of Target Analytes**

| analytes | molecular formula | $t_R$ (min) | $[M + H]^+$ | collision energy (V) | MS/MS | concentrations (mg/g) | | |
|---|---|---|---|---|---|---|---|---|
| | | | | | | DST | DS | TC |
| dihydrotanshinone I | $C_{18}H_{14}O_3$ | 3.778 | 279.1031 | 20 | 179.0904;167.0855;223.0711 | 0.06 | 1.02 | 1.97 |
| tanshinone I | $C_{18}H_{12}O_3$ | 4.694 | 277.0878 | 20 | 167.0857;179.0854;249.0873 | 0.02 | 1.43 | 4.67 |
| cryptotanshinone | $C_{19}H_{20}O_3$ | 4.778 | 297.1506 | 20 | 239.1205;281.0580;283.0518 | 0.11 | 1.69 | 5.68 |
| tanshinone IIA | $C_{19}H_{18}O_3$ | 5.912 | 295.1352 | 25 | 265.0828;268.5011;280.1182 | 0.26 | 3.61 | 9.61 |


dx.doi.org/10.1021/jf5029625 | J. Agric. Food Chem. 2014, 62, 9683−9689

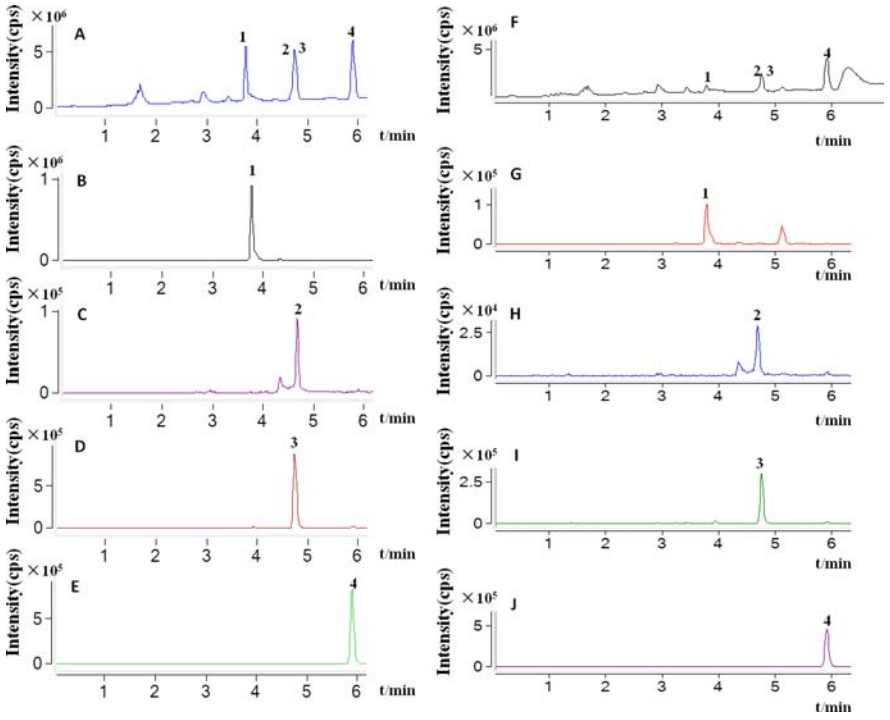


**Figure 8.** Total ion chromatograms (TICs) of standard solution (analytes concentrations of 25 ng/mL) (A) and DST sample solution (F). Extracted ion chromatograms (EICs) of dihydrotanshinone I (B), tanshinone I (C), cryptotanshinone (D), and tanshinone IIA (E) in standard solution; EICs of dihydrotanshinone I (G), tanshinone I (H), cryptotanshinone (I), and tanshinone IIA (J) in sample solution. Analytes: (1) dihydrotanshinone I, (2) tanshinone I, (3) cryptotanshinone, and (4) tanshinone IIA.

## AUTHOR INFORMATION


### Corresponding Author

*E-mail: caojun91@163.com. Phone: +86-571-28867909. Fax: +86-571-28867909.

### Author Contributions

§These authors contributed equally to this work.



### Funding

This study was supported by General Program of National Natural Science Foundation of China (No.81274065), Research on Public Welfare Technology Application Projects of Zhejiang Province (No.2014C37069), Changjiang Scholars and Innovative Research Team in Chinese University (IRT 1231), Young and Middle-Aged Academic Leaders of Hangzhou (2013-45), Scientific Research Foundation of Hangzhou Normal University (2011QDL33), and the new-shoot Talents Program of Zhejiang province (2013R421044, 2014R421019).


### Notes

The authors declare no competing financial interest.

## REFERENCES


(1) Li, W.; Zhao, D. Y. An overview of the synthesis of ordered mesoporous materials. *Chem. Commun.* **2013**, *49*, 943−946.

(2) Joshi, M. D.; Ho, T. D.; Cole, W. T. S.; Anderson, J. L. Determination of polychlorinated biphenyls in ocean water and bovine milk using crosslinked polymeric ionic liquid sorbent coatings by solid-phase microextraction. *Talanta* **2014**, *118*, 172−179.

(3) Jafari, M. T.; Saraji, M.; Sherafatmand, H. Polypyrrole/montmorillonite nanocomposite as a new solid phase microextraction fiber combined with gas chromatography-corona discharge ion mobility spectrometry for the simultaneous determination of diazinon and fenthion organophosphorus pesticides. *Anal. Chim. Acta* **2014**, *814*, 69−78.

(4) Chao, Y. Y.; Lee, C. H.; Chien, T. Y.; Shih, Y. H.; Lu, Y. A.; Kuo, T. H.; Huang, Y. L. Effects of push/pull perfusion and ultrasonication on the extraction efficiencies of phthalate esters in sports drink samples using on-line hollow-fiber liquid-phase microextraction. *J. Agric. Food Chem.* **2013**, *61*, 8063−8071.

(5) Ge, D.; Lee, H. K. Ionic liquid based hollow fiber supported liquid phase microextraction of ultraviolet filters. *J. Chromatogr. A* **2012**, *1229*, 1−5.

(6) Costas-Mora, I.; Romero, V.; Pena-Pereira, F.; Lavilla, I.; Bendicho, C. Quantum dot-based headspace single-drop microextraction technique for optical sensing of volatile species. *Anal. Chem.* **2011**, *83*, 2388−2393.

(7) Jiao, J.; Ma, D. H.; Gai, Q. Y.; Wang, W.; Luo, M.; Fu, Y. J.; Ma, W. Rapid analysis of Fructus forsythiae essential oil by ionic liquids-assisted microwave distillation coupled with headspace single-drop microextraction followed by gas chromatography-mass spectrometry. *Anal. Chim. Acta* **2013**, *804*, 143−150.

(8) Ruan, E. D.; Aalhus, J. L.; Summerfelt, S. T.; Davidson, J.; Swift, B.; Juárez, M. Determination of off-flavor compounds, 2-methyl-isoborneol and geosmin, in salmon fillets using stir bar sorptive extraction-thermal desorption coupled with gas chromatography-mass spectrometry. *J. Chromatogr. A* **2013**, *1321*, 133−136.

(9) Malowicki, S. M. M.; Martin, R.; Qian, M. C. Volatile composition in raspberry cultivars grown in the pacific northwest determined by stir bar sorptive extraction-gas chromatography-mass spectrometry. *J. Agric. Food Chem.* **2008**, *56*, 4128−4133.

(10) Li, T. H.; Joshi, M. D.; Ronning, D. R.; Anderson, J. L. Ionic liquids as solvents for in situ dispersive liquid-liquid microextraction of DNA. *J. Chromatogr. A* **2013**, *1272*, 8−14.

(11) Pinto, E.; Melo, A.; Ferreira, I. M. P. L. V. O. Sensitive quantitation of polyamines in plant foods by ultrasound assisted benzoylation and dispersive liquid−liquid microextraction with the aid of experimental designs. *J. Agric. Food Chem.* **2014**, *62*, 4276−4284.

(12) Wang, J.; Yang, C.; Li, H. J.; Piao, X. F.; Li, D. H. Gas purge-microsyringe extraction: a rapid and exhaustive direct microextraction technique of polycyclic aromatic hydrocarbons from plants. *Anal. Chim. Acta* **2013**, *805*, 45−53.

(13) Galán-Cano, F.; Lucena, R.; Cárdenas, S.; Valcárcel, M. Dispersive micro-solid phase extraction with ionic liquid-modified silica for the determination of organophosphate pesticides in water by ultra performance liquid chromatography. *Microchem. J.* **2013**, *106*, 311−317.
(14) Jiménez-Soto, J. M.; Cárdenas, S.; Valcárcel, M. Evaluation of single-walled carbon nanohorns as sorbent in dispersive micro solid-phase extraction. *Anal. Chim. Acta* **2012**, *714*, 76−81.
(15) Jiménez-Soto, J. M.; Cárdenas, S.; Valcárcel, M. Dispersive micro solid-phase extraction of triazines from waters using oxidized single-walled carbon nanohorns as sorbent. *J. Chromatogr. A* **2012**, *1245*, 17−23.
(16) Giannoulis, K. M.; Tsogas, G. Z.; Giokas, D. L.; Vlessidis, A. G. Dispersive micro-solid phase extraction of ortho-phosphate ions onto magnetite nanoparticles and determination as its molybdenum blue complex. *Talanta* **2012**, *99*, 62−68.
(17) Fu, S. C.; Tzing, S. H.; Chen, H. C.; Wang, Y. C.; Ding, W. H. Dispersive micro-solid phase extraction combined with gas chromatography-chemical ionization mass spectrometry for the determination of N-nitrosamines in swimming pool water samples. *Anal. Bioanal. Chem.* **2012**, *402*, 2209−2216.
(18) Skorek, R.; Zawisza, B.; Marguí, E.; Queralt, I.; Sitko, R. Dispersive micro solid-phase extraction using multiwalled carbon nanotubes for simultaneous determination of trace metal ions by energy-dispersive X-ray fluorescence spectrometry. *Appl. Spectrosc.* **2013**, *67*, 204−209.
(19) Zhao, J.; Deng, J. W.; Chen, Y. W.; Li, S. P. Advanced phytochemical analysis of herbal tea in China. *J. Chromatogr. A* **2013**, *1313*, 2−23.
(20) Cao, J.; Wei, Y. J.; Qi, L. W.; Li, P.; Qian, Z. M.; Luo, H. W.; Chen, J.; Zhao, J. Determination of fifteen bioactive components in Radix et Rhizoma Salviae Miltiorrhizae by high-performance liquid chromatography with ultraviolet and mass spectrometric detection. *Biomed. Chromatogr.* **2008**, *22*, 164−172.
(21) Shi, Z. H.; He, J. T.; Yao, T. T.; Chang, W. B.; Zhao, M. P. Simultaneous determination of cryptotanshinone, tanshinone I and tanshinone IIA in traditional Chinese medicinal preparations containing Radix salvia miltiorrhiza by HPLC. *J. Pharmaceut. Biomed.* **2005**, *37*, 481−486.
(22) Wan, A. K. S.; Leung, S. W. S.; Zhu, D. Y.; Man, R. Y. K. Vascular effects of different lipophilic components of "Danshen", a traditional Chinese medicine, in the isolated porcine coronary artery. *J. Nat. Prod.* **2008**, *71*, 1825−1828.
(23) Cao, J.; Chen, J.; Yi, L.; Li, P.; Qi, L. W. Comparison of oil-in-water and water-in-oil microemulsion electrokinetic chromatography as methods for the analysis of eight phenolic acids and five diterpenoids. *Electrophoresis* **2008**, *29*, 2310−2320.
(24) Shi, Y. F.; Li, B.; Wang, P.; Dua, R.; Zhao, D. Y. Micelle swelling agent derived cavities for increasing hydrophobic organic compound removal efficiency by mesoporous micelle@silica hybrid materials. *Microporous Mesoporous Mater.* **2012**, *155*, 252−257.
(25) Jafari, M. T.; Saraji, M.; Yousefi, S. Negative electrospray ionization ion mobility spectrometry combined with microextraction in packed syringe for direct analysis of phenoxyacid herbicides in environmental waters. *J. Chromatogr. A* **2012**, *1249*, 41−47.

In plants, flavonoids are contained in most compartments of cells, including the cytosol, vacuoles, endoplasmic reticulum (ER), chloroplasts, nucleus, and extracellular space, although the sites of flavonoid biosynthesis, storage, and usage are all separate. This observation indicates the presence of efficient systems that transport flavonoids across endomembranes and plasma membranes in plants.[13] Recent studies have implicated multidrug and toxic compound extrusion transporters (MATEs), which are major proteins involved in the transport of plant secondary metabolites, including flavonoids.[14] MATEs are found on vacuolar membranes in plant cells and mediate flavonoid uptake using electrochemical gradients across membranes, which are generated by proton pumps, including P-type ATPase, vacuolar V-type ATPase, and $H^+$-pyrophosphatase. MATEs have been found in the vacuolar membranes of various plant species, with various substrate specificities. For example, MATE from *Arabidopsis* and *Medicago truncatula* transports epicatechin-3-*O*-glucoside, whereas a grapevine MATE transports cyanidine-3-*O*-glucoside to the inside of the vacuole.[14]

Interestingly, MATE orthologs are also highly expressed in humans, particularly in the kidney, adrenal gland, liver, and skeletal muscle. Human MATE1 has 95% amino acid sequence homology compared to that of *Arabidopsis*. To date, the major role of human MATE1 is thought to be in the transport of various organic cationic drugs, such as tetraethylammonium, 1-methyl-4-phenylpyridinium, and metformin.[15] However, some anionic compounds, including estrone sulfate, acyclovir, and ganciclovir, have also been reported to be MATE1 substrates.[16]

The purpose of this study was to investigate whether MATE1 could take up dietary flavonoids in metabolically active mammalian cells, such as hepatocytes. To assess this, we first demonstrated the cellular localization of MATE1, in both mouse and human liver and intestine, via immunofluorescence microscopy. We then assessed intracellular flavonoid accumulation in cultured hepatocytes and HEK293 cells overexpressing MATE1, using eight representative dietary flavonoids (quercetin, kaempferol, luteolin, apigenin, and their glycosides). Experiments with MATE1 gene knockdown and MATE1 inhibitors were performed to demonstrate MATE1-specific flavonoid transport.

## MATERIALS AND METHODS

**Cell Culture.** HepG2 and HEK293T cells (Korean Cell Line Bank, Seoul, Korea) were grown in Dulbecco's modified Eagle's medium (DMEM) containing 10% heat-inactivated fetal bovine serum and 1% penicillin−streptomycin at 37 °C in 5% $CO_2$. To establish a MATE1-overexpressing stable cell line (hMATE1), human MATE1 plasmid DNA (Origene, Rockville, MD) in a neomycin-resistance vector was transfected into HEK293T cells. Cells that stably expressed MATE1 were selected in medium containing G418 (Sigma-Aldrich, St. Louis, MO) for five rounds of subculture, and the expression of hMATE1 was confirmed with reverse transcription polymerase chain reaction (RT-PCR) (inset of Figure 2F).

**Cellular Flavonoid Accumulation Assay.** Quercetin, kaempferol, luteolin, apigenine, and quercetin-3-*O*-glucoside were purchased from Sigma-Aldrich (St. Louis, MO). Kaempferol-3-*O*-glucoside was purchased from Extrasynthese (Genay, France). Luteolin-7-*O*-glucoside and apigenine-7-*O*-glucoside were purchased from the Indofine Chemical Company (Hillsborough, NJ). HEK293T and hMATE1 cells were seeded in 12-well plates at $5 \times 10^5$ cells/well the day before treatment. Cells were stimulated with flavonoids for 0, 2, 4, 6, 8, and 10 min, and then the cellular flavonoid concentration was quantified using spectrofluorometry as described previously.[17] After washing cells twice with phosphate-buffered saline (PBS), cellular flavonoids were extracted with methanol (1 mL/well) at 65 °C for 1 h, followed by centrifugation at 17 000 rpm for 2 min. The supernatants were concentrated with a SpeedVac concentrator (N-Biotek, Bucheon, Korea) and then dissolved in 200 μL of 4′,6-diamidino-2-phenylindole, which contained dimethyl sulfoxide (DMSO), in a fluoro 96-well plate. The intensity of the fluorescence signal was measured with an excitation/emission of 485/535 nm using a Victor X2 multilabel plate reader (PerkinElmer, Waltham, MA). The flavonoid concentrations were calculated using a standard curve that was generated with known concentrations of the examined flavonoids.

**Effects of MATE1 Gene Knockdown, Overexpression, and Inhibitors on Cellular Quercetin Accumulation.** siRNA of the MATE1 gene was purchased from Santa Cruz Biotechnology, Inc. (Santa Cruz, CA). HEK293T cells were transfected with MATE1 siRNA (20 pmol/$5 \times 10^5$ cells) and incubated for 1 day before experiments. The knockdown of MATE1 gene expression was confirmed by immunoblot analysis. In the assays with transporter inhibitors, phenylmethylsulfonyl fluoride (PMSF, 100 μM), cyclopiazonic (50 μM), pyrimethamine (1 μM), and bafilomycin A1 (100 nM) were incubated for 30 min before quercetin stimulation. Cellular flavonoid quantification was performed according to the method described in the section above.

**Immunofluorescence Assay.** HepG2 and hMATE1 cells were cultured on polylysine-coated glass slides for 24 h and fixed with 4% paraformaldehyde for 20 min. Mouse liver and intestine tissues from C57BL/6J mice were fixed in 4% paraformaldehyde, embedded in optimal cutting temperature (OCT) compounds, and sectioned on a cryotome at −25 °C (10−20 μM thickness, CM3050S, Leica, Wetzlar, Germany). The human tissue sections were purchased from Genetex (San Antonio, TX). For immunofluorescence staining, fixed cells and tissues were incubated with 5% bovine serum albumin (BSA) in PBS for 30 min and immunostained with a rabbit polyclonal MATE1 antibody (Abcam, Cambridge, MA), together with an antibody for a marker protein of intracellular organelles, for 1 h. Antibodies for mouse monoclonal pan-cadherin, goat polyclonal prohibitin, mouse monoclonal lysosome-associated membrane protein-1 (LAMP1), goat polyclonal calnexin, goat polyclonal peroxin, and goat polyclonal catalase were purchased from Santa Cruz Biotechnology, Inc. (Santa Cruz, CA). As a secondary fluorescent antibody, Alexa Fluor 532 goat anti-rabbit was used and incubated for another 1 h with either Alexa Fluor 488 goat anti-mouse or Alexa Fluor 488 donkey anti-goat antibody. The coverslips were embedded in anti-fade mounting medium after staining with 4′,6-diamidino-2-phenylindole. Image analysis was performed using a Zeiss LSM510 META confocal microscope and the Zeiss LSM510 version 3.2 software (Carl Zeiss, Jena, Germany). Co-localized spots were quantified using ImageJ software [version 1.47, National Institutes of Health (NIH), Bethesda, MD] and calculated using [co-localization (%) = yellow spots/total spots × 100].

**Immunoblotting.** Plasma membrane, ER, and peroxisomal fractions were isolated from mouse livers using density gradient centrifugation as described previously.[18,19] The protein concentration was determined using the Bradford reagent, with BSA as a standard. Protein samples (40 μg) in Laemmli sample buffer were boiled for 5 min and separated on 8−10% sodium dodecyl sulfate−polyacrylamide gel electrophoresis (SDS−PAGE) gels. Separated proteins were electrophoretically transferred onto nitrocellulose membranes. Nonspecific binding was blocked with 5% nonfat dry milk in Tris-buffered saline with Tween-20 (TBST) buffer for 1 h at room temperature (RT), and membranes were incubated with primary antibodies. After washing several times with 1% TBST wash buffer, membranes were incubated with the secondary antibody for 1 h at RT. Immunoreactive bands were detected by enhanced chemiluminescence western blot detection reagents and quantified by the ChemiDoc XRS system (Bio-Rad, Hercules, CA) using the Quantity One software (version 4.6.9, Bio-Rad). The enzyme-linked immunosorbent assay (ELISA) assay for MATE1 protein quantification was performed according to the instructions of the manufacturer (Cusabio, Wuhan, China).

**Measurement of Cellular Lipids, Peroxidation, and Glucose Uptake.** Oleic acid was dissolved in ethanol at 100 mM for use as a

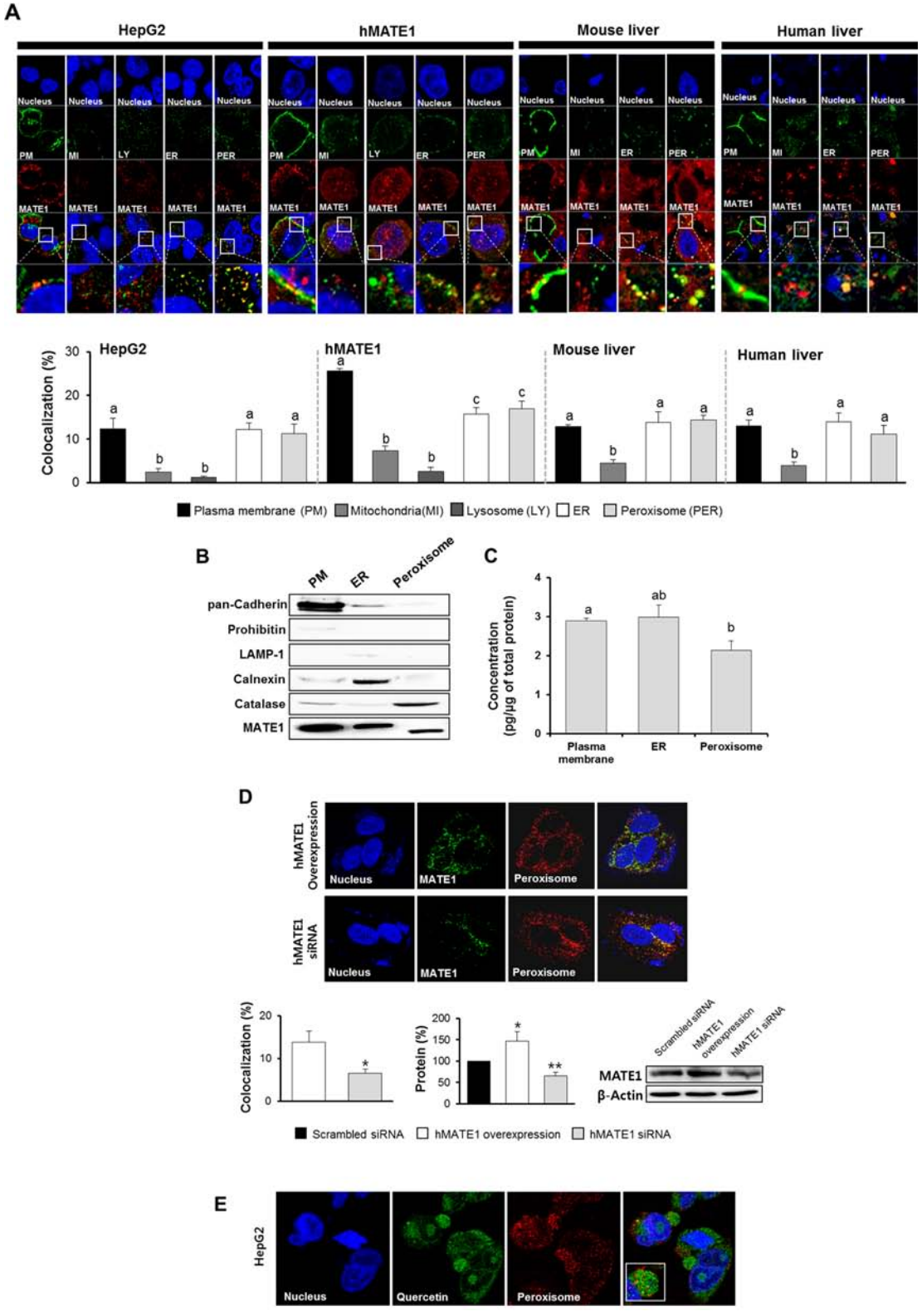


**Figure 1.** Cellular localization of MATE1 in cultured cells and tissues. (A) Localization of MATE1 in HepG2, hMATE1 cells, and mouse and human tissues. Antibodies against pan-cadherin [plasma membrane (PM)], prohibitin [mitochondria (MI)], LAMP-1 [lysosome (LY)], calnexin (ER), and peroxin [peroxisome (PER)] labeled cellular organelles. Blue, green, and red signals indicate nuclei, cellular organelles, and MATE1, respectively. Images were taken using a confocal microscope. (B) Immunoblotting of MATE1 with cellular organelles from the mouse liver. (C) Concentrations of MATE1 in mouse liver plasma, ER, and peroxisomal membrane determined by ELISA. (D) Localization of MATE1 (green) on peroxisome (catalase, red) in MATE1 overexpressed and knockdown HepG2 cells. (E) Co-localization of cellular quercetin (green) and catalase (red), a marker for peroxisomes in HepG2 cells. The values are the mean ± SEM. Statistical significance was analyzed using a one-way ANOVA and Student's *t* test. $p < 0.05$ was considered statically significant.


dx.doi.org/10.1021/jf500916d | J. Agric. Food Chem. 2014, 62, 9690−9698

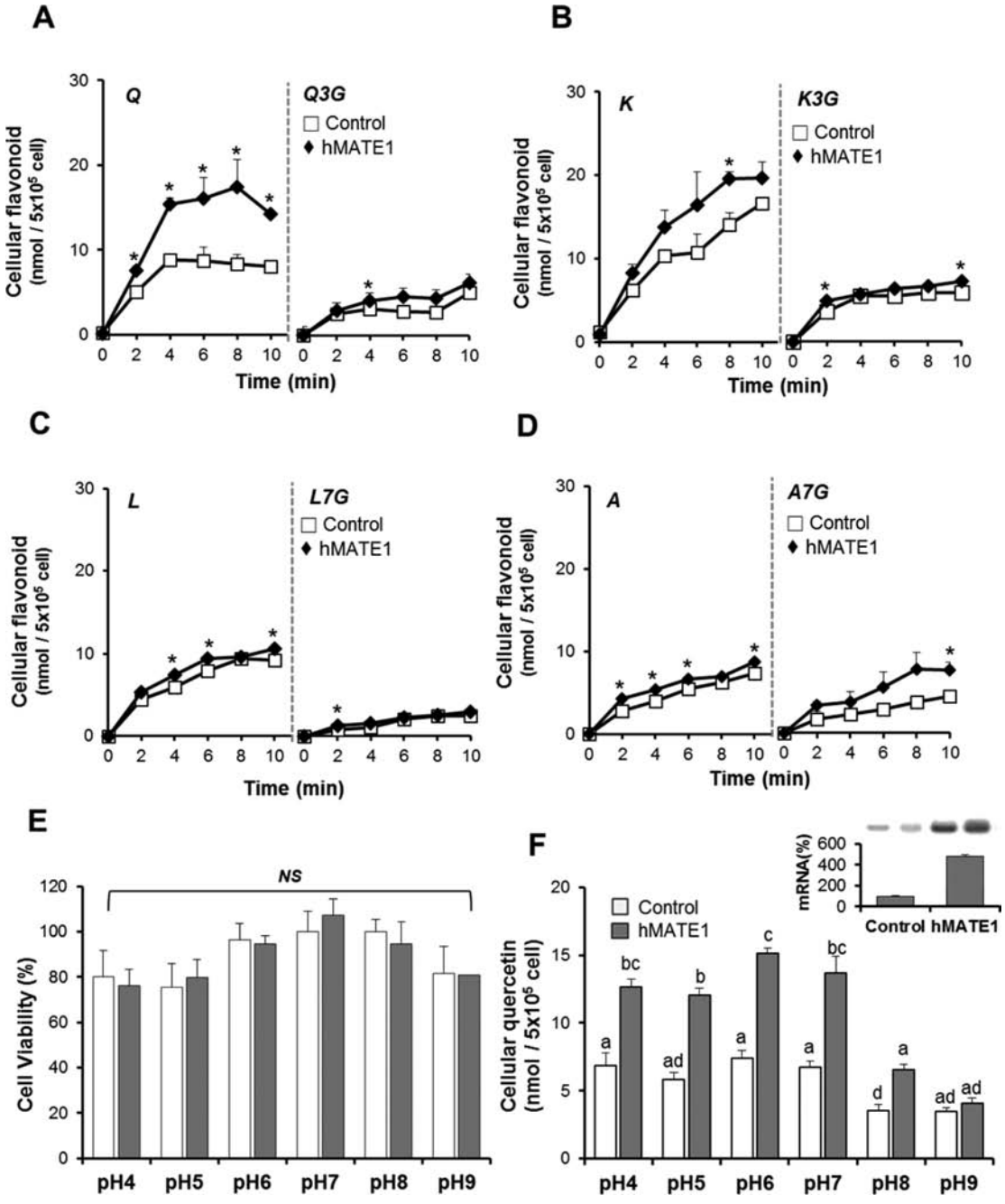


**Figure 2.** Effect of MATE1 overexpression on cellular flavonoid accumulation. (A–D) Time-course accumulation of intracellular flavonoids. Quercetin (Q), kaempferol (K), luteolin (L), and apigenin (A) were incubated (100 $\mu$M each) with control HEK293T or hMATE1 cells for 10 min. The cellular flavonoids were quantified every 2 min as described in the Materials and Methods. The values are the mean ± SEM. (*) $p < 0.05$ versus the control. (E) Cell viability. Control (HEK293T) and hMATE1 cells were incubated in PBS buffer at pH 4–9 for 5 min. (F) Intracellular quercetin accumulation at various pH values. The values are the mean ± SEM. The group comparison was performed using a one-way ANOVA. QG, quercetin-3-*O*-glucoside; KG, kaempferol-3-*O*-glucoside; LG, luteolin-7-*O*-glucoside; and AG, apigenine-7-*O*-glucoside.

stock solution. To make lipid-loading media, the oleic acid stock solution was diluted to 400 $\mu$M in serum-free media, which included 0.5% BSA. Control and hMATE1 cells were seeded in 6-well plates at a concentration of $5 \times 10^5$ cells/well and stimulated with normal media, oleic acid-containing media, or oleic acid- and flavonoid-containing media for 10 min. Cells were washed with PBS, and 2 mL of hexane/isopropanol (2:1) was added and incubated for 30 min. The solvent was then collected and evaporated under vacuum. Extracts were dissolved in 80% ethanol, and total cholesterol and triacylglycerol contents were measured using a Cobas C111 automatic analyzer (Roche, Basel, Switzerland). Lipid peroxidation was measured using a thiobarbituric acid reactive substances (TBARS) assay as described previously.[20] For the glucose uptake assay, a previous study and the instructions of the manufacturer were followed (Cayman, Ann Arbor, MI).[21]

**Statistical Analysis.** The data are expressed as the mean ± standard error of the mean (SEM). Differences were considered statistically significant at $p < 0.05$ or by a one-way analysis of variation (ANOVA) test. Each experiment was performed at least in triplicate.

## RESULTS

**Cellular Localization of MATE1 in the Liver.** The tissue distribution of MATE1 expression in mice revealed substantial


dx.doi.org/10.1021/jf500916d | J. Agric. Food Chem. 2014, 62, 9690–9698

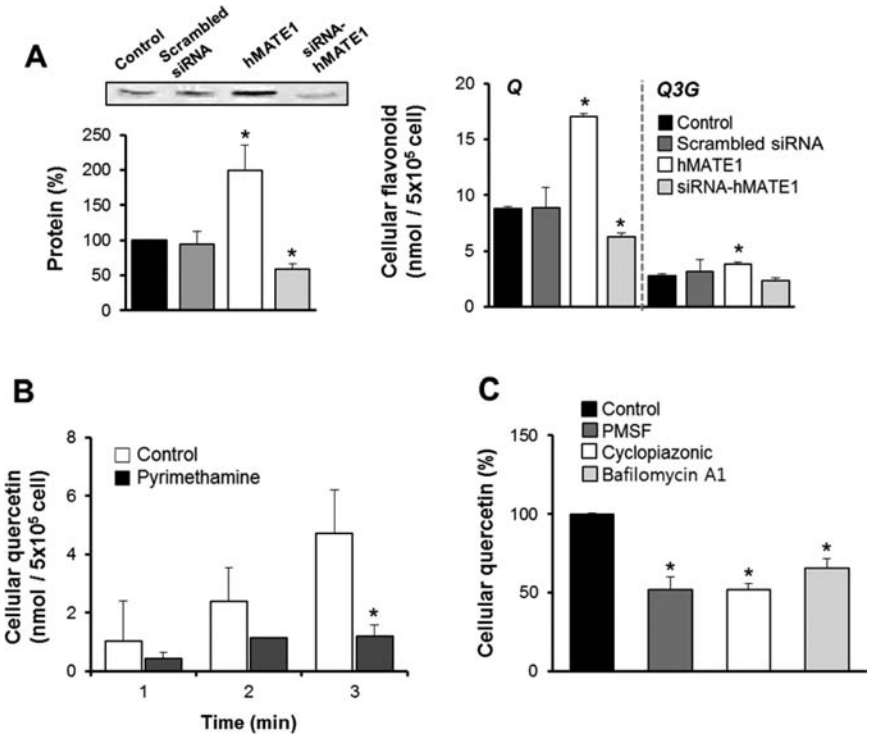


**Figure 3.** Quercetin accumulation in cells with hMATE1 knockdown and MATE inhibitor treatment. (A) HEK293T cells were transfected with the hMATE1 expression vector or MATE1 siRNA, respectively. Then, intracellular quercetin concentrations were measured as described in the Materials and Methods. The knockdown and overexpression efficiencies were assessed with immunoblotting analysis. Quercetin (100 $\mu$M) was incubated for 3 min, and the intracellular accumulation was quantified. (B) Effect of pyrimethamine on cellular flavonoid accumulation. HepG2 cells were incubated with quercetin (100 $\mu$M) for 3 min with or without pyrimethamine (1 $\mu$M). (C) Effects of PMSF, cyclopiazonic, and bafilomycin A1 on flavonoid accumulation in HepG2 cells. Cells were incubated with quercetin (100 $\mu$M) for 5 min with or without the membrane transporter inhibitors. The values are the mean ± SEM. (*) $p < 0.05$ versus the control.

gene expression of MATE1 in the liver and several other tissues, such as the kidney, which suggests that MATE1 may play a role in the cellular accumulation of the flavonoid quercetin in the liver (see Figure S1 of the Supporting Information). Immunofluorescence analysis investigated the subcellular localization of MATE1 in mouse and human liver tissues as well as in cultured cells with antibodies for marker proteins of plasma (pan-cadherin), mitochondrial (prohibitin), lysosomal (LAMP), ER (calnexin), and peroxisomal (peroxin or catalase) membranes (Figure 1). Our results indicate that the MATE1 protein is expressed in liver tissues. The expression levels were similar in both mice and human tissues. Immunofluorescence analysis suggested that MATE1 is primarily expressed in the plasma, ER, and peroxisomal membranes in cultured hepatocytes, hMATE1 cells, and both mouse and human liver tissues (Figure 1A). These results were confirmed with isolated membrane fractions from mouse liver using immunoblotting analysis and ELISA (panels B and C of Figure 1). Analysis with intestinal tissues was confirmed (see Figure S2 of the Supporting Information). To confirm the MATE1 expression on peroxisome, HepG2 cells were transfected with MATE1 siRNA and were analyzed with immunofluorescence analysis (Figure 1D). Result confirmed the reduction of MATE1 expression in cells with MATE1 knockdown (−56% versus MATE1 overexpression; $p < 0.05$). Next, we performed immunofluorescent microscopy to localize the subcellular accumulation of quercetin (Figure 1E). The results suggest that a significant amount of quercetin is accumulated in the peroxisome. The accumulation of quercetin in peroxisomes may be due to uptake by MATE1 in the peroxisomal membrane. A significant amount of quercetin was also found in the nucleus.

**Effect of MATE1 on Flavonoid Transport.** Because MATE1 was highly expressed in the liver tissue, we next investigated cellular flavonoid uptake by MATE in HEK293 cells overexpressing hMATE1. Eight representative flavonoids that are abundant in common dietary plants[22] were examined for cellular accumulation (panels A–D of Figure 2). The flavonoid concentration used in this study was chosen on the basis of preliminary assay results (see Figure S3 of the Supporting Information). Cellular flavonoid uptake occurs rapidly, and of the tested compounds, quercetin exhibited the most efficient uptake by MATE1, which was determined by comparing the uptake in hMATE1 and control cells. The quercetin concentration at 8 min was increased by 110% in hMATE1 cells when compared to the controls (17 versus 8 nmol/5 × $10^5$ cell in hMATE1 and controls, respectively; $p < 0.05$). Kaempferol was transported by MATE1 to a lesser degree than quercetin. The intracellular accumulations of quercetin-3-*O*-glucoside, kaempferol-3-*O*-glucoside, luteolin, luteolin-7-*O*-glucoside, apigenin, and apigenine-7-*O*-glucoside were marginally but significantly altered by hMATE1 overexpression, which suggested that MATE1 might transport diverse flavonoids, including both aglycones and glycosides, with different affinities.

It is difficult to predict the substrate specificity of MATE1, as evidenced by our results. However, four factors appear to determine the efficiency of MATE1-dependent flavonoid uptake: molecular weight, the number of hydrogen bond donors and acceptors, hydrophobicity, and ionization status.

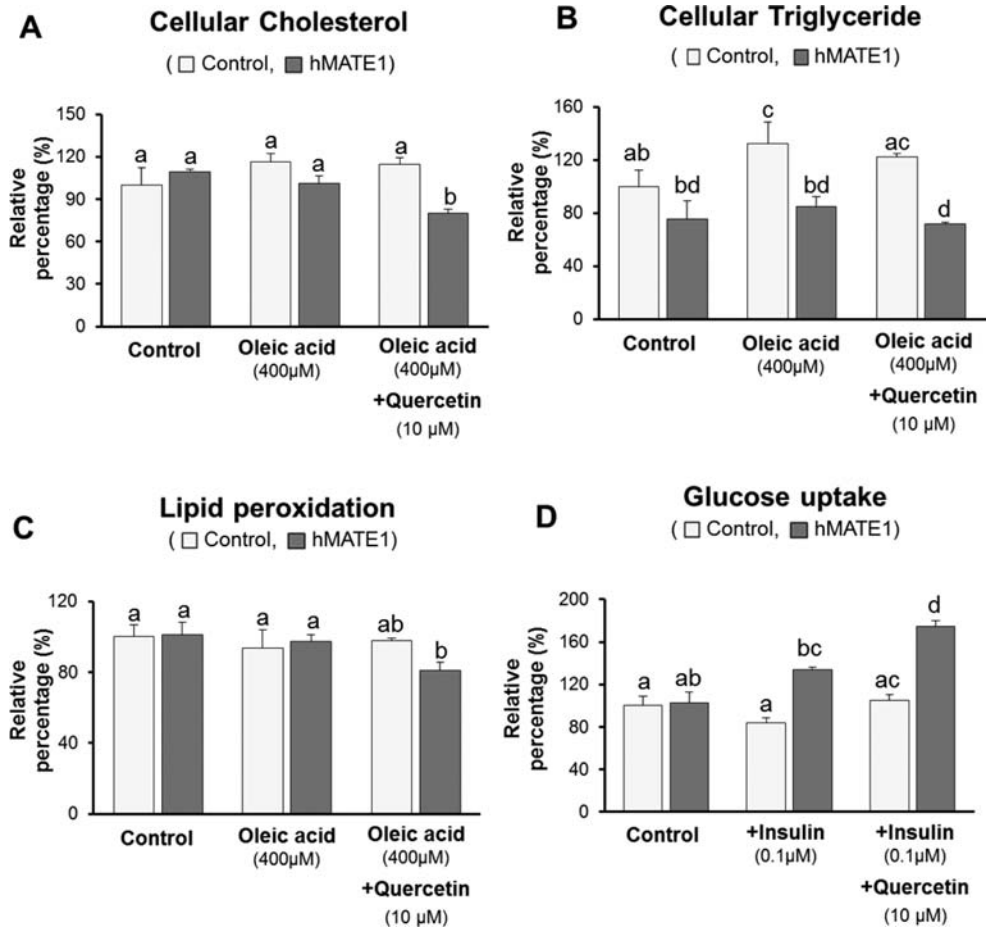


**Figure 4.** Effects of MATE1 overexpression on lipid metabolism. (A and B) Cellular cholesterol and triglyceride concentrations in lipid-loaded cells. (C) Lipid peroxidation levels in lipid-loaded cells with quercetin treatment. Lipid peroxidation was measured using the TBARS assay. (D) Insulin sensitivity test in lipid-loaded cells. Lipid-loaded cells were stimulated with insulin, and then cellular glucose uptake was quantified. The values are the mean ± SEM. Statistical significance was analyzed using a one-way ANOVA.

First, our results demonstrate that aglycones were superior substrates for MATE1 compared to glycosides and exhibited greater cellular uptake. The reason for this is not clear; however, it is possible that flavonoid glycosides may be too large for MATE1, because most known substrates for MATE1 have a molecular weight of less than 300 g/mol. Additionally, aglycones with a greater number of hydrogen bond donors and acceptors and a lower degree of hydrophobicity showed greater cellular uptake. Thus, quercetin showed the highest level of cellular uptake among all of the tested flavonoids because it is a small aglycone and shows the lowest hydrophobicity among tested flavonoid aglycone (see Table S1 of the Supporting Information).

Finally, the ionization of flavonoid aglycones, at a basic pH, hindered cellular uptake. Flavonoids are not ionized at a neutral pH ($pK_a$ = 6.74−7.76), but hydroxyl groups progressively remove protons in accordance with increasing pH.[23] In quercetin, cell viability was reduced slightly at various pH values compared to at pH 7, but the reductions were not statistically significant (Figure 2E). Cellular quercetin uptake was pH-dependent and greatest at pH 6, at which quercetin is not ionized. The quercetin concentration was increased in hMATE1 cells by 105% compared to controls, at this pH value ($p < 0.001$; Figure 2F). In contrast, at pH 9, the cellular quercetin accumulation was markedly reduced in comparison to at pH 6 and was only moderately higher in hMATE1 cells compared to controls. These findings demonstrate that a negative charge on flavonoids may prohibit uptake by MATE1.

**Quercetin Accumulation in Cells with hMATE1 Knockdown in HEK293T Cells and MATE Inhibitor Treatment in HepG2 Cells.** Transfection with hMATE1 siRNA knocked down its protein expression in HEK293T cells by −41% compared to the control (Figure 3A). Cellular flavonoid accumulation was decreased by 29% with statistical significance in siRNA hMATE1 cells compared to the control ($p < 0.05$; Figure 3A). Next, the effects of several inhibitors of membrane transporters were investigated in HepG2 cells. Pyrimethamine is a competitive and specific inhibitor of MATE1.[9] In HepG2 cells that were stimulated with pyrimethamine, quercetin uptake was dramatically reduced by 75% at 3 min when compared to controls ($p < 0.05$ versus the control; Figure 3B). We also quantified quercetin transport in hMATE1 cells that were stimulated with PMSF, cyclopiazonic acid, and bafilomycin A1 (Figure 3C), which are inhibitors for bilitranslocase and P- and V-type ATPases, respectively.[9,24,25] PMSF significantly blocked quercetin accumulation by up to 48%, as reported previously ($p < 0.05$). Cyclopiazonic acid and bafilomycin A1 reduced intracellular quercetin accumulation by 48 and 35%, respectively, when compared to controls ($p < 0.05$). These results suggest that multiple membrane proteins, which include MATE1 and bilitranslocase, mediate intracellular hepatic quercetin transport. Additionally, the data also suggest


dx.doi.org/10.1021/jf500916d | J. Agric. Food Chem. 2014, 62, 9690−9698

that quercetin uptake by MATE1 is mediated by secondary active transport, which requires the activity of both P- and V-type ATPases as well as a proton gradient across the membrane.

**Biological Activity of Quercetin in Lipid-Loaded hMATE1 Cultured Cells.** Quercetin ameliorates symptoms of metabolic syndrome, including dyslipidemia, insulin sensitivity, and obesity. Hepatic lipid accumulation is one of the common symptoms in metabolic syndrome; thus, we investigated the effect of hMATE1 expression on hepatic lipid accumulation. hMATE1 cells that were stimulated with quercetin had intracellular cholesterol and triglyceride concentrations that were significantly reduced by 30 and 41%, respectively, compared to control cells ($p < 0.05$; panels A and B of Figure 4). The antioxidative activity of quercetin (10 $\mu$M) increased in hMATE1 cells when compared to controls; thus, the levels of lipid peroxides were reduced after lipid loading ($p < 0.05$; Figure 4C). In addition, insulin-mediated cellular glucose uptake was improved in lipid-loaded hMATE1 cells when compared to the control (Figure 4D).

## DISCUSSION

Flavonoids are plant-specific; approximately 8000 different types have been isolated from various plants. Quercetin, which is one of the most abundant flavonoids, has been intensively studied for its various biological activities in humans, including its hypolipidemic effects and regulation of metabolic syndrome symptoms.[26,27] However, considering the amount of biological activity studies with flavonoids, including quercetin, their cellular transport mechanism in mammals remains unknown.

The mechanism of flavonoid transport has been investigated intensively in plant tissues, and MATE1 has been reported to carry out the vacuolar transport of anthocyanin in *Arabidopsis*. Interestingly, human MATE1 is expressed at high levels in the kidney, liver, and intestine.[15] Human MATE1 has 95% amino acid sequence homology compared to that expressed in *Arabidopsis*. It has been reported that the major role of human MATE1 is to transport various organic cations; however, some anionic drugs, including estrone sulfate, are also MATE1 substrates.[15,16]

The results of our study demonstrate that MATE1 mediates cellular flavonoid accumulation in cultured cells overexpressing MATE1. Among eight selected flavonoid aglycones and glycosides, quercetin aglycone showed the highest cellular accumulation in cells that overexpressed MATE1, which suggests that MATE1 is a cellular quercetin transporter. Kaempferol, luteolin, and apigenin uptake were moderately enhanced with MATE1 overexpression. Knocking down the expression of MATE1 with siRNA diminished the cellular quercetin accumulation. Additionally, treatment of cells with pyrimethamine, which is a MATE inhibitor, reduced cellular flavonoid accumulation by 75%, demonstrating the critical role of MATE1 in cellular flavonoid accumulation. A reduction of quercetin accumulation in cells that were incubated with V- and P-type ATPase inhibitors also confirmed the secondary active transport of human MATE1. The hypolipidemic, antioxidative, and cellular glucose uptake activities of quercetin in cultured hepatocytes were exaggerated in cells that overexpressed MATE1, which suggests that the increased bioavailability of quercetin enhanced its biological activity. An immunoblotting analysis with isolated subcellular membranous organelles revealed that MATE1 is highly expressed in both the liver and intestine, especially in peroxisomes and the ER as well as in the plasma membrane. Immunohistochemistry with mouse and human liver tissues as well as with cultured hepatocytes demonstrated a similar subcellular localization of MATE1, which was consistent with the immunoblotting analysis. Finally, the fluorescent staining analysis revealed that quercetin was co-localized in peroxisomes and the nucleolus, which suggests the potential accumulation of quercetin in the corresponding organelles, in which peroxisomal accumulation is mediated by MATE1 at least in peroxisome.

In plant tissues, MATE1 has a high affinity for glycoside forms of flavonoids, such as epicatechin-3-*O*-glucoside and cyanidine-3-*O*-glucoside, over the corresponding aglycones. However, the present data demonstrate that aglycones showed higher levels of cellular accumulation than glycosides in cells that overexpressed hMATE1, except for apigenin-7-*O*-glycoside.[13,14] The reasons for the differences in substrate specificity between human and plant MATE1 are unclear at present. Minor differences in amino acid sequence may be associated with differential substrate specificity in human and plant MATE1. It appears that human MATE1 has broad substrate specificity. MATE1 is thought to be involved in the transport of various organic cations, including tetraethylammonium, 1-methyl-4-phenylpyridinium, and metformin,[15] as well as some anionic compounds, including estrone sulfate, acyclovir, and ganciclovir.[16] In this study, we demonstrate that MATE1 also transports flavonoid aglycones with high affinity.

Prediction of the common structural components of MATE1 substrates appears to be highly problematic. However, Wittwer et al. described the major physicochemical parameters of MATE1 substrates in animal cells, including molecular weight, the number of hydrogen bond donors, and degree of hydrophobicity,[28] as being in line with our results pertaining to flavonoid transport. We demonstrated that flavonoid aglycones are superior substrates for MATE1 compared to their glycosides, suggesting that molecular weight may be the key determinant of MATE1 substrate specificity. Among the tested flavonoid aglycones, those with a higher number of hydrogen bond donors and acceptors, together with low hydrophobicity (assessed via the log *P* value), were superior substrates for MATE1. As such, quercetin demonstrated the highest uptake, followed by kaempferol, luteolin, and apigenin. These prerequisites for MATE1 substrate specificity were applied to explain other drug-based substrates for MATE1, such as metformin and 1-methyl-4-phenylpyridinium.[29]

In the MATE1 inhibitor and gene knockdown experiments, the basal level of quercetin uptake was maintained, which indicated that the uptake of quercetin and potentially other flavonoids occurs in a highly complex manner through multiple cellular transporters. With regard to quercetin, we know that MATE1 and bilitranslocase mediate the cellular uptake of quercetin; however, HepG2 cells that were incubated simultaneously with two inhibitors, namely, PMSF and pyrimethamine, revealed slightly increased quercetin accumulation (data not shown), which suggested that there may be an additional low-capacity, high-affinity cellular transporter.

The subcellular localization of MATE1 revealed that MATE1 is also expressed in intracellular organelles, including the ER and peroxisomal membrane as well as the plasma membrane. To our knowledge, this study is the first to confirm the expression of MATE1 in subcellular organelles in animal cells. Previously, Otsuka et al. reported the localization of human MATE1 in the liver, which suggested the expression of MATE1 in the canalicular and apical membranes of bile ducts. The

authors reported that MATE1 may be a polyspecific exporter for various types of organic compounds into the bile canaliculi with multidrug resistant gene-1.[30] Another study also claimed the expression of MATE1 in the brush border membrane of the proximal tubule of the kidney.[31] However, both studies did not report the intracellular localization of MATE1 in humans, which was previously confirmed in plant tissues. The findings of the expression of MATE1 in hepatic subcellular organelles and the accumulation of cellular flavonoids in organelles add a novel function for human MATE1, in addition to the previously reported role of exporting organic cations.

In conclusion, MATE1 is a novel flavonoid transporter in mammalian cells, particularly for quercetin in the liver and intestine. MATE1 is mainly expressed in plasma, ER, and peroxisomal membranes, and increased cellular flavonoid accumulation was observed in hMATE1 cells. Cellular quercetin accumulation in mammalian MATE1 eliminates lipid and glucose disorders. Owing to the limited bioavailability of dietary quercetin, the control of quercetin bioavailability through regulation of MATE1 expression may optimize its health benefits.

## ■ ASSOCIATED CONTENT

### Supporting Information

Tissue distribution of MATE1 gene expression in different mouse tissues (Figure S1), cellular localization of MATE1 in mouse and human intestine (Figure S2), concentration-dependent flavonoid uptake in hMATE cells (Figure S3), and chemical properties of tested flavonoid and cellular flavonoid accumulation in hMATE1 cells (Table S1). This material is available free of charge via the Internet at http://pubs.acs.org.

## ■ AUTHOR INFORMATION

### Corresponding Author

*Telephone: +82-2-3290-3029. Fax: +82-2-3290-3653. E-mail: junelee@korea.ac.kr.

### Funding

This study was supported by the "Global Ph.D. Fellowship Project" of the National Research Foundation of Korea (NRF) and the "Cooperative Research Program for Agriculture Science and Technology Development (Project PJ010528032014)" of the Rural Development Administration, Republic of Korea.

### Notes

The authors declare no competing financial interest.

## ■ ABBREVIATIONS USED

ER, endoplasmic reticulum; LAMP, lysosome-associated membrane protein; MATE1, multidrug and toxic compound extrusion transporter-1; PMSF, phenylmethylsulfonyl fluoride; TBARS, thiobarbituric acid reactive substances; TBST, tris-buffered saline with Tween-20

## ■ REFERENCES

(1) Winkel-Shirley, B. Flavonoid biosynthesis. A colorful model for genetics, biochemistry, cell biology, and biotechnology. *Plant Physiol.* **2001**, *126* (2), 485−493.

(2) RiceEvans, C. A.; Miller, N. J.; Paganga, G. Structure−antioxidant activity relationships of flavonoids and phenolic acids. *Free Radical Biol. Med.* **1996**, *21* (3), 417−417.

(3) Middleton, E.; Kandaswami, C.; Theoharides, T. C. The effects of plant flavonoids on mammalian cells: Implications for inflammation, heart disease, and cancer. *Pharmacol. Rev.* **2000**, *52* (4), 673−751.

(4) Rivera, L.; Moron, R.; Sanchez, M.; Zarzuelo, A.; Galisteo, M. Quercetin ameliorates metabolic syndrome and improves the inflammatory status in obese Zucker rats. *Obesity* **2008**, *16* (9), 2081−2087.

(5) Egert, S.; Bosy-Westphal, A.; Seiberl, J.; Kurbitz, C.; Settler, U.; Plachta-Danielzik, S.; Wagner, A. E.; Frank, J.; Schrezenmeir, J.; Rimbach, G.; Wolffram, S.; Muller, M. J. Quercetin reduces systolic blood pressure and plasma oxidised low-density lipoprotein concentrations in overweight subjects with a high-cardiovascular disease risk phenotype: A double-blinded, placebo-controlled cross-over study. *Br. J. Nutr.* **2009**, *102* (7), 1065−1074.

(6) Davis, H. R.; Zhu, L. J.; Hoos, L. M.; Tetzloff, G.; Maguire, M.; Liu, J. J.; Yao, X. R.; Iyer, S. P. N.; Lam, M. H.; Lund, E. G.; Detmers, P. A.; Graziano, M. P.; Altmann, S. W. Niemann-Pick C1 like 1 (NPC1L1) is the intestinal phytosterol and cholesterol transporter and a key modulator of whole-body cholesterol homeostasis. *J. Biol. Chem.* **2004**, *279* (32), 33586−33592.

(7) Wu, Q. W.; Ortegon, A. M.; Tsang, B.; Doege, H.; Feingold, K. R.; Stahl, A. FATP1 is an insulin-sensitive fatty acid transporter involved in diet-induced obesity. *Mol. Cell. Biol.* **2006**, *26* (9), 3455−3467.

(8) Dawson, P. A.; Lan, T.; Rao, A. Bile acid transporters. *J. Lipid Res.* **2009**, *50* (12), 2340−2357.

(9) Maestro, A.; Terdoslavich, M.; Vanzo, A.; Kuku, A.; Tramer, F.; Nicolin, V.; Micali, F.; Decorti, G.; Passamonti, S. Expression of bilitranslocase in the vascular endothelium and its function as a flavonoid transporter. *Cardiovasc. Res.* **2010**, *85* (1), 175−183.

(10) Passamonti, S.; Terdoslavich, M.; Franca, R.; Vanzo, A.; Tramer, F.; Braidot, E.; Petrussa, E.; Vianello, A. Bioavailability of flavonoids: A review of their membrane transport and the function of bilitranslocase in animal and plant organisms. *Curr. Drug Metab.* **2009**, *10* (4), 369−394.

(11) Morris, M. E.; Zhang, S. Z. Flavonoid−drug interactions: Effects of flavonoids on ABC transporters. *Life Sci.* **2006**, *78* (18), 2116−2130.

(12) Yi, W. G.; Akoh, C. C.; Fischer, J.; Krewer, G. Absorption of anthocyanins from blueberry extracts by Caco-2 human intestinal cell monolayers. *J. Agric. Food Chem.* **2006**, *54* (15), 5651−5658.

(13) Zhao, J.; Dixon, R. A. The 'ins' and 'outs' of flavonoid transport. *Trends Plant Sci.* **2010**, *15* (2), 72−80.

(14) Zhao, J.; Dixon, R. A. MATE transporters facilitate vacuolar uptake of epicatechin 3′-*O*-glucoside for proanthocyanidin biosynthesis in *Medicago truncatula* and *Arabidopsis*. *Plant Cell* **2009**, *21* (8), 2323−2340.

(15) Astorga, B.; Ekins, S.; Morales, M.; Wright, S. H. Molecular determinants of ligand selectivity for the human multidrug and toxin extruder proteins MATE1 and MATE2-K. *J. Pharmacol. Exp. Ther.* **2012**, *341* (3), 743−755.

(16) Tanihara, Y.; Masuda, S.; Sato, T.; Katsura, T.; Ogawa, O.; Inui, K. Substrate specificity of MATE1 and MATE2-K, human multidrug and toxin extrusions/$H^+$-organic cation antiporters. *Biochem. Pharmacol.* **2007**, *74* (2), 359−371.

(17) Lee, J. H.; Kim, Y. J.; Hoang, M. H.; Jun, H. J.; Lee, S. J. Rapid quantification of cellular flavonoid levels using quercetin and a fluorescent diphenylboric acid 2-amino ethyl ester probe. *Food Sci. Biotechnol.* **2014**, *23* (1), 75−79.

(18) Graham, J.; Ford, T.; Rickwood, D. The preparation of subcellular organelles from mouse liver in self-generated gradients of iodixanol. *Anal. Biochem.* **1994**, *220* (2), 367−373.

(19) Tuma, P. L.; Hubbard, A. L. Isolation of rat hepatocyte plasma membrane sheets and plasma membrane domains. *Current Protocols in Cell Biology*; John Wiley and Sons, Inc.: Hoboken, NJ, 2001; Chapter 3, Unit 3.2, DOI: 10.1002/0471143030.cb0302s02.

(20) Chen, L.; Yang, X.; Jiao, H.; Zhao, B. Tea catechins protect against lead-induced cytotoxicity, lipid peroxidation, and membrane fluidity in HepG2 cells. *Toxicol. Sci.* **2002**, *69* (1), 149−156.

(21) Vidyashankar, S.; Sandeep Varma, R.; Patki, P. S. Quercetin ameliorate insulin resistance and up-regulates cellular antioxidants

during oleic acid induced hepatic steatosis in HepG2 cells. *Toxicol. In Vitro* **2013**, *27* (2), 945−953.
(22) Miean, K. H.; Mohamed, S. Flavonoid (myricetin, quercetin, kaempferol, luteolin, and apigenin) content of edible tropical plants. *J. Agric. Food Chem.* **2001**, *49* (6), 3106−3112.
(23) Jovanovic, S. V.; Steenken, S.; Tosic, M.; Marjanovic, B.; Simic, M. G. Flavonoids as antioxidants. *J. Am. Chem. Soc.* **1994**, *116* (11), 4846−4851.
(24) Seidler, N. W.; Jona, I.; Vegh, M.; Martonosi, A. Cyclopiazonic acid is a specific inhibitor of the $Ca^{2+}$-ATPase of sarcoplasmic reticulum. *J. Biol. Chem.* **1989**, *264* (30), 17816−17823.
(25) Furuchi, T.; Aikawa, K.; Arai, H.; Inoue, K. Bafilomycin A1, a specific inhibitor of vacuolar-type $H^+$-ATPase, blocks lysosomal cholesterol trafficking in macrophages. *J. Biol. Chem.* **1993**, *268* (36), 27345−27348.
(26) Ross, J. A.; Kasum, C. M. Dietary flavonoids: Bioavailability, metabolic effects, and safety. *Annu. Rev. Nutr.* **2002**, *22*, 19−34.
(27) Panchal, S. K.; Poudyal, H.; Brown, L. Quercetin ameliorates cardiovascular, hepatic, and metabolic changes in diet-induced metabolic syndrome in rats. *J. Nutr.* **2012**, *142* (6), 1026−1032.
(28) Wittwer, M. B.; Zur, A. A.; Khuri, N.; Kido, Y.; Kosaka, A.; Zhang, X. X.; Morrissey, K. M.; Sali, A.; Huang, Y.; Giacomini, K. M. Discovery of potent, selective multidrug and toxin extrusion transporter 1 (MATE1, SLC47A1) inhibitors through prescription drug profiling and computational modeling. *J. Med. Chem.* **2013**, *56* (3), 781−795.
(29) Hillgren, K. M.; Keppler, D.; Zur, A. A.; Giacomini, K. M.; Stieger, B.; Cass, C. E.; Zhang, L. Emerging transporters of clinical importance: an update from the international transporter consortium. *Clin. Pharmacol. Ther.* **2013**, *94* (1), 52−63.
(30) Omote, H.; Hiasa, M.; Matsumoto, T.; Otsuka, M.; Moriyama, Y. The MATE proteins as fundamental transporters of metabolic and xenobiotic organic cations. *Trends Pharmacol. Sci.* **2006**, *27* (11), 587−593.
(31) Terada, T.; Inui, K. I. Physiological and pharmacokinetic roles of $H^+$/organic cation antiporters (MATE/SLC47A). *Biochem. Pharmacol.* **2008**, *75* (9), 1689−1696.

Table 1. Flavonoid Content in 16 Genotypes of Common Bean by LC-qMS[a]

| genotype | type of grain | origin | μg/g dry weight of seed flour | | | | | | |
|---|---|---|---|---|---|---|---|---|---|
| | | | DA | GE | KA | M | Q | CM | DA + GE |
| Arc 1 | B | M | 6.82 ± 0.95 | 6.38 ± 0.78 | 2.28 ± 0.19 | nd | 2.56 ± 0.44 | 7.75 ± 0.33 | 13.20 |
| IAC Diplomata | B | M | nd | 1.10 ± 0.80 | 0.78 ± 0.06 | nd | 1.09 ± 0.17 | 2.32 ± 0.09 | |
| Raz 55 | B | M | 8.05 ± 1.83 | 5.98 ± 0.89 | 5.40 ± 0.78 | 26.15 ± 22.86 | 8.34 ± 0.91 | 17.67 ± 4.40 | 14.03 |
| TU | B | M | nd | 0.98 ± 0.17 | 4.85 ± 3.53 | 78.94 ± 13.94 | 15.85 ± 3.57 | 0.75 ± 0.14 | |
| IPR Uirapuru | B | M | nd | 1.45 ± 0.06 | 2.82 ± 0.39 | nd | 4.37 ± 3.80 | 2.60 ± 0.21 | |
| IAC Una | B | M | 2.30 ± 0.28 | 2.95 ± 0.13 | 1.58 ± 0.74 | nd | 2.80 ± 0.94 | 5.95 ± 0.40 | 5.25 |
| IAC Alvorada | C | M | nd | nd | 1.64 ± 1.18 | nd | nd | nd | |
| IAC Carioca Comum | C | M | nd | 1.17 ± 0.15 | 35.09 ± 2.55 | nd | nd | 1.19 ± 0.16 | |
| IAC Formoso | C | M | nd | 8.93 ± 0.67 | 60.07 ± 3.17 | nd | 9.88 ± 3.04 | 16.85 ± 0.81 | |
| IAC Pérola | C | M | nd | 0.82 ± 0.65 | 16.37 ± 11.53 | nd | nd | 3.31 ± 2.87 | |
| IAC Harmonia | S | A/M | nd | nd | 0.40 ± 0.32 | nd | nd | nd | |
| IAC Boreal | S | A/M | nd | nd | 2.69 ± 0.40 | nd | nd | nd | |
| Brancão Argentino | W | A | nd | nd | nd | nd | nd | nd | |
| IAC Jabola | Bo | A/M | nd | 1.39 ± 0.09 | 117.65 ± 5.09 | nd | 2.79 ± 0.65 | 4.50 ± 1.04 | |
| IAC Esperança | Bo | A/M | nd | 2.16 ± 0.29 | 72.13 ± 1.06 | nd | nd | 2.53 ± 0.36 | |
| Flor de Mayo | R | A | nd | 1.93 ± 0.33 | 6.47 ± 0.59 | nd | nd | nd | |
| Soja | | | 62.66 ± 2.68 | 77.80 ± 8.38 | nd | nd | nd | nd | 140.46 |

[a]Values shown are means of three repetitions. Type of grain: B, black; C, carioca; S, striped; W, white; Bo, bolinha; R, red. Origin: A, Andean; M, Mesoamerican. Isoflavonoids: DA, daidzein, and GE, genistein. Flavonols: KA, kaempferol, M, myricetin, and Q, quercetin. CM, coumestrol. nd, not detected.

was to assess the flavonoid and coumestrol content in germplasm with a broad genetic base of the species, for the purpose of introducing new nutraceutical parameters in the crop breeding program.

## MATERIALS AND METHODS

**Plant Material.** The study was carried out at the Campinas (SP) (22° 54′ 20″ S, 47° 03′ 39″ W) during the rainy season (December–May) with 16 common bean genotypes from the two major gene pools with different seed coats and grain sizes, and one soybean genotype used as a reference (Table 1, Figure 1). Seeds of each cultivar were sown in a 5-m-length row (10 plants/m) for a total area of 105 $m^2$. After 3 months, grains from all genotypes were collected and kept in an air-circulation laboratory oven at 30 °C for drying to constant weight, and afterward ground in a mill and stored with protection against moisture.

**Standards.** Authentic standard daidzein, daidzin, genistein, and genistin (isoflavonoids); quercetin, kaempferol, and myricetin (flavonols); coumestrol (coumestan); and chrysin were purchased from Sigma Chemical Co. (St. Louis, MO). Stock solutions were prepared by dissolving the standards in MeOH–$H_2O$ (1:1) for a final concentration of 10 mg/mL.

**Solvents.** All solvents used were HPLC-grade and were purchased from Sigma Chemical Co. (St. Louis, MO).

**Extraction and Purification of Flavonoids.** Portions (2 g) of dry and ground grains were extracted with 60 mL of 70% ethanol (pH 2.0, adjusted with formic acid) for 24 h at ambient temperature.[21] The extracts were partitioned with 60 mL of hexane, and the aqueous phase was evaporated under reduced pressure to dryness. The residue of each extract was resuspended in MeOH–$H_2O$ (1:1), filtered through a 13 mm PTFE membrane filter of 0.45 μm, and kept at −20 °C up to the time of analysis. Each extract was prepared and analyzed in triplicate.

**Identification and Quantification of Flavonoids.** Quantification of all compounds was conducted from construction of a calibration curve with chrysin as internal standard. Individual identification of the flavonoids (negative mode) was performed on the basis of retention times, spectroscopic data, and mass-to-charge ratio ($m/z$) of each standard by use of 10 points of concentration, 0.005–5 μg/mL, containing the internal standard at a final concentration of 4 μg/mL (Table 2). Results were expressed as milligrams per gram dry weight of seed flour.

Figure 1. Seed coat colors of the 16 genotypes evaluated. (A) Arc1, (B) IAC Diplomata, (C) Raz 55, (D) TU, (E) IPR Uirapuru, (F) IAC Una, (G) IAC Alvorada, (H) IAC Carioca Comum, (I) IAC Formoso, (J) IAC Pérola, (K) IAC Harmonia, (L) IAC Boreal, (M) Brancão Argentino, (N) IAC Jabola, (O) IAC Esperança, and (P) Flor de Mayo.

**Analytical Techniques and Equipment.** The LC-ESI-QTOF-MS MicroTOF-QII Bruker equipped with an autosampler, binary pump, thermostated column compartment, and multiple-wavelength detector was used. Separations of flavonoids were achieved on a 150 × 2.0 mm i.d, 5 μm C18 Luna column (Phenomenex, Torrence, CA) at 30 °C. Injection volume was 20 μL at a flow rate of 0.25 mL/min. Linear gradient elution was performed with solvent A (methanol/formic acid, 95:5 v/v) and solvent B (5% formic acid in water, v/v) at


dx.doi.org/10.1021/jf5033312 | J. Agric. Food Chem. 2014, 62, 9699–9704

**Table 2. LC-qMS and Calibration Parameters of Flavonoids**

| compd | $t_R$ (min) | $[M - H]^-$ ($m/z$) | $r^2$ | concn ($\mu$M) |
|---|---|---|---|---|
| daidzein | 13.39 | 253 | 0.976 | 0.02−19.7 |
| genistein | 13.39 | 269 | 0.991 | 0.02−18.5 |
| quercetin | 15.56 | 301 | 0.996 | 0.02−16.5 |
| kaempferol | 17.47 | 285 | 0.995 | 0.02−17.5 |
| myricetin | 13.10 | 317 | 0.999 | 0.01−15.7 |
| coumestrol | 18.19 | 267 | 0.991 | 0.02−18.7 |
| chrysin | 20.25 | 253 | | 0.02−19.7 |

30% A/70% B from 0 to 4 min, 100% A from 4 to 50 min, and 30% A/70% B from 50 to 65 min. Chromatograms were recorded by UV detection at 254, 270, and 330 nm and by ESI-MS in negative-ion scan mode (100−600 $m/z$) with nitrogen as nebulizer gas at 58 psi and 4.5 kV capillary voltage at 350 °C. Identification of flavonoids and coumestan was based on the following ions ($[M - H]^-$, $m/z$) for each analyte: 253 for daidzein, 269 for genistein, 415 for daidzin, 431 for genistin, 301 for quercetin, 285 for kaempferol, 317 for myricetin, 267 for coumestrol, and 253 for chrysin.

**Data Analysis.** Descriptive statistics were used to characterize the data overall and across factors. To identify statistical differences in flavonoid content among factors, ANOVA and canonical analysis methods were employed. Statistical analyses were performed by use of the Genes program.[22]

## RESULTS AND DISCUSSION

**Identification of Bean Flavonoids and Coumestrol.** The maximum and minimum temperatures of the location where the plant material was grown ranged from 17.6 to 27.5 °C (Figure 2) with mean monthly rainfall of 7.14 mm

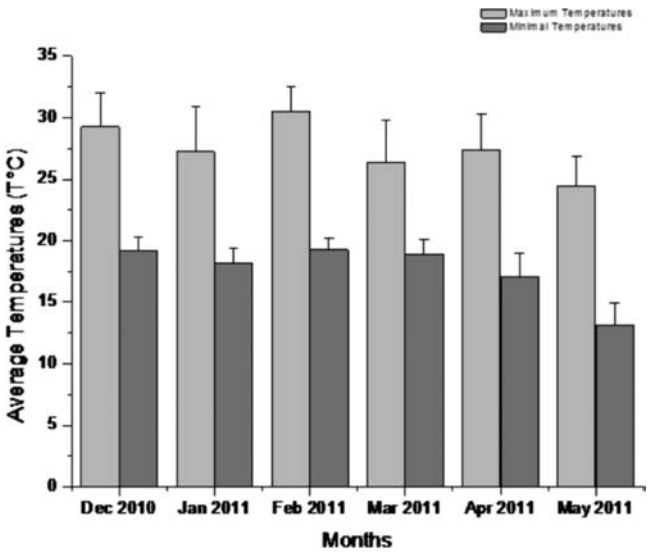


**Figure 2.** Average maximum and minimum temperature during the growth biological assay.

(December 2010−May 2011). Studies on genetic and environmental effects, performed on soybean in locations where mean temperatures ranged from 19 to 27 °C, manifested a strong influence of the environment on isoflavonoid contents.[23,24]

In all 16 genotypes assessed, we found the flavonoids quercetin (Q), myricetin (M), and kaempferol (KA) and the nonglycosylated forms of isoflavonoids daidzein (DA) and genistein (GE), both of greater occurrence among the legumes, as well as coumestrol, all with wide variation of occurrence among the genotypes of the study (Table 1).[25]

With the exceptions of IAC Alvorada (carioca seed coat), IAC Boreal and IAC Harmonia (striped seed coat), and Brancão Argentino (white seed coat), all the genotypes exhibited genistein (GE), ranging from 0.82 (IAC Pérola) to 8.93 (IAC Formoso) $\mu$g/g.

Among the types of grains, the genotypes of black seed coat and Mesoamerican origin stood out: in addition to containing GE, they were the only ones to also exhibit daidzein (DA), as in the case of IAC Una (2.30 ± 0.28 $\mu$g/g), Arc 1 (6.82 ± 0.95 $\mu$g/g), and Raz 55 (8.05 ± 1.83 $\mu$g/g). A similar result was reported by Romani et al.,[26] who observed the presence of these isoflavonoids in a local variety of black bean, and by Díaz-Batalla et al.[25] in assessment of cultivated and wild Mexican common beans. Liggins et al.[10] also reported levels of daidzein and genistein in beans with red seed coat. IAC Una, Arc 1, and Raz 55 were the only ones to show DA and GE at higher levels. IAC Una is considered to be the main Brazilian cultivar for resistance to the anthracnose pathogen (*Colletotrichum lindemuthianum*).[27] In Arc 1 and Raz55, the presence of the protein arcelin was observed, which is considered to be the main source of resistance to *Zabrotes subfasciatus*, one of the main pests of stored grains that occurs in common bean.[28]

With variation from 0.82 to 14.03 $\mu$g/g isoflavonoids for the genotypes assessed, the results obtained were similar to those reported in common bean, where contents from 6 to 14 $\mu$g/g were found for different landraces, from 8.3 to 13.4 $\mu$g/g for striped common beans, and from 7.1 to 11.4 $\mu$g/kg of isoflavonoids (daidzein and genistein) in haricot bean.[26,27,29]

In soybean, a microbial toxic action of the glycosides daidzein and genistein was proposed in resistance to fungus infection of seeds and seedlings.[30] In the genus *Phaseolus*, Adesanya et al.[31] tested isoflavones, isoflavonones, pterocarpans, and coumestan from five species against *Aspergillus niger* and *Cladosporium cucumericum* and observed the importance of at least a phenolic function to activate the fungitoxic activity of these compounds, making assessment of the structure−fungitoxic activity relationships within these groups of isoflavonoids possible.

Corroborating the results found by Beninger et al.,[32] flavonols occurred in all the genotypes assessed, except for the genotype Brancão Argentino (Table 1). The highest occurrence of the flavonol kaempferol (KA) was seen in grains with a light-colored seed coat like those of the bolinha and carioca types. IAC Jabola and IAC Esperança, both with bolinha and carioca seed coat types, such as IAC Carioca Comum, IAC Formoso, and IAC Pérola (all of Mesoamerican origin), exhibited kaempferol contents that ranged from 16.37 to 117.65 $\mu$g/g (Table 1). A similar profile was found by Ranilla et al.[6] in assessment of 25 Brazilian common bean cultivars as a function of color of the seed coat and of the cotyledon. This flavonol modifies a series of cell signaling pathways acting with less toxicity in comparison to standard chemotherapies.[33]

Quercetin (Q) and myricetin (M) occurred preferentially in black grains, ranging from 1.09 to 15.85 $\mu$g/g and from 26.15 to 78.94 $\mu$g/g, respectively. Díaz-Batalla et al.[25] found a similar occurrence of quercetin in black grains and kaempferol in lighter-colored grains. In fact, quercetin and kaempferol are the most abundant flavonols in foods and are antioxidant and chelating compounds with beneficial effects on health.[34] They are also associated with the function of protecting seeds against pathogens and predators.[35] An explanation for the fact of common bean being considered a source of flavonols was the high occurrence of quercetin and kaempferol in the cultivar


dx.doi.org/10.1021/jf5033312 | J. Agric. Food Chem. 2014, 62, 9699−9704

IAC Formoso, exhibiting contents from 9.88 ± 3.04 to 60.07 ± 3.17 μg/g.[11]

Genotypes of Mesoamerican origin with black and carioca seed coats and of Andean origin with bolinha seed coat manifested coumestrol (Table 1). Coumestrol is an important compound which contains high levels of estrogenic activity, 30−100 times greater than that of the isoflavones, and it was identified in all the black grains (Table 1), ranging from 0.75 (TU) to 17.67 (Raz 55) μg/g.[18] Among the grains with carioca seed coat, IAC Formoso presented the greatest content of this coumestan (16.85 ± 0.81 μg/g). Konar[36] assessed common bean and lentils through LC-MS/MS and found this coumestan in common bean (18.5 μg/kg) and a mean value of 16.9 μg/kg in yellow, green, and red lentils. Moreover, by LC-MS/MS and with standards marked with $^{13}C$, Kuhnle et al.[37] found contents ranging from 1 to 10 μg/100 g for common bean, values considered very inferior to ours, even when it is taken into account that the authors expressed their results by fresh weight.

IAC Formoso exhibited the greatest concentration of genistein among all the genotypes assessed (8.93 ± 0.67 μg/g), around 11% of the total presented by the soybean control. Genistein is considered to be the isoflavone with greatest biological activity and is furthermore classified as an inducible phytoalexin.[21] In addition, IAC Formoso exhibited the second greatest concentration of coumestrol (16.85 ± 0.81 μg/g), a compound that has been reported as an estrogen receptor twice as powerful as genistein and, furthermore, a modulator in hormone production of the thymus.[38]

**Grouping Common Bean According to Seed Coat Color.** Canonical variable analysis (CVA) was applied to the values of flavonoid content of the genotypes assessed. This multivariate analysis is similar to principal component analysis, and it is especially used in discriminating analyses with replication of observations because it is based on the variances of these replications.

The first three canonical variables explained 97.5% of the total variance among the 16 genotypes and showed the formation of three groups in accordance with the flavonoid and coumestrol content (Figure 3). A first group gathered the genotypes Arc 1 and Raz 55, both with a black seed coat and of Mesoamerican origin and with the greatest isoflavonoid contents found in the study. A second group was composed of IAC Jabola and IAC Esperança, both with bolinha type grains and the greatest concentrations of the flavonol kaempferol, which occurred preferentially in light-colored grains. All the other genotypes were in a third group.

Canonical variable 1 (VC1), with 78.8% of the total variance, differentiated the genotypes of the study in accordance with daidzein and genistein content. Thus, Arc 1 and Raz 55 were differentiated from IAC Jabola and IAC Esperança, by presenting the highest and lowest contents of daidzein and genistein, respectively (Table 1). Canonical variable 2 (VC2) represents 13.2% of the variation and showed the separation of the genotypes in two groups with contrasting values of concentration of total flavonoids. In VC2, the first group gathered IAC Carioca comum, IAC Jabola, IAC Esperança, IAC Formoso, IAC Una, TU, Arc 1 and Raz 55. A second group was formed by IAC Diplomata, IPR Uirapuru, IAC Alvorada, IAC Pérola, IAC Harmonia, IAC Boreal, Flor de Mayo, and Brancão Argentino.

The variability found for flavonoid content in the grains of 16 genotypes assessed under field conditions may be explained by how these materials arose. Thus, factors such as seed coat type

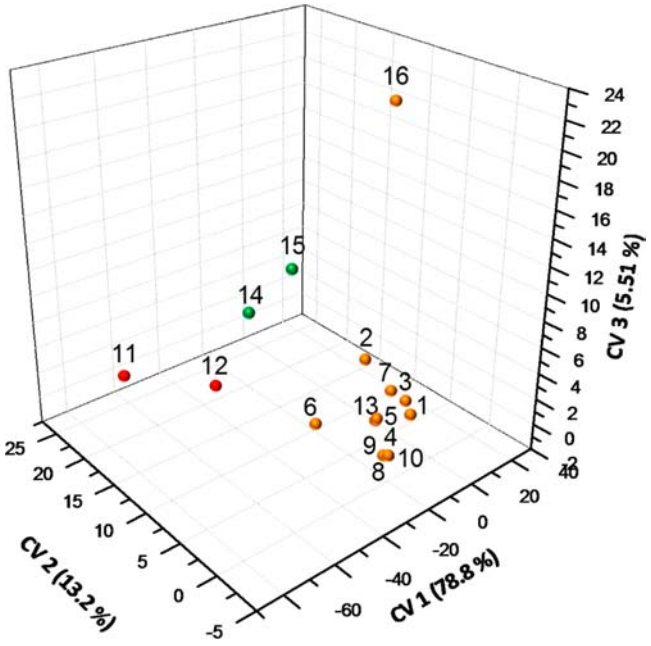


**Figure 3.** Multivariate exploratory analysis for 16 genotypes of common bean. Three groups were formed after canonical analysis: the yellow group contained IAC Diplomata (1), IAC Una (2), IPR Uirapuru (3), IAC Alvorada (4), IAC Pérola (5), IAC Carioca comum (6), TU (7), IAC Harmonia (8), IAC Boreal (9), Brancão Argentino (10), Flor de Mayo (13) and IAC Formoso (16) genotypes; The red group contained IAC Jabola (11) and IAC Esperança (12) genotypes; and the green group contained Arc1 (14) and Raz 55 (15) genotypes.

and selection for tolerance to biotic and abiotic stresses may explain the different concentrations of metabolites found. Related studies reinforce this hypothesis, where differences in the variability of isoflavonoids and flavonoids in accordance with the type of seed coat, genotype, and genotype−environmental interaction were cited by various authors.[23,39,40]

Important levels of flavonoids were observed in the germplasm of common bean grown under the same environmental conditions and high variability between groups with different seed coat colors. Among the beans with carioca-type seed coat, which represents nearly all of the common beans grown, IAC Formoso, a cultivar recently introduced for planting on a commercial scale, showed high values of flavonoids and coumestrol. This result suggests that this cultivar may be used in the genealogy of future genetic materials with a view toward adoption of nutraceutical characteristics in common bean.

## AUTHOR INFORMATION

### Corresponding Author

*Telephone (+5519) 35213105; fax (+5519) 35213023; e-mail paula.lima@iqm.unicamp.br.

### Notes

The authors declare no competing financial interest.

## ACKNOWLEDGMENTS

This work was financially supported by FAPESP. C.A.C., A.F.C., M.J.K., and S.A.M.C. thank the Conselho Nacional de Desenvolvimento Científico e Tecnológico (CNPq) for granting fellowships.

## ■ ABBREVIATIONS

ANOVA, analysis of variance; DA, daidzein; GE, genistein; HPLC, high-performance liquid chromatography; KA, kaempferol; LC-ESI-QTOF-MS, liquid chromatography−electrospray ionization quadrupole time-of-flight mass spectrometry; M, myricetin; PTFE, poly(tetrafluoroethylene); Q, quercetin

## ■ REFERENCES


(1) Angioi, S. A.; Rau, D.; Attene, G.; Nanni, L.; Bellucci, E.; Logozzo, G.; Negri, V.; Spagnoletti-Zeuli, P. L.; Papa, R. Beans in Europe: Origin and structure of the European landraces of *Phaseolus vulgaris* L. *Theor. Appl. Genet.* **2010**, *121*, 829−843.

(2) Carbonell, S. A. M.; Chiorato, A. F.; Carvalho, C. R. L.; Júnior, E. U. R.; Ito, M. A.; Borges, W. L. B.; Ticelli, M.; Santos, N. C. B.; Gallo, P. B. IAC Formoso: New carioca common bean cultivar. *Crop Breed. Appl. Biotechnol.* **2010**, *10*, 374−376.

(3) Espinosa-Alonso, L. G.; Lygin, A.; Widholm, J. M.; Valverde, M. E.; Paredes-Lopez, O. Polyphenols in wild and weedy Mexican common beans (*Phaseolus vulgaris* L.). *J. Agric. Food Chem.* **2006**, *54*, 4436−4444.

(4) Boniglia, C.; Carratú, B.; Gargiulo, R.; Giammarioli, S.; Mosca, M.; Sanzini, E. Content of phytoestrogens in soy-based dietary supplements. *Food Chem.* **2009**, *115*, 1389−1392.

(5) Kuhnle, G. G. C.; Dell'Aquila, C.; Runswick, S. A.; Bingham, S. A. Variability of phytoestrogen content in foods from different sources. *Food Chem.* **2009**, *113*, 1184−1187.

(6) Ranilla, L. G.; Genovese, M. I.; Lajolo, F. M. Polyphenols and antioxidant capacity of seed coat and cotyledon from Brazilian and Peruvian bean cultivars (*Phaseolus vulgaris* L.). *J. Agric. Food Chem.* **2007**, *55*, 90−98.

(7) Broughton, W. J.; Hernández, G.; Blair, M. W.; Beebe, S. Beans (*Phaseolus* spp.) - Model food legumes. *Plant Soil* **2003**, *252*, 55−128.

(8) Dong, M.; He, X.; Liu, R. H. Phytochemicals of black bean seed coats: Isolation, structure elucidation, and their antiproliferative and antioxidative activities. *J. Agric. Food Chem.* **2007**, *55*, 6044−6051.

(9) Pascual-Teresa, S.; Hallundb, J.; Talbotc, D.; Schrootd, J.; Williamse, C. M.; Bugelb, S.; Cassidy, A. Absorption of isoflavones in humans: effects of food matrix and processing. *J. Nutr. Biochem.* **2006**, *17*, 257−264.

(10) Liggins, L.; Bluck, L. J. C.; Runswick, S.; Atkinson, C.; Coward, W. A.; Bingham, S. A. Daidzein and genistein contents of vegetables. *Br. J. Nutr.* **2000**, *84*, 717−725.

(11) Dinelli, G.; Bonetti, A.; Minelli, M.; Marotti, I.; Catizone, P.; Mazzanti, A. Content of flavonols in Italian bean (*Phaseolus vulgaris* L.) ecotypes. *Food Chem.* **2006**, *99*, 105−114.

(12) Kuhnle, G. G. C.; Dell'Aquila, C.; Low, Y. L.; Kussmaul, M.; Bingham, S. A. Extraction and quantification of phytoestrogens in foods using automated solid-phase extraction and LC/MS/MS. *Anal. Chem.* **2007**, *79*, 9234−9239.

(13) Boué, S. M.; Burow, M. E.; Wiese, T. E.; Shih, B. Y.; Elliott, S.; Carter-Wientjes, C. H.; McLachlan, J. A.; Bhatnagar, D. Estrogenic and antiestrogenic activities of phytoalexins from red kidney bean (*Phaseolus vulgaris* L.). *J. Agric. Food Chem.* **2004**, *59*, 112−120.

(14) Wang, H.; Murphy, P. A. Isoflavone content in commecial soybean foods. *J. Agric. Food Chem.* **1994**, *42*, 1666−1673.

(15) Eldridge, A. C.; Kwolek, W. F. Soybean isoflavones: Effect of environment and variety on composition. *J. Agric. Food Chem.* **1983**, *31*, 394−396.

(16) Morris, P. F.; Savard, M. E.; Ward, E. W. B. Identification and accumulation of isoflavonoids and isoflavone glucosides in soybean leaves and hypocotyls in resistance responses to *Phytophthora megasperma* f.sp. *glycinea*. *Physiol. Mol. Plant Pathol.* **1991**, *39*, 229−244.

(17) Hong, Y. H.; Wang, S. C.; Hsu, C.; Lin, B. F.; Kuo, Y. H.; Huang, C. J. Phytoestrogenic compounds in alfalfa sprout (*Medicago sativa*) beyond coumestrol. *J. Agric. Food Chem.* **2011**, *59*, 131−137.

(18) Bacaloni, A.; Cavaliere, C.; Faberi, A.; Foglia, P.; Samperi, R.; Lagana, A. Determination of isoflavones and coumestrol in river water and domestic wastewater sewage treatment plants. *Anal. Chim. Acta* **2005**, *531*, 229−237.

(19) Lee, Y.-H.; Yuk, H. J.; Park, K.-H.; Bae, Y.-S. Coumestrol induces senescence through protein kinase CKII inhibition-mediated reactive oxygen species production in human breast cancer and colon cancer cells. *Food Chem.* **2013**, *141*, 381−388.

(20) Saijo, K.; Collier, J. G.; Li, A. C.; Katzenellenbogen, J. A.; Glass, C. K. An ADIOL-ERbeta-CtBP trans repression pathway negatively regulates microglia-mediated inflammation. *Cell* **2011**, *145*, 584−595.

(21) Romani, A.; Vignolini, P.; Galardi, C.; Aroldi, C.; Vazzana, C.; Heimler, D. Polyphenolic content in different plant parts of soy cultivars grown under natural conditions. *J. Agric. Food Chem.* **2003**, *51*, 5301−5306.

(22) Cruz, C. D. *Programa Genes - Análise multivariada e simulação*. 1st ed.; Editora UFV, Universidade Federal de Viçosa: Viçosa, Brazil, 2006; Vol. *1*.

(23) Carrão-Panizzi, M. C.; Del Pino Beleia, A.; Kitamura, K.; Oliveira, M. C. N. Effects of genetics and environment on isoflavone content of soybean from different regions of Brazil. *Pesqui. Agropecu. Bras.* **1999**, *34*, 1787−1795.

(24) Tsukamoto, C.; Shimada, S.; Igita, K.; Kudou, S.; Kokubun, M.; Okubo, K.; Kitamura, K. Factors affecting isoflavone content in soybean seeds: Changes in isoflavones, saponins, and composition of fatty acids at different temperatures during seed development. *J. Agric. Food Chem.* **1995**, *43*, 1184−1192.

(25) Díaz-Batalla, L.; Widholm, J. M.; Fahey, G. C.; Costano-Tostado, E.; Paredez-López, O. Chemical components with health implications in wild and cultivated Mexican common bean seeds (*Phaseolus vulgaris* L.). *J. Agric. Food Chem.* **2006**, *54*, 2045−2052.

(26) Romani, A.; Vignolini, P.; Galardi, C.; Mulinacci, N.; Benedettelli, S.; Heimler, D. Germplasm characterization of Zolfino landraces (*Phaseolus vulgaris* L.) by flavonoid content. *J. Agric. Food Chem.* **2004**, *52*, 3838−3842.

(27) Carbonell, S. A. M.; Ito, M. F.; Pompeu, A. S.; Francisco, F. G.; Ravagnani, S.; Almeida, A. L. L. Raças fisiológicas de *Colletotrichum lindemuthianum* e reação de linhagens e cultivares de feijoeiro no Estado de São Paulo. *Fitopatol. Bras.* **1999**, *24*, 60−65.

(28) Ribeiro-Costa, C. S.; Pereira, P. R. V. S.; Zulovski, L. Desenvolvimento de *Zabrotes subfasciatus* (Boh.) (Coleoptera: Chrysomelidae, Bruchinae) em genótipos de *Phaseolus vulgaris* L. (Fabaceae) cultivados no estado do Paraná e contendo arcelina. *Neotrop. Entomol.* **2007**, *36*, 560−564.

(29) Konar, N.; Poyrazoglu, E. S.; Demir, K.; Artik, N. Determination of conjugated and free isoflavones in some legumes by LC-MS/MS. *J. Food Compos. Anal.* **2012**, *25*, 173−178.

(30) Graham, T. L.; Kim, J. E.; Graham, M. Y. Role of constitutive isoflavone conjugates in the accumulation of glyceollin in soybean infected with *Phytophthora megasperma*. *Mol. Plant-Microbe Interact.* **1990**, *3*, 157−166.

(31) Adesanya, S. A.; O'Neill, M. J.; Roberts, M. F. Structure-related fungitoxicity of isoflavonoids. *Physiol. Mol. Plant Pathol.* **1986**, *29*, 95−103.

(32) Beninger, C. W.; Hosfield, G. L.; Bassett, M. J. Flavonoid composition of three genotypes of dry bean (*Phaseolus vulgaris*) differing in seed coat color. *J. Am. Hortic. Sci.* **1999**, *124*, 514−518.

(33) Zhang, Y.; Chen, A. Y.; Li, M.; Chen, C.; Yao, Q. *Ginkgo biloba* extract kaempferol inhibits cell proliferation and induces apoptosis in pancreatic cancer cells. *J. Surg. Res.* **2008**, *148*, 17−23.

(34) Heim, K. E.; Tagliaferro, A. R.; Bobilya, D. J. Flavonoid antioxidants: Chemistry, metabolism and structure-activity relationships. *J. Nutri. Biochem.* **2002**, *13*, 572−584.

(35) Islam, F. M. A.; Rengifo, J.; Redden, R. J.; Basford, K. E.; Beebe, S. E. Association between seed coat polyphenolics (tannins) and disease resistance in common bean. *Plant Food Hum. Nutr.* **2003**, *58*, 285−297.

(36) Konar, N. Non-isoflavone phytoestrogenic compound contents of various legumes. *Eur. Food Res. Technol.* **2013**, *236*, 523−530.

(37) Kuhnle, G. G. C.; Dell'Aquila, C.; Aspinall, S. M.; Runswick, S. A.; Joosen, A. M. C. P.; Mulligan, A. A.; Bingham, S. A. Phytoestrogen

content of fruits and vegetables commonly consumed in the UK based on LC-MS and $^{13}$C-labelled standards. *Food Chem.* **2009**, *116*, 542−554.

(38) Ndebele, K.; Graham, B.; Tchouwou, P. B. Estrogenic activity of coumestrol, DDT, and TCDD in human cervical cancer cells. *Int. J. Environ. Res. Public. Health* **2010**, *7*, 2045−2056.

(39) Lee, S. J.; Seguin, P.; Kim, J. J.; Moond, H. I.; Ro, H. M.; Kim, E. H.; Seo, S. H.; Kang, E. Y.; Ahn, J. K.; Chung, I. M. Isoflavones in Korean soybeans differing in seed coat and cotyledon color. *J. Food Compos. Anal.* **2010**, *23*, 160−165.

(40) Kim, J. K.; Kim, E. H.; Lee, O. K.; Park, S. Y.; Lee, B.; Kim, S. H.; Park, I.; Chung, I. M. Variation and correlation analysis of phenolic compounds in mung bean (*Vigna radiata* L.) varieties. *Food Chem.* **2013**, *141*, 2988−2997.

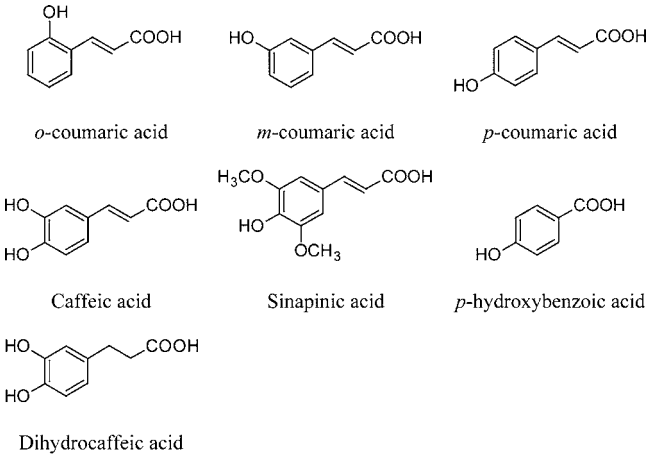


**Figure 1.** Chemical structures of coumaric acids and related compounds.

of the mechanism and kinetics of a series of oxidation reactions between CAs and different •OX species (•OH, •OOH, •$OCH_3$, and •$OOCH_3$) using the density function theory (DFT) is the ultimate goal of this work.

## COMPUTATIONAL DETAILS

DFT calculations were carried out using the Gaussian09 (rev. C.01) set of programs.[46] The reagent, transition state (TS), and molecular complex (MC) geometries were optimized at the M06-2X level,[47] along with the 6-311+G** basis set. M06-2X is especially recommended for thermodynamic and kinetic calculations.[47,48] An initial conformational analysis was carried out for the reagents to obtain the lowest energy conformation. The nature of the stationary points was assessed by means of the normal vibration frequencies calculated from the analytical second derivatives of the energy. The first-order saddle points, which are related to transition states, must show an imaginary value for the frequency associated with the eigenvector primarily describing the product formation step, whereas the real minima of the potential energy hypersurface, which are related to stable species, have to show positive real values for all of the vibrational frequencies. In addition, intrinsic reaction coordinate (IRC) calculations at the M06-2X/6-311+G** level were carried out to assess each reaction pathway.

The rate constants ($k_{TST}$) were calculated through the thermodynamic formulation of the transition state theory (TST). Gibbs free energy barriers were computed at 298.15 K. The tunneling effect along the reaction coordinate has been accounted for by means of the transmission coefficient $\chi(T)$ given by Wigner's model

$$\chi(T) = 1 + \frac{1}{24}\left(\frac{h|\omega^*|}{k_B T}\right)^2 \quad (5)$$

where $\omega^*$ and $k_B$ are the TS imaginary frequency and the Boltzmann constant, respectively.[49−52] Thus, the final expression for the rate constant ($k_{TST/W}$) becomes

$$k_{TST/W} = \chi(T) k_{TST} \quad (6)$$

## RESULTS AND DISCUSSION

Figure 1S (in the Supporting Information) summarizes the most favored conformers obtained from the initial conformational analysis for the three coumaric acids studied in this work. As discussed above, the oxidation of hydroxycinnamic acid derivatives with reactive oxygen species is expected to be carried out via addition to the double bond or H abstraction. To simplify the study (there are a considerable number of chemically different hydrogen atoms in the studied compounds) and because the most labile hydrogen atoms correspond to the hydroxyl and carboxylic groups, we decided not to consider more H abstraction pathways than those related to these two groups. The transition states corresponding to the addition pathways were computed only on one side of the reagent because coumaric acids show planar structures (see Figure 2) in which both sides are chemically equivalents.

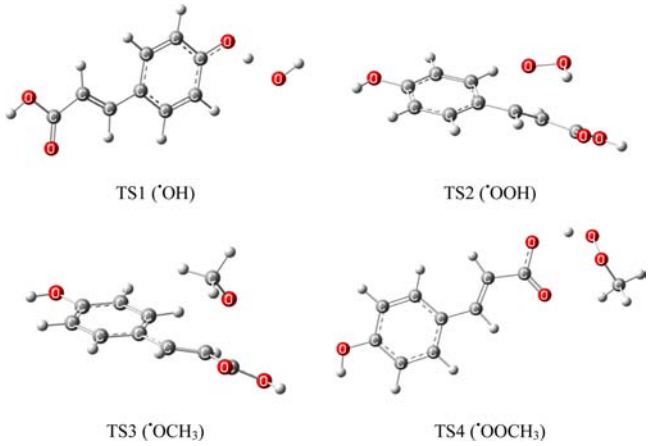


**Figure 2.** Some of the different transitions states found for the reactions of *p*-coumaric acid with reactive oxygen species. Geometries were optimized at the M06-2X/6-311+G** level.

Different transition states were named TS*n*, where *n* indicates the position attacked by the •OX species. Thus, TS1 and TS4 correspond to the transition states in which •OX abstracts the H atom from the −OH and −COOH groups, respectively, whereas the addition mechanism occurs through both TS2 and TS3. Figure 2 shows some examples of the different transitions states found for the reactions of *p*-coumaric acid with •OX. Detailed information on the main geometrical parameters for all of the computed transition states can be found in the Supporting Information. For the H abstraction mechanism, TSs involving •OH radicals show some differences with respect to the rest of TSs. TS1s involving •OH show geometries close to the reagents in which the breaking O···H bond length is within 1.02−1.03 Å, whereas the forming H···O bond is significantly longer (1.40−1.42 Å). For the rest of the TS1s, differences between the lengths of the breaking and forming bonds are significantly smaller, lying within 0.01−0.18 Å. The geometries of TS4s involving •OH are also different from the rest of the TS4s. In the first ones, the difference between the lengths of the breaking and forming bonds are ≤0.09 Å, whereas the other TS4s are within the range of 0.32−0.61 Å. Besides, for TS4s involving •OH and •OOH radicals, the short lengths (≤2.05 Å) between the hydrogen atom from •OX and the carbonyl oxygen from the acid group, compared to the sum of van der Waals radii (2.6 Å),[53] suggest possible stabilizing interactions. This fact may lead to the formation of 5- and 6-membered pseudorings for TS4s involving •OH and •OOH radicals (see Tables 1S−6S in the Supporting Information). No significant differences were observed for TS2 and TS3 with respect to the sort of •OX species chosen. •OX interacts with an unsaturated carbon with a C═C···O angle within 87−110° and with an O···C bond length within 1.88−2.18 Å. Two examples of IRC profiles for H abstraction and addition pathways of the *m*-coumaric acid + •OH reaction can be seen in Figure 3.


dx.doi.org/10.1021/jf5011148 | J. Agric. Food Chem. 2014, 62, 9705−9710

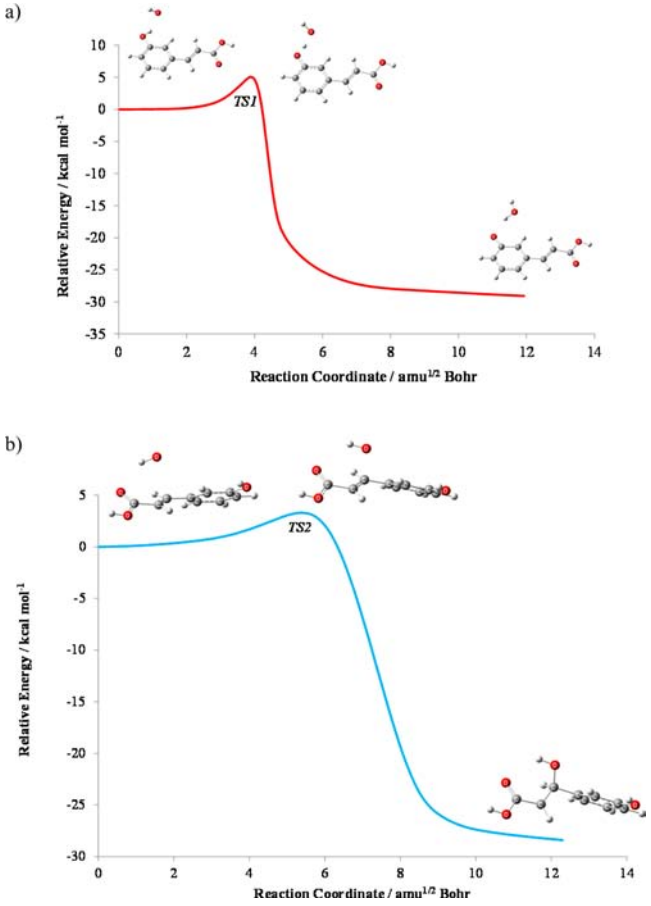


**Figure 3.** IRC calculations for both an H abstraction and an addition channel of the *m*-coumaric acid + •OX reaction computed at the M06-2X/6-311+G** level: (a) pathway through TS1; (b) pathway through TS2.

Table 1 summarizes the activation ($\Delta G^{\ddagger}$) and reaction ($\Delta_r G$) Gibbs free energies calculated for each considered reaction pathway. $\Delta G^{\ddagger}$ increases following the order •OH < $^{\bullet}OCH_3$ < •OOH < $^{\bullet}OOCH_3$, where the most significant rise is observed for the peroxide radicals. The lowest free energy barriers were calculated for TS1 and TS3 in all of the reactions, whereas TS4 shows significantly higher $\Delta G^{\ddagger}$ values than the rest of the pathways. The addition mechanism through TS3 is the pathway with the lowest free energy barriers for the reactions involving •OH. This was expected because the addition of a radical at the 2′-position of C═C via TS3 led to a benzylic radical, which is more stable than that formed after the addition at the 1′-position of the double bond. In a previous DFT study, Leopoldini et al. have also been reported that the addition mechanism is thermodynamically and kinetically favored over the H-abstraction for the reaction of caffeic acid with •OH, being the 2′-position favored over the 1′-position.[41] For the reactions involving $^{\bullet}OCH_3$, •OOH, and $^{\bullet}OOCH_3$, the $\Delta G^{\ddagger}$ values calculated for the TS1 pathways (H abstraction mechanism) are at least 1.7 kcal mol$^{-1}$ lower than the corresponding reaction pathways through TS3 (addition mechanism). In this sense, a DFT study from Galano et al.[32] also reported that the main mechanism for the reaction of •OOH with a related compound, sinapinic acid, should be H abstraction through TS1. In general, H abstraction reactions show a lower free energy barrier for *o*- and *p*-coumaric acids than for *m*-coumaric acid, whereas addition reactions do not show a clear trend. Negative $\Delta_r G$ values were calculated for all pathways considered in coumaric acid reactions with •OH and $^{\bullet}OCH_3$ radicals, in contrast with the positive values computed for reactions involving peroxide radicals.

Kinetic rate constants using the TST were estimated at 298.15 K and are shown in Table 1. In this table, $k_{TST/W}$ values include tunneling coefficient corrections, whereas $k_{TST}$ values do not. Substantial differences in the rate constant values were obtained for reactions involving different •OX species. Those values follow the inverse order of the free energy barrier heights (•OH > $^{\bullet}OCH_3$ > •OOH > $^{\bullet}OOCH_3$). For coumaric acid + •OH reactions, $k_{TST}$ values for the addition mechanism through TS3 are at least 60% higher than the corresponding TS1 H abstraction pathway (for *m*-coumaric acid + •OH reaction, the difference for both $k_{TST}$ values becomes an order of magnitude). However, these differences are reduced or even inverted with the use of tunneling coefficient corrections because the small imaginary frequencies (see Table 2) computed for the different TS1s ($\upsilon < 1600i$ cm$^{-1}$) lead to $\chi(T)$ coefficients from 3 to 4 times larger than those calculated for the addition pathways. Hence, both addition through TS3 and H abstraction through TS1 can be considered pathways with a comparable weight in the global reaction mechanism. Here, it is worth noting that each addition pathway presents two equivalent reaction points because of the planarity of the molecule. For the reactions involving the rest of •OX species studied, H abstraction at the hydroxyl group should be the main reaction mechanism. In these cases, values estimated for $k_{TST/W}$ corresponding to TS1 are ≥2 orders of magnitude higher than $k_{TST/W}$ values estimated for the rest of pathways.

The lowest rate constants were estimated for *m*-coumaric acid reactions with any •OX, which agrees with the experimental observations reported by Nenadis et al.[54] In that work, the highest radical scavenging activity (RSA), using the 2,2-diphenyl-1-picrylhydrazyl (DPPH•) assay, was measured for both *o*-coumaric and *p*-coumaric acid with respect to the *m*-isomer. Nevertheless, the trolox antioxidant activity (TEAC), using the 2,2′-azinobis(3-ethylbenzothiazoline-6-sulfonic acid) ($ABTS^{\bullet+}$) assay, determined for *p*-coumaric acid highlights the rest of the studied compounds (TEAC is about 2 times higher for the *p*-isomer than for the *o*- and *m*-isomers). Comparable TEAC values have been reported for *o*- and *m*-coumaric acids. These differences in the antioxidant activity could not be explained by Nenadis et al.[54] on the basis of bond dissociation energies and ionization energies. Thus, the kind of •OX species seems to play a role in the order of reactivity of coumaric acids, which is consistent with our results. According to our calculations, *p*-coumaric acid may be the most reactive with •OH within the studied compounds, the addition to an unsaturated carbon being the main reaction mechanism. In contrast, *o*-coumaric should be the most reactive with •OOH, $^{\bullet}OCH_3$, and $^{\bullet}OOCH_3$, and in this case, the H abstraction from the hydroxyl group seems to be the main reaction mechanism. As mentioned before, previous theoretical studies on the reactions of related hydroxycinnamic acids with radicals also suggest that the reaction mechanism is controlled by addition for the reactions with •OH and by H abstraction for the reactions with •OOH.[41] Unfortunately, the addition mechanism was not considered in other previous theoretical works on the antioxidant activity of hydroxycinnamic acids such as *p*-coumaric, caffeic, and sinapinic acids.[26,29,40] Mantzavinos et al. determined the reaction intermediates of *p*-coumaric acid


dx.doi.org/10.1021/jf5011148 | J. Agric. Food Chem. 2014, 62, 9705−9710

**Table 1. Activation ($\Delta G^{\ddagger}$) and Reaction ($\Delta_r G$) Gibbs Free Energies Calculated for the Most Relevant Pathways of the Studied Reactions[a]**

| | | | | | | | $k_{TST/W}$ (L mol$^{-1}$ s$^{-1}$) | |
|---|---|---|---|---|---|---|---|---|
| compound | radical | pathway | $\Delta G^{\ddagger}$ (kcal mol$^{-1}$) | $\Delta_r G$ (kcal mol$^{-1}$) | $k_{TST}$ (L mol$^{-1}$ s$^{-1}$) | $\chi(T)$ | individual reaction pathway | global mechanism |
| *o*-coumaric acid | $^{\bullet}$OH | TS1 | 6.25 | −30.58 | $1.63 \times 10^{8}$ | 4.35 | $7.07 \times 10^{8}$ | $1.30 \times 10^{9}$ |
| | | TS2 | 8.44 | −21.63 | $4.03 \times 10^{6}$ | 1.22 | $4.93 \times 10^{6}$ | |
| | | TS3 | 5.98 | −24.35 | $2.59 \times 10^{8}$ | 1.13 | $2.92 \times 10^{8}$ | |
| | | TS4 | 10.79 | −4.85 | $7.60 \times 10^{4}$ | 3.89 | $2.95 \times 10^{5}$ | |
| | $^{\bullet}$OOH | TS1 | 16.95 | 0.74 | 2.34 | 5.81 | $1.36 \times 10^{1}$ | $1.36 \times 10^{1}$ |
| | | TS2 | 22.66 | 4.47 | $1.51 \times 10^{-4}$ | 1.55 | $2.35 \times 10^{-4}$ | |
| | | TS3 | 20.20 | 2.27 | $9.69 \times 10^{-3}$ | 1.43 | $1.39 \times 10^{-2}$ | |
| | | TS4 | 34.99 | 26.47 | $1.39 \times 10^{-13}$ | 2.14 | $2.98 \times 10^{-13}$ | |
| | $^{\bullet}$OCH$_3$ | TS1 | 9.24 | −16.20 | $1.05 \times 10^{6}$ | 4.49 | $4.74 \times 10^{6}$ | $4.74 \times 10^{6}$ |
| | | TS2 | 16.35 | −9.34 | 6.46 | 1.36 | 8.80 | |
| | | TS3 | 13.92 | −9.75 | $3.88 \times 10^{2}$ | 1.28 | $4.94 \times 10^{2}$ | |
| | | TS4 | 21.59 | 9.54 | $9.34 \times 10^{-4}$ | 1.81 | $1.69 \times 10^{-3}$ | |
| | $^{\bullet}$OOCH$_3$ | TS1 | 17.26 | 2.51 | 1.38 | 6.10 | 8.43 | 8.65 |
| | | TS2 | 24.62 | 8.18 | $5.62 \times 10^{-6}$ | 1.54 | $8.63 \times 10^{-6}$ | |
| | | TS3 | 18.93 | 4.14 | $8.25 \times 10^{-2}$ | 1.34 | $1.11 \times 10^{-1}$ | |
| | | TS4 | 37.31 | 28.25 | $2.77 \times 10^{-15}$ | 2.07 | $5.72 \times 10^{-15}$ | |
| *m*-coumaric acid | $^{\bullet}$OH | TS1 | 7.28 | −26.93 | $2.88 \times 10^{7}$ | 3.68 | $1.06 \times 10^{8}$ | $9.09 \times 10^{8}$ |
| | | TS2 | 8.36 | −22.92 | $4.61 \times 10^{6}$ | 1.18 | $5.45 \times 10^{6}$ | |
| | | TS3 | 5.79 | −25.55 | $3.55 \times 10^{8}$ | 1.12 | $3.96 \times 10^{8}$ | |
| | | TS4 | 11.16 | −4.12 | $4.10 \times 10^{4}$ | 3.74 | $1.54 \times 10^{5}$ | |
| | $^{\bullet}$OOH | TS1 | 18.68 | 4.39 | $1.27 \times 10^{-1}$ | 5.98 | $7.56 \times 10^{-1}$ | $7.57 \times 10^{-1}$ |
| | | TS2 | 22.46 | 3.69 | $2.12 \times 10^{-4}$ | 1.51 | $3.21 \times 10^{-4}$ | |
| | | TS3 | 22.52 | 1.54 | $1.93 \times 10^{-4}$ | 1.46 | $2.81 \times 10^{-4}$ | |
| | | TS4 | 36.34 | 27.20 | $1.44 \times 10^{-14}$ | 2.06 | $2.97 \times 10^{-14}$ | |
| | $^{\bullet}$OCH$_3$ | TS1 | 10.31 | −12.55 | $1.73 \times 10^{5}$ | 4.53 | $7.85 \times 10^{5}$ | $7.89 \times 10^{5}$ |
| | | TS2 | 15.83 | −11.04 | $1.56 \times 10^{1}$ | 1.32 | $2.06 \times 10^{1}$ | |
| | | TS3 | 13.12 | −11.75 | $1.49 \times 10^{3}$ | 1.29 | $1.92 \times 10^{3}$ | |
| | | TS4 | 22.09 | 10.27 | $4.02 \times 10^{-4}$ | 1.67 | $6.73 \times 10^{-4}$ | |
| | $^{\bullet}$OOCH$_3$ | TS1 | 19.77 | 6.16 | $2.02 \times 10^{-2}$ | 6.37 | $1.29 \times 10^{-1}$ | $1.29 \times 10^{-1}$ |
| | | TS2 | 24.18 | 7.12 | $1.17 \times 10^{-5}$ | 1.50 | $1.76 \times 10^{-5}$ | |
| | | TS3 | 22.42 | 5.27 | $2.30 \times 10^{-4}$ | 1.46 | $3.37 \times 10^{-4}$ | |
| | | TS4 | 38.26 | 28.97 | $5.65 \times 10^{-16}$ | 1.95 | $1.10 \times 10^{-15}$ | |
| *p*-coumaric acid | $^{\bullet}$OH | TS1 | 6.24 | −29.97 | $1.66 \times 10^{8}$ | 4.04 | $6.70 \times 10^{8}$ | $2.05 \times 10^{9}$ |
| | | TS2 | 8.14 | −22.10 | $6.73 \times 10^{6}$ | 1.19 | $8.03 \times 10^{6}$ | |
| | | TS3 | 5.46 | −25.08 | $6.22 \times 10^{8}$ | 1.10 | $6.82 \times 10^{8}$ | |
| | | TS4 | 10.90 | −4.62 | $6.37 \times 10^{4}$ | 3.85 | $2.45 \times 10^{5}$ | |
| | $^{\bullet}$OOH | TS1 | 17.55 | 1.35 | $8.54 \times 10^{-1}$ | 6.22 | 5.31 | 5.34 |
| | | TS2 | 22.25 | 3.95 | $3.02 \times 10^{-4}$ | 1.53 | $4.62 \times 10^{-4}$ | |
| | | TS3 | 20.22 | 2.50 | $9.33 \times 10^{-3}$ | 1.41 | $1.31 \times 10^{-2}$ | |
| | | TS4 | 35.11 | 26.70 | $1.14 \times 10^{-13}$ | 2.08 | $2.37 \times 10^{-13}$ | |
| | $^{\bullet}$OCH$_3$ | TS1 | 9.58 | −15.59 | $5.87 \times 10^{5}$ | 4.60 | $2.70 \times 10^{6}$ | $2.71 \times 10^{6}$ |
| | | TS2 | 15.88 | −10.40 | $1.42 \times 10^{1}$ | 1.33 | $1.89 \times 10^{1}$ | |
| | | TS3 | 12.68 | −11.64 | $3.13 \times 10^{3}$ | 1.26 | $3.94 \times 10^{3}$ | |
| | | TS4 | 21.64 | 9.76 | $8.52 \times 10^{-4}$ | 1.74 | $1.49 \times 10^{-3}$ | |
| | $^{\bullet}$OOCH$_3$ | TS1 | 17.88 | 3.12 | $4.87 \times 10^{-1}$ | 6.72 | 3.27 | 3.27 |
| | | TS2 | 24.35 | 7.47 | $8.78 \times 10^{-6}$ | 1.51 | $1.33 \times 10^{-5}$ | |
| | | TS3 | 22.04 | 5.44 | $4.36 \times 10^{-4}$ | 1.43 | $6.23 \times 10^{-4}$ | |
| | | TS4 | 37.61 | 28.47 | $1.69 \times 10^{-15}$ | 2.02 | $3.42 \times 10^{-15}$ | |

[a]TST rate constants estimated at 298.15 K are also appended including ($k_{TST/W}$) or not ($k_{TST}$) tunneling coefficient corrections. The level of theory used was M06-2X/6-311+G**.

oxidation in different conditions by high-performance liquid chromatography (HPLC). The authors suggested that the oxidation at pH 3.5 starts through two main routes: (i) oxygen attack to the nonaromatic double bond to form glyoxylic acid and *p*-hydroxybenzoic acid (see Figure 1); (ii) decarboxylation reaction leading to *p*-vinylphenol. Under acidic conditions (pH 1) and in the presence of homogeneous catalyst ions such as $Fe^{2+}$, $Cu^{2+}$, $Zn^{2+}$, and $Co^{2+}$, a decarboxylation mechanism is favored.[55,56] Andreozzi et al. also determined the reaction intermediates of *p*-coumaric acid oxidation with ozone by


dx.doi.org/10.1021/jf5011148 | J. Agric. Food Chem. 2014, 62, 9705−9710

**Table 2. Calculated Imaginary Frequencies ($cm^{-1}$) for the Studied Transition States at the M06-2X/6-311+G** Level**

| | | radical | | | |
|---|---|---|---|---|---|
| compound | pathway | $^{\bullet}OH$ | $^{\bullet}OOH$ | $^{\bullet}OCH_3$ | $^{\bullet}OOCH_3$ |
| *o*-coumaric acid | TS1 | −1857.3 | −2227.3 | −1897.2 | −2293.5 |
| | TS2 | −478.8 | −755.2 | −611.6 | −743.0 |
| | TS3 | −360.3 | −666.6 | −533.1 | −593.1 |
| | TS4 | −1724.5 | −1081.7 | −912.1 | −1049.2 |
| *m*-coumaric acid | TS1 | −1662.3 | −2264.6 | −1908.3 | −2352.3 |
| | TS2 | −434.2 | −727.3 | −573.1 | −721.1 |
| | TS3 | −344.9 | −685.3 | −544.7 | −692.1 |
| | TS4 | −2352.3 | −1044.9 | −832.8 | −991.8 |
| *p*-coumaric acid | TS1 | −1771.1 | −2318.4 | −1925.9 | −2428.8 |
| | TS2 | −445.7 | −737.6 | −580.1 | −727.7 |
| | TS3 | −316.4 | −647.9 | −516.2 | −665.5 |
| | TS4 | −1715.0 | −1054.8 | −875.3 | −1026.5 |

HPLC and proposed that the initial oxidation step arises from the electrophilic attack of ozone to the nonaromatic double bond.[57] Therefore, the addition mechanism should be considered in theoretical studies on oxidation reactions of phenolic acids containing nonaromatic double bonds with reactive oxygen species.

## ■ ASSOCIATED CONTENT

### Ⓢ Supporting Information

Figure 1S and Tables 1S−6S. This material is available free of charge via the Internet at http://pubs.acs.org.

## ■ AUTHOR INFORMATION


### Corresponding Author

*(A.G.) E-mail: andres.garzon@uclm.es.


### Notes

The authors declare no competing financial interest.

## ■ ACKNOWLEDGMENTS

We gratefully thank Supercomputing Service of Castilla−La Mancha University for allocation of computational resources.

## ■ REFERENCES


(1) Kim, K. H.; Tsao, R.; Yang, R.; Cui, S. W. Phenolic acid profiles and antioxidant activities of wheat bran extracts and the effect of hydrolysis conditions. *Food Chem.* **2006**, *95*, 466−473.

(2) Mattila, P.; Pihlava, J. M.; Hellström, J. Contents of phenolic acids, alkyl- and alkenylresorcinols, and avenanthramides in commercial grain products. *J. Agric. Food Chem.* **2005**, *53*, 8295−8295.

(3) Dykes, L.; Rooney, L. W. Phenolic compounds in cereal grains and their health benefits. *Cereal Foods World* **2007**, *52*, 97−111.

(4) Carrasco Pancorbo, A.; Cruces-Blanco, C.; Segura Carretero, A.; Fernández Gutiérrez, A. Sensitive determination of phenolic acids in extra-virgin olive oil by capillary zone electrophoresis. *J. Agric. Food Chem.* **2004**, *52*, 6687−6693.

(5) García, A.; Brenes, M.; Romero, C.; García, P.; Garrido, A. Study of phenolic compounds in virgin olive oils of the Picual variety. *Eur. Food Res. Technol.* **2002**, *215*, 407−412.

(6) Berzas Nevado, J. J.; Castañeda Peñalvo, G.; Rodríguez Robledo, V.; Vargas Martínez, G. New CE-ESI-MS analytical method for the separation, identification and quantification of seven phenolic acids including three isomer compounds in virgin olive oil. *Talanta* **2009**, *79*, 1238−1246.

(7) Nergiz, C.; Ünal, K. Determination of phenolic acids in virgin olive oil. *Food Chem.* **1991**, *39*, 237−240.

(8) Tsimidou, M.; Papadopoulos, G.; Boskou, D. Phenolic compounds and stability of virgin olive oil−Part I. *Food Chem.* **1992**, *45*, 141−144.

(9) Servili, M.; Montedoro, G. F. Contribution of phenolic compounds to virgin olive oil quality. *Eur. J. Lipid Sci. Technol.* **2002**, *104*, 602−613.

(10) Baderschneider, B.; Winterhalter, P. Isolation and characterization of novel benzoates, cinnamates, flavonoids, and lignans from Riesling wine and screening for antioxidant activity. *J. Agric. Food Chem.* **2001**, *49*, 2788−2798.

(11) Rodríguez-Delgado, M. A.; Malovaná, S.; Pérez, J. P.; Borges, T.; García Montelongo, F. J. Separation of phenolic compounds by high-performance liquid chromatography with absorbance and fluorimetric detection. *J. Chromatogr., A* **2001**, *912*, 249−257.

(12) Buiarelli, F.; Cartoni, G.; Coccioli, F.; Levetsovitou, Z. Determination of phenolic acids in wine by high-performance liquid chromatography with a microbore column. *J. Chromatogr., A* **1995**, *695*, 229−235.

(13) Serra Bonvehí, J.; Soliva Torrentó, M.; Centelles Lorente, E. Evaluation of polyphenolic and flavonoid compounds in honeybee-collected pollen produced in Spain. *J. Agric. Food Chem.* **2001**, *49*, 1848−1853.

(14) Kassim, M.; Achoui, M.; Mustafa, M. R.; Ali Mohd, M.; Yusoff, K. M. Ellagic acid, phenolic acids, and flavonoids in Malaysian honey extracts demonstrate in vitro anti-inflammatory activity. *Nutr. Res. (N.Y.)* **2010**, *30*, 650−659.

(15) Cai, Y.; Luo, Q.; Sun, M.; Corke, H. Antioxidant activity and phenolic compounds of 112 traditional Chinese medicinal plants associated with anticancer. *Life Sci.* **2004**, *74*, 2157−2184.

(16) Rice-Evans, C. A.; Miller, N. J.; Paganga, G. Structure-antioxidant activity relationships of flavonoids and phenolic acids. *Free Radical Biol. Med.* **1996**, *20*, 933−956.

(17) Sroka, Z.; Cisowski, W. Hydrogen peroxide scavenging, antioxidant and anti-radical activity of some phenolic acids. *Food Chem. Toxicol.* **2003**, *41*, 753−758.

(18) Silva, F. A. M.; Borges, F.; Guimarães, C.; Lima, J. L. F. C.; Matos, C.; Reis, S. Phenolic acids and derivatives: studies on the relationship among structure, radical scavenging activity, and physicochemical parameters. *J. Agric. Food Chem.* **2000**, *48*, 2122−2126.

(19) Soobrattee, M. A.; Neergheen, V. S.; Luximon-Ramma, A.; Aruoma, O. I.; Bahorun, T. Phenolics as potential antioxidant therapeutic agents: mechanism and actions. *Mutat. Res.* **2005**, *579*, 200−213.

(20) Fernández, M. A.; Sáenz, M. T.; García, M. D. Anti-inflammatory activity in rats and mice of phenolic acids isolated from *Scrophularia frutescens*. *J. Pharm. Pharmacol.* **1998**, *50*, 1183−1186.

(21) de Barros, M. P.; Lemos, M.; Luis Maistro, E.; Leite, M. F.; Barreto Sousa, J. P.; Kennup Bastos, J.; Faloni de Andrade, S. Evaluation of antiulcer activity of the main phenolic acids found in Brazilian green propolis. *J. Ethnopharmacol.* **2008**, *120*, 372−377.

(22) Rice-Evans, C. A.; Miller, N. J.; Paganga, G. Antioxidant properties of phenolic compounds. *Trend Plant Sci.* **1997**, *2*, 152−159.

(23) Cheng, J. C.; Dai, F.; Zhou, B.; Yang, L.; Liu, Z.-L. Antioxidant activity of hydroxycinnamic acid derivatives in human low density lipoprotein: mechanism and structure−activity relationship. *Food Chem.* **2007**, *104*, 132−139.

(24) Kikuzaki, H.; Hisamoto, M.; Hirose, K.; Akiyama, K.; Taniguchi, H. Antioxidant properties of ferulic acid and its related compounds. *J. Agric. Food Chem.* **2002**, *50*, 2161−2168.

(25) Zheng, W.; Wang, S. Y. Antioxidant activity and phenolic compounds in selected herbs. *J. Agric. Food Chem.* **2001**, *49*, 5165−5170.

(26) Hotta, H.; Nagano, S.; Ueda, M.; Tsujino, Y.; Koyama, J.; Osakai, T. Higher radical scavenging activities of polyphenolic

antioxidants can be ascribed to chemical reactions following their oxidation. *Biochim. Biophys. Acta* **2002**, *1572*, 123−132.
(27) Mohajeri, A.; Somayeh Asemani, S. Theoretical investigation on antioxidant activity of vitamins and phenolic acids for designing a novel antioxidant. *J. Mol. Struct.* **2009**, *930*, 15−20.
(28) Zhang, H. Y.; Ji, H. F. How vitamin E scavenges DPPH radicals in polar protic media. *New J. Chem.* **2006**, *30*, 503−504.
(29) Leopoldini, M.; Prieto Pitarch, I.; Russo, N.; Toscano, M. Structure, conformation, and electronic properties of apigenin, luteolin, and taxifolin antioxidants. A first principle theoretical study. *J. Phys. Chem. A* **2004**, *108*, 92−96.
(30) Leopoldini, M.; Marino, T.; Russo, N.; Toscano, M. Antioxidant properties of phenolic compounds: H-atom versus electron transfer mechanism. *J. Phys. Chem. A* **2004**, *108*, 4916−4922.
(31) Wright, J. S.; Johnson, E. R.; Di Labio, G. A. Predicting the activity of phenolic antioxidants: theoretical method, analysis of substituent effects, and application to major families of antioxidants. *J. Am. Chem. Soc.* **2001**, *123*, 1173−1183.
(32) Galano, A.; Francisco-Márquez, M.; Alvarez-Idaboy, J. R. Mechanism and kinetics studies on the antioxidant activity of sinapinic acid. *Phys. Chem. Chem. Phys.* **2011**, *13*, 11199−11205.
(33) Galano, A.; Macías-Ruvalcaba, N. A.; Medina Campos, O. N.; Pedraza-Chaverri, J. Mechanism of the OH radical scavenging activity of nordihydroguaiaretic acid: a combined theoretical and experimental study. *J. Phys. Chem. B* **2010**, *114*, 6625−6635.
(34) Leopoldini, M.; Russo, N.; Toscano, M. The molecular basis of working mechanism of natural polyphenolic antioxidants. *Food Chem.* **2011**, *125*, 288−306.
(35) Galano, A.; Álvarez-Diduk, R.; Ramírez-Silva, M. T.; Alarcón-Ángeles, G.; Rojas-Hernández, A. Role of the reacting free radicals on the antioxidant mechanism of curcumin. *Chem. Phys.* **2009**, *363*, 13−23.
(36) Nikolic, K. M. Theoretical study of phenolic antioxidants properties in reaction with oxygen-centered radicals. *J. Mol. Struct. THEOCHEM* **2006**, *774*, 95−105.
(37) Trouillas, P.; Marsal, P.; Siri, D.; Lazzaroni, R.; Duroux, J. L. A DFT study of the reactivity of OH groups in quercetin and taxifolin antioxidants: the specificity of the 3-OH site. *Food Chem.* **2006**, *97*, 679−688.
(38) Thavasi, V.; Peng Leong, L.; Anthony Bettens, R. P. Investigation of the influence of hydroxy groups on the radical scavenging ability of polyphenols. *J. Phys. Chem. A* **2006**, *110*, 4918−4923.
(39) Mendoza-Wilson, A. M.; Glossman-Mitnik, D. Theoretical study of the molecular properties and chemical reactivity of (+)-catechin and (−)-epicatechin related to their antioxidant ability. *J. Mol. Struct. THEOCHEM.* **2006**, *761*, 97−106.
(40) Urbaniak, A.; Molski, M.; Szeląg, M. Quantum-chemical calculations of the antioxidant properties of *trans*-*p*-coumaric acid and *trans*-sinapinic acid. *Comput. Methods Sci. Technol.* **2012**, *18*, 117−128.
(41) Leopoldini, M.; Chiodo, S. G.; Russo, N.; Toscano, M. Detailed investigation of the OH radical quenching by natural antioxidant caffeic acid studied by quantum mechanical models. *J. Chem. Theory Comput.* **2011**, *7*, 4218−4233.
(42) Chiodo, S. G.; Leopoldini, M.; Russo, N.; Toscano, M. The inactivation of lipid peroxide radical by quercetin. A theoretical insight. *Phys. Chem. Chem. Phys.* **2010**, *12*, 7662−7670.
(43) Alberto, M. E.; Russo, N.; Grand, A.; Galano, A. A physicochemical examination of the free radical scavenging activity of Trolox: mechanism, kinetics and influence of the environment. *Phys. Chem. Chem. Phys.* **2013**, *15*, 4642−4650.
(44) Litwinienko, G.; Ingold, K. U. Abnormal solvent effects on hydrogen atom abstraction. 2. Resolution of the curcumin antioxidant controversy. The role of sequential proton loss electron transfer. *J. Org. Chem.* **2004**, *69*, 5888−5896.
(45) Foti, M. C.; Daquino, C.; Geraci, C. Electron-transfer reaction of cinnamic acids and their methyl esters with the DPPH$^{\bullet}$ radical in alcoholic solutions. *J. Org. Chem.* **2004**, *69*, 2309−2314.
(46) Frisch, M. J.; Trucks, G. W.; Schlegel, H. B.; Scuseria, G. E.; Robb, M. A.; Cheeseman, J. R.; Scalmani, G.; Barone, V.; Mennucci, B.; Petersson, G. A.; Nakatsuji, H.; Caricato, M.; Li, X.; Hratchian, H. P.; Izmaylov, A. F.; Bloino, J.; Zheng, G.; Sonnenberg, J. L.; Hada, M.; Ehara, M.; Toyota, K.; Fukuda, R.; Hasegawa, J.; Ishida, M.; Nakajima, T.; Honda, Y.; Kitao, O.; Nakai, H.; Vreven, T.; Montgomery, J. A., Jr.; Peralta, J. E.; Ogliaro, F.; Bearpark, M.; Heyd, J. J.; Brothers, E.; Kudin, K. N.; Staroverov, V. N.; Kobayashi, R.; Normand, J.; Raghavachari, K.; Rendell, A.; Burant, J. C.; Iyengar, S. S.; Tomasi, J.; Cossi, M.; Rega, N.; Millam, N. J.; Klene, M.; Knox, J. E.; Cross, J. B.; Bakken, V.; Adamo, C.; Jaramillo, J.; Gomperts, R.; Stratmann, R. E.; Yazyev, O.; Austin, A. J.; Cammi, R.; Pomelli, C.; Ochterski, J. W.; Martin, R. L.; Morokuma, K.; Zakrzewski, V. G.; Voth, G. A.; Salvador, P.; Dannenberg, J. J.; Dapprich, S.; Daniels, A. D.; Farkas, Ö.; Foresman, J. B.; Ortiz, J. V.; Cioslowski, J.; Fox, D. J. *Gaussian 09*; Gaussian, Inc.: Wallingford, CT, USA, 2009.
(47) Zhao, Y.; Truhlar, D. G. The M06 suite of density functionals for main group thermochemistry, thermochemical kinetics, noncovalent interactions, excited states, and transition elements: two new functionals and systematic testing of four M06-class functionals and 12 other functionals. *Theor. Chem. Acc.* **2008**, *120*, 215−241.
(48) Zhao, Y.; Truhlar, D. G. Applications and validations of the Minnesota density functionals. *Chem. Phys. Lett.* **2011**, *502*, 1−13.
(49) Alvarez-Idaboy, J. R.; Mora-Díez, N.; Boyd, R. J.; Vivier-Bunge, A. On the importance of prereactive complexes in molecule−radical reactions: hydrogen abstraction from aldehydes by OH. *J. Am. Chem. Soc.* **2001**, *123*, 2018−2024.
(50) Chandra, A. K.; Uchimaru, T. Kinetics of hydrogen abstraction from chloromethanes by the hydroxyl radical: a computational study. *J. Phys. Chem. A* **2000**, *104*, 8535−8539.
(51) El-Nahas, A. M.; Uchimaru, T.; Sugie, M.; Tokuhashi, K.; Sekiya, A. Hydrogen abstraction from dimethyl ether (DME) and dimethyl sulfide (DMS) by OH radical: a computational study. *J. Mol. Struct. THEOCHEM.* **2005**, *722*, 9−19.
(52) Rodríguez, A.; Rodríguez, D.; Garzón, A.; Soto, A.; Aranda, A.; Notario, A. Kinetics and mechanism of the atmospheric reactions of atomic chlorine with 1-penten-3-ol and (*Z*)-2-penten-1-ol: an experimental and theoretical study. *Phys. Chem. Chem. Phys.* **2010**, *12*, 12245−12258.
(53) Levine, I. N. *Physical Chemistry*, 6th ed.; McGraw Hill: New York, 2009.
(54) Nenadis, N.; Wang, L. F.; Tsimidou, M.; Zhang, H. Y. Estimation of scavenging activity of phenolic compounds using the ABTS$^{\bullet+}$ assay. *J. Agric. Food Chem.* **2004**, *52*, 4669−4674.
(55) Mantzavinos, D.; Hellenbrand, R.; Livingston, A. G.; Metcalfe, I. S. Catalytic wet oxidation of *p*-coumaric acid: partial oxidation intermediates, reaction pathways and catalyst leaching. *Appl. Catal. B: Environ.* **1996**, *7*, 379−396.
(56) Mantzavinos, D.; Hellenbrand, R.; Metcalfe, I. S.; Livingston, A. G. Partial wet oxidation of *p*-coumaric acid: oxidation intermediates, reaction pathways and implications for wastewater treatment. *Water Res.* **1996**, *30*, 2969−2976.
(57) Andreozzi, R.; Caprio, V.; D'Amore, M. G.; Insola, A. *p*-Coumaric acid abatement by ozone in aqueous solution. *Water Res.* **1995**, *29*, 1−6.

In a preliminary experiment, FCO seed ethanol extract inhibited NF-κB activation in LPS-stimulated peritoneal macrophages. Therefore, we isolated the primary anti-inflammatory constituent, ursolic acid, from the seed of FCO and investigated its anti-inflammatory effect in LPS- or peptidoglycan-stimulated peritoneal macrophages and 2,4,6-trinitrobenzenesulfonic acid (TNBS)-induced colitis mice.

## MATERIALS AND METHODS

**Chemicals.** RPMI 1640, peptidoglycan purified from *Staphylococcus aureus*, LPS purified from *Escherichia coli* O111:B4, and TNBS were purchased from Sigma-Aldrich (St. Louis, MO). Antibodies for cyclooxygenase (COX)-2, inducible NO synthetase (iNOS), and β-actin were purchased from Santa Cruz Biotechnology (Santa Cruz, CA). Antibodies for IRAK-4, IRAK-1, p-IRAK-1, IκB-α, p-IKK-β, ERK, p-ERK, JNK, p-JNK p38, p-p38, p65, and p-p65 were purchased from Cell Signaling Technology (Danvers, MA). Enzyme-linked immunosorbent assay (ELISA) kits for cytokines and prostaglandin E2 (PGE2) were from R&D Systems (Minneapolis, MN). 3,3′-Diaminobenzidine tetrahydrochloride substrate was purchased from Thermo Scientific (Rockford, IL).

**Isolation of Ursolic Acid.** The dried seed of FCO (500 g) was extracted 3 times with hexane (3 L) at room temperature and 80% ethanol (2.5 L) in boiling water, successively, and evaporated under reduced pressure (35.2 g). The ethanol extract was suspended in distilled water, fractionated with BuOH twice, and evaporated under reduced pressure (21.5 g). The BuOH-soluble fraction was subjected to silica gel column chromatography (40 × 5 cm) with a gradient of $CHCl_3$/MeOH (100:1, 50:1, 25:1, 20:1, 10:1, 5:1, and 0:1, each 1.2 L) to afford seven subfractions. Of them, subfraction E2 (2.5 g) most potently inhibited NF-κB activation in LPS-stimulated peritoneal macrophages. Therefore, it was applied for isolation of the active constituents. Subfraction E2 was subjected to silica gel column chromatography (30 × 5 cm) with a gradient of $CHCl_3$/MeOH (40:1−10:1) to give four subfractions (E2.1−E2.4). Of them, the most potent anti-inflammatory constituent E2.2 (53 mg) was obtained as crystals in MeOH. The isolated compound was identified to be ursolic acid by instrumental analysis [nuclear magnetic resonance (NMR), Varian UNITY INOV-500 spectrophotometer, API-2000 spectrometer] and compared to an authentic standard, as reported in the literature.[14]

*Ursolic Acid (Purity of >95%).* Amorphous white powder. IR $\nu_{max}$ ($cm^{-1}$): 1692, 2928, 3421. Electrospray ionization mass spectrometry (ESI−MS) (*m*/*z*): [$M^+$] 456. $^1H$ NMR ($CDCl_3$, 500 MHz) δ: 5.52 (1H, t, *J* = 3.5 Hz, H-12), 3.48 (1H, dd, *J* = 10.5 and 4.0 Hz, H-3), 2.63 (1H, d, *J* = 3.5 Hz, H-18), 1.27, 1.26, 1.10, 1.08 (each 3H, s H-23, 27, 26, 24), 1.02 (3H, d, *J* = 6.5 Hz, H-30), 0.98 (3H, d, *J* = 6.5 Hz, H-29), 0.89 (3H, s, H-25). $^{13}C$ NMR ($CDCl_3$, 125 MHz) δ: 180.1 (C-28), 139.7 (C-13), 126.1 (C-12), 78.6 (C-3), 56.2 (C-18), 53.8 (C-5), 47.1 (C-17), 42.3 (C-14), 39.6 (C-4), 39.4 (C-1), 37.5 (C-22), 34.6 (C-10), 33.6 (C-7), 29.1 (C-19, C-20), 29.0 (C-15), 26.4 (C-21), 24.2 (C-27), 24.1 (C-11), 24.1 (C-2), 24.0 (C-23, C-30), 23.8 (C-16), 21.7 (C-29), 19.1 (C-6), 16.9 (C-24, C-25), 16.0 (C-26).

**Animals.** All animal experiments were approved by the Committee for the Care and Use of Laboratory Animals in the College of Pharmacy, Kyung Hee University (KHP-2012-11-01-R1) and performed according to the Kyung Hee University guides for Laboratory Animals Care and Usage.

Male C57BL/6J mice (male, 19−23 g, 6 weeks old) and TLR4-deficient C57BL/10ScNJ mice (male, 19−23 g, 6 weeks old) were purchased from Jackson Laboratory (Bar Harbor, ME). All animals were fed standard laboratory chow (Samyang Co., Seoul, South Korea), housed in wire cages at 20−22 °C and 50 ± 10% relative humidity, and allowed water *ad libitum*.

**Isolation and Culture of Peritoneal Macrophages.** The mice were intraperitoneally injected with 4% thioglycolate solution (2 mL) and sacrificed on the fourth day after injection, and their peritoneal cavities were rinsed with RPMI 1640 (10 mL).[15] The peritoneal lavage fluid was centrifuged at 200*g* for 10 min. Collected cells were resuspended with RPMI 1640 and seeded in a 12-well microplate. After incubation for 1 h at 37 °C, the cells were washed 3 times and non-adherent cells were removed by aspiration. Attached cells were used as peritoneal macrophages. The cells ($0.5 \times 10^6$ cells/well) were cultured in 24-well plates at 37 °C for 3 days in RPMI 1640 plus 10% fetal bovine serum (FBS). To count the number of macrophage cells, the adherent macrophages were then scraped with a rubber policeman, suspended into fresh phosphate-buffered saline (PBS), stained with Giemsa, and counted by a hemocytometer. To examine the anti-inflammatory effect of ursolic acid, macrophages were cultured in the absence or presence of ursolic acid (dissolved in 0.1% dimethyl sulfoxide) with 100 ng/mL LPS or peptidoglycan.

**ELISA and Immunoblotting in Peritoneal Macrophages.** For the assay of NF-κB activation-inhibitory activity of FCO ethanol extract, peritoneal macrophages ($0.5 \times 10^6$ cells) were stimulated with LPS (100 ng/mL) for 90 min in the presence or absence of FCO ethanol extract (10 or 20 μg/mL), then lysed, and centrifuged at 2000*g* for 10 min.[15] The macrophages ($0.5 \times 10^6$ cells) were also stimulated with LPS (100 ng/mL) or peptidoglycan (100 ng/mL) for 90 min (for the assay of IRAK-4, IRAK-1, p-IKK-β, IκB-α, p65, p-p65, p38, p-p38, ERK, p-ERK, JNK, p-JNK, and β-actin) or 20 h (for the assay of COX-2, iNOS, and β-actin) in the presence or absence of ursolic acid (10 and 20 μM) (dissolved in 0.1% dimethyl sulfoxide), then lysed, and centrifuged at 2000*g* for 10 min. Cell supernatants were used for immunoblot and ELISA analyses. Cytokine levels were assayed using an ELISA kit. Protein expression was analyzed by immunoblotting. Briefly, the supernatants were separated by 10% sodium dodecyl sulfate−polyacrylamide gel electrophoresis (SDS−PAGE) and transferred onto polyvinylidene difluoride membranes. The membranes were blocked with 5% nonfat dried-milk proteins in phosphate-buffered saline containing 0.05% Tween 20 (PBST, Biosesang, Inc., Seoul, Korea) and then probed with COX-2, iNOS, IRAK-4, IRAK-1, p-IKK-β, IκB-α, p65, p-p65, p38, p-p38, ERK, p-ERK, JNK, p-JNK, or β-actin antibodies. After washing with PBST, proteins were detected by incubating with horseradish peroxidase (HRP)-conjugated secondary antibodies for 50 min. Bands were visualized using an enhanced chemiluminescence reagent (Millipore Cooperation, Billerica, MA).[15]

**Immunofluorescent Confocal Microscopy.** For the assay of LPS/TLR4 complex formation, peritoneal macrophages plated on cover slides were cultured at 37 °C for 20 h. Cells were treated with Alexa Fluor 594-conjugated LPS (100 ng/mL, Invitrogen) for 60 min in the absence or presence of ursolic acid (10 and 20 μM), as previously reported.[16] Cells were fixed with 4% formaldehyde and 3% sucrose for 20 min, then treated with rabbit polyclonal anti-TLR4 antibody (Santa Cruz Biotechnology) for 90 min at 4 °C, and incubated with Alexa Fluor 488-conjugated secondary antibodies (Invitrogen) for 1 h. Stained cells were observed with a confocal microscope.

**Flow Cytometry.** Peritoneal macrophages ($1 \times 10^5$ cells) were incubated with or without Alexa Fluor 448-conjugated LPS (10 μg/mL) in the absence or presence of ursolic acid (5, 10, and 20 μM) for 30 min. Cells were fixed in PBS containing 3% sucrose and 4% paraformaldehyde for 20 min, as previously reported,[16] and then analyzed by flow cytometer (C6 Flow Cytometer System, Ann Arbor, MI).

**Transient Transfection of Small Interfering RNA (siRNA).** Peritoneal macrophages were seeded at $3 \times 10^5$ cells/well in 24-well plates and allowed to rest for 2 days prior to transfection. Cells were transfected with 100 nM siRNA for TLR4 (Dharmacon, Chicago, IL) or MyD88 (Santa Cruz Biotechnology) using Lipofectamine 2000 (Invitrogen, Carlsbad, CA) according to the protocol of the manufacturer. At 48 h after transfection, cells were treated with or without ursolic acid (10 and 20 μM) and/or LPS (100 ng/mL).

**Preparation of Experimental Colitis in Mice.** To investigate the curative effect of ursolic acid against colitis in mice, mice were divided into five groups: normal control and TNBS-induced colitis groups treated in the absence or presence of ursolic acid (10 and 20 mg/kg) or mesalazine (10 mg/kg) dissolved in 2% Tween 80.[21] Each group consisted of six mice. TNBS-induced colitis was induced by intrarectal

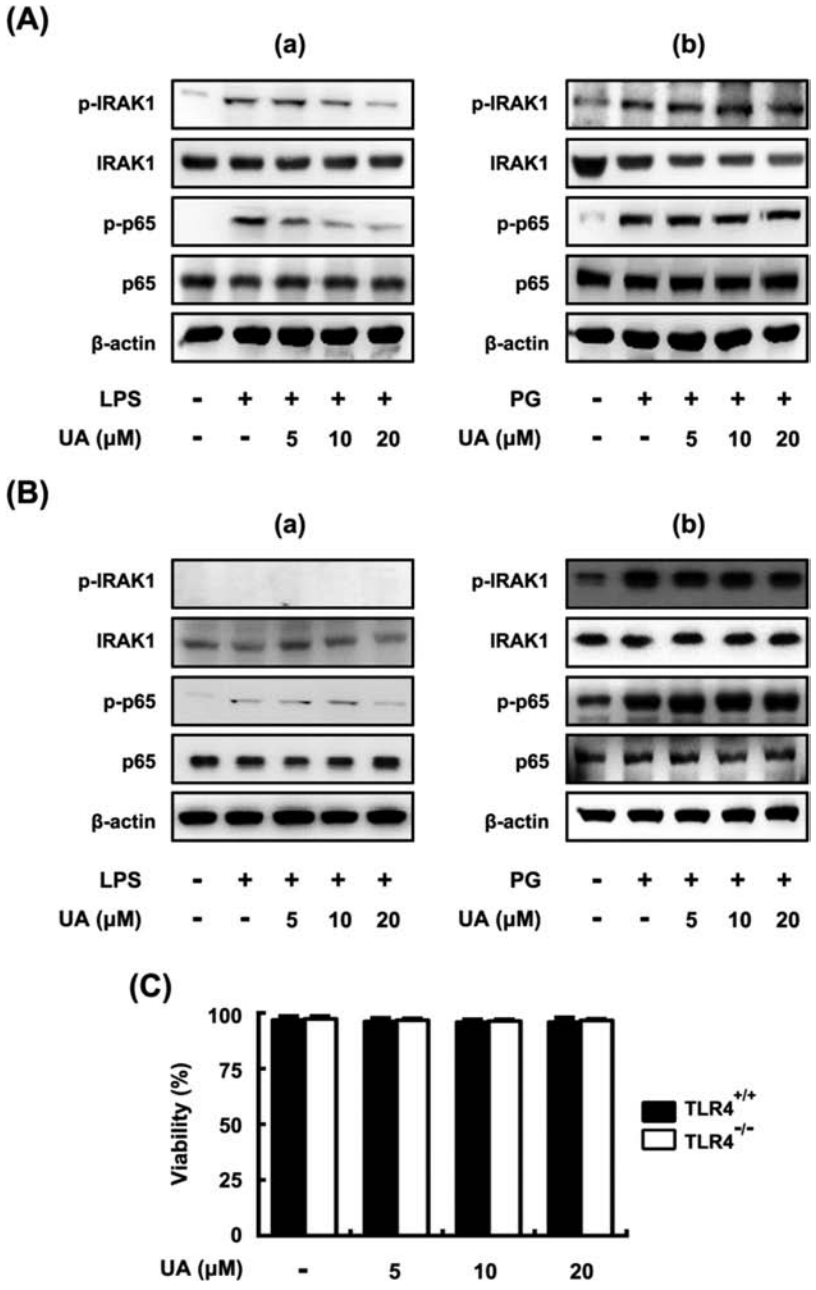


**Figure 1.** Effect of ursolic acid (UA) on IRAK1 phosphorylation and NF-κB activation in normal TLR4$^{+/+}$ and TLR4$^{-/-}$ peritoneal macrophages stimulated with lipopolysaccharide (LPS) or peptidoglycans (PG). (A) Effect in (a) LPS- or (b) PG-stimulated TLR4$^{+/+}$ peritoneal macrophages. (B) Effect in (a) LPS- or (b) PG-stimulated TLR4$^{-/-}$ peritoneal macrophages. Peritoneal macrophages were isolated from TLR4$^{+/+}$ and TLR4$^{-/-}$ mice and then incubated with LPS (100 ng/mL) or PG (100 ng/mL) in the absence or presence of UA (5, 10, or 20 μM) for 60 min. Protein expression of IRAK1, p-IRAK1, p65, p-p65, and β-actin was assayed by immunoblotting. (C) Cell viability of UA for (a) TLR4$^{+/+}$ and (b) TLR4$^{-/-}$ peritoneal macrophages. Cell viability was measured by a tryphan blue staining assay. Ursolic acid was treated for 48 h. All data are expressed as the mean ± SD ($n$ = 4 in a single experiment).

injection of 2.5% (w/v) TNBS solution (100 μL) in 50% ethanol into the colon of lightly anesthetized (with ether) mice via a thin round-tip needle equipped with a 1 mL syringe.[15] The normal control group was treated with vehicle alone instead of TNBS and test agents. A needle was inserted to 3.5−4 cm proximal to anal verge. To distribute agents within the entire colon, the mice were held in a vertical position for 30 s after injection. Using this procedure, >96% of the mice retained the TNBS enema. If an animal quickly excreted the TNBS−ethanol solution, it was excluded. Ursolic acid (10 and 20 mg/kg) or mesalazine (10 mg/kg) was orally administered once a day for 3 days from the first day after TNBS treatment. Mice were sacrificed 18 h after the final administration of test agents. The colon was removed quickly, then opened longitudinally, and gently washed by PBS. Macroscopic assessment of the colitis grade was scored: 0, no ulcer and no inflammation; 1, no ulceration and local hyperemia; 2, ulceration without hyperemia; 3, ulceration and inflammation at one site only; 4, two or more sites of ulceration and inflammation; and 5, ulceration extending more than 2 cm, as previously described.[21] The colon was then stored at −80 °C for immunoblotting and ELISA. For histological exams, the colon was fixed with 4% paraformaldehyde and then stored in 30% sucrose solution.

For histologic exams, colons were fixed in 10% buffered formalin solution, embedded in paraffin, cut into 7 μm sections, stained with hematoxylin−eosin, and then observed under a light microscope.


dx.doi.org/10.1021/jf501487v | J. Agric. Food Chem. 2014, 62, 9711−9721

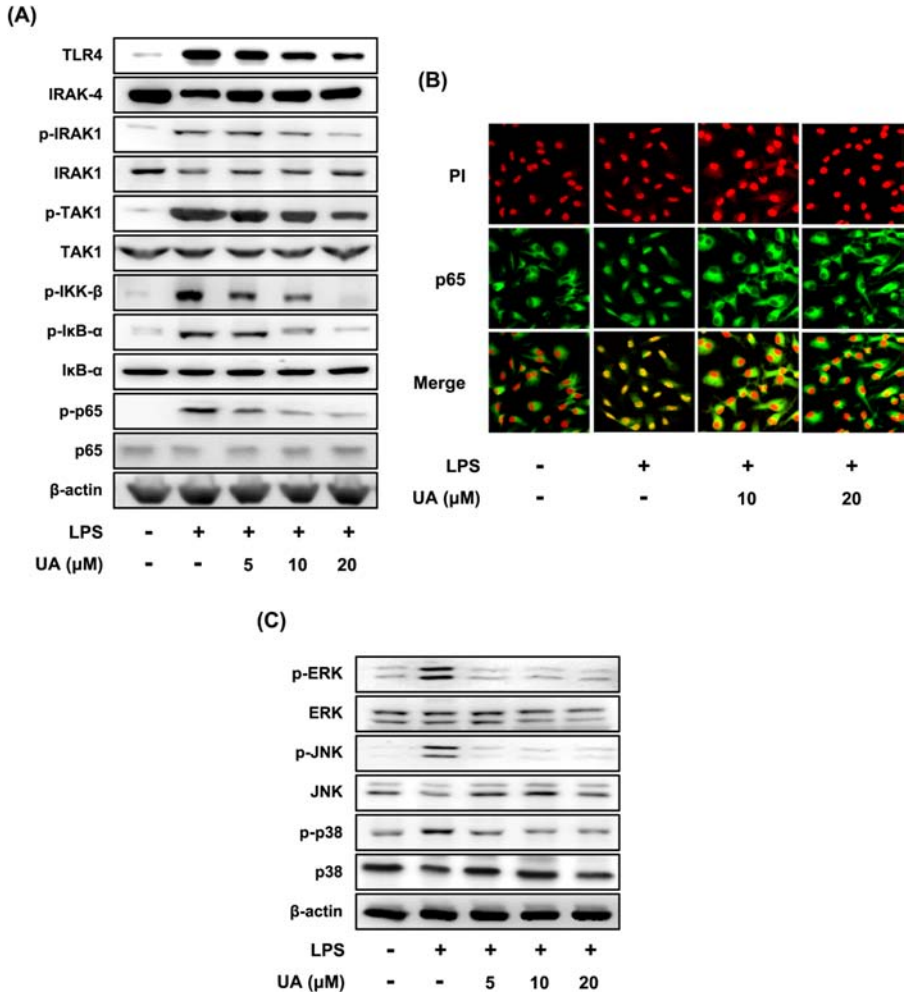


**Figure 2.** Effect of ursolic acid (UA) on the activation of TLR4/NF-κB and MAPKs in lipopolysaccharide (LPS)-stimulated peritoneal macrophages. (A) Effect on TLR4/NF-κB signaling pathway. (B) Effect on translocation of NF-κB into the nuclei. (C) Effect on the activation of MAPKs. Peritoneal macrophages were incubated with LPS (100 ng/mL) in the absence or presence of UA (10 and 20 μM) for 60 min. Protein expressions were assayed by immunoblotting.

**Assay of Myeloperoxidase (MPO) Activity.** Colons were homogenized in 10 mM potassium phosphate buffer (pH 7.0) containing 0.5% hexadecyl trimethylammonium bromide and then centrifuged at 15000*g* and 4 °C for 20 min.[16] The supernatant (50 μL) was added in a reaction mixture preincubated at 37 °C for 5 min, which contained 0.1 mM $H_2O_2$ and 1.6 mM tetramethylbenzidine and scanned at 650 nm at 37 °C for 10 min. MPO activity was defined as the enzyme quantity degrading 1 μmol of hydrogen peroxide/mg of protein. The amount of protein was determined by the Bradford protein assay kit, as previously reported.[16]

**Determination of Cytokines, PGE2, and Nitrite in the Colons of Mice.** Cytokine and PGE2 levels were determined using an ELISA kit. Briefly, colons were homogenized in ice-cold RIPA lysis buffer (1 mL) containing 1% phosphatase inhibitor cocktail and 1% protease inhibitor cocktail. The lysate was centrifuged at 15000*g* and 4 °C for 10 min, and the resulting supernatant was used for immunoblotting and ELISA, as previously described.[16]

Nitrite was measured using Griess reagent.[15] The supernatant (100 μL) was mixed with 100 μL of Griess reagent [the mixture of an equal volume of 1% sulfanilamide in 5% $H_3PO_4$ and 0.1% *N*-(1-naphthyl)ethylenediamine dihydrochloride in $H_2O$] in a 96-well plate, and then the absorbance was spectrophotometrically measured at 550 nm. The concentration of nitrite was determined, using a sodium nitrite, as a standard.

**Statistical Analysis.** Data are presented as the mean ± standard deviation (SD) and were statistically analyzed using one-way analysis of variation (ANOVA) and Turkey's multiple comparison tests (12.0K for Windows, SPSS, Inc., Chicago, IL). *p* values of 0.05 or less were considered statistically significant.

## RESULTS

**Inhibitory Effect of Ursolic Acid on the Expression of Inflammatory Mediators in LPS- or Peptidoglycan-Stimulated Peritoneal Macrophages.** In a preliminary study, FCO seed 80% ethanol extract potently inhibited NF-κB activation in LPS-stimulated peritoneal macrophages (see Supplemental Figure S1 of the Supporting Information). Therefore, we isolated ursolic acid, a potent inhibitor for NF-κB activation, through activity-guided fractionation and investigated the inhibitory effect of ursolic acid on LPS-linked TLR4/NF-κB activation in $TLR4^{+/+}$ or $TLR4^{-/-}$ peritoneal macrophages activated with LPS or peptidoglycan. The stimulation of LPS or peptidoglycan increased IRAK1 phosphorylation and NF-κB activation in $TLR4^{+/+}$ cells (Figure 1A). Treatment with ursolic acid inhibited LPS-induced IRAK1 phosphorylation and NF-κB activation. In contrast, ursolic acid did not inhibit peptidoglycan-induced IRAK1 phosphorylation and NF-κB activation in $TLR4^{+/+}$ cells. However, the stimulation of LPS failed to significantly activate IRAK1 and NF-κB in TLR4-deficient ($TLR^{-/-}$) cells, but the stimulation of


dx.doi.org/10.1021/jf501487v | J. Agric. Food Chem. 2014, 62, 9711−9721

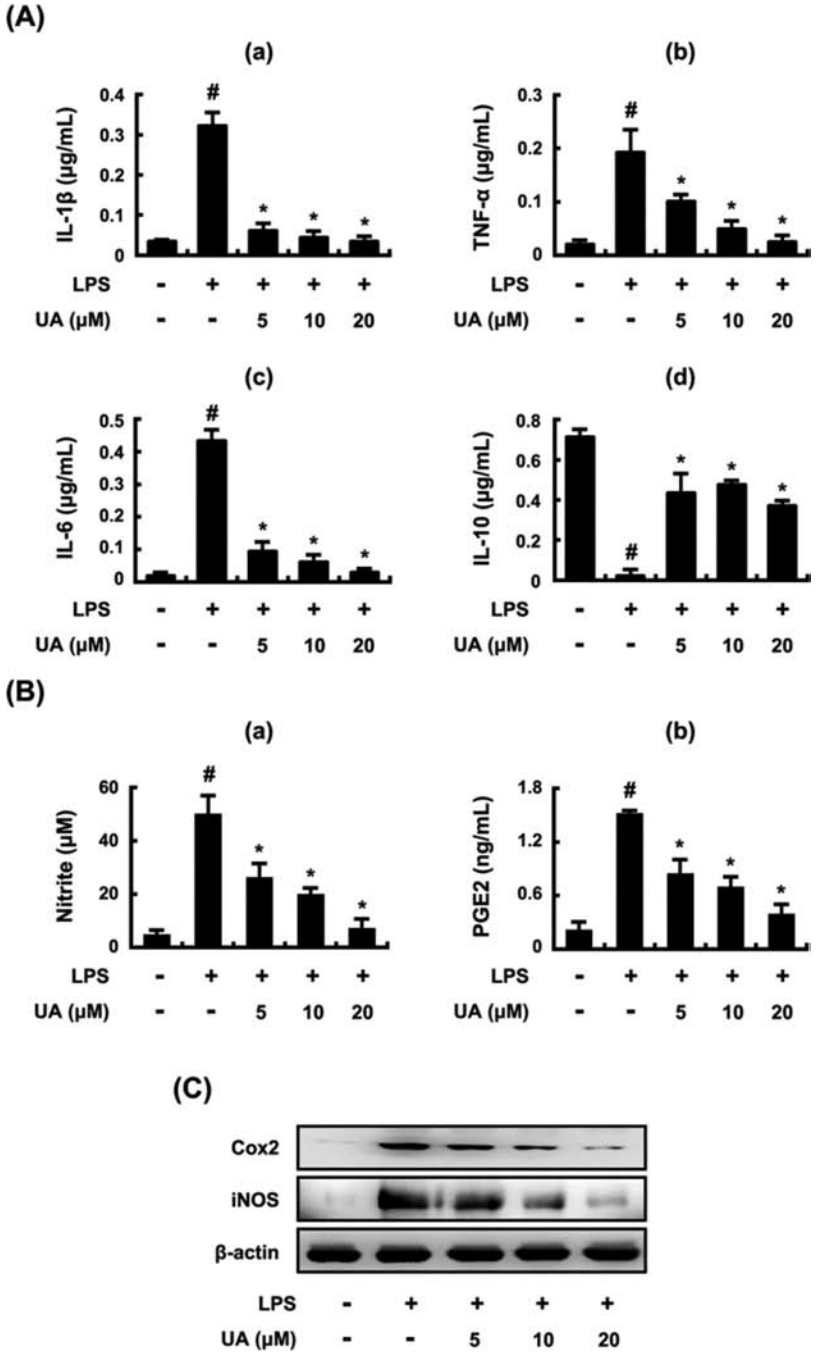


**Figure 3.** Effect of ursolic acid (UA) on the expression of inflammatory markers in peritoneal macrophages stimulated with lipopolysaccharide (LPS). (A) Effect on TNF-$\alpha$, IL-1$\beta$, IL-6, and IL-10. (B) Effect on the production of PGE2 and NO. (C) Effect on the expression of iNOS and COX-2. Peritoneal macrophages were incubated with LPS (100 ng/mL) in the absence or presence of UA (10 or 20 $\mu$M) for 20 h. Cytokines and PGE2 were assayed by ELISA. iNOS and COX-2 were assayed by immunoblotting. NO was assayed, using Griess reagent. All data are the mean ± SD ($n$ = 4). (#) Significantly different versus the normal group ($p < 0.05$). (*) Significantly different versus the control group ($p < 0.05$).

peptidoglycan significantly increased IRAK1 phosphorylation and NF-$\kappa$B activation (Figure 1B). Notably, ursolic acid could not inhibit peptidoglycan-induced IRAK1 and NF-$\kappa$B activation in the TLR4-deficient cells.

To investigate the cytotoxicity of ursolic acid, peritoneal macrophages were treated with ursolic acid (10 and 20 $\mu$M) for 48 h. Cells were then trypsinized, stained with Trypan blue solution, and assessed for viability. No cytotoxic effect of ursolic acid was observed under the experimental conditions (Figure 1C).

Phosphorylation of inhibitor of nuclear factor $\kappa$B kinase subunit $\beta$ (IKK$\beta$) and I$\kappa$B$\alpha$ (through ubiquitination and proteolytic degradation) leads to the translocation of NF-$\kappa$B into the nuclei.[17] Therefore, we measured the effect of ursolic acid on phosphorylation of TAK1, IKK$\beta$, and I$\kappa$B$\alpha$ and degradation of IRAK1 and IRAK4 in LPS-stimulated peritoneal macrophages (Figure 2A). Treatment with LPS significantly induced these processes. Ursolic acid significantly inhibited the phosphorylation of these proteins. To confirm the inhibitory effect of ursolic acid on NF-$\kappa$B activation, we measured its


dx.doi.org/10.1021/jf501487v | J. Agric. Food Chem. 2014, 62, 9711−9721

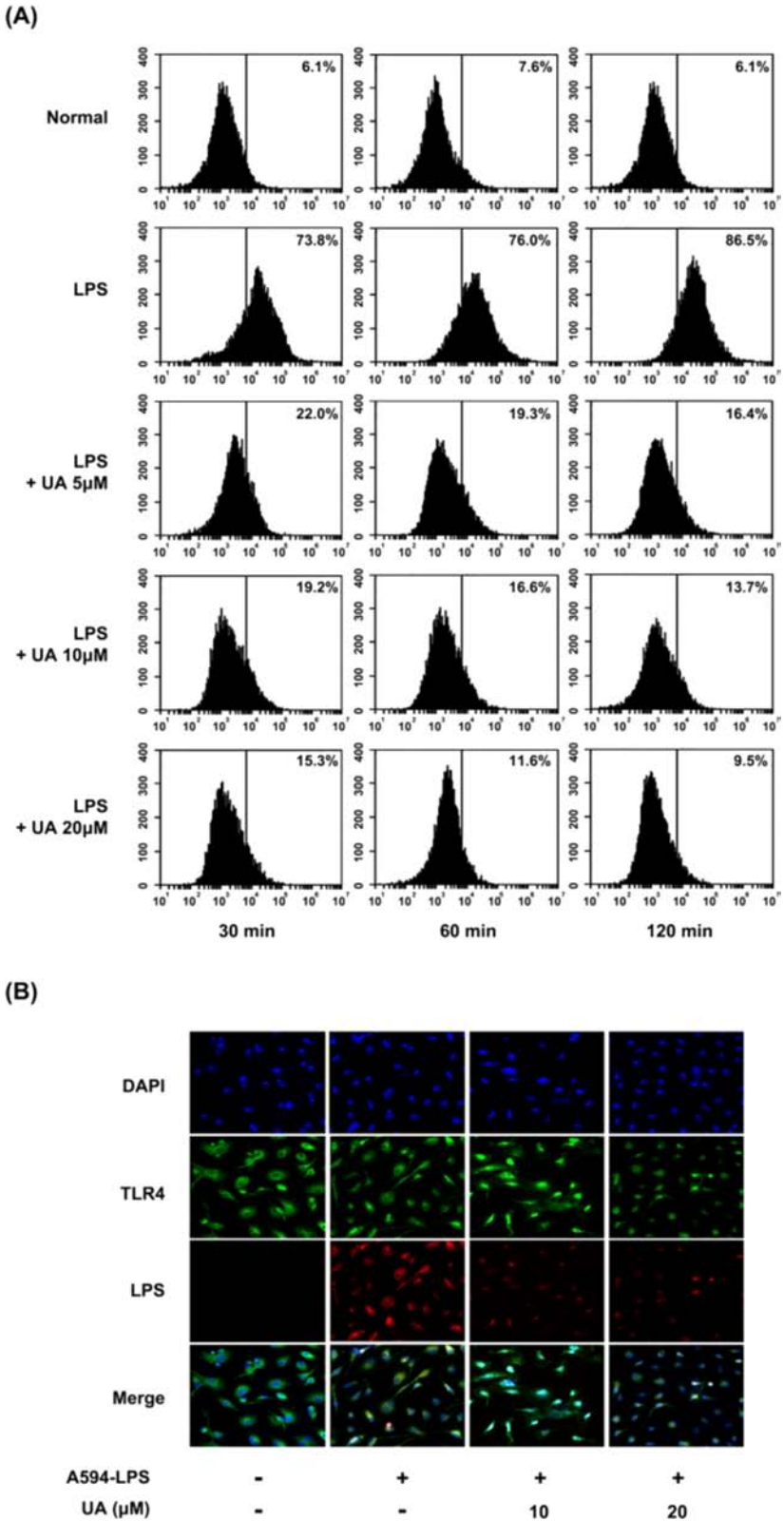


**Figure 4.** Inhibitory effect of ursolic acid (UA) on the binding of LPS to TLR4 in peritoneal macrophages. Peritoneal macrophages isolated from mice were incubated with Alexa Fluor 488-conjugated LPS for 30 min for a flow cytometry or 60 min for a confocal microscopy in the absence or presence of UA (5, 10, and 20 $\mu$M), and the cells were stained with rabbit polyclonal anti-TLR4 antibody for 2 h at 4 °C, incubated with secondary antibodies conjugated with TRITC for 1 h, and then analyzed using a (A) flow cytometer and (B) confocal microscope. The normal group was treated with vehicle alone instead of LPS and UA.

inhibitory effect on the translocation of NF-$\kappa$B into the nuclei in LPS-stimulated peritoneal macrophages (Figure 2B). LPS significantly increased the translocation of NF-$\kappa$B into the nuclei, which was significantly inhibited by ursolic acid. We also


dx.doi.org/10.1021/jf501487v | J. Agric. Food Chem. 2014, 62, 9711−9721

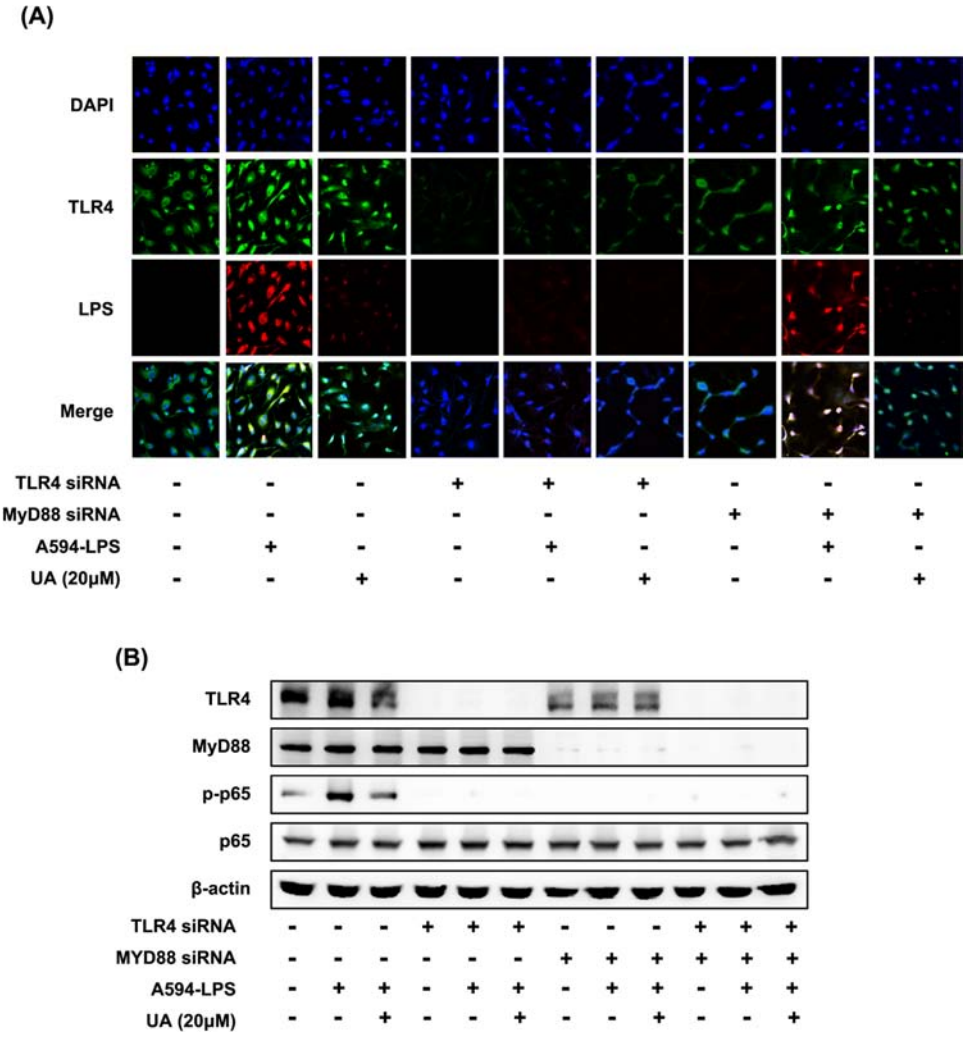


**Figure 5.** Effect of ursolic acid (UA) on the expression of TLR4 and MyD88 and activation of NF-κB in peritoneal macrophages transfected with or without TLR4 siRNA and/or MyD88 siRNA. (A) Peritoneal macrophages isolated from mice were incubated with Alexa Fluor 594-conjugated LPS (100 ng/mL) for 30 min in the absence or presence of UA (10 and 20 μM), and then LPS binding on the surface of TLR4 and/or MyD88 siRNA-transfected peritoneal macrophages was measured using a confocal microscope. (B) Effect on NF-κB activation. TLR4, MyD88, p65, p-p65, and β-actin proteins were assayed by immunoblotting.

investigated the effect of ursolic acid on MAPK activation in LPS-stimulated peritoneal macrophages (Figure 2C). LPS stimulation activated ERK, JNK, and p38. However, ursolic acid significantly suppressed their phosphorylation.

Next, we measured the effect of ursolic acid on the expression of proinflammatory cytokines IL-1β, IL-6, and TNF-α in LPS-stimulated peritoneal macrophages (Figure 3A). LPS significantly increased the expression of these cytokines. Treatment with ursolic acid inhibited TNF-α, IL-1β, and IL-6 expression. Urosolic acid also decreased LPS-induced PGE2 and NO production (Figure 3B). Further, ursolic acid suppressed LPS-induced COX-2 and iNOS expression (Figure 3C).

**Ursolic Acid Inhibits the Binding of LPS to TLR4.** Treatment with ursolic acid (5, 10, and 20 μM) inhibited the phosphorylation of IRAK1, IκBα, and p65 in LPS-stimulated peritoneal macrophages. Therefore, we examined the ability of ursolic acid to inhibit LPS binding to TLR4 on peritoneal macrophages using a flow cytometer (Figure 4A). Treatment of peritoneal macrophages with Alexa Fluor 488-conjugated LPS induced a significant shift. However, treatment with ursolic acid remarkably restored the Alexa Fluor 488-conjugated LPS-mediated shift of macrophages. Next, we examined the ability of ursolic acid to inhibit LPS binding to TLR4 on peritoneal macrophages using a confocal microscope (Figure 4B). Alexa Fluor 488-conjugated TLR4 antibody was found to bind the macrophages, and this binding was unaffected by ursolic acid treatment. Alexa Fluor 594-conjugated LPS was also found to potently bind to macrophages. However, ursolic acid treatment significantly inhibited the binding of Alexa Fluor 594-conjugated LPS to the macrophages.

To further confirm whether ursolic acid inhibits LPS binding to TLR4 on peritoneal macrophages, the macrophages were transiently transfected with TLR4 or MyD88 siRNA for 48 h and then protein expression of TLR4 and MyD88 was detected (Figure 5). Knockdown efficiencies of TLR4 and MyD88 were 93 and 89%, respectively, as determined by immunoblotting. When the cells were treated with Alex 594-conjugated LPS, the LPS did not bind to the macrophages transfected with TLR4 siRNA. Ursolic acid did not influence the binding of LPS to TLR4 or MyD88 siRNA-transfected macrophages (data not shown). However, it was observed that LPS was bound to


dx.doi.org/10.1021/jf501487v | J. Agric. Food Chem. 2014, 62, 9711−9721

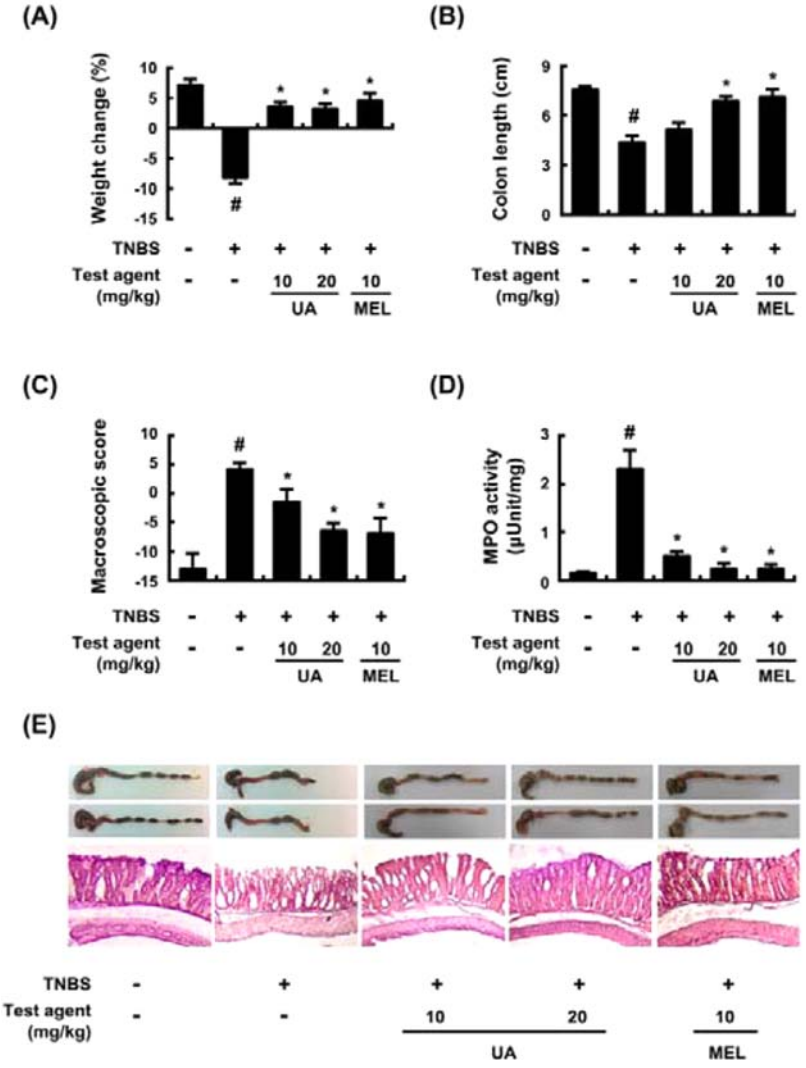


**Figure 6.** Effect of ursolic acid (UA) on (A) body weight, (B) colon length, (C) macroscopic score, (D) peritoneal MPO activity, and (E) histology in the colon tissues of TNBS-induced colitic mice. TNBS (2.5% TNBS in 50% ethanol) was intrarectally administered in mice. Test agents (TNBS, vehicle alone; UA10, 10 mg/kg of UA; UA20, 20 mg/kg of UA; and MEL, 10 mg/kg of mesalazine) were orally administered. The normal group (NOR) was treated with vehicle alone in normal mice. Test agents (dissolved in 2% Tween 80) were orally administered once daily for 3 days after TNBS treatment. Mice were sacrificed 18 h after the final administration of test agents. Colons were stained with hematoxylin−eosin and then assessed by light microscopy. All data are the mean ± SD ($n$ = 6). (#) Significantly different versus the normal group ($p < 0.05$). (*) Significantly different versus the control group ($p < 0.05$).

MyD88 siRNA-transfected cells. Nevertheless, LPS did not activate NF-κB. When ursolic acid (20 μM) was treated prior to stimulation with LPS in MyD88 siRNA-transfected macrophages, ursolic acid potently inhibited the binding of LPS to TLR4 on these cells.

**Ursolic Acid Inhibits the Expression of Proinflammatory Cytokines and Activation of NF-κB in TNBS-Induced Colitic Mice.** We also investigated the inhibitory effect of ursolic acid on TNBS-induced colitis in mice. When TNBS was intrarectally injected in mice, colitis was caused, as observed in previous reports.[15] Oral administration of ursolic acid significantly inhibited TNBS-induced colon shortening and increased the macroscopic score (Figure 6). Ursolic acid (20 mg/kg) inhibited the TNBS-induced MPO activity by 92% compared to normal mice treated with TNBS alone ($p < 0.05$). Histologic examination of the colon in TNBS-induced colitic mice showed edema, dense infiltration of the superficial layers of the mucosa, and epithelial cell disruption by large ulcerations. Orally administered ursolic acid suppressed edema and epithelial cell disruption. We also measured the levels of proinflammatory cytokines, IL-1β, IL-6, and TNF-α, and an anti-inflammatory cytokine, IL-10, in the colons of TNBS-treated mice (Figure 7A). TNBS significantly increased TNF-α, IL-1β, IL-6, and IL-10 expression. Ursolic acid inhibited the expression of pro-inflammatory cytokines TNF-α, IL-1β, and IL-6, although β-actin expression was not affected. Thus, ursolic acid (20 mg/kg) inhibited expression of these cytokines by 93% for IL-1β ($p < 0.05$), 86% for TNF-α ($p < 0.05$), and 85% for IL-6 ($p < 0.05$). However, ursolic acid reversed the TNBS-mediated downregulation of IL-10 expression to 79% of the normal control group ($p < 0.05$). Treatment with TNBS also increased the expression of COX-2 and iNOS, the degradation of IRAK1 and IRAK4, and the activation of IRAK1, IKKβ, and NF-κB (p-p65) (Figure 7B), all of which were blocked by ursolic acid. Further, ursolic acid inhibited the degradation of IRAK1 and IRAK4.

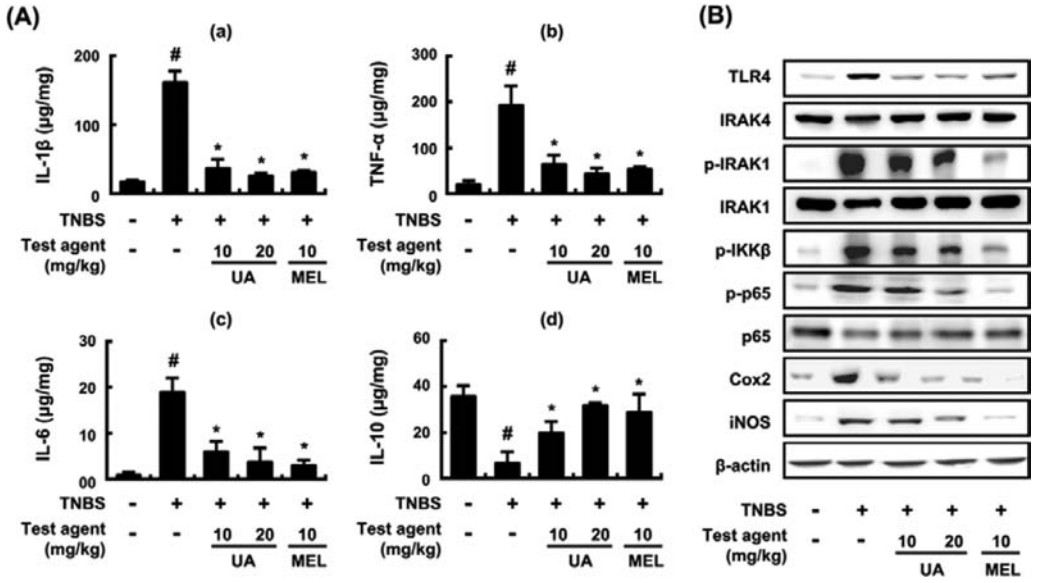


**Figure 7.** Effect of ursolic acid (UA) on the expression of inflammatory cytokines IL-1$\beta$, IL-6, and TNF-$\alpha$, iNOS, and COX-2 and the activation of NF-$\kappa$B in the colon tissues of TNBS-induced colitic mice. TNBS was intrarectally administered in control (2.5% TNBS in 50% ethanol), UA (10 or 20 mg/kg), and mesalazine (MEL, 10 mg/kg) groups; the normal group was treated with vehicle alone. Mice were sacrificed 18 h after the final administration of test agents. (A) Effect on the expression of proinflammatory cytokines. Cytokines were assayed by ELISA. (B) Effect on the expression of TLR4, iNOS, and COX-2 and the activation of NF-$\kappa$B, as determined by immunoblotting. All data values are the mean ± SD ($n$ = 6). (#) Significantly different versus the normal group ($p < 0.05$). (∗) Significantly different versus the control group ($p < 0.05$).

## DISCUSSION

Inflammation is a complex, highly sequential series of events provoked by a variety of stimuli, including pathogens.[18] Inflammation is classified as acute or chronic. Acute inflammation is a normal and beneficial response to injury or infection. However, chronic inflammation is excessive and persistent. This chronically inflammatory response causes progressive injuries to the body, resulting in a variety of severe inflammatory diseases, such as colitis and rheumatoid arthritis.[19,20] The inflammatory process is usually tightly regulated by inflammatory mediators, such as TNF-$\alpha$, IL-1$\beta$, and IL-6, and immune cells, such as neutrophils, monocytes, and lymphocytes.[1] Of these inflammatory mediators, TNF-$\alpha$ and IL-1$\beta$ are activated through NF-$\kappa$B, which consists of five members, including RelA, cRel, RelB, p50, and p52.[3,21] There are canonical and non-canonical NF-$\kappa$B signaling pathways. The canonical NF-$\kappa$B is primarily involved in natural immunity and most inflammation, while non-canonical NF-$\kappa$B plays a role in B-cell maturation and autoimmune diseases. NF-$\kappa$B is an essential transcription factor for immune functions. However, excessive NF-$\kappa$B activation often causes inflammation.[4] Bacterial lipopolysaccharides or peptidoglycans increase blood IL-1$\beta$ and TNF-$\alpha$ levels via canonical and non-canonical TLR-linked NF-$\kappa$B signaling pathways and cause inflammation, although blood IL-1$\beta$ and TNF-$\alpha$ levels are hardly detectable in mice without any stimuli or treatment.[5,22] Therefore, to regulate the expression of proinflammatory cytokines via the canonical NF-kB signaling pathway in macrophages, many constituents isolated from natural products, including saponins and flavonoids, have recently been applied.[23,24]

In a preliminary study, FCO seed 80% ethanol extract potently inhibited NF-$\kappa$B activation in LPS-stimulated peritoneal macrophages. We isolated ursolic acid as a potent inhibitor for NF-$\kappa$B activation from FCO seed. Ursolic acid, which is distributed in vegetables and functional foods as a main constituent, inhibits carrageenan-induced paw edema in rats[25] as well as TPA/croton oil-induced ear edema.[26] Ursolic acid also inhibits LPS-induced cognitive deficits by suppressing p38/NF-$\kappa$B mediated inflammatory pathways,[27] LPS-stimulated lung inflammation via NF-$\kappa$B activation,[28] ovalbumin-induced airway inflammation,[29] and zymosan-induced acute inflammation in mice.[30]

Therefore, we investigated the anti-inflammatory effect on TNBS-stimulated colitis in mice. We found that ursolic acid inhibited the expression of inflammatory enzymes, COX-2 and iNOS, as well as activation of their transcription factor NF-$\kappa$B. Ursolic acid also inhibited the expression of pro-inflammatory cytokines, TNF-$\alpha$ and IL-1$\beta$, but increased the expression of anti-inflammatory cytokine, IL-10, which was reduced by TNBS. These results suggest that ursolic acid may inhibit colitis by inhibiting NF-$\kappa$B activation as well as the activation of Th1 cells, which are activated by pro-inflammatory cytokines TNF-$\alpha$ and IL-1$\beta$,[31] rather than Th2 cells, which are activated by IL-4 and IL-10.[31] This suggestion is supported by previous studies showing that ursolic acid protects $CCl_4$-induced inflammation by inhibiting MAPK, STAT3, and NF-$\kappa$B signaling pathways.[32] Ursolic acid also inhibits Th1 cytokine IL-2 production and induces Th2 cytokine IL-10 production in murine primary splenocytes.[33]

In the present study, we found that ursolic acid inhibited the expression of inflammatory markers COX-2, iNOS, TNF-$\alpha$, and IL-1$\beta$ as well as activation of NF-$\kappa$B and MAPKs in LPS-stimulated peritoneal macrophages, as previously reported in RAW264.7 cells.[34,35]

Ursolic acid inhibits the expression of proinflammaotry cytokines in murine T cells, B cells, and macrophages as well as activation of NF-$\kappa$B in T cells.[36] Ursolic acid also inhibits TPA-induced COX-2 expression and PGE2 synthesis in human mammary epithelial cells via the protein kinase C/MAPK signaling pathway[37] as well as the leucine-stimulated mROC1 signaling pathway in C2C12 myotube cells by suppressing mTOR localization to lysosome.[38]

However, its anti-inflammatory mechanism has not been thoroughly studied.

To understand the anti-inflammatory mechanism of ursolic acid, we investigated its effect on IRAK phosphorylation and binding of LPS to TLR4 in macrophages. Ursolic acid not only inhibited the binding of LPS to TLR4 on peritoneal macrophages transfected with or without MyD88 siRNA but also suppressed the phosphorylation of IRAK1 and IκBα and the degradation of IRAK1 and IRAK4. Further, ursolic acid inhibited the expression of proinflammatory cytokines TNF-α, IL-1β, and IL-6 as well as activation NF-kB and MAPKs. However, ursolic acid did not inhibit IP-10 synthesis in T84 colon carcinoma cells.[39] These results suggest that ursolic acid may suppress NF-κB and MAPK signaling pathways by inhibiting the binding of LPS to TLR4 on immune cells, such as macrophages. Additionally, we investigated the effect of ursolic acid on systemic inflammation and septic death in mice peritoneally injected with LPS (see Supplemental Figure S2 of the Supporting Information). Ursolic acid [10 mg/kg, *per os* (po)] significantly reduced LPS-induced blood proinflammatory cytokines IL-1β and TNF-α levels. Further, Ursolic acid inhibited LPS-induced septic death (systemic inflammation). These results also suggest that ursolic acid may inhibit LPS-stimulated inflammatory responses.

On the basis of these findings, we conclude that ursolic acid may ameliorate inflammatory diseases, such as colitis, by regulating NF-κB and MAPK signaling pathways via the inhibition of LPS binding to TLR4 on immune cells.

## ■ ASSOCIATED CONTENT

### Supporting Information

Effect of *C. officinalis* seed 80% ethanol extract (FCO) on NF-κB activation in lipopolysaccharide-stimulated peritoneal macrophages (Supplemental Figure S1) and Inhibitory effect of ursolic acid (UA) on IL-1β and TNF-α production and septic death in mice intraperitoneally injected with LPS (Supplemental Figure S2). This material is available free of charge via the Internet at http://pubs.acs.org.

## ■ AUTHOR INFORMATION

### Corresponding Author

*Telephone: +82-2-961-0357. Fax: +82-2-957-5030. E-mail: dhkim@khu.ac.kr.

### Funding

This study was supported by a grant from BK21 Plus Program through the National Research Foundation of Korea funded by the Ministry of Education, Science and Technology (2013).

### Notes

The authors declare no competing financial interest.

## ■ ABBREVIATIONS USED

COX, cyclooxygenase; ELISA, enzyme-linked immunosorbent assay; FBS, fetal bovine serum; IKK-β, inhibitor of nuclear factor κB kinase subunit β; IL, interleukin; iNOS, inducible NO synthetase; IRAK, interleukin 1 receptor-associated kinase; LPS, lipopolysaccharide; MPO, myeloperoxidase; NF-κB, nuclear factor κ light-chain enhancer of activated B cells; TLR, toll-like receptor; TNBS, 2,4,6-trinitrobenzenesulfonic acid; TNF, tumor necrosis factor

## ■ REFERENCES

(1) Sotolongo, J.; Ruiz, J.; Fukata, M. The role of innate immunity in the host defense against intestinal bacterial pathogens. *Curr. Infect. Dis. Rep.* **2012**, *14*, 15−23.

(2) Lawrence, T. The nuclear factor NF-κB pathway in inflammation. *Cold Spring Harbor Perspect. Biol.* **2009**, *1*, No. a001651.

(3) Perkins, N. D.; Gilmore, T. D. Good cop, bad cop: The different faces of NF-kB. *Cell Death Differ.* **2006**, *13*, 759−771.

(4) Li, Q.; Verma, I. M. NF-κB regulation in the immune system. *Nat. Rev. Immunol.* **2002**, *2*, 331−367.

(5) Sacre, S. M.; Lundberg, A. M.; Andreakos, E.; Taylor, C.; Feldmann, M.; Foxwell, B. M. Selective use of TRAM in lipopolysaccharide (LPS) and lipoteichoic acid (LTA) induced NF-κB activation and cytokine production in primary human cells: TRAM is an adaptor for LPS and LTA signaling. *J. Immunol.* **2007**, *178*, 2148−2154.

(6) Takeuchi, O.; Akira, S. Toll-like receptors; their physiological role and signal transduction system. *Int. Immunopharmacol.* **2001**, *1*, 625−635.

(7) Stuart, L. M.; Deng, J.; Silver, J. M.; Takahashi, K.; Tseng, A. A.; Hennessy, E. J.; Ezekowitz, R. A.; Moore, K. J. Response to *Staphylococcus aureus* requires CD36-mediated phagocytosis triggered by the COOH-terminal cytoplasmic domain. *J. Cell. Biol.* **2005**, *170*, 477−485.

(8) Zughaier, S. M. *Neisseria meningitidis* capsular polysaccharides induce inflammatory responses via TLR2 and TLR4-MD-2. *J. Leukocyte Biol.* **2011**, *89*, 469−480.

(9) Li, X.; Jiang, S.; Tappingm, R. I. Toll-like receptor signaling in cell proliferation and survival. *Cytokine* **2010**, *49*, 1−9.

(10) Chan, M. M.; Huang, H. I.; Fenton, M. R.; Fong, D. In vivo inhibition of nitric oxide synthase gene expression by curcumin, a cancer preventive natural product with anti-inflammatory properties. *Biochem. Pharmacol.* **1998**, *55*, 1955−1962.

(11) Jang, S. E.; Hyam, S. R.; Jeong, J. J.; Han, M. J.; Kim, D. H. Penta-*O*-galloyl-β-D-glucose ameliorates inflammation by inhibiting MyD88/NF-κB and MyD88/MAPK signaling pathways. *Br. J. Pharmacol.* **2013**, *170*, 1078−1091.

(12) Lin, M. H.; Liu, H. K.; Huang, W. J.; Huang, C. C.; Wu, T. H.; Hsu, F. L. Evaluation of the potential hypoglycemic and β-cell protective constituents isolated from *Corni fructus* to tackle insulin-dependent diabetes mellitus. *J. Agric. Food Chem.* **2011**, *59*, 7743−7751.

(13) Kim, S. H.; Kim, B. K.; Lee, Y. C. Effects of *Corni fructus* on ovalbumin-induced airway inflammation and airway hyper-responsiveness in a mouse model of allergic asthma. *J. Inflammation (London, U. K.)* **2012**, *9*, 9.

(14) Fu, L.; Zhang, S.; Li, N.; Wang, J.; Zhao, M.; Sakai, J.; Hasegawa, T.; Mitsui, T.; Kataoka, T.; Oka, S.; Kiuchi, M.; Hirose, K.; Ando, M. Three new triterpenes from *Nerium oleander* and biological activity of the isolated compounds. *J. Nat. Prod.* **2005**, *68*, 198−206.

(15) Lee, I. A.; Hyam, S. R.; Jang, S. E.; Han, M. J.; Kim, D. H. Ginsenoside Re ameliorates inflammation by inhibiting the binding of lipopolysaccharide to TLR4 on macrophages. *J. Agric. Food Chem.* **2012**, *60*, 9595−9602.

(16) Lee, I. A.; Park, Y. J.; Joh, E. H.; Kim, D. H. Soyasaponin Ab ameliorates colitis by inhibiting the binding of lipopolysaccharide (LPS) to toll-like receptor (TLR)4 on macrophages. *J. Agric. Food Chem.* **2011**, *59*, 13165−13172.

(17) Shuto, T.; Xu, H.; Wang, B.; Han, J.; Kai, H.; Gu, X. X.; Murphy, T. F.; Lim, D. J.; Li, J. D. Activation of NF-κB by nontypeable *Hemophilus influenzae* is mediated by toll-like receptor 2-TAK1-dependent NIK-IKKα/β-IκBα and MKK3/6-p38 MAP kinase signaling pathways in epithelial cells. *Proc. Natl. Acad. Sci. U. S. A.* **2001**, *17*, 8774−8779.

(18) Mahida, Y. R. The key role of macrophages in the immunopathogenesis of inflammatory bowel disease. *Inflammatory Bowel Dis.* **2000**, *6*, 21−33.

(19) Cominelli, F.; Kam, L. Inflammatory mediators of inflammatory bowel disease. *Curr. Opin. Gastroenterol.* **1993**, *9*, 534−543.

(20) Simmonds, R. E.; Foxwell, B. M. Signalling, inflammation and arthritis: NF-κB and its relevance to arthritis and inflammation. *Rheumatology (Oxford, U. K.)* **2008**, *47*, 584−590.
(21) Lee, I. A.; Park, Y. J.; Yeo, H. K.; Han, M. J.; Kim, D. H. Soyasaponin I attenuates TNBS-induced colitis in mice by inhibiting NF-κB pathway. *J. Agric. Food Chem.* **2010**, *58*, 10929−10934.
(22) Andreakos, E.; Sacre, S.; Foxwell, B. M.; Feldmann, M. The toll-like receptor-nuclear factor κB pathway in rheumatoid arthritis. *Front. Biosci.* **2005**, *10*, 2478−2488.
(23) Chen, S. Natural products triggering biological targets—A review of the anti-inflammatory phytochemicals targeting the arachidonic acid pathway in allergy asthma and rheumatoid arthritis. *Curr. Drug Targets* **2011**, *12*, 288−301.
(24) Ikeda, Y.; Murakami, A.; Ohigashi, H. Ursolic acid: An anti- and pro-inflammatory triterpenoid. *Mol. Nutr. Food Res.* **2008**, *52*, 26−42.
(25) Miceli, N.; Taviano, M. F.; Giuffrida, D.; Trovato, A.; Tzakou, O.; Galati, E. M. Anti-inflammatory activity of extract and fractions from *Nepeta sibthorpii* Bentham. *J. Ethnopharmacol.* **2005**, *97*, 261−266.
(26) Altinier, G.; Sosa, S.; Aquino, R. P.; Mencherini, T.; Della Loggia, R.; Tubaro, A. Characterization of topical antiinflammatory compounds in *Rosmarinus officinalis* L. *J. Agric. Food Chem.* **2007**, *55*, 1718−1723.
(27) Wang, Y. J.; Lu, J.; Wu, D. M.; Zheng, Z. H.; Zheng, Y. L.; Wang, X. H.; Ruan, J.; Sun, X.; Shan, Q.; Zhang, Z. F. Ursolic acid attenuates lipopolysaccharide-induced cognitive deficits in mouse brain through suppressing p38/NF-κB mediated inflammatory pathways. *Neurobiol. Learn. Mem.* **2011**, *96*, 156−165.
(28) Chen, X.; Wan, Y.; Zhou, T.; Li, J.; Wei, Y. Ursolic acid attenuates lipopolysaccharide-induced acute lung injury in a mouse model. *Immunotherapy* **2013**, *5*, 39−47.
(29) Kim, S. H.; Hong, J. H.; Lee, Y. C. Ursolic acid, a potential PPARγ agonist, suppresses ovalbumin-induced airway inflammation and Penh by down-regulating IL-5, IL-13, and IL-17 in a mouse model of allergic asthma. *Eur. J. Pharmacol.* **2013**, *701*, 131−143.
(30) Kang, S. Y.; Yoon, S. Y.; Roh, D. H.; Jeon, M. J.; Seo, H. S.; Uh, D. K.; Kwon, Y. B.; Kim, H. W.; Han, H. J.; Lee, H. J.; Lee, J. H. The anti-arthritic effect of ursolic acid on zymosan-induced acute inflammation and adjuvant-induced chronic arthritis models. *J. Pharm. Pharmacol.* **2008**, *60*, 1347−1354.
(31) Burger, D.; Dayer, J. M. Cytokines, acute-phase proteins, and hormones: IL-1 and TNF-α production in contact-mediated activation of monocytes by T lymphocytes. *Ann. N. Y. Acad. Sci.* **2002**, *966*, 464−473.
(32) Ma, J. Q.; Ding, J.; Zhang, L.; Liu, C. M. Ursolic acid protects mouse liver against CCl4-induced oxidative stress and inflammation by the MAPK/NF-κB pathway. *Environ. Toxicol. Pharmacol.* **2014**, *37*, 975−983.
(33) Ku, C. M.; Lin, J. Y. Anti-inflammatory effects of 27 selected terpenoid compounds tested through modulating Th1/Th2 cytokine secretion profiles using murine primary splenocytes. *Food Chem.* **2013**, *141*, 1104−1113.
(34) Ryu, S. Y.; Oak, M. H.; Yoon, S. K.; Cho, D. I.; Yoo, G. S.; Kim, T. S.; Kim, K. M. Antiallergic and anti-inflammatory triterpenes from the herb of *Prunella vulgaris*. *Planta Med.* **2000**, *66*, 358−360.
(35) Ikeda, Y.; Murakami, A.; Ohigashi, H. Ursolic acid promotes the release of macrophage migration inhibitory factor via ERK2 activation in resting mouse macrophages. *Biochem. Pharmacol.* **2005**, *70*, 1497−1505.
(36) AAChecker, R.; Sandur, S. K.; Sharma, D.; Patwardhan, R. S.; Jayakumar, S.; Kohli, V.; Sethi, G.; Aggarwal, B. B.; Sainis, K. B. Potent anti-inflammatory activity of ursolic acid, a triterpenoid antioxidant, is mediated through suppression of NF-κB, AP-1 and NF-AT. *PLoS One* **2012**, *7*, No. e31318.
(37) Subbaramaiah, K.; Michaluart, P.; Sporn, M. B.; Dannenberg, A. J. Ursolic acid inhibits cyclooxygenase-2 transcription in human mammary epithelial cells. *Cancer Res.* **2000**, *60*, 2399−2404.
(38) Ou, X.; Liu, M.; Luo, H.; Dong, L. Q.; Liu, F. Ursolic acid inhibits leucine-stimulated mTORC1 signaling by suppressing mTOR localization to lysosome. *PLoS One* **2014**, *9*, No. e95393.
(39) Mueller, D.; Triebel, S.; Rudakovski, O.; Richling, E. Influence of triterpenoids present in apple peel on inflammatory gene expression associated with inflammatory bowel disease (IBD). *Food Chem.* **2013**, *139*, 339−346.

capacity has been studied using different assays,[6,9] and high amounts of phenolic compounds and high antioxidant activities were observed. In addition, research on other *Myrica* species has been performed. *Myrica esculenta* (syn. *Myrica nagi*) has also been reported to be rich in antioxidant compounds and to present several medicinal applications and satisfactory antioxidant and anticancer activities.[14−16] However, no studies have been published regarding the chemical composition or antioxidant capacity of *Myrica faya*. Considering the high antioxidant activity reported in previous studies regarding other *Myrica* species, special attention should be paid to the chemical composition of *M. faya* and other underutilized plants.

In this work we present, for the first time, a report on the phytochemical content and antioxidant activity of *Myrica faya*. The methanolic extracts of its fruits and leaves were characterized by HPLC-DAD/ESI-MS$^n$, putting special emphasis on the phenolic composition. In addition, its antioxidant capacity was evaluated using radical scavenging methods (ABTS and DPPH) and analyzing its L-ascorbic acid (L-AA) content. The obtained results were compared to the previous ones reported for other *Myrica* species, the main goal of this work being to find out if the chemical composition of *M. faya* makes it a valuable plant from the health and economic points of view.

## MATERIAL AND METHODS

**Chemicals and Instruments.** All reagents and standards were of analytical reagent (AR) grade. L-Ascorbic acid (L-AA) (purity: 99%), quercetin hydrated (99%), potassium iodate (99%), Folin−Ciocalteu's phenol reagent (FCR), gallic acid (99%), rutin (≥98%), and potassium acetate (>99.5%) were purchased from Panreac (Madrid, Spain). Ellagic acid (≥96%), 6-hydroxy-2,5,7,8-tetramethylchroman-2-carboxylic acid (Trolox) (>99.8%), 2,2′-azinobis(3-ethylbenzthiazoline-6-sulfonic acid) (ABTS) (≥99%), and 2,2-diphenyl-1-picrylhydrazyl (DPPH) (>95%) were obtained from Fluka (Lisbon, Portugal). Apigenin (≥99%) and (+)catechin hydrated (>99%) were purchased from Extrasynthese (Genay, France). Caffeic acid (≥98%), potassium persulfate (99%), sodium carbonate (p.a.), metaphosphoric acid (MPA) (33.5−36.5%), and formic acid (98%) were obtained from Sigma-Aldrich (St. Louis, MO); aluminum chloride hexahydrated (98%) and potassium iodine (98%) were from Riedel-de Haën (Hanover, Germany). Acetic acid (99.8%), ethylenediaminetetraacetic acid disodium salt (EDTA) (98%), and starch (98%) were supplied by Merck (Darmstadt, Germany). Cyanidin-3-glucoside (C3G) chloride (>98%) was obtained from Biopurify phytochemicals LTD (Chengdu, China). The methanol (99.9%) used for the extraction of *M. faya* was purchased from Fisher (Lisbon, Portugal). LC−MS grade acetonitrile ($CH_3CN$) (99%) (LabScan; Dublin, Ireland) and ultrapure water (Milli-Q Waters purification system; Millipore; Milford, MA) were used for analysis.

**Sample Preparation.** Samples of *Myrica faya* were collected in the wild in Machico (Madeira Island) in July 2013 and identified by taxonomist Fátima Rocha. Voucher specimens have been stored at Madeira Botanical Garden Herbarium (Funchal, Madeira) (voucher: MADJ 13165). For analysis, plant material was separated into leaves and berries (fully ripe), destemmed, and washed. Then, samples were lyophilized to dryness (Savant vapor trap RVT400; Thermo Scientific Inc.; Waltham, MA), ground to powder, and stored at −20 °C.

**Extraction of Phenolic Compounds.** Before the samples were subjected to evaluation, an extraction procedure was optimized. Acetone and methanol were tested as extraction solvents. Briefly, 5 g of leaf powder and 100 mL of solvent were submitted to ultrasound sonication (Bandelin Sonorex; Germany) at 35 Hz and 200 W for 60 min (room temperature). Then, extracts were filtered and concentrated to dryness under reduced pressure in a rotary evaporator (Buchi Rotavapor R-114) at 40 °C. The efficiency of the different extraction conditions was determined by means of total phenolic content assay (described below). On the basis of the results, the concentration of solvent in water (%, v/v) and influence of extraction duration were also tested (60, 30, and 15 min). Finally, the optimal conditions found were applied to the target plant material, and the resulting extracts were stored at 4 °C until further analysis.

**Chromatographic Conditions.** The HPLC analysis was performed on a Dionex ultimate 3000 series instrument (Thermo Scientific Inc.) coupled to a binary pump, a diode-array detector (DAD), an autosampler, and a column compartment (kept at 20 °C). Separation was achieved on a Phenomenex Gemini $C_{18}$ column (5 μm, 250 mm × 3.0 mm i.d.) using a mobile phase composed by $CH_3CN$ (A) and water/formic acid (0.1%, v/v) at a flow rate of 0.4 mL min$^{-1}$. The following gradient program was used: 20% A (0 min), 25% A (10 min), 25% A (20 min), 50% A (40 min), 100% A (42−47 min), and 20% A (49−55 min). Spectral data for all peaks were accumulated in the range 190−520 nm. A solution with concentration (w/v) of 5 mg mL$^{-1}$ was prepared by dissolving the dried extract in the initial HPLC mobile phase, filtered through 0.45 μm PTFE membrane filters, and 10 μL was injected. The chromatographic analysis was performed in triplicate ($n$ = 3) for each sample.

For HPLC-DAD/ESI-MS$^n$ analysis, a Bruker Esquire model 6000 ion trap mass spectrometer (Bremen, Germany) with an ESI source was used. MS$^n$ analysis worked in negative and positive mode, and scan range was set at $m/z$ 100−1000 with speed of 13 000 Das$^{-1}$. The conditions of ESI were as follows: drying and nebulizer gas ($N_2$) flow rate and pressure, 10 mL min$^{-1}$ and 50 psi; capillary temperature, 325 °C; capillary voltage, 4.5 keV; collision gas (He) pressure and energy, 1 × 10$^{-5}$ mbar and 40 eV. The acquisition of MS$^n$ data was made in auto MS$^n$ mode, with isolation width of 4.0 $m/z$, and fragmentation amplitude of 1.0 V (MS$^n$ up to MS$^4$). Esquire control software was used for the data acquisition and Data Analysis for processing.

**Quantification of Phenolic Compounds.** For this quantitative analysis, one polyphenol was selected as the standard for each group, and was used to calculate individual concentrations by HPLC-DAD. Caffeic and gallic acids were used for hydroxycinnamic and hydroxybenzoic acids, respectively. Anthocyanins standard was cyanidin 3-*O*-glucoside. Quercetin and apigenin were the standards used for the flavonols and flavones, respectively. (+)-Catechin hydrate and ellagic acid were used as standards for quantification of flavanols and ellagitannins. Stock standard solutions (1000 mg/L) were prepared in methanol, and calibration curves were prepared by diluting the stock solutions with the initial mobile phase. Six concentrations (5−100 mg/L) were used for the calibration, plotting peak area versus concentration, obtaining $R^2 \geq 0.967$ in all cases. Peak area was used as the analytical signal for polyphenol quantification. Total individual phenolic contents (TIPC) was defined as the sum of the quantified phenolic compounds.

**Analysis of L-AA Content and Sugars.** Fresh berries were homogenized in a blender, and the pH was measured directly in the pulp using a Metrohm 7444 pH-meter (calibrated with standard buffer solutions of pH 7 and pH 9, respectively). The total soluble solids (TSS) were determined using an Atago RX-1000 refractometer, and the results were reported as Brix degrees (°Brix).

L-AA determination was carried out using the procedure indicated in our previous work.[17] Briefly, 10 mL of extraction solution (30 g L$^{-1}$ MPA−80 mL L$^{-1}$ acetic acid−1 mmol L$^{-1}$ EDTA) was added to 3 mL of pulp, and the mixture was centrifuged (4000 rpm; 20 min; 4 °C). The resulting extract was immediately analyzed by iodometric titration: 1 mL of 10 g L$^{-1}$ starch solution and 1 mL of 100 g L$^{-1}$ potassium iodide solution were added to fruit extract (diluted 1:10 with deionized water). Then, the samples were titrated with 0.002 mol L$^{-1}$ potassium iodate solution, until the mixture became dark blue and the color persisted for more than 60 s. This procedure was repeated in triplicate.

**TPC, TFC, and Antioxidant Capacities Assays.** *Total Phenolic Content (TPC).* The total phenolic content was determined by the Folin−Ciocalteu method.[18] Briefly, 50 μL aliquots (5 mg mL$^{-1}$ of dried extract dissolved in methanol) were mixed with 1.25 mL of FCR (diluted 1:10) and 1 mL of 7.5% $Na_2CO_3$ solution. After 30 min in darkness and room temperature, the absorbance was measured at 765


dx.doi.org/10.1021/jf503540s | J. Agric. Food Chem. 2014, 62, 9722−9735

nm ($n$ = 3) in a PerkinElmer UV−vis Lambda 2 spectrophotometer. The amounts of total phenolics were expressed as mg gallic acid equivalents (GAE)/100 g of dried extract (DE).

*Total Flavonoid Content (TFC).* The total flavonoid content was evaluated using the aluminum chloride colorimetric method:[18] 0.5 mL of methanolic extract (2.5 mg $mL^{-1}$) was mixed with 1.5 mL of methanol, 2.8 mL of distilled water, 0.1 mL of $CH_3COOK$ (1 mol $L^{-1}$), and 0.1 mL of $AlCl_3{\cdot}6H_2O$. The absorbance was measured at 415 nm after 30 min of reaction. The final results were expressed as mg of rutin equivalent (RUE)/100 g DE.

*ABTS Radical Scavenging Activity.* The $ABTS^{\bullet+}$ assay was performed according to Gouveia et al.[18]For each analysis, 40 $\mu$L of methanolic solution was added to 1.96 mL of $ABTS^{\bullet+}$ solution (diluted in phosphate buffered saline, PBS; absorbance 0.700 ± 0.021). The reduction of absorbance at 734 nm was measured during 10 min, and the results were expressed as $\mu$mol Trolox equivalent (TE)/100 g DE.

*DPPH Radical Scavenging Activity.* The DPPH assay followed a method previously reported:[18] 100 $\mu$L of methanolic solution (5 mg $mL^{-1}$) were added to 3.5 mL of DPPH radical solution (0.06 mol $L^{-1}$). The decrease in absorbance at 516 nm was measured every minute during 30 min. The DPPH results were expressed as $\mu$mol Trolox equivalent (TE)/100 g DE.

**Statistical Analysis.** Analysis of variance (ANOVA) was used to evaluate the results obtained in L-AA, TPC, TFC, and antioxidant assays determinations (IBM SPSS Statistics 20, SPSS, Inc.).

## RESULTS AND DISCUSSION

In this study, we aimed to establish, for the first time, the phenolic profile from different morphological parts of *Myrica faya*. Prior to the phenolic characterization, the influence of different experimental variables on the extraction procedure (solvent type, concentration, and duration of extraction) was investigated to increase the extraction efficiency of phenolics.

The results from the extraction experiments are shown in Figure 1.

A significant difference ($p$ < 0.05) was found between extraction with pure methanol or pure acetone, with a higher extraction yield using pure methanol (Figure 1a). Our results contradict those of Saini et al., who reported that acetone was more efficient than methanol for the extraction of phenolics from *M. esculenta*.[16] On the basis of our data, methanol was chosen for further investigations, and results showed that an increase in the percentage of this solvent influenced positively the extraction efficiency (Figure 1b). Significant differences ($p$ < 0.05) were observed between the different concentrations of methanol, except for 90% and 80%. Moreover, the yields of phenolic content were equal ($p$ > 0.05) when using aqueous methanol (80%) and acetone as the extraction solvents. Taking this fact into account, pure methanol was used to evaluate the influence of extraction time, and the results indicated that increasing the extraction duration had a positive effect on the extraction efficiency ($p$ < 0.05) (Figure 1c). Thus, an extraction time of 60 min with 100% methanol was considered as optimum.

**HPLC-DAD-ESI/$MS^n$ Screening.** Figure 2 shows the chromatogram obtained during the analysis of the methanolic extracts from *Myrica faya* by HPLC-DAD-ESI/$MS^n$. The identification of compounds was carried out by comparison of their UV−vis spectra and mass spectrometric data obtained under negative electrospray ionization ($ESI^-$) conditions with the data available in scientific literature.

The method achieved a good separation, and no relevant variation was observed in the three determinations performed for each sample. In general, in the $MS^1$ spectrum the most

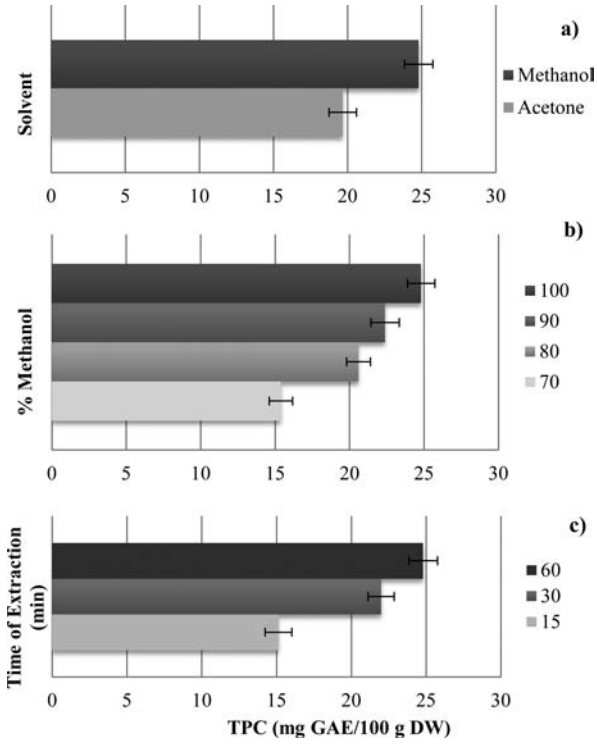


**Figure 1.** Extraction efficiency of different extraction conditions determined by TPC (mg/100 g DW) in *Myrica faya* leaves: (a) effect of solvent (methanol versus acetone); (b) effect of methanol concentration (v/v); (c) effect of extraction time. All extractions procedures were repeated three times ($n$ = 3).

intense peak corresponded to the deprotonated molecular ion $[M - H]^-$. The mass spectra of the conjugated form of the phenolic compounds showed the aglycone ion as a result of the loss of moieties like hexosyl, deoxyhexosyl, pentosyl, rutinosyl, caffeoyl, and glucuronyl (−162, −146, −132, −308, −162, and −176 Da, respectively). The identification of the compounds detected in leaf and berries extracts is presented in Tables 1 and 2, respectively, and their chemical structures are shown in Figure 3.

Compounds were numbered by their elution order, since most of them were not found in both samples (leaves and berries). More than 50 different compounds were detected and classified into two main groups: flavonoids (flavan-3-ols, flavones, isoflavones, and flavonols) and phenolic acids (hydroxybenzoic and hydroxycinnamic acids). Quinic acid and derivatives were also relevant in leaves. Additionally, mass spectra data from the positive ionization mode ($ESI^+$) was used for confirmation of the anthocyanidin compounds, namely cyanidin-3-glucoside and delphinidin-*O*-hexoside, in berries. A characteristic esterification with gallic acid was found in the majority of the compounds, representing the dominant group bound to polyphenols of leaves and berries.

The phenolic profiles obtained by our HPLC-UV/DAD-$MS^n$ analysis were similar to previous reports on *Myrica*.[6−8,10−13,15] In addition, we were still able to identify for the first time in this genus 26 compounds, namely flavones, ellagitannins, lignans, terpenoids, among others. The analysis showed that leaves of *M. faya* were significantly more complex when compared to berries, most of the identified compounds exclusively being detected in the leaf extracts. Nevertheless, some compounds were only detected in berries (**2**, **4**, **6**, **9**, **13**, **16**, **19**, **24**, and **26**).

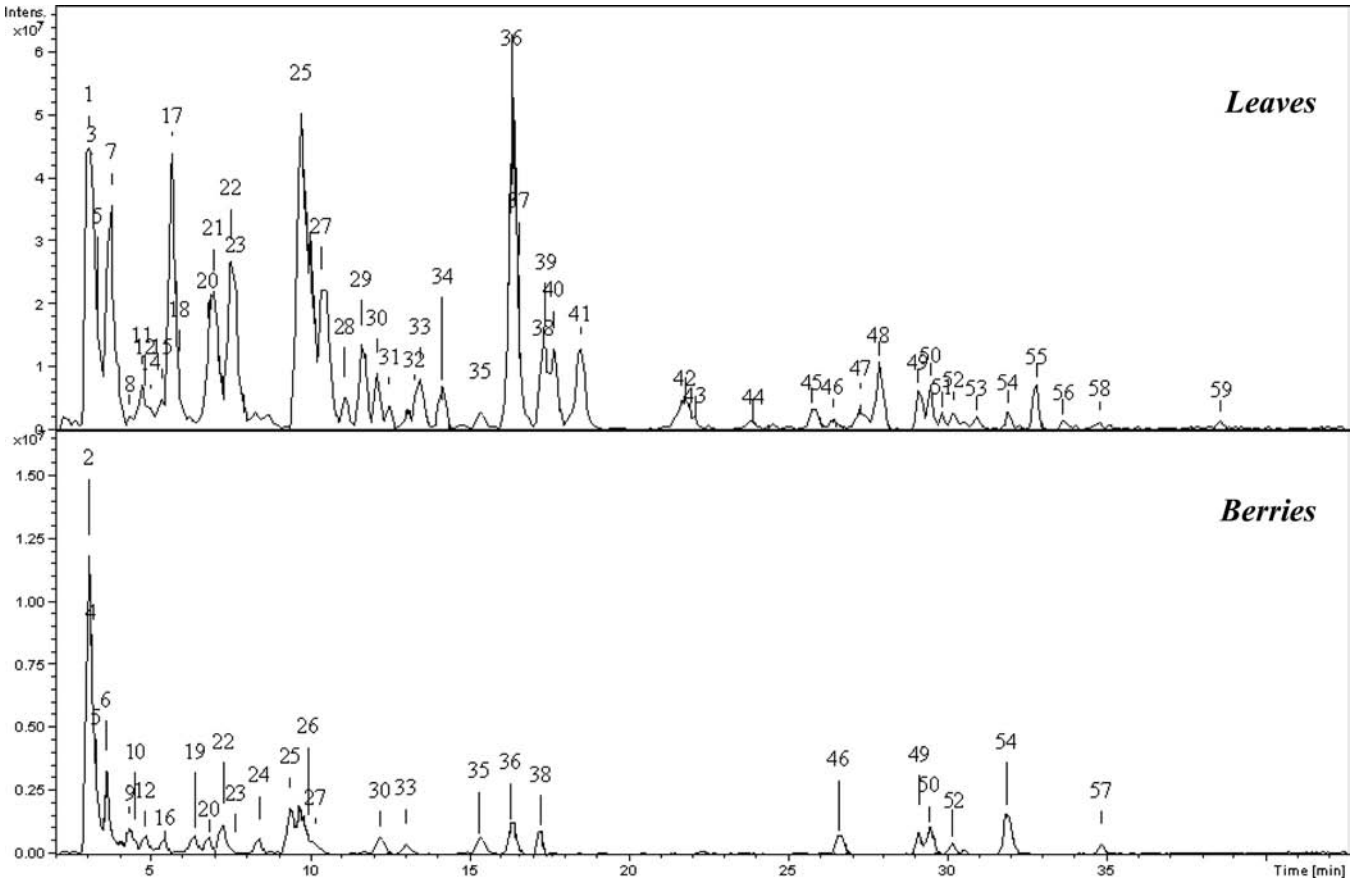


**Figure 2.** HPLC-DAD-ESI/MS$^n$ base peak chromatograms (BPC) of the methanolic extracts from *Myrica faya*: leaves and berries.

*Negative Mode Ionization.* For the analysis of the phenolic composition of *M. faya*, both the positive and negative ionization modes were used. However, the majority of the information was obtained using the negative mode, and the positive mode was mainly used for confirmation purposes.

*Identification of Phenolic Acids.* Compound **4** presented $[M - H]^-$ ion at $m/z$ 341. It suffered the neutral loss of 162 Da (hexoside), producing a fragment ion at $m/z$ 179. This ion suffered further fragmentation, producing fragment ions at $m/z$ 161 and 135, which are typical from caffeic acid, so the compound was identified as caffeic acid *O*-hexoside.[19]

Compound **29** exhibited a $[M - H]^-$ ion at $m/z$ 415 and was characterized as a caffeic acid derivative. Its MS$^n$ spectrum was identical to that described previously in *H. obconicum*[19] by our group. To our best knowledge, the presence of caffeic acid derivatives has not been reported, so far, in *Myrica*.

Compound **17** displayed a $[M - H]^-$ ion at $m/z$ 421, which gave origin to an ion at $m/z$ 385 (by loss of 36 Da). Further fragmentation led to sinapic acid aglycone at $m/z$ 223 (by loss of 162 Da),[10] being characterized as sinapic acid-*O*-hexoside derivative.

Compounds **37** and **39**, showing $[M - H]^-$ ions at $m/z$ 511 and 481, were identified, for the first time in *Myrica*, as derivatives of sinapic acid-*O*-hexoside and ferulic acid-*O*-hexoside, respectively. Both showed identical neutral losses at $MS^2$ (126 + 162 Da), but the presence of sinapic and ferulic acids led to different characterizations. While the 162 Da loss are attributed to hexoside units attached to the aglycones, the 126 Da loss could not be identified.

Compound **6** with $[M - H]^-$ at $m/z$ 331 was plausibly identified as galloyl-*O*-hexoside, according to previous studies in pomegranate.[20,21]

Compound **8** exhibited $[M - H]^-$ ion at $m/z$ 467 and fragmented into ion at $m/z$ 169 [gallic acid $- H]^-$ due to loss of 298 Da. In the absence of more specific data, **8** was assigned as a gallic acid derivative.

Compound **18**, with $[M - H]^-$ at $m/z$ 285, was identified as protocatechuic acid-*O*-pentoside based on bibliographic data.[22] The presence of this hydroxybenzoic acid in *Myrica* species is consistent with previous reports.[13]

*Flavonoids.* In this study, flavonoids (flavones, flavonols, and flavan-3-ols) were detected in their glycosylated form and/or esterified with acyl groups and were the most abundant components identified.

Compound **11** had an $[M - H]^-$ ion at $m/z$ 761 and displayed typical product ions for galloyl-di(epi)gallocatechin at $m/z$ 609 $[M - 152 - H]^-$, 591 $[M - 170 - H]^-$, and 423 $[M - 170 - 168 - H]^-$, which corresponded to losses of galloyl moieties (170 and 152 Da) and retro-Diels–Alder reaction product ion (168 Da), respectively. This fragmentation behavior is congruent with the previously published[11] for this compound in *Myrica rubra*.

Compound **12** was assigned as gallo(epi)catechin with characteristic $[M - H]^-$ ion at $m/z$ 305, based on previous characterization on pomegranate.[21]

Compound **13** displayed $[M - H]^-$ ion at $m/z$ 483 and gave origin to a product ion at $m/z$ 447 (by loss of 36 Da). Sequential loss of a hexoside moiety produced luteolin aglycone


dx.doi.org/10.1021/jf503540s | J. Agric. Food Chem. 2014, 62, 9722–9735

**Table 1. Characterization of Phenolic and Organic Compounds of the Methanolic Extracts of Leaves from *Myrica faya***

| no. | $t_R$ (min) | $\lambda_{max}$[a] (nm) | $[M - H]^-$ ($m/z$) | HPLC-DAD-ESI/$MS^n$ $m/z$ (% base peak) | assigned identity |
|---|---|---|---|---|---|
| 1 | 3.0 | 234, 273 | 683 $[2M - H]^-$ | $MS^2$ [683]: 341 (100), 342 (10.3) | unknown |
| | | | | $MS^3$ [683→341]: 179 (100), 161 (24.1), 143 (17.7), 119 (15.5), 113 (18.0) | |
| | | | | $MS^4$ [683→341→179]: 161 (29.7), 149 (22.7), 143 (87.7), 113 (48.8), 101 (30.1), 89 (100) | |
| 3 | 3.1 | | 533 | $MS^2$ [533]: 191 (100) | quinic acid derivative |
| | | | | $MS^3$ [533→191]: 173 (100), 127 (64.9), 109 (32.8), 99 (50.1), 93 (59.0), 85 (42.1) | |
| | | | | $MS^4$ [533→191→173]: 109 (100) | |
| 5 | 3.3 | | 191 | $MS^2$ [191]: 173 (58.2), 127 (100), 111 (40.5), 109 (23.8), 93 (41.7), 85 (37.1), 109 (23.8) | quinic acid |
| | | | | $MS^3$ [191→127]: 109 (100), 99 (53.9), 85 (39.8) | |
| 7 | 3.8 | | 383 $[2M - H]^-$ | $MS^2$ [383]: 191 (100) | quinic acid dimer |
| | | | | $MS^3$ [383→191]: 127 (100), 85 (69.8), 93 (58.4), 109 (60.4), 111 (43.0), 173 (24.5) | |
| 8 | 4.3 | 213, 273 | 467 | $MS^2$ [467]: 436 (36.6), 391 (52.4), 301 (42.1), 275 (71.9), 169 (100) | gallic acid derivative |
| | | | | $MS^3$ [467→169]: 125 (100), 123 (41.5) | |
| 11 | 4.7 | 207, 276 | 761 | $MS^2$ [761]: 635 (17.8), 609 (69.0), 575 (36.6), 591 (51.2), 593 (33.8), 423 (100), 305 (38.4) | galloyl(epi)gallocatechin dimer |
| | | | | $MS^3$ [761→423]: 305 (51.2), 297 (61.7), 283 (100), 255 (77.4), 243 (36.5) | |
| | | | | $MS^4$ [761→423→283]: 255 (33.5), 241 (100) | |
| 12 | 4.8 | | 305 | $MS^2$ [305]: 261 (54.6), 221 (34.0), 219 (85.6), 204 (21.7), 179 (100), 166 (17.0), 139 (16.5), 137 (63.1) | gallo(epi)catechin[b] |
| | | | | $MS^3$ [305→179]: 163 (100), 152 (45.5), 151 (77.3), 135 (32.1) | |
| 14 | 5.0 | | 935 | $MS^2$ [935]: 917 (20.9), 659 (21.2), 633 (100), 615 (36.7), 571 (18.5), 329 (25.4), 301 (21.9), 299 (49.4) | galloyl-bis-HHDP-*O*-hexoside (Casuarinin)[b] |
| | | | | $MS^3$ [935→633]: 615 (76.5), 571 (100), 481 (44.3), 383 (31.7), 329 (76.1), 301 (28.7), 299 (97.9), 275 (26.5) | |
| 15 | 5.3 | | 447 | $MS^2$ [447]: 401 (100) | benzyl alcohol hexose pentose (formate adduct)[b] |
| | | | | $MS^3$ [447→401]: 269 (100), 179 (48.2), 161 (38.9), 159 (14.7) | |
| | | | | $MS^4$ [447→401→269]: 161 (100), 143 (32.5), 99 (17.5) | |
| 17 | 5.6 | | 421 | $MS^2$ [421]: 386 (68.4), 385 (100), 305 (12), 205 (90.2), 153 (14.1) | sinapic acid-*O*-hexoside derivative |
| | | | | $MS^3$ [421→385]: 326 (22.4), 265 (23.5), 224 (13.6), 223 (100), 205 (23.1) | |
| | | | | $MS^4$ [421→385→223]: 208 (46.4), 179 (79), 164 (100) | |
| 18 | 5.9 | 209, 277 | 285 | $MS^2$ [285]: 154 (11.8), 153 (100), 152 (21.2), 109 (12.0) | protocathechuic acid-*O*-pentoside |
| | | | | $MS^3$ [285→153]: 109 (77.0), 108 (100) | |
| 20 | 6.8 | | 457 | $MS^2$ [457]: 331 (19.8), 319 (14.8), 305 (12.4), 193 (16.3), 169 (100) | gallo(epi)catechin-*O*-gallate |
| | | | | $MS^3$ [457→169]: 125 (100) | |
| 21 | 7.0 | 209, 275 | 915 $[2M - H]^-$ | $MS^2$ [915]: 458 (14.6), 457 (100) | gallo(epi)catechin-*O*-gallatedimer |
| | | | | $MS^2$ [915→457]: 331 (27.4), 305 (33.1), 193 (16.2), 169 (100) | |
| | | | | $MS^3$ [915→457→169]: 125 (100) | |
| 22 | 7.5 | 209, 268, 359 | 479 | $MS^2$ [479]: 317 (100), 316 (92.3), 179 (16.0) | myricetin-*O*-hexoside |
| | | | | $MS^3$ [479→317]: 287 (30.6), 271 (81.6), 193 (40.6), 179 (100) | |
| 23 | 7.7 | | 631 | $MS^2$ [631]: 479 (39.7), 318 (12.7), 317 (100) | myricetin-*O*-(*O*-galloyl)hexoside |
| | | | | $MS^3$ [631→317]: 179 (100), 151 (39.1) | |
| 25 | 9.7 | 209, 262, 349 | 463 | $MS^2$ [463]: 318 (10.1), 317 (100), 316 (64.5) | myricetin-*O*-deoxyhexoside |
| | | | | $MS^3$ [463→317]: 288 (11.4), 287 (24.7), 272 (27.2), 271 (59.7), 270 (35.9), 179 (100), 151 (10.7) | |
| 27 | 10.3 | 207, 358 | 615 | $MS^2$ [615]: 302 (14.7), 301 (100), 313 (16.6), 463 | galloylquercetin-*O*- hexoside[b] |
| | | | | $MS^3$ [615→301]: 179 (100), 193 (15.5), 151 (63.4) | |
| | | | | $MS^4$ [615→301→179]: 257 (11.5), 151 (100), 169 (64.3) | |
| 28 | 11.0 | | 593 | $MS^2$ [593]: 285 (100), 286 (18.8) | kaempferol-*O*-rutinoside[b] |
| | | | | $MS^3$ [593→285]: 257 (100), 241 (58.8), 229 (35.9), 197 (17.6), 169 (23.2), 163 (39.6), 93 (30.3) | |
| | | | | $MS^4$ [593→285→257]: 255 (22.1), 151 (100) | |
| 29 | 11.6 | | 415 | $MS^2$ [415]: 369 (65.9), 225 (30.0), 179 (100), 161 (11.4), 149 (10.7), 143 (12.2) | caffeic acid derivative (formate adduct) |
| | | | | $MS^3$ [415→179]: 161 (100), 135 (48.4), 89 (49.6) | |
| 30 | 12.1 | 208, 267, 343 | 447 | $MS^2$ [447]: 285 (91.8), 284 (100), 255 (22.0), 256 (16.8) | kaempferol-*O*-hexoside[b] |

**Table 1. continued**

| no. | $t_R$ (min) | $\lambda_{max}$[a] (nm) | $[M - H]^-$ ($m/z$) | HPLC-DAD-ESI/$MS^n$ $m/z$ (% base peak) | assigned identity |
|---|---|---|---|---|---|
| | | | | $MS^3$ [447→285]: 255 (100), 227 (42.3), 256 (22.7), 257 (17.4), 239 (16.1), 223 (103.), 151 (10.4) | |
| | | | | $MS^4$ [447→284→255]: 255 (16.2), 229 (100), 227 (25.7), 211 (38.7), 167 (46.0) | |
| 31 | 12.5 | | 579 | $MS^2$ [579]: 534 (16.7), 533 (100), 372 (22.5), 371 (99.5) | phylligenin-*O*-hexoside[b] (formate adduct) |
| | | | | $MS^3$ [579→533]: 372 (15.9), 371 (100) | |
| | | | | $MS^3$ [579→371]: 342 (18.1), 341 (100), 340 (61.9), 297 (13.1) | |
| | | | | $MS^4$ [579→533→371]: 357 (29.2), 356 (100), 342 (18.3), 341 (68.7), 297 (13.1) | |
| 32 | 13.2 | 208, 265, 347 | 599 | $MS^2$ [599]: 313 (100), 285 (98.5), 314 (22.6), 286 (12.3) | kaempferol-*O*-(*O*-galloyl)hexoside[b] |
| | | | | $MS^3$ [599→313]: 169 (100), 125 (36.0), 152 (34.0), 211 (29.3) | |
| 33 | 13.4 | | 447 | $MS^2$ [447]: 301 (100), 300 (24.9), 302 (14.8) | quercetin-*O*-deoxyhexoside |
| | | | | $MS^3$ [447→301]: 273 (22.8), 271 (14.8), 255 (10.7), 211 (21.3), 179 (76.6), 169 (32.5), 151 (100) | |
| | | | | $MS^4$ [447→301→179]: 169 (28.3), 151 (100) | |
| 34 | 14.1 | | 539 | $MS^2$ [539]: 378 (13.5), 377 (64.0), 308 (29.3), 307 (100), 275 (71.0) | oleuropein[b] |
| | | | | $MS^3$ [539→307]: 276 (13.2), 275 (100), 223 (56.8), 149 (39.8), 139 (13.8) | |
| 35 | 15.3 | | 633 | $MS^2$ [633]: 488 (16.5), 487 (12.2), 470 (18.7), 469 (100), 347 (50.7) | benzoyl-*p*-dicoumaryl- 2,7-anhydro-3-deoxy-2-octulopyranosonic acid[b] |
| | | | | $MS^3$ [633→469]: 347 (76.0), 323 (56.3), 303 (20.4), 259 (33.1), 235 (15.7), 163 (100), 145 (50.9) | |
| | | | | $MS^4$ [633→469→163]: 119 (100) | |
| 36 | 16.3 | 211, 267, 345 | 615 | $MS^2$ [615]: 318 (16.8), 317 (100), 463 (41.8) | myricetin-*O*-(*O*-galloyl)deoxyhexoside |
| | | | | $MS^3$ [615→317]: 227 (11.6), 193 (16.2), 191 (12.6), 180 (12.4), 179 (100), 151 (33.3), 137 (16.7) | |
| | | | | $MS^4$ [615→317→179]: 151 (100) | |
| 37 | 16.5 | | 511 | $MS^2$ [511]: 385 (31.4), 287 (29.3), 269 (12.8), 224 (13.2), 223 (100), 163 (13.5) | sinapic acid-*O*-hexoside derivative[b] |
| | | | | $MS^3$ [511→223]: 208 (69.4), 179 (100), 178 (43.3), 209 (50.0), 164 (32.3) | |
| | | | | $MS^4$ [511→223→179]: 164 (100) | |
| 38 | 17.3 | 211, 267, 345 | 615 | $MS^2$ [615]: 463 (31.2) 318 (13.2), 317 (100) | myricetin-*O*-(*O*-galloyl)deoxyhexoside |
| | | | | $MS^3$ [615→317]: 271 (10.7), 255 (10.9), 193 (16.3), 192 (15.5), 179 (100), 151 (60.7), 137 (25.0) | |
| | | | | $MS^4$ [615→317→179]: 169 (22.6), 151 (100) | |
| 39 | 17.4 | 209, 329 | 481 | $MS^2$ [481]: 463 (15.2), 355 (15.5), 287 (24.2), 193 (100), 161 (13.5) | ferulic acid-*O*-hexoside derivative[b] |
| | | | | $MS^3$ [481→193]: 178 (93.3), 149 (100), 134 (44.8) | |
| 40 | 17.6 | | 431 | $MS^2$ [431]: 286 (16.7), 285 (100), 284 (28.4), 255 (10.5) | kaempferol-*O*-rhamnoside[b] |
| | | | | $MS^3$ [431→285]: 257 (61.7), 255 (100), 239 (32.5), 229 (52.5), 197 (30.7), 163 (19.4) | |
| | | | | $MS^4$ [431→285→255]: 229 (46.7), 213 (20.3), 189 (13.3), 185 (10.5), 151 (100), 93 (38.7) | |
| 41 | 18.5 | | 549 | $MS^2$ [549]: 505 (23.7), 504 (24.9), 503 (100), 324 (15.4), 323 (89.2) | unknown |
| | | | | $MS^3$ [549→503]: 413 (81.0), 324 (10.9) 323 (100), 161 (33.0) | |
| | | | | $MS^4$ [549→503→323]: 308 (34.6), 295 (48.8), 292 (38.0), 279 (47.2), 265 (48.5), 263 (71.8), 247 (68.9), 235 (47.8), 233 (100) | |
| 42 | 21.7 | | 489 | $MS^2$ [489]: 454 (32.3), 447 (36.5), 445 (39.0), 403 (38.6), 301 (100), 300 (25.8) | quercetin-*O*-acetylrhamnoside |
| | | | | $MS^3$ [489→301]: 151 (100), 243 (63.0), 271 (84.2) | |
| 43 | 22.0 | | 565 | $MS^2$ [565]: 358 (22.3), 357 (100) | dichotomitin-*O*-hexoside[b] |
| | | | | $MS^3$ [565→357]: 343 (20.4), 342 (100), 327 (41.9), 299 (21.6) | |
| | | | | $MS^3$ [565→357]: 343(16.6), 342 (60.5), 327 (100) | |
| | | | | $MS^4$ [565→357→342]: 328 (22.3), 327 (100), 299 (34.5) | |
| | | | | $MS^4$ [565→357→327]: 299 (100), 268 (87.9), 228 (48.1), 227 (87.1) | |
| 44 | 23.8 | | 599 | $MS^2$ [599]: 553 (28.3), 485 (25.8), 447 (45.6), 301 (100), 299 (11.1), 297 (18.7) | quercetin-*O*-(*O*-galloyl)deoxyhexoside |
| | | | | $MS^3$ [599→301]: 273 (15.5), 187 (12.9), 179 (57.7), 151 (100) | |
| | | | | $MS^4$ [599→301→179]: 151 (100) | |
| 45 | 25.7 | | 507 | $MS^2$ [507]: 461 (100), 443 (38.5), 294 (10.5), 293 (64.0) | lactiflorin[b] (formate adduct) |
| | | | | $MS^3$ [507→461]: 443 (29.5), 293 (100), 149 (58.9), 131 (23.9) | |
| | | | | $MS^4$ [507→461→293]: 149 (100), 122 (47.9) | |


dx.doi.org/10.1021/jf503540s | J. Agric. Food Chem. 2014, 62, 9722−9735

**Table 1. continued**

| no. | $t_R$ (min) | $\lambda_{max}$[a] (nm) | $[M - H]^-$ ($m/z$) | HPLC-DAD-ESI/$MS^n$ $m/z$ (% base peak) | assigned identity |
|---|---|---|---|---|---|
| 46 | 26.6 | | 491 | $MS^2$ [491]: 371 (12.9), 330 (28.5), 330 (20.3), 329 (100), 314 (10.7) | tricin-*O*-hexoside[b] |
| | | | | $MS^3$ [491→329]: 315 (53.0), 314 (100) | |
| | | | | $MS^3$ [491→329→314]: 300 (40.3), 299 (100) | |
| 47 | 27.3 | | 491 | $MS^2$ [491]: 330 (26.9), 329 (100) | tricin-*O*-hexoside[b] |
| | | | | $MS^3$ [491→329]: 315 (14.3), 314 (100), 136 (38.6), 135 (40.1) | |
| | | | | $MS^4$ [491→329→314]: 300 (43.1), 299 (100) | |
| 48 | 27.8 | | 555 | $MS^2$ [555]: 417 (21.7), 305 (32.9), 287 (27.1), 269 (100), 267 (22.4), 223 (54.3), 161 (22.2) | baicalein derivative[b] |
| | | | | $MS^3$ [555→269]: 251 (20.5), 241 (38.8), 227 (45.9), 226 (51.3), 225 (32.3), 223 (100), 197 (48.9), 195 (33.5), 179 (17.1) | |
| | | | | $MS^4$ [555→269→223]: 197 (100) | |
| 49 | 29.1 | | 491 | $MS^2$ [491]: 473 (20.8), 330 (15.2), 329 (100) | tricin-*O*-hexoside[b] |
| | | | | $MS^3$ [491→329]: 314 (100), 299 (70.5), 271 (52.1), 193 (48.3), 181 (62.0), 135 (51.6) | |
| 50 | 29.4 | | 563 | $MS^2$ [563]: 356 (11.0), 355 (100) | conidendrin-*O*-hexoside[b] |
| | | | | $MS^3$ [563→355]: 341 (12.8), 340 (100), 325 (43.4) | |
| | | | | $MS^4$ [563→355→340]: 326 (15.2), 325 (100), 296 (79.8), 281 (36.7), 212 (27.6) | |
| | | | | $MS^4$ [563→355→325]: 296 (100), 281 (79.8), 212 (27.6) | |
| 51 | 29.8 | | 583 | $MS^2$ [583]: 286 (17.7), 285 (100) | kaempferol derivative |
| | | | | $MS^3$ [583→285]: 267 (55.6), 257 (100), 241 (43.8), 151 (93.5), 169 (48.8) | |
| 52 | 30.4 | | 535 | $MS^2$ [535]: 490 (31.6), 489 (100) | 5,7-dihydroxy-6,8-dimethoxyflavone-7-*O*-glucuronide[b] |
| | | | | $MS^3$ [535→489]: 327 (46.0), 313 (100), 298 (55.5), 283 (33.6) | |
| | | | | $MS^4$ [535→489→313]: 298 (100), 283 (22.7), 269 (32.4), 254 (29.4) | |
| 53 | 30.9 | | 677 | $MS^2$ [677]: 593 (75.0), 575 (61.3), 285 (100), 284 (99.2), 268 (17.7), 255 (22.3), 229 (19.3) | kaempferol-*O*-rutinoside |
| | | | | $MS^3$ [677→285]: 283 (51.6), 257 (100), 255 (65.6), 241 (74.3), 229 (38.5), 197 (49.1) | derivative[b] |
| 54 | 31.9 | | 779 | $MS^2$ [779]: 634 (26.5), 633 (100), 616 (26.2), 615 (74.3), 469 (38.7) | benzoyl-*p*-tricoumaryl- 2,7-anhydro-3-deoxy-2-octulopyranosonic acid[b] |
| | | | | $MS^3$ [779→633]: 488 (18.7), 487 (17.9), 470 (35.0), 469 (100), 325 (17.3), 265 (11.1) | |
| | | | | $MS^4$ [779→633→469]: 307 (88.9), 163 (100), 145 (49.5) | |
| 55 | 32.8 | | 695 | $MS^2$ [695]: 488 (25.6), 487 (100) | unknown |
| | | | | $MS^3$ [695→487]: 421 (31.1), 410 (48.3), 409 (100), 401 (35.3), 391 (59.4), 390 (16.2) | |
| | | | | $MS^4$ [695→487→409]: 392 (15.7), 391 (35.2), 380 (34.7), 379 (100), 377 (25.2), 359 (24.2) | |
| 56 | 33.6 | | 673 | $MS^2$ [673]: 638 (23.4), 637 (100), 655 (22.6), 619 (15.2), 611 (15.7), 595 (16.7) | unknown |
| | | | | $MS^3$ [673→637]: 609 (54.4), 401 (26.0), 365 (37.7), 332 (28.9), 209 (100), 203 (64.2) | |
| 58 | 34.8 | | 515 | $MS^2$ [515]: 454 (55.9), 269 (100), 243 (18.2), 241 (28.1), 227 (71.6), 183 (40.5) | unknown |
| | | | | $MS^3$ [515→269]: 228 (100), 213 (80.2), 149 (14.8) | |
| 59 | 38.5 | | 515 | $MS^2$ [515]: 285 (43.9), 284 (100), 255 (23.0) | kaempferol derivative |
| | | | | $MS^3$ [515→284]: 257 (19.2), 256 (25.0), 255 (100), 242 (34.0), 195 (21.1) | |

[a]Wavelengths not provided when the UV spectrum was not properly observed due to low intensity. [b]Compound identified for the first time in *Myrica* genus.

($m/z$ 285). Thus, **13** was identified as a luteolin-*O*-hexoside derivative, reported for the first time in *Myrica*.

(epi)Catechin monomer and (epi)catechin-*O*-gallate (compounds **19** and **26**) displayed $[M - H]^-$ ions at $m/z$ 289 and 441, respectively, and were assigned according to previous characterizations[23] in grape pomace. Catechin has been previously detected in *M. esculenta* by an HPLC-PDA method.[15]

Compound **20** exhibited a $[M - H]^-$ ion at $m/z$ 457 and was assigned as gallocatechin-*O*-gallate, on the basis of previous studies in *M. rubra*.[11] Although compound **20** was detected before in leaves of bayberry, we report here for the first time its presence in fruits of this genus. With $[M - H]^-$ ion at $m/z$ 915 and $MS^2$ product ion at $m/z$ 457, compound **21** was plausibly identified as a dimer of gallo(epi)catechin-*O*-gallate.

Conjugates of myricetin (compounds **22**, **23**, **25**, **36**, and **38**), quercetin (compounds **33**, **42**, and **44**), and kaempferol (compounds **28**, **30**, **32**, and **40**) were characterized according to the sugar moieties attached to their aglycones (at $m/z$ 317, 301, and 285, respectively). The characterizations of these compounds in *Myrica faya* were supported by previous reports in *M. rubra*[6−8,11,13] and pomegranate.[20] Myricetin derivatives were reported as the major flavonoids in extracts of *M. rubra*'s leaves and berries. Besides kaempferol-*O*-hexoside (**30**), all

**Table 2. Characterization of Phenolic and Organic Compounds of the Methanolic Extracts of Berries from *Myrica faya***

| no. | $t_R$ (min) | $\lambda_{max}$[a] (nm) | $[M - H]^-$ ($m/z$) | HPLC-DAD-ESI/$MS^n$ $m/z$ (% base peak) | assigned identity |
|---|---|---|---|---|---|
| 2 | 3.0 | 219, 280, 516 | 449 (+) | $MS^2$ [449]: 288 (14.1), 287 (100) | cyanidin-3-glucoside |
| | | | | $MS^3$ [449→287]: 241 (87.2), 213 (100), 193 (58.2), 185 (47.6), 175 (57.5), 169 (50.1) 165 (24.1), 161 (31.3), 137 (69.0) | |
| | | | | $MS^4$ [449→287→213]: 167 (100) | |
| 4 | 3.2 | 234, 274 | 341 | $MS^2$ [341]: 179 (100), 135 (22.7) | caffeic acid-*O*-hexoside[b] |
| | | | | $MS^3$ [341→179]: 161 (11.7), 135 (100) | |
| 5 | 3.3 | | 191 | $MS^2$ [191]: 173 (58.2), 127 (100), 111 (40.5), 109 (23.8), 93 (41.7), 85 (37.1), 109 (23.8) | quinic acid |
| | | | | $MS^3$ [191→127]: 109 (100), 99 (53.9), 85 (39.8) | |
| 6 | 3.4 | | 331 | $MS^2$ [331]: 271 (30.5), 169 (100), 125 (29.7) | galloyl-*O*-hexoside[b] |
| | | | | $MS^3$ [331→169]: 125 (100) | |
| 9 | 4.3 | 280, 519 | 465 (+) | $MS^2$ [465]: 304 (17.7), 303 (100) | delphinidin-*O*-hexoside[b] |
| | | | | $MS^3$ [465→303]: 258 (22.3), 257 (100), 247 (11.8), 229 (80.5), 163 (10.3), 135 (31.4) | |
| | | | | $MS^4$ [465→303→257]: 229 (56.4), 213 (100), 173 (63.4) | |
| 10 | 4.5 | | 405 | $MS^2$ [405]: 388 (11.6), 387 (16.7), 191 (100) | quinic acid derivative |
| | | | | $MS^3$ [405→191]: 173 (23.3), 127 (100), 111 (14.0), 93 (10.2) | |
| 13 | 4.8 | | 483 | $MS^2$ [483]: 448 (20.6), 447 (100) | luteolin-*O*-hexoside derivative[b] |
| | | | | $MS^3$ [483→447]: 286 (17.8), 285 (100), 284 (20.5) | |
| | | | | $MS^4$ [483→447→285]: 243 (100), 241 (55.0), 217 (29.2), 199 (16.8), 167 (41.9), 125 (37.7) | |
| 16 | 5.4 | | 431 | $MS^2$ [431]: 386 (41.1), 385 (100), 384 (22.1), 175 (17.4) | roseoside[b] (formate adduct) |
| | | | | $MS^3$ [431→385]: 223 (100), 153 (30.1), 138 (11.4) | |
| | | | | $MS^4$ [431→385→223]: 206 (47.0), 153 (100), 147 (39.9) | |
| 19 | 6.4 | | 289 | $MS^2$ [289]: 247 (19.3), 245 (100), 205 (48.0), 203 (16.2), 179 (14.6), 161 (15.7) | (epi)catechin[b] |
| | | | | $MS^3$ [289→245]: 205 (40.1), 204 (85.6), 203 (100), 202 (47.2), 187 (53.4), 162 (17.2), 121 (56.3) | |
| 20 | 6.8 | | 457 | $MS^2$ [457]: 331 (19.8), 319 (14.8), 305 (12.4), 193 (16.3), 169 (100) | gallo(epi)catechin-*O*-gallate[b] |
| | | | | $MS^3$ [457→169]: 125 (100) | |
| 22 | 7.5 | 209, 268, 359 | 479 | $MS^2$ [479]: 317 (100), 316 (92.3), 179 (16.0) | myricetin-*O*-hexoside[b] |
| | | | | $MS^3$ [479→317]: 287 (30.6), 271 (81.6), 193 (40.6), 179 (100) | |
| | | | | $MS^4$ [479→317→179]: 169 (100) | |
| 23 | 7.7 | | 631 | $MS^2$ [631]: 479 (39.7), 318 (12.7), 317 (100) | myricetin-*O*-(*O*-galloyl)hexoside |
| | | | | $MS^3$ [631→317]: 179 (100), 151 (39.1) | |
| | | | | $MS^4$ [631→317→179]: 169 (28.6), 151 (100) | |
| 24 | 8.4 | | 597 | $MS^2$ [597]: 477 (45.0), 459 (15.3), 417 (25.2), 388 (17.3), 387 (53.6), 358 (20.0), 357 (100) | glucaric acid derivative[b] |
| | | | | $MS^3$ [597→357]: 300 (15.3), 209 (100), 123 (12.1),121 (25.4) | |
| | | | | $MS^4$ [597→357→209]: 191 (70.5), 165 (48.0), 147 (100) | |
| 26 | 10.2 | 207, 265, 352 | 441 | $MS^2$ [441]: 289 (100), 290 (21.5), 169 (17.5), 331 (11.6) | (epi)catechin-*O*-gallate[b] |
| | | | | $MS^2$ [441→289]: 245 (100), 179 (28.3), 161 (27.4), 135 (17.6), 85 (13.0) | |
| | | | | $MS^3$ [441→289→245]: 203 (100), 202 (39.7), 204 (65.1), 205 (43.4), 188 (53.4) | |
| 27 | 10.3 | 207, 358 | 615 | $MS^2$ [615]: 302 (14.7), 301 (100), 313 (16.6), 463 | galloylquercetin-*O*- hexoside[b] |
| | | | | $MS^3$ [615→301]: 179 (100), 193 (15.5), 151 (63.4) | |
| | | | | $MS^4$ [615→301→179]: 257 (11.5), 151 (100), 169 (64.3) | |
| 30 | 12.1 | 208, 267, 343 | 447 | $MS^2$ [447]: 285 (91.8), 284 (100), 255 (22.0), 256 (16.8) | kaempferol-*O*-hexoside |
| | | | | $MS^3$ [447→285]: 255 (100), 227 (42.3), 256 (22.7), 257 (17.4), 239 (16.1), 223 (103.), 151 (10.4) | |
| | | | | $MS^4$ [447→284→255]: 255 (16.2), 229 (100), 227 (25.7), 211 (38.7), 167 (46.0) | |
| 33 | 13.4 | | 447 | $MS^2$ [447]: 301 (100), 300 (24.9), 302 (14.8) | quercetin-*O*-deoxyhexoside |
| | | | | $MS^3$ [447→301]: 273 (22.8), 271 (14.8), 255 (10.7), 211 (21.3), 179 (76.6), 169 (32.5), 151 (100) | |
| | | | | $MS^4$ [447→301→179]: 169 (28.3), 151 (100), | |
| 35 | 15.3 | | 633 | $MS^2$ [633]: 488 (16.5), 487 (12.2), 470 (18.7), 469 (100), 347 (50.7) | benzoyl-*p*-dicoumaryl- 2,7-anhydro-3-deoxy-2-octulopyranosonic acid[b] |
| | | | | $MS^3$ [633→469]: 347 (76.0), 323 (56.3), 303 (20.4), 259 (33.1), 235 (15.7), 163 (100), 145 (50.9) | |


dx.doi.org/10.1021/jf503540s | J. Agric. Food Chem. 2014, 62, 9722−9735

**Table 2. continued**

| no. | $t_R$ (min) | $\lambda_{max}$[a] (nm) | $[M - H]^-$ ($m/z$) | HPLC-DAD-ESI/$MS^n$ $m/z$ (% base peak) | assigned identity |
|---|---|---|---|---|---|
| | | | | $MS^4$ [633→469→163]: 119 (100) | |
| 36 | 16.3 | 211, 267, 345 | 615 | $MS^2$ [615]: 318 (16.8), 317 (100), 463 (41.8) | myricetin-*O*-(*O*-galloyl)deoxyhexoside |
| | | | | $MS^3$ [615→317]: 227 (11.6), 193 (16.2), 191 (12.6), 180 (12.4), 179 (100), 151 (33.3), 137 (16.7) | |
| | | | | $MS^4$ [615→317→179]: 151 (100) | |
| 38 | 17.3 | 211, 267, 345 | 615 | $MS^2$ [615]: 463 (31.2) 318 (13.2), 317 (100) | myricetin-*O*-(*O*-galloyl)deoxyhexoside |
| | | | | $MS^3$ [615→317]: 271 (10.7), 255 (10.9), 193 (16.3), 192 (15.5), 179 (100), 151 (60.7), 137 (25.0) | |
| | | | | $MS^4$ [615→317→179]: 169 (22.6), 151 (100) | |
| 40 | 17.6 | | 431 | $MS^2$ [431]: 286 (16.7), 285 (100), 284 (28.4), 255 (10.5) | kaempferol-*O*-rhamnoside[b] |
| | | | | $MS^3$ [431→285]: 257 (61.7), 255 (100), 239 (32.5), 229 (52.5), 197 (30.7), 163 (19.4) | |
| | | | | $MS^4$ [431→285→255]: 229 (46.7), 213 (20.3), 189 (13.3), 185 (10.5), 151 (100), 93 (38.7) | |
| 46 | 26.6 | | 491 | $MS^2$ [491]: 371 (12.9), 330 (28.5), 330 (20.3), 329 (100), 314 (10.7) | tricin-*O*-hexoside[b] |
| | | | | $MS^3$ [491→329]: 315 (53.0), 314 (100) | |
| | | | | $MS^3$ [491→329→314]: 300 (40.3), 299 (100) | |
| 49 | 29.1 | | 491 | $MS^2$ [491]: 473 (20.8), 330 (15.2), 329 (100) | tricin-*O*-hexoside[b] |
| | | | | $MS^3$ [491→329]: 314 (100), 299 (70.5), 271 (52.1), 193 (48.3), 181 (62.0), 135 (51.6) | |
| 50 | 29.4 | | 563 | $MS^2$ [563]: 356 (11.0), 355 (100) | conidendrin-*O*-hexoside[b] |
| | | | | $MS^3$ [563→355]: 341 (12.8), 340 (100), 325 (43.4) | |
| | | | | $MS^4$ [563→355→340]: 326 (15.2), 325 (100), 296 (79.8), 281 (36.7) , 212 (27.6) | |
| | | | | $MS^4$ [563→355→325]: 296 (100), 281 (79.8), 212 (27.6) | |
| 52 | 30.4 | | 535 | $MS^2$ [535]: 490 (31.6), 489 (100) | 5,7-dihydroxy-6,8-dimethoxyflavone-7-*O*-glucuronide[b] (formate adduct) |
| | | | | $MS^3$ [535→489]: 327 (46.0), 313 (100), 298 (55.5), 283 (33.6) | |
| | | | | $MS^4$ [535→489→313]: 298 (100), 283 (22.7), 269 (32.4), 254 (29.4) | |
| 54 | 31.9 | | 779 | $MS^2$ [779]: 634 (26.5), 633 (100), 616 (26.2), 615 (74.3), 469 (38.7) | benzoyl-*p*-tricoumaryl- 2,7-anhydro-3-deoxy-2-octulopyranosonic acid[b] |
| | | | | $MS^3$ [779→633]: 488 (18.7), 487 (17.9), 470 (35.0), 469 (100), 325 (17.3), 265 (11.1) | |
| | | | | $MS^4$ [779→633→469]: 307 (88.9), 163 (100), 145 (49.5) | |
| 57 | 34.7 | | 327 | $MS^2$ [327]: 311 (27.9), 294 (13.1), 293 (18.7), 229 (100), 211 (72.1), 183 (14.5), 171 (12.4) | oxo-dihydroxy-octadecenoic acid[b] |
| | | | | $MS^3$ [327→229]: 211 (100), 209 (32.3), 165 (16.9), 127 (32.2), 125 (67.3) | |

[a]Wavelengths not provided when the UV spectrum was not properly observed due to low intensity. [b]Compound identified for the first time in *Myrica* genus.

other kaempferol conjugates have never been characterized in *Myrica* species.

Compound **27**, with $[M - H]^-$ at $m/z$ 615, was plausibly identified as galloylquercetin-*O*-hexoside after sequential loss of 152 and 162 Da.[24] This compound has been previously characterized in tropical fruits, but not in *Myrica*.

Compound **51** exhibited $[M - H]^-$ at $m/z$ 583, and its $MS^2$ fragmentation revealed kaempferol aglycone at $m/z$ 285 (by loss of 298 Da). However, complete identification of **51** was not achieved, being characterized as a kaempferol derivative.

Compound **53** displayed $[M - H]^-$ at $m/z$ 677 and $MS^2$ base peak at $m/z$ 285, due to the loss of 392 Da. Product ions at $m/z$ 593 and 575 corroborated kaempferol-*O*-rutinoside and dehydrated kaempferol-*O*-rutinoside, with **53** being identified as a kaempferol-*O*-rutinoside derivative.

Compound **43** exhibited a $[M - H]^-$ ion at $m/z$ 565 and a direct loss of 208 Da (46 + 162 Da) that suggested a formate adduct plus hexoside moiety. Further fragmentation showed identical behavior as dichtomitin, an isoflavone, with product ions at $m/z$ 342 $[M - H - CH_3]^-$, 327 $[M - H - CH_3 \times 2]^-$, and 299 $[M - H - CH_3 \times 2 - CO]^-$.[25] Thus, **43** was plausibly classified as dichtomitin-*O*-hexoside, for the first time in *Myrica*.

Compounds **46** and **52** exhibited $[M - H]^-$ ions at $m/z$ 491 and 535 and showed neutral losses of 162 and 208 Da, respectively. The sequential fragmentation allowed for the identification of two losses of 15 Da each in both compounds, due to two methoxyl groups. Their fragmentation behaviors were consistent with those described before in herbs[18] for tricin-*O*-hexoside (dihydroxy-dimethoxy-*O*-hexoside flavones) (**46**) and 5,7-dihydroxy-6,8-dimethoxy-7-*O*-glucuronide flavone (**52**).[26] With longer retention times, compounds **47** ($t_R$ = 27.3 min) and **49** ($t_R$ = 29.1 min) exhibited similar fragmentation pattern as **46**, being also assigned as tricin-*O*-hexoside. On the basis of only $MS^n$ data, the stereochemical structures of the sugar moieties could not be elucidated.

Compound **48** exhibited $[M - H]^-$ ion at $m/z$ 555 and product ion at $m/z$ 269, due to loss of 286 Da. Further fragmentation produced characteristic ions of baicalein: at $m/z$ 251 $[M - H_2O - H]^-$, 241 $[M - CO - H]^-$, and 223 $[M - H_2O - CO - H]$, according to Han et al.[27] Thus, **48** was

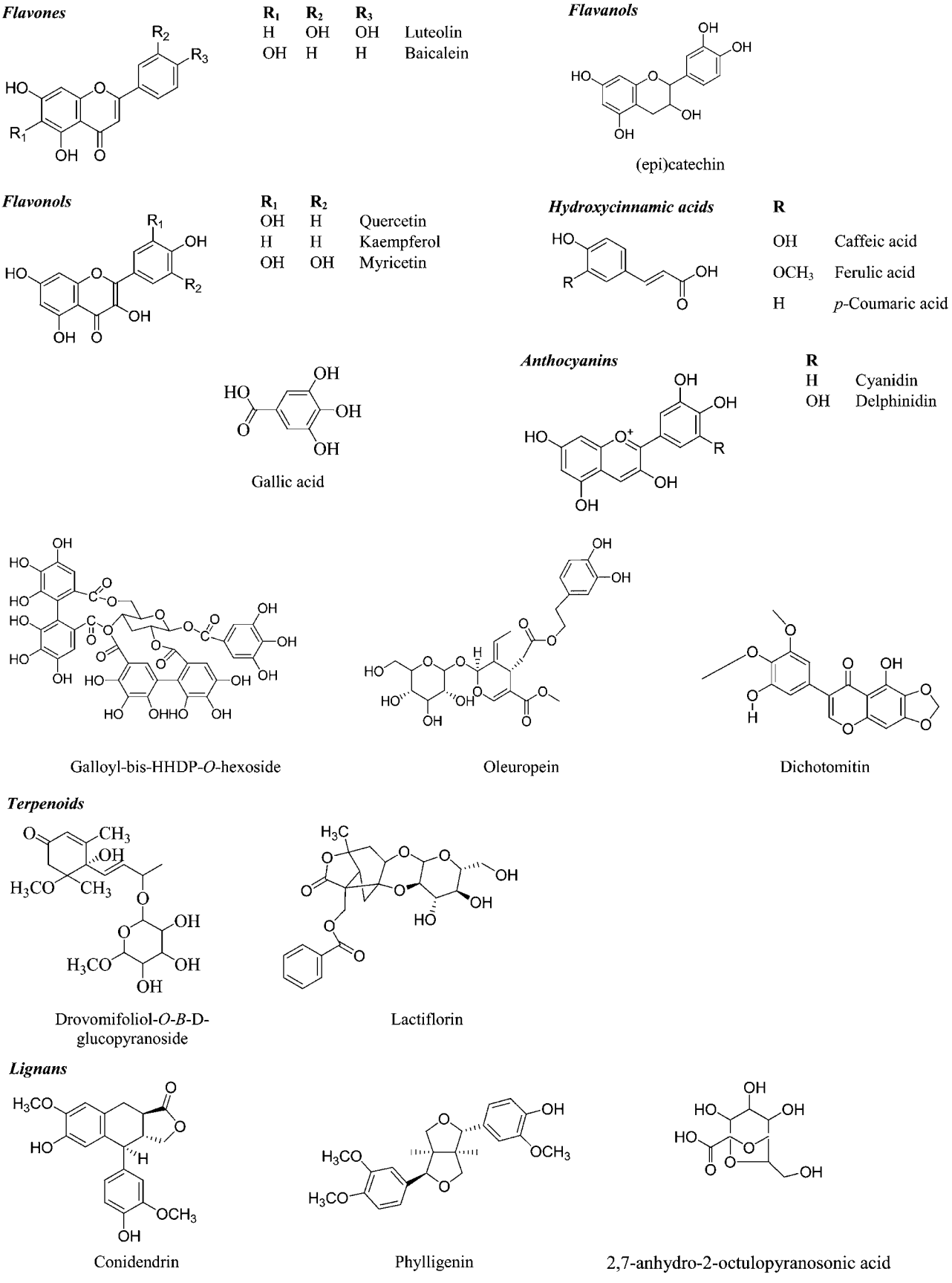


**Figure 3.** Chemical structures of the main phytochemicals detected in the methanolic extracts from *Myrica faya* (leaves and berries).

identified as a baicalein derivative, detected for the first time in *Myrica*.

Compound **59** displayed $[M - H]^-$ ion at $m/z$ 515, and produced kaempferol aglycone at $m/z$ 284 (by loss of 231 Da).


dx.doi.org/10.1021/jf503540s | J. Agric. Food Chem. 2014, 62, 9722−9735

In the absence of more specific data, **59** was characterized as a kaempferol derivative.

*Lignans.* Compounds **31** and **50** displayed $[M - H]^-$ ions at $m/z$ 579 and 563. In $MS^2$ both compounds showed a loss of 208 Da (possibly formic acid plus hexoside moieties). Further $MS^n$ data were in accordance with those previously described in pomegranate for pylligenin and conidendrin.[28] Thus, **31** and **50** were characterized as phylligenin-*O*-hexoside and conidendrin-*O*-hexoside, respectively. To our best knowledge, we report here for the first time the presence of lignans in *Myrica*.

*Other Compounds.* Galloyl-bis-hexahydroxydiphenoyl-(HHDP)-*O*-hexoside (compound **14**) was plausibly identified in leaves according to previous findings.[20] It showed $[M - H]^-$ ion at $m/z$ 935 and main fragment at $m/z$ 633 (HHDP-galloylhexoside) along with other product ions at $m/z$ 615 (dehydrated derivative), 481 (HHDP-hexoside), and 299 (ellagic acid). This finding marks the first report of an ellagitannin in *Myrica* species.

Additionally, some other nonphenolic compounds were detected in this analysis: organic acids, monoterpenes, phenylethanoids, and fatty acids.

Quinic acid showed $[M - H]^-$ at $m/z$ 191 (compound **5**) and was plausibly characterized according to literature data.[19] Quinic acid dimer (compound **7**) with $[M - H]^-$ at $m/z$ 383 showed a direct loss of 191 Da, with further fragmentation behavior identical to compound **5**.

Compound **3**, with $[M - H]^-$ ion at $m/z$ 533, exhibited a fragment ion at $m/z$ 191, which displayed the typical fragmentation pattern of quinic acid. Without further information, it was identified as a quinic acid derivative.

Benzyl alcohol hexose pentose (compound **15**) displayed $[M + HCOO]^-$ ion at $m/z$ 447, and sequential losses of 46 (formate) and 132 (pentose) Da were observed. This fragmentation pattern was similar to that previously described in *Melicoccus bijugatus* Jacq. fruits.[29]

Compound **16** exhibited $[M + HCOO]^-$ ion at $m/z$ 431 and suffered the loss of 46 Da (formate) to produce the ion at $m/z$ 385, which was identified as a roseoside (vomifoliolglucoside). It produced a fragment ion at $m/z$ 223 by loss of a sugar moiety (162 Da), and followed the exact behavior reported by Liet al. to what they called drovomifoliol-*O*-*B*-D-glucopyranoside (a terpenoid).[30] Roseoside has been previously identified in *Myrica*'s barks and leaves, but not in fruits.[14]

Another monoterpene was characterized (compound **45**), with ions at $m/z$ 507 $[M + HCOO]^-$, 461 $[M - H]^-$, 443 $[M - H - H_2O]^-$, and 293 $[M - H - C_7H_6O_2]^-$. It followed the exact same pattern described for lactiflorin,[31] being documented here for the first time in this genus.

Compound **24** displayed an $[M - H]^-$ ion at $m/z$ 597, and its sequential fragmentation led to typical glucaric acid ions (at $m/z$ 209, 191, 147).[32] Thus, with no other information available, **24** was identified as a glucaric acid derivative, reported here for the first time in *Myrica*.

The $MS^n$ spectrum of compound **34** showed an $[M - H]^-$ ion at $m/z$ 539 which produced fragment ions at $m/z$ 377 $[M - 162 - H]^-$ and 307 $[M - 162 - C_4H_6O - H]^-$. Sequential fragmentation was consistent with that reported for oleuropein.[33] This compound is one of the major phenolics (phenylethanoid) present in olive leaves and pulp and to our best knowledge have not been reported, so far, in *Myrica.*

Compound **35** exhibited $[M - H]^-$ at $m/z$ 633 and during $MS^2$ fragmentation lost 163 Da, which could be attributed to a coumaric acid. Further fragmentation gave product ions at $m/z$ 347 and 323, which corroborated the presence of benzoyl and coumaroyl groups (122 and 146 Da, respectively). This behavior was similar to that reported for benzoyl-*p*-coumaryl-2,7-anhydro-3-deoxy-2-octulopyranosonic acid,[34,35] with **35** being identified as this compound. With an extra neutral loss of 146 Da, compound **54** displayed $[M - H]^-$ ion at $m/z$ 779 and was characterized as benzoyl-*p*-tricoumaryl-2,7-anhydro-3-deoxy-2-octulopyranosonic acid. The presence of another coumaryl group instead of a rhamnose unit attached to the molecule was consistent with the longer retention time ($t_R$ = 31.9 min). To our best knowledge, octulosonic acid derivatives were reported here, for the first time, in *Myrica*.

Compound **57** showed $[M - H]^-$ ion at $m/z$ 327. The neutral loss of 98 Da in $MS^2$ corresponded to the loss of an end-group HO—CH═CH$(CH_2)_3CH_3$ from an oxylipin molecule.[36] Compound **57** was thus identified as an oxo-dihydroxyoctadecenoic acid (oxo-DHODE). This compound, together with trihydroxyoctacedenoic acid (THODE), has been found by our group in the leaves of other species from Madeira endemic flora (unpublished results).

Other peaks (compounds **1**, **41**, **55**, **56**, and **58**) were detected, but their UV and $MS^n$ data did not provide any valuable information about their chemical nature. Thus, their structures could not be elucidated.

*Positive Mode Ionization.* *Faya* berries are red or dark in color, attributed mainly to anthocyanins, which are more easily characterized with electrospray ionization operating in the positive mode ($ESI^+$) in combination to the characteristic UV-DAD absorptions.[20,21] The $ESI^+$ analysis was only relevant for the berries extracts.

Compound **2** gave an $[M + H]^+$ ion at $m/z$ 449, and the main $MS^2$ fragment ion was observed at $m/z$ 287, corresponding to the neutral loss of 162 Da. Further fragmentation of the ion at $m/z$ 287 suggested that the aglycone was cyanidin based on literature data.[13] Thus, **2** was characterized as cyanidin-3-glucoside, which has been reported as the dominant anthocyanin (95% of total anthocyanins) present in *Myrica rubra* fruits.

Compound **9** exhibited $[M - H]^-$ ion at $m/z$ 465, forming a fragment ion at $m/z$ 303 (by the loss of 162 Da). $MS^n$ fragment ions at $m/z$ 257 and 229 were consistent with those reported for delphinidin.[37] Therefore, **9** was characterized for the first time in *Myrica* as delphinidin-*O*-hexoside.

**Quantification of Phenolic Compounds.** In the present study, 21 polyphenols were quantified by HPLC-DAD using the corresponding standards for calibration for each group, and the obtained results are shown in Table 3.

The phenolic composition of leaves and berries varied quantitatively. The results indicated that flavonols, flavanols, and phenolic acids were the most abundant compounds in the leaves. Myricetin-*O*-deoxyhexoside presented the highest concentration in leaves, which is in agreement with bibliographic data on *M. rubra*.[11] Leaves were also rich in myricetin-*O*-(*O*-galloyl)deoxyhexoside, gallo(epi)catechin-*O*-gallate dimer, and galloyl-bis-HHDP-*O*-hexoside (casuarin). TIPC of the leaves was comparable to those reported previously in *M. rubra* (1133−2255 mg GAE/100 g of dried leaves).

For berries, anthocyanins, flavonols, and flavones represented the dominant class of polyphenols. C3G was the major compound, followed by myricetin-*O*-hexoside and luteolin-*O*-hexoside derivative. Previous work[7,8,13] on juice and pomace from *M. rubra* also reported C3G as one of the main polyphenols in berries. Flavonoids (in particular flavonols)

**Table 3. Contents of Total and Individual Phenolic Compounds (mg/100 g DW) in Leaves and Berries from *Myrica faya*[a]**

| phenolic compounds | leaves | berries |
|---|---|---|
| Phenolic Acids | | |
| caffeic acid-*O*-hexoside | | 45.73 ± 0.97 |
| protocatechuic acid-*O*-pentoside | 7.53 ± 0.9 | |
| total | 7.53 ± 0.9 | 45.73 ± 0.97 |
| Flavanols | | |
| galloyl-di(epi)-gallocatechin | 43.42 ± 0.98 | |
| (epi)catechin | 2.56 ± 0.41 | nd |
| gallo(epi)catechin-*O*-gallate dimer | 132.06 ± 8.27 | |
| (epi)catechin-*O*-gallate | | 37.80 ± 1.22 |
| total | 178.04 ± 4.33 | 37.80 ± 1.22 |
| Flavonols | | |
| myricetin-*O*-hexoside | 62.79 ± 2.15 | 80.98 ± 2.65 |
| myricetin-O-(O-galloyl)hexoside | 53.59 ± 1.59 | nd |
| myricetin-*O*-deoxyhexoside | 770.35 ± 11.31 | 44.20 ± 1.23 |
| galloylquercetin-*O*-hexoside | 33.88 ± 2.11 | 41.73 ± 2.06 |
| kaempferol-*O*-rutinoside | 13.25 ± 0.85 | - |
| kaempferol-*O*-hexoside | 16.65 ± 1.94 | 8.44 ± 0.46 |
| kaempferol-*O*-(*O*-galloyl)hexoside | 14.35 ± 0.79 | |
| quercetin-*O*-deoxyhexoside | 16.86 ± 0.86 | 33.95 ± 1.35 |
| myricetin-*O*-(*O*-galloyl) deoxyhexoside | 233.98 ± 6.55 | 59.51 ± 2.64 |
| kaempferol-*O*-rhamnoside | 26.27 ± 2.69 | nd |
| total | 1241.97 ± 10.79 | 268.81 ± 9.43 |
| Flavones | | |
| luteolin-*O*-hexoside derivative | | 77.68 ± 5.44 |
| tricin-*O*-hexoside | 26.38 ± 1.48 | 5.01 ± 0.94 |
| total | 26.38 ± 1.48 | 82.69 ± 4.79 |
| Ellagitannins | | |
| galloyl-bis-HHDP-*O*-hexoside (casuarin) | 86.46 ± 6.75 | |
| total | 86.46 ± 6.75 | |
| Anthocyanins | | |
| cyanidin-*O*-hexoside | | 368.57 ± 5.42 |
| delphinidin-*O*-hexoside | | 16.52 ± 0.36 |
| total | | 385.09 ± 6.61 |
| TIPC | 1540.38 ± 87.76 | 820.11 ± 46.71 |

[a]nd = not detected.

were also present in higher amounts than phenolic acids. (epi)Catechin, myricetin-*O*-(*O*-galloyl)hexoside, and kaempferol-*O*-rhamnoside were not quantified in berries due to their low concentration.

The TIPC of leaves and berries was lower than those determined by the Folin−Ciocalteu method (Table 4). This difference is attributed to the fact that the Folin−Ciocalteu method tends to overestimate the contents of total phenolics, since it gives positive answer to other substances, and also because not all the identified compounds could be quantified.

**Analysis of L-AA Content.** The data regarding L-AA content, pH, and °Brix of *faya* berries are presented in Table 4.

The amounts of L-AA present in *M. faya* berries had not been determined before and were within the range of those reported for bayberries (Table 4). No data were found about vitamin C content in *M. esculenta*. Apart from *Myrica* species, the L-AA contents obtained here were higher than others reported previously in other berry fruits like blackberry, blueberry, chokeberry, raspberry, and redcurrant, but lower than in blackcurrant and strawberry.[17,38] The sugar content, evaluated through the °Brix, was higher than in *M. rubra* and within the range reported for most commercial berries (usually between 10 and 18), and the acidity was low.

**TPC, TFC, and Antioxidant Capacity Tests.** The results obtained for total phenolic and flavonoid contents of *Myrica faya* leaves and berries are presented in Table 3. L-AA is a powerful antioxidant, and its presence in plant extracts produces inaccurate estimations of TPC values because L-AA reduces FCR. One approach to improve the TPC values is the calculation of a corrected TPC value based on the L-AA reducing activity present in the extract.[39,40] The L-AA standard was tested for TPC using the same procedure previously described and it was found to present reducing activity of 0.683 mg GAE/g L-AA. So, for each sample, L-AA contribution was calculated by multiplying the L-AA content by 0.683. The corrected TPC of the samples, calculated by subtracting L-AA contribution, is also shown in Table 4.

Our tests revealed that leaves had a much higher content of total phenolics than berries, which is in agreement with previous literature reports for other subspecies of *Myrica*. TPC values of *Myrica faya* (leaves and berries) are comparable to those reported for other *Myrica* species (with *faya* showing a slightly higher content). Compared with other commonly consumed berries, *faya* presented higher TPC values than blackberry, blueberry, raspberry, and strawberry.[17,38] For TFC assay the same pattern was observed; however, no data regarding flavonoid content of leaves was found in the literature for comparison. Rawat et al. reported TFC values of *M. esculenta* (131−238 mg quercetin equivalent/100 g of dried weight), but those results were expressed in different units, which makes a comparison difficult.[15]

**Table 4. Overview of L-AA, pH, TSS, TPC, TFC, and Antioxidant Capacity Assays (ABTS, DPPH) Determinations in *Myrica faya* (Leaves and Berries)[a]**

| | faya (*Myrica faya*) | | bayberry (*Myrica rubra*) | | box myrtle (*Myrica esculenta*) | |
|---|---|---|---|---|---|---|
| parameters | leaves | berries | leaves | berries | leaves | berries |
| pH | | 4.02 | | | | |
| TSS (°Brix) | | 14.87 | | 11.6−13.4[41] | | |
| L-AA content (mg/100 g FW) | | 48.42 ± 1.93 | | 11−114[41] | 4.16 | |
| TPC (g GAE/100 g DE) | 24.80 ± 0.28 | 5.26 ± 0.13 | 8.14−19.63[11] | 0.07−4.74[6−8,12,13] | 15[15] | 0.18−2.86[15,16] |
| TPC (g GAE/100 g DE)[b] | | 5.23 ± 0.13 | | | | |
| TFC (g RUE/100 g DE) | 12.72 ± 0.16 | 4.21 ± 0.12 | | 0.01−0.12[6,12] | | |
| ABTS (g TE/100 g DE) | 24.10 ± 0.13 | 12.51 ± 0.15 | | 0.33−10.06[6,8,12] | 38.45[15] | |
| DPPH (g TE/100 g DE) | 20.36 ± 0.12 | 9.24 ± 0.11 | | 0.74−9.10[12,13] | | |

[a]All measurements were performed in triplicate (mean ± SD). [b]corrected TPC value (subtracted L-AA contribution).

In this study, both ABTS and DPPH were used to evaluate the antioxidant capacity of *Myrica faya*, and the results are shown in Table 4. *Myrica faya* presented a considerable free-radical scavenging capacity, with leaves showing a stronger reducing power than fruits, which corroborated the measured phenolic and flavonoid contents.

The values obtained for *M. faya* in the ABTS assay were slightly higher than the range of values reported for *M. rubra*, but lower than those from *M. esculenta*. *Faya* berries were much more active than, for instance, strawberries (1455.50 μmol TE) evaluated in the same experimental conditions (data to be published elsewhere). According to Sun et al.,[9] many structure−activity relationship studies have confirmed that the strong antioxidant capacities of *Myrica* species are attributed to the high content of galloyl esters that enhance such properties and confer high radical scavenging activities.[9]

In conclusion, over 50 compounds were characterized, for the first time, in different morphological parts of *Myrica faya* by means of an HPLC-DAD-ESI/MS$^n$ method. *M. faya* shared some characteristics in phenolic profile with other *Myrica* species. Nevertheless, we reported for the first time the presence of some flavonoids, ellagitannins, lignans, phenylethanoids, and other organic compounds in this genus. The levels of L-AA and C3G observed in the berries were high, so they can constitute a good source of these nutrients when compared to other fruits. This study provides scientific evidence that *M. faya* is a rich source of bioactive compounds with great potential as natural antioxidants. *Faya* berries are underutilized, mainly due to the lack of scientific studies about their potential health benefits, and consumption and marketing deserve promotion, representing an opportunity for growers and collectors to reach niche markets to increase their revenues.

## AUTHOR INFORMATION


### Corresponding Author

*Phone: +351 291 705 102. E-mail: castilho@uma.pt.



### Funding

V.S. is grateful to Fundação para a Ciência e Tecnologia (FCT, Portugal) for a Ph.D. grant SFRH/BD/84672/2012. This research was supported by FCT with funds from the Portuguese Government (Project PEst-OE/QUI/UI0674/2011). The mass spectrometer used in this work is part of the Portuguese National Mass Spectrometry Network (Contract RNEMREDE/1508/REM/2005) and was purchased in the framework of the National Programme for Scientific Re-equipment, with funds from POCI 2010 (FEDER) and FCT. E.J.L.-M. also acknowledges the financial support from Campus de Excelencia Internacional Agroalimentario (ceiA3) and University of Jaén, from Spain.


### Notes

The authors declare no competing financial interest.

## ABBREVIATIONS USED

FCR, Folin−Ciocalteu's phenol reagent; trolox, 6-hydroxy-2,5,7,8-tetramethylchroman-2-carboxylic acid; ABTS, 2,2′-azinobis(3-ethylbenzthiazoline-6-sulfonic acid); DPPH, 2,2-diphenyl-1-picrylhydrazyl; MPA, metaphosphoric acid; EDTA, ethylenediaminetetraacetic acid disodium salt; DAD, diode-array detector; AR, analytical reagent; L-AA, L-ascorbic acid; $CH_3CN$, acetonitrile; TSS, total soluble solids; $Na_2CO_3$, sodium carbonate; $CH_3COOK$, sodium acetate; $AlCl_3{\cdot}6H_2O$, aluminum chloride hexahydrated; PBS, phosphate buffered saline; DE, dried extract; ANOVA, analysis of variance; TE, trolox equivalent; RUE, rutin equivalent; GA, gallic acid equivalent; HPLC-DAD-ESI/MS$^n$, high performance liquid chromatography with online UV and electrospray ionization mass spectrometric detection; SD, standard deviation

## REFERENCES


(1) Amira, A. M. A. Oxidative stress and disease: An updated review. *Res. J. Immunol.* **2011**, *3*, 129−145.

(2) Gouveia, S.; Spínola, V.; Castilho, P. C., Phenolic compounds and antioxidant capacity of medicinal plants: A review. In *Medicinal Plants: Antioxidant Properties, Traditional Uses and Conservation Strategies*; Nova Science Publishers, Inc.: Hauppauge, NY, 2013; pp 1−40.

(3) Shan, B.; Cai, Y.-Z.; Brooks, J. D.; Corke, H. The *in vitro* antibacterial activity of dietary spice and medicinal herb extracts. *Int. J. Food Microbiol.* **2007**, *117*, 112−119.

(4) GISD (Global Invasive Species Database): *Morella faya* (tree, shrub). http://www.issg.org/database/species/ecology.asp?si=100 (accessed Sept 20 2013).

(5) Pérez, M. Á. C. *Native Flora of the Canary Islands*. Editorial Everest: Leon, Spain, 2000.

(6) Bao, J.; Cai, Y.; Sun, M.; Wang, G.; Corke, H. Anthocyanins, flavonols, and free radical scavenging activity of Chinese bayberry (*Myrica rubra*) extracts and their color properties and stability. *J. Agric. Food Chem.* **2005**, *53*, 2327−2332.

(7) Fang, Z.; Zhang, M.; Wang, L. HPLC-DAD-ESIMS analysis of phenolic compounds in bayberries (*Myrica rubra* Sieb. et Zucc.). *Food Chem.* **2007**, *100*, 845−852.

(8) Fang, Z.; Zhang, Y.; Lüa, Y.; Ma, G.; Chen, J.; Liu, D.; Ye, X. Phenolic compounds and antioxidant capacities of bayberry juices. *Food Chem.* **2009**, *113*, 884−888.

(9) Sun, C.; Huang, H.; Xu, C.; Li, X.; Chen, K. Biological activities of extracts from Chinese bayberry (*Myrica rubra* Sieb. et Zucc.): A review. *Plant Foods Hum. Nutr.* **2013**, *68*, 97−106.

(10) Wang, C.; Zhao, J.; Chen, F.; Cheng, Y.; Guo, A. Separation, identification, and quantitation of phenolic acids in Chinese waxberry (*Myrica rubra*) Juice by HPLC-PDA-ESI-MS. *J. Food Sci.* **2012**, *77*, C272−C277.

(11) Yang, H.; Ge, Y.; Sun, Y.; Liu, D.; Ye, X.; Wu, D. Identification and characterisation of low-molecular-weight phenolic compounds in bayberry (*Myrica rubra* Sieb. et Zucc.) leaves by HPLC-DAD and HPLC-UV-ESIMS. *Food Chem.* **2011**, *128*, 1128−1135.

(12) Zhang, W.; Li, X.; Zheng, J.; Wang, G.; Sun, C.; Ferguson, I.; Chen, K. Bioactive components and antioxidant capacity of Chinese bayberry (*Myrica rubra* Sieb. and Zucc.) fruit in relation to fruit maturity and postharvest storage. *Eur. Food Res. Technol.* **2008**, *227*, 1091−1097.

(13) Zhou, S. H.; Fang, Z. X.; Lü, Y.; Chen, J. C.; Liu, D. H.; Ye, X. Q. Phenolics and antioxidant properties of bayberry (*Myrica rubra Sieb. et Zucc.*) pomace. *Food Chem.* **2009**, *112*, 394−399.

(14) Panthari, P.; Kharkwal, H.; Joshi, D. D. *Myrica nagi*: A review on active constituents, biological and therapeutic effects. *Int. J. Pharm. Pharm. Sci.* **2012**, *4*, 38−42.

(15) Rawat, S.; Jugran, A.; Giri, L.; Bhatt, I. D.; Rawal, R. S. Assessment of antioxidant properties in fruits of *Myrica esculenta*: A popular wild edible species in Indian Himalayan region. *J. Evidence-Based Complementary Altern. Med.* **2011**, *2011*.

(16) Saini, R.; Garg, V.; Dangwal, K. Effect of extraction solvents on polyphenolic composition and antioxidant, antiproliferative activities of Himalyan bayberry (*Myrica esculenta*). *Food Sci. Biotechnol.* **2013**, *22*, 887−894.

(17) Spínola, V.; Mendes, B.; Câmara, J. S.; Castilho, P. C. Effect of time and temperature on vitamin C stability in horticultural extracts. UHPLC-PDA vs iodometric titration as analytical methods. *LWT—Food Sci. Technol.* **2013**, *50*, 489−495.

(18) Gouveia, S.; Castilho, P. C. Antioxidant potential of *Artemisia argentea* L'Hér alcoholic extract and its relation with the phenolic composition. *Food Res. Int.* **2011**, *44*, 1620−1631.

(19) Gouveia, S.; Castilho, P. C. Characterisation of phenolic acid derivatives and flavonoids from different morphological parts of *Helichrysum obconicum* by a RP-HPLC-DAD-(−)-ESI-MS$^n$ method. *Food Chem.* **2011**, *129*, 333−344.
(20) Fischer, U. A.; Carle, R.; Kammerer, D. R. Identification and quantification of phenolic compounds from pomegranate (*Punica granatum* L.) peel, mesocarp, aril and differently produced juices by HPLC-DAD-ESI/MS$^n$. *Food Chem.* **2011**, *127*, 807−821.
(21) Mena, P.; Calani, L.; Dall'Asta, C.; Galaverna, G.; García-Viguera, C.; Bruni, R.; Crozier, A.; Del Rio, D. Rapid and comprehensive evaluation of (poly)phenolic compounds in pomegranate (*Punica granatum* L.) juice by UHPLC-MSn. *Molecules* **2012**, *17*, 14821−14840.
(22) Calani, L.; Beghè, D.; Mena, P.; Del Rio, D.; Bruni, R.; Fabbri, A.; Dall'Asta, C.; Galaverna, G. Ultra-HPLC−MSn (poly)phenolic profiling and chemometric analysis of juices from ancient Punica granatum L. Cultivars: A nontargeted approach. *J. Agric. Food Chem.* **2013**, *61*, 5600−5609.
(23) Rockenbach, I. I.; Jungfer, E.; Ritter, C.; Santiago-Schübel, B.; Thiele, B.; Fett, R.; Galensa, R. Characterization of flavan-3-ols in seeds of grape pomace by CE, HPLC-DAD-MS$^n$ and LC-ESI-FTICR-MS. *Food Res. Int.* **2012**, *48*, 848−855.
(24) Gordon, A.; Jungfer, E.; da Silva, B. A.; Maia, J. G. S.; Marx, F. Phenolic constituents and antioxidant capacity of four underutilized fruits from the Amazon region. *J. Agric. Food Chem.* **2011**, *59*, 7688−7699.
(25) Zhang, Y.-Y.; Wang, Q.; Qi, L.-W.; Qin, X.-Y.; Qin, M.-J. Characterization and determination of the major constituents in *Belamcandae* Rhizoma by HPLC−DAD−ESI-MS$^n$. *J. Pharm. Biomed. Anal.* **2011**, *56*, 304−314.
(26) Li, J.; Wang, Y.-H.; Smillie, T. J.; Khan, I. A. Identification of phenolic compounds from Scutellaria lateriflora by liquid chromatography with ultraviolet photodiode array and electrospray ionization tandem mass spectrometry. *J. Pharm. Biomed. Anal.* **2012**, *63*, 120−127.
(27) Han, J.; Ye, M.; Xu, M.; Sun, J.; Wang, B.; Guo, D. Characterization of flavonoids in the traditional Chinese herbal medicine-Huangqin by liquid chromatography coupled with electrospray ionization mass spectrometry. *J. Chromatogr. B: Anal. Technol. Biomed. Life Sci.* **2007**, *848*, 355−362.
(28) Fischer, U. A.; Jaksch, A. V.; Carle, R.; Kammerer, D. R. Determination of lignans in edible and nonedible parts of pomegranate (*Punica granatum* L.) and products derived therefrom, particularly focusing on the quantitation of isolariciresinol Using HPLC-DAD-ESI/MS$^n$. *J. Agric. Food Chem.* **2012**, *60*, 283−292.
(29) Bystrom, L. M.; Lewis, B. A.; Brown, D. L.; Rodriguez, E.; Obendorf, R. L. Characterisation of phenolics by LC−UV/Vis, LC−MS/MS and sugars by GC in *Melicoccus bijugatus* Jacq. 'Montgomery' fruits. *Food Chem.* **2008**, *111*, 1017−1024.
(30) Li, X.; Zhang, Y.; Zeng, X.; Yang, L.; Deng, Y. Chemical profiling of bioactive constituents in *Sarcandra glabra* and its preparations using ultra-high-pressure liquid chromatography coupled with LTQ Orbitrap mass spectrometry. *Rapid Commun. Mass Spectrom.* **2011**, *25*, 2439−2447.
(31) Xu, S.-j.; Yang, L.; Zeng, X.; Zhang, M.; Wang, Z.-t. Characterization of compounds in the Chinese herbal drug *Mu-Dan-Pi* by liquid chromatography coupled to electrospray ionization mass spectrometry. *Rapid Commun. Mass Spectrom.* **2006**, *20*, 3275−3288.
(32) Simirgiotis, M. J.; Caligari, P. D. S.; Schmeda-Hirschmann, G. Identification of phenolic compounds from the fruits of the mountain papaya *Vasconcellea pubescens* A. DC. grown in Chile by liquid chromatography−UV detection−mass spectrometry. *Food Chem.* **2009**, *115*, 775−784.
(33) Savarese, M.; De Marco, E.; Sacchi, R. Characterization of phenolic extracts from olives (*Olea europaea* cv. Pisciottana) by electrospray ionization mass spectrometry. *Food Chem.* **2007**, *105*, 761−770.
(34) Wang, Y.-F.; Hu, L.-M.; Liu, Y.-N.; Pan, X.-P.; Pan, G.-X.; Chang, Y.-X.; Gao, X.-M. A rapid method for qualitative and quantitative analysis of major constituents in Dengzhanxixin injection by LC-DAD-ESI-MS$^n$. *Chromatographia* **2010**, *71*, 845−853.
(35) Zhang, Y.; Shi, P.; Qu, H.; Cheng, Y. Characterization of phenolic compounds in *Erigeron breviscapus* by liquid chromatography coupled to electrospray ionization mass spectrometry. *Rapid Commun. Mass Spectrom.* **2007**, *21*, 2971−2984.
(36) Van Hoyweghen, L.; De Bosscher, K.; Haegeman, G.; Deforce, D.; Heyerick, A. In vitro inhibition of the transcription factor NF-κB and cyclooxygenase by bamboo extracts. *Phytother. Res.* **2014**, *28*, 224−230.
(37) Lätti, A. K.; Riihinen, K. R.; Jaakola, L. Phenolic compounds in berries and flowers of a natural hybrid between bilberry and lingonberry (*Vaccinium* × *intermedium* Ruthe). *Phytochemistry* **2011**, *72*, 810−815.
(38) Szajdek, A.; Borowska, E. J. Bioactive compounds and health-promoting properties of berry fruits: A review. *Plant Foods Hum. Nutr.* **2008**, *63*, 147−156.
(39) Isabelle, M.; Lee, B. L.; Lim, M. T.; Koh, W.-P.; Huang, D.; Ong, C. N. Antioxidant activity and profiles of common vegetables in Singapore. *Food Chem.* **2010**, *120*, 993−1003.
(40) Sanchez-Rangel, J. C.; Benavides, J.; Heredia, J. B.; Cisneros-Zevallos, L.; Jacobo-Velazquez, D. A. The Folin-Ciocalteu assay revisited: improvement of its specificity for total phenolic content determination. *Anal. Methods* **2013**, *5*, 5990−5999.
(41) Chen, K.; Xu, C.; Zhang, B.; Ferguson, I. B. Red bayberry: Botany and horticulture. In *Horitcultural Reviews*; Janick, J., Ed.; John Wiley & Sons: New York, 2004.

stimulates glucose-dependent insulin secretion from pancreatic beta-cells and suppresses glucagon release from alpha-cells, thereby improving glucose control.[10] Recent observations suggested the direct protective role of DPP-4 inhibitor beyond its glucose-lowering potential. DPP-4 inhibition improved albumin excretion and associated renal parameters in streptozotocin (STZ)-induced diabetic animals, while the effects were independent of blood glucose or systolic blood pressure.[11,12] In the clinical trial, DPP-4 inhibitors lower the albuminuria in type 2 diabetic patients, independent of the level of HbA1C.[13] Among the approved DPP-4 inhibitors, the excretion of linagliptin in the urine is particularly low, which may be a beneficial property in diabetic patients suffering from renal impairment.

*Hibiscus sabdariffa*, whose calyces are used as a daily drink in North Africa and Middle and South Asia, was shown to be bioeffective in many ways.[14,15] At least 18 phenolic compounds were found in the polyphenol extracts of *Hibiscus sabdariffa* L. calyx (HPE).[16] Our previous publications have shown the antidiabetic potential of HPE.[16,17] Using the type 2 diabetic rats exhibiting insulin resistance,[18] we demonstrated that HPE has a benefit in diabetic nephropathy by inhibiting albuminuria and hyperfiltration, and reversing the renal fibrosis and associated biomarkers.[19] Recently, we reported that HPE attenuates renal EMT as inhibiting high glucose-induced vimentin and loss of cell junction. HPE recovered the basement membrane surrounding tubular region in diabetic kidneys.[20]

In the present study, using the in vitro and in vivo model, we aim to investigate if insulin resistance signal and DPP-4 could be involved in renal EMT, and further explore the putative role of HPE on this mechanism for preventing diabetic nephropathy.

## MATERIALS AND METHODS

**Preparation of HPE.** *Hibiscus sabdariffa* L. calyx was purchased from Taitung Area Farmer's association. HPE was prepared as previously reported, and its chemical composition was analyzed with liquid chromatography−tandem mass spectrometry. Phenolic compounds including gallic acid, galloyl ester, protocatechuic acid, caffeic acid, caffeoyl quinic acid, chlorogenic acid, and quercetin derivative were found in HPE (shown in the Supporting Information).[16]

**Cell Culture.** HK-2 cells purchased from Food Industry Research and Development Institute were cultured in keratinocyte serum free medium (Gibco BRL) with 5 ng/mL epidermal growth factor and 50 μg/mL bovine pituitary extract. The cells were grown in a humidified incubator at 37 °C in an atmosphere of 5% $CO_2$ and 95% air. HK-2 cells were inoculated into a 6 cm dish at a density of $5 \times 10^5$ cells for 24 h and then treated with 30 mM glucose with or without various concentrations (0.05−5 mg/mL) of HPE for 48 h.

**Cytotoxicity Assay.** HK-2 cells were seeded at a density of $1 \times 10^6$ cells/mL in a 24-well plate and incubated with linagliptin at various concentrations (1−100 μM) for 24 h. Thereafter, the medium was changed and cells were incubated with 3-(4,5-dimethylthiazol-2-yl)-2,5-diphenyltetrazolium bromide (MTT, 0.5 mg/mL) for 4 h. The viable cell was directly proportional to the production of formazan. Following dissolution in isopropanol, the result was read at 563 nm with a spectrophotometer (Hitachi, U-3210).

**Western Blot Analysis.** Cells were harvested into lysis buffer containing 50 mM Tris-HCl (pH 6.8), 10% glycerol, 2% SDS, and 5% mercaptoethanol and then lysed by sonication. Cell lysate was centrifuged at 9300*g* for 20 min at 4 °C, and the supernatant was collected as the protein sample. After quantifying, equal amounts of protein samples (50 μg) were subjected to 10% SDS−polyacrylamide gel electrophoresis and transferred to nitrocellulosemembranes (Millipore, Bedford, MA). Membranes were blocked with 5% nonfat milk powder with 0.1% Tween-20 in TBS and then incubated with the primary antibody at 4 °C overnight against the following targets. IRS-1: Santa Cruz (1:1000). pIRS-1 (S307): Cell Signaling (1:500). DPP4: Abcam (1:1000). PI3K: Santa Cruz (1:1000). pPI3K (p85, Tyr 458): Cell Singaling (1:500). Antibodies of IRS-1 and PI3K were purchased from Santa Cruz (Santa Cruz, CA), and DPP4 was from Abcam (Cambridge, U.K.). Antibodies of pIRS-1 (S307) and pPI3K were from Cell Singaling, Danvers, MA. Afterward, membranes were washed three times with 0.1% Tween-20 in TBS and incubated with the secondary antibody (1:5000) conjugated to horseradish peroxidase (GE Healthcare, Little Chalfont, Buckinghamshire, U.K.). Band detection was thereafter revealed by enhanced chemiluminescence using ECL Western blotting detection reagents and exposed in FUJFILM Las-3000 (Tokyo, Japan). Protein quantitative was determined by densitometry using FUJFILM-Multi Gauge V2.2 software.

**Assay for DPP-4 Activity.** Cells were seeded on 96-well plate ($1 \times 10^6$/well). After treatment under various conditions, cells of each well were lysed with 100 μL of NP-40 lysis buffer (containing 10 mM HEPES (pH 7.5), 142.5 mM KCl, 5 mM $MgCl_2$, 1 mM EGTA, and 0.2% NP-40) and centrifuged at 9300*g* for 20 min at 4 °C. The supernatants were collected, and the protein concentrations were determined with the Bradford assay. DPP4 activity was measured by DPP4/CD26 Assay Kit for Biological Samples (Enzo Life Sciences). Briefly, H-Gly-Pro-pNA, a chromogenic substrate of DPP-4, is hydrolyzed into the dipeptide Gly-Pro and the product 4-nitroaniline, whose rate of appearance would be measured spectrophotometrically at 405 nm. The activity was normalized with protein concentration, then in proportion to the control. Linagliptin, a gift from Boehringer Ingelheim, was used as DPP4 inhibitor in the experiment.

**siRNA Transfection.** HK-2 cells were seeded at $1 \times 10^5$ cells in each 6 cm Petri dish and incubated for 24 h. Transfection of siRNA (IRS-1 of human) was performed by the Lipofectamine 2000 Reagent Protocol. The final concentration of siRNA (SR302452A: rGrGrArU-rArGrGrArCrArArArUrUrCrArGrUrArArArCrAGG) in transfection medium (keratinocyte serum-free medium without bovine pituitary extract and EGF) was 45 nM; incubation was carried out for 6 h. The transfection medium was subsequently replaced with normal cultured medium and incubated for another 12 h. After that, cells were treated with different conditions. Cell proteins were then extracted and prepared for Western blotting.

**Animal Experiment.** The animal experimental project was approved by the Animal Model Experimental Ethics Committee of Chung-Shan Medical University based on the European Community guidelines (IACUC approval No: 1007). A type 2 diabetic model was carried out according to our previous publication.[16,18] Briefly, male Sprague−Dawley rats (weight 250 ± 20 g) obtained from LuxBiotech Co., Taiwan, were divided into several groups ($n = 8$ for each group), including the control (normal diet), FAT + STZ (high fat diet and streptozotocin injection), FAT + STZ + low HPE (with 100 mg/kg HPE added), and FAT + STZ + high HPE (with 200 mg/kg HPE added). Seven weeks later, when the average body weight attained 425 ± 15 g, the FAT groups were injected with a dose of STZ 35 mg/kgbw. About 2 weeks later, when the hyperglycemic status was confirmed, rats were tube-fed with or without different doses of HPE. The metabolic features, histological findings, and biomolecule expression of this model have been shown in our previous reports.[16,19] Safety evaluation revealed that HPE did no harm to liver, kidney, or cardiovascular tissue. After rats were sacrificed, the kidney chops were added to radioimmunoprecipitation assay (RIPA) buffer and protein inhibitors and homogenized at 4 °C. The tissue homogenates were centrifuged at 9300*g* for 20 min at 4 °C, and the resulting supernatants (whole-tissue extracts) were used for Western blot analysis.

**Immunohistochemistry.** The kidneys were fixed in 4% paraformaldehyde, embedded in paraffin, sectioned into 4 μm, and processed for IHC examination. The primary antibody of pIRS-1 (S307) was from Novus, Littleton, CO. Immunostaining was completed using the UltraSensitive S-P kit (Maxim Co., streptavidin peroxidase method).

**Statistical Analysis.** The statistical software SPSS v.12.0 was used to analyze the data. One-way ANOVA was performed ($p < 0.05$), while Bonferroni's multiple comparison was used for post-test.

## RESULTS

**HPE Inhibits the High Glucose-Induced Expression of Vimentin and Phosphorylation of IRS-1 (S307).** Compared with the control, high glucose increased nearly 3-fold of the vimentin, while HPE inhibited the expression dose-dependently. HPE at 0.5 and 1 mg/mL reduced 45% and 55% of vimentin, respectively (Figure 1A). As well, the phosphorylation of IRS-1 (S307) was increased 2-fold by high glucose. Treatment of HPE inhibited the phosphorylation significantly (Figure 1B). These results implicate that there might be a correlation between EMT and the insulin resistance signals; both are attenuated by HPE. Treatment with HPE has been tested by cytotoxicity assay, and it is nontoxic for HK-2 cells.[20]

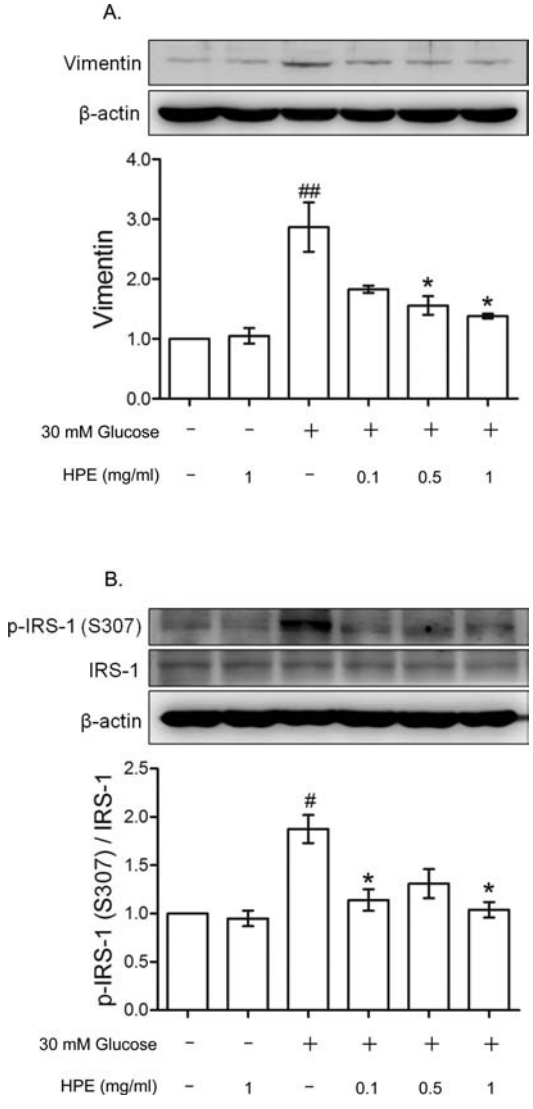


**Figure 1.** Effect of HPE on vimentin and IRS-1 (S307). HK-2 cells were incubated for 48 h under normal or high glucose (30 mM) conditions with or without different concentrations of HPE. Cell proteins were extracted and analyzed with Western blot: (A) vimentin; (B) IRS-1 (S307). Protein levels of vimentin and the ratio of IRS-1 (S307)/IRS-1 were calculated as fold compared with the control. Data are presented as means ± SD ($n = 3$) and analyzed with ANOVA. $^{\#}p < 0.05$, $^{\#\#}p < 0.01$ compared with the control. $^{*}p < 0.05$, compared with the high glucose-treated.

**HPE Inhibits DPP-4 Activity Induced by High Glucose.** Figure 2A showed that neither high glucose nor HPE affect the DPP-4 protein level. However, by measuring DPP-4 activity, the alteration was discovered significantly. High glucose stimulated the activation of DPP-4 about 2.6-fold. Although the dose 0.1 mg/mL could not suppress the activation, 0.5 and 1 mg/mL HPE showed a good inhibitory effect to decrease DPP-4 activity even below that in the control (Figure 2B). Hence DPP-4 could be involved in the high glucose and HPE-regulated signals.

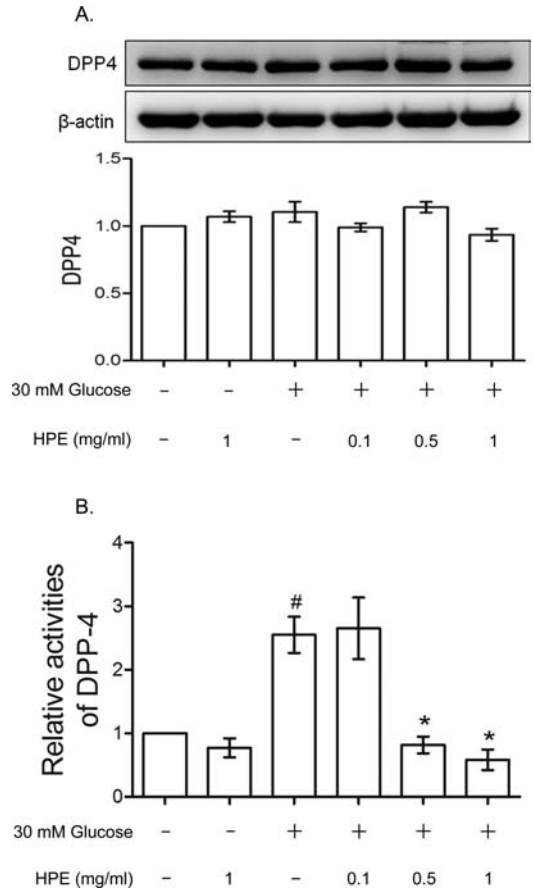


**Figure 2.** Effect of HPE on DPP-4. HK-2 cells were incubated for 48 h under normal or high glucose (30 mM) conditions with or without different concentrations of HPE. (A) DPP-4 proteins were extracted and analyzed with Western blot. (B) DPP-4 activity was analyzed. Protein levels and activity were calculated as fold compared with the control. Data are presented as means ± SD ($n = 3$) and analyzed with ANOVA. $^{\#}p < 0.05$, compared with the control. $^{*}p < 0.05$, compared with the high glucose-treated.

**Linagliptin Was Revealed To Be Nontoxic and Effectively Inhibited DPP-4.** Linagliptin was used as DPP-4 inhibitor to investigate the putative role of DPP-4. The test of cytotoxicity assay revealed that linagliptin is nontoxic under 2 $\mu$M (Figure 3A). In comparison with the control, 1 $\mu$M linagliptin reduced 80% of DPP-4 activity (Figure 3B). Hence it was the dose chosen in the following experiment.

**DPP-4 Mediates the Regulation of Vimentin, IRS-1 (S307), and PI3K.** Figure 4 shows that high glucose-induced vimentin and IRS-1 (S307) phosphorylation were significantly


dx.doi.org/10.1021/jf5024092 | J. Agric. Food Chem. 2014, 62, 9736−9743

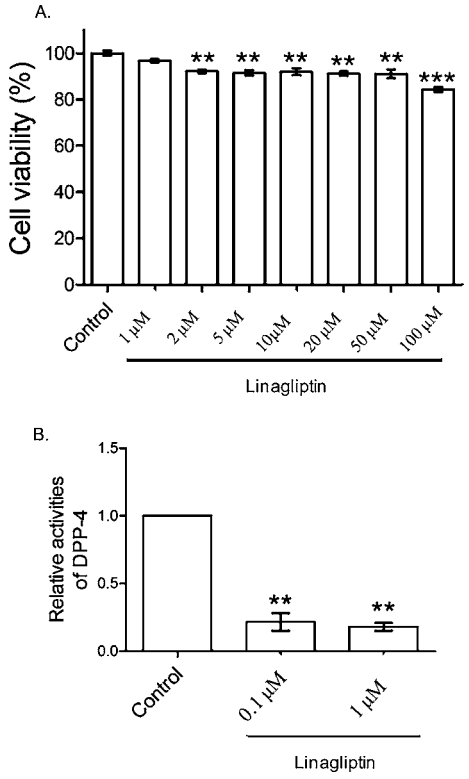


**Figure 3.** Cytotoxicity and DPP-4 inhibitory effect of linagliptin. (A) HK-2 cells were incubated for 48 h with or without different concentrations of linagliptin. Cell viability was calculated as percentage compared with the control group. (B) DPP-4 activity was analyzed. Data are presented as means ± SD ($n$ = 3) and analyzed with ANOVA. $^{**}p < 0.01$, $^{***}p < 0.001$, compared with the control.

reduced by 1 $\mu$M linagliptin or 1 mg/mL HPE. Noticeably, especially IRS-1 (S307) phosphorylation was inhibited by linagliptin or HPE even below that in the control. In contrast, PI3K, a normal response signal transmitting insulin sensitivity, was decreased about 20% by high glucose while recovered by either linagliptin or HPE. These results indicate that DPP-4 activation mediates the downstream resistance and EMT signals, while HPE has potential to improve the pathogenic markers (Figure 4).

**IRS-1 Plays the Pivotal Role To Mediate Downstream Expression of Vimentin.** For illustrating if vimentin elevation could be downstream of IRS-1, si-RNA of IRS-1 was transfected into the high glucose-incubated tubular cells. Figure 5A shows that the knockdown blocked most of the IRS-1 expression and reduced about 75% of the IRS-1 protein. High glucose-induced vimentin was significantly attenuated by the si-RNA (Figure 5B), indicating that IRS-1 and its phosphorylation could be an essential mediator of downstream EMT.

In addition to the resistance marker, we have further tested if glucose uptake could be involved (shown in the Supporting Information). The finding revealed that no matter whether glucose uptake is significantly altered or not, DPP-4/insulin resistance signal is the critical mediator of renal EMT.

**pIRS-1 (S307) and Vimentin Are Coordinately Increased in the Diabetic Kidneys.** Immunochemical staining demonstrated that pIRS-1 (S307) appeared rich in type 2 diabetic rats, especially surrounding the tubular region (Figure 6A–C). As previously indicated,[20] vacuole fusions and lipid accumulation were also found in the diabetic tubular

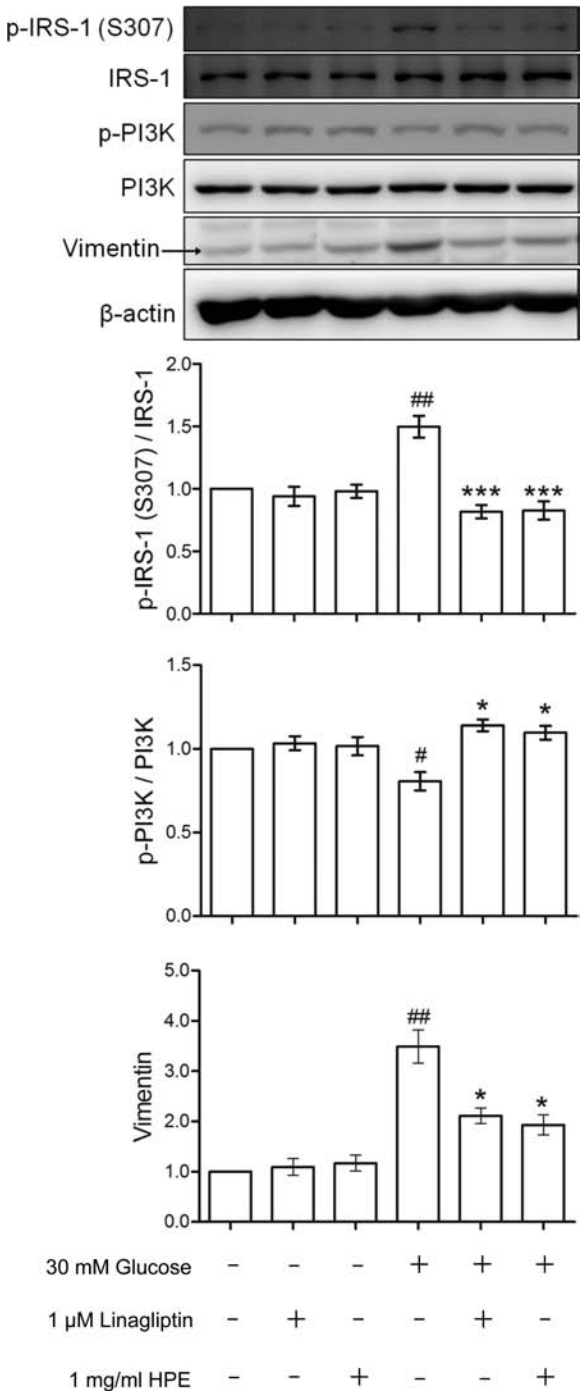


**Figure 4.** Effect of HPE on IRS-1 (S307), p-PI3K, and vimentin. HK-2 cells were incubated for 48 h under normal or high glucose (30 mM) conditions with or without different concentrations of HPE. Cell proteins were extracted and analyzed with Western blot. The ratios of IRS-1 (S307)/IRS-1 and p-PI3K/PI3K and the level of vimentin were calculated as fold compared with the control. Data are presented as means ± SD ($n$ = 3) and analyzed with ANOVA. $^{\#}p < 0.05$, $^{\#\#}p < 0.01$ compared with the control. $^{*}p < 0.05$, $^{***}p < 0.001$, compared with the high glucose-treated.

region, accompanied by the destroyed basement membrane. As well, the protein level of vimentin significantly increased 1.5-fold in diabetic kidneys (Figure 6D). Treatment of HPE, especially at the dose of 200 mg/kg, ameliorated the resistance


dx.doi.org/10.1021/jf5024092 | J. Agric. Food Chem. 2014, 62, 9736–9743

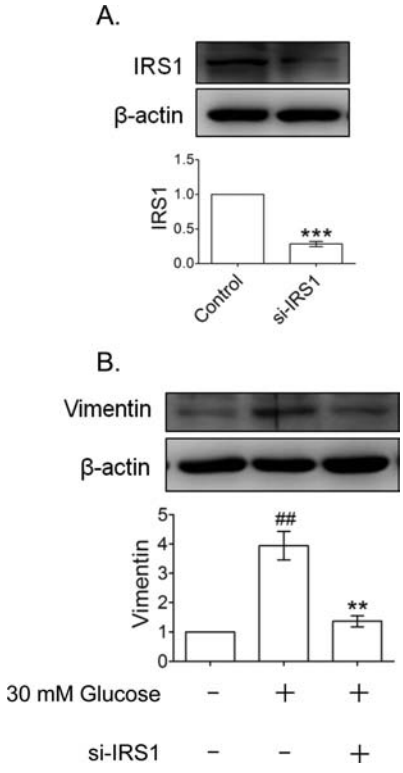


**Figure 5.** Signal cascades of IRS-1 and vimentin. HK-2 cells were transfected with siRNA and then incubated under different conditions. Cell proteins were extracted and analyzed with Western blot: (A) IRS-1; (B) vimentin. Protein levels were calculated as fold compared with the control. Data are presented as means ± SD ($n$ = 3) and analyzed with ANOVA. $^{\#\#}p < 0.01$, compared with the control. $^{**}p < 0.01$, $^{***}p < 0.001$, compared with the high glucose-treated.

signal, and it reduced the EMT marker even below that in the control, thereby improving the histological changes.

## DISCUSSION

We demonstrated the concomitant expression of the pivotal markers of EMT and insulin resistance in renal tubular cells. Treatment of HPE or linagliptin inhibited the high glucose-induced activation of DPP-4, thereby regulating vimentin and phosphorylation of IRS-1(S307), while recovering the signals of PI-3K. Blocking IRS-1 inhibited the elevation of vimentin, suggesting that an essential role of IRS-1 mediates between DPP-4 and the downstream EMT. In the diabetic rat, pIRS-1 (Ser 307) was abundantly expressed especially surround the tubular region, accompanied by increased vimentin in the kidney. Treatment of HPE ameliorated the EMT and resistance and improved the histological change.

EMT is an important process for embryonic development. Moreover, it occurs under pathological conditions, including cancer cell invasion and renal fibrosis.[21−23] EMT involves loss of epithelial cell adhesion, disrupted basement membrane, enhanced cell migration, and invasion.[24] With increasing vimentin, tubular epithelial cells undergo a phenotypic transformation into matrix-producing fibroblasts.[25] Besides measuring the protein markers, we have performed the morphologic observation to identify EMT. Scanning electromicroscopy and immunohistochemical stain proved that high glucose induced typical features of EMT, while HPE attenuated the alteration.[20] In diabetes, transitioned tubular epithelial cells are associated with interstitial fibrosis and renal dysfunction.[26] Our previous report demonstrated the effect of HPE on inhibiting renal fibrosis of type 2 diabetic rats,[19] which should partly be attributed to the improvement of EMT.

IRS-1 (S307), which is phosphorylated via several mechanisms, including insulin-stimulated kinases or stress-activated kinases like JNK1, is a serine residue located near the phosphotyrosine-binding domain of IRS-1. The phosphorylation of Ser307 leading to a conformational change disrupts the interaction between the catalytic domain of the insulin receptor and the phosphotyrosine-binding domain of IRS-1, and thus inhibits insulin signaling and stimulating the phosphatidylinositol 3-kinase and MAPK cascades.[27] IRS-1 (S307) phosphorylation is viewed as a hallmark of insulin resistance in biologically insulin-responsive cells or tissues.[28]

Cellular insulin resistance predominantly affects adipose and muscle cells. However, a spectrum of renal disease is associated with increased markers of insulin resistance, although direct causal mechanisms are not known.[29] Among a variety of kidney cells, podocyte, with kinetics similar to that of muscle cells, was shown to be insulin sensitive with respect to glucose uptake only if nephrin is expressed.[30] Palmitate blocks insulin-stimulated glucose uptake in human podocytes by dysregulating the phosphorylation of the insulin receptor, IRS-1 and PKB, and leads to impaired translocation of GLUT4 to the cell surface.[29] The resistance signals were also found in human embryonic kidney cells.[9] In the present study, high glucose-induced EMT and resistance marker were concomitantly rescued by HPE or linagliptin in renal tubular cells, implying that insulin resistance could get involved in the interstitial fibrosis and diabetic nephropathy. The mediating role was confirmed with IRS knockdown. Moreover, this phenomenon was proved in kidneys of type 2 diabetic rats. Our findings suggest that insulin resistance, attenuated by HPE, should pivotally associate with renal tubular EMT.

Many previous studies showed that DPP-4 inhibitor improved renal function parameters including albuminuria and creatinine clearance, or improved the histological changes of interstitial volume and glomerular basement membrane thickness, while the effects appeared to be independent of blood glucose lowering.[12,13] DPP-4 inhibition on top of angiotensin receptor blocker treatment significantly reduced urinary albumin excretion and oxidative stress in diabetic eNOS knockout mice, and the results were independent of blood glucose or systolic blood pressure.[11] Treatment with DPP-4 inhibitor significantly improved hyperglycemia and insulin resistance in SHR/NDmcr-cp rats, as evidenced by oral glucose tolerance test and homeostasis model assessment for insulin resistance, respectively.[31] In adults with metabolic symdrome, DPP-4 decrease was associated with insulin sensitivity following exercise training and weight loss.[32] There is evidence that DPP-4 inhibitors directly act on collagen metabolism and modulate the fibrosis marker such as transforming growth factor $\beta$.[33,34] We recently showed that HPE inhibit the angiotensin receptor-1/transforming growth factor $\beta$1 mediated EMT.[20] The cascades could be downstream of DPP-4 and even the subsequent resistance signal. Furthermore, the usual dose of linagliptin (MW = 472.54) for type 2 DM is 2.5 mg daily per os, which corresponds to 5.3 $\mu$mol. Taking the serum volume to be approximately 4 L per capita for human, the transient blood concentration could yield 1.325 $\mu$M. In the present study, 1.0 $\mu$M of linagliptin was used as DPP-4 inhibitor of the experiment, which is indeed correct and feasible.

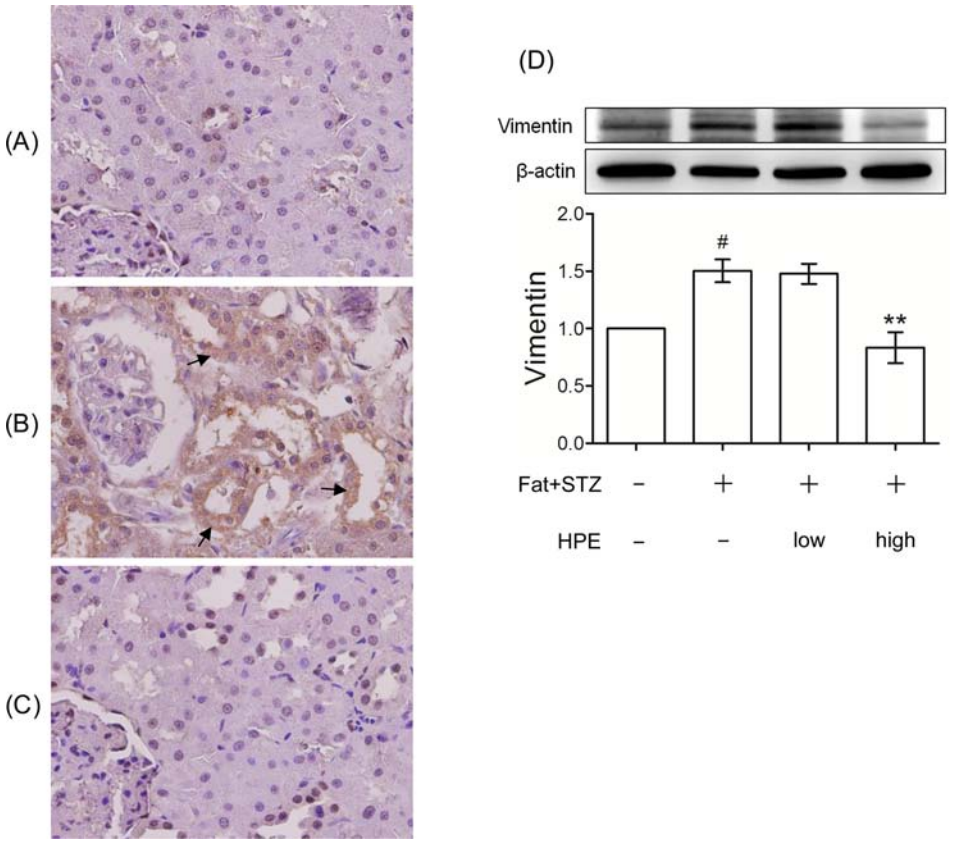


**Figure 6.** Effect of HPE on the diabetic kidneys. Kidneys of normal and type 2 diabetic rats with or without HPE treatment were examined by IHC (200×) and Western blot. (A–C) Histological expressions of IRS-1 Ser (307) (brown staining as arrow-indicated) in normal, diabetic, and 200 mg/kg HPE treated diabetic groups, respectively. (D) Protein levels of vimentin in the diabetic kidneys. $^{\#}p < 0.05$, compared with the control. $^{**}p < 0.01$, compared with the diabetic group.

In the present study, we have tested some of the components of HPE (shown in the Supporting Information). Although caffeic acid, protocatechuic acid, chlorogenic acid, and gallic acid all have the potential to inhibit DPP-4, a low dose of caffeic acid especially inhibits EMT of renal tubular cells. Gallic acid and cholorogenic acid could also exert some effect in triggering DPP-4 and the downstream EMT. The synergistic effects should be considered. In fact, all the tested compounds were reported to be antidiabetic. Caffeic acid promoted glycolysis and glycogen synthesis, but inhibited gluconeogenesis in insulin-resistant hepatocytes.[35] Caffeic acid protected the kidney from diabetic injuries, reducing blood glucose, HbA1c, blood urine nitrogen, urine output, renal advanced glycation end product (AGE), and inflammatory cytokines, while improving clearance of creatinine.[36] Treatment of protocatechuic acid also reduced plasma HbA1c, urinary glycative albumin, renal AGEs, and receptor of AGE.[37] Chlorogenic acid lowered fasting plasma glucose, TBARS, and lipid hydroperoxides in diabetic rats.[38] Gallic acid stimulated insulin secretagogue by regenerating pancreas $\beta$-islets, thus increasing plasma insulin and glucose tolerance.[39] Galloyl ester decreased oxidative stress and AGEs, and improved hepatic and renal function in type 2 diabetic db/db mice.[40]

In conclusion, HPE improves insulin resistance signals and EMT, which is implicated in the pathogenesis of diabetic nephropathy. HPE deserves further investigation and could be an adjuvant to prevent diabetic renal damage.

## ■ ASSOCIATED CONTENT

### Supporting Information

Table of retention time, UV–vis, and mass spectral characteristics for the phenolics identified in HPE (S1); graphic depicting glucose uptake assay (S2); and graphics depicting DPP-4 inhibited by the phenolics of HPE and vimentin reduced by the phenolics of HPE (S3). This material is available free of charge via the Internet at http://pubs.acs.org.

## ■ AUTHOR INFORMATION

### Corresponding Author

*Institute of Medicine, Chung-Shan Medical University, Number 110, Section 1, Chien-Kuo North Road, Taichung 402, Taiwan. E-mail: cshy049@csh.org.tw. Fax: 866-4-24739220.

### Funding

Funding for this research was provided by Chung-Shan Medical University Hospital, under CSH-2014-C006, and National Science Council, Taiwan, under MOST 103-2320-B-241-002.

### Notes

The authors declare no competing financial interest.

## ■ ABBREVIATIONS USED

DPP-4, type 4 dipeptidyl peptidase; EMT, epithelial to mesenchymal transition; HPE, polyphenol extracts of *H. sabdariffa*; IRS-1 (S307), phosphorylation of Ser307 of insulin receptor substrate-1; PI3K, phosphatidylinositol 3-kinase; STZ, streptozotocin

## REFERENCES


(1) Wolf, G.; Ziyadeh, F. N. The role of angiotensin II in diabetic nephropathy: Emphasis on nonhemodynamic mechanisms. *Am. J. Kidney Dis.* **1997**, *29*, 153−163.

(2) Yamamoto, T.; Noble, N. A.; Cohen, A. H.; Nast, C. C.; Hishida, A.; Gold, L. I.; Border, W. A. Expression of transforming growth factor-beta isoforms in human glomerular diseases. *Kidney Int.* **1996**, *49*, 461−469.

(3) Remuzzi, G.; Benigni, A.; Remuzzi, A. Mechanisms of progression and regression of renal lesions of chronic nephropathies and diabetes. *J. Clin. Invest.* **2006**, *116*, 288−296.

(4) Strutz, F. M. EMT and proteinuria as progression factors. *Kidney Int.* **2009**, *75*, 475−481.

(5) Balakumar, P.; Arora, M. K.; Reddy, J.; Anand-Srivastava, M. B. Pathophysiology of diabetic nephropathy: Involvement of multifaceted signaling mechanism. *J. Cardiovasc. Pharmacol.* **2009**, *54*, 129−138.

(6) Chaykovska, L.; von Websky, K.; Rahnenführer, J.; Alter, M.; Heiden, S.; Fuchs, H.; Runge, F.; Klein, T.; Hocher, B. Effects of DPP-4 inhibitors on the heart in a rat model of uremic cardiomyopathy. *PLoS One* **2011**, *6*, e27861.

(7) Choi, K.; Kim, Y. B. Molecular mechanism of insulin resistance in obesity and type 2 diabetes. *Korean J. Int. Med.* **2010**, *25*, 119−129.

(8) Lin, C. L.; Lin, J. K. Epigallocatechin gallate (EGCG) attenuates high glucose-induced insulin signaling blockade in human hepG2 hepatoma cells. *Mol. Nutr. Food Res.* **2008**, *52*, 930−939.

(9) Jiang, G.; Dallas-Yang, Q.; Liu, F.; M?ller, D. E.; Zhang, B. B. Salicylic acid reverses phorbol 12-myristate-13-acetate (PMA)- and tumor necrosis factor alpha (TNFalpha)-induced insulin receptor substrate 1 (IRS1) serine 307 phosphorylation and insulin resistance in human embryonic kidney 293 (HEK293) cells. *J. Biol. Chem.* **2003**, *278*, 180−186.

(10) Hocher, B.; Reichetzeder, C.; Alter, M. L. Renal and Cardiac Effects of DPP-4 Inhibitors—from Preclinical Development to Clinical Research. *Kidney Blood Pressure Res.* **2012**, *36*, 65−84.

(11) Alter, M. L.; Ott, I. M.; von Websky, K.; Tsuprykov, O.; Sharkovska, Y.; Krause-Relle, K.; Raila, J.; Henze, A.; Klein, T.; Hocher, B. DPP-4 Inhibition on Top of Angiotensin Receptor Blockade Offers a New Therapeutic Approach for Diabetic Nephropathy. *Kidney Blood Pressure Res.* **2012**, *36*, 119−130.

(12) Liu, W. J.; Xie, S. H.; Liu, Y. N.; Kim, W.; Jin, H. Y.; Park, S. K.; Shao, Y. M.; Park, T. S. Dipeptidyl peptidase IV inhibitor attenuates kidney injury in streptozotocin-induced diabetic rats. *J. Pharmacol. Exp. Ther.* **2012**, *340*, 248−255.

(13) Groop, P. H.; Cooper, M. E.; Perkovic, V.; Emser, A.; Woerle, H. J.; von Eynatten, M. Linagliptin lowers albuminuria on top of recommended standard treatment in patients with type 2 diabetes and renal dysfunction. *Diabetes Care* **2013**, *36*, 3460−3468.

(14) Lin, H. H.; Chen, J. H.; Wang, C. J. Chemopreventive properties and molecular mechanisms of the bioactive compounds in *Hibiscus Sabdariffa* Linne. *Curr. Med. Chem.* **2011**, *18*, 1245−1254.

(15) Chen, C. C.; Hsu, J. D.; Wang, S. F.; Chiang, H. C.; Yang, M. Y.; Kao, E. S.; Ho, Y. C.; Wang, C. J. *Hibiscus sabdariffa* extract inhibits the development of atherosclerosis in cholesterol-fed rabbits. *J. Agric. Food Chem.* **2003**, *51*, 5472−5477.

(16) Peng, C. H.; Chyau, C. C.; Chan, K. C.; Chan, T. H.; Wang, C. J.; Huang, C. N. *Hibiscus sabdariffa* polyphenolic extract inhibits hyperglycemia, hyperlipidemia, and glycation-oxidative stress while improving insulin resistance. *J. Agric. Food Chem.* **2011**, *59*, 9901−9909.

(17) Huang, C. N.; Chan, K. C.; Lin, W. T.; Su, S. L.; Wang, C. J.; Peng, C. H. *Hibiscus sabdariffa* inhibits vascular smooth muscle cell proliferation and migration induced by high glucoses—A mechanism involves connective tissue growth factor signals. *J. Agric. Food Chem.* **2009**, *57*, 3073−3079.

(18) Peng, C. H.; Ker, Y. B.; Weng, C. F.; Peng, C. C.; Huang, C. N.; Lin, L. Y.; Peng, R. Y. Insulin secretagogue bioactivity of finger citron fruit (*Citrus medica* L. var. *Sarcodactylis* Hort, Rutaceae). *J. Agric. Food Chem.* **2009**, *57*, 8812−8819.

(19) Yang, Y. S.; Huang, C. N.; Wang, C. J.; Lee, Y. J.; Chen, M. L.; Peng, C. H. Polyphenols of *Hibiscus sabdariffa* improved diabetic nephropathy via regulating the pathogenic markers and kidney functions of type 2 diabetic rats. *J. Funct. Foods* **2013**, *5*, 810−819.

(20) Yang, Y. S.; Wang, C. J.; Huang, C. N.; Chen, M. L.; Chen, M. J.; Peng, C. H. Polyphenols of *Hibiscus sabdariffa* improved diabetic nephropathy via attenuating renal epithelial mesenchymal transition. *J. Agric. Food Chem.* **2013**, *61*, 7545−7551.

(21) Xu, J.; Zhu, W.; Xu, W.; Yao, W.; Zhang, B.; Xu, Y.; Ji, S.; Liu, C.; Long, J.; Ni, Q.; Yu, X. Up-Regulation of MBD1 promotes pancreatic cancer cell epithelial-mesenchymal transition and invasion by epigenetic down-regulation of E-cadherin. *Curr. Mol. Med.* **2013**, *13*, 387−400.

(22) Dai, X.; Ge, J.; Wang, X.; Qian, X.; Zhang, C.; Li, X. OCT4 regulates epithelial-mesenchymal transition and its knockdown inhibits colorectal cancer cell migration and invasion. *Oncol. Rep.* **2013**, *29*, 155−160.

(23) Aresu, L.; Benali, S.; Garbisa, S.; Gallo, E.; Castagnaro, M. Matrix metalloproteinases and their role in the renal epithelial mesenchymal transition. *Histol. Histopathol.* **2011**, *26*, 307−313.

(24) Neilson, E. G. Mechanisms of disease: Fibroblasts– A new look at an old problem. *Nat. Clin. Pract. Nephrol.* **2006**, *2*, 101−108.

(25) Li, J.; Qu, X.; Bertram, J. F. Endothelial−myofibroblast transition contributes to the early development of diabetic renal interstitial fibrosis in streptozotocin-induced diabetic mice. *Am. J. Pathol.* **2009**, *175*, 1380−1388.

(26) Guarino, M.; Tosoni, A.; Nebuloni, M. Direct contribution of epithelium to organ fibrosis: Epithelial−mesenchymal transition. *Hum. Pathol.* **2009**, *40*, 1365−1376.

(27) Aguirre, V.; Werner, E. D.; Giraud, J.; Lee, Y. H.; Shoelson, S. E.; White, M. F. Phosphorylation of Ser307 in insulin receptor substrate-1 blocks interactions with the insulin receptor and inhibits insulin action. *J. Biol. Chem.* **2002**, *277*, 1531−1537.

(28) Le Marchand-Brustel, Y.; Gual, P.; Gremeaux, T.; Gonzalez, T.; Barres, R.; Tanti, J. F. Fatty acid-induced insulin resistance: role of insulin receptor substrate 1 serine phosphorylation in the retro-regulation of insulin signalling. *Biochem. Soc. Trans.* **2003**, *31*, 1152−1156.

(29) Lennon, R.; Pons, D.; Sabin, M. A.; Wei, C.; Shield, J. P.; Coward, R. J.; Tavare, J. M.; Mathieson, P. W.; Saleem, M. A.; Welsh, G. I. Saturated fatty acids induce insulin resistance in human podocytes: implications for diabetic nephropathy. *Nephrol,. Dial., Transplant.* **2009**, *24*, 3288−3296.

(30) Coward, R. J.; Welsh, G. I.; Koziell, A.; Hussain, S.; Lennon, R.; Ni, L.; Tavaré, J. M.; Mathieson, P. W.; Saleem, M. A. Nephrin is critical for the action of insulin on human glomerular podocytes. *Diabetes* **2007**, *56*, 1127−1135.

(31) Nakagami, H.; Pang, Z.; Shimosato, T.; Moritani, T.; Kurinami, H.; Koriyama, H.; Tenma, A.; Shimamura, M.; Morishita, R. The dipeptidyl peptidase-4 inhibitor teneligliptin improved endothelial dysfunction and insulin resistance in the SHR/NDmcr-cp rat model of metabolic syndrome. *Hypertens. Res.* **2014**, *37*, 629−635.

(32) Malin, S. K.; Huang, H.; Mulya, A.; Kashyap, S. R.; Kirwan, J. P. Lower dipeptidyl peptidase-4 following exercise training plus weight loss is related to increased insulin sensitivity in adults with metabolic syndrome. *Peptides* **2013**, *47*, 142−147.

(33) Jost, M. M.; Lamerz, J.; Tammen, H.; Menzel, C.; De Meester, I.; Lambeir, A. M.; Augustyns, K.; Scharpé, S.; Zucht, H. D.; Rose, H.; Jürgens, M.; Schulz-Knappe, P.; Budde, P. *In vivo* profiling of DPP4 inhibitors reveals alterations in collagen metabolism and accumulation of an amyloid peptide in rat plasma. *Biochem. Pharmacol.* **2009**, *77*, 228−237.

(34) Chaykovska, L.; von Websky, K.; Rahnenführer, J.; Alter, M.; Heiden, S.; Fuchs, H.; Runge, F.; Klein, T.; Hocher, B. Effects of DPP-4 inhibitors on the heart in a rat model of uremic cardiomyopathy. *PLoS One* **2011**, *6*, e27861.

(35) Huang, D. W.; Shen, S. C. Caffeic acid and cinnamic acid ameliorate glucose metabolism via modulating glycogenesis and

gluconeogenesis in insulin-resistant mouse hepatocytes. *J. Funct. Foods* **2012**, *4*, 358−366.
(36) Chao, C. Y.; Mong, M. C.; Chan, K. C.; Yin, M. C. Antiglycative and anti-inflammatory effects of caffeic acid and ellagic acid in kidney of diabetic mice. *Mol. Nutr. Food Res.* **2010**, *54*, 388−395.
(37) Lin, C. Y.; Tsai, S. J.; Huang, C. S.; Yin, M. C. Antiglycative effects of protocatechuic acid in the kidneys of diabetic mice. *J. Agric. Food Chem.* **2011**, *59*, 5117−5124.
(38) Karthikesan, K.; Pari, L.; Menon, V. P. Protective effect of tetrahydrocurcumin and chlorogenic acid against strep tozotocin−nicotinamide generated oxidative stress induce d diabetes. *J. Funct. Foods* **2010**, *2*, 134−142.
(39) Latha, R. C.; Daisy, P. Insulin-secretagogue, antihyperlipidemic and other protective effects of gallic acid isolated from *Terminalia bellerica* Roxb. in streptozotocin-induced diabetic rats. *Chem.-Biol. Interact.* **2011**, *189*, 112−118.
(40) Park, C. H.; Noh, J. S.; Yamabe, N.; Kang, K. S.; Tanaka, T.; Yokozawa, T. Beneficial effect of 7-O-galloyl-D-sedoheptulose on oxidative stress and hepatic and renal changes in type 2 diabetic db/db mice. *Eur. J. Pharmacol.* **2010**, *640*, 233−242.

determination of the bioactivity contribution ratio of certain compounds from a complex extract (7).

Therefore, the present study aimed to figure out the key phenolic compounds accounting for the antioxidant effects of longan seed extract using a combination of Fourier transform ion cyclotron resonance mass spectrometry (FT-ICR−MS), high-performance liquid chromatography electrospray ionization mass spectrometry (HPLC−ESI−MS) analysis, online fishing or knockout, and antioxidant-based screening strategies. Detailed information on the chemical structure−antioxidant activity relationship of longan seed extract will allow us to exploit it as a potentially beneficial phytonutrient.

## MATERIALS AND METHODS

**Plant Materials.** Fresh and fully mature longan fruits (cv. Shixia), which were harvested from south China, were transported to the laboratory for subsequent processing. The longan seeds from non-disease fruits were collected and freeze-dried at −60 °C for 48 h. All of the samples were homogenized to a powder using a stainless-steel grinder and then stored at −20 °C prior to analysis.

**Chemicals.** Analytical or high-performance liquid chromatography (HPLC)-grade solvents and reagents were used. Methanol, acetonitrile, and formic acid were purchased from Fisher Scientific (Waltham, MA). Trolox, fluorescein disodium, and 2,2-diphenylpicrylhydrazyl (DPPH) were obtained from Sigma-Aldrich (St. Louis, MO). 2,2′-Azobis(2-amidinopropane) dihydrochloride (AAPH) was purchased from Wako Chemicals USA (Richmond, VA). D3520 macroporous resin was purchased from Nankai Chemical Plant (Tianjin, China).

**Preparation of Longan Seed Polyphenols (LSPs).** LSPs were extracted according to the modified method by Soong et al.[6] A total of 5 g of dried longan seed powder was refluxed in 100 mL of aqueous ethanol (90%, v/v) at 70 °C for 1.5 h, using a heating mantle to control the temperature and a water-jacketed condenser to return the vapor to the pot. The extract was filtered with a 30 μm Whatman filter paper under vacuum, and the residue was extracted 2 more times. The extract was evaporated under reduced pressure at 35 °C to remove the solvent before lyophilization. The crude polyphenol extract was purified on D3520 macroporous resin.[10] Approximately 10 g of the crude extract was dissolved in 50 mL of 40% ethanol and loaded on a glass column (4.2 × 60 cm) packed with D3520 macroporous resin. Then, 1000 mL of distilled water was used to remove the sugar, and 1000 mL of 40% ethanol was used to elute the phenols at a flow rate of 1.5 mL/min. After elution, the solvent was removed using a rotary evaporator under vacuum, the residue was lyophilized, and LSPs were obtained. Samples were dissolved in methanol to 1 mg/mL prior to HPLC analysis.

**FT-ICR−MS Analysis.** FT-ICR mass spectra were collected on a Bruker Apex-Qe-FT-ICR mass spectrometer equipped with a 9.4 T superconducting magnet (Bruker Co., Chicago, IL). The LSP extract was dissolved in methanol at 0.1 μg/μL. Then, 100 μL of the solution was imported into an electrospray ionization (ESI) technique at a flow rate of 100 μL/h, with the temperature at 180 °C. Mass spectra were obtained in negative-ion mode, and the mass scale ranged from $m/z$ 100 to 2000.

**HPLC−ESI−MS Analysis.** The separation of LSPs by HPLC was performed on an Agilent 1100 liquid chromatograph system (Santa Clara, CA) with a ZORBAX TC-C18 (4.6 × 250 mm, 5 μm, Agilent) column. Separation was accomplished at 30 °C with 0.4% formic acid in water (solvent A) and methanol (solvent B) at 1.0 mL/min using a gradient as follows: 0−10 min, 5−25% B; 10−20 min, 25−55% B; 20−30 min, 55% B; 30−35 min, 55−5% B; and re-equilibration with 5% B for 5 min. Samples were filtered through a 0.45 μm cellulose acetate spin filter before injecting 10 μL, and the eluate was monitored at 280 nm.

Electrospray ionization mass spectroscopy (ESI−MS) analysis was conducted on an Agilent 1100 LC−MS spectrometer (Santa Clara, CA) equipped with a diode array detector and an Agilent 6300 ion trap (Santa Clara, CA) in negative-ion mode. The mobile phase and gradient were the same as HPLC analysis described above. For mass spectroscopy (MS), the heated capillary temperature and spray needle voltage were 350 °C and 4 kV, respectively. The drying gas ($N_2$) flow rate was set at 10 L/min, and mass spectra scale ranged from $m/z$ 100 to 2000.

**Online Knockout.** The strategy included two main steps: (1) screening out the target fractions/peaks in an extract fingerprint and (2) knocking out target fractions/peaks. In this strategy, any component in an extract can be fished or knocked out. On the basis of the method reported by Liu et al.,[7] the online knockout experiments of LSPs were conducted on a SHIMADZU liquid chromatograph system (Shimadzu Co., Kyoto, Japan) with a semi-preparative HPLC column (ZORBAX SB-C18, 9.4 × 250 mm, 5 μm, Agilent). Samples were dissolved in methanol at 50 mg/mL before injecting 20 μL into the system. The mobile phase and gradient were the same as described above for analytical HPLC, except that the flow rate was 4 mL/min. Different ingredients of the extract were separated by the liquid chromatography (LC) column and eluted out from the detector cell. We collected different fractions/peaks manually. To collect accurately, we connected the detector cell with a short PEEK tubing with a narrow inner diameter (Agilent, inner diameter of 0.13 mm). When the elution began, the eluate was collected from the PEEK tube in a brown container to keep away from light. As soon as the target fraction/peak appeared, the target fraction/peak was collected in another flask separately. Once the collection of the target fraction/peak was finished, the residual components were collected in the former container continuously. All of the target fractions or peaks were completely fished from the total extract by repeating this step. Different kinds of samples collected by the online fishing or knockout method were using a rotary evaporator under vacuum to remove solvent and stored at 4 °C for HPLC analysis and antioxidant activity assays.

**Assays for Antioxidant Activity.** *Determination of the Reducing Power.* The ferric-reducing antioxidant power (FRAP) assay was according to the methods by Dudonne et al. and Ozgen et al.,[11,12] with some modification. LSPs were dissolved in methanol to give various concentrations (20, 40, 60, 80, and 100 μg/mL). A total of 1 mL of various LSP solutions was mixed with 0.2 M phosphate buffer (0.2 mL, pH 6.6) and 0.3% potassium ferricyanide (1.5 mL) in a test tube. The mixture was kept in a water bath at 50 °C for 20 min. Then, 10% trichloroacetic acid (1 mL), 0.3% ferric chloride (0.5 mL), and distilled water (3 mL) were added to the mixture before the absorbance was measured at 700 nm.

*Determination of the DPPH-Scavenging Activity.* The DPPH-scavenging activity of LSPs was evaluated according to the methods by Cervato et al.[13] and Goupy et al.[14] A total of 2 mL of sample (10 μg/mL) dissolved in methanol was mixed with 2 mL of 0.2 mM DPPH solution. The mixture was incubated in the dark at 25 °C for 30 min before the absorbance was measured at 517 nm. The reaction mixture without a test sample was used as the control. The scavenging capacity of LSPs was calculated as follows: scavenging rate (%) = (1 − absorbance of sample/absorbance of control) × 100. The activity loss of each sample with target fraction/peak missing was calculated as follows: activity loss (%) = (1 − scavenging rate of sample with one fraction or peak missing/scavenging rate of sample before knockout) × 100.

*Determination of the Oxygen Radical Absorbance Capacity (ORAC).* The measurement of the ORAC assay was based on the method by Huang et al.[15] A total of 25 μL of sample solution (0.1 mg/mL, dissolved in methanol) was transferred to a 96-well polystyrene plate. Then, 150 μL of $8.16 \times 10^{-5}$ mM fluorescein solution diluted in 75 mM phosphate buffer (pH 7.4) was added. The plate was covered with a lid to maintain a constant temperature and preincubated (37 °C) for 10 min. The reaction was initiated by adding 25 μL of 153 mM AAPH. The result was recorded on a fluorescent reader every 5 min for 80 min, with the excitation wavelength at 485 nm and emission wavelength at 530 nm. The standard curve was obtained using Trolox (a water-soluble derivative of vitamin E with antioxidant property) as a standard. The Trolox standard was prepared as follows: 0.250 g of Trolox was dissolved in 50 mL of 75 mM phosphate buffer (pH 7.4)


dx.doi.org/10.1021/jf502995z | J. Agric. Food Chem. 2014, 62, 9744−9750

to give a 0.02 M stock solution. The stock solution was diluted with the same phosphate buffer to 50, 25, 12.5, 6.25, and 3.125 $\mu$M working solutions. The net area under the curve (AUC) of the standard and samples was calculated as

$$\mathrm{AUC} = 0.5 + f_1/f_0 + \ldots + f_i/f_0 + \ldots + f_{15}/f_0 + 0.5(f_{16}/f_0)$$

where $f_0$ is the initial fluorescence reading at 0 min and $f_i$ is the fluorescence reading at time $i$. Final ORAC values were expressed as micromoles of Trolox equivalents per liter of samples.

**Data Analysis.** All of the determinations were performed in triplicate. Data were expressed as the mean ± standard deviation (SD) and evaluated by one-way analysis of variation (ANOVA) of SPSS 19.0 (SPSS, Inc., Chicago, IL) with Duncan's multiple range test. $p$ values of <0.05 were considered as significant.

## RESULTS AND DISCUSSION

We extracted the phenolic compounds from longan seed with 90% ethanol. Polyphenols were enriched by selective treatment with D3520 macroporous resin. HPLC analysis revealed that LSPs were a very complex mixture, with more than 20 peaks being eluted out. Because of the complicated composition of LSPs, we divided it into three fractions, as indicated in Figure 2, and then further analyzed each fraction by the FT-ICR−MS method, which is a powerful tool for characterizing complex compounds.[16,17] FT-ICR−MS spectra of fraction 1 showed two strong signals of $[M - H]^-$ at $m/z$ 169.0106 and 339.0319 (Figure 1a). The former was 0.99 ppm error contrasted to the molecular mass of gallic acid ($C_7H_6O_5$), and the latter was corresponding to $[2M - H]^-$ ion of gallic acid,[18] indicating that gallic acid was the main composition of fraction 1, which was identified in longan seeds by Soong et al. and Sudjaroen et al. previously.[6,18] Similarly, we obtained two strong signals of $[M - H]^-$ at $m/z$ 300.9958 and 602.9996 on the spectra of fraction 3 (Figure 1c). The signal of $[M - H]^-$ at $m/z$ 300.9958 was identified as ellagic acid ($C_{14}H_6O_8$), with the molecular weight error of 1.28 ppm paralleled with the theoretical value, and the signal of $[M - H]^-$ at $m/z$ 602.9996 was corresponding to the $[2M - H]^-$ ion of ellagic acid, suggesting that fraction 3 was mainly composed of ellagic acid.[6]

In comparison to fractions 1 and 3, fraction 2 was more complex (Figure 1b), with three strong signals of $[M - H]^-$ at $m/z$ 387.1631, 469.0584, and 633.0711 and nine weak signals of $[M - H]^-$ at $m/z$ 197.0421, 283.2610, 319.0429, 433.0379, 513.0967, 801.0757, 863.1814, 907.0769, and 951.0717 being observed. Ethyl gallate, 2-*O*-galloyl-$\beta$-D-xylopyranosyl, myricetin, ellagic acid 4-*O*-$\alpha$-l-arabinofuranoside, corilagin, isomallotinic acid, proanthocyanidin trimer (A type), and geraniin (hemiacetal forms) with the $[M - H]^-$ ions of 197, 283, 319, 433, 633, 801, 863, and 951, respectively, were reported in longan seeds and other plant materials.[18−23] Our results provided primary evidence for their probable existence in longan seeds. However, besides these eight known compounds, structures of other signals of fraction 2 as well as their contributions to the antioxidant activity of LSPs were needed to be further elucidated by other means.

The FT-ICR−MS data suggested that LSPs may contain high levels of free and conjugated forms of gallic and ellagic acids. However, the current studies concerning the antioxidant contributions of gallic and ellagic acids to LSPs are inconsistent. For example, Soong et al.[6] suggested that free forms of gallic and ellagic acids had great contribution to the antioxidant activity of LSPs, while Rangkadilok et al.[1] revealed that gallic and ellagic acids might not be the main contributors for the potent antioxidant properties of LSPs. They suggested that the strong antioxidant activity of LSPs may be derived from other unknown phenols. These inconsistent results promoted us to figure out which fraction of LSPs (the gallic-acid-rich fraction 1, the ellagic-acid-rich fraction 3, or the more complex fraction 2) was responsible for the potent antioxidant activity of LSPs. We used the online fishing/knockout technology[7] to screen the bioactive compound group that represented the efficacy of LSPs. According to the online knockout method,[7] three remaining fractions of LSPs (missing fractions 1, 2, and 3) were obtained from HPLC separation. As shown in Figure 2, it was clear that, after the online knockout program, the target fraction in LSPs disappeared completely.

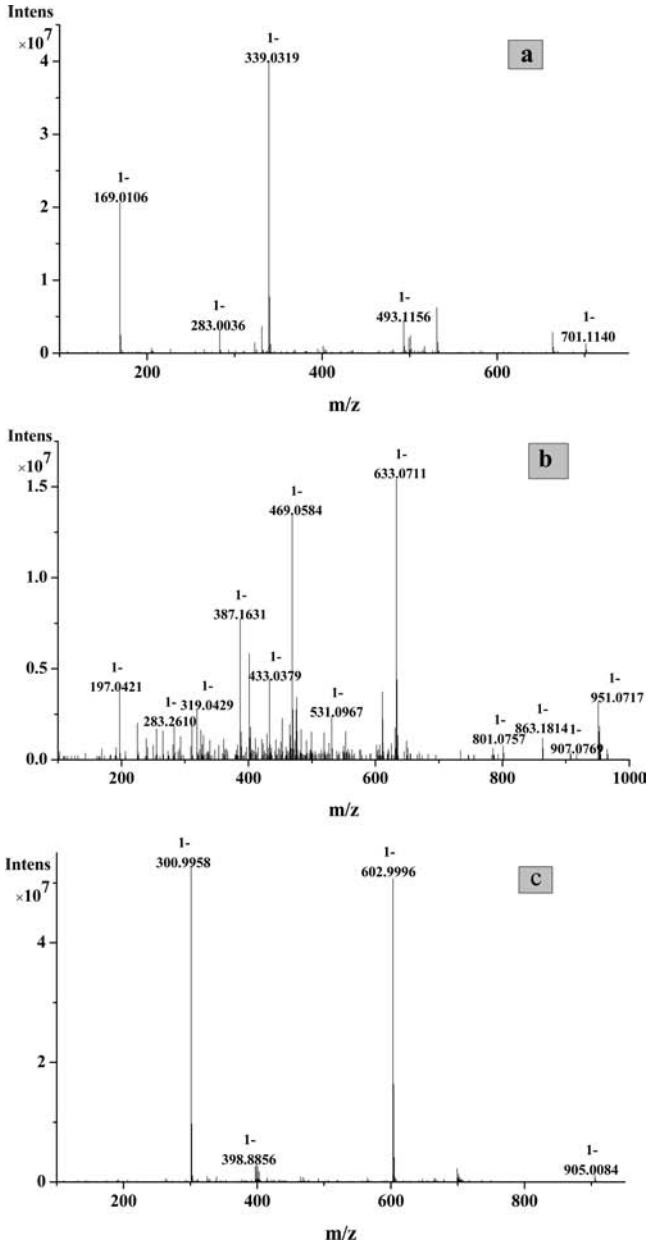


**Figure 1.** FT-ICR mass spectrum of fractions 1, 2, and 3 of LSPs.

The DPPH and FRAP assays were used to evaluate the antioxidant activity of LSPs and their three remaining fractions after knockout. By comparison of the DPPH scavenging rates (Table 1), it was easy to see that the effect of fraction 1 on the DPPH-scavenging activity was little, indicating that fraction 1 had a small contribution to the antioxidant efficiency of LSPs,

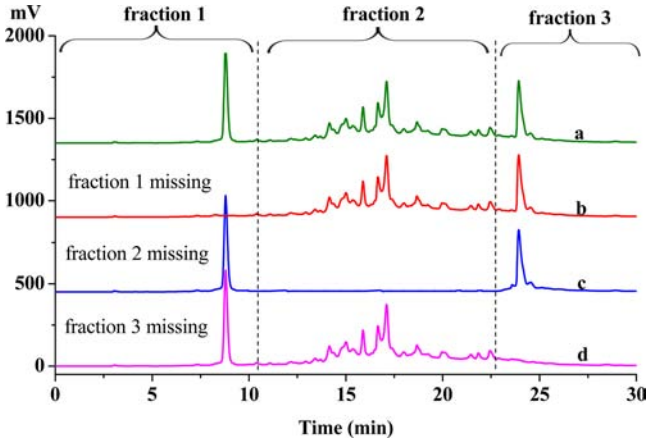


**Figure 2.** Chromatograms of fraction knockout under the same HPLC conditions: (a) chromatogram with total polyphenols of longan seed, (b) chromatogram with fraction 1 knockout, (c) chromatogram with fraction 2 knockout, and (d) chromatogram with fraction 3 knockout.

**Table 1. Scavenging Rate and Activity Loss of the Samples against the DPPH Radical**[a]

| sample by online knockout | scavenging rate (%) | activity loss (%) |
|---|---|---|
| total LSPs | 70.29 ± 0.96 a | |
| sample 1 (fraction 1 missing) | 64.65 ± 1.31 b | 8.03 ± 0.02 b |
| sample 2 (fraction 2 missing) | 56.23 ± 1.44 c | 20.00 ± 0.02 a |
| sample 3 (fraction 3 missing) | 58.42 ± 1.39 c | 16.89 ± 0.02 a |

[a]The data are given as the mean ± SD ($n$ = 3). Mean values in the same column with unlike letters are significantly different ($p$ < 0.05).

while fractions 2 and 3 played important roles in the DPPH-scavenging effect of LSPs. The contribution rate of each fraction to the DPPH-scavenging effect of LSPs was expressed as the activity loss of the correspondent sample before knockout. The contribution order of each fraction to the antioxidant activity of LSPs was fraction 2 > fraction 3 > fraction 1. The same results were also obtained in the FRAP assay (Figure 3). Our results suggested that fraction 1 had very little contribution to the antioxidant activity of LSPs, which was in line with the results by Rangkadilok et al.[1] Therefore, we ignored it in the following study. As described above, fraction 3 was mainly composed of ellagic acid, which was reported to

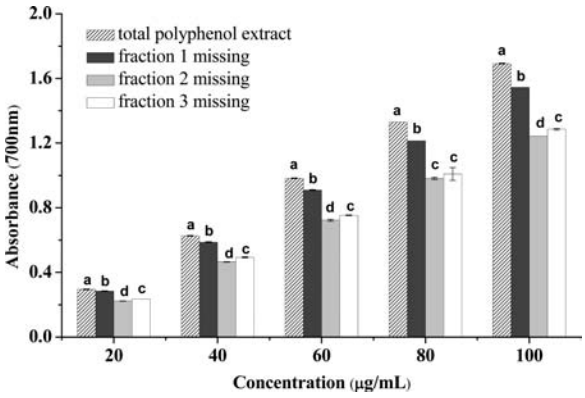


**Figure 3.** Reducing power of total polyphenols, sample 1 (fraction 1 missing), sample 2 (fraction 2 missing), and sample 3 (fraction 3 missing). Bars with different letters at the same concentration differ significantly ($p$ < 0.05).

exert an antioxidant effect *in vitro*,[16] and its prominent effect was due to the special structure unit, catechol hydroxyl, which can produce stable phenoxy radicals by the 1,2-benzoquinone unit after hydrogen abstraction.

According to the results mentioned above, fraction 2 had the highest contribution to the antioxidant properties of LSPs but was a complex mixture. To figure out the main active constituents accounting for the antioxidant properties in fraction 2, we continued to separate it into three fractions by the knockout method. As shown in Figure 4, it was evident that

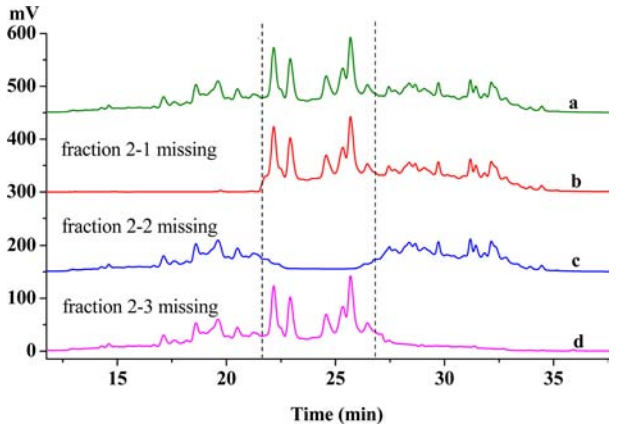


**Figure 4.** Chromatograms of fraction knockout under the same HPLC conditions: (a) chromatogram with fraction 2, (b) chromatogram with fraction 2-1 knockout, (c) chromatogram with fraction 2-2 knockout, and (d) chromatogram with fraction 2-3 knockout.

three fractions (2-1, 2-2, and 2-3) were fishing out successively. Likewise, both the DPPH scavenging and FRAP assays were performed to further evaluate the antioxidant contribution of each missing fraction. Table 2 illustrated that the DPPH

**Table 2. Scavenging Rate and Activity Loss of Fraction 2 and Different Samples against the DPPH Radical**[a]

| sample by online knockout | scavenging rate (%) | activity loss (%) |
|---|---|---|
| fraction 2 | 41.13 ± 0.004 a | |
| sample 4 (fraction 2-1 missing) | 34.89 ± 0.012 b | 15.16 ± 0.028 b |
| sample 5 (fraction 2-2 missing) | 24.68 ± 0.025 c | 40.00 ± 0.06 a |
| sample 6 (fraction 2-3 missing) | 34.11 ± 0.006 b | 17.05 ± 0.016 b |

[a]The data are expressed as the mean ± SD ($n$ = 3). Mean values in the same column with unlike letters are significantly different ($p$ < 0.05).

scavenging effect of each sample with target fraction knockout was in the following order: sample 4 (fraction 2-1 missing) > sample 6 (fraction 2-3 missing) > sample 5 (fraction 2-2 missing), which meant that the order of the contribution of each fraction was fraction 2-2 > fraction 2-3 > fraction 2-1. When fraction 2-2 was knocked out, the scavenging effect of sample 5 (fraction 2-2 missing) reduced significantly, demonstrating that fraction 2-2 had vital contribution to the total radical scavenging activity of fraction 2, while the missing of fractions 2-1 and 2-3 did not affect the scavenging rate notably. The FRAP assay (Figure 5) provided further support for the above conclusion. These findings have led to a conclusion that fraction 2-2 was the target bioactive group in longan seed extract. However, a further online fishing or knockout program was needed to screen the target bioactive compounds.


dx.doi.org/10.1021/jf502995z | J. Agric. Food Chem. 2014, 62, 9744−9750

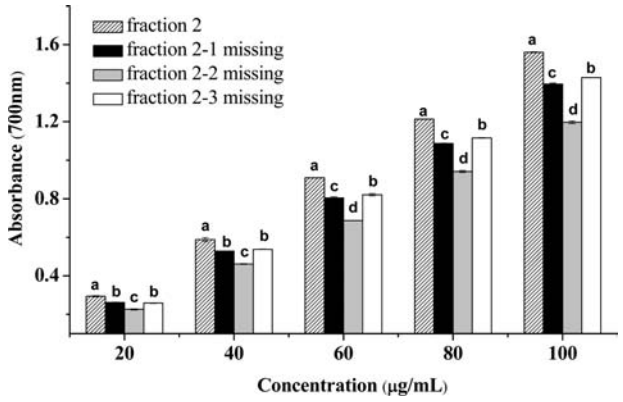


**Figure 5.** Reducing power of fraction 2, sample 4 (fraction 2-1 missing), sample 5 (fraction 2-2 missing), and sample 6 (fraction 2-3 missing). Bars with unlike letters at the same concentration are significantly different ($p < 0.05$).

We obtained good separation of fraction 2-2 by adjusting the HPLC elution program as follows: the mobile phase consisted of 0.4% formic acid mixed with double distilled water (solvent A) and methanol/acetonitrile (50:50, v/v) (solvent B); the gradient program started from 0 min (5% B) to 10 min (25% B) and 20 min (32% B) and then was re-equilibrated for 10 min with 5% B for the next analysis. The HPLC fingerprint of fraction 2-2 was finally obtained with favorable separation.

Likewise, peaks 1−8 in fraction 2-2 were knocked out one by one. By comparison of the obtained chromatograms (Figure 6),

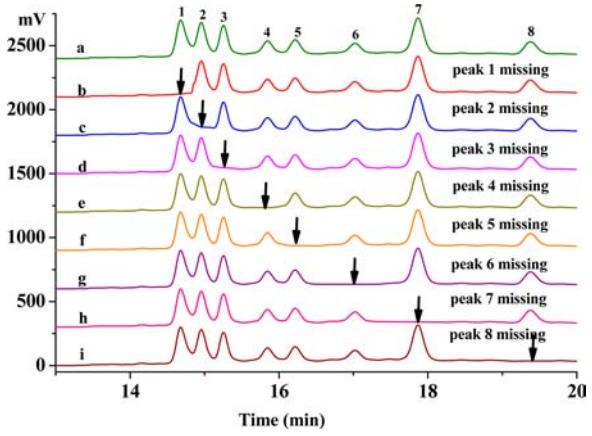


**Figure 6.** Chromatograms of peak knockout under the same HPLC conditions: (a) chromatogram with fraction 2-2, (b) chromatogram with peak 1 knockout, (c) chromatogram with peak 2 knockout, (d) chromatogram with peak 3 knockout, (e) chromatogram with peak 4 knockout, (f) chromatogram with peak 5 knockout, (g) chromatogram with peak 6 knockout, (h) chromatogram with peak 7 knockout, and (i) chromatogram with peak 8 knockout.

it was obvious that the target peaks in fraction 2-2 were knocked out completely. Similarly, DPPH and ORAC assays were used to screen and evaluate the possible target bioactive compounds in fraction 2-2. The scavenging rates of all of the collections with target peaks missing were summarized in Table 3. The DPPH scavenging property of each collection declined as follows: collections 8 (peak 8 missing) > 7 (peak 7 missing) > 2 (peak 2 missing) > 3 (peak 3 missing) > 5 (peak 5 missing) > 6 (peak 6 missing) > 4 (peak 4 missing) > 1 (peak 1 missing), consistent with the results of contribution rates

**Table 3. Scavenging Rate and Activity Loss of Fraction 2-2 and Different Collections against the DPPH Radical[a]**

| collection by online knockout | scavenging rate (%) | activity loss (%) |
|---|---|---|
| fraction 2-2 | 81.54 ± 0.008 a | |
| collection 1 (peak 1 missing) | 28.37 ± 0.007 h | 65.20 ± 0.009 a |
| collection 2 (peak 2 missing) | 54.55 ± 0.008 d | 33.10 ± 0.01 e |
| collection 3 (peak 3 missing) | 41.72 ± 0.007 e | 48.83 ± 0.009 d |
| collection 4 (peak 4 missing) | 34.23 ± 0.008 g | 58.02 ± 0.01 b |
| collection 5 (peak 5 missing) | 40.19 ± 0.005 f | 50.71 ± 0.006 c |
| collection 6 (peak 6 missing) | 35.16 ± 0.011 g | 56.88 ± 0.013 b |
| collection 7 (peak 7 missing) | 57.27 ± 0.008 c | 29.77 ± 0.01 f |
| collection 8 (peak 8 missing) | 69.31 ± 0.007 b | 15.00 ± 0.009 g |

[a]The data are expressed as the mean ± SD ($n = 3$). Mean values in the same column with different letters are significantly different ($p < 0.05$).

(peaks 1 > 4 > 6 > 5 > 3 > 2 > 7 > 8). It was evident that peaks 1, 4, and 6 performed a great contribution to the total antioxidant activity of fraction 2-2. Besides, the contribution rates of peaks 5 and 3 were 50.71 and 48.83%, respectively, which were a little lower than those of peaks 1, 4, and 6. However, very limited decreases on the DPPH-scavenging effects of collections with peaks 2, 7, and 8 knockout were observed, revealing that the three peaks had a small contribution to the bioactivity of fraction 2-2 in comparison to other peaks.

The ORAC assay was used to further confirm the contribution of each peak to the antioxidant activity of fraction 2-2. As illustrated in Figure 7, the ORAC value of each

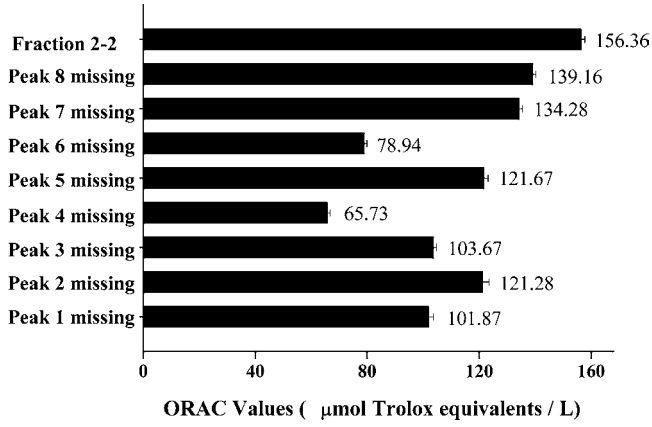


**Figure 7.** ORAC values of fraction 2-2 and different collections with target peak knockout. All of the results are expressed as micromoles of Trolox equivalents per liter.

collection was in the following order: collections 8 (peak 8 missing) > 7 (peak 7 missing) > 5 (peak 5 missing) > 2 (peak 2 missing) > 3 (peak 3 missing) > 1 (peak 1 missing) > 6 (peak 6 missing) > 4 (peak 4 missing), demonstrating that the contribution of each peak to the antioxidant activity of fraction 2-2 declined as follows: peaks 4 > 6 > 1 > 3 > 2 > 5 > 7 > 8. The minor discrepancy between the results of DPPH and ORAC assays may be due to the different systems.[2,24] Taken together, DPPH and ORAC analyses suggested that peaks 1, 4, and 6 could be the main contributors to the total antioxidant activity of fraction 2-2. These specific bioactive compounds may represent the remarkable antioxidant effect of polyphenols in longan seeds.


dx.doi.org/10.1021/jf502995z | J. Agric. Food Chem. 2014, 62, 9744−9750

Table 4. HPLC−ESI−MS Analysis for Individual Phenolic Compounds of Fraction 2-2 of Longan Seed Extract

| peak number | retention time (min) | $[M - H]^-$ ($m/z$) | $MS^2$ ions ($m/z$) | compound |
|---|---|---|---|---|
| 1 | 13.41 | 291 | 247, 205, 161 | unknown |
| 2 | 13.63 | 291 | 247, 205, 161 | unknown |
| 3 | 14.01 | 633 | 463, 301, 275 | corilagin |
| 4 | 14.65 | 387 | 369, 207, 163, 119 | *p*-coumaric acid glycoside |
| 5 | 14.91 | 469 | 425, 301 | (*S*)-flavogallonic acid |
| 6 | 15.77 | 611 | 397, 301, 229 | ellagic acid derivative |
| 7 | 16.61 | 477 | 462, 301, 169 | methyl-ellagic acid glucopyranoside |
| 8 | 17.97 | 197 | 169, 125 | ethyl gallate |

Therefore, we used HPLC−ESI−MS to explore the structures of peaks 1−8 in fraction 2-2. The results are summarized in Table 4.

HPLC−MS analysis in negative-ion mode revealed that peaks 1 and 2 had a common molecular mass and fragmentation pattern, suggesting a pair of isomers. The molecular ion $[M - H]^-$ was observed at $m/z$ 291. Fragment ions were found at $m/z$ 247, 205, and 161 in the $MS^2$ spectrum. The fragment at $m/z$ 247 corresponded to a loss of 44 amu resulting from the elimination of a $CO_2$ molecule from the molecular ion. The fragment ion at $m/z$ 205 was derived from the loss of two ethenone, and the fragment ion at $m/z$ 161 came from the further loss of a $CO_2$ molecule. The ESI−MS fragmentation patterns of peaks 1 and 2 were very similar to that of catechin but with dominant peaks Δ2 amu larger than that of catechin. It was reported to exist in strawberry fruits in a previous study,[25] but the detailed structure was unknown.

Peak 3 showed a distinct molecular ion at $m/z$ 633, and its three characteristic $MS^2$ fragments ions were observed at $m/z$ 463, 301, and 275, indicating that it was galloyl-HHDP-glucopyranose (corilagin).[21] The fragment at $m/z$ 463 was attributed to the loss of a galloyl unit from the parent molecule, and the ion at $m/z$ 301 was defined as ellagic acid.[26] It was also reported to be one of the major polyphenol components of longan seeds by Sudjaroen et al.[18]

The molecular ion of peak 4 was at $m/z$ 387. Four characteristic fragment ions were found at $m/z$ 369, 207, 163, and 119, in the $MS^2$ spectrum of $m/z$ 387. The first fragment ion ($[M - H - 18]^-$) at $m/z$ 369 resulted from the elimination of a water molecule from the parent molecule. The fragment ions at $m/z$ 207 ($[M - H - 18 - 162]^-$) and $m/z$ 163 ($[M - H - 18 - 162 - 44]^-$) corresponded to the further loss of a glucosyl moiety and the continuing loss of a $CO_2$ molecule. The fragment ion at $m/z$ 163, with its typical production ion at $m/z$ 119, was identified as *p*-coumaric acid.[27,28] Thus, it was deduced that peak 4 was probably a *p*-coumaric acid−glucose conjugate linked by a carboxyl group, but further work is needed to verify the structure of this compound.

Peak 5 presented a molecular ion $[M - H]^-$ at $m/z$ 469 with two characteristic $MS^2$ fragment ions at $m/z$ 425 and 301, respectively. The former came from the neutral loss of $CO_2$, and the latter was identified as ellagic acid at $m/z$ 301. On the basis of the mass spectra data,[23] peak 5 was identified as (*S*)-flavogallonic acid.

Peak 6 showed a molecular ion at $m/z$ 611 and two strong fragment ions at $m/z$ 397 and 301. Besides, the fragment ion at $m/z$ 229 was observed, which is indicative of the presence of ellagic acid ($m/z$ 301). Because no more structural information was available, we deduced that this compound could be an ellagic acid derivative.

Peak 7, with a $m/z$ of 477, was identified as methyl-ellagic acid glucopyranoside on the basis of a previous study[29] and the observed mass spectra. The fragment ions at $m/z$ 462 ($[M - H - 15]^-$) and $m/z$ 301 ($[M - H - 15 - 161]^-$) corresponded to the loss of a methyl unit and a glucosyl unit, respectively. Ellagic acid at $m/z$ 301 was also identified.

Peak 8, with a $m/z$ of 197, was determined to be ethyl gallate, which yielded the characteristic fragment ion at $m/z$ 169 (gallic acid) by losing an ethyl unit. The fragment ion at $m/z$ 125 resulted from the continuing loss of $CO_2$, further confirming the proposed structure.[30,31] This compound was previously identified in longan seeds by Zheng et al.[2]

In summary, the combination of FT-ICR−MS analysis, HPLC−ESI−MS analysis, online fishing or knockout, and antioxidant-based screening strategies was used to screen the key phenolic compounds accounting for the potent antioxidant effects of longan seeds for the first time. Ellagic acid and its derivative were proven to have important contribution to the antioxidant activity of LSPs. A new compound, probably *p*-coumaric acid-glycoside, had the greatest contribution to the antioxidant capacity of LSPs, while gallic acid, corilagin, (*S*)-flavogallonic acid, methyl-ellagic acid glucopyranoside, and ethyl gallate did not affect the potent antioxidant activity of LSPs, showing a small contribution to the total bioactivity. Further work on the detailed structures of the newly found phenolic compounds of *p*-coumaric acid-glycoside and ellagic acid derivative with high antioxidant activity and their structure−activity relationships is needed.

## AUTHOR INFORMATION

### Corresponding Author

*Telephone/Fax: 86-27-87282966. E-mail: lichmyl@mail.hzau.edu.cn.

### Funding

This study was supported by the National Science and Technology Pillar Program during the 12th Five-Year Plan Period (2012BAD31B03), the Chinese Ministry Program for New Century Excellent Talents in University (NCET-12-0865), and the Fundamental Research Funds for the Central Universities (2013PY022).

### Notes

The authors declare no competing financial interest.

## REFERENCES

(1) Rangkadilok, N.; Sitthimonchai, S.; Worasuttayangkurn, L.; Mahidol, C.; Ruchirawat, M.; Satayavivad, J. Evaluation of free radical scavenging and antityrosinase activities of standardized longan fruit extract. *Food Chem. Toxicol.* **2007**, *45*, 328−336.

(2) Zheng, G.; Xu, L.; Wu, P.; Xie, H.; Jiang, Y.; Chen, F.; Wei, X. Polyphenols from longan seeds and their radical-scavenging activity. *Food Chem.* **2009**, *116*, 433−436.

(3) Soong, Y. Y.; Barlow, P. J. Isolation and structure elucidation of phenolic compounds from longan (*Dimocarpus longan* Lour.) seed by high-performance liquid chromatography−electrospray ionization mass spectrometry. *J. Chromatogr. A* **2005**, *1085*, 270−277.
(4) Rangkadilok, N.; Worasuttayangkurn, L.; Bennett, R. N.; Satayavivad, J. Identification and quantification of polyphenolic compounds in longan (*Euphoria longana* Lam.) fruit. *J. Agric. Food Chem.* **2005**, *53*, 1387−1392.
(5) Soong, Y.-Y.; Barlow, P. J. Antioxidant activity and phenolic content of selected fruit seeds. *Food Chem.* **2004**, *88*, 411−417.
(6) Soong, Y.; Barlow, P. Quantification of gallic acid and ellagic acid from longan (*Dimocarpus longan* Lour.) seed and mango (*Mangifera indica* L.) kernel and their effects on antioxidant activity. *Food Chem.* **2006**, *97*, 524−530.
(7) Liu, Y.; Zhou, J. L.; Liu, P.; Sun, S.; Li, P. Chemical markers' fishing and knockout for holistic activity and interaction evaluation of the components in herbal medicines. *J. Chromatogr. A* **2010**, *1217*, 5239−5245.
(8) Wu, J.-H.; Huang, C.-Y.; Tung, Y.-T.; Chang, S.-T. Online RP-HPLC−DPPH screening method for detection of radical-scavenging phytochemicals from flowers of *Acacia confusa*. *J. Agric. Food Chem.* **2007**, *56*, 328−332.
(9) Bandoniene, D.; Murkovic, M. On-line HPLC−DPPH screening method for evaluation of radical scavenging phenols extracted from apples (*Malus domestica* L.). *J. Agric. Food Chem.* **2002**, *50*, 2482−2487.
(10) Xu, X.; Xie, B.; Pan, S.; Yang, E.; Wang, K.; Cenkowski, S.; Hydamake, A. W.; Rao, S. A new technology for extraction and purification of proanthocyanidins derived from sea buckthorn bark. *J. Sci. Food Agric.* **2006**, *86*, 486−492.
(11) Dudonne, S.; Vitrac, X.; Coutiere, P.; Woillez, M.; Merillon, J.-M. Comparative study of antioxidant properties and total phenolic content of 30 plant extracts of industrial interest using DPPH, ABTS, FRAP, SOD, and ORAC assays. *J. Agric. Food Chem.* **2009**, *57*, 1768−1774.
(12) Ozgen, M.; Reese, R. N.; Tulio, A. Z.; Scheerens, J. C.; Miller, A. R. Modified 2,2-azino-bis-3-ethylbenzothiazoline-6-sulfonic acid (ABTS) method to measure antioxidant capacity of selected small fruits and comparison to ferric reducing antioxidant power (FRAP) and 2,2′-diphenyl-1-picrylhydrazyl (DPPH) methods. *J. Agric. Food Chem.* **2006**, *54*, 1151−1157.
(13) Cervato, G.; Carabelli, M.; Gervasio, S.; Cittera, A.; Cazzola, R.; Cestaro, B. Antioxidant properties of oregano (*Origanum vulgare*) leaf extracts. *J. Food Biochem.* **2000**, *24*, 453−465.
(14) Goupy, P.; Dufour, C.; Loonis, M.; Dangles, O. Quantitative kinetic analysis of hydrogen transfer reactions from dietary polyphenols to the DPPH radical. *J. Agric. Food Chem.* **2003**, *51*, 615−622.
(15) Huang, D.; Ou, B.; Hampsch-Woodill, M.; Flanagan, J. A.; Prior, R. L. High-throughput assay of oxygen radical absorbance capacity (ORAC) using a multichannel liquid handling system coupled with a microplate fluorescence reader in 96-well format. *J. Agric. Food Chem.* **2002**, *50*, 4437−4444.
(16) Aharoni, A.; Ric de Vos, C.; Verhoeven, H. A.; Maliepaard, C. A.; Kruppa, G.; Bino, R.; Goodenowe, D. B. Nontargeted metabolome analysis by use of Fourier transform ion cyclotron mass spectrometry. *OMICS* **2002**, *6*, 217−234.
(17) Gougeon, R. D.; Lucio, M.; Frommberger, M.; Peyron, D.; Chassagne, D.; Alexandre, H.; Feuillat, F.; Voilley, A.; Cayot, P.; Gebefügi, I. The chemodiversity of wines can reveal a metabologeography expression of cooperage oak wood. *Proc. Natl. Acad. Sci. U. S. A.* **2009**, *106*, 9174−9179.
(18) Sudjaroen, Y.; Hull, W. E.; Erben, G.; Wurtele, G.; Changbumrung, S.; Ulrich, C. M.; Owen, R. W. Isolation and characterization of ellagitannins as the major polyphenolic components of Longan (*Dimocarpus longan* Lour.) seeds. *Phytochemistry* **2012**, *77*, 226−237.
(19) Atoui, A. K.; Mansouri, A.; Boskou, G.; Kefalas, P. Tea and herbal infusions: Their antioxidant activity and phenolic profile. *Food Chem.* **2005**, *89*, 27−36.
(20) Li, C.; Leverence, R.; Trombley, J. D.; Xu, S.; Yang, J.; Tian, Y.; Reed, J. D.; Hagerman, A. E. High molecular weight persimmon (*Diospyros kaki* L.) proanthocyanidin: A highly galloylated, A-linked tannin with an unusual flavonol terminal unit, myricetin. *J. Agric. Food Chem.* **2010**, *58*, 9033−9042.
(21) Hager, T. J.; Howard, L. R.; Liyanage, R.; Lay, J. O.; Prior, R. L. Ellagitannin composition of blackberry as determined by HPLC−ESI−MS and MALDI−TOF−MS. *J. Agric. Food Chem.* **2008**, *56*, 661−669.
(22) Li, S.; Xiao, J.; Chen, L.; Hu, C.; Chen, P.; Xie, B.; Sun, Z. Identification of A-series oligomeric procyanidins from pericarp of *Litchi chinensis* by FT-ICR−MS and LC−MS. *Food Chem.* **2012**, *135*, 31−38.
(23) Pfundstein, B.; El Desouky, S. K.; Hull, W. E.; Haubner, R.; Erben, G.; Owen, R. W. Polyphenolic compounds in the fruits of Egyptian medicinal plants (*Terminalia bellerica*, *Terminalia chebula* and *Terminalia horrida*): Characterization, quantitation and determination of antioxidant capacities. *Phytochemistry* **2010**, *71*, 1132−1148.
(24) Hsieh, M.-C.; Shen, Y.-J.; Kuo, Y.-H.; Hwang, L. S. Antioxidative activity and active components of longan (*Dimocarpus longan* Lour.) flower extracts. *J. Agric. Food Chem.* **2008**, *56*, 7010−7016.
(25) Simirgiotis, M. J.; Theoduloz, C.; Caligari, P. D.; Schmeda-Hirschmann, G. Comparison of phenolic composition and antioxidant properties of two native Chilean and one domestic strawberry genotypes. *Food Chem.* **2009**, *113*, 377−385.
(26) Lee, J.-H.; Johnson, J. V.; Talcott, S. T. Identification of ellagic acid conjugates and other polyphenolics in muscadine grapes by HPLC−ESI−MS. *J. Agric. Food Chem.* **2005**, *53*, 6003−6010.
(27) Owen, R.; Haubner, R.; Hull, W.; Erben, G.; Spiegelhalder, B.; Bartsch, H.; Haber, B. Isolation and structure elucidation of the major individual polyphenols in carob fibre. *Food Chem. Toxicol.* **2003**, *41*, 1727−1738.
(28) Fang, N.; Yu, S.; Prior, R. L. LC/MS/MS characterization of phenolic constituents in dried plums. *J. Agric. Food Chem.* **2002**, *50*, 3579−3585.
(29) He, N.; Wang, Z.; Yang, C.; Lu, Y.; Sun, D.; Wang, Y.; Shao, W.; Li, Q. Isolation and identification of polyphenolic compounds in longan pericarp. *Sep. Purif. Technol.* **2009**, *70*, 219−224.
(30) Lee, R. J.; Lee, V. S.; Tzen, J. T.; Lee, M. R. Study of the release of gallic acid from (−)-epigallocatechin gallate in old oolong tea by mass spectrometry. *Rapid Commun. Mass Spectrom.* **2010**, *24*, 851−858.
(31) Yilmaz, Y.; Toledo, R. T. Major flavonoids in grape seeds and skins: Antioxidant capacity of catechin, epicatechin, and gallic acid. *J. Agric. Food Chem.* **2004**, *52*, 255−260.

However, one of the questions that arise when phenolic compounds are esterified as the polar head of phospholipids would be whether the derived structure would be digested and bioaccesible during gastrointestinal digestion, as the first step before any other physiological action beyond intestinal tissues.

The *in vitro* intestinal models of lipid digestion are an interesting tool for obtaining preliminary and valuable information concerning digestion of lipid species. Due to their utility, the use of *in vitro* digestion models in the study of bioactive compounds has increased, becoming a well-accepted analytical tool.[18] However, as far as we know, all the models of *in vitro* lipid digestion have been developed for the major lipid dietary forms, namely, triglycerides (TG), whereas the *in vitro* digestion models focused on phospholipids have not been extensively investigated. In general, we consider that the development of a model that closely simulates the *in vivo* conditions is especially essential when performing the digestion of novel or unknown lipids under *in vitro* conditions, in order to accurately understand obtained results and to avoid misinterpretations due to the own methodology used. Therefore, a reliable *in vitro* digestion model for phospholipids should be previously developed before the application of the model to the experimental molecule PHT.

Concerning the general digestion process of phospholipids, this is mainly catalyzed by the enzyme phospholipase A2 (PLA2) at the intestinal level, which hydrolyzes fatty acids from the sn-2 location almost completely to release lyso-phospholipids and free fatty acids (FFA).[17] After hydrolysis, a high bioaccessibility has been described for phospholipids, which means that their lipid products are easily solubilized within the micellar phase for absorption.[17] Together with the simulation of these events and results, an *in vitro* model of intestinal digestion of phospholipids should also take into account the coexistence of dietary exogenous phospholipids together with endogenous biliary phospholipids. Furthermore, the simultaneous presence of other dietary fats together with phospholipids should also be considered, in order to mimick a real intake of dietary lipids, where phospholipids are minor compounds compared to TG.

Therefore, the aim of the present research was to perform a simulation of the intestinal digestion of PHT under *in vitro* conditions. First, the *in vitro* intestinal digestion model was optimized for the digestion of phospholipids, in order to be certain that the model reflected physiological intestinal digestion for these compounds, and to reject that any artifact or the own conditions of the digestion method would not interfere with the results obtained for PHT. Furthermore, the bioaccessibility of HT esterified as PHT after digestion was compared with that of free HT, or HT premixed with phospholipids. Finally, the impact of digestion on the antioxidant ability of PHT compared to HT was also assayed.

## MATERIALS AND METHODS

**Reagents and Materials.** HT (purity higher than 90% w/w) was acquired from Seprox Biotech (Madrid, Spain). PHT (86% PHT, 8% HT, and 6% fully hydrogenated phosphatidylcholine) was synthesized by enzymatic transphosphatidilation of HT and phosphatidylcholine (Phospholipon 90H, Lipoid, Switzerland). The detailed procedure of the synthesis of PHT was already described.[15] A commercial olive oil was used as a representative of dietary typical oil.

Trizma, maleic acid, pancreatin from porcine pancreas, bile salts, and ammonium hydroxide solution 30% were from Sigma-Aldrich Chemie GmbH (Steinheim, Germany). Phosphatidylcholine (PC) from egg yolk (98%) was purchased from Lipoid (Ludwigshafen, Germany). Sodium sulfate anhydrous, sodium chloride, calcium chloride, and ethanol absolute were purchased from Panreac (Barcelona, Spain). Ortho-phosphoric acid was purchased from Scharlab (Sentmenat, Barcelona). All solvents used were of HPLC grade from Lab-Scan (Dublin, Ireland).

***In Vitro* Lipid Digestion.** A previously developed model for TG[19] was adapted to simulate the simultaneous presence of dietary TG, dietary phospholipids, and endogenous biliary phospholipids. Briefly, the adapted model consisted of a sample of 0.5 g of olive oil and 0.1 g of phospholipid which were mixed with 16 mL of Trizma−maleate buffer 0.1 M pH 7.5. In the case of control digestions and optimization of the *in vitro* model, the sample was the same phospholipid used for the synthesis of PHT (Phospholipon 90H, PL). In the case of PHT, this was added at the same equivalent weight used for the digestion of PL. The prepared medium was pre-emulsified by homogenization for 2 min at 3500 rpm.

On the other hand, a solution trying to simulate biliary secretion was prepared by mixing 0.1 g of PC, 0.25 g of bile salts, 0.02 g of cholesterol, 0.5 mL of a 325 mM $CaCl_2$ solution, 1.5 mL of a 3.25 mM NaCl solution, and 10 mL of Trizma−maleate buffer, and this mixture was homogenized for 2 min at 3500 rpm. Then, the pre-emulsified sample and the simulated biliary secretion were mixed and homogenized together for 2 min at 3500 rpm. The whole media was placed in a thermostatically controlled vessel at 37 °C and continuously stirred by a magnetic stir bar at 1000 rpm. The simulation of intestinal digestion was started by the addition of fresh pancreatin extract (0.5 g of pancreatine in 3 mL of Trizma−maleate buffer, stirred for 10 min and centrifuged at 1600 × *g* for 15 min). The enrichment with PLA2 was carried out by addition of 5 mg of a food grade PLA2 from *Streptomyces violaceoruber* ($10^3$ U/mg) from Nagase Chemtex Corporation (Fukuchiyama Factory, Kyoto, Japan). After addition of enzymes, reaction was continued for 60 min. In order to study the evolution of lipid products throughout the hydrolytic process, aliquots were taken at 0, 5, 10, 30, and 60 min of reaction.

Additional digestions were performed in order to compare the bioaccessibility of PHT with that of HT, or with that of a premixed HT with a dose of dietary PL (HT+PL). In both cases, HT was added to the media at equivalent weights as those added by PHT. Furthermore, in both cases, the coexistence with olive oil was kept.

*In vitro* digestion of each experiment was performed at least in triplicate.

**Separation of Phases after in Vitro Lipid Digestion.** At the end of digestion, the medium was submitted to centrifugation at 4000 rpm for 40 min at 37 °C (5810R Eppendorf Iberica, Madrid, Spain) according to Soler-Rivas et al.[20] After centrifugation, an upper oily phase (OP), a lower aqueous or micellar phase (MP), and a minor precipitated phase (PP) were obtained. The lipid composition of each phase was analyzed. In the case of the MP, aliquots were collected for quantification of micellar structures by using a light microscope and a Neubauer cell counter chamber (Brand, Germany).[20]

**Lipid Extraction.** The total lipids from samples were extracted twice by a mixture of chloroform/methanol/ortho-phosphoric acid (100:80:4, v/v/v) at a ratio of solvent to sample of 3:1 (v/v). Ortho-phosphoric acid was necessary for a proper recovery of the lyso-PL species. The mixture was vortexed for 1 min and centrifuged for 10 min at 13500 rpm (ScanSpeed mini, Micro Centrifuge). The organic phase containing the separated lipids was collected, and anhydrous sodium sulfate was added before further analysis.

**Analysis of Lipid Products.** *Polar Lipids.* The polar lipid composition was determined on a Luna 5 μm HILIC diol column (250 mm, 4.6 mm, Phenomenex, Torrance, California, USA) coupled to an HPLC Agilent 1200 Series containing a thermostatized column compartment, a quaternary pump, an autosampler, a vacuum degasser, and an evaporative light scattering detector. The used method was based on Casado et al.[15] with brief modifications. The flow rate was 1.5 mL $min^{-1}$. A splitter valve was used after the thermostatized column compartment and part of the mobile phase was directed through the detector (3.5 bar and 55 °C). The column temperature was maintained at 55 °C. The mobile phase utilized consisted of a ternary gradient of (A) hexane/2-propanol/acetic acid/triethylamine (815/

170/15/0.5 v/v/v/v), (B) 2-propanol/Milli-Q $H_2O$/acetic acid/triethylamine (840/140/15/0.5 v/v/v/v), and (C) hexane. The method starts at 50% A and 50% C increasing up to 100% A in 5.1 min, and reaching 12% B and 88% A in 20 min. This percentage is maintained for 15 min, and then is changed up to 40% B and 60% A in 0.5 min. Finally, the gradient returns to initial conditions and is maintained for 20 min.

This methodology was used to analyze phospholipid and lysophospholipid species, HT, and bile salts. Identification and quantification was carried out by using standards for each lipid class. In the case of lyso-PHT, a purification procedure of this standard was previously necessary as described later. In order to minimize error when using HPLC with ELSD, rigorous calibration curves utilizing the appropriated standards were developed for each set of samples injected, since the detector response was nonlinear and specific to each compound.

*Neutral Lipids.* The neutral lipids composition was determined on an Agilent poroshell 120 (2.7 $\mu$m, 100 × 4.6 mm$^2$) coupled to an HPLC Agilent 1200 Series (Avondale, PA) containing a thermostated column compartment (35 °C), a quaternary pump, an autosampler, a vacuum degasser, and an evaporative light scattering detector (ELSD). Conditions of the ELSD were 3.5 bar and 35 °C. A split valve was used after the column, and only 50% of the mobile phase was directed through the detector. The column temperature was maintained at 35 °C. The ternary gradient has already been detailed by Vazquez, Fernandez, Martin, Reglero, and Torres.[21]

This methodology was used to analyze TG, diglycerides (DG), monoglycerides (MG), and FFA. Identification and quantification was carried out by using standards for each lipid class. In order to minimize error when using HPLC with ELSD, rigorous calibration curves utilizing appropriated commercial standards were developed for each set of samples injected, since the detector response was nonlinear and specific to each compound.

**Purification of Lyso-PHT for Analysis of Digestion Products.** For a proper quantification of digestion products from PHT, the major hydrolysis product lyso-PHT was necessary as pure as possible to perform the corresponding standard calibration curves. To obtain this standard, it was necessary to (1) develop a protocol to hydrolyze PHT to lyso-PHT up to enough amounts necessary for the study and (2) develop a protocol for the subsequent purification of the released lyso-PHT.

*Hydrolysis Reaction of PHT to Lyso-PHT.* Taking the digestion model of PL as a reference, diverse modifications were performed in order to reach as complete hydrolysis as possible of PHT up to lyso-PHT. Preliminary assays showed that either other lipids in the medium, as well as other surface active agents, such as bile salts or MG, were necessary for a proper hydrolysis of PL and PHT in general. Therefore, olive oil was kept in the reaction, and MG was used instead of bile salts. This was done because the later separation of bile salts from lyso-PHT and lyso-PL in general during the purification procedure was complicated, contrary to isolation from MG.

Briefly, the hydrolysis medium consisted of 80 mg of PHT mixed with 80 mg of olive oil, 60 mg of MG, 0.4 mL of $CaCl_2$ (325 mM), 1.2 mL of NaCl (3.25 mM), and 20.6 mL of Trizma−maleate buffer pH 7.5. The mixture was homogenized (Ultra-Turrax IKA T18) for 4 min at 3500 rpm. The reaction was started with the addition of fresh pancreatin extract (0.3 g of pancreatin in 1.8 mL of Trizma−maleate buffer pH 7.5, stirred for 10 min and centrifuged at 1600 g for 15 min) and PLA2 solution (0.2 g of PLA2 in 2 mL of Trizma−maleate buffer pH 7.5, vortexed for 1 min). The hydrolysis reaction was performed in a thermostatically controlled shaker (IKA KS 4000 ic control) at 37 °C and 250 rpm for 120 min. Finally, the total lipids from the reaction were extracted by chloroform/methanol (2:1, v/v) for subsequent analysis and purification. Under these conditions, around 95% of PHT was hydrolyzed to lyso-PHT and FFA.

*Purification of Lyso-PHT by SPE.* After the hydrolysis reaction, the obtained mixture of lipid compounds consisted of FFA (45%) and lyso-PHT (35%) as major products, together with minor levels of residual PHT, lyso-PL, and MG. The purification of lyso-PHT was performed by SPE. The method of Mateos et al.[22] to separate phenolic compounds of vegetable oils was combined with the method of Carelli et al.[23] to separate classes of phospholipids of vegetable oils.

Initially, the procedure of Mateos et al.[22] was followed. Briefly, a 500 mg diol-bonded phase cartridge (Isolute, Biotage, UK) was conditioned with 6 mL of methanol and 6 mL of hexane, consecutively. The lipid sample (1 mL, 40 mg/mL in chloroform) was added to the cartridge. Most glycerides (mainly MG, and residual DG and TG in case) were first eluted with 6 mL of hexane. Then, most FFA were eluted with 4 mL of hexane: ethyl acetate (90:10, v/v). The next step of the method of Mateos et al.[22] used methanol for elution of phenolic compounds. However, we modified this step by mixing methanol with ammonium hydroxide (15 mL of methanol/ammonium hydroxide solution 99.5:0.5, v/v) for the proper elution of the polar lipids (lyso-PHT, lyso-PL, and residual PHT), according to the procedure of Carelli et al.[23] This modification was necessary because it was tested that only methanol was not useful to elute lyso-PHT, although it effectively eluted HT. Only the mixture with ammonium hydroxide allowed a proper recuperation of lyso-PHT. Curiously, the complete method of Carelli et al.[23] (without combination with the method of Mateos et al.[22]) was not useful for recovering lyso-PHT, although we tested that it was effective for lyso-PL purification. Finally, we found that the combination of the first steps of the method of Mateos et al.[22] with the last step of Carelli et al.[23] were the most proper conditions to a successful recovery of lyso-PHT. At the end of the procedure, the solvent fraction containing polar lipids was evaporated under $N_2$ at 40 °C and redissolved in chloroform/methanol (2:1 v/v) for subsequent analysis. The purity of the lyso-PHT product obtained by the developed protocol was closer to 80%, together with minor levels of FFA, MG, and lyso-PL.

**Antioxidant Activity of Compounds by DPPH Test.** The antioxidant activity of the intestinal medium containing PHT or HT was measured at 0 and 60 min of digestion by DPPH test. An aliquot (50 $\mu$L) of ethanol solution containing 5−30 $\mu$g/mL of intestinal media was added to 1950 $\mu$L of DPPH in ethanol (23.5 $\mu$g/mL). The reaction was completed after 90 min at room temperature and darkness, and absorbance was measured at 517 nm. The remaining DPPH concentration in the reaction medium was estimated by proper calibration curves of DPPH. The scavenging activities were expressed as 50% of inhibitory concentration (EC50), which denotes the concentration of HT (mM) (expressed as the equivalent concentration of HT in PHT) required for giving a 50% reduction of DPPH concentration relative to that of a DPPH control.

Control experiments of the digestion media in the absence of the tested compounds were also performed, and the lack of change in DPPH concentration was measured.

**Statistical Analysis.** Statistical analyses were performed by means of the general linear model procedure of the SPSS 17.0 statistical package (SPSS Inc., Chicago, IL, USA) by one-way analysis of variance. Differences were considered significant at $p \leq 0.05$. Posthoc Tukey's tests were performed in order to establish significant differences.

## RESULTS AND DISCUSSION

**Development of an *in Vitro* Intestinal Model for Digestion of Phospholipids.** Previous to *in vitro* digestion of PHT, an intestinal digestion model for phospholipids was first developed, in order to be certain that the model reflected the physiological intestinal lipid digestion of these lipids, and to reject that any artifact or the own conditions of the digestion method would not interfere with the results obtained for the PHT hydrolysis.

One of the main problems to optimize a reliable *in vitro* model for phospholipids is the imprecise data in the scientific literature on basic and general parameters such as the typical hydrolysis degree of these lipids, the habitual amount of luminal phospholipids and PLA2, or the exact degree of bioaccessibility. Therefore, as a reference of physiological criteria, we considered the data of Borgström[17] that stated that

phospholipids are absorbed efficiently, that conversion to lysophospholipids is essential for absorption to occur, and that the luminal concentration of PLA2 is high enough for hydrolysis to lysophospholipids.

A previously developed model for TG[19] was adopted as a starting point. Such a model was considered useful because we already demonstrated that it closely reflected the physiological results found in the intraluminal phase in man during fat digestion, namely, TG. However, some modifications would be necessary in order to simulate a proper digestion for phospholipids.

The developed model for intestinal digestion of TG uses the pancreatin as the source of digestive enzymes. Pancreatin is a pancreatic extract that contains most of the digestive enzymes responsible for digestion of major macromolecules at intestinal lumen. In the specific case of lipid digestion, pancreatic lipase is the major enzyme found in pancreatin. Although pancreatic lipase may partially hydrolyze phospholipids, most hydrolysis is catalyzed by PLA2. However, both the presence and the level of PLA2 in pancreatin for proper hydrolysis are not stated in the product specifications.

On the other hand, the developed digestion model for TG was adapted to simulate the simultaneous presence of dietary exogenous phospholipids and TG, as well as endogenous biliary phospholipids. Concerning exogenous dietary phospholipids, those were included at a proper ratio to TG. This is difficult data to establish, because the dietary intake of phospholipids reported in the scientific literature is quite variable, taking into account the variable amount of phospholipids that can be found depending on a meal. Thus, ratios from 1 to 10% of total daily fat intake has been reported.[16,24] A high-phospholipid meal was simulated in the model. Concerning endogenous biliary phospholipids, the included dose was proportional to bile salts and cholesterol, taking into account the gallbladder bile lipid secretion during a fed state.[25]

Furthermore, a separation of the preparation of both fractions of phospholipids at different stages was considered. This is because exogenous phospholipids are found mixed with TG in the aqueous digestion medium, where the phospholipids are found as a surface component of the TG emulsion.[17] On the other hand, the endogenous phospholipids are found as a dispersion in bile salts as lamellar aggregates or mixed micellar aggregates.[17] Therefore, we considered that such different phases should be prepared separately, trying to simulate the pre-emulsion of dietary lipids that would enter later the intestinal lumen to be mixed with the preformed biliary secretion.

Figure 1a shows the *in vitro* digestion initially performed by the use of pancreatin. As shown, the level of pancreatin effectively hydrolyzed TG forms up to the physiologically considered level at duodenal lumen; namely, around 75% was degraded to the main hydrolysis products (FFA and MG). On the contrary, both the hydrolysis of phospholipids and the level of the product lysophospholipids were minor, suggesting that pancreatin does not have enough hydrolytic activity to effectively digest phospholipids. Therefore, the enrichment with PLA2 was considered necessary.

As far as we know, previous information on typical physiological levels of PLA2 has not been clearly reported, so we considered as criteria of PLA2-dose optimization the statement of Borgstrom,[17] who suggested that the luminal concentration of PLA2 is high enough for a complete hydrolysis of phospholipids to lysophospholipids. Therefore, several

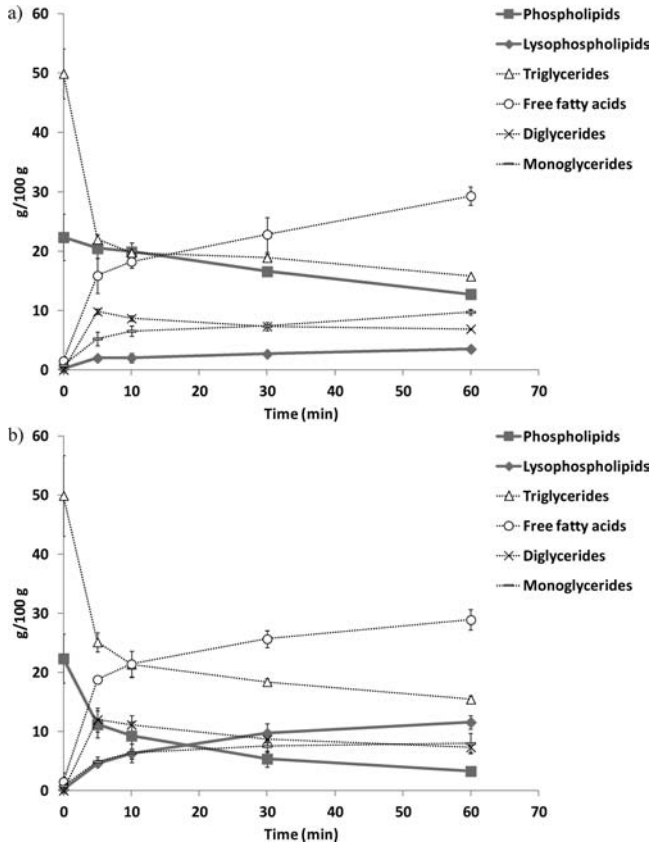


**Figure 1.** Course of *in vitro* intestinal digestion by (a) pancreatin or (b) PLA2-enrichment of pancreatin.

commercial PLA2's added at variable levels were tested (data not shown) up to reaching a quantitative hydrolysis level of phospholipids. As shown in Figure 1b, the final optimized method with a proper dose of PLA2 progressively hydrolyzed phospholipids up to almost complete digestion, releasing lysophospholipid as the major hydrolysis product, together with residual nonhydrolyzed phospholipids. Furthermore, the digestion of the rest of the lipids was not influenced by the presence of PLA2. These results were closer to *in vivo* physiological digestion of phospholipids,[17] so the *in vitro* model that was developed was considered useful to test the intestinal digestion of the experimental molecule PHT. The detailed procedure of the *in vitro* model after performing all the explained modifications was that described in the Materials and Methods section.

***In Vitro* Intestinal Digestion of Phosphatidylhydroxytyrosol.** To perform the digestion of PHT, it was not as easy as replacing total phospholipids of the media by PHT. This is because the fraction of phospholipids from biliary secretion should be kept in order to reproduce a physiological situation. Therefore, the PHT was included in the media as dietary phospholipid, but it coexisted together with the endogenous phospholipid of the medium during the hydrolysis process.

The evolution of *in vitro* intestinal digestion of PHT is shown in Figure 2. It can be observed that PHT was progressively hydrolyzed to lyso-PHT. However, the rate of digestion was slower than the phospholipid control sample (Figure 1b). Thus, at the end of digestion, only around 50% of PHT was hydrolyzed.

To compare the digestion of PHT in the presence and in the absence of endogenous phospholipids, additional experiments

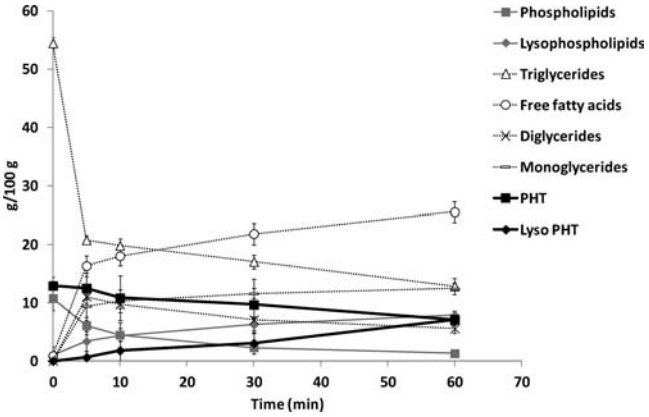


**Figure 2.** Course of *in vitro* intestinal digestion of PHT.

were performed. Thus, PHT as the only form of phospholipid substrate for PLA2 was added to the media, which means that biliary PC was removed and that PHT was added both as dietary and biliary phospholipid. For comparative purposes, the same procedure was performed for PL. The release of lysophospholipid species was considered to compare the rate of hydrolysis. As shown in Figure 3, the rate of digestion of

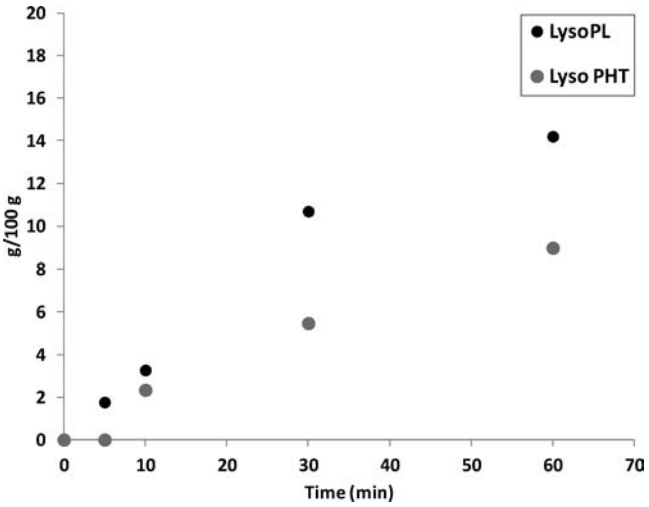


**Figure 3.** Lyso-PL or lyso-PHT releasing during *in vitro* intestinal digestion of PL or PHT, respectively, without coexistence of other phospholipids in the media.

PHT was slower than the hydrolysis of the control PL. Therefore, this experiment showed that the slower digestion of PHT would be related to the own molecule PHT.

The explanation of this result is complex, because previous information on the digestion of phospholipids with a modified polar-head with so atypical structures is scarce. Nevertheless, it has been described that there are different factors that determine the rate and extent of enzymatic hydrolysis of any phospholipid in general. According to scientific literature, the aggregation of the substrate under the form of mixed micelles, lamellar structures, liposomes, or emulsions is necessary, since this appears to facilitate the interaction of the sn-2 fatty acid ester with the catalytic site of the enzyme.[26−28] However, the specific type of aggregation determines the hydrolysis rate. Furthermore, the presence of other lipids which influences the packing of the fatty acid chains and the headgroup are also related to the action of PLA2.[28] Whether PHT determined differences on these factors is unknown but might be considered as potential reasons of the different results on the rate of hydrolysis. According to Scott et al.[27] on the contribution of the sn-3 substituent on the PLA2 binding affinity, these authors stated that the own nature of the phosphatidyl ester affects the physical chemistry of the aggregates, such as surface charge distribution or the state of aggregation. In this respect, it is important to remark that PL and PHT might show a different surface charge distribution, taking into account that the former would be a neutral PL, whereas PHT should be an anionic phospholipid due to the removal of choline. Related to the different state of aggregation, the numbers of micellar structures formed after *in vitro* digestion of PL and PHT were determined. According to Figure 4, a lower number of micellar structures were detected for PHT digestion when compared to PL, which seemed to be in agreement with the lower hydrolysis of PHT.

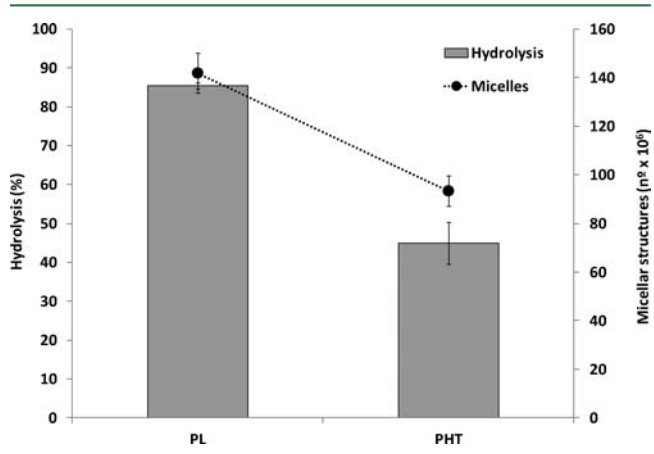


**Figure 4.** Hydrolysis of PL and PHT versus the number of micellar structures.

**Bioaccessibility of Phosphatidylhydroxytyrosol.** During intestinal digestion of dietary fat, it has been shown that the intraluminal content is structured as an oily phase (OP) dispersed in a micellar bile salt solution (MP).[29] This OP mainly contains undigested TG and DG, whereas the MP contains bile salts and the end products of enzymatic hydrolysis, namely, MG, FFA, and lysophospholipids. All of these lipid products are aggregated as mixed micelles, micelles, vesicles, or emulsion droplets.[30,31] Absorption of lipid products takes place supported by this MP, which enhances the transport of lipid products to the enterocytes throughout the unstirred water layer close to the microvillous membrane, where they are absorbed.[32] Furthermore, a minor fraction of insoluble calcium soaps of fatty acids liberated during the pancreatic digestion can be formed, which are not absorbable, tend to precipitate, and are wasted in faeces. The analysis of lipid products of these three phases, MP, OP, and PP, contributes to the study of bioaccessibility, defined as the fraction of a compound that is released from its matrix in the gastrointestinal tract and thus becomes available for intestinal absorption.[33]

According to Figure 5, most hydrolysis products, including neutral and polar lipids, were found distributed within the bioaccessible fraction MP, suggesting a high bioaccessibility. In the case of the control PL samples, a significant OP was isolated (16% of total lipid products), and a minor PP was also detected. The specific distribution of total lipid products within the three phases is detailed in Figure 6. As shown in Figure 6a,


dx.doi.org/10.1021/jf503477h | J. Agric. Food Chem. 2014, 62, 9751−9759

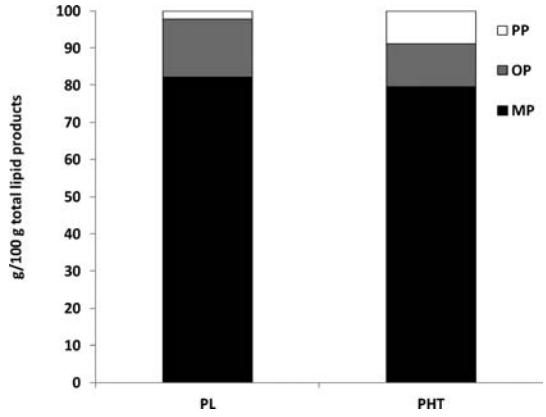


**Figure 5.** Partition of total lipid products between the isolated fractions MP, OP, and PP after 60 min of *in vitro* intestinal digestion.

the polar lipids from hydrolysis of PL (lyso-PL and residual nondigested PL) were totally included in the MP, suggesting a high bioaccessibility of PL. These results were in agreement with the expected physiological data of phospholipids, so these obtained results also validated the *in vitro* model developed on the ability to reproduce *in vivo* physiological results on bioaccessibility of phospholipids, and lipids in general.

Some differences were observed in the case of the sample containing PHT. As shown in Figure 5, the distribution of lipid products within the OP was lower (around 12% of total lipid products), and the PP increased instead (around 9% of total lipid products precipitated) compared to the PL sample. At any case, most lyso-PHT and residual PHT were found within the bioaccessible fraction MP.

As detailed in Figure 6b, the observed increase in the PP fraction was mainly due to an increased precipitation of FFA and a fraction of nondigested PHT. In fact, the bioaccessibility of the FFA changed from 92% in the case of PL samples to 80% in the case of PHT samples. This unexpected a priori result is difficult to explain, attending to the fact that both PL and PHT samples had the same amount and fatty acid profile. In general, any precipitation of FFA during intestinal digestion should be related to a limited solubilization within micellar structures and formation of calcium soaps that cannot be solubilized in the aqueous media. Taking into account that the assays of PHT samples produced a lower amount of micellar structures than PL samples (Figure 4), this might determine the differences on nonmicellated fatty acids between both samples. It was also significant that around 8% of total PHT was precipitated

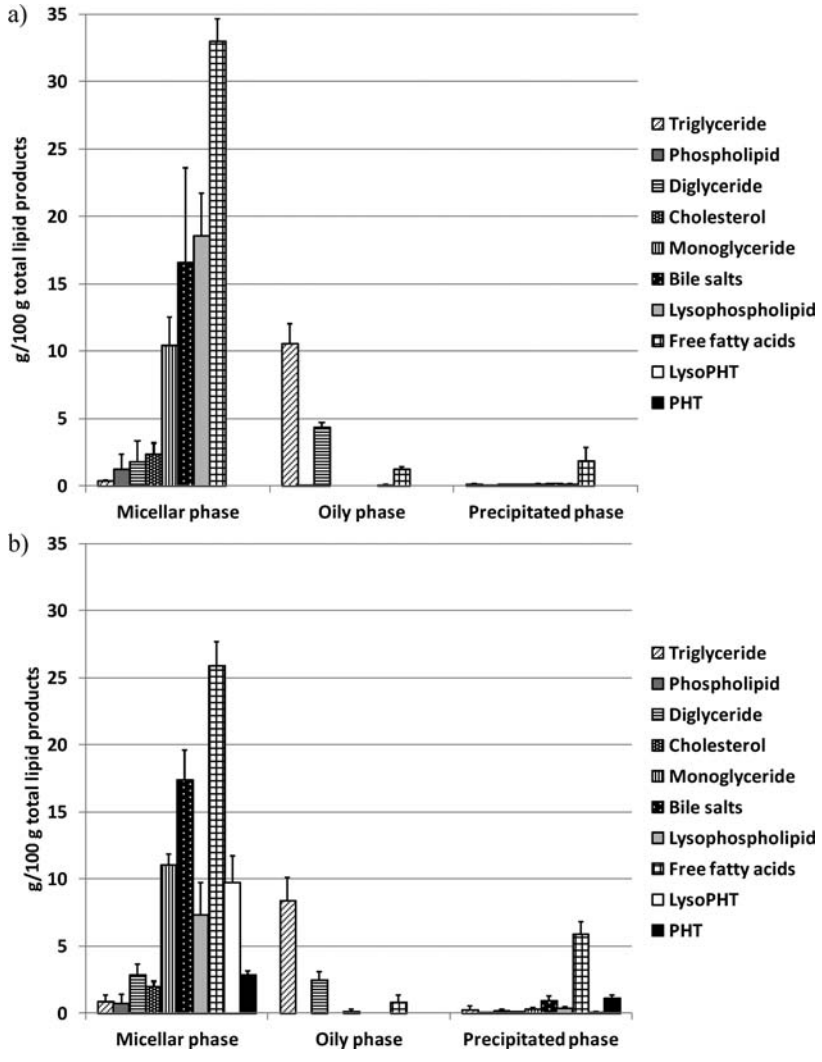


**Figure 6.** Partition of individual lipid products between the isolated fractions MP, OP, and PP after 60 min of *in vitro* intestinal digestion.


dx.doi.org/10.1021/jf503477h | *J. Agric. Food Chem.* 2014, 62, 9751−9759

together with FFA, whereas nondigested PL did not precipitate in the case of PL sample. A minor fraction of precipitated bile salts was also measured for the PHT sample contrary to the PL sample. Therefore, the particular molecule PHT might be related to these results.

In order to evaluate the magnitude of PHT as a carrier of HT, its bioaccessibility as the esterified form was compared to that of HT. Furthermore, a comparative study with a premixture HT+PL was considered of interest in order to compare the bioaccessibility of HT when it coexisted with a dose of dietary PL, with that of HT under the esterified form as PL (PHT). According to Figure 7, most HT was included

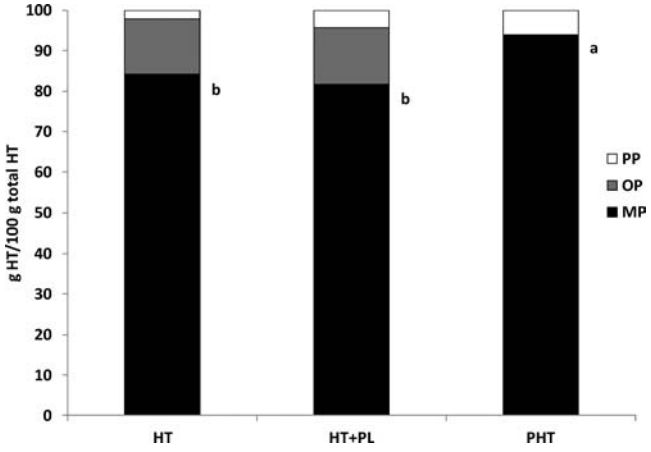


**Figure 7.** Partition of total HT between the isolated fractions MP, OP, and PP after 60 min of *in vitro* intestinal digestion.

within the bioaccessible fraction MP for the three forms of HT addition, suggesting a high bioaccessibility. Nevertheless, the portion of HT within the MP under the form of PHT was slightly superior to the other forms of addition of HT. Such a difference was due to a fraction of HT within the OP that was not detected for the PHT sample. These results would suggest that a portion of HT would not be so easily dispersed in the aqueous media when this phenolic compound was free or premixed with PL, contrary to the esterified forms of HT as PHT. Probably, the amphiphilic properties of PHT as a phospholipid allowed its dispersion in the aqueous media, which in turn indirectly allowed the dispersion of the vehiculated HT. Furthermore, a minor precipitated fraction of HT was found for all samples, which was not significantly different. These results contributed to the study of the potential of PHT as well as to the general behavior of the phenolic HT. Previous detailed information on the fractionation of HT, or combinations HT+PL, between the different phases of the intestinal medium under *in vitro* conditions was not found.

Concerning the bioaccessibility of PHT, it should be noted that Borgström[17] stated that conversion of phospholipids to lysophospholipids is essential for absorption to occur. Therefore, according to the obtained results, despite that most of the digested PHT was found within the bioaccessible MP fraction, PHT would be only partially absorbed as lyso-PHT. However, this fact remains unclear and should be elucidated, since it has also been reported that there is no abnormality in phospholipid absorption in the case of deficiency in PLA2 (nonhydrolyzed phospholipids).[24] Therefore, further studies concerning bioavailability of PHT would be of interest in order to validate whether PHT would be effectively recognized by intestinal mucosa for absorption and subsequent metabolism, and its validation as a potential vehicle of HT.

**Effect of *in Vitro* Digestion on the Antioxidant Activity of Phosphatidylhydroxytyrosol.** In a recent study, we have successfully shown a significant antioxidant activity of PHT in diverse edible oils, which was comparable or even superior to HT.[4] Taking such evidence of antioxidant ability of PHT into account, the antioxidant effect was explored in the current study when it was affected by the intestinal digestion process. This was considered of interest, especially taking into account that PHT was mainly degraded to lyso-PHT after intestinal digestion, and this would be the major bioaccessible molecule. Furthermore, the modification of the antioxidant activity of diverse phenolic compounds after the process and conditions of gastrointestinal digestion has been previously described, including HT;[34] hence, the interest in producing carriers of these compounds that could protect their activity during the gastrointestinal transit.

As shown in Figure 8, either PHT or digested PHT showed a lower antioxidant activity than HT at any moment of digestion.

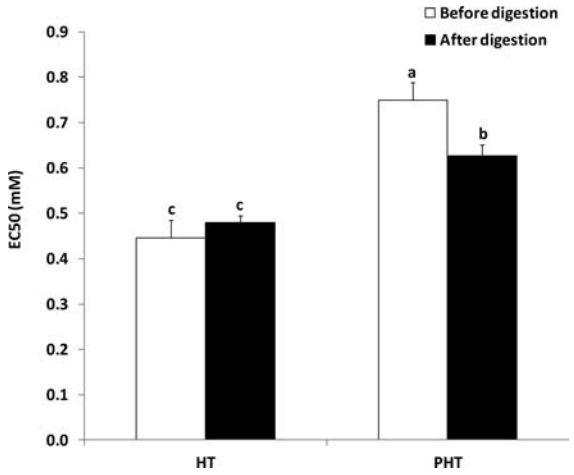


**Figure 8.** Scavenging activity of HT and equivalent concentration of HT under the form of PHT, before and after digestion.

Furthermore, the antioxidant activity of the control HT did not seem to be affected by the digestion process. An interesting finding was that the EC50 value of digested PHT was significantly inferior to that observed before digestion. This result might suggest that the digestion products, mainly the major lyso-PHT, might show better antioxidant ability than the former PHT. This could be considered reasonable, taking into account the simpler and more hydrophilic molecule of lyso-PHT compared to PHT. Thus, after intestinal digestion, a closer value of EC50 between digested PHT and HT was achieved (0.6 and 0.5 mM, respectively).

As a summary, the present study showed that the synthetic phosphatidyl derivative of HT is recognized by phospholipases during the simulation of intestinal digestion but less efficiently than the analogous PL. At any case, both the major hydrolysis product, namely, lyso-PHT, and most of the nondigested PHT were found within the bioaccessible aqueous fraction; hence, most of the esterified HT was potentially bioaccessible. On the other hand, the digested PHT might be a more superior antioxidant than the nonhydrolyzed PHT. Nevertheless, the evaluation of the potential bioactivity of PHT and its digested

product would be necessary in further studies, in order to validate the carriers of HT under the form of phospholipids.

## AUTHOR INFORMATION


### Corresponding Author

*Phone: +34 910017930. E-mail: diana.martin@uam.es.



### Funding

This work was supported by the Ministerio de Economía y Competitividad (INNSAOLI, project number IPT-2011-1248-060000, Subprograma INNPACTO) and the Comunidad de Madrid (ALIBIRD, project number S2009/AGR-1469). The contract of M.I.M.-V. was also supported by the INNSAOLI project and is also acknowledged.


### Notes

The authors declare no competing financial interest.

## ABBREVIATIONS USED

DG, diglycerides; FFA, free fatty acids; HT, hydroxytyrosol; MG, monoglycerides; MP, micellar phase; OP, oily phase; PC, phosphatidylcholine; PHT, phosphatidylhydroxytyrosol; PL, Phospholipon 90H; PLA2, phospholipase A2; PP, precipitated phase; TG, triglycerides

## REFERENCES


(1) Cornwell, D. G.; Ma, J. Nutritional benefit of olive oil: the biological effects of hydroxytyrosol and its arylating quinone adducts. *J. Agric. Food Chem.* **2008**, *56*, 8774−8786.

(2) Granados-Principal, S.; Quiles, J. L.; Ramirez-Tortosa, C. L.; Sanchez-Rovira, P.; Ramirez-Tortosa, M. C. Hydroxytyrosol: from laboratory investigations to future clinical trials. *Nutr. Rev.* **2010**, *68*, 191−206.

(3) Killeen, M. J.; Pontoniere, P.; Crea, R. Hydroxytyrosol. An examination of its potential role in cardiovascular disease, inflammation, and longevity. *Agro Food Ind. Hi-Tech* **2011**, *22*, 16−19.

(4) Martin, D.; Garcia-Serrano, A.; Casado, V.; Vázquez, L.; Reglero, G.; Torres, C. F. Antioxidant activity of phosphatidyl derivatives of hydroxytyrosol in edible oils. *Eur. J. Lipid Sci. Technol.* **2014**, *116*, 1035−1043.

(5) D'Angelo, S.; Manna, C.; Migliardi, V.; Mazzoni, O.; Morrica, P.; Capasso, G.; Pontoni, G.; Galletti, P.; Zappia, V. Pharmacokinetics and metabolism of hydroxytyrosol, a natural antioxidant from olive oil. *Drug Metab. Dispos.* **2001**, *29*, 1492−1498.

(6) De la Torre, R. Bioavailability of olive oil phenolic compounds in humans. *Inflammopharmacology* **2008**, *16*, 245−247.

(7) Rubió, L.; Macià, A.; Castell-Auví, A.; Pinent, M.; Blay, M. T.; Ardévol, A.; Motilva, M. J. Effect of the co-occurring olive oil and thyme extracts on the phenolic bioaccesibility and bioavailability assessed by in vitro digestion and cell models. *Food Chem.* **2014**, *149*, 277−284.

(8) Grasso, S.; Siracusa, L.; Spatafora, C.; Renis, M.; Tringali, C. Hydroxytyrosol lipophilic analogues: Enzymatic synthesis, radical scavenging activity and DNA oxidative damage protection. *Bioorg. Chem.* **2007**, *35*, 137−152.

(9) Torres de Pinedo, A.; Peñalver, P.; Rondón, D.; Morales, J. C. Efficient lipase-catalyzed synthesis of new lipid antioxidants based on a catechol structure. *Tetrahedron* **2005**, *61*, 7654−7660.

(10) Trujillo, M.; Mateos, R.; Collantes de Teran, L.; Espartero, J. L.; Cert, R.; Jover, M.; Alcudia, F.; Bautista, J.; Cert, A.; Parrado, J. Lipophilic hydroxytyrosyl esters. Antioxidant activity in lipid matrices and biological systems. *J. Agric. Food Chem.* **2006**, *54*, 3779−3785.

(11) Laguerre, M.; López Giraldo, L. J.; Lecomte, J.; Figueroa-Espinoza, M. C.; Baréa, B.; Weiss, J.; Decker, E. A.; Villeneuve, P. Relationship between hydrophobicity and antioxidant ability of "phenolipids" in emulsion: a parabolic effect of the chain length of rosmarinate esters. *J. Agric. Food Chem.* **2010**, *58*, 2869−2876.

(12) Madrona, A.; Pereira-Caro, G.; Mateos, R.; Rodríguez, G.; Trujillo, M.; Fernández-Bolaños, J.; Espartero, J. L. Synthesis of hydroxytyrosyl alkyl ethers from olive oil waste waters. *Molecules* **2009**, *14*, 1762−1772.

(13) Pereira-Caro, G.; Mateos, R.; Traka, M. H.; Bacon, J. R.; Bongaerts, R.; Sarriá, B.; Bravo, L.; Kroon, P. A. Hydroxytyrosyl ethyl ether exhibits stronger intestinal anticarcinogenic potency and effects on transcript profiles compared to hydroxytyrosol. *Food Chem.* **2013**, *138*, 1172−1182.

(14) Pereira-Caro, G.; Mateos, R.; Saha, S.; Madrona, A.; Espartero, J. L.; Bravo, L.; Kroon, P. A. Transepithelial transport and metabolism of new lipophilic ether derivatives of hydroxytyrosol by enterocyte-like Caco-2/TC7 cells. *J. Agric. Food Chem.* **2010**, *58*, 11501−11509.

(15) Casado, V.; Reglero, G.; Torres, C. F. Novel and efficient solid to solid transphosphatidylation of two phenylalkanols in a biphasic GRAS medium. *J. Mol. Catal. B: Enzym.* **2014**, *99*, 14−19.

(16) Espinosa-Salinas, I.; Rodriguez-Casado, A.; Molina, S.; Rodriguez-Gonzalez, A.; Ordovas, J. M.; Ramirez de Molina, A. Beneficial effects of bioactive phospholipids: genomic bases. *Curr. Nutr. Food Sci.* **2011**, *7*, 145−154.

(17) Borgström, B. Luminal digestion of fats. In *The Pancreas: Biology, Pathobiology, and Disease*; Go, V. L. W., Dimagno, E. P., Gardner, J. D., Lebenthal, E., Reber, H. A., Scheele, G. A., Eds.; Raven Press: New York, 1993; pp 475−488.

(18) Minekus, M.; Alminger, M.; Alvito, P.; Balance, S.; Bohn, T.; Bourlieu, C.; Carriere, F.; et al. A standardised static in-vitro digestion method suitable for food − an international consensus. *Food Funct.* DOI: 10.1039/C3FO60702J.

(19) Martín, D.; Morán-Valero, M. I.; Señoráns, F. J.; Reglero, G.; Torres, C. F. In vitro intestinal bioaccessibility of alkylglycerols versus triacylglycerols as vehicles of butyric acid. *Lipids* **2011**, *46*, 277−285.

(20) Soler-Rivas, C.; Marin, F. R.; Santoyo, S.; Garcia-Risco, M. R.; Senorans, F. J.; Reglero, G. Testing and enhancing the in vitro bioaccessibility and bioavailability of Rosmarinus officinalis extracts with a high level of antioxidant abietanes. *J. Agric. Food Chem.* **2010**, *58*, 1144−1152.

(21) Vázquez, L.; Fernandez, O.; Martin, D.; Reglero, G.; Torres, C. F. Comparison of molecular distillation and liquid $CO_2$ extraction for monoolein purification. 104th AOCS, Annual Meeting & Expo. Montreal, Canada, 2013.

(22) Mateos, R.; Espartero, J. L.; Trujillo, M.; Rios, J. J.; León-Camacho, M.; Alcudia, F.; Cert, A. Determination of phenols, flavones, and lignans in virgin olive oils by solid-phase extraction and high-performance liquid chromatography with diode array ultraviolet detection. *J. Agric. Food Chem.* **2001**, *49*, 2185−2192.

(23) Carelli, A. A.; Brevedan, M. I.; Crapiste, G. H. Quantitative determination of phospholipids in sunflower oil. *J. Am. Oil Chem. Soc.* **1997**, *74*, 511−514.

(24) Cohn, J. S.; Kamili, A.; Wat, E.; Chung, R. W.; Tandy, S. Dietary phospholipids and intestinal cholesterol absorption. *Nutrients* **2010**, *2*, 116−127.

(25) Duane, W. C.; Ginsberg, R. L.; Bennion, L. J. Effects of fasting on bile acid metabolism and biliary lipid composition in man. *J. Lipid Res.* **1976**, *17*, 211−219.

(26) Dijkstra, B. W.; Drenth, J.; Kalk, K. H. Active site and catalytic mechanism of phospholipase A2. *Nature* **1981**, *289*, 604−606.

(27) Scott, D. L.; White, S. P.; Otwinowski, Z.; Yuan, W.; Gelb, M. H.; Sigler, P. B. Interfacial catalysis: the mechanism of phospholipase A2. *Science* **1990**, *250* (4987), 1541.

(28) Carey, M. C.; Small, D. M.; Bliss, C. M. Lipid digestion and absorption. *Annu. Rev. Physiol.* **1983**, *45*, 651−677.

(29) Hofmann, A.; Borgstrom, B. The intraluminal phase of fat digestion in man: the lipid content of the micellar and oil phases of intestinal content obtained during fat digestion and absorption. *J. Clin. Invest.* **1964**, *43*, 247−257.

(30) Porter, C.; Charman, W. In vitro assessment of oral lipid based formulations. *Adv. Drug Delivery Rev.* **2001**, *50*, s127−s147.

(31) Fatouros, D.; Bergenstahl, B.; Mullertz, A. Morpholigal observations on a lipid-based drug delivery system during in vitro digestion. *Eur. J. Pharm. Sci.* **2007**, *31*, 85−94.
(32) Ramirez, M.; Amate, L.; Gil, A. Absorption and distribution of dietary fatty acids from different sources. *Early Hum. Dev.* **2001**, *65*, s95−s101.
(33) Fernandez-Garcia, E.; Carvajal-Lerida, I.; Perez-Galvez, A. In vitro bioaccessibility assessment as a prediction tool of nutritional efficiency. *Nutr. Res.* **2009**, *29*, 751−760.
(34) Pereira-Caro, G.; Sarriá, B.; Madrona, A.; Espartero, J. L.; Escuderos, M. E.; Bravo, L.; Mateos, R. Digestive stability of hydroxytyrosol, hydroxytyrosyl acetate and alkyl hydroxytyrosyl ethers. *Int. J. Food Sci. Nutr.* **2012**, *63*, 703−707.

prepared by dissolving chitosan flakes in HCl to achieve a final pH of 5−6. The solutions of catechol and mediator were prepared in phosphate buffer (0.1 M, pH 7.0).

**Preparation of the Clove−Chitosan Film.** To obtain an insoluble clove fraction, clove (5, 30, or 60 mg/mL) was suspended in water, vortexed, and then, centrifuged (3200*g* for 5 min). After discarding the upper brown solution, the settled clove was suspended in fresh water and again centrifuged. This process was repeated until the upper solution showed no absorbance peaks (300−700 nm) where phenolic antioxidants would be expected (see Figure S1, Supporting Information). The insoluble clove fraction was next suspended in aqueous solutions containing chitosan (0.5%, pH 5.5), and then, small amounts of this suspension (20 $\mu$L) were spread onto a standard gold electrode (area ~ 0.0314 $cm^2$). The film was vacuum-dried at 37 °C for 30 min and then immersed in phosphate buffer (pH 7.0; 30 min). This buffer treatment partially deprotonates the primary amines of chitosan and converts the film into a water-insoluble form. In most experiments, films containing insoluble clove were compared against control chitosan films (lacking clove).

**Electrochemical Instruments.** Electrochemical measurements (cyclic voltammetry and chronocoulometry) were performed using a three-electrode system (CHI Instruments 6273C electrochemical analyzer). The working electrode was the standard gold electrode (with chitosan film, area = 0.03 $cm^2$), the reference electrode was Ag/AgCl, and the counter electrode was a Pt wire. All electrochemical experiments were done in a mixed solution of 50 $\mu$M Fc and 50 $\mu$M $Ru^{3+}$ in phosphate buffer (0.1 M, pH 7.0). Air was excluded by purging $N_2$ during the experiment. For measurement of antioxidant and pro-oxidant activities, the gold-coated silicon wafer was used as a working electrode because its larger surface area (0.9 $cm^2$) increased sensitivities of these measurements.

**Antioxidant Assay.** Antioxidant activity was measured by adapting the standard oxygen radical absorbance capacity (ORAC) method that probes a hydrogen atom transfer mechanism. We used this method to probe if/how antioxidant properties varied depending on whether the clove−chitosan film was poised in an oxidized or reduced state. In this case, the film-coated electrode was electrochemically poised in an oxidized or reduced state (see the text for details) and then incubated in a solution (200 $\mu$L) of fluorescein (10 nM) in 0.1 M phosphate buffer (pH 7.0) followed by the rapid addition of the AAPH solution (20 mM). The mixture was incubated for a fixed time of 30 min at 37 °C, and then, the fluorescence was recorded using a fluorescence plate reader (SpectraMax M2, Molecular Devices, CA).

**Assay for Pro-oxidant Activity.** The film-coated electrodes were electrochemically poised in either oxidized or reduced states, dried with $N_2$, and then, incubated in air-saturated water for 15 min. The $H_2O_2$ generated in this aqueous solution was assayed using Amplex Red reagent (Amplex Red Hydrogen Peroxide/Peroxidase Assay Kit, Invitrogen, OR), and the results were measured using a fluorescence plate reader.

**Statistical Analysis.** All experiments were carried out in triplicate. Statistical analyses were performed using one-way analysis of variance compared with control.

## RESULTS AND DISCUSSION

**Initial Evidence of Redox Activity.** Scheme 1a illustrates the experimental approach for preparing a chitosan film containing insoluble clove. The photograph shows a standard gold electrode while the schematic illustrates that a clove−chitosan film is prepared directly adjacent to this electrode. Scheme 1a also illustrates the structure of this film with the insoluble clove particles entrapped within the chitosan network. Previously, we studied chitosan films containing insoluble melanin particles[36] and chitosan films with grafted catechol moieties.[40] Results from these earlier studies can be used to compare observations with insoluble clove.

Scheme 1b shows the electrochemical system used to probe the redox activities of the clove−chitosan film. This film-coated

**Scheme 1. Experimental Sample, System, and Electrochemical Redox Cycling**[a]

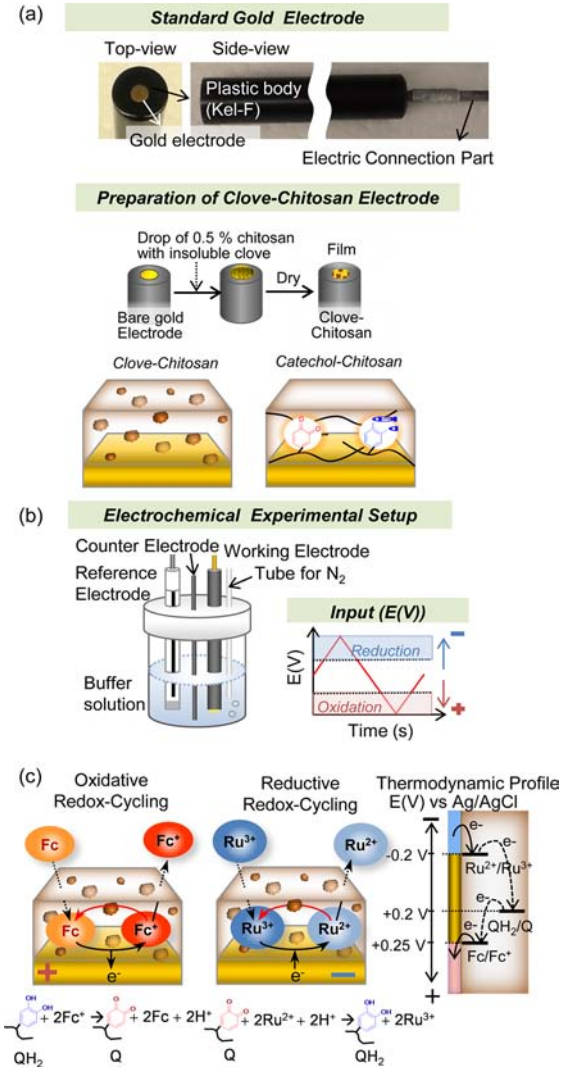


[a](a) Standard gold electrode and preparation of film with insoluble clove entrapped within a chitosan matrix (films with covalently grafted catechol moieties are used for illustrative and comparative purposes). (b) Electrochemical system used for cyclic voltammetry (cyclic input potentials are imposed). (c) Redox cycling of electrochemical mediators (Fc and $Ru^{3+}$) and chemical mechanism proposed for the case of catechol−chitosan films.[40]

"working" electrode is inserted into a buffered solution (0.1 M phosphate; pH 7.0) along with the reference (Ag/AgCl) and counter electrodes. As illustrated, an input potential ($E$; volts) can be imposed to the underlying gold electrode, and the basis of this electrochemical analysis is to infer redox activities from the observed output currents. In initial studies, this clove−chitosan film was probed by cyclic voltammetry such that the potential ($E$) of the electrode was controllably cycled between oxidative values (more positive values of $E$) and reductive values (more negative values of $E$). If a chemical species can access the electrode and undergo redox reactions with the electrode, then oxidation is observed as a negative current while reduction is observed as a positive current. (Note: cyclic voltammetry data is commonly displayed as a plot of current vs potential without explicitly showing time.)


dx.doi.org/10.1021/jf503479d | J. Agric. Food Chem. 2014, 62, 9760−9768

Chemical intuition suggests several expectations for this initial cyclic voltammetry experiment. First, minimal oxidation or reduction currents should be observed if the clove−chitosan film is probed in a buffer solution that lacks diffusible redox-active species. In this case, there are no accessible electrons to exchange with the electrode: chitosan is not redox-active and cannot conduct electrons, and the insoluble clove particles are entrapped too far from the electrode surface for direct electron exchange. The first control in Figure 1a is for a chitosan film prepared with the insoluble fraction of clove and probed in the absence of soluble mediators. As expected, the cyclic voltammograms (CVs) for this control show no oxidation or reduction peaks.

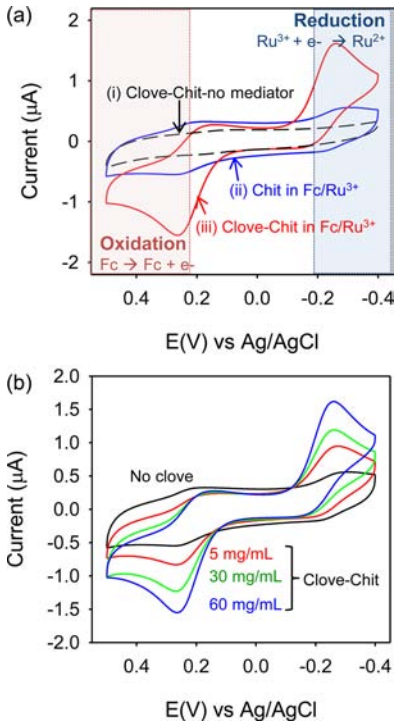


**Figure 1.** CVs provide initial evidence that insoluble clove has redox activity (scan rate = 50 mV/s). (a) CVs for electrodes coated with chitosan films: (i) clove−chitosan control incubated without mediators shows neither chitosan nor clove are conducting (no peak currents are observed); (ii) chitosan control incubated with both Fc and $Ru^{3+}$ mediators (50 $\mu$M each) shows that the chitosan film is permeable to these mediators (the small peak currents correspond to the diffusion of mediators); (iii) clove−chitosan incubated with both mediators shows amplified peak currents consistent with redox cycling. (b) CVs for electrodes coated with chitosan films containing varying clove levels show amplified peak currents increase with increasing clove levels.

In order for oxidation or reduction currents to be observed, a soluble redox mediator must be incorporated in the buffer, and this mediator must be able to diffuse through the film to access the electrode. We incorporate two electrochemical mediators in the buffer: Fc typically exists in its reduced state but can be readily and reversibly oxidized when the potential is cycled near its $E^{\circ}$ (+0.25 V vs Ag/AgCl); and $Ru^{3+}$ typically exists in its oxidized state but can be readily and reversibly reduced near its $E^{\circ}$ (−0.2 V vs Ag/AgCl). A second expectation is that, if these two mediators are added into the buffer, then they should be capable of diffusing through the films to exchange electrons directly with the underlying electrode and thus oxidation and reduction currents should be observed in the CVs. The second control in Figure 1a is for a chitosan film (without clove) that was incubated in the presence of these two mediators. When the potential for this chitosan-coated electrode was cycled to oxidative voltages, a small oxidation peak current was observed near +0.27 V consistent with the expected Fc oxidation. Figure 1a shows that, when the potential for this chitosan-coated electrode was cycled to reductive voltages, a small reduction peak current was observed near −0.27 V consistent with the expected $Ru^{3+}$ reduction.

If the insoluble clove particles entrapped in the chitosan film can exchange electrons with the mediators, then a third expectation is that the oxidation and/or reduction currents observed in the CVs should be altered compared to those observed with the chitosan control film. The experimental sample in Figure 1a is the clove−chitosan film incubated in the presence of both Fc and $Ru^{3+}$ mediators. Considerable amplification of the Fc-mediated oxidation currents and the $Ru^{3+}$-mediated reduction currents are observed in Figure 1a. If the observed amplification of mediator currents is due to redox interactions with the entrapped clove particles, then a further expectation is that amplification should vary with the amount of entrapped clove. As expected, the CVs in Figure 1b show that amplification of the Fc-oxidation and $Ru^{3+}$-reduction currents increases with increasing amounts of clove incorporated into the films. These results provide initial evidence that the insoluble components of clove can undergo redox interactions with the soluble Fc and $Ru^{3+}$ mediators.

A possible mechanistic explanation for the above observations is provided in Scheme 1c that was proposed in earlier studies with catechol-modified chitosan films.[41] Specifically, the Fc mediator can diffuse from solution through the film and undergo oxidation at the electrode to generate $Fc^{+}$ species. The oxidized $Fc^{+}$ species can either diffuse out of the film into solution or undergo redox interactions with the insoluble clove incorporated in the film. The observed amplification of the oxidation currents suggests the clove donates electrons to the $Fc^{+}$ to regenerate the Fc species that can undergo oxidative redox cycling with the electrode. Similarly, Scheme 1c illustrates that amplification of the reducing currents is indicative of reductive redox cycling of the $Ru^{3+}$ mediator such that it accepts electrons at the electrode but donates these electrons to the insoluble clove. In previous studies, we proposed that the observed redox cycling involved a switching between the reduced catechols ($QH_2$) and oxidized *o*-quinones (Q) as illustrated by the reactions in Scheme 1c.[41] The thermodynamic plot in Scheme 1c shows that electron transfer occurs from more negative to more positive potentials.

**Switching the Films to Oxidized or Reduced States.** A convenient feature of electrochemical methods is that arbitrarily complex input potentials can be imposed on a sample. As illustrated in Scheme 2, we use step changes in the input potential in the presence of the Fc and $Ru^{3+}$ mediators to switch the redox state of the film. To switch the film to a reduced state, Scheme 2a shows that the potential is stepped to provide reducing conditions (−0.4 V vs Ag/AgCl). As illustrated by the schematic, this step change would drive the $Ru^{3+}$ reductive-redox-cycling reaction to mediate the transfer of electrons from the electrode to the sample (e.g., to quinone moieties). Over time, this reduction (or charging) step should "saturate" the sample with electrons. To switch the film to an oxidized state, Scheme 2b shows that the potential is stepped to an oxidative value (+0.5 V vs Ag/AgCl) to drive the Fc


dx.doi.org/10.1021/jf503479d | J. Agric. Food Chem. 2014, 62, 9760−9768

**Scheme 2. Step Changes in Input Potential Can Be Used to (a) Engage $Ru^{3+}$ Reductive Redox Cycling to Charge the Film with Electrons, (b) Engage Fc Oxidative Redox Cycling to Discharge the Film, and (c) Quantify Redox Capacity by Chronocoulometry (Impose a Constant Potential and Quantify Electron Transfer)**

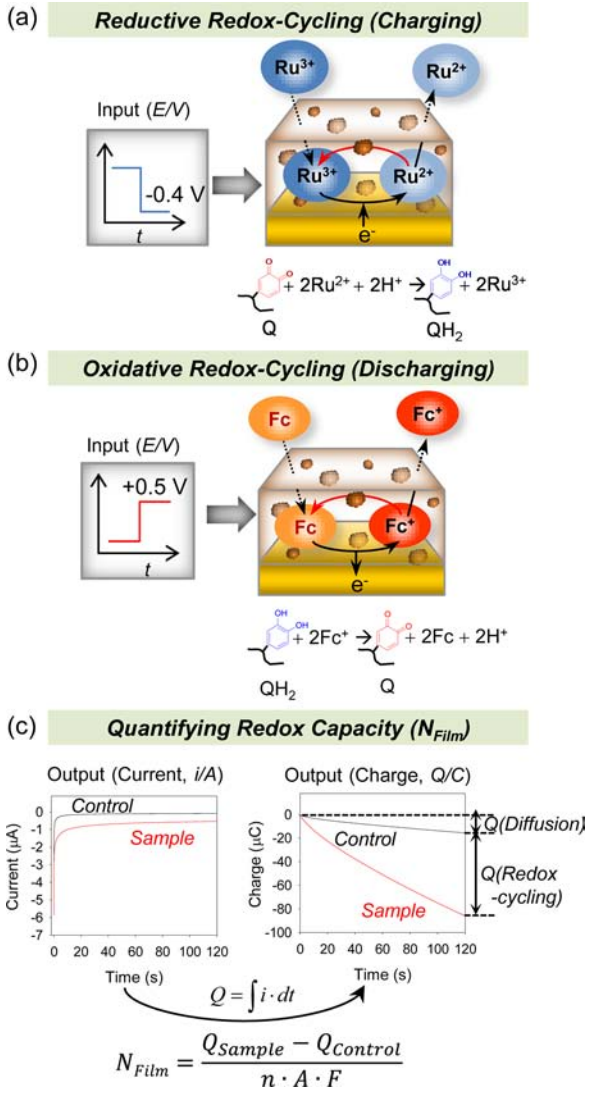


oxidative-redox-cycling reaction to mediate electron transfer from the sample to the electrode (i.e., to discharge electrons from the sample).

**Quantifying Redox Capacity.** We used such step changes in input potential to quantify the redox capacity of the clove entrapped within the chitosan film. Initially, the film was charged with electrons using a reducing potential step (−0.4 V; 2 min). After charging, the potential was stepped to an oxidative value (+0.5 V; 2 min) to allow Fc to discharge the film. During discharging, the electrode current ($i$) was measured, and the electron transfer ($Q$) was calculated by integration of the measured current as illustrated in Scheme 2c (this method of imposing a constant potential and measuring $Q$ is referred to as chronocoulometry). The redox capacity of the film is determined by comparing an experimental sample (clove−chitosan film) against a control chitosan film. As illustrated in Scheme 2c, the charge transfer observed for the control chitosan film ($Q_{control}$) is attributed to the oxidation of the Fc mediator that diffuses from the bulk solution through the film to the electrode surface. The charge transfer for the clove−chitosan film ($Q_{sample}$) is attributed to both Fc diffusion and Fc redox cycling in the film. The difference between these values is used to calculate the redox capacity ($N_{film}$) of the film as illustrated in Scheme 2c.

Experimental results for samples prepared with differing levels of clove are shown in Figure 2a. As expected, the

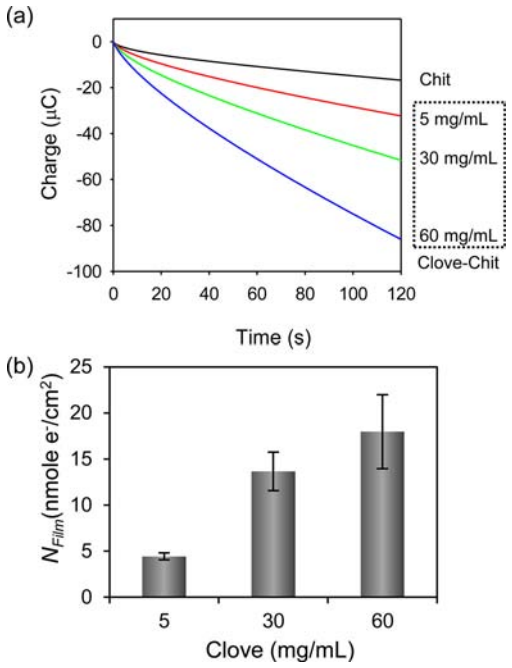


**Figure 2.** Electrochemical method (chronocoulometry) to quantify the redox capacity of the films ($N_{film}$). (a) Experimental results for the Fc-mediated oxidative charge transfer in response to a step input of oxidative potential (from an open circuit potential to +0.5 V vs Ag/AgCl that is maintained constant for 2 min). (b) The redox capacity for clove−chitosan films increases with increasing levels of insoluble clove.

observed charge transfer during this 2 min discharging step was greater when the sample contained more insoluble clove incorporated into the chitosan films. Figure 2b shows the calculated values of redox capacity and demonstrates that the insoluble clove possesses considerable redox capacity. To provide some estimate of the significance of these measured redox capacities, we consider a clove−chitosan film prepared by applying 20 $\mu$L of a 30 mg/mL solution to a working electrode area of 0.03 $cm^2$ to obtain ≈20 mg clove/$cm^2$. If the redox capacity is attributed to a two-electron transfer involving a quinone−catechol couple, then the measured value of 13 nmole $e^-/cm^2$ corresponds to ≈0.7 $\mu g/cm^2$ catechol. Thus, the observed redox capacity could be the result of ≈0.04 $\mu$g/mg catechol equivalence in this insoluble clove sample. It is important to emphasize that, while the above estimate is stoichiometric, redox cycling can act catalytically for transferring electrons from a reductant to an oxidant.[40]

There are two important caveats to the method for calculating $N_{film}$. First, particulate samples (e.g., insoluble clove) can be difficult to completely charge or discharge because of limitations in the abilities of the mediators to diffuse into and access redox-active moieties within the particles.[36] Thus, the measured redox capacities are operational measures


dx.doi.org/10.1021/jf503479d | J. Agric. Food Chem. 2014, 62, 9760−9768

useful for comparison but an underestimation of the true ability of the sample to accept, store, and donate electrons.

Second, our method probes a comparatively small window of redox potentials that is most relevant to the reversible oxidation and reduction of catecholic moieties. We believe this potential region is important given the redox gradients in the gut[42] and the ability of reversible redox cycling in this milieu to provide a means for redox interactions among the microbiota and the epithelium.[43] We do not expect these imposed potentials are sufficiently aggressive to oxidize monophenolics (e.g., eugenol is a major component of clove[39]) that can undergo irreversible reactions important to radical scavenging activities.[44] Again, while this narrow potential region allows us to focus on reversible redox interactions, we are underestimating the true redox capacity of a sample.

**Repeatable Redox Switching.** In addition to using cyclic voltammetry to provide initial evidence for redox activities (Scheme 1 and Figure 1) and chronocoulometry to provide semiquantitative measure of redox capacity (Scheme 2 and Figure 2), we are developing a third electrochemical method to assess the reversibility of these redox interactions. Specifically, we collected CVs for numerous oxidation and reduction cycles to observe the repeatability of redox cycling. In principle, this approach is analogous to approaches used in control theory in which oscillating inputs are used to impose to small perturbations to a system and the resulting oscillating outputs provide information on the response of the system to these inputs. If the response of the system is fully reversible, then the oscillating outputs are expected to be "steady"; the amplitude and frequency should remain constant over time (provided the oscillating input remained the same).

Experimentally, we tested film-coated electrodes (either chitosan or clove−chitosan films) in solutions containing both the Fc and $Ru^{3+}$ mediators with the imposed cyclic input potentials indicated in Figure 3a. Visual inspection of the output currents shows no noticeable changes over the eight cycles of this experiment and provides initial evidence that the output is steady. Steady output currents would indicate that the redox activities being probed by this method are fully reversible (i.e., the oxidation and reduction reactions of clove are reversible). A more subtle implication of steady outputs is that, during each cycle, the Fc-mediated oxidative redox cycling of clove is nearly balanced by the $Ru^{3+}$-mediated reductive redox-cycling reduction of clove.

To more rigorously analyze the results in Figure 3a, we focus on the current versus potential curves (i.e., the CVs) for each cycle as illustrated in Scheme 3. A CV from an individual cycle serves as the "signal" that is divided into four quadrants based on whether the currents are oxidizing or reducing and how the currents are assigned, to the oxidative redox cycler (e.g., Fc) or reductive redox cycler (e.g., $Ru^{3+}$). (We should note that the assignment of each quadrant to activities of a single chemical entity is useful for processing the information although such an assignment is a simplification of the underlying chemistries.) As indicated by the upper equation in Scheme 3b, the charge transfer for each quadrant is calculated by integration of the current for that quadrant ($Q = \int i\, dt$). If the redox reactions being detected by this method are fully reversible, then one expectation is that the charge-transfer values should remain constant over time. Figure 3b shows the calculated Q for the two largest quadrants of Scheme 3a were nearly constant for the eight cycles of the experiment.

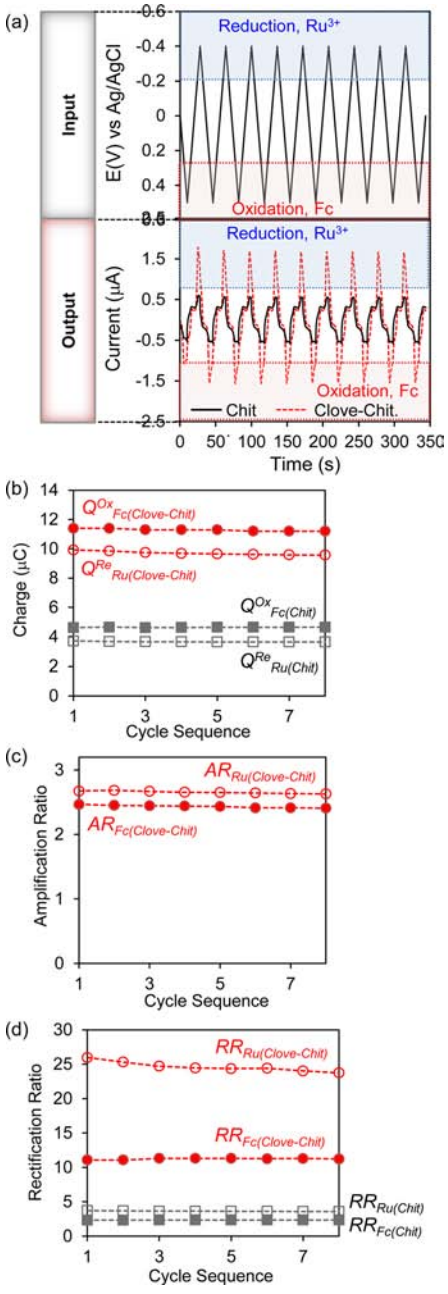


**Figure 3.** Repeatability of the redox cycling of clove with the Fc−$Ru^{3+}$ system (scan rate = 50 mV/s; 60 mg/mL clove). (a) The cyclic potential input allows the Fc and $Ru^{3+}$ mediators (50 $\mu$M each) to sequentially oxidize and reduce the clove (see Scheme 3 for signal analysis). (b) Charge transfer ($Q$) for Fc oxidation and $Ru^{3+}$ reduction with clove−chitosan remains relatively constant over the eight cycles tested. (c) Amplification ratios for Fc oxidation and $Ru^{3+}$ reduction with clove−chitosan exceed 2 and are nearly constant. (d) Rectification ratios for Fc oxidation and $Ru^{3+}$ reduction with clove−chitosan are large (>10) and nearly constant.

Previous studies have shown characteristic signatures of redox cycling emerge by considering the two sets of ratios indicated in Scheme 3b.[37] The amplification ratios (ARs) compare the charge transfer ($Q$) in a given quadrant for the clove−chitosan film to an equivalent $Q$ for the unmodified chitosan film (control). The AR contains information on redox cycling, since a film that can redox cycle (e.g., clove−chitosan) is expected to have an amplified output current compared to a


dx.doi.org/10.1021/jf503479d | J. Agric. Food Chem. 2014, 62, 9760−9768

**Scheme 3. Signal Analysis of Results from the Individual CV Cycles**[a]

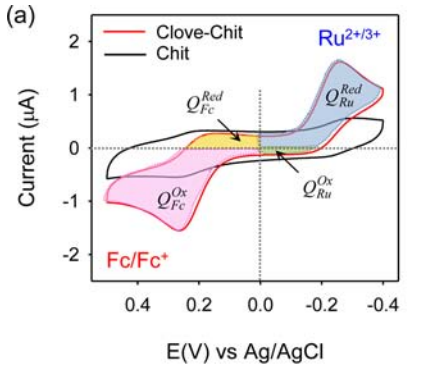


(b)

**Charge Transfer**

$$Q = \int i\,dt = \int \frac{i}{v}\,dE \left( v = \frac{dE}{dt} = Scan\ rate \right)$$

**Amplification Ratio (AR)**

$$AR_{Fc} = \frac{(Q_{Fc}^{Ox})_{Clove-Chitosan}}{(Q_{Fc}^{Ox})_{Chitosan}}$$

$$AR_{Ru} = \frac{(Q_{Ru}^{Red})_{Clove-Chitosan}}{(Q_{Ru}^{Red})_{Chitosan}}$$

**Rectification Ratio (RR)**

$$RR_{Fc} = Q_{Fc}^{Ox} / Q_{Fc}^{Red}$$

$$RR_{Ru} = Q_{Ru}^{Red} / Q_{Ru}^{Ox}$$

[a]Scan rate = 50 mV/s; 60 mg/mL clove. (a) The "signal" for each cycle is analyzed by dividing the CVs into quadrants, calculating the charge transfer ($Q$) for each quadrant, and assigning these values to activities of a single mediator. (b) Calculation procedure for determining charge transfer ($Q$), amplification ratios (ARs), and rectification ratios (RRs).

relevant control film that cannot redox cycle (e.g., unmodified chitosan film). Figure 3c shows a 2−3-fold amplification of both Fc oxidation and $Ru^{3+}$ reduction currents for the clove−chitosan, and these ARs are nearly constant over the course of the eight cycles.

The second ratios in Scheme 3b are the rectification ratios (RRs) that are more subtle and consider how (a) electrode currents in the Fc region are primarily oxidative ($Fc^+$ reduction by redox cycling in the film decreases the amount of $Fc^+$ reduction occurring at the electrode) and (b) electrode currents in the $Ru^{3+}$ region are primarily reductive ($Ru^{2+}$ oxidation by redox cycling in the film decreases the amount of $Ru^{2+}$ oxidation occurring at the electrode). In essence, the RR considers the linkage between Fc-mediated oxidative redox cycling and $Ru^{3+}$-mediated reductive redox cycling; reductive redox cycling charges the sample with electrons that are subsequently removed during the oxidative redox-cycling portion of the cycle. Thus, samples that can sequentially engage these oxidative and reductive redox-cycling reactions would be expected to have large and constant RRs.[37] Figure 3d shows that large RRs are observed for the clove−chitosan film and again these ratios remain nearly constant over the course of the eight cycles.

In summary, the results in Figure 3 demonstrate that the electrochemical mediators Fc and $Ru^{3+}$ can repeatedly oxidize and reduce components in insoluble clove; that is, insoluble clove residue is redox-active and can be repeatedly and reversibly cycled between oxidized and reduced states.

**Antioxidant Behavior.** A method commonly used to examine antioxidant radical scavenging activities is to incubate a sample with the radical generator AAPH ($E^\circ$ = +0.8 V vs Ag/AgCl) and fluorescein. Fluorescein is readily damaged by the resulting free radical while a sample with free radical scavenging activities protects fluorescein. In the next study, we used this method to test whether the radical scavenging antioxidant properties of clove depended on whether it was poised in a reduced or oxidized state. As illustrated in Scheme 2, it is possible to use an electrochemical method to poise the film to either an oxidized or reduced state to investigate this question. In these experiments, we used a gold-coated silicon wafer as our electrode to allow a larger sample area to be probed (0.9 vs 0.03 $cm^2$ for the standard gold electrode of Scheme 1a) and to facilitate comparison with previous studies. To poise the sample in an oxidized or reduced state, the clove-containing film is incubated in the presence of both the Fc and $Ru^{3+}$ mediators. To reduce the sample (i.e., to charge it with electrons), a reducing potential is imposed to the underlying electrode (−0.4 V; 30 min) to allow $Ru^{3+}$ reductive redox cycling to transfer electrons from the electrode to the insoluble clove. To oxidize the sample (i.e., to discharge its electrons), an oxidizing potential was imposed to the underlying electrode (+0.5 V; 30 min) to allow Fc oxidative redox cycling to transfer electrons from the insoluble clove. (Note: we used longer charging and discharging times to facilitate comparison with previous studies[36] and repeated chronocoulometric determinations of $N_{film}$ under these conditions.) These films were then incubated with fluorescein and AAPH for 30 min after which the fluorescence of fluorescein was measured.

The first two entries in Figure 4a are for the negative and positive controls that show no or complete loss of fluorescence of fluorescein. The third entry in Figure 4a shows that chitosan (without insoluble clove) offers little protection from free radical damage. The final two entries in Figure 4a show that insoluble clove offers substantial antioxidant protection and the oxidized and reduced states of insoluble clove offer comparable protection. This result demonstrates the well-known antioxidant properties of clove but further demonstrates that this antioxidant property is not sensitive to whether clove is in an oxidized or reduced state. As mentioned above, the redox window used to poise clove in its oxidized or reduced state is likely too mild to alter the redox state of eugenol that is believed to be a major component of the antioxidant activity of clove.[39] This result suggests that at least some of the moieties that confer radical scavenging antioxidant activities (e.g., eugenol) are not responsible for the reversible redox activities being observed by our electrochemical method.

Figure 4b shows results for samples prepared with differing levels of clove and further indicates that the radical scavenging antioxidant properties are insensitive to redox state. Previous studies with other insoluble phenolic matrices (i.e., melanin) show comparable results: the radical scavenging antioxidant properties are insensitive to the redox state at least for the moieties changed by our electrochemical method.[36]

For comparison with results from studies with other phenolic materials,[36,40] we replot our antioxidant activities in terms of redox capacity as shown in Figure 4c. This normalization

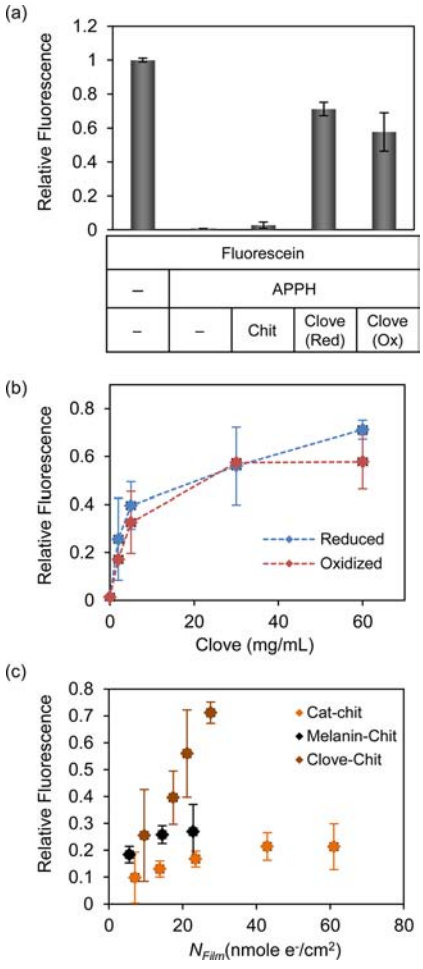


**Figure 4.** Radical scavenging antioxidant activities do not depend on the redox state of insoluble clove. (a) Films (60 mg/mL insoluble clove) poised in either oxidized or reduced states were observed to have similar abilities to protect fluorescein from free radical oxidative damage by APPH. (b) Films prepared with differing contents of insoluble clove have greater free radical scavenging antioxidant activities, and these activities are observed irrelevant to whether the films are poised in an oxidized or reduced state. (c) Comparison of antioxidant activities and redox capacities for chitosan films with either entrapped melanin or clove or chemically modified with catechol (data for melanin- and catechol-modified chitosan are reproduced from prior work).[36]

assesses how the antioxidant activities correlate to redox activities among various materials (note: the comparatively large error bars for the insoluble clove presumably reflects the particulate nature of these samples). While the incorporation of greater amounts of materials (e.g., phenolics) in the film increases both redox and antioxidant activities, the slopes of the curves vary among the different materials. The large slope for the clove–chitosan sample reflects its high antioxidant activities while the low slope for the catechol–chitosan sample indicates that its high redox activity is not accompanied by high radical scavenging antioxidant activities. Presumably, differences in the behavior between clove–chitosan and catechol–chitosan reflect differences in chemical components—that clove has different chemical moieties that confer radical scavenging antioxidant activity. The important observation is that antioxidant and redox activities are not exclusively linked to each other.

**Pro-oxidant Activity: $H_2O_2$ Generation.** In a final experiment, we prepared films on gold-coated silicon wafers (as described in Figure 4), poised the films in either an oxidized or a reduced state, exposed them to air, and examined their abilities to spontaneously generate $H_2O_2$. For these studies, the poised films were exposed to air-saturated water for 15 min, after which the solution was assayed for $H_2O_2$. Figure 5a shows

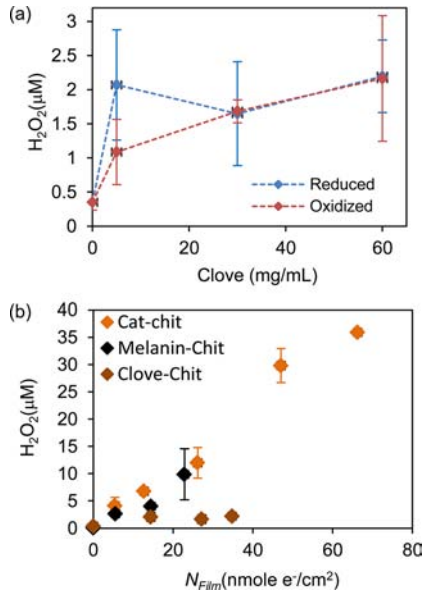


**Figure 5.** Pro-oxidant activities (as measured by $H_2O_2$ generation) for insoluble clove are low and do not depend on the redox state. (a) Clove–chitosan films poised in either an oxidized or a reduced state showed limited ability to generate $H_2O_2$ upon a 15 min exposure to air. (b) Comparison of $H_2O_2$ generation and redox capacities for chitosan films with either entrapped melanin or clove or chemically modified with catechol (data for melanin- and catechol-modified chitosan reproduced from prior work).[36]

relatively low levels of $H_2O_2$ were generated in these experiments and $H_2O_2$ generation was independent of whether samples were in an oxidized or reduced state. This result differs from previous observations with catechol-modified films or melanin-containing films that showed considerable $H_2O_2$-generating abilities but only when the films had been poised in a reduced state.[36,40]

Finally, we compare the $H_2O_2$ generation of clove–chitosan against results previously observed with other phenolic materials.[36,40] In comparison to melanin–chitosan and catechol–chitosan, Figure 5b shows that clove is unusual in that its reversible redox activity is not accompanied by an equivalent ability to generate $H_2O_2$. Presumably, this difference reflects differences in the chemical components in the insoluble clove sample. Possibly the high antioxidant and low pro-oxidant activities of clove may be important in putative health beneficial effects.

In conclusion, electrochemical methods were used to probe the redox activities of a model insoluble dietary antioxidant (i.e., clove), and we report two immediately interesting observations. First, we observed that insoluble clove possesses redox activities and can be rapidly and repeatedly switched between oxidized and reduced states. Recent literature indicates that considerable amounts of dietary antioxidant phenolics pass through the small intestine in an insoluble form and suggest that standard analytical methods may not fully account for their contribution


dx.doi.org/10.1021/jf503479d | J. Agric. Food Chem. 2014, 62, 9760–9768

to health benefits.[45−47] The observation that insoluble clove can undergo redox reactions with soluble mediators (electron shuttles) suggests that dietary antioxidants may participate in redox interactions in the intestine and thus affect redox homeostasis and health even in the absence of solubilization or absorption.[48] Second, we observed that insoluble clove (even when poised in a reduced state) has considerably less ability to generate $H_2O_2$ compared to other catechol-based matrices (e.g., melanin). This observation suggests that insoluble clove may possess little pro-oxidant activities although we should note that (i) we only measured the most stable ROS ($H_2O_2$) while other pro-oxidant species may have been generated; and (ii) we used relatively mild oxidation conditions to focus on reversible redox activities while the literature indicates that, under more aggressive oxidation conditions, eugenol can behave as a pro-oxidant.[49,50] Overall, we suggest that electrochemical methods may provide new and important opportunities to study redox homeostasis and oxidative stress.

## ■ ASSOCIATED CONTENT

### Supporting Information

Additional description of the insoluble clove fraction including the UV−visible spectra of the filtrates. This material is available free of charge via the Internet at http://pubs.acs.org.

## ■ AUTHOR INFORMATION

### Corresponding Author

*Phone: (301) 405-8389; fax: (301) 314-9075; e-mail: gpayne@umd.edu.

### Funding

The authors gratefully acknowledge financial support from the Robert W. Deutsch Foundation and the Defense Threat Reduction Agency (HDTRA1-13-0037).

### Notes

The authors declare no competing financial interest.

## ■ REFERENCES

(1) Zamora-Ros, R.; Fedirko, V.; Trichopoulou, A.; Gonzalez, C. A.; Bamia, C.; Trepo, E.; Nothlings, U.; Duarte-Salles, T.; Serafini, M.; Bredsdorff, L.; Overvad, K.; Tjonneland, A.; Halkjaer, J.; Fagherazzi, G.; Perquier, F.; Boutron-Ruault, M. C.; Katzke, V.; Lukanova, A.; Floegel, A.; Boeing, H.; Lagiou, P.; Trichopoulos, D.; Saieva, C.; Agnoli, C.; Mattiello, A.; Tumino, R.; Sacerdote, C.; Bueno-de-Mesquita, H. B.; Peeters, P. H. M.; Weiderpass, E.; Engeset, D.; Skeie, G.; Arguelles, M. V.; Molina-Montes, E.; Dorronsoro, M.; Tormo, M. J.; Ardanaz, E.; Ericson, U.; Sonestedt, E.; Sund, M.; Landberg, R.; Khaw, K. T.; Wareham, N. J.; Crowe, F. L.; Riboli, E.; Jenab, M. Dietary flavonoid, lignan and antioxidant capacity and risk of hepatocellular carcinoma in the European prospective investigation into cancer and nutrition study. *Int. J. Cancer* **2013**, *133*, 2429−2443.

(2) Finley, J. W.; Kong, A. N.; Hintze, K. J.; Jeffery, E. H.; Ji, L. L.; Lei, X. G. Antioxidants in foods: State of the science important to the food industry. *J. Agric. Food Chem.* **2011**, *59*, 6837−6846.

(3) Madamanchi, N. R.; Vendrov, A.; Runge, M. S. Oxidative stress and vascular disease. *Arterioscler., Thromb., Vasc. Biol.* **2005**, *25*, 29−38.

(4) Steinhubl, S. R. Why have antioxidants failed in clinical trials? *Am. J. Cardiol.* **2008**, *101*, 14D−19D.

(5) Scalbert, A.; Manach, C.; Morand, C.; Remesy, C.; Jimenez, L. Dietary polyphenols and the prevention of diseases. *Crit. Rev. Food Sci. Nutr.* **2005**, *45*, 287−306.

(6) Scalbert, A.; Williamson, G. Dietary intake and bioavailability of polyphenols. *J. Nutr.* **2000**, *130*, 2073S−2085.

(7) Pietta, P.-G. Flavonoids as antioxidants. *J. Nat. Prod.* **2000**, *63*, 1035−1042.

(8) Tomas-Barberan, F. A.; Andres-Lacueva, C. Polyphenols and health: Current state and progress. *J. Agric. Food Chem.* **2012**, *60*, 8773−8775.

(9) Quideau, S.; Deffieux, D.; Douat-Casassus, C.; Pouysegu, L. Plant polyphenols: Chemical properties, biological activities, and synthesis. *Angew. Chem., Int. Ed.* **2011**, *50*, 586−621.

(10) Baur, J. A.; Sinclair, D. A. Therapeutic potential of resveratrol: The in vivo evidence. *Nat. Rev. Drug Discovery* **2006**, *5*, 493−506.

(11) El-Seedi, H. R.; El-Said, A. M. A.; Khalifa, S. A. M.; Goransson, U.; Bohlin, L.; Borg-Karlson, A. K.; Verpoorte, R. Biosynthesis, natural sources, dietary intake, pharmacokinetic properties, and biological activities of hydroxycinnamic acids. *J. Agric. Food Chem.* **2012**, *60*, 10877−10895.

(12) Wright, J. S.; Johnson, E. R.; DiLabio, G. A. Predicting the activity of phenolic antioxidants: Theoretical method, analysis of substituent effects, and application to major families of antioxidants. *J. Am. Chem. Soc.* **2001**, *123*, 1173−1183.

(13) Bast, A.; Haenen, G. Ten misconceptions about antioxidants. *Trends Pharmacol. Sci.* **2013**, *34*, 430−436.

(14) Jones, D. P.; Go, Y. M. Redox compartmentalization and cellular stress. *Diabetes, Obes. Metab.* **2010**, *12*, 116−125.

(15) Popa-Wagner, A.; Mitran, S.; Sivanesan, S.; Chang, E.; Buga, A. M. ROS and brain diseases: The good, the bad, and the ugly. *Oxid. Med. Cell. Longevity* **2013**, *2013*, 1−14.

(16) Huang, D. J.; Ou, B. X.; Prior, R. L. The chemistry behind antioxidant capacity assays. *J. Agric. Food Chem.* **2005**, *53*, 1841−1856.

(17) Prior, R. L.; Wu, X. L.; Schaich, K. Standardized methods for the determination of antioxidant capacity and phenolics in foods and dietary supplements. *J. Agric. Food Chem.* **2005**, *53*, 4290−4302.

(18) Weseler, A. R.; Bast, A. Pleiotropic-acting nutrients require integrative investigational approaches: The example of flavonoids. *J. Agric. Food Chem.* **2012**, *60*, 8941−8946.

(19) Flohé, L.; Brigelius-Flohé, R.; Saliou, C.; Traber, M. G.; Packer, L. Redox regulation of NF-kappa B activation. *Free Radical Biol. Med.* **1997**, *22*, 1115−1126.

(20) Dalton, T. D.; Shertzer, H. G.; Puga, A. Regulation of gene expression by reactive oxygen. *Annu. Rev. Pharmacol. Toxicol.* **1999**, *39*, 67−101.

(21) MacDonald, R. S.; Wagner, K. Influence of dietary phytochemicals and microbiota on colon cancer risk. *J. Agric. Food Chem.* **2012**, *60*, 6728−6735.

(22) Hwang, S. L.; Shih, P. H.; Yen, G. C. Neuroprotective effects of citrus flavonoids. *J. Agric. Food Chem.* **2012**, *60*, 877−885.

(23) Schafer, F. Q.; Buettner, G. R. Redox environment of the cell as viewed through the redox state of the glutathione disulfide/glutathione couple. *Free Radical Biol. Med.* **2001**, *30*, 1191−1212.

(24) Circu, M. L.; Aw, T. Y. Reactive oxygen species, cellular redox systems, and apoptosis. *Free Radical Biol. Med.* **2010**, *48*, 749−762.

(25) Nathan, C.; Cunningham-Bussel, A. Beyond oxidative stress: An immunologist's guide to reactive oxygen species. *Nat. Rev. Immunol.* **2013**, *13*, 349−361.

(26) Ray, P. D.; Huang, B. W.; Tsuji, Y. Reactive oxygen species (ROS) homeostasis and redox regulation in cellular signaling. *Cell. Signal.* **2012**, *24*, 981−990.

(27) Go, Y. M.; Jones, D. P. Cysteine/cystine redox signaling in cardiovascular disease. *Free Radical Biol. Med.* **2011**, *50*, 495−509.

(28) Rose, S.; Melnyk, S.; Pavliv, O.; Bai, S.; Nick, T. G.; Frye, R. E.; James, S. J. Evidence of oxidative damage and inflammation associated with low glutathione redox status in the autism brain. *Transl. Psychiatry* **2012**, *2*, e134.

(29) Na, H. K.; Surh, Y. J. Modulation of Nrf2-mediated antioxidant and detoxifying enzyme induction by the green tea polyphenol EGCG. *Food Chem. Toxicol.* **2008**, *46*, 1271−1278.

(30) Kemp, M.; Go, Y. M.; Jones, D. P. Nonequilibrium thermodynamics of thiol/disulfide redox systems: A perspective on redox systems biology. *Free Radical Biol. Med.* **2008**, *44*, 921−937.

(31) Go, Y. M.; Jones, D. P. The redox proteome. *J. Biol. Chem.* **2013**, *288*, 26512−26520.

(32) Moriarty-Craige, S. E.; Jones, D. P. Extracellular thiols and thiol/disulfide redox in metabolism. *Annu. Rev. Nutr.* **2004**, *24*, 481−509.
(33) Kim, E.; Gordonov, T.; Bentley, W. E.; Payne, G. F. Amplified and in situ detection of redox-active metabolite using a biobased redox capacitor. *Anal. Chem.* **2013**, *85*, 2102−2108.
(34) Kim, E.; Gordonov, T.; Liu, Y.; Bentley, W. E.; Payne, G. F. Reverse engineering to suggest biologically relevant redox activities of phenolic materials. *ACS Chem. Biol.* **2013**, *8*, 716−724.
(35) Liu, Y.; Kim, E.; Lee, M. E.; Zhang, B.; Elabd, Y. A.; Wang, Q.; White, I. M.; Bentley, W. E.; Payne, G. F. Enzymatic writing to soft films: Potential to filter, store, and analyze biologically relevant chemical information. *Adv. Funct. Mater.* **2014**, 480−491.
(36) Kim, E.; Liu, Y.; Leverage, W. T.; Yin, J.-J.; White, I. M.; Bentley, W. E.; Payne, G. F. Context-dependent redox properties of natural phenolic materials. *Biomacromolecules* **2014**, *15*, 1653−1662.
(37) Liu, Y.; Kim, E.; White, I. M.; Bentley, W. E.; Payne, G. F. Information processing through a bio-based redox capacitor: Signatures for redox-cycling. *Bioelectrochemistry* **2014**, *98*, 94−102.
(38) Perez-Jimenez, J.; Neveu, V.; Vos, F.; Scalbert, A. Identification of the 100 richest dietary sources of polyphenols: An application of the Phenol-Explorer database. *Eur. J. Clin. Nutr.* **2010**, *64*, S112−S120.
(39) Jirovetz, L.; Buchbauer, G.; Stoilova, I.; Stoyanova, A.; Krastanov, A.; Schmidt, E. Chemical composition and antioxidant properties of clove leaf essential oil. *J. Agric. Food Chem.* **2006**, *54*, 6303−6307.
(40) Kim, E.; Liu, Y.; Baker, C. J.; Owens, R.; Xiao, S.; Bentley, W. E.; Payne, G. F. Redox-cycling and $H_2O_2$ generation by fabricated catecholic films in the absence of enzymes. *Biomacromolecules* **2011**, *12*, 880−888.
(41) Kim, E.; Liu, Y.; Shi, X.-W.; Yang, X.; Bentley, W. E.; Payne, G. F. Biomimetic approach to confer redox activity to thin chitosan films. *Adv. Funct. Mater.* **2010**, *20*, 2683−2694.
(42) Espey, M. G. Role of oxygen gradients in shaping redox relationships between the human intestine and its microbiota. *Free Radical Biol. Med.* **2013**, *55*, 130−140.
(43) Circu, M. L.; Aw, T. Y. Intestinal redox biology and oxidative stress. *Semin. Cell Dev. Biol.* **2012**, *23*, 729−737.
(44) Lin, X.; Ni, Y.; Kokot, S. Electrochemical mechanism of eugenol at a Cu doped gold nanoparticles modified glassy carbon electrode and its analytical application in food samples. *Electrochim. Acta* **2014**, *133*, 484−491.
(45) Saura-Calixto, F. Dietary fiber as a carrier of dietary antioxidants: An essential physiological function. *J. Agric. Food Chem.* **2011**, *59*, 43−49.
(46) Saura-Calixto, F. Concept and health-related properties of nonextractable polyphenols: The missing dietary polyphenols. *J. Agric. Food Chem.* **2012**, *60*, 11195−11200.
(47) Perez-Jimenez, J.; Torres, J. L. Analysis of nonextractable phenolic compounds in foods: The current state of the art. *J. Agric. Food Chem.* **2011**, *59*, 12713−12724.
(48) Celik, E. E.; Gokmen, V.; Fogliano, V. Soluble antioxidant compounds regenerate the antioxidants bound to insoluble parts of foods. *J. Agric. Food Chem.* **2013**, *61*, 10329−10334.
(49) Fujisawa, S.; Atsumi, T.; Kadoma, Y.; Sakagami, H. Antioxidant and prooxidant action of eugenol-related compounds and their cytotoxicity. *Toxicology* **2002**, *177*, 39−54.
(50) Atsumi, T.; Iwakura, I.; Fujisawa, S.; Ueha, T. Reactive oxygen species generation and photo-cytotoxicity of eugenol in solutions of various pH. *Biomaterials* **2001**, *22*, 1459−1466.

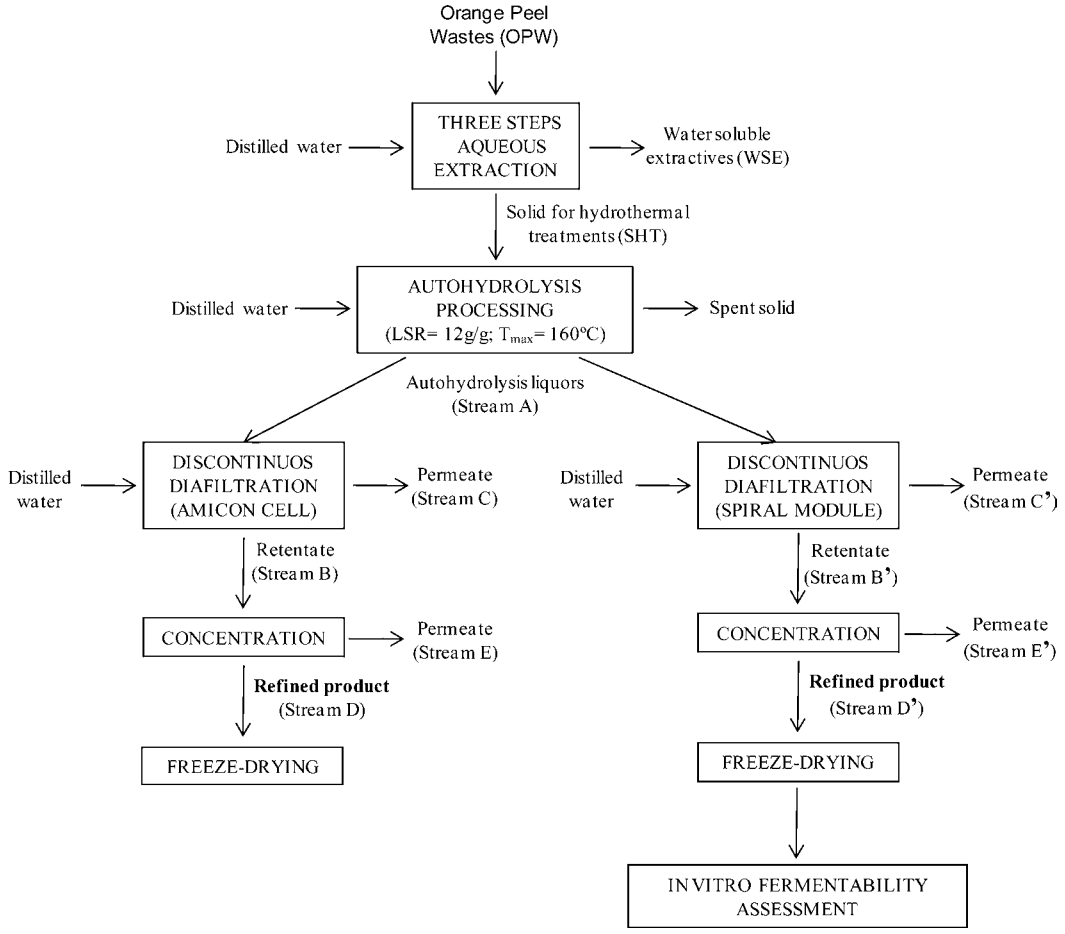


**Figure 1.** Scheme of the process.

and/or concentrating the mixtures of oligosaccharides (OS) generated by hydrothermolysis.[8,12−15]

On the other hand, orange peel wastes (OPW) is also used as raw material for pectin production, which is used in the food industry as an ingredient of drugs used to treat gastrointestinal disorders, diabetes, and high blood pressure or to reduce blood cholesterol.[16−18]

This work deals with (i) the manufacture of POS mixtures obtained from OPW by hydrothermal processing and their refining using membranes; (ii) characterization of the chemical composition and structure of POS; (iii) evaluation of the prebiotic potential of refined POS by in vitro fermentation with human fecal inocula; and (iv) comparison of the POS prebiotic properties with those of orange pectin and commercial FOS. The prebiotic potential of the various substrates was assessed by measuring the dynamics of selected microbial populations using the fluorescent in situ hybridization (FISH) technique, as well as by measuring gas generation, pH, and production of short-chain fatty acids (SCFAs).

## MATERIALS AND METHODS

**Raw Material.** OPW samples were kindly supplied by Indulleida S.A. (Lleida, Spain). To avoid variations in the composition of the raw material, all of the samples were mixed in a single lot, which was stored at −18 °C until use. When necessary, a portion of this lot was defrosted, milled, and used for analytical determinations or processing according to the methods listed below.

**Production and Purification of Pectin-Derived Oligosaccharides.** POS-containing liquors were obtained by OPW hydrothermal treatment under conditions reported as optimal (maximum temperature, 160 °C; severity factor of 288 min)[6] and purified by a two-step membrane process (discontinuous diafiltration and concentration) according to the scheme shown in Figure 1 and following the same method indicated by Gómez et al.[8] previously. The diafiltered solution was subjected to membrane concentration to reach a volume concentration ratio (VCR) of 3.60.

To assess the scaling of membrane purification, samples were purified in an experimental setup made up of the following elements: a spiral wound membrane (regenerated cellulose, 1 kDa, reference TFF6 from Millipore), a 30 L feed-tank with a coil for temperature control, a diaphragm pump (Hydra-cell, Wanner Engineering Inc.), two pressure gauges at the membrane inlet and outlet to measure the transmembrane pressure (TMP), a needle valve located after the membrane to achieve the desired TMP, and a flowmeter to measure the recirculation flow. Operation was performed at TMP = 4 bar. A total volume of 27 L (4.5 L of stream A and 22.5 L of distilled water) was treated in this setup. The refined product (stream D′) was freeze-dried and used as a carbon source for fermentation.

**Pectin Extraction.** OPW samples were extracted with water to reduce the free sugar content,[6] and pectin was obtained from the insoluble fraction by acid extraction as described Hwang et al.[19]

**POS Mixtures Fractionation by Semipreparative Anion Exchange Chromatography.** A freeze-dried sample from stream D was diluted with water (10.2 mL) to a solute content of 5 g/L, and the solution was loaded into a column (30 × 2.6 cm) containing DEAE-Sepharose CL 6B pre-equilibrated with distilled water. The system was eluted sequentially with distilled water, 0.1 M NaCl, 0.2 M NaCl, and 0.3 M NaCl (1 mL/min, 750 min per solution). Fractions of the eluate (9 mL) were collected and assayed for uronic acids. Four pools were prepared by mixing the appropriate fractions. NaCl-containing pools

were desalted and concentrated by nanofiltration through a 300 Da molecular weight cutoff in the Amicon cell before analysis.

**In Vitro Fermentation Assays.** Samples of refined POS (stream D′ in Figure 1) and orange pectin were assayed for in vitro fermentability according the method of Gullón et al.[15] FOS (Sigma) were included as a positive control, and medium without carbon source was used as negative control. Gas generation was measured by inserting a sterile needle into the butyl rubber septum of each tube, and the pressure buildup in the headspace was measured in milliliters. Cells were harvested by centrifugation (10000 rpm), and the supernatants were filtered through 0.20 mm cellulose acetate membranes (Sartorius stedim biotech, Germany) before HPLC analysis and pH measurement. Cell pellets were used for counting the selected bacterial groups by FISH. All additions and inoculations were carried out under anaerobic conditions, in a cabinet flushed with a gas stream containing 5% $H_2$, 10% $CO_2$, and 85% $N_2$.

*Fluorescent in Situ Hybridization.* Changes in bacterial populations were measured by FISH using synthetic oligonucleotide probes targeting specific regions of the 16S rRNA molecule, labeled with the fluorescent dye Cy3 (Sigma). Assays were performed for the following groups: *Bifidobacterium* (Bif164 probe), *Lactobacillus/Enterococcus* (Lab158 probe), *Bacteroides/Prevotella* (Bac303 probe), *Clostridium histolyticum* group clusters I and II (Chis150 probe), *Atopobium* cluster (Ato291 probe), *Clostridium coccoides/Eubacterium rectale* group (*Clostridium* clusters XIVa+b; Erec482 probe), *Faecalibacterium prausnitzii* and relatives (Fpra655 probe), and *Roseburia intestinalis* subcluster (Rint623 probe).[20,21] Total cell counts were performed by staining with 4′,6-diamidino-2-phenylindole (DAPI). At least 15 fields per sample were considered.

*Statistical Analysis.* Differences in bacterial populations and acid concentrations were tested using one-way analysis of variance (ANOVA) and Tukey's post hoc test. Differences were considered significant when $p < 0.05$.

**Enzymatic Degradation of Refined POS and Pectin.** Five milligrams of refined POS (stream D′) was dissolved into 1 mL of sodium acetate buffer (50 mM, pH 5.4) and incubated in shaken flasks at 40 °C sequentially with pectin lyase (PL) from *Aspergillus niger* for 6 h and endopolygalacturonase (PG) from *Kluyveromyces fragilis* for 18 h.[22] The amount of enzymes was selected to produce low-DP GalA oligomers. After incubation, enzymes were inactivated by heating at 100 °C for 5 min, the digest was centrifuged for 10 min at 19500*g*, and the supernatant was analyzed by high-performance anion exchange chromatography (HPAEC).

**Analytical Methods.** *Analysis of Liquors.* As a first approach, samples of streams A, B, D, B′, and D′ were centrifuged, filtered through 0.45 $\mu$m cellulose acetate membranes, and assayed for GalA, glucose, galactose, arabinose, and acetic acid by HPLC. Analyses were performed using a 1260 series Agilent chromatograph fitted with a refractive index detector and a Bio-Rad Aminex HPX- 87H column, which was eluted with 0.003 M $H_2SO_4$ at 50 °C at 0.6 mL/min. Galactose and arabinose peaks can also include traces of xylose and rhamnose, respectively. The content of nonvolatile compounds (NVC), other nonvolatile compounds (ONVC), and oligomers was calculated as described previously.[8]

To get a more complete information, sugar composition of the final POS stream D′ was also quantified by GC as alditol acetates and the uronic acids were determined colorimetrically with 3-phenylphenol using an automated analyzer.[23] The degree of methylesterification (DM) was determined by a colorimetric method[24] after saponification with 1 M NaOH at room temperature, whereas the degree of acetylation (DA) was analyzed using the Megazyme acetic acid kit.[22] Orange pectin samples were subjected to the same analyses.

*High-Performance Anion-Exchange Chromatography with Pulsed Amperometric Detection (HPAEC-PAD).* The neutral sugar constituents of POS pools (from stream D) isolated by column chromatography were determined by HPAEC-PAD after acid posthydrolysis (4 g sulfuric acid/100 g solution at 121 °C for 20 min).[8] Uronic acids were quantitated by using the method mentioned above (see results in Figure 2).

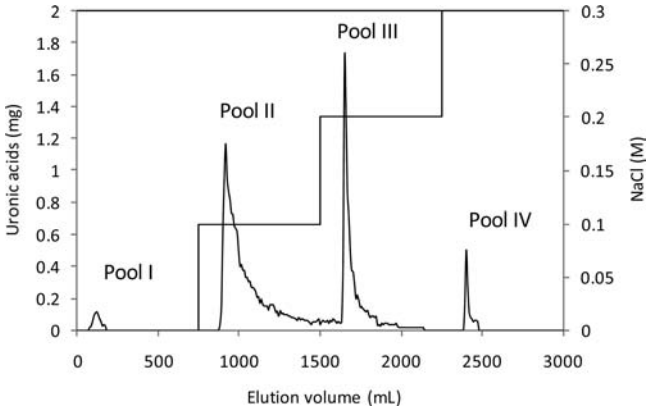


**Figure 2.** Elution profile of GalA (sample from stream D). Pools: eluted with distilled water (pool I), eluted with 0.1 M NaCl (pool II), eluted with 0.2 M NaCl (pool III), and eluted with 0.3 M NaCl (pool IV).

POS in the various process streams were analyzed by HPAEC using an ICS5000 HPAEC instrument (Dionex Corp., Sunnyvale, CA, USA) fitted with pulsed amperometric and diode array detectors (HPAEC-PAD/UV), with a CarboPac PA-1 column (2 mm i.d. × 250 mm) and a CarboPac PA guard column (2 mm i.d. × 25 mm). The flow rate was 0.3 mL/min, and the column temperature was 20 °C. The mobile phases were (A) 0.1 M NaOH and (B) 1 M NaOAc in 0.1 M NaOH. The elution profile was as follows: 0−15 min, 0−5% B; 15−60 min, 5−70% B; 60−65 min, 70−100% B; 65−70 min, 100% B; 70−70.1 min, 100−0% B; and finally column re-equilibration by 0% B from 70.1 to 85 min. Saturated (DP 2−5) and unsaturated (DP 2−6) OGalA and neutral (AraOS and GalOS) standards were used for identification and quantification. The quantification of higher DP OGalA was carried out using the equation

$$\frac{\text{PAD peak area}}{\text{GalA concn}} = k \times \text{DP}^n$$

which relates PAD peak area, GalA concentration, and DP being $k$ = 0.733 and $n$ = −1.06 for saturated OGalA and $k$ = 0.938 and $n$ = −1.42 for unsaturated OGalA.

*High-Performance Size Exclusion Chromatography (HPSEC).* Stream D′ and pectin samples were analyzed by HPSEC using an Ultimate 3000 system (Dionex). A set of four TSK-Gel super AW columns (Tosoh Bioscience, Tokyo, Japan) was used in series: one guard column (6 mm i.d. × 40 mm) and the three separation columns 4000, 3000, and 2500 (6 mm × 150 mm). The column temperature was set at 55 °C, and samples (20 $\mu$L, 2.5 mg/mL) were eluted with filtered 0.2 M $NaNO_3$ at a flow rate of 0.6 mL/min. Elution was monitored using a refractive index detector (Shodex RI 101; Showa Denko K.K., Kawasaki, Japan). Pectin standards were included (82000, 63900, and 51400 Da).

*Hydrophilic Interaction Liquid Chromatography (HILIC).* Pools II and III from stream D were diluted (1:1 v/v) with acetonitrile and analyzed using an Accela UHPLC system (Thermo Scientific, Waltham, MA, USA) coupled to an evaporative light scattering detector (Agilent 1200 series, Gen Tech Scientific Inc., Arcade, NY, USA) and an ESI-IT-MS-detector (LTQ Velos Pro ion trap MS, Thermo Scientific) as described previously by Remoroza et al.[25] Elution was performed at a flow rate of 300 $\mu$L/min and the column temperature was kept at 35 °C. The injection volume was 5 $\mu$L.

The elution profile used was slightly modified: 0−1 min, isocratic 80% B; 1−31 min, linear from 80 to 60% B; followed by column washing, 31−35 min, linear from 60 to 40% B; 35−36 min, 40% B; column re-equilibration; 36−36.1 min, linear from 40 to 80% B; and 36.1−45 min, 80% B.

*Matrix-Assisted Laser Desorption/Ionization-Time of Flight Mass Spectrometry (MALDI-TOF MS).* Pool I was diluted with Millipore water at 1 mg/mL and desalted with AG 50W-X8 resin (Bio-Rad Laboratories, Hercules, CA, USA) (a small amount with a spatula spoon to 50 uL of each sample and desalting was allowed for ∼30 min). After centrifugation for 10 min, 1 $\mu$L of the desalted sample solution was mixed

Table 1. Chemical Composition and Recovery Yields of Process Streams (Expressed as Kilograms per Kilogram NVC)[a]

| | | Amicon cell | | | spiral wound module | | |
|---|---|---|---|---|---|---|---|
| component | feed (stream A) | diafiltrate (stream B) | final retentate (stream D) | recovery yield[b] (%) | diafiltrate (stream B′) | final retentate (stream D′) | recovery yield[b] (%) |
| glucose | 0.060 | 0.013 | 0.003 | 3.57 | 0.013 | 0.004 | 4.14 |
| galactose | 0.064 | 0.014 | 0.004 | 3.78 | 0.014 | 0.005 | 4.29 |
| arabinose | 0.017 | 0.004 | 0.001 | 3.62 | 0.003 | 0.001 | 3.12 |
| galacturonic acid | 0.007 | 0.001 | 0.001 | 8.73 | 0.002 | 0.002 | 13.99 |
| acetic acid | 0.004 | 0.001 | 0.000 | 0.00 | 0.001 | 0.000 | 4.26 |
| GlcOS | 0.020 | 0.014 | 0.009 | 30.69 | 0.011 | 0.006 | 18.6 |
| GalOS | 0.120 | 0.158 | 0.165 | 92.98 | 0.152 | 0.158 | 76.84 |
| AraOS | 0.180 | 0.247 | 0.253 | 91.80 | 0.238 | 0.243 | 78.88 |
| AcO | 0.011 | 0.012 | 0.013 | 80.03 | 0.013 | 0.013 | 71.40 |
| OGalA | 0.378 | 0.493 | 0.534 | 95.42 | 0.453 | 0.480 | 74.18 |
| ONVC | 0.144 | 0.046 | 0.017 | 8.11 | 0.100 | 0.088 | 35.93 |

[a]NVC content in stream A, 0.041 kg NVC/kg liquor; NVC content in stream B, 0.030 kg NVC/kg liquor; NVC content in stream D, 0.098 kg NVC/kg liquor; NVC content in stream B′, 0.031 kg NVC/kg liquor; NVC content in stream D′, 0.103 kg NVC/kg liquor. [b]Taking into account both stages of diafiltration and concentration.

on a MALDI plate (Bruker Daltonics, Bremen, Germany) with 1 μL of matrix solution (25 mg/mL 2,5-dihydroxy benzoic acid, Bruker Daltonics) in 50% (v/v) acetonitrile and dried under an air stream. MALDI-TOF MS analysis was performed using an Ultraflex workstation (Bruker Daltonics) equipped with a nitrogen laser of 337 nm, operated in positive mode with a laser power intensity of 60%. After a delayed extraction time of 350 ns, the ions were accelerated to a kinetic energy of 22 kV before detection. The mass spectrometer was calibrated with a mixture of maltodextrins (Avebe, Foxhol, The Netherlands; MD20; mass range $m/z$ 500−2000). The data were processed using the Bruker Daltonics flexAnalysis software.

*Determination of Carbohydrates and Fermentation Products in Cell-Free Supernatants.* Supernatants from the anaerobic culture tubes inoculated with fecal inocula were filtered through 0.2 μm cellulose acetate membranes and analyzed by HPLC for monosaccharides, OS, formate, lactate, succinate, and SCFA (acetic, propionic, and butyric acids) using the method described under (Analysis of Liquors).

## RESULTS AND DISCUSSION

**Production, Purification, and Chemical Characterization of POS.** The hydrothermal processing of OPW led to a POS-containing liquid phase, which was refined by membrane filtration to obtain a purified product with prebiotic potential. Figure 1 shows the general flow of the process, and Table 1 lists compositional and recovery data.

Stream D was enriched in OS (AraOS, 25.3%; OGalA, 53.4%; and GalOS, 16.5%) and presented a low content of nonvolatile, nonsaccharide compounds (1.7 g ONVC/100 g NVC), at high OS recovery yields (91.8−95.4%). In comparison, >90% of ONVC were removed. These results confirmed the suitability of the process considered in this study for manufacturing high-purity POS.

Figure 2 shows the elution profile of OGalA determined for the refined product (stream D). The samples corresponding to the four main peaks were combined in four pools (I−IV), obtained by elution with distilled water and a stepwise NaCl gradient. Table 2 shows the monomer composition of the various samples. Pool I contained 94.6% of neutral oligomers, whereas other pools were characterized by high contents of acidic oligomers (especially pool II, with about 85% GalA present). The presence of oligomer compounds in pools I−III was confirmed by HPSEC analysis (data not shown). Pools II and III accounted for 40.2 and 29.3%, respectively, of the refined product (stream D), whereas pool IV was of minor importance in quantitative terms (5.1%).

Table 2. Yields and Compositions of Pools of the Refined Product in Stream D

| | pool I | pool II | pool III | pool IV | refined product (stream D) |
|---|---|---|---|---|---|
| yield[a] (%) | 26.1 | 40.2 | 29.3 | 5.1 | |
| monomer composition (%) | | | | | |
| rhamnose | 1.36 | 1.30 | 4.27 | 6.89 | 2.4 |
| arabinose | 65.21 | 5.21 | 7.31 | 6.88 | 23.2 |
| galactose | 20.41 | 6.99 | 18.28 | 10.88 | 14.9 |
| glucose | 3.12 | 0.19 | 0.06 | 0.17 | 1.2 |
| xylose | 4.47 | 0.98 | 0.79 | 2.74 | 1.8 |
| acetic acid | 0.00 | 0.43 | 1.10 | 15.89 | 1.3 |
| galacturonic acid | 5.43 | 84.91 | 68.18 | 56.54 | 54.5 |

[a]Yield expressed as mg saccharides/100 mg refined product applied to column.

As expected, arabinose was the major component of pool I (65.2%), followed by galactose (20.4%). Rhamnose accounted for 6.89 wt % of pool IV, in comparison with 1.36 and 1.30 wt % for pools I and II, respectively.

Additional information on the structure and molar mass distribution of pools I, II, and III was obtained by HPAEC-PAD analysis (pool IV was not analyzed because of its low relative abundance). In agreement with the compositional data in Table 2, the elution profiles in Figure 3 confirmed the presence of both AraOS of DP 4−11 (and higher but showing minor response areas) and several types of GalOS (DP > 5) in pool I as identified by available standards. Pools II and III showed rather similar elution profiles (but with different relative responses, being higher in pool II), characterized by the presence of both saturated and unsaturated OGalA of DP 2−12. As reported previously,[8,26] the explanation of finding similar peaks in both chromatograms could be related to the DM; its value affects the order of elution in a DEAE-Sepharose CL 6B column. In fact, the average DM was higher for oligomers in pool II than in pool III (65.4 vs 59.3%). However, other different compounds could be present in both pools; HPSEC profiles (data not shown) demonstrated the presence of higher molecular weight compounds in pool III.

Additional information for pools II and III was obtained by HILIC-ELSD-MS. Figure 4 shows the HILIC chromatograms. The major peaks in pool II corresponded to $GalA_4Me$ ($4^{10}$), $UGalA_7Me_3$ ($U7^{30}$), $GalA_8Me_4$ ($8^{40}$), and $GalA_8Me_3$ ($8^{30}$),


dx.doi.org/10.1021/jf503475b | J. Agric. Food Chem. 2014, 62, 9769−9782

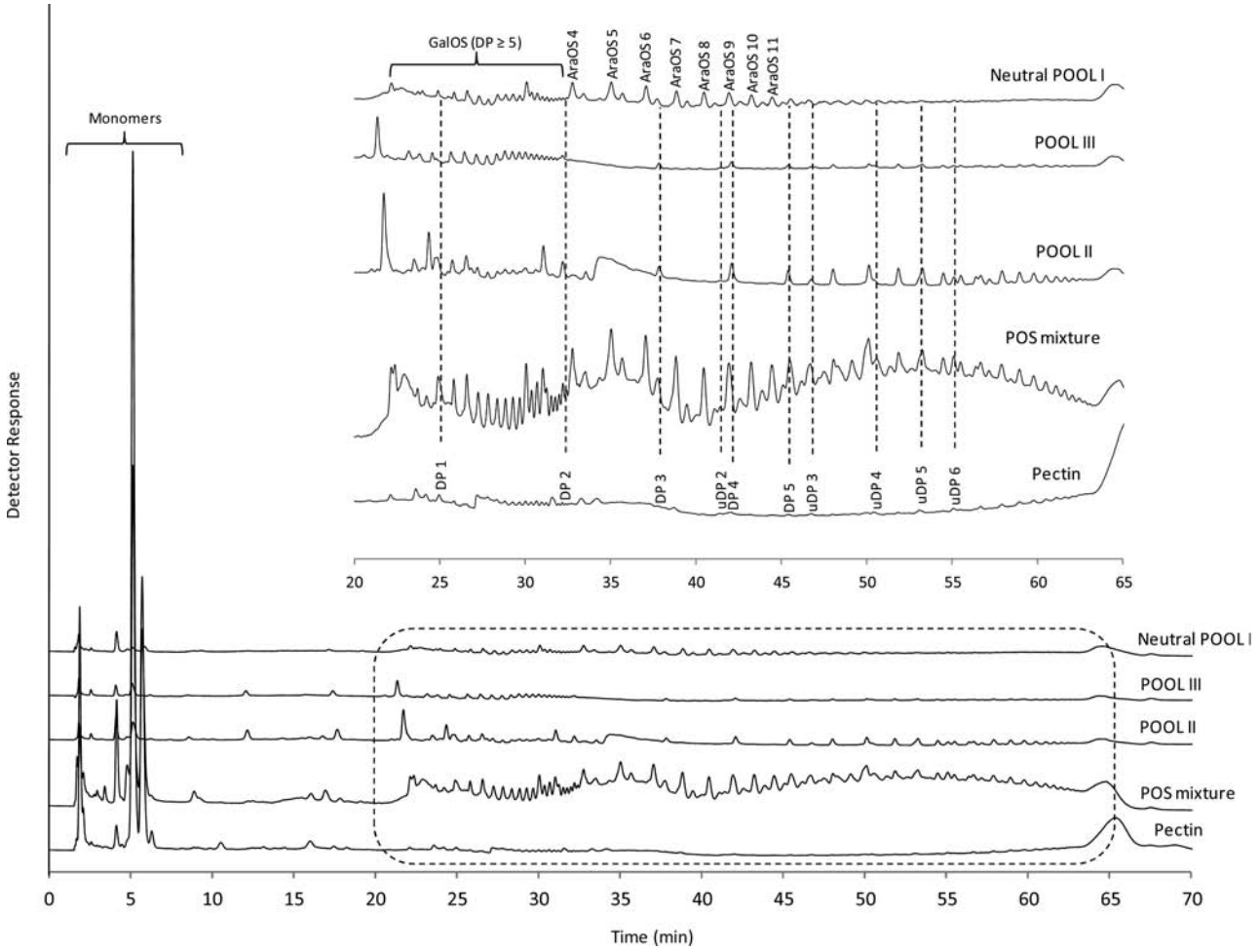


**Figure 3.** HPAEC-PAD chromatograms recorded for pectin, POS, pools I–III (from stream D), and standards (GalOS, AraOS, and OGalA).

| RT (min) | 13.47 | 18.10 | 22.40 | 23.67 | 25.40 | 26.05 | 28.95 | 29.69 | 30.81 | 31.71 | 33.71 | 35.19 | 35.51 | 35.66 | 36.30 | 36.78 | 36.87 | 41.42 |
|---|---|---|---|---|---|---|---|---|---|---|---|---|---|---|---|---|---|---|
| m/z | 1680.86 | 711.26 | 369.09 | 559.09 | 749.18 | 907.18 | 645.26 | 545.17 | 735.18 | 638.26 | 922.26 | 550.17 | 740.18 | 1553.69 | 733.26 | 1106.27 | 1596.78 | 1777.28 |
| Structure | $Hex_7Pent_4$ | - | $2^{00}$ | $3^{10}$ | $4^{20}$ | $U5^{20}$ | $U7^{40}$ | $3^{00}$ | $4^{10}$ | $U7^{30}$ | $5^{20}$ | $6^{20}$ | $8^{40}$ | - | $8^{30}$ | $12^{60}$ | $U9^{10}$ | $10^{00}$ |

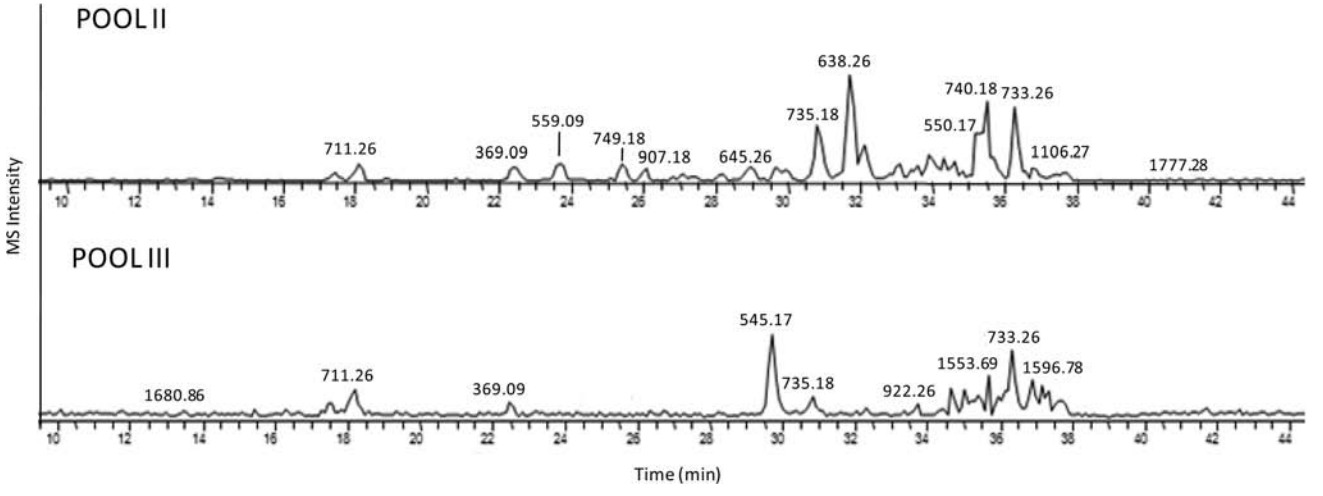


**Figure 4.** HILIC elution profile determined for acidic pools II and III. Structure annotation: $U5^{20}$ DP 5; two O-methyl esters and 0 *O*-acetyl group; U, unsaturated GalA.


dx.doi.org/10.1021/jf503475b | *J. Agric. Food Chem.* 2014, 62, 9769–9782

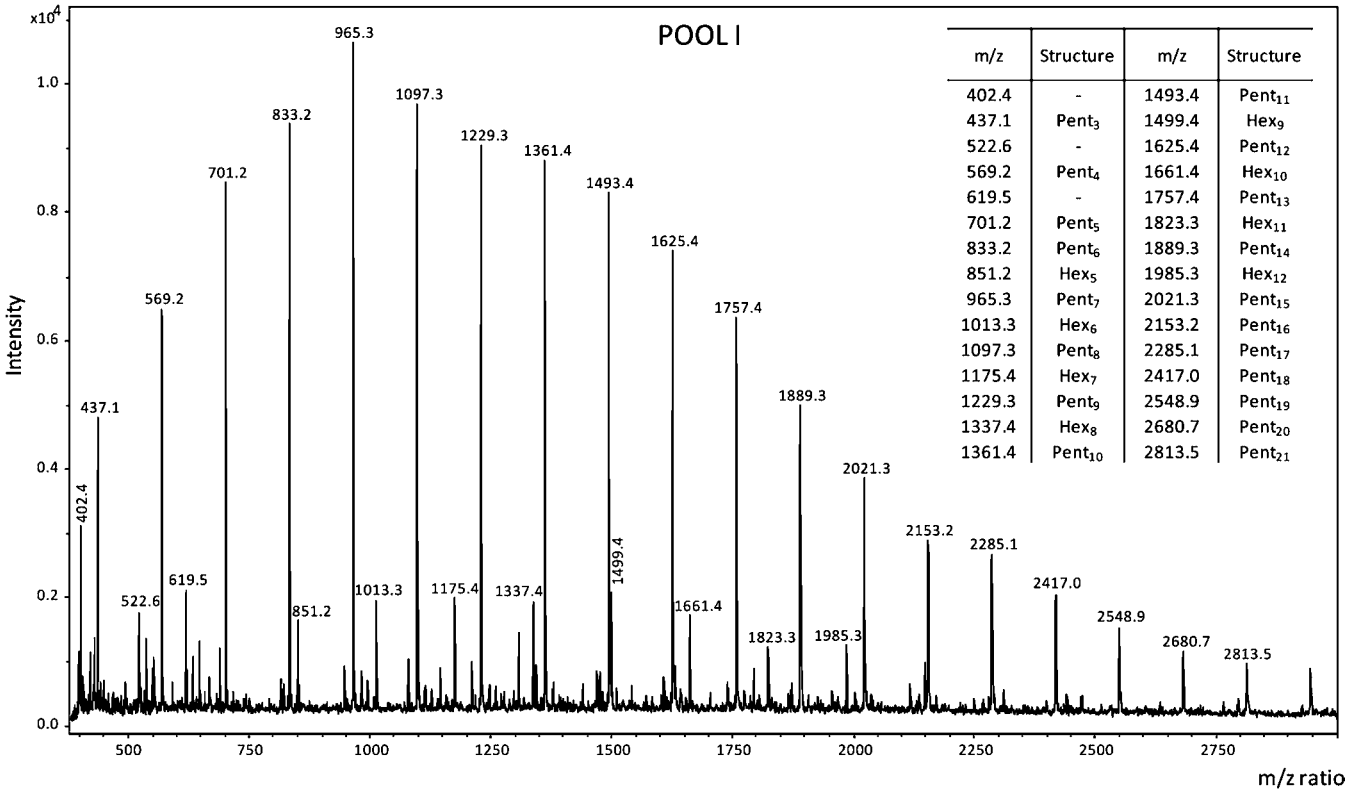


| m/z | Structure | m/z | Structure |
|---|---|---|---|
| 402.4 | - | 1493.4 | $Pent_{11}$ |
| 437.1 | $Pent_3$ | 1499.4 | $Hex_9$ |
| 522.6 | - | 1625.4 | $Pent_{12}$ |
| 569.2 | $Pent_4$ | 1661.4 | $Hex_{10}$ |
| 619.5 | - | 1757.4 | $Pent_{13}$ |
| 701.2 | $Pent_5$ | 1823.3 | $Hex_{11}$ |
| 833.2 | $Pent_6$ | 1889.3 | $Pent_{14}$ |
| 851.2 | $Hex_5$ | 1985.3 | $Hex_{12}$ |
| 965.3 | $Pent_7$ | 2021.3 | $Pent_{15}$ |
| 1013.3 | $Hex_6$ | 2153.2 | $Pent_{16}$ |
| 1097.3 | $Pent_8$ | 2285.1 | $Pent_{17}$ |
| 1175.4 | $Hex_7$ | 2417.0 | $Pent_{18}$ |
| 1229.3 | $Pent_9$ | 2548.9 | $Pent_{19}$ |
| 1337.4 | $Hex_8$ | 2680.7 | $Pent_{20}$ |
| 1361.4 | $Pent_{10}$ | 2813.5 | $Pent_{21}$ |

**Figure 5.** MALDI-TOF mass spectrum of neutral pool I.

whereas $GalA_2$ ($2^{00}$), $GalA_3Me$ ($3^{10}$), $GalA_4Me_2$ ($4^{20}$), $UGalA_5Me_2$ ($U5^{20}$), $UGalA_7Me_4$ ($U7^{40}$), and $GalA_{12}Me_6$ ($12^{60}$) appeared in minor amounts. Pool III contained some of these components, together with $GalA_3$ ($3^{00}$) and $UGalA_9Me$ ($U9^{10}$).

The components of pool I were characterized by MALDI-TOF MS. Figure 5 illustrates the structure of neutral oligosaccharides. High-intensity signals appeared at intervals of 132 $m/z$ units, corresponding to pentose moieties. On the basis of the compositional data in Table 2, it can be inferred that these oligomers correspond to AraOS with DP in the range of 3−21. In addition, lower signals separated by 162 $m/z$ units (corresponding to hexose units) also appeared, confirming the presence of DP 5−12 oligomers mainly made up of galactose.

The use of an Amicon module has an important drawback: its low capacity to produce sufficient amounts of refined product to carry out extensive in vitro and/or in vivo studies on their biological properties or to commercialize it. Therefore, in both situations, a scaleup is needed and, in this work, a spiral wound module was employed (see details under Production and Purification of Pectin-Derived Oligosaccharides).

The POS obtained with the spiral wound membrane (stream D′) contained 89.4 wt % of oligosaccharides (excluding GlcOS), a value in the range reported for commercial prebiotics and in agreement with reported results.[8] Figure 6A shows the HPSEC response for both pectin and stream D′, which presented a wide DP range. Because of this, a sample of POS was subjected to enzymatic degradation with PL and PG. Figure 6B shows the HPAEC chromatogram determined for the hydrolyzed sample. Using both saturated (DP 2−5) and unsaturated (DP 2−6) OGalA standards and the equation mentioned under HPAEC-PAD, in the sample from the D′ stream just 22.31% of the total GalA could be quantified as oligomers with DP ≤ 12, in comparison with 83.90% in the enzymatically hydrolyzed sample. Therefore, >61% of OGalA showed a DP > 12.

In conclusion, AraOS (DP 3-21), GalOS (DP 5−12), and OGalA (DP 2−12, with variable DM) were identified in POS mixtures, in which long-chain products are also present.

**In Vitro Fermentability of POS from OPW.** To evaluate the prebiotic potential of the refined POS contained in stream D′, a comparative in vitro fermentability study was carried out. FOS (which is accepted as the "gold standard" of a prebiotic ingredient) and orange pectin were also employed as fermentation substrates. The effects of the various substrates on the metabolic activity and on the dynamics of the microbial populations were studied in media inoculated with human fecal samples from three healthy adult volunteers (donors A, B, and C).

Figure 7 shows the concentration profiles determined for the various types of OS, which showed the following relative susceptibility to fermentation: GlcOS > GalOS > AraOS > OGalA. During the first 5 h of fermentation, the concentration of GalOS dropped markedly to reach about 50% of the initial value. Oppositely, OGalA presented an almost flat profile in the first hours of fermentation. GlcOS were almost completely consumed after 10 h, whereas the concentrations of GalOS, AraOS, and OGalA decreased to 12, 16, and 33% of the respective initial amounts. Some variability was observed in the data from individual donors: for example, the media inoculated with samples from donor B presented a lower fermentation rate for all of the considered substrates (data not shown).

GalOS, AraOS, and OGalA were progressively consumed: the concentrations were reduced to 8 and 5% of the initial values after 18 and 24 h, respectively. The observed OS consumption pattern was in agreement with reported results.[15] The slow assimilation kinetics of POS suggests that fermentation of these OS in humans may proceed (at least, in part) in the distal part of the


dx.doi.org/10.1021/jf503475b | J. Agric. Food Chem. 2014, 62, 9769−9782

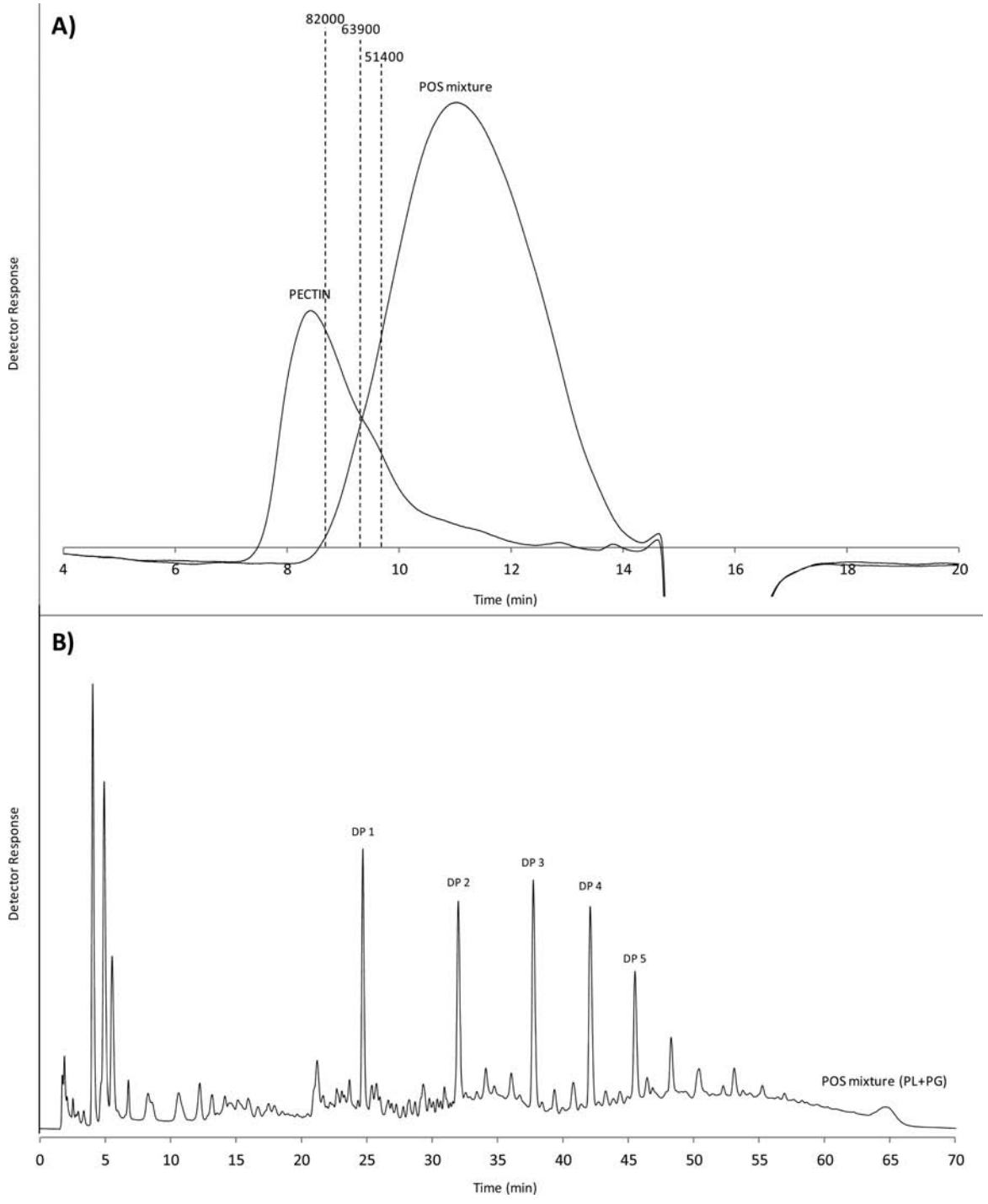


**Figure 6.** (A) HPSEC chromatograms of pectin and POS (stream D′) and (B) HPAEC-PAD chromatogram of POS generated by partial enzymatic hydrolysis. Pectin standards (MW: 82000, 63900, and 51400 Da) are included.

**Table 3. Composition of Stream D′ and Pectin (Data Obtained after Hydrolysis and Monomer Determination by GC as Alditol Acetates)**

| | sugar composition (w/w %) | | | | | | | | |
|---|---|---|---|---|---|---|---|---|---|
| substrate | Rham | Ara | Xyl | Man | Gal | Glc | GalA | DM (%) | DA (%) |
| stream D′ | 0.73 | 19.10 | 0.57 | 1.79 | 13.43 | 2.41 | 42.75 | 59.5 | 8.5 |
| pectin | 0.81 | 9.21 | 0.31 | 0.42 | 6.69 | 2.25 | 49.30 | 56.1 | 3.6 |

colon, where protein fermentation results in the production of potentially harmful compounds such as ammonia, phenol, indols, thiols, amines, and sulfides. Increased SCFA production in the distal colon is expected to result in protective effects.[27]

The chemical structure of oligosaccharides (defined by degree of polymerization, sugar composition, type of linkages, or degree of esterification) is influential in the fermentation rate,[28] becausse defined species and strains of microorganisms show predilection


dx.doi.org/10.1021/jf503475b | J. Agric. Food Chem. 2014, 62, 9769−9782

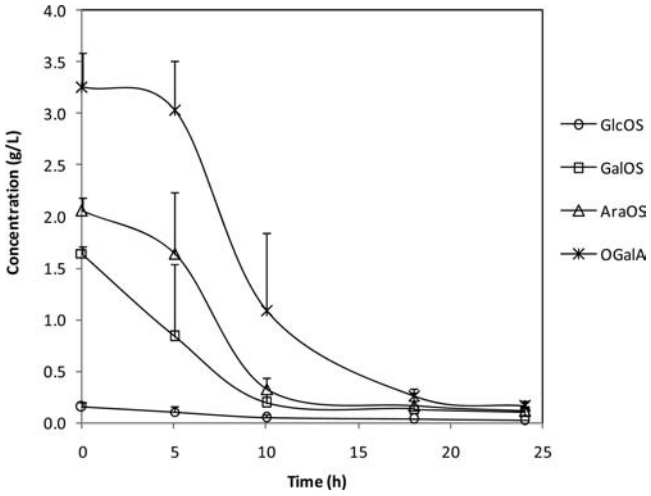


**Figure 7.** Concentration profiles obtained in the in vitro fermentation of the various substrates.

for defined substrates.[29] Fermentation clearly resulted in microbial growth and formation of lactate, gas, SFCA, and other organic acids. Gas production was similar in experiments with POS and FOS (data not shown), with a maximum accumulated production of 22 mL total gas after 48 h. Hernandez-Hernandez et al.[30] and Sarbini et al.[31] also reported on gas generation upon fermentation, which (if excessive) may become an undesirable side effect of prebiotic ingestion.

*Effects on the Microbial Populations.* Table 4 lists the results of bacterial counts corresponding to the various fermentation experiments.

*(a) Total Bacteria (DAPI).* There is strong evidence that the colonic fermentation of prebiotics is influential in the gut function. Fermentation results in increased bacterial mass, increased stool weight (by osmotic water binding), increased stool frequency, and softer stools.[32] The data in Table 4 show that the total cell counts increased markedly with time in media containing suitable carbon sources. In the control experiment, bacterial growth was observed just in the first 5 h of fermentation. In media containing FOS, POS, and pectin, the total cell counts increased by factors of 27−38, with no significant differences among them ($p > 0.05$). This finding is in agreement with data reported for experiments using neutral oligomers and polymers, as well as OGalA and PGalA, as carbon sources.[29]

Lactobacilli, bifidobacteria, and eubacteria are considered to cause health-promoting functions on host health such as inhibition of growth of exogenous and/or harmful bacteria and stimulation of inmune functions and synthesis of vitamins. Clostridia are mainly harmful bacteria, whereas enterococci, bacteroides, and streptococci may cause positive or harmful effects,[33] making individual assessments on the growth pattern of representative bacterial groups necessary.

*(b) Bifidobacterium Genus (Bif164 Probe).* Increased proportions of bifidobacteria and lactobacilli (which are able to convert carbohydrates into acids and generally lack toxicity)[32] are thought to be associated with healthier microbial compositions. The data in Table 4 confirmed a preferential growth of bifidobacteria on the various cultures, (including the control, although statistically significant differences were observed with media containing suitable carbon sources).

In cultures with FOS, orange pectin, and POS, the bifidobacteria counts increased after 24 h by a similar factor (30 on average), confirming the bifidogenic properties of all substrates. This finding is in agreement with the results reported using FOS, apple pectin, and POS derived from apple pectin.[9] The ratio between the counts of bifidobacteria and total cells (expressed as percent) was fairly constant (11.8% at the beginning of the experiment and 11.3% on average during fermentation). The results determined for FOS are in agreement with the data from Onumpai et al.[29] The same authors reported on the inability of acid oligomers to promote bifidobacteria growth, whereas Gullón et al.[15] found that pure bifidobacteria cultures can assimilate neutral OS, but not OGalA. In fact, bifidobacteria can degrade a variety of arabinose and galactose polysaccharides and oligosaccharides.[29] On this basis, the growth of bifidobacteria on POS is preferentially ascribed to utilization of the neutral constituents of oligomers, which account for about 40% of the total. This idea is in agreement with the profiles determined for neutral sugar consumption and relative increase in bifidobaceria counts: both of them took place mainly in the first 5 h or fermentation, a period in which OGalA were scarcely assimilated (see Figure 7). However, other factors (such as structural features of the substrate and individual differences among donors) may also be influential. In a related study, Leijdekkers et al.[34] did not found a clear bifidogenic effect in experiments with POS from sugar beet pulp containing GalOS, AraOS, and mixtures of acidic oligosaccharides (mainly made up of rhamnogalacturonan and homogalacturonan oligosaccharides distinct from the classes of sugar beet POS used previously for in vitro fermentation studies).

*(c) Lactobacillus−Enterococcus Group (Lab158 Probe).* The counts increased upon fermentation of the various substrates, which behave differently. Progressive increases in numbers were observed during fermentations in cultures with pectin and FOS, whereas no significant increases were observed after 5 h in cultures containing POS. This finding is in agreement with the data reported for POS derived from apple.[9] After 24 h of fermentation, the *Lactobacillus−Enterococcus* numbers increased by factors of 76 and 93 in cultures containing FOS and POS, respectively, whereas less marked effects were observed in pectin-containing media (in which the counts increased by a factor of 52). In related studies, Chen et al.[9] reported on the ability of apple-derived POS (sugar composition: GalA, 29.6% w/w; Ara, 18.4%; Gal, 21.1%; Xyl, 8.4%) and FOS for promoting *Lactobacillus* growth, whereas significant effects of inulin and GalOS on *Lactobacillus* growth were also reported.[29] In this latter study, oligorhamnogalacturonides and DP 5 OGalA were found to exert just transient effects. FOS and POS promoted a selective growth of the *Lactobacillus−Enterococcus* group with respect to total cells, increasing its relative proportion from 6.8% at the beginning of fermentations up to 16.2% after 24 h. Considering as a whole the counts of healthy bacteria (*Bifidobacteria* and *Lactobacillus−Enterococcus*), POS and FOS boosted the growth from 18.5 to 27%, whereas the effect of pectin was poorer (accounting for 19.2% of total counts after 24 h).

*(d) Bacteroides−Prevotella Group (Bac303 Probe).* The genus *Bacteroides* is part of the phylum Bacteroidetes, which together with Firmicutes account for about 90% of the human intestinal microbiota. *Bacteroides* may ferment carbohydrates into acetic acid and propionic acid. This latter is considered as a healthy compound that can inhibit the synthesis of cholesterol. However, *Bacteroides* can also produce harmful reactions (for example, amine generation from proteins). From the point of view of this study, this group is important because *Bacteroides* are major carbohydrate-degrading organisms in the gut, which can

**Table 4. Bacterial Populations (Expressed as Log Cells per Milliliter) in Fecal Batch Cultures Using Human Inocula and Different Substrates[a]**

| | | substrate | | | |
|---|---|---|---|---|---|
| probe/stain[b] | time (h) | POS | pectin | FOS | control |
| DAPI | 0 | 8.26 (0.06) | 8.26 (0.06) | 8.26 (0.06) | 8.26 (0.06) |
| | 5 | 9.52 (0.08)b | 9.38 (0.05)b | 9.16 (0.18)b | 8.63 (0.09)b, 2 |
| | 10 | 9.69 (0.01)b, c | 9.62 (0.03)c | 9.60 (0.06)b, c | 8.77 (0.06)b, 2 |
| | 24 | 9.85 (0.03)c | 9.84 (0.02)d | 9.70 (0.09)c | 8.87 (0.03)b, 2 |
| Bif164 | 0 | 7.33 (0.03) | 7.33 (0.03) | 7.33 (0.03) | 7.33 (0.03) |
| | 5 | 8.68 (0.22)b | 8.54 (0.16)b | 8.45 (0.16)b | 8.09 (0.12)b |
| | 10 | 8.78 (0.10)b | 8.74 (0.07)b | 8.76 (0.13)b | 7.98 (0.10)b, 2 |
| | 24 | 8.87 (0.11)b | 8.84 (0.05)b | 8.83 (0.14)b | 8.10 (0.14)b, 2 |
| Lab158 | 0 | 7.09 (0.10) | 7.09 (0.10) | 7.09 (0.10) | 7.09 (0.10) |
| | 5 | 8.63 (0.16)b | 8.30 (0.04)b, 1, 2 | 8.42 (0.15)b | 7.73 (0.15)b, 2 |
| | 10 | 8.79 (0.09)b | 8.61 (0.04)c | 8.69 (0.06)b, c | 7.78 (0.08)b, 2 |
| | 24 | 9.06 (0.03)b | 8.81 (0.03)c, 2 | 8.97 (0.06)c, 1, 2 | 7.95 (0.07)b, 3 |
| Bac303 | 0 | 7.45 (0.02) | 7.45 (0.02) | 7.45 (0.02) | 7.45 (0.02) |
| | 5 | 8.58 (0.10)b | 8.62 (0.13)b | 8.09 (0.13)b, 1, 2 | 7.81 (0.13)a, b, 2 |
| | 10 | 8.76 (0.02)b, c | 8.94 (0.10)b, c | 8.61 (0.06)c | 8.06 (0.13)b, 2 |
| | 24 | 8.89 (0.02)c | 9.07 (0.05)c | 8.89 (0.02)c | 8.12 (0.06)b, 2 |
| Chis150 | 0 | 7.48 (0.06) | 7.48 (0.06) | 7.48 (0.06) | 7.48 (0.06) |
| | 5 | 8.64 (0.11)b | 8.73 (0.13)b | 8.37 (0.25)b, 1, 2 | 7.86 (0.09)a, b, 2 |
| | 10 | 8.97 (0.06)c | 9.00 (0.08)b, c | 8.84 (0.08)b | 8.02 (0.13)b, 2 |
| | 24 | 9.16 (0.02)c, 1, 2 | 9.30 (0.04)c | 8.84 (0.11)b, 2 | 7.87 (0.14)a, b, 3 |
| Ato291 | 0 | 7.28 (0.05) | 7.28 (0.05) | 7.28 (0.05) | 7.28 (0.05) |
| | 5 | 8.52 (0.12)b | 8.47 (0.12)b | 7.98 (0.11)b, 2 | 7.75 (0.06)b, 2 |
| | 10 | 8.56 (0.12)b | 8.37 (0.06)b | 8.21 (0.09)b, 1, 2 | 7.89 (0.04)b, 2 |
| | 24 | 8.75 (0.03)b | 8.56 (0.07)b | 8.43 (0.15)b | 7.84 (0.07)b, 2 |
| Erec482 | 0 | 7.40 (0.13) | 7.40 (0.13) | 7.40 (0.13) | 7.40 (0.13) |
| | 5 | 8.69 (0.15)b | 8.49 (0.19)b | 8.25 (0.17)b, 1, 2 | 7.81 (0.01)2 |
| | 10 | 8.91 (0.05)b | 8.81 (0.11)b | 8.91 (0.12)c | 7.80 (0.23)2 |
| | 24 | 8.81 (0.09)b | 8.89 (0.06)b | 8.75 (0.07)b, c | 7.95 (0.07)2 |
| Fpra655 | 0 | 7.40 (0.14) | 7.40 (0.14) | 7.40 (0.14) | 7.40 (0.14) |
| | 5 | 8.63 (0.11)b | 8.51 (0.16)b | 8.17 (0.12)b, 1, 2 | 7.68 (0.04)a, b, 2 |
| | 10 | 8.84 (0.14)b | 8.59 (0.13)b | 8.50 (0.08)b, 1, 2 | 7.98 (0.12)b, 2 |
| | 24 | 8.77 (0.06)b | 8.79 (0.09)b | 8.59 (0.07)b | 7.96 (0.03)b, 2 |
| Rint623 | 0 | 7.25 (0.22) | 7.25 (0.22) | 7.25 (0.22) | 7.25 (0.22) |
| | 5 | 8.49 (0.15)b | 8.23 (0.17)b | 7.99 (0.06)b, 1, 2 | 7.39 (0.23)2 |
| | 10 | 8.62 (0.13)b | 8.40 (0.17)b | 8.61 (0.12)c | 7.78 (0.07)2 |
| | 24 | 8.67 (0.04)b | 8.51 (0.09)b | 8.68 (0.03)c | 7.86 (0.13)2 |

[a]Standard error is shown in parentheses ($n$ = 3). Different letters for the same probe and same substrate indicate significant differences (Tukey's test, $p < 0.05$) between different time points (no letter = a). Different numbers in the same row indicate significant differences between different substrates (no number = 1). [b]DAPI, 4′,6-diamidino-2-phenylindole; Bif164, *Bifidobacterium*; Lab158, *Lactobacillus/Enterococcus*; Bac303, *Bacteroides/Prevotella*; Chis150, *Clostridium histolyticum* clusters I and II; Ato291, *Atopobium*; Erec482, *Clostridium coccoides/Eubacterium rectale*; Fpra655, *Faecalibacterium prausnitzii*; Rint623, *Roseburia intestinalis*.

degrade pectins.[29] According to the results in Table 4, the population of *Bacteroides*−*Prevotella* in media containing the considered substrates increased significantly and progressively with time. The highest increase in counts (by a factor of 32) was determined for pectin, even if the differences among substrates were not significant after 24 h. Onumpai et al.[29] reported on the ability of this group to grow on a number of acid substrates (PGalA, methylated pectin, DP 9 OGalA, and methylated OGalA) and compounds with neutral chains (including GalOS, AraOS, the corresponding polymers and inulin). In relative terms, the population accounted for a fairly constant fraction of total counts (15.5% at the beginning of experiments and 14.5% after 24 h).

*(e) Clostridium histolyticum Group Clusters I and II (Chis150 Probe).* The data in Table 4 show that proliferation of this group was significant in cultures with FOS during the first


dx.doi.org/10.1021/jf503475b | J. Agric. Food Chem. 2014, 62, 9769−9782

5 h of fermentation, whereas a progressive evolution was observed in media containing pectin or POS. The data obtained after 10 and 24 h revealed no significant count differences between POS and FOS cultures, whereas pectin led to the highest result. In a related study, Salazar et al.[20] reported increased counts of these clusters after 10 h in media containing inulin, whereas significant increases from PGalA (but not from acidic or neutral oligomers and polymers of neutral sugars) have been reported.[29]

Concerning the ratio between the number of this group of cells and the total counts, scarce effects were observed after 24 h in media containing FOS and POS, whereas a higher value was achieved using pectin as a carbon source. From the point of view of the biological effects, this means that the behavior observed for POS is more favorable than the one determined for pectin; in general, clostridia are considered as harmful bacteria.[33]

*(f) Atopobium Cluster (Ato291 Probe).* The *Atopobium* cluster corresponds to a dominant group of human bacteria, but its role is still undefined.[35] Increased counts of the *Atopobium* cluster upon FOS ingestion were reported.[36] In this work, significant population increases were observed after 5 h. After 10 or 24 h, no significant differences among substrates were found, even if the highest values corresponded to POS cultures. The average factor for population increase after 24 h was 21. In relative terms, the ratio with respect to total counts decreased upon fermentation from 0.105 to 0.062.

The results achieved with the major bacterial groups able to produce butyrate from polysaccharides (or from acetic acid or lactic acid by a cross-feeding mechanism) are listed in the next paragraphs. Many investigations have illustrated the beneficial role of butyrate on gut health.[37−39]

*(g) Clostridium coccoides/Eubacterium rectale Group (Clostridium Clusters XIVa+b, Erec482 Probe).* Bacteria of cluster XIVa are considered beneficial because of their ability to produce butyrate from acetate, lactate, and polysaccharides.[28] The data in Table 4 show significant increases in counts during the first 5 h of fermentation, with no significant differences among the various carbon sources. After 24 h, the number of bacteria belonging to this group increased in media containing FOS, POS, or pectin by an average factor of 26. Their ratio with respect to the total counts increased from 0.138 to 0.175 after 10 h, with a further decrease (0.105 after 24 h). Onumpai et al.[29] reported increases in the counts of this type of bacteria in fermentation using AraOS as substrates.

*(h) Part of Clostridium Cluster IV (Faecalibacterium prausnitzii Group, Fpra655 Probe).* *F. prausnitzii* belongs to the *Clostridium* IV cluster, which includes important butyrogenic bacteria, a deficit of which has been related to the recurrence of imflammatory bowel disease and to ulcerative colitis. Significant increases in counts were observed in the period 0−5 h, with variations of minor importance at longer fermentation times. No significant differences among substrates were observed. On average, the numbers of this group of bacteria increased by a factor of 20 upon fermentation, and their ratio with respect to the total counts decreased from 0.138 at the beginning to 0.105 after 10 h and to 0.083 after 24 h. Literature data indicated increased counts of this group when methylated OGalA was fermented and slight decreases when OGalA with DP 5−9 were grown,[29] whereas important increases of *Faecalibacterium* in experiments using POS from sugar beet as a carbon source have also been reported.[34]

*(i) Roseburia intestinalis (Rint623 Probe).* *R. intestinalis* produces butyric acid (a desired and healthy product as it is the major source of energy of epithelial cells and can contribute to the cell proliferation and differentiation) of which counts increased during the first 5 h in experiments with POS and pectin and in the first 10 h in experiments with FOS. The data in Table 4 confirm that the population increased upon fermentation by a factor of 23 as an average for the three substrates, whereas the count ratio respect to total cells decreased from 0.098 to 0.609 upon fermentation.

Finally, it is worth remarking that the sum of the counts of the individual groups determined in this work accounted for 96.2−98.5% of the total cell counts determined by DAPI.

*Effects of the Substrate on Organic Acid Production and pH.* Table 5 lists data concerning SCFA production (averages and standard errors) during the fermentation of the various types of media. All substrates were utilized, causing pH drops that were more marked in experiments with POS and FOS (1.9 and 2.2 units, respectively) than in assays with pectin (pH drop = 1.5 units). The higher pH decrease observed in FOS cultures is in agreement with literature data[34] and is ascribed to the comparatively high lactic acid concentration (a compound of comparatively low $pK_a$). The fairly constant pH observed in the control is ascribed to the limited SCFA production and to the possible neutralization with ammonia produced from protein.

Scarce production of succinic acid was observed, with maximal concentrations (in the range of 1.25−2.2 mM) that were achieved at short fermentation times.

The lactic acid concentration profile showed differences for individual substrates and donors. Low lactic acid concentrations were achieved in the control and in assays with POS and pectin, whereas progressively growing concentrations (up to 22−24 mM in assays with inocula from donors B and C or 14 mM for inocula from donor A) were achieved in FOS cultures. Dependence of the concentration patterns on the considered donor have been reported using inulin as a substrate.[20] The limited lactate concentrations in cultures containing POS or pectin are in agreement with previous studies,[4,15] and its depletion can be due to utilization by other common intestinal bacteria acting as an intermediary metabolite for the formation of additional acetate, propionate, and/or butyrate.[40,41]

Formic acid is an intermediary product mainly produced by bifidobacteria. The data in Table 5 show scarce formic acid production in the control experiment, but significant concentrations in the case of the cultures with FOS, POS, and pectin. Although the cultures with the three carbon sources led to different formic acid concentrations, the observed variations were not statistically significant. The highest final concentrations were achieved in cultures with FOS and pectin, whereas the concentration profiles depended on the considered donor. In experiments with FOS, the cultures with inocula from the various donors led to profiles of similar shape (a fast increase in formic acid concentration followed by a plateau), but the highest final concentration (28 mM) corresponded to the inocula from donor. In experiments with pectin, the maximum concentrations were achieved after 18 h, but the corresponding values were strongly affected by the donor. The fermentation pattern of POS-containing media was similar in media inoculated with samples from donors A and B (steadily increasing concentrations up to a final value in the range of 8.5−13.8 mM), but different from the media made with samples from donor C (in which the concentration reached a maximum value after 10 h and then dropped markedly).

Figure 8 lists data concerning the production of SCFA (acetate, propionate, and butyrate). For a given substrate, the profiles of the total SCFA concentration (including acetate, propionate, and butyrate) were similar in experiments with

Table 5. Concentrations of Formate, Lactate, and Short-Chain Fatty Acids (Millimolar) and pH of Fermentation Media[a]

| | | carbon source | | | |
|---|---|---|---|---|---|
| organic acid | time (h) | POS | pectin | FOS | control |
| lactate | 0 | 0.28 (0.16) | 0.03 (0.01) | 0.07(0.03) | 0.04 (0.01) |
| | 5 | 2.52 (1.23) | 1.77 (0.49) | 4.08 (1.90) | 0.01 (0.00) |
| | 10 | 0.12 (0.12) | 1.49 (0.46) | 10.48 (4.81) | 0.00 (0.00) |
| | 18 | 0.05 (0.03) | 0.00 (0.00) | 16.22 (6.22)b | 0.04 (0.04) |
| | 24 | 0.00 (0.00) | 0.00 (0.00) | 16.03 (7.35) | 0.00 (0.00) |
| | 32 | 0.00 (0.00) | 0.00 (0.00) | 16.84 (8.17) | 0.00 (0.00) |
| | 48 | 0.00 (0.00) | 0.00 (0.00) | 15.62 (7.66) | 0.00 (0.00) |
| formate | 0 | 0.50 (0.25) | 2.12 (0.23)b | 0.00 (0.00) | 0.02 (0.01) |
| | 5 | 2.99 (0.86)a, b | 6.52 (1.75) | 3.65 (1.42)a, b | 0.06 (0.04)b |
| | 10 | 7.32 (1.48)a, b | 15.52 (4.22) | 11.99 (0.90) | 0.21 (0.10)b |
| | 18 | 8.21 (3.26)a, b | 16.42 (4.81) | 16.34 (1.76) | 0.07 (0.03)b |
| | 24 | 6.34 (2.62)a, b | 15.32 (5.31) | 16.70 (2.83) | 0.03 (0.02)b |
| | 32 | 8.06 (3.93)a, b | 11.57 (5.46)a, b | 17.56 (3.12) | 0.00 (0.00)b |
| | 48 | 7.42 (3.57)a, b | 7.06 (3.50)a, b | 18.36 (4.94) | 0.00 (0.00)b |
| acetate | 0 | 3.69 (1.09) | 2.44 (0.42) | 0.49 (0.19) | 3.34 (1.66) |
| | 5 | 19.66 (5.96) | 15.58 (5.17) | 12.68 (4.63) | 4.15 (0.58) |
| | 10 | 55.43 (8.72) | 38.07 (7.85)a, b | 32.22 (3.40)a, b | 10.82 (1.38)b |
| | 18 | 73.32 (1.76) | 48.82 (3.37)b | 44.05 (3.72)b | 20.66 (0.65)c |
| | 24 | 70.18 (8.98) | 54.23 (0.77)a,b | 40.37 (4.59)b, c | 24.27 (0.59)c |
| | 32 | 75.71 (4.70) | 57.60 (0.40)a, b | 40.60 (6.34)b, c | 28.63 (2.57)c |
| | 48 | 78.07 (2.68) | 60.72 (1.42)b | 39.22 (4.42)c | 31.89 (0.66)c |
| propionate | 0 | 0.38 (0.23) | 2.38 (0.17)b | 0.55 (0.40) | 1.17 (0.71)a, b |
| | 5 | 1.04 (0.33) | 4.01 (0.54)b | 1.34 (0.76)a, b | 1.25 (0.77)a, b |
| | 10 | 4.78 (1.36)a, b | 7.98 (1.41) | 3.55 (0.95)a, b | 1.82 (0.22)b |
| | 18 | 7.90 (1.82) | 11.01 (1.72) | 6.92 (2.22) | 4.00 (0.97) |
| | 24 | 8.06 (1.98) | 12.88 (2.80) | 7.10 (1.64) | 4.57 (0.99) |
| | 32 | 9.46 (1.40)a, b | 14.13 (1.81) | 7.47 (1.62)a, b | 5.35 (0.91)b |
| | 48 | 9.17 (1.54) | 15.64 (0.55)b | 8.49 (1.14) | 5.74 (1.08) |
| butyrate | 0 | 0.85 (0.23) | 0.52 (0.14) | 0.49 (0.49) | 0.77 (0.42) |
| | 5 | 2.97 (0.6) | 1.85 (0.74) | 2.78 (0.87) | 0.94 (0.18) |
| | 10 | 9.03 (1.41)a, b | 4.19 (1.57) | 13.10 (3.05)b | 2.50 (0.71) |
| | 18 | 15.17 (1.39) | 7.60 (1.23)a, c | 24.46 (2.94)b | 4.92 (0.72)c |
| | 24 | 15.07 (0.44)a, b | 8.99 (1.12)a, b | 26.08 (7.81) | 5.60 (0.86)b |
| | 32 | 17.58 (1.39)a, b | 10.11 (1.39)a, b | 26.98 (8.53) | 6.48 (0.17)b |
| | 48 | 18.06 (1.22)a, b | 12.28 (1.29)a, b | 27.42 (7.78) | 6.95 (0.58)b |
| total SCFA | 0 | 4.92 (1.52) | 5.33 (0.74) | 1.53 (0.35) | 5.29 (2.30) |
| | 5 | 23.68 (6.50) | 21.43 (6.26) | 16.80 (5.93) | 6.34 (1.44) |
| | 10 | 69.24 (9.11) | 50.24 (8.75) | 48.87 (5.64) | 15.14 (2.29)b |
| | 18 | 96.39 (1.90) | 67.44 (3.03)b | 75.43 (3.68)b | 29.59 (1.31)c |
| | 24 | 93.31 (11.12) | 76.10 (2.49) | 73.55 (2.96) | 34.44 (1.14)b |
| | 32 | 102.75 (4.73) | 81.83 (1.95)b | 75.05 (3.04)b | 40.46 (2.33)c |
| | 48 | 105.30 (2.70) | 88.63 (0.11)b | 75.13 (2.40)c | 44.58 (1.81)d |
| pH | 0 | 6.88 | 7.51 | 6.93 | 6.94 |
| | 5 | 6.37 | 6.76 | 6.41 | 6.91 |
| | 10 | 5.13 | 6.08 | 5.00 | 6.86 |
| | 18 | 5.00 | 5.96 | 4.79 | 6.93 |
| | 24 | 5.00 | 6.11 | 4.80 | 7.00 |
| | 32 | 5.03 | 6.05 | 4.72 | 6.88 |
| | 48 | 5.00 | 5.98 | 4.91 | 6.92 |

[a]Starting concentrations of the test substrates were 1% (w/v). Standard error is shown in parentheses ($n$ = 3). Different letters indicate significant differences ($P < 0.05$) for the same acid and time (no letter = a). Substrates were compared for seven points of fermentation (0, 5, 10, 18, 24, 32, and 48 h).


dx.doi.org/10.1021/jf503475b | J. Agric. Food Chem. 2014, 62, 9769−9782

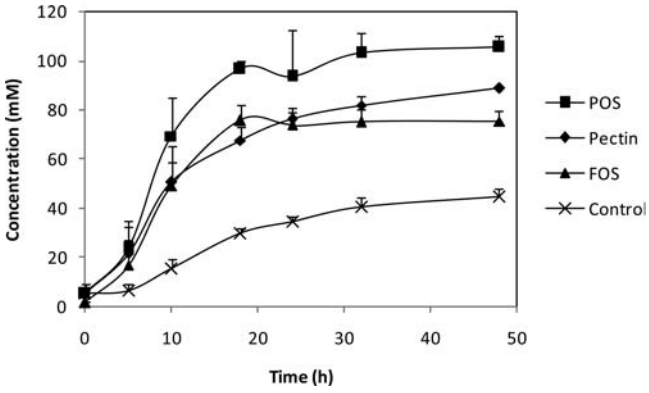


**Figure 8.** Time course of total SCFA production during fermentations.

inocula from the various donors (data not shown). In experiments with FOS, the highest concentration was achieved after 18 h, whereas the assays with pectin and POS showed slower kinetics. The highest SCFA concentration after 48 h (105.3 mM) was obtained using POS, in comparison with 88.6 mM using pectin and 75.1 mM using FOS. Leijdekkers et al.[34] also found higher SCFA concentrations in experiments with POS than with FOS.

Even though the total SCFA concentration profiles presented similar patterns in assays with inocula from the various donors, the product distribution depended on the considered substrate. Acetate was the major individual acid in all cases and was generated mainly in the period 0−18 h, reaching significantly different concentrations in assays with each of the three substrates. The highest concentrations (78.07 mM from POS, 60.72 mM from pectin, and 39.22 mM from FOS) were achieved after 48 h.

A number of studies have confirmed the beneficial effects of butyrate and propionate in gut health. As a consequence, it is important to identify and characterize prebiotics promoting the growth of bacterial groups able to produce butyrate and propionate selectively.

Propionate is mainly produced by *Bacteroides* and other bacteria with the *Clostridium* IX cluster. Propionic acid plays a significant role in lipid metabolism, and the combination of high propionate levels with low acetate/propionate ratios is indicative of hypolipidemic effects.[42] The data in Table 5 show similar propionate concentration profiles in experiments with POS and FOS, whereas the experiments with pectin led to the highest concentration after 48 h, which was statistically different from the ones obtained from POS and FOS. Both the kinetics and the maximum concentrations depended on the considered donor. In general, the media inoculated with samples from donor A exhibited slower kinetics and achieved lower propionate concentrations than in the rest of the cases.

Butyrate, mainly produced by eubacteria and some clostridia, is the major energy source of colonic epithelial cells and may have an impact on growth and cell differentiation. The differences in concentration achieved after 24 h in experiments with the three carbon sources were not significant. The general patterns of the butyrate concentration profiles were similar in experiments with POS, pectin, and FOS, but this latter substrate led to higher a maximum concentration (42 mM) in media inoculated with samples from donor A than in media made with samples from donors B and C (about 19 mM). High butyrate production from POS and FOS has also been reported.[34] In comparative terms, the mass concentration ratio butyrate/SCFA was 0.17 after 24 h, a result significantly higher than the ones reported for assays with POS (concentration ratios below 0.10).[29]

Acetate and butyrate were the major organic acids in POS and FOS fermentation, a finding in agreement with previous studies.[11,13,15] However, when pectin was used as a carbon source, the maximum propionate concentration was higher than the one of butyrate. On the basis of the data listed in Table 4 for the counts of the *Bacteroides*−*Prevotella* group, this finding is ascribed to the metabolic activity of bacteria belonging to the *Bacteroides* group, which are known to be able to produce propionate from carbohydrates[43] and to degrade pectins.[29]

**Conclusions.** POS were manufactured by hydrothermal treatment of orange peel wastes and purified using membranes to yield a refined product containing up to 90% of oligosaccharides. Its prebiotic potential was assessed by in vitro fermentation using human fecal inocula. For comparison, the same type of experimental work was performed using pectin and commercial FOS as carbon sources. The evolution of selected microbial populations was measured during fermentations by FISH. Gas generation, pH, and production of SCFA were also measured.

The various types of carbohydrates making part of the POS concentrates were utilized by microorganisms at different rates, the slowest reaction corresponding to OGalA. All of the tested groups of bacteria increased their populations during fermentation, but their relative proportions with respect to total counts were significantly different. POS boosted particularly the growth of lactobacilli, in a way that the ratio between the joint counts of lactobacilli and bifidobacteria and the total cell number increased from 0.17 to 0.27 upon fermentation. POS fermentation resulted in a remarkable generation of SCFA (maximum concentration = 105 mM after 48 h), with a concentration profile defined by the following sequence: acetate > butyrate > propionate. The same sequence was observed for FOS cultures, whereas pectin fermentation led to propionate concentrations higher than the ones of butyrate.

In general terms, fermentation of POS and FOS resulted in similar SCFA distributions, but the kinetics of acid generation was slower for POS, suggesting that they could be fermented (at least in part) in the distal part of the colon, where the associated healthy effects could be more important.

## AUTHOR INFORMATION

### Corresponding Author

*(J.L.A.) Fax: +34 988 38 70 01. E-mail: xluis@uvigo.es.

### Funding

We are grateful to the Spanish Ministry of Science and Innovation (Project Ref. CTQ2008-05322/PPQ) and to Xunta de Galicia (INBIOMED Project) for the financial support of this work. Both projects were partially funded by the FEDER Program of the European Union ("Unha maneira de facer Europa"). B. Gómez thanks the Spanish Ministry of Education, Culture and Sports for her FPU research grant, and B. Gullón thanks the FCT (Fundação para a Ciência e Tecnologia) for her postdoctoral fellowship (Reference SFRH/BPD/79941/2011).

### Notes

The authors declare no competing financial interest.

## ABBREVIATIONS USED

AcO = acetyl substituents in oligomers
AraOS = arabino-oligosaccharides
DAPI = 4′,6-diamidino-2-phenylindole
DA = degree of acetylation
DM = degree of methylation
DP = degree of polymerization

FISH = fluorescent in situ hybridization
FOS = fructo-oligosaccharides
GalA = galacturonic acid
GalOS = galacto-oligosaccharides
GlcOS = gluco-oligosaccharides
HILIC-ELSD MS = hydrophilic interaction liquid chromatography, evaporative light scattering detector mass spectrometry
HPAEC-PAD = high-performance anion exchange chromatography-pulsed amperometric detector
HPLC = high-performance liquid chromatography
HPSEC = high-performance size exclusion chromatography
MALDI-TOF = matrix-assisted laser desorption/ionization-time-of-flight
NVC = nonvolatile compounds
OGalA = oligogalacturonides
ONVC = other nonvolatile compounds
OPW = orange peel wastes
PG = endopolygalacturonase
PGalA = polygalacturonic acid
PL = pectin lyase
POS = pectic oligosaccharides
SCFA = short-chain fatty acids
TMP = transmembrane pressure
VCR = volume concentration ratio

## REFERENCES


(1) Gibson, G. R.; Scott, K. P.; Rastall, R. A.; Tuohy, K. M.; Hotchkiss, A.; Dubert-Ferrandon, A.; Gareau, M.; Murphy, E. F.; Saulnier, D.; Loh, G.; Macfarlane, S.; Delzenne, N.; Ringel, Y.; Kozianowski, G.; Dickmann, R.; Lenoir-Wijnkoop, I.; Walker, C.; Randal, B. Dietary prebiotics: current status and new definition. *Food Sci. Technol. Bull.: Funct. Foods* **2010**, *7*, 1−19.

(2) Gullón, B.; Gómez, B.; Martínez-Sabajanes, M.; Yáñez, R.; Parajó, J. C.; Alonso, J. L. Pectic oligosaccharides: manufacture and functional properties. *Trends Food Sci. Technol.* **2013**, *30*, 153−161.

(3) Mandalari, G.; Nueno Palop, C.; Tuohy, K.; Gibson, G. R.; Bennett, R. N.; Waldron, K. W.; Bisignano, G.; Narbad, A.; Faulds, C. B. *In vitro* evaluation of the prebiotic activity of a pectic oligosaccharide-rich extract enzymatically derived from bergamot peel. *Appl. Microbiol. Biotechnol.* **2007**, *73*, 1173−1179.

(4) Gómez, B.; Gullón, B.; Veiga, A.; Parajó, J. C.; Alonso, J. L. *Searching for New Prebiotics for Elderly: Production and in Vitro Evaluation of Pectic Oligosaccharides from Apple Pomace. The Intestinal Microbiota and Gut Health: Contribution of the Diet, Bacterial Metabolites, Host Interactions and Impact on Health and Disease (ENGIHR)*; IATA (CSIC): Valencia, Spain, Sept 18−20, 2013.

(5) Grohmann, K.; Cameron, R. G.; Buslig, B. S. Fractionation and pretreatment of orange peel by dilute acid hydrolysis. *Bioresour. Technol.* **1995**, *4*, 129−141.

(6) Martínez, M.; Yáñez, R.; Alonso, J. L.; Parajó, J. C. Chemical production of pectic oligosaccharides from orange peel wastes. *Ind. Eng. Chem. Res.* **2010**, *49*, 8470−8476.

(7) Martínez Sabajanes, M.; Yáñez, R.; Alonso, J. L.; Parajó, J. C. Pectic oligosaccharides production from orange peel waste by enzymatic hydrolysis. *Int. J. Food Sci. Technol.* **2012**, *47*, 747−754.

(8) Gómez, B.; Gullón, B.; Yañez, R.; Parajó, J. C.; Alonso, J. L. Pectic-oligosacharides from lemon peel wastes: production, purification and chemical characterization. *J. Agric. Food Chem.* **2013**, *61*, 10043−10053.

(9) Chen, J.; Liang, R.-H.; Liu, W.; Li, T.; Liu, C.-M.; Wu, S.-S.; Wang, Z.-J. Pectic-oligosaccharides prepared by dynamic high-pressure microfluidization and their *in vitro* fermentation properties. *Carbohydr. Polym.* **2013**, *91*, 175−182.

(10) Hotchkiss, A. T.; Olano-Martin, E.; William, E. G.; Gibson, G. R.; Rastall, R. A. Pectic oligosaccharides as prebiotics (Oligosaccharides in Food and Agriculture). *ACS Symp. Ser.* **2003**, *No. 849*, 54−62.

(11) Manderson, K.; Pinart, M.; Tuohy, K. M.; Grace, W. E.; Hotchkiss, A. T.; Widmer, W.; Yadhav, M. P.; Gibson, G. R.; Rastall, R. A. *In vitro* determination of prebiotic properties of oligosaccharides derived from an orange juice manufacturing by-product stream. *Appl. Environ. Microbiol.* **2005**, *71*, 8383−8389.

(12) Vegas, R.; Luque, S.; Álvarez, J. R.; Alonso, J. L.; Domínguez, H.; Parajó, J. C. Membrane-assisted processing of xylooligosaccharide-containing liquors. *J. Agric. Food Chem.* **2006**, *54*, 5430−5436.

(13) Gullón, P.; González-Muñoz, M. J.; van Gool, M. P.; Schols, H. A.; Hirsch, J.; Ebringerová, A.; Parajó, J. C. Production, refining, structural characterization and fermentability of rice husk xylooligosaccharides. *J. Agric. Food Chem.* **2010**, *58*, 3632−3641.

(14) González-Muñoz, M. J.; Santos, V.; Parajó, J. C. Purification of oligosaccharides obtained from *Pinus pinaster* hemicelluloses by diafiltration. *Desalin. Water Treat.* **2011**, *27*, 48−53.

(15) Gullón, B.; Gullón, P.; Sanz, Y.; Alonso, J. L.; Parajó, J. C. Prebiotic potential of a refined product containing pectic oligosaccharides. *LWT−Food Sci. Technol.* **2011**, *44*, 1687−1696.

(16) Paulsen, B. S.; Barsett, H. Bioactive pectic polysaccharides. *Adv. Polym. Sci.* **2005**, *186*, 69−101.

(17) Yamada, H.; Kiyohara, H. Immunomodulating activity of plant poly-saccharides structures. *Comprehensive Glycoscience*; Voragen, A. G. J., Ed.; Elsevier: Amsterdam, The Netherlands, 2007; pp 663−693.

(18) Matsumoto, T.; Moriya, M.; Sakurai, M. H.; Kiyohara, H.; Tabuchi, Y.; Yamada, H. Stimulatory effect of a pectic polysaccharide from a medicinal herb, the roots of *Bupleurum falcatum* L., on G-CSF secretion from intestinal epitherial cells. *Int. Immunopharmacol.* **2008**, *8*, 581−588.

(19) Hwang, J. K.; Kim, C. J.; Kim, C. T. Extrusion of apple pomace facilitates pectin extraction. *J. Food Sci.* **1998**, *63*, 841−844.

(20) Salazar, N.; Ruas-Madiedo, P.; Kolida, S.; Collins, M.; Rastall, R.; Gibson, G.; de los Reyes-Gavilán, C. G. Exoplysaccharides produced by *Bifidobacterium longum* IPLA E44 and *Bifidobacterium animalis* subsp. *lactis* IPLA R1 modify the composition and metabolic activity of human faecal microbiota in pH-controlled batch cultures. *Int. J. Food Microbiol.* **2009**, *135*, 260−267.

(21) Hold, G. L.; Schwiertz, A.; Aminov, R. I.; Blaut, M.; Flint, H. J. Oligonucleotide probes that detect quantitatively significant groups of butyrate-producing bacteria in human feces. *Appl. Environ. Microbiol.* **2003**, *69*, 4320−4324.

(22) Remoroza, C.; Cord-Landwehr, S.; Leijdekkers, A. G. M.; Moerschbacher, B. M.; Schols, H. A.; Gruppen, H. Combined HILIC-ELSD/ESI-MS*n* enables the separation, identification and quantification of sugar beet pectin derived oligomers. *Carbohydr. Polym.* **2012**, *90*, 41−48.

(23) Kühnel, S.; Schols, H. A.; Gruppen, H. Aiming for the complete utilization of sugar-beet pulp: examination of the effects of mild acid and hydrothermal pretreatment followed by enzymatic digestion. *Biotechnol. Biofuels* **2011**, *4*, 14.

(24) Guillotin, S. E.; Van Loey, A.; Boulenguer, P.; Schols, H. A.; Voragen, A. G. J. Rapid HPLC method to screen pectins for heterogeneity in methyl-esterification and amidation. *Food Hydrocolloids* **2007**, *21*, 85−91.

(25) Remoroza, C.; Buchholt, H. C.; Gruppen, H.; Schols, H. A. Descriptive parameters for revealing substitution patterns of sugar beet pectins using pectolytic enzymes. *Carbohydr. Polym.* **2014**, *101*, 1205−1215.

(26) Ralet, M. C.; Cabrera, J. C.; Bonnin, E.; Quéménér, B.; Hellín, P.; Thibault, J. F. Mapping sugar beet pectin acetylation pattern. *Phytochemistry* **2005**, *66*, 1832−1843.

(27) Yang, J.; Maldonado-Gómez, M. X.; Hutkins, R. W.; Rose, D. J. Production and *in vitro* fermentation of soluble, non-digestible, feruloylated oligo- and polysaccharides from maize and wheat brans. *J. Agric. Food Chem.* **2014**, *62*, 159−166.

(28) Cardelle-Cobas, A.; Olano, A.; Corzo, N.; Villamiel, N.; Collins, M.; Kolida, S.; Rastall, R. A. *In vitro* fermentation of lactulose-derived oligosaccharides by mixed fecal microbiota. *J. Agric. Food Chem.* **2012**, *60*, 2024−2032.

(29) Onumpai, C.; Kolida, S.; Bonnin, E.; Rastall, R. A. Microbial utilization and selectivity of pectin fractions with various structures. *Appl. Environ. Microbiol.* **2011**, *77*, 5747−5754.
(30) Hernandez-Hernandez, O.; Côté, G. L.; Kolida, S.; Rastall, R. A.; Sanz, M. L. *In vitro* fermentation of alternansucrase raffinose-derived oligosaccharides by human gut bacteria. *J. Agric. Food Chem.* **2011**, *59* (20), 10901−10906.
(31) Sarbini, S. R.; Kolida, S.; Naeye, T.; Einerhand, A. W.; Gibson, G. R.; Rastall, R. A. The prebiotic effect of $\alpha$-1,2 branched, low molecular weight dextran in the batch and continuous faecal fermentation system. *J. Funct. Foods* **2013**, *5*, 1938−1946.
(32) Nino Bins, 2013; www.sepyp.es (last accessed June 2014).
(33) Ladirat, S. E. Galacto-oligosaccharides to counter the side effects of antibiotic treatments. Ph.D. Thesis, Wageningen University (ISBN 978-94-6173-839-4), 2014.
(34) Leijdekkers, A. G. M.; Aguirre, M.; Venema, K.; Bosch, G.; Gruppen, H.; Schols, H. A. In vitro fermentability of sugar beet pulp derived oligosaccharides using human and pig fecal inocula. *J. Agric. Food Chem.* **2014**, *62*, 1079−1087.
(35) Jia, J.; Frantz, N.; Khoo, C.; Gibson, G. R.; Rastall, R. A.; McCartney, A. L. Investigation of the faecal microbiota associated with canine chronic diarrhea. *FEMS Microbiol. Ecol.* **2010**, *71*, 304−312.
(36) Saulnier, D. M.; Gibson, G. R.; Kolida, S. *In vitro* effects of selected synbiotics on the human faecal microbiota composition. *FEMS Microbiol. Ecol.* **2008**, *66*, 516−527.
(37) Pryde, S. E.; Duncan, S. H.; Hold, G. L.; Stewart, C. S.; Flint, H. J. The microbiology of butyrate formation in the human colon. *FEMS Microbiol. Lett.* **2002**, *217*, 133−139.
(38) Hamer, H. M.; Jonkers, D.; Venema, K.; Vanhoutvin, S.; Troost, F. J.; Brummer, R.-J. Review article: The role of butyrate on colonic function. *Aliment. Pharmacol. Ther.* **2008**, *27*, 104−119.
(39) Scott, K. P.; Martin, J. C.; Duncan, S. H.; Flint, H. J. Prebiotic stimulation of human colonic butyrate-producing bacteria and bifidobacteria *in vitro*. *FEMS Microbiol. Ecol.* **2014**, *87*, 30−40.
(40) Belenguer, A.; Duncan, S. H.; Graham Calder, A.; Holtrop, G.; Louis, P.; Lobley, G. E. Two routes of metabolic cross-feeding between *Bifidobacterium adolescentis* and butyrate producing anaerobes from the human gut. *Appl. Environ. Microbiol.* **2006**, *72*, 3593−3599.
(41) Bourriaud, C.; Robins, R. J.; Martin, L.; Kozlowski, F.; Tenailleau, E.; Cherbut, C.; Michel, C. Lactate is mainly fermented to butyrate by human intestinal microfloras but inter-individual variation is evident. *J. Appl. Microbiol.* **2005**, *99*, 201−212.
(42) Delzenne, N. M.; Kok, N. Effects of fructans-type prebiotics on lipid metabolism. *Am. J. Clin. Nutr.* **2001**, *73*, 456S−458S.
(43) Hughes, S. A.; Shewry, P. R.; Gibson, G. R.; McCleary, B. V.; Rastall, R. A. *In vitro* fermentation of oat and barley derived $\beta$-glucans by human faecal microbiota. *FEMS Microbiol. Ecol.* **2008**, *64*, 482−493.

regulate protein translation.[34] Because broiler chicks go through intensive protein synthesis during the growth, it is not only novel but also relevant to determine effects of the dietary microalgal biomass inclusion on their functional expression of signal proteins involved in the mTOR pathway.

Just as broiler chicks, weanling pigs grow at a fast rate with intensive protein metabolism.[35] Likewise, our previous research[13] showed that weanling pigs grew well with diets containing 7.5% DFA to replace corn and soybean meal, but not with 15% DFA replacing corn and soybean meal or 7.5% DFA replacing soybean meal. Subsequently, the same question arose as to whether weanling pigs could tolerate higher inclusion levels of the other apparently "superior" types of defatted microalgal biomass. However, there were different considerations of the pig experiment from those of the broilers. Comparatively, effects of the added microalgal biomass on plasma biochemical measures of nutritional status including tartrate-resistant acid phosphatase (TRAP), alkaline phosphatase (AKP), and alanine aminotransferase (ALT)[8] were less certain than those in the broiler studies. Meanwhile, plasma urea nitrogen (PUN) and amino acid profiles are often used to estimate nutritional values of feed proteins.[36] Apparently, it is more difficult and expensive to sample tissues from pigs than from chicks to study the metabolic regulation of the full production cycle that is likely very different between weanling and finishing pigs.[37,38] Although various sources of NSPases are increasingly added into swine diets containing nonconventional ingredients,[39,40] the general notion remains that these enzymes are more consistently effective[41] in diets for poultry.

Therefore, we conducted two parallel pig and broiler experiments to determine nutritional and metabolic values of a newly acquired defatted green microalgal (DGM, *Desmodesmus* sp., Cellana, Kailua-Kona, HI, USA) biomass from biofuel research that contained 31.2% crude protein. The objective of the pig experiment (I) was to determine impacts of including 10% DGM and (or) 0.06% protease on growth performance and plasma levels of TRAP, AKP, ALT, urea nitrogen, uric acid, and amino acids. The objective of the chick experiment (II) was to determine impacts of including 15% DGM and (or) 0.06% protease or NSP enzymes on growth performance, plasma levels of uric acid and amino acids, and production of signal proteins related to the mTOR pathway in liver and muscle.

## MATERIALS AND METHODS

**Chemicals.** The nutrient composition of the DGM is presented in Table 1. Protease Ronozyme ProAct and NSPase mixture (50% Roxazyme G2, 40% Ronozyme A, and 10% Ronozyme WX) were obtained from DSM Nutritional Products Inc. (Parsippany, NJ, USA). Phthaldehyde complete solution reagent was purchased from Sigma-Aldrich (St. Louis, MO, USA). Kits for determining uric acid, urea nitrogen, and alanine aminotransferase (ALT) were obtained from Thermo Scientific, Inc. (Waltham, MA, USA). Rabbit-anti-$\beta$-actin (4967), rabbit-anti-mTOR (7C10), rabbit-antiphospho-mTOR (S2448), rabbit-anti-S6 (5G10), rabbit-antiphospho-S6 (S235/236), rabbit-anti-S6K1 (49D7), rabbit-antiphospho-S6K1 (T389), rabbit-antiphospho-4E-BP1 (S65), and rabbit-anti-eIF4E (C46H6) monoclonal antibodies were purchased from Cell Signaling Technology, Inc. (Danvers, MA, USA).

**Pig Experiment.** *Experimental Design, Growth Performance, and Blood Sample Collection.* All animal experimental procedures were approved by the Cornell University Institute Animal Care and Use Committee. Weanling Yorkshire × Hampshire × Landrace pigs ($n$ = 32) were allotted into one of four treatment groups in a 2 (DGM: 0 or 10%, on an "as is" basis) × 2 (ProAct: 0 or 0.06%) factorial arrangement ($n$ = 8 pigs per treatment). The experimental diet compositions are presented in Table 2. The inclusion rate of ProAct was based on our previous experiment.[5] All diets were formulated to meet the nutrient requirements of weanling pigs.[42] Pigs were housed in individual pens with a feeder and nipple water drinker. Appropriate feed was weighed out each morning to minimize the amount of spillage. Any spillage was collected and weighed the following morning prior to the addition of fresh feed. Individual pig weights were recorded biweekly for determination of body weight gain and feed conversion efficiency. Blood samples were collected biweekly from the anterior vena cava into heparinized tubes and kept on ice until analyses were completed on the same day.

**Table 1. Nutritional Composition of Defatted Green Marine Microalgal DGM (*Desmodesmus* sp.) Biomass[a]**

| nutrient | % "as is" | amino acid | % "as is" |
|---|---|---|---|
| dry matter | 96.0 | alanine | 2.27 |
| crude protein | 31.2 | arginine | 1.45 |
| crude fat | 1.50 | aspartic acid | 2.69 |
| acid detergent fiber | 15.4 | cysteine | 0.33 |
| neutral detergent fiber | 23.2 | glutamic acid | 2.93 |
| ash | 17.1 | glycine | 1.72 |
| calcium (Ca) | 0.33 | histidine | 0.50 |
| phosphorus (P) | 0.65 | hydroxylysine | 0.37 |
| sodium (Na) | 3.24 | hydroxyproline | 0.07 |
| potassium (K) | 0.89 | isoleucine | 1.10 |
| magnesium (Mg) | 0.63 | leucine | 2.29 |
| | | lysine | 1.61 |
| **mineral** | **mg/kg** | methionine | 0.48 |
| iron (Fe) | 1900 | ornithine | 0.04 |
| copper (Cu) | 16.0 | phenylalanine | 1.34 |
| manganese (Mn) | 154 | proline | 2.73 |
| zinc (Zn) | 34.0 | serine | 1.10 |
| molybdenum (Mo) | 2.4 | taurine | 0.02 |
| selenium (Se) | 0.12 | threonine | 1.26 |
| | | tryptophan | 0.43 |
| | | tyrosine | 1.01 |
| | | valine | 1.59 |

[a]Proximate analysis was carried out by Dairy One Coop Inc. (Ithaca, NY, USA), and amino acids were determined by the Agricultural Experiment Station Chemical Laboratories at the University of Missouri (Columbia, MO, USA).

*Plasma Biochemical Analyses.* Blood samples were centrifuged at 1500$g$ for 20 min to collect plasma. Plasma AKP activity was determined according to the method of Bowers and McComb.[43] Plasma TRAP activity was determined according to the method of Lau et al.[44] with a modification of pH to 5.8. Total plasma amino acid concentration was determined using a modified $o$-phthaldehyde (OPA) derivatization assay. Briefly, phthaldehyde complete reagent was added at equal volume to a plasma aliquot, vortexed, and read within 2 min at 340 nm on a 96-well plate reader (Biotek Instruments, Inc., Winooski, VT, USA). Plasma uric acid, urea nitrogen, and ALT were assayed using the above-described commercial kits.

**Broiler Experiment.** *Experimental Design, Growth Performance, and Sample Collection.* Ross 308 broiler chicks were received at 1 day of age and assigned to one of six treatment groups in a randomized complete block design. A 2 (DGM: 0 or 15%, on an "as is" basis) × 3 (enzyme: none, ProAct, and NSPase) factorial arrangement was used within each block. Each treatment consisted of five battery cages (five birds/cage), and each cage was considered a replicate. The compositions of the control and the DGM-containing diets are shown in Table 3. Both protease and NSPase were incorporated at 0.06% on the basis of our previous experiments.[5] Birds were housed within Petersime battery cages and allowed ad libitum access to feed and water. Birds were fed the starter diet from day 1 to day 21 and the grower diet from day 22 to day 42 (Table 3). All diets were formulated

**Table 2. Nutritional Composition of Swine Experimental Diets**

| ingredient | control | control + protease | DGM[a] | DGM + protease |
|---|---|---|---|---|
| corn (yellow) (%) | 64.0 | 64.0 | 62.3 | 62.3 |
| soybean meal (48.5% CP) (%) | 28.1 | 28.1 | 20.0 | 20.0 |
| DGM (%) | 0.00 | 0.00 | 10.0 | 10.0 |
| corn oil (%) | 2.00 | 2.00 | 3.00 | 3.00 |
| dicalcium phosphate (%) | 1.50 | 1.50 | 1.50 | 1.50 |
| plasma protein (%) | 0.00 | 0.00 | 1.20 | 1.20 |
| limestone (%) | 0.70 | 0.70 | 0.70 | 0.70 |
| L-lysine HCl (%) | 0.25 | 0.25 | 0.35 | 0.35 |
| DL-methionine (%) | 0.01 | 0.01 | 0.01 | 0.01 |
| L-threonine (%) | 0.10 | 0.10 | 0.10 | 0.10 |
| salt (%) | 0.18 | 0.18 | 0.00 | 0.00 |
| vitamin/mineral mix[b] (%) | 0.20 | 0.20 | 0.20 | 0.20 |
| choline (%) | 0.10 | 0.10 | 0.10 | 0.10 |
| enzyme[c] or corn starch (%) | 2.36 | 2.36 | 0.06 | 0.06 |
| antibiotic[d] (%) | 0.50 | 0.50 | 0.50 | 0.50 |
| total (%) | 100 | 100 | 100 | 100 |
| | | | | |
| nutritional composition | | | | |
| ME (kcal/kg) | 3380 | 3380 | 3370 | 3370 |
| protein (%) | 18.0 | 18.0 | 18.1 | 18.1 |
| lysine | 1.09 | 1.09 | 1.11 | 1.11 |
| methionine + cysteine | 0.64 | 0.64 | 0.64 | 0.64 |
| threonine | 0.70 | 0.70 | 0.65 | 0.65 |

[a]DGM, defatted green microalgal (*Desmodesmus* sp.) biomass (Cellana, Kailua-Kona, HI, USA) that contained 31.2% crude protein. [b]Vitamin and mineral premix supplied the following amounts (per kilogram of diet): vitamin A, 2200 IU; vitamin $D_3$, 220 IU; vitamin E, 16 IU; vitamin K, 0.5 mg; biotin, 0.05 mg; choline, 0.5 g; folacin, 0.3 mg; niacin, 15 mg; pantothenic acid, 10 mg; riboflavin, 3.5 mg; thiamin, 1 mg; vitamin $B_6$, 1.5 mg; vitamin $B_{12}$, 17.5 μg; Cu, 6 mg; I, 0.14 mg; Mn, 4 mg; Zn 100 mg; Se, 0.3 mg; Mg, 0.4 mg; and Fe, 80 mg. [c]Ronozyme ProAct (DSM Nutritional Products Inc., Parsippany, NJ, USA). Protease activity was measured in PROT units, where 1 unit is defined as the amount of enzyme that releases 1 μmol of *p*-nitroaniline from 1 μM substrate (Suc-Ala-Ala-Pro-Phe-*p*-nitroaniline) per minute at pH 9.0 and 37 °C. [d]Antibiotic additive (Tylan 10) contained tylosin (as tylosin phosphate) at 22 g/kg.

**Table 3. Nutritional Composition of Poultry Experimental Diets**

| ingredient | control starter | DGM[a] starter | control grower | DGM grower |
|---|---|---|---|---|
| corn (yellow) (%) | 57.0 | 49.0 | 54.4 | 48.2 |
| soybean meal (48.5% CP) (%) | 36.9 | 28.0 | 37.0 | 28.2 |
| DGM[a] (%) | 0.00 | 15.0 | 0.00 | 15.0 |
| corn oil (%) | 1.74 | 3.45 | 4.25 | 5.30 |
| dicalcium phosphate (%) | 1.95 | 1.19 | 1.95 | 1.19 |
| limestone (%) | 1.30 | 1.90 | 1.30 | 1.90 |
| L-lysine HCl (%) | 0.30 | 0.75 | 0.30 | 0.00 |
| DL-methionine (%) | 0.35 | 0.50 | 0.35 | 0.00 |
| salt (%) | 0.25 | 0.00 | 0.25 | 0.00 |
| mineral[b]/vitamin[c] premix (%) | 0.05 | 0.05 | 0.05 | 0.05 |
| choline (%) | 0.10 | 0.10 | 0.10 | 0.10 |
| enzyme[d] or starch (%) | 0.06 | 0.06 | 0.06 | 0.06 |
| total (%) | 100 | 100 | 100 | 100 |
| | | | | |
| nutritional composition | | | | |
| ME (kcal/kg) | 2970 | 3030 | 3100 | 3160 |
| protein (%) | 21.8 | 21.6 | 21.6 | 21.7 |
| lysine (%) | 1.49 | 1.46 | 1.50 | 1.20 |
| methionine + cysteine (%) | 1.07 | 1.19 | 1.10 | 0.70 |
| threonine (%) | 0.95 | 0.95 | 0.84 | 0.85 |
| Ca (%) | 1.05 | 1.07 | 1.10 | 1.10 |
| available P (%) | 0.40 | 0.40 | 0.40 | 0.40 |

[a]Defatted green microalgal (*Desmodesmus* sp.) biomass (Cellana, Kailua-Kona, HI, USA) that contained 31.2% crude protein. [b]Provided (in mg//kg of diet): $CuSO_4 \cdot 5H_2O$, 31.42; KI, 0.046; $FeSO_4 \cdot 7H_2O$, 224.0; $MnSO_4 \cdot H_2O$, 61.54; $Na_2SeO_3$, 0.13; ZnO, 43.56; $Na_2MoO_4 \cdot 2H_2O$, 1.26. [c]Provided (in IU/kg of diet): vitamin A, 6500; vitamin $D_3$, 3500; vitamin E, 25; and (in mg/kg of diet) riboflavin, 25; D-calcium pantothenate, 25; nicotinic acid, 150; cyanocobalamin, 0.011; choline chloride, 1250; biotin, 1.0; folic acid, 2.5; thiamin hydrochloride, 7.0; pyridoxine hydrochloride, 25.0; menadione sodium bisulfite, 5.0; and ethoxyquin, 66. [d]Each of the four experimental diets contains either starch (control) or protease (Ronozyme ProAct, DSM Nutritional Products Inc., Parsippany, NJ, USA) or NSPase (a mixture of 50% Roxazyme G2, 40% Ronozyme A, and 10% Ronozyme WX (DSM Nutritional Products Inc., Parsippany, NJ, USA). Protease activity was measured in PROT units, where 1 unit is defined as the amount of enzyme that releases 1 μmol of *p*-nitroaniline from 1 μM substrate (Suc-Ala-Ala-Pro-Phe-*p*-nitroaniline) per minute at pH 9.0 and 37 °C. Ronozyme WX activity was measured in FXU units, where the minimum activity of the endo-1,4-β-xylanase is 1000 FXU/g, where an FXU unit is the amount of enzyme that releases 7.8 μmol of reducing sugar (xylose equivalents) from azo-wheat arabinoxylan per minute at pH 6.0 and 50 °C. Roxazyme G2 contains a minimum of 8000 U/g of endo-1,3-β-glucanase, 18000 U/g of endo-1,3(4)-β-glucanase, and 26000 U/g of endo-1,4-β-xylanase, where 1 U is the amount of enzyme that liberates 0.1 μmol of glucose from carboxymethylcellulose, barley β-glucan, or oat spelt xylan per minute at pH 5.0 and 40 °C, for each enzyme, respectively. Ronozyme A (CT) consisted of 200 kilo-Novo α-amylase units and 350 fungal β-glucanase units/g of enzyme concentrate.

to meet the nutrient requirements for both periods[45] except for no supplemental lysine or methionine in the DGM grower diets to test the maximal potential of the microalgal protein. Body weight and feed intake were recorded weekly by cage. Feed spillage was collected and weighed daily. Blood samples (~1−3 mL, not exceeding 10% of blood volume) were collected at days 21 and 42 via right wing vein in heparinized needles. At day 42, one bird per cage was euthanized by $CO_2$ asphyxiation and the liver and right pectoralis muscle were excised and immediately frozen for protein quantitation and Western blot analysis.

*Plasma Biochemical and Western Blot Analyses.* Blood samples were centrifuged at 1500*g* for 20 min to collect plasma. Total plasma amino acid content and uric acid were assayed using the same methods described above under Pig Experiment. Frozen liver and muscle samples were ground in liquid nitrogen. Powdered tissue (10 mg) was then homogenized on ice with ice-cold buffer (80 μL) containing 20 mM 4-(2-hydroxyethyl)-1-piperazineethanesulfonic acid (HEPES), 100 mM KCl, 50 mM NaF, 1 mM dithiothreitol, 0.5 mM sodium orthovanate, 0.2 mM ethylenediaminetetraacetic acid (EDTA), 0.1 mM phenylmethanesulfonyl fluoride (PMSF), and 1 mM benzamidine. Homogenates were centrifuged at 1000*g* for 30 min at 4 °C, and the supernatant was centrifuged at 10000*g* for 10 min at 4 °C. The final supernatants were aliquoted and stored at −80 °C. Tissue lysates (50 μg of protein) were subjected to sodium dodecyl sulfate−polyacrylamide gel electrophoresis (SDS-PAGE) and Western blotting using the appropriate antibody (Supplemental Table 1 in the Supporting Information).

Table 4. Effects of Defatted Green Microalgal Biomass (DGM) and Protease on Growth Performance of Pigs[a]

| diet: | control | | DGM | | | P value | | |
|---|---|---|---|---|---|---|---|---|
| enzyme: | none | protease | none | protease | SEM | DGM | enzyme | interaction |
| body weight, kg | | | | | | | | |
| day 0 | 9.49 | 9.63 | 9.66 | 9.95 | 0.15 | 0.47 | 0.55 | 0.73 |
| day 14 | 18.0 | 17.2 | 17.5 | 18.4 | 0.26 | 0.51 | 0.94 | 0.14 |
| day 28 | 28.6 | 26.2 | 26.7 | 28.1 | 0.45 | 0.96 | 0.60 | 0.03[b] |
| body weight gain, g/day | | | | | | | | |
| days 0−14 | 609 | 538 | 562 | 600 | 15.4 | 0.77 | 0.58 | 0.09 |
| days 14−28 | 757 | 648 | 648 | 695 | 18.6 | 0.39 | 0.39 | 0.24 |
| days 0−28 | 683 | 593 | 605 | 648 | 15.0 | 0.71 | 0.40 | 0.02[b] |
| feed intake, g/day | | | | | | | | |
| days 0−14 | 1040 | 1020 | 935 | 1070 | 26.7 | 0.58 | 0.22 | 0.17 |
| days 14−28 | 1220 | 1190 | 1100 | 1140 | 33.7 | 0.25 | 0.90 | 0.66 |
| days 0−28 | 1130 | 1110 | 1020 | 1110 | 27.1 | 0.32 | 0.51 | 0.36 |
| gain/feed efficiency | | | | | | | | |
| days 0−14 | 0.59 | 0.54 | 0.61 | 0.56 | 0.02 | 0.44 | 0.10 | 1.00 |
| days 4−28 | 0.62 | 0.55 | 0.60 | 0.61 | 0.02 | 0.52 | 0.34 | 0.17 |
| days 0−28 | 0.61 | 0.54 | 0.60 | 0.59 | 0.01 | 0.45 | 0.15 | 0.45 |

[a]Data are expressed as mean ($n$ = 7−8). Main effects of DGM, protease, and their interaction were analyzed by two-way ANOVA. [b]The significant interactions indicate that the protease exerted negative effects in the control diet but positive effects in the DGM diet. However, Duncan's multiple-range test showed no significant difference among the treatment means.

Table 5. Effects of Defatted Green Microalgal Biomass (DGM) and Protease on Plasma Biochemical Indicators of Pigs[a]

| diet: | control | | DGM | | | P value | | |
|---|---|---|---|---|---|---|---|---|
| enzyme: | none | protease | none | protease | SEM | DGM | enzyme | interaction |
| tartrate-resistant acid phosphatase, U/L | | | | | | | | |
| day 0 | 168 | 169 | 162 | 160 | 4.13 | 0.39 | 0.99 | 0.86 |
| day 14 | 202 | 189 | 183 | 175 | 4.22 | 0.05[b] | 0.92 | 0.47 |
| day 28 | 145 | 145 | 146 | 145 | 0.32 | 0.51 | 0.34 | 0.53 |
| alkaline phosphatase, U/L | | | | | | | | |
| day 0 | 87.1 | 86.9 | 86.9 | 82.3 | 1.45 | 0.44 | 0.44 | 0.47 |
| day 14 | 224 | 175 | 222 | 179 | 11.6 | 0.95 | 0.05[c] | 0.92 |
| day 28 | 94.5 | 80.0 | 122 | 111 | 6.88 | 0.03[d] | 0.36 | 0.66 |
| alanine aminotransferase, U/L | | | | | | | | |
| day 0 | 16.8 | 14.2 | 13.5 | 15.8 | 0.77 | 0.54 | 0.88 | 0.13 |
| day 14 | 14.0 | 17.0 | 13.5 | 16.6 | 0.67 | 0.73 | 0.02[e] | 0.78 |
| day 28 | 16.0 | 16.1 | 16.9 | 15.0 | 0.68 | 0.89 | 0.60 | 0.54 |
| uric acid, μmol/L | | | | | | | | |
| day 0 | 19.2 | 16.8 | 18.2 | 15.3 | 0.67 | 0.40 | 0.06 | 0.70 |
| day 14 | 30.8a | 23.5ab | 24.5ab | 16.7b | 1.74 | 0.07 | 0.03[f] | 0.44 |
| day 28 | 36.0 | 27.5 | 27.0 | 28.3 | 1.01 | 0.38 | 0.62 | 0.22 |
| urea nitrogen, mg/dL | | | | | | | | |
| day 0 | 8.3 | 9.9 | 8.8 | 7.5 | 0.40 | 0.27 | 0.80 | 0.07 |
| day 14 | 5.9 | 7.3 | 5.5 | 5.2 | 0.32 | 0.04[g] | 0.39 | 0.14 |
| day 28 | 7.3a | 7.7a | 6.2ab | 4.6b | 0.37 | 0.01[h] | 0.45 | 0.10 |
| amino acid, μmol/mL | | | | | | | | |
| day 0 | 9.7 | 9.6 | 9.7 | 9.7 | 0.15 | 0.91 | 1.00 | 0.82 |
| day 14 | 17.8 | 17.2 | 17.5 | 17.8 | 0.28 | 0.74 | 0.79 | 0.48 |
| day 28 | 27.4 | 26.2 | 26.6 | 27.6 | 0.51 | 0.79 | 0.94 | 0.34 |

[a]Data are expressed as mean ($n$ = 7−8). Main effects of DGM, protease, and their interaction were analyzed by two-way ANOVA. Treatment means in the same row without a common letter differ, $P < 0.05$, according to Duncan's multiple-range test. [b]DGM effect, $P < 0.05$: control, 196 vs DGM, 179 U/L, $n$ = 14−16. [c]Protease effect, $P < 0.05$: none, 223 vs protease, 177 U/L, $n$ = 14−16. [d]DGM effect, $P < 0.03$: control, 87 vs DGM, 117 U/L, $n$ = 14−16. [e]Protease effect, $P < 0.02$: none, 13.8 vs protease, 16.8 U/L, $n$ = 14−16. [f]Protease effect, $P < 0.03$: none, 27.7 vs protease, 20.1 μmol/L, $n$ = 14−16. [g]DGM effect, $P < 0.04$: control, 6.60 vs DGM, 5.35 mg/dL, $n$ = 14−16. [h]DGM effect, $P < 0.01$: control, 7.50 vs DGM, 5.40 mg/dL, $n$ = 14−16.

**Statistical Analyses.** Data were analyzed with the GLM procedure of PC-SAS 8.1 (SAS Institute, Cary, NC, USA). The overall main effects of DGM and the enzymes and their interactions were determined using two-way ANOVA (2 × 2 factorial for the pig experiment and 2 × 3 factorial for the chick experiment). Growth parameters were analyzed as time-repeated measurements. Mean comparisons were conducted using Duncan's multiple-range test. If there was an interaction between DGM and the enzyme(s), only conditional (within the same level of the other variable) treatment mean comparisons were considered. Due to the semiquantitative

Table 6. Effects of Defatted Green Microalgal Biomass (DGM) and Hydrolytic Enzymes on Growth Performance of Broilers[a]

| diet: | control | | | DGM | | | | *P* value | | |
|---|---|---|---|---|---|---|---|---|---|---|
| enzyme: | none | protease | NSPase | none | protease | NSPase | SEM | DGM | enzyme | interaction |
| weight gain, g/week·chick | | | | | | | | | | |
| days 0–21 | 221 | 236 | 227 | 221 | 239 | 216 | 3.70 | 0.73 | 0.16 | 0.73 |
| days 22–42 | 493b | 569a | 554ab | 525ab | 539ab | 418b | 12.2 | 0.02 | 0.01 | 0.01[b] |
| days 0–42 | 384b | 436a | 423ab | 404ab | 419ab | 338c | 7.80 | 0.02 | 0.01 | 0.01[b] |
| feed intake, g/week·chick | | | | | | | | | | |
| days 0–21 | 360a | 360a | 356a | 291b | 358a | 338ab | 7.80 | 0.05[c] | 0.16 | 0.13 |
| days 22–42 | 828b | 910ab | 888ab | 1004a | 939ab | 973ab | 21.4 | 0.03[d] | 0.95 | 0.34 |
| days 0–42 | 596 | 635 | 622 | 647 | 648 | 656 | 10.4 | 0.13 | 0.68 | 0.75 |
| feed efficiency | | | | | | | | | | |
| days 0–21 | 0.58b | 0.62b | 0.59b | 0.80a | 0.68b | 0.65b | 0.02 | 0.01 | 0.10 | 0.03[b] |
| days 22–42 | 0.76a | 0.82a | 0.82a | 0.76a | 0.78a | 0.59b | 0.02 | 0.02 | 0.10 | 0.03[b] |
| days 0–42 | 0.67bc | 0.71ab | 0.72ab | 0.78a | 0.73ab | 0.62c | 0.01 | 0.59 | 0.03 | 0.01[b] |

[a]Data are expressed as mean ($n$ = 5). Main effects of DGM, enzyme, and their interaction were analyzed by two-way ANOVA. Treatment means in the same row without a common letter differ, $P < 0.05$, according to Duncan's multiple-range test. [b]With significant interactions between DGM and enzyme, only conditional treatment mean comparisons should be considered: comparing the DGM effect at each of three enzyme treatments and the enzyme effect within each of the two diets (control and DGM). [c]DGM effect, $P < 0.05$: control, 359 vs DGM, 329 g/week·chick, $n$ = 15. [d]DGM effect, $P < 0.03$: control, 875 vs DGM, 972 g/week·chick, $n$ = 15.

Table 7. Effects of Defatted Green Microalgal Biomass (DGM) and Hydrolytic Enzymes on Plasma Biochemical Indicators of Broilers[a]

| diet: | control | | | DGM | | | | *P* value | | |
|---|---|---|---|---|---|---|---|---|---|---|
| enzyme: | none | protease | NSPase | none | protease | NSPase | pooled SEM | DGM | enzyme | interaction |
| plasma amino acids, μmol/mL | | | | | | | | | | |
| day 21 | 0.32b | 0.66a | 0.26b | 0.40b | 0.29b | 0.38b | 0.04 | 0.01[b] | 0.03 | 0.01[c] |
| day 42 | 3.72a | 1.53b | 2.12ab | 2.20ab | 2.36ab | 3.53a | 0.25 | 0.60 | 0.12 | 0.01[c] |
| plasma uric acid, mmol/L | | | | | | | | | | |
| day 21 | 0.25ab | 0.21b | 0.28ab | 0.27ab | 0.24b | 0.31a | 0.01 | 0.07 | 0.02 | 1.00 |
| day 42 | 0.51 | 0.57 | 0.52 | 0.54 | 0.48 | 0.53 | 0.01 | 0.68 | 0.98 | 0.08 |

[a]Data are expressed as mean ($n$ = 5). Main effects of DGM, enzyme, and their interaction were analyzed by two-way ANOVA. Treatment means in the same row without a common letter differ, $P < 0.05$, according to Duncan's multiple-range test. [b]Enzyme effect: none, 0.26ab; protease, 0.24b; and NSPase, 0.30a mmol/L. Means without a common letter differ, $P < 0.05$, $n$ = 10. [c]With significant interactions between DGM and enzyme, only conditional treatment mean comparisons should be considered: comparing the DGM effect at each of three enzyme treatments and the enzyme effect within each of the two diets (control and DGM).

nature and limited sample size ($n$ = 3) of the Western blot analyses, only selected treatment effects were directly compared with the respective controls using the $t$ test. Data are expressed as means ± SEM, and $P < 0.05$ was considered statistically significant.

## RESULTS

**Pig Experiment.** Neither the 10% DGM nor the 0.06% protease addition alone affected body weight, average daily gain, average daily feed intake, or feed efficiency at any time points of the 28 day experiment (Table 4). However, there was an interaction between DGM and protease on the day 28 body weight ($P$ = 0.03) and overall average body weight gain for the entire 28 day experiment ($P$ = 0.02), showing a beneficial trend of the protease to both measures in the presence of DGM, but an adverse effect in the control diet. The DGM inclusion decreased ($P < 0.05$) the day 14 plasma TRAP activity by 9%, increased ($P < 0.03$) the day 28 plasma AKP activity by 34%, decreased the day 14 plasma uric acid concentrations ($P$ = 0.07) by 32%, and decreased the day 14 and 28 plasma urea nitrogen concentrations ($P < 0.05$) by 23 and 39%, respectively (Table 5). The protease addition decreased ($P$ = 0.05) the day 14 plasma AKP activity by 26%, increased ($P < 0.05$) the day 14 plasma ALT activity by 22%, and decreased ($P < 0.05$) the day 14 plasma uric acid concentrations by 38%, respectively. Plasma amino acid concentrations were not affected by either the DGM or the protease inclusion.

**Broiler Experiment.** There were significant ($P < 0.02$) effects of DGM, enzyme, and their interaction on body weight gains of chicks during the grower period (days 22–42) and (or) the entire period (days 0–42) (Table 6). The gains for both periods were improved ($P < 0.05$) by the protease addition into the control diet, but the gain for the entire period decreased ($P < 0.05$) with NSPase addition to the DGM diet. Chicks fed the DGM diet had 9% lower ($P < 0.05$) feed intake than those fed the control diet during the starter period (days 0–21), but this difference was reversed with an 11% increase during the grower period. Thus, there was no difference in the overall feed intake between these two diets. There were significant interactions of DGM and enzyme ($P < 0.03$) on the gain/feed ratios for all of the assayed periods. During the starter period and the entire period, chicks fed the DGM diet without the enzyme supplementation had 38 and 16% greater ($P < 0.05$) gain/feed efficiency, respectively, than those fed the control diet. Supplementing the NSPase to the DGM diets decreased ($P < 0.05$) the gain/feed efficiencies for all three periods, whereas supplementing the protease to the DGM diets decreased ($P < 0.05$) the gain/feed efficiency for the starter period. The enzyme supplementations in the control diets

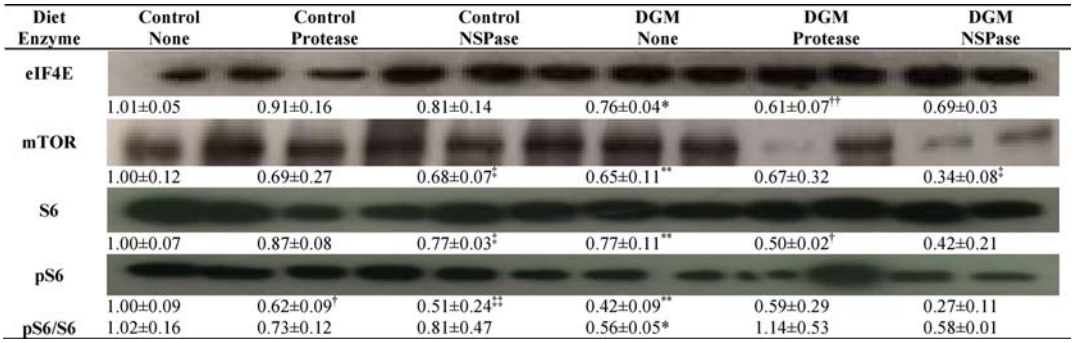


**Figure 1.** Effects of defatted green microalgal biomass (DGM) and hydrolytic enzymes on protein and phosphorylation levels of protein biosynthesis regulators in livers of broilers. Data are expressed as means ± SE ($n$ = 3). Values are expressed as a ratio to $\beta$-actin and then normalized to the control. Blots are representative of three independent replicate gels. (*) Significant effect of DGM versus control ($P$ < 0.05), (**) trending effect of DGM versus control ($P$ < 0.10), (†) significant effect of protease versus treatment control ($P$ < 0.05), (††) trending effect of protease versus treatment control ($P$ < 0.10), (‡) significant effect of NSPase versus treatment control ($P$ < 0.05), (‡‡) trending effect of NSPase versus treatment control ($P$ < 0.10). eIF4E, eukaryotic initiation factor 4E; p70, p70 S6 kinase; S6, S6 ribosomal protein; pS6, phospho-S6 ribosomal protein; mTOR, mammalian target of rapamycin.

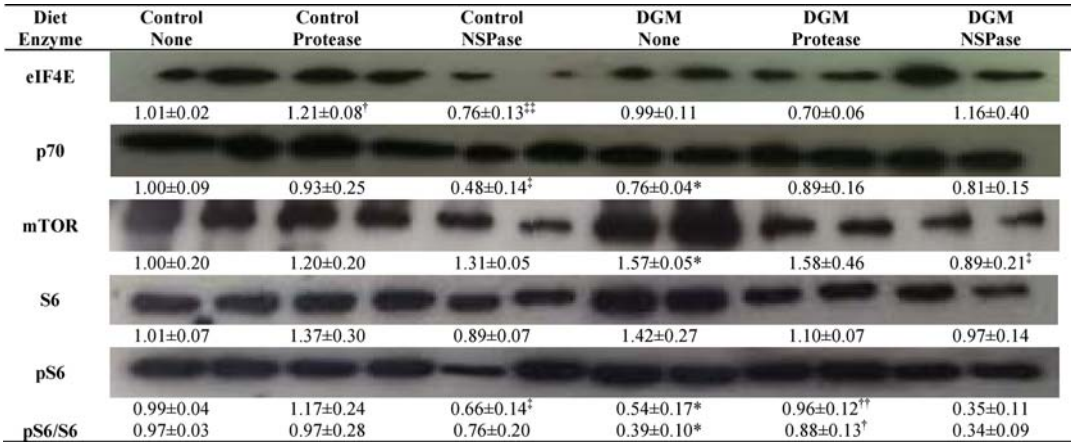


**Figure 2.** Effects of defatted green microalgal biomass (DGM) and hydrolytic enzymes on protein and phosphorylation levels of protein biosynthesis regulators in muscles of broilers. Data are expressed as means ± SE ($n$ = 3). Values are expressed as a ratio to $\beta$-actin and then normalized to the control. Blots are representative of three independent replicate gels. (*) Significant effect of DGM versus control ($P$ < 0.05), (**) trending effect of DGM versus control ($P$ < 0.10), (†) significant effect of protease versus treatment control ($P$ < 0.05), (††) trending effect of protease versus treatment control ($P$ < 0.10), (‡) significant effect of NSPase versus treatment control ($P$ < 0.05), (‡‡) trending effect of NSPase versus treatment control ($P$ < 0.10). eIF4E, eukaryotic initiation factor 4E; p70, p70 S6 kinase; S6, S6 ribosomal protein; pS6, phospho-S6 ribosomal protein; mTOR, mammalian target of rapamycin.

showed no such effects on the gain/feed efficiency. Plasma amino acid concentrations were elevated ($P$ < 0.05) and decreased ($P$ < 0.05) by the addition of the protease into the control diet on days 21 and 42, respectively (Table 7). Plasma uric acid concentrations at day 21 appeared to be decreased by protease, but the only significant difference ($P$ < 0.05) was seen between the two enzyme-supplemented DGM diets.

The inclusion of DGM consistently decreased ($P$ < 0.05−0.1) all four proteins (eIF4E, mTOR, S6, and pS6) and the ratio of pS6/S6 in the liver compared with the control diet without supplemental enzymes (Figure 1). However, the same inclusion exhibited variable effects on the same four proteins, the ratio of pS6/S6, and p70 in the breast muscle (Figure 2). Supplementing NSPase into the control diet decreased hepatic mTOR ($P$ < 0.05), S6 ($P$ < 0.05), and pS6 ($P$ < 0.1) and muscle eIF4E ($P$ < 0.1), p70 ($P$ < 0.05), and pS6 ($P$ < 0.05), respectively. Supplementing NSPase into the DGM diet decreased ($P$ < 0.05) both hepatic and muscle mTOR levels. Supplementing the protease into the control diet decreased ($P$ < 0.05) hepatic pS6 level and elevated ($P$ < 0.05) muscle eIF4E level, whereas supplementing the same enzyme into the DGM diet decreased ($P$ < 0.05) hepatic eIF4E and S6 levels and enhanced muscle pS6 ($P$ < 0.1) and the ratio of pS6/S6 ($P$ < 0.05).

## DISCUSSION

The main finding of the pig experiment was that the 10% inclusion of DGM produced no appreciable adverse effects on growth performance of the pigs except for numerically a 7% decrease in the body weight at day 28 and a 13% decrease in overall daily body weight gain. Interestingly, these decreases were restored by the supplemental protease in the DGM-containing diet. These data are in agreement with past reports that pigs tolerate moderate levels of various species of microalgal inclusion.[6,8,46] As shown in our previous broiler,[5] hen,[12] and pig[13] experiments, feeding weanling pigs with the 10% DGM diet did not alter their plasma ALT activity. Although pigs fed the DGM diet showed elevated plasma AKP activity at day 28 and decreased plasma TRAP activity at day 14, these changes were neither consistent nor sufficient to

suggest altered phosphorus nutrition status.[47] Our previous studies[5] also supported this notion. Apparently, digestibility and bioavailability of phosphorus in this and other sources of microalgal biomass need to be determined directly.

Effects of supplemental DGM and protease on dietary protein digestion and utilization in pigs were assessed by the responses of plasma uric acid, urea nitrogen, and amino acid concentrations. Whereas the DGM diet did not alter plasma amino acid concentration, it lowered substantially plasma uric acid and urea nitrogen concentrations. These favorable decreases seem to indicate that pigs utilized their ingested N more efficiently from the DGM-containing diet than from the control diet. As plasma urea nitrogen is highly correlated with urinary nitrogen excretion rate,[36] its decrease may result in attenuated nitrogen excretion to the environment from the swine production. It is worth mentioning that 1.2% plasma protein was added in the DGM-containing diet to match the protein and amino acid concentrations of the control diet. It is unknown if the superior plasma protein[48,49] helped overcome any possible deficiencies of the DGM-containing diet. Meanwhile, supplementing 0.06% protease in both control and DGM-containing diet also improved plasma uric acid concentration. Along with the above-described positive effect on growth performance of pigs, these improvements suggest an enhanced proteolysis by the extrinsic protease in the DGM-containing diet.

Results of the broiler experiment showed a potential of the inclusion of 15% DGM to improve growth performance of chicks. Gain/feed efficiency of chicks fed the DGM-containing diet was indeed greater than that of chicks fed the control diet during the starter and the entire 42 day period. The decreased feed intake during the starter period followed by an elevated feed intake during the grower period in chicks fed the DGM-containing diet, compared with those fed the control diet, might reflect an adaptation of the animals to the microalgal biomass. Notably, synthetic lysine and methionine were added into the DGM-containing diet only during the starter period. The DGM-containing grower diet was formulated to match only the protein but not the two limiting amino acids of the control diet, which was designed to determine the maximum potential of the DGM protein. Remarkably, chicks fed such grower diet displayed a growth performance similar to that of those fed the control diet. In comparison with the compromised body weight and body weight gain in the weanling pigs fed only 10% DGM, the tolerance of the broiler chicks to the inclusion of 15% DGM without exogenous lysine or methionine implied their better capacity to utilize DGM than shown by the weanling pigs. Nevertheless, thought should be given to possible confounding effects of the rather different lysine and methionine profiles between the control and DGM grower diets and (or) a slight extra methionine supplementation in the DGM starter diets. Along with the positive control diet as used in the present study, an additional negative control diet may be formulated to match the lower levels of lysine and methionine of the DGM grower diet for the future exploration of the full potential and mechanism of DGM in meeting protein and amino acid requirements for chicks and pigs.

Supplementing protease and NSPase to the broiler diets produced mixed or opposite effects on their growth performance. Protease supplementation to the control diets led to an increased weight gain. However, the same supplementation to the DGM-containing diet, as in the case of 7.5% DFA supplementation in our previous research,[5] showed little or no consistent effects. Presumably, the DGM contained a high level of NSPs within the cell wall structure.[50] Because NSPs possess antinutritive activity even at low levels (<50 g/kg) in broiler diets,[51] feeding DGM might alter the intestinal transit time, the intestinal mucosa, and hormonal regulations.[52] Intriguingly, NSPase supplementation to the DGM-containing diet consistently decreased growth performance. The mechanism responsible for this counterintuitive response remains unclear to us. Similar to the results seen at day 14 in the pig experiment, the supplemental protease decreased plasma uric acid concentrations of chicks, suggesting improved dietary nitrogen utilization.[10,11] However, the DGM inclusion, unlike in the case of DFA,[5] did not decrease plasma uric acid concentration of chicks in the present study. The inclusions of DGM and protease exerted a stronger effect on plasma amino acid concentrations at day 21 than at day 42. This time difference may reflect an adaptation of chicks to the microalgal protein and (or) a less dependence on exogenous enzymes to hydrolyze dietary proteins.[41]

The strong impacts of DGM inclusion on the protein production of the five key signal molecules in the pathway of mTOR in both liver and muscle of chicks are novel. Likewise, supplemental protease or NSPase also affected protein levels of these molecules in the two tissues to various extents. Because these proteins are key regulators of cell growth, protein synthesis, and energy metabolism,[51] the inclusions of DGM or enzyme-mediated decreases of these proteins, in particular in liver, were not well correlated with the dietary treatment effects on growth performance or plasma measures unless there was a feedback mechanism at the time-point of our tests. Clearly, these observations should not be used to draw sound conclusions, but regarded as a starting point to stimulate more systematic research. It will be fascinating to determine if any unique composition of protein and amino acids in the DGM and specific hydrolytes produced by the supplemental enzymes mediate the changes of these mTOR pathway-related proteins. It will also be necessary to confirm the tissue and (or) signal protein discrepancies in response to the DGM and enzyme supplementations. Eventually, these molecular regulations should be directly linked to the metabolic outcomes and production traits of animals fed the DGM and enzyme-supplemented diets.

Overall, weanling pigs and broiler chicks performed well with dietary inclusions of 10 and 15% DGM, respectively. The biomass feeding decreased plasma uric acid and urea nitrogen concentrations in pigs and improved feed use efficiency in chicks. Supplemental protease demonstrated moderate benefits on growth performance or certain biochemical indicators in pigs and (or) chicks, whereas supplemental NSPase showed little or somewhat negative effects. Dietary inclusions of DGM or enzymes affected hepatic and muscle protein production of the mTOR pathway, but metabolic implications and molecular mechanisms of the observed effects require future research.

## ■ ASSOCIATED CONTENT

### Ⓢ Supporting Information

Supplementary Table 1. This material is available free of charge via the Internet at http://pubs.acs.org.

## ■ AUTHOR INFORMATION

### Corresponding Author

*(X.G.L.) Phone: (607) 254-4703. Fax: (607) 255-9829. E-mail: XL20@cornell.edu.

## Funding

This study was supported in part by a USDA/DOE Biomass R&D Initiative grant and a Hatch grant from Cornell University.

## Notes

The authors declare no competing financial interest.

## REFERENCES

(1) Cromwell, G. L. Soybean meal - the gold standard. *Farmer's Pride, KPPA News* **1999**, *11* (20), http://www.uky.edu/Ag/AnimalSciences/swine/swineresearchupdates.html.

(2) Olson, R. D. *Below Cost Feed Crops: An Indirect Subsidy for Industrial Animal Factories*; Institute for Agriculture and Trade Policy: Minneapolis, MN, USA, 2006.

(3) Grau, C. R.; Klein, N. W. Sewage-grown algae as a feedstuff for chicks. *Poult. Sci.* **1957**, *36*, 1046−1051.

(4) Mokady, S.; Yannai, S.; Einav, P.; Berk, Z. Algae grown on wastewater as a source of protein for young chickens and rats. *Nutr. Rep. Int.* **1979**, *9*, 383−390.

(5) Austic, R. E.; Mustafa, A.; Jung, B.; Gatrell, S.; Lei, X. G. Potential and limitation of a new defatted diatom microalgal biomass in replacing soybean meal and corn in diets for broiler chickens. *J. Agric. Food Chem.* **2013**, *61*, 7341−7348.

(6) Hintz, H. F.; Heitman, H. Sewage-grown algae as a protein supplement for swine. *Anim. Prod.* **1967**, *9*, 135.

(7) Yap, T. N.; Wu, J. F.; Pond, W. G.; Krook, L. Feasibility of feeding *Spirulina maxima*, *Arthrospira platensis* or *Chlorella* sp. to pigs weaned to a dry diet at 4 to 8 days of age. *Nutr. Rep. Int.* **1982**, *25*, 543−552.

(8) Isaacs, R.; Roneker, K. R.; Huntley, M.; Lei, X. G. A partial replacement of soybean meal by whole or defatted algal meal in diet for weanling pigs does not affect their plasma biochemical indicators. *J. Anim. Sci.* **2011**, *89*, 723−723.

(9) Chisti, Y. Biodiesel from microalgae. *Biotechnol. Adv.* **2007**, *25*, 294−306.

(10) Donsbough, A. L.; Powell, S.; Waguespack, A.; Bidner, T. D.; Southern, L. L. Uric acid, urea, and ammonia concentrations in serum and uric acid concentration in excreta as indicators of amino acid utilization in diets for broilers. *Poult. Sci.* **2010**, *89*, 287−294.

(11) Hernandez, F.; Lopez, M.; Martinez, S.; Megias, M. D.; Catala, P.; Madrid, J. Effect of low-protein diets and single sex on production performance, plasma metabolites, digestibility, and nitrogen excretion in 1- to 48-day-old broilers. *Poult. Sci.* **2012**, *91*, 683−692.

(12) Leng, X.; Hsu, K.; Austic, R.; Lei, X. G. Effect of dietary defatted diatom biomass on egg production and quality of laying hens. *J. Anim. Sci. Biotechnol.* **2014**, *5*, 3.

(13) Lum, K. K.; Roneker, K. R.; Lei, X. G. Effects of various replacements of corn and soy by defatted microalgal meal on growth performance and biochemical status of weanling pigs. *J. Anim. Sci.* **2012**, *90*, 701−701.

(14) Simbaya, J.; Slominski, B.; Guenter, W.; Morgan, A.; Campbell, L. The effects of protease and carbohydrase supplementation on the nutritive value of canola meal for poultry: in vitro and in vivo studies. *Anim. Feed Sci. Technol.* **1996**, *61*, 219−234.

(15) Ghazi, S.; Rooke, J.; Galbraith, H.; Bedford, M. The potential for the improvement of the nutritive value of soya-bean meal by different proteases in broiler chicks and broiler cockerels. *Br. Poult. Sci.* **2002**, *43*, 70−77.

(16) Coppedge, J.; Klein, J.; Brown, B.; Ratliff, B.; Ruch, F.; Lee, J. T. Effects of co-administration of phytase and NSPase on broiler performance and bone ash. *Int. J. Poult. Sci.* **2011**, *10*, 933−939.

(17) Edney, M.; Campbell, G.; Classen, H. The effect of $\beta$-glucanase supplementation on nutrient digestibility and growth in broilers given diets containing barley, oat groats or wheat. *Anim. Feed Sci. Technol.* **1989**, *25*, 193−200.

(18) Viveros, A.; Brenes, A.; Pizarro, M.; Castano, M. Effect of enzyme supplementation of a diet based on barley, and autoclave treatment, on apparent digestibility, growth performance and gut morphology of broilers. *Anim. Feed Sci. Technol.* **1994**, *48*, 237−251.

(19) Vranjes, M. V.; Wenk, C. The influence of extruded vs. untreated barley in the feed, with and without dietary enzyme supplement on broiler performance. *Anim. Feed Sci. Technol.* **1995**, *54*, 21−32.

(20) Steenfeldt, S.; Müllertz, A.; Fris Jensen, J. Enzyme supplementation of wheat-based diets for broilers: 1. Effect on growth performance and intestinal viscosity. *Anim. Feed Sci. Technol.* **1998**, *75*, 27−43.

(21) Wang, Z.; Qiao, S.; Lu, W.; Li, D. Effects of enzyme supplementation on performance, nutrient digestibility, gastrointestinal morphology, and volatile fatty acid profiles in the hindgut of broilers fed wheat-based diets. *Poult. Sci.* **2005**, *84*, 875−881.

(22) Brown, M.; Jeffrey, S.; Volkman, J.; Dunstan, G. Nutritional properties of microalgae for mariculture. *Aquaculture* **1997**, *151*, 315−331.

(23) Chen, C.; Zhao, X.; Yen, H.; Ho, S.; Cheng, C.; Lee, D.; Bai, F.; Chang, J. Microalgae-based carbohydrates for biofuel production. *Biochem. Eng. J.* **2013**, *78*, 1−10.

(24) Northcote, D. H.; Goulding, K. J.; Horne, R. W. The chemical composition and structure of the cell wall of *Hydrodictyon africanum* Yaman. *Biochem. J.* **1958**, *70*, 391.

(25) Fu, C.; Hung, T.; Chen, J.; Su, C.; Wu, W. Hydrolysis of microalgae cell walls for production of reducing sugar and lipid extraction. *Bioresour. Technol.* **2010**, *101*, 8750−8754.

(26) Takeda, H. Classification of *Chlorella* strains by means of the sugar components of the cell wall. *Biochem. Syst. Ecol.* **1988**, *16*, 367−371.

(27) Venkataraman, L.; Somasekaran, T.; Becker, E. Replacement value of blue-green alga (*Spirulina platensis*) for fishmeal and a vitamin-mineral premix for broiler chicks. *Br. Poult. Sci.* **1994**, *35*, 373−381.

(28) Becker, E. W. Micro-algae as a source of protein. *Biotechnol. Adv.* **2007**, *25*, 207−210.

(29) Sarbassov, D. D.; Ali, S. M.; Sabatini, D. M. Growing roles for the mTOR pathway. *Curr. Opin. Cell Biol.* **2005**, *17*, 596−603.

(30) Boussaid-Om Ezzine, S.; Métayer-Coustard, S.; Collin, A.; Rideau, N.; Leterrier, C.; Bouvarel, I.; Seiliez, I.; Tesseraud, S. Regulators of protein metabolism are affected by cyclical nutritional treatments with diets varying in protein and energy content. *J. Nutr. Biochem.* **2012**, *23*, 1467−1473.

(31) Kimball, S. R.; Jefferson, L. S. Control of protein synthesis by amino acid availability. *Curr. Opin. Clin. Nutr. Metab. Care* **2002**, *5*, 63−67.

(32) Kimball, S. R.; Jefferson, L. S. Signaling pathways and molecular mechanisms through which branched-chain amino acids mediate translational control of protein synthesis. *J. Nutr.* **2006**, *136*, 227S−231S.

(33) Luo, J.; Chen, D.; Yu, B. Effects of different dietary protein sources on expression of genes related to protein metabolism in growing rats. *Br. J. Nutr.* **2010**, *104*, 1421.

(34) Wang, X.; Proud, C. G. The mTOR pathway in the control of protein synthesis. *Physiology* **2006**, *21*, 362−369.

(35) Robison, O. W. Growth patterns in swine. *J. Anim. Sci.* **1976**, *42*, 1024−1035.

(36) Kohn, R.; Dinneen, M.; Russek-Cohen, E. Using blood urea nitrogen to predict nitrogen excretion and efficiency of nitrogen utilization in cattle, sheep, goats, horses, pigs, and rats. *J. Anim. Sci.* **2005**, *83*, 879−889.

(37) Suryawan, A.; Escobar, J.; Frank, J. W.; Nguyen, H. V.; Davis, T. A. Developmental regulation of the activation of signaling components leading to translation initiation in skeletal muscle of neonatal pigs. *Am. J. Physiol. Endocrinol. Metab.* **2006**, *291*, E849−E859.

(38) Escobar, J.; Frank, J. W.; Suryawan, A.; Nguyen, H. V.; Davis, T. A. Amino acid availability and age affect the leucine stimulation of protein synthesis and eIF4F formation in muscle. *Am. J. Physiol. Endocrinol. Metab.* **2007**, *293*, E1615−E1621.

(39) Ao, X.; Meng, Q.; Yan, L.; Kim, H.; Hong, S.; Cho, J.; Kim, I. Effects of non-starch polysaccharide-degrading enzymes on nutrient

digestibility, growth performance and blood profiles of growing pigs fed a diet based on corn and soybean meal. *Asian−Aust. J. Anim. Sci.* **2010**, *23*, 1632−1638.
(40) Owusu-Asiedu, A.; Kiarie, E.; Peron, A.; Woyengo, T. A.; Simmins, P. H.; Nyachoti, C. M. Growth performance and nutrient digestibilities in nursery pigs receiving varying doses of xylanase and β-glucanase blend in pelleted wheat- and barley-based diets. *J. Anim. Sci.* **2012**, *90* (Suppl. 4), 92−94.
(41) Adeola, O.; Cowieson, A. J. Board-Invited Review: Opportunities and challenges in using exogenous enzymes to improve nonruminant animal production. *J. Anim. Sci.* **2011**, *89*, 3189−3218.
(42) National Research Council. *Nutrient Requirements of Swine*; National Academies Press: Washington, DC, USA, 2012.
(43) Bowers, J. N.; McComb, R. B. Measurement of total alkaline phosphatase activity in human serum. *Clin. Chem.* **1975**, *21*, 1988−1995.
(44) Lau, K. H.; Onishi, T.; Wergedal, J. E.; Singer, F. R.; Baylink, D. J. Characterization and assay of tartrate-resistant acid phosphatase activity in serum: potential use to assess bone resorption. *Clin. Chem.* **1987**, *33*, 458−462.
(45) NRC. *Nutrient Requirements of Poultry*, 9th revised ed.; National Academies Press: Washington, DC, USA, 1994.
(46) Fevrier, C.; Seve, B. Incorporation of a spiruline (*Spirulina maxima*) in swine food. *Ann. Nutr. Aliment.* **1975**, *29*, 625−650.
(47) Koch, M. E.; Mahan, D. C. Biological characteristics for assessing low phosphorus intake in finishing swine. *J. Anim. Sci.* **1986**, *62*, 163−172.
(48) Kats, L.; Nelssen, J.; Tokach, M.; Goodband, R.; Hansen, J.; Laurin, J. The effect of spray-dried porcine plasma on growth performance in early weaned pig. *J. Anim. Sci.* **1994**, *72*, 2075−2081.
(49) Grinstead, G.; Goodband, R.; Dritz, S.; Tokach, M.; Nelssen, J.; Woodworth, J.; Molitor, M. Effects of a whey protein product and spray dried animal plasma on growth performance of weanling pigs. *J. Anim. Sci.* **2000**, *78*, 647−657.
(50) Domozych, D. S.; Ciancia, M.; Fangel, J. U.; Mikkelsen, M. D.; Ulvskov, P.; Willats, W. G. The cell walls of green algae: a journey through evolution and diversity. *Front. Plant Sci.* **2012**, *3*, 82.
(51) Annison, G.; Choct, M. Anti-nutritive activities of cereal non-starch polysaccharides in broiler diets and strategies minimizing their effects. *World's Poult. Sci. J.* **1991**, *47*, 232−242.
(52) Vahouny, G. V. Dietary fiber, lipid metabolism, and atherosclerosis. *Fed. Proc.* **1982**, *41*, 2801−2806.

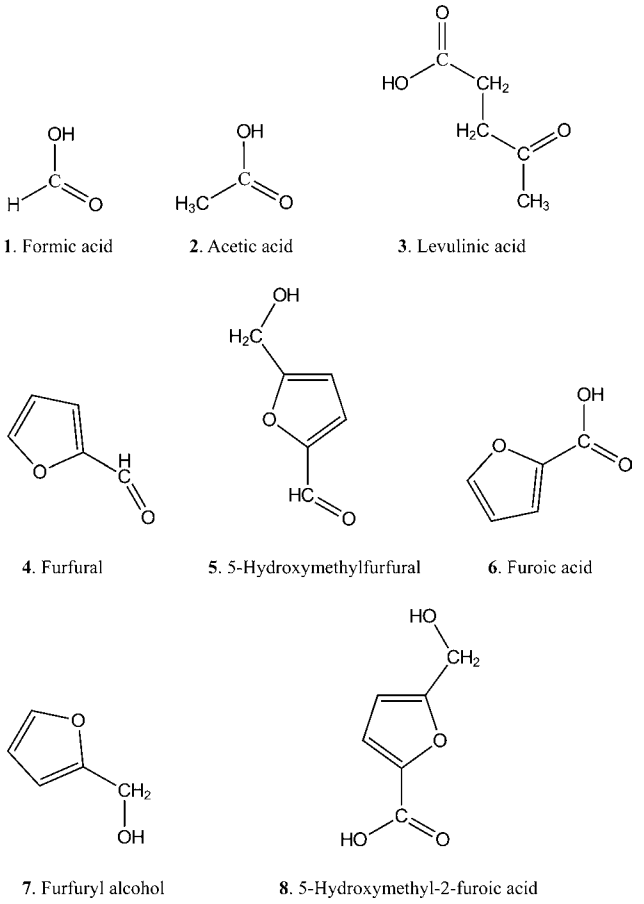


**Figure 1.** Structures of model inhibitors and related conversion compounds: (**1**) formic acid; (**2**) acetic acid; (**3**) levulinic acid; (**4**) furfural; (**5**) 5-hydroxymethylfurfural; (**6**) furoic acid; (**7**) furfuryl alcohol; (**8**) 5-hydroxymethyl-2-furoic acid.

important aliphatic acids and furan aldehydes on cultures of *G. xylinus*.

The influences of formic acid, acetic acid, levulinic acid, furfural, and 5-hydroxymethylfurfural on static cultures of *G. xylinus* were investigated during a period of 7 days when cell proliferation, sugar consumption, the pH of the cultures, and the concentration of the inhibitor were monitored daily by using modern analytical techniques including fluorescence staining, high-performance anion-exchange chromatography (HPAEC), and high-performance liquid chromatography−UV diode array detection (HPLC-UV-DAD). At the end of the cultivation, the yield of BNC was determined, and bioconversion products derived from furan aldehydes were identified and quantitated. This is the first study of the effects of specific lignocellulose-derived aliphatic acids and furan aldehydes on BNC production by *G. xylinus*, and it is also the first demonstration of the ability of *G. xylinus* to convert furan aldehydes. Studies in this area give a better understanding of the properties of *G. xylinus* and can give important information regarding suitable detoxification methods and directions for efficient production of BNC from lignocellulosic feedstocks.

## MATERIALS AND METHODS

**Chemicals and Microorganism.** Reagent grade chemicals purchased from Sigma-Aldrich (St. Louis, MO, USA) were used in the experiments. The substances added to the bacterial cultures were formic acid, **1**, acetic acid, **2**, levulinic acid, **3**, furfural, **4**, and 5-hydroxymethylfurfural, **5** (Figure 1). *G. xylinus* strain ATCC 23770 was obtained from the American Type Culture Collection (Manassas, VA, USA).

**Cultivation of *G. xylinus*.** The liquid seed medium, which was prepared using ultrapure water, contained 3.0 g/L yeast extract, 5.0 g/L tryptone, and 25 g/L glucose. The pH of all media was adjusted to 5.0. The fermentation medium was prepared by dissolving 0.75 g of glucose, 0.15 g of tryptone, and 0.09 g of yeast extract in 23.2 mL of ultrapure water.

Pre-inoculum for all experiments was prepared by transferring a bacterial colony grown on agar seed medium into 100 mL of liquid seed medium. After 24 h of agitated cultivation at 30 °C, 1.8 mL of cell suspension was introduced into a 100 mL Erlenmeyer flask containing 23.2 mL of the fermentation medium. The culture was then incubated at 30 °C with agitation for another 24 h to ensure that the bacterial cells were in the exponential growth phase before the addition of inhibitory substances.

Before the addition of the inhibitors, aqueous stock solutions were prepared and the pH of the stock solutions was adjusted to 5 with $H_2SO_4$ and NaOH. The concentration of the stock solutions of the aliphatic acids was 6 times higher than the concentration in the cultivation medium. For each of the aliphatic acids, 5 mL of the stock solution was added to obtain 25, 100, 175, and 250 mM in the resulting media. Triplicates were performed for each aliphatic acid. Five milliliters of autoclaved ultrapure water was added to reference cultures without inhibitors. The 100 mL Erlenmeyer flasks containing 30 mL of bacterial culture were incubated statically at 30 °C for 7 days. Samples (2 mL) from each flask were taken aseptically every 2 days during this time period. The samples were stored at −20 °C until analyzed.

Distilled furfural was added directly to the culture medium to reach final concentrations of 10, 20, 30, and 40 mM. A stock solution of 5-hydroxymethylfurfural (0.15 g/mL) was prepared in ultrapure water and was then added into the medium to reach the same final concentrations as for furfural. Triplicates were performed for each aliphatic acid.

**Determination of BNC Yield.** Production of BNC was quantitated gravimetrically on the basis of the dry weight of the insoluble BNC obtained at the end of cultivation. The BNC was collected after the incubation and dried to constant weight at 105 °C. After that, the BNC was weighed for calculation of the volumetric yield (g/L) and the yield on consumed sugar (g/g). The yield of BNC on consumed sugar (g/g) was calculated by using the following equation:

$$\text{BNC yield on consumed sugar (g/g)} = \frac{\text{BNC (g)}}{\text{glucose on first day (g)} - \text{residual glucose (g)}}$$

**Analysis of Glucose.** The concentration of glucose during the cultivations was monitored by using an Accu-Chek Aviva glucometer (Roche Diagnostics GmbH, Mannheim, Germany). The consumption rate of the glucose during cultivation was calculated by using the following equation:

$$\text{glucose consumption rate (g/[L·day])} = \frac{\text{glucose on first day (g/L)} - \text{residual glucose (g/L)}}{\text{cultivation time (days)}}$$

**Analysis of Aliphatic Acids.** Quantitation of formic acid, acetic acid, and levulinic acid was done using HPAEC. Before analysis, all samples were filtered through a 0.20 μm Millex-GN syringe-driven filter unit (Millipore, County Cork, Ireland) and diluted with ultrapure water. The HPAEC analysis was performed with a Dionex ICS-3000 system with a conductivity detector. The analytical column used was a 250 mm × 4 mm i.d., 9 μm, IonPac AS15, with a 50 mm × 4 mm i.d., 9 μm, IonPac AG15 guard column (Dionex, Sunnyvale, CA, USA). Isocratic elution with 35 mM sodium hydroxide at a flow rate of 1.2 mL/min was used for separation of the anions. The total run time of the analysis was 16 min. For quantitation of aliphatic acids, standard


dx.doi.org/10.1021/jf502623s | J. Agric. Food Chem. 2014, 62, 9792−9799

curves covering the range from 0.5 to 50 ppm were prepared using reference standards.

**Analysis of Furan Derivatives.** The concentrations of the furan aldehydes **4** and **5** were analyzed using high-performance liquid chromatography (HPLC) with an Agilent series 1200 instrument equipped with a G1315D diode array multiple wavelength detector (Agilent Technologies, Santa Clara, CA, USA). Samples (10 $\mu$L) were diluted 20-fold with ultrapure water and filtered through 0.2 $\mu$m Millex-GN syringe-driven filter units (Millipore). A volume of 2 $\mu$L of each diluted sample was injected into a column. The column used was a 50 mm × 3.0 mm i.d., 1.8 $\mu$m, Zorbax RRHT SB-C18 (Agilent Technologies), and the flow rate was 0.5 mL/min. Elution was performed with a gradient made of a mixture of ultrapure water and acetonitrile, both of which contained 0.1% formic acid. The gradient started with 3% acetonitrile for 3 min, after which the acetonitrile content increased linearly to 10% after 5 min. The column temperature was maintained at 40 °C. For quantitation of furan aldehydes **4** and **5**, standard curves covering the range from 0.5 to 50 ppm were prepared using reference standards. The wavelength used for quantitation of **4** and **5** was 280 nm.

The possible bioconversion of furfural and 5-hydroxymethylfurfural to corresponding acids and alcohols was investigated using HPLC-UV-DAD, and retention times and spectra of reference standards for 2-furoic acid (furan-2-carboxylic acid), **6**, furfuryl alcohol (2-furanmethanol), **7**, and 5-hydroxymethyl-2-furoic acid, **8** (Figure 1). The wavelength for quantitation of **6** and **8** was 254 nm, and the wavelength for quantitation of **7** was 210 nm.

**Analysis of Bacterial Viability.** The bacterial cells were collected by filtration through Durapore membrane filters in a 1225 sampling manifold (Millipore) and were then resuspended in saline. The viability of the bacterial cells was determined by using a BacLight live/dead bacterial viability fluorescence staining kit (Invitrogen, Grand Island, NY, USA) and a Synergy H4 hybrid microplate reader (BioTek Instruments, Winooski, VT, USA). The protocol for microplate assays supplied by the manufacturer was followed. A standard curve for the relative fluorescence value (RFV) and the number of bacterial cells was made before analysis of samples from the bacterial cultures from experimental series with inhibitors.

## RESULTS AND DISCUSSION

**Effects of Aliphatic Acids.** The effects of the three aliphatic acids **1**, **2**, and **3** (Figure 1) were evaluated in the concentration range of 25−250 mM. Figure 2 shows the effects of acid **1** on sugar consumption, cell viability, and the pH of bacterial cultures. When the concentration of acid **1** was 25 mM, *G. xylinus* could consume glucose at a rate of 3.1 g/(L·day), which was similar to the rate observed for cultures grown in the reference medium (Table 1; Figure 2). During the 7 days of cultivation after the addition of acid **1**, the pH of cultures with 25 mM acid **1** decreased from 4.4 to 3.1, which was slightly higher than the 2.7 in the reference medium. The concentration of live bacteria in the culture with 25 mM acid **1** reached the maximal value, 16.8 × $10^6$ cells/mL, at the fourth day, when acid **1** was exhausted. After that, there was a slight decrease in the concentration of live bacteria (Figure 2C). The volumetric yield of BNC in the medium containing 25 mM acid **1** was 3.2 g/L, whereas it was 3.5 g/L in the reference medium (Table 1). The BNC yield on consumed glucose was 0.15 g/g, whereas it was 0.16 g/g in the reference medium (Table 1).

When the initial dosage of acid **1** was increased to 100 mM or higher, the consumption rate of glucose decreased to ≤0.18 g/(L·day) (Table 1) and the pH value did not change much (Figure 2B). Low concentrations of live bacterial cells were observed in the media, and the concentration of acid **1** was constant (Figure 2). There was no synthesis of BNC in the media with 100 mM or higher concentrations of acid **1** (Table 1). Thus, *G. xylinus* could tolerate 25 mM formic acid, but at 100 mM or higher concentrations there was a complete inhibition of both the production of BNC and the growth of the bacterial cells.

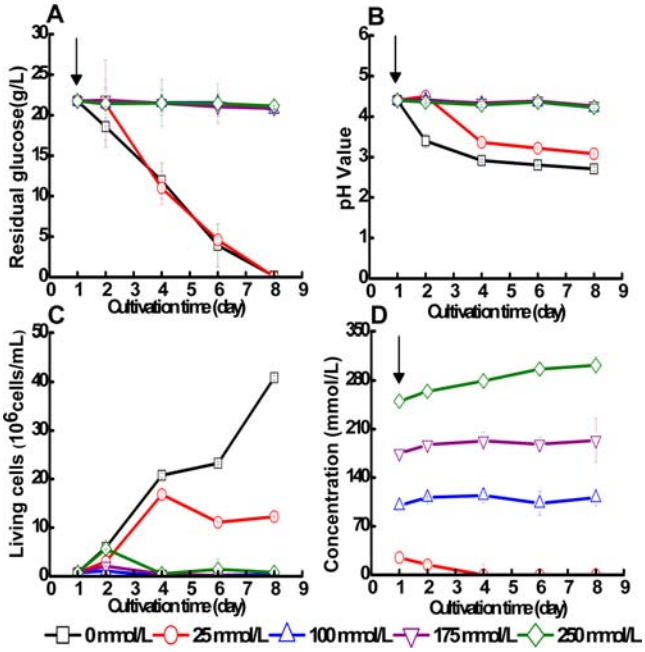


**Figure 2.** Changes in (A) glucose concentration, (B) pH value, (C) cell growth, and (D) formic acid concentration during cultivation of *G. xylinus* in media supplemented with formic acid. The arrows indicate the time for addition of formic acid. Error bars show standard errors of means of three replicates.

Concentrations of acid **2** up to 250 mM did not stop the growth of *G. xylinus* or the production of BNC (Figure 3; Table 1). The glucose was consumed gradually during the cultivation (Figure 3). In the first 3 days after the addition of acid **2**, the consumption rates of glucose for cultures with acid additions of 25, 100, and 175 mM were 4.8, 5.1, and 4.9 g/(L·day), respectively. These were higher than that for the cultures grown in reference medium, which had a glucose consumption rate of 3.3 g/(L·day) after 3 days. At the end of the cultivation, there was little glucose left in the media except for cultures with an initial addition of 250 mM acetic acid, which contained 3.2 g/L (Figure 3A). The average glucose consumption rate during the 7 day cultivation in media with 25−175 mM acetic acid was 3.1 g/(L·day), which was the same as for cultures grown in reference medium (Table 1). For cultures in medium with 250 mM acid **2**, the average glucose consumption rate was 2.6 g/(L·day), which shows a decrease ($p < 0.05$, $t$ test) compared to cultures grown in reference medium. The volumetric yield of BNC in the media with acetic acid did not differ significantly ($p < 0.05$) from the yield of the cultures in reference medium except for cultures with an initial addition of 250 mM acid **2**, for which it decreased to 3.1 g/L. Even though the glucose consumption rate and the volumetric yield of BNC were lower for medium with 250 mM, the BNC yield on consumed glucose (0.17 g/g) was slightly higher than that of the cultures in reference medium (0.16 g/g). It can be concluded that high concentrations of acetic acid tend to inhibit the proliferation of *G. xylinus*, but not its ability to produce BNC. The pH decreased gradually, but the pH in the medium with high concentration of acetic acid did not drop as much as that in the


dx.doi.org/10.1021/jf502623s | J. Agric. Food Chem. 2014, 62, 9792−9799

**Table 1. Yield of Bacterial Nanocellulose and Glucose Consumption Rate in 7 Day Cultures Supplemented with Aliphatic Acids**

| | concentration | | | | |
|---|---|---|---|---|---|
| acid | 0 mM | 25 mM | 100 mM | 175 mM | 250 mM |
| | | | **Volumetric Yield of Bacterial Nanocellulose (g/L)** | | |
| **1** | 3.5 ± 0.3 | 3.2 ± 0.2 | ND[a] | ND | ND |
| **2** | 3.5 ± 0.3 | 3.4 ± 0.7 | 3.5 ± 0.9 | 3.6 ± 0.5 | 3.1 ± 0.3 |
| **3** | 3.5 ± 0.3 | 3.5 ± 0.5 | 5.0 ± 0.9 | 4.2 ± 0.9 | 3.8 ± 0.5 |
| | | | **Bacterial Nanocellulose Yield on Consumed Glucose (g/g)** | | |
| **1** | 0.16 ± 0.01 | 0.15 ± 0.01 | ND | ND | ND |
| **2** | 0.16 ± 0.01 | 0.16 ± 0.03 | 0.16 ± 0.04 | 0.17 ± 0.02 | 0.17 ± 0.01 |
| **3** | 0.16 ± 0.01 | 0.16 ± 0.02 | 0.23 ± 0.04 | 0.20 ± 0.04 | 0.18 ± 0.02 |
| | | | **Glucose Consumption Rate (g/(L·day))** | | |
| **1** | 3.1 ± 0.1 | 3.1 ± 0.1 | 0.18 ± 0.30 | 0.13 ± 0.10 | 0.09 ± 0.01 |
| **2** | 3.1 ± 0.1 | 3.1 ± 0.1 | 3.1 ± 0.1 | 3.1 ± 0.1 | 2.6 ± 0.1 |
| **3** | 3.1 ± 0.1 | 3.1 ± 0.1 | 3.1 ± 0.1 | 3.1 ± 0.1 | 3.1 ± 0.1 |

[a]None detected.

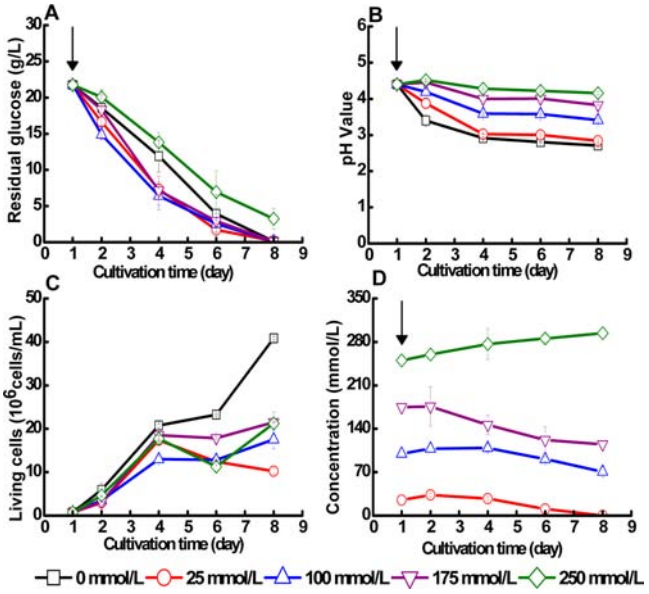


**Figure 3.** Changes in (A) glucose concentration, (B) pH value, (C) cell growth, and (D) acetic acid concentration during cultivation of *G. xylinus* in media supplemented with acetic acid. The arrows indicate the time for addition of acetic acid. Error bars show standard errors of means of three replicates.

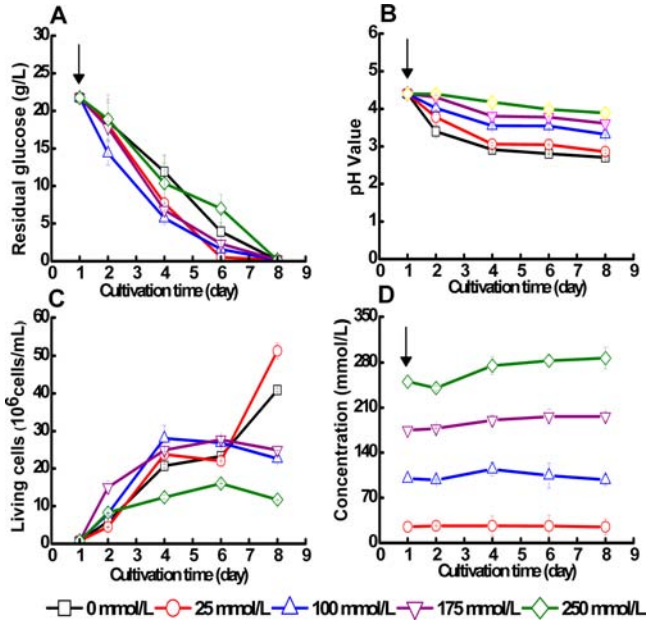


**Figure 4.** Changes in (A) glucose concentration, (B) pH value, (C) cell growth, and (D) levulinic acid concentration during cultivation of *G. xylinus* in media supplemented with levulinic acid. The arrows indicate the time for addition of levulinic acid. Error bars show standard errors of means of three replicates.

medium with low concentration of acetic acid. This can be attributed to the buffering capacity of acetic acid, which has a p$K_a$ of 4.76, close to the initial pH of the cultures. *G. xylinus* consumed acetic acid when the initial concentration was 175 mM or lower (Figure 3D). The concentration of acetic acid increased slightly in cultures with an initial concentration of 250 mM (Figure 3). This may be due to evaporation of water during the cultivation and to the bacterium not being able to convert as much acetic acid as in the other media.

Results obtained with acid **3** are shown in Figure 4 and Table 1. After the addition of acid **3** to the medium, there was a sharp decrease in the concentration of glucose during the first 3 days of cultivation (Figure 4A). The average glucose consumption rate in cultures with 25, 100, 175, and 250 mM levulinic acid during the first 3 days were 4.7, 5.3, 5.0, and 3.8 g/(L·day), respectively. They were higher than that of the reference medium (3.3 g/(L·day)). At the end of the cultivation, there was little glucose left in the media (Figure 4A). The average glucose consumption rate during the 7 days of cultivation with levulinic acid was 3.1 g/(L·day) for all media (Table 1). The pH value in all media decreased gradually, although the decrease of pH in media with higher concentrations of levulinic acid was smaller than that in media with lower concentrations or no levulinic acid. The buffering effect of levulinic acid (Figure 4B) may explain the slightly more rapid initial glucose consumption rates of cultures containing levulinic acid (Figure 4A). The bacterium grew well in media with levulinic acid (Figure 4C), and the maximum concentration of live bacteria ($51.3 \times 10^6$ cells/mL) was observed in the medium with 25 mM levulinic acid. This concentration was even higher than that in the reference medium, which was $40.8 \times 10^6$ cells/mL. The lowest concentration of live cells, $11.7 \times 10^6$ cells/mL, was obtained in the medium with 250 mM levulinic acid. The concentration of levulinic acid did not change during the cultivation (Figure 4D), which indicates that *G. xylinus* was not


dx.doi.org/10.1021/jf502623s | J. Agric. Food Chem. 2014, 62, 9792−9799

able to utilize levulinic acid. The concentration of levulinic acid in cultures with an initial concentration of 250 mM increased slightly at the end of the cultivation, which can be attributed to evaporation of water in combination with the inability of *G. xylinus* to utilize levulinic acid. The volumetric yield of BNC increased significantly ($p < 0.05$) as the concentration of levulinic acid got higher. The maximum yield of BNC, 5.0 g/L, was obtained with an initial concentration of levulinic acid of 100 mM, whereas cultures with reference medium reached only 3.5 g/L (Table 1). Even cultures with an initial concentration of 250 mM gave higher yields than cultures with reference medium (Table 1). There was a similar trend for the BNC yield on consumed glucose (Table 1). The BNC yield on consumed glucose in medium with 100 mM, 0.23 g/g, was the highest value for media with or without aliphatic acids (Table 1).

The results demonstrate that formic acid is more inhibitory to *G. xylinus* than acetic acid, whereas inhibitory concentrations of levulinic acid were not reached in the interval studied. The result is in one way similar to results obtained in experiments with a baker's yeast strain, where formic acid was found to be more inhibitory than levulinic acid or acetic acid.[17] Larsson et al.[17] found that concentrations exceeding around 100 mM tended to decrease the ethanol yield, whereas lower concentrations instead stimulated ethanol production at the expense of biomass synthesis. There are also differences, as levulinic acid was found to be more inhibitory to yeast than acetic acid[18] and the effects of acetic acid and levulinic acid on *G. xylinus* were positive at least up to 175 mM (this work).

Acids may be inhibitory for several reasons. One possibility is that the protonated form of the acid passes across the plasma membrane and releases the proton in the cytoplasm, where the pH is higher than in the surrounding medium.[19,20] To maintain a constant intracellular pH value, protons are pumped out of the cell by a plasma membrane ATPase. This may lead to excessive consumption of ATP and, in the long run, to depletion of the pool of ATP. Another possibility is that they would act as uncouplers, amphiphilic molecules that dissolve in the inner mitochondrial membrane of eukaryotes or in the plasma membrane of prokaryotes and transfer protons across the membrane, which would uncouple the respiratory chain and the oxidative phosphorylation and disturb the regeneration of ATP. However, the anions of formic acid, acetic acid, and levulinic acid are hydrophilic and could not readily traverse the cell membrane.[21] A third possibility could be intracellular anion accumulation. After dissociation, the anionic form of the acid would be captured in the cell.[19] It has been speculated that formic acid would have higher anion toxicity to yeast.[17] It has also been suggested that formic acid would increase the membrane leakage of ethanologenic *Escherichia coli* LY01.[22]

There are several studies of the effect of weak acids on *Acetobacter*, another genus of acetic acid bacteria, which is characterized by a strong ability to oxidize alcohols and sugars to acetic acid and by high resistance to the acid.[23] An efflux pump of *Acetobacter aceti* IFO 3283 has been reported to enable the bacterium to grow in the presence of high concentrations of acetic acid.[24] Addition of acetic acid to cultures of *Acetobacter xylinum* strain DA has been shown to enhance the cellulose yield from glucose.[25] Glucose is catabolized to generate energy for bacterial anabolism and can be used as a building block in the synthesis of bacterial cellulose. If glucose is partly substituted by another carbon source (such as acetic acid), the conversion of glucose to cellulose may be improved.[25] This is a possible explanation for some of our results with *G. xylinus*, where relatively low concentrations of bacteria in media with high concentrations of acetic acid gave similar yields of BNC as obtained with the reference medium (Table 1; Figure 3C).

**Effects of Aldehydes.** As shown in Figure 5, furfural (**4**, Figure 1) had a very clear negative effect on *G. xylinus*. Only 5.6

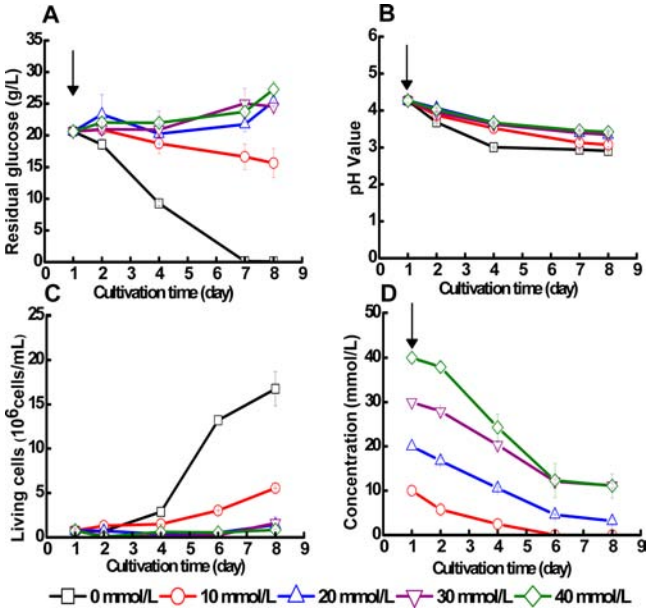


**Figure 5.** Changes in (A) glucose concentration, (B) pH value, (C) cell growth, and (D) furfural concentration during cultivation of *G. xylinus* in media supplemented with furfural. The arrows indicate the time for addition of furfural. Error bars show standard errors of means of three replicates.

$\times 10^6$ live cells/mL were found in cultures with an initial furfural concentration of 10 mM, which can be compared to $16.8 \times 10^6$ live cells/mL in cultures with reference medium. With an addition of 10 mM furfural, the average consumption rate of glucose was 0.71 g/(L·day), only 24% of the rate observed for cultures in reference medium (Table 2). With 10 mM furfural, a BNC yield of 1.1 g/L was achieved, which was 20% of the yield obtained with reference medium. The decreased volumetric yield of BNC in the presence of furfural was mainly due to the reduction of the concentration of live bacteria, although the BNC yield on consumed glucose was also lower (0.22 g/g) than in cultures with reference medium (0.27 g/g). When the concentration of furfural was increased to 20 mM, there was no glucose consumption in the cultures (Figure 5A) and there were hardly any live bacteria in the culture medium (Figure 5C). The slight increase in glucose concentration in cultures with an initial furfural concentration between 20 and 40 mM can be explained by evaporation of water during the incubation (Figure 5A).

Figure 5D indicates that the concentration of furfural decreased as the cultivation continued. This could be due not only to bioconversion of furfural by *G. xylinus* but also to evaporation of furfural. In cultures with furfural, furoic acid was identified as a main product (Table 3). Furoic acid (**6**, Figure 1) was formed in all cultures to which furfural was added, but the highest yield, 88%, was observed in cultures with an initial furfural concentration of 10 mM. No furfuryl alcohol was detected in the culture media. Control experiments with medium with furfural but without bacterial inoculum were


dx.doi.org/10.1021/jf502623s | J. Agric. Food Chem. 2014, 62, 9792−9799

**Table 2. Yield of Bacterial Nanocellulose and Glucose Consumption Rate in 7 Day Cultures Supplemented with Furan Aldehydes**

| | concentration | | | | |
|---|---|---|---|---|---|
| aldehyde | 0 mM | 10 mM | 20 mM | 30 mM | 40 mM |
| | **Volumetric Yield of Bacterial Nanocellulose (g/L)** | | | | |
| **4** | 5.6 ± 0.8 | 1.1 ± 0.5 | ND[a] | ND | ND |
| **5** | 5.6 ± 0.8 | 4.3 ± 0.1 | 0.81 ± 0.01 | ND | ND |
| | **Bacterial Nanocellulose Yield on Consumed Glucose (g/g)** | | | | |
| **4** | 0.27 ± 0.04 | 0.22 ± 0.01 | ND | ND | ND |
| **5** | 0.27 ± 0.04 | 0.31 ± 0.01 | 0.22 ± 0.02 | ND | ND |
| | **Glucose Consumption Rate (g/(L·day))** | | | | |
| **4** | 2.9 ± 0.1 | 0.71 ± 0.33 | ND | ND | ND |
| **5** | 2.9 ± 0.1 | 2.0 ± 0.2 | 0.34 ± 0.20 | ND | ND |

[a]None detected.

**Table 3. Conversion of Furan Aldehydes in Bacterial Cultures**

| | | | | |
|---|---|---|---|---|
| initial concentration of **4** (mM) | 10 | 20 | 30 | 40 |
| yield of **6** (%) | 88 | 62 | 42 | 34 |
| initial concentration of **5** (mM) | 10 | 20 | 30 | 40 |
| yield of **8** (%) | 76 | 32 | 15 | 12 |

performed. No conversion products from furfural were detected in the medium, which indicates that the furoic acid formed in media with bacteria was a bioconversion product and not a product caused by oxidation by air or by other media components. Apart from bioconversion, the decrease of the concentration of furfural in the culture media (Table 3) can be attributed to evaporation of furfural. Experiments with acid wood hydrolysates have shown that furfural easily evaporates. After evaporation of 10% of the volume, the concentration of furfural was reduced with 37%, whereas the concentration of 5-hydroxymethylfurfural, which is much less volatile than furfural, was unchanged.[18]

The effects of 5-hydroxymethylfurfural (**5**, Figure 1) on the bacterial cultures are shown in Figure 6 and Table 2. When the initial concentration of 5-hydroxymethylfurfural was 10 mM, the growth rate increased rapidly from the fourth day, and the maximum concentration of viable cells, $13.3 \times 10^6$ cells/mL, was obtained on day 7. The average consumption rate of glucose was 2.0 g/(L·day), which was lower than for the culture in control medium (2.9 g/(L·day)). When the initial concentration of 5-hydroxymethylfurfural was increased to 20 mM, the consumption rate of glucose decreased sharply to 0.34 g/(L·day). As the initial concentration of 5-hydroxymethylfurfural was increased further, the growth of the bacteria diminished and the glucose consumption rate was negligible. The pH value decreased gradually during the cultivation. When the initial 5-hydroxymethylfurfural concentrations were 10 and 20 mM, the yields of BNC were 0.31 and 0.22 g/g, respectively (Table 2). As the yield of BNC in the reference medium was 0.27 g/g, low concentrations of 5-hydroxymethylfurfural may have a positive effect on the production of BNC. The data in Table 2 and Figure 6 indicate that 5-hydroxymethylfurfural was less toxic than furfural to *G. xylinus*.

When the initial concentration of 5-hydroxymethylfurfural was 10 mM, all of the 5-hydroxymethylfurfural could be converted by the bacteria (Figure 6D). When the initial concentration of 5-hydroxymethylfurfural was higher, the conversion rate seemed to decline. Analyses of the culture

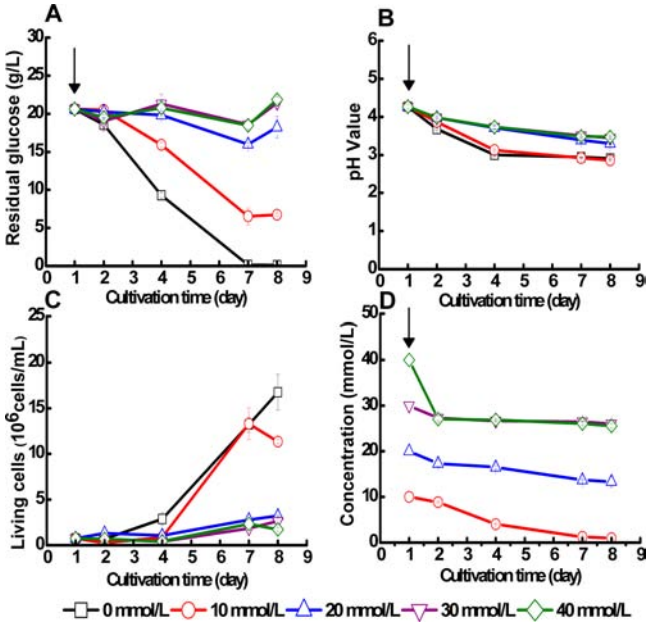


**Figure 6.** Changes in (A) glucose concentration, (B) pH value, (C) cell growth, and (D) 5-hydroxymethylfurfural concentration during cultivation of *G. xylinus* in media supplemented with 5-hydroxymethylfurfural. The arrows indicate the time for addition of 5-hydroxymethylfurfural. Error bars show standard errors of means of three replicates.

fluid indicated formation of 5-hydroxymethyl-2-furoic acid (**8**, Figure 1). The yield of 5-hydroxymethyl-2-furoic acid was highest (76%) in cultures with an initial concentration of 5-hydroxymethylfurfural of 10 mM (Table 3), which clearly indicates that it was the predominant bioconversion product. At higher initial concentrations of 5-hydroxymethylfurfural, the yield of 5-hydroxymethyl-2-furoic acid dropped. It is noteworthy that there was formation of 5-hydroxymethyl-2-furoic acid (12% yield) even when the initial concentration of 5-hydroxymethylfurfural was as high as 40 mM, and there were no clear signs of glucose consumption, the concentration of viable cells was low, and there were only minor changes in pH indicating low metabolic activity (Figure 6). Control experiments (without inoculation but with addition of 5-hydroxymethylfurfural) showed no conversion products from 5-hydroxymethylfurfural, which supports the conclusion that 5-hydroxymethyl-2-furoic acid was formed by biocatalytic conversion.


dx.doi.org/10.1021/jf502623s | J. Agric. Food Chem. 2014, 62, 9792−9799

The inhibition by furan aldehydes of ethanologenic microorganisms, such as *S. cerevisiae*, has been studied extensively.[14,15] *S. cerevisiae* would typically be expected to reduce furfural to furfuryl alcohol[26] and 5-hydroxymethylfurfural to 5-hydroxymethylfurfuryl alcohol (2,5-bis-hydroxymethylfuran).[27] However, during respiratory growth *S. cerevisiae* exclusively converted furfural to furoic acid.[28] Under both aerobic and anaerobic conditions, 5-hydroxymethylfurfural was mainly reduced to 5-hydroxymethyl furfuryl alcohol by yeast and only small amounts of 5-hydroxymethyl furoic acid were found.[27] Methanobacteria have been found to convert furfural to furfuryl alcohol,[29] whereas *Clostridium acetobutylicum* was found to reduce both furfural and 5-hydroxymethylfurfural to the corresponding alcohols.[30] Wahlbom and Hahn-Hägerdal[31] studied *S. cerevisiae* TMB 3001 and found that the reduction of furfural was associated with consumption of NADH, whereas the reduction of 5-hydroxymethylfurfural was associated with the consumption of NADPH. NADH plays an important part in many cellular reactions, including respiratory and fermentative catabolism, whereas NADPH is mainly utilized in biosynthetic reactions. NADPH may also function as an essential cofactor for enzymes involved in protection against oxidative stress. Besides intracellular redox balance, stress also affects energy metabolism, as many stress-responsive processes are dependent on ATP availability. The ability of *G. xylinus* to oxidize furan aldehydes has not been reported before. Biotransformation by oxidation is not self-evident, as *G. xylinus* has been found to reduce phenolic aldehydes to the corresponding alcohols.[16]

NAD(P)H- and $NAD(P)^+$-dependent reactions have also been studied in *G. xylinus*.[1] *A. aceti* MIM2000/28 has been reported to have the ability to convert polyconjugated aldehydes to the corresponding acids, an ability that has been used for a number of selective bio-oxidations.[32] The probable reaction behind conversion of furfural by *G. xylinus* would be

$$\text{furfural} + H_2O + NAD(P)^+ \rightarrow \text{furoic acid} + NAD(P)H + H^+$$

Similarly, 5-hydroxymethylfurfural would probably be oxidized to 5-hydroxymethyl-2-furoic acid in a reaction involving the reduction of $NAD(P)^+$. Assuming that these reactions have relatively high priority, as indicated by furan aldehyde bioconversion taking place (Table 3) without concurrent glucose catabolism or BNC production at the higher furan aldehyde concentrations studied (Table 2), the furan aldehydes would be expected to interfere with critical cellular reactions involving oxidized nicotinamide adenine dinucleotides. It is a possibility that the furoic acids are less toxic than the corresponding aldehydes, and in that case the reactions indicated above would represent detoxification reactions, but that possibility needs to be addressed in future investigations.

Kubiak et al.[33] identified a megaplasmid of *G. xylinus* E25 and found some genes connected to oxidoreductases. Megaplasmids may be important for the survival of bacteria under stress. Oxidoreductases would probably be involved in the catalysis of oxidation of furan aldehydes to the corresponding carboxylic acids. The potential effects of *G. xylinus* oxidoreductases on furan aldehydes warrant attention in future studies.

In summary, the effects of presumed inhibitors, three aliphatic carboxylic acids and two furan aldehydes, on cultures of *G. xylinus* have been elucidated. Whereas formic acid, furfural, and 5-hydroxymethylfurfural had an inhibitory effect, appropriately high concentrations of levulinic acid and acetic acid were found to stimulate BNC production. The sensitivity of *G. xylinus* to furan aldehydes differed from that observed for other microorganisms, such as *S. cerevisiae*, which indicates that results obtained with other microorganisms cannot be extrapolated to *G. xylinus*. The main bioconversion products of furfural and 5-hydroxymethylfurfural were found to be the corresponding carboxylic acids. The effects of carboxylic acids need to be further investigated using pH-controlled cultures. Information provided by the current study paves the way for future studies on potential synergistic effects of different inhibitory compounds. A better understanding of inhibitory and stimulatory effects of lignocellulose-derived compounds will facilitate the development of robust processes for the production of BNC from lignocellulosic resources.

## AUTHOR INFORMATION

### Corresponding Author

*(F.H.) E-mail: fhong@dhu.edu.cn. Phone: +86-21-67792649. Fax: +86-21-67792649.

### Funding

This investigation was funded by the Program for New Century Excellent Talents in University (NCET-12-0828), by the National Natural Science Foundation of China (51373031), the Science and Technology Commission of Shanghai Municipality (12 nm0500600 and 11230700600), the Fundamental Research Funds for the Central Universities, the Kempe Foundations, the Swedish Energy Agency (35367-1), the Swedish Research Council (621-2011-4388), and Bio4Energy (www.bio4energy.se). S.Z. was supported by the Innovation Foundation of Donghua University for Doctoral Candidates (no. 12D11322).

### Notes

The authors declare no competing financial interest.

## ABBREVIATIONS USED

BNC, bacterial nanocellulose; HPAEC, high-performance anion-exchange chromatography; HPLC, high-performance liquid chromatography; HPLC-UV-DAD, high-performance liquid chromatography−UV diode array detection; RFV, relative fluorescence value

## REFERENCES

(1) Bielecki, S.; Krystynowicz, A.; Turkiewicz, M.; Kalinowska, H. Bacterial cellulose. In *Biopolymers (Polysaccharides I: Polysaccharides from Prokaryotes)*; Vandamme, J., Baets, S. D., Steinbüchel, A., Eds.; Wiley-VCH Verlag: Weinheim, Germany, 2002; Vol. 5, pp 37−90.

(2) Chawla, P. R.; Bajaj, I. B.; Survase, S. A.; Singhal, R. S. Microbial cellulose: fermentative production and applications. *Food Technol. Biotechnol.* **2009**, *47*, 107−124.

(3) Fu, L.; Zhang, J.; Yang, G. Present status and applications of bacterial cellulose-based materials for skin tissue repair. *Carbohydr. Polym.* **2013**, *92*, 1432−1442.

(4) Jiang, G.; Qiao, J.; Hong, F. Application of phosphoric acid and phytic acid-doped bacterial cellulose as novel proton-conducting membranes to PEMFC. *Int. J. Hydrogen Energy* **2012**, *37*, 9182−9192.

(5) Lu, X.; Tang, S.; Huang, B.; Shen, X.; Hong, F. Preparation and characterization of bacterial cellulose/hydroxypropyl chitosan blend as-spun fibers. *Fiber Polym.* **2013**, *14*, 935−940.

(6) Wei, B.; Yang, G.; Hong, F. Preparation and evaluation of a kind of bacterial cellulose dry films with antibacterial properties. *Carbohydr. Polym.* **2011**, *84*, 533−538.

(7) Hong, F.; Guo, X.; Zhang, S.; Han, S. F.; Yang, G.; Jonsson, L. J. Bacterial cellulose production from cotton-based waste textiles: enzymatic saccharification enhanced by ionic liquid pretreatment. *Bioresour. Technol.* **2012**, *104*, 503−508.

(8) Hong, F.; Qiu, K. An alternative carbon source from konjac powder for enhancing production of bacterial cellulose in static cultures by a model strain *Acetobacter aceti* subsp *xylinus* ATCC 23770. *Carbohydr. Polym.* **2008**, *72*, 545−549.
(9) Chen, L.; Hong, F.; Yang, X.; Han, S. Biotransformation of wheat straw to bacterial cellulose and its mechanism. *Bioresour. Technol.* **2013**, *135*, 464−468.
(10) Hong, F.; Zhu, Y. X.; Yang, G.; Yang, X. X. Wheat straw acid hydrolysate as a potential cost-effective feedstock for production of bacterial cellulose. *J. Chem. Technol. Biotechnol.* **2011**, *86*, 675−680.
(11) Cavka, A.; Guo, X.; Tang, S. J.; Winestrand, S.; Jönsson, L. J.; Hong, F. Production of bacterial cellulose and enzyme from waste fiber sludge. *Biotechnol. Biofuels* **2013**, *6*, 25.
(12) Guo, X.; Cavka, A.; Jönsson, L. J.; Hong, F. Comparison of methods for detoxification of spruce hydrolysate for bacterial cellulose production. *Microb. Cell Fact.* **2013**, *12*, 93.
(13) Jönsson, L. J.; Alriksson, B.; Nilvebrant, N. O. Bioconversion of lignocellulose: inhibitors and detoxification. *Biotechnol. Biofuels* **2013**, *6*, 16.
(14) Nevoigt, E. Progress in metabolic engineering of *Saccharomyces cerevisiae*. *Microbiol. Mol. Biol. Rev.* **2008**, *72*, 379−412.
(15) Pienkos, P.; Zhang, M. Role of pretreatment and conditioning processes on toxicity of lignocellulosic biomass hydrolysates. *Cellulose* **2009**, *16*, 743−762.
(16) Zhang, S.; Winestrand, S.; Guo, X.; Chen, L.; Hong, F.; Jönsson, L. J. Effects of aromatic compounds on the production of bacterial nanocellulose by *Gluconacetobacter xylinus*. *Microb. Cell Fact.* **2014**, *13*, 62.
(17) Larsson, S.; Palmqvist, E.; Hahn-Hägerdal, B.; Tengborg, C.; Stenberg, K.; Zacchi, G.; Nilvebrant, N. O. The generation of fermentation inhibitors during dilute acid hydrolysis of softwood. *Enzyme Microb. Technol.* **1999**, *24*, 151−159.
(18) Larsson, S.; Reimann, A.; Nilvebrant, N. O.; Jönsson, L. J. Comparison of different methods for the detoxification of lignocellulose hydrolyzates of spruce. *Appl. Biochem. Biotechnol.* **1999**, *77*−*79*, 91−103.
(19) Piper, P.; Calderon, C. O.; Hatzixanthis, K.; Mollapour, M. Weak acid adaptation: the stress response that confers yeasts with resistance to organic acid food preservatives. *Microbiology* **2001**, *147*, 2635−2642.
(20) Russell, J. B. Another explanation for the toxicity of fermentation acids at low pH: anion accumulation versus uncoupling. *J. Appl. Microbiol.* **1992**, *73*, 363−370.
(21) Casal, M.; Cardoso, H.; Leao, C. Mechanisms regulating the transport of acetic acid in *Saccharomyces cerevisiae*. *Microbiology* **1996**, *142*, 1385−1390.
(22) Zaldivar, J.; Ingram, L. O. Effect of organic acids on the growth and fermentation of ethanologenic *Escherichia coli* LY01. *Biotechnol. Bioeng.* **1999**, *66*, 203−210.
(23) Fukaya, M.; Takemura, H.; Okumura, H.; Kawamura, Y.; Horinouchi, S.; Beppu, T. Cloning of genes responsible for acetic acid resistance in *Acetobacter aceti*. *J. Bacteriol.* **1990**, *172*, 2096−2104.
(24) Matsushita, K.; Inoue, T.; Adachi, O.; Toyama, H. *Acetobacter aceti* possesses a proton motive force-dependent efflux system for acetic acid. *J. Bacteriol.* **2005**, *187*, 4346−4352.
(25) Toda, K.; Asakura, T.; Fukaya, M.; Entani, E.; Kawamura, Y. Cellulose production by acetic acid-resistant *Acetobacter xylinum*. *J. Ferment. Bioeng.* **1997**, *84*, 228−231.
(26) Palmqvist, E.; Almeida, J. S.; Hahn-Hägerdal, B. Influence of furfural on anaerobic glycolytic kinetics of *Saccharomyces cerevisiae* in batch culture. *Biotechnol. Bioeng.* **1999**, *62*, 447−454.
(27) Taherzadeh, M. J.; Gustafsson, L.; Niklasson, C.; Liden, G. Physiological effects of 5-hydroxymethylfurfural on *Saccharomyces cerevisiae*. *Appl. Microbiol. Biotechnol.* **2000**, *53*, 701−708.
(28) Sárvári, H. I.; Franzén, C. J.; Taherzadeh, M. J.; Niklasson, C.; Lidén, G. Effects of furfural on the respiratory metabolism of *Saccharomyces cerevisiae* in glucose-limited chemostats. *Appl. Environ. Microbiol.* **2003**, *69*, 4076−4086.
(29) Deppenmeier, U. The unique biochemistry of methanogenesis. *Prog. Nucleic Acid Res.* **2002**, *71*, 223−283.
(30) Zhang, Y.; Han, B.; Ezeji, T. C. Biotransformation of furfural and 5-hydroxymethyl furfural (HMF) by *Clostridium acetobutylicum* ATCC 824 during butanol fermentation. *New Biotechnol.* **2012**, *29*, 345−351.
(31) Wahlbom, C. F.; Hahn-Hägerdal, B. Furfural, 5-hydroxymethyl furfural, and acetoin act as external electron acceptors during anaerobic fermentation of xylose in recombinant *Saccharomyces cerevisiae*. *Biotechnol. Bioeng.* **2002**, *78*, 172−178.
(32) Pini, E.; Bertacche, V.; Molinari, F.; Romano, D.; Gandolfi, R. Direct conversion of polyconjugated compounds into their corresponding carboxylic acids by *Acetobacter aceti*. *Tetrahedron* **2008**, *64*, 8638−8641.
(33) Kubiak, K.; Kurzawa, M.; Jędrzejczak-Krzepkowska, M.; Ludwicka, K.; Krawczyk, M.; Migdalski, A.; Kacprzak, M. M.; Loska, D.; Krystynowicz, A.; Bielecki, S. Complete genome sequence of *Gluconacetobacter xylinus* E25 strain − valuable and effective producer of bacterial nanocellulose. *J. Biotechnol.* **2014**, *176*, 18−19.

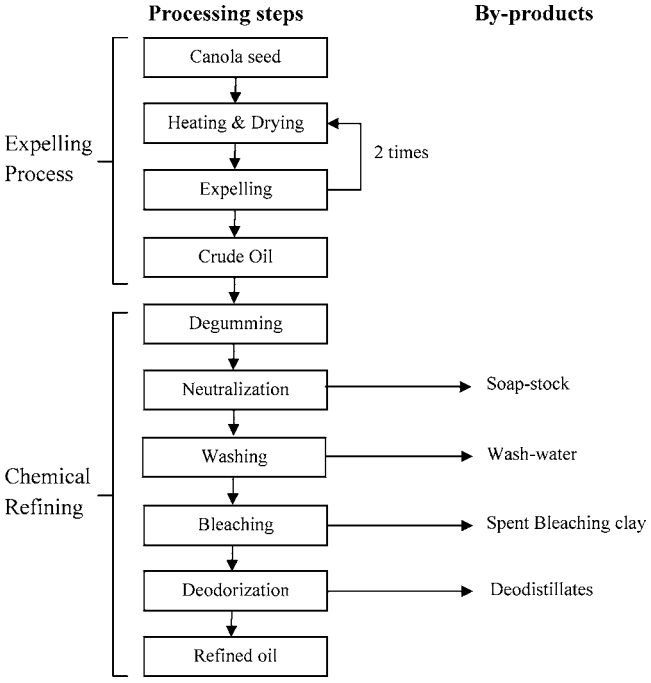


**Figure 2.** Expeller-pressing process for canola oil and the corresponding chemical refining and residual byproducts.

ingredient, raw material for animal feed, and/or a novel source for biodiesel production.[16] The utilization of soap stock to recover other bioactive compounds is an emerging area to add value to the edible oil processing and refining sector. After neutralization, water is commonly added to the oil to reduce the soap content. This soapy water containing the neutralized lipids is a commercial byproduct and is referred to in the present study as wash water. After these refining steps, bleaching and deodorization follow. Spent bleaching clay is generated as a byproduct during bleaching. Finally, edible oil deodorization is conducted to remove off flavors utilizing steam distillation under elevated temperature and vacuum conditions.[17] This results in the production of another byproduct, deodistillates or deodorization distillates, which are a rich source of many bioactive compounds, including tocochromanols, phytosterols, and polyphenols. For instance, a novel canolol dimer, beside sinapic acid and canolol, was detected in significant amounts (3500 mg/kg).[18] Thus, the economic values of the oil refining byproducts can be increased by recovering these valuable bioactive components such as tocopherols and the sinapic acid derivatives.[18,19]

Another implication of the refining processes is that bioactive antioxidants of the edible oils are lost, possibly degraded or even leached during the high-temperature processing of refining.[18,20] The majority of antioxidants found in canola are polyphenols with a hydrophilic nature[21] and, thus, may leach into wash water or soap stock. There are only a few studies associating the antioxidant compositions and their oil refining byproducts.[8,18,19,22] Ortega-García et al.[9] reported many polyphenols in the olive oil refining byproducts (819.9 mg/kg of soap stock and 134.4 mg/kg of wash water samples). The reports that these endogenous antioxidants are being removed by the adsorbent during the bleaching process make the corresponding byproduct, the spent bleaching clay, a candidate for a further recovery study.[22]

These polyphenols and tocopherols have added value by being both abundant and naturally occurring for potential use in cosmetic, food, and pharmaceutical applications.[23−25] Although several studies have been conducted to evaluate the loss of these antioxidants from edible oil refining,[8−13] only a few of these studies explored the possibility of recovering them from the corresponding refining byproducts. Thus, this paper is the first ever attempt to characterize and quantitate the retention and loss of sinapic acid derivatives and tocopherols in the corresponding byproducts associated with the refining processes. In addition, characterization and quantification of antioxidant phenolics of expeller-pressed canola oils at different stages of refining were also studied. Furthermore, the rapid extraction techniques of these bioactive phenolics were also examined to highlight the value-added potential of byproducts of refining.

## MATERIALS AND METHODS

**Industrial Samples and Chemicals.** Canola oils from different refining stages (crude, degummed, neutralized, bleached, and deodorized oils) and corresponding byproducts including soap stock, wash water, spent bleaching clay, and deodistillates were supplied by Vittera Canola Processing Inc. (Winnipeg, Canada). All samples were collected from the same batch of processed oil and stored at −20 °C before analysis. All chemicals used in this study were purchased from Sigma-Aldrich and of analytical grade.

**Extraction of Sinapic Acid Derivatives.** *Canola Oils.* Canola oils were extracted with aqueous methanol (70%) as previously described.[7] Briefly, 2 g of each sample was dissolved in 5 mL of extraction solvent, and the mixture was vortexed for 3 min followed by centrifugation at 5000 for 5 min under refrigerated conditions. The supernatant was collected, and the residue was re-extracted following the same procedure one more time. The supernatants were pooled, and the mixture was then made up to 10 mL using 70% aqueous methanol.

*Refining Byproducts.* Wash water and deodistillates were extracted using the method described above to produce "Extract 1". Additionally, they were also extracted with 50% aqueous methanol to produce "Extracts 2−5" as previously described.[19] Briefly, samples (2 g) were solubilized with 10 mL of hexane (1:5 w/v), followed by extraction using 50% methanol (3 mL) three times. Instead of hexane, other nonpolar solvents such as chloroform, cyclohexane, and toluene were used for solubilization prior to extraction. The methanolic extracts were pooled and made up to 10 mL using 50% methanol.

Spent bleaching clay was defatted using a Soxtec 2050 (Foss-Tecator, Foss North America) and the oil was extracted as described elsewhere. The defatted spent bleaching clay was extracted following the procedure described by Khattab et al.[26] Briefly, spent bleaching clay sample (1 g) was extracted with 9 mL 70% methanol with ultrasound treatment for 1 min twice. The filtrates were pooled and made up to 30 mL.

The soap-stock samples (pH 12) were adjusted to two different pH levels (7 and 2) using 2 M HCl and extracted with 10 mL of ethyl acetate thrice. The extracts were pooled, concentrated in a rotary evaporator at 50 °C to dryness, and then redissolved in 5 mL of 70% methanol.

**Extraction of Tocopherols.** The oils, wash water, or deodistillate samples were extracted directly with absolute methanol and methanol/2-propanol (1:1, v/v) mixture for several times.[27] Briefly, 2 g of oil or byproduct sample were first extracted with 10 mL of absolute methanol for 3 min. The residue was extracted with 10 mL of methanol/2-propanol mixture (1:1, v/v) three times. The supernatants were pooled and made up to 40 mL, filtered using a Whatman No. 1 filter paper, and evaporated to dryness under $N_2$, and the residue was redissolved in 5 mL of the methanol/2-propanol mixture.

**Synthesis of Canolol.** The synthesis of canolol was carried following a previously reported method[28] with slight modifications. Syringaldehyde and malonic acid were mixed and microwave irradiated


dx.doi.org/10.1021/jf502428z | J. Agric. Food Chem. 2014, 62, 9800−9807

Table 1. Effect of Chemical Refining Steps on the Phenolic and Tocopherol Compositions of Expeller-Pressed Canola Oils[a]

| antioxidant composition | crude oil | degummed oil | neutralized oil | bleached oil | deodorized oil |
|---|---|---|---|---|---|
| sinapic acid (μg/g) | 30.5 ± 0.5 a | 36.2 ± 3.5 a | ND b | ND b | ND b |
| canolol (μg SAE/g) | 697 ± 17 a | 547 ± 11 b | 644 ± 91 ab | 26.8 ± 0.9 c | ND d |
| sinapine (μg SAE/g) | TA | TA | TA | ND | ND |
| α-tocopherol (mg/kg) | 159 ± 3 a | 163 ± 13 a | 164 ± 7 a | 177 ± 9 a | 113 ± 15 b |
| γ-tocopherol (mg/kg) | 472 ± 3 a | 473 ± 30 a | 477 ± 12 a | 419 ± 15 b | 246 ± 9 c |
| TPC-HPLC (μg SAE/g)[b] | 727 ± 172 a | 583 ± 110 b | 644 ± 91 b | 26.8 ± 0.9 c | ND d |
| TPC-FC (μg SAE/g)[c] | 107 ± 14 a | 89.1 ± 11.1 b | 83.8 ± 12.2 b | 2.7 ± 0.3 c | ND d |
| total tocopherol (mg/kg) | 631 ± 6 a | 636 ± 43 ab | 641 ± 19 a | 596 ± 24 b | 359 ± 24 c |

[a]All data are expressed as mean ± standard deviation ($n = 6$). Mean values in each row that share the same letter are not significantly different ($p < 0.05$). ND = not detected. TA = trace amount. SAE = sinapic acid equivalent. [b]Total phenolic content calculated by adding the major phenolic peaks in HPLC: sinapic acid + canolol. [c]Total phenolic content calculated by the Folin−Ciocalteu assay.

for 5 min with piperidine−acetic acid mixture as condensing agent using a domestic microwave oven. The highly viscous reaction mixture was diluted with 70% methanol and filtered using syringe filters (0.45 μm) prior to HPLC quantification. The purity of the obtained canolol was approximately 82%.

**HPLC Analyses of Sinapic Acid Derivatives and Tocopherols.** Sinapic acid derivatives were quantified using a reversed-phase HPLC-DAD (Dionex, Sunnyvale, CA), as described previously,[27] with an 80 mm × 4.0 mm i.d., 4 μm, Synergi Fusion-RP column (Phenomenex, Torrance, Canada). Standards of sinapine, sinapic acid, and synthetic canolol were used to authenticate the retention time and UV absorption spectra. The contents of all sinapic acid derivatives were expressed as sinapic acid equivalents (SAE) in μg/g of sample, wherein sinapine and sinapic acid were detected at 330 nm and canolol was detected at 270 nm. Standard of sinapic acid was prepared in concentrations between 50 and 500 μg/mL.

The chromatographic separation of tocopherols was performed on a 150 mm × 4.6 mm i.d., 5 μm, C18 Prodigy ODS-2 column (Phenomenex, Torrance, Canada) as described previously,[27] with slight modifications. The elution solvents used were (A) 1% acetic acid/water (1:99) and (B) 1% acetic acid/methanol (1:99). An isocratic elution was performed with 1% A and 99% B for 30 min. The column was maintained at 25 °C with a flow rate of 1.0 mL/min. The injection volume was 20 μL. Chromatograms were acquired at 294 nm; identification of tocopherols was achieved by comparing the relative retention times and spectrum with the standards of α-, β-, and γ-tocopherols. Triplicate samples were analyzed with duplicate injections of each sample for statistical validation of results.

**Estimation of Total Phenolic Content.** Total phenolic contents in the extracts of oil and their corresponding refining byproducts were estimated using the Folin−Ciocalteu reagent as described,[21,29] using a DU 800 UV/vis spectrophotometer (Beckman Coulter Inc., Mississauga, Canada). An authentic standard of sinapic acid was used for calibration purposes, and the results of duplicate analyses were expressed as μg SAE/g of sample.

**Estimation of Antioxidant Activity.** The antioxidant activity of the phenolic extract was determined by the free radical scavenging activity using DPPH (2,2-diphenyl-1-picrylhydrazyl) according to the method proposed by Brand-Williams et al.[30] with slight modifications. Briefly, 1 mL of extract was added to 2.9 mL of 0.1 mM DPPH ethanolic solution and reacted for 10 min, and the absorbance was measured at 516 nm. The linear range of the calibration curve of sinapic acid standard was prepared from 10 to 500 μM, and the antioxidant activity was expressed as μM SAE/g of sample.

**Statistical Analyses.** All extractions were carried out in triplicate with duplicate analysis of samples, and results are presented as mean ± SD (Microsoft Excel, Version 2010). One-way analysis of variance (ANOVA) was done using SAS 9.4 software (SAS Institute Inc.). Statistical significance was determined using least significant difference *t*-test. Statistical significance was accepted at $p < 0.05$. Regression analysis was carried out using Microsoft Excel (Version 2010).

## RESULTS AND DISCUSSION

**Effect of Refining on Sinapic Acid Derivatives and Tocopherol Contents of Expeller-Pressed Canola Oil.** The contents of endogenous phenolics of the various canola oils are indicated in Table 1. With respect to sinapic acid derivatives, crude expeller-pressed canola oil retained canolol (697 μg SAE/g), sinapic acid (30.5 μg/g oil), and sinapine (beyond detection limit) in agreement with the levels observed by Koski et al.[7] The amount of canolol in canola oil was slightly decreased during the degumming process, while the concentration of sinapic acid was not significantly affected. Sinapic acid decreased to an undetectable level in the canola oils during neutralization, while the concentration of canolol was slightly increased. In the industrial oil refining practices, neutralization of oil is commonly conducted by converting free fatty acid to soaps by adding caustic soda solutions and the neutralized oil is normally obtained after soap stock separation, oil washing, and drying. The increase of canolol content in neutralized oil might be attributed partially due to the conversion of sinapic acid and other precursors, accelerated by higher temperatures during the drying of washed oil. Thermal decarboxylation and cleavage of sinapic acid have been previous reported for different heat treatments,[2,31] but further studies are required to confirm the cause of this increase. This contradicted the findings of Zacchi and Eggers[14] that polyphenol content was reduced after neutralization; however, the neutralization process in that[14] study was simulated under laboratory conditions, which may be different from industrial practices. Also, different conditions of neutralization, such as the type and concentration of caustic solution, and varieties of oilseeds may have significant influence on the content of polyphenols in oils.[22] A significant amount of canolol was lost during the bleaching process (about >90%), which was further reduced to an undetectable level during deodorization. Substantial reductions in rapeseed oil polyphenols during bleaching and deodorization processes have been previously reported;[14] the authors related this to the high adsorptive activity of the bleaching clay and the elevated temperatures of the deodorization process.

With respect to the total phenolic content, solvent-extracted crude canola oils contain about 125 ppm (as gallic acid equivalents) of total phenolics, and this included sinapine, sinapic acid, and 4-vinyl-2,6-dimethoxyphenol (canolol).[22] In the current study, total phenolic contents of expeller-pressed canola oil extracts were assessed using HPLC-DAD and the Folin−Ciocalteu method. The phenolic contents estimated by these two different methods were compared to determine the correlation. The HPLC-DAD-based total phenolic content was the highest in the crude oil and decreased slightly during


dx.doi.org/10.1021/jf502428z | J. Agric. Food Chem. 2014, 62, 9800−9807

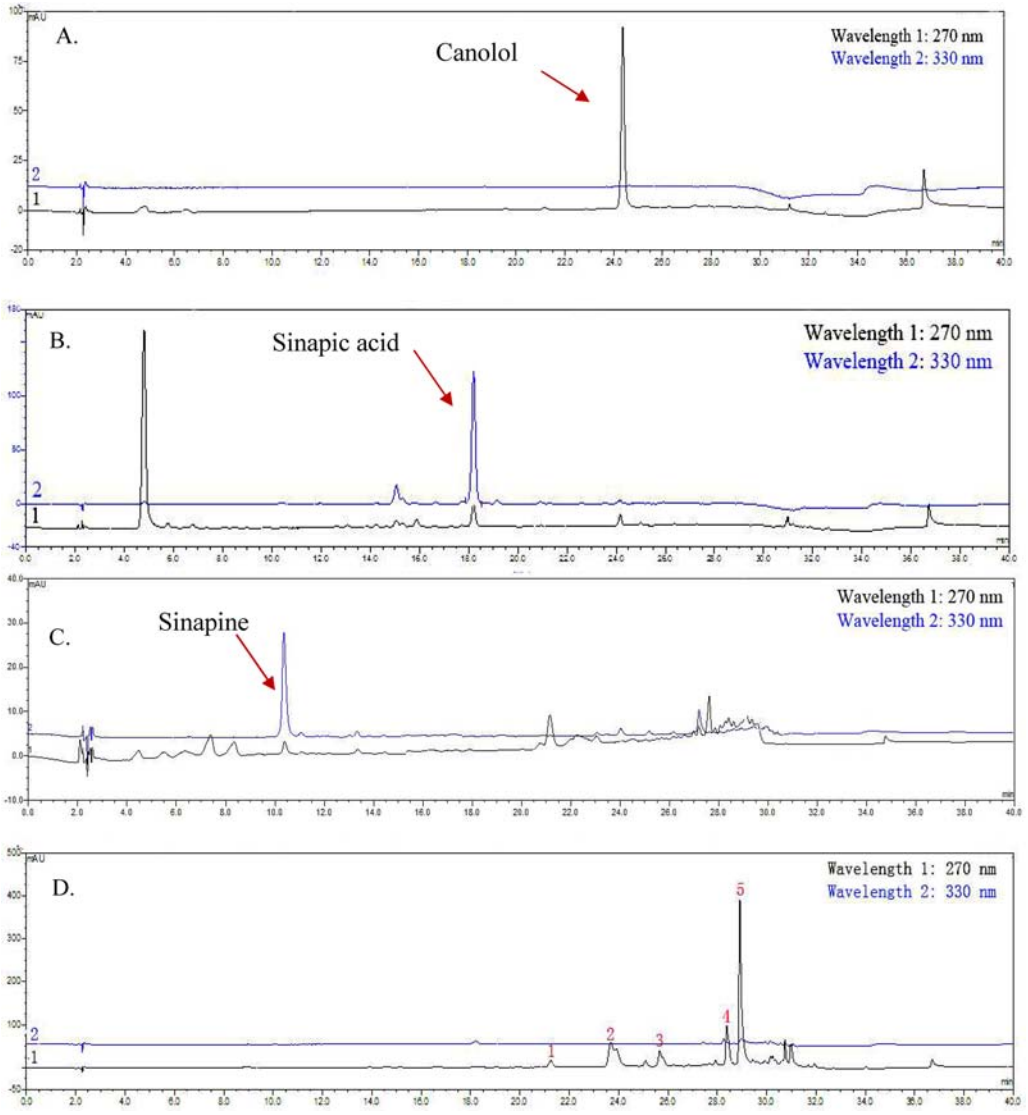


**Figure 3.** HPLC-DAD chromatograms of phenolic extracts obtained from canola oil refining byproducts: (A) wash water, (B) soap stock, (C) spent bleaching clay, and (D) deodistillates.

degumming and neutralization (Table 1). Bleaching and deodorization further reduced the total phenolic content to negligible amounts. The total phenolics quantified by the Folin−Ciocalteu method showed a similar trend, although the values were much lower than the total phenolics detected through the DAD-HPLC method. The Folin−Ciocalteu assay is a well-known method used to determine total phenolic content; however, it is not efficient to measure the decarboxylation products of the hydroxycinnamates.[32] Previous studies were in agreement that the Folin−Ciocalteu method could underestimate canolol.

With respect to tocopherols, another class of antioxidants, the total tocopherol content in crude expeller-pressed canola oil was estimated to be 631 mg/kg with $\alpha$- and $\gamma$-tocopherol in an approximate ratio of 1:3, and $\delta$-tocopherol was absent. Degumming and neutralization had little or no effect on the tocopherols, but bleaching resulted in a slight reduction of $\gamma$-tocopherol in canola oil. This study was consistent with earlier studies on other vegetable oils,[11,33,34] which showed that bleaching resulted in a slight reduction (6%) and deodorization led to the most significant loss (about 37.6%) of total tocopherols.

**Sinapic Acid Derivatives and Tocopherol Profiles in Refining Byproducts.** *Soap Stock.* Sinapic acid was the only phenolic compound detected in the soap stock used in this study (Figure 3B). The amount of sinapic acid in soap stock ranged from 17.1 to 42.9 $\mu$g/g, depending on the extraction pH. Although many studies have noted that high amounts of polyphenols are extractable from soap stocks of some vegetable oils, such as rice bran[35,36] and olive[8] oils, the potential of obtaining sinapic acid from canola oil soap stock was not considered. Our results provide the first data showing the recovery of sinapic acid from canola soap stock. Acid treatment increased the extraction efficiency through solubilization of sinapic acid from soap stocks by 1.8 and 2.5 times at pH values of 7 and 2, when compared to pH 12 (Table 3). The total phenolics obtained with the Folin−Ciocalteu assay (TPC-FC) also supported this trend. These result conformed with previous observations[37] that the acid treatments of phenolic extracts helped to prevent the oxidation of sinapic acid. The TPC-FC values of soap stock extracts were higher than that


dx.doi.org/10.1021/jf502428z | J. Agric. Food Chem. 2014, 62, 9800−9807

**Table 2. Phenolic and Tocopherol Compositions of Expeller-Pressed Canola Oil Refining Byproducts[a]**

| antioxidant composition | bleaching clay | wash water | soapstock | deodistillates |
|---|---|---|---|---|
| sinapine (μg SAE/g) | 199.3 ± 58.5 a | ND b | ND b | ND b |
| sinapic acid (μg/g) | ND b | ND b | 42.9 ± 2.7 a | ND b |
| canolol (μg SAE/g) | 1.42 ± 0.02 b | 365.2 ± 20.9 a | ND c | ND c |
| α-tocopherol (mg/kg) | 9.64 ± 0.25 c | 168.6 ± 2.1 b | ND d | 647 ± 6 a |
| γ-tocopherol (mg/kg) | 14.84 ± 0.16 c | 278.4 ± 2.0 b | ND d | 3104 ± 16 a |
| TPC-HPLC (μg SAE/g)[b] | 201 ± 58 c | 365.2 ± 20.9 b | 42.9 ± 2.7 d | 2766 ± 2 a |
| TPC-FC (μg SAE/g)[c] | 677 ± 179 a | 167.2 ± 10.3 b | 147 ± 15 b | 526 ± 11 a |
| total tocopherol (mg/kg) | 24.5 ± 0.5 c | 446.8 ± 2.8 b | ND d | 3751 ± 21 a |
| DPPH (μM SAE/g) | 140 ± 15 bc | 173.5 ± 10.7 bb | 106.7 ± 11.7 c | 350 ± 15 a |

[a]All data are expressed as mean ± standard deviation ($n = 6$). Mean values in each row that share the same letter are not significantly different ($p < 0.05$). ND = not detected; SAE = sinapic acid equivalent. [b]Total phenolic content calculated by adding the major phenolic peaks in HPLC: sinapine + sinapic acid + canolol + unidentified polor compound. [c]Total phenolic content calculated by Folin-Ciocalteu assay.

**Table 3. Effect of Different Conditions on the Phenolic Extraction Efficiency and DPPH Radical Scavenging Activity of Canola Oil Refining Byproducts[a]**

| refining byproducts | extraction conditions | TPC-HPLC (μg SAE/g) | TPC-FC (μg SAE/g) | DPPH (μM SAE/g) |
|---|---|---|---|---|
| wash water | hexane | 448 ± 74 d | 190 ± 21 c | 189 ± 15 c |
| | choloroform | 69.8 ± 0.1 f | 29.0 ± 3.2 e | 18.6 ± 3.0 f |
| | cyclohexane | 419 ± 31 d | 178 ± 5 c | 168 ± 12 c |
| | toluene | 167 ± 7 e | 60.2 ± 11.3 d | 54.2 ± 23.3 e |
| | direct methanol extraction | 365 ± 21 d | 167 ± 10 c | 174 ± 11 d |
| deodistillates | hexane | 2537 ± 28 a | 525 ± 10 a | 336 ± 11 a |
| | choloroform | 54.1 ± 5.0 f | 79 ± 46 d | 168 ± 67 c |
| | cyclohexane | 2065 ± 129 b | 523 ± 20 a | 345 ± 12 a |
| | toluene | 649 ± 114 c | 354 ± 60 b | 295 ± 28 b |
| | direct methanol extraction | 2766 ± 2 a | 542 ± 36 a | 350 ± 14 a |
| soap stock | pH = 2 | 42.9 ± 2.7 f | 147 ± 15 c | 107 ± 2 d |
| | pH = 7 | 31.2 ± 4.3 g | 89.4 ± 23.6 d | 96.5 ± 17.3 d |
| | pH = 12 | 17.07 ± 0.22 h | 69.2 ± 11.9 d | 22.6 ± 6.4 e |

[a]All data are expressed as mean ± standard deviation ($n = 6$). Mean values in each column that share the same letter are not significantly different ($p < 0.05$).

determined by HPLC, which may be attributed to the Folin–Cioacalteu-reactive phenolics and other interfering compounds.

Sinapic acid present in the crude and degummed oils was lost during neutralization, perhaps either leached or adsorbed in soap stock. The storage of soap stocks at room temperature is also of special interest, as the alkaline pH might contribute toward unavoidable side reactions, thereby affecting the composition of minor components including antioxidants and their stability.[38] This instability could be partially avoided by neutralization or acidification of samples by facilitating a rapid extraction and recovery of stable antioxidants.

*Wash Water.* A considerable amount of phenolics (365 μg SAE/g) was also observed in the canola oil wash water in the present study (Table 2). Similar results have been reported by many investigators assessing the polyphenol content of wash water from olive oil refining.[9,39] Canolol was the predominant phenolic compound present in the wash water sample (69.8–448 μg SAE/g) with minor variations based on the solvent used for solubilizing it prior to methanolic extraction (Figure 3A and Table 3). For example, solubilization of the wash water sample with hexane and cyclohexane resulted in higher yield of canolol (448 and 419 μg SAE/g, respectively) compared with chloroform (69.8 μg SAE/g) and toluene (167 μg SAE/g). The presence of canolol in wash water is because of the high lipid content (>50%) in the sample, associating more of the fat-soluble antioxidants. The results also indicated that canolol was retained during neutralization.

This study demonstrated a rapid method to extract and identify sinapic acid derivatives in edible oil refining wash water. Results support that the wash water retains canolol. The tocopherol composition of these samples was also assessed, and the result showed that it was similar to that of degummed or neutralized oils. The concentrations of α- and γ-tocopherol in wash water were 169 and 278 mg/kg, respectively (Table 2). The retention of canolol and tocopherols in the wash water could be attributed to the minor amount of neutralized oil that was carried through in the wash water. Neutralized oils retained canolol and tocopherols, as discussed above.

*Spent Bleaching Clay.* Total phenolic content (Folin–Ciocalteu assay) of spent bleaching clay was determined to be 677.9 μg SAE/g, and the tocopherol compositions are summarized in Table 2. A substantial amount of sinapine (199 μg SAE/g) was present in the spent bleaching clay. It might be due to the occurrence of sinapine in neutralized oil which is carried to the bleaching clay. Sinapine might be concentrated in the bleaching clay due to the high adsorptive activities of bleaching clay. Bleaching clay has been primarily used to remove color pigments such as chlorophyll and carotenoids from vegetable oils,[22] and the high polyphenol adsorption efficiency of the clay has been reported previously.[40,41] The absence of sinapine in bleached and deodorized oils also confirmed this result (Table 1). However, phenolics including sinapic acid and canolol were not detected

in the bleaching clay. Low amounts of tocopherols were detected in the spent bleaching clay.

It has been suggested by Loh et al.[42] that the residual oil in spent bleaching clay should ideally be extracted and used for industrial applications in order to reduce the cost of oil processing. Unlike the palm oil refining process, canola oil refining may not generate high residual oil in the bleaching clay, but it could be used as a novel source for recovering sinapine, as demonstrated by our results.

*Deodistillates.* Total phenolic content (Folin−Ciocalteu assay) of deodistillates was 525.7 μg SAE/g, the highest among of all the refining byproducts (Table 2). In the extracts of deodistillates, all peaks were identified at 270 nm and the chromatograms are presented in Figure 3C. There are five unidentified peaks eluting between 21 and 29 min, which have not been previously reported. The UV spectra (maximum absorbance) of these peaks are summarized in Table 4. The highest concentrations of the phenolic compounds were observed for the peaks detected at 28−29 min (peak 4, 349.7 μg SAE/g; peak 5, 1708.6 μg SAE/g). The major peak (peak 5, $t_R$ ∼ 28.9 min) exhibited maximum absorbance at 279 nm and did not correspond to any phenolic compounds present in canola seed or canola oil. The spectrum of peak 4 had two wavelength maxima at 209 and 281 nm. It is likely that these phenolic compounds are derivatives of canolol or other sinapates. A previous study reported canolol dimer as the predominant phenolic compound in commercial rapeseed deodistillates based on the dimerization at high temperature or in acid-catalyzed conditions.[17] The phenolic compounds found in the current study might be oligomers of canolol; however, further studies are required for their structural elucidation and characterization.

**Table 4. Concentration and UV Spectra Data of Phenolic Peaks of Deodistillates Extracts Detected at 270 nm**

| peak number[a] | $t_R$ (min) | UV maximum absorbance wavelength (nm) | concn (μg SAE/g) |
|---|---|---|---|
| 1 | 21.3 | 217, 275 | 52.42 ± 2.67 |
| 2 | 23.6 | 282 | 180.6 ± 3.5 |
| 3 | 25.6 | 206, 273 | 182.3 ± 23.7 |
| 4 | 28.4 | 209, 281 | 349.7 ± 20.0 |
| 5 | 28.9 | 279 | 1708.6 ± 21.6 |

[a]Peak numbers refer to the peaks in Figure 2D.

The polarities of various extraction solvents have a tremendous effect on the solubility and, therefore, extraction efficiency[43] of phenolics. The efficacy of different nonpolar solvents to optimally and rapidly extract deodistillate phenolic compounds was investigated (Table 3). The results were similar to that of phenolic extraction in wash water, where solubilization with hexane and cyclohexane followed by methanolic extraction produced a higher amount of phenolics (2537 and 2065 μg SAE/g) from deodistillates than predissolution with chloroform and toluene. Direct methanol extraction of deodistillates resulted in the highest yield of phenolics compared to presolvent solubilization of deodistillates. However, presolvent solubilization showed advantages in improving extraction yield (37% improvement) for large-scale extractions, as reported in a previous study.[4]

The present study also identified deodistillates as a rich source of tocopherols in addition to other phenolics. Both α- and γ-tocopherols were detected in the deodistillates at 2:1 ratio. The deodistillate extract contained 647 mg of α-tocopherol and 3104 mg of γ-tocopherol per kg of deodistillate, a quantity that is greater than those in any crude vegetable oil. These amounts conformed with the values obtained from rapeseed oil deodistillates.[16]

The study indicated a 2-fold potential of deodistillates. First, deodistillate was the best source for recovery of tocopherols among the oil-refining byproducts investigated. The tocopherol content of canola oil at various processing stages supported that the maximum tocopherol losses occurred during the deodor-

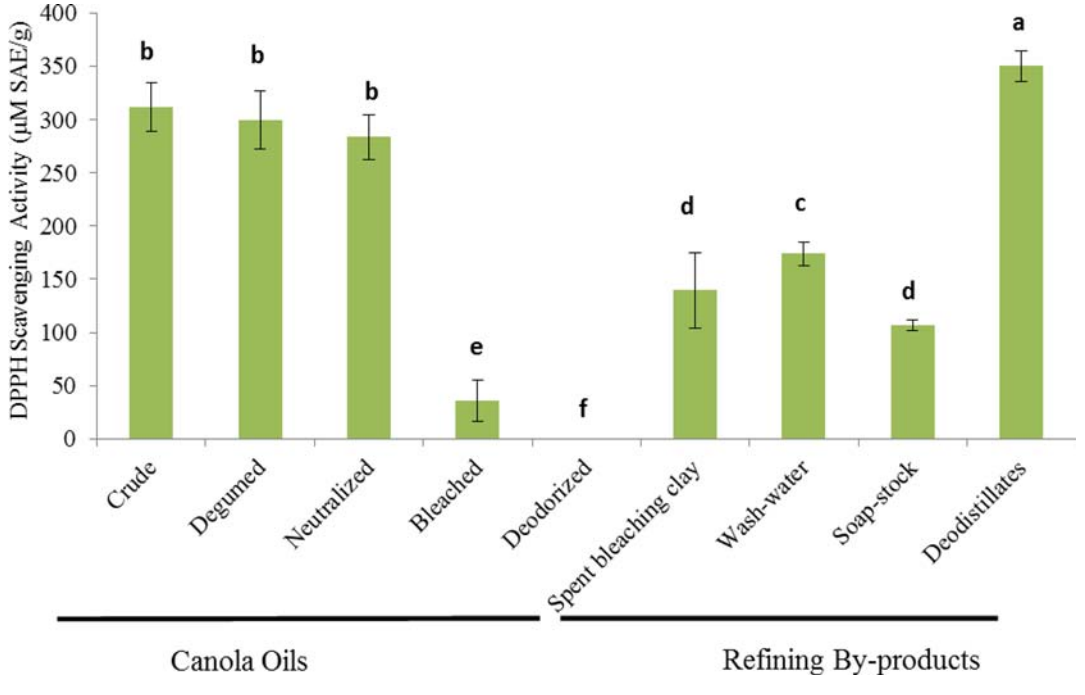


**Figure 4.** DPPH antioxidant activities of expeller canola oils and refining byproducts.

ization process. Second, the extracts of deodistillate showed several phenolic compounds that were not reported until now, requiring further studies for adequate characterization.

**Antioxidant Activity of Phenolic Extracts of Canola Oil and Refining Byproducts.** The antioxidant capacity of expeller-pressed canola oils and refining byproducts were evaluated using the DPPH radical scavenging activities. In the present study, the crude canola oil showed the highest antioxidant activity at a DPPH free radical activity equivalent of 311.9 ± 23.1 $\mu$M SAE/g. These values decreased slightly after degumming and neutralization while reducing rapidly to less than 50 $\mu$M SAE/g after the bleaching step (Figure 4). The decrease was mainly attributed to the loss of endogenous phenolics and tocopherols from expeller-pressed canola oil during refining. Previously, Wakamatsu et al.[2] reported a significant reduction in the anti-ROO• activity of canola oil with each refining stage. The loss of antioxidant activity of oils was translated to a high antioxidant potential of the corresponding refining byproduct in the present study. Among various oil-refining byproducts, deodistillates exhibited the highest radical scavenging activity ($\mu$M SAE/g) of 350.3, followed by wash water (173.5), bleaching clay (139.7), and soap stock (106.7) (Figure 4). This order corroborated with the concentration of the active phenolic compounds contained in the corresponding refining byproducts.

In order to further examine the radical scavenging activity of the phenolic compounds recovered from canola oils and the corresponding refining byproducts, the correlation of the sum of phenolic compounds and antioxidant activity was calculated. There were strong correlations between the total phenolic content and radical scavenging activity in all refining byproducts as well as canola oil ($R^2$ = 0.88−0.99). In addition, the radical scavenging activity of soap stock phenolic extract increased rapidly (slope = 5.670) as the concentration of phenolics (majorly sinapic acid) increased. While this slope of increase was lower in canola oil (0.414) and wash water (0.458) extracts, it was the lowest in deodistillate (0.298) extracts. This result indicated that the DPPH radical scavenging activity of sinapic acid might be more apparent than for sinapine, canolol, and canolol derivatives at the same concentration. A previous study asserted that the 4-vinyl derivatives of hydroxycinnamic acids exhibited lower antioxidant activity than their corresponding phenolic acids.[32] Other studies reported the opposite trend when evaluating the antioxidant potential in different systems such as emulsion[44] and cell culture.[45] Canolol and its polymerized derivatives found in the canola oil refining byproducts could be extracted and potentially used as antioxidants in various food systems.

Renewed interest in utilization of oil-processing byproducts as sources of various high-value coproducts, such as phenolics, phytosterol, protein, and lipids, persists. Processes have been developed to extract phytosterols and tocopherols from refining byproducts of different vegetable oils. The recovery of valuable phenolics with proven bioactivities can improve the economic feasibility of edible oil refining. Given this context, our results provide new knowledge on the byproducts of canola oil subjected to different stages of refining. Sinapic acid (42.9 $\mu$g/g), sinapine (199 $\mu$g/g), and canolol (344 $\mu$g/g) were found in the refining byproducts, namely, soap stock, spent bleaching clay, and wash water, for the first time. Tocopherols (3.75 mg/g) and other nonidentified phenolic compounds (2.7 mg SAE/g) were found in deodistillates. In conclusion, this is the first study showing the retention and recovery of the sinapic acid derivatives and tocopherols using byproducts generated in a commercial expeller-pressed facility. This approach opens up opportunities for utilization of these byproducts as new side streams for commercial utilization in the context of canola and rapeseed oil refining. More studies are recommended to unfold the recovery, extraction, and mechanisms of structural changes of these endogenous biophenols using byproducts of edible oil refining.

## ■ ASSOCIATED CONTENT

### Ⓢ Supporting Information

Correlation of the sum of phenolic compounds in expeller-pressed canola oil and refining byproducts with DPPH radical scavenging activity. This material is available free of charge via the Internet at http://pubs.acs.org.

## ■ AUTHOR INFORMATION

### Corresponding Author

*Tel: +1-204-474-9976. Fax: +1-204-474-7592. E-mail: Usha.Thiyam@umanitoba.ca.

### Funding

This study was funded by the Natural Sciences and Engineering Research Council of Canada (NSERC) as part of ENGAGE project and was supported by Viterra Canola Inc.

### Notes

The authors declare no competing financial interest.

## ■ ACKNOWLEDGMENTS

Bryan Allison and Mike Adelino, both from Viterra Canola Inc., are greatly acknowledged for their contribution toward discussion of results and project management. Dr. N. A. Michael Eskin is gratefully acknowledged for his technical input.

## ■ REFERENCES

(1) Subramanian, R.; Nakajima, M.; Kimura, T.; Maekawa, T. Membrane process for premium quality expeller-pressed vegetable oils. *Food Res. Int.* **1998**, *31*, 587−593.

(2) Wakamatsu, D.; Morimura, S.; Sawa, T.; Kida, K.; Nakai, C.; Maeda, H. Isolation, identification, and structure of a potent alkyl-peroxyl radical scavenger in crude canola oil, canolol. *Biosci. Biotechnol., Biochem.* **2005**, *69*, 1568−1574.

(3) Vuorela, S.; Meyer, A. S.; Heinonen, M. Quantitative analysis of the main phenolics in rapeseed meal and oils processed differently using enzymatic hydrolysis and HPLC. *Eur. Food Res. Technol.* **2003**, *217*, 517−523.

(4) Aachary, A. A.; Chen, Y.; Eskin, N. A. M.; Thiyam-Hollander, U. Crude canolol and canola distillate extracts improve the stability of refined canola oil during deep-fat frying. *Eur. J. Lipid Sci. Technol.* **2014**, DOI: 10.1002/ejlt.201300498.

(5) Kuwahara, H.; Kanazawa, A.; Wakamatu, D.; Morimura, S.; Kida, K.; Akaike, T.; Maeda, H. Antioxidative and antimutagenic activities of 4-vinyl-2,6-dimethoxyphenol (canolol) isolated from canola oil. *J. Agric. Food Chem.* **2004**, *52*, 4380−4387.

(6) Cao, X.; Tsukamoto, T.; Seki, T.; Tanaka, H.; Morimura, S.; Cao, L.; Tatematsu, M. 4-Vinyl-2,6-dimethoxyphenol (canolol) suppresses oxidative stress and gastric carcinogenesis in *Helicobacter pylori*-infected carcinogen-treated Mongolian gerbils. *Int. J. Cancer.* **2008**, *122*, 1445−1454.

(7) Koski, A.; Pekkarinen, S.; Hopia, A.; Wähälä, K.; Heinonen, M. Processing of rapeseed oil: Effects on sinapic acid derivative content and oxidative stability. *Eur. Food Res. Technol.* **2003**, *217*, 110−114.

(8) McGinely, L. Analysis and quality control for processing and processed fats. *Anal. Oilseeds Fats Fatty Foods* **1991**, 460−470.

(9) Ortega-García, J.; Gámez-Meza, N.; Noriega-Rodriguez, J. A.; Dennis-Quiñonez, O.; García-Galindo, H. S.; Angulo-Guerrero, J. O.; Medina-Juárez, L. A Refining of high oleic safflower oil: Effect on the sterols and tocopherols content. *Eur. Food Res. Technol.* **2006**, *223*, 775−779.
(10) Tasan, M.; Demirci, M. Total and individual tocopherol contents of sunflower oil at different steps of refining. *Eur. Food Res. Technol.* **2005**, *220*, 251−254.
(11) Ferrari, R. A.; Schulte, E.; Esteves, W.; Brühl, L.; Mukherjee, K. D. Minor constituents of vegetable oils during industrial processing. *J. Am. Oil Chem. Soc.* **1996**, *73*, 587−592.
(12) Van Hoed, V.; Depaemelaere, G.; Ayala, J. V.; Santiwattana, P.; Verhé, R.; De Greyt, W. Influence of chemical refining on the major and minor components of rice brain oil. *J. Am. Oil Chem. Soc.* **2006**, *83*, 315−321.
(13) McLaughlin, P. J.; Weihrauch, J. L. Vitamin E content of foods. *J. Am. Diet. Soc.* **1979**, *75*, 647−665.
(14) Zacchi, P.; Eggers, R. High temperature pre-conditioning of rapeseed: A polyphenol enriched oil and the effect of refining. *Eur. J. Lipid Sci. Technol.* **2008**, *110*, 111−119.
(15) Zeldenrust, R. S. Edible oil processing-alkali refining. *AOCS Lipid Library* **2012**; http://lipidlibrary.aocs.org/processing/alkrefining/index.htm (assessed January 10, 2014).
(16) Luxem, F. J.; Troy, W. M. Method of making alkyl esters using pressure. U.S. Patent 6768015, 2004.
(17) Dudrow, F. A. Deodorization of edible oil. *J. Am. Oil Chem. Soc.* **1983**, *60*, 272−274.
(18) Harbaum-Piayda, B.; Oehlke, K.; Sönnichsen, F. D.; Zacchi, P.; Eggers, R.; Schwarz, K. New polyphenolic compounds in commercial deodistillate and rapeseed oils. *Food Chem.* **2010**, *123*, 607−615.
(19) Nogala-Kalucka, M.; Korczak, J.; Wagner, K. H.; Elmadfa, I. Tocopherol composition of deodorization distillates and their antioxidative activity. *Food/Nahrung* **2004**, *48*, 34−37.
(20) Cvengros, J. Physical refining of edible oils. *J. Am. Oil Chem. Soc.* **1995**, *72*, 1193−1196.
(21) Thiyam, U.; Stöckmann, H.; Zum Felde, T.; Schwarz, K. Antioxidative effect of the main sinapic acid derivatives from rapeseed and mustard oil by-products. *Eur. J. Lipid Sci. Technol.* **2006**, *108*, 239−248.
(22) Ghazani, S. M.; Marangoni, A. G. Minor components in canola oil and effects of refining on these constituents: A review. *J. Am. Oil Chem. Soci.* **2013**, *90*, 923−932.
(23) Wanasundara, U. N.; Shahidi, F. Canola extract as an alternative natural antioxidant for canola oil. *J. Am. Oil Chem. Soc.* **1994**, *71*, 817−822.
(24) Vuorela, S.; Salminen, H.; Mäkelä, M.; Kivikari, R.; Karonen, M.; Heinonen, M. Effect of plant phenolics on protein and lipid oxidation in cooked pork meat patties. *J. Agric. Food Chem.* **2005**, *53*, 8492−8497.
(25) Jiang, J.; Cao, D. H.; Tsukamoto, T.; Wang, G. Q.; Jia, Z. F.; Suo, J.; Cao, X. Y. Anticancer effects of 4-vinyl-2,6-dimethoxyphenol (canolol) against SGC-7901 human gastric carcinoma cells. *Oncol. Lett.* **2013**, *5*, 1562−1566.
(26) Khattab, R.; Eskin, M.; Aliani, M.; Thiyam, U. Determination of sinapic acid derivatives in canola extracts using high-performance liquid chromatography. *J. Am. Oil Chem. Soc.* **2010**, *87*, 147−155.
(27) Tasioula-Margari, M.; Okogeri, O. Simultaneous determination of phenolic compounds and tocopherols in virgin olive oil using HPLC and UV detection. *Food Chem.* **2001**, *74*, 377−383.
(28) Sinha, A. K.; Sharma, A.; Joshi, B. P. One-pot two-step synthesis of 4-vinylphenols from 4-hydroxy substituted benzaldehydes under microwave irradiation: A new perspective on the classical Knoevenagel−Doebner reaction. *Tetrahedron* **2007**, *63*, 960−965.
(29) Swain, T.; Hillis, W. E. The phenolic constituents of *Purmus domestica*. 1. The quantitative analysis of phenolic constituents. *J. Sci. Food. Agric.* **1959**, *10*, 63−68.
(30) Brand-Williams, W.; Cuvelier, M. E.; Berset, C. L. W. T. Use of a free radical method to evaluate antioxidant activity. *LWT Food Sci. Technol.* **1995**, *28*, 25−30.
(31) Bernini, R.; Mincione, E.; Barontini, M.; Provenzano, G.; Setti, L. Obtaining 4-vinylphenols by decarboxylation of natural 4-hydroxycinnamic acids under microwave irradiation. *Tetrahedron* **2007**, *63*, 9663−9667.
(32) Terpinc, P.; Polak, T.; Šegatin, N.; Hanzlowsky, A.; Ulrih, N. P.; Abramovič, H. Antioxidant properties of 4-vinyl derivatives of hydroxycinnamic acids. *Food Chem.* **2011**, *128*, 62−69.
(33) Čmolík, J.; Pokorný, J.; Réblová, Z.; Svoboda, Z. Tocopherol retention in physically refined rapeseed oil as a function of deodorization temperature. *Eur. J. Lipid Sci. Technol.* **2008**, *110*, 754−759.
(34) Naz, S.; Sherazi, S. T. H.; Talpur, F. N. Changes of total tocopherol and tocopherol species during sunflower oil processing. *J. Am. Oil Chem. Soc.* **2011**, *88*, 127−132.
(35) Seetharamaiah, G. S.; Prabhakar, J. V. Oryzanol content of Indian rice bran oil and its extraction from soap stock. *J. Food Sci. Technol.* **1986**, *23*, 270−273.
(36) Rao, K. V. S. A.; Rao, B. V. S. K.; Thengumpillil, N. B. K. U.S. Patent 6,410,762, 2002.
(37) Prapakornwiriya, N.; Diosady, L. L. Recovery of sinapic acid from a waste stream in the processing of yellow mustard protein isolate. *J. Food Process Eng.* **2008**, *31*, 173−185.
(38) Ruenroengklin, N.; Zhong, J.; Duan, X.; Yang, B.; Li, J.; Jiang, Y. Effects of various temperatures and pH values on the extraction yield of phenolics from litchi fruit pericarp tissue and the antioxidant activity of the extracted anthocyanins. *Int. J. Mol. Sci.* **2008**, *9*, 1333−1341.
(39) Fki, I.; Allouche, N.; Sayadi, S. The use of polyphenolic extract, purified hydroxytyrosol and 3, 4-dihydroxyphenyl acetic acid from olive mill wastewater for the stabilization of refined oils: A potential alternative to synthetic antioxidants. *Food Chem.* **2005**, *93*, 197−204.
(40) Pollard, S. J.; Sollars, C. J.; Perry, R. A clay−carbon adsorbent derived from spent bleaching earth: Surface characterisation and adsorption of chlorophenols from aqueous solution. *Carbon* **1992**, *30*, 639−645.
(41) Eroğlu, E.; Eroğlu, İ.; Gündüz, U.; Yücel, M. Effect of clay pretreatment on photofermentative hydrogen production from olive mill wastewater. *Bioresour. Technol.* **2008**, *99*, 6799−6808.
(42) Loh, S. K.; Stephen, J.; Muzzamil, N.; Kah, Y. C.; Yuen, M. C.; Weng, S. L. Enhancement of palm oil refinery waste—Spent bleaching earth (SBE) into bio organic fertilizer and their effects on crop biomass growth. *Ind. Crop Prod.* **2013**, *49*, 775−781.
(43) Chen, C. W.; Ho, C. T. Antioxidant properties of polyphenols extracted from green and black teas. *J. Food Lipids.* **1995**, *2*, 35−46.
(44) Galano, A.; Francisco-Márquez, M.; Alvarez-Idaboy, J. R. Canolol: A promising chemical agent against oxidative stress. *J. Phys. Chem. B* **2011**, *115*, 8590−8596.
(45) Cao, X.; Tsukamoto, T.; Seki, T.; Tanaka, H.; Morimura, S.; Cao, L.; Tatematsu, M. 4-Vinyl-2,6-dimethoxyphenol (canolol) suppresses oxidative stress and gastric carcinogenesis in *Helicobacter pylori*-infected carcinogen-treated Mongolian gerbils. *Int. J. Cancer.* **2008**, *122*, 1445−1454.

17 months) and final live weight (around 665 kg) to avoid weight and age effects on muscle characteristics and beef meat quality.

All bulls were directly transported in a lorry (3 × 2 m) from the experimental farm to the experimental abattoir situated at 1 km from the rearing building, with two bulls of the same home pen per transport to avoid social isolation stress. After unloading, they were slaughtered within 3 min in the slaughterhouse of INRA institute (Saint-Genès-Champanelle, France) in compliance with the current ethical guidelines for animal welfare. Bulls were stunned by captive bolt prior to exsanguination.

Muscle samples from Longissimus thoracis (LT, mixed fast oxido-glycolytic muscle 23% of type I fibers, 36% IIA, and 39% of IIX) and Semitendinosus (ST, mixed fast glycolytic 8% of type I fibers, 24% of IIA, and 64% of IIX) were excised from the carcass of each animal within 15 min after slaughter. Muscle samples were immediately frozen in liquid nitrogen and stored at −80 °C until protein extraction for protein marker quantification. Samples of the two muscles for sensory evaluation and mechanical measurement were cut into steaks 24 h after slaughter and placed in sealed plastic bags under vacuum and kept between 2 and 4 °C for 14 days for aging, then frozen, and stored at −20 °C until analysis.

**Meat Quality Evaluation.** LT and ST samples were grilled on a preheated grill at 310 °C, resulting in an internal cooked temperature of 55 °C. For sensory analysis, a trained sensory panel (12 experienced panelists) evaluated the steak samples of the same muscle. The panel evaluated overall tenderness attribute on a continuous and unstructured scale with scores from 0 to 10 (0 = hard, 10 = tender).[16,17]

Toughness of cooked meat was further evaluated instrumentally by Warner−Bratzler shear force (WBSF) using an Instron 5944 as described by Lepetit and Culioli.[18] Force at rupture during shear compression testing was expressed in N/cm$^2$.

Sensory and mechanical values of tenderness were used to compute a synthetic tenderness index by combining standardized normal sensory and mechanical tenderness/toughness values.[19] This was calculated for each muscle as the difference within each breed between the standardized values of tenderness score minus the standardized value of the WBSF measure. This index was suggested to take into account the very close genetic correlation underlying the moderate phenotypic correlation observed between both traits,[20] suggesting both traits are under the control of common genes.

**Dot-Blot Analysis.** The 21 proteins analyzed are described in Table 1. The conditions for use and specificity of primary antibodies against these 21 proteins in bovine muscle have been determined previously by Guillemin et al.[21] using Western blot techniques (Table 2).

Total protein extractions were performed according to the method of Bouley et al.[22] in a denaturation extraction buffer (8.3 M urea, 2 M thiourea, 1% DTT, 2% CHAPS). The protein concentration was determined using the Bradford protein assay.[23] Protein extractions were stored at −20 °C.

Relative abundances of proteins were evaluated following the dot-blot technique as described by Guillemin et al.[21] Briefly, protein samples were spotted in quadruplicate on a nitrocellulose membrane with the Minifold I dot blot from Schleicher & Schuell Biosciences (Germany) and hybridized with the specific antibody of each protein, with conditions described in Table 2. Secondary fluorescent-conjugated IRDye 800CW antibodies (anti-mouse, anti-sheep, and anti-rabbit) were supplied by LI-COR Biosciences (Lincoln, NE, USA) and used at 1/20000. Subsequently, membranes were scanned by an Odyssey (LI-COR Biosciences) scanner at 800 nm. Protein relative abundance for each sample, given in arbitrary units, was normalized by comparison to a reference sample constituted by mixing all samples from young bulls from this experiment in equal proportions. The technical coefficient of variation of this technique is on average 9%.[21]

**Statistical Analysis.** Analysis of variance was performed using the GLM procedure of SAS for repeated measures (version 9.1, 2002; SAS Institute Inc.). The effects of breed, muscle type (LT vs ST), and breed × muscle type interaction are reported. When significant effects were detected, differences were evaluated by the PDIFF option of SAS.

**Table 1. 21 Protein Biomarkers of Beef Tenderness Investigated in This Study[a]**

| protein name | gene | UniProt ID |
|---|---|---|
| hea shock proteins | | |
| αB-crystallin | CRYAB | P02511 |
| Hsp20 | HSPB6 | O14558 |
| Hsp27 | HSPB1 | P04792 |
| Hsp40 | DNAJA1 | P31689 |
| Hsp70-1A/B | HSPA1B | P08107 |
| Hsp70-8 | HSPA8 | P11142 |
| Hsp70-Grp75 | HSPA9 | P38646 |
| metabolism | | |
| Eno3 (enolase 3) | ENO3 | P13929 |
| LDH-B (lactate dehydrogenase chain B) | LDHB | P07195 |
| MDH1 (malate dehydrogenase 1) | MDH1 | P40925 |
| structure | | |
| CapZ-β (F-actin-capping protein subunit β) | CAPZB | P47756 |
| α-actin | ACTA1 | P68133 |
| MyLC-1F (myosin light chain 1F) | MYL1 | P05976 |
| MyBP-H (myosin binding protein H) | MYBPH | Q13203 |
| MyHC-I (myosin heavy chain-I) | MYH7 | P12883 |
| MyHC-II (MyHC IIa + IIx + IIb)) | MYH2 | Q9UKX2 |
| MyHC-IIx (myosin heavy chain-IIx) | MYH1 | P12882 |
| oxidative resistance | | |
| DJ-1 (Parkinson disease protein 7) | PARK7 | Q99497 |
| PRDX6 (*cis*-peroxiredoxin) | PRDX6 | P30041 |
| SOD1 (superoxide dismutase Cu/Zn) | SOD1 | P00441 |
| proteolysis | | |
| μ-calpain | CAPN1 | P07384 |

[a]Protein biomarkers of beef tenderness established by our group in previous proteomic studies (for reviews see Guillemin et al.,[27] and Picard et al.[6,8,10,11]).

Principal component analyses (PCAs) were performed using the factor procedure of SAS to study the overall relationships between the studied variables (tenderness traits and protein relative abundances).

Multiple regression analyses were carried out using XLStat 2009 software to explain overall tenderness, WBSF, and tenderness index traits for the two muscles separately, presenting the 21 protein biomarkers as potential explanatory variables, as well as breed. The "optimal model" explaining maximal variability option was used with "maximal four variables". The percentage of variability in meat quality parameter explained by proteins is based on the adjusted $r^2$ value of the regression analysis × 100%.

Absence of collinearity was verified for each model. Condition indices and variance proportions were produced using the COLLIN option of SAS, with components identified as collinear if they possessed both a high condition index >10 and a proportion of variation >0.5 for two or more variables.

## RESULTS

**Tenderness Traits.** The values of tenderness evaluated in three ways are presented in Table 3. For the LT muscle, significant breed effects were found for overall tenderness only, AA bulls being more tender than BA and LI bulls (Table 3). In the ST muscle, significant differences between breeds were observed for the WBSF and the tenderness index. A significant muscle × breed interaction was observed for the WBSF and the tenderness index, Limousin ST muscle being tougher than BA, whereas AA had intermediate values (Table 3). Overall tenderness (Table 3) was much higher in the LT. For the WBSF, this was only a tendency.

**Table 2. Suppliers and Conditions for Each Primary Antibody Used in This Study**

| target protein | antibody references | dilution[a] |
|---|---|---|
| heat shock proteins | | |
| αB-crystallin | monoclonal anti-bovine assay designs SPA-222 | 1/500 |
| Hsp20 | monoclonal anti-human Santa Cruz HSP20-11:SC51955 | 1/200 |
| Hsp27 | monoclonal anti-human Santa Cruz HSP27 (F-4):SC13132 | 1/3000 |
| Hsp40 | monoclonal anti-human Santa Cruz HSP40-4 (SPM251):SC-56400 | 1/250 |
| Hsp70-1A/B | monoclonal anti-human Abnova HSPA1B (M02), clone 3B7 | 1/2000 |
| Hsp70-8 | monoclonal anti-bovine Santa Cruz HSC70 (BRM22):SC-59572 | 1/250 |
| Hsp70-Grp75 | monoclonal anti-human RD systems clone 419612 | 1/250 |
| metabolism | | |
| Eno3 | monoclonal anti-human Abnova Eno3 (M01), clone 5D1 | 1/45000 |
| LDH-B | monoclonal anti-human Novus LDHB NB110-57160 | 1/50000 |
| MDH1 | monoclonal anti-pig Rockland 100-601-145 | 1/1000 |
| structure | | |
| CapZ-β | monoclonal anti-human Abnova CAPZB (M03), clone 4H8 | 1/250 |
| α-actin | monoclonal anti-rabbit Santa Cruz α-actin (5C5):SC-58670 | 1/1000 |
| MyLC-1F | polyclonal anti-human Abnova MYL1 (A01) | 1/1000 |
| MyBP-H | monoclonal anti-human Abnova MYBPH (M01), clone 1F11 | 1/4000 |
| MyHC-I | monoclonal anti-bovine Biocytex 5B9 | 1/2000 |
| MyHC-II[b] | monoclonal anti-bovine Biocytex 15F4 | 1/4000 |
| MyHC-IIx | monoclonal anti-bovine Biocytex 8F4 | 1/500 |
| oxidative resistance | | |
| DJ-1 | polyclonal anti-human Santa Cruz DJ-1 (FL-189):SC-32874 | 1/250 |
| PRDX6 | monoclonal anti-human Abnova PRDX6 (M01), clone 3A10-2A11 | 1/500 |
| SOD1 | polyclonal anti-rat Acris SOD1 APO3021PU-N | 1/1000 |
| proteolysis | | |
| μ-calpain | monoclonal anti-bovine Alexis μ-calpain 9A4H8D3 | 1/1000 |

[a]Dilution of each antibody was defined according to Guillemin et al.[27] [b]MyHC II corresponds to fast MyHC: IIa+IIx+IIb isoforms.

**Protein Relative Abundances.** Significant breed effects were found for at least one of the two muscles for most of the proteins except for Hsp70-1B, MyBP-H, and SOD1 (Table 4). The two muscles of AA bulls presented higher levels of αB-crystallin, Hsp27, Eno3, and PRDX6 and lower levels of MyHC-IIx. Most proteins showed an effect of muscle or a muscle × breed interaction, apart from MyLC-1F, MyBP-H, SOD1, and μ-calpain (Table 4).

**Relationships between Biomarkers and Tenderness Traits.** *Descriptive Analysis.* The PCA illustrating the relationships between relative abundances of protein biomarkers and tenderness traits evaluated by (i) sensory analysis (overall tenderness), (ii) Warner−Bratzler shear force (WBSF), and (iii) tenderness index are presented in Figure 1. In the two muscles, overall tenderness and tenderness index were positively correlated, and both were negatively correlated with the WBSF

*(a) LT Muscle.* As illustrated in Figure 1a, high overall tenderness scores were positively associated with small Hsp proteins (Hsp27, Hsp20, αB-crystallin), Eno3, structural protein CapZ-β, and antioxidants PRDX6 and DJ-1 when considered across breeds. Low tenderness scores were associated with proteins of the Hsp70 family (Hsp70-8, Hsp70-1A/B, and Hsp70/Grp75) or related to fast glycolytic muscle fibers (e.g., LDH-B, MyHC-IIx). The average loadings of the different breeds (Figure 1b) differed on the first axis (BA < LI < AA; $P = 0.0001$), and on the second axis, the AA bulls differed from the other breeds (AA > LI, BA; $P = 0.001$). Compared to LI and BA, LT muscles of AA bulls were characterized by higher abundances of small Hsp (Hsp27, Hsp20, αB-crystallin), Hsp40, Eno3, CapZ-β, PRDX6, and DJ-1 and lower abundances of LDH-B and MyHC-IIx (cf. Table 4).

*(b) ST Muscle.* In the ST muscles, overall tenderness scores were positively associated with LDH-B and MyHC-IIx (Figure 1c) and negatively with small Hsps (Hsp27, Hsp20, αB-crystallin), Hsp40, Eno3, MyHC-I, CapZ-β, PRDX6, and DJ-1. On the first axis (Figure 1d), AA differed significantly ($P < 0.0001$) from the other breeds (LI, BA < AA), and on the second axis all breeds differed significantly (AA < LI < BA; $P < 0.01$). As in the LT, AA were characterized by higher abundances of small Hsp, Hsp40, Eno3, MyHC-I, CapZ-β, PRDX6, and DJ-1 and lower abundances of LDH-B and MyHC-IIx.

*(c) Comparison of the PCAs of the LT and ST Muscles.* The PCA demonstrates inverse relationships between some proteins

**Table 3. Effect of Breed and Muscle on Beef Tenderness Trait Evaluated Using Three Analysis Methods**

| | | breed (B)[a] | | | | muscle (M)[c] | | significance[d] | | |
|---|---|---|---|---|---|---|---|---|---|---|
| variable | muscle | AA 21 | BA 25 | LI 25 | SEM[b] | LT 70 | ST 68 | B | M | B × M |
| overall tenderness | LT[e] | 5.27a | 4.85b | 4.75b | 0.08 | 4.94a | 4.58b | * | ** | ns |
| | ST | 4.58 | 4.66 | 4.49 | 0.05 | | | ns | | |
| WBSF[f] | LT | 40.62 | 44.24 | 41.69 | 1.27 | 42.27 | 44.90 | ns | t | * |
| | ST | 45.91ab | 41.35b | 47.80a | 1.01 | | | * | | |
| tenderness index | LT | 0.67 | −0.14 | −0.26 | 0.20 | 0.04 | −0.03 | ns | ns | * |
| | ST | −0.14ab | 0.58a | −0.56b | 0.18 | | | * | | |

[a]Breed designation: AA, Aberdeen Angus; BA, Blond d'Aquitaine; LI, Limousin. [b]Standard error of mean. [c]Muscle designation: LT, Longissimus thoracis; ST, Semitendinosus [d]$t$, <0.1; *, <0.05; **, <0.001. [e]Least-square means in the same row for breed and muscle effects not followed by a common letter (a, b) differ significantly: $P < 0.05$. [f]Warner−Bratzler shear force test.

**Table 4. Breed, Muscle, and Breed × Muscle Interaction Effects on the 21 Protein Biomarkers of Beef Tenderness**

| | | breed (B)[a] | | | | muscle (M)[c] | | significance[d] | | |
|---|---|---|---|---|---|---|---|---|---|---|
| variable | muscle | AA 21 | BA 25 | LI 25 | SEM[b] | LT 71 | ST 69 | B | M | B × M |
| αB-crystallin[e] | LT | 26.5a | 16.1b | 18.4b | 0.84 | 20.0a | 8.9b | *** | *** | * |
| | ST | 12.5a | 7.0b | 7.9b | 0.45 | | | *** | | |
| Hsp20 | LT | 20.2 | 17.5 | 17.9 | 0.51 | 18.5a | 13.2b | t | *** | ns |
| | ST | 13.6 | 12.9 | 13.3 | 0.35 | | | ns | | |
| Hsp27 | LT | 28.7a | 19.0b | 21.4b | 1.08 | 22.7a | 16.0b | ** | *** | ns |
| | ST | 21.0a | 13.7b | 14.3b | 0.60 | | | *** | | |
| Hsp40 | LT | 18.1a | 17.1ab | 16.1b | 0.26 | 17.0a | 13.0b | ** | *** | ns |
| | ST | 13.8 | 12.8 | 12.6 | 0.22 | | | * | | |
| Hsp70-1A/B | LT | 17.6 | 17.8 | 19.3 | 0.46 | 18.3a | 12.5b | ns | *** | ns |
| | ST | 12.0 | 12.6 | 12.8 | 0.29 | | | ns | | |
| Hsp70-8 | LT | 15.8b | 17.5a | 16.6ab | 0.22 | 16.7a | 15.6b | * | ** | ns |
| | ST | 15.0 | 16.0 | 15.8 | 0.19 | | | t | | |
| Hsp70/Grp75 | LT | 9.1c | 16.6a | 12.6b | 0.44 | 13.0 | 12.6 | *** | ns | *** |
| | ST | 13.3 | 12.6 | 12.0 | 0.24 | | | ns | | |
| Eno3 | LT | 17.5a | 14.9ab | 13.4b | 0.56 | 15.1a | 13.4b | * | * | ns |
| | ST | 15.5a | 13.3b | 12.9b | 0.35 | | | ** | | |
| LDH-B | LT | 10.2c | 19.1a | 14.2b | 0.59 | 14.7 | 13.4 | *** | t | ** |
| | ST | 11.2c | 15.0a | 13.5b | 0.33 | | | *** | | |
| MDH1 | LT | 12.3b | 15.4a | 14.1ab | 0.45 | 14.1 | 14.9 | * | ns | * |
| | ST | 15.4 | 15.1 | 14.2 | 0.37 | | | ns | | |
| CapZ-β | LT | 19.3a | 15.9b | 15.4b | 0.42 | 16.7a | 14.0b | ** | *** | * |
| | ST | 14.9 | 13.4 | 13.8 | 0.28 | | | ns | | |
| α-actin | LT | 16.9b | 19.5a | 16.3b | 0.40 | 17.6 | 17.6 | ** | ns | ** |
| | ST | 17.5 | 17.4 | 17.9 | 0.31 | | | ns | | |
| MyLC-1F | LT | 14.9ab | 15.5a | 14.3b | 0.20 | 14.9 | 15.2 | * | ns | ns |
| | ST | 15.0 | 15.7 | 15.0 | 0.18 | | | ns | | |
| MyBP-H | LT | 14.9 | 13.3 | 13.7 | 0.84 | 14.0 | 12.7 | ns | ns | ns |
| | ST | 13.8 | 12.4 | 12.0 | 0.36 | | | ns | | |
| MyHC-I | LT | 17.7 | 16.9 | 18.4 | 0.33 | 17.7a | 12.4b | ns | *** | ** |
| | ST | 14.3a | 10.2c | 12.4b | 0.35 | | | *** | | |
| MyHC-II | LT | 13.7c | 16.5a | 15.0b | 0.30 | 15.1b | 16.8a | ** | *** | * |
| | ST | 16.3 | 16.9 | 17.2 | 0.22 | | | ns | | |
| MyHC-IIx | LT | 4.2c | 23.3a | 14.3b | 1.08 | 14.5b | 24.34a | *** | *** | ** |
| | ST | 18.4c | 28.6a | 24.8b | 0.74 | | | *** | | |
| DJ-1 | LT | 17.1 | 16.0 | 16.6 | 0.33 | 16.5a | 13.5b | ns | *** | ns |
| | ST | 14.6a | 13.1b | 13.0b | 0.26 | | | * | | |
| PRDX6 | LT | 15.5a | 13.4b | 13.3b | 0.22 | 14.0b | 16.1a | *** | *** | ns |
| | ST | 17.7a | 15.6b | 15.2b | 0.23 | | | *** | | |
| SOD1 | LT | 17.6 | 15.8 | 15.6 | 0.42 | 16.3 | 16.7 | ns | ns | ns |
| | ST | 16.1 | 10.2 | 12.4 | 1.22 | | | ns | | |


dx.doi.org/10.1021/jf501528s | J. Agric. Food Chem. 2014, 62, 9808−9818

**Table 4. continued**

| variable | muscle | breed (B)[a] AA 21 | BA 25 | LI 25 | SEM[b] | muscle (M)[c] LT 71 | ST 69 | significance[d] B | M | B × M |
|---|---|---|---|---|---|---|---|---|---|---|
| $\mu$-calpain | LT | 14.2b | 15.9a | 14.0b | 0.28 | 14.7 | 14.4 | ** | ns | ns |
| | ST | 13.6b | 15.2a | 14.1ab | 0.26 | | | * | | |

[a]Breed designation: AA, Aberdeen Angus; BA, Blond d'Aquitaine; LI, Limousin. [b]Standard error of mean. [c]Muscle designation: LT, Longissimus thoracis; ST, Semitendinosus [d]$t$, <0.1; *, <0.05. **, <0.001; ***, <0.0001. [e]Least-squares means in the same row for breed and muscle effects not followed by a common letter (a–c) differ significantly: $P < 0.05$.

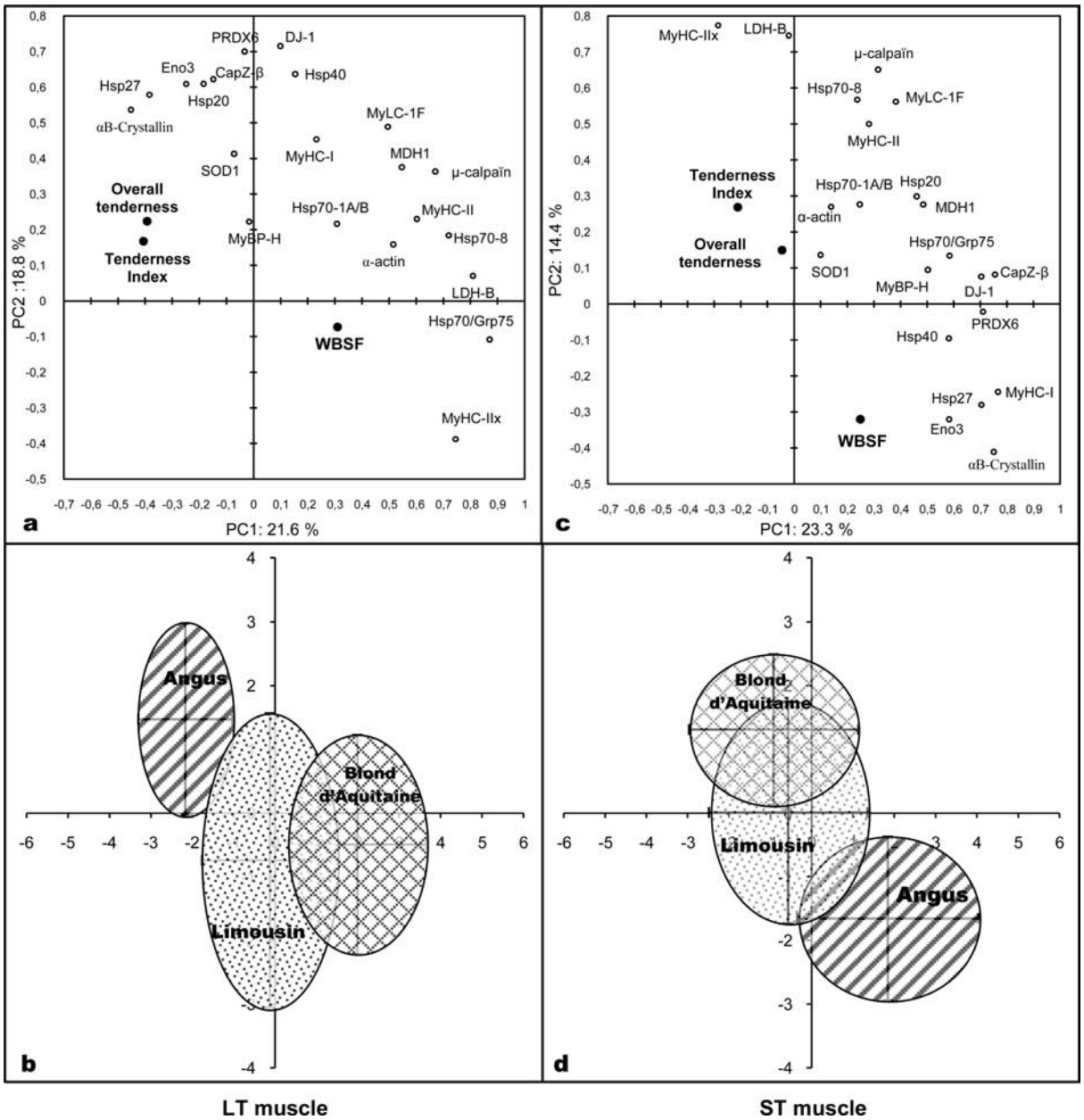


**Figure 1.** Principal component analysis: (a, c) distribution of protein abundance and meat tenderness traits (overall tenderness, WBSF, and tenderness index) for the LT and ST muscles, respectively; (b, d) distribution of the three breeds on the first two principal axes (mean ± standard errors) for LT and ST muscles, respectively.

and tenderness in the two muscles. MyHC-IIx and LDH-B were positively associated with tenderness in ST muscle and negatively in LT. In contrast, proteins from the small Hsp family, Eno3, Hsp40, CapZ-$\beta$, PRDX6, and DJ-1, were negatively correlated with tenderness in ST and positively in LT muscle. In addition, the graphs show that the Angus breed was associated with high tenderness values in LT muscle and with low tenderness in the ST muscle.

*Regression Analyses.* Multiple regression analyses carried out on the pooled data of the three breeds showed that, for the

**Table 5. Equations of Best Models (Parameters Including the Direction and Level of Significance) To Predict Overall Tenderness across Breeds and for Each Breed**

| breed[a] | parameter 1 | *P* value[b] | parameter 2 | *P* value | parameter 3 | *P* value | parameter 4 | *P* value | predictive power[3] | *P* value model |
|---|---|---|---|---|---|---|---|---|---|---|
| **Semitendinosus Muscle** | | | | | | | | | | |
| AA | + PRDX6 | ** | − Eno3 | * | − α-actin | § | | | 43 | * |
| BA | − Hsp70-1A/B | * | + replicate | * | | | | | 39 | * |
| LI | + MyHC-II | *** | − PRDX6 | ** | + Hsp70/Grp75 | ‡ | | | 53 | ** |
| all breeds | − Hsp20 | * | + LDH-B | § | + PRDX6 | § | − Hsp70-1A/B | * | 14 | * |
| **Longissimus thoracis Muscle** | | | | | | | | | | |
| AA | − MyLC-1F | ** | + MyHC-IIx | § | + replicate | ‡ | | | 35 | § |
| BA | + DJ-1 | *** | − MyBP-H | § | + replicate | * | | | 40 | * |
| LI | − Hsp70-1A/B | * | + MyLC-F1 | * | | | | | 35 | * |
| all breeds | − MyHC-IIx | § | + Hsp20 | § | − Hsp70-1A/B | § | | | 17 | * |

[a]Breed designation: AA, Aberdeen Angus; BA, Blond d'Aquitaine; LI, Limousin. [b]Significance of differences: ‡: $P = 0.06$; §, $P < 0.05$; *: $P < 0.01$; **: $P < 0.001$; ***: $P < 0.0001$. [3](%) of variability between animals explained by the model.

**Table 6. Equations of Best Models (Parameters Including the Direction and Level of Significance) To Predict WBSF across Breeds and for Each Breed**

| breed[a] | parameter 1 | *P* value[b] | parameter 2 | *P* value | parameter 3 | *P* value | predictive power[c] | *P* value model |
|---|---|---|---|---|---|---|---|---|
| **Semitendinosus Muscle** | | | | | | | | |
| AA | − αB-crystallin | § | + Eno3 | * | + Hsp70-1A/B | § | 36 | § |
| BA | − MyHC-IIx | ± | + Eno3 | ‡ | − α-actin | § | 22 | § |
| LI | − MyHC-IIx | * | − MyHC-II | § | − replicate | *** | 60 | *** |
| all breeds | − MyHC-IIx | * | + Hsp70-1A/B | § | | | 15 | * |
| **Longissimus thoracis Muscle** | | | | | | | | |
| AA | | | | | | | | |
| BA | − α-actin | § | | | | | 21 | § |
| LI | + LDH-B | ** | − MDH1 | ** | + Hsp70-1A/B | ** | 60 | *** |
| all breeds | + Hsp70-1A/B | * | + replicate | § | | | 10 | * |

[a]Breed designation: AA, Aberdeen Angus; BA, Blond d'Aquitaine; LI, Limousin. [b]Significance of differences: ‡, $P = 0.1$; §, $P < 0.05$; *, $P < 0.01$; **, $P < 0.001$; ***, $P < 0.0001$. [c]Percent of variability between animals explained by the model.

**Table 7. Equations of Best Models (Parameters Including the Direction and Level of Significance) To Predict Tenderness Index across Breeds and for Each Breed**

| breed[a] | parameter 1 | *P* value[b] | parameter 2 | *P* value | parameter 3 | *P* value | parameter 4 | *P* value | predictive power[c] | *P* value model |
|---|---|---|---|---|---|---|---|---|---|---|
| **Semitendinosus Muscle** | | | | | | | | | | |
| AA | + αB-crystallin | § | + PRDX6 | § | − Eno3 | * | | | 47 | * |
| BA | − Hsp70-1A/B | § | + replicate | § | | | | | 24 | * |
| LI | − αB-crystallin | * | + Hsp40 | * | + MyHC-II | ** | − PRDX6 | ** | 73 | *** |
| all breeds | + MyHC-IIx | § | + replicate | * | | | | | 12 | * |
| **Longissimus thoracis Muscle** | | | | | | | | | | |
| AA | − Eno3 | § | + Hsp27 | * | − CapZ-β | + | | | 29 | * |
| BA | − CapZ-β | § | + Hsp40 | ‡ | + α-actin | * | − Hsp70-8 | * | 28 | § |
| LI | − LDH-B | *** | + MDH1 | ** | + CapZ-β | * | − Hsp70-1A/B | *** | 66 | *** |
| all breeds | + α-actin | § | − Hsp70-1A/B | * | − MyHC-IIx | * | | | 17 | ** |

[a]Breed designation: AA, Aberdeen Angus; BA, Blond d'Aquitaine; LI, Limousin. [b]Significance of differences: ‡, $P = 0.1$; §, $P < 0.05$; *, $P < 0.01$; **, $P < 0.001$; ***, $P < 0.0001$. [c]Percent of variability between animals explained by the model.

LT and ST muscles, the proteins explained only 10−17% of the variability of the three tenderness measurements (Tables 5−7). The models for overall tenderness retained (Table 5) LDH-B, PRDX6, Hsp20, and Hsp70-1A/B for the ST muscle and Hsp20, MyHC-IIx, and Hsp70-1B for the LT muscle. The models for WBSF retained Hsp70-1B for the two muscles and MyHC-IIx for the ST muscle (Table 6). The models of the tenderness index retained MyHC-IIx for the ST and LT muscles. The LT tenderness index was further correlated with α-actin and with Hsp70-1A/B (Table 7).

When breeds were considered separately, the prediction power (adjusted $r^2$) improved, although it varied according to breed and tenderness measurement (Tables 5−7). The models for LI bulls had the most predictive power. The model of overall tenderness of the ST muscle of LI bulls retained (Table 5) fast MyHC, Hsp70/Grp75, and PRDX6, explaining 53% of the variability between animals. MyLC-1F and Hsp70-1A/B explained 35% of variability in overall tenderness of the LT muscle between LI bulls. The model for WSBF explained even 60% of the variability of the LI breed in both muscles (Table 6). Proteins retained in the models were MyHC-IIx and -II for

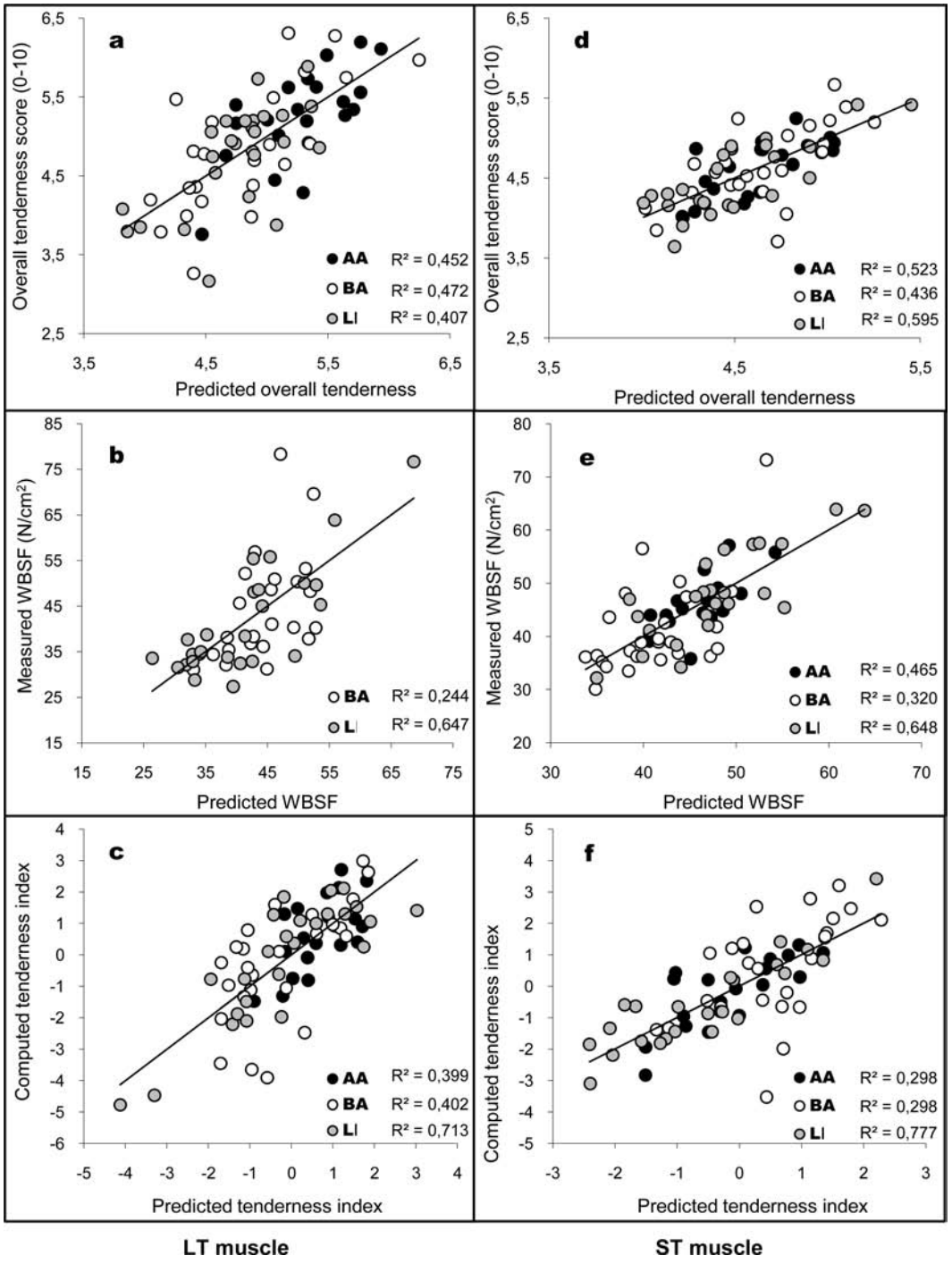


**Figure 2.** Correlations between predicted and measured beef tenderness traits (for tenderness, WBSF, and tenderness index) using best models for the three breeds among LT (a–c) and ST muscles (d–f). Adjusted *r*-squares corresponding to the prediction equations shown in Tables (5–7) for each breed are given. Breed designation: AA, Aberdeen Angus; BA, Blond d'Aquitaine; LI, Limousin.

the ST muscle and LDH-B, Hsp70-1A/B, and MDH1 for the LT muscle (Table 6). The model for the tenderness index for both muscles had high predictive power, explaining 73 and 66% of the variability for the ST and LT, respectively (Table 7).

Correlations between predicted and measured values for each tenderness trait among the two studied muscles are shown (Figure 2).

For the AA bulls, none of the 21 quantified protein biomarkers could predict the WBSF of the LT muscle (Table 6). In the ST muscle, the WBSF was predicted by Eno3 and Hsp70-1A/B (positively) and by αB-crystallin (negatively). Overall tenderness and tenderness index were better predicted in the ST than in the LT muscle.

For the BA bulls, prediction powers were similar in the two muscles with better prediction for overall tenderness by Hsp70-1A/B (negatively) in ST and by DJ-1 (positively) and MyBP-H (negatively) in LT muscle (Table 5). The predictions of WBSF and tenderness index were lower than in the two other breeds (Tables 6 and 7).


dx.doi.org/10.1021/jf501528s | J. Agric. Food Chem. 2014, 62, 9808–9818

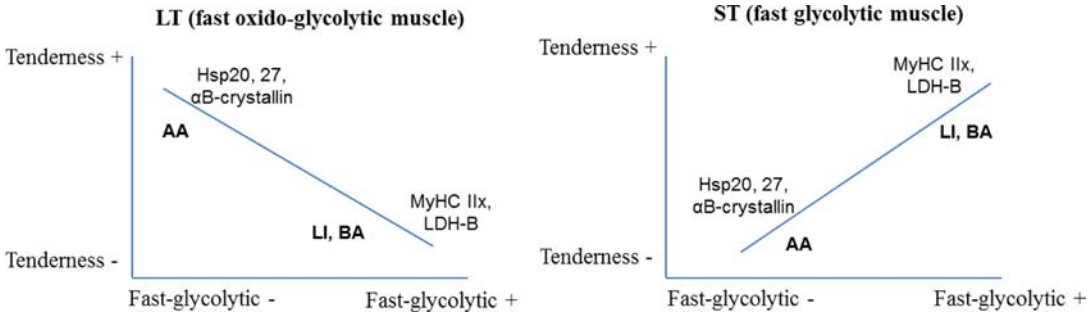


**Figure 3.** Schematic illustration of the relationships between muscle metabolic and contractile properties and tenderness depending on the muscle. (Left) For the Longissimus thoracis (fast oxido-glycolytic muscle), higher degrees of fast glycolytic properties are associated with lower tenderness. (Right) For the Semitendinous (fast glycolytic muscle) higher degrees of fast glycolytic properties are associated with higher tenderness. Consequently, biomarkers associated with contractile and metabolic properties of the muscles such as MyHC IIx and LDH-B are positively or negatively associated with tenderness of the ST and LT muscles, respectively. The opposite is found for other biomarkers such as small Hsps (Hsp20, Hsp27, $\alpha$B-crystallin). ST and LT muscles from Angus breed (AA) have lower levels of fast glycolytic properties than those of Limousin (LI) and Blond d'Aquitaine (BA) breeds. Therefore, their LT and ST muscles are more and less tender, respectively, than those of the LI and BA breeds.

Overall, the results demonstrate that among the 21 quantified proteins, Hsp70-1A/B was often retained in the prediction models of the different breeds and negatively correlated with the different tenderness measurements in both muscles. Proteins representing fast glycolytic fiber types such as MyHC-IIx or LDH-B were correlated with tenderness in the two muscles for the three tenderness traits, but the direction of the correlation depended on the muscle, as also illustrated in the PCA (Figure 1): they were positively correlated with tenderness measurements in the ST and negatively correlated in the LT muscle. The glycolytic Eno3 enzyme was correlated with the three tenderness indicators in the ST muscle of the AA bulls. PRDX6 was correlated with ST overall tenderness and tenderness index but never with WBSF.

## ■ DISCUSSION

The first objective of this study was to determine in two different muscles of young Aberdeen Angus, Limousin, and Blond d'Aquitaine bulls the relationships between tenderness indicators and several protein biomarkers previously identified as good predictors of meat tenderness.[6] The second objective was to propose prediction equations of tenderness based on the abundances of the biomarkers. Among the quantified proteins, Hsp70-1A/B was the only protein associated with the different tenderness indicators in the two muscles and the three breeds. Other proteins including LDH-B, MyHC-IIx, and various small Hsps were associated with tenderness, but oppositely in the ST compared to the LT muscle. These data suggest that different mechanisms underlie tenderness, some which are common between both muscles, whereas others differ. The underlying mechanisms appear to be related to the contractile and metabolic properties of the muscle, and they differ in the sense that the direction of the correlation with tenderness depends on the muscle.

**Muscle- and Breed-Specific Biomarkers of Tenderness.** Our findings show that MyHC-IIx and LDH-B are positively and negatively correlated with tenderness of the ST muscle (fast glycolytic) and LT muscle (fast oxido-glycolytic, respectively. These opposite correlations are in agreement with earlier studies. For example, Chaze et al.[19] showed in young bulls from three main French beef breeds that in the LT muscle several proteins representing fast glycolytic properties were negatively correlated with tenderness and several proteins corresponding to slow oxidative properties were positively correlated with tenderness. Studying the same muscle in young Blond d'Aquitaine, Morzel et al.[24] found succinate dehydrogenase, an oxidative enzyme, to be a good marker of tenderness. In Charolais young bulls, fast proteins such as Troponin T fast isoforms, phosphoglucomutase, fast MyHC, and glycogen phosphorylase were found to be potential biomarkers of toughness, and slow MyHC, ATP synthase $\beta$, and ApoBEC were associated with increased tenderness.[12] Other studies based on fiber types and enzyme activities showed positive relationships between slow oxidative fiber types and tenderness in the LT and a negative relationships in the ST muscle.[2] This was further confirmed in a meta-analysis combining more than 332,000 data on fiber types and enzyme activities of these two muscles in several types of cattle.[4] The present results indicate also that in the case of a fast glycolytic muscle such as ST, muscles containing a greater proportion of fast glycolytic fibers will produce more tender meat and, in the case of a more oxidative muscle such as LT, muscles containing a greater proportion of slow oxidative fibers will produce more tender meat. In the present study, LT meat of AA bulls was more tender and ST meat was less tender compared to the LI and BA breeds. This is coherent with the opposite correlations described above. Irrespective of breed, for the LT muscle, the more glycolytic it is, the less tender it is, and for the ST muscle, the more glycolytic it is, the more it is tender. The LT of AA was less glycolytic compared to the other breeds and, consequently, more tender. The ST of AA was less glycolytic compared to the other breeds and, consequently, less tender. Other factors, such as lipid content, may of course also play a significant role.

The positive correlation between MyHC-IIx and tenderness observed in the LT muscle of the AA bulls may seem to contrast with the above idea. Other authors found similarly positive relationships between fast glycolytic type and tenderness in LT muscle from animals with muscles with oxidative characteristics. For example, D'Allessandro et al.[25] in Longissimus dorsi from Chianina beef cattle observed that the tender meat group on the basis of WBSF was characterized by higher levels of glycolytic enzymes.

Overall, existing results demonstrate that the contractile and metabolic properties of muscle play a major role in the elaboration of tenderness.

The present study found other opposite associations between proteins and tenderness according to the muscle or breed. Thus, proteins from the small Hsp family (Hsp20, Hsp27, and αB-crystallin) were inversely associated with tenderness depending on the two muscles. These proteins were negatively associated with tenderness in the ST muscle and positively in the LT muscle. These data are in agreement with the results of Guillemin et al.,[26] who demonstrated that in the ST muscle, Hsp from both the Hsp70 family and small sHsp family were inversely correlated with tenderness as observed in the present study. Nevertheless, these Hsps were not correlated with tenderness of the LT muscle. In a previous experiment with Blond d'Aquitaine young bulls, we found inverse relationships between sHsp abundances and tenderness in ST and LT muscles.[10] This could demonstrate that the functions of sHsp depend on the contractile and metabolic properties of the muscle. Guillemin et al.[27] showed that slow oxidative fibers have the highest abundance of αB-crystallin. This is in accordance with our data showing higher abundances in LT than in ST muscle and earlier data reported by Guillemin et al.[26] showing higher abundances in Charolais young bulls and AA than in LI and BA.

Overall, these results allow understanding why the correlations between one biomarker and tenderness could be reversed as described in the literature. Our results give explanations as described in Figure 3. These relationships according to muscle and breed types need to be confirmed in other muscles and animal types.

In the present study, PRDX6, an antioxidant enzyme, was associated with tenderness mainly of the ST muscle, but in opposite directions, depending on the breed. This is in accordance with earlier results. Guillemin et al.[27] found that PRDX6 is a biomarker of low tenderness of the ST muscle in young Charolais bulls, whereas Jia et al.[28] reported an overexpression of PRDX6 in tender meat in young Norwegian Red bulls. The antioxidant action of PRDX6 is based on the hydrolysis of hydrogen peroxides and facilitation of the repair of damaged cell membranes via reduction of peroxidized phospholipids.[7,29] Antioxidant enzymes such as PRDX6 and also SOD1 are involved in the protection of the cell against oxidative stress, which is causal of free radicals of oxygen, resulting in the formation of protein aggregates.[30] These aggregates may hamper the tenderization process of the meat. In agreement with this finding, D'Alessandro et al.[25] proposed that oxidative stress promotes meat tenderness and elicits heat shock protein responses. Ouali and co-workers[7,31] proposed that the first step of the conversion of muscle into meat is the onset of apoptosis. This death process is energy dependent and involves a large number of proteins including Hsp families. D'Alessandro et al.[25] discusses the possible causes of opposite relationships between abundances of oxidative enzymes and tenderness. The authors speculate that post-mortem metabolism in tender and tough meat is subtly modulated via higher levels of specific enzymes and amino acidic residue phosphorylation in a breed-specific fashion. Results of the present study showing that PRDX6 is positively associated with overall tenderness in AA and negatively in LI young bulls are in accordance with this suggestion. Guillemin et al.[27] showed that the relationship between antioxidant enzymes such as PRDX6 and also SOD1 was more significant in Charolais steers than in young bulls, suggesting that gender may also play a role. They showed that SOD1 was correlated with tenderness only in steers, which may explain the absence of an association between tenderness and SOD1 in the present study.

Overall, these data demonstrate that the contractile and metabolic properties of muscles play a major role in the elaboration of tenderness. It is likely that mechanisms underlying the determinism of tenderness involve several biological processes such as apoptosis, oxidative stress, and proteolysis, which depend probably on these muscle properties.

**Hsp70-1A/B Is a Good Candidate Biomarker of Meat Tenderness in the Three Breeds.** Proteins from the Hsp70 family (Hsp70-1A/B, Hsp70-8, GRP 75) were recently found to be related to tenderness.[8] In the present study, among Hsp70s, only Hsp70-1A/B (gene HSPA1B), also called Hsp70-2 depending on species, was negatively associated with overall tenderness and tenderness index and positively with WBSF in the two muscles across the three breeds.

The members of the Hsp70 family serve a variety of roles: (i) they act as molecular chaperones facilitating the assembly of multiprotein complexes, (ii) they participate in the translocation of polypeptides across cell membranes and to the nucleus, and (iii) they help in the proper folding of nascent polypeptide chains.[32] In the Diaphragma muscle from Holstein−Friesian cattle, Sugimoto et al.[33] showed that misfolding of energy-related proteins due to Hsp70 deficiency might lead to protein aggregation and muscle fiber degeneration. This is in coherence with the negative association with tenderness observed in the present study. Moreover, the study of Crawford and Horowits[34] showed that, in particular, scaffolding proteins and chaperone proteins such as Hsp90 and Hsp70 are required for individual steps in the assembly of myofibril. The study of Miyabara et al.[35] showed that Hsp70 improves structural and functional recovery of skeletal muscle after disuse atrophy. This is in agreement with several studies showing that Hsp70 is one of the most important heat shock proteins for maintenance of cell integrity during normal cellular growth as well as under pathophysiological conditions.[36,37] These data suggest that Hsp70 is important for maintaining structural, ultrastructural, and functional properties of skeletal muscle. Possibly, Hsp70-1A/B plays also an important role in structural modifications during post-mortem aging. Hsp70-1A/B has further an antiapoptotic role in skeletal muscle. Gao et al.[36] reported a function of Hsp70-1A/B in regulating TNF-α-induced cell apoptosis. By forming the complex Hsp70/CHIP/ASK1, Hsp70 promotes ASK1 proteasomal degradation and prevents TNF-α-induced cell apoptosis. Hsp70 proteins are also known to sequester pro-apoptotic factors such as BCL-2.[38] These data are in agreement with the important role of apoptosis in meat aging.[7,39]

The present study found that in contrast to Hsp70-1A/B, the association between the relative abundance of the other Hsp70s and tenderness traits differed according to breed and muscle. This may be explained by different regulation of the expression of these Hsp70s in the muscle. In the present study, Hsp70/Grp75 and Hsp70-8 were less abundant in AA than in BA, particularly in the LT muscle. However, Hsp70-1A/B abundance did not differ between breeds in the two muscles. These data are in agreement with the results of Guillemin et al.,[27] who showed no effect of gender on Hsp70-1A/B abundance between steers and young bulls. This would explain the association between Hsp70-1A/B and tenderness across muscles and breeds observed in the present study. The lack of consistent associations between tenderness and Hsp70/Grp75 may be explained by the fact that it is exclusively expressed in

the mitochondrial matrix and that it is involved in the translocation and folding of nascent polypeptide chains of both nuclear and mitochondrial origin.[40]

These findings suggest that Hsp70-1A/B could be a relatively general biomarker of tenderness in different muscles and breeds compared to proteins discussed earlier, which appear to be quite strongly muscle- or breed-specific.

In conclusion, this study shows that some biomarkers of tenderness such as MyHC IIx, LDH-B, and small Hsp are dependent on the contractile and metabolic properties of the muscle (cf. Figure 3), explaining their opposite relationships with tenderness in the ST compared to the LT muscle and in AA compared to LI and BA bulls. It further shows that Hsp70-1A/B is a biomarker of low beef tenderness across the breeds and muscles studied. All of these biomarkers need further testing in various muscles from cattle of different genders and breeds before they can be used as biomarkers in routine immunological testing.

## AUTHOR INFORMATION


### Corresponding Author

*(B.P.) Phone: 0033473624056. Fax: 0033473624639. E-mail: brigitte.picard@clermont.inra.fr.



### Funding

This work was part of the EU FP6 Integrated Project ProSafeBeef, contract no. FOODCT-2006-36241. Funding by the European Union is gratefully acknowledged with respect to animal production and laboratory analyses. We are further thankful to Constantine 1 University, INATAA Institute (Algeria), for the financial support given to M.G.


### Notes

The authors declare no competing financial interest.

## ACKNOWLEDGMENTS


We thank INRA-Le Magneraud for the sensory analysis and INRA UERT (Theix) for animal management and slaughter. We thank all of the persons involved in this project for their assistance in data collection, the management and slaughtering of animals, muscle sampling, and the dot-blot and Warner–Bratzler assays.


## REFERENCES


(1) Verbeke, W.; Van Wezemael, L.; de Barcellos, M. D.; Kugler, J. O.; Hocquette, J. F.; Ueland, O.; Grunert, K. G. European beef consumers' interest in a beef eating-quality guarantee Insights from a qualitative study in four EU countries. *Appetite* **2010**, *54*, 289–296.

(2) Picard, B.; Jurie, C.; Bauchart, D.; Dransfield, E.; Ouali, A.; Martin, J. F.; Jailler, R.; Lepetit, J.; Culioli, J. Muscle and meat characteristics from the main beef breeds of the Massif Central. *Sci. Aliments* **2007**, *27*, 168–180.

(3) Renand, G.; Picard, B.; Touraille, C.; Berge, P.; Lepetit, J. Relationships between muscle characteristics and meat quality traits of young Charolais bulls. *Meat Sci.* **2001**, *59*, 49–60.

(4) Chriki, S.; Renand, G.; Picard, B.; Micol, D.; Journaux, L.; Hocquette, J. F. Meta-analysis of the relationships between beef tenderness and muscle characteristics. *Livest. Sci.* **2013**, *155*, 424–434.

(5) Hocquette, J. F.; Lehnert, S.; Barendse, W.; Cassar-Malek, I.; Picard, B. Recent advances in cattle functional genomics and their application to beef quality. *Animal* **2007**, *1*, 159–173.

(6) Picard, B.; Berri, C.; Lefaucheur, L.; Molette, C.; Sayd, T.; Terlouw, C. Skeletal muscle proteomics in livestock production. *Brief Funct. Genomics* **2010**, *9*, 259–78.

(7) Ouali, A.; Gagaoua, M.; Boudida, Y.; Becila, S.; Boudjellal, A.; Herrera-Mendez, C. H.; Sentandreu, M. A. Biomarkers of meat tenderness: present knowledge and perspectives in regards to our current understanding of the mechanisms involved. *Meat Sci.* **2013**, *95*, 854–870.

(8) Picard, B.; Gagaoua, M.; Kammoun, M.; Terlouw, C.; Hocquette, J. F.; Micol, D. Biomarkers of beef tenderness in young bulls of three breeds. In *Proceedings of the 59th International Congress of Meat Science and Technology*, Izmir, Turkey; Elsevier: Amsterdam, The Netherlands, 2013; p 4.

(9) Gagaoua, M.; Boudida, Y.; Becila, S.; Picard, B.; Boudjellal, A.; Herrera-Mendez, C. H.; Sentandreu, M.; Ouali, A. Serine protease inhibitors as good predictors of meat tenderness: which are they and what are their functions? *Crit. Rev. Food Sci. Nutr.* **2014**, DOI: 10.1080/10408398.2012.741630 .

(10) Picard, B.; Lefevre, F.; Lebret, B. Meat and fish flesh quality improvement with proteomic applications. *Anim. Front.* **2012**, *2*, 18–25.

(11) Picard, B.; Meunier, B.; Barboiron, C.; Dunoyer, N.; Guillemin, N.; Micol, D., From protein markers to phenotyping tools for evaluation of beef tenderness. In *Farm Animal Proteomics*; Rodrigues, P., Eckersall, D., Almeida, A., Eds.; Wageningen Academic Publishers: Wageningen, The Netherlands, 2012; pp 165–168.

(12) Guillemin, N.; Bonnet, M.; Jurie, C.; Picard, B. Functional analysis of beef tenderness. *J. Proteomics* **2011**, *75*, 352–365.

(13) Listrat, A.; Picard, B.; Jailler, R.; Collignon, H.; Peccatte, J. R.; Micol, D.; Geay, Y.; Dozias, D. Grass valorisation and muscular characteristics of blonde d'Aquitaine steers. *Anim. Res.* **2001**, *50*, 105–118.

(14) Jurie, C.; Picard, B.; Micol, D.; Listrat, A.; Kammoun, M.; Hocquette, J. F. Muscle characteristics from young bulls of different beef breeds. In *57th International Congress of Meat Science and Technology*, Ghent, Belgium, Aug 7– 12, 2011; Elsevier: Amsterdam, The Netherlands, 2011.

(15) Guillemin, N.; Meunier, B.; Jurie, C.; Cassar-Malek, I.; Hocquette, J. F.; Levéziel, H.; Picard, B. Validation of a dot-blot quantitative technique for large-scale analysis of beef tenderness biomarkers. *J. Physiol. Pharmacol.* **2009**, *60*, 91–97.

(16) Dubost, A.; Micol, D.; Picard, B.; Lethias, C.; Andueza, D.; Bauchart, D.; Listrat, A. Structural and biochemical characteristics of bovine intramuscular connective tissue and beef quality. *Meat Sci.* **2013**, *95*, 555–561.

(17) Gagaoua, M.; Micol, D.; Richardson, R. I.; Hocquette, J. F.; Terlouw, E. M. C.; Meteau, K.; Juin, H.; Moloney, A. P.; Nuernberg, K.; Scollan, N. D.; Boudjellal, A.; Picard, B. Relationships between overall liking score and sensory meat attributes in different types of beef cattle. In *Proceedings of the 59th International Congress of Meat Science and Technology*, Izmir, Turkey; Elsevier: Amsterdam, The Netherlands, 2013; pp 1–4.

(18) Lepetit, J.; Culioli, J. Mechanical properties of meat. *Meat Sci.* **1994**, *36*, 203–237.

(19) Chaze, T.; Hocquette, J.-F.; Meunier, B.; Renand, G.; Jurie, C.; Chambon, C.; Journaux, L.; Rousset, S.; Denoyelle, C.; Lepetit, J.; Picard, B. Biological markers for meat tenderness of the three main French beef breeds using 2-DE and MS approach. In *Proteomics in Foods*; Toldrá, F., Nollet, L. M. L., Eds.; Springer: New York, 2013; Vol. 2, pp 127–146.

(20) Allais, S.; Levéziel, H.; Hocquette, J.; Rousset, S.; Denoyelle, C.; Journaux, L.; Renand, G. Fine mapping of quantitative trait loci underlying sensory meat quality traits in three French beef cattle breeds. *J. Anim. Sci.* **2014**, DOI: 10.2527/jas.2014-7868.

(21) Guillemin, N.; Meunier, B.; Jurie, C.; Cassar-Malek, I.; Hocquette, J. F.; Leveziel, H.; Picard, B. Validation of a dot-blot quantitative technique for large scale analysis of beef tenderness biomarkers. *J. Physiol. Pharmacol* **2009**, *60* (Suppl. 3), 91–97.

(22) Bouley, J.; Chambon, C.; Picard, B. Mapping of bovine skeletal muscle proteins using two-dimensional gel electrophoresis and mass spectrometry. *Proteomics* **2004**, *4*, 1811–1824.

(23) Bradford, M. M. A rapid and sensitive method for the quantitation of microgram quantities of protein utilizing the principle of protein-dye binding. *Anal. Biochem.* **1976**, *72*, 248–254.

(24) Morzel, M.; Terlouw, C.; Chambon, C.; Micol, D.; Picard, B. Muscle proteome and meat eating qualities of Longissimus thoracis of "Blonde d'Aquitaine" young bulls: a central role of HSP27 isoforms. *Meat Sci.* **2008**, *78*, 297−304.
(25) D'Alessandro, A.; Marrocco, C.; Rinalducci, S.; Mirasole, C.; Failla, S.; Zolla, L. Chianina beef tenderness investigated through integrated omics. *J. Proteomics* **2012**, *75*, 4381−4398.
(26) Guillemin, N.; Jurie, C.; Renand, G.; Hocquette, J. F.; Micol, D.; Lepetit, J.; Picard, B. Different phenotypic and proteomic markers explain variability of beef tenderness across muscles. *Int. J. Biol.* **2012**, *4*, 26−38.
(27) Guillemin, N.; Jurie, C.; Cassar-Malek, I.; Hocquette, J. F.; Renand, G.; Picard, B. Variations in the abundance of 24 protein biomarkers of beef tenderness according to muscle and animal type. *Animal* **2011**, *5*, 885−894.
(28) Jia, X.; Veiseth-Kent, E.; Grove, H.; Kuziora, P.; Aass, L.; Hildrum, K. I.; Hollung, K. Peroxiredoxin-6 − a potential protein marker for meat tenderness in bovine longissimus thoracis muscle. *J. Anim Sci.* **2009**, *87*, 2391−2399.
(29) Manevich, Y.; Fisher, A. B. Peroxiredoxin 6, a 1-Cys peroxiredoxin, functions in antioxidant defense and lung phospholipid metabolism. *Free Radical Biol. Med.* **2005**, *38*, 1422−1432.
(30) Morzel, M.; Gatellier, P.; Sayd, T.; Renerre, M.; Laville, E. Chemical oxidation decreases proteolytic susceptibility of skeletal muscle myofibrillar proteins. *Meat Sci.* **2006**, *73*, 536−543.
(31) Ouali, A.; Herrera-Mendez, C. H.; Coulis, G.; Becila, S.; Boudjellal, A.; Aubry, L.; Sentandreu, M. A. Revisiting the conversion of muscle into meat and the underlying mechanisms. *Meat Sci.* **2006**, *74*, 44−58.
(32) Daugaard, M.; Rohde, M.; Jaattela, M. The heat shock protein 70 family: highly homologous proteins with overlapping and distinct functions. *FEBS Lett.* **2007**, *581*, 3702−3710.
(33) Sugimoto, M.; Furuoka, H.; Sugimoto, Y. Deletion of one of the duplicated Hsp-0 genes causes hereditary myopathy of diaphragmatic muscles in Holstein-Friesian cattle. *Anim. Genet.* **2003**, *34*, 191−197.
(34) Crawford, G. L.; Horowits, R. Scaffolds and chaperones in myofibril assembly: putting the striations in striated muscle. *Biophys. Rev.* **2011**, *3*, 25−32.
(35) Miyabara, E. H.; Nascimento, T. L.; Rodrigues, D. C.; Moriscot, A. S.; Davila, W. F.; AitMou, Y.; deTombe, P. P.; Mestril, R. Overexpression of inducible 70-kDa heat shock protein in mouse improves structural and functional recovery of skeletal muscles from atrophy. *Pfluegers Arch: Eur. J. Physiol.* **2012**, *463*, 733−741.
(36) Gao, Y.; Han, C.; Huang, H.; Xin, Y.; Xu, Y.; Luo, L.; Yin, Z. Heat shock protein 70 together with its co-chaperone CHIP inhibits TNF-$\alpha$ induced apoptosis by promoting proteasomal degradation of apoptosis signal-regulating kinase1. *Apoptosis* **2010**, *15*, 822−833.
(37) Kundrat, L.; Regan, L. Identification of residues on Hsp70 and Hsp90 ubiquitinated by the cochaperone CHIP. *J. Mol. Biol.* **2010**, *395*, 587−594.
(38) Beere, H. M.; Green, D. R. Stress management − heat shock protein-70 and the regulation of apoptosis. *Trends Cell Biol.* **2001**, *11*, 6−10.
(39) Gagaoua, M.; Boudida, Y.; Becila, S.; Picard, B.; Boudjellal, A.; Sentandreu, M. A.; Ouali, A. New caspases' inhibitors belonging to the serpin superfamily: a novel key control point of apoptosis in mammalian tissues. *Adv. Biosci. Biotechnol.* **2012**, *3*, 740−750.
(40) Arakawa, A.; Handa, N.; Shirouzu, M.; Yokoyama, S. Biochemical and structural studies on the high affinity of Hsp70 for ADP. *Protein Sci.* **2011**, *20*, 1367−1379.

proteins, sorghum protein bodies are more highly cross-linked, leading to increased levels of covalent bonding and protein polymerization in the matrix.[8,9] This increased level of cross-linking reduces overall protein digestibility, which compounds nutritional deficiencies of sorghum, such as low inherent levels of lysine and threonine, and often needs to be supplemented in food and feed.[13]

Identification and characterization of endosperm proteins and the elements regulating their synthesis, localization, and degradation facilitates enhancement of amino acid content and starch accessibility for improved grain nutritional value.[14] This study involves the evaluation of grain protein composition in sorghum lines with allelic variation in kafirin storage proteins using a range of proteomic tools, including reversed-phase HPLC (RP-HPLC), lab on a chip (LOC), SDS-PAGE, and liquid chromatography−tandem mass spectrometry (LC−MS/MS). The focus of the work is to identify candidate proteins, which may impact on quality traits, particularly those which are differentially expressed across the genotypes.

## MATERIALS AND METHODS

**Plant Material.** Twenty-eight inbred sorghum lines, with previously determined allelic variation in the $\beta$-, $\gamma$-, and $\delta$-kafirin storage proteins, were included in the study.[15] The primary focus of the analysis was on comparisons between the $\beta$-kafirin null line QL12 and 296B, an important food line of Indian origin. Plants were cultivated under field conditions at the University of Queensland, Gatton campus, QLD, Australia, over the 2008/2009 and 2011/2012 summer growing seasons.

**Protein Extractions.** *Albumin/Globulin (A/G).* Wholegrain flour (100 mg) prepared from kernels ground in liquid nitrogen using a mortar and pestle was mixed in 1 mL of extraction solvent (50 mM Tris·HCl pH 7.8, 100 mM KCl, and 5 mM EDTA). The sample was vortexed and centrifuged, and a 500 $\mu$L aliquot of supernatant was removed to a new tube.[16] The process was repeated by adding an additional 1 mL of extraction solvent to the pellet, repeating the extraction process and removing an additional 500 $\mu$L of supernatant to the same tube.

*Prolamin.* The A/G pellet from the above extraction procedure was retained and washed with 1 mL of distilled water ($dH_2O$), and 1 mL of solvent was added (60% *tert*-butyl alcohol, 0.5% sodium acetate w/v, and 2% $\beta$-mercaptoethanol ($\beta$-ME) v/v). The pellet was then vortexed and centrifuged, and 500 $\mu$L of supernatant was transferred to a new tube. The procedure was repeated once, and a further 500 $\mu$L of supernatant was removed to the same tube.

*Glutelin/Residual Proteins.* The pellet from the prolamin extraction was washed with 1 mL of $dH_2O$ and 1 mL of sodium borate buffer (125 mM pH 10.0 containing 1% SDS w/v and 1% $\beta$-ME v/v) was added to the pellet. The suspension was vortexed and centrifuged, and 500 $\mu$L of supernatant was transferred to a new tube. The procedure was repeated once, and a further 500 $\mu$L of supernatant was removed to the same tube.

**Reversed-Phase HPLC (RP-HPLC).** Protein samples were analyzed using an Agilent 1100 HPLC system (Agilent, Foster City, CA), fitted with a Poroshell column of varying stationary phases (as indicated below for the various protein fractions). The system employed a binary gradient with a constant flow rate of 0.7 mL/min, and a column temperature was maintained at 55 °C. Solvents for RP-HPLC included water containing 0.1% trifluoroacetic acid (TFA) w/v (A), and acetonitrile (ACN) containing 0.07% TFA w/v (B), with gradient flow specifications as follows: 0−18 min, 45%−60% B; 18−19 min, decreased to 45% B; followed by a 7 min post run. Absorbance was measured with a UV detector at 214 nm.

*Albumin/Globulins.* After extraction, 250 $\mu$L A/G aliquots were freeze-dried in a SpeedVac overnight. Prior to RP-HPLC analysis, the aliquots were resuspended in 100 $\mu$L of 50% ethylene glycol to stabilize proteins.[17] Samples (5 $\mu$L) were analyzed using a 2.1 × 75 mm Poroshell 300 SB C3 column.

*Prolamins.* After extraction, protein samples (1 mL) were alkylated by adding 33 $\mu$L of 4-vinylpyridine and vortexed for 10 min. Samples (5 $\mu$L) were then injected directly for RP-HPLC analysis using 2.1 × 75 mm Poroshell 300 SB C18 column.[16] Proteins were detected by UV at 214 nm.

**Lab on a Chip (LOC).** The lab-on-a-chip procedure was carried out on an Agilent 2100 Bioanalyser using the Protein 80 assay kit (Agilent Technologies, Palo Alto, CA). A 1:1 mixture of protein to denaturing buffer was used.

**Sodium Dodecyl Sulfate Polyacrylamide Gel Electrophoresis (SDS-PAGE).** *Protein Sample Cleanup.* Samples were cleaned and concentrated with a 2-D Clean-Up Kit (GE Healthcare Ltd.). Concentrations were measured using a 2-D Quant Kit (GE Healthcare Ltd.) according to the manufacturer's instructions.

*One-Dimensional (1D) SDS-PAGE.* A 10 $\mu$L sample was resuspended in 5 $\mu$L of 3X loading buffer (100 mM Tris, 1% SDS (w/v), 0.01% bromophenol blue, 15% glycerol, 0.05% $\beta$-ME), and heated to 95 °C, and then chilled on ice and loaded onto a small format precast anyKd (10−250 kDa range) gradient gel (Bio-Rad, Hercules, CA), with 15 $\mu$L of ColorPlus prestained marker (broad range 7−175 kDa) added to the first and last wells. Gels were run in SDS buffer (25 mM Tris, 200 mM glycine, 0.1% SDS w/v) at 200 V for 40 min until the loading dye front reached the bottom of the gel. Gels were fixed in 50% MeOH, 7% acetic acid for 1 h with shaking, and then stained in ∼50 mL of Coomassie stain overnight. Gels were destained in 1% acetic acid for 30 min, and then rinsed with $dH_2O$ and scanned.

*Two-Dimensional (2D) Isoelectric focusing.* A rehydration solution containing 100 $\mu$g of protein was prepared to a total volume of 125 $\mu$L (20 $\mu$L of protein [concentration 5 $\mu$g/$\mu$L], 100 $\mu$L of rehydration buffer [7 M urea, 2 M thiourea, 2% CHAPS, 0.5% (v/v) IPG buffer, 0.0002% bromophenol blue], 4 $\mu$L of fresh 1 M dithiothreitol (DTT), 1.25 $\mu$L of carrier ampholytes [pH 3−11]). The sample mixture was loaded onto 7 cm IPG strip (3−11 nonlinear gradient (NL) small strips), placed in a carrier coffin, and 0.8 mL of dry strip cover fluid was applied to minimize evaporation and urea crystallization. IEF was run for a total of ∼16 000 V h at 20 °C on the IPGphor with the following program settings: 30 V for 14 h (rehydration), 100 V for 2 h (Step-n-hold), 500 V for 1.5 h (Step-n-hold), 1000 V for 1.5 h (Step-n-hold), 5000 V for 1 h (gradient), 5000 V for 2 h (Step-n-hold), and 50 V (hold). It was ensured that the voltage reached at least 5000 V to achieve a standard protein gradient. Strips were removed from the coffin and either used immediately for 2D SDS-PAGE gel analysis or stored at −20 °C until required.

*Two-Dimensional SDS-PAGE.* IPG strips were saturated with MES running buffer [50 mM 2-morpholinoethanesulfonate (MES), 50 mM Tris base, 0.01% SDS w/v, 1 mM EDTA], 6 M urea, 30% glycerol, 2% SDS w/v, and 0.001% bromophenol blue by first equilibrating in MES buffer plus 50 mg/mL (DTT) for 15 min with shaking to reduce disulfide bonds, and then soaking strips in MES buffer plus 125 mg/mL iodoacetamide (IAA) for 15 min with shaking to alkylate the free cysteine residues. IPG strips were fitted into Bis/Tris small format precast gels (15%) (Invitrogen, Carlsbad, CA). The loading well was then sealed with ∼0.8 mL agarose sealing solution (0.5% agarose, 0.001% bromophenol blue). The gel was run in 1X MES running buffer at low voltage (25−50 V) for 30 min, and then the voltage was increased to 125 V and run until the loading dye front disappeared off the bottom of the gel (approximately 1.5−2 h). Gels were fixed in 50% MeOH, 7% acetic acid for 1 h with shaking, and then transferred to a Sypro Ruby silver stain solution overnight with shaking and destained for 30 min (10% MeOH, 7% acetic acid) prior to scanning using a Typhoon 9400 (GE Healthcare). The gel was then stained in Coomassie overnight with shaking to visualize spots for excision from gel and subsequent mass spectrometric analysis. Coomassie stained gels were destained in 1% acetic acid and scanned with Odyssey at 700 nm.

**Mass Fingerprinting (LC−MS/MS).** *Reduction/Alkylation of Gel Pieces.* Protein spots were manually excised from gels and destained in 50 mM ammonium bicarbonate (ABC)/50% acetonitrile (ACN), 2 × 200 $\mu$L, with shaking for 3−4 h or overnight. For 1D gel pieces, buffer/destain was removed from gel pieces with pipetting and the sample was soaked in 40 $\mu$L of 10 mM DTT to reduce cysteine residues. Gel pieces were incubated at 60 °C for 30 min, DTT solution was removed, and 40 $\mu$L of 55 mM fresh IAA was added. Samples were then incubated at room temperature for 30 min in the dark. IAA was discarded and (for 1D

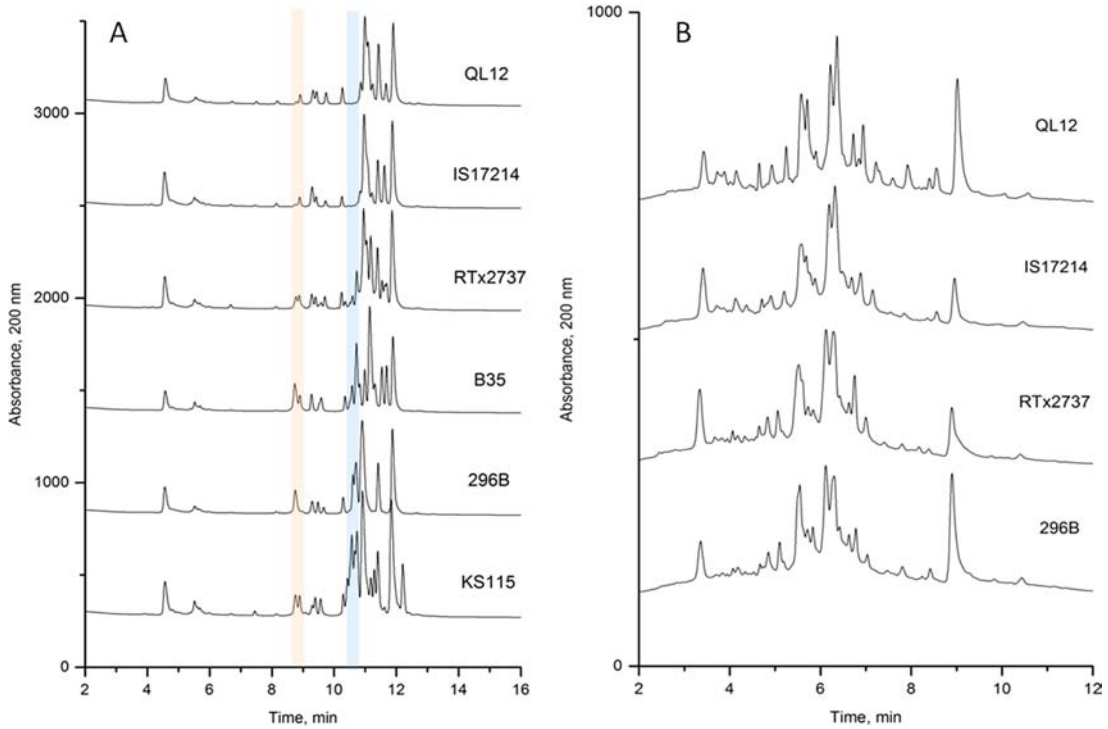


**Figure 1.** RP-HPLC profiles for the (A) alcohol-soluble (prolamin) fraction and (B) water/salt-soluble (albumin/globulin) fraction across $\beta$-kafirin null allelic variants QL12, 1517214, and RTx2737, and lines with normal $\beta$-kafirin content, including B35, 296B, and KS115. In the prolamin fraction $\beta$-kafirin null lines showed a reduction in the size of a peak eluted at 9 min (outlined in orange). Peak distribution profiles at 10−11 min elution times were similar across lines with normal $\beta$-kafirin content, while a significant proportion of protein in this area of the chromatogram was missing in the $\beta$-kafirin null mutants (outlined in blue).

and 2D gel pieces), 100 $\mu$L of 50 mM ammonium bicarbonate (ABC) was added, with vortexing/shaking for 1−2 min, removal of solution, and repeated washing. Gel pieces were then dehydrated in 50 $\mu$L of 100% ACN for 5 min, with vortexing.

*Enzymatic Digestion and Peptide Extraction.* Gel pieces were rehydrated in a 50 mM ABC solution containing 8 $\mu$L of trypsin (10 ng/$\mu$L) (sequencing-grade modified trypsin, Promega, Madison, WI) for 10−20 min at 4 °C. An additional volume (6−16 $\mu$L) of 50 mM ABC buffer was then added, depending on the size of the gel piece, and samples were incubated overnight at 37 °C. Then, 50 $\mu$L of 50% ACN/0.1% TFA was added to of gel pieces and samples were sonicated in a water bath for 10 min, and centrifuged briefly, and supernatant was transferred to a new tube. An additional 50 $\mu$L aliquot of 50% ACN/0.1% TFA was added, sonication was repeated, and supernatant was combined with the first extract. Supernatant was lyophilized in a SpeedVac at 45 °C, and peptides were resuspended in 10 $\mu$L of 5% ACN/0.1% TFA. A Ziptip cleanup was carried out according to the manufacturer's instructions (Millipore) for removal of acrylamide contamination prior to MS analysis.

*LC−MS/MS.* Digested peptides were run on LC−MS/MS using an ESI-QTOF instrument. MS parameters were similar to those in Kappler and Nouwens,[18] with the following modifications: Samples were desalted for 5 min on an Agilent C18 trap (0.3 × 5 mm, 5 $\mu$m), followed by separation on a Vydac Everest C18 column (300 A, 5 $\mu$m, 150 mm × 150 $\mu$m) at a flow rate of 1 $\mu$L/min, using a gradient of 10−60% buffer B over 30 min, where buffer A = 1% ACN/0.1% formic acid and buffer B = 80% ACN/0.1% formic acid. Eluted peptides were directly analyzed on a TripleTof 5600 mass spectrometer (ABSciex) using a Nanospray III interface. Gas and voltage were set as required. MS TOF scan across $m/z$ 350−1800 was performed for 0.5 s, followed by data-dependent acquisition of 20 peptides with intensity above 100 counts across $m/z$ 40−1800 (0.05 s per spectrum) with rolling collision energy. MS data were converted to Mascot generic format and submitted to Mascot.

*MS Data Analysis.* The automated Mascot search engine (Matrix Science, London, U.K.) was used to identify best matched protein sequences to the peptides detected by MS. Trypsin was specified as the proteolytic enzyme, and carbamidomethyl (C) of cysteine and oxidation (M) of methionine residues were taken into account. Charged states of 2+, 3+, and 4+ were considered for parent ions. Using a Ludwig-based search of plant species, a profile of best matched protein(s) was generated employing an algorithm to rank the proteins identified based on their peptide mass fingerprints. Individual ion scores were calculated as $-10 \times 10g(P)$, where $P$ is the probability that the observed match is a random event. Peptides identified with an ion score of >40 were considered to indicate identity or extensive similarity. Each of the peptide identifications was manually inspected and verified to ensure that the spectra were composed of a wide series of intense fragments, which could be designated as major fragments (b or y) of the proposed peptide. Each protein match also generated a protein score in the MS/MS search report, which is the sum of the highest ions scores for each distinct sequence. The exponentially Modified Protein Abundance Index (emPAI) provided an approximate, relative quantification of the proteins present in the sample. Functionally characterized homologues to putative uncharacterized sorghum proteins identified with MS were identified through BLAST searches based on FASTA sequences derived through queries to the Uniprot database.

**Statistical Analysis.** Absorbance values from RP-HPLC of alcohol-soluble proteins were interpolated by a spline method, and absorbance area values were calculated to 0.01 min intervals using MATLAB (release 2012a, The MathWorks, Natick, MA). Linear correlation coefficients were calculated between an individual absorbance area and digestibility and shown as a continuous spectrum over RP-HPLC retention time.

## RESULTS AND DISCUSSION

**RP-HPLC Profiling of Seed Proteins.** Profiling of alcohol-soluble prolamin (Figure 1A and Supporting Information, Figure S1) and water/salt-soluble albumin/globulin (A/G) (Figure 1B


dx.doi.org/10.1021/jf5022847 | J. Agric. Food Chem. 2014, 62, 9819−9831

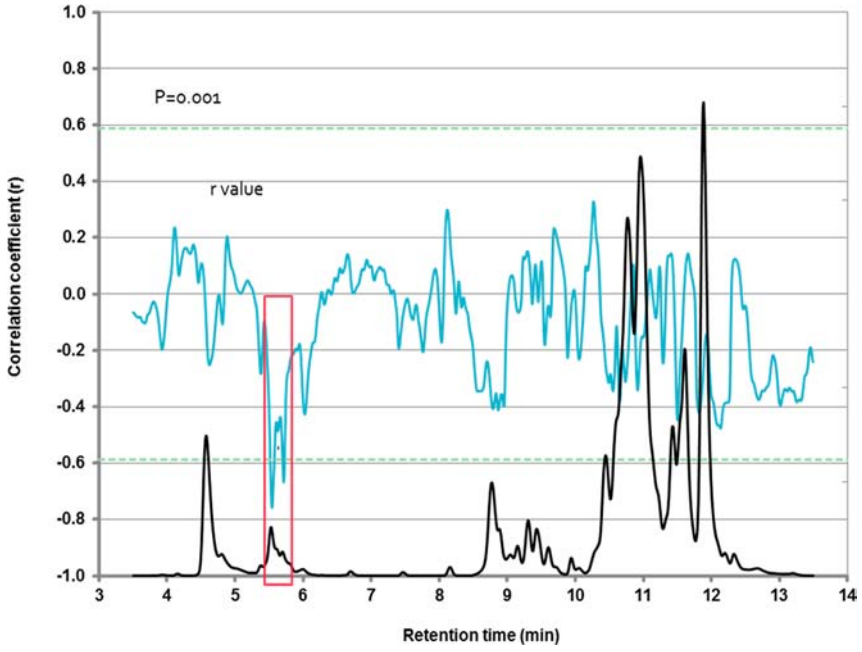


**Figure 2.** RP-HPLC analysis showing a significant negative correlation between protein digestibility (%) and an alcohol-soluble kafirin protein peak eluting at 5.5−6 min on the chromatogram (outlined in red). Analysis was carried out across 26 diverse sorghum lines (listed in Table 1), including the genotypes evaluated for ethanol conversion by Cremer et al.[20]

**Table 1. Total Protein, % Protein Digestibility, and Total Starch Measurements for Sorghum Grain Lines with Diverse Kafirin Allelic Backgrounds**

| | | | | uncooked | | cooked | | | |
|---|---|---|---|---|---|---|---|---|---|
| genotype/line | $\beta$ | $\gamma$ | $\delta$ | total protein (%) | digestibility (%) | total protein (%) | digestibility (%) | starch (%) | moisture |
| RTx7000/FF-RTx7000 | 1 | 2 | 1 | 12.5 | 51.5 | 14.3 | 21.2 | 70.1 | 8.1 |
| IS22457C | 2 | 1 | 1 | 11.9 | 60.2 | 13.4 | 24.0 | 54.9 | 7.3 |
| IS8525 | 1 | 4 | 2 | 13.9 | 18.1 | 15.1 | 7.6 | 62.2 | 6.6 |
| QL12 | 3 | 1 | 2 | 14.6 | 58.4 | 15.5 | 25.3 | 56.3 | 7.9 |
| IS12572C/FF-6214E | 1 | 1 | 2 | 10.6 | 30.8 | 14.0 | 26.0 | 62.9 | 10.4 |
| Ai4 | 1 | 3 | 2 | 12.7 | 45.1 | 13.8 | 21.8 | 62.5 | 10.5 |
| BTx3197 | 1 | 2 | 2 | 12.8 | 40.5 | 15.4 | 25.4 | 66.5 | 10.3 |
| Hegari/Early Hegari | 4 | 1 | 1 | 11.8 | 54.4 | 15.2 | 29.0 | 71.0 | 7.5 |
| ISCV745 | 1 | 1 | 1 | 10.3 | 60.2 | 12.1 | 32.0 | 70.4 | 10.7 |
| B923296 | 1 | 1 | 2 | 11.9 | 61.2 | 13.3 | 22.3 | 64.0 | 7.6 |
| ISCV400 | 4 | 1 | 1 | 11.9 | 56.9 | 13.6 | 29.6 | 68.1 | 7.6 |
| QL39 | 2 | 1 | 1 | 11.0 | 40.1 | 13.3 | 17.0 | 67.3 | 9.5 |
| Karper 669 | 1 | 1 | 1 | 12.6 | 55.3 | 14.0 | 25.6 | 67.3 | 9.7 |
| QL41 | 1 | 2 | 2 | 10.7 | 51.6 | 12.5 | 22.7 | 68.0 | 9.7 |
| R931945-2-2 | 1 | 2 | 1 | 11.6 | 62.3 | 12.9 | 17.3 | 66.8 | 6.1 |
| R89562/R890562-1-1 | 1 | 1 | 1 | 13.2 | 46.9 | 14.9 | 18.7 | 67.3 | 6.6 |
| M35-1/FF-BM351 | 1 | 3 | 2 | 12.9 | 48.7 | 14.3 | 15.8 | 67.1 | 9.2 |
| KS115 | 1 | 4 | 2 | 16.5 | 40.8 | 18.1 | 16.8 | 64.1 | 9.6 |
| IS17214 | 3 | 1 | 2 | 11.4 | 59.2 | 13.5 | 33.8 | 61.9 | 10.8 |
| SC1270-6-8/FF-SC1270-6-8 | 2 | 1 | 1 | 12.0 | 59.0 | 14.0 | 17.3 | 62.5 | 9.6 |
| LR91918 | 2 | 3 | 2 | 10.3 | 56.0 | 12.6 | 26.4 | 63.1 | 9.4 |
| IS12611C-F-F_ SC11114E | 2 | 1 | 1 | 11.3 | 54.0 | 13.8 | 22.5 | 64.7 | 8.1 |
| R9733 | 4 | 2 | 1 | 14.6 | 59.6 | 16.8 | 14.7 | 66.8 | 5.8 |
| BOK11/FF-BPK11 | 1 | 2 | 2 | 11.7 | 65.0 | 13.5 | 15.9 | 60.5 | 7.2 |
| BTx623/FF-BTx623 | 2 | 2 | 1 | 12.9 | 50.8 | 15.3 | 15.3 | 64.9 | 9.9 |
| B35/FF-B35 | 1 | 2 | 1 | 11.7 | 51.4 | 13.4 | 19.2 | 63.0 | 8.8 |
| 296B/FF-296B | 1 | 3 | 1 | 10.0 | 68.2 | 12.8 | 28.6 | 58.2 | 10.8 |
| RTx2737/FF-BTx2737 | 3 | 1 | 1 | 13.3 | 58.1 | 15.2 | 19.0 | 59.3 | 7.9 |

and Supporting Information, Figure S2) protein fractions across 28 sorghum lines using RP-HPLC revealed a range of diversity, particularly in the alcohol-soluble kafirin-containing fraction. Variation observed across wild-type and mutant lines could


dx.doi.org/10.1021/jf5022847 | J. Agric. Food Chem. 2014, 62, 9819−9831

contribute to phenotypic differences, such as increased flour viscosity and fermentation efficiency.[19,20] Among the β-kafirin null lines QL12, IS17214, and RTx2737, a high degree of similarity was observed in the alcohol-soluble peak distributions compared to lines with functional β-kafirin alleles. An approximately 50% reduction in the height of a peak eluting at 9 min was observed in β-kafirin null lines compared to wild type (Figure 1A, highlighted in orange), indicating a likely elution profile for β-kafirin (under the analysis conditions described here) and presenting a potential marker for the protein. Alternately, the β-kafirin peak could have been masked by a series of larger peaks eluting from the column at 10−11 min, which were absent in null lines (Figure 1A, highlighted in blue). Further work to positively identify the β-kafirin in RP-HPLC separations under these exact conditions is needed. RP-HPLC analysis of the water/salt-soluble fraction showed less similarity among peak profiles for the β-kafirin null mutants relative to other lines. However, substantial quantitative differences in peak heights were observed among the genotypes and there was a high level of variability across the sample set in a peak eluting at 9 min, which was unrelated to fluctuations in total sample protein concentration.

Interestingly, a statistically significant negative correlation was identified between a set of protein peaks eluted in the kafirin fraction and protein digestibility across sorghum grain lines, providing evidence for links between seed protein composition and end-use traits (Figure 2). Further research is needed to identify the protein(s) present in this peak; however, given the sequential extraction procedure utilized in this work, it is likely that this is a member of the kafirin family.

**Lab-on-a-Chip (LOC) Analysis of Seed Proteins.** LOC analysis, employing microfluidic chip−capillary electrophoresis, generated size-separated protein profiles for alcohol-soluble (prolamin) (Figure 3) and water/salt-soluble (A/G) fractions (Supporting Information, Figure S3). The prolamin fraction showed a large set of peaks present in the 22−26 kDa size range, representing the previously characterized α- and γ-kafirins. Small peaks were also visible at 11 and 19 kDa, with the 19 kDa peak representing the β-kafirins and the 11 kDa peak potentially representing the δ-kafirins. The β-kafirin peak was diminished in size in β-kafirin nulls, but, interestingly, a peak or set of peaks was visible at 19−20 kDa across all lines. This indicates that an additional protein of a similar size to β-kafirin may be present in the peak. This protein could represent a different protein, such as peptidyl-prolyl cis/trans isomerase (PPIase), identified in the same band/spot as β-kafirin through SDS-PAGE and LC−MS/MS, as outlined in the section SDS-PAGE and LC−MS/MS Protein Profiling. Chip profiles indicate that several cultivars in addition to the β-kafirin null mutants contain relatively low levels of β-kafirin, including 296B, a highly digestible line.[20] LOC analysis also revealed the presence of a small peak visible at 46 kDa in alcohol-soluble samples, which could represent a high molecular weight kafirin or kafirin dimer. In subsequent analysis, a protein spot extracted from the corresponding size range on 2D gels was identified through LC−MS/MS as a ∼36 kDa γ-prolamin homologue (Supporting Information, Figure S4 and Supplementary Table 1), thus providing sequence information for this kafirin entity at the protein level. As observed with RP-HPLC, the LOC profiling of the water/salt-soluble fraction shows that QL12 contains a relatively high content and diversity of A/G's compared to other genotypes (Supporting Information, Figure S3). High-lysine sorghum varieties, such as P721, exhibit an elevated A/G content, with increased nutritional value.[21] This indicates that QL12, among other lines, may contain increased levels of lysine and other essential amino acids due to a high A/G content.

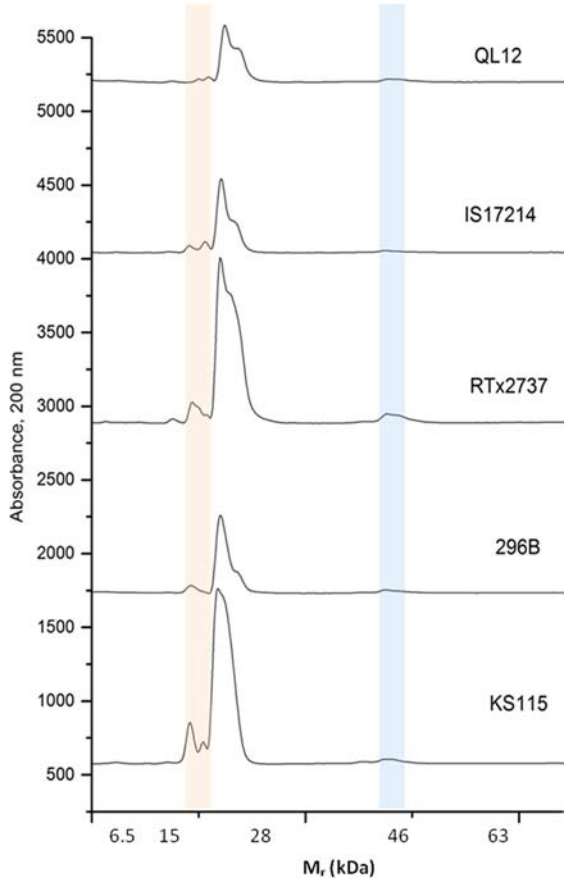


**Figure 3.** Alcohol-soluble proteins visualized on lab on a chip (LOC) across β-kafirin null lines QL12, 1517214, and RTx2737, and normal β-kafirin lines 296B and M35. A 19 kDa β-kafirin peak (highlighted in orange) precedes a set of large 22−25 kDa α- and γ-kafirin peaks, and a HMW prolamin is visible across the genotypes as a small peak at ∼50 kDa (highlighted in blue).

**SDS-PAGE and LC−MS/MS Protein Profiling.** Profiling of water/salt-soluble (A/G), alcohol-soluble (prolamin), and alkali-soluble (glutelin) protein fractions across the β-kafirin null mutant QL12 and wild-type line 296B using SDS-PAGE gel separation methods, coupled with mass spectrometry (LC−MS/MS) (Figure 4 and Supporting Information, Figure S4 and Supplementary Table 1), identified a range of proteins involved in storage protein biochemistry and starch metabolism. One-dimensional gel separation of each of the protein fractions by size (Figure 4) showed that the A/G fraction contains a highly concentrated, complex array of proteins present across a broad size range, similar to profiles generated in previous studies.[22] The prolamin fraction was less complex and more concentrated within the 23−26 kDa size range, which contains the more abundant α-kafirin storage proteins. The alkali-soluble glutelin fraction exhibited some similarities to the prolamin fraction, likely due to incomplete extraction of the prolamin fraction, but contained a wider diversity of protein bands visible across a greater size range, which was also verified on 2D gels, and has been reported in previous studies.[23,24] It is hypothesized that the glutelin proteins are more diverse because they both play a role in connecting the protein:starch matrix and provide a source of


dx.doi.org/10.1021/jf5022847 | J. Agric. Food Chem. 2014, 62, 9819−9831

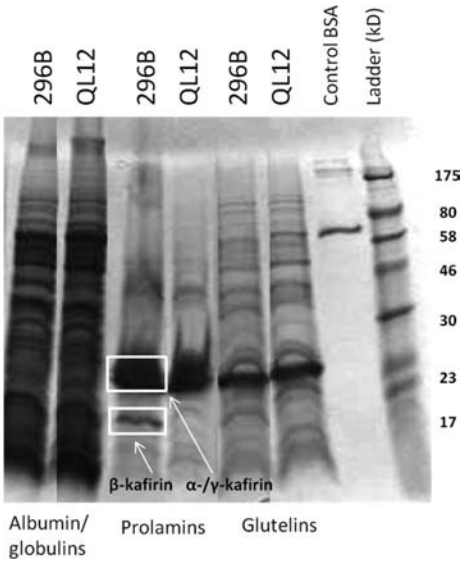


**Figure 4.** One-dimensional SDS-PAGE separation of water/salt-soluble (albumin/globulins), alcohol-soluble (prolamins), and alkali-soluble (glutelins) from normal $\beta$-kafirin allelic variant 296B, and $\beta$-kafirin null QL12. Excised protein bands (outlined in white) were digested with trypsin and analyzed using LC−MS/MS (results listed in Supporting Information, Supplementary Table 1). Ladder: P7709V ColorPlus Prestained Protein Marker, Broad Range (7−175 kDa) Mw ladder.

hydrolytic enzymes for the breakdown of starch and protein during germination.[25]

**Characterization of Kafirin Subclasses and the $\beta$-Kafirin Null Mutation.** Each kafirin subclass in the alcohol-soluble fraction was isolated using SDS-PAGE and identified through LC−MS/MS. $\alpha$- and $\gamma$-kafirins were visualized within the 22−25 kDa size range on the 1D SDS-PAGE gel (Figure 4, outlined in white). Using 2D SDS-PAGE separation of proteins by both size and charge, the $\delta$-kafirin protein was isolated in the prolamin fraction for genotype 296B (spot 11) (Supporting Information, Figure S4 and Supplementary Table 1). Matches to $\alpha$- and $\gamma$-kafirins were also generated on 2D gels in prolamin gel spots 8 and 11 for genotype QL12, and with spot 9 returning $\alpha$-kafirin as a top hit. Differential expression of the $\beta$-kafirin protein was detected in the alcohol-soluble fraction across mutant and wild-type germplasm. This provided a positive control for the MS technique and allowed for further characterization of the mutant at the protein level. One-dimensional separation of the prolamin fraction revealed altered expression of $\beta$-kafirin in a 19 kDa protein band, present in 296B and absent in QL12 (Figure 4, outlined in white), as predicted based on previous molecular characterization.[15] On 2D gels differential expression of $\beta$-kafirin was identified in 296B prolamin spot 11 and glutelin spot 4 (Supporting Information, Figure S4 and Supplementary Table 1). Identification of $\beta$-kafirin in the glutelin fraction (296B spot 4) may reflect the incomplete sequential extraction of alcohol-soluble proteins in the previous step.[26] $\beta$-Kafirin was completely absent in QL12, with the exception of a weak hit in the 2D prolamin spot 1, which had a low Mascot score achieved across two peptide matches and was discarded due to poor-quality spectral data. This match may represent a truncated form of the protein, as it was identified in a smaller size range on the gel. Although protein expression was generally similar across the genotypes within the range of spots analyzed on 2D gels, differential expression of a low molecular weight thioredoxin (Trx) enzyme was identified in the water/salt-soluble fraction, where spot 4 was present in 296B and absent in QL12. This was the only Trx identified across the protein fractions analyzed in the study, with the finding replicated in triplicate (Figure 5 and Supporting Information , Supplementary Table 1). Trx catalyzed the conversion of seed proteins from the oxidized to the reduced state during germination, with significant impacts on protein digestibility and grain nutrition.

**Sorghum Homologue to 50 kDa $\gamma$-Prolamin.** High molecular weight (HMW) $\gamma$-prolamins (~50 kDa) have been identified and characterized across a range of plant species,

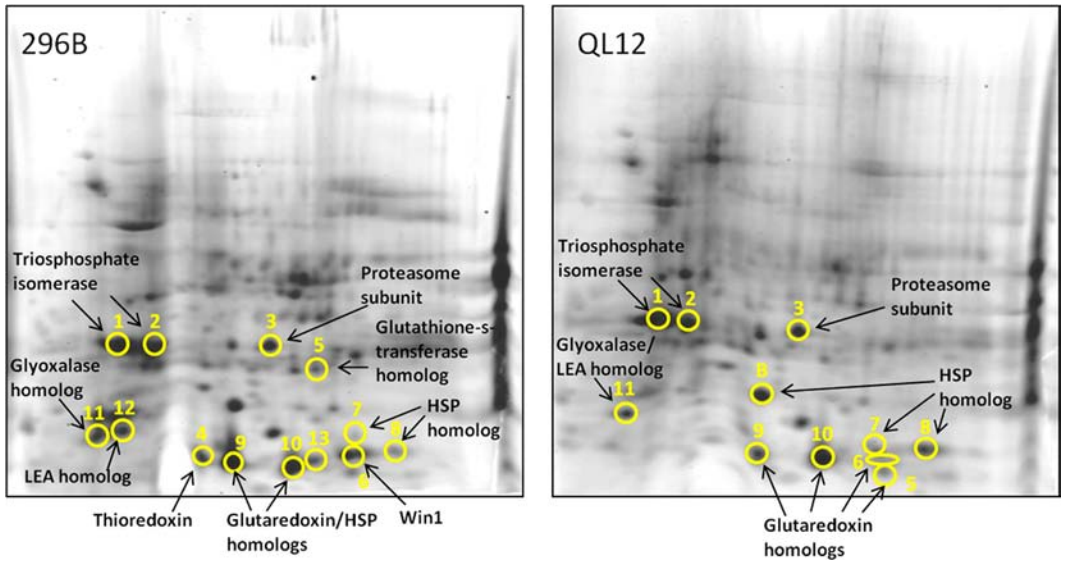


**Figure 5.** Two-dimensional SDS-PAGE analysis of the water/salt-soluble protein fraction in $\beta$-kafirin null allelic variant compared with wild-type 296B. Protein samples were loaded onto 7 cm IPG strips (3−11 NL) and run on IPGphor machine for isoelectric focusing. SDS-PAGE gels (4−12% Bis/Tris small format precast) were utilized for separation of proteins by size (Mw). Protein spots (circled in yellow) were excised across a range of size and pI, digested with trypsin, and identified with LC−MS/MS. Spot 4 was identified as a differentially expressed thioredoxin, present in 296B and absent in QL12.


dx.doi.org/10.1021/jf5022847 | J. Agric. Food Chem. 2014, 62, 9819−9831

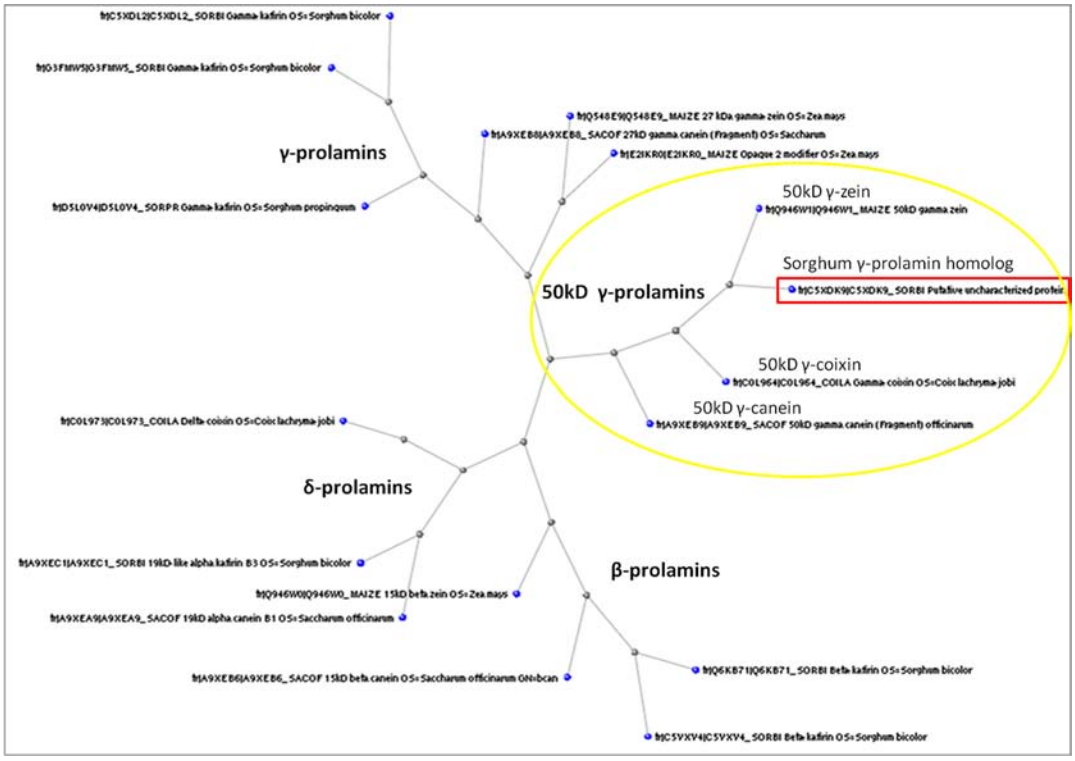


**Figure 6.** Phylogenetic neighbor joining tree view of the alignment of protein sequences representing prolamin subclasses across grass species using the Grishin protein method. Uncharacterized sorghum γ-prolamin homologue groups with 50 kDa γ-zein and γ-canein of maize and sugarcane, and groups away from the LMW γ-prolamins.

including maize and wheat.[27,28] Previous studies on sorghum have identified a protein band at ∼45 kDa in the alcohol-soluble fraction using 1D SDS-PAGE. However, this protein has not yet been characterized at the genetic level.[15] The HMW protein band was previously reported as a kafirin dimer because it diminishes in intensity upon treatment with increasing concentrations of reducing agent, indicating that it can be broken down into smaller peptides.[8,29] However, because the original 45 kDa band is still intact on reduced gels, it has also been suggested that the protein may be linked by bonds that are not broken by reducing agents.[30] In the present study, this HMW protein was visible in reduced alcohol-soluble protein samples from both genotypes QL12 and 296B, on 1D and 2D gels. LC−MS/MS data indicate that this protein represents a homologue to HMW γ-prolamin identified in closely related species (Supporting Information, Figure S4 and Supplementary Table 1). Across both genotypes, 2D prolamin spot 4 returned a match for a putative uncharacterized sorghum protein (accession number C5XDK9), exhibiting homology to 50 kDa γ-zein, γ-canein, and γ-coixin (Figure 6). The sorghum γ-prolamin homologue is larger than any previously characterized kafirin, with a calculated Mw 36 615 Da. LOC analysis of the prolamin fraction revealed the presence of two small peaks at ∼44 and 46 kDa across the majority of the sample collection (Figure 3, highlighted in blue), which may correspond to two genetic variants of the HMW γ-prolamin.[8,27] In a previous study using LOC, similar peak profiles were also observed for the HMW prolamin peak in reduced alcohol-soluble protein samples extracted from three grain genotypes (QL12, QL41, and 296B) from the kafirin allelic variant sample set, which had been harvested in a previous growing season.[31] Across our data set, quantitative peak area values were attained through LOC for the peaks in the 44−46 kDa size range and these data were aligned with readings for grain quality parameters. The general structure and distribution of prolamins in the protein bodies has been shown to be uniform across maize and sorghum. In maize, 50 kDa γ-zeins localize to the periphery of the protein bodies, similar to other γ-zeins.[27] Immunocytochemistry shows that γ-kafirins also localize to the periphery of protein bodies, and may prevent proteolysis of internally positioned α-kafirins.[32] Sorghum lines with increased digestibility exhibit a change in the protein body structure from spherical to invaginated, with the γ-kafirins located from the periphery to the folds of the structure, resulting in an increased exposure of the α-kafirins to proteolytic breakdown.[33] In maize, a clear physical distribution of zein classes is observed within the seed. Protein bodies in the subaleurone layer are smaller and contain mainly β- and γ-zeins, while those encapsulating starch in the inner endosperm are larger and contain continuous central regions of α-zeins with β- and γ-zeins located on the periphery.[34] Construction of mutant γ-zein proteins has pinpointed the proline-rich N-terminal domain as being critical in wild-type protein body development.[35] Furthermore, deletion of a cysteine-rich γ-zein domain results in abnormally structured protein bodies. The different kafirin classes exhibit variable solubilities according to their degree of polymerization and cross-linking.[29] Interactions between β- and γ-kafirins on the periphery of protein bodies may limit enzyme accessibility to α-kafirin, impeding digestion of protein and starch encased in the matrix. This study presents evidence for the seed-specific expression of a high molecular weight γ-prolamin homologue in sorghum. Characterization of this protein in sorghum could enhance efforts to further distinguish the roles of the different classes of kafirins in maintaining endosperm connectivity and access to starch.

**Identification of Proteins with Potential Impacts on Grain Quality.** Profiling of water/salt-, alcohol-, and alkali-soluble proteins across the sample population of kafirin allelic

variants using mass spectrometry identified proteins with potential various impacts on the structure of the protein−starch matrix, such as enzymes functioning in protein cross-linking and the mobilization of starch during germination[36,37] (Table 2, Figure 5−7, and Supporting Information, Figure S4 and Supplementary Table 1). Identification and localization of these proteins in the mature grain indicates they may have an impact on endosperm development and/or germination. Deciphering the precise activities of these proteins in sorghum will involve additional analysis of the transcriptome and proteome throughout grain development.

*Thioredoxins (Trx) and Glutaredoxins (Grx).* Thioredoxins are small proteins containing a site with a redox-active disulfide, which functions in the reversible oxidation of protein SH groups to a disulfide bridge[38] (Table 2). Differential expression of a sorghum Trx protein, C5XB72, homologous to maize Trx B6SX54, was observed in the A/G fraction, with 2D protein spot 4 present in 296B and absent in QL12 (Figure 5). Matches to sorghum Trx had a high emPAI protein quantification score, pI 5.79, and Mw 13 061 Da. Trx labeling studies have shown in vitro and in vivo that the enzyme catalyzes the reduction of seed proteins during germination.[39] Therefore, Trx has been linked to enhanced grain digestibility in wheat and sorghum.[40,41] Alternate expression of Trx in this study may be associated with the *β*-kafirin null mutation and could have potential downstream impacts on digestibility, in addition to effects of the mutation.

The sorghum homologue to a maize glutaredoxin Grx_C2.2−glutaredoxin subgroup 1 was identified in the A/G fraction in 296B spots 9 and 10, and in QL12 spots 5 and 6, which localized to the same size range (Mw ∼13 kDa) (Figure 5). Grx, including the maize Grx_C2.2 identified in this study, catalyze the enzymatic reaction where proteins with reduced sulfide groups are converted to those with oxidized disulfide bonds (Table 2). Grx have been implicated in the oxidative stress response through regeneration of enzymes involved in peroxide and methionine sulfoxide reduction.[42] These proteins therefore have dual roles in protein aggregation and stress responses, creating opportunities for the development of streamlined grain improvement strategies affecting multiple traits.

*Protein Disulfide Isomerases (PDIs).* PDIs function as molecular chaperones in disulfide-mediated protein folding. They contain two Trx domains with a redox site.[43] Matches to HMW PDI from maize (C0PLF0 and A5A5E7) were generated in glutelin spot 2 across both genotypes (Supporting Information, Figure S5 and Supplementary Table 2). These proteins appear to migrate to the same location on A/G and prolamin gels, but the spots were not analyzed in this fraction using LC−MS/MS. However, it is possible that they share the same identity as the PDIs identified in the glutelin fraction because their distribution on the gel is similar. Again, the presence of these spots across multiple fractions may be a result of incomplete sequential extraction of the proteins.

Previous studies indicate that PDI mutations can result in irregular starch granule formation and chalky grain phenotypes.[44] The rice mutant *esp2* lacks protein disulfide isomerase-like (PDIL) 1:1, but shows enhanced expression of the thiol disulfide oxidoreductase OsEro1.[45] The grain exhibits altered seed storage protein compartmentalization through inhibition of disulfide bond formation. It has been proposed that the formation of native disulfide bonds in proglutelins also depends on an electron transfer pathway involving the OsEro1 and the PDI-like OsPDIL.[46] In the *floury2* mutant, PDIL is up-regulated, where a mutation in a signaling peptide results in the abnormal

**Table 2. Protein Candidates Identified in Sorghum Grain with Reported Effects on Protein−Starch Matrix Structure, Grain Quality, and Stress Responses**

| accession no. | protein | 296B spot | QL12 spot | protein fraction | homologues | function |
|---|---|---|---|---|---|---|
| C5XB72/C5YGL1 (sorghum) | thioredoxin | 4 | absent | A/G | B6SX54_maize | converts seed proteins from the oxidized to the reduced state during germination |
| C5YBX1 (sorghum) | glutaredoxin Grx_C2.2−glutaredoxin subgroup 1 | 9 and 10 | 5 and 6 | A/G | B6THA1_maize | converts proteins with reduced sulfide groups to those with oxidized disulfide bonds |
| F2DDK1 (barley) | peroxiredoxin | 5 | 5 | prolamin | HB6T2Y1_maize and PR2E1_ORYSJ (rice) | interacts with glutaredoxins, thioredoxins, and cyclophilin as both reductants and non-dithio−disulfide exchange proteins |
| C5XT06, B3GQV9, and C5Z9C6 (sorghum) | peptidyl-prolyl cis/trans isomerase (PPIase) | 9, 10, and 11 | 9 and 10 | prolamin/glutelin | maize B4FZZ2 and B4FY3T, wheat AZLM55, sugarcane C7E3V7 | facilitates protein folding through slow isomerization of peptide bonds in oligopeptides and through the amino acid proline in cellular proteins |
| A5A5E7 (maize) | protein disulfide isomerase (PDI) | 2 | 2 | glutelin | maize C0PLF0 and A5A5E7 | promotes the correct disulfide pairing in proteins |
| P81368 (sorghum) | α-amylase inhibitor | 1, 2, 8, and 11 | 1 and 2 | prolamin | IAA5_SORI (sorghum) | slows the conversion of starch to sugars (and ethanol) |


dx.doi.org/10.1021/jf5022847 | J. Agric. Food Chem. 2014, 62, 9819−9831

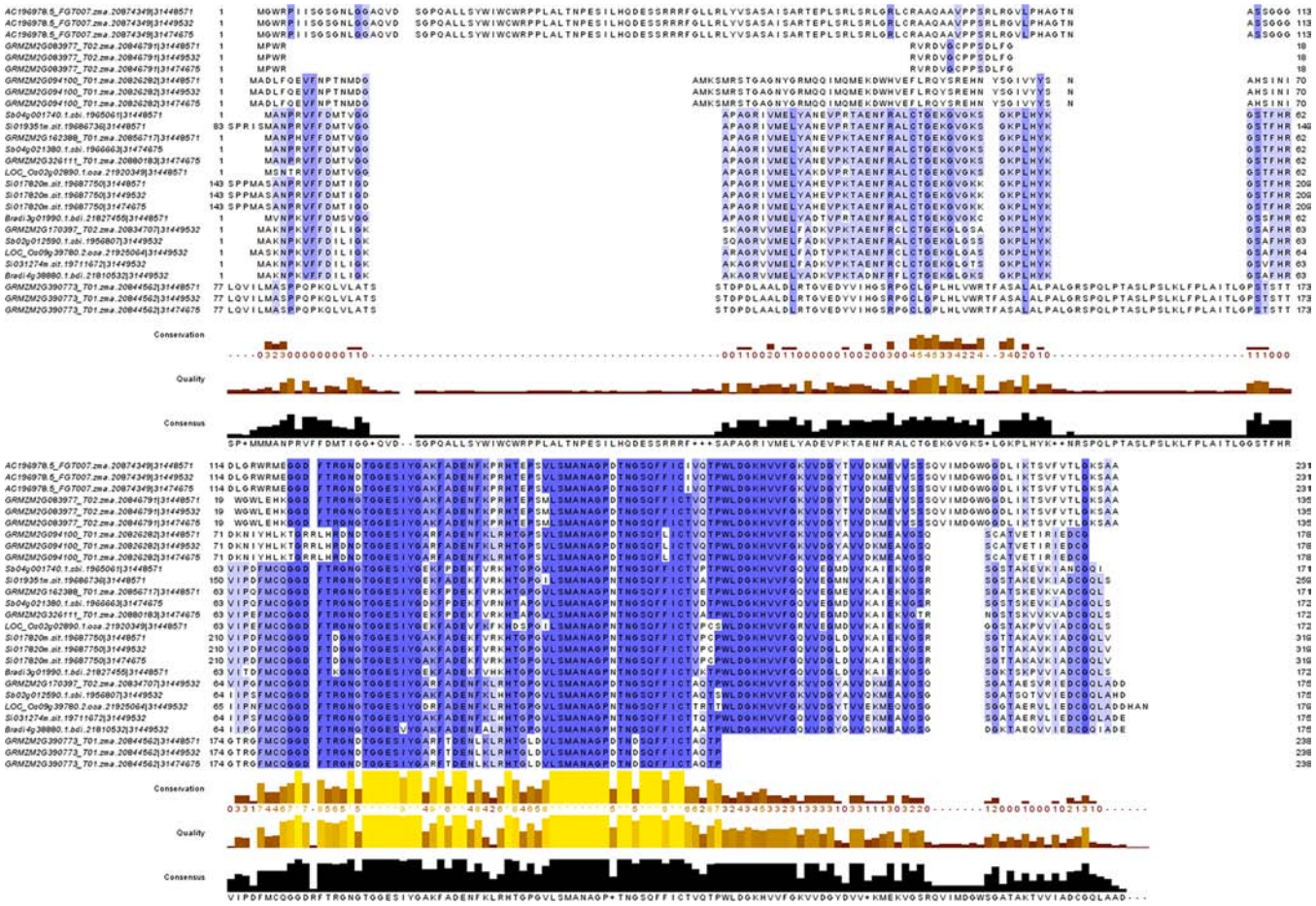

**Figure 7.** ClustalW alignment of peptidyl-prolyl cis/trans isomerase (PPIase) peptide sequences across major grass species, illustrating a high level of sequence homology. PPIases identified in sorghum grain prolamin and glutelin protein fractions (Supporting Information, Figure S4 and Supplementary Table 1) are included. Dark purple indicates exact homology; light purple indicates highly conserved homology.

processing and accumulation of small precursor $\alpha$-zeins and high levels of luminal binding protein (BiP) in irregularly shaped protein bodies.[47] Mutations in sorghum protein isomerases, such as PDI, may have a similar effect on protein body formation.

*Peptidyl-prolyl cis/trans Isomerases (PPIases).* PPIases catalyze protein folding through isomerization of peptide bonds in oligopeptides and on proline residues in cellular proteins.[43,48,49] PPIases were identified in the 19 kDa band colocalized with $\beta$-kafirin on the 296B 1D prolamin gel, as well as in the 26 kDa band, colocalized with $\alpha$-kafirin (Figure 4). On 2D gels, PPIases were detected in the 296B prolamin fraction gel spots 9, 10 and 11, and in QL12 gel spots 9 and 10, as well as in the QL12 glutelin fraction spot 4 (Supporting Information, Figure S4 and Supplementary Table 1). Sorghum PPIases identified in the study (accession numbers C5XT06, C5Z9C6, and B3GQV9), consistently localized to the same size region (~18 kDa) on 1D and 2D PAGE gels, and within the same pI range pH 8–9. PPIases colocalized with $\beta$- and $\delta$-kafirins in the 296B 2D prolamin gel spot 11 and with $\alpha$-kafirin in QL12 spot, as well as in the prolamin fraction on the 1D SDS-PAGE gel, indicating that they are hydrophobic enzymes, which may interact with the kafirins.

The PPIase family is encoded by multiple genes, exhibiting some redundancy in plants.[50] An alignment of the sorghum PPIases identified in this study, with orthologues from closely related species, reveals a high level of sequence homology at the protein level (Figure 7). The sorghum PPIases exhibited close homology to their counterparts in *Zea mays* (B4FZZ2 and B4FY3T), *Triticum aestivum* (AZLM55), *Saccharum officinarum* (C7E3V7), *Citrus sinensis* (D0ELH5) and *Gerbera* (A8CYN7). PIN1-type PPIases are encoded by multiple genes and are present in a wide variety of plant species. A four amino acid insertion site is situated next to the phosphor-specific recognition site of the active site, regulating the activity of the enzyme.[51] The PPIase activity of cyclophilins is regulated by thioredoxin,[52] also identified in this study and discussed above. PIN1At in *Arabidopsis* encodes a PPIase, which regulates flowering time through phosphorylation-dependent prolyl cis/trans isomerization of key regulatory pathway specific transcription factors.[53] Alterations to protein folding status catalyzed by PPIases with the cis/trans isomerization of proline imidic peptide bonds could also affect protein body composition in sorghum and other grain crops.[54]

*Heat Shock Protein (HSP)/Luminal Binding Protein (BiP).* HSP/BiP chaperones are key regulators of protein body biogenesis, with significant impacts on grain quality traits and composition[55] (Table 2). HSPs/BiPs were isolated predominantly from the water/salt-soluble (A/G) and alkali-soluble (glutelin) protein fractions across both genotypes (Figure 5 and Supporting Information, Figure S5 and Supplementary Table 2). A/G spot 2 produced a strong match to sorghum protein (accession number C5XY25), which exhibits homology to the *Oryza sativa* 19 kDa class II HSP. The protein has a calculated Mw 19 982 Da and pI 5.71, appropriate to its position on the gel.


dx.doi.org/10.1021/jf5022847 | J. Agric. Food Chem. 2014, 62, 9819–9831

A sorghum homologue to a maize 16.9 kDa class I heat shock protein was also identified (C5XQR9) in a lower molecular weight region of the gel within a more basic pI range, relative to spot 2 discussed above. The HSP homologue C5XQR9 localized to an appropriate position on the gel, corresponding to Mw 17 121 Da and pI 6.18. Matches to C5XQR9 were observed in 296B spots B, 7, 8, 9, and 10, and in QL12 spots B and 7. QL12 spot 8 contained an additional sorghum homologue (accession number C5XML7) to a maize 17.5 kDa class II HSP.

In addition, several HMW (50−75 kDa) putative uncharacterized proteins with homology to HSP chaperones or luminal binding proteins (BiPs) were identified in the alkali-soluble glutelin fraction across both 296B and QL12 genotypes (accession numbers C5YU58, C5WNX8, and C5XPN2). Sorghum HSP C5YU58 has also been identified in grain proteomic analyses carried out by other researchers.[56] In maize, elevated HSP/BiP levels during development are linked to mutations in $\alpha$- and $\gamma$-zeins resulting in an opaque or floury phenotype.[55,57,58] BiP has been found to associate with the surface of rice protein bodies, assisting in prolamin deposition through disulfide bonding at specific cysteine residues.[59] In wheat, these chaperones are localized to the interior, rather than on the surface of protein bodies, indicating diverse roles for HSP/BiP in protein body aggregation across different plant species.[60]

*α-Amylase Inhibitors.* Sorghum $\alpha$-amylase inhibitors were isolated from the prolamin fraction in both genotypes (Figure 5, Table 2). The enzyme was isolated from a low molecular weight (10−15 kDa) size range, within pI 7−8. The inhibitor was identified in 296B gel spots 1, 2, 8, and 11, and in QL12 spots 1 and 2, which was observed across duplicate gels. The activity of $\alpha$-amylase inhibitors in the grain affects starch digestion into glucose, slowing the conversion of starch to ethanol during the fermentation process.[61] Lines expressing low levels of $\alpha$-amylase inhibitor may be appropriate candidates for the biofuels industry. $\alpha$-Amylase inhibitors also play a role in plant defense, where they deter crop destruction by snails and birds in tannin-containing sorghum and have been shown to enhance insect resistance in wheat.[62−64]

**Non-Prolamin Proteins in the Protein−Starch Matrix.** Non-prolamin proteins, such as albumins and globulins, are rich in essential amino acids, including lysine and tryptophan, and provide the embryo with additional readily accessible nitrogen reserves during germination. Sorghum homologues to the major nonkafirin storage proteins were identified across all protein solubilities (Supporting Information, Figure S4 and Supplementary Table 1). In the water/salt-soluble fractions sorghum homologues to globulin and cupin-like proteins in *Zea mays* were abundant, including accession numbers C5WY16 and C5WQD2.

Globulins are saline-soluble secondary storage proteins, with many belonging to the cupin superfamily. For example, 7S globulins function exclusively as storage proteins, but are not required for normal seed function.[65] Globulin S-1 (63 kDa) and globulin S-2 (45 kDa) collectively represent ∼20% of seed protein content in maize and share amino acid sequence similarity with the 7S seed proteins of wheat and legumes.[66] These proteins have significant impacts on the nutritional quality of the grain.

Proteins identified in the alkali-soluble glutelin fraction included a range of vicilin- and legumin-like storage proteins. The sorghum homologue to uncleaved maize legumin, accession number C5YY38, and the globulin/vicilin-like sorghum homologue C5WUN6, were identified in this fraction. Immuno-localization studies in *Medicago trunculata* using antivicilin antibodies show preferential targeting of vicilins to the periphery of the protein bodies.[67] Sorghum glutelins have not yet been extensively characterized, but it is hypothesized that they may form complex highly linked protein networks encasing protein bodies and providing additional structure to the protein−starch matrix.[68,69] Protein members of the legumin superfamily are most abundant in legumes, oats, and rice. Wheat legumin-like protein, or triticin, accumulates in globulin inclusion bodies at the periphery of prolamin bodies. Overexpression of pea legumin in wheat forms crystalline patterns contributing to the altered structure of the protein−starch matrix.[70,71]

A range of proteins were identified in the glutelin fraction in addition to legumin and vicillin, which included HSPs/BiPs, cell division cycle proteins, homologues to maize caleosin, glutathione *S*-transferases, RuBisCo large subunit binding protein, and wheat MOTHER OF FT AND TFL1 (MFT), which regulates seed dormancy and the onset of germination.[72] Significant amounts of $\alpha$-, $\beta$-, and $\delta$-kafirins were also identified in this fraction, although quantification scores indicate that their concentrations were considerably less than in the prolamin fraction, and their presence may be due to incomplete sequential extraction of the alcohol-soluble fraction as previously noted.

Across the study, protein spots excised from HMW areas of 2D gels generally produced matches specifically to HMW proteins, while spots excised from LMW areas tended to produce matches to both high and low molecular weight proteins. This indicates that spots in LMW areas of the gel may contain a mix of intact proteins and protein subunits, or cleaved products of larger proteins. For example, sorghum homologues to HMW globulin S-1 and S-2 (C5WY16 and C5WQD2), cupin family proteins (C5WUN and C5X0T3), and uncleaved legumin (C5YY38) were isolated from every protein fraction, from both high and low molecular weight areas of the gel, whereas LMW proteins (∼13 kDa), such as thioredoxin, glutaredoxin, and $\alpha$-amylase inhibitors, were isolated exclusively from the lower molecular weight area of the gel. Highly abundant sorghum homologues to glyceraldehyde-3-phosphate dehydrogenase as well as various HSPs were detected in the glutelin fraction. These proteins were generally found in the area of their calculated pI values, but localized across a broader size range. Because the presence of these proteins was so widespread, the matches were not listed in results tables (Supporting Information, Supplementary Table 1), unless they represented the only quality match returned for a protein spot.

**Sorghum Proteomics.** Our proteomic analysis compiles sequence and biochemical information describing a range of proteins affecting sorghum endosperm structure and composition. The derived data set will further augment annotation of the sorghum proteome and facilitate identification of potential targets for improved grain quality. Furthermore, the data provide a basis for comparative analysis with other major grain crops. Possible avenues for utilizing protein sequence data include the development of high-lysine varieties with increased A/G content for enhanced nutritional quality, as well as the modification of enzyme-regulated protein aggregation in the endosperm for increased starch availability.

Differential regulation of thioredoxin in the $\beta$-kafirin null mutant QL12 indicates that expression of the enzyme may be either directly or indirectly linked to the $\beta$-kafirin mutation. Evaluation of Trx expression at the RNA/protein level across additional $\beta$-kafirin mutants and at varying stages of development

could provide further insights into this relationship. Future research on previously uncharacterized proteins identified in this study may reveal elements related to grain quality parameters, such as digestibility and flour pasting properties. In particular, the HMW $\gamma$-prolamin homologue identified provides an interesting candidate for further functional analysis as it has been shown to localize to the periphery of the protein bodies in maize, possibly limiting enzymatic access to internally located $\alpha$-zeins and starch. Identification of proteins with desirable amino acid content and enhanced digestibility will also benefit future research initiatives to improve sorghum grain nutritional value and palatability.

The commercial success of grain crops with altered protein composition, such as high lysine and increased digestibility lines, can be limited by negative pleiotropic effects accompanying changes in the amino acid profile. For example, maize endosperm protein mutants, *o2* (*opaque2*) and *fl2* (*floury2*) have an improved amino acid content, but exhibit a number of undesirable traits such as reduced grain yield and increased susceptibility to diseases and pests. This work supports the development of high throughput screening methods for biomarkers associated with grain quality and endeavors for the genetic improvement and biofortification of sorghum through molecular breeding and transformation. The identification and characterization of proteins impacting on various grain quality parameters in sorghum, such as nutritional quality, grain hardness, and stress resistance, will assist breeders in their introgression of genetic factors associated with these traits into established breeding lines. The rapid introgression and selection of desirable grain quality traits will require the linking of the proteome with the genome. Next generation genome resequencing[73] and genotyping by selection[74] tools are now publically available and are being incorporated into sorghum prebreeding for other grain quality traits such as digestibility.[75] This will ultimately lead to more cost-effective and efficient plant breeding for improved sorghum varieties tailored to specific end uses.

## ■ ASSOCIATED CONTENT

### Supporting Information

Supplementary Table 1 contains a list of protein matches to LC−MS/MS generated peptide profiles. Figure S1 contains RP-HPLC peak profiles of the alcohol-soluble (prolamin) proteins, and Figure S2 contains RP-HPLC profiles for the water/salt-soluble protein fraction across sorghum grain samples. Figure S3 contains LOC profiling of the A/G fraction in $\beta$-kafirin null variants compared to wild type. Figure S4 presents 2D SDS-PAGE gels for A/G, prolamin, and glutelin fractions for wild-type 296B and $\beta$-kafirin null QL12. Figure S5 and Supplementary Table 2 show 2D SDS PAGE/LC−MS/MS identification HMW alkali-soluble (glutelin) proteins. This material is available free of charge via the Internet at http://pubs.acs.org.

## ■ AUTHOR INFORMATION

### Corresponding Author

*Tel.: +61-3365-2141. Fax: +61-3365-2141. E-mail: j.cremer@uq.edu.au.

### Funding

The work is supported by funding from an ARC linkage grant with Pacific Seeds, by the Andersons Research Program, and by the USDA—ARS, Manhattan, KS, USA.

### Notes

Names are necessary to report factually on available data; however, the U.S. Department of Agriculture neither guarantees nor warrants the standard of the product, and use of the name by the U.S. Department of Agriculture implies no approval of the product to the exclusion of others that may also be suitable. USDA is an equal opportunity provider and employer.

The authors declare no competing financial interest.

## ■ ACKNOWLEDGMENTS

Extensive support in proteomic techniques was kindly provided by Dr. Amanda Nouwens at the SCMB protein facility (The University of Queensland). Identification of proteins with LC−MS/MS was facilitated through open access queries to the Mascot server.

## ■ ABREVIATIONS USED

A/G, albumin/globulins; BiP, luminal binding proteins; Grx, glutaredoxins; HPLC, high performance liquid chromatography; IEF, isoelectric focusing; HSP, heat shock proteins; HMW, high molecular weight; kDa, kilodalton; LMW, low molecular weight; LC−MS/MS, liquid chromatography−tandem mass spectrometry; LOC, lab on a chip; MS, mass spectrometry; Mw, molecular weight; PDI, protein disulfide isomerase; PPIase, peptidyl-prolyl cis/trans isomerase; SDS-PAGE, sodium dodecyl sulfate polyacrylamide gel electrophoresis; Trx, thioredoxin

## ■ REFERENCES

(1) United Nations. *World Population to 2300*; United Nations: New York, 2004.

(2) Rijsberman, F. R. Water scarcity: Fact or fiction? *Agric. Water Manage.* **2006**, *80*, 5−22.

(3) Ortiz, R.; Iwanaga, M.; Reynolds, M. P.; Wu, H.; Crouch, J. H. Overview on Crop Genetic Engineering for Drought-prone Environments. *J. SAT Agric. Res.* [Online] **2007**, *4* (1), 30 pp. http://www.icrisat.org/journal/SpecialProject/sp3.pdf.

(4) Steduto, P.; Katerji, N.; Puertos-Molina, H.; Unlu, M.; Mastrorilli, M.; Rana, G. Water-use efficiency of sweet sorghum under water stress conditions Gas-exchange investigations at leaf and canopy scales. *Field Crops Res.* **1997**, *54*, 221−234.

(5) Kim, M.; Day, D. F. Composition of Sugar Cane, Energy Cane, and Sweet Sorghum Suitable for Ethanol Production at Louisiana Sugar Mills. *J. Ind. Microbiol. Biotechnol.* **2011**, *38*, 803−807.

(6) Wong, J. H.; Lau, T.; Cai, N.; Singh, J.; Pedersen, J. F.; Vensel, W. H.; Hurkman, W. J.; Wilson, J. D.; Lemaux, P. G.; Buchanan, B. B. Digestibility of protein and starch from sorghum (Sorghum bicolor) is linked to biochemical and structural features of grain endosperm. *J. Cereal Sci.* **2009**, *49*, 73−82.

(7) Rooney, L. W. Sorghum and Millets. In *Cereal Grain Quality*, Henry, R. J., Kettlewell, P. S., Eds.; Chapman and Hall: Dordrecht, Netherlands, 1996; pp 153−177.

(8) Belton, P. S.; Delgadillo, I.; Halford, N. G.; Shewry, P. R. Kafirin structure and functionality. *J. Cereal Sci.* **2006**, *44*, 272−286.

(9) De Mesa-Stonestreet, N. J.; Alavi, S.; Bean, S. R. Sorghum Proteins: The Concentration, Isolation, Modification, and Food Applications of Kafirins. *J. Food Sci.* **2010**, *75*, R90−R104.

(10) Shull, J. M.; Watterson, J. J.; Kirleis, A. W. Proposed nomenclature for the alcohol-soluble proteins (kafirins) of Sorghum bicolor (L. Moench) based on molecular weight, solubility, and structure. *J. Agric. Food Chem.* **1991**, *39*, 83−87.

(11) Xu, J. H.; Messing, J. Amplification of prolamin storage protein genes in different subfamilies of the Poaceae. *Theor. Appl. Genet.* **2009**, *119*, 1397−412.

(12) Song, R.; Llaca, V.; Linton, E.; Messing, J. Sequence, Regulation, and Evolution of the Maize 22-kD $\alpha$ Zein Gene Family. *Genome Res.* **2001**, *11*, 1817−1825.

(13) Luis, E. S.; Sullivan, T. W.; Nelson, L. A. Nutrient Composition and Feeding Value of Proso Millets, Sorghum Grains, and Corn in Broiler Diets. *Poultry Sci.* **1982**, *61*, 311−320.

(14) Matta, N.; Singh, A.; Kumar, Y. Manipulating seed storage proteins for enhanced grain quality in cereals. *Afr. J. Food Sci.* **2009**, *3*, 439−446.
(15) Laidlaw, H.; Mace, E.; Williams, S.; Sakrewski, K.; Mudge, A.; Prentis, P.; Jordan, D.; Godwin, I. Allelic variation of the beta-, gamma- and delta-kafirin genes in diverse *Sorghum* genotypes. *Theor. Appl. Genet.* **2010**, *121*, 1227−1237.
(16) Bean, S. R.; Ioerger, B. P.; Blackwell, D. L. Separation of Kafirins on Surface Porous Reversed-Phase High-Performance Liquid Chromatography Columns. *J. Agric. Food Chem.* **2011**, *59*, 85−91.
(17) Bean, S. R.; Tilley, M. Separation of Water-Soluble Proteins from Cereals by High-Performance Capillary Electrophoresis (HPCE). *Cereal Chem.* **2003**, *80*, 505−510.
(18) Kappler, U.; Nouwens, A. S. The molybdoproteome of Starkeya novella—insights into the diversity and functions of molybdenum containing proteins in response to changing growth conditions. *Metallomics* **2013**, *5*, 325−334.
(19) Shewayrga, H.; Sopade, P. A.; Jordan, D. R.; Godwin, I. D. Characterisation of grain quality in diverse sorghum germplasm using a Rapid Visco-Analyzer and near infrared reflectance spectroscopy. *J. Sci. Food Agric.* **2012**, *92*, 1402−1410.
(20) Cremer, J. E.; Liu, L.; Bean, S. R.; Ohm, J. B.; Tilley, M.; Wilson, J. D.; Kaufman, R. C.; Vu, T. H.; Gilding, E. K.; Godwin, I. D.; Wang, D. Impacts of kafirin allelic diversity, starch content and protein digestibility on ethanol conversion efficiency in grain sorghum. *Cereal Chem.* **2014**, *91*, 218−227.
(21) Guiragossian, V.; Chibber, B. A. K.; Van Scoyoc, S.; Jambunathan, R.; Mertz, E. T.; Axtell, J. D. Characteristics of proteins from normal, high lysine, and high tannin sorghums. *J. Agric. Food Chem.* **1978**, *26*, 219−223.
(22) Reddy, N. P. E.; Vauterin, M.; Frankard, V.; Jacobs, M. Biochemical Characterisation and Cloning of α-Kafirin Gene from Sorghum (Sorghum bicolor L Moench). *J. Plant Biochem. Biotechnol.* **2001**, *10*, 101−106.
(23) Vendemiatti, A.; Rodrigues Ferreira, R.; Humberto Gomes, L.; Oliveira Medici, L.; Antunes Azevedo, R. Nutritional Quality of Sorghum Seeds: Storage Proteins and Amino Acids. *Food Biotechnol.* **2008**, *22*, 377−397.
(24) Wilson, C. M.; Shewry, P. R.; Miflin, B. J. Maize endosperm proteins compared by sodium dodecyl sulphate gel electrophoresis and isoelectric focussing. *J. Cereal Chem.* **1981**, *58*, 275−281.
(25) Wu, Y. V.; Wall, J. S. Lysine content of protein increased by germinating of normal and high lysine sorghum. *J. Agric. Food Chem.* **1980**, *28*, 455−458.
(26) Taylor, J. R. N.; Novellie, L.; Liebenberg, N. v. d. W. Sorghum protein body composition and ultrastructure. *J. Cereal Chem.* **1984**, *61*, 69−73.
(27) Woo, Y.-M.; Hu, D. W.-N.; Larkins, B. A.; Jung, R. Genomics Analysis of Genes Expressed in Maize Endosperm Identifies Novel Seed Proteins and Clarifies Patterns of Zein Gene Expression. *Plant Cell* **2001**, *13*, 2297−2317.
(28) Ferrante, P.; Masci, S.; D'Ovidio, R.; Lafiandra, D.; Volpi, C.; Mattei, B. A proteomic approach to verify in vivo expression of a novel γ-gliadin containing an extra cysteine residue. *Proteomics* **2006**, *6*, 1908−1914.
(29) Wang, Y.; Tilley, M.; Bean, S.; Sun, X. S.; Wang, D. Comparison of Methods for Extracting Kafirin Proteins from Sorghum Distillers Dried Grains with Solubles. *J. Agric. Food Chem.* **2009**, *57*, 8366−8372.
(30) Mokhawa, G.; Kerapeletswe-Kruger, C. K.; Ezeogu, L. I. Electrophoretic analysis of malting degradability of major sorghum reserve proteins. *J. Cereal Sci.* **2013**, *58*, 191−199.
(31) Pandit, P. *Molecular characterisation of the alpha-kafirin multigene family for the genetic improvement of sorghum grain quality*. Dissertation, The University of Queensland, Brisbane, 2008.
(32) Oria, M. P.; Hamaker, B. R.; Shull, J. M. Resistance of Sorghum α-, β-, and γ-Kafirins to Pepsin Digestion. *J. Agric. Food Chem.* **1995**, *43*, 2148−2153.
(33) Oria, M. P.; Hamaker, B. R.; Axtell, J. D.; Huang, C.-P. A highly digestible sorghum mutant cultivar exhibits a unique folded structure of endosperm protein bodies. *Proc. Natl. Acad. Sci. U.S.A.* **2000**, *97*, 5065−5070.
(34) Lending, C. R.; Larkins, B. A. Changes in the zein composition of protein bodies during maize endosperm development. *Plant Cell* **1989**, *1*, 1011−1023.
(35) Geli, M. I.; Torrent, M.; Ludevid, D. Two structural domains mediate two sequential events in [gamma]-zein targeting: Protein endoplasmic reticulum retention and protein body formation. *Plant Cell* **1994**, *6*, 1911−1922.
(36) Cho, M.-J.; Wong, J. H.; Marx, C.; Jiang, W.; Lemaux, P. G.; Buchanan, B. B. Overexpression of thioredoxin h leads to enhanced activity of starch debranching enzyme (pullulanase) in barley grain. *Proc. Natl. Acad. Sci. U.S.A.* **1999**, *96*, 14641−14646.
(37) Alkhalfioui, F.; Renard, M.; Vensel, W. H.; Wong, J.; Tanaka, C. K.; Hurkman, W. J.; Buchanan, B. B.; Montrichard, F. Thioredoxin-Linked Proteins Are Reduced during Germination of Medicago truncatula Seeds. *Plant Physiol.* **2007**, *144*, 1559−1579.
(38) Holmgren, A. Thioredoxin catalyzes the reduction of insulin disulfides by dithiothreitol and dihydrolipoamide. *J. Biol. Chem.* **1979**, *254*, 9627−9632.
(39) Alkhalfioui, F.; Renard, M.; Montrichard, F. Unique properties of NADP-thioredoxin reductase C in legumes. *J. Exp. Bot.* **2007**, *58*, 969−978.
(40) Wong, J. H.; Cai, N.; Tanaka, C. K.; Vensel, W. H.; Hurkman, W. J.; Buchanan, B. B. Thioredoxin Reduction Alters the Solubility of Proteins of Wheat Starchy Endosperm: An Early Event in Cereal Germination. *Plant Cell Physiol.* **2004**, *45*, 407−415.
(41) Sahoo, L.; Lindquist, D. J. L.; Pedersen, J. F.; Kaur, R.; Wong, J. H.; Buchanan, B. B.; Lemaux, P. G. Effect Of Transgenes From Sorghum On The Fitness Of Shattercane x Sorghum Hybrids. In *62nd Annual Meeting of the North Central Weed Science Society 2007*; Curran Associates: Red Hook, NY, 2007; p 45.
(42) Rouhier, N.; Lemaire, S. D.; Jacquot, J. P. The role of glutathione in photosynthetic organisms: Emerging functions for glutaredoxins and glutathionylation. *Annu. Rev. Plant Biol.* **2008**, *59*, 143−166.
(43) Freedman, R. B. A protein with many functions? *Nature* **1989**, *337*, 407−408.
(44) Kim, Y.; Yeu, S.; Park, B.; Koh, H.-J.; Song, J.; Seo, H. Protein Disulfide Isomerase-Like Protein 1−1 Controls Endosperm Development through Regulation of the Amount and Composition of Seed Proteins in Rice. *PLoS One* **2012**, *7* (9), e44493.
(45) Takemoto, Y.; Coughlan, S. J.; Okita, T. W.; Satoh, H.; Ogawa, M.; Kumamaru, T. The Rice Mutant esp2 Greatly Accumulates the Glutelin Precursor and Deletes the Protein Disulfide Isomerase. *Plant Physiol.* **2002**, *128*, 1212−1222.
(46) Onda, Y.; Kumamaru, T.; Kawagoe, Y. ER membrane-localized oxidoreductase Ero1 is required for disulfide bond formation in the rice endosperm. *Proc. Natl. Acad. Sci. U.S.A.* **2009**, *106*, 14156−14161.
(47) Li, C.; Larkins, B. Expression of protein disulfide isomerase is elevated in the endosperm of the maize floury-2 mutant. *Plant Mol. Biol.* **1996**, *30*, 873−882.
(48) Gething, M.-J.; Sambrook, J. Protein folding in the cell. *Nature* **1992**, *355*, 35−45.
(49) Brandts, J.; Halvorsen, H.; Brennan, M. Consideration of the possibility that the slow step in protein denaturation reactions is due to cis-trans isomerism of proline residues. *Biochemistry* **1975**, *14*, 4953−4963.
(50) He, Z.; Li, L.; Luan, S. Immunophilins and Parvulins. Superfamily of Peptidyl Prolyl Isomerases in Arabidopsis. *Plant Physiol.* **2004**, *134*, 1248−1267.
(51) Yao, J.-L.; Kops, O.; Lu, P.-J.; Lu, K. P. Functional Conservation of Phosphorylation-specific Prolyl Isomerases in Plants. *J. Biol. Chem.* **2001**, *276*, 13517−13523.
(52) Motohashi, K.; Koyama, F.; Nakanishi, Y.; Ueoka-Nakanishi, H.; Hisabori, T. Chloroplast Cyclophilin Is a Target Protein of Thioredoxin: Thiol Modulation of the Peptidyl-prolyl cis-trans Isomerase Activity. *J. Biol. Chem.* **2003**, *278*, 31848−31852.

(53) Wang, Y.; Liu, C.; Yang, D.; Yu, H.; Liou, Y.-C. Pin1At Encoding a Peptidyl-Prolyl cis/trans Isomerase Regulates Flowering Time in Arabidopsis. *Mol. Cell* **2010**, *37*, 112−122.
(54) Duodu, K. G.; Tang, H.; Grant, A.; Wellner, N.; Belton, P. S.; Taylor, J. R. N. FTIR and solid state 13C spectroscopy of proteins of wet cooked and popped sorghum and maize. *J. Cereal Sci.* **2001**, *33*, 261−269.
(55) Zhang, F.; Boston, R. Increases in binding protein (BiP) accompany changes in protein body morphology in three high-lysine mutants of maize. *Protoplasma* **1992**, *171*, 142−152.
(56) Buckner, R. J. *Developmental and crosslinking factors related to low protein digestibility of sorghum grain*. Dissertation, Purdue University, West Lafayette, IN, 1997.
(57) Kim, C. S.; Gibbon, B. C.; Gillikin, J. W.; Larkins, B. A.; Boston, R. S.; Jung, R. The maize Mucronate mutation is a deletion in the 16-kDa γ-zein gene that induces the unfolded protein response1. *Plant J.* **2006**, *48*, 440−451.
(58) Kim, C. S.; Hunter, B. G.; Kraft, J.; Boston, R. S.; Yans, S.; Jung, R.; Larkins, B. A. A Defective Signal Peptide in a 19-kD α-Zein Protein Causes the Unfolded Protein Response and an Opaque Endosperm Phenotype in the Maize De*-B30 Mutant. *Plant Physiol.* **2004**, *134*, 380−387.
(59) Muench, D. G.; Wu, Y.; Zhang, Y.; Li, X.; Boston, R. S.; Okita, T. W. Molecular Cloning, Expression and Subcellular Localization of a BiP Homolog from Rice Endosperm Tissue. *Plant Cell Physiol.* **1997**, *38*, 404−412.
(60) Levanony, H.; Rubin, R.; Altschuler, Y.; Galili, G. Evidence for a novel route of wheat storage proteins to vacuoles. *J. Cell Biol.* **1992**, *119*, 1117−1128.
(61) Dreher, M. L.; Dreher, C. J.; Berry, J. W.; Fleming, S. E. Starch digestibility of foods: A nutritional perspective. *Crit. Rev. Food Sci. Nutr.* **1984**, *20*, 47−71.
(62) Farmer, E.; Ryan, C. Inter plant communication: air-borne methyl jasmonate induces synthesis of proteinase inhibitors in plant leaves. *Proc. Natl. Acad. Sci. U.S.A.* **1990**, *87*, 7713−7716.
(63) Gatehouse, A.; Fenton, K.; Jepson, I.; Pavey, D. The effects of a-amylase inhibitors on insect storage pests: inhibition of a-amylase in vitro and effects on development in vivo. *J. Sci. Food Agric.* **1986**, *37*, 727−734.
(64) Yetter, M.; Saunders, R.; Boles, H. Alpha-amylase inhibitors from wheat kernels as factors in resistance to postharvest insects. *Cereal Chem.* **1979**, *56* (4), 243.
(65) Kriz, A. L.; Wallace, N. H. Characterisation of the maize globulin-2 gene and analysis of 2 null alleles. *Biochem. Genet.* **1991**, *29*, 241−254.
(66) Belanger, F. C.; Kriz, A. L. Molecular Characterization of the Major Maize Embryo Globulin Encoded by the *Glb1* Gene. *Plant Physiol.* **1989**, *91*, 636−643.
(67) Abiraches-Darmency, M.; Dessaint, F.; Benlicha, E.; Schneider, C. Biogenesis of protein bodies during vicilin accumulation in Medicago truncatula immature seeds. *BMC Res. Notes* **2012**, *5*, 409.
(68) Shull, J. M.; Watterson, J. J.; Kirleis, A. W. Purification and immunocytochemical localization of kafirins in Sorghum bicolor (L. Moench) endosperm. *Protoplasma* **1992**, *171*, 64−74.
(69) Taylor, J.; Taylor, J. R. N. Protein Biofortified Sorghum: Effect of Processing into Traditional African Foods on Their Protein Quality. *J. Agric. Food Chem.* **2011**, *59*, 2386−2392.
(70) Arcalis, E.; Marcel, S.; Altmann, F.; Kolarich, D.; Drakakaki, G.; Fischer, R.; Christou, P.; Stoger, E. Unexpected Deposition Patterns of Recombinant Proteins in Post-Endoplasmic Reticulum Compartments of Wheat Endosperm. *Plant Physiol.* **2004**, *136*, 3457−3466.
(71) Stöger, E.; Parker, M.; Christou, P.; Casey, R. Pea Legumin Overexpressed in Wheat Endosperm Assembles into an Ordered Paracrystalline Matrix. *Plant Physiol.* **2001**, *125*, 1732−1742.
(72) Nakamura, S.; Abe, F.; Kawahigashi, H.; Nakazono, K.; Tagiri, A.; Matsumoto, T.; Utsugi, S.; Ogawa, T.; Handa, H.; Ishida, H.; Mori, M.; Kawaura, K.; Ogihara, Y.; Miura, H. A Wheat Homolog of MOTHER OF FT AND TFL1 Acts in the Regulation of Germination. *Plant Cell* **2011**, *23*, 3215−3229.
(73) Mace, E. S.; Tai, S.; Gilding, E. K.; Li, Y.; Prentis, P. J.; Bian, L.; Campbell, B. C.; Hu, W.; Innes, D. J.; Han, X.; Cruickshank, A.; Dai, C.; Frère, C.; Zhang, H.; Hunt, C. H.; Wang, X.; Shatte, T.; Wang, M.; Su, Z.; Li, J.; Lin, X.; Godwin, I. D.; Jordan, D. R.; Wang, J. Whole-genome sequencing reveals untapped genetic potential in Africa's indigenous cereal crop sorghum. *Nat. Commun.* **2013**, *4*, No. 2320.
(74) Morris, G. P.; Ramu, P.; Deshpande, S. P.; Hash, C. T.; Shah, T.; Upadhyaya, H. D.; Riera-Lizarazu, O.; Brown, P. J.; Acharya, C. B.; Mitchell, S. E.; Harriman, J.; Glaubitz, J. C.; Buckler, E. S.; Kresovich, S. Population genomic and genome-wide association studies of agro-climatic traits in sorghum. *Proc. Natl. Acad. Sci. U.S.A.* **2013**, *110*, 453−458.
(75) Gilding, E. K.; Frère, C. H.; Cruickshank, A.; Rada, A. K.; Prentis, P. J.; Mudge, A. M.; Mace, E. S.; Jordan, D. R.; Godwin, I. D. Allelic variation at a single gene increases food value in a drought-tolerant staple cereal. *Nat. Commun.* **2013**, *4*, 1483.

Table 1. PPO Purification from Manila Mango Fruit (*Mangifera indica* cv. Manila)[a]

| purification step | volume (mL) | activity (units/mL) | total activity (units) | protein content (mg/mL) | specific activity (units/mg protein) | purification (fold) | yield (%) |
|---|---|---|---|---|---|---|---|
| crude extract | 920 | 779 | 717048 | 19.10 | 41 | 1 | 100 |
| $(NH_4)_2SO_4$ precipitation 30−85% | 800 | 804 | 643200 | 4.95 | 162 | 4 | 90 |
| phenyl-Sepharose | 20 | 4366 | 87320 | 1.03 | 4205 | 103 | 12 |
| ion exchange | 16 | 1399 | 22384 | 0.15 | 8839 | 216 | 3 |

[a]These values were obtained in a typical purification.

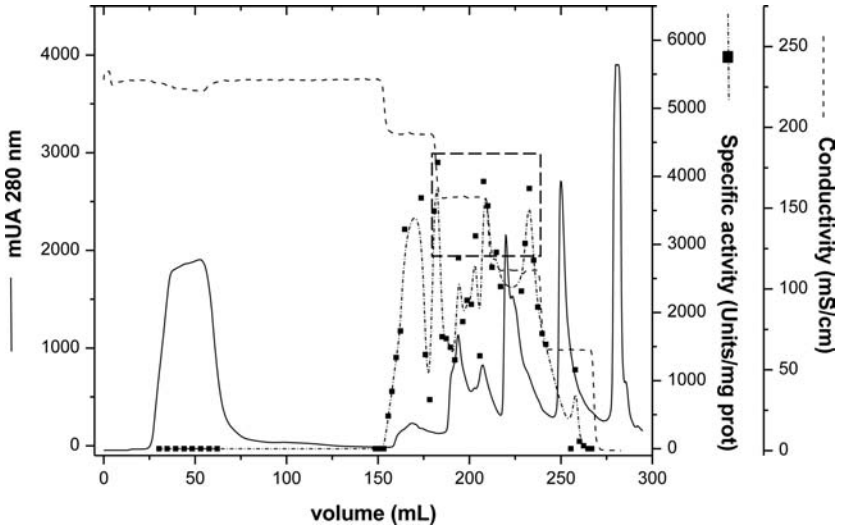


**Figure 1.** Elution profile by hydrophobic interaction. The column used was a phenyl-Sepharose 4-fast flow. Polyphenol oxidase activity was determined in collected fractions. Absorbance at 280 nm (mAU) (solid lines), specific activity (■), and conductivity (mS/cm) (dashed lines) are shown. Fractions with the highest specific activity are framed with dashed lines.

York, NY, USA). All other reagents were from Sigma-Aldrich (St. Louis, MO, USA).

**Extraction Procedure.** PPO crude extract was obtained from 350 g of Manila mango pulp mixed with 700 mL of 0.2 M sodium phosphate buffer, pH 7.0, 1% w/v poly(vinylpolypyrolidone) (PVPP), 1% v/v Triton X-100, and protease inhibitors (0.33 mg/100 mL aprotinin and 0.1 mM phenylmethanesulfonyl fluoride (PMSF)). PPO crude extract was left to rest overnight and centrifuged at 10650*g* for 30 min. The supernatant obtained was filtered and aprotinin (0.33 mg/100 mL) was added. All extraction procedures were carried out at 4 °C.

**PPO Activity Assay.** PPO activity assay was performed in (1 mL) 0.2 M sodium phosphate buffer, pH 7.0, containing 50 mM catechol or pyrogallol as substrate; 33 μL of the enzyme solution was added to initiate the reaction. PPO assay was performed at 25 °C using an Agilent 8453 UV−vis (New York, NY, USA) diode array spectrophotometer. $\Delta Abs_{420\ nm}$ was recorded every 5 s during 5 min. One unit of PPO activity was defined as the change in absorbance of 0.001 $min^{-1}$ $mL^{-1}$ of enzyme.[15]

**Purification Procedure.** PPO was purified as described by[10] briefly, filtered crude extract was subjected to $(NH_4)_2SO_4$ precipitation (30−85% saturation) at 4 °C, then centrifuged at 10650*g*, 30 min. The precipitate was resuspended in a small volume of phosphate buffer (50 mM sodium phosphate, pH 7.0), 1.2 M ammonium sulfate, and 0.6 M potassium chloride and dialyzed overnight against three changes of the same buffer. The dialyzed solution was centrifuged at 34500*g* for 30 min and the supernatant collected. Aprotinin (0.33 mg/100 mL) was added to the supernatant. Protein concentration was determined by UV absorbance at 280 nm.

Chromatography was carried out at room temperature using a Fast Protein Liquid Chromatography (FPLC) system from GE. The supernatant was loaded onto an XK 16/20 column packed with phenyl-Sepharose 4-fast flow previously equilibrated with buffer used in dialysis (equilibrium buffer). Then, the column was washed with equilibrium buffer (70 mL) to remove unbound proteins. The equilibrium buffer was displaced stepwise from 100 to 0% with distilled water, and the bound proteins were eluted. Flow rate was 1.0 mL/min, and fractions (2.5 mL) were collected. PPO activity and protein concentration were determined, obtaining the elution profile. Fractions showing high specific activity were pooled and then dialyzed overnight against three changes of buffer A (20 mM Tris-HCl, pH 7.0) at 4 °C. Aprotinin (0.33 mg/100 mL) was added to the dialyzed enzyme.

After that, the suspension was loaded onto anion exchange column Mono Q HR 10/10, previously equilibrated by washing with low ionic buffer A (40 mL) followed by high ionic buffer B (80 mL 20 mM Tris-HCl pH 7.0, containing 1.0 M KCl) and finally with low ionic buffer A (80 mL). The flow rate was 2 mL/min,and fractions (2 mL) were collected. Protein was eluted by linearly increasing the ionic strength; four linear gradients were used in the elution process: (a) from 0 to 16% in 34 mL, (b) from 16 to 19% in 10 mL, (c) from 19 at 25% in 40 mL, and (d) from 25 to 100% in 40 mL. Then the column was washed with 100% elution buffer by using a volume of 24 mL. PPO activity and protein concentration were determined in each fraction, and the elution profile was obtained.

**PPO Molecular Weight (MW) Determination.** Column chromatography was used for MW determination of the native enzyme and carried out at room temperature using an FPLC system. Briefly, a Superdex 200 10/300 GL column was washed with distilled water (50 mL) and then with elution buffer (50 mL of 50 mM phosphate, pH 7.0, and 0.15 M KCl) at a flow rate of 0.5 mL/min. After that, 350 μL of purified PPO was loaded onto the column and eluted with elution buffer (30 mL); fractions (1 mL) were collected, and for each fraction activity was determined. PPO molecular weight was determined by extrapolation of the PPO elution time in a calibration curve generated using a set of proteins with different molecular weights.


dx.doi.org/10.1021/jf5029784 | J. Agric. Food Chem. 2014, 62, 9832−9840

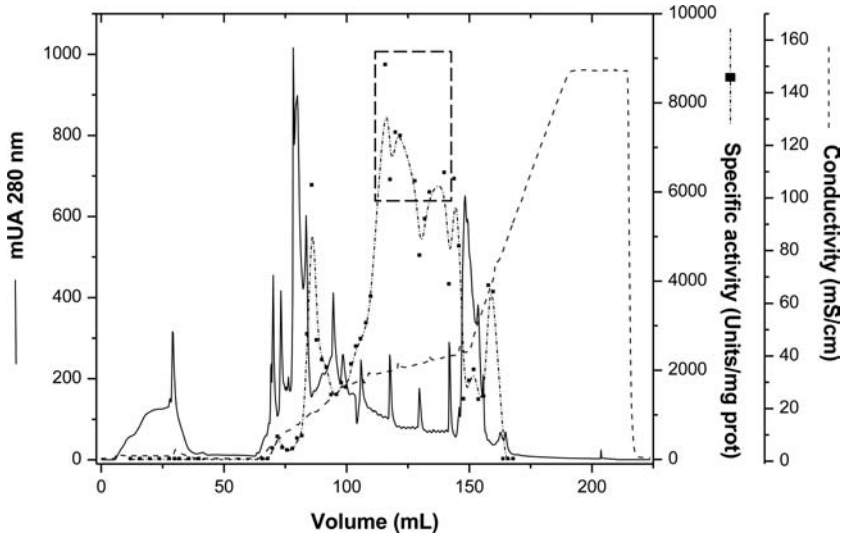


**Figure 2.** Elution profile by ion exchange chromatography. The column used was a Mono Q HR. Polyphenol oxidase activity was determined in collected fractions. Absorbance at 280 nm (mAU) (solid lines), specific activity (■), and conductivity (mS/cm) (dashed lines) are shown. Fractions with the highest specific activity are framed with dashed lines.

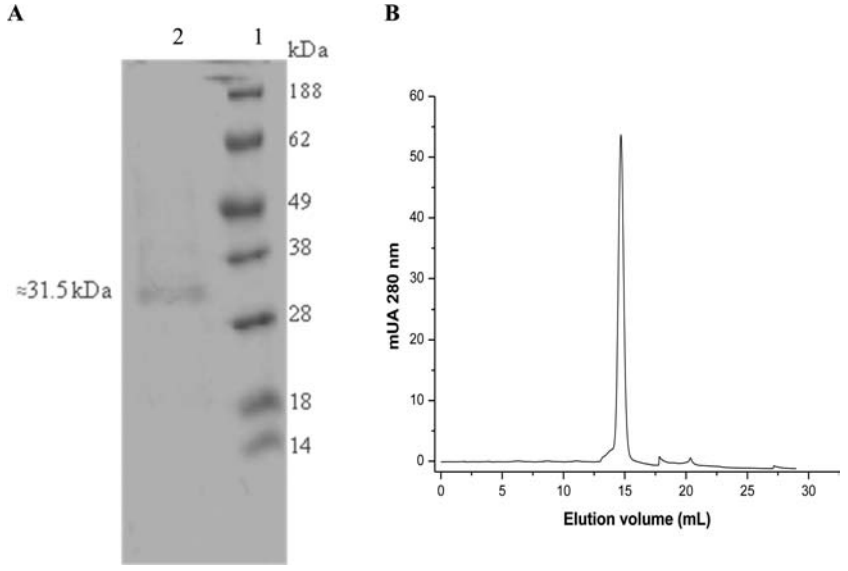


**Figure 3.** (A) SDS-PAGE of PPO purified from Manila mango: lane 1, molecular weight markers; lane 2, purified enzyme. (B) Elution profile by gel filtration from mango PPO.

**Gel Electrophoresis (SDS-PAGE).** Enzyme purity was determined at different purification steps using SDS-PAGE.[16] The concentration of the separating gel was 12%, and that of the stacking gel was 4%. Protein standard molecular weight markers were used.

**pH Dependence of PPO Activity.** The effect of pH on PPO activity was measured in 1 mL of 50 mM catechol in 0.1 M citric acid−0.2 M sodium phosphate buffer and in 2.5−8.0 M borate buffer, pH range 8.5−12.0 at 25 °C. Reaction was started by the addition of 33 $\mu$L of the isolated PPO. PPO specific activity (U/mg protein) was determined as described above.

**Optimum Temperature.** PPO activity was assayed in 1 mL, by incubating 33 $\mu$L of the enzyme in 0.1 M citric acid−0.2 M sodium phosphate buffer, pH 6.0, containing 50 mM catechol or pyrogallol for 30 min at different temperatures (20−80 °C). PPO activity was determined as described above.

**Determination of PPO Kinetic Parameters.** PPO velocity ($v$) at different substrate concentrations was measured in 0.2 M sodium phosphate buffer, pH 7.0, and various concentrations of substrates catechol, pyrogallol, and 4-methylcatecol (1−150 mM). The Michaelis−Menten constant ($K_m$) and maximum catalytic velocity ($V_{max}$) for each substrate were determined by Lineweaver−Burk and nonlinear regression.

**PPO Substrate Specificity.** PPO substrate specificity was determined using eight different substrates. PPO activity was monitored as the change in substrate absorbance (ΔAbs) at a given wavelength ($\lambda$) as follows: catechol, pyrogallol, 4-methylcatecol, epicatechin, caffeic acid, ferulic acid, and phenol at $\lambda$ = 420 nm; L-3,4-dihydroxyphenylalanine (DL-dopa) at $\lambda$ = 480 nm. PPO activity assay solution was prepared in 0.2 M sodium phosphate buffer, pH 7.0, and variable concentrations of the given substrate (1, 2.5, and 10 mM).[9,10] PPO specific activity (U/mg protein) was determined as described above.

**Effect of Inhibitors on PPO Activity.** PPO activity was measured with 50 mM catechol (substrate) in 0.2 M sodium phosphate buffer, pH 7.0, in the presence of different concentrations of inhibitor (0.1, 1, and 10 mM): tropolone, kojic acid, ascorbic acid, sodium chloride, sodium metabisulfite, citric acid, EDTA disodium salt, succinic acid,


dx.doi.org/10.1021/jf5029784 | J. Agric. Food Chem. 2014, 62, 9832−9840

benzoic acid, and potassium sorbate. The effect of inhibitors on PPO specific activity (U/mg protein) was determined as described above.

**Effect of Metal Ions on PPO Activity.** PPO activity was measured with 50 mM catechol in 0.2 M sodium phosphate buffer, pH 7.0, and the presence of different concentrations (0.1, 1, and 10 mM) of the following salts: KCl, $CaCl_2$, $Na_2SO_4$, $MgSO_4$, $MgCl_2$, $ZnSO_4$, and $MnSO_4$. For $CuSO_4$ the concentrations used were 0.5, 2.5, 5, and 10 mM. PPO specific activity (U/mg protein) in the presence of ions was determined as described above.

## RESULTS AND DISCUSSION

**PPO Extraction from Manila Mango.** In plants, PPO is a plastid enzyme; in contrast, their phenolic substrates are located in vacuoles. The extraction of PPO from Manila mango was performed by using Triton X-100, a nonionic detergent. Triton X-100 is widely used in the recovery of membrane constituents as it provides a mild nondenaturing condition for proteins. In addition, PVPP was included in the PPO extraction buffer to minimize *o*-quinone formation and prevent phenol–protein interactions.[17] Increased recovery in PPO activity has been observed by the addition of protease inhibitors to the extraction buffer, usually aprotinin (trasylol), PMSF, and/or benzamide.[18] Therefore, it was decided also to include aprotinin and PMSF in the PPO extraction buffer. After extraction was performed, the determined specific activity for Manila mango PPO (crude extract) was 41 U/mg protein, in contrast to those reported for PPOs from other fruits and vegetables such as Badami mango peel (1.34 U/mg protein),[13] Kensington mango (1.8 U/g fresh weight),[19] Haden mango (0.1 U/min·mL),[11] mamey (22 U/mg protein),[10] persimmon (8.8 U/mg protein),[20] and banana (20.7 U/mg protein).[8]

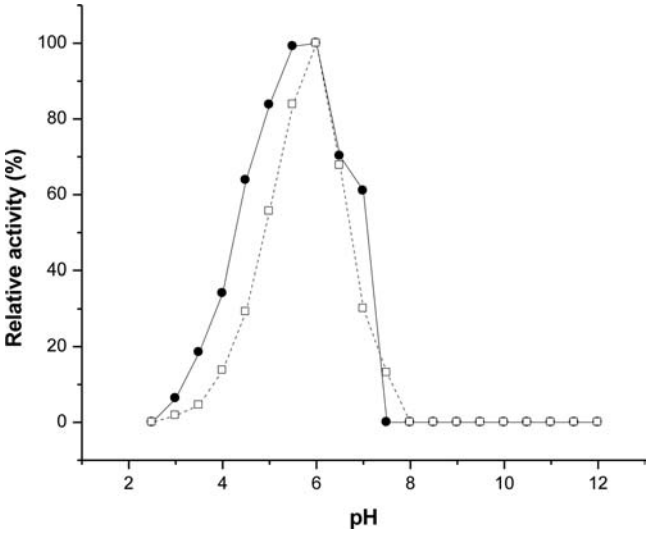


**Figure 4.** PPO activity from Manila mango dependence on pH. Catechol (□) and pyrogallol (●) were used as substrate in 0.1 M acid citric–0.2 M disodium phosphate buffer (pH 2.5–8.0) and 0.2 M borate (pH 8.5–12). Activity was expressed as relative activity (%) compared with high activity determined. Lines are drawn to aid visualization. Values are means from three replicates. Standard deviations were <5%.

**PPO Purification.** Ammonium sulfate precipitation (30–85%) resulted in a 4-fold increase in PPO purity (Table 1). Then, hydrophobic interaction chromatography was performed using phenyl-Sepharose 4-fast flow; this technique has been used previously in the purification of PPOs from different vegetables and fruits, that is, in apple,[9] mamey,[10] d'Anjou pear,[21] and peach,[22] but has not been used in mango PPO.

Figure 1 shows the elution profile of PPO. Unbound proteins were eluted at initial fractions, between 25 and 75 mL as monitored by absorbance at 280 nm. Then, the bound proteins began to be eluted at ≈195 mS/cm (fractions above 150 mL) (Figure 1). PPO activity was determined in collected fractions, and the highest activity was observed in fractions eluting at ≈160 mS/cm (182–232 mL). At this purification step, PPO showed a 103-fold increase in purity (Table 1). Fractions showing the highest specific activity were pooled and dialyzed against 20 mM Tris-HCl buffer, pH 7.0. Then, the dialyzed enzyme was loaded onto a Mono Q HR 10/10 anion exchange column and eluted; the above procedure has been useful in the purification of PPO from different sources including mamey,[10] Goldnugget loquat,[23] apple,[9] banana pulp,[8] Badami mango peel,[13] and Raspuri mango sap (latex) (DEAE-Sephacel).[24] On the other hand, in Kensington mango PPO sap and skin have been partially purified by Sephadex G-25.[19]

The elution profile (absorbance at 280 nm) showed a protein peak that elutes before the salt concentration increases (Figure 2). However, highly absorbing (280 nm) peaks were observed during elution with salt gradient; PPO activity was determined in collected fractions, and the highest PPO activities were located in fractions eluting between 32 and 42 mS/cm (108–150 mL) (Figure 2). At this purification step, PPO was purified 216-fold (Table 1).

**Electrophoresis and PPO MW Determination.** PPO purity was determined by sodium dodecyl sulfate–polyacrylamide gel electrophoresis (SDS-PAGE) and protein stained with Coomassie brilliant blue. The Manila mango PPO was essentially pure as observed in SDS-PAGE and showed a MW of ≈31.5 kDa; however, a MW of 65 kDa was determined by gel filtration (GF) (Figure 3). Therefore, the Manila mango PPO seems to be a dimer in its native state. After GF elution, PPO was collected and enzyme activity assayed and, importantly, the eluted enzyme showed a specific activity similar to that previously loaded. PPO MW determination by combining both SDS-PAGE and GF has been used before in other PPOs from different plant sources with confident results: (a) MW for PPO from mamey was ≈18 kDa by SDS-PAGE and 16.1 kDa by GF, a monomer;[10] (b) MW for PPO from loquat fruit was 58 kDa by SDS-PAGE and 55 kDa by GF, a monomer;[25] (c) MW for PPO from pineapple was ≈25 kDa by SDS-PAGE and ≈104 kDa by GF, a tetramer;[26] and (d) MW for PPO from Raspuri mango sap was ≈105 kDa by SDS-PAGE and ≈100 kDa by GF, a monomer.[24] In this regard, most PPOs from plants are monomers, but it has been found that some fungi PPOs are mainly oligomers (tetramers with small subunits).[27]

**Effect of pH on PPO Activity.** The activity of purified PPO was determined at different pH values using catechol and pyrogallol as substrates. PPO activity was observed in the pH range between 3.0 and 7.0 with both substrates. The maximum PPO activity was observed at pH 6.0 with 100% activity. Therefore, it may be considered that the optimum pH for PPO activity is 6.0 (Figure 4). At pH >7.5, PPO activity decreased drastically. Interestingly, PPO from Manila mango showed the highest activity at pH 6.0 with both substrates. As shown in Table 2, usually PPOs from fruits are more active at neutral or slightly acid pH.[26] For example, in PPO in flesh from varieties Tainong and Haden mango, the optimum pH values were shown at 7.0 and 6.0,[11,12] respectively; on the other hand, for

Table 2. Optimum pH, Temperature, and $K_m$ for PPO from Different Sources

| source | substrate | pH | temperature (°C) | $K_m$ (mM) | ref |
|---|---|---|---|---|---|
| Manila mango | catechol | 6 | 65 | 15.1 | this study |
| | pyrogallol | 6 | 65 | 2.7 | |
| | 4-methylcatechol | ND[a] | ND | 3.1 | |
| Tainong mango | catechol | 7 | 30 | 6.3 | 12 |
| | pyrogallol | ND | ND | 47.8 | |
| Haden mango | catechol | 6 | ND | ND | 11 |
| Chokanan mango peel | catechol | 5.5 | 55 | ND | 14 |
| Badami mango peel | catechol | 5.4 | 50 | 3.5 | 13 |
| | epicatechin | ND | ND | 2 | |
| | dopamine | ND | ND | 6.9 | |
| | caffeic acid | ND | ND | 12.4 | |
| Kensington mango sap, skin | 4-methylcatechol | 5.3 | 70−80 | ND | 19 |
| | 4-methylcatechol | 5.8 | 30 | ND | |
| atemoya | catechol | 7 | 28 | 79.3 | 29 |
| | 4-methylcatechol | 6 | 35 | 5.5 | |
| mamey | catechol | 7 | 35 | 44 | 10 |
| | pyrogallol | ND | ND | 1.3 | |
| Medlar | catechol | 6.8 | 55 | 5.7 | 23, 33 |
| | 4-methylcatechol | 6.5 | 35 | 7.5 | |
| | 3-(3,4-dihydroxyphenyl-alanine) propionic acid | ND | ND | 1.9 | |
| | epicatechin | ND | ND | 4 | |
| banana pulp | dopamine | 6.5 | 30 | 2.8 | 8 |
| Izmir grape | catechol | 7.2 | 25 | 3.65 | 30 |

[a]ND, not determined.

PPO in peel from varieties Chokanan and Badami mango, the optimum pH values were presented at 5.5 and 5.4, respectively,[13,14] using catechol as substrate in all cases. However, for PPO in the sap and skin from Kensington mango, the optimum pH values were 5.3 and 5.8, respectively, using 4-methylcatechol.[19] In this regard, it has been observed that the optimum pH for PPO activity seems to be dependent on the type of substrate, enzyme localization into the cell, plant source, and extraction method.

**Optimum Temperature.** The optimum temperature for PPO activity was analyzed by assaying the enzyme at temperatures ranging from 20 to 80 °C for catechol and pyrogallol using 0.1 M citric acid−0.2 M sodium phosphate buffer, pH 6.0, because at this pH was obtained the highest activity. PPO activity was maintained within the temperature range of 20−70 °C with catechol as substrate. On the other hand, maximum PPO activity with pyrogallol was in the range of 60−70 °C, with the highest activity observed at 65 °C for both substrates. PPO activity decreased when the temperature was increased above 70 °C. However, at 80 °C PPO activity was zero due to thermal inactivation (Figure 5). High temperatures disrupted the three-dimensional structure of the enzyme, leading to its denaturation.[17] Activity dependence on temperature has been studied in PPOs from different plant sources (Table 2). In the case of mango, PPO in flesh from Tainong mango showed highest activity at 30 °C using catechol as substrate,[12] but in Badami and Chokanan mango peel the highest activities were observed at 50 and 55 °C, respectively,[13,14] using the same substrate. In PPO from Kensington mango sap (latex) the highest activity was presented at 70−80 °C and in skin at 30 °C, using 4-methylcatechol.[19] The optimum temperature for PPO activity usually depends on the environmental condition where the fruit grows, plant species, and/or variety. However, it may be affected also by the type of substrate used in the activity assay.[17]

**PPO Kinetic Parameters.** The dependence of PPO velocity on substrate concentration was studied. Three different substrates were chosen: catechol, pyrogallol, and 4-methylcatechol.The lowest $K_m$ (highest affinity) was observed for pyrogallol (2.77 mM), followed by 4-methylcatechol (3.14 mM) and catechol (15.14 mM). The $K_m$ for pyrogallol was similar to that observed for PPO from mamey,[10] but very low when compared to that for Tainong mango ($K_m$ = 47.81 mM);[12] for PPO from Badami mango peel it was observed that epicatechin presented the highest affinity ($K_m$ = 2.0 mM),[13] followed by catechol, dopamine, and caffeic acid. Kinetic parameters have not been studied for varieties Haden, Chokanan, and Kensington mango.[11,14,19] Catechol seems to be the least preferred substrate for PPOs from most fruits and vegetables except Medlar ($K_m$ = 5.7 mM) (Table 2). In this

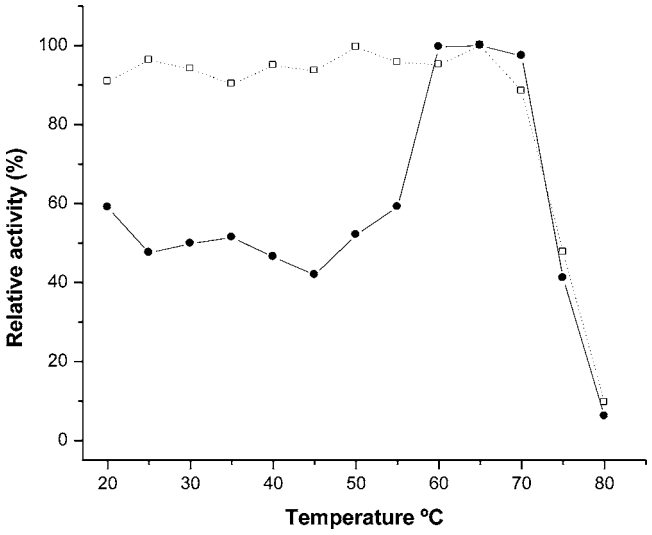


**Figure 5.** Optimum temperature of PPO from Manila mango. Catechol (□) and pyrogallol (●) were used in 0.1 M acid citric−0.2 M disodium phosphate buffer, pH 6.0. Pyrogallol also was probed. The results are very similar (data not shown). Activity was expressed as relative activity (%) compared with high activity determined. Lines are drawn to aid visualization. Values are means from three replicates. Standard deviations were <5%.

**Table 3. Substrate Specificity from Manila Mango PPO[a]**

| substrate | concentration (mM) | relative activity[b] (%) |
|---|---|---|
| catechol | 10 | 100 |
| | 2.5 | 17 |
| | 1 | 0 |
| pyrogallol | 10 | 145 |
| | 2.5 | 120 |
| | 1 | 95 |
| 4-methylcatechol | 10 | 62 |
| | 2.5 | 23 |
| | 1 | 14 |
| DL-dopa | 10 | 19 |
| | 2.5 | 0 |
| | 1 | 0 |

[a]Values are means from three replicates. Standard deviations were <5%. Also, caffeic acid, ferulic acid, epicatechin, and phenol were measured, showing no activity. [b]Activities are expressed as relative activity (%) compared with activity determined with 10 mM catechol. Substrates were prepared in 0.2 M sodium phosphate buffer, pH 7.0.

**Table 4. Effect of Inhibitors on PPO Activity from Manila Mango[a]**

| compound | concentration (mM) | relative activity[b] (%) |
|---|---|---|
| tropolone | 0.1 | 0 |
| | 1.0 | 0 |
| | 10.0 | 0 |
| ascorbic acid | 0.1 | 0 |
| | 1.0 | 0 |
| | 10.0 | 0 |
| sodium metabisulfite | 0.1 | 0 |
| | 1.0 | 0 |
| | 10.0 | 0 |
| kojic acid | 0.1 | 52 |
| | 1.0 | 24 |
| | 10.0 | 0 |
| sodium chloride | 0.1 | 45 |
| | 1.0 | 43 |
| | 10.0 | 41 |
| benzoic acid | 0.1 | 69 |
| | 1.0 | 64 |
| | 10.0 | 48 |
| citric acid | 0.1 | 70 |
| | 1.0 | 71 |
| | 10.0 | 67 |
| potassium sorbate | 0.1 | 77 |
| | 1.0 | 74 |
| | 10.0 | 63 |
| succinic acid | 0.1 | 82 |
| | 1.0 | 76 |
| | 10.0 | 69 |
| EDTA | 0.1 | 90 |
| | 1.0 | 89 |
| | 10.0 | 79 |

[a]Values are means from three replicates. Standard deviations were <5%. [b]Activities are expressed as relative activity (%) compared with activity determined with 50 mM catechol. The compounds were prepared with 0.2 M disodium phosphate buffer 7.0 in catechol 50 mM.

regard, PPOs from plants and fruits have different affinities toward diverse substrates. The active site of the enzyme seems to interact in different ways with substrates where the proper −R group structure and position provide the advantage for efficient binding and catalysis. However, the main criterion for choosing the best substrate is by the highest catalytic efficiency ($V_{max}/K_m$). In this regard, the $V_{max}/K_m$ (U $mM^{-1}$ $min^{-1}$) ratio for pyrogallol was 1926 followed by 1162 for 4-methylcatechol and 376 for catechol. Therefore, in this study pyrogallol seems to be the most effective substrate for Manila mango PPO.

**Substrate Specificity.** Substrate specificity for Manila mango PPO was studied using eight different substrates (Table 3). Relative activities were compared with activity observed in the presence of catechol (100%). The highest activity was found using pyrogallol (a trihydroxyphenol), followed by catechol, 4-methylcatechol, and DL-dopa (dihydroxyphenols) (Table 3). In contrast, no activity was detected for dihydroxyphenols epicatechin and caffeic acid or for monohydroxyphenols ferulic acid and phenol. Some authors suggest that the most common substrates for PPOs are catechol, 4-methylcatechol, chlorogenic acid, and catechins.[17,28] In this regard, it has been observed that pyrogallol is the best substrate for PPO from mamey,[10] whereas 4-methylcatechol has been shown to be the best substrate for PPO from atemoya[29] and Bramley's Seedling apple.[9] In contrast, catechol has been observed to be the best substrate for PPO from Izmir grape[30] and Tainong mango.[12] These differences maybe due to


dx.doi.org/10.1021/jf5029784 | J. Agric. Food Chem. 2014, 62, 9832−9840

Table 5. Effect of Metal Ions on PPO Activity from Manila Mango[a]

| compound | concentration (mM) | relative activity[b] (%) |
|---|---|---|
| KCl | 0.1 | 113 |
| | 1.0 | 118 |
| | 10.0 | 120 |
| $CaCl_2$ | 0.1 | 168 |
| | 1.0 | 197 |
| | 10.0 | ND |
| $MgCl_2$ | 0.1 | 90 |
| | 1.0 | 90 |
| | 10.0 | 89 |
| $Na_2SO_4$ | 0.1 | 89 |
| | 1.0 | 141 |
| | 10.0 | 195 |
| $MgSO_4$ | 0.1 | 123 |
| | 1.0 | 128 |
| | 10.0 | 149 |
| $MnSO_4$ | 0.1 | 93 |
| | 1.0 | 136 |
| | 10.0 | 177 |
| $ZnSO_4$ | 0.1 | 114 |
| | 1.0 | 134 |
| | 10.0 | 182 |
| $CuSO_4$ | 0.5 | 13 |
| | 2.5 | 33 |
| | 5.0 | 44 |
| | 10.0 | 51 |

[a]Values are means from three replicates. Standard deviations were <5%. [b]Activities are expressed as relative activity (%) compared with activity determined with 50 mM catechol. The compounds were prepared with 0.2 M disodium phosphate buffer 7.0 in catechol 50 mM. ND, not determined.

either plant species (and cultivars), the substrate, or the chemical structure of the side chain, number of hydroxyl groups, and position in the benzene ring.[17]

Natural phenols have been found in mango fruit; some of these are (a) cinnamic acid derivatives such as chlorogenic acid and ferulic acid; (b) flavonol derivates such as xanthone-*C*-glycosides, epicatechin gallate, and flavonol glycosides; (c) gallic acid derivatives such as gallotannins; (d) hydroxybenzoic acid derivates such as gallic acid, protocatechuic acid, and vanillic acid; and (e) xanthones such as mangiferin and mangostin, benzophenones, and ellagic acid.[31] In this regard, the observed relative abundance of phenolic compounds in fruits is as follows: cinnamic acid derivatives > catechins ≈ leucoanthocyanidins (flavan-3,4-diols) > flavonols. Many phenolic compounds are excellent as browning substrates and antioxidants. However, as antioxidants they are usually present at relative low concentrations such that at high concentration they are susceptible to autoxidation; however, they are found in fruits and vegetables in all structural parts. The presence of phenolic compounds in foods is considered beneficial for human health. In biological systems, they appear to react with oxygen species, whereas PPO causes most of the oxidative damage in foods when phenolic compounds act as substrates.[32]

**PPO Inhibition Profile.** PPO activity inhibition was determined in the presence of the following molecules: tropolone, kojic acid, ascorbic acid, sodium chloride, sodium metabisulfite, citric acid, ethylenediaminetetraacetic acid (EDTA) disodium salt, succinic acid, benzoic acid, and potassium sorbate. Complete inhibition was observed with tropolone, ascorbic acid, and sodium metabisulfite at 0.1 mM. Kojic acid also inhibited completely PPO activity but at 10 mM, whereas sodium chloride, benzoic acid, citric acid, succinic acid, potassium sorbate, and EDTA inhibited PPO but to a lower degree (Table 4).

PPO inhibitors are classified on the basis of the inhibition mechanism as follows: (a) reducing agents, (b) chelating agents, (c) complexing agents, (d) acidulants, (e) enzyme inhibitors, and (f) enzyme modifiers. All of them inhibit the formation of melanin by preventing the accumulation of *o*-quinones or by forming stable colorless products.[17]

Ascorbic acid inhibits PPO by reacting specifically with histidine residues, but it is commonly used also as an antibrowning agent.[17] Manila mango PPO exhibited 100% inhibition by ascorbic acid, and the same inhibition degree has been observed for PPOs from mamey[10] and Tainong mango.[12] The most effective inhibitor of enzymatic browning is known to be sodium metabisulfite. In agreement with the above, in the present study PPO showed 100% inhibition by metabisulfite. A similar result has been observed in PPOs from mamey,[10] atemoya,[29] Bramley's Seedling apple,[9] and medlar fruit,[33] with potassium metabisulfite. Sulfites act by reducing molecular oxygen present in the food system, thus making it unavailable for oxidative reactions. In addition, sulfites react with *o*-quinones and intermediate molecules in the browning reaction, preventing thus the formation of colored complexes. The use of this preservative has several disadvantages such as negative effects on texture, development of unpleasant flavors, and possible corrosion of containers.[34] Many inhibitors of PPO are known, but only a few have been considered as potential alternatives to sulfites. Kojic acid is a chelator of transition metal ions as well as a free radical scavenger. Kojic acid inhibits PPO from several *Aspergillus* species, mushrooms, and some plants and crustaceans and also inhibits effectively the formation rate of pigments and oxygen uptake.[35] Tropolone is structurally analogous to *o*-diphenol substrates and also acts as an effective copper chelator; that is, tropolone behaves as a potent competitive inhibitor in enzymes such as dopamine-$\beta$-hydroxylase and PPO from mushroom.[36] In this regard, PPO from Manila mango was 100% inhibited by tropolone (0.1 mM) and kojic acid (10 mM). In contrast, in PPO from Dominga grape, tropolone and kojic acid (1 mM) showed 85 and 12% activity inhibition, respectively;[37] in PPO from banana, tropolone and kojic acid (1 mM) inhibited the enzyme 80 and 10%, respectively;[38] in PPO from persimmon, tropolone (1 mM) inhibited completely the enzyme;[20] and in PPO from mamey, tropolone and kojic acid (10 mM) showed 100% activity inhibition.[10]

Sodium chloride, benzoic acid, citric acid, succinic acid, potassium sorbate, and EDTA were found to be the less effective inhibitors in Manila mango PPO. Similar results were observed in PPOs from mamey[10] and Bramley's Seedling apple.[9] EDTA is well-known as a metal ion chelator but displays low specificity for copper; however, in some cases it may inhibit PPO, whereas high salt (NaCl) concentration

enhances hydrophobic interactions, causing enzyme aggregation and consequently a loss in activity.[39] Some isolated PPOs seem to be relatively unaffected by inhibitors.[28]

PPOs from various sources have been studied in the presence of nonclassical inhibitors; that is, Tainong mango,[12] Haden mango,[11] Izmir grape,[30] and atemoya[29] were tested with β-mercaptoethanol, L-cysteine, glycine, diethyldithiocarbamate, sodium azide, thiourea, erythorbic acid, and resorcylic acid. In this regard, β-mercaptoethanol and L-cysteine exhibit high inhibition efficiency. However, β-mercaptoethanol may not be used in the food industry because of its toxicity concerns. L-Cysteine acts by readily forming complexes with quinones, thus inhibiting PPOs through formation of side products with *o*-quinone and 4-methylcatechol.[40]

**Effect of Metal Ions on PPO Activity.** The effect of metal ions on PPO activity is shown in Table 5. The presence of salts resulted in the increase (almost twice in some cases) of PPO activity; KCl has little effect on the PPO activity. The exceptions were $MgCl_2$ and $CuSO_4$, which caused inhibitory effects of ≈10 and >50%, respectively. A similar result was observed for $Mg^{2+}$ in PPO from atemoya, where both $MgCl_2$ and $MgSO_4$ caused inhibition of 20%.[29] In the presence of $MgCl_2$ Chokanan mango peel decreased 18% its PPO activity.[14] In contrast, $CuSO_4$, $FeSO_4$, and $MnCl_2$ have no measurable effect on PPO activity.[29] $BaCl_2$, $ZnSO_4$, $MnCl_2$, and $CuSO_4$ have no effect on enzyme activity as it just decreases ≈3% in PPO from banana.[8] Some of these metal ions probably combine with substrate and/or PPO, thus favoring the binding to active site and enhancing enzyme catalysis and resulting in increased activity.[39]

## AUTHOR INFORMATION


### Corresponding Author

*(H.N.) Phone/fax: (+52) 55 58146537. E-mail: hnajerap@gmail.com.



### Funding

This work was partially supported by scholarship ICYTDF (SRI/PB/55/2012) to G.P.-O., grants from CONACYT (156497) and PROMEP (UASLP-PTC-301) to J.G.S., and grants from CONACYT (105532) and PROMEP (UAM-PTC-144) to H.N.


### Notes

The authors declare no competing financial interest.

## REFERENCES


(1) Galán Saúco, V. *El Cultivo del Mango*, 2nd ed.; Mundi-Prensa: Madrid, Spain, 2009; Chapters 1 and 2.

(2) SIAP. Agricultural production from mango (*Mangifera*) Mexico, http://www.siap.gob.mx/index.php?option=com_wrapper&view=wrapper&Itemid=351.

(3) Ndiaye, C.; Xu, S. Y.; Wang, Z. Steam blanching effect on polyphenoloxidase, peroxidase and colour of mango (*Mangifera indica* L.) slices. *Food Chem.* **2009**, *13*, 92−95.

(4) Alija, C. M.; Bhat, S. G.; Prasada Rao, U. J. S. Valuable components of raw and ripe peels from two Indian mango varieties. *Food Chem.* **2007**, *102*, 1006−1011.

(5) Prieto, H.; Utz, D.; Castro, A.; Aguirre, C.; Gonzalez-Aguero, M.; Valdes, H.; Cifuentes, N.; Defilippi, B. G.; Zamora, P.; Zuniga, G.; Campos-Vargas, R. Browning in *Annona cherimola* fruit: role of polyphenol oxidase and characterization of a coding sequence of the enzyme. *J. Agric. Food Chem.* **2007**, *55*, 9208−9218.

(6) Ciou, J. Y.; Lin, H. H.; Chiang, P. Y.; Wang, C. C.; Charles, A. L. The role of polyphenol oxidase and peroxidase in the browning of water caltrop pericarp during heat treatment. *Food Chem.* **2011**, *127*, 523−527.

(7) Mayer, A. M. Polyphenol oxidases in plants and fungi: going places? *Phytochemistry* **2006**, *67*, 2318−2331.

(8) Yang, C. P.; Fujita, S.; Ashrafuzzaman, M.; Nakamura, N.; Hayashi, N. Purification and characterization of polyphenol oxidase from banana (*Musa sapientum* L.) pulp. *J. Agric. Food Chem.* **2000**, *48*, 2732−2735.

(9) Ni Eidhin, M. D.; Murphy, E.; O'Beirne, D. Polyphenol oxidase from apple (*Malus domestica* Borkh. cv Bramley's Seedling): purification strategies and characterization. *J. Food Sci.* **2006**, *71*, C51−C58.

(10) Palma-Orozco, G.; Ortiz-Moreno, A.; Dorantes-Alvarez, L.; Sampedro, J. G.; Najera, H. Purification and partial biochemical characterization of polyphenol oxidase from mamey (*Pouteria sapota*). *Phytochemistry* **2011**, *72*, 82−88.

(11) Park, Y. K.; Sato, H. H.; Almeida, T. D.; Moretti, R. H. Polyphenol oxidase of mango (*Mangifera indica* var. Haden). *J. Food Sci.* **1980**, *45*, 1619−1621.

(12) Wang, J.; Jiang, W.; B, W.; Liu, S.; Gong, Z.; Luo, Y. Partial properties of poliphenol oxidase in mango (*Mangifera indica* L. cv. 'Tainong') pulp. *J. Food Biochem.* **2007**, *31*, 45−55.

(13) Prabha, T. N.; Patwardhan, M. V. Purification and properties of polyphenoloxidase of mango peel (*Mangifera indica*). *J. Biosci.* **1982**, *4*, 69−78.

(14) Mehrnoush, A.; Shuhaimi, M.; Yazid, A. M. M. Characterization of polyphenol oxidase from mango (*Mangifera indica* L. cv. Chokanan) peel. *J. Food Agric. Environ.* **2012**, *10*, 109−112.

(15) Oktay, M.; Küfreviolğlu, I.; Kocaçalişkan, I.; Şakiroğlu, H. Polyphenol oxidase from Amasya apple. *J. Food Sci.* **1995**, *60*, 494−496.

(16) Laemmli, U. K. Cleavage of structural proteins during the assembly of the head of bacteriophage T4. *Nature* **1970**, *227*, 680−685.

(17) Yoruk, R.; Marshall, M. R. Physicochemical properties and function of plant polyphenol oxidase. *J. Food Biochem.* **2003**, *27*, 361−422.

(18) Gauillard, F.; Richard-Forguet, F. Polyphenoloxidases from Williams pear (*Pyrus communis* L., cv Williams): activation, purification and some properties. *J. Sci. Food Agric.* **1997**, *74*, 49−56.

(19) Robinson, S. P.; Loveys, B. R.; Chacko, E. K. Polyphenol oxidase enzymes in the sap and skin of mango fruit. *Aust. J. Plant Physiol.* **1993**, *20*, 99−107.

(20) Núñez-Delicado, E.; Sojo, M. M.; García-Carmona, F.; Sánchez-Ferrer, A. Partial purification of latent persimmon fruit polyphenol oxidase. *J. Agric. Food Chem.* **2003**, *51*, 2058−2063.

(21) Wissemann, K. W.; Montgomery, M. W. Purification of d'Anjou pear (*Pyrus communis* L.) polyphenol oxidase. *Plant Physiol.* **1985**, *78*, 256−262.

(22) Flurkey, W. H.; Jen, J. J. Purification of peach polyphenol oxidase in the presence of added protease inhibitors. *J. Food Biochem.* **1980**, *4*, 29−41.

(23) Şener, A.; Ümit Ünal, M.; Aksay, S. Purification and characterization of polyphenol oxidase from goldnugget loquat (*Eriobotrya japonica* cv. Goldnugget). *J. Food Biochem.* **2011**, *35*, 1568−1575.

(24) John, K. S.; Bhat, S. G.; Rao, U. J. S. P. Isolation and partial characterization of phenol oxidases from *Mangifera indica* L. sap (latex). *J. Mol. Catal. B−Enzym.* **2011**, *68*, 30−36.

(25) Ding, C. K.; Chachin, K.; Ueda, Y.; Imahori, Y. Purification and properties of polyphenol oxidase from loquat fruit. *J. Agric. Food Chem.* **1998**, *46*, 4144−4149.

(26) Das, J. R.; Bhat, S. G.; Gowda, L. R. Purification and characterization of a polyphenol oxidase from the kew cultivars of Indian pinneapple fruit. *J. Agric. Food Chem.* **1997**, *45*, 2031−2035.

(27) Flurkey, W. H.; Inlow, J. K. Proteolytic processing of polyphenol oxidase from plants and fungi. *J. Inorg. Biochem.* **2008**, *102*, 2160−2170.

(28) Mayer, A. M. Polyphenol oxidases in plants and fungi: going places? *Phytochemistry* **2006**, *67*, 2318−2331.
(29) Rodrígues Cháves, I.; Ferreira, E.; da Silva, M. A.; Neves, V. A. Polyphenoloxidase from atemoya fruit (*Annona cherimola* Mill. × *Annona squamosa* L.). *J. Food Biochem.* **2011**, *35*, 1583−1592.
(30) Önez, Z.; KarakuŞ, E.; Pekyardimci, Ş. Izmir grape polyphenol oxidase (*Vitis vinifera* L.): partial purification and some kinetic properties. *J. Food Biochem.* **2008**, *32*, 396−414.
(31) Manthey, J. A.; Perkins-Veazie, P. Influences of harvest date and location on the levels of β-carotene, ascorbic acid, total phenols, the in vitro antioxidant capacity, and phenolic profiles of five commercial varieties of mango (*Mangifera indica* L.). *J. Agric. Food Chem.* **2009**, *57*, 10825−10830.
(32) Robards, K.; Prenzler, P. D.; Tucker, G.; Swatsitang, P.; Glover, W. Phenolic compounds and their role in oxidative processes in fruits. *Food Chem.* **1999**, *66*, 401−436.
(33) Dincer, B.; Colak, A.; Aydin, N.; Kadioglu, A.; Güner, S. Characterization of polyphenoloxidase from medlar fruitd (*Mespilus germanica* L., Rosaceae). *Food Chem.* **2002**, *77*, 1−7.
(34) Almeida, M. E.; Nogueira, J. N. The control of polyphenol oxidase activity in fruits and vegetables. A study of the interactions between the chemical compounds used and heat treatment. *Plant Foods Hum. Nutr.* **1995**, *47*, 245−256.
(35) Kahn, V.; Ben-Shalom, N.; Zakin, V. Effect of kojic acid on the oxidation of *N*-acetyldopamine by mushroom tyrosinase. *J. Agric. Food Chem.* **1997**, *45*, 4460−4465.
(36) Espín, J. C.; Wichers, H. J. Slow-binding inhibition of mushroom (*Agaricus bisporus*) tyrosinase isoforms by tropolone. *J. Agric. Food Chem.* **1999**, *47*, 2638−2644.
(37) Núñez-Delicado, E.; Serrano-Megías, M.; Pérez-López, A. J.; López-Nicolás, J. M. Polyphenol oxidase from Dominga table grape. *J. Agric. Food Chem.* **2005**, *53*, 6087−6093.
(38) Sojo, M. M.; Núñez-Delicado, E.; García-Carmona, F.; Sánchez-Ferrer, A. Partial purification of a banana polyphenol oxidase using triton X-114 and PEG 8000 for removal of polyphenols. *J. Agric. Food Chem.* **1998**, *46*, 4924−4930.
(39) Sun, H. J.; Wang, J.; Tao, X. M.; Shi, J.; Huang, M. Y.; Chen, Z. Purification and characterization of polyphenol oxidase from rape flower. *J. Agric. Food Chem.* **2012**, *60*, 823−829.
(40) Janovitz-Klapp, A. H.; Richard-Forget, F. C.; Goupy, P. M.; Nicolas, J. J. Inhibition studies on apple polyphenol oxidase. *J. Agric. Food Chem.* **1990**, *38*, 926−931.

$$\frac{\partial C(x, t)}{\partial t} = D_e \frac{\partial^2 C(x, t)}{\partial x^2} \quad (1)$$

To solve eq 1, the following boundary conditions were set: $x = \pm a$, $C = C_o$ and $-a < x < a$, $C = f(t)$, with sample thickness $2a$.

The geometry of apple slices can be reduced to a slab, i.e., a "thin film with negligible edge effects". This means that diffusional mass transport through the edges of the film is negligible compared to that through the main surface of the film[18] (Figure 1). The solution proposed by Crank[19] for slab geometry is

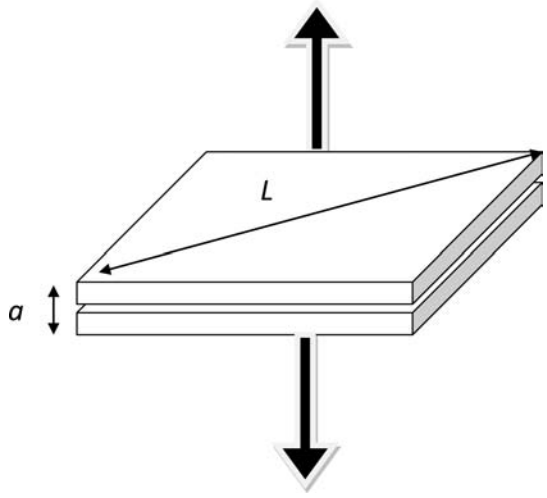


**Figure 1.** Scheme of diffusion from slab ($4a < L$) (→, solute leaching direction).

$$\frac{C(t) - C_\infty}{C_o - C_\infty} = \frac{8}{\pi^2} \sum_{n=1}^{n\to\infty} \frac{1}{(2n+1)^2} \exp\left(-\frac{D_e(2n+1)^2}{2a^2}\pi^2 t\right) \quad (2)$$

$$\frac{C(t) - C_\infty}{C_o - C_\infty} = \frac{8}{\pi^2} \exp\left(-\frac{D_e}{2a^2}\pi^2 t\right) \quad (3)$$

where $C$ is the average solute concentration at time $t$ of sampling, $C_o$ is the initial uniform concentration, and $C_\infty$ is the solute concentration after time $t$.

It is generally assumed that, for a Fourier number ($-D_e/4a^2\pi^2$) greater than 0.1,[20] only the first term in the series becomes significant. When this condition is attained, the effective diffusivity can be calculated by plotting $\ln(Y)$ against time ($t$). $Y$ is the dimensionless concentration (eq 5).

Linear behavior must be observed in accordance with

$$\ln Y = \ln \frac{8}{\pi^2} - \frac{D_e}{2a^2}\pi^2 t \quad (4)$$

with

$$Y = \frac{C(t) - C_\infty}{C_o - C_\infty} \quad (5)$$

For each set of conditions, the adjustable parameters of each model for decreases in sugar and polyphenols were determined.

## MATERIALS AND METHODS

**Plant Materials.** Two varieties of dessert apple (Golden Delicious and Granny Smith), purchased in a local supermarket (Auchan, Avignon, France), were used for the experiments. Tissue from the parenchyma zone of the apple was chosen after manually removing the peel and core. Planar pieces 20 mm high were cut from the parenchyma tissue; four slices were obtained per fruit. To prevent any polyphenol oxidation, the apple slices were sprayed with a solution of 40 g/L sodium fluoride (NaF). A total of 10 fruits per cultivar were used for each leaching run, with different batches of 10 fruits replicated 3 times in leaching experiments.

**Determination of the Isotonic Point.** Cylindrical samples of diameter 1 cm were cut with a core borer from the flesh side of the section, trimmed to a length of 4.70 cm using a double-bladed razor, and then soaked overnight in a mannitol solution (from 0 to 0.8 M). For each mannitol concentration, six apple cylinders coming from six different apples were used. To minimize cellular degradation of tissue strength during the experiment because of pH variation and following the method described by Lin and Pitt,[21] the mannitol solutions were buffered at pH 7 with $K_2HPO_4$ (0.02 M) and $KH_2PO_4$ (0.02 M).

Samples represented approximately 30% of solution volume. Before and after the soaking, weight and dimensions (diameter and height) of the samples were determined using an analytical balance (±0.01 g, CP124S, Sartorius, Germany) and digital calliper (Absolute Digimatic, Mitutoyo, U.K.). The apple tissue cylinders were carefully blotted with tissue paper to remove excess water before the measurements. The isotonic point was calculated by interpolation to zero weight gain or volume change from the weight gain or loss of tissue as a function of the mannitol concentration. The water potential ($\Psi$) in the cell after soaking was estimated from the molarity of the solution using the ideal gas law

$$\Psi = -MRT \quad (6)$$

where $M$ is the molarity, $T$ is the temperature (K), and $R = 0.008\,314$ kJ mol$^{-1}$ K$^{-1}$.

To estimate the osmotic pressure ($\Psi_{op}$) of the cell contents in any solution, the osmotic pressure at incipient plasmolysis ($\Psi_{op}{}^0$) was first determined. $V^0$ is the sample volume at incipient plasmolysis, and $V$ is the sample volume in the given solution. The turgor pressure ($P_c$) in a given solution was obtained from

$$\Psi_{op} = \Psi_{op}{}^0 (V^0/V) \quad (7)$$

$$P_c = \Psi - \Psi_{op}{}^0 \quad (8)$$

**Mass-Transfer Experiment.** Mannitol was used as the osmotic agent. A solid/liquid ratio of 1:20 was used under magnetic stirring. Experiments were run at a constant temperature (20 °C) in stainless-steel vessels, each containing a different concentration of osmotic solution, namely, 0.2, 0.4, and 0.6 M. An additional vessel of distilled water was used as a control. Apple pieces were retrieved for biochemical analysis after 1, 2, 4, and 6 h.

Matrix mass changes were monitored to determine water gain, after each immersion time during soaking experiments. The measurements were repeated 3 times, with a different batch of apple each time.

Water gain percentage ($W_g$)

$$W_g\,(\%) = \frac{M(t) - M_o}{M_o} \times 100 \quad (9)$$

where $M_o$ is the matrix weight (g) before the experiment and $M(t)$ is the matrix weight (g) during the experiment at a time $t$.

**Biochemical Analyses.** Biochemical analyses were performed on powdered product after freeze-drying. All of the samples were freeze-dried in a USIFROID SMH 15 freeze-dryer (Usifroid, France) for 48–72 h.

*Solvents and Chemicals.* Methanol, acetonitrile, and acetone of chromatographic quality were provided by Fisher Scientific (Fair Lawn, NJ), and toluene-α-thiol was provided by Sigma-Aldrich (Deisenhofen, Germany). Deionized water was obtained with a


dx.doi.org/10.1021/jf503100d | J. Agric. Food Chem. 2014, 62, 9841–9847

Milli-Q water system (Millipore, Bedford, MA). (+)-Catechin, (−)-epicatechin, caffeoylquinic acid, mannitol, glucose, and fructose were also provided by Sigma-Aldrich. Phloretin and *p*-coumaric acid were from Extrasynthese (Lyon, France). Phloridzin was from Fluka (Buchs, Switzerland).

*Quantification of Sugar.* Fruit parenchyma freeze-dried powder (5 g) was added to 20 mL of distilled water and homogenized with a polytron homogenizer for 1 min. The homogenates were centrifuged at 9000*g* for 10 min at 4 °C. The supernatant was collected to analyze sugars by a colorimetric enzymatic method as described by Bureau et al.[12]

*Quantification of Polyphenols by High-Performance Liquid Chromatography (HPLC) after Thioacidolysis.* Polyphenols were quantified by HPLC after thioacidolysis as described by Bureau et al.[12] The average degree of polymerization ($DP_n$) was measured by calculating the molar ratio of all of the flavan-3-ol units (thioether adducts plus terminal units) to (−)-epicatechin and (+)-catechin corresponding to terminal units. A HPLC system equipped with a diode array detector (SPD-M20A, Schimadzu, Inc., Kyoto, Japan) and a Lichro 250 × 4 mm column, Lichrospher 100 RP-18.5 $\mu$m (25 cm × 4.6 mm), were used. Quantification was performed by the external standard method. Results were expressed in milligrams per kilogram of fresh weight (FW). Losses of phenolic compounds (MC) were calculated, using eq 10 and expressed as percentage (w/w) of the initial concentration

$$\mathrm{MC}\ (\%) = \frac{\mathrm{DM}(0)C(0) - \mathrm{DM}(t)C(t)}{\mathrm{DM}(0)C(0)} \times 100 \qquad (10)$$

where $C(0)$ is the initial phenolic compound concentration in the sample (mg/kg of dry weight), $C(t)$ is the phenolic compound concentration in the sample at time $t$ (mg/kg of dry weight), DM(0) is the initial dry matter of the sample (g/100 g of FW), and DM($t$) is the dry matter of the sample at time $t$ (g/100 g of FW)

**Statistical Analysis.** Data underwent statistical analysis using the analysis of variance (ANOVA) test with SPSS (version 7.0, IBM, Chicago IL) Windows 7 software. Means were compared using Duncan's multiple range tests. Pooled standard deviations (SDs) were also estimated.[22] Pooled SDs were calculated using the sum of individual variances weighted by the individual degrees of freedom of each series of replicates.[23] A multiple regression analysis module was also used to determine raw material characteristics on the response to osmotic variation. To obtain the model parameters, the R (version 3.0.1, free license) nonlinear regression tool was used.

## RESULTS AND DISCUSSION

**Determination of the Isotonic Point.** Figure 2 presents matrix length changes as a function of the mannitol concentration. Turgor and osmotic pressure values in soaking solution were calculated. Osmotic pressure increased and turgor pressure decreased as the mannitol concentration increased. A relationship between the solution osmotic pressure and cell turgor pressure was observed. The isotonic points of Granny Smith and Golden Delicious were determined by plotting the sample volume variation against the mannitol concentration. The point of equilibrium of Granny Smith was 0.43 M, and the point of equilibrium of Golden Delicious was 0.61 M. Therefore, the value of the isotonic point for Granny Smith was −1.15 MPa, and the value of the isotonic point for Golden Delicious was −1.49 MPa. Similar results were found by Lin and Pitt[21] and Alamar et al.[24] on apple slices in various mannitol solution concentrations. We can assume that variety and composition effects explain differences in isotonic point values.

**Effects on Dry Matter (DM) Changes.** During the leaching process, the DM content at different immersion durations was experimentally obtained over a range of concentrations (0, 0.2, 0.4, and 0.6 M). In Figure 3, for both

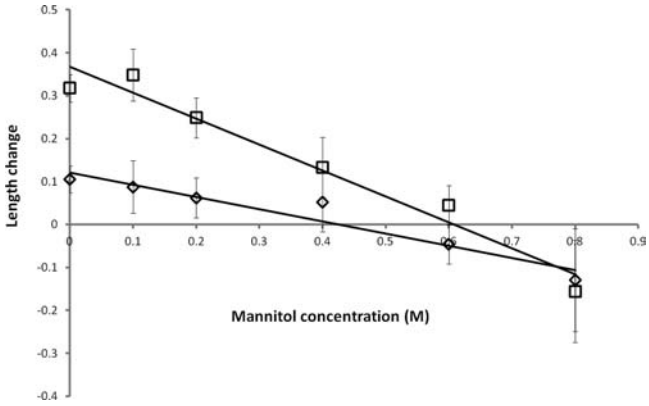


**Figure 2.** Parenchyma tissue length changes in various mannitol solutions (three biological replicates). Two apple varieties were used (□, Golden Delicious; ◇, Granny Smith). Isotonic points were determined by linear regression. Pooled SD values were 0.026 for Golden Delicious and 0.039 for Granny Smith, respectively.

apples, DM data means are plotted against time. The rates of matter loss were determined from the graph. Water entry into the sample was also monitored, as presented in Figure 3. Water gain resulted in a weight increase from 12 to 16% in apple matrix in 0 M mannitol solution (pure water). No data are available for other mannitol solutions. Similar results were reported by Linn and Pitt[21] in hypotonic solution. Two simultaneous phenomena, DM loss and water entrance, took place during the leaching process. Their combined effect could explain DM losses according to immersion time. Apparent diffusivity and equilibrium matter content ($C_\infty/C_o$) were therefore determined.

For Golden Delicious, DM decreased at 0 and 0.2 M mannitol contents. No changes were observed for higher mannitol concentrations. For Granny Smith, a DM decrease was observed only at 0 M. The losses of DM were probably due to diffusion mostly of sugars in soaking solution. According to the isotonic point of each apple variety, the leaching occurred only for a difference of at least 0.4 M between cells and external solution. DM losses were closely linked to differences in osmotic pressure between fruit and external solution.

Apparent diffusivity values were estimated from analytical solutions by Crank[19] by fitting DM. Apparent diffusivity was then determined. Table 1 presents diffusivity values as a function of the mannitol concentration. DM losses occurred only from 0 to 0.2 M for Golden Delicious and 0 M for Granny Smith. The apparent diffusivity values were therefore determined. DM losses decreased with increasing the mannitol concentration. The decrease in turgor pressure between cells and aqueous solution seemed to limit DM losses.

**Effect on the Total Sugar Content.** The majority of the DM in ripe apple is made up of simple sugars. Figure 4 shows the plots of the sugar concentration versus immersion time. For both apples, total sugar losses decreased as mannitol in the solution increased from 0 to 0.6 M. The total sugar retained in the matrix then went from 5.3 to 7.7 g/100 g of FW for Golden Delicious and from 6.7 to 9.5 g/100 g of FW for Granny Smith. The losses depended upon the mannitol concentration in the medium. As in previous results, sugar leaching in solution could also be due to an osmotic pressure difference. The experimental data were then fitted to estimate apparent diffusivity from eq 2, with only the first term of the series being retained. The results presented in Table 1 show that the decrease in apparent

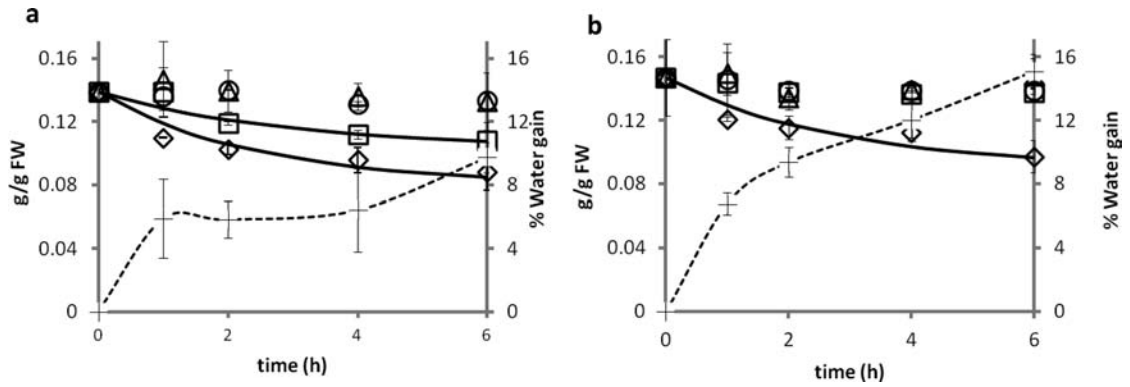


**Figure 3.** DM changes in different osmotic solutions (◇, 0 M; □, 0.2 M; △, 0.4 M; and ○, 0.6 M) against time for two apple varieties: (a) Golden Delicious and (b) Granny Smith. Water gain (+) percentage against time in different osmotic solutions.

**Table 1. Apparent Diffusivity with Equilibrium Content ($C_\infty/C_o$) for DM and Sugars Leaching from Apple Slices in Mannitol Solutions (Three Biological Replicates)**

| | Granny Smith | | | | Golden Delicious | | | |
|---|---|---|---|---|---|---|---|---|
| | DM | | total sugars | | DM | | total sugars | |
| mannitol concentration (M) | $D_e$ ($\times 10^{-9}$) | $C_\infty/C_o$ | $D_e$ ($\times 10^{-9}$) | $C_\infty/C_o$ | $D_e$ ($\times 10^{-9}$) | $C_\infty/C_o$ | $D_e$ ($\times 10^{-9}$) | $C_\infty/C_o$ |
| 0 | 1.81 ± 0.39[a] | 0.65 | 2.48 ± 0.31 | 0.67 | 2.20 ± 0.19 | 0.63 | 1.8 ± 0.43 | 0.53 |
| 0.2 | | 0.91 | | 0.95 | 0.73 ± 0.29 | 0.78 | 1.31 ± 1.90 | 0.77 |
| 0.4 | | 0.96 | | 0.75 | | 0.96 | | 0.64 |
| 0.6 | | 0.93 | | 0.85 | | 0.99 | 0.29 ± 0.38 | 0.67 |

[a]Standard error.

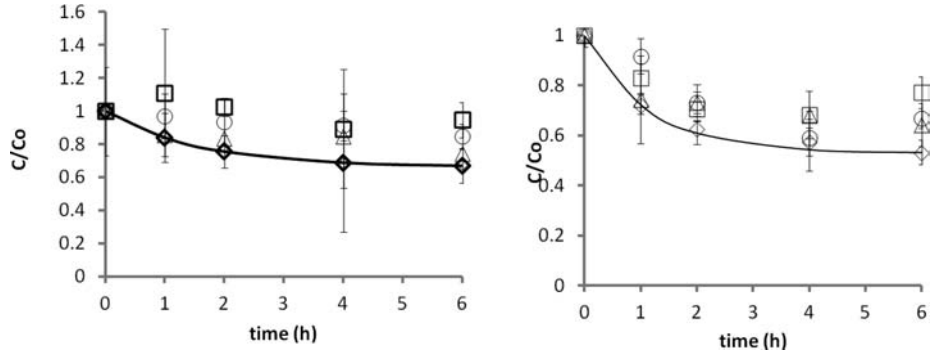


**Figure 4.** Total sugar concentration changes in different osmotic solutions (◇, 0 M; □, 0.2 M; △, 0.4 M; and ○, 0.6 M) against time for two apple varieties: (a) Granny Smith and (b) Golden Delicious. Models of diffusion are represented by full lines.

**Table 2. Concentration of Phenolic Compounds (mg/kg of FW) in Parenchyma Tissue of the Apple Cultivar Samples[a]**

| apple variety | CAT | EPI | PCA | $DP_n$ | CQA | *p*CQ | XPL | PLZ | PT |
|---|---|---|---|---|---|---|---|---|---|
| Golden Delicious | 26 ± 25 | 70 ± 37 | 580 ± 280 | 7.17 ± 0.01 | 87 ± 13 | 1.5 ± 0.8 | 11 ± 4 | 12 ± 3 | 780 ± 30 |
| Granny Smith | 20 ± 17 | 58 ± 25 | 760 ± 50 | 6.52 ± 2.26 | 56 ± 9 | 10 ± 0.7 | 7 ± 1 | 9 ± 2 | 910 ± 100 |

[a]Data are expressed as the mean ± SD for three biological replicates. CAT, (+)-catechin; EPI, (−)-epicatechin; PRO, procyanidins; $DP_n$, average degree of polymerization of procyanidins; CQA, cafeoylquinic acid; *p*CQ, *para*-coumarylquinic acid; XPL, phloretin xyloglucoside; PLZ, phloridzin; and PT, total polyphenols.

diffusivity was from 1.8 to 0.3 × $10^{-9}$ $m^2$ $s^{-1}$ for Golden Delicious and only 2.5 × $10^{-9}$ $m^2$ $s^{-1}$ for Granny Smith. No apparent diffusivity value was determined for the sugar content, which did not decrease significantly. The model did not apply. The values of $D_e$ were found to depend upon the mannitol solution concentration, with no effect of the apple variety. Total sugars were decreased during the leaching process. However, the increase of the solution concentration by an osmotic agent, such as mannitol, could preserve total sugar losses.

This conclusion agrees with results obtained for the extraction of total sugar in similar conditions for apple in different concentrations of osmotic solution.[25,26]

The different behaviors of total sugar may reflect the mechanism of transport in the cell.[25] As reported by Lin and Pitt[21] in distilled water, cell rupture because of high turgor pressure caused cytolysis. According to the apple variety, an increase in the mannitol concentration in aqueous solution decreased total sugar losses. This may be linked to the extent of cytolysis or the slope of the concentration gradient.


dx.doi.org/10.1021/jf503100d | J. Agric. Food Chem. 2014, 62, 9841−9847

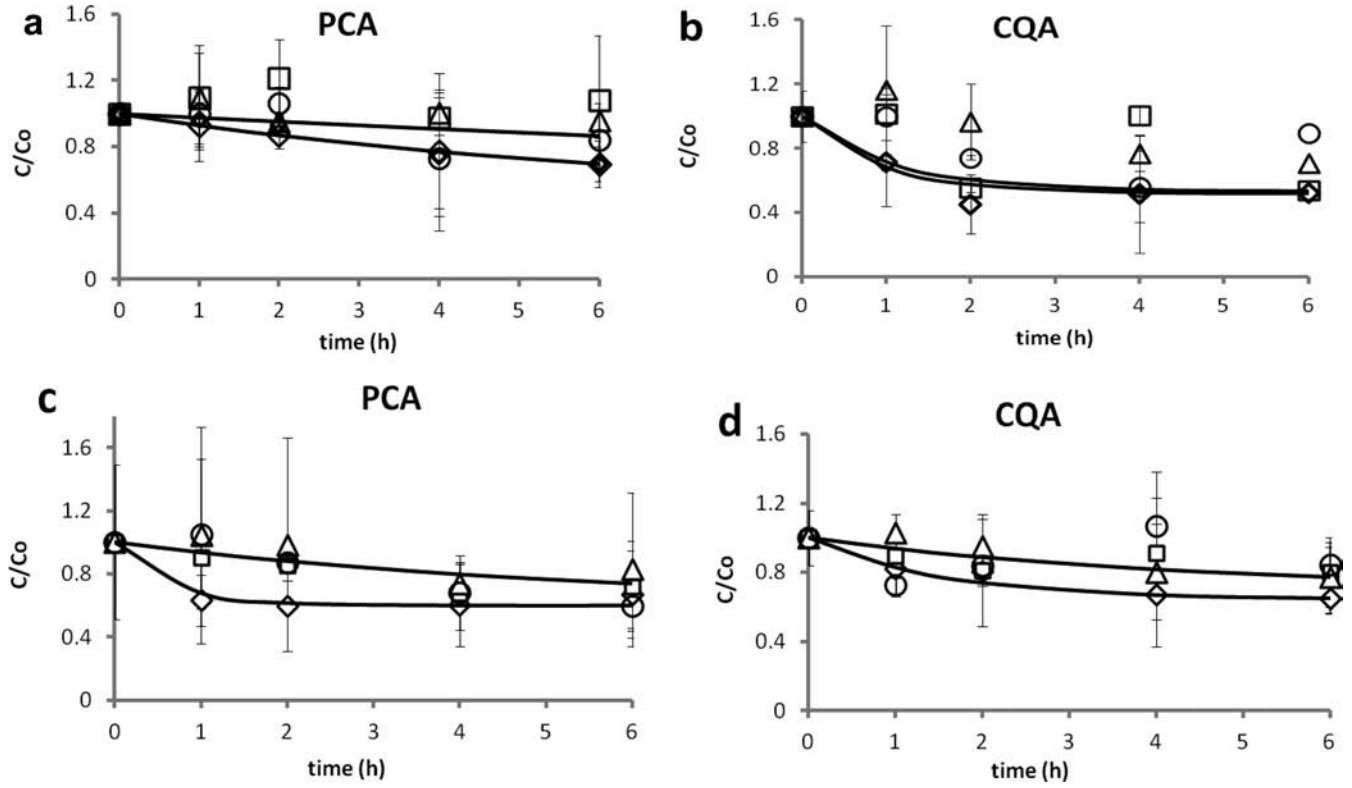


**Figure 5.** Changes in phenolic compounds in different osmotic solutions (◇, 0 M; □, 0.2 M; △, 0.4 M; and ○, 0.6 M) according to time for two apple varieties: (a and b) Granny Smith and (c and d) Golden Delicious (three biological replicates). Models of diffusion are represented by full lines. PCA, procyanidins; CQA, caffeoylquinic acids.

**Characterization of the Polyphenol Composition in Fresh Fruit.** The two dessert apple varieties were selected for their different phenolic contents and concentrations; the initial measurements are presented in Table 2. The main antioxidants in Golden Delicious and Granny Smith are polyphenols. Marked differences in total polyphenol content were found as a function of cultivar. Granny Smith contained more polyphenols than Golden Delicious. Our results were similar to those of previous studies.[14]

HPLC individual identification found polyphenols from three subclasses in the flesh of both apples: (1) flavan-3-ols (monomeric catechins and procyanidins), (2) hydroxycinnamic acids (chlorogenic acid and *para*-coumaroylquinic acid), and (3) dihydrochalcones (phloretin xyloglucoside and phloridzin).

In agreement with previous studies,[14] procyanidins were the main phenolic compounds, representing 74 and 84% of total polyphenols in Granny Smith and Golden Delicious, respectively. Their degree of polymerization ($DP_n$) of 7.2 and 6.6 for Golden Delicious and Granny Smith, respectively, were also close to those reported earlier.[14] Monomeric flavan-3-ols, accounted for 12 and 8% of total polyphenol in Golden Delicious and Granny Smith parenchyma, respectively. Caffeoylquinic acid, the main hydroxycinnamic acid, represented 11 and 6% of total polyphenols in Golden Delicious and Granny Smith parenchyma, respectively. Finally, dihydrochalcones represented less than 3% of the phenolic compounds in both apple varieties.

**Effects of Osmotic Solutions on Polyphenol Leaching.** Because slices were pretreated by NaF, a potent inhibitor of polyphenol oxidase, no oxidation was expected to occur, and within the time scale of the experiment, auto-oxidation was not significant. Losses of phenolic compounds from apple tissues in this experiment were therefore solely due to leaching.

Osmolarity of mannitol solutions affected polyphenol leaching. Figure 5 presents the evolution of concentrations (relative to FW) of procyanidins and caffeoylquinic acid. Losses of phenolic compounds were estimated by the difference in their concentrations relative to FW of slices before and after leaching.

*Flavan-3-ol Subclass.* For the Granny Smith variety, (+)-catechin decreased during the first 4 h of the treatment in distilled water and fell to 15% of the initial content. However, no (+)-catechin losses could be quantified in mannitol solutions, regardless of the mannitol concentrations. Losses of (−)-epicatechin were 47% in distilled water, with again no losses in the different mannitol solutions. Similar results were also found with losses of 31% procyanidins in distilled water and no losses in different mannitol solutions.

In Golden Delicious, (+)-catechin decreased by 47% in distilled water but only very slightly in mannitol solutions. Similar results were obtained for (−)-epicatechin and procyanidins.

*Hydroxycinnamic Acid Subclass.* In the Granny Smith variety, caffeoylquinic acid losses decreased with increasing the mannitol concentration. For *p*-coumaroylquinic acids, the opposite behavior was observed.

For the Golden Delicious variety, caffeoylquinic acid losses were also observed. However, no losses of *p*-coumaroylquinic acids were observed. The results present few different trends as a function of apple cultivar.

*Dihydrochalcones.* In the Golden Delicious variety, phloridzin losses were 30 and 35% in 0 and 0.2 M mannitol solutions, respectively. No losses were observed at higher


dx.doi.org/10.1021/jf503100d | J. Agric. Food Chem. 2014, 62, 9841−9847

**Table 3. Apparent Diffusivity of Phenolic Compounds from Apple Parenchymatous Tissues in Different Osmotic Solutions (Three Biological Replicates)[a]**

| phenolic compound | mannitol concentration (M) | GD ($\times 10^{-9}$, $m^2$ $s^{-1}$) | $C_\infty/C_0$ | GS ($\times 10^{-9}$, $m^2$ $s^{-1}$) | $C_\infty/C_0$ |
|---|---|---|---|---|---|
| CAT | 0 | 0.28 ± 0.04[b] | 0.66 | 0.07 ± 0.15 | 0.87 |
| | 0.2 | 0.20 ± 0.05 | 0.70 | nd[c] | nd |
| | 0.4 | 0.06 ± 0.04 | 0.70 | nd | nd |
| | 0.6 | nd | 0.81 | nd | nd |
| EPI | 0 | 0.25 ± 0.06 | 0.60 | 0.28 ± 0.16 | 0.53 |
| | 0.2 | 0.17 ± 0.09 | 0.66 | nd | nd |
| | 0.4 | 0.19 ± 0.04 | 0.69 | nd | nd |
| | 0.6 | 0.04 ± 0.20 | 0.81 | nd | nd |
| PCA | 0 | 0.17 ± 0.15 | 0.72 | 0.20 ± 0.03 | 0.69 |
| | 0.2 | 0.18 ± 0.04 | 0.69 | 0.01 ± 0.01 | nd |
| | 0.4 | nd | 0.79 | nd | nd |
| | 0.6 | nd | 0.62 | nd | 0.65 |
| CQA | 0 | 0.21 ± 0.04 | 0.60 | 0.37 ± 0.18 | 0.67 |
| | 0.2 | 0.14 ± 0.05 | 0.77 | 0.20 ± 0.19 | 0.70 |
| | 0.4 | nd | 0.75 | 0.21 ± 0.07 | 0.66 |
| | 0.6 | nd | 0.85 | nd | 0.67 |
| PT | 0 | 0.19 ± 0.12 | 0.62 | 0.20 ± 0.02 | 0.67 |
| | 0.2 | 0.16 ± 0.04 | 0.69 | nd | nd |
| | 0.4 | nd | 0.79 | nd | nd |
| | 0.6 | nd | 0.62 | nd | 0.85 |

[a]CAT, (+)-catechin; EPI, (−)-epicatechin; CQA, caffeoylquinic acid; PT, total polyphenols; GD, Golden Delicious; GS, Granny Smith; and $C/C_o$, equilibrium polyphenol content. [b]Standard error. [c]Not determined.

mannitol solutions. Phloretin xyloglucoside decreased by 15% in pure water, while no changes appeared in mannitol solutions. For the Granny Smith variety, phloridzin losses were 50% in pure water. No losses were observed in mannitol solutions. Phloretin xyloglucoside losses were 30% in 0 and 0.2 M mannitol solution, but in 0.4 and 0.6 M, losses fell to 20%.

Monomeric catechins, hydroxycinnamic acids, and dihydrochalcones were either preserved or had limited losses in mannitol solution. The same trends were found for procyanidins.

The decreases in the leaching of phenolic compounds in the presence of mannitol were due to physiological barriers in cells. Cell structural integrity thus affected polyphenol diffusion. Difference in osmotic pressure caused changes in cell structure integrity.

The losses found here were considerably lower than those observed by Renard,[27] who studied diffusion to water of thermally treated pear slices. Devic et al.,[5] after 3 h in an optical density (OD) system, i.e., with very high sugar contents in the external solution, observed very limited diffusion of polyphenols. The differences between monomeric phenols (catechins, hydroxycinnamic acids, or dihydrochalcones) and procyanidins could be explained by their affinity with cell walls, as stated by Renard et al.[28] and Le Bourvellec et al.[29] A further indication for the involvement of this mechanism is an increase in the degree of polymerization for the retained procyanidins (up to 7.2 in Golden Delicious and 7.4 in Granny Smith after 6 h). Le Bourvellec et al.[30] found that procyanidins were mainly bound to pectins. Watrelot et al.[31] also found that stronger association was obtained with longer procyanidin molecules interacting with highly methylated pectins.

*Estimation of Apparent Diffusivity of Polyphenols.* The experimental data were also fitted, and results are presented in Table 3. Apparent diffusivity values were determmined when changes in polyphenol content were significant.

Apparent diffusivity values decreased with increasing the mannitol solution concentration. Total phenolic values varied from 0.1 to 0.2 × $10^{-9}$ $m^2$ $s^{-1}$ for Golden Delicious and from 0.2 to 0.3 × $10^{-9}$ $m^2$ $s^{-1}$ for Granny Smith. Total phenolic compound apparent diffusivities depended upon the osmotic solution concentration and were lower than those observed for total sugars. Sugars present in cells seem to leach faster than polyphenols, possibly owing to their lower molecular weight but also their physiological role in the plant.

Phenols must thus overcome the physiological barriers, mainly cell membranes, which provide dominant resistance for phenol release and influence mass transfer.[32] Different cell states in osmotic solution as reported[21,26] also seemed to affect polyphenol migration out of the matrix. Procyanidins presented lowest diffusivities, possibly owing to their high molecular weight[33] and non-covalent interaction with cell wall materials.[34]

Sugar and polyphenol concentrations decreased during the immersion of apple slices in mannitol solution depending upon a certain level of the mannitol concentration. The changes were probably due to leaching into the soaking solution. The application of Fick's second law allowed for the determination of apparent diffusivity. The link found between the decrease in solute loss and increase in the mannitol concentration could be associated with integrity of the cell structure. In all cases, the concentration of phenolic compounds changed according to the difference in osmotic pressure of the soaking solution. In raw fruit, leaching occurs if cell integrity is lost. Some of the difference in phenolic compound leaching was found to be a function of apple variety.

## AUTHOR INFORMATION

### Corresponding Author

*Telephone: +33-4-32-72-24-94. Fax: +33-4-32-72-24-92. E-mail: catherine.renard@avignon.inra.fr.

### Funding

The authors thank the Ministry of Higher Education and Research of Côte d'Ivoire for grants to Mouhamadou Kebe. The research leading to these results received funding from the European Community's Seventh Framework Program (FP7/2007-2013) under Grant Agreement FP7-222-654 DREAM.

### Notes

The authors declare no competing financial interest.

## ■ ACKNOWLEDGMENTS

The authors thank the SQPOV Laboratory (Fruit Team) for their assistance and technical expertise.

## ■ REFERENCES

(1) Knorr, D.; Zenter, M.; Heinz, V.; Lee, D.-U. Applications and potential of uultrasonic in food processing. *Trends Food Sci. Technol.* **2004**, *15*, 261−266.

(2) Lindley, M. G. The impact of food processing on antioxidants in vegetable oils, fruits and vegetables. *Trends Food Sci. Technol.* **1998**, *9*, 336−340.

(3) Devic, E.; Guyot, S.; Daudin, J.-D.; Bonazzi, C. Effect of temperature and cultivar on polyphenol retention and mass transfer during osmotic dehydrated of apples. *J. Agric. Food Chem.* **2010**, *58*, 606−614.

(4) Singh, B.; Kumar, A.; Gupta, A. K. Study of mass transfer kinetics and effective diffusivity during osmotic dehydration of carrot cubes. *J. Food Sci.* **2007**, *79*, 471−480.

(5) Devic, E.; Guyot, S.; Daudin, J.-D.; Bonazzi, C. Kinetics of polyphenol losses during soaking and drying of cider apples. *Food Bioprocess Technol.* **2010**, *3*, 867−877.

(6) Kaymak-Ertekin, F.; Sultanoglu, M. Modelling of mass transfer during osmotic dehydration of apples. *J. Food Eng.* **2000**, *46*, 243−250.

(7) Rastogi, N. K.; Raghavarao, K. S. M. S.; Niranjan, K.; Knorr, D. Recent developments in osmotic dehydration: Methods to enhance mass transfer. *Trends Food Sci. Technol.* **2002**, *13*, 48−59.

(8) Macheix, J.-J.; Fleuriet, A.; Sarni-Manchado, P. Composés phénoliques dans la plante—Structure, biosynthèse, répartition et rôles. In *Les Polyphénols en Agroalimentaire*; Sarni-Manchado, P., Cheynier, V., Eds.; Tec & Doc-Lavoisier: Paris, France, 2003.

(9) Boyer, J.; Liu, R. H. Apple phytochemicals and their health benefits. *Nutr. J.* **2004**, *3* (5), 1−15.

(10) Ader, P.; Grenacher, B.; Langguth, P.; Scharrer, E.; Wolffram, S. Cinnamate uptake by rat small intestine: Transport kinetics and transepithelial transfer. *Exp. Physiol.* **1996**, *81*, 943−955.

(11) Bernards, M. A.; Lewis, N. G. The macromolecular aromatic domain in suberized tissue: A changing paradigm. *Phytochemistry* **1998**, *47*, 915−933.

(12) Bureau, S.; Scibisz, I.; Le Bourvellec, C.; Renard, C. M. G. C. Effect of sample preparation on the measurement of sugars, organic acids, and polyphenols in apple fruit by mid-infared spectroscopy. *J. Agric. Food Chem.* **2012**, *60*, 3551−3563.

(13) Guyot, S.; Marnet, N.; Sanoner, P.; Drilleau, J. F. Direct thiolysis on crude apple materials for high-performance liquid chromatography characterization and quantification of polyphenols in cider apple tissues and juices. *Methods Enzymol.* **2001**, *335*, 57−70.

(14) Guyot, S.; Marnet, N.; Drilleau, J. Procyanidins are the most abundant polyphenols in dessert apples at maturity. *Lebensm.-Wiss. Technol.* **2002**, *51*, 6240−6247.

(15) Soliva-Fortuny, R. C.; Martin-Belloso, O. New advances in extending the shelf-life of fresh-cut fruits. *Trends Food Sci. Technol.* **2003**, *14*, 341−353.

(16) Varzakas, T. H.; Leach, G. C.; Israilides, C. J. Theoretical and experimental approaches towards the determination of solute effective diffusivities in foods. *Enzyme Microb. Technol.* **2005**, *37*, 29−41.

(17) Paradisia, P.; Cesaric, R.; Mainardid, F.; Tampierib, F. The fractional Fick's law for non-local transport processes. *Phys. A* **2001**, *293*, 130−142.

(18) Siepmann, J.; Siepmann, F. Modeling of diffusion controlled drug delivery. *J. Controlled Release* **2012**, *16*, 351−362.

(19) Crank, J. *The Mathematics of Diffusion*, 2nd ed.; Clarendon Press: Oxford, U.K., 1975; pp 1−27.

(20) Sineiro, J.; Domfnguez, H.; Ntifiez, M. J.; Lema, J. M. Ethanol extraction of polyphenols in an immersion extractor. Effect of pulsing flow. *J. Am. Oil Chem. Soc.* **1996**, *73*, 1121−1125.

(21) Lin, T. T.; Pitt, R. E. Rheology of apple and potato tissue as affected by cell turgor pressure. *J. Texture Stud.* **1986**, *17*, 291−313.

(22) Thalheimer, W.; Cook, S. How to calculate effect sizes from published research articles: A simplified methodology. *Work Learn. Res.* **2002**, 1−9.

(23) Box, W. G.; Hunter, G. E.; Hunter, J. S. *Statistics for Experimenters, an Introduction to Design, Data Analysis and Model Building*; John Wiley and Sons: Hoboken, NJ, 1978; pp 352.

(24) Alamar, M. C.; Vanstreels, E.; Oey, M. L.; Molto, E.; Nicolaï, B. M. Micromechanical behaviour of apple tissue and compression tests: Storage conditions and cultivar effect. *J. Food Eng.* **2008**, *86*, 324−333.

(25) Lazarides, N. H.; Gekash, V.; Mavroudis, N. Apparent mass diffusivities in fruit and vegetable tissues undergoing osmotic processing. *J. Food Eng.* **1997**, *31*, 315−324.

(26) Rodrigues, A. E.; Mauro, M. A. Effective diffusion coefficients behavior in osmotic dehydration of apple slices considering shrinking and local concentration dependence. *J. Food Process Eng.* **2007**, *31*, 207−228.

(27) Renard, C. M. G. C. Effects of conventional boiling on the polyphenols and cell walls of pears. *J. Sci. Food Agric.* **2005**, *318*, 310−318.

(28) Renard, C. M. G. C.; Baron, A.; Guyot, S.; Drilleau, J.-F. Interactions between apple cell walls and native apple polyphenols: Quantification and some consequences. *Int. J. Biol. Macromol.* **2001**, *29*, 115−125.

(29) Le Bourvellec, C.; Le Quéré, J.-M.; Renard, C. M. G. C. Impact of non-covalent interactions between condensed tannin and apple cell walls: Elaboration of a quantitative model and its application to transfer from fruit to juice. *J. Agric. Food Chem.* **2007**, *55*, 7896−7904.

(30) Le Bourvellec, C.; Guyot, S.; Renard, C. M. G. C. Interactions between apple (*Malus* × *domestica* Borkh.) polyphenols and cell walls modulate the extractability of polysaccharides. *Carbohydr. Polym.* **2009**, *75*, 251−261.

(31) Watrelot, A. A.; Le Bourvellec, C.; Imberty, I.; Renard, C. M. G. C. Interactions between pectic compounds and procyanidins are iinfluence by methylation and chain length. *Biomacromolecules* **2013**, *14*, 709−718.

(32) Kays, S. J. *Postharvest Physiology and Handling of Perishable Plant Products*; Van Nostrand Reinhold: New York, 1991; pp 526.

(33) Sanoner, P. Les polyphénols de la pomme à cidre: Diversité variétale et oxydation. Ph.D. Thesis, Université de Caen/Basse-Normandie, Caen, France, 2001 (in French).

(34) Le Bourvellec, C.; Guyot, S.; Renard, C. M. G. C. Interaction between procyanidins and the apple cell wall material. Part 1: Effects of some environmental parameters. *Biochim. Biophys. Acta* **2004**, *1672*, 192−202.

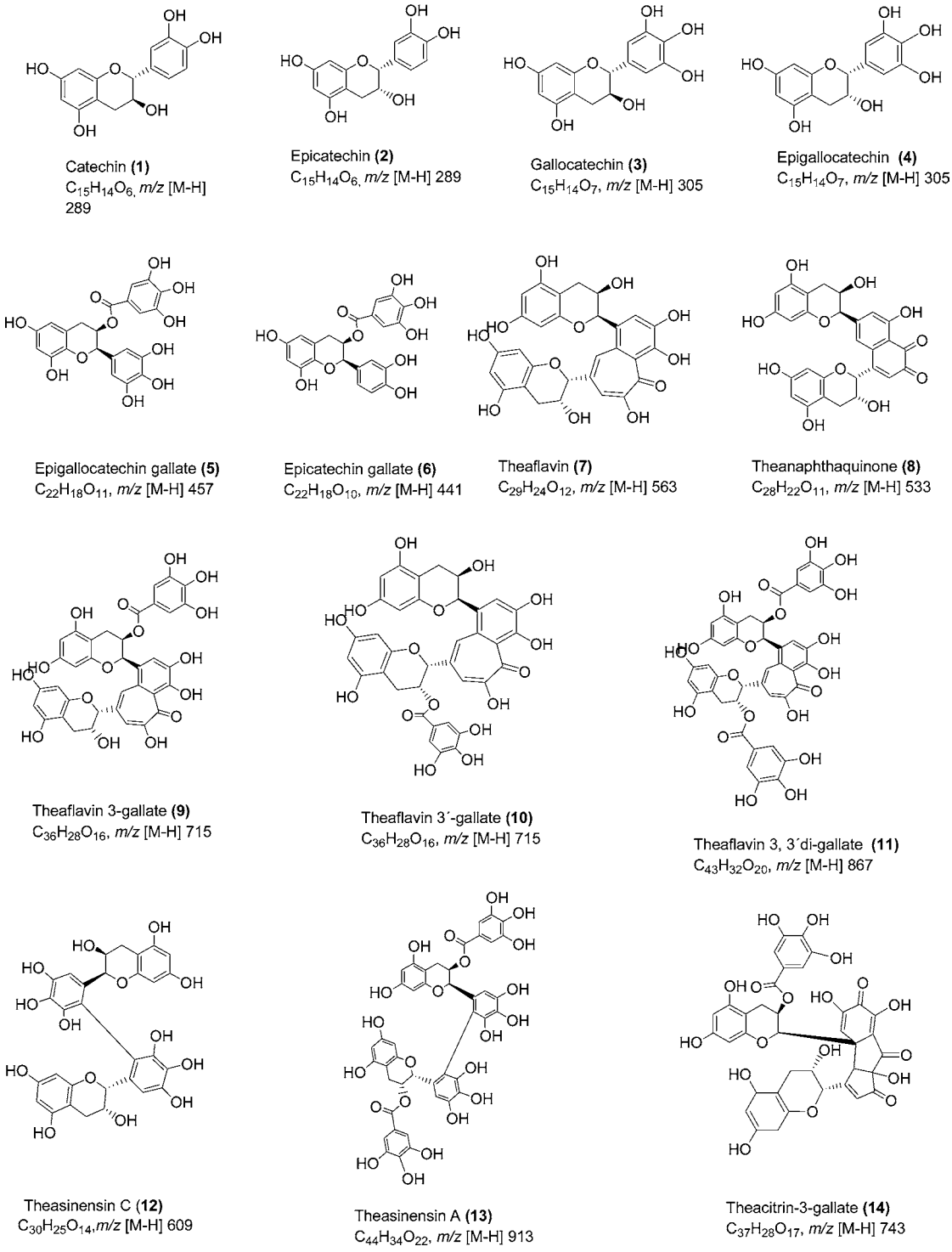


**Figure 1.** Structures of catechins and their formal dimers previously identified in black tea.

(O), hydrogen ($H_2$), gallates ($C_7H_5O_4$), and catechins in various oxygenation degrees acting as main building blocks in black tea chemistry. According to the data generated, oxygen insertion was observed as mass increment in the largest number.[16] However, the type and nature of the compounds were still unknown. Later, on the basis of initial ESI-FTICR-MS data[17,18] from targeted tandem LC-MS experiments, the data revealed that a significant fraction of thearubigins consists of polyhydroxylated derivatives of catechin dimers (a stepwise increase of oxygen increments within the dimeric structures), the so-called "homologous series".[9] On the basis of the experimental data, the oxidative cascade hypothesis was proposed. This hypothesis proposes the formation of the *o*-quinones of different dimeric and oligomeric structures in the oxidation process, where these could be followed by nucleophilic addition of water in the fermentation process, leading to polyhydroxylated structures, and this continues until all aromatic hydrogens are replaced by OH functionalities, thus increasing the number of the components within the thearubigin fractions. Previous investigations carried out on


dx.doi.org/10.1021/jf502220c | J. Agric. Food Chem. 2014, 62, 9848−9859

the oxidative cascade hypothesis revealed the presence of homologous series of theaflavins (TFs), their gallate esters theaflavin mono- and digallates, and theacitrin (TC) structures.[16,17] Kuhnert et al. additionally showed that a significant portion of these compounds are in redox equilibrium with their quinone counterparts.[17] MALDI-MS experiments on TRs[18] and detailed tandem MS investigations by Yassin et al. additionally showed that trimers and teramers of flavan-3-ols are major products of oxidative tea fermentation.[18]

The aim of this study is to further confirm the second level of the oxidative cascade hypothesis and to structurally elucidate the novel thearubigin components. For this investigation electrospray ionization tandem mass spectrometry (ESI-LC-ion trap-MS) was employed for characterizing thearubigins in homologous series reaching $m/z$ 1000. A particular emphasis was put on derivatives of theasinensins (TSs, also referred to as bisflavanones) and theanaphthaquinones (TNQs), the two dimeric catechin derivatives so far not investigated. The experimental strategy used was based on generating extracted ion chromatograms EIC at the mass of the parent ion and their corresponding hydroxylated derivatives, where the signals are strong enough to obtain $MS^2$ and $MS^3$ spectra. In this approach, the different $m/z$ signals of the parent ion of theanaphthaquinone and theasinensin C dimeric structures and their hydroxylated components were obtained in the homologous series, where several regioisomers were detected at distinct retention times, increasing the structural variety of the newly identified thearubigin compounds.

Furthermore, interestingly a new series of compounds could be also identified for the first time revealing the presence of $H_2O_2$ as a contributor in the fermentation process.[19] Previous studies done by Sinkar et al. confirmed the presence of $H_2O_2$ and its important role in the oxidation process leading to the formation of thearubigins in the presence of peroxidase enzyme.[20] In this investigation, by focusing on the ESI-LC-tandem mass $MS^n$ measurements, the homologous series of dimeric structures theasinensin C and theanaphthaquinone are obtained, and a new series containing epoxide derivatives of theasinensin A that has not been previously investigated are reported.

## MATERIALS AND METHODS

**Chemicals and Reagents.** All chemicals and reagents were purchased from Sigma-Aldrich. Black tea samples of Ceylon, Assam, and Indian tea varieties were purchased from a local supermarket and provided from the Unilever Excellence Center.

**Preparation of Thearubigins.** Freshly ground black tea leaves (8 g) were added to 150 mL of freshly boiled water and kept for 10 min in a Thermos flask, which was inverted every 30 s. The flask contents were filtered through a Whatman no. 4 filter paper to remove the leaves, and the remaining brew was allowed to cool to room temperature. Caffeine sufficient to achieve 20 mM was added to the brew, stirred to ensure dissolution, allowed to stand at 4 °C for 2 h, and centrifuged at 23300*g* for 20 min. The resulting precipitate was recovered and suspended in boiling water and partitioned against aliquots of ethyl acetate (40 mL) until no further color was extracted (usually five times).

The ethyl acetate supernatant was removed and evaporated to dryness under nitrogen below 35 °C, and the residue (TF fraction) was recovered in 10 mL of distilled water. The aqueous phase was partitioned at 80 °C against 2 volumes of chloroform, and the decaffeinated liquid was stored overnight at −80 °C and freeze-dried. The freeze-dried material (TR fraction) was stored at −20 °C until required and reconstituted as required for the analysis. The yield of thearubigins in this method was mainly 10% and obtained as orange to light brown fluffy powders.

**LC-$MS^n$ Method.** The extracted thearubigin solutions were reconstituted to a 0.5 mg/mL concentration in 1:1 methanol/water, filtered through a 0.45 $\mu$m HPLC filter, and analyzed by LC-MS method using Aligent 1100 series LC equipment and a DAD detector with a light pipe flow cell (recording at 400 and 245 nm and scanning from 200 to 600 nm). This was coupled to an ion trap mass spectrometer fitted with an ESI source (Bruker Daltonics HCT Ultra) operating in the negative ion Auto $MS^n$ mode to obtain fragment ion $m/z$. Separations were achieved on a Polaris 5-C18-A column (length, 250 mm; diameter, 3 mm; particle size, 5 $\mu$m) with a step gradient elution employing acetonitrile (MeCN) and water containing 0.005% formic acid, as follows: 8% MeCN from 0 to 50 min, then changing to 31% MeCN for 10 min, then changing to 25% MeCN for a further 5 min. The column eluent was first directed to the UV detector and then to the ESI interface operating with a capillary voltage of 1 V, and fragmentation amplitude was set starting at 30% and ending at 200%. The capillary temperature was also set at 300 °C. Nitrogen gas was used here as nebulizing and drying gas at a flow rate of 10 L/min and a pressure of 10 psi, respectively.

**High-Resolution LC-MS.** High-resolution LC-MS in the negative ion mode was carried out using the same HPLC equipped with a MicrOTOF Focus mass spectrometer (Bruker Daltonics) fitted with an ESI source, and internal calibration was achieved with 10 mL of 0.1 M sodium formate solution injected through a six-port valve prior to each chromatographic run. Calibration was carried out using the enhanced quadratic calibration mode. It should be noted that in TOF calibration the intensities of the measured peaks have a significant influence on the magnitude of the mass error with high-intensity peaks, resulting in detector saturation displaying larger mass errors. Where necessary, this was avoided by using a more dilute sample. All MS measurements were carried out in the negative ion mode.

**HPLC Analysis.** The extracted thearubigins were analyzed by HPLC using an Agilent 1200 HPLC pump with a 5 $\mu$L loop, coupled to an Agilent 1100 autosampler and an Agilent 1100 DAD-UV−vis detector. Black tea extracts and thearubigin extracts were reconstituted at 5 mg/mL in 1:1 MeOH/$H_2O$ and filtered through a 0.45 $\mu$m HPLC filter prior to injection of a volume of 3 $\mu$L. HPLC analysis used a Polaris 5-C18-A column (length, 250 mm; diameter, 3 mm; particle size, 5 $\mu$m) with a step gradient elution employing acetonitrile (MeCN) and water containing 0.005% formic acid, as follows: 8% MeCN from 0 to 50 min, then changing to 31% MeCN for 10 min, then changing to 25% MeCN for a further 5 min.

**Data Analysis.** Data were analyzed using Bruker Data Analysis 4.0 software. Micro TOF data were analyzed (TICs, EICs) after external enhanced quadratic calibration. Ion trap data were analyzed in terms of EICs, TICs, and neutral loss chromatograms (NLCs) using the implemented software routines.

## RESULTS AND DISCUSSION

For further investigating the hydroxylation process of the dimeric components and confirming their presence within the oxidative cascade hypothesis in thearubigin fractions, ESI-LC-$MS^n$ experiments were carried out on the homologous series of theasinensin C (**12**) and its gallate ester theasinensin A (**13**) (Figure1). These structures are formed via dimerization of two catechin derivatives. Additionally, a homologous series of theanaphthaquinones (**8**) (Figure 1) were investigated, which is formed via further oxidation of theaflavin. Both dimeric structures are likely implicated in the thearubigin formation.

LC−tandem MS experiments were performed on the selected $m/z$ parent ions expected for these compounds, which are potentially the first member of the anticipated homologous series. Extracted ion chromatograms (EICs) were created from the $m/z$ values of hypothetical members of the homologous series, and in case strong signals were observed at the corresponding $m/z$ values, targeted fragmentation experi-

Table 1. Homologous Series for Theanaphthaquinone Confirming the Presence of the Hydroxylated Derivatives with Their Selected $MS^2$ and $MS^3$ Fragment Ions and Neutral Losses Observed[a]

| | molecular formula | RT[b] (min) | LC-MS [M − H] ($m/z$) | fragment ion LC-$MS^2$ ($m/z$) | neutral loss $\delta$M(S1 − S2)[c] (Da) | fragment ion LC-$MS^3$ ($m/z$) |
|---|---|---|---|---|---|---|
| **8** | $C_{28}H_{21}O_{11}$ | 47.9 | 533 | **514.8 (100%)**, 464.6 (55.9%), 396.6 (31.6%) | 18.2, 69, 137 | 304.7 (100%), 376.8 (40%) |
| **8** + $O_2$ | $C_{28}H_{21}O_{13}$ | 50.1 | 565.1 | **544.9 (100%)**, 494.5 (40.5%) | 20.7, 70.1 | 240.6 (100%) |
| **8** + $O_3$ | $C_{28}H_{21}O_{14}$ | 53.5 | 581.2 | **512.5 (100%)**, 444.5 (33.1%) | 69, 138 | 444.5 (100%), 376.5 (18%) |
| | | 43 | 581.3 | **512.5 (100%)**, 444.5 (19%) | 69, 137 | 444.5 (100%), 376.5 (25%) |
| | | 34.7 | 581.3 | **512.5 (100%)**, 444.5 (20%) | 69, 137 | 444.5 (100%) |
| | | 30.9 | 581.2 | **512.5 (100%)**, 444.5 (31.4%) | 69, 137 | 444.5 (100%), 376.4 (21.3%) |
| **8** + $O_4$ | $C_{28}H_{21}O_{15}$ | 48.4 | 597 | **528.5 (100%)** | 69 | 402.5 (100%) |
| **8** + $O_5$ | $C_{28}H_{21}O_{16}$ | 39 | 613.2 | **544.5 (100%)**, 476.5 (5%) | 69, 137 | 402.5 (100%) |
| | | 28.1 | 613.1 | **544.5 (100%)**, 476.5 (5.2%) | 69, 137 | 402.5 (100%) |

[a]$MS^2$ fragment ions highlighted in bold are subjected for further fragmentation for $MS^3$ fragment ions. [b]RT, retention time (min). [c]$\delta$M(S1 − S2), mass loss (Da).

ments were carried out corresponding to $MS^2$ and $MS^3$ spectra. The presence of fragment ions with their neutral losses was located; therefore, the fragmentation pattern and its mechanism have been determined for the parent structure forming the first member of each homologous series. Later, oxygen mass increments were introduced, and different signals at $m/z$ values corresponding to the majority of predicted hydroxylated derivatives were established. The interpretation here was based on the fragment ions and the neutral losses for the parent ions observed, where the mechanism of fragmentation has been previously established either from investigation of authentic reference compounds or from literature precedents.[16] The assumption for identifying the homologous series of different hydroxylated parent ions was based on their $m/z$ values and their $MS^2$ fragment spectra observed. An identical fragmentation mechanism has to be obtained for the whole homologous series. For example, theaflavins (**7** shown in Figure 1) undergo fragmentation with a neutral loss of an enone of $m/z$ 137 ($C_7H_6O_3$), which can be rationalized in terms of retro Diels-Alder fragmentation (RDA) at one of the benzopyran moieties.[21] It has been confirmed that the whole homologous series of this compound underwent the same fragmentation.[16] On the other hand, its gallate esters, for example, theaflavin mono/digallates (**9**, **10**, and **11** in Figure 1) underwent losses of 152 and 170 Da, indicating the loss of galloyl moieties. The whole series underwent oxygen insertions within the sites of the fragment ions obtained or within the available sites of the galloyl neutral losses having the same fragmentation mechanism. Hence, it was suggested that it is reasonable to expect that a similar fragmentation mechanism will apply to all members of the homologous series investigated. There is ample evidence in the literature for many classes of compounds, where minor structural changes do not alter the basic fragmentation pathways.[22,23] Therefore, the hydroxylated derivative will fragment by the same mechanism as the parent compound. It was anticipated that generally retention time on reversed phase packings would decrease relative to the parent compound as hydroxylation increased unless internal hydrogen bonding significantly increased the hydrophobicity.[16]

**Theanaphthaquinone and Its Homologous Series.** Theanaphthaquinone (**8**) showed an MS spectrum at $m/z$ 533 characterized by its $MS^2$ fragment ions: at $m/z$ 514 as a base peak revealing the loss of $H_2O$; at $m/z$ 464 having a neutral loss of 69 Da, which is rationalized by the loss of $C_3HO_2$ from the quinone part of this compound; a fragment ion of a very weak intensity at $m/z$ 396 showing a neutral loss of 137 Da indicating a RDA fragmentation occurring on one of the catechin moieties of this molecule. The EIC of theanaphthaquinone and its fragment spectra are shown in Figure 1 in the Supporting Information. Theanaphthaquinones have different sites available to hydroxylation, and to evaluate the assignment of these peaks as hydroxy-theanaphthaquinone, EICs were prepared to their corresponding predicted masses and the data are exhibited in Table 1. Furthermore, by using constant neutral loss analysis of the tandem mass, the presence of particular fragment ions and their neutral losses corresponding to their chromatographic peaks could be located and tentative structures assigned.

EICs were created for the predicted polyhydroxylated compounds of theanaphthaquinone (**8** + $O_x$). These showed the presence of $m/z$ values corresponding to the components with two oxygen insertions at $m/z$ 565.1 ($C_{28}H_{21}O_{13}$), three oxygen insertions at $m/z$ 581.2 ($C_{28}H_{21}O_{14}$), four oxygen insertions at $m/z$ 597 ($C_{28}H_{21}O_{15}$), and five oxygen insertions at $m/z$ 613.1 ($C_{28}H_{21}O_{16}$). However, these were of low intensity when compared to other signals corresponding to members of homologous series of TFs and TCs previously reported.[17] The high-resolution masses of all TNQ derivatives were in line with data from previous FT-ICR-MS data and confirmed the elemental composition of these ions.[9]

Only a single chromatographic peak was detected for $m/z$ 565.4 corresponding to **8** + $O_2$ for the predicted dihydroxylated derivative at a retention time of 50.1 min. Tandem mass experiment of this compound gave $MS^2$ fragment ions at $m/z$ 544.9, revealing a loss of $H_2O$ molecule, and a characteristic fragment ion at $m/z$ 494.5, revealing a loss of $C_3HO_2$. The same fragmentation was previously observed in the parent ion, thus showing that this compound belongs to the homologous series of theanaphthaquinone with two oxygen insertions. This peak was tentatively assigned as a dihydroxylated derivateive of TNQ (**8** + $O_2$).

Four chromatographic peaks were detected in the EIC at the $m/z$ 581.2 (**8** + $O_3$) at different retention times of 53.5, 43, 34.7, and 30.9 min, as expected for the trihydroxylated theanaphthaquinone. All exhibited an $MS^2$ fragment ion at $m/z$ 512.5 as a base peak revealing a loss of 69 Da, thus


dx.doi.org/10.1021/jf502220c | J. Agric. Food Chem. 2014, 62, 9848−9859

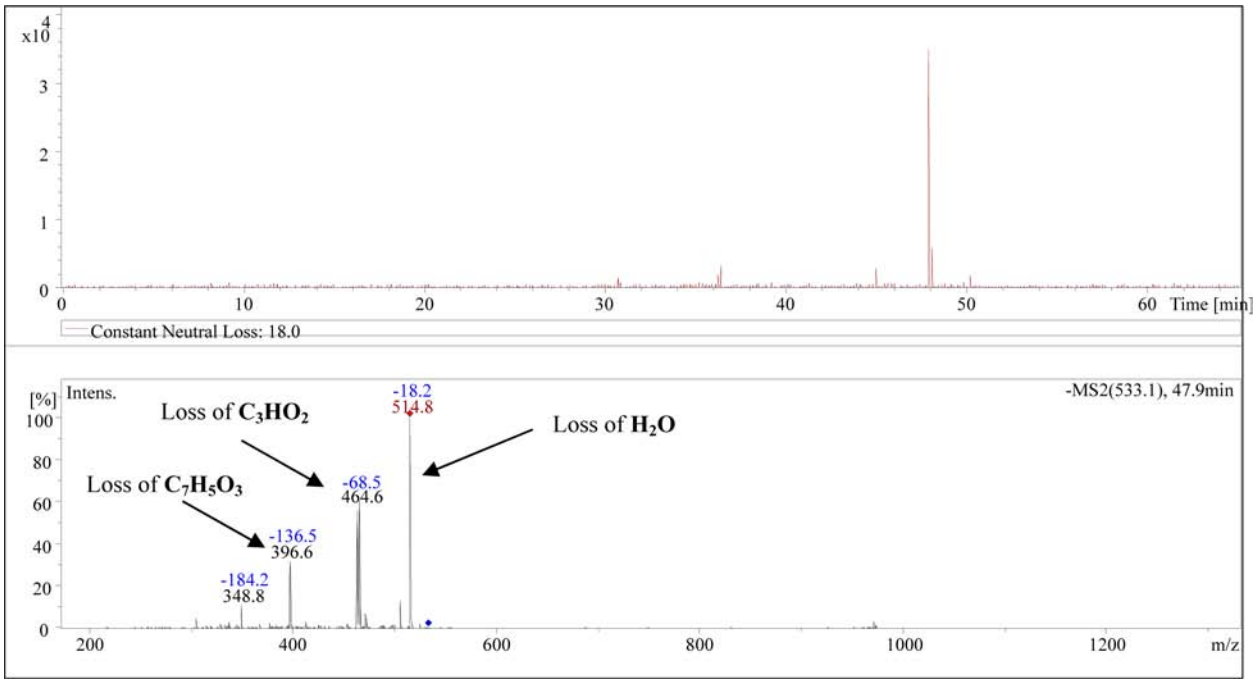


**Figure 2.** Neutral losses of $H_2O$ and $C_3HO_2$ for theanaphthaquinone (**8**) at *m/z* 533.

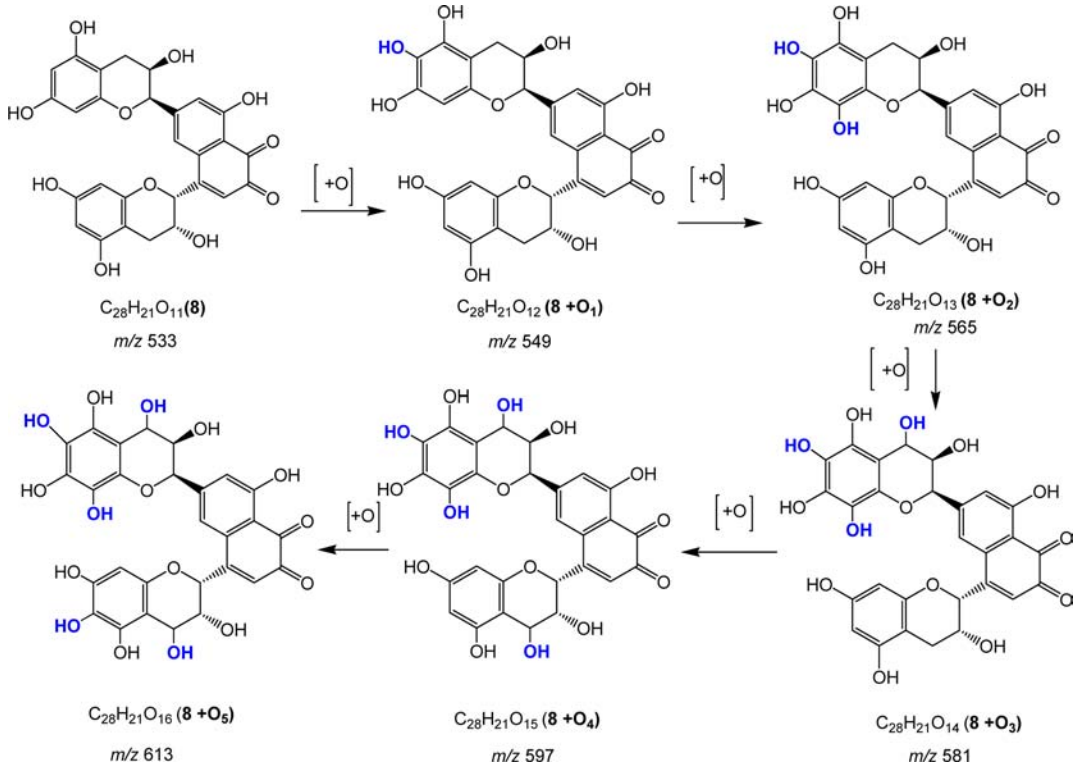


**Figure 3.** Homologous series of theanaphthaquinone (**8**) with successive oxygen insertion (regioisomers selected randomly).

corresponding to the loss of $C_3HO_2$ and revealing three oxygen insertions within the compound. Minor fragment ions with different intensities at *m/z* 444.5 were also observed revealing RDA fragmentation as previously identified in the parent ion. These four peaks were tentatively assigned as tetrahydroxylated derivatives of TNQ (**8** + $O_4$).

One chromatographic peak was detected for the *m/z* 597 at a retention time of 48.4 min corresponding to **8** + $O_4$. Tandem mass experiments showed a transition of this precursor ion to a fragment $MS^2$ ion at *m/z* 528.5 as a base peak characterized by a neutral loss of 69 Da of $C_3HO_2$ and revealing four oxygen insertions within this compound.

Two chromatographic peaks were detected for the *m/z* 613 at retention times of 39 and 28.1 min as expected for the pentahydroxylated theanaphthaquinone. Tandem mass fragmentation experiments showed a main fragment ion $MS^2$ at *m/*


dx.doi.org/10.1021/jf502220c | *J. Agric. Food Chem.* 2014, 62, 9848−9859

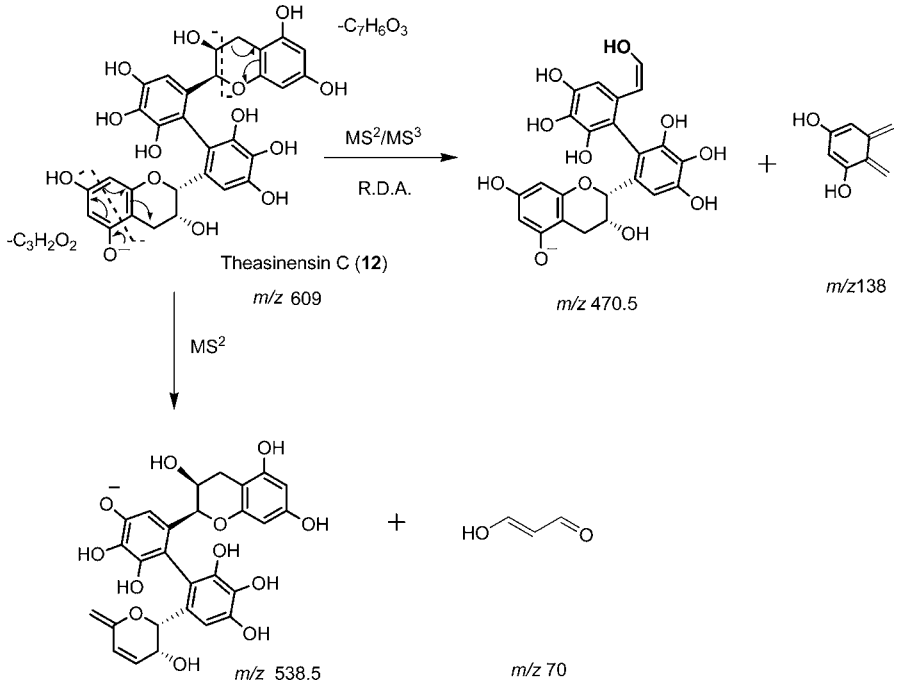


**Figure 4.** Fragmentation mechanism of theasinensin C (**12**) at $m/z$ 609 undergoing loss of $C_3H_2O_2$ and retro-Diels–Alder fragmentation. (The sites of deprotonation in $[M - H]^-$ have been selected randomly.)

**Table 2. Homologous Series for Theasinensin C (12) Confirming the Presence of the Hydroxylated Derivatives with Their Selected $MS^2$ and $MS^3$ Fragment Ions and Neutral Losses Observed**[a]

| | molecular formula | LC-MS $[M - H]m/z$ | RT[b] (min) | fragment ions LC-$MS^2$ $m/z$ | neutral loss $\delta M(S^1 - S^2)$[c] (Da) | fragment ions LC-$MS^3$ $m/z$ |
|---|---|---|---|---|---|---|
| **12** | $C_{30}H_{25}O_{14}$ | 609.0 | 34.6 | 538.6 (67.8%), 456.9 (22.56%), 438.9 (41.1%) | 70.4, 152.1, 170.1 | |
| | | 609.0 | 34.1 | **538.5 (100%)**, 470.5 (15.56%) | 70., 138.5 | 470.5 (100%) |
| **12** + $O_2$ | $C_{30}H_{25}O_{16}$ | 641.0 | 33.2 | 604.8 (100%), **570.5 (92%)** | 36.2, 70 | 504.5 (100%), 436.5 (26.2%) |
| | | | | 504.5 (21.5%) | 137 | |
| **12** + $O_4$ | $C_{30}H_{25}O_{18}$ | 673.1 | 20.1 | 654.1 (7%), **602.5 (100%)** | 19, 70 | 544.5 (100%) |
| | | 673.1 | 40.1 | **604.5 (100%)**, 535.5 (20.4%) | 69, 136.6 | 544.5 (100%), 492.8 (15.8%) |
| | | 673 | 40.9 | **655 (100%)**, 626.6, 604.5 (22.3%) | 18,46, 69 | 502.9 (100%) |
| **12** + $O_6$ | $C_{30}H_{25}O_{20}$ | 705.6 | 47.8 | **636.4 (100%)** | 69.2 | 578.4 (100%), 520.5 (28.3%) |

[a] $MS^2$ fragment ions highlighted in bold are subjected for further fragmentation for $MS^3$ fragment ions. [b] RT, retention time (min). [c] $\delta M(S1 - S2)$: mass loss (Da).

$z$ 544.5 having a neutral loss of 69 Da of $C_3HO_2$, thus indicating all of the oxygens are inserted in the fragment ion, which corresponds to **8** + $O_5$.

The main neutral losses of all the chromatographic peaks identified revealing losses of $H_2O$, loss of $C_3HO_2$, and weak RDA fragmentation are shown in Figures 2 and 3, thus confirming the assignment made. Therefore, theanaphthaquinone undergoes nucleophilic addition of $H_2O$ in the fermentation process for TR formation, where successive oxygen insertion takes place, giving its polyhydroxylated derivatives. These are exhibited in Figure 3, showing the hydroxylation process. Again, it should be noted that in the absence of authentic reference compounds, assignments of detailed structures are tentative and information on the regiochemistry of oxygen insertion is speculative with structures shown corresponding to positions of random oxygen insertion. Therefore, a new homologous series of theanaphthaquinone was observed within the oxidative cascade hypothesis extending the members of the thearubigin family.[16,17]

**Theasinensin C and Its Homologous Series.** Another systematic search for homologous series was carried out on theasinensin C ($C_{30}H_{25}O_{14}$) (**12**) shown in Figure 1 as a parent compound. Signals corresponding to $m/z$ values of polyhydroxylated theasinensins were previously identified in FT-ICR-MS and MALDI-MS data of TR extracts.[16,24] EICs were also generated for the mass of parent ions expected for this homologous series. Theasinensin C (**12**) is characterized by it mass spectrum with $[M - H]$ ion at $m/z$ 609, revealing the presence of two isomers at different retention times of 34.6 and 48.1 min, with the major chromatographic peak of this compound detected at 34.6 min as shown in Figure 2 in the Supporting Information. Performing tandem MS experiments with the precursor ion at $m/z$ 609 gave a $MS^2$ fragment spectra characterized by a base peak at $m/z$ 538.6 exhibiting a neutral loss of 70 Da, thus indicating a loss of $C_3H_2O_2$. Further $MS^3$


dx.doi.org/10.1021/jf502220c | J. Agric. Food Chem. 2014, 62, 9848–9859

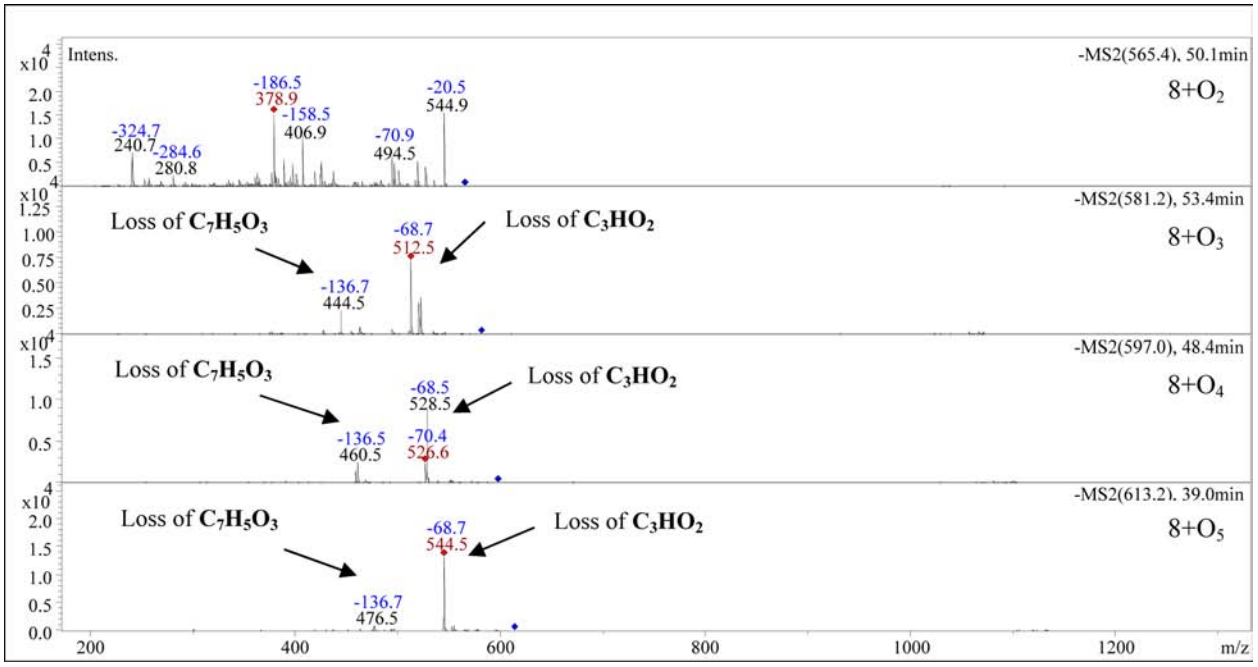


**Figure 5.** Constant neutral losses for the hydroxylated components of theanaphthaquinones (**8** + $O_x$): *m*/*z* 565.4, 581.2, 597.2, and 613.2 exhibiting losses of $H_2O$, $C_3HO_2$, and retro-Diels–Alder fragmentation.

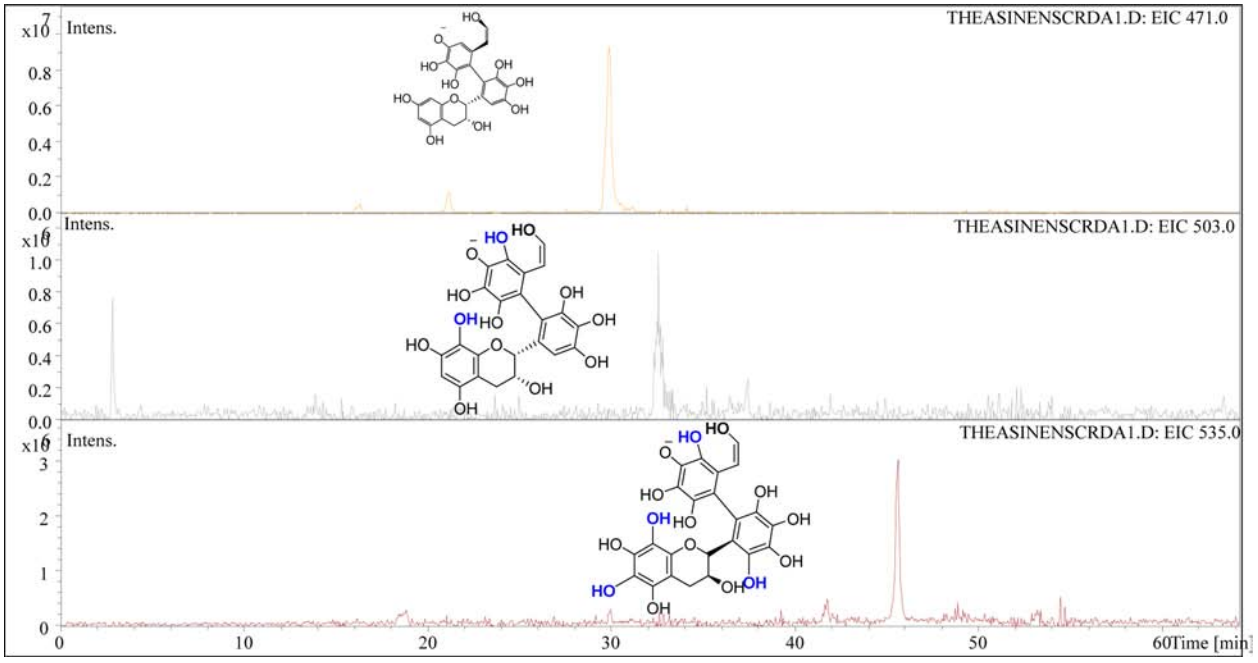


**Figure 6.** Extracted ion chromatograms EICs showing the retro-Diels–Alder (RDA) fragment ions in the homologous series of theasinensin C (**12**); (a, top) EIC at *m*/*z* 471; (b, middle) EIC at *m*/*z* 503; (c, bottom) EIC at *m*/*z* 535. (The sites of deprotonation in $[M - H]^-$ and regioisomers are selected randomly.)

tandem mass experiments with a precursor ion at *m*/*z* 538.6 gave the characteristic $MS^3$ fragment ion at *m*/*z* 470.5 corresponding to a loss of 138 amu, and this indicates that the molecule underwent first a loss of $C_3H_2O_2$, with fragmentation on one of the two benzopyran A-ring moieties followed by a RDA fragmentation with the loss of an enone fragment. The fragmentation mechanism is shown in Figure 4.

It is worth noting that while theasinensins have a biphenyl connection on the catechol B-rings, proanthocyanidins (another dimeric catechin structure) are connected from the resorcinol A-ring to the C-ring as indicated in Figure 5 in the Supporting Information. Both classes of compounds are constitutional isomers of one another with proanthocyanidins as well reported previously in tea chemistry. Both can be identified and differentiated by their different $MS^2$ fragment ions obtained in LC tandem MS. Proanthocyanidins show different $MS^2$ fragment spectra characterized by retro Diels–Alder fragmentation R.D.A. with a neutral loss of 168 Da giving *m*/*z* 441, Quinide Methide fission Q.M. giving *m*/*z* 305, and heterolytic ring fission H.R.F. giving an *m*/*z* 483 with a neutral


dx.doi.org/10.1021/jf502220c | J. Agric. Food Chem. 2014, 62, 9848–9859

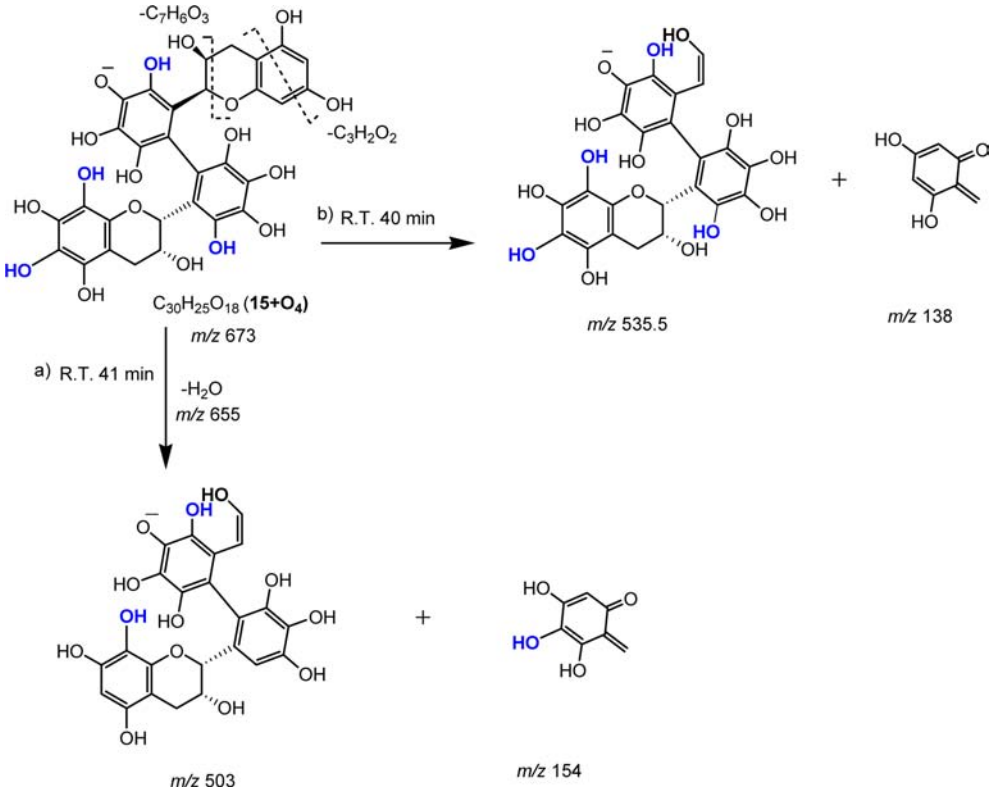


**Figure 7.** Mechanism of retro-Diels–Alder fragmentations (RDA) of a selected member of theasinensin C of the tetrahydroxylated derivative at *m/z* 673 showing the oxygen insertion process occurring. (The sites of deprotonation in $[M - H]^-$ and regioisomers are selected randomly.)

loss of 126 Da. Further details for differentiating between these two isomeric structures are shown in the fragmentation mechanism of the proanthocyanidin isomeric structure in Figure 6 in the Supporting Information.

To evaluate the assignment of the hydroxylated components within the homologous series of theasinensin C (**12**), EICs were prepared for their corresponding expected *m/z* values. Whereas theasinensin C (**12**) $C_{30}H_{25}O_{14}$ was detected at *m/z* 609, the EICs of its hydroxylated components were detected at *m/z* 641 for $C_{30}H_{25}O_{16}$, at *m/z* 673.1 for $C_{30}H_{25}O_{18}$, and at *m/z* 705.6 for $C_{30}H_{25}O_{20}$. The identity of the molecular formulas was previously established by FT-ICR-MS.[9] A detailed study for the hydroxylated derivatives of this compound and their $MS^2$ and $MS^3$ fragment ions is exhibited in Table 2.

One chromatographic peak was identified for *m/z* 641 $C_{30}H_{25}O_{16}$, corresponding to theasinensin C with two oxygen insertions (**15** + $O_2$), eluting at a retention time of 33.2 min. This compound gave a fragment ion at *m/z* 604.8 as a major peak exhibiting a neutral loss of 36 amu, corresponding to a loss of two $H_2O$ molecules from this ion, and another characteristic $MS^2$ ion at *m/z* 570.5 revealing the loss of $C_3H_2O_2$. Further fragmentation gave $MS^3$ as base peak at *m/z* 504.5 revealing the further RDA fragmentation occurring in this compound. Hence, the fragmentation pattern observed match fragment ions expected for a dihydroxylated theasinensin derivative.

Three isomers in the EIC with *m/z* 673 were detected at different retention times of 20.1, 40.1, and 40.9 min, corresponding to the predicted tetrahydroxylated theasinensin **12** + $O_4$ ($C_{30}H_{25}O_{18}$). One of them eluting at 20.1 min showed a transition from *m/z* 673.1 to a fragment ion at *m/z* 602.5 as a base peak, indicating the loss of $C_3H_2O_2$ and the oxygen insertions within the dimeric ring. The second isomer of the *m/z* 673 eluting at 40.1 min showed a transition from *m/z* 673 to 604.5 and 535.5, exhibiting a major loss of $C_3H_2O_2$ on the benzopyran ring and a minor loss of 136.6 amu due to RDA fragmentation occurring, whereas all of the hydroxyl groups are inserted within the fragment ion of the theasinensin C ring. The third isomer of the *m/z* 673 was eluting at 40.9 min showing a transition from *m/z* 673 to 655 exhibiting a neutral loss of 18 amu, which is the loss of water, and indicating three hydroxyl insertions within this compound. A further $MS^3$ fragmentation for this compound gave a transition of the $MS^2$ fragment ion at *m/z* 655 to $MS^3$ at *m/z* 503, which indicates that two hydroxyl groups are inserted within the theasinensin fragment ion and one hydroxyl insertion was occurring within the eliminated benzopyran moiety, whereas this molecule was undergoing a loss of water at the same time. This is briefly illustrated in Figure 7. Hence the fragmentation pattern observed matches the fragment ions expected for the tetrahydroxylated theasinensin derivative. In a part of fragmentation pattern of these compounds a loss of water was observed, which has not been observed in the parent compound. An additional set of EICs were created in the all $MS^n$ mode searching for fragment ions that would be characteristic for hydroxylated theasinensins. Representative data are shown in Figure 6. Here fragment ions originating from RDA fragmentations at *m/z* 471, 503, and 535 were observed corresponding to bisflavanol-like compounds with two or four oxygens inserted, respectively. These observed fragment ions point toward the presence of hydroxylated theasinensins. It should as well be noted that the fragment spectra obtained showing frequently loss of two water molecules from the precursor ion might as well correspond to hydroxylated theasinensin derivatives, in which, due to a


dx.doi.org/10.1021/jf502220c | J. Agric. Food Chem. 2014, 62, 9848–9859

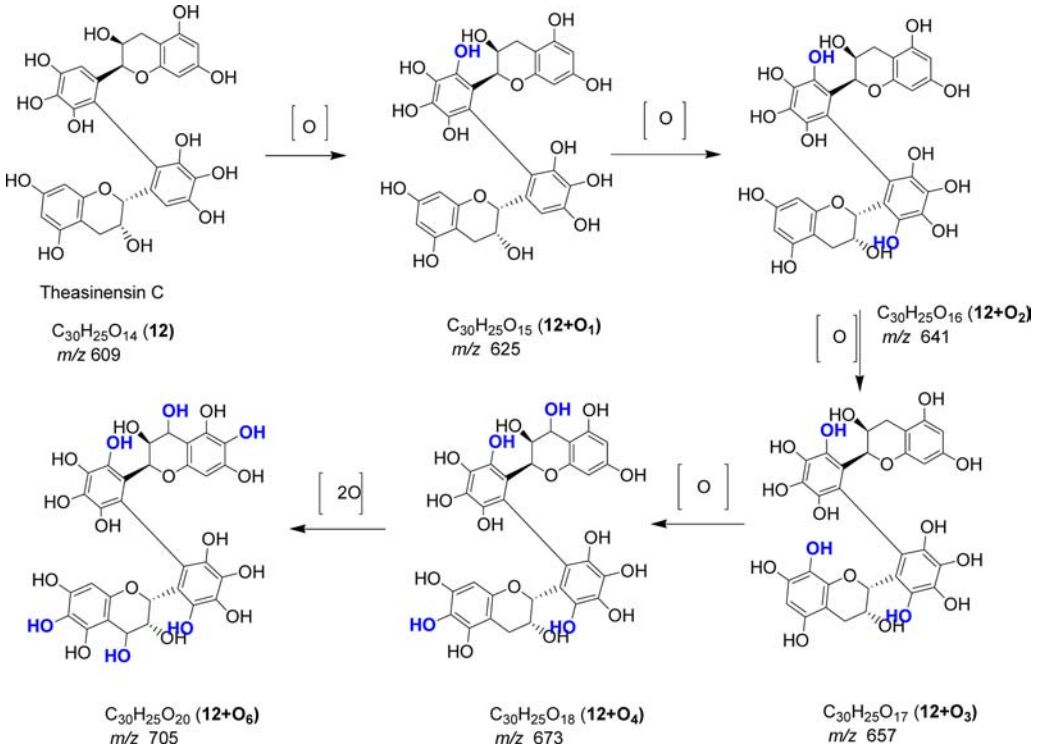


**Figure 8.** Homologous series of theasinensin C (**12**) with successive oxygen insertion. (Regioisomers are selected randomly.)

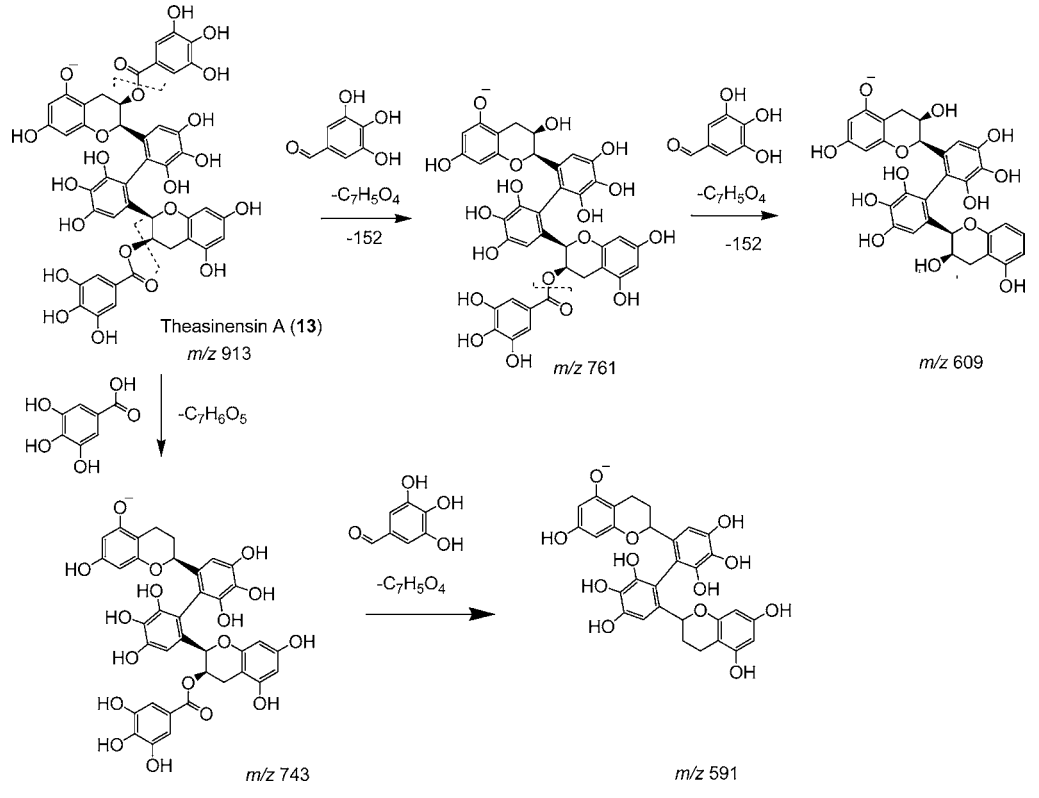


**Figure 9.** Mechanism of fragmentation for theasinensin A (**12**) at $m/z$ 913.1 exhibiting its characteristic fragment ions. (The sites of deprotonation in $[M - H]^-$ and regioisomers are selected randomly.)

change of the aromatic substitution pattern, the fragmentation pathway is altered.

Only one isomer of $C_{30}H_{25}O_{20}$ corresponding to **15** + $O_6$ was observed at $m/z$ 705.6, giving a transition to $m/z$ 636.4 as a major peak intensity, which reveals a loss of $C_3H_2O_2$ from the A-ring and indicating all of the hydroxyl groups are inserted within the theasinensin fragment.

All of the above-mentioned results are exhibited in Table 2, confirming the presence of a new homologous series for theasinensin C present in thearubigin fraction. Tetntative


dx.doi.org/10.1021/jf502220c | J. Agric. Food Chem. 2014, 62, 9848−9859

Table 3. New Class of Compounds for Theasinensin A (13) Detected with Their Selected Tandem Mass Spectral Data and Their Neutral Losses, Showing Different Fragmentation Mechanisms Compared to the Parent Ion

| | molecular formula | LC-MS [M − H] $m/z$ | RT[a] (min) | fragment ions LC-MS$^2$ $m/z$ | neutral loss $\delta$M($S^1 - S^2$)[b] (Da) |
|---|---|---|---|---|---|
| **13** | $C_{44}H_{33}O_{22}$ | 913.2 | 22.1 | 761.2 (28%), 743.2 (40.59%), 609.1 (5.44%), 591.2 (100%) | 152, 170, 304, 322 |
| | | | 16.3 | 761.2 (34.01%), 743.2 (23%), 609 (14.92%), 591.2 (100%) | 152, 170, 304, 322 |
| | | | 15.7 | 761.2 (39.67%), 743.2 (33.17),, 609.2 (15.1%), 591.2 (100%) | 152, 170, 304, 322 |
| | | | 1.7 | 761.1 (32.29%), 743.2 (31.27%), 609.2 (13.98%), 591.2 (100%) | 152, 170, 304, 322 |
| **13** + $O_1$ | $C_{44}H_{33}O_{23}$ | 929.0 | 32.6 | 913.3 (76.06%), 870.7 (100%) | 16, 58.3 |
| **13** + $O_2$ | $C_{44}H_{33}O_{24}$ | 945.0 | 52.3 | 926.6 (11.78%), 909.1 (100%), 657.2 (8%) (609 + 3O) | 18, 36, 287.8 |
| | | 945.3 | 47.8 | 909.2 (26%), 886.6 (100%) | 36, 58.4 |
| **13** + $O_3$ | $C_{44}H_{33}O_{25}$ | 960.9 | 64 | 916.9 (100%), 657 (12.4%) (609 + 3O) | 44, 304 |
| **13** + $O_4$ | $C_{44}H_{33}O_{26}$ | 977.1 | 51.2 | 959.4 (19.1%), 920.6 (100%) | 17.5, 56 |
| | | 977.3 | 32.8 | 918.5 (57.8%), 863.6 (22.68%) | 58.1, 113 |
| **13** + $O_5$ | $C_{44}H_{33}O_{27}$ | 993.3 | 49 | 961.2 (19.2%), 934.6 (100%) | 32, 58.4 |

[a]RT, retention time (min). [b]$\delta$M(S1 − S2), mass loss (Da).

structures of the homologous series of theasinensin C are shown in Figure 8.

**Theasinensin A and Its Homologous Series.** Theasinensin A (**13**) as indicated in Figure 1 is characterized by its mass spectrum with a pseudomolecular ion at $m/z$ 913.2 [M − H] in the negative ion mode, exhibiting different characteristic fragment ions. In the EIC of $m/z$ 913 as shown in Figure 8 in the Supporting Information, three signals are observed at different retention times of 1.7, 16.3, and 22.5 min. The first fragment ion was observed at $m/z$ 761.2 with a neutral loss of 152 amu, and a second fragment ion was also observed at $m/z$ 743.2 with a neutral loss of 170 amu, both revealing the loss of one of the galloyl moieties of this compound. A third fragment ion was observed at $m/z$ 609.1, exhibiting a loss of 304 amu, which can be rationalized due to a loss of two galloyl moieties from both parts of theasinensin A. A base peak fragment ion was exhibited in the MS$^2$ spectra at $m/z$ 591.2, indicating the loss of one galloyl group from one part of the molecule and another gallate ester from the second part. The fragmentation of this compound and its mechanism are shown briefly in Figure 9.

To evaluate the assignment of the hydroxylated components within the homologous series of theasinensin A (**13**), EICs were prepared for their corresponding expected $m/z$ values. Whereas theasinensin A (**13**) was detected at $m/z$ 913.2 ($C_{44}H_{33}O_{22}$), EICs for its predicted hydroxylated components were prepared at $m/z$ 929 ($C_{44}H_{33}O_{23}$), at $m/z$ 945 ($C_{44}H_{33}O_{24}$), at $m/z$ 961 ($C_{44}H_{33}O_{25}$), at $m/z$ 977.1 ($C_{44}H_{33}O_{26}$), and at $m/z$ 993.3 ($C_{44}H_{33}O_{27}$). These results are shown in Table 3. Targeted tandem MS experiments of the hypothetical hydroxylated components of theasinensin A (**13**) were carried out for evaluating the presence of oxygen insertions within these compounds, to confirm whether a homologous series of theasinensin A is present.

As shown in Table 3, the EIC at $m/z$ 929 showed a single peak at a retention time of 32.6 min corresponding to a theasinensin A with one oxygen inserted (**13** + $O_1$). The precursor ion at $m/z$ 929.1 displayed a MS$^2$ fragment ion at $m/z$ 913.3 as a base peak having a neutral loss of only 16 amu. However, such MS$^2$ fragmentation did not show a similar fragmentation as the parent ion of theasinensin A, undergoing the neutral losses of the galloyl moieties, which is its characteristic fragmentation mechanism. Hence, this could not be in agreement with the hypothesis of the homologous series as previously described by which the whole series undergoes similar if not identical fragmentation as described for the parent ion. Neutral loss of 16 amu is characteristic for either peroxide functionalities or epoxide functionalities, so that the compound observed was tentatively assigned to a peroxo or epoxy derivative of a bisflavanol.

Two chromatographic peaks corresponding to the predicted dihydroxylated component of theasinensin A (**13** + $O_2$) were detected in the EIC at $m/z$ 945.0. The first peak was observed at a retention time of 52.3 min, where its MS$^2$ spectrum exhibited fragment ions at $m/z$ 926.6 showing a loss of $H_2O$, a base peak at $m/z$ 909.1 with a neutral loss of 36 amu, thus indicating a further loss of $H_2O$ molecule, and a characteristic fragment ion with a very weak intensity at $m/z$ 657.2, revealing a loss of two galloyl moieties from this compound undergoing a loss of oxygen ($2C_7H_5O_4 - O$) and three oxygen insertions within the fragment ion, which is in agreement as the fragmentation pathway of the parent ion theasinensin A. A second isomer of $m/z$ 945 was detected at a retention time of 47.8 min; the MS$^2$ spectrum of this compound gave a fragment ion with a medium intensity at $m/z$ 909.2 revealing a loss of two molecules of $H_2O$.

Only one chromatographic peak in the EIC at $m/$ 961 corresponding to three oxygen insertions (**13** + $O_3$) was observed at 64.0 min. Its MS$^2$ spectrum showed a characteristic base peak at $m/z$ 916.9 suffering a neutral loss of 44 Da (loss of $CO_2$), and further fragment ions were observed, one of which was detected coeluting with a low intensity at $m/z$ 657 exhibiting a neutral loss of 304 Da, which indicates the loss of the two galloyl groups from this compound as in the parent ion and three oxygen insertions within the fragment ion. The latter fragment ion is in agreement with a trihydroxylated theasinensin structure.

Two chromatographic signals in the EIC at $m/z$ 977.1 for the predicted tetrahydroxylated derivatives of theasinensin A (**13** + $O_4$) were detected. The first one was observed at a retention time of 51.2 min, exhibiting MS$^2$ fragment spectra characterized by a weak fragment ion at $m/z$ 959.4 having a neutral loss of 17.5, which corresponds to a loss of one hydroxyl group, and another characteristic MS$^2$ ion with high intense peak was identified at $m/z$ 920.6 having a neutral loss of 56 Da ($-C_3H_4O$) characteristic for flavanol C-ring cleavage. The second isomer at $m/z$ 977.3 was observed eluting at 32.8 min, and the latter showed no characteristic fragmentation of


dx.doi.org/10.1021/jf502220c | J. Agric. Food Chem. 2014, 62, 9848−9859

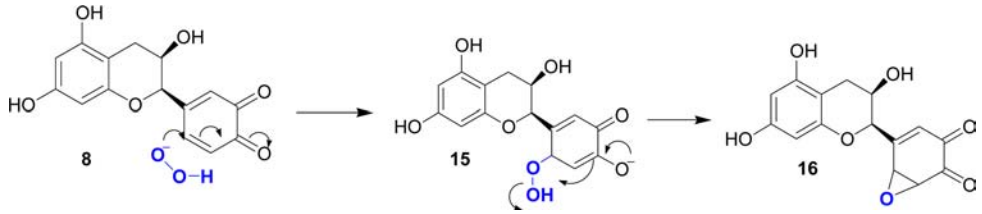


**Figure 10.** Proposed mechanism undergoing oxygen insertion by nucleophilic addition of $H_2O_2$.

theasinensin A. Thus, these two mentioned isomeric compounds could not be considered as a part of the homologous series of theasinensin A, so no tetrahydroxylated components of this series are present.

A single chromatographic peak was observed in the EIC at $m/z$ 993.3, a value predicted for a pentahydroxylated derivative of theasinensin A (**13** + $O_5$). The $MS^2$ spectrum of this component exhibited a characteristic fragment ion at $m/z$ 961.2 showing a neutral loss of 32 amu, which indicates the loss of two oxygens, whereas only three oxygens were inserted within the fragment ions of this compound. As in the previously identified compounds, this new component did not undergo the same fragmentation as the parent compound, theasinensin A, thus indicating that this compound does not belong to the homologous series suggested.

Accordingly, this observation can be rationalized by suggesting that a new series of oxidation products in thearubigin formation may exist. These new compounds undergo mainly oxygen losses (−32 Da, $-O_2$) during $MS^2$ is a characteristic for peroxides or epoxides. It is proposed that these compounds can be formed in the presence of $H_2O_2$ in black tea thearubigin fractions, with hydrogen peroxide acting as a nucleophile adding to *o*-quinone moieties. It should be noted that due to the $\alpha$-effect hydrogen peroxide is around 1000 times more nucleophilic if compared to water, the conventional nucleophile involved in thearubigin chemistry. The existence of $H_2O_2$ in black tea has been previously discussed and confirmed by Sinkar et al. in an attempt to investigate the biochemistry and chemistry of thearubigins using polyphenol oxidase and peroxidase enzymes.[20] In his work, Sinkar demonstrated that TPPO, while oxidizing catechins, generates $H_2O_2$ in concentrations of 290−390 $\mu$M, which may play a role in the oxidation process in the thearubigin formation. In this part of research, we were able to identify a further oxygenation process taking place but here by nucleophilic addition of $H_2O_2$ as the second suggested mechanism in the oxidation process for the formation of new peroxide intermediate (**15**) or epoxide structures (**16**) by nucleophilic attack of the enolate moiety in peroxo intermediate (**15**). The new suggested mechanism is shown in Figure 10.

**Alternative Graphical Representation in Modified Kendrick Plot of Homologous Series.** In our study new thearubigin components were clearly characterized by employing tandem LC-$MS^n$ experiments. The data generated in the homologous series of theanaphthoquinone and theasinensin C were consistent with the hypothesis previously formulated, in which polyhydroxylated dimers of catechins are formed by nucleophilic addition of water to the quinone oxidized counterparts of catechins. On the other hand, new compounds containing oxygen insertions in the series of theasinensin A were identified, where the latter were rationalized according to the nucleophilic addition of hydrogen peroxide, thus forming thearubigin components of a different structural class. Data on the homologous series of theasinensin A were inconclusive, with MS data not allowing tentative structure suggestions. In summary, this study has complemented previous knowledge on thearubigin chemistry and added evidence for the presence of homologous series of formal oxygen insertion for the two previously not studied dimers of catechins, theasinensins and theanaphthaquinone. Most TR components identified so far must be considered as belonging to the class of flavonoids originating from flavonoid precursors all possessing at least one characteristic C6−C3−C6 moisty.

In previous work we have used conventional Kendrick diagrams using Kendrick masses plotted against Kendrick mass deficits as visual display tools.[9,16] However, this type of representation seems inadequate for black tea chemistry or in general any other processed food. Therefore, we introduce at this stage a modified graphical representation of homologous series reminiscent of a mass deficit diagram in Figure 11. In the

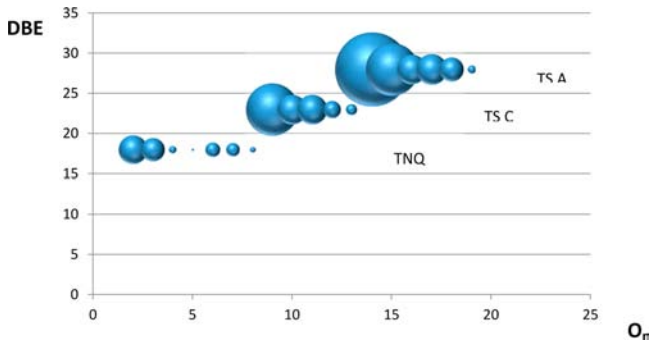


**Figure 11.** Modified Kendrick diagram with numbers of oxygens $O_n$ plotted against double-bond equivalents (DBE) displaying homologous series of theanaphthoquinone (TNQ) and theasinensins A and C (TS A and TS C) with bubble size corresponding to absolute intensities from direct infusion mass spectral data in the negative ion mode (see ref 16).

case of TR components homologous series differ in number of oxygen atoms, which are plotted on the *x*-axis. On the *y*-axis a compound class-specific parameter needs to be chosen. We suggest using double-bond equivalents (DBEs) as such a parameter. In certain cases, for example, if comparing TFs with TSs, the number of DBE (18 in this case) is identical, so for such situations we suggest using as a compound class-specific parameter, the number of carbon atoms $C_n$ divided by DBEs. As an additional third parameter in Figure 11 the intensity of the mass spectral peak corresponding to the member of the homologous series is shown in a bubble plot with intensity corresponding to the diameter of the bubble.

Such a modified Kendrick diagram with numbers of oxygens $O_n$ plotted against DBE displaying homologous series of theanaphthoquinone (TNQ) and theasinensins A and C (TS A


dx.doi.org/10.1021/jf502220c | J. Agric. Food Chem. 2014, 62, 9848−9859

and TS C) with bubble size corresponding to absolute intensities on parallel lines to the *x*-axis from direct infusion mass spectral data in the negative ion mode[16] is introduced here.

## ■ ASSOCIATED CONTENT

### Supporting Information

Supplementary Figures 1−5. This material is available free of charge via the Internet at http://pubs.acs.org.

## ■ AUTHOR INFORMATION

### Corresponding Author

*(N.K.) E-mail: n.kuhnert@jacobs-university.de. Phone: 0049 421 200 3120.

### Notes

The authors declare no competing financial interest.

## ■ ACKNOWLEDGMENTS

We thank Anja Mueller for technical assistance.

## ■ ABBREVIATIONS USED

ESI/LC-MS$^n$, electrospray ionization/high-performance liquid chromatography−tandem mass spectrometry; EIC, extracted ion chromatograms; TRs, thearubigins

## ■ REFERENCES

(1) Poulter S. Daily Mail online, dailymail, UK, June 27, 2008.
(2) FAO Web site with data from 2013:, http://www.fao.org/news.
(3) Drynan, J. W.; Clifford, M. N.; Obuchowicz, J.; Kuhnert, N. The chemistry of low molecular weight black tea polyphenols. *Nat. Prod. Rep.* **2010**, *27* (3), 417−462.
(4) Kuhnert, N.; Dairpoosh, F.; Yassin, G.; Golon, A.; Jaiswal, R. What is under the hump? Mass spectrometry based analysis of complex mixtures in processed food − lessons from the characterisation of black tea thearubigins, coffee melanoidines and caramel. *Food Funct.* **2013**, *4*, 1130−1147.
(5) Roberts, E. A. H.; Wood, D. J. Separation of tea polyphenols on paper chromatograms. *Biochem. J.* **1953**, *53*, 332−336.
(6) Kallithraka, S.; Bakker, J.; Clifford, M. N. Evaluation of bitterness and astringency of (+)-catechin and (−)-epicatechin in red wine and in model solution. *J. Sens. Stud.* **1997**, *12*, 25−37.
(7) Bruschi, L.; Copeland, E. L.; Clifford, M. N. Unexpected hyperchromic interactions during the chromatography of theafulvins and simple flavonoids. *Food Chem.* **1999**, *67*, 143−146.
(8) Gardener, E. J.; Ruxton, C. H. S.; Leeds, A. R. Black tea − helpful or harmful? A review of the evidence. *Eur. J. Clin. Nutr.* **2006**, 1−16.
(9) Kuhnert, N. Unraveling the structure of the black tea thearubigins. *Arch. Biochem. Biophys.* **2010**, *501*, 37−51.
(10) Wu, Z. G.; Rodgers, R. P.; Marshall, A. G. Compositional determination of acidic species in Illinois no. 6 coal extracts by electrospray ionization Fourier transform ion cyclotron resonance mass spectrometry. *Energy Fuels* **2004**, *18*, 1424−1428.
(11) Kim, S.; Kramer, R. W.; Hatcher, P. G. Graphical method for analysis of ultrahigh-resolution broadband mass spectra of natural organic matter, the van Krevelen diagram. *Anal. Chem.* **2003**, *75*, 5336−5344.
(12) Kendrick, E.; Mass, A. Scale based on $CH_2$ = 14.0000 for high resolution mass spectrometry of organic compounds. *Anal. Chem.* **1963**, *35*, 2146−2152.
(13) Hughey, C. A.; Rodgers, R. P.; Marshall, A. G. Resolution of 11000 compositionally distinct components in a single electrospray ionization Fourier transform ion cyclotron resonance mass spectrum of crude oil. *Anal. Chem.* **2002**, *74*, 4145−4149.
(14) Hughey, C. A.; Galasso, S. A.; Zumberge, J. E. Detailed compositional comparison of acidic NSO compounds in biodegraded reservoir and surface crude oils by negative ion electrospray Fourier transform ion cyclotron resonance mass spectrometry. *Fuel* **2007**, *86*, 758−768.
(15) Koch, B. P.; Dittmar, T.; Witt, M.; Kattner, G. Fundamentals of molecular formula assignment to ultrahigh resolution mass data of natural organic matter. *Anal. Chem.* **2007**, *79*, 1758−1763.
(16) Kuhnert, N.; Drynan, J. W.; Obuchowicz, J.; Clifford, M. N.; Witt, M. Mass spectrometric characterization of black tea thearubigins leading to an oxidative cascade hypothesis for thearubigin formation. *Rapid Commun. Mass Spectrom.* **2010**, *24*, 3387−3404.
(17) Kuhnert, N.; Clifford, M. N.; Mueller, A. Oxidative cascade reactions yielding polyhydroxy-theaflavins and theacitrins in the formation of black tea thearubigins: evidence by tandem LC-MS. *Food Funct.* **2010**, *1*, 180−199.
(18) Yassin, G.; Koek, J.; Kuhnert, N. Identification of trimeric and tertameric flavan-3-ol derivatives in the SII black tea thearubigin fraction of black tea using ESI-tandem and MALDI-TOF mass spectrometry. *Food Res. Int.* **2014**, DOI: 10.1016/j.foodres.2014.04.010.
(19) Nakayama, T.; Ichiba, M.; Kuwabara, M.; Kajiya, K.; Kumazawa, S. Mechanisms and structural specificity of hydrogen peroxide formation during oxidation of catechins. *Food Sci. Technol. Res.* **2002**, *8*, 261−267.
(20) Subramanian, N.; Venkatesh, P.; Ganguli, S.; Sinkar, V. P. Role of polyphenol oxidase and peroxidase in the generation of black tea theaflavins. *J. Agric. Food Chem.* **1999**, *47*, 2571−2578.
(21) Mulder, T. P. J.; van Platerink, C. J.; Schuyl, P. J. W.; van Amelsvoort, J. M. M. Analysis of theaflavins in biological fluids using liquid chromatography-electrospray mass spectrometry. *J. Chromatogr., B* **2001**, *760*, 271−279.
(22) Cuyckens, F.; Claeys, M. Mass spectrometry in the structural analysis of flavonoids. *J. Mass Spectrom.* **2004**, *39*, 1−15.
(23) Cren-Olive, C.; Deprez, S.; Lebrun, S.; Coddeville, B.; Rolando, C. Characterization of methylation site of monomethylflavan-3-ols by liquid chromatography/electrospray ionization tandem mass spectrometry. *Rapid Commun. Mass Spectrom.* **2000**, *14*, 2312−2319.
(24) Drynan, J. W.; Clifford, M. N.; Obuchowicz, J.; Kuhnert, N. MALDI-TOF mass spectrometry: avoidance of artifacts and analysis of caffeine-precipitated sill thearubigins from 15 commercial black teas. *J. Agric. Food Chem.* **2012**, *60*, 4514−4525.

antibodies were obtained from Novus (Littleton, CO). Anti-ERK, anti-pERK, anti-acetyl-CoA carboxylase (ACC), and C/EBP$\beta$ were purchased from Cell Signaling (Danvers, MA). Anti-perilipin A and anti-PPAR$\gamma$ were obtained from Chemicon International (Billerica, MA) and Cayman (Ann Arbor, MI), respectively. Goat anti-rabbit peroxidase-conjugated antibody was purchased from Jackson ImmunoResearch (West Grove, PA).

**Cell Culture.** 3T3-L1 preadipocytes (BCRC 60159) purchased from Bioresource Collection and Research Center (BCRC) of Food Industry Research and Development Institute (Hsinchu, Taiwan) were cultured in DMEM supplemented with 10% CBS at 37 °C in a humidified atmosphere containing 5% $CO_2$. At 2 days after confluence, cells were cultured in FBS-containing DMEM (10%, v/v) with the addition of insulin (0.862 $\mu$M), DEX (1 $\mu$M), and IBMX (0.5 mM) to induce differentiation (day 0). On day 2, the medium was substituted by DMEM with 10% FBS and insulin (0.862 $\mu$M) for another 2 days. On day 4, the medium was changed to DMEM with 10% FBS only, and the same medium was provided again on day 6. 2,4,5-TMBA dissolved in DMSO was added in the medium (final concentration of 0.5 mM) at specific time periods. Control samples were prepared by the addition of isovolumetric dimethyl sulfoxide (DMSO) to the medium.

**Oil Red O Staining of Adipocytes and Quantification of Triglyceride Accumulation.** The formation of lipid droplets in adipocytes was observed by Oil Red O staining. Cells were washed twice with phosphate-buffered saline (PBS) before the addition of 10% formaldehyde at room temperature. After 10 min, formaldehyde was removed. Cells were then fixed with fresh 10% formaldehyde for 1 h, followed by the washes with water twice and with 60% isopropanol for 5 min. The cells were completely dry at room temperature before they were stained with Oil Red O (three parts of 0.35% Oil Red O dye in isopropanol and two parts of water) for 15 min at room temperature with shaking and then washed 4 times with water before photographed under a microscope. For the measurement of lipid accumulated in adipocytes, the isopropanol-washed and completely dried cells were shaken with 100% isopropanol for 10 min. The dissolved lipid was quantified by measuring the absorbance at 500 nm. The results were expressed as the lipid accumulation relative to that of the control group.

**Measurement of PPAR$\gamma$ Activation.** Activation of PPAR$\gamma$ in cells harvested at the second and eighth days of adipogenesis was measured by an enzyme-linked immunosorbent assay (ELISA) kit (Signosis, Sunnyvale, CA). Briefly, the nuclear extracts prepared from culture cells by an extraction kit (Signosis, Sunnyvale, CA) were added to the 96-well plate, which was pre-immobilized with PPAR$\gamma$ consensus sequencing oligo. The activated PPAR$\gamma$ was detected with the specific antibody against the PPAR$\gamma$ subunit and a horseradish peroxidase (HRP)-conjugated secondary antibody. The colorimetric detection was measured by a spectrophotometer at 450 nm.

**Western Blotting.** Cells were washed with cold phosphate-buffered saline (PBS) twice, harvested, and centrifuged at 936$g$ for 5 min. The pellets were resuspended in lysis buffer containing 150 mM sodium chloride, 1% Nonidet P 40, and 50 mM Tris-HCl at pH 7.5. The cell suspension was centrifuged at 16805$g$ at 4 °C for 30 min. After centrifugation, the supernatant was collected for analysis and its protein content was determined by a DC Protein Assay Kit (Bio-Rad, Hercules, CA). Equal amounts of proteins from each sample were denatured and separated by gel electrophoresis before being transferred to polyvinylidene fluoride (PVDF) membranes (PerkinElmer, Waltham, MA). The membranes were blocked with 5% nonfat dry milk in Tris-buffered saline containing Tween (TBST) (137 mM NaCl, 0.1% Tween-20, and 20 mM Tris-HCl at pH 8.3) for 1 h before sequentially incubated with primary antibody overnight in a cold room and HRP-conjugated secondary antibody for 1 h at room temperature. Immunoreactive proteins were detected using an enhanced chemiluminescence kit (ECL, PerkinElmer, Waltham, MA), and the film was analyzed using ImageQuant software (Molecular Dynamics, Sunnyvale, CA) to obtain densitometric values. For stripping and reprobing, the membrane was incubated with stripping buffer [0.2 M glycine, 3.5 mM sodium dodecyl sulfate (SDS), and 0.1% Tween-20 at pH 2.2] at room temperature for 10 min. After the buffer was discarded, the membrane was incubated with fresh stripping buffer for another 10 min, followed by two 10 min washes by PBS buffer and two 5 min washes by TBST buffer. After striping, the blocking and probing were performed as mentioned above. The relative expression of each protein was calculated as the "densitometric value of protein/densitometric value of $\beta$-actin collocated". The ratio of phosphorylated proteins to total proteins was calculated by the comparison of relative expression.

**Statistical Analysis.** Statistical analysis was carried out using Statistical Analysis System (SAS Institute, Cary, NC). Analysis of variance (ANOVA) and Student−Newmann−Keuls multiple range test were performed to evaluate the differences among groups ($\alpha$ = 0.05).

## RESULTS

**Effect of the Incubation Period of 2,4,5-TMBA on Adipogenesis.** To figure out the time period critically affected by 2,4,5-TMBA during adipogenesis, preadipocytes were cultured with 2,4,5-TMBA specifically at post-induction days 0−2, 2−4, 4−6, or 6−8 only (Figure 1A). At day 8, photos were taken for each group under a microscope and the relative accumulation of lipids was estimated. As shown in panels B and C of Figure 1, preadiopcytes were poorly differentiated without the presence of adipogenic factors ("−IDI") but well-differentiated with the presence of adiogenic factors ("+IDI"). When preadipocytes were treated with 2,4,5-TMBA at different time periods in the presence of adipogenic factors, relative lipid accumulation was decreased by 67.93, 34.65, 49.56, and 34.32% for days 0−2, 2−4, 4−6, and 6−8 groups, respectively (Figure 1D). The most significant inhibitory effect was observed when 2,4,5-TMBA was present in the medium at days 0−2. Withdrawal of 2,4,5-TMBA from the medium did not restore adipogenesis.

**Effect of 2,4,5-TMBA on the Expression of MEK and ERK during Adipogenesis.** Different from the study design for Figure 1 (Figure 1A), the study design for Figures 2−4 (Figure 2A) was to investigate the expression of signaling molecules and transcription factors at different stages when 2,4,5-TMBA was co-cultured with preadipocytes during the differentiation process. The cells were harvested at post-induction days 2, 4, 6, and 8 (Figure 2A).

Phosphorylation of the MEK/ERK signaling pathway is crucial for the differentiation of preadipocytes. To study how MEK/ERK is affected during adipogenesis, preadipocytes cultured with 2,4,5-TMBA were harvested at post-induction days 2, 4, 6, and 8 (Figure 2A). 2,4,5-TMBA decreased the level of phosphorylated MEK at the early stage but increased the level at the late stage (Figure 2B). ERK1 but not ERK2 is specifically required for the differentiation of 3T3-L1. During adipogenesis, ERK1 has to be turned on by phosphorylation at the initial stage but shut off later on.[7] Because activation of MEK leads to the phosphorylation of ERK1, the effect of 2,4,5-TMBA on ERK1 phosphorylation was in accordance with the result of MEK phosphorylaiton; the expression of phosphorylated ERK1 was suppressed initially but enhanced at the terminal period (Figure 2C), which is opposite to the conditions required for adipogenesis.

**Effect of 2,4,5-TMBA on the Expression of C/EBP$\alpha$, $\beta$, and $\delta$ and PPAR$\gamma$ during Adipogenesis.** Activation of ERK is followed by the expression of C/EBP$\beta$ and C/EBP$\delta$, which further induces the expression of PPAR$\gamma$ and C/EBP$\alpha$.[5,6] As the study design shown in Figure 2A, the expression of C/EBP$\alpha$, $\beta$, and $\delta$ and PPAR$\gamma$ was determined when 2,4,5-TMBA-

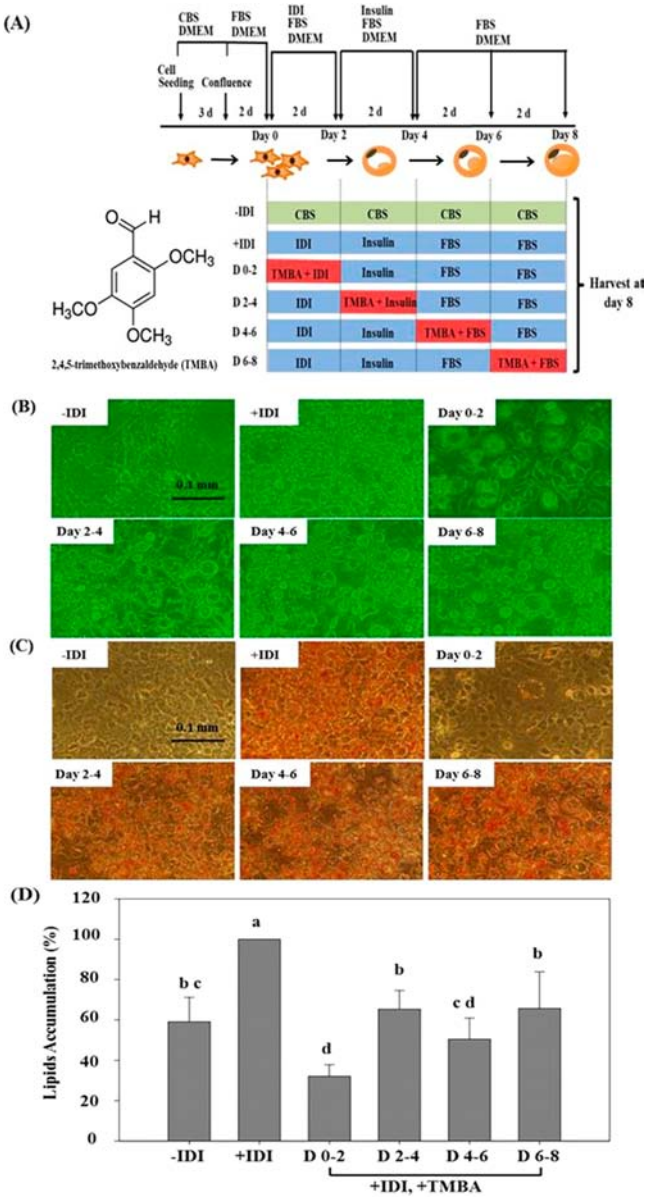


**Figure 1.** Effect of the incubation period of 2,4,5-TMBA on adipogenesis. (A) Study design. "−IDI" refers to the absence of adipogenic factors (insulin, dexamethasone, and isobutylmethylxanthine) in DMEM. "+IDI" refers to the presence of adipogenic factors in culture medium. "D 0−2" to "D 6−8" groups refer to the specific post-induction period for the addition of 2,4,5-TMBA (0.5 mM) to medium containing adiopgenic factors. CBS, calf bovine serum; FBS, fetal bovine serum. (B) Photos taken under a microscope at day 8 (200×). (C) Photos taken under a microscope after Oil Red O staining at day 8 (200×). (D) Relative lipid accumulation at day 8. Values are means of three replicated cultures. Groups with the same letter are not significantly different ($\alpha$ = 0.05).

treated preadipocytes were harvested at post-induction days 2, 4, 6, and 8. When preadipocytes were cultured without the presence of 2,4,5-TMBA, the levels of C/EBP$\beta$ and C/EBP$\delta$ gradually increased throughout the intermediate to terminal differentiation periods. However, the treatment of 2,4,5-TMBA downregulated the overall expression of both proteins (panels A and B of Figure 3).

PPAR$\gamma$2 but not PPAR$\gamma$1 is required for the activation of adipogenesis.[12] Phosphorylation of PPAR$\gamma$2 by ERK at the late stage of adipogenesis decreases the transcription activity of PPAR$\gamma$2 and suppresses differentiation of preadipocytes.[13,14] Without the treatment of 2,4,5-TMBA, the ratio of PPAR$\gamma$2 being phosphorylated was lower at the late stage than that at the early stage; however, culture with 2,4,5-TMBA increased the level of phosphorylated PPAR$\gamma$2 at the late stage (Figure 3C), which decreased the transcription activity of PPAR$\gamma$2, as shown in Figure 3D. The pattern of C/EBP$\alpha$ expression was similar to that of C/EBP$\beta$ and C/EBP$\delta$. The level of C/EBP$\alpha$ gradually increased during adipogenesis, but the expression was suppressed in the presence of 2,4,5-TMBA (Figure 3E).

**Effect of 2,4,5-TMBA on the Expression of ACC, FAS, and Perilipin A.** ACC is the rate-limiting enzyme in fatty acid *de novo* synthesis, providing malonyl-CoA substrate for the biosynthesis of fatty acids.[15] FAS is a multifunctional protein with the function of catalyzing the synthesis of long-chain saturated fatty acids from acetyl-CoA and malonyl-CoA.[16] As the study design shown in Figure 2A, the expression of ACC, FAS, and perilipin A was determined when 2,4,5-TMBA-treated preadipocytes were harvested at post-induction days 2, 4, 6, and 8, respectively. Without the presence of 2,4,5-TMBA, expression of ACC and FAS in preadipocytes was elevated along the process of adipogenesis. However, when preadipocytes were cultured with 2,4,5-TMBA, expression of ACC and FAS was suppressed at the terminal stage of adipogenesis, an important stage for lipid accumulation (panels A and B of Figure 4).

At the late stage of lipid droplet formation and maturation, perilipin replaces the other droplet-coating proteins and becomes the only coating protein to reside on the large lipid droplets. Perilipin A is the predominant isoform of perilipin proteins found in mature adipocytes.[17,18] Without the treatment of 2,4,5-TMBA, expression of perilipin A gradually increased during adipogenesis, reaching the maximum when the cells were fully differentiated (Figure 4C). Although a similar pattern was observed in 2,4,5-TMBA-treated cells, the overall expression of perilipin A was attenuated.

## DISCUSSION

Previously, we showed that 2,4,5-TMBA suppresses the differentiation of preadipocytes.[11] In this study, preadipocytes were co-cultured with 2,4,5-TMBA specifically at post-induction days 0−2, 2−4, 4−6, or 6−8 only to further figure out the stages that are critically affected by 2,4,5-TMBA during adipogenesis. Moreover, preadipocytes were co-cultured with 2,4,5-TMBA during the differentiation process and harvested at days 2, 4, 6, and 8 to study the expression of signaling molecules and transcription factors at different stages of adipogenesis (Figure 5).

Although several signal transduction pathways are involved in adipogenesis, transient activation of the MEK/MAPKs signaling pathway is required for the differentiation of preadipocytes.[19] Activation of MEK by adipogenic stimuli leads to the phosphorylation of MAPKs: ERK, c-Jun amino-terminal kinase (JNK), and p38 MAPK. ERK1 and ERK2 isoforms have distinct biological functions. ERK1 has been clearly linked to the regulation of preadipocyte differentiation and adiposity. Using *ERK1*$^{-/-}$ mice, Bost et al. demonstrated that *ERK1*$^{-/-}$ mice have fewer adipocytes and decreased adiposity than those of wild-type animals. In addition, *ERK1*$^{-/-}$ mice challenged with a high-fat diet are protected from obesity and insulin resistance.[20] Bost et al. also showed that preadiocytes isolated from *ERK1*$^{-/-}$ mice exhibit impaired differentiation.[7]


dx.doi.org/10.1021/jf503344v | J. Agric. Food Chem. 2014, 62, 9860−9867

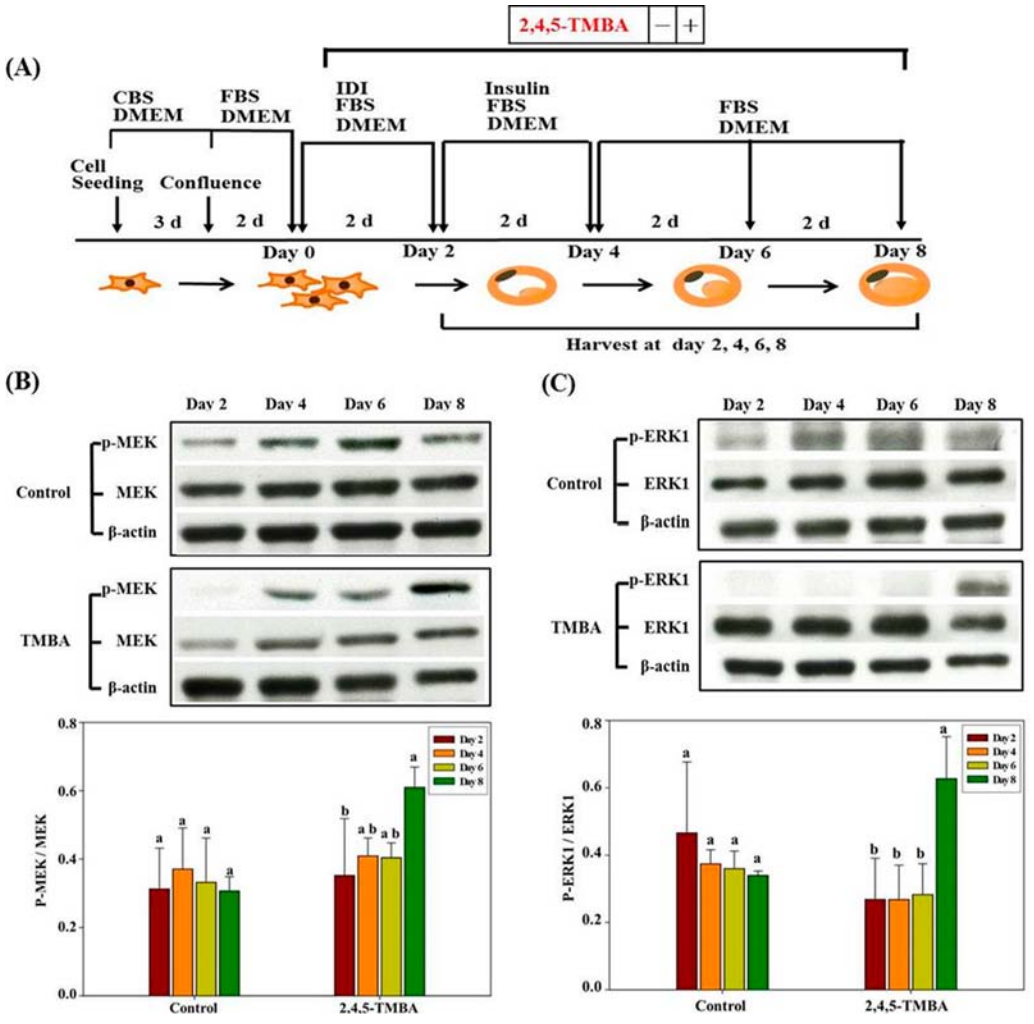


**Figure 2.** Effects of 2,4,5-TMBA on the expression of MEK and ERK during adipogenesis. (A) Study design. 2,4,5-TMBA (0.5 mM) was supplemented to culture medium during the adipogenic process. The cells were harvested at days 2, 4, 6, and 8. (B) Protein expression of phosphorylated MEK (pMEK) and MEK. (C) Protein expression of phosphorylated ERK (pERK) and ERK. Relative expression of proteins was calculated according to the reference band of $\beta$-actin. The ratio of phosphorylated proteins to total proteins was calculated by the comparison of relative expression. Values are means of three replicated cultures. Groups with the same letter are not significantly different ($\alpha = 0.05$). MEK, MAP kinase kinase; ERK, extracellular signal-regulated kinase.

Phosphorylation at specific threonine and tyrosine residues by MEK leads to the activation of ERK1, and the activation needs to be timely regulated during adipogenesis.[7,21] ERK1 has to be turned on at the early stage for a proliferative process but to be shut off later on to prevent the phosphorylation of PPAR$\gamma$.[7,20] PPAR$\gamma$ is a substrate of ERK, and its phosphorylation by ERK decreases its transcription activity.[14,22] Prusty et al. observed a rapid induction of ERK1 phosphorylation following the exposure of preadipocyte to adipogenic stimuli, but the level of phosphorylation gradually declines during adipogenesis.[23] Lii et al. showed that diallyl trisulfide, the second most abundant organosulfide in garlic oil, suppresses the differentiation of 3T3-L1 preadipocytes through prolonging ERK phosphorylation along adipogenesis.[24] Turpin et al. reported carbamazepine, a dibenzazepine, strongly inhibited adipogenesis through activation of the ERK pathway.[25] Moreover, both evodiamine (a major alkaloidal compound extracted from the fruit of *Evodia fructus*) and EGCG [(−)-epigallocatechin gallate] suppress preadipocyte differentiation through the ERK pathway.[26,27] In this current study, treatment of 2,4,5-TMBA attenuated ERK phosphorylation at the early stage but elevated the phosphorylation during terminal differentiation, which is opposite to the conditions required for adipogenesis.

The cytotoxic effect of 2,4,5-TMBA was estimated in our previous study.[11] When preadiopcytes were co-cultured with 0.5 mM 2,4,5-TMBA during differentiation, the cell viability was decreased by 25.82% at the end of the 8 day differentiation period. On the basis of the results, the inhibition on adipogenesis observed in this study mostly resulted from the action of 2,4,5-TMBA instead of cytotoxicity. When the rats were orally administered with 100 mg/kg 2,4,5-TMBA, the serum concentration of 2,4,5-TMBA reached 5.44, 8.39, 9.09, and 5.64 $\mu$g/mL at 30, 60, 120, and 240 min, respectively (data not shown). Because rats did not show toxicity when gavaged with 2,4,5-TMBA at a dose of 2000 mg/kg,[28] a serum concentration close to 0.5 mM (100 $\mu$g/mL) might be reached *in vivo* by administering a higher dose of 2,4,5-TMBA.

Activation of MEK/MAPKs in preadipocyte is rapidly followed by the expression of C/EBP$\beta$ and C/EBP$\delta$, which further induces the expression of PPAR$\gamma$ and C/EBP$\alpha$, the two transcription factors that oversee the terminal differentiation


dx.doi.org/10.1021/jf503344v | J. Agric. Food Chem. 2014, 62, 9860−9867

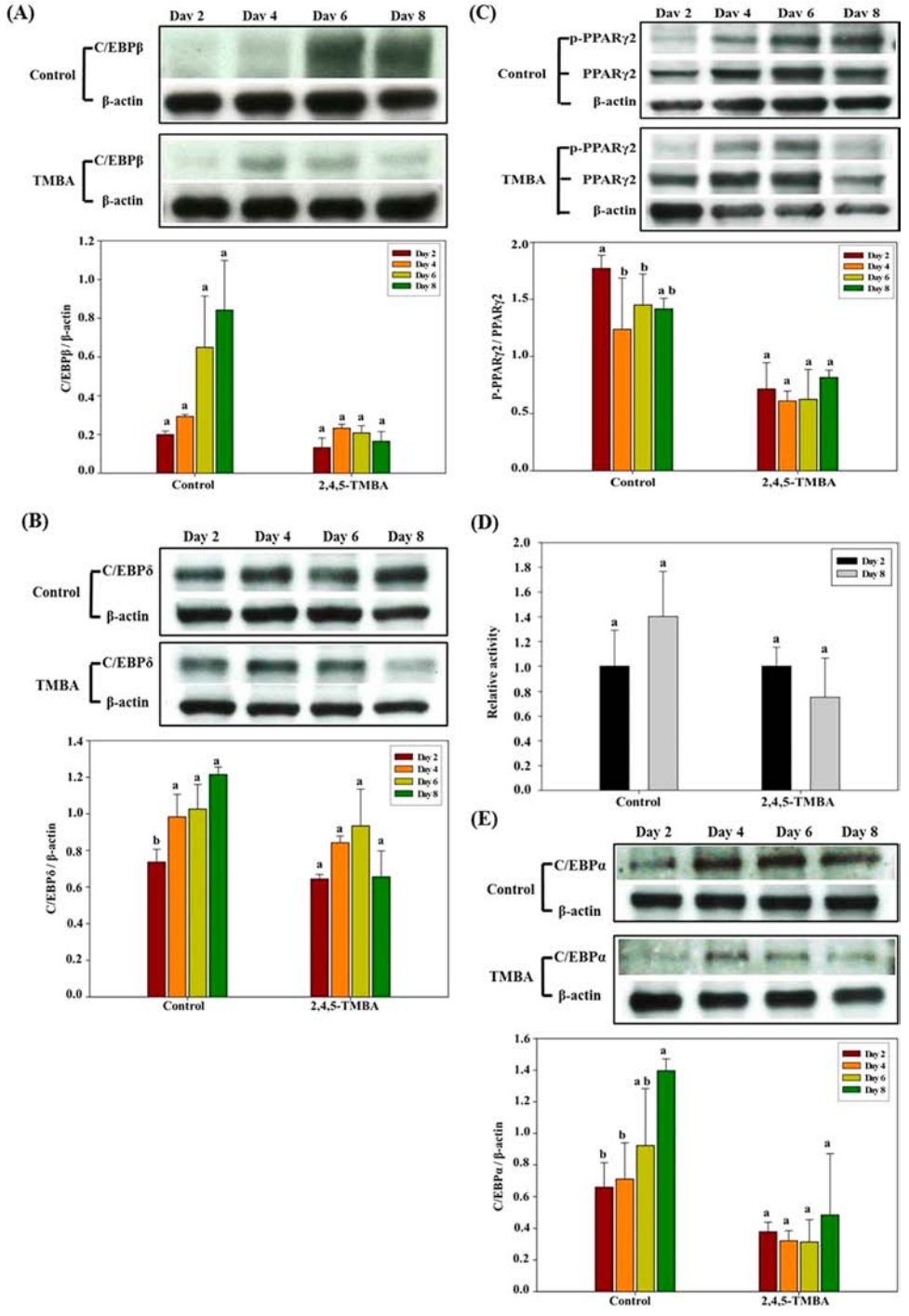


**Figure 3.** Effects of 2,4,5-TMBA on the expression of transcription factors. The cells were cultured with 2,4,5-TMBA (0.5 mM) and harvested at days 2, 4, 6, and 8. Expression of (A) C/EBP$\beta$, (B) C/EBP$\delta$, (C) PPAR$\gamma$2, and (E) C/EBP$\alpha$. (D) Result of PPAR$\gamma$ activation. Relative expression of proteins was calculated according to the reference band of $\beta$-actin. The ratio of phosphorylated proteins to total proteins was calculated by the comparison of relative expression. Values are means of three replicated cultures. Groups with the same letter are not significantly different ($\alpha = 0.05$). C/EBP, CCAAT/enhancer binding protein; PPAR, peroxisome proliferator-activated receptor.

process.[29] C/EBP$\beta$ and C/EBP$\delta$ play a synergistic role in preadipocyte differentiation. Embryonic fibroblasts derived from mice lacking either C/EBP$\beta$ or C/EBP$\delta$ do not differentiate into mature adipocytes.[30] PPAR$\gamma$ is the master regulator of adipogenesis.[31] Activated PPAR$\gamma$ enhances the expression of C/EBP$\alpha$, and then both factors synergistically induce the genes responsible for the maturation of adipocytes. PPAR$\gamma$ can promote adipogenesis in C/EBP$\alpha$-deficient cells, but C/EBP$\alpha$ has no ability to promote adipogenesis in the absence of PPAR$\gamma$.[32] PPAR$\gamma$2 but not PPAR$\gamma$1 is required for the activation of adipogenesis.[12] *PPAR$\gamma$2*$^{-/-}$ mouse embryonic fibroblasts showed a dramatically reduced capacity for adipogenesis compared to wild-type mouse embryonic fibroblasts.[33] Phosphorylation of PPAR$\gamma$2 by ERK decreases its transcription activity.[14] In this study, co-culture with 2,4,5-TMBA down-regulated the overall expression of C/EBPs and PPAR$\gamma$2 but elevated the ratio of PPAR$\gamma$2 being phosphorylated at the terminal stage (panels A–C and E of Figure 3), which results in


dx.doi.org/10.1021/jf503344v | J. Agric. Food Chem. 2014, 62, 9860–9867

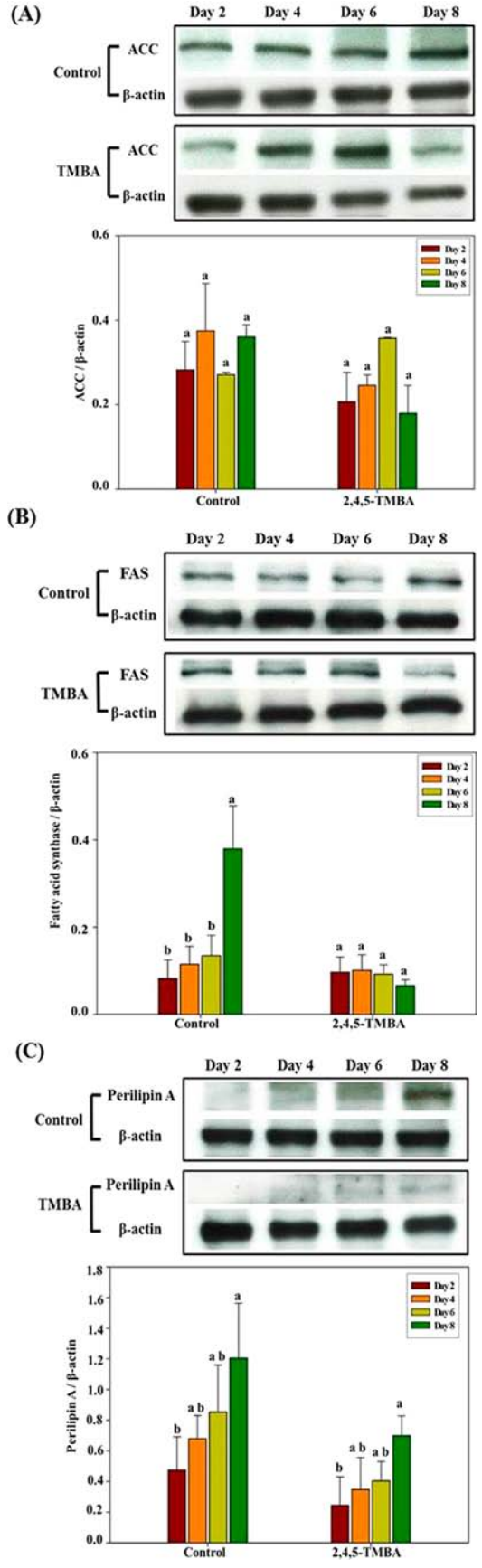


**Figure 4.** Effects of 2,4,5-TMBA on the expression of lipogenic enzymes and lipid droplet-coating protein. The cells were cultured with 2,4,5-TMBA (0.5 mM) and harvested at days 2, 4, 6, and 8. Expression of (A) ACC, (B) FAS, and (C) perilipin A. Relative expression of proteins was calculated according to the reference band of $\beta$-actin. Values are means of three replicated cultures. Groups with the same letter are not significantly different ($\alpha = 0.05$). ACC, acetyl-CoA carboxylase; FAS, fatty acid synthase.

a decreased transcription activity of PPAR$\gamma$2 (Figure 3D), leading to the attenuation of adipogenesis. This increased phosphorylation of PPAR$\gamma$2 resulted from enhanced ERK1 phosphorylation by 2,4,5-TMBA at the terminal stage.

The increase in size of adipocytes arises in part from progressive lipid accumulation during adipogenesis. Both ACC and FAS play crucial roles in *de novo* lipogenesis in mammals.[15,16] The study by Wu et al. showed that husk extract, punicalagin, and ellagic acid exhibit FAS inhibitory activity. When 3T3-L1 adiocytes were incubated with these extracts and compounds, adipogenesis was inhibited.[34] Lower levels of ACC and FAS were also observed in carbamazepine-treated preadipocytes, which showed impaired lipid accumulation.[25] Loftus et al. have demonstrated that animals with lowered ACC and FAS activities showed significantly reduced adiposity.[35] In a previous study, we showed that incubation with 2,4,5-TMBA decreased the amount of lipid accumulated in adipocytes.[11] Results of this current study show that the inhibitory effect of 2,4,5-TMBA on the expression of ACC and FAS is mainly observed at the late period of adipogenesis, an important stage for lipid accumulation.

One characteristic of mature adipocytes is the formation and enlargement of intracellular lipid droplets. The proteins that coat lipid droplets change during droplet biogenesis and play critical roles in the maintenance of the lipid droplet structure and regulation of lipid metabolism. At the late stage of lipid droplet formation and maturation, perilipins become the only coating protein and perilipin A is the predominant isoform found in mature adipocytes.[18] In obese subjects, expression of perilipin A in adipose tissue is elevated.[36] However, lipid accumulation in adipocytes is significantly decreased in *perilipin* null mice.[37] In this study, we observed an inhibition on the expression of perilipin A when preadipocytes were cultured with 2,4,5-TMBA. Suppression of perilipin A could impair the formation of lipid droplets and maturation, leading to a decreased lipid accumulation as observed in 2,4,5-TMBA-treated cells.

Taken together, our results showed that 2,4,5-TMBA may suppress adipogenesis through the regulation of ERK1 phosphorylation. 2,4,5-TMBA inhibited the phosphorylaton of ERK1 at the early stage of the adipogenic process but enhanced it at the late stage, which is opposite the conditions required for adipogenesis. Although all of the effects observed might be coincidental and not yet mechanistically interdependent, the opposite effects of 2,4,5-TMBA on ERK at the early and late stages of the 8 day adipogenic process may be mediated by the modulation of scaffolding protein AEBP-1 and phosphatases MKP-1 and MKP-3. AEBP-1 protects the ERK from specific phosphatase and is downregulated at the late stage of adipogenesis. Conversely, expression of MKP-1 and MKP-3 is upregulated in mature adipocytes.[38−40] Prospectively, the interaction of 2,4,5-TMBA with AEBP-1, MKP-1, and MPL-3 will be worth studying. Moreover, application of microarray technology to monitor global changes in gene expression


dx.doi.org/10.1021/jf503344v | J. Agric. Food Chem. 2014, 62, 9860−9867

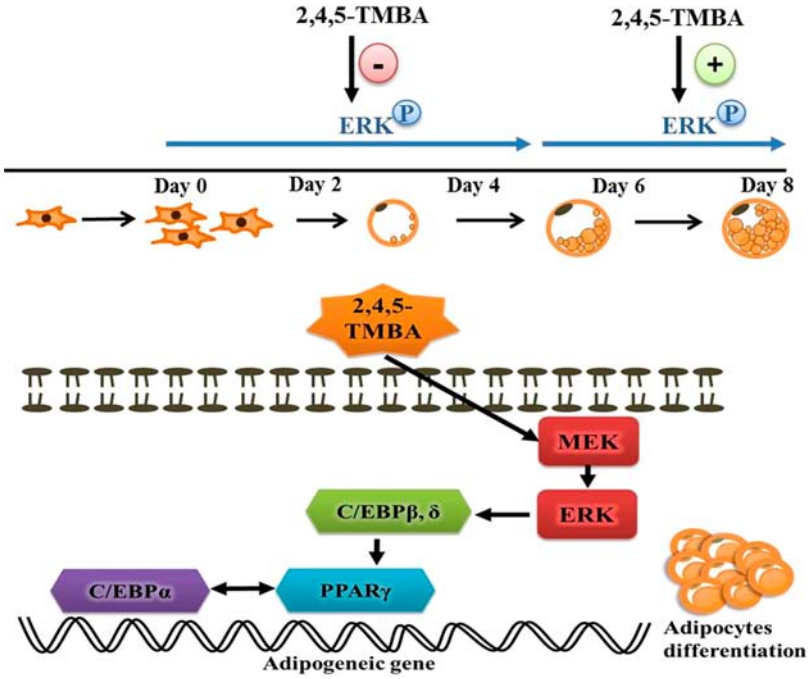


**Figure 5.** Proposed mechanism for the suppression of adipogenesis by 2,4,5-TMBA.

profiles during 3T3-L1 differentiation will help to elucidate the mode of regulation by 2,4,5-TMBA.

Obesity results from the hypertropy of adipocytes and the recruitment of new adipocytes from preadipocytes. Both processes are significantly dependent upon the regulation of adipogenesis. Although results from *in vitro* studies cannot be directly extrapolated into clinical effects, our study will help to elucidate the anti-adipogenic potential of 2,4,5-TMBA.

## AUTHOR INFORMATION

### Corresponding Author

*Telephone: 886-2-25381111, ext. 6214. Fax: 886-2-25334789. E-mail: drkuo@mail.usc.edu.tw.

### Funding

This study was supported by the National Science Council (NSC 101-2313-B-158-001) and Shih Chien University (USC-101-05-02001).

### Notes

The authors declare no competing financial interest.

## REFERENCES

(1) Tang, Q. Q.; Otto, T. C.; Lane, M. D. Mitotic clonal expansion: A synchronous process required for adipogenesis. *Proc. Natl. Acad. Sci. U. S. A.* **2003**, *100*, 44−49.

(2) Feve, B. Adipogenesis: Cellular and molecular aspects. *Best Pract. Res., Clin. Endocrinol. Metab.* **2005**, *19*, 483−499.

(3) Otto, T. C.; Lane, M. D. Adiopose development: From stem cell to adipocyte. *Annu. Rev. Biochem. Mol. Biol.* **2012**, *40*, 229−242.

(4) Yeh, W. C.; Cao, M.; Casson, M.; Mcknight, S. L. Cascade regulation of adipocyte terminal differentiation by three members of the C/EBP family of leucine zipper proteins. *Genes Dev.* **1995**, *15*, 168−181.

(5) Feve, B. Adipogenesis: Cellular and molecular aspects. *Best Pract. Res., Clin. Endocrinol. Metab.* **2005**, *19*, 483−499.

(6) Prusty, D.; Park, B.-H.; Davis, K. E.; Farmer, S. R. Activation of MEK/ERK signaling promotes adipogenesis by enhancing peroxisome proliferator-activated receptor $\gamma$ (PPAR)$\gamma$ and C/EBP$\alpha$ gene expression during the differentiation of 3T3-L1 preadipocytes. *J. Biol. Chem.* **2002**, *277*, 46226−46232.

(7) Bost, F.; Aouadi, M.; Caron, L.; Even, P.; Belmonte, N.; Prot, M.; Dani, C.; Hofman, P.; Pages, G.; Marchand-Brustel, Y. L.; Binetruy, B. The extracellular signal-regulated kinase isoform ERK1 is specifically required for in vitro and in vivo adipogenesis. *Diabetes* **2005**, *54*, 402−411.

(8) Momin, R. A.; De Witt, D. L.; Nair, M. G. Inhibition of cyclooxygenase (COX) enzymes by compounds from *Daucus carota* L. seeds. *Phytother. Res.* **2003**, *17*, 976−979.

(9) Fajas, L.; Miard, S.; Briggs, M. R.; Auwerx, J. Selective cyclo-oxygenase-2 inhibitors impair adipocyte differentiation through inhibition of the clonal expansion phase. *J. Lipid Res.* **2003**, *44*, 1652−1659.

(10) Ghoshal, S.; Trivedi, D. B.; Graf, G. A.; Loftin, C. D. Cyclooxygenase-2 deficiency attenuates adipose tissue differentiation and inflammation in mice. *J. Biol. Chem.* **2011**, *286*, 889−898.

(11) Wu, M. R.; Hou, M. H.; Lin, Y. L.; Kuo, C. F. 2,4,5-TMBA, an inhibitor of cyclooxygenase-2, suppresses adipogenesis and enhances lipolysis in 3T3-L1 adipocytes. *J. Agric. Food Chem.* **2012**, *60*, 7262−7269.

(12) Ren, D.; Collingwood, T. N.; Rebar, E. J.; Wolffe, A. P.; Camp, H. PPAR$\gamma$ knockdown by engineered transcription factors: Exogenous PPAR$\gamma$2 but not PPAR$\gamma$1 reactivates adipogenesis. *Cenes Dev.* **2002**, *16*, 27−32.

(13) Hu, E.; Kim, J. B.; Sarraf, P.; Spiegelman, B. M. Inhibition of adipogenesis through MAP kinas-mediated phosphorylation of PPAR$\gamma$. *Science* **1996**, *274*, 2100−2103.

(14) Camp, H. S.; Tafuri, S. R. Regulation of peroxisome proliferator-activated receptor gamma activity by mitogen-activated protein kinase. *J. Biol. Chem.* **1997**, *272*, 10811−10816.

(15) Lane, M. D.; Moss, J.; Plalkis, S. E. Acetyl coenzyme A carboxylase. *Curr. Top. Cell. Regul.* **1974**, *8*, 139−195.

(16) Wakil, S. J.; Stoops, J. K.; Joshi, V. C. Fatty acid synthase and its regulation. *Annu. Rev. Biochem.* **1983**, *52*, 537−579.

(17) Wolins, N. E.; Quaynor, B. K.; Skinner, J. R.; Schoenfish, M. J.; Tzekov, A.; Bicket, P. E. S3-12, adipophilin, and TIP47 package lipid in adipocytes. *J. Biol. Chem.* **2005**, *280*, 19146−19155.

(18) Brasaemle, D. L. The perilipin family of structural lipid droplet proteins: Stabilization of lipid droplets and control of lipolysis. *J. Lipid Res.* **2007**, *48*, 2547−2559.

(19) Bost, F.; Aouadi, M.; Caron, L.; Binetruy, B. The role of MAPKs in adipocyte differentiation and obesity. *Biochimie* **2005**, *87*, 51−56.
(20) Bost, F.; Caron, L.; Marchetti, I.; Dani, C.; Le Marchand-Brustel, Y.; Binetruy, B. Retinoic acid activation of the ERK pathway is required for embryonic stem cell commitment into adipocyte lineage. *Biochem. J.* **2002**, *361*, 621−627.
(21) Elion, E. A. Routing MAP kinase cascades. *Science* **1998**, *281*, 1625−1626.
(22) Adams, M.; Reginato, M. J.; Shao, D.; Lazar, M. A.; Chatterjee, V. K. Transcriptional activation by peroxisome proliferator-activated receptor gamma is inhibited by phosphorylation at a consensus mitogen-activated protein kinase site. *J. Biol. Chem.* **1997**, *272*, 5128−5132.
(23) Prusty, D.; Park, B.-H.; Davis, K. E.; Farmer, S. R. Activation of MEK/ERK signaling promotes adipogenesis by enhancing peroxisome proliferator-activator $\gamma$ (PPAR$\gamma$) and C/EBP$\alpha$ gene expression during the differentiation of 3T3-L1 preadipocytes. *J. Biol. Chem.* **2002**, *277*, 46226−46232.
(24) Lii, C.-K.; Huang, C.-Y.; Chen, H.-W.; Chow, M.-Y.; Lin, Y.-R.; Huang, C.-S.; Tsai, C.-W. Diallyl trisulfide suppresses the adipogenesis of 3T3-L1 preadipocytes through ERK activation. *Food Chem. Toxicol.* **2012**, *50*, 478−484.
(25) Turpin, E.; Muscat, A.; Vatier, C.; Chetrite, G.; Corruble, E.; Moldes, M.; Fève, B. Carbamaze directly inhibits adipocyte differentiation through activation of the ERK 1/2 pathway. *Br. J. Pharmacol.* **2013**, *168*, 139−150.
(26) Wang, T.; Wang, Y.; Yamashita, H. Evodiamine inhibits adipogenesis via the EGFR-PKC$\alpha$-ERK signaling pathway. *FEBS Lett.* **2009**, *583*, 3655−3659.
(27) Kim, H.; Sakamoto, K. (−)-Epigallocatechin gallate suppresses adipocyte differentiation through the MEK/ERK and PI3K/Akt pathways. *Cell Biol. Int.* **2012**, *36*, 147−153.
(28) Chen, C. C.; Kuo, C. F. Acute limit oral toxicity study of 2,4,5-trimethoxybenzaldehyde in rats. In *Nutrition, Functional and Sensory Properties of Foods*; Ho, C.-T., Mussinan, C., Shahidi, F., Contis, E. T., Eds.; Royal Society of Chemistry: London, U.K., 2013; pp 324−329.
(29) Farmer, S. R. Transcriptional control of adipocyte formation. *Cell Metab.* **2006**, *4*, 263−273.
(30) Tanaka, T.; Yoshida, N.; Kishimoto, T.; Akira, S. Defective adipocyte differentiation in mice lacking the C/EBP-$\beta$ and/or C/EBP-$\delta$ gene. *EMBO J.* **1997**, *16*, 7432−7443.
(31) Farmer, S. R. Regulation of PPAR$\gamma$ activity during adipogenesis. *Int. J. Obes.* **2005**, *29*, S13−S16.
(32) Rosen, E. D.; Hsu, C. H.; Wang, X.; Sakai, S.; Freeman, M. W.; Gonzalez, F. J.; Spiegelman, B. M. C/EBP$\alpha$ induces adipogenesis through PPAR$\gamma$: A united pathway. *Genes Dev.* **2002**, *16*, 22−26.
(33) Zhang, J.; Fu, M.; Cui, T.; Xiong, C.; Xu, K.; Zhong, W.; Xiao, Y.; Floyd, D.; Liang, J.; Song, Q.; Chen, Y. E. Selective disruption of PPAR$\gamma$2 impairs the development of adipose tissue and insulin sensitivity. *Proc. Natl. Acad. Sci. U. S. A.* **2004**, *101*, 10703−10708.
(34) Wu, D.; Ma, X.; Tian, W. Pomegranate husk exract, punicalagin and ellagic acid inhibit fatty acid synthase and adipogenesis of 3T3-L1 adipocyte. *J. Funct. Food* **2013**, *5*, 633−641.
(35) Loftus, T. M.; Jaworsky, D. E.; Frehywot, G. L.; Townsend, C. A.; Ronnett, G. V.; Lane, M. D.; Kuhajda, F. P. Reduced food intake and body weight in mice treated with fatty acid synthase inhibitors. *Science* **2000**, *288*, 2379−2381.
(36) Kern, P. A.; Di Gregorio, G.; Lu, T.; Rassouli, N.; Ranganathan, G. Perilipin expression in human adipose tissue is elevated with obesity. *J. Clin. Endocrinol. Metab.* **2004**, *89*, 1352−1358.
(37) Tansey, J. T.; Sztalryd, C.; Gruia-Gray, J.; Roush, D. L.; Zee, J. V.; Gavrilova, O.; Reitman, M. L.; Deng, C.-X.; Li, C.; Kimmel, A. R.; Londos, C. Perilipin ablation results in a lean mouse with aberrant adipocyte lipolysis, enhanced leptin production, and resistance to diet-induced obesity. *Proc. Natl. Acad. Sci. U. S. A.* **2001**, *98*, 6494−6499.
(38) Kim, S. W.; Muise, A. M.; Lyons, P. J.; Ro, H. S. Regulation of adipogenesis by a transcriptional repressor that modulates MAPK activation. *J. Biol. Chem.* **2001**, *276*, 10199−10206.
(39) Sun, H.; Charles, C. H.; Lau, L. F.; Tonks, N. K. MKP-1 (3CH134), an immediate early gene product, is a dual specificity phosphatase that dephosphorulates MAP kinase in vivo. *Cell* **1993**, *75*, 487−493.
(40) Muda, M.; Boschert, U.; Dickinson, R.; Martinou, J.-C.; Martinou, I.; Camps, M.; Schlegel, W.; Arkinstall, S. MKP-3, a novel cytosolic protein-tyrosine phosphatase that exemplifiers a new class of mitogen-activated protein kinase phosphatase. *J. Biol. Chem.* **1996**, *271*, 4319−4326.

reduced browning tendency of treated wines after a maderization test, which they assumed to be due to the removal of up to 30% procyanidins and cinnamates.

More recently, a winemaking process with a modified chitosan-based biofilm was patented,[30] claimed to protect wine from oxidation thanks to the presence of phenolic compounds grafted onto the chitosan film, with this latter inserted in the bottle just before bottling.

However, taking into consideration all of the reported activities for unmodified chitosan, in particular those linked to the antiradical and antioxidant properties, it would be interesting to test the effect of this polysaccharide on phenol oxidative kinetics in wine-like conditions, in view to hypothesize its use in musts and wines with reduced levels of sulfur dioxide and at different vinification stages.

The aim of this work was, hence, to compare the efficacy of chitosan and sulfur dioxide in controlling the browning of air-saturated white wine model solutions containing (+)-catechin, metal ions, and tartaric acid. The color of the solutions and the generation of brownish xanthylium cations and intermediate phenolic species were monitored by means of high-performance liquid chromatography with diode array detection and mass spectrometry (HPLC−DAD/MS). In addition, the protecting capacity of the two additives toward the chemical oxidation of three varietal thiols was further evaluated by gas chromatography/mass spectrometry (GC/MS).

## MATERIALS AND METHODS

**Chemicals.** HPLC-grade acetonitrile and acetic acid were obtained from Merck (Darmstadt, Germany). Water was of Milli-Q quality. (+)-Catechin, (+)-tartaric acid, $Fe^{II}$ sulfate heptahydrate, $Cu^{II}$ sulfate pentahydrate, potassium metabisulfite, low-molecular-weight 75−85% deacylated chitosan (product 448869), 5,5′-dithiobis(2-nitrobenzoic acid), and 3-mercapto-3-methylbutan-1-ol (3MMB) were obtained from Sigma-Aldrich (Milan, Italy). 3-Mercaptohexan-1-ol (3MH) and 3-mercaptohexyl acetate (3MHA) were purchased from Interchim (Montluçon, France). 4-Methoxy-2-methylbutane-2-thiol (4MMB) was provided by Oxford Chemical (Hartlepool, U.K.). High-purity nitric acid (Suprapur, Merck, Germany) was used for the inductively coupled plasma−optical emission spectroscopy (ICP−OES) analysis.

**Model Wine Solutions.** A total of 4 L of a solution containing 5 g/L (+)-tartaric acid and 12% (v/v) ethanol was prepared. The pH was adjusted to 3.6 with 2 M NaOH before bringing to the mark progressively by adding water.

The solution was stirred at room temperature in open air until saturated with $O_2$ (1 h),[31] before (+)-catechin addition at 100 mg/L. To this solution, 5 nM/L 3MH, 3MHA, and 3MMB were further added (from bulk standard solutions, according to Ellmann's method[32]).

Trials were arranged by transferring aliquots (80 mL) of the above-cited solution in 125 mL inert glass bottles (Supelco, Bellefonte, PA), leaving air in the headspace with the aim to accelerate the oxidation phenomena. A total of 80 μL of an aqueous solution containing $Fe^{II}$ sulfate heptahydrate (5 g/L) and $Cu^{II}$ sulfate pentahydrate (300 mg/L) was added to each bottle to give a final concentration of 5 mg/L Fe and 0.30 mg/L Cu. When appropriate, 80 mg/L sulfur dioxide (as potassium metabisulfite) and 1 g/L chitosan were separately added, to constitute the following solutions: MS (model solution), $SO_2$ (model solution + sulfur dioxide), and Kt (model solution + chitosan). The bottles, closed with a silicone septum (Supelco, Bellefonte, PA) and crimped with airtight aluminum caps (Supelco, Bellefonte, PA), were stored at room temperature (22 °C), in the dark.

Because of chitosan insolubility, once closed, Kt samples were mechanically shook (Roller 6, IKA, Germany) for 5 min to permit a homogeneous distribution of the polisaccharides. A total of 5 min of shaking was also performed, on Kt samples, each 2 days all along the experiment.

With the aim to deepen both the adsorption efficacy of chitosan on oxidized phenols and the chelating capacity on metals, at day 21, a portion of each MS solution was transferred to a 25 mL inert glass bottle, added with 1g/L chitosan, ermetically closed with aluminum caps and mechanically shook for 30 h (samples Kt 30 h). These solutions were analyzed for their browning level and phenolic and metal content using the methods outlined below.

**Browning and $SO_2$ Measurement.** The experimentation lasted 21 days, during which three bottles, prepared identically for each trial (MS, $SO_2$, and Kt), were taken at time points 0, 3, 7, 14, and 21 days, for the analytical determinations to be carried out in triplicate. The browning development of the samples was followed measuring the increase in absorbance at 440 nm (1 cm optical path) using a Jasco 810 spectrophotometer (Tokyo, Japan), after filtration (0.45 μm, cellulose filters). Total $SO_2$ concentrations were determined in accordance with the official International Organization of Vine and Wine (OIV) method.[33]

**Reversed-Phase (RP)-HPLC/Electrospray Ionization (ESI)−MS Analysis of (+)-Catechin and Other Phenols Generated during Its Oxidation.** HPLC separation and identification of (+)-catechin and phenolic compounds generated during its oxidation were performed on a Agilent LC-MSD 1100 series single quadrupole (Agilent Technologies, Palo Alto, CA), equipped with an autosampler and a diode array UV−vis detector, according to a previous method.[31] The column was a Poroshell 120 SB C18, 2.7 μm, 150 × 4.6 mm inner diameter, operating at 30 °C with a flow of 0.9 mL/min. Elution solvents were 2% acetic acid in HPLC-grade water (eluent A) and 2% acetic acid in HPLC-grade acetonitrile (eluent B). Gradient elution was as follow: from 98 to 95% A in 9 min, from 95 to 90% A in 6 min, from 90 to 82% A in 4 min, from 82 to 80% A in 3 min, from 80 to 70% A in 3 min, from 70 to 50% A in 3 min, from 50 to 0% A in 2 min, and from 0 to 98% A in 3 min. A post-run time of 5 min was further applied. Mass detection was carried out using an ESI interface operating in positive mode, scanning from $m/z$ 100 to 1000 and using the following conditions: drying gas flow, 9.0 L/min; nebulizer pressure, 50 psi; gas drying temperature, 350 °C; capillary voltage, 4000 V; and fragmentor voltage, 15 V. Identification of (+)-catechin was accomplished by comparison of the UV spectrum and retention time of the standard compound. Phenolic compounds generated by (+)-catechin oxidative decay, which lacked of available standards, were identified on the basis of the UV and MS spectrum already reported in other studies.[31,34] Quantification of residual (+)-catechin in the samples was performed at 280 nm using an external calibration curve built by injecting solutions of known concentrations. Other phenols were monitored according to their maximum absorption wavelength (280 nm for carboxymethine-linked dimers and xantene and 440 nm for xanthylium ions and their esters) and quantified in a semi-quantitative fashion as peak area. Before injection, synthetic wines were filtered at 0.45 μm with a cellulose filter. All analysis were performed in duplicate.

**Extraction of Volatile Thiols.** Thiols were quantified after solid-phase extraction (SPE) separation as proposed by Fedrizzi et al.,[35] with little modifications. A 50 mL sample volume containing 0.1 mL of internal standard (4MMB at 50 μM/L in 50% hydroalcoholic solution) was percolated through an Isolute ENV+ cartridges (1 g/6 mL) (IST, Ltd., Mid Glamorgan, U.K.) previously conditioned with methanol (15 mL) and 12% hydroalcolic solution (20 mL) in that order. Analytes were recovered by passing 30 mL of $CH_2Cl_2$. The extract was added with 60 mL of *n*-pentane, dried with $Na_2SO_4$, and distilled to about 100 μL with a small vigreux column.

**GC/MS Analysis of Thiols.** A total of 2 μL of the extract were injected in the splitless mode (splitless time of 1 min) into a Thermo Scientific Trace GC ultra gas chromatograph (Waltham, MA), equipped with a Thermo Scientific Trace DSQ selective mass detector and a fused silica capillary Stabilwax DA column (Restek, Bellefonte, PA) (30 m, 0.25 mm inner diameter, and 0.25 μm film thickness), under the following working conditions: GC-grade helium as the carrier gas at a flow rate (constant flow, vacuum compensation) of 1.0 mL/min; column temperature program, 40 °C heated at 1 °C/min to 45 °C, then at 3 °C/min to 100 °C, and finally heated at 5 °C/min to


dx.doi.org/10.1021/jf5025664 | J. Agric. Food Chem. 2014, 62, 9868−9875

240 °C. The injection temperature was 250 °C. Detection was carried out by electron ionization (EI) mode, using an ionization energy of 70 eV. The transfer line was heated at 220 °C, and the ionization source was heated at 250 °C. 3MH, 3MHA, 3MMB, and the internal standard (4MMB) were detected in single ion monitoring (SIM) mode by monitoring the following ions: $m/z$ 134 and 100 for 3MH and 4MMB (internal standard), $m/z$ 120, 86, and 75 for 3MMB, and $m/z$ 116, 101, and 88 for 3MHA. The quantification ions were $m/z$ 134 for both 3MH and the internal standard, $m/z$ 86 for 3MMB, and $m/z$ 116 for 3MHA. The content of each single thiol in the solutions has been expressed as the relative chromatographic area with respect to the area of the internal standard.

**Metal Content.** ICP−OES analysis of Fe and Cu was carried out on a Spectro Archos apparatus (Kleve, Germany) equipped with a 1.8 mm torch and a side on plasma interface (SPI). Radio frequency (RF) power was 1350 W; plasma flow was 12.5 L/min; auxiliary flow was kept at 0.5 L/min; nebulizer flow was 0.8 L/min; and the pump rate was kept at 1.5 mL/min. Total iron and copper were monitored at wavelengths of 324.754 and 238.204 nm, respectively, and plasma view was in radial mode. Because of the relatively simple composition of the samples, the analysis was performed by directly aspirating the filtered solutions (0.22 $\mu$m, cellulose filters), without prior digestion.

Standard calibration curves were prepared from 1000 $\mu$g/mL single-element solutions (Alfa Aesar, Germany) in 1% $HNO_3$ (v/v).

**Statistical Analysis.** One-way analysis of variation (ANOVA) was performed using Statistica 6 (StatSoft Italia srl, Italy) software package. In the case of significant differences, the Tukey honest significant difference (HSD) test at $p < 0.05$ was used to evaluate differences between means of each treatment.

## RESULTS AND DISCUSSION

**Browning of White Wine Model Solutions.** The color development of the solutions all along the entire duration of the trial was spectrophotometrically monitored at 440 nm (Figure 1), that is, at the maximum absorption wavelength of brown pigments generated by the oxidative decay of (+)-catechin.[10] All of the solutions remained virtually colorless for the first 7 days, after which a steady increase in browning was observed for the MS solutions. At our conditions, hence, this could be thought of as the time necessary to generate the xanthylium cations in "not protected" model wines (as was the case of MS samples).

$SO_2$ and Kt samples shared a common evolution in color development until day 14, with a moderate increase in browning [<0.040 absorbance (ABS) units] with respect to days 3 and 7. However, at day 21, $SO_2$ solutions were significantly more oxidized than the Kt solutions. This likely is the consequence of the almost complete consumption of sulfites in the former solutions, which, at the 14th and 21st days, were found to contain 12.8 and <0.6 mg/L of total $SO_2$, respectively (data not shown). For experimental conditions similar to the conditions that we used in this work, the fast browning of model wine solutions once sulfites had been completely oxidized has already been reported.[31]

In the same Figure 1, it is possible to appreciate the changes in absorbance at 280 nm of the model wines. The contribution to this absorbance mainly comes from (+)-catechin, but other colorless intermediates (carboxymethine-linked dimers and xanthenes, both coming from (+)-catechin oxidation) may significantly contribute, depending upon their amounts in solutions. The figure clearly shows that, at day 3, chitosan provoqued a relevant reduction in absorbance, which remained substantially unchanged after the 7th day of conservation onward. This trend of absorbancies could well be due to the initial adsorption of (+)-catechin and phenolic intermediates on the chitosan chain and/or the lack in generation of the latter.

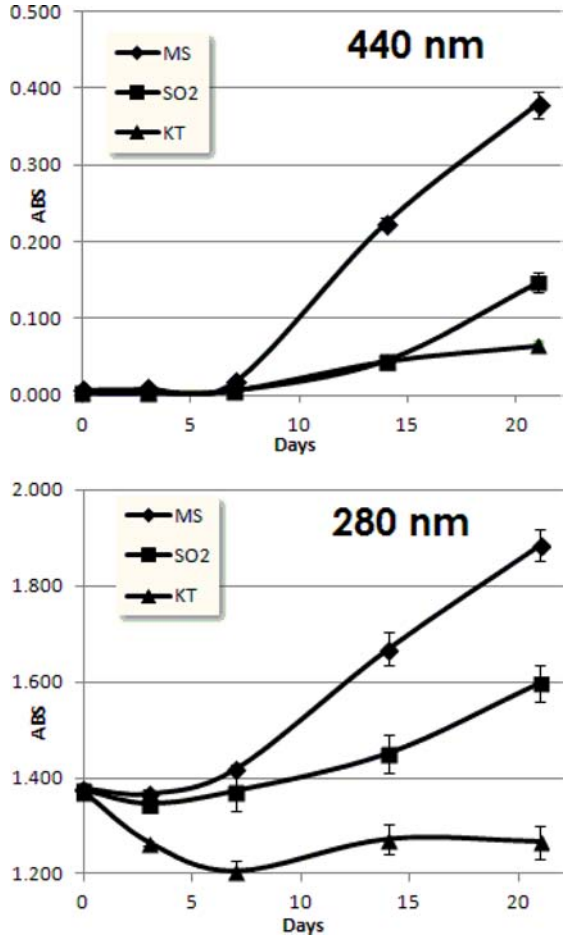


**Figure 1.** Changes in absorbance at 440 and 280 nm of MS, $SO_2$, and Kt solutions during 21 days of oxidation. MS, model solution; $SO_2$, sulfur dioxide; and Kt, chitosan.

On the contrary, $SO_2$ solutions and to a significantly greater extent MS, increased their absorbance at 280 nm likely because of the progressive generation of oxidized dimers. Further comments on these data will be given in the continuing of the discussion.

Overall, Figure 1 shows that, when individually present in solutions, 1g/L chitosan and 80 mg/L free $SO_2$ exerted an apparently comparable antibrowning ability. As previously mentioned, two other works,[28,29] aimed to evaluate the effects of different fining agents on white wine oxidation, outlined the reduced tendency to browning of white wines added with up to 4 g/L chitosan. In those papers, the treated wines were filtered and submitted to an accelerated oxidation (2−5 days at 50 °C) at the end of which chitosan performed comparably (or marginally worse) to polyvinylpolypyrrolidone (PVPP) or potassium caseinate. Even though the authors only linked this results to the ability of chitosan to adsorb phenols (preferentially hydroxycinnamic acids), other concomitant antibrowning mechanisms could not be excluded.

In addition, specific information on the effect of chitosan on the generation of intermediate oxidized compounds in environments pertinent to wine is totally lacking in the literature.

To deepen this latter subject, the presence of phenolic compounds [e.g., (+)-catechin and dimers generated from its

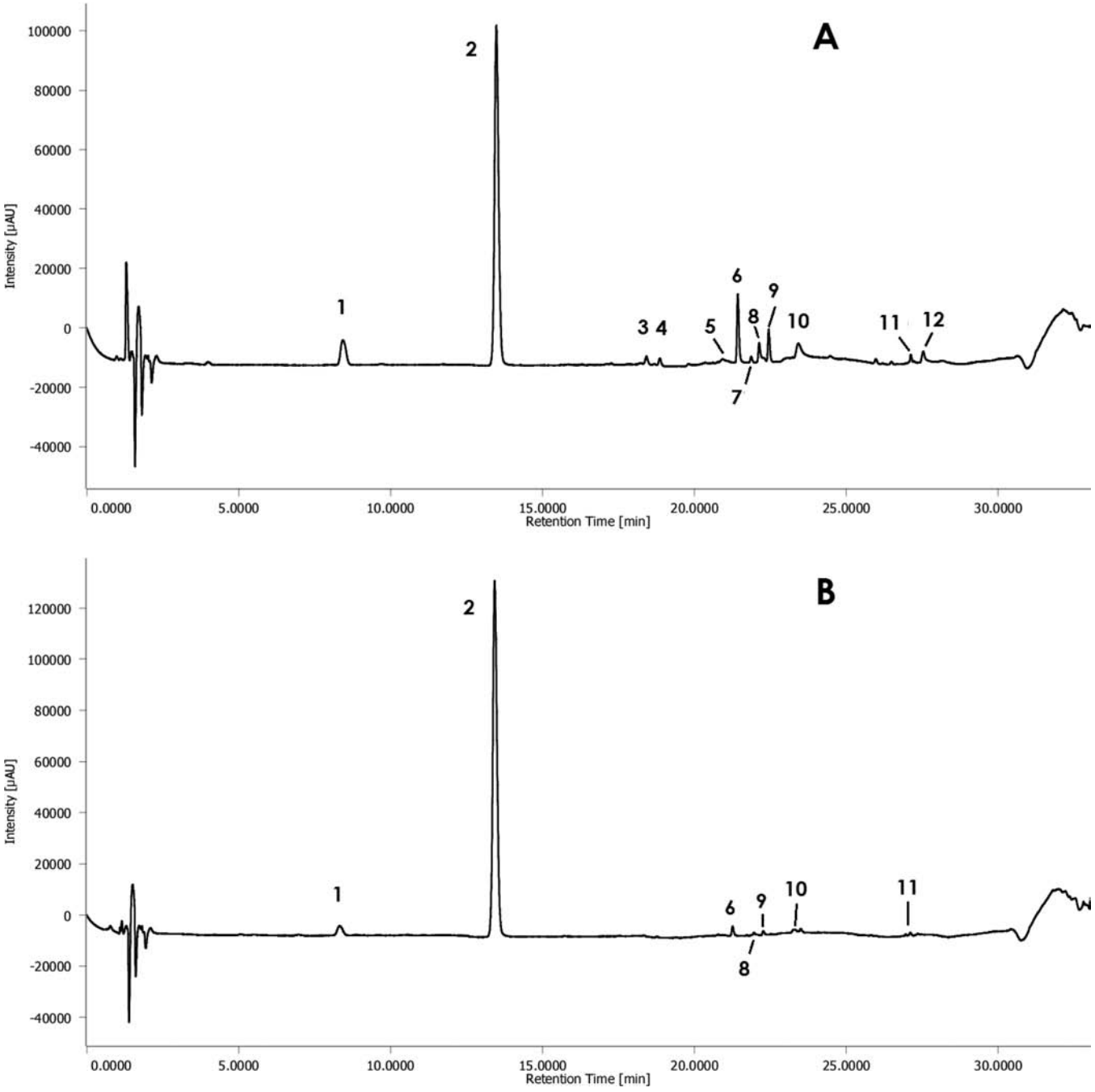


**Figure 2.** HPLC traces at 280 nm of phenolic compounds present in model white wines after 21 days of oxidation: (A) MS sample (model solution) and (B) Kt sample (chitosan). Peak identification: 1, 3, 4, and 7, carboxymethine-linked (+)-catechin dimers; 2, (+)-catechin; 5, 6, 8, and 9, xanthylium cation isomers; 10, xanthenes; and 11 and 12, xanthylium cation ethyl esters.

oxidation] in the solutions was monitored by means of HPLC–DAD/MS, all along the trial.

In Figure 2, two representative chromatograms of MS and Kt solutions (panels A and B, respectively) at day 21 are depicted. A total of 12 compounds were identified according to previous works,[31,34] including 4 carboxymethine-linked isomers, 4 xanthylium cation isomers, 2 xanthylium cation ethyl esters, and 1 peak corresponding to xanthene. This pattern of compounds could give a full representation of the kinetics underlying the browning development of model wines, because it is now accepted that glyoxylic-mediated oxidation of (+)-catechin ensues the following steps: (1) tartaric acid oxidation to give glyoxylic acid, (2) generation of glyoxylic-acid-bridged (+)-catechin dimers, (3) dehydration of dimers to generate xanthene derivatives, and (4) oxidation of xanthene giving rise to xanthylium cations.[10]

As shown in Figure 3A and independent from the sample considered, no dimers where formed before day 3. A very fast generation in MS samples followed, bringing those solutions to accumulate the maximum amount of pigment precursors at day 7, just in coincidence with the beginning of the browning (Figure 1), even if to a much lesser extent, also Kt samples showed the formation of carboxymethine-linked dimers, indicating the occurrence of the first step of the oxidative


dx.doi.org/10.1021/jf5025664 | J. Agric. Food Chem. 2014, 62, 9868–9875

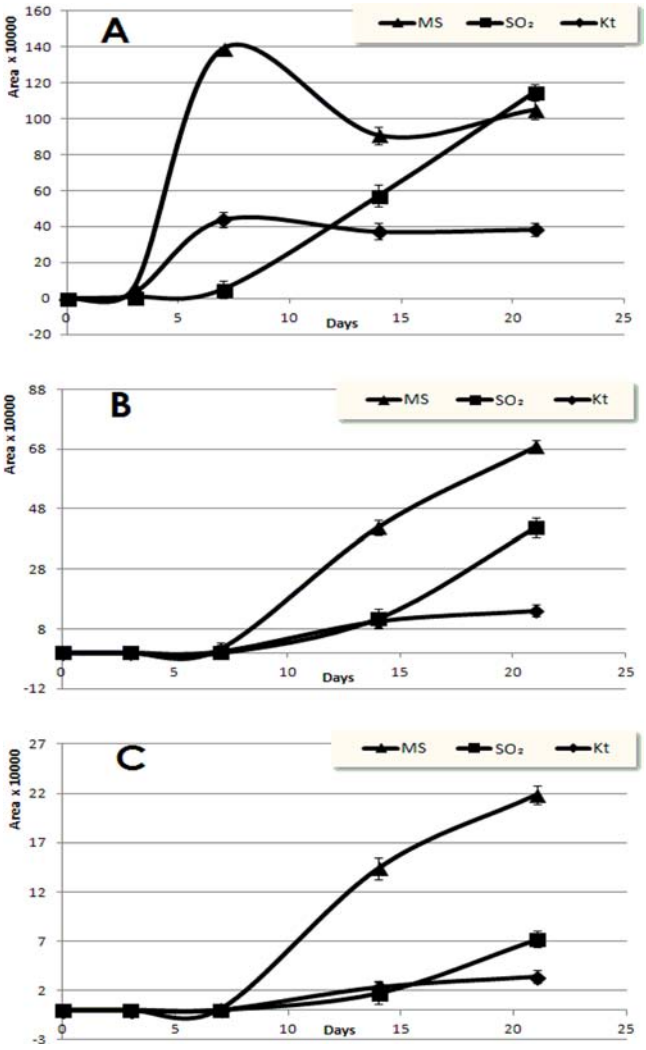


**Figure 3.** Change in the peak area of (a) carboxymethine-linked (+)-catechin dimers (sum of peaks 1, 3, 4, and 7 from Figure 2), (b) xanthene (peak 10 from Figure 2), and (c) xanthylium cations (sum of peaks 5, 6, 8, 9, 11, and 12 from Figure 2) during the experiment. All peaks were detected at 280 nm, except xanthylium cations and corresponding esters (440 nm).

ladder. Interestingly, in these solutions, the amounts of dimers remained unchanged until the end of the trial. For what concern $SO_2$, it effectively inhibited the formation of dimers up to day 7. This capacity could be attributed to both the trapping of glyoxylic acid[36] and the scavenging of RSO generated by the metal redox cycle and hydrogen peroxide.[8] However, at day 14, the content of carboxymethine-bridged dimers in the samples containing sulfites significantly increased, exceeding the amount found in Kt solutions. This imply that, even in the presence of sulfites, radical-mediated tartaric acid oxidation occurred, which is in accordance with Elias and Waterhouse,[37] who found that, to completely inhibit the Fenton reaction, more than 64 mg/L free $SO_2$ was needed, although 32 mg/L did inhibit the production of radical adducts by 87% compared to the control. At the end of the observed period (day 21), because of the complete oxidation of sulfites, the carboxymethine-bridged dimer amount in $SO_2$ samples further increased, equalizing the content of MS solutions.

Panels B and C of Figure 3 depict the generation of xanthenes and xanthylium cations, respectively. It is shown that these compounds followed a common kinetic, being produced apparently simultaneously after day 7 and increasing with time according to the amount of carboxymethine-linked dimers present in each solution (Figure 3A). It seems, hence, that, while, for the production of xanthenes from its precursors, a 4 day period is needed (compare panels A and B of Figure 3), the next oxidative step, driving to yellow pigments, is considerably faster. It is also apparent that, for each sample, the xanthylium cation concentration is perfectly reflected in the browning level, as shown in Figure 1.

Table 1 reports the data relative to the residual amount of (+)-catechin in the solutions.

**Table 1. Residual (+)-Catechin Content (mg/L) in Model Wine Solutions During the Trial**[a]

| | days | | | |
|---|---|---|---|---|
| | 3 | 7 | 14 | 21 |
| MS | 94.7 ± 2.6 a | 82.0 ± 3.1 a | 69.4 ± 2.6 a | 58.9 ± 1.3 a |
| $SO_2$ | 97.5 ± 3.0 b | 93.0 ± 2.7 b | 80.2 ± 2.1 b | 64.4 ± 1.8 b |
| Kt | 92.7 ± 2.8 a | 79.8 ± 2.2 a | 77.3 ± 2.4 b | 73.6 ± 1.4 c |

[a]In each column, significant differences ($p < 0.05$) are identified with different letters. MS, model solution; $SO_2$, sulfur dioxide; and Kt, chitosan.

Sulfited solutions consistently had the highest amount of residual (+)-catechin (at least up to day 14, i.e., when suitable amounts of additive were still detected), confirming the ability of this additive to protect flavanols from oxidation.[13] In accordance with UV absorbancies at 280 nm of Kt samples (Figure 1), chitosan initially provoqued a decline in (+)-catechin content (Table 1) likely because of the interaction of this latter with the polysaccharide chain. However, at day 14, those solutions had the same (+)-catechin content as the $SO_2$ samples, suggesting that chitosan may have reduced the (+)-catechin oxidative decay in those solutions.

**Interaction of Chitosan with Metals, (+)-Catechin, and Products of Its Oxidation.** Stimulated by the intriguing results, a further experiment was carried out to estimate both the extent of the adsorption of oxidized phenolic compounds on chitosan and the chelating aptitude of this additive (e.g., two mechanisms that could have contributed to the reduced browning of Kt solutions). To do this, the oxidized MS solutions withdrawn at day 21 were added to 1 g/L chitosan and continuously stirred for 30 h. On these samples, the analysis of phenols and metals was performed and reported in Figure 4 and Table 2, respectively.

According to the results from phenol analysis (Figure 4), chitosan appeared to have a relevant interaction with xanthylium cations, carboxymethine dimers, and (+)-catechin, whose amounts in solutions were reduced by 70, 45, and 15%, respectively, while no interaction was found with xanthene and ethyl esters of xanthylium cations. These interactions entailed a reduction in absorbance at 280 and 440 nm as high as 33 and 72%, respectively (data not shown), and suggest that at least a portion of the observed antibrowning capacity of chitosan could be due to the removal of intermediate compounds and xanthylium pigments eventually formed through the oxidative ladder.

The different behaviors of chitosan with respect to phenolic compounds are the consequence of several interaction mechanisms described for it. In fact, it contains functional groups, such as amino, acetamido, and hydroxy, that are prone

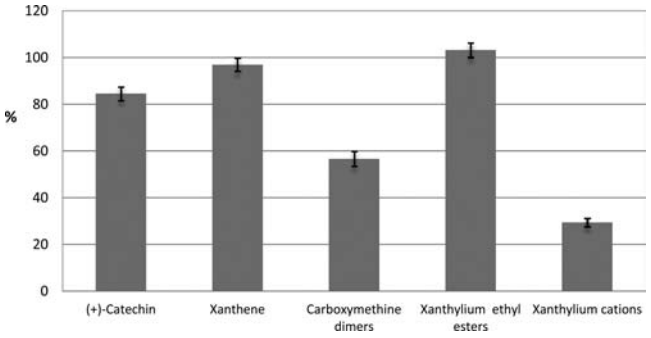


**Figure 4.** Percentage of residual phenolic compounds in MS samples (sampled at day 21) after the addition of 1 g/L chitosan and stirring for 30 h.

**Table 2. Metal Concentration (mg/L) in Model Wines at Day 21**[a]

| | Cu | Fe | percentage of residual Cu (%) | percentage of residual Fe (%) |
|---|---|---|---|---|
| MS | 0.318 ± 0.005 | 5.090 ± 0.068 | 101 | 100 |
| $SO_2$ | 0.320 ± 0.002 | 5.130 ± 0.058 | 101 | 101 |
| Kt | 0.227 ± 0.005 | 1.480 ± 0.021 | 71 | 29 |
| Kt (30 h)[b] | 0.162 ± 0.001 | 0.865 ± 0.013 | 51 | 17 |

[a]In the third and fourth columns, residual percentages are given with respect to the same sample at day 0. MS, model solution; $SO_2$, sulfur dioxide; and Kt, chitosan. [b]Sample Kt (30 h) identifies MS solutions (sampled at day 21) after the addition of 1 g/L chitosan and 30 h of stirring.

to link molecules by ion exchanges, van der Waals interactions, and hydrogen bonds, also as a function of pH.[38] It was found that the lower the pH, the higher the phenol adsorption efficiency, because of the electrostatic interaction exerted by ammonium groups on phenolate anions.[38] In addition, Spagna et al. proposed the "cooperative" nature of the phenomena involving chitosan and hydroxycinnamic acids, where adsorption is favored by the presence of compounds already adsorbed on the polysaccharide surface.[28] As a matter of fact, on the basis of the results shown in Figure 4 and considering that the compounds that did not interact with chitosan eluted later in RP-HPLC conditions (Figure 2), it is possible to hypothize that hydrophilicity may play a further role.

The chelating activity of chitosan was also evaluated, and the results are shown in Table 2. In this table, the residual metal content of MS, $SO_2$, and Kt samples after 21 days of conservation have been compared to that of the same MS samples added with 1 g/L chitosan and stirred for 30 h.

It could be highlighted that, at day 21, Kt samples had about 30 and 70% residual amounts of Fe and Cu, respectively, if compared to the initial concentration. Even more significant results were obtained in the solutions stirred for 30 h, where the reduction in metals was of 83 and 49% for Fe and Cu, respectively. Our results indicate the higher affinity of chitosan for Fe, with respect to Cu, and confirm the findings by Bornet and collegues,[26] who reported chelation activities up to 90% for Fe and 65% for Cu after the addition of 2 g/L chitosan in both white and red wines. On the basis of these results, hence, a further explanation for chitosan antibrowning efficacy could be the trapping of transition metals and the consequent suppression of Fenton chemistry.

**Decay of Varietal Thiols in White Wine Model Solutions.** Apart from phenols, oxidation may involve other reactive molecules constitutive of wines. Thiols, in particular, are highly sensitive to oxidation and may concurrently undergo either nucleophilic addition with (+)-catechin *o*-quinones or autoxidation, catalized by metals and hydroxyl radicals, which gives disulfides.[39] In both of these reactions, the presence of radical species generated by the transition metal redox cycle plays a primary role.[8] Accordingly, to compare the efficacy of sulfites and chitosan in protecting thiols from oxidation, the bulk model wine solution had been added 3MH, 3MHA, and 3MMB, three varietal thiols already identified as aromatic markers in Sauvignon Blanc.[40]

Figure 5 shows the residual amounts (as a percentage of the chromatographic area with respect to day 0) of each thiol in

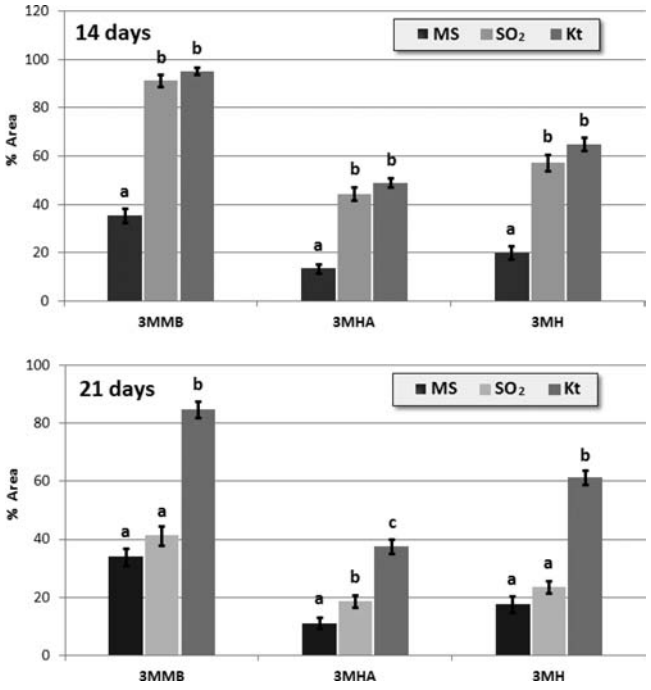


**Figure 5.** Percentage of the residual amount of 3MMB, 3MHA, and 3MH in sample solutions after 14 and 21 days of oxidation. Relative peak areas (with respect to internal standard 4MMB) are diagramed. For each cluster, significant differences ($p < 0.05$) are identified with different letters.

samples after 14 and 21 days of conservation. As a general consideration and independent from the sample, 3MMB, probably because of the weak nucleophilic character of its tertiary SH group,[39] demonstrated to be the least oxidizable thiol, being reduced by about 6, 9, and 64% after 14 days in Kt, $SO_2$, and SM solutions, respectively. On the contrary, the 3MHA amount decreased to the highest extent. For this ester, in fact, acid-catalyzed hydrolysis as a loss mechanism should be considered together with oxidation of the thiol moiety.[7] From Figure 5, it is evident that the highest protective effect is exerted by sulfite up to 14 days, as the consequence of its ability to both reduce back or quench *o*-quinones,[8] and reacts with oxygen radicals.[14] In another study on aerated model wines, 50 mg/L $SO_2$ protected 3MH for a 7 day period, after which a quick oxidation took place, making those samples not dissimilar to the samples not containing $SO_2$.[39] At our experimental conditions, this happened after 21 days of conservation (sample


dx.doi.org/10.1021/jf5025664 | J. Agric. Food Chem. 2014, 62, 9868−9875

$SO_2$ in Figure 5), because of the complete disappearence of sulfites in solutions. For what concern Kt model wines, at day 14, they had the same thiol amount of the $SO_2$ samples. In addition, the prolonged presence of chitosan in the sample permitted the highest protection of these volatiles even after 21 days of conservation (Figure 5). It is possible to hypothesize that these findings are, at least in part, due to the antiradical activity of chitosan, which can lower the amount of reactive species in the medium, in this way reducing the generation of *o*-quinones and/or the direct oxidation of thiols. It is worth mentioning that a significant radical scavenging activity of chitosan toward superoxide ($O_2^{\bullet}$) and hydroxyl ($OH^{-\bullet}$) radicals and hydrogen peroxide has already been reported.[23,41]

Overall, the results obtained in this work demonstrate the efficacy of chitosan in controlling the oxidative decay of (+)-catechin in model white wines submitted to air exposure. The antibrowning capacity of 1 g/L of this polysaccharide has been found to be comparable to that of 80 mg/L free $SO_2$ for at least 14 days, i.e., until the additives were present in the solutions. Afterward, following the complete oxidation of sulfites, those samples added to $SO_2$ became significantly darker than the samples containing chitosan. The chitosan antibrowning activity is proposed to be the result of a series of concurrent mechanisms, including phenolic adsorption, metal chelation, and radical scavenging, which cooperate in lowering the oxidative strength of the solution, with respect to (+)-catechin. In addition, chitosan effectively protected thiols from oxidation and did not appear to interact with them. To our knowledge, this is the first investigation on the mechanisms subtended to the antioxidant activity of chitosan in a model environment pertinent to wine.

Our results suggest that chitosan could be a potential candidate in view to find technological alternatives to sulfite in winemaking. Trials on real wines are now needed to verify its efficacy as, for example, a stabilizing treatment before bottling or during conservation in tanks. Its use in $SO_2$-free fermenting grape musts and/or in specific steps of the winemaking process is currently under investigation by our group.

## AUTHOR INFORMATION

### Corresponding Author

*Telephone: +39-0547338124. Fax: +39-0547338103. E-mail: fabio.chinnici@unibo.it.

### Notes

The authors declare no competing financial interest.

## REFERENCES

(1) Tao, Y.; García, J. F.; Sun, D.-W. Advances in wine aging technologies for enhancing wine quality and accelerating wine aging process. *Crit. Rev. Food Sci. Nutr.* **2014**, *54*, 817−835.

(2) Gómez-Plaza, E.; Cano-López, M. A review on micro-oxygenation of red wines: Claims, benefits and the underlying chemistry. *Food Chem.* **2011**, *125*, 1131−1140.

(3) Waterhouse, A. L.; Laurie, V. F. Oxidation of wine phenolics: A critical evaluation and hypotheses. *Am. J. Enol. Vitic.* **2006**, *57*, 306−313.

(4) Oliveira, C. M.; Ferreira, A. C. S.; De Freitas, V.; Silva, A. M. S. Oxidation mechanisms occurring in wines. *Food Res. Int.* **2011**, *44*, 1115−1126.

(5) Bueno, M.; Culleré, L.; Cacho, J.; Ferreira, V. Chemical and sensory characterization of oxidative behavior in different wines. *Food Res. Int.* **2010**, *43*, 1423−1428.

(6) Ugliano, M. Oxygen contribution to wine aroma evolution during bottle aging. *J. Agric. Food Chem.* **2013**, *61*, 6125−6136.

(7) Herbst-Johnstone, M.; Nicolau, L.; Kilmartin, P. A. P. A. Stability of varietal thiols in commercial Sauvignon Blanc wines. *Am. J. Enol. Vitic.* **2011**, *62*, 495−502.

(8) Danilewicz, J. C. Interaction of sulfur dioxide, polyphenols, and oxygen in a wine-model system: Central role of iron and copper. *Am. J. Enol. Vitic.* **2007**, *58*, 53−60.

(9) Clark, A. C.; Scollary, G. R. Copper(II)-mediated oxidation of (+)-catechin in a model white wine system. *Aust. J. Grape Wine Res.* **2002**, *8*, 186−195.

(10) Es-Safi, N.-E.; Le Guernevé, C.; Fulcrand, H.; Cheynier, V.; Moutounet, M. Xanthylium salts formation involved in wine colour changes. *Int. J. Food Sci. Technol.* **2000**, *35*, 63−74.

(11) Es-Safi, N.-E.; Le Guernevé, C.; Fulcrand, H.; Cheynier, V.; Moutounet, M. New polyphenolic compounds with xanthylium skeletons formed through reaction between (+)-catechin and glyoxylic acid. *J. Agric. Food Chem.* **1999**, *47*, 5211−5217.

(12) Barril, C.; Clark, A. C.; Prenzler, P. D.; Karuso, P.; Scollary, G. R. Formation of pigment precursor (+)-1″-methylene-6″-hydroxy-2*H*-furan-5″-one-catechin isomers from (+)-catechin and a degradation product of ascorbic acid in a model wine system. *J. Agric. Food Chem.* **2009**, *57*, 9539−9546.

(13) Danilewicz, J. C. Mechanism of autoxidation of polyphenols and participation of sulfite in wine: Key role of iron. *Am. J. Enol. Vitic.* **2011**, *62*, 319−328.

(14) Danilewicz, J. C. Interaction of sulfur dioxide, polyphenols, and oxygen in a wine-model system: Central role of iron and copper. *Am. J. Enol. Vitic.* **2007**, *58*, 53−60.

(15) Sayavedra-Soto, L. A.; Montgomery, M. W. Inhibition of polyphenoloxidase by sulfite. *J. Food Sci.* **1986**, *51*, 1531−1536.

(16) Ough, C. S.; Were, L. Sulfur dioxide and sulfites. In *Antimicrobials in Food*, 3rd ed.; Davidson, P. M., Sofos, J. N., Branen, A. L., Eds.; CRC Press (Taylor and Francis Group): Boca Raton, FL, 2005; pp 143−160.

(17) European Food Safety Authority (EFSA). *Opinion of the Scientific Panel on Dietetic Products, Nutrition and Allergies on a Request from the Commission Relating to the Evaluation of Allergenic Foods for Labelling Purposes*; EFSA: Parma, Italy, 2004; http://www.efsa.europa.eu/de/efsajournal/doc/32.pdf (accessed March 14, 2014).

(18) Santos, M. M. C.; Nunes, C.; Saraiva, J. A.; Coimbra, M. A. Chemical and physical methodologies for the replacement/reduction of sulfur dioxide use during winemaking: Review of their potentialities and limitations. *Eur. Food Res.* **2012**, *234*, 1−12.

(19) Comuzzo, P.; Zironi, R. Biotechnological strategies for controlling wine oxidation. *Food Eng. Rev.* **2013**, *5*, 217−229.

(20) Luo, Y.; Wang, Q. Recent advances of chitosan and its derivatives for novel applications in food science. *J. Food Process. Beverages* **2013**, *1*, 13.

(21) Dutta, P. K.; Dutta, J.; Tripathi, V. S. Chitin and chitosan: Chemistry, properties and applications. *J. Sci. Ind. Res.* **2004**, *63*, 20−31.

(22) Yen, M.-T.; Yang, J.-H.; Mau, J.-L. Antioxidant properties of chitosan from crab shells. *Carbohydr. Polym.* **2008**, *74*, 840−844.

(23) Chien, P.-J.; Sheu, F.; Huang, W.-T.; Su, M.-S. Effect of molecular weight of chitosans on their antioxidative activities in apple juice. *Food Chem.* **2007**, *102*, 1192−1198.

(24) European Union (EU). Commission regulation (EU) 53/2011 of 21 January 2011. *Off. J. Eur. Union* **2011**, L19/1−L19/6.

(25) Quintela, S.; Villarán, M. C.; López De Armentia, I.; Elejalde, E. Ochratoxin A removal from red wine by several oenological fining agents: bentonite, egg albumin, allergen-free adsorbents, chitin and chitosan. *Food Addit. Contam., Part A* **2012**, *29*, 1168−1174.

(26) Bornet, A.; Teissedre, P. L. L. Chitosan, chitin-glucan and chitin effects on minerals (iron, lead, cadmium) and organic (ochratoxin A) contaminants in wines. *Eur. Food Res. Technol.* **2007**, *226*, 681−689.

(27) Bornet, A.; Teissedre, P. L. Intérêt de l'utilisation de chitine, chitosane et de leurs dérivés en œnologie. *J. Int. Sci. Vigne Vin* **2005**, *39*, 199−207.

(28) Spagna, G.; Barbagallo, R. N.; Pifferi, P. G. Fining treatments of white wines by means of polymeric adjuvants for their stabilization against browning. *J. Agric. Food Chem.* **2000**, *48*, 4619−4627.
(29) Spagna, G.; Pifferi, P. G.; Rangoni, C.; Mattivi, F.; Nicolini, G.; Palmonari, R. The stabilization of white wines by adsorption of phenolic compounds on chitin and chitosan. *Food Res. Int.* **1996**, *29*, 241−248.
(30) Da Silva, M. A. C. R.; Nunes, C. S. C.; Maricato, E. S. O.; Da Cunha, A. M. M. V.; Barroso, S. A. L. V. M.; Da Silva, J. A. L. Winemaking process without sulfur dioxide addition using chitosan-based films. EU Patent CA2854282 A1, May 10, 2013.
(31) Chinnici, F.; Sonni, F.; Natali, N.; Riponi, C. Oxidative evolution of (+)-catechin in model white wine solutions containing sulfur dioxide, ascorbic acid or gallotannins. *Food Res. Int.* **2013**, *51*, 59−65.
(32) Ellman, G. L. Tissue sulfhydryl groups. *Arch. Biochem. Biophys.* **1959**, *82*, 70−77.
(33) International Organization of Vine and Wine (OIV). *Compendium of International Methods of Wine and Must Analysis*; OIV: Paris, France, 2013.
(34) Clark, A. C.; Prenzler, P. D.; Scollary, G. R. The role of copper(II) in the bridging reactions of (+)-catechin by glyoxylic acid in a model white wine. *J. Agric. Food Chem.* **2003**, *51*, 6204−6210.
(35) Fedrizzi, B.; Versini, G.; Lavagnini, I.; Nicolini, G.; Magno, F. Gas chromatography−mass spectrometry determination of 3-mercaptohexan-1-ol and 3-mercaptohexyl acetate in wine: A comparison of headspace solid phase microextraction and solid phase extraction methods. *Anal. Chim. Acta* **2007**, *596*, 291−297.
(36) Sonni, F.; Moore, E. G.; Clark, A. C.; Chinnici, F.; Riponi, C.; Scollary, G. R. Impact of glutathione on the formation of methylmethine- and carboxymethine-bridged (+)-catechin dimers in a model wine system. *J. Agric. Food Chem.* **2011**, *59*, 7410−7418.
(37) Elias, R. J.; Waterhouse, A. L. Controlling the fenton reaction in wine. *J. Agric. Food Chem.* **2010**, *58*, 1699−1707.
(38) Milhome, M. A. L.; de Keukeleire, D.; Ribeiro, J. P.; Nascimento, R. F.; Carvalho, T. V.; Queiroz, D. C. Removal of phenol and conventional pollutants from aqueous effluent by chitosan and chitin. *Quim. Nova* **2009**, *32*, 2122−2127.
(39) Nikolantonaki, M.; Chichuc, I.; Teissedre, P.-L.; Darriet, P. Reactivity of volatile thiols with polyphenols in a wine-model medium: Impact of oxygen, iron, and sulfur dioxide. *Anal. Chim. Acta* **2010**, *660*, 102−109.
(40) Tominaga, T.; Furrer, A.; Henry, R.; Dubourdieu, D. Identification of new volatile thiols in the aroma of *Vitis vinifera* L. var. Sauvignon Blanc wines. *Flavour Fragrance J.* **1998**, *162*, 159−162.
(41) Xing, R.; Liu, S.; Guo, Z.; Yu, H.; Wang, P.; Li, C.; Li, Z.; Li, P. Relevance of molecular weight of chitosan and its derivatives and their antioxidant activities in vitro. *Bioorg. Med. Chem.* **2005**, *13*, 1573−1577.

amine, $N^{\alpha}$-*t*-BOC-lysine, $N^{\varepsilon}$-formyl-L-lysine, *N*-formyl-L-proline, *o*-phenylenediamine (OPD), quinoxaline (Q), 2-quinoxalinol, sodium cyanoborohydride, $D_2O$, methanol (HPLC gr., VWR Chemicals, Darmstadt, Germany), TLC plates, dipotassium hydrogen phosphate trihydrate, potassium dihydrogen phosphate, dimethyl sulfoxide, diethylenetriaminepentaacetic acid (Merck, Darmstadt, Germany), heptafluorobutyric acid (ACROS Organics, Geel, Belgium), formic acid (Grüssing GmbH, Filsum, Germany), $CDCl_3$ (ARMAR Chemicals, Leipzig/Döttingen, Germany), and hydroxymethylfurfural (Alfa Aeser, Karlsruhe, Germany). $N^{\varepsilon}$-Carboxymethyl-L-lysine was synthesized according to the literature.[14] Quinoxaline reference standards (maltosone-Q, threosone-Q, 1-deoxypentosone-Q, 3-deoxymaltosone-Q, 3,4-dideoxypentosone-Q, 4-deoxyglucosone-Q, 1,4-dideoxyglucosone-Q, 1,5-dideoxymaltosone-4-ene-Q, 3-deoxygalactosone-Q, 5,6-dihydroxy-2,3-dioxohexanal-Q, 1-deoxymaltosone-Q, 3-deoxyglucosone-Q, glucosone-Q, 1-deoxyglucosone-Q, 3-deoxypentosone-Q, 1-deoxytheosone-Q, 3-deoxythreosone-Q) were isolated and characterized in previous work.[9,15]

**Beer Samples.** For the present study 11 commercially available Pilsner type beer samples were obtained. Analyses of the fresh beer samples were carried out in duplicate. Aging was conducted for one beer sample under aerated and deaerated conditions at 50 °C for 2 weeks. Aeration was achieved by opening the bottles, flushing the headspace shortly with air, and capping it again. Samples from the aging experiment were analyzed in triplicate. Aliquots were taken directly after cooling down. Samples were degassed by filtration for further processing.

***N*-(Furan-2-ylmethyl)naphthalene-1-amine (Furfural-N).** One millimole of furfural was dissolved in 50 mL of water. A mixture of 2 mmol of 1-naphthylamine in 25 mL of 15% acetic acid and dimethyl sulfoxide (50:50, v/v) and a solution of 5 mmol of sodium cyanoborohydride in 25 mL of water were added. The reaction mixture was stirred overnight at 40 °C. The reaction mixture was extracted twice with 100 mL of hexane, and the organic phase was concentrated under vacuum. The crude product was further purified by column chromatography (silica gel 60, hexane−acetone 8:1). Fractions containing furfural-N (TLC (silica gel): $R_f$ 0.4, hexane−acetone (8:1), UV detection) were concentrated under vacuum to obtain the compound as a brownish oil. (0.9 mmol, 87%). $^1$H NMR (500 MHz, $CDCl_3$): $\delta$ [ppm] = 4.51 (s, 2H), 6.34 (dd, $^3J$ = 3.2, $^4J$ = 0.8 Hz, 1H), 6.38 (dd, $^3J$ = 3.2, $^3J$ = 1.8 Hz, 1H), 6.73 (d, $^3$ =7.5 Hz, 1H), 7.31 (d, $^3J$ = 8,5 Hz 1H), 7.38 (pt, $^3J$ = 7.5 Hz, $^3J$ = 8.5 Hz, 1H), 7.44 (dd, $^3J$ = 1.8 Hz, $^4J$ = 0.8 Hz, 1H), 7.50−7.45 (m, 2H), 7.86−7.81 (m, 2H). $^{13}$C NMR (125 MHz, $CDCl_3$): $\delta$ [ppm] = 41.9, 105.1, 107.4, 110.6, 118.3, 120.1, 123.7, 124.9, 125.9, 126.6, 128.8, 134.4, 142.2, 142.9, 152.6. HR-MS: *m*/*z* 224.1070 (found); *m*/*z* 224.1070 (calculated for $C_{15}H_{14}NO$ $[M + H]^+$).

**5-(Naphthalene-1-aminomethyl)-2-furanmethanol (HMF-N).** The synthesis of HMF-N was carried out as described above. One millimole of hydroxymethylfurfural was used as the educt. The crude product was extracted with 100 mL of $CHCl_3$, concentrated under vacuum, and purified by column chromatography (silica gel 60 using hexane−acetone 5:2). Fractions HMF-N (TLC (silica gel): $R_f$ 0.26, hexane−acetone (5:2), UV detection) were concentrated under vacuum to obtain the compound as white crystals (0.7 mmol, 70%). $^1$H NMR (500 MHz, $CDCl_3$): $\delta$ [ppm] = 4.46 (s, 2H), 4.57 (s, 2H), 6.23 (d, $^3J$ = 3.2 Hz, 1H), 6.25 (d, $^3J$ = 3.2 Hz, 1H), 6.70 (dd, $^3J$ = 7.5, $^4J$ = 0.8 Hz, 1H), 7.29 (d, $^3J$ = 8.5, 1H), 7.35 (pt, $^3J$ = 8.5, $^3J$ = 7.5 Hz 1H), 7.44−7.41 (m, 1H), 7.48−7.45 (m, 1H), 7.81−7.79 (m, 1H), 7.85−7.82 (m, 1H). $^{13}$C NMR (125 MHz, $CDCl_3$): $\delta$ [ppm] = 41.9, 57.5, 105.2, 108.3, 108.8, 118.4, 120.1, 123.8, 125.0, 125.9, 126.5, 128.8, 134.4, 142.8, 152.5, 153.8. HR-MS: *m*/*z* 254.1176 (found); *m*/*z* 254.1176 (calculated for $C_{16}H_{16}NO_2$ $[M + H]^+$).

***N*-Carboxymethyl-L-proline (CMP).** CMP was synthesized according to the literature with some modifications.[16] Twenty millimoles of chloroacetic acid was cooled to −18 °C and stirred under argon atmosphere. To this was added dropwise 2.5 g of potassium hydroxide dissolved in 10 mL of water. Twenty millimoles of L-proline and 1.2 g of potassium hydroxide were dissolved in 5 mL of water and added dropwise to the reaction mixture. The solution was then heated to 80 °C, and the temperature was held for 4 h. Within this time 0.28 g of potassium hydroxide in 5 mL of water was added dropwise. The reaction mixture was cooled down and neutralized with 6 M hydrochloric acid. CMP was extracted from the reaction mixture with a strong anion exchanger (Amberlite IRA-410, Sigma-Aldrich, Munich/Steinheim, Germany). After elution with 1 M hydrochloric acid, the solution was dried and the crude product was further purified by column chromatography (cellulose, *n*-butanol−acetic acid−water 20:3:5). The fractions containing CMP (TLC (cellulose), $R_f$ 0.28, same solvent, detection with bromcresol green) were concentrated under vacuum, redissolved in water, and lyophilized to give CMP as a white powder (5.9 mmol, 30%). $^1$H NMR (500 MHz, $D_2O$): $\delta$ [ppm] = 1.84 (m, H), 1.97 (m, 2H), 2.30 (m, 1H), 3.12 (m, 1H), 3.53 (m, 1H), 3.88 (d, 1H, $^2J$ = 16.7 Hz), 4.08 (d, 1H, $^2J$ = 16.7 Hz), 4.16 (dd, 1H, $^3J$ = 6.1 Hz; $^3J$ = 6.3 Hz). $^{13}$C NMR (500 MHz, $D_2O$): $\delta$ [ppm] = 22.7, 28.2, 54.5, 54.7, 65.8, 168.7, 171.1. HR-MS: *m*/*z* 172.0613 (found); *m*/*z* 172.0615 (calculated for $C_7H_{10}NO_4$ $[M - H]^-$).

**Incubation of Carbohydrates.** In general, incubations were conducted in 0.1 M phosphate buffer at two different pH levels (pH 5 and pH 7) and 50 °C for up to 7 days. Maltose, maltotetraose, maltopentaose, maltohexaose, and maltoheptaose (42 mM) were incubated individually with either $N^{\alpha}$-*t*-BOC-lysine (42 mM) or L-proline (42 mM). Incubations were performed under aerated and deaerated conditions. Deaeration was achieved by degassing of the buffer with helium, addition of 1 mM diethylenetriaminepentaacetic acid, and using minimum headspace volume during incubation. Samples of maltotetraose were prepared in triplicate and incubated up to 7 days, the rest in duplicate for 7 days, respectively. Data for all target analytes showed coefficients of variation <5%.

**Enzymatic Assay of Formic Acid.** For the quantitation of formic acid in maltotetraose incubations an enzyme test kit obtained from R-Biopharm AG (Darmstadt, Germany) was used.

**Analytical HPLC-FLD (Fluorescence Detection) for Carbohydrates.** Derivatization of carbohydrates was carried out following the method of Rakete and Glomb.[3] The derivatized samples were diluted with eluent B to concentrations appropriate for detection. Eluents were water (A) and a mixture of methanol and demineralized water (7:3, v/v; B). Heptafluorobutyric acid (0.6 mL/L) was added to both eluents as ion pair reagent. Analyses were carried out on a Waters HPLC system consisting of a Waters 600-MS pump, a Waters 470 fluorescence detector, and a Waters 712 WISP autosampler (Waters Corp., Milford, MA, USA). Chromatographic separations were performed on a stainless steel column (Knauer, Eurospher 100-5 C18, 250 × 4.6 mm, 5 $\mu$m, Berlin, Germany) using a flow rate of 1 mL min$^{-1}$ at 20 °C (Jetstream 2 column oven, Jasco, Groß-Umstadt, Germany). The wavelengths of excitation and emission were adjusted to 318 and 440 nm, respectively. The separation started at 65:35 (A:B). After 75 min, B was raised to 100% in 5 min to flush the column for 15 min. Within 5 min the composition of the eluents was changed to starting conditions and equilibrated for 15 min prior to injection of the next analysis.

**Analytical HPLC-MS$^2$.** A Jasco PU-2080 Plus quaternary gradient pump with degasser and a Jasco AS-2057 Plus autosampler (Jasco, Gross-Umstadt, Germany) were used. Chromatographic separations were performed on a stainless steel column (KNAUER, Eurospher 100-5 C18, 250 × 4.6 mm, 5 $\mu$m, Berlin, Germany) using a flow rate of 1 mL min$^{-1}$. The mass analyses were performed using an Applied Biosystems API 4000 quadrupole instrument (Applied Biosystems, Foster City, CA, USA) equipped with an API source using an electrospray ionization (ESI) interface in the positive mode. The LC system was connected directly to the probe of the mass spectrometer. Nitrogen was used as sheath and auxiliary gas. All compounds were analyzed by scheduled multiple reaction monitoring (sMRM). Quantitation was based on the standard addition method. More precisely, increasing concentrations of authentic reference compounds were added to aliquots of the sample (50:50, v/v). A regression of response versus concentration was used to determine the concentration of the analyte in the sample. Calibration with this method resolves potential matrix interferences.

Table 1. Mass Spectrometric Parameters for AGEs and Derivatized Furfural (Furfural-N) and Hydroxymethylfurfural (HMF-N)[a]

| | mass (amu) | | | | | |
|---|---|---|---|---|---|---|
| | Q1 | Q3 | retention time (min) | DP (V) | CE (eV) | CXP (V) |
| *N*-formyllysine (FL) | 175.1 | 112.1 | 11.6 | 40 | 20 | 13 |
| *N*-carboxymethyllysine (CML) | 205.1 | 130.2 | 8.4 | 50 | 17 | 9 |
| $N^{\varepsilon}$-formylproline (FP) | 144.1 | 98.1 | 14.8 | 45 | 32 | 11 |
| $N^{\varepsilon}$-carboxymethylproline (CMP) | 174.2 | 128.1 | 4.9 | 35 | 41 | 11 |
| furfural-N | 224.2 | 53.1 | 13.6 | 86 | 55 | 8 |
| HMF-N | 254.3 | 111.1 | 8.0 | 83 | 35 | 14 |

[a]MRM mode. DP: declustering potential. CE: collision energy. CXP: cell exit potential.

*α-Dicarbonyl Compounds.* Sample aliquots were reincubated with *o*-phenylenediamine (OPD, 5 mM) for 5 h at 25 °C. OPD was added at the time of sampling to avoid artifacts. The derivatized samples were diluted with water to concentrations appropriate for detection. The mobile phase used consisted of water (solvent A) and methanol/water (7:3 (v/v), solvent B). To both solvents (A and B) was added 0.6 mL/L heptafluorobutyric acid (HFBA). Chromatographic parameters were according to Henning et al.[17] Elution of quinoxalines (1-deoxymaltosone-Q at 8.3 min, maltosone-Q at 8.7 min, glucosone-Q at 9.8 min, 1-deoxyglucosone-Q at 12.0 min, 3-deoxymaltosone-Q at 11.1 min, threosone-Q at 14.5 min, 1,5-dideoxymaltoson-4-ene-Q at 11.4 min, 4-deoxyglucosone-Q at 13.6 min, 3-deoxyglucosone-Q at 13.9 min, glyoxylic acid-Q at 17.1 min, 1-deoxypentosone-Q at 17.3 min, 3-deoxypentosone-Q at 16.7 min, 3-deoxygalactosone at 14.4 min, 5,6-dihydroxy-2,3-dioxohexanal-Q (1) at 17.4 min, 5,6-dihydroxy-2,3-dioxohexanal-Q (2) at 18.3 min, 1,4-dideoxyglucosone-Q at 18,4 min, 3-deoxythreosone-Q at 18,8 min, 1-deoxythreosone-Q at 19.3 min, glyoxal-Q at 20.6 min, 3,4-dideoxypentosone-Q at 20.0 min, methylglyoxal-Q at 22.1 min, and diacetyl-Q at 23.4 min) was monitored by mass spectrometry. The optimized parameters for mass spectrometry as well as limits of detection and quantitation for all compounds monitored were according to previous work.[9]

*AGEs.* Prior to injection into the HPLC-$MS^2$ system, solutions were diluted to appropriate concentrations with water. For deprotection of the $N^{\alpha}$-BOC protection group an equal volume of 6 M hydrochloric acid was added to the sample and kept at room temperature for 30 min. The mobile phase used consisted of water (solvent A) and methanol/water (7:3 (v/v), solvent B). To both solvents (A and B) was added 1.2 mL/L HFBA. Samples were injected at 1% B, and gradient was then changed to 20% B within 15 min and to 100% B after 2 min (held 8 min). Then gradient was changed to 1% B within 2 min and held for 7 min. The optimized parameters for mass spectrometry and retention times are shown in Table 1.

*Furfural and Hydroxymethylfurfural.* Derivatization of furfural and hydroxymethylfurfural was carried out analogously to carbohydrate derivatization.[3] However, samples were reincubated for only 1 h at 20 °C and diluted to appropriate concentrations with methanol prior to injection into the HPLC-$MS^2$ system. The mobile phase used consisted of water (solvent A) and methanol/water (7:3 (v/v), solvent B). To both solvents (A and B), 0.8 mL/L formic acid was added. Samples were injected at 90% B, and gradient was then changed to 100% B within 10 min and held for 15 min. Then the mobile phase was changed to 90% B within 1 min and equilibrated for 7 min prior to injection of the next analysis. The optimized parameters for mass spectrometry and retention times are shown in Table 1.

**Identification of *N*-Formylproline (FP) and *N*-Carboxymethylproline (CMP) in Beer.** Filtrated beer was subjected to several analytical HPLC runs as mentioned above. Fractions containing FP and CMP were combined and dried in a vacuum concentrator (Savant Speed-Vac Plus SC 110 A combined with a Vapor Trap RVT 400, Thermo Fisher Scientific GmbH, Dreieich, Germany). The residue was dissolved in water and injected into the HPLC-$MS^2$ system performing a CID experiment. The fragmentation spectra of the authentic references were obtained with the same parameters (declustering potential (DP), collision cell exit potential (CXP)) as in Table 1. Parameters for collision energy (CE) were as follows: FP, 19 eV; CMP, 21 eV).

**Nuclear Magnetic Resonance Spectroscopy (NMR).** $^{1}H$ and $^{13}C$ NMR spectra were recorded on a Varian Unity Inova 500 instrument operating at 500 MHz for $^{1}H$ and 125 MHz for $^{13}C$. $SiMe_4$ was used as a reference for calibrating the chemical shift.

**High Resolution Mass Determination (HR-MS).** The positive and negative ion high resolution ESI mass spectra were obtained from an Orbitrap Elite mass spectrometer (Thermofisher Scientific, Bremen, Germany) equipped with an HESI electrospray ion source (spray voltage 4 kV; capillary temperature 275 °C, source heater temperature 40 °C; FTMS resolution >30.000). Nitrogen was used as sheath and auxiliary gas. The sample solutions were introduced continuously via a 500 μL Hamilton syringe pump with a flow rate of 5 μL $min^{-1}$. The data were evaluated by the Xcalibur software 2.7 SP1.

## RESULTS AND DISCUSSION

Since dextrins represent the predominant carbohydrates and proline is the most relevant free amino acid in beer, they are the major source for Maillard induced carbohydrate degradation. The formation of α-dicarbonyl compounds, furfural, and hydroxymethylfurfural (HMF) has been previously studied in beer and numerous model incubations. Nevertheless, this is the first time mechanistic investigations of amine induced degradation of dextrins up to maltoheptaose were performed and compared directly to changes during beer aging. Maltotetraose as the major carbohydrate in beer was investigated in more detail. The formation of Maillard reaction products derived from maltose and dextrins in the presence of proline and lysine was followed in a defined aqueous model system under aerated and deaerated conditions at pH 7 and pH 5. To compare results to previous findings of Smuda et al., especially the formation of α-dicarbonyls, incubations were also performed in the presence of $N^{\alpha}$-*t*-BOC-lysine, later referred to as lysine.[9] All parameters were also monitored in 11 fresh and commercially available Pilsner type beers as well as in two artificially aged beers, of which one was additionally exposed to oxidative stress. Though beer normally is not exposed to temperatures above 30 °C, the aging experiment conducted at 50 °C delivered conclusive results and was comparable to other aging procedures found in the literature. However, reaction kinetics may differ in comparison to lower temperatures.

**Changes in the Carbohydrate Profile.** The breakdown of dextrins was studied in model incubations. As shown in Table 2, formation of glucose, maltose (Mal), and maltotriose (M3) during incubation of maltotetraose (M4) with proline at pH 7 and pH 5 revealed significantly higher amounts of M3 vs Mal and glucose. Levels of glucose, Mal, and M3 were throughout higher under aerated than deaerated conditions. The degradation of higher molecular dextrins maltopentaose (M5), maltohexaose (M6), and maltoheptaose (M7) showed

**Table 2. Formation of Glucose, Maltose, and Maltotriose during Degradation of Maltotetraose (M4) with Proline in mmol/mol M4 after 7 d under Aerated (a) and Deaerated (d) Conditions**

| | glucose | | maltose | | maltotriose | |
|---|---|---|---|---|---|---|
| pH | a | d | a | d | a | d |
| 7 | 0.19 | 0.09 | 0.25 | 0.08 | 0.71 | 0.42 |
| 5 | 0.18 | 0.09 | 0.25 | 0.08 | 0.68 | 0.27 |

a similar depolymerization down to glucose (data not shown). The results for lysine were quite similar (Supporting Information). The change in the carbohydrate profile during aging of beer is given in Table 3. Unfortunately, M3 could not be separated from isomaltose and, thus, was not quantitated in beer. Levels of M4 to M7 slightly decreased during aging but showed no significant change between fresh and aged beer. In agreement with the model incubations, much higher amounts for glucose and Mal were found in aged samples. The ratio of glucose to Mal was two to one detected in fresh samples. Mal increased 9-fold during aging, glucose only 2-fold. In contrast to the model incubations the impact of aeration on the degradation and formation of carbohydrates was negligible in beer samples.

**Table 3. Changes in the Carbohydrate Profile of Beer during Forced Aging (mmol/L)**

| | fresh | deaerated | aerated |
|---|---|---|---|
| maltoheptaose | 0.77 | 0.78 | 0.78 |
| maltohexaose | 1.04 | 1.01 | 0.98 |
| maltopentaose | 1.67 | 1.61 | 1.59 |
| maltotetraose | 7.1 | 7.0 | 6.9 |
| maltose | 0.03 | 0.33 | 0.31 |
| glucose | 0.07 | 0.14 | 0.14 |

**Formation of α-Dicarbonyl Compounds.** The α-dicarbonyls were trapped postincubation with *o*-phenylenediamine as their corresponding quinoxalines following an established method.[9] The concentrations of the α-dicarbonyls formed during the degradation of all used carbohydrates in the presence of proline at pH 7 are summarized in Table 4. In general, formation of α-dicarbonyl compounds monitored during model incubations of maltotetraose to maltoheptaose was in good agreement with the results found for maltose.[9] However, in contrast to Smuda and Glomb, only ten α-dicarbonyls were identified in oligosaccharide incubations. Levels of 1-deoxyglucosone, threosone, and 1-deoxypentosone were under the limit of quantitation or detection, respectively. These α-dicarbonyls are formed by glucose degradation in maltose incubations, which only has a minor impact in oligosaccharide incubations. As expected, the maltose derived α-dicarbonyls 1-deoxymaltosone, 3-deoxymaltosone, 1,5-dideoxymaltoson-4-ene, and maltosone were only quantitated in maltose incubations and, thus, are not listed. For higher oligosaccharides reference compounds with the complete carbon backbone are not available.

Formation of α-dicarbonyls in the presence of lysine at pH 7 was up to ten times higher compared to proline incubations, showing the same response to oxidative conditions. Obviously, lysine represents a better nucleophile than proline. Moreover, the degradation of the Amadori product of proline may require more activation energy.[18] As proline represents the most abundant free amino acid in beer, data of lysine incubations are given in the Supporting Information. When the experiments were conducted at pH 5, some α-dicarbonyls could not be quantitated. However, most α-dicarbonyls showed a similar response to oxidative conditions but at much lower concentrations (factor 3 to 10). The effect of pH value has been shown to have significant impact on reaction rates and mechanistic pathways of the Maillard reaction.[19] Due to protonation of amino functions the reaction rate decreases with decreasing pH. Nevertheless, at the approximate pH of beer (4 to 5), α-dicarbonyls are still formed and degraded during aging at 50 °C while their absolute concentrations remain relatively low. Thus, we decided to only show the results for pH 7, with one exception. Interestingly, 3-deoxyglucosone and 3-deoxygalactosone showed higher amounts at pH 5. 3-Deoxygalactosone had its maximum even after 3 days and decreased afterward (Table 5). Moreover, 3-deoxyglucosone was formed at approximately equal concentrations in incubations containing either lysine or proline, strongly suggesting an acid−base catalyzed formation pathway involving dextrins in addition to the amine induced degradation of glucose. 3-Deoxyglucosone along with 3-deoxygalactosone were also the predominant α-dicarbonyls detected in beer. Formation of 3-deoxygalactosone by epimerization of 3-deoxyglucosone was previously described in the literature.[20,21]

**Table 4. Formation of α-Dicarbonyls (mmol/mol Carbohydrate) during Degradation of Maltose (Mal), Maltotetraose (M4), Maltopentaose (M5), Maltohexaose (M6), and Maltoheptaose (M7) with Proline under Aeration (a) and Deaeration (d) (pH 7, 7 d)**

| | Mal | | M4 | | M5 | | M6 | | M7 | |
|---|---|---|---|---|---|---|---|---|---|---|
| | a | d | a | d | a | d | a | d | a | d |
| glyoxal | 4.3 | 0.28 | 7.3 | 0.38 | 8.85 | 0.48 | 10.0 | 0.7 | 13.59 | 0.6 |
| methylglyoxal | 0.041 | 0.039 | 0.041 | 0.038 | 0.048 | 0.047 | 0.048 | 0.052 | 0.057 | 0.057 |
| glyoxylic acid | <LOQ[a] | <LOQ | 0.005 | <LOQ | 0.011 | <LOQ | 0.016 | <LOQ | 0.027 | <LOQ |
| diacetyl | 0.013 | 0.033 | 0.012 | 0.027 | 0.012 | 0.034 | 0,014 | 0.038 | 0.014 | 0.038 |
| 1-deoxythreosone | 0.004 | 0.003 | 0.005 | 0.004 | 0.005 | 0.004 | 0.005 | 0.005 | 0.006 | 0.006 |
| 3-deoxythreosone | 0.091 | 0.001 | 0.070 | 0.001 | 0.062 | 0.001 | 0.062 | 0.001 | 0.072 | 0.001 |
| 3-deoxypentosone | 0.107 | 0.007 | 0.116 | 0.007 | 0.124 | 0.012 | 0.139 | 0.018 | 0.140 | 0.015 |
| 3,4-dideoxypentosone | 0.005 | 0.04 | 0.009 | 0.056 | 0.027 | 0.098 | 0.016 | 0.086 | 0.006 | 0.080 |
| 5,6-dihydroxy-2,3-dioxohexanal | 0.001 | 0.003 | 0.001 | 0.004 | 0.002 | 0.006 | 0.002 | 0.007 | 0.002 | 0.007 |
| 4-deoxyglucosone | 0.2 | 0.3 | 0.4 | 0.5 | 0.4 | 0.6 | 0.4 | 0.4 | 0.3 | 0.6 |

[a]LOQ: limit of quantification.


dx.doi.org/10.1021/jf503038c | J. Agric. Food Chem. 2014, 62, 9876−9884

**Table 5. Comparison of 3-Deoxyglucosone and 3-Deoxygalactosone (Each mmol/mol Maltotetraose) Formed during Incubations of Maltotetraose (M4) with Proline (pro) or Lysine (lys) at pH 5 and 7**

| | | 3-deoxyglucosone | | 3-deoxygalactosone | |
|---|---|---|---|---|---|
| | pH | aerated | deaerated | aerated | deaerated |
| pro | 7 | <LOQ[a] | <LOQ | <LOQ | <LOQ |
| pro | 5 | 0.025[b] | 0.023[b] | 0.041[b] | 0.039[b] |
| lys | 7 | <LOQ | <LOQ | <LOQ | <LOQ |
| lys | 5 | 0.021[b] | 0.028[b] | 0.037[c] | 0.038[c] |

[a]LOQ: limit of quantitation. [b]At 7 d. [c]At 3 d.

Analogously, 3-deoxyglucosone and 3-deoxygalactosone may also be formed from 3-deoxyosones derived from carbohydrate degradation of dextrins. This should be the subject of future investigations since 3-deoxyglucosone and 3-deoxygalactosone represent the direct precursors of HMF. At either pH, some α-dicarbonyls also showed a strong influence of the degree of polymerization, in particular glyoxal and glyoxylic acid. Most other α-dicarbonyls also increased, but to a much lesser extent. This must be caused by the quality of the leaving group, which obviously improves with increasing degree of polymerization. Alternatively, continuous depolymerization of dextrins down to glucose may also generate new sources for α-dicarbonyls, but has to be estimated to be only of minor importance.

In general, the results of model incubations at pH 7 were in support of the changes observed during beer aging. The α-dicarbonyls determined in beer are given in Table 6. Contrary to the model incubations, 21 α-dicarbonyls were found in beer. It is noteworthy that, based on preparation of mash and wort, glucose and maltose derived α-dicarbonyls are indeed present in fresh beer. Especially, α-dicarbonyls generated in the presence of oxygen, e.g., maltosone, glucosone, 3-deoxypentosone, and 3-deoxythreosone, were in good agreement. About half of the α-dicarbonyls measured in fresh samples decreased during aging. Especially 3-deoxyglucosone and 3-deoxygalactosone as well as 3-deoxypentosone and 1-deoxyglucosone showed considerably lower amounts after thermal processing. Others occurred at larger quantities compared to their concentrations measured in fresh beer. Vanderhaegen et al. reported an impact on the formation of Maillard reaction products in the presence of oxygen.[6] However, due to the respective beer matrix it is rather difficult to predict the behavior of highly reactive intermediates such as α-dicarbonyls. Bravo et al. demonstrated the extent of α-dicarbonyl formation and their effect on flavor deterioration during extended shelf life.[4] In particular, they depicted that a variety of these compounds are already preformed during preparation of beer and therefore found in the final product while both formation and degradation still continue during shelf life. Levels detected for 3-deoxypentosone, 3-deoxyglucosone, 1-deoxypentosone, 1-deoxyglucosone, methylglyoxal, and diacetyl in fresh beer were in good agreement with their results.

Formation of α-dicarbonyls was studied in detail in incubations of M4 with proline at pH 7. Levels of methylglyoxal were almost identical under aerated and deaerated conditions (0.041 vs 0.038 mmol/mol M4, Figure 1). Methylglyoxal also increased slightly during beer aging, revealing a negligible effect of aeration. Glyoxal showed an 18-fold higher concentration

**Table 6. Concentrations of α-Dicarbonyls, Furfural, HMF, and AGEs Determined in Beer**

| | | forced aging experiment (μM)[b] | | |
|---|---|---|---|---|
| | range[a] (μM) | fresh | deaerated | aerated |
| glyoxal | 5−8 | 5.2 ± 0.3 | 4.3 ± 0.1*[c] | 4.98 ± 0.05* |
| methylglyoxal | 1.7−3.5 | 1.73 ± 0.09 | 1.9 ± 0.1 | 2.2 ± 0.1 |
| glyoxylic acid | <LOQ[d] | <LOQ | <LOQ | <LOQ |
| diacetyl | 1−8 | 0.602 ± 0.005 | 0.849 ± 0.004* | 1.09 ± 0.053* |
| threosone | 0.05−0.20 | 0.2 ± 0.004 | 0.107 ± 0.004* | 0.175 ± 0.003* |
| 3-deoxythreosone | 0.05−0.56 | 0.049 ± 0.002 | 0.081 ± 0.001* | 0.17 ± 0.02* |
| 1-deoxythreosone | 0.10−0.37 | 0.104 ± 0.004 | 0.120 ± 0.003 | 0.109 ± 0.004 |
| 3,4-dideoxypentosone | <LOQ | <LOQ | <LOQ | <LOQ |
| 1-deoxypentosone | 0.28−0.63 | 0.28 ± 0.03 | <LOQ | <LOQ |
| 3-deoxypentosone | 1−6 | 1.38 ± 0.08 | 0.84 ± 0.03* | 1.1 ± 0.04* |
| glucosone | 0.3−0.7 | 0.67 ± 0.02 | 0.51 ± 0.01* | 0.80 ± 0.08* |
| 1-deoxyglucosone | 3−11 | 3.4 ± 0.1 ± 0.1 | 0.46 ± 0.008 | 0.46 ± 0.01 |
| 3-deoxyglucosone | 50−100 | 48.6 ± 0.7 | 36.6 ± 0.6 | 40 ± 3 |
| 1,4-dideoxyglucosone | 0.7−0.25 | 0.066 ± 0.008 | 0.049 ± 0.001 | 0.052 ± 0.003 |
| 5,6-dihydroxy-2,3-dioxohexanal | <LOQ | <LOQ | <LOQ | <LOQ |
| 4-deoxyglucosone | 0.3−1.5 | 0.36 ± 0.07 | 0.03 ± 0.01 | 0.12 ± 0.05 |
| 3-deoxygalactosone | 20−80 | 28 ± 1 | 18.6 ± 0.7 | 21 ± 1 |
| 1-deoxymaltosone | 2−8 | 4.4 ± 0.2 | 2.47 ± 0.07 | 2.7 ± 0.1 |
| 3-deoxymaltosone | 3−12 | 3 ± 0.1 | 5.2 ± 0.2 | 5.3 ± 0.2 |
| maltosone | 0.24−0.5 | 0.321 ± 0.007 | 0.227 ± 0.001* | 0.343 ± 0.005* |
| 1,5-dideoxymaltoson-4-ene | 0.4−4.2 | 0.37 ± 0.01 | 0.34 ± 0.04 | 0.4 ± 0.02 |
| *N*-formylproline (FP) | 1.8−4.4 | 2.98 ± 0.01 | 3.04 ± 0.04 | 3.08 ± 0.06 |
| *N*-carboxymethylproline (CMP) | 0.21−0.59 | 0.305 ± 0.001 | 0.310 ± 0.002* | 0.37 ± 0.01* |
| furfural | 0.2−0.4 | 0.26 ± 0.01 | 4.2 ± 0.2* | 5.5 ± 0.2* |
| hydroxymethylfurfural (HMF) | 2−5 | 2.2 ± 0.1 | 19.3 ± 0.3 | 21 ± 2 |

[a]11 fresh samples, replicate analyses $n = 2$. [b]1 sample ± SD, replicate analyses $n = 3$. [c]Values marked with an asterisk (*) showed a significant difference between deaerated and aerated samples with $p < 0.05$. [d]LOQ, limit of quantitation.


dx.doi.org/10.1021/jf503038c | J. Agric. Food Chem. 2014, 62, 9876−9884

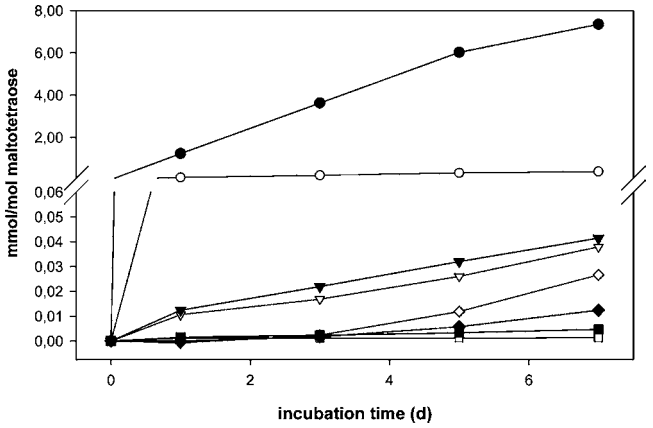


**Figure 1.** Formation of $C_2$−$C_4$ $\alpha$-dicarbonyl compounds in maltotetraose/proline incubations at pH 7 under aerated (closed symbols) and deaerated (open symbols) conditions: methylglyoxal (▼), glyoxal (●), glyoxylic acid (■), diacetyl (◆).

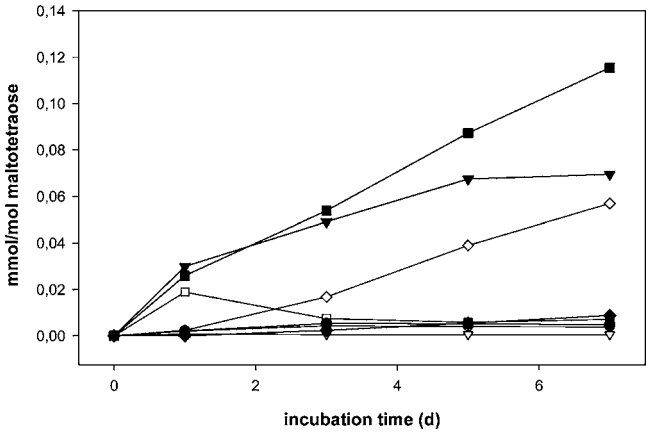


**Figure 2.** Formation of $C_4$−$C_5$ $\alpha$-dicarbonyl compounds in maltotetraose/proline incubations at pH 7 under aerated (closed symbols) and deaerated (open symbols) conditions: 1-deoxythreosone (●), 3-deoxythreosone (▼), 3-deoxypentosone (■), 3,4-dideoxypentosone (◆).

under aeration (7.3 vs 0.38 mmol/mol M4) in model incubations and increased from maltose to maltoheptaose. During beer aging glyoxal levels decreased, but significantly responded to aeration. Glyoxylic acid was found only in small quantities under aeration (0.005 mmol/mol M4) and considerably increased with increasing degree of polymerization. In contrast to the findings of Smuda et al. for maltose degradation, glyoxylic acid revealed significantly higher amounts under aeration from dextrins. This supports the findings of Velisek et al., who described glyoxylic acid as an oxidation product of glyoxal.[22] This hypothesis is further facilitated by the fact that concentrations of glyoxylic acid increased with levels of glyoxal at approximately the same rate from maltose to maltoheptaose. Glyoxylic acid was not quantitated in fresh beer or during aging. However, this may be explained by reaction of glyoxylic acid with other compounds in beer and also by its extremely low levels of formation as shown in model incubations. Levels of diacetyl doubled under nonoxidative conditions (0.012 vs 0.027 mmol/mol M4) in model incubations. In contrast, diacetyl levels in beer behaved differently and revealed higher amounts under aeration during aging. This suggests other chemical pathways like the oxidation of 2,3-butanediole or acetoin to be of major importance. Threosone, which was not detectable in dextrin incubations, was identified in beer and responded to aeration.

Investigations on $\alpha$-dicarbonyls with a backbone consisting of four and five carbon atoms are shown in Figure 2. Only small amounts of 1-deoxythreosone were found in model incubations, and they showed only minor differences between aeration and deaeration. Levels also hardly changed during beer aging. 3-Deoxythreosone revealed a strong response to aeration (0.070 mmol/mol M4). Under deaeration levels measured were at the limit of quantitation. A similar picture was found for the beer aging experiment, where 3-deoxythreosone levels increased especially under aeration. Levels of 3-deoxypentosone, the precursor of furfural, responded considerably to aerated conditions (0.116 vs 0.007 mmol/mol M4). Though 3-deoxypentosone decreased during beer aging, levels in aerated beer were significantly higher. 3,4-Dideoxypentosone increased under deaerated conditions (0.056 mmol/mol M4), whereas amounts formed under aeration remained low (0.009 mmol/mol M4). In contrast, 3,4-dideoxypentosone was only found in traces in beer. This may be explained by the high reactivity of the structure itself or, more likely, of its unknown precursor. Mavric et al. are so far the only authors proposing a possible mechanism considering 4-deoxyglucosone as the educt.[23] 1-Deoxypentosone represents a specific fragmentation product of glucose, hence, we were able to detect small amounts in fresh beer and only traces after thermally induced stress.[15]

Formation of $\alpha$-dicarbonyl compounds with a backbone consisting of six carbon atoms is shown in Figure 3. 5,6-Dihydroxy-2,3-dioxohexanal, 4-deoxyglucosone, and 1,4-dideoxyglucosone were already mentioned as specific degradation products of oligosaccharides with 1,4-glycosidic linkage.[23−25] 5,6-Dihydroxy-2,3-dioxohexanal was found to be lower under aeration than deaeration. Based on its structure, 5,6-dihydroxy-2,3-dioxohexanal is prone to further fragmentation, explaining the low amounts detected in beer. Levels of 4-deoxyglucosone were slightly higher under deaerated conditions in model incubations (0.4 vs 0.5 mmol/mol M4). During beer aging, 4-deoxyglucosone decreased and displayed a lower concentration in aerated samples, which is rather contrary to model incubations and must be explained by oxidative degradation. In incubations formation of 1,4-dideoxyglucosone responded

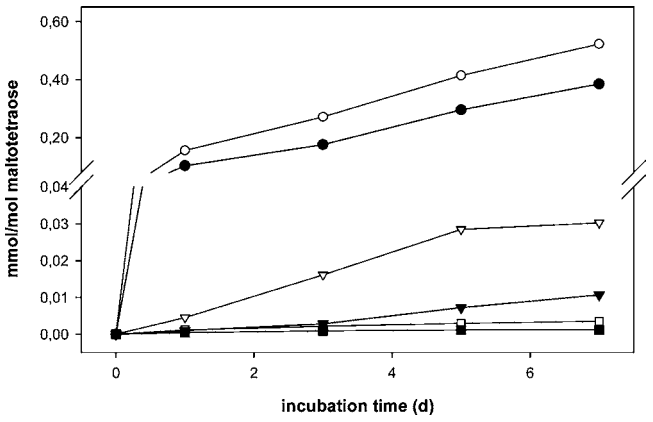


**Figure 3.** Formation of $C_6$ $\alpha$-dicarbonyl compounds in maltotetraose/proline incubations at pH 7 under aerated (closed symbols) and deaerated (open symbols) conditions: 5,6-dihydroxy-2,3-dioxohexanal (■), 4-deoxyglucosone (●), 1,4-dideoxyglucosone (▼).


dx.doi.org/10.1021/jf503038c | J. Agric. Food Chem. 2014, 62, 9876−9884

considerably to nonoxidative conditions and was found to be low under aeration (0.011 vs 0.030 mmol/mol M4). Contrary to the findings of Bravo et al., only small amounts of 1,4-dideoxyglucosone were found in beer, and they slightly decreased during beer aging. Glucosone responded strongly to the aeration of beer and increased during aging while levels were found to be lower in normal aged beer.

For the first time maltosone, 1-deoxymaltosone, 3-deoxymaltosone, and 1,5-dideoxymaltoson-4-ene were quantitated as specific Mal derived degradation products in beer. As their concentrations remained below the limit of detection during incubation of maltotetraose and higher molecular weight dextrins, they refer solely to the Maillard chemistry of Mal.[9] 1,5-Dideoxymaltoson-4-ene, among other $\alpha$-dicarbonyls, was previously identified by Bravo et al. in beer.[4] It is again important to note that these degradation products of maltose are already formed during mash preparation and wort boiling, reflecting the high concentrations of Mal in mash and wort. During aging, Mal was formed in relatively high amounts by depolymerization of oligomeric dextrins, suggesting a net increase in the formation of $\alpha$-dicarbonyls mentioned above. This is supported by the accumulation of 3-deoxymaltosone as a relatively stable intermediate. On the other hand, concentrations of maltosone and 1,5-dideoxymaltoson-4-ene remained almost unchanged during beer aging, and 1-deoxymaltosone was even degraded significantly. These results must be explained by the high reactivity of these compounds as their degradation exceeds their formation.

**Formation of Furfural and Other Follow-Up Products.** Besides the formation of $\alpha$-dicarbonyls a range of other Maillard reaction products was analyzed in model incubations (Table 7) and beer (Table 6). Formation of furfural with 3-deoxypentosone as the immediate precursor is well described for pentose and hexose degradation in the literature.[26,27] Furthermore, 3-deoxypentosone has been described as a predominating $\alpha$-dicarbonyl derived from the degradation of oligosaccharides.[28] However, more recent studies strongly suggest the formation of 3-deoxypentosone via hydrolytic $\beta$-dicarbonyl cleavage of oxyosones.[9,15] Furthermore, amine induced cleavage leading to amides may also be of importance.[25] Consequently 3-deoxypentosone and therefore furfural should also be formed by oxidative degradation of dextrins as shown in Figure 4. The oxidation of dextrins leads to oxyosones. The nucleophilic cleavage of the 1,3-tautomer at the C1 position leads to formation of formic acid as well as of *N*-formylproline (FP). The emerging 1,2-enediol will immediately cleave off substituents at position 3 to give 3-deoxypentosone and subsequently, after cyclization and dehydration, furfural. As described above, the preferred formation of 3-deoxypentosone and depolymerization of dextrins under aerated conditions supported the given mechanism. In further accordance with this mechanism furfural was found in much higher concentrations in aerated M4 incubations (1.04 $\mu$mol/mol vs 0.25 $\mu$mol/mol M4). The results for M4/lysine incubations were quite similar (Supporting Information). Levels of furfural detected in fresh beer were in accordance with the literature.[29] Furfural increased up to 20-fold (0.26 $\pm$ 0.01 $\mu$M, fresh, vs 4.2 $\pm$ 0.2 $\mu$M, deaerated, vs 5.5 $\pm$ 0.2 $\mu$M, aerated) after thermal processing of beer, exceeding the degradation of 3-deoxypentosone (decreased by 20 to 40%) and therefore suggesting a simultaneous net increase of 3-deoxpentosone. Again in line with the mechanism shown in Figure 4, concentrations of furfural were significantly higher under aeration than deaeration and strongly suggested a major participation of Maillard mechanisms in the formation of furfural during beer aging. As counterparts of the hydrolytic $\beta$-dicarbonyl cleavage shown in Figure 4, formic acid and FP must be found in the aerated model incubations, too. Indeed, both structures were formed in higher yields under aerated conditions (4.1 vs 3.0 mmol/mol M4 and 0.89 vs 0.64 mmol/mol M4, respectively), showing almost the same ratio between deaerated and aerated conditions (Table 7). This supports the proposed parallel mechanism of formation by hydrolytic $\beta$-dicarbonyl cleavage. Interestingly, formation also occurred under deaeration, which must be explained by fragmentation of other reactive intermediates. Levels of formic acid were significantly higher than those of FP because the hydroxide ion represents a better nucleophile compared to proline. Unfortunately, the sensitivity of the formic acid enzyme assay was not sufficient for the determination in incubations at pH 5. FP levels at pH 5 were about 20 times lower compared to pH 7, nevertheless, showing the same ratio between aeration and deaeration. Formation of FP increased from Mal to M7 and displayed an increasing deviation between aerated and deaerated conditions (data not shown). Levels of FP in beer (2.98 $\pm$ 0.01 $\mu$M, fresh, vs 3.04 $\pm$ 0.04 $\mu$M, deaerated, vs 3.08 $\pm$ 0.06 $\mu$M, aerated) showed no noticeable changes during aging. Thus, FP must be primarily generated during beer production before bottling. FP was also confirmed in beer by $MS^2$ spectra (Supporting Information). The lysine analogue $N^{\varepsilon}$-formyllysine (FL) was also determined in model incubations displaying an almost similar behavior compared to FP (Supporting Information). As lysine levels in beer are very low, FL was not detectable in beer samples.[30]

**Table 7. Levels of Furfural ($\mu$mol/mol Maltotetraose), *N*-Formylproline (FP), *N*-Carboxymethylproline (CMP), and Formic Acid Concentrations (Each mmol/mol Maltotetraose) in Incubation Mixtures of Maltotetraose (M4) with Proline at pH 7 and pH 5 (7 d)**

| | pH 7 | | pH 5 | |
|---|---|---|---|---|
| | aerated | deaerated | aerated | deaerated |
| furfural | 1.04 | 0.25 | na[a] | na |
| FP | 0.089 | 0.064 | 0.004 | 0.003 |
| formic acid | 4.1 | 3.0 | na | na |
| CMP | 0.560 | 0.059 | 0.170 | 0.049 |

[a]na: not analyzed.

HMF was already found in relatively high amounts in nonincubated solutions of M4 and decreased during incubation. This is most likely caused by impurities of the used carbohydrates, where HMF could be generated during the preparation of the carbohydrates and then degraded during incubation. Levels of HMF detected in fresh beer were in accordance with the literature.[29] During aging, levels of HMF increased 10-fold (2.2 $\pm$ 0.1 $\mu$M, fresh, vs 19.3 $\pm$ 0.3 $\mu$M, deaerated, vs 21 $\pm$ 2 $\mu$M, aerated). As implied above, epimerization of 3-deoxyglucosone to 3-deoxygalactosone may impair the formation of HMF. Instead, the strong increase of HMF supports a high formation and degradation rate from both 3-deoxyglucosone and 3-deoxygalactosone, regardless of the presence of oxygen during thermal processing of beer.

$N^{\varepsilon}$-Carboxymethyllysine (CML) is one of the most commonly identified AGEs in foodstuffs.[31] However, analogously to FP, *N*-carboxymethylproline (CMP) must be

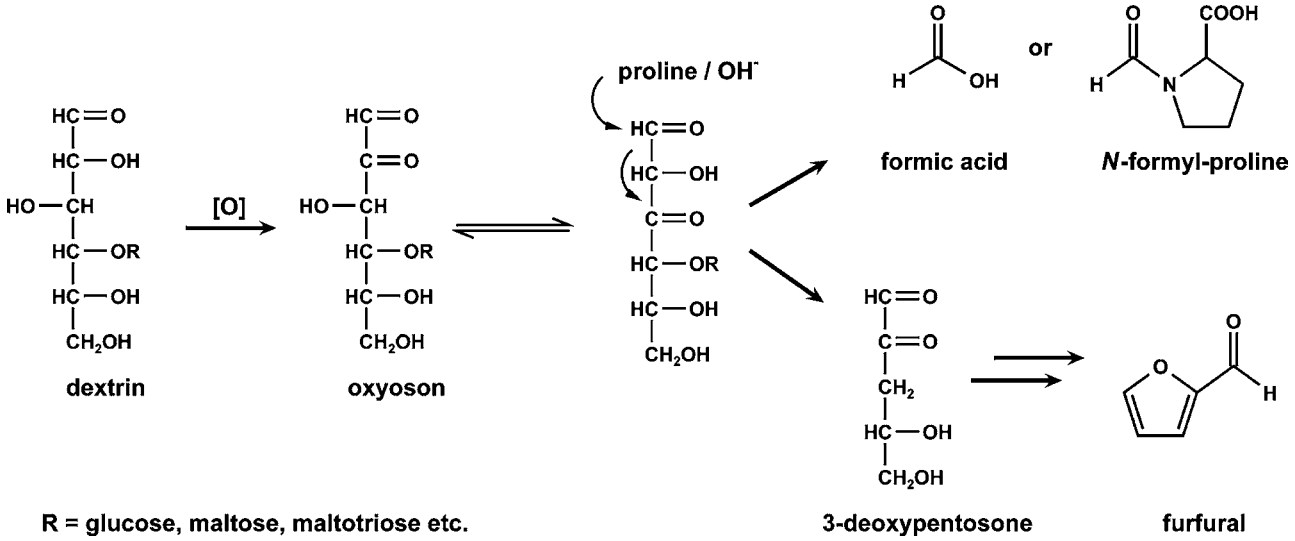


**Figure 4.** Oxidation of oligosaccharides leads to the formation of formic acid, *N*-formylproline, and 3-deoxypentosone by hydrolytic $\beta$-dicarbonyl cleavage of the oxyosone. 3-Deoxypentosone gives furfural after cyclization and dehydration.

regarded as more important in the context of beer. Similar to the formation of CML, CMP can be formed by oxidative fragmentation of the proline Amadori compound or by reaction with glyoxal and glycolaldehyde.[14,32] This was confirmed as CMP was almost exclusively generated under oxidative conditions in model incubations (0.560 vs 0.059 mmol/mol M4). At pH 5 relatively high levels of CMP were still found (0.170 vs 0.049 mmol/mol M4). In contrast to FP, the accumulation of CMP responded considerably to aging of beer and the impact of oxidative stress. CMP was also confirmed in beer by $MS^2$ spectra (Supporting Information). The results of incubations of M4 with lysine showed a very similar behavior of CML to CMP (Supporting Information). However, CML was not detectable in beer samples, reflecting again the low lysine concentrations in beer.[30]

In conclusion, we were able to identify significant changes in the formation of Maillard specific compounds involving oxygen dependent mechanisms. Dextrins were shown to be the major source for $\alpha$-dicarbonyl formation in bottled beer. As shown by the rapid formation of furfural and HMF during forced beer aging, $\alpha$-dicarbonyls are still formed at high rates at low pH values. In contrast to HMF, formation of furfural was unequivocally enhanced under oxidative conditions from dextrin degradation. The underlying mechanism of hydrolytic $\beta$-dicarbonyl cleavage also entailed the established formation of formic acid and FP. On the other hand, the formation of CMP must be attributed to the oxidative fragmentation of the proline Amadori product. In a first attempt to assess the importance of the novel proline AGEs CMP and FP, solely CMP must be recommended as a marker for oxidative stress in beer. Thus, these results will now allow a better evaluation of the chemical processes during processing and aging of beer.

## ■ ASSOCIATED CONTENT

### Supporting Information

Additional results for model incubations and mass spectrometry. This material is available free of charge via the Internet at http://pubs.acs.org.

## ■ AUTHOR INFORMATION

### Corresponding Author

*Phone: ++049-345-5525784. E-mail: marcus.glomb@chemie.uni-halle.de.

### Notes

The authors declare no competing financial interest.

## ■ ACKNOWLEDGMENTS

We thank Dr. D. Ströhl from the Institute of Organic Chemistry, Halle, Germany, for recording NMR spectra and Dr. J. Schmidt from the Leibniz Institute of Plant Biochemistry, Halle, Germany, for performing accurate mass determination.

## ■ REFERENCES

(1) De Schutter, D. The Chemistry of Aging Beer. *Beer Health Dis. Prev.* **2009**, 374−388.

(2) Baert, J. J.; De Clippeleer, J.; Hughes, P. S.; De Cooman, L.; Aerts, G. On the Origin of Free and Bound Staling Aldehydes in Beer. *J. Agric. Food Chem.* **2012**, *60*, 11449−11472.

(3) Rakete, S.; Glomb, M. A. A Novel Approach for the Quantitation of Carbohydrates in Mash, Wort, and Beer with RP-HPLC Using 1-Naphthylamine for Precolumn Derivatization. *J. Agric. Food Chem.* **2013**, *61*, 3828−3833.

(4) Bravo, A.; Herrera, J. C.; Scherer, E.; Ju-Nam, Y.; Rübsam, H.; Madrid, J.; Zufall, C.; Rangel-Aldao, R. Formation of $\alpha$-Dicarbonyl Compounds in Beer during Storage of Pilsner. *J. Agric. Food Chem.* **2008**, *56*, 4134−4144.

(5) Madigan, D.; Perez, A.; Clements, M. Furanic aldehyde analysis by HPLC as a method to determine heat-induced flavor damage to beer. *J. Am. Soc. Brew. Chem.* **1998**, 146−151.

(6) Vanderhaegen, B.; Neven, H.; Coghe, S.; Verstrepen, K. J.; Verachtert, H.; Derdelinckx, G. Evolution of Chemical and Sensory Properties during Aging of Top-Fermented Beer. *J. Agric. Food Chem.* **2003**, *51*, 6782−6790.

(7) Carneiro, J. R.; Guido, L. F.; Almeida, P. J.; Rodrigues, J. A.; Barros, A. A. The impact of sulphur dioxide and oxygen on the behaviour of 2-furaldehyde in beer: an industrial approach. *Int. J. Food Sci. Technol.* **2006**, *41*, 545−552.

(8) Varmuza, K.; Steiner, I.; Glinsner, T.; Klein, H. Chemometric evaluation of concentration profiles from compounds relevant in beer ageing. *Eur. Food Res. Technol.* **2002**, *215*, 235−239.

(9) Smuda, M.; Glomb, M. A. Novel Insights into the Maillard Catalyzed Degradation of Maltose. *J. Agric. Food Chem.* **2011**, *59*, 13254−13264.
(10) Glomb, M. A.; Rösch, D.; Nagaraj, R. H. Nδ-(5-Hydroxy-4,6-dimethylpyrimidine-2-yl)-L-ornithine, a Novel Methylglyoxal−Arginine Modification in Beer. *J. Agric. Food Chem.* **2001**, *49*, 366−372.
(11) Tressl, R.; Helak, B.; Koeppler, H.; Rewicki, D. Formation of 2-(1-pyrrolidinyl)-2-cyclopentenones and cyclopent(b)azepin-8(1H)-ones as proline specific Maillard products. *J. Agric. Food Chem.* **1985**, *33*, 1132−1137.
(12) Tressl, R.; Helak, B.; Kersten, E.; Rewicki, D. Formation of proline- and hydroxyproline-specific Maillard products from [1−13C]glucose. *J. Agric. Food Chem.* **1993**, *41*, 547−553.
(13) Tressl, R.; Rewicki, D.; Helak, B.; Kamperschroer, H. Formation of pyrrolidines and piperidines on heating L-proline with reducing sugars. *J. Agric. Food Chem.* **1985**, *33*, 924−928.
(14) Glomb, M. A.; Monnier, V. M. Mechanism of protein modification by glyoxal and glycolaldehyde, reactive intermediates of the Maillard reaction. *J. Biol. Chem.* **1995**, 10017−10026.
(15) Gobert, J.; Glomb, M. A. Degradation of Glucose: Reinvestigation of Reactive α-Dicarbonyl Compounds. *J. Agric. Food Chem.* **2009**, *57*, 8591−8597.
(16) Tribet, M.; Covelo, B.; Sicilia-Zafra, A. G.; Navarrete-Casas, R.; Choquesillo-Lazarte, D.; González-Pérez, J. M.; Castiñeiras, A.; Niclós-Gutiérrez, J. Ternary copper(II) complexes with N-carboxymethyl-l-prolinato(2−) ion and imidazole or creatinine: A comparative study of the interligand interactions influencing the molecular recognition and stability. *J. Inorg. Biochem.* **2005**, *99*, 1424−1432.
(17) Henning, C.; Liehr, K.; Girndt, M.; Ulrich, C.; Glomb, M. A. Extending the Spectrum of α-Dicarbonyl Compounds in Vivo. *J. Biol. Chem.* **2014**, DOI: 10.1074/jbc.M114.563593.
(18) Zhang, P.-J.; Zhao, Z.-G.; Yu, S.-J.; He, S.-Z. Degradation of N-(1-Deoxy-D-xylulos-1-yl)glycine and N-(1-Deoxy-D-xylulos-1-yl)-proline using thermal treatment. *Int. J. Food Sci. Technol.* **2012**, *47*, 475−481.
(19) Martins, S. I.; Van Boekel, M. A. J. S. Kinetics of the glucose/glycine Maillard reaction pathways: influences of pH and reactant initial concentrations. *Food Chem.* **2005**, *92*, 437−448.
(20) Hellwig, M.; Degen, J.; Henle, T. 3-Deoxygalactosone, a "New" 1,2-Dicarbonyl Compound in Milk Products. *J. Agric. Food Chem.* **2010**, *58*, 10752−10760.
(21) Degen, J.; Hellwig, M.; Henle, T. 1,2-Dicarbonyl Compounds in Commonly Consumed Foods. *J. Agric. Food Chem.* **2012**, *60*, 7071−7079.
(22) Velisek, J.; Davidek, J.; Pokorny, J.; Grundova, K.; Janicek, G. Reactions of Glyoxal with Glycine. II. Influence of Reaction Conditions on the Course of Reaction. *Z. Lebensm.-Unters. Forsch.* **1972**, 323−329.
(23) Mavric, E.; Henle, T. Isolation and identification of 3,4-dideoxypentosulose as specific degradation product of oligosaccharides with 1,4-glycosidic linkages. *Eur. Food Res. Technol.* **2006**, *223*, 803−810.
(24) Hollnagel, A.; Kroh, L. W. Degradation of Oligosaccharides in Nonenzymatic Browning by Formation of α-Dicarbonyl Compounds via a "Peeling Off" Mechanism. *J. Agric. Food Chem.* **2000**, *48*, 6219−6226.
(25) Smuda, M.; Voigt, M.; Glomb, M. A. Degradation of 1-Deoxy-D-erythro-hexo-2,3-diulose in the Presence of Lysine Leads to Formation of Carboxylic Acid Amides. *J. Agric. Food Chem.* **2010**, *58*, 6458−6464.
(26) Antal, M. J.; Leesomboon, T.; Mok, W. S.; Richards, G. N. Mechanism of formation of 2-furaldehyde from D-xylose. *Carbohydr. Res.* **1991**, *217*, 71−85.
(27) Ahmad, T.; Kenne, L.; Olsson, K.; Theander, O. The formation of 2-furaldehyde and formic acid from pentoses in slightly acidic deuterium oxide studied by 1H NMR spectroscopy. *Carbohydr. Res.* **1995**, *276*, 309−320.
(28) Hollnagel, A.; Kroh, L. W. 3-Deoxypentosulose: An α-Dicarbonyl Compound Predominating in Nonenzymatic Browning of Oligosaccharides in Aqueous Solution. *J. Agric. Food Chem.* **2002**, *50*, 1659−1664.
(29) Li, M.; Yang, Z.; Yang, M.; Shan, L.; Dong, J. Determination of Furfural in Beer by High-Performance Liquid Chromatography with Solid-Phase Extraction. *J. Inst. Brew.* **2009**, *115* (3), 226−231.
(30) Vanderhaegen, B.; Neven, H.; Verstrepen, K. J.; Delvaux, F. R.; Verachtert, H.; Derdelinckx, G. Influence of the Brewing Process on Furfuryl Ethyl Ether Formation during Beer Aging. *J. Agric. Food Chem.* **2004**, *52*, 6755−6764.
(31) Hull, G. L.; Woodside, J. V.; Ames, J. M.; Cuskelly, G. J. Nε-(Carboxymethyl)lysine content of foods commonly consumed in a Western style diet. *Food Chem.* **2012**, *131*, 170−174.
(32) Dunn, J. A.; Ahmed, M. U.; Murtjahaw, M. H.; Richardson, J. M.; Walla, M. D.; Thorpe, S. R.; Baynes, J. W. Reaction of Ascorbate with Lysine and Protein under Autoxidizing Conditions: Formation of N-epsilon-(Carboxymethyl)lysine by Reaction between Lysine and Products of Autoxidation of Ascorbate. *Biochemistry* **1990**, *29*, 10964−10970.

Table 1. Ana-rLOX Effect on Farinograph Characteristics of Wheat Flour[a]

| ana-rLOX (U/g) | water absorption (%) | development time (min) | stability time (min) | degree of softening (ICC) |
|---|---|---|---|---|
| 0 | 57.70 ± 0.10a | 3.70 ± 0.10c | 7.00 ± 0.20a | 74.50 ± 1.30b |
| 5 | 58.00 ± 0.20b | 4.20 ± 0.10d | 7.70 ± 0.10b | 78.60 ± 1.40c |
| 10 | 59.70 ± 0.10c | 4.70 ± 0.10e | 8.80 ± 0.20c | 93.20 ± 1.70d |
| 20 | 65.00 ± 0.20d | 3.80 ± 0.10c | 9.50 ± 0.20d | 97.10 ± 1.50e |
| 30 | 65.20 ± 0.30d | 3.20 ± 0.10b | 9.50 ± 0.30d | 97.50 ± 1.70e |
| 40 | 57.60 ± 0.10a | 2.40 ± 0.10a | 7.10 ± 0.10a | 71.30 ± 1.10a |

[a]Data are expressed as means ± SD, $n = 3$, $p < 0.05$.

It was found that the C-terminus of the allene oxide synthase (AOS)−LOX fusion gene from *Anabaena* sp. PCC 7120 belonged to the LOX family.[16] Previously, we successfully cloned, expressed, and secreted an ana-rLOX from *Anabaena* sp. PCC 7120 in *Bacillus subtilis*.[17] The recombined ana-rLOX exhibited ability as a flour improver to form peroxidation radical in the presence of polyunsaturated fatty acid[12] and improve the quality of wheat flour.[10] However, the mechanism of improving the quality of wheat flour by adding ana-rLOX was not clear. Therefore, the protein component and dough properties of wheat flour were investigated by measuring their farinograph and extensograph parameters and analyzed by HPLC-MS/MS in this study.

## MATERIALS AND METHODS

**Raw Materials.** Wan 44 wheat used in this study was a medium-gluten variety bred in Anhui province of China, and it was suitable for noodle-making (protein content, 11.7%; wet gluten, 36.5%; gluten index, 75.7). Measurement methods are described in detailed in the next paragraph. These cultivars were milled into flour by using a Brabender Laboratory Mill (Brabender, Duisburg, Germany) according to the AACC-approved method 26-21A (AACC 2000).[18] The flours were stored at 4 °C until further use. Purified ana-rLOX was used in the work, and the enzyme activity was 30000 U/mg.

**Measurement of Dough Property.** The farinograph parameters of flour were measured by using a Brabender Farinograph (mixer bowl, 300 g; Brabender), according to the standard method. Ana-rLOX was added into 300 g of wheat flour (Wan 44), reaching final enzyme activities of 10, 20, 30, and 40 U/g flour, respectively. Then, these flours were mixed in the farinograph bowl at 63 rpm and 30 °C for 20 min. The parameters of water absorption and stability time were automatically exported from the farinograph device.

The extensograph parameters of flour were measured by using a Brabender extensograph. A piece of dough (150 g) was cut into a standard cylindrical shape by using the extensograph. The test piece was allowed to rest for 45 min in the extensograph rest cabinet at 30 °C. After that, the dough was stretched by the extensograph hook until rupture occurred. The characteristics were described as proposed by the extensograph, according to the standard method (AACC, 2000). Resistance to extension ($R$, mm), dough extensibility ($E$, mm), and $R/E$ values at 45, 90, and 135 min were indicated.

**Protein Extraction and Concentration Measurements.** Protein was extracted from wheat flour on the basis of its solubility using a modified Osborne procedure.[19] The protein extracts were further purified through dialysis and lyophilization and stored at 4 °C until use. Protein content was assayed by the colorimetric Bradford method using bovine serum albumin (BSA) as standard. Analyses were carried out at wavelength $\lambda$= 595 nm (UV−vis spectrophotometer (Shimadzu, UV-2450, Japan). To determine protein concentration, the standard curve based on BSA was made ($y = 0.492x$; $R^2 = 0.9966$).

**FT-IR Measurements.** An FT-IR spectrum of glutenin was collected between 4000 and 500 $cm^{-1}$(mid-infrared region) on a PerkinElmer Spectrum 100 FTIR spectrometer (Thermo Nicolet Corp., Avatar 360, USA) with 256 scans at a resolution of 4 $cm^{-1}$. The sample was ground with spectroscopic grade potassium bromide (KBr) powder and then pressed into 1 mm pellets (2 mg of sample per 200 mg dry KBr). A blank KBr disk was used as background. The FT-IR spectrum was smoothed and the baseline was corrected automatically by using the built-in software of the spectrophotometer.

**Detection of Total Proteins in the Dough by HPLC.** The total protein from 100 mg of dough was extracted stepwise three times with 1.5 mL of Tris-HCl (pH 8.5), vortexed for 2 min at room temperature, and incubated for 60 min at 40 °C with shaking. Samples were centrifuged at 10000$g$ for 3 min. Supernatants were collected, mixed all together, and filtered through a 0.45 $\mu$m nylon filter. The protein extracts were analyzed on a Waters chromatography system (600S controller, 616 pumps, and 717 autosampler) (Waters Corp., New Castle, DE, USA), controlled with Millennium software by using a procedure similar to that of Marchylo et al. Twenty microliters of the filtered extract was injected into a 300SB-$C_8$ reverse phase analytical column (4.6 × 250 mm, 5 $\mu$m particle size, 300 Å pore size; Agilent Technologies), and separation was carried out at 60 °C by using a linear gradient of aqueous acetonitrile containing 0.1% TFA at a flow rate of 1 mL/min. The acetonitrile concentration was increased from 24 to 50% over 80 min and held constant thereafter. Absorbance was monitored at 210 nm. To determine protein concentration, the standard curve based on BSA was made ($y = 0.492x$; $R^2 = 0.9966$).

**Determination of Protein Component in the Dough by MS/MS.** One hundred microliters from the HPLC fraction was vacuum concentrated (Speed Vac) to complete dryness and redissolved in 5 $\mu$L of 50% acetonitrile containing 0.1% TFA. Then, 5 $\mu$L of 100 mM ammonium hydrogen carbonate was added into the solution to optimize conditions for tryptic digestion. The proteins were reduced by adding 1.1 $\mu$L of 100 mM dithiothreitol (DTT), followed by incubation in a water bath at 60 °C for 45 min with intermittent vortex every 10 min. The reduced proteins were alkylated by adding 11.1 $\mu$L of 100 mM iodoacetamide and keeping the solution in the dark for 30 min with intermittent vortex every 10 min. The reduced and alkylated proteins were incubated with 1.5 $\mu$L of trypsin (100 ng/ul) at 37 °C for 20 h. Tryptic digests (1 $\mu$L) were deposited on a metal surface sample plate, and 160 mg/mL 2,5-dihydroxybenzoic acid (DHB) (1 $\mu$L) was added on the top with air-drying.[20] Samples were then analyzed in positive ion mode by using a MALDI with hybrid quadruple time-of-flight tandem mass spectrometry (QqToF-MS) prototype instrument constructed in collaboration with MDS SCIEX (model PBS-II, Ciphergen Biosystems Inc., Fremont, CA, USA). Peptide spectra were obtained using 600−1200 shots, whereas MS/MS spectra were obtained using 4000−6000 shots.

**Statistical Analysis.** Data were reported as means ± standard deviations (SD) for triplicate treatments. One-way analysis of variance (ANOVA) was performed using SPSS for Windows (version 10.0.5; SPSS Inc., Chicago, IL, USA).

## RESULTS AND DISCUSSION

**Effects of Ana-rLOX on the Index of a Flour's Quality Property.** The dough rheological properties are considered to predict the processing behavior and control the quality of food products. The farinograph is used to estimate the water absorption of flour, the formation time, the stability time, and the degree of softening of dough during mixing. These parameters are often used as indices to evaluate flour quality. The improvement effects of ana-rLOX on flour quality were

Table 2. Ana-rLOX Effect on Extensogram Characteristics of Wheat Dough[a]

| | 0 U/g ana-rLOX | | | 30 U/g ana-rLOX | | |
|---|---|---|---|---|---|---|
| index | 45 min | 90 min | 135 min | 45 min | 90 min | 135 min |
| extension area ($cm^2$) | 110.0 ± 0.8 | 122.0 ± 0.8 | 117.0 ± 0.5 | 112.0 ± 0.9 | 132.0 ± 1.3 | 118.0 ± 1.1 |
| resistance (BU) | 471.0 ± 2.3 | 648.0 ± 5.8 | 401.0 ± 2.0 | 500.0 ± 5.5 | 712.0 ± 2.1 | 749.0 ± 6.7 |
| extensibility (mm) | 155.0 ± 2.4 | 150.0 ± 1.5 | 136.0 ± 2.1 | 137.0 ± 2.9 | 122.0 ± 2.5 | 107.0 ± 3.3 |
| ratio ($R/E$) | 2.5 | 3.1 | 3.7 | 3.7 | 5.8 | 7.0 |

[a]Data are expressed as means ± SD, $n$ = 3. BU, Brabender unit; ratio $R/E$, resistance/extensibility.

investigated by using the farinograph, and the results are shown in Table 1.

The water absorption of the dough was significantly increased after the addition of 30 U/g of ana-rLOX to wheat flour, reaching the maximum of 65.2%. However, the water absorption decreased when 40 U/g ana-rLOX was added to the flour. Flour water absorption is the percent of weight gain after the flour soaked in water under 30 °C. Higher water absorption reflected higher production rate. The increase of water absorption in wheat food could soften the core of the food and prolong the shelf life.[21]

The dough development time (DDT) reached the longest at 10 U/g enzyme, and then it decreased by 13% with increasing ana-rLOX to 40 U/g. For pure wheat flour, DDT reflects the total energy amount that is needed to develop the gluten network.[22] The increase in the DDT showed that the dough became a more compact gluten network. However, DDT has an effect on the productivity; therefore, longer DDT for the dough should be avoided to improve output.[23]

The dough stability time was an indicator of the strength of flour. A higher value represents a stronger dough property. The dough stability time increased from 7 to 9.5 min when ana-rLOX was added to wheat flours from 0 to 30 U/g. This showed that the addition of ana-rLOX increased the stability time of the dough. In addition, the softening degree, also called mixing tolerance index, was applied to determine the degree to which dough would soften over a period of mixing. In this study, the softening degree of dough increased with the addition of ana-rLOX and reached the maximum of 97 at 30 U/g, an increase of 31.1% compared to that without ana-rLOX. The result suggested that the gluten network was strengthened with the addition of ana-rLOX, which led to cross-linking of inter/intra-proteins of the rough. From the above result, it was found that the indices of the quality property of flour were improved and so the strength of the dough increased when a certain range of ana-rLOX was added to the flour. However, an overdose of ana-rLOX would shorten the development time and stability time and yield a poor-quality dough because overadding ana-rLOX could cause excessive cross-linking of the wheat protein and prevent the flour from absorbing water.

**Effects of Ana-rLOX on Extensograph Parameters of Flour Dough.** The extensograph measures the extensibility and resistance of dough to stretch. A higher resistance to extension indicates that the dough requires a larger force to stretch. Table 2 presents the ana-rLOX effect on the extensograph parameters of the dough at 45, 90, and 135 min of fermentation time. The extension area and maximum resistance of the dough with addition of ana-rLOX were larger than those without enzyme. The maximum resistance reached 749.0 ± 6.7 BU at 135 min, which was a 34.73% improvement as compared to no enzyme. However, the extensibility of the dough with ana-rLOX was lower than that without enzyme.

$R/E$ of the dough with ana-rLOX was larger than that without enzyme and approached around 7.0 at 135 min, which indicated that the strength of the dough was significantly improved. It is generally known that the strength of dough and its three-dimensional network depends on the arrangement and number of disulfide bonds and sulfhydryl groups of the proteins, and most of the changes in dough-mixing properties are caused by thiol−disulfide interchange reactions.[24] It has been reported that LOX reacted with the molecular oxygen and polyunsaturated fatty acids and formed the peroxides and hydroperoxides, which could oxidize the thiol groups of the proteins to form inter- and intramolecular disulfide bonds.[12] Thus, the improvement of stretching ability of the dough could be because of cross-linking between the flour proteins by ana-rLOX in the work.

**Ana-rLOX Effect on Protein Component in the Dough.** Various kinds of proteins in dough were extracted to investigate the change of quality properties of the flour by adding ana-rLOX. As shown in Figure 1, it was found that the glutenin in

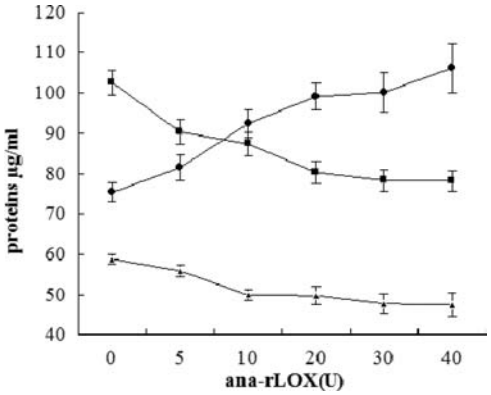


**Figure 1.** Effect of ana-rLOX on the protein component of the dough: (▲) albumin globulin; (■) gliadin; (●) gluten.

the dough was increased, whereas the levels of gliadin, albumin, and globulin were decreased, with the increase of ana-rLOX activity from 5 to 40 U/g, indicating that the protein component was changed after the addition of ana-rLOX. Part of albumin and globulin was combined with glutenin turned into glutenin copolymers; therefore, the resistance of dough was improved. The protein component of wheat flour influenced mixing and baking properties. Gliadins and glutenins were the two primary storage proteins in wheat. Glutenin shows elastic property and enhanced cohesive strength of flour dough, and gliadin exhibits a viscous property and increases the extensibility of the gluten phase.[25] This could also demonstrate that ana-rLOX could improve the rheological properties of wheat flour dough.

**Ana-rLOX Effect on FT-IR Spectroscopy of Glutenin.** FT-IR spectra of the glutenin have several bands due to

different vibrations of the peptide moiety. Amide I and amide III bands are the most frequently used to assign secondary structures of proteins. Amide I originates from C═O stretching vibration of the amide group, whereas amide III comes from C—N stretching and N—H bending.[26] In this work, the effect of ana-rLOX on the glutenin structure was evaluated through the two bands around 1660 and 1231 $cm^{-1}$ and assigned to amides I and III, respectively.

Figure2 shows that the amide I band at around 1660 $cm^{-1}$ correlated to the $\alpha$-helix conformation shifted to 1653 $cm^{-1}$,[27]

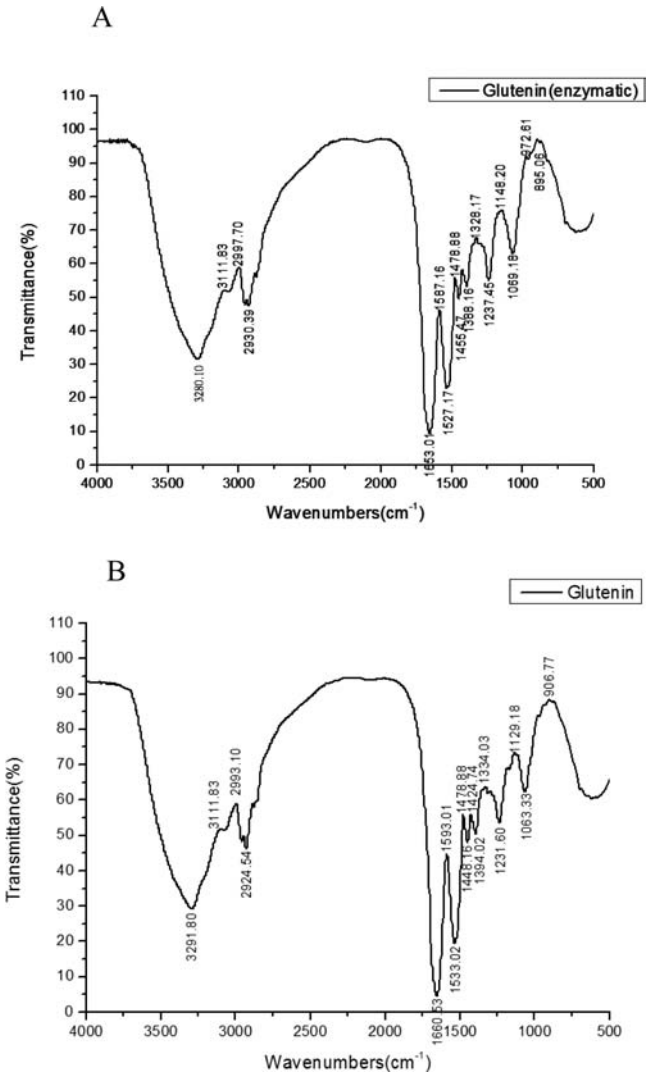


**Figure 2.** FT-IR spectra of glutenin from wheat dough before and after the addition of ana-rLOX: (A) glutenin with ana-rLOX; (B) glutenin without ana-rLOX.

indicating that the $\alpha$-helix conformation in the glutenin of the dough with ana-rLOX was decreased as compared to that without ana-rLOX. However, the amide III band (1200−1300 $cm^{-1}$) at around 1231 $cm^{-1}$ correlating to the $\beta$-sheet conformation was shifted to 1237 $cm^{-1}$,[28] which indicated that the $\beta$-sheet conformation in the dough glutenin modified by ana-rLOX tended to increase. The $\alpha$-helix conformation of the protein has a more compact and stable structure, whereas the structure of the $\beta$-sheet conformation of protein is less compact and stable.[27] Belton et al. reported that $\beta$-sheet was related to high chain mobility produced by an increase of hydration glutenin.[26] The observed result could explain the enhancement of the water absorption in wheat flour modified with ana-rLOX as being due to the increased flexibility of the glutenin molecule by the shift of amide I and III bands. A similar effect of NaCl on $\beta$-sheet conformations was observed by FT-IR in glutenin proteins.[29]

**Analysis of Protein Component of Dough Modified with Ana-rLOX by HPLC and MS/MS.** HPLC coupled with mass spectrometry is a very powerful analytical technique due to its high sensitivity and accuracy. In HPLC, the proteins are eluted according to different surface hydrophobicities. Total protein in wheat dough before and after the addition of ana-rLOX was extracted and determined by HPLC to understand the change of the protein components. Figure 3 shows that

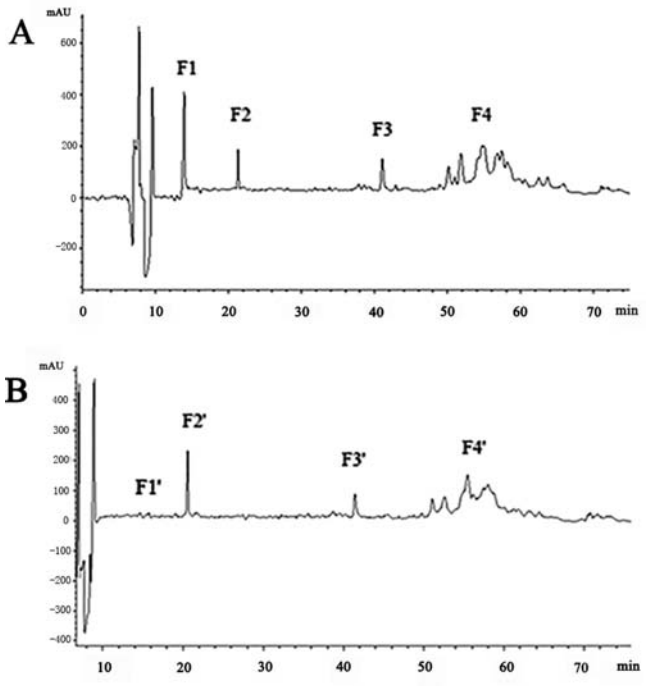


**Figure 3.** HPLC chromatograms of the protein extracts from wheat dough before and after the addition of ana-rLOX: (A) non-ana-rLOX; (B) 30 U/g ana-rLOX.

there were four protein peak regions in the dough without the addition of ana-rLOX. However, the F1 peak at 14 min was not shown in the dough with ana-rLOX, indicating that the protein component could be altered with the addition of ana-rLOX. Generally, as the elution time increased, the polarity of the substances eluted out gradually decreased in gradient elution. Thus, the protein at 14 min could be considered as a polar and hydrophilic substance, such as albumins or globins with better water solubility.

Then, each fraction was analyzed by MS/MS to determine the protein component to investigate why the protein at F1 peak did not show in the dough with ana-rLOX. The protein kinds, their molecular weights, and the characteristics of these fractions are summarized in Tables 3 and 4.

The fractions at 14 min (F1), 20 min (F2), and 55 min (F4) peaks were analyzed by MS/MS. Seventeen peptide adductions $[M + H]^+$ ($m/z$ 1189.6, 1189.6, 1064.6, 2426.1, 1360.7, 1906.0, 1822.9, 1189.6, 1012.4, 991.5, 1280.6, 1028.6, 3164.4, 1813.9, 1522.8, 1311.6, 1362.5, and 1346.5) for fraction F1 were


dx.doi.org/10.1021/jf503238h | J. Agric. Food Chem. 2014, 62, 9885−9892

**Table 3. Identification of Wheat Proteins for F1, F2, and F4 Peaks by MS/MS**

| reference scan(s) | protein peptide sequence[a] | M/H$^+$ | accession[b] Rsp[c] |
|---|---|---|---|
| F1 peak | | | |
| 1. globulin-3A | | | 390979705 |
| (*Triticum aestivum*) | | | |
| 7623 | ***K.ALRPFDEVSR.L*** | 1189.6 | 4 |
| 7629 | ***K.ALRPFDEVSR.L*** | 1189.6 | 5 |
| 7520 | K.ILHTISVPGK.F | 1064.6 | 1 |
| 6720 | ***R.AKDQQDEGFVAGPEQQQEHER.G*** | 2426.1 | 1 |
| 8769 | ***R.DTFNLLEQRPK.I*** | 1360.7 | 1 |
| 9309 | ***R.GSAFVVPPGHPVVEIASSR.G*** | 1906.0 | 1 |
| 9793 | ***R.GSSNLQVVCFEINAER.N*** | 1822.9 | 3 |
| 4758 | ***R.HEQEEQGR.G*** | 1012.4 | 1 |
| 6959 | R.RPYVFGPR.S | 991.5 | 1 |
| 6410 | ***R.SFHALAQHDVR.V*** | 1280.6 | 1 |
| 7775 | R.VAIMEVNPR.A | 1028.6 | 1 |
| 2. globulin 1 | | | 110341790 |
| (*Triticum aestivum*) | | | |
| 7069 | ***R.QEVQGGQYGSETGGSQQQQQGGGYHGVTVGR.G YHGVTVGR.G*** | 3164.4 | 1 |
| 10720 | ***R.AGEGAVGVPLFQAQWGAR.E*** | 1813.9 | 1 |
| 3. S48186 grain softness | | | 1086237 |
| 11732 | ***K.AIWTSIQGDLSGFK.G*** | 1522.8 | 1 |
| 12343 | ***K.DM*PLSWFFPR.T*** | 1311.6 | 1 |
| 6735 | ***K.VDSCSDYVM*DR.C*** | 1362.5 | 1 |
| 6734 | ***K.VDSCSDYVMDR.C*** | 1346.5 | 1 |
| F2 peak | | | 133741924 |
| 1. $\gamma$-gliadin | | | |
| (*Triticum aestivum*) | | | |
| 9657 | R.DALLQQCSPVADM*SFLR.S | 1966.9 | 1 |
| 11457 | R.DALLQQCSPVADMSFLR.S | 1950.9 | 1 |
| 8748 | R.SQAVQPRSCLVM*WEQCCQQLK.A | 2652.2 | 1 |
| 8759 | R.SQAVQPRSCLVM*WEQCCQQLK.A | 2652.2 | 2 |
| 9145 | R.SQAVQPRSCLVMWEQCCQQLK.A | 2636.2 | 2 |
| 2. gliadin/avenin-like | | | 281335538 |
| 6955 | R.SAWEPQHPSSPEHQPTPQPQEHPVPHQK.L | 3217.5 | 1 |
| 8759 | R.SQVVQHSSCLVM*WEQCCQQLK.A | 2651.2 | 1 |
| 9145 | R.SQVVQHSSCLVMWEQCCQQLK.A | 2635.2 | 1 |
| 3. gliadin/avenin-like | | | 281335544 |
| 7847 | R.CQAIHNVVESIR.Q | 1425.7 | 1 |
| 7848 | R.CQAIHNVVESIR.Q | 1425.7 | 1 |
| 7258 | R.M*SLHTLPSMCK.I | 1320.6 | 1 |
| 7347 | R.QQQHHQPQQEVQLEGLR.M | 2083.0 | 1 |
| F4 peak | | | 121455 |
| 1. glutenin (wheat), low molecular weight | | | |
| 9277 | K.VFLQQQCIPVAMQR.C | 1717.9 | 1 |
| 9419 | R.SQMLQQSICHVMQQQCCQQLR.Q | 2691.2 | 1 |
| 2. low-molecular-weight glutenin subunit | | | 336092119 |
| (*Triticum aestivum*) | | | |
| 8707 | K.VFLQQQCSPVAM*PQSLAR.S | 2076.0 | 1 |
| 8694 | K.VFLQQQCSPVAM*PQSLAR.S | 2076.0 | 1 |
| 9568 | K.VFLQQQCSPVAMPQSLAR.S | 2060.0 | 1 |
| 9558 | K.VFLQQQCSPVAMPQSLAR.S | 2060.0 | 1 |

[a]Italic and bold indicate the occurrence in wheat proteins before and after the addition of ana-rLOX. [b]GenBank accession number. [c]Rank of preliminary score.

obtained. The peptides were matched with those in *Triticum aestivum* database and were identified as globulin-3A, globulin 1, and grain softness protein of *T. aestivum*, respectively (Table 3).

**Table 4. Identification of Wheat Protein with Added Ana-rLOX for F2′ and F4′ Peaks by MS/MS**

| reference scan(s) | protein peptide sequence[a] | M/H$^+$ | accession[b] Rsp[c] |
|---|---|---|---|
| F2′ peak | | | |
| 1. globulin 3A (*Triticum aestivum*) | | | 390979705 |
| 6579 | ***R.AKDQQDEGFVAGPEQQQEHER.G*** | 2426.1 | 1 |
| 8535 | R.DTFNLLEQRPK.I | 1360.7 | 1 |
| 9018 | ***R.GSAFVVPPGHPVVEIASSR.G*** | 1906.0 | 1 |
| 9639 | ***R.GSSNLQVVCFEINAER.N*** | 1822.9 | 1 |
| 4445 | ***R.HEQEEQGR.G*** | 1012.4 | 1 |
| 4798 | R.RGSGSESEEEQDQQR.Y | 1721.7 | 1 |
| 6342 | ***R.SFHALAQHDVR.V*** | 1280.6 | 1 |
| 2. S48186 grain softness | | | 1086237 |
| 11732 | ***K.AIWTSIQGDLSGFK.G*** | 1522.8 | 1 |
| 12343 | K.DM*PLSWFFPR.T | 1311.6 | 1 |
| 6735 | ***K.VDSCSDYVM*DR.C*** | 1362.5 | 1 |
| 6734 | ***K.VDSCSDYVMDR.C*** | 1346.5 | 1 |
| 3. γ-gliadin | | | 133741924 |
| 9657 | R.DALLQQCSPVADM*SFLR.S | 1966.9 | 1 |
| 11457 | R.DALLQQCSPVADMSFLR.S | 1950.9 | 1 |
| 8748 | R.SQAVQPRSCLVM*WEQCCQQLK.A | 2652.2 | 1 |
| 8759 | R.SQAVQPRSCLVM*WEQCCQQLK.A | 2652.2 | 2 |
| 9145 | R.SQAVQPRSCLVMWEQCCQQLK.A | 2636.2 | 2 |
| 4. gliadin/avenin-like seed protein (*Triticum aestivum*) | | | 281335538 |
| 6955 | R.SAWEPQHPSSPEHQPTPQPQEHPVPHQK.L | 3217.5 | 1 |
| 8759 | R.SQVVQHSSCLVM*WEQCCQQLK.A | 2651.1 | 1 |
| 9145 | R.SQVVQHSSCLVMWEQCCQQLK.A | 2635.2 | 1 |
| 5. gliadin/avenin-like seed protein (*Triticum aestivum*) | | | 281335544 |
| 7847 | R.CQAIHNVVESIR.Q | 1425.7 | 1 |
| 7848 | R.CQAIHNVVESIR.Q | 1425.7 | 1 |
| 7258 | R.M*SLHTLPSMCK.I | 1320.6 | 1 |
| 7347 | R.QQQHHQPQQEVQLEGLR.M | 2083.0 | 1 |
| 6. globulin 1 (*Triticum aestivum*) | | | 110341801 |
| 7102 | R.QEVQGGQYGSETGGGQQQGGGYHGVTVGR.G HGVTVGR.G | 2878.3 | 1 |
| 7777 | R.DYEQSMPPLGEGR.H | 1478.7 | 1 |
| 7. globulin 1 (*Triticum aestivum*) | | | 110341790 |
| 7069 | ***R.QEVQGGQYGSETGGSQQQQQGGGYHGVTVGR.G GYHGVTVGR.G*** | 3164.4 | 1 |
| 10720 | ***R.AGEGAVGVPLFQAQWGAR.E*** | 1813.9 | 1 |
| 8. A27319 gliadin- wheat | | | 100783 |
| 6638 | R.DVVLQQHNIAHAR.S | 1500.8 | 1 |
| 8222 | R.NLALQTLPR.M | 1025.6 | 1 |
| F4′ peak | | | |
| 1. S48186 wheat softness protein 1a, 15K | | | 1086237 |
| 11902 | K.AIWTSIQGDLSGFK.G | 1522.8 | 1 |
| 12484 | ***K.DM*PLSWFFPR.T*** | 1311.6 | 1 |
| 12977 | K.DMPLSWFFPR.T | 1295.6 | 1 |
| 6860 | K.VDSCSDYVMDR.C | 1346.5 | 1 |
| 2. wheat softness protein-1B2 | | | 60652218 |
| 12093 | K.DM*PLSWIFPR.T | 1277.6 | 1 |
| 6483 | K.LDSCSDYVM*DR.C | 1376.5 | 1 |
| 7243 | K.LDSCSDYVMDR.C | 1360.5 | 1 |

**Table 4. continued**

| reference scan(s) | protein peptide sequence[a] | M/H$^+$ | accession[b] Rsp[c] |
|---|---|---|---|
| 3. LMW wheat glutenin subunit | | | 121455 |
| 9277 | K.VFLQQQCIPVAMQR.C | 1717.9 | 1 |
| 9419 | R.SQMLQQSICHVMQQQCCQQLR.Q | 2691.2 | 1 |
| 4. LMW glutenin | | | 336092119 |
| 8707 | K.VFLQQQCSPVAM*PQSLAR.S | 2076.0 | 1 |
| 8694 | K.VFLQQQCSPVAM*PQSLAR.S | 2076.0 | 1 |
| 9568 | K.VFLQQQCSPVAMPQSLAR.S | 2060.0 | 1 |
| 9558 | K.VFLQQQCSPVAMPQSLAR.S | 2060.0 | 1 |
| 5. globulin-3A (*Triticum aestivum*) | | | 390979705 |
| 7665 | ***K.ALRPFDEVSR.L*** | 1189.6 | 12 |
| 8743 | ***R.DTFNLLEQRPK.I*** | 1360.7 | 1 |

[a]Italic and bold indicate the occurrence in wheat proteins before and after the addition of ana-rLOX. [b]GenBank accession number. [c]Rrank of preliminary score.

Twelve peaks at $m/z$ 1966.9, 1950.9, 2652.2, 2636.2, 2652.2, 3217.5, 2651.2, 2635.2, 1425.7, 1425.7, 1320.6, and 2083.0 were assigned to the peptide adduction $[M + H]^+$ in fraction F2 at the 20 min peak. The compounds of the fraction F2 were identified as three major proteins, namely, γ-gliadin and two gliadin/avenin-like seed proteins (Table 3). However, the protein component was changed in the protein fraction F2′ by adding ana-rLOX (Table 4), and the new protein moleculed such as globulin 3A, globulin 1, and grain softness protein besides γ-gliadin and two gliadin/avenin-like seed proteins were found in fraction F2′. This observation indicated that the hydrophilic globulin could be integrated into the gliadin owing to the peroxidation radicals initialized by ana-rLOX.

In the protein fraction F4 at the 55 min peak, six of the peptides adductions ($m/z$ 1717.9, 2691.2, 2076.0, 2676.0, 2060.0, and 2060.0) were found and were identified as low-molecular-weight glutenin and GLTA-wheat glutenin from *T. aestivum*. In fraction F4′, new protein molecules, such as S48186 grain softness protein 1a, grain softness protein 1B2, and globulin 3A, were also observed. This result demonstrated that the hydrophilic protein component in wheat flour was combined into glutenin by enzymatic reaction after the addition of ana-rLOX.

The oxidative polymerization of the proteins to HMW fractions was an important prerequisite to obtain strong gluten. In our previous study, we had already observed that the flour treated with ana-rLOX improved the dough quality in terms of higher strength and tenacity, which have shown an increase of disulfide bond content because of the oxidation of free −SH groups.[17] Moreover, these results provided clear evidence that ana-rLOX from *Anabaena* sp. PCC 7120 could make globulin cross-link with gliadin and LMW glutenin, which improved the rheologcal properties of the dough. Some studies have shown that LOX affected the flour quality by inducing S−S bond formation of glutenin,[30] but this study demonstrated that ana-rLOX could make glutenin cross-link with other kinds of proteins, such as globulin-3A, globulin 1, and S48186 grain softness protein 1a, and 15K, forming HMW glutenin. These results not only provided clear evidence that ana-rLOX influenced the protein component of wheat flour but also explained the mechanism of its improving effect on the farinograph and extensograph parameters of wheat flour.

## AUTHOR INFORMATION


### Corresponding Author

*(Z.L.) Phone/fax: +86-25-84396583. E-mail: fmb@njau.edu.cn.



### Funding

This work was funded by the National Natural Science Foundation of China (31071605; 31470095), the Chinese "863 High-Tech" Program (2012AA022207), the Science and Technology Support Program of Jiangsu Province (BE2011390), and the project funded by the Priority Academic Program Development of Jiangsu Higher Education Institutions (PAPD).


### Notes

The authors declare no competing financial interest.

## REFERENCES


(1) Karin, A.; Kristiina, K.; Antti, K. Kinetics of transglutaminase-induced cross-linking of wheat proteins in dough. *J. Agric. Food Chem.* **2005**, *53*, 1039−1045.

(2) Shewry, P. R.; Popineau, Y.; Lafiandra, D.; Belton, P. Wheat glutenin subunits and dough elasticity: findings of the EUROWHEAT Project. *Trends Food Sci. Technol.* **2001**, *11*, 433−441.

(3) Osborne, T. B.; Harris, I. F. The chemistry of the proteins of the wheat kernel. II. Preparation of proteins in sufficient amount for hydrolysis. *Fresenius' J. Anal. Chem.* **1907**, *46*, 749−756.

(4) Weegels, P. L.; Hamer, R. J.; Schofield, J. D. Critical review: functional properties of wheat glutenin. *J. Cereal Sci.* **1996**, *23*, 1−18.

(5) Wieser, H.; Kieffer, R. Correlations of the amount of gluten protein types to the technological properties of wheat flours determined on a micro-scale. *J. Cereal Sci.* **2001**, *34*, 19−27.

(6) Jekle, M.; Becker, T. Dough microstructure: novel analysis by quantification using confocal laser scanning microscopy. *Food Res. Int.* **2011**, *44*, 984−991.

(7) Alessandro, A.; Concha, C. Small and large deformation viscoelastic behaviour of selected fibre blends with gelling properties. *Food Hydrocolloids* **2009**, *23*, 742−748.

(8) Anil, M. Using of hazelnut testa as a source of dietary fiber in breadmaking. *J. Food Eng.* **2007**, *80*, 61−67.

(9) Dunnewind, B.; van Vliet, T.; Orsel, R. Effect of oxidative enzymes on bulk rheological properties of wheat flour doughs. *J. Cereal Sci.* **2002**, *36*, 357−366.

(10) Zhang, C.; Zhang, S.; Lu, Z. X.; Bie, X. M.; Zhao, H. Z.; Wang, X. M.; Lu, F. X. Effects of recombinant lipoxygenase on wheat flour, dough and bread properties. *Food Res. Int.* **2013**, *54*, 26−32.

(11) Faubion, J. M.; Hoseney, R. C. Lipoxygenase: its biochemistry and role in breadmaking. *Cereal Chem.* **1981**, *58*, 175−180.

(12) Wang, X. M.; Lu, F. X.; Zhang, C.; Lu, Y. J.; Bie, X. M.; Ren, D.; Lu, Z. X. Peroxidation radical formation and regiospecificity of recombinated *Anabaena* sp. lipoxygenase and its effect on modifying wheat proteins. *J. Agric. Food Chem.*. **2014**, *62*, 1713−1719.
(13) Huang, Y. R.; Hua, Y. F.; Qiu, A. Y. Soybean protein aggregation induced by lipoxygenase catalyzed linoleic acid oxidation. *Food Res. Int.* **2006**, *39*, 240−249.
(14) Godovac-Zimmermann, J.; Brown, L. R. Perspectives for mass spectrometry and functional proteomics. *Mass Spectrom. Rev.* **2001**, *20*, 51−57.
(15) Cunsolo, V.; Foti, S.; Saletti, R.; Gilbert, S.; Tatham, A.; Shewry, P. R. Structural studies of glutenin subunits 1Dy10 and 1Dy12 by matrix-assisted laser desorption/ionization mass spectrometry and high-performance liquid chromatography/electrospray ionization mass spectrometry. *Rapid Commun. Mass Spectrom.* **2003**, *17*, 442−454.
(16) Schneider, C.; Niisuke, K.; Boeglin, W. E.; Voehler, M.; Stec, D. F.; Proter, N. A.; Brash, A. R. Enzymatic synthesis of a bicyclobutane fatty acid by a hemoprotein−lipoxygenase fusion protein from the cyanobacterium *Anabaena* PCC 7120. *Proc. Natl. Acad. Sci. U.S.A.* **2007**, *48*, 18941−18945.
(17) Zhang, C.; Tao, T. T.; Ying, Q.; Zhang, D. L.; Lu, F. X.; Bie, X. M.; Lu, Z. X. Extracellular production of lipoxygenase from *Anabaena* sp. PCC 7120 in *Bacillus subtilis* and its effect on wheat protein. *Appl. Microbiol. Biotechnol.* **2012**, *94*, 949−958.
(18) American Association of Cereal Chemists. *Approved Methods of the AACC*, 11th ed.; AACC: St. Paul, MN, USA, 2000.
(19) Weegels, P. L.; Hamer, R. J.; Schofield, J. D. RP-HPLC and capillary electrophoresis of subunits from glutenin isolated by SDS and Osborne fractionation. *J. Cereal Sci.* **1995**, *22*, 211−224.
(20) Qian, Y. W.; Preston, K.; Krokhin, O.; Mellish, J.; Ens, W. Characterization of wheat gluten proteins by HPLC and MALDI TOF mass spectrometry. *J. Am. Soc. Mass Spectrom.* **2008**, *19*, 1542−1550.
(21) Sroan, B. S.; Bean, S. R.; MacRitchie, F. Mechanism of gas cell stabilization in bread making. I. The primary gluten-starch matrix. *J. Cereal Sci.* **2009**, *49*, 32−40.
(22) Rieder, A.; Holtekjølen, A. K.; Sahlstrøm, S.; Moldestad, A. Effect of barley and oat flour types and sourdoughs on dough rheology and bread quality of composite wheat bread. *J. Cereal Sci.* **2012**, *55*, 44−52.
(23) Ding, S. Y.; Yang, J. The fluence of emulsifiers on the rheological properties of wheat flour dough and quality of fried instant noodles. *LWT − Food Sci. Technol.* **2013**, *53*, 61−69.
(24) Breuillet, C.; Yildiz, E.; Cuq, B.; Kokini, J. L. Study of the anomalous capillary bagley factor behavior of three types of wheat flour doughs at two moisture contents. *J. Texture Stud.* **2002**, *33*, 315−340.
(25) Koehler, P.; Kieffer, R.; Wieser, H. Effect of hydrostatic pressure and temperature on the chemical and functional properties of wheat gluten III. Studies on gluten films. *J. Cereal Sci.* **2010**, *51*, 140−145.
(26) Belton, P. S.; Colquhoun, I. J.; Grant, A.; Wellner, N.; Field, J. M.; Shewry, P. R. FTIR and NMR studies on the hydration of a high-Mr subunit of glutenin. *Int. J. Biol. Macromol.* **1995**, *17*, 74−80.
(27) Correa, M. J.; Ferrer, E.; Anon, M. C.; Ferrero, C. Interaction of modified celluloses and pectins with gluten proteins. *Food Hydrocolloids* **2014**, *35*, 91−99.
(28) Herrero, A. M. Raman spectroscopy for monitoring protein structure in muscle food systems. *Crit. Rev. Food Sci. Nutr* **2008**, *48* (6), 512−529.
(29) Ukai, T.; Matsumura, Y.; Urade, R. Disaggregation and reaggregation of gluten proteins by sodium chloride. *J. Agric. Food Chem.* **2008**, *56*, 1122−1130.
(30) Borrell, G. M.; Ficco, D. B. M.; Di Fonzo, N.; Fares, C. Effects of lipoxygenase and of chemical oxidising agent potassium iodate on rheological properties of durum dough. *Int. J. Food Sci. Technol.* **2006**, *41*, 639−645.

temperature (RT) with 10 times their weight of distilled water. Using a kitchen mixer, the soybean seeds were homogenized at low speed for 1 min. Soybean milk was obtained from the resulting slurry by the removal of an insoluble residue (soy pulp fiber) by filtration (FILTER-LAB qualitative filter paper, pore size 43−48 $\mu$m). The soybean milk was heated in boiling water for 15 min and then cooled to RT.

**Protein Extraction.** The three protocols used to prepare the protein extracts, one for soybean seed samples and two for the soybean milk samples, are outlined in Figure 1.

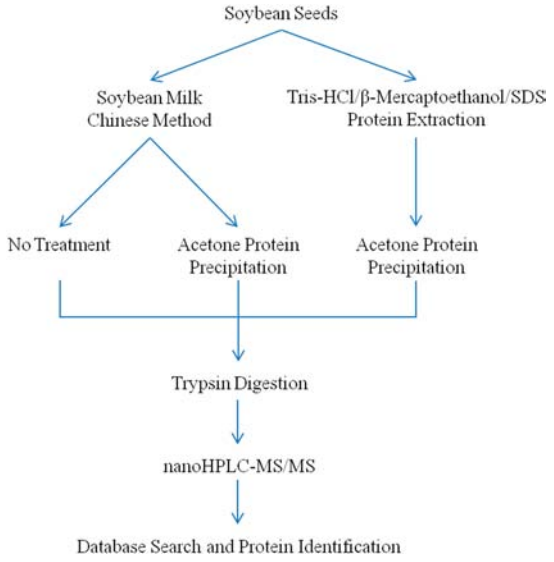


**Figure 1.** Workflow diagram for the experimental procedure.

*Extraction of Proteins from Soybean Seeds.* Soybean seeds were shortly sterilized with 70% ethanol for 10 s and then washed with distilled water three times. Dry seeds (ca. 1 g) were frozen in liquid nitrogen and ground to a fine powder in a precooled mortar with pestle. The powder (0.1 g) was defatted three times with 1 mL of petroleum ether, shaking gently and thoroughly for 15 min. Then, the proteins were extracted with 1 mL of a solution containing 50 mmol $L^{-1}$ Tris-HCl pH 8.8, 1.5 mmol $L^{-1}$ KCl, 0.07% $\beta$-mercaptoethanol, 1% protease inhibitor cocktail, and 1% (w/v) sodium dodecyl sulfate (SDS). The samples were incubated on ice for 1 h with intermittent mixing with vortex (1 min) every 15 min, and insoluble materials were removed by centrifugation at 4 °C for 15 min at 11 000*g*. The supernatant was transferred to a new centrifuge tube, four volumes of cold acetone with 0.07% (*v*/*v*) $\beta$-mercaptoethanol were added, and then the sample was mixed thoroughly and incubated at −20 °C overnight. The precipitate was collected by centrifugation (18 400*g* for 15 min at 4 °C), washed three times with acetone containing 0.07% (v/v) $\beta$-mercaptoethanol, air-dried, and solubilized in urea buffer pH 8.5 (8 mol $L^{-1}$ urea in 50 mmol $L^{-1}$ $NH_4HCO_3$). The proteins were quantified by Bradford assay using BSA standard[17] and stored at −80 °C until the trypsin digestion. Three experimental replicates were performed.

*Proteins from Soybean Milk without Any Treatment.* From a 10 mL aliquot of soybean milk, prepared as described above, the proteins were directly quantified by Bradford assay using BSA standard[17] and stored at −80 °C until further processing.

*Acetone Precipitation of Proteins from Soybean Milk.* The soybean milk (10 mL) was placed in acetone-compatible tube, and four volumes of cold (−20 °C) acetone with 0.07% (v/v) $\beta$-mercaptoethanol were added. The tube was vortex-mixed and incubated overnight at −20 °C. The precipitated proteins from soybean milk were collected by centrifugation (18 400*g* for 15 min at 4 °C), washed three times with acetone containing 0.07% (v/v) $\beta$-mercaptoethanol, air-dried, and solubilized in urea buffer pH 8.5 (8 mol $L^{-1}$ urea in 50 mmol $L^{-1}$ $NH_4HCO_3$). The protein content was quantified by Bradford assay using BSA standard[17] and stored at −80 °C until the trypsin digestion. Three experimental replicates were performed.

**Enzymatic Digestion and Off-Line Desalting.** Aliquots from soybean seed samples, soybean milk samples, and precipitated proteins from soybean milk samples were reduced, alkylated, and digested with trypsin. For the digestion of the proteins from soybean milk without any treatment, we added urea to the soybean milk to reach a 8 mol $L^{-1}$ concentration in order to denature the proteins. Reduction of disulfide bonds was performed with dithiothreitol (DTT, 200 mmol $L^{-1}$) in incubation at 37 °C for 1 h, under slight agitation. Carbamidomethylation of thiol groups was performed by addition of iodoacetamide (IAA, 200 mmol $L^{-1}$) and incubation for 1 h in the dark at RT. To consume any leftover alkylating agent and to avoid trypsin alkylation, DTT (200 mmol $L^{-1}$) was added, and samples were incubated at 37 °C for 1 h, under slight agitation. The samples were then diluted with $NH_4HCO_3$, pH 8.5 (50 mmol $L^{-1}$) to obtain a final 1 mol $L^{-1}$ urea concentration. Sequencing-grade modified tryspin was added (1:20, w/w, enzyme to protein ratio), and the samples were incubated overnight at 37 °C. Enzymatic digestion was quenched with trifluoroacetic acid (TFA). Digested samples were desalted using SPE C18 cartridges conditioned with ACN and rinsed with 0.1% TFA aqueous solution. Peptides were eluted from the SPE column with ACN/dd$H_2O$ (50/50, v/v) containing 0.05% TFA, and were dried in a Speed-Vac SC 250 Express (Thermo S 164 avant, Holbrook, NY, U.S.A.). Each sample was reconstituted with 0.1% HCOOH aqueous solution and stored at −80 °C until analysis.

**NanoHPLC-MS/MS Analysis.** Nano high-performance liquid chromatography (nanoHPLC) coupled to tandem mass spectrometry (MS/MS) analysis was performed on a hybrid linear ion trap-Orbitrap mass spectrometer (model Orbitrap Elite, Thermo Scientific, Bremen, Germany) equipped with a nanoelectrospray ion source. Peptide mixtures were separated by reversed-phase (RP) chromatography using the Dionex Ultimate 3000 (Dionex Corporation Sunnyvale, CA, U.S.A.). The LC system was connected to a manufactured 25 cm fused-silica nanocolumn, 75 $\mu$m i.d., packed in-house with Acclaim-C18 2.2 $\mu$m silica microparticles, with outlet frit prepared using Kasil. Peptide mixtures were enriched on a 300 $\mu$m i.d. × 5 mm Acclaim PepMap 100 C18 (5 $\mu$m particle size, 100 Å pore size) precolumn (Dionex), employing a premixed mobile phase $H_2O$/ACN 98:2 (v/v) (from loading pump) containing 0.1% (v/v) HCOOH at a flow-rate of 10 $\mu$L $min^{-1}$. LC gradient was optimized to detect the largest set of peptides, using $H_2O$/HCOOH (99.9:0.1, v/v) as mobile phase A and ACN/HCOOH (99.9:0.1, v/v) as mobile phase B. After an isocratic step at 1% B for 5 min, B was linearly increased to 11% within 2 min and then to 31% within 120 min; afterward, phase B was maintained at 31% within 10 min, and increased to 80% within the following 10 min. Then, phase B was maintained at 80% for 10 min to rinse the column. Finally, B was lowered to 1% over 1 min and the column re-equilibrated for 22 min (180 min total

run time). MS spectra of tryptic digests were collected over an $m/z$ range of 380−2000, using a resolution setting of 60 000 (full width at half-maximum, fwhm, at $m/z$ 400), operating in the data-dependent mode to automatically switch between Orbitrap-MS and linear ion trap-MS/MS acquisition. MS/MS spectra were collected for the 20 most abundant ions in each MS scan. Rejection of +1, and unassigned charge states was enabled. All MS/MS spectra were collected using normalized collision energy of 30%, and an isolation window of 2 $m/z$. Ion trap and Orbitrap maximum ion injection times were set to 100 and 200 ms, respectively. Automatic gain control (AGC) was used to prevent overfilling of the ion traps and was set to $1 \times 10^6$ for full FTMS scan, and $1 \times 10^4$ ions in $MS^n$ mode for the linear ion trap. To minimize redundant spectral acquisitions, dynamic exclusion was enabled with a repeat count of 1 and a repeat duration of 30 s with exclusion duration of 70 s. In order to increase the number of identified peptides/proteins, we performed three technical replicates (nanoHPLC-MS/MS runs) for each of the three experimental replicates.

**Database Searching and Protein Identification.** Raw MS/MS data files from Xcalibur software (version 2.2 SP1.48, Thermo Fisher Scientific) were submitted to Proteome Discoverer software (version 1.3, Thermo Scientific) with the Mascot (v.2.3.2, Matrix Science) search engine for peptide/protein identification. The searches were performed against Swiss-Prot database (Release 01-2014, 541 954 sequences). The search was limited to proteins from species of the *Other Green Plants* (18 092 sequences) taxonomy entries and performed using the built-in decoy search option of Mascot. Enzymatic digestion with trypsin was selected, together with maximum of 2 missed cleavages, peptide charges from +2 to +5, a precursor mass tolerance of 10 ppm and a fragment mass tolerance of 0.8 Da; acetylation (N-term), oxidation (M), and deamidation (N, Q) were used as dynamic modifications, whereas carbamidomethylation (C) was used as static modification.

**Scaffold Analysis.** Scaffold software (version Scaffold 3.4.3, Proteome Software Inc., Portland, OR, U.S.A.)[18] was used to validate MS/MS based peptide and protein identification. The additional X! Tandem search engine (The GPM, Cyclone version 2010.12.01.1) was also used, keeping the same parameters previously used for Mascot. According to the Peptide and Protein Prophet algorithms[19,20] implemented into Scaffold, identifications were accepted if they could be established at a probability greater than 95% and 99% for proteins and peptides, respectively, and if proteins contained at least 2 unique peptides, resulting in a false discovery rate of 0.02% for peptides and 2.1% for proteins. Proteins that contained similar peptides and could not be differentiated on the basis of MS/MS analysis alone were grouped to satisfy the principles of parsimony.

## RESULTS AND DISCUSSION

**Design of the Experiment and Proteomic Approach.** The objective of this study was to characterize the protein profile of mature seeds of soybean and soybean milk obtained from the seeds themselves using the Chinese method. Furthermore, precipitation with acetone was also evaluated in order to assess whether the protein precipitation of soybean milk could improve the subsequent nanoHPLC-MS/MS analysis and the identification of proteins. Therefore, a shotgun proteomic approach was employed. The proteins extracted from the mature soybean seeds, the proteins of the soybean milk and those obtained from soybean milk by precipitation with acetone were digested with trypsin, and the resulting peptides were characterized using nanoHPLC-MS/MS analysis and database search. Figure 1 shows a workflow diagram for the experimental procedures.

**Proteins Identified in Mature Soybean Seeds and Soybean Milk.** This is the first study reporting the comparison of protein profiles of mature soybean seed and soybean milk by a shotgun proteomic approach. The analysis of the protein profile of the three systems under investigation led to the identification of 209 proteins in seeds, 200 in milk, and 183 in precipitated soybean milk. Figure 2 shows a Venn diagram in which the protein profiles of the three systems investigated are compared. From a first analysis, the protein profiles of the three systems apparently showed some differences. The Venn diagram shows 19 unique proteins for the seeds, 15 unique proteins for the soybean milk, and 13 unique proteins for the precipitated soybean milk. These differences are, however, misleading. The milk samples, and in particular the precipitated milk samples, cannot present unique proteins, because they derive from the same seeds, the proteome of which was also characterized (see Supporting Information file). Thus, the unique proteins identified for the milk and the precipitated milk samples are to be ascribed to the three different approaches for obtaining the protein samples and to the statistical variability of the LC-MS/MS experiments.

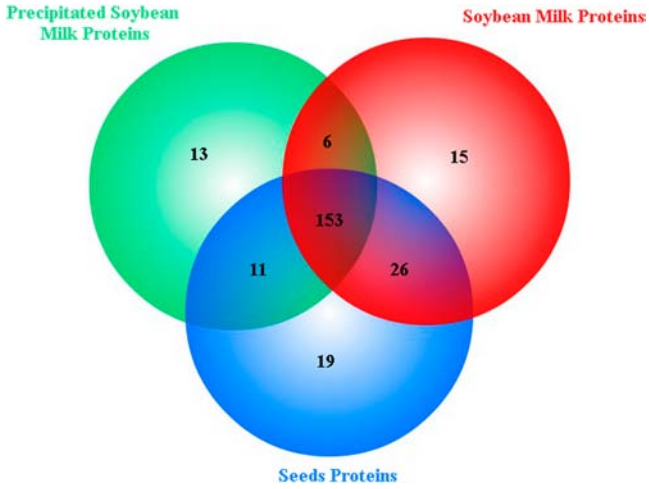


**Figure 2.** Venn diagram of the differentially identified proteins in soybean seeds, soybean milk, and precipitated soybean milk.

Proteins extracted from the mature soybean seeds were obtained with a standard extraction procedure, which requires the use of specific reagents (Tris-HCl, KCl, $\beta$-mercaptoethanol, protease inhibitor cocktail, and SDS) and a precipitation step with acetone (Figure 1); on the contrary, the soybean milk proteins were obtained with a simple but effective extraction from the aqueous phase at RT (Figure 1). In our opinion, the two protein extraction methods provide comparable results; the few differences exhibited by protein profiles (unique proteins) are due to the statistical variability of the experiments. Indeed, small changes in the signal intensity of a peptide (especially if present at low concentration) affect its selection for MS/MS spectrum acquisition, which can therefore be different between different LC-MS experiments. The quality of the MS/MS experiments can also vary, leading to successful identification in some cases but not in others.[21] Therefore, this shotgun

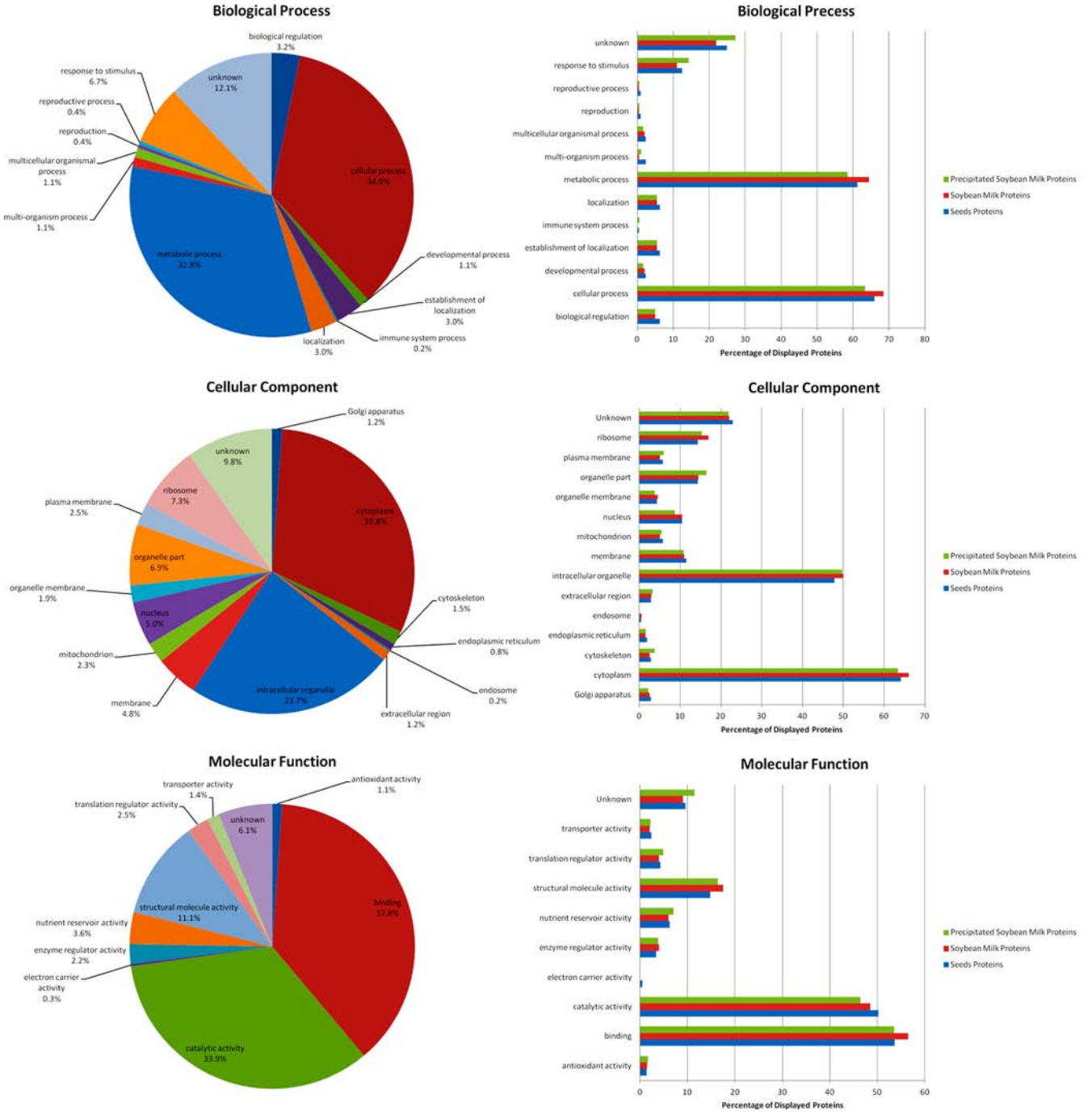


**Figure 3.** Gene Ontology annotation according to biological process, cellular component, and molecular function of the 243 nonredundant identified proteins and relative distribution of the seed proteins, soybean proteins, and precipitated soybean milk proteins.

proteomics analysis showed substantial equivalence of the soluble protein composition in mature soybean seeds and prepared soybean milk.

The largest differences presented by the third system (precipitated soybean milk) compared to the other two (Figure 2) are mainly due to the different procedure by which the proteins were obtained (i.e., the precipitation from soybean milk with acetone).

Precipitation is frequently used to concentrate proteins and to remove interfering compounds which could be responsible for irreproducible results. This is the case, for example, of most agriculturally interesting species, where the precipitation step is necessary to remove secondary metabolite compounds, which are present in large amounts. The precipitation with acetone or, even more significantly, the precipitation with acetone/TCA definitely improve the results obtained by two-dimensional polyacrylamide gel electrophoresis (2D-PAGE) analysis because it allows a better resolution.[14] However, in the shotgun proteomics approach, the precipitation leads to a loss of information, i.e. a smaller number of identified proteins (Figure 2). Our study showed that the prepared soybean milk, which contains sugars, lipids, and secondary metabolic compounds over proteins, can be analyzed by the shotgun proteomics approach directly, without any precipitation step with acetone.


dx.doi.org/10.1021/jf5034152 | J. Agric. Food Chem. 2014, 62, 9893−9899

The protein profile of the mature soybean seeds provided in this study is the most comprehensive one to the authors' best knowledge. Ten years ago, two studies based on 2D-PAGE, which is an extremely time-consuming technique, were published on the proteomic analysis of mature soybean seeds; Herman et al.[11] identified 111 protein spots, and Mooney et al.[13] identified 44 protein spots. A more recent study, based on nanoUPLC-MS$^E$ technique,[22] identified 113 proteins; Gomes et al.[15] identified 117 proteins with one-dimensional gel electrophoresis followed by MS and MS/MS analysis. Our results far exceed the low number of proteins identified in these previous works and provide additional identifications for the proteins present at low amounts in addition to those particularly abundant, such as the seed storage proteins. However, recently, Miernyck et al.[23] reported the identification of proteins in different stages of maturation only in the testa from developing soybean seeds. In almost every maturation stage Miernyck et al.[23] identified a larger number of proteins then the one obtained from the proteomic analysis of the whole mature soybean seed. This difference can be explained by several reasons: (i) In the mature whole seeds, 70−80% of the protein content is made up of storage proteins, which are highly abundant and thus hinder the detection of the lower abundance proteins, (ii) although in this work, a specific database for *Glycine max* was not employed; SwissProt was used, instead, because it is a high quality, curated, annotated, and non-redundant protein sequence database. Despite this, our results (243 identified proteins) are not excessively lower than the ones reported by Miernyck et al.[23] for the last stages of development of the testa (193 identified proteins in S8 and 272 identified proteins in S9).

This study demonstrated that a shotgun proteomics approach with in solution digestion is not sensitive to the presence of lipids, saccharides, and secondary metabolites that are in the soybean milk. Vice versa, a 2D-PAGE analysis would have been sensitive to the presence of contaminants of any nature and therefore requires a precipitation step that improves the resolution and reproducibility of the gels but leads to loss of information, with fewer identified proteins.

**Protein Classification.** In the present study, a total of 243 nonredundant proteins was identified (Figure 2). However, 161 proteins were annotated with a taxonomy other than *Glycine max*, like *Nicotiana tabacum*, *Pisum sativum*, or *Zea mays*. This could be ascribed to the fact that soybean is a newly sequenced species and several proteins are still not annotated in SwissProt. Consequently, we blasted all the proteins in the entire UniProtKB database, filtering the results by *Glycine max* only. All the blast searches gave good results (the majority with more than 85% of identity and maximal E-values of $10^{-18}$) with proteins of soybean present only in TrEMBL section (see Supporting Information, Tab: BLAST).

The identified proteins were classified by the Gene Ontology (GO) terms in three broader domains: biological process, cellular component, and molecular function, and according to the Scaffold's system, each protein displayed in the samples may have one or many GO terms (Figure 3). With regard to the molecular function domain, the two most represented categories are binding and catalytic activity, with a large number of proteins belonging to both categories. This finding is in agreement with the classification based on the biological process, where the two most represented categories are cellular process and metabolic process, and also in this case many proteins belong to both categories. These proteins are often referred to as "housekeeping" proteins, which are essential for the maintenance of normal cell metabolism and involved in seed development, and some of these proteins are enzymes or enzyme inhibitors. The housekeeping protein fraction is made up of relatively small amounts of numerous protein species.

The other important category of proteins in molecular function domain is nutrient reservoir activity (Figure 3), better known as storage proteins. The two major seed storage proteins from soybean are multimeric with Svedberg coefficients of 7S and 11S. The 7S globulins are composed of $\beta$-conglycinin subunits, whereas 11S globulins are composed of glycinin proteins.[24−26] The storage proteins account for the major part of the seed proteins, 70−83% of the total proteins in terms of abundance, and are represented by relatively few different species of proteins. The main characteristics of seed storage proteins are that (i) they accumulate in seeds in large quantities, (ii) they are tissue-specific and occur only in the seed, (iii) they are synthesized during seed development, (iv) they are often sequestered in membrane-bound organelles (protein bodies), and (v) they are hydrolyzed to release their constituent amino acids during germination.

There are several housekeeping proteins, but they are present in a small amount; vice versa, the storage proteins comprise only few proteins, but they are present in a large amount, as confirmed by MS/MS data (Supporting Information). Indeed, the storage proteins showed high values of spectral counts, whereas the housekeeping proteins showed low values of spectral counts.

Liu et al.[27] demonstrated a linear relationship between the spectral count and the relative protein abundance over a dynamic range of 2 orders of magnitude. The spectral counting method relies on the simple concept that an increase in protein abundance can increase the number of its detectable proteolytic peptides (i.e., the total number of MS/MS spectra that are acquired for that peptide).

With regard to domain cellular component, the two most represented categories are cytoplasm and intracellular organelle. This result confirms that most of the seed proteins are storage proteins. Storage proteins primarily accumulate in the protein storage vacuoles of terminally differentiated cells of the embryo and endosperm and as protein bodies (PBs) directly assembled within the endoplasmic reticulum.

PBs form as a consequence of developmentally regulated events that induce storage protein synthesis in specialized cells and promote storage protein accumulation in specific organelles. Storage proteins may remain in the endoplasmic reticulum or be transported through the endomembrane system to distal sites. The major seed vacuolar storage proteins, (i.e., 7S and 11S globulins) form dimers, trimers, and tetramers in the endoplasmic reticulum lumen shortly after synthesis.

Figure 3 shows that the relative distribution of the seed proteins, soybean proteins and precipitated soybean milk proteins, on the basis of GO classification, is substantially equivalent.

**Identified Allergens in Soybean.** The soybean, a legume of high nutritional value, is also known to be one of the major allergenic foods. Identification and characterization of specific protein components linked to soybean allergy has been the focus of several studies. The results of these investigations have shown that a heterogeneous group of proteins are IgE-binding and are potential allergens. In the present study, some of the proteins already described as allergens were found (Table 1).

**Table 1. Identified Allergens in Soybean**

| no. | identified proteins | entry name |
|---|---|---|
| 1 | hydrophobic seed protein | HPSE_SOYBN |
| 2 | profilin 1[a] | PROF1_SOYBN |
| 3 | profilin 2[a] | PROF2_SOYBN |
| 4 | stress-induced protein SAM22 | SAM22_SOYBN |
| 5 | beta-conglycinin, alpha chain | GLCA_SOYBN |
| 6 | 34 kDa maturing seed protein | P34_SOYBN |
| 7 | glycinin | GLYG5_SOYBN |
| 8 | 2S albumin | 2SS_SOYBN |
| 9 | lectin (agglutinin) | LEC_SOYBN |
| 10 | trypsin inhibitor A | ITRA_SOYBN |

[a]Profilin was found with only one unique peptide and thus is not reported in the Supporting Information file.

The hydrophobic seed proteins are a group of proteins with low molecular weight which belong to the lipid transfer proteins (LTP) family,[28] the role of which is to transport the phospholipids from liposomes to mitochondria. It has been observed that these proteins are responsible for soybean epidemic asthma,[29] but they are not responsible for asthma that affects the workers of intermediate products of the soybean, which is instead due to proteins at higher molecular weight.[30]

Profilin 1 and profilin 2 are proteins involved in the growth process of actin microfilaments and belong to a group of structural and metabolic proteins. The sequences that are capable of binding to IgE are maintained in all the proteins belonging to the family of profilin. They are the main cause of the allergic response to pollen. Rihs et al.[31] have shown that the ability of profilin to bind IgE depends on the structural and conformational integrity.

Stress-induced protein SAM22 belongs to the BetVI family. It is involved in defense response of the plant. This protein is the leading cause of allergy to soybean in patients with birch pollinosis. Mittag et al.,[32] through a clinical investigation, revealed that 96% of patients reacting to *Bet v* 1 have also *Glym* 4-specific IgE and that 64% of them recognized other soybean proteins.

Beta-conglycinin is a seed storage glycoprotein which is accumulated during the seed growth and stored in order to be later hydrolyzed and used as a source of carbon and nitrogen atoms for the plant. The alpha-subunit of beta-conglycinin is responsible for the allergic response.[33]

The 34 kDa maturing seed protein, also known as P34, is considered a major allergenic protein of soybean seeds.[34] It belongs to the peptidase C1 family and is involved in the hydrolysis of peptide bonds by a mechanism in which the sulfide group of an amino acid residue of the protein behaves as a nucleophile.

Glycinin is the most widespread storage protein in soybean, as well as one of the major allergens. The glycinin belongs to the globulins family, and as the Beta-conglycinin, each subunit is composed of an acidic and a basic chain. Pedersen et al.[35] reported IgE-binding to all of the native acidic subunits of glycinin but little or none to the basic subunits.

2S albumin is also a storage protein, but it belongs to the 2S seed storage albumins family and is formed by two chains linked by a disulfide bridge. As LTP, it is classified in the prolamin superfamily having a similar structure of alpha helices. The allergenicity of this protein also depends on this similarity.

Lectin is a protein found in the seeds of plants, mainly of leguminous plants. It is formed by four subunits, 30 kDa each, and it is able to bind sugars. It is involved in carbohydrate recognition by a virus membrane and plays an important role in the immune system of plants. Barnett et al.[36] have investigated the possible role of lectin binding of IgE in RAST of legume and wheat extracts. They reported that there was significant immune binding of some of the lectins by specific IgE, and they concluded that these lectins may be important in expression of IgE-mediated allergic responses.

Trypsin inhibitor A belongs to the protease inhibitor I3 (leguminous Kunitz-type inhibitor) family, and it has endopeptidase and protease inhibitor activity. This protein is part of the defense system of the plant. Hypersensitivity to trypsin inhibitor is also documented by inhalation and was reported for the first time on soybean mill workers. Quirce et al.[37] have shown a relationship between a skin and a bronchial response to purified soybean KTI and work-related asthma in two bakers who were occupationally exposed to soybean flour.

Despite their well-documented allergenicity, soybean derivatives continue to be increasingly used in a variety of food products due to their well-documented health benefits. In this context, the knowledge of the protein profile of the soybean milk becomes important for a conscious consumption. We believe that proteomics should be considered a powerful tool in the functional characterization of the proteome as well as in the assessment of food safety. Indeed proteomic analysis could help to define specific allergenic proteins present in complex matrices, such as soybean seeds or soybean milk.

## ■ ASSOCIATED CONTENT

### Supporting Information

Proteins identified in soybean seeds, soybean milk, and soybean milk by precipitation; GO terms pie charts: GO annotation in biological process, cellular component and molecular function of the 243 nonredundant identified proteins and relative distribution of the seeds proteins, soybean proteins and precipitated soybean milk proteins; result of BLAST search in Uniprot. This material is available free of charge via the Internet at http://pubs.acs.org.

## ■ AUTHOR INFORMATION

### Corresponding Author

*E-mail: chiara.cavaliere@uniroma1.it. Fax: +39 06 490631. Phone: +39 06 49913834.

### Notes

The authors declare no competing financial interest.

## ■ ACKNOWLEDGMENTS

We thank Consorzio Agrario dell'Emilia (Società Cooperativa, San Giorgio di Piano, BO, Italy), Dr. (Dott.) Stefano Monari and Dr. (Dott.ssa) Silvia Forapani for the kind donation of soybean seeds and soybean milk employed in this study.

## ■ ABBREVIATIONS USED

2D-PAGE, two-dimensional polyacrylamide gel electrophoresis; AGC, automatic gain control; DTT, dithiothreitol; fwhm, full width at half-maximum; GO, gene ontology; IAA, iodoacetamide; LTP, lipid transfer protein; PBs, protein bodies; RT, room temperature; SDS, sodium dodecyl sulfate; SPE, solid phase extraction; TCA, trichloroacetic acid; TFA, trifluoroacetic acid

## REFERENCES


(1) Paucar-Menacho, L. M.; Amaya-Farfán, J.; Berhow, M. A.; Mandarino, J. M. G.; Mejia, E. G.; Chang, Y. K. A high-protein soybean cultivar contains lower isoflavones and saponins but higher minerals and bioactive peptides than a low-protein cultivar. *Food Chem.* **2010**, *120*, 15−21.

(2) Cavaliere, C.; Cucci, F.; Foglia, P.; Guarino, C.; Samperi, R.; Laganà, A. Flavonoid Profile in Soybeans by High Performance Liquid Chromatography−Tandem Mass Spectrometry. *Rapid Commun. Mass Spectrom.* **2007**, *21*, 2177−2187, DOI: 10.1002/rcm.3049.

(3) Derbyshire, E.; Wright, D. J.; Boulter, D. Legumin and vicilin storage protein of legume seeds. *Phytochem.* **1976**, *15*, 3−24.

(4) Spector, D.; Anthony, M.; Alexander, D.; Arab, L. Soy consumption and colorectal cancer. *Nutr. Cancer.* **2003**, *47*, 1−12.

(5) Badger, T. M.; Ronis, M. J. J.; Simmen, R. C. M.; Simmen, F. A. Soy protein isolate and protection against cancer. *J. Am. Coll. Nutr.* **2005**, *24*, 146S−149S.

(6) IUIS Allergen Nomenclature Sub-Committee. http://www.allergen.org/search.php?allergensource=Glycine+max (accessed July 2014).

(7) Kuppannan, K.; Julka, S.; Karnoup, A.; Dielman, D.; Schafer, B. 2DLC-UV/MS Assay for the Simultaneous Quantification of Intact Soybean Allergens Gly m 4 and Hydrophobic Protein from Soybean (HPS). *J. Agric. Food. Chem.* **2014**, *62*, 4884−4892.

(8) Holzhauser, T.; Wackermann, O.; Ballmer-Weber, B. K.; Bindslev-Jensen, C.; Scibilia, J.; Perono-Garoffo, L.; Utsumi, S.; Poulsen, L. K.; Vieths, S. Soybean (Glycine max) allergy in Europe: Gly m (*β*-conglycinin) and Gly m 6 (glycinin) are potential diagnostic markers for severe allergic reactions to soy. *J. Allergy Clin. Immunol.* **2009**, *123*, 452−458.

(9) Kuo, H. Y.; Chen, S. H.; Yeh, A. I. Preparation and Physicochemical Properties of Whole-Bean Soymilk. *J. Agric. Food Chem.* **2014**, *62*, 742−749.

(10) Magni, C.; Ballabio, C.; Restani, P.; Sironi, E.; Scarafoni, A.; Poiesi, C.; Duranti, M. Two-dimensional electrophoresis and Western-blotting analyses with anti Ara h 3 basic subunit IgG evidence the cross-reacting polypeptides of *Arachis hypogaea*, *Glycine max*, and *Lupinus albus* seed proteomes. *J. Agric. Food. Chem.* **2005**, *53*, 2275−2281.

(11) Herman, E. M.; Helm, R. M.; Jung, R.; Kinney, A. J. Genetic modification removes an immunodominant allergen from soybean. *Plant Physiol.* **2003**, *132*, 36−43.

(12) Hajduch, M.; Ganapathy, A.; Stein, J. W.; Thelen, J. J. A systematic proteomic study of seed filling in soybean. Establishment of high-resolution two-dimensional reference maps, expression profiles, and an interactive proteome database. *Plant Physiol.* **2005**, *137*, 1397−1419.

(13) Mooney, B. P.; Thelen, J. J. High-throughput peptide mass fingerprinting of soybean seed proteins: automated workflow and utility of UniGene expressed sequence tag databases for protein identification. *Phytochem.* **2004**, *65*, 1733−1744.

(14) Natarajan, S.; Xu, C.; Caperna, T. J.; Garret, W. M. Comparison of protein solubilization methods suitable for proteomic analysis of soybean seed proteins. *Anal. Biochem.* **2005**, *342*, 214−220.

(15) Gomes, L. S.; Senna, R.; Sandim, V.; Silva-Neto, M. A. C.; Perales, J. E. A.; Zingali, R. B.; Soares, M. R.; Fialho, E. Four Conventional Soybean [*Glycine max* (L.) Merrill] Seeds Exhibit Different Protein Profiles As Revealed by Proteomic Analysis. *J. Agric. Food Chem.* **2014**, *62*, 1283−1293.

(16) Natarajan, S.; Luthria, D.; Bae, H.; Lakshman, D.; Mitra, A. Transgenic soybeans and soybean protein analysis: an overview. *J. Agric. Food Chem.* **2013**, *61*, 11736−11743.

(17) Bradford, M. M. A rapid and sensitive method for the quantitation of microgram quantities of protein utilizing the principle of protein dye binding. *Anal. Biochem.* **1976**, *72*, 248−253.

(18) Searle, B. C. Scaffold: a bioinformatic tool for validating MS/MS-based proteomic studies. *Proteomics* **2010**, *10*, 1265−1269.

(19) Nesvizhskii, A. I.; Kolker, E.; Aebersold, R. Empirical statistical model to estimate the accuracy of peptide identifications made by MS/MS and database search. *Anal. Chem.* **2002**, *74*, 5383−5392.

(20) Nesvizhskii, A. I.; Keller, A.; Kolker, E.; Aebersold, R. A statistical model for identifying proteins by tandem mass spectrometry. *Anal. Chem.* **2003**, *75*, 4646−4658.

(21) Berg, M.; Parbel, A.; Pettersen, H.; Fenyö, D.; Björkesten, L. Reproducibility of LC-MS-based protein identification. *J. Exp. Bot.* **2006**, *57*, 1509−1514.

(22) Murad, A. M.; Rech, E. L. NanoUPLC-MS$^E$ proteomic data assessment of soybean seeds using the Uniprot database. *BMC Biotechnol.* **2012**, *12*, 82.

(23) Miernyk, J. A.; Johnston, M. L. Proteomic analysis of the testa from developing soybean seeds. *J. Proteomics* **2013**, *89*, 265−72.

(24) Roberts, R. C.; Briggs, D. R. Isolation and characterization of the 7S component of soybean globulins. *Cereal Chem.* **1965**, *42*, 71−85.

(25) Hill, J. E.; Breidenbach, R. W. Proteins of soybean seeds. II. Accumulation of the major protein components during seed development and maturation. *Plant Physiol.* **1974**, *53*, 747−751.

(26) Thanh, V. H.; Shibasaki, K. Heterogeneity of beta-conglycinin. *Biochim. Biophys. Acta* **1976**, *181*, 404−409.

(27) Liu, H.; Sadygov, R. G.; Yates, J. R., III A model for random sampling and estimation of relative protein abundance in shotgun proteomics. *Anal. Chem.* **2004**, *76*, 4193−4201.

(28) Gonzalez, R.; Varela, J.; Carreira, J.; Polo, F. Soybean hydrophobic protein and soybean hull allergy. *Lancet* **1995**, *346*, 48−49.

(29) Gonzalez, R.; Polo, F.; Zapatero, L.; Caravaca, F.; Carreira, J. Purification and characterization of major inhalant allergens from soybean hulls. *Clin. Exp. Allergy* **1992**, *22*, 748−755.

(30) Quirce, S.; Polo, F.; Figueredo, E.; Gonzalez, R.; Sastre, J. Occupational asthma caused by soybean flour in bakers-difference with soybean-induced epidemic asthma. *Clin. Exp. Allergy* **2000**, *30*, 839−846.

(31) Rihs, H. P.; Chen, Z.; Rueff, F.; Petersen, A.; Rozynek, P.; Heimann, H.; Baur, X. IgE binding of the recombinant allergen soybean profilin (rGly m 3) is mediated by conformational epitopes. *J. Allergy Clin. Immunol.* **1999**, *104*, 1293−1301.

(32) Mittag, D.; Vieths, S.; Vogel, L.; Becker, W. M.; Rihs, H. P.; Helbling, A.; Wuthrich, B.; Ballmer-Weber, B. K. Soybean allergy in patients allergic to birch pollen: clinical investigation and molecular characterization of allergens. *J. Allergy Clin. Immunol.* **2004**, *113*, 148−154.

(33) Ogawa, T.; Bando, N.; Tsuji, H.; Nishikawa, K.; Kitamura, K. *α*-Subunit of *β*-conglycinin, an allergenic protein recognised by IgE antibodies of soybean-sensitive patients with atopic dermatitis. *Biosci. Biotechnol. Biochem.* **1995**, *59*, 831−833.

(34) Yaklich, R. W.; Helm, R. M.; Cockrell, G.; Herman, E. M. Analysis of the distribution of the major soybean seed allergens in a core collection of Glycine max accessions. *Crop Sci.* **1999**, *39*, 1444−1447.

(35) Pedersen, H. S.; Djurtoft, R. Antigenic and allergenic properties of acidic and basic peptide chains from glycinin. *Food Agric. Immunol.* **1989**, *1*, 101−109.

(36) Barnett, D.; Howden, M. E. H. Lectins and the radio-allergosorbent test. *J. Allergy Clin. Immunol.* **1987**, *80*, 558−561.

(37) Quirce, S.; Fernandez-Nieto, M.; Polo, F.; Sastre, J. Soybean trypsin inhibitor is an occupational inhalant allergen. *J. Allergy Clin. Immunol.* **2002**, *109*, 178.

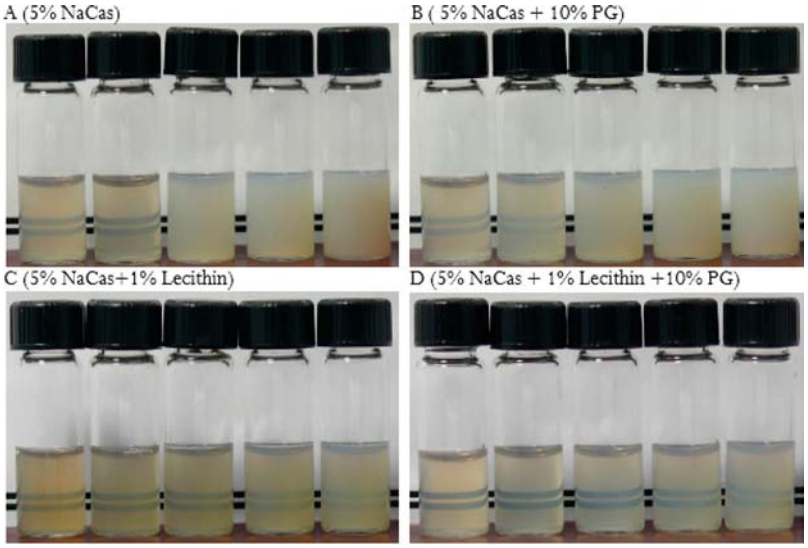


**Figure 1.** Appearance of thyme oil nanoemulsions prepared with various combinations of 5% w/v NaCas, 10% v/v PG, and 1% w/v lecithin. Thyme oil concentration in each image is 0.5, 1.0, 1.5, 2.0, and 2.5% w/v from left to right.

**Preparation of Emulsions.** NaCas was hydrated at 5% w/v in deionized water overnight at room temperature (21 °C). Four sets of thyme oil emulsions were prepared. In the first set, different amounts of thyme oil (0.5, 1.0, 1.5, 2.0, and 2.5% w/v) were directly emulsified in 10 mL of NaCas solution (9 mL of 5% NaCas and 1 mL of deionized water) at 15,000 rpm for 3 min using a model Cyclone I.Q.$^2$ microprocessor homogenizer (The VirTis Company, Inc., Gardiner, NY). In the second set, same amounts of thyme oil were dissolved in 1 mL of PG, which was then mixed with 9 mL of the 5% w/v NaCas solution and emulsified as above. In the third set, 0.1 g of lecithin was added into 9 mL of the 5% w/v NaCas solution, vortexed for 30 min, and then mixed with thyme oil and homogenized as in the first set. In the fourth set, lecithin was mixed with the NaCas solution as in the third set, and thyme oil predissolved in PG was homogenized as in the second set. Emulsions as prepared in the fourth set were also studied for NaCas (2.5% and 5% w/v) and lecithin (0, 0.5, and 1.0% w/v) concentrations in the aqueous phase.

**Turbidity.** The absorbance of thyme oil emulsions was measured at 600 nm ($Abs_{600}$) as an indicator of turbidity using a UV−vis spectrophotometer (model Biomate 5, Thermo Electron Corp., Woburn, MA).

**Particle Size and Zeta Potential Measurements.** The dynamic light scattering experiments were conducted using a Delas Nano-Zeta Potential and submicron particle size analyzer (Beckman Coulter, Inc., Brea, CA). The emulsion samples were diluted 20 times in 0.01 M phosphate-buffered saline (PBS, pH 7) at ambient temperature prior to analysis. The zeta potentials of thyme oil emulsions were measured using the same instrument for samples diluted 100 times in deionized water and adjusted to pH 7.0. Two emulsion replicates were tested three times each.

**Atomic Force Microscopy (AFM).** The morphology of thyme oil emulsions was characterized using a Multimode VIII microscope (Bruker Corp., Santa Barbara, CA). Emulsions containing 1% thyme oil prepared with NaCas and lecithin were diluted $10^5$ times using 0.01 M PBS at pH 7. Four microliters of each sample was spread evenly onto a freshly cleaved mica sheet that was mounted on a sample disk (Bruker Corp., Santa Barbara, CA) and air-dried for >2 h. The samples were scanned using a rectangular cantilever probe (Bruker Nanoprobe, Camarillo, CA) with aluminum reflective coating on the back side and a quoted force constant of 2.80 N/m. The topography images were collected at the tapping mode.

**Quantification of Protein Surface Load.** The amount of NaCas on thyme oil droplet surface was quantified to investigate the effect of lecithin on surface adsorption of NaCas. To facilitate the separation of oil droplets, an excess amount (10% w/v) of thyme oil was directly emulsified in the aqueous phase with various combinations of NaCas (0, 2.5, and 5% w/v) and lecithin (0, 0.5, and 1.0% w/v). Particle sizes were measured right after homogenization and after storage at room temperature (21 °C) for 15 days. Emulsions before and after storage were centrifuged at 12550*g* for 60 min using an Eppendorf MiniSpin plus centrifuge (Hamburg, Germany). The bottom aqueous phase was filtrated through a 0.22 $\mu$m polyvinyl difluoride membrane filter. To minimize the interference of thyme oil compounds such as thymol on protein assay, 50 $\mu$L of the permeate was mixed with 500 $\mu$L of an acetone−hexane (1:1, v:v) mixture[29] to extract thyme oil and precipitate protein. After vigorous mixing and centrifugation at 6700*g* for 10 min, the supernatant (organic phase) was discarded, and the bottom protein precipitate was redissolved in 600 $\mu$L of 100 mM NaOH and was quantified using the bicinchoninic acid (BCA) method (Thermo Fisher Scientific Inc., Morris Plains, NJ). NaCas was used as a reference protein in the BCA assay. The surface load ($\Gamma_s$, mg/m$^2$) of protein and the volume−area ($d_{3,2}$) mean diameters were calculated using eq 1 and 2, respectively.

$$\Gamma_s = \frac{M_s d_{3,2}}{6V_{oil}} \quad (1)$$

where $M_s$ is the mass of NaCas adsorbed on oil droplets, and $V_{oil}$ is the volume of thyme oil. The thymol oil density used in calculation was 0.932 g/mL.[30]

$$d_{3,2} = \frac{\sum_{i=1} n_i d_i^3}{\sum_{i=1} n_i d_i^2} \quad (2)$$

where $d_i$ is the diameter of the $i$th group of droplets and $n_i$ is the corresponding number of droplets.

**Statistical Analysis.** Two independent emulsion replicates were studied throughout. Analysis of variance (ANOVA) testing was conducted using the SPSS 16.0 statistical analysis system (SPSS Inc., Chicago, IL). The least significant difference (LSD) test was used to determine the significant difference of mean values at a $P$ level of 0.05.

## RESULTS AND DISCUSSION

**Turbidity of Emulsions.** Photographs of thyme oil emulsions prepared with various combinations of 5% w/v NaCas, 1% w/v lecithin, and 10% v/v PG are shown in Figure 1. The treatments with 5% w/v NaCas alone and its combination with 10% v/v PG were only capable of emulsifying 1.0% w/v thyme oil as transparent or translucent dispersions. In comparison, after addition of 1% w/v lecithin, emulsions with


dx.doi.org/10.1021/jf5034366 | J. Agric. Food Chem. 2014, 62, 9900−9907

up to 2.5% w/v thyme oil were translucent when prepared with 5% w/v NaCas, and the clarity further improved with 10% v/v PG. The appearance generally agreed with the $Abs_{600}$ (Figure 2). Since PG is fully miscible with water, predissolving thyme

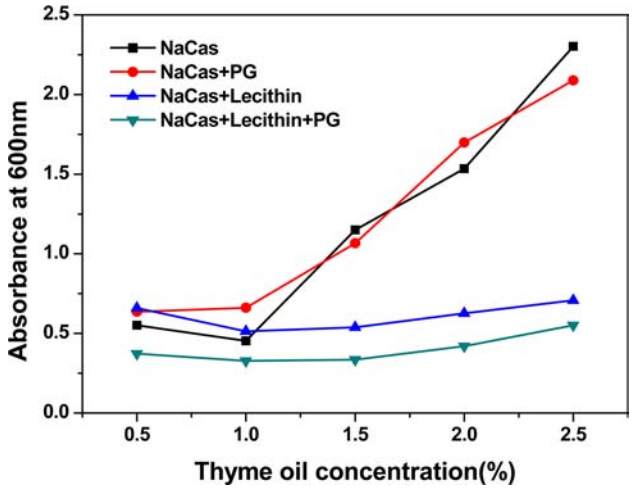


**Figure 2.** Absorbance at 600 nm of nanoemulsions with 0.5−2.5% w/v thyme oil prepared with various combinations of 5% w/v NaCas, 10% v/v PG, and 1% w/v lecithin.

oil in PG before emulsification likely reduces the oil/water interfacial tension, which is a main mechanism of cosurfactants facilitating the formation of nanoemulsions.[31] Furthermore, PG had no significant impact on emulsion formation by NaCas but facilitated emulsion formation for the NaCas−lecithin blend. This is likely due to the impacts on solubility of surfactants: NaCas is water-soluble, while lecithin (phosphatidylcholines) is not.

Subsequently, two concentrations (1.0 and 2.0% w/v) of thyme oil were emulsified using various combinations of NaCas (2.5% w/v) and lecithin (0.5 or 1% w/v) concentrations. Photographs are shown in Figure 3, while the $Abs_{600}$ is

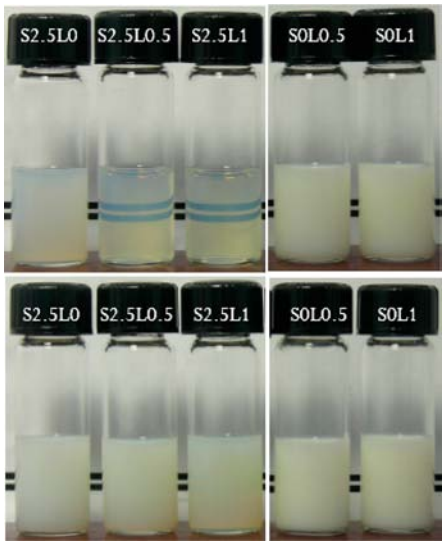


**Figure 3.** Appearance of nanoemulsions with 1.0% w/v (top) or 2.0% w/v (bottom) thyme oil emulsified by 2.5% w/v NaCas, 0.5 or 1% w/v lecithin, or both. All samples contained 10% v/v PG. Labels on vial caps: S, NaCas; L, lecithin; numbers, surfactant concentrations.

compiled in Table 1. With 1.0% w/v thyme oil, emulsions prepared with combinations of NaCas and lecithin were all

**Table 1. Absorbance at 600 nm of 1 or 2% w/v Thyme Oil Emulsified by 2.5% w/v NaCas and 0−1.0% w/v Lecithin[a]**

| thyme oil (% w/v) | lecithin (% w/v) | $Abs_{600}$ |
|---|---|---|
| 1.0 | 0 | 1.48 ± 0.14 c |
| 1.0 | 0.5 | 0.30 ± 0.01 d |
| 1.0 | 1.0 | 0.27 ± 0.01 d |
| 2.0 | 0 | 2.44 ± 0.10 a |
| 2.0 | 0.5 | 2.21 ± 0.16 b |
| 2.0 | 1.0 | 1.35 ± 0.01 c |

[a]All samples contained 10% v/v PG. Numbers are mean ± standard deviation from duplicates. Different letters represent significant differences in the mean.

transparent, while those with 2.5% NaCas or (0.5 or 1.0% w/v) lecithin alone were turbid. As thyme oil concentration increased to 2.0% w/v, all samples were turbid. The $Abs_{600}$ of thyme oil emulsions in Table 1 showed that addition of lecithin significantly decreased the turbidity of thyme oil emulsions prepared with NaCas ($P < 0.05$).

**Hydrodynamic Diameters of Emulsions.** Mean hydrodynamic diameters of thyme oil emulsions are compiled in Table 2. Emulsions prepared with NaCas−lecithin blend had significantly smaller particles than those prepared with NaCas or lecithin alone ($P < 0.05$). For example, compared to treatments with 1.0% w/v thyme oil emulsified by 1.0% w/v lecithin (mean diameter = 179.7 nm) or 5.0% w/v NaCas alone (mean diameter = 105.5 nm), the corresponding nanoemulsion prepared with the NaCas−lecithin blend had much smaller droplets with a mean diameter of 66.6 nm ($P < 0.05$). These results were consistent with the visual appearance (Figure 3) and $Abs_{600}$ (Table 1). Similar results have been reported for emulsions made with blends of NaCas and sucrose esters (with lipids being mono-, di-, and tristearate or palmitate).[35] Small molecular weight surfactants may coadsorb with NaCas or displace NaCas on droplet surfaces and therefore alter the composition and properties of interfaces, and the reduction of interfacial tension may facilitate the formation of smaller droplets.[32]

**Emulsion Structures Studied by AFM.** Emulsions containing 1.0% w/v thyme oil prepared with 2.5% w/v NaCas, 0.5% w/v lecithin, or both were imaged using AFM (Figure 4). Relatively bigger particles were observed for the emulsions prepared with NaCas or lecithin alone (Figures 4A and 4B) when compared to the treatment prepared with the surfactant blend (Figure 4C). The average particle dimension estimated in AFM was 134.3, 147.3, and 76.9 nm for emulsions prepared with NaCas only, lecithin only, and both, respectively. These results were generally in agreement with those obtained using dynamic light scattering (Table 2).

**Zeta-Potential of Emulsions.** Zeta-potentials of emulsions prepared with 1.0% w/v thyme oil emulsified by NaCas alone, lecithin alone, and their blend were measured at pH 7 (Table 3). The emulsion prepared with 1% w/v lecithin only had a highly negative zeta-potential (−58.2 ± 1.2 mV), which is attributed to the phosphate group of lecithin.[33] In comparison, the zeta-potential of the emulsion prepared with 2.5% w/v NaCas only had a significantly smaller magnitude (−25.8 ± 6.8 mV) than that with lecithin only ($P < 0.05$). When 5% w/v NaCas was used in homogenization, the zeta-potential


dx.doi.org/10.1021/jf5034366 | J. Agric. Food Chem. 2014, 62, 9900−9907

**Table 2. Mean Hydrodynamic Diameters (nm) of 1% and 2% w/v Thyme Oil Emulsified by NaCas, Lecithin, or Both, before and after Storage at Room Temperature for 120 Days[a]**

| | | hydrodynamic diam (nm) | | | | | |
|---|---|---|---|---|---|---|---|
| | | 0% NaCas | | 2.5% w/v NaCas | | 5.0% w/v NaCas | |
| thyme oil (% w/v) | lecithin (% w/v) | day 0 | day 120 | day 0 | day 120 | day 0 | day 120 |
| 1.0 | 0 | N/A | N/A | 150.2 ± 6.6 c | N/A | 105.5 ± 3.5 d | N/A |
| | 0.5 | 177.5 ± 3.0 bc | 188.5 ± 2.4 abc | 77.1 ± 5.4 fg | 80.7 ± 0.7 efg | 74.7 ± 0.4 fg | 75.4 ± 1.0 fg |
| | 1.0 | 179.7 ± 2.2 bc | 203.6 ± 5.9 a | 67.5 ± 0.8 g | 83.9 ± 13.7[efg] | 66.6 ± 2.1 g | 71.8 ± 4.5 g |
| 2.0 | 0 | N/A | N/A | 206.5 ± 10.5 a | N/A | 180.7 ± 12.6 bc | N/A |
| | 0.5 | 170.3 ± 2.9 c | 184.3 ± 6.0 abc | 115.9 ± 10.1 d | 113.0 ± 0.8 d | 79.1 ± 1.8 efg | 86.1 ± 10.6 efg |
| | 1.0 | 177.7 ± 4.6 bc | 196.3 ± 11.5 ab | 95.2 ± 2.4 def | 101.6 ± 4.9 de | 68.4 ± 2.3 g | 72.7 ± 1.7 fg |

[a]All samples contained 10% v/v PG. Numbers are mean ± standard deviation from duplicates. Different letters represent significant differences in the mean.

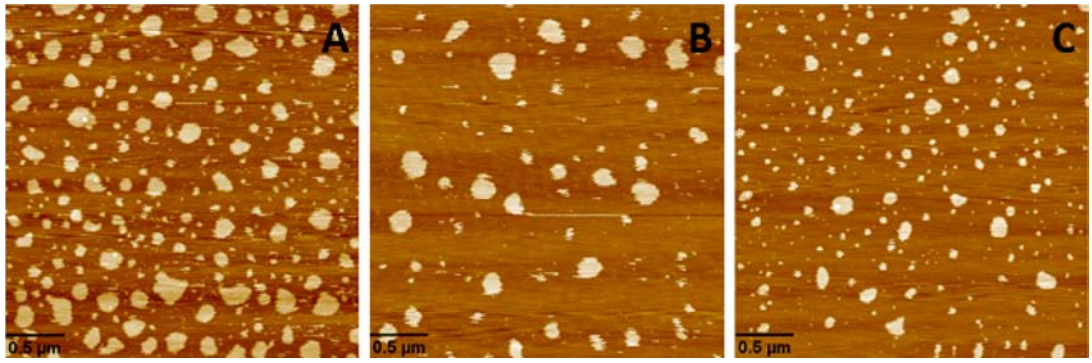


**Figure 4.** AFM images of thyme oil (1.0% w/v) nanoemulsions prepared with 2.5% w/v NaCas (A), 0.5% w/v lecithin (B), or both (C). All samples contained 10% v/v PG.

**Table 3. Zeta-Potential (mV) of Thyme Oil (1.0% w/v) Nanoemulsions Prepared with NaCas with and without Lecithin at pH 7.0[a]**

| | zeta-potential (mV) | | |
|---|---|---|---|
| lecithin (% w/v) | 0% NaCas | 2.5% w/v NaCas | 5.0% w/v NaCas |
| 0 | | −25.8 ± 6.8 c | −39.7 ± 1.2 b |
| 1.0 | −58.2 ± 1.2[a] | −44.6 ± 2.6 b | −41.7 ± 2.4 b |

[a]All emulsions contained 10% v/v PG. Numbers are mean ± standard deviation from duplicates. Different letters represent significant differences in the mean.

magnitude (−39.7 ± 1.2 mV) was higher than that prepared with 2.5% NaCas and was close to the zeta-potential of NaCas solution,[34] which may suggest a significant amount of free NaCas in the aqueous phase. For the nanoemulsion prepared with 2.5% w/v NaCas and 1% w/v lecithin, the magnitude of zeta-potential (−44.6 ± 2.6 mV) was between those prepared with lecithin and NaCas alone. Since free NaCas was not removed, the zeta-potential data in Table 3 did not provide straightforward information about interfacial structures. It however should be noted that the electrostatic attraction between negatively charged phosphate group of lecithin and positively charged amine groups of NaCas is still possible at neutral acidity despite that both are overall negatively charged, as previously demonstrated for pectin and NaCas.[14]

**Effect of Lecithin on Surface Adsorption of NaCas.** The protein content on unit surface area of emulsion droplets ($\Gamma_s$, mg/m$^2$) is commonly determined to study the surface activity of proteins and the impacts by competing or coadsorbing surfactants. For 10% thyme oil emulsified by 2.5% w/v NaCas and 0−1% w/v lecithin, an increase in lecithin content decreased the droplet dimension but not the amount of adsorbed NaCas ($P > 0.05$), resulting in the reduced $\Gamma_s$ (Table 4). Because a larger surface area (smaller droplets) requires the coverage by a greater amount of surfactants, the data suggest the coadsorption of NaCas and lecithin. The $\Gamma_s$ did not change significantly after 15-day storage at 21 °C, suggesting that there was no detachment of NaCas. With the gradual increase in lecithin content, the droplet dimension decreased to near those prepared with lecithin only. Therefore, lecithin is more surface-active than NaCas in emulsifying thyme oil. For emulsions prepared with 5% w/v NaCas, the droplet size ($P < 0.05$) and the percentage of adsorbed NaCas ($P > 0.05$) were smaller than those for emulsions prepared with 2.5% NaCas, corresponding to similar $\Gamma_s$ ($P > 0.05$). The $\Gamma_s$ of treatments prepared with 5% w/v NaCas and 0 and 0.5% lecithin decreased ($P < 0.05$) after storage for 15 days. Because the droplet dimension of these two emulsions did not change after storage, the results indicated the detachment of NaCas. Conversely, the treatment prepared with 5% NaCas and 1% lecithin showed insignificant changes in both droplet dimension and $\Gamma_s$ ($P > 0.05$).

The competitive surface adsorption and possible displacement of NaCas by more surface-active lecithin are dependent on their overall concentrations and molar ratios.[22,35,36] In a study coemulsifying 20% w/w soybean oil by 0.2−2% w/w NaCas and lecithin at lecithin:casein molar ratios of 0.7:1−49:1,[22] the gradual reduction of $\Gamma_s$ of NaCas with increases in lecithin concentration was similar to the findings of the present study (Table 4), but their $\Gamma_s$ increased with increases in NaCas concentration and were all below 3.5 mg/m$^2$. The $\Gamma_s$ in the present study was much higher than that in ref 22 and was not significantly different at two (2.5 and 5% w/v) NaCas


dx.doi.org/10.1021/jf5034366 | J. Agric. Food Chem. 2014, 62, 9900−9907

Table 4. Volume−Area Mean Diameter $d_{3,2}$ (nm), Polydispersity Index, Percentage of Adsorbed NaCas, and Surface Load of NaCas in Emulsions with 10% w/v Thyme Oil Prepared with NaCas, Lecithin, or Both, before and after Storage at 21 °C for 15 Days[a]

| NaCas (% w/v) | lecithin (% w/v) | $d_{3,2}$ (nm) | | polydispersity index | | adsorbed NaCas (%) | | protein surface load ($\Gamma_s$ mg/m$^2$) | |
|---|---|---|---|---|---|---|---|---|---|
| | | day 0 | day 15 | day 0 | day 15 | day 0 | day 15 | day 0 | day 15 |
| 0 | 0.5 | 175.28 ± 6.97 c | 182.37 ± 7.32 c | 0.28 ± 0.02 ab | 0.27 ± 0.02 bc | N/A | N/A | N/A | N/A |
| | 1.0 | 163.14 ± 15.22 c | 161.38 ± 27.09 c | 0.23 ± 0.00 c | 0.22 ± 0.02 c | N/A | N/A | N/A | N/A |
| 2.5 | 0 | 307.96 ± 10.54 ab | 350.80 ± 12.12 a | 0.31 ± 0.02 ab | 0.30 ± 0.01 ab | 69.82 ± 3.36 a | 69.27 ± 0.33 a | 8.35 ± 0.40 ab | 9.43 ± 0.04 a |
| | 0.5 | 282.66 ± 12.89 b | 350.48 ± 8.65 a | 0.32 ± 0.01 a | 0.30 ± 0.01 ab | 68.56 ± 2.91 a | 64.50 ± 2.14 ab | 7.53 ± 0.32 abc | 8.78 ± 0.29 a |
| | 1.0 | 182.42 ± 8.52 c | 181.18 ± 19.96 c | 0.28 ± 0.01 ab | 0.29 ± 0.01 ab | 67.84 ± 1.23 a | 61.23 ± 0.22 abc | 4.81 ± 0.09 e | 4.31 ± 0.02 e |
| 5.0 | 0 | 172.93 ± 11.04 c | 170.64 ± 11.12 c | 0.28 ± 0.01 ab | 0.26 ± 0.01 bc | 64.15 ± 1.93 abc | 52.22 ± 2.13 cd | 8.62 ± 0.26 a | 6.92 ± 0.28 bcd |
| | 0.5 | 159.78 ± 9.82 c | 143.11 ± 13.98 c | 0.26 ± 0.02 bc | 0.26 ± 0.02 bc | 62.51 ± 1.32 abc | 48.68 ± 4.12 d | 7.75 ± 0.16 ab | 5.41 ± 0.46 de |
| | 1.0 | 144.02 ± 0.29 c | 143.53 ± 7.30 c | 0.27 ± 0.01 bc | 0.28 ± 0.02 ab | 54.64 ± 7.31 bcd | 46.67 ± 1.43 d | 6.11 ± 0.82 cde | 5.20 ± 0.16 e |

[a]Numbers are mean ± standard deviation from duplicates. Different letters represent significant differences in the mean.

concentrations (Table 4) although the lecithin:casein molar ratios (2.8−11.4:1) in this work were within their range. The differences in their and the present studies can result from differences in the droplet dimension (300−800 nm in ref 22), emulsification conditions, polarity of oil, and overall NaCas and lecithin concentrations. As for the interfacial structure, Fang and Dalgleish[22] proposed that the thickness of the adsorbed casein layer could increase when lecithin concentration increases gradually and, when there is a sufficient amount of lecithin, the oil droplets are directly covered mostly by lecithin that can be adsorbed by caseins protruding to the continuous aqueous phase. At their studied conditions, Fang and Dalgleish[22] did not observe surface displacement of NaCas by lecithin, which is mostly in agreement with the present study (Table 4). However, in our case, $\Gamma_s$ decreased for nanoemulsions prepared with 5% w/v NaCas and 0 and 0.5% w/v lecithin that also showed a decrease in droplet dimension after storage (Table 4). Since the thickness of the NaCas layer increases with its bulk concentration,[22] the observations from these two emulsions can result from the detachment of caseins rather than the displacement by lecithin. The speculation however requires experimental verifications.

**Emulsion Stability.** One common concern about essential oil nanoemulsions is their stability against Ostwald ripening because of the water solubility of essential oil components being higher than that of lipids composed of medium- or long-chain fatty acids.[31] Physically, compounds in smaller particles have a higher solubility, which results in the continuous dissolving and eventual disappearance of smaller particles, and the dissolved compounds join bigger particles that grow during storage.[37] Nonpolar substances such as corn oil[38] can be blended with essential oils in emulsion preparation to serve as inhibitors of Ostwald ripening.[31] Ripening inhibitors however lower the loading level and antimicrobial activity of essential oils.

Emulsions with 1 and 2% thyme oil were studied for storage stability at 21 °C for 120 days. Creaming was observed for emulsions prepared with NaCas alone after 2- or 3-day storage at room temperature and became more significant after longer storage. Creaming can be contributed by increases in overall particle dimension due to depletion flocculation (by unadsorbed NaCas) or particle growth due to coalescence and/or Ostwald ripening.[4] In contrast, nanoemulsions prepared with 1 and 2% thyme oil and NaCas−lecithin blend appeared transparent or translucent throughout storage.

When particle size distributions of emulsions prepared with lecithin only or NaCas−lecithin blend were compared before and after 4-month storage at room temperature (Figure 5), several trends were observed. Emulsions prepared with NaCas−lecithin blend exhibited smaller particles with narrower distributions than that prepared with lecithin only, indicating the better emulsifying activity of the blend. For these emulsions, the interfacial layer next to thyme oil is likely composed of both lecithin and NaCas, different from the model of sequential layers of lecithin and NaCas as proposed by Fang and Dalgleish[22] that would otherwise result in bigger droplets for emulsions prepared with both surfactants. The growth of particle size was observed for all emulsions, and the growth was much smaller for emulsions prepared with the blend than those with lecithin alone, suggesting the better stabilizing ability of the blend. The growth of average hydrodynamic diameter (Table 2) however was overall not statistically significant ($P > 0.05$).

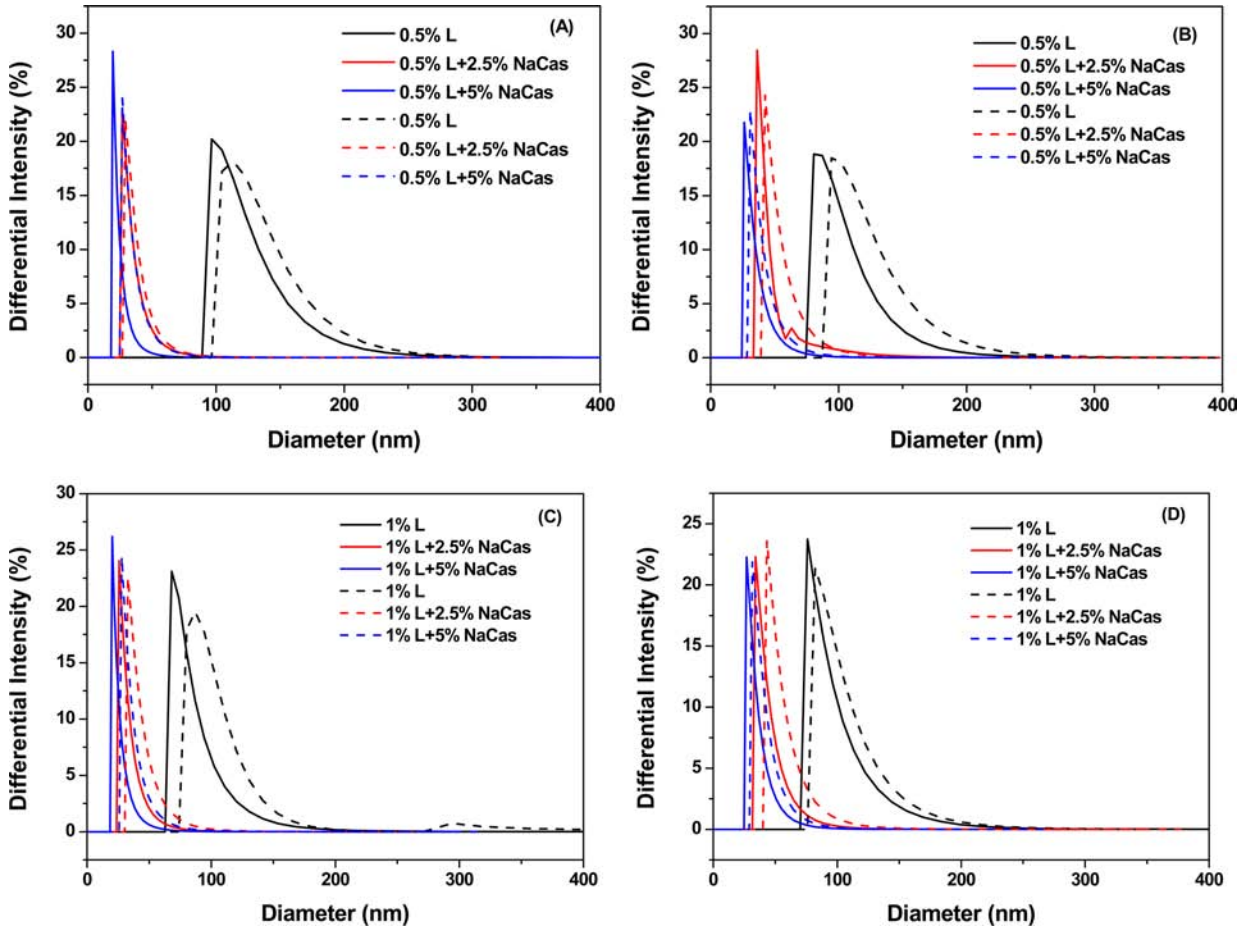


**Figure 5.** Particle size distributions of nanoemulsions with 1.0% w/v (A and C) or 2% w/v (B and D) thyme oil emulsified by lecithin and NaCas–lecithin blend before (solid curves) and after (dashed curves) storage at room temperature (21 °C) for 4 months.

In addition to Ostwald ripening discussed above, coalescence can also cause the growth of particles during storage, particularly for small molecular surfactants such as lecithin with a small headgroup.[39] Coalescence is initiated by the aggregation of two oil droplets controlled by colloidal interactions. In the present study, emulsions prepared with lecithin only had a higher magnitude of zeta-potential (Table 3) than those with the NaCas–lecithin blend. Since emulsions prepared with lecithin only and the NaCas–lecithin blend had insignificant increase in mean particle diameter (Table 2), it may suggest that the electrostatic repulsion is effective in preventing particle aggregation. The protrusion of NaCas in the continuous phase of emulsions prepared with the surfactant blend may have provided additional steric repulsion that resulted in smaller net growth of droplets after storage than emulsions prepared with lecithin only (Table 2). Similar phenomena were reported for orange oil emulsions prepared with lysolecithin and sucrose monopalmitate.[29] Therefore, it is likely that Ostwald ripening is the major mechanism responsible for particle growth of emulsions in the present study, and the narrower particle size distribution and thicker interface of emulsions prepared with the NaCas–lecithin blend both resulted in less significant particle size changes than those prepared with NaCas or lecithin only.

The stability of emulsions prepared with a mixture of proteins and small molecular surfactants has been widely studied. In some cases, the interaction or displacement between emulsifiers resulted in the significantly decreased stability. For example, combinations of caseinate and Tween 20 at certain ratios led to severe flocculation and creaming, which was attributed to the depletion flocculation by unabsorbed protein.[40] Combinations of lecithin with other small molecular surfactants also have been shown to improve the stability of emulsions. Lecithin added in emulsions stabilized by sucrose monopalmitate strengthened the electrostatic repulsion at acid conditions and resulted in the excellent stability of emulsions against Ostwald ripening, flocculation, and coalescence.[41] Emulsifying soybean oil by combinations of lecithin and nonionic steric surfactants such as polyethylene glycol hexadecyl ether (Brij) increased the stability of emulsions at increased ionic strengths when compared to those prepared with lecithin only.[42] This is because, although the surfactant blend reduced the zeta-potential magnitude of droplets when compared to those stabilized by lecithin, Brij provided steric repulsion to stabilize emulsions.[42]

In summary, technological advancement has been shown in the present work for stable and transparent thyme oil nanoemulsions prepared using combinations of GRAS emulsifiers NaCas and lecithin. These transparent nanoemulsions had mean diameters smaller than ~100 nm at neutral pH. The clearer and smaller droplets of nanoemulsions prepared with the NaCas–lecithin blend than those with individual surfactants suggested that NaCas and lecithin synergistically emulsified thyme oil rather than the preferential adsorption and displacement of NaCas by more surface-active lecithin. The interface composed of both NaCas and lecithin


dx.doi.org/10.1021/jf5034366 | J. Agric. Food Chem. 2014, 62, 9900–9907

provided repulsive electrostatic and also likely steric interactions against destabilization mechanisms of creaming, flocculation, and coalescence and, together with narrow particle size distributions, minimized Ostwald ripening. These transparent nanoemulsions prepared from GRAS ingredients have great potential to incorporate lipophilic antimicrobials such as thyme oil in transparent beverages to enhance the microbiological safety.

## AUTHOR INFORMATION


### Corresponding Author

*Department of Food Science and Technology, The University of Tennessee, 2510 River Drive, Knoxville, TN 37996. Phone: (865) 974-6196. Fax: (865) 974-7332. E-mail: qzhong@utk.edu.



### Funding

This work was supported by the University of Tennessee and the USDA National Institute of Food and Agriculture.


### Notes

The authors declare no competing financial interest.

## REFERENCES


(1) Rao, J.; McClements, D. J. Food-grade microemulsions, nanoemulsions and emulsions: Fabrication from sucrose monopalmitate & lemon oil. *Food Hydrocolloids* **2011**, *25*, 1413−1423.

(2) Relkin, P.; Jung, J.-M.; Ollivon, M. Factors affecting vitamin degradation in oil-in-water nano-emulsions. *J. Therm. Anal. Calorim.* **2009**, *98*, 13−18.

(3) Donsì, F.; Annunziata, M.; Sessa, M.; Ferrari, G. Nanoencapsulation of essential oils to enhance their antimicrobial activity in foods. *LWT—Food Sci. Technol.* **2011**, *44*, 1908−1914.

(4) McClements, D. J. *Food Emulsions: Principles, Practices and Techniques*; 2nd ed.; CRC Press: Boca Raton, FL, 2005.

(5) Holley, R. A.; Patel, D. Improvement in shelf-life and safety of perishable foods by plant essential oils and smoke antimicrobials. *Food Microbiol.* **2005**, *22*, 273−292.

(6) Weiss, J.; Gaysinsky, S.; Davidson, M.; McClements, J. Nanostructured encapsulation systems: food antimicrobials. In *Global Issues in Food Science and Technology*; Barbosa-Canovas, G. V., Mortimer, A., Lineback, D., Spiess, W., Buckle, K., Colonna, P., Eds.; Academic Press: London, England, 2009; pp 425−479.

(7) Smith-Palmer, A.; Stewart, J.; Fyfe, L. Antimicrobial properties of plant essential oils and essences against five important food-borne pathogens. *Lett. Appl. Microbiol.* **1998**, *26*, 118−122.

(8) Elgayyar, M.; Draughon, F.; Golden, D.; Mount, J. Antimicrobial activity of essential oils from plants against selected pathogenic and saprophytic microorganisms. *J. Food Prot.* **2001**, *64*, 1019−1024.

(9) Donsì, F.; Annunziata, M.; Vincensi, M.; Ferrari, G. Design of nanoemulsion-based delivery systems of natural antimicrobials: Effect of the emulsifier. *J. Biotechnol.* **2012**, *159*, 342−350.

(10) Kralova, I.; Sjöblom, J. Surfactants used in food industry: a review. *J. Dispersion Sci. Technol.* **2009**, *30*, 1363−1383.

(11) Liu, L.; Zhao, Q.; Liu, T.; Kong, J.; Long, Z.; Zhao, M. Sodium caseinate/carboxymethylcellulose interactions at oil−water interface: Relationship to emulsion stability. *Food Chem.* **2012**, *132*, 1822−1829.

(12) Dickinson, E. Caseins in emulsions: interfacial properties and interactions. *Int. Dairy J.* **1999**, *9*, 305−312.

(13) Dickinson, E.; Semenova, M. G.; Antipova, A. S. Salt stability of casein emulsions. *Food Hydrocolloids* **1998**, *12*, 227−235.

(14) Surh, J.; Decker, E. A.; McClements, D. J. Influence of pH and pectin type on properties and stability of sodium-caseinate stabilized oil-in-water emulsions. *Food Hydrocolloids* **2006**, *20*, 607−618.

(15) Dalgleish, D. G.; Srinivasan, M.; Singh, H. Surface properties of oil-in-water emulsion droplets containing casein and Tween 60. *J. Agric. Food Chem.* **1995**, *43*, 2351−2355.

(16) Dickinson, E.; McClements, D. J. *Advances in Food Colloids*; Springer: 1995.

(17) Hu, M.; McClements, D. J.; Decker, E. A. Lipid oxidation in corn oil-in-water emulsions stabilized by casein, whey protein isolate, and soy protein isolate. *J. Agric. Food Chem.* **2003**, *51*, 1696−1700.

(18) McClements, D. J. Protein-stabilized emulsions. *Curr. Opin. Colloid Interface Sci.* **2004**, *9*, 305−313.

(19) Hunt, J. A.; Dalgleish, D. G. Heat stability of oil in water emulsions containing milk proteins: effect of ionic strength and pH. *J. Food Sci.* **1995**, *60*, 1120−1123.

(20) van Nieuwenhuyzen, W.; Tomás, M. C. Update on vegetable lecithin and phospholipid technologies. *Eur. J. Lipid Sci. Technol.* **2008**, *110*, 472−486.

(21) Arnold, G.; Schuldt, S.; Schneider, Y.; Friedrichs, J.; Babick, F.; Werner, C.; Rohm, H. The impact of lecithin on rheology, sedimentation and particle interactions in oil-based dispersions. *Colloids Surf., B* **2012**, *418*, 147−156.

(22) Fang, Y.; Dalgleish, D. G. Casein adsorption on the surfaces of oil-in-water emulsions modified by lecithin. *Colloids Surf., B* **1993**, *1*, 357−364.

(23) Gaysinsky, S.; Davidson, P. M.; McClements, D. J.; Weiss, J. Formulation and characterization of phytophenol-carrying antimicrobial microemulsions. *Food Biophys.* **2008**, *3*, 54−65.

(24) Center for the Evaluation of Risks to Human Reproduction. NTP-CERHR Expert Panel report on the reproductive and developmental toxicity of propylene glycol. *J. Reprod. Toxicol.* **2004**, *18*, 533−579.

(25) El Maghraby, G. M. Transdermal delivery of hydrocortisone from eucalyptus oil microemulsion: effects of cosurfactants. *Int. J. Pharm.* **2008**, *355*, 285−292.

(26) Kale, N. J.; Allen, L. V., Jr Studies on microemulsions using Brij 96 as surfactant and glycerin, ethylene glycol and propylene glycol as cosurfactants. *Int. J. Pharm.* **1989**, *57*, 87−93.

(27) Rao, J.; McClements, D. J. Formation of flavor oil microemulsions, nanoemulsions and emulsions: influence of composition and preparation method. *J. Agric. Food Chem.* **2011**, *59*, 5026−5035.

(28) Xue, J.; Davidson, P. M.; Zhong, Q. Thymol nanoemulsified by whey protein-maltodextrin conjugates: The enhanced emulsifying capacity and anti-listerial properties in milk by propylene glycol. *J. Agric. Food Chem.* **2013**, *61*, 12720−12726.

(29) McClements, D. J.; Decker, E. A.; Choi, S. J. Impact of environmental stresses on orange oil-in-water emulsions stabilized by sucrose monopalmitate and lysolecithin. *J. Agric. Food Chem.* **2014**, *62*, 3257−3261.

(30) Wu, J.-E.; Lin, J.; Zhong, Q. Physical and antimicrobial characteristics of thyme oil emulsified with soluble soybean polysaccharide. *Food Hydrocolloids* **2014**, *39*, 144−150.

(31) McClements, D. J.; Rao, J. Food-grade nanoemulsions: formulation, fabrication, properties, performance, biological fate, and potential toxicity. *Crit. Rev. Food Sci. Nutr.* **2011**, *51*, 285−330.

(32) Tual, A.; Bourles, E.; Barey, P.; Houdoux, A.; Desprairies, M.; Courthaudon, J.-L. Effect of surfactant sucrose ester on physical properties of dairy whipped emulsions in relation to those of O/W interfacial layers. *J. Colloid Interface Sci.* **2006**, *295*, 495−503.

(33) Chuah, A. M.; Kuroiwa, T.; Kobayashi, I.; Nakajima, M. Effect of chitosan on the stability and properties of modified lecithin stabilized oil-in-water monodisperse emulsion prepared by microchannel emulsification. *Food Hydrocolloids* **2009**, *23*, 600−610.

(34) Chen, H.; Zhong, Q. Processes improving the dispersibility of spray-dried zein nanoparticles using sodium caseinate. *Food Hydrocolloids* **2014**, *35*, 358−366.

(35) Courthaudon, J. L.; Dickinson, E.; Christie, W. W. Competitive adsorption of lecithin and. beta.-casein in oil-in-water emulsions. *J. Agric. Food Chem.* **1991**, *39*, 1365−1368.

(36) Fang, Y.; Dalgleish, D. G. Competitive adsorption between dioleoylphosphatidylcholine and sodium caseinate on oil-water interfaces. *J. Agric. Food Chem.* **1996**, *44*, 59−64.

(37) Taylor, P. Ostwald ripening in emulsions. *Adv. Colloid Interface Sci.* **1998**, *75*, 107−163.

(38) Ziani, K.; Chang, Y.; McLandsborough, L.; McClements, D. J. Influence of surfactant charge on antimicrobial efficacy of surfactant-stabilized thyme oil nanoemulsions. *J. Agric. Food Chem.* **2011**, *59*, 6247−6255.
(39) Pan, L.; Tomás, M.; Añón, M. Effect of sunflower lecithins on the stability of water-in-oil and oil-in-water emulsions. *J. Surfactants Deterg.* **2002**, *5*, 135−143.
(40) Dickinson, E.; Ritzoulis, C.; Povey, M. J. Stability of emulsions containing both sodium caseinate and Tween 20. *J. Colloid Interface Sci.* **1999**, *212*, 466−473.
(41) Choi, S. J.; Decker, E. A.; Henson, L.; Popplewell, L. M.; Xiao, H.; McClements, D. J. Formulation and properties of model beverage emulsions stabilized by sucrose monopalmitate: Influence of pH and lyso-lecithin addition. *Food Res. Int.* **2011**, *44*, 3006−3012.
(42) De Vleeschauwer, D.; Van der Meeren, P. Colloid chemical stability and interfacial properties of mixed phospholipid−non-ionic surfactant stabilised oil-in-water emulsions. *Colloids Surf., A* **1999**, *152*, 59−66.

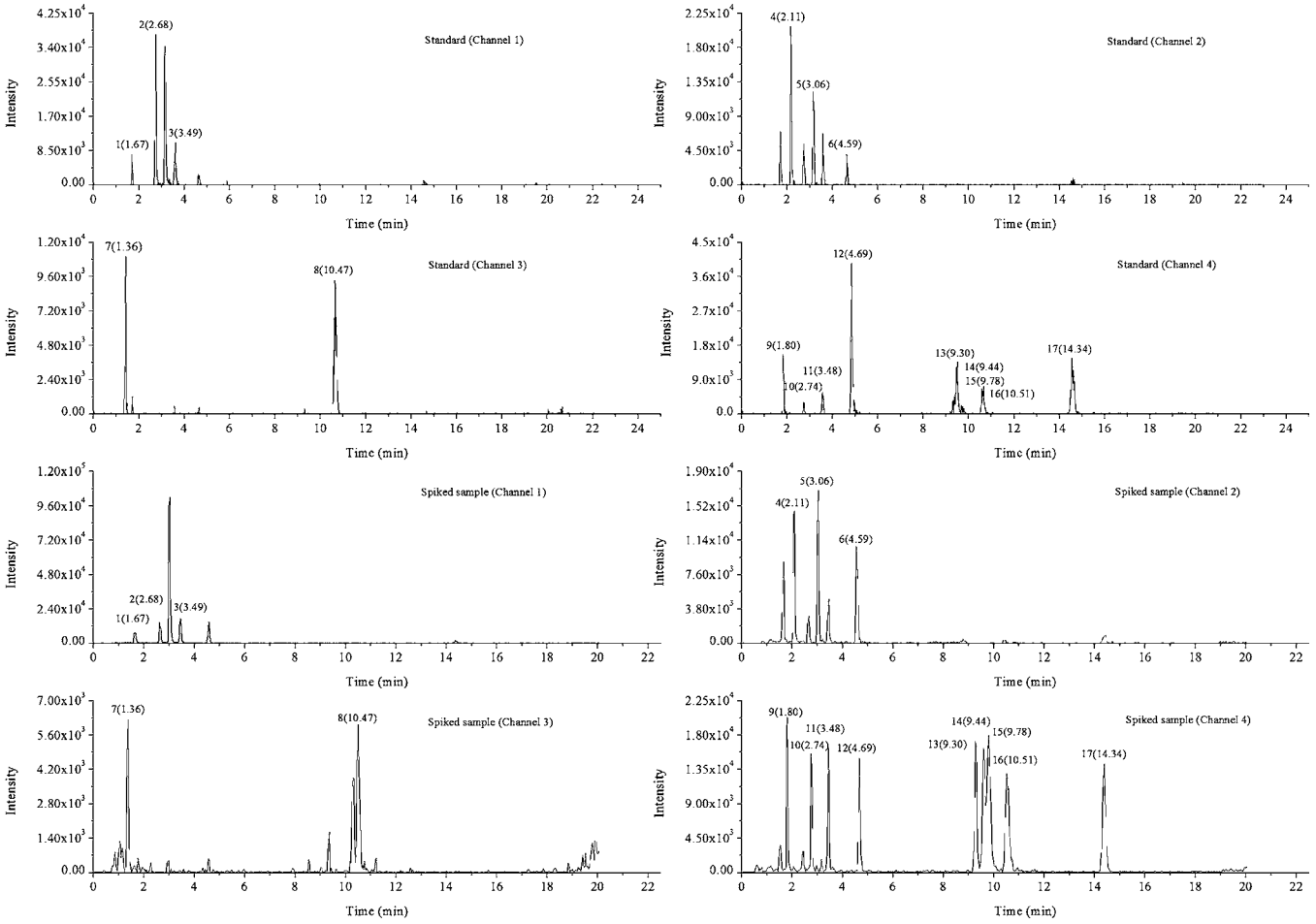


**Figure 1.** UPLC-MS/MS chromatograms of a standard solution (125 $\mu$g/mL) and a beef patty spiked with 180 $\mu$L of 30 ng/mL mixed standard solution containing all 17 HAs from all seven HA categories: **1**. IQ[4,5-*b*] ($m/z$ 199 → $m/z$ 184); **2**. MeIQ ($m/z$ 213→ $m/z$ 198); **3**. 4,8-DiMeIQx ($m/z$ 228 → $m/z$ 213); **4**. MeIQx ($m/z$ 214 → $m/z$ 199); **5**. 7,8-DiMeIQx ($m/z$ 228 → $m/z$ 187); **6**. IQ ($m/z$ 199 → $m/z$ 184); **7**. IQx ($m/z$ 200 → $m/z$ 185); **8**. A$\alpha$C ($m/z$ 184 → $m/z$ 167); **9**. DMIP ($m/z$ 163 → $m/z$ 148); **10**. 1,5,6-TMIP ($m/z$ 177 → $m/z$ 162); **11**. Glu-P-1($m/z$ 199 → $m/z$ 92); **12**. 4,7,8-TriMeIQx ($m/z$ 242 → $m/z$ 227); **13**. PhIP ($m/z$ 225 → $m/z$ 210); **14**. Harman ($m/z$ 183 → $m/z$ 115); **15**. Norharman ($m/z$ 169 → $m/z$ 115); **16**. Phe-P-1 ($m/z$ 171 → $m/z$ 127); **17**. MeA$\alpha$C ($m/z$ 198 → $m/z$ 181).

used to make a patty using a Petri dish (6 cm × 1.5 cm) to ensure uniformity. Neither fat nor oil was used for roasting. A RATIONAL SCC 61E Self-cooking Center (Landsberg, Munich, Germany) was used to roast (only dry heat) the beef patties. The hot plate was preheated for 5 min to 230 °C. The patties were put into the preheated oven, and roasted for 10 min on each side. The internal temperature was measured by inserting an accessary digital contact thermometer into the geometric center of each ground beef patty. The core temperature of the patties immediately after cooking was 85 °C. After completing the cooking processes, the beef patties were cooled at room temperature and the cooked meat samples were cut into small pieces, freeze-dried, and stored at −20 °C until used.

**Extraction of HAs.** The HAs were extracted using a modified method originally developed by Gross and Grueter.[20] Three grams of minced, freeze-dried meat was dissolved in 3 mL of 1 mol/L NaOH and homogenized for 1 min. The alkaline solution was mixed with 13 g of diatomaceous earth. Then, 50 mL of ethyl acetate was added and ultrasonic extracted twice for 30 min. The ethyl acetate extracts of the HAs were added into a Waters Oasis MCX cartridge, which was preconditioned with 6 mL of methanol, 6 mL of distilled water, and 6 mL of 0.1 mol/L HCl. The cartridge was sequentially rinsed with 6 mL of 0.1 mol/L HCl and 6 mL of methanol. The retained analytes were eluted with 6 mL of a methanol−ammonia (19:1, v/v) mixture. The eluted mixtures were evaporated to dryness under nitrogen, and the final extracts were dissolved in 250 $\mu$L of methanol just before measurement.

**Identification and Quantification of HAs.** The HAs were identified and quantified using an UPLC equipped with a triple quadripole mass spectrometer (Waters, Milford, MA, USA) using positive electrospray ionization. HA chromatography of HAs was performed on an ACQUITY UPLC BEH $C_{18}$ reversed-phase column (1.7 $\mu$m particle size, 2.1 mm × 50 mm) at 35 °C. The A solvent was 10 mM ammonium acetate (pH 6.8), and the B solvent was acetonitrile. The solvent composition was 0−0.1 min, 90% A; 0.1−18 min, 10−30% B; 18−20 min, 30−100% B; 20−20.1 min, 100−10% B. The flow rate was 0.3 $\mu$L/min, and the injection volume was 1 $\mu$L. The mass spectrometric detection was conducted in the multireaction monitoring (MRM) scan mode. The mass spectrometry operating conditions were capillary voltage 3.5 kV, ion source temperature 120 °C, and desolvation temperature 350 °C. The HAs were quantified with calibration curves of each kind of HA at eight calibrant levels, ranging from 0.2 to 30.0 ng/mL.

**Statistics.** Three independent repeated experiments were used for standard calibration. The averages from duplicate beef patties were calculated for each HA. Student's *t*-tests were performed in SPSS (SPSS Inc., Chicago, IL) to detect significant differences between the quantities of HA in the spiced and control beef patties. PCA was performed for visualizing the effects of spices on HA profiles. For PCA analysis, the contents of HAs that could be detected and quantified in all beef patties were employed to generate a data matrix, in which the rows and columns represent the observations (samples of beef patties with spices) and the variables (contents of HAs in the same

**Table 1. Working Linear Range, Calibration Curve, Determination Coefficients ($R^2$), Recoveries, Precision (% RSD), and LODs for the Quantification of 17 HAs from Seven Categories in the Spiked Beef Patties by UPLC-MS/MS[a]**

| category | compound | working linear range (ng/mL) | calibration curve[b] | determination coefficients ($R^2$) | recoveries (%) | precision (% RSD, $n$ = 3) | LOD (ng/mL) |
|---|---|---|---|---|---|---|---|
| $\alpha$-carbolines | A$\alpha$C | 0.8−193.9 | $y$ = 13.4767$x$ + 8.4644 | 0.9948 | 83.2 ± 0.9 | 1.08 | 0.34 |
| | MeA$\alpha$C | 2.2−550.0 | $y$ = 4.3739$x$ + 70.6418 | 0.9951 | 84.4 ± 13.3 | 15.78 | 4.39 |
| $\beta$-carbolines | Harman | 0.4−183.8 | $y$ = 15.9752$x$ − 17.2985 | 0.9973 | 106.6 ± 3.7 | 3.49 | 2.32 |
| | Norharman | 0.5−249.5 | $y$ = 12.4056$x$ − 6.9619 | 0.9997 | 108.4 ± 14.5 | 13.38 | 1.09 |
| $\delta$-carbolines | Glu-P-1 | 1.2−616.2 | $y$ = 7.3127$x$ − 17.2221 | 0.9992 | 59.5 ± 16.6 | 27.95 | 3.42 |
| imidazopyridines | PhIP | 0.9−442.5 | $y$ = 9.8884$x$ + 2.0035 | 0.9996 | 71.0 ± 6.9 | 9.72 | 0.57 |
| | DMIP | 0.8−424.5 | $y$ = 11.3769$x$ − 2.8979 | 0.9992 | 36.9 ± 3.0 | 8.23 | 0.48 |
| | 1,5,6-TMIP | 1.0−508.0 | $y$ = 4.9683$x$ − 26.9904 | 0.9917 | 68.6 ± 4.0 | 5.84 | 0.70 |
| imidazoquinolines | IQ | 4.3−411.0 | $y$ = 9.3589$x$ − 4.4315 | 0.9999 | 62.2 ± 4.3 | 6.94 | 2.81 |
| | MeIQ | 0.5−552.0 | $y$ = 10.5729$x$ − 13.6313 | 0.9993 | 75.6 ± 5.2 | 6.86 | 0.24 |
| | IQ[4,5-$b$] | 0.6−77.2 | $y$ = 46.1976$x$ − 0.1045 | 0.9998 | 62.6 ± 1.4 | 2.26 | 0.07 |
| imidazoquinoxalines | IQx | 2.1−1054.0 | $y$ = 4.3582$x$ − 2.4828 | 0.9997 | 54.2 ± 9.3 | 17.13 | 1.00 |
| | MeIQx | 1.0−517.0 | $y$ = 3.5604$x$ + 13.6990 | 0.9968 | 59.6 ± 2.9 | 4.80 | 0.68 |
| | 4,8-DiMeIQx | 0.5−131.5 | $y$ = 43.2758$x$ − 0.3099 | 0.9991 | 86.4 ± 13.2 | 15.23 | 0.29 |
| | 7,8-DiMeIQx | 4.3−511.9 | $y$ = 1.8635$x$ − 6.9893 | 0.9999 | 53.6 ± 6.5 | 12.20 | 9.81 |
| | 4,7,8-TriMeIQx | 0.5−259.5 | $y$ = 53.1091$x$ + 0.4951 | 0.9998 | 65.8 ± 4.0 | 6.02 | 0.38 |
| phenylpyridine | Phe-P-1 | 0.7−94.0 | $y$ = 33.2624$x$ + 6.2996 | 0.9995 | 95.9 ± 17.0 | 17.70 | 0.41 |

[a]Recoveries were performed by adding 70, 120, and 180 $\mu$L of 30 ng/mL mixed standard solutions to control samples. Recoveries were represented as means ± standard deviations ($n$ = 3). [b]Eight levels ($n$ = 3) of each kind of HAs were employed for calculating the calibration curve. $y$ is the peak area of HA, and $x$ is the corresponding concentration (ng/mL).

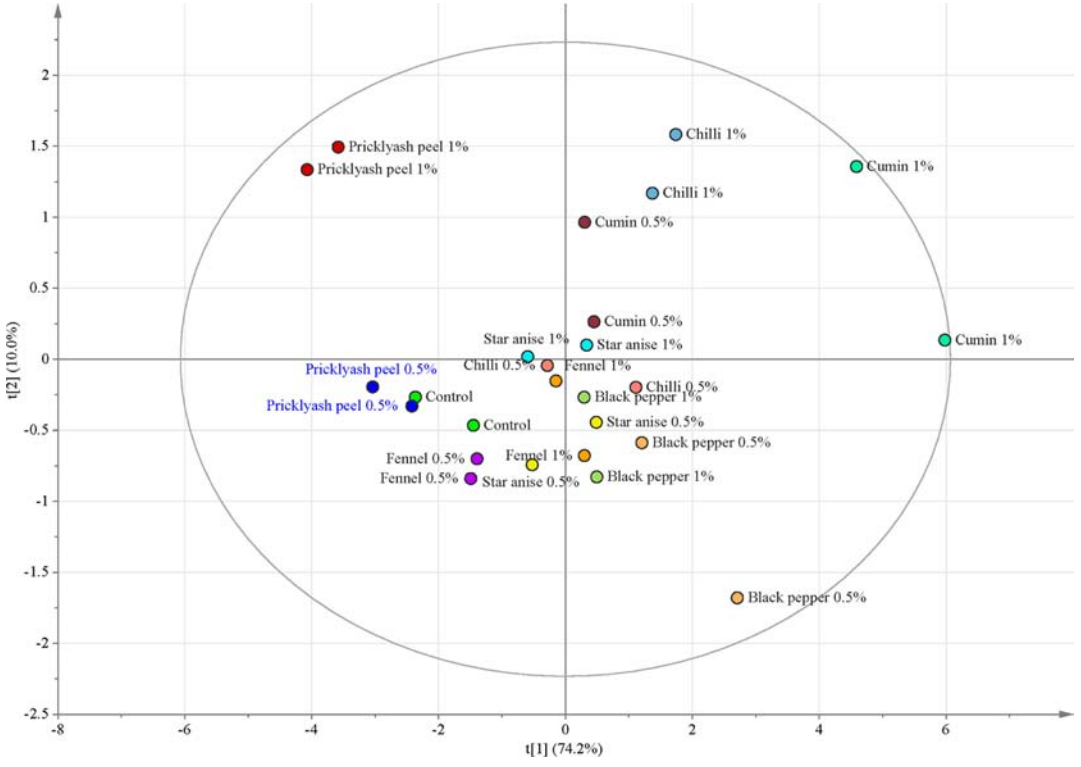


**Figure 2.** PCA score plot (PC1 versus PC2) of the HA profiles of the imidazopyridines (PhIP, DMIP, and 1,5,6-TMIP), imidazoquinoxalines (MeIQx and 4,8-DiMeIQx), and $\beta$-carbolines (harman and norharman).

chromatograms of a single beef patty). The resulting data matrix was then imported into SIMCA-P+13 (UMETRICS, Umea, Sweden) for PCA analysis. Two principal components were used for calculating the PCA models, and the normal distribution of the variables was checked first to ensure that the data were suitable for conducting a PCA.

## RESULTS AND DISCUSSION

**Quantification of the HA Profiles by UPLC-MS/MS.** The profiles of seven HA categories, the $\alpha$-carbolines (A$\alpha$C and MeA$\alpha$C), $\beta$-carbolines (harman and norharman), $\delta$-carbolines (Glu-P-1), imidazopyridines (PhIP, DMIP, and 1,5,6-TMIP), imidazoquinolines (IQ, MeIQ, and IQ[4,5-$b$]), imidazoquinoxalines (IQx, MeIQx, 4,8-DiMeIQx, 7,8-DiMexIQx, and 4,7,8-TriMeIQx), and phenylpyridines (Phe-P-1), were inves-


dx.doi.org/10.1021/jf503682j | J. Agric. Food Chem. 2014, 62, 9908−9915

tigated to assess the effects of six spices commonly used in China, pricklyash peel, star anise, fennel, cumin, chilli, and black pepper, on HA formation in roast beef patties. The patties were either made with no spice, or 0.5 or 1% of one of these spices.

HAs in each patty were extracted and quantified by UPLC-MS/MS. The imidazopyridines (PhIP, DMIP, and 1,5,6-TMIP), imidazoquinoxalines (MeIQx and 4,8-DiMeIQx), and $\beta$-carbolines (harman and norharman) were detected in all of the samples. The $\alpha$-carbolines (A$\alpha$C and MeA$\alpha$C), $\delta$-carbolines (Glu-P-1), imidazoquinolines (MeIQ), and imidazoquinoxalines (7,8-DiMeIQx) were not detected in any of the samples. The signal-to-noise ratios of the phenylpyridines (Phe-P-1), imidazoquinolines (IQ, IQ[4,5-*b*]), and imidazoquinoxalines (IQx and 4,7,8-TriMeIQx) were too low to allow detection in the control samples; however, for these HAs, quantifiable amounts were found after addition of spices.

Figure 1 shows the UPLC-MS/MS chromatograms of a standard solution and a beef patty spiked with a standard solution containing 17 HAs from all seven categories. The HA recoveries were between 54.2 and 108.4%, except for DMIP, which was 36.9%. The HA recoveries were higher than those reported by Gross and Grueter (33−85%).[20] Although the harman and norharman recoveries were larger than 100%, the values were reasonable considering the variances caused by the heterogenicity and complexity of the beef matrix, and the very low levels of HAs,[21] and are in agreement with previously reported values.[22,23]

The precision for all 17 HAs upon repeated samples showed good repeatability, as illustrated in Table 1. Most of the coefficients of the HA standard curves were above 0.999, indicating good linearity of the levels of each HA under certain peak areas. The results showed that the developed method was suitable for assessing the effects of spices on the HA profiles of roast beef patties. The rest of the analysis focused on seven HAs from the imidazopyridine, imidazoquinoxaline, and $\beta$-carboline categories, which were found in all of the samples.

**Effects of Chinese Spices on the HA Profiles.** PCA was used to examine the differences between the control and spiced samples' HA profiles. The first and second principal components (PCs) explained 74.2 and 10.0% of the systematic variation, respectively. The score plot of PC1 versus PC2 is displayed in Figure 2. As shown in the figure, most of the samples scatter into each other, which may indicate that the HA profiles of those samples were similar. The samples with 1% pricklyash peel, chilli, or cumin are located far away from the other samples in the figure, including the controls. These spices may therefore have had large effects on the HA profiles.

Table 2 shows the total HA levels. The total HA mean value of the 1% pricklyash peel samples was significantly ($p < 0.05$) lower than that of the control samples, representing an inhibition of 35%. In contrast, the total HA mean values of the 1% cumin and chilli samples were significantly ($p < 0.05$) higher than the control samples, representing a promotion of 175 and 88%.

Many studies have reported that spices can inhibit HA formation to a certain extent. For example, 20% ethanolic extracts of rosemary in beef patties were reported to inhibit PhIP by 85.3% and MeIQx by 91.7%.[24] The Asian spices turmeric, fingerroot, and galangal were shown to significantly decrease HA formation by 39.2, 33.5, and 18.4%, respectively.[17] Black pepper was also found to have an inhibitory effect on the total HA amount of between 12 and 100%.[15] However, the results for the effects of spices on HA formation have not

**Table 2. Heterocyclic Amine Levels (ng/g) of Control and Spice Beef Patties[a]**

| | | PhIP | DMIP | 1,5,6-TMIP | imidazopyridines | MeIQx | 4,8-DiMeIQx | imidazoquinoxalines | Harman | Norharman | $\beta$-carbolines | total HAs |
|---|---|---|---|---|---|---|---|---|---|---|---|---|
| control | | 13.7 ± 2.82 | 0.27 ± 0.07 | 0.36 ± 0.00 | 14.3 ± 2.04 | 0.83 ± 0.09 | 0.33 ± 0.06 | 1.16 ± 0.11 | 0.81 ± 0.19 | 5.45 ± 0.17 | 6.26 ± 0.26 | 21.8 ± 2.40 |
| pricklyash peel | 0.5% | 11.0 ± 1.70 | 0.42 ± 0.04 | 0.00 ± 0.00[b] | 11.4 ± 1.17 | 0.69 ± 0.13 | 0.25 ± 0.01 | 0.93 ± 0.10 | 0.73 ± 0.16 | 5.12 ± 0.72 | 5.84 ± 0.63 | 18.2 ± 1.90 |
| | 1% | 6.06 ± 0.44 | 0.00 ± 0.00 | 0.00 ± 0.00[b] | 6.06 ± 0.32 | 0.34 ± 0.05[b] | 0.24 ± 0.04 | 0.57 ± 0.06[b] | 0.96 ± 0.22 | 6.51 ± 0.32 | 7.47 ± 0.38 | 14.1 ± 0.76 |
| star anise | 0.5% | 19.1 ± 3.55 | 0.76 ± 0.04[b] | 0.39 ± 0.06 | 20.2 ± 2.59 | 0.87 ± 0.00 | 0.64 ± 0.07[b] | 1.51 ± 0.05 | 1.37 ± 0.23[b] | 4.64 ± 1.07 | 6.01 ± 0.92 | 27.8 ± 3.56 |
| | 1% | 15.8 ± 0.02 | 0.59 ± 0.10 | 0.38 ± 0.05 | 16.7 ± 0.12 | 0.88 ± 0.17 | 0.60 ± 0.14 | 1.49 ± 0.03 | 1.78 ± 0.41 | 5.38 ± 1.28 | 7.15 ± 1.20 | 25.4 ± 1.35 |
| fennel | 0.5% | 11.9 ± 0.87 | 0.36 ± 0.08 | 0.39 ± 0.07 | 12.7 ± 0.51 | 0.91 ± 0.04 | 0.62 ± 0.01 | 1.54 ± 0.04 | 0.85 ± 0.02 | 3.62 ± 0.00[b] | 4.47 ± 0.02 | 18.7 ± 0.53 |
| | 1% | 15.7 ± 0.21 | 0.64 ± 0.11 | 0.67 ± 0.05 | 17.0 ± 0.19 | 0.91 ± 0.11 | 0.71 ± 0.06[b] | 1.62 ± 0.12[b] | 1.31 ± 0.03 | 5.37 ± 0.22 | 6.68 ± 0.13 | 25.3 ± 0.44 |
| cumin | 0.5% | 16.3 ± 1.15 | 0.58 ± 0.13 | 0.43 ± 0.10 | 17.3 ± 0.79 | 0.80 ± 0.11 | 0.95 ± 0.05[b] | 1.76 ± 0.12[b] | 1.30 ± 0.08 | 12.6 ± 0.54[b] | 13.9 ± 0.44 | 33.0 ± 1.11 |
| | 1% | 28.6 ± 4.01 | 1.30 ± 0.06[b] | 1.18 ± 0.25 | 31.1 ± 3.06[b] | 1.32 ± 0.27 | 1.04 ± 0.01[b] | 2.36 ± 0.20[b] | 2.21 ± 0.01 | 24.2 ± 1.18[b] | 26.4 ± 0.82[b] | 59.9 ± 2.44[b] |
| chilli pepper | 0.5% | 20.5 ± 3.20[b] | 0.74 ± 0.15 | 0.50 ± 0.10 | 21.7 ± 2.30 | 0.73 ± 0.11 | 0.94 ± 0.19 | 1.67 ± 0.21 | 1.08 ± 0.23 | 8.60 ± 1.70 | 9.68 ± 1.36 | 33.1 ± 3.87 |
| | 1% | 21.6 ± 0.63 | 0.56 ± 0.07 | 0.93 ± 0.04[b] | 23.0 ± 0.52 | 0.71 ± 0.06 | 0.92 ± 0.03[b] | 1.63 ± 0.07 | 1.69 ± 0.34 | 14.6 ± 0.97[b] | 16.3 ± 0.44[b] | 41.0 ± 0.01 |
| black pepper | 0.5% | 25.1 ± 4.08[b] | 0.85 ± 0.19 | 0.83 ± 0.09 | 26.8 ± 3.08 | 1.14 ± 0.23 | 0.94 ± 0.10[b] | 2.08 ± 0.23 | 1.35 ± 0.09 | 7.22 ± 1.02 | 8.58 ± 0.65 | 37.4 ± 3.97 |
| | 1% | 20.5 ± 1.18 | 0.76 ± 0.10 | 0.45 ± 0.09 | 21.7 ± 0.83 | 0.88 ± 0.18 | 0.83 ± 0.09[b] | 1.71 ± 0.06 | 1.07 ± 0.08 | 8.08 ± 0.15 | 9.14 ± 0.16 | 32.6 ± 0.60 |

[a]Comparisons are made to control within the same column. [b]Provides statistical significance at $p$ value = 0.05. Means ± standard deviations; $n$ = 6 for all treatments.


dx.doi.org/10.1021/jf503682j | J. Agric. Food Chem. 2014, 62, 9908−9915

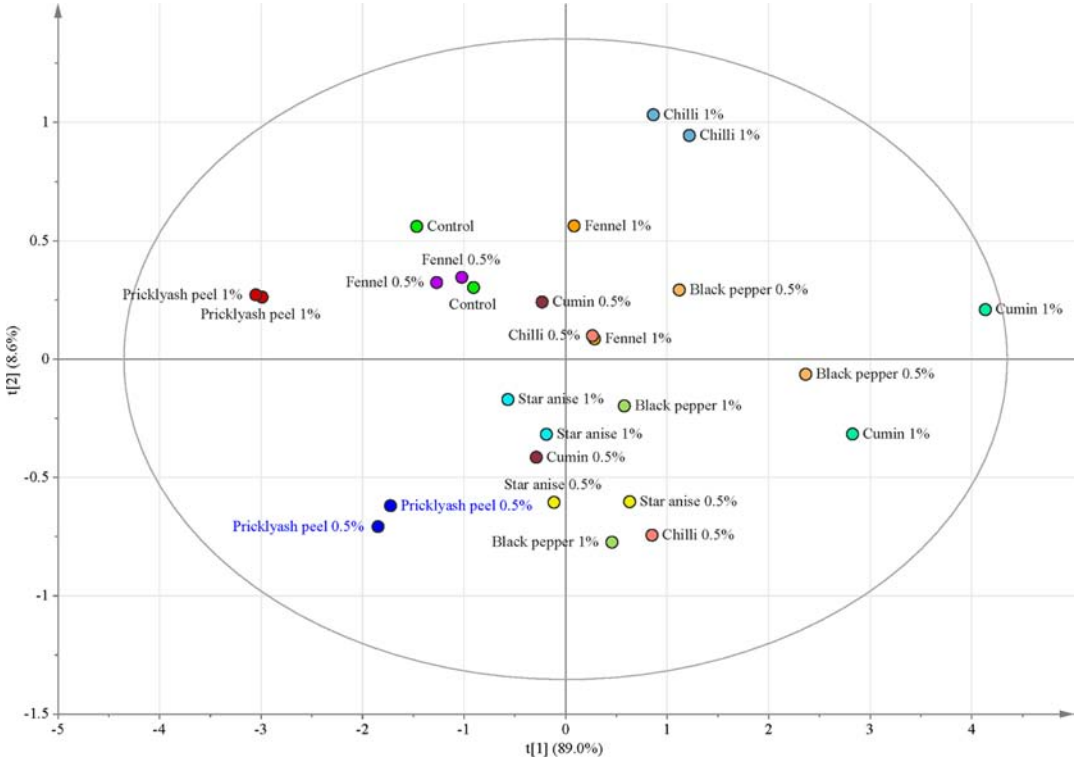


**Figure 3.** PCA score plot (PC1 versus PC2) of the imidazopyridine profiles (PhIP, DMIP, and 1,5,6-TMIP).

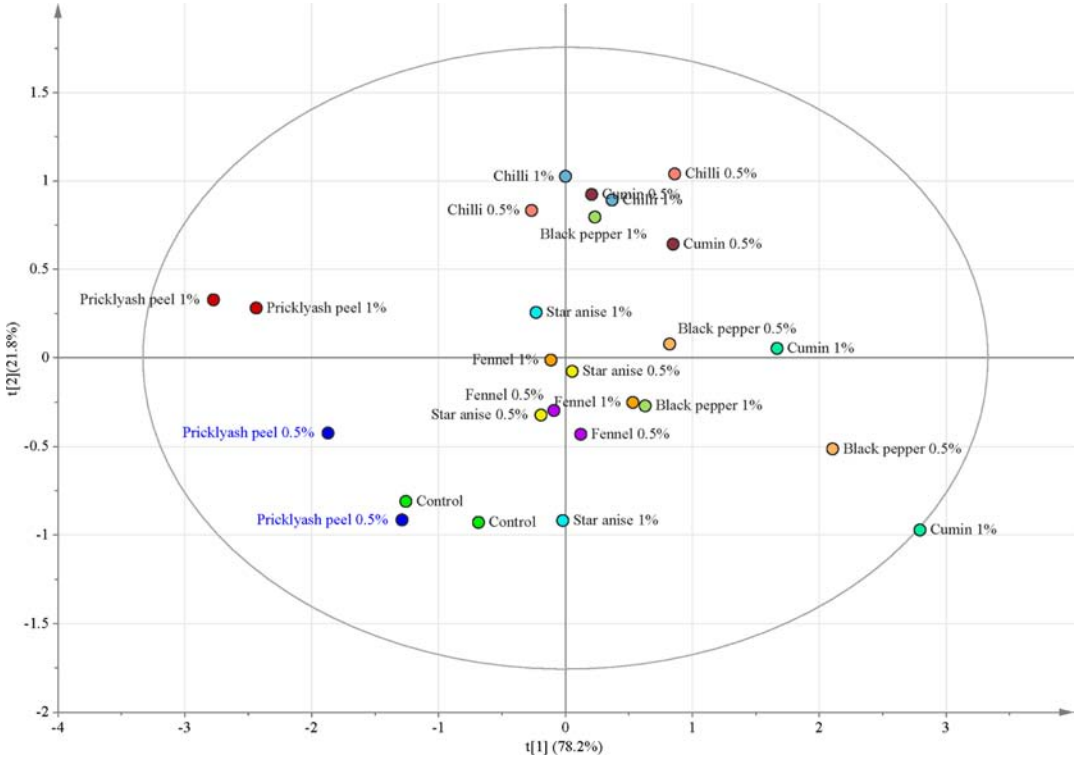


**Figure 4.** PCA score plot (PC1 versus PC2) of the imidazoquinoxaline profiles (MeIQx and 4,8-DiMeIQx).

always agreed. For instance, oregano and basil extracts were reported to increase PhIP.[21]

In contrast to most previous findings, most of the spices studied here promoted rather than inhibited the formation of HAs. The results may be attributed to the specificity of the interactions between individual HAs and the recipe of added spices. Many antioxidants that act protectively in low amounts may act as pro-oxidants in higher concentrations.[25] Furthermore, HAs have stability problems at high temperatures and start to degrade.[26]

The formation of HAs is dependent on the heating temperature and time. However, the main purpose of this


dx.doi.org/10.1021/jf503682j | J. Agric. Food Chem. 2014, 62, 9908−9915

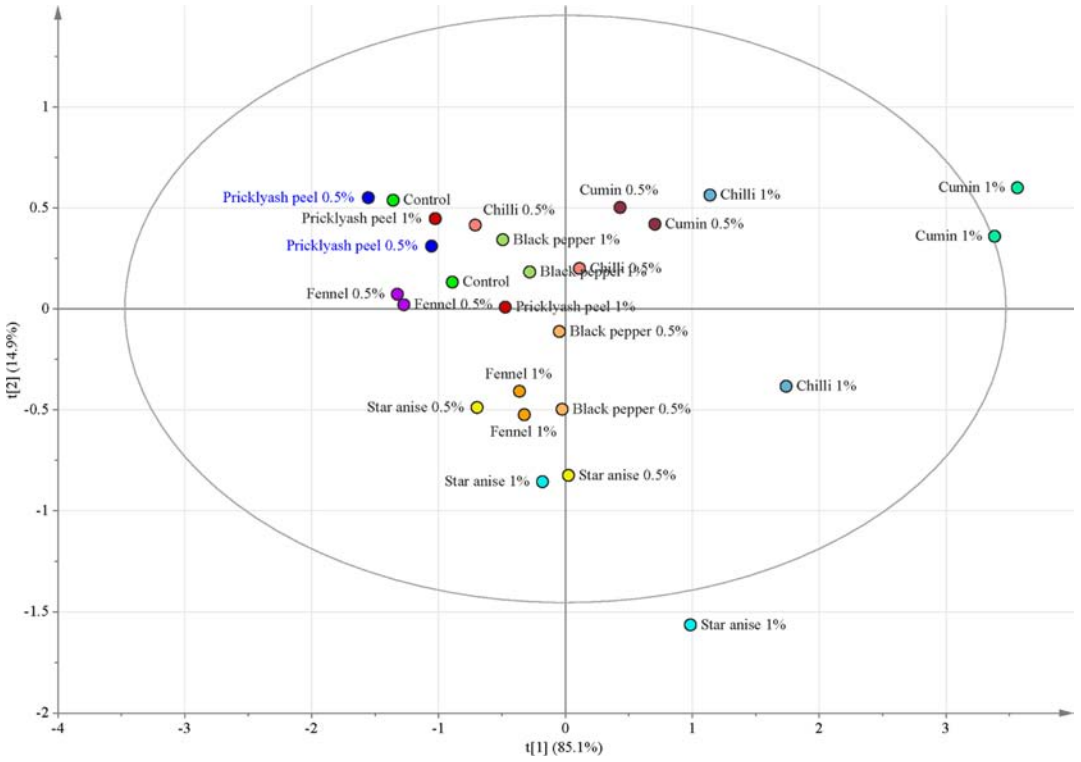


**Figure 5.** PCA score plot (PC1 versus PC2) of the $\beta$-carboline profiles (harman and norharman).

study is to evaluate the effects of commonly used Chinese spices on HA profiles. In future studies, we will examine how the cooking parameters, such as temperature and time, moderate the effects of Chinese spices on HA profiles. The changes in HA precursors after the roasting of control and spiced patties will also be examined.

**Effects of Chinese Spices on the Imidazopyridine Profiles.** The imidazopyridines PhIP, DMIP, and 1,5,6-TMIP were detected in all of the samples. PCA was used to evaluate the effects of adding spices on the imidazopyridine profiles. Figure 3 shows the score plot (PC1 versus PC2) of the control and spiced samples. The first two PCs explained 97.6% of the systematic variation. In Figure 3, the data points corresponding to the 1% pricklyash peel, chilli, and cumin samples are located far away from the other samples' data points, as in the score plot of all of the HA profiles in Figure 2. We can conclude that these spices greatly affected the imidazopyridine profiles. Table 2 shows that 1% pricklyash peel significantly inhibited the total imidazopyridine levels ($p < 0.05$) by 58%, whereas 1% chilli and 1% cumin significantly ($p < 0.05$) promoted the total imidazopyridine levels by 61 and 117%, respectively.

In the literature, PhIP is usually quantified to assess the effects of spices; however, limited studies have mentioned DMIP and 1,5,6-TMIP. For example, Puangsombat demonstrated that the addition of 0.2% cumin slightly decreased PhIP formation.[17] However, we found that 0.5 and 1% cumin both promoted the formation of PhIP, although the increase was only significant for 1% cumin. Previous research has suggested that the antioxidant effect may depend on the concentration of the antioxidant and the heating time.[24] We used larger amounts of spices (0.5 and 1% versus 0.2%) and longer roasting times (10 min/side versus 5 min/side), which may have resulted in the different effects on PhIP formation.

**Effects of Chinese Spices on the Imidazoquinoxaline Profiles.** Figure 4 shows the PCA score plot (PC1 versus PC2) of the imidazoquinoxaline profiles, including the MeIQx and 4,8-DiMeIQx. The first two PCs explained 78.2 and 21.8% of the systematic variation, respectively. Figure 4 shows that the samples containing 1% pricklyash peel and 1% cumin are situated relatively far away from the other samples. These spices may therefore have had a great effect on the imidazoquinoxaline profiles. The mean of the total imidazoquinoxaline levels on the addition of 1% pricklyash peel was significantly ($p < 0.05$) lower than in the control samples, indicating inhibition of 51%. The mean value on addition of 1% cumin was remarkably ($p < 0.05$) higher than in the control samples, indicating promotion of 103%.

Imidazoquinoxalines such as MeIQx and 4,8-DiMeIQx have been widely detected in beef.[14,27,28] Black pepper (at 1% level) has been reported to inhibit 4,8-DiMeIQx completely in high-fat meatball at 225 °C,[15] whereas the addition of 0.2% cumin had little effect on MeIQx and total HAs at 204 °C in beef patties.[17] However, our results showed that cumin and black pepper promoted both MeIQx and 4,8-DiMeIQx formation, except for 0.5% cumin. The differences may be due to different cooking temperatures and times.

**Effects of Chinese Spices on the $\beta$-Carboline Profiles.** The PCA scores plot (PC1 versus PC2) of the $\beta$-carboline (harman and norharman) profiles is shown in Figure 5. The first two PCs explained 85.1 and 14.9% of the systematic variation. In Figure 5, most of the samples are dispersed, but the samples containing 1% cumin lie far away from the rest of the samples. It is therefore likely that 1% cumin had a great effect on the $\beta$-carboline profiles in the roast beef patties. The mean of the total $\beta$-carboline values in samples with 1% cumin was significantly ($p < 0.05$) larger than in the control samples, a promotion of 322%. Although the two $\beta$-carbolines harman and


dx.doi.org/10.1021/jf503682j | J. Agric. Food Chem. 2014, 62, 9908−9915

norharman have been detected in beef,[22] little is known about the effects of spices on their formation.

In conclusion, pricklyash peel primarily inhibits the formation of all of the HA categories, whereas other spices primarily promote HA formation. Furthermore, the total HA and imidazopyridine profiles are significantly affected by 1% pricklyash peel, chilli, and cumin; the imidazoquinoxaline profiles are significantly influenced by 1% pricklyash peel and cumin; and the $\beta$-carboline profiles are only significantly affected by 1% cumin. These results shed light on the selection of spices for use in meat processing.

## AUTHOR INFORMATION


### Corresponding Author

*Phone: +86 510 85329032. Fax: +86 510 85919065. E-mail: chenjie@jiangnan.edu.cn.



### Funding

This work was supported financially by the National Natural Science Foundation of China (Grant No. 31101287), National Basic Research Program of China (Grant No. 2012CB720801), and National Key Scientific Instrument and Equipment Development Project (Grant No. 2011YQ170067).


### Notes

The authors declare no competing financial interest.

## ABBREVIATIONS USED

HA, heterocyclic amine; PCA, principal component analysis; PC, principal component; A$\alpha$C, 2-amino-9*H*-pyrido[2,3-*b*]-indole; MeA$\alpha$C, 2-amino-3-methyl-9*H*-pyrido[2,3-*b*]indole; Harman,1-methyl-9*H*-pyrido[3,4-*b*]indole; Norharman, 9*H*-pyrido[3,4-*b*]indole; Glu-P-1, 2-amino-6-methyldipyrido-[1,2-*a*:3′,2′-*d*]imidazole; IQ, 2-amino-3-methyl-imidazo[4,5-*f*]-quinoline; MeIQ, 2-amino-3,4-dimethyl-imidazo[4,5-*f*]-quinoline; IQ[4,5-*b*], 2-amino-1-methyl-imidazo[4,5-*b*]-quinoline; PhIP, 2-amino-1-methyl-6-phenylimidazo[4,5-*b*]pyridine; DMIP, 2-amino-1,6-dimethylimidazo[4,5-*b*]pyridine; 1,5,6-TMIP, 2-amino-1,5,6-trimethylimidazo[4,5-*b*]pyridine; Phe-P-1, 2-amino-5-phenylpyridine; IQx, 2-amino-3-methylimidazo[4,5-*f*]quinoxaline; MeIQx, 2-amino-3,8-dimethylimidazo[4,5-*f*]-quinoxaline; 4,8-DiMeIQx, 2-amino-3,4,8-trimethylimidazo-[4,5-*f*]quinoxaline; 7,8-DiMeIQx, 2-amino-3,7,8-trimethylimidazo[4,5-*f*]quinoxaline; 4,7,8-TriMeIQx, 2-amino-3,4,7,8-tetramethylimidazo[4,5-*f*]quinoxaline

## REFERENCES


(1) Sugimura, T. Overview of carcinogenic heterocyclic amines. *Mutat. Res.* **1997**, *376*, 211−219.

(2) Alaejos, M. S.; Afonso, A. M. Factors that affect the content of heterocyclic aromatic amines in foods. *Compr. Rev. Food Sci. Food Saf.* **2011**, *10*, 52−108.

(3) Felton, J. S.; Malfatti, M. A.; Knize, M. G.; Salmon, C. P.; Hopmans, E. C.; Wu, R. W. Health risks of heterocyclic amines. *Mutat. Res.* **1997**, *376*, 37−41.

(4) Knize, M. G.; Felton, J. S. Formation and human risk of carcinogenic heterocyclic amines formed from natural precursors in meat. *Nutr. Rev.* **2005**, *63*, 158−165.

(5) Sugimura, T. Carcinogenicity of mutagenic heterocyclic amines formed during the cooking process. *Mutat. Res.* **1985**, *150*, 33−41.

(6) Sugimura, T.; Wakabayashi, K.; Nakagama, H.; Nagao, M. Heterocyclic amines: mutagens/carcinogens produced during cooking of meat and fish. *Cancer Sci.* **2004**, *95*, 290−299.

(7) Knize, M. G.; Dolbeare, F. A.; Carroll, K. L.; Moore, D. H.; Felton, J. S. Effect of cooking time and temperature on the heterocyclic amine content of fried beef patties. *Food Chem. Toxicol.* **1994**, *32*, 595−603.

(8) Solyakov, V.; Skog, K. Screening for heterocyclic amines in chicken cooked in various ways. *Food Chem. Toxicol.* **2002**, *40*, 1205−1211.

(9) Kikugawa, K. Involvement of free radicals in the formation of heterocyclic amines and prevention by antioxidants. *Cancer Lett.* **1999**, *143*, 123−126.

(10) Hasaniya, N.; Youn, K.; Xu, M. R.; Hernaez, J.; Dashwood, R. Inhibitory activity of green and black tea in a free radical-generating system using 2-amino-3-methylimidazo[4,5-*f*]quinolone as substrate. *Jpn. J. Cancer Res.* **1997**, *88*, 553−558.

(11) Srinivasan, K. Antioxidant potential of spices and their active constituents. *Crit. Rev. Food Sci. Nutr.* **2014**, *54*, 352−372.

(12) Rubio, L.; Motilva, M. J.; Romero, M. P. Recent advances in biologically active compounds in herbs and spices: a review of the most effective antioxidant and anti-inflammatory active principles. *Crit. Rev. Food Sci. Nutr.* **2013**, *53*, 943−953.

(13) Palma, A.; Montoya, M. R.; Arteaga, J. F.; Rodriguez Mellado, J. M. Determination of antioxidant activity of spices and their active principles by differential pulse voltammetry. *J. Agric. Food Chem.* **2014**, *62*, 582−589.

(14) Keskekoglu, H.; Uren, A. Inhibitory effects of pomegranate seed extract on the formation of heterocyclic aromatic amines in beef and chicken meatballs after cooking by four different methods. *Meat Sci.* **2014**, *96*, 1446−1451.

(15) Oz, F.; Kaya, M. The inhibitory effect of black pepper on formation of heterocyclic aromatic amines in high-fat meatball. *Food Control* **2011**, *22*, 596−600.

(16) Gibis, M.; Weiss, J. Antioxidant capacity and inhibitory effect of grape seed and rosemary extract in marinades on the formation of heterocyclic amines in fried beef patties. *Food Chem.* **2012**, *134*, 766−774.

(17) Puangsombat, K.; Jirapakkul, W.; Smith, J. S. Inhibitory activity of Asian spices on heterocyclic amines formation in cooked beef patties. *J. Food Sci.* **2011**, *76*, T174−T180.

(18) Lu, M.; Yuan, B.; Zeng, M. M.; Chen, J. Antioxidant capacity and major phenolic compounds of spices commonly consumed in China. *Food Res. Int.* **2011**, *44*, 530−536.

(19) Chen, Q. Q.; Gan, Z. L.; Zhao, J. H.; Wang, Y.; Zhang, S. M.; Li, J. M.; Ni, Y. Y. *In vitro* comparison of antioxidant capacity of cumin (*Cuminum cyminum L.*) oils and their main components. *Food Sci. Technol.* **2014**, *55*, 632−67.

(20) Gross, G. A.; Grueter, A. Quantitation of mutagenic/carcinogenic heterocyclic aromatic amines in food products. *J. Chromatogr.* **1992**, *592*, 271−278.

(21) Damasius, J.; Venskutonis, P. R.; Ferracane, R.; Fogliano, V. Assessment of the influence of some spice extracts on the formation of heterocyclic amines in meat. *Food Chem.* **2011**, *126*, 149−156.

(22) Yao, Y.; Peng, Z. Q.; Wan, K. H.; Shao, B.; Shi, J. M.; Zhang, Y. W.; Wang, F. L.; Hui, T. Determination of heterocyclic amines in braised sauce beef. *Food Chem.* **2013**, *141*, 1847−1853.

(23) Lu, Q. F.; Chu, X. G.; Li, J.; Sun, L.; Ling, Y.; Yang, M. L.; Wang, X. J.; Ding, F.; Xu, C. B. Simultaneous determination of 15 heterocyclic amines in grilled fish using solid phase extraction and ultra performance liquid chromatography with electrospray ionization tandem mass spectrometry. *Chin. J. Anal. Chem.* **2011**, *39*, 501−505.

(24) Puangsombat, K.; Smith, J. S. Inhibition of heterocyclic amine formation in beef patties by ethanolic extracts of rosemary. *J. Agric. Food Chem.* **2010**, *75*, T40−T47.

(25) Lan, C. M.; Kao, T. H.; Chen, B. H. Effects of heating time and antioxidants on the formation of heterocylic amines in marinated foods. *J. Chromatogr., B* **2004**, *802*, 27−37.

(26) Arvidsson, P.; Van Boekel, M. A. J. S.; Skog, K.; Jagerstad, M. Kinetics of formation of polar heterocyclic amines in a meat model system. *J. Food Sci.* **2011**, *62*, 911−916.

(27) Jinap, S.; Mohd-Mokhtar, M. S.; Farhadian, A.; Hasnol, N. D. S.; Jaafar, S. N.; Hajeb, P. Effects of varying degrees of doneness on the

formation of heterocyclic aromatic amines in chicken and beef satay. *Meat Sci.* **2013**, *94*, 202−207.
(28) Wong, D.; Wang, M. F. Inhibitory activities of some vitamins on the formation of cholesterol oxidation products in beef patties. *J. Agric. Food Chem.* **2013**, *61*, 8471−8476.

comprehensive approach to evaluating the biological context of statistically significant differences.

A statistical tolerance interval is derived from a sample distribution to estimate the population range (Figure 1). The

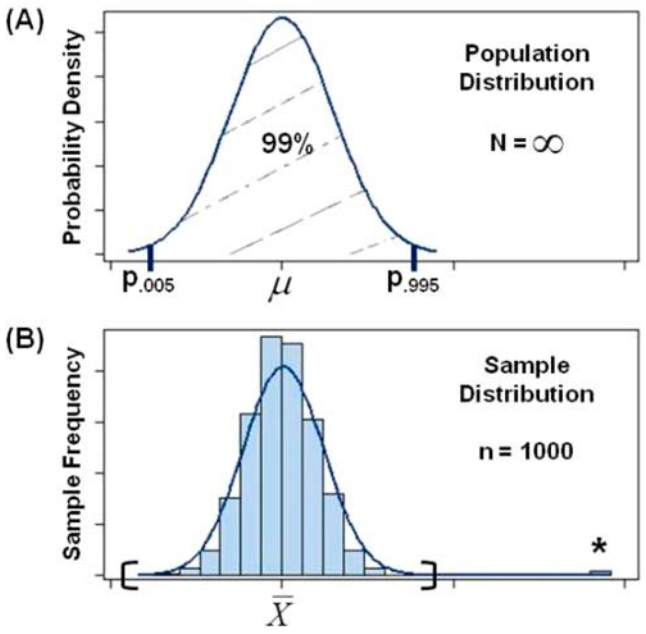


**Figure 1.** Conceptual illustration of a 99%-content, 95%-confidence tolerance interval. (A) Theoretical population distribution where $p_{.005}$ and $p_{.995}$ represent the 0.5th and 99.5th percentile points, respectively. Between $p_{.005}$ and $p_{.995}$ lie 99% of the population values. The population distribution is based on an infinite number of population values (i.e., $N = \infty$), where $\mu$ represents the center of the distribution or the population mean. (B) Sample distribution is based on a finite number of sample values (e.g., $n = 1000$), where $\bar{X}$ represents the center of the distribution or the sample mean. The 99%-content, 95%-confidence tolerance interval, denoted by the brackets on the $x$-axis, is generated on the basis of the sample distribution to infer the range between the 0.5th and 99.5th percentile points of the population distribution. In practice, there can be extreme sample values, also known as outliers. The asterisk (*) denotes an example of an extreme value, which is not included in the tolerance interval.

better the sampling of natural variability associated with a crop population, the better the true population can be modeled using a tolerance interval. For the compositional equivalence evaluation, a statistical tolerance interval for each analyte can be computed from the cumulative historical data to infer the natural range of analyte values from the crop population with a history of safe use. A tolerance interval is a statistically constructed interval that is expected to contain at least a specified proportion (i.e., percent content) of the population, with a specified confidence level.[15,16] For example, a 99%-content tolerance interval with 95% confidence for a specific analyte is intended to contain at least 99% of the population values for this analyte, with a confidence level of 95%. Figure 1 illustrates the concept of a 99%-content, 95%-confidence tolerance interval. The tolerance interval is generated using the sample data distribution to infer the range between the 0.5th and 99.5th percentiles of the population distribution.

There are varied approaches to the computation of tolerance intervals. Both the classical parametric approach[17,18] and the nonparametric approach[19] have been used to compute tolerance intervals for composition data. These two approaches assume data values are identically and independently distributed (*iid*).[15,16] However, data values from multisite field studies are not independent from each other and tend to be highly correlated. Additionally, data sets from multisite field studies are typically unbalanced due to unequal allocation of genotypes to environments. These tolerance interval approaches failed to consider the data structure when applied to composition data.

In this paper, we describe a model-based parametric approach to derive a statistical tolerance interval from cumulative historical data. A linear mixed model, which has been widely used to statistically analyze data from agricultural experiments involving multisite studies,[20] is applied to estimate parameter values that are subsequently needed for the tolerance interval computation. The theoretical basis underlying this tolerance interval approach is presented and compared to other currently employed approaches used to represent natural variation observed in conventional crop composition. An example of the use of this tolerance interval approach is demonstrated using maize grain cumulative historical data, both as an overall composition data set and in the context of two specific analytes.

## MATERIALS AND METHODS

**Maize Grain Samples from Multisite Field Studies for Compositional Analyses.** Maize grain samples were collected from 61 unique Pioneer brand non-GM commercial hybrid maize lines, which ranged in comparative relative maturity (Pioneer CRM) rating from 75 to 119 (Figure 2). Commercial launch of these hybrid

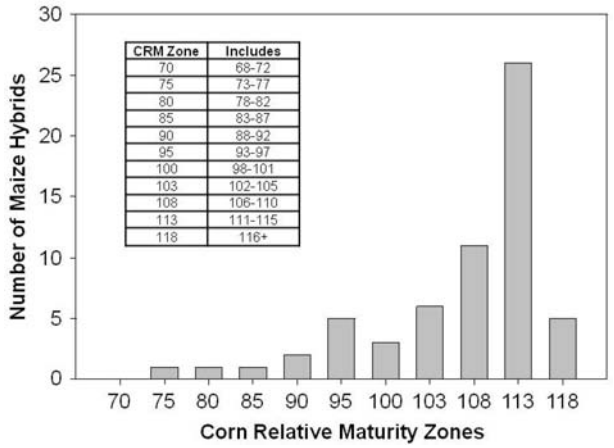


**Figure 2.** Distribution of corn relative maturity zones of the 61 Pioneer brand non-genetically modified commercial maize hybrids used to generate tolerance intervals. Comparative relative maturity (CRM) ratings of individual maize lines are grouped into zones as shown.

lines occurred between 1989 and 2011 (Figure 3). The maize grain samples were collected from eight multisite field studies between 2003 and 2011. These field sites consisted of 47 unique environments representative of commercial maize-growing regions of the United States, Canada, Chile, and Argentina (Table 1). Each field site, season, and planting date combination represents one unique environment. The experimental design utilized at each field site was a randomized complete block design with either three or four blocks.

Maize production at each field site was conducted using standard agronomic practices in accordance with local practices and recommendations. A summary of monthly temperature, precipitation, and irrigation data from each location is provided in Supporting Information (Supplementary Tables 1−5). Grain samples were


dx.doi.org/10.1021/jf502158q | J. Agric. Food Chem. 2014, 62, 9916−9926

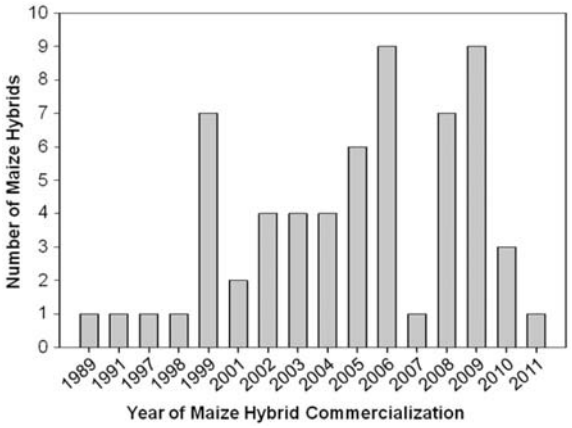


**Figure 3.** Distribution of commercialization year of the 61 Pioneer brand non-genetically modified commercial maize hybrids used to generate tolerance intervals.

collected after reaching physiological maturity (R6 growth stage),[21] where five previously self-pollinated ears per plot (one ear per plant) were husked, shelled, and pooled to make one grain sample per plot. Grain samples were shipped frozen to EPL Bio Analytical Services (EPL BAS, Niantic, IL, USA). Samples were stored frozen prior to and after grinding.

**Compositional Analyses of Maize Grain Samples.** Compositional analyses of processed samples were conducted in accordance with guidance from the Organisation for Economic Co-operation and Development (OECD) maize composition consensus document[22] and included an assessment of proximate, fiber, fatty acid, amino acid, mineral, vitamin, secondary metabolite, and antinutrient analyte concentrations. For an in-depth illustration of substantial equivalence assessment of composition data, discussion herein is limited to the two individual analytes tryptophan and oleic acid.

Compositional analyses of the processed samples were conducted by EPL BAS using validated methods. For tryptophan analysis, samples were hydrolyzed with lithium hydroxide and quantified using reverse phase high-performance liquid chromatography (HPLC) with ultraviolet (UV) detection (HPLC-UV).[23] The HPLC-UV instrument was calibrated using external standards. For oleic acid analysis, ether extraction and base hydrolysis were conducted on the samples, followed by conversion of free fatty acids to fatty acid methyl esters (FAME). FAME concentrations were quantified using gas chromatography with flame ionization detection (GC-FID). The GC-FID instrument was calibrated using external standards.[24−26] A molecular weight conversion was performed to convert the FAME concentration value to a fatty acid concentration value.

**Construction of Statistical Tolerance Intervals for Composition Data Derived from Multisite Field Studies.** For a given composition analyte, the response value $y_{ijk}$ from the $i$th environment, $j$th genotype, and $k$th block was modeled as

**Table 1. Summary of Location, Planting Date, and Soil Texture for the 47 Unique Environments from Which Maize Grain Samples Were Collected for Compositional Analyses**

| year | location[a] | planting date | soil texture |
|---|---|---|---|
| 2003 | Chula, Georgia, USA | May 30 | sandy loam |
| | Bagley, Iowa, USA | June 5 | loam |
| | Larned, Kansas, USA | May 31 | sandy loam |
| | York, Nebraska, USA | May 30 | silt loam |
| | New Holland, Ohio, USA | June 10 | silt loam |
| | Hereford, Pennsylvania, USA | June 17 | loam |
| 2007 | Quitman, Georgia, USA | May 18 | fine sandy loam |
| | Richland, Iowa, USA | May 11 | loam |
| | Larned, Kansas, USA | May 18 | loam |
| | York, Nebraska, USA | May 11 | silt loam |
| | Branchton, Ontario, Canada | May 14 | silt loam |
| | Germansville, Pennsylvania, USA | May 24 | loam |
| 2009−2010 | Peumo, Cachapoal, Chile | December 2 | silt loam |
| | Colina, Chacabuco, Chile | November 19 | loam |
| | Buin, Maipo, Chile | November 23 | loam |
| | Loreto, Maipo, Chile | November 27 | loam |
| 2010 | Stewardson, Illinois, USA | May 25 | silt loam |
| | Wyoming, Illinois, USA | May 25 | silt loam |
| | Rockville, Indiana, USA | May 6 | silty clay loam |
| | Sheridan, Indiana, USA | May 6 | silt loam |
| | Atlantic, Iowa, USA | May 24 | clay loam |
| | Bagley, Iowa, USA | May 21 | loam |
| | Dana, Iowa, USA | May 20 | clay loam |
| | Lime Springs, Iowa, USA | May 19 | clay loam |
| | Richland, Iowa, USA | May 6 | silt loam |
| | Larned, Kansas, USA | May 24 | loamy sand |
| | Deerfield, Michigan, USA | June 7 | silty clay loam |
| | Geneva (1), Minnesota, USA | May 17 | clay loam |
| | Geneva (2), Minnesota, USA | May 26 | clay loam |
| | Brunswick, Nebraska, USA | May 5 | loamy fine sand |
| | York (1), Nebraska, USA | April 28 | silt loam |
| | York (2), Nebraska, USA | May 4 | silt loam |
| | York (3), Nebraska, USA | May 27 | silt loam |
| | Hinton, Oklahoma, USA | May 12 | sandy loam |
| | Branchton (1), Ontario, Canada | May 7 | silt loam |
| | Branchton (2), Ontario, Canada | May 28 | silt loam |
| | Thorndale, Ontario, Canada | May 19 | loam |
| | Germansville, Pennsylvania, USA | June 4 | loam |
| | Groom (1), Texas, USA | May 4 | silty clay loam |
| | Groom (2), Texas, USA | June 15 | clay loam |
| | Verona, Wisconsin, USA | May 24 | silt loam |
| 2010−2011 | Gahan, Buenos Aires, Argentina | October 24 | silt loam |
| | Inés Indart, Buenos Aires, Argentina | October 23 | silt loam |
| | Tacuarí, Buenos Aires, Argentina | October 24 | silt loam |
| | Olivar, Cachapoal, Chile | December 2 | sandy loam |
| | Popeta, Cahcapoal, Chile | December 7 | clay loam |
| | Colina, Chacabuco, Chile | December 14 | loam |

[a]Location is the closest town to the field trial site. Locations followed by numbers in parentheses differentiate between unique environments.


dx.doi.org/10.1021/jf502158q | J. Agric. Food Chem. 2014, 62, 9916−9926

$$y_{ijk} = \mu + \text{environment}_i + \text{genotype}_j + (\text{genotype} \times \text{environment})_{ji} + \text{block(environment)}_{ki} + \varepsilon_{ijk}$$

where $\mu$ represents the grand mean; random effect environment$_i$ is identically and independently distributed (*iid*) $N(0,\sigma_E^2)$; random effect genotype$_j$ is *iid* $N(0,\sigma_G^2)$; interaction effect (genotype × environment)$_{ji}$ is *iid* $N(0,\sigma_{G\times E}^2)$; random effect block(environment)$_{ki}$ is *iid* $N(0,\sigma_B^2)$; and the plot error term $\varepsilon_{ijk}$ is *iid* $N(0,\sigma_\varepsilon^2)$. Other than the grand mean being a fixed effect, all other terms in the model are random effects. This linear mixed model (LMM) is also known as a random effects model. On the basis of the LMM configuration described above, the variance of $y_{ijk}$ is the sum of variance components from all identified sources in the model, denoted as

$$Var(y_{ijk}) = \sigma_E^2 + \sigma_G^2 + \sigma_{G\times E}^2 + \sigma_B^2 + \sigma_\varepsilon^2 \equiv \sigma_{total}^2$$

A two-sided 99%-content tolerance interval was constructed with 95% confidence for the distribution of $N(\mu,\sigma_{total}^2)$. With $\hat{\mu}$, $\hat{\sigma}_E^2$, $\hat{\sigma}_G^2$, $\hat{\sigma}_{G\times E}^2$, $\hat{\sigma}_B^2$, and $\hat{\sigma}_\varepsilon^2$ denoted as the restricted maximum likelihood estimates of the grand mean and the variance components of the LMM, the estimate of total variance $\hat{\sigma}_{total}^2$ was computed as

$$\hat{\sigma}_{total}^2 = \hat{\sigma}_E^2 + \hat{\sigma}_G^2 + \hat{\sigma}_{G\times E}^2 + \hat{\sigma}_B^2 + \hat{\sigma}_\varepsilon^2$$

Let $R_0$ represent the ratio of $\sigma_{total}^2$ over the variance of $\hat{\mu}$ and assume that $R_0$ is known. It follows from sections 2.3.1 and 4.5.1 of Krishnamoorthy and Mathew[27] that the lower and upper tolerance limits (*LTL* and *UTL*, respectively) for the two-sided 100(1-$\gamma$)%-content, 100(1-$\alpha$)%-confidence tolerance interval are

$$LTL = \hat{\mu} - \hat{\sigma}_{total}\sqrt{\frac{m\cdot\chi_{1;1-\gamma}^2(1/R_0)}{\chi_{m;\alpha}^2(0)}} \qquad (1.0)$$

$$UTL = \hat{\mu} + \hat{\sigma}_{total}\sqrt{\frac{m\cdot\chi_{1;1-\gamma}^2(1/R_0)}{\chi_{m;\alpha}^2(0)}}$$

where

$$m = 2\frac{(\hat{\sigma}_{total}^2)^2}{\mathbf{J}\hat{\Delta}\mathbf{J}'}$$

Here $\chi_{1;1-\gamma}^2(1/R_0)$ represents the 100(1 − $\gamma$)th percentile of a noncentral chi-square distribution with the degree of freedom being 1 and the noncentrality parameter being $1/R_0$; $\chi_{m;\alpha}^2(0)$ represents the 100$\alpha$th percentile of a central chi-square distribution with $m$ degrees of freedom; $m$ originates from the Satterthwaite approximation[28] to the degrees of freedom of $\hat{\sigma}_{total}^2$; $\hat{\Delta}$ is the estimated variance−covariance matrix of ($\hat{\sigma}_E^2$, $\hat{\sigma}_G^2$, $\hat{\sigma}_{E\times G}^2$, $\hat{\sigma}_B^2$, $\hat{\sigma}_\varepsilon^2$); $\mathbf{J}$ is a row vector of 1; and $\mathbf{J}'$ is a column vector of 1.

Following the approach taken by Bagui, Bhaumick, and Parnes,[29] here the unknown parameter $R_0$ (the ratio of the variance of the population over the variance of the grand mean estimator $\mu$) was approximated by its point estimate $\hat{R}_0 = \hat{\sigma}_{total}^2/\hat{V}ar(\hat{\mu})$, with $\hat{V}ar(\hat{\mu})$ being the estimated variance of the grand mean. This results in a two-sided tolerance interval that is narrower than the true two-sided 100(1-$\gamma$)%-content, 100(1-$\alpha$)%-confidence tolerance interval.

The SAS (SAS Institute Inc., Cary, NC, USA) code for constructing the tolerance interval is provided in the Supporting Information (Supplementary Method).

## RESULTS AND DISCUSSION

**Justification for Model-Based Tolerance Interval Approach.** The parametric tolerance interval approach, which incorporates the linear mixed model described here, is superior to a classical parametric or nonparametric approach for unbalanced data generated from multisite field studies. Both the classical parametric and nonparametric approaches assume data values are identically and independently distributed (*iid*). However, data values from multisite field studies are not *iid* and tend to be highly correlated. Data from multisite field studies are correlated on several levels: data values collected from the same genotype at the same field site are apt to be highly correlated, data values collected from different genotypes at the same field site are more likely correlated than those grown at different field sites, and data values collected from the same genotype at different field sites are likely correlated as well. Data from multisite field studies conducted over multiple seasons (referred to as cumulative historical data) are unbalanced in structure due to an unequal allocation of genotypes to environments. Our linear mixed model, which is a random effects model, considers and accommodates the correlated and unbalanced data structure resulting from multisite field studies conducted over multiple seasons. The linear mixed model incorporated into this parametric tolerance interval approach has been widely used to statistically analyze data from agricultural experiments involving multisite field studies.[20]

The conventional formula for the classical parametric tolerance interval was developed assuming responses are *iid* following a normal distribution,[15] and our model-based parametric tolerance interval approach degenerates into the classical parametric solution under those conditions. When the data values are *iid* normal with sample size $n$, then $m$ equals $n - 1$ and $R_0$ equals $n$, and formula 1.0 is simplified into the conventional formula for the two-sided tolerance interval.[27]

When employing random effects models for unbalanced data, construction of the tolerance interval becomes substantially more complicated, but our approach is computationally feasible and straightforward to execute via SAS (see Supplementary Method in the Supporting Information) or other appropriate statistical software. Compared to simple cases such as those with normally distributed *iid* data, analytical formulas for the tolerance limits are not available for unbalanced and correlated data, and numerical methods or approximations become necessary.[27] For a one-way random effect model with balanced data, the unknown $R_0$ is approximated by its lower confidence limit to achieve the desired content with the nominal confidence level.[30] However, "no guidelines are given regarding the choice of the confidence level" for unbalanced data.[27] Alternatively, with a one-way random effect model, the tolerance interval has been successfully developed using generalized pivotal quantity machinery.[31,32] This approach involves statistical resampling and heavy computation, which is difficult for most practitioners to implement. To our knowledge, an extension from the one-way random effect model to a two-way random effects model is not available with a generalized pivotal quantity approach.[27] Our random effects model is multiway, as it involves more than two random effects and our data sets are unbalanced; therefore, instead of solving for an unbiased solution using heavy computation, the unknown $R_0$ is simply replaced with its point estimate. As a result, our tolerance interval is expected to be narrower than a true 99%-content, 95%-confidence tolerance interval, and as such is conservative in the context of a GM crop safety assessment.

A simulation study was conducted to demonstrate that the actual coverage of our tolerance interval is indeed narrower than the nominal coverage level. The tolerance interval coverage was evaluated according to the approach of Liao.[33] In this exercise, 5000 data sets were simulated following an experimental design similar to the cumulative historical data set

and a given set of variance component values. For each of the simulated data sets (data not shown), the actual content of the computed tolerance interval was recorded and compared to the nominal content level (i.e., 99%). Of the 5000 sets of tolerance intervals, 94.24% of the sets had an actual content of at least 99%. With the size of the simulation ($n$ = 5000), the standard error associated with 94.24% is 0.3295%. This result, which is less than the nominal confidence level of 95%, demonstrates that our tolerance interval is indeed narrower than a true 99%-content, 95%-confidence tolerance interval.

**Sample Size.** In the context of a cumulative historical data set with a correlated data structure, a recommended minimum sample size in terms of total number of data points is impractical because our tolerance interval solution is a complex function of various factors. Using the tolerance interval formula 1.0, the width of a tolerance interval (represented by the minimum and maximum calculated limits) is a function of three factors: $\hat{\sigma}^2_{\text{total}}$ (the estimated total variance), $m$ (the Satterthwaite degrees of freedom), and $\hat{R}_0$ (the estimated ratio of $\hat{\sigma}^2_{\text{total}}$ over the variance of the estimated grand mean $\hat{\mu}$). As the natural variation of the population ($\hat{\sigma}^2_{\text{total}}$) increases, so does the width of the tolerance interval. Parameter $R_0$ can be considered the effective sample size of the population, as it is the ratio of the variance of the population ($\hat{\sigma}^2_{\text{total}}$) over the variance of the grand mean estimator $\mu$ (formula 1.0). As $R_0$ is dependent on each of the individual variance factors that make up the total variance of the population, $R_0$ would be different for each analyte of an individual data set. Therefore, it is not straightforward to determine a universal minimum sample size $n$ that could be applied to all analytes. In contrast, we recommend minimum values for the two parameters $m$ and $R_0$ associated with our tolerance interval approach.

Minimum $m$ and $R_0$ values were determined by plotting the functional relationship for critical components of the tolerance interval formula versus $m$ and $R_0$, with recommended minimum values corresponding to when the respective plot converges. For data collected under multisite field studies over multiple seasons with unbalanced allocations of genotypes to environments, both $m$ and $R_0$ are increasing functions with respect to the number of unique environments, number of genotypes at each environment, and number of blocks within environments. Due to the unbalanced nature of cumulative historical data, it is cumbersome to provide an explicit formula for $m$ and $R_0$ as functions of the number of unique environments and genotypes. As a result, it is impractical to provide a recommendation for the minimally required number of genotypes or environments. Additionally, $m$ and $R_0$ are determined by the estimated variance components as well as the variance−covariance matrix of the estimated variance. Instead, it is more feasible to investigate the empirical behavior of the tolerance limits using functional curves that examine the relationship between $m/\chi^2_{m;\alpha}(0)$ and $m$ and the relationship between $\chi^2_{1;1-\gamma}(1/R_0)$ and $R_0$ (Figure 4). As both $m$ and $R_0$ approach infinity, the calculated tolerance interval stabilizes and the tolerance limits approach the true percentiles of the population.

As illustrated in Figure 4, $m/\chi^2_{m;\alpha}(0)$ starts to stabilize when $m$ approaches 60, and $\chi^2_{1;1-\gamma}(1/R_0)$ starts to stabilize when $R_0$ approaches 50; therefore, we recommend a minimum $m$ of 60 for the Satterthwaite degrees of freedom and a minimum $R_0$ of 50 for the effective sample size when tolerance intervals are constructed from data derived from multisite field studies. In the context of composition data, $m$ and $R_0$ are estimated

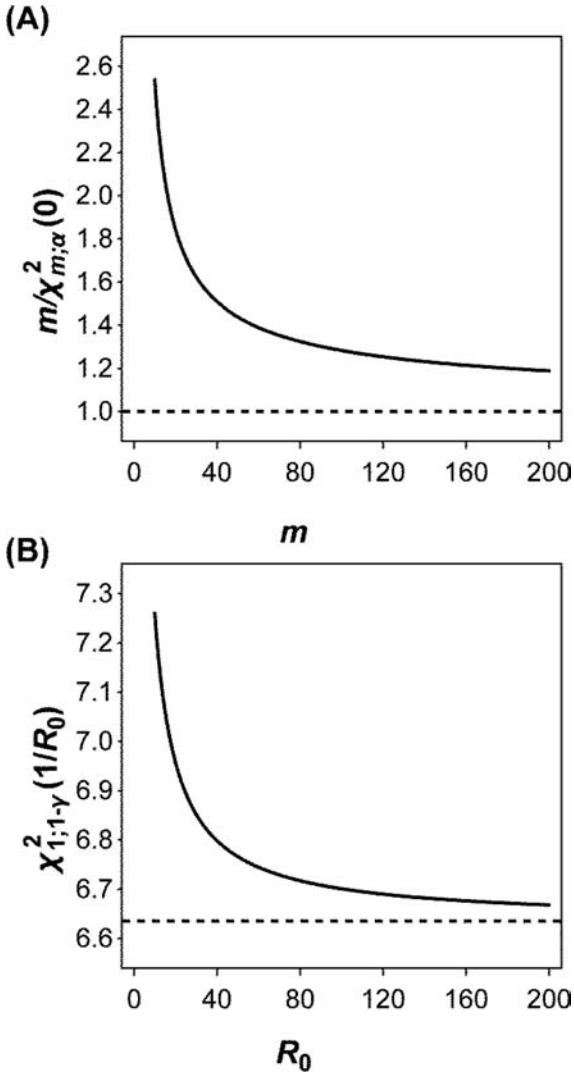


**Figure 4.** (A) Plot of $m/\chi^2_{m;\alpha}(0)$ versus $m$. Solid line corresponds to $m/\chi^2_{m;\alpha}(0)$. Dashed line corresponds to the limit of $m/\chi^2_{m;\alpha}(0)$ as $m$ approaches infinity. (B) Plot of $\chi^2_{1;1-\gamma}(1/R_0)$ versus $R_0$. Solid line corresponds to $\chi^2_{1;1-\gamma}(1/R_0)$. Dashed line corresponds to the limit of $\chi^2_{1;1-\gamma}(1/R_0)$ as $R_0$ approaches infinity. $m$ is the Satterthwaite degrees of freedom, and $R_0$ is the estimated ratio of the total variance over the variance of the grand mean. $m/\chi^2_{m;\alpha}(0)$ and $\chi^2_{1;1-\gamma}(1/R_0)$ are two critical components of the tolerance interval equation that determine the width of a tolerance interval (represented by the minimum and maximum calculated limits).

individually for each analyte, and then estimated $m$ and $R_0$ values are examined across analytes to evaluate the adequacy of the data set for the purpose of generating tolerance intervals. For example, $m$ and $R_0$ were estimated for each individual analyte in a data set composed of cumulative maize grain data from 2003 to 2011 (referred to here as the 2003−2011 maize grain cumulative historical data set; data not shown). The minimum estimated $m$ value for a given analyte in this cumulative historical data set was 76, which exceeded the recommended minimum of 60. The estimated $R_0$ values for 2 of 55 analytes in the 2003−2011 maize grain cumulative historical data set were below the recommended minimum of 50, and the lower of the two $R_0$ values was 47. Therefore, this cumulative historical data set was deemed adequate for generating tolerance intervals for maize grain analytes.

**Tolerance Interval Construction and Results.** Tolerance intervals are constructed by estimating parameters (grand mean and variance components) using linear mixed model analysis and subsequently using these parameter values in formula 1.0. Within the 2003−2011 maize grain cumulative historical data set, two analytes (tryptophan and oleic acid) are used as examples to illustrate how tolerance intervals are constructed. For each individual variance component that contributed to the total variance of tryptophan and oleic acid, the estimated values are provided in Table 2, along with the corresponding

**Table 2. Variance Components**

| | tryptophan | | oleic acid | |
|---|---|---|---|---|
| source of variation | variation | % total variation | variation[a] | % total variation |
| genotype | $6.70 \times 10^{-6}$ | 6.7 | 0.0131 | 55.6 |
| environment | $7.11 \times 10^{-5}$ | 71.6 | 0.00387 | 16.4 |
| genotype × environment | $3.51 \times 10^{-6}$ | 3.5 | 0.00206 | 8.7 |
| block (environment) | 0 | 0.0 | 0 | 0.0 |
| residual | $1.80 \times 10^{-5}$ | 18.1 | 0.00456 | 19.3 |

[a]Variance component estimates were obtained on the log-transformed scale.

percentages of the total variance. Environmental variance was the largest contributor to the total variation of tryptophan values (71.6% of the total variance), whereas genotypic variation was the largest contributor to the total variation of oleic acid values (55.6% of the total variance). Any given composition analyte has a natural variation that is influenced by various individual contributors (e.g., genotypic factors, environmental factors). However, it is important to recognize that the natural variation is the sum of these variation sources and the key objective here is to capture and estimate the total variation, not to characterize or quantify the individual factors that make up the total variation.

Tolerance intervals (99%-content, 95%-confidence) were constructed on the basis of the grand mean and the total variance estimated from the linear mixed model analysis. Tolerance interval results for tryptophan and oleic acid are presented in Table 3 along with the corresponding range of

**Table 3. Tolerance Interval Results**

| analyte | tolerance interval | data range |
|---|---|---|
| tryptophan[a] | 0.0344−0.0940 | 0.0348−0.0927 |
| oleic acid[b] | 18.1−44.0 | 17.0−42.8 |

[a]Percent dry weight. [b]Percent total fatty acids.

individual data values for each analyte. To illustrate the reasonableness of the tolerance interval coverage, the tryptophan and oleic acid tolerance interval results were compared to the individual data points for each multisite field study included in the cumulative historical data set using dot plots (Figure 5). Of the 1038 samples included in the cumulative historical data set, all of the tryptophan sample values were within the respective tolerance interval, and all but three of the oleic acid sample values were within the respective tolerance interval. It is expected that 1% of all data values from a population would fall outside a 99%-content tolerance interval. However, a sample set such as the 2003−2011 maize grain cumulative historical data set is unlikely to cover all

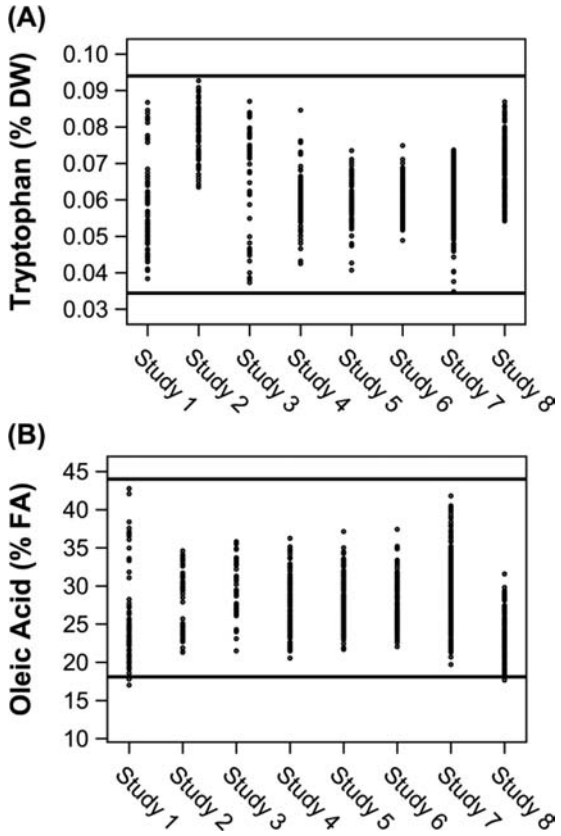


**Figure 5.** Dot plots for (A) tryptophan (% dry weight) and (B) oleic acid (% total fatty acids). The horizontal lines are tolerance interval limits constructed from the 2003−2011 maize grain cumulative historical data set for (A) tryptophan (0.0344, 0.0940) and (B) oleic acid (18.1, 44.0).

extremes of the population and may have <1% of data values outside the calculated tolerance interval for a given analyte. The same sample set may also have >1% of data values outside the calculated tolerance interval for a different analyte due to the random nature of sampling. As shown in Figure 5, this tolerance interval approach appropriately reflects the natural variation observed in this cumulative historical data set without over-extrapolation.

**Tolerance Interval Application.** During a substantial equivalence assessment, tolerance intervals can be used to interpret statistical differences within the biological context of natural variation. A statistically significant difference between the GM crop and the non-GM comparator in the compositional assessment may not be biologically relevant. Like any statistical test, the statistical power (i.e., the power of detecting a difference) is driven by the size of the study and the variation in the study data,[34] and detection of a statistical difference does not address whether the difference is biologically relevant. Composition data may vary more or less for some analytes compared to other analytes. Therefore, individual analytes end up having different statistical powers, and some analytes may be statistically overpowered due to smaller data variation. For any statistical comparison, there is a possibility of identifying a statistically significant difference by chance (known as type I error or false-positive error). In other words, across all composition analytes for which statistical comparisons are conducted between a GM crop and a non-GM comparator at the significance level of 0.05, statistically significant differences


dx.doi.org/10.1021/jf502158q | J. Agric. Food Chem. 2014, 62, 9916−9926

are expected to be identified for 5% of the analytes due to false-positive error. Additionally, even if a statistically significant difference could be attributed to the genetic modification, the magnitude of the difference is usually negligible when compared to the influence from genetics and environments as demonstrated previously in compositional equivalence evaluations of GM crops.[35−37] Consequently, it is critical to place any statistical difference within biological context. Tolerance intervals derived from cumulative historical data are a powerful tool to examine biological relevance of significant differences because the data are collected from the population with a history of safe use. Our tolerance interval approach makes statistical inference to the natural range of population values for a given analyte. This inferred natural range then becomes the basis of biological context for compositional equivalence evaluation.

To provide an example of how a tolerance interval is utilized to assist with the substantial equivalence assessment of GM crop composition data, one multisite field study is presented here. This study (identified as study 4 in Figure 5) was conducted in North America during the 2010 growing season at nine field sites. The study contained four GM maize hybrids and one non-GM near-isogenic control maize hybrid (referred to as control maize hybrid). All GM maize hybrids and the control maize hybrid were from the same genetic background. The study also contained six non-GM commercial maize hybrids (referred to as reference maize hybrids). At each site, three of the six reference maize hybrids were randomized together with all four GM maize hybrids and the control maize hybrid in a randomized complete block design according to European Food Safety Authority (EFSA) guidance.[38] The resulting grain composition data were statistically analyzed to compare the across-site means of each of the four GM maize hybrids to the across-site mean of the control maize hybrid.

Tryptophan and oleic acid concentrations are summarized in side-by-side box plots for each GM and control maize hybrid, as well as for the pooled data from the six reference maize hybrids (Figure 6). The tryptophan and oleic acid tolerance intervals constructed from the 2003−2011 maize grain cumulative historical data set are also provided in Figure 6. For tryptophan, a statistically significant difference (at the significance level of 0.05) was identified between one GM maize hybrid and the control maize hybrid (identified as GM2 and COMP91, respectively, in Figure 6A). When the mean values designated by the diamond within each box plot are compared, the statistical difference between the GM2 and control means for tryptophan is not visually obvious, with a magnitude of <4% (GM2 mean = 0.0610% dry weight, control mean = 0.0632% dry weight). For oleic acid, a statistically significance difference was identified for three of the GM maize hybrids (identified as GM2, GM3, and GM4 in Figure 6B) compared to the control maize hybrid (COMP91). The statistical difference between each GM mean compared to the control mean for oleic acid was <20% (GM2 mean = 31.0% total fatty acid, GM3 mean = 31.4% total fatty acid, GM4 mean = 32.7% total fatty acid, control mean = 27.3% total fatty acid); this magnitude of difference is more visually obvious when the mean values designated by the diamond within each box plot are compared.

The next step in the substantial equivalence assessment was to compare any relevant GM maize line data ranges to the corresponding tolerance interval for each identified statistically significant difference, to examine the statistical difference in the context of the crop population with an established history of safe use. For both analytes, all box plots fell within the respective tolerance interval (constructed from the 2003−2011 maize grain cumulative historical data set). Because the tryptophan and oleic acid data ranges of the corresponding GM maize hybrids fell within the respective range of natural variation for the analyte, it can be concluded that the statistical differences are not biologically relevant.

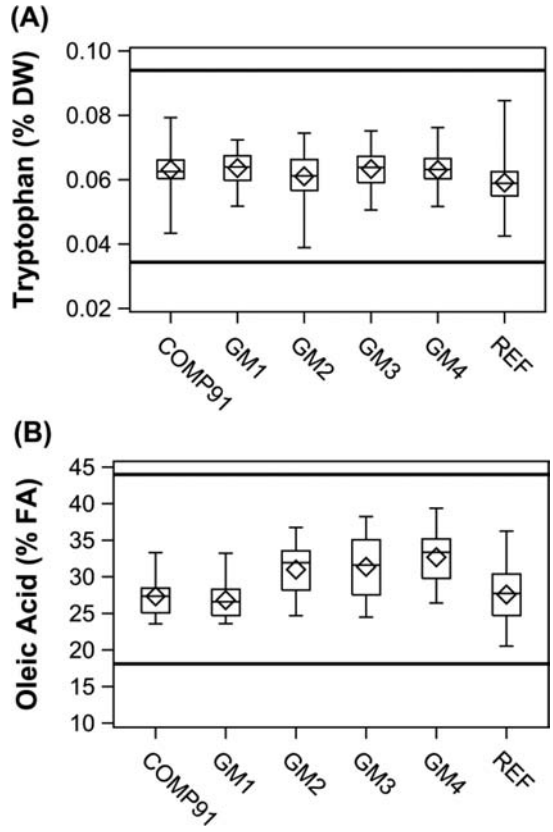


**Figure 6.** Box plots by genotype for (A) tryptophan (% dry weight) and (B) oleic acid (% total fatty acids) in a single study (study 4 in Figure 5). Data were plotted for the near-isogenic control maize hybrid (coded COMP91), the four genetically modfied maize hybrids (coded GM1, GM2, GM3, and GM4), and combined data from the six reference maize hybrids (coded REF). The diamond within each box plot represents the mean value. The whiskers were drawn from the first quartile and third quartile to the minimum and maximum data points, respectively. The horizontal lines are tolerance interval limits constructed from the 2003−2011 maize grain cumulative historical data set for (A) tryptophan (0.0344, 0.0940) and (B) oleic acid (18.1, 44.0).

Additionally, Figure 6 illustrates a limitation of sampling commercial reference data in a single study, in that the interquartile ranges for the pooled data from the reference maize hybrids are not noticeably larger than those of the individual GM or control maize hybrids. The limited number of environments and genotypes represented in one multisite field study conducted in a single year results in reference data that do not adequately represent the population. This reference data may even be a biased sample set due to extreme environmental conditions experienced in that particular year. As illustrated in Table 4, $m$ and $R_0$ values derived from the single-study reference hybrids are well below the recommended minimums of 60 and 50, respectively. The best way to ensure that individual $m$ and $R_0$ values for a given data set are above the recommended minimums is to include more extensive sampling

**Table 4. Comparison of Key Parameters for Sample Size Adequacy**

| | cumulative historical data[a] | | single study data | |
|---|---|---|---|---|
| analyte | $m$[b] | $R_0$[c] | $m$ | $R_0$ |
| tryptophan | 81 | 57 | 23 | 12 |
| oleic acid | 140 | 66 | 22 | 12 |

[a]The 2003−2011 maize grain cumulative historical data set. [b]$m$ is the Satterthwaite degrees of freedom. [c]$R_0$ is the estimated ratio of the total variance over the variance of the grand mean.

from a large number of genotypes and representative environments, which may require multiple years of data accumulation.

**Importance of Cumulative Historical Data.** A cumulative historical data set provides a greater number of environments (i.e., field sites) and a greater diversity of environmental and other site-specific factors including soil characteristics (e.g., soil type, pH, organic matter), environmental conditions (e.g., temperatures, precipitation, solar radiation, humidity, wind), management practices (e.g., crop history, tillage practices, pesticide applications, fertilizer applications, irrigation), and biotic factors (e.g., insects, pathogens, weeds). For example, the environmental diversity of the North American sites used in the 2003−2011 maize grain cumulative historical data set is illustrated in Figure 7. An environmental classification system that defines long-term abiotic macroenvironment types for maize production[39] was used to construct Figure 7. Cumulative historical data also incorporate increased genotypic diversity compared to a single-year multisite field study because of the availability and inclusion of more genotypes over time. Tolerance intervals generated from cumulative historical data are more robust than reference data from a single study due to sample size adequacy and increased environmental and genotypic diversity and are, therefore, more representative of the actual corresponding range of values for the population.

Over the past few years, some interest has been expressed in the application of an equivalence testing approach to the substantial equivalence assessment of GM crops. One approach is to grow non-GM commercial reference lines in the same study at the same field sites as the corresponding GM and non-GM near-isogenic control lines and to utilize the resulting non-GM commercial reference composition data to generate an equivalence interval for each analyte.[38] The purpose of the equivalence test is to assess whether the mean of the GM crop (i.e., 90% confidence interval of the mean) for each given analyte falls within the corresponding equivalence interval at a given level of statistical confidence (i.e., 95%). This approach is conceptually appealing but has a number of limitations.

As discussed previously, the limited number of environments and genotypes contained in a single multisite field study results in an inadequate representation of the population. This particular equivalence interval approach relies heavily on the estimated value of genotypic variance (i.e., parameter $\sigma_G^2$ is the key component of the equivalence interval), but without extensive testing of the genotypes under their relevant environments, it is impossible to obtain an accurate estimate of the genotypic variance. In the previously described single multisite field study, the non-GM near-isogenic control maize, although considered as safe as the non-GM commercial reference lines, has a tryptophan mean confidence interval (0.0607% dry weight, 0.0649% dry weight) that does not entirely fall within the equivalence interval (0.0530% dry weight, 0.0646% dry weight) established by the non-GM commercial reference lines within the study. It is therefore

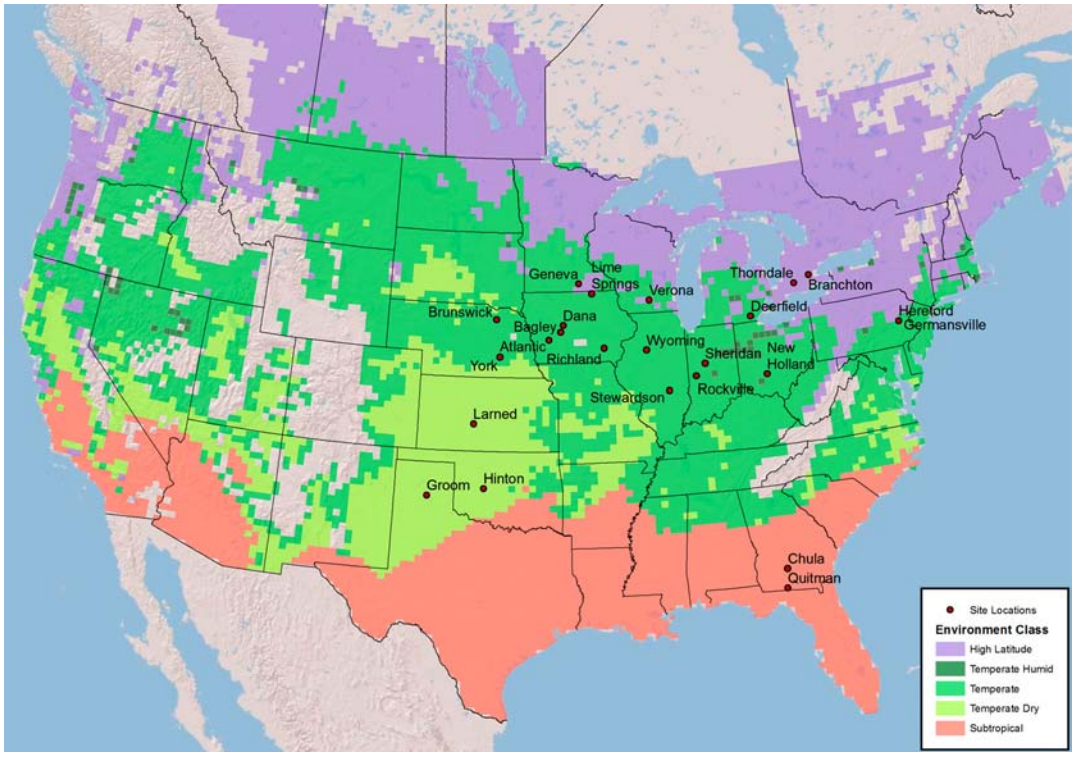


**Figure 7.** Environmental classification of long-term abiotic macroenvironment types for maize production in North America using the classification system described by Löffler et al.[39] and 30 year (1982−2012) weather data.


dx.doi.org/10.1021/jf502158q | J. Agric. Food Chem. 2014, 62, 9916−9926

noted that the equivalence test, as well as any statistical test, cannot be relied on as the sole tool to evaluate the compositional equivalence of a GM crop. In fact, because the equivalence limits are estimated values that depend on which reference lines are included in a given study, this particular equivalence testing approach is not a legitimate statistical equivalence test. A classical equivalence test requires the equivalence limits to be fixed a priori.[40] Tolerance intervals generated from cumulative historical data are more robust and provide a more adequate inference to the natural ranges of the population values compared to equivalence intervals generated from a single multisite field study.

**Advantages of Tolerance Interval Approach.** Environmental and genotypic variances are generally large contributors to the overall total variation of composition data values.[9−11,13] Appropriate and adequate sampling of both environments and genotypes is critical to accurately estimating the total variance of the population and the resulting tolerance intervals. Our model-based parametric tolerance interval approach has many advantages over other approaches for use in substantial equivalence assessment of a given GM crop. This approach considers the correlated and unbalanced data structure of multisite field studies over multiple seasons, as opposed to nonparametric and classical parametric approaches, which assume the data are *iid*. The approach can be executed using SAS or other appropriate statistical software and is more computationally feasible than some other alternatives that require statistical resampling and heavy computation. The approach is conservative in that it provides a tolerance interval narrower than a true 99%-content, 95%-confidence tolerance interval. The conservative nature of this approach is acceptable in the context of GM crop safety assessment because it is less likely to incorrectly conclude that a statistical difference is not biologically relevant. The two parameters associated with this tolerance interval approach, $m$ and $R_0$, can be used to evaluate the adequacy of a data set in the context of the correlated and unbalanced data structure. The use of $m$ and $R_0$ for data set evaluation is of greater practical value compared to a universal minimum sample size $n$ applied to all composition analytes regardless of data structure. Tolerance intervals generated from cumulative historical data are more robust than reference data ranges or equivalence intervals derived from a single study, because cumulative historical data provide a more adequate sample size as well as greater environmental and genotypic diversity. It is appropriate to use these tolerance intervals as reference ranges to evaluate biological relevance of statistical differences identified during substantial equivalence assessment of a GM crop.

The use of literature ranges in a substantial equivalence assessment is a complementary way to evaluate the biological context of statistical differences. In the case of the 2003−2011 maize grain cumulative historical data set, some tolerance intervals were narrower than the corresponding literature ranges, and some were wider (data not shown). The width of a given literature range may be influenced by the number of maize genotypes represented (which may be larger or smaller than the number of genotypes represented by Pioneer brand non-GM commercial maize lines in the corresponding tolerance interval derived from the 2003−2011 maize grain cumulative historical data set). The width of the literature range may also be restricted by the infrequent updates of existing data sources, such as the International Life Sciences Institute (ILSI) Crop Composition Database (which is a compilation of non-GM crop composition data from a number of companies engaged in the agricultural biotechnology industry),[41,42] or by the lack of recent publications to add to the literature ranges. Because access to a diverse range of non-GM commercial lines can be restricted due to proprietary concerns, and given the premise that all non-GM commercial lines have a history of safe use, it is therefore worthwhile to consider establishing a common set of tolerance intervals and/or equivalence intervals across the agricultural biotechnology industry. Currently, the necessary information for model-based tolerance interval construction is not available from the ILSI Crop Composition Database[42] (e.g., distinguishing between different lines and different locations). There might be future opportunity to expand the existing ILSI Crop Composition Database with this additional information or to establish a different database that is suitable for this purpose.

In conclusion, under the substantial equivalence framework for crop composition assessment, it is important to acknowledge the value of cumulative historical data. One way to utilize cumulative historical data is to generate a set of tolerance intervals using an approach that appropriately considers the correlated data structure. Our tolerance interval approach has a solid theoretical basis, provides an ease of implementation, and offers a practical solution to the representation of natural variation derived from crop populations with an established history of safe use for practitioners in the field of GM crop safety assessment.

## ■ ASSOCIATED CONTENT

### Supporting Information

Supplementary method, SAS code for construction of the tolerance interval, and weather data in Supplementary Tables 1−5. This material is available free of charge via the Internet at http://pubs.acs.org.

## ■ AUTHOR INFORMATION

### Corresponding Author

*(B.H.) Phone: (515) 535-4920. Fax: (515) 535-7279. E-mail: Bonnie.Hong@Pioneer.com.

### Notes

The authors declare no competing financial interest.

## ■ ACKNOWLEDGMENTS

We express appreciation to Qing Kang for work contributing to the development of the model-based tolerance interval approach and for statistical discussion; to Yiwei Wang and Xiaoxiao Kong for simulation study conduct; to Brian Baumhover and Chris Linderblood for maize hybrid and unique environment identification, respectively; to Brian Baumhover, Chris Linderblood, Wayne Mehre, Emily Moellring, Lee Prochaska, Brad Atchison, and David Roberts for their work conducting field studies from which data were used in constructing tolerance intervals; to Emily Huang and Tim Andersen for figure preparation; to Nancy Wilmeth and Anne Carlson for manuscript preparation and quality control review, respectively; and to Hiroshi Omori with the University of Tokyo for manuscript development and preparation.

## ■ ABBREVIATIONS USED

GM, genetically modified; *iid*, identically and independently distributed; CRM, comparative relative maturity; OECD, Organisation for Economic Co-operation and Development;

HPLC-UV, high-performance liquid chromatography with ultraviolet detection; FAME, fatty acid methyl esters; GC-FID, gas chromatography with flame ionization detection; LMM, linear mixed model; SAS, Statistical Analysis System; EFSA, European Food Safety Authority; ILSI, International Life Sciences Institute

## REFERENCES


(1) Codex Alimentarius Commission. *Guideline for the Conduct of Food Safety Assessment of Foods Derived from Recombinant-DNA Plants*; Codex Alimentarius: Rome, Italy, 2008; CAC/GL 45-2003.

(2) Organisation for Economic Co-operation and Development (OECD). *Safety Evaluation of Foods Derived by Modern Biotechnology: Concepts and Principles*; OECD: Paris, France, 1993.

(3) Kuiper, H. A.; Kleter, G. A.; Noteborn, H. P. J. M.; Kok, E. J. Substantial equivalence − an appropriate paradigm for the safety assessment of genetically modified foods? *Toxicology* **2002**, *181−182*, 427−431.

(4) Organisation for Economic Co-operation and Development (OECD). *Report of the OECD Workshop on the Toxicological and Nutritional Testing of Novel Foods*; OECD: Paris, France, 1998; SG/ICGB(1998)1/FINAL.

(5) Codex Alimentarius Commission. *Foods Derived from Biotechnology*; Food and Agriculture Organization of the United Nations, World Health Organization: Rome, Italy, 2003.

(6) World Health Organization (WHO). *Application of the Principles of Substantial Equivalence to the Safety Evaluation of Foods or Food Components from Plants Derived by Modern Biotechnology*; Report of a WHO Workshop; WHO: Geneva, Switzerland, 1995; WHO/FNU/FOS/95.1.

(7) International Life Sciences Institute (ILSI). *The Safety Assessment of Novel Foods*, Guidelines Prepared by the ILSI Europe Novel Food Task Force; ILSI: Brussels, Belgium, 1995.

(8) Food and Agiculture Organization of the United Nations (FAO)/World Health Organization (WHO). *Safety Aspects of Genetically Modified Foods of Plant Origin*; Report of a Joint FAO/WHO Expert Consultation on Foods Derived from Biotechnology; WHO: Geneva, Switzerland, 2000; WHO/SDE/PHE/FOS/00.6.

(9) Reynolds, T. L.; Nemeth, M. A.; Glenn, K. C.; Ridley, W. P.; Astwood, J. D. Natural variability of metabolites in maize grain: differences due to genetic background. *J. Agric. Food Chem.* **2005**, *53* (26), 10061−10067.

(10) Harrigan, G. G.; Stork, L. G.; Riordan, S. G.; Reynolds, T. L.; Ridley, W. P.; Masucci, J. D.; MacIsaac, S.; Halls, S. C.; Orth, R.; Smith, R. G.; Wen, L.; Brown, W. E.; Welsch, M.; Riley, R.; McFarland, D.; Pandravada, A.; Glenn, K. C. Impact of genetics and environment on nutritional and metabolite components of maize grain. *J. Agric. Food Chem.* **2007**, *55* (15), 6177−6185.

(11) Harrigan, G. G.; Lundry, D.; Drury, S.; Berman, K.; Riordan, S. G.; Nemeth, M. A.; Ridley, W. P.; Glenn, K. C. Natural variation in crop composition and the impact of transgenesis. *Nat. Biotechnol.* **2010**, *28* (5), 402−404.

(12) Jaureguy, L. M.; Rodriguez, F. L.; Zhang, L.; Chen, P.; Brye, K.; Oosterhuis, D.; Mauromoustakos, A.; Clark, J. R. Planting date and delayed harvest effects on soybean seed composition. *Crop Sci.* **2013**, *53* (5), 2162−2175.

(13) Privalle, L. S.; Gillikin, N.; Wandelt, C. Bringing a transgenic crop to market: where compositional analysis fits. *J. Agric. Food Chem.* **2013**, *61* (35), 8260−8266.

(14) Kitta, K. Availability and utility of crop composition data. *J. Agric. Food Chem.* **2013**, *61* (35), 8304−8311.

(15) Graybill, F. A. Applications of the general linear model. In *Theory and Application of the Linear Model*; Duxbury Press: Boston, MA, USA, 1976; pp 270−275.

(16) Hahn, G.; Meeker, W. Q. Distribution-free statistical intervals. In *Statistical Intervals: A Guide for Practitioners*; Wiley: Hoboken, NJ, USA, 1991; pp 75−99, 325−327.

(17) Ridley, W. P.; Sidhu, R. S.; Pyla, P. D.; Nemeth, M. A.; Breeze, M. L.; Astwood, J. D. Comparison of the nutritional profile of glyphosate-tolerant corn event NK603 with that of conventional corn (*Zea mays* L.). *J. Agric. Food Chem.* **2002**, *50* (25), 7235−7243.

(18) Berman, K. H.; Harrigan, G. G.; Riordan, S. G.; Nemeth, M. A.; Hanson, C.; Smith, M.; Sorbet, R.; Zhu, E.; Ridley, W. P. Compositions of seed, forage, and processed fractions from insect-protected soybean MON 87701 are equivalent to those of conventional soybean. *J. Agric. Food Chem.* **2009**, *57* (23), 11360−11369.

(19) Herman, R. A.; Scherer, P. N.; Phillips, A. M.; Storer, N. P.; Krieger, M. Safe composition levels of transgenic crops assessed via a clinical medicine model. *Biotechnol. J.* **2010**, *5* (2), 172−182.

(20) Smith, A. B.; Cullis, B. R.; Thompson, R. The analysis of crop cultivar breeding and evaluation trials: an overview of current mixed model approaches. *J. Agric. Sci.* **2005**, *143* (06), 449−462.

(21) Abendroth, L. J.; Elmore, R. W.; Boyer, M. J.; Marlay, S. K. *Corn Growth and Development*; Iowa State University Extension: Ames, IA, USA, 2011; PMR 1009.

(22) Organisation for Economic Co-operation and Development (OECD). *Consensus Document on Compositional Considerations for New Varieties of Maize (Zea mays): Key Food and Feed Nutrients, Anti-nutrients and Secondary Plant Metabolites*; Series on the Safety of Novel Foods and Feeds, No. 6; OECD: Paris, France, 2002; ENV/JM/MONO(2002)25.

(23) Rogers, S. R.; Pesti, G. M. Determination of tryptophan from feedstuffs using reverse phase high-performance liquid chromatography. *J. Micronutr. Anal.* **1990**, *7* (1), 27−35.

(24) Association of Official Analytical Chemists (AOAC). Fat acidity − grains. Method 939.05. In *Official Methods of Analysis of AOAC International*, 17th ed.; Horowitz, W., Ed.; AOAC International: Gaithersburg, MD, USA, 2000.

(25) American Oil Chemists' Society (AOCS). Preparation of methyl esters of fatty acids. Method Ce 2-66. In *Official Methods and Recommended Practices of the American Oil Chemists' Society*, 5th ed.; Firestone, D., Ed.; AOCS: Champaign, IL, USA, 1997.

(26) American Oil Chemists' Society (AOCS). Determination of fatty acids in edible oils and fats by capillary GLC. Method Ce 1e-91. In *Official Methods and Recommended Practices of the American Oil Chemists' Society*, 5th ed.; Firestone, D., Ed.; AOCS: Champaign, IL, USA, 2000.

(27) Krishnamoorthy, K.; Mathew, T. *Statistical Tolerance Regions: Theory, Applications, and Computation*; Wiley: Hoboken, NJ, USA, 2009.

(28) Fai, A. H. T.; Cornelius, P. L. Approximate F-tests of multiple degree of freedom hypotheses in generalized least squares analyses of unbalanced split-plot experiments. *J. Stat. Comput. Simul.* **1996**, *54* (4), 363−378.

(29) Bagui, S. C.; Bhaumik, D. K.; Parnes, M. One-sided tolerance limits for unbalanced m-way random-effects ANOVA models. *J. Appl. Stat. Sci.* **1996**, *3* (2/3), 135−148.

(30) Mee, R. W. $\beta$-expectation and $\beta$-content tolerance limits for balanced one-way ANOVA random model. *Technometrics* **1984**, *26* (3), 251−254.

(31) Liao, C. T.; Lin, T. Y.; Iyer, H. K. One- and two-sided tolerance intervals for general balanced mixed models and unbalanced one-way random models. *Technometrics* **2005**, *47* (3), 323−335.

(32) E, L.; Hannig, J.; Iyer, H. Fiducial intervals for variance components in an unbalanced two-component normal mixed linear model. *J. Am. Stat. Assoc.* **2008**, *103* (482), 854−865.

(33) Liao, C. T.; Iyer, H. K. A tolerance interval for the normal distribution with several variance components. *Stat. Sinica* **2004**, *14* (1), 217−229.

(34) Lovell, D. P. Biological importance and statistical significance. *J. Agric. Food Chem.* **2013**, *61* (35), 8340−8348.

(35) Herman, R. A.; Phillips, A. M.; Collins, R. A.; Tagliani, L. A.; Claussen, F. A.; Graham, C. D.; Bickers, B. L.; Harris, T. A.; Prochaska, L. M. Compositional equivalency of Cry1F corn event TC6275 and conventional corn (*Zea mays* L.). *J. Agric. Food Chem.* **2004**, *52* (9), 2726−2734.

(36) Lundry, D. R.; Burns, J. A.; Nemeth, M. A.; Riordan, S. G. Composition of grain and forage from insect-protected and herbicide-tolerant corn, MON 89034 × TC1507 × MON 88017 × DAS-59122-7 (Smartstax), is equivalent to that of conventional corn (*Zea mays* L.). *J. Agric. Food Chem.* **2013**, *61* (8), 1991−1998.
(37) Venkatesh, T. V.; Breeze, M. L.; Liu, K.; Harrigan, G. G.; Culler, A. H. Compositional analysis of grain and forage from MON 87427, an inducible male sterile and tissue selective glyphosate-tolerant maize product for hybrid seed production. *J. Agric. Food Chem.* **2014**, *62* (8), 1964−1973.
(38) European Food Safety Authority (EFSA) Panel on Genetically Modified Organisms (GMO). Guidance for risk assessment of food and feed from genetically modified plants. *EFSA J.* **2011**, *9* (5), 2150.
(39) Löffler, C. M.; Wei, J.; Fast, T.; Gogerty, J.; Langton, S.; Bergman, M.; Merrill, B.; Cooper, M. Classification of maize environments using crop simulation and geographic information systems. *Crop Sci.* **2005**, *45* (5), 1708−1716.
(40) Wellek, S. *Testing Statistical Hypotheses of Equivalence*; Chapman and Hall/CRC Press: Boca Raton, FL, USA, 2003.
(41) Ridley, W. P.; Shillito, R. D.; Coats, I.; Steiner, H.-Y.; Shawgo, M.; Phillips, A.; Dussold, P.; Kurtyka, L. Development of the International Life Sciences Institute crop composition database. *J. Food Compos. Anal.* **2004**, *17* (3−4), 423−438.
(42) Alba, R.; Phillips, A.; Mackie, S.; Gillikin, N.; Maxwell, C.; Brune, P.; Ridley, W.; Fitzpatrick, J.; Levine, M.; Harris, S. Improvements to the International Life Sciences Institute crop composition database. *J. Food Compos. Anal.* **2010**, *23* (7), 741−748.

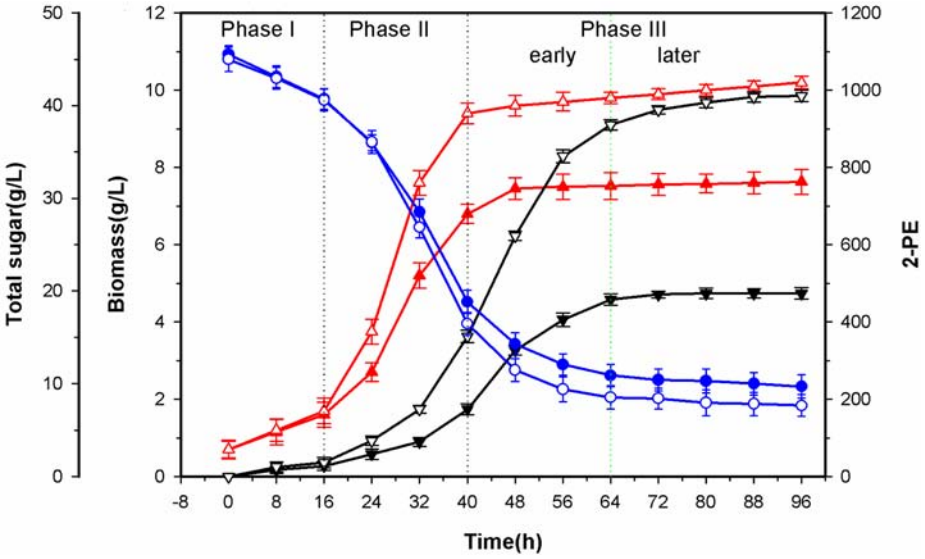


**Figure 1.** Time course profiles of key fermentation parameters (dry cell weight, total sugar, and 2-PE concentration) with 2 L airlift loop reactors. Red triangles represent dry cell weight, black inverted triangles represent 2-PE production, and blue circles represent total sugar. Solid and open symbols represent C1 and C2 conditions, respectively. Values shown represent the means of five independent experiments, and error bars represent standard deviations of five values.

understanding of the influences of intracellular metabolites on 2-PE production, as well as revealing the mechanism of MMC high-producing 2-PE at a systematic level, becomes increasingly important.

Here, the MMC utilizing CMW were employed to produce 2-PE under different conditions. Differences in 2-PE production and cell growth are presented, and comparative metabolomics was applied to analyze the differences for overall intracellular metabolites of microbes. Feeding experiments were further carried out to verify the analysis results, and the metabolic mechanism hypothesis of the MMC high-producing 2-PE was proposed eventually.

## MATERIALS AND METHODS

**Wastewater.** Cane molasses wastewater (CMW), discharged in the pretreatment of cane molasses and alcohol fermentation process, was obtained from a cane sugar refinery in Nanning, Guangxi Province, China. CMW was centrifuged at 10000*g* for 10 min, the insoluble impurities were removed, and then an appropriate concentration of ammonium sulfate and sodium dihydrogen phosphate at the ratio chemical oxygen demand (COD):N:P = 100:2:1, as well as 6 g/L Phe, were added into the supernatant.

**Chemicals.** Succinic acid was purchased from Fluka (Buchs, Switzerland). Spectroscopic-grade methanol, acetonitrile, and trichloroacetic acid were purchased from Concord (Tianjin, China). *N*-Methyl-*N*-(trimethylsilyl)trifluoroacetamide (MSTFA) was purchased from J&K Scientific. Pyridine, methoxyamine hydrochloride, glucose 6-phosphate, ribulose 5-phosphate, ribose 5-phosphate, and fructose 6-phosphate were obtained from Sigma–Aldrich (St. Louis, MO). Distilled water was purified by use of the Milli-Q20 system (Millipore, Billerica, MA).

**Microbes and Culture Conditions.** The strains used in this study were derived from Mu et al.[18] in our previous work. They were identified as *Bacillus* sp., *Pseudomonas* sp., *Candida tropicalis*, *A. niger*, *S. cerevisiae*, *Kluyveromyces hubeiensis*, *Rhodotorula glutinis*, and *Issatchenkia orientalis*. All the fungi in this study were proposed as main 2-PE producers.[2,6] The eight strains could tolerate high concentrations of 2-PE, and mutual cooperation between the strains could well decolorize the wastewater and achieve resource ultilization.[18]According to the Kyoto Encyclopedia of Genes and Genomes (KEGG) database, each of the microbes contains six basic metabolic pathways: Embden–Meyerhof–Parnas (EMP) pathway, tricarboxylic acid (TCA) cycle, pentose phosphate pathway (PPP), shikimate pathway, amino acid metabolism, and fatty acid metabolism.

Airlift loop reactors with 2 L volume were used in the experiments, and 1.2 L of fermentation broth was transferred into each reactor. The initial operating conditions (C1) were set as temperature 30 °C, pH 5.0 ± 0.1, and air flow rate 0.4 vvm. The optimized operating conditions (C2) were kept as the temperature 35 °C, pH 7.0 ± 0.1, and air flow 0.8 vvm.

**Analysis Method.** The reactor operated for 96 h in batch cultivation mode. Five parallel cultures were sampled with 10 mL aliquots regularly. Biomass, calculated by dry cell weight, was measured by filtering through a preweighed 45 μm pore size filter, washing with 0.9% NaCl (w/w), and then drying to a constant weight at 80 °C.[19] Total sugar concentration in the fermentation broth was determined by anthrone colorimetry.[20] 2-PE was quantified by gas chromatography (GC, Agilent 6890N); conditions were set as PEG-20 M capillary column (30 m, 0.32 mm internal diameter, 0.25 μm film thickness, China) at 210 °C with a nitrogen carrier gas flow rate of 90 mL/min. A flame ionization detector was employed with hydrogen flow rate of 500 mL/min and air flow rate of 50 mL/min. The detection and sample temperatures were 210 and 240 °C, respectively.

**Sampling, Quenching, and Extraction of Intracellular Metabolites.** Samples (10 mL) for metabolic profiling were harvested at 24, 40, 64, and 80 h from the initial inoculation. The mixed cells were quenched and extracted as in previous reports[16,21] with slight modifications. For metabolite extraction, 1 mL of cold methanol–water solution (50% v/v, −40 °C) was added into cells, which were then frozen in liquid nitrogen for 1 min. The freeze–thaw cycle was repeated three times. After centrifugation at 5000*g* for 3 min, the supernatant was collected. Another 2.5 mL of cold methanol–water solution (60% v/v, −40 °C) was added into the precipitate for further extraction. After mixing and centrifugation at 10000*g* for 3 min, the extract was pooled with the former one, and the combined sample was centrifuged at 10000*g* for 5 min again. Finally, 100 μL extracts, mixed with 10 μL of succinic acid-$d_4$ (0.1 mg/mL) as internal standard, were lyophilized (D307 Christ, Germany) at −40 °C for 3–4 h and stored at −80 °C for further processing.

**Determination of Intracellular Metabolites.** Intracellular metabolites were determined by gas chromatography–mass spectrometry (GC-MS) and liquid chromatography–tandem mass spectrometry (LC-MS/MS). The apparatus, specific process, and parameter selection were performed according to Xia et al.[19] with slight changes

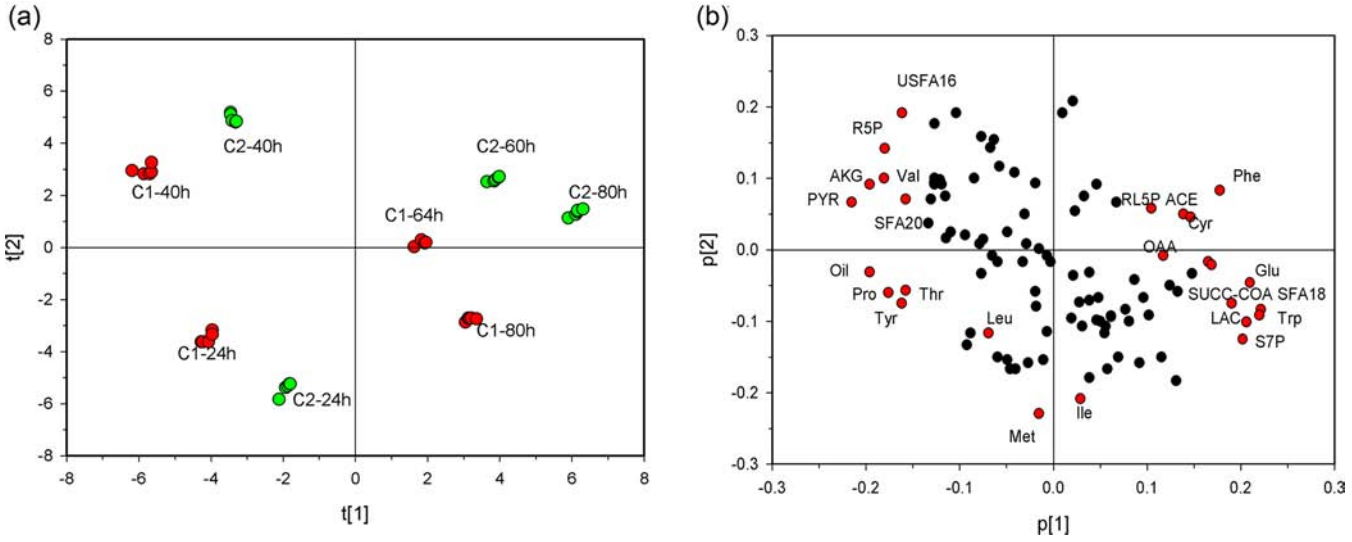


**Figure 2.** (a) PCA score and (b) loading plots.

in parameter settings. Derivatized sample (1 $\mu$L) was injected with a split ratio of 1:10, and scan range was set as 50−800 $m/z$ to acquire mass spectra in GC-MS.

High-performance liquid chromatography−electrospray ionization tandem mass spectrometry (HPLC-ESI-MS/MS) analysis was performed to quantify CoA esters. Extraction and analysis of intracellular CoA esters was carried out according to the method described by Park et al.[22] Parameters of selective ion scan of ester coenzyme A ($m/z$ parent > $m/z$ daughter) were monitored as a series of chromatograms: acetyl-CoA for 810/303, succinyl-CoA for 868/361. The area of each metabolite peak was normalized with the internal standard and cell biomass on the same chromatograph.

The generated normalized peak areas (variables) were imported into SIMCA-P v 11.0 (Umetrics, Umea, Sweden) for multivariate statistical analysis. Principal component analysis (PCA) and partial least-squares (PLS) discriminant analysis were carried out to investigate intracellular metabolite profiles. PCA, an unsupervised method, can gain insight into the nature of multivariate data. The PCA score plot was used to judge the similarities and differences among the samples by similar scores clustering together and different scores scattering. In the loading plot, each data point represented a unique metabolite, which was important to discriminate metabolic differences.[19] PLS analysis, a supervised method, was subsequently applied to evaluate the relationship between metabolites and products.[23] The variable importance in the projection (VIP) index was introduced to estimate the contribution of each metabolite variable to the pattern recognition quantitatively. Generally, a metabolite with VIP value greater than 1 illustrates a significant contribution to the separation of sample groups within the PLS model, and the higher the VIP value of a metabolite, the greater contribution it has.[19]

**Statistical Analysis.** Two-tailed $t$-tests were performed on specific metabolites by Microsoft Excel. At least a $P$ value < 0.01 was considered statistically different. Five replicates were used to perform multivariate analysis for each sample. Data were shown as the mean ± standard deviations for each analyzed sample.

## RESULTS AND DISCUSSION

**Performance of MMC Fermentation under C1 and C2 Conditions.** Fermentation performance under C1 and C2 conditions is shown in Figure 1. According to the change of biomass, the entire fermentation process could be divided into lag phase (phase I, 0−16 h), logarithmic phase (phase II, 16−40 h), and stationary phase (phase III, 40−96 h).

In lag phase, the mixed microbes were adapting themselves to the substrates, and the utilization of corresponding substrates and synthesis of some enzymes were being activated.[24] The biomass and total sugar consumption under the two conditions showed no significant difference. The biomass increased to 0.18 (C1) and 0.19 (C2) g/L. Little 2-PE was detected (Figure 1). In logarithmic phase, the highest biomass was achieved, up to 6.8 and 9.4 g/L under C1 and C2 conditions, respectively. The total sugar concentration decreased from 45 to 18.8 (C1) and 16.5 (C2) g/L. The production of 2-PE accumulated up to 175 (C1) and 361 (C2) mg/L, beginning to present significant differences. But it was not the main phase of 2-PE biosynthesis (Figure 1). During this period, some preferable nitrogen source ammonium sulfate existing in wastewater was first absorbed to facilitate the rapid growth of MMC but contributed little to 2-PE biosynthesis. When ammonium sulfate was depleted, the uptake of Phe was begun to synthesize 2-PE.[9] In stationary phase (phase III), cell growth stopped. As the main nitrogen source, Phe was utilized for 2-PE synthesis. During 40−64 h, the productivity of 2-PE was 0.01 (C1) and 0.02 (C2) $g{\cdot}L^{-1}{\cdot}h^{-1}$. The 2-PE concentration reached 459 (C1) and 910 (C2) mg/L, 2.62- and 2.52-fold higher compared to phase II, respectively. However, during 64−96 h, the production of 2-PE remained invariable with extremely low substrate consumption. The final concentration of 2-PE under C2 conditions (987 mg/L) was 2.07-fold higher than that under C1 conditions (477 mg/L). Therefore, based on the variation of 2-PE biosynthesis, phase III was divided into early stationary phase (40−64 h) and later stationary phase (64−96 h) for discussion below. Results indicated that the biosynthesis of 2-PE under two conditions mainly occurred in early stationary phase, and the MMC presented a perfect performance in production of 2-PE under C2 conditions.

Taken together, the MMC exhibited different fermentation behaviors under C1 and C2 conditions. To explore the reason why microbes had higher production under C2 conditions, it is necessary to study the intracellular metabolite profile of the mixed microbes. Hence, the changing of MMC intracellular metabolites would be profiled, and the metabolic mechanism hypothesis of MMC high-producing 2-PE could be proposed eventually.

**Identification of Key Metabolites and Metabolic Pathways Closely Associated with 2-PE Biosynthesis.** In total, 102 intracellular metabolites were identified by GC-


dx.doi.org/10.1021/jf502239d | J. Agric. Food Chem. 2014, 62, 9927−9935

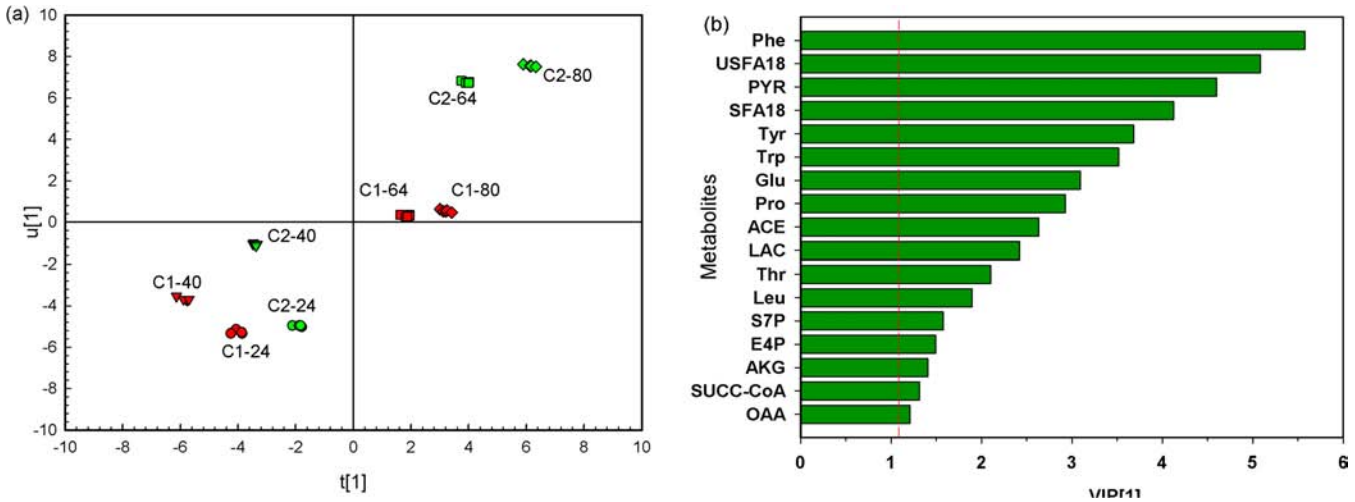


**Figure 3.** Results of PLS analysis: (a) PLS score plot $t[1]/u[1]$; (b) VIP plot.

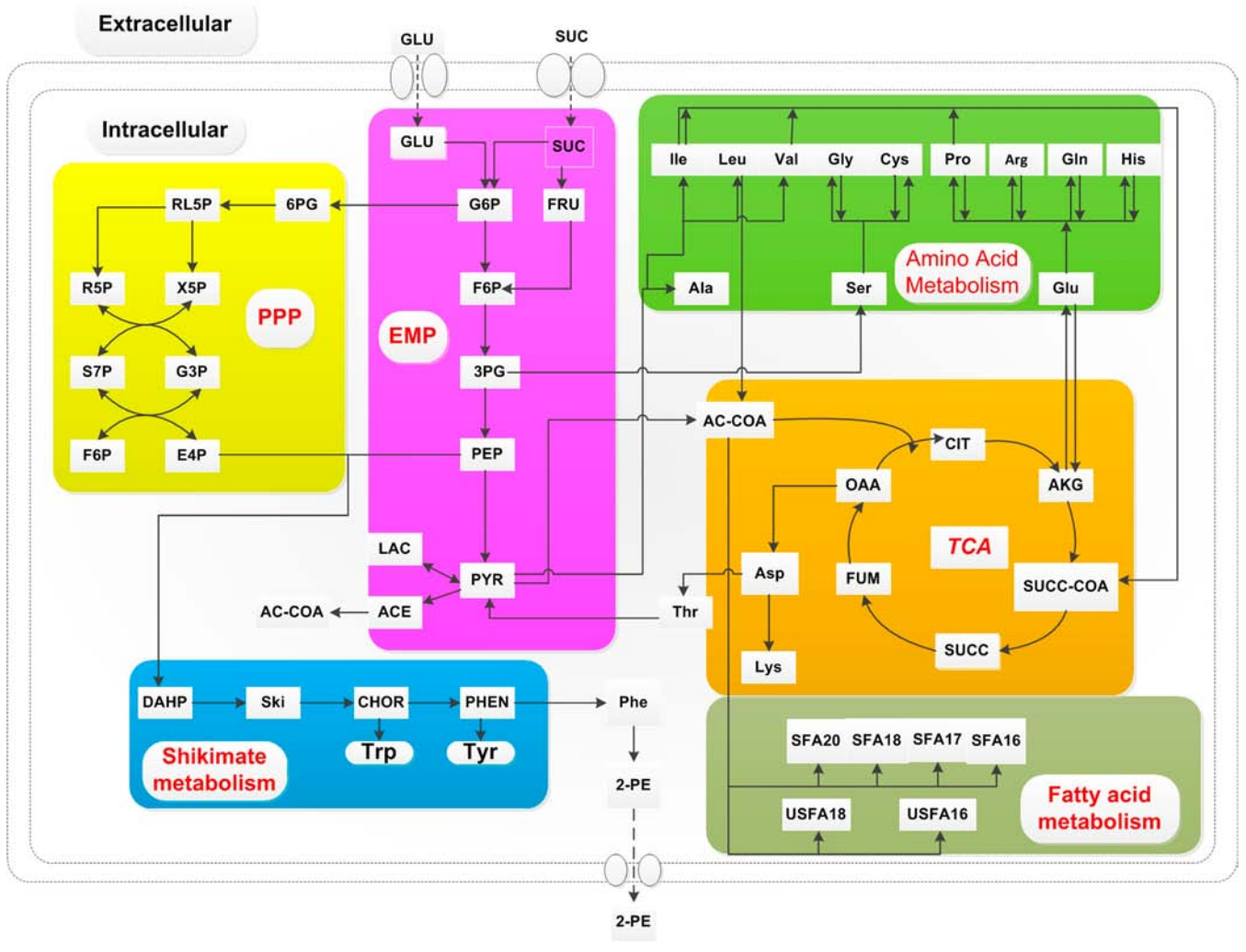


**Figure 4.** Schematic diagram of main metabolites in key pathways.

MS, LC-MS/MS, and HPLC-ESI-MS/MS, including sugars, organic acids, alcohols, amino acids, fatty acids, amines, and other compounds (see Table S1 in Supporting Information). The intracellular metabolic differences under C1 and C2 conditions were analyzed by multivariate statistical analysis. Initially, PCA ($R^2$ = 0.91, $Q^2$ = 0.94) was performed. A tight clustering of five parallels for individual time points and a clear separation between the different conditions revealed quite clear discrimination between samples under different culture conditions and fermentation times (Figure 2a). The result


dx.doi.org/10.1021/jf502239d | J. Agric. Food Chem. 2014, 62, 9927−9935

indicated that metabolomics was suitable to monitor culture processes and metabolic characteristics under different conditions.[25] In the loading plot (Figure 2b), each data point represented a unique metabolite and reflected the contribution of a specific component to the loading value. It demonstrated that the intermediate metabolites (represented by red circles in Figure 2b) from the EMP pathway, TCA cycle, PPP, shikimate pathway, amino acid metabolism, and fatty acid metabolism contributed most to the separate clustering.

In addition, PLS was applied to further verify the differences and identify the metabolites mainly responsible for discrimination between the two conditions. Owing to relatively high 2-PE production under C2 conditions, the samples were located in the upper right quadrant at 64 and 80 h, while the other samples were located in the lower left quadrant of the plot (Figure 3a). The significant discrimination on the PLS score plot profiling reflected the MMC metabolic differences under different conditions and stages. The contribution of each intracellular metabolite to 2-PE was shown by VIP score. Metabolites correlated to the first component (VIP score >1) were selected for further investigation. A total of 17 identified metabolites including lactate (LAC), pyruvate (PYR), acetate (ACE), oxaloacetate (OAA), succinyl-CoA (SUCC−COA), α-ketoglutarate (AKG), sedoheptulose-7-phosphate (S7P), erythrose 4-phosphate (E4P), L-tyrosine (Tyr), L-tryptophan (Trp), L-phenylalanine (Phe), L-glutamate (Glu), L-proline (Pro), L-leucine (Leu), L-threonine (Thr), stearic acid (SFA18), and oleic acid (USFA18) were found to be the key metabolites that were responsible for differentiation between the two conditions (Figure 3b). Those metabolites were involved in six basic metabolic pathways stated above (Figure 4) and will be discussed below in detail.

**Analysis of Six Basic Metabolic Pathways.** *Embden−Meyerhof−Parnas Pathway.* As illustrated in Figure 5, EMP

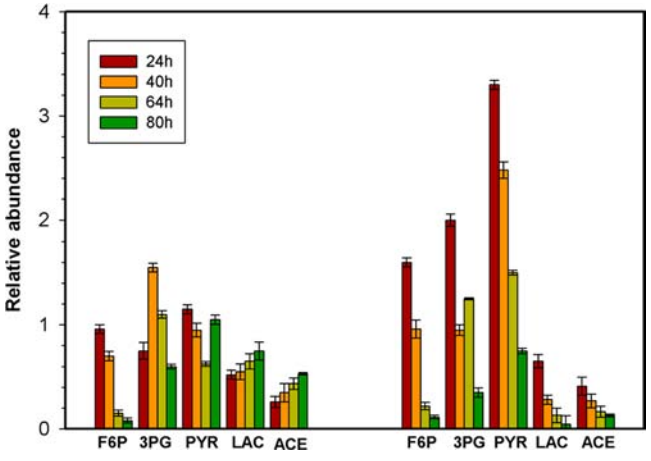


**Figure 5.** Relative abundance of intracellular metabolites in EMP pathway under (left) C1 and (right) C2 conditions. F6P, fructose 6-phosphate; 3PG, 3-phosphoglyceric acid; PYR, pyruvate; LAC, lactate; ACE, acetate.

metabolite levels under C2 conditions were higher than those under C1 conditions at 24 and 40 h. However, few differences could be seen in the EMP pathway at 40 and 80 h. In the whole fermentation process, 3-phosphoglyceric acid (3PG) presented different trends between C1 and C2. The relative abundance of 3PG under C1 conditions rose from 0.75 (24 h) to 1.55 (40 h) and then decreased to 0.6 (80 h). But under C2 conditions, it declined from 2 (24 h) to 0.95 (40 h), then rose slightly up to 1.25 (64 h), and eventually fell to 0.35 (80 h). The change of 3PG was closely related to levels of its derivatives such as serine, glycine, and cysteine (Figure 4). During 24−40 h, with 3PG being consumed rapidly, amino acids were quickly synthesized under C2 conditions. During stationary phase, synthetic rates of amino acids slowed down with the accumulation of 3PG; afterward 3PG was consumed for maintaining the survival of microbes. The relative abundance of pyruvate under C2 conditions was obviously higher than that under C1 conditions at 24 and 40 h. Then it dropped sharply in the entire fermentation process, falling from 3.3 to 0.75. But no significant change was found for C1. However, lactate and acetic acid under C1 conditions were accumulated, and the relative abundance reached 0.75 and 0.53, respectively, at 80 h. Conversely, the relative abundance of lactate and acetate under C2 conditions was extremely low at 80 h: 0.043 and 0.13, respectively. According to the carbon metabolic network of microorganisms, pyruvate flux could be toward lactate, acetate, amino acids, or acetyl-CoA. These metabolic branches competed with each other for carbon flux, and the flux distribution determined the metabolic state of MMC.[26] Results indicated that some pyruvate metabolic flows under C1 conditions distributed to lactate and acetate, resulting in accumulation of lactate and acetate during stationary phase. However, under C2 conditions, pyruvate was mainly expended in anabolism or converted to acetyl-CoA, and intracellular lactate and acetate were utilized. The high VIP from PLS suggested that lactate (VIP = 2.3), acetate (VIP = 2.5), and pyruvate (VIP = 4.37) were significant relevant to 2-PE biosynthesis. Therefore, feeding experiments were carried out to prove the analysis above, under the premise that carbon flux distribution to acetyl-CoA under C2 conditions was still insufficient. Pyruvate (5 g/L), lactate (2 g/L), and acetate (0.5 g/L) were added at 16 h under C2 conditions, since their high concentration would make the pH drop and cause microorganism overload.[27] It was found that 2-PE production was increased to 1077, 1204, and 1180 mg/L, respectively, suggesting that an improvement of carbon flux distribution to acetyl-CoA would benefit the accumulation of 2-PE.

*Tricarboxylic Acid Cycle.* TCA cycle metabolite levels under C2 conditions were apparently higher than those under C1 conditions at 24 and 40 h (Figure 6). It demonstrated that the intracellular metabolites NADH and ATP under C2 conditions were higher at 24 and 40 h, providing more material, reduction−oxidation, and energy to maintain microbe energetics and keep the 2-PE synthesis system highly efficient.[28] The levels of OAA, AKG, SUCC−COA, and FUM dropped at 64 and 80 h compared to those at 24 h. Furthermore, the relative abundance of intracellular OAA under C2 conditions was lower than that under C1 at 64 and 80 h, reflecting the weak TCA cycle under C2 conditions during stationary phase. No obvious differences were found for FUM and CIT between C1 and C2. However, AKG and SUCC−COA under C2 conditions were much higher than under C1 conditions. Since AKG and SUCC−COA were correlated with TCA cycle as well as amino acid (Glu and Pro) metabolism (Figure 4), higher AKG and SUCC−COA level as well as lower citric acid level indirectly reflected the higher catabolism of Glu and Pro. Furthermore, not only could AKG provide NADH for microbes when AKG converted to SUCC−COA, but it could also be regarded as the ammonia receptor in the deamination process of Phe. Therefore, a higher intracellular AKG level under C2

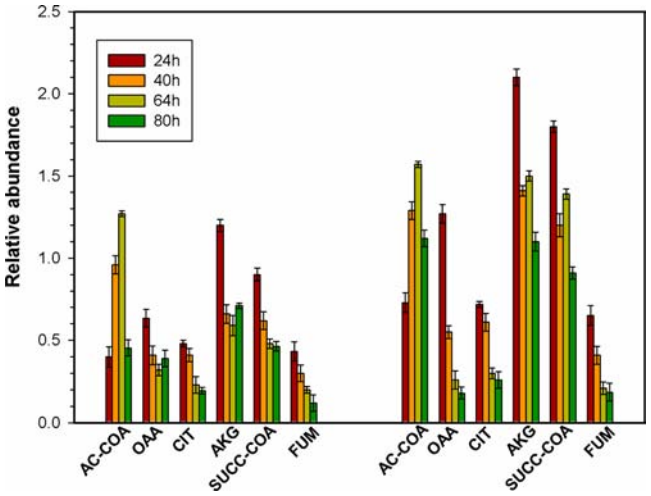


**Figure 6.** Relative abundance of TCA cycle intracellular metabolites under (left) C1 and (right) C2 conditions. AC−COA, acetyl-CoA; OAA, oxaloacetate; CIT, citrate; AKG, $\alpha$-ketoglutarate; SUCC−COA, succinyl-CoA; FUM, fumarate.

conditions during stationary phase contributed to 2-PE biosynthesis.

*Pentose Phosphate Pathway.* PPP metabolites under C2 conditions were at higher levels than under C1 conditions at 24 h (Figure 7). However, the relative abundance of 6-

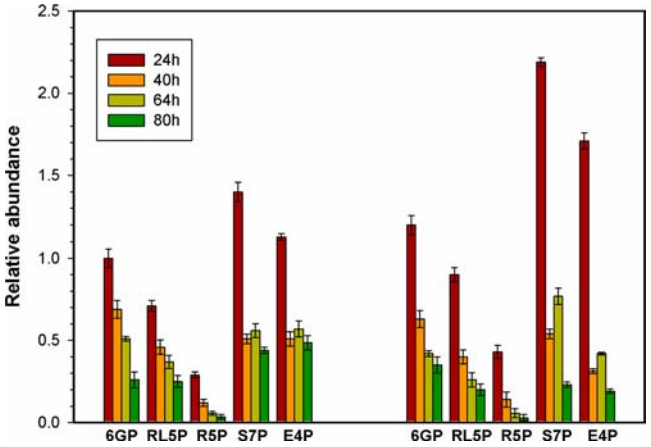


**Figure 7.** Relative abundance of intracellular metabolites in PPP under (left) C1 and (right) C2 conditions. 6PG, glucose 6-phosphate; RL5P, ribulose 5-phosphate; R5P, ribose 5-phosphate; S7P, sedoheptulose 7-phosphate; E4P, erythrose 4-phosphate.

phosphogluconic acid (6PG), ribulose 5-phosphate (RL5P), and ribose 5-phosphate (R5P) under both conditions declined in the entire metabolic process. As precursors of nucleotide synthesis, 6PG, RL5P, and R5P were rapidly consumed in nucleotide synthesis. The level of sedoheptulose 7-phosphate (S7P) and erythrose 4-phosphate (E4P) under C2 conditions declined at 40 h and then slightly increased at 64 h. E4P is a precursor of aromatic amino acid biosynthesis. The level change of S7P and E4P was opposite to that of intracellular aromatic amino acids. This phenomenon might be related to the process where anabolism of aromatic amino acids was repressed and turned into catabolism.[29] It was accompanied by rapid catabolism of Phe and biosynthesis of 2-PE. Therefore, S7P and E4P declined during logarithmic phase, with a slight accumulation during early stationary phase. It could be concluded that S7P and E4P influenced 2-PE biosynthesis by influencing the metabolism of the shikimate pathway indirectly.

*Shikimate Pathway.* The relative abundance of shikimic acid presented similar variation under both conditions. It first increased from 0.45 (24 h) to 0.82 (40 h) and then gradually decreased to 0.35 (80 h) under C2 conditions, and it increased from 0.23 (24 h) to 0.41 (40 h) and then decreased to 0.33 (80 h) under C1 conditions (Figure 8). It can be seen that shikimic

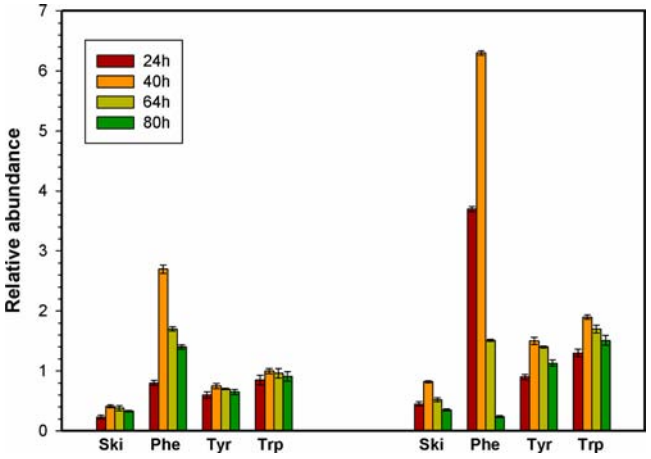


**Figure 8.** Relative abundance of intracellular metabolites in shikimate pathway under (left) C1 and (right) C2 conditions. Ski, shikimic acid; Phe, L-phenylalanine; Tyr, L-tyrosine; Trp, L-tryptophan.

acid was rapidly synthesized during logarithmic phase, which was confirmed by the simultaneous increment of intracellular aromatic amino acids. During stationary phase, the anabolic rate of shikimic acid declined, which could be seen from the decline of intracellular shikimic acid concentration. Meanwhile, the relative abundance of aromatic amino acids Tyr and Trp slowly decreased under both C1 and C2 conditions. It might be that accumulation of excessive aromatic amino acids at 40 h generated feedback inhibition on the activity of key enzymes in the shikimic acid anabolic pathway.[29] As a result, shikimic acid synthesis was repressed and the metabolism of aromatic amino acids was shifted from anabolism to catabolism, promoting 2-PE biosynthesis. The relative abundance of Phe under C2 conditions declined notably from 6.3 at 40 h to 0.14 at 80 h. Phe under C1 conditions also declined in some degree, from 2.7 to 1.4. It was thought that the Ehrlich pathway was activated, leading to rapid decline of Phe as well as biosynthesis of 2-PE during the process.[30] At 40 h, the intracellular Phe level under C2 was higher than that under C1. It may be because metabolism of MMC under C2 conditions was more active, and more nitrogen (Phe) uptake from the environment was needed.[9,31] Subsequently, intracellular Phe was consumed to biosynthesize 2-PE and thus declined sharply.[32]

To prove the analysis above, feeding experiments were performed, with the assumption that the uptake of amino acids from the environment by cells did not saturate. Phe (12 g/L), Tyr (1 g/L), and Trp (1 g/L) were supplied at 32 h under C2 conditions, since a high concentration of Tyr and Trp could compete with Phe for catabolism, which would reduce 2-PE production.[33] The results showed that 2-PE production was increased to 1341, 1200, and 1169 mg/L, for enhancement of 36%, 21.6%, and 18.4%, respectively. This suggested that the appropriate accumulation of intracellular Tyr and Trp could


dx.doi.org/10.1021/jf502239d | J. Agric. Food Chem. 2014, 62, 9927−9935

facilitate the shift of aromatic amino acids from anabolism to catabolism, and high Phe concentration could promote 2-PE biosynthesis through the Ehrlich pathway at the end of logarithmic phase.

*Amino Acid Metabolism.* For amino acid metabolism, changes of various amino acids are shown in Figure 9. These

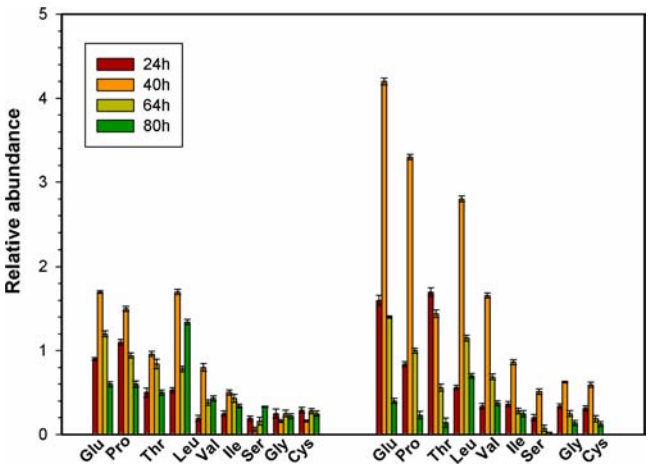


**Figure 9.** Relative abundance of intracellular metabolites in amino acid metabolic pathway under (left) C1 and (right) C2 conditions. Glu, L-glutamate; Pro, L-proline; Thr, L-threonine; Leu, L-leucine; Val, L-valine; Ile, L-isoleucine; Ser, L-serine; Gly, L-glycine; Cys, L-cysteine.

detected amino acids required biosynthetic precursors involved in central carbon metabolism (EMP pathway, TCA cycle, and PPP) and were linked to the synthesis of new cellular components or energy sources needed in fermentation at the expense of the amino acid pool. For example, Gly, Ser, Cys, Leu, and Ile could derive from the EMP pathway. Glu, Pro, and Val could flow to TCA, and Thr could flow to the EMP pathway. PLS analysis demonstrated that Glu, Pro, Thr, and Leu, with VIP values greater than 1, were correlated with 2-PE biosynthesis.

Glu and Pro are important carbon skeletons for AKG by catabolism (Figure 4).[34] The relative abundance of Glu and Pro under C2 conditions was 4.2 and 3.3 at 40 h and then significantly fell to 0.4 and 0.23, respectively. However, the maximum relative abundance of Glu and Pro under C1 conditions was just 1.7 and 1.5 and subsequently declined to 0.6 and 0.6, respectively. It could be inferred that intracellular Glu and Pro under C2 conditions were consumed rapidly during the 2-PE biosynthesis period. Apart from supporting protein synthesis and cell growth, Glu and Pro are also catabolized for AKG regeneration, which is consistent with the analysis result of TCA. Thr is an important amino acid for pyruvate synthesis. The alteration of Thr level directly reflected its metabolic flux state toward the EMP pathway.[35] Under C1 conditions, relative abundance of Thr remained below 1, without obvious fluctuation. On the contrary, under C2 conditions, the abundance of Thr changed dramatically from 1.7 at 24 h to 0.2 at 80 h, indicating that Thr was consumed to provide some metabolites related to the EMP pathway and maintain cells' normal metabolism during stationary phase. The sharp decline of Thr under C2 conditions reflected the urgent need of microbes for catabolism, and indirectly influenced 2-PE biosynthesis. Leu could be derived from pyruvate and degraded to acetyl-CoA, which was closely associated with fatty acid synthesis (Figure 4).[36] The abundance of Leu may reflect the level of EMP pathway and metabolic flux to fatty acid pathway. At 40 h, the relative abundance of Leu was up to 2.8 under C2 and 1.7 under C1, demonstrating that intracellular metabolic flux of EMP pathway was higher under C2 during logarithmic phase. However, the relative abundance of Leu under C2 decreased to 1.6 at 80 h. The sharp decline of Leu under C2 conditions might correlate with the precursor supplement of fatty acid synthesis and promote the synthesis of membrane lipid composition to tolerate 2-PE toxicity.[37]

Therefore, feeding those amino acids in the early stage could provide precursors for metabolism. However, as the adding time was delayed, those amino acids, regarded as nitrogen, could compete with Phe for nitrogen utilization,[32] which would result in the drop of 2-PE production. Complex amino acids (2 g/L Glu, Pro, Thr, and Leu, mixed in equal proportion) were added to wastewater at 16 h under C2 conditions. The 2-PE production was increased to 1133 mg/L, demonstrating that Glu, Pro, Thr, and Leu would affect 2-PE biosynthesis.

*Fatty Acid Metabolism.* In fatty acid metabolism, the levels of metabolites such as eicosanoic acid (SFA20), stearic acid (SFA18), heptadecanoic acid (SFA17), and palmitic acid (SFA16) under C2 conditions were significantly lower than under C1 conditions (Figure 10). However, the levels of

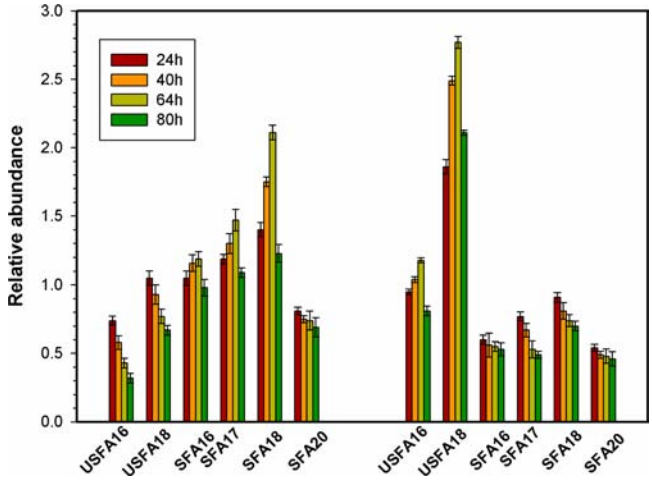


**Figure 10.** Relative abundance of intracellular metabolites in fatty acid metabolic pathway under (left) C1 and (right) C2 conditions. USFA16, palmitoleic acid; USFA18, oleic acid; SFA16, palmitic acid; SFA17, heptadecanoic acid; SFA18, stearic acid; SFA20, eicosanoic acid.

palmitoleic acid (USFA16) and oleic acid (USFA18) were higher than under C1 conditions. During the whole fermentation process, the average relative abundance of SFA18 under C2 conditions was only 0.49-fold of that under C1, and USFA18 was 2.7-fold of that under C1 conditions. The ratio of unsaturated fatty acids (USFA) to saturated fatty acids (SFA) under C2 conditions was obviously higher than that under C1 conditions. A high USFA/SFA ratio is conducive to the cell membrane gaining a strong capacity to resist the tough outside environment.[38] It is the main mechanism for microbes to adapt to environmental stress. 2-PE was toxic to microbes. One of the toxicity mechanisms is that aromatic alcohol could change the liquidity of the membrane, leading to easy permeability. Then the transport systems of sugars and amino acids in cytoplasmic membrane are affected, the passive diffusion of ions and small metabolites through the membrane


dx.doi.org/10.1021/jf502239d | J. Agric. Food Chem. 2014, 62, 9927−9935

is accelerated, and the gradient of transmembrane protons is disturbed, thus leading to leakage of intracellular ions and reduced intake of amino acids and sugars.[1] It was reported that oleic acid could prevent alcohol poisoning of cells by regulating the liquidity of the cell membrane.[39] Thus, unsaturated fatty acid played a significant role in improving the capacity of cell membrane to resist the toxicity of 2-PE. However, it also had been reported that a high concentration of oleic acid could inhibit the growth of microorganisms.[40] During early growth phase, oleic acid existing in the medium would be toxic to microbes.[41] Therefore, 15% (v/v) oleic acid was added to the CMW at 40 h under C2 conditions. Finally, 2-PE production was elevated to 1378 mg/L, increased by 39.6% compared to the control group without oleic acid supplement. The results suggested that cell membranes of 2-PE high-producers had a strong capacity to resist outside toxicity by increasing the ratio between intracellular unsaturated and saturated fatty acid concentrations.

**Metabolic Mechanism Hypothesis for High 2-PE Production by MMC Utilizing CMW.** From the analysis above, it was found that EMP pathway, TCA cycle, PPP, shikimate pathway, and amino acid pathway presented high metabolic levels during logarithmic phase, which was beneficial for absorbing nutrition for cell growth and promoting Phe uptake from the wastewater. During stationary phase, the metabolic levels of EMP and TCA cycle weakened. To maintain basic metabolism, the catabolism of intracellular amino acids was accelerated and the intracellular Phe was predominantly used to transaminate and synthesize 2-PE through the Ehrlich pathway.

On the basis of metabolic profiling analysis, during logarithmic phase, the metabolic flux of intracellular pyruvate, lactate, and acetate for high-producing MMC was converted to acetyl-CoA, improving the metabolic flux related to acetyl-CoA, which facilitated the uptake of Phe by cells for 2-PE biosynthesis. In the shikimate pathway, an appropriate accumulation of intracellular Tyr and Trp as well as an increase of intracellular Phe for microbes at the end of logarithmic phase could inhibit de novo synthesis of 2-PE, leading to 2-PE biosynthesized in quantity through the Ehrlich pathway. In amino acid metabolism, Glu, Pro, Thr, and Leu, associated with central carbon metabolism and fatty acid metabolism, indirectly reflected the cell metabolic state. In fatty acid metabolism, the resistance of cell membrane to 2-PE toxicity could be strengthened by increasing USFA/SFA. Those findings provided theoretical guidance for species domestication and selection as well as medium optimization when MMC utilized CMW to produce 2-PE.

## ■ ASSOCIATED CONTENT

### Supporting Information

One table listing intracellular metabolites and VIP score order of PLS analysis under C1 and C2 conditions. This material is available free of charge via the Internet at http://pubs.acs.org.

## ■ AUTHOR INFORMATION


### Corresponding Author

*Telephone and fax +86-22-27892061; e-mail jpwen@tju.edu.cn.

### Author Contributions

§X.P. and H.Q. contributed equally to this work.



### Funding

This research was financially supported by the National 973 Project of China (2013CB733600), the Key Program of National Natural Science Foundation of China (21236005), and the Program of Introducing Talents of Discipline to Universities (B06006).


### Notes

The authors declare no competing financial interest.

## ■ ABBREVIATIONS

MMC, microbial mixed cultures; CMW, cane molasses wastewater; 2-PE, 2-phenyethanol; Phe, phenylalanine; Tyr, tyrosine; Thr, tryptophan; LAC, lactate; PYR, pyruvate; ACE, acetate; SUCC−COA, succinyl-CoA; Glu, glutamate; Pro, proline; Leu, leucine; Thr, threonine; Ser, serine; Gly, glycine; Cys, cysteine; Val, valine; Ile, isoleucine; E4P, erythrose 4-phosphate; S7P, sedoheptulose 7-phosphate; 3PG, 3-phosphoglyceric acid; OAA, oxaloacetate; AKG, $\alpha$-ketoglutarate; SFA18, stearic acid; USFA18, oleic acid; USFA16, palmitoleic acid; SFA17, heptadecanoic acid; SFA16, palmitic acid; SFA20, eicosanoic acid; USFA, unsaturated fatty acids; SFA, saturated fatty acids; EMP, Embden−Meyerhof−Parnas pathway; TCA, tricarboxylic acid cycle; PPP, pentose phosphate pathway; C1, initial operating conditions; C2, optimized operating conditions; COD, chemical oxygen demand; PCA, principal component analysis; PLS, partial least-squares method; VIP, variable importance in projection; GC-MS, gas chromatography−mass spectrometry; LC-MS/MS, liquid chromatography−mass spectrometry/mass spectrometry; HPLC-ESI-MS/MS, high-performance liquid chromatography−electrospray ionization tandem mass spectrometry

## ■ REFERENCES


(1) Hua, D.; Lin, S.; Li, Y.; Chen, H.; Zhang, Z. B.; Du, Y.; Zhang, X. H.; Xu, P. Enhanced 2-phenylethanol production from L-phenylalanine via in situ product adsorption. *Biocatal. Biotransform.* **2010**, *28*, 259−266.

(2) Etschmann, M.; Sell, D.; Schrader, J. Screening of yeasts for the production of the aroma compound 2-phenylethanol in a molasses-based medium. *Biotechnol. Lett.* **2003**, *25*, 531−536.

(3) Kadota, H.; Ishida, Y. Production of volatile sulfur compounds by microorganisms. *Annu. Rev. Microbiol.* **1972**, *26*, 127−138.

(4) Abraham, B. G.; Berger, R. G. Higher fungi for generating aroma components through novel biotechnologies. *J. Agric. Food. Chem.* **1994**, *42*, 2344−2348.

(5) Fabre, C. E.; Blanc, P. J.; Goma, G. Production of benzaldehyde by several strains of *Ischnoderma bensoinum*. *Sci. Aliment.* **1996**, *16*, 61−68.

(6) Lomascolo, A.; Lesage-Meessen, L.; Haon, M.; Navarro, D.; Antona, C.; Faulds, C.; Marcel, A. Evaluation of the potential of *Aspergillus niger* species for the bioconversion of L-phenylalanine into 2-phenylethanol. *World J. Microbiol. Biotechnol.* **2001**, *17*, 99−102.

(7) Mei, J. F.; Min, H.; Lu, Z. M. Biocatalytic synthesis of 2-phenylethanol by yeast cells. *Chin. J. Catal.* **2007**, *28*, 993−998.

(8) Etschmann, M.; Sell, D.; Schrader, J. Medium optimization for the production of the aroma compound 2-phenylethanol using a genetic algorithm. *J. Mol. Catal. B: Enzym.* **2004**, *29*, 187−193.

(9) Eshkol, N.; Sendovski, M.; Bahalul, M.; Katz-Ezov, T.; Kashi, Y.; Fishman, A. Production of 2-phenylethanol from L-phenylalanine by a stress tolerant *Saccharomyces cerevisiae* strain. *J. Anal. Microbiol.* **2009**, *106*, 534−542.

(10) Bader, J.; Mast-Gerlach, E.; Popović, M. K.; Bajpai, R.; Stahl, U. Relevance of microbial coculture fermentations in biotechnology. *J. Appl. Microbio.* **2010**, *109*, 371−387.

(11) Kleerebezem, R.; van Loosdrecht, M. Mixed culture biotechnology for bioenergy production. *Curr. Opin. Biotechnol.* **2007**, *18*, 207−212.
(12) Satyawali, Y.; Balakrishnan, M. Wastewater treatment in molasses-based alcohol distilleries for COD and color removal: a review. *J. Environ. Manage.* **2008**, *86*, 481−497.
(13) Brahimi-Horn, M. C.; Mickelson, C. A.; Gaal, A. M.; Guglielmino, M. G.; Sparrow, L. G. Lipolytic activity produced by *Pseudomonas aeruginosa* and *Acinetobacter calcoaceticus* strains grown in wool-scour effluent. *Enzyme Microb. Technol.* **1991**, *13*, 740−746.
(14) Ding, M. Z.; Wang, X.; Yang, Y.; Yuan, Y. J. Comparative metabolic profiling of parental and inhibitors-tolerant yeasts during lignocellulosic ethanol fermentation. *Metabolomics* **2012**, *8*, 232−243.
(15) Bundy, J. G.; Davey, M. P.; Viant, M. R. Environmental metabolomics: a critical review and future perspectives. *Metabolomics* **2009**, *5*, 3−21.
(16) Yu, S.; Huang, D.; Wen, J.; Li, S.; Chen, Y.; Jia, X. Metabolic profiling of a *Rhizopus oryzae* fumaric acid production mutant generated by femtosecond laser irradiation. *Bioresour. Technol.* **2012**, *114*, 610−615.
(17) Wang, G.; Huang, D.; Qi, H.; Wen, J.; Jia, X.; Chen, Y. Rational medium optimization based on comparative metabolic profiling analysis to improve fumaric acid production. *Bioresour. Technol.* **2013**, *137*, 1−8.
(18) Mu, L.; Hu, X. G.; Liu, X. W.; Zhao, Y. J.; Xu, Y. P. Production of 2-phenylethanol by microbial mixed cultures allows resource recovery of cane molasses wastewater. *Fresen. Environ. Bull.* **2014**, *23*, 1356−1365.
(19) Xia, M.; Huang, D.; Li, S.; Wen, J.; Jia, X.; Chen, Y. Enhanced FK506 production in *Streptomyces tsukubaensis* by rational feeding strategies based on comparative metabolic profiling analysis. *Biotechnol. Bioeng.* **2013**, *110*, 2717−2730.
(20) Tian, S.; Zhou, X.; Gong, H.; Ma, X.; Zhang, F. Orthogonal test design for optimization of the extraction of polysaccharide from *Paeonia sinjiangensis* KY Pan. *Pharmacogn. Mag.* **2011**, *7*, 4.
(21) Ding, M. Z.; Zhou, X.; Yuan, Y. J. Metabolome profiling reveals adaptive evolution of *Saccharomyces cerevisiae* during repeated vacuum fermentations. *Metabolomics* **2010**, *6*, 42−55.
(22) Park, J. W.; Jung, W. S.; Park, S. R.; Park, B. C.; Yoon, Y. J. Analysis of intracellular short organic acid-coenzyme A esters from actinomycetes using liquid chromatography-electrospray ionization-mass spectrometry. *J. Mass Spectrom.* **2007**, *42*, 1136−1147.
(23) Yang, H.; Pang, W.; Lu, H.; Cheng, D.; Yan, X.; Cheng, Y.; Jiang, Y. Comparison of metabolic profiling of cyanidin-3-O-galactoside and extracts from blueberry in aged mice. *J. Agric. Food Chem.* **2011**, *59*, 2069−2076.
(24) Yates, G. T.; Smotzer, T. On the lag phase and initial decline of microbial growth curves. *J. Theor. Biol.* **2007**, *244*, 511−517.
(25) Dietmair, S.; Hodson, M. P.; Quek, L. E.; Timmins, N.; Chrysanthopoulos, P.; Jacob, S.; Gray, P.; Nielsen, L. Metabolite profiling of CHO cells with different growth characteristics. *Biotechnol. Bioeng.* **2012**, *109*, 1404−1414.
(26) Cao, Y.; Cao, Y.; Lin, X. Metabolically engineered *Escherichia coli* for biotechnological production of four-carbon 1, 4-dicarboxylic acids. *J. Ind. Microbiol. Biotechnol.* **2011**, *38*, 649−656.
(27) Narendranath, N. V.; Thomas, K. C.; Ingledew, W. M. Effects of acetic acid and lactic acid on the growth of *Saccharomyces cerevisiae* in a minimal medium. *J. Ind. Microbiol. Biotechnol.* **2001**, *26*, 171−177.
(28) Fernie, A. R.; Carrari, F.; Sweetlove, L. J. Respiratory metabolism: glycolysis, the TCA cycle and mitochondrial electron transport. *Curr. Opin. Biotechnol.* **2004**, *7*, 254−261.
(29) Wang, H.; Di, Z. F. Regulation of shikimic acid biosynthesis pathway. *Biotechnol. Bull.* **2009**, *3*, 50−53.
(30) Atsumi, S.; Hanai, T.; Liao, J. C. Non-fermentative pathways for synthesis of branched-chain higher alcohols as biofuels. *Nature* **2008**, *451*, 86−89.
(31) Wittmann, C.; Hans, M.; Bluemke, W. Metabolic physiology of aroma-producing *Kluyveromyces marxianus*. *Yeast* **2002**, *19*, 1351−1363.
(32) Etschmann, M.; Bluemke, W.; Sell, D.; Schrader, J. Biotechnological production of 2-phenylethanol. *Appl. Microbiol. Biotechnol.* **2002**, *59*, 1−8.
(33) Hua, D.; Xu, P. Recent advances in biotechnological production of 2-phenylethanol. *Biotechnol. Adv.* **2011**, *29*, 654−660.
(34) Takagi, H. Proline as a stress protectant in yeast: physiological functions, metabolic regulations, and biotechnological applications. *Appl. Microbiol. Biotechnol.* **2008**, *81*, 211−223.
(35) Morris, J. G. Utilization of L-threnonine by a pseudomonad: a catabolic role for L-threonine aldolase. *Biochem. J.* **1969**, *115*, 603.
(36) Kohlhaw, G. B. Leucine biosynthesis in fungi: entering metabolism through the back door. *Microbiol. Mol. Biol. Rev.* **2003**, *67*, 1−15.
(37) Mahmud, T.; Bode, H. B.; Silakowski, B.; Kroppenstedt, R.; Xu, M.; Nordhoff, S. A novel biosynthetic pathway providing precursors for fatty acid biosynthesis and secondary metabolite formation in myxobacteria. *J. Biol. Chem.* **2002**, *277*, 32768−32774.
(38) Mannazzu, I.; Angelozzi, D.; Belviso, S.; Budroni, M. Behaviour of *Saccharomyces cerevisiae* wine strains during adaptation to unfavourable conditions of fermentation on synthetic medium: Cell lipid composition, membrane integrity, viability and fermentative activity. *Int. J. Food Microbiol.* **2008**, *121*, 84−91.
(39) You, K. M.; Rosenfield, C. L.; Knipple, D. C. Ethanol tolerance in the yeast *Saccharomyces cerevisiae* is dependent on cellular oleic acid content. *Appl. Environ. Microbiol.* **2003**, *69*, 1499−1503.
(40) Marounek, M.; Savka, O.; Skrivanova, V. Effect of caprylic, capric and oleic acid on growth of rumen and rabbit caecal bacteria. *J. Anim. Feed Sci.* **2002**, *11*, 507−516.
(41) Stark, D.; Münch, T.; Sonnleitner, B. Extractive bioconversion of 2-phenylethanol from l-phenylalanine by *Saccharomyces cerevisiae*. *Biotechnol. Prog.* **2002**, *18*, 514−523.

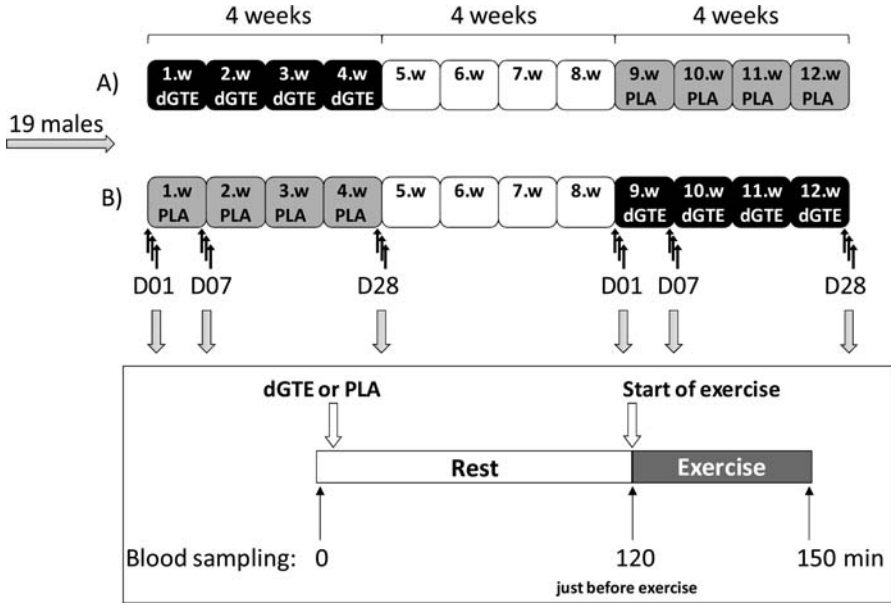


**Figure 1.** Study design: (A, B) study arms. PLA, placebo; dGTE, decaffeinated green tea extract; w, week; D01, D07, D28, day 1, 7, or 28 of the respective supplementation period.

useful in capturing the multifactorial and subtle influences of complex dietary ingredients on overall metabolism.

Therefore, in the present study, we applied GC-MS- and LC-MS-based untargeted four-phase metabolite profiling and targeted profiling of catecholamines to human plasma to compare the metabolic effects (i) between cGTE and dGTE supplementation and (ii) between 1, 7, and 28 days of dGTE ingestion at rest and during exercise.

## MATERIALS AND METHODS

**Study Design.** The study was designed as a double-blind, crossover, counterbalanced study (Figure 1) and has been described previously.[26] In brief, 20 healthy, physically active, habitual caffeine-consuming, male participants [mean ± SD age, 21 ± 2 years; weight, 75.0 ± 7.0 kg; body mass index (BMI), 23.2 ± 2.2 kg/m$^2$; maximal oxygen consumption ($\dot{V}O_{2max}$), 55.4 ± 4.6 mL·mL·kg$^{-1}$·min$^{-1}$] completed two 28 day supplementation periods of dGTE and PLA ingestion, separated by a 28 day wash-out period. One subject dropped out of the study. Each supplementation period included three experimental days, namely, on the first day (dGTE_D01 or PLA_D01), after 7 days (dGTE_D07 or PLA_D07), and after 28 days (dGTE_D28 or PLA_D28) of supplementation. Before each experimental day, the subjects followed a 24 h controlled diet (consisting of three meals each containing ∼50% carbohydrate, ∼35% fat, and ∼15% protein, total energy intake = 2700 kcal) and were asked to refrain from any physical activity and not consume alcohol- or caffeine-based beverages. On each experimental day, a resting blood sample (5 mL) was taken at baseline ($t$ = 0 min) after a 12 h overnight fast. Then the participants consumed two capsules of dGTE or PLA with 200 mL of water, rested for 2 h in a seated position and subsequently completed a 30 min cycle exercise bout at 50% $W_{max}$ (55 $\dot{V}O_{2max}$). Blood samples were taken before the exercise bout commenced ($t$ = 120 min) and at 30 min during the exercise bout. Participants ingested four capsules per day containing dGTE or PLA for a total of 28 days, respectively. Two capsules were consumed an hour before lunch (or 2 h before the exercise bout on the experimental days), and two additional capsules were consumed an hour before dinner. The dGTE was Sunphenon 90 DCF-T (lot 003191) obtained from Taiyo Europe (Fiderstadt, Germany). Each dGTE capsule contained 156 ± 3 mg of EGCG, 284 ± 6 mg of total catechins, and ∼3 mg of caffeine. (The catechin composition has been reported in ref 28.) The total catechin ingestion was 1136 ± 24 mg per day. The PLA capsule contained 273 ± 25 mg of cellulose.

All participants gave written informed consent to participate in the study. The study was approved by the Life and Sciences Ethical Review Committee at the University of Birmingham.

All blood samples were collected in EDTA-containing tubes and stored on ice for no longer than 35 min. Subsequently, plasma was separated by centrifugation (3500 rpm, 15 min, 4 °C), aliquoted in 1 mL samples, and stored at −80 °C.

**Data Acquisition.** *Plasma Analysis of Polyphenols.* Polyphenol concentrations in plasma from 19 subjects were analyzed at $t$ = 0 min and $t$ = 120 min on all six experimental days. In total, 225 samples (3 samples were missing) were measured by high-performance liquid chromatography multiple-reaction monitoring mass spectrometry (HPLC-MRM-MS) with prior enzymatic deconjugation of glucuronides and sulfates, as described previously.[23] In total, 9 phenolic compounds were quantified by means of 10-point calibration curves using external standards. They included (−)-catechin (C), (−)-epicatechin (EC), (−)-gallocatechin (GC), (−)-epigallocatechin (EGC), (−)-epicatechin gallate (ECG), (−)-epigallocatechin gallate (EGCG), 3/4-*O*-methylgallic acid (3/4-OMGA), 5-(3′,4′-dihydroxyphenyl)-γ-valerolactone (3,4-diOH-VL), and 5-(3′-methoxy-4′-hydroxyphenyl)-γ-valerolactone (3-MeO-4-OH-VL). The concentrations of 3-*O*-methylgallic acid (3-OMGA) and 4-*O*-methylgallic acid (4-OMGA) were combined to 3/4-OMGA because they could not be fully separated. Similarly, combined ECG values were reported for ECG and CG.

*Metabolite Profiling.* Plasma metabolite profiles from 19 subjects were acquired from samples collected at $t$ = 0, 120, and 150 min on four experimental days (dGTE_D01, dGTE7_D07, dGTE_D28, PLA_D28), respectively.

Four-phase metabolite profiling and quantification of catecholamines were performed on human plasma samples at Metanomics Health GmbH, Berlin, Germany. Three types of mass spectrometry analyses were applied. GC-MS (gas chromatography−mass spectrometry; Agilent 6890 GC coupled to an Agilent 5973 MS-System, Agilent, Waldbronn, Germany) and LC-MS/MS (liquid chromatography-MS/MS; Agilent 1100 HPLC-System (Agilent) coupled to an Applied Biosystems API4000 MS/MS-System (Applied Biosystems, Darmstadt, Germany)) were used for broad profiling, as described by van Ravenzwaay et al.[29] SPE-LC-MS/MS (solid phase extraction-LC-MS/MS; Symbiosis Pharma (Spark, Emmen, The Netherlands) coupled to an Applied Biosystems API4000 MS/MS-System (Applied Biosystems, Darmstadt, Germany) was used for the determination of catecholamine concentrations. Two hundred and one metabolites fulfilled the quality criteria for relative quantification, and absolute quantification was

performed for additional 10 metabolites. From a total of 211 metabolites, 184 were known metabolites and 27 were not chemically identified with sufficient certainty (i.e., thus considered in the present study to be unknown analytes). The known metabolites belonged to different metabolite (ontology) classes: 22 amino acids; 17 metabolites related to amino acids; 12 carbohydrates and related metabolites; 84 complex lipids, fatty acids, and related metabolites; 16 metabolites related to energy metabolism; 13 hormones, signal substances, and related metabolites; 4 nucleobases and related metabolites; 7 vitamin, cofactors, and related metabolites; and 9 miscellaneous metabolites.

Technical reference samples were measured in parallel with the study samples to allow the relative quantification of metabolites in the study samples. These technical reference samples were generated by pooling aliquots of plasma from all study samples. Relative quantification for each metabolite was obtained by normalizing peak intensity in the study samples to the median peak intensity of the corresponding metabolite in the technical reference samples measured in the same batch.

For the metabolite profiling by GC-MS and LC-MS/MS, proteins were removed from plasma samples (60 $\mu$L) by precipitation. Subsequently, polar and nonpolar plasma fractions were separated for both GC-MS and LC-MS/MS analysis by adding water and a mixture of ethanol and dichloromethane. For GC-MS analyses, the nonpolar fraction was treated with methanol under acidic conditions to yield the fatty acid methyl esters derived from both free fatty acids and hydrolyzed complex lipids. The polar and nonpolar fractions were further derivatized with *O*-methyl-hydroxyamine hydrochloride (20 mg/mL in pyridine, 50 $\mu$L) to convert oxo groups to *O*-methyloximes and subsequently with a silylating agent (MSTFA, 50 $\mu$L) before GC-MS analysis.[30] For LC-MS/MS analyses, both fractions were reconstituted in appropriate solvent mixtures. High-performance LC (HPLC) was performed by gradient elution using methanol/water/formic acid on reversed phase separation columns. Mass spectrometric detection technology was applied as described in U.S. patent 7196323, which allows targeted and high-sensitivity "multiple reaction monitoring" profiling in parallel to a full screen analysis.

For the lipid phase, the broad profiling technology determines, for example, fatty acid concentrations after acid/methanol treatment, which is essential for derivatization preceding GC-MS analysis. As a consequence, complex lipids are hydrolyzed to components of the lipid backbone (i.e., glycerol) and fatty acids. Hence, the concentration of a fatty acid determined by this procedure represents the sum of its occurrence in free and in lipid-bound form. Components of the backbone can be recognized by the term ("lipid fraction") added to the metabolite name. As an example "glycerol, lipid fraction" represents glycerol liberated from complex lipids; in contrast, "glycerol, polar fraction" represents glycerol that had been present originally in the biological sample. The use of "additional" (add) indicates that quantification can be affected by the co-occurrence of metabolites exhibiting identical characteristics in the analytical methods. Literature data and/or comparison with alternative methods (e.g., LC-MS/MS, GC-MS) suggest that such metabolites are present at minor concentrations only.

Catecholamines and their related metabolites were measured by online SPE-LC-MS/MS, as described by Yamada et al.[31] Quantification was performed using stable isotope-labeled standards.

**Data Analysis of Metabolite Profiles.** The data set included 215 metabolite profiles. (One subject was excluded because of protocol violation. Another sample was missing.) Analysis of the four-phase metabolite profiles and the catecholamines were based on pool-normalized ratios and on absolute concentrations in nanograms per milliliter, respectively. For the multivariate and univariate statistical analysis, the data were log-transformed to better match normal distribution.

Principal component analysis (PCA) was performed using SIMCA P + version 12 software (Umetrics, Umea, Sweden). Data were centered and scaled to unit variance to introduce a common scale for all metabolites independent of their absolute variance. The explorative unsupervised multivariate analysis method PCA was used for the detection of trends, patterns, and groupings among samples and variables. PCA revealed outliers that belonged to samples from one subject and thus were excluded from further analysis.

Single-metabolite analysis of variance (ANOVA) analysis was performed using the R-software package nlme.[32,33] For this analysis, additional six samples were excluded, because their plasma catechin concentrations significantly deviated from average concentrations. The analysis was performed for in total 211 metabolites including all SQ metabolites from four-phase metabolite profiling and all catecholamines quantified by targeted profiling. A mixed-effects ANOVA model was built using the factors *treatment* (PLA_D28, dGTE_D01, dGTE_D07, dGTE_D28), *time* (0, 120, 150), *study arm* (A, B) and *subject*. All possible secondary and tertiary interactions between fixed factors were evaluated in the model refinement process. Model diagnostics was performed to ensure adequacy of the model structure. To this end, residuals were inspected visually by scatter plots of standardized residuals versus fitted values. Additionally, factors or interactions resulting in a number of significantly changed metabolites beneath the expected false-positive rate were excluded. Inclusion of all other factors and interactions ensured that residuals did not correlate with fitted values and showed homogeneous variance. No interaction between the factors *time* and *study arm* was considered. Thus, the following model was used (R annotation):

$$\text{fixed: } \sim(\text{treatment} + \text{time})^2 + \text{study arm}$$

$$\text{random: } \sim 1|\text{subject}$$

The *t* statistics results of the ANOVA models comprised estimates, standard deviations, *t* values, and *p* values and *q* values corrected according to the methods of Benjamini-Hochberg (*q* value) or Bonferroni (qval.Bonf). The resulting numbers of significantly changed metabolites were evaluated by binomial test to account for false positives due to multiple hypotheses testing.

## RESULTS

**Effect of dGTE on Exogenous Metabolites.** To check the compliance, the concentrations of several catechins were measured in plasma after deconjugation of glucuronides and sulfates at baseline ($t$ = 0 min) and 2 h after the ingestion of two capsules of dGTE or PLA ($t$ = 120 min) on D01, D07, and D28, respectively. Six individual samples were identified as outliers, and thus removed, because they did not confirm dGTE exposure in the dGTE condition or indicated dGTE exposure in the PLA condition.

The concentrations of the remaining 219 samples are shown as box plots in Figure 2. As expected, the concentrations of EGCG, EGC, EC, and ECG/CG significantly increased 2 h after dGTE ingestion. These catechins accumulated in plasma following 7 days of dGTE ingestion, as shown by the increased baseline levels at D07 when compared to D01. However, there was no further accumulation, because the baseline levels after 7 and 28 days dGTE intake were similar. The plasma concentrations of GC, C, and GCG were <10 ng/mL and did not show significant effects of dGTE (data not shown).

Besides the catechins, slight increases in 3/4-OMGA and salicylic acid (detected by the four-phase metabolite profiling) were found 2 h after dGTE ingestion. These metabolites appeared early in plasma, because 3/4-OMGA can be formed by methylation of gallic acid in the liver and salicylic acid may be present in dGTE, as it has been earlier identified in green tea infusion.[34] In contrast, the gut microbial metabolites 3,4-diOH-VL, pyrogallol, and hippuric acid (detected by the four-phase metabolite profiling) did not increase 2 h after dGTE ingestion, because they enter into the circulation at a later time. However, 3,4-diOH-VL and pyrogallol were increased at baseline after 7 and 28 days of dGTE ingestion, showing that these metabolites circulate in a steady state in plasma. The baseline concentrations of 3/4-OMGA, salicylic acid, pyrogallol, and hippurate after PLA

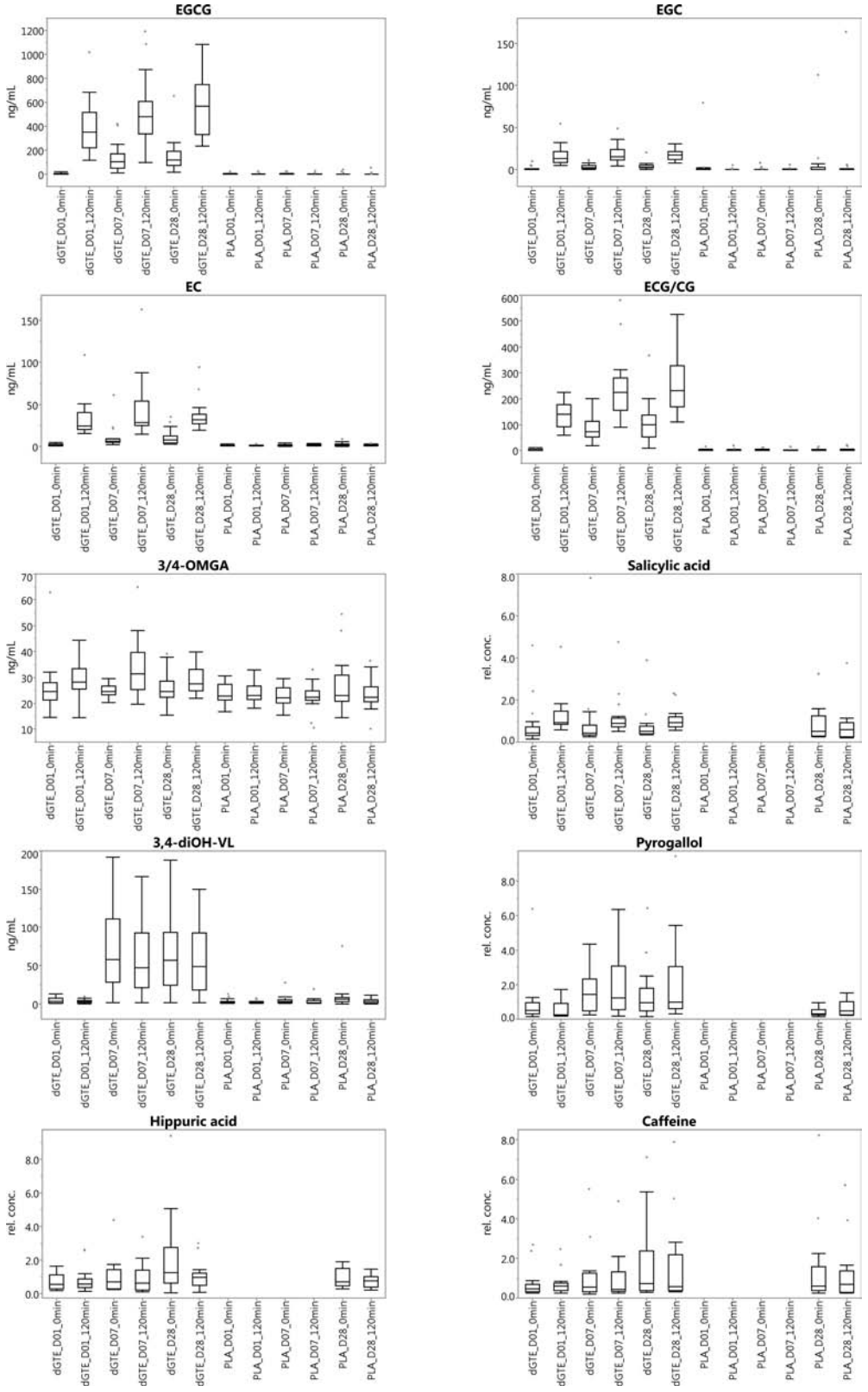


**Figure 2.** Concentrations of exogenous metabolites in plasma after deconjugation of glucuronides and sulfates at baseline ($t$ = 0 min) and 2 h after intake of two capsules of dGTE or PLA ($t$ = 120 min) on D01, D07, or D08, respectively. (−)-Epicatechin (EC), (−)-epigallocatechin (EGC), (−)-epi/catechin gallate (ECG/GC), (−)-epigallocatechin gallate (EGCG), 3/4-*O*-methylgallic acid (3,4-OMGA), and 5-(3′,4′-dihydroxyphenyl)-$\gamma$-valerolactone (3/4-diOH-VL) were measured in absolute concentrations. Salicylic acid, pyrogallol, hippurate, and caffeine were measured in relative concentrations and not on D01 and D07 after PLA ingestion.

ingestion can be explained by the intake of other polyphenol-containing food sources.

In addition to the catechin metabolites, caffeine was relatively quantified from the four-phase metabolite profiles. The caffeine


dx.doi.org/10.1021/jf502764r | J. Agric. Food Chem. 2014, 62, 9936−9943

**Table 1. ANOVA Estimate for Effect of dGTE on Plasma Metabolites at Baseline ($t$ = 0 min) under Fasting and Resting Condition**

| | Control | Effects after 7 Days | | Effects after 28 Days | |
|---|---|---|---|---|---|
| Treatment | dGTE_D01 | dGTE_D07 | dGTE_D07 | dGTE_D28 | dGTE_D28 |
| Reference Treatment | PLA_D28 | PLA_D28 | dGTE_D01 | PLA_D28 | dGTE_D01 |
| METABOLITE NAME | Ratio | Ratio | Ratio | Ratio | Ratio |
| Alanine | | | | 0.91 | 0.90 |
| Arginine | | 0.90 | 0.94 | | |
| Citrulline | | 0.90 | 0.88 | | |
| 3-Hydroxyisobutyrate | | 1.24 | 1.17 | 1.20 | |
| p-Cresol sulfate (add: m/o-Cresol sulfate) | | 1.76 | 2.52 | | |
| Glucose-1-phosphate (add: Glucose) | | 1.20 | | 1.15 | 1.09 |
| Cholesterylester C16:0 | 1.12 | 0.89 | 0.79 | 1.16 | |
| Cholesta-2,4,6-triene | | | | 0.87 | 0.86 |
| TAG (C16:0,C16:1) | | | | 0.86 | 0.90 |
| TAG (C18:2,C18:3) | | | | 0.80 | 0.77 |
| myo-Inositol, lipid fraction | | | | 0.92 | 0.87 |
| Phosphatidylcholine (C16:1,C18:2) | | 0.94 | | 0.88 | 0.91 |
| Phosphatidylcholine (C16:0,C18:2) | | | | | 1.03 |
| Dodecanoylcarnitine | | | | 1.26 | 1.38 |
| 3-Hydroxybutyrate | | 1.66 | 1.46 | 2.00 | 1.76 |
| Homovanillic acid | | 1.14 | 1.18 | | |
| Pyrogallol | | 3.11 | 3.12 | 2.40 | 2.40 |
| Pseudouridine | | 1.05 | 1.08 | | |
| Coenzyme Q10 | | 0.86 | 0.86 | | |
| Coenzyme Q9 | | 0.75 | 0.84 | 0.72 | 0.81 |

Data were transformed to ratio scale (10^x);
color coding: ratio > 1 & p-value < 0.01 (•)
ratio > 1 & 0.01 ≤ p-value < 0.05 (•)
ratio > 1 & 0.05 ≤ p-value < 0.10 (•)
ratio < 1 & 0.05 ≤ p-value < 0.10 (•)
ratio < 1 & 0.01 ≤ p-value < 0.05 (•)
ratio < 1 & p-value < 0.01 (•)
Font coding: black & bold: ( ratio < 0.5 ) or ( ratio >2 )
black & normal: ( 0.5 ≤ ratio < 0.9 ) or ( 1.1 < ratio ≤ 2 )
grey & normal: 0.9 ≤ ratio ≤ 1.1.

concentrations in plasma were indeed lower after dGTE ingestion when compared to our previous study performed with cGTE,[13] as demonstrated by the different ratios of 120 to 0 min upon dGTE and cGTE ingestion (dGTE_D07, 1.0; vs cGTE, 2.47). Moreover, no significant differences in caffeine concentrations were observed between the PLA and dGTE ingestion, also confirming that the caffeine concentrations in the dGTE capsules were negligible. Yet, a slight increase of caffeine was observed at baseline after 28 days of dGTE ingestion when compared to D01, which may be explained by a lower compliance to refrain from caffeinated products on the day before the experimental trials.

**Effect of dGTE on Endogenous Metabolites at Baseline under Resting Conditions ($t$ = 0 min).** A total of 211 metabolites including 184 known and 27 unknown (not chemically identified) metabolites from different ontology classes were measured in plasma of 18 healthy males after 1 day (D01), 7 days (D07), and 28 days (D28) of dGTE ingestion and 28 days of PLA ingestion using four-phase metabolite profiling and quantitative targeted analysis of catecholamines. (Samples from one subject were excluded because they were identified as outliers in PCA.)

Initially, the effects of 7 and 28 day dGTE ingestion were compared at baseline ($t$ = 0 min) under fasting and resting conditions to both the 28 day PLA ingestion (PLA) and the first day of dGTE ingestion (dGTE_D01). Both samples can be used as references, because two capsules of dGTE or PLA were consumed only after the collection of the baseline sample on D01. The comparison between dGTE_D01 and PLA thus served as control. Table 1 shows only those significant effects that were consistently observed for both comparisons (reference to PLA and to dGTE_D01) to avoid overinterpretation of the data. The table including all significant effects is given in the Supporting Information (Table S1). After both 7 and 28 days of dGTE ingestion, increases in 3-hydroxybutyrate and pyrogallol, and a reduction in coenzyme Q9 were observed. Moreover, some effects were different between 7 and 28 days of dGTE ingestion: After 7 days of dGTE ingestion, reductions in arginine, citrulline, and coenzyme Q10 as well as increases in 3-hydroxyisobutyrate, cresol sulfate, homovanillic acid, and pseudouridine were observed. After 28 days of dGTE ingestion, reductions in alanine, cholesta-2,4,6-triene, triacylglycerides (TAG C16:0, C16:1; TAG C18:2, C18:3), *myo*-inositol liberated from complex lipids and phosphatidylchloline (C16:1, C18:2) as well as increases in glucose-1-phosphate, phosphatidylchloline (C16:0, C18:2), and dodecanoylcarnitine were found.

**Acute and Acute-on-Chronic Effects of dGTE on Endogenous Metabolites at Rest ($t$ = 120 min).** The acute and acute-on-chronic effects were assessed 2 h after the ingestion of two capsules of dGTE on D01 (acute), D07 (acute-on-chronic), and D28 (acute-on-chronic) or PLA on day 28 ($t$ = 120 min) under resting conditions. The changes occurring within these 2 h on D01, D07, and D28 after dGTE ingestion were compared with those after PLA ingestion. In addition, the effects of dGTE ingestions on D01, D07, and D28 were compared to PLA at $t$ = 120 min. All significant metabolite changes are summarized in the Supporting Information (Table S2). In addition, plots of mean concentrations versus time are depicted for the most relevant metabolites in Figure S1. The 2 h resting period induced significant effects on the metabolism: When comparing the effects at $t$ = 120 min to $t$ = 0 min after PLA ingestion, reductions in many metabolites were observed, including, for example, some amino acids and related metabolites (glutamate, phenylalanine, tyrosine, isoleucine, valine, sytine, taurine, keutoleucine, citrulline, ornithine), catecholamines (2,3-dihydroxyphenylacetatate (DOPAC), 5-hydroxy-3-methoxymandelic acid, normetanephrine, homovanillic acid), cortisol, 3-hydroxybutyrate, lactate, succinate, and some lysophosphatidylcholines. Moreover, 2-hydroxybutyrate, pyruvate, citrate, and glucose liberated from complex lipids were significantly increased. Similar changes were observed on D01, D07, and D28 after dGTE ingestion, indicating that dGTE did not significantly affect these metabolites. There were only a few consistent effects that could be attributed to the dGTE ingestion. Apart from the significant increase in salicylic acid, which is most likely an exogenous metabolite, as already mentioned above, only phosphate and glucose liberated from complex lipids were reduced at $t$ = 120 min on D01, D07, and D28 after dGTE ingestion when compared to PLA because their concentrations were increased 2 h after the PLA ingestion. Moreover, a slightly stronger increase in 4-hydroxy-3-methoxyphenylglycol (HMPG) and a slightly stronger reduction in *myo*-inositol were observed after the 2 h of both acute and acute-on-chronic (7 and 28 days) dGTE ingestion when compared to their changes after PLA ingestion. However, these changes resulted only in marginally at 120 min on one of the dGTE treatment days when compared to PLA (D01 for HMPG and D28 for *myo*-inositol). In addition, the reductions of some carnitines (dodecanoylcarnitine, oleoylcarnitine, tetradecanoylcarnitine) were stronger after 2 h of dGTE ingestion, in particular on D28 due to their higher baseline values. Furthermore, the increases in cholesterol esters may potentially be attributed to the acute dGTE ingestion. Cholesterol ester C18:1 levels were significantly increased at $t$ = 120 min on D01, D07, and D28 after dGTE ingestion when compared to PLA and their baseline values. However, such changes were not consistently found for all cholesterol esters or on all dGTE treatment days. Likewise, several other metabolite changes such as for 4-hydroxyphenylpyruvate, cysteine, pyruvate, DOPAC, pyrogallol, some fatty acids, and sphingomyelins were observed only on specific treatment days but not consistently on D01, D07, and


dx.doi.org/10.1021/jf502764r | J. Agric. Food Chem. 2014, 62, 9936−9943

D28. Other statistically significant differences between dGTE and PLA treatment at $t$ = 120 min such as those found for phosphatidylcholine (C16:1, C18:2), *trans*-4-hydroxproline, asparagine, glucose-1-phosphate, and homovanillic acid can mainly be attributed to differences in baseline values rather than significant changes induced within 2 h after dGTE or PLA ingestion. All together, the endogenous metabolic effects observed upon acute and acute-on-chronic (D07 and D2) dGTE ingestion were either inconsistent or could be attributed to baseline effects or did not allow for a clear biological interpretation.

**Acute and Acute-on-Chronic Effects of dGTE on Endogenous Metabolites during Exercise ($t$ = 150 min).** The acute and acute-on-chronic effects of dGTE during exercise were assessed by comparing the metabolite changes after 30 min of moderate intensity exercise ($t$ = 150 min) to those observed just prior to exercise under resting conditions at $t$ = 120 min. This comparison was carried out on D01 (acute), D07 (acute-on-chronic), and D28 (acute-on-chronic) following dGTE ingestion and on D28 following PLA ingestion. In addition, the effects of dGTE ingestions on D01, D07, and D28 were compared to PLA at $t$ = 150 min. All significant metabolite changes are summarized in the Supporting Information (Table S2). In addition, plots of mean concentrations versus time are depicted for the most relevant metabolites in Figure S1. The comparison following PLA ingestion reflected the effects of moderate intensity exercise alone on the metabolism. Many metabolites were up-regulated, in particular, those that were related to adrenergic stimulation and energy metabolism.

Resting and exercise had opposite effects on several metabolites. For example, glutamate, taurine, glycerol, and cortisol were reduced under resting conditions, but increased during exercise. In contrast, 2-hydrxobutyrate was increased at rest and decreased during exercise. The effects of exercise were similar on D01, D07, and D28 following dGTE ingestion, indicating that exercise was the dominating effect and that the exercise test was reproducible.

When the effects of dGTE on D01, D07, and D28 were compared to PLA during exercise, dGTE did not induce consistent changes in metabolites related to energy metabolism such as markers of lipolysis and glycolysis, catecholamines, and tricarboxylic acid (TCA) cycle metabolites. Most metabolite changes during exercise were scattered, meaning that they were observed either on D01, D07, or D28 (i.e., glucose-1-phosphate, lactate, allantoin, 2-hydroxybutyrate, 3-indoxylsulfate, sphingomyelin (C18:1, C24:0)) or not substantiated by other metabolites from the same pathway. Therefore, it is questionable whether these changes can unambiguously be attributed to dGTE ingestion. Only a stronger increase in uridine was consistently observed during 30 min of exercise after acute and acute-on-chronic (7 and 28 days) dGTE ingestion, when compared to the change after PLA ingestion. Other differences between dGTE and PLA ingestion at $t$ = 150 min such as those for cholesterol esters, 3-hydroxybutyrate, and some fatty acids were due to differences in concentrations at $t$ = 120 min rather than differences in slopes during exercise. No statistically significant effects of dGTE were found when the data were normalized to $t$ = 120 min, except for the scattered results of 3-indoxylsufate and sphingomyelin (C18:1, C24:0).

## DISCUSSION

The present results suggest that sustained dGTE ingestion increases metabolic markers of fat oxidation under resting conditions but not during exercise. Together with our previous study,[16,27] we have now shown that 7 days of ingestion of dGTE and cGTE both increase 3-hydroxybutyrate at baseline under fasting and resting conditions. The production of this ketone body is indicative of augmented fat oxidation. However, in contrast to our previous results with cGTE, no increases in glycerol[27] and nonesterfied fatty acids[26] were observed after 7 days of dGTE ingestion, indicating that dGTE did not enhance lipolysis. Furthermore, like cGTE, dGTE also did not increase markers of fat oxidation during exercise.

After 28 days of dGTE ingestion, 3-hydroxybutyrate was still increased at baseline. In addition, an increase in dodecanoylcarnitine was found, indicating enhanced mitochondrial fatty acid oxidation. An increase in fat oxidation may also be related to the reductions in certain TAGs observed after 28 days of ingestion of dGTE. In agreement with this, reduced TAG levels at baseline have been found in our previous study using cGTE[27] and in another study in which overweight and obese adults consumed a beverage containing GT catechins or a caffeine-matched, catechin-free beverage for 12 weeks.[35] However, there is still limited and inconsistent evidence on the effect of GTE on lipid metabolism from in vivo studies, although many in vitro and animal models have already proposed several modes of actions such as decreased adipocyte differentiation and lipogenesis, increased $\beta$-oxidation, and decreased lipid absorption.[17,36]

Interestingly, the concentrations of coenzyme Q9 were reduced at baseline after 7 and 28 days of dGTE ingestion. In addition, reductions in coenzyme Q10 were observed after 7 days of dGTE ingestion. Coenzymes Q function as electron carrier for the production of cellular energy[37] and as endogenous antioxidants in protecting lipoproteins against peroxidation.[38] They are considered as early markers of oxidative damage. Thus, the reductions in coenzymes Q may provide indirect evidence of the pro/antioxidant activity of green tea catechins.[39] This activity seems to be stronger after 7 days of dGTE ingestion than after 28 days not only because of the reduction in coenzyme Q10 but also because of the slight reductions in arginine and citrillune, which are also known to be involved in radical scavenging.[40]

In this study, we could not confirm the acute metabolic effects observed in our previous study using cGTE.[23] Two hours after the ingestion of a single dose of dGTE or PLA, no consistent changes in taurine, 3,4-dihydroxyphenylethylene-glycol, serotonin, some cholesteryl esters, fatty acids, triglycerides, sphingosines, and any other metabolites were found in plasma, which may be explained not only by the absence of caffeine but also by different catechin concentrations in the plasma. Despite the same dose of total catechins administered in both studies, average concentrations at $t$ = 120 min for ECGC and (E)CG were, respectively, 2.1- and 1.5-fold higher and for EGC and EC, 0.17- and 0.42-fold lower, in this study when compared to our previous study. Differences in the food format (previous study: drink; this study: capsules) and in the composition of the GTE (e.g. 312 mg of EGCG in two capsules, 207 mg of EGCG in 330 mL of drink) may have led to differences in the bioavailability of the catechins and to different effects on the endogenous metabolism.

Further to the effects observed at rest, dGTE did not elicit significant and consistent changes on the endogenous metabolites in plasma during exercise, neither after acute nor for acute-on-chronic (7 and 28 days) ingestion of dGTE. This result is in line with our findings on whole body fat oxidation rates,[26] yet differ from our earlier metabolomics results showing that cGTE induced subtle changes on metabolites related to energy metabolism during exercise (increase in pyruvate, lactate and alanine, and reduction in 3-hydyroxybutyrate).

Taken together, there is evidence from two studies that both dGTE and cGTE ingestion induced increases in 3-hydroxybutyrate, a marker of fat oxidation. suggesting that catechins, and not caffeine, are the main actives driving this effect. The absence of caffeine in dGTE, however, also abolished some other significant metabolic effects related to energy metabolism under resting and exercise conditions that were previously seen with cGTE. For example, using dGTE no metabolic changes related to lipolysis were observed at rest. Considering that ketone body homeostasis in humans is determined by lipolysis, intrahepatic ketogenesis, and peripheral ketone body utilization, the results from our studies with dGTE and cGTE may suggest that caffeine alters the free fatty acid supply liberated from adipose tissue or that GT catechins promote hepatic ketone body production. These processes are regulated by hormones such as insulin, catecholamines, and thyroid hormones. Yet, changes in insulin (data not shown) and catecholamines were not observed at baseline after 7 days of ingestion of either dGTE or cGTE. Thus, neither study supports the hypothesis that catechins enhance fat oxidation through the inhibition of catechol-*O*-methyl-transferase (which degrades norepinephrine, thereby prolonging the action of sympathetically released norepinephrine[36]).

Our metabolomics approach clearly provided comprehensive insights into the sensitive regulation of the plasma metabolome. The metabolic effects induced by resting and moderate-intensity exercise clearly dominated over those induced by dGTE. Various metabolites related to glycolysis (pyruvate, lactate), fatty acid oxidation (carnitines, glycerol, 3-hydroxybutyrate), TCA cycle (succinate, malate), stress (catecholamines, cortisol), amino acid catabolism (alamine, glutamate, taurine, ketoleucine), inflammation (sphingosines) were involved in regulating the metabolism during moderate-intensity exercise. Many of these metabolites have already been discussed in relation to exercise in other studies.[41−46] Most metabolite changes were consistently observed on all four experimental days, showing that the effects of exercise and resting were reproducible. On the other hand, several effects were statistically significant yet inconsistent, indicating either that the plasma metabolome is sensitive to unknown factors that were not controlled in the study or that dGTE itself induced irregular effects. The fact that the daily ingestion of high doses of dGTE was able to elicit only subtle effects on the endogenous metabolism hampers a clear distinction between effects induced by dGTE or other factors. The findings of our studies suggest that consistent metabolic effects of GTE may be reliably captured and compared only from well-controlled studies. Moreover, there is a clear need to further assess whether the GTE-induced increase in the metabolic marker of fat oxidation is relevant for whole body fat oxidation rates under sedentary conditions.

## ■ ASSOCIATED CONTENT

### Supporting Information

Figures S1 and Tables S1 and S2. This material is available free of charge via the Internet at http://pubs.acs.org.

## ■ AUTHOR INFORMATION


### Corresponding Author

*(D.M.J.) Phone: +31 10 460 5987. Fax: +31 10 460 5310. E-mail: doris.jacobs@unilever.com.


### Author Contributions

A.E.J., A.B.H., R.K.R., D.M.J., and S.L. conceived and designed study; A.B.H. and R.K.R performed the study; K.M.-J.-T, U.G., and D.M.J. analyzed the data; D.M.J., S.L., and D.J.M. wrote the paper; A.E.J. and D.J.M. provided significant advice.


### Funding

This research was funded by Unilever R&D.


### Notes

The authors declare no competing financial interest.

## ■ ACKNOWLEDGMENTS

We thank Metanomics-Health GmbH for analyzing the samples.

## ■ REFERENCES


(1) Kovacs, E. M.; Mela, D. J. Metabolically active functional food ingredients for weight control. *Obes. Rev.* **2006**, *7* (1), 59−78.

(2) Westerterp-Plantenga, M. S. Green tea catechins, caffeine and body-weight regulation. *Physiol. Behav.* **2010**, *100* (1), 42−46.

(3) Sae-tan, S.; Grove, K. A.; Lambert, J. D. Weight control and prevention of metabolic syndrome by green tea. *Pharmacol. Res.* **2011**, *64* (2), 146−154.

(4) Bohn, S. K.; Ward, N. C.; Hodgson, J. M.; Croft, K. D. Effects of tea and coffee on cardiovascular disease risk. *Food Funct.* **2012**, *3* (6), 575−591.

(5) Moore, R. J.; Jackson, K. G.; Minihane, A. M. Green tea (*Camellia sinensis*) catechins and vascular function. *Br. J. Nutr.* **2009**, *102* (12), 1790−1802.

(6) Hursel, R.; Viechtbauer, W.; Westerterp-Plantenga, M. S. The effects of green tea on weight loss and weight maintenance: a meta-analysis. *Int. J. Obes. (London)* **2009**, *33* (9), 956−961.

(7) Auvichayapat, P.; Prapochanung, M.; Tunkamnerdthai, O.; Sripanidkulchai, B. O.; Auvichayapat, N.; Thinkhamrop, B.; Kunhasura, S.; Wongpratoom, S.; Sinawat, S.; Hongprapas, P. Effectiveness of green tea on weight reduction in obese Thais: a randomized, controlled trial. *Physiol. Behav.* **2008**, *93* (3), 486−491.

(8) Berube-Parent, S.; Pelletier, C.; Dore, J.; Tremblay, A. Effects of encapsulated green tea and Guarana extracts containing a mixture of epigallocatechin-3-gallate and caffeine on 24 h energy expenditure and fat oxidation in men. *Br. J. Nutr.* **2005**, *94* (3), 432−436.

(9) Dulloo, A. G.; Duret, C.; Rohrer, D.; Girardier, L.; Mensi, N.; Fathi, M.; Chantre, P.; Vandermander, J. Efficacy of a green tea extract rich in catechin polyphenols and caffeine in increasing 24-h energy expenditure and fat oxidation in humans. *Am. J. Clin. Nutr.* **1999**, *70* (6), 1040−1045.

(10) Harada, U.; Chikama, A.; Saito, S.; Takase, H.; Nagao, T.; Hase, T.; Tokimitsu, I. Effects of the long-term ingestion of tea catechins on energy expenditure and dietary fat oxidation in healthy subjects. *J. Health Sci.* **2005**, *51* (2), 248−252.

(11) Ichinose, T.; Nomura, S.; Someya, Y.; Akimoto, S.; Tachiyashiki, K.; Imaizumi, K. Effect of endurance training supplemented with green tea extract on substrate metabolism during exercise in humans. *Scand. J. Med. Sci. Sports* **2010**, *21* (4), 598−605.

(12) Venables, M. C.; Hulston, C. J.; Cox, H. R.; Jeukendrup, A. E. Green tea extract ingestion, fat oxidation, and glucose tolerance in healthy humans. *Am. J. Clin. Nutr.* **2008**, *87* (3), 778−784.

(13) Hodgson, A. B.; Randell, R. K.; Jeukendrup, A. E. The effect of green tea extract on fat oxidation at rest and during exercise: evidence of efficacy and proposed mechanisms. *Adv. Nutr.* **2013**, *4* (2), 129−140.

(14) Diepvens, K.; Kovacs, E. M.; Nijs, I. M.; Vogels, N.; Westerterp-Plantenga, M. S. Effect of green tea on resting energy expenditure and substrate oxidation during weight loss in overweight females. *Br. J. Nutr.* **2005**, *94* (6), 1026−1034.

(15) Eichenberger, P.; Colombani, P. C.; Mettler, S. Effects of 3-week consumption of green tea extracts on whole-body metabolism during cycling exercise in endurance-trained men. *Int. J. Vitam. Nutr. Res.* **2009**, *79* (1), 24−33.

(16) Randell, R. K.; Hodgson, A. B.; Lotito, S. B.; Jacobs, D. M.; Boon, N.; Mela, D. J.; Jeukendrup, A. E. No effect of 1 or 7 d of green tea extract ingestion on fat oxidation during exercise. *Med. Sci. Sports Exerc.* **2013**, *45* (5), 883−891.

(17) Wang, S.; Moustaid-Moussa, N.; Chen, L.; Mo, H.; Shastri, A.; Su, R.; Bapat, P.; Kwun, I.; Shen, C. L. Novel insights of dietary polyphenols and obesity. *J. Nutr. Biochem.* **2014**, *25* (1), 1−18.
(18) Astrup, A.; Toubro, S.; Cannon, S.; Hein, P.; Breum, L.; Madsen, J. Caffeine: a double-blind, placebo-controlled study of its thermogenic, metabolic, and cardiovascular effects in healthy volunteers. *Am. J. Clin. Nutr.* **1990**, *51* (5), 759−767.
(19) Dulloo, A. G.; Geissler, C. A.; Horton, T.; Collins, A.; Miller, D. S. Normal caffeine consumption: influence on thermogenesis and daily energy expenditure in lean and postobese human volunteers. *Am. J. Clin. Nutr.* **1989**, *49* (1), 44−50.
(20) Hursel, R.; Viechtbauer, W.; Dulloo, A. G.; Tremblay, A.; Tappy, L.; Rumpler, W.; Westerterp-Plantenga, M. S. The effects of catechin rich teas and caffeine on energy expenditure and fat oxidation: a meta-analysis. *Obes. Rev.* **2011**, *12* (7), e573−e581.
(21) Dulloo, A. G.; Seydoux, J.; Girardier, L.; Chantre, P.; Vandermander, J. Green tea and thermogenesis: interactions between catechin-polyphenols, caffeine and sympathetic activity. *Int. J. Obes. Relat. Metab. Disord.* **2000**, *24* (2), 252−258.
(22) Hursel, R.; Westerterp-Plantenga, M. S. Catechin- and caffeine-rich teas for control of body weight in humans. *Am. J. Clin. Nutr.* **2013**, *98* (6 Suppl.), 1682S−1693S.
(23) Hodgson, A. B.; Randell, R. K.; Mahabir, J. T. K.; Lotito, S.; Mulder, T.; Mela, D. J.; Jeukendrup, A. E.; Jacobs, D. M. Acute effects of green tea extract intake on exogenous and endogenous metabolites in human plasma. *J. Agric. Food Chem.* **2014**, *62* (5), 1198−1208.
(24) Achten, J.; Jeukendrup, A. E. Relation between plasma lactate concentration and fat oxidation rates over a wide range of exercise intensities. *Int. J. Sports Med.* **2004**, *25* (1), 32−37.
(25) Graham, T. E.; Helge, J. W.; MacLean, D. A.; Kiens, B.; Richter, E. A. Caffeine ingestion does not alter carbohydrate or fat metabolism in human skeletal muscle during exercise. *J. Physiol.* **2000**, *529* (Part 3), 837−847.
(26) Randell, R. K.; Hodgson, A. B.; Lotito, S. B.; Jacobs, D. M.; Rowson, M.; Mela, D. J.; Jeukendrup, A. E. Variable duration of decaffeinated green tea extract ingestion on exercise metabolism. *Med. Sci. Sports Exerc.* **2013**, *46* (6), 1185−1193.
(27) Hodgson, A. B.; Randell, R. K.; Boon, N.; Garczarek, U.; Mela, D. J.; Jeukendrup, A. E.; Jacobs, D. M. Metabolic response to green tea extract during rest and moderate-intensity exercise. *J. Nutr. Biochem.* **2013**, *24* (1), 325−334.
(28) Glube, N.; van Moos, L.; Duchateau, G. Capsule shell material impacts the *in vitro* disintegration and dissolution behaviour of a green tea extract. *Results Pharma Sci.* **2013**, *3*, 1−6.
(29) van Ravenzwaay, B.; Cunha, G. C.; Leibold, E.; Looser, R.; Mellert, W.; Prokoudine, A.; Walk, T.; Wiemer, J. The use of metabolomics for the discovery of new biomarkers of effect. *Toxicol. Lett.* **2007**, *172* (1−2), 21−28.
(30) Roessner, U.; Wagner, C.; Kopka, J.; Trethewey, R. N.; Willmitzer, L. Technical advance: simultaneous analysis of metabolites in potato tuber by gas chromatography-mass spectrometry. *Plant J.* **2000**, *23* (1), 131−142.
(31) Yamada, H.; Yamahara, A.; Yasuda, S.; Abe, M.; Oguri, K.; Fukushima, S.; Ikeda-Wada, S. Dansyl chloride derivatization of methamphetamine: a method with advantages for screening and analysis of methamphetamine in urine. *J. Anal. Toxicol.* **2002**, *26* (1), 17−22.
(32) Pinheiro, J.; Bates, D.; DebRoy, S.; Sarkar, D. *The R Core Team nlme: Linear and Nonlinear Mixed Effects Models*; R Foundation for Statistical Computing: Vienna, Austria, 2009.
(33) *R Development Core Team R: A Language and Environment for Statistical Computing*; R Foundation for Statistical Computing: Vienna, Austria, 2008.
(34) Gruz, J.; Novák, O.; Strnad, M. Rapid analysis of phenolic acids in beverages by UPLC-MS/MS. *Food Chem.* **2008**, *111* (3), 789−794.
(35) Maki, K. C.; Reeves, M. S.; Farmer, M.; Yasunaga, K.; Matsuo, N.; Katsuragi, Y.; Komikado, M.; Tokimitsu, I.; Wilder, D.; Jones, F.; Blumberg, J. B.; Cartwright, Y. Green tea catechin consumption enhances exercise-induced abdominal fat loss in overweight and obese adults. *J. Nutr.* **2009**, *139* (2), 264−270.
(36) Wolfram, S.; Wang, Y.; Thielecke, F. Anti-obesity effects of green tea: from bedside to bench. *Mol. Nutr. Food Res.* **2006**, *50* (2), 176−187.
(37) Crane, F. L. Biochemical functions of coenzyme Q10. *J. Am. Coll. Nutr.* **2001**, *20* (6), 591−598.
(38) Stocker, R.; Bowry, V. W.; Frei, B. Ubiquinol-10 protects human low density lipoprotein more efficiently against lipid peroxidation than does alpha-tocopherol. *Proc. Natl. Acad. Sci. U.S.A.* **1991**, *88* (5), 1646−1650.
(39) Kim, H. S.; Quon, M. J.; Kim, J. A. New insights into the mechanisms of polyphenols beyond antioxidant properties; lessons from the green tea polyphenol, epigallocatechin 3-gallate. *Redox Biol.* **2014**, *2*, 187−195.
(40) Fang, Y. Z.; Yang, S.; Wu, G. Free radicals, antioxidants, and nutrition. *Nutrition* **2002**, *18* (10), 872−879.
(41) Brugnara, L.; Vinaixa, M.; Murillo, S.; Samino, S.; Rodriguez, M. A.; Beltran, A.; Lerin, C.; Davison, G.; Correig, X.; Novials, A. Metabolomics approach for analyzing the effects of exercise in subjects with type 1 diabetes mellitus. *PLoS One* **2012**, *7* (7), No. e40600.
(42) Chorell, E.; Moritz, T.; Branth, S.; Antti, H.; Svensson, M. B. Predictive metabolomics evaluation of nutrition-modulated metabolic stress responses in human blood serum during the early recovery phase of strenuous physical exercise. *J. Proteome Res.* **2009**, *8* (6), 2966−2977.
(43) Lehmann, R.; Zhao, X.; Weigert, C.; Simon, P.; Fehrenbach, E.; Fritsche, J.; Machann, J.; Schick, F.; Wang, J.; Hoene, M.; Schleicher, E. D.; Haring, H. U.; Xu, G.; Niess, A. M. Medium chain acylcarnitines dominate the metabolite pattern in humans under moderate intensity exercise and support lipid oxidation. *PLoS One* **2010**, *5* (7), No. e11519.
(44) Lewis, G. D.; Farrell, L.; Wood, M. J.; Martinovic, M.; Arany, Z.; Rowe, G. C.; Souza, A.; Cheng, S.; McCabe, E. L.; Yang, E.; Shi, X.; Deo, R.; Roth, F. P.; Asnani, A.; Rhee, E. P.; Systrom, D. M.; Semigran, M. J.; Vasan, R. S.; Carr, S. A.; Wang, T. J.; Sabatine, M. S.; Clish, C. B.; Gerszten, R. E. Metabolic signatures of exercise in human plasma. *Sci. Transl. Med.* **2010**, *2* (33), 33−37.
(45) Morris, C.; Grada, C. O.; Ryan, M.; Roche, H. M.; De, V. G.; Gibney, M. J.; Gibney, E. R.; Brennan, L. The relationship between aerobic fitness level and metabolic profiles in healthy adults. *Mol. Nutr. Food Res.* **2013**, *57* (7), 1246−1254.
(46) Pohjanen, E.; Thysell, E.; Jonsson, P.; Eklund, C.; Silfver, A.; Carlsson, I. B.; Lundgren, K.; Moritz, T.; Svensson, M. B.; Antti, H. A multivariate screening strategy for investigating metabolic effects of strenuous physical exercise in human serum. *J. Proteome Res.* **2007**, *6* (6), 2113−2120.

differences,[19] metabolic effect to dietary intervention,[20] and information about gut health status.[21−23] Thus, assessment of metabolic changes in feces using metabolomics may be a unique approach to disect gut microbe interactions in the complex gut system and identify metabolic changes induced by the intake of fibers and prebiotics.

The aim of the present study is to extend a previous investigation evaluating the impact of PDX on fecal microbiota in humans by Costabile et al.[24] In this previous study, PDX consumption was shown to significantly increase butyrate-producing *Ruminoccus intestinalis* and *Clostridium Cluster* I, II, and IV. In addition, PDX fermentation was shown to reduce the genotoxicity of fecal water and affect the bowel habits of human subjects. Consequently, the findings from the previous study encouraged us to learn more about the effects of PDX intake on the gut metabolome. For this purpose, high-resolution nuclear magnetic resonance (NMR) spectroscopy-based metabolomics was performed on feces from the study by Costabile et al.[24] In addition, the relationship between the fecal metabolome and gut microbial profiles was investigated to elucidate the potential of NMR-based metabolomics to decipher the specific metabolic activity of the gut microbiota.

## MATERIALS AND METHODS

**Sampling and Sample Material.** Samples from an intervention with a double-blind, randomized, placebo-controlled crossover design were used.[24] A total of 31 volunteers from the area of Reading, United Kingdom (U.K.) were involved in the original study; however, because of sample scarcity, we could only include samples from 12 healthy volunteers (4 males and 8 females) aged 18 to 50 years. For anthropometric measures, see Table 1. During each intervention period, subjects were not allowed to intake prebiotics, probiotics, antibiotics, or drugs active on gastrointestinal motility, such as laxatives. All subjects consumed PDX powder (Litesse Ultra, 8 g/day; Danisco UK, Redhill, U.K.) or an equivalent placebo (maltodextrin powder, 8 g/day, Syral, Marckolsheim, France) for 3 weeks followed by a 3-week washout period, and then crossover occurred. Fecal samples were collected from each volunteer at five different time points, before PDX intake at baseline, following PDX treatment, following washout 1, following maltodextrin intake, and following washout 2 (Figure 1). The study protocol was approved by the Ethics and Research Committee of the University of Reading and conducted according to the guidelines in the Declaration of Helsinki.

**Table 1. Anthropometric Characteristics of the Subjects[a]**

| characteristics | |
|---|---|
| age (years) | 33.9 ± 8.3 |
| BMI (kg/m$^2$) | 23.8 ± 2.4 |
| waist (cm) | 80.66 ± 9.3 |

[a]Values are means ± standard deviation.

**Preparation of Fecal Water Samples.** The extraction was performed and described previously by Costabile et al.[24] Fecal water was extracted 1:1 (w/v) in 1 M-ice-cold phosphate buffer saline (PBS, pH 7.4). The samples were homogenized in a stomacher bag for 2 min, and the aliquots were ultracentrifuged at 64000 *g* for 2 h at 4 °C (Beckman Optima L90K Ultracentrifuge; Beckman Limited, High Wycombe, U.K.). The supernatants were carefully removed and stored in a 1.5 mL Eppendorf tube at −70 °C until analysis.

**$^1$H NMR Spectroscopic Analyses.** Fecal water samples extracted in 1:1 (w/v) PBS were thawed and diluted with an equal amount of PBS. Further dilution was performed due to the limited amount of samples available for NMR analysis. The diluted mixture was vortexed (10 s) and centrifuged at 10000*g* for 15 min at 4 °C. A volume of 500 μL of clear supernatant was transferred to a 5 mM NMR tube and 100 μL of deuterium oxide ($D_2O$) containing 0.025 mg/mL of 3-(Trimethylsilyl) propionicacid-$d_4$ sodium salt (TSP) was added as a lock solvent. One dimensional NMR experiments were conducted using a Bruker Advance DRX 600 MHz spectrometer equipped with a 5 mm triple resonance (TXI) probe at a temperature of 298 K. The Noespr1d (90°-d1−90°-$d_{mix}$-90°-FID, Bruker, Rheinstetten, Germany) sequence was performed to suppress signals from water molecules where d1 is a 4 μs delay time and $d_{mix}$ is the mixing time. The spectra was acquired with 64 scans, a spectral width of 7288 Hz collected into 32K data points, an acquisition time of 2.24 s, and a relaxation delay of 5 s. The obtained free induction decay (FID) was multiplied by 0.3 Hz of line broadening before Fourier transformation. The spectra were referenced to TSP (chemical shift 0 ppm), phased, and baseline corrected in the Topspin 3.0 software (Bruker). Relative quantification of selected $^1$H resonance was performed by integration of peak areas using Topspin 3.0 (Bruker). The integrals were normalized to the concentration of TSP added as an external reference. Assignments of $^1$H NMR signals were carried out using Chenomx NMR Suite 7.7 (Chenomx, Canada) and according to the Human Metabolome Database[25] and the literature.[20] In addition, the heteronuclear single quantum correlation (HSQC) 2D NMR technique was applied to confirm the identity of the given metabolites. The 2D experiment was acquired with a spectral width of 6127 Hz in the $^1$H dimension and 27164 Hz in the $^{13}$C dimension, a matrix with size of 4096 × 1024, 512 transients per increment and a relaxation delay of 2 s.

**Data Analysis.** NMR spectra were imported to MATLABR2010b (The Mathworks, Inc.), and the misalignments of the spectra were corrected using the algorithm icoshift based on the correlational shifting of spectral intervals.[26] The spectrum with the highest correlation to the rest of the spectra in the matrix was used as a reference. The algorithm for icoshift is open-source and available at

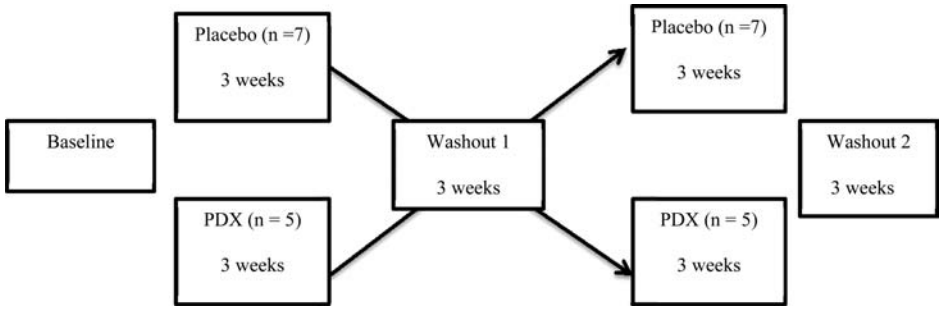


**Figure 1.** Schematic of the crossover intervention design. Each box represents a group of human subjects in the crossover design. The first group consumed PDX powder for 3 weeks, and then after a 3-week washout period, they consumed the equivalent placebo for 3 weeks. The second group received first the placebo (maltodextrin) for 3 weeks, and then after a 3-week washout period, PDX powder for another 3-week treatment period. The fecal samples were collected at five time points from each subject; before PDX intake at baseline, following PDX treatment, following washout 1, following placebo, and following washout 2.[24]


dx.doi.org/10.1021/jf5031218 | J. Agric. Food Chem. 2014, 62, 9944−9951

www.model.life.ku.dk/icoshift. Both the unwanted region (12 to 9 ppm, 0.5 to −1.2 ppm) and the region containing the water resonance (5 to 4.7 ppm) were removed from the aligned spectra. The spectra were normalized to unit area and pareto-scaled. Multivariate data analysis was performed to explore whether the PDX intervention led to systematic metabolic changes and to identify which metabolites were the most differentiating biomarkers between the PDX treated and placebo samples.

Initially, principal component analysis (PCA) of the preprocessed NMR spectra ($n$ = 60) was performed to visualize general grouping, trend, and outliers in the data. Subsequently, supervised partial least-squares discriminant analysis (PLS-DA) was performed to discriminate between the treated and placebo samples ($n$ = 24). In addition, PLS regressions between NMR spectra from the PDX and placebo-treated subjects ($X$ variable) and the bacterial cell count ($\log_{10}$, $Y$ variable) were used to elucidate the relationship between the NMR metabolic profile and bacterial cell count. PLS-DA and PLS models were performed on unit-normalized NMR spectra using full cross validation. Enumeration of bacterial cells was performed and previously described by Costabile et al.[24] PCA, PLSDA, and PLS-regression were conducted using the PLS Toolbox (eigenvector Research) in MATLAB2009b. Furthermore, statistical total correlation spectroscopy (STOCSY) analysis was performed in multiple samples from PDX treated spectra ($n$ = 12) in MATLABR2010b. Kirill Veselkov, Imperial College 2009, wrote the script for STOCSY.[27]

## RESULTS

**NMR Metabolite Profiles of Fecal Samples.** The $^1$H NMR spectra of fresh fecal samples revealed a wide range of metabolites. Figure 2 shows a representative spectrum of a fecal sample extracted in PBS buffer. The use of buffer during extraction allowed us to reduce the chemical shift inconsistency between the samples. The obtained $^1$H NMR spectra contained resonances from SCFA (predominantly acetate, propionate, and butyrate), branched chain fatty acids, biogenic amines, bile acids, organic acids, carbohydrate, and amino acids (Table 2). A pronounced effect of PDX intake was observed on the NMR profile. Visual inspection of spectra showed that samples collected after PDX intervention had a markedly different fecal metabolite profile than baseline, placebo, and washout samples. The difference can be ascribed to the presence of undigested PDX material (3.5−4.5 ppm) and compounds in the spectral region of 5.0−5.5 ppm (Figure 3), which are assigned to oligomers of glucose (alpha anomeric protons) and other unidentified carbohydrates, appearing as a result of cleavage of PDX. This assignment was confirmed from $^1$H NMR spectra obtained on a pure standard of PDX (10 mg/L) (data shown in Supporting Information Figure S1).

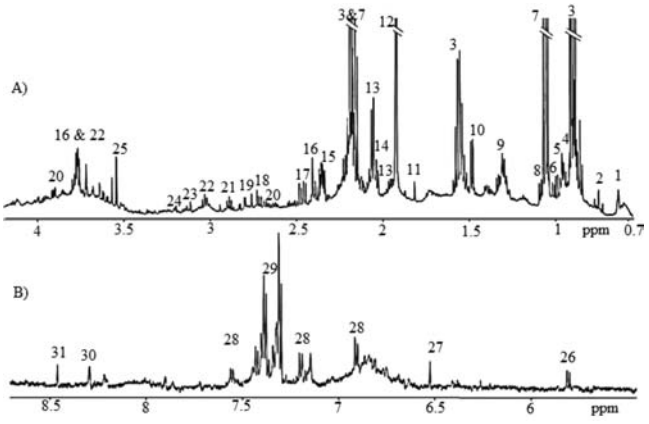


**Figure 2.** Representative $^1$HNMR spectrum of a human fecal sample extracted in PBS buffer: (A) 0.8−4.2 ppm and (B) 5.5−8.6 ppm. The aromatic region in the spectrum (5.5−8.6 ppm) has been magnified three times compared to the aliphatic region. Keys to the figure are given in Table 2.

**Table 2. $^1$H NMR Chemical Shifts and Signal Assignments of Metabolites Found in Fecal Extracts**

| no. | compound | proton chemical shift in ppm and multiplicity |
|---|---|---|
| 1 | deoxycholate | 0.72(s), 0.93(s), 0.97(s) |
| 2 | unknown | 0.8(t) |
| 3 | *n*-butyrate | 0.9(t), 1.56(t), 2.16(t) |
| 4 | leucine | 0.96(d), 0.97(d), 1.7(m) |
| 5 | iso-leucine | 0.94(t), 1.02(d), 1.27(m) |
| 6 | valine | 0.99(d), 1.05(d), 2.3(m) |
| 7 | propionate | 1.06(t), 2.19(m) |
| 8 | 3-methyl-2oxovalerate[a] | 0.9(t), 1.1(d), 1.4(m), 1.7(m), 2.9(m) |
| 9 | *n*-valerate | 0.88(t), 1.31(m), 1.53(m), 2.18(m) |
| 10 | alanine | 1.48(d), 3.78(q) |
| 11 | glutarate | 1.8(t), 2.19(t) |
| 12 | acetate | 1.92(s) |
| 13 | iso-valerate | 0.91(d), 1.96(m), 2.06(d) |
| 14 | *N*-acetylglutamate[a] | 1.87(s), 2.02(s), 2.2(t), 4.1(m) |
| 15 | glutamate | 2.14(m), 2.46(m), 3.78(m) |
| 16 | succinate | 2.41(s) |
| 17 | *N*-cabromoylaspartate[a] | 2.44(d), 2.46(d), 2.65(d), 2.67(d) |
| 18 | sarcosine[a] | 2.71(s), 3.6(s) |
| 19 | dimethylamine | 2.72(s) |
| 20 | aspartate[a] | 2.69(dd), 2.82(dd), 3.91(dd) |
| 21 | trimethylamine | 2.87(s) |
| 22 | lysine | 3.03(t) |
| 23 | malonate[a] | 3.13(s) |
| 24 | choline | 3.2(s), 3.53(m) |
| 25 | glycine | 3.57(s) |
| 26 | uracil | 5.82(d), 7.54(d) |
| 27 | fumarate | 6.5(s) |
| 28 | tyrosine | 6.91(d), 7.2(d) |
| 29 | phenylacetate | 3.54(s), 7.31(m), 7.37(m) |
| 30 | imidiazol[a] | 8.3(s) |
| 31 | formate | 8.46(s) |

[a]Tentative assignment with best matched signals.

**Multivariate Data Analysis.** To determine and characterize the global metabolic effect of PDX on the human gut metabolome, multivariate data analysis was applied on the NMR spectra. In total, 60 NMR spectra from 12 subjects were included in the data analysis. PCA was performed on the pareto-scaled normalized $^1$H NMR spectra to explore the metabolic difference between baselines, PDX treated, wash out 1, placebo, and wash out 2 samples. The score plot shows that the PDX treated samples have distinct clustering along PC1 explaining 30.46% of the total variation (Figure 4A), and the corresponding loading reveals that the clustering could mainly be ascribed to the presence of undigested residuals PDX in the region 3.5 to 4.5 ppm of the spectra (Figure 4B). It is also apparent from the loading plot that propionate, butyrate, and acetate varied between the samples; however, these metabolites were not indicative to any distinct clusters but represented a sample-to-sample variation.

To minimize the sample-to-sample variation, PCA was also performed including only the $^1$H NMR spectra from the PDX and placebo samples. The score plot depicts two distinct


dx.doi.org/10.1021/jf5031218 | J. Agric. Food Chem. 2014, 62, 9944−9951

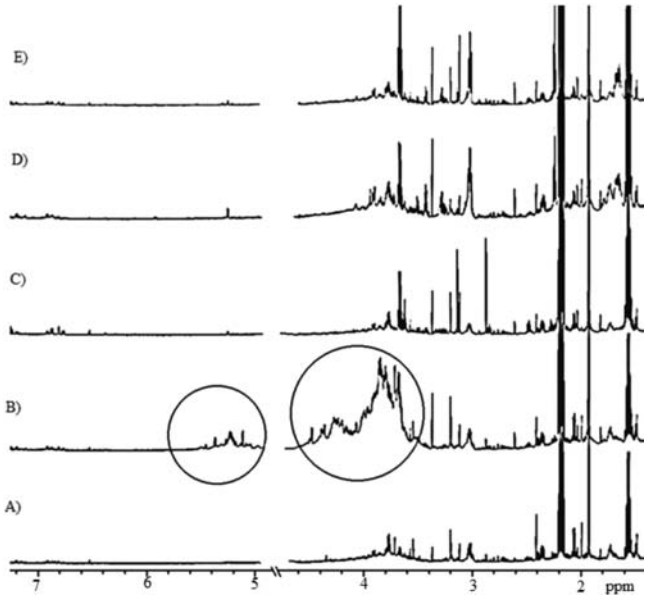


**Figure 3.** Typical 600 MHz $^1$HNMR spectra of fecal samples extracted in PBS buffer. Each spectrum represents fecal samples collected from the same human subject at five different time points: (A) baseline, (B) PDX treated, (C) washout 1, (D) placebo, and (E) washout 2. The large circle region (Figure 3B, 3.5−4.5 ppm) in the spectra represents the broad signals from PDX + other unidentified carbohydrates and a smaller circled region (Figure 3B, 5−5.5 ppm) represents alpha anomeric protons of PDX + other unidentified carbohydrates.

clusters along PC1 (Figure 4C). From the corresponding loading, the metabolites contributing to this clustering included succinate, lysine, phenylacetate, acetate, propionate, and butyrate, which were all decreased while signals from residual PDX and oligomers of glucose (alpha anomeric protons) and other unidentified carbohydrates were increased for the PDX-treated samples (Figure 4D). In addition, PLS-DA was performed on the $^1$H NMR spectra excluding the 3.5−5.5 ppm region in the spectra in order to discover potential metabolic differences between the PDX-treated and placebo samples. However, the model had more than 50% of classification error, indicating that the generated models were not sufficiently robust (data not shown).

**Targeted Analyses of Metabolite Concentrations.** The relative concentrations of fecal SCFA (acetate, butyrate, and propionate), branched chain fatty acids (iso-valerate), biogenic amine (dimethyl amine), organic acid (succinate), and amino acid (phenylacetate) were quantified from the $^1$H NMR spectra (Table 3). No significant changes in any of the fecal metabolites were observed after PDX or placebo treatment. This finding is in agreement with the previous study by Costabile et al.[24] and is supported by the correlation between the NMR and GC MS derived content for acetate, butyrate, and propionate (data shown in the Supporting Information Table S1).

**Correlation Analysis.** To identify intervariable correlations, STOCSY analysis was performed on $^1$H NMR spectra of multiple PDX-treated samples ($n$ = 12). The STOCSY approach enables the detection of highly correlated peaks whose concentrations are interdependent or under some common regulatory mechanism.[27] In one-dimensional STOCSY analysis, variables are correlated to a given chemical shift value (for instance $\delta$ = 5.25 ppm). The positive and negative values between the covariance of variables indicate the association to the 5.25 ppm variable that represents the particular signal from a molecule in the spectrum. The covariance pattern is indicated in a color code which represents the strength of statistical associations (red high and blue low). The STCOSY analysis shows (Figure 5) that the oligomers of glucose (alpha anomeric protons) and other unidentified carbohydrates in the 5 to 5.5 ppm region (covariance $\delta$ = 5.25 ppm) of the PDX treated spectra were positively correlated with the broad signal at 3.5 to 4.5 ppm from PDX, propionate, and acetate signals. The highest statistical associations (significance level of $p < 0.05$) were observed for the 3.5 to 4.5 ppm PDX signal and propionate. Thus, STOCSY enables us to identify associations between PDX and other fecal metabolites.

Furthermore, PLS regressions were performed to elucidate the relationship between the NMR metabolite profile (placebo and PDX treated, $n$ = 24) and bacterial cell count ($\log_{10}$) for bacteria in the fecal extract. From PLS regressions between the NMR metabolite profile and fecal bacterial count, the highest level of correlation could be established with *Bifidobacterium* ($R^2$ = 0.66) (Table 4). Intriguingly, the regression coefficient plot (Figure 6A) shows that succinate, acetate, and propionate were negatively correlated with the amount of *bifidobacteria* while butyrate and malonate content are positively correlated with *bifidobacteria* in feces. The variable importance for projection (VIP) plot was used to rank the importance of the variables. The VIP plot showed acetate and succinate to be the most influential variable. In addition to *Bifidobacterium*, regression analysis also showed positive correlation of *Bacteroides* ($R^2$ = 0.45) with acetate content in the feces (Figure 6B). Similar results were obtained when correlations between bacterial cell count and the data from previous gas chromatography-mass spectrometry (GC-MS) analyses were performed (described in Supporting Information). This finding substantiates that changes in the *Bifidobacterium* and *Bacteroides* populations in the colon could be correlated to succinate and acetate concentrations in feces.

## DISCUSSION

Previous studies have shown a prebiotic potential of PDX;[8,10,11,24,28] however, little is known about the global metabolic impact of PDX in the human gut. $^1$H NMR-based metabolite profiling enabled identification of a wide range of metabolites such as SCFA (acetate, butyrate, and propionate), organic acids (succinate, fumarate), branched chain fatty acids (iso-butyrate, iso-valerate), biogenic amines (trimethylamine, dimethyl amine), carbohydrates, and amino acids (phenyl-acetate, tyrosine) in feces. Thus, a broad view of the diet-induced metabolite changes could be explored using the approach conducted here compared to the gas chromatography analysis performed earlier.[24]

PCA (Figure 4A) showed a distinct clustering of PDX-treated samples when compared with the corresponding metabolite profile from the baseline, placebo, and washout samples. The clustering could mainly be ascribed to residual PDX and unknown oligosaccharides in the feces. Thus, the present study reveals a very strong effect of PDX intake on the NMR metabolome due to the presence of residual PDX and partly degraded PDX products. Previous studies have also shown that during gastrointestinal transit, a proportion of undigested PDX is excreted in the feces.[24,28,11] Our data provide additional and strong evidence of undigested PDX as we could visually identify the presence of residual PDX in the

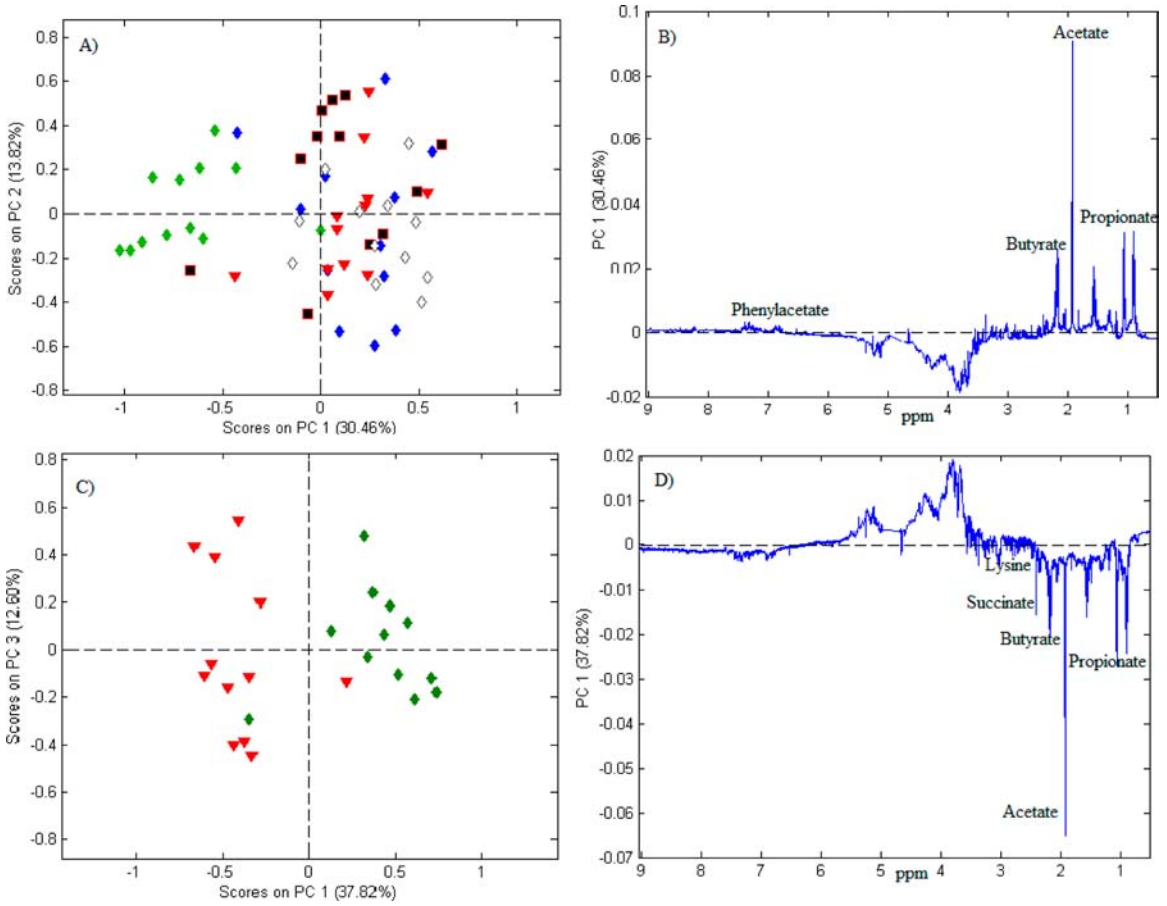


**Figure 4.** PCA score plots and loadings: (A) score plot of the first and second principal component (PC) from 60 fecal samples (black quare with red outline) baseline samples, (green diamond) PDX treated samples, (blue diamond) wash out 1 sample, (downward pointing red triangle) placebo treated, and (white diamond) washout 2 samples. (B) Loading profile of first principal component from 60 fecal samples. (C) Score plot illustrating (downward pointing red triangle) placebo and (green diamond) PDX treated samples. (D) Loading profile of first PC.

**Table 3. Relative Quantification of Fecal Metabolites**[a]

| metabolite | control mean (±) SE | PDX treated mean (±) SE | *P*-value |
|---|---|---|---|
| phenylacetate | 0.10 ± 0.01 | 0.05 ± 0.05 | 0.12 |
| succinate | 0.19 ± 0.01 | 0.52 ± 0.01 | 0.21 |
| acetate | 6.46 ± 0.22 | 5.71 ± 0.22 | 0.29 |
| butyrate | 2.29 ± 0.01 | 1.90 ± 0.07 | 0.42 |
| alanine | 0.46 ± 0.02 | 0.45 ± 0.29 | 0.82 |
| propionate | 2.97 ± 0.12 | 2.78 ± 0.11 | 0.35 |
| isovalerate[b] | 0.52 ± 0.02 | 0.51 ± 0.01 | 0.23 |
| dimethylamine[b] | 0.52 ± 0.02 | 0.03 ± 0.01 | 0.90 |
| malonate[b] | 0.13 ± 0.01 | 0.20 ± 0.01 | 0.52 |

[a]The values are integrals relative to the TSP signal in the spectra. [b]Resonance signals below detection limit are not included.

NMR spectra of the feces (Figure 3). The results imply that NMR could be a very useful method to determine whether the subject consumed PDX. Thus, compliance of PDX consumption by a subject during intervention studies can be confirmed by NMR analysis, which commonly is a challenge for dietary intervention studies. In this context, NMR spectroscopy is simple, rapid, reproducible, and less labor intensive than many other analytical techniques.[29,30]

The results from this study demonstrate that depolymerized products of PDX were present in the feces of PDX-treated subjects. This finding provides evidence that the fermentation of PDX is continued until the distal part of the colon. Saccharolytic activity in the distal colon has been associated with a specific health benefit due to a reduction of proteolytic activities, which are linked to production of genotoxin and carcinogenic effects.[31] Costabile et al. also showed that the genotoxicity of the fecal water was significantly reduced due to PDX fermentation.[24]

PDX intake has been found to increase the production of SCFA in studies on rats,[11,32] dogs,[9] in vitro models,[32,10] and humans.[8] In particular, levels of butyrate and acetate have been highly elevated in the previous studies due to PDX fermentation; however, such changes were not observed in this study. Nevertheless, the STOCSY analysis performed on multiple $^1$H NMR spectra obtained after PDX consumption showed that residual PDX could be correlated with acetate and propionate and that the correlation was significant ($p < 0.05$). This correlation suggests that the concentration of acetate and propionate might be interdependent or under some regulative mechanism with bacterial degradation of PDX. Thus, it is likely that high inter- and intrasample variation in the subjects might have masked any additional effects of PDX consumption. Additionally, the diet, genotype of the individuals, lifestyle, environmental factors, or gut microbial variation might have had a higher impact on the metabolic outcome than the PDX treatment. To overcome the masking effect, we believe further, controlled studies with a larger number of individuals are

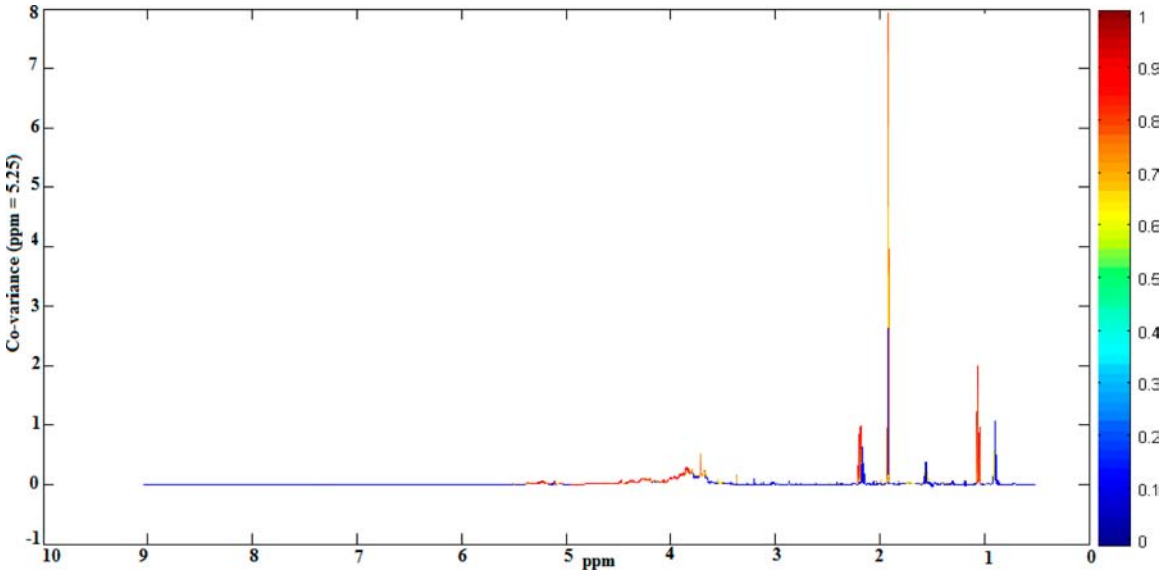


**Figure 5.** One-dimensional STOCSY analysis to identify intensity variables correlated to the chemical shift, $\delta$ = 5.25 ppm. The positive and negative values between the covariance of variables indicate the association to the 5.25 ppm variable that represents PDX. The color code of covariance patterns indicates the strength of statistical associations.

**Table 4. Correlation of Bacterial Cell Count ($\log_{10}$) and NMR Data Obtained from PLS Regression**

| S/N | species | $R^2$ | $\log_{10}$ max | $\log_{10}$ min |
|---|---|---|---|---|
| 1 | *Atopobium* group | 0.13 | 10.22 | 8.45 |
| 2 | *Bacteroides* genus | 0.46 | 10.45 | 9.23 |
| 3 | *Bifidobacterium* genus | 0.66 | 10.14 | 7.09 |
| 4 | *Eubacterium rectale* group | 0.01 | 10.58 | 9.61 |
| 5 | *Lactobacillus/Enterococcus* genera | 0.14 | 10.12 | 8.23 |

needed to establish the link between metabolic response and PDX consumption.

There is an increasing interest in understanding how fibers and prebiotics affect specific gut bacteria and the gut fermentation pattern.[33−36] PLS regression analyses between NMR fecal metabolite profiles and the bacterial cell count of individual bacteria showed a strong correlation between the fecal metabolite profile and the amount of *bifidobacteria* present in feces. Intriguingly, the VIP loading revealed a negative correlation between the content of *bifidobacteria* and levels of succinate and acetate. In parallel, the *Bacteroides* content had a positive correlation with acetate in the feces (Figure 6). This finding is consistent with the fact that acetate and succinate are associated with carbohydrate metabolism and major metabolites of *Bacteroides*.[37] The result indicates that carbohydrate metabolism in the colon is affected by varying numbers of *bifidobacteria* and *Bacteroides* populations in the gut. Recently, production of succinate by *Bifidobacterium* has also been demonstrated, but their ability to produce succinate was found to be dependent on energy source and the presence of different *bifidobacterial* species.[38] On the basis of our results, we suggest the negative correlation between *bifidobacteria* and the level of succinate might be due to alterations in the *bifidobacteria* species in the colon. Thus, the potential to correlate the fecal metabolome and microbial groups demonstrated in the present study suggests great promise for NMR based metabolomics to explore correlations between the microbial community and their activity expressed as the metabolites that are present.

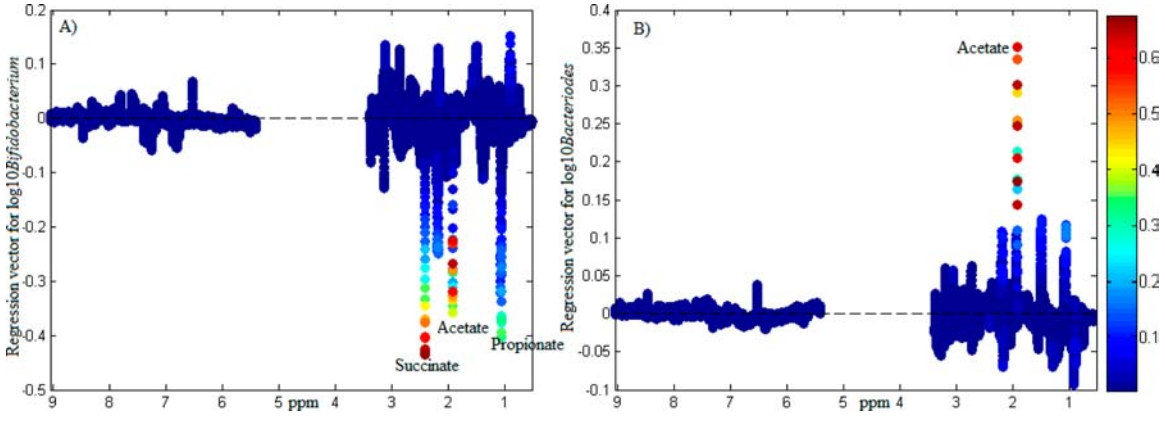


**Figure 6.** Results from PLS regression analysis. (A) Regression coefficients from PLS regression analysis show that succinate, acetate, and propionate contents were negatively correlated with the *Bifidobacterium* content while butyrate and malonate were positively correlated with *Bifidobacterium* content. (B) Regression coefficients from PLS regression analysis show that acetate content is positively correlated with the *Bacteroides* content in feces.


dx.doi.org/10.1021/jf5031218 | J. Agric. Food Chem. 2014, 62, 9944−9951

While a correlation could be established between the fecal metabolome and bacterial cell counts of *Bifidobacterium* and *Bacteroides*, correlations could not be established for other bacterial groups (Table 4). This result could be due to low variations in the content of these bacteria between the subjects and that they were not influenced by the intervention with PDX,[24] or for a bacterial genus such as *Lactobacillus*. The lack of correlations for other bacterial groups may be because other bacteria do not produce any of the metabolites that may also be because it is not producing any of the metabolites that vary in the $^1$H NMR spectra.

In conclusion, the present study demonstrated that NMR-based metabolomics is a useful and efficient technique for metabolite profiling of feces and to test compliance to a dietary intervention with PDX. It is anticipated that the approach could be applied to other dietary fibers. In addition, through the application of STOCSY, novel associations between PDX and the metabolites acetate and propionate could be identified, demonstrating the potential of metabolomics to unravel intermolecular interactions and small metabolite alterations that may not appear as significant treatment effects. Finally, the establishment of a correlation between the fecal metabolome and the levels of *Bifidobacterium* and *Bacteroides* demonstrates the potential of NMR-based metabolomics to elucidate metabolic activity of specific bacteria in the gut.

## ■ ASSOCIATED CONTENT

### Supporting Information

Typical 600 MHz $^1$HNMR spectra of PDX (Figure S1) and correlations between NMR and GC-MS data (Table S1) and between metabolite concentration and bacterial cell count (Table S2). This material is available free of charge via the Internet at http://pubs.acs.org.

## ■ AUTHOR INFORMATION

### Corresponding Author

*E-mail: hannec.bertram@agrsci.dk. Phone: 004587158353.

### Funding

The present study is part of the Ph.D. work of Santosh Lamichhane and was financially supported by DuPont, Food Future Innovation (FFI), and Aarhus University. The authors also wish to thank the Danish research council FTP for financial support through the project "Advances in food and nutrition research through implementation of metabolomics technologies" (Grant No. 274-09-0107).

### Notes

The authors declare the following competing financial interest(s): This work was partly funded by Danisco, who are marketing polydextrose. The authors Sofia Forssten, Arthur C. Ouwehand, Markku Saarinen, and Henrik Max Jensen were employees of Danisco at the time of the study.

## ■ REFERENCES

(1) Kanauchi, O.; Andoh, A.; Mitsuyama, K. Effects of the modulation of microbiota on the gastrointestinal immune system and bowel function. *J. Agric. Food Chem.* **2013**, *61*, 9977−9983.

(2) Hedin, C.; Whelan, K.; Lindsay, J. O. Evidence for the use of probiotics and prebiotics in inflammatory bowel disease: A review of clinical trials. *Proc. Nutr. Soc.* **2007**, *66*, 307−315.

(3) Geier, M. S.; Butler, R. N.; Howarth, G. S. Probiotics, prebiotics and synbiotics: A role in chemoprevention for colorectal cancer? *Cancer Biol. Ther.* **2006**, *5*, 1265−1269.

(4) Lomax, A. R.; Calder, P. C. Prebiotics, immune function, infection and inflammation: A review of the evidence. *Br. J. Nutr.* **2009**, *101*, 633−658.

(5) El Oufir, L.; Flourié, B.; Bruley Des Varannes, S.; Barry, J. L.; Cloarec, D.; Bornet, F.; Galmiche, J. P. Relations between transit time, fermentation products, and hydrogen consuming flora in healthy humans. *Gut* **1996**, *38*, 870−877.

(6) Lahtinen, S. J.; Knoblock, K.; Drakoularakou, A.; Jacob, M.; Stowell, J.; Gibson, G. R.; Ouwehand, A. C. Effect of molecule branching and glycosidic linkage on the degradation of Polydextrose by gut microbiota. *Biosci., Biotechnol. Biochem.* **2010**, *74*, 2016−2021.

(7) Hull, S.; Re, R.; Tiihonen, K.; Viscione, L.; Wickham, M. Consuming Polydextrose in a mid-morning snack increases acute satiety measurements and reduces subsequent energy intake at lunch in healthy human subjects. *Appetite* **2012**, *59*, 706−712.

(8) Jie, Z.; Bang-yao, L.; Ming-jie, X.; Hai-wei, L.; Zu-kang, Z.; Ting-song, W.; Craig, S. A. S. Studies on the effects of Polydextrose intake on physiologic funtions in Chinese people. *Am. J. Clin. Nutr.* **2000**, *72*, 1503−1509.

(9) Beloshapka, A. N.; Wolff, A. K.; Swanson, K. S. Effects of feeding Polydextrose on faecal characteristics, microbiota and fermentative end products in healthy adult dogs. *Br. J. Nutr.* **2012**, *108*, 638−644.

(10) Mäkivuokko, H.; Kettunen, H.; Saarinen, M.; Kamiwaki, T.; Yokoyama, Y.; Stowell, J.; Rautonen, N. The effect of cocoa and Polydextrose on bacterial fermentation in gastrointestinal tract simulations. *Biosci., Biotechnol. Biochem.* **2007**, *71*, 1834−1843.

(11) Figdor, S. K.; Rennhard, H. H. Caloric utilization and disposition of [14C]Polydextrose in the rat. *J. Agric. Food Chem.* **1981**, *29*, 1181−1189.

(12) Guarner, F.; Malagelada, J. R. Gut flora in health and disease. *Lancet* **2003**, *361*, 512−519.

(13) Nicholson, J. K.; Holmes, E.; Kinross, J.; Burcelin, R.; Gibson, G.; Jia, W.; Pettersson, S. Host-gut microbiota metabolic interactions. *Science* **2012**, *336*, 1262−1267.

(14) David, L. A.; Maurice, C. F.; Carmody, R. N.; Gootenberg, D. B.; Button, J. E.; Wolfe, B. E.; Ling, A. V.; Devlin, A. S.; Varma, Y.; Fischbach, M. A.; Biddinger, S. B.; Dutton, R. J.; Turnbaugh, P. J. Diet rapidly and reproducibly alters the human gut microbiome. *Nature* **2014**, *505*, 559−563.

(15) Blaut, M.; Clavel, T. Metabolic diversity of the intestinal microbiota: implications for health and disease. *J. Nutr.* **2007**, *137*, 751S−755S.

(16) Egert, M.; De Graaf, A. A.; Smidt, H.; De Vos, W. M.; Venema, K. Beyond diversity: Functional microbiomics of the human colon. *Trends Microbiol.* **2006**, *14*, 86−91.

(17) Rezzi, S.; Ramadan, Z.; Fay, L. B.; Kochhar, S. Nutritional metabonomics: Applications and perspectives. *J. Proteome Res.* **2007**, *6*, 513−525.

(18) Martin, F. P. J.; Sprenger, N.; Montoliu, I.; Rezzi, S.; Kochhar, S.; Nicholson, J. K. Dietary modulation of gut functional ecology studied by fecal metabonomics. *J. Proteome Res.* **2010**, *9*, 5284−5295.

(19) Saric, J.; Wang, Y.; Li, J.; Coen, M.; Utzinger, J.; Marchesi, J. R.; Keiser, J.; Veselkov, K.; Lindon, J. C.; Nicholson, J. K.; Holmes, E. Species variation in the fecal metabolome gives insight into differential gastrointestinal function. *J. Proteome Res.* **2008**, *7*, 352−360.

(20) Jacobs, D. M.; Deltimple, N.; van Velzen, E.; van Dorsten, F. A.; Bingham, M.; Vaughan, E. E.; van Duynhoven, J. 1H NMR metabolite profiling of feces as a tool to assess the impact of nutrition on the human microbiome. *NMR Biomed.* **2008**, *21*, 615−626.

(21) Marchesi, J. R.; Holmes, E.; Khan, F.; Kochhar, S.; Scanlan, P.; Shanahan, F.; Wilson, I. D.; Wang, Y. Rapid and noninvasive metabonomic characterization of inflammatory bowel disease. *J. Proteome Res.* **2007**, *6*, 546−551.

(22) Yap, I. K. S.; Li, J. V.; Saric, J.; Martin, F. P.; Davies, H.; Wang, Y.; Wilson, I. D.; Nicholson, J. K.; Utzinger, J.; Marchesi, J. R.; Holmes, E. Metabonomic and microbiological analysis of the dynamic effect of vancomycin-lnduced gut microbiota modification in the mouse. *J. Proteome Res.* **2008**, *7*, 3718−3728.

(23) Le Gall, G.; Noor, S. O.; Ridgway, K.; Scovell, L.; Jamieson, C.; Johnson, I. T.; Colquhoun, I. J.; Kemsley, E. K.; Narbad, A. Metabolomics of fecal extracts detects altered metabolic activity of gut microbiota in ulcerative colitis and irritable bowel syndrome. *J. Proteome Res.* **2011**, *10*, 4208−4218.
(24) Costabile, A.; Fava, F.; Röytiö, H.; Forssten, S. D.; Olli, K.; Klievink, J.; Rowland, I. R.; Ouwehand, A. C.; Rastall, R. A.; Gibson, G. R.; Walton, G. E. Impact of Polydextrose on the faecal microbiota: A double-blind, crossover, placebo-controlled feeding study in healthy human subjects. *Br. J. Nutr.* **2012**, *108*, 471−481.
(25) Wishart, D. S.; Knox, C.; Guo, A. C.; Eisner, R.; Young, N.; Gautam, B.; Hau, D. D.; Psychogios, N.; Dong, E.; Bouatra, S.; Mandal, R.; Sinelnikov, I.; Xia, J.; Jia, L.; Cruz, J. A.; Lim, E.; Sobsey, C. A.; Shrivastava, S.; Huang, P.; Liu, P.; Fang, L.; Peng, J.; Fradette, R.; Cheng, D.; Tzur, D.; Clements, M.; Lewis, A.; de souza, A.; Zuniga, A.; Dawe, M.; Xiong, Y.; Clive, D.; Greiner, R.; Nazyrova, A.; Shaykhutdinov, R.; Li, L.; Vogel, H. J.; Forsythei, I. HMDB: A knowledgebase for the human metabolome. *Nucleic Acids Res.* **2009**, *37*, 603−610.
(26) Savorani, F.; Tomasi, G.; Engelsen, S. B. icoshift: A versatile tool for the rapid alignment of 1D NMR spectra. *J. Magn. Reson.* **2010**, *202*, 190−202.
(27) Cloarec, O.; Dumas, M. E.; Craig, A.; Barton, R. H.; Trygg, J.; Hudson, J.; Blancher, C.; Gauguier, D.; Lindon, J. C.; Holmes, E.; Nicholson, J. Statistical total correlation spectroscopy: An exploratory approach for latent biomarker identification from metabolic 1H NMR data sets. *Anal. Chem.* **2005**, *77*, 1282−1289.
(28) Achour, L.; Flourié, B.; Briet, F.; Pellier, P.; Marteau, P.; Rambaud, J. C. Gastrointestinal effects and energy value of Polydextrose in healthy nonobese men. *Am. J. Clin. Nutr.* **1994**, *59*, 1362−1368.
(29) Kim, H. K.; Choi, Y. H.; Verpoorte, R. NMR-based plant metabolomics: Where do westand, where do we go? *Trends Biotechnol.* **2011**, *29*, 267−275.
(30) Bertram, H. C.; Malmendal, A.; Petersen, B. O.; Madsen, J. C.; Pedersen, H.; Nielsen, N. C.; Hoppe, C.; Mølgaard, C.; Michaelsen, K. F.; Duus, J. Ø. Effect of magnetic field strength on NMR-based metabonomic human urine data. Comparative study of 250, 400, 500, and 800 MHz. *Anal. Chem.* **2007**, *79*, 7110−7115.
(31) Rowland, I. R.; Mallett, A. K.; Wise, A. The effect of diet on the mammalian gut flora and its metabolic activities. *Crit. Rev. Toxicol.* **1985**, *16*, 31−103.
(32) Weaver, C. M.; Martin, B. R.; Story, J. A.; Hutchinson, I.; Sanders, L. Novel fibers increase bone calcium content and strength beyond efficiency of large intestine fermentation. *J. Agric. Food Chem.* **2010**, *58*, 8952−8957.
(33) Hernot, D. C.; Boileau, T. W.; Bauer, L. L.; Middelbos, I. S.; Murphy, M. R.; Swanson, K. S.; Fahey, G. C., Jr. In vitro fermentation profiles, gas production rates, and microbiota modulation as affected by certain fructans, galactooligosaccharides, and Polydextrose. *J. Agric. Food Chem.* **2009**, *57*, 1354−1361.
(34) Aura, A. M.; Niemi, P.; Mattila, I.; Niemelä, K.; Smeds, A.; Tamminen, T.; Faulds, C.; Buchert, J.; Poutanen, K. Release of small phenolic compounds from Brewer's spent grain and its lignin fractions by human intestinal microbiota in vitro. *J. Agric. Food Chem.* **2013**, *61*, 9744−9753.
(35) Koecher, K. J.; Noack, J. A.; Timm, D. A.; Klosterbuer, A. S.; Thomas, W.; Slavin, J. L. Estimation and interpretation of fermentation in the Gut: Coupling results from a 24 h batch in vitro system with fecal measurements from a human intervention feeding study using fructo-oligosaccharides, inulin, gum acacia, and pea fiber. *J. Agric. Food Chem.* **2014**, *62*, 1332−1337.
(36) Yang, J.; Maldonado-Gómez, M. X.; Hutkins, R. W.; Rose, D. J. Production and in Vitro fermentation of soluble, non-digestible, feruloylated oligo- and polysaccharides from maize and wheat brans. *J. Agric. Food Chem.* **2014**, *62*, 159−166.
(37) Fischbach, M. A.; Sonnenburg, J. L. Eating for two: How metabolism establishes interspecies interactions in the gut. *Cell Host Microbe* **2011**, *10*, 336−347.
(38) Van Der Meulen, R.; Adriany, T.; Verbrugghe, K.; De Vuyst, L. Kinetic analysis of bifidobacterial metabolism reveals a minor role for succinic acid in the regeneration of NAD+ through its growth-associated production. *Appl. Environ. Microbiol.* **2006**, *72*, 5204−5210.

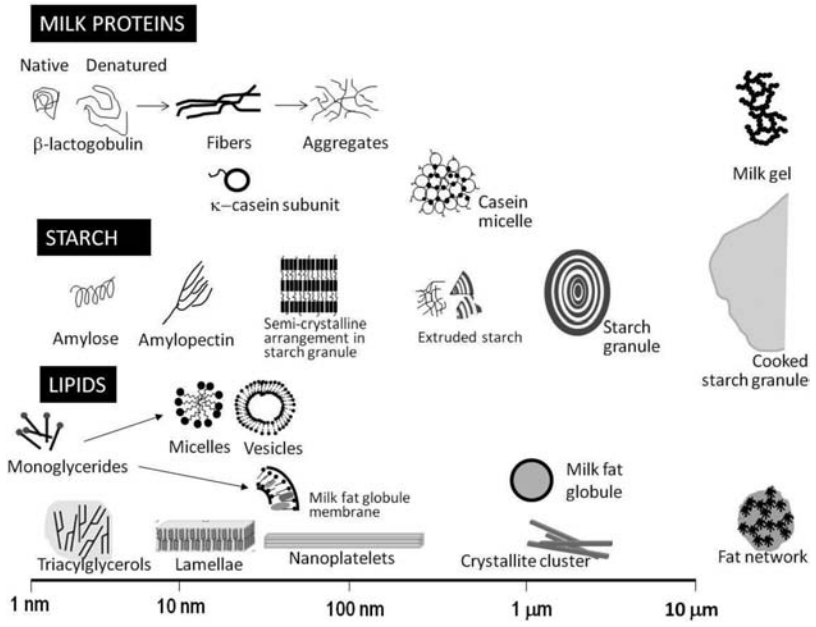


**Figure 1.** Proteins, starches, and lipids undergo major transformations at several length scales during processing and cooking. Casein micelles and fat globules in milk enter the kitchen already as micrometer or submicrometer structures to later give rise to a myriad of dairy products. Starch granules must be cooked so that amylose and amylopectin are released from their natural semicrystalline arrangement of nanosize dimensions. Lipid molecules may form nanostructures (monoglycerides) or become hierarchically assembled into fat crystal networks (triacylglycerols). (Approximate scales.)

pH (Figure 2a).[7] Denatured globular proteins in milk form coaggregates with casein, resulting in stiff gels (e.g., yogurt).

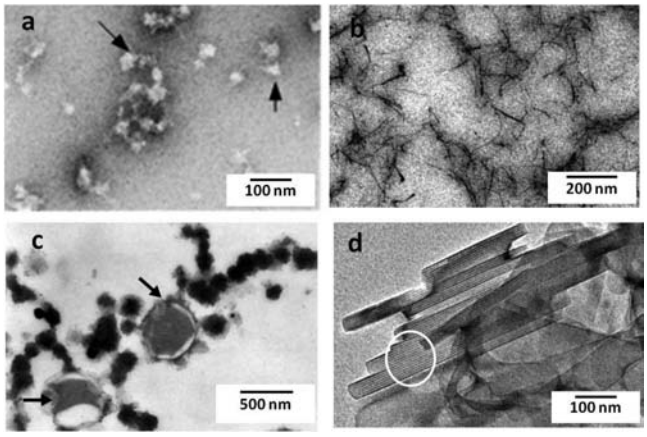


**Figure 2.** Images of some food structures at the nanoscale: (a) protein aggregates (arrows) produced by heating native $\beta$-lactoglobulin at 80 °C and pH 6.0[7] (these types of aggregates may also be formed when milk is heated); (b) TEM image of a 1% $\kappa$-carrageenan gel;[10] (c) yogurt-type gel showing two milk fat globules (arrows) and casein micelles arranged as a string of beads[2] (note anchoring of the strands to the globules' surface); (d) cross section of nanoplatelets (circle) in a fat crystal network.[13] All images were acquired by transmission electron microscopy.

Incidentally, $\alpha$-lactalbumin has the ability to form nanotubules, but their presence in dairy products has not been reported.[8] Wheat flour has two unique proteins: the macropolymer glutenin (approximate length of 50 nm and diameter of 1.8 nm) and the monomeric units of gliadin. During kneading the long glutenin chains associate via physical entanglements into a large network and further interact with space-filling gliadins to form the thin films that give the unique viscoelastic properties and gas-holding capacity to wheat dough.[9] Polysaccharide gels trap abundant water inside a polymer or colloidal network, turning liquid foods into a semisolid material. Electron micrographs show that some polysaccharide gels, such as those of $\kappa$-carrageenan that may be present in flans and puddings, have fine and long filaments a few nanometers in diameter (Figure 2b).[10] Conversely, casein gels, the basic structures in cheeses and yogurts, have thick strands formed by casein micelles attached as a string of beads (Figure 2c).

All starches in cereals and legumes (and roots as well) are present in the form of densely packed granules 5−50 $\mu$m in size. Inside the granule, the branched polysaccharide amylopectin is ordered as neat semicrystalline layers 10 nm in thickness holding amylose molecules in inner spaces (Figure 1). Cooking in the presence of abundant water hydrates and swells the starch granules, obliterating their native structure and releasing both polymers. Thus, a cake mix may now set in the oven into a firm matrix formed by gluten proteins interspersed with swollen starch granules, fat, and sugar that harbors many gas cells. However, most cereal foods are metastable amorphous materials, and the released starch biopolymers may recrystallize on cooling into domains 10−20 nm in size, as those found in stale bakery products or cooled potatoes.[11] Con-Conversely, expanded snacks are produced by heating and shearing a low-moisture starchy flour inside an extruder-cooker, physically fragmenting the granules to submicrometer sizes and breaking down amylose and amylopectin into dextrins. Upon exiting the extruder's die, the melt is blown up by the released steam, resulting in a spongy and soft material characteristic of extruded snacks.[12]

Lipids in oilseeds are stored in discrete subcellular organelles called lipid bodies, <1 $\mu$m in size, surrounded by proteins that act as natural emulsifiers. Most lipids that we consume are triacylglycerol molecules (triglycerides) that may crystallize


dx.doi.org/10.1021/jf5016939 | J. Agric. Food Chem. 2014, 62, 9953−9956

from the molten state as nanoplatelets 30−40 nm thick and extending for around 370 nm (Figure 2d).[13] In turn, stacks of nanoplatelets form crystallites that cluster together into aggregates, eventually developing a fat network that occludes portions of liquid fat resulting in a plastic structure typical of butter and margarine (Figure 1). Monoglycerides and phospholipids are used as emulsifiers due to their amphiphilic nature. In an aqueous phase they may self-associate into a multitude of nanosized structures, for example, micelles and vesicles, which may be found in emulsions such as salad dressings (Figure 1).[14]

Two-phase systems in foods such as emulsions and liquid foams owe their existence to interfacial liquid films stabilized by amphiphilic lipids and/or proteins. Adsorption at oil/water (O/W) interfaces in protein-stabilized food emulsions occurs at dimensions of 10 nm.[15] The stability of beer foam (head) depends on the interaction of proteins and polypeptides extracted from malt and iso-$\alpha$-acids from hops to form an elastic film around 10 nm thick at the liquid/air interface. Although the channels separating adjacent bubbles (lamellae) may have initially an average thickness of around 1 $\mu$m, liquid continuously drains from them until thinning leads to the eventual collapse of the foam.[16]

Solid particles and droplets produced by mechanical size reduction are present in several foods and ingredients. From a sensorial viewpoint soft foods containing solid particles >40 $\mu$m are described as having a "sandy texture", thus the need for fine milling. Grinding and homogenization involve a kinetics of size reduction that yields a particle or droplet size distribution usually characterized by a mean value that in O/W emulsions (e.g., dressings and mayonnaise) produced by high-pressure homogenization may be around 300 nm.[17] Most particles in a commercial chocolate enrobing mass, for instance, are between 8 and 40 $\mu$m, but ca. 0.5% have sizes <1 $\mu$m.[18] This may seem a low volume fraction, but it represents a large number of particles due to their tiny size. The shelves in our kitchens store food powders that tend to agglomerate, so amorphous silica particles are a permitted additive to avoid caking. Some commercial samples of food-grade $SiO_2$ contain aggregates in the range of 50−200 nm with a mode of 70−120 nm.[19] Titanium dioxide nanoparticles, used to enhance the whiteness of a wide variety of foods (e.g., candy and chewing gum), are <300 nm in at least one dimension and 30% of them are <100 nm.[20] They are eliminated in the urine and feces. However, some inorganic nanoparticles have been demonstrated to have biological activity at the cellular and subcellular levels when they are neither soluble in water or oil nor degraded in the gastrointestinal tract nor readily excreted.

Several food components crystallize during processing or storage. The size of crystals increases continuously with time after nucleation, whereas the reverse occurs as they become dissolved in saliva or in the gastrointestinal fluids. Heat and mass transfer limitations during crystallization result in a distribution of sizes whose tail representing small crystals may well intrude into the nanorange. A domestic ice cream machine produces ice crystals 30−40 $\mu$m in size that may be perceived as sandiness on the tongue. However, pouring liquid nitrogen (−196 °C) directly into the cream mix under vigorous agitation causes the formation of tiny ice crystals <1 $\mu$m, giving ice cream a smooth texture that fascinates modern chefs.[21] On the contrary, it has been known for more than a century that the grittiness we appreciate in some cheeses corresponds to crystals of different amino acids that develop during aging (e.g., Roquefort cheese and tyrosine crystals).[22] Crystals (mainly of calcium oxalate) have also been found in many edible plants, but they are probably dissolved during cooking or digestion.[23]

Nanoprocessing of foods does not end in the kitchen but continues inside our bodies. Different from most other materials of our daily life, the "utility" of food structures lies in the rate and extent to which they are broken down and disintegrated. It is quite likely that as nutrients become liberated from the food matrix during digestion they will participate in interactions among them and with other molecules, thus forming new nanosized particles,[24] complex aggregates,[25] and self-assembled colloidal nanostructures,[26] a phenomenon that we are just starting to understand.

Nanoparticles may unintentionally find their way into our foods, for example, after being released from food packaging, coatings of processing equipment, or products of plant or animal origin. Some nanoparticles, particularly those of inorganic sources, have been shown to transverse the gastrointestinal mucosa, getting into some organs and reaching the cellular level.[27] In vivo studies on the cytotoxicity or genotoxicity of these nanomaterials, generally conducted in mice and rats, are scarce, and most of them fail at adequately characterizing the materials utilized; thus, no generalizations could be made of their biological activity.[28] Despite efforts from food regulatory agencies and institutions (e.g., FAO/WHO), gaps continue to exist as to the methodologies to be used in evaluating the safety of these nanomaterials and the relevance of the data generated.[29]

## ■ CONCLUSIONS

There are many identifiable nanostructures in the foods we eat. These edible nanostructures are assembled by nature, created during processing or cooking, intentionally added as ingredients, and perhaps incorporated inadvertently from the surroundings (e.g., nanoparticles in the air beaten into food foams). So far, they have proven to be either soluble, degradable in the gut, or eliminated from our bodies and nontoxic, conditions expected to be satisfied also by fabricated nanostructures added to foods. Increasing knowledge of the nanostructures present in our foods may provide a basis for the rational design of structures at the nanoscale to impart desired taste/texture attributes, thus replacing the trial-and-error approaches presently used. Conceivably, food scientists may be inspired by how these "natural" nanostructures come into being to develop novel and functional products from the "bottom-up". Meanwhile, the toolbox provided by the nanosciences is assisting not only in our understanding of the nanoscale phenomena of the materials we eat and digest but also in our assessment of the potential implications of new food nanotechnologies.[30]

## ■ AUTHOR INFORMATION

### Corresponding Author

*Foreign member, U.S. National Academy of Engineering. Phone: 562 2354-4256. E-mail: jmaguile@ing.puc.cl.

### Notes

The authors declare no competing financial interest.

## ■ REFERENCES

(1) Institute of Medicine. Safety and efficacy of nanomaterials in food products. In *Nanotechnology in Food Products*; National Academy Press: Washington, DC, USA, 2009; pp 55−83.

(2) Aguilera, J. M. Food materials and structures. In *Edible Structures: The Basic Science of What We Eat*; CRC Press/Taylor and Francis: Boca Raton, FL, USA, 2012; pp 53−105.
(3) Heid, H. W.; Keenan, T. W. Intracellular origin and secretion of fat globules. *Eur. J. Cell Biol.* **2005**, *84*, 245−258.
(4) Michalski, M.-C.; Januel, C. Does homogenization affect the human health properties of cow's milk? *Trends Food Sci. Technol.* **2006**, *17*, 423−437.
(5) Lepetit, J. Collagen contribution to meat toughness: theoretical aspects. *Meat Sci.* **2008**, *80*, 960−967.
(6) Donald, A. Food for thought. *Nat. Mater.* **2004**, *3*, 579−581.
(7) Zuñiga, R. N.; Tolkach, A.; Kulozik, U.; Aguilera, J. M. Kinetics of formation and physicochemical characterization of thermally-induced β-lactoglobulin aggregates. *J. Food Sci.* **2010**, *75*, E261−E268.
(8) Graveland-Bikker, J. F.; de Kruif, C. G. Unique milk protein based nanotubes: food and nanotechnology meet. *Trends Food Sci. Technol.* **2006**, *17*, 196−203.
(9) Veraverbeke, W. S.; Delcour, J. A. Wheat protein composition and properties of wheat glutenin in relation to breadmaking functionality. *Crit. Rev. Food Sci.* **2002**, *42*, 179−208.
(10) Walther, B.; Lorén, N.; Nydén, M.; Hermansson, A.-M. Influence of κ-carrageenan gel structures on diffusion of probe molecules determined by transmission electron microscopy and NMR diffusometry. *Langmuir* **2006**, *22*, 8221−8228.
(11) Chung, H.-J.; Liu, Q. Impact of molecular structure of amylase and amylopectin on amylase association during cooling. *Carbohydr. Polym.* **2009**, *77*, 807−815.
(12) Barron, C.; Bouchet, B.; Della Valle, G.; Gallant, D. J.; Planchot, V. Microscopical study of the destructuring of waxy maize and smooth pea starches by shear and heat at low hydration. *J. Cereal Sci.* **2001**, *33*, 289−300.
(13) Acevedo, N. C.; Marangoni, A. G. Characterization of the manoscale in triacylglycerol crystal networks. *Cryst. Growth Des.* **2010**, *10*, 3327−3333.
(14) Mezzenga, R.; Schurtenberger, P.; Burbidge, A.; Michel, M. Understanding foods as soft materials. *Nat. Mater.* **2005**, *4*, 729−740.
(15) Dagleish, D. G. Food emulsions − their structures and structure-forming properties. *Food Hydrocolloids* **2006**, *20*, 415−422.
(16) Mileva, E.; Tchoukov, P.; Exerowa, E. Amphiphilic nanostructures in thin liquid films. *Adv. Colloid Interfac. Sci.* **2005**, *114−115*, 47−52.
(17) Schubert, H.; Ax, K.; Behrend, O. Product engineering of dispersed systems. *Trends Food Sci. Technol.* **2003**, *14*, 9−16.
(18) Servais, C.; Jones, R.; Roberts, I. The influence of particle size distribution on the processing of foods. *J. Food Eng.* **2002**, *51*, 201−208.
(19) Contardo, C.; Ravani, L.; Passarella, M. Size characterization by sedimentation field flow fractionation of silica particles used as food additives. *Anal. Chim. Acta* **2013**, *788*, 183−192.
(20) Weir, A.; Westerhoff, P.; Fabricius, L.; Hristovski, K.; von Goetz, N. Titanium dioxide nanoparticles in food and personal care products. *Environ. Sci. Technol.* **2012**, *46*, 2242−2250.
(21) http://blog.khymos.org/2012/09/09/gastrophysics-symposium-in-copenhagen/ (accessed Dec 9, 2013).
(22) Dox, A. W. The occurrence of tyrosine crystals in Roquefort cheese. *J. Am. Chem. Soc.* **1911**, *33*, 423−425.
(23) Nakata, P. A. Advances in our understanding of calcium oxalate crystal formation and function in plants. *Plant Sci.* **2003**, *164*, 901−909.
(24) Monro, J. A.; Mishra, S.; Hardacre, A. Glycemic impact regulation based on progressive geometric changes in starch-based food particles during digestion. *Food Dig.* **2011**, *2*, 1−12.
(25) Mackie, A.; Macierzanka, A. Colloidal aspects of protein digestion. *Curr. Opin. Colloid Interface Sci.* **2010**, *15*, 102−108.
(26) Porter, J. H.; Trevaskis, N. L.; Charman, W. N. Lipids and lipid-based formulations: optimizing the oral delivery of lipophylic drugs. *Nat. Rev. Drug Discovery* **2007**, *6*, 231−248.
(27) Casals, E.; Vázquez-Campos, S.; Bastús, N. G.; Puntes, V. Distribution and potential toxicity of engineered inorganic nanoparticles and carbon nanostructures in biological systems. *Trends Anal. Chem.* **2008**, *27*, 672−683.
(28) Magnuson, B. A.; Jonaitis, T. S.; Card, J. W. A brief review of the occurrence, use, and safety of food-related nanomaterials. *J. Food Sci.* **2011**, *76*, R126−R133.
(29) Takeuchi, M.; Kojima, M.; Luetzow, M. State of the art on the initiatives and activities relevant to risk assessment and risk management of nanotechnologies in the food and agriculture sectors. *Food Res. Intl.* **2014**, *64*, 976−981.
(30) Maynard, A.; Bowman, D.; Hodge, G. The problem of regulating sophisticated materials. *Nat. Mater.* **2011**, *10*, 554−557.

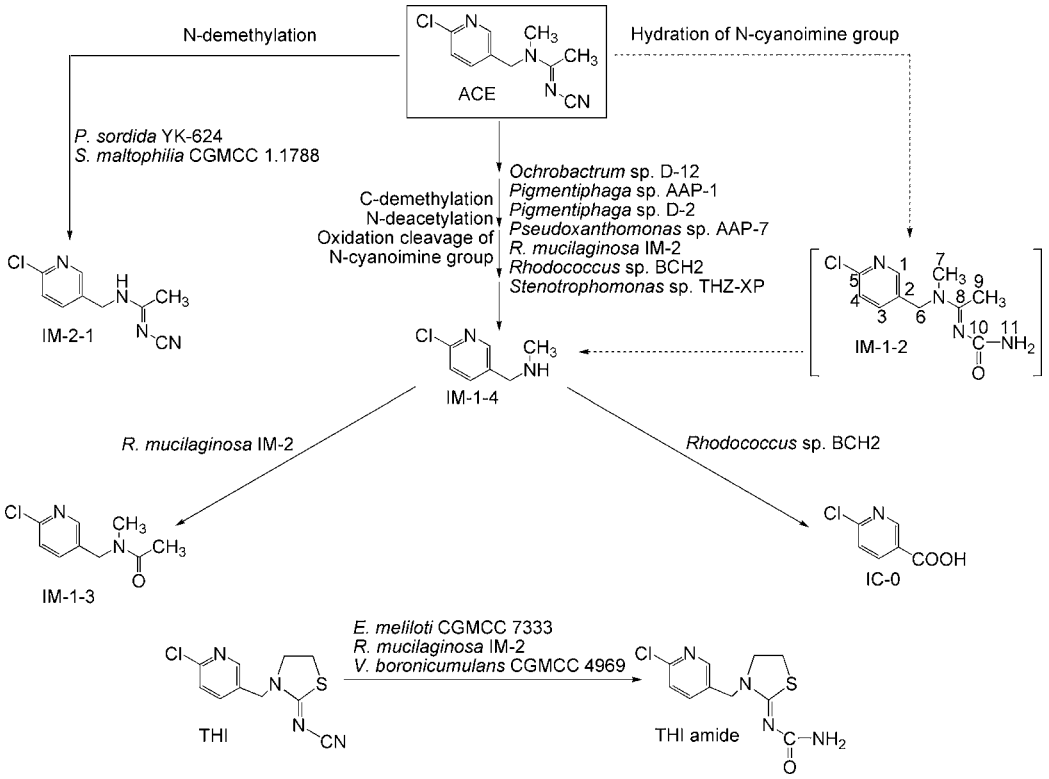


**Figure 1.** Molecular structures of ACE and its metabolites and the pathway in microbial metabolism.

*Phanerochaete sordida* YK-624 metabolize ACE via N-demethylation to IM-2-1.[17,18] The bacteria *Ochrobactrum* sp. D-12, *Pigmentiphaga* sp. AAP-1, D-2, *Pseudoxanthomonas* sp. AAP-7, *Rhodococcus* sp. BCH2, and *Stenotrophomonas* sp. THZ-XP and the yeast *Rhodotorula mucilaginosa* IM-2 metabolize ACE via the proposed N-deacetylation, C-demethylation, or oxidative cleavage of the *N*-cyanoimine group to IM-1-4, which is further metabolized by *Rhodococcus* sp. BCH2 to IC-0 or by *R. mucilaginosa* IM-2 to IM-1-3.[10,19−23] Notably, the formation pathway of the *N*-carbamoylimine metabolite IM-1-2 in plants, animals, and soils was not detected in the microbial ACE degradation pathways listed above. Nevertheless, although the metabolism of ACE in plants, animals, and soil has been clearly described, as have a few cases of microbial degradation, the corresponding enzymatic mechanism of ACE degradation by potentially useful environmental microorganisms has not yet been explored.

The seven major commercial neonicotinoid insecticides contain three structural components: an *N*-heterocyclyl-methyl moiety (A), a heterocyclic or acyclic spacer (B), and an *N*-nitroimine, nitromethylene, or *N*-cyanoimine pharmacophore (C).[14] It is interesting that the same structural components in related chemical compounds are metabolized by the same microbes; for example, *S. maltophilia* CGMCC 1.1788 hydroxylates the same site of component B, that is, the imidazolidine ring in IMI and imidaclothiz and also the thiazolidine ring of THI.[24] *Pseudomonas* sp. 1G transforms IMI and TMX at the component C *N*-nitroimine group via a nitro reduction pathway.[25] THI has the same *N*-cyanoimine group as ACE, and we isolated four THI-degrading bacteria, *Variovorax boronicumulans* CGMCC 4969, *Ensifer meliloti* CGMCC 7333, *Ensifer adhaerens* 6315, and *Ensifer* sp. SCL3-19, with the ability to hydrate THI by converting an *N*-cyanoimine group to an amide metabolite.[26,27] Therefore, we examined these four strains for their ability to degrade ACE and identified the metabolic pathway of ACE transformation used by these ACE-degrading bacteria. Metabolites were then tested for bioefficacy against the horse bean aphid, and the corresponding enzymatic conversion of ACE was further studied. The present study will help to elucidate the environmental fate of ACE, the toxicity of its metabolites, and the mechanism of enzymatic ACE degradation.

## MATERIALS AND METHODS

**Chemicals.** ACE was provided by Professor Jueping Ni of the Jiangsu Pesticide Research Institute, Nanjing, China (98% purity). HPLC grade acetonitrile (part no. AB1124-134) and methanol (part no. MS1922-001) were purchased from TEDIA (Fairfield, OH, USA). All other reagents were of analytical grade and purchased from Sinopharm Chemical Reagent Co., Ltd. (Shanghai, China).

**Strains and Media.** The wild bacteria *E. meliloti* CGMCC 7333,[27] *Ensifer* sp. SCL3-19,[27] *E. adhaerens* CGMCC 6315,[28] and *V. boronicumulans* CGMCC 4969[26] were isolated from soil and identified by 16S rRNA gene analysis. *Ensifer* sp. SCL3-19 was stored in our laboratory, and the other strains were deposited in the China General Microbiological Culture Collection Center (CGMCC) (Beijing, China). *Escherichia coli* Rosetta (DE3), the host for nitrile hydratase (NHase) gene expression, was maintained in our laboratory. Luria−Bertani (LB) medium (pH 7.2) for cell cultivation contained 10.0 g of peptone, 5.0 g of yeast extract, and 10.0 g of NaCl in 1.0 L of deionized water.

**Biodegradation of ACE by the Four THI-Degrading Bacteria, Resting *E. coli* Rosetta (DE3) Cells Overexpressing the NHase Gene from CGMCC 7333, and Purified NHase.** To evaluate the ability of resting bacterial cells to biotransform ACE, a single bacterial colony grown on an LB agar plate was inoculated into a 100 mL flask containing 10 mL of LB broth. The broth was incubated in a rotary shaker at 220 rpm and 30 °C for 24 h. Then, 1 mL of this culture was inoculated into a 500 mL flask containing 100 mL of LB broth and 0.1 mmol/L $CoCl_2$ and incubated using the same culture conditions for 12 h. Subsequently, 5 mL of cultivated broth was sampled, and cells were


dx.doi.org/10.1021/jf503557t | J. Agric. Food Chem. 2014, 62, 9957−9964

harvested with centrifugation at 6000*g* for 10 min. The cell pellet was washed with 0.2 mol/L sodium phosphate buffer (pH 7.5) and resuspended in a 50 mL plastic centrifuge tube containing 5 mL of the same buffer with 500 mg/L ACE. These cell suspensions were used for resting-cell ACE transformation. Meanwhile, phosphate buffer inoculated with either bacteria or dissolved ACE alone was used as control.

The NHase gene cluster from CGMCC 7333 was 1671 bp in length and contained $\alpha$- and $\beta$-subunits of 642 and 660 bp in length, respectively, and an accessory protein gene of 387 bp in length.[27] The GenBank accession numbers for the NHase $\alpha$-subunit, $\beta$-subunit, and accessory protein-coding genes from *E. meliloti* CGMCC 7333 are KF601242, KF601243, and KF601244. Overexpression of recombinant NHase in *E. coli* Rosetta (DE3) and purification of the NHase protein with His-tag affinity chromatography were performed according to the manufacturer's (Takara Bio Co., Dalian, China) protocols. The ACE biotransformation protocol was identical for the THI-degrading bacteria. To test the transformation of ACE by NHase, 10 $\mu$L of NHase was sampled and added to 1 mL of 0.2 mol/L phosphate buffer (pH 7.5) with 500 mg/L of ACE added in a 1.5 mL plastic centrifuge tube and covered.

Transformations were conducted under the above cultivation conditions for the indicated times. The samples were centrifuged at 10000*g* for 10 min to remove residual cells. The supernatant was collected, subjected to filtration with a 0.22 $\mu$m pore-size membrane, and diluted 10-fold for HPLC analysis of substrates and metabolites.

**Preparation of Metabolites.** ACE biotransformation by resting *E. coli* Rostta (DE3) cells overexpressing the NHase from *E. meliloti* CGMCC 7333 was scaled to a 1 L flask containing 300 mL of transformation broth and cultivated in a rotary shaker at 220 rpm and 30 °C until the ACE substrate was completely converted as determined by HPLC analysis. Cell residue was removed by centrifuging the mixture at 10000*g* for 20 min. The supernatant was extracted three times with equal volumes of ethyl acetate. The organic fraction was dehydrated with anhydrous sodium sulfate, after which the organic phase was filtered using a 0.22 $\mu$m pore-size organic membrane. Samples were then concentrated in a rotary vacuum evaporator at a temperature of 40 °C and crystallized in a vacuum dryer. The metabolite crystals were checked for purity using HPLC.

**HPLC, Liquid Chromatography–Mass Spectrometry (LC-MS), and Nuclear Magnetic Resonance (NMR) Analyses.** An Agilent 1260 HPLC system (Agilent Technologies, Santa Clara, CA, USA) equipped with a reverse-phase HC-C18 guard column (4.6 × 12.5 mm, 5 $\mu$m particle size, part no. 520518-904, Agilent Technologies, Wilmington, DE, USA) and an HC-C18 column (4.6 × 250 mm, 5 $\mu$m particle size, part no. 588905-902, Agilent Technologies, Wilmington, DE, USA) was used to analyze the transformation of ACE and its metabolites. Elution was conducted at a flow rate of 1 mL/min in a mobile phase that contained water, acetonitrile, and 0.01% acetic acid (water/acetonitrile, 65:35). The signal was monitored at a wavelength of 235 nm using an Agilent G1314A UV detector. LC-MS was conducted using an Agilent 1290 infinity LC with a G1315B diode array detector and an Agilent 6460 triple-quadrupole LC-MS system equipped with an electrospray ion (ESI) source (Agilent Technologies, Wilmington, DE, USA) that was operated in the positive ion mode. The column, mobile phase, and its proportion were similar to those mentioned for HPLC. The flow rate of elution was set to 0.6 mL/min, and the monitored wavelength of the metabolites formed in the biotransformation of ACE and IM-1-2 was set to 270 and 250 nm, respectively. $^{13}$C and $^{1}$H NMR spectra for the metabolite were obtained in DMSO-$d_6$ using a Bruker AV-400 NMR spectrometer (Bruker, Faellanden, Switzerland) operating at 100 and 400 MHz, respectively. Chemical shifts were referenced against internal tetramethylsilane. Several NMR techniques were used to assign proton and carbon atom chemical shifts ($\delta$), including distortionless enhancement by polarization transfer (DEPT), heteronuclear multiple bond correlation (HMBC), and heteronuclear single-quantum correlation spectroscopy (HSQC).

**Half-Life of ACE Degradation.** Half-life values for the degradation of ACE and its metabolites were determined by plotting $\ln(I/I_0)$ against time using the equation $\ln(I/I_0) = -kt$, where $I_0$ and $I$ represent the initial and residual concentrations. The half-life was calculated as

$$t_{1/2} = (\ln 2)/k$$

where $t_{1/2}$ is the half-life and $k$ is the apparent elimination constant. In all cases, the first-order equation provided a satisfactory fit for the data ($r > 0.9$) and thus provided the basis for the half-life calculation.[21]

**Bioefficacy of ACE Metabolites.** Bioefficacy assays were conducted at the National Pesticide Research and Development South Centre, Nanjing, China, during October 2013. Horse bean plants and the aphid *Aphis craccivora* Koch were used for bioefficacy tests. Oral ingestion and contact bioassays were performed using methods described by Buchholz and Nauen.[29]

## RESULTS

### Biodegradation of ACE by Resting *V. boronicumulans* CGMCC 4969, *E. meliloti* CGMCC 7333, *E. adhaerens*

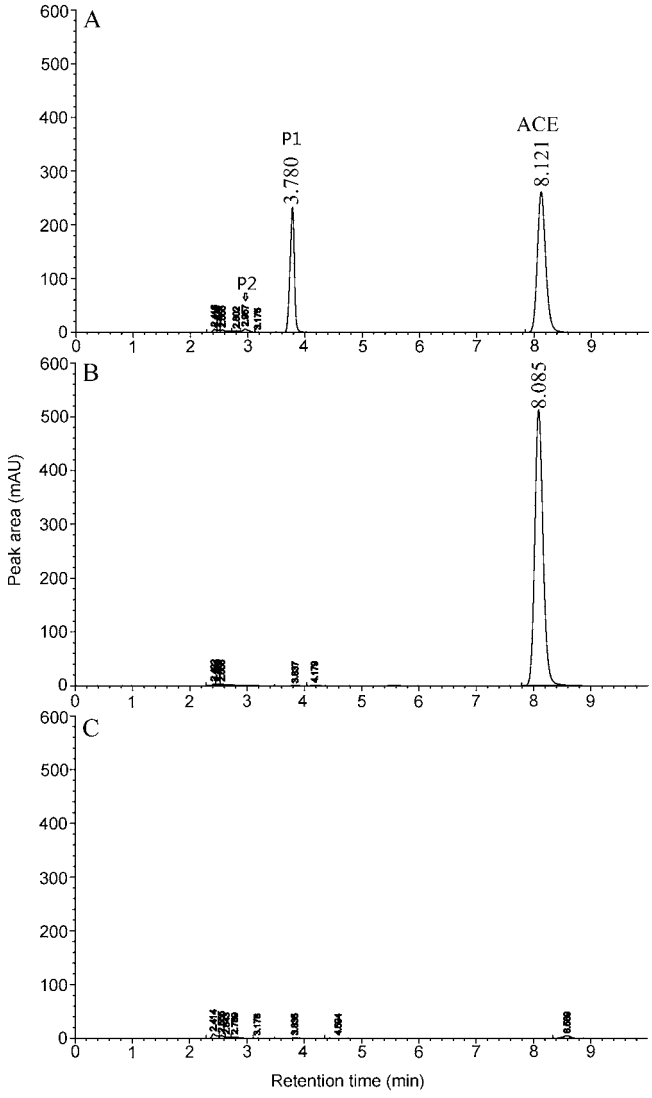


**Figure 2.** HPLC spectra of ACE biodegradation by resting *E. meliloti* CGMCC 7333 cells: (A) phosphate buffer containing 500 mg/L ACE and CGMCC 7333; (B) phosphate buffer containing 500 mg/L ACE; (C) phosphate buffer containing CGMCC 7333. Elution rate of the mobile phase was 1 mL/min, and the detection wavelength was 235 nm; the $OD_{600}$ value of the resting cell suspensions was 5; and the sampled time was 96 h.


dx.doi.org/10.1021/jf503557t | J. Agric. Food Chem. 2014, 62, 9957–9964

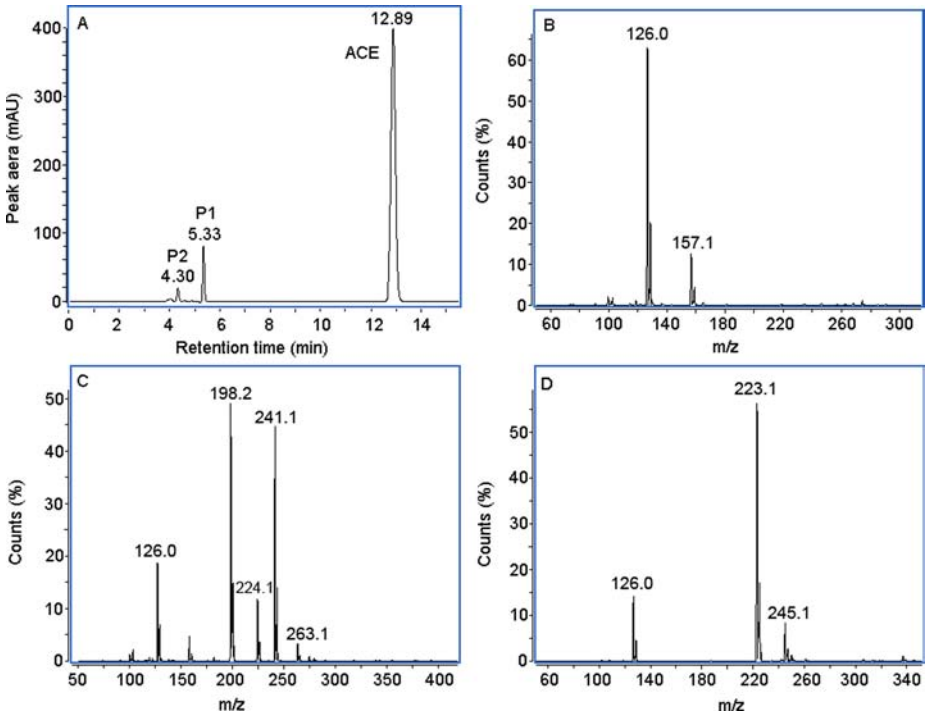


**Figure 3.** LC-MS data for the biotransformation of ACE by *E. meliloti* CGMCC 7333: (A) HPLC spectrum of ACE degradation for 4 days; (B, C, D) mass data of the metabolite peaks P1 and P2 and the substrate ACE at retention times of 4.30, 5.33, and 12.89 min, respectively. Elution rate of the mobile phase was 0.6 mL/min, and the detection wavelength was 250 nm.

**Table 1. $^{13}$C NMR and $^{1}$H NMR Chemical Shift Assignments for Metabolites in DMSO-$d_6$**

| position | $^{13}$C NMR | $^{1}$H NMR |
|---|---|---|
| C1 | 149.4 | 8.33 (d), 1H, $J$ = 1.6 Hz |
| C2 | 133.7 | |
| C3 | 139.5 | 7.76 (dd), 1H, $J$ = 8.0 Hz, $J$ = 1.6 Hz |
| C4 | 124.5 | 7.48 (d), 1H, $J$ = 8.0 Hz |
| C5 | 149.5 | |
| C6 | 49.2 | 4.61 (s), 2H |
| C7 | 36.1 | 2.91 (s), 3H |
| C8 | 160.8 | |
| C9 | 16.4 | 2.12 (s), 3H |
| C10 | 165.4 | |
| N11 | | 6.28, 6.13 (b), 2H |

**CGMCC 6315, and *Ensifer* sp. SCL3-19 Cells.** The four THI-hydrating bacterial strains *V. boronicumulans* CGMCC 4969,[26] *E. adhaerens* CGMCC 6315,[28] *E. meliloti* CGMCC 7333, and *Ensifer* sp. SCL3-19[27] were tested for ACE degradation. After transformation for 60 h, *V. boronicumulans* CGMCC 4969, *E. meliloti* CGMCC 7333, and *E. adhaerens* 6315 degraded 23 ± 2, 45 ± 5, and 8 ± 1% of ACE, respectively, whereas *Ensifer* sp. SCL3-19 did not degrade ACE. *E. meliloti* CGMCC 7333, which degraded THI at the highest level,[27] also degraded ACE the most efficiently of the tested bacteria. Therefore, this bacterium was used for further studies.

**Identification of Metabolites Formed during ACE Biotransformation.** ACE biotransformation by resting *E. meliloti* CGMCC 7333 cells resulted in the formation of an apparent new peak (P1) with an HPLC retention time of 3.78 min (Figure 2A). This peak could be detected in 12, 24, 36, 48, and 60 h, and no comparable peak was observed upon analysis of controls containing ACE (Figure 2B) or inoculated bacterium alone (Figure 2C). After transformation for 48 h, another new small peak (P2) with a retention time of 2.96 min was observed in the transformation broth. Peaks P1 and P2 with retention times of 4.30 and 5.33 min, respectively, were observed in LC-MS analysis of the biotransformation of ACE in 96 h (Figure 3A). As shown in Figure 3B, metabolite P2 displayed a protonated parent ion (M + H) at $m/z$ 157 and a major fragment ion (M − $CH_4N$) at $m/z$ 126. Thus, P2 could be assigned to IM-1-4 (Figure 1), a major metabolite that appears in soil, plant, and microbial metabolism of ACE.[10,20,23,30] Metabolite P1 (Figure 3C) displayed a protonated parent ion (M + H) at $m/z$ 241, a sodiated adduct (M + Na) at $m/z$ 263, a fragment ion (M − O) at $m/z$ 224, an unknown fragment ion at $m/z$ 198, and a fragment ion (M − $C_4H_8N_3O$) at $m/z$ 126. The unknown fragment ion at $m/z$ 198 also appeared in the spectrum of the gas chromatography−mass spectrometry (GC-MS) analysis of IM-1-2 reported by Yeter and Aydin.[31] The mass of metabolite P1 was enhanced by the addition of a water molecule to the substrate ACE (M + H) at $m/z$ 223 (Figure 3D) and was identical to the mass data reported for IM-1-2 by Yeter and Aydin[31] and Kamel et al.[32] Resting *E. coli* Rosetta cells overexpressing CGMCC 7333 NHase also hydrolyzed ACE to a metabolite with the same HPLC retention time as metabolite P1, and this metabolite showed the same mass as P1 in LC-MS analysis (data not shown). This *E. coli* strain transformed ACE completely in 2 h and was thus used for preparation of metabolite P1. The purified P1 was then used for NMR analysis. As is shown in Table 1, there are 10 carbon atoms in the $^{13}$C NMR spectrum, which was identical to the parent ACE. Therefore, the previously reported metabolites IM-2-1 (nine carbon atoms), IM-1-4 (seven carbon atoms), and IM-1-3 (nine carbon atoms) could be excluded.[17,20,23] There were 13 protons in the $^{1}$H NMR spectrum of the ACE metabolite P1, which was an


dx.doi.org/10.1021/jf503557t | J. Agric. Food Chem. 2014, 62, 9957−9964

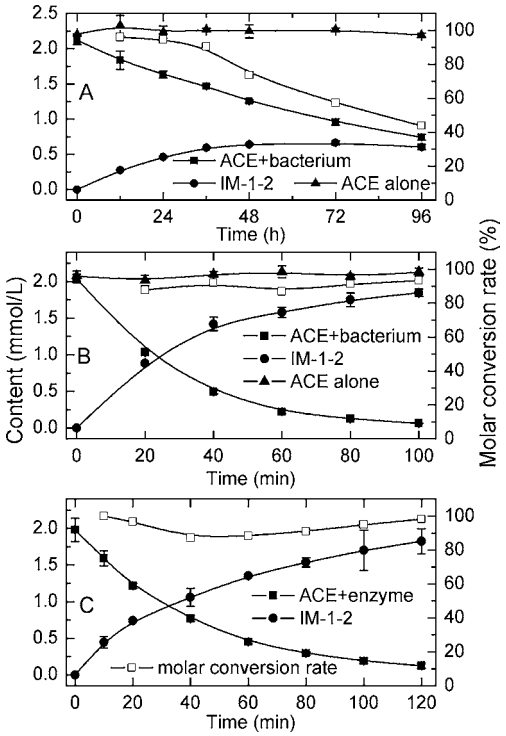


**Figure 4.** Time course of ACE degradation by *E. meliloti* CGMCC 7333 (A), *E. coli* Rosetta overexpressing NHase (B), and pure NHase (C). Preparation of resting *E. meliloti* CGMCC 7333 and *E. coli* Rosetta (DE3) cells is described under Materials and Methods. The $OD_{600}$ value of resting cell suspensions was 5. The NHase concentration was 67.9 μg/mL in 0.2 mol/L phosphate buffer (pH 7.5) with the addition of 0.1 mmol/L $CoCl_2$, and the reaction conditions were the same as for the resting-cell transformation of ACE. Average values and standard deviations were calculated from three parallel cultures tested three times ($n$ = 9).

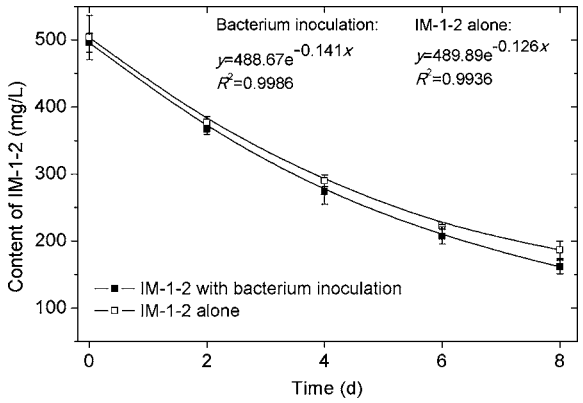


**Figure 5.** Degradation of IM-1-2 by *E. meliloti* CGMCC 7333. IM-1-2 was used as a substrate for transformation. The transformation conditions were the same as for ACE. The control was not inoculated with bacteria, and therefore any IM-1-2 degradation was spontaneous.

increase of 2 protons relative to the ACE substrate. The 2 new protons had chemical shifts of $\delta$ 6.13 and 6.28, respectively. These two protons had no correlation with the carbon atom in HSQC analysis. Therefore, they were assigned to the protons of the amide moiety. Meanwhile, a chemical shift was not observed for the C10 carbon atom of ACE in the $^{13}C$ NMR spectrum, and a new chemical shift ($\delta$ 165.4) appeared in metabolite P1 that could be assigned to the carbon atom of the amide moiety. On the basis of MS and NMR data, ACE metabolite P1 was the *N*-carbamoylimine derivate previously called IM-1-2.[15]

**Kinetics of ACE Transformation by Resting *E. meliloti* CGMCC 7333 Cells, the *E. coli* Rosetta (DE3) Strain Overexpressing the NHase Gene from *E. meliloti* CGMCC 7333, and Purified NHase.** Time course analyses of ACE hydration by resting *E. meliloti* CGMCC 7333 cells (Figure 4A) indicated that the quantity of ACE declined from 2.12 to 0.74 mmol/L in 96 h with an ACE degradation ratio of 65.1%. ACE degradation fitted first-order dissipation kinetics ($R$ = 0.99) with a half-life of 63.0 h. For ACE biodegradation, the molar conversion rates (the amount of IM-1-2 formed divided by the amount of ACE lost) at 12, 24, 36, 48, 72, and 96 h were 96.0, 94.6, 90.5, 73.7, 57.2, and 43.8%, respectively. In the initial 36 h, the molar conversion rate was >90%, which indicated that ACE hydration was the primary pathway of ACE degradation.

As is shown in Figure 4B, the quantity of ACE in the NHase overexpressing *E. coli* Rosetta (DE3) reaction declined from 2.04 to 0.06 mmol/L in 100 min with a degradation ratio of 97.1%. The half-life of ACE degradation was calculated to be 19.7 min ($R$ = 0.99). The molar conversion rates of ACE degradation by NHase overexpressing *E. coli* Rosetta cells at 20, 40, 60, 80, and 100 min were 87.7, 92.1, 86.8, 91.3, and 93.3%, respectively.

The quantity of ACE in the pure NHase reaction (Figure 4C) declined from 1.98 to 0.12 mmol/L in 120 min with a degradation ratio of 93.9%. The half-life of ACE degradation was calculated to be 30.1 min ($R$ = 0.99). The molar conversion rates of ACE degradation by NHase at 10, 20, 40, 60, 80, 100, and 120 min were 98.1, 96.8, 87.2, 88.3, 91.0, 94.9, and 98.2%, respectively. These results indicated that the NHase from *E. meliloti* CGMCC 7333 was responsible for the conversion of ACE to IM-1-2.

**Degradation of IM-1-2.** We previously reported that *E. meliloti* CGMCC 7333 hydrolyzed THI to THI amide with a molar conversion rate of >90% at every sampled time.[27] Interestingly, the molar conversion rate of ACE degradation declined significantly after transformation for 36 h. This result indicated that the IM-1-2 formed by hydration of ACE by *E. meliloti* CGMCC 7333 may have been further degraded. Therefore, IM-1-2 was used as a substrate for transformation by *E. meliloti* CGMCC 7333 to explore whether further IM-1-2 degradation was mediated by the bacterium. As shown in Figure 5, both the experimental group with bacterial inoculation and the control without CGMCC 7333 inoculation showed apparent IM-1-2 degradation. After incubation for 8 days, the amount of IM-1-2 was reduced by 1.40 and 1.32 mmol/L with bacterial inoculation and with IM-1-2 alone, respectively, and the corresponding degradation rates were 67.5 and 62.9%, respectively. The half-lives for IM-1-2 degradation for the experimental and control groups were fitted into first-order dissipation kinetics ($R^2$ = 0.9986 and 0.9936, respectively) and were calculated to be 4.9 and 5.5 days, respectively. There was no significant difference ($P$ > 0.05) in IM-1-2 degradation between the experimental and control groups at any sampled time. These results indicate that IM-1-2 degradation did not result from bacterial transformation and instead resulted from spontaneous chemical degradation.

As shown in Figure 6A, three new peaks with retention times of 4.26, 4.53, and 6.84 min, respectively, were observed in the LC-MS analysis of the control group sample without bacterial inoculation after incubation for 8 days. It can be observed that


dx.doi.org/10.1021/jf503557t | J. Agric. Food Chem. 2014, 62, 9957−9964

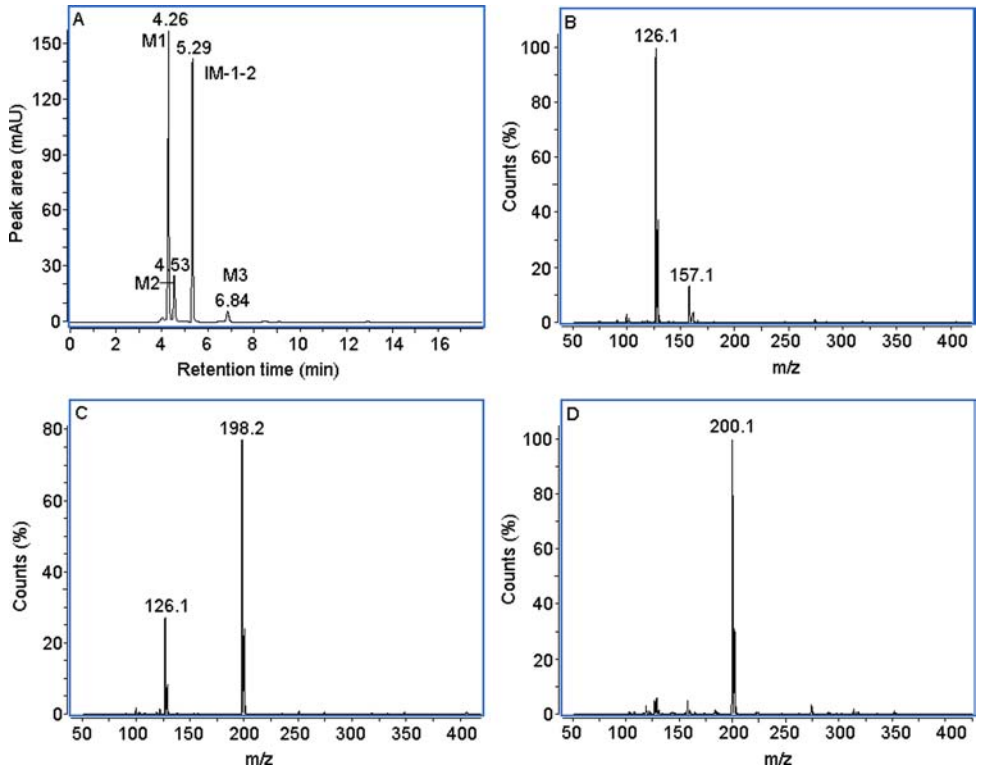


**Figure 6.** LC-MS data for the degradation of IM-1-2 in phosphate buffer without CGMCC 7333 inoculation: (A) HPLC spectrum of IM-1-2 degradation for 8 days without bacterial inoculation (substrate IM-1-2 peaked at a retention time of 5.29 min); (B, C, D) mass data of the metabolite peaks M1, M2, and M3 at retention times of 4.26, 4.53, and 6.84 min, respectively. The elution rate of the mobile phase was 0.6 mL/min, and the detection wavelength was 270 nm.

**Table 2. Bioefficacy of IM-1-2 against the Horse Bean Aphid *A. craccivora***

| compound | content (mg/L) | total insects tested | mortality[a] (%) |
|---|---|---|---|
| IM-1-2 | 1.0000 | 59 | 13.56 ± 5.85 |
| | 0.2500 | 50 | 12.00 ± 1.24 |
| | 0.0625 | 65 | 7.69 ± 0.85 |
| | 0.0156 | 73 | 8.22 ± 4.22 |
| ACE | 0.2500 | 51 | 100.00 ± 0.00 |
| | 0.0625 | 67 | 100.00 ± 0.00 |
| | 0.0156 | 70 | 87.14 ± 4.57 |
| control | 0 | 71 | 5.63 ± 0.94 |

[a]Mortality is expressed using the mean ± standard error from three parallel tests. Mortality was examined at 72 h after application of ACE or IM-1-2.

M1 (Figure 6B) has a protonated parent ion (M + H) at $m/z$ 157 and a major fragment ion (M − $CH_4N$) at $m/z$ 126. These mass data were identical to product P2 (Figure 3B), which was thus assigned to IM-1-4. M2 has a protonated parent ion (M + H) at $m/z$ 198 and could be attributed to the metabolite resulting from cleavage of the *N*-carbamoylimine group in IM-1-2. This metabolite has been detected in mice and plant metabolism of ACE and was named ACE-NH.[33] M3 had a parent ion (M + H) at $m/z$ 200 and could be attributed to the metabolite resulting from the reduction of the C═NH group in ACE-NH to form a C—$NH_2$ group. M3 was not reported previously[33] and was named ACE-$NH_2$. Metabolites M1, M2, and M3 will be purified and subjected to NMR analyses in future studies.

**Laboratory Bioassays of IM-1-2 against the Horse Bean Aphid *A. craccivora*.** The insecticidal activities of metabolites produced by microbial transformation contribute to the bioefficacy persistence of neonicotinoid insecticides.[8] ACE is recommended as a plant foliar spray, and IM-1-2 is one of its plant metabolites.[33] Therefore, we examined the bioefficacy of IM-1-2 against the horse bean aphid *A. craccivora*. As is shown in Table 2, ACE showed perfect and acute insecticidal activity in both the contact and oral ingestion bioassays. At applied concentrations of 0.2500, 0.0625, and 0.0156 ppm, aphid mortalities were 100, 100, and 87.14%, respectively. At the same tested concentrations, the mortality rates of IM-1-2 were only 12.00, 7.69, and 8.22%, respectively. Even when the concentration of IM-1-2 was increased to 1 ppm, the mortality level was only 13.56%. Laboratory bioassays indicated that IM-1-2 had dramatically reduced activity against the aphid *A. craccivora*. Similar results were observed for the bioassay of the THI amide, which reduced insecticidal activity by at least 1 order of magnitude when compared with the THI parent.[19] The above data indicated that the replacement of the crucial pharmacophore cyano group in ACE and THI with an amide group results in a significant reduction in insecticidal activity.

## DISCUSSION

ACE is stable in buffered solutions at pH 5.0−8.0 and in sunlight. It is degraded slowly at pH 9 and 45 °C.[34] However, ACE was degraded rapidly by aerobic soil metabolism, with a half-life ranging from 1 to 8.2 days in studies of various U.S., European, and Chinese soils and varied from 16 to 17 days under field conditions in Indian soils.[17,32] In our present study, ACE was readily degraded by *E. meliloti* CGMCC 7333, the

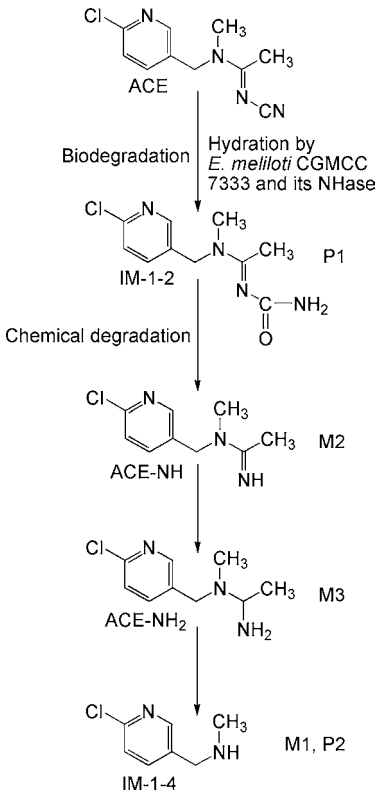


**Figure 7.** Proposed metabolic degradation pathways for ACE by *E. meliloti* CGMCC 7333 and further degradation of IM-1-2.

CGMCC 7333 NHase overexpressing *E. coli*, and the purified CGMCC 7333 NHase with half-lives of 63.0 h, 19.7 min, and 30.1 min, respectively. LC-MS and NMR analyses indicated that CGMCC 7333 NHase mediated the hydration of ACE to metabolite IM-1-2. IM-1-2 is unstable in phosphate-buffered solutions with a half-life of 5.5 days, and this chemical degradation resulted in cleavage of the *N*-carbamoylimine group to an ACE-NH derivate. ACE-NH was then converted to ACE-$NH_2$, which was subsequently cleaved to IM-1-4. The proposed pathway of ACE metabolism by *E. meliloti* CGMCC 7333 and chemical degradation of IM-1-2 are presented in Figure 7. Apparently, ACE degradation via the IM-1-2 pathway mediated by NHase and the chemical degradation of IM-1-2 resulted in the rapid degradation fo ACE in soil.

Metabolites of neonicotinoid insecticides have been shown to contribute to the toxicity of these insecticides.[7] For example, olefin metabolite of IMI was noted to be >10 times more toxic than the parent IMI,[35,36] whereas ACE metabolites, including IM-2-1, IC-0, IM-O (6-chloro-3- pyridiylmethanol), IM-1-4, and IM-1-3, were found to exhibit lower toxicity than ACE.[17,19,37] In our present study, we further proved that one of the major metabolites of ACE degradation, IM-1-2, also showed a dramatic reduction in toxicity (Table 2). Therefore, the rapid biotransformation and detoxification of the metabolites leading to the cyano-group-containing ACE is less toxic than the nitro-group-containing IMI against certain insects.[37] However, the selectivity of neonicotinoids to insect nAChR could be attributed to the pharmacophore group nitroimine (=N—$NO_2$) and cyanoimine (=N—CN), because they have a much higher affinity for insects, when compared with vertebrate nAChRs, and the loss of a nitro or cyano group to the imine metabolite (=NH) can completely reverse the selective toxicity of neonicotinoid insecticides to insects over vertebrates.[38] As shown in Figure 7, IM-1-2 can be spontaneously converted to the imine group containing metabolite ACE-NH and, therefore, ACE degradation via IM-1-2 pathway to form ACE-NH may increase the risk of ACE toxicity to vertebrates. Our present results may help to explore the mechanism of the adverse effect of ACE and IMI on human health.[11]

The molecular structures of ACE and THI have 6-chloro-3-pyridinylmethyl and *N*-cyanoamidine groups in common, but differ in their cyclic thiazolidine and acyclic methyl moieties (Figure 1). *E. meliloti* CGMCC 7333 hydrolyzes ACE and THI to the corresponding *N*-carbamoylimine derivatives despite the molecular differences between these two molecules. *Ensifer* sp. SCL3-19 hydrolyzes only the cyclic THI, not the acyclic ACE. We speculate that this difference in substrate selectivity between *E. meliloti* CGMCC 7333 and *Ensifer* sp. SCL3-19 may be attributed to differences in NHase structure between the two *Ensifer* species. The full NHase gene from *Ensifer* sp. SCL3-19 is being cloned and expressed, and site-specific mutation of various NHase genes will be conducted in the future to explore NHase function and the specific hydrolysis of the neonicotinoid insecticides ACE and THI.

Among ACE-degrading bacteria, *Rhodococcus* sp. BCH2 has been reported to degrade ACE, and three metabolites were observed in HPLC spectra. Two of these metabolites were determined to be IM-1-4 and IC-0 by GC-MS analysis. The authors assumed that ACE was degraded via IM-1-2 because they found an *N*-carbamoylimine group in the extraction of the mixed metabolites by Fourier transform infrared spectrum analysis, although they did not identify IM-1-2 itself by LC-MS or NMR analysis.[10] The present findings suggest that IM-1-2 cannot be directly detected as a product of ACE metabolism by *Rhodococcus* sp. BCH2, perhaps because IM-1-2 is hydrolyzed in this preparation process. In addition, it is known that the NHase of *Rhodococcus* catalyzes the conversion of the nitrile compound acrylonitrile to acrylamide in industrial processes,[39] and therefore it has been suggested that ACE degradation by *Rhodococcus* sp. BCH2 requires further study.

In conclusion, our present study first found that the nitrogen-fixing bacterium *E. meliloti* CGMCC 7333 and its NHase specifically transform the neonicotinoid insecticide ACE to IM-1-2. IM-1-2 is unstable due to chemical hydrolysis and produces the metabolites ACE-NH, ACE-$NH_2$, and IM-1-4. The present findings will improve our understanding of the environmental fate of ACE and the corresponding enzymatic mechanisms.

## AUTHOR INFORMATION

### Corresponding Authors

*(L.-J.Z.) E-mail: zlj@nies.org.
*(Y.-J.D.) E-mail: daiyijun@njnu.edu.cn

### Funding

This research was financed by the Priority Academic Program Development (PAPD) of Jiangsu Higher Education Institutions, National Science Foundation of China (31370143), the Professional and Public Project of National Environmental Protection (201009033), and the Academic Natural Science Foundation of Jiangsu Province (14KJA180004).

### Notes

The authors declare no competing financial interest.

## REFERENCES


(1) Jeschke, P.; Nauen, R.; Schindler, M.; Elbert, A. Overview of the status and global strategy for neonicotinoids. *J. Agric. Food Chem.* **2011**, *59*, 2897−2908.

(2) Elbert, A.; Haas, M.; Springer, B.; Thielert, W.; Nauen, R. Applied aspects of neonicotinoid uses in crop protection. *Pest Manage. Sci.* **2008**, *64*, 1099−1105.

(3) Stokstad, E. Pesticides under fire for risks to pollinators. *Science* **2013**, *340*, 674−676.

(4) Zeng, G.; Chen, M.; Zeng, Z. Risks of neonicotinoid pesticides. *Science* **2013**, *340*, 1403.

(5) Taira, K.; Fujioka, K.; Aoyama, Y. Qualitative profiling and quantification of neonicotinoid metabolites in human urine by liquid chromatography coupled with mass spectrometry. *PLoS One* **2013**, *8*, No. e80332.

(6) Gupta, M.; Shanker, A. Persistence of acetamiprid in tea and its transfer from made tea to infusion. *Food Chem.* **2008**, *111*, 805−810.

(7) Blacquiere, T.; Smagghe, G.; van Gestel, C. A.; Mommaerts, V. Neonicotinoids in bees: a review on concentrations, side-effects and risk assessment. *Ecotoxicology* **2012**, *21*, 973−992.

(8) Liu, Z.; Dai, Y.; Huang, G.; Gu, Y.; Ni, J.; Wei, H.; Yuan, S. Soil microbial degradation of neonicotinoid insecticides imidacloprid, acetamiprid, thiacloprid and imidaclothiz and its effect on the persistence of bioefficacy against horsebean aphid *Aphis craccivora* Koch after soil application. *Pest Manage. Sci.* **2011**, *67*, 1245−1252.

(9) Kocaman, A. Y.; Topaktaş, M. In vitro evaluation of the genotoxicity of acetamiprid in human peripheral blood lymphocytes. *Environ. Mol. Mutagen.* **2007**, *48*, 483−490.

(10) Phugare, S. S.; Jadhav, J. P. Biodegradation of acetamiprid by isolated bacterial strain *Rhodococcus* sp. BCH2 and toxicological analysis of its metabolites in silkworm (*Bombax mori*). *CLEAN−Soil, Air, Water* **2013**, DOI: 10.1002/clen.201200563.

(11) Kimura-Kuroda, J.; Komuta, Y.; Kuroda, Y.; Hayashi, M.; Kawano, H. Nicotine-like effects of the neonicotinoid insecticides acetamiprid and imidacloprid on cerebellar neurons from neonatal rats. *PLoS One* **2012**, *7*, No. e32432.

(12) Singh, T. B.; Mukhopadhayay, S. K.; Sar, T. K.; Ganguly, S. Acetamiprid induces toxicity in mice under experimental conditions with prominent effect on the hematobiochemical parameters. *J. Drug Metab. Toxicol.* **2012**, *3*, 134 DOI: 10.4172/2157-7609.1000134.

(13) Brunet, J. L.; Badiou, A.; Belzunces, L. P. In vivo metabolic fate of [$^{14}$C]-acetamiprid in six biological compartments of the honeybee, *Apis mellifera* L. *Pest Manage. Sci.* **2005**, *61*, 742−748.

(14) Casida, J. E. Neonicotinoid metabolism: compounds, substituents, pathways, enzymes, organisms, and relevance. *J. Agric. Food Chem.* **2011**, *59*, 2923−2931.

(15) Tokieda, M.; Tanaka, T.; Ozawa, M.; Gomyo, T. High performance liquid chromatographic determination of acetamiprid and its degradation products in soil. *J. Pestic. Sci.* **1998**, *23*, 296−299.

(16) Omar, S.; Abdel-Sater, M. Microbial populations and enzyme activities in soil treated with pesticides. *Water, Air, Soil Pollut.* **2001**, *127*, 49−63.

(17) Chen, T.; Dai, Y.-J.; Ding, J.-F.; Yuan, S.; Ni, J.-P. N-demethylation of neonicotinoid insecticide acetamiprid by bacterium *Stenotrophomonas maltophilia* CGMCC 1.1788. *Biodegradation* **2008**, *19*, 651−658.

(18) Wang, J.; Hirai, H.; Kawagishi, H. Biotransformation of acetamiprid by the white-rot fungus *Phanerochaete sordida* YK-624. *Appl. Microbiol. Biotechnol.* **2012**, *93*, 831−835.

(19) Dai, Y.-J.; Ji, W.-W.; Chen, T.; Zhang, W.-J.; Liu, Z.-H.; Ge, F.; Yuan, S. Metabolism of the neonicotinoid insecticides acetamiprid and thiacloprid by the yeast *Rhodotorula mucilaginosa* strain IM-2. *J. Agric. Food Chem.* **2010**, *58*, 2419−2425.

(20) Tang, H.; Li, J.; Hu, H.; Xu, P. A newly isolated strain of *Stenotrophomonas* sp. hydrolyzes acetamiprid, a synthetic insecticide. *Process Biochem.* **2012**, *47*, 1820−1825.

(21) Wang, G.; Chen, X.; Yue, W.; Zhang, H.; Li, F.; Xiong, M. Microbial degradation of acetamiprid by *Ochrobactrum* sp. D-12 isolated from contaminated soil. *PLoS One* **2013**, *8*, No. e82603.

(22) Yang, H.; Wang, X.; Zheng, J.; Wang, G.; Hong, Q.; Li, S.; Li, R.; Jiang, J. Biodegradation of acetamiprid by *Pigmentiphaga* sp. D-2 and the degradation pathway. *Int. Biodeterior. Biodegrad.* **2013**, *85*, 95−102.

(23) Wang, G.; Yue, W.; Liu, Y.; Li, F.; Xiong, M.; Zhang, H. Biodegradation of the neonicotinoid insecticides acetamiprid by bacterium *Pigmentiphaga* sp. strain AAP-1 isolated from soil. *Bioresour. Technol.* **2013**, *138*, 359−368.

(24) Dai, Y.; Zhao, Y.; Zhang, W.; Yu, C.; Ji, W.; Xu, W.; Ni, J.; Yuan, S. Biotransformation of thianicotinyl neonicotinoid insecticides: diverse molecular substituents response to metabolism by bacterium *Stenotrophomonas maltophilia* CGMCC 1.1788. *Bioresour. Technol.* **2010**, *101*, 3838−3843.

(25) Pandey, G.; Dorrian, S. J.; Russell, R. J.; Oakeshott, J. G. Biotransformation of the neonicotinoid insecticides imidacloprid and thiamethoxam by *Pseudomonas* sp. 1G. *Biochem. Biophys. Res. Commun.* **2009**, *380*, 710−714.

(26) Zhang, H.-J.; Zhou, Q.-W.; Zhou, G.-C.; Cao, Y.-M.; Dai, Y.-J.; Ji, W.-W.; Shang, G.-D.; Yuan, S. Biotransformation of the neonicotinoid insecticide thiacloprid by the bacterium *Variovorax boronicumulans* strain J1 and mediation of the major metabolic pathway by nitrile hydratase. *J. Agric. Food Chem.* **2011**, *60*, 153−159.

(27) Ge, F.; Zhou, L.-Y.; Wang, Y.; Ma, Y.; Zhai, S.; Liu, Z.-H.; Dai, Y.-J.; Yuan, S. Hydrolysis of the neonicotinoid insecticide thiacloprid by the $N_2$-fixing bacterium *Ensifer meliloti* CGMCC 7333. *Int. Biodeterior. Biodegrad.* **2014**, *93*, 10−17.

(28) Zhou, G.-c.; Wang, Y.; Zhai, S.; Ge, F.; Liu, Z.-h.; Dai, Y.-j.; Yuan, S.; Hou, J.-y. Biodegradation of the neonicotinoid insecticide thiamethoxam by the nitrogen-fixing and plant-growth-promoting rhizobacterium *Ensifer adhaerens* strain TMX-23. *Appl. Microbiol. Biotechnol.* **2013**, *97*, 4065−4074.

(29) Buchholz, A.; Nauen, R. Translocation and translaminar bioavailability of two neonicotinoid insecticides after foliar application to cabbage and cotton. *Pest Manage. Sci.* **2002**, *58*, 10−16.

(30) Tokieda, M.; Iiyoshi, K.; Sugioka, K.; Gomyo, T. Residue determination method for the insecticide acetamiprid in crops by gas chromatography. *J. Pestic. Sci.* **1997**, *22*, 77−83.

(31) Yeter, O.; Aydın, A. Determination of acetamiprid and IM-1-2 in post-mortem human blood, liver, stomach contents by HPLC-DAD. *J. Forensic Sci.* **2014**, *59*, 287−292.

(32) Kamel, A.; Qian, Y.; Kolbe, E.; Stafford, C. Development and validation of a multiresidue method for the determination of neonicotinoid and macrocyclic lactone pesticide residues in milk, fruits, and vegetables by ultra-performance liquid chromatography/MS/MS. *J. AOAC Int.* **2010**, *93*, 389−399.

(33) Ford, K. A.; Casida, J. E. Comparative metabolism and pharmacokinetics of seven neonicotinoid insecticides in spinach. *J. Agric. Food Chem.* **2008**, *56*, 10168−10175.

(34) Gupta, S.; Gajbhiye, V. T.; Gupta, R. K. Effect of light on the degradation of two neonicotinoids viz acetamiprid and thiacloprid in soil. *Bull. Environ. Contam. Toxicol.* **2008**, *81*, 185−189.

(35) Nauen, R.; Ebbinghaus-Kintscher, U.; Schmuck, R. Toxicity and nicotinic acetylcholine receptor interaction of imidacloprid and its metabolites in *Apis mellifera* (Hymenoptera: Apidae). *Pest Manage. Sci.* **2001**, *57*, 577−586.

(36) Dai, Y. J.; Yuan, S.; Ge, F.; Chen, T.; Xu, S. C.; Ni, J. P. Microbial hydroxylation of imidacloprid for the synthesis of highly insecticidal olefin imidacloprid. *Appl. Microbiol. Biotechnol.* **2006**, *71*, 927−934.

(37) Iwasa, T.; Motoyama, N.; Ambrose, J. T.; Roe, M. R. Mechanism for the differential toxicity of neonicotinoid insecticides in the honey bee *Apis mellifera*. *Crop Prot.* **2004**, *23*, 371−378.

(38) Tomizawa, M.; Casida, J. E. Selective toxicity of neonicotinoids attributable to specificity of insect and mammalian nicotinic receptors. *Annu. Rev. Entomol.* **2003**, *48*, 339−364.

(39) Kobayashi, M.; Shimizu, S. Nitrile hydrolases. *Curr. Opin. Chem. Biol.* **2000**, *4*, 95−102.

Table 1. Chemical Composition of the Clinoptilolite (Cp) Used in the Study

| oxide | $SiO_2$ | $Al_2O3$ | $Fe_2O_3$ | CaO | MgO | $TiO_2$ | $Na_2O$ | $K_2O$ | loi |
|---|---|---|---|---|---|---|---|---|---|
| % (w/w) | 63.60 | 11.81 | 1.74 | 7.35 | 0.69 | 0.40 | 4.40 | 0.169 | 9.81 |

Table 2. Chemical Composition of the Phosphate Rock (PR) Used in the Study

| oxide | $P_2O_5$ | $SiO_2$ | $Fe_2O_3$ | $Al_2O_3$ | $TiO_2$ | CaO | MgO | $Na_2O$ | $K_2O$ | S | V | loi |
|---|---|---|---|---|---|---|---|---|---|---|---|---|
| % (w/w) | 9.72 | 52.29 | 3.39 | 3.57 | 0.45 | 18.04 | 0.32 | 0.16 | 2.76 | 0.3 | 0.011 | 4.87 |

from Lisina together with natural and $NH_4$−Cp as an effective natural fertilizer mixture. Artificial neural network (ANN) models are recognized as a good modeling tool because they provide solutions to the problems from a set of experimental data and are capable of handling complex systems with nonlinearities and interactions between decision variables.[23,24] The main aim of this research was to determine how the processing time and changes in composition of the mixtures affect the PR dissolution and, further, whether the test mixtures have the potential to be adequate sources of nutrients required for plant growth. Using principal component analysis (PCA) and sensitivity analysis, solution concentrations of elements were tested against the impact of process variables. Empirical models of given systems were developed in the form of second-order polynomial (SOP) and ANN models. Characterization of the utilized minerals was also performed.

## MATERIAL AND METHODS

**Characterization of Materials.** The zeolite tuff (Cp), originating from deposit Baia Mare, Romania, and PR, apatite from ore deposit Lisina, near Bosilegrad, Serbia, were used in the experiment. Selected characteristics of the Cp and PR samples are presented in Tables 1 and 2. The CEC of the Cp using EPA method no. 9081 was 158.2 mequiv/100 g of zeolite (out of which $Ca^{2+}$ 92 mequiv, $K^+$ 51.5 mequiv, $Na^+$ 8.85 mequiv, and $Mg^{2+}$ 5.84 mequiv). To obtain $NH_4$−Cp, a partial saturation of Cp with $NH_4^+$ was performed according to the procedure described by Mihajlović et al.[25] at 1:7.5 ratios.

Powder X-ray diffraction (XRD) method was used to determine the phase composition of the Cp, $NH_4$−Cp, and PR. The XRD patterns of used natural Cp and $NH_4$−Cp were obtained on a Philips PW 1710 automated diffractometer using a Cu tube operated at 40 kV and 30 mA (for method details, see Mihajlović et al.[26]). Energy-dispersing spectroscopy (EDS) on scanning electron microscopy (JEOL JSM−6610LV SEM) was used to determine the composition of the starting materials.

**Experimental Procedure.** Two groups of several batch experiments were performed to investigate the solubility and ion-exchange relationships between Cp and PR. The purified Cp fraction (50−100 $\mu$m) and the PR coarse silt fractions (<37 $\mu$m) were used. The first group was composed of Cp/PR mixtures, and the second was composed of $NH_4$−Cp/PR mixtures. Both mixture groups were assembled in three different ratios of Cp and PR, 5:1, 10:1, and 15:1, and each system initially contained 4 g of PR. The mixtures in three replicates were placed in a 300 mL volumetric flask to which 200 mL of distilled water was added. Samples were shaken on a rotary shaker for 24, 48, and 72 h at 220 rpm After being drained, the resulting solutions were examined for contents of $Ca^{2+}$, $K^+$, $Na^+$, and $Mg^{2+}$ using the "Perkin Elmer AAS "703". Solution P concentration was determined by colorimetric method,[27] using SPEKOL 1300 UV VIS spectrophotometer.

**Exploratory Data Analysis.** Descriptive statistical analyses of the results were expressed as the mean ± standard deviation (SD). Analysis of variance (ANOVA) and the following posthoc Tukey's HSD were performed using StatSoft Statistica 10.0 software.

**Principal Component Analysis.** PCA is a multivariate analytical procedure extensively used in exploratory data analysis, in which the data are transformed into orthogonal components (principal components) that are linear combinations of the original variables.[28] This transformation is defined in such a way that the first principal component accounts for the largest variance in the data set. Consecutively, each of the following principal components accounts for the maximum of the remaining variance in the data set. In this research PCA analysis was used (i) to outline differences between the analyzed samples (mixture groups) by calculating score plots and (ii) to find correlations between the processes parameters (design variables) and measured solution concentrations of the cations (measured variables) by calculating correlation loading plots. All PCA calculations were performed by using The Unscrambler (version 10.1, CAMO Process AS, Oslo, Norway) and in-house developed routines written in MATLAB (version R2010a, The MathWorks, Natick, MA).

**Second-Order Polynomial Model.** The SOP model was used to estimate the main effect of the process parameters on the final concentrations of the investigated elements. The independent variables were processing time and composition of the fertilizer mixtures. All SOP models were fitted to data assembled by experimental measurements. The models of the following form were developed to relate 5 dependent outputs ($Y$) to 2 process variables ($X$):

$$Y_k = \beta_{k0} + \sum_{i=1}^{2} \beta_{ki} X_i + \sum_{i=1}^{2} \beta_{kii} X_i^2 + \beta_{k12} X_1 X_2, \quad k = 1, 2, 3, 4, 5 \tag{2}$$

where $\beta_{k0}$, $\beta_{ki}$, $\beta_{kii}$, and $\beta_{k12}$ are constant regression coefficients; $Y_k$ is the concentration of either P, $Ca^{2+}$, $K^+$, $Na^+$, or $Mg^{2+}$; and $X_i$ are either the processing time or the zeolite share in the mixture. Significant terms in the model were found using ANOVA for each dependent variable. The SOP models were obtained for each dependent variable, where factors were rejected when their significance level was $p > 0.05$. SOP modeling was performed by using StatSoft Statistica 10.0 software.

**Artificial Neural Network Modeling.** According to StatSoft Statistica's recommendations, the database was randomly divided into training data (60%), cross-validation data (20%), and testing data (20%). The cross-validation data set was used to test the performance of the network while training was in progress as an indicator of the level of generalization and the time at which the network has begun to overtrain. To improve the behavior of the ANN, the data set was normalized. To obtain good network behavior, it was necessary to make a trial-and-error procedure and to choose the number of hidden layers, together with the number of neurons within. The use of only one layer is advisible, because more layers worsens the problem of local minima.[29] According to Taylor,[30] multilayer perceptron models (MLPs) with three layers (input, hidden, and output) are the most flexible and general-purpose kind of ANN and, therefore, were used in this study. The MLP neural network learns using the "back-propagation" algorithm. The Levenberg−Marquardt algorithm was proved to be the fastest and suitable for networks of moderate size. The Broyden−Fletcher−Goldfarb−Shanno (BFGS) algorithm, implemented in StatSoft Statistica's evaluation routine, was used for ANN modeling.

**Training, Testing, and System Implementation.** After defining the architecture of ANN, the training step was initiated. Because of the high degree of parameters' variability, the training process was repeated several times to obtain the best performance of the ANN. It

was accepted that successful training was achieved when learning and cross-validation curves (sum of squares—SOS vs training cycles) approached zero. Testing was carried out with the best weights stored during the training step. Coefficient of determination ($r^2$) and SOS were used as parameters to check the performance (i.e., the accuracy) of the obtained ANNs. Finally, the best-behaved ANN was chosen and the model was implemented by using an algebraic system of equations to predict solution P, Ca, K, Na, and Mg concentrations in both fertilizer mixtures.

**Sensitivity Analysis.** ANNs were tested using sensitivity analysis to determine whether and under what circumstances the obtained models might result in an ill-conditioned system.[30] Sensitivity analysis is used for more precise defining of the influence of processing variables on the observed responses. The infinitesimal amount (+0.0001%) was added to each input variable in 10 equally spaced individual points encompassed by minimum and maximum of the training data, according to StatSoft Statistica's default. These signals were normally distributed with constant intensity and frequency.

## RESULTS AND DISCUSSIONS

**Mineral Characterization.** The XRD analyses confirmed that the major mineralogical component of the Cp and the $NH_4$−Cp was clinoptilolite (>75%) (Figures 1 and 2). The Cp

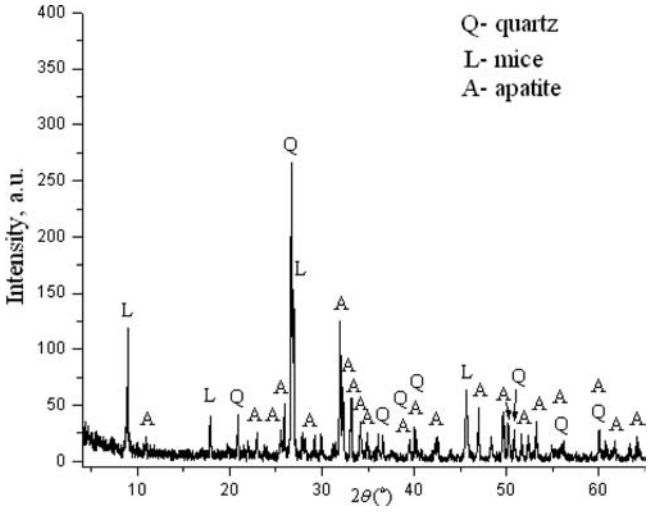


**Figure 1.** Diffractogram of the phosphate rock.

samples predominantly contained zeolite minerals from the group heulandites−clinoptilolites (HEUs) and feldspars, with smaller amounts of quartz, carbonates, and mica. The $NH_4$−Cp samples predominantly contained zeolite minerals from the group HEUs and smaller amounts of quartz and mica. A fraction of volcanic glass in both samples was significant, and the degree of crystallinity was very low. The XRD spectra of used natural Cp and $NH_4$−Cp could be found elsewhere.[26] The mineral composition of the analyzed PR sample mainly contained apatite and smaller amounts of quartz and mica (Figure 1).

Scanning electromicrographs illustrate the morphology of the analyzed zeolites and PR samples (Figure 2a, b, and c). The photomicrograph of the Cp sample shows that the crystal assemblage occurs as plates clustered closely together (Figure 2a). Clinoptilolite generally exists in the coffin-shaped crystals of monoclinic symmetry.[31] The flaky material coexisting with the crystals indicates the possible presence of mica and clay, which is consistent with the XRD analysis. The corresponding SEM energy-dispersive X-ray (EDX) spectrum shows that, apart from the gold (Au) peak, the main chemical elements (Al, Si, O, K, Mg, Ca, and Fe) are present in the Cp structure, which is in agreement with its chemical composition (Table 1). The SEM micrograph of the $NH_4$−Cp sample shows that the crystals maintained their original form after saturation, with a detectable content of impurities (Figure 2b). The matching SEM-EDX spectrum proved the presence of Si, Al, O, and K, but with smaller amounts of Ca and the absence of Mg compared to the untreated Cp EDX spectrum. The SEM micrograph of the PR particle is shown in Figure 2c, also with an obvious presence of flaky impurities. The matching EDX confirms the presence of the basic structural elements of the ore (P, Ca, and F) as well as the presence of Si and Al probably from quartz and mica, which is in agreement with the XRD spectra.

**Experimental Results.** *Reaction Time.* The reaction times in the present study were chosen on the basis of the proposed equilibrium times of similar batch experiments with zeolite and PR.[8,20,22] To assess the effect of mixture composition on nutrient availability, three ratios of Cp to PR, 5:1, 10:1, and 15:1, were used. The concentrations of P, $Ca^{2+}$, $K^+$, $Na^+$, and $Mg^{2+}$ in the solution, after shaking the Cp/PR and $NH_4$−Cp/PR mixtures for various durations of time, are shown in Tables 3 and 4, respectively. Obtained element concentrations were compared to the time-related concentrations liberated from PR alone.

In the Cp/PR mixtures a sudden increase in the concentration of all nutrients for the first 24 h of shaking was observed, followed by a significantly different but moderate increase up to 72 h for all three Cp/PR ratios (Table 3). Allen et al.[22] reported a similar small improvement in cation exchange in the Cp/PR mixture, after a rapid increase for the first 16 h. Also, after 72 h cation exchange has nearly ceased up to 96 h.[22] From Table 3 a gradual increase in concentrations of all nutrients as the ratio of the Cp/PR mixture increases can be observed. This finding is in accordance with previous results for P but in contrast to the behavior of $Ca^{2+}$ reported by Allen et al.[22] and Barbarick et al.[8] In the $NH_4$−Cp/PR mixtures, a rapid increase of solution P concentration in the first 24 h was followed by a slow increase up to 72 h (Table 4). This finding is also in accordance with the results of Allen et al.[32] where, after an initial phase of 6 h, the rate of P release decreased with time, despite the further PR dissolution. Solution P concentrations found in the $NH_4$−Cp/PR mixtures were about 2- to 3-fold higher than the P concentrations released from the correspondent Cp/PR mixtures. Similarly, three times higher P concentrations released from the $NH_4$−Cp/PR mixture compared to the Cp/PR mixture have been reported by Lai and Eberl.[20] Solution Ca concentrations after 24 h showed a tendency to decrease with time in the $NH_4$−Cp/PR mixtures and were 25 times higher than the $Ca^{2+}$ concentrations found in the respective Cp/PR mixtures. These results support the conclusions that have been previously published by Lai and Eberl,[20] where the released $Ca^{2+}$ from the PR, driven by cation exchange with $NH_4^+$, has been partially sequestered by the zeolite before equilibrium. The decrease in Ca promotes further dissolution of PR. Therefore, the $NH_4$−Cp contributes more to the dissolution of PR than the natural Cp. Solution Na and K concentrations increased by 2-fold with an increase of $NH_4$−Cp/PR ratio and varied over time around similar values. Solution Mg concentrations rapidly increased with time and with an increase of $NH_4$−Cp/PR ratio and were ∼70 times higher than the correspondent Mg concentrations released from the Cp/PR mixture. These results suggest a potentially

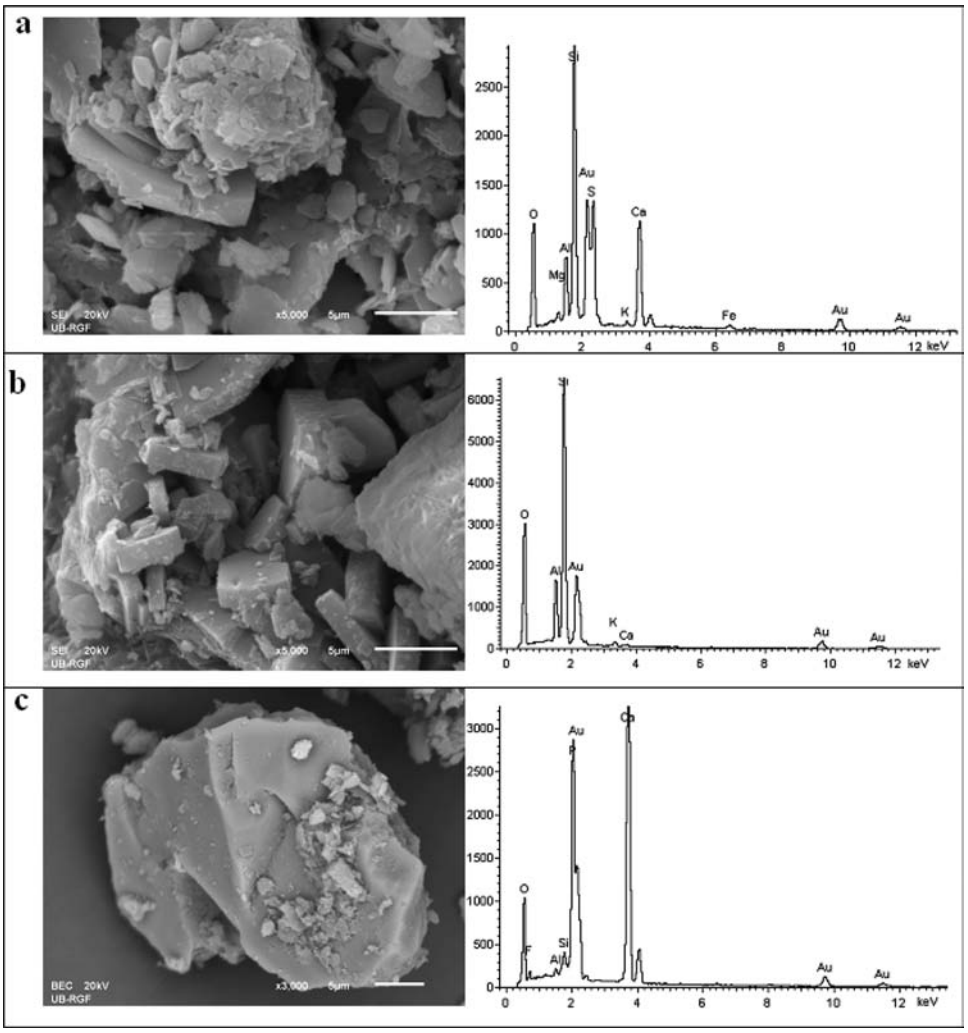


**Figure 2.** SEM photomicrograph and the correspondent EDX spectra of (a) natural Cp, (b) $NH_4$−Cp, and (c) PR from Lisina.

**Table 3. Mean Concentrations ± SD of P, $Ca^{2+}$, $K^+$, $Na^+$, and $Mg^{2+}$ in the Solution, Following the Different Mixing Times and Compositions of the Cp/PR Mixture**[a]

| no. | *t* (h) | Cp/PR ratio | P (mg $L^{-1}$) | Ca (mg $L^{-1}$) | K (mg $L^{-1}$) | Na (mg $L^{-1}$) | Mg (mg $L^{-1}$) | pH |
|---|---|---|---|---|---|---|---|---|
| 1 | 24 | 0:1 | 0.00 ± 0.00 a | 5.00 ± 0.08 c | 3.53 ± 0.04 a | 0.21 ± 0.00 a | 0.11 ± 0.00 a | 7.45 |
| 2 | 24 | 5:1 | 0.15 ± 0.00 e | 11.00 ± 0.04 d | 7.85 ± 0.09 b | 20.05 ± 0.17 c | 0.33 ± 0.00 d | 7.53 |
| 3 | 24 | 10:1 | 0.17 ± 0.00 f | 16.50 ± 0.24 b | 9.63 ± 0.10 c | 25.40 ± 0.53 b | 0.61 ± 0.01 c | 7.55 |
| 4 | 24 | 15:1 | 0.18 ± 0.00 c | 20.50 ± 0.54 h | 10.16 ± 0.20 d | 25.65 ± 0.48 b | 0.88 ± 0.02 h | 7.62 |
| 5 | 48 | 0:1 | 0.00 ± 0.00 a | 6.00 ± 0.05 a | 3.60 ± 0.06 a | 0.25 ± 0.00 a | 0.13 ± 0.00 a,b | 7.47 |
| 6 | 48 | 5:1 | 0.18 ± 0.00 c | 12.50 ± 0.19 e | 7.84 ± 0.12 b | 20.95 ± 0.18d | 0.38 ± 0.01 e | 7.55 |
| 7 | 48 | 10:1 | 0.20 ± 0.00 b,d | 16.50 ± 0.37 b | 9.62 ± 0.16 c | 25.50 ± 0.26 b | 0.63 ± 0.01 c | 7.66 |
| 8 | 48 | 15:1 | 0.20 ± 0.00 b | 22.50 ± 0.34 i | 10.33 ± 0.21 d | 28.05 ± 0.43 f | 0.91 ± 0.02 i | 7.70 |
| 9 | 72 | 0:1 | 0.01 ± 0.00 a | 6.60 ± 0.04 a | 3.71 ± 0.06 a | 0.28 ± 0.00 a | 0.15 ± 0.00 b | 7.46 |
| 10 | 72 | 5:1 | 0.20 ± 0.00 d | 13.50 ± 0.31 f | 7.87 ± 0.04 b | 22.95 ± 0.32 e | 0.45 ± 0.01 f | 7.59 |
| 11 | 72 | 10:1 | 0.21 ± 0.00 b | 18.50 ± 0.26 g | 9.28 ± 0.13 c | 24.95 ± 0.20 b | 0.69 ± 0.00 g | 7.61 |
| 12 | 72 | 15:1 | 0.26 ± 0.00 g | 24.50 ± 0.57 j | 10.34 ± 0.21 d | 29.50 ± 0.42 g | 0.95 ± 0.01 j | 7.75 |

[a]Values printed in one column with the same letters (a−j) are not statistically different at the $p < 0.05$ level, 95% confidence limit, according to Tukey's HSD test.

important role of $Mg^{2+}$ in the PR-dissolution process. Allen et al.[22] referred to the complex mechanism of $NH_4$−Cp−PR interaction, despite the fact that the simplified eq 1 describing the mechanism of PR dissolution was assumed to be sufficient.

**$NH_4^+$ in Soil Solution.** The typical range of $NH_4^+$ in soil solutions of agricultural soils varies between 0.36 and 3.60 mg $L^{-1}$.[33] According to numerous literature data points, the optimum N concentrations for maximum yield production of various plants ranges between 150 and 300 mg $L^{-1}$.[34−38] By applying chemical fertilizers, plants are supplied with inorganic N via two basic forms: inorganic nitrate nitrogen ($NO_3^{2-}$−N) and ammonium nitrogen ($NH_4^+$−N). A satisfactory plant yield

Table 4. Mean Concentrations ± SD of P, $Ca^{2+}$, $K^+$, $Na^+$, and $Mg^{2+}$ in the Solution, Following the Different Mixing Times and Compositions of the $NH_4$−Cp/PR Mixture[a]

| no. | t (h) | PR/$NH_4$−Cp ratio | P (mg $L^{-1}$) | Ca (mg $L^{-1}$) | K (mg $L^{-1}$) | Na (mg $L^{-1}$) | Mg (mg $L^{-1}$) | pH |
|---|---|---|---|---|---|---|---|---|
| 13 | 24 | 0:1 | 0.00 ± 0.00 a | 5.00 ± 0.09 a | 3.53 ± 0.04 a | 0.21 ± 0.00a | 0.11 ± 0.00 a | 7.45 |
| 14 | 24 | 5:1 | 0.36 ± 0.00 f | 155.00 ± 2.99 e | 21.35 ± 0.48 c | 3.78 ± 0.02 b | 12.65 ± 0.18 d | 8.53 |
| 15 | 24 | 10:1 | 0.42 ± 0.01 d | 372.50 ± 4.05 b | 32.95 ± 0.29 d | 6.11 ± 0.09 c | 33.00 ± 0.88 f | 8.55 |
| 16 | 24 | 15:1 | 0.53 ± 0.01 b,c | 700.50 ± 7.29 h | 37.13 ± 0.54 e | 6.06 ± 0.10 c | 45.89 ± 0.68 b | 8.62 |
| 17 | 48 | 0:1 | 0.00 ± 0.00 a | 6.00 ± 0.17 a | 3.60 ± 0.05 a | 0.25 ± 0.00 a | 0.13 ± 0.00 a | 7.47 |
| 18 | 48 | 5:1 | 0.41 ± 0.01 d | 112.50 ± 3.40 c | 19.45 ± 0.32 b | 3.59 ± 0.02 b | 11.25 ± 0.10 c | 8.55 |
| 19 | 48 | 10:1 | 0.52 ± 0.01 b | 470.00 ± 7.85 b | 33.25 ± 0.55 d | 6.27 ± 0.09 c | 46.25 ± 0.39 b | 8.66 |
| 20 | 48 | 15:1 | 0.57 ± 0.01 e | 552.50 ± 3.80 f | 41.07 ± 0.70 g | 6.41 ± 0.12 d | 47.94 ± 0.61 g | 8.70 |
| 21 | 72 | 0:1 | 0.01 ± 0.00 a | 6.60 ± 0.15 a | 3.71 ± 0.04 a | 0.28 ± 0.00 a | 0.15 ± 0.00 a | 7.46 |
| 22 | 72 | 5:1 | 0.53 ± 0.01 b,c | 135.00 ± 1.95 d | 20.15 ± 0.33 b,c | 3.78 ± 0.08 b | 15.60 ± 0.34 e | 8.59 |
| 23 | 72 | 10:1 | 0.55 ± 0.02 c,e | 480.00 ± 6.56 b | 31.45 ± 0.19 f | 6.48 ± 0.13 d | 53.50 ± 0.07 h | 8.61 |
| 24 | 72 | 15:1 | 0.82 ± 0.02 g | 602.50 ± 14.96 g | 35.82 ± 0.49e | 6.27 ± 0.08 c | 61.69 ± 1.01 i | 8.75 |

[a]Values printed in one column with the same letters (a−i) are not statistically different at the $p < 0.05$ level, 95% confidence limit, according to Tukey's HSD test.

may be achieved by a combination of both N types and sometimes with $NH_4^+$−N alone.[38] It was also demonstrated that plants adjust to acidic soils and that soils with low redox potential favor $NH_4^+$ ions.[39] When considering the degree of saturation of used Cp,[25,27] recalculated total contents of $NH_4^+$ from Cp-exchange sites in the $NH_4$−Cp/PR mixtures were 4, 8, and 12 g $L^{-1}$ for 5:1, 10:1, and 15:1 ratios, respectively. Thus, all three $NH_4$−Cp/PR mixtures that were used in this study have the potential to meet the necessity of plants for nitrogen even at a very low level of $NH_4^+$ discharge. This has already been confirmed by previous experiments with the $NH_4$−Cp/PR mixtures of similar composition.[8,21,22,32,40]

**Solution Cation Concentrations.** *Potassium.* As was shown by Tisdale et al.,[41] the optimum soil solution K concentrations are in the range between 8.6 and 60.0 mg $L^{-1}$. The concentration of $K^+$ found in the solution of the Cp/PR and $NH_4$−Cp/PR mixtures were near the lower and middle part of the range, giving further support to the ability of the test mixtures to provide K (Tables 3 and 4). The highest concentration of $K^+$ in the solution (41.07 mg $L^{-1}$) was detected in the $NH_4$−Cp/PR mixture with the maximum Cp abundance (Table 4).

*Phosphorus.* According to Tisdale et al.,[41] soil solution P concentrations adequate for a variety of crops range from 0.2 to 0.3 mg $L^{-1}$. Solution P concentrations in this study were between 0.15 and 0.28 mg $L^{-1}$ in the Cp/PR mixtures and between 0.36 and 0.82 mg $L^{-1}$ in the $NH_4$−Cp/PR mixtures (Tables 3 and 4). Allen et al.[22] reported that the Cp/PR mixtures of similar composition have provided between 0.465 and 12.1 mg $L^{-1}$ of P in the solution when reactive North Carolina (NC) and Tennessee (TN) PRs were used. Even though the solubility of PR from Lisina was lower compared to the NC and TN PRs, the prepared substrates have the potential to provide sufficient levels of P to support plant growth, especially the $NH_4$−Cp/PR mixtures.

*Calcium.* In well-balanced, flowing nutrient solutions, maximal growth rates of ryegrass and tomato were obtained at Ca concentrations of 0.1 and 4.0 mg $L^{-1}$, respectively.[38] According to Asher and Edwards,[42] the $Ca^{2+}$ concentrations required for plant growth have to be substantially higher in soil solutions than in balanced flowing nutrient solutions. Typical soil solution Ca concentrations necessary for a high yield of agricultural crops has been reported to be from 8 to 45 mg $L^{-1}$ and should not be lower than 14.8 mg $L^{-1}$.[41] Solution Ca concentrations in the Cp/PR substrates in this study ranged from 11.0 to 24.5 mg $L^{-1}$ (Table 3). In the $NH_4$−Cp/PR mixtures the intensities of Ca were between 112.5 and 700.5 mg $L^{-1}$ (Table 4). These results indicate that a sufficient amount of $Ca^{2+}$ can be supplied by the $NH_4$−Cp/PR test mixtures. Further, obtained solution Ca concentrations released from the $NH_4$−Cp/PR mixtures were substantially higher than previously reported.[22,40] This can be attributed to the difference in physicochemical composition of the raw materials, but also to the fact that in this experiment partially saturated $NH_4$−Cp was used, which preparation has been previously proposed.[25] Thus, obtained $NH_4$−Cp contains a sufficient amount of residual Ca that may be released in further ion-exchange reactions.

*Sodium.* In temperate regions, the typical Na concentration in soil solution is on average 2.3−23.0 mg $L^{-1}$. In semiarid and arid regions the concentrations of $Na^+$ in soil solution are 50-fold higher and may have a damaging effect on the growth of most crop plants due to saline stress. The growth response to $Na^+$ significantly varies among plant species as well as genotypes within a species.[37] The concentrations of $Na^+$ in the Cp/PR mixture solution in this study varied between 20.05 and 29.50 mg $L^{-1}$ and from 3.59 to 6.48 mg $L^{-1}$ in the $NH_4$−Cp/PR mixtures (Tables 1 and 2). Both substrates are therefore low in Na and do not induce saline stress in plants. In arid regions the $NH_4$−Cp/PR mixtures could prove to be good soil conditioners. Although $Na^+$ is essential for many, but not all, plant species, the conclusions on $Na^+$ as a beneficial nutrient are relatively scarce.[43]

*Magnesium.* The optimal concentration of $Mg^{2+}$ in soil equilibrium solutions is ∼0.94 mg $L^{-1}$.[37] Solution Mg concentrations in this study ranged from 0.33 to 0.95 mg $L^{-1}$ in the Cp/PR mixtures and from 11.25 to 61.69 mg $L^{-1}$ in the $NH_4$−Cp/PR mixtures, indicating that the ample Mg will be supplied by the test substrates even when the unsaturated zeolite is used (Tables 3 and 4).

*Solution pH Values.* In the Cp/PR mixtures the pH values ranged between 7.53 and 7.75 and were slightly increased compared to the pH values of the PR alone (Table 3). The same trend of solution pH values between natural Cp and PR alone has been reported in ref 20. Because the solution pH values of the $NH_4$−Cp/PR mixtures increase as the mixture ratio increases, the pH values of the measured mixtures increased from 8.53 to 8.75 (Table 4). According to Allen et

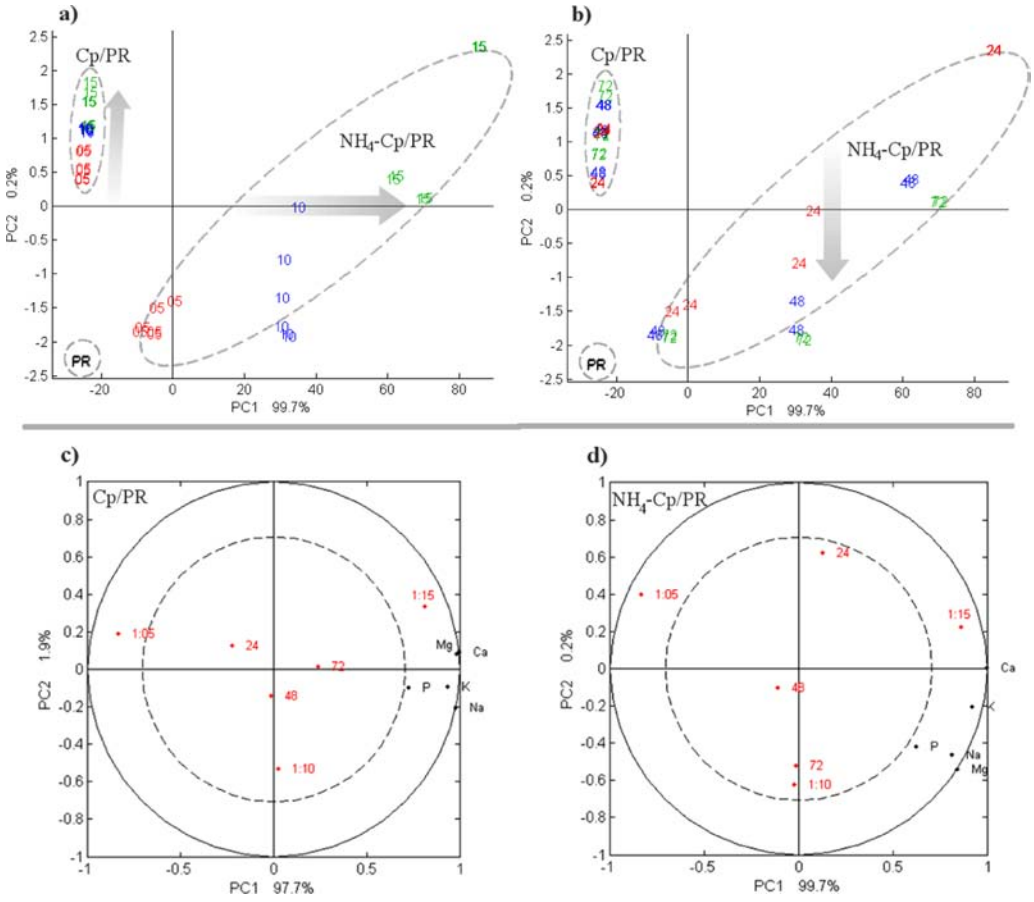


**Figure 3.** Score plots of the PCA model obtained on the whole data set with samples labeled in accordance with (a) the zeolite/PR ratio (where 05 designates 5:1, 10 designates 10:1, and 15 designates 15:1 ratio) and (b) the duration of mixing time (24, 48, and 72 h). Correlation loading plots of the PCA model for (c) the Cp/PR mixtures where design variables are presented in red and solution cation concentrations are presented in black color and (d) the $NH_4$−Cp/PR mixtures where variables are presented as in (c).

al.,[22] better dissolution of PR promoted by $NH_4$−Cp released more $OH^-$ into solution as the Cp/PR ratio increased (eq 1).

**Principal Component Analysis.** PCA was performed on the whole data set (Tables 3 and 4) to analyze the main variation patterns caused by the experimental design, and the results are presented as score plots in Figure 3a and b.[44] To obtain a better overview of the effects of mixing time and $NH_4$−Cp/PR ratio on solution cation concentrations in different substrates, two additional principal component analyses were performed on the subsets of data: one for Cp/PR substrate samples and one for $NH_4$−Cp/PR substrate samples (presented as correlation loading plots in Figure 3c and d).[44]

*Effect of Zeolite/PR Ratio.* The PCA score plot with samples labeled in accordance with the zeolite/PR ratio is presented in Figure 3a. The first two principal components account for 99.9% of the variation in the data set, and along these principal components the separation between substrates of different composition is observed: pure PR samples are separated in the farthest down-left part of the score plot, Cp/PR samples in the upper left, and the $NH_4$−Cp/PR substrate samples are separated in the right part of the score plot. Furthermore, a clear separation between the $NH_4$−Cp/PR substrates of different composition is visible along the first principal component. Along with that, the variance between the Cp/PR substrates of different composition is also observed along the second principal component but is significantly less pronounced than for the $NH_4$−Cp/PR substrates. This indicates that the composition of the mixture has a much stronger effect on the $NH_4$−Cp/PR mixture. Moreover, the highest zeolite share has the strongest influence on solution cation concentrations (Figure 3a).

*Effect of Mixing Time.* A PCA score plot with samples labeled in accordance with the duration of mixing time is presented in Figure 3b. A separation between the $NH_4$−Cp/PR substrates that were mixed for different durations of time can be observed along the second principal component (emphasized with gray downward arrow). It can also be seen that the influence of mixing time increases as the zeolite/PR ratio increases, meaning that the strongest effect of mixing time is observed for the substrates with 15:1 zeolite/PR ratio (e.g., these samples are more separated than the rest). Conversely, the influence of the mixing time has a very weak effect on the Cp/PR substrates and PR alone.

*Correlation Loading Plots.* From the correlation loading plots calculated for both substrates (Figure 3c and d), it can be observed that the highest zeolite/PR ratio exhibits the strongest influence on solution P, Ca, K, Na, and Mg concentrations. Moreover, the concentration of $Ca^{2+}$ in the solution is most affected by the $NH_4$−Cp/PR ratio of 15:1, while P is being the least affected by the same. In contrast to the Cp/PR mixture, a positive correlation between solution P concentrations, mixing time of 72 h, and $NH_4$−Cp/PR ratio of 10:1 was observed. Although these variables are positioned in the inner circle of the


dx.doi.org/10.1021/jf502704j | J. Agric. Food Chem. 2014, 62, 9965−9973

**Table 5. ANOVA of the Cp/PR Mixtures**

| | df | P | Ca | K | Na | Mg |
|---|---|---|---|---|---|---|
| $t$ | 1 | 0.04[a] | 1918.90 | 1.83 | 95.60 | 192.96[b] |
| $t^2$ | 1 | 0.00 | 3506.58[b] | 3.12 | 30.23 | 5.46 |
| Cp | 1 | 0.58[a] | 641431.56[a] | 1997.52[a] | 339.44[a] | 5201.31[a] |
| Cp $^2$ | 1 | 0.06[a] | 11 913.30[a] | 94.95[a] | 22.63 | 22.25 |
| $t \times$ Cp | 1 | 0.02[a] | 2049.19 | 0.57 | 167.22[b] | 105.07 |
| error | 6 | 0.04 | 5818.80 | 13.94 | 202.34 | 328.96 |
| $r^2$ | | 0.899 | 0.984 | 0.988 | 0.764 | 0.897 |

[a]Significant at $p < 0.05$ level. [b]Significant at $p < 0.10$, level, 95% confidence limit, error terms were found statistically insignificant; df = degrees of freedom.

correlation loading plot (<50% of explained variance), the positive correlation found between them can be taken as an indication that the highest concentration of P in the solution can be achieved with longer mixing times and the moderate $NH_4$−Cp share in the mixture.

**ANOVA and SOP Models.** ANOVA was conducted for obtained SOP models, and solution P, Ca, K, Na, and Mg concentrations were tested against the impact of process variables (Tables 5 and 6). According to ANOVA of SOP models for Cp/PR mixtures, calculation of solution P, Ca, K, Na and Mg concentrations was mostly affected by the linear term of the Cp share in the mixture, which is statistically significant at $p < 0.05$ level, 95% confidence limit (Table 5). The quadratic term of the Cp share was also found to be very influential for the calculation of P, Ca, and K at $p < 0.05$ level. The linear term of t was found to be significant for calculation of P ($p < 0.05$).

**Table 6. ANOVA of the $NH_4$−Cp/PR Mixtures**

| | df | P | Ca | K | Na | Mg |
|---|---|---|---|---|---|---|
| t | 1 | 0.00 | 12.75[a] | 0.00 | 5.07 | 0.01[a] |
| $t^2$ | 1 | 0.00 | 0.05 | 0.01 | 0.01 | 0.00 |
| $NH_4$−Cp | 1 | 0.06[a] | 449.36[a] | 70.22[a] | 1120.44[a] | 1.01[a] |
| $NH_4$−Cp $^2$ | 1 | 0.02[a] | 0.96 | 9.05[a] | 260.03[a] | 0.00 |
| t × $NH_4$−Cp | 1 | 0.00 | 1.12[b] | 0.00 | 1.60 | 0.00 |
| error | 6 | 0.00 | 1.90 | 0.53 | 41.91 | 0.00 |
| $r^2$ | | 0.905 | 0.992 | 0.988 | 0.946 | 0.997 |

[a]Significant at $p < 0.05$ level. [b]Significant at $p < 0.10$ level, 95% confidence limit, error terms were found to be statistically insignificant; df = degrees of freedom.

According to ANOVA of SOP models for $NH_4$−Cp/PR mixtures, calculation of solution P, Ca, K, Na, and Mg concentrations was mostly affected by the linear term of the $NH_4$−Cp share in the mixture, which is statistically significant at $p < 0.05$ level, 95% confidence limit (Table 6). The quadratic term of the $NH_4$−Cp share was also found to be very influential for the calculation of P, K, and Na, $p < 0.05$ level. The linear term of t was found to be significant for calculation of Ca (at $p < 0.05$ level).

The residual variance, marked as error in Tables 5 and 6, presents the model disagreement with the experimental values (contributions of other members that are not described in the SOP model). All developed models showed statistically insignificant deviation from the experimental values of the model, which confirmed their suitability. Analysis revealed that

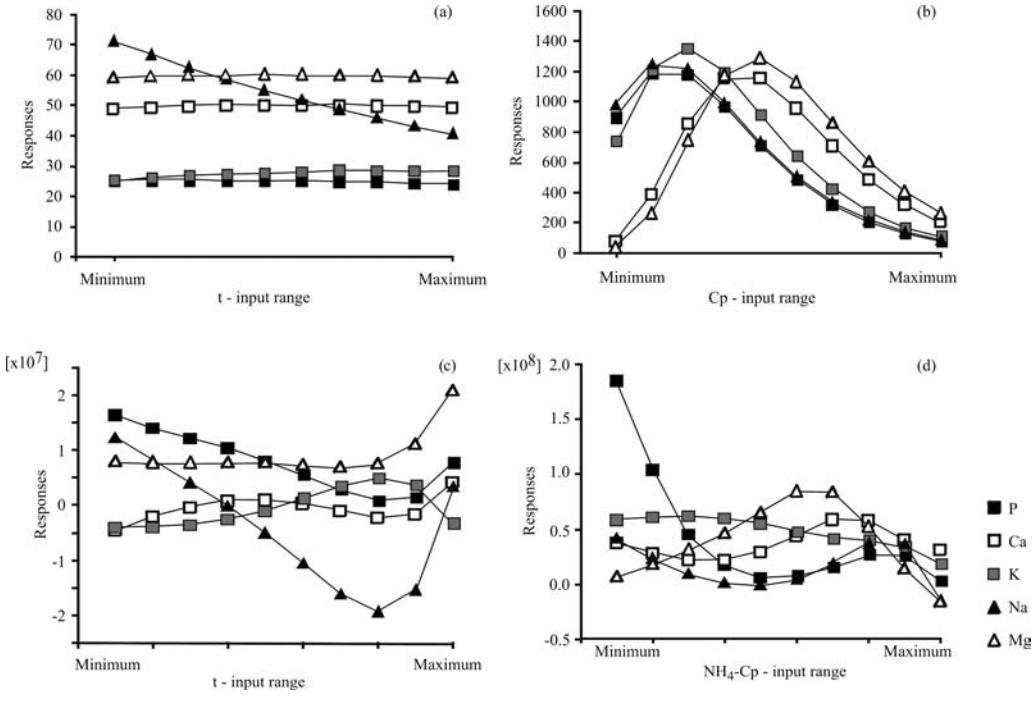


**Figure 4.** Sensitivity analysis for infinitesimal changes of process parameters in the Cp/PR mixtures (a, b) and the $NH_4$−Cp/PR mixtures (c, d).

linear, quadratic, as well as interchange terms considerably influenced forming SOP models. It is concluded that all of the obtained models were statistically significant and in agreement with the experimental results.

**Neurons in the ANN Hidden Layer.** All variables considered in the ANOVA analysis were also used for the ANN modeling. The optimum number of hidden neurons in this case was chosen upon minimizing the difference between the predicted ANN values and the measured solution concentrations of the elements, using SOS during testing as the performance indicator. According to ANN, the optimal number of neurons in the hidden layer was 3 (network MLP 2−3−5) for the Cp/PR mixture and 9 (network MLP 2−9−5) for the $NH_4$−Cp/PR mixture application, as well as when obtaining high values of $r^2$ and low values of SOS.

**Simulation of the ANNs.** ANN models were used to predict experimental variables (solution P, Ca, K, Na, and Mg concentrations). An optimal network, used for the Cp/PR mixture application, was able to predict all process outputs for a broad range of the process variables (coefficients of determination reached 0.986 for P; 0.993 for $Ca^{2+}$; 0.998 for $K^+$; 0.994 for $Na^+$; and 0.997 for $Mg^{2+}$) during the testing period. The accuracy of solution P, Ca, K, Na, and Mg concentrations' prediction of the $NH_4$−Cp/PR mixtures was also very good (0.998 for P; 0.999 for $Ca^{2+}$; 0.999 for $K^+$; 0.999 for $Na^+$; and 0.999 for $Mg^{2+}$ calculations). The predicted values were very close to the measured values in most cases, in terms of $r^2$ value. It is noteworthy that these coefficients of determination values are higher than those $r^2$ associated with the SOP model. Although ANN models are more complex (29−77 weight biases for the solution P, Ca, K, Na, and Mg concentration model of both the Cp/PR and $NH_4$−Cp/PR experimental mixtures) than SOPs; ANNs performed a bit better because of the high nonlinearity of the developed system. The mean of residuals for the Cp/PR mixture application model were 0.040 for P, 0.006 for $Ca^{2+}$, 0.019 for $K^+$, 0.015 for $Na^+$, and 0.010 for $Mg^{2+}$ content. The mean of residuals for the $NH_4$−Cp/PR mixture application model were 0.051 for P, 0.006 for $Ca^{2+}$, 0.028 for $K^+$, 0.025 for $Na^+$, and 0.012 for $Mg^{2+}$. These results showed a good approximation to normal distribution around zero with a probability of 95% (2 × SD), which delineates a good generalization ability of ANN model for the range of observed experimental values.

**Sensitivity Analysis.** For better access to the concentration changes of the elements, due to variations of process parameters, a sensitivity analysis was performed. The greater effect observed in outputs means greater sensitivity with respect to the process parameters.[45] Herein, the influence of the infinitesimal changes in process parameters (inputs) over solution P, Ca, K, Na, and Mg concentrations (outputs) was observed (Figure 4). The calculated changes in outputs corresponded to the level of experimental errors and showed how processing time and composition of the mixtures influence solution P, Ca, K, Na, and Mg concentrations.

Solution P, Ca, K, and Mg concentrations in the Cp/PR mixtures were not affected by the duration of the experiment, while prolongation of mixing negatively affects the Na concentration (Figure 4a). In contrast to this, in the $NH_4$−Cp/PR mixtures, solution P, Ca, K, Na, and Mg concentrations were affected by infinitesimal changes especially at a higher value of *t*. The concentrations of P, $Ca^{2+}$, $Na^+$, and $Mg^{2+}$ were increasing, while the concentration of $K^+$ in the solution was lowering at the upper input range limit (Figure 4c). In the Cp/PR mixtures all elemental concentrations in the solution were increased by small positive changes in Cp input between the minimum and medium input range (Figure 4b). The medium Cp input led to higher responses of P, Ca, K, Na, and Mg. The changes in $NH_4$−Cp share in the mixture led to complex phenomena, with it being most evident at the middle and upper limits of the input range, which is in accordance with PCA. Similar to $NH_4$−Cp system, responses to P, Ca, K, Na, and Mg concentration decrease with the Cp share increase, as the system approaches equilibrium. The highest response of P was observed close to the minimum of the Cp and $NH_4$−Cp input range, which is in accordance with PCA and ANOVA analysis, as well as with experimental findings.

## AUTHOR INFORMATION


### Corresponding Author

*Dr. Marija L. Mihajlović, Central Laboratory for Testing, Institute for Technology of Nuclear and Other Mineral Raw Materials, 86 Franchet d'Esperey St., 11000 Belgrade, Serbia. Tel.: +381 11 3691 722. E-mail: m.mihajlovic@itnms.ac.rs.



### Funding

The authors are grateful to the Serbian Ministry of Science and Technological Development for the financial support of this investigation included in the projects TR 31003 and TR 31055, project cycle 2011−2014.


### Notes

The authors declare no competing financial interest.

## REFERENCES


(1) Leon, L. A.; Fenster, W. E.; Hammond, L. L. Agronomic potential of eleven phosphate rocks from Brazil, Colombia, Peru and Venezuela. *Soil Sci. Soc. Am. J.* **1986**, *50*, 798−802.

(2) Chien, S. H.; Prochnow, L. I.; Mikkelsen, R. Agronomic Use of Phosphate Rock for Direct Application. *Better Crops* **2010**, *94*, 21−23.

(3) Hart, M. R.; Quin, B. F.; Nguyen, M. L. Phosphorus runoff from agricultural land and direct fertilizer effects: A review. *J. Environ. Qual.* **2004**, *33*, 1954−1972.

(4) Marić, S.; Nikolić, J. Ore deposits of Yugoslavia. The phosphate deposits of Lisina. *Bull. - Inst. Geol. Geophys. Res., Ser. A* **1969**, 339−350.

(5) Notholt, J. G.; Sheldon, R. P.; Davidson, D. F. *Phosphate Deposits of the World: Phosphate Rock Resources*; Cambridge Earth Science Series; Cambridge University Press: New York, 2005; Vol. 2.

(6) Chien, S. H. Factors Affecting the Agronomic Effectiveness of Phosphate Rock for Direct Application. In *Direct Application of Phosphate Rock and Related Technology: Latest Development and Practical Experiences*; Rajan, S. S. S., Chien, S. H., Ed.; Special Publications IFDCSP- 37; IFDC: Muscle Shoals, AL, 2003; pp 50−62.

(7) Smalberger, S. A.; Singh, U.; Chien, S. H.; Henao, J.; Wilkens, P. W. Development and validation of a phosphate rock decision support system. *Agron. J.* **2006**, *98*, 471−483.

(8) Barbarick, K. A.; Lai, T. M.; Eberl, D. D. Exchange fertilizer (phosphate rock plus ammonium zeolite) effects on sorghum-sudangrass. *Soil Sci. Soc. Am. J.* **1990**, *54*, 911−916.

(9) de Campos Bernardi, A. C.; Oliviera, P. P. A.; de Melo Monte, M. B.; Souza-Barros, F. Brazilian sedimentary zeolite use in agriculture. *Microporous Mesoporous Mater.* **2013**, *167*, 16−21.

(10) Perego, C.; Bagatin, R.; Tagliabue, M.; Vignola, R. Zeolites and related mesoporous materials for multi-talented environmental solutions. *Microporous Mesoporous Mater.* **2013**, *166*, 37−49.

(11) Ming, D.; Mumpton, E. Zeolites in soils. In *Minerals in Soil Environments*, 2nd ed.; Dixon, J.B., Weed, S.B., Ed.; Soil Science Society of America: Madison, WI, 1989; pp 873−911.

(12) Gruener, J. E.; Ming, D. W.; Henderson, K. E.; Galindo, C., Jr. Common ion effects in zeoponic substrates: Wheat plant growth experiment. *Microporous Mesoporous Mater.* **2003**, *61*, 223−230.

(13) Gruener, J. E.; Ming, D. W.; Henderson, K. E.; Galindo, C., Jr.; Golden, D. C. Plant productivity and characterization of zeoponic substrates after three successive crops of radish (Raphanus sativus L.). *Microporous Mesoporous Mater.* **2007**, *105*, 279−284.
(14) Arcoya, A.; Gonzalez, J. A.; Llabre, G.; Seoane, X. L.; Travieso, N. Role of the counteractions on the molecular sieve properties of a clinoptilolite. *Microporous Mater.* **1996**, *7*, 1−13.
(15) Kalló, D. Applications of natural zeolites in water and wastewater treatment. In *Natural Zeolites: Occurrence, Properties, Applications, Reviews in Mineralogy and Geochemistry*; Bish, D. L., Ming, D.W., Eds.; Mineralogical Society of America: Washington, DC, 2001; Vol. *45*, pp 519−550.
(16) Stamatakis, G.; Tsantila, N.; Samiotaki, M.; Panayotou, G. N.; Dimopoulos, A.; Halvadakis, C.; Demopoulos, C. Detection and Isolation of Antiatherogenic and Antioxidant Substances Present in Olive Mill Wastes by a Novel Filtration System. *J. Agric. Food Chem.* **2009**, *57*, 10554−10564.
(17) Malekian, R.; Abedi-Koupai, J.; Eslamian, S. S.; Mousavi, S. F.; Abbaspour, K. C.; Afyuni, M. Ion-exchange process for ammonium removal and release using natural Iranian zeolite. *Appl. Clay Sci.* **2011**, *51*, 323−329.
(18) Xu, W.; Li, L. Y.; Grace, J. R. Zinc removal from acid rock drainage by clinoptilolite in a slurry bubble column. *Appl. Clay Sci.* **2010**, *50*, 158−163.
(19) Smičiklas, I.; Dimović, S.; Plećaš, I. Removal of $Cs^{1+}$, $Sr^{2+}$ and $Co^{2+}$ from aqueous solutions by adsorption on natural clinoptilolite. *Appl. Clay Sci.* **2007**, *35*, 139−144.
(20) Lai, T.; Eberl, D. Controlled and renewable release of phosphorus in soils from mixtures of phosphate rock and $NH_4$-exchanged clinoptilolite. *Zeolites* **1986**, *6*, 129−132.
(21) Pickering, W.; Menzies, N.; Hunter, M. Zeolite/rock phosphate—A novel slow release phosphorus fertiliser for potted plant production. *Sci. Hortic.* **2002**, *94*, 333−343.
(22) Allen, E. R.; Hossner, L. R.; Ming, D. W.; Henninger, D. L. Solubility and cation exchange in phosphate rock and ammonium- and potassium-saturated clinoptilolite mixtures. *Soil Sci. Soc. Am. J.* **1993**, *57*, 1368−1374.
(23) Zheng, H.; Jiang, L.; Lou, H.; Hu, Y.; Kong, X.; Lu, H. Application of Artificial Neural Network (ANN) and Partial Least-Squares Regression (PLSR) to Predict the Changes of Anthocyanins, Ascorbic Acid, Total Phenols, Flavonoids, and Antioxidant Activity during Storage of Red Bayberry Juice Based on Fractal Analysis and Red, Green, and Blue (RGB) Intensity Values. *J. Agric. Food Chem.* **2011**, *59*, 592−600.
(24) Śliwińska, M.; Wiśniewska, P.; Dymerski, T.; Namieśnik, J.; Wardencki, W. Food Analysis Using Artificial Senses. *J. Agric. Food Chem.* **2014**, *62*, 1423−1448.
(25) Mihajlović, M.; Stojanović, M.; Lopičić, Z.; Petrović, M.; Milojković, J.; Šoštarić T.Lačnjeva, Č. Sustainable agriculture: Obtaining $NH_4$-zeolite fertilizer supplement. The 45th International October Conference on Mining and Metallurgy, Bor Lake, Bor, Serbia, October 16−19, 2013.
(26) Mihajlović, M.; Stojanović, M.; Lopičić, Z.; Milojković, J.; Šoštarić, T.; Petrović, M. In search for adequate $NH_4$-clinoptilolite fertilizer supplement: Parameter optimization. 5th Serbian, Croatian, Slovenian Symposium on Zeolites, Zlatibor, Serbia, 2013; pp 108−112.
(27) Koenig, R. A.; Johnson, C. R. Colorimetric Determination of Phosphorus in Biological Materials. *Ind. Eng.* **1942**, *14*, 155−156.
(28) Pearson, K. On lines and planes of closest fit to systems of points in space. *Philos. Mag.* **1901**, *2*, 559−572.
(29) Arsenović, M.; Radojević, Z.; Stanković, S.; Lalić, Ž.; Pezo, L. What to expect from heavy clay? *Ceram. Int.* **2013**, *39*, 1667−1675.
(30) Taylor, B. *Methods and Procedures for the Verification and Validation of Artificial Neural Networks*; Springer Science+Business Media: New York, 2006.
(31) Sand, L. B.; Mumpton, F. A. *Natural Zeolites: Occurrences, Properties, Use*; Pergamon Press: USA, 1976; p 356.
(32) Allen, E. R.; Hossner, L. R.; Ming, D. W.; Henninger, D. L. Release rates of phosphorus, ammonium and potassium in clinoptilolite-phosphate rock systems. *Soil Sci. Soc. Am. J.* **1996**, *60*, 1467−1472.
(33) Owen, A. G.; Jones, D. L. Competition for amino acids between wheat roots and rhizosphere microorganisms and the role of amino acids in plant N acquisition. *Soil Biol. Biochem.* **2001**, *33*, 651−657.
(34) Aloni, B.; Karni, L.; Rylski, I.; Zaidman, Z. The effect of nitrogen fertilization and shading on the incidence of "colour spots" in sweet pepper (*Capsicum annuum*) fruit. *J. Hortic. Sci.* **1994**, *69*, 767−773.
(35) Schon, M. K.; Compton, M. P.; Bell, E.; Burns, I. Nitrogen concentrations affect pepper yield and leachate nitrate-nitrogen from rockwool culture. *Hortic. Sci.* **1994**, *29*, 1139−1142.
(36) Qawasmi, W.; Mohamad, M. J.; Najim, H.; Qubursi, R. Response of bell pepper grown inside plastic house to nitrogen fertilization. *Commun. Soil Sci. Plant Anal.* **1999**, *30*, 2499−2509.
(37) Bryson, G. M.; Barker, A. V. Determination of optimal fertilizer concentration range for tomatoes grown in peat-based medium. *Commun. Soil Sci. Plant Anal.* **2002**, *33*, 759−777.
(38) Marschner, P. *P. Marschner's Mineral Nutrition of Higher Plants*, third ed.; Elsevier Ltd.: Amsterdam, The Netherlands, 2012.
(39) Lee, J. A. The calcicole-calcifuge problem revisited. *Adv. Bot. Res.* **1999**, *29*, 1−30.
(40) Beiersdorfer, R. E.; Ming, D. W.; Galindo, C., Jr. Solubility and cation exchange properties of zeoponic substrates. *Mesoporous Mater.* **2003**, *61*, 231−247.
(41) Tisdale, S. L.; Nelson, W. L.; Beaton, J. D. *Soil fertility and fertilizers*; Macmillan Publ. Co.: New York, 1985.
(42) Asher, C. J; Edwards, D. G. In *Encyclopedia of Plant Physiology, New Series*; Läuchli, A., Bieleski, R. L., Eds.; Springer-Verlag: Berlin and New York, 1983; pp 94−119.
(43) Pilon-Smits, E. A. H.; Quinn, C. F.; Tapken, W.; Malagoli, M.; Schiavon, M. Physiological functions of beneficial elements. *Curr. Opin. Biotechnol.* **2009**, *12*, 267−274.
(44) Martens, H.; Næs, T. *Multivariate Calibration*; Wiley: Chichester, U.K., 1989.
(45) Pezo, L.; Arsenović, M.; Radojević, Z. ANN model of brick properties using LPNORM calculation of minerals content. *Ceram. Int.* **2014**, *40*, 9637−9645.

soils in response to different environmental gradients, such as redox status, soil porosity, and water contents.[19] The changes in PLFAs also permit study of the mechanism of persistent organic pollutant biodegradation in soils.[20−22] Bardgett et al. reported that total PLFAs decreased with increasing soil depth in both grazed and ungrazed grasslands.[23] From the soil surface down to 2 m, the ratios of cyclopropyl/monoenoic precursors and total saturated/monounsaturated fatty acids increased with soil depth, suggesting that the microorganisms inhabiting the deeper soil horizons are more carbon limited than surface-dwelling microbes.[24] The focus of the present work is to study the influence of electron donors and acceptors on the PLFAs.

The aims of this study were (a) to study the dissipation of PCP and follow the evolution of its metabolites in vertical profiles of flooded paddy soil (0−50 mm); (b) to determine the effects of external electron donors and acceptors on the vertical profiles of PCP dissipation and microbial community structure; and (c) to establish a link between soil microbial community structures (PLFAs), PCP dissipation, and redox reaction.

## MATERIALS AND METHODS

**Soil.** The soil was taken from the surface layer (0−20 cm) of a paddy soil in Jiaxing city, Zhejiang province, China. After sampling, the soil was air-dried, ground, and sieved to <1 mm prior to use. The soil contained 22.2% clay, 53.1% silt, and 24.7% sand. The soil pH, organic carbon, and amorphous Fe were 5.8, 31.3 g $kg^{-1}$, and 6.1 g $kg^{-1}$, respectively.

**Chemicals.** Pentachlorophenol (PCP, >98% purity) and 3,4,5-trichlorophenol (3,4,5-TCP, >98% purity) were obtained from Sigma-Aldrich (St. Louis, MO, USA). Methanol (>99.9% purity) was obtained from Merck KGaAb (Darmstadt, Germany). The other analytical grade chemicals were obtained from Sinopharm Chemical Reagent Co., Ltd., Shanghai, China.

**Electron Acceptors and Donors.** $Na_2SO_4$ and $NaNO_3$ were used to supply $SO_4^{2-}$ and $NO_3^-$ as electron acceptors. The concentrations of $Na_2SO_4$ and $NaNO_3$ were 2.8 and 1.7 g $kg^{-1}$ soil. The concentrations adopted were those normally used to create $SO_4^{2-}$ and $NO_3^-$ reducing conditions in soil−water systems.[5,25]

Crop residues were used to supply electron donors. They were rice straw (*Oryza sativa* L.), wheat straw (*Triticum aestivum* L.), canola residue (*Brassica chinensis* L.), and Chinese milk vetch (*Astragalus sinicus* L.). They were collected from field sites, oven-dried at 65 °C for 24 h, and then ground to <1 mm. Some of the residues were used for determination of chemical composition, and the remainder were stored for incubation experiments. Their chemical compositions (including total C, N, S, TOC, $NH_4^+$-N, $NO_3^-$-N) were analyzed following previously described methods[26,27] and are shown in Table S1 of the Supporting Information (SI). Details can be found in the SI.

**Analytical Methods.** Soil pH was determined in a suspension of 1:2.5 soil/water ratio (w/v). Soil organic carbon (OC) was measured by dichromate digestion. Soil particle size was determined using a hydrometer method. Soil-dissolved organic carbon (DOC) was extracted by Milli-Q water (soil/water, 1:2.5, w/v), determined by a TOC Analyzer (Multi N/C 3100, Jena Analytical, Jena, Germany). Soil $NH_4^+$ extracted by 1 M KCl (shaking 1 h at 20 °C, soil/extractant, 1:10) was analyzed colorimetrically using a continuous colorimetric flow system (Skalar SAN$^{++}$System, Breda, The Netherlands). $SO_4^{2-}$ was determined by shaking soils (0.5 g, freeze-dried) with 5 mL of Milli-Q water for 15 min. The suspensions were filtered through 0.22 $\mu$m Millipore membranes followed by analysis using a Dionex ICS-2000 ion chromatography system (Dionex, Sunnyvale, CA, USA) equipped with an ASRS Ultra II self-regenerating suppressor. The column used was IonPac AS11-HC, and the mobile phase was 10 mM aqueous potassium hydroxide. $Na_2SO_4$ was used as the standard for $SO_4^{2-}$ detection. The average recovery ($n$ = 3) of the analytic method for $SO_4^{2-}$ was 89.0 ± 3.0%.

**Experiment Design.** To prepare xenobiotic spiked soil, PCP solution in methanol was mixed with a portion of soil. The spiked soil was thereafter vented for 24 h for the methanol to vaporize and then mixed thoroughly with a large portion of uncontaminated soil (1:19, w/w). Then, the $NaNO_3$, $Na_2SO_4$, and crop residues were added to the PCP-polluted soils at 1.7, 2.8, and 15 g $kg^{-1}$ soil, respectively, and mixed thoroughly to establish eight treatments: (A) PCP unspiked control (CK1); (B) PCP without other addition (CK2); (C) PCP + $NaNO_3$; (D) PCP + $Na_2SO_4$; (E) PCP + wheat; (F) PCP + rice; (G) PCP + canola; (H) PCP + vetch. Finally, both amended and unamended soils were transferred to 250 mL beakers to provide 7 cm thick soil depths and equilibrated in a greenhouse for 7 days; Milli-Q water was added to create a 2 mm thick water layer covering the soil surface. The daytime temperature was between 30 and 35 °C, the night-time temperature was between 25 and 30 °C; soils were sampled at 30, 60, and 120 days after incubation by sacrificing individual replicates. Four days before sampling, flooded water above the soil surface in three duplicate beakers was allowed to evaporate and then to reach almost soil saturation. A 20 mL syringe with the top cut off was used to take samples from four profiles (0−10, 10−20, 20−30, and 30−50 mm) separately. Evaporated water was refilled with Milli-Q water every 2 days.

**PCP and Intermediate Analyses.** The concentration of PCP in soils was determined by ultrasonic extraction and solid phase enrichment, followed by HPLC analysis.[5] Soil samples (2 g, freeze-dry weight) were adjusted to pH 4 with sulfuric acid and extracted in 10 mL of methanol by ultrasonics (60 kHz, 25 °C) for 15 min. After centrifugation at 3000 rpm for 10 min, the supernatants were collected. The soil residues were then extracted twice more, as above. The supernatant extracts from each soil sample were then combined and concentrated to 1 mL by rotary evaporation. The concentrated extracts were then transferred to an SPE C18 cartridge (6 mL, 500 mg) with 10 mL of Milli-Q water followed by elution with 10 mL of methanol and concentrated to 2 mL under $N_2$. Finally, each sample was filtered through a 0.22 $\mu$m Millipore membrane (ANPEL, 13 mm diameter) prior to analysis. Details of the HPLC analysis were described in our previous study.[5] All measurements were in triplicates with a variation generally <5%. Procedural blanks were determined by going through the same extraction and cleanup procedures for each series of samples. The average recovery ($n$ = 3) and the determined limits for PCP detection were 95.0 ± 2.1% and 0.01 mg $kg^{-1}$, respectively.

The sample preparation and the extractants used for intermediate analysis were as described earlier by Chen et al.[2] with small modifications. Briefly, soil (2 g, freeze-dry weight) was extracted with 10 mL of methanol followed by centrifuging, and the supernatants were collected. The procedure was performed three times, and the supernatants were combined. The supernatants were concentrated to 1 mL by rotary evaporation and $N_2$ and then derivatized by mixing with $K_2CO_3$ (10 mL, 0.2 M) and acetic anhydride (0.5 mL). The derivatizations were then extracted using 4 mL of hexane. The determination of intermediates was performed using a GC-MS (N6890/5975B, Agilent, Santa Clara, CA, USA) equipped with an HP-5MS capillary column of 30 m × 250 $\mu$m × 0.25 $\mu$m film thickness. The temperature ramp was as follows: 80 °C for 2 min, from 80 to 250 °C at 10 °C $min^{-1}$, held for 5 min.

**PLFA Extraction and Analysis.** The microbial community structure was determined by PLFA analysis. The PLFAs were extracted from soils using a single-phase chloroform−methanol−citrate buffer system.[28] Then, phospholipids were separated from neutral lipids and glycolipids on a solid-phase extraction column (Supelco, Inc., Bellefonte, PA, USA). Methyl myristate fatty acid (19:0) was added as internal standard, and PLFAs were subsequently derivatized by mild alkali methanolysis. The resulting fatty acid methyl esters were identified by GC (N6890, Agilent) fitted with a MIDI Sherlocks microbial identification system (version 4.5, MIDI, USA). Fatty acids are described according to the nomenclature of He et al.[21] Details can be found in the SI. Main taxa, including bacteria, Gram-positive bacteria, Gram-negative bacteria, fungi, actinomycetes, sulfate-reducing bacteria, aerobic bacteria, anaerobic bacteria, and cyanobacteria, were identified by their specific individual PLFA biomarkers.[29−31] PLFAs that contributed <1% of the total amount of extracted sample or PLFAs that were observed in only one sample were eliminated from the data set.

**Statistical Analysis.** Statistical analysis and principle component analysis (PCA) of soil PLFAs were conducted with the SPSS 16.0

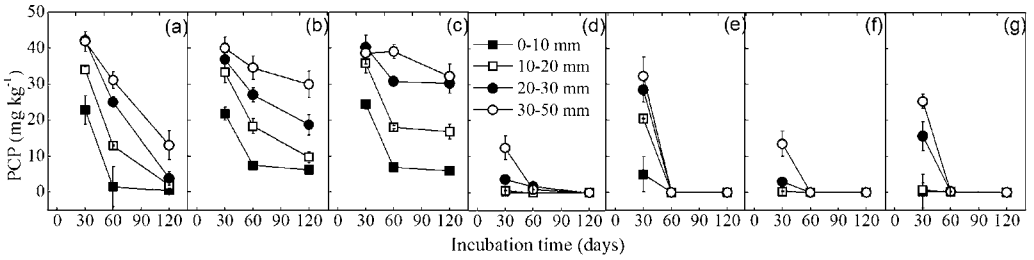


**Figure 1.** Dissipation of PCP in soil profiles amended with different electron acceptors and donors: (a) control; (b) $NO_3^-$; (c) $SO_4^{2-}$; (d) wheat straw; (e) rice straw; (f) canola residue; (g) Chinese milk vetch. Error bars represent standard deviation of triplicate measurements.

**Table 1. Concentration (Milligrams per Kilogram) of 3,4,5-Trichlorophenol (3,4,5-TCP) in Soils**

| incubation time (days) | soil depth (mm) | control | $NO_3^-$ | $SO_4^{2-}$ | wheat | rice | canola | vetch |
|---|---|---|---|---|---|---|---|---|
| 30 | 0–10 | ND[a] | ND | ND | 3.9 (0.6)[b] | 8.7 (1.6) | 12.2 (1.2) | 19.8 (1.4) |
| | 10–20 | ND | ND | ND | 7.2 (1.2) | 8.9 (0.3) | 2.0 (0.2) | 10.8 (0.5) |
| | 20–30 | ND | ND | ND | 5.1 (1.4) | 3.8 (0.2) | 1.2 (0.1) | 4.6 (0.5) |
| | 30–50 | ND | ND | ND | 2.2 (0.2) | 1.4 (0.0) | 1.2 (0.1) | 2.4 (0.1) |
| 60 | 0–10 | 1.7 (0.1) | 0.39 (0.0) | 3.87 (0.3) | 1.6 (0.3) | 12.7 (1.2) | 10.9 (0.4) | 16.1 (1.1) |
| | 10–20 | 1.0 (0.0) | 0.19 (0.0) | 4.78 (0.3) | 1.5 (0.1) | 20.5 (2.9) | 20.9 (1.0) | 21.8 (2.1) |
| | 20–30 | 1.7 (0.1) | 0.27 (0.0) | 2.54 (0.1) | 1.1 (0.0) | 24.7 (0.4) | 21.8 (2.7) | 27.6 (0.5) |
| | 30–50 | ND | 0.99 (0.0) | 0.46 (0.0) | 0.9 (0.0) | 26.7 (2.1) | 21.2 (5.5) | 28.0 (1.8) |
| 120 | 0–10 | 4.7 (0.5) | 0.65 (0.0) | 0.44 (0.0) | 1.0 (0.0) | 8.6 (0.3) | 4.0 (0.1) | 9.1 (0.4) |
| | 10–20 | 12.9 (1.6) | 2.53 (0.2) | 0.48 (0.0) | 1.7 (0.1) | 16.1 (1.1) | 15.9 (1.9) | 14.8 (0.5) |
| | 20–30 | 9.4 (0.6) | 2.32 (0.3) | 0.44 (0.0) | 1.1 (0.0) | 23.2 (0.5) | 21.2 (1.3) | 23.9 (0.4) |
| | 30–50 | 1.3 (0.0) | 1.64 (0.2) | 0.33 (0.0) | 1.1 (0.0) | 26.6 (1.5) | 26.1 (0.4) | 27.3 (0.2) |

[a]ND, tot detected. [b]Mean value (standard deviation).

correlate and factor procedures. Treatment effects were tested by one-way ANOVA. In addition, Pearson correlation analysis was applied to study the relationship between PCP/3,4,5-TCP and the microbial community. Correlation analysis was performed using SPSS 16.0 for windows. All values are the means of triplicate determinations.

## RESULTS

**PCP Dissipation in Soil Profiles.** The dissipation of PCP in soil profiles is shown in Figure 1. Changes in PCP concentrations varied widely following the addition of electron donors and acceptors but showed a general trend in the initial 30 days of incubation, in which PCP decreased with increasing soil depth in all treatments. However, electron donors and acceptors showed opposite influences on the PCP dissipation. The addition of $NO_3^-$ and $SO_4^{2-}$ significantly ($p < 0.05$) inhibited the dissipation of PCP in the deep layer (20–50 mm) with increasing incubation time (Figure 1b,c), whereas the crop residues (Figure 1d–g) enhanced PCP dissipation in all soil profiles. By the end of the incubation, the PCP concentrations were 0.5–13.3, 6.3–30.0, and 6.0–32.2% for the control, $NO_3^-$, and $SO_4^{2-}$ treatments, respectively. As with all of the crop residue treatments, the PCP concentrations were <0.01 mg $kg^{-1}$ in all soil profiles (Figure 1d–g). No significant differences were observed between the four crop residue treatments.

**Formation of Intermediates during Dissipation.** 3,4,5-TCP was produced as a major intermediate of PCP dissipation during the incubation (Table 1). During the initial 30 days of incubation, 3,4,5-TCP was produced in the electron donor treatments, whereas it was not found in the control or electron acceptor treatments. The 3,4,5-TCP concentration showed the same trend in all of the electron donor treatments, which decreased with increasing soil depth. After 60 days of incubation, 3,4,5-TCP could almost be found in all of the treatments, but the variation trends were markedly different. In the electron donor treatments, the concentration increased with increasing soil depth except the wheat residue treatment in which the 3,4,5-TCP concentration was too low to have any significant difference between soil profiles. The 3,4,5-TCP concentrations in the electron donor treatments remained unchanged until the end of incubation. At the end, 3,4,5-TCP was also found in the other treatments, especially the control treatment, in which approximately 12.9 mg $kg^{-1}$ of 3,4,5-TCP was found in the 10–20 mm soil layer.

**Variations of Electron Acceptors and Donors in Soil Profiles.** The variations of dissolved organic carbon (DOC), $SO_4^{2-}$, and $NH_4^+$ in soil profiles are shown in Figure 2. The addition of crop residues greatly increased the release of DOC in the order Chinese milk vetch > rice > wheat > canola (Figure 2A). The spatial variations of DOC in the soil profiles showed the same trend during the entire incubation. The main trend was that the DOC increased with increasing soil depth during the entire incubation period. In the crop residue treatments, DOC decreased sharply from 30 to 60 days and maintained a slow decline until the end of incubation. However, in the control and electron acceptor treatments, the DOC concentration showed a slow decline from 30 to 60 days and remained constant by the end of incubation at 120 days, especially in the deep layers.

The vertical distribution of $SO_4^{2-}$ increased with increasing soil depth during 30 days of incubation, but the trend was opposite by the end of incubation at 120 days (Figure 2B) except for the $SO_4^{2-}$ treatment (Figure 2Bc). The addition of $NO_3^-$ inhibited the $SO_4^{2-}$ reduction compared to the control treatment. In contrast, the dissipation of $SO_4^{2-}$ markedly increased with the


dx.doi.org/10.1021/jf502746n | J. Agric. Food Chem. 2014, 62, 9974–9981

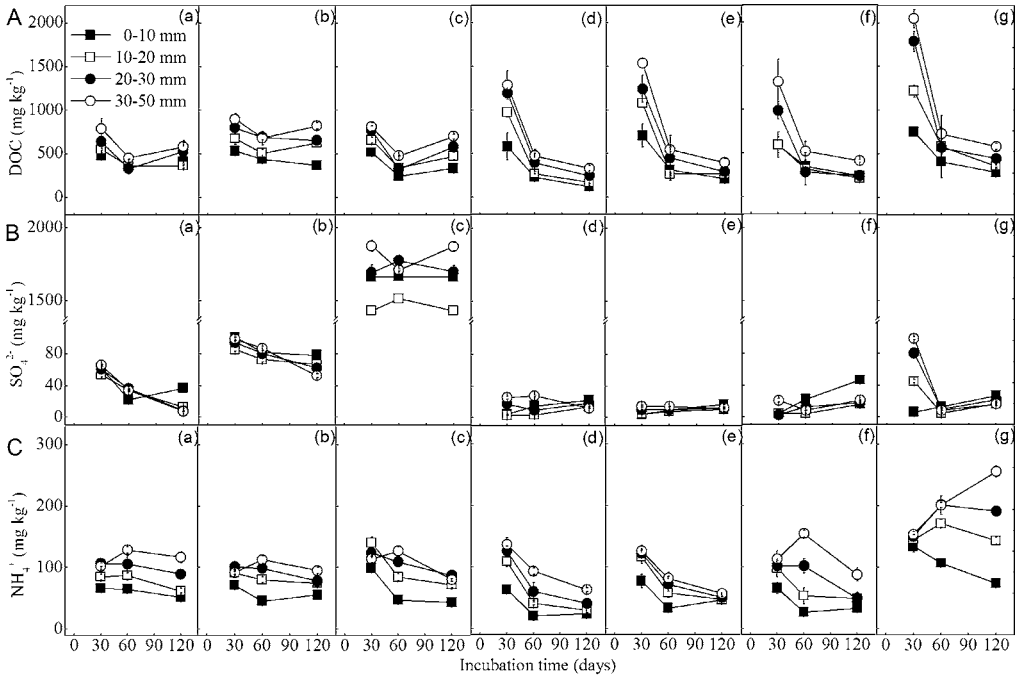


**Figure 2.** Variations of (A) DOC, (B) $SO_4^{2-}$, and (C) $NH_4^+$ in soil profiles: (a) control; (b) $NO_3^-$; (c) $SO_4^{2-}$; (d) wheat straw; (e) rice straw; (f) canola residue; (g) Chinese milk vetch. Error bars represent standard deviation of triplicate measurements.

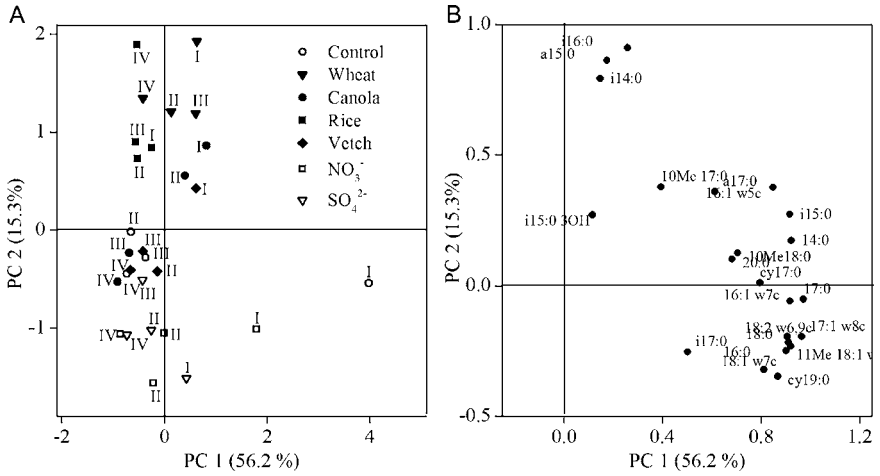


**Figure 3.** Principal component analysis of PLFAs in soil amended with different electron donors/acceptors: (A) soil sample PCA scores; (B) loadings of individual PLFAs. Soil profiles: (I) 0−10 mm; (II) 10−20 mm; (III) 20−30 mm; (IV) 30−50 mm.

addition of wheat straw, rice straw, and canola residue, whereas the vetch residue increased the soil $SO_4^{2-}$ content. However, the final concentrations of $SO_4^{2-}$ were 10.5−46.8 and 7.6−36.8 mg $kg^{-1}$ for the electron donor treatments and control treatment, respectively.

The $NH_4^+$ in the soil profiles showed the same trend in all treatments during the entire incubation time and decreased with increasing soil depth (Figure 2C). In the electron acceptor treatments, the addition of $SO_4^{2-}$ (2.8 g $kg^{-1}$ soil) markedly increased the $NH_4^+$ formation, whereas the addition of $NO_3^-$ (1.7 g $kg^{-1}$) had no effect. The Chinese milk vetch also increased the soil $NH_4^+$ content, whereas the other electron donor treatments enhanced the dissipation of $NH_4^+$ during the incubation.

**Soil Microbial Community Structure.** PCA is a multivariate technique that analyzes a data table in which observations are described by several intercorrelated quantitative dependent variables. Its goal is to extract the important information from the table, to represent it as a set of new orthogonal variables called principal components, and to display the pattern of similarity of the observations and of the variables as points in maps.[32] In this study, PCA was used to analyze the changes in soil PLFA patterns in response to the addition of electron acceptors and donors and the variation of soil depth (Figure. 3). The PCA was conducted with 25 individual PLFAs that were present in all of the treatments (Table 2 of the Supporting Information). The first principal component (PC1) accounted for 56.2% of the variation, whereas the second principal component (PC2) accounted for 15.3% of variation in the data. It was found that PC1 was responsible for the variation of PLFA values versus the soil depth, whereas PC2 was responsible for the respective variation of PLFA values versus the addition of electron donors and acceptors (Figure 3A). All of the individual PLFAs had positive PC1 values, which indicated that the abundance of PLFA


dx.doi.org/10.1021/jf502746n | J. Agric. Food Chem. 2014, 62, 9974−9981

**Table 2. PLFA Ratios in Soil Profiles with and without Amendment of Electron Donors and Acceptors**

| | CK1[a] | | | | CK2 | | | | $NO_3^-$ | | | | $SO_4^{2-}$ | | | |
|---|---|---|---|---|---|---|---|---|---|---|---|---|---|---|---|---|
| PLFA[b] | I[c] | II[c] | III[c] | IV[c] | I | II | III | IV | I | II | III | IV | I | II | III | IV |
| cy/pre | 0.31 | 0.31 | 0.22 | 0.46 | 0.20 | 0.67 | 0.46 | 0.87 | 0.29 | 0.41 | 0.25 | 0.50 | 0.25 | 0.43 | 0.39 | 0.74 |
| i/a | 2.41 | 1.73 | 1.60 | 1.47 | 2.67 | 1.60 | 1.70 | 1.74 | 2.31 | 1.91 | 2.07 | 1.83 | 2.34 | 2.12 | 1.77 | 1.88 |
| F/B | 0.14 | 0.50 | 0.16 | 0.33 | 0.36 | 0.11 | 0.14 | 0.12 | 0.51 | 0.29 | 0.23 | 0.11 | 0.38 | 0.46 | 0.11 | 0.09 |
| S/M | 1.36 | 0.81 | 1.32 | 0.90 | 1.90 | 1.19 | 0.94 | 1.37 | 0.89 | 0.92 | 0.79 | 1.03 | 2.26 | 1.17 | 0.93 | 1.21 |
| | wheat | | | | rice | | | | canola | | | | vetch | | | |
| PLFA | I | II | III | IV | I | II | III | IV | I | II | III | IV | I | II | III | IV |
| cy/pre | 0.34 | 0.36 | 0.34 | 0.65 | 0.37 | 0.36 | 0.33 | 0.47 | 0.28 | 0.30 | 0.37 | 0.46 | 0.25 | 0.19 | 0.50 | 0.50 |
| i/a | 1.52 | 1.45 | 1.46 | 1.19 | 0.89 | 0.76 | 0.73 | 0.71 | 1.69 | 1.28 | 1.24 | 1.31 | 1.60 | 1.30 | 1.44 | 1.52 |
| F/B | 0.13 | 0.22 | 0.53 | 0.11 | 0.12 | 0.13 | 0.13 | 0.08 | 0.33 | 0.44 | 0.27 | 0.20 | 0.27 | 0.25 | 0.24 | 0.30 |
| S/M | 0.96 | 1.08 | 1.13 | 1.29 | 0.87 | 0.87 | 0.88 | 1.26 | 0.78 | 0.91 | 1.04 | 1.14 | 0.95 | 0.95 | 1.24 | 1.50 |

[a]CK1, PCP unspiked control; CK2, PCP without other addition. [b]cy/pre, ratio of cyclopropyl fatty acids to monoenoic precursor; i/a, ratio of iso to anteiso branched PLFAs; F/B, ratio of fungi to bacteria PLFAs; S/M, ratio of saturated to monounsaturated PLFAs. [c]Soil profiles: (I) 0−10 mm; II, 10−20 mm; III, 20−30 mm; IV, 30−50 mm.

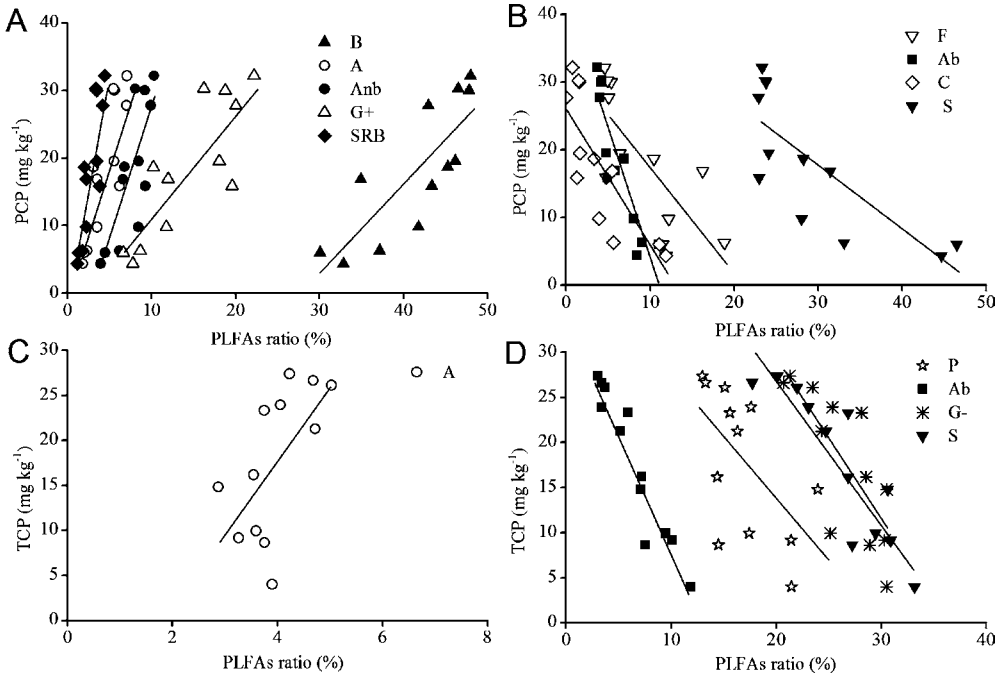


**Figure 4.** Correlation between PCP/3,4,5-TCP and microbial community: (A, B) relationship between PCP and ratio of PLFA signature groups to total PLFAs (%) in the electron acceptor and control treatments; (C, D) relationship between 3,4,5-TCP and ratio of PLFA signature group in the electron donor treatments. Symbols: B, bacteria; A, actinomycetes; Anb, anaerobic bacteria; G+, Gram-positive bacteria; SRB, sulfate reducing bacteria; F, fungi; Ab, aerobic bacteria; C, cyanobacteria; S, saturated PLFAs; P, precursors of cyclopropyl fatty acids; G-, Gram-negative bacteria.

decreased with increasing soil depth. The 17:1$\omega$8c and 17:0 had the highest PC1 values, which achieved 0.965 and 0.972, respectively (Figure 3B). The $NO_3^-$ and $SO_4^{2-}$ treatments clustered together and had much lower values in PC2 than the crop residue treatments. The order was electron acceptors, Chinese milk vetch, canola, rice, and wheat from negative to positive scores of PC2 (Figure 3A). cy19:0, 18:1$\omega$7c, and 17:1$\omega$8c represented aerobic bacteria clustered on the negative PC2, and i14:0, a15:0 and i16:0 represented anaerobic bacteria clustered on the positive PC2.

Ratios of particular PLFAs were changed with soil depth and varied significantly, with different responses to the addition of electron acceptors and donors (Table 2). In all treatments, the 30−50 mm soil layer had the highest cy/pre value, whereas the 0−10 mm soil layer had the highest i/a value. The S/M value increased with decreasing soil depth in the electron donor treatments, whereas no regularity could be found in the control and electron acceptor treatments.

**Correlation between PCP/3,4,5-TCP and Microbial Community.** Pearson correlation analysis is defined as a parametric linear correlation analysis based on Pearson's $r$ statistic and performed on raw data between two variables of observation.[33] The relationships between PCP/3,4,5-TCP and microbial community are shown in Figure 4. Pearson correlation analysis was used to demonstrate the relationship between PCP dissipation and PLFAs in the control, $NO_3^-$, and $SO_4^{2-}$ treatments because high residual PCP concentration was found in these treatments by the end of incubation. The results showed that PCP concentration was significantly and positively related ($p < 0.05$) to bacteria, actinomycetes, anaerobic bacteria, Gram-positive bacteria, and sulfate-reducing bacteria (Figure 4A), but negatively related to fungi, aerobic bacteria, cyanobacteria, and

saturated PLFAs (Figure 4B). In the crop residue treatments, PCP dissipated completely by the end and resulted in the production of 3,4,5-TCP. Therefore, here, we analyzed the correlation between 3,4,5-TCP and PLFAs. The 3,4,5-TCP concentration was significantly and positively correlated ($p < 0.05$) with actinomycetes (Figure 4C), but negatively correlated with the precursors of cyclopropyl fatty acids, anaerobic bacteria, Gram-negative bacteria, and saturated PLFAs (Figure 4D).

## DISCUSSION

**PCP Dissipation and 3,4,5-TCP Production.** The electron donors and acceptors showed significantly different effects on the dissipation of PCP in soil profiles (Figure 1). The inhibition of electron acceptors to PCP dissipation might be caused by competition for electron donors with PCP or increased soil redox potential, which finally inhibited PCP reduction. This was similar to other work.[5,25] The oxidation of electron donors was necessary for the anaerobic reduction of PCP, $SO_4^{2-}$, and $NO_3^-$. Dissolved organic carbon is an important complex electron donor that supports many redox reactions in flooded soils.[11,15] Hence, the PCP, $SO_4^{2-}$, and the DOC released from the decomposition of crop residues decreased with increasing incubation time (Figures 1 and 2). In addition, the decomposition of crop residues may also increase soil fertility, which might increase microbial activity involved in PCP dissipation.

The dissipation of PCP resulted in the accumulation of 3,4,5-TCP (Table 1). The inhibition of further 3,4,5-TCP dissipation might be due to the depletion of DOC (Figure 2A). Alletto et al.[34] found that isoxaflutole mineralization was significantly influenced by the nature of crop residues. The application of green manure to flooded soil resulted in the selective pathway of reductive dechlorination of DDT to DDD without enhanced formation of DDE.[35] In this study, 3,4,5-TCP was the major intermediate produced during the dissipation of PCP. The final accumulation of 3,4,5-TCP in soil profiles may be due to the deficiency of the meta and para positions of dehalogenase, which are both involved in the dechlorination of 3,4,5-TCP. Bouchard et al.[8] reported that the dechlorination of PCP by *Desulfitobacterium frappieri* resulted in the rapid production of 3,4,5-TCP, but further dechlorination was inhibited. However, 3,4,5-TCP showed greater toxicity than PCP.[8] In this study, the application of crop residues resulted in the accumulation of 3,4,5-TCP, a more toxic intermediate of PCP degradation. Hence, the accumulation of 3,4,5-TCP might inhibit bacterial growth.

Even though the addition of electron donors can increase the dissipation of PCP, it can also produce more toxic intermediate products. The decomposition of crop residues in soil can enrich soil fertility and simultaneously can also supply electron donors for redox reactions, including organic pollutants. Clearly, the negative effects should not be ignored.

**Soil Microbial Community Structure Response to External Electron Donors and Acceptors.** PLFA analysis is widely used to quantitatively assess the microbial community composition of soils.[29−31] In this study, the soil depth had the most effect on the PLFAs even in the small distance from 0 to 50 mm depth (Figure 3A). This significant difference in PLFA composition might be attributed to the flooded conditions. After flooding, oxygen could be consumed in a few hours followed by the reduction of $NO_3^-$, Fe(III), and $SO_4^{2-}$.[10] This might result in the formation of aerobic/anaerobic gradients from the surface to the deeper layers of soil profiles, possibly accounting for the difference in the PLFA composition. The PCA also showed that the composition of the microbial community was decreased with soil depth. Sundh et al.[36] reported that the total concentration of PLFAs decreased with depth in most profiles of both wet and dry boreal peat lands, but the decrease was steeper for wet sites than dry ones. This indicated a greater abundance of aerobic than anaerobic microorganisms. In this study, cyanobacteria were significantly and negatively related to PCP concentration (Figure 4B). Cyanobacteria could promote bacterial degradation of organic contaminants by increasing the oxygen supply or alternative organic substrates to promote bacterial growth.[37] In addition, cyanobacteria play an important role in the uptake and removal of insecticides.[37] Hence, in our study, the rapid dissipation of PCP (Figure 1) and 3,4,5-TCP (Table 1) in the surface layer might be partly caused by stimulation of the growth of cyanobacteria.

The predominant PLFAs differed significantly under different conditions (Figure 3). The monounsaturated PLFAs, such as cy19:0, 18:1$\omega$7c, and 17:1$\omega$8c, clustered on the negative PC2, which represented anaerobic bacteria, whereas the terminally branched PLFAs, i14:0, a15:0, and i16:0, clustered on the positive PC2, which represented aerobic bacteria (Figure 3B). The results indicated the successive shift from aerobic bacteria to anaerobic bacteria when electron acceptors were changed to electron donors. Among the Gram-negative bacteria, terminally branched PLFAs are more commonly found in anaerobes than in aerobes. Compared to wheat and rice treatments, the PCA clusters of vetch and canola treatments were much closer to the electron acceptor treatments (Figure 3A). This could be caused by the mineralization of S and N contained in vetch and canola residues (Table 1 of the Supporting Information; Figure 2Bg,Cg). The $SO_4^{2-}$ released during the decomposition of the crop residue also could be used as electron acceptors for soil microorganisms. The mineralization of organic N could release $NH_4^+$ under anaerobic condition and release $NO_3^-$ under aerobic conditions. Thus, both $SO_4^{2-}$ and $NO_3^-$ released from vetch and canola residues would have inhibited the formation of reducing environments due to a lack of electron donors.[5]

The ratios of specific PLFAs could be used to analyze the microbial stress response to substrate availability, water limitations, and contamination.[22,38] In this study, the values of cy/pre ratio were higher in the 30−50 mm layer, which might be caused by the higher DOC in the deep layer. As suggested by Feng and Simpson,[38] substrate availability has a large influence on the ratio of cy/pre. However, the cy/pre ratio decreased after the addition of electron donors. Similarly, Hammesfahr et al.[39] reported a decrease of cy/pre under manure addition. The decrease in S/M ratios indicated that the physiological and nutritional stress of the microbial community was relieved due to the increase in soluble substances.[40,41] However, our results were the opposite, in that the S/M ratios (Table 2) showed the same trend with DOC (Figure 2A) in soil profiles when amended with electron donors. A lower S/M ratio may be attributed to the higher rate of nutrient turnover.[29] 3,4,5-TCP is more toxic to bacteria and fungi than PCP.[42,43] In this study, the S/M ratio increased with soil depth, which probably implied that the nutrient turnover in soils declined after the accumulation of 3,4,5-TCP. In addition, the monounsaturated fatty acids also represent aerobic bacteria, which dominant in the surface and decrease with increasing soil depth.

In conclusion, this study provided an improved understanding of reductive dechlorination of PCP through investigating the dissipation of PCP and the variation in the microbial community in vertical soil profiles under flooded conditions with the

amendment of electron donors and acceptors. The addition of crop residues significantly enhanced PCP dissipation by supplying DOC as electron donors, whereas the addition of $NO_4^-$ and $SO_4^{2-}$ inhibited it by competition for electron donors with PCP or prevented the decrease in soil redox potential. The variety of PLFAs was decreased with increasing soil depth. Electron donors and acceptors showed significantly different effects on the soil microbial community. It shifted from aerobic to anaerobic bacteria when electron acceptors were changed to electron donors. Increases in the S/M ratio with soil depth probably implied that the nutrient turnover ability in soils declined after the accumulation of 3,4,5-TCP. However, further research is required to elucidate and exploit the links between electron donors/acceptors, PCP intermediates, and functional microorganisms involved.

## ■ ASSOCIATED CONTENT

### Supporting Information

Crop residue extraction and analysis; Table S1 (chemical composition of the plant materials used in this study); nomenclature of PLFAs; Table S2 (25 identified PLFAs and their attribute microbial species). This material is available free of charge via the Internet at http://pubs.acs.org.

## ■ AUTHOR INFORMATION

### Corresponding Authors

*(J.X.) Phone: +86 571 88982069. Fax: +86 571 88982069. E-mail: jmxu@zju.edu.cn.

*(Y.H.) Phone: +86 571 88982065. E-mail: yhe2006@zju.edu.cn.

### Funding

This work was financially supported by the National Natural Science Foundation of China (41090284, 41130532) and the Fundamental Research Funds for the Central Universities.

### Notes

The authors declare no competing financial interest.

## ■ ABBREVIATIONS USED

PCP, pentachlorophenol; 3,4,5-TCP, 3,4,5-trichlorophenol; HPLC, high-performance liquid chromatography; DOC, dissolved organic carbon; PLFAs, phospholipid fatty acids; cy/pre, cyclopropyl fatty acids to monenoic precursors; i/a, iso to anteiso; F/B, ratio of fungi to bacteria PLFAs; S/M, ratio of saturated to monounsaturated PLFAs

## ■ REFERENCES

(1) He, Y.; Xu, J.; Lv, X.; Ma, Z.; Wu, J.; Shi, J. Does the depletion of pentachlorophenol in root-soil interface follow a simple linear dependence on the distance to root surfaces? *Soil Biol. Biochem.* **2009**, *41*, 1807−1813.

(2) Chen, M.; Shih, K.; Hu, M.; Li, F.; Liu, C.; Wu, W.; Tong, H. Biostimulation of indigenous microbial communities for anaerobic transformation of pentachlorophenol in paddy soils of southern China. *J. Agric. Food Chem.* **2012**, *60*, 2967−2975.

(3) Ruder, A. M.; Yiin, J. H. Mortality of US pentachlorophenol production workers through 2005. *Chemosphere* **2011**, *83*, 851−861.

(4) Yu, H.; Wang, Y.; Chen, P.; Li, F.; Chen, M.; Hu, M.; Ouyang, X. Effect of nitrate addition on reductive transformation of pentachlorophenol in paddy soil in relation to iron(III) reduction. *J. Environ. Manage.* **2014**, *132*, 42−48.

(5) Lin, J.; He, Y.; Xu, J. Changing redox potential by controlling soil moisture and addition of inorganic oxidants to dissipate pentachlorophenol in different soils. *Environ. Pollut.* **2012**, *170*, 260−267.

(6) Field, J. A.; Sierra-Alvarez, R. Microbial degradation of chlorinated phenols. *Rev. Environ. Sci. Biol.* **2008**, *7*, 211−241.

(7) Meade, T.; D Angelo, E. M. [$^{14}$C]Pentachlorophenol mineralization in the rice rhizosphere with established oxidized and reduced soil layers. *Chemosphere* **2005**, *61*, 48−55.

(8) Bouchard, B.; Beaudet, R.; Villemur, R.; McSween, G.; Lepine, F.; Bisaillon, J. G. Isolation and characterization of *Desulfitobacterium frappieri* sp *nov*, an anaerobic bacterium which reductively dechlorinates pentachlorophenol to 3-chlorophenol. *Int. J. Syst. Bacteriol.* **1996**, *46*, 1010−1015.

(9) Yoshida, N.; Yoshida, Y.; Handa, Y.; Kim, H.; Ichihara, S.; Katayama, A. Polyphasic characterization of a PCP-to-phenol dechlorinating microbial community enriched from paddy soil. *Sci. Total Environ.* **2007**, *381*, 233−242.

(10) Lin, J.; Xu, Y.; Brookes, P. C.; He, Y.; Xu, J. Spatial and temporal variations in pentachlorophenol dissipation at the aerobic-anaerobic interfaces of flooded paddy soils. *Environ. Pollut.* **2013**, *178*, 433−440.

(11) Lin, J.; He, Y.; Shi, J.; Liu, X.; Xu, J. The release of dissolved organic carbon in paddy soils under contrasting redox status. In *Functions of Natural Organic Matter in Changing Environment*, 1st ed.; Xu, J., Wu, J., He, Y., Eds.; Springer: Dordrecht, The Netherlands, 2013; pp 313−317.

(12) Coates, J. D.; Cole, K. A.; Chakraborty, R.; O'Connor, S. M.; Achenbach, L. A. Diversity and ubiquity of bacteria capable of utilizing humic substances as electron donors for anaerobic respiration. *Appl. Environ. Microbiol.* **2002**, *68*, 2445−2452.

(13) Hall, S. J.; Silver, W. L. Iron oxidation stimulates organic matter decomposition in humid tropical forest soils. *Global Change Biol.* **2013**, *19*, 2804−2813.

(14) Xu, H.; Cai, Z. C.; Li, X. P.; Tsuruta, H. Effect of antecedent soil water regime and rice straw application time on $CH_4$ emission from rice cultivation. *Aust. J. Soil Res.* **2000**, *38*, 1−12.

(15) Bi, R.; Yuan, T.; Lu, Q.; Yuan, Y.; Zhou, S. Electron donor capacity of reducing dissolved organic matter from crop residue decomposition as probed by chronoamperometry. *Chemosphere* **2013**, *93*, 1665−1671.

(16) Li, Q.; Ding, Y.; Zhang, W.; Wang, X.; Ji, G.; Zhou, Y. Sorptive interaction between goethite and strongly reducing organic substances from anaerobic decomposition of green manures. *Soil Biol. Biochem.* **2008**, *40*, 2922−2927.

(17) Kijjanapanich, P.; Annachhatre, A. P.; Esposito, G.; Lens, P. N. L. Use of organic substrates as electron donors for biological sulfate reduction in gypsiferous mine soils from Nakhon Si Thammarat (Thailand). *Chemosphere* **2014**, *101*, 1−7.

(18) Wang, P.; Wang, H.; Wu, L.; Di, H.; He, Y.; Xu, J. Influence of black carbon addition on phenanthrene dissipation and microbial community structure in soil. *Environ. Pollut.* **2012**, *161*, 121−127.

(19) Burke, D. J.; Smemo, K. A.; López-Gutiérrez, J. C.; DeForest, J. L. Soil fungi influence the distribution of microbial functional groups that mediate forest greenhouse gas emissions. *Soil Biol. Biochem.* **2012**, *53*, 112−119.

(20) Ding, N.; Guo, H.; Hayat, T.; Wu, Y.; Xu, J. Microbial community structure changes during Aroclor 1242 degradation in the rhizosphere of ryegrass (*Lolium multiflorum* L.). *FEMS Microbiol. Ecol.* **2009**, *70*, 149−158.

(21) He, Y.; Xu, J.; Ma, Z.; Wang, H.; Wu, Y. Profiling of PLFA: implications for nonlinear spatial gradient of PCP degradation in the vicinity of *Lolium perenne* L. roots. *Soil Biol. Biochem.* **2007**, *39*, 1121−1129.

(22) Vryzas, Z.; Papadakis, E. N.; Oriakli, K.; Moysiadis, T. P.; Papadopoulou-Mourkidou, E. Biotransformation of atrazine and metolachlor within soil profile and changes in microbial communities. *Chemosphere* **2012**, *89*, 1330−1338.

(23) Bardgett, R. D.; Leemans, D. K.; Cook, R.; Hobbs, P. J. Seasonality of the soil biota of grazed and ungrazed hill grasslands. *Soil Biol. Biochem.* **1997**, *29*, 1285−1294.

(24) Fierer, N.; Schimel, J. P.; Holden, P. A. Variations in microbial community composition through two soil depth profiles. *Soil Biol. Biochem.* **2003**, *35*, 167−176.

(25) Chang, B.; Zheng, J.; Yuan, S. Effects of alternative electron donors, acceptors and inhibitors on pentachlorophenol dechlorination in soil. *Chemosphere* **1996**, *33*, 313−320.

(26) Xiao, K.; Xu, J.; Tang, C.; Zhang, J.; Brookes, P. C. Differences in carbon and nitrogen mineralization in soils of differing initial pH induced by electrokinesis and receiving crop residue amendments. *Soil Biol. Biochem.* **2013**, *67*, 70−84.
(27) Wang, Y.; Tang, C.; Wu, J.; Liu, X.; Xu, J. Impact of organic matter addition on pH change of paddy soils. *J. Soil Sediment.* **2013**, *13*, 12−23.
(28) He, Y.; Ding, N.; Shi, J.; Wu, M.; Liao, H.; Xu, J. Profiling of microbial PLFAs: implications for interspecific interactions due to intercropping which increase phosphorus uptake in phosphorus limited acidic soils. *Soil Biol. Biochem.* **2013**, *57*, 625−634.
(29) Yao, Z.; Wang, H.; Wu, L.; Wu, J.; Brookes, P. C.; Xu, J. Interaction between microbial community and invading *Escherichia coli* O157:H7 in soils from vegetable fields. *Appl. Environ. Microbiol.* **2014**, *80*, 70−76.
(30) Coleman, M. L.; Hedrick, D. B.; Lovley, D. R.; White, D. C.; Pye, K. Reduction of Fe(III) in sediments by sulphate-reducing bacteria. *Nature* **1993**, *361*, 436−438.
(31) Hill, G. T.; Mitkowski, N. A.; Aldrich-Wolfe, L.; Emele, L. R.; Jurkonie, D. D.; Ficke, A.; Maldonado-Ramirez, S.; Lynch, S. T.; Nelson, E. B. Methods for assessing the composition and diversity of soil microbial communities. *Appl. Soil Ecol.* **2000**, *15*, 25−36.
(32) Abdi, H.; Williams, L. J. Principal component analysis. *WIREs Comput. Stat.* **2010**, *2*, 433−459.
(33) Dutilleul, P.; Stockwell, J. D.; Frigon, D.; Legendre, P. The Mantel test versus Pearson's correlation analysis: assessment of the differences for biological and environmental studies. *J. Agric., Biol., Environ. Stat.* **2000**, *5*, 131−150.
(34) Alletto, L.; Coquet, Y.; Bergheaud, V.; Benoit, P. Water pressure head and temperature impact on isoxaflutole degradation in crop residues and loamy surface soil under conventional and conservation tillage management. *Chemosphere* **2012**, *88*, 1043−1050.
(35) Mitra, J.; Raghu, K. Influence of green manuring on the persistence of DDT in soil. *Environ. Technol. Lett.* **1988**, *9*, 847−852.
(36) Sundh, I.; Nilsson, M.; Borga, P. Variation in microbial community structure in two boreal peatlands as determined by analysis of phospholipid fatty acid profiles. *Appl. Environ. Microbiol.* **1997**, *63*, 1476−1482.
(37) Subashchandrabose, S. R.; Ramakrishnan, B.; Megharaj, M.; Venkateswarlu, K.; Naidu, R. Mixotrophic cyanobacteria and microalgae as distinctive biological agents for organic pollutant degradation. *Environ. Int.* **2013**, *51*, 59−72.
(38) Feng, X.; Simpson, M. J. Temperature and substrate controls on microbial phospholipid fatty acid composition during incubation of grassland soils contrasting in organic matter quality. *Soil Biol. Biochem.* **2009**, *41*, 804−812.
(39) Hammesfahr, U.; Heuer, H.; Manzke, B.; Smalla, K.; Thiele-Bruhn, S. Impact of the antibiotic sulfadiazine and pig manure on the microbial community structure in agricultural soils. *Soil Biol. Biochem.* **2008**, *40*, 1583−1591.
(40) Zhao, C.; Xing, M.; Yang, J.; Lu, Y.; Lv, B. Microbial community structure and metabolic property of biofilms in vermifiltration for liquid-state sludge stabilization using PLFA profiles. *Bioresour. Technol.* **2014**, *151*, 340−346.
(41) Hueso, S.; García, C.; Hernández, T. Severe drought conditions modify the microbial community structure, size and activity in amended and unamended soils. *Soil Biol. Biochem.* **2012**, *50*, 167−173.
(42) Ruckdeschel, G.; Renner, G. Effects of pentachlorophenol and some of its known and possible metabolites on fungi. *Appl. Environ. Microbiol.* **1986**, *51*, 1370−1372.
(43) Ruckdeschel, G.; Renner, G.; Schwarz, K. Effects of pentachlorophenol and some of its known and possible metabolites on different species of bacteria. *Appl. Environ. Microbiol.* **1987**, *53*, 2689−2692.

244 °C. IR ($\nu$) (KBr), $cm^{-1}$: 3500, 3350 ($NH_2$), 1690 (CO), 1660 (CO). $^1H$ NMR ($CDCl_3$) $\delta$: 7.0−7.4 (m, 4H, Ar-H), 5.6 (br s, 2H, $NH_2$), 3.8 (s, 3H, $OCH_3$), 2.0 (s, 3H, $CH_3$), 1.3−1.5 (t, 3H, $CH_3$). Elemental analysis calculated for $C_{18}H_{15}N_2NaO_4S$ (%): C, 57.14; H, 4.00; N, 7.40; S, 8.47. Found (%): C, 57.39; H, 4.44; N, 7.57; S, 8.70.

**Synthetic Procedure for Piperidinium 3,5-Dicyano-2-oxo-4-spirocyclopentane-1,2,3,4-tetrahydro-pyridine-6-thiolate (3).** To a mixture of cyclopentanone (0.88 mL, 10 mmol), cyanothioacetamide (1.0 g, 10 mmol), and ethyl cyanoacetate (1.06 mL, 10 mmol) in ethanol (15 mL), 1.0 mL (10 mmol) of piperidine was added. The reaction mixture was stirred at room temperature for 2 h. The resulting precipitate was filtered off and recrystallized from ethanol as white needles of compound **3**. Yield: 76%. mp: 198−199 °C. IR ($\nu$) (KBr), $cm^{-1}$: 3195 (NH), 2181, 2250 (2CN), 1674 (CO). $^1H$ NMR (DMSO-$d_6$) $\delta$: 9.41 (s, 1H, NH), 8.30 (s, 2H $NH_2$), 4.13 (s, 1H, $C_{(5)}H$), 3.01−3.04 (t, 4H, $N(CH_2)_2$), 1.56−1.82 (m, 14H, $7CH_2$). Elemental analysis calculated for $C_{16}H_{22}N_4OS$ (%): C, 60.35; H, 6.96; N, 17.59; S, 10.07. Found (%): C, 59.99; H, 6.95; N, 17.50; S, 9.29.

**General Synthetic Procedure for Compounds 4 and 5.** To a suspension of compound C or D (10 mmol) in ethanol (25 mL), 1.0 mL (10 mmol) of piperidine was added. The reaction mixture was heated under reflux for 5 min and then allowed to cool. The crystalline solid that formed was collected by filtration, washed with ethanol, and air-dried to give yellow needles of compounds **4** or **5**.

**Piperidinium 5-Acetyl-3-cyano-4-(4′-methoxyphenyl)-6-methylpyridine-2-thiolate (4).** Yield: 87%. mp: 242−243 °C. IR ($\nu$) (KBr), $cm^{-1}$: 2217 (CN), 1704 (CO). $^1H$ NMR (DMSO-$d_6$) $\delta$: 7.17−7.19 (d, $J$ = 8 Hz, 2H, Ar-H), 7.02−7.04 (d, $J$ = 8 Hz, 2H, Ar-H), 3.81 (s, 3H, $OCH_3$), 3.04−3.07 (t, 3H, $CH_2N^+CH_2$), 2.21 (s, 3H, $CH_3CO$), 1.70 (s, 3H, $CH_3$), 1.65−1.68 (m, 10H, $5CH_2$). Elemental analysis calculated for $C_{21}H_{25}N_3O_2S$ (%): C, 65.77; H, 6.57; N, 10.96; S, 8.36. Found (%): C, 65.86; H, 6.93; N, 10.77; S, 8.75.

**Piperidinium 5-Acetyl-4-(4′-chlorophenyl)-3-cyano-6-methylpyridine-2-thiolate (5).** Yield: 84%. mp: 198−199 °C. IR ($\nu$) (KBr), $cm^{-1}$: 2217 (CN), 1704 (CO). $^1H$ NMR ($CDCl_3$) $\delta$: 7.99 (br s, 2H, $N^+H_2$), 7.35−7.37 (d, $J$ = 8 Hz, 2H, Ar-H), 7.20−7.22 (d, $J$ = 8 Hz, 2H, Ar-H), 3.19−3.22 (t, 4H, $CH_2NCH_2$), 2.27 (s, 3H, $CH_3CO$), 1.77−1.80 (m, 4H, $2CH_2$), 1.75 (s, 3H, $CH_3$), 1.56−1.60 (m, 2H, $CH_2$). Elemental analysis calculated for $C_{20}H_{22}ClN_3OS$ (%): C, 61.92; H, 5.72; N, 10.83; S, 8.27. Found (%): C, 61.78; H, 5.68; N, 10.69; S, 8.51.

**Insect Field Strain.** The field strain of cowpea aphids, *A. craccivora*, was collected from fava bean, *Vicia faba*, fields of Assiut University Experimental Farm during the 2013/2014 season.

**Laboratory Bioassay.** The activities of insecticidal compounds against nymphs and adults of cowpea aphid were tested by the leaf dip bioassay method.[10] Reported here are the results of laboratory tests to determine the concentration of these chemical compounds that is required to kill 50% ($LC_{50}$) of nymphs and adults, with a modification in the toxicity tests. Six concentrations of aqueous solution of each compound plus 0.1% Triton X-100 as a surfactant were used. A total of 20 apterous adults and 20 nymphs, approximately of the same size, were dipped for 10 s in each concentration 3 times. The treated aphids were allowed to dry at room temperature for about 0.5 h. Control batches of aphids were similarly dipped in a solution of distilled water plus 0.1% Triton X-100. After the treated batches of aphids had dried, they were individually transferred to Petri dishes (9 cm diameter) and held for 24 h at 22 + 2 °C, 60 + 5% relative humidity, and photoperiod of 12:12 (light/dark). Aphid mortality was recorded 24 and 48 h after treatment with a binocular microscope. An aphid was considered dead if it was incapable of coordinated forward movement. The toxicity experiment of each compound was repeated twice, and the results were corrected by Abbott's formula.[11] Median lethal concentrations ($LC_{50}$) and slope values of chemical compounds were determined by the Probit regression analysis program and expressed in parts per million (ppm).[12]

## RESULTS AND DISCUSSION

**Synthesis.** The synthetic procedures for the title compounds are outlined in Scheme 1. The intermediate compounds **A**,[13] **B**,[14] **C**, and **D**[15] were prepared following the procedures reported previously.

**Scheme 1**

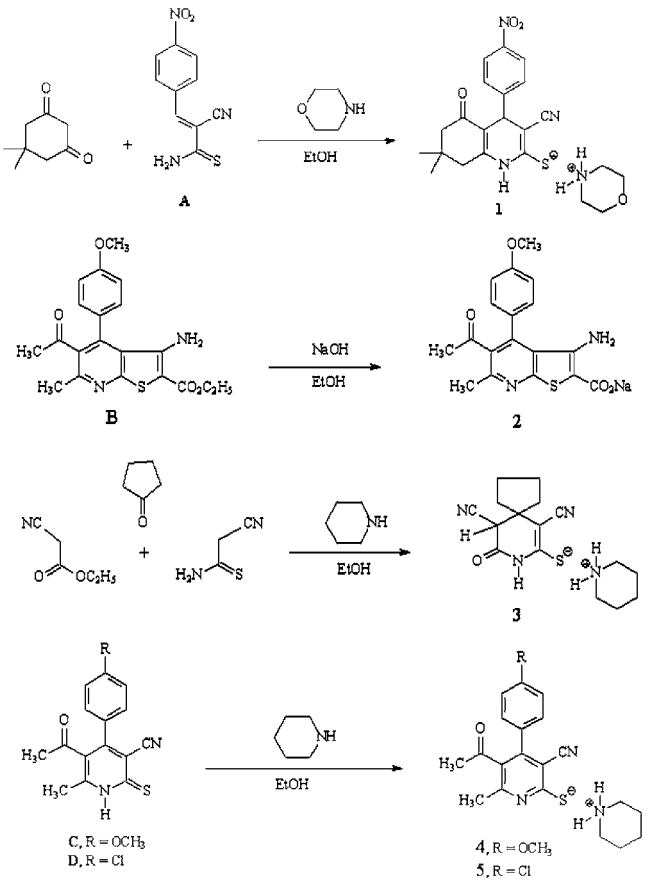


The structure of the synthesized compounds was elucidated and confirmed on the basis of their spectral and elemental analyses.

*Toxicity Test for the Cowpea Aphid Nymphs.* Insecticidal activities against the nymphs of cowpea aphid are shown in Table 1 and Figure 1. One of the tested compounds showed excellent insecticidal activities against nymphs of cowpea aphid, and others exhibit moderate to strong activities compared to acetamiprid. The $LC_{50}$ values of compounds **1**, **2**, **3**, **4**, and **5** were 0.004, 0.013, 0.180, 0.570, and 2.050 ppm, respectively, while that of acetamiprid was 0.010 ppm after 24 h of treatment. It was found that all compounds showed higher toxicity after 48 h treatment, with $LC_{50}$ values of 0.0001, 0.0030, 0.0100, 0.0100, and 0.0230, respectively, whereas that of acetamiprid was 0.0004 ppm. The above results revealed that the insecticidal activity of compound **1** against nymphs of cowpea aphid was 2.5- and 4.0-fold that of acetamiprid after 24 and 48 h of treatment.

*Toxicity Test for the Cowpea Aphid Adults.* Insecticidal activities against the adults of cowpea aphid are shown in Table 2 and Figure 2. All of the tested compounds showed low to excellent insecticidal activities against cowpea aphid adults after 24 h of treatment. Compound **1**, which has a $LC_{50}$ value of 0.010 ppm, was more active than acetamiprid itself, which


dx.doi.org/10.1021/jf503992y | J. Agric. Food Chem. 2014, 62, 9982−9986

**Table 1. Insecticidal Activity of Acetamiprid and Compounds 1, 2, 3, 4, and 5 against the Nymphs of Cowpea Aphid, *A. craccivora*, after 24 and 48 h of Treatment**

| | 24 h | | | 48 h | | |
|---|---|---|---|---|---|---|
| compound | slope ± SE | $LC_{50}$ (ppm) | toxic ratio[a] | slope ± SE | $LC_{50}$ (ppm) | toxic ratio[a] |
| acetamiprid | 0.24 ± 0.02 | 0.010 | 1 | 0.36 ± 0.03 | 0.0004 | 1 |
| **1** | 0.37 ± 0.03 | 0.004 | 2.5 | 0.37 ± 0.04 | 0.0001 | 4 |
| **2** | 0.22 ± 0.02 | 0.013 | 0.76 | 0.29 ± 0.03 | 0.0030 | 0.13 |
| **3** | 0.19 ± 0.03 | 0.180 | 0.05 | 0.19 ± 0.03 | 0.0100 | 0.04 |
| **4** | 0.16 ± 0.03 | 0.570 | 0.02 | 0.24 ± 0.03 | 0.0100 | 0.04 |
| **5** | 0.16 ± 0.02 | 2.050 | 0.004 | 0.24 ± 0.03 | 0.0230 | 0.02 |

[a]The toxic ratio is defined as the ratio of the $LC_{50}$ value of acetamiprid for baseline toxicity and the $LC_{50}$ value of the compound.

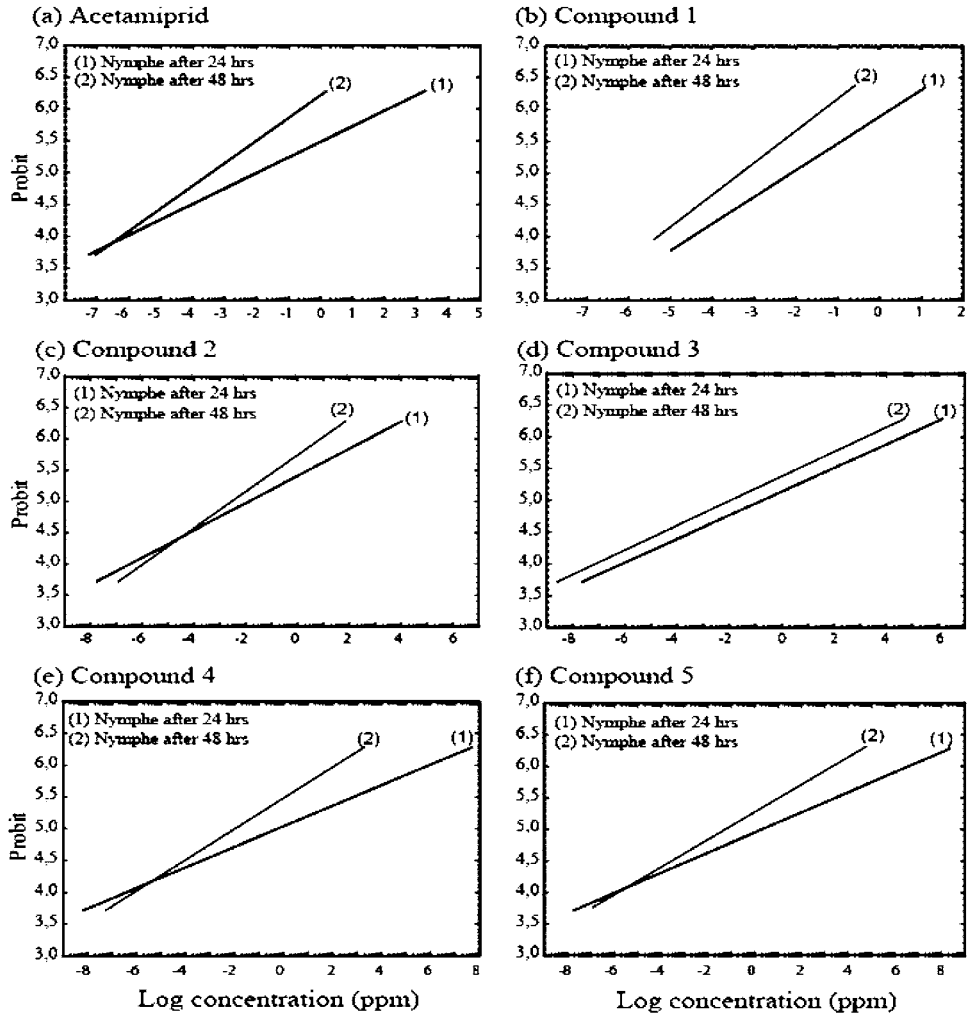


**Figure 1.** Insecticidal activities of acetamiprid and compounds **1**, **2**, **3**, **4**, and **5** against the nymphs of cowpea aphid, *A. craccivora*, after 24 and 48 h of treatment.

exhibits a $LC_{50}$ value of 0.041 ppm. The compounds **2**, **3**, **4**, and **5** showed low activity, with $LC_{50}$ values of 3.330, 2.270, 19.590, and 19.650 ppm, respectively. Compounds **1**, **2**, **3**, **4**, and **5** and acetamiprid showed higher toxicity after 48 h of treatment, with $LC_{50}$ values of 0.0005, 0.2300, 0.2900, 0.0800, 0.1340, and 0.0030, respectively. The Insecticidal activity of compound **1** against cowpea aphid adults was about 4.0- and 6.0-fold that of acetamiprid after 48 h of treatment.

Finally, It is interesting to note that (i) the highest activity associated with compound **1** may be due to the presence of the nitro group in its molecular structure because a number of neonicotinoids contain this group, (ii) the presence of the cyano group has no effect on the insecticidal activity of the tested compounds because compound **2**, which lack this cyano group, showed higher activity than each of compounds **3** (which possess two cyano groups), **4**, and/or **5**, (iii) the thienopyridine moiety in compound **2** may anticipate the insecticidal activity because this compound ranks second in the order of toxicity after compound **1**, and (iv) compound **4**, which contains the methoxyl group, showed relatively higher activity than its chloro analogue **5**, and this is an unexpected result, where the presence of the chlorine atom in the molecule often promoted the activity.


dx.doi.org/10.1021/jf503992y | J. Agric. Food Chem. 2014, 62, 9982−9986

**Table 2. Insecticidal Activity of Acetamiprid and Compounds 1, 2, 3, 4, and 5 against the Adults of Cowpea Aphid, *A. craccivora*, after 24 and 48 h of Treatment**

| | 24 h | | | 48 h | | |
|---|---|---|---|---|---|---|
| compound | slope ± SE | $LC_{50}$ (ppm) | toxic ratio[a] | slope ± SE | $LC_{50}$ (ppm) | toxic ratio[a] |
| acetamiprid | 0.224 ± 0.03 | 0.041 | 1 | 0.28 ± 0.03 | 0.0030 | 1 |
| **1** | 0.50 ± 0.05 | 0.010 | 4.10 | 0.35 ± 0.04 | 0.0005 | 6 |
| **2** | 0.20 ± 0.02 | 3.330 | 0.01 | 0.23 ± 0.02 | 0.2300 | 0.01 |
| **3** | 0.20 ± 0.03 | 2.270 | 0.02 | 0.19 ± 0.03 | 0.2900 | 0.01 |
| **4** | 0.17 ± 0.03 | 19.590 | 0.002 | 0.20 ± 0.03 | 0.0800 | 0.04 |
| **5** | 0.16 ± 0.03 | 19.650 | 0.002 | 0.18 ± 0.03 | 0.1340 | 0.022 |

[a]The toxic ratio is defined as the ratio of the $LC_{50}$ value of acetamiprid for baseline toxicity and the $LC_{50}$ value of the compound.

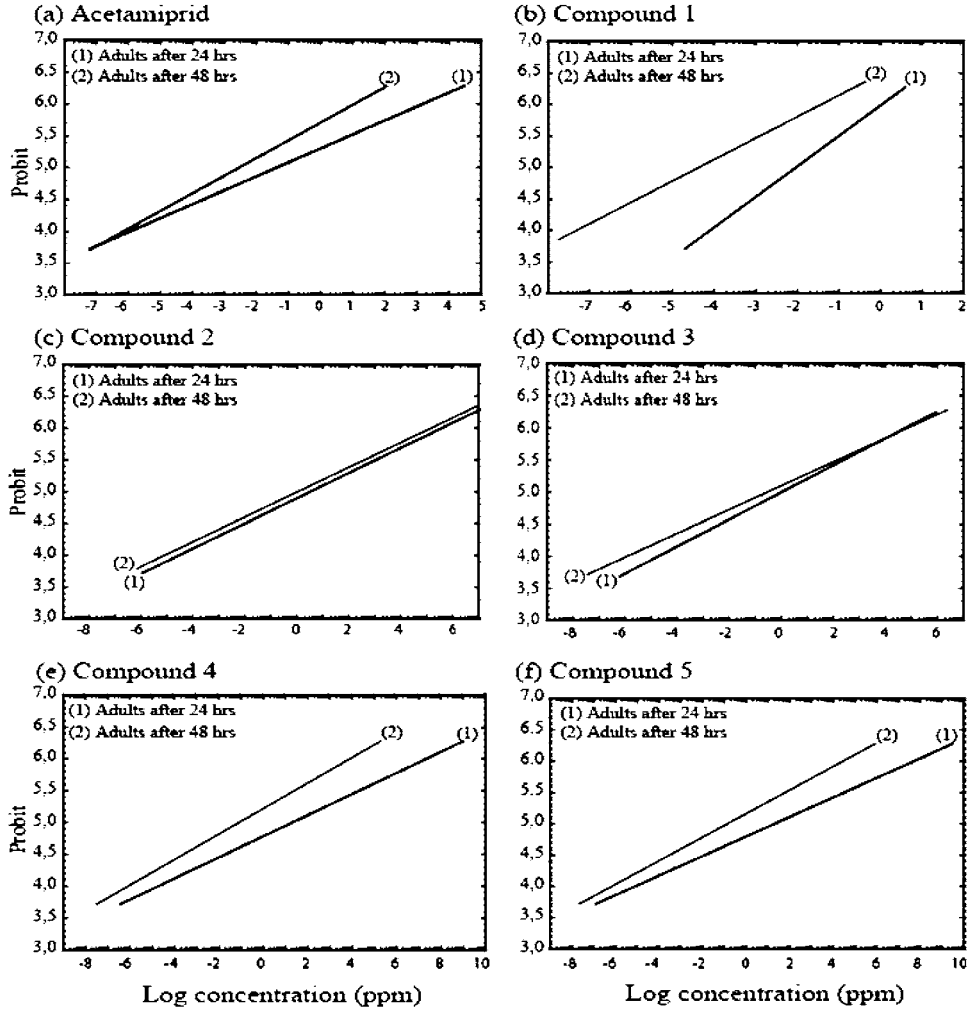


**Figure 2.** Insecticidal activities of acetamiprid and compounds **1**, **2**, **3**, **4**, and **5** against the adults of cowpea aphid, *A. craccivora*, after 24 and 48 h of treatment.

## AUTHOR INFORMATION

### Corresponding Author

*E-mail: ebakhite@yahoo.com.

### Notes

The authors declare no competing financial interest.

## REFERENCES

(1) Liu, M. C.; Lin, T. S.; Cory, J. G.; Cory, A. H.; Sartorelli, A. C. Synthesis and biological activity of 3- and 5-amino derivatives of pyridine-2-carboxaldehyde thiosemicarbazone. *J. Med. Chem.* **1996**, *39*, 2586−2593.

(2) Finkelstein, B. L.; Martz, M. A.; Strock, C. Synthesis and insecticidal activity of novel pyridine methanesulfonates. *J. Pestic. Sci.* **1997**, *50*, 319−323.

(3) Li, G.; Qian, X.; Cui, J.; Huang, Q.; Zhang, R.; Guan, H. Synthesis and herbicidal activity of novel 3-aminocarbonyl-2-oxazolidinethione derivatives containing a substituted pyridine ring. *J. Agric. Food Chem.* **2006**, *54*, 125−129.

(4) Jo, Y. W.; Im, W. B.; Rhee, J. K.; Shim, M. J.; Kim, W. B.; Choi, E. C. Synthesis and antibacterial activity of oxazolidinones containing pyridine substituted with heteroaromatic ring. *Bioorg. Med. Chem.* **2004**, *12*, 5909−5915.

(5) Tomizawa, M.; Maltby, D.; Medzihradszky, K. F.; Zhang, N.; Durkin, K. A.; Presly, J.; Talley, T. T.; Taylor, P.; Burlingame, A. L.;

Casida, J. E. Defining nicotinic agonist binding surfaces through photo affinity labeling. *Biochemistry* **2007**, *46*, 8798−8806.
(6) Nauen, R.; Ebbinghaus-Kintscher, U.; Elbert, A.; Jeschke, P.; Tietjen, K. Acetylcholine receptors as sites for developing neonicotinoid insecticides. In *Biochemical Sites Important in Insecticide Action and Resistance*; Ishaaya, I.; Ed.; Springer Verlag: Berlin, Germany, 2001; pp 70−105.
(7) Elbert, A.; Becker, B.; Hartwig, J.; Erdelen, C. Imidacloprid, a new systemic insecticide. *Pflanzenschutz-Nachr. Bayer* **1991**, *44*, 113−136.
(8) Zian, Z.; Shao, X.; Li, Z.; Qian, X.; Huang, Q. Synthesis, insecticidal activity and QSAR of novel nitromethylene neonicotinoids with tetrahydropyridine fixed *cis* configuration and exo-ring ether modification. *J. Agric. Food Chem.* **2007**, *55*, 2288−2292.
(9) Sharanin, Yu. A.; Goncharenko, M. P.; Shestopalov, A. M.; Litvinov, V. P.; Turov, A. V. Condensed pyridines. IX. Synthesis and properties of substituted 3-cyano-5,6,7,8-tetrahydro-2(1*H*)-quinolie-thiones. *Zh. Org. Khim.* **1991**, *27*, 1996−2008.
(10) O'Brien, P. J.; Abdel-Aal, Y. A.; Ottea, J. A.; Graves, J. B. Relationship of insecticide resistance to carboxylesterases in *Aphis gossypii* (Homoptera: Aphididae) from Midsouth cotton. *J. Econ. Entomol.* **1992**, *85*, 651−657.
(11) Abbott, W. S. A method of computing the effectiveness of an insecticide. *J. Econ. Entomol.* **1925**, *18*, 265−267.
(12) *Probit Analysis: A Statistical Treatment of the Sigmoid Response Curve*; Finney, D. J., Ed.; Cambridge University Press: Cambridge, U.K., 1962.
(13) Brunskill, J. S. A.; De, A.; Ewing, D. F. Dimerisation of 3-ayl-2-cyanothioacrylamides: A [2 + 4] cycloaddition to give substituted 3,4-dihydro-2*H*-thiopyrans. *J. Chem. Soc., Perkin Trans. 1* **1978**, 629−633.
(14) Bakhite, E. A.; Abdel-Rahman, A. E.; Al-Taifi, E. A. Synthesis of new thiopyridines, thienopyridines, pyridothienopyrimidines and pyranothienopyridines with anticipated biological activity. *J. Chem. Res.* **2003**, *6*, 320−321.
(15) Abdel-Rahman, A. E.; Bakhite, E. A.; Al-Taifi, E. A. Synthesis and antimicrobial activity of new pyridothienopyrimidines and pyridothienotriazines. *J. Chin. Chem. Soc.* **2002**, *49*, 223−231.

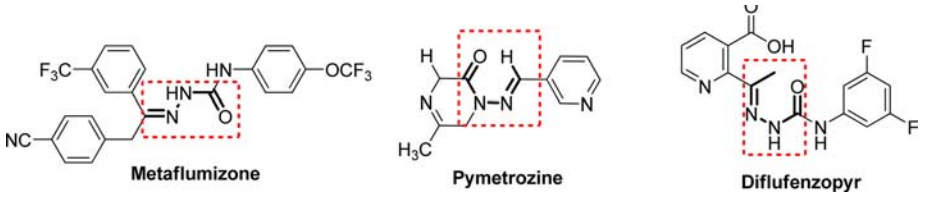


**Figure 1.** Acylhydrazone compounds.

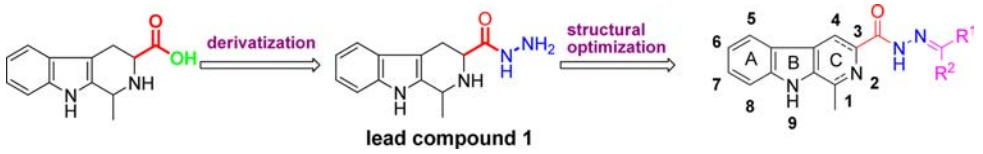


**Figure 2.** Design of target compounds.

**General Synthesis.** All anhydrous solvents were dried and purified by standard techniques. The synthetic routes are given in Scheme 2.

**Synthesis of (3*S*)-1-Methyl-2,3,4,9-tetrahydro-1*H*-pyrido-[3,4-*b*]indole-3-carbohydrazide (1).** This compound was synthesized by the method[17] reported in 99% yield: mp =100−103 °C; $^1$H NMR (400 MHz, $CDCl_3$) $\delta$ 8.15 (s, 1H, NH), 7.90 (s, 1H, NHCO), 7.50 (d, $^3J_{HH}$ = 7.6 Hz, 1H, Ar−H), 7.32 (d, $^3J_{HH}$ = 8.0 Hz, 1H, Ar−H), 7.17 (t, $^3J_{HH}$ = 7.2 Hz, 1H, Ar−H), 7.11 (t, $^3J_{HH}$ = 7.2 Hz, 1H, Ar−H), 4.18−4.23 (m, 1H, C**H**$CH_3$), 3.93 (br, 2H, $NH_2$), 3.65 (q, $^3J_{HH}$ = 8.4 Hz, 1H, C**H**CO), 3.26−3.32 (m, 1H, C$\mathbf{H}_2$), 2.71−2.78 (m, 1H, C$\mathbf{H}_2$), 1.48 (d, $^3J_{HH}$ = 6.8 Hz, 3H, C$\mathbf{H}_3$); $^{13}$C NMR (100 MHz, DMSO-$d_6$) $\delta$ 172.0, 137.9, 135.8, 126.9, 120.5, 118.3, 117.4, 110.9, 106.2, 56.1, 48.2, 25.4, 20.0; HRMS (ESI) calcd for $C_{13}H_{17}N_4O$ [M + H]$^+$ 245.1397, found 245.1398.

**Synthesis of 1-Methyl-9*H*-carbazole-3-carboxylic Acid Hydrazide (2).** A mixture of ethyl 1-methyl-9*H*-pyrido[3,4-*b*]indole-3-carboxylate[18] (2.00 g, 7.86 mmol) and hydrazine hydrate (80%) (3.15 g, 5.04 mmol) in a mixed solvent of alcohol (80 mL) and DMF (25 mL) was heated at reflux for 24 h; then the mixture was concentrated in vacuo. Solid was precipitated out and collected by filtration. The cake was extracted with boiling alcohol (each 30 mL) for several times until the filter cake did not dissolve in hot alcohol any more. The combined extract was concentrated to give **2** as a light-pink solid (0.90 g, 48%): mp =242−244 °C; $^1$H NMR (300 MHz, DMSO-$d_6$) $\delta$ 11.92 (s, 1H, NH), 9.51 (s, 1H, O═C-NH), 8.64 (s, 1H, Ar−H), 8.35 (d, $^3J_{HH}$ = 8.1 Hz, 1H, Ar−H)), 7.64 (d, $^3J_{HH}$ = 8.1 Hz, 1H, Ar−H), 7.57 (t, $^3J_{HH}$ = 7.2 Hz, 1H, Ar−H), 7.28 (t, $^3J_{HH}$ = 7.2 Hz, 1H, Ar−H), 4.55 (s, 2H, $NH_2$), 2.82 (s, 3H, C$\mathbf{H}_3$); $^{13}$C NMR (100 MHz, DMSO-$d_6$) $\delta$ 164.1, 141.0, 140.7, 138.7, 135.7, 128.3, 127.3, 122.2, 121.4, 119.9, 112.2, 111.9, 20.4; HRMS (ESI) calcd for $C_{13}H_{13}N_4O$ [M + H]$^+$ 241.1084, found 241.1084.

**Synthesis of *N*′-Benzylidene-(3*S*)-1-methyl-2,3,4,9-tetrahydro-1*H*-pyrido[3,4-*b*]indole-3-carbohydrazide (3).** To a slurry of compound **1** (0.50 g, 2.05 mmol) in toluene (35 mL) was added dropwise benzaldehyde (0.44 g, 4.10 mmol) at room temperature, Then the reaction mixture was heated to reflux. After 5 h, TLC analysis showed the complete consumption of compound **1**. The reaction solution was cooled to room temperature, and solid was precipitated out. The solid was filtrated and washed with toluene and then stirred in absolute ether for 1.5 h to remove the remaining toluene. Filtered once again to give **3** as a yellow solid (0.50 g, 74%): mp = 200−204 °C; $^1$H NMR (400 MHz, DMSO-$d_6$) $\delta$ 11.48 and 11.35 (s, 1H, NH), 10.84 and 10.81 (s, 1H, O═C-NH), 8.34 and 8.06 (s, 1H, N═CH), 7.71 and 7.61 (dd, $^3J_{HH}$ = 7.6 Hz, $^4J_{HH}$ = 1.6 Hz, 1H, Ph-H), 7.49−7.42 (m, 2H, Ph-H), 7.42−7.33 (m, 2H, Ph-H and Ar−H), 7.31 and 7.30 (d, $^3J_{HH}$ = 8.0 Hz, 1H, Ar−H), 7.03 (t, $^3J_{HH}$ = 7.2 Hz, 1H, Ar−H), 6.95 and 6.92 (t, $^3J_{HH}$ = 7.2 Hz, 1H, Ar−H), 4.48 and 3.61 (dd, $^3J_{HH}$ = 10.8 Hz, 3.6 Hz, 1H, C**H**), 4.15 (q, $^3J_{HH}$ = 8.0 Hz, 1H, C**H**), 2.98−2.89 (m, 1H, C$\mathbf{H}_2$), 2.71 and 2.62 (ddd, $^2J_{HH}$ = 14.4 Hz, $^3J_{HH}$ = 11.6 Hz, $^4J_{HH}$ = 2.0 Hz, 1H, C$\mathbf{H}_2$), 1.45 (d, $^3J_{HH}$ = 6.8 Hz, 3H, C$\mathbf{H}_3$); $^{13}$C NMR (100 MHz, DMSO-$d_6$) $\delta$ 174.6 and 169.1, 147.0 and 143.4, 137.9, 135.8, 134.4 and 134.1, 130.0 and 129.8, 128.9 and 128.8, 127.1 and 126.7, 126.9 and 126.9, 120.6, 118.4, 117.5, 111.0, 106.2 and 106.1, 56.7 and 53.3, 48.4 and 47.7, 25.5 and 25.4, 20.0; HRMS (ESI) calcd for $C_{20}H_{21}N_4O$ [M + H]$^+$ 333.1710, found 333.1715.

Compounds **4**−**26** were synthesized using the similar procedure as compound **3**.

*Data for 1-Methyl-9H-b-carboline-3-carboxylic Acid Benzylidene-hydrazide (**4**).* This compound was obtained as a yellow solid in 91% yield: mp = 303−306 °C; $^1$H NMR (300 MHz, DMSO-$d_6$) $\delta$ 12.05 (s, 1H, NH), 11.85 (s, 1H, O═C-NH), 8.82 (s, 1H, N═CH), 8.69 (s, 1H, Ar−H), 8.41 (d, $^3J_{HH}$ = 7.8 Hz, 1H, Ar−H), 7.77 (d, $^3J_{HH}$ = 6.3 Hz, 2H, Ph-H), 7.67 (d, $^3J_{HH}$ = 8.1 Hz, 1H, Ar−H), 7.60 (t, $^3J_{HH}$ = 7.2 Hz, 1H, Ar−H), 7.55−7.41 (m, 3H, Ph-H), 7.31 (t, $^3J_{HH}$ = 7.2 Hz, 1H, Ar−H), 2.92 (s, 3H, C$\mathbf{H}_3$); $^{13}$C NMR (100 MHz, DMSO-$d_6$) $\delta$ 161.2, 147.9, 141.1, 140.8, 138.2, 136.1, 134.6, 129.9, 128.9, 128.4, 127.5, 127.1, 122.3, 121.4, 120.1, 113.2, 112.3, 20.4; HRMS (ESI) calcd for $C_{20}H_{17}N_4O$ [M + H]$^+$ 329.1397, found 329.1402.

*Data for N′-Benzylidene-(3R)-1-methyl-2,3,4,9-tetrahydro-1H-pyrido[3,4-b]indole-3-carbohydrazide (**5**).* This compound was obtained as a light yellow solid in 76% yield: mp = 197−200 °C; $^1$H NMR (400 MHz, DMSO-$d_6$) $\delta$ 11.67 and 11.47 (s, 1H, NH), 10.98 and 10.86 (s, 1H, O═C−NH), 8.35 and 8.09 (s, 1H, N═CH), 7.75−7.69 (m, 1H, Ph-H), 7.66−7.60 (m, 1H, Ph-H), 7.50−7.41 (m, 2H, Ph-H), 7.41−7.36 (m, 2H, Ph-H and Ar−H), 7.33 and 7.31 (d, $^3J_{HH}$ = 8.8 Hz, 1H, Ph-H), 7.06 and 7.04 (t, $^3J_{HH}$ = 7.2 Hz, 1H, Ar−H), 7.00−6.92 (m, 1H, Ar−H), 4.70−4.61 and 3.69 (dd, $^3J_{HH}$ = 10.4 Hz, 3.6 Hz, 1H, C**H**), 4.42−4.14 (m, 1H, C**H**), 3.08 and 2.98 (dd, $^2J_{HH}$ = 14.8 Hz, $^3J_{HH}$ = 2.8 Hz, 1H, C**H**), 2.79−2.67 (m, 1H, C$\mathbf{H}_2$), 1.53 and 1.48 (d, $^3J_{HH}$ = 6.8 Hz, 3H, C$\mathbf{H}_3$); $^{13}$C NMR (100 MHz, DMSO-$d_6$) $\delta$ 173.4 and 168.8, 147.2 and 144.1, 137.2, 136.0 and 135.9, 134.3 and 134.0, 130.0 and 130.0, 128.8, 127.1, 126.8 and 126.6, 120.9 and 120.7, 118.6 and 118.5, 117.7 and 117.5, 111.1 and 111.1, 106.0 and 105.7, 56.6 and 53.6, 48.5 and 48.1, 25.3 and 24.7, 19.7 and 19.0; HRMS (ESI) calcd for $C_{20}H_{21}N_4O$ [M + H]$^+$ 333.1710, found 333.1708.

*Data for N′-(4-tert-Butylbenzylidene)-(3S)-1-methyl-2,3,4,9-tetrahydro-1H-pyrido[3,4-b]indole-3-carbohydrazide (**6**).* This compound was obtained as a yellow solid in 72% yield: mp = 139−143 °C; $^1$H NMR (400 MHz, DMSO-$d_6$) $\delta$ 11.47 and 11.32 (s, 1H, NH), 10.87 and 10.82 (s, 1H, O═C-NH), 8.31 and 8.03 (s, 1H, N═CH), 7.88 and 7.70−7.27 (m, 6H, Ph-H and Ar−H), 7.04 (t, $^3J_{HH}$ = 6.8 Hz, 1H, Ar−H), 6.96 (t, $^3J_{HH}$ = 7.2 Hz, 1H, Ar−H), 4.48 and 3.62 (dd, $^3J_{HH}$ = 10.4 Hz, 7.2 Hz, 1H, C**H**), 4.27−4.08 (m, 1H, C**H**), 3.02−2.88 (m, 1H, C$\mathbf{H}_2$), 2.77−2.59 (m, 1H, C$\mathbf{H}_2$), 1.52−1.35 (m, 3H, C$\mathbf{H}_3$), 1.30 and 1.24 (s, 9H, C$\mathbf{H}_3$); $^{13}$C NMR (100 MHz, DMSO-$d_6$) $\delta$ 174.3 and 168.9, 152.8 and 152.6, 147.0 and 143.3, 137.8, 135.8, 131.6 and 131.4, 129.2, 126.9 and 126.5, 125.7 and 125.6, 120.6 and 120.6, 118.4, 117.5 and 117.5, 111.0, 106.2 and 106.0, 56.7 and 53.5, 48.4 and 47.7, 34.6 and 34.5, 31.0 and 30.9, 25.5 and 25.2, 19.9 and 19.9; HRMS (ESI) calcd for $C_{24}H_{29}N_4O$ [M + H]$^+$ 389.2336, found 389.2338.

*Data for N′-(4-(Dimethylamino)benzylidene)-(3S)-1-methyl-2,3,4,9-tetrahydro-1H-pyrido[3,4-b]indole-3-carbohydrazide (**7**).*


dx.doi.org/10.1021/jf503794g | J. Agric. Food Chem. 2014, 62, 9987−9999

This compound was obtained as a yellow solid in 73% yield: mp = 215−220 °C; $^1$H NMR (400 MHz, DMSO-$d_6$) $\delta$ 11.20 and 11.05 (s, 1H, NH), 10.84 and 10.80 (s, 1H, O═C-NH), 8.16 and 7.92 (s, 1H, N═CH), 7.52 and 7.36 (d, $^3J_{HH}$ = 7.6 Hz, 2H, Ph-H), 7.44−7.38 (m, 1H, Ar−H), 7.30 (d, $^3J_{HH}$ = 6.4 Hz, 1H, Ar−H), 7.03 (t, $^3J_{HH}$ = 6.8 Hz, 1H, Ar−H), 6.95 (t, $^3J_{HH}$ = 6.8 Hz, 1H, Ar−H), 6.75 and 6.67 (d, $^3J_{HH}$ = 7.6 Hz, 2H, Ph-H), 4.44 and 3.57 (d, $^3J_{HH}$ = 8.8 Hz, 1H, C**H**), 4.23−4.08 (m, 1H, C**H**), 3.07−2.86 (m, 7H, N−C**H**$_3$ and C**H**$_2$), 2.74−2.56 (m, 1H, C**H**$_2$), 1.52−1.38 (m, 3H, C**H**$_3$); $^{13}$C NMR (100 MHz, DMSO-$d_6$) $\delta$ 173.8 and 168.5, 151.5 and 151.3, 147.8 and 144.2, 137.8, 135.8, 128.4 and 127.9, 126.9, 121.6 and 121.5, 120.6 and 120.5, 118.4, 117.5, 111.9 and 111.8, 111.0, 106.2 and 106.1, 56.6 and 53.5, 48.4 and 47.7, 39.8, 25.6 and 25.2, 19.9; HRMS (ESI) calcd for $C_{22}H_{26}N_5O$ [M + H]$^+$ 376.2132, found 376.2137.

*Data for N′-(4-Nitrobenzylidene)-(3S)-1-methyl-2,3,4,9-tetrahydro-1H-pyrido[3,4-b]indole-3-carbohydrazide (**8**).* This compound was obtained as a yellow solid in 74% yield: mp = 222−227 °C; $^1$H NMR (400 MHz, DMSO-$d_6$) $\delta$ 11.81 and 11.68 (s, 1H, NH), 10.87 and 10.82 (s, 1H, O═C-NH), 8.46 and 8.17 (s, 1H, N═CH), 8.31 and 8.22 (d, $^3J_{HH}$ = 8.4 Hz, 2H, Ph-H), 7.98 and 7.88 (d, $^3J_{HH}$ = 8.4 Hz, 2H, Ph-H), 7.41 and 7.36 (d, $^3J_{HH}$ = 7.6 Hz, 1H, Ar−H), 7.31 (d, $^3J_{HH}$ = 6.4 Hz, 1H, Ar−H), 7.04 (t, $^3J_{HH}$ = 7.2 Hz, 1H, Ar−H), 6.96 (t, $^3J_{HH}$ = 7.6 Hz, 1H, Ar−H), 4.55 and 3.67 (d, $^3J_{HH}$ = 8.8 Hz, 1H, C**H**), 4.25−4.10 (m, 1H, C**H**), 2.96 (d, $^2J_{HH}$ = 13.6 Hz, 1H, C**H**$_2$), 2.79−2.60 (m, 1H, C**H**$_2$), 1.47 (d, $^3J_{HH}$ = 6.4 Hz, 3H, C**H**$_3$); $^{13}$C NMR (100 MHz, DMSO-$d_6$) $\delta$ 174.8 and 169.6, 147.8 and 147.7, 144.6, 140.7 and 140.4, 137.8 and 137.5, 135.9, 128.0 and 127.7, 126.9, 124.1, 120.7 and 120.6, 118.5, 117.6 and 117.5, 111.0, 106.1 and 106.0, 56.8 and 53.2, 48.5 and 47.8, 25.4 and 25.4, 19.9 and 19.8; HRMS (ESI) calcd for $C_{20}H_{20}N_5O_3$ [M + H]$^+$ 378.1561, found 378.1563.

*Data for N′-(4-Chlorobenzylidene)-(3S)-1-methyl-2,3,4,9-tetrahydro-1H-pyrido[3,4-b]indole-3-carbohydrazide (**9**).* This compound was obtained as a yellow solid in 81% yield: mp = 140−145 °C; $^1$H NMR (400 MHz, DMSO-$d_6$) $\delta$ 11.62 and 11.51 (s, 1H, NH), 10.91 and 10.85 (s, 1H, O═C-NH), 8.35 and 8.07 (s, 1H, N═CH), 7.74 and 7.64 (d, $^3J_{HH}$ = 7.2 Hz, 2H, Ph-H), 7.58−7.35 (m, 3H, Ph-H and Ar−H), 7.35−7.28 (m, 1H, Ar−H), 7.10−7.00 (m, 1H, Ar−H), 7.00−6.90 (m, 1H, Ar−H), 4.56 and 3.66 (d, $^3J_{HH}$ = 9.6 Hz, 1H, C**H**), 4.30−4.12 (m, 1H, C**H**), 3.03−2.90 (m, 1H, C**H**$_2$), 2.79−2.62 (m, 1H, C**H**$_2$), 1.54−1.39 (m, 3H, C**H**$_3$); $^{13}$C NMR (100 MHz, DMSO-$d_6$) $\delta$ 174.2 and 169.1, 145.8 and 142.4, 137.6 and 135.9, 134.5 and 134.3, 133.3 and 133.0, 129.0, 128.7, 128.4, 126.9 and 126.8, 120.7 and 120.6, 118.5 and 118.4, 117.6 and 117.5, 111.0, 106.1 and 105.9, 56.7 and 53.3, 48.5 and 47.8, 25.4 and 25.1, 19.8 and 19.6; HRMS (ESI) calcd for $C_{20}H_{20}N_4OCl$ [M + H]$^+$ 367.1320, found 367.1323.

*Data for N′-(2,4-Dichlorobenzylidene)-(3S)-1-methyl-2,3,4,9-tetrahydro-1H-pyrido[3,4-b]indole-3-carbohydrazide (**10**).* This compound was obtained as a light yellow solid in 85% yield: mp = 211−213 °C; $^1$H NMR (400 MHz, DMSO-$d_6$) $\delta$ 11.82 and 11.77 (s, 1H, NH), 10.91 and 10.84 (s, 1H, O═C-NH), 8.71 and 8.42 (s, 1H, N═CH), 8.00 and 7.85 (d, $^3J_{HH}$ = 8.4 Hz, 1H, Ph-H), 7.73 and 7.71 (d, $^4J_{HH}$ = 2.0 Hz, 1H, Ph-H), 7.53 and 7.43−7.35 (dd, $^3J_{HH}$ = 8.4 Hz, $^4J_{HH}$ = 2.0 Hz, 1H, Ph-H), 7.41 and 7.37 (d, $^3J_{HH}$ = 8.0 Hz, 1H, Ar−H), 7.32 and 7.31 (d, $^3J_{HH}$ = 8.0 Hz, 1H, Ar−H), 7.04 (t, $^3J_{HH}$ = 7.2 Hz, 1H, Ar−H), 6.96 and 6.94 (t, $^3J_{HH}$ = 7.2 Hz, 1H, Ar−H), 4.65−4.56 and 3.66 (dd, $^3J_{HH}$ = 10.4 Hz, 3.6 Hz, 1H, C**H**), 4.35−4.13 (m, 1H, C**H**), 3.06−2.91 (m, 1H, C**H**$_2$), 2.78−2.64 (m, 1H, C**H**$_2$), 1.54−1.43 (m, 3H, C**H**$_3$); $^{13}$C NMR (100 MHz, DMSO-$d_6$) $\delta$ 174.0 and 169.2, 142.0 and 139.0, 137.5 and 137.5, 135.9, 135.0 and 134.9, 133.8 and 133.7, 130.8 and 130.4, 129.4 and 129.4, 128.1 and 128.1, 128.1 and 127.8, 126.8 and 126.7, 120.8 and 120.6, 118.5 and 118.5, 117.7 and 117.5, 111.1 and 111.0, 106.1 and 105.8, 56.7 and 53.4, 48.5 and 48.0, 25.3 and 25.0, 19.8 and 19.3; HRMS (ESI) calcd for $C_{20}H_{19}N_4OCl_2$ [M + H]$^+$ 401.0931, found 401.0929.

*Data for N′-(3,4-Dichlorobenzylidene)-(3S)-1-methyl-2,3,4,9-tetrahydro-1H-pyrido[3,4-b]indole-3-carbohydrazide (**11**).* This compound was obtained as a light yellow solid in 79% yield: mp = 189−193 °C; $^1$H NMR (400 MHz, DMSO-$d_6$) $\delta$ 11.84 and 11.67 (s, 1H, NH), 10.98 and 10.86 (s, 1H, O═C-NH), 8.34 and 8.07 (s, 1H, N═CH), 7.94 and 7.88 (s, 1H, Ph-H), 7.72 and 7.64 (s, 2H, Ph-H), 7.41 and 7.39 (d, $^3J_{HH}$ = 8.4 Hz, 1H, Ar−H), 7.33 and 7.31 (d, $^3J_{HH}$ = 8.4 Hz, 1H, Ar−H), 7.06 and 7.04 (t, $^3J_{HH}$ = 7.2 Hz, 1H, Ar−H), 6.96 and 6.96 (t, $^3J_{HH}$ = 7.2 Hz, 1H, Ar−H), 4.68 and 3.70 (dd, $^3J_{HH}$ = 10.4 Hz, 4.4 Hz, 1H, C**H**), 4.38 and 4.19 (q, $^3J_{HH}$ = 6.4 Hz, 1H, C**H**), 3.06 and 2.98 (dd, $^2J_{HH}$ = 14.4 Hz, $^3J_{HH}$ = 3.6 Hz, 1H, C**H**$_2$), 2.80−2.66 (m, 1H, C**H**$_2$), 1.53 and 1.48 (d, $^3J_{HH}$ = 6.4 Hz, 3H, CH$_3$); $^{13}$C NMR (100 MHz, DMSO-$d_6$) $\delta$ 173.5 and 169.0, 144.5 and 141.6, 137.2, 135.9 and 135.9, 135.2 and 134.8, 132.2 and 132.1, 131.7, 131.1, 128.6 and 128.5, 126.9 and 126.8, 126.6 and 126.4, 120.9 and 120.7, 118.6 and 118.5, 117.7 and 117.5, 111.1 and 111.0, 105.9 and 105.6, 56.6 and 53.5, 48.5 and 48.1, 25.3 and 24.7, 19.6 and 18.9; HRMS (ESI) calcd for $C_{20}H_{19}N_4OCl_2$ [M + H]$^+$ 401.0931, found 401.0934.

*Data for N′-(4-Methoxybenzylidene)-(3S)-1-methyl-2,3,4,9-tetrahydro-1H-pyrido[3,4-b]indole-3-carbohydrazide (**12**).* This compound was obtained as a yellow solid in 69% yield: mp = 138−143 °C; $^1$H NMR (400 MHz, DMSO-$d_6$) $\delta$ 11.35 and 11.22 (s, 1H, NH), 10.84 and 10.81 (s, 1H, O═C-NH), 8.27 and 8.00 (s, 1H, N═CH), 7.65 and 7.55 (d, $^3J_{HH}$ = 8.0 Hz, 2H, Ph-H), 7.40 and 7.36 (d, $^3J_{HH}$ = 7.6 Hz, 1H, Ar−H), 7.30 (d, $^3J_{HH}$ = 7.6 Hz, 1H, Ar−H), 7.08−6.89 (m, 4H, Ar−H and Ph-H), 4.45 and 3.59 (d, $^3J_{HH}$ = 8.8 Hz, 1H, C**H**), 4.20−4.08 (m, 1H, C**H**), 3.81 and 3.74 (s, 3H, O−C**H**$_3$), 2.93 (d, $^2J_{HH}$ = 14.4 Hz, 1H, C**H**$_2$), 2.76−2.56 (m, 1H, C**H**$_2$), 1.45 (d, $^3J_{HH}$ = 6.0 Hz, 3H, C**H**$_3$); $^{13}$C NMR (100 MHz, DMSO-$d_6$) $\delta$ 174.3 and 168.8, 160.8 and 160.6, 146.9 and 143.2, 137.9, 135.8 and 135.8, 128.6 and 128.2, 127.0 and 126.9, 126.7, 120.5, 118.4, 117.5, 114.3, 111.0, 106.2 and 106.1, 56.7 and 53.3, 55.3 and 55.2, 48.4 and 47.6, 25.5 and 25.4, 20.0 and 19.9; HRMS (ESI) calcd for $C_{21}H_{23}N_4O_2$ [M + H]$^+$ 363.1816, found 363.1819.

*Data for N′-(3-Methoxybenzylidene)-(3S)-1-methyl-2,3,4,9-tetrahydro-1H-pyrido[3,4-b]indole-3-carbohydrazide (**13**).* This compound was obtained as yellow solid in 63% yield: mp = 186−190 °C; $^1$H NMR (400 MHz, DMSO-$d_6$) $\delta$ 11.54 and 11.39 (s, 1H, NH), 10.87 and 10.83 (s, 1H, O═C-NH), 8.32 and 8.03 (s, 1H, N═CH), 7.45−7.11 (m, 5H, Ph-H and Ar−H), 7.08−6.89 (m, 3H, Ar−H and Ph-H), 4.48 and 3.63 (d, $^3J_{HH}$ = 8.0 Hz, 1H, C**H**), 4.25−4.10 (m, 1H, C**H**), 3.81 and 3.69 (s, 3H, O−C**H**$_3$), 3.02−2.89 (m, 1H, C**H**$_2$), 2.77−2.60 (m, 1H, C**H**$_2$), 1.46 (d, $^3J_{HH}$ = 5.2 Hz, 3H, C**H**$_3$); $^{13}$C NMR (100 MHz, DMSO-$d_6$) $\delta$ 174.3 and 169.2, 159.6, 147.1 and 143.4, 137.8 and 137.5, 135.9 and 135.8, 135.6, 130.0 and 130.0, 126.9, 120.7 and 120.6, 120.0 and 119.1, 118.4, 117.5, 116.2 and 115.4, 112.0 and 111.3, 111.0, 106.2 and 106.0, 56.7 and 53.6, 55.2 and 55.1, 48.5 and 47.8, 25.5 and 25.2, 19.9 and 19.8; HRMS (ESI) calcd for $C_{21}H_{23}N_4O_2$ [M + H]$^+$ 363.1816, found 363.1818.

*Data for N′-(2-Methoxybenzylidene)-(3S)-1-methyl-2,3,4,9-tetrahydro-1H-pyrido[3,4-b]indole-3-carbohydrazide (**14**).* This compound was obtained as yellow solid in 82% yield: mp = 180−183 °C; $^1$H NMR (400 MHz, DMSO-$d_6$) $\delta$ 11.52 and 11.46 (s, 1H, NH), 10.90 and 10.84 (s, 1H, O═C-NH), 8.66 and 8.41 (s, 1H, N═CH), 7.84 and 7.68 (d, $^3J_{HH}$ = 7.2 Hz, 1H, Ph-H), 7.41 (d, $^3J_{HH}$ = 7.6 Hz, 1H, Ar−H), 7.37 (d, $^3J_{HH}$ = 7.6 Hz, 1H, Ar−H), 7.31 (dd, $^3J_{HH}$ = 8.0 Hz, 4.0 Hz, 1H, Ph-H), 7.14−6.86 (m, 4H, Ph-H and Ar−H), 4.54 and 3.61 (dd, $^3J_{HH}$ = 10.0 Hz, 2.8 Hz, 1H, C**H**), 4.30−4.10 (m, 1H, C**H**), 3.86 and 3.84 (s, 3H, O−C**H**$_3$), 3.04−2.89 (m, 1H, C**H**$_2$), 2.77−2.60 (m, 1H, C**H**$_2$), 1.55−1.37 (m, 3H, C**H**$_3$); $^{13}$C NMR (100 MHz, DMSO-$d_6$) $\delta$ 173.9 and 168.9, 157.7 and 157.6, 142.5 and 139.3, 137.6, 135.8, 131.5 and 131.4, 126.9 and 126.8, 125.6 and 125.2, 122.3 and 122.1, 120.7 and 120.7, 120.6, 118.5 and 118.4, 117.6 and 117.5, 111.8, 111.0, 106.1 and 105.9, 56.6 and 53.5, 55.7, 48.4 and 47.8, 25.5 and 25.1, 19.9 and 19.6; HRMS (ESI) calcd for $C_{21}H_{23}N_4O_2$ [M + H]$^+$ 363.1816, found 363.1823.

*Data for N′-(3,4-Dimethoxybenzylidene)-(3S)-1-methyl-2,3,4,9-tetrahydro-1H-pyrido[3,4-b]indole-3-carbohydrazide (**15**).* This compound was obtained as light yellow solid in 91% yield: mp = 203−206 °C; $^1$H NMR (400 MHz, DMSO-$d_6$) $\delta$ 11.47 and 11.27 (s, 1H, NH), 10.89 and 10.83 (s, 1H, O═C-NH), 8.25 and 7.99 (s, 1H, N═CH), 7.43−7.36 (m, 1H, Ar−H), 7.34−7.27 and 7.22−7.15 (m, 3H, Ar−H and Ph-H), 7.07−6.91 (m, 3H, Ar−H and Ph-H), 4.49 and 3.67−3.59 (dd, $^3J_{HH}$ = 11.2 Hz, 3.6 Hz, 1H, C**H**), 4.33−4.11 (m, 1H, C**H**), 3.82 and 3.75 (s, 3H, O−C**H**$_3$), 3.81 and 3.64 (s, 3H, O−C**H**$_3$), 3.03 and 2.94 (dd, $^2J_{HH}$ = 14.8 Hz, $^3J_{HH}$ = 2.8 Hz, 1H, C**H**$_2$), 2.76−

2.65 (m, 1H, C$\mathbf{H}_2$), 1.48 and 1.46 (d, $^3J_{HH}$ = 6.8 Hz, 3H, C$\mathbf{H}_3$); $^{13}$C NMR (100 MHz, DMSO-$d_6$) $\delta$ 173.7 and 168.8, 150.7 and 150.5, 149.1 and 148.9, 147.4 and 143.7, 137.7, 135.9, 127.0, 126.9 and 126.9, 121.8 and 120.7, 120.6 and 120.4, 118.4, 117.5, 111.7 and 111.5, 111.0, 109.2 and 108.3, 106.1 and 106.0, 56.6 and 53.8, 55.6 and 55.5, 55.5 and 55.3, 48.4 and 48.0, 25.5 and 24.9, 19.9 and 19.6; HRMS (ESI) calcd for $C_{22}H_{25}N_4O_3$ $[M + H]^+$ 393.1921, found 393.1918.

*Data for N′-(Benzo[d][1,3]dioxol-5-ylmethylene)-(3S)-1-methyl-2,3,4,9-tetrahydro-1H-pyrido[3,4-b]indole-3-carbohydrazide (**16**).* This compound was obtained as yellow solid in 83% yield: mp = 199−203 °C; $^1$H NMR (400 MHz, DMSO-$d_6$) $\delta$ 11.41 and 11.26 (s, 1H, NH), 10.86 and 10.81 (s, 1H, O═C-NH), 8.24 and 7.96 (s, 1H, N═CH), 7.40 and 7.36 (d, $^3J_{HH}$ = 7.6 Hz, 1H, Ar−H), 7.31 and 7.30 (d, $^3J_{HH}$ = 8.0 Hz, 1H, Ar−H), 7.28 and 7.17 (s, 1H, Ph-H), 7.15 and 7.09 (d, $^3J_{HH}$ = 8.0 Hz, 1H, Ph-H), 7.06−6.96 (m, 2H, Ar−H and Ph-H), 6.94 (t, $^3J_{HH}$ = 7.6 Hz, 1H, Ar−H), 6.10 (s, 1H, O−C$\mathbf{H}_2$), 6.02 (d, $^2J_{HH}$ = 4.8 Hz, 1H, O−C$\mathbf{H}_2$), 4.49 and 3.60 (dd, $^3J_{HH}$ = 10.8 Hz, 3.6 Hz, 1H, C$\mathbf{H}$), 4.22 and 4.13 (m, 1H, C$\mathbf{H}$), 2.99−2.87 (m, 1H, C$\mathbf{H}_2$), 2.75−2.57 (m, 1H, C$\mathbf{H}_2$), 1.45 (d, $^3J_{HH}$ = 6.4 Hz, 3H, C$\mathbf{H}_3$); $^{13}$C NMR (100 MHz, DMSO-$d_6$) $\delta$ 174.2 and 168.9, 149.1 and 148.9, 148.0 and 147.9, 146.9 and 143.2, 137.8, 135.8, 128.8 and 128.6, 126.9, 123.3 and 122.8, 120.6 and 120.6, 118.4, 117.5, 111.0, 108.5, 106.2 and 106.0, 105.1 and 105.0, 101.6 and 101.5, 56.7 and 53.3, 48.4 and 47.7, 25.5 and 25.2, 19.9 and 19.8; HRMS (ESI) calcd for $C_{21}H_{21}N_4O_3$ $[M + H]^+$ 377.1608, found 377.1615.

*Data for N′-((2,3-Dihydrobenzo[b][1,4]dioxin-6-yl)methylene)-(3S)-1-methyl-2,3,4,9-tetrahydro-1H-pyrido[3,4-b]indole-3-carbohydrazide (**17**).* This compound was obtained as yellow solid in 81% yield: mp = 204−207 °C; $^1$H NMR (400 MHz, DMSO-$d_6$) $\delta$ 11.44 and 11.26 (s, 1H, NH), 10.89 and 10.82 (s, 1H, O═C-NH), 8.21 and 7.94 (s, 1H, N═CH), 7.40 and 7.36 (d, $^3J_{HH}$ = 7.6 Hz, 1H, Ar−H), 7.32 and 7.30 (d, $^3J_{HH}$ = 8.0 Hz, 1H, Ar−H), 7.20 and 7.10 (s, 1H, Ph-H), 7.19 and 7.09 (d, $^3J_{HH}$ = 7.6 Hz, 1H, Ph-H), 7.07−7.01 (m, 1H, Ar−H), 6.99−6.83 (m, 2H, Ar−H and Ph-H), 4.51 and 3.61 (dd, $^3J_{HH}$ = 10.8 Hz, 3.6 Hz, 1H, C$\mathbf{H}$), 4.35−4.09 (m, 5H, C$\mathbf{H}$ and O−C$\mathbf{H}_2$-C$\mathbf{H}_2$-O), 3.03−2.89 (m, 1H, C$\mathbf{H}_2$), 2.76−2.60 (m, 1H, C$\mathbf{H}_2$), 1.53−1.43 (m, 3H, C$\mathbf{H}_3$); $^{13}$C NMR (100 MHz, DMSO-$d_6$) $\delta$ 173.8 and 168.8, 146.8, 145.2 and 145.1, 143.6 and 143.6, 143.2, 137.7 and 137.1, 135.9 and 135.8, 127.7 and 127.5, 126.9 and 126.8, 120.7 and 120.7, 120.6 and 120.3, 118.5 and 118.4, 117.6 and 117.5, 115.3 and 114.9, 111.1 and 111.0, 106.2 and 105.9, 64.3 and 64.3, 64.1 and 64.0, 56.6 and 53.6, 48.5 and 47.9, 25.5 and 25.0, 19.9 and 19.6; HRMS (ESI) calcd for $C_{22}H_{23}N_4O_3$ $[M + H]^+$ 391.1765, found 391.1763.

*Data for N′-((6-Hydroxynaphthalen-2-yl)methylene)-(3S)-1-methyl-2,3,4,9-tetrahydro-1H-pyrido[3,4-b]indole-3-carbohydrazide (**18**).* This compound needed recrystallization from methanol to removed the remaining aldehyde. This compound was obtained as yellow solid in 70% yield: mp = 275−278 °C; $^1$H NMR (400 MHz, DMSO-$d_6$) $\delta$ 11.46 and 11.35 (s, 1H, NH), 10.85 and 10.81 (s, 1H, O═C-NH), 9.98 (s, 1H, OH), 8.42 and 8.16 (s, 1H, N═CH), 7.99 and 7.91 (s, 1H, Naphthalene-H), 7.85 (d, $^3J_{HH}$ = 9.2 Hz, 1H, Naphthalene-H), 7.80 and 7.61 (d, $^3J_{HH}$ = 8.8 Hz, 1H, Naphthalene-H), 7.74 and 7.70 (d, $^3J_{HH}$ = 8.8 Hz, 1H, Naphthalene-H), 7.42 and 7.37 (d, $^3J_{HH}$ = 7.6 Hz, 1H, Ar−H), 7.16 and 7.08 (s, 1H, Naphthalene-H), 7.15−7.09 (m, 1H, Naphthalene-H), 7.04 (t, $^3J_{HH}$ = 7.6 Hz, 1H, Ar−H), 7.00−6.90 (m, 1H, Ar−H), 4.52 and 3.63 (d, $^3J_{HH}$ = 8.4 Hz, 1H, C$\mathbf{H}$), 4.25−4.10 (m, 1H, C$\mathbf{H}$), 3.02−2.90 (m, 1H, C$\mathbf{H}_2$), 2.73 and 2.65 (t, $^2J_{HH}$ = 12.8 Hz, 1H, C$\mathbf{H}_2$), 1.47 (d, $^3J_{HH}$ = 6.0 Hz, 3H, C$\mathbf{H}_3$); $^{13}$C NMR (100 MHz, DMSO-$d_6$) $\delta$ 174.5 and 169.0, 156.5 and 156.5, 147.4 and 144.0, 137.9, 135.8 and 135.8, 135.6 and 135.4, 130.1 and 130.0, 129.0, 128.7 and 128.7, 127.3 and 127.3, 127.0 and 126.9, 126.9 and 126.8, 123.0 and 122.3, 120.6, 119.2 and 119.2, 118.4, 117.5, 111.0, 109.1, 106.1 and 106.0, 56.7 and 53.3, 48.4 and 47.7, 25.6 and 25.4, 20.0 and 20.0; HRMS (ESI) calcd for $C_{24}H_{23}N_4O_2$ $[M + H]^+$ 399.1816, found 399.1822.

*Data for N′-(Pyridin-4-ylmethylene)-(3S)-1-methyl-2,3,4,9-tetrahydro-1H-pyrido[3,4-b]indole-3-carbohydrazide (**19**).* This compound was obtained as yellow solid in 79% yield: mp = 235−239 °C; $^1$H NMR (400 MHz, DMSO-$d_6$) $\delta$ 11.84 and 11.69 (s, 1H, NH), 10.90 and 10.84 (s, 1H, O═C-NH), 8.65 and 8.57 (d, $^3J_{HH}$ = 5.6 Hz, 2H, Py-H), 8.35 and 8.05 (s, 1H, N═CH), 7.65 and 7.57 (d, $^3J_{HH}$ = 5.6 Hz, 2H, Py-H), 7.41 and 7.37 (d, $^3J_{HH}$ = 7.6 Hz, 1H, Ph-H), 7.34−7.29 (m, 1H, Ar−H), 7.04 (t, $^3J_{HH}$ = 7.6 Hz, 1H, Ar−H), 6.95 (t, $^3J_{HH}$ = 7.6 Hz, 1H, Ar−H), 4.58 and 3.67 (dd, $^3J_{HH}$ = 10.8 Hz, 3.6 Hz, 1H, C$\mathbf{H}$), 4.26 and 4.16 (q, $^3J_{HH}$ = 6.4 Hz, 1H, C$\mathbf{H}$), 3.05−2.91 (m, 1H, C$\mathbf{H}_2$), 2.80−2.62 (m, 1H, C$\mathbf{H}_2$), 1.48 (d, $^3J_{HH}$ = 6.4 Hz, 3H, $CH_3$); $^{13}$C NMR (100 MHz, DMSO-$d_6$) $\delta$ 174.5 and 169.4, 150.3, 144.7, 141.6, 141.3 and 141.2, 137.7 and 135.8, 126.9 and 126.8, 121.0, 120.7 and 120.6, 118.5 and 118.4, 117.6 and 117.5, 111.0, 106.0 and 105.9, 56.7 and 53.3, 48.5 and 47.9, 25.4 and 25.2, 19.8 and 19.6; HRMS (ESI) calcd for $C_{19}H_{20}N_5O$ $[M + H]^+$ 334.1662, found 334.1663.

*Data for N′-(pyridin-3-ylmethylene)-(3S)-1-methyl-2,3,4,9-tetrahydro-1H-pyrido[3,4-b]indole-3-carbohydrazide (**20**).* This compound was obtained as yellow solid in 72% yield: mp = 205−209 °C; $^1$H NMR (400 MHz, DMSO-$d_6$) $\delta$ 11.74 and 11.58 (s, 1H, NH), 10.91 and 10.84 (s, 1H, O═C-NH), 8.84 and 8.79 (s, 1H, Py-H), 8.62 and 8.55 (d, $^3J_{HH}$ = 4.0 Hz, 1H, Py-H), 8.41 and 8.12 (s, 1H, N═CH), 8.12 and 8.03 (d, $^3J_{HH}$ = 4.0 Hz, 1H, Py-H), 7.49 and 7.44−7.35 (m, 2H, Py-H and Ar−H), 7.33 and 7.31 (d, $^3J_{HH}$ = 7.6 Hz, 1H, Ph-H), 7.04 (t, $^3J_{HH}$ = 7.6 Hz, 1H, Ar−H), 6.96 (t, $^3J_{HH}$ = 7.6 Hz, 1H, Ar−H), 4.59 and 3.66 (dd, $^3J_{HH}$ = 10.8 Hz, 3.6 Hz, 1H, C$\mathbf{H}$), 4.32 and 4.12 (m, 1H, C$\mathbf{H}$), 3.05−2.92 (m, 1H, C$\mathbf{H}_2$), 2.78−2.63 (m, 1H, C$\mathbf{H}_2$), 1.53−1.39 (m, 3H, C$\mathbf{H}_3$); $^{13}$C NMR (100 MHz, DMSO-$d_6$) $\delta$ 169.1, 150.7 and 150.5, 148.7 and 148.5, 144.4 and 140.9, 137.6 and 135.8, 133.4 and 133.2, 130.3, 130.0, 126.9 and 126.8, 124.0 and 124.0, 120.7 and 120.6, 118.5 and 118.4, 117.6 and 117.5, 111.0, 106.0 and 105.9, 56.7 and 53.4, 48.5 and 47.9, 25.4 and 25.1, 19.8 and 19.5; HRMS (ESI) calcd for $C_{19}H_{20}N_5O$ $[M + H]^+$ 334.1662, found 334.1664.

*Data for N′-(Pyridin-2-ylmethylene)-(3S)-1-methyl-2,3,4,9-tetrahydro-1H-pyrido[3,4-b]indole-3-carbohydrazide (**21**).* This compound was obtained as yellow solid in 85% yield: mp = 245−249 °C; $^1$H NMR (400 MHz, DMSO-$d_6$) $\delta$ 11.69 and 11.65 (s, 1H, NH), 10.85 and 10.82 (s, 1H, O═C-NH), 8.62 and 8.57 (d, $^3J_{HH}$ = 4.8 Hz, 1H, Py-H), 8.36 and 8.10 (s, 1H, N═CH), 7.95 and 7.80 (d, $^3J_{HH}$ = 8.0 Hz, 1H, Py-H), 7.88 and 7.75 (td, $^3J_{HH}$ = 7.6 Hz, $^4J_{HH}$ = 1.2 Hz, 1H, Py-H), 7.44−7.33 (m, 2H, Py-H and Ar−H), 7.31 and 7.30 (d, $^3J_{HH}$ = 7.6 Hz, 1H, Ar−H), 7.03 (t, $^3J_{HH}$ = 7.2 Hz, 1H, Ar−H), 6.95 and 6.92 (t, $^3J_{HH}$ = 7.2 Hz, 1H, Ar−H), 4.50 and 3.63 (dd, $^3J_{HH}$ = 10.8 Hz, 4.0 Hz, 1H, C$\mathbf{H}$), 4.16 (q, $^3J_{HH}$ = 8.0 Hz, 1H, C$\mathbf{H}$), 2.94 (ddd, $^2J_{HH}$ = 14.8 Hz, $^3J_{HH}$ = 4.4 Hz, $^4J_{HH}$ = 1.6 Hz, 1H, C$\mathbf{H}_2$), 2.72 and 2.63 (ddd, $^2J_{HH}$ = 14.8 Hz, $^3J_{HH}$ = 10.8 Hz, $^4J_{HH}$ = 2.0 Hz, 1H, C$\mathbf{H}_2$), 1.46 and 1.45 (d, $^3J_{HH}$ = 6.8 Hz, 3H, C$\mathbf{H}_3$); $^{13}$C NMR (100 MHz, DMSO-$d_6$) $\delta$ 174.8 and 169.5, 153.4 and 153.0, 149.5, 147.2 and 143.9, 137.8 and 137.8, 136.9 and 136.9, 135.8 and 135.8, 126.9 and 126.9, 124.4 and 124.2, 120.6, 119.9 and 119.6, 118.4, 117.5 and 117.5, 111.0, 106.1 and 106.0, 56.8 and 53.2, 48.5 and 47.7, 25.5, 19.9; HRMS (ESI) calcd for $C_{19}H_{20}N_5O$ $[M + H]^+$ 334.1662, found 334.1666.

*Data for N′-(Furan-2-ylmethylene)-(3S)-1-methyl-2,3,4,9-tetrahydro-1H-pyrido[3,4-b]indole-3-carbohydrazide (**22**).* The crude product was chromatographed on silica gel (DCM/MeOH = 40:1 → 30:1 → 20:1) to give two compounds. Compound **22a** was obtained as yellow solid in 55% yield: mp = 144−148 °C; $^1$H NMR (400 MHz, $CDCl_3$) $\delta$ 10.33 and 10.20 (s, 1H, NH), 8.26 and 8.11 (s, 1H, O═C-NH), 8.04 and 7.72 (s, 1H, N═CH), 7.51−7.38 (m, 2H, Ar−H and furan-H), 7.34 and 7.31 (d, $^3J_{HH}$ = 7.6 Hz, 1H, Ar−H), 7.14 (t, $^3J_{HH}$ = 6.8 Hz, 1H, Ar−H), 7.08 (t, $^3J_{HH}$ = 7.2 Hz, 1H, Ar−H), 6.77 and 6.62 (s, 1H, furan-H), 6.45 and 6.42 (s, 1H, furan-H), 4.65 and 3.69 (d, $^3J_{HH}$ = 7.6 Hz, 1H, C$\mathbf{H}$), 4.32−4.11 (m, 1H, C$\mathbf{H}$), 3.30 and 3.19 (d, $^2J_{HH}$ = 13.6 Hz, 1H, C$\mathbf{H}_2$), 2.79 (t, $^2J_{HH}$ = 13.2 Hz, 1H, C$\mathbf{H}_2$), 1.97 (br, 1H, NH), 1.52 and 1.46 (d, $^3J_{HH}$ = 6.4 Hz, 3H, C$\mathbf{H}_3$); $^{13}$C NMR (100 MHz, DMSO-$d_6$) $\delta$ 174.4 and 169.1, 149.5 and 149.1, 145.1 and 144.9, 137.8 and 137.7, 136.9, 135.8, 126.9 and 126.9, 120.6, 118.4, 117.5, 113.6 and 113.3, 112.2 and 112.1, 111.0, 106.2 and 106.1, 56.7 and 53.2, 48.5 and 47.7, 25.5 and 25.4, 19.9; HRMS (ESI) calcd for $C_{18}H_{19}N_4O_2$ $[M + H]^+$ 323.1503, found 323.1505.

Compound **22b** was obtained as yellow solid in 3% yield: mp = 154−157 °C; $^1$H NMR (400 MHz, $CDCl_3$) $\delta$ 12.00 and 10.44 (s, 1H, NH), 8.00 and 7.94 (s, 1H, O═C-NH), 7.64 and 7.60 (s, 1H, N═CH), 7.52 and 7.46 (d, $^3J_{HH}$ = 7.6 Hz, 1H, Ar−H), 7.40−7.30 (m, 2H, Ar−H and furan-H), 7.16 (t, $^3J_{HH}$ = 7.2 Hz, 1H, Ar−H), 7.11 (t, $^3J_{HH}$

= 7.2 Hz, 1H, Ar−H), 6.78 and 6.70 (s, 1H, furan-H), 6.60 and 6.55 (s, 1H, furan-H), 4.67 and 3.82 (d, $^3J_{HH}$ = 8.8 Hz, 1H, C**H**), 4.36−4.25 (m, 1H, C**H**), 3.30 and 3.20 (d, $^2J_{HH}$ = 15.2 Hz, 1H, C**H**$_2$), 2.92−2.75 (m, 1H, C**H**$_2$), 1.72 (br, 1H, NH), 1.61−1.49 (m, 3H, C**H**$_3$); $^{13}$C NMR (100 MHz, DMSO-$d_6$) $\delta$ 169.4, 147.8, 145.6, 138.2, 135.8, 130.8, 127.0, 120.6, 118.4, 117.6, 116.2, 112.5, 111.0, 106.8, 56.9, 48.8, 24.4, 19.9; HRMS (ESI) calcd for $C_{18}H_{19}N_4O_2$ [M + H]$^+$ 323.1503, found 323.1509.

*Data for N′-((1H-Pyrrol-2-yl)methylene)-(3S)-1-methyl-2,3,4,9-tetrahydro-1H-pyrido[3,4-b]indole-3-carbohydrazide (**23**).* This compound was obtained as red solid in 75% yield: mp = 207−209 °C; $^1$H NMR (400 MHz, DMSO-$d_6$) $\delta$ 11.52 and 11.31 (s, 1H, NH), 11.16 and 11.05 (s, 1H, Pyrrole-NH), 10.83 and 10.80 (s, 1H, O═C-NH), 8.15 and 7.88 (s, 1H, N═CH), 7.45−7.35 (m, 1H, Ar−H), 7.30 (d, $^3J_{HH}$ = 7.2 Hz, 1H, Ar−H), 7.03 (t, $^3J_{HH}$ = 7.2 Hz, 1H, Ar−H), 6.95 (t, $^3J_{HH}$ = 7.2 Hz, 1H, Ar−H), 6.90 and 6.83 (s, 1H, Pyrrole-H), 6.45 and 6.39 (s, 1H, Pyrrole-H), 6.13 and 6.08 (s, 1H, Pyrrole-H), 4.60 and 3.58 (d, $^3J_{HH}$ = 8.8 Hz, 1H, C**H**), 4.24−4.08 (m, 1H, C**H**), 2.98−2.88 (m, 1H, C**H**$_2$), 2.70−2.59 (m, 1H, C**H**$_2$), 1.50−1.45 (m, 3H, C**H**$_3$); $^{13}$C NMR (100 MHz, DMSO-$d_6$) $\delta$ 173.9 and 168.4, 140.2, 137.8, 136.4, 135.8, 127.0 and 126.9, 121.9, 120.6 and 120.6, 118.4, 117.7 and 117.5, 113.3 and 112.8, 111.0, 109.2 and 109.1, 106.4 and 106.2, 56.6 and 52.6, 48.4 and 47.7, 25.6 and 25.1, 19.9 and 19.7; HRMS (ESI) calcd for $C_{18}H_{20}N_5O$ [M + H]$^+$ 322.1662, found 322.1668.

*Data for N′-(Thiophen-2-ylmethylene)-(3S)-1-methyl-2,3,4,9-tetrahydro-1H-pyrido[3,4-b]indole-3-carbohydrazide (**24**).* This compound was obtained as yellow solid in 76% yield: mp = 139−141 °C; $^1$H NMR (400 MHz, DMSO-$d_6$) $\delta$ 11.55 and 11.39 (s, 1H, NH), 10.90 and 10.83 (s, 1H, O═C-NH), 8.56 and 8.24 (s, 1H, N═CH), 7.67 and 7.54 (d, $^3J_{HH}$ = 4.8 Hz, 1H, Thiophene-H), 7.47−7.35 (m, 2H, Thiophene-H and Ar−H), 7.35−7.28 (m, 1H, Ar−H), 7.14 and 7.09 (t, $^3J_{HH}$ = 4.4 Hz, 1H, Thiophene-H), 7.04 (t, $^3J_{HH}$ = 7.2 Hz, 1H, Ar−H), 7.00−6.90 (m, 1H, Ar−H), 4.38 and 3.62 (dd, $^3J_{HH}$ = 8.8 Hz, 4.0 Hz, 1H, C**H**), 4.29−4.10 (m, 1H, C**H**), 3.04−2.89 (m, 1H, C**H**$_2$), 2.77−2.61 (m, 1H, C**H**$_2$), 1.54−1.38 (m, 3H, C**H**$_3$); $^{13}$C NMR (100 MHz, DMSO-$d_6$) $\delta$ 173.6 and 168.9, 142.3, 139.1 and 138.9, 138.6 and 137.6, 135.9 and 135.8, 130.8 and 130.4, 128.8 and 128.4, 128.0 and 127.9, 126.9 and 126.8, 120.7 and 120.6, 118.5 and 118.4, 117.5, 111.1 and 111.0, 106.1 and 105.9, 56.7 and 53.7, 48.5 and 47.9, 25.4 and 25.0, 19.8 and 19.6; HRMS (ESI) calcd for $C_{18}H_{19}N_4OS$ [M + H]$^+$ 339.1274, found 339.1278.

*Data for N′-((1H-imidazol-2-yl)methylene)-(3S)-1-methyl-2,3,4,9-tetrahydro-1H-pyrido[3,4-b]indole-3-carbohydrazide (**25**).* This compound was obtained as green solid in 81% yield: mp = 188−190 °C; $^1$H NMR (400 MHz, DMSO-$d_6$) $\delta$ 14.10, 13.33, 12.81, and 12.57 (s, 1H, Imidzole-NH), 12.93 and 11.47 (s, 1H, NH), 10.84 and 10.81 (s, 1H, O═C-NH), 8.45, 8.26, 7.95, and 7.44 (s, 1H, N═CH), 7.42−6.88 (m, 6H, Ar−H and Imidzole-H), 4.65, 4.50, 3.69, and 3.63 (m, 1H, C**H**), 4.37 and 4.17 (m, 1H, C**H**), 3.03 and 2.95 (d, $^2J_{HH}$ = 14.0 Hz, 1H, C**H**$_2$), 2.78−2.56 (m, 1H, C**H**$_2$), 1.52−1.42 (m, 3H, C**H**$_3$); $^{13}$C NMR (100 MHz, DMSO-$d_6$) $\delta$ 174.9, 174.7, 170.4 and 169.2, 142.6, 142.5, 141.1 and 141.0, 139.0, 138.2, 137.8 and 137.7, 135.8 and 135.2, 129.6 and 129.3, 127.0, 126.9, 126.9 and 126.8, 120.6 and 120.6, 118.4, 117.7 and 117.5, 111.0 and 111.0, 106.5, 106.4, 106.2 and 106.0, 57.2, 56.8, 53.1 and 52.5, 48.7, 48.5, 47.9 and 47.7, 25.6, 25.3, 25.3 and 25.1, 20.0, 20.0, 19.8 and 19.8; HRMS (ESI) calcd for $C_{17}H_{19}N_6O$ [M + H]$^+$ 323.1615, found 323.1620.

*Data for (N′-((E)-But-2-enylidene)-(3S)-1-methyl-2,3,4,9-tetrahydro-1H-pyrido[3,4-b]indole-3-carbohydrazide (**26**).* The crude produt was chromatographed on silica gel to give **26** as a yellow solid in 79% yield: mp = 145−148 °C; $^1$H NMR (400 MHz, $CDCl_3$) $\delta$ 10.10 and 9.63 (s, 1H, NH), 8.23 and 8.15 (s, 1H, O═C-NH), 7.72 and 7.37 (d, $^3J_{HH}$ = 8.4 Hz, 1H, N═CH), 7.43 (d, $^3J_{HH}$ = 6.8 Hz, 1H, Ar−H), 7.35−7.27 (m, 1H, Ar−H), 7.20−7.00 (m, 2H, Ar−H), 6.42−5.94 (m, 2H, C**H**C**H**), 4.57−4.48 and 3.70−3.58 (m, 1H, C**H**), 4.31−4.06 (m, 1H, C**H**), 3.27 and 3.12 (d, $^2J_{HH}$ = 14.4 Hz, 1H, C**H**$_2$), 2.85−2.66 (m, 1H, C**H**$_2$), 2.09 (br, 1H, NH), 1.92−1.75 (m, 3H, C**H**$_3$), 1.50 and 1.43 (d, $^3J_{HH}$ = 5.6 Hz, 3H, C**H**$_3$); $^{13}$C NMR (100 MHz, $CDCl_3$) $\delta$ 175.5 and 169.2, 150.3 and 147.2, 139.7 and 138.9, 136.8, 136.0 and 135.9, 128.5 and 128.1, 127.3 and 127.2, 121.8 and 121.7, 119.6 and 119.5, 118.3 and 118.1, 111.1, 107.9 and 107.7, 57.2 and 54.1, 49.4 and 48.0, 25.7 and 25.2, 20.2 and 20.2, 18.7 and 18.6; HRMS (ESI) calcd for $C_{18}H_{20}N_5O$ [M + H]$^+$ 297.1710, found 297.1714.

**Synthesis of *N′*-(Butylidene)-(3*S*)-1-methyl-2,3,4,9-tetrahydro-1*H*-pyrido[3,4-*b*]indole-3-carbohydrazide (27).**[19] To a solution of compound **1** (0.50 g, 2.05 mmol) in THF (35 mL) was added dropwise *n*-butanal (0.30 g, 4.10 mmol) at room temperature, After 3 h, TLC analysis showed the complete consumption of compound **1**. Then the mixture was concentrated in vacuo, and the crude product was purified by column chromatography on silica gel eluted with DCM/MeOH (25:1 → 10:1) to give **27** as a yellow solid in 71% yield: mp = 113−117 °C; $^1$H NMR (400 MHz, DMSO-$d_6$) $\delta$ 11.04 and 10.97 (s, 1H, NH), 10.82 and 10.80 (s, 1H, O═C-NH), 7.59 and 7.42−7.33 (m, 2H, N═CH and Ar−H), 7.30 (d, $^3J_{HH}$ = 7.6 Hz, 1H, Ph-H), 7.03 (t, $^3J_{HH}$ = 6.8 Hz, 1H, Ar−H), 6.95 (t, $^3J_{HH}$ = 6.8 Hz, 1H, Ar−H), 4.28 and 3.51 (d, $^3J_{HH}$ = 9.6 Hz, 1H, C**H**), 4.19−4.04 (m, 1H, C**H**), 2.89 (d, $^2J_{HH}$ = 14.0 Hz, 1H, C**H**$_2$), 2.67 and 2.57 (t, $^2J_{HH}$ = 12.8 Hz, 1H, C**H**$_2$), 2.25−2.10 (m, 2H, C**H**$_2$), 1.55−1.40 (m, 5H, C**H**$_3$ and C**H**$_2$), 0.92 and 0.86 (t, $^3J_{HH}$ = 6.8 Hz, 3H, C**H**$_3$); $^{13}$C NMR (100 MHz, DMSO-$d_6$) $\delta$ 173.9 and 168.7, 151.3 and 147.8, 137.8 and 137.7, 135.9, 126.9, 120.6, 118.4, 117.5 and 117.5, 111.0, 106.2 and 106.1, 56.5 and 53.3, 48.4 and 47.7, 33.9 and 33.7, 25.5 and 25.2, 20.0, 19.5 and 19.2, 13.7 and 13.5; HRMS (ESI) calcd for $C_{17}H_{23}N_4O$ [M + H]$^+$ 299.1866, found 299.1870.

Compounds **28** and **29** were synthesized using a similar procedure as compound **27**.

*Data for N′-(Octylidene)-(3S)-1-methyl-2,3,4,9-tetrahydro-1H-pyrido[3,4-b]indole-3-carbohydrazide (**28**).* The crude product was purified by column chromatography on silica gel eluted with DCM/MeOH (40:1 → 30:1 → 10:1) to give **28** as a yellow solid in 78% yield: mp = 68−71 °C; $^1$H NMR (400 MHz, $CDCl_3$) $\delta$ 9.94 and 9.02 (s, 1H, NH), 7.90 and 7.50 (s, 1H, N═CH), 7.50 and 7.46 (d, $^3J_{HH}$ = 8.0 Hz, 1H, Ar−H), 7.34 and 7.32 (d, $^3J_{HH}$ = 8.4 Hz, 1H, Ar−H), 7.17 (t, $^3J_{HH}$ = 7.2 Hz, 1H, Ar−H), 7.11 (t, $^3J_{HH}$ = 7.2 Hz, 1H, Ar−H), 4.53 and 3.70 (dd, $^3J_{HH}$ = 11.2 Hz, 4.4 Hz, 1H, C**H**), 4.33−4.17 (m, 1H, C**H**), 3.37 and 3.13 (dd, $^2J_{HH}$ = 14.4 Hz, $^3J_{HH}$ = 2.8 Hz, 1H, C**H**$_2$), 2.83−2.72 (m, 1H, C**H**$_2$), 2.38 and 2.22 (q, $^3J_{HH}$ = 7.2 Hz, 2H, C**H**$_2$), 1.96 (br, 1H, NH), 1.58−1.43 (m, 4H, C**H**$_2$ and C**H**$_3$), 1.42−1.18 (m, 9H, C**H**$_2$), 0.95−0.81 (m, 3H, C**H**$_3$); $^{13}$C NMR (100 MHz, $CDCl_3$) $\delta$ 175.2 and 168.6, 152.8 and 148.8, 136.7 and 136.6, 135.9 and 135.9, 127.3 and 127.2, 122.0 and 121.8, 119.7 and 119.5, 118.4 and 118.1, 111.0, 108.4 and 107.9, 57.3 and 54.1, 49.5 and 47.9, 32.4 and 32.1, 31.7 and 31.7, 29.3, 29.1 and 29.0, 26.7 and 26.3, 25.6 and 25.1, 22.6 and 22.6, 20.2, 14.1 and 14.1; HRMS (ESI) calcd for $C_{21}H_{31}N_4O$ [M + H]$^+$ 355.2493, found 355.2492.

*Data for N′-(Cyclohexylmethylene)-(3S)-1-methyl-2,3,4,9-tetrahydro-1H-pyrido[3,4-b]indole-3-carbohydrazide (**29**).* The crude product was purified by column chromatography on silica gel eluted with DCM/MeOH (100:1 → 40:1 → 20:1) to give **29** as a yellow solid in 92% yield: mp = 123−126 °C; $^1$H NMR (400 MHz, $CDCl_3$) $\delta$ 9.88 and 9.21 (s, 1H, NH), 7.98 and 7.96 (s, 1H, N═CH), 7.49 and 7.47 (d, $^3J_{HH}$ = 8.0 Hz, 1H, Ar−H), 7.38−7.29 and 7.05 (m, 2H, Ar−H and O═C-NH), 7.16 and 7.16 (t, $^3J_{HH}$ = 7.2 Hz, 1H, Ar−H), 7.10 (t, $^3J_{HH}$ = 7.2 Hz, 1H, Ar−H), 4.52 and 3.66 (dd, $^3J_{HH}$ = 10.8 Hz, 4.4 Hz, 1H, C**H**), 4.28 and 4.18 (q, $^3J_{HH}$ = 6.8 Hz, 1H, C**H**), 3.35 and 3.12 (dd, $^2J_{HH}$ = 15.6 Hz, $^3J_{HH}$ = 2.8 Hz, 1H, C**H**$_2$), 2.85−2.72 (m, 1H, C**H**$_2$), 2.47−2.35 and 2.23−2.13 (m, 1H, C**H**), 1.94 (br, 1H, NH), 1.87−1.58 (m, 4H, C**H**$_2$), 1.53 and 1.48 (d, $^3J_{HH}$ = 10.8 Hz, 3H, C**H**$_3$), 1.38−1.11 (m, 6H, C**H**$_2$), 0.95−0.81 (m, 3H, C**H**$_3$); $^{13}$C NMR (100 MHz, $CDCl_3$) $\delta$ 175.3 and 168.6, 156.3 and 152.2, 136.9 and 136.6, 135.9 and 135.8, 127.4 and 127.3, 122.0 and 121.7, 119.8 and 119.5, 118.4 and 118.1, 110.9, 108.5 and 108.0, 57.4 and 54.2, 49.5 and 47.9, 40.8 and 40.4, 30.2, 30.0 and 30.0, 25.9 and 25.8, 25.6 and 25.4, 25.3 and 25.1, 20.3 and 20.3; HRMS (ESI) calcd for $C_{20}H_{27}N_4O$ [M + H]$^+$ 339.2180, found 339.2179.

**Synthesis of *N′*-(2,2-Dimethylpropylidene)-(3*S*)-1-methyl-2,3,4,9-tetrahydro-1*H*-pyrido[3,4-*b*]indole-3-carbohydrazide (30).**[19] To a solution of compound **1** (0.38 g, 1.56 mmol) in THF (35 mL) was added dropwise trimethylacetaldehyde (0.27 g, 3.11 mmol)

**Scheme 1. Synthesis of Compound 1**

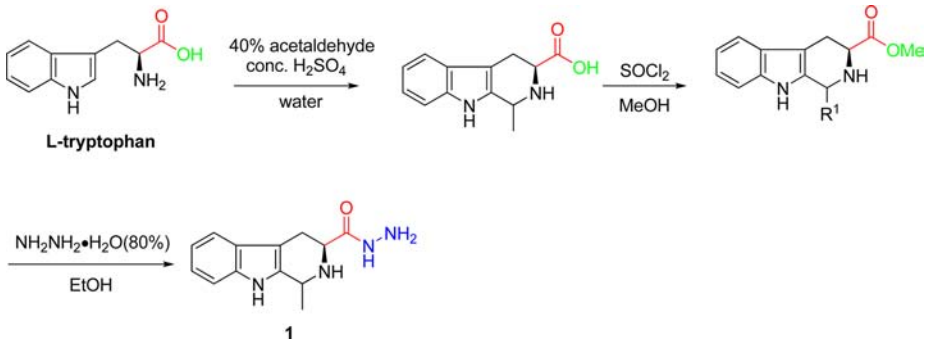


**Scheme 2. Synthesis of Compounds 3 and 5−33**

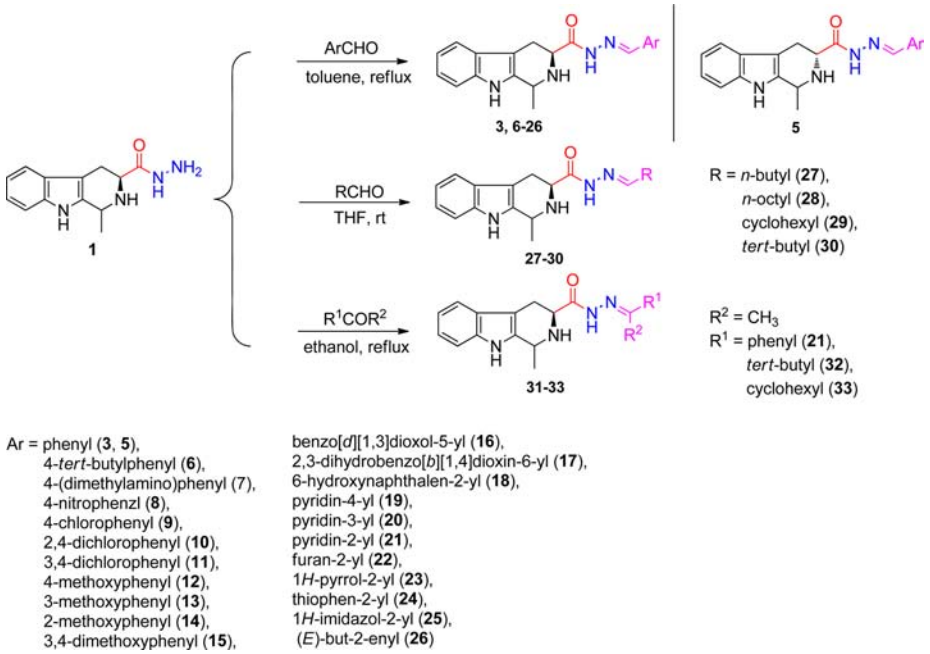


at room temperature, After 6 h, TLC analysis showed the complete consumption of compound **1**. Then the mixture was concentrated in vacuo and dried without further operation to give **30** as a yellow solid in 95% yield: mp = 140−141 °C; $^1$H NMR (100 MHz, $CDCl_3$) $\delta$ 9.93 and 9.39 (s, 1H, NH), 8.13 and 8.09 (s, 1H, N═CH), 7.53−7.02 (m, 4H, Ar−H), 4.51 and 3.67 (d, $^3J_{HH}$ = 8.4 Hz, 1H, C**H**), 4.37−4.16 (m, 1H, C**H**), 3.33 and 3.13 (d, $^2J_{HH}$ = 14.4 Hz, 1H, C**H**$_2$), 2.79 (t, $^2J_{HH}$ = 13.2 Hz, 1H, C**H**$_2$), 2.09 (br, 1H, NH), 1.58−1.41 (m, 3H, C**H**$_3$), 1.15 and 1.06 (s, 9H, C**H**$_3$); $^{13}$C NMR (100 MHz, $CDCl_3$) $\delta$ 176.0 and 169.3, 160.9 and 156.5, 137.3, 136.7 and 136.6, 128.1 and 127.9, 122.6 and 122.4, 120.4 and 120.2, 119.1 and 118.8, 111.7, 109.0 and 108.5, 58.1 and 55.1, 50.2 and 48.7, 35.8 and 35.6, 31.0 and 27.9, 28.1 and 28.0, 26.1 and 25.8, 20.9; HRMS (ESI) calcd for $C_{18}H_{25}N_4O$ [M + H]$^+$ 313.2023, found 313.2028.

**Synthesis of *N*′-(1-Phenylethylidene)-(3*S*)-1-methyl-2,3,4,9-tetrahydro-1*H*-pyrido[3,4-*b*]indole-3-carbohydrazide (31).**[20] To a solution of compound **1** (0.50 g, 2.05 mmol) in EtOH (35 mL) was added acetophenone (0.27 g, 2.25 mmol), and then the reaction mixture was heated to reflux. After 6 h, the reaction was complete detected by TLC. The mixture was concentrated in vacuo, and the crude product was purified by column chromatography on silica gel eluted with DCM/MeOH (30:1 → 10:1) to give **31** as a light yellow solid in 56% yield: mp = 221−224 °C; $^1$H NMR (400 MHz, DMSO-$d_6$) $\delta$ 10.84 and 10.81 (s, 1H, N−H), 10.69 and 10.48 (s, 1H, O═C-NH),7.89−7.77 and 7.76−7.67 (m, 2H, Ph-H), 7.48−7.27 (m, 5H, Ph-H and Ar−H), 7.08−6.88 (m, 2H, Ar−H), 4.53 and 3.78 (dd, $^3J_{HH}$ = 10.8 Hz, 3.6 Hz, 1H, C**H**), 4.23−4.11 (m, 1H, C**H**), 3.03−2.93 (m, 1H, C**H**$_2$), 2.76−2.59 (m, 1H, C**H**$_2$), 3.31 and 3.30 (s, 3H, C**H**$_3$), 1.46 (d, $^3J_{HH}$ = 6.4 Hz, 3H, C**H**$_3$); $^{13}$C NMR (100 MHz, DMSO-$d_6$) $\delta$ 175.3 and 169.2, 151.9 and 148.0, 138.1, 137.9 and 137.6, 135.8 and 135.8, 129.3 and 129.1, 128.4 and 128.4, 126.9, 126.4 and 125.9, 120.6, 118.4, 117.5 and 117.5, 111.0, 106.4 and 106.1, 56.5 and 53.7, 48.4 and 47.7, 25.5 and 25.3, 19.9, 13.7 and 13.4; HRMS (ESI) calcd for $C_{21}H_{23}N_4O$ [M + H]$^+$ 347.1867, found 347.1872.

Compounds **32** and **33** were synthesized using a similar procedure as compound **31**.

*Data for N′-(3,3-Dimethylbutan-2-ylidene)-(3S)-1-methyl-2,3,4,9-tetrahydro-1H-pyrido[3,4-b]indole-3-carbohydrazide (32).* The crude product was purified by column chromatography on silica gel eluted with DCM/MeOH (30:1 → 10:1) to give **32** as a yellow solid in 63% yield: mp = 103−107 °C; $^1$H NMR (400 MHz, DMSO-$d_6$) $\delta$ 10.80 and 10.79 (s, 1H, N−H), 10.18 and 10.02 (s, 1H, O═C-NH),7.40 and 7.35 (d, $^3J_{HH}$ = 7.6 Hz, 1H, Ar−H), 7.29 (d, $^3J_{HH}$ = 8.0 Hz, 1H, Ar−H), 7.03 (t, $^3J_{HH}$ = 7.2 Hz, 1H, Ar−H), 6.95 and 6.93 (t, $^3J_{HH}$ = 6.8 Hz, 1H, Ar−H), 4.26 and 3.65 (dd, $^3J_{HH}$ = 10.8 Hz, 4.0 Hz, 1H, C**H**), 4.16−4.07 (m, 1H, C**H**), 2.94 (dd, $^2J_{HH}$ = 14.8 Hz, $^3J_{HH}$ = 2.8 Hz, 1H, C**H**$_2$), 2.70−2.53 (m, 1H, C**H**$_2$), 1.87 and 1.85 (s, 3H, C**H**$_3$), 1.43 (d, $^3J_{HH}$ = 6.4 Hz, 3H, C**H**$_3$), 1.12 and 1.04 (s, 9H, C**H**$_3$); $^{13}$C NMR (100 MHz, DMSO-$d_6$) $\delta$ 174.7 and 168.6, 163.2 and 158.5, 137.9 and 137.5, 135.8, 126.9, 120.6 and 120.5, 118.4, 117.5 and 117.4, 111.0, 106.5 and 106.2, 56.6 and 54.4, 48.4 and 47.8, 38.5 and 38.3, 27.6 and 27.5, 26.0, 25.3 and 24.8, 20.0 and 19.9, 12.0 and 11.8;


dx.doi.org/10.1021/jf503794g | J. Agric. Food Chem. 2014, 62, 9987−9999

HRMS (ESI) calcd for $C_{19}H_{27}N_4O$ $[M + H]^+$ 327.2180, found 327.2186.

*Data for N′-Cyclohexylidene-(3S)-1-methyl-2,3,4,9-tetrahydro-1H-pyrido[3,4-b]indole-3-carbohydrazide (**33**).* The crude product was purified by column chromatography on silica gel eluted with DCM/MeOH (30:1 → 10:1) to give **33** as a yellow solid in 60% yield: mp = 131−135 °C; $^1$H NMR (400 MHz, DMSO-$d_6$) $\delta$ 10.81 and 10.78 (s, 1H, NH), 10.39 and 10.24 (s, 1H, O═C-NH),7.39 and 7.36 (d, $^3J_{HH}$ = 8.0 Hz, 1H, Ar−H), 7.29 (d, $^3J_{HH}$ = 7.6 Hz, 1H, Ar−H), 7.02 (t, $^3J_{HH}$ = 7.2 Hz, 1H, Ar−H), 6.94 (t, $^3J_{HH}$ = 7.2 Hz, 1H, Ar−H), 4.36 and 3.62 (dd, $^3J_{HH}$ = 10.0 Hz, 3.6 Hz, 1H, C**H**), 4.18−4.04 (m, 1H, C**H**), 2.94−2.84 (m, 1H, C**H**$_2$), 2.69−2.58 (m, 1H, C**H**$_2$), 2.40−2.12 (m, 4H, C**H**$_2$), 1.71−1.51 (m, 6H, C**H**$_2$), 1.42 (d, $^3J_{HH}$ = 6.0 Hz, 3H, C**H**$_3$); $^{13}$C NMR (100 MHz, DMSO-$d_6$) $\delta$ 168.7, 161.5, 137.8, 135.8, 126.9 and 126.8, 120.6 and 120.5, 118.4, 117.5, 111.0, 106.3, 56.3 and 53.3, 48.3 and 47.7, 35.2 and 35.0, 27.0 and 26.8, 25.7 and 25.5, 25.1, 19.9 and 19.8; HRMS (ESI) calcd for $C_{19}H_{25}N_4O$ $[M + H]^+$ 325.2023, found 325.2023.

**Biological Assay.** The anti-TMV and fungicidal and insecticidal activities of the synthesized compounds were tested using our previously reported methods.[21,22]

**Field Trials.** The experiments were carried out between June and July in 2014. The trial against TMV was performed in the trial area of Institute of Environment and Resources, Yunnan Provincial Academy of Agricultural Sciences, Kunming, Yunnan Province, China. The experimental design was a randomized complete block with three treatments. The untreated plots served as a blank control. The formulation of compounds **9** (1% EC) and **29** (1% ME) was prepared in our lab. They were diluted to 10, 50, or 100 g(ai)/ha (weight (gram) of active ingredient/hectare) before use. The formulation of moroxydine hydrochloride−cupric acetate (20% WP) and amino-oligosaccharins (5% aqueous solution) were obtained from Wansheng Biological Pesticide Co., Ltd. (Shandong, China) and Hainan zhengye zhong nong Co., Ltd. (Hainan, China) respectively. The incidence was surveyed 10 days after the third time spraying. The severity of the virus disease was divided into 0−4 grade. The disease index and control effect can be calculated by using the following formulas:

disease index

$$I\% = [\sum (N_n n)/(N4)] \times 100$$

$$\text{control effect } (\%) = 1 - (I'_{bc}I)/(I_{bc}I') \times 100$$

where $N_n$ is the number of diseased plants of each relative level values, $n$ is the relative level values ($n$ = 0−4), $N$ is the total number of diseased plants, $I'_{bc}$ is the disease index of the blank control area before spraying, $I_{bc}$ is the disease index of the blank control area 10 days after the third time spraying, $I'$ is the disease index of the spraying area before spraying; and $I$ is the disease index of the spraying area 10 days after the third time spraying.

## RESULTS AND DISCUSSION

**Synthesis.** The synthesis of the lead compound **1** is shown in Scheme 1. Using L-tryptophan as starting material, the tetrahydrocarboline skeleton of **1** was constructed through Pictet−Spengler cyclization, and then the given carboxylic acid reacted with thionyl chloride and methanol to form methyl ester, which subsequently reacted with hydrazine hydrate to give compound **1**.

**Scheme 3. Synthesis of Compounds 2 and 4**

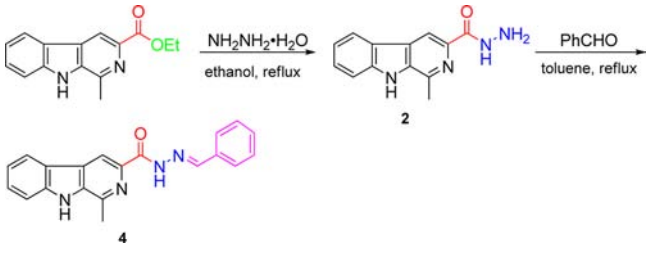


**Scheme 4. Prediction of the Configuration**

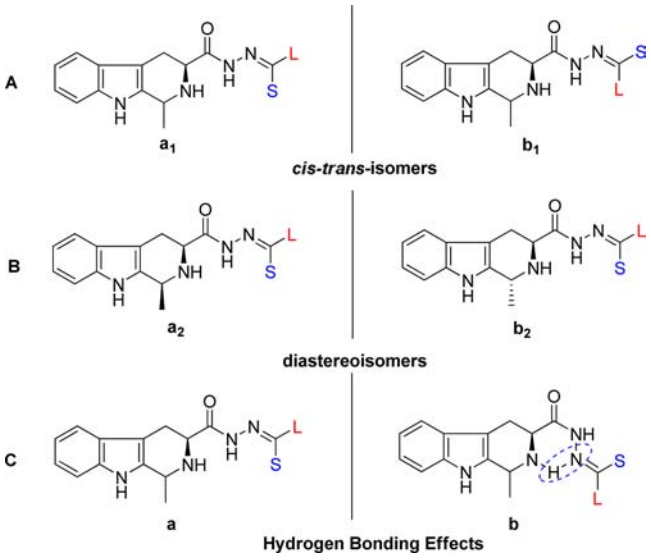


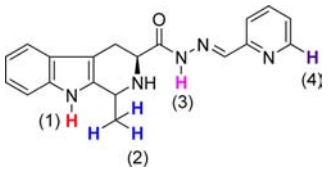


**Figure 3.** Compound **21**.

The compounds **3** and **6−33** containing the acylhydrazone fragment all can be synthesized from lead compound **1** by reaction with the corresponding aldehydes or ketones under different reaction conditions (Scheme 2). To be specific, when aromatic aldehydes were used as starting materials, the corresponding reactions were carried out in toluene under reflux conditions. When the reaction was complete, the reaction system was cooled to room temperature, and the solid products precipitated because of their poor solubility in toluene. By this approach, compounds **3** and **6−26** could be easily obtained in 60%−91% yields. When aliphatic aldehydes were used as starting materials, the corresponding reactions were carried out in tetrahydrofuran at room temperature. When the reaction was complete, compounds **27−30** could be obtained by column chromatography in 71%−95% yields. When ketones were used, these reactions were carried out in ethanol under reflux conditions. When the reaction was complete, compounds **31−33** could be obtained by column chromatography in 56%−63% yields.

In addition, 1-methyl-9*H*-carbazole-3-carboxylic acid hydrazide **2** could be prepared from ethyl 1-methyl-9*H*-pyrido[3,4-*b*]indole-3-carboxylate, which was synthesized from tryptophan through a literature protocol.[17] Compound **2** reacted with benzaldehyde using a similar procedure as the preparation of compound **3** to give **4** in 91% yield (Scheme 3).

**Configuration.** At room temperature, the $^1$H and $^{13}$C NMR spectra of most of target compounds exhibited two sets of signals, which aroused our attention. Initially, this phenomenon was thought to be due to the presence of *cis−trans* isomers (prediction A, Scheme 4); however, in the $^1$H NMR spectrum


dx.doi.org/10.1021/jf503794g | J. Agric. Food Chem. 2014, 62, 9987−9999

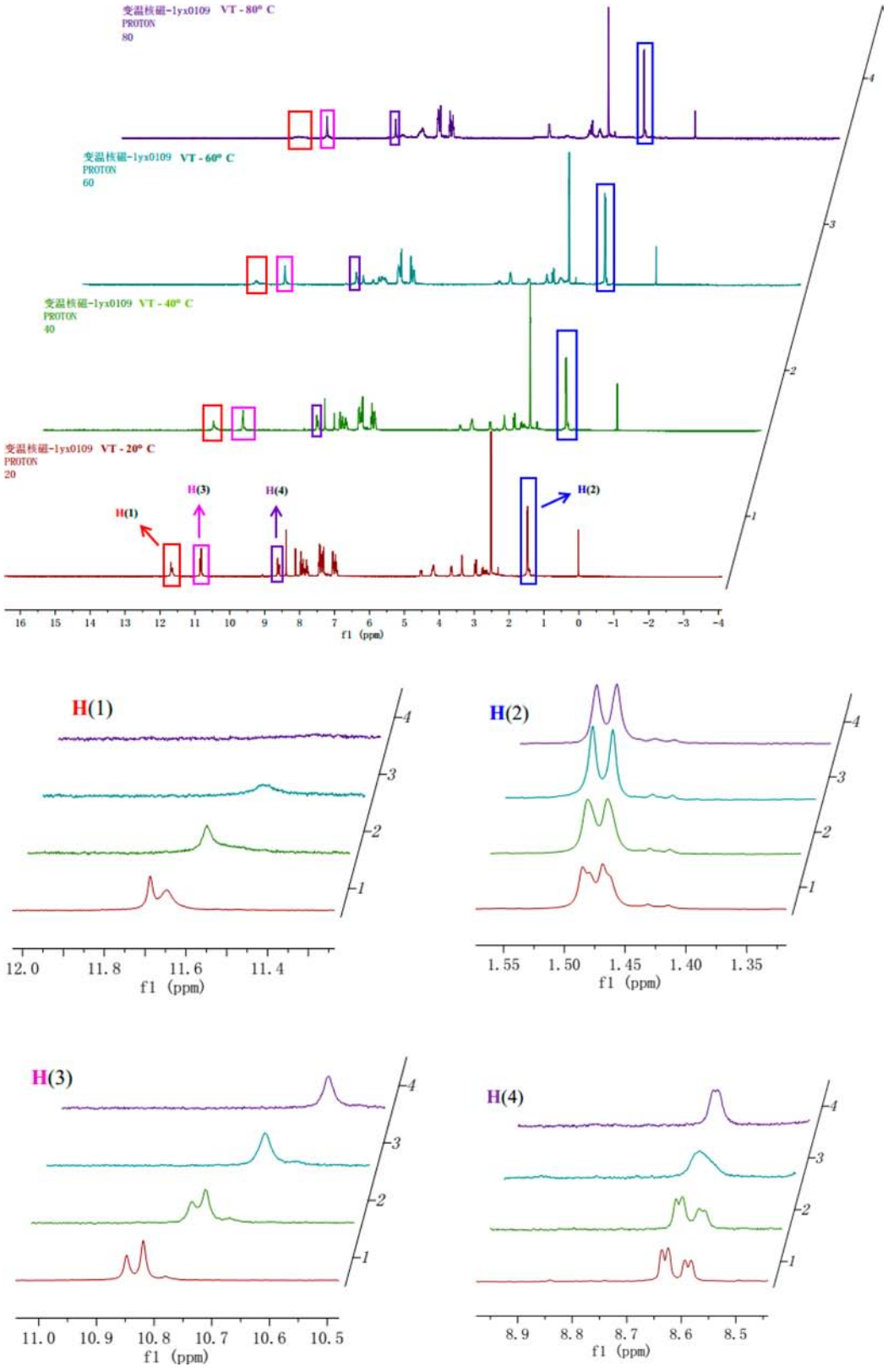


**Figure 4.** $^{1}$H NMR of Compound **21** at Different Temperatures.

of **4** only one set of signals was observed, which suggested such phenomenon resulted from other reasons. Meanwhile, the presence of diastereoisomers (prediction B, Scheme 4) as a possible reason was excluded (the $^{1}$H NMR spectra of precursor **1** as well as compound **21** (Figures 3, 4 and 5) clearly showed the presence of diastereoisomeric mixtures, and the ratio is 10:1). Eventually, hydrogen-bonding effects (prediction C, Scheme 4) was put forward, and variable-temperature (VT) $^{1}$H NMR studies (Figures 4 and 5) of compound **21** were performed in order to confirm this


dx.doi.org/10.1021/jf503794g | J. Agric. Food Chem. 2014, 62, 9987−9999

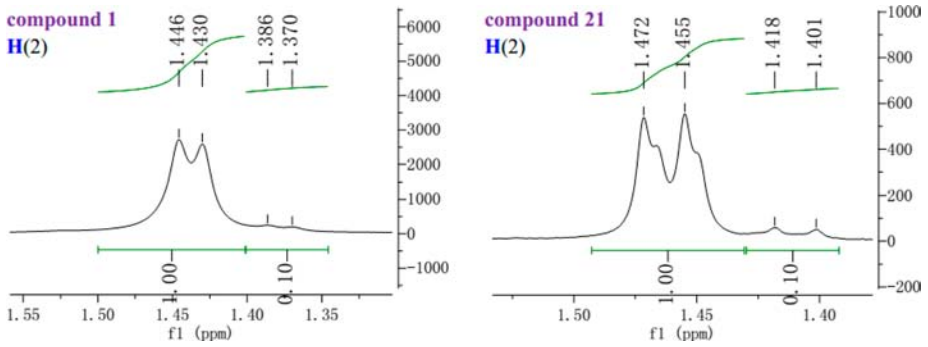


**Figure 5.** $^{1}$H NMR (H2) of compounds **1** and **21**.

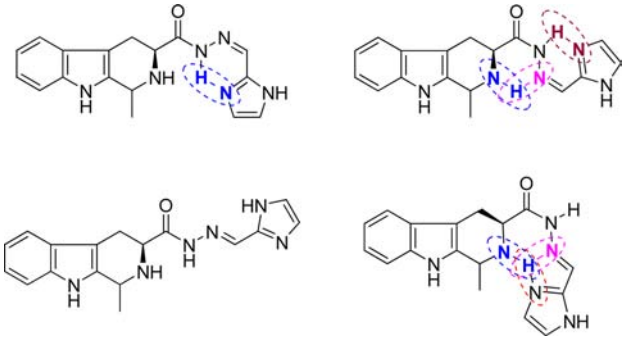

**Figure 6.** Hydrogen-bonding effects of compound **25**.

hypothesis. As we can see, the coalescence of signals was observed in the entire $^{1}$H NMR spectrum with the rise of the temperature (20 → 40 → 60 → 80 °C). Therefore, the VT $^{1}$H NMR studies indicated that the doubling of signals in the $^{1}$H and $^{13}$C NMR spectra was very likely due to hydrogen-bonding effects. In addition, it also could explain the appearance of four sets of signals in compound **25** (Figure 6).

**Antiviral Activities.** In our previous work, high antiviral lead compound **1** was found, on the basis of which, a series of derivatives containing acylhydrazone structure were synthesized to investigate the influence of the variation in the basic skeleton of **1**. The acylhydrazone compounds exhibited excellent antiviral activity. The antiviral results *in vitro* and *in vivo* (protection, inactivation, and curative) are listed in Tables 1 and 2. Overall, compared with ribavirin, most of the newly designed compounds exhibited desirable anti-TMV activity *in vitro*. Compounds **8**, **9**, **12**, **16**, **28**, **29**, and **30** showed much higher inhibition than that of ribavirin and their precursor **1** at 500 and 100 μg/mL. Especially, the activity of compound **16** was 36.9% at 100 μg/mL, which was very close to that of Ribavirin (40%) at 500 μg/mL.

When the C ring (Figure 3) was tetrahydropyridine, the in vitro activity of compound **1** (40.4%, 500 μg/mL) was a little lower than that of the β-carboline compound **2** (43.9%, 500 μg/mL); however, activity of compound **3** (55.8%, 500 μg/mL) was obviously higher than that of compound **4** (41.8%, 500 μg/mL). On the other hand, the activity of compound **1** (40.4%, 500 μg/mL) showed obviously lower inhibition than that of compound **3** (55.8%, 500 μg/mL), which proved that it is advantageous to improve the activity if the hydrazide structure at the 3-position of tetrahydrogen-β-carboline was changed to acylhydrazone. Hence, a representative set of compounds containing acylhydrazone structure were designed to search for better-activity compounds. Additionally, the

**Table 1. *In Vitro* Antiviral Activities of Compounds 1−33 against TMV**

| compd | concn (μg/mL) | inhibition rate (%) | compd | concn (μg/mL) | inhibition rate (%) |
|---|---|---|---|---|---|
| 1 | 500 | 40.4 | 18 | 500 | 40.9 |
| | 100 | 14.9 | | 100 | 0 |
| 2 | 500 | 43.9 | 19 | 500 | 36.6 |
| | 100 | 23.8 | | 100 | 0 |
| 3 | 500 | 55.8 | 20 | 500 | 33.3 |
| | 100 | 28.4 | | 100 | 0 |
| 4 | 500 | 41.8 | 21 | 500 | 32.7 |
| | 100 | 10.5 | | 100 | 0 |
| 5 | 500 | 49.6 | 22 | 500 | 48.8 |
| | 100 | 10.8 | | 100 | 15.4 |
| 6 | 500 | 52.4 | 23 | 500 | 49.5 |
| | 100 | 17.6 | | 100 | 8.8 |
| 7 | 500 | 56.8 | 24 | 500 | 58.5 |
| | 100 | 20.4 | | 100 | 23 |
| **8** | **500** | **62.8** | 25 | 500 | 42.4 |
| | 100 | 19.6 | | 100 | 0 |
| **9** | **500** | **67.3** | 26 | 500 | 35.2 |
| | **100** | **30.8** | | 100 | 0 |
| 10 | 500 | 56.8 | 27 | 500 | 32.6 |
| | 100 | 20.1 | | 100 | 7.8 |
| 11 | 500 | 50.7 | **28** | **500** | **61.3** |
| | 100 | 15.1 | | **100** | **23.2** |
| **12** | **500** | **62.5** | **29** | 500 | 59.6 |
| | **100** | **28.7** | | **100** | **31.2** |
| 13 | 500 | 53.2 | **30** | **500** | **64.4** |
| | 100 | 13.2 | | **100** | **27.5** |
| 14 | 500 | 38.5 | 31 | 500 | 30.2 |
| | 100 | 0 | | 100 | 9.2 |
| 15 | 500 | 37.2 | 32 | 500 | 58.1 |
| | 100 | 7.8 | | 100 | 25.6 |
| **16** | **500** | **72.6** | 33 | 500 | 43.4 |
| | **100** | **36.9** | | 100 | 8.6 |
| 17 | 500 | 46.5 | Ribavirin | 500 | 40 |
| | 100 | 19.8 | | 100 | 12.9 |

structure−activity relationship (SAR) demonstrated that the chirality at the 3-position of tetrahydrogen-β-carboline affected slightly the antiviral activity; for instance, compound **3** (3*S*,


dx.doi.org/10.1021/jf503794g | J. Agric. Food Chem. 2014, 62, 9987−9999

Table 2. *In Vivo* Antiviral Activities of Compounds 1−33 against TMV

| compd | concn (μg/mL) | inactivation effect (%) | curative effect (%) | protection effect (%) |
|---|---|---|---|---|
| 1 | 500 | 40 | 42.3 | 39.6 |
| | 100 | 8.5 | 10.3 | 13.4 |
| 2 | 500 | 55.4 | 58.9 | 49.7 |
| | 100 | 21.4 | 16.9 | 19.2 |
| 3 | 500 | 56.8 | 53.1 | 58.4 |
| | 100 | 23.4 | 26.5 | 24.7 |
| 4 | 500 | 47.1 | 45 | 47.9 |
| | 100 | 13.8 | 7.9 | 19.4 |
| 5 | 500 | 51.7 | 47.6 | 48.2 |
| | 100 | 12.3 | 19.5 | 8.9 |
| 6 | 500 | 50.3 | 47 | 53.8 |
| | 100 | 13.3 | 18.2 | 21.7 |
| **7** | **500** | **64.5** | **60.4** | **62.4** |
| | **100** | **25** | **23.1** | **18.9** |
| 8 | 500 | 58.3 | 57.1 | 61.5 |
| | 100 | 27.4 | 20.8 | 21.4 |
| **9** | **500** | **70.4** | **71.5** | **64.2** |
| | **100** | **35.9** | **29.2** | **34.1** |
| **10** | **500** | **66.7** | **60.4** | **57.2** |
| | **100** | **28.5** | **31.5** | **18.6** |
| 11 | 500 | 55.2 | 48.9 | 48.1 |
| | 100 | 20.4 | 23.5 | 14.8 |
| **12** | **500** | **69.1** | **66.4** | **70** |
| | **100** | **30.4** | **34.8** | **31.8** |
| 13 | 500 | 59.2 | 54 | 54.7 |
| | 100 | 22.1 | 16.5 | 20.6 |
| 14 | 500 | 43.2 | 36.4 | 34.8 |
| | 100 | 0 | 10.9 | 0 |
| 15 | 500 | 47.1 | 40.5 | 42.3 |
| | 100 | 20.3 | 16.2 | 11 |
| **16** | **500** | **74.5** | **69** | **68.1** |
| | **100** | **33.6** | **30.2** | **35.8** |
| 17 | 500 | 43.6 | 48.1 | 46 |
| | 100 | 15.2 | 18.6 | 10.3 |
| 18 | 500 | 45.6 | 43.9 | 47.8 |
| | 100 | 16.9 | 8.2 | 0 |
| 19 | 500 | 43.4 | 39.6 | 37.5 |
| | 100 | 8.8 | 12.9 | 0 |
| 20 | 500 | 41 | 36.9 | 33.6 |
| | 100 | 11.2 | 5.7 | 0 |
| 21 | 500 | 38.9 | 36.8 | 31.4 |
| | 100 | 9.2 | 0 | 0 |
| 22 | 500 | 54.6 | 44.2 | 47.5 |
| | 100 | 18.2 | 9.3 | 11.5 |
| **23** | **500** | **61.3** | **63.4** | **54.7** |
| | **100** | **20.2** | **27.8** | **30** |
| 24 | 500 | 59.1 | 52.3 | 61.3 |
| | 100 | 29.6 | 25.1 | 31.8 |
| 25 | 500 | 49.6 | 45.3 | 48.1 |
| | 100 | 21.3 | 12.6 | 18.5 |
| 26 | 500 | 47 | 33.2 | 37.1 |
| | 100 | 8.5 | 0 | 6.7 |
| 27 | 500 | 47.1 | 41.3 | 40.5 |
| | 100 | 13.4 | 10.4 | 11.3 |
| **28** | **500** | **73.4** | **70.9** | **59.6** |
| | **100** | **32.8** | **31.7** | **27.3** |
| **29** | **500** | **75.8** | **62.8** | **69.2** |
| | **100** | **36.3** | **30.4** | **25.7** |
| **30** | **500** | **63.7** | **68.2** | **66.8** |
| | **100** | **28.9** | **36.8** | **33.4** |
| 31 | 500 | 39.5 | 34.8 | 37.2 |
| | 100 | 13.6 | 11.1 | 7.9 |
| 32 | 500 | 59.7 | 55.4 | 56.8 |
| | 100 | 21.3 | 16.7 | 18.9 |
| 33 | 500 | 33 | 41.9 | 46.2 |
| | 100 | 12.8 | 10.9 | 14.3 |
| Ribavirin | 500 | 37.6 | 39.4 | 37.9 |
| | 100 | 12.3 | 11.9 | 14 |

55.8%, 500 μg/mL) was slightly more active than compound **5** (3*R*, 49.6%, 500 μg/mL).

Furthermore, it was noteworthy that the substituents of the acylhydrazone moiety had a significant impact on anti-TMV activity.

When $R^2$ was hydrogen and $R^1$ was a benzene ring, it was universally advantageous to anti-TMV activity if substituents were introduced to the 4-position of the benzene ring such as **7** (56.8%, 500 μg/mL), **8** (62.8%, 500 μg/mL), **9** (67.3%, 500 μg/mL), and **12** (62.5%, 500 μg/mL). Monosubstitution or multisubstitution on the benzene ring affected anti-TMV activity to a certain extent, for instance, compared with compounds **10** (56.8%, 500 μg/mL) and **11** (50.7%, 500 μg/mL), the monosubstituted compound **9** exhibited significantly higher activity. In addition, the position of the substituent group also was favored to increase anti-TMV activity; the activity of compound **12** (62.5%, 500 μg/mL) was much better than that of **13** (53.2%, 500 μg/mL) and **14** (38.5%, 500 μg/mL), the order of their activities was para > meta > ortho. However, the activity was greatly reduced when the benzene ring was changed to a naphthalene ring, such as **18** (40.9%, 500 μg/mL).

Interestingly, compound **16** (72.6%, 500 μg/mL) exhibited excellent inhibitory effect; in contrast, compounds **15** (37.2%, 500 μg/mL) and **17** (46.5%, 500 μg/mL) were far less effective. We speculated it could be ascribed to the tension on the five-membered ring of **16**, which inhibited the conjugation of the lone-pair electrons of oxygen atoms with the benzene ring.

When $R^2$ was hydrogen and $R^1$ was a heterocyclic ring, the anti-TMV activities of these compounds (**19**−**25**) reduced obviously compared with those of compounds with substituted benzene (**3**, **5**−**18**).

When $R^2$ was hydrogen and $R^1$ was an aliphatic substituent, both the length of the aliphatic chain and the number of branched chains affected anti-TMV activity; the more branched and the longer was the aliphatic chain, the better was the


dx.doi.org/10.1021/jf503794g | J. Agric. Food Chem. 2014, 62, 9987−9999

**Table 3. Fungicidal Activity of Compounds 1−4 and Compounds 6−33 against Fourteen Kinds of Phytopathogens**

| compd | fungicidal activity (%)/50 mg/kg | | | | | | | | | | | | | |
|---|---|---|---|---|---|---|---|---|---|---|---|---|---|---|
| | F.C.[a] | C.H | P.P | A.S | F.G | F.M | S.S | P.C | R.C | B.M | W.A | P.I | R.S | B.C |
| 1 | 13.6 | 18.2 | 39.4 | 9.5 | 38.5 | 29.4 | 30.8 | 51.5 | 54.1 | 24.0 | 24.0 | 26.1 | 4.2 | 27.8 |
| 2 | 34.6 | 35.3 | 55.6 | 25.0 | 24.1 | 0.0 | 11.8 | 7.9 | 43.1 | 12.0 | 11.1 | 16.0 | 13.2 | 13.6 |
| **3** | 36.4 | **72.7** | 36.4 | **57.1** | **53.8** | **58.8** | 26.9 | **69.7** | **86.5** | **60.0** | **52.0** | 30.4 | 48.6 | **88.9** |
| 4 | 15.4 | 17.6 | 55.6 | 20.0 | 44.8 | 7.1 | 35.3 | 18.4 | 43.1 | 12.0 | 14.8 | 16.0 | 13.2 | 36.4 |
| **6** | **65.4** | **82.4** | **97.2** | **70.0** | **41.4** | **57.1** | **94.1** | **73.7** | **98.0** | **84.0** | **77.8** | **76.0** | **88.2** | **86.4** |
| 7 | 38.5 | 76.5 | **97.2** | 65.0 | 31.0 | 35.7 | 41.2 | **78.9** | **96.1** | **64.0** | 48.1 | 72.0 | 63.2 | **72.7** |
| 8 | 38.5 | 58.8 | **72.2** | 45.0 | 58.6 | 42.9 | **88.2** | **78.9** | **88.2** | **60.0** | 48.1 | 52.0 | 59.2 | **72.7** |
| **9** | **61.5** | **76.5** | **97.2** | **55.0** | **75.9** | **64.3** | **88.2** | **81.6** | **94.1** | **68.0** | **77.8** | **80.0** | **81.6** | **59.1** |
| 10 | 27.3 | 45.5 | **48.5** | 42.9 | 53.8 | 47.1 | 46.2 | **60.6** | **56.8** | **56.0** | 60.0 | 39.1 | 45.8 | **52.8** |
| **11** | **77.3** | **72.7** | **97.0** | **71.4** | **76.9** | **70.6** | **84.6** | **84.8** | **97.3** | **80.0** | **80.0** | **65.2** | **62.5** | **80.6** |
| 12 | 23.1 | 64.7 | **72.2** | 30.0 | 65.5 | 64.3 | **94.1** | **73.7** | **84.3** | **68.0** | 55.6 | 52.0 | 59.2 | **59.1** |
| 13 | 34.6 | 58.8 | **69.4** | 65.0 | 41.4 | 57.1 | **88.2** | **81.6** | **92.2** | **48.0** | 40.7 | 40.0 | 68.4 | **68.2** |
| 14 | 26.9 | 23.5 | **88.9** | 45.0 | 72.4 | 21.4 | **64.7** | **63.2** | **78.4** | **56.0** | 40.7 | 44.0 | 32.9 | **77.3** |
| 15 | 22.7 | 45.5 | **66.7** | 52.4 | 30.8 | 47.1 | **21.2** | **84.8** | **89.2** | **52.0** | 72.0 | 30.4 | 44.4 | **66.7** |
| 16 | 31.8 | 63.6 | **63.6** | 52.4 | 53.8 | 58.8 | **44.2** | **81.8** | **86.5** | **56.0** | 48.0 | 39.1 | 50.0 | **88.9** |
| 17 | 22.7 | 45.5 | **66.7** | 52.4 | 30.8 | 47.1 | **21.2** | **84.8** | **89.2** | **52.0** | 72.0 | 30.4 | 44.4 | **66.7** |
| 18 | 19.2 | 47.1 | **77.8** | 30.0 | 10.3 | 28.6 | **88.2** | **84.2** | **86.3** | **56.0** | 48.1 | 44.0 | 28.9 | **72.7** |
| 19 | 23.1 | 35.3 | **52.8** | 15.0 | 27.6 | 21.4 | **64.7** | 28.9 | **66.7** | 28.0 | 29.6 | 24.0 | 23.7 | 36.4 |
| 20 | 38.5 | 41.2 | **83.3** | 15.0 | 62.1 | 50.0 | 35.3 | 26.3 | **80.4** | 32.0 | 40.7 | 52.0 | 39.5 | 54.5 |
| 21 | 23.1 | 23.5 | **75.0** | 20.0 | 20.7 | 21.4 | 5.9 | 18.4 | **41.2** | 16.0 | 25.9 | 12.0 | 21.1 | 36.4 |
| 22 | 11.5 | 52.9 | **69.4** | 35.0 | 6.9 | 28.6 | **64.7** | 39.5 | **68.6** | 20.0 | 33.3 | 36.0 | 32.9 | 81.8 |
| 23 | 23.1 | 23.5 | **97.2** | 15.0 | 41.4 | 14.3 | **58.8** | 42.1 | **74.5** | 28.0 | 29.6 | 24.0 | 32.9 | 22.7 |
| 24 | 26.9 | 47.1 | **55.6** | 45.0 | 62.1 | 28.6 | **88.2** | 68.4 | **72.5** | 44.0 | 44.4 | 36.0 | 46.1 | 72.7 |
| 25 | 34.6 | 47.1 | **97.2** | 15.0 | 27.6 | 28.6 | 35.3 | 18.4 | **64.7** | 12.0 | 25.9 | 24.0 | 15.8 | 36.4 |
| 26 | 26.9 | 29.4 | **52.8** | 30.0 | 20.7 | 14.3 | 41.2 | 31.6 | **64.7** | 36.0 | 22.2 | 32.0 | 6.6 | 40.9 |
| 27 | 19.2 | 17.6 | **69.4** | 45.0 | 6.9 | 0.0 | 64.7 | 5.3 | 43.1 | 12.0 | 14.8 | 20.0 | 6.6 | 9.1 |
| 28 | 9.1 | 36.4 | 24.2 | 19.0 | 61.5 | 35.3 | 46.2 | 18.2 | 29.7 | 36.0 | 32.0 | 17.4 | 22.2 | 44.4 |
| 29 | 4.5 | 0.0 | 33.3 | 19.0 | 30.8 | 41.2 | 21.2 | 9.1 | 29.7 | 36.0 | 24.0 | 17.4 | 5.6 | 66.7 |
| 30 | 4.5 | 18.2 | 36.4 | 19.0 | 46.2 | 29.4 | 15.4 | 12.1 | 48.6 | 20.0 | 24.0 | 17.4 | 8.3 | 36.1 |
| 31 | 0.0 | 36.4 | 39.4 | 33.3 | 61.5 | 29.4 | 11.5 | 36.4 | 51.4 | 36.0 | 52.0 | 26.1 | 15.3 | 69.4 |
| 32 | 4.5 | 36.4 | 36.4 | 14.3 | 53.8 | 23.5 | 3.8 | 18.2 | 48.6 | 28.0 | 32.0 | 30.4 | 8.3 | 41.7 |
| 33 | 0.0 | 18.2 | 9.1 | 19.0 | 46.2 | 29.4 | 7.7 | 12.1 | 48.6 | 32.0 | 32.0 | 26.1 | 15.3 | 52.8 |
| **carbendazim** | <50 | <50 | <50 | <50 | 100 | <50 | 100 | <50 | 100 | 100 | 100 | 100 | 100 | <50 |
| **chlorothalonil** | 100 | 73.3 | 100 | 73.3 | <50 | 100 | <50 | 100 | 100 | 91.3 | 91.3 | 86.4 | 100 | 100 |

[a] *F.C., Fusarium oxysporum* sp. *cucumeris*; *C.H., Cercospora arachidicola* Hori; *P.P., Physalospora piricola*; *A.S., Alternaria solani*; *F.G., Fusarium graminearum*; *F.M., Fusarium moniliforme*; *S.S., Sclerotinia sclerotiorum*; *P.C., Phytophthora capsici*; *R.C., Rhizoctonia cerealis*; *B.M., Bipolaris maydis*; *W.A.*, watermelon anthracnose; *P.I., Phytophthora infestans*; *R.S., Rhizoctonia solani*; *B.C., Botrytis cinerea*.

**Table 4. Insecticidal Activity of Compounds 1−4 and Compound 6−33 against Four Kinds of Insects**

| compd | larvicidal activity (%) at concn (mg/kg) | | | | |
|---|---|---|---|---|---|
| | *M. separata* | *H. armigera* | *O. nubilalis* | *C. pipiens pallens* | |
| | 600 mg/kg | 600 mg/kg | 600 mg/kg | 10 mg/kg | 5 mg/kg |
| 1 | 20 | 20 | 30 | 40 | — |
| 2 | 45 | 40 | 40 | 100 | 40 |
| **3** | **75** | **55** | **60** | **100** | **80** |
| 4 | 5 | 30 | 0 | 15 | — |
| 6 | 10 | 30 | 5 | 20 | — |
| 7 | 25 | 40 | 30 | 55 | — |
| 8 | 30 | 35 | 35 | 65 | — |
| 9 | 25 | 25 | 20 | 50 | — |
| 10 | 45 | 35 | 40 | 100 | 20 |
| 11 | 5 | 30 | 5 | 10 | — |
| 12 | 20 | 35 | 15 | 35 | — |
| 13 | 35 | 30 | 40 | 75 | — |
| 14 | 25 | 30 | 30 | 50 | — |
| 15 | 65 | 40 | 55 | 100 | 40 |
| 16 | 15 | 30 | 15 | 15 | — |
| 17 | 30 | 15 | 35 | 60 | — |
| 18 | 40 | 35 | 45 | 75 | — |
| 19 | 15 | 15 | 20 | 30 | — |
| 20 | 20 | 10 | 30 | 40 | — |
| 21 | 25 | 20 | 20 | 50 | — |
| 22 | 10 | 20 | 15 | 25 | — |
| **23** | **70** | **50** | **60** | **100** | **80** |
| 24 | 35 | 20 | 30 | 75 | — |
| 25 | 40 | 45 | 35 | 85 | — |
| 26 | 40 | 20 | 50 | 85 | — |
| 27 | 15 | 10 | 10 | 35 | — |
| 28 | 45 | 20 | 50 | 100 | 10 |
| 29 | 45 | 20 | 55 | 100 | 10 |
| 30 | 25 | 20 | 30 | 55 | — |
| 31 | 20 | 30 | 30 | 40 | — |
| 32 | 45 | 45 | 40 | 100 | 20 |
| 33 | 20 | 25 | 15 | 45 | — |

activity. For example, compound **26** containing an unsaturated aliphatic chain (35.2%, 500 μg/mL) and **27** (32.6%, 500 μg/mL) containing a saturated short-chain displayed lower anti-TMV activities than **28** (61.3%, 500 μg/mL), **29** (59.6%, 500 μg/mL), and **30** (64.4%, 500 μg/mL). When $R^2$ was methyl, the compounds **31** (30.2%, 500 μg/mL), **32** (58.1%, 500 μg/mL), and **33** (43.4%, 500 μg/mL) exhibited much lower antiviral activities than **3** (55.8%, 500 μg/mL), **30** (64.4%, 500 μg/mL), and **29** (59.6%, 500 μg/mL), which meant that the hydrogen-bond in N**H**═CH played an important role in the anti-TMV activity.

Further bioassay was conducted to investigate their inactivation, curative, and protection effect *in vivo* (Table 2). These results also showed that most of the compounds exhibited excellent antiviral activity and similar structure−activity relationship as the activities *in vitro*. Especially the activities of compounds **9** (70.4%, 71.5%, and 64.2% at 500 μg/mL), **12** (69.1%, 66.4%, and 70% at 500 μg/mL), **16** (74.5%, 69%, and 68.1% at 500 μg/mL), **28** (73.4%, 70.9%, and 59.6% at 500 μg/mL), **29** (75.8%, 62.8%, and 69.2% at 500 μg/mL), and **30** (63.7%, 68.2%, and 66.8% at 500 μg/mL) were much superior to ribavirin (37.6%, 39.4%, and 37.9% at 500 μg/mL). What is more, their anti-TMV activities (≥30%) at 100 μg/mL were close to ribavirin at 500 μg/mL.

**Fungicidal Activity.** The fungicidal results are listed in Table 3. Most of β-carboline, tetrahydrogen-β-carboline alkaloids, and their derivatives showed good fungicidal activities against 14 kinds of phytopathogens; especially compounds **6**, **9**, and **11** exhibited desirable fungicidal activities against each of the phytopathogens. Additionally, tetrahydrogen-β-carboline derivatives exhibited higher activities than β-carboline derivatives. When the skeleton was tetrahydrogen-β-carboline (C ring was tetrahydropyridine), the fungicidal activities were greatly affected by the substituents ($R^1$ and $R^2$) on the acylhydrozone. The compounds with one hydrogen and one aryl group (**3**, **5**−**25**) exhibited high activities against fungi; whereas the compounds with no hydrogen or with at least one alkyl group (**26**−**33**) exhibited relatively poor activities. Noteworthily, the compounds containing aryl groups exhibited fungicidal activities to certain fungi selectively; they showed apparently higher activities against *Physalospora piricola*, *Sclerotinia sclerotiorum*, *Phytophthora capsici*, *Rhizoctonia cerealis*, *Bipolaris maydi*, and *Botrytis cinerea* than the others.


dx.doi.org/10.1021/jf503794g | J. Agric. Food Chem. 2014, 62, 9987−9999

**Table 5. Results of Anti-TMV Activities of Field Trial in 2014 after 10 Days of Application of 9, 29, Amino-oligosaccharins, and Moroxydine Hydrochloride−Cupric Acetate**

| compd[a] | concn (gai/ha) | $I'_{eq}$ [b] | $I_{eq}$ [c] | $E$[d] (%) |
|---|---|---|---|---|
| **9** (1% EC) | 10 | 1.14 | 1.52 | 65.28 |
| | 50 | 1.86 | 4.92 | 80.82 |
| | 100 | 0.00 | 0.00 | 100.00 |
| **29** (1% ME) | 10 | 1.10 | 1.52 | 70.91 |
| | 50 | 0.79 | 0.00 | 100.00 |
| | 100 | 0.00 | 0.00 | 100.00 |
| blank control | | 2.56 | 5.23 | |
| amino-oligosaccharins (5% aqueous solution) | 100 | 3.33 | 3.33 | 66.67 |
| moroxydine hydrochloride−cupric acetate (20% WP) | 600 | 1.23 | 2.67 | 66.67 |

[a]EC, emulsifiable concentrate; ME, microemulsion; WP, wettable powder. [b]$I'_{eq}$, the average disease index of the spraying area before spraying. [c]$I_{eq}$, the average disease index of the spraying area 10 days after the third time spraying. [d]$E$, the average control effect 10 days after the third time spraying.

**Figure 7.** Effect of anti-TMV activities in field trials of compounds **9** and **29**.

**Insecticidal Activity.** These derivatives also showed broad-spectrum insecticidal activities (Table 4). What is more, compounds **3** and **23**, which contain a phenyl group or a pyrryl group, respectively, exhibited moderate insecticidal activity against the four kinds of insects (*Mythimna separata*, *Helicoverpa armigera*, *Ostrinia nubilalis*, and *Culex pipiens pallens*).

**Field Trials.** Because compounds **9** and **29** exhibited excellent anti-TMV activity in laboratory, 1% EC of compound **9** and 1% ME of compound **29** were evaluated for their anti-TMV activities in Tengchong County, Yunnan Province, China. Their efficacy was compared with the amino-oligosaccharins, moroxydine hydrochloride−cupric acetate, and an untreated control. Table 5 presents part of the results of field trials. Compounds **9** and **29** (Figure 7) exhibited better activities than control plant virus inhibitors. The results showed that the series of compounds, especially compound **29**, are promising for plant virus control.

In summary, we designed and synthesized a series of novel tetrahydrogen-$\beta$-carboline and $\beta$-carboline derivatives containing an acylhydrazide or acylhydrazone moiety at the 3-position. The hydrogen bonding effect was verified via variable-temperature (VT) $^1$H NMR studies. What is more, the target compounds exhibited good anti-TMV activity in the laboratory; especially, *in vivo*, inactivation, curative, and protection activities of compounds **8**, **9**, **12**, **16**, **28**, **29**, and **30** were much higher (57.1−75.8% at 500 $\mu$g/mL) than that of ribavirin (37.6%, 37.6%, 39.4%, and 37.9% at 500 $\mu$g/mL) and the lead compound **1** (40.4%, 40.0%, 42.3%, and 39.6% at 500 $\mu$g/mL), and the relevant SAR was summarized. At the same time, field trials of compounds **9** and **29** further demonstrated the antiviral efficacy against TMV. In addition, we were pleased to find that these compounds also showed broad-spectrum of fungicidal activity and insecticidal activity. For instance, compounds **3**, **6**, **9**, and **11** exhibited good inhibition of the 14 kinds of phytopathogens; compounds **3** and **23** exhibited moderate insecticidal activity against four kinds of investigated insects. Further studies on structural optimization are in progress in our laboratory.

## AUTHOR INFORMATION


### Corresponding Author

*Qingmin Wang. Tel: +86-(0)22-23503952; Fax: +86-(0)22-23503952; E-mail: wang98h@263.net; wangqm@nankai.edu.cn.


### Notes

The authors declare no competing financial interest.

## ACKNOWLEDGMENTS


This work was supported by the National Natural Science Foundation of China (Grants 21132003, 21121002, 21372131, and 21102077), the Specialized Research Fund for the Doctoral Program of Higher Education (Grant 20130031110017), and the Science Technology Plan Project of China Tobacco Yunnan Company (Grants 2012YN08, 2012YN11, and 2013YN37).


## REFERENCES


(1) El-Wakeil, N. E. Botanical Pesticides and Their Mode of Action. *Gesunde Pflanz.* **2013**, *65*, 125−149.

(2) Jacobson, M. Botanical pesticides, past, present, and future. *ACS Symp. Ser.* **1989**, *387*, 1−10.

(3) Isman, M. B. Botanical insecticides: For richer, for poorer. *Pest Manage. Sci.* **2008**, *64* (1), 8−11.

(4) Massaro, E. J. *Handbook of Neurotoxicology*; Humana Press: Totowa, NJ, USA, 2002; p 237.

(5) Callaway, J. C.; McKenna, D. J.; Grob, C. S.; Brito, G. S.; Raymon, L. P.; Poland, R. E.; Andrade, E. N.; Andrade, E. O.; Mash, D. C. Pharmacokinetics of Hoasca alkaloids in healthy humans. *J. Ethnopharmacol.* **1999**, *65* (3), 243−256.

(6) Reniers, J.; Robert, S.; Frederick, R.; Masereel, B.; Vincent, S.; Wouters, J. Synthesis and evaluation of $\beta$-carboline derivatives as potential monoamine oxidase inhibitors. *Bioorg. Med. Chem.* **2011**, *19* (1), 134−144.

(7) Srivastava, S. K.; Agarwal, A.; Chauhan, P. M. S.; Agarwal, S. K.; Bhaduri, A. P.; Singh, S. N.; Fatima, N.; Chatterjee, R. K. Potent 1,3-disubstituted-9*H*-pyrido[3,4-*b*]indoles as new lead compounds in antifilarial chemotherapy. *J. Med. Chem.* **1999**, *42* (9), 1667−1672.

(8) Tang, J. G.; Wang, Y. H.; Wang, R. R.; Dong, Z. J.; Yang, L. M.; Zheng, Y. T.; Liu, J. K. Synthesis of analogues of flazin, in particular, flazinamide, as promising anti-HIV agents. *Chem. Biodiversity* **2008**, *5* (3), 447−460.

(9) Miller, J. F.; Turner, E. M.; Sherrill, R. G.; Gudmundsson, K.; Sethna, A. S. P.; Brown, K. W.; Harvey, R.; Romines, K. R.; Golden, P. Substituted tetrahydro-$\beta$-carbolines as potential agents for the treatment of human papillomavirus infection. *Bioorg. Med. Chem. Lett.* **2010**, *20* (1), 256−259.

(10) Zhao, P. L.; Li, J.; Yang, G. F. Synthesis and insecticidal activity of chromanone and chromone analogues of diacylhydrazines. *Bioorg. Med. Chem.* **2007**, *15*, 1888−1895.

(11) Chen, Q.; Liu, Z. M.; Chen, C. N.; Jiang, L. L.; Yang, G. F. Synthesis and fungicidal activities of new 1,2,4-triazolo[1,5-*a*]-pyrimidines. *Chem. Biodiversity* **2009**, *6*, 1254−1265.

(12) Jin, Y.-X.; Zhong, A.-G.; Zhang, Y.-J.; Pan, F.-Y. Synthesis, crystal structure, spectroscopic properties, antibacterial activity and theoretical studies of a novel difunctional acylhydrazone. *J. Mol. Struct.* **2011**, *1002* (1−3), 45−50.
(13) Liu, X. H.; Liu, H. J.; Tan, C. X.; Weng, J. Q. Application of acylhydrazonederivatives as fungicide. Faming Zhuanli Shenqing, CN 101874496 A 2010.
(14) Fuog, D.; Fergusson, S. J.; Flückiger, C. Pymetrozine: A novel insecticide affecting aphids and whiteflies. In *Insecticides with Novel Modes of Action*. Springer: Berlin Heidelberg, 1998; pp 40−49.
(15) Jose, L.; Armes, N. J.; Farlow, R.; Aldridge, K.; Robin, F.; Tedeschi, L. Metaflumizone, a new broad-spectrum insecticide for crop protection. *Congress Proceedings 2007 of the XVI International Plant Protection Congress*; British Crop Protection Council: Hampshire, U.K., 2007; Vol. *1*, pp 74−81.
(16) Lym, R. G.; Christianson, K. M. Diflufenzopyr increases perennial weed control with auxin herbicides. *Proceedings of the Western Society of Weed Science (USA)*; Western Society of Weed Science: Las Cruces, NM, 1998.
(17) Yao, K.; Zhao, M.; Zhang, X. Y.; Wang, Y. J.; Li, L.; Zheng, M. Q.; Peng, S. Q. A class of oral *N*-[(1*S*,3*S*)-1-methyl-1,2,3,4-tetrahydro-*β*-carboline-3-carbonyl]-*N*′-(amino-acid-acyl)hydrazine: Discovery, synthesis, in *vitro* anti-platelet aggregation/in *vivo* anti-thrombotic evaluation and 3D QSAR analysis. *Eur. J. Med. Chem.* **2011**, *46*, 3237−3249.
(18) Song, H. J.; Liu, Y. X.; Liu, Y. X.; Wang, L. Z.; Wang, Q. M. Synthesis and antiviral and fungicidal activity evaluation of *β*-carboline, dihydro-*β*-carboline, tetrahydro-*β*-carboline alkaloids, and their derivatives. *J. Agric. Food Chem.* **2014**, *62* (5), 1010−1018.
(19) Takemiya, A.; Hartwig, J. F. Palladium-Catalyzed Synthesis of Aryl Ketones by Coupling of Aryl Bromides with an Acyl Anion Equivalent. *J. Am. Chem. Soc.* **2006**, *128* (46), 14800−14801.
(20) Joshi, S. D.; Vagdevi, H. M.; Vaidya, V. P.; Gadaginamath, G. S. Synthesis of new 4-pyrrol-1-yl benzoic acid hydrazide analogs and some derived oxadiazole, triazole and pyrrole ring systems: A novel class of potential antibacterial and antitubercular agents. *Eur. J. Med. Chem.* **2008**, *43*, 1989−1996.
(21) Wang, K. L.; Su, B.; Wang, Z. W.; Wu, M.; Li, Z.; Hu, Y. N.; Fan, Z. J.; Mi, N.; Wang, Q. M. Synthesis and antiviral activities of phenanthroindolizidine alkaloids and their derivatives. *J. Agric. Food Chem.* **2010**, *58* (5), 2703−2709.
(22) Zhao, H. P.; Liu, Y. X.; Cui, Z. P.; Beattie, D.; Gu, Y. C.; Wang, Q. M. Design, Synthesis, and Biological Activities of Arylmethylamine Substituted Chlorotriazine and Methylthiotriazine Compounds. *J. Agric. Food Chem.* **2011**, *59* (21), 11711−11717.

In this paper, modified hemicellulose-*graft*-carboxylic azobenzene hydrogels were prepared, which showed multiresponsive behaviors to light, pH, and water/ethanol alternating solutions. The chemical structures of the xylan-type hemicellulose derivative, azobenzene monomers, and the synthesized hydrogels were investigated using FT-IR and $^1$H and $^{13}$C NMR. The morphologies of the resulting hydrogels were characterized by using SEM. The water swelling ratios and swelling/deswelling behaviors of the hydrogels in different solvents were investigated. Furthermore, the in vitro drug release behaviors of the synthesized hydrogels were also studied by using vitamin $B_{12}$ ($VB_{12}$) as a model drug.

## MATERIALS AND METHODS

**Materials.** Xylan-type hemicelluloses were extracted from bamboo (*Dendrocalamus membranaceus* Munro, *Dm*M) according to our previous work.[29] The obtained xylan-type hemicelluloses mainly consisted of xylose (86.58%), arabinose (5.65%), glucose (1.97%), mannose (1.75%), galactose (0.69%), and glucuronic acid (2.80%). Glycidyl methacrylate (GMA), *p*-aminobenzoic acid, acryloyl chloride, 4-dimethylaminopyridine (DMAP), and azobis(isobutyronitrile) (AIBN) were purchased from Aladdin Reagent Co., Ltd., Shanghai, China. Other chemicals and solvents were of analytical reagent grade and used as received.

**Methods.** The scheme for the preparation of xylan-type hemicellulose-based hydrogel is illustrated in Scheme 1. The experimental details are given below.

**Scheme 1. Scheme for Preparation of Xylan-Type Hemicellulose-Based Hydrogel**

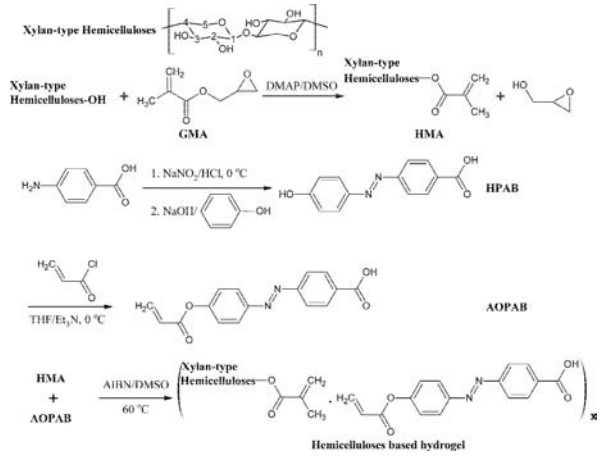


**Synthesis of Hemicellulose Methacrylate (HMA).** HMA was synthesized according to the method reported by De Smedt et al.[30] 10.0 g of dried xylan-type hemicelluloses was added into the flask with 90 mL of DMSO under magnetic stirring. The mixture was stirred vigorously at 90 °C for 0.5 h. After that, the temperature was adjusted to room temperature and 2.0 g of DMAP was added. Then 3.60 g of GMA was added to the solution corresponding to a ratio of 1 mol of GMA per 3 mol of anhydroxylose units. The reaction was carried out at room temperature for 48 h. At the end of the reaction, the mixture was added dropwise into 500 mL of ethanol under vigorous stirring. The separation, purification, and dehydration of HMA were performed according to the process reported in the literature.[30]

**Synthesis of 4-[(4′-Hydroxy)phenylazo]benzoic Acid (HPAB) and 4-[(4-Acryloyloxyphenyl)azo]benzoic Acid (AOPAB).** HPAB was synthesized according to the method reported by Chen et al.[28] A solution of $NaNO_2$ (4.14 g, 60 mmol) in 60 mL of $H_2O$ was added dropwise to a solution of 4-aminobenzoic acid (8.23 g, 60 mmol) in 24 mL of HCl (37%) in an ice water bath. The solution was stirred for 30 min and diluted with 300 mL of ice water. Then phenol (5.92 g, 63 mmol) and NaOH (2.52 g, 63 mmol) mixture in 30 mL of $H_2O$ was added dropwise at 0−5 °C. The mixture was stirred for 2 h, and the NaOH solution was added to precipitate the product, which was then washed with water and dried in a vacuum oven at 50 °C for 24 h. The structure of the orange product obtained was determined using $^1$H NMR. $^1$H NMR (DMSO-$d_6$): 7.01 (d, 2H), 7.85 (d, 2H), 7.89 (d, 2H), 8.12 (d, 2H). The $^1$H NMR spectrum of HPAB is illustrated in Figure S1 in the Supporting Information.

AOPAB was prepared by the reaction between acryloyl chloride and HPAB according to the method reported by Haitjema et al.[31] HPAB (3.63 g, 15 mmol) and triethylamine (5.06 g, 50 mmol) were dissolved in dry tetrahydrofuran (THF, 50 mL) and cooled in an ice water bath. A solution of acryloyl chloride (4.50 g, 50 mmol) in dry THF (15 mL) was added over 2 h, and the temperature was fixed at 0−5 °C and stirred for 48 h. At the end of reaction, the mixture was added dropwise to water. After filtration, the yellow precipitate was first dissolved in boiling acetic acid and subsequently crystallized during cooling down of the solution. The structure of the yellow product obtained was determined using $^1$H NMR. $^1$H NMR (DMSO-$d_6$): 6.22 (d, 1H), 6.46 (dd, 1H), 6.60 (d, 1H), 7.47 (d, 2H), 8.00 (dd, 4H), 8.16 (d, 2H). The $^1$H NMR spectrum of AOPAB is illustrated in Figure S2 in the Supporting Information.

**Preparation of Xylan-Type Hemicellulose-*graft*-photoisomeric Azobenzene Hydrogels.** HMA (1.0 g) and AOPAB (0.02, 0.04, 0.08, 0.12, and 0.16 g) were added into the test tube with 20 mL of DMSO, respectively. The mixture was shaken vigorously on a vortex mixer until completely homogeneous. Then AIBN (0.02 g) was added into the mixture as an initiator with nitrogen bubbling for 15 min. After mixing, the test tube was placed in a water bath at 60 °C for 24 h. The resultant hydrogels were cut into a single slice about 2 mm thick and first immersed in ethanol for 3 days and then dialyzed in deionized water for 1 week. The prepared hydrogels were freeze-dried in a freeze drier at −50 °C. The conditions of synthesizing the hydrogels are illustrated in Table 1.

**Table 1. Synthesis Conditions of the Prepared Hydrogels**

| samples | HMA/g | AOPAB/wt %[a] | AIBN/g |
|---|---|---|---|
| H1 | 1.0 | 2 | 0.02 |
| H2 | 1.0 | 4 | 0.02 |
| H3 | 1.0 | 8 | 0.02 |
| H4 | 1.0 | 12 | 0.02 |
| H5 | 1.0 | 16 | 0.02 |

[a]The mass ratio of AOPAB to HMA.

**Characterizations.** The composition of neutral sugars and uronic acids in the xylan-type hemicelluloses was detected by high-performance anion-exchange chromatography (HPAEC, Dionex ICS3000, U.S.) with pulsed amperometric detector, a Carbopac PA-20 column (4 × 250 mm, Dionex), and a guard PA-20 column (3 × 30 mm, Dionex). 18 mM NaOH was used as mobile phase at a flow rate of 0.4 mL/min.[32] FT-IR spectra of xylan-type hemicelluloses, HMA, and prepared hydrogels were recorded on a Bruker Tensor 27 spectrophotometer in the range of 4000−400 cm$^{-1}$ with a resolution of 4 cm$^{-1}$. A KBr disk containing 1% finely ground sample was used for measurement. $^1$H NMR spectra of HPAB and AOPAB and $^{13}$C NMR spectra of xylan-type hemicelluloses and HMA were carried out on a Bruker DRX-400 spectrometer operating at 400.12 MHz for $^1$H NMR and 100.62 MHz for $^{13}$C NMR. Xylan-type hemicelluloses in 1.0 mL of $D_2O$ and HPAB, AOPAB, HMA in 1.0 mL of DMSO-$d_6$ was used for NMR measurement (20 mg for $^1$H NMR, 80 mg for $^{13}$C NMR), respectively. A scanning electron microscope (ZEISS EVO 18, Germany) was used to record the morphologies of the hydrogels. The accelerating voltage of the instrument was maintained at 10.00 kV. Ultraviolet visible spectroscopy (S-3100, Scinco) was used to measure the time-dependent light sensitive behavior of the hydrogel and drug concentration in PBS.

**Measurement of Time- and pH-Dependent Swelling Ratios.** The swelling ratio of the hydrogel in distilled water as a function of

time was measured as follows. Preweighed dried hydrogel ($m_0$) was immersed into excessive distilled water, and the mass of the wet hydrogel ($m_t$) was determined at regular intervals after removal of the surface water with filter paper. The swelling experiments were performed twice to check the reproducibility. The swelling ratio (SR) was calculated by the following equation:

$$SR = (m_t - m_0)/m_0 \quad (1)$$

where $m_0$ and $m_t$ were the weights of dried and swollen hydrogels, respectively.

The pH sensitivity of the hydrogel was investigated by immersing about 1.0 g of sample into phosphate buffer solutions of pH 2.0, 4.0, 5.9, 7.4, 9.0, and 10.8 for 48 h at 37 °C to reach equilibrium. Since the SR of the hydrogel is also influenced by the ionic strength of the solution, the ionic strengths of these phosphate buffer solutions with various pH values were adjusted to 0.1 M with NaCl. The SR values of the hydrogels in various pH buffer solutions were measured using a similar method for water absorption and calculated according to eq 1.

**Swelling and Deswelling Behaviors of Hydrogel in Different Buffer Solutions.** The swelling and deswelling behaviors of the hydrogel in response to pH were carried out in different buffer solutions (pH 2.0 and 7.4). The swollen samples in water were first immersed in buffer solution of pH 7.4 for 30 min and weighed. Then the swollen samples were soaked in the buffer solution with pH 2.0 for another 30 min and weighed again. The procedure was repeated to record the swelling and deswelling performances of the hydrogel in buffer solutions of different pH values.

**Swelling and Deswelling Behaviors of Hydrogel in Water/Ethanol Alternating Solutions.** The swelling and deswelling behaviors of the hydrogel in response to water/ethanol alternating solutions were carried out as follows. The swollen samples in water were first immersed in ethanol and weighed per 100 s. After 10 min, the swollen samples were soaked in water and weighed per 100 s for another 10 min. The procedure was repeated to record the swelling and deswelling performances of the hydrogel in different solvents.

**Light Response Behavior of Hydrogel.** Dried hydrogel was first ground into a fine powder by using a Mikro-dismembrator S homogenizer (Sartorius, Goettingen, Germany) for light response test. Then it was transferred into plenty of distilled water for 48 h. The hydrogel was recovered by filtration and washed with plenty of distilled water. Next the hydrogel was dispersed into a certain amount of distilled water again. UV irradiation was carried out in an ultraviolet analyzer, which could emit UV light at 365 nm. The UV/vis spectra of the hydrogels as a function of irradiation time were recorded by ultraviolet visible spectroscopy (S-3100, Scinco).

**The Maximum Drug Release and in Vitro Drug Release Behavior of Hydrogel.** The maximum drug release was carried out by swelling the preweighed hydrogel in sufficient vitamin $B_{12}$ ($VB_{12}$) solution (0.5 mg/mL). After swelling in the solution for 48 h, the hydrogel was taken out and freeze-dried. To determine the maximum drug release, the hydrogel was first ground into fine powder. Then, the powder was put into a certain amount of water to maximize the drug release. The solution was filtered through a 0.22 $\mu$m filter, and the filtrate was determined by measuring its absorbance at 375 nm using a UV spectrophotometer to calculate the maximum drug release of the hydrogel. The drug concentrations were calculated based on the determined calibration curves.

In this work, $VB_{12}$ was used as a model hydrophilic drug to investigate the release behavior of the synthesized hydrogel in vitro. First, 20 mL of PBS (pH 7.4 or pH 2.2) was added into 50 mL of transparent tube and maintained in an incubator at 37 ± 0.3 °C with or without UV irradiation at 365 nm. Then, a certain amount of dried $VB_{12}$ loaded hydrogel was put into the PBS solution. The hydrogel was immersed in 20 mL of PBS (pH 7.4 or pH 2.2) and shaken at 100 rpm at 37 °C. At specific time intervals, 1.0 mL of PBS solution was removed and replaced by 1.0 mL of fresh PBS solution. After centrifugation at 10,000 rpm for 10 min, the supernatant of the PBS solution was collected and stored at −20 °C for further analysis. The collected supernatants were detected on a UV spectrophotometer at 375 nm to determine the concentration of $VB_{12}$. The drug cumulative release profiles were plotted as a function of time.

## RESULTS AND DISCUSSION

**FT-IR Analysis of Xylan-Type Hemicelluloses, HMA, and Prepared Hydrogels.** The FT-IR spectra of xylan-type hemicelluloses, HMA, and the prepared hydrogel (H3) were recorded and are illustrated in Figure 1. The strong and wide

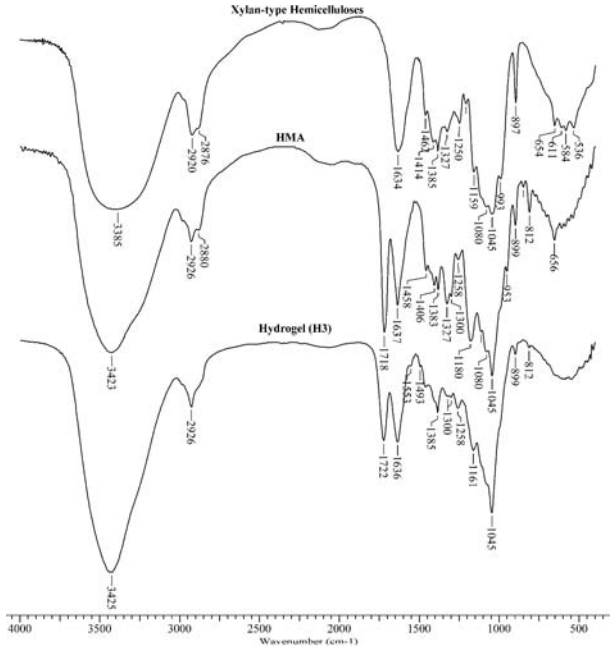


**Figure 1.** FT-IR spectra of xylan-type hemicelluloses, HMA, and the synthesized hydrogel (H3).

absorption at 3423 $cm^{-1}$ is attributed to the hydroxyl stretching vibration, and the bands at 2926 and 2880 $cm^{-1}$ are related to the C−H asymmetric and symmetrical vibrations of alkanes, respectively. These signals in the spectra are originated from the anhydrosugar unit of xylan-type hemicelluloses. The strong bands in the region 1200−1000 $cm^{-1}$ in xylan-type hemicelluloses are mainly from the ring vibrations and C−O−C glycosidic bond vibration overlapped with C−OH group stretching vibration.[33] The absorption band at 1634 $cm^{-1}$ in the spectrum of xylan-type hemicelluloses is assigned to the bending mode of the absorbed water. However, the band at 1637 $cm^{-1}$ in the spectrum of HMA is much sharper than that in xylan-type hemicelluloses. This is very likely related to the C═C in HMA, which shows the sharp C═C stretching signals at around 1630 $cm^{-1}$. Furthermore, HMA displays much stronger bands at 1327, 1300, and 1180 $cm^{-1}$ than xylan-type hemicelluloses, which originate from the C−H in-plane bending vibration of alkenes and C−O−C stretching of carboxylic esters. The small sharp band at 812 $cm^{-1}$ in HMA is related to the $CH_2$ out of plane bending of alkenes, and it can be seen that this band is absent in the xylan-type hemicelluloses. Two small absorption signals at 1553 and 1493 $cm^{-1}$ in the synthesized hydrogel originate from the aromatic skeletal vibration of aromatic structures. Signals at 1327, 1300, and 812 $cm^{-1}$ related to the C═C groups in hydrogel are much lower than those in HMA, suggesting that, during the preparation of the hydrogels, most C═C groups of HMA react with AOPAB by free radical reaction. These signal changes observed in the

FT-IR spectra preliminarily confirmed the successful synthesis of HMA and the target hydrogel.

**$^{13}$C NMR Analysis of Xylan-Type Hemicelluloses and HMA.** In this work, HMA is an important intermediate in the preparation of xylan-type hemicellulose-based hydrogel. The introduction of C═C groups into hemicelluloses makes HMA easy to polymerize with AOPAB. In order to ensure the accurate structure of HMA, $^{13}$C NMR spectra of xylan-type hemicelluloses and HMA were performed and are illustrated in Figure 2.

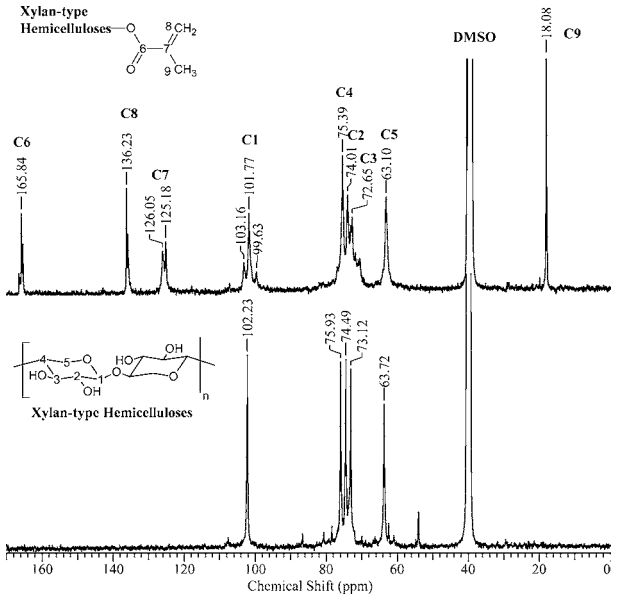


**Figure 2.** $^{13}$C NMR spectra of xylan-type hemicelluloses and HMA.

As seen in the $^{13}$C NMR spectrum of xylan-type hemicelluloses, five strong signals at 101.73, 76.43, 74.27, 68.25, and 63.02 ppm originating from the main 1,4-linked $\beta$-D-xylopyranosyl units can be observed apparently, which are assigned to the C1, C2, C3, C4, and C5 positions of the xylan backbone, respectively. In the $^{13}$C NMR spectrum of HMA, except the signals from xylan backbone, signals from acrylate groups also appear. Chemical shifts at 165.84, 136.23, 126.05 (125.18), and 18.08 ppm originate from C6, C8, C7, and C9 of HMA, respectively. These signals are all assigned and shown in Figure 2. In addition, the signal splitting of C7 (126.05 and 125.18 ppm) and C1 (103.16, 101.77, and 99.63) is likely caused by the substituted position difference of acrylate in the xylan backbone, and a similar phenomenon had been reported in other hemicelluloses derivatives.[34]

**Morphology of Hydrogels.** Figure 3 shows the SEM images of the cross section of the freeze-dried hydrogels with different contents of AOPAB. Honeycomb-like architecture could be observed in H1−H4, while cracklike structure can be found in H5 due to its high crossing density. Furthermore, as the content of AOPAB increased, the observed pore volume decreased significantly. The decrease of hydrogel pore volume was further confirmed by the swelling behavior later. This is likely related to the reactivity ratio of HMA and AOPAB. There are still visible residual C═C groups in the FT-IR spectrum of the hydrogel after reaction at 60 °C for 24 h, suggesting that the poor self-polymerization rate of HMA and AOPAB might be responsible for this phenomenon. It was assumed that the copolymerization between HMA and AOPAB could have led to an increase in cross-linking density and then caused the pore volume decrease.

**Time-Dependent Swelling Behaviors of Hydrogels.** The swelling ability is one of the most important factors of a hydrogel, which is correlated with many of its properties, such as permeability, drug loading, and mechanical characteristics.[35] Therefore, the swelling ability of the prepared hydrogels with different contents of AOPAB in deionized water was measured as a function of time and is illustrated in Figure 4.

The swelling ratios of the dried hydrogels increased at a fast rate during the first 3 h and then achieved a swelling equilibrium about 4 h later. The maximum swelling degrees of these hydrogels (from H1 to H5) were 9.8, 8.4, 6.7, 2.8, and 2.2 g/g in deionized water, respectively, which were in accordance with the pore volume decrease of hydrogels with the increase of AOPAB content, as observed in their SEM images. It indicated that AOPAB content showed a significant effect on the swelling process of the hydrogels. As the dried hydrogels were immersed in water, partial carboxylic groups (−COOH) originating from AOPAB were gradually ionized into carboxylate groups (−COO$^-$). The formation of anion−anion electrostatic repulsion forces within the three-dimensional polymer structure caused the hydrogel network sustained expansion. As the carboxylic group further reached its

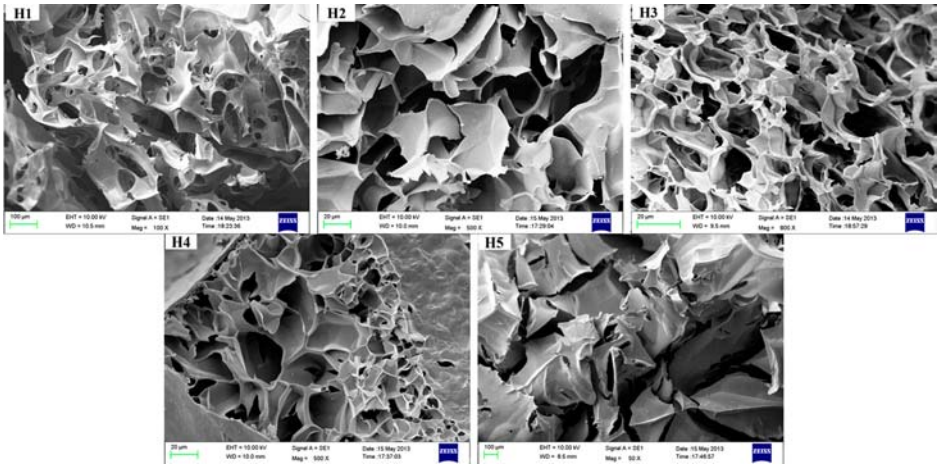


**Figure 3.** SEM images of the cross section of the freeze-dried hydrogels with different contents of AOPAB.

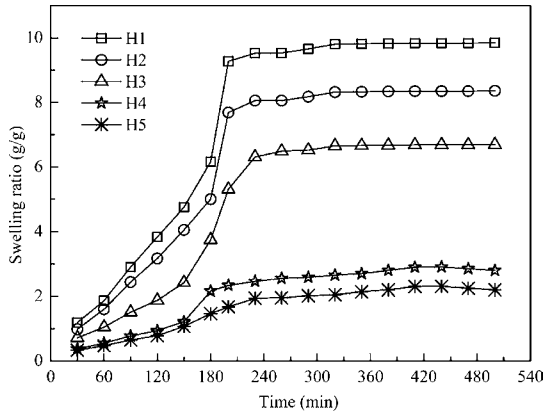


**Figure 4.** Swelling behavior of the hydrogels in water as a function of time.

ionization equilibrium, the swelling of the hydrogel also achieved a maximum.

**pH-Dependent Swelling Behaviors of Hydrogels.** Stimulus-responsive behavior is an important property of a hydrogel. Figure 5 illustrates the equilibrium swelling ratios

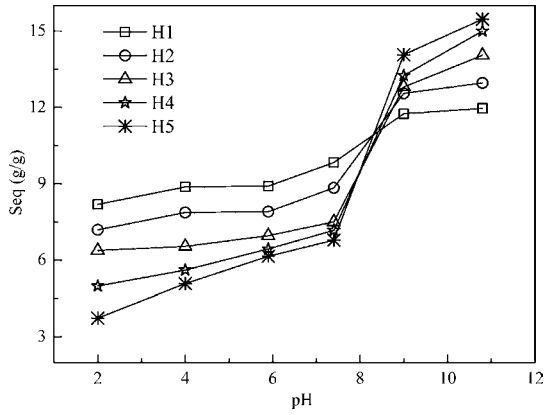


**Figure 5.** Equilibrium swelling ratios of the obtained hydrogels as a function of pH.

($S_{eq}$) of the obtained hydrogels with different amounts of AOPAB in solutions of different pH values. The equilibrium swelling ratio of all hydrogels increased with the pH of the initial solution. It was assumed that as the pH increased from 2.0 to 10.8, more −COOH groups in the hydrogel were ionized into $-COO^-$ groups. The anion−anion electrostatic repulsion forces were strengthened and the hydrogel networks were expanded gradually, thus resulting in the high swelling ratio of the hydrogel at the high pH value.

In the pH range of 2.0 to 7.4, the hydrogels containing a lower content of AOPAB showed higher $S_{eq}$ values. A similar result was found in their water absorption test. However, as compared with $S_{eq}$ in pH 2.0−7.4, the hydrogels showed opposite swelling capacities as the pH increased to 9.0 and 10.8. It was observed that in the solution of pH 9.0 and 10.8, the higher the AOPAB content was, the lower the $S_{eq}$ value was. The $S_{eq}$ value of H5 in pH 10.8 was 4.15 times higher than that in pH 2.0, while this value was only 1.46 for H1. It can be deduced that, at lower pH value, almost all carboxyl groups exist in the COOH form, and the solution absorption capacity mainly depends on the pore volume of the hydrogel. The $S_{eq}$ values are well in line with the pore changes observed in their SEM images. However, most carboxyl groups exist in the $-COO^-$ form in alkaline solution, thus the electrostatic repulsion forces will dominate the solution absorption capacity of the hydrogel. High AOPAB content will lead to high $S_{eq}$ value of hydrogel. Therefore, the hydrogel with a higher content of AOPAB showed a stronger pH responsive behavior.

**Swelling and Deswelling Behaviors of Hydrogel in Buffers.** Reusability is another important factor that is associated with the applications of hydrogel. In this study, the swelling and deswelling behaviors of the hydrogel (H5) in the buffer solutions with pH 2.0 and 7.4 at 37 °C are shown in Figure 6. When the swollen hydrogel in the buffer of pH 7.4

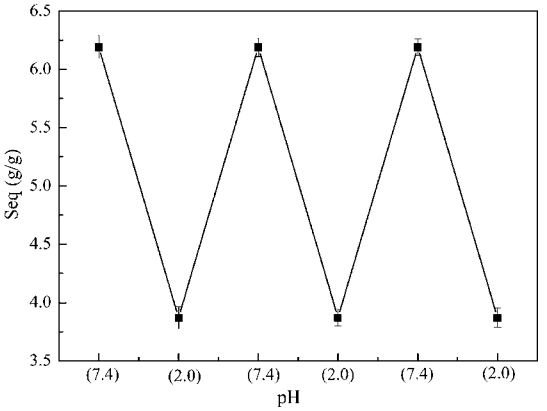


**Figure 6.** Swelling and deswelling ability of the hydrogel (H5) in the buffer solutions of pH 2.0 and 7.4.

was transferred into the solution of pH 2.0, the swelling ratio of H5 decreased from ∼6.2 g/g to ∼3.9 g/g. According to the results from pH-dependent swelling test, the carboxylates ($-COO^-$) would be generally protonated into carboxyl groups with the pH decrease and further resulted in the deswelling of the hydrogel. When the hydrogel was put into the solution of pH 7.4 again, these carboxyl groups would be ionized into $-COO^-$ again and the electrostatic repulsion forces induced the expansion of the hydrogel network and finally led to the reswelling of the hydrogel. After three swelling and deswelling cycles, no obvious decrease in swelling could be observed. A similar result was also reported in other hemicellulose-based poly(acrylic acid) hydrogel.[11]

**Swelling and Deswelling Behaviors of Hydrogel in Water and Ethanol Alternating Solutions.** To investigate the response behavior of the hydrogel in organic solvent and its recycle performance, the swelling and deswelling behaviors of the hydrogel (H1) in distilled water and ethanol alternating solutions are shown in Figure 7. As can be seen, the swollen hydrogel in distilled water rapidly deswelled in ethanol. When the shrunken hydrogel was put into distilled water again, it would expand again within a short period. It was reported that the swelling capacity of the hydrogel in organic solvents was closely related to the solubility parameter of the solvent and dielectric constant as well as the interaction between the polar groups of solvents and the ionic groups in the polymer network.[11,36,37] The Hildebrand solubility parameter and the relative dielectric constant of water and ethanol are 23.4 and 12.9 $cal^{1/2}$ $cm^{-3/2}$, respectively.[38] According to the Hildebrand equation, to dissolve a polymer in a solvent, the solubility parameter values must be close to each other.[37] To our best knowledge, almost all hydrogels with hydrophilic groups


dx.doi.org/10.1021/jf504040s | J. Agric. Food Chem. 2014, 62, 10000−10007

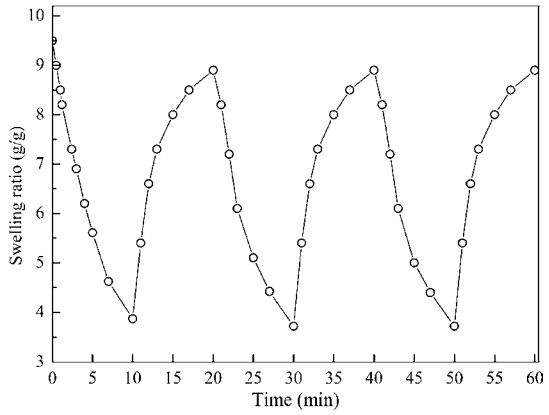


**Figure 7.** Swelling and deswelling behavior of the hydrogel (H1) in water/ethanol alternating solutions.

showed higher swelling ratios in water than in organic solvent,[11,36] suggesting that the solubility parameters of these hydrogels were much closer to that of water. Furthermore, ethanol possesses a much lower dielectric constant than water, which can significantly reduce the electrical double layer thickness and the dissociation abilities of the carboxyl groups.[39] Therefore, the synthesized hydrogel showed much lower swelling ratio in ethanol than in water. In addition, during the swelling and deswelling recycles, the adsorption and desorption process is reversible, which makes the repeated utilization of hydrogels possible.

**Time-Dependent Light Response Behavior of Hydrogel.** To investigate the light responsive behavior of hydrogel, finely ground hydrogel suspended in deionized water after being irradiated with UV light for different periods was subjected to UV/vis spectroscopy. The UV/vis spectra of the hydrogel solutions (H3) after UV irradiation were recorded and are illustrated in Figure 8. It was reported that the maximum

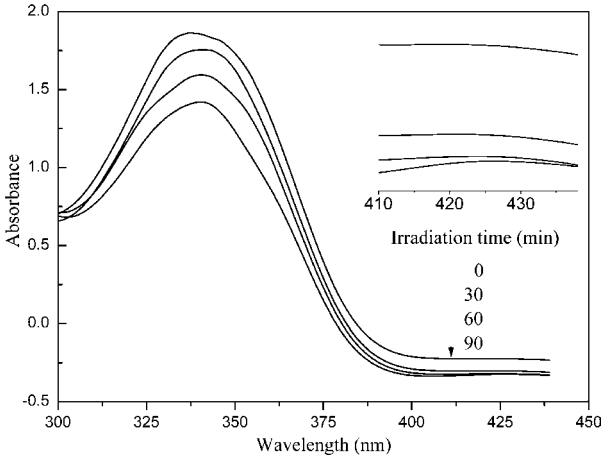


**Figure 8.** UV/vis spectra of the hydrogel (H3) solution after UV irradiation for 0, 30, 60, and 90 min, respectively (from the top down).

absorption peak of *trans*-azobenzene appeared at around 350 nm, which was associated with $\pi-\pi^*$ transition of *trans*-azobenzene, while *cis*-azobenzene showed a maximum absorption band near 440 nm, which was assigned to the $n-\pi^*$ transition of *cis*-azobenzene.[23,27] As seen in Figure 8, the absorption at around 340 nm originating from *trans*-azobenzene ($\pi-\pi^*$ transition) decreased with increasing UV irradiation time, while the absorption band at around 430 nm ($n-\pi^*$ transition of *cis*-azobenzene) appeared with very weak intensity, which can be observed in the top right corner of Figure 8. The signal change suggested the *trans*−*cis* photoisomerization of the azobenzene units in the synthesized hydrogel. Furthermore, a previous report showed that *trans*−*cis* photoisomerization of the azobenzene would change the hydrophilic/hydrophobic balance of material.[40] Therefore, the light response behavior of synthesized hydrogel might have potential in drug delivery application.

**Drug Release Behaviors of Hydrogel.** In order to investigate whether the synthesized hydrogel had special drug release behavior, vitamin $B_{12}$ ($VB_{12}$) was used as a model drug to record its in vitro release behavior at 37 °C. The influences of release medium pH and UV irradiation on the release behaviors of the prepared hydrogel were tested. The cumulative release data were summarized and are plotted in Figure 8. As seen in Figure 8, the initial release of $VB_{12}$ was very fast in the first 2 h, and then the release of $VB_{12}$ slowed down and moved toward release equilibrium. Additionally, pH value of medium and UV irradiation both had obvious effects on the release of $VB_{12}$. Over the releasing process, the cumulative release value of $VB_{12}$ in neutral medium was always higher than that in acidic medium. Without UV irradiation, the final cumulative release rates of the hydrogel in acidic medium and neutral medium were 78.2% and 89.3%, respectively. This is very likely related to the difference in swell ratios of the hydrogel in different mediums. Because the SR value of the hydrogel in neutral medium was much higher than that in acidic medium, the diffuse of drug was much faster.

As previously mentioned, the synthesized hydrogel showed a light response behavior under the UV irradiation. The thermodynamically stable *trans*-conformation of azobenzene structure would convert into the *cis*-conformation under UV irradiation.[23,40] However, as the *cis*-conformation of azobenzene was exposed to visible light or deposited in the dark, it would transfer into the *trans*-conformation again, resulting in a shift of the hydrophilic/hydrophobic balance arising from the *trans*−*cis* isomerization.[40] From Figure 9, it was found that the cumulative release of hydrophilic $VB_{12}$ from the hydrogel under UV irradiation was higher than that without UV irradiation. It can be explained by following reasoning. As the $VB_{12}$ loaded hydrogel was placed into the release medium, due to the

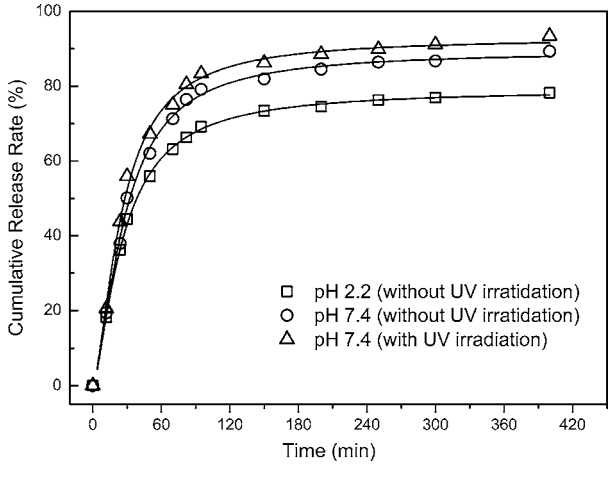


**Figure 9.** Vitamin $B_{12}$ ($VB_{12}$) in vitro cumulative release behavior of the synthesized hydrogel (H3) at 37 °C.


dx.doi.org/10.1021/jf504040s | J. Agric. Food Chem. 2014, 62, 10000−10007

different concentrations of $VB_{12}$ in the hydrogel and the release medium, the $VB_{12}$ started to gradually diffuse toward the release medium accompanied by the expansion of the hydrogel. However, the UV irradiation would change the hydrophilic/hydrophobic balance and make the hydrogel more hydrophobic, which would drive the hydrophilic $VB_{12}$ into the release medium and finally result in a higher cumulative release rate.

To conclude, a novel hemicellulose-based hydrogel with multiresponse behaviors to pH, solvent, and light was prepared by free radical copolymerization of xylan-type hemicellulose glycidyl methacrylate with 4-[(4-acryloyloxyphenyl)azo]-benzoic acid. The swelling ratio of the synthesized hydrogel ranged from 2.2 to 9.8 g/g in distilled water, which decreased generally with the increase of AOPAB content. The swelling capacity was closely associated with the strong electrostatic repulsion among carboxylic groups ($-COO^-$). The stimulus-response behaviors indicated that the hydrogel could be easily controlled by changing solvent pH and solvent type. Furthermore, the prepared hydrogel also showed good swelling and deswelling recycling performance. Results from light response test showed that the *trans*-conformation of azobenzene in hydrogel would generally convert into the *cis*-conformation under UV irradiation. Furthermore, this light response hydrogel was applied as a drug delivery device to monitor its drug release behavior, and results indicated that the hydrogel under UV irradiation showed higher drug cumulative release rate than that without UV irradiation.

## ■ ASSOCIATED CONTENT

### Ⓢ Supporting Information

$^1H$ NMR spectra of HPAB and AOPAB. This material is available free of charge via the Internet at http://pubs.acs.org.

## ■ AUTHOR INFORMATION


### Corresponding Authors

*(X.P.) Tel/fax: +86 20 87111861. E-mail: fexwpeng@scut.edu.cn.

*(R.S.) Tel/fax: +86 20 87111861. E-mail: ynsun@scut.edu.cn.



### Funding

The project is supported by the National Natural Science Foundation of China (21404043), Research Fund for the Doctoral Program of Higher Education (20130172120024), Guangdong Natural Science Foundation (S2013040015055), Science and Technology Project of Guangzhou City in China (2014J2200063), and Fundamental Research Funds for the Central Universities.


### Notes

The authors declare no competing financial interest.

## ■ REFERENCES


(1) Yang, H.; Liu, H.; Kang, H.; Tan, W. Engineering target-responsive hydrogels based on aptamer−target interactions. *J. Am. Chem. Soc.* **2008**, *130*, 6320−6321.

(2) Qiu, Y.; Park, K. Environment-sensitive hydrogels for drug delivery. *Adv. Drug Delivery Rev.* **2012**, *64*, 49−60.

(3) Peppas, N. A.; Bures, P.; Leobandung, W.; Ichikawa, H. Hydrogels in pharmaceutical formulations. *Eur. J. Pharm. Biopharm.* **2000**, *50*, 27−46.

(4) Chung, H. J.; Park, T. G. Self-assembled and nanostructured hydrogels for drug delivery and tissue engineering. *Nano Today* **2009**, *4*, 429−437.

(5) Yoshida, R. Design of functional polymer gels and their application to biomimetic materials. *Curr. Org. Chem.* **2005**, *9*, 1617−1641.

(6) Hamidi, M.; Azadi, A.; Rafiei, P. Hydrogel nanoparticles in drug delivery. *Adv. Drug Delivery Rev.* **2008**, *60*, 1638−1649.

(7) Kopecek, J. Hydrogel biomaterials: A smart future? *Biomaterials* **2007**, *28*, 5185−5192.

(8) Richter, A.; Paschew, G.; Klatt, S.; Lienig, J.; Arndt, K. F.; Adler, H. J. P. Review on hydrogel-based pH sensors and microsensors. *Sensors* **2008**, *8*, 561−581.

(9) Kabiri, K.; Omidian, H.; Hashemi, S. A.; Zohuriaan-Mehr, M. J. Synthesis of fast-swelling superabsorbent hydrogels: effect of cross-linker type and concentration on porosity and absorption rate. *Eur. Polym. J.* **2003**, *39*, 1341−1348.

(10) Sadeghi, M.; Hosseinzadeh, H. Synthesis of starch-poly(sodium acrylate-co-acrylamide) superabsorbent hydrogel with salt and pH-responsiveness properties as a drug delivery system. *J. Bioact. Compat. Polym.* **2008**, *23*, 381−404.

(11) Peng, X. W.; Ren, J. L.; Zhong, L. X.; Peng, F.; Sun, R. C. Xylan-rich hemicelluloses-graft-acrylic acid ionic hydrogels with rapid responses to pH, salt, and organic solvents. *J. Agric. Food Chem.* **2011**, *59*, 8208−8215.

(12) Kandile, N. G.; Nasr, A. S. Environment friendly modified chitosan hydrogels as a matrix for adsorption of metal ions, synthesis and characterization. *Carbohydr. Polym.* **2009**, *78*, 753−759.

(13) Kono, H.; Zakimi, M. Preparation, water absorbency, and enzyme degradability of novel chitin- and cellulose/chitin-based superabsorbent hydrogels. *J. Appl. Polym. Sci.* **2013**, *128*, 572−581.

(14) Chiu, H. C.; Hsiue, G. H.; Lee, Y. P.; Huang, L. W. Synthesis and characterization of pH-sensitive dextran hydrogels as a potential colon-specific drug delivery system. *J. Biomater. Sci., Polym. Ed.* **1999**, *10*, 591−608.

(15) Markland, P.; Zhang, Y. H.; Amidon, G. L.; Yang, V. C. A pH- and ionic strength-responsive polypeptide hydrogel: Synthesis, characterization, and preliminary protein release studies. *J. Biomed. Mater. Res.* **1999**, *47*, 595−602.

(16) Guo, B.; Finne-Wistrand, A.; Albertsson, A. C. Facile synthesis of degradable and electrically conductive polysaccharide hydrogels. *Biomacromolecules* **2011**, *12*, 2601−2609.

(17) Saha, B. Hemicellulose bioconversion. *J. Ind. Microbiol. Biotechnol.* **2003**, *30*, 279−291.

(18) Söderqvist Lindblad, M.; Ranucci, E.; Albertsson, A. C. Biodegradable polymers from renewable sources. New hemicellulose-based hydrogels. *Macromol. Rapid Commun.* **2001**, *22*, 962−967.

(19) Peng, X. W.; Zhong, L. X.; Ren, J. L.; Sun, R. C. Highly effective adsorption of heavy metal ions from aqueous solutions by macroporous xylan-rich hemicelluloses-based hydrogel. *J. Agric. Food Chem.* **2012**, *60*, 3909−3916.

(20) Li, X. M.; Pan, X. J. Hydrogels based on hemicellulose and lignin from lignocellulose biorefinery: A mini-review. *J. Biobased Mater. Bioenergy* **2010**, *4*, 289−297.

(21) Matsumoto, S.; Yamaguchi, S.; Wada, A.; Matsui, T.; Ikeda, M.; Hamachi, I. Photo-responsive gel droplet as a nano- or pico-litre container comprising a supramolecular hydrogel. *Chem. Commun.* **2008**, 1545−1547.

(22) Peng, K.; Tomatsu, I.; Kros, A. Light controlled protein release from a supramolecular hydrogel. *Chem. Commun.* **2010**, *46*, 4094−4096.

(23) Liu, X. K.; Jiang, M. Optical switching of self-assembly: Micellization and micelle-hollow-sphere transition of hydrogen-bonded polymers. *Angew. Chem., Int. Ed.* **2006**, *45*, 3846−3850.

(24) Natansohn, A.; Rochon, P. Photoinduced Motions in Azo-Containing Polymers. *Chem. Rev.* **2002**, *102*, 4139−4176.

(25) Ikeda, T.; Tsutsumi, O. Optical switching and image storage by means of azobenzene liquid-crystal films. *Science* **1995**, *268*, 1873−1875.

(26) Ikeda, T.; Mamiya, J. I.; Yu, Y. Photomechanics of liquid-crystalline elastomers and other polymers. *Angew. Chem., Int. Ed.* **2007**, *46*, 506−528.

(27) Zhao, Y. L.; Stoddart, J. F. Azobenzene-based light-responsive hydrogel system. *Langmuir* **2009**, *25*, 8442−8446.
(28) Chen, D.; Liu, H.; Kobayashi, T.; Yu, H. Multiresponsive reversible gels based on a carboxylic azo polymer. *J. Mater. Chem.* **2010**, *20*, 3610−3614.
(29) Peng, X. W.; Ren, J. L.; Zhong, L. X.; Cao, X. F.; Sun, R. C. Microwave-induced synthesis of carboxymethyl hemicelluloses and their rheological properties. *J. Agric. Food Chem.* **2010**, *59*, 570−576.
(30) De Smedt, S. C.; Lauwers, A.; Demeester, J.; Van Steenbergen, M. J.; Hennink, W. E.; Roefs, S. P. F. M. Characterization of the network structure of dextran glycidyl methacrylate hydrogels by studying the rheological and swelling behavior. *Macromolecules* **1995**, *28*, 5082−5088.
(31) Haitjema, H. J.; Buruma, R.; Van Ekenstein, G. O. R. A.; Tan, Y. Y.; Challa, G. New photoresponsive (meth)acrylate (co)polymers containing azobenzene pendant sidegroups with carboxylic and dimethylamino substituents—I. Synthesis and characterization of the monomers. *Eur. Polym. J.* **1996**, *32*, 1437−1445.
(32) Sun, S. N.; Li, M. F.; Yuan, T. Q.; Xu, F.; Sun, R. C. Effect of Ionic Liquid Pretreatment on the Structure of Hemicelluloses from Corncob. *J. Agric. Food Chem.* **2012**, *60*, 11120−11127.
(33) Kacurakova, M.; Capek, P.; Sasinkova, V.; Wellner, N.; Ebringerova, A. FT-IR study of plant cell wall model compounds: pectic polysaccharides and hemicelluloses. *Carbohydr. Polym.* **2000**, *43*, 195−203.
(34) Cao, X.; Sun, S.; Peng, X.; Zhong, L.; Sun, R. Synthesis and characterization of cyanoethyl hemicelluloses and their hydrated products. *Cellulose* **2013**, *20*, 291−301.
(35) Zhang, H.; Zhao, C.; Cao, H.; Wang, G.; Song, L.; Niu, G.; Yang, H.; Ma, J.; Zhu, S. Hyperbranched poly(amine-ester) based hydrogels for controlled multi-drug release in combination chemotherapy. *Biomaterials* **2010**, *31*, 5445−5454.
(36) Liu, Y.; Xie, J. J.; Zhu, M. F.; Zhang, X. Y. A study of the synthesis and properties of AM/AMPS copolymer as superabsorbent. *Macromol. Mater. Eng.* **2004**, *289*, 1074−1078.
(37) Pourjavadi, A.; Soleyman, R.; Barajee, G. R. Novel nanoporous superabsorbent hydrogel based on poly(acrylic acid) grafted onto salep: Synthesis and swelling behavior. *Starch/Staerke* **2008**, *60*, 467−475.
(38) Huang, J. B.; Zhu, B. Y.; Zhao, G. X.; Zhang, Z. Y. Vesicle formation of a 1:1 catanionic surfactant mixture in ethanol solution. *Langmuir* **1997**, *13*, 5759−5761.
(39) Adelnia, H.; Riazi, H.; Saadat, Y.; Hosseinzadeh, S. Synthesis of monodisperse anionic submicron polystyrene particles by stabilizer-free dispersion polymerization in alcoholic media. *Colloid Polym. Sci.* **2013**, *291*, 1741−1748.
(40) Tong, X.; Wang, G.; Soldera, A.; Zhao, Y. How can azobenzene block copolymer vesicles be dissociated and reformed by light? *J. Phys. Chem. B* **2005**, *109*, 20281−20287.

subsequent settling or from grape cell walls prior to or during fermentation. Whereas polysaccharides have been shown to contribute to the perceived viscosity of model wine,[2,5] their role in the mouthfeel and taste of white wine, where they have the potential to form complex colloids with other macromolecules and phenolics, is less clear.

A variety of juice extraction and handling options are used in the production of white wines: whole bunch pressing, free run juice, pressing fraction juice, prefermentation skin contact, and juice hyperoxidation. A simultaneous comparison of the effects of these winemaking options on white wine composition and their effect on the broad range of mouthfeel attributes encountered in white wine has not been conducted to date. This study aimed first to investigate the effects of the commonly applied juice extraction and processing methods used in white winemaking on wine phenolic composition and, second, to examine the relationships between phenolic composition and other aspects of the wine matrix, pH, total polysaccharides, glycerol and alcohol concentrations, on the mouthfeel profile of white wine.

## MATERIALS AND METHODS

**Grape Sources and Winemaking.** Handpicked bunches (3 t) of Riesling from Eden Valley, South Australia (harvested February 25, 2010), Viognier from the Adelaide Hills, South Australia (harvested March 11, 2010), and Chardonnay from Lyndoch, South Australia (harvested February 11, 2010) were sourced (hereafter referred to as "grape sources"). Potassium metabisulfite was added at picking at 50 mg/L on the basis of an estimated yield of 700 L/t. The grapes were transported for a maximum of 2 h in 0.5 t bins before being chilled overnight. The grapes were subsequently destemmed and crushed using a Diemme 4t/h destemmer-crusher. An amount of 1.75 t of the resultant must from each grape source was pressed by a 2.5 t capacity Willmes membrane press (Willmes "Merlin", 1 t whole bunch and 2.5 t crushed capacity) to yield three fractions: free run juice (FR) at <0.5 bar pressure, light pressings (LP) at 0.5−1.0 bar, and hard pressings (HP) at 1.0−2.0 bar.

A portion of the FR juice was extensively hyperoxidized (HOX) by sparging with 100% oxygen at 8−10 L/min until reaching 40 mg/L free dissolved oxygen (Nomasense PSt3, Nomacorc LLC, Zebulon, NC, USA). Skin-contacted (SC) treatments were produced by blending free run and press fractions obtained from must held in press for 60 h at 5 °C and pressed as described above. Whole bunch pressed juice (WB) was also obtained by pressing 0.5 t of whole bunches at 1.0−2.0 bar.

The juices were cold settled with the aid of pectolytic enzymes (Novozyme, Vinoclear Classic, Dittingen, Switzerland) for 24−48 h and acid adjusted using tartaric acid. Duplicate 30 L fermentation vessels were filled with each juice and inoculated with *Saccharomyces cereviseae* strain EC1118. The ferments proceeded at 0.5−1.0 Baumé per day until dryness. Thereafter, 60 mg/L $SO_2$ was added, and the wines were cold stabilized by seeding with 4 g/L potassium bitartrate at 4 °C. Protein stability was achieved by adding 1 g/L sodium bentonite to the juice prior to fermentation and by adding additional sodium bentonite after cold stabilization at a rate determined by the 80 °C/2 h test.[14] The stabilized wines were sparged with nitrogen and argon to attain a dissolved oxygen level of <0.6 mg/L, bottled in 375 mL antique green bottles under Sarin-tin screw caps, and stored at 15 °C prior to analysis and sensory assessment.

**Sensory Assessment of Mouthfeel and Taste.** Eleven tasters (five males and six females) were used. All but one had experience in profiling the mouthfeel and tastes in white wine. Taster training was conducted over five sessions to generate and define mouthfeel and taste attributes appropriate to the wines and to identify attribute redundancies. Tasters were trained using a subset of the wines used in the study and a high-phenolic white wine made by fermenting juice in the presence of skins. The attribute descriptions agreed upon to represent the tastes and mouthfeel characteristics of the training wines were 'astringency (drying)', drying or mouth puckering; 'viscosity', body, weight, or thickness; 'hotness', warmth perceived after expectorating; 'acidity', sourness/tartness while in the mouth; 'sweet', sweetness while in the mouth; 'bitter', bitterness in the mouth. Bitterness and acidity after expectorating were also selected by the panel as relevant descriptors, but were subsequently found to correlate strongly with in-mouth sensations so they were deemed redundant.

Standards for 'astringency (drying)' (0.5 g/L aluminum potassium sulfate, Ajax Finechem, Sydney, NSW, Australia), 'viscosity' (3 g/L carboxymethyl cellulose, sodium salt, Sigma-Aldrich, St. Louis, MO, USA), "bitter" (15 mg/L quinine sulfate, Sigma-Aldrich), 'hotness' (20% v/v ethanol, Tarac Industries, Nuriootpa, SA, Australia), and 'acidity' (2 g/L tartaric acid, Ajax Finechem, Sydney, Australia) in water were also presented for discussion during training. The tasters were familiarized with the use of the unstructured line scale used in the formal assessment by rating six of the experimental wines in duplicate on the chosen attributes. The line scale was 15 cm long with "low" and "high" anchor points placed at 1.5 and 13.5 cm along the scale.

The perceived intensity of the taste and mouthfeel attributes of all wines (3 grape sources × 6 treatments × 2 fermentation replicates) were assessed in triplicate using the line scale used in training. Twenty wines were tasted per day over six sessions that extended over 14 days. Thirty milliliters of wine was tasted from clear ISO tasting glasses under natural lighting and at room temperature (22 ± 1 °C). The tasters were forced to rest for 1 min between wines and for 10 min after every fourth wine. Sensory assessment was conducted 1 month after bottling. Basic wine analysis was conducted at the time of bottling, and polysaccharide concentration and phenolic profiles were evaluated 4 months after bottling.

**Wine Analysis.** *Phenolics.* Total phenolics (TP) and total hydroxycinnamates (HCA) were determined on the basis of absorbance at 280 and 320 nm.[15] Absorbance at 370 nm ($A_{370}$) was also measured to assess the concentration of flavonol compounds. As the variation in TP, HCA, and $A_{370}$ between replicate ferments was low (CV < 2.5%), one fermentation replicate from each of the three grape sources was further analyzed for phenolic composition by HPLC with an Agilent 1100 chromatography system under the following conditions. Tandem (2×) Phenomenex Gemini C6-Phenyl columns (2.1 mm × 150 mm, 3 μm) were used with 20 μL injections of wine at 45 °C. Gradient composition and flow rates were as follows: 2% formic acid in water (v/v, solvent A) and 2% formic acid in methanol (v/v, solvent B); 0.5% B from 0 to 5 min, to 20% B from 5 to 70 min, to 98% B from 70 to 110 min (0−110 min, 0.16 mL/min), 98% B from 110 to 115 min (0.13 mL/min), and 0.5% B from 110 to 120 min (0.16 mL/min).

The phenolic compounds from a mixture of wines from the three grape sources were identified using HPLC-ESI-QTOF. Identification was made on the basis of accurate masses (mass difference <5 mDa) and isotope ratios (mSigma <20) of the respective $[M - H]^-$ ions to the assigned elemental composition as well as their MS/MS and UV spectra. The identities of some phenolic compounds were confirmed by comparison with the MS/MS and UV spectra of corresponding reference compounds (Supportying Information). For quanitification, benzoic acids and flavanols were expressed in gallic acid equivalents, hydroxycinnamates and GRP as ferulic acid equivalents, and flavones and flavanonols as quercetin-3-glucoside equivalents.

*Polysaccharides and Glycerol.* For polysaccharide determination, 240 mL of wine was reduced to 60 mL under vacuum at 30 °C (in triplicate) and 180 mL of ethanol added (96% v/v, Tarac Industries, Nuriootpa, SA, Australia). The precipitate was removed by centrifugation and washed twice with ethanol, dissolved in Milli-Q water, and extensively dialyzed at 23 °C against Milli-Q water for 36 h (3.5 kDa MW cutoff tubing, Thermo Scientific, Rockford, IL, USA) before being freeze-dried and weighed. Size exclusion chromatography (Phenomenex BioSep-SEC-S 2000, 300 × 7.8 mm, 40 μL injection, 40 °C, 0.1 M $NaNO_3$ as mobile phase, 1 mL/min. RI and UV−vis detection at 280 nm. MW estimated using Pullulan standards 100, 48, 23.7, and 12.2 kDa, Showa Denko, Japan) was used to confirm the

**Table 1. Wine Composition**[a]

| treatment | Glu+Fru (g/L) | pH | TA (g/L) | ethanol (% v/v) | glycerol (g/L) | PS (mg/L) | TP $A_{280}$ (au) | HCA $A_{320}$ (au) | $A_{370}$ (au) |
|---|---|---|---|---|---|---|---|---|---|
| WB | 0.55 (0.09) | 3.06 (0.02) | 7.4 (0.3) | 13.1 (0.1) | 6.47 (0.16) | 154 (1) | 0.655 (0.132) | 2.147 (0.308) | 0.513 (0.033) |
| HOX | 0.77 (0.08) | 3.04 (0.05) | 7.4 (0.3) | 13.2 (0.1) | 6.41 (0.13) | 160 (2) | 0.527 (0.096) | 1.591 (0.194) | 0.530 (0.052) |
| FR | 0.79 (0.10) | 3.11 (0.03) | 7.3 (0.3) | 13.4 (0.1) | 6.43 (0.06) | 154 (2) | 1.569 (0.266) | 3.300 (0.470) | 0.598 (0.042) |
| LP | 0.45 (0.08) | 3.17 (0.01) | 7.2 (0.2) | 13.2 (0.1) | 6.79 (0.17) | 155 (1) | 2.281 (0.315) | 3.270 (0.578) | 0.678 (0.054) |
| HP | 0.55 (0.09) | 3.18 (0.02) | 7.3 (0.2) | 13.2 (0.1) | 6.81 (0.27) | 146 (2) | 2.643 (0.234) | 3.283 (0.486) | 0.716 (0.059) |
| SC | 0.58 (0.04) | 3.15 (0.06) | 7.6 (0.2) | 13.0 (0.2) | 6.71 (0.08) | 167 (3) | 4.029 (0.394) | 5.499 (0.819) | 0.919 (0.087) |
| P | 0.008 | n/a[b] | n/a | <0.001 | 0.003 | 0.029 | <0.001 | <0.001 | <0.001 |

[a]Two standard errors are shown in parentheses ($n = 6$). [b]n/a indicates juices were acid adjusted with tartaric acid so effects cannot be attributed to treatment.

absence of low molecular weight carbohydrates and low molecular weight phenolic compounds in the lyophilized material. Glycerol concentration was determined by HPLC as previously described.[16]

**Statistical Analysis.** *Wine Composition.* The effects of juice extraction and handling methods (hereafter referred to as winemaking) on the concentrations of total polysaccharides, glycerol, TP, HCA, and $A_{370}$ were analyzed by ANOVA with winemaking as factors with fermentation replicates nested within them. Winemaking was considered fixed and fermentation replicates, random factors. Concentrations of phenolic classes, benzoic acids, tyrosol and resveratrols, hydroxycinnamic acids, GRP, flavanols, flavonols, flavononols, and flavanones, were analyzed by ANOVA with replications provided by grape sources.

*Sensory Attribute Ratings.* Taster ratings were analyzed by ANOVA with winemaking and assessors as factors, with fermentation replicates nested within winemaking treatments. Assessors and fermentation replicates were treated as random factors and winemaking as fixed factors.

*Relationships between Wine Composition and Sensory Ratings.* Mean sensory intensities were modeled on wine pH, titratable acidity, ethanol, total polysaccharides, glycerol, and glucose and fructose concentrations, on the concentrations of major phenolic classes, and on TP, HCA, and $A_{370}$ using orthogonal scores partial least-squares regression (PLS).

ANOVA were conducted using MINITAB 14 (Minitab Inc., State College, PA, USA). PLS regression analysis was conducted using Unscrambler 10.2 (CAMO Software AS, Oslo, Norway).

## RESULTS AND DISCUSSION

**Winemaking.** The experimental winemaking protocol produced wines with analytical parameters generally expected of white wine (Table 1). Although juices from press fractions are more likely to be selected for hyperoxidization in commercial practice than free run juices, the inclusion of a hyperoxidized free run treatment was produced in this study with the intention of producing wines with phenolic concentrations at the lower end that may be found in commercial practice. Conversely, the extended period of skin contact (60 h at 5 °C) was applied to produce phenolic concentrations typical of high-phenolic white wines. It should also be noted that as the juices were pH adjusted by tartaric acid addition, the differences in pH and TA among wines given in Table 1 and the perceived acidity and sweetness of the wines do not necessarily reflect the effect of the winemaking treatments applied.

**Phenolic Composition.** The free run (FR) treatment represents a logical "control" treatment because on a volume basis it is the most widely used method of white wine production. Juice extraction and handling significantly affected TP, HCA, and $A_{370}$ ($p < 0.05$) as well as benzoic acid, hydroxycinnamic acid, flavanol, flavanonol, flavonol, flavanone, and phenol concentrations ($P < 0.1$) (Figures 1 and 2).

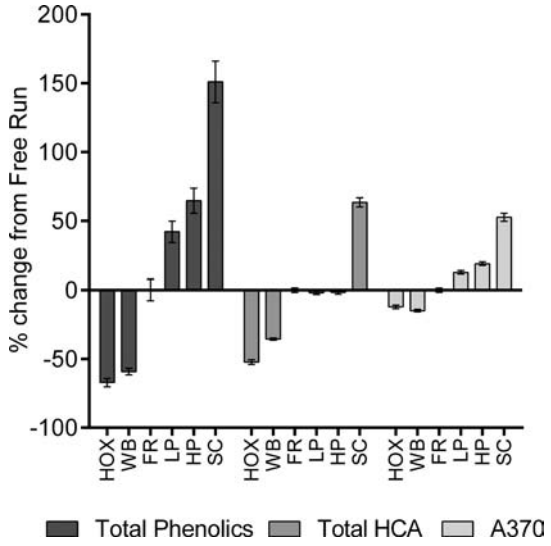


**Figure 1.** Difference in total phenolics, total hydroxycinnamates, and $A_{370}$ of wines as a percentage of wines made from free run juice. HOX, hyperoxidised free run; WB, whole bunch press; FR, free run; LP, light pressings; HP, hard pressings; SC, 60 h skin contact prefermentation. Error bars represent 2 standard errors.

The whole bunch pressed (WB) wines contained significantly lower TP than the free run wines (Figure 1), which resulted from lower concentrations of benzoic acids, hydroxycinnamic acids (Figure 2A), and flavanols (Figure 2B). Lower concentrations of flavanols were expected in the whole bunch pressed wines as the process results in less disruption to the berry than do crushing and draining. The lower HCA in the whole bunch pressed wines may be explained by less contact with the two possible sources of HCA, grape pulp solids and skins.[17]

The hard pressing (HP) wines in this study did not differ in their concentrations of either HCA or their oxidative products (GRP) (Figure 2A) compared with the free run wines, which suggests either that they were not released from the skins during pressing or that they were subsequently removed possibly via fining type actions of other macromolecules released during pressing or following other condensation reactions during fermentation.

Hyperoxidation of free run juice (HOX) resulted in significantly lower TP and HCA compared to the free run control[1] (Figure 1). The reduction in TP resulted from significantly reduced concentrations of hydroxycinnamic acids, flavanols, and flavanonols (Figure 2). The higher concentration of GRP (albeit not statistically significant) in the hyperoxidized wines relative to the free run wines suggests that some caftaric

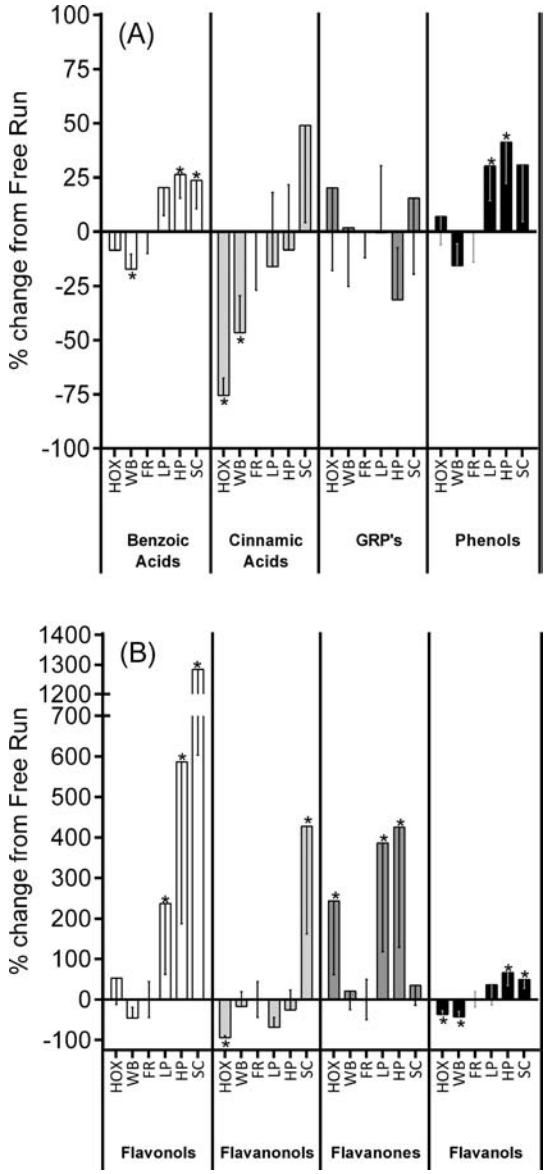


**Figure 2.** Difference in concentrations of major phenolic classes as a percentage of those in the corresponding free run wines: (A) nonflavonoids; (B) flavonoids. Error bars represent 2 standard errors. ∗ indicates significant difference from free run control.

acid was converted to GRP. Similarly, the significantly lower concentrations of flavanols in the hyperoxidized wines compared with the free run wines may be attributed to polyphenol oxidase catalyzed oxidation.[18] Reduced flavanonol concentration resulting from hyperoxidation has not previously been reported. However, given that flavanonols and flavanols both contain catechol 3′,4′-dihydroxyl electron-donating groups, their reduction may attributable to the same oxidative mechanism. The hyperoxidation regimen used in this study could be considered to be extreme in that the juice was extensively saturated using pure oxygen. Whether flavanonol concentration is similarly affected when a more commercially representative oxygenation regimen is applied is yet to be tested.

The wines made from pressings (LP and HP) and skin-contacted juice (SC) were higher in TP than those made from free run juices (Figure 1). The pressing and skin contact treatments were similar in that they both involved some form of interaction between juice and skins, and therefore both would be expected to result in greater extraction of phenolics from the skins.[19,20] However, the wines made from the juices produced from pressing skins and those made by skin contact had significantly different phenolic profiles (Figure 2). Specifically, extensive prefermentation skin contact resulted in wines with significantly higher flavanonol concentrations than the free run wines, but the light and hard pressing wines did not differ in this regard, whereas the pressing wines contained significantly higher concentrations of flavanones than did either the free run or skin contacted wines. The different phenolic profiles between the pressings and skin contact wines suggest that mechanisms other than simple extraction were involved during skin contact and pressing. The skin contact juices were in contact with skins for a substantially longer period than those of pressings juices, which may have favored enzymatically catalyzed oxidative processes such as the C-4 hydroxylation and dehydrogenation of flavanols into flavanonols.[21] The lower proportional increase in flavanones in the skin-contacted wines compared with that of the pressing wines is worthy of further investigation given that these compounds are known to be the primary contributors of bitterness in other foods and beverages.[22] In citrus, flavanones are enzymatically biotransformed to flavanonols via flavonol intermediates.[23] The concomitant lower concentrations of flavanones and higher concentrations of flavanonols and flavonols observed in the skin-contacted wines compared with the pressing wines may suggest that extensive skin contact could similarly involve enzymatic transformation of flavanones into flavononols. Keeping juice in contact with skins prior to fermentation has been shown to increase total hydroxycinnamates when done under conditions similar to those of this study, that is, at low temperature and under the action of pectolytic enzymes.[24,25] However, the contrasting effect of skin contact and pressing with respect to wine HCA concentration is worthy of further investigation.

The tyrosol concentration was higher in the pressings and wines than the free run wines. This was most likely the result of greater extraction of tyrosine from the skins, which is metabolized by yeast during primary fermentation to produce tyrosol.[26]

**Glycerol and Polysaccharide Concentration.** Wines made from pressings and skin-contacted juice had significantly higher ($p$ = 0.003) glycerol concentrations that those made from whole bunch pressed or free run juice (Table 1). However, the range in mean glycerol concentrations among treatments was <10% of the range of glycerol concentrations that have been reported in surveys of commercial dry white wines.[12,27] The small practical differences in glycerol concentration between wines from juices obtained from different juice extraction methods are expected as it is known that glycerol production depends primarily on yeast strain and fermentation conditions,[28] which were the same across all winemaking treatments.

The total polysaccharide concentrations of wine made primarily from juice deriving mostly from the grape pulp (whole bunch pressed, free run, and hyperoxidized free run) were similar. Skin-contacted wines were significantly higher in total polysaccharides, possibly due to skin-bound pectins being released during maceration, adding to the polysaccharides already present in the juice (Table 1). Wines made from hard pressings contained significantly lower polysaccharide concentrations than the other treatments, which suggest that

polysaccharides may form condensation products with phenolics under the action of hard pressing.

**Mouthfeel and Taste Effects of Juice Extraction and Relationships to Wine Composition.** The mean sensory attribute intensity ratings with treatments ordered from lowest to highest mean TP are given in Figure 3. 'Astringency (drying)' generally decreased with increasing TP. Under the classical protein−phenolic binding model of astringency, wines with higher phenolics should be more, rather than less, astringent. However, it may be that the monomeric phenolics in white wine may not have a sufficient number of hydrogen bonding sites that are required to extensively cross-link salivary proteins with phenolics and therefore elicit astringency. Analogously, chlorogenic acid, which is structurally similar to and contains the same number of hydrogen bonding sites as caftaric acid, was also found not to elicit astringency in model studies.[29] Organic acids are capable of producing drying astringent-like sensations in their own right with pH being a greater influence than titratable acidity.[30] The acidity parameters of pH and titratable acidity were very strongly correlated with 'astringency (drying)', with lower pH ($r$ = −0.87, $p$ < 0.001) and higher TA ($r$ = 0.53, $p$ < 0.001) wines being more 'astringent (drying)'. These correlations and PLS results (Figure 4) strongly suggest that the astringent (drying) sensation perceived in these wines resulted from acidity rather than phenolic concentration. Adding white wine phenolics to a white wine of pH 3.3 increased its astringency, but the same addition of phenolics did not increase the astringency of the same wine that had been previously been adjusted to pH 3.0.[31] However, consistent with the results of this study, lower pH wines were generally perceived to be more astringent than higher pH wines regardless of their phenolic content.[31]

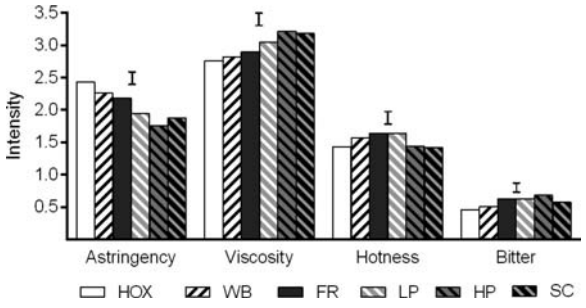


**Figure 3.** Mean ratings of mouthfeel and taste attribute ratings by juice extraction and handling treatment. Bars represent LSD 5%.

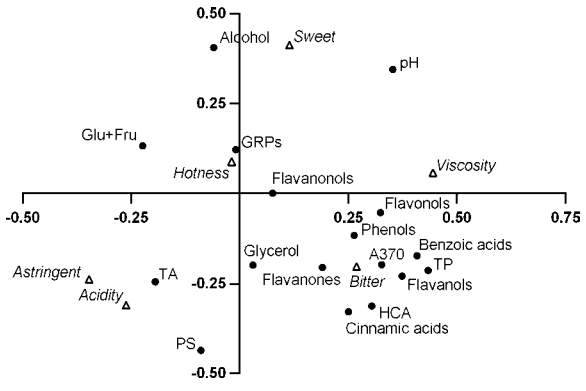


**Figure 4.** Partial least-squares regression correlation loadings of sensory attributes and total phenolics (TP), total hydroxycinnamates (HCA), $A_{370}$, total polysaccharides (PS), glucose and fructose (Glu +Fru), titratable acidity (TA), phenolic classes, pH, ethanol and glycerol concentrations.

Astringency can be modulated by viscosity,[32] which could explain why the wines perceived as more viscous were rated as less astringent (Figure 3). However, as perceived viscosity was positively correlated with total phenolic concentration, which under the classic protein−phenolic precipitation model would be expected to increase astringency, it is likely that variations in astringency/drying in these wines were due to factors other than total phenolic concentration.

Perceived viscosity was positively associated with TP, $A_{370}$, and pH ($p$ < 0.001, Table 2). PLS analysis also suggests that both pH and phenolics contribute to perceived viscosity (Figure 4). Oral perception of viscosity has previously been attributed to pH-induced changes in oral surface rheology.[33] Adding whole phenolics from white wine has also recently been shown to increase the perceived viscosity of white wine.[31] Perceived viscosity was most strongly correlated with benzoic acid ethyl ester ($r$ = 0.48, $p$ = 0.032), cinnamic acid ethyl ester ($r$ = 0.57, $p$ = 0.009), and flavonol ethyl ester ($r$ = 0.42, $p$ = 0.063) concentrations. Phenolic acid ethyl esters are formed during the course of alcoholic fermentation and are ubiquitous in alcohol beverages including wine,[34] but as both their formation through esterification and degradation by hydrolysis are pH dependent, their role in perceived viscosity remains speculative.

Despite the potential for glycerol and polysaccharides to increase the perceived viscosity by increasing physical viscosity,[13,35] neither glycerol nor polysaccharide concentrations were positively associated with perceived viscosity in these wines (Table 2; Figure 4). Whereas this may have been due to the small relative differences in glycerol and polysaccharide concentrations among treatments (Table 1), various studies have suggested that perceived viscosity in white wine or model wine is either unaffected or nominally affected by glycerol or polysaccharide concentrations within those typical of dry white wines[2,4,13,36]

'Hotness' was not significantly associated with any compositional variable, including ethanol concentration (Table 2). In other studies, adding either ethanol,[3] or phenolics[31] derived from white wines made white wine perceptively hotter. The lack of a correlation between 'hotness' and ethanol concentration may have resulted either from the narrow range of ethanol concentration among samples or by suppression by other wine components.

Juice extraction and handling had a significant effect on bitterness ($p$ = 0.013; Figure 3), with bitterness increasing with total phenolic concentration ($r$ = 0.460, $p$ = 0.034; Table 2). PLS analysis also suggested that phenolics contributed to bitterness in these wines (Figure 4). Bitterness was strongly associated with flavanol concentration ($r$ = 0.722, $p$ < 0.001). Flavanols have been shown to elicit bitterness,[37] and their role in bitterness perception has recently been confirmed following the discovery that they activate known bitter receptors on the tongue.[38] Benzoic acids and their derivatives were also positively associated with bitterness ($r$ = 0.417, $p$ = 0.034), which has been observed in red wines.[39] Flavanone concentrations were related to greater bitterness ($r$ = 0.470, $p$ = 0.018), which is consistent with findings related to other foodstuffs.[23] However, as flavanone concentration was strongly correlated with flavanol concentration ($r$ = 0.730, $p$ < 0.001),

Table 2. Correlations between Wine Composition and Mouthfeel and Taste Attributes[a]

| | Glu+Fru | pH | TA | ethanol | glycerol | PS | TP | HCA | $A_{370}$ |
|---|---|---|---|---|---|---|---|---|---|
| astringency(drying) | 0.29 | −0.87*** | 0.53*** | −0.21 | 0.16 | 0.39* | −0.39* | −0.09 | −0.15 |
| viscosity | −0.20 | 0.70*** | −0.34* | −0.02 | 0.02 | −0.34* | 0.55*** | 0.32* | 0.53*** |
| hotness | −0.07 | −0.03 | −0.07 | 0.25 | 0.24 | −0.14 | −0.11 | −0.06 | −0.02 |
| acidity | 0.25 | −0.74*** | 0.59*** | −0.10 | 0.23 | 0.39* | −0.27 | −0.06 | −0.13 |
| bitter | −0.25 | 0.12 | −0.12 | −0.16 | 0.03 | 0.16 | 0.46** | 0.39* | 0.31 |
| sweet | 0.02 | 0.73*** | −0.62*** | 0.39* | −0.29 | −0.53** | −0.03 | −0.24 | −0.12 |

[a]*, **, and *** indicate significance at $p < 0.05$, 0.01, and 0.001, respectively.

the interpretation that flavanones contribute to bitterness remains speculative. Hydroxycinnammic acids in white wine did not influence bitterness perception even when added to concentrations well above that found in white wines,[40] which is inconsistent with the positive association ($r = 0.417$, $p = 0.034$) between summed concentrations of hydroxycinnamic acids and their derivatives and bitterness observed in this study. One possible reason is that the previous studies assessed the effect of individual hydroxycinnamics, whereas in this study bitterness was equated to the summed presence of free hydroxycinnamic acids and their tartaric acid and ethyl esters.

Prefermentation skin contact resulted in wines with significantly higher TP than the pressing wines, but they tended to be less bitter. This may have been the result of different phenolic profiles (Figure 2) as some phenolic classes may elicit more bitterness than others.[41] Alternatively, the lower bitterness in the skin-contacted wines may be the result of masking by acidity or polysaccharides (Table 1).

Sweetness perception and glucose and fructose concentraiond were unrelated, which could be due to the narrow range of concentrations (0.2−1.0 g/L) and masking by acidity ($r$ sweetness with TA = −0.62, $p < 0.001$). Whereas polysaccharide concentration was negatively associated with sweetness (Table 2; Figure 4), a direct effect cannot be attributed as polysaccharide concentration was correlated with pH ($r = 0.67$, $p < 0.001$). However, there is a potential for polysaccharides to act as sweetness antagonists as their extensive and complex structures provide the possibility that they have glycophores of size and shape similar to those of small molecular weight sweet compounds in white wine.

In conclusion, different methods of juice extraction and handling techniques resulted in significant differences in overall phenolic content and phenolic profiles, but only small differences in glycerol and polysaccharide concentrations. White wine bitterness was nominally affected by overall phenolic concentration and by the relative concentrations of phenolic compounds present. The perception of palate astringency or drying sensation could best be accounted for by pH differences rather than phenolics and, therefore, could be influenced by winemaking methods used to modify acidity. pH in combination with phenolic content influenced perceived viscosity, with higher pH and more phenolic wines having more apparent viscosity, which is an important attribute when fuller bodied styles of white wine are required.

## ■ ASSOCIATED CONTENT

### Supporting Information

Chromatographic and spectral characteristics of pure reference phenolic compounds analyzed by HPLC-DAD; phenolic compounds determined by HPLC-ESI-QTOF-MS/MS. This material is available free of charge via the Internet at http://pubs.acs.org.

## ■ AUTHOR INFORMATION


### Corresponding Author

*(R.G.) Phone: +61 8 3136630. Fax: +61 8 3136600. E-mail: richard.gawel@awri.com.au.

### Present Addresses

†(S.C.V.S.) Department of Biological Sciences, Macquarie University, New South Wales 2109, Australia.

‡(E.J.W.) Australian Grape and Wine Authority, Kent Town, South Australia 5067, Australia.



### Funding

The work was funded by Australia's grapegrowers and winemakers through their investment body, the Australian Grape and Wine Authority, with matching funds from the Australian government, and by Orlando Wines.

### Notes

The authors declare no competing financial interest.


## ■ REFERENCES


(1) Cejudo-Bastante, M. J.; Castro-Vázquez, L.; Hermosín-Gutiérrez, I.; Pérez-Coello, M. S. Combined effects of preferementative skin maceration and oxygen addition of must on color-related phenolics, volatile composition, and sensory characteristics of Airén white wine. *J. Agric. Food Chem.* **2011**, *59*, 12171−12182.

(2) Jones, P. R.; Gawel, R.; Francis, I. L.; Waters, E. J. The influence of interactions between major white wine components on the aroma, flavour and texture of model white wine. *Food Quality Pref.* **2008**, *19*, 596−607.

(3) Gawel, R.; Van Sluyter, S.; Waters, E. J. The effects of ethanol and glycerol on the body and other sensory characteristics of Riesling wines. *Aust. J. Grape Wine Res.* **2007**, *13*, 38−45.

(4) Nurgel, C.; Pickering, G. Contribution of glycerol, ethanol and sugar to the perception of viscosity and density elicited by model white wine. *J. Texture Stud.* **2005**, *36*, 303−323.

(5) Vidal, S.; Courcoux, P.; Francis, L.; Kwiatkowski, M.; Gawel, R.; Williams, P.; Waters, E.; Cheynier, V. Use of an experimental design approach for evaluation of key wine components on mouth-feel perception. *Food Quality Pref.* **2004**, *15*, 209−217.

(6) Darias-Martín, J.; Díaz-González, D.; Díaz-Romero, C. Influence of two pressing processes on the quality of must in white wine production. *J. Food Eng.* **2004**, *63*, 335−340.

(7) Cheynier, V.; Souquet, J.-M.; Samson, A.; Moutounet, M. Hyperoxidation: influence of various oxygen supply levels on oxidation kinetics of phenolic compounds and wine quality. *Vitis* **1991**, *30*, 107−115.

(8) Di Lecce, G.; Arranz, S.; Jáuregui, O.; Tresserra-Rimbau, A.; Quifer-Rada, P.; Lamuela-Raventós, R. M. Phenolic profiling of the skin, pulp and seeds of Albarino grapes using hybrid quadrupole time-of-flight and triple-quadrupole mass spectrometry. *Food Chem.* **2014**, *145*, 874−882.

(9) Trousdale, E. K.; Singleton, V. L. Astilbin and engeletin in grape and wine. *Phytochemistry* **1983**, *22*, 619−620.

(10) Edwards, T. L.; Singleton, V. L.; Boulton, R. Formation of ethyl esters of tartaric acid during wine aging: chemical and sensory effects. *Am. J. Enol. Vitic.* **2004**, *36*, 118−124.

(11) Ramey, D. D.; Ough, C. S. Volatile ester hydrolysis or formation during storage of model solutions and wines. *Am. J. Enol. Vitic.* **1980**, *28*, 928−934.
(12) Nieuwoudt, H. H.; Prior, B. A.; Pretorious, I. S.; Bauer, F. F. Glycerol in South African table wines: an assessment of its relationship to wine quality. *S. Afr. J. Enol. Vitic.* **2002**, *23*, 22−30.
(13) Runnenbaum, R. C.; Boulton, R. B.; Powell, R. L.; Heymann, H. Key constituents affecting wine body − an exploratory study. *J. Sensory Stud.* **2011**, *26*, 62−70.
(14) Pocock, K. F.; Waters, E. J. Protein haze in bottled white wines: how well do stability tests and bentonite fining trials predict haze formation during storage and transport? *Aus. J. Grape Wine Res.* **2008**, *12*, 212−220.
(15) Somers, T. C.; Ziemelis, G. Spectral evaluation of total phenolic components in *Vitis vinifera* grapes and wines. *J. Sci. Food Agric.* **1985**, *36*, 1275−1284.
(16) Nissen, T. L.; Schulze, U.; Nielsen, J.; Villadsen, J. Flux distribution in anaerobic, glucose-limited continuous cultures of *Saccharomyces cerevisiae*. *Microbiology* **1997**, *143*, 203−218.
(17) Somers, T. C.; Pocock, K. F. Phenolic assessment of white musts: varietal differences in free-run juices and pressings. *Vitis* **1991**, *30*, 189−201.
(18) Guyot, S.; Cheynier, V.; Souquet, J.-M.; Moutounet, M. Influence of pH on the enzymatic oxidation of (+)-catechin in model systems. *J. Agric. Food Chem.* **1995**, *43*, 2458−2462.
(19) Singleton, V. L.; Zaya, J.; Truesdale, E. White table wine quality and polyphenol composition as affected by must $SO_2$ content and pomace contact time. *Am. J. Enol. Vitic.* **1980**, *31*, 14−20.
(20) Darias-Martín, J. J.; Rodríguez, O.; Díaz, E.; Lamuela-Raventós, R. M. Effect of skin contact on the antioxidant phenolics in white wine. *Food Chem.* **2000**, *71*, 483−487.
(21) Matsuda, M.; Otsuka, Y.; Jin, S.; Wasaki, J.; Watanabe, J.; Watanabe, T.; Osaki, M. Biotransformation of (+)-catechin into taxifolin by a two-step oxidation: primary stage of (+)-catechin metabolism by a novel (+)-catechin-degrading bacteria, *Burkholderia* sp. KTC-1, isolated from tropical peat. *Biochem. Biophys. Res. Commun.* **2008**, *366*, 414−419.
(22) Horowitz, R. M.; Gentili, B. Taste and structure in phenolic glycosides. *J. Agric. Food Chem.* **1969**, *17*, 696−700.
(23) Moriguchi, T.; Kita, M.; Tomono, Y.; Endo-Inagaki, T.; Omura, M. Gene expression in flavonoid biosynthesis: correlation with flavonoid accumulation in developing citrus fruit. *Physiol. Plant.* **2001**, *111*, 66−74.
(24) Fernández-Zurbano, P.; Ferreira, V.; Peña, C.; Escudero, A.; Cacho, J. Effects of maceration time and pectolytic enzymes added during maceration on the phenolic composition of must. *Food Sci. Technol. Int.* **1999**, *5*, 319−325.
(25) Hernanz, D.; Recamales, A. F.; Gonzáles-Miret, M. L.; Gómez-Míguez, M. J.; Vicario, I. M.; Heredia, F. J. Phenolic composition of white wines with a prefermentative maceration at experimental and industrial scale. *J. Food Eng.* **2007**, *80*, 327−335.
(26) Singleton, V. L.; Trousdale, E. White wine phenolics: varietal and processing differences as shown by HPLC. *Am. J. Enol. Vitic.* **1983**, *34*, 27−34.
(27) Rankine, B. C.; Bridson, D. A. Glycerol in Australian wines and factors influencing its formation. *Am. J. Enol. Vitic.* **1971**, *22*, 6−12.
(28) Erasmus, D. J.; Cliff, M.; Van Vuuren, H. J. J. Impact of yeast strain on the production of acetic acid, glycerol and the sensory attributes of icewine. *Am. J. Enol. Vitic.* **2004**, *55*, 371−378.
(29) Naish, M.; Clifford, M. N.; Birch, G. G. Sensory astringency of 5-*O*-caffeoylquinic acid, tannic acid and grape seed tannin by a time intensity procedure. *J. Sci. Food Agric.* **1993**, *61*, 57−64.
(30) Lawless, H. T.; Horne, J.; Giasi, P. Astringency of organic acids is related to pH. *Chem. Senses* **1996**, *21*, 397−403.
(31) Gawel, R.; Van Sluyter, S. C.; Smith, P. A.; Waters, E. J. Effect of pH and alcohol on perception of phenolic character in white wine. *Am. J. Enol. Vitic.* **2013**, *64*, 425−429.
(32) Peleg, H.; Noble, A. C. Effect of viscosity, temperature and pH on astringency in cranberry juice. *Food Qual. Pref.* **1999**, *10*, 343−347.
(33) Nordbo, H.; Darwish, S.; Bhatnagar, R. S. Salivary viscosity and lubrication: Influence of pH and calcium. *Scand. J. Dental Res.* **1984**, *92*, 306−314.
(34) Hashizume, K.; Ito, T.; Shimohashi, M.; Kokita, A.; Tokiwano, T.; Okuda, M. Taste-guided fractionation and instrumental analysis of hydrophobic compounds in saki. *Biosci., Biotechnol., Biochem.* **2012**, *76*, 1291−1295.
(35) Weaver, L.; Yu, L. P.; Rollings, J. E. Weighted intrinsic viscosity relationships for polysaccharide mixtures in dilute aqueous solutions. *J. Appl. Polym. Sci.* **1988**, *35*, 1631−1637.
(36) Gawel, R.; Waters, E. J. The effect of glycerol on the perceived viscosity of dry white table wine. *J. Wine Res.* **2008**, *19*, 109−114.
(37) Narukawa, M.; Noga, C.; Ueno, Y.; Sato, T.; Misaka, T.; Watanabe, T. Evaluation of the bitterness of green tea catechins by a cell-based assay with the human bitter taste receptor hTAS2R39. *Biochem. Biophys. Res. Commun.* **2011**, *405*, 620−625.
(38) Soares, S.; Kohl, S.; Thalmann, S.; Mateus, N.; Meyerhof, W.; De Freitas, V. Different phenolic compounds activate distinct human bitter taste receptors. *J. Agric. Food Chem.* **2013**, *61*, 1525−1533.
(39) Hufnagel, J. C.; Hofmann, T. Orosensory-directed identification of astringent mouthfeel and bitter-tasting compounds in red wine. *J. Agric. Food Chem.* **2008**, *56*, 1376−1386.
(40) Verétte, E.; Noble, A. C.; Somers, T. C. Hydroxycinnamates of *Vitis vinifera*: sensory assessment in relation to bitterness in white wines. *J. Sci. Food Agric.* **1988**, *45*, 267−272.
(41) Maga, J. A.; Lorenz, K. Taste threshold values for phenolic acids which can influence flavor properties of certain flours, grains and oilseeds. *Cereal Sci. Today* **1973**, *18*, 326−330.

**Table 1. Wines Analyzed in the Experiment Including Origin, Age, Varietal Composition, and Some Basic Compositional Parameters**

| wine | denomination of origin | vintage year | grape variety | oak aging | alcohol % (v/v) | pH | TA[a] (g/L) | VA[b] (g/L) | RS[c] (g/L) | TPI[d] | CI[e] | astringency[f] (g/L) |
|---|---|---|---|---|---|---|---|---|---|---|---|---|
| R1 | Rioja | 2009 | Tempranillo, Graciano, Mazuelo | 12 | 13.20 | 3.57 | 4.60 | 0.44 | 2.09 | 53.30 | 7.75 | 0.21 |
| R2 | Rioja | 2010 | Tempranillo | 0 | 12.50 | 3.60 | 5.29 | 0.20 | 1.52 | 47.40 | 7.98 | 0.14 |
| R3 | Rioja | 2006 | Tempranillo, Viura | 18 | 13.00 | 3.42 | 5.04 | 0.51 | 2.23 | 51.20 | 7.88 | 0.20 |
| R4 | Rioja | 2010 | Tempranillo, Garnacha | 0 | 14.00 | 3.98 | 4.52 | 0.45 | 1.77 | 62.40 | 11.79 | 0.26 |
| R5 | Rioja | 2010 | Tempranillo (100%) | 0 | 12.50 | 3.67 | 5.01 | 0.44 | 2.32 | 60.30 | 9.55 | 0.36 |
| R6 | Rioja | 2009 | Tempranillo, Garnacha | 18 | 12.60 | 3.64 | 5.10 | 0.59 | 1.67 | 51.50 | 7.18 | 0.25 |
| R8 | Rioja | 2010 | Graciano (100%) | 8 | 14.20 | 3.53 | 5.56 | 0.44 | 2.31 | 66.60 | 16.92 | 0.15 |
| A7 | Arlanza | 2008 | Tempranillo | 12 | 13.00 | 3.69 | 5.49 | 0.60 | 1.98 | 55.60 | 8.45 | 0.33 |
| V10 | Valdepusa | 2005 | Cabernet Sauvignon | 12 | 14.20 | 3.66 | 5.23 | 0.60 | 4.35 | 85.80 | 18.34 | 0.87 |
| C11 | Cariñena | 2007 | Garnacha, Tempranillo, Cabernet Sauvignon | 18 | 12.90 | 3.56 | 5.59 | 0.86 | 3.81 | 54.60 | 8.63 | 0.47 |
| C12 | Cariñena | 2005 | Merlot, Tempranillo, Cabernet Sauvignon | 10 | 13.00 | 3.45 | 5.51 | 0.73 | 3.39 | 78.50 | 11.40 | 0.56 |
| C13 | Cariñena | 2010 | Garnacha, Tempranillo, Cabernet Sauvignon | 0 | 13.00 | 3.61 | 5.23 | 0.57 | 2.57 | 69.80 | 14.52 | 0.31 |
| B9 | Campo de Borja | 2010 | Garnacha (100%) | 4 | 13.90 | 3.39 | 5.79 | 0.46 | 3.61 | 74.10 | 13.54 | 0.28 |
| B14 | Campo de Borja | 2007 | Garnacha (100%) | 15 | 13.10 | 3.47 | 5.31 | 0.55 | 4.34 | 62.10 | 10.17 | 0.34 |
| B15 | Campo de Borja | 2010 | Garnacha (70%), Syrah (20%), Tempranillo (10%) | 0 | 13.80 | 3.65 | 5.08 | 0.46 | 2.68 | 61.20 | 12.36 | 0.07 |
| D16 | Ribera del Duero | 2008 | Tempranillo (100%) | 18 | 13.60 | 3.63 | 5.18 | 0.48 | 1.71 | 61.70 | 9.57 | 0.45 |

[a]Total acidity expressed in g/L of tartaric acid. [b]Volatile acidity expressed in g/L of acetic acid. [c]Reducing sugars expressed in g/L. [d]Total polyphenol index, expressed in absorbance × 100. [e]Color index, expressed as $(A_{420} + A_{520} + A_{620})$ [f]Expressed as tannic acid.

wine oxidation and ultimately determining the specific aldehyde production rate of a given wine is therefore large. The list includes transition metals catalyzing the formation of quinones,[34−36] amino acids, alcohols, α-dicarbonyls, wine polyphenols,[32,37,38] and sulfur dioxide, known to act as antioxidant[39−41] and as a carbonyl binder.[42]

Reduction problems are associated with the accumulation of volatile sulfur compounds (VSCs),[43−45] particularly $H_2S$ and methanethiol (MeSH),[14] during bottle aging in conditions of minimum oxygen ingress through the bottle closure.[13,16,46−48] It is believed that the major source of VSCs in wine is yeast metabolism. The formation of small amounts of $H_2S$ are inherent to fermentation[49] and related to multiple factors.[50−52] The formation of MeSH and EtSH has been related to yeast catabolism of methionine and cysteine,[53] although it could be also related to amino acid synthesis.[54] The levels of these compounds are controlled by some treatments such as copper finning, aeration, and/or addition of lees.[9,55] The reasons why these molecules accumulate during bottle aging, more often in those wines suffering of high VSCs levels during fermentation, are not clearly known,[9] although several hypotheses such as the hydrolysis of thioacetates,[56] the reduction of disulfides,[57] the reaction between cysteine and wine α-dicarbonyls,[33] the transition-metal-catalyzed reduction of sulfate or sulfite,[58] or the hydrolysis of thioacetals[36] were formulated long time ago. The potential role of transition metal ions in amino acid transamination, racemization, and desulfhydration is well-documented in the classical chemistry literature,[59−61] but only a recent report has shown that wines spiked with transition metals can accumulate during storage in oxygen-free containers with higher levels of $H_2S$ and MeSH.[55] Therefore, the list of compounds potentially determining the wine tendency to form VSCs during wine bottle aging includes again transition metals, α-dicarbonyls, disulfides and thioacetates, sulfite and sulfate, and sulfur-containing amino acids.

The major aim of the present work is to search for relationships between some key chemical compositional parameters of the wines and the rates of production or depletion of oxidation- and reduction-related compounds along with bottling storage under different oxidation regimes.

## MATERIALS AND METHODS

**Wines, Reagents, Standards, and Materials.** *Wines.* Sixteen different commercial Spanish red wines from six different Spanish denominations of origin were used in the present study, as detailed in Table 1.

*Solvents.* Dichloromethane, methanol, pentane, hexane, and diethyl ether (gas chromatography quality) were purchased from Merck (Darmstadt, Germany). Ethanol was from Panreac (Barcelona, Spain). Water with resistance of 18.2 MΩ·cm at 25 °C was purified in a Milli-Q system from Millipore (Bedford, Germany).

*SPE Cartridge Materials.* LiChrolut EN resins (styrene/divinylbenzene copolymer) and 1 mL internal volume polypropylene cartridges were supplied by Merck. Carboxen-polydimethylsiloxane (CAR-PDMS) fibers were supplied by Supelco (Bellefonte, PA, U.S.A.). Semiautomated solid-phase extraction was carried out with a VAC ELUT 20 station system from Varian (Wallnut Creek, CA, U.S.A.) and automated solid-phase extraction was carried out with a GX-274 Liquid Handler from Gilson (Middleton, WI, U.S.A.).

*Chemical Standards.* The chemical standards used for the analytical characterization of wines were supplied by Merck (Darmstadt, Germany), Panreac (Barcelona, Spain), Lancaster (Eastgate, U.K.), Scharlau (Barcelona, Spain), SAFC (Steinheim, Germany), Aldrich (Madrid, Spain), Fluka (Madrid, Spain), ChemService (West Chester, PA, U.S.A.) and Oxford Chemicals (Hartlepool, U.K.). Purity of chemical standards is over 95% in all cases, and most of them are over 99%. Specific details can be obtained from method references.[15,62−73]

**Storage of Wine Samples under Different Oxygen Regimes.** The original wine bottles were opened inside a glovebox from Jacomex (Dagneux, France) in which oxygen was under 0.002%. The content of four bottles was mixed in a big beaker and stirred until the oxygen level in the wine dropped to 0.00 mg/L (in general, initial oxygen content for the recently opened bottle was under 0.01 mg $L^{-1}$), as measured with a fluorescence oxygen meter OptiOx SG-9 from Mettler Toledo (Barcelona, Spain). Then, 17 different samples of each wine (140 mL of wine with 8 mL of Argon headspace) were prepared in airtight amber vials (Aldrich Sure-Seal bottles) supplied by Sigma-Aldrich (Madrid, Spain). The vials were closed with an internal silicone septum, a strong crimp cap and an external screw cap. The internal septum of the bottles was intentionally pierced to different extents (in three bottles 0 times and in two 1, 2, 3, 4, 5, 6, and 8 times) in order to provoke different oxygen penetration rates. Vials were further sealed into plastic bags with known oxygen permeability (<9 cc/$m^2$ 24 h) supplied by Amcor (Barcelona, Spain). The efficiency of this procedure was assessed in preliminary trials in which solutions of 12% ethanol (v/v) in water were stored for 2 months, and the oxygen level was determined by measuring the dissolved oxygen as previously explained. The 272 vials (16 wines × 17 samples/wine) so prepared were stored at 25 °C in the dark for 6 months in an incubator Climas GROW 360 (Climas, Barcelona, Spain). In all cases, we were able to produce the same wine with quite different levels of oxidation after 6 months of storage. The total amount of oxygen taken by the samples was indirectly measured through the change in absorbance at 420 nm (from 2 to 60 mg $O_2$/L).

The relationship between absorbance at 420 nm and oxygen consumption was assessed in an independent experiment in which the wines were poured into a 60 mL screw-capped clear glass tubes containing PreSense Pst3 oxygen sensors from Presense (Regensburg, Germany). The wines were then saturated with atmospheric air until the measurement of dissolved oxygen reached 6 mg/L. Oxygen level was monitored with the Nomasense oxygen analyzer from Nomacorc S.A. (Aubel, Belgium). Wines were stored in the dark at 25 °C until the wine dissolved oxygen content dropped below 1 mg/L. Then the wine was saturated again with oxygen and the process was repeated along five saturation cycles. After each cycle, the wine absorbance at 420 nm was measured.

**Analytical Characterization of the 16 Original Samples and of the 17 Specimens Produced Per Wine Sample.** An extensive analytical characterization of the 16 original samples was carried out including basic enological chemical parameters, metallic elements, chemical astringency, amino acids, volatile carbonyls, VSCs, sotolon, general aroma composition, low molecular weight polyphenols, and polymeric pigments, as detailed below. In these samples, 2 (3 in the case of VSCs) analytical replicates were carried out per sample. In addition, absorbance at 420 nm, free and total $SO_2$, amino acids, volatile carbonyls, VSCs, and the general aroma composition were also analyzed in the 272 specimens derived from the 16 samples after the 6 months of storage. In these cases, a single analytical replicate was carried out in the analysis.

*Conventional Enological Parameters.* Conventional enological parameters of wines were determined in accordance with official OIV practices.[62] Total polyphenol index (TPI) was estimated as absorbance at 280 nm.[63] For all absorbance measurements the UV−vis spectrophotometer UV-17000 Pharma Spec from Shimadzu (Duisburg, Germany) was used.

*Determination of Free and Total Sulfur Dioxide.* Free and total sulfur dioxide was determined following the Rippert methodology (iodometry using starch as indicator). Wine, 15 mL, was titrated with $I_2$ 0.02 N until a bluish-violet tonality appeared. These procedures are described in ref 62. Combined sulfur dioxide levels have been calculated as the difference between total and free $SO_2$.

*Quantitative Analysis of Metallic Elements.* Microwave-assisted digestion in a closed vessel was used to mineralize wine samples. Samples were further analyzed by inductively coupled plasma optical emission spectrometry (ICP-OES), as described by Gonzalvez et al.[64] The elements analyzed are given in Table 2.

**Table 2. Ranges and Mean Concentrations in the Initial 16 Spanish Red Wines of Amino Acids and Alcohols Potentially Precursors for Oxidation Aldehydes and Some Trace Mineral Elements with Potential Catalytic Activity upon the Oxidation Processes**

| parameter | concentration range (mg/L) | average (mg/L) | median (mg/L) | SD |
|---|---|---|---|---|
| amino acid precursors | | | | |
| threonine | 27.3−390 | 146 | 108 | 97.7 |
| γ-aminobutyric acid | 9.37−109 | 37.50 | 24.00 | 29.5 |
| valine | 3.47−28.9 | 15.70 | 13.50 | 7.22 |
| methionine | 1.14−7.26 | 3.56 | 3.24 | 1.64 |
| isoleucine | 3.36−22.6 | 11.50 | 10.40 | 5.25 |
| leucine | 5.07−72.5 | 35.10 | 35.80 | 18.4 |
| phenylalanine | 7.91−33.4 | 18.40 | 18.10 | 6.64 |
| alcohol precursors | | | | |
| isobutanol | 37.2−76.1 | 53.60 | 49.60 | 11.5 |
| 1-butanol | 0.94−1.76 | 1.28 | 1.27 | 0.23 |
| isoamyl alcohol | 187−438 | 276 | 270 | 66 |
| 1-hexanol | 0.96−3.16 | 1.96 | 1.88 | 0.58 |
| methionol | 0.58−4.94 | 1.72 | 1.49 | 1.03 |
| benzyl alcohol | 0.01−0.17 | 0.05 | 0.04 | 0.04 |
| β-phenylethanol | 19.1−104 | 41.5 | 37.5 | 20.4 |
| trace elements | | | | |
| Al | 0.40−1.95 | 1.08 | 1.18 | 0.46 |
| Cr | <0.63 | | | |
| Cu | <0.09−1.75 | 0.25 | 0.09 | 0.42 |
| Fe | 1.47−4.96 | 2.77 | 2.78 | 0.90 |
| Mn | 0.34−1.19 | 0.80 | 0.85 | 0.25 |
| Mo | <0.23 | | | |
| Ni | <0.09−1.67 | 0.74 | 0.21 | 0.69 |
| S | 118−357 | 205 | 186 | 67.8 |
| Ti | <0.08−0.15 | 0.09 | 0.08 | 0.03 |
| V | <0.51 | | | |
| Zn | 0.23−0.89 | 0.58 | 0.63 | 0.16 |

*Chemical Astringency Determination.* The analysis was carried out by the method published by Llaudy et al.[65] using ovoalbumin as the precipitation agent and tannic acid solutions as standards.

*Quantitative Analysis of Amino Acids.* A precolumn derivatization procedure with aminoquinolyl-*N*-hydrosysuccinimidyl carbamate (AQC) for the determination of amino acids levels in wines using a quaternary high-performance liquid chromatography (HPLC) eluent system was followed as it is described in ref 66.

*Quantitative Analysis of Carbonyl Compounds.* Carbonyl compounds were extracted following an automated (GX-274 Liquid Handler from Gilson −Middleton WI, U.S.A.) solid-phase extraction (SPE) method and analyzed in a gas chromatography−mass spectrometry (GC-MS) system with negative chemical ionization (NCI), using a variation of the method described in the literature.[67] This method is based on the derivatization with *O*-(2,3,4,5,6-pentafluorobencyl)-hydroxylamine hydrochloride (PFBHA). Derivatives are formed in the SPE cartridge in which the analytes have been previously isolated. In our case, cartridges had 100 mg of LiChrolut EN resins, which implies that only half of wine, reagents, cleaning solvents, and derivatizating agent aqueous solution were necessary. Before the derivatization process, 20 μL of 5-chloro-2-pentanone 10 mg/L standard solution in ethanol, prepared daily, were loaded onto the wine. Derivatization reagent aqueous solution (5 mg/mL PFBHA) was prepared daily also. Derivatization was carried out at room temperature for 15 min. Derivatized analytes were eluted with 1 mL of 10% diethyl ether (v/v) in hexane and finally 30 μL of 2,3,6-trichloroanisole 17.5 mg/L were added as internal standard.

*Quantitative Analysis of Volatile Sulfur Compounds.* The quantitative determination of wine sulfur compounds is described in the method proposed by Lopez et al.[68] The method dilutes the sample in brine, and the sample headspace is preconcentrated with automated headspace solid-phase microextraction (HS-SPME) with a CAR-PDMS fiber and subsequently analyzed by gas chromatography-pulsed flame photometric detection (GC-PFPD)

*Quantitative Analysis of Sotolon.* This analyte was quantified by using SPE extraction coupled with a GC-MS analysis described in reference.[15] The instrumental conditions are described by Ferreira et al.[71]

*Quantitative Analysis of Major Aroma Compounds.* This analysis was carried out by the method published by Ortega et al.[69] The strategy followed a liquid−liquid microextraction with dichloromethane and the use of several internal standards to correct for matrix effects. The method is based on gas-chromatographic−flame ionization detection analysis of the dichloromethane microextracts.

*Quantitative Analysis of Minor and Trace Aroma Compounds.* The method is described in ref 70. The wine was extracted in a SPE cartridge filled with LiChrolut EN resins. The elution was carried out with dichloromethane containing 5% methanol (v/v). These extracts were directly analyzed by gas chromatography with ion trap mass spectrometry detection without further concentration.

*Quantification of Non-Volatile Compounds by UPLC-MS.* Individual nonvolatile compounds with low molecular weight (anthocyanin-derived pigments such as glycosylated, acylated, pyranoathocyanins or anthocyanin-flavonol dimers; flavonols; phenolic acids and esters; trans-resveratrol) were first isolated by preparative gel permeation chromatography (GPC). The preparative column was formed by TSK Toyopearl gel, which was packed in a HW-50F Millipore (Bedford, MA, U.S.A.) Vantage L column (120 mm × 12 mm i.d.) at atmospheric pressure as described elsewhere.[72] Two milliliters of wine were directly injected in the column and flow rate was regulated at 1 mL/min using a peristaltic pump. The first fraction containing the compounds of low molecular weight were eluted with 60 mL of ethanol/water/trifluoroacetic acid (55:45:0.05, v/v/v). This fraction was brought to dryness under vacuum, redissolved in 2 mL of formic acid/water (5:95, v/v), and further analyzed by UPLC-MS.

UPLC analyses were performed using a Waters Acquity Ultra Performance LC system (Milford, MA, U.S.A.) by direct injection of wine samples, previously filtered with 0.22 μm nylon discs. UPLC separation was achieved using an acquity BEH C18 column (100 mm × 2.1 mm, i.d., 1.7 μm particle size, Waters), kept at 40 °C. Mobile phase flow rate was 0.45 mL/min and the injection volume was 7.5 μL. Solvents were (A) water/formic acid (0.1%), and (B) acetonitrile/formic acid (0.1%). The gradient program employed was as follows: 0−4 min, 99−92% A; 4−11 min, 92−70% A; 11−13.5 min, 70−0% A; 13.5−14.5 min, 0−99% A. The UPLC system was coupled to a microTOF II high-resolution mass spectrometer (Bruker Daltonik, Germany) equipped with an Apollo II ESI (electrospray) source and controlled by Bruker Daltonics Data Analysis software. The ESI source was operated in negative mode recorded in the range of $m/z$ 150 and 1500. The optimized conditions of the ESI source were as follows: capillary voltage, 3.5 kV; ESI source temperature, 180 °C; desolvation temperature, 200 °C; cone gas flow, 9 L/min; the nebulizer gas was set at 3 bar and 25 °C. LC−MS was performed operating in both (continuum) MS mode and in MS/MS mode. The spectra were acquired at the speed of 2 scan/s. Fragmentor voltage for MS/MS acquisition mode was 35 eV.

The identity assignation of compounds was carried out by comparison of their retention time ($t_R$), MS and MS/MS spectra with those of their respective commercially available standards. Quantification was performed by UPLC-MS and using the response (peak area) ratio for each compound. The calibration curves were prepared by calculating the peak area of the different standards and were used to determine linearity and instrumental detection (LOD) and quantification (LOQ) limits. LOD and LOQ were calculated using 3 S/m and 10 S/m ($S$ is the standard deviation of the response; $m$ is the slope of the calibration curve), respectively. Calibration curves were prepared in methanol. The estimated concentrations of anthocyanin derivatives have been expressed as malvidin-3-*O*-glucosyde equivalents (mg/L of malvidin-3-*O*-glucosyde), Hydroxicinnamic acids and esters as caftaric acid equivalents (mg/L of caftaric acid).[72]

*Analysis of Polymeric Pigments.* The procedure for polymeric pigments determination was based on that developed by Habertson et al.[73] In accordance with the method, two tubes for each sample were required. The first tube was made up by dispensing 1 mL of an acetic/NaCl buffer (200 mM acetic acid and 170 mM adjusted to pH 3.3 with HCl) into the tube and then adding 500 μL of wine. One milliliter of the mixture was transferred to a cuvette. Then, 80 μL of 0.36 M potassium metabisulfite was added and the absorbance at 520 nm was determined after 10 min of incubation (reading A).

For the second tube, 1 mL of acetic/NaCl buffer containing bovin serum albumin (1 mg/L) was put into the tube together with 500 μL of wine. The mixture was allowed to incubate at room temperature for 15 min with slow agitation. After incubation, the sample was centrifuged 10 min at 2000 rpm to pellet the protein−tannin precipitate. One milliliter of the supernatant was put into the cuvette, then 80 μL of 0.36 M potassium metabisulfite was added, and after a 10 min incubation the absorbance was determined at 520 nm (reading B). The absorbance due to SPP (small polymeric pigments) and LPP (large polymeric pigments) is given as B and (A-B),

Table 3. Carbonyl Compounds and VSCs Concentration Ranges and Mean Concentrations of the Initial 16 Red Wines

| | concentration range (μg/L) | | average (μg/L) | median (μg/L) | odor threshold (μg/L) |
|---|---|---|---|---|---|
| | lower limit | upper limit | | | |
| carbonyl compounds | | | | | |
| methional | 0.76 | 8.51 | 2.49 | 1.90 | 0.50[21] |
| phenylacetaldehyde | 5.09 | 39.20 | 14.40 | 10.40 | 1.00[22] |
| 2-methylpropanal | 10.60 | 81.50 | 44.80 | 42.60 | 6.00[22] |
| 2-methylbutanal | 3.65 | 38.40 | 11.80 | 8.34 | 16[22] |
| 3-methylbutanal | 9.75 | 39.30 | 26.20 | 26.00 | 4.60[22] |
| (*E*)-2-hexenal | 0.02 | 0.09 | 0.04 | 0.04 | 4.00[22] |
| (*E*)-2-heptenal | 0.02 | 0.10 | 0.05 | 0.03 | 4.60[22] |
| (*E*)-2-octenal | 0.04 | 0.19 | 0.10 | 0.08 | 3.00[22] |
| (*E*)-2-nonenal | 0.02 | 0.20 | 0.09 | 0.07 | 0.60[22] |
| 1-octen-3-one | 0.006 | 0.07 | 0.02 | 0.02 | 0.02[90] |
| benzaldehyde | <0.08 | 6.93 | 1.21 | 0.08 | 2000[91] |
| vanillin | <0.6 | 470 | 91.50 | 35.70 | 200[92] |
| sotolon | 5.12 | 12.40 | 9.01 | 8.25 | 15[93] |
| volatile sulfur compounds (VSCs) | lower limit | upper limit | average | median | odor threshold |
| hydrogen sulfide | <4.00 | 110.00 | 33.40 | 24.00 | 1.10−1.60[94] |
| methanethiol | <0.8 | 2.94 | 1.79 | 1.93 | 1.80−3.10[95] |
| ethanethiol | <1.00 | | | | 1.10[96] |
| dimethylsulfide | 5.61 | 31.40 | 11.60 | 9.60 | 25[96] |
| diethylsulfide | <0.50 | | | | 0.90[96] |
| dimethyldisulfide | <0.60 | | | | 29[96] |
| diethyldisulfide | <0.10 | | | | 4.30[96] |

respectively. The sum of SPP and LPP was named "polymeric pigments" in the present manuscript.

**Statistical Analysis and Data Treatment.** *Determination of Carbonyl Formation Rates.* For each one of the 17 specimens derived from a single wine, the increments of a given carbonyl were determined by subtracting the carbonyl content of the original wine. Then, those 17 increments from that given carbonyl from that wine were represented versus the corresponding 420 nm absorbance increments, and a straight regression line was calculated using least-squares regression analysis. The slope of such regression line is the formation rate of such given carbonyl in that wine and the uncertainty of such slope is the uncertainty of the carbonyl formation rate. These calculations were carried out using Regression analysis of Excel 2013 (Microsoft). Comparison between carbonyl formation rates were carried out via *t* test analysis assuming dissimilar variances.

*Determination of VSCs Depletion Rates.* These were calculated as described for the carbonyls. Principal component analysis (PCA) was carried out using the statistical software The Unscrambler 9.7. from Camo (Norway).

## RESULTS AND DISCUSSION

**Characterization of the Initial Wines.** The basic enological parameters of the 16 original red wines used in the study are given in Table 1. Values of ethanol (12.5−14.2%), reducing sugars (below 4.35 g/L), pH (3.42−3.98), and titratable acidity (4.52−5.79 g/L are normal among Spanish red wines. Volatile acidity was mostly below 0.6 g/L, and only two samples (C11 and C12) have slightly higher values (0.86 and 0.73 g/L), which may be due to long storage in oak barrels (18 and 10 months, respectively).

Table 2 presents a summary of the wine contents in potential aroma precursors of carbonyls (amino acids and alcohols) and in trace mineral elements (the complete set of data is given as Supporting Information). As seen in the table, the amino acids with highest variation ranges (higher than 1 magnitude order) are threonine, γ-aminobutyric acid, and leucine, while the least variable is phenylalanine for which the highest level is just 4.2 times above the smallest. Alcohol levels are less variable, and in most cases, the ratios between the highest and the smallest are below 3. Exceptions are benzyl alcohol, methionol, and β-phenylethanol, for which such ratios are 16, 8.6, and 5.4, respectively. As for the trace elements, in all cases, their contents are low. The ubiquitous iron is in all cases below 5 mg/L, while copper levels only exceeded 1 mg/L in a single wine. The median content of this element was just 0.092 mg/L. Leaving aside aluminum and nickel, median levels were in all cases below 1 mg/L. Elemental sulfur was included in the list as a potential general precursor for VSCs.

Table 3 summarizes (the complete set of data is given as Supporting Information) the levels of carbonyls and VSCs measured in the original wines before the aging experiment. As can be seen, initial wines already contain Strecker aldehydes—methional, phenylacetaldehyde, 2-methylpropanal, 2-methylbutanal and 3-methylbutanal—at levels above their corresponding thresholds, as already noted in previous works,[15,22] while their contents in lipid-related alkenals are very low. The wines also contain small but suprathreshold amounts of 1-octen-3-one, which is a lipid-related aroma compound. It has been identified as a major contributor to the fungus type aroma observed in grape berries contaminated by mildew,[74] but it has been also identified in hydrolisates obtained from fractions of glycosidic aroma precursors extracted from noninfected grapes.[75] The wines also contained small amounts of sotolon, which can be formed by oxidation from threonine,[76] of benzaldeyde, a common grape and wine product usually found under its odor threshold, and of vanillin, which mostly comes from the oak used in winemaking.

As for VSCs, median contents in the set of wines are relatively low, as shown in Table 3. It is clear, however, that some wines contained hydrogen sulfide and methanethiol at

levels high enough to show "reduced" character. Results for $H_2S$ are comparable to those presented by Siebert et al.,[77] although 3 out of the 16 wines showed maxima levels (see Supporting Information). Similarly, concentration ranges of MeSH and DMS are similar to those reported previously.[68,78] EtSH, diethylsulfide (DES), dimethyldisulfide (DMDS), and diethyldisulfide (DEDS) were not detected, in accordance with data given in previous works.[77,78]

**Oxidation in Terms of Absorbance at 420 nm.** The present study involves the storage of wines in recipients with different oxygen permeabilities and requires a measurement of the total amount of oxygen consumed by the wine during the storage time. Due to limitations in the availability of standardized materials with different and known oxygen permeabilities, we decided to produce such recipients in a relatively rough way by piercing more or less the internal septa of our amber vials. The degree of oxygen consumed by of our samples was just indirectly controlled by the absorbance at 420 nm, which is commonly used to assess the degree of wine color oxidation. In order to validate this procedure, the 16 wines were oxidized (at 5 consecutive oxygen saturations) in clear glass tubes containing oxygen sensors (see methods) so that we could measure the real wine oxygen consumption and relate it with its change in absorbance at 420 nm. The 16 wine × 5 oxygen levels/wine = 80 pairs of points were graphically represented revealing a good linear relationship ($R^2$ = 0.81, significant at $P < 4.2 \times 10^{-30}$) and showing that on average, the consumption of 10 mg/L of oxygen implies an increase of 0.46 units of absorbance. This value is in relatively good agreement with the increase of 0.52 found by Ferreira et al. in white wines.[79] In the present experiment, and given that the maximum absorbance increments were around 2.6 absorbance units, we can conclude that our samples consumed along the 6 month period between nothing and around 56 mg of oxygen per liter.

**Rates of Production of Carbonyls upon Wine Oxidation.** For each one of the wines, the levels of carbonyls produced during the 6 months of storage increased in approximately a linear way with the amount of oxygen consumed, as shown in Figure 1 for the case of methional and three different samples (wines R2, B14, and C12). The ordinates of the figure are the increments of methional measured in the 17 different specimens obtained from the wines R2, B14, and C12 after the 6 months of storage under different oxygen regimes. Such increments are represented versus the measured increment in absorbance at 420 nm of the corresponding specimens. The existence of such linear relationships (significant in the three cases at $P < 0.008$, $<1.3 \times 10^{-8}$, and $<1.5 \times 10^{-8}$, respectively), makes it possible to determine the methional formation rate (MFR) of each wine as simply the slope of the regression line together with its uncertainty. As can be seen, these wines produced on average 26.3 ± 2.4, 11.2 ± 1.0, and 0.74 ± 0.24 μg/L of methional, per unit of increment of absorbance at 420 nm, respectively. The differences between those MFR are highly significant ($P < 1.8 \times 10^{-5}$ and $<2 \times 10^{-8}$ for the consecutive paired comparisons) and relevant, as will be later commented. Taking into account the relationship between absorbance and mg/L of oxygen consumed previously estimated, it can be estimated that these wines produced 1.21, 0.51, and 0.011 μg/L of methional per mg/L of oxygen consumed, respectively. In molar terms, this implies that per mol of oxygen consumed the wines produced 372, 158, and 10.4 μmol of methional, respectively.

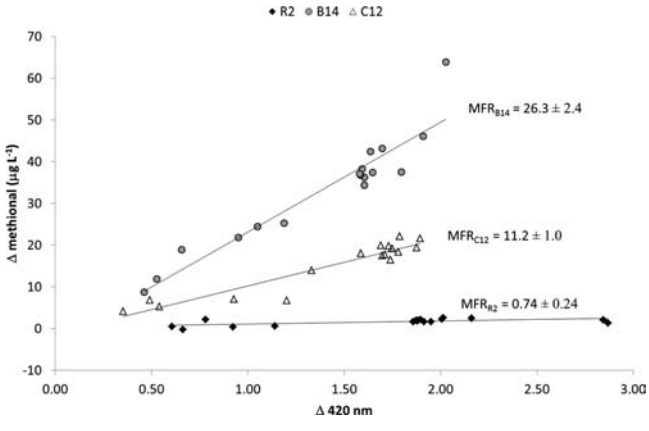


**Figure 1.** Linear relationships between the increments of methional measured in the 17 specimens obtained after the 6 month storage under different oxygen levels of wines B14, R2, and C12, vs the corresponding increments in absorbance at 420 nm of the specimens. The methional formation rates (MFR) are the slopes of the least-square regression lines.

As the linear pattern was observed for most wines and carbonyls, it is possible to estimate the specific rates of production of each aldehyde for each particular wine as shown before. Those data are summarized in Table 4, while more detailed data are given in the Supporting Information. Table 4 gives the ranges and medians of aldehyde formation rates per unit of oxygen consumed. For comparison purposes, the last column of the table gives the median increment in odor activity value (OAV) after the wine has consumed 25 mg/L of oxygen. Such parameter confirms previous findings about the utmost importance of methional and phenylacetaldehyde on the sensory characteristics of aged wines[15,22,80] and reveals that alkenals are rather unimportant oxidation compounds in the slow oxidation taking place during bottle aging, in contrast to what happened in an accidental oxidation with unlimited access to air.[22] The branched aldehydes, 2-methylpropanal, and 3-methylbutanal also have median increments of several units in OAV terms. Surprisingly, 1-octen-3-one and vanillin, which usually are not considered aging-related aroma compounds, showed consistent and potentially sensory relevant increases with the oxidation level. A recent work from Balboa-Lagunero et al.[80] reports an increase of vanillin levels upon oxidation as well. Benzaldehyde is also formed during oxidation but it is far from reaching the odor threshold. Another relevant observation is the absence of sotolon in the table, due to the fact that this compound was not found to increase with the oxidation level and hence it was not possible to estimate any sotolon formation rate, in agreement with the findings of Silva Ferreira et al.,[18,23] who found that this compound was readily formed only at 60 °C.

As ranges in Table 4 reveal, there are large differences in the aldehyde formation rates between wines. In the case of methional, for instance, the wine-forming maxima amounts of this aldehyde (1.57 μg/L per mg/L of $O_2$ consumed), forms it 57 times faster than the wine forming the minimum amount. Differences for phenylacetaldehyde are smaller (a factor 7), and for branched aldehydes difference factors lie between 11 and 27. Differences in the case of 1-octen-3-one are extreme (>600). These data indicate that the rate of production of carbonyls upon wine oxidation is an intrinsic characteristic of each wine. Aldehyde formation rates in the table would be

**Table 4. Minimum, Maximum, and Median Carbonyl Formation Rates Per Unit of Oxygen Consumed in the 16 Wines of the Study and Potential Sensory Significance[a]**

| | min | max | median | max/min | median[b] | OAV[c] |
|---|---|---|---|---|---|---|
| methional | 0.03 | 1.57 | 0.45 | 57.00 | 137.00 | 22.00 |
| phenylacetaldehyde | 0.35 | 2.49 | 0.97 | 7.00 | 259.00 | 24.00 |
| 2-methylpropanal | 0.13 | 2.72 | 1.17 | 21.00 | 776.00 | 4.90 |
| 2-methylbutanal | 0.14 | 1.58 | 0.60 | 11.00 | 222.00 | 0.93 |
| 3-methylbutanal | 0.14 | 3.88 | 1.59 | 27.00 | 589.00 | 8.60 |
| (*E*)-2-hexenal | 0.000005 | 0.004 | 0.0005 | 780.00 | 0.15 | 0.00 |
| (*E*)-2-heptenal | 0.00001 | 0.002 | 0.0005 | 180.00 | 0.15 | 0.00 |
| (*E*)-2-octenal | 0.0002 | 0.007 | 0.0012 | 29.00 | 0.29 | 0.01 |
| (*E*)-2-nonenal | 0.0002 | 0.019 | 0.0037 | 106.00 | 0.85 | 0.15 |
| 1-octen-3-one | 0.00001 | 0.009 | 0.0006 | 683.00 | 0.13 | 0.89 |
| benzaldehyde | 0.19 | 8.56 | 2.49 | 45.00 | 750.00 | 0.03 |
| vanillin | 0.51 | 17.65 | 4.26 | 35.00 | 896.00 | 0.53 |

[a]Except where indicated, data are expressed as $\mu$g/L of carbonyl per mg/L of oxygen consumed. [b]Expressed in $\mu$mol/L of carbonyl per mol/L of oxygen consumed. [c]Odor activity units formed for the median formation rate after the consumption of 25 mg/L of oxygen.

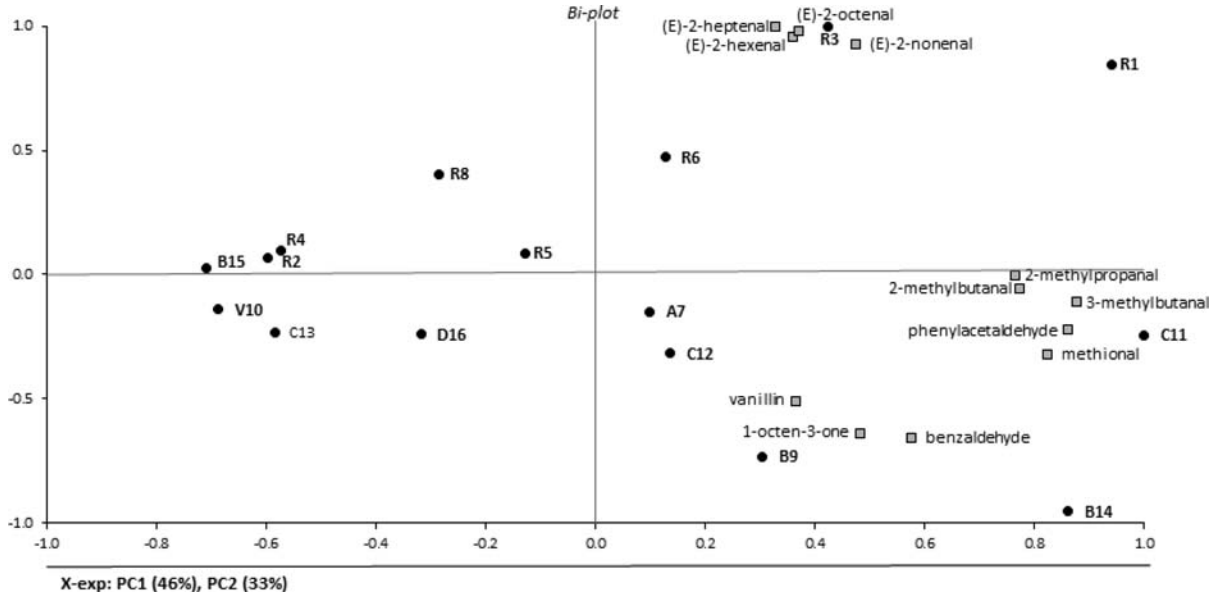


**Figure 2.** PCA showing the projection of samples and variables in terms of their general ability to produce carbonyl compounds.

**Table 5. Relevant Correlations Between (a) Strecker Aldehyde Formation Rates, (b) Wine Initial Concentrations of Strecker Aldehydes, with Different Types of Potential Precursors or Reaction Intermediates**

(a)

| formation rates | wine amino acid | | wine alcohol | | wine diacetyl | | combined $SO_2$ | |
|---|---|---|---|---|---|---|---|---|
| | *r* | *p* | *r* | *p* | *r* | *p* | *r* | *p* |
| methional | 0.62 | 0.01 | 0.23 | 0.39 | −0.38 | 0.15 | 0.62 | 0.01 |
| phenylacetaldehyde | 0.68 | 0.004 | 0.33 | 0.21 | −0.33 | 0.22 | 0.56 | 0.03 |
| 2-methylpropanal | 0.50 | 0.04 | 0.16 | 0.56 | −0.27 | 0.31 | 0.43 | 0.10 |
| 2-methylbutanal | 0.40 | 0.12 | | | −0.31 | 0.25 | 0.41 | 0.11 |
| 3-methylbutanal | 0.57 | 0.02 | 0.09 | 0.74 | −0.21 | 0.45 | 0.76 | 0.001 |

(b)

| adehydes initial concentration | wine amino acid | | wine alcohol | |
|---|---|---|---|---|
| | *r* | *p* | *r* | *p* |
| methional | 0.31 | 0.24 | 0.72 | 0.001 |
| phenylacetaldehyde | 0.24 | 0.37 | 0.25 | 0.34 |
| 2-methylpropanal | 0.22 | 0.41 | 0.12 | 0.67 |
| 2-methylbutanal | 0.48 | 0.06 | | |
| 3-methylbutanal | 0.01 | 0.96 | 0.13 | 0.63 |

**Table 6. Relevant Correlations Between Carbonyl Formation Rates and Phenolic Composition**

| | meth[a] | phen[b] | 2mprop[c] | 2mbut[d] | 3mbut[e] | E2hex[f] | E2hep[g] | E2oct[h] | E2non[i] | 1o3one[j] | benz[k] | van[l] |
|---|---|---|---|---|---|---|---|---|---|---|---|---|
| IPT[m] | ns[n] | ns | ns | ns | ns | −0.52 | −0.51 | −0.50 | −0.59 | ns | ns | ns |
| pigment molecules | | | | | | | | | | | | |
| anthocyanin-3-glucoside | ns | ns | ns | ns | ns | ns | ns | ns | ns | ns | ns | ns |
| anthocyanin acylated | ns | ns | ns | ns | ns | ns | ns | ns | ns | ns | ns | ns |
| pyranoanthocyanin | −0.48 | −0.53 | −0.68 | −0.63 | −0.58 | ns | ns | ns | ns | ns | ns | ns |
| anthocyanin-flavanol | −0.54 | −0.54 | −0.68 | −0.54 | −0.72 | ns | ns | ns | ns | ns | ns | ns |
| polymeric pigments | Ns | ns | −0.43 | ns | ns | −0.46 | −0.51 | −0.49 | −0.61 | ns | ns | ns |
| flavonols | | | | | | | | | | | | |
| total flavonols | −0.46 | −0.45 | −0.53 | −0.53 | −0.56 | ns | ns | ns | −0.52 | ns | ns | ns |
| myricetin-3-glucoside | ns | ns | ns | ns | ns | −0.58 | −0.66 | −0.61 | −0.66 | ns | 0.61 | ns |
| quercetin-3-galactoside | ns | −0.43 | ns | ns | −0.49 | ns | ns | ns | −0.46 | ns | ns | ns |
| quercetin-3-glucuronide | ns | ns | −0.45 | ns | ns | ns | ns | ns | −0.51 | ns | ns | ns |
| quercetin-3-glucopiranosido | ns | −0.52 | ns | −0.48 | ns | −0.48 | ns | ns | −0.55 | ns | ns | ns |
| kaempferol-3-glucoside | ns | ns | ns | ns | ns | ns | ns | ns | −0.43 | ns | ns | ns |
| syringentin-3-glu | ns | −0.45 | −0.51 | ns | −0.49 | ns | ns | ns | ns | ns | −0.48 | ns |
| isorhamnetin-3-glucoside | ns | ns | ns | ns | ns | −0.45 | −0.49 | −0.43 | −0.46 | ns | ns | ns |
| myricetin-3-glucoside | ns | ns | ns | ns | ns | ns | ns | −0.45 | −0.54 | ns | ns | ns |
| quercetin | ns | ns | −0.46 | ns | ns | ns | ns | ns | −0.47 | ns | ns | ns |
| kaempferol | ns | ns | −0.55 | ns | ns | ns | ns | −0.46 | −0.57 | ns | ns | ns |
| phenolic acids and esters | | | | | | | | | | | | |
| gallic | ns | ns | ns | ns | ns | ns | ns | ns | ns | ns | 0.63 | ns |
| ellagic | ns | ns | ns | ns | ns | −0.49 | −0.58 | ns | −0.49 | 0.53 | ns | 0.66 |
| protocatechuic | ns | ns | ns | ns | ns | ns | ns | 0.43 | 0.50 | ns | ns | ns |
| protocatechuic ethyl ester | ns | ns | ns | ns | ns | 0.53 | 0.50 | 0.54 | 0.59 | ns | ns | ns |
| *cis*-caftaric | ns | ns | ns | ns | ns | ns | ns | ns | ns | ns | ns | 0.49 |
| *trans*-caftaric | ns | ns | ns | ns | ns | ns | ns | ns | ns | ns | ns | 0.67 |
| *trans*-coumaric | ns | −0.46 | ns | ns | ns | ns | ns | ns | ns | ns | ns | ns |
| ferulic | ns | ns | ns | ns | ns | ns | ns | ns | ns | 0.47 | ns | 0.57 |
| caffeic acid ethyl ester | 0.50 | 0.58 | ns | ns | 0.54 | ns | ns | ns | ns | 0.88 | 0.69 | 0.52 |
| stilbene | | | | | | | | | | | | |
| *trans*-resveratrol | ns | ns | ns | ns | ns | 0.76 | 0.89 | 0.87 | 0.78 | ns | ns | ns |

[a]Methional. [b]Phenylacetaldehyde. [c]2-Methylpropanal. [d]2-Methylbutanal. [e]3-Methylbutanal. [f](*E*)-2-Hexenal. [g](*E*)-2-Heptenal. [h](*E*)-2-Octenal. [i](*E*)-2-Nonenal. [j]1-Octen-3-one. [k]Benzaldehyde. [l]Vanillin. [m]Total polyphenol index. [n]Not significant.

consistent with aldehyde contents of normal aged nonoxidized wines,[15,22] provided that they have taken up to 50 mg/L oxygen.

The pattern of carbonyl production upon wine oxidation during bottle aging is revealed in the principal component analysis shown in Figure 2. As shown in the figure, all carbonyls have positive loadings on the PC1, which means that this component arranges wines attending to their general ability to produce carbonyls upon oxidation. Samples C11 and R1 are the samples showing in all cases maxima carbonyl production rates. The second component separates wines attending to their individual ability to form alkenals on the one hand and vanillin, benzaldehyde and 1-octen-3-one on the other. Taking into account the large differences in aldehyde production rates, the plot tells us that wines on the left (samples V10, B15...) can undergo prolonged oxidative bottling aging periods without noticeable formation of aldehydes, while samples on the right of the plane, such as R1 and C11, will develop very quickly oxidation-related carbonyls, which will undoubtedly cause them to lose their freshness very soon.

**Formation from Precursors and Role of Intermediates and Catalysts.** As shown in Table 5a, the production rates of Strecker aldehydes are significantly correlated (except 2-methylbutanal) to the wine initial levels in the corresponding amino acid, but not to the wine initial levels in the corresponding alcohol. This suggests that wine amino acids act as primary active precursors for those aldehydes during wine oxidation, confirming previous hypotheses and observations.[21,30] Amino acid levels did not decrease significantly with oxidation, in agreement with a previous report[30] and with the low amount of aldehyde produced.

In the particular case of methional, however, the formation of the aldehyde from the alcohol, methionol, should not be ruled out, because as shown in Table 5b, the initial wine content of this aldehyde is strongly correlated to the wine initial level of methionol. The oxidation of methionol to methional seems, however, not to be the single oxidative degradation pathway of this molecule, because the levels of this alcohol were found to significantly decrease by oxidation (data not shown), while the concomitant increases of methional observed explained only between 4 and 14% of the decrease in methionol. Methionol could be also oxidized to its corresponding *S*-oxide, as recently suggested by Fedrizzi et al.[81]

Carbonyl production rates were significantly correlated to some metallic elements. Methional and phenylacetaldehyde production rates were significantly correlated to the wine content in Zn ($r = 0.51$, $p < 0.05$). The rates of formation of 2-methylpropanal and 2-methylbutanal were significantly correlated to the combined wine content in Fe, Zn, and Cu ($r = 0.58$ and 0.63; $p < 0.05$ and <0.01, respectively). Such correlations were not observed for 3-methylbutanal. In the case of (*E*)-2-alkenals, their production seems to be positively correlated with

Ni levels ($r$ = 0.59 and 0.57, both $p < 0.05$ for (*E*)-2-nonenal and (*E*)-2-octenal, respectively) and negatively with Mn ($r$ = −0.51 and $r$ = −0.51, both $p < 0.05$ for (*E*)-2-nonenal and (*E*)-2-heptenal, respectively). Carbonyl production rates were not correlated to the wine levels in the single dicarbonyl measured in the present study: diacetyl.

In the case of polyphenolic material, several correlations were found, as shown in Table 6. The rates of production of Strecker aldehydes are, in general, negatively correlated to pyroanthocyanidins, anthocyanin-flavanol adducts, flavonols, and *p*-coumaric acid, while they are positively correlated with the ethyl ester of caffeic acid. The rates of production of alkenals are even more strongly correlated to the wine phenolic composition. Negative correlations with TPI, polymeric pigments, flavonols, and ellagic acid and positive correlations with protocatechic acid, its ethyl ester, and *trans*-resveratrol were observed.

It is worth mentioning that anthocyanin pigments formed at the end of the alcoholic fermentation and during wine aging are negatively correlated to Strecker aldehyde and alkenal production rates. Despite their very different chemical structure, those anthocyanin-derived pigments have in common that the 4-position of the heterocycle is occupied, making them more stable and resistant to the action of the bisulfite ions than the anthocyanins from which they originate. An increase in the formation of these pigments is linked to a decrease of anthocyanins combined with $SO_2$, which would result in more color and more available $SO_2$, which could explain the negative correlation. Furthermore, Strecker aldehyde and alkenal production rates keep a negative correlation to flavonols, regardless of whether the determination of these polyphenols is carried out globally by molecular absorption spectroscopy or individually by UPLC-MS. These phenolic compounds are known to be the most effective antioxidant flavonoids,[82] due to the keto group and the OH at the 3-position of the heterocycle.

Benzaldehyde and vanillin mainly show a significant positive correlation with phenolic acids. Benzaldehyde is correlated with gallic acid, and vanillin with caftaric, ferulic, and ellagic acid. Caftaric and ferulic acid come from grapes, the source of ellagic acid is the aging barrel, and gallic acid comes from both sources.

In the case of pH, evidence suggests that less aldehyde (per unit of change in absorbance) is formed at higher pHs. This relationship only reaches the statistical significance level in the case of 2-methylbutanal ($p < 0.02$), but in all cases, the slopes were negative, suggesting that even if the wines oxidize faster at higher pHs, such oxidation is more efficiently producing carbonyls at acid pHs.

**Release from Bisulfite Adducts?** The rates of carbonyl formation during oxidation are in many instances significantly correlated with the combined $SO_2$ level of the original wine. This is the case of methional, phenylacetaldehyde, and 3-methylbutanal, as shown in Table 5, but these correlations were also observed in the cases of (*E*)-2-hexenal ($r$ = 0.530, $p < 0.05$), (*E*)-2-octenal ($r$ = 0.546, $p < 0.05$), (*E*)-2-nonenal ($r$ = 0.517, $p < 0.05$) and 1-octen-3-one ($r$ = 0.546, $p < 0.05$). Combined $SO_2$ includes all the different forms of sulfur dioxide that cannot be purged by a stream of air from an acidic portion of the sample at room temperature. In wine, carbonyls form relatively stable adducts with $SO_2$.[30,42] Those complexes would affect their liquid−gas transfer coefficients and hence their concentration in the headspaces above wine. The correlation between carbonyl formation rates and combined $SO_2$ make us hypothesize that a certain fraction of the oxidation-related carbonyls are in fact already formed in the initial wine trapped under the form of bisulfite adducts. From this point of view, then it follows that the observed formation of aldehydes upon oxidation would not be, at least in part, the direct result of the oxidation of precursor molecules but the simple result of the oxidation of sulfur dioxide itself that would provoke the liberation of the already present bisulfite-trapped aldehydes. In order to assess to what extent the observed formation of aldehydes is real formation from the direct oxidation of precursors, or just release from trapped forms upon depletion of sulfur dioxide, more refined analytical procedures, including the ability to separate between bonded and free forms of aldehydes, will be required.

**VSCs Production and Depletion.** VSCs have been measured by a previously developed method specifically designed for avoiding matrix effects by means of a strong dilution of the wine matrix in brine.[68] Therefore, VSCs measurements truly reflect levels of these compounds in wine rather than the free amounts present in the headspace, which is usually what is measured.[16,77,83] This difference should be taken into account in the interpretation of the results.

As it was previously done, the levels of the three relevant VSCs measured ($H_2S$, MeSH, and DMS) in each one of the 17 specimens produced from each wine sample have been plotted versus the absorbance at 420 nm, and regression lines have been estimated. Two different types of patterns emerge out of the data. In the case of hydrogen sulfide, in all the cases there is a clear decrease with respect to the original wines even in the samples whose oxidation level was very small; that is, in no single case could we appreciate any real accumulation of this molecule, and in all cases, the level of this molecule decreased concomitantly with the level of oxidation. In the cases of MeSH and DMS, on the contrary, we could detect an increment between the levels of the original wine and the levels of the wines after 6 months of storage with low level of oxidation. The effect of oxidation in these two cases was, generally speaking, also a decrease of the molecule with the level of oxidation. All these data are summarized in Table 7.

As shown in Table 7, degradation rates of hydrogen sulfide range from −0.25 to −2.3 μg/L per mg/L $O_2$ consumed (233 to 2160 μmol/L per mol/L oxygen consumed). Hydrogen sulfide degradation rates are strongly correlated to the own initial level of hydrogen sulfide ($r$ = −0.99), which basically suggests that the oxidation kinetics of this molecule follow a second-order kinetic model, according to which oxidation rate would be proportional to both the concentration of initial product ($H_2S$) and of reactant (a wine quinone, hydrogen peroxide, or other reactive oxygen species), being the kinetic constant very similar in all the wines. The strong correlation with the initial concentration of hydrogen sulfide is explained because what is measured in the present work is the degradation rate per oxidation unit, meaning that hydrogen sulfide is oxidized following the main wine oxidation pathway, which is consistent with its highest reaction rates to quinones, as recently measured.[31] Notwithstanding this affirmation, degradation rates are strongly correlated to copper ($r$ = −0.85, $p < 0.0001$) and iron ($r$ = −0.60; $p < 0.05$) levels. A closer look at these data revealed that the three wines with the highest levels of copper contained also the highest levels of hydrogen sulfide, which may just be the result of the industrial use of $Cu^{2+}$ to remove an excess of $H_2S$ caused by a problematic fermentation.[55] The fact that we could not observe

**Table 7. Degradation Rates of VSCs upon Oxidation and Increments (When Applicable) Consequence of Bottle Storage[a]**

| sample | $H_2S$ degradation rate | MeSH average increment | MeSH degradation rate | DMS average increment | DMS degradation rate |
|---|---|---|---|---|---|
| R1 | −0.41 | 1.10 | −0.02 | 5.60 | −0.21 |
| R2 | −0.37 | 1.90 | −0.06 | 4.80 | −0.17 |
| R3 | −0.39 | 0.90 | ns[b] | 5.00 | −0.24 |
| R4 | −0.35 | 2.60 | ns | 21.00 | −0.32 |
| R5 | −0.50 | 2.30 | −0.04 | 12.00 | −0.21 |
| R6 | −0.60 | 1.90 | −0.04 | 8.70 | −0.23 |
| A7 | −2.30 | 3.30 | −0.14 | 22.00 | −0.56 |
| R8 | −0.65 | ns | ns | ns | ns |
| B9 | −0.49 | 4.50 | −0.08 | ns | −0.23 |
| V10 | −0.25 | 3.70 | −0.02 | 5.70 | −0.28 |
| C11 | −1.78 | ns | ns | 8.40 | −0.24 |
| C12 | −0.57 | ns | ns | 9.00 | −0.49 |
| C13 | −1.63 | ns | ns | 8.50 | −0.14 |
| B14 | −0.78 | 3.90 | ns | 4.30 | ns |
| B15 | −0.36 | 4.00 | −0.11 | 9.50 | ns |
| D16 | −0.35 | 6.90 | ns | 8.40 | ns |

[a]Degradation rates are μg/L of VSC degraded per mg/L of oxygen consumed, and increments are μg/L of VSC. [b]Not significant.

any increment on the levels of hydrogen sulfide even at the lowest oxygen levels, would suggest that there are no specific precursors for this molecule in these wines in apparent contrast to the increments very often observed along bottle aging.[14] As was mentioned previously, this disagreement could be related to the nature of our analytical method.

In the case of methanethiol, and in clear contrast to the case of hydrogen sulfide, a small but significant increment on the levels of this molecule has been measured in 12 out of the 16 wines, which suggests that this molecule can be formed from some precursor. Interestingly, methanethiol increments are positively correlated to the wine levels in several amino acids. Although the maximum degree of correlation has been found with the amino acid arginine ($r = 0.72$, $p < 0.01$), the most relevant is the one found with methionine ($r = 0.53$, $p < 0.05$), because this amino acid could be a specific precursor for methanethiol, as recently demonstrated for soy proteins[84] in a reaction mediated by hydroxyl radicals.[85] Furthermore, a negative correlation appears between methanethiol formation and resveratrol levels ($-0.58$, $p < 0.05$), whose activity as reactive oxygen species (ROSs) scavenger, in particular toward hydroxyl radicals, is well documented.[86] It is also worth mentioning the observed correlation between MeSH formation and total proanthocyanidin levels ($r = 0.60$, $p < 0.05$), which may suggest that these compounds compete by the quinones that react and destroy MeSH. A significant negative correlation with aluminum levels ($r = -0.59$, $p < 0.05$) has been also found, in contrast to the low effects found for this cation in methanethiol production.[55]

Methanethiol levels, as previously observed in the case of $H_2S$, decrease with oxidation. As no disulfide was detected in this study, the main degradation route should be the reaction of the mercaptan with a quinone produced along with oxidation.[31,39] Decreases are smaller than those observed for $H_2S$, because levels of methanethiol were in all cases smaller, in many instances close to the method detection limits, and because the reaction rate is smaller.[31] As in the $H_2S$ case, there is a significant negative correlation with copper ($r = -0.59$, $p < 0.05$) and iron levels ($r = -0.67$, $p < 0.01$), which is consistent with the central role played by these cations in wine oxidation.[39] The correlation, however, is strongly influenced by the single wine with the highest levels of these metals, which also had the maximum degradation rate. There is a sound correlation with Mn levels ($r = -0.67$, $p < 0.01$), suggesting that this cation also has a responsibility in the oxidative degradation of methanethiol. This should be further studied, because although the implication of Mn in wine oxidation was experimentally demonstrated in the past,[87] there are no recent reports addressing the role of this cation in wine oxidation.

Dimethylsulfide levels increase after 6 months of storage, as the most likely consequence of the hydrolysis of its known precursor, *S*-methylmethionine.[88] This precursor was not measured in this study. We should note a positive correlation with pH ($r = 0.73$, $p < 0.01$) consistent with the known higher speed of the hydrolytical process at higher pHs. Dimethylsulfide levels also decreased significantly in most cases upon wine oxidation as shown in Table 7, in contrast to what is stated in a recent review,[2] but in agreement with some other reports.[89] Further experiments would be required to clarify the fate of DMS upon oxidation.

## ■ ASSOCIATED CONTENT

### Supporting Information

Concentrations of the initial 16 Spanish red wines of amino acids, alcohols potentially precursors for aldehydes, some trace elements which potential catalytic activity upon oxidation processes, carbonyl compounds and VSCs. Carbonyl formation rates of the 16 wines upon their oxidation. This material is available free of charge via the Internet at http://pubs.acs.org

## ■ AUTHOR INFORMATION

### Corresponding Author

*E-mail: vferre@unizar.es. Fax: 34 976761292. Phone: 34976 762067.

### Funding

This work has been funded by the Spanish Ministry of Economy and Competitiveness (Project AGL2010 230183). E.F-L. has received a grant from DGA, and M.B. has received a grant from the Spanish FPI program.

### Notes

The authors declare no competing financial interest.

## ■ REFERENCES

(1) Gambuti, A.; Rinaldi, A.; Ugliano, M.; Moio, L. Evolution of Phenolic Compounds and Astringency during Aging of Red Wine: Effect of Oxygen Exposure before and after Bottling. *J. Agric. Food Chem.* **2013**, *61*, 1618−1627.

(2) Ugliano, M. Oxygen Contribution to Wine Aroma Evolution during Bottle Aging. *J. Agric. Food Chem.* **2013**, *61*, 6125−6136.

(3) Chira, K.; Jourdes, M.; Teissedre, P. L. Cabernet sauvignon red wine astringency quality control by tannin characterization and polymerization during storage. *Eur. Food Res. Technol.* **2012**, *234*, 253−261.

(4) Chira, K.; Pacella, N.; Jourdes, M.; Teissedre, P. L. Chemical and sensory evaluation of Bordeaux wines (Cabernet-Sauvignon and Merlot) and correlation with wine age. *Food Chem.* **2011**, *126*, 1971−1977.

(5) McRae, J. M.; Kassara, S.; Kennedy, J. A.; Waters, E. J.; Smith, P. A. Effect of Wine pH and Bottle Closure on Tannins. *J. Agric. Food Chem.* **2013**, *61*, 11618−11627.

(6) Fulcrand, H.; Benabdeljalil, C.; Rigaud, J.; Cheynier, V.; Moutounet, M. A new class of wine pigments generated by reaction

between pyruvic acid and grape anthocyanins. *Phytochemistry* **1998**, *47*, 1401−1407.
(7) Perez-Magarino, S.; Jose, M. Evolution of flavanols, anthocyanins, and their derivatives during the aging of red wines elaborated from grapes harvested at different stages of ripening. *J. Agric. Food Chem.* **2004**, *52*, 1181−1189.
(8) Wirth, J.; Morel-Salmi, C.; Souquet, J. M.; Dieval, J. B.; Aagaard, O.; Vidal, S.; Fulcrand, H.; Cheynier, V. The impact of oxygen exposure before and after bottling on the polyphenolic composition of red wines. *Food Chem.* **2010**, *123*, 107−116.
(9) Ugliano, M.; Kwiatkowski, M. J.; Travis, B.; Francis, I. L.; Waters, E. J.; Herderich, M. J.; Pretorius, I. S. Post-bottling management of oxygen to reduce off-flavour formation and optimize wine style. *Aust. N. Z. Wine Ind. J.* **2009**, *24*, 24−28.
(10) Hofmann, T.; Schieberle, P.; Grosch, W. Model studies on the oxidative stability of odor-active thiols occurring in food flavors. *J. Agric. Food Chem.* **1996**, *44*, 251−255.
(11) Blanchard, L.; Darriet, P.; Dubourdieu, D. Reactivity of 3-mercaptohexanol in red wine: Impact of oxygen, phenolic fractions, and sulfur dioxide. *Am. J. Enol. Vitic.* **2004**, *55*, 115−120.
(12) Herbst-Johnstone, M.; Nicolau, L.; Kilmartin, P. A. Stability of Varietal Thiols in Commercial Sauvignon blanc Wines. *Am. J. Enol. Vitic.* **2011**, *62*, 495−502.
(13) Lopes, P.; Silva, M. A.; Pons, A.; Tominaga, T.; Lavigne, V.; Saucier, C.; Darriet, P.; Teissedre, P. L.; Dubourdieu, D. Impact of Oxygen Dissolved at Bottling and Transmitted through Closures on the Composition and Sensory Properties of a Sauvignon Blanc Wine during Bottle Storage. *J. Agric. Food Chem.* **2009**, *57*, 10261−10270.
(14) Ugliano, M.; Kwiatkowski, M.; Vidal, S.; Capone, D.; Siebert, T.; Dieval, J. B.; Aagaard, O.; Waters, E. J. Evolution of 3-Mercaptohexanol, Hydrogen Sulfide, and Methyl Mercaptan during Bottle Storage of Sauvignon blanc Wines. Effect of Glutathione, Copper, Oxygen Exposure, and Closure-Derived Oxygen. *J. Agric. Food Chem.* **2011**, *59*, 2564−2572.
(15) San Juan, F.; Cacho, J.; Ferreira, V.; Escudero, A. Aroma Chemical Composition of Red Wines from Different Price Categories and Its Relationship to Quality. *J. Agric. Food Chem.* **2012**, *60*, 5045−5056.
(16) He, J.; Zhou, Q.; Peck, J.; Soles, R.; Qian, M. C. The effect of wine closures on volatile sulfur and other compounds during post-bottle ageing. *Flavour Fragrance J.* **2013**, *28*, 118−128.
(17) Escudero, A.; Asensio, E.; Cacho, J.; Ferreira, V. Sensory and chemical changes of young white wines stored under oxygen. An assessment of the role played by aldehydes and some other important odorants. *Food Chem.* **2002**, *77*, 325−331.
(18) Ferreira, A. C. S.; Oliveira, C.; Hogg, T.; de Pinho, P. G. Relationship between potentiometric measurements, sensorial analysis, and some substances responsible for aroma degradation of white wines. *J. Agric. Food Chem.* **2003**, *51*, 4668−4672.
(19) Singleton, V. L.; Kramling, T. E. Browning of white wines and an accelerated test for browning capacity. *Am. J. Enol. Vitic.* **1976**, *27*, 157−160.
(20) Wildenradt, H. L.; Singleton, V. L. The production of aldehydes as a result of oxidation of polyphenolic compounds and its relation to wine aging. *Am. J. Enol. Vitic.* **1974**, *25*, 119−126.
(21) Escudero, A.; Hernandez-Orte, P.; Cacho, J.; Ferreira, V. Clues about the role of methional as character impact odorant of some oxidized wines. *J. Agric. Food Chem.* **2000**, *48*, 4268−4272.
(22) Cullere, L.; Cacho, J.; Ferreira, V. An assessment of the role played by some oxidation-related aldehydes in wine aroma. *J. Agric. Food Chem.* **2007**, *55*, 876−881.
(23) Ferreira, A. C. S.; Hogg, T.; de Pinho, P. G. Identification of key odorants related to the typical aroma of oxidation-spoiled white wines. *J. Agric. Food Chem.* **2003**, *51*, 1377−1381.
(24) Cutzach, I.; Chatonnet, P.; Henry, R.; Pons, M.; Dubourdieu, D. Etude sur l'arôme des vins doux naturels non muscatés. 2$^{e}$ partie: Dosages de certains composés volatils intervenant dans l'arôme des vins doux naturels au cours de leur élevage et de leur vieillissement. *J. Int. Sci. Vigne Vin* **1998**, *32*, 211−221.
(25) Escudero, A.; Cacho, J.; Ferreira, V. Isolation and identification of odorants generated in wine during its oxidation: a gas chromatography-olfactometric study. *Eur. Food Res. Technol.* **2000**, *211*, 105−110.
(26) Schneider, R.; Baumes, R.; Bayonove, C.; Razungles, A. Volatile compounds involved in the aroma of sweet fortified wines (vins doux naturels) from Grenache Noir. *J. Agric. Food Chem.* **1998**, *46*, 3230−3237.
(27) Pons, A.; Lavigne, V.; Darriet, P.; Dubourdieu, D. Role of 3-Methyl-2,4-nonanedione in the Flavor of Aged Red Wines. *J. Agric. Food Chem.* **2013**, *61*, 7373−7380.
(28) Saijo, R.; Takeo, T. The formation of aldehydes from amino acids by tea leaves extracts. *Agric. Biol. Chem.* **1970**, *34*, 227−233.
(29) Rizzi, G. P. Formation of Strecker aldehydes from polyphenol-derived quinones and alpha-amino acids in a nonenzymic model system. *J. Agric. Food Chem.* **2006**, *54*, 1893−1897.
(30) Grant-Preece, P.; Fang, H. J.; Schmidtke, L. M.; Clark, A. C. Sensorially important aldehyde production from amino acids in model wine systems: Impact of ascorbic acid, erythorbic acid, glutathione and sulphur dioxide. *Food Chem.* **2013**, *141*, 304−312.
(31) Nikolantonaki, M.; Waterhouse, A. L. A Method To Quantify Quinone Reaction Rates with Wine Relevant Nucleophiles: A Key to the Understanding of Oxidative Loss of Varietal Thiols. *J. Agric. Food Chem.* **2012**, *60*, 8484−8491.
(32) Singleton, V. L. Oxygen with phenols and reated reactions in musts, wines, and model system. Observations and practical inplications. *Am. J. Enol. Vitic.* **1987**, *38*, 69−77.
(33) Pripis-Nicolau, L.; deRevel, G.; Bertrand, A.; Maujean, A. Formation of flavor components by the reaction of amino acid and carbonyl compounds in mild conditions. *J. Agric. Food Chem.* **2000**, *48*, 3761−3766.
(34) Danilewicz, J. C. Review of reaction mechanisms of oxygen and proposed intermediate reduction products in wine: Central role of iron and copper. *Am. J. Enol. Vitic.* **2003**, *54*, 73−85.
(35) Danilewicz, J. C.; Seccombe, J. T.; Whelan, J. Mechanism of interaction of polyphenols, oxygen, and sulfur dioxide in model wine and wine. *Am. J. Enol. Vitic.* **2008**, *59*, 128−136.
(36) Waterhouse, A.; Laurie, V. Oxidation of wine phenolics: A critical evaluation and hypotheses. *Am. J. Enol. Vitic.* **2006**, *57*, 306−313.
(37) Kilmartin, P. A.; Zou, H. L.; Waterhouse, A. L. A cyclic voltammetry method suitable for characterizing antioxidant properties of wine and wine phenolics. *J. Agric. Food Chem.* **2001**, *49*, 1957−1965.
(38) Li, H.; Guo, A.; Wang, H. Mechanisms of oxidative browning of wine. *Food Chem.* **2008**, *108*, 1−13.
(39) Danilewicz, J. C. Interaction of sulfur dioxide, polyphenols, and oxygen in a wine-model system: Central role of iron and copper. *Am. J. Enol. Vitic.* **2007**, *58*, 53−60.
(40) Elias, R. J.; Waterhouse, A. L. Controlling the Fenton Reaction in Wine. *J. Agric. Food Chem.* **2010**, *58*, 1699−1707.
(41) Makhotkina, O.; Kilmartin, P. A. Electrochemical Oxidation of Wine Polyphenols in the Presence of Sulfur Dioxide. *J. Agric. Food Chem.* **2013**, *61*, 5573−5581.
(42) de Azevedo, L. C.; Reis, M. M.; Motta, L. F.; da Rocha, G. O.; Silva, L. A.; de Andrade, J. B. Evaluation of the formation and stability of hydroxyalkylsulfonic acids in wines. *J. Agric. Food Chem.* **2007**, *55*, 8670−8680.
(43) Majcenovic, A. B.; Schneider, R.; Lepoutre, J. P.; Lempereur, V.; Baumes, R. Synthesis and stable isotope dilution assay of ethanethiol and diethyl disulfide in wine using solid phase, microextraction. Effect of aging on their levels in wine. *J. Agric. Food Chem.* **2002**, *50*, 6653−6658.
(44) Mestres, M.; Busto, O.; Guasch, J. Analysis of organic sulfur compounds in wine aroma. *J. Chromatogr. A* **2000**, *881*, 569−581.
(45) Park, S. K.; Boulton, R. B.; Bartra, E.; Noble, A. C. Incidence of volatile sulfur-compounds in Califronia wines. A preliminary survey. *Am. J. Enol. Vitic.* **1994**, *45*, 341−344.
(46) Kwiatkowski, M. J.; Skouroumounis, G. K.; Lattey, K. A.; Waters, E. J. The impact of closures, including screw cap with three

different headspace volumes, on the composition, colour and sensory properties of a Cabernet Sauvignon wine during two years storage. *Aust. J. Grape Wine Res.* **2007**, *13*, 81−94.
(47) Skouroumounis, G. K.; Kwiatkowski, M. J.; Francis, I. L.; Oakey, H.; Capone, D. L.; Duncan, B.; Sefton, M. A.; Waters, E. J. The impact of closure type and storage conditions on the composition, colour and flavour properties of a Riesling and a wooded Chardonnay wine during five years' storage. *Aust. J. Grape Wine Res.* **2005**, *11*, 369−384.
(48) Ugliano, M.; Dieval, J.-B.; Siebert, T. E.; Kwiatkowski, M.; Aagaard, O.; Vidal, S.; Waters, E. J. Oxygen Consumption and Development of Volatile Sulfur Compounds during Bottle Aging of Two Shiraz Wines. Influence of Pre- and Postbottling Controlled Oxygen Exposure. *J. Agric. Food Chem.* **2012**, *60*, 8561−8570.
(49) Schutz, M.; Kunkee, R. E. Formation of hydrogen-sulfide from elemental sulfur during fermentation by wine yeast. *Am. J. Enol. Vitic.* **1977**, *28*, 137−144.
(50) Giudici, P.; Kunkee, R. E. The effect of nitrogen deficiency and sulfur-containing amino-acids on the reduction of sulfate to hydrogen-sulfide by wine yeasts. *Am. J. Enol. Vitic.* **1994**, *45*, 107−112.
(51) Jiranek, V.; Langridge, P.; Henschke, P. A. Regulation of hydrogen-sulfide liberation in wine-producing Saccharomyces-Cerevisiae strains by assimilable nitrogen. *Appl. Environ. Microb.* **1995**, *61*, 461−467.
(52) Linderholm, A. L.; Findleton, C. L.; Kumar, G.; Hong, Y.; Bisson, L. F. Identification of genes affecting hydrogen sulfide formation in Saccharomyces cerevisiae. *Appl. Environ. Microb.* **2008**, *74*, 1418−1427.
(53) Spinnler, H. E.; Berger, C.; Lapadatescu, C.; Bonnarme, P. Production of sulfur compounds by several yeasts of technological interest for cheese ripening. *Int. Dairy J.* **2001**, *11*, 245−252.
(54) Landaud, S.; Helinck, S.; Bonnarme, P. Formation of volatile sulfur compounds and metabolism of methionine and other sulfur compounds in fermented food. *Appl. Microbiol. Biot.* **2008**, *77*, 1191−1205.
(55) Viviers, M. Z.; Smith, M. E.; Wilkes, E.; Smith, P. Effects of Five Metals on the Evolution of Hydrogen Sulfide, Methanethiol, and Dimethyl Sulfide during Anaerobic Storage of Chardonnay and Shiraz Wines. *J. Agric. Food Chem.* **2013**, *61*, 12385−12396.
(56) Leppanen, O. A.; Denslow, J.; Ronkainen, P. P. Determination of thiolacetates and some other volatile sulfur-compounds in alcoholic beverages. *J. Agric. Food Chem.* **1980**, *28*, 359−362.
(57) Bobet, R. A.; Noble, A. C.; Boulton, R. B. Kinetics of the ethanethiol and diethyl disulfide interconversion in wine-like solutions. *J. Agric. Food Chem.* **1990**, *38*, 449−452.
(58) Swiegers, J. H.; Bartowsky, E. J.; Henschke, P. A.; Pretorius, I. S. Yeast and bacterial modulation of wine aroma and flavour. *Aust. J. Grape Wine Res.* **2005**, *11*, 139−173.
(59) Gruenwedel, D. W.; Patnaik, R. K. Release of hydrogen sulfide and methyl mercaptan from sulfur-containing amino acids. *J. Agric. Food Chem.* **1971**, *19*, 775−9.
(60) Metzler, D. E.; Olivard, J.; Snell, E. E. Transamination of pyridoxamine and amino acids with glyoxylic acid. *J. Am. Chem. Soc.* **1954**, *76*, 644−648.
(61) Olivard, J.; Metzler, D. E.; Snell, E. E. Catalytic racemization of amino acids by pyridoxal and metal salts. *J. Biol. Chem.* **1952**, *199*, 669−674.
(62) *Recueil des méthodes internationales d'analyse des vins et des moûts*; Office International de la Vigne et du Vin: Paris, 1990.
(63) Ribéreau-Gayon, P. Le dosage des composes phénoliques totaux dans les vins rouges. *Chim. Anal.* **1970**, *52*, 627−631.
(64) Gonzalvez, A.; Armenta, S.; Pastor, A.; de la Guardia, M. Searching the most appropriate sample pretreatment for the elemental analysis of wines by inductively coupled plasma-based techniques. *J. Agric. Food Chem.* **2008**, *56*, 4943−4954.
(65) Llaudy, M. C.; Canals, R.; Canals, J. M.; Rozes, N.; Arola, L.; Zamora, F. New method for evaluating astringency in red wine. *J. Agric. Food Chem.* **2004**, *52*, 742−746.
(66) Hernandez-Orte, P.; Ibarz, M. J.; Cacho, J.; Ferreira, V. Amino acid determination in grape juices and wines by HPLC using a modification of the 6-aminoquinolyl-N-hydroxysuccinimidyl carbamate (AQC) method. *Chromatographia* **2003**, *58*, 29−35.
(67) Zapata, J.; Mateo-Vivaracho, L.; Cacho, J.; Ferreira, V. Comparison of extraction techniques and mass spectrometric ionization modes in the analysis of wine volatile carbonyls. *Anal. Chim. Acta* **2010**, *660*, 197−205.
(68) Lopez, R.; Lapena, A. C.; Cacho, J.; Ferreira, V. Quantitative determination of wine highly volatile sulfur compounds by using automated headspace solid-phase microextraction and gas chromatography-pulsed flame photometric detection - Critical study and optimization of a new procedure. *J. Chromatogr. A* **2007**, *1143*, 8−15.
(69) Ortega, C.; Lopez, R.; Cacho, J.; Ferreira, V. Fast analysis of important wine volatile compounds Development and validation of a new method based on gas chromatographic-flame ionisation detection analysis of dichloromethane microextracts. *J. Chromatogr. A* **2001**, *923*, 205−214.
(70) Lopez, R.; Aznar, M.; Cacho, J.; Ferreira, V. Determination of minor and trace volatile compounds in wine by solid-phase extraction and gas chromatography with mass spectrometric detection. *J. Chromatogr. A* **2002**, *966*, 167−177.
(71) Ferreira, V.; Jarauta, I.; Lopez, R.; Cacho, J. Quantitative determination of sotolon, maltol and free furaneol in wine by solid-phase extraction and gas chromatography-ion-trap mass spectrometry. *J. Chromatogr. A* **2003**, *1010*, 95−103.
(72) Saenz-Navajas, M. P.; Tao, Y. S.; Dizy, M.; Ferreira, V.; Fernandez-Zurbano, P. Relationship between Nonvolatile Composition and Sensory Properties of Premium Spanish Red Wines and Their Correlation to Quality Perception. *J. Agric. Food Chem.* **2010**, *58*, 12407−12416.
(73) Harbertson, J. F.; Picciotto, E. A.; Adams, D. O. Measurement of polymeric pigments in grape berry extracts and wines using a protein precipitation assay combined with bisulfite bleaching. *Am. J. Enol. Vitic.* **2003**, *54*, 301−306.
(74) Darriet, P.; Pons, M.; Henry, R.; Dumont, O.; Findeling, V.; Cartolaro, P.; Calonnec, A.; Dubourdieu, D. Impact odorants contributing to the fungus type aroma from grape berries contaminated by powdery mildew (Uncinula necator); Incidence of enzymatic activities of the yeast Saccharomyces cerevisiae. *J. Agric. Food Chem.* **2002**, *50*, 3277−3282.
(75) Lopez, R.; Ezpeleta, E.; Sanchez, I.; Cacho, J.; Ferreira, V. Analysis of the aroma intensities of volatile compounds released from mild acid hydrolysates of odourless precursors extracted from Tempranillo and Grenache grapes using gas chromatography-olfactometry. *Food Chem.* **2004**, *88*, 95−103.
(76) Cutzach, I.; Chatonnet, P.; Dubourdieu, D. Study of the formation mechanisms of some volatile compounds during the aging of sweet fortified wines. *J. Agric. Food Chem.* **1999**, *47*, 2837−2846.
(77) Siebert, T. E.; Solomon, M. R.; Pollnitz, A. P.; Jeffery, D. W. Selective Determination of Volatile Sulfur Compounds in Wine by Gas Chromatography with Sulfur Chemiluminescence Detection. *J. Agric. Food Chem.* **2010**, *58*, 9454−9462.
(78) Fang, Y.; Qian, M. C. Sensitive quantification of sulfur compounds in wine by headspace solid-phase microextraction technique. *J. Chromatogr. A* **2005**, *1080*, 177−185.
(79) Ferreira, A. C. S.; Guedes de Pinho, P.; Rodrigues, P.; Hogg, T. Kinetics of Oxidative Degradation of White Wines and How They are Affected by Selected Technological Parameters. *J. Agric. Food Chem.* **2002**, *50*, 5919−5924.
(80) Balboa-Lagunero, T.; Arroyo, T.; Cabellos, J. M.; Aznar, M. Sensory and Olfactometric Profiles of Red Wines after Natural and Forced Oxidation Processes. *Am. J. Enol. Vitic.* **2011**, *62*, 527−535.
(81) Fedrizzi, B.; Zapparoli, G.; Finato, F.; Tosi, E.; Turri, A.; Azzolini, M.; Versini, G. Model Aging and Oxidation Effects on Varietal, Fermentative, and Sulfur Compounds in a Dry Botrytized Red Wine. *J. Agric. Food Chem.* **2011**, *59*, 1804−1813.
(82) Berset, C. Antioxydants phénoliques − Structure, propiétés et sources végétales. In *Les polyphenols en agroalimentaire*; Sarni-Manchado, P., Cheynier, V., Eds. Lavoisier: Paris, 2006; pp 265−290.

(83) Herszage, J.; Ebeler, S. E. Analysis of Volatile Organic Sulfur Compounds in Wine Using Headspace Solid-Phase Microextraction Gas Chromatography with Sulfur Chemiluminescence Detection. *Am. J. Enol. Vitic.* **2011**, *62*, 1−8.
(84) Lei, Q.; Boatright, W. L. Methionine is the methyl group donor for sulfite-associated methanethiol formation in isolated soy proteins. *J. Food Sci.* **2006**, *71*, C527−C531.
(85) Spasojevic, I.; Pristov, J. B.; Vujisic, L.; Spasic, M. The reaction of methionine with hydroxyl radical: reactive intermediates and methanethiol production. *Amino Acids* **2012**, *42*, 2439−2445.
(86) Leonard, S. S.; Xia, C.; Jiang, B. H.; Stinefelt, B.; Klandorf, H.; Harris, G. K.; Shi, X. L. Resveratrol scavenges reactive oxygen species and effects radical-induced cellular responses. *Biochem. Biophys. Res. Commun.* **2003**, *309*, 1017−1026.
(87) Cacho, J.; Castells, J. E.; Esteban, A.; Laguna, B.; Sagrista, N. Iron, copper, and manganese influence on wine oxidation. *Am. J. Enol. Vitic.* **1995**, *46*, 380−384.
(88) Loscos, N.; Segurel, M.; Dagan, L.; Sommerer, N.; Marlin, T.; Baumes, R. Identification of S-methylmethionine in Petit Manseng grapes as dimethyl sulphide precursor in wine. *Anal. Chim. Acta* **2008**, *621*, 24−29.
(89) Vasserot, Y.; Jacopin, C.; Jeandet, P. Effect of bottle capacity and bottle-cap permeability to oxygen on dimethylsulfide formation in champagne wines during aging on the lees. *Am. J. Enol. Vitic.* **2001**, *52*, 54−55.
(90) Cullere, L.; Cacho, J.; Ferreira, V. Validation of an analytical method for the solid phase extraction, in cartridge derivatization and subsequent gas chromatographic-ion trap tandem mass spectrometric determination of 1-octen-3-one in wines at ngL(−1) level. *Anal. Chim. Acta* **2006**, *563*, 51−57.
(91) Peinado, R. A.; Moreno, J.; Bueno, J. E.; Moreno, J. A.; Mauricio, J. C. Comparative study of aromatic compounds in two young white wines subjected to pre-fermentative cryomaceration. *Food Chem.* **2004**, *84*, 585−590.
(92) Guth, H. Quantitation and Sensory Studies of Character Impact Odorants of Different White Wine Varieties. *J. Agric. Food Chem.* **1997**, *45*, 3027−3032.
(93) Martin, B.; Etievant, P. X.; Lequere, J. L.; Schlich, P. More clues about sensory impact of sotolon in some flor sherry wines. *J. Agric. Food Chem.* **1992**, *40*, 475−478.
(94) Siebert, T. E.; Bramley, B.; Solomon, M. R. Hydrogen sulfide: aroma detection threshods study in red and white wine. *AWRI Technol. Rev.* **2009**, *183*, 14−16.
(95) Solomon, M. R.; Geue, J.; Osidazc, P.; Siebert, T. Aroma detection threshold study of methanethiol in white and red wine. *AWRI Technol. Rev.* **2010**, *186*, 8−10.
(96) Goniak, O. J.; Noble, A. C. Sensory study of selected volatile sulfur-compounds in white wine. *Am. J. Enol. Vitic.* **1987**, *38*, 223−227.

**Table 1. Details of the Target Compounds**

| no. | analyte | CAS Registry No. | usage | SML[a] (mg kg$^{-1}$) | log$P^b$ |
|---|---|---|---|---|---|
| 1 | Cyasorb UV-1164 | 2725-22-6 | light stabilizer | 5 | 11.43 |
| 2 | Irgafos 168 | 31570-04-4 | antioxidant | 60 | 15.71 |
| 3 | Irganox 1010 | 6683-19-8 | antioxidant | 60 | 19.29 |
| 4 | Irganox 3114 | 27676-62-6 | antioxidant | 5 | 13.17 |
| 5 | Irganox 3790 | 40601-76-1 | antioxidant | 6 | 12.75 |
| 6 | Irganox 565 | 991-84-4 | antioxidant | 30 | 13.37 |
| 7 | Tinuvin 1577 | 147315-50-2 | light stabilizer | 0.05 | 8.59 |
| 8 | Tinuvin 234 | 70321-86-7 | light stabilizer | 2 | 8.41 |
| 9 | Tinuvin 326 | 3896-11-5 | light stabilizer | 30[c] | 5.33 |
| 10 | Tinuvin 327 | 3864-99-1 | light stabilizer | 30[c] | 6.49 |
| 11 | Tinuvin P | 2440-22-4 | light stabilizer | 30[c] | 3.19 |

[a]Specific migration limits of the target compounds according to 10/2011[1] [b]Values predicted by MarvinSketch. [c]The SMLs are given for the sum of these substances.

preparation techniques and the development of specific applications with these techniques are time-consuming and expensive ways to remove matrices or to enrich compounds. Liquid−liquid extraction with low-temperature purification is a practical technique for eliminating fat[38−40] as it freezes out while the target compounds remain dissolved in the organic phase.

The aim of this study was to develop and validate an LC-MS/MS method to measure the concentration of Cyasorb UV-1164, Tinuvin P, Tinuvin 234, Tinuvin 326, Tinuvin 327, and Tinuvin 1577 (UV stabilizers) and Irgafos 168, Irganox 1010, Irganox 3114, Irganox 3790, and Irganox 565 (antioxidants) in milk. To remove the fat content of the milk extracts liquid−liquid extraction with low-temperature purification was chosen because of its simplicity. In the course of method development different solvents, extraction volumes, and pH values were investigated to maximize recoveries. Injection volume was optimized to minimize the matrix effect. Because of the lack of isotope-labeled internal standards, both external and matrix calibrations were checked. During method development milk samples with low fat content were used. However, robustness was checked using fattier samples.

## MATERIALS AND METHODS

**Chemicals and Materials.** Irganox 565 (99%) was purchased from Chemos GmbH (RK Tech, Hungary); Tinuvin P (99.3%), Tinuvin 326 (98%), and Tinuvin 324 (98%) from Tokyo Chemical Indrustry Co. (RK Tech, Hungary); Cyasorb UV-1164 (97%), Irganox 3114 (97%), and Tinuvin 1577 (99%) from Toronto Research Chemicals Inc. (RK Tech, Hungary); and Tinuvin 327 (98%), Irganox 3790 (97%), Irgafos 168 (98%), and Irganox 1010 (98%) from Sigma-Aldrich Co. (Hungary).

2-Propanol (HPLC grade), tetrahydrofuran (HPLC grade), dichloromethane (GC grade), formic acid (Suprapur), acetic acid (Suprapur), NaCl, and ammonium acetate (ReagPhEur) were purchased from Merck Ltd. (Hungary). Acetonitrile (HPLC grade), methanol (HPLC grade), ethyl acetate (Picograde), and acetone (Picograde) were purchased from LGC Promochem Ltd. (Hungary). Ammonium solution (25%; Normapur) was obtained from VWR International, LLC. Ammonium formate (LC-MS grade) was bought from Fluka (Sigma-Aldrich Co., Hungary).

Mixed stock solution of the standards was prepared in dichloromethane at a concentration of 500 $\mu$g/mL for every target compound. The working solution was prepared by 10-fold dilution with tetrahydrofuran. One gram spiked milk samples were prepared by adding 100 $\mu$L of working solution.

UHT milk samples in Tetra Pak containers with fat contents of 1.5 and 3.5% were purchased in local food stores and, until analyzed, stored in a refrigerator at 5 °C.

**Instrumentation.** HPLC separation was performed on an Agilent 1100 HPLC equipped with a degasser (G1322A), a binary pump (G1312A), an autosampler (G1313A), a column thermostat (G1316A), and a variable-wavelength detector (G1314A). Mass spectrometric detection was carried out by using an Applied Biosytems API 2000 triple quadrupole. Data acquisition and evaluation were performed using Analyst version 1.6.1 software.

For centrifugation Z206A and Z230A Hermle centrifuges were used. HPLC grade water was prepared by a Direct-Q 5 (Millipore) system. A Julabo FT902 cryostat with acetone was used for liquid−liquid extraction with low-temperature purification. Dry residue weights of the extracts were measured with a Mettler Toledo AB135-S/FACT balance. To avoid contamination, only glass labware was allowed to come in contact with the sample.

**Recovery and Matrix Effect.** Recovery and matrix effect were optimized separately. Good recoveries are necessary for low limits of detection, yet good recoveries combined with high matrix effect indicate poor accuracy, especially for external calibration. Matrix effects (ME) and recoveries (RE) can be calculated by using eqs 1 and 2:[41]

$$\mathrm{ME}\ (\%) = \frac{B}{A} \times 100 \quad (1)$$

$$\mathrm{RE}\ (\%) = \frac{C}{B} \times 100 \quad (2)$$

$A$ is the peak area of the standard solution, $B$ is the peak area of the standard in the sample spiked after the extraction, and $C$ is the peak area of the standard in the sample spiked before the extraction. If ME is 100%, there is no matrix effect. If ME is >100%, there is a signal enhancement, and if ME is <100%, there is signal suppression. For all milk samples, A, B, and C samples were prepared with three parallel and mean values substituted into the above-described formulas.

After optimization of the sample preparation procedure based on recoveries, 1, 2, and 5 $\mu$L injection volumes were tested to minimize matrix effect.

**Chromatography and Mass Spectrometry Method Development.** Columns of different types, selectivities, and dimensions were tested to reach medium retention, acceptable peak symmetry, and narrow peaks. The tested columns were as follows: GL Sciences InertSustain C18 (100 mm × 2.1 mm × 3 $\mu$m); Phenomenex Synergi 4u Polar-RP 80A (150 mm × 2.0 mm × 4 $\mu$m); YMC-UltraHT Hydrosphere C18 (50 mm × 3.0 mm × s-2 $\mu$m); YMC-Triart C18 (100 mm × 2.1 mm × 3 $\mu$m); Thermo Hypersil Gold C18 (30 mm × 2.0 mm × 1.9 $\mu$m); Kinetex C18 (100 mm × 2.1 mm × 2.6 $\mu$m); Kinetex pentafluorophenyl (PFP) (100 mm × 2.1 mm × 2.6 $\mu$m). Gradient elution was performed during the studies of the columns with 0.25 mL/min flow. Water-based eluent was called "A" and the organic modifier, "B". Gradient was started at 90% A, held for 2 min.

Table 2. Ionization Mode and MRM Transitions of the Target UV Stabilizers and Antioxidants by LC-MS/MS

| | | precursor ion | | | | | | product ion | | |
|---|---|---|---|---|---|---|---|---|---|---|
| no. | analyte | structure | $m/z$ | DP[a] | FP[a] | EP[a] | CEP[a] | $m/z$ | CE[a] | CXP[a] |
| 1 | Cyasorb UV-1164 | $(M + H)^+$ | 510.2 | 106 | 350 | 12 | 18 | 136.1 | 59 | 4 |
| | | | | | | | | 132.2 | 59 | 4 |
| 2 | Irgafos 168 | $(M + H)^+$ | 647.4 | 111 | 360 | 12 | 20 | 147.2 | 69 | 6 |
| | | | | | | | | 235.0 | 79 | 12 |
| 3 | Irganox 1010 | $(M + NH_4)^+$ | 1195.0 | 111 | 280 | 12 | 60 | 219.0 | 117 | 8 |
| | | | | | | | | 163.0 | 121 | 8 |
| 4 | Irganox 3114 | $(M + NH_4)^+$ | 801.5 | 51 | 370 | 11 | 80 | 219.2 | 51 | 8 |
| | | | | | | | | 203.2 | 111 | 6 |
| 5 | Irganox 3790 | $(M + NH_4)^+$ | 717.2 | 51 | 370 | 9 | 34 | 191.2 | 37 | 8 |
| | | | | | | | | 135.2 | 81 | 4 |
| 6 | Irganox 565 | $(M + H)^+$ | 589.3 | 146 | 310 | 11 | 22 | 250.1 | 69 | 6 |
| | | | | | | | | 57.1 | 101 | 4 |
| 7 | Tinuvin 1577 | $(M + H)^+$ | 426.2 | 131 | 230 | 11 | 18 | 104.2 | 63 | 2 |
| | | | | | | | | 136.0 | 55 | 4 |
| 8 | Tinuvin 234 | $(M + H)^+$ | 448.2 | 41 | 370 | 10.5 | 18 | 91.2 | 77 | 2 |
| | | | | | | | | 119.1 | 51 | 4 |
| 9 | Tinuvin 326 | $(M + H)^+$ | 316.0 | 41 | 350 | 11 | 12 | 260.0 | 31 | 6 |
| | | | | | | | | 105.0 | 59 | 2 |
| 10 | Tinuvin 327 | $(M + H)^+$ | 358.0 | 66 | 340 | 10.5 | 14 | 57.2 | 51 | 4 |
| | | | | | | | | 302.3 | 31 | 10 |
| 11 | Tinuvin P | $(M + H)^+$ | 226.0 | 41 | 370 | 9.5 | 14 | 120.1 | 27 | 4 |
| | | | | | | | | 107.1 | 29 | 4 |

[a]DP, declustering potential (V); FP, focusing potential (V); EP, entrance potential; CEP, collision entrance potential (V); CE, collision energy (eV); CXP, collision exit potential (V).

Linear gradient was applied to increase B to 90% in 8 min; 90% B was held for 10 min. Fourteen minutes was needed to equilibrate the system before the next injection. During optimization of chromatographic and mass spectrometric parameters, 5 $\mu$L was injected from a 500 ng/mL standard methanol solution onto the columns three times.

Different compositions of the mobile phase were tested. Formic acid (0.1 v/v %) both in Direct-Q water and in organic modifiers was used on every column. Both acetonitrile and methanol were tested as organic modifiers. Ammonium acetate (20 mmol/L; pH adjusted to 5.00) was also examined with both methanol and acetonitrile on all of the columns. On the Kinetex PFP column also the amount of buffer was tested with 1, 5, and 20 mmol/L ammonium formate (pH adjusted to 2.80 with formic acid). In these experiments 0.1 v/v % formic acid in methanol was used as organic eluent. Effects of the pH were studied on Kinetex PFP with pH 2.80 ammonium formate (20 mmol/L) and pH 5.00 ammonium acetate (20 mmol/L) in Direct-Q water. Methanol was used as the organic modifier in these experiments.

**Optimization of Sample Preparation.** In our method, liquid–liquid extraction was used to remove proteins and carbohydrates and low-temperature purification to remove fats from milk samples. The fat content of the extracts is usually removed by freezing for 12 h in a freezer at −20 °C.[38−40] The freezing process can be accelerated at lower temperature by liquid nitrogen, liquid nitrogen combined with an organic solvent, or a cryostat. We used a cryostat at −50 °C with acetone. Liquid–liquid extraction with low-temperature purification is usually combined with filtration. Even though syringe filtration would have been practical, we had to avoid any plastic tools. Thus, centrifugation, which is an easy and cheap way to remove particles from liquids, was used instead.

Optimization was started with a pretrial with extraction of the target compounds from 5 mL aqueous solutions into 5 mL of acetonitrile with three parallel samples to find out if basic or acidic conditions provide higher recoveries for the target compounds. Phase separation was obtained by adding 0.25 g of NaCl. For pH modification 0.1 v/v % formic acid and 0.1 v/v % ammonia solutions were used. Recoveries were tested without any pH modification as well. Because the alkaline media proved to be the best, the optimization of sample preparation was started with 25 $\mu$L of 25% ammonia solution for pH adjustment of the 1 g milk samples before extraction with 4 mL of solvent.

Acetonitrile, acetone, tetrahydrofuran, ethyl acetate, and 2-propanol were tested on milk samples using liquid–liquid extraction with low-temperature purification. After the extraction solvent, the extraction volume was optimized. One gram of milk was extracted with 2, 5, and 10 mL of the selected solvent.

The variety of functional groups contained by the target compounds necessitated a finer setting of the pH later: 50 $\mu$L of either 2 mol/L (pH ∼13), $2 \times 10^{-2}$ mol/L (pH ∼11), or $2 \times 10^{-4}$ mol/L (pH ∼9) NaOH solution was added to 1 g of spiked milk samples to determine the effects of the pH on recoveries.

Two microliters was injected from every sample during the development of sample preparation. Finally, the lipid-removing efficiency of low-temperature purification was tested using the validated sample preparation method, detailed in the next paragraph.

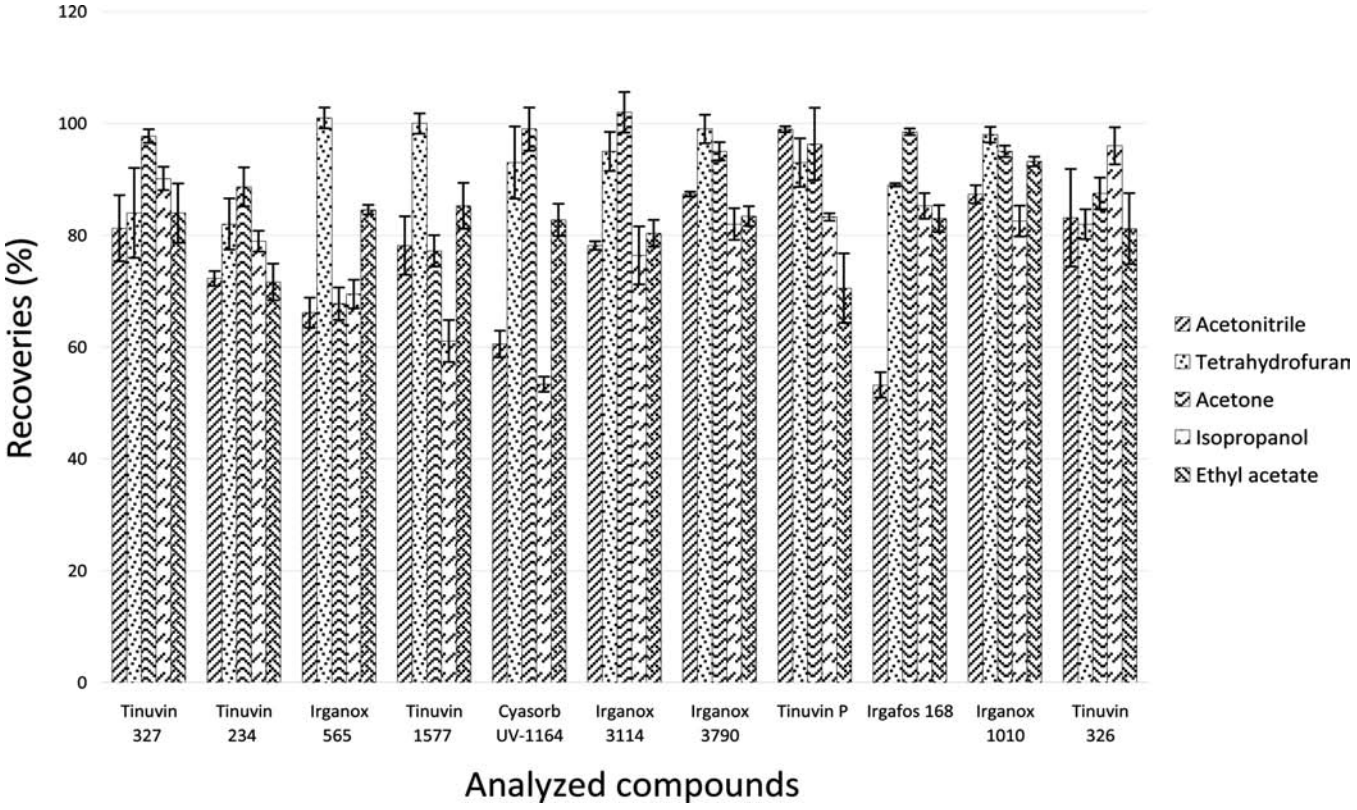


**Figure 1.** Recoveries for liquid−liquid extraction with low-temperature purification using different solvents on 1.5% fat milk. Error bars represent the mean ± standard deviation of recoveries calculated using average peak areas of the standard in the sample spiked after the extraction, $n = 3$.

For this purpose dry residue weights of 0.5 mL extracts were determined before and after low-temperature purification with five parallel samples. Measurements were performed from both 1.5 and 3.5% fat-containing milk. For the determination of dry residue weight, samples were dried to constant weight at 102 °C.

**Validated Method.** One gram of milk was weighed into a 40 mL vial. First, 50 μL $2 \times 10^{-2}$ mol/L NaOH (pH ∼11) solution was added to the sample. This was followed by 5 mL of tetrahydrofuran and 0.25 g of NaCl. The sample was vortexed for a minute and sonicated for a further 10 min. After the extraction, sample was centrifuged for 10 min at 410*g*. A 1.5 mL aliquot of the upper phase was transferred to a 2 mL HPLC vial that was sealed afterward. The vial was placed into a 15 mL centrifuge tube filled with 2.15 mL of −50 °C acetone then kept at −50 °C by cryostat for 30 min for the fat content to freeze out. In this centrifuge tube the sample was centrifuged for 2 min at 3300*g*. After centrifugation for 2 min, 0.5 mL of the fat-free supernatant was transferred to another HPLC vial from which the injection took place.

Gradient elution was carried out at a flow rate of 0.25 mL/min using 1 mmol/L ammonium formate (pH adjusted to 2.80 with formic acid) buffer in water as eluent A and 0.1 v/v % formic acid in methanol as eluent B. The gradient separation was started at 10% B, and then by a linear gradient B was increased to 95% within 3 min. This composition was held for 13 min, and then the eluent composition was lowered to 10% B immediately. Before the next run was begun, 14 min of equilibration time was necessary.

In the case of external calibration 1 μL, otherwise 5 μL, sample aliquots were injected with needle wash (vial wash in acetonitrile) onto a 100 mm × 2.1 mm × 2.6 μm PFP (Kinetex, Phenomenex, Hungary) core−shell column equipped with an in-line filter containing replacement frits (2 mm, 0.2 μm). The column temperature was kept at 30 °C during the analysis.

Electrospray ion source was used in positive mode. The sample was ionized and nebulized with 4500 V (IS voltage). The curtain gas, the nebulizer gas in the ion spray and the auxiliary gas, which helps to evaporate the spray droplets, were all nitrogen set to CUR 10, GS1 40, and GS2 60, respectively. The temperature of GS2 (TEM) was set to 550 °C. Nitrogen was used also as collision gas for collision-activated dissociation (CAD 7). Positive ions were acquired in multiple reaction monitoring (MRM) mode. For all compounds two transitions were monitored. Details of the MRM transitions are presented in Table 2. Dwell time was 50 ms for all transitions. Component-dependent parameters were acquired by measuring $NH_4^+$ adduct in the case of Irganox 1010, Irganox 3114, and Irganox 3790.

**Method Validation.** The method was validated with 1 g spiked negative milk samples (milk sample that did not contain any of the target polymer additives in detectable amount) with fat content of 1.5%. MDLs were determined with a series of spiked negative milk samples as the least detectable amount of analyte with a signal-to-noise ratio above 3. External standard calibration was performed from 125 μg/kg to 25 mg/kg concentration and matrix calibration between 25 μg/kg and 2.5 mg/kg. Because linear regression is suitable for only 1 order of magnitude, quadratic regression was applied. Accuracies and precisions were calculated at two concentration levels (500 μg/kg and 5 mg/kg) for external calibration for both 1.5 and 3.5% fat containing milk samples with three parallel samples. In the case of matrix calibration, accuracies and precisions were tested on all calibration levels with three parallels. Accuracies are given as percentages comparing the concentration calculated from the calibration curves with that of the spiked milk samples. To quantify intraday precision values relative standard deviation (RSD) was calculated from the average concentration and their standard deviation. To check the robustness of the method with regard to the fat content of the sample, accuracies and intraday precision values were determined also for fattier milk samples (3.5%) at 100 μg/kg and 1 mg/kg.

## RESULTS AND DISCUSSION

**Optimization of LC-MS/MS Conditions.** Most of the UV stabilizers can be protonated and measured by ESI.[25] Although atmospheric pressure chemical ionization (APCI)[6,8,9] or atmospheric pressure photoionization (APPI)[9] mode is

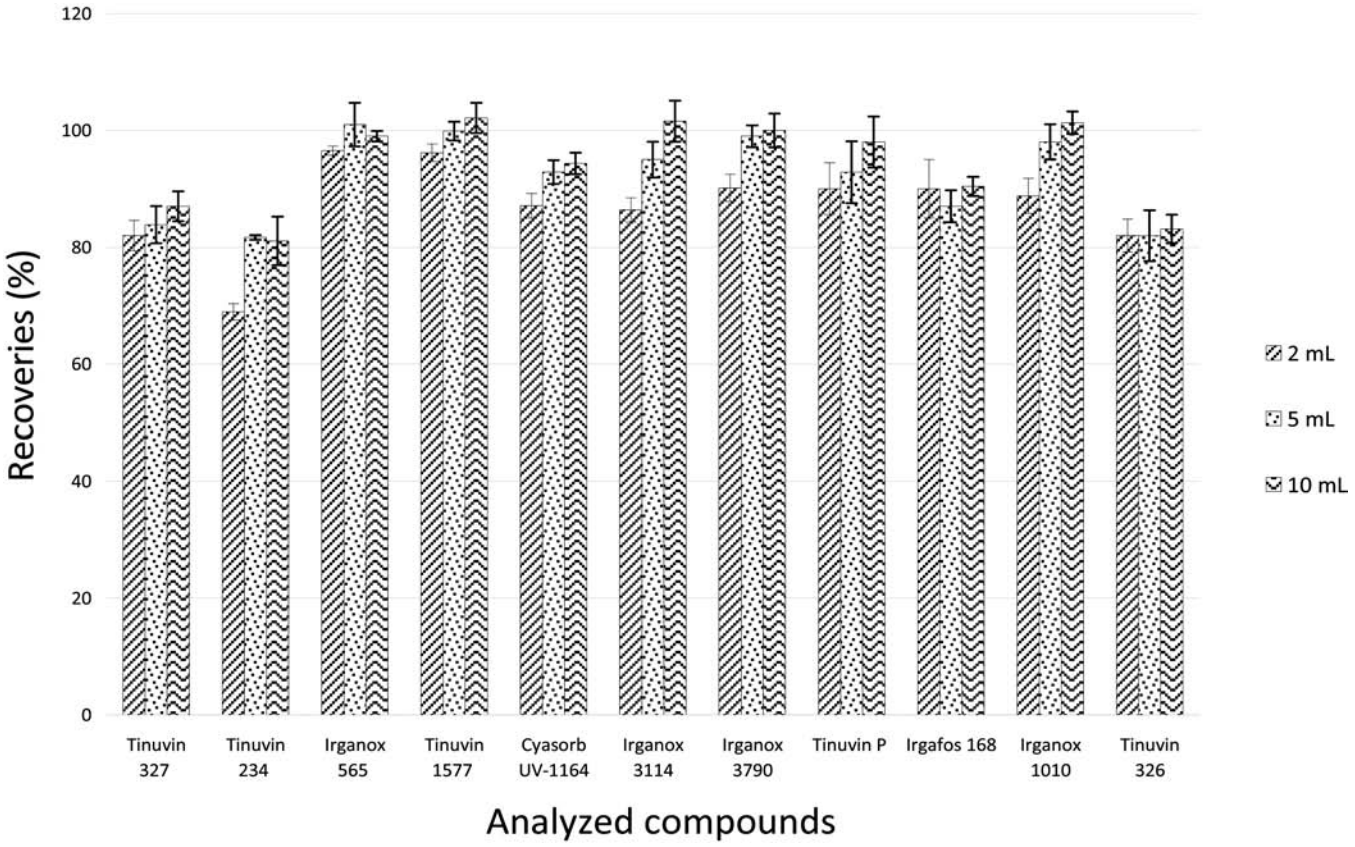


**Figure 2.** Recoveries for liquid–liquid extraction with low-temperature purification using different volumes of tetrahydrofuran on 1.5% fat milk. Error bars represent the mean ± standard deviation of recoveries calculated using average peak areas of the standard in the sample spiked after the extraction, $n = 3$.

advisable for some of the target compounds, mostly for the antioxidants, ESI was preferred in our method because it grants satisfying intensity for all compounds.

The first tests of columns and eluents showed that 0.1 v/v % formic acid in Direct-Q water and acetonitrile cannot elute Irganox 565 and Cyasorb UV-1164 from the GL Sciences InertSustain C18, YMC-UltraHT Hydrosphere C18, and YMC-Triart C18 columns. From the Kinetex C18 only Irganox 565 could not be eluted. Such problems did not occur with the Phenomenex Synergi 4u Polar-RP 80A, Thermo Hypersil Gold C18, and Kinetex PFP columns. On the Synergi 4u Polar-RP 80A and on the Thermo Hypersil Gold C18 the last peaks broadened severely compared to the Kinetex PFP. Kinetex PFP is made using core–shell technology that guaranteed high plate number and effective separation and therefore better signal-to-noise ratio compared to a fully porous column. Kintex PFP was chosen for further experiments. These initial experiments also revealed that with regard to sensitivity Tinuvin 327, Tinuvin 326, and Tinuvin P are the critical compounds.

Using methanol–water instead of acetonitrile–water granted higher abundance for most compounds but also higher back pressure and longer retention time. Methanol is a weaker eluent compared to acetonitrile, but it increased the signal so methanol was used for further experiments.

Effects of the pH of the eluent were studied with pH 2.80 ammonium formate (20 mmol/L) and pH 5.00 ammonium acetate (20 mmol/L) in water. Lower pH granted higher abundance for all of the compounds. The increment of the signal of Tinuvin P was the lowest: it gave only a 1.14 times bigger peak at pH 2.8 compared to that at pH 5.00. The highest increment was measured for Tinuvin 1577, giving a 3.9 ratio. (See the Supporting Information, Figure S1.)

Finally, the amount of ammonium formate was optimized. The abundance of the compounds measured as ammonium adduct increased with increasing amount of ammonium formate, but the three critical compounds suffered ion suppression. Ammonium formate (1 mmol/L) was chosen to minimize ion suppression and still provide enough ammonium ion for the sensitive and reproducible measurement of Irganox 1010, Irganox 3114, and Irganox 3790 peaks in the form of ammonium adduct. (See the Supporting Information, Figure S2.)

On the basis of these results and considerations, positive electrospray ion source (ESI) and a 100 mm × 2.1 mm × 2.6 $\mu$m PFP core–shell column with gradient elution using 1 mmol/L ammonium formate (pH 2.80) buffer and methanol with 0.1 v/v % formic acid as eluents was chosen.

**Optimization of Sample Preparation.** As potential extraction solvent, acetonitrile, acetone, 2-propanol, ethyl acetate, and tetrahydrofuran were tested on alkalinized milk samples. The observed recoveries are shown in Figure 1. Recoveries were >50% for all compounds with every solvent. The lowest recoveries were observed with acetonitrile and 2-propanol. Acetone, ethyl acetate, and tetrahydrofuran provided acceptable recoveries. Using acetone, the recoveries were >87% except for Irganox 565 (68%) and Tinuvin 1577 (77%). Extractions with ethyl acetate resulted <80% only for Tinuvin 234 (72%) and Tinuvin P (71%). Tetrahydrofuran provided >82% recoveries for all compounds. Thus, tetrahydrofuran was chosen for further studies.

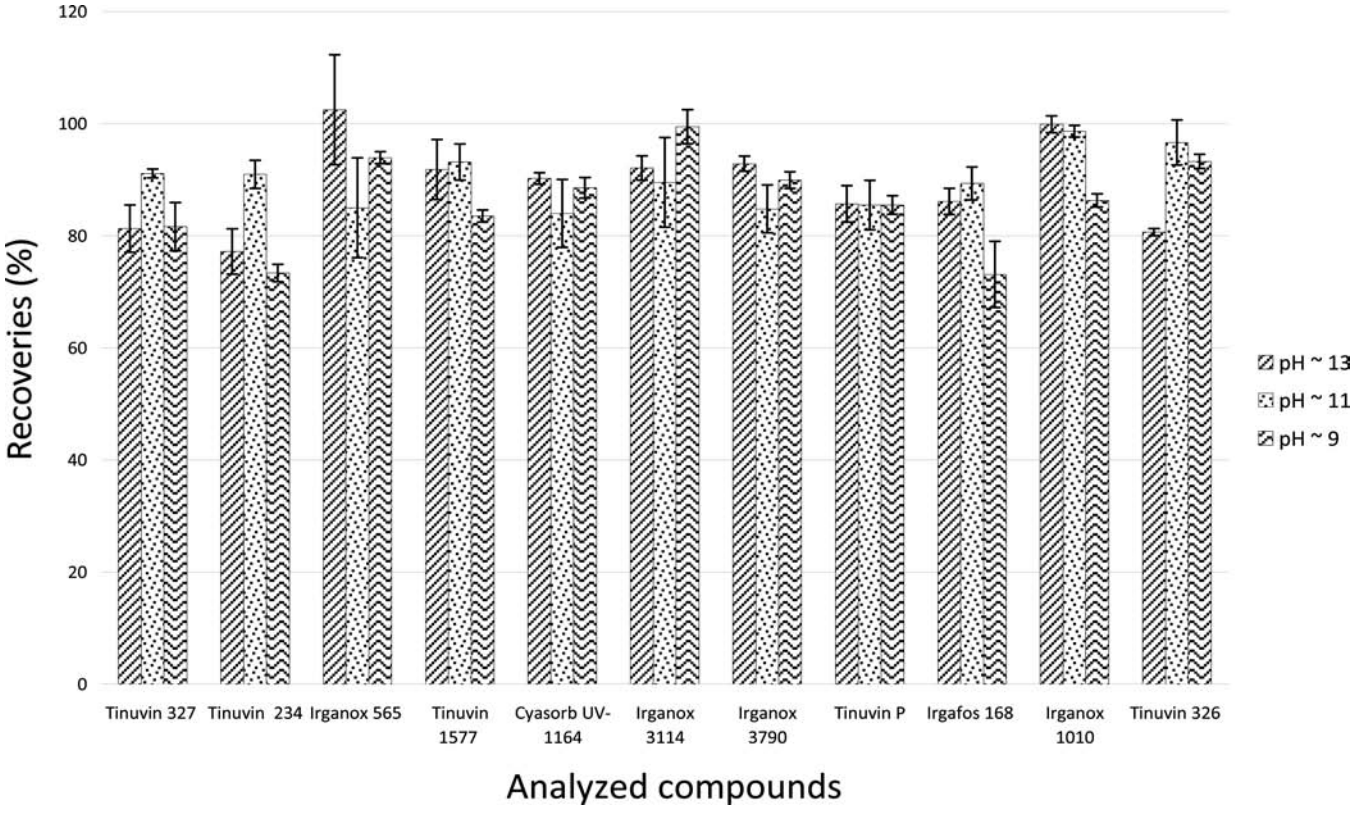


**Figure 3.** Recoveries for liquid−liquid extraction with low-temperature purification at different pH values using tetrahydrofuran on 1.5% fat milk. Error bars represent the mean ± standard deviation of recoveries calculated using average peak areas of the standard in the sample spiked after the extraction, $n = 3$.

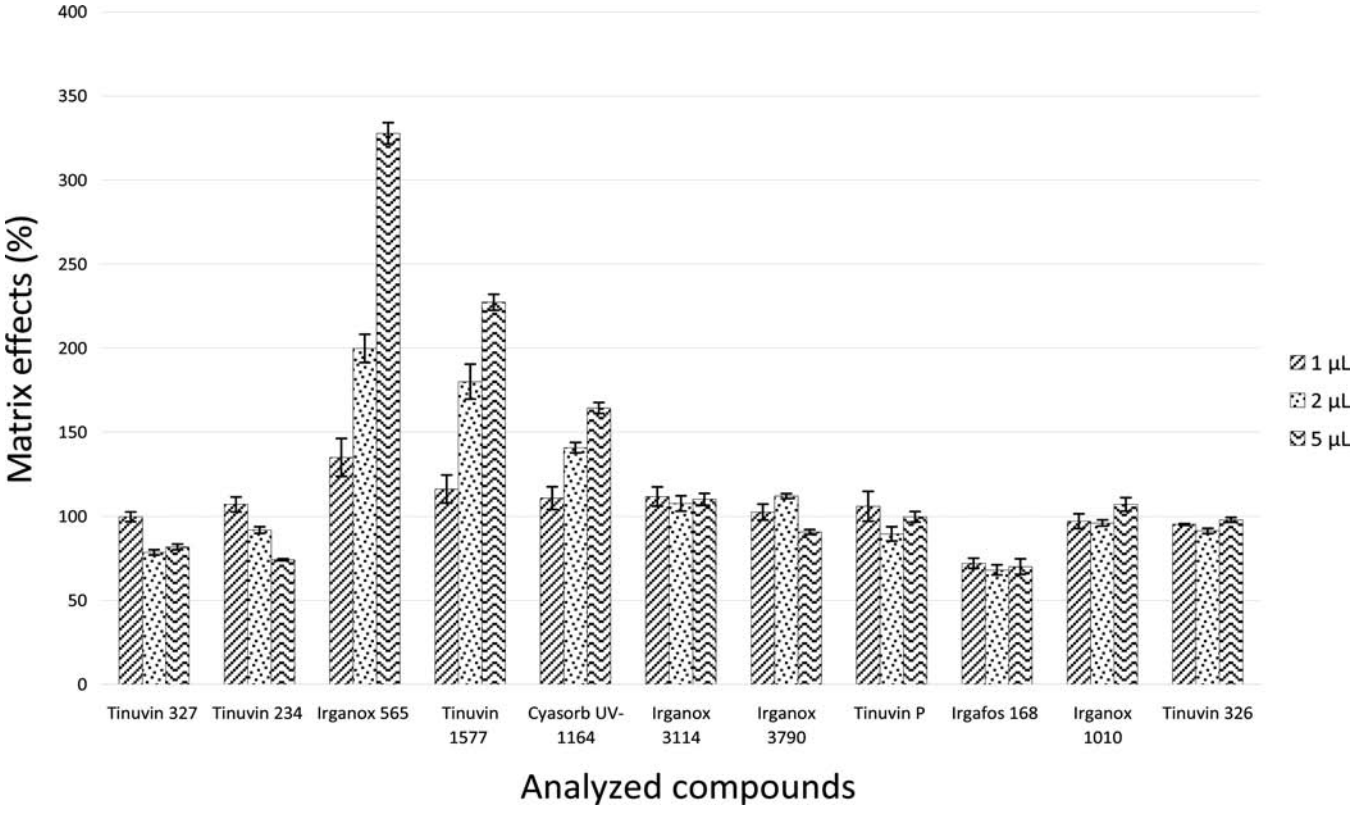


**Figure 4.** Matrix effects using liquid−liquid extraction with low-temperature purification on 1.5% fat milk with different injection volumes. Error bars represent the mean ± standard deviation of matrix effects calculated using average peak areas of the standard solution, $n = 3$.


dx.doi.org/10.1021/jf503110v | J. Agric. Food Chem. 2014, 62, 10028−10037

Table 3. Validation Results Using External Calibration

| | accuracy (RSD%) | | | | | |
|---|---|---|---|---|---|---|
| | 1.5% fat | | 3.5% fat | | | |
| analyte | 500 μg/kg | 5 mg/kg | 500 μg/kg | 5 mg/kg | determination coefficient | MDL[a] (μg/kg) |
| Cyasorb UV-1164 | 125 (8) | 148 (16) | 117 (9) | 152 (17) | 0.9972 | 2.5 |
| Irgafos 168 | 64 (4) | 67 (5) | 67 (7) | 68 (12) | 0.9974 | 5 |
| Irganox 1010 | 100 (9) | 114 (12) | 113 (7) | 126 (7) | 0.9926 | 5 |
| Irganox 3114 | 98 (11) | 97 (8) | 96 (12) | 94 (10) | 0.9920 | 2.5 |
| Irganox 3790 | 100 (5) | 95 (5) | 96 (4) | 96 (4) | 0.9982 | 2.5 |
| Irganox 565 | 133(6) | 127 (9) | 129 (12) | 127 (10) | 0.9904 | 2.5 |
| Tinuvin 1577 | 129 (7) | 136 (11) | 135 (14) | 118 (16) | 0.9942 | 5 |
| Tinuvin 234 | 90 (8) | 91 (8) | 89 (13) | 94 (7) | 0.9928 | 2.5 |
| Tinuvin 326 | 97 (3) | 92 (7) | 98 (5) | 95 (9) | 0.9972 | 25 |
| Tinuvin 327 | 80 (12) | 75 (9) | 81 (12) | 78 (10) | 0.9966 | 25 |
| Tinuvin P | 97 (1) | 97 (5) | 94 (3) | 95 (5) | 0.9986 | 25 |

[a]MDL, method detection limits.

The volume of tetrahydrofuran necessary for the extraction was tested at 2, 5, and 10 mL. Two milliliters of extraction solvent granted good recoveries for most of the compounds. (See Figure 2.) The recoveries were >80% except for Tinuvin 234. Increasing the extraction volume from 2 to 5 mL increased the recoveries, especially for Tinuvin 234, Cyanosorb-UV 1164, Irganox 3114, Irganox 1010, and Irganox 3790. With 5 mL of tetrahydrofuran the average recovery was 92%, and with 10 mL it was 94%. Anyhow, using 10 mL instead of 5 mL did not result in such a big increase in recoveries that it would be beneficial to use that much solvent with regard to environmental and financial reasons. Hence, 5 mL was used in the process of validation.

Because the target compounds have various functional groups, optimization of the pH of the extraction was indispensable. At first extraction from water, 0.1 v/v % formic acid, and 0.1 v/v % ammonia solutions to acetonitrile as the organic phase were tested. Without pH modification lower recoveries were reached than with either formic acid or ammonia solution. Acidic condition provided the best recoveries for Irganox 3790, Irganox 3114, and Tinuvin 326. In this medium recoveries were <70% for Irganox 565, Cyasorb UV-1164, and Irgafos 168. Recoveries were >75% with ammonia solution for every compound. Because an alkaline environment gave acceptable recoveries for the biggest number of target compounds, milk samples were set to pH 9, 11, and 13 with NaOH (Figure 3). At pH 13 recovery for Tinuvin 234 was 77%. At pH 9 it was 73% as well as for Irgafos 168. pH 11 was found to be the most suitable for the extraction of most analytes: it provided >84% recoveries for all of the compounds. For further studies pH 11 was applied.

On the basis of these results 50 μL of a $2 \times 10^{-2}$ mol/L NaOH solution was added to milk samples to adjust the pH for extraction. To reach the highest recoveries, 5 mL of tetrahydrofuran was used for the extraction.

The efficiency of low-temperature purification was tested by measuring the dry residue weight of the tetrahydrofuran extracts before and after the purification. In the case of 1.5% fat milk, the dry residue of a given amount of extract before low-temperature purification is 1.67 mg; that of the same amount of extract after low-temperature purification is 1.39, so the decrease (0.28) is 16.7% of the original dry residue weight (1.67).

**Matrix Effect.** Measurement error originating from ion suppression/enhancement can be eliminated by using internal standards or matrix calibration. Isotope-labeled internal standards offer an expensive way to decrease the matrix effects; moreover, for our target compounds we could not find any in commercial trade. Nonlabeled internal standards ought to resemble the corresponding target compound regarding ionization efficiency, functional groups, polarity, and retention time. Finding suitable nonlabeled internal standards that meet all of the mentioned criteria is almost impossible. On the other hand, matrix calibration is a time-consuming technique, so after minimization of the matrix effect, it is worthwhile to test external calibration first.

Instead of dilution lower matrix effect can be obtained by applying lower injection volumes; 1, 2, and 5 μL of injected volume were tested (Figure 4). Significant ion enhancement was experienced in the cases of Irganox 565, Cyasorb UV-1164, and Tinuvin 1577. By contrast, ion suppression took place in the case of Tinuvin 234. With 1 μL injection volume, the matrix effect could be decreased to 116% in the case of Tinuvin 1577, to 135% in the case of Irganox 565, and to 111% in the case of Cyasorb UV-1164. For the remaining compounds decreasing the matrix amount (i.e., injection volume) did not result in remarkable changes. One microliter injection volume was chosen.

**Method Validation.** Specificity was found to be satisfactory without any chromatographic interference at the retention time of the compounds. MRM chromatograms for negative milk and spiked negative milk samples are shown in the Supporting Information (Figures S3−S13).

**External Calibration.** Validation data obtained with external calibration are summarized in Table 3. Calibration curves ranged from 125 μg/kg to 25 mg/kg. The lowest determination coefficient was 0.9904 (Irganox 565). Parameters of the calibration curves are given in the Supporting Information (Table S1). The MDLs were in the range from 2.5 to 25 μg/kg. These detection limits are at least 1 order of magnitude lower than the corresponding SMLs.

Using external calibration, no significant effect of the fat content of the milk samples on accuracy and precision was observed. Good accuracy and precision values were obtained for Tinuvin P, Tinuvin 326, Irganox 3114, Irganox 3790, and Tinuvin 234 with both types of milk samples (1.5 and 3.5% fat contents). In this group the lowest accuracy was 89%, whereas

Table 4. Validation Results Using Matrix Calibration

| | accuracy (RSD%) | | | | | | | | |
|---|---|---|---|---|---|---|---|---|---|
| | 1.5% fat | | | | | 3.5% fat | | | |
| analyte | 25 μg/kg | 100 μg/kg | 500 μg/kg | 1 mg/kg | 2.5 mg/kg | 100 μg/kg | 1 mg/kg | determination coefficient | MDL[a] (μg/kg) |
| Cyasorb UV-1164 | 93 (3) | 98 (6) | 102 (7) | 99 (4) | 100 (3) | 82 (4) | 93 (2) | 0.9988 | 0.25 |
| Irgafos 168 | 95 (3) | 103 (2) | 99 (8) | 100 (2) | 100 (2) | 92 (0.4) | 100 (1) | 0.9992 | 2.5 |
| Irganox 1010 | 100 (7) | 96 (11) | 100 (13) | 100 (4) | 100 (6) | 98 (2) | 99 (5) | 0.9958 | 0.25 |
| Irganox 3114 | 109 (3) | 106 (8) | 95 (11) | 102 (10) | 100 (9) | 108 (12) | 92 (12) | 0.9914 | 0.5 |
| Irganox 3790 | 108 (6) | 109 (11) | 94 (13) | 102 (4) | 100 (2) | 92 (12) | 87 (7) | 0.9980 | 0.5 |
| Irganox 565 | 107 (1) | 104 (2) | 96 (5) | 101 (4) | 100 (3) | 93 (2) | 95 (3) | 0.9990 | 0.25 |
| Tinuvin 1577 | 94 (5) | 100 (3) | 102 (1) | 99 (9) | 100 (4) | 91 (2) | 101 (2) | 0.9978 | 0.25 |
| Tinuvin 234 | 95 (2) | 102 (8) | 98 (2) | 101 (3) | 100 (3) | 100 (4) | 100 (3) | 0.9992 | 0.25 |
| Tinuvin 326 | 97 (8) | 101 (1) | 100 (3) | 100 (4) | 100 (3) | 87 (12) | 101 (3) | 0.9990 | 2.5 |
| Tinuvin 327 | 103 (2) | 101 (4) | 99 (5) | 100 (4) | 100 (2) | 107 (2) | 102 (1) | 0.9990 | 10 |
| Tinuvin P | 95 (11) | 97 (3) | 98 (4) | 101 (5) | 100 (5) | 94 (6) | 101 (4) | 0.9980 | 2.5 |

[a]MDL, method detection limits.

the highest was 100%. For these components the highest RSD was 12% (for Irganox 3114). For Tinuvin 327 the accuracies were between 75 and 81% and the RSD values between 10 and 12%. On the basis of the goal of the measurement, these values can also be acceptable.

For Irganox 565, Cyasorb UV-1164, Tinuvin 1577, and Irganox 1010 the accuracies were >110% due to matrix effects. For Irgafos 168 the accuracy was <70% due to ion suppression. Because of these unsatisfactory results external calibration is not applicable for the measurement of Irganox 565, Cyasorb UV-1164, Tinuvin 1577, Irganox 1010, and Irgafos 168. Anyhow, even for these compounds external calibration is suitable for screening of migration problems. On the other hand, the method was successfully validated for Tinuvin P, Tinuvin 234, Tinuvin 326, Tinuvin 327, Irganox 3114, and Irganox 3790 using external calibration and 1 μL injection volume. For these compounds MDLs were lower than the SML values in Regulation 10/2011/EC by 3 orders of magnitude.

**Matrix Calibration.** Validation data obtained with matrix calibration are summarized in Table 4. Calibration curves ranged from 25 μg/kg to 2.5 mg/kg. The lowest determination coefficient was 0.9914 (Irganox 3114) Parameters of the calibration curves are shown in the Supporting Information (Table S1). Due to the larger injection volume (and signal enhancement for some compounds) the MDLs were lower than in the case of external calibration.

Matrix calibration provided excellent accuracies and RSD values for milk samples containing 1.5% fat. Accuracies were between 93 and 109%, and RSD values were <13%. Using the matrix calibration on 3.5% fat milk at 100 μg/kg and 1 mg/kg concentrations, the accuracies were between 82 and 108% and the RSD values were <12% which are also acceptable.

Although liquid−liquid extraction combined with low-temperature purification provided good recoveries, the matrix effect still caused some difficulties regarding accuracy and precision. Because of the lack of isotope-labeled internal standards both external and matrix calibrations were tested. For Irganox 565, Cyasorb UV-1164, Tinuvin 1577, Irganox 1010, and Irgafos 168 acceptable accuracy and precision could be achieved only using matrix calibration. However, for all of the compounds MDLs were lower than the SML values in Regulation 10/2011/EC by 1−3 order(s) of magnitude. As a result, the presented analytical method using matrix calibration can be advised for determination of all targeted compounds (Cyasorb UV-1164, Irgafos 168, Irganox 1010, Irganox 3114, Irganox 3790, Irganox 565, Tinuvin 1577, Tinuvin 234, Tinuvin 326, Tinuvin 327, and Tinuvin P) in milk samples. With external calibration it can be used for the determination of Irganox 3114, Irganox 3790, Tinuvin 234, Tinuvin 326, Tinuvin 327, and Tinuvin P, whereas it can be used for the screening of Irganox 565, Cyasorb UV-1164, Tinuvin 1577, Irganox 1010, and Irgafos 168.

## ■ ASSOCIATED CONTENT

### Supporting Information

Figure S1, effects of pH; Figure S2, effects of buffer amount in the eluent from the point of view of the peak area; Figures S3−S13, chromatograms for negative milk and spiked milk samples; Table S1, parameters of the calibration curves for both external and matrix calibration. This material is available free of charge via the Internet at http://pubs.acs.org.

## ■ AUTHOR INFORMATION

### Corresponding Author

*(Z.E.) E-mail: eke.zsuzsanna@wirec.eu. Phone: +36 30 5980300.

### Funding

We gratefully acknowledge Wessling International Research and Educational Center (WIREC) for providing financial support.

### Notes

The authors declare no competing financial interest.

## ■ ACKNOWLEDGMENTS

We gratefully acknowledge Wessling International Research and Educational Center (WIREC) for providing the LC-MS/MS instrument.

## ■ REFERENCES

(1) Commission Regulation (EU) no. 10/2011 on 14 January 2011 on plastic materials and articles intended to come into contact with food.

(2) Gao, Y.; Gu, Y.; Wei, Y. Determination of polymer additives−antioxidants and ultraviolet (UV) absorbers by high-performance liquid chromatography coupled with UV photodiode array detection in food simulants. *J. Agric. Food Chem.* **2011**, *59*, 12982−12989.

(3) Dopico-Garcia, M. S.; Lopez-Vilarino, J. M.; Gonzalez-Rodriguez, M. V. Antioxidant content of and migration from commercial

polyethylene, polypropylene, and polyvinyl chloride packages. *J. Agric. Food Chem.* **2007**, *55*, 3225−3231.
(4) Marcato, B.; Guerra, S.; Vianello, M.; Scalia, S. Migration of antioxidant additives from various polyolefinic plastics into oleaginous vehicles. *Int. J. Pharm.* **2003**, *257*, 217−225.
(5) Farajzadeh, M. A.; Vardast, M. R.; Bahram, M. Optimization of dispersive liquid−liquid microextraction of Irganox 1010 and Irgafos 168 from polyolefins before liquid chromatographic analysis. *Chromatographia* **2009**, *69*, 409−419.
(6) Farajzadeh, M. A.; Bahram, M.; Jönsson, J. A. Dispersive liquid−liquid microextraction followed by high-performance liquid chromatography-diode array detection as an efficient and sensitive technique for determination of antioxidants. *Anal. Chim. Acta* **2007**, *591*, 69−79.
(7) Duderstadt, R. E.; Fischer, S. Effect of organic mobile phase composition on signal responses for selected polyalkene additive compounds by liquid chromatography−mass spectrometry. *J. Chromatogr., A* **2008**, *1193*, 70−78.
(8) Baner, A.; Guggenberger, A. Analysis of Tinuvin 1577 polymer additive in edible oils using on-line coupled HPLC-GC. *J. High Resolut. Chromatogr.* **1997**, *20*, 669−673.
(9) Block, C.; Wynants, L.; Kelchtermans, M.; De Boer, R.; Compernolle, F. Identification of polymer additives by liquid chromatography−mass spectrometry. *Polym. Degrad. Stab.* **2006**, *91*, 3163−3173.
(10) Reingruber, E.; Himmelsbach, M.; Sauer, C.; Buchberger, W. Identification of degradation products of antioxidants in polyolefins by liquid chromatography combined with atmospheric pressure photoionisation mass spectrometry. *Polym. Degrad. Stab.* **2010**, *95*, 740−745.
(11) Nerin, C.; Fernandez, C.; Domeno, C.; Salafrance, J. Determination of potential migrants in polycarbonate containers used for microwave ovens by high-performance liquid chromatography with ultraviolet and fluorescence detection. *J. Agric. Food Chem.* **2003**, *51*, 5647−5653.
(12) Dopico-Garcia, M. S.; Lopez-Vilarino, J. M.; González-Rodriguez, M. V. Determination of antioxidant migration levels from low-density polyethylene films into food simulants. *J. Chromatogr., A* **2003**, *1018*, 53−62.
(13) Nakata, H.; Murata, S.; Filatreau, J. Occurrence and concentrations of benzotriazole UV stabilizers in marine organisms and sediments from the Ariake Sea, Japan. *Environ. Sci. Technol.* **2009**, *43*, 6920−6926.
(14) Garde, J. A.; Catala, R.; Gavara, R. Global and specific migration of antioxidants from polypropylene films into food simulants. *J. Food Prot.* **1998**, *61*, 1000−1006.
(15) Reinas, I.; Oliveira, J.; Pereira, J.; Machado, F.; Pocas, M. F. Migration of two antioxidants from packaging into a solid food and into Tenax®. *Food Control* **2012**, *28*, 333−337.
(16) Carpinteiro, I.; Abuin, B.; Rodriguez, I.; Ramil, M.; Cela, R. Pressurized solvent extraction followed by gas chromatography tandem mass spectrometry for the determination of benzotriazole light stabilizers in indoor dust. *J. Chromatogr., A* **2010**, *1217*, 3729−3735.
(17) Kameda, Y.; Kimura, K.; Miyazaki, M. Occurrence and profiles of organic sun-blocking agents in surface waters and sediments in Japanese rivers and lakes. *Environ. Pollut.* **2011**, *159*, 1570−1576.
(18) Reddy, C. M.; Quinn, J. G.; King, J. W. Free and bound benzotriazoles in marine and freshwater sediments. *Environ. Sci. Technol.* **2000**, *34*, 973−979.
(19) Carpinteiro, I.; Abuin, B.; Ramil, M.; Rodriguez, I.; Cela, R. Matrix solid-phase dispersion followed by gas chromatography tandem mass spectrometry for the determination of benzotriazole UV absorbers in sediments. *Anal. Bioanal. Chem.* **2012**, *402*, 519−527.
(20) Garde, J. A.; Catala, R.; Gavara, R.; Hernandez, R. J. Characterizing the migration of antioxidants from polypropylene into fatty food simulants. *Food Addit. Contam.* **2001**, *18*, 750−762.
(21) Camacho, W.; Karlsson, S. Quality-determination of recycled plastic packaging waste by identification of contaminants by GC−MS after microwave assisted extraction (MAE). *Polym. Degrad. Stab.* **2001**, *71*, 123−134.
(22) Hilder, E. F.; Klampfl, C. W.; Buchberger, W.; Haddad, P. R. Separation of hydrophobic polymer additives by microemulsion electrokinetic chromatography. *J. Chromatogr., A* **2001**, *922*, 293−302.
(23) Zhou, L. Y.; Ashraf-Khorassani, M.; Taylor, L. T. Comparison of methods for quantitative analysis of additives in low-density polyethylene using supercritical fluid and enhanced solvent extraction. *J. Chromatogr., A* **1999**, *858*, 209−218.
(24) Daimon, H.; Hirata, Y. Directly coupled supercritical-fluid extraction/capillary supercritical-fluid chromatography of polymer additives. *Chromatographia* **1991**, *32*, 549−554.
(25) Ashraf-Khorassani, M.; Levy, J. M. Quantitative analysis of polymer additives in low density polyethylene using supercritical fluid extraction/supercritical fluid chromatography. *J. High Resolut. Chromatogr.* **1990**, *13*, 742−747.
(26) Montesdeoca-Esponda, S.; Vega-Morales, T.; Sosa-Ferrera, Z.; Santana-Rodríguez, J. J. Extraction and determination methodologies for benzotriazole UV stabilizers in personal-care products in environmental and biological samples. *Trends Anal. Chem.* **2013**, *51*, 23−32.
(27) Nász, S.; Debreczeni, L.; Rikker, T.; Eke, Z. Development and validation of a liquid chromatographic-tandem mass spectrometric method for determination of eleven coccidiostats in milk. *Food Chem.* **2012**, *133*, 536−543.
(28) Liu, T.; Cao, P.; Geng, J.; Li, J.; Wang, M.; Wang, M.; Li, X.; Yin, D. Determination of triazine herbicides in milk by cloud point extraction and high-performance liquid chromatography. *Food Chem.* **2014**, *142*, 358−364.
(29) Socas-Rodriguez, B.; Asension-Ramos, M.; Hernández-Borges, J.; Rodriguez-Delgado, M. Á. Analysis of oestrogenic compounds in dairy products by hollow-fibre liquid-phase microextraction coupled to liquid chromatography. *Food Chem.* **2014**, *149*, 319−325.
(30) Liu, X.; Yu, Y.; Zhao, M.; Zhang, H.; Li, Y.; Duan, G. Solid phase extraction using magnetic core mesoporous shell microspheres with C18-modified interior pore-walls for residue analysis of cephalosporins in milk by LC−MS/MS. *Food Chem.* **2014**, *150*, 206−212.
(31) Malone, E. M.; Elliott, C. T.; Kennedy, D. G.; Regan, L. Rapid confirmatory method for the determination of sixteen synthetic growth promoters and bisphenol A in bovine milk using dispersive solid-phase extraction and liquid chromatography−tandem mass spectrometry. *J. Chromatogr., B* **2010**, *878*, 1077−1084.
(32) Carro, A. M.; González, P.; Lorenzo, R. A. Simultaneous derivatization and ultrasound-assisted dispersive liquid−liquid microextraction of chloropropanols in soy milk and other aqueous matrices combined with gas-chromatography−mass spectrometry. *J. Chromatogr., A* **2013**, *1319*, 35−45.
(33) Maragou, N. C.; Lampi, E. N.; Thomaidis, N. S.; Koupparis, M. A. Determination of bisphenol A in milk by solid phase extraction and liquid chromatography−mass spectrometry. *J. Chromatogr., A* **2006**, *1129*, 165−173.
(34) Casajuana, N.; Lacorte, S. New methodology for the determination of phthalate esters, bisphenol A, bisphenol A diglycidyl ether, and nonylphenol in commercial whole milk samples. *J. Agric. Food Chem.* **2004**, *52*, 3702−3707.
(35) Tso, J.; Aga, D. S. A systematic investigation to optimize simultaneous extraction and liquid chromatography tandem mass spectrometry analysis of estrogens and their conjugated metabolites in milk. *J. Chromatogr., A* **2010**, *1217*, 4784−4795.
(36) Huang, L. C.; Zheng, N.; Zheng, B. Q.; Wen, F.; Cheng, J. B.; Han, R. W.; Xu, X. M.; Li, S. L.; Wang, J. Q. Simultaneous determination of aflatoxin $M_1$, ochratoxin A, zearalenone and $\alpha$-zearalenol in milk by UHPLC−MS/MS. *Food Chem.* **2014**, *146*, 242−249.
(37) Shao, B.; Zhao, R.; Meng, J.; Xue, Y.; Wu, G.; Hu, J.; Tu, X. Simultaneous determination of residual hormonal chemicals in meat, kidney, liver tissues and milk by liquid chromatography−tandem mass spectrometry. *Anal. Chim. Acta* **2005**, *548*, 41−50.
(38) Goulart, S. M.; de Queiroz, M. E. L. R.; Neves, A. A.; de Queiroz, J. H. Low-temperature clean-up method for the determi-

nation of pyrethroids in milk using gas chromatography with electron capture detection. *Talanta* **2008**, *75*, 1320−1323.
(39) Rübensam, G.; Barreto, F.; Hoff, R. B.; Kist, T. L.; Pizzolato, T. M. A liquid−liquid extraction procedure followed by a low temperature purification step for the analysis of macrocyclic lactones in milk by liquid chromatography−tandem mass spectrometry and fluorescence detection. *Anal. Chim. Acta* **2011**, *705*, 24−29.
(40) Andrade, P. D.; Silva, J. L. G.; da Caldas, E. D. Simultaneous analysis of aflatoxins B1, B2, G1, G2, M1 and ochratoxin A in breast milk by high-performance liquid chromatography/fluorescence after liquid−liquid extraction with low temperature purification (LLE−LTP). *J. Chromatogr., A* **2013**, *1304*, 61−68.
(41) Gosetti, F.; Mazzucco, E.; Zampieri, D.; Gennaro, M. C. Signal suppression/enhancement in high-performance liquid chromatography tandem mass spectrometry. *J. Chromatogr., A* **2010**, *1217*, 3929−3937.

Millipore (Billerica, MA, USA). Trifluoroacetic acid, HPLC grade, was purchased from Sigma-Aldrich (St. Louis, MO, USA). MALDI matrix (sinapinic acid) was obtained from BrukerDaltonik GmbH (Bremen, Germany) (purity of 99%).

**Procyanidin B3 Synthesis.** Procyanidin B3 was obtained by hemisynthesis between (+)-taxifolin and (+)-catechin.[12] Taxifolin (100 mg, 0.986 mmol) and catechin (186 mg, 1.58 mmol) were dissolved in ethanol (20 mL), and this solution was degassed under Ar for 10 min. A sodium borohydrate solution previously degassed under argon was dropped under not oxidized conditions (Ar), and the solution was left for 15 min under magnetic agitation. After that, degassed (Ar) distilled water (13.5 mL) was added and the pH was adjusted to 4.5 using an acetic acid 5% v/v solution. Finally, procyanidin B3 was extracted with ethyl acetate and purified by Toyopearl gel column according to previous experiments.[13] The B3 obtained had a purity >90% determined by LC-MS.

**Saliva Collection and Treatment.** Saliva was collected from three healthy nonsmoking volunteers, and they were named saliva A, saliva B, and saliva C. Triplicates were collected for each saliva sample. The saliva samples were mixed with 10% TFA (final concentration = 0.1%) to precipitate several high molecular weight salivary proteins (such as $\alpha$-amylases, mucins, carbonic anhydrase, and lactoferrin) and to preserve sample protein composition (histatins, PRPs, and statherins), because TFA partially inhibits intrinsic protease activity. After centrifugation (8000$g$ for 5 min), supernatant was separated from the precipitate and used for the following experiments.

**HPLC-UV Saliva Analysis.** Saliva samples were analyzed by HPLC-DAD prior to mass spectrometry analysis according to previous studies.[11,14] An HPLC-DAD Elite Lachrom system (L-2130) equipped with a Vydac C8 column, with 5 $\mu$m particle diameter (column dimensions 150 × 2.1 mm), was used. Detection was carried out at 214−280 nm, using a diode array detector (L-2455). The HPLC solvents were (eluent A) 0.2% aqueous TFA and (eluent B) 0.2% TFA in ACN/water 80:20 (v/v). The gradient applied was linear from 10 to 40% (eluent B) in 60 min, at a flow rate of 0.30 mL/min. After this first elution program, the column was washed with 100% eluent B for 20 min to elute S-type cystatins and other late-eluting proteins. After washing, the column was stabilized in the initial conditions.

**Mass Spectrometry Analysis.** Mass spectrometry analysis was used to identify salivary proteins and to assess the tannin−protein aggregate formation. The method described as follows is based on that of a previous study.[17]

**ESI-MS Analysis.** An aliquot of each assay was injected by flow injection analysis (FIA) into an LTQ-OrbitrapXL mass spectrometer, from ThermoFisher Scientific (Waltham, MA, USA). Sample was pumped at 5 $\mu$L/min using nitrogen as sheath gas at a flow of 5 (arbitrary unit system). Electrospray conditions from 3 kV spray voltage, 270 °C capillary temperature, and tube lens are established at 100 V at optimal analysis conditions. Samples were diluted into a methanol/acetonitrile/TFA 0.01% (5:5:90 v/v) mixture 1:10 prior to analysis. Xcalibur 2.2 software was used to control the analysis and to interpret the data obtained. Because proteins acquire different charge states in the interface, after the mass spectrometry analysis, spectra were subjected to a deconvolution process using the charge ratio analysis method (CRAM) by MagTram 1.03 software.

**MALDI-TOF Analysis.** One microliter of saliva or tannin−saliva sample (dilution 1:10) was applied onto a stainless steel target plate (MTP 394 target plate Ground steel BC, BrukerDaltonik GmbH), overlaid with 1 $\mu$L of matrix solution containing 10 mg/mL sinapic acid in acetonitrile, water, and TFA (50:47.5:2.5, v/v), and finally air-dried. Samples were spotted in triplicates.

Mass spectra were automatically acquired on an UltrafleXtream MALDI-TOF-TOF mass spectrometer (BrukerDaltonics) operating in linear positive ion detection mode with laser SmartBeam-III and under FlexCompass 1.4 software control (BrukerDaltonics). For each sample the mass spectra (range from 500 to 50 000 Da) of 1000 laser shots were accumulated with 2000 Hz frequency.

**B3−Human Salivary Protein Aggregation.** Three different salivas (A, B, and C) were mixed with procyanidin B3. The differences in salivary protein profiles between samples were evaluated by HPLC. Further aggregation was studied by mass spectrometry (ESI-MS and MALDI-TOF). This experimental study was designed to establish differences in the aggregation process between salivas with different protein profiles and tannin at different concentrations. Differences in B3−salivary protein aggregates were established at two tannin concentrations (0.5 and 1 mg/mL procyanidin B3). Saliva A and saliva C were treated with 0.5 and 1 mg/mL B3, respectively, whereas saliva B was treated with both B3 concentrations. For all assays, 50 $\mu$L of B3 was added to 150 $\mu$L of saliva sample. After vortexing for 5 min, the samples were maintained for 30 min at room temperature prior to analysis.

**Kinetics Stability of Tannin−Protein Aggregates.** Fifty microliters of B3(1 mg/mL) was added to 150 $\mu$L of saliva C to study the aggregates tannin−salivary protein and follow their evolution in time after 1, 6, and 20 h.

All binding assays were analyzed in triplicates both by MALDI-TOF and by ESI-MS. Results obtained by FIA-ESI-MS were submitted to a deconvolution process. Blank subtraction with saliva control was made prior to the introduction of data into the MagTram software. Thus, the information obtained by ESI-MS was simplified, and the tannin−salivary protein complex deconvolution mass spectra became clearer.

Phyton is a program language that is used in a wide variety of application domains, often in mass spectrometry to compare or handle spectra.[15] It was employed as an identification bioinformatic tool to elucidate the structure of new tannin−protein aggregates. In this case, Phyton was used to reckon the different links between the different tannins assayed and the salivary proteins. This software works by matching the new $m/z$ values with the different protein $m/z$ values present in the control and each tannin added $m/z$ value. Adducts and loss of ions such as $H_3O^+$ or $NH_4^+$ as well as reduction or oxidation processes have been considered. After running Python, several matches were hypothesized for each assay. Only the aggregate identifications matched by the two analytical techniques used (MALDI-TOF and ESI-MS) were considered. MALDI-TOF sensitivity decreased as higher analysis ratios were used. When B3−salivary protein aggregate stability was evaluated over time, higher aggregates were formed; thus, this phenomenon was worsened. ESI-MS was, therefore, the main technique chosen to discern the evaluation of aggregates formed over time.

**Statistical Treatment.** All data values obtained empirically were treated statistically to observe significant differences. Graphpad Prism 6.1 was the software used in data statistical treatment. The Tukey test was used to establish differences in a single-step multiple comparison (it compares every mean with every other mean). The Tukey test gave a more precise value for scatter (mean square of residuals), which was reflected in more degrees of freedom. When mean A is compared to mean C, the test compares the difference between means to the amount of scatter, quantified using information from all of the groups, not just groups A and C. This gives more power to detect differences and made sense under the assumption that all of the data are sampled from populations with the same standard deviation, even if the means were different.

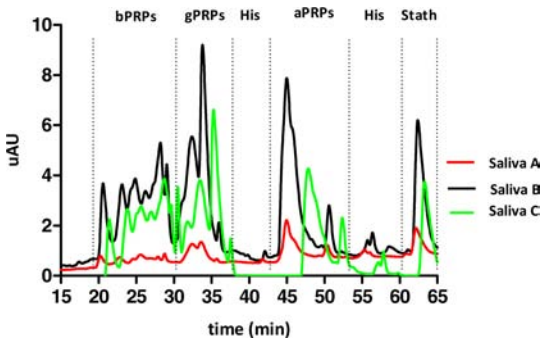


**Figure 1.** Salivary protein chromatographic profile from three salivas (A, B, and C). bPRPs, basic proline-rich proteins; gPRPs, glucosylated proline-rich proteins; His, histatins; aPRPs, acidic proline-rich proteins; Stath, statherins.

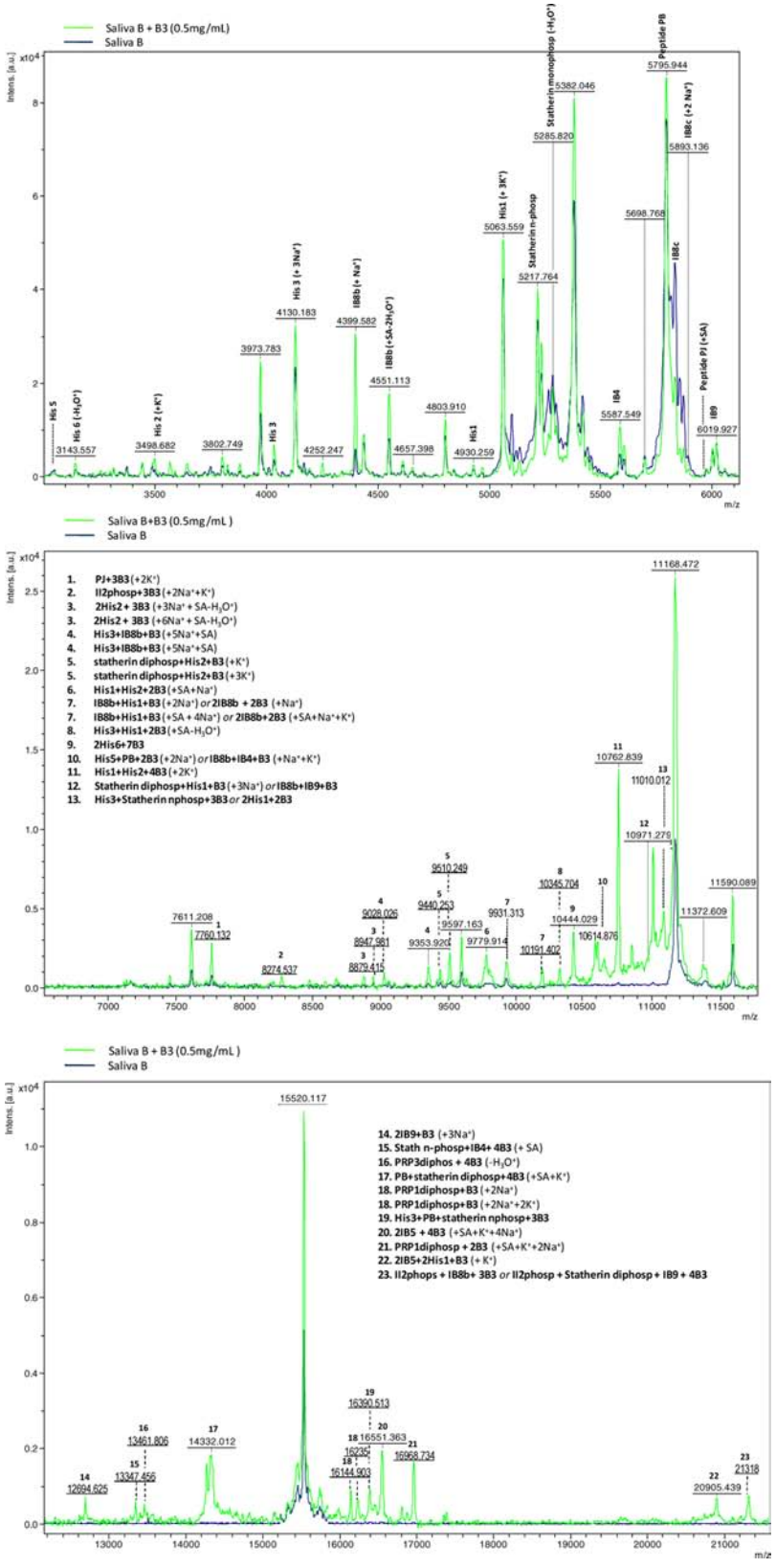


**Figure 2.** MALDI-TOF B3—human salivary protein aggregates profile. aPRP, acidic proline-rich protein; PRP3diphosphate, proline-rich protein 3 diphosphate; PRP1diphosphate, proline-rich protein 1 diphosphate; gPRP, acidic proline-rich protein; IB1, glucosidic proline-rich peptide IB1; II-2phosphate, glucosidic proline rich peptide II-2phosphate; IB8c, basic proline-rich peptide IB8c; IB8b, basic proline-rich peptide IB8b; PJ, basic proline-rich peptide PJ; IB6, basic proline-rich peptide IB6; IB9, basic proline-rich peptide IB9; IB5, basic proline-rich peptide IB5; IB4, basic proline-rich peptide IB4; His, histatins; His2, histatin 2; His 3, histatin 3; His 1, histatin 1; His 6, histatin 6; His 5, histatin 5; PB, statherin peptide PB; Statherin diphosp, Statherin diphosphate; Statherin monophosp, Statherin monophosphate; Statherin nphosp, Statherin n-phosphate.


dx.doi.org/10.1021/jf5033284 | J. Agric. Food Chem. 2014, 62, 10038−10045

## RESULTS

The aggregation between procyanidin B3 and human saliva (A, B, C) with different protein profiles was studied by mass spectrometry.

Figure 1 shows the overlaid chromatographic protein profile (HPLC-DAD) of salivas A, B, and C. After HPLC-DAD analysis, some chromatographic differences were evident between the different salivas. The chromatographic protein profile was identified on the basis of previous studies.[14] The different groups of proteins appeared characterized in the chromatogram by different parts according to their elution times. The first eluted peaks constituted the bPRPs (20−30 min), the second eluted peaks corresponded to gPRPs (30−35 min), the third chromatographic zone corresponded to aPRPs (45−50 min), and the last one contained the statherins (Stath) (60−65 min). Histatins (His) eluted at different retention times along the chromatogram, but they are mainly embedded at times around 40 and 55 min.[12,14]

The salivary protein content is described in Table 1 for all samples analyzed. Several quantitative changes were observed between saliva samples. The salivary protein content was expressed as relative percentage area values. To compare the relative protein concentrations between saliva samples, saliva B was considered as being 100% due to its highest chromatographic peak area. Significant differences in the salivary proteins were observed between samples. Saliva A and saliva C have relative amounts of 10.25 and 75.44% of saliva B, respectively. In saliva A, the aPRPs comprised the group of salivary protein with higher area values followed by statherins, bPRPs, gPRPs, and histatins. However, in saliva B and C, the bPRPs was the salivary protein with higher area followed by gPRPs, aPRPs, statherins and histatins (Table 1).

**Table 1. Percent Area of Salivary Proteins (PRPs, Statherins, and Histatins) from Three Different Saliva Samples (A, B, and C)**

| | | saliva A | saliva B | saliva C |
|---|---|---|---|---|
| PRPs | bPRPs | 18.31 | 39.27 | 37.15 |
| | gPRPs | 14.75 | 31.93 | 31.97 |
| | aPRPs | 33.73 | 18.34 | 19.97 |
| histatins | | 9.66 | 2.73 | 1.59 |
| statherins | | 23.55 | 7.73 | 9.32 |
| total salivary proteins (referred to saliva B[a]) | | 10.25 | 100 | 75.44 |

[a]Saliva B was considered as being 100% due to its highest chromatographic area.

The soluble B3−salivary protein aggregates formed with these three saliva samples were characterized by mass spectrometry. MALDI-TOF was used to identify the B3−salivary protein spectra profile, and all data results were confirmed by ESI-MS.

Forty-eight soluble B3−protein aggregates were identified (Supporting Information Table S1). The major soluble B3−protein aggregates according to the MALDI-TOF spectrum profile for saliva B are shown in Figure 2. Twenty-three major B3−salivary protein aggregates and some adducts are shown in the mass spectra. The majority of B3−salivary protein aggregates are embedded in the $m/z$ 8000−16000 range (1−13 aggregates) and the $m/z$ 20000−22000 range (14−23 aggregates). The majority of aggregates had His in their composition (mass peaks 3, 4, 5, 6, 7, 8, 9, 10, 11, 12, 13, 19, and 22). Mass peaks 1, 4, 7, 10, 14, 20, 22, and 23 had bPRPs in their composition, and mass peaks 5, 10, 12, 13, 15, 17, 19, and 23 were formed by Stath. aPRPs and gPRPs are supposed to be part of only two major aggregates, 18 and 21 and 2 and 23, respectively.

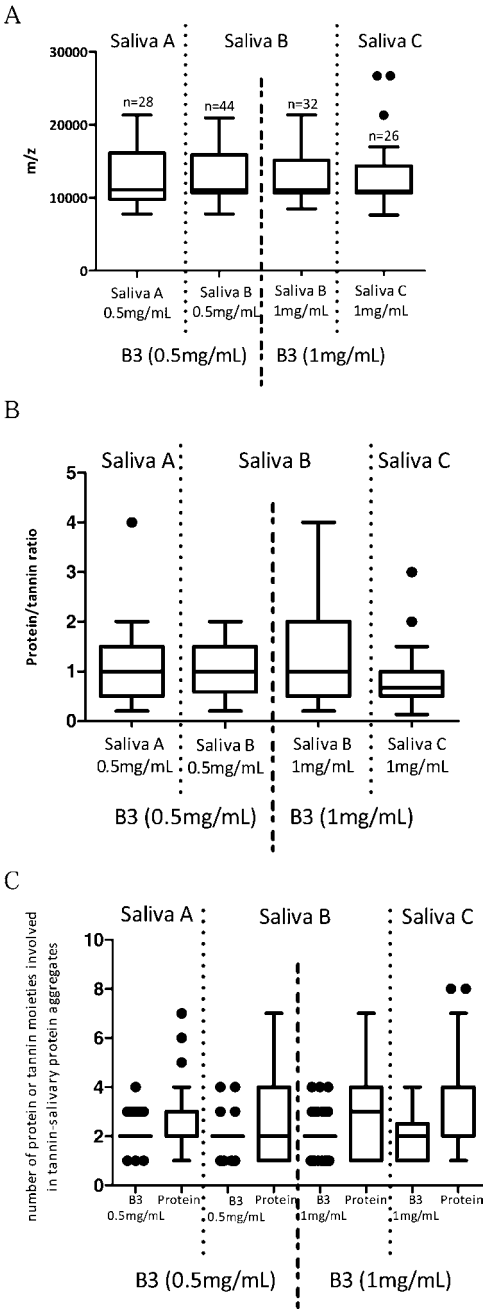


**Figure 3.** B3−salivary protein aggregates comparison between different salivas at different tannin concentrations: number and molecular mass of aggregates (A); protein/tannin ratio (B); number of proteins or tannins involved in aggregate formation (C).

Figure 3A shows the differences of number and molecular mass of all soluble B3−salivary protein aggregates identified after statistical data treatment. All aggregates had molecular masses in the range from 8000 to 25000 Da. The median molecular mass of soluble B3−salivary protein aggregates formed was the same regardless of the saliva sample and tannin concentration tested (≈11000 Da). Nevertheless, little differences can be observed. At higher B3 concentration, saliva B yielded B3−salivary protein aggregates with higher molecular weight mass range than saliva C except the three aggregates (symbolized by points)


dx.doi.org/10.1021/jf5033284 | J. Agric. Food Chem. 2014, 62, 10038−10045

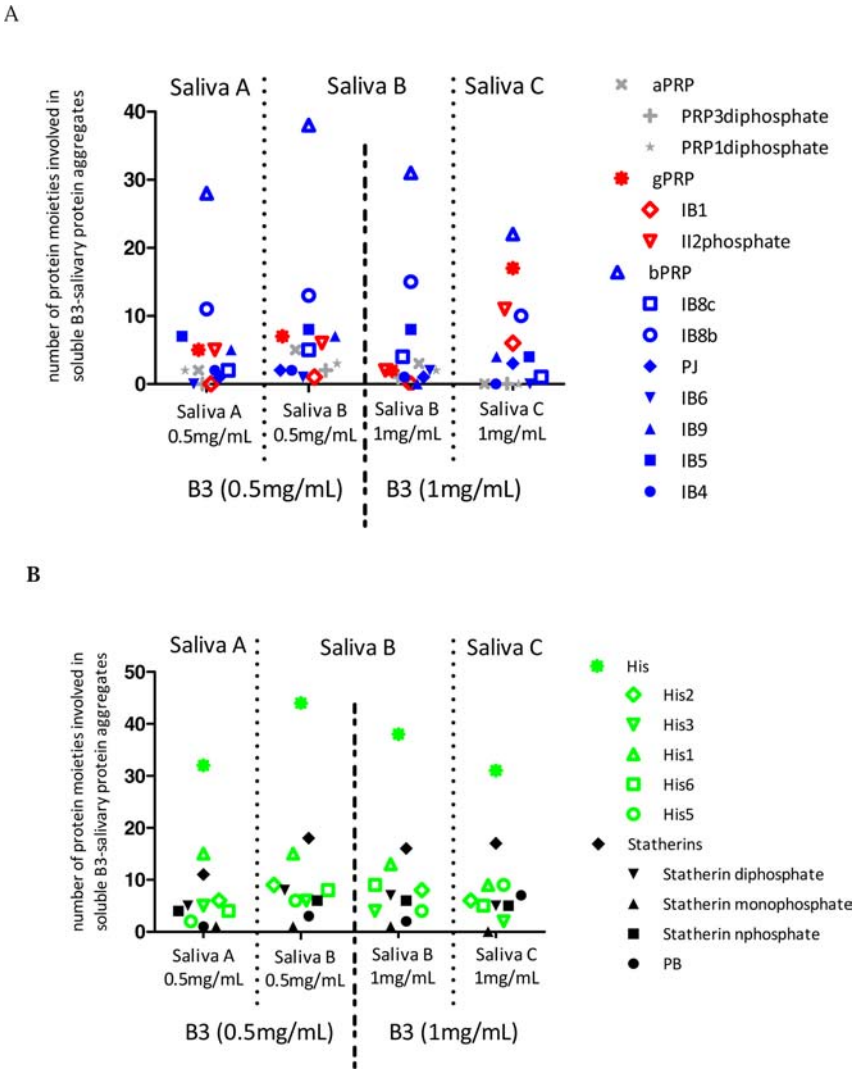


**Figure 4.** B3−salivary protein aggregates between different salivas at different tannin concentrations: occurrence of PRPs (A) and histatins and statherins (B). aPRP, acidic proline-rich protein; PRP3diphosphate, proline-rich protein 3 diphosphate; PRP1diphosphate, proline-rich protein 1 diphosphate; gPRP, acidic proline-rich protein; IB1, glucosidic proline-rich peptide IB1; II-2phosphate, glucosidic proline-rich peptide II-2phosphate; IB8c, basic proline-rich peptide IB8c; IB8b, basic proline-rich peptide IB8b; PJ, basic proline-rich peptide PJ; IB6, basic proline-rich peptide IB6; IB9, basic proline-rich peptide IB9; IB5, basic proline-rich peptide IB5; IB4, basic proline-rich peptide IB4; His, histatins; His2, histatin 2; His 3, histatin 3; His 1, histatin 1; His 6, histatin 6; His 5, histatin 5; PB, statherin peptide PB.

that appeared disperse with a molecular mass ≥20000. At lower B3 concentration, no differences were observed in the size of aggregates formed. Furthermore, no difference was observed in the molecular mass of the aggregates identified when two different tannin concentrations were tested (saliva B). Even though little or no differences were observed in the molecular mass, several differences were observed in the amount of aggregates identified. Forty-four aggregates were identified in saliva B, whereas saliva A yielded only 28 soluble B3−salivary protein aggregates at low tannin concentration. At higher tannin concentration, saliva B yielded 32 soluble B3−salivary protein aggregates and 26 were identified in saliva C.

The differences in protein/tannin ratio depending on the saliva or tannin concentration tested are shown in Figure 3B. At lower tannin concentration (0.5 mg/mL B3), there were no significant differences in protein/tannin ratio of soluble B3−salivary protein aggregates regardless of the saliva tested. Nevertheless, at higher tannin concentration (1 mg/mL B3) the median protein/tannin ratio of soluble B3−salivary protein aggregates yielded with saliva C was lower than those obtained with saliva B. Moreover, at higher B3 concentration, the range of protein/tannin ratio was higher for saliva B. The protein/tannin ratio reached values rounding 4, whereas saliva C did not achieve a value of 2. The protein/tannin ratio of soluble B3−salivary protein aggregates tended to be higher with higher tannin concentration when the same saliva was tested (Figure 3B).

As described in Figure 3C, the number of tannin and protein moieties involved in soluble B3−salivary protein aggregate formation at lower B3 concentration was almost the same. At higher tannin concentration (1 mg/mL), the number of protein moieties was higher than the number of B3 units in the aggregate formation either in different salivas or in the same saliva.

As aforementioned, the major aggregates had His in their composition, followed by bPRPs. Figure 4 shows the occurrence of salivary proteins in soluble B3−salivary protein aggregates depending on the saliva and/or tannin concentration used. No differences were found in salivary proteins that yielded the majority of soluble B3−salivary protein aggregates either with different

saliva or with different tannin concentrations. The protein group with higher occurrence in soluble B3−salivary protein aggregates was the His followed by bPRPs, Stath, gPRPs, and aPRPs.

**Time Stability of Soluble B3−Human Salivary Protein Aggregates.** Aggregation between B3 and salivary proteins was studied by mass spectrometry analysis (ESI-MS and MALDI-TOF) over time. MALDI-TOF and ESI-MS spectra showed trending for new mass peaks to appear at higher molecular mass range (data not shown). The aggregates formed during reaction time are described in Table S2 in the Supporting Information. Figure 5 shows the evolution over time in terms of number and molecular mass of the aggregates formed, protein/tannin ratio, and the scrutiny of proteins and tannin moieties involved in the formation of B3−human salivary protein aggregates. After 1 h of incubation time at room temperature, the number of aggregates found in saliva C increased from 26 to 42; it further increased exponentially after 6 h, leading to a maximum of 166 B3−human salivary protein aggregates, and it went down to 130 at 20 h. The median of molecular mass of aggregates also experienced some changes over time. Most of the aggregates decreased their size from 11000 to 7500 Da during the first hour of incubation time. At 6 h their size increased to a median of 18000 Da, and it further decreased to 13000 Da after 20 h of incubation. Although the median molecular mass followed a path first decreasing, increasing, and then decreasing once again, the trend was to form higher aggregates with time, but these aggregates appeared statistically scattered (symbolized by points) (Figure 5A).

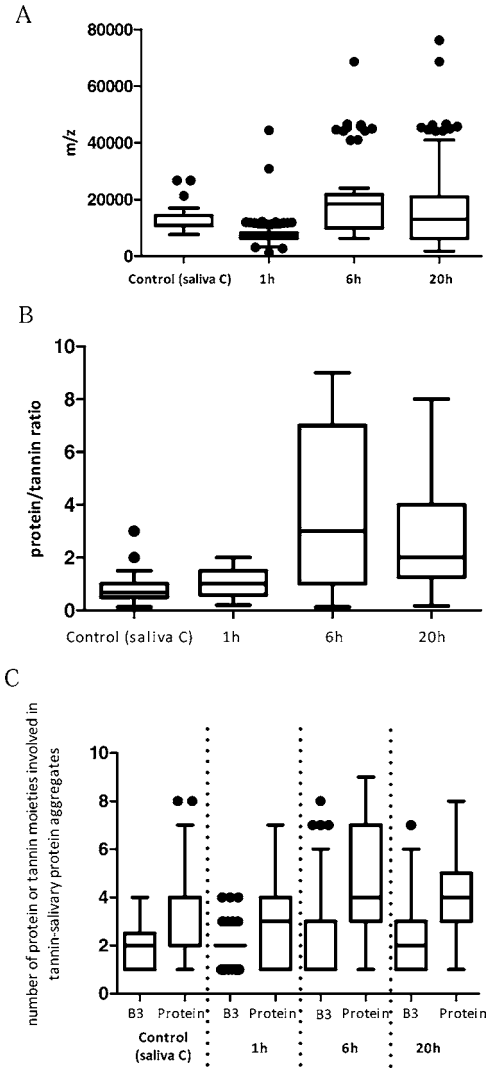


**Figure 5.** B3−salivary protein aggregate stability over time: number and molecular mass of aggregates (A); ratio protein/tannin (B); number of proteins or tannins involved in aggregate formation (C).

It should be noted that after 6 h, slight turbidity was observed in samples, probably resulting from the formation of insoluble complexes, and the homogeneity of samples was lost.

The number and molecular mass of aggregates has evolved over time, leading to new B3−human salivary protein aggregates, but some stable complexes were maintained over time. After 6 h of incubation time, six B3−salivary protein complexes did not evolve, appearing at the same signal spectra; they are the B3−statherin n-phosphate, 6B3−His6, B3−IB9, 3B3−statherin n-phosphate, 5B3−statherin monophosphate, and 4B3−PJ. At 20 h only two aggregates were maintained, the B3−IB9 ($m/z$ 6623) and 3B3−statherin n-phosphate ($m/z$ 6992).

On the other hand, the trend after 6 h was for major aggregates to be composed of more than five proteins and only one or two tannin moieties. The median protein/tannin ratio of B3−salivary protein aggregates was maintained from control to 1 h, then it increased to a maximum median value at 6 h, and finally decreased after 20 h of incubation (Figure 5B). These differences in protein/tannin ratio of B3−salivary protein aggregates are given by the change in protein moieties involved in B3−salivary protein aggregate formation among time (Figure 5C). As Figure 5C shows, the trend is to increase the number of protein moieties involved in aggregation process from control to 1 and 6 h, and then the number of protein moieties involved in B3−salivary protein aggregates was maintained until 20 h of incubation. On the other hand, the number of tannin moieties involved in aggregation changed only at 6 h, decreasing to a median value of 1 per soluble aggregate.

Figure 6 shows the scrutiny of proteins involved in aggregate formation. From control to 1 h no difference was observed in the scrutiny of proteins involved in the aggregate formation. The protein group with higher occurrence in B3−salivary protein aggregates was His, followed by bPRPs, Stath, gPRPs, and aPRPs. After 6 h, His are no longer the group of proteins with higher occurrence in the soluble B3−human salivary protein aggregates. The bPRPs became the group of proteins that yielded higher number of aggregates followed by Stath. Furthermore, most of the aggregates were only formed, in descending order, by IB8b, His6, PRP3diphosp, Stath monophosphate, Stath n-phosphate, IB9, peptide PB, and peptide PJ. After 20 h, most of the aggregates were formed by the same proteins but the order was altered. The proteins involved in higher number of aggregates after 20 h were, in descending order, PB, PJ, His6, IB9, Stath monophosphate, IB8b, Stath n-phosphate, and PRP3diphosp, respectively.

## ■ DISCUSSION

Individual chromatographic differences between samples were verified from salivas A, B, and C. This fact could influence differences in the B3−salivary protein aggregation process at the two tannin concentrations tested (0.5 and 1 mg/mL). The median molecular mass rounded 11000 Da regardless of the saliva or tannin concentration used. Several differences were found in the number of aggregates formed at different tannin concentrations and saliva samples tested. In general, it could be assumed that the number of soluble aggregates formed was higher at lower B3 concentration. On the other hand, a higher number of aggregates was observed at higher salivary protein

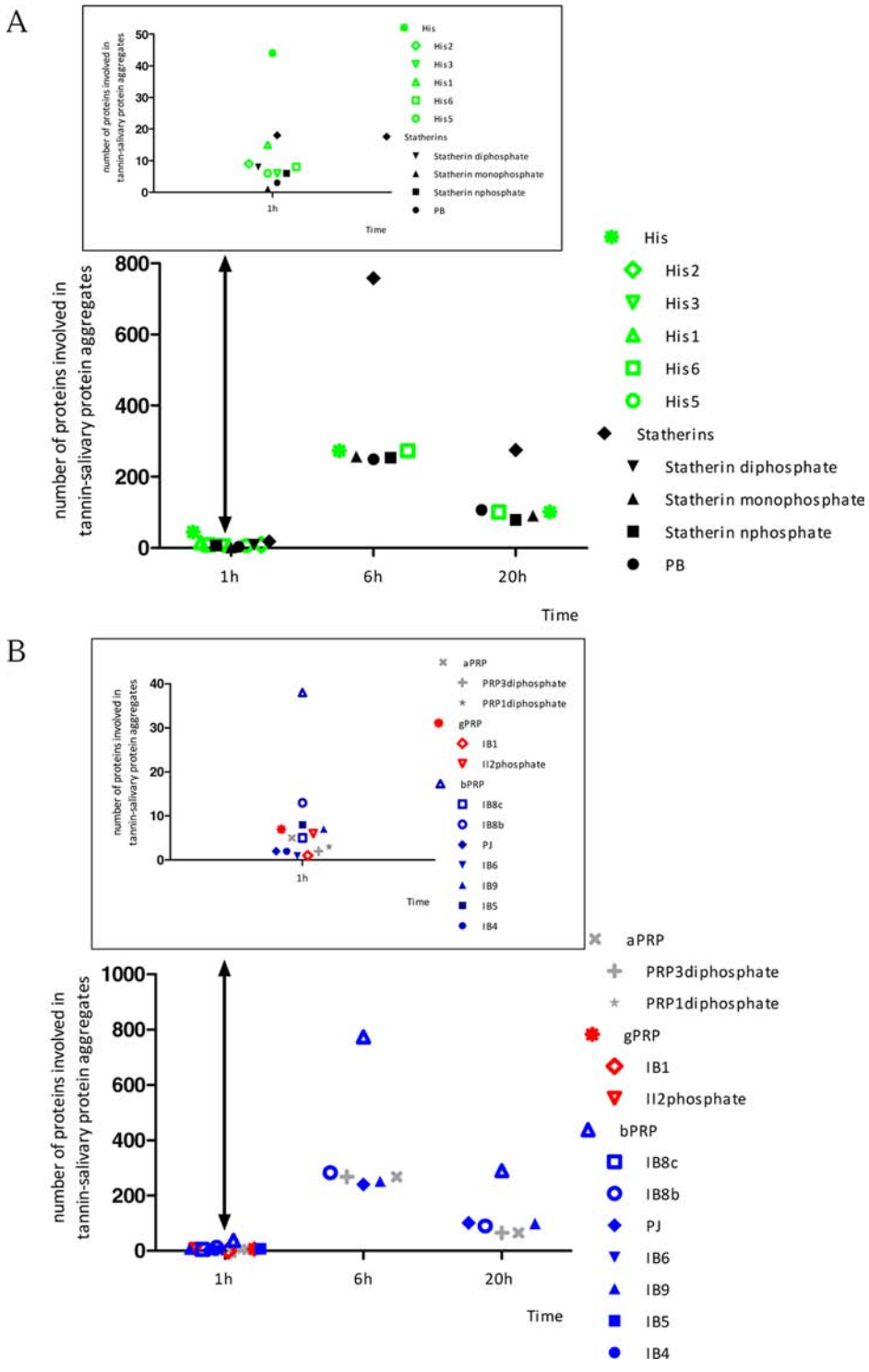


**Figure 6.** B3−salivary protein aggregates stability over time: occurrence of PRPs (A) and histatins and statherins (B). aPRP, acidic proline-rich protein; PRP3diphosphate, proline-rich protein 3 diphosphate; PRP1diphosphate, proline-rich protein 1 diphosphate; gPRP, acidic proline-rich protein; IB1, glucosidic proline-rich peptide IB1; II-2phosphate, glucosidic proline-rich peptide II-2phosphate; IB8c, basic proline-rich peptide IB8c; IB8b, basic proline-rich peptide IB8b; PJ, basic proline-rich peptide PJ; IB6, basic proline-rich peptide IB6; IB9, basic proline-rich peptide IB9; IB5, basic proline-rich peptide IB5; IB4, basic proline-rich peptide IB4; His, histatins; His2, histatin 2; His 3, histatin 3; His 1, histatin 1; His 6, histatin 6; His 5, histatin 5; PB, statherin peptide PB.

concentration (area values). The results presented herein also confirmed that for the same saliva sample at higher tannin concentration, the number of protein moieties involved in B3−salivary protein aggregate formation was also higher. These results are in agreement with previous studies. Cannon et al.[8] verified that at lower tannin concentrations at least, half of the protein added did not bind to tannin. According to Lorenz et al.,[16] increasing the tannin concentration decreases the protein solubility, so this fact could complicate the formation of a higher number of aggregates.


dx.doi.org/10.1021/jf5033284 | J. Agric. Food Chem. 2014, 62, 10038−10045

The protein and/or tannin selectivity was also verified regardless of the saliva samples and tannin concentration tested. The same group of salivary proteins yielded the higher number of aggregates despite some salivary protein chromatographic differences between samples. These results are in agreement with previous studies because His was the group of proteins that produced a higher number of aggregates when saliva was treated with B3.[17] Although His was the group of proteins that formed a higher number of soluble B3−salivary protein aggregates studied by mass spectrometry, it should be pointed out that Stath and aPRPs were the more reactive groups of proteins and led to a higher precipitation to form insoluble complexes.[14,18]

Stability over time was also studied showing that the B3−salivary protein aggregates evolved in time. After 1 h of incubation, the trend was to decrease the molecular mass of the B3−salivary protein aggregates. It is well-known that protein−tannin noncovalent aggregation is a reversible process in aqueous models.[19−21] After 1 h, new B3−salivary protein aggregates were formed, whereas the first B3−salivary protein aggregates were broken up. The trend after 6 h within the following 20 h was to increase the number of protein moieties involved in the aggregation process, and only a few aggregates were maintained. These results are in agreement with previous studies in which the number of protein moieties forming aggregates increased over time.[8] On the other hand, it should be noted that the group of proteins involved in aggregates changed over time. Whereas His was the protein group with higher selectivity from the initial aggregation process to 1 h, after 6 h, the bPRPs and Stath yielded the higher number of aggregates. Hence, the B3−salivary protein aggregates changed not only in number but also in the type of proteins involved in their composition. The results presented herein highlight the effect of the tannin concentration in the formation of different soluble B3−salivary protein aggregates. Furthermore, the individual effect of the different salivas has been exhibited. The differences in B3−salivary protein aggregates were based primarily in the number of complexes formed and hence not their molecular masses. Moreover, the protein/tannin ratio barely varied between different saliva samples or tannin concentration, but the number of tannin moieties involved in the aggregation process was higher at higher B3 concentrations.

On the other hand, the evolution of B3−salivary protein was revealed because a higher number with higher size was formed and their stoichiometry also changed over time.

## ■ ASSOCIATED CONTENT

### Ⓢ Supporting Information

FIA-ESI-MS spectra of human saliva protein and B3−human saliva protein complexes as well as MALDI-TOF spectra accuracy and sensibility. This material is available free of charge via the Internet at http://pubs.acs.org.

## ■ AUTHOR INFORMATION

### Corresponding Author

*(V.D.F.) Phone: +351 220 402 558. Fax: 351 220 402 659. E-mail: vfreitas@fc.up.pt.

### Funding

We thank the Fundaçao para a Ciencia e Tecnologia (FCT), which funded this work by a postdoctoral fellowship (SFRH/BPD/85293/2012) and by a research project grant (NORTE-07-0162-FEDER-000048).

### Notes

The authors declare no competing financial interest.

## ■ REFERENCES

(1) Huq, N. L.; Cross, K. J.; Ung, M.; Myroforidis, H.; Veith, P. D.; Chen, D.; Stanton, D.; He, H.; Ward, B. R.; Reynolds, E. C. A review of the salivary proteome and peptidome and saliva-derived peptide therapeutics. *Int. J. Pept. Res. Ther.* **2007**, *13*, 547−564.

(2) Hagerman, A. E.; Rice, M. E.; Ritchard, N. T. Mechanisms of protein precipitation for two tannins, pentagalloyl glucose and epicatechin$_{16}$ (4→8) catechin (procyanidin). *J. Agric. Food Chem.* **1998**, *46*, 2590−2595.

(3) Poncet-Legrand, C.; Edelmann, A.; Putaux, J.-L.; Cartalade, D.; Sarni-Manchado, P.; Vernhet, A. Poly(L-proline) interactions with flavan-3-ols units: influence of the molecular structure and the polyphenol/protein ratio. *Food Hydrocolloids* **2006**, *20*, 687−697.

(4) Siebert, K. J.; Troukhanova, N. V.; Lynn, P. Y. Nature of polyphenol-protein interations. *J. Agric. Food Chem.* **1996**, *44*, 80−85.

(5) Hagerman, A. E.; Butler, L. G. The specificity of proanthocyanidin-protein interactions. *J. Biol. Chem.* **1981**, *256*, 4494−4497.

(6) Erel-Unal, I.; Sukhishvili, S. A. Hydrogen-bonded multilayers of a neutral polymer and a polyphenol. *Macromolecules* **2008**, *41*, 3962−3970.

(7) Hagerman, A. E.; Robbins, C. T. Implications of soluble tannin-protein complexes for tannin analysis and plant defense mechanisms. *J. Chem. Ecol.* **1987**, *13*, 1243−1259.

(8) Canon, F.; Paté, F.; Cheynier, V.; Sarni-Manchado, P.; Giuliani, A.; Pérez, J.; Durand, D.; Li, J.; Cabane, B. Aggregation of the salivary proline-rich protein IB5 in the presence of the tannin EgCG. 6. *Langmuir* **2013**, *29*, 1926−1937.

(9) Peleg, H.; Gacon, K.; Schlich, P.; Noble, A. C. Bitterness and astringency of flavan-3-ol monomers, dimers and trimers. *J. Sci. Food Agric.* **1999**, *79*, 1123−1128.

(10) Kallithraka, S.; Barker, J.; Clifford, M. N. Evidence that salivary proteins are involved in astringency. *J. Sens. Stud.* **1998**, *13*, 29−43.

(11) De Freitas, V.; Carvalho, E.; Mateus, N. Study of carbohydrate influence on protein-tannin aggregation by nephelometry. *Food Chem.* **2003**, *81*, 503−509.

(12) Geissmen, T. A.; Yoshimura, N. N. Synthetic proanthocyanidin. *Tetrahedron Lett.* **1996**, *7*, 2669−2673.

(13) De Freitas, V. A. P.; Glories, Y.; Laguerre, M. Incidence of molecular structure in oxidation of grape seed procyanidins. *J. Agric. Food Chem.* **1998**, *46*, 376−382.

(14) Soares, S.; Mateus, N.; de Freitas, V. Interaction of different classes of salivary proteins with food tannins. *Food Res. Int.* **2012**, *49*, 807−813.

(15) Bald, T.; Barth, J.; Niehues, A.; Specht, M.; Hippler, M.; Fufezan, C. pymzML − Python module for high-throughput bioinformatics on mass spectrometry data. *Bioinformatic* **2012**, *28*, 1052−1053.

(16) Lorenz, M. M.; Alkhafadji, L.; Stringano, E.; Staffan, N.; Mueller-Harvey, I.; Udén, P. Relationship between condensed tannin structures and their ability to precipitate feed proteins in the rumen. *J. Sci. Food Agric.* **2014**, *94*, 963−968.

(17) Perez-Gregorio, M. R.; Mateus, N.; de Freitas, V. Rapid screening and identification of new soluble tannin-salivary protein aggregates in saliva by mass spectrometry (MALDI-TOF-TOF and FIA-ESI-MS). *Langmuir* **2014**, *30*, 8528−8537.

(18) Soares, S.; Vitorino, R.; Osório, H.; Fernandes, A.; Venâncio, A.; Mateus, N.; Amado, F.; De Freitas, V. Reactivity of human salivary proteins families toward food polyphenols. *J. Agric. Food Chem.* **2011**, *59*, 5535−5547.

(19) Hagerman, A. E. Fifty years of polyphenol−protein complexes. In *Recent Advances in Polyphenol Researc*, 1st ed.; Cheynier, V., Sarni-Manchado, P., Quideau, S., Eds.; Wiley-Blackwell: Oxford, UK, 2012; Vol. 3.

(20) De Freitas, V. A. P.; Mateus, N. Structural features of procyanidin interactions with salivary proteins. *J. Agric. Food Chem.* **2001**, *49*, 940−945.

(21) De Freitas, V.; Mateus, N. Nephelometric study of salivary protein−tannin aggregates. *J. Sci. Food Agric.* **2001**, *82*, 113−119.

more, the most abundant tea catechin, EGCG, has also been shown to exhibit hepatoprotective effects against liver injury by ethanol and carbon tetrachloride ($CCl_4$)-induced liver injury.[14,15] To the best of our knowledge, most studies on EGCG3″Me have focused on its antioxidant and inhibitory activities to allergies, and little information about the hepatoprotective effect of EGCG3″Me against alcohol-induced toxicity is available. Therefore, the main objective of the present study was to evaluate the hepatoprotective effects of EGCG3″Me. First, high-purity EGCG3″Me was prepared through extraction from Chinese oolong tea and simple purification procedures by using polyamide and Toyopearl HW-40S column chromatography. Then, the hepatoprotective effects of EGCG3″Me were evaluated by the antioxidant and hepatoprotective activity in alcohol-induced hepatotoxicity in the HepG2 cell line and mice.

## MATERIALS AND METHODS

**Chemicals.** Toyopearl HW-40S resin was purchased from Tosoh Corp. (Tokyo, Japan), and polyamide resin was obtained from Qingdao Ocean Chemical Co., Ltd. (Qingdao, China). 2,2-Diphenyl-1-picrylhydrazyl (DPPH) and 2,2′-azinobis(3-ethylbenzothiazoline-6-sulfonic acid) diammonium salts (ABTS) were obtained from Sigma Chemical Co. (St. Louis, MO, USA). 2,4,6-Tri(2-pyridyl)-*s*-triazine (TPTZ) was obtained from Fluka (Buchs, Swiltzerland). Standards of EGCG and EGCG3″Me were prepared according to our reported methods.[16,17] Human hepatic cancer HepG2 cells were obtained from the Cell Bank of Shanghai Institute of Cell Biology (Shanghai, China). 3-(4,5-Dimethylthiazol-2-yl)-2,5-diphenyl tetrazolium bromide (MTT), penicillin, and streptomycin were purchased from Sigma Chemical Co. Fetal bovine serum (FBS), trypsin, and RPMI-1640 media were purchased from Gibco/Invitrogen (Grand Island, NY, USA). Male Kunming mice were obtained from the Experimental Animal Centre of Academy of the Military Medical Sciences (Beijing, China). Analytical kits for aspartate aminotransferase (AST), alanine aminotransferase (ALT), glutathione peroxidase (GSH-Px), superoxide dismutase (SOD), and malondialdehyde (MDA) were obtained from Nanjing Jiancheng Bioengineering Research Institute (Nanjing, China). All other chemicals and reagents were of analytical grade.

**Tea Samples.** Oolong tea was purchased from a local market in Guangzhou, China. The fresh tea leaves picked were given a solar withering process for 2 h, followed by indoor withering for 4 h, and then 5 cycles of hand rolling for 20 min. The final steps consisted of 2 h of fermentation, followed by 5 min of killing, 5 min of kneading, and 5 h of roasting.[18] The oolong tea manufacturing process was replicated five times. After the manufacture, the water content of oolong tea is 4.05 ± 0.24%. The oolong tea sample was ground into powder using a milling machine, and the material that passed through a 40 mesh sieve was kept in sealed polyethylene bags at −20 °C until use.

**Preparation of Tea Catechins.** EGCG and EGCG3″Me were prepared from oolong tea according to the reported method with some modifications.[16,17] Briefly, 2 kg of tea powder was extracted with 32 L of distilled water at 96 °C for 40 min. Upon extraction, the extract was centrifuged at 4500*g* for 15 min, and the resulting insoluble residue was treated again as described above. The supernatants, which were extraction solutions of 2 times, were combined and concentrated by using rotary evaporators under vacuum. The resulting residue was dissolved, filtered, and applied to a column wet-packed polyamide resin. After reaching adsorptive saturation, the column was washed by distilled water and then eluted by 80% ethanol. The effluent of the ethanol solution was collected and concentrated, affording the crude extract for further purification.

The crude extract was dissolved and loaded onto a Toyopearl HW-40S column pre-equilibrated with 80% ethanol. The column was eluted with 80% ethanol, and the elution was monitored by measuring the absorbance at 280 nm and autocollected. The eluted fractions were analyzed by high-performance liquid chromatography with a diode array detector (HPLC-DAD), and the desired fractions were collected, concentrated, loaded onto the Toyopearl HW-40S column, respectively, and treated as described above. As results, the fractions containing EGCG and EGCG3″Me were concentrated and freeze-dried by a freeze-dry system respectively, affording EGCG and EGCG3″Me.

**Analysis and Characterization of EGCG3″Me.** The contents of tea catechins were determined according to the reported method using an Agilent 1100 series HPLC (Agilent, Santa Clara, CA, USA).[17] The separation was achieved on a TSKgel ODS-100Z column (4.6 × 150 mm, 5 μm; Tosoh). The mobile phase consisted of formic acid solution (pH 2.5, A) and methanol (B). Elution was performed with a linear gradient as follows: 0−15 min, A from 82 to 40%. The injection volume was 20 μL. The temperature of column oven was set at 40 °C, and the flow rate was set at 1.0 mL/min.

The structures of tea catechin monomers isolated from oolong tea were characterized by ESI-MS/MS and $^1$H NMR. ESI-MS/MS analysis was performed by using a TSQ Quantum Ultra triple -quadrupole mass spectrometer (Thermo Scientific) in positive mode. The operation parameters of the ESI ion source were as follows: drying gas, $N_2$; temperature, 270 °C; flow rate of drying gas, 4 L/min; pressure of nebulizer gas ($N_2$), 9.0 psi; and capillary voltage, 4 kV. ESI-TOF-MS spectra and $^1$H NMR spectrum were recorded on an Applied Biosystems mass spectrometer. $^1$H NMR spectrum was recorded by a Bruker DRX-500 spectrometer operated at 300 K with $D_2O$ as solvent. Chemical shifts ($\delta$) are given in parts per million, and $J$ values are given in hertz.

**DPPH Assay.** The DPPH free radical scavenging activity of each sample was determined according to the reported method.[19] The percentage of DPPH$^\bullet$ that was scavenged was calculated using

$$\text{scavenging activity (\%)} = (\text{Abs}_{\text{cont}} - \text{Abs}_{\text{samp}})/\text{Abs}_{\text{cont}} \times 100$$

where $\text{Abs}_{\text{cont}}$ is the absorbance of the control and $\text{Abs}_{\text{samp}}$ is the absorbance of the sample. The DPPH free radical scavenging activity was expressed by $IC_{50}$ value, which is the concentration of extract required to decrease the absorbance at 517 nm by 50%. Measurements were performed at least in triplicate.

**ABTS Assay.** The ABTS free radical scavenging activity of each sample was determined according to the method described by Stratil et al.[20] The radical cation ABTS$^{\bullet+}$ was generated by persulfate oxidation of ABTS, and the ABTS$^{\bullet+}$ scavenging rate was calculated to express the antioxidant ability of the sample. $IC_{50}$ values calculated denote the concentration of sample required to decrease the absorbance at 734 nm by 50%.

**FRAP Assay.** The ability to reduce ferric ions was measured using a modified version of the method described by Benzie and Strain.[21] The antioxidant capacity based on the ability to reduce ferric ions of sample was calculated from the linear calibration curve and expressed as millimoles of $FeSO_4$ equivalents per gram of sample (DW).

**Cell Culture.** The human hepatoma cell line HepG2 was cultured in the RPMI-1640 medium supplemented with FBS (10%), penicillin (100 U/mL), and streptomycin (100 μg/mL). This was incubated at 37 °C in a humidified 5% $CO_2$ incubator; cells were diluted to a density of 1 × $10^5$ cells/mL and fed every 2 days with fresh medium. Under these conditions the generation time of HepG2 cells was approximately 36 h. At subconfluence the Petri dishes were carefully washed with serum-free culture medium and treated for the following investigations.

**In Vitro Cytotoxicity Assay.** The $CTC_{50}$ (50% cytotoxic concentration) was determined by estimating mitochondrial synthesis using the tetrazolium assay.[22] Briefly, HepG2 cells were pipetted into a 96-well flat-bottom plate (100 μL/well) at a density of 1 × $10^5$ cells/mL. After 12 h of incubation at 37 °C in a humidified 5% $CO_2$ incubator, nonadherent cells were removed by washing with serum-free culture medium. Then, fresh medium (100 μL/well, control group) or test sample (100 μL/well, EGCG3″Me at a final concentration of 25, 50, 100, or 200 μg/mL) was added to each well, and the cells were incubated for 24, 48, and 72 h, respectively. After incubation, MTT solution (10 μL/well, 5 mg/mL) was added to each well, and the plate was incubated for an additional 4 h at 37 °C.

Finally, 100 μL of 10% sodium dodecyl sulfate (SDS) in 0.01 N HCl was added to each well, and the plate was kept overnight for the dissolution of formazan crystals. The absorbance of each well at 570 nm was measured. The inhibition rate was calculated according to the following formula:

$$\text{inhibition rate (\%)} = 100 - (\text{mean OD of individual test group} / \text{mean OD of control group}) \times 100$$

A concentration−response curve was generated using inhibition rate (%) and EGCG3″Me sample concentration (μg/mL). The $CTC_{50}$ value is calculated from the concentration−response curve.

**Alcohol-Induced Toxicity in HepG2 Cell Line.** To each well of the 96-well flat-bottom plate was added 100 μL of diluted HepG2 cell suspension ($1.0 \times 10^5$ cells/mL). After 12 h, when a partial monolayer was formed, the supernatant was removed and the monolayer was washed once with serum-free culture medium. Bifendate, a synthetic intermediate of schisandrin C with protective effect against drug-induced liver injury in rodents, is often used for the treatment of hepatitis as well as regarded as a positive control for exploring other hepatoprotective drugs.[23] Therefore, bifendate was adopted for the evaluation of the hepatoprotective effect of EGCG3″Me as positive control. The cells were treated with 100 μL of toxicant (medium containing 1% (v/v) alcohol), 100 μL of positive control (medium containing 1% (v/v) alcohol and bifendate (10, 20, and 40 μg/mL)), 100 μL of sample (medium containing 1% (v/v) alcohol and EGCG3″Me (10, 20, and 40 μg/mL)), and 100 μL of control (medium, medium and EGCG3″Me (40 μg/mL)), medium, and bifendate (40 μg/mL) for various time intervals of 3, 6, 12, and 24 h, and the following assays were carried out to observe time-dependent changes.

**Cell Viability.** Cell viability after alcohol treatment was evaluated by using a MTT-based colorimetric method as mentioned under in Vitro Cytotoxicity Assay. Briefly, after the cells were treated with 1% (v/v) alcohol for 24 h, MTT solution was added to each well, and the plate was incubated for an additional 4 h at 37 °C. Finally, 100 μL of 10% SDS in 0.01 M HCl was added to each well, and the plate was kept overnight for the dissolution of formazan crystals. The absorbance of each well at 570 nm was measured, and the viability rate was calculated according to the formula below:

$$\text{viability (\%)} = (\text{Abs}_{\text{samp}}/\text{Abs}_{\text{cont}}) \times 100\%$$

**Biochemical Assays of Alcohol-Induced Toxicity in HepG2 Cell Line.** The 96-well flat-bottom plates were centrifuged at 500*g* for 5 min at 4 °C, and the culture medium and cells were collected separately. The medium (0.2 mL) was used for measuring AST and ALT activities. AST and ALT activities in sera were measured using commercial reagent kits from Nanjing Jiancheng Bioengineering Institute. The level of MDA and activity of GSH-Px in HepG2 cells were also determined by using commercial reagent kits from the same institute according to the instruction manuals.

**Animals and Experimental Design.** The hepatoprotective effect of EGCG3″Me against alcohol-induced acute liver damage in mice was evaluated according to the reported method with proper modifications.[24] Furthermore, all procedures involving animals were conducted in strict accordance with Chinese legislation on the use and care of laboratory animals during the entire experimental period. Male Kunming mice (8 weeks old) with body weights (BW) of about 20 g were used in the present study. They were maintained in a room with a controlled temperature of 22 ± 0.5 °C and a normal day/night cycle and allowed free access to basal pellet diet and tap water.

After adapting to the environment for 7 days, these mice were randomly divided into six groups of eight each: (I) normal control group; (II) alcohol model control group; (III) positive control group; (IV−VI) EGCG3″Me treatment groups. Mice in the normal control group and alcohol model control group were given 1.0 mL of physiological saline and 50% alcohol solution, respectively, once daily. Bifendate and EGCG3″Me were both dissolved in physiological saline. Mice in the positive control group were given 0.5 mL of bifendate (10 mg/kg BW) per day. Mice in EGCG3″Me treatment groups were respectively fed 0.5 mL of EGCG3″Me solution in three different doses (25, 50, and 100 mg/kg BW) once daily. For positive control and EGCG3″Me treatment groups, they were fed 0.5 mL of 50% alcohol solution before given bifendate and EGCG3″Me, respectively. All administrations were conducted by gastric gavage for 14 consecutive days. After 10 h of fasting following the last administration, the mice were killed by decapitation. Blood samples were collected immediately and centrifuged at 3000 rpm for 10 min at 4 °C to afford the sera. The sera were stored at −70 °C until the determination of AST and ALT activities. The liver was excised and homogenized in 0.1 g/mL wet weight of ice-cold physiological saline. The homogenate was centrifuged at 3000 rpm for 10 min, and the supernatant was collected for determination of SOD and GSH-Px activities and the level of MDA.

**Biochemical Assays of Alcohol-Induced Toxicity in Mice.** The activities of AST and ALT in serum and the levels of MDA, SOD, and GSH-Px activities in liver were determined by using commercial reagent kits from Nanjing Jiancheng Bioengineering Institute according to the instruction manuals.

**Histopathological Evaluation.** Livers from mice in different groups were fixed in 10% neutral formalin solution, dehydrated in graded alcohol, and embedded in paraffin. Thin sections of 5 μm thickness of liver tissue were cut and mounted on glass slides and then were counter-stained with hematoxylin−eosin (H&E).[25] Then, thin sections of liver were made into permanent slides and were examined for possible histopathological changes under a high-resolution microscope with photographic facility.

**Statistical Analysis.** Data were analyzed by SPSS and expressed as mean ± standard deviation (SD) for at least three replicates. Significance was determined at $P < 0.05$ by ANOVA followed by Duncan's multiple-comparison tests.

## RESULTS

**Preparation of EGCG3″Me.** In the present study, EGCG3″Me was prepared from Chinese oolong tea by extraction and purification of column chromatography.[17] As shown in Figure 2, peaks 1−13 in the HPLC chromatogram of oolong tea infusion were identified to be gallic acid, (−)-gallocatechin, theobromine, (−)-epigallocatechin, (−)-catechin, theophylline, EGCG, caffeine, (−)-epicatechin, GCG

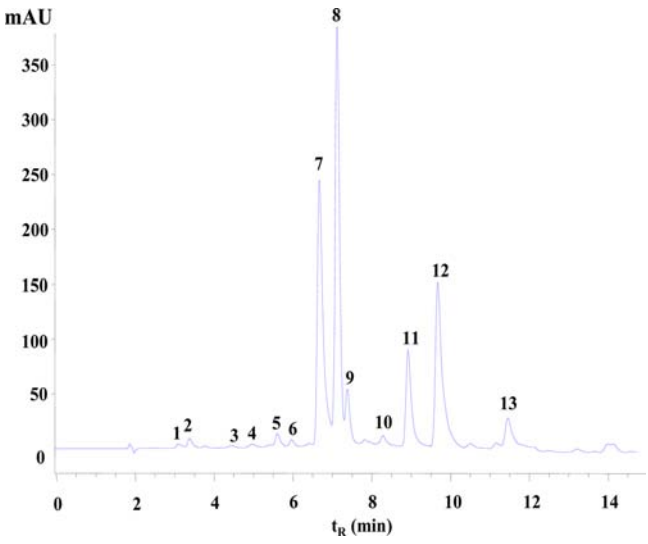


**Figure 2.** HPLC chromatograms of tea catechins, gallic acid, caffeine, theobromine, and theophylline from oolong tea (1, gallic acid; 2, (−)-gallocatechin; 3, theobromine; 4, (−)-epigallocatechin; 5, (−)-catechin; 6, theophylline; 7, EGCG; 8, caffeine; 9, (−)-epicatechin; 10, GCG; 11, EGCG3″Me; 12, (−)-epicatechin gallate; 13, (−)-catechin gallate).


dx.doi.org/10.1021/jf5016335 | J. Agric. Food Chem. 2014, 62, 10046−10054

((−)-gallocatechin gallate), EGCG3″Me, (−)-epicatechin gallate, and (−)-catechin gallate according to the retention times and online DAD spectra of authentic standards. In our previous study, EGCG3″Me as standard was obtained from Japanese green tea. Here, we found that Chinese oolong tea from Guangdong province contained relatively higher contents of EGCG, GCG, and EGCG3″Me. The contents of EGCG, GCG, and EGCG3″Me in Chinese oolong tea and Japanese green tea were 49.6 ± 0.82, 3.26 ± 0.23, and 11.9 ± 0.48 mg/g and 41.7 ± 0.91, 2.05 ± 0.12, and 8.07 ± 0.29 mg/g, respectively. Therefore, the infusion of oolong tea was loaded onto polyamide and Toyopearl HW-40S columns, respectively, affording high purity (>99%) of EGCG3″Me.

The structure of the resulting EGCG3″Me was characterized by ESI-TOF-MS and $^1$H NMR. Positive-mode MS for it gave molecular ion signals at $m/z$ 495.2 for $[M + Na]^+$ and at $m/z$ 473.2 for $[M + H]^+$. The results indicated that its molecular weight is 472.2, corresponding to that of EGCG3″Me.

$^1$H NMR data for EGCG3″Me: 7.01 (1 H, d, H-2″), 6.98 (1H, d, H-6″), 6.49 (2H, s, H-2′, H-6′), 5.87 (1H, d, H-8), 5.83 (1H, d, H-6), 5.56 (1H, s, H-2), 5.35 (1H, bs, 3-OH), 5.24 (1H, d, H-3), 3.82 (3H, s, $OCH_3$), 3.10 (1H, dd, H-4 ax), 2.85 (1H, dd, H-4 equiv).

The $^1$H NMR spectrum was similar to that of EGCG except for the presence of a methoxyl proton signal at $\delta$ 3.82 (3H, s) and two aromatic proton signals at $\delta$ 6.98 (1H, d) and 7.01 (1H, d).[26] On irradiation of the methoxyl proton signal, a nuclear Overhauser effect was observed at the aromatic proton signal at $\delta$ 6.98. From these data it was assumed to be EGCG3″Me and was assigned by comparison of the reported NMR data.[27]

**Determination of Antioxidant Activity of EGCG3″Me.** DPPH free radical scavenging activities of EGCG3″Me and EGCG are shown in Figue 3A. EGCG3″Me showed high scavenging activity on superoxide radical, and it increased with the increase of sample concentration. At concentrations ranging from 0.2 to 0.8 mg/mL, the scavenging activity increased rapidly with the increase of concentration; after that, it increased slowly. The EGCG3″Me showed DPPH radical scavenging activity with an $IC_{50}$ of 0.37 mg/mL. The free radical scavenging activity of EGCG3″Me was less than that of EGCG ($IC_{50}$ = 0.31 mg/mL), which exhibited high antioxidative property.

The antioxidant abilities of EGCG3″Me and EGCG determined by using the ABTS method are shown in Figure 3B. In our results, EGCG exhibited considerably higher activity than EGCG3″Me. In addition, the $ABTS^{\bullet+}$ scavenging rates of EGCG3″Me and EGCG increased with the increase of concentration in our study.

The trends for ferric ion reducing activities of EGCG3″Me and EGCG are shown in Figure 3C. For EGCG3″Me and EGCG, the absorbance increased clearly, due to the formation of the $Fe^{2+}$−TPTZ complex with increasing concentration. Similar to the results of the DPPH and ABTS assays, the reducing activity for EGCG was higher than that of EGCG3″Me.

**Determination of Hepatoprotective Activity of EGCG3″Me.** To ascertain the extent of toxicity caused by 1% of alcohol in HepG2 cells, we quantified the cell viability (Figure 4A) and AST (Figure 4B) and ALT (Figure 4C) levels at various time intervals of 3, 6, 12, and 24 h. MDA formed (Figure 4D) and GSH-Px content (Figure 4E) were also determined. It can be seen that no significant changes in cell

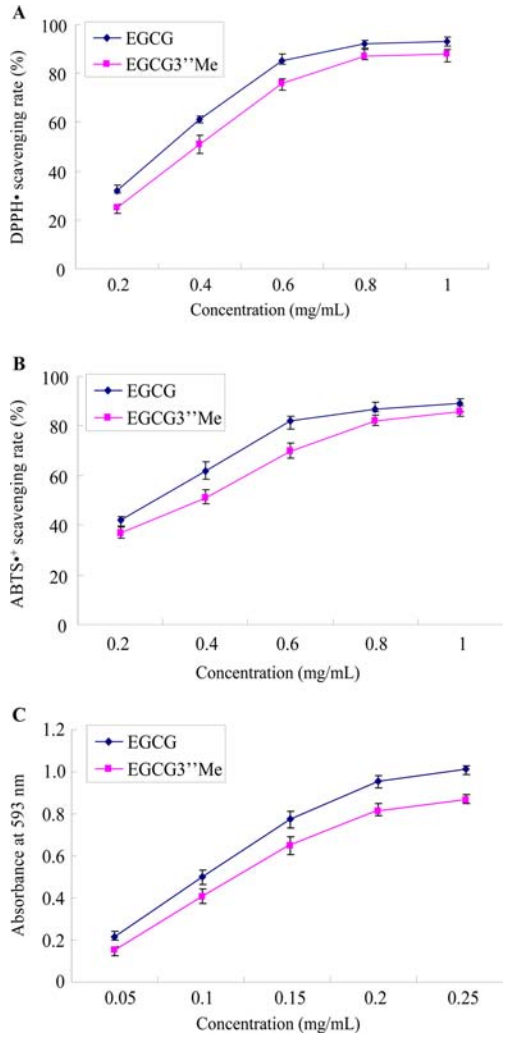


**Figure 3.** Antioxidant activities of EGCG and EGCG3″Me made from Chinese oolong tea determined by DPPH free radical-scavenging assay (A), ABTS assay (B), and FRAP assay (C).

viability, AST and ALT levels, lipid peroxidation, and glutathione depletion were observed until an exposure period of 3 h when compared with normal control, thus overruling any direct solvent-mediated damage by alcohol in HepG2 cells. Thereafter, a time-dependent significant ($P < 0.05$) increased leakage of AST and ALT and loss of cell viability were observed. Similarly, a significant ($P < 0.05$) increased lipid peroxidation with concurrent decrease in GSH-Px content was noted compared with normal control when cells were incubated for 6, 12, and 24 h.

The cytotoxicity of EGCG3″Me was studied by in vitro cytotoxicity assay, and it showed the $CTC_{50}$ value of EGCG3″Me was 94.2, 156, and 190 $\mu$g/mL for 24, 48, and 72 h, respectively, which showed EGCG3″Me had no cytotoxicity for the HepG2 cell line in this study.

Table 1 depicts the protective effect of EGCG3″ and bifendate on alcohol-induced toxicity in the HepG2 cell line. A significant decrease in cell viability and significant increases in AST and ALT levels were observed in HepG2 cells exposed to alcohol as compared with the normal control group. Both EGCG3″Me and bifendate treatments along with alcohol significantly increased the viability of cells. The middle concentration of bifendate (20 $\mu$g/mL) was more effective


dx.doi.org/10.1021/jf5016335 | J. Agric. Food Chem. 2014, 62, 10046−10054

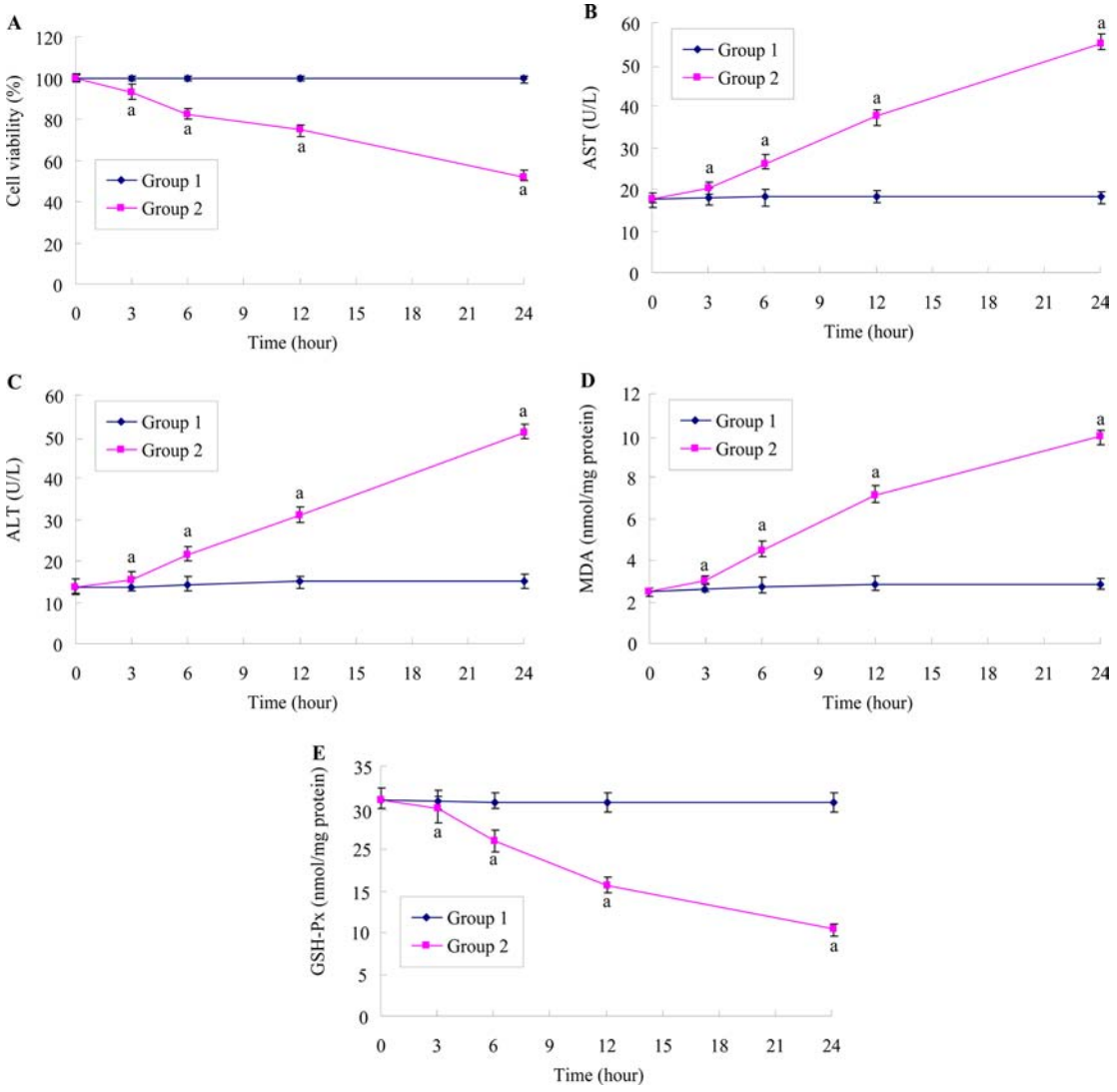


**Figure 4.** Time-dependent changes observed in (A) cell viability, (B) AST and (C) ALT leakage, and (D) MDA and (E) GSH-Px levels after exposure to 1% of alcohol in HepG2 cells. Group 1, normal control; group 2, alcohol control (1%, v/v). Results are expressed as mean ± SEM ($n$ = 5). Level of significance $P < 0.05$. [a]Compared with normal control.

**Table 1. Protective Effect of EGCG3″Me and Bifendate on Alcohol-Induced Toxicity in HepG2 Cell Line[a]**

| group | exptl group | cell viability (%) | AST (U/L) | ALT (U/L) | MDA (nmol/mg protein) | GSH-Px (nmol/mg protein) |
|---|---|---|---|---|---|---|
| (I) control | | | | | | |
| 1 | normal control | 99.9 ± 0.24 | 17.9 ± 0.34 | 12.0 ± 0.21 | 2.08 ± 0.11 | 32.5 ± 0.15 |
| 2 | EGCG3″Me control (40 μg/mL) | 99.5 ± 0.19 | 17.8 ± 0.22 | 12.0 ± 0.31 | 2.14 ± 0.13 | 32.0 ± 0.19 |
| 3 | bifendate control (40 μg/mL) | 99.8 ± 0.30 | 18.0 ± 0.18 | 12.2 ± 0.14 | 2.16 ± 0.20 | 32.1 ± 0.24 |
| (II) toxin treatment | | | | | | |
| 4 | alcohol control (1%, v/v) | 48.5 ± 0.69a | 53.9 ± 0.85a | 36.2 ± 1.47a | 7.91 ± 0.38a | 10.3 ± 0.43a |
| (III) EGCG3″Me treatment | | | | | | |
| 5 | alcohol (1%, v/v) + EGCG3″Me (10 μg/mL) | 61.4 ± 1.19b | 42.8 ± 1.44b | 29.2 ± 1.13b | 6.80 ± 0.36b | 26.7 ± 0.78f |
| 6 | alcohol (1%, v/v) + EGCG3″Me (20 μg/mL) | 66.8 ± 1.04c | 39.1 ± 0.31c | 27.4 ± 0.85c | 6.22 ± 0.24c | 22.7 ± 1.74e |
| 7 | alcohol (1%, v/v) + EGCG3″Me (40 μg/mL) | 75.3 ± 1.75d | 33.0 ± 0.60d | 20.7 ± 1.38f | 5.31 ± 0.16f | 16.7 ± 1.03c |
| (IV) bifendate treatment | | | | | | |
| 8 | alcohol (1%, v/v) + bifendate (10 μg/mL) | 67.8 ± 1.43c | 38.9 ± 0.75c | 26.6 ± 1.21d | 6.02 ± 0.35d | 22.6 ± 1.26e |
| 9 | alcohol (1%, v/v) + bifendate (20 μg/mL) | 78.3 ± 2.30e | 32.2 ± 0.81e | 21.4 ± 0.63e | 5.52 ± 0.61e | 17.7 ± 0.69d |
| 10 | alcohol (1%, v/v) + bifendate (40 μg/mL) | 87.3 ± 1.61f | 24.7 ± 1.05f | 16.5 ± 1.09g | 4.87 ± 0.22g | 13.8 ± 0.43b |

[a]Results are expressed as mean ± SEM ($n$ = 5). No significant difference was noted between groups 1, 2, and 3. Data in the same column (group 4–10) with different letters are significantly different at $P < 0.05$ among different treatments.


dx.doi.org/10.1021/jf5016335 | J. Agric. Food Chem. 2014, 62, 10046–10054

when compared with all concentrations of EGCG3″Me. Increased release of intracellular enzymes AST and ALT was observed at >3 h exposure to alcohol. This indicated membrane damage and instability owing to oxidative injury created by alcohol. Likewise, alcohol caused an increase in the level of MDA with a concurrent decrease in GSH-Px content in HepG2 cells. The alcohol-induced changes in the HepG2 cells were ameliorated by cotreatment of the toxin along with both EGCG3″Me and bifendate. It was observed that when treated with different concentrations (10, 20, and 40 $\mu$g/mL) of EGCG3″Me, the cells showed a significant restoration of the altered biochemical parameters toward normal compared with the toxin-treated group in a concentration-dependent manner.

Effects of EGCG3″Me pretreatment on alcohol-induced alteration in body weight and relative organ weight in mice are shown in Table 2. It can be seen that body weights of mice were not affected by the treatment of alcohol, bifendate, or EGCG3″Me, for no differences were observed for body weights among different groups. However, significant increases of the relative weights of liver, spleen, and thymus were observed for the mice in the alcohol control group, indicating that alcohol induced hypertrophy of these organ tissues in mice. On the contrary, the pretreatment of bifendate showed a remarkable decrease in elevated relative organ weights when compared with the model control group. Moreover, the administration of EGCG3″Me significantly reduced the relative weight of liver and spleen and, notably, a similar effect was observed for the relative weight of thymus in mice pretreated with EGCG3″Me at a medium or high dose.

**Table 2. Effects of EGCG3″Me Pretreatment on Alcohol-Induced Alteration in Body Weight and Relative Organ Weight in Mice[a]**

| | | relative weight (g/g body weight, %) | | |
|---|---|---|---|---|
| group | body weight (g) | liver | spleen | thymus |
| I | 35.3 ± 2.04 | 4.38 ± 0.20a | 0.24 ± 0.02a | 0.21 ± 0.02a |
| II | 34.4 ± 1.28 | 5.62 ± 0.33e | 0.37 ± 0.04d | 0.28 ± 0.01c |
| III | 34.6 ± 1.39 | 4.39 ± 0.34a | 0.27 ± 0.03b | 0.20 ± 0.01a |
| IV | 35.2 ± 2.23 | 5.47 ± 0.27d | 0.34 ± 0.03c | 0.27 ± 0.02c |
| V | 36.3 ± 1.87 | 4.45 ± 0.16b | 0.26 ± 0.02b | 0.21 ± 0.02b |
| VI | 35.1 ± 2.08 | 4.58 ± 0.19c | 0.27 ± 0.02b | 0.22 ± 0.02b |

[a]Groups I, II, and III represent the normal control, model control, and positive control, respectively. Groups IV, V, and VI represent the groups pretreated with EGCG3″Me at doses of 25, 50, and 100 mg/kg BW per day, respectively. Each value is presented as the mean ± SD ($n$ = 8). Different lower case letters indicate significant difference from the model group at the level of $P < 0.05$.

Table 3 shows the effects of EGCG3″Me pretreatment on alcohol-induced alteration in serum enzyme activities of AST and ALT and hepatic SOD, GSH-Px, and MDA levels in mice. Apparently, significant increases in AST and ALT activities were observed in sera of the alcohol model group when compared with the normal control group, indicating that the alcohol-induced hepatotoxicity in mice was well-established. The elevated AST and ALT levels were reduced significantly in a concentration-dependent manner in mice pretreated with EGCG3″Me. Compared with those in the model control group, the levels of AST and ALT decreased 38.9 and 38.7%, respectively, at a dose of 100 mg/kg BW per day of EGCG3″Me. There was also a significant decrease in SOD and GSH-Px activities and an increase in MDA level in the alcohol model group when compared with the normal control group. As shown in Table 3, the administration of EGCG3″Me significantly enhanced SOD and GSH-Px activities but decreased MDA levels when compared with the model control group. At a high dose of EGCG3″Me, SOD and GSH-Px activities in the liver were restored by 5.67 and 32.4% in alcohol-induced liver injury mice. However, there was no significant difference of SOD activity for mice pretreated by EGCG3″Me at a medium or high dose. The level of MDA was significantly reduced in a concentration-dependent manner in the mice pretreated with EGCG3″Me. At a dose of 100 mg/kg BW per day of EGCG3″Me, the level of MDA in mice was 0.77 ± 0.03 nmol/mg protein, which was 32.5% lower than that of the alcohol model group.

The effects of EGCG3″Me and bifendate on liver histopathology of alcohol-treated mice are presented in Figure 5. In the normal control group (Figure 5I), the liver sections showed normal hepatic cells with well-preserved cytoplasm, prominent nucleus, and clear central vein (CV), whereas in the model control group, massive inflammation, infiltration, and many ballooned hepatocytes (blue arrow) were observed around the CV (Figure 5II). For the positive control group, bifendate (10 mg/kg) exhibited a significant protective effect evidenced by showing a clear CV and similar liver tissue compared with the normal group (Figure 5III). In addition, similar protection from alcohol-induced inflammation and infiltration in liver tissues was observed by the pretreatment with EGCG3″Me in a dose-dependent manner (Figure 5IV–VI). In Figure 5IV, a moderate inflammation area with color changes around the CV and fewer ballooned hepatocytes were observed; in Figure 5V, less inflammation and infiltration around CV and trace ballooned hepatocytes were presented, whereas Figure 5IV shows a clear CV and similar tissue structure when compared with the normal control group.

**Table 3. Effects of EGCG3″Me Pretreatment on Alcohol-Induced Alteration in Serum Enzyme Activities of AST and ALT and Hepatic SOD, GSH-Px, and MDA Levels in Mice[a]**

| group | AST (U/L) | ALT (U/L) | SOD (U/mg) | GSH-Px (nmol/mg protein) | MDA (nmol/mg protein) |
|---|---|---|---|---|---|
| I | 28.6 ± 2.72a | 19.9 ± 1.43a | 275 ± 11.4a | 10.3 ± 0.26a | 0.58 ± 0.03a |
| II | 64.6 ± 3.17f | 97.6 ± 3.78f | 247 ± 20.1e | 6.12 ± 0.17f | 1.14 ± 0.08e |
| III | 33.8 ± 2.44b | 53.5 ± 3.18b | 268 ± 10.4b | 8.89 ± 0.22b | 0.78 ± 0.03b |
| IV | 51.6 ± 1.98e | 82.5 ± 2.71e | 255 ± 21.8d | 6.76 ± 0.09e | 1.02 ± 0.03d |
| V | 47.6 ± 2.72d | 67.1 ± 3.44d | 259 ± 10.4c | 6.99 ± 0.05d | 0.88 ± 0.04c |
| VI | 39.6 ± 2.72c | 59.6 ± 3.02c | 261 ± 9.98c | 8.10 ± 0.03c | 0.77 ± 0.03b |

[a]Groups I, II, and III represent the normal control, model control, and positive control, respectively. Groups IV, V, and VI represent the group pretreated with EGCG3″Me at doses of 25, 50, and 100 mg/kg BW per day, respectively. Each value is presented as the mean ± SD ($n$ = 8). Different lower case letters are significantly different from the model group at the level of $P < 0.05$.

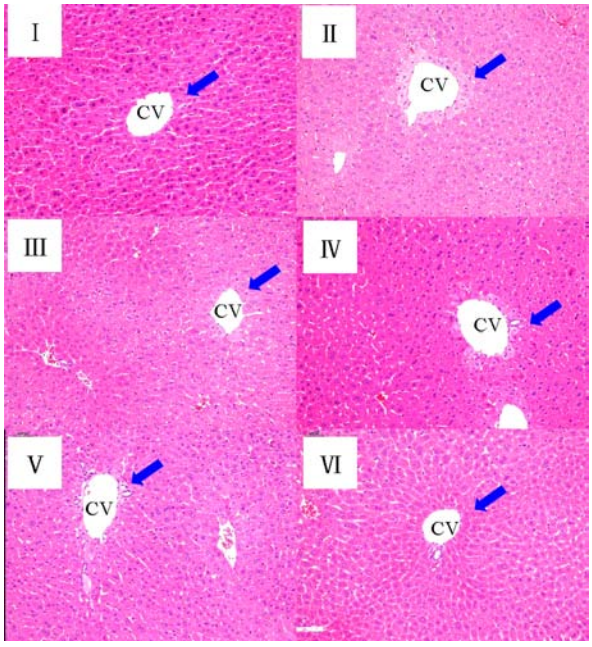


**Figure 5.** Photomicrographs of liver sections stained with hematoxylin−eosin: (I) liver from a mouse in normal control group pretreated with physiological saline; (II) liver from a mouse in model control group pretreated with physiological saline followed by alcohol treatment; (III) liver from a mouse in positive control group pretreated with bifendate (10 mg/kg) followed by alcohol treatment; (IV) liver from a mouse in the group pretreated with EGCG3″Me (25 mg/kg) followed by alcohol treatment; (V) liver from a mouse in the group pretreated with EGCG3″Me (50 mg/kg) followed by alcohol treatment; (VI) liver from a mouse in the group pretreated with EGCG3″Me (100 mg/kg) followed by alcohol treatment. CV, central vein.

## DISCUSSION

Oolong tea is reported to have a wide range of health benefits, and its polyphenols have been considered as promising active ingredients responsible for the effects. However, previous studies have not connected the hepatoprotective effects to the phenolic constituents of oolong tea. In this study, we for the first time explored the hepatoprotective efficacy of EGCG3″Me from Chinese oolong tea.

EGCG3″Me is generally prepared from limited oolong tea or green tea by extraction with water and purification with HP-20 column chromatography and preparative HPLC.[26] In the present study, EGCG3″Me of high purity was successfully prepared from Chinese oolong tea through water extraction and simple purification procedures of polyamide and Toyopearl HW-40S column chromatography. Obviously, it is a simple and efficient procedure for the preparation of EGCG3″Me compared with reported methods.

In our study, we demonstrated that the in vitro antioxidant activity of EGCG is greater than that of EGCG3″Me. EGCG is the main component of tea polyphenols, which has been shown to have significant biological activity. However, for the low bioavailability, EGCG is rapidly metabolized to a variety of derivative products after absorption, including glycosylation, sulfation, and methylated derivatives.[28] These derivatives are likely to play an important role in vivo and show higher biological activity.[29,30] Currently, the function, mechanism, and biotransformation of these derivatives in vivo are still to be investigated and clarified. In this test, EGCG3″Me showed high antioxidant activity, which may also have excellent hepatoprotective ability as EGCG.

Recently, the in vitro cytotoxicity and hepatoprotective activity of plant extracts have gained importance for primary level screening. HepG2 cells possess many morphological and biochemical features of normal hepatocytes. Because it retains many of the phenotypic and genotypic characteristics of liver cells, this cell line has been used in various studies related to medicinal plants for their liver-protecting property.[31,32] Therefore, the present study was designed to ascertain the hepatoprotective activity of EGCG3″Me against alcohol in the HepG2 cell line.

Alcohol-mediated liver injury in vitro is reported in the literature to be caused by two components, a direct solvent effect or the generation of free radicals and subsequent lipid peroxidation depending on its concentration, the duration of exposure, and the sensitivity of the in vitro system to which it is added.[33,34] During alcohol exposure, superoxide radical is believed to play a central role in alcohol-induced liver injury. It can be produced readily by numerous processes and reacts through catalytic pathways in cells to form potent oxidants, including hydroxyl radical, hydrogen peroxide, and peroxynitrite.[35] In this study, our results in conjunction with other reports proved that hepatotoxin caused a time-dependent production of reactive oxygen species (ROS) and subsequent lipid peroxidation in HepG2 cells, which was found to be maximum after an incubation period of 24 h.[36] Therefore, HepG2 cells were incubated with alcohol for 24 h to study the protective effects of EGCG3″Me against alcohol-induced toxicity. Increased release of intracellular enzymes AST and ALT was observed at 24 h of exposure to alcohol. This indicated membrane damage and instability owing to oxidative injury created by the hepatotoxin. Likewise, alcohol treatment caused significant increase in the level of MDA, with a concurrent decrease in SOD and GSH-Px contents in HepG2 cells. When treated with different concentrations of EGCG3″Me, HepG2 cells showed a significant restoration of the altered biochemical parameters toward the normal compared with model control group. The possible underlying mechanism for the hepatoprotective effect of EGCG3″Me in a dose-dependent manner is its ability to inhibit lipid peroxidation and maintenance of GSH-Px and SOD by virtue of its antioxidative powers. Due to the nontoxic and hepatoprotective nature of EGCG3″Me, it was thought pertinent to assess its hepatoprotective potential in vivo using a mouse model.

Alcohol administration in animal models has been used as a test for potential hepatoprotective agents frequently. In the present study, a remarkably increased relative organ weight was observed in the model control group compared with the normal control group (Table 2). Furthermore, we found a dramatic elevation of AST and ALT activities in the model control group when compared with other groups (Table 3). The results indicated that alcohol induced hepatotoxicity in animal organs and disorders of enzyme activities. In recent times, much evidence has demonstrated that increases of serum AST and ALT activities caused by hepatotoxin are related to hepatic structural damage because these entities are normally localized to the cytoplasm and are released into the circulation after cellular damage occurred.[37,38] However, both relative organ weights and AST and ALT activities decreased dramatically in mice pretreated with bifendate when compared with those in the model control group (Table 2), and similar results have

been obtained by the pretreatment of EGCG3″Me. The results suggested that EGCG3″Me might have a protective effect against alcohol-induced liver injury in mice.

The accumulation of alcohol-induced radicals leads to a free radical mediated lipid peroxidation and cell necrosis, which causes liver injury, and the level of MDA provides an indirect index of lipid peroxidation. In the present study, the increase in MDA levels suggests enhanced lipid peroxidation leading to tissue damage and failure of antioxidant defense mechanisms to prevent formation of excessive free radicals. In our study, the pretreatment of EGCG3″Me inhibited alcohol-induced hepatotoxicity effectively by reducing the formation of MDA in the liver. At a dose of 100 mg/kg BW per day of EGCG3″Me, the MDA level reached the same level as the positive control group. This suggested that EGCG3″Me might have a hepatoprotective effect by decreasing oxidative stress in the liver of alcohol-induced mice. These results are also in good agreement with histopathological results. As shown in Figure 5, marked and widespread inflammation and infiltration areas were depicted in the model control group, whereas those of the bifendate treatment group and EGCG3″Me treatment group with a high dose reversed alcohol-induced liver injury, indicating that EGCG3″Me was effective against alcohol-induced hepatotoxic effect. In the model control group, SOD and GSH-Px activities were very low, whereas the mice of the positive control group showed higher activities when compared with the model control group. Notably, the activities of SOD and GSH-Px were also elevated markedly by the pretreatment of EGCG3″Me, especially at a dose of 100 mg/kg BW per day. It has been reported that the decrease in the activity of SOD, the increase in the lipid peroxidation, and the breakdown of the GSH-dependent antioxidant defense system are obviously seen along with the liver damage induced by hepatotoxin.[39] Oxidative stress has been considered as a major molecular mechanism involved in alcohol toxicity; in our study, EGCG3″Me showed excellent antioxidant and hepatoprotective activities in a dose-dependent manner, and the present results were in good agreement with other results.[37−39]

According to the results stated above, it is believed that the hepatoprotective effect of polyphenol is related to its antioxidant activity. Cui et al. reported the protective effects of polyphenol-enriched extract from green tea, including epigallocatechin, rutin, and epicatechin, against $CCl_4$-induced liver injury in mice, and emphasized the importance of a high content of polyphenols for guarding intact endogenous cellular antioxidant defense systems.[40] The most abundant tea catechin, EGCG, has also been shown to exhibit hepatoprotective effects against liver injury by ethanol and carbon tetrachloride.[14,15] Although EGCG has also been shown to exhibit hepatoprotective effects against liver injury, some studies demonstrated that high doses of EGCG can lead to mild liver injury.[41] During digestion and transfer across the small intestine, and in the liver, EGCG is rapidly metabolized by phase II enzymes to various *O*-sulfated, *O*-glucuronidated, and *O*-methylated forms, which may play an important role in vivo.[28] In the present study, the antioxidant and hepatoprotective effects of EGCG3″Me from Chinese oolong tea were confirmed.

In conclusion, high-purity EGCG3″Me was successfully prepared from Chinese oolong tea by extraction with hot water and simple purification procedures of polyamide and Toyopearl HW-40S column chromatography. In an in vitro antioxidant study, EGCG3″Me exhibited potential antioxidant activity. For hepatoprotective activity in vitro, it was observed that EGCG3″Me effectively alleviated the changes induced by alcohol in a concentration-dependent manner. On the basis of the in vivo alcohol-induced liver injury model, we demonstrated that the administration of EGCG3″Me significantly decreased AST and ALT levels in the serum and the liver level of MDA and remarkably restored the liver activities of SOD and GSH-Px in alcohol-induced liver injury mice. Accordingly, this suggested that EGCG3″Me had a significant hepatoprotective effect on alcohol-induced liver injury possibly via its antioxidant activity to protect biological systems against oxidative stress. These results provided evidence that EGCG3″Me might be an important active substance responsible for the hepatoprotective effect of Chinese oolong tea; therefore, EGCG3″Me could be developed as a potential functional food ingredient for liver injury and the maintenance of human health.

## AUTHOR INFORMATION

### Corresponding Author

*(X.Z.) Phone: +86-574-87609573. Fax: +86-574-87608347. E-mail: zhangxin@nbu.edu.cn.

### Funding

This work is sponsored by K. C. Wong Magna Fund in Ningbo University.

### Notes

The authors declare no competing financial interest.

## ABBREVIATIONS USED

EGCG, (−)-epigallocatechin gallate; EGCG3″Me, (−)-epigallocatechin 3-*O*-(3-*O*-methyl) gallate; GCG, (−)-gallocatechin gallate; ALD, alcoholic liver disease; $CCl_4$, carbon tetrachloride; DPPH, 2,2-diphenyl-1-picrylhydrazyl; ABTS, 2,2′-azinobis(3-ethylbenzothiazoline-6-sulfonic acid) diammonium salts; TPTZ, 2,4,6-tri(2-pyridyl)-*s*-triazine; MTT, 3-(4,5-dimethylthiazol-2-yl)-2,5-diphenyl tetrazolium bromide; FBS, fetal bovine serum; AST, aspartate aminotransferase; ALT, alanine aminotransferase; GSH-Px, glutathione peroxidase; SOD, superoxide dismutase; MDA, malondialdehyde; HPLC-DAD, high-performance liquid chromatography with diode array detector; ESI-MS/MS, electrospray ionization tandem mass spectrometry; ESI-TOF-MS, electrospray ionization time-of-flight mass spectrometry; NMR, nuclear magnetic resonance; $CTC_{50}$, 50% cytotoxic concentration; SDS, sodium dodecyl sulfate; OD, optical density or absorbance; BW, body weight; H&E, hematoxylin−eosin; SD, standard deviation; SEM, standard error of the mean; CV, central vein

## REFERENCES

(1) Gramza, A.; Korczak, J. Tea constituents (*Camellia sinensis* L.) as antioxidants in lipid systems. *Trends Food Sci. Technol.* **2005**, *16*, 351−358.

(2) Song, J. M.; Lee, K. H.; Seong, B. L. Antiviral effect of catechins in green tea on influenza virus. *Antivir. Res.* **2005**, *68*, 66−74.

(3) Yuan, J. M.; Sun, C.; Butler, L. M. Tea and cancer prevention: epidemiological studies. *Pharmacol. Res.* **2011**, *64*, 123−135.

(4) Singh, B. N.; Shankar, S.; Srivastava, R. K. Green tea catechin, epigallocatechin-3-gallate (EGCG): mechanisms, perspectives and clinical applications. *Biochem. Pharmacol.* **2011**, *82*, 1807−1821.

(5) Maeda-Yamamoto, M.; Ema, K.; Monobe, M.; Tokuda, Y.; Tachibana, H. Epicatechin-3-*O*-(3″-*O*-methyl)-gallate content in various tea cultivars (*Camellia sinensis* L.) and its in vitro inhibitory effect on histamine release. *J. Agric. Food Chem.* **2012**, *60*, 2165−2170.

(6) Gao, B.; Bataller, R. Alcoholic liver disease: pathogenesis and new therapeutic targets. *Gastroenterology* **2011**, *141*, 1572−1585.

(7) Lima, C. F.; Fernandes-Ferreira, M.; Pereira-Wilson, C. Phenolic compounds protect HepG2 cells from oxidative damage: relevance of glutathione levels. *Life Sci.* **2006**, *79*, 2056−2068.
(8) Wang, D. Y.; Zhao, Y.; Sun, Y. F.; Yang, X. B. Protective effects of Ziyang tea polysaccharides on $CCl_4$-induced oxidative liver damage in mice. *Food Chem.* **2014**, *143*, 371−378.
(9) Lu, X. S.; Zhao, Y.; Sun, Y. F.; Yang, S.; Yang, X. B. Characterisation of polysaccharides from green tea of *Huangshan Maofeng* with antioxidant and hepatoprotective effects. *Food Chem.* **2013**, *141*, 3415−3423.
(10) Augustyniak, A.; Waszkiewicz, E.; Skrzydlewska, E. Preventive action of green tea from changes in the liver antioxidant abilities of different aged rats intoxicated with ethanol. *Nutrition* **2005**, *21*, 925−932.
(11) Casey, C. A.; McVicker, B. L.; Donohue, T. M.; McFarland, M. A.; Wiegert, R. L. Liver asialoglycoprotein receptor levels correlate with severity of alcoholic liver damage in rats. *J. Appl. Physiol.* **2004**, *96*, 76−80.
(12) Cederbaum, A. I.; Lu, Y. K.; Wu, D. F. Role of oxidative stress in alcohol-induced liver injury. *Arch. Toxicol.* **2009**, *83*, 519−548.
(13) Das, S. K.; Vasudevan, D. M. Alcohol-induced oxidative stress. *Life Sci.* **2007**, *81*, 177−187.
(14) Oliva, J.; Bardag-Gorce, F.; Tillman, B.; French, S. W. Protective effect of quercetin, EGCG, catechin and betaine against oxidative stress induced by ethanol in vitro. *Exp. Mol. Pathol.* **2011**, *90*, 295−299.
(15) Tipoe, G. L.; Leung, T. M.; Liong, E. C.; Lau, T. Y.; Fung, M. L.; Nanji, A. A. Epigallocatechin-3-gallate (EGCG) reduces liver inflammation, oxidative stress and fibrosis in carbon tetrachloride ($CCl_4$)-induced liver injury in mice. *Toxicology* **2010**, *273*, 45−52.
(16) Zhang, X.; Xu, F.; Gao, Y.; Wu, J.; Sun, Y.; Zeng, X. X. Optimising the extraction of tea polyphenols, (−)-epigallocatechin gallate and theanine from summer green tea by using response surface methodology. *Int. J. Food Sci. Technol.* **2012**, *47*, 2151−2157.
(17) Zhang, X.; Zhu, X. L.; Sun, Y. K.; Hu, B.; Sun, Y.; Jabbar, S.; Zeng, X. X. Fermentation *in vitro* of EGCG, GCG and EGCG3″Me isolated from oolong tea by human intestinal microbiota. *Food Res. Int.* **2013**, *54*, 1589−1595.
(18) Chen, Y. L.; Jiang, Y. M.; Duan, J.; Shi, J.; Xue, S.; Kakuda, Y. Variation in catechin contents in relation to quality of '*Huang Zhi Xiang*' oolong tea (*Camellia sinensis*) at various growing altitudes and seasons. *Food Chem.* **2010**, *119*, 648−652.
(19) Liu, L. X.; Sun, Y.; Laura, T.; Liang, X. F.; Ye, H.; Zeng, X. X. Determination of polyphenolic content and antioxidant activity of kudingcha made from *Ilex kudingcha* C.J. Tseng. *Food Chem.* **2009**, *112*, 35−41.
(20) Stratil, P.; Klejdus, B.; Kubán, V. Determination of total content of phenolic compounds and their antioxidant activity in vegetables-evaluation of spectrophometic methods. *J. Agric. Food Chem.* **2006**, *54*, 607−616.
(21) Benzie, I. F.; Strain, J. J. The ferric reducing ability of plasma (FRAP) as a measure of "antioxidant power": the FRAP assay. *Anal. Biochem.* **1996**, *239*, 70−76.
(22) Mossmann, T. Rapid colorimetric assay for cellular growth and survival: application to proliferation and cytotoxic assays. *J. Immunol. Methods* **1983**, *65*, 55−63.
(23) Pan, S.; Yang, R.; Dong, H.; Yu, Z.; Ko, K. Bifendate treatment attenuates hepatic steatosis in cholesterol/bile salt- and high-fat diet-induced hypercholesterolemia in mice. *Eur. J. Pharmacol.* **2006**, *552*, 170−175.
(24) Wang, M. C.; Zhu, P. L.; Jiang, C. X.; Ma, L. P.; Zhang, Z. J.; Zeng, X. X. Preliminary characterization, antioxidant activity *in vitro* and hepatoprotective effect on acute alcohol-induced liver injury in mice of polysaccharides from the peduncles of *Hovenia dulcis*. *Food Chem. Toxicol.* **2012**, *50*, 2964−2970.
(25) Nada, S. A.; Omara, E. A.; Abdel-Salam, O. M. E.; Zahran, H. G. Mushroom insoluble polysaccharides prevent carbon tetrachloride-induced hepatotoxicity in rat. *Food Chem. Toxicol.* **2010**, *48*, 3184−3188.
(26) Sano, M.; Suzuki, M.; Miyase, T.; Yoshino, K.; Maeda-Yamamoto, M. Novel antiallergic catechin derivatives isolated from oolong tea. *J. Agric. Food Chem.* **1999**, *47*, 1906−1910.
(27) Davis, A. L.; Cai, Y.; Davies, A. P.; Lewis, J. R. $^1H$ and $^{13}C$ NMR assignments of some green tea polyphenols. *Magn. Reson. Chem.* **1996**, *34*, 887−890.
(28) Selma, M. V.; Espín, J. C.; Tomás-Barberán, F. A. Interaction between phenolics and gut microbiota: role in human health. *J. Agric. Food Chem.* **2009**, *57*, 6485−6501.
(29) Huo, C. D.; Yang, H. J.; Cui, Q. Z.; Dou, Q. P.; Chan, T. H. Proteasome inhibition in human breast cancer cells with high catechol-*O*-methyltransferase activity by green tea polyphenol EGCG analogs. *Bioorg. Med. Chem.* **2010**, *18*, 1252−1258.
(30) Dueñas, M.; González-Manzano, S.; González-Paramás, A.; Santos-Buelga, C. Antioxidant evaluation of *O*-methylated metabolites of catechin, epicatechin and quercetin. *J. Pharm. Biomed.* **2010**, *51*, 443−449.
(31) Vidyashankar, S.; Sandeep Varma, R.; Patki, P. S. Quercetin ameliorate insulin resistance and up-regulates cellular antioxidants during oleic acid induced hepatic steatosis in HepG2 cells. *Toxicol. In Vitro* **2013**, *27*, 945−953.
(32) Mersch-Sundermann, V.; Knasmüller, S.; Wu, X. J.; Darroudi, F.; Kassie, F. Use of a human-derived liver cell line for the detection of cytoprotective, antigenotoxic and cogenotoxic agents. *Toxicology* **2004**, *198*, 329−340.
(33) Wang, Y. H.; Liu, Y. L.; Kirpich, I.; Ma, Z. H.; Wang, C. L.; Zhang, M.; Suttles, J.; McClain, C.; Feng, W. K. *Lactobacillus rhamnosus* GG reduces hepatic TNF$\alpha$ production and inflammation in chronic alcohol-induced liver injury. *J. Nutr. Biochem.* **2013**, *24*, 1609−1615.
(34) Li, R.; Liang, T.; He, Q. L.; Guo, C.; Xu, L. Y.; Zhang, K. F.; Duan, X. Q. Puerarin, isolated from *Kudzu root* (Willd.), attenuates hepatocellular cytotoxicity and regulates the GSK-3$\beta$/NF-$\kappa$B pathway for exerting the hepatoprotection against chronic alcohol-induced liver injury in rats. *Int. Immunopharmacol.* **2013**, *17*, 71−78.
(35) Tsukamoto, H.; Horne, W.; Kamimura, S.; Niemelä, O.; Parkkila, S.; Ylä-Herttuala, S.; Brittenham, G. M. Experimental liver cirrhosis induced by alcohol andiron. *J. Clin. Invest.* **1995**, *96*, 620−630.
(36) Krithika, R.; Mohankumar, R.; Verma, R. J.; Shrivastav, P. S.; Mohamad, I. M.; Gunasekaran, S.; Narasimhan, S. Isolation, characterization and antioxidative effect of phyllanthin against $CCl_4$-induced toxicity in HepG2 cell line. *Chem.−Biol. Interact.* **2009**, *181*, 351−358.
(37) Dhanasekaran, M.; Ignacimuthu, S.; Agastian, P. Potential hepatoprotective activity of ononitol monohydrate isolated from *Cassia tora* L on carbon tetrachloride induced hepatotoxicity in wistar rats. *Phytomedicine* **2009**, *16*, 891−895.
(38) Hwang, Y. P.; Choi, J. H.; Jeong, H. G. Protective effect of the *Aralia continentalis* root extract against carbon tetrachloride-induced hepatotoxicity in mice. *Food Chem. Toxicol.* **2009**, *47*, 75−81.
(39) Gan, D.; Ma, L. P.; Jiang, C. X.; Wang, M. C.; Zeng, X. X. Medium optimization and potential hepatoprotective effect of mycelial polysaccharides from *Pholiota dinghuensis* Bi against carbon tetrachloride-induced acute liver injury in mice. *Food Chem. Toxicol.* **2012**, *50*, 2681−2688.
(40) Cui, Y. M.; Yang, X. B.; Lu, X. S.; Chen, J. W.; Zhao, Y. Protective effects of polyphenols-enriched extract from Huangshan Maofeng green tea against $CCl_4$-induced liver injury in mice. *Chem.−Biol. Interact.* **2014**, *220*, 75−83.
(41) Saleh, I. G.; Ali, Z.; Abe, N.; Wilson, F. D.; Hamada, F. M.; Abd-Ellah, M. F.; Walker, L. A.; Khan, I. A.; Ashfaq, M. K. Effect of green tea and its polyphenols on mouse liver. *Fitoterapia* **2013**, *90*, 151−159.

stability, bioaccessibility, and permeability of ginsenosides in WG and RG during in vitro digestion was conducted using a Caco-2 cell culture model coupled with an oral, gastric, and small intestinal simulated digestion. The overall design of the study is outlined in Figure S1 in the Supporting Information.

## MATERIALS AND METHODS

**Materials and Chemicals.** Standard ginsenosides, including the compounds Rg1, Re, Rf, Rg2 (20*S*), Rg2 (20*R*), Rb1, Rc, Rb2, Rd, Rg6, F4, Rk3, Rh4, Rg3 (20*S*), Rg3 (20*R*), Rk1, and Rg5, were purchased from the Ambo Institute (Daejeon, Korea). $\alpha$-Amylase, pepsin, pancreatin, pancreatic lipase, and bile extract were purchased from Sigma-Aldrich (St. Louis, MO, USA) for simulated digestion. All cell culture reagents including Dulbecco's modified Eagle's medium (DMEM), fetal bovine serum, 1 M 4-(2-hydroxyethyl)-1-piperazineethanesulfonic acid (HEPES), phosphate buffer saline (PBS), 100× penicillin and streptomycin, and trypsin/EDTA were obtained from Gibco (Carlsbad, CA, USA). Hanks' balanced salt solution (HBSS) and 100× nonessential amino acids were purchased from Sigma-Aldrich. Transwell permeable polycarbonate inserts (0.4 $\mu$m) and 12-well cell culture plates were obtained from Corning Inc. The solvents used for ultraperformance liquid chromatography (UPLC) were purchased from Fisher Scientific (Springfield, NJ, USA). Unless indicated, all other chemicals were supplied by Sigma-Aldrich.

**Sample Preparation.** Freshly harvested 6-year-old Korean ginseng (*P. ginseng* C.A. Meyer) roots cultivated in Geumsan, South Korea, were selected for this study. They were washed and dried at 60 °C for 2 days using a forced airflow oven (WFO-400, EYELA, Japan) to produce WG. The RG was also prepared by steam cooking at 95 ± 5 °C for 18 h and dried under the same conditions as stated above for WG. Then, the dried WG and RG were pulverized and passed through a 350 $\mu$m screen (Chunggyesanggongsa, Korea) to prepare homogeneous powder samples, and the WG and RG powders were immediately stored at −20 °C until analysis.

**Simulated Digestion of WG and RG.** Simulated digestion was performed according to the method described by Garrett et al.[17] with minor modifications. Briefly, WG and RG powders (2 g) were homogenized in 10 mL of saline solution containing 120 mM NaCl, 5 mM KCl, and 6 mM $CaCl_2$. Then, 1000 units of $\alpha$-amylase was added, and the pH was adjusted to 6.5. After the addition of saline solution to a volume of 12.5 mL, the samples were incubated at 37 °C for 5 min in a shaking water bath (Lab Companion, Jeio Tech, Korea) at 95 rpm for the simulated oral phase of digestion. To mimic the gastric phase of human digestion, the pH of the sample was acidified to 2.5 with HCl and 0.5 mL of porcine pepsin solution (0.075 g/mL in 0.1 N HCl) was added. The samples were filled with saline solution to a volume of 15 mL and incubated at 37 °C for 2 h in a shaking water bath at 95 rpm. To simulate the intestinal phase more accurately and specifically, its phase was separated into three intestinal parts (duodenum, jejunum, and ileum). In the duodenum part, 250 mg of bile extract, 0.5 mL of pancreatic lipase (0.01 g/mL of 0.1 M sodium bicarbonate), and 0.5 mL of pancreatin (0.08 g/mL saline) were added, and the pH was increased to 4.5 by adding 1 M sodium bicarbonate. Samples were incubated for 30 min at 37 °C (final volume = 20 mL). In the jejunum part, the pH was adjusted to 5.5 and incubated for 90 min at 37 °C (final volume = 22.5 mL). Finally, the pH was adjusted to 6.5 and incubated for 300 min at 37 °C (final volume = 25 mL) to mimic the ileum part. At the end of each digestion, the aqueous supernatant, that is, the bioaccessible fraction (100 $\mu$L) was collected through a 0.2 $\mu$m PVDF syringe filter (Whatman, UK) for bioaccessibility measurement of ginsenosides. To measure the digestive stability of ginsenosides, the final digestates were added to ethanol (25 mL) and extracted by sonication for 1 h. After the ethanol mixtures of the aqueous fraction or digestate were centrifuged at 12300*g* for 10 min, their supernatants were recollected and filtered through a 0.2 $\mu$m filter prior to ultraperformance liquid chromatography−mass spectrometry (UPLC-MS) analysis. For the permeability test, the soluble fractions (5 mL) from ileum digestion of WG and RG were prepared through a 0.2 $\mu$m filter and immediately treated with a Caco-2 cell monolayer.

**Permeability of Micellar Ginsenosides by Caco-2 Human Intestinal Cells.** Caco-2 cells (HTB-37, American Type Culture Collection, Rockville, MD, USA) were maintained for cellular transport experiments, according to the method of Hubatsch et al.[25] For the experiments, cells were seeded at a density of $3 \times 10^5$ cells $cm^{-2}$ on the tissue culture-treated polycarbonate filter in 12-transwell plates. The cultures were grown for 21−29 days to obtain a differentiated intestinal cell monolayer. Transepithelial electrical resistance (TEERS) measurements were taken twice weekly using a Millipore Millicell-ERS system (Millipore Corp., Bedford, MA, USA) to ensure the monolayer was intact. Once the TEER values reached 600−1000 $\Omega/cm^2$, the monolayer was used for transport study.

To initiate the transport experiments, the culture media in the donor and receiving compartments were carefully aspirated, and the cells were rinsed with prewarmed transport medium (HBSS supplemented with 25 mM HEPES, pH 7.4). Following a 30 min equilibration with the transport medium at 37 °C, the cells were incubated with the ginsenoside-rich micellar solutions from simulated digestion, which were diluted 5 times with transport medium. The transport studies were performed in both directions for 2 h as follows. For apical-to-basolateral transport (a to b), 1.2 mL of transport medium was added in the basolateral part, and 0.45 mL of each diluted micellar solution was added into the apical part, and a 0.05 mL sample ($C_0$) was immediately withdrawn into a collection tube. After 2 h, 0.6 mL of basolateral transport medium was withdrawn for the analysis and replenished with an equal volume of fresh transport medium. For basolateral-to-apical transport (b to a), 1.25 mL of each diluted aqueous solution was added in the basolateral part and a 0.05 mL sample was immediately withdrawn, followed by 0.4 mL of transport medium being added into the apical part. Then, 0.2 mL of apical transport medium was withdrawn after 2 h and replenished with the same volume of fresh transport medium. The TEER values were measured after cell integrity was confirmed. All of the collected samples were added with the same volume of acetonitrile to increase the stability of ginsenosides prior to UPLC-MS analysis. The apparent permeability coefficient ($P_{app}$) was calculated as

$$P_{app} = \frac{\partial Q}{AC_0\partial t}$$

where $\partial Q \partial t$ is the permeability rate, $A$ is the surface area of the membrane filter, and $C_0$ is the initial concentration in the donor compartment (the apical compartment in the a to b transport study and basolateral compartment in the b to a transport study).

**UPLC-MS Analysis.** The quantitative analysis of ginsenosides in WG and RG was performed using the UPLC-MS (Thermofisher Scientific, Fremont, CA, USA) method according to a previous paper by Wang et al.[12] with a slight modification to avoid the overlay of each analyte. The UPLC system was equipped with an ACCELA pump, ACCELA autosampler, and ACCELA PDA detector. Chromatographic separation was carried out at 35 °C on a reversed-phase YMC-ultraHT Pro C18 column (50 × 2.0 mm, 2.0 $\mu$m, YMC Inc., USA). The mobile phase was acetonitrile (A) and 0.1% formic acid in water (B). Gradient elution started with 18% of solvent A and 82% of solvent B, which was changed to 22% A for 10 min, then to 35% A for 10 min, then to 45% A for 8 min, then to 65% A for 4 min, and held for 3 min; then it was changed to 90% A for 5 min. The flow rate was kept at 0.4 mL/min, and the sample volume to be injected was set at 1 $\mu$L. UPLC-ion trap-MS analysis was performed in full-scan mode with an LCQ FLEET ion trap mass spectrometer, which was equipped with an electrospray ionization (ESI) source. The mass spectra were acquired in negative mode using a scan range of the charge ratio ($m/z$) 100−1500. The conditions used for the ESI source were as follows: heater temperature, 200 °C; sheath gas flow rate, 40 bar; spray voltage, 5 kV; capillary temperature, 300 °C; capillary voltage, 45 V; and tube lens, 125 V. Data analysis was performed using Xcalibur 2.2 software (Thermofisher Scientific). Seventeen ginsenosides, Rg1, Re, Rf, Rg2 (20*S*), Rg2 (20*R*), Rb1, Rc, Rb2, Rd, Rg6, F4, Rk3, Rh4, Rg3 (20*S*), Rg3 (20*R*), Rk1, and Rg5, were identified by comparing the retention time with reference standards and the molecular weight with previous

**Table 1. Stability in Each Digestate Generated by Simulated Oral, Gastric, and Small Intestinal Digestion of WG[a]**

| | recovery in digestion phase (%) | | | | | |
|---|---|---|---|---|---|---|
| ginsenoside | food[b] | mouth | stomach | duodenum | jejunum | ileum |
| **T-PPD** | **2.30 ± 0.15** | **96 ± 7** | **97 ± 9** | **99 ± 5** | **100 ± 3** | **108 ± 11** |
| Rb1 | 1.17 ± 0.26 | 93 ± 8 | 100 ± 3 | 104 ± 2 | 97 ± 7 | 103 ± 5 |
| Rb2 | 0.47 ± 0.05 | 98 ± 3 | 99 ± 7 | 88 ± 8 | 101 ± 2 | 113 ± 5* |
| Rc | 0.52 ± 0.13 | 99 ± 2 | 89 ± 7 | 95 ± 5 | 106 ± 5 | 114 ± 4* |
| Rd | 0.14 ± 0.03 | 102 ± 3 | 95 ± 4 | 103 ± 2 | 101 ± 2 | 110 ± 8 |
| **T-PPT** | **4.17 ± 0.26** | **98 ± 6** | **100 ± 11** | **105 ± 7** | **103 ± 4** | **100 ± 5** |
| Re | 2.08 ± 0.27 | 99 ± 5 | 100 ± 3 | 104 ± 8 | 100 ± 2 | 97 ± 7 |
| Rf | 0.50 ± 0.09 | 95 ± 7 | 91 ± 6 | 100 ± 5 | 102 ± 5 | 93 ± 4 |
| Rg1 | 1.14 ± 0.29 | 98 ± 4 | 96 ± 9 | 103 ± 5 | 102 ± 3 | 103 ± 3 |
| Rg2 (20*S*) | 0.28 ± 0.08 | 96 ± 5 | 118 ± 4* | 117 ± 5* | 123 ± 8* | 114 ± 3* |
| Rg2 (20*R*) | 0.17 ± 0.06 | 98 ± 3 | 130 ± 16* | 123 ± 8* | 123 ± 4* | 113 ± 3* |
| **T-G** | **6.47 ± 0.33** | **98 ± 6** | **99 ± 10** | **103 ± 6** | **102 ± 4** | **103 ± 8** |

[a]T-PPD, T-PPT, and T-G represent the sum quantities of protopanaxdiol type ginsenosides, protopanaxtriol type ginsenosides, and all ginsenosides, respectively. Data represent the mean ± SD from four independent experiments. Recovery (%) was calculated from percentage of the ginsenoside concentrations in digestates of each digestion phase on food material. Mean values in rows for each digestion phase show statistically significant differences in Tukey's test. *, $p < 0.05$ compared to food. [b]The ginsenoside content in food material was expressed as mg/g of dry weight.

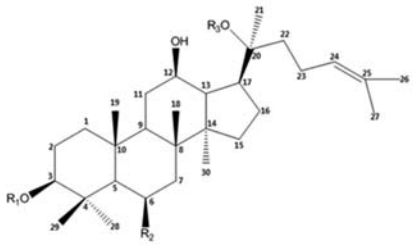

| | Ginsenoside | $R_1$ | $R_2$ | $R_3$ |
|---|---|---|---|---|
| PPD type | **Rb1** | Glc(1→2)Glc- | H | Glc(1→6)Glc- |
| | **Rb2** | Glc(1→2)Glc- | H | Arap(1→6)Glc- |
| | **Rc** | Glc(1→2)Glc- | H | Araf(1→6)Glc- |
| | **Rd** | Glc(1→2)Glc- | H | Glc |
| | **(R,S)-Rg3** | Glc(1→2)Glc- | H | H |
| PPT type | **Re** | H | -OGlc(2→1)Rha | Glc |
| | **Rf** | H | -OGlc(2→1)Glc | H |
| | **Rg1** | H | -OGlc | Glc |
| | **(R,S)-Rg2** | H | -OGlc(2→1)Rha | H |

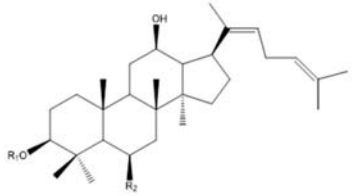

| | Ginsenoside | $R_1$ | $R_2$ |
|---|---|---|---|
| PPD type | **Rk1** | Glc(1→2)Glc- | H |
| PPT type | **F4** | H | -OGlc(2→1)Rha |
| | **Rh4** | H | -OGlc |

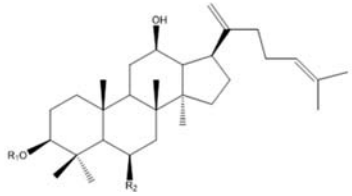

| | Ginsenoside | $R_1$ | $R_2$ |
|---|---|---|---|
| PPD type | **Rg5** | Glc(1→2)Glc- | H |
| PPT type | **Rg6** | H | -OGlc(2→1)Rha |
| | **Rk3** | H | -OGlc |

**Figure 1.** Chemical structures of ginsenosides identified in white and red ginsengs. Glc, *β*-D-gluco-pyranosyl; Araf, *α*-L-arabino-furanosyl; Arap, *α*-L-arabino-pyranosyl; Rha, *α*-L-rhamno-pyranosyl.

published data[3,26] (Figures S2 and S3 and Table S1 in the Supporting Information). All calibration curves were plotted on the basis of linear regression analysis of the integrated peak areas in the total ion chromatogram (TIC) versus concentrations of the four different concentrations in a range from 2 to 200 *μ*g/mL. The regression equations and correlation coefficients for the analysis of the 17 marker constituents were obtained. A high linearity ($r^2 > 0.982$) was obtained for each standard curve (data not shown).

**Statistical Analysis.** All data are expressed as the mean ± standard deviation (SD). Statistical analysis was performed by a one-way analysis of variance (ANOVA) followed by Tukey's honestly significant difference (HSD) test using IBM SPSS statistics 21. *P* values < 0.05 were considered statistically significant.

## RESULTS AND DISCUSSION

**Stability of Ginsenosides during Simulated Digestion of WG and RG.** Information about the stability and bioaccessibility of ginsenosides from ginseng during transit through the gut is still limited. To assess the stability of ginsenosides during in vitro digestion of WG and RG, the ginsenosides present in the ingredients during simulated oral, gastric, and small intestinal digestion as well as food materials in

Table 2. Stability in Each Digestate Generated by Simulated Oral, Gastric, and Small Intestinal Digestion of RG[a]

| | recovery in digestion phase (%) | | | | | |
|---|---|---|---|---|---|---|
| ginsenoside | food[b] | mouth | stomach | duodenum | jejunum | ileum |
| **T-PPD** | **8.10 ± 0.45** | **95 ± 5** | **98 ± 6** | **99 ± 3** | **95 ± 4** | **97 ± 4** |
| Rb1 | 3.30 ± 0.27 | 95 ± 1 | 99 ± 3 | 96 ± 2 | 90 ± 2* | 92 ± 1* |
| Rb2 | 1.14 ± 0.10 | 96 ± 4 | 91 ± 6 | 97 ± 3 | 89 ± 3* | 91 ± 2* |
| Rc | 1.08 ± 0.16 | 96 ± 3 | 96 ± 2 | 94 ± 2 | 89 ± 2* | 91 ± 2* |
| Rd | 0.32 ± 0.0 | 97 ± 3 | 94 ± 6 | 96 ± 2 | 94 ± 4 | 97 ± 6 |
| Rg 3(20*S*) | 1.10 ± 0.21 | 93 ± 8 | 105 ± 4 | 109 ± 8 | 98 ± 5 | 99 ± 3 |
| Rg3 (20*R*) | 0.44 ± 0.02 | 92 ± 9 | 100 ± 3 | 100 ± 4 | 101 ± 1 | 103 ± 2 |
| Rk1 | 0.35 ± 0.05 | 96 ± 6 | 105 ± 3 | 114 ± 5* | 141 ± 8** | 162 ± 4** |
| Rg5 | 0.36 ± 0.0 | 95 ± 7 | 108 ± 8 | 107 ± 5 | 106 ± 4 | 107 ± 6 |
| **T-PPT** | **3.72 ± 0.18** | **97 ± 4** | **100 ± 2** | **104 ± 5** | **97 ± 5** | **99 ± 2** |
| Re | 0.67 ± 0.05 | 93 ± 8 | 90 ± 8 | 104 ± 5 | 94 ± 6 | 96 ± 4 |
| Rf | 0.49 ± 0.06 | 105 ± 5 | 104 ± 7 | 96 ± 8 | 102 ± 7 | 103 ± 5 |
| Rg1 | 0.38 ± 0.04 | 97 ± 4 | 93 ± 4 | 92 ± 7 | 97 ± 2 | 98 ± 5 |
| Rg2 (20*S*) | 1.25 ± 0.17 | 96 ± 3 | 104 ± 5 | 107 ± 8 | 98 ± 3 | 100 ± 3 |
| Rg2 (20*R*) | 0.44 ± 0.09 | 95 ± 7 | 105 ± 5 | 106 ± 6 | 92 ± 7 | 98 ± 3 |
| Rg6 | 0.076 ± 0.005 | 98 ± 3 | 101 ± 2 | 100 ± 1 | 103 ± 4 | 106 ± 5 |
| F4 | 0.11 ± 0.02 | 95 ± 6 | 106 ± 4 | 102 ± 2 | 104 ± 5 | 109 ± 8 |
| Rk3 | 0.11 ± 0.01 | 97 ± 2 | 98 ± 2 | 98 ± 1 | 100 ± 2 | 98 ± 2 |
| Rh4 | 0.19 ± 0.03 | 95 ± 5 | 102 ± 3 | 105 ± 5 | 97 ± 3 | 98 ± 4 |
| **T-G** | **11.82 ± 0.46** | **95 ± 5** | **99 ± 4** | **101 ± 4** | **95 ± 5** | **98 ± 3** |

[a]Data represent the mean ± SD from four independent experiments. Mean values in rows for each digestion phase show statistically significant differences in Tukey's test. *, $p < 0.05$ compared to food; **, $p < 0.01$ compared to food. [b]The ginsenoside content in food material was expressed as mg/g of dry weight.

the WG and RG powders were identified and quantitated by UPLC-MS analysis. As shown in Figure S2 (Supporting Information), nine ginsenosides were detected in WG powder. The total ginsenoside content of WG was 6.47 ± 0.33 mg/g dry weight (Table 1). Ginsenoside Re (2.08 ± 0.27 mg/g) was most abundant, followed by Rb1, Rg1, Rb2, Rc, and Rf, and there were traces of Rg2 and Rd. The PPD/PPT ratio was 0.55. These results were similar to the total ginsenoside content (7.4 mg/g) and PPD/PPT ratio (0.46) of WG reported by Choi et al.[27] There were no differences in the composition of ginsenosides when compared to the results of Kim et al.[28] and Sun et al.,[8] but the total quantities of ginsenosides were somewhat different. The PPD/PPT ratio also differed as it ranged from 0.5 to 1.5. This is thought to be influenced by the cultivated areas, growth years, and harvest time of ginseng. Meanwhile, 17 ginsenosides were detected in RG powder (Figure S2 and Figure 1). The total ginsenoside content of RG was 11.82 ± 0.46 mg/g, 1.8-fold higher than that of WG (Table 2). Unlike WG, the main ginsenoside of RG was Rb1 (3.30 ± 0.27 mg/g). The levels of polar PPT type ginsenosides, such as Re and Rg1, decreased, and levels of all of the ginsenosides of the PPD type, such as Rb1, Rb2, Rc, Rd, Rg3 (*S*,*R*), Rk1, and Rg5, and the less polar ginsenosides of the PPT type, such as Rg2 (*S*,*R*), Rg6, F4, Rk3, and Rh4, increased. The mechanisms involved were deduced to be the demalonylation of malonyl ginsenosides in WG[27] and the loss of a glycosyl moiety at C-20−OH of dammarane type ginsenosides through thermal hydrolysis by steam processing.[3] Thus, the PPD/PPT ratio increased to 2.18. The formation of less polar ginsenosides (Rg2 (20*S*), Rg2 (20*R*), Rg3 (20*S*), Rg3 (20*R*), Rg5, Rg6, Rh1, Rh4, F4, Rk1, and Rk3) in steamed ginseng has been reported for Korean ginseng.[7,29] Recently, many studies had been conducted on the quantitative analysis of ginsenosides in RG. The ginsenoside contents varied by preparation method, such as the steaming temperature, steaming time, and number of steaming repetitions for RG,[3,27] and by the type of ginseng and its country of origin.[8] According to papers by Choi et al.[27] and Kim et al.,[28] the PPD/PPT ratio of RG ranged from 1.5 to 3.5. Our results are also within this range. However, the contents and profiles of the ginsenosides varied considerably compared to other studies.[3,4,8,28] These results suggest that the difference may be due to not only the steaming and drying conditions during RG preparation but also the contents and constituents present in WG itself.

Most of the ginsenosides in the WG powders in each digestion phase were stable with a >95% recovery rate (Table 1). In addition, the recoveries of ginsenosides Rb2 and Rc as well as Rg2 (20*S*) and Rg2 (20*R*) in the ileum phase were significantly increased to 113−114%. When the WG was incubated with a digestive fluid that did not contain enzymes, the results differed from those shown in Table 1 (data not shown). The increase of the recovery of ginsenosides Rb2, Rc, and Rg2 in the intestinal phase was thought to be due to the increase of extraction rate by intestinal enzymes during digestion. In contrast, the recovery of ginsenoside from the RG powders in each digestion phase was mostly >90%, except for ginsenoside Rk1 (Table 2). Thus, the recovery of ginsenosides Rb1, Rb2, and Rc was significantly decreased, whereas that of Rk1 was remarkably increased from the duodenum to the ileum. It was reported that PPD type ginsenosides such as Rb1, Rb2, and Rc were mainly converted to Rk1 and Rg5 through Rg3 (Figure 2).[26] In the above result, the change in the recovery rate was thought to be due to the conversion of Rb1, Rb2, and Rc to Rk1 during simulated digestion. Kim et al.[23] reported that stability of the ginsenosides in red ginseng extract was observed when they were placed in a 37 °C water bath for 4 h, and no significant changes in the ginsenoside composition were found. Moreover, the ginsenosides Rb1 and Rg1 added to serum samples in rats were stable as the recovery range was 90.13−105.66%.[16] Serventi et al.[19]

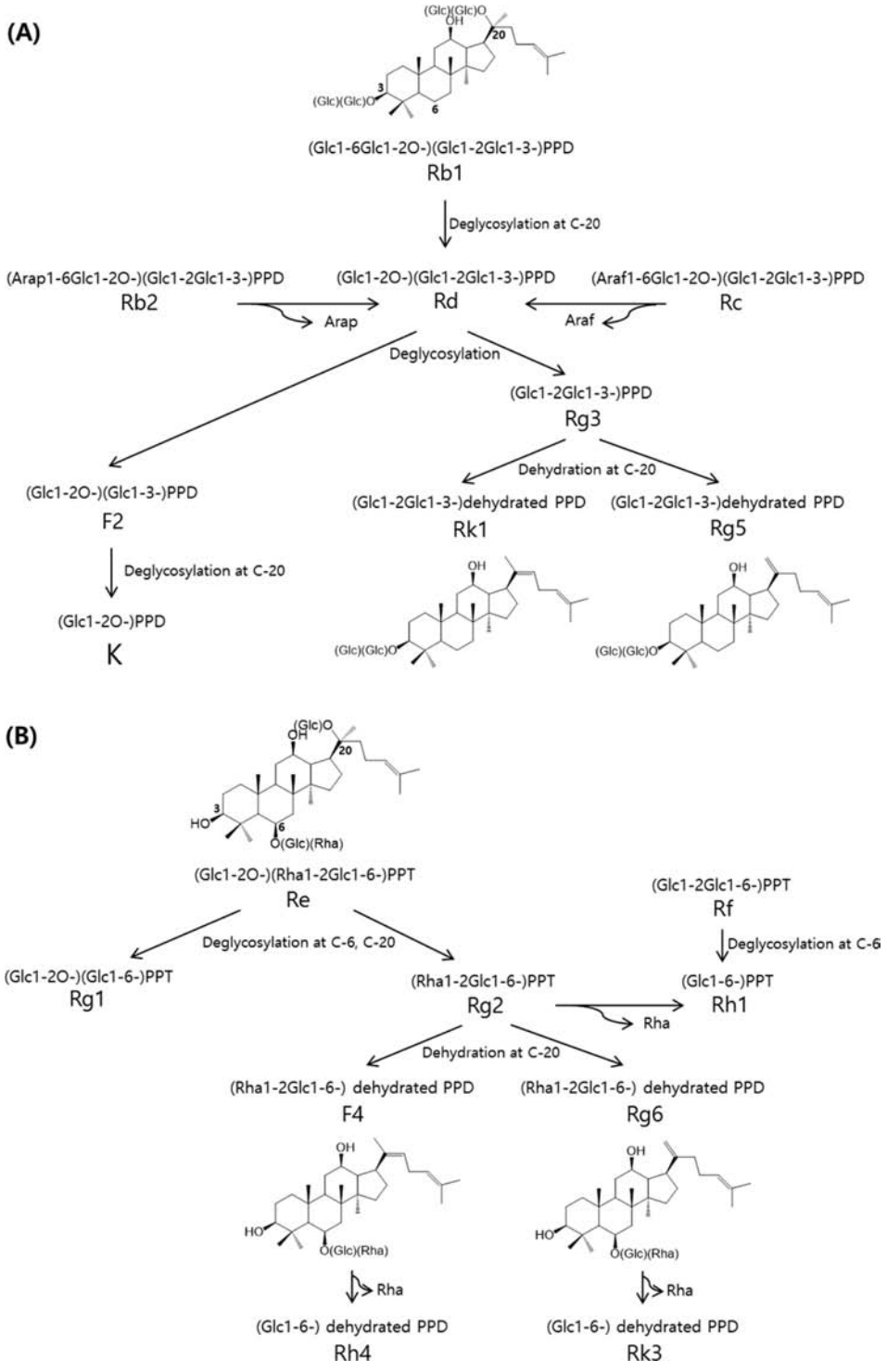


**Figure 2.** Possible enzymatic or chemical bioconversion of protopanaxadiol (A) and protopanaxatriol (B) type ginsenosides.

observed that the recovery of total saponins in soy bread was 83% during in vitro digestion, although recovery of saponins differed considerably by saponin type. In addition, the recovery of carotenoids in meals was >70% during in vitro digestion.[17] Therefore, these results indicate that most of the ginsenosides in RG and WG were relatively stable during in vitro digestion.

**Bioaccessibility of Ginsenosides during Simulated Digestion of WG and RG.** Bioaccessibility refers to the amount of a constituent in a food or supplement that is released from the matrix during digestion to a potentially absorbable form.[30] The aqueous or bioaccessible fractions from undigested material were separated through centrifugation from digestates in each phase generated during simulated digestion. The bioaccessibility of ginsenosides in the aqueous fraction from the food to the small intestinal phase of the simulated digestion of WG (Table 3) and RG (Table 4) generally increased. Among the nine ginsenosides in WG, the bioaccessibility of ginsenoside Re in the food phase (prior to the early stage of enzyme addition in the mouth) had the highest level, at 90% of the food matrix. The ginsenosides Rg1, Rg2 (20*S*), Rf, and Rg2 (20*R*)

Table 3. Bioaccessibility of PPD and PPT Ginsenosides from Each Digestate Generated during Simulated Digestion of WG[a]

| | bioaccessibility in digestion phase (%) | | | | | |
|---|---|---|---|---|---|---|
| ginsenoside | food | mouth | stomach | duodenum | jejunum | ileum |
| **T-PPD** | **60 ± 2.9c** | **63 ± 4.3c** | **73 ± 2.6b** | **71 ± 2.7b** | **78 ± 2.7a** | **80 ± 2.6a** |
| Rb1 | 60 ± 2.7b | 57 ± 5.0b | 74 ± 1.9a | 71 ± 5.7a | 71 ± 2.9a | 74 ± 2.6a |
| Rb2 | 59 ± 2.8c | 67 ± 3.9b | 70 ± 4.0b | 67 ± 2.0b | 85 ± 5.0a | 87 ± 0.1a |
| Rc | 60 ± 1.2c | 70 ± 3.7b | 75 ± 1.9b | 71 ± 0.3b | 83 ± 1.4a | 86 ± 4.4a |
| Rd | 71 ± 4.7b | 78 ± 4.5b | 72 ± 2.4b | 78 ± 2.9b | 89 ± 1.3a | 88 ± 3.1a |
| **T-PPT** | **85 ± 3.9** | **86 ± 3.8** | **85 ± 5.8** | **84 ± 3.2** | **89 ± 3.9** | **91 ± 3.0** |
| Re | 90 ± 6.3 | 90 ± 3.8 | 89 ± 5.0 | 89 ± 2.3 | 91 ± 2.4 | 92 ± 5.0 |
| Rf | 77 ± 2.5b | 83 ± 3.4ab | 82 ± 0.5ab | 89 ± 2.0a | 90 ± 5.2a | 91 ± 3.2a |
| Rg1 | 82 ± 4.3a | 84 ± 5.4a | 83 ± 7.5a | 76 ± 4.6ab | 85 ± 2.7a | 89 ± 1.9a |
| Rg2 (20*S*) | 80 ± 5.3 | 84 ± 4.8 | 86 ± 10.8 | 82 ± 5.8 | 88 ± 6.4 | 89 ± 3.3 |
| Rg2 (20*R*) | 75 ± 0.9ab | 76 ± 1.5ab | 69 ± 5.4ab | 70 ± 1.5b | 79 ± 2.6a | 81 ± 1.4a |
| **T-G** | **76 ± 1.2b** | **78 ± 2.5ab** | **81 ± 4.4ab** | **79 ± 3.0ab** | **85 ± 3.3a** | **87 ± 2.8a** |

[a]Bioaccessibility (%) was calculated from percentage of the ginsenoside concentrations in digestates of each digestion phase on white ginseng. Values represent mean ± SD from four independent experiments. Significant differences at digestion phase of individual ginsenosides as determined by Tukey's test ($p < 0.05$) are indicated by different letters.

Table 4. Bioaccessibility of PPD and PPT Ginsenosides from Each Digestate Generated during Simulated Digestion of RG[a]

| | bioaccessibility in digestion phase (%) | | | | | |
|---|---|---|---|---|---|---|
| ginsenoside | food | mouth | stomach | duodenum | jejunum | ileum |
| **T-PPD** | **54 ± 2.8d** | **62 ± 4.3c** | **56 ± 3.1d** | **56 ± 3.9d** | **75 ± 3.4b** | **85 ± 3.0a** |
| Rb1 | 60 ± 2.7b | 69 ± 5.0a | 60 ± 1.9b | 58 ± 5.7b | 74 ± 2.9a | 82 ± 2.6a |
| Rb2 | 60 ± 2.2b | 70 ± 3.9a | 53 ± 4.0b | 53 ± 4.5b | 72 ± 5.0a | 80 ± 0.1a |
| Rc | 62 ± 4.7b | 71 ± 3.7a | 46 ± 2.8c | 55 ± 3.0b | 71 ± 1.4a | 79 ± 4.4a |
| Rd | 65 ± 1.2b | 73 ± 4.5a | 64 ± 2.4b | 63 ± 2.9b | 76 ± 1.3a | 85 ± 3.1a |
| Rg3 (20*S*) | 37 ± 2.3d | 44 ± 3.8c | 57 ± 5.0b | 58 ± 2.3b | 79 ± 2.4a | 86 ± 5.0a |
| Rg3 (20*R*) | 34 ± 2.5e | 43 ± 3.4d | 65 ± 0.5b | 52 ± 2.0c | 71 ± 5.2b | 95 ± 3.2a |
| Rk1 | 32 ± 3.3d | 39 ± 5.4c | 38 ± 3.2c | 43 ± 4.6c | 91 ± 2.7b | 131 ± 1.9a |
| Rg5 | 36 ± 3.5d | 43 ± 4.8cd | 53 ± 5.0c | 50 ± 5.8c | 79 ± 6.4b | 91 ± 3.3a |
| **T-PPT** | **64 ± 2.4c** | **69 ± 2.9c** | **64 ± 5.0c** | **56 ± 2.8d** | **75 ± 3.4b** | **84 ± 2.9a** |
| Re | 85 ± 2.8a | 85 ± 1.5a | 84 ± 5.4a | 68 ± 1.5b | 73 ± 2.6b | 84 ± 1.4a |
| Rf | 63 ± 3.4b | 75 ± 7.3a | 71 ± 2.2b | 51 ± 4.0c | 70 ± 3.0b | 85 ± 3.6a |
| Rg1 | 77 ± 2.1 | 81 ± 5.2 | 70 ± 10.5 | 77 ± 0.5 | 73 ± 2.4 | 78 ± 2.8 |
| Rg2 (20*S*) | 62 ± 3.2c | 65 ± 1.9c | 63 ± 3.6c | 54 ± 2.6c | 80 ± 1.8b | 88 ± 4.0a |
| Rg2 (20*R*) | 61 ± 1.1b | 66 ± 4.0b | 56 ± 2.7c | 56 ± 3.3c | 76 ± 4.5a | 81 ± 1.1a |
| Rg6 | 36 ± 0.8c | 43 ± 1.2b | 25 ± 6.4d | 27 ± 2.6d | 78 ± 2.4a | 83 ± 2.4a |
| F4 | 30 ± 2.5c | 37 ± 0.8b | 34 ± 4.8bc | 29 ± 4.1c | 68 ± 5.6a | 75 ± 5.5a |
| Rk3 | 39 ± 1.6c | 45 ± 2.0b | 35 ± 5.5c | 35 ± 3.7c | 71 ± 3.7a | 79 ± 3.3a |
| Rh4 | 38 ± 3.8d | 44 ± 2.2c | 38 ± 4.0d | 30 ± 2.5e | 66 ± 4.3b | 77 ± 1.74a |
| **T-G** | **57 ± 2.6d** | **64 ± 3.6c** | **58 ± 4.1d** | **56 ± 3.3d** | **75 ± 3.4b** | **85 ± 2.9a** |

[a]Bioaccessibility (%) was calculated from percentage of the ginsenoside concentrations in digestates of each digestion phase on red ginseng. Values represent mean ± SD from four independent experiments. Significant differences at digestion phase of individual ginsenosides as determined by Tukey's test ($p < 0.05$) are indicated by different letters.

ranged from 75 to 82%, and ginsenoside Rd constituted 71% of the matrix, whereas Rb1, Rc, and Rb2 had the lowest level at about 60%. The release percentages of total PPD (T-PPD) and PPT (T-PPT) were 60 and 85%, respectively. In the early phase, the bioaccessibility of ginseng saponins from the food matrix was higher for the PPT type, including Re, Rf, Rg1, and Rg2 (*S*,*R*) than for the PPD type, including Rb1, Rb2, Rc, and Rd. Moreover, the percentages of most of the ginsenosides transferred to the bioaccessible fraction after termination of the small intestinal phase (ileum = final stage) of simulated digestion increased to >85%, except for Rb1 (74%) and Rg2 (20*R*) (81%). The release percentages for T-PPD and T-PPT were 80 and 90%, respectively. The gap between the T-PPD and T-PPT types in the ileum phase (10%) was lower than that in the food phase (25%) during in vitro digestion. The ginsenosides are classified as belonging to the two major groups according to their structures. The PPD type had sugar moieties attached to the C-3 and/or C-20, and the PPT type has sugar moieties at C-6 and/or C-20 (Figure 1).[3] The polarity of PPT, having two hydrophilic tails (sugar moieties) and an additional hydroxyl group, is greater than that of PPD. Thus, the results implied that PPD ginsenosides were more slowly released during the digestion process than the PPT type.

Meanwhile, the release of ginsenosides in the aqueous fraction during simulated digestion of the RG increased, especially in the jejunum and ileum (Table 4). Among the 17 ginsenosides in RG, ginsenoside Re (85%) showed the highest bioaccessibility in the food phase as with the WG, followed by ginsenoside Rg1 (77%) > Rb1, Rb2, Rc, Rd, Rf, Rg2 (20*S*), and Rg2 (20*R*) (60%) > Rg3 (*S*,*R*), Rk1, Rg5, Rg6, F4, Rk3, and

Rh4 (30−40%), in decreasing order. Namely, the bioaccessibility of ginsenoside components present in WG itself was >60%, whereas the less polar RG ginsenosides exhibited low bioaccessibility at <40%. Ginsenosides Rg6 and F4 were presumed to be generated through deglycosylation of Re to Rg2 and a dehydration reaction at the C-20 (21) or C-20 (22) of Rg2 (20*S*). Subsequently, ginsenosides Rh4 and Rk3 were generated, respectively, through eliminating the terminal glycosyl moiety at the C-6 position of ginsenosides F4 and Rg6, whereas ginsenoside Rg3 was deduced to be generated through elimination of the terminal glycosyl moiety at the C-20−OH of Rb1, Rb2, and Rc to Rd and through removal of the remaining glycosyl moiety at the C-20 position of Rd. Next, ginsenosides Rg5 and Rk1 were generated, respectively, through a dehydration reaction at the C-20 (21) or C-20 (22) of Rg2 (20S), which was consistent with the findings reported by others (Figure 2).[3,7,24,26] The newly generated ginsenosides via deglycosylation and dehydration from Rb1, Rb2, Rc, Rd, Re, and Rg1 by WG steaming were less polar, and these unique, less polar RG ginsenosides were rapidly released after the jejunum phase. Bioaccessibility of ginsenoside Rk1 was increased only up to 131%. The results suggest that the particular ginsenosides in RG were greatly influenced by intestinal enzymes and bile extract compared with the polar ginsenosides in WG. Kim et al.[23] observed that the compositions of the red ginseng extracts remarkably changed after in vitro digestion; the proportions of the polar ginsenosides, such as ginsenosides Rg1, Re, Rb1, Rc, Rb2, Rb3, and Rd, decreased in contents, whereas the less polar ginsenosides, such as ginsenosides Rh1, Rg2, Rg3, Rk1, and Rg5, increased. These results suggested that ginsenosides are influenced only by gastric fluid and not by intestinal fluid. The bioaccessibility of total ginsenosides (T-G) in the food phase of RG (57%) was lower than that of WG (76%), but the bioaccessibility of RG (85%) was similar to that of WG (87%) in the final ileum phase of simulated digestion (Tables 3 and 4). These results suggest that the total RG ginsenosides were slowly liberated due to the generation of less polar ginsenosides and an increase in PPD ginsenosides. Therefore, these findings suggest that ginsenoside structure and the composition of WG and RG were influenced by the bioaccessibility of ginsenosides at each phase during in vitro digestion.

**Permeability of Ginsenosides by Caco-2 Cells.** A close correlation between the in vitro permeability across Caco-2 cell monolayers and the in vivo human absorption after oral administration has been obtained for several compounds.[31−33] Thus, the bidirectional permeability of ginsenosides in chyme generated by simulated digestion of WG and RG using Caco-2 cell monolayers was assessed. As shown in Table 5, the permeability coefficients of Rg1, Re, Rc, Rf, and Rb1 in the a to b direction for WG were determined as $5.17 \times 10^{-7}$, $3.60 \times 10^{-7}$, $3.02 \times 10^{-7}$, $3.00 \times 10^{-7}$, and $1.33 \times 10^{-7}$ cm/s in 2 h in descending order, respectively, whereas ginsenosides Rb2, Rd, and Rg2 (*S*,*R*) were not detected. It is well-known that compounds with $P_{app}$ values of $<1 \times 10^{-6}$ cm/s, between $1 \times 10^{-6}$ and $10 \times 10^{-6}$ cm/s, and $>10 \times 10^{-6}$ cm/s are considered to have low (<20%), moderate (20−70%), and high (70−100%) absorption respectively.[31,34] According to these criteria, the ginsenosides with a $P_{app}$ value of $<1 \times 10^{-6}$ cm/s in Caco-2 cell monolayers are likely to be poorly absorbed from the intestine in humans. The $P_{app}$ values in the b to a direction were >10-fold greater than those in the a to b direction, and the $P_{app}$ values for ginsenosides Rb2 and Rg2 (20*S*) in the b to a direction were only $10.6 \times 10^{-7}$ and $33.0 \times 10^{-7}$ cm/s, respectively. Subsequently, the permeability coefficients of Rg1, Re, Rf, Rc, and Rb1 in the a to b direction for RG were determined as $5.92 \times 10^{-7}$, $4.68 \times 10^{-7}$, $2.47 \times 10^{-7}$, $1.61 \times 10^{-7}$, and $0.91 \times 10^{-7}$ cm/s in descending order, respectively, indicating that most of the RG ginsenosides have a poor permeability and absorption rate in vivo. The other RG ginsenosides were not detected. The permeability in the b to a direction was more than 10-fold greater than that in the a to b direction, except for Rc. Overall, even though the bioavailability of the same ginsenosides in WG and RG was slightly different, it suggest that the permeability of several ginsenosides were influenced by some different components in food matrix of WG and RG powder. Both the PPD and PPT groups of ginsenosides exhibited low bioavailability at less than 5%, and but PPT ginsenosides, including Re, Rf, Rg1 and Rg2, had better bioavailability than PPD ginsenosides, including Rb1, Rb2 and Rc, perhaps because PPD ginsenosides degrade faster than PPT ginsenosides.[16] These results were similar to those found in previous studies.[9] Study with cultures of Caco-2 human intestinal cells on soy saponins showed that trans-epithelial transport of soy saponin Bb during a 4 h incubation were quite limited (<3% from medium with $P_{app}$ $<4 \times 10^{-6}$ cm/s).[19,36] Thus, the permeability of ginsenoside Rg1 (>3%) only was higher than that of soy saponin Bb, another ginsenosides were similar to soy saponin Bb. The permeability of ginsenosides such as Rb2, Rd, Rg3, Rk1, Rg5, Rg6, F4, Rk3, and Rh4 in WG and RG by Caco-2 cells was not detected because of the relatively small amounts of these components in WG and RG. Compound K, the main metabolite of the PPD ginsenosides, was detected mostly in the plasma and urine of

**Table 5. Permeability of Ginsenosides in Chyme Generated by Simulated Digestion of WG and RG by Caco-2 Cells[a]**

| | $P_{app}$ ($\times 10^{-7}$ cm/s) | | |
|---|---|---|---|
| ginsenoside | apical to basolateral | basolateral to apical | permeability (%) |
| **White Ginseng** | | | |
| Rb1 | 1.33 ± 0.27c | 32.6 ± 2.56c | 0.80 ± 0.16c |
| Rb2 | ND | 10.6 ± 3.21d | ND |
| Rc | 3.02 ± 0.34b | 32.5 ± 4.74c | 1.83 ± 0.21b |
| Re | 3.60 ± 0.85b | 48.1 ± 5.23b | 2.18 ± 0.52ab |
| Rf | 3.00 ± 0.72b | 47.2 ± 2.08b | 1.82 ± 0.44b |
| Rg1 | 5.17 ± 1.20a | 63.3 ± 5.83a | 3.12 ± 0.72a |
| Rg2 (20*S*) | ND | 33.0 ± 3.72c | ND |
| **Red Ginseng** | | | |
| Rb1 | 0.91 ± 0.25c | 13.8 ± 2.37d | 0.55 ± 0.15c |
| Rb2 | ND | 9.10 ± 0.65d | ND |
| Rc | 1.61 ± 0.19bc | 10.2 ± 1.24 | 0.98 ± 0.30c |
| Re | 4.68 ± 0.78a | 60.9 ± 4.88a | 2.83 ± 0.47ab |
| Rf | 2.47 ± 0.17b | 40.1 ± 5.41b | 1.49 ± 0.10b |
| Rg1 | 5.92 ± 1.33a | 77.9 ± 2.07a | 3.58 ± 0.80a |
| Rg2 (20*S*) | ND | 29.4 ± 2.87c | ND |
| Rg2 (20*R*) | ND | 33.2 ± 4.56c | ND |

[a]Permeability coefficient ($P_{app}$) was calculated as $P_{app} = \partial Q/AC_0\partial t$, where $\partial Q\partial t$ is the permeability rate, $A$ is the surface area of the membrane filter, and $C_0$ is the initial concentration in the donor compartment (apical compartment in a to b transport study and basolateral compartment in b to a transport study). Permeability (%) was calculated from volume contrast percentage of the ginsenoside concentrations appeared in the receiver side on donor compartment. Data represent the means ± SD from four independent experiments. Different letters in columns for each compound show statistically significant differences in Tukey's test ($p < 0.05$).

humans after oral administration.[10,11] Compound K was not found in our results, and this was presumed to be because the in vitro digestion system excluded enterobacterium. Recent studies have reported that the polar ginsenosides exhibited poor bioavailability following oral administration in vivo, and less polar ginsenosides generated via internal metabolism exhibited potent anticancer, antiobesity, and anti-inflammatory bioactivities.[23,35] However, little is known about the comparative study of the bioavailability of various ginsenosides present in ginseng. This study is the first report on the wide bioavailability of ginsenoside components in WG and RG powders using a Caco-2 cell culture model coupled with in vitro digestion. However, as the main metabolism of ginsenosides in ginseng is reported to take place in the small and large intestines, future studies should evaluate the bioavailability of ginsenosides by intestinal microflora in the small and large intestine model and develop a method to improve the poor bioavailability of ginsenosides.

In conclusion, the results obtained in the present study demonstrate that all of the ginsenosides in WG and RG were highly stable during simulated digestion. In addition, the bioaccessibility of ginsenosides from WG and RG during oral, gastric, and small intestinal digestion gradually increased. Even though the bioaccessibility was different according to the ginsenoside compositions of WG and RG, it was comparatively good at 85% in the final ileum phase. However, all of the ginsenosides in WG and RG had poor absorption through the Caco-2 cell monolayers. Hence, a further study on the bioavailability of ginsenosides in an in vivo model system and a method for enhancing the absorption of ginsenosides are required.

## ■ ASSOCIATED CONTENT

### Ⓢ Supporting Information

Figures S1−S3 and Table S1. This material is available free of charge via the Internet at http://pubs.acs.org.

## ■ AUTHOR INFORMATION


### Corresponding Authors

*(C.-H.P.) Phone: 82-33-650-3652. Fax: 82-33-650-3679. E-mail: cheolpan@gmail.com.

*(B.-H.U.) Phone: 82-33-650-3601. Fax: 82-33-650-3629. E-mail: albertum@kist.re.kr.



### Funding

This work was supported by an intramural grant (2Z04222) from the Korean Institute of Science and Technology, Gangneung Institute.


### Notes

The authors declare no competing financial interest.

## ■ ABBREVIATIONS USED

WG, white ginseng; RG, red ginseng; PPD, protopanaxadiol; PPT, protopanaxatriol; T-PPD, total quantities of protopanaxadiol type ginsenosides; T-PPT, total quantities of protopanaxatriol type ginsenosides; T-G, total ginsenosides; a to b, apical-to-basolateral transport; b to a, basolateral-to-apical transport; $P_{app}$, permeability coefficient; UPLC-MS, ultraperformance liquid chromatography−mass spectrometry

## ■ REFERENCES


(1) Park, H. J.; Kim, D. H.; Park, S. J.; Kim, J. M.; Ryu, J. H. Ginseng in traditional herbal prescriptions. *J. Ginseng Res.* **2012**, *36*, 225−241.

(2) Kim, W. Y.; Kim, J. M.; Han, S. B.; Lee, S. K.; Kim, N. D.; Park, M. K. Steaming of ginseng at high temperature enhances biological activity. *J. Nat. Prod.* **2000**, *63*, 1702−1704.

(3) Xie, Y. Y.; Luo, D.; Cheng, Y. J.; Ma, J. F.; Wang, Y. M.; Liang, Q. L. Steaming-induced chemical transformations and holistic quality assessment of red ginseng derived from *Panax ginseng* by means of HPLC-ESI-MS/MS($n$)-based multicomponent quantification fingerprint. *J. Agric. Food Chem.* **2012**, *60*, 8213−8224.

(4) Chu, C.; Xu, S.; Li, X.; Yan, J.; Liu, L. Profiling the ginsenosides of three ginseng products by lc-q-tof/ms. *J. Food Sci.* **2013**, *78*, C653−C659.

(5) Tang, W.; Zhang, Y.; Gao, J.; Ding, X.; Gao, S. The anti-fatigue effect of 20($R$)-ginsenoside Rg3 in mice by intranasally administration. *Biol. Pharm. Bull.* **2008**, *31*, 2024−2027.

(6) Wee, J. J.; Mee Park, K.; Chung, A. S. Biological activities of ginseng and its application to human health. In *Herbal Medicine: Biomolecular and Clinical Aspects*; Benzie, I. F. F., Wachtel-Galor, S., Eds.; CRC Press: Boca Raton, FL, USA, 2011; pp157−174.

(7) Chan, E. C.; Yap, S. L.; Lau, A. J.; Leow, P. C.; Toh, D. F.; Koh, H. L. Ultra-performance liquid chromatography/time-of-flight mass spectrometry based metabolomics of raw and steamed *Panax notoginseng*. *Rapid Commun. Mass Spectrom.* **2007**, *21*, 519−528.

(8) Sun, S.; Qi, L. W.; Du, G. J.; Mehendale, S. R.; Wang, C. Z.; Yuan, C. S. Red notoginseng: higher ginsenoside content and stronger anticancer potential than Asian and American ginseng. *Food Chem.* **2011**, *125*, 1299−1305.

(9) Qi, L. W.; Wang, C. Z.; Du, G. J.; Zhang, Z. Y.; Calway, T.; Yuan, C. S. Metabolism of ginseng and its interactions with drugs. *Curr. Drug Metab.* **2011**, *12*, 818−822.

(10) Lee, J.; Lee, E.; Kim, D.; Lee, J.; Yoo, J.; Koh, B. Studies on absorption, distribution and metabolism of ginseng in humans after oral administration. *J. Ethnopharmacol.* **2009**, *122*, 143−148.

(11) Tawab, M. A.; Bahr, U.; Karas, M.; Wurglics, M.; Schubert-Zsilavecz, M. Degradation of ginsenosides in humans after oral administration. *Drug Metab. Dispos.* **2003**, *31*, 1065−1071.

(12) Wang, C. Z.; Kim, K. E.; Du, G. J.; Qi, L. W.; Wen, X. D.; Li, P. Ultra-performance liquid chromatography and time-of-flight mass spectrometry analysis of ginsenoside metabolites in human plasma. *Am. J. Chin. Med.* **2011**, *39*, 1161−1171.

(13) Gu, Y.; Wang, G. J.; Sun, J. G.; Jia, Y. W.; Wang, W.; Xu, M. J. Pharmacokinetic characterization of ginsenoside Rh2, an anticancer nutrient from ginseng, in rats and dogs. *Food Chem. Toxicol.* **2009**, *47*, 2257−2268.

(14) Han, M.; Fu, S.; Fang, X. L. Comparison between the characteristics of absorption and pharmacokinetic behavior of ginsenoside Rg1 and ginsenoside Rb, of *Panax notoginseng* saponins. *Yao Xue Xue Bao* **2007**, *42*, 849−853.

(15) Han, M.; Han, L. M.; Wang, Q. S.; Bai, Z. H.; Fang, X. L. Mechanism of oral absorption of *Panax notoginseng* saponins. *Yao Xue Xue Bao* **2006**, *41*, 498−505.

(16) Xu, Q. F.; Fang, X. L.; Chen, D. F. Pharmacokinetics and bioavailability of ginsenoside Rb1 and Rg1 from *Panax notoginseng* in rats. *J. Ethnopharmacol.* **2003**, *84*, 187−192.

(17) Garrett, D. A.; Failla, M. L.; Sarama, R. J. Development of an in vitro digestion method to assess carotenoid bioavailability from meals. *J. Agric. Food Chem.* **1999**, *47*, 4301−4309.

(18) Liu, C. S.; Glahn, R. P.; Liu, R. H. Assessment of carotenoid bioavailability of whole foods using a Caco-2 cell culture model coupled with an in vitro digestion. *J. Agric. Food Chem.* **2004**, *52*, 4330−4337.

(19) Serventi, L.; Chitchumroonchokchai, C.; Riedl, K. M.; Kerem, Z.; Berhow, M. A.; Vodovotz, Y.; Schwartz, S. J.; Failla, M. L. Saponins from soy and chickpea: stability during bread making and in vitro bioaccessibility. *J. Agric. Food Chem.* **2013**, *61*, 6703−6710.

(20) Sabboh-Jourdan, H.; Valla, F.; Epriliati, I.; Gidley, M. J. Organic acid bioavailability from banana and sweet potato using an in vitro digestion and Caco-2 cell model. *Eur. J. Nutr.* **2011**, *50*, 31−40.

(21) Gautam, S.; Platel, K.; Srinivasan, K. Higher bioaccessibility of iron and zinc from food grains in the presence of garlic and onion. *J. Agric. Food Chem.* **2010**, *58*, 8426−8429.
(22) Seiquer, I.; Delgado-Andrade, C.; Haro, A.; Navarro, M. P. Assessing the effects of severe heat treatment of milk on calcium bioavailability: in vitro and in vivo studies. *J. Dairy Sci.* **2010**, *93*, 5635−5643.
(23) Kim, S. N.; Lee, J. H.; Shin, H.; Son, S. H.; Kim, Y. S. Effects of in vitro-digested ginsenosides on lipid accumulation in 3T3-L1 adipocytes. *Planta Med.* **2009**, *75*, 596−601.
(24) Kong, H.; Wang, M.; Venema, K.; Maathuis, A.; van der Heijden, R.; van der Greef, J. Bioconversion of red ginseng saponins in the gastro-intestinal tract in vitro model studied by high-performance liquid chromatography-high resolution Fourier transform ion cyclotron resonance mass spectrometry. *J. Chromatogr., A* **2009**, *1216*, 2195−2203.
(25) Hubatsch, I.; Ragnarsson, E. G.; Artursson, P. Determination of drug permeability and prediction of drug absorption in Caco-2 monolayers. *Nat. Protoc.* **2007**, *2*, 2111−2119.
(26) Sun, B. S.; Xu, M. Y.; Li, Z.; Wang, Y. B.; Sung, C. K. UPLC-Q-TOF-MS/MS analysis for steaming times-dependent profiling of steamed *Panax quinquefolius* and its ginsenosides transformations induced by repetitious steaming. *J. Ginseng Res.* **2012**, *36*, 277−290.
(27) Choi, J. E.; Nam, K. Y.; Li, X.; Kim, B. Y.; Cho, H. S.; Hwang, K. B. Changes of chemical compositions and ginsenoside contents of different root parts of ginsengs with processing method. *Korean J. Med. Crop Sci.* **2010**, *18*, 118−125.
(28) Kim, S. N.; Ha, Y. W.; Shin, H.; Son, S. H.; Wu, S. J.; Kim, Y. S. Simultaneous quantification of 14 ginsenosides in *Panax ginseng* C.A. Meyer (Korean red ginseng) by HPLC-ELSD and its application to quality control. *J. Pharm. Biomed. Anal.* **2007**, *45*, 164−170.
(29) Kwon, S. W.; Han, S. B.; Park, I. H.; Kim, J. M.; Park, M. K.; Park, J. H. Liquid chromatographic determination of less polar ginsenosides in processed ginseng. *J. Chromatogr., A* **2001**, *921*, 335−339.
(30) Fernandez-Garcia, E.; Carvajal-Lerida, I.; Perez-Galvez, A. In vitro bioaccessibility assessment as a prediction tool of nutritional efficiency. *Nutr. Res. (N.Y.)* **2009**, *29*, 751−760.
(31) Yee, S. In vitro permeability across Caco-2 cells (colonic) can predict in vivo (small intestinal) absorption in man − fact or myth. *Pharm. Res.* **1997**, *14*, 763−766.
(32) Artursson, P.; Karlsson, J. Correlation between oral drug absorption in humans and apparent drug permeability coefficients in human intestinal epithelial (Caco-2) cells. *Biochem. Biophys. Res. Commun.* **1991**, *175*, 880−885.
(33) Gres, M. C.; Julian, B.; Bourrie, M.; Meunier, V.; Roques, C.; Berger, M.; Boulenc, X.; Berger, Y.; Fabre, G. Correlation between oral drug absorption in humans, and apparent drug permeability in TC-7 cells, a human epithelial intestinal cell line: comparison with the parental Caco-2 cell line. *Pharm. Res.* **1998**, *15*, 726−733.
(34) Zhang, B.; Zhu, X. M.; Hu, J. N.; Ye, H.; Luo, T.; Liu, X. R. Absorption mechanism of ginsenoside compound K and its butyl and octyl ester prodrugs in Caco-2 cells. *J. Agric. Food Chem.* **2012**, *60*, 10278−10284.
(35) Wang, C. Z.; Aung, H. H.; Zhang, B.; Sun, S.; Li, X. L.; He, H. Chemopreventive effects of heat-processed *Panax quinquefolius* root on human breast cancer cells. *Anticancer Res.* **2008**, *28*, 2545−2551.
(36) Hu, J.; Reddy, M. B.; Hendrich, S.; Murphy, P. A. Soysaponin I and sapongenol B have limited absorption by Caco-2 intestinal cells and limited bioavailability in women. *J. Nutr.* **2004**, *134*, 1867−1873.

nutrients,[9] and mycorrhization[2,34] on polyphenolics profile of basil have also been studied. These studies have been carried out using conventional pot (CP system) grown plants in the greenhouse[2,4,18,19,32,34] or in hydroponic systems.[6,7] Several studies also report collection of plants from wild or market bought samples for polyphenolics study.[2,3] For the screening of large and diverse collection of cultivars of *Ocimum basilicum*, use of a conventional pot system as a screening platform is a large, cumbersome, and voluminous technique requiring high cost and physical operations. Therefore, a system which can be managed in less space and observed throughout with visibility of the root system, as is not the case in a conventional pot system, is needed for screening studies of *Ocimum basilicum*.

For the selection of basil cultivars to be used for medicinal and food applications, determination of antioxidant potential also plays an important role. Conventionally, determination of antioxidant potential utilizes spectrophotometric assays based on 2,2-diphenyl-1-picrylhydrazyl radical ($DPPH^{\bullet}$) and 2,2′-azinobis(3-ethylbenzothioazoline-6-sulfonic acid) radical cation ($ABTS^{\bullet+}$) chromogens.[35] To increase the efficiency of detection these assays have been coupled with a HPLC postcolumn separation where the antioxidant potential of individual constituents can be assessed.[35−37] Postcolumn detection using the conventional chromogens has the disadvantage of long processing times, which results in poor resolution of the resulting chromatogram.[36] Chemiluminescence signals produced by the use of an acidic potassium permanganate assay overcome this issue due to the fast nature of the light producing reaction involved, and this technology has been used for polyphenolics analysis in many studies.[35−42]

Assays based on chemiluminescence offer selectivity to antioxidants, high sensitivity, ease of chemical preparation, long shelf life of the reagent, fast analysis time, and simple instrumentation. A positive correlation between the acidic potassium permanganate and the traditional DPPH assay has been also observed, making this technology an ideal replacement for the cumbersome online DPPH assay.[35] Further to this a direct correlation between acidic potassium permanganate chemiluminescnce signal and bioactive potential in muscle cell culture has been determined.[39] The distinct advantages of chemiluminescence based assays enable them to be used as a test for estimation of total antioxidant potential and for the assessment of individual chromatographically separated components.

This study developed a new "in vitro" true to type (as offspring plants raised are phenotypically and metabolically similar to the parent plant) system for plant growth in a controlled environment that allowed morphotyping, screening, and selection of the high yielding cultivars of *Ocimum basilicum* for three marker compounds rosmarinic, chicoric, and caffeic acids (referred to as polyphenolics in this study). Acidic potassium permanganate chemiluminescence detection was used to determine the antioxidant activity for whole extracts and key compounds of interest. We believe that the system has distinct advantages of uniformity, high reproducibility, and efficiency over the CP system approaches currently used in plant science for screening and selection studies.

## MATERIALS AND METHODS

**Plant Material.** Seeds of 15 different *Ocimum basilicum* cultivars from five different countries (India, Germany, Spain, United States of America, and Australia) were used in this study for representation of morphological variability and chemical diversity. Seeds were purchased from seed suppliers and research institutes. The seeds of each cultivar were tested for viability by first washing with 0.1% (v/v) Tween 20 for 3 min, then with tap water to remove excess detergent, followed by surface sterilization with 0.01% $HgCl_2$ two times for 2 min followed by washing with sterile distilled water three times. The surface sterilized seeds were placed on Murashige and Skoog (MS) medium within 90 mm diameter Petri plates (25 seeds in each plate). The plates were then incubated in the dark in a plant growth room at 25 ± 2 °C at 60% relative humidity. After 10−20 d the percentage germination for each seed lot was determined and seed lots were characterized on the basis of germination percentage as high (70−100%), medium (31−69%), low (21−30%), and very low or nil (0−20%).

**Chemicals.** Mercuric chloride ($HgCl_2$) and Tween 20 used for seed sterilization and standards of gallic acid, rosmarinic acid, chicoric acid, and caffeic acid were obtained from Sigma-Aldrich (Castle Hill, Australia), and Murashige and Skoog medium was prepared following the method of Murashige and Skoog.[43]

Ethanol and 85% *o*-phosphoric acid (AR grade) were obtained from Merck (Kilsyth, Australia). HPLC grade methanol was obtained from BDH Chemicals (Poole, England). Millipore Millex-HN (syringe filters; 0.45 μm) that were used for filtration of samples were obtained from Merck (Darmstadt, Germany).

For the chemiluminescence assays, potassium permanganate was obtained from Chem Supply (Gillman, Australia), sodium polyphosphate was obtained from Sigma-Aldrich (Castle Hill, Australia), and analytical grade sulfuric acid was from Merck (Kilsyth, Australia).

MS medium was prepared by dissolving $KNO_3$ (0.37 M), $NH_4NO_3$ (0.41 M), $MgSO_4{\cdot}7H_2O$ (0.06 M), $KH_2PO_4$ (0.02 M), $CaCl_2{\cdot}2H_2O$ (0.08 M), $MnSO_4{\cdot}4H_2O$ (0.01 M), $ZnSO_4{\cdot}4H_2O$ (0.04 M), $H_3BO_3$ (0.01 M), KI ($4.81 \times 10^{-4}$ M), $Na_2MoO_4$ ($1.21 \times 10^{-4}$ M), $CuSO_4{\cdot}5H_2O$ ($1.57 \times 10^{-5}$ M), $CoCl_2{\cdot}6H_2O$ ($1.93 \times 10^{-3}$ M), $Na_2EDTA$ (0.01 M), $FeSO_4{\cdot}7H_2O$ (0.01 M) (all from Merck), glycine (0.002 M), nicotinic acid ($4.06 \times 10^{-4}$ M), pyridoxine hydrochloride ($2.95 \times 10^{-4}$ M), thiamine hydrochloride ($2.96 \times 10^{-5}$ M), and myoinositol (0.05 M) in 1 L of distilled water with 2.5% phytagel (all from Sigma-Aldrich, St. Louis, MO), and the pH was maintained at 5.8. The prepared medium was then autoclaved at 121 °C, 15 psi for 15−20 min.

***In Vitro* System.** An *in vitro* [true to type] whole plant system was developed. A 90 mm diameter Petri dish containing MS medium was used as the plant growth substrate. To enable plant growth from the sterile substrate, a hole was made in the lid of the dish. A germinated seedling at the two leaf stage was transferred using forceps and inserted leaf first through the hole in the lid of the Petri plate that had been removed from the base. The lid containing the inserted seedling was then gently placed back on the base which contained the MS medium so that the root was in contact with the medium. After successful transfer any space around the stem was sealed with sterile silicone grease. The Petri dish containing a seedling was placed on a flat bench, and then the plate was covered with a black paper sheet that had a hole in the center from which the stem emerged (Figure 1A). The black sheet was used to minimize light incidence on the developing root system. The same steps were repeated for each of 15 cultivars that were arranged in a completely randomized block design with three replicates for each. The plants were grown under controlled conditions at 25 ± 2 °C under cool white fluorescent lights (Thermoline Scientific, Wetherill Park, NSW, Australia) that had a photosynthetic photon flux density of 100−120 $\mu M\ m^{-2}\ s^{-1}$ for a photoperiod of 16 h light and 8 h dark with 60% humidity.

**Conventional Plant System (CP System).** For comparison with the in vitro whole plant growth system, a conventional pot experimental system was also set up. For this purpose, seeds were surface sterilized using the procedure previously described and then sown in trays in sterilized commercially obtained soil (Loess soil) mixed with absorbent granules (TERRA-GREEN, Greenscape Aeration Company, Atascadero, CA) and kept in the dark. After germination one seedling at the two leaf stage was transferred to a 5 L black plastic pot containing the soil:granule mix. The experiment was set up with all cultivars with three replicates each in a completely randomized block design in a greenhouse at 25−28 °C. The plants

**Figure 1.** *Ocimum basilicum* cultivars grown in the *in vitro* setup developed in a 90 mm Petri dish. Four different morphotypes were observed in the study: (A) large (lettuce) leaf and robust type; (B) purple colored type; (C) tall and slender type; (D) dwarf leaf type. There were four types of flower found in the study: (E) light purple; (F) white flower; (G) dark purple flower; and (H) purple flower.

were watered to pot capacity on a daily basis and fertilized fortnightly with Hoagland solution.[44]

**Plant Harvesting, Morphotyping, and Lyophilization.** Plants were grown to maturity in both systems and examined for variation in aerial morphology. The morphology of each cultivar was classified according to the traits used by Carović-Stanko et al.,[21] who used the morphological traits developed by the International Union for the Protection of New Varieties of Plants for *Ocimum basilicum L* (UPOV 2003).[45] Plant height and internodal distance was measured on harvested plants from the base of the stem to the apical bud using a standard mm scale. After harvest, samples were lyophilized (Labconco lyophilizer, Kansas City, MO, United States of America) at −94.3 °C and 141 kPa for 48 h, and then the lyophilized weight was recorded (data not shown).

**Extraction for Total Phenolics, Individual Polyphenolics, and Antioxidant Potential Analysis.** For total phenolics, individual polyphenolics (rosmarinic chicoric and caffeic acids), total antioxidant, and individual antioxidant potential studies using postcolumn chemiluminescence assay, 50 mg of lyophilized plant material (aerial and root) was homogenized separately in 500 μL of 60% ethanol. To the homogenized mixture was added 14.5 mL of 60% ethanol, and the mixture was sonicated at 25 °C using an ultrasonicator (Branson Ultrasonics, Danbury, CT, United States of America) for 10 min. The sonicated extract was then centrifuged at 10,000 rpm for 5 min, the supernatant was collected in a 25 mL volumetric flask, and the leftover residue was re-extracted in 10 mL of 60% ethanol for 5 min and then centrifuged as previously. The supernatant was then pooled in volumetric flasks that contained the first fraction, and the final volume was made up to 25 mL with 60% ethanol. The extracts were then filtered and stored in the dark at −80 °C in HPLC vials for total phenolics, individual polyphenolics, and chemiluminescence studies.

**Determination of Total Phenolics.** For the determination of total phenolics, a modified Folin−Ciocalteau colorimetric assay[46] was used. Briefly, to 100 μL of the ethanolic extract were added 400 μL of distilled water, 250 μL of Folin−Ciocalteau reagent, and 1.25 mL of 2.1% aqueous sodium carbonate, the mixture was incubated in the dark for 30 min, and the absorbance of the resulting mixture was taken at 735 nm using a microplate reader (SPECTRAmax 340 PC$^{384}$ Microplate Spectrophotometer, Sunnyvale, CA, United States of America) against the same mixture without sample. The total phenolic concentration was quantified from a standard curve prepared for gallic acid within the range of 20−100 mg/L, and the final concentration of total phenolics in a sample is reported as gallic acid equilvalents (GAE mg/g DW).

**Determination of Rosmarinic, Chicoric, and Caffeic Acid Contents by HPLC Analysis.** Chromatographic analysis was carried out using HPLC (Agilent Technologies 1200 series liquid chromatography system), equipped with a quaternary pump, solvent degasser system, autosampler, and diode array detector (Agilent Technologies, Victoria, Australia). Inbuilt software (Hewlett-Packard Chemstation, Agilent Technologies) was used to control the HPLC pump and acquire data from the diode array, UV−vis absorbance, and chemiluminescence detectors. Separations were performed on an Apollo TM C 18 (150 mm × 4.60 mm × 5 μm particle diameter) column.

For separation of individual polyphenolics the mobile phase used was HPLC grade water + 0.1% OPA (mobile phase A) and methanol + 0.1% OPA (mobile phase B). A gradient program was developed for RA quantitation: 0−2 min isocratic 0% B, 2−5 min linear gradient to 40% B, 5−10 min a linear gradient to 50% B, 10−18 min isocratically maintained at 50% B, 18−23 min a decreasing gradient from 50% to 40%, and finally 23−25 min 0% B for column washing. The flow rate of the mobile phase was 1.0 mL/min, and the wavelength used for detection of all three acids was 280 nm with an injection volume of 20 μL. Unknown samples were identified by comparison of the retention times with those of commercial standard. For the sensitivity study of RA, ChA, and CA, 20 standard samples were prepared between $1 \times 10^{-3}$ M and $1 \times 10^{-12}$ M. Quantification of unknown samples was determined by comparison of integrated peak area for each sample with a standard calibration curve of rosmarinic, chicoric, and caffeic acids.

**Determination of Total Antioxidant Potential.** Total antioxidant potential was determined using acidic potassium permanganate chemiluminescence detection coupled to an Agilent 1200 HPLC system. The HPLC system (without a column in place) was coupled with a Minipuls 3 peristaltic pump, bridged PVC tubing, and custom built luminometer (which functions similarly to a conventional flow injection analysis system). Both the in vitro and CP system whole plant samples were diluted 100 times using deionized water before injection of 50 μL of the sample at flow rate of 3 mL min$^{-1}$ and merging with acidic potassium permanganate ($1 \times 10^{-3}$ M), and the peak area was recorded. The acidic potassium permanganate was prepared by dissolution of potassium permanganate in 1% sodium polyphosphate solution adjusted to pH 2 with sulfuric acid.

**Determination of Individual Antioxidant Potential by Chemiluminescence Assay.** In vitro grown plant sample extracts were subjected to postcolumn acidic potassium permanganate assay to assess the contribution of individual polyphenolic compounds. All polyphenolic standards ($1 \times 10^{-3}$ M to $1 \times 10^{-12}$ M) were prepared in 100% analytical grade methanol and appropriately diluted with the same solvent. Postcolumn acidic potassium permanganate assay was performed using the system previously described.[36] Postcolumn acidic potassium permanganate chemiluminescence was generated using an in house built manifold. The reagent, propelled at a flow rate of 3 mL min$^{-1}$ using a Gilson Minipuls 3 peristaltic pump (John Morris Scientific, Balwyn, Australia) with bridged PVC tubing (DKSH), merged with the HPLC eluate at a T-piece, and the light emitted from the reacting mixture was detected with a custom built flow-through

luminometer, which consisted of a coiled flow cell comprising 80 cm × 0.8 mm i.d., transparent PTFE-PFA tubing (DKSH), mounted flush against the window of an Electron Tubes photomultiplier tube (model 9828SB, ETP) set at a constant voltage of 900 V from a stable power supply (PM20D, ETP) via a voltage divider (C611, ETP). The flow cell photomultiplier tube and voltage divider were encased in a padded light-tight housing, and a Hewlett-Packard analogue to digital interface box (Agilent Technologies) was used to convert the signal from the chemiluminescence detector.

**Statistical Analysis.** All data presented in this study is expressed in terms of mean ± SEM. Raw data was analyzed using a commercial statistical package (GraphPad Prism 6). One-way analysis of variance with a Tukey HSD test of significance at $p < 0.05$ was used to determine the effect of cultivar on the quantified morphological traits, total phenolic content, individual polyphenolics content, and antioxidant potential for both systems.

Two-way ANOVA analysis using Sidak's multiple comparison test was used to examine the difference between the two growth systems for total phenolics, the individual polyphenolics, and total antioxidant potential. Correlation between total polyphenolics, total polyphenolic antioxidant potential, and rosmarinic acid antioxidant potential was tested using Pearson test at a significance level of 0.05.

Hierarchical cluster analysis was performed using IBM SPSS Statistics 22 to determine if there was a relationship between the cultivars grown in the in vitro system and their polyphenolic constituents. Data used was standardized using $Z$ score and between group linkages were analyzed using squared Euclidean distance and represented in the form of a dendrogram.

## RESULTS AND DISCUSSION

**Germination Rates of Seeds from Selected Cultivars.** Seeds were collected from different seed suppliers and research institutes from five countries. Of the 29 cultivars collected 14 showed no or very low germination and were not used further in this study. Thus, 15 cultivars were used for the analyses (Table 1).

**Morphotyping of Cultivars.** There are 27 traits mentioned in the UPOV guidelines for *Ocimum basilicum*.[45] They can be classified into four major groups, namely, plant type (habitat; height; density), stem type (color; pubescence; number of flowering shoots), leaf type (blade length; pubescence; color; margin; glossiness), and flower type (corolla color; bract hairiness; color of style). Collected cultivars were assessed against these major qualitative and quantitative traits (Table 2). The collected cultivars were broadly classified into large (lettuce) leaf and robust type, dwarf leaf type, purple colored type, or tall and slender type (Figure 1). All the cultivars grew successfully in both the in vitro and CP systems. Plants were healthy at maturity and progressed to flowering (approximately 90 days for the CP system grown plants). Flowering in the in vitro system was either accelerated, with some cultivars flowering at 60 days (for example B2, B8, and B10), or delayed, with flowering after 90 days. Plant height in the CP system was generally much greater than that in the in vitro system, with some cultivars grown in the CP system 20 times the height of those in the in vitro system (for example, B1 3.37 ± 0.44 cm in vitro and 74.83 ± 3.17 cm in the CP system). Height difference was reflected in the greater number of nodes, branches, and internodal distances found for the CP system grown plants. Traits shown in Table 2 align with other studies of *Ocimum basilicum*[18] where morphological diversity is reported.

**Table 1. Seed Collection and Screening of the *Ocimum basilicum* Cultivars for the Study Based on Their Germination Percentage[a]**

| code | cultivar | country |
|---|---|---|
| B1 | Cim Saumya | India |
| B2 | Turkmaniya Basil | India |
| B3 | Subja | India |
| B4 | Ban Tulsi | India |
| B5 | Basilicum Breitblattriges | Germany |
| B6 | Basil Genovese | India |
| B7 | Basil Genovese | Spain |
| B8 | Basil Minimum | Spain |
| B9 | Organic Cinnamon | Australia |
| B10 | Organic Thai Basil | Australia |
| B11 | Basil Stella | Australia |
| B12 | Holey Green | Australia |
| B13 | Red Rubin | Australia |
| B14 | Basil Genovese America | United States of America |
| B15 | Sweet Basil | United States of America |

[a]29 cultivars of *Ocimum basilicum* were collected for the study. B16−B29 (not shown in this table) showed no or very low germination (0−20%) and were not used in the study. B7, B8, B12, and B13 showed low germination percentage (21−30%); B1, B2, B3, B5, and B6 showed medium germination percentage (31−69%); and B3, B9, B14, and B15 showed high germination percentage (70−100%).

**Standardization of a Method for Extraction of Rosmarinic Acid.** Lyophilization of plant samples was determined, through preliminary analysis, to yield the highest concentration of polyphenolics (data not shown). This result concurs with that found previously[3] in a comparison of basil that was lyophilized with fresh, quick frozen or blanched and frozen samples. The removal of water concentrates polyphenolics in the dried plant samples. For *Ocimum basilicum,* RA is the major metabolite of interest, thus our extraction method was developed for its isolation. We tested a number of extraction protocols using ethanol, homogenization, and two forms of sonication (water bath assisted or ultrasonication) to optimize yields of RA from lyophilized samples. The highest yields of RA, 33.58 ± 0.95 mg/g DW and 31.45 ± 0.68 mg/g DW (Figure 2), were found when 80% v/v ethanol in water or 60% v/v ethanol in water respectively was used as the extraction solvent in combination with water bath sonication. Routinely, 60% v/v ethanol in water was used with the sonication processing of all samples. This protocol was found to be time efficient, required minimal resources, and was easy to perform.

**Comparison of the in Vitro and CP System.** *Total Phenolics.* The Folin−Ciocalteau phenolic assay was used to quantitate the total phenolic content of samples derived from the in vitro and CP growth systems for whole plant and was expressed in terms of gallic acid equivalents per gram (Figure 3). There was a significant difference ($p < 0.05$) found in total phenolic content between the two growth systems. It was also found that cultivars grown in the CP system had higher total phenolic contents; for example, the highest phenolic content was found in three of the cultivars, B12 (156.15 ± 6.19 mg/g GAE DW), B13 (127.41 ± 3.11 mg/g GAE DW), and B14 (126.41 ± 0.72 mg/g GAE DW), while the lowest was found for B10 (73.86 ± 1.29 mg/g GAE DW). The in vitro system showed a similar trend of phenolic content among cultivars, and the highest was found in B12 (69.69 ± 2.83 mg/g GAE DW), B13 (67.79 ± 0.82 mg/g GAE DW), and B7 (65.71 ± 2.14 mg/g GAE DW) while the significantly lowest level was found in B15 (41.78 ± 0.99 mg/g GAE DW). The highest

**Table 2. Morphotyping of the 15 Cultivars of *Ocimum basilicum* Grown in the *in Vitro* System and the CP System[a]**

| | in vitro system | | | | CP system | | | |
|---|---|---|---|---|---|---|---|---|
| code | plant height (cm) | no. of nodes | no. of branches | internodal distance (cm) | plant height (cm) | no. of nodes | no. of branches | internodal distance (cm) |
| B1 | 3.37 ± 0.44 c | 6.33 ± 0.33 cde | 12.71 ± 0.66 abc | 0.33 ± 0.08 c | 74.83 ± 3.17 bcde | 12.00 ± 0.58 c | 24.00 ± 1.15 c | 8.77 ± 0.27 ab |
| B2 | 4.31 ± 0.15 bc | 9.00 ± 0.57 bc | 18.00 ± 1.15 abc | 0.50 ± 0.05 c | 75.00 ± 0.58 bcde | 11.33 ± 0.33 cd | 22.67 ± 0.67 cd | 9.17 ± 0.18 ab |
| B3 | 5.53 ± 0.38 abc | 9.00 ± 0 c | 18.00 ± 0 abc | 0.31 ± 0.05 c | 101.70 ± 6.98 ab | 14.67 ± 1.86 bc | 29.33 ± 3.71 bc | 8.60 ± 1.10 ab |
| B4 | 5.12 ± 0.28 abc | 9.00 ± 0 bc | 18.00 ± 0 abc | 0.43 ± 0.03 c | 69.36 ± 5.83 de | 11.33 ± 0.33 cd | 22.67 ± 0.67 cd | 8.23 ± 0.32 ab |
| B5 | 4.93 ± 0.37 abc | 7.67 ± 0.33 bcde | 15.32 ± 0.66 abc | 0.41 ± 0.05 c | 88.83 ± 2.59 abcd | 19.33 ± 0.88 ab | 38.67 ± 1.76 ab | 6.13 ± 0.19 bcd |
| B6 | 4.51 ± 0.37 abc | 8.33 ± 0.33 bcd | 16.71 ± 0.66 abc | 0.42 ± 0.05 c | 79.60 ± 7.41 abcd | 14.33 ± 0.88 bc | 28.67 ± 1.76 bc | 6.87 ± 0.70 bc |
| B7 | 3.47 ± 0.20 c | 7.67 ± 0.33 bcde | 15.31 ± 0.74 ab | 0.93 ± 0.08 abc | 85.20 ± 7.05 abcd | 16.00 ± 0.58 abc | 32.00 ± 1.15 abc | 6.40 ± 0.56 bc |
| B8 | 8.13 ± 1.41 abc | 7.67 ± 0.37 bcde | 15.33 ± 0.66 a | 0.93 ± 0.08 abc | 51.86 ± 4.68 ef | 21.33 ± 2.96 a | 42.67 ± 5.93 a | 2.20 ± 0.36 d |
| B9 | 6.50 ± 0.45 abc | 12.71 ± 1.20 a | 25.31 ± 2.41 abc | 1.57 ± 0.12 a | 94.30 ± 1.64 abcd | 15.67 ± 1.45 abc | 31.33 ± 2.91 abc | 11.83 ± 0.83 a |
| B10 | 9.60 ± 2.79 ab | 9.33 ± 0.88 b | 18.72 ± 1.76 bc | 0.81 ± 0.50 abc | 26.86 ± 7.95 f | 5.33 ± 0.88 d | 10.67 ± 1.76 d | 3.73 ± 0.89 cd |
| B11 | 9.73 ± 2.15 a | 6.67 ± 0.66 bcde | 13.31 ± 1.33 bc | 1.00 ± 0.11 abc | 72.16 ± 9.31 cde | 14.00 ± 1.15 bc | 27.33 ± 2.91 bc | 6.93 ± 0.23 bc |
| B12 | 5.93 ± 0.44 abc | 5.67 ± 0.33 de | 11.33 ± 0.66 c | 1.41 ± 0.21 ab | 78.70 ± 4.31 abcde | 11.33 ± 0.33 cd | 22.67 ± 0.67 cd | 9.13 ± 1.95 ab |
| B13 | 6.41 ± 0.37 abc | 6.67 ± 0.33 bcde | 13.31 ± 0.66 abc | 0.86 ± 0.12 abc | 92.66 ± 1.09 abcd | 17.33 ± 0.88 abc | 34.67 ± 1.76 abc | 6.07 ± 0.28 bcd |
| B14 | 5.17 ± 0.68 abc | 8.00 ± 0.33 bcde | 15.32 ± 0.66 bc | 0.61 ± 0.11 bc | 105.23 ± 3.47 a | 16.33 ± 0.88 abc | 32.67 ± 1.76 abc | 8.13 ± 0.47 ab |
| B15 | 3.43 ± 0.33 c | 5.00 ± 0.57 e | 10.00 ± 1.15 c | 0.66 ± 0.17 bc | 99.00 ± 3.06 abc | 17.00 ± 0.58 abc | 30.67 ± 3.53 abc | 7.57 ± 1.03 bc |

[a]Data represented as mean ± SEM of each of three replicates ($n = 3$). Different letters indicate significant differences ($p \leq 0.05$) according to Tukey's HSD. Plant habitat: All erect type except for B8, showing intermediate habitat. Plant density: Varies from loose (B1, B2, B4) to medium (B9, B10, B15) to dense (B3, B5, B6, B7, B8, B12, B13, B14). Stem type: Stem color in all cultivars was green except for B9 and B13, and hairs were present in all. Leaf type: Variants in leaf morphology including ovate/dark green/less hairy/serrated/flat (B1, B2, B4), ovate/green/hairy/serrated/undulate (B9), lanceolate/purple/serrated/flat (B13), broad ovate/green/hairy/serrated/undulate (B12), small ovate/dark green/serrated/flat/less hairy (B8), broad ovate/green/serrated/undulate/flat/glossy (B3, B5, B6, B7, B11, B14, B15) and lanceolate/green/serrated/less hairy (B15) were observed. Flower type: Four types of flower colors, light purple (B1, B2, B4, B10), white (B3, B5, B6, B7, B8, B11, B14, B15), dark purple (B9, B13), and purple type (B12), were found in this study.



dx.doi.org/10.1021/jf502709e | J. Agric. Food Chem. 2014, 62, 10064−10075

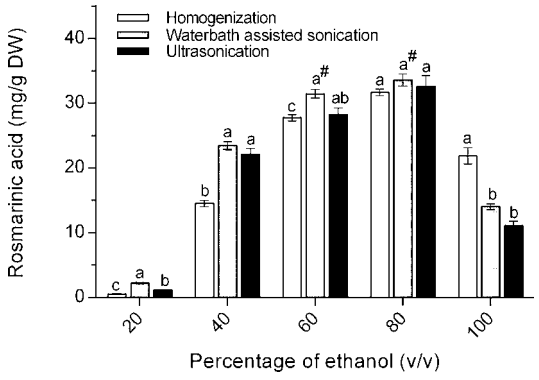


**Figure 2.** Comparison between homogenization, water bath sonication and ultrasonication at five different percentages of ethanol for standardization, and selection of extraction methodology for rosmarinic acid. Data are presented as the mean ± SEM of each of three replicates ($n$ = 3). Different letters indicate significant differences ($p \leq 0.05$) between methods, within percentage of ethanol according to Tukey's HSD. # shows no significant difference ($p \leq 0.05$) between 60% ethanol and 80% ethanol with water bath sonication.

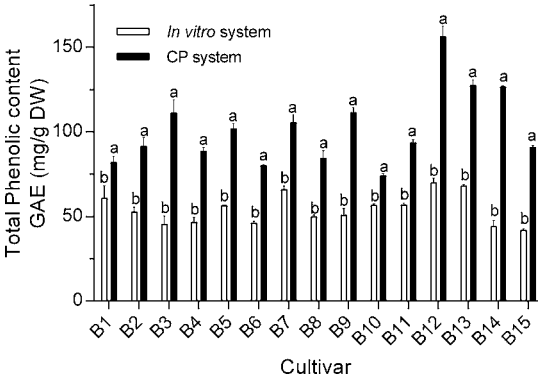


**Figure 3.** Total phenolic content for 15 *Ocimum basilicum* cultivars grown in the *in vitro* system and the CP system. Total phenolic content is reported in gallic acid equivalents, GAE (mg/g DW). Data are presented as mean ± SEM of each of three replicates ($n$ = 3) for the whole plant. Different letters indicate significant differences ($p \leq 0.05$) between the two growth systems, within cultivars according to Sidak's multiple comparison test.

phenolic content was thus found in B12 and B13 for both growth systems. This analysis clearly shows the effect of cultivar on the total phenolic content which correlates well with reports for this species and other studies.[4,47]

Our values for CP system grown samples are of the same magnitude as those reported by Jaysinghe et al.[19] for different fractions used by them. Total phenolic content is dependent on age and state of plant material (dry/fresh), and the contents found in mature plants in our study were much higher than those found for four week old plants (17.58 mg/g GAE DW) in the study reported by Kwee and Niemeyer[4] and Lee and Scagel.[2] Even though determination of total phenolics in plant cultivar samples is a useful comparative measure and may correlate well with antioxidant activity, it provides little indication of the responsible compounds.

*Individual Polyphenolic Content.* HPLC was used to determine the concentrations of RA, ChA, and CA in both the aerial parts and roots of the different cultivars of *Ocimum basilicum* grown in the in vitro and CP systems. A characteristic chromatogram (Figure 4) of extracts from the aerial part and

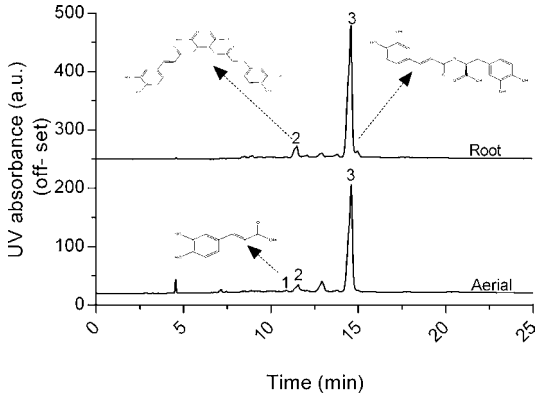


**Figure 4.** Typical HPLC chromatogram for the aerial and root samples of *Ocimum basilicum* using UV absorbance detection (280 nm). Peak 1: caffeic acid (10.6 min). Peak 2: chicoric acid (11.6 min). Peak 3: rosmarinic acid (14.5 min).

roots of B13 showed distinct peaks for RA (14.5 min), ChA (11.6 min), and CA (10.9 min). Analytical figures of merit for three polyphenolics are shown in Table 3. As reported by

**Table 3. Analytical Figures of Merit for Polyphenolics Found in This Study**

| | UV detection | | chemiluminescence | |
|---|---|---|---|---|
| polyphenolic | $R^2$ | LOD ($\mu$M) | $R^2$ | LOD ($\mu$M) |
| rosmarinic acid | 0.9988 | 0.5 | 0.9984 | 0.75 |
| chicoric acid | 0.9900 | 0.2 | 0.9870 | 0.1 |
| caffeic acid | 0.9922 | 10 | 0.9985 | 5 |

earlier studies, RA was found as the major polyphenolic in the ethanolic extract of these cultivars. The highest and lowest RA producing cultivars for whole plants were the same for both growth systems. No significant difference ($p < 0.05$) in RA content of whole plants was found for 11 out of the 15 cultivars grown in both systems. For four of the cultivars there was a significantly higher level of RA in CP system grown plants compared with those grown in vitro. B13, B12, and B7 were found to be high producing cultivars in both systems whereas B3, B5, and B11 emerged as low producing cultivars in both systems. RA content found in whole plants grown in the in vitro system ranged from as low as 24.20 ± 2.31 mg/g DW in B3 to 89.44 ± 1.49 mg/g DW in B13. B13 (89.44 ± 1.49 mg/g DW), B12 (78.00 ± 2.69 mg/g DW), and B7 (52.09 ± 6.38 mg/g DW) were the highest producing cultivars in the in vitro system while B3 (24.20 ± 2.31 mg/g DW), B14 (26.39 ± 0.82 mg/g DW), and B5 (28.46 ± 1.27 mg/g DW) were identified as the lowest producing cultivars (Figure 5A).

As shown in Tables 4 and 5 the aerial parts are found to be the major reserve of RA in both the in vitro system (10/15 cultivars) and the CP system (11/15 cultivars). The RA content found in the aerial parts is higher on a mg/g DW basis than that previously reported[2,4,9,32,34] while our results show similarity to the amounts reported (4–25 mg/g DW) by Kiferle[6] for leaves obtained from hydroponically grown plants.

The utility of the aerial parts of *Ocimum basilicum* and other plants belonging to the Lamiaceae family are well recognized for their RA content,[48] but to our knowledge only three studies, namely, Kiferle et al.,[6] Scagel and Lee,[34] and Toussaint et al.,[49] have studied roots as a source of RA. Interestingly, in our study roots of B13 in both systems showed an equal content of RA.

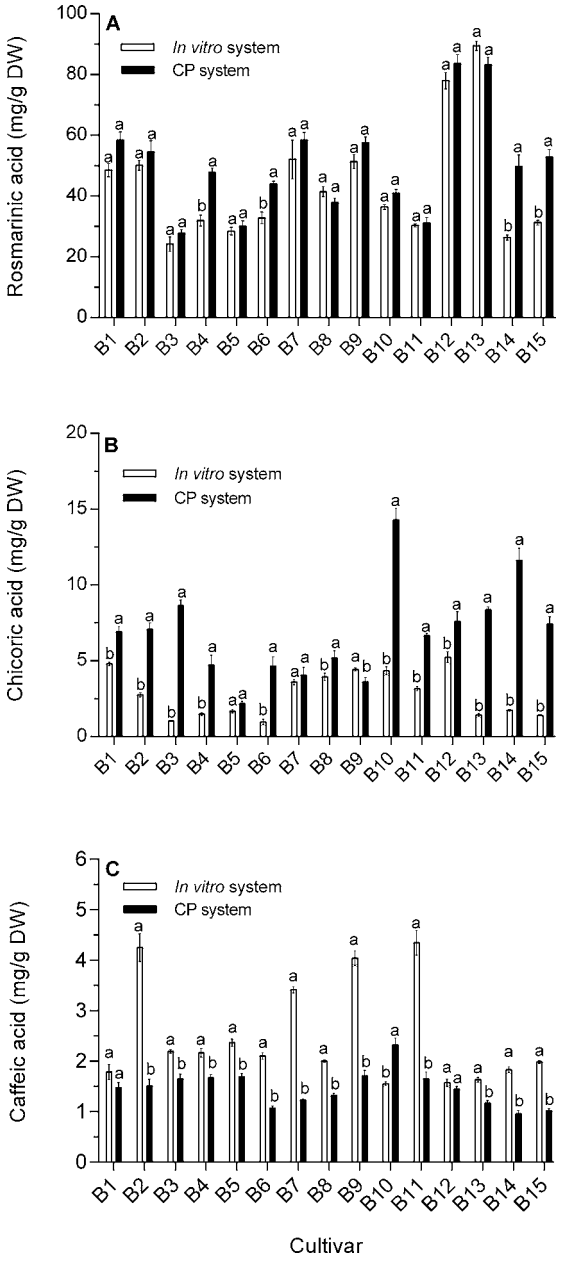


**Figure 5.** Concentrations of polyphenolics detected by HPLC analysis in the 15 *Ocimum basilicum* cultivars for the whole plant grown in the *in vitro* system and CP system. Comparison of (A) rosmarinic acid, (B) chicoric acid, and (C) caffeic acid (mg/g DW) content between the two growth systems. Data are presented as mean ± SEM of each of three replicates ($n$ = 3) for the whole plant. Different letters indicate significant differences ($p \leq 0.05$) between the two growth systems, within cultivars according to Sidak's multiple comparison test.

On the other hand, roots of cultivars such as B6, B3, B7, and B5 grown in the in vitro system produced up to three times more RA than in the CP system. Roots are clearly an alternative and rich source of RA. Kiferle et al.[6] reported high values of RA in roots of three cultivars at full bloom for plants growing in a hydroponic system and showed levels of RA similar to those found for two cultivars used in our study (B14, 27.32 ± 0.94 mg/g DW, and B7, 21.32 ± 0.85 mg/g DW). B13 in the in vitro system had RA content in the aerial parts of 45.33 ± 0.65 and in the roots of 44.11 ± 0.87 mg/g DW, showing that it has great potential as a source of RA and for selection studies. For all cultivars, similarity in RA profile for 11 cultivars between the CP system and the in vitro system shows that the in vitro system is very useful as a screening and selection tool for RA.

While the focus of this research was on quantification of RA in cultivars of *Ocimum basilicum*, the analysis of ChA and CA also offered insights into the contribution of other polyphenolics in the same cultivar and their antioxidant potential. Unlike RA, ChA content (Figure 5B) showed significant ($p < 0.05$) differences between both of the growth systems for all cultivars except for B5, B7, and B9. In the CP system B3 showed 8 times higher levels of ChA than in the in vitro growth system. The amount of ChA for the whole plant found in the in vitro growth system ranged from the highest level (5.24 ± 0.37 mg/g DW ChA) in B12 to the lowest level (0.98 ± 0.16 mg/g DW ChA) in B7. B12 (5.24 ± 0.37 mg/g DW ChA), B1 (4.80 ± 0.11 mg/g DW ChA), and B9 (4.44 ± 0.10 mg/g DW ChA) were found as high ChA producing cultivars in the in vitro system while B6 (0.98 ± 0.16 mg/g DW ChA), B3 (1.04 ± 0.04 mg/g DW ChA), and B15 (1.41 ± 0.04 mg/g DW ChA) were found as low producing cultivars. Similar to RA, aerial parts were found to be major sources of ChA in both systems (Tables 3 and 4). The amount of ChA (7.59 ± 0.37 mg/g DW ChA) found in B12 for the CP system and the amount found, 5.24 ± 0.37 mg/g ChA DW, in the in vitro system showed that this cultivar can be selected as a common high yielding cultivar.

The quantities of ChA reported in the in vitro and CP systems are higher than that reported in five studies to date on *Ocimum basilicum* and ChA.[2−4,9,34] Concentrations of ChA found in our study for B10 for the CP system are as much as 3.9 and 4.5 times higher than that reported in two previous studies.[29,4] Difference in growing conditions, age of harvest, extraction procedure, and analytical conditions can be defined as possible reasons for such a variable observation.[50] Although plants were grown for the same duration as in the studies conducted by Lee and Scagel[2] and Scagel and Lee,[34] the use of fresh samples and differences in cultivar type and extraction procedures may account for the differences of their values (0.114−0.885 mg/g FW and 0.05−0.01 mg/g FW) in comparison to our study. To the best of our knowledge, we have reported for the first time ChA in roots of *Ocimum basilicum.* No ChA was found in roots of B4, while the highest levels were found in B1 (2.45 ± 0.12 mg/g ChA) for plants grown in the in vitro system.

For CA in the in vitro system (Figure 5C) higher concentrations were found than in the CP system except for B10, which produced 1.4 times more CA. Cultivar type showed a significant effect on CA in both of the growth systems. The values found in this study ranged from 4.35 ± 0.25 mg/g CA DW in B11 to 1.55 ± 0.04 mg/g CA DW in B10. In the in vitro system high levels of CA were found in B11 (4.35 ± 0.25 mg/g CA DW), B2 (4.25 ± 0.27 mg/g CA DW), and B9 (4.04 ± 0.15 mg/g CA DW) while the lowest values were reported in B10 (1.55 ± 0.04 mg/g CA DW), B12 (1.58 ± 0.07 mg/g CA DW), and B13 (1.63 ± 0.04 mg/g CA DW). A low level of CA in B12 and B13 cultivars corresponds to the highest levels of RA in the same cultivars. As CA is a precursor to RA, low levels of CA compared to RA may indicate high biosynthetic turnover of CA. Similarly to RA and ChA, the aerial parts showed higher production of CA in 13 of the cultivars. Another possibility that may account for the higher levels of RA and ChA found compared with the levels of CA is that polyphenolic synthesis is altered during maturation and this may also account for the low

Table 4. Average Individual Polyphenolic Content in the 15 Cultivars of *Ocimum basilicum* Grown in the *in Vitro* System[a]

| | rosmarinic acid (mg/g DW) | | chicoric acid (mg/g DW) | | caffeic acid (mg/g DW) | |
|---|---|---|---|---|---|---|
| code | aerial parts | roots | aerial parts | roots | aerial parts | roots |
| B1 | 26.92 ± 0.75 d | 21.64 ± 2.29 de | 2.35 ± 0.10 cd | 2.45 ± 0.12 a | 1.45 ± 0.14 def | 0.34 ± 0.02 f |
| B2 | 35.10 ± 1.57 bc | 15.02 ± 0.20 efg | 1.82 ± 0.07 de | 0.94 ± 0.07 c | 2.36 ± 0.18 bc | 1.89 ± 0.12 b |
| B3 | 6.36 ± 0.17 f | 17.83 ± 2.18 def | 0.71 ± 0.08 g | 0.33 ± 0.05 ef | 1.45 ± 0.02 def | 0.74 ± 0.04 cde |
| B4 | 29.62 ± 1.81 cd | 2.34 ± 0.36 h | 1.49 ± 0.10 ef | nil | 1.74 ± 0.06 de | 0.43 ± 0.03 ef |
| B5 | 10.10 ± 0.09 f | 18.36 ± 1.27 def | 1.29 ± 0.11 efg | 0.39 ± 0.03 de | 1.94 ± 0.06 cd | 0.42 ± 0.02 ef |
| B6 | 7.93 ± 0.92 f | 24.87 ± 1.24 cd | 0.63 ± 0.13 g | 0.35 ± 0.03 de | 1.67 ± 0.09 de | 0.43 ± 0.03 ef |
| B7 | 17.06 ± 1.91 e | 35.04 ± 4.47 b | 3.30 ± 0.19 ab | 0.31 ± 0.02 ef | 2.60 ± 0.07 b | 0.81 ± 0.04 cd |
| B8 | 25.79 ± 0.70 d | 15.70 ± 1.10 efg | 2.98 ± 0.16 abc | 0.96 ± 0.09 c | 1.51 ± 0.04 de | 0.49 ± 0.03 def |
| B9 | 38.87 ± 1.97 b | 12.52 ± 0.78 fg | 2.27 ± 0.01 cd | 2.17 ± 0.11 a | 1.46 ± 0.02 def | 2.58 ± 0.16 a |
| B10 | 26.97 ± 0.49 d | 9.47 ± 0.72 gh | 3.35 ± 0.23 ab | 1.01 ± 0.04 c | 1.00 ± 0.02 fgh | 0.55 ± 0.03 def |
| B11 | 16.64 ± 0.77 e | 13.70 ± 0.61 efg | 2.71 ± 0.16 bc | 0.45 ± 0.04 de | 3.56 ± 0.23 a | 0.79 ± 0.06 cd |
| B12 | 47.79 ± 2.33 a | 30.21 ± 0.43 bc | 3.47 ± 0.27 a | 1.78 ± 0.10 b | 0.59 ± 0.03 h | 0.98 ± 0.05 c |
| B13 | 45.33 ± 0.65 a | 44.11 ± 0.87 a | 0.95 ± 0.08 fg | 0.47 ± 0.06 de | 0.93 ± 0.01 gh | 0.71 ± 0.03 cde |
| B14 | 17.51 ± 0.22 e | 8.89 ± 0.80 gh | 1.05 ± 0.08 fg | 0.69 ± 0.04 cd | 1.47 ± 0.04 def | 0.36 ± 0.01 f |
| B15 | 17.17 ± 0.73 e | 14.10 ± 0.53 efg | 1.09 ± 0.07 fg | 0.33 ± 0.04 ef | 1.35 ± 0.07 efg | 0.64 ± 0.08 def |

[a]Data represented as mean ± SEM of each of three replicates ($n = 3$) at a concentration of mg/g DW. Different letters indicate significant differences ($p \leq 0.05$) according to Tukey's HSD.

Table 5. Average Individual Polyphenolic Content in the 15 Cultivars of *Ocimum basilicum* Grown in the CP System[a]

| | rosmarinic acid (mg/g DW) | | chicoric acid (mg/g DW) | | caffeic acid (mg/g DW) | |
|---|---|---|---|---|---|---|
| code | aerial parts | roots | aerial parts | roots | aerial parts | roots |
| B1 | 39.60 ± 2.61 ab | 18.85 ± 0.25 c | 5.60 ± 0.24 cdef | 1.33 ± 0.08 cd | 1.18 ± 0.11 bc | 0.30 ± 0.01 fg |
| B2 | 32.69 ± 2.46 bcd | 21.83 ± 1.51 bc | 6.20 ± 0.26 cd | 0.88 ± 0.05 def | 1.00 ± 0.09 bcde | 0.50 ± 0.06 abcde |
| B3 | 16.11 ± 0.53 ghi | 11.71 ± 0.81 de | 6.89 ± 0.09 bc | 1.75 ± 0.13 c | 0.95 ± 0.10 bcde | 0.70 ± 0.03 a |
| B4 | 28.26 ± 1.31 def | 19.52 ± 0.70 c | 4.09 ± 0.37 fgh | 0.63 ± 0.01 ef | 1.15 ± 0.03 bcd | 0.52 ± 0.03 abcde |
| B5 | 13.60 ± 1.45 hi | 16.53 ± 0.58 cd | 1.65 ± 0.06 i | 0.53 ± 0.01 f | 1.19 ± 0.09 b | 0.50 ± 0.02 abcde |
| B6 | 32.04 ± 0.95 bcd | 11.92 ± 0.38 de | 3.66 ± 0.38 gh | 0.97 ± 0.04 def | 0.69 ± 0.01 efg | 0.38 ± 0.04 efg |
| B7 | 37.17 ± 1.69 abc | 21.32 ± 0.85 c | 3.47 ± 0.31 gh | 0.59 ± 0.07 ef | 0.80 ± 0.02 cdef | 0.42 ± 0.02 cdefg |
| B8 | 20.40 ± 0.96 fgh | 17.46 ± 1.10 cd | 4.45 ± 0.20 efg | 0.73 ± 0.09 def | 0.86 ± 0.03 cdef | 0.46 ± 0.01 bcdef |
| B9 | 36.29 ± 0.88 abcd | 21.23 ± 1.52 c | 2.80 ± 0.10 hi | 0.81 ± 0.07 def | 1.10 ± 0.08 bcd | 0.61 ± 0.05 abc |
| B10 | 30.52 ± 0.96 cde | 10.46 ± 0.39 e | 12.59 ± 0.30 a | 1.70 ± 0.14 c | 1.93 ± 0.14 a | 0.40 ± 0.02 defg |
| B11 | 11.60 ± 0.80 i | 19.52 ± 1.21 c | 5.47 ± 0.22 cdef | 1.18 ± 0.13 cde | 1.22 ± 0.10 b | 0.43 ± 0.03 cdefg |
| B12 | 44.71 ± 1.62 a | 38.89 ± 1.85 a | 3.43 ± 0.18 gh | 4.16 ± 0.23 a | 0.85 ± 0.02 bcdef | 0.60 ± 0.05 abc |
| B13 | 39.40 ± 1.74 ab | 43.84 ± 2.13 a | 4.66 ± 0.18 defg | 3.72 ± 0.07 ab | 0.53 ± 0.01 gh | 0.65 ± 0.04 ab |
| B14 | 22.46 ± 2.97 efg | 27.32 ± 0.94 b | 8.38 ± 0.75 b | 3.25 ± 0.29 b | 0.36 ± 0.05 h | 0.59 ± 0.08 abcd |
| B15 | 30.78 ± 1.46 cde | 22.08 ± 1.10 bc | 5.71 ± 0.27 cde | 1.71 ± 0.07 c | 0.77 ± 0.03 def | 0.25 ± 0.01 g |

[a]Data represented as mean ± SEM of each of three replicates ($n = 3$) at a concentration of mg/g DW. Different letters indicate significant differences ($p \leq 0.05$) according to Tukey's HS.

concentration of caffeic acid in comparison to RA and ChA as observed in our study.[18]

In the CP system plants were grown in the natural conditions and the light exposure was given equally and consistently to every unit by regular shifting. Similarly, in the in vitro system plants were grown under cool white fluorescent lights having qualities close to natural light and every unit was provided with uniform and consistent light conditions by regular shifting. Since the light conditions were consistent and the medium was consistent in each system, the polyphenolic response produced in the present study can be considered due to plant property in relation to the medium and light conditions. Additionally, the objective of the present work was to compare and find out whether an alternate system to the CP system can be evolved, and as the results have shown a similar trend for the major polyphenolic (RA), we presume that the developed technique is true to type to a greater extent.

Significant differences were found between the two growth systems for the four cultivars in RA and 13 out of 15 cultivars in ChA and CA profile. Conventional pot system was found to have higher amount of RA and ChA. Differences in the growth substrates, regular nutrient supplementation, and early flowering for all cultivars growing in conventional pot system can be hypothesized as the reasons for high RA and ChA content in the CP system and its significant difference from the in vitro system.[9,29,32] Additionally, as the extraction methodology was optimized for RA in the present study, it can be concluded that separate and targeted extraction of ChA and CA is needed to correlate the effects of growth substrate, growth parameters, and extraction methodology on their content in the two systems.

In the present study chicoric and caffeic acids are the minor polyphenolics found in the cultivars of *Ocimum basilicum*. The CP system is found as a better system for ChA while the in vitro system is found to be better for CA, clearly indicating that the amount of minor polyphenolic is differently affected by the growth substrate and growth parameters in basil in comparison to the major polyphenolics such as RA. The reasons for such an

observation can be studied in the future with extraction methodology optimized for these minor metabolites. It can be further postulated that parameters such as light quality, humidity, and temperature strongly affect the biosynthetic pathway for expression of minor polyphenolics in basil.

*Total Antioxidant Potential and Individual Polyphenolic Antioxidant Potential.* Antioxidant potential can be defined as the capacity of chemical moieties to act as inhibitors of free radicals, donators of hydrogen, quenchers of singlet oxygen, or molecules which can interrupt the oxidation process.[7] Thus, the identification of antioxidants from complex matrices is of significant importance to food, agriculture, and pharmaceutical industries. Detection of antioxidants by conventional antioxidant assays such as DPPH and FRAP assay is time-consuming. Acidic potassium permanganate reacts with potential antioxidant molecules to produce light due to excitation of manganese II species. The signals produced by the acidic potassium permanganate assay show good agreement with conventionally used assays thus its use has been advocated as an excellent alternative.[35]

Polyphenolics react with acidic potassium permanganate,[41] which is a distinct advantage of the chemiluminescence based assay over conventional assays. The method used in our study for total antioxidant assessment was as described by McDermott et al.[36] but modified and applied, for the first time to our knowledge, to *Ocimum basilicum* plant extracts. Total antioxidant content varied among the 15 cultivars for both growth systems. For the in vitro grown plant samples antioxidant potential was higher in comparison to CP grown plants. Similarly, in terms of total antioxidant content (Figure 6) no significant difference was found for the same 11 cultivars

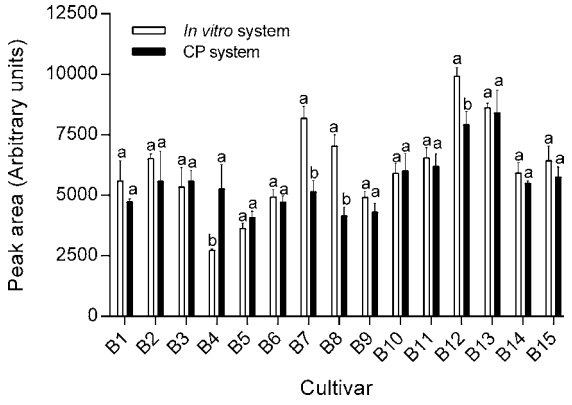


**Figure 6.** Total antioxidant potential found in 15 *Ocimum basilicum* cultivars grown in the *in vitro* system and the CP system by chemiluminescence analysis. Total antioxidant potential is expressed in terms of peak area. Data are presented as mean ± SEM of each of three replicates ($n$ = 3) for the whole plant. Different letters indicate significant differences ($p \leq 0.05$) between the two growth systems, within cultivars according to Sidak's multiple comparison test.

grown in both of the growth systems. B13 and B12 cultivars showed the highest chemiluminescence signals for plants growing in both growth systems.

It is important to identify individual polyphenolics within a complex matrix which may be responsible for antioxidant activity. To assess the contribution of individual polyphenolics, an enhanced acidic permanganate assay, a postcolumn technique, coupled with HPLC was performed on extracts from all cultivars growing in the in vitro growth system. RA antioxidant detection by the acidic potassium permanganate assay has been reported earlier by our group,[35,36] and in the present study its contribution to total antioxidant content was determined by comparing the peak area of RA with the peak area of total antioxidants. The highest antioxidant activity was found in association with RA for high yielding cutlivars such as B13 (Red Rubin), B12 (Holy Green), and B7 (Basil Genovese) cultivars growing in the in vitro system. RA associated antioxidant activity contributed to 44.7%, 44.4%, and 33.6% of the total antioxidant potential in these three cultivars while ChA (2.8%, 3.9%, and 5.8%) and CA (1.0%, 1.1%, and 1.7%) showed a lower percentage of total signal. RA is the major antioxidant compound detected in this study followed by ChA and CA. A positive correlation between the total polyphenolic content (RA + ChA + CA) detected by HPLC and the total polyphenolic antioxidant potential (RA + ChA + CA) and antioxidant potential of RA detected by chemiluminescence was found in this study (Figure 7). The presence of two catechol

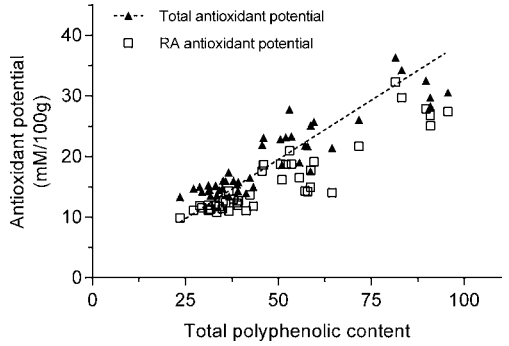


**Figure 7.** Correlation between antioxidant potential (total polyphenolic antioxidant potential and rosmarinic acid antioxidant potential) detected by chemiluminescence assay and total polyphenolic content detected by HPLC analysis for the 15 *Ocimum basilicum* cultivars grown in the in vitro system. The Pearson correlation coefficient ($r$) for antioxidant potential with total polyphenolic content response was 0.910 and 0.912 ($R^2$ = 0.828, 0.832) respectively. Antioxidant potential detected by chemiluminescence assay is expressed as mM/100 g. Data are presented as mean ± SEM of each of three replicates ($n$ = 3) for the whole plant.

rings with a carboxylic acid group gives rise to the antioxidant potential of RA.[5] The acidic potassium permanganate chemiluminescence detection and the subsequent determination of the antioxidant characteristics of ChA were observed for the first time in this study. The chemiluminescence assay is a sensitive and efficient method for determination of antioxidant activity that we propose as a tool for quick selection and screening of conventionally or in vitro grown samples. Our results indicated that polyphenolics content and antioxidant potential detected by chemiluminescence were positively correlated and significantly affected by cultivar type.

**Correlation between Morphotype and Individual Polyphenolic Content.** The contents of RA, ChA, and CA in aerial parts and roots of all cultivars were subjected to hierarchical cluster analysis to examine similarities and differences between the cultivars. Two distinct groups were generated based on the polyphenolic content analysis (Figure 8), and within the two main groups several subgroups were evident. Two main groups were primarily separated on flower color, which was highly correlated with plant morphology (leaf shape, leaf surface, stem type, plant habit) and RA content.

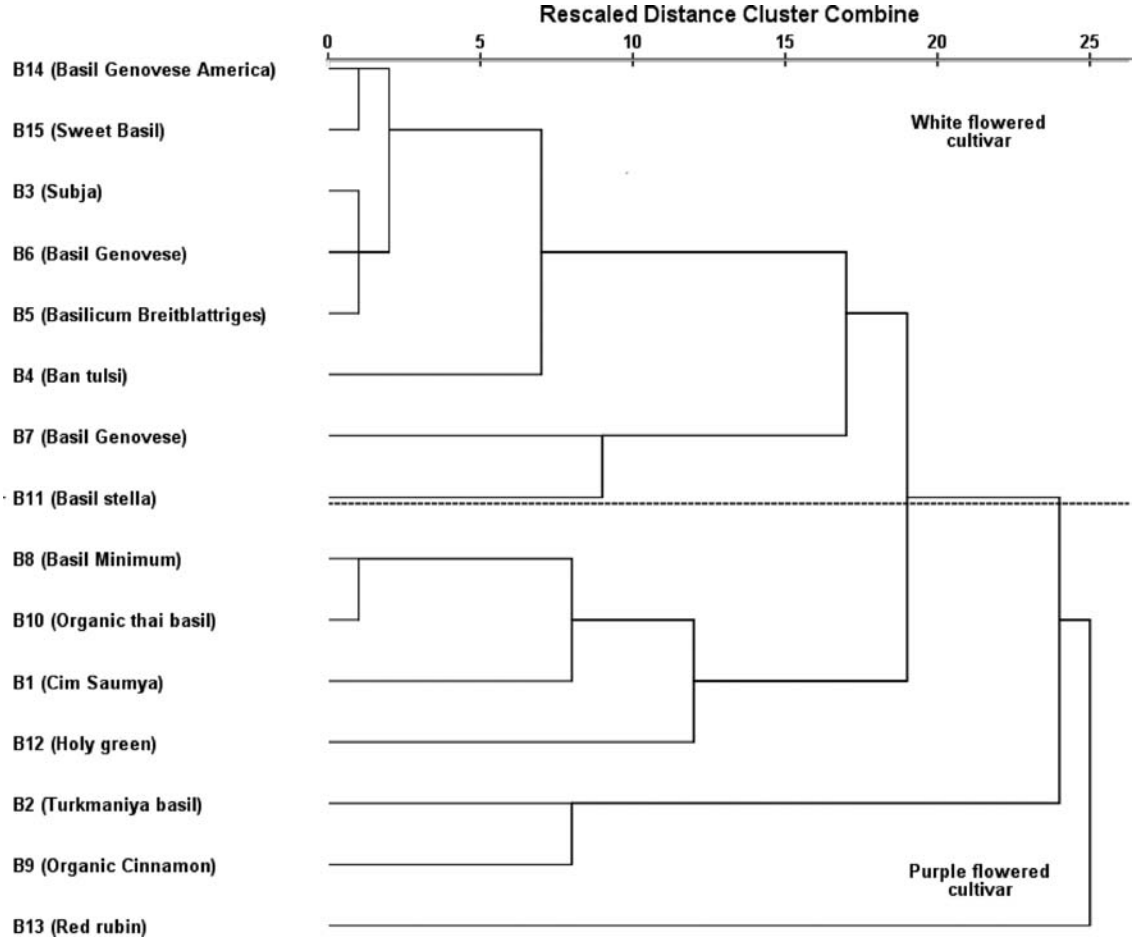


**Figure 8.** Clustering of 15 *Ocimum basilicum* cultivars grown in the *in vitro* system based on rosmarinic acid, chicoric acid, and caffeic acid content found in aerial parts and roots. Data used was standardized with *Z*-score using squared Euclidean distance, and dendrogram was drawn using SPSS 22 statistical computer package. Purple flowered cultivars showed higher contents of rosmarinic acid in comparison to white flowered cultivars. Dashed lines represent the division between the white and purple flowered cultivars.

Those cultivars with the highest RA content were purple flowered, and those with lower RA content were white flowered except for B4, which is a purple flowered cultivar that fell into the white flowered cluster.

**Merits of the in Vitro System.** The advantages of the developed in vitro screening system over conventional pot system include use of sterile, transparent (ease of observation), and precisely defined medium for root growth, no additional nutrient supplementation, and less labor and physical space requirement. These advantages allow for ease of downstream processing and nondestructive sampling for fast and reproducible screening of officinal plants. Additionally, the proposed in vitro system also shows advantages over hydroponics as a screening system as it does not requires use of specialized instrumentation, technical skills, labor, and energy.

Our study identified B13 (Red Rubin), B12 (Holy Green), and B7 (Basil Genovese) as high yielding cultivars in terms of high polyphenolic (RA) content and total polyphenolic antioxidant potential. Rosmarinic acid is the major metabolite found in the cultivars tested, and we have discovered that, in addition to its presence in the aerial parts of plants, roots are a viable and alternative source of RA. A distinct relationship in morphology and polyphenolic content was also revealed in this study, and purple flowered cultivars were found to be a rich source of RA compared with white flowered cultivars. We propose that the screening method described here will be applicable for the screening of a wide variety of secondary metabolites in a range of herbaceous annuals and that the method lends itself to the rapid determination of antioxidant activity in plant extracts.

## AUTHOR INFORMATION

### Corresponding Author

*Tel: +91 11 2468 2100, 2631, 2628. Fax: +91 11 2468 2145. E- mail: aloka@teri.res.in.

### Funding

Deakin University provided a postgraduate scholarship to S.S.

### Notes

The authors declare no competing financial interest.

## ACKNOWLEDGMENTS

We duly acknowledge the assistance from Shailendra Kumar for managing the greenhouse experiments at TERI and Dr. Hashmath Hussain, Deakin University, for assistance with use of Graph Pad Prism 6. Infrastructure support provided by TERI, India, and Deakin University, Australia, is also duly acknowledged.

## ABBREVIATIONS USED

CP, conventional pot; RA, rosmarinic acid; ChA, chicoric acid; CA, caffeic acid; OPA, *o*-phosphoric caid; DPPH$^{\bullet}$, 2,2-diphenyl-1-picrylhydrazyl radical; ABTS$^{\bullet+}$, 2,2′- azinobis(3-ethylbenzothioazoline-6-sulfonic acid) radical cation; HPLC, high performance liquid chromatography; GAE, gallic acid equivalents

## REFERENCES


(1) Gobalakrishnan, R.; Kulandaivelu, M.; Bhuvaneswari, R.; Kandavel, D.; Kannan, L. Screening of wild plant species for antibacterial activity and phytochemical analysis of *Tragia involucrata L. J. Pharm. Anal.* **2013**, *3*, 460−465.

(2) Lee, J.; Scagel, C. F. Chicoric acid found in basil (*Ocimum basilicum L.*) leaves. *Food Chem.* **2009**, *115* (2), 650−656.

(3) Lee, J. Caffeic acid derivatives in dried Lamiaceae and *Echinacea purpurea* products. *J. Funct. Foods* **2010**, *2*, 158−162.

(4) Kwee, E. M.; Niemeyer, E. D. Variations in phenolic composition and antioxidant properties among 15 basil (*Ocimum basilicum L.*) cultivars. *Food Chem.* **2011**, *128* (4), 1044−1050.

(5) Del Baño, M. J.; Lorente, J.; Castillo, J.; Benavente-García, O.; del Río, J. A.; Ortuño, A.; Quirin, K.-W.; Gerard, D. Phenolic diterpenes, flavones, and rosmarinic acid distribution during the development of leaves, flowers, stems and roots of *Rosmarinus officinalis*. antioxidant activity. *J. Agric. Food Chem.* **2003**, *51*, 4247−4253.

(6) Kiferle, C.; Lucchesini, M.; Mensuali-Sodi, A.; Maggini, R.; Raffaelli, A.; Pardossi, A. Rosmarinic acid content in basil plants grown *in vitro* and in hydroponics. *Cent. Eur. J. Biol.* **2011**, *6*, 946−957.

(7) Sgherri, C.; Cecconami, S.; Pinzino, C.; Navari-Izzo, F.; Izzo, R. Levels of antioxidants and nutraceuticals in basil grown in hydroponics and soil. *Food Chem.* **2010**, *123* (2), 416−422.

(8) Treutter, D. Significance of flavonoids in plant resistance: a review. *Environ. Chem. Lett.* **2006**, *4*, 147−157.

(9) Nguyen, P. M.; Kwee, E. M.; Niemeyer, E. D. Potassium rate alters the antioxidant capacity and phenolic concentration of basil (*Ocimum basilicum L.*) leaves. *Food Chem.* **2010**, *123* (4), 1235−1241.

(10) Zgórka, G.; Głowniak, K. Variation of free phenolic acids in medicinal plants belonging to the Lamiaceae family. *J. Pharm. Biomed. Anal.* **2001**, *26* (1), 79−87.

(11) Tepe, B.; Eminagaoglu, O.; Akpulat, H. A.; Aydin, E. Antioxidant potentials and rosmarinic acid levels of the methanolic extracts of *Salvia verticillata (L.)* subsp. *verticillata* and *S. verticillata (L.) subsp. amasiaca* (Freyn & amp; Bornm.) Bornm. *Food Chem.* **2007**, *100* (3), 985−989.

(12) Park, J. B. Identification and quantification of a major anti-oxidant and anti-inflammatory phenolic compound found in basil, lemon thyme, mint, oregano, rosemary, sage, and thyme. *Int. J. Food Sci. Nutr.* **2011**, *62*, 577−584.

(13) Karam, N.; Jawad, F.; Arikat, N.; Shibl, R. Growth and rosmarinic acid accumulation in callus, cell suspension, and root cultures of wild *Salvia fruticosa*. *Plant Cell, Tissue Organ Cult.* **2003**, *73*, 117−121.

(14) Makri, O.; Kintzios, S. *Ocimum sp.* (Basil): botany, cultivation, pharmaceutical properties, and biotechnology. *J. Herbs, Spices Med. Plants* **2008**, *13*, 123−150.

(15) Carović-Stanko, K.; Orlić, S.; Politeo, O.; Strikić, F.; Kolak, I.; Milos, M.; Satovic, Z. Composition and antibacterial activities of essential oils of seven *Ocimum* taxa. *Food Chem.* **2010**, *119* (1), 196−201.

(16) Umar, A.; Zhou, W.; Abdusalam, E.; Tursun, A.; Reyim, N.; Tohti, I.; Moore, N. Effect of *Ocimum basilicum L.* on cyclo-oxygenase isoforms and prostaglandins involved in thrombosis. *J. Ethnopharmacol.* **2014**, *152*, 151−155.

(17) Hussain, A. I.; Anwar, F.; Hussain Sherazi, S. T.; Przybylski, R. Chemical composition, antioxidant and antimicrobial activities of basil (*Ocimum basilicum*) essential oils depends on seasonal variations. *Food Chem.* **2008**, *108* (3), 986−995.

(18) Javanmardi, J.; Khalighi, A.; Kashi, A.; Bais, H. P.; Vivanco, J. M. Chemical characterization of basil (*Ocimum basilicum L.*) found in local accessions and used in traditional medicines in Iran. *J. Agric. Food Chem.* **2002**, *50*, 5878−5883.

(19) Jayasinghe, C.; Gotoh, N.; Aoki, T.; Wada, S. Phenolics composition and antioxidant activity of Sweet Basil (*Ocimum basilicum L.*). *J. Agric. Food Chem.* **2003**, *51*, 4442−4449.

(20) Umar, A.; Imam, G.; Yimin, W.; Kerim, P.; Tohti, I.; Berké, B.; Moore, N. Antihypertensive effects of *Ocimum basilicum L.* (OBL) on blood pressure in renovascular hypertensive rats. *Hypertens. Res.* **2010**, *33*, 727−730.

(21) Carović-Stanko, K.; Šalinović, A.; Grdiša, M.; Liber, Z.; Kolak, I.; Satovic, Z. Efficiency of morphological trait descriptors in discrimination of *Ocimum basilicum L.* accessions. *G. Bot. Ital.* **2011**, *145*, 298−305.

(22) Labra, M.; Miele, M.; Ledda, B.; Grassi, F.; Mazzei, M.; Sala, F. Morphological characterization, essential oil composition and DNA genotyping of *Ocimum basilicum* L. cultivars. *Plant Sci.* **2004**, *167* (4), 725−731.

(23) Bulgakov, V. P.; Inyushkina, Y. V.; Fedoreyev, S. A. Rosmarinic acid and its derivatives: biotechnology and applications. *Crit. Rev. Biotechnol.* **2012**, *32*, 203−217.

(24) Petersen, M.; Simmonds, M. S. Rosmarinic acid. *Phytochemistry* **2003**, *62* (2), 121−125.

(25) Braidy, N.; Matin, A.; Rossi, F.; Chinain, M.; Laurent, D.; Guillemin, G. Neuroprotective effects of rosmarinic acid on ciguatoxin in primary human neurons. *Neurotoxic. Res.* **2014**, *25*, 226−234.

(26) Azevedo, M. F.; Lima, C. F.; Fernandes-Ferreira, M.; Almeida, M. J.; Wilson, J. M.; Pereira-Wilson, C. Rosmarinic acid, major phenolic constituent of Greek sage herbal tea, modulates rat intestinal SGLT1 levels with effects on blood glucose. *Mol. Nutr. Food Res.* **2011**, *55*, S15−S25.

(27) Tai, J.; Cheung, S.; Wu, M.; Hasman, D. Antiproliferation effect of Rosemary (*Rosmarinus officinalis*) on human ovarian cancer cells *in vitro*. *Phytomedicine* **2012**, *19*, 436−443.

(28) Peev, G.; Penchev, P.; Peshev, D.; Angelov, G. Solvent extraction of rosmarinic acid from lemon balm and concentration of extracts by nanofiltration: Effect of plant pre-treatment by supercritical carbon dioxide. *Chem. Eng. Res. Des.* **2011**, *89*, 2236−2243.

(29) Lee, J.; Scagel, C. F. Chicoric acid: chemistry, distribution, and production. *Front. Chem.* **2013**, *1* (40), 1−17.

(30) Schlernitzauer, A.; Oiry, C.; Hamad, R.; Galas, S.; Cortade, F.; Chabi, B.; Casas, F.; Pessemesse, L.; Fouret, G.; Feillet-Coudray, C. Chicoric acid is an antioxidant molecule that stimulates AMP kinase pathway in L6Myotubes and extends lifespan in *Caenorhabditis elegans*. *PLoS One* **2013**, *8* (11), 1−11.

(31) Casanova, L. M.; da Silva, D.; Sola-Penna, M.; de Magalhães Camargo, L. M.; de Moura Celestrini, D.; Tinoco, L. W.; Costa, S. S. Identification of chicoric acid as a hypoglycemic agent from *Ocimum gratissimum* leaf extract in a biomonitoring *in vivo* study. *Fitoterapia* **2014**, *93*, 132−141.

(32) Koroch, A. R.; Juliani, H. R.; Sims, C.; Simon, J. E. Antioxidant activity, total phenolics, and rosmarinic acid content in different basils (*Ocimum spp.*). *Isr. J. Plant Sci.* **2010**, *58*, 191−195.

(33) Shiga, T.; Shoji, K.; Shimada, H.; Hashida, S.-N.; Goto, F.; Yoshihara, T. Effect of light quality on rosmarinic acid content and antioxidant activity of sweet basil, *Ocimum basilicum L. Plant Biotechnol.* **2009**, *26*, 255−259.

(34) Scagel, C. F.; Lee, J. Phenolic composition of basil plants is differentially altered by plant nutrient status and inoculation with mycorrhizal fungi. *HortScience* **2012**, *47*, 660−671.

(35) Francis, P. S.; Costin, J. W.; Conlan, X. A.; Bellomarino, S. A.; Barnett, J. A.; Barnett, N. W. A rapid antioxidant assay based on acidic potassium permanganate chemiluminescence. *Food Chem.* **2010**, *122* (3), 926−929.

(36) McDermott, G. P.; Conlan, X. A.; Noonan, L. K.; Costin, J. W.; Mnatsakanyan, M.; Shalliker, R. A.; Barnett, N. W.; Francis, P. S. Screening for antioxidants in complex matrices using high performance

liquid chromatography with acidic potassium permanganate chemiluminescence detection. *Anal. Chim. Acta* **2011**, *684* (1), 134−141.
(37) Shi, S.-Y.; Zhang, Y.-P.; Jiang, X.-Y.; Chen, X.-Q.; Huang, K.-L.; Zhou, H.-H.; Jiang, X.-Y. Coupling HPLC to on-line, post-column (bio) chemical assays for high-resolution screening of bioactive compounds from complex mixtures. *Trends Anal. Chem.* **2009**, *28* (7), 865−877.
(38) Niederländer, H. A.; van Beek, T. A.; Bartasiute, A.; Koleva, I. I. Antioxidant activity assays on-line with liquid chromatography. *J. Chromatogr. A* **2008**, *1210* (2), 121−134.
(39) Conlan, X. A.; Stupka, N.; McDermott, G. P.; Barnett, N. W.; Francis, P. S. Correlation between acidic potassium permanganate chemiluminescence and *in vitro* cell culture assay: Physiologically meaningful antioxidant activity. *Anal. Methods* **2010**, *2*, 171−173.
(40) Costin, J. W.; Barnett, N. W.; Lewis, S. W.; McGillivery, D. J. Monitoring the total phenolic/antioxidant levels in wine using flow injection analysis with acidic potassium permanganate chemiluminescence detection. *Anal. Chim. Acta* **2003**, *499* (1), 47−56.
(41) Bellomarino, S.; Parker, R.; Conlan, X.; Barnett, N.; Adams, M. Partial least squares and principal components analysis of wine vintage by high performance liquid chromatography with chemiluminescence detection. *Anal. Chim. Acta* **2010**, *678* (1), 34−38.
(42) Adcock, J. L.; Francis, P. S.; Barnett, N. W. Acidic potassium permanganate as a chemiluminescence reagent—A review. *Anal. Chim. Acta* **2007**, *601* (1), 36−67.
(43) Murashige, T.; Skoog, F. A revised medium for rapid growth and bio-assays with tobacco tissue cultures. *Physiol. Plant.* **1962**, *15*, 473−497.
(44) Hoagland, D. R.; Arnon, D. I. The water-culture method for growing plants without soil. *Circ.—Calif. Agric. Exp. Stn.* **1950**, 347.
(45) UPOV. 2003. Basil (*Ocimum basilicum L.*): Guidelines for the conduct of tests for distinctness, uniformity and stability Geneva: UPOV. (http://www.upov.int/edocs/tgdocs/en/tg200.doc).
(46) Singleton, V. L.; Rossi, J. A. Colorimetry of total phenolics with phosphomolybdic- phosphotungstic acid reagents. *Am. J. Enol. Vitic.* **1965**, *16*, 144−158.
(47) Poiroux-Gonord, F.; Bidel, L. P. R.; Fanciullino, A.-L.; Gautier, H.; Lauri-Lopez, F.; Urban, L. Health benefits of vitamins and secondary metabolites of fruits and vegetables and prospects to increase their concentrations by agronomic approaches. *J. Agric. Food Chem.* **2010**, *58*, 12065−12082.
(48) Hakkim, F. L.; Shankar, C. G.; Girija, S. Chemical composition and antioxidant property of holy basil (*Ocimum sanctum L.*) leaves, stems, and inflorescence and their *in vitro* callus cultures. *J. Agric. Food Chem.* **2007**, *55*, 9109−9117.
(49) Toussaint, J. P.; Smith, F. A.; Smith, S. E. The effect of the arbuscular mycorrhizal symbiosis on the production of phytochemicals in basil. Ph.D. Thesis, The University of Adelaide, 2008.
(50) Lee, J.; Scagel, C. F. Chicoric acid levels in commercial basil (*Ocimum basilicum*) and *Echinacea purpurea* products. *J. Funct. Foods* **2010**, *2* (1), 77−84.

**Fig Leaves.** Five fig varieties (Masui Dauphine, Horaishi, Kadota, Violette de Solies, and Negronne) cultivated in our orchard (Kawanishi, Hyogo, Japan) were used in this study. From the middle of June to early July, leaves at the nodes from the tip of the shoot to the fifth node were obtained. After a washing with water, the leaves were cut with a ceramic kitchen knife into 1.5 cm squares. The cut leaves were packaged in polyethylene bag with nitrogen gas and stored in an MDF-393AT freezer (Panasonic Healthcare, Tokyo, Japan) at −80 °C.

**Preparation of Leaf Extract.** The frozen leaves were freeze-dried by using an FDU-2100 freeze-dryer equipped with a DRC-3L dry chamber (Tokyo Rikakikai, Tokyo, Japan). Immediately after freeze-drying, leaves were pulverized to powder with a food mill (IFM-300SG, Iwatani, Osaka, Japan) four times for 10 s. Methanol or a mixture of water/methanol/acetone = 1:1:1 (v/v) was used as the extractant. Leaf powder (0.2 g) was placed in an Erlenmeyer flask, and 30 mL of extractant was added. The flask was shaken in a circular motion at 120 rpm using an NR-30 rotary shaker (Taitec, Saitama, Japan) for 3 h at room temperature. The atmosphere in the chamber of the food mill and in the flask was replaced by nitrogen. After centrifugation at 17000*g* for 10 min with a CR21G II centrifuge (Hitachi High-Technologies, Tokyo, Japan), the supernatant was collected. The residue was resuspended in 10 mL of extractant and centrifuged again under the same conditions. This process was repeated, and the collected supernatant was combined and made to be the volume of 50 mL by adding the extractant. The extract was filtered using a syringe filter (PTFE membrane, pore size = 0.45 μm) and stored at −20 °C.

**Identification of Phenylpropanoids.** *LC-DAD-MS/MS Analysis.* Analysis was carried out according to the method described by Kammerer et al.[25] with some modifications in equipment, column, and gradient program to reduce analysis time. An LC20ADXR HPLC with a diode array detector (DAD) system (Shimadzu, Kyoto, Japan) and a micrOTOF-Q II quadrupole-time-of-flight tandem mass spectrometer fitted with an ESI ion source (Bruker Daltonics, Billerica, MA, USA) were utilized. The UV−vis spectrum was recorded from 200 to 800 nm by DAD. A Synergi Hydro-RP column (particle size = 2.5 μm; 100 mm × 3 mm i.d., Phenomenex, Torrance, CA, USA) was employed for the separation of the phenylpropanoids. The mobile phase was (A) 2% acetic acid and (B) 0.5% acetic acid/acetonitrile = 1:1. The gradient began with 10% B and was varied to 24% B at 8 min, 30% B at 16 min, 55% B at 24 min, 100% B at 30 min, 100% B isocratic from 30 to 33.2 min, and 10% B from 34 to 36 min. The flow rate of the mobile phase was 0.4 mL/min. The temperature of the column oven was 40 °C, and the sample injection volume was 5 μL. Mass spectrometry was carried out using the following conditions: mass range, $m/z$ 50−1000; spectra rate, 1 Hz; nebulizing gas, nitrogen (1.6 bar); drying gas, nitrogen (180 °C, 7 L/min); capillary voltage, −4500 V for positive ion and +2800 V for negative ion; hexapole RF, 100 Vpp; quadrupole ion energy, 5 eV; collision gas, nitrogen (1.6 bar); collision energy, 10 eV; collision RF, 100 Vpp.

*Separation of HPLC Peak Fractions.* A semipreparative HPLC system equipped with a Delta 600 solvent pump (Waters, Milford, MA, USA) and AQUA C18 column (particle size = 5 μm; 250 × 10 mm i.d., Phenomenex) was used. The mobile phase was the same as that utilized for LC-DAD-MS/MS. The gradient started with 10% B and was varied to 24% B at 20 min, 30% B at 40 min, 55% B at 60 min, 100% B at 75 min, 100% B isocratic from 75 to 83 min, and 10% B from 84 to 90 min. The flow rate of the mobile phase was 4.7 mL/min. The temperature of the column oven was 30 °C. The extract was concentrated by evaporation, and 250 μL was injected into the system. The peaks that adsorbed at 320 nm were collected. The separated peak fractions were evaporated to remove the organic solvent. The dried fractions were dissolved in water and freeze-dried.

*NMR Measurements.* $^{1}$H NMR (400 MHz), $^{13}$C NMR (100 MHz), distortionless enhancement by polarization transfer (DEPT), double quantum filtered correlated spectroscopy (DQF-COSY), heteronuclear multiple-quantum coherence (HMQC), and heteronuclear multiple-bond connectivity (HMBC) NMR spectra were recorded with a JNM-ECA400 spectrometer (JEOL, Tokyo, Japan) in deuterated methanol ($CD_3OD$) using a 5 mm NMR tube. The chemical shifts were given on a $\delta$ (parts per million) scale with tetramethylsilane as an internal standard.

*Analysis of Sugar in Glycosides.* The freeze-dried HPLC peak fraction (1 mg) was dissolved in 5 mL of methanol, and HCl was added to reach 6 N. The mixture was heated at 90 °C for 4 h to hydrolyze the glycosides. After neutralization with NaOH, the sugar released from the glycoside was labeled by an ABEE (4-amino benzoic acid ethyl ester) labeling kit (J-oil mills, Tokyo, Japan) and was analyzed by HPLC. An LC-10A HPLC system (Shimadzu) and XBridge Phenyl (particle size = 5 μm; 150 mm × 4.6 mm i.d., Waters) were used for the analysis of the ABEE-labeled sugar. The mobile phase was 0.2 M potassium borate buffer (pH 8.9)/acetonitrile = 93:7 (v/v). The flow rate was 1.0 mL/min. The column oven temperature was 30 °C. The injection volume was 10−30 μL, and the peak was detected by monitoring the absorbance at 305 nm.

**Quantitative Determination of Phenylpropanoids.** An 1100 system HPLC-DAD (Agilent Technologies, Santa Clara, CA, USA) was used for determination of the phenylpropanoids. The column, mobile phase, and analytical conditions for HPLC were the same as those utilized for LC-DAD-MS/MS. Caffeoylmalic acid was detected by absorbance at 320 nm. Rutin, psoralen, bergapten, and psoralic acid glucoside were detected by absorbance at 250 nm. The calibration curves were made from standard chemicals, except for that of psoralic acid glucoside, which was made from the separated material from the fig leaves. All measurements were performed in triplicate.

**Evaluation of Antioxidative Activities.** *Superoxide Anion Radical ($O_2^{\bullet-}$) Scavenging Activity.* Following the method described by Saito et al.,[26] $O_2^{\bullet-}$ generated from the reaction of HPX and XOD was measured by ESR spin trapping with DMPO as the spin trapping agent. The ESR measurement conditions (JES-FA100, JEOL) were as follows: microwave power, 4 mW; field sweep, 330.5−340.5 mT; field modulation frequency, 100 kHz; field modulation width, 0.07 mT; sweep time, 2 min; time constant, 0.1 s. Fifty microliters of 2 mM HPX was placed in a test tube, and 30 μL of DMSO, 50 μL of sample, 20 μL of 4.45 M DMPO were added. The mixture was added to 50 μL of 0.4 U/mL XOD and vortexed for 20 s. The mixture was transferred to an ESR spectrometry liquid cell, and the DMPO−OOH spin adduct was quantified 100 s after the addition of XOD. The measurements were performed in duplicate. The $O_2^{\bullet-}$ scavenging activity was expressed as superoxide dismutase (SOD)-like activity from the calibration curve of standard SOD. Additionally, $IC_{50}$ values of samples were measured and the reaction rate constants with $O_2^{\bullet-}$ of samples ($k_2$) were calculated using eq 1, according to the method described by Mitsuta et al.[27]

$$k_2\ (\mathrm{M^{-1}\,s^{-1}}) = k_1 \times [\mathrm{DMPO}]/\mathrm{IC_{50}} \quad (1)$$

$k_1$ is the reaction rate constant with DMPO and $O_2^{\bullet-}$. The literature value used for the calculation was 15.7 $M^{-1}$ $s^{-1}$.[28] [DMPO] indicates the final concentration of DMPO, and the utilized value was 445 mM.

*Oxygen Radical Absorbance Capacity (ORAC).* The assay was carried out according to the method described by Dávalos et al.[29] with some modifications. In brief, 25 μL of the sample and 150 μL of phosphate buffer ($^1/_{15}$ M, pH 7.4) containing 100 nM fluorescein were placed in each well of a 96-well black, flat-bottom microwell plate (Thermo Fisher Scientific NUNC, Roskilde, Denmark). After preincubation at 37 °C for 30 min, 25 μL of 480 mM AAPH was added to the mixture using an onboard pipettor of plate reader (FLUOstar OPTIMA, BMG Labtech, Offenburg, Germany). From 270 s before the AAPH addition, the emission at 520 nm of each well was measured using a plate reader every 90 s for 60 intervals, with an excitation of 485 nm. The microwell plate was incubated at 37 °C during the measurements and was stirred prior to each measurement. The measurements were performed in triplicate. The area under the curve (AUC; calculated as an integral of the fluorescence intensity during measurement) of each sample was calculated, and activity was expressed as the trolox equivalent (μmol TE/g).

## RESULTS AND DISCUSSION

**Identification of Phenylpropanoids in Fig Leaves.** HPLC chromatograms of the MeOH and water/MeOH/acetone = 1:1:1 (v/v) extracts from Masui Dauphine leaves are shown as an example in Figure 1. The chromatogram profile

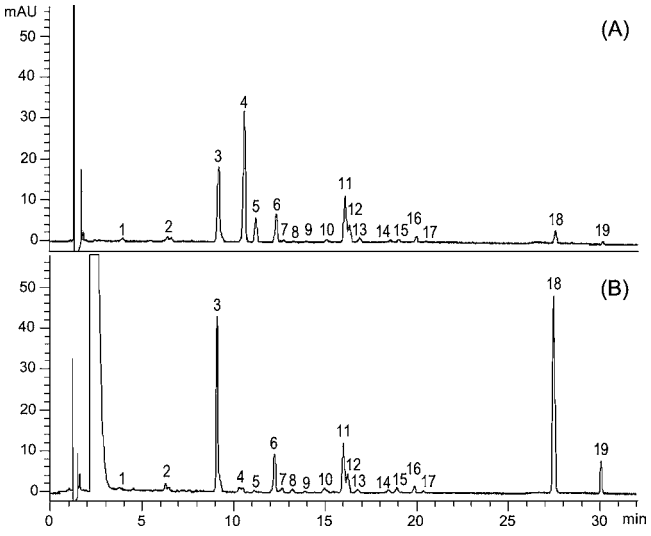


**Figure 1.** HPLC separation of phenylpropanoids from fig leaves: (A) MeOH extract; (B) water/MeOH/acetone = 1:1:1 extract of Masui Dauphine leaves. Peak detection was carried out at 280 nm. For peak assignment see Table 1.

differed depending on the extractant. Peaks 4 and 5 were reduced in the water/MeOH/acetone extract. Peaks 3, 18, and 19 of the water/MeOH/acetone extract were bigger than those in the MeOH extract. The LC-DAD-MS/MS results and corresponding identification of each peak are shown in Table 1. These peaks were detected from the five varieties examined. The intensities of the precursor ion (molecular ion) of peak 3, 4, and 5 detected in negative ion mode were >10 times than those detected in the positive ion mode. On the other hand, the intensities of the precursor ions of peaks 18 and 19 in the positive ion mode were about 30-fold higher than in the negative mode. In other peaks, the differences of the intensity of precursor ion were 0.7- to 1.2-fold between positive ion mode and negative ion mode.

Compound **2** showed a retention time (RT) of 6.5 min in HPLC, a molecular ion with $m/z$ 353 $[M - H]^-$, and a product ion with $m/z$ 191 in MS/MS. The formula of the molecular ion was calculated to be $C_{16}H_{17}O_9$. By matching the data with those of the standard chemical, compound **2** was identified as chlorogenic acid (Figure 2).

Compound **3** afforded a RT of 9.3 min in HPLC, a molecular ion with $m/z$ 295 $[M - H]^-$, and product ions with $m/z$ 133 (100%), 115 (85%), and 135 (75%) in MS/MS. The formula of the molecular ion was calculated to be $C_{13}H_{12}O_8$. These values matched with those of caffeoylmalic acid (CMA). Furthermore, NMR was used to confirm the planar structure (Figure 3; Table 2). Therefore, compound **3** was identified as CMA.

Compound **4** afforded a RT of 10.3 min in HPLC analysis, a molecular ion with $m/z$ 365 $[M - H]^-$, and a product ion with $m/z$ 159 in MS/MS. The formula of the molecular ion was calculated to be $C_{17}H_{17}O_9$. From the data obtained by NMR (Table 3), compound **4** was found to have the planar structure shown in Figure 4. Psoralen and sugar were generated by the

**Table 1. LC-MS Data of Phenylpropanoids from Fig Leaf Extract**

| peak | compound | retention time (min) | MS precursor ion $m/z$ | MS/MS product ions $m/z$ (%) |
|---|---|---|---|---|
| | **Negative Ion Mode $[M - H]^-$** | | | |
| 1 | unknown | 4.0 | 343 | 137 (100), 181 (47) |
| 2 | chlorogenic acid | 6.5 | 353 | 191 (100) |
| 3 | caffeoylmalic acid (CMA) | 9.3 | 295 | 133 (100), 115 (85), 135 (75) |
| 4 | psoralic acid-glucoside (PAG) | 10.3 | 365 | 159 (100) |
| 5 | unknown | 11.3 | 395 | 201 (100), 189 (65) |
| 6 | isoschaftoside | 12.4 | 563 | 353 (100), 383 (78), 443 (56) |
| 7 | unknown | 12.7 | 447 | 357 (100), 327 (90) |
| 8 | unknown | 13.3 | 163 | 119 (100), 98 (60) |
| 9 | unknown | 14.0 | 423 | 201 (100), 89 (25) |
| 10 | unknown | 15.0 | 193 | 134 (100) |
| 11 | rutin (quercetin 3-*O*-rutinoside) | 16.1 | 609 | 300 (100) |
| 12 | unknown | 16.3 | 365 | 159 (100) |
| 13 | isoquercetin (quercetin 3-*O*-glucoside) | 16.9 | 463 | 300 (100) |
| 14 | unknown | 18.3 | 467 | ND |
| 15 | quercetin 3-*O*-(6″-*O*-malonyl)-glucoside | 19.1 | 549 | 300 (100), 505 (30) |
| 16 | unknown | 20.1 | 593 | 285 (100) |
| 17 | astragalin (kaempferol 3-*O*-glucoside) | 20.5 | 447 | 284 (100) |
| | **Positive Ion Mode $[M + H]^+$** | | | |
| 18 | psoralen | 27.7 | 187 | 131 (100) |
| 19 | bergapten (5-methoxypsoralen) | 30.3 | 217 | 202 (100), 174 (45) |

hydrolysis of the compound **4** with hydrochloric acid. This sugar was identified as glucose by HPLC analysis using the ABEE labeling method. As such, compound **4** was determined to be (2*Z*)-3-[6-(β-D-glucopyranosyloxy)-1-benzofuranyl]-2-propenoic acid (psoralic acid-glucoside).

Compound **5** exhibited a RT of 11.3 min in HPLC, a molecular ion with $m/z$ 395 $[M - H]^-$, and product ions with $m/z$ 201 (100%) and 189 (65%) in MS/MS. The formula of the molecular ion was calculated to be $C_{18}H_{19}O_{10}$. The chemical composition was equivalent to psoralic acid glucoside (PAG) with an additional methoxy group ($CHO_3$−, FW 31.03). Furthermore, bergapten and glucose were generated by hydrolysis of the compound **5** fraction with hydrochloric acid. Thus, compound **5** was determined to be a PAG derivative with an additional methoxy group in the aglycone.

Compound **6** showed a RT of 12.4 min in HPLC, a molecular ion with $m/z$ 563 $[M - H]^-$, and product ions with $m/z$ 353 (100%), 383 (78%), and 443 (56%) in MS/MS. The formula of the molecular ion was calculated to be $C_{26}H_{27}O_{14}$. By matching the data to that of a standard chemical, compound **6** was identified as isoschaftoside (Figure 2). Schaftoside, the structural isomer of isoschaftoside, afforded a different product ion pattern ($m/z$ 353, 100%; 383, 83%; 443, 72%), but the


dx.doi.org/10.1021/jf5025938 | J. Agric. Food Chem. 2014, 62, 10076−10083

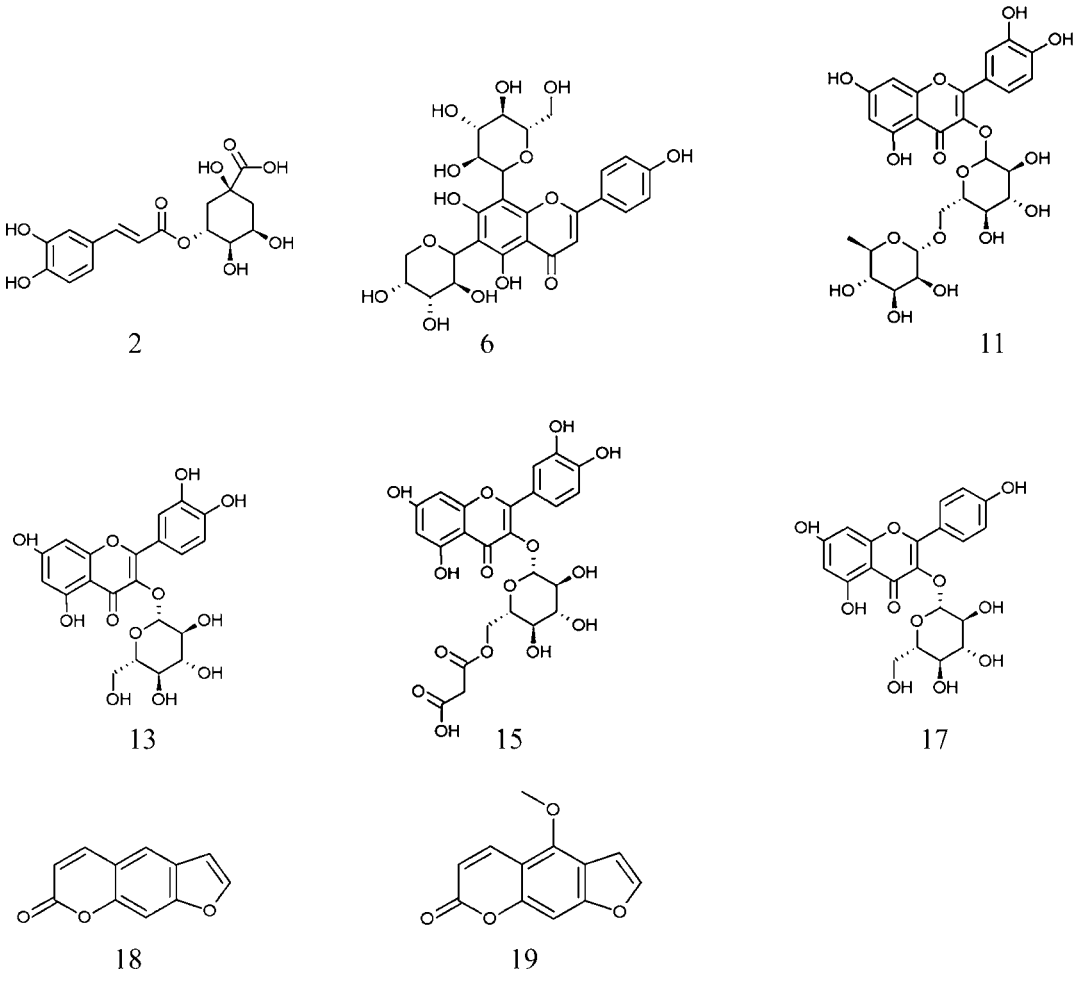


**Figure 2.** Identified compounds in fig leaf extract (except compounds **3** and **4**): compound **2**, chlorogenic acid; compound **6**, isoschaftoside; compound **11**, rutin; compound **13**, isoquercetin; compound **15**, quercetin 3-*O*-(6″-*O*-malonyl)-glucoside; compound **17**, astragalin; compound **18**, psoralen; compound **19**, bergapten.

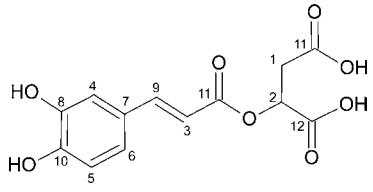

**Figure 3.** Chemical structure of compound **3**. For atom numbering see Table 2.

same RT. Thus, it is possible that a small amount of schaftoside was present in fig leaves.

Compound **11** showed a RT of 16.1 min in HPLC, a molecular ion with $m/z$ 609 $[M - H]^-$, and a product ion with $m/z$ 300 in MS/MS. The formula of the molecular ion was calculated to be $C_{27}H_{29}O_{16}$. By comparison to the standard, compound **11** was identified as rutin (quercetin 3-*O*-rutinoside, Figure 2).

Compound **12** showed a RT of 16.3 min in HPLC and the same molecular ion as PAG in MS/MS. The formula of the molecular ion was the same as that of PAG ($C_{18}H_{19}O_{10}$). Therefore, compound **12** was thought to be an isomeric form of PAG.

Compound **13** showed a RT of 16.9 min in HPLC, a molecular ion with $m/z$ 463 $[M - H]^-$, and a product ion with $m/z$ 300 in MS/MS. The formula of the molecular ion was calculated to be $C_{21}H_{19}O_{12}$. By comparison with the standard, compound **13** was identified as isoquercetin (quercetin 3-*O*-glucoside, Figure 2).

Compound **15** presented a RT of 19.1 min in HPLC, a molecular ion with $m/z$ 549 $[M - H]^-$, and product ions with $m/z$ 300 (100%) and 505 (30%) in MS/MS. The formula of the molecular ion was calculated to be $C_{24}H_{21}O_{15}$. Compound

**Table 2. NMR Spectroscopic Data of Compound 3 ($\delta$ in $CD_3OD$)**

| | $^1$H | | $^{13}$C |
|---|---|---|---|
| | $\delta$ | multiplicity ($J$ in Hz) | $\delta$ |
| 1 | 2.911 | m | 37.47 |
| 2 | 5.453 | dd (3.7,8.7) | 70.64 |
| 3 | 6.313 | d (15.6) | 114.49 |
| 4 | 7.055 | d (2.3) | 115.19 |
| 5 | 6.776 | d (8.2) | 116.55 |
| 6 | 6.958 | dd (1.8, 8.2) | 123.20 |
| 7 | | | 127.73 |
| 8 | | | 146.87 |
| 9 | 7.586 | d (16.0) | 147.75 |
| 10 | | | 149.79 |
| 11 | | | 168.24 |
| 12 | | | 173.42 |


dx.doi.org/10.1021/jf5025938 | J. Agric. Food Chem. 2014, 62, 10076−10083

**Table 3. NMR Spectroscopic Data of Compound 4 ($\delta$ in $CD_3OD$)**

| | $^1$H | | $^{13}$C |
|---|---|---|---|
| | $\delta$ | multiplicity ($J$ in Hz) | $\delta$ |
| 1 | 3.713 | dd (119, 5.0) | 62.53 |
| | 3.905 | dd (11.9, 1.8) | |
| 2 | 3.407−3.430 | m | 71.35 |
| 3 | 3.455−3.536 | m | 74.96 |
| 4 | 3.455−3.536 | m | 78.14 |
| 5 | 3.455−3.536 | m | 78.27 |
| 6 | 7.380 | s | 99.98 |
| 7 | 4.960 | d (7.3) | 103.31 |
| 8 | 6.754 | d (1.4) | 107.55 |
| 9 | 5.971 | d (12.8) | 120.82 |
| 10 | | | 122.96 |
| 11 | | | 123.13 |
| 12 | 7.859 | s | 123.63 |
| 13 | 7.371 | d (12.4) | 139.67 |
| 14 | 7.664 | d (2.3) | 146.58 |
| 15 | | | 155.04 |
| 16 | | | 157.31 |
| 17 | | | 170.76 |

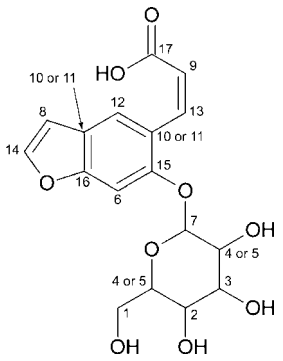


**Figure 4.** Chemical structure of compound **4**. For atom numbering see Table 3.

**15** was identified as quercetin 3-*O*-(6″-*O*-malonyl)-glucoside (Figure 2) by comparison with the standard.

Compound **17** exhibited a RT of 20.5 min in HPLC, a molecular ion with $m/z$ 447 $[M - H]^-$, and a product ion with $m/z$ 284 in MS/MS. The formula of the molecular ion was calculated to be $C_{21}H_{19}O_{11}$. By matching to the standard, compound **17** was identified as astragalin (kaempferol 3-*O*-glucoside, Figure 2).

Compound **18** presented a RT of 27.7 min in HPLC, a molecular ion with $m/z$ 187 $[M + H]^+$, and a product ion with $m/z$ 131 in MS/MS. The formula of the molecular ion was calculated to be $C_{11}H_7O_3$. Compound **18** was identified as psoralen (Figure 2) by comparison to the standard.

Compound **19** showed a RT of 30.3 min in HPLC, a molecular ion with $m/z$ 217 $[M + H]^+$, and product ions with $m/z$ 202 (100%) and 174 (45%) in MS/MS. The formula of the molecular ion was calculated to be $C_{12}H_9O_4$. By matching to the standard, compound **19** was identified as bergapten (5-methoxypsoralen, Figure 2).

**Phenylpropanoid Composition in Fig Leaves.** The amounts of some identified phenylpropanoids with comparatively large peak areas in the UV chromatograms were measured for five varieties including Masui Dauphine and Horaishi, the major varieties in Japan (Table 4).

Among the polyphenols, the CMA content ranged from 14.4 (Negronne) to 20.6 mg/g dry weight (DW) (Violette de Solies). The rutin content ranged from 7.2 (Negronne) to 11.4 mg/g DW (Violette de Solies), which was around 50−60% of the CMA content. CMA was the most abundant polyphenol in the fig leaves. CMA was reported to be found in plants such as *Chelidonium majus* L., *Corydalis lutea* L.,[30] lettuce (*Lactuca sativa* L.),[31] and nettle (*Urtica dioica* L.).[32] However, we found that fig leaves contained CMA for the first time. The second most abundant polyphenol, rutin, has been identified in many other plants. Additionally, some studies detected rutin in fig leaves.[17,18,20] Isoschaftoside was also previously identified in fig leaves,[33] and it was also considered a major polyphenol in addition to CMA and rutin. The HPLC-UV peak areas of other polyphenols were considerably small.

Among the furanocoumarins, the psoralen content ranged from 3.8 (Horaishi) to 23.0 mg/g DW (Violette de Solies). The bergapten content was only 12−22% of the psoralen content in the five varieties. The PAG content ranged from 6.7 (Horaishi) to 42.2 mg/g DW (Violette de Solies), which was approximately twice the psoralen content. Psoralen was regarded as the primary furanocoumarin in fig leaves. Because psoralen and glucose were generated in the hydrolysis of PAG, PAG may be a precursor of psoralen in fig leaves. PAG was identified in *Psoralea plicata* L.[34] and *Psoralea corylifolia* L.[35] We found that fig leaves contained PAG for the first time. One mole of psoralen (molecular weight (MW) 186) and glucose (MW 180) was generated by the hydrolysis of one mole of PAG (MW 366).[35] In fig leaves, the PAG content was approximately equivalent to the psoralen content by mole. Therefore, the potential psoralen content in fig leaves may be increased by approximately 2 times. Furthermore, a precursor of bergapten was also detected. Kasajima et al. reported a similar compound from methanol extracts of fig leaves.[18]

**Varietal Characteristics of Phenylpropanoid Composition.** Violette de Solies contained the greatest amounts of CMA, rutin, psoralen, bergapten, and PAG in the leaves among the five varieties of fig investigated in this study. The CMA and rutin contents differed between 1.4 and 1.6 times among the five fig varieties. Moreover, the furanocoumarin and PAG

**Table 4. Major Phenylpropanoid Content (Milligrams per Gram DW)[a] from Leaves of 5 Fig Varieties**

| variety | CMA[b] | PAG[b] | rutin | psoralen | bergapten |
|---|---|---|---|---|---|
| Masui Dauphine | 16.6 ± 0.6 | 18.0 ± 1.4 | 9.7 ± 0.4 | 10.2 ± 0.5 | 1.4 ± 0.1 |
| Horaishi | 17.6 ± 0.3 | 6.7 ± 0.2 | 11.3 ± 0.2 | 3.8 ± 0.0 | 0.8 ± 0.0 |
| Kadota | 18.7 ± 0.1 | 14.0 ± 0.6 | 8.7 ± 0.1 | 7.0 ± 0.1 | 1.1 ± 0.0 |
| Violette de Solies | 20.6 ± 0.6 | 42.2 ± 0.9 | 11.4 ± 0.4 | 23.0 ± 0.5 | 5.0 ± 0.1 |
| Negronne | 14.4 ± 0.7 | 15.4 ± 0.6 | 7.2 ± 0.4 | 9.2 ± 0.3 | 1.1 ± 0.0 |

[a]Mean ± standard deviation ($n$ = 3). [b]CMA, caffeoylmalic acid, PAG, psoralic acid-glucoside.

contents of the Violette de Solies leaves were more than double those of Masui Dauphin.

It was reported that large doses (15 mg/person) of furanocoumarins administered orally induced photodermatitis in humans.[36] Therefore, caution should be exercised with oral ingestion of furanocoumarins from fig leaves. The leaves of Violette de Solies may have more risks for human health than other varieties with high concentrations of furanocoumarin and PAG. Horaishi is thought to be a low-risk variety because the leaves contain a lower amount of furanocoumarins and PAG.

There are a large number of fig varieties, so investigation of other varieties is necessary to elucidate the varietal characteristics of phenylpropanoid composition in fig leaves. If a variety with a low furanocoumarin-related compound content and high polyphenol content is found, it may be suitable for consumption.

**Antioxidant Activity of Phenylpropanoids in Fig Leaves.** Because CMA and PAG were the most abundant phenylpropanoids in the fig leaves, their $O_2^{\bullet-}$ scavenging activities were measured by ESR spin trapping. The SOD-like activities of CMA and PAG separated from fig leaves were 70604 and 3776 U/g, respectively.

The $O_2^{\bullet-}$ scavenging activities at various concentrations and $IC_{50}$ values were measured, and the reaction rate constants with $O_2^{\bullet-}$ ($k_2$) were calculated for CMA (standard chemical and separated material) and rutin (standard chemical) (Table 5).

**Table 5. $O_2^{\bullet-}$ Scavenging Activity and ORAC of CMA, Rutin, and PAG from Fig Leaves**

| | $O_2^{\bullet-}$ scavenging activity[a] | | ORAC[b] | |
|---|---|---|---|---|
| compound | $IC_{50}$ ($\mu$M) | $k_2$ ($M^{-1}s^{-1}$) | $\mu$mol TE[c]/g DW | $\mu$mol TE/$\mu$mol |
| CMA (standard) | 12.0 | $5.8 \times 10^5$ | 12043 ± 258 | 3.57 ± 0.08 |
| CMA (separated[d]) | 33.2 | $2.1 \times 10^5$ | 11130 ± 558 | 3.30 ± 0.17 |
| rutin (standard) | 17.4 | $4.0 \times 10^5$ | 14856 ± 2229 | 9.07 ± 0.36 |
| PAG (separated) | –[e] | – | 2156 ± 452 | 0.79 ± 0.17 |

[a]Mean ($n$ = 2). [b]Mean ± standard deviation ($n$ = 2). [c]Trolox equivalent. [d]Separated from fig leaves of Masui Dauphine variety. [e]Not measured because of low activity.

The $IC_{50}$ values of standard and separated CMA were 12 and 33.2 $\mu$M, respectively. The $k_2$ values of standard and separated CMA were $5.8 \times 10^5$ and $2.1 \times 10^5$ $M^{-1}$ $s^{-1}$, respectively. Impurities in the CMA separated from the fig leaves may have led to the lower $k_2$ value as compared to the standard compound. The $O_2^{\bullet-}$ scavenging activity of rutin (standard chemical; $IC_{50}$ = 17.4 $\mu$M and $k_2 = 4.0 \times 10^5$ $M^{-1}$ $s^{-1}$) was equivalent to that of CMA.

CMA is the compound that coupled with caffeic acid and malic acid. The $k_2$ values of caffeic acid and chlorogenic acid (caffeoylquinic acid) were reported to be $9.6 \times 10^5$ and $16.7 \times 10^5$ $M^{-1}$ $s^{-1}$, respectively.[37] Rutin is the glycoside of quercetin with rutinose. The $O_2^{\bullet-}$ scavenging activity of rutin is approximately equivalent to that of quercetin.[38] The $k_2$ values of catechin, epicatechin, epicatechin gallate, epigallocatechin and epigallocatechin gallate were reported to be $(0.4–0.6) \times 10^5$, $(0.5–0.7) \times 10^5$, $(3.8–4.3) \times 10^5$, $(4.1–7.7) \times 10^5$, and $(7.3–14.2) \times 10^5$ $M^{-1}$ $s^{-1}$, respectively.[38,39] Vitamin C has a high $O_2^{\bullet-}$ scavenging activity with a reported reaction rate constant of $(2.7–3.5) \times 10^5$ $M^{-1}$ $s^{-1}$.[40−42] Therefore, the $O_2^{\bullet-}$ scavenging activities of CMA and rutin were higher than or equivalent to those of other catechins and vitamin C, but lower than those of chlorogenic acid and epigallocatechin gallate.

ORAC is one method that is used to evaluate the suppression of peroxy radicals in vitro. The ORAC values by weight of CMA (standard chemical and separated material), rutin, and PAG were 12043, 11130, 14856, and 2156 $\mu$mol TE/g, respectively (Table 5). The ORAC values by mole of the aforementioned compounds were 3.57, 3.30, 9.07, and 0.79 $\mu$mol TE/$\mu$mol, respectively. The ORAC value of PAG was <25% that of CMA, and it was a tendency similar to the SOD-like activity.

The value of the separated CMA from fig leaves was moderately lower than that of the standard CMA. Impurities in the separated CMA may have led to the lower activity. CMA and rutin showed equivalent ORAC values per weight. However, rutin exhibited an ORAC value that was approximately 3 times higher than that of CMA per mole. The difference in molecular structure, including the number or placement of binding hydroxyl groups, may have led to a different affinity with the radical derived from AAPH among the compounds. Ou et al. reported the ORAC values of caffeic acid, chlorogenic acid, quercetin, rutin, and catechin to be 4.37, 3.14, 7.28, 6.01, and 6.76 $\mu$mol TE/$\mu$mol, respectively.[43] The ORAC level of CMA was equivalent to those of caffeic acid and chlorogenic acid and was moderately lower than those of quercetin, rutin, and catechin. The ORAC level of rutin was higher than those of caffeic acid and chlorogenic acid and was equivalent to those of quercetin and catechin.

In fig leaves, CMA and rutin were the major polyphenols and were found in relatively high concentrations. Therefore, both compounds are thought to contribute to the antioxidant activity. PAG is the most abundant phenylpropanoid in fig leaves, but the $O_2^{\bullet-}$ scavenging activity and ORAC of PAG were significantly lower in comparison with CMA and rutin. Isoschaftoside was the third most abundant compound, but the contribution to antioxidant activity was small because apigenin, the aglycon of isoschaftoside, showed low $O_2^{\bullet-}$ scavenging activity (data abbreviated). Similarly, because the contents of other polyphenols (chlorogenic acid and quercetin glycosides) were significantly less than that of CMA and rutin, the contribution to $O_2^{\bullet-}$ antioxidant activity was thought to be small.

**Potential of Fig Leaves as Functional Food Material.** Many papers have described the various physiological functions of polyphenols. The reduction effect of rheumatalgia was reported in CMA-rich nettle extracts.[44] Other caffeic acid derivatives, such as chlorogenic acid, were shown to reduce obesity, diabetes, and inflammation in animals.[45−48] The palliation of cerebral ischemia disorder in rats[49] and mitigation of convulsions induced by kainic acid in mice[50] were reported as effects of rutin. The fruit of *Psoralea corylifolia* L. containing PAG composes "Buguzhi", a euphoriant in Chinese medicine. Ossiferous promotion was reported with Buguzhi extracts,[51] but the exact effect of PAG on human health is unknown. When fig leaf extract is taken orally, the amount of furanocoumarins may increase in the stomach. When using fig leaves as food, it is necessary to examine how PAG will be hydrolyzed in the human body.

Fig leaf extracts exhibited high antioxidant activities, but the activity was less than that of green tea or coffee according to the

phenylpropanoid content found in this investigation. To elucidate the functionalities of fig leaves, further studies in the influence of CMA and PAG on human health are necessary. Moreover, a greater number of fig varieties should be evaluated in regard to phenylpropanoid content and antioxidant activity of the extracts. Similarly, the influence of various processing and extraction methods on the residual rate of the components in fig leaves should also be investigated.

## AUTHOR INFORMATION


### Corresponding Author

*(T.T.) Phone: +81-72-740-3300. Fax: +81-72-758-6934. E-mail: tooru_takahashi@shokuken.or.jp.


### Notes

The authors declare no competing financial interest.

## REFERENCES


(1) Zohary, D.; Spiegel-Roy, P. Beginnings of fruit growing in the world. *Science* **1975**, *187*, 319−327.

(2) Kislev, M. E.; Hartmann, A.; Bar-Yosef, O. Early domesticated fig in the Jordan valley. *Science* **2006**, *312*, 1372−1374.

(3) Ryo, H. *Toho Eiyo Shinsho*; Medical Yukon: Kyoto, Japan, 2005; pp 70−71.

(4) Lee, K.-H.; Wang, H.-K.; Itokawa, H.; Morris-Natschke, S. L. Current perspectives on Chinese medicines and dietary supplements in China, Japan and the United States. *J. Food Drug Anal.* **2000**, *8*, 219−228.

(5) Abbasi, A. M.; Khan, M. A.; Shah, M. H.; Shah, M. M.; Pervez, A.; Ahmad, M. Ethnobotanical appraisal and cultural values of medicinally important wild edible vegetables of lesser Himalayas-Pakistan. *J. Ethnobiol. Ethnomed.* **2013**, *9*, 66−79.

(6) Takahashi, T.; Saito, K.; Mokudai, T.; Kohno, M. Antioxidant capacity and related compounds of fig leaf. *Rep. Toyo College Food Technol. Toyo Inst. Food Technol.* **2009**, *27*, 21−27.

(7) Konyalıoğlu, S.; Sağlam, H.; Kıvçak, B. $\alpha$-Tocopherol, flavonoid, and phenol contents and antioxidant activity of *Ficus carica* leaves. *Pharm. Biol.* **2005**, *43*, 683−686.

(8) Serraclara, A.; Hawkins, F.; Pérez, C.; Domínguez, E.; Campillo, J. E.; Torres, M. D. Hypoglycemic action of an oral fig-leaf decocton in type-I diabetic patients. *Diabetes Res. Clin. Pract.* **1998**, *39*, 19−22.

(9) Pérez, C.; Domínguez, E.; Ramiro, J. M.; Romero, A.; Campillo, J. E.; Torres, M. D. A study on the glycaemic balance in streptozotocin-diabetic rats treated with an aqueous extract of *Ficus carica* (fig tree) leaves. *Phytother. Res.* **1996**, *10*, 82−83.

(10) Canal, J. R.; Torres, M. D.; Romero, A.; Pérez, C. A chloroform extract obtained from a decoction of *Ficus carica* leaves improves the cholesterolaemic status of rats with streptozotocin-induced diabetes. *Acta Physiol. Hung.* **2000**, *87*, 71−76.

(11) Pérez, C.; Canal, J. R.; Campillo, J. E.; Romero, A.; Torres, M. D. Hypotriglyceridaemic activity of *Ficus carica* leaves in experimental hypertriglyceridaemic rats. *Phytother. Res.* **1999**, *13*, 188−191.

(12) Patil, V. V.; Bhangale, S. C.; Patil, V. R. Evaluation of anti-pyretic potential of *Ficus carica* leaves. *Int. J. Pharm. Sci. Rev. Res.* **2010**, *2*, 48−50.

(13) Patil, V. V.; Patil, V. R. Evaluation of anti-inflammatory activity of *Ficus carica* Linn. leaves. *Indian J. Nat. Prod. Resources.* **2011**, *2*, 151−155.

(14) Parr, A. J.; Bolwell, G. P. Phenols in the plant and in man. The potential for possible nutritional enhancement of the diet by modifying the phenols content or profile. *J. Sci. Food Agric.* **2000**, *80*, 985−1012.

(15) Manach, C.; Williamson, G.; Morand, C.; Scalbert, A.; Remesy, C. Bioavailability and bioefficacy of polyphenols in humans. I. Review of 97 bioavailability studies. *Am. J. Clin. Nutr.* **2005**, *81*, 230S−243S.

(16) Arts, I. C.; Hollman, P. H. Polyphenols and disease risk in epidemiologic studies. *Am. J. Clin. Nutr.* **2005**, *81*, 317−325.

(17) Teixeira, D. M.; Patao, R. F.; Coelho, A. V.; Da Costa, C. T. Comparison between sample disruption methods and solid-liquid extraction (SLE) to extract phenolic compounds from *Ficus carica* leaves. *J. Chromatogr.* **2006**, *1103*, 22−28.

(18) Kasajima, N.; Furutake, T.; Shiota, S.; Kaneda, M. *55th (Year 2008) Annual Meeting of the Japanese Society of Pharmacognosy*; Nagasaki Abstract Papers; Japanese Society of Pharmacognosy: Tokyo, Japan, 2008; pp 238.

(19) Singab, A. N.; Ayoub, N. A.; Ali, E. N.; Mostafa, N. M. Antioxidant and hepatoprotective activities of Egyptian Moraceus plants against carbon tetrachloride-induced oxidative stress and liver damage in rats. *Pharm. Biol.* **2010**, *48*, 1255−1264.

(20) Mawa, S.; Husain, H.; Jantan, I. *Ficus carica* L. (Moraceae): phytochemistry, traditional uses and biological activities. *Evidence-Based Complement. Altern. Med.* **2013**, 1−8.

(21) Tani, M. Dermatopathy caused by the chemical substance. 36. Phytophototoxic contact dermatitis due to the plant. *Med. Drug J.* **2002**, *38*, 2398−2405.

(22) Ho, P. C.; Saville, D. J. Inhibition of human CYP3A4 activity by grapefruit flavonoids, furanocoumarins and related compounds. *J. Pharm. Pharm. Sci.* **2001**, *4*, 217−227.

(23) Vo-Dinh, T.; White, D. A.; O'Malley, M. A.; Seligman, P. J.; Beier, R. C. Fluorescence detection of phototoxic psoralens in vegetable products. *J. Agric. Food Chem.* **1988**, *36*, 333−337.

(24) Hussein, A.; Shugaev, I. Phototoxic response to *Ficus carica* leaf and shoot saps. *Israel Med. Assoc. J.* **2012**, *14*, 399−400.

(25) Kammerer, D.; Claus, A.; Carle, R.; Schieber, A. Polyphenol screening of pomace from red and white grape varieties (*Vitis vinifera* L.) by HPLC-DAD-MS/MS. *J. Agric. Food Chem.* **2004**, *52*, 4360−4367.

(26) Saito, K.; Kohno, M.; Yoshizaki, F.; Niwano, Y. Extensive screening for edible herbal extracts with potent scavenging activity against superoxide anions. *Plant Foods Hum. Nutr.* **2008**, *63*, 65−70.

(27) Mitsuta, K.; Mizuta, Y.; Kohno, M.; Hiramatsu, M.; Mori, A. The application of ESR spin-trapping technique to the evaluation of SOD-like activity of biological substances. *Bull. Chem. Soc. Jpn.* **1990**, *63*, 187−191.

(28) Finkelstein, E.; Rosen, G. M.; Rauckman, E. J. Spin trapping kinetics of the reaction of superoxide and hydroxyl radicals with nitrones. *J. Am. Chem. Soc.* **1980**, *102*, 4994−4999.

(29) Dávalos, A.; Gómez-Cordovés, C.; Bartolomé, B. Extending applicability of the oxygen radical absorbance capacity (ORAC-fluorescein) assay. *J. Agric. Food Chem.* **2004**, *52*, 48−54.

(30) Boegge, S. C.; Kesper, S.; Verspohl, E. J.; Nahrstedt, A. Redution of ACh-induced contraction of rat isolated ileum by coptisine, (+)-caffeoylmalic acid, *Chelidonium majus*, and *Corydalis lutea* extracts. *Planta Med.* **1996**, *2*, 173−174.

(31) Baur, S.; Klaiber, R. G.; Koblo, A.; Carle, R. Effect of different washing procedures on phenolic metabolism of shredded packaged iceberg lettuce during storage. *J. Agric. Food Chem.* **2004**, *52*, 7017−7025.

(32) Pinelli, P.; Ieri, F.; Vignolini, P.; Bacci, L.; Baronti, S.; Romani, A. Extraction and HPLC analysis of phenolic compounds in leaves, stalks, and textile fibers of *Urtica dioica* L. *J. Agric. Food Chem.* **2008**, *56*, 9127−9132.

(33) Siewek, F.; Herrmann, K. Isomeric di-*C*-glycosylflavones in fig (*Ficus carica* L.). *Z. Naturforsch. C* **1985**, *40*, 8−12.

(34) Hamed, A. I.; Springuel, I.; El-Emary, N. A.; Mitome, H.; Yamada, Y. A phenolic cinnamate dimer from *Psoralea plicata*. *Phytochemistry* **1997**, *45*, 1257−1261.

(35) Qiao, C.-F.; Han, Q.-B.; Mo, S.-F.; Song, J.-Z.; Xu, L.-J.; Chen, S.-L.; Yang, D.-J.; Kong, L.-D.; Kung, H.-F.; Xu, H.-X. Psoralenoside and isopsoralenoside, two new benzofuran glycosides from *Psoralea corylifolia*. *Chem. Pharm. Bull.* **2006**, *54*, 714−716.

(36) Schlatter, J.; Zimmerli, B.; Dick, R.; Panizzon, R.; Schlatter, C. Dietary intake and risk assessment of phototoxic furocoumarins in humans. *Food Chem. Toxicol.* **1991**, *29*, 523−530.

(37) Kono, Y.; Kobayashi, K.; Tagawa, S.; Adachi, K.; Ueda, A.; Sawa, Y.; Shibata, H. Antioxidant activity of polyphenolics in diets rate constants of reactions of chlorogenic acid and caffeic acid with reactive

species of oxygen and nitrogen. *Biochim. Biophys. Acta* **1997**, *1335*, 335−342.
(38) Jovanovic, S. V.; Simic, M. G. Antioxidants in nutrition. *Ann. N.Y. Acad. Sci.* **2000**, *899*, 326−334.
(39) Suzuki, N.; Goto, A.; Oguni, I.; Mashiko, S.; Nomoto, T. Reaction rate constants of tea leaf catechines wih superoxide: superoxide-dismutase (SOD)-like activity measured by *Cypridina* luciferin analogue chemiluminescence. *Chem. Express.* **1991**, *6*, 655−658.
(40) Nishikimi, N. Ascorbic acid with superoxide anion generated by the xanthine-xanthine oxidase system. *Biochem. Biophys. Res. Comun.* **1975**, *63*, 463−468.
(41) Hashizume, H.; Tsujimoto, Y. Evaluation of superoxide radical scavenging activity of dental phenolic compounds by ESR spin-trapping technique. *Jpn. J. Conservative Dentistry* **1992**, *35*, 1053−1058.
(42) Goto, N.; Niki, E. Rates of interactions of superoxide with vitamin E, vitamin C and related compounds as measured by chemiluminescence. *Biochim. Biophys. Acta* **1992**, *1115*, 201−207.
(43) Ou, B.; Hampsch-Woodill, M.; Prior, R. L. Development and validation of an improved oxygen radical absorbance capacity assay using fluorescein as the fluorescent probe. *J. Agric. Food Chem.* **2001**, *49*, 4619−4626.
(44) Chrubasik, S.; Wink, M. Treatment of osteoarthritic pain with herbal drugs. *Proceedings of the 8th World Congress on Pain*; International Association for the Study of Pain: Washington, DC, USA, 1998; pp 507−514.
(45) Cho, A. S.; Jeon, S. M.; Kim, M. J.; Yeo, J.; Seo, K. I.; Choi, M. S.; Lee, M. K. Chlorogenic acid exhibits anti-obesity property and improves lipid metabolism in high-fat diet-induced-obese mice. *Food Chem. Toxicol.* **2010**, *48*, 937−943.
(46) Li, S. Y.; Chang, C. Q.; Ma, F. Y.; Yu, C. L. Modulating effects of chlorogenic acid on lipids and glucose metabolism and expression of hepatic peroxisome proliferator-activated receptor-alpha in golden hamsters fed on high fat diet. *Biomed. Environ. Sci.* **2009**, *22*, 122−129.
(47) Meng, S.; Cao, J.; Feng, Q.; Peng, J.; Hu, Y. Roles of chlorogenic acid on regulating glucose and lipids metabolism: A review. *Evidence-Based Complement. Alternat. Med.* **2013**, No. 801457.
(48) dos Santos, M. D.; Almeida, M. C.; Lopes, N. P.; de Souza, G. E. Evaluation of the anti-inflammatory, analgesic and antipyretic activities of the natural polyphenol chlorogenic acid. *Biol. Pharm. Bull.* **2006**, *29*, 2236−2240.
(49) Pu, F.; Mishima, K.; Irie, K.; Motohashi, K.; Tanaka, Y.; Egawa, T.; Kitamura, Y.; Egashira, N.; Iwasaki, K.; Fujiwara, M. Neuroprotective effects of quercetin and rutin on spatial memory impairment in an 8-arm radial maze task and neuronal death induced by repeated cerebral ischemia in rats. *J. Pharmacol. Sci.* **2007**, *104*, 329−334.
(50) Nassiri-Asi, M.; Farivar, T. N.; Abbasi, E.; Sadeghnia, H. R.; Sheikhi, M.; Lotfizadeh, M.; Bazahang, P. Effects of rutin on oxidative stress in mice with kainic acid-induced seizure. *J. Integrative Med.* **2013**, *11*, 337−342.
(51) Wong, R. W. K.; Rabie, A. B. M. Effect of buguzhi (*Psoralea corylifolia* fruit) extract on bone formation. *Phytother. Res.* **2010**, *24*, 155−160.

concentrations higher than 95% in some orange varieties. For other citrus species, such as grapefruit, the proportion can be lower (between 80−90%), and in lemon, it can be even lower (bellow 75%). In the case of lemon, the presence of other monoterpene hydrocarbons, such as $\beta$-pinene and $\gamma$-terpinene, allows attainment of similar amounts of monoterpene hydrocarbons, as in orange. Other compounds, such as oxygenated monoterpenes (alcohols and aldehydes), also show interspecific variation.

The biological activity of citrus essential oils has been widely recognized.[30] For fruit flies, larval toxicity of some of their compounds has been reported for *C. capitata*,[26,31] and in general monoterpene hydrocarbons show less toxicity than oxygenated monoterpenes.[31] In addition, the proportions of monoterpenes and other compounds of the essential oils vary according to senescence of the fruit. These changes have been associated both with host acceptance[32] and with a reduction in peel extracts toxicity.[26]

The interaction of all the resistance mechanisms offered by the plant results in a variation between species and cultivars in their suitability as hosts. For example, lemon has been reported as the poorest host citrus for larval survival of *C. capitata*[24,23] and the Caribbean fruit fly, *Anastrepha suspensa* (Loew).[22] For *A. fraterculus* populations from Argentina, the absence of larval development allows proposing that lemon is not a host,[33] yet the mechanisms involved have not been investigated. In addition, the inability of the Mexican morphotype of *A. fraterculus* to successfully develop in the Valencia orange and the Ruby Red grapefruit renders the status of Mexican *A. fraterculus* as a pest of citrus in Mexico unsubstantiated.[34] In contrast, grapefruit has been reported as a good host for *A. suspensa*[22] and the Mexican fruit fly, *Anastrepha ludens* (Loew.),[35] and it was found naturally infested by *A. fraterculus* and *C. capitata* in Argentina.[17,18] For the case of *A. ludens*, it has been argued that its long ovipositor allows the females to lay the eggs in the albedo area of the peel, thus preventing the contact of the newly emerged larvae with the toxic compounds present in the essential oil glands from the flavedo on their way to the pulp.[36] Moreover, the susceptibility of citrus to *A. suspensa* was found to vary according to the senescence of the fruit.[22,37]

Given the relevance of understanding the resistance mechanisms of the plants that can affect host use in fruit flies, we investigated the role of peel extracts of lemon and grapefruit on the survival of the immature stages of *A. fraterculus*. We used an integrative approach and evaluated the insecticidal activity of the ether extracts obtained from the peel of the two citrus species as well as the toxicity of the major constituent of the essential oil (limonene) and one oxygenated monoterpene (citral). In addition, we evaluated the impact of the ripening stage of the fruit on the toxicity. We also evaluated another fruit fly species, *C. capitata,* from which extensive research has been done for comparison. Finally, we characterized the chemical composition of the extracts to allow identification of putative responsible compounds in case we found a differential mortality.

## MATERIALS AND METHODS

**Insects.** Eggs and first instar larvae of *A. fraterculus* and *C. capitata* were obtained from colonies established at the Agriculture Zoology laboratories of Estación Experimental Agroindustrial Obispo Colombres (EEAOC), Tucumán, Argentina. *Anastrepha fraterculus* colony was initiated in 1997 with pupae obtained from infested guavas, collected in the vicinity of Tafí Viejo, Tucumán province (northwest Argentina).[38] Wild individuals were introduced into the laboratory and were maintained following standard procedures.[38,39] *Ceratitis capitata* colony was initiated with wild individuals obtained from infested oranges collected at different localities in northwest Argentina (Salta and Jujuy provinces) and held under artificial rearing conditions using standard procedures. For the bioassays, eggs were collected from the rearing cages for 4 h. To evaluate the egg stage, eggs were used right after collection. For the larval stage, eggs were incubated for 48 to 72 h in a chamber at 25 ± 2 °C and 60 ± 20% relative humidity to obtain the larvae. All the experiments were conducted in the laboratory.

**Plant Material.** The citrus varieties used were lemon, *C. limon* var. Eureka, and grapefruit, *C. paradisi* var. Foster Seedless. Fruit were collected in May 2011 and in August 2012 from the experimental orchard at EEAOC (26°47′15,45″/65°11′23,72″) in Las Talitas, Tucumán, Argentina. These periods corresponded to two different ripening stages of the fruit; the fruit from May was at the stage in which it is harvested for its commercialization (the fruit is already ripening and is turning from green to yellow) while the fruit from August corresponded to the overripe stage. Fruits were randomly selected from different plants; however, special precaution was taken to avoid damaged fruit or with symptoms of illness or pests.

**Extraction of Ether Extracts.** One day after harvest, the fruits were washed with tap water and dried at room temperature. The flavedo was removed from the peel with a metal grater and placed in a glass Erlenmeyer. Peel compounds were extracted with ethyl ether by immersion. The flask was covered with a cotton plug and was placed on a shaker for 40 min. Ether extracts were filtered, and the solvent was evaporated using a rotary evaporator at room temperature.

**Chemical Compounds.** Two compounds were also evaluated. The monoterpene hydrocarbon limonene was selected, since it is the predominant compound of essential oil citrus extracts; the oxygenated monoterpene citral was selected because it is a component that exhibited high toxicity against *C. capitata* larvae.[26,31] (*R*)-Limonene (98%) and citral (mixture of neral and geranial) (95%) were purchased from Sigma-Aldrich, Buenos Aires, Argentina.

**Chemical Characterization of the Ether Extracts from the Peel.** The chemical characterization of the extracts was performed at the Laboratory for Research and Analytical Services (LISA) from Facultad de Bioquímica, Química y Farmacia, Universidad Nacional de Tucumán (FBQF-UNT) (Tucumán, Argentina). The ether extracts were analyzed by gas chromatography (GC) using an Ultra Trace gas chromatograph with DB-1 column-MS 25 mm × 0.25 mm ID, temperature ramp of 60 to 300 °C (3 °C/min), and an injection temperature of 270 °C. The mass spectrometer used was a Polaris Q, EI (+) 70 eV with an ion trap analyzer as detector. Individual peaks were identified by the retention time and retention rates. At least two independent analyses were performed for each extract. The results were processed to obtain the percentage of the area occupied by each compound, and this value was averaged in each extract. The components were identified by the comparison of their retention index (RI) with reference to a homologous series of *n*-alkanes (C9−C25), by comparing their mass spectra with those reported in the literature, and by computer matching with the Adams 31[40] library.

**Bioassays.** *Fumigant Toxicity Assessment. Eggs.* Fumigant toxicity was determined by exposing the eggs to the volatiles of the ether extracts or to the pure compounds. For each experimental unit, 20 eggs were deposited with the aid of a fine brush on a piece of black filter paper (2 cm × 2 cm) which was in turn placed over a dampened cloth (5 cm × 5 cm) inside a glass Petri dish of 10 cm diameter (90 $cm^3$ volume). The cloth was used to avoid the dehydration of the eggs. On the other side of the Petri dish, and without being in contact with the damp cloth, a square of filter paper (3 cm × 3 cm), previously impregnated with the extract or the corresponding compound, was placed. The Petri dish was sealed with parafilm and incubated at 25 °C for 24 h. Then the damp cloth and the filter paper with the eggs were placed in an untreated plastic Petri dish of 10 cm diameter and left for incubation. After 5 days, the number of chorions (corresponding to those individuals that survived the embryonic developmental stage)

**Table 1. Chemical Compositions of the Ether Extracts from Citrus Peel of Ripe and Overripe Fruit of Lemon and Grapefruit, and Their Relative Proportions (% Area)**

| | | ripe | | overripe | |
|---|---|---|---|---|---|
| compound | RI[a] | *C. limon* | *C. paradisi* | *C. limon* | *C. paradisi* |
| α-thujene | 935 | 0.25 ± 0.02[b] | | | |
| α-pinene | 942 | 1.20 ± 0.17 | 0.22 | 0.69 ± 0.17 | |
| camphene | 957 | 1.27 ± 0.17 | 0.33 ± 0.06 | | |
| sabinene | 983 | | | 1.13 ± 0.23 | 0.28 ± 0.06 |
| β-pinene | 988 | 6.08 ± 0.73 | 0.21 ± 0.05 | 5.94 ± 0.59 | 0.23 ± 0.31 |
| myrcene | 1000 | 1.54 ± 0.17 | 1.36 ± 0.12 | 1.11 ± 0.21 | 1.30 ± 0.26 |
| octanal | 1010 | 0.02 ± 0.01 | 0.58 ± 0.3 | | |
| pseudolimonene | 1018 | tr[c] | | | |
| *o*-cimene | 1032 | 0.18 ± 0.25 | | 0.66 ± 0.13 | 0.07 |
| *d*-limonene | 1042 | 71.50 ± 1.37 | 82.70 ± 0.98 | 64.3 ± 4.58 | 88.5 ± 0.88 |
| (ε)-β-ocimene | 1055 | 0.11 | 0.23 ± 0.05 | | |
| γ-terpinene | 1068 | 9.38 ± 0.43 | 0.10 ± 0.01 | 11 ± 0.6 | 0.34 ± 0.49 |
| *cis*-sabinene hydrate | 1075 | 0.08 ± 0.02 | 0.33 ± 0.44 | | |
| terpinolene | 1097 | 0.32 ± 0.01 | 0.07 ± 0.05 | | |
| linalool | 1107 | 0.27 ± 0.05 | 0.43 ± 0.28 | | |
| nonanal | 1111 | 0.09 ± 0.01 | 0.12 ± 0.08 | | |
| camphor | 1158 | 0.04 ± 0.01 | 0.12 ± 0.06 | | |
| (ε)-isocitral | 1190 | 0.38 ± 0.05 | 0.43 ± 0.31 | 0.56 ± 0.12 | 0.12 ± 0.02 |
| decanal | 1209 | 0.02 ± 0.01 | 0.71 ± 0.3 | | |
| nerol | 1229 | 0.32 ± 0.03 | 0.14 ± 0.09 | 0.86 ± 0.2 | 0.02 |
| neral | 1240 | 1.25 ± 0.11 | 0.17 ± 0.11 | 1.13 ± 0.19 | 0.05 ± 0 |
| geraniol | 1252 | 0.23 ± 0.02 | 0.10 ± 0.08 | 0.9 ± 0.2 | 0.04 ± 0.04 |
| geranial | 1267 | 1.82 ± 0.16 | 0.36 ± 0.22 | 1.7 ± 0.29 | 0.08 ± 0.03 |
| undecanal | 1299 | 0.03 ± 0.01 | 0.07 ± 0.04 | | |
| neryl acetate | 1357 | 0.44 ± 0.02 | 0.02 | 1.53 ± 0.25 | 0.03 ± 0.01 |
| α-copaene | 1368 | | 0.27 ± 0.03 | | |
| geranyl acetate | 1375 | 0.25 ± 0.01 | 0.16 ± 0.07 | | |
| β-elemenene | 1381 | 0.01 | 0.23 ± 0.03 | | |
| dodecanal | 1398 | | 0.06 ± 0.03 | | |
| β-caryophillene | 1409 | 0.33 ± 0.01 | 0.65 ± 0.01 | 0.39 ± 0.08 | 1.05 ± 0.22 |
| trans-α-bergamotene | 1425 | | | 1.17 ± 0.16 | 0.02 |
| α-humulene | 1442 | 0.03 ± 0.01 | 0.11 ± 0.02 | | |
| bicyclo germacrene | 1482 | 0.05 ± 0.02 | 0.07 ± 0.03 | | |
| β-bisabolene | 1494 | 0.72 ± 0.03 | | 1.88 ± 0.35 | |
| δ-cadinene | 1506 | tr | 0.3 ± 0.01 | | |
| hexadecanoic acid | 1865 | 0.02 ± 0.01 | 0.10 ± 0.01 | | |
| citroptene | 1875 | 0.24 ± 0.15 | 0.01 | 0.28 ± 0.07 | |
| bergamotene | 1929 | 0.01 | 0.09 ± 0.01 | | |
| ostole | 1989 | | 0.19 ± 0.01 | | |
| coumarin | 2056 | 0.01 | 0.35 ± 0.47 | | |
| oxypseucedanin | 2063 | | 5.69 ± 1.82 | | |
| prangenin | 2210 | | 0.23 ± 0.01 | | |
| auraptene | 2292 | | 1.56 | | |
| unidentified | 2304 | 0.05 | 1.03 ± 0.76 | | |
| *monoterpene hydrocarbons* | | 91.86 | 85.55 | 85.58 | 90.75 |
| *sesquiterpene hydrocarbons* | | 1.14 | 1.63 | 4.02 | 1.57 |
| *alcohols* | | 0.90 | 0.99 | 2.24 | 0.24 |
| *aldehydes* | | 3.61 | 2.48 | 3.38 | 0.35 |
| *esters* | | 0.69 | 0.18 | | |
| *coumarins* | | 0.25 | 1.66 | 0.28 | 0.1 |
| *total* | | 98.57 | 99.86 | 95.12 | 92.09 |

[a]Retention index on a DB-1MS column relative to homologous series of *n*-alkanes. [b]Mean ± SE. [c]tr, trace, <0.01%.

and turgid eggs (corresponding to dead individuals) were quantified. In the controls, the filter paper was clean.

*Larvae.* The experimental design was similar to that used for eggs; each experimental unit consisted of 20 larvae that were placed on a black filter paper which, in this case, was placed over a pile of five pieces of white filter paper (2 cm × 3 cm) moistened with a sugar solution 10% (w/v). The extract or compound was applied on another piece of filter paper, placed at the opposite end of the Petri dish. The plate was sealed with parafilm and incubated for 24 h, the time at which larval mortality was registered (each larva was considered dead

**Table 2. Fumigant Activity of the Ether Extracts of Lemon cv. Eureka and Grapefruit cv. Foster Seedless and Two Monoterpenes in Eggs and Larval Stages of *Anastrepha fraterculus***

| stage | compound | $n$ | $LC_{50}$[a] (95% CL[b]) $\mu L/cm^3$ air | | $LC_{90}$[a] (95% CL[b]) $\mu L/cm^3$ air | | $\chi^2$ (d.f.) |
|---|---|---|---|---|---|---|---|
| egg | lemon ether extract | 597 | 0.23 a[c] | (0.20−0.26) | 0.36 | (0.32−0.42) | 0.56 (3) |
| | grapefruit ether extract | 601 | 0.28 a | (0.23−0.33) | 0.62 | (0.50−0.87) | 0.12 (2) |
| | limonene | 599 | 0.16 b | (0.14−0.18) | 0.27 | (0.24−0.31) | 1.71 (3) |
| | citral | 599 | 0.04 c | (0.02−0.06) | 0.16 | (0.09−0.42) | 2.25 (2) |
| larva | lemon ether extract | 1060 | 0.07 c | (0.03−0.12) | 0.34 | (0.16−6.19) | 8.90 (3) |
| | grapefruit ether extract | 1017 | 0.08 c | (0.05−0.11) | 0.40 | (0.19−7.38) | 3.88 (3) |

[a]Lethal concentration. [b]Confidence limits. [c]Values followed by different letters are significantly different ($p < 0.05$).

**Table 3. Fumigant Toxicity of the Ether Extracts of Ripe and Overripe Lemon cv. Eureka and Grapefruit cv. Foster Seedless on Eggs of *Anastrepha fraterculus***

| compound | ripening stage | $n$ | $LC_{50}$[a] (95% CL[b]) $\mu L$ extract/$cm^3$ air | | $LC_{90}$[a] (95% CL[b]) $\mu L$ extract/$cm^3$ air | | $\chi^2$ (d.f.) |
|---|---|---|---|---|---|---|---|
| lemon ether extract | ripe | 1078 | 0.16 ab[c] | (0.14−0.18) | 0.24 | (0.22−0.28) | 0.30 (2) |
| | overripe | 893 | 0.19 a | (0.17−0.21) | 0.27 | (0.24−0.34) | 0.01 (1) |
| grapefruit ether extract | ripe | 1068 | 0.14 b | (0.12−0.15) | 0.21 | (0.19−0.25) | 0.06 (2) |
| | overripe | 1074 | 0.16 ab | (0.14−0.17) | 0.23 | (0.21−0.28) | 0.56 (2) |

[a]Lethal concentration. [b]Confidence limits. [c]Values followed by different letters are significantly different ($p < 0.05$).

when it remained immobile even after touching it gently with a brush). The control was performed similarly but without applying any extract or compound.

*Contact Toxicity Assessment. Eggs.* Contact toxicity was evaluated by incubating the eggs in an emulsion of water with a sodium salt of carboxymethylcellulose containing the extract or compound.[41] The eggs were obtained and manipulated as described previously. Once the black filter paper with the 20 eggs was placed in the damp cloth, 100 $\mu$L of the emulsion was applied with a micropipette (Eppendorf ). The Petri dish was sealed with parafilm and incubated at 25 °C for 5 days. The control was performed similarly, but the emulsion contained no extract or compound. Mortality was assessed as described for fumigant toxicity bioassays.

*Larvae.* Contact toxicity also involved the use of an emulsion which, in this case, contained sugar to provide food. Larvae were obtained and manipulated as described in the fumigant toxicity section. After applying the emulsion (100 $\mu$L), the Petri dish was sealed with parafilm. For the controls, the larvae were imbibed in the emulsion that lacked any extract or compound. Larval mortality was registered after 24 h of exposure. Both bioassays were performed in compliance with the appropriate laws and institutional guidelines to meet security standards and adequate animal handling.

**Experiments and Treatments.** *Experiment 1. Fumigant Toxicity of Lemon and Grapefruit Ether Extracts and Limonene and Citral on Egg and Larval Stages.* For the egg stage, the concentrations used were 0.07, 0.14, 0.28, 0.56, 1.11, and 2.22 $\mu$L extract/$cm^3$ air for the lemon and grapefruit extracts; 0.11, 0.21, 0.42, 0.83, and 1.11 $\mu L/cm^3$ air for limonene and 0.01, 0.11, 0.22, 0.44, and 0.89 $\mu L/cm^3$ air for citral. The number of individuals evaluated for each concentration ranged between 60 and 100, involving three to five independent repetitions. For the larval stage, the concentrations used were 0.014, 0.028, 0.056, 0.111, and 0.222 $\mu$L extract/$cm^3$ air. The number of individuals evaluated for each concentration ranged between 100 and 200, involving five to ten independent repetitions.

*Experiment 2. Fumigant Toxicity of Extracts Obtained at Different Ripening Stages from Lemon and Grapefruit on Egg Stage.* The concentrations used were 0.07, 0.14, and 0.28 $\mu$L extract/$cm^3$ air for the extracts of ripe lemon and grapefruit. The number of individuals evaluated for each concentration in each extract ranged between 60 and 100, involving three and five independent repetitions. The concentrations for overripe fruit were 0.07, 0.14, 0.28, and 0.55 $\mu$L extract/$cm^3$ air. The number of individuals evaluated for each concentration in each extract ranged between 60 and 100, involving three and five independent repetitions.

*Experiment 3. Comparative Analysis between A. fraterculus and C. capitata.* The comparative analysis between *A. fraterculus* and *C. capitata* involved peel extracts of lemon and grapefruit and limonene and citral. A contact assay for eggs and larvae was performed. For eggs, dilutions were performed at 50%, starting from an emulsion containing 100 $\mu$L of fruit extract or limonene, while for citral, they were performed starting from an emulsion containing 20 $\mu$L per mL. Eight concentrations were used: 1.56, 5, 6.25, 12.5, 25, 50, 75, and 100 $\mu$L per mL for extracts or compound in eggs of *A. fraterculus*, seven concentrations of lemon or grapefruit extract were evaluated on *C. capitata*: 6.25, 12.5, 25, 50, 100, 200, and 400 $\mu$L per mL for extracts. Dilutions for limonene started from an emulsion containing 100 $\mu$L per mL, and seven concentrations were used. One to four replicates were performed for each extract. For the larvae, dilutions were also performed at 50%, starting with an emulsion containing 20 $\mu$L of extract or compound per mL of solution. A total of nine concentrations were applied: 0.156, 0.3125, 0.625, 1.25, 2.5, 5, 6.25, 12.5, and 20 $\mu$L per mL.

**Data Analysis.** Data were analyzed by a probit analysis to obtain $LC_{50}$ and $LC_{90}$ values. Mortality was corrected in those cases in which the control cages had dead individuals (mortality attributable to a reason not related to the toxicity of the essential oil). The significance of the model was determined by a goodness of fit $\chi$-square test estimated with maximum likelihood. In all cases, the statistical package POLO Plus V1 (Software LeOra 2002−2003)[42] was used. Differences between $LC_{50}$ values were considered significant when the respective Confidence Intervals 95% (CI95%) did not overlap.

## RESULTS

**Chemical Characterization of the Ether Extracts from Lemon and Grapefruit.** The chemical characterization of the different extracts is presented in Table 1. For all extracts, the major chemical group was monoterpene hydrocarbons, and within this group, the major compound was D-limonene (higher than 70%), except in the extract from overripe lemon. The remaining chemicals ranged from 10.96% to 0.01%. The main constituents (more than 1% of the total area) of the extract of ripe lemon were D-limonene, $\gamma$-terpinene, $\beta$-pinene, geranial, myrcene, camphene, neral, and $\alpha$-pinene. In the case of grapefruit extract, the major compounds were limonene, oxypseucedanin, auraptene, and myrcene. The extract of the overripe lemon was characterized by D-limonene, $\gamma$-terpinene, $\beta$-pinene, $\beta$-bisabolene, geranial, neryl acetate, $\alpha$-*trans*-berga-

**Table 4. Contact Toxicity of the Lemon Ether Extract cv. Eureka and Grapefruit Ether Extract cv. Foster Seedless, and Compounds Limonene and Citral in *Anastrepha fraterculus* and *Ceratitis capitata* Eggs**

| compound | species | $n$ | $LC_{50}$[a] (95% CL[b]) μL/mL | | $LC_{90}$ (95% CL) μL/mL | | $\chi^2$ (df) |
|---|---|---|---|---|---|---|---|
| lemon ether extract | *A. fraterculus* | 520 | 18.12 ac[c] | (6.11−26.03) | 36.87 | (25.53−58.46) | 9.95 (6) |
| | *C. capitata* | 177 | 113.46 b | (68.15−158.75) | 323.94 | (231.62−596.73) | 2.43 (4) |
| grapefruit ether extract | *A. fraterculus* | 802 | 26.25 c | (17.83−35.59) | 57.64 | (41.93−97.99) | 8.21 (4) |
| | *C. capitata* | 264 | 72.94 bd | (41.13−111.50) | 240.43 | (150.60−632.98) | 9.16 (5) |
| limonene | *A. fraterculus* | 258 | 34.04 cd | (25.38−42.74) | 80.37 | (60.30−146.11) | 5.68 (6) |
| | *C. capitata* | 140 | 77.06 b | (55.35−95.27) | 119.64 | (96.47−241.28) | 3.33 (5) |
| citral | *A. fraterculus* | 717 | 12.82 a | (11.26−14.36) | 16.79 | (14.95−19.75) | 4.25 (5) |
| | *C. capitata* | 712 | 22.44 c | (19.37−34.21) | 41.76 | (29.77−193.58) | 1.46 (5) |

[a]Lethal concentration. [b]Confidence limits. [c]Values followed by different letter are significantly different ($p < 0.05$).

**Table 5. Contact Toxicity of the Lemon Ether Extract cv. Eureka and Grapefruit Ether Extract cv. Foster Seedless, and Compounds Limonene and Citral in *Anastrepha fraterculus* and *Ceratitis capitata* Larvae**

| compound | species | $n$ | $LC_{50}$[a] (95% CL[b]) μL/mL | | $LC_{90}$ (95% CL) μL/mL | | $\chi^2$ (df) |
|---|---|---|---|---|---|---|---|
| lemon ether extract | *A. fraterculus* | 234 | 0.43 a[c] | (0.14−0.73) | 2.07 | (1.20−7.92) | 0.789 (4) |
| | *C. capitata* | 148 | 0.44 a | (0.34−0.55) | 0.84 | (0.65−1.42) | 2.867 (4) |
| grapefruit ether extract | *A. fraterculus* | 253 | 0.61 ab | (0.25−1.06) | 3.51 | (1.94−12.09) | 6.084 (5) |
| | *C. capitata* | 155 | 0.60 a | (0.40−0.76) | 1.16 | (0.91−1.92) | 0.272 (5) |
| limonene | *A. fraterculus* | 171 | 0.84 abc | (0.04−2.57) | 23.93 | (6.30−9012.32) | 6.419 (4) |
| | *C. capitata* | 451 | 2.30 bc | (0.88−4.80) | 2.28 | (1.54−4.40) | 21.726 (5) |
| citral | *A. fraterculus* | 258 | 1.62 abc | (0.28−2.77) | 4.98 | (2.93−21.32) | 4.538 (4) |
| | *C. capitata* | 453 | 3.18 c | (2.29−4.01) | 7.69 | (4.96−35.86) | 6.315 (5) |

[a]Lethal concentration. [b]Confidence limits. [c]Values followed by different letters are significantly different ($p < 0.05$).

motene, neral, sabinene, and myrcene. Overripe grapefruit contained D-limonene, NI compound, myrcene, and β-caryophyllene.

**Fumigant Toxicity of Different Citrus Ether Extracts and Pure Compounds.** The volatile phases from lemon and grapefruit extracts were equally toxic to eggs of *A. fraterculus* ($p > 0.05$) (Table 2). Citral was four times more toxic than limonene, with their $LC_{50}$ values (0.04 and 0.16 μL/cm$^3$ air, respectively) being significantly different ($p < 0.05$). Additionally, limonene was significantly more toxic than both lemon and grapefruit extracts ($p < 0.05$). In agreement with what was found in eggs, larval mortality was equal for lemon and grapefruit extracts ($p > 0.05$) (Table 2).

**Fumigant Toxicity of Ether Extracts Obtained at Different Ripening Stages from Lemon and Grapefruit.** The extract from overripe lemon was slightly less toxic than the extract from ripe lemon, but the difference between their $LC_{50}$ values was not significant ($p > 0.05$). The extracts of ripe and overripe grapefruit were equally toxic ($p > 0.05$) (Table 3).

**Comparative Analysis between *A. fraterculus* and *C. capitata*.** *Eggs.* Lemon extract was six times more toxic to eggs of *A. fraterculus* than to eggs of *C. capitata* with their $LC_{50}$ values (18.12 and 113.46, respectively) being significantly different ($p < 0.05$) (Table 4). Grapefruit extract was also significantly more toxic to eggs of *A. fraterculus* than to eggs of *C. capitata* ($LC_{50}$ 26.25 and 72.94, respectively) (Table 4). Eggs of *A. fraterculus* were significantly more susceptible to limonene and citral than those of *C. capitata* ($p < 0.05$) (Table 4).

*Larvae.* Toxicity values of lemon and grapefruit extracts as well as of limonene and citral revealed no differences in sensitivity between *A. fraterculus* and *C. capitata* ($p > 0.05$) (Table 5). Contrary to what was found for eggs, citral was equally as toxic as limonene ($p > 0.05$).

## DISCUSSION

The presence of toxic compounds in the citrus essential oils from the citrus peel has been proposed as the main resistance mechanism of citrus species against fruit flies. Our integrative approach allowed us to evaluate the toxicity of lemon and grapefruit peel extracts in *A. fraterculus* eggs and larvae, the toxicity of limonene (the major compound of both citrus species essential oils) and citral (one highly toxic oxygenated monoterpene), and the effect of fruit ripening on the toxicity from the extracts of the citrus peel. Moreover, with this approach we were able to compare *A. fraterculus* susceptibility with that from *C. capitata*, from which host records in citrus and resistance mechanisms are better known.

Extracts from the peels of lemon and grapefruit proved toxic to *A. fraterculus* eggs and larvae. This is in agreement with what has been found for *A. suspensa*[22] and *C. capitata*[26,31] and confirms, by contact and fumigant bioassays, the occurrence of chemical resistance mechanisms. Other works extended the detrimental effects of several essential oils to the adult stage as an attempt to find organic insecticides.[7,30] Evaluations involved essential oils from citrus species such as *C. arantium* L. against *C. capitata* and the olive fly, *Bactrocera oleae* (Gmelin),[27] and from other plants such as *Hyptis suaveolens* (L.) Poiteau, *Rosmarinus officinalis* L., *Lavandula angustifolia* Miller and *Thuja occidentalis* L.,[41] and *Tagetes* spp.[43] in *C. capitata*. There is even one case of development of a novel packaging system controlling the release of essential oils from *Eugenia caryophyllata* Thumb against *C. capitata*.[44] Here, we did not explore if the extracts were toxic to the adult stage given that our main objective was to study insect−plant interaction and the role of chemical resistance mechanisms present in the fruit as a determinant of its status as a host of *A. fraterculus*. Our

results provide good evidence to sustain that lemon has chemically mediated resistance mechanisms.

Lemon and grapefruit extracts showed the same levels of toxicity within and between fruit fly species. This was confirmed in the fumigant (*A. fraterculus* only) and contact (*A. fraterculus* and *C. capitata*) bioassays and at both the egg and larval stages. Comparative studies between citrus species in *A. suspensa* larvae showed the same trend; grapefruit, orange, and lemon oils were equally toxic.[22] In contrast, studies conducted in *C. capitata* larvae showed that lemon oil from the variety Maglini was less toxic than the oil of three varieties of sweet orange (Merlin, Artas, and New Hall) and the oil of bitter orange (*Citrus aurantium L.* (Rootstock)).[31] The authors attributed this difference to the presence of $\alpha$- and $\beta$-pinene (less toxic than limonene) and to the low concentration of limonene in the lemon oil (less than 75%), while in the orange varieties evaluated, limonene was always above 95%. In our study, even when the amount of limonene in the extract from Eureka lemon (71%) was also lower when compared with the extract of Foster Seedless grapefruit (83%), the toxicity was similar. The chemical profiles of Maglini (Table 1)[31] and Eureka (this study, Table 1) lemons presented similar amounts of monoterpene hydrocarbons (91.7% and 91.9% for Papachristos et al.[31] and for our work, respectively) and oxygenated monoterpenes (6.4% and 5.2% for Papachristos et al.[31] and for our work, respectively). However, we did not evaluate extracts with limonene levels higher than 95%, whereas Papachristos et al.[31] evaluated different orange varieties that contained limonene levels higher than 95%. On the other hand, the work presented by Greany et al.[22] lacks information on oils chemical composition. In conclusion, more studies involving more citrus species are needed in order to assess different susceptibility among fruit fly species attributable to different limonene amounts.

The toxicities of limonene and citral were different and depended on the stage evaluated. For eggs, limonene was less toxic than citral, for both *A. fraterculus* (fumigant and contacts bioassays) and *C. capitata* (contact bioassays). For larvae, the confidence intervals of the $LC_{50}$ obtained for *A. fraterculus* and *C. capitata* had a great overlap, suggesting that limonene and citral were equally toxic. This is not in agreement with what was found by Papachristos et al.[31] for *C. capitata* larvae. One possible explanation could be the interaction of some compounds with the media in which they are presented. In the case of Papachristos et al.,[31] compounds were dispensed in the larval diet while in our case they were applied in a sugar solution.

Overripe lemon extract was marginally less toxic to *A. fraterculus* eggs than that from ripe lemon. This can be explained by the fact that, in overripe lemon, limonene showed values below 70% of the area. It could be proposed that mixtures containing less than 70% of limonene will be less toxic than mixtures with higher values of this compound. This could be one reason for the senescence-related susceptibility of grapefruit to *A. suspensa* infestation.[37] However, our inferences are based on tests that evaluated fumigant activity. The extract from overripe lemon had equal content of citroptene compared to that of ripen fruit. This compound, being less volatile than limonene, could have not been available at the same amounts in the fumigant tests as in the contact. In addition, our asseveration needs further confirmation, since the confidence intervals had a slight overlap. As for grapefruit, the chemical profile was similar to that from the lemon, and this may be the main reason for the similar toxicity.

Larvae were more sensitive than eggs. This was shown in both the fumigant and contact evaluations. In the fumigant tests, larvae were approximately three times more sensitive while, for the contact tests, the relationship was much higher (approximately 45 times more sensitive). A major susceptibility in larvae compared to eggs has been reported for *C. capitata* after topical application of *Fueniculum vulgarem* Mill. oil.[45] In a study that evaluated the effect of egg age on fumigant toxicity of the essential oil from *Lavandula hybrid* Rev., *Rosmarinus officinalis* L., and *Eucalyptus globules* Labill in the beetle *Acanthoscelides obtectus* (Say), it was demonstrated that as the eggs aged, and consequently the embryo developed, the susceptibility to the toxic compounds from the essential oils increased.[46] The authors attributed this to the fact that monoterpenes act against insects as neurotoxins; thus, the ovicidal activity could only be apparent when the nervous system begins to develop. In our case, the exposure to toxic compounds was done to fresh eggs, so embryonic development is expected to have been at an early stage. Therefore, it would be necessary to test older eggs to confirm this hypothesis. Another possible and nonmutually exclusive explanation could be the importance of the chorion as a barrier to penetration of toxic compounds.

The comparison between *A. fraterculus* and *C. capitata* revealed differences between the two species. Eggs of *A. fraterculus* were more sensitive than eggs of *C. capitata* to the effect not only of lemon and grapefruit extracts but also of limonene and citral. In contrast, for the larvae, the toxicities in both species were similar. The differences found in eggs could be explained by differences in the permeability of the egg shell or the susceptibility to certain compounds or chemical groups. It is worth wondering whether the differences in egg sensitivity between species had an impact on the immature performance of the fruit. To express this difference, it is necessary that eggs are exposed to the essential oils, and this can happen if the females lay their eggs in the glands of the flavedo. It has been proposed that females can adjust their oviposition behavior and prefer laying their eggs in the less toxic area of the albedo to avoid the toxic flavedo. However, this can be possible only on those species in which the female has a long ovipositor. Birke et al.[36] have already proposed this as an explanation why *A. ludens* can infest different citrus species. In the same line of evidence, it has been indicated that the resistance that lemon exhibits to the attack of *A. suspensa*[22] would be related to the thickness of the flavedo, the high concentration of oxygenated terpenoids, such as linalool, and the absolute amount of oil present in the peel. Under this hypothesis, we should expect that *A. fraterculus* will not survive or will have a poor performance in citrus with thin albedo such as lemon and oranges and will be able to develop better in fruits with a thicker albedo such as grapefruit and bitter orange, since it has a long ovipositor. Field infestation data[17−19] and laboratory experiments[47] seem to support this hypothesis.

Conclusively, we showed that extracts from the citrus peel are toxic to *A. fraterculus* immature stages and this contributes to the nonhost condition of lemon for *A. fraterculus*. It is probable that this condition is attained by a combination of the presence of chemical resistance mechanisms, as shown here, and the structure of the lemon peel that enhances the chances of the eggs or the larvae to enter in contact with the essential oil. Our results and those from Augier et al.,[48] with thorough

inspections of field and packing houses, as well as those of Gastaminza et al.,[33] with fruit-infestation laboratory and field experiments, provide good evidence and follow the guidelines to determine the host condition of a given species and variety of fruit to a given fruit fly species.[49,50] The recognition of the nonhost status of lemon will surely contribute to improve trade agreements.

## AUTHOR INFORMATION


### Corresponding Author

*Telephone: (+54) 381 4390003. Fax: (+54) 381 4364156. E-mail: josefinaruiz2802@hotmail.com.



### Funding

Financial support was provided by grants BID-PICTO 2005 32932 and BID-PICT 2006 1747 from Agencia Nacional de Promoción Cientacuífica y Tecnológica, ANPCyT, and research contracts 13015 and 11894 from the International Atomic Energy Agency, IAEA.


### Notes

The authors declare no competing financial interest.

## ACKNOWLEDGMENTS


We appreciate the valuable technical help of all the personnel from the Agriculture Zoology laboratories of Estación Experimental Agroindustrial Obispo Colombres (EEAOC) for their collaboration along the course of this study. We thank Dr. Nikos Papadopoulos for his valuable comments in an earlier version of the manuscript and three anonymous reviewers for all the constructive input during the revision process of the manuscript.


## REFERENCES


(1) Christenson, L. D.; Foote, R. H. Biology of fruit flies. *Annu. Rev. Entomol.* **1960**, *5*, 171−192.

(2) White, I. M.; Elson-Harris, M. M. *Fruit Flies of Economic Significance: their Identification and Bionomics*; C.A.B. International in association with Australian Centre for International Agricultural Research (ACIAR): Wallingford, Oxon, U.K., 1992; p 601.

(3) Greany, P. D. Host plant resistance to tephritids: an under-exploited control strategy. In *Fruit flies: Their Biology, Natural Enemies and Control*; Robinson, A. S., Hooper, G., Eds.; Elsevier: Amsterdam, The Netherlands, 1989; Vol. 3*A*, pp 353−362.

(4) Aluja, M. R. *Manejo Integrado de la Mosca de la Fruta*; Trillas Ed.: Mexico, 1993; p 251.

(5) Aluja, M. R. Bionomics and management of *Anastrepha*. *Annu. Rev. Entomol.* **1994**, *39*, 155−178.

(6) Follett, P. A.; Neven, L. G. Current trends in quarantine entomology. *Annu. Rev. Entomol.* **2006**, *51*, 359−385.

(7) Isman, M. B. Botanical insecticides, deterrents and repellents in modern agriculture and an increasingly regulated world. *Annu. Rev. Entomol.* **2006**, *51*, 45−66.

(8) Devorshak, C. Area-Wide Integrated Pest Management Programmes and Agricultural Trade: Challenges and Opportunities for Regulatory Plant Protection. In *Area-Wide Control of Insect Pests. From Research to Field Implementation*, 1 st ed.; Vreysen, M. J. B., Robinson, A. S., Hendrichs, J., Eds.; Springer: The Netherlands, 2007; pp 407−415.

(9) Guillén, D.; Sánchez, R. Expansion of the national fruit fly control programme in Argentina. In *Area-Wide Control of Insect Pests. From Research to Field Implementation*, 1 st ed.; Vreysen, M. J. B., Robinson, A. S., Hendrichs, J., Eds.; Springer: The Netherlands, 2007; pp 653−660.

(10) Hernández-Ortiz, V.; Aluja, M. Listado de especies del género neotropical *Anastrepha* (Diptera: Tephritidae) con notas sobre su distribución y plantas hospederas. *Folia Entomol. Mex.* **1993**, *88*, 89−105.

(11) Malavasi, A.; Zucchi, A.; Sugayama, R. Biogeografía. In *Moscas-das-frutas de Importância Econômica no Brasil. Conhecimento básico e aplicado*, 1 st ed.; Malavasi, A., Zucchi, R. A., Eds.; Holos: Ribeirão Preto, 2000; pp 93−98.

(12) Norrbom, A. L.; Kim, K. C. A list of the reported host plant of the species of *Anastrepha* (Diptera: Tephritidae). U.S. Dept. Agric. Animal Plant Health Inspection Service. *Miscellaneous Publication 81(USA)* **1988**, 52.

(13) Norrbom, A. L. *Host plant database for Anastrepha and Toxotrypana (Diptera: Tephritidae: Toxotrypanini), Diptera Data Dissemination Disk*; North American Dipterist's Society: Washington, DC, 2003.

(14) FAO/IAEA. Distribution map of Ceratitis capitata. 2013. http://nucleus.iaea.org/sites/naipc/twd/PublishingImages/Forms/DispForm.aspx?ID=50 (September 16, 2014 most recent access date).

(15) Liquido, N. J.; Barr, P. G.; Cunningham, R. T. MEDHOST, an encyclopedic bibliography of the host plants of the Mediterranean fruit fly, *Ceratitis capitata* (Wiedemann), version 1; *Fruit fly expert identification system and systematic information database, Diptera dissemination disk*; 2013, vol. *1*.

(16) Federcitrus. La actividad citrícola argentina. Informe Anual. Federación Argentina del Citrus, Buenos Aires, Argentina. 2014. http://www.federcitrus.org/noticias/upload/informes/Act%20Citricola%2014.pdf (September 16, 2014 most recent access date).

(17) Ovruski, S. M.; Schliserman, P.; Aluja, M. Native and introduced host plants of *Anastrepha fraterculus* and *Ceratitis capitata* (Diptera: Tephritidae) in Northwestern Argentina. *J. Econ. Entomol.* **2003**, *96*, 1108−1118.

(18) Segura, D. F.; Vera, T.; Cagnotti, C.; Vaccaro, N.; De Coll, O.; Ovruski, S.; Cladera, J. Relative abundance of *Ceratitis capitata* and *Anastrepha fraterculus* (Diptera: Tephritidae) in diverse host species and localities of Argentina. *Ann. Entomol. Soc. Am.* **2006**, *99*, 70−83.

(19) Oroño, L. E.; Albornoz-Medina, P.; Núñez-Campero, S.; van Nieuwenhove, G. A.; Bezdjian, L. P.; Martin, C. B.; Schliserman, P.; Ovruski, S. M. Update of host plant list of *Anastrepha fraterculus* and *Ceratitis capitata* in Argentina. In *Fruit Flies of Economic Importance: From Basic to Applied Knowledge*; Sugayama, R. L., Zucchi, R. A., Ovruski, S. M., Sivinski, J., Eds; Biofábrica: Moscamed Brazil, Salvador, Bahia, Brazil, 2008; pp 207−225.

(20) Back, E. A.; Pemberton, C. E. Susceptibility of citrus fruits to the attack of the Mediterranean fruit fly. *J. Agric. Res.* **1915**, *3*, 311−330.

(21) Papachristos, D. P.; Papadopoulos, N. T. Are citrus species favorable hosts for the Mediterranean fruit fly? A demographic perspective. *Entomol. Exp. Appl.* **2009**, *132*, 1−12.

(22) Greany, P. D.; Styer, S. C.; Davis, P. L.; Shaw, P. E.; Chambers, D. L. Biochemical resistance of citrus to fruit flies. Demonstration and elucidation of resistance to the Caribbean fruit fly. *Anastrepha suspensa*. *Entomol. Exp. Appl.* **1983**, *34*, 40−50.

(23) Papachristos, D. P.; Papadopoulos, N. T.; Nanos, G. D. Survival and development of immature stages of the Mediterranean fruit fly (Diptera: Tephritidae) in citrus fruit. *J. Econ. Entomol.* **2008**, *101*, 866−872.

(24) Spitler, G. H.; Armstrong, J. W.; Couey, H. M. Mediterranean fruit fly (Diptera: Tephritidae) host status of commercial lemon. *J. Econ. Entomol.* **1984**, *77*, 1441−1444.

(25) Bodenheimer, F. S. *Citrus Entomology in the Middle East*; Junk: Gravenhage, The Netherlands, 1951; p 663.

(26) Salvatore, A.; Borkosky, S.; Willink, E.; Bardón, A. Toxic effects of lemon peel constituents on *Ceratitis capitata*. *J. Chem. Ecol.* **2004**, *30*, 323−333.

(27) Siskos, E. P.; Konstantopoulou, M. A.; Mazomenos, B. E. Insecticidal activity of *Citrus aurantium* peel extract against *Bactrocera oleae* and *Ceratitis capitata* adults (Diptera: Tephritidae). *J. Appl. Entomol.* **2009**, *133*, 108−116.

(28) Kouloussis, N. A.; Katsoyannos, B. I.; Papadopoulos, N. T.; Ioannou, C. S.; Iliadis, I. V. Enhanced mating competitiveness of

*Ceratitis capitata* males following exposure to citrus compounds. *J. Appl. Entomol.* **2013**, *137* (Suppl.1), 30−38.
(29) Jing, L.; Lei, Z.; Li, L.; Xie, R.; Xi, W.; Guan, Y.; Sumner, L. W.; Zhou, Z. Antifungal activity of citrus essential oils. *J. Agric. Food Chem.* **2014**, *62*, 3011−3033.
(30) Regnault-Roger, C.; Vincent, C.; Arnason, J. Essential oils in insect control: low-risk products in a highstakes world. *Annu. Rev. Entomol.* **2012**, *57*, 405−424.
(31) Papachristos, D. P.; Kimbaris, A. C.; Papadopoulos, N. T.; Polissiou, M. G. Toxicity of citrus essential oils against *Ceratitis capitata* (Diptera: Tephritidae) larvae. *Ann. Appl. Biol.* **2009**, *155*, 381−389.
(32) Ioannou, C. S.; Papadopoulos, N. T.; Kouloussis, N. A.; Tananaki, C. I.; Katsoyannos, B. I. Essential oils of citrus fruit stimulate oviposition in the Mediterranean fruit fly *Ceratitis capitata* (Diptera: Tephritidae). *Physiol. Entomol.* **2012**, *37*, 330−339.
(33) Gastaminza, G.; Augier, L.; Villagrán, M. E.; Villagrán, M. F.; Willink, E. Determinación de la condición del limón como hospedero de *Ceratitis capitata* y *Anastrepha fraterculus*. In *Moscas de los Frutos y su Relevancia Cuarentenaria en la Citricultura del Noroeste de Argentina. Once años de investigaciones 1996−2007*; Estación Experimental Agroindustrial Obispo Colombres: Tucumán, Argentina, 2007, http://www.eeaoc.org.ar/publicaciones/categoria/18/81/LZ- (September 16, 2014 most recent access date).
(34) Aluja, M.; Pérez-Staples, D.; Macías-Ordóñez, R.; Piñeiro, J.; McPheron, B.; Hernández-Ortiz, V. Nonhost status of *Citrus sinensis* cultivar Valencia and *C. paradisi* cultivar Ruby Red to Mexican *Anastrepha fraterculus* (Diptera: Tephritidae). *J. Econ. Entomol.* **2003**, *96*, 1693−1703.
(35) Leyva, J. L.; Browning, H. W.; Gilstrap, F. E. Development of *Anastrepha ludens* (Diptera: Tephritidae) in several host fruit. *Environ. Entomol.* **1991**, *20*, 1160−1165.
(36) Birke, A.; Aluja, M.; Greany, P.; Bigurra, E.; Pérez-Staples, D.; McDonald, R. Long aculeus and behavior of *Anastrepha ludens* render gibberellic acid ineffective as an agent to reduce 'Ruby Red' grapefruit susceptibility to the attack of pestiferous fruit fly in commercial groves. *J. Econ. Entomol.* **2006**, *99*, 1184−1193.
(37) Greany, P. D.; Shaw, P. E.; Davis, P. L.; Hatton, T. T. Senescence-related susceptibility of Marsh grapefruit to laboratory infestation by *Anastrepha suspensa*. *Fla. Entomol.* **1985**, *68*, 144−150.
(38) Jaldo, H. E.; Gramajo, C.; Willink, E. Mass rearing of *Anastrepha fraterculus* (Diptera: Tephritidae): a preliminary strategy. *Fla. Entomol.* **2001**, *84*, 716−718.
(39) Vera, M. T.; Abraham, S.; Oviedo, A.; Willink, E. Demographic and quality control parameters of *Anastrepha fraterculus* (Diptera: Tephritidae) artificial rearing. *Fla. Entomol.* **2007**, *90*, 53−57.
(40) Adams, R. P. *Identification of essential oil components by gas chromatography quadrupole mass spectroscopy*; Allured Publishers: Carol Stream, IL, 2001.
(41) Benelli, G.; Flamini, G.; Canale, A.; Cioni, P. L.; Conti, B. Toxicity of some essential oil formulations against the Mediterranean fruit fly *Ceratitis capitata* (Wiedemann) (Diptera Tephritidae). *Crop Prot.* **2012**, *42*, 223−229.
(42) LeOra Software 2002−2003. Polo Plus. Probit and Logit Analysis. Versión 1.
(43) López, S. B.; López, M. L.; Aragon, L. M.; Tereschuk, M. L.; Slanis, A. C.; Feresin, G. E.; Zygadlo, J. A.; Tapia, A. A. Composition and anti-insect activity of essential oils from *Tagetes* L. species (Asteraceae, Helenieae) on *Ceratitis capitata* Wiedemann and *Triatoma infestans* Klug. *J. Agric. Food Chem.* **2011**, *59*, 5286−5292.
(44) Arancibia, M.; Rabossi, A.; Bochicchio, P. A.; Moreno, S.; López-Caballero, M. E.; Gómez-Guillén, M. C.; Montero, P. Biodegradable films containing clove or citronella essential oils against the Mediterranean fruit fly *Ceratitis capitata* (Diptera: Tephritidae). *J. Agric. Food. Technol.* **2013**, *3*, 1−7.
(45) Oliveira, F. Q. D.; Malaquias, J. B.; Figueiredo, W. R. D.S.; Batista, J. D. L.; Beserra, E. B.; Oliveira, R. D. Insecticidal activity of bioproducts on *Ceratitis capitata* Wiedemann (Diptera: Tephritidae). *Afr. J. Biotechnol.* **2014**, *13*, 1430−1438.
(46) Papachristos, D. P.; Stamopoulos, D. C. Fumigant toxicity of three essential oils on the eggs of *Acanthoscelides obtectus* (Say) (Coleoptera: Bruchidae). *J. Stored Prod Res.* **2004**, *40*, 517−525.
(47) Ruiz, M. J. *Mecanismos de resistencia química del limón al ataque de Anastrepha fraterculus (Diptera: Tephritidae)*. Ph.D. Thesis. Universidad Nacional de Tucumán, Argentina. 2013.
(48) Augier, L.; Gastaminza, G.; Villagrán, M. E.; Villagrán, M. F.; Zaia, G.; Willink, E.; Stein, B. Detección de la presencia de los estados juveniles de *Ceratitis capitata* y *Anastrepha fraterculus* en frutos de limón. In *Moscas de los Frutos y su Relevancia Cuarentenaria en la Citricultura del Noroeste de Argentina. Once años de investigaciones 1996−2007*; Estación Experimental Agroindustrial Obispo Colombres: Tucumán, Argentina, 2007, http://www.eeaoc.org.ar/publicaciones/categoria/18/79/LZ-Deteccion-de-la-presencia-de-los-estados-juveniles-de-mosca-en-limon---cap-7.html (September 16, 2014 most recent access date).
(49) Cowley, J. M.; Backer, R. T.; Harte, D. S. Definition and determination of host status for multivoltine fruit fly (Diptera: Tephritidae) species. *J. Econ. Entomol.* **1992**, *85*, 312−317.
(50) Aluja, M.; Mangan, R. L. Fruit fly (Diptera: Tephritidae) host status determination: critical conceptual, methodological, and regulatory considerations. *Annu. Rev. Entomol.* **2008**, *53*, 473−502.

A characterization of food thermal damage can be achieved through the indirect measurement of the lysine APs such as lactulosyl-lysine or maltulosyl-lysine during acid hydrolysis by measuring furosine[27,28] or bound HMF.[29,30] More recently, some techniques allowed the direct measurement of the APs through LC/ESI-MS with or without labeled internal standard.[4,31−33] Other two routinely indicators of thermal damage are CML and CEL, which can be analyzed by MALDI-TOF/MS,[34] LC-MS/MS after acidic hydrolysis stable isotope dilution assay,[35,36] and GC-MS.[37] This last technique is commonly used for the determination and accurate quantification of MR volatile compounds such as hydroxycarbonyls, glycolaldehyde, acetol, and acetoin, or off-flavor compounds such as methional and 2-acetyl-2-thiazoline.[38−41] Last, but not least, a broad range of publications focuses on the determination of $\alpha$-dicarbonyls by using different derivatizing agents.[42,43]

The control of the MR in food using functional ingredients can promote the formation of compounds having the desired color and flavor, and it can reduce the concentration of off-flavors and potential toxic molecules. During the past years several approaches have been proposed to inhibit MR development in milk,[44] specifically by using green tea extract or catechins.[45,46] The mechanism behind the trapping activity of phenolic rings has been elucidated, and the chemical structure of the epicatechin−methylglyoxal adduct has been identified.[47,48] Recently, response surface methodology has been used to investigate the dose−response relationship of a catechin, genistein, and diadzein mixture as a prethermal processing technique to reduce the formation of reactive carbonyl species (RCSs) such as glyoxal, methylglyoxal, and 3-deoxyglucosone in ultrahigh-temperature (UHT) milk.[49] Twenty compounds having an aromatic ring substituted with at least one hydroxyl group have been reacted with methylglyoxal: results about the trapping efficiency can be transferred to milk product to verify the possibility of producing new better quality milk beverages.[50]

Olive mill wastewater is a byproduct of the olive oil production process and represents an abundant source of phenolic compounds.[51] olive mill wastewater typically contains 98% total phenols originally present in the olive, only a minor part being recovered in olive oil.[52] olive mill wastewater contains >60 phenolic compounds, among which the most relevant are secoiridoid derivatives, such as hydroxytyrosol and the dialdehydic form of decarboxymethyl oleuropein aglycone along with tyrosol and verbascoside.[53] The biological properties of its main components have been accurately reviewed;[52] olive mill wastewater has been proposed for a wide range of applications including the production of nutraceuticals,[54] the formulation of fish feed,[55] and stabilization during lard production;[56] however, its activity in preventing MR development in foods was never investigated.

In this paper, the ability of an ingredient obtained from olive mill wastewater through ultrafiltration and successive spray-drying in controlling the MR in UHT milk was examined. Olive mill wastewater activity was tested in laboratory-scale UHT milk to verify its effectiveness in the reduction of early-stage MR products, such as free APs, protein-bound APs, and RCSs, in the reduction of off-flavor formation and in the inhibition of CML formation.

## MATERIAL AND METHODS

**Chemicals.** Acetonitrile, methanol, and water for solid phase extraction (SPE) and LC-MS/MS determination were obtained from Merck (Darmstadt, Germany). The ion pairing agent perfluoropentanoic acid, trichloroacetic acid, hydrochloric acid (37%), sodium borohydride, sodium hydroxide, the analytical standards L-lysine hydrochloride, [4,4,5,5-$d_4$]-L-lysine hydrochloride ($d_4$-Lys), tyrosol (2-(4-hydroxyphenyl)ethanol, 98%), 3-hydroxytyrosol 98%, and verbascoside 98% along with glyoxal 40% solution in water, methylglyoxal 40% solution in water, and diacetyl (2,3-butanedione, 97%) as well as glycolaldehyde, acetoin, acetol, *o*-phenylenediamine (o-PD, 99.5%), and formic acid (MS grade 98%) were purchased from Sigma-Aldrich (St. Louis, MO, USA). Analytical standards *N*-$\varepsilon$-(2-furoylmethyl)-L-lysine (furosine), *N*-$\varepsilon$-(carboxymethyl)-L-lysine (CML), and its respective deuterated standard *N*-$\varepsilon$-(carboxy[$^2H_2$]-methyl)-L-lysine ($d_2$-CML) were obtained from Polypeptide Laboratories (Strasbourg, France), whereas 3-deoxyglucosone, $^{13}C_4$-acetoin, and $^{13}C_4$-diacetyl were obtained from TRC (Toronto Research Chemicals, Ontario, Canada).

**Formulation of OMW.** Olive oil mill wastewater polyphenol powders (OMW) were prepared from the water fraction resulting from olive oil production as follows. Olive water collected after olive paste centrifugation was treated with pectinases and fractionated by a filtration plant made up with three membranes at different cutoffs at 37 °C. Olive water was forced to pass through microfiltration (cutoff 25 kDa), ultrafiltration (cutoff 8 kDa), and nanofiltration (cutoff 0.3 kDa) membranes. At each stage a retentate containing the compounds not passing the membrane pores was collected. The ultrafiltration (UFR) retentate was concentrated by inverse osmosis (cutoff 0.1 kDa) up to 20% dry weight and spray-dried by adding maltodextrin and acacia fiber in a ratio 1:1 with the dry weight. A fine pale yellow powder with mild olive flavor was obtained and used in this study.

**OMW Characterization.** The phenolic profile of OMW was characterized by reversed phase HPLC-UV−vis to quantify the phenylethanoids: hydroxytyrosol, tyrosol, and verbascoside. Briefly, 100 mg of powder was dissolved in 10 mL of water, and after the complete melting of the coating material (5 min, room temperature under continuous stirring), 1 mL was purified on a preactivated C-18 cartridge (1 $cm^3$, 30 mg; Phenomenex, Torrance, CA, USA). Samples were eluted according to the method described by Kokkinidou and Peterson,[49] and after drying, they were reconstituted in a mixture of water/methanol 95:5 (v/v); 20 $\mu$L was injected onto a Prodigy ODS3 250 mm × 4.6 reversed phase C-18 (Phenomenex). The UPLC system consisted of two binary pumps (LC-20A, Shimadzu, Kyoto, Japan) equipped with an UV−vis detector (SPD20A, Shimadzu). The mobile phases were water/0.1% formic acid (A) and methanol (B). Hydroxytyrosol, tyrosol, and verbascoside were separated according to the gradient 0 min, 5% B; 5 min, 5% B; 40 min, 70% B; 42 min, 70% B; 45 min, 5% B; 50 min, 5% B; and the typical retention times were 20, 23, and 28 min, respectively. The three analytes were quantified by the external standard technique and the results reported as milligrams per gram of powder.

**Laboratory-Scale UHT Milk Treatment.** Raw milk (protein, 3.5%; fat, 1%) was obtained from a local market, and OMW was added to obtain final concentrations of 0.5 and 1 mg/mL. The three samples, one control and two samples with OMW, were homogenized, and after the complete dispersion of the powder (5 min, room temperature under continuous stirring) thermally treated in a laboratory-scale UHT milk system. It was constituted by three different tanks: two with oil, set at 180 and 140 °C, respectively, and another one with water at 6 °C. All of the samples were simultaneously treated, and one vial was used as reference. Along with 5 mL of milk, a thermocouple was inserted inside the reference headspace vial to control the time/temperature profile of each set. The high temperature of the first batch allowed a rapid increase of the temperature in the vial; instead, the second tank stabilized the temperature at 140 °C for 5 s. At the end of the thermal process the samples were rapidly moved into the last tank where the cooling phase blocked the extent of the MR. Finally, as soon as the samples reached 15 °C, they were rapidly frozen in dry ice in ethanol and stored at −20 °C until the analysis.

**CML, Total Lysine, and Furosine Analysis.** Total lysine and its derivatives *N*-$\varepsilon$-(carboxymethyl)lysine (CML) and *N*-$\varepsilon$-(2-furoylmethyl)-L-lysine (furosine) were analyzed according to the methods of

Fenaille et al., Delatour et al., and Troise et al. with some modifications.[35,36,57] Briefly, 100 μL of milk was mixed along with 0.45 mL of sodium borohydride (1 M in 0.1 N NaOH) and 0.5 mL of borate buffer (pH 9.2). The mixture was incubated for 4 h at room temperature to reduce the fructosyl-lysine in hexitol-lysine, and 1 mL of TCA (20% final concentradtion) was added to promote protein precipitation. Finally, 2 mL of 6 N HCl was added after careful removal of the supernatant. The mixture was incubated for 24 h at 110 °C in a forced-air circulating oven, and 400 μL was evaporated under a gentle flow of nitrogen. The samples were reconstituted in 380 μL of water, and 10 μL of the internal standard $d_2$-CML and 10 μL of $d_4$-lysine were added to obtain a final concentration of 50 ng/mL for both standards. Samples were loaded onto equilibrated Oasis HLB 1 $cm^3$ cartridges (Waters, Wexford, Ireland) and eluted according to the method previously described; finally, 5 μL was analyzed by ion pairing liquid chromatography coupled to MS/MS.[57] Furosine, CML, lysine, and the respective internal standard separation was achieved on a reversed phase core−shell column (Kinetex C18, 2.1 mm × 100 mm, Phenomenex) with a C-18 precolumn (3.0 × 4.0 mm, Phenomenex) using the following mobile phases: (A) 5 mM perfluoropentanoic acid and (B) acetonitrile/5 mM perfluoropentanoic acid. Compounds were eluted at 200 μL/min through the following gradient of solvent B: 0 min, 10% B; 2 min, 10% B; 5 min, 70% B; 7 min, 70% B; 9 min, 90% B; 10 min, 90% B; 12 min, 10% B; 15 min, 10% B. With the above-described chromatographic conditions, typical retention times for CML and $d_2$-CML were 6.8 min; for $d_4$-lysine and lysine, 7.03 min; and for furosine, 7.31 min. The MS/MS system was an API3000 (Applied Biosystems, Carlsbad, CA, USA); positive electrospray ionization was used for detection, and the source parameters were selected as follows: spray voltage, 5.0 kV; capillary temperature, 350 °C; dwell time, 100 ms. The chromatographic profile was recorded in multiple reaction monitoring mode, and the characteristic transitions were monitored to improve selectivity: for CML, furosine and lysine, the respective transitions of $m/z$ 205−84.1, $m/z$ 255.1−130.2, and $m/z$ 147.2−130.2 were used as quantifier, whereas $m/z$ 205−130.2, $m/z$ 255.1−84, and $m/z$ 147.2−84.1 were used as qualifier. CML was quantified using $d_2$-CML as internal standard ($m/z$ 207−144.1 and 207−84 for quantification and confirmation, respectively), whereas for furosine and lysine, $d_4$-lysine was used ($m/z$ 151.2−134.1 and 151.1−88 for quantification and confirmation, respectively).

**Free Amadori Products.** For the detection of free Amadori products (APs), each milk sample was diluted 10 times with water and ultracentrifuged (14800 rpm, 10 min, 4 °C), and then the supernatants were accurately filtered (RC 0.45 μm, Phenomenex) and injected. For the chromatographic separation a reversed phase core−shell column (Kinetex C18, 2.1 mm × 100 mm, Phenomenex) with a C-18 precolumn (3.0 × 4.0 mm, Phenomenex) was used. The mobile phases consisted of 5 mM NFPA in water (solvent A) and 5 mM NFPA in acetonitrile (solvent B). The following gradient of solvent B was used: 0 min, 10% B; 2 min, 10% B; 5 min, 50% B; 7 min, 50% B; 9 min, 10% B; 12 min, 10% B; 15 min, 10% B. The flow rate was set to 200 μL/min, and the injection volume was 5 μL. The U-HPLC was directly interfaced to an Exactive Orbitrap high-resolution mass spectrometer (HRMS) equipped with a heated electrospray interface (HESI). Mass spectrometer was operated in the full spectra positive ionization acquisition mode, in the mass range of $m/z$ 65−500; the mass spectrometry parameters were set up according to Troise et al.[58]

**Quantification of Reactive Carbonyl Species (RCSs).** Methylglyoxal, glyoxal, 3-deoxyglucosone, and diacetyl (2,3-butanedione) as well as glycolaldehyde, acetoin, and acetol were quantified using the synthesized stable isotopes $^{13}C_4$-acetoin and $^{13}C_4$-diacetyl as internal standards. Each internal standard (0.5 mM) was added to 5 mL of milk, followed by 500 μL of 10% trichloroacetic acid. The samples were then vortexed and centrifuged at 3904*g* for 20 min at 4 °C (Beckman Coulter, Allegra X-22R), and the supernatant was collected. Solid phase extraction (SPE) method was used to isolate the compounds of interest and avoid interference from phenolic compounds and adducts. A derivatization method followed, and samples were analyzed using an Acquity UPLC system interfaced with a Quattro Premier XE micromass mass spectrometer (Waters Co., Milford, MA, USA). An Acquity UPLC 2.1 × 100 mm BEH Phenyl 1.7 μm column with a VanGuard 2.1 × 5 mm BEH Phenyl 1.7 μm precolumn was used for separation, and all experiments were performed in triplicate. Analytes were detected using electrospray positive ionization−multiple reaction monitoring (MRM) using methods previously developed and reported by Kokkinidou and Peterson and specifically designed to avoid quantitative interference from phenolic compounds and adducts.[49]

**Quantification of Maillard Related Off-Flavor Volatiles.** A dynamic headspace method was developed for the quantification of off-flavor markers, namely, 2-acetyl-2-thiazoline and methional. Analysis was performed using a 6890 GC equipped with a 5973 mass selective detector (Agilent Technologies), thermal desorption unit (TDU, Gerstel), PTV inlet (CIS 4, Gerstel), and MPS 2 (Gerstel). Briefly, 2 mL of nanopure water and 1 M sodium chloride were added to 5 mL of UHT milk (control and treatments) spiked with deuterated standards. Sample was then purged with nitrogen, dry-purged to eliminate water, and then transferred to a thermal desorption unit. Measurements were performed 24 h after UHT processing using the analytical parameters summarized in Table 1.

**Table 1. Analysis Conditions Used for Identification and Quantification of Maillard-Related Off-Flavor Markers**

| | Analysis Conditions |
|---|---|
| PTV | solvent vent (20 mL/min) at 7.1 psi |
| | solvent vent (0.5 min), 20 °C (0.5 min); 10 °C/s; 290 °C (4 min) |
| column | DB5-MS, 30 m × 0.25 mm × 0.25 μm |
| | He, constant flow = 1 mL/min |
| oven | 40 °C (2 min); 4 °C/min; 160 °C |
| | 30 °C/min; 250 °C (5 min) |
| MSD | SIM, 104 + 48 (methional), 107 + 51 ($d_3$-methional), 129 (2-acetyl-2-thiazoline), 133 ($d_4$-2-acetyl-2-thiazoline) |
| | **Dynamic Headspace Component** |
| chemical trap | Tenax TA |
| DHS unit | trap temperature: ambient, 40 °C sample incubation temperature (10 min) |
| | 1000 mL purge volume, 50 mL/min purge flow |
| | 320 mL dry volume, 40 mL/min dry flow |
| TDU unit | solvent venting 20 °C (1 min); 720 °C/min; 290 °C (4 min) |

**Statistical Analysis.** Each thermal treatment was repeated twice to improve the reliability of the laboratory-scale UHT system, whereas each sample was analyzed twice and injected two times. Results were reported as nanograms per milliliter of milk for RCSs, milligrams per 100 g of protein for furosine, lysine, and CML, and percent inhibition toward the control samples for free APs. Data were analyzed by ANOVA, and means were compared by Tukey's test ($\alpha = 0.05$) using XLStat statistical software (Addinsoft, New York, NY, USA).

## RESULTS AND DISCUSSION

The use of a OMW ingredient obtained from ultrafiltered and spray-dried olive mill wastewater was evaluated for its ability to control the overall extent of the MR. The functional aspects of OMW were tested using a laboratory-scale UHT milk, and the selected outcomes were the MR aroma key odorants, the reduction of early-stage MRPs such as APs, the formation of protein-bound MRPs such as furosine and CML, and the ability to trap RCSs.

The first part of the work involved the production of OMW by four subsequent steps: the starting material was made by the water resulting after oil separation, which was treated with pectinases and fractionated by three different membranes to obtain three different retentate fractions.[59,60] The ultrafiltration

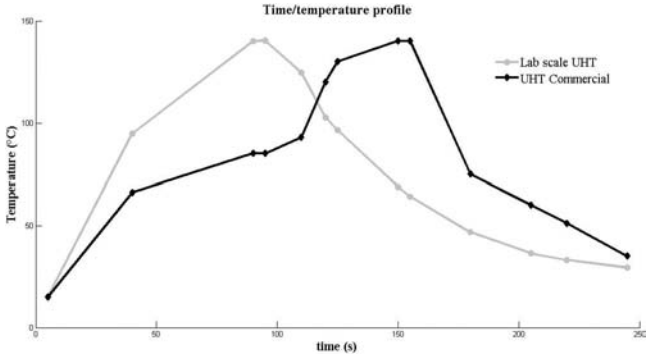


**Figure 1.** Comparison between laboratory-scale UHT system and commercial indirect tubular UHT system. The holding time used was the same for direct UHT processing and UHT plaque sterilization.

retentate was concentrated by inverse osmosis up to 67% dry matter and spray-dried with acacia fiber and maltodextrin in a molar ratio of 1:1 to obtain a fine pale yellow powder.[61] The phenolic profile of OMW was characterized by reversed phase UPLC-UV−vis to quantify the main constituents: hydroxytyrosol, tyrosol, and verbascoside. The concentrations of the three compounds in the OMW were 31 ± 0.2, 1.9 ± 0.1, and 2.8 ± 0.09 mg/g, respectively, in line with previous papers dealing with the composition of olive mill wastewater.[51,53,62]

Two different concentrations of OMW (0.05 and 0.1% w/v) were dissolved in raw cow's milk, and their impact on thermal damage was investigated by monitoring several intermediates and end-products of MR. A laboratory-scale UHT treatment was developed for this purpose: the thermal profile of the treatment confirmed that the thermal load closely simulated those of a commercial indirect tubular UHT processing method as highlighted in Figure 1. In the system here developed the time/temperature profile was similar to the ones previously reported for commercial indirect tubular UHT processing, direct UHT processing, and plaque UHT sterilization.[63,64] The sterilization factors were calculated according to Morales et al. using as reference temperature 127 °C and as $z$ value 30 °C.[65] They were 1.55 and 1.51 min for commercial UHT milk and laboratory-scale UHT milk, respectively. To compare the two concentrations of OMW, a control sample (without OMW) was simultaneously heated and several MRPs and RCSs were measured. In these conditions the final concentration of olive polyphenols reached a maximum of 36.1 mg/L without evident effects on milk sensory properties.

Off-flavor formation in UHT milk was already investigated in different papers.[12,66,67] According to the previous literature methional and 2-acetyl-2-thiazoline, commonly used as markers of off-flavor formation or aroma active compounds, were selected to verify the activity of OMW on this parameter. As shown in Figure 2 the concentration of methional was reduced from 4.08 ± 0.33 ng/mL for control UHT milk to 3.09 ± 0.26 and 2.15 ± 0.28 ng/mL for OMW 0.05% and OMW 0.1%, respectively. Furthermore, the concentration of 2-acetyl-2-thiazoline was reduced from 0.87 ± 0.09 ng/mL for control UHT milk to 0.74 ± 0.11 and 0.48 ± 0.08 ng/mL for OMW 0.05% and OMW 0.1%, respectively. This means that compared to control UHT milk, OMW 0.05% reduced by 24.3 and 16.9% the concentrations of methional and 2-acetyl-2-thiazoline, respectively, albeit those reductions were not statistically significant. Increasing the OMW concentration to 0.1% reduced the concentrations of methional and 2-acetyl-2-thiazoline by 47.3 and 46.1%, respectively, when compared to control UHT milk. This reduction was significant, indicating a concentration-dependent effectiveness of the phenolic mixture in reducing off-flavor generation during thermal processing. Data clearly showed that increasing the added OMW concentration prior to thermal processing can significantly decrease the concentration of off-flavor markers when compared to control UHT milk. These results were in line with those previously reported for the milk off-flavor and the potential role of added polyphenol.[67−69]

The trapping activity of OMW toward RCSs was evaluated by monitoring the concentrations of hydroxycarbonyl and dicarbonyl compounds in UHT milk with and without added OMW prior to thermal processing. The target RCSs monitored were glycoaldehyde, acetoin, and acetol for hydroxycarbonyls and glyoxal, methylglyoxal, 3-deoxyglucosone, and 2,3-butanedione for $\alpha$-dicarbonyls as they have been extensively studied for their contribution to AGE generation and carbonyl stress. Results are presented in Figures 3 and 4: the concentration of glycoaldehyde decreased from 246.03 ± 26.74 to 135.71 ± 30.63 and 105.36 ± 25.11 ng/mL for control UHT milk, OMW 0.05%, and OMW 0.1%, respectively, corresponding to reductions of 44.8 and 57.2% for samples containing OMW 0.05 and 0.1%. Similarly, OMW reduced the concentration of acetoin from 2293.73 ± 165.35 to 1897.91 ± 201.41 and 1321.86 ± 86.11 ng/mL for control UHT milk, OMW 0.05%, and OMW 0.1%, respectively, corresponding to reductions of 17.3 and 42.4% of acetoin for OMW 0.05 and 0.1% treatments. On the contrary, OMW did not show any reactivity toward acetol as no significant difference was observed between control UHT milk and OMW samples. These results can be explained on the basis of chemical reactivity as it follows the electophilicity of hydroxycarbonyl

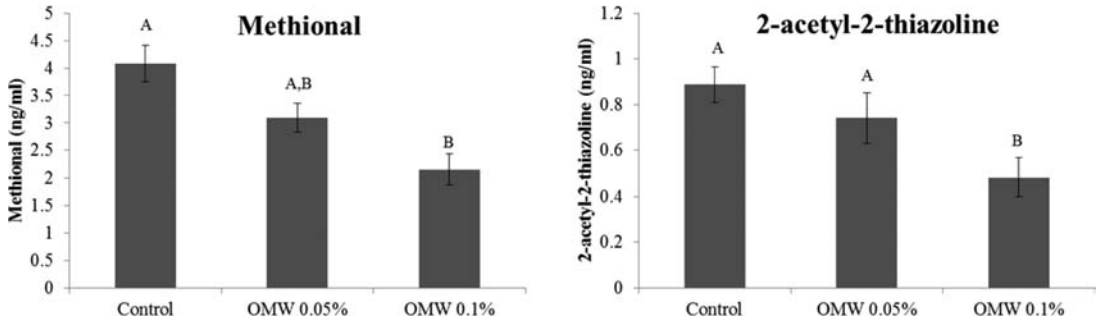


**Figure 2.** Methional and 2-acetyl-2-thiazoline concentration in control UHT milk, milk with 0.05% OMW, and milk with 0.1% OMW. Different letters correspond to significant differences (Tukey test, $\alpha$ = 0.05).

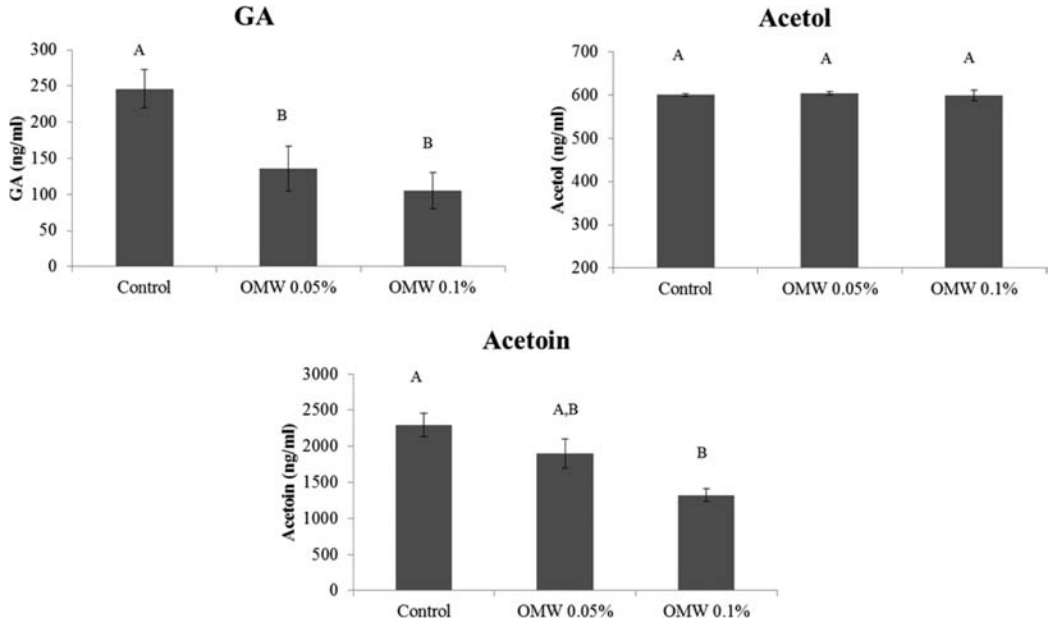


**Figure 3.** Hydroxycarbonyl concentration in control UHT milk, milk with 0.05% OMW, and milk with 0.1% OMW. Different letters correspond to significant differences (Tukey test, $\alpha = 0.05$). GA, glycoaldehyde.

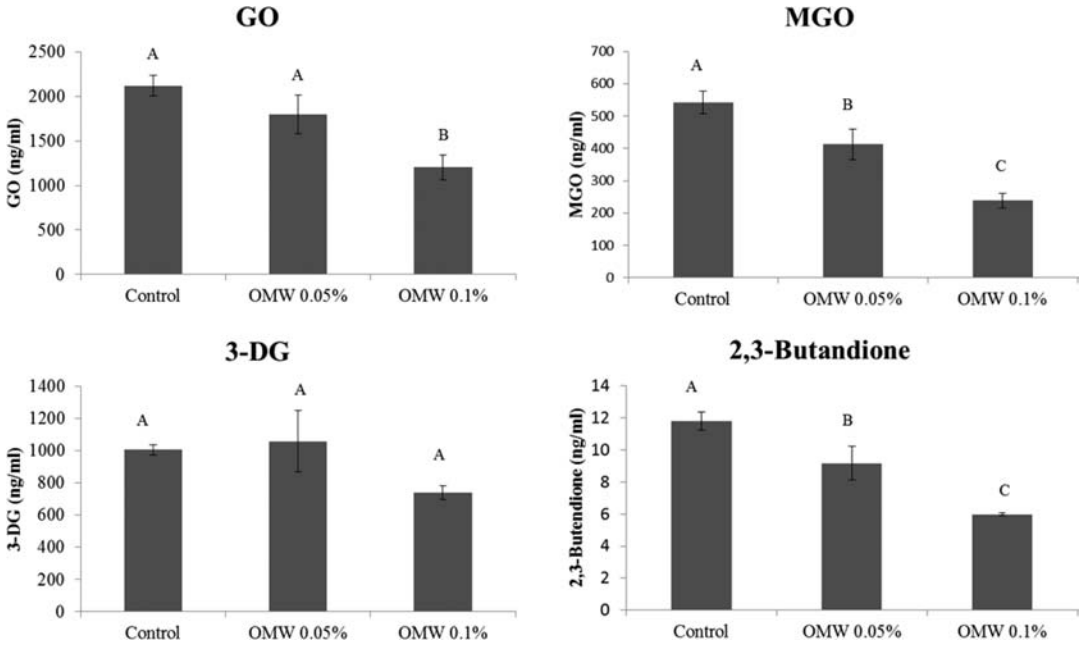


**Figure 4.** $\alpha$-Dicarbonyl concentration in control UHT milk, milk with 0.05% OMW, and milk with 0.1% OMW. Different letters correspond to significant differences (Tukey test, $\alpha = 0.05$).

compounds and thus the reactivity of phenolic compounds toward trapping them: the electron-rich phenols present in OMW can easily react with electrophilic hydroxycarbonyl compounds due to the presence of a hydroxyl group in position $\alpha$.

Slight differences in the concentration of $\alpha$-hydroxycarbonyls from previously reported papers can be ascribed to external factors such as microbial activity, starting material, and thermal treatments.[69−71]

The concentration of glyoxal was reduced from 2118.71 ± 113.94 ng/mL in control UHT milk to 1798.04 ± 218.49 and 1201.36 ± 136.73 ng/mL after the addition of OMW at 0.05 and 0.1%, respectively. This means reductions of 15.1 and 43.3% for glyoxal in samples with OMW 0.05 and 0.1% added, respectively. Methylglyoxal values were also reduced by 23.8 and 55.9% with OMW 0.05 and 0.1% addition, respectively. Both electrophilic dicarbonyls can give hydroxyalkylation of phenolic rings: Figure 4 suggests a higher activity of OMW toward methylglyoxal with respect to glyoxal, and this can be also due to the fact that the latter can polymerize in aqueous media, resulting in a lower affinity toward phenols.[72] For both compounds the observed reductions were in line with those previously reported.[49,50]

The concentration of 2,3-butanedione was reduced from 11.79 ± 0.55 ng/mL for control UHT milk to 9.16 ± 1.04 and 5.98 ± 0.09 ng/mL for OMW 0.05% and 0.1%, respectively,

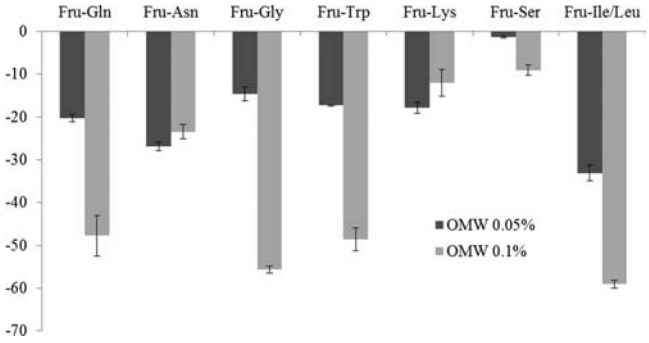


**Figure 5.** Amadori product mean percent inhibition in control UHT milk, milk with 0.05% OMW, and milk with 0.1% OMW.

and 3-deoxyglucosone was modified only by the addition of the higher concentration of OMW as no significant difference was observed between control UHT milk and milk treated with OMW 0.05%. It can be hypothesized that the trapping activity toward 3-deoxyglucosone is affected by the partial charge on the oxygen of the carbon carbonyl in position 2, by the presence of other carbons that can stabilize the structure, and by steric hindrance. From this first set of experiments it can be concluded that OMW treatment was not very effective in trapping C6 sugar fragments, whereas a significative reactivity of phenolic compounds in OMW mixture was observed toward methylglyoxal, diacetyl, and glycoladehyde.

All of the RCSs monitored are of interest not only for their contribution to MR pathways and carbonyl stress but also because they can contribute to the generation of off-flavor compounds; thus, their suppression can both directly and indirectly lead to a reduction in off-flavor generation.

The effect of OMW was tested also in the reduction of free APs, which can be measured without protein hydrolysis, thanks to the relatively high content of free amino acids in milk.[73] The formation of the AP was the central hub for the forthcoming steps of MR, so the presence of the phenolic rings favored the reduction of the AP formation and in turn of many MRPs via direct reaction with an amino group or via glyoxal trapping.

As shown in Figure 5, the reduction of AP formation was particularly evident for hydrophobic glycated amino acids, such as isoleucine/leucine and glycine. This can be explained by the high concentration of these amino acids and their APs and by the lower reactivity relative to that of other amino acids toward reducing sugars. The best known compounds are the Amadori products *N*-ε-fructosyl-lysine and furosine. The effect of OMW on free *N*-ε-fructosyl-lysine formation was significant at both concentrations: 12.1 and 17.8% over the control sample for OMW 0.1% and OMW 0.05%, respectively.

Finally the ability of OMW to reduce the formation of protein-bound CML and furosine was investigated. Results in Figure 6 show that after acidic hydrolysis the reduction of protein-bound MRPs was more pronounced for furosine; the reductions were 25.4 and 47.4% when OMW 0.05% and OMW 0.1% of phenolic powder were added, respectively. For CML the reductions were 11.2 and 16.2%, showing significant differences between the two phenolic powder concentrations and the control samples. Data on furosine showed that its concentration decreased from 10.962 ± 0.805 mg/100 g protein in the control UHT milk to 8.162 ± 0.794 and 5.761 ± 0.924 mg/100 g protein for OMW 0.05 and 0.1%, respectively.

The differences between CML and furosine reduction can be tentatively explained in two ways. First, the two MRPs could follow two different pathways. Furosine is formed by cyclization through the C-6 hydroxyl group and dehydration reaction, and it reflects the protein-bound Amadori products of lysine, because the free *N*-ε-fructosyl-lysine is destroyed by acidic hydrolysis.[4] CML can be formed by two mechanisms: the enediol form of the *N*-ε-fructosyl-lysine can undergo oxidative cleavage to produce CML and erythronic acid via free radical generation with simultaneous oxygen consumption, and glyoxal can easily block the amino group on the side chain via the Namiki pathway.[74] Second, as shown in Figure 7, the reduction of both protein-bound and free MRPs can be associated not

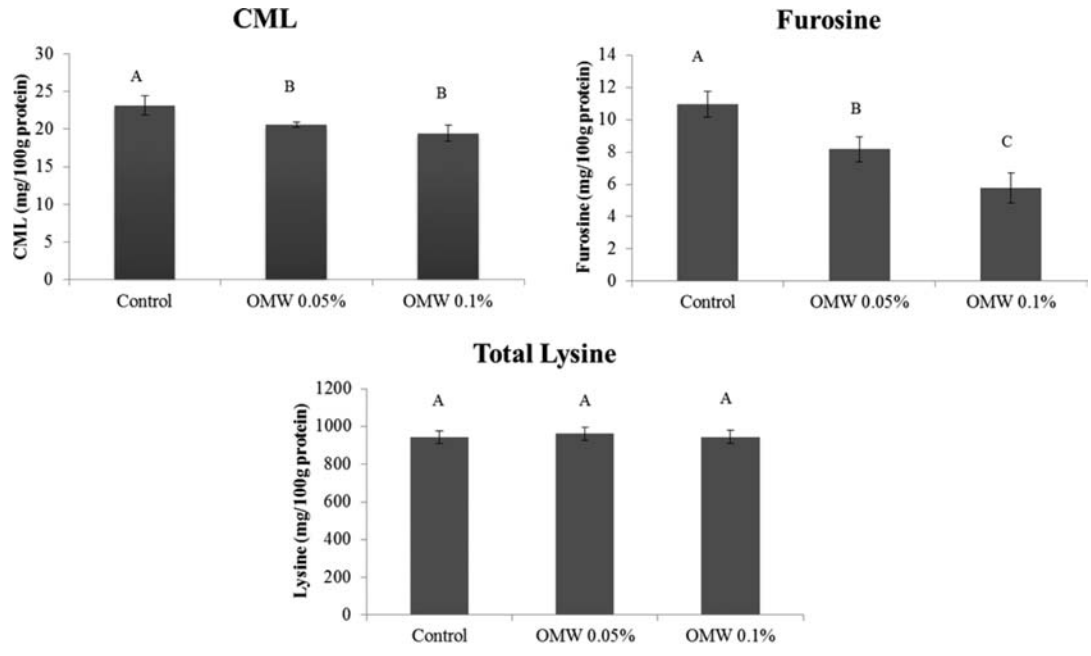


**Figure 6.** CML, furosine, and total lysine concentrations in control UHT milk, milk with 0.05% OMW, and milk with 0.1% OMW. Different letters correspond to significant differences (Tukey test, $\alpha = 0.05$).

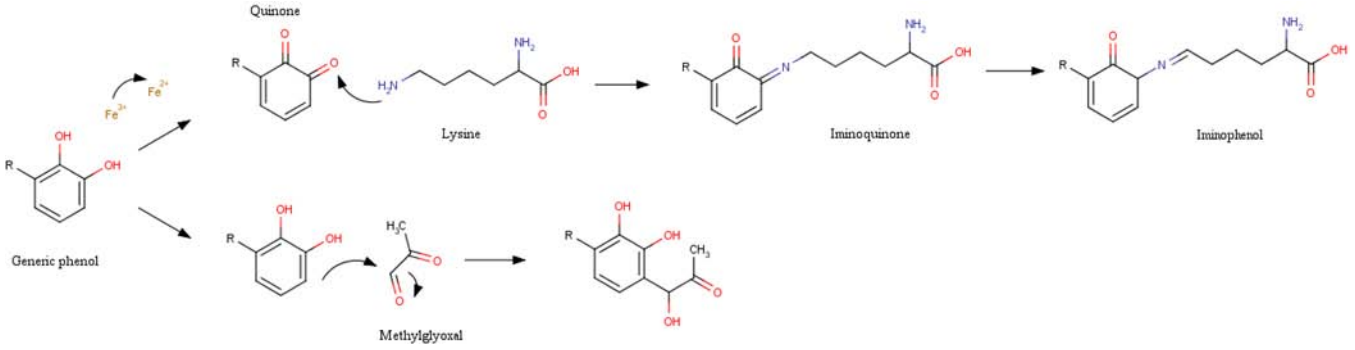


**Figure 7.** Proposed mechanism of MRP reduction by phenolic compounds adapted from Totlani and Peterson,[47] Estévez,[76] and Guerra and Yaylayan.[77]

only with the reduction of the Amadori product of lysine and glucose but also with the above-described trapping activity. A trisubstituted phenolic ring with an *o*-dihydroxy function can easily react with dicarbonyls by hydroxyalkylation and aromatic substitution reaction, thus showing trapping activity toward methylglyoxal and glyoxal.[47,48,75] Moreover, in the presence of reactants such as ascorbic acid or iron, the phenolic ring can be oxidized to quinone, whose reaction with side chain of lysine and other amino group can lead to the formation of iminoquinone and iminophenol via Schiff bases as highlighted by Estévez[76] and Guerra and Yaylayan.[77] The results on CML and furosine fully confirmed those previously obtained by other groups.[27,35,78]

In conclusion, in this paper it was demonstrated that OMW besides its potential nutritional functionality could also help in the production of superior quality food and can provide an effective strategy in the control of the MR. The result was achieved on a broad range of MRPs that contributed to the final chemical composition of the UHT milk. Interestingly, these results were obtained in conditions not leading to easily detectable modifications of either physical properties (viscosity or color) or sensory properties (bitterness, astringency, olive flavor). However, the sensory acceptability of the addition of OMW should be further investigated.

## AUTHOR INFORMATION

### Corresponding Author

*(V.F.) Phone: +31 (0)317 485171. Fax: +31 (0)317 485171. E-mail: vincenzo.fogliano@wur.nl.

### Funding

This work was funded by the program PON01_ 02863 "Incapsulazione di principi attivi per il miglioramento di qualità e sicurezza degli alimenti" funded by the Italian Ministry of University and Scientific Research (MIUR).

### Notes

The authors declare no competing financial interest.

## ABBREVIATIONS USED

MR, Maillard reaction; APs, Amadori products; RCSs, reactive carbonyl species; OMW, olive mill wastewater phenolic powder

## REFERENCES

(1) Awuah, G. B.; Ramaswamy, H. S.; Economides, A. Thermal processing and quality: principles and overview. *Chem. Eng. Process.* **2007**, *46*, 584−602.

(2) van Boekel, M.; Fogliano, V.; Pellegrini, N.; Stanton, C.; Scholz, G.; Lalljie, S.; Somoza, V.; Knorr, D.; Jasti, P. R.; Eisenbrand, G. A review on the beneficial aspects of food processing. *Mol. Nutr. Food Res.* **2010**, *54*, 1215−1247.

(3) Maillard, L. C. Action of amino acids on sugars. Formation of melanoidins in a methodical way. *Compt. Rend.* **1912**, *154*, 66−68.

(4) Yaylayan, V. A.; Huyghues-Despointes, A. Chemistry of Amadori rearrangement products: analysis, synthesis, kinetics, reactions, and spectroscopic properties. *Crit. Rev. Food Sci.* **1994**, *34*, 321−369.

(5) Hodge, J. E. Dehydrated foods, chemistry of browning reactions in model systems. *J. Agric. Food Chem.* **1953**, *1*, 928−943.

(6) Nursten, H. E. *The Maillard Reaction: Chemistry, Biochemistry, and Implications*; Royal Society of Chemistry: Cambridge, UK, 2005.

(7) Pischetsrieder, M.; Henle, T. Glycation products in infant formulas: chemical, analytical and physiological aspects. *Amino Acids* **2012**, *42*, 1111−1118.

(8) van Boekel, M. A. J. S. Effect of heating on Maillard reactions in milk. *Food Chem.* **1998**, *62*, 403−414.

(9) Finot, A. P. Nutritional and metabolic aspects of protein modification during food processing. In *Modification of Proteins: Food, Nutritional, and Pharmacological Aspects*; Feeney, R. E., Whitaker, J. R., Eds.; American Chemical Society: Washington, DC, USA, 1982; Vol. 198.

(10) Leclere, J.; Birlouez-Aragon, I. The fluorescence of advanced Maillard products is a good indicator of lysine damage during the Maillard reaction. *J. Agric. Food Chem.* **2001**, *49*, 4682−4687.

(11) Monti, S. M.; Ritieni, A.; Graziani, G.; Randazzo, G.; Mannina, L.; Segre, A. L.; Fogliano, V. LC/MS analysis and antioxidative efficiency of Maillard reaction products from a lactose-lysine model system. *J. Agric. Food Chem.* **1999**, *47*, 1506−1513.

(12) van Boekel, M. A. J. S. Formation of flavour compounds in the Maillard reaction. *Biotechnol. Adv.* **2006**, *24*, 230−233.

(13) Zhang, Y. G.; Dorjpalam, B.; Ho, C. T. Contribution of peptides to volatile formation in the Maillard reaction of casein hydrolysate with glucose. *J. Agric. Food Chem.* **1992**, *40*, 2467−2471.

(14) Calligaris, S.; Manzocco, L.; Anese, M.; Nicoli, M. C. Effect of heat-treatment on the antioxidant and pro-oxidant activity of milk. *Int. Dairy J.* **2004**, *14*, 421−427.

(15) Morales, F. J.; Jimenez-Perez, S. Free radical scavenging capacity of Maillard reaction products as related to colour and fluorescence. *Food Chem.* **2001**, *72*, 119−125.

(16) Jiang, Z. M.; Brodkorb, A. Structure and antioxidant activity of Maillard reaction products from α-lactalbumin and β-lactoglobulin with ribose in an aqueous model system. *Food Chem.* **2012**, *133*, 960−968.

(17) Chen, Y. J.; Liang, L.; Liu, X. M.; Labuza, T. P.; Zhou, P. Effect of fructose and glucose on glycation of β-lactoglobulin in an intermediate-moisture food model system: analysis by liquid chromatography-mass spectrometry (LC-MS) and data-independent acquisition LC-MS (LC-MSE). *J. Agric. Food Chem.* **2012**, *60*, 10674−10682.

(18) Rizzi, G. P. Chemical structure of colored Maillard reaction products. *Food Rev. Int.* **1997**, *13*, 1−28.

(19) Morales, F. J.; van Boekel, M. A. J. S. A study on advanced Maillard reaction in heated casein/sugar solutions: colour formation. *Int. Dairy J.* **1998**, *8*, 907−915.
(20) Somoza, V. Five years of research on health risks and benefits of Maillard reaction products: an update. *Mol. Nutr. Food Res.* **2005**, *49*, 663−672.
(21) Tessier, F. J.; Birlouez-Aragon, I. Health effects of dietary Maillard reaction products: the results of ICARE and other studies. *Amino Acids* **2012**, *42*, 1119−1131.
(22) Sebekova, K.; Somoza, V. Dietary advanced glycation end-products (AGEs) and their health effects − PRO. *Mol. Nutr. Food Res.* **2007**, *51*, 1079−1084.
(23) Thornalley, P. J. Dietary AGEs and ALEs and risk to human health by their interaction with the receptor for advanced glycation endproducts (RAGE) − an introduction. *Mol. Nutr. Food Res.* **2007**, *51*, 1107−1110.
(24) Vanholder, R.; De Smet, R.; Glorieux, G.; Argiles, A.; Baurmeister, U.; Brunet, P.; Clark, W.; Cohen, G.; De Deyn, P. P.; Deppisch, R.; Descamps-Latscha, B.; Henle, T.; Jorres, A.; Lemke, H. D.; Massy, Z. A.; Passlick-Deetjen, J.; Rodriguez, M.; Stegmayr, B.; Stenvinkel, P.; Tetta, C.; Wanner, C.; Zidek, W. Review on uremic toxins: classification, concentration, and interindividual variability. *Kidney Int.* **2003**, *63*, 1934−1943.
(25) Henle, T. Protein-bound advanced glycation endproducts (AGEs) as bioactive amino acid derivatives in foods. *Amino Acids* **2005**, *29*, 313−322.
(26) Klenovics, K. S.; Boor, P.; Somoza, V.; Celec, P.; Fogliano, V.; Sebekova, K. Advanced glycation end products in infant formulas do not contribute to insulin resistance associated with their consumption. *PLoS One* **2013**, *8*, No. e53056.
(27) Henle, T.; Zehetner, G.; Klostermeyer, H. Fast and sensitive determination of furosine. *Z. Lebensm. Unters. Forsch.* **1995**, *200*, 235−237.
(28) Erbersdobler, H. F.; Somoza, V. Forty years of furosine − forty years of using Maillard reaction products as indicators of the nutritional quality of foods. *Mol. Nutr. Food Res.* **2007**, *51*, 423−430.
(29) Morales, F. J.; Romero, C.; Jimenez-Perez, S. Chromatographic determination of bound hydroxymethylfurfural as an index of milk protein glycosylation. *J. Agric. Food Chem.* **1997**, *45*, 1570−1573.
(30) Morales, F. J.; Jimenez-Perez, S. Study of hydroxymethylfurfural formation from acid degradation of the Amadori product in milk-resembling systems. *J. Agric. Food Chem.* **1998**, *46*, 3885−3890.
(31) Vinale, F.; Fogliano, V.; Schieberle, P.; Hofmann, T. Development of a stable isotope dilution assay for an accurate quantification of protein-bound *N*-ε-(1-deoxy-D-fructos-1-yl)-L-lysine using a C-13-labeled internal standard. *J. Agric. Food Chem.* **1999**, *47*, 5084−5092.
(32) Vinale, F.; Monti, S. M.; Panunzi, B.; Fogliano, V. Convenient synthesis of lactuloselysine and its use for LC-MS analysis in milk-like model systems. *J. Agric. Food Chem.* **1999**, *47*, 4700−4706.
(33) Yeboah, F. K.; Alli, I.; Yaylayan, V. A.; Konishi, Y.; Stefanowicz, P. Monitoring glycation of lysozyme by electrospray ionization mass spectrometry. *J. Agric. Food Chem.* **2000**, *48*, 2766−2774.
(34) Kislinger, T.; Humeny, A.; Peich, C. C.; Becker, C. M.; Pischetsrieder, M. Analysis of protein glycation products by MALDI-TOF/MS. *Ann. N. Y. Acad. Sci.* **2005**, *1043*, 249−259.
(35) Fenaille, F.; Parisod, V.; Visani, P.; Populaire, S.; Tabet, J. C.; Guy, P. A. Modifications of milk constituents during processing: a preliminary benchmarking study. *Int. Dairy J.* **2006**, *16*, 728−739.
(36) Delatour, T.; Hegele, J.; Parisod, V.; Richoz, J.; Maurer, S.; Steven, M.; Buetler, T. Analysis of advanced glycation endproducts in dairy products by isotope dilution liquid chromatography-electrospray tandem mass spectrometry. The particular case of carboxymethyllysine. *J. Chromatogr., A* **2009**, *1216*, 2371−2381.
(37) Charissou, A.; Ait-Ameur, L.; Birlouez-Aragon, I. Evaluation of a gas chromatography/mass spectrometry method for the quantification of carboxymethyllysine in food samples. *J. Chromatogr., A* **2007**, *1140*, 189−194.
(38) Schlutt, B.; Moran, N.; Schieberle, P.; Hofmann, T. Sensory-directed identification of creaminess-enhancing volatiles and semi-volatiles in full-fat cream. *J. Agric. Food Chem.* **2007**, *55*, 9634−9645.
(39) Pripis-Nicolau, L.; de Revel, G.; Bertrand, A.; Maujean, A. Formation of flavor components by the reaction of amino acid and carbonyl compounds in mild conditions. *J. Agric. Food Chem.* **2000**, *48*, 3761−3766.
(40) Munch, P.; Hofmann, T.; Schieberle, P. Comparison of key odorants generated by thermal treatment of commercial and self-prepared yeast extracts: Influence of the amino acid composition on odorant formation. *J. Agric. Food Chem.* **1997**, *45*, 1338−1344.
(41) Schieberle, P.; Hofmann, T. Evaluation of the character impact odorants in fresh strawberry juice by quantitative measurements and sensory studies on model mixtures. *J. Agric. Food Chem.* **1997**, *45*, 227−232.
(42) Degen, J.; Hellwig, M.; Henle, T. 1,2-Dicarbonyl compounds in commonly consumed foods. *J. Agric. Food Chem.* **2012**, *60*, 7071−7079.
(43) Smuda, M.; Glomb, M. A. Fragmentation pathways during Maillard-induced carbohydrate degradation. *J. Agric. Food Chem.* **2013**, *61*, 10198−10208.
(44) Troise, A. D.; Fogliano, V. Reactants encapsulation and Maillard reaction. *Trends Food Sci. Technol.* **2013**, *33*, 63−74.
(45) Schamberger, G. P.; Labuza, T. P. Effect of green tea flavonoids on Maillard browning in UHT milk. *LWT−Food Sci. Technol.* **2007**, *40*, 1410−1417.
(46) Colahan-Sederstrom, P. M.; Peterson, D. G. Inhibition of key aroma compound generated during ultrahigh-temperature processing of bovine milk via epicatechin addition. *J. Agric. Food Chem.* **2005**, *53*, 398−402.
(47) Totlani, V. M.; Peterson, D. G. Reactivity of epicatechin in aqueous glycine and glucose Maillard reaction models: quenching of C(2), C(3), and C(4) sugar fragments. *J. Agric. Food Chem.* **2005**, *53*, 4130−4135.
(48) Totlani, V. M.; Peterson, D. G. Influence of epicatechin reactions on the mechanisms of Maillard product formation in low moisture model systems. *J. Agric. Food Chem.* **2007**, *55*, 414−420.
(49) Kokkinidou, S.; Peterson, D. G. Response surface methodology as optimization strategy for reduction of reactive carbonyl species in foods by means of phenolic chemistry. *Food Funct.* **2013**, *4*, 1093−1104.
(50) Lo, C. Y.; Hsiao, W. T.; Chen, X. Y. Efficiency of trapping methylglyoxal by phenols and phenolic acids. *J. Food Sci.* **2011**, *76*, H90−H96.
(51) De Marco, E.; Savarese, M.; Paduano, A.; Sacchi, R. Characterization and fractionation of phenolic compounds extracted from olive oil mill wastewaters. *Food Chem.* **2007**, *104*, 858−867.
(52) Obied, H. K.; Allen, M. S.; Bedgood, D. R.; Prenzler, P. D.; Robards, K.; Stockmann, R. Bioactivity and analysis of biophenols recovered from olive mill waste. *J. Agric. Food Chem.* **2005**, *53*, 823−837.
(53) Servili, M.; Baldioli, M.; Selvaggini, R.; Miniati, E.; Macchioni, A.; Montedoro, G. High-performance liquid chromatography evaluation of phenols in olive fruit, virgin olive oil, vegetation waters, and pomace and 1D- and 2D-nuclear magnetic resonance characterization. *J. Am. Oil Chem. Soc.* **1999**, *76*, 873−882.
(54) Angelino, D.; Gennari, L.; Blasa, M.; Selvaggini, R.; Urbani, S.; Esposto, S.; Servili, M.; Ninfali, P. Chemical and cellular antioxidant activity of phytochemicals purified from olive mill waste waters. *J. Agric. Food Chem.* **2011**, *59*, 2011−2018.
(55) Zabetakis, I.; Nasopoulou, C. Agricultural and aquacultural potential of olive pomace. A review. *J. Agric. Sci.* **2013**, *5*, 116.
(56) De Leonardis, A.; Macciola, V.; Lembo, G.; Aretini, A.; Nag, A. Studies on oxidative stabilisation of lard by natural antioxidants recovered from olive-oil mill wastewater. *Food Chem.* **2007**, *100*, 998−1004.
(57) Troise, A. D.; Dathan, N. A.; Fiore, A.; Roviello, G.; Di Fiore, A.; Caira, S.; Cuollo, M.; De Simone, G.; Fogliano, V.; Monti, S. M. Faox enzymes inhibited Maillard reaction development during storage

both in protein glucose model system and low lactose UHT milk. *Amino Acids* **2013**, *46*, 279−288.
(58) Troise, A. D.; Fiore, A.; Roviello, G.; Monti, S. M.; Fogliano, V. Simultaneous quantification of amino acids and Amadori products in foods through ion pairing liquid chromatography high resolution mass spectrometry. *Amino Acids* **2014**, DOI: 10.1007/s00726-014-1845-5.
(59) Akdemir, E. O.; Ozer, A. Investigation of two ultrafiltration membranes for treatment of olive oil mill wastewater. *Desalination* **2009**, *249*, 660−666.
(60) Gkoutsidis, P. E.; Petrotos, K. B.; Kokkora, M. I.; Tziortziou, A. D.; Christodouloulis, K.; Goulas, P. Olive mill waste water (OMWW) treatment by diafiltration. *Desalin. Water Treat.* **2011**, *30*, 237−246.
(61) Fang, Z. X.; Bhandari, B. Encapsulation of polyphenols − a review. *Trends Food Sci. Technol.* **2010**, *21*, 510−523.
(62) Visioli, F.; Romani, A.; Mulinacci, N.; Zarini, S.; Conte, D.; Vincieri, F. F.; Galli, C. Antioxidant and other biological activities of olive mill waste waters. *J. Agric. Food Chem.* **1999**, *47*, 3397−3401.
(63) Birlouez-Aragon, I.; Sabat, P.; Gouti, N. A new method for discriminating milk heat treatment. *Int. Dairy J.* **2002**, *12*, 59−67.
(64) Datta, N.; Elliott, A. J.; Perkins, M. L.; Deeth, H. C. Ultra-high-temperature (UHT) treatment of milk: comparison of direct and indirect modes of heating. *Aust J. Dairy Technol.* **2002**, *57*, 211−227.
(65) Morales, F. J.; Romero, C.; Jimenez-Perez, S. Characterization of industrial processed milk by analysis of heat-induced changes. *Int. J. Food Sci. Technol.* **2000**, *35*, 193−200.
(66) Vazquez-Landaverde, P. A.; Velazquez, G.; Torres, J. A.; Qian, M. C. Quantitative determination of thermally derived off-flavor compounds in milk using solid-phase microextraction and gas chromatography. *J. Dairy Sci.* **2005**, *88*, 3764−3772.
(67) Karagul-Yuceer, Y.; Cadwallader, K. R.; Drake, M. Volatile flavor components of stored nonfat dry milk. *J. Agric. Food Chem.* **2002**, *50*, 305−312.
(68) Karagul-Yuceer, Y.; Drake, M.; Cadwallader, K. R. Aroma-active components of nonfat dry milk. *J. Agric. Food Chem.* **2001**, *49*, 2948−2953.
(69) Kokkinidou, S.; Peterson, D. G. Control of Maillard-type off-flavor development in ultra high temperature processed milk by phenolic chemistry. *J. Agric. Food Chem.* **2014**, *62*, 8023−8033.
(70) Ostlie, H. M.; Treimo, J.; Narvhus, J. A. Effect of temperature on growth and metabolism of probiotic bacteria in milk. *Int. Dairy J.* **2005**, *15*, 989−997.
(71) Callon, C.; Berdague, J. L.; Dufour, E.; Montel, M. C. The effect of raw milk microbial flora on the sensory characteristics of Salers-type cheeses. *J. Dairy Sci.* **2005**, *88*, 3840−3850.
(72) Wang, Y.; Ho, C. T. Flavour chemistry of methylglyoxal and glyoxal. *Chem. Soc. Rev.* **2012**, *41*, 4140−4149.
(73) Gandolfi, I.; Palla, G.; Delprato, L.; Denisco, F.; Marchelli, R.; Salvadori, C. D-Amino acids in milk as related to heat-treatments and bacterial-activity. *J. Food Sci.* **1992**, *57*, 377−379.
(74) Ahmed, M. U.; Thorpe, S. R.; Baynes, J. W. Identification of *N*-ε-carboxymethyllysine as a degradation product of fructoselysine in glycated protein. *J. Biol. Chem.* **1986**, *261*, 4889−4894.
(75) Lo, C. Y.; Li, S. M.; Tan, D.; Pan, M. H.; Sang, S. M.; Ho, C. T. Trapping reactions of reactive carbonyl species with tea polyphenols in simulated physiological conditions. *Mol. Nutr. Food Res.* **2006**, *50*, 1118−1128.
(76) Estevez, M. Protein carbonyls in meat systems: a review. *Meat Sci.* **2011**, *89*, 259−279.
(77) Guerra, P. V.; Yaylayan, V. A. Interaction of flavanols with amino acids: postoxidative reactivity of the B-ring of catechin with glycine. *J. Agric. Food Chem.* **2014**, *62*, 3831−3836.
(78) Hull, G. L. J.; Woodside, J. V.; Ames, J. M.; Cuskelly, G. J. *N*-ε-(Carboxymethyl)lysine content of foods commonly consumed in a Western style diet. *Food Chem.* **2012**, *131*, 170−174.

## NOTE ADDED AFTER ASAP PUBLICATION

This paper was published ASAP on October 3, 2014, with an error to Figure 4A. The corrected version was reposted on October 6, 2014.

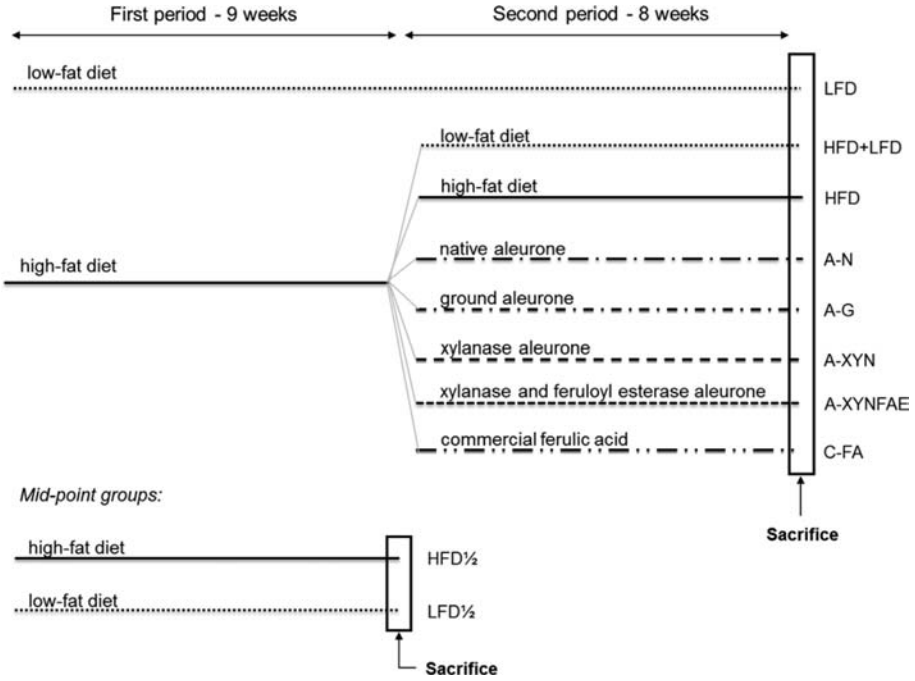


**Figure 1.** Experimental design of this study. Low-fat diet was provided during the whole period to the LFD group. High-fat diet was provided to the other groups during the first period (9 weeks), and during the second period (8 weeks) the diet was switched to the following diets: low-fat (HFD + LFD group), high-fat (HFD group), native aleurone (A-N group), ground aleurone (A-G group), xylanase treated aleurone (A-XYN group), xylanase and feruloyl esterase treated aleurone (A-XYNFAE), or commercial ferulic acid (C-FA group). Midpoint groups received either high-fat (HFD1/2) or low-fat (LFD1/2) diets and were sacrificed in the end of the first period (9 weeks).

**Table 1. Composition of the Diets: Carbohydrate, Fat, Protein, Cellulose, Mineral, Vitamin, Arabinoxylans (AX; Total, Insoluble, and Soluble), and Ferulic Acid (FA; Bound, Conjugated, and Free) Expressed as grams per 100 g[a]**

| | control diets | | aleurone diets | | | | FA diet |
|---|---|---|---|---|---|---|---|
| | HFD | LFD | A-N | A-G | A-XYN | A-XYNFAE | C-FA |
| carbohydrate | 41.4 | 67.3 | 39.5 | 39.3 | 39.7 | 39.5 | 41.4 |
| fat | 23.6 | 4.3 | 22.5 | 22.4 | 22.6 | 22.5 | 23.6 |
| protein | 23.7 | 19.2 | 22.5 | 22.4 | 22.7 | 22.6 | 23.7 |
| cellulose | 5.0 | 5.0 | 0.0 | 0.0 | 0.0 | 0.0 | 5.0 |
| mineral mix | 1.0 | 1.0 | 1.0 | 1.0 | 1.0 | 1.0 | 1.0 |
| vitamin mix | 1.0 | 1.0 | 1.0 | 1.0 | 1.0 | 1.0 | 1.0 |
| total AX | 0.52 ± 0.01 | 0.42 ± 0.00 | 3.80 ± 0.01 | 3.88 ± 0.15 | 3.75 ± 0.07 | 3.42 ± 0.2 | 0.57 ± 0.03 |
| insoluble AX | 0.49 ± 0.01 | 0.39 ± 0.00 | 3.61 ± 0.02 | 3.63 ± 0.16 | 2.28 ± 0.08 | 0.84 ± 0.27 | 0.54 ± 0.03 |
| soluble AX | 0.03 ± 0.00 | 0.03 ± 0.00 | 0.19 ± 0.02 | 0.25 ± 0.02 | 1.47 ± 0.03 | 2.58 ± 0.15 | 0.03 ± 0.00 |
| total FA | 0.0 ± 0.0 | 0.0 ± 0.0 | 0.11 ± 0.0 | 0.11 ± 0.0 | 0.09 ± 0.0 | 0.07 ± 0.04 | 0.10 ± 0.04 |
| bound FA | 0.0 ± 0.0 | 0.0 ± 0.0 | 0.10 ± 0.0 | 0.11 ± 0.0 | 0.05 ± 0.0 | 0.01 ± 0.06 | 0.00 ± 0.00 |
| conjugated FA | 0.0 ± 0.0 | 0.0 ± 0.0 | 0.00 ± 0.0 | 0.01 ± 0.0 | 0.03 ± 0.0 | 0.02 ± 0.03 | 0.01 ± 0.02 |
| free FA | 0.0 ± 0.0 | 0.0 ± 0.0 | 0.00 ± 0.0 | 0.00 ± 0.0 | 0.01 ± 0.0 | 0.04 ± 0.01 | 0.08 ± 0.00 |
| antioxidant capacity | 10.7 ± 1.0 | 10.8 ± 0.8 | 14.1 ± 0.6 | 15.1 ± 2.0 | 22.9 ± 4.0 | 27.5 ± 3.1 | 25.9 ± 1.4 |

[a]The antioxidant capacity is expressed as mmol of TEAC/kg. Arabinoxylans, ferulic acid contents, and antioxidant capacity are reported as means ± SD. Amounts of carbohydrate, fat, protein, minerals, and vitamins in aleurone diets were added to match the energy content similar to that of the high-fat diet. For HFD-, A-N-, A-G-, A-XYN-, A-XYNFAE-, and C-FA-enriched diets: carbohydrate = corn starch (21%), maltodextrin (29%), and sucrose (50%); fat = soybean oil (12.3%) and lard (87.7%); protein = casein (98.5%) and L-cystine (1.5%). For LFD: carbohydrate = corn starch (45%), maltodextrin (5%), and sucrose (50%); fat = soybean oil (55.6%) and lard (44.4%); protein = casein (98.5%) and L-cystine (1.5%).

and wet processes to increase the bioaccessibility and bioavailability of bioactive compounds. Ultrafine dry grinding of the wheat bran and aleurone layer improved indeed their antioxidant capacity and fermentability and increased the bioavailability of their phenolic compounds.[17−21] The inner part of aleurone obtained by debranning and air classification also presented higher bioaccessibility of phenolic compounds and vitamins compared to the outer part of aleurone or the unfractionated bran.[22] Enzymatic treatment of aleurone improved to a larger extent its antioxidant capacity[19] and also allowed greater and faster metabolism of FA in an *in vitro* gut fermentation model.[20] Bioprocessed wheat bran had higher bioavailability of its phenolics *in vitro* and *ex vivo*.[23,24]

The aim of this work was to investigate the capacity of differently processed wheat aleurone fractions (native, finely ground, or enzymatically treated) to counteract metabolic disorders in a diet-induced-obesity mouse model. The design of this study consisted of first inducing obesity in mice (first

period, 9 weeks fed with high-fat diet) and then providing the processed aleurone fractions (second period −8 weeks fed with high-fat diet enriched with aleurone) (Figure 1). The aleurone was added in the diet of mice in order to provide 5% of the dietary fiber, which is a common level used in mice studies. Besides aleurone-enriched diets, high- and low-fat diets without aleurone were also provided during the whole experiment (first + second periods) as two control groups. The effects of the different aleurone-enriched diets were evaluated by recording obesity (body weight gain, adiposity), fasting blood glucose, fasting plasma insulin and leptin, pro- and anti-inflammation markers, and oxidative stress.

## MATERIALS AND METHODS

**Wheat Aleurone Layer Treatments.** The native aleurone-rich fraction (85% aleurone) was obtained by dry processing of bran provided by Bühler AG (Uzwil, Switzerland). Its chemical composition is described by Rosa et al.[19] (39.7 g of dietary fiber, 22.2 g of protein, 13.3 g of ash, 9.8 g of fat, and 5.8 g of starch in 100 g of wheat aleurone dry matter). The native aleurone had 192 $\mu$m mean particle size ($d_{50}$) and 24.3 and 0.6 g of total AX and total FA/(100 g), respectively. AX of native aleurone was present mainly in insoluble form (96.3%), and FA was mainly esterified to polysaccharides (98.5%). Three treatments were applied on the native aleurone to obtain three modified aleurone fractions: (i) finely ground aleurone, (ii) xylanase treated aleurone, and (iii) xylanase and feruloyl esterase treated aleurone.[20] The finely ground aleurone, which was obtained by ultrafine grinding with an impact mill in cryogenic conditions, had 65 $\mu$m mean particle size. The finely ground aleurone had amounts of insoluble AX and bound FA similar to that of the native one. Both enzymatic treated aleurones had amounts of total AX and total FA similar to that the native aleurone, but the proportions of soluble AX and free FA were higher in these treated fractions. The aleurone fractions were prepared in UMR IATE (Montpellier, France), and their total composition was described in our previous work.[20]

**Study Diets.** Each aleurone fraction was added at concentration 13% (w/w) in a commercial high-fat diet with 45% of energy from fat (D12451 high-fat diet; Research Diets Inc., New Brunswick, NJ, USA). High-fat diet ingredients and aleurone fraction were mixed and then extruded into pellets using a cold extrusion process. The pellets were manufactured by Research Diets. The total composition of each pellet is displayed in Table 1. Pellets will be called diet throughout this work. Based on the initial chemical composition of native aleurone, all of the aleurone-enriched diets were designed to match the commercial high-fat diet with calorie density, the amount of macronutrients, and the total fiber content (5%). The diets and study groups receiving the aleurone fractions, native, finely ground, xylanase treated, and xylanase plus feruloyl esterase treated, were named as A-N, A-G, A-XYN and A-XYNFAE, respectively. Commercial FA (Sigma, St. Louis, MO, USA) was also added into the high-fat diet (named as group C-FA) in the same concentration as the FA content of the AN diet. Phenolic acids (bound to polysaccharides, conjugated to mono- or oligosaccharides, and in the free form) and AX (insoluble and soluble forms) contents were determined in the pellets after the addition of aleurone fractions in order to check that these compounds were not lost or deconjugated during the extrusion process and to measure the exact amount of AX and FA consumed by mice in each diet. The total antioxidant capacity of the pellets was also determined. All of the methodologies used are described by Rosa et al.[18,20] The pellets were stocked into bags under vacuum at 4 °C and protected from light to avoid oxidation during the experiment.

**Animals and Experimental Design.** C57BL/6J male mice were obtained from the National Laboratory Animal Center (Kuopio, Finland) at the age of 9 weeks (initial weight = 23.8 ± 0.2 g). The mice were acclimatized for 1 week and housed 3−4 animals per cage during the weeks 1−12 and in single cages from week 13 until the end of the study (week 17). The conditions in the animal house were controlled: temperature, 22 ± 1 °C; relative air humidity, 55 ± 15%; 12 h/12 h light/dark cycle with lights on at 7 am. The experimental design is showed in Figure 1. After 1 week of acclimatization, mice ($n$ = 85) were fed ad libitum a commercial high-fat diet (D12451, Research Diets) for 9 weeks to induce obesity and related metabolic disorders. The control group ($n$ = 20) was fed ad libitum a commercial low-fat control diet (D12450B, Research Diets). After 9 weeks of prefeeding, 10 mice receiving high-fat diet and 10 mice receiving low-fat diet were sacrificed (midpoint groups HFD1/2 and LFD1/2). These midpoint groups were used in order to evaluate the metabolic status of mice in the end of the first period. The rest of the mice receiving high-fat diets were randomized into 7 study groups ($n$ = 9−14 per group) and were fed either with D12451 (high-fat diet control, HFD, $n$ = 14), D12450B (group switched from high- to low-fat diet, named as lifestyle control group HFD + LFD, $n$ = 9), the D12451 diets enriched with aleurone fractions (A-N, A-G, A-XYN, and A-XYNFAE diets, $n$ = 10, 11, 10, and 11, respectively) or commercial ferulic acid (C-FA diet, $n$ = 11) for 8 weeks. The group receiving the low-fat diet (LFD, $n$ = 10) remained on the same diet until the end of the study to serve as a "healthy control". The lifestyle control group (HFD + LFD) was used in order to compare the effects of the consumption of aleurone-enriched diets with a energy-restricted diet.

At the end of the experiment, the mice were fasted for 7.5−8.5 h and sacrificed by decapitation after being made unconscious by $CO_2$ gas. Venous blood was collected into ethylenediametetraacetic acid (EDTA) tubes (K2-EDTA Microtainer Tubes with BD Microgard Closure, Beckton Dickinson Oy) and centrifuged for 10 min × 16000g at room temperature. Plasma was frozen on dry ice and stored at −70 °C in smaller aliquots. Tissues including liver were dissected immediately after blood collection, rinsed with physiological saline, wrapped into aluminum foil, snap frozen in liquid nitrogen, and stored at −70 °C until further processing. The animal experiments were approved by the Institutional Animal Care and Use Committee of the Provincial Government of Finland (permission no. 041003).

**Monitoring of the Body Weight and Feed Intake.** The body weight of the mice was measured weekly. Feed intake was also monitored weekly (always on the same day of the week) by determining the difference between the pellets supplied and the amount of pellets left on the grid and taking the spillage of the pellets into account. The energy intake was calculated based on the feed intake and the energy density of the diet. The average feed intake was calculated based on the diet consumption of each mouse during the first (weeks 1−9) and second (weeks 10−17) periods of the experiment.

**Assays of Plasma Samples.** Blood glucose was measured by LifeScan OneTouch Ultra glucometer from the venous blood drops immediately after decapitation. The following analyses were performed in the frozen plasma which was thawed just before carrying out the experiments. C-reactive protein (CRP), pro-inflammatory cytokines (IL-6 and IL-1$\beta$), anti-inflammatory cytokines (IL-10), tumor necrosis factors $\alpha$ (TNF$\alpha$), leptin, and insulin were measured from the plasma using Multiplex Biomarker Immunoassays for Luminex xMAP technology (Millipore, Billerica, MA, USA) following the instructions of the manufacturer. The CRP was assessed by MAP2MAG-76K kit; cytokines IL-1$\beta$, IL-6, IL-10, and TNF$\alpha$ were measured by MCYTOMAG-70K kit, and leptin together with insulin, by MMHMAG-44K-02 kit. For measurement of the cytokines, the lowest concentration of the calibration curve was 3.2 mg/L. However, some plasma samples presented concentrations under this limit of detection, and an arbitrary medium value of 1.6 mg/L was attributed to them.

**Measurement of Liver Oxidative Stress Markers.** Livers were cryo-ground in 10 mL grinding steel jars with a stainless steel ball for 60 s with 15 Hz using TissueLyser II (Qiagen). The obtained liver powder was used for the oxidative stress marker analyses. The amounts of total (TGSH) and oxidized (GSSG) gluthathione were determined spectrophotometrically as described previously.[25] Lipid peroxidation level was evaluated by thiobarbituric acid−reactive substances (TBARS) and lipid hydroperoxydes (LPO), which were measured according to the method of Sunderman et al.[26] and Kinnunen et al.,[27] respectively. Sulfhydryl groups (SH) was measured according to Faure and Lafond[28] and protein carbonyls using the ELISA method as

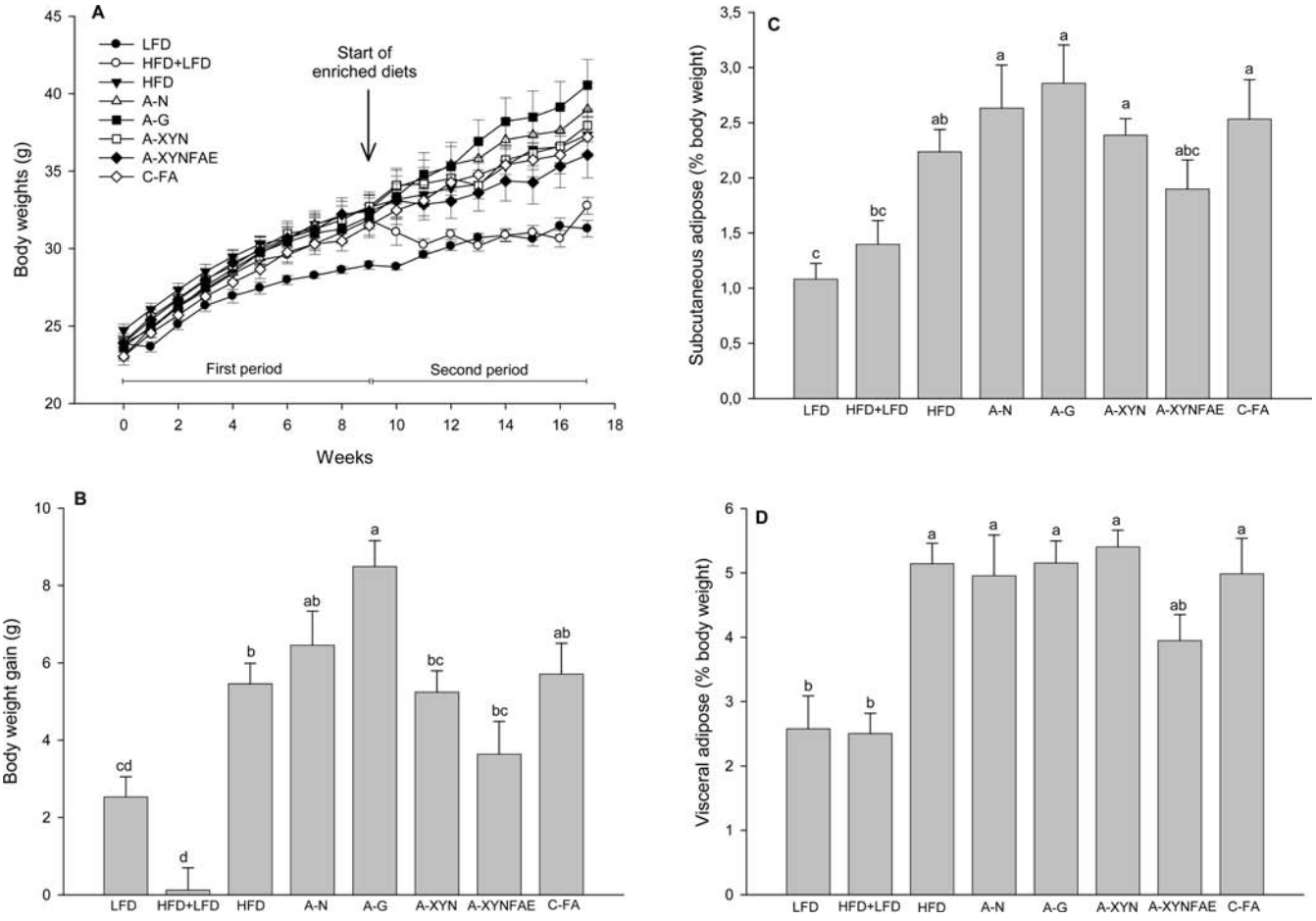


**Figure 2.** (A) Development of body weights of mice during the first (9 weeks) and second (8 weeks) periods. (B) Body weight gain during the second period (weeks 10−17). Weights for subcutaneous (C) and visceral (D) adipose tissues (percent body weight) at the end of the experiment (week 17). The values are reported as means ± SEM ($n$ = 10, 9, 14, 10, 11, 10, 11, and 11 for LFD, HFD + LFD, HFD, A-N, A-G, A-XYN, A-XYNFAE, and C-FA, respectively). Values not significantly different ($p > 0.05$) are designated by pairs of letters.

previously described by Oksala et al.[29] Oxygen radical absorbance capacity (ORAC) was used for the measurement of the antioxidant capacity, which was performed using a multiwell plate reader according to the methods described previously.[30] The activity of antioxidant enzymes catalase (CAT), glutathione peroxidase (GPx), and superoxide dismutase (SOD) was measured according to the method of Beers and Sizer,[31] Flohe and Gunzler,[32] and Marklund,[33] respectively. Protein carbonyls and ORAC measurements were performed in triplicate, and the other markers were measured in duplicates.

**Statistical Analysis.** Results were expressed as means ± standard error of the mean (SEM). Statistical analysis based on one-way ANOVA was applied followed by a Tukey−Kramer honest significant difference (HSD) posthoc test at 95% confidence level ($p < 0.05$) for the data following a normal distribution and having similar variance. The student's $t$-test at 95% confidence level ($p < 0.05$) was also applied in pairs between the HFD control group and each aleurone-enriched group. Correlation analyses were carried out by the Pearson's correlation method with a 95% confidence interval. For the analysis of the midpoint groups (HFD1/2 and LFD1/2), the student's $t$-test ($p < 0.05$) was applied.

## RESULTS

**Characterization of the Aleurone-Enriched Diets.** The total amounts of AX in the aleurone-enriched diets (A-N, A-G, A-XYN, and A-XYNFAE) were around 3.4−3.9 g/(100 g) (Table 1). Both diets A-N and A-G contained AX mainly in insoluble form (95%). The enzymatic process applied on aleurone efficiently solubilized AX, and thus the diets A-XYN and A-XYNFAE had higher proportion of AX in soluble form (39 and 75%, respectively). The total amount of FA in the aleurone-enriched diets was around 0.07−0.1 g/(100 g), which was equivalent to the amount of commercial FA in the C-FA diet (0.1 g/(100 g), mainly in free form). Both diets A-N and A-G had 95% of FA as bound to AX polysaccharides (Table 1). A-XYN and A-XYNFAE diets contained higher amounts of FA in both conjugated and free forms (41 and 84% for A-XYN and A-XYNFAE, respectively). The controls (HFD and LFD) and C-FA diets contained traces of AX, which came from the cellulose fraction added in these diets. Any traces of FA were detected in the control diets. The antioxidant capacity of the diets was measured and expressed in Trolox equivalent antioxidant capacity (TEAC). HFD and LFD had similar antioxidant capacity (10.8 mmol of TEAC/kg). Enrichment of the diets with either enzymatically treated aleurone fractions (A-XYN and A-XYNFAE diets) or free FA (C-FA diet) clearly increased the antioxidant capacity of the high-fat diets (2.5- and 2.1-fold for A-XYN and A-XYNFAE diets, respectively; Table 1). The diets A-N and A-G had slightly higher antioxidant capacity (1.3- and 1.4-fold, respectively) as compared to HFD alone (Table 1).

**Metabolic Status after 9 week High-Fat Feeding.** The high-fat diet resulted in significantly ($p < 0.05$) higher body weight after 9 weeks of feeding (31.4 ± 0.9 vs 28.2 ± 0.4 g for HFD1/2 and LFD1/2 groups, respectively; see the Supporting

Information Table S1). The adiposity index, i.e., the amount of adipose tissue (subcutaneous and visceral) in relation to the body weight, was significantly ($p < 0.05$) higher in the HFD1/2 group (4.8 vs 2.6% for HFD1/2 and LFD1/2, respectively) at the end of the first period. The plasma fasting insulin (1.7 ± 0.3 vs 0.9 ± 0.1 μg/mL for HFD1/2 and LFD1/2 groups, respectively) and leptin levels (14.9 ± 5 vs 3.9 ± 1 μg/mL for HFD1/2 and LFD1/2 groups, respectively) were also significantly ($p < 0.05$) increased in the HFD1/2 group, while no significant difference was observed in the fasting blood glucose concentration between the midpoint groups. Both groups presented similar levels of oxidative stress and inflammatory markers, except for the GSSG/TGSH ratio and IL-6 (pro-inflammatory) which were significantly ($p < 0.05$) higher in the HFD1/2 group (Supporting Information Table S1).

**Body Weight, Body Fat Content, and Intestinal Tissue Weight.** The development of body weights of mice during both periods of the study was displayed in Figure 2A. The body weight gain during the second period of the experiment (weeks 10−17), i.e., the difference of weight between week 17 and week 10, was calculated and shown in Figure 2B. The body weight gain of the HFD control group was significantly higher than that of the LFD group (Figure 2B). The HFD control group also had twice the weight of subcutaneous and visceral adipose tissues as compared to the LFD group (Figure 2C,D). The change from the high-fat diet to low-fat diet for the second period (HFD + LFD or "lifestyle" group) resulted in a rapid weight loss within the first 2 weeks after the dietary change (Figure 2A) and in the reduction of the weight of the adipose tissues (Figure 2C,D), reaching levels similar to the low-fat-diet control group (LFD).

The group receiving the high-fat diet enriched with the ultrafine ground wheat aleurone (A-G group) had the highest increase in body weight gain, which was significantly different ($p < 0.05$, ANOVA) from the body weight gain in the HFD control group (Figure 2B). Groups receiving high-fat diets enriched with native aleurone, enzymatically treated aleurone fractions, or commercial FA had body weight gain similar to that of the HFD control group (Figure 2B). In addition, there were no significant differences in the weights of the adipose tissues between the HFD control group and aleurone- or FA-enriched diets (Figure 2C,D). Although the group receiving aleurone treated with xylanase and feruloyl esterase (A-XYNFAE) had results statistically similar to those of HFD, a tendency toward reduced body weight gain (33% reduction, $p = 0.07$ $t$-test) and lower visceral adipose tissue amount (23% reduction, $p = 0.004$ $t$-test) was observed when comparing only these two groups (A-XYNFAE and HFD) by the $t$-test. Body weight gain and adipose tissue accumulation in the A-XYNFAE group was indeed found statistically similar to that of the LFD control (Figure 2B−D). All groups receiving high-fat diet had similar energy intake regardless of aleurone enrichment (Table 2). Only the low-fat-fed groups (LFD and lifestyle HFD + LFD group) had significantly lower energy intake ((kcal/mouse)/day) as compared to HFD groups (Table 2).

All diets enriched with wheat aleurone preparations produced intestinal tissue of similar weight of compared those from HFD, except A-XYNFAE which had significant ($p < 0.05$, ANOVA) higher weight of intestinal tissue than the HFD control (Table 2). Cecal and colon tissue weights were not significantly changed by enriched aleurone diets or free FA compared to the HFD control group.

**Table 2. Body Weight, Weights of Intestinal, Caecum, and Colon Tissues, and Fasting Plasma Glucose of Mice in the End of the Second Period[a]**

| | LFD | HFD + LFD | HFD | A-N | A-G | A-XYN | A-XYNFAE | C-FA |
|---|---|---|---|---|---|---|---|---|
| final body weight (g) | 31.3 ± 0.5c | 32.7 ± 0.5bc | 37.4 ± 1.2ab | 39.0 ± 1.7ab | 40.5 ± 1.7a | 37.9 ± 1.0ab | 36.0 ± 1.5abc | 37.2 ± 1.3ab |
| food intake (g/day) | 3.69 ± 0.07a | 3.62 ± 0.08ab | 3.33 ± 0.06cd | 3.43 ± 0.08abc | 3.25 ± 0.07cd | 3.38 ± 0.07bcd | 3.17 ± 0.06cd | 3.12 ± 0.06d |
| energy intake (kcal/day) | 14.2 ± 0.3bc | 13.9 ± 0.3c | 15.5 ± 0.3a | 15.4 ± 0.3ab | 14.6 ± 0.2abc | 15.5 ± 0.3ab | 14.5 ± 0.2abc | 14.6 ± 0.2abc |
| intestinal tissue (g) | 0.85 ± 0.05abc | 0.89 ± 0.05abc | 0.77 ± 0.05bc | 0.96 ± 0.05abc | 0.96 ± 0.07abc | 0.98 ± 0.06ab | 1.07 ± 0.04a | 0.74 ± 0.03c |
| cecum tissue (g) | 0.091 ± 0.01a | 0.077 ± 0.01ab | 0.064 ± 0.00ab | 0.088 ± 0.01ab | 0.079 ± 0.0ab | 0.086 ± 0.01ab | 0.089 ± 0.01a | 0.057 ± 0.00b |
| colon tissue (g) | 0.17 ± 0.01a | 0.15 ± 0.01a | 0.15 ± 0.01a | 0.17 ± 0.01a | 0.17 ± 0.01a | 0.17 ± 0.01a | 0.17 ± 0.01a | 0.15 ± 0.01a |
| glucose (mmol/L) | 8.1 ± 0.6a | 9.0 ± 0.5a | 10.2 ± 0.5a | 10.9 ± 0.6a | 10.4 ± 0.7a | 10.5 ± 0.9a | 9.9 ± 0.4aa | 9.4 ± 0.7a |

[a]Food intake and energy intake are the average consumption during the second period. The values are reported as means ± SEM. The values not significantly different ($p > 0.05$) are designated by the same letter.


dx.doi.org/10.1021/jf503314a | J. Agric. Food Chem. 2014, 62, 10101−10109

**Blood Plasma Parameters (Glucose, Insulin, and Leptin Levels).** The fasting blood glucose level was similar between all the groups (Table 2). The fasting insulin levels were doubled in the HFD group as compared to the LFD group (Figure 3A). The change from the high-fat diet to low-fat

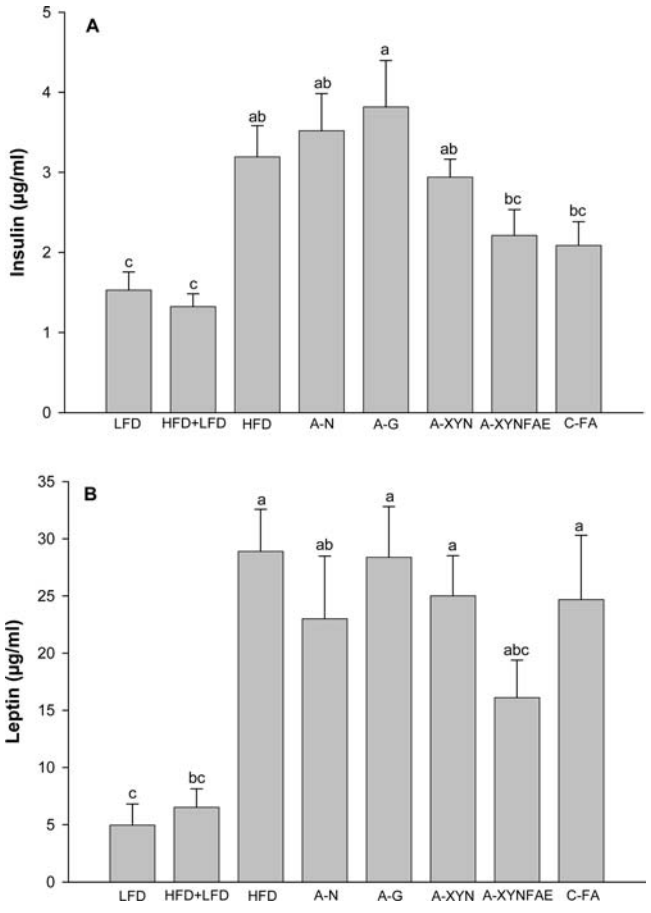


**Figure 3.** Plasma levels of (A) insulin and (B) leptin at the end of the experiment (week 17). The values are reported as means ± SEM. Values not significantly different ($p > 0.05$) are designated by pairs of letters.

diet (HFD + LFD lifestyle group) normalized the fasting insulin levels to the level observed in the LFD control group. Enrichment with aleurone preparations or commercial FA had no significant effect on insulin levels compared to the control HFD group (Figure 3A). However, A-XYNFAE had a tendency toward lowered fasting insulin levels (30% reduction, $p = 0.07$ *t*-test) compared to the HFD control group. A similar trend was observed for the C-FA group (35% reduction, $p = 0.03$ *t*-test) compared to the HFD control group.

The level of plasma leptin was 5.8-fold higher in the HFD group than in the LFD group (Figure 3B). The change from the high-fat diet to low-fat diet (HFD + LFD lifestyle group) resulted in reduction of leptin concentrations to the same level as in the LFD group. No significant differences in leptin levels were found between the HFD and aleurone-enriched groups. The group A-XYNFAE was the only one that had a tendency toward a reduced leptin level (44% reduction, $p = 0.02$ *t*-test) as compared to the HFD control group (Figure 3b). The level of leptin in all groups was positively correlated with the amount of adipose tissue in mice ($r = 0.98$ and 0.93 for visceral and subcutaneous, respectively).

**Oxidative Stress and Inflammation.** All of the data for oxidative and inflammatory markers are displayed in the Supporting Information (Table S2). High-fat diet feeding did not result in significant changes of the oxidative or inflammatory markers as compared to the LFD control group. Neither the aleurone-enriched diets nor C-FA-enriched diet had any beneficial impact on the levels of protein oxidation, the total antioxidant capacity, TBARS, TGSH, GSSG, GSSG/TGSH, CRP, pro (IL-1$\beta$, IL-6), or anti-inflammatory cytokines (IL-10) as compared to HFD. The only oxidative marker affected by the diets was the LPO. The aleurone-enriched diet A-XYN (LPO = 15.9 ± 1.9 nmol/g) and the C-FA (LPO = 16.4 ± 0.8 nmol/g) diet reduced the LPO levels significantly ($p < 0.05$, ANOVA) by 25% and 22%, respectively, as compared to the HFD control diet (LPO = 21.1 ± 0.8 nmol/g). The LPO levels did not change in the other groups (LPO = 18−20 nmol/g). Furthermore, no differences in the activity of the antioxidant enzymes catalase, GPx, and SOD were observed between the study groups.

## DISCUSSION

In the present work, the structure of the wheat aleurone was disrupted (by physical and enzymatic methods), and the effects of this disintegration on obesity and associated metabolic disorders in DIO mice were studied in a curative design. A curative design means that aleurone-enriched diets were provided to mice previously induced to develop obesity by feeding for 9 weeks with a high-fat diet. The amount of aleurone (13%) added in the high-fat diet provided a diet with 5% dietary fiber to mice, which is a common fiber (usually cellulose) level used in mice studies.

**Effects of Native and Processed Aleurone on Obese Mice.** Enrichment of the high-fat diet with 13% native wheat aleurone (group A-N) had no impact on the reversal of obesity in DIO mice. Other studies have also observed that high-fat diet supplemented with aleurone in corresponding amounts to those used in this study (10% for 3 weeks)[14] or wheat bran (16.5% for 12 weeks)[34] did not reduce the obesity of mice or rats in a preventive design. A preventive design means that no prefeeding period with high-fat diet was performed; i.e., the studied compound was added to the diet already in the beginning of the experiment. On the other hand, a recent study by Neyrinck et al.[12] showed that a high-fat diet (60E%) supplemented with purified AX from wheat (10% (w/w)) for 4 weeks in a preventive design decreased adiposity, body weight gain, serum and hepatic cholesterol accumulation, and insulin resistance in mice and that these effects were related to changes in the gut microbiota. The difference of the results obtained by Neyrinck et al.[12] as compared to the results found in our study could be attributed to the higher amount of purified AX (around 2.5-fold higher) and/or the preventive design of the study. If native aleurone had no impact on the reversal of obesity in DIO mice in our study, the ultrafine ground aleurone (group A-G) surprisingly increased ($p < 0.05$, Figure 2B) the body weight gain of mice as compared to the HFD control. The native and ground aleurones had a similar amount of insoluble AX and bound FA. Ultragrinding increased the aleurone particle surface area exposed to digestive enzymes, probably rendering the digestion more efficient. This could have led mice to increase their gain of weight when supplemented with ultraground aleurone instead of a native one or only a high-fat diet.

The disruption of aleurone by enzymatic treatment with the xylanase and feruloyl esterase (A-XYNFAE group) only showed a tendency ($p = 0.07$, *t*-test) toward reduced body weight gain as compared to the HFD group. A similar tendency toward lower visceral adipose tissue and secretion of leptin was observed when comparing only A-XYNFAE and HFD by *t*-test ($p = 0.004$ and $p = 0.02$ for visceral adipose tissue and leptin, repectively). A-XYNFAE diet had the highest proportion of soluble AX (75%) and conjugated and free forms of ferulic acid (85% of the total FA, respectively) in comparison to other aleurone fractions. Free and conjugated FA forms were reported to be bioavailable already in the upper part of the intestinal tract of humans and mice and beneficial against obesity in rodents.[35,36] Son et al.[37] observed that mice fed during 7 weeks with a free FA enriched high-fat diet in a preventive design reduced their body weight gain. In our work, however, mice fed the C-FA diet (100% free FA) did not have any significant reduction in the body weight gain or adiposity. This discrepancy between the two studies might be due to the 5-fold lower FA dose we administrated and to the curative design of our work. Since C-FA diet had no effect on the body weight gain of mice, the A-XYNFAE tendency could be more related to the high amount of soluble AX in this fraction. Soluble fiber can reduce the obesity by contributing to the viscosity of digesta in the small intestine delaying gastric emptying and decreasing the rate of lipid and carbohydrate absorption in the digestive tract.[38,39] Soluble AX fibers were also demonstrated to impact on the microbial metabolism (i.e., the formation of SCFA, gases, and phenolic metabolites) using an *in vitro* gut model with faecal microbiota as an inoculum.[20] However, the beneficial effects of the enzymatic solubilization of AX on mice obesity remained here as a minor trend, and it might be more pronounced adding the A-XYNFAE diet in a preventive way.

Obesity is associated with an increased risk of developing insulin resistance and type 2 diabetes. In our study the 17 weeks high-fat diet feeding tended to increase fasting blood glucose as compared to the low-fat control group ($p = 0.02$, *t*-test), but neither aleurone- nor FA-enriched diets had any effect on the fasting blood glucose. However, AXYNFAE and C-FA groups had a tendency toward lower fasting plasma insulin level compared to HFD ($p = 0.07$ for AXYNFAE and $p = 0.03$ for C-FA, *t*-test). This tendency to better insulin sensitivity might be related to the high amount of bioacessible FA in both groups rather than to their soluble AX fiber contents, as the C-FA diet contained only cellulose as fiber. Free FA has been previously shown to improve insulin sensitivity in diabetic rats,[40] suggesting that the different effects observed might be due the dose, longer feeding period (19 weeks), and preventive design.

**Effects of Native and Processed Aleurone on Oxidative Stress and Inflammatory Status.** There were no significant differences between the aleurone fractions, C-FA, and control groups for most of the markers for oxidative stress or inflammation. Similarly in healthy humans, the enrichment of the diet with aleurone (amount of aleurone corresponding to 1% of the diet, which provided around 15 g of dietary fiber from aleurone) during a 4 week period did not change the plasma antioxidant activity or markers of inflammation, CRP being the only one decreased after consuming aleurone.[16] In our study, the only marker significantly affected by the diets was the lipid peroxidation byproduct lipidhydroperoxides (LPO). The significant decrease in the LPO levels in A-XYN and C-FA groups ($p = 0.01$ and $p = 0.03$, respectively, ANOVA) may be related to the high antioxidant capacity of these diets due to the high amount of bioaccessible FA, which was shown to scavenge free radicals from the lipid phase and quench the lipid peroxides.[41] However, the fact that the A-XYNFAE diet did not reduce LPO levels despite its high antioxidant capacity remains unclear. Other studies have also shown that supplementation with free FA and feruloyl oligosaccharides from wheat bran decreases oxidative stress biomarkers in high-cholesterol, diabetic, and normal rats.[42−44]

Even though the HFD control group had higher levels of obesity, fasting plasma insulin and leptin compared to LFD throughout the experiment, HFD did not have any significant impact on the degree of oxidative stress or the inflammatory marker levels as compared to LFD. Similarly to our results, Hogan et al.[45] also observed that 12 weeks of a high fat diet feeding was not enough to induce oxidative stress in C57BL/6J mice when compared to a normal diet. It is noteworthy that despite the high amount of fat (45 E%), mainly saturated lard, present in the high-fat diet used in our study, the diet also contained adequate amounts of vitamins and minerals which can help the body metabolism to cope with potential oxidative stress. Therefore, more robust models of feeding trials such as cafeteria diets might be useful in future studies.[46]

In conclusion, this study showed that enrichment of diet with native aleurone reduced neither obesity nor oxidative stress and inflammatory status of DIO mice, but high-fat diets enriched with processed aleurone could impact some parameters of mice metabolism. Disruption of the physical structure of aleurone by ultrafine grinding was not beneficial, as it slightly increased the body weight gain of mice. Disintegration of aleurone at the molecular level showed some trends to reduce body weight gain, visceral adiposity, leptin level, and fasting insulin level in DIO mice, probably related to their higher content in soluble fiber, bioaccessible FA, and other phytochemicals. Considering the cost of aleurone milling and enzymatic treatments, it seems that the use of native or processed aleurone to counteract the metabolic disorders caused by obesity is limited. The lack of significant improvements was probably due to the curative design of this study, which aimed to reverse mice obesity by aleurone-enriched diets. The trends toward improvements of obesity observed by enzymatic treated aleurone indicates that it might be of interest to study the nutritional potential of processed aleurone on healthy mice fed with a high-fat diet in a preventive design.

## ■ ASSOCIATED CONTENT

### Supporting Information

Status of mice in the end of the first period (midpoint groups HFD1/2 and LFD1/2; Table S1) and oxidative and inflammatory markers of mice fed high-fat diet enriched with aleurone fractions (end of the second period; Table S2). This material is available free of charge via the Internet at http://pubs.acs.org.

## ■ AUTHOR INFORMATION

### Corresponding Author

*E-mail: micard@supagro.inra.fr. Tel.: +33 4 99 61 28 89. Fax: +33 4 99 61 30 76.

### Funding

The project was financed by the price Chercheur d'Avenir 2009 (Région Languedoc-Roussillon) awarded to V. M,. and it was

also supported by Agropolis Foundation, OCDE and AFFRST. P.h.D funding for N.N.R. was provided by the French National Education Ministry. J.P. is grateful to the The Finnish Graduate School on Applied Biosciences: Bioengineering, Food & Nutrition, Environment. J.P., K.H., and H.M. are grateful to the Nordforsk Nordic Centre of Excellence project "HELGA—Whole grains and health". Support from the Academy of Finland to K.P. is gratefully acknowledged.

### Notes

The authors declare no competing financial interest.

## ■ ACKNOWLEDGMENTS

We thank A. Putois (UMR IATE-Montpellier), B. Bonnafos (UMR Dynamique Musculaire et Métabolisme-Montpellier), and S. Martilla (UEF-Kuopio) for skilful technical assistance. W. von Reding (Bühler SA, Switzerland) is thanked for providing the native wheat aleurone. J. F. Sørensen (Danisco, Denmark) and C. Faulds (IFR, Norwich, U.K.) are thanked for kindly providing the enzymes Grindamyl Powerbake 950 and feruloyl esterase, respectively.

## ■ ABBREVIATIONS

A-N, native aleurone diet; A-G, ground aleurone diet; A-XYN, xylanase treated aleurone diet:; A-XYNFAE, xylanase and feruloyl esterase treated aleurone diet; AX, arabinoxylans; C-FA, commercial ferulic acid diet; DIO, diet-induced obesity; FA, ferulic acid; HFD, high-fat diet; LFD, low-fat diet; TEAC, Trolox equivalent antioxidant capacity

## ■ REFERENCES

(1) Eckel, R. H.; Grundy, S. M.; Zimmet, P. Z. The metabolic syndrome. *Lancet* **2005**, *365*, 1415−1428.

(2) Vincent, H. K.; Taylor, A. G. Biomarkers and potential mechanisms of obesity-induced oxidant stress in humans. *Int. J. Obes.* **2006**, *30*, 400−418.

(3) McKeown, N. M.; Yoshida, M.; Shea, M. K.; Jacques, P. F.; Lichtenstein, A. H.; Rogers, G.; Booth, S. L.; Saltzman, E. Whole-grain intake and cereal fiber are associated with lower abdominal adiposity in older adults. *J. Nutr.* **2009**, *139*, 1950−1955.

(4) Bazzano, L. A.; Song, Y. Q.; Bubes, V.; Good, C. K.; Manson, E.; Liu, S. Dietary intake of whole and refined grain breakfast cereals and weight gain in men. *Obes. Res.* **2005**, *13*, 1952−1960.

(5) Fardet, A. New hypotheses for the health-protective mechanisms of whole-grain cereals: What is beyond fibre? *Nutr. Res. Rev.* **2010**, *23*, 65−134.

(6) Brouns, F.; Hemery, Y.; Price, R.; Anson, N. M. Wheat aleurone: Separation, composition, health aspects, and potential food use. *Crit. Rev. Food Sci. Nutr.* **2012**, *52*, 553−568.

(7) Hemery, Y.; Rouau, X.; Lullien-Pellerin, V.; Barron, C.; Abecassis, J. Dry processes to develop wheat fractions and products with enhanced nutritional quality. *J. Cereal Sci.* **2007**, *46*, 327−347.

(8) Saulnier, L.; Sado, P. E.; Branlard, G.; Charmet, G.; Guillon, F. Wheat arabinoxylans: Exploiting variation in amount and composition to develop enhanced varieties. *J. Cereal Sci.* **2007**, *46*, 261−281.

(9) Barron, C.; Surget, A.; Rouau, X. Relative amounts of tissues in mature wheat (Triticum aestivum L.) grain and their carbohydrate and phenolic acid composition. *J. Cereal Sci.* **2007**, *45*, 88−96.

(10) Garcia, A. L.; Otto, B.; Reich, S. C.; Weickert, M. O.; Steiniger, J.; Machowetz, A.; Rudovich, N. N.; Möhlig, M.; Katz, N.; Speth, M.; Meuser, F.; Doerfer, J.; Zunft, H.-F.; Pfeiffer, A. H. F.; Koebnick, C. Arabinoxylan consumption decreases postprandial serum glucose, serum insulin and plasma total ghrelin response in subjects with impaired glucose tolerance. *Eur. J. Clin. Nutr.* **2007**, *61*, 334−341.

(11) Lu, Z. X.; Walker, K. Z.; Muir, J. G.; O'Dea, K. Arabinoxylan fibre improves metabolic control in people with Type II diabetes. *Eur. J. Clin. Nutr.* **2004**, *58*, 621−628.

(12) Neyrinck, A. M.; Possemiers, S.; Druart, C.; Van de Wiele, T.; De Backer, F.; Cani, P. D.; Larondelle, Y.; Delzenne, N. M. Prebiotic effects of wheat arabinoxylan related to the increase in bifidobacteria, Roseburia and Bacteroides/Prevotella in diet-induced obese mice. *PLoS One* **2011**, *6*, 20944−20944.

(13) Zhao, Z. H.; Moghadasian, M. H. Chemistry, natural sources, dietary intake and pharmacokinetic properties of ferulic acid: A review. *Food Chem.* **2008**, *109*, 691−702.

(14) Neyrinck, A. M.; De Backer, F.; Cani, P. D.; Bindels, L. B.; Stroobants, A.; Portetelle, D.; Delzenne, N. M. Immunomodulatory properties of two wheat bran fractions—aleurone-enriched and crude fractions—in obese mice fed a high fat diet. *Int. Immunopharmacol.* **2008**, *8*, 1423−1432.

(15) Sagara, M.; Mori, M.; Mori, H.; Tsuchikura, S.; Yamori, Y. Effect of dietary wheat aleurone on blood pressure and blood glucose and its mechanisms in obese spontaneously hypertensive rats: Preliminary report on comparison with a soy diet. *Clin. Exp. Pharmacol. Physiol.* **2007**, *34*, S37−S39.

(16) Price, R. K.; Wallace, J. M. W.; Hamill, L. L.; Keaveney, E. M.; Strain, J. J.; Parker, M. J.; Welch, R. W. Evaluation of the effect of wheat aleurone-rich foods on markers of antioxidant status, inflammation and endothelial function in apparently healthy men and women. *Br. J. Nutr.* **2012**, *108*, 1644−1651.

(17) Hemery, Y. M.; Anson, N. M.; Havenaar, R.; Haenen, G. R. M. M.; Noort, M. W. J.; Rouau, X. Dry-fractionation of wheat bran increases the bioaccessibility of phenolic acids in breads made from processed bran fractions. *Food Res. Int.* **2010**, *43*, 1429−1438.

(18) Rosa, N. N.; Barron, C.; Gaiani, C.; Dufour, C.; Micard, V. Ultra-fine grinding increases the antioxidant capacity of wheat bran. *J. Cereal Sci.* **2013**, *57*, 84−90.

(19) Rosa, N. N.; Dufour, C.; Lullien-Pellerin, V.; Micard, V. Exposure or release of ferulic acid from wheat aleurone: Impact on its antioxidant capacity. *Food Chem.* **2013**, *141*, 2355−2362.

(20) Rosa, N. N.; Aura, A. M.; Saulnier, L.; Holopainen-Mantila, U.; Poutanen, K.; Micard, V. Effects of disintegration on in vitro fermentation and conversion patterns of wheat aleurone in a metabolical colon model. *J. Agric. Food Chem.* **2013**, *61*, 5805−5816.

(21) Stewart, M. L.; Slavin, J. L. Particle size and fraction of wheat bran influence short-chain fatty acid production *in vitro*. *Br. J. Nutr.* **2009**, *102*, 1404−1407.

(22) Zaupa, M.; Scazzina, F.; Dall'Asta, M.; Calani, L.; Del Rio, D.; Bianchi, M. A.; Melegari, C.; De Albertis, P.; Tribuzio, G.; Pellegrini, N.; Brighenti, F. In vitro bioaccessibility of phenolics and vitamins from durum wheat aleurone fractions. *J. Agric. Food Chem.* **2014**, *62*, 1543−1549.

(23) Mateo Anson, N.; Aura, A.-M.; Selinheimo, E.; Mattila, I.; Poutanen, K.; van den Berg, R.; Havenaar, R.; Bast, A.; Haenen, G. R. M. M. Bioprocessing of wheat bran in whole wheat bread increases the bioavailability of phenolic acids in men and exerts antiinflammatory effects ex vivo. *J. Nutr.* **2011**, *141*, 137−43.

(24) Mateo Anson, N.; Selinheimo, E.; Havenaar, R.; Aura, A.-M.; Mattila, I.; Lehtinen, P.; Bast, A.; Poutanen, K.; Haenen, G. R. M. M. Bioprocessing of wheat bran improves in vitro bioaccessibility and colonic metabolism of phenolic compounds. *J. Agric. Food Chem.* **2009**, *57*, 6148−6155.

(25) Lappalainen, Z.; Lappalainen, J.; Oksala, N. K.; Laaksonen, D. E.; Khanna, Z. S.; Sen, C. K.; Atalay, M. Diabetes impairs exercise training-associated thioredoxin response and glutathione status in rat brain. *J. Appl. Physiol.* **2009**, *106*, 461−467.

(26) Sunderman, F. W., Jr.; Marzouk, A.; Hopfer, S. M.; Zaharia, O.; Reid, M. C. Increased lipid peroxidation in tissues of nickel chloride-treated rats. *Ann. Clin. Lab. Sci.* **1985**, *15*, 229−236.

(27) Kinnunen, S.; Oksala, N. K. J.; Hyyppä, S.; Sen, C. K.; Radak, Z.; Laaksonen, D. E.; Szabo, B.; Jakus, J.; Atalay, M. Alpha-Lipoic acid modulates thiol antioxidant defenses and attenuates exercise-induced

oxidative stress in standardbred trotters. *Free Radical Res.* **2009**, *43*, 697−705.
(28) Faure, P.; Lafond, J. Measurement of plasma sulfhydryl and carbonyl groups as a possible indicator of protein oxidation. In *Analysis of free radicals in biological systems*; Favier, A., Cadet, J., Kalyanaraman, B., Fontecave, M., Pierre, J., Eds.; Birkhauser Verlag: Basel, Switzerland, 1995; pp 237−248.
(29) Oksala, N. K. J.; Paimela, H.; Alhava, E.; Atalay, M. Heat shock preconditioning induces protein carbonylation and alters antioxidant protection in superficially injured guinea pig gastric mucosa *in vitro*. *Dig. Dis. Sci.* **2007**, *52*, 1897−1905.
(30) Kinnunen, S.; Hyyppa, S.; Lehmuskero, A.; Oksala, N.; Mäenpää, P.; Hänninen, O.; Atalay, M. Oxygen radical absorbance capacity (ORAC) and exercise-induced oxidative stress in trotters. *Eur. J. Appl. Physiol.* **2005**, *95*, 550−556.
(31) Beers, R.; Sizer, I. A spectrophotometric method for measuring the breakdown of hydrogen peroxide by catalase. *J. Biol. Chem.* **1952**, *195*, 133−140.
(32) Flohe, L.; Gunzler, W. A. Assays of glutathione peroxidase. *Methods Enzymol.* **1954**, *105*, 114−121.
(33) Marklund, S. Spectrophotometric study of spontaneous disproportionation of superoxide anion radical and sensitive direct assay for superoxide dismutase. *J. Biol. Chem.* **1976**, *251*, 7504−7507.
(34) Belobrajdic, D. P.; Lam, Y. Y.; Mano, M.; Wittert, G. A.; Bird, A. R. Cereal based diets modulate some markers of oxidative stress and inflammation in lean and obese Zucker rats. *Nutr. Metab.* **2011**, *8*, 27.
(35) Andreasen, M. F.; Kroon, P. A.; Williamson, G. Esterase activity able to hydrolyze dietary antioxidant hydroxycinnamates is distributed along the intestine of mammals. *J. Agric. Food Chem.* **2001**, *49*, 5679−5684.
(36) Hsu, C.-L.; Yen, G.-C. Phenolic compounds: Evidence for inhibitory effects against obesity and their underlying molecular signaling mechanisms. *Mol. Nutr. Food Res.* **2008**, *52*, 53−61.
(37) Son, M. J.; Rico, C. W.; Nam, S. H.; Kang, M. Y. Influence of oryzanol and ferulic acid on the lipid metabolism and antioxidative status in high fat-fed mice. *J. Clin. Biochem. Nutr.* **2010**, *46*, 150−156.
(38) Brennan, C. S. Dietary fibre, glycaemic response, and diabetes. *Mol. Nutr. Food Res.* **2005**, *49*, 560−570.
(39) Davidson, M. H.; McDonald, A. Fiber: Forms and functions. *Nutr. Res. (N. Y., NY, U. S.)* **1988**, *18*, 617−624.
(40) Choi, R.; Kim, B. H.; Naowaboot, J.; Lee, M. Y.; Hyun, M. R.; Cho, E. J.; Lee, E. S.; Lee, E. Y.; Yang, Y. C.; Chung, C. H. Effects of ferulic acid on diabetic nephropathy in a rat model of type 2 diabetes. *Exp. Mol. Med.* **2011**, *43*, 676−683.
(41) Srinivasan, M.; Rukkumani, R.; Sudheer, A. R.; Menon, V. P. Ferulic acid, a natural protector against carbon tetrachloride-induced toxicity. *Fundam. Clin. Pharmacol.* **2005**, *19*, 491−496.
(42) Ou, S. Y.; Jackson, G. M.; Jiao, X.; Chen, J.; Wu, J.-Z.; Huang, X.-S. Protection against oxidative stress in diabetic rats by wheat bran feruloyl oligosaccharides. *J. Agric. Food Chem.* **2007**, *55*, 3191−3195.
(43) Wang, J.; Sun, B.; Cao, Y. Wheat bran feruloyl oligosaccharides enhance the antioxidant activity of rat plasma. *Food Chem.* **2010**, *123*, 472−476.
(44) Yeh, Y. H.; Lee, Y. T.; Hsieh, H. S.; Hwang, D. F. Dietary caffeic acid, ferulic acid and coumaric acid supplements on cholesterol metabolism and antioxidant activity in rats. *J. Food Drug Anal.* **2009**, *17*, 123−132.
(45) Hogan, S.; Canning, C.; Sun, S.; Sun, X.; Zhou, K. Effects of grape pomace antioxidant extract on oxidative stress and inflammation in diet induced obese mice. *J. Agric. Food Chem.* **2010**, *58*, 11250−11256.
(46) Sampey, B. P.; Vanhoose, A. M.; Winfield, H. M.; Freemerman, A. J.; Muehlbauer, M. J.; Fueger, P. T.; Newgard, C. B.; Makowski, L. Cafeteria diet is a robust model of human metabolic syndrome with liver and adipose inflammation: Comparison to high-fat diet. *Obesity* **2011**, *19*, 1109−1117.

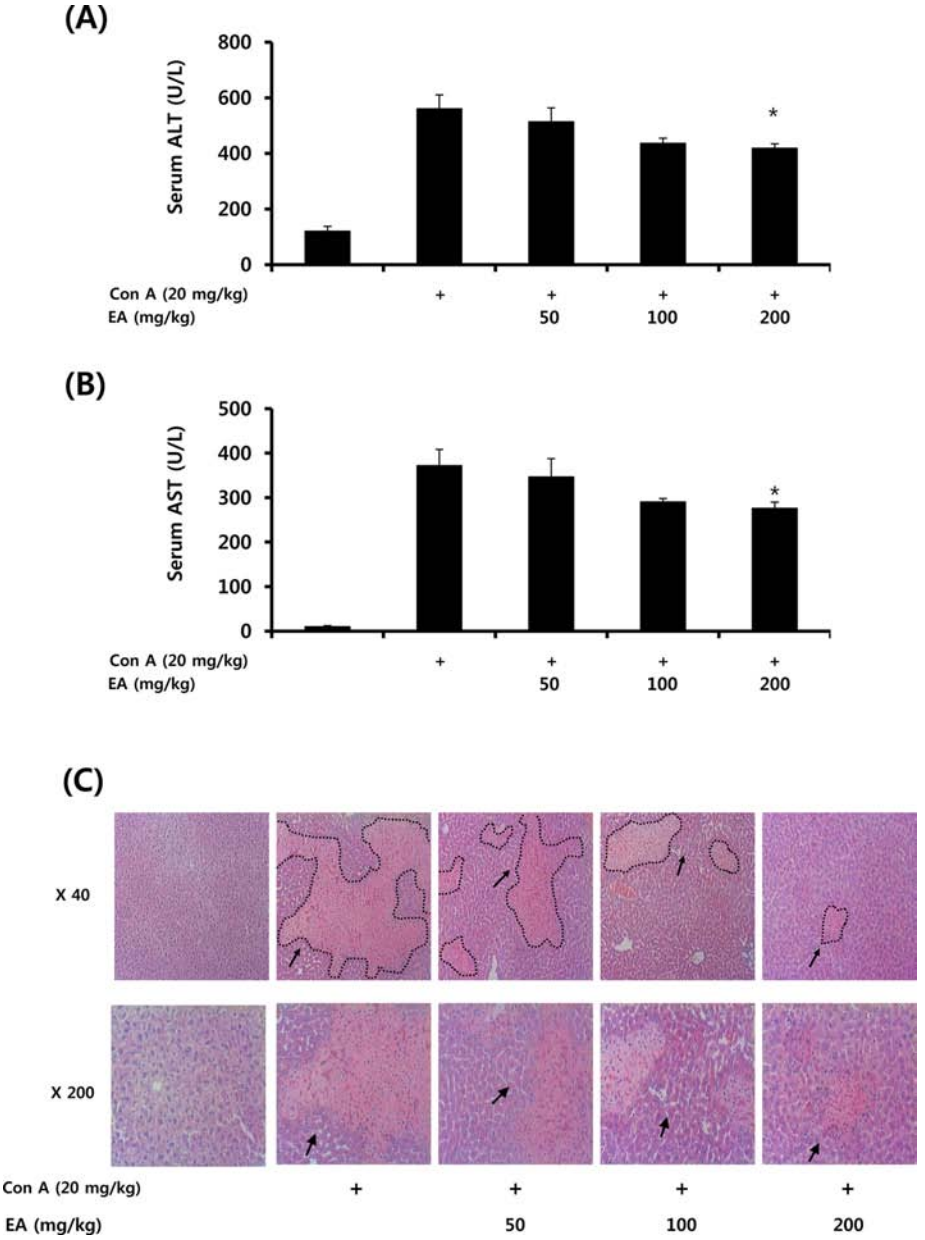


**Figure 1.** Hepatoprotective effects of EA in Con A-induced liver dysfunction. Mice were pretreated with EA (50, 100, or 200 mg/kg) at both 12 and 1 h before challenge with Con A. The control mice were given distilled water. (A) Serum ALT levels were determined 8 h after Con A injection. (B) Serum AST levels were determined 8 h after Con A injection. Bar represents the mean ± SD ($n$ = 4 mice per group). (*) $p < 0.05$ versus Con A. (C) Liver sections obtained 24 h after Con A injection were assessed by H&E staining (original magnification, 40×, and 200×).

is involved in TLR2 and TLR4 expression and MAPK/NF-κB signaling pathways.

## MATERIALS AND METHODS

**Animals.** Pathogen-free male BALB/c mice (8 weeks old; weight, 23 ± 2 g) were purchased from Orient Bio, Inc. (Seoul, Korea). The animals were acclimated for 1 week before the experiments. They were allowed free access to laboratory-standard food and water on a 12 h light/12 h dark cycle in a temperature (22 ± 2 °C) and humidity (50 ± 5%) controlled environment. All procedures and animal treatments were performed in a clean animal laboratory room according to the guidelines for laboratory animal experimentation specified by Chung-Ang University. This work was approved by the appropriate ethics committees for the use of laboratory animals at Chung-Ang University.

**Animal Treatment.** Con A was dissolved in pyrogen-free normal saline at a concentration of 25 mg/mL and intravenously injected at a dose of 20 mg/kg of body weight to induce hepatitis, as previously described.[25] EA was dissolved in 0.01 N NaOH[26] at concentrations of 5, 10, or 20 mg/mL and administered by gavage at doses of 50, 100, or 200 mg/kg of body weight.[27,28] The mice were randomized into five groups ($n$ = 4/group; total = 30) as follows: (i) sham group as the vehicle control, including oral administration of the phosphate-buffered saline (PBS) and a tail vein injection with the same volume of saline, (ii) Con A administration group that received no EA treatment, (iii) EA 50 (50 mg/kg) group, (iv) EA 100 (100 mg/kg) group, and (v) EA 200 (200 mg/kg) group. Mice, deprived of food 24 h before Con A treatment with free access to water, were administered with respective doses of EA at both 12 and 1 h before challenge with Con A. Liver samples were obtained 24 h after Con A injection.

**Serum Transaminase Activity Assays.** Blood was obtained from individual mice at 8 h after Con A injection. Serum levels of AST and ALT were used as markers of liver injury. Alanine aminotransaminase (ALT) and aspartate aminotransaminase (AST) concentrations were measured using an IDTox ALT color endpoint assay kit and an IDTox

AST color endpoint assay kit (ID Laboratories, Inc., London, Ontario, Canada), respectively, according to the instructions of the manufacturer, and absorbance was measured using a spectrophotometer.

**Histopathological Examination of the Liver.** The liver tissues were excised, fixed in 10% neutral buffered formalin, and embedded in paraffin. We prepared 4 $\mu$m thick slices stained with hematoxylin and eosin (H&E) according to standard procedures. The slides were examined using light microscopy.

**RNA Isolation, cDNA Synthesis, and Real-Time Quantitative Polymerase Chain Reaction (qPCR) Amplification.** Liver tissues were stored at −80 °C until required. RNA was extracted using Trizol reagent (Invitrogen, Carlsbad, CA). For real-time qPCR, 0.1 $\mu$g of total RNA was reverse-transcribed using a SuperScript III First-Strand Synthesis System for reverse transcription (RT)-PCR (Invitrogen). Real-time PCR was performed in triplicate using the MyiQ Single-Color Real-Time PCR Detection System and an iQ SYBR Green Supermix (Bio-Rad, Hercules, CA). Relative expression was normalized to glyceraldehyde 3-phosphate dehydrogenase (GAPDH) levels. The primer sequences used were as follows: GAPDH, forward, 5-TTC ACC ACC ATG GAG AAG GC-3 and reverse, 5-GGC ATG GAC TGT GGT CAT GA-3; TLR2, forward, 5-AAG ATG TCG TTC AAG GAG GTG CG-3 and reverse, 5-ATC CTC TGA GAT TTG ACG CTT TG-3; TLR4, forward, 5-GGT GTG AAA TTG AGA CAA TTG AAA AC-3 and reverse, 5-GTT TCC TGT CAG TAC CAA GGT TGA-3; tumor necrosis factor $\alpha$ (TNF-$\alpha$), forward, 5-GGC AGG TCT ACT TTG GAG TC-3 and reverse, ACA TTC GAG GCT CCA GTG AA-3; interleukin 6 (IL-6), forward, 5-ACC GCT ATG AAG TTC CTC TC-3 and reverse, 5-CCT CTG TGA AGT CTC CTC TC-3; and interleukin 1$\beta$ (IL-1$\beta$), forward, 5-TCA TGG GAT GAT GAT GAT AAC CTG CT-3 and reverse, 5-CCC ATA CTT TAG GAA GAC ACG GAT T-3. The thermal cycling conditions were as follows: pre-denaturation at 95 °C for 5 min, denaturation at 95 °C for 10 s, annealing at 58 °C for 15 s, and extension at 72 °C for 20 s.

**Isolation of Cytoplasmic and Nuclear Proteins and Immunoblotting.** Frozen liver tissues were weighed and homogenized in ice-cold hypotonic buffer [25 mM Tris (pH 7.5), 150 mM NaCl, 1 mM ethylenediaminetetraacetic acid (EDTA), 2 mM sodium orthovanadate, 50 mM sodium fluoride, 1 mM phenylmethylsulfonyl fluoride (PMSF), 0.1% Triton-X 100, phosphatase inhibitor cocktail tablets, and protease inhibitor cocktail tablets]. Homogenates were incubated for 10 min on ice and centrifuged (12500*g* for 10 min at 4 °C). Cytoplasmic proteins were collected from the supernatants, and nuclear proteins were collected from the pellets. Cytoplasmic fractions were stored at −70 °C. Nuclear proteins were released by dropwise addition of a high-salt buffer [25 mM Tris (pH 7.5), 500 mM NaCl, 10% glycerol, 1 mM EDTA, 2 mM sodium orthovanadate, 50 mM sodium fluoride, 1 mM PMSF, 0.2% Triton-X 100, phosphatase inhibitor cocktail tablets, and protease inhibitor cocktail tablets]. Samples were incubated on ice for 30 min with smooth shaking. The nuclei-containing suspension was then centrifuged (16000*g* for 30 min at 4 °C). The supernatant fraction was collected as the nuclear extract. This extract was stored in aliquots at −70 °C for the subsequent NF-$\kappa$B assay. Protein concentrations of the homogenate were determined using the BCA protein assay with bovine serum albumin as a standard. Equal amounts of whole protein extracts (50 $\mu$g) were separated on 10% acrylamide gels using sodium dodecyl sulfate−polyacrylamide gel electrophoresis. Then, the proteins were transferred onto polyvinylidene fluoride (PVDF) membranes and incubated overnight at 4 °C with specific primary antibodies, namely, rabbit polyclonal anti-TLR2 (Santa Cruz Biotechnology, Santa Cruz, CA) at a dilution of 1:500, rabbit polyclonal anti-TLR4 (Santa Cruz Biotechnology) at a dilution of 1:500, rabbit polyclonal anti-JNK and anti-p-JNK (Cell Signaling Technology, Beverly, MA) at a dilution of 1:2000, rabbit polyclonal anti-ERK and anti-p-ERK (Cell Signaling Technology) at a dilution of 1:2000, rabbit polyclonal anti-p38 and anti-p-p38 (Cell Signaling Technology) at a dilution of 1:2000, rabbit polyclonal anti-I$\kappa$B-$\alpha$ (Santa Cruz Biotechnology) at a dilution of 1:2000, rabbit polyclonal anti-p65 (Cell Signaling Technology) at a dilution of 1:2000, and rabbit polyclonal anti-inducible nitric oxide synthase (iNOS, Santa Cruz Biotechnology) at a dilution of 1:2000. Each filter was then washed 3 times for 10 min and incubated for 2 h at room temperature with horseradish peroxidase (HRP)-labeled secondary anti-rabbit antibody (Cell Signaling Technology) containing blocking solution. To ensure equal loading, the blots were analyzed for GAPDH expression using an anti-GAPDH antibody (Santa Cruz Biotechnology). Immunodetection was performed using Amersham ECL western blotting detection reagents (GE Healthcare, U.K.). Densitometric data were studied after normalization with the control (housekeeping gene). The signals were analyzed and quantified using ImageJ software [National Institutes of Health (NIH), Bethesda, MD].

**Liver Tissue Immunofluorescence.** The liver tissues were fixed in 4% paraformaldehyde, dehydrated, paraffin-embedded, and cut into 4−5 $\mu$m thick sections. After antigen retrieval, the slides were stained with primary TLR2 or TLR4 antibodies (Santa Cruz) and a fluorescently labeled secondary antibody and counterstained with 4′-6-diamidino-2-phenylindole (DAPI). Confocal images were collected in fluorescence mode followed by electronic image merging.

**Statistical Analysis.** Results are represented as the mean ± standard deviation (SD) and were analyzed statistically with analysis of variance (ANOVA), and differences between groups were determined with the Turkey method. Statistical significance was accepted when $p < 0.05$.

## RESULTS

**Hepatoprotective Effect of EA on Con A-Induced Hepatitis.** Acute hepatitis was induced in BALB/c mice by

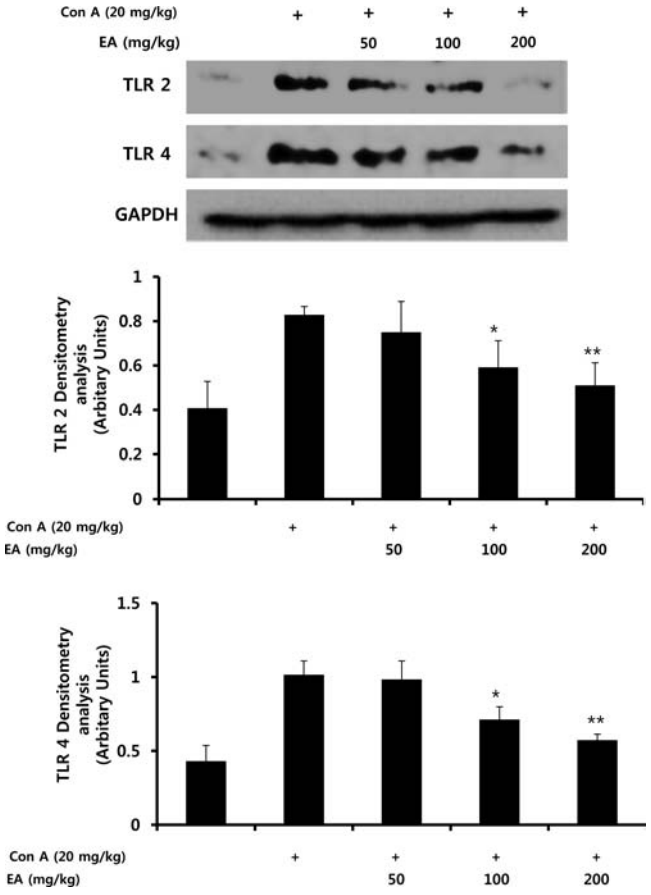


**Figure 2.** Effect of EA on the Con A-induced expression of TLR2 and TLR4 in mouse liver. Hepatic TLR2 and TLR4 protein levels were determined by immunoblotting. Densitometry was performed following normalization to the control (GADPH). Bar represents the mean ± SD ($n$ = 4 mice per group). (*) $p < 0.05$ versus Con A. (**) $p < 0.01$ versus Con A.

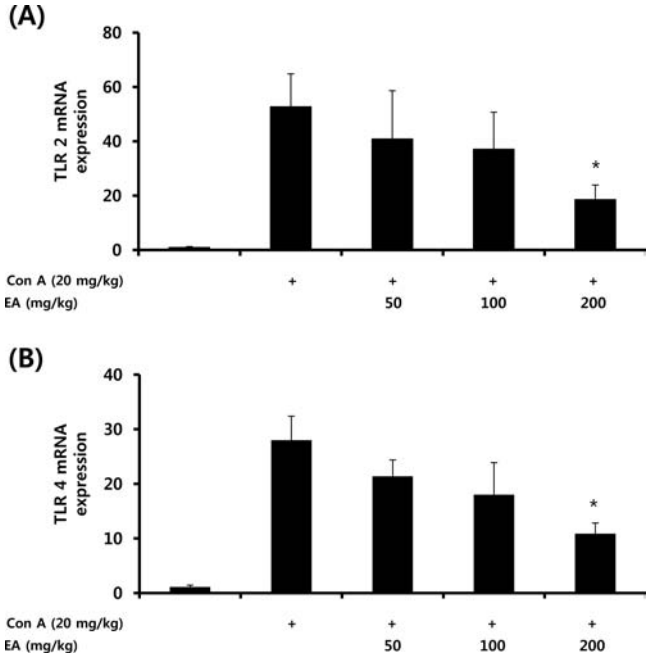


**Figure 3.** Effect of EA treatment on the expression of (A) TLR2 and (B) TLR4 mRNAs in the liver was examined by real-time qPCR. TLR2 and TLR4 mRNA levels were normalized to GAPDH expression in each sample. Bar represents the mean ± SD ($n$ = 4 mice per group). (*) $p < 0.05$ versus Con A.

intravenous injection of Con A. Plasma levels of AST and ALT were significantly increased at 8 h after injection of Con A (Figure 1). In comparison to the vehicle-treated group, the groups receiving oral administration of EA at doses of 50, 100, or 200 mg/kg at both 12 and 1 h before Con A injection showed a significant and dose-dependent decrease in the plasma levels of AST and ALT. Histopathological examination of the liver tissue was used to determine the effects of EA on Con A-induced liver injury. Light microscopy examination showed extensive inflammatory infiltration and large areas of necrosis in the livers of Con A-treated mice. In contrast, mice pretreated with EA showed dose-dependent reduction in liver damage (Figure 1C). This histopathologic evidence of liver damage was positively correlated with increased serum levels of liver enzymes. Taken together, pretreatment with EA showed a protective effect on Con A-induced hepatitis.

**Effects of EA on the TLR2 and TLR4 Expression in Con A-Induced Hepatitis.** We examined the effect of EA on the expression of TLR2 and TLR4 in Con A-induced hepatitis. We observed very low expression levels of TLR2 and TLR4 in the vehicle group. However, the Con A-treated group showed a significant increase of TLR2 and TLR4 expression levels (Figures 2 and 3). TLR2 and TLR4 were highly expressed, which suggested that both receptors were involved in the pathological sequelae of Con A-induced acute liver injury. EA-treated groups showed reduced expression levels of TLR2 and TLR4 in a dose-dependent manner (Figures 2 and 3). In immunofluorescence analysis, TLR2 and TLR4 were reduced in EA-treated groups in a dose-dependent manner (Figure 4).

**Effect of EA on the JNK, ERK1/2, and p38 Signaling Pathways in Con A-Induced Hepatitis.** TLR signaling pathways are involved in the activation of MAPKs. These molecules play a key role in inducing gene expression, which initiates inflammatory responses. We investigated the effect of EA on the Con A-induced hepatitis-associated activation of JNK, ERK1/2, and p38. We detected JNK, ERK1/2, and p38 MAPK protein phosphorylation using western blotting in the cytosolic extracts of liver tissues using phospho-specific MAPK antibodies. Con A treatment increases phosphorylation of JNK, ERK1/2, and p38; however, the EA treatment group showed a strong inhibition of phosphorylation of JNK, ERK1/2, and p38 (panels A–C of Figure 5). These results suggested that the activation of JNK, ERK1/2, and p38 could be induced at the acute stage of hepatitis caused by Con A and treatment with EA significantly decreased the phosphorylation levels of p38, JNK, and ERK1/2.

**EA Inhibits NF-κB Activation and IκB-α Degradation in Con A-Induced Hepatitis.** We further investigated the effect of EA on NF-κB activation and IκB degradation in a mouse model of Con A-induced hepatitis. EA pretreatment inhibits NF-κB activation and IκB-α degradation in an EA dose-dependent manner (panels A and B of Figure 6).

**EA Pretreatment Inhibits the Expression of Pro-inflammatory Cytokines and iNOS in Con A-Induced Hepatitis.** TNF-α, IL-6, and IL-1β have been shown to play critical roles in the progression of Con A-induced liver injury. To investigate whether EA influences the production of these cytokines, we measured the mRNA expression of TNF-α, IL-6, and IL-1β in Con A-induced hepatitis. The levels of TNF-α, IL-6, and IL-1β mRNA significantly increased in the control group

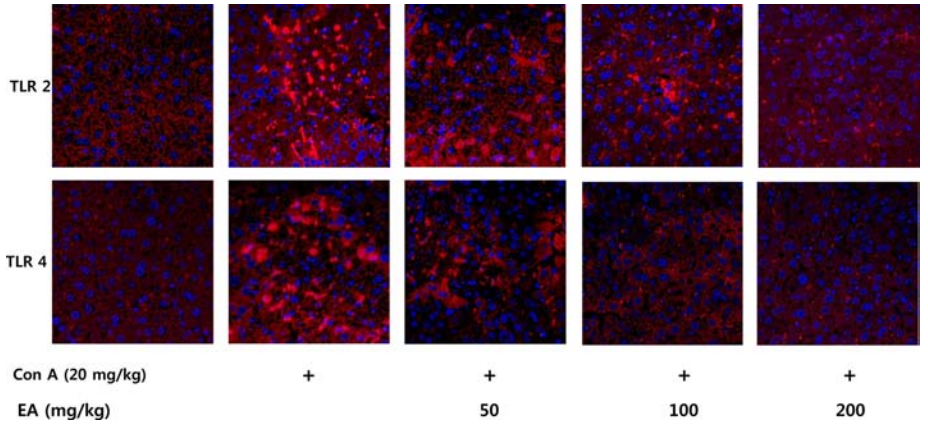


**Figure 4.** TLR2 and TLR4 localization in murine liver by immunofluorescence microscopy after administration of Con A for 24 h (original magnification and 300×).

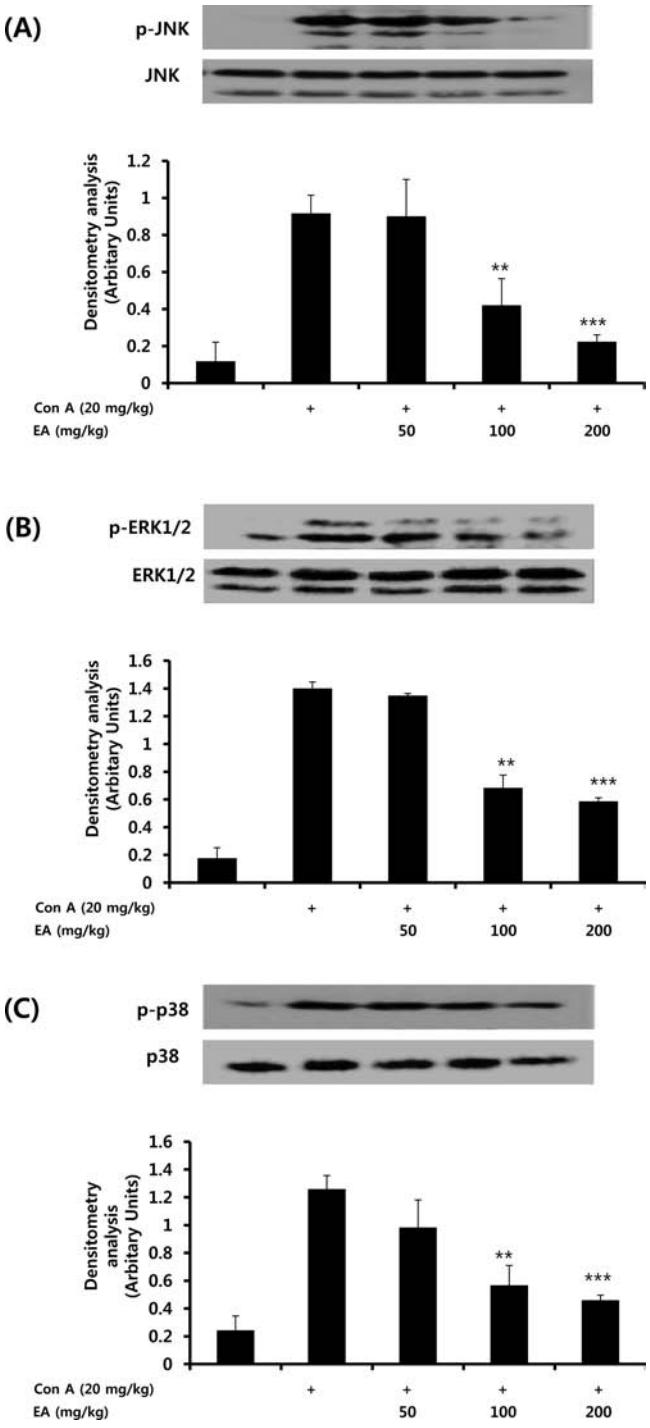


**Figure 5.** Hepatic (A) p-JNK, (B) p-ERK, and (C) p-p38 protein levels determined by immunoblotting. Densitometry was performed following normalization to the control (JNK, ERK, and p38 housekeeping genes, respectively). Bar represents the mean ± SD ($n$ = 4 mice per group) (∗) $p < 0.05$ versus Con A. (∗∗) $p < 0.01$ versus Con A. (∗∗∗) $p < 0.001$ versus Con A.

(panels A–C of Figure 7). EA pretreatment decreased the expression of TNF-$\alpha$, IL-6, and IL-1$\beta$ in the livers of Con A-treated groups. These data suggest that EA suppresses the expression of inflammatory cytokines in Con A-induced hepatitis. iNOS is a protein that is predominantly expressed on the sites of inflammation. We measured the cytosolic iNOS expression levels in the liver using western blotting. Exposure of

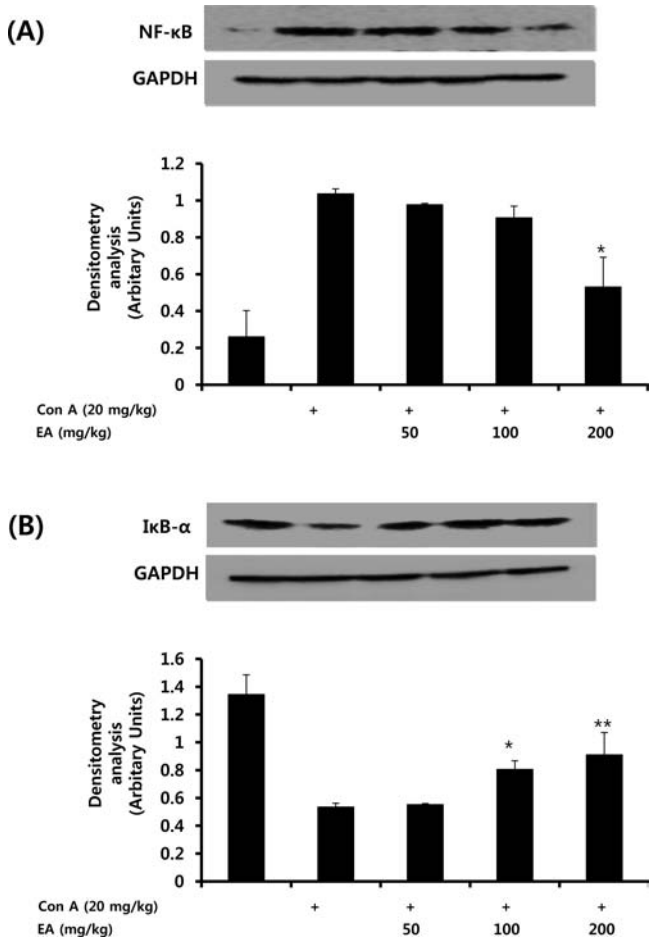


**Figure 6.** Effect of EA on the NF-κB pathway in Con A-induced liver injury. Hepatic (A) NF-κB and (B) IκB-$\alpha$ protein levels determined by immunoblotting. Densitometry was performed following normalization to the control (GADPH). Bar represents the mean ± SD ($n$ = 4 mice per group). (∗) $p < 0.05$ versus Con A. (∗∗) $p < 0.01$ versus Con A. (∗∗∗) $p < 0.001$ versus Con A.

the liver to Con A caused strong iNOS expression, which indicated that these proteins could be induced in the acute stage of hepatitis. Pretreatment of EA significantly decreased this upregulation of iNOS protein expression in a dose-dependent manner (Figure 7D).

## DISCUSSION

A recent study showed that the ALT and AST levels decreased after treatment with EA in Balb/C mice after Con A-induced fulminant liver failure.[24] However, the exact mechanism underlying this effect remains unclear. To determine the mechanisms underlying the protective effects of EA, we examined the TLR pathway. TLR expression may be associated with the production of proinflammatory cytokines because the activation of these receptors stimulates signaling pathways, which result in activation of NF-κB and MAPK phosphorylation (Figure 8).

Con A-induced hepatitis is an experimental model of immune-mediated liver disease in humans.[29] Con A was originally identified as a mitogen in T lymphocytes and activates macrophages and neutrophils.[30,31] The hepatitis induced by intravenous injection of Con A is mainly dependent upon T-cell activation.[2] Hepatic injury caused by Con A disrupts the hepatocellular plasma membrane, and the enzymes

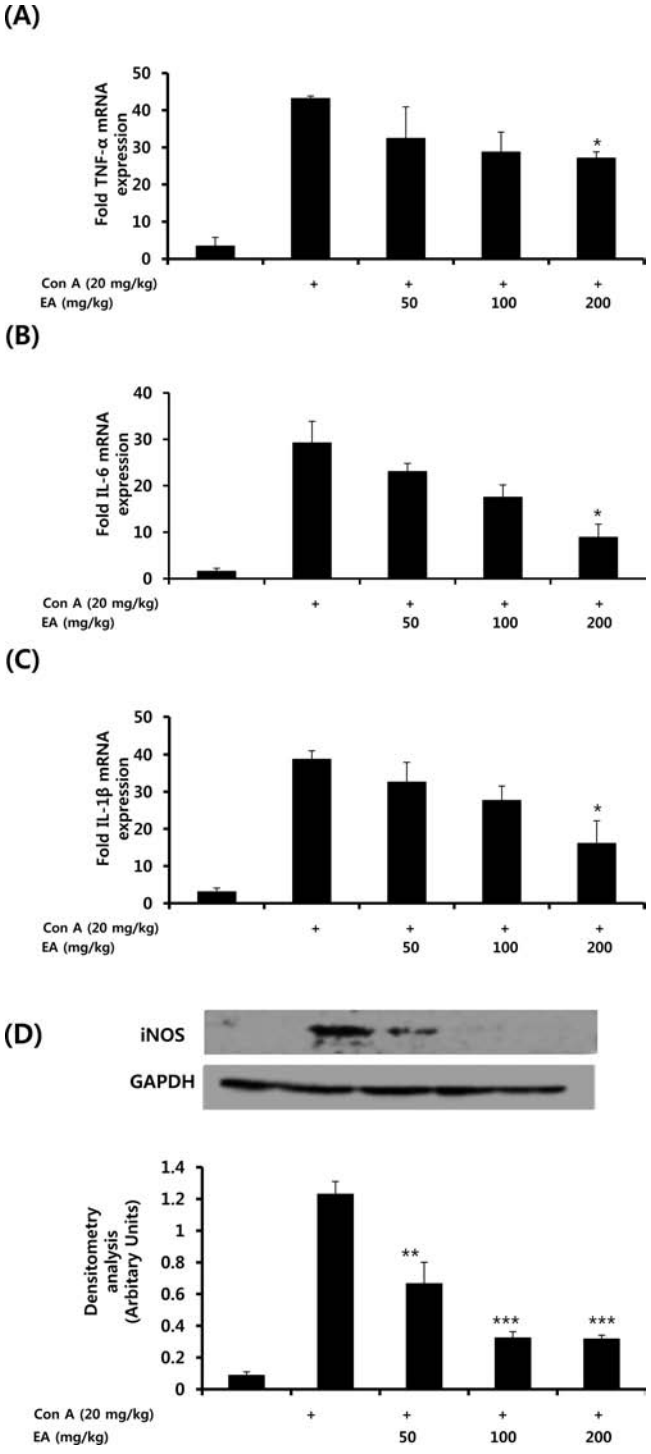


**Figure 7.** Effect of EA on the expression of proinflammatory cytokines and iNOS protein in the liver after Con A administration. Expression of (A) TNF-$\alpha$, (B) IL-6, and (C) IL-1$\beta$ mRNAs in the liver were examined by real-time qPCR. TNF-$\alpha$, IL-6, and IL-1$\beta$ mRNA levels were normalized to GAPDH expression in each sample. (D) iNOS protein levels determined by immunoblotting. Densitometry was performed following normalization to the control (GADPH). Bar represents the mean ± SD ($n$ = 4 mice per group). (*) $p < 0.05$ versus Con A.

normally present in the cytosol are released into the bloodstream.[32] In the present study, the ALT and AST levels in the Con A-treated mice returned to normal after pretreatment with EA, which showed the hepatoprotective

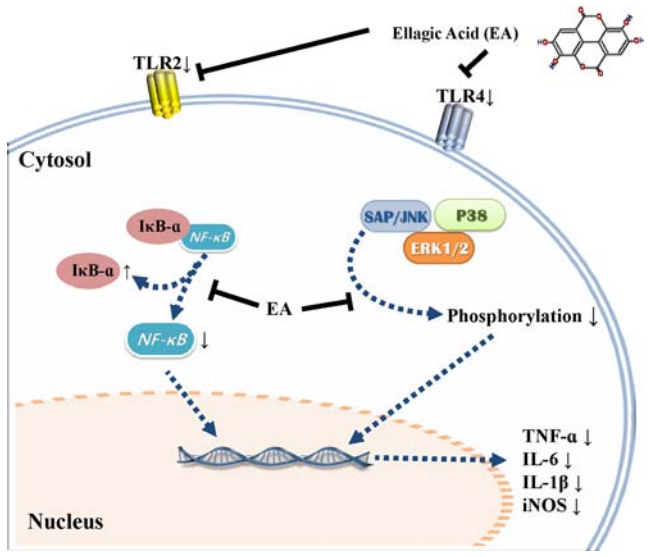


**Figure 8.** Hypothetic mechanism of the EA protective effect against hepatitis via TLR and MAPK/NF-$\kappa$B signaling pathways. EA decreased TLR2 and TLR4 levels (Figures 2–4). EA decreased the phosphorylation of JNK, ERK1/2, and p38 (Figure 5). EA suppressed NF-$\kappa$B and increased I$\kappa$B-$\alpha$ (Figure 6). EA suppressed inflammatory cytokines (Figure 7).

activity of EA. In the previous studies, EA was administered at doses of 50, 100, or 200 mg/kg of body weight.[27,28] In this study, we set the optimal dose range of the EA (0, 50, 100, or 200 mg/kg of body weight) and have shown the hepatoprotective effect of EA. Additionally, on the basis of previous studies,[33−38] we chose the optimal time points of EA treatment at 12 and 1 h prior to an injection of Con A. Soyasapogenol A, which has protective effects on a Con A-induced hepatitis model, was administered at 2 and 14 h prior to an intravenous injection of Con A. In other studies, therapeutic compounds, including allicin, Inchinko-to, and coumarin derivatives, were treated 1 h before Con A injection. Additionally, the Gal-3 inhibitor, which attenuates Con A-induced hepatitis, was intraperitoneally administered 2 h before and immediately after Con A injection.[33−38]

Previous studies indicated that the pathogenesis of Con A-induced hepatitis was mainly mediated by the release of inflammatory cytokines. TNF-$\alpha$, IL-6, and IL-1$\beta$ play crucial roles in the development of Con A-induced hepatitis.[39,40] These studies suggested that inhibition of TNF-$\alpha$, IL-6, and IL-1$\beta$ tended to alleviate liver injury. In the present study, we found that pretreatment with EA decreased the hepatic mRNA expression of TNF-$\alpha$, IL-6, and IL-1$\beta$ in Con A-induced liver injury. Therefore, we propose that EA exerts its hepatoprotective effects through the inhibition of TNF-$\alpha$, IL-6, and IL-1$\beta$ production.

In a recent study, the TLR signaling pathway was shown to be the predominant pathway in the early phase in a model of Con A-induced hepatitis.[4] The expression of TLR2 and TLR4 was increased in the liver during Con A-induced hepatitis.[1] Furthermore, TLR signaling stimulates the production of type I cytokines and, thus, recruits and activates T/NK cells. Activated T/NK cells exert cytotoxic effects on hepatocytes through induction of death receptor-mediated apoptosis, which results in liver injury.

Activation of TLR2 and TLR4 results in the recruitment of MyD88, an adaptor molecule, which subsequently facilitates the

activation of downstream signaling pathways. Two major kinase-mediated signaling pathways are activated after TLR stimulation, the MAPK and IκB kinase (IKK) complex pathways, which transduce various upstream signals to the activation of AP-1 and NF-κB transcription factors. Both of these are essential for the expression of activation-induced inflammatory mediators, including chemokines and cytokines.[17] Recent studies have shown that, in comparison to wild-type mice, TLR2 or TLR4 knockout mice are protected from Con A-induced hepatic injury.[9,41] Furthermore, MyD88-knockout mice develop less severe Con A-induced hepatitis with less production of proinflammatory cytokines.[42] These studies have provided evidence that TLR2 and TLR4 play an important role in Con A-induced hepatitis. Intervention via the regulation of TLR2 and TLR4 expression may therefore represent a therapeutic target for Con A-induced hepatitis.

In the present study, we showed that TLR2 and TLR4 expression in liver tissues, at the mRNA and protein levels, was significantly reduced by EA pretreatment (Figures 2−4). This might be attributed, at least in part, to the amelioration of liver injury and changes in cytokine production in mice. These data are new and relevant, because the effect of EA on these receptors has not been reported thus far. We propose that EA may have general anti-inflammatory effects in diseases associated with TLR signaling.

The liver is constantly exposed to bacterial peptidoglycans and LPS from the intestines via the hepatic portal vein.[16] After ligand binding, the TLRs activate downstream signaling pathways via recruitment of a group of intracellular TIR-domain-containing adaptors, including MyD88.[17] Recruitment of MyD88 leads to the activation of MAPKs, including ERK, JNK, and p38, and the transcription factor NF-κB, all of which regulate the expression of genes encoding the inflammatory cytokines.[14,18]

The transcription factor NF-κB consists of a heterodimer of p50 and p65, which is retained in the cytoplasm via the masking of a nuclear localization signal by the inhibitor IκB-α. Upon activation, IKK phosphorylates IκB-α, which promotes its translocation to the nucleus and results in the expression of various proinflammatory cytokines, including IL-2, IL-6, IL-8, IL-1β, and TNF-α.[43] In addition, NF-κB activation mediates the transcription of proinflammatory genes, such as *iNOS*. Many studies have suggested that NF-κB may be a key regulator of inflammation in liver injury.[44] Thus, inflammatory mechanisms play an important role in T-cell-mediated liver disease associated with increased activity of NF-κB. Inhibiting the activation of NF-κB exerts protective effects against liver injury; therefore, we propose that EA acts on NF-κB via the inhibition of IκB-α, which results in the prevention of NF-κB translocation into the nucleus in acute hepatitis. Furthermore, our findings show that EA can reduce the expression of the proinflammatory gene *iNOS*. Other important downstream signaling targets of TLRs are the MAPKs. The three major groups of MAPKs identified in mammalian cells are p38 MAPK, JNK kinase, and ERK.[45] MAPKs are key modulators of several target genes that ultimately regulate innate and adaptive immunity, cell motility, and cell proliferation.[46,47] Three different types of MAPKs contribute to the induction of AP-1 activity through phosphorylation of a different substrate. Activator protein (AP)-1 largely controls T-cell activation in the liver after binding of foreign antigens to the T-cell receptor, which leads to the secretion of cytokines, such as TNF-α, IL-6, and IL-1β.[46,47] ERK, JNK, and p38 MAPK pathways may therefore represent potential targets for inhibiting the progression of liver fibrosis. Similarly, inhibition of the phosphorylation of JNK, ERK, and p38 has protective effects in hepatitis. To our knowledge, this is the first study in which the protective effect of EA mediated by the inhibition of p38, JNK, and ERK MAPKs in hepatitis has been described.

In conclusion, we showed that EA attenuates Con A-induced hepatitis. One of the possible mechanisms underlying this effect is inhibition of TLR2 and TLR4 expression, which may decrease the expression of inflammatory cytokines and, in turn, inhibit the phosphorylation of MAPK and nuclear translocation NF-κB. This may account for a reduction in TNF-α, IL-6, and IL-1β expression by inhibition of NF-κB-mediated transcriptional activation and IκB-α degradation and prevention of p38, JNK, and ERK MAPK phosphorylation. Therefore, our findings suggest that TLR2, TLR4, NF-κB, and MAPK may be the specific molecular targets of EA in its protective effects against Con A-induced hepatitis.

## AUTHOR INFORMATION

### Corresponding Author

*Telephone: 82-2-820-5610. Fax: 82-2-3280-5610. E-mail: proteinlab@hanmail.net.

### Funding

This research was supported by the Chung-Ang University Excellent Student Scholarship and the Public Welfare and Safety Research Program through the National Research Foundation of Korea (NRF), as funded by the Ministry of Science, ICT and Future Planning (NRF-2010-0020844).

### Notes

The authors declare no competing financial interest.

## REFERENCES

(1) Ajuebor, M. N.; Carey, J. A.; Swain, M. G. CCR5 in T cell-mediated liver diseases: What's going on? *J. Immunol.* **2006**, *177* (4), 2039−2045.

(2) Tiegs, G.; Hentschel, J.; Wendel, A. A T cell-dependent experimental liver injury in mice inducible by concanavalin A. *J. Clin. Invest.* **1992**, *90* (1), 196−203.

(3) Ojiro, K.; et al. MyD88-dependent pathway accelerates the liver damage of concanavalin A-induced hepatitis. *Biochem. Biophys. Res. Commun.* **2010**, *399* (4), 744−749.

(4) Cao, Q. Y.; et al. A microarray analysis of early activated pathways in concanavalin A-induced hepatitis. *J. Zhejiang Univ., Sci., B* **2010**, *11* (5), 366−377.

(5) Tu, C. T.; et al. Curcumin attenuates concanavalin A-induced liver injury in mice by inhibition of toll-like receptor (TLR)2, TLR4 and TLR9 expression. *Int. Immunopharmacol.* **2012**, *12* (1), 151−157.

(6) Chen, Y.; Sun, R. Toll-like receptors in acute liver injury and regeneration. *Int. Immunopharmacol.* **2011**, *11* (10), 1433−1441.

(7) Soares, J. B.; et al. Increased hepatic expression of TLR2 and TLR4 in the hepatic inflammation-fibrosis-carcinoma sequence. *Innate Immun.* **2012**, *18* (5), 700−708.

(8) Berzsenyi, M. D.; et al. Hepatic TLR2 and TLR4 expression correlates with hepatic inflammation and TNF-α in HCV and HCV/HIV infection. *J. Viral Hepatitis* **2011**, *18* (12), 852−860.

(9) Xu, J.; et al. Extracellular histones are mediators of death through TLR2 and TLR4 in mouse fatal liver injury. *J. Immunol.* **2011**, *187* (5), 2626−2631.

(10) Bourke, E.; et al. The toll-like receptor repertoire of human B lymphocytes: Inducible and selective expression of TLR9 and TLR10 in normal and transformed cells. *Blood* **2003**, *102* (3), 956−963.

(11) Bosisio, D.; et al. Stimulation of toll-like receptor 4 expression in human mononuclear phagocytes by interferon-γ: A molecular basis for

priming and synergism with bacterial lipopolysaccharide. *Blood* **2002**, *99* (9), 3427−3431.
(12) Kadowaki, N.; et al. Subsets of human dendritic cell precursors express different toll-like receptors and respond to different microbial antigens. *J. Exp. Med.* **2001**, *194* (6), 863−869.
(13) Muzio, M.; et al. Differential expression and regulation of toll-like receptors (TLR) in human leukocytes: Selective expression of TLR3 in dendritic cells. *J. Immunol.* **2000**, *164* (11), 5998−6004.
(14) Schwabe, R. F.; Seki, E.; Brenner, D. A. Toll-like receptor signaling in the liver. *Gastroenterology* **2006**, *130* (6), 1886−1900.
(15) Akira, S.; Uematsu, S.; Takeuchi, O. Pathogen recognition and innate immunity. *Cell* **2006**, *124* (4), 783−801.
(16) Seki, E.; Brenner, D. A. Toll-like receptors and adaptor molecules in liver disease: Update. *Hepatology* **2008**, *48* (1), 322−335.
(17) Akira, S.; Takeda, K. Toll-like receptor signalling. *Nat. Rev. Immunol.* **2004**, *4* (7), 499−511.
(18) Antosz, H.; Choroszynska, D. Negative regulation of toll-like receptor signalling. *Postepy Hig. Med. Dosw.* **2013**, *67*, 339−350.
(19) Suzuki, N.; et al. Ellagic acid inhibits pancreatic fibrosis in male Wistar Bonn/Kobori rats. *Dig. Dis. Sci.* **2009**, *54* (4), 802−810.
(20) Chao, P. C.; Hsu, C. C.; Yin, M. C. Anti-inflammatory and anti-coagulatory activities of caffeic acid and ellagic acid in cardiac tissue of diabetic mice. *Nutr. Metab.* **2009**, *6*, 33.
(21) Rogerio, A. P.; et al. Anti-inflammatory effects of *Lafoensia pacari* and ellagic acid in a murine model of asthma. *Eur. J. Pharmacol.* **2008**, *580* (1−2), 262−270.
(22) Bell, C.; Hawthorne, S. Ellagic acid, pomegranate and prostate cancer—A mini review. *J. Pharm. Pharmacol.* **2008**, *60* (2), 139−144.
(23) Falsaperla, M.; et al. Support ellagic acid therapy in patients with hormone refractory prostate cancer (HRPC) on standard chemotherapy using vinorelbine and estramustine phosphate. *Eur. Urol.* **2005**, *47* (4), 449−454.
(24) Hwang, J. M.; et al. Ellagic acid protects hepatocytes from damage by inhibiting mitochondrial production of reactive oxygen species. *Biomed. Pharmacother.* **2010**, *64* (4), 264−270.
(25) Bozza, M.; et al. Interleukin-11 reduces T-cell-dependent experimental liver injury in mice. *Hepatology* **1999**, *30* (6), 1441−1447.
(26) Atessahin, A.; et al. Modulatory effects of lycopene and ellagic acid on reproductive dysfunction induced by polychlorinated biphenyl (Aroclor 1254) in male rats. *Basic Clin. Pharmacol. Toxicol.* **2010**, *106* (6), 479−489.
(27) Girish, C.; Pradhan, S. C. Hepatoprotective activities of picroliv, curcumin, and ellagic acid compared to silymarin on carbon-tetrachloride-induced liver toxicity in mice. *J. Pharmacol. Pharmacother.* **2012**, *3* (2), 149−155.
(28) Singh, K.; Jaggi, A. S.; Singh, N. Exploring the ameliorative potential of *Punica granatum* in dextran sulfate sodium induced ulcerative colitis in mice. *Phytother. Res.* **2009**, *23* (11), 1565−1574.
(29) Kaneko, Y.; et al. Augmentation of V$\alpha$14 NKT cell-mediated cytotoxicity by interleukin 4 in an autocrine mechanism resulting in the development of concanavalin A-induced hepatitis. *J. Exp. Med.* **2000**, *191* (1), 105−114.
(30) Cameron, A. R.; Nelson, J.; Forman, H. J. Depolarization and increased conductance precede superoxide release by concanavalin A-stimulated rat alveolar macrophages. *Proc. Natl. Acad. Sci. U. S. A.* **1983**, *80* (12), 3726−3728.
(31) Boldt, D. H.; MacDermott, R. P.; Jorolan, E. P. Interaction of plant lectins with purified human lymphocyte populations: Binding characteristics and kinetics of proliferation. *J. Immunol.* **1975**, *114* (5), 1532−1536.
(32) Rajesh, M. G.; Latha, M. S. Preliminary evaluation of the antihepatotoxic activity of Kamilari, a polyherbal formulation. *J. Ethnopharmacol.* **2004**, *91* (1), 99−104.
(33) Volarevic, V.; et al. Galectin-3 deficiency prevents concanavalin A-induced hepatitis in mice. *Hepatology* **2012**, *55* (6), 1954−1964.
(34) Itoh, A.; et al. Hepatoprotective effect of syringic acid and vanillic acid on concanavalin A-induced liver injury. *Biol. Pharm. Bull.* **2009**, *32* (7), 1215−1219.
(35) Bruck, R.; et al. Allicin, the active component of garlic, prevents immune-mediated, concanavalin A-induced hepatic injury in mice. *Liver Int.* **2005**, *25* (3), 613−621.
(36) Okamoto, T.; et al. Inhibition of concanavalin A-induced mice hepatitis by coumarin derivatives. *Jpn. J. Pharmacol.* **2001**, *85* (1), 95−97.
(37) Yamashiki, M.; et al. Effects of the Japanese herbal medicine 'Inchinko-to' (TJ-135) on concanavalin A-induced hepatitis in mice. *Clin. Sci.* **2000**, *99* (5), 421−431.
(38) Kuzuhara, H.; et al. Protective effects of soyasapogenol A on liver injury mediated by immune response in a concanavalin A-induced hepatitis model. *Eur. J. Pharmacol.* **2000**, *391* (1−2), 175−181.
(39) Sass, G.; et al. Cytokine expression in three mouse models of experimental hepatitis. *Cytokine* **2002**, *19* (3), 115−120.
(40) Kesherwani, V.; Sodhi, A. Quantitative role of p42/44 and p38 in the production and regulation of cytokines TNF-$\alpha$, IL-1$\beta$ and IL-12 by murine peritoneal macrophages in vitro by concanavalin A. *Cytokine* **2007**, *37* (1), 62−70.
(41) Gong, Q. A.; et al. High-mobility group box 1 exacerbates concanavalin A-induced hepatic injury in mice. *J. Mol. Med.* **2010**, *88* (12), 1289−1298.
(42) Ojiro, K.; et al. MyD88-dependent pathway accelerates the liver damage of concanavalin A-induced hepatitis. *Biochem. Biophys. Res. Commun.* **2010**, *399* (4), 744−749.
(43) Ghosh, S.; Hayden, M. S. New regulators of NF-$\kappa$B in inflammation. *Nat. Rev. Immunol.* **2008**, *8* (11), 837−848.
(44) He, G.; Karin, M. NF-$\kappa$B and STAT3—Key players in liver inflammation and cancer. *Cell Res.* **2011**, *21* (1), 159−168.
(45) De Keulenaer, G. W.; et al. Convergence of redox-sensitive and mitogen-activated protein kinase signaling pathways in tumor necrosis factor-$\alpha$-mediated monocyte chemoattractant protein-1 induction in vascular smooth muscle cells. *Arterioscler., Thromb., Vasc. Biol.* **2000**, *20* (2), 385−391.
(46) Wang, X. J.; et al. B7-H4 treatment of T cells inhibits ERK, JNK, p38, and AKT activation. *PLoS One* **2012**, DOI: 10.1371/journal.-pone.0028232.
(47) Plotnikov, A.; et al. The MAPK cascades: Signaling components, nuclear roles and mechanisms of nuclear translocation. *Biochim. Biophys. Acta, Mol. Cell Res.* **2011**, *1813* (9), 1619−1633.

China. Fruits were harvested when fully mature according to commercial practice and immediately transported to the laboratory. The clusters were selected on the basis of uniform color, size, and firmness, and blemished and diseased fruits were discarded. SA with a concentration of 1 mM was chosen for this experiment on the basis of a previous study.[7] Treatments were performed as follows: (i) grape berries immersed in sterile distilled water at 20 °C for 10 min were designated the control; (ii) grape berries immersed in 1 mM SA solution at 20 °C for 10 min were designated the SA treatment. Following treatments, fruits were placed on kraft paper and allowed to dry at 20 °C for 20 h. Both control and treated grape berries were then stored in a temperature-controlled chamber at 2 °C with a relative humidity of 95% for 45 days. At 0, 15, and 45 days of storage, three samples (30 grape berries for each) were taken randomly from each treatment for biochemical and proteomic analysis.

**Measurement of Weight Loss, Flesh Firmness, and Membrane Leakage.** Weight loss was recorded by subtracting final weight from the initial weight of the clusters and then expressed as percent weight loss with reference to the initial weight. Fruit firmness was determined using a TX-XT2i texture analyzer (Stable Micro Systems, Surrey, UK) with a 5 mm diameter probe at a speed of 1 mm/s and expressed in newtons (N). Measurements were carried out on two opposite sides of each individual fruit (15 grapes randomly selected from each treatment) after removal of the peel. Membrane leakage was determined according to the previously described method[21] using a digital conductivity meter (DDB-6200, Shanghai Leici Apparatus, Shanghai, China) and expressed as percentage of the conductivity of total tissue electrolyte.

**Protein Extraction.** Protein extraction was performed according to the method described by Yuan et al.[22] Deseeded grape berries tissues (approximately 10 g) taken from at least 15 fruits were ground to a fine powder in liquid nitrogen with a mortar and pestle. The ground tissue was suspended in 5 mL of extraction buffer containing 0.8 M sucrose, 0.1 M Tris-HCl, pH 7.5, 10 mM EDTA, 0.1 M KCl, 2 mM phenylmethanesulfonyl fluoride, and 2% $\beta$-mercaptoethanol, incubated by shaking for 1 h at 4 °C. Afterward, an equal volume of Tris-saturated phenol (pH 7.9) was added, and the mixture was incubated on a shaker for another 30 min at room temperature. Samples were then centrifuged for 10 min at 9000*g*. The resulting upper phenol phase was collected and washed twice with extraction buffer. The phenol phase was carefully transferred to a new centrifuge tube, and 5 volumes of ice-cold methanol containing 0.1 M ammonium acetate was added. Tubes were mixed by gentle inversion and then kept at −20 °C overnight. After that, samples were centrifuged at 9000*g* for 30 min, and the precipitated protein pellets were washed three times with cooled methanol containing 0.1 M ammonium acetate and finally twice with cooled acetone. The pellets were dried under vacuum at room temperature and resolubilized in lysis buffer containing 7 M urea, 2 M thiourea, 4% 3-[(3-cholamidopropyl)dimethylammonio]-1-propanesulfonate, 1% dithiothrietol (DTT), and 1% carrier ampholytes (pH 3−10).

**Two-Dimensional Gel Electrophoresis.** 2-DE was performed as described by Wang et al.[23] A Protean IEF Cell instrument (Bio-Rad, Hercules, CA, USA) was used for isoelectric focusing (IEF) with precast immobilized pH gradient (IPG) strips (pH 4−7, 17 cm). Samples of 300 $\mu$L containing 700 $\mu$g of protein were loaded by passive in-gel rehydration. The strips were subjected to IEF using the following program: at 500 V for 0.5 h, at 1000 V for 1 h, at 4000 V for 1 h, at 8000 V for 2 h, and focusing at 8000 V until a final volt-hours of 60000 was reached. After IEF, strips were equilibrated in 10 mL of SDS equilibration buffer (7 M urea, 2% SDS, 0.075 M Tris-HCl, pH 8.8, 30% glycerol), first with buffer containing 1% DTT for 15 min and afterward with buffer containing 2.5% iodoacetamide for 15 min. The second-dimensional electrophoresis was run on a 12% polyacrylamide gel in an Ettan DALT System (GE Healthcare, Piscataway, NJ, USA). Gel electrophoresis was first conducted at 5 W/gel for 0.5 h and then at 15 W/gel for 5.5 h. Proteins spots in 2-DE gels were visualized by Coomassie blue staining. Three replicate gels were run for each sample. Image analysis was performed with PDQuest software (version 7.2; Bio-Rad). Data were normalized as a percentage of the total density of all valid spots on the corresponding gel. Normalized spot volumes were compared between the control and treatment samples on each gel, and only those spots with an average fold change >1.5 at least at one time point after cold storage, as well as exhibiting the same expression pattern among the three replicates, were considered as differentially expressed proteins.[22]

**In-Gel Digestion and Mass Spectrometric Analysis.** Differentially expressed protein spots were manually excised from the gels and destained with 50 mM $NH_4HCO_3$ in 50% (v/v) acetonitrile. The gel pieces were then reduced in 10 mM DTT for 45 min at 55 °C and alkylated in 55 mM iodoacetamide for 45 min at room temperature. After washing with 0.025 mM $NH_4HCO_3$ in 50% (v/v) acetonitrile, the dried gels were incubated in 10 $\mu$L of 10 ng/mL trypsin (Sigma-Aldrich, Shanghai, China) at 37 °C overnight. The supernatant was collected for mass spectrometry analysis.

Mass spectrometry data were obtained using an ultraflex matrix-assisted laser desorption/ionization time-of-flight (MALDI-TOF) mass spectrometer (Bruker, Bremen, Germany). The resulting peptide mass fingerprinting (PMF) were queried against the NCBInr database using MASCOT software (http://www.matrixscience.com). The following parameters were used for database searches: taxonomy, Viridiplantae (green plant); cleavage specificity, trypsin with up to one missed cleavage; allowed modifications, carbamidomethylation of cysteine; peptide tolerance, ±0.2 Da; mass value, $MH^+$ and monoisotopic.

**Sugar Measurement.** GC-MS analyses of sugar contents were performed according to the method of Yun et al.,[24] with minor modification. Briefly, grape berry (10 g) tissue taken from at least 15 fruits was ground in a mortar with liquid $N_2$, and 600 mg of the resulting powder was suspended in 8.4 mL of cooled methanol. A total of 600 $\mu$L of 0.2 mg/mL ribitol was added as a quantification internal standard. The resulting extract was incubated in 90 $\mu$L of methoxamine hydrochloride (20 mg/mL in pyridine) by shaking at 50 °C for 45 min, followed by a 30 min treatment at 60 °C using 100 $\mu$L of *N*-methyl-*N*-trimethylsilyl-trifluoroacetamide containing 1% trimethylchlorosilane. The derivatized samples were analyzed by a Thermo Scientific TRACE GC Ultra system (Waltham, MA, USA) equipped with a fused-silica capillary column (30 m × 0.25 mm, Thermo Scientific) chemically bonded with 0.25 $\mu$m TR-5MS stationary phase. The injector temperature was 250 °C with a carrier helium gas flow rate of 1 mL/min. The column temperature was initially kept at 100 °C for 1 min and then increased to 184 °C at a rate of 3 °C/min, increased to 190 °C at a rate of 0.5 °C/min, and increased to 280 °C at a rate of 15 °C/min, at which it was held for 5 min. The column effluent was introduced into the ion source of a Thermo Scientific ITQ 1100 MS. Ions were generated by a 70 eV electron, and ion source temperature was set at 250 °C. Total ion current spectra were recorded from $m/z$ 45 to 600 in scanning mode. The compound was identified by comparing the mass spectrum with that in the NIST library 2005. The quantitative results were processed into Microsoft Word using the toolbox in Thermo Xcalibur. For comparative purposes, within each chromatogram the peak areas of the compounds were normalized by the sample fresh weight and by the peak area from the internal ribitol standard, resulting in a relative response ratio for each compound.

**Determination of Energy Charge.** Extraction and measurement of ATP, ADP, and AMP contents were conducted according to the previously described method.[25] Flesh tissue (2 g) of grape berries was homogenized with 5 mL of 0.6 mol/L perchloric acid. After centrifugation at 20000*g* for 15 min, a volume of 3 mL of supernatant was taken and quickly adjusted to pH 6.5 using KOH solution and passed through a 0.45 $\mu$m filter. Liquid assays of ATP, ADP, and AMP contents were performed on a Shimadzu SPD-M20A HPLC system (Kyoto, Japan) equipped with a DAD detector and a Shim-pack VP-ODS column (250 mm × 4.6 mm, Shimadzu). Mobile phases consisted of A (0.06 mol/L $K_2HPO_4$ and 0.04 mol/L $KH_2PO_4$ solution, pH 7.0) and B (acetonitrile) with a flow rate of 1.2 mL/min. The gradient program was as follows: 0−2 min, 2% B; 2−4 min, 5% B; 4−5 min, 20% B; 5−6 min, 25% B; 6−9 min, 2% B. The injection volume was 20 $\mu$L, and the detection wavelength was 254

nm. Standard curves of each reference compound were used to quantify ATP, ADP, and AMP concentrations. Energy charge was calculated as [ATP + $^1/_2$ ADP]/[ATP + ADP + AMP].

**Statistical Analysis.** One-way analysis of variance (ANOVA) was carried out to estimate differences using the software package SPSS version 17.0, and minimum significant differences were calculated by using Duncan's test ($\alpha$ = 0.05). Data presented were expressed as means ± standard deviation (SD).

## RESULTS

**Evaluation of Postharvest Quality of SA-Treated Grape Berries.** Weight loss was effectively reduced by SA treatment with values of 4.1 ± 0.1 and 2.5 ± 0.0% for control and treated fruits after 45 days of storage, respectively (Figure 1a). The same behavior was also found for fruit firmness

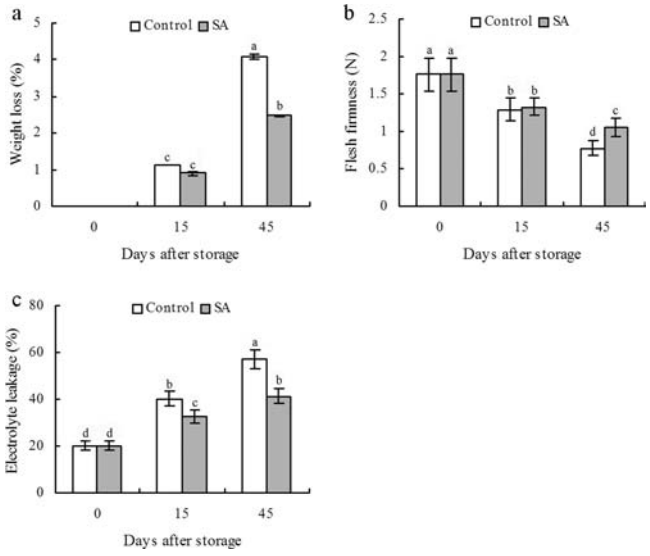


**Figure 1.** Changes of weight loss (a), flesh firmness (b), and electrolyte leakage (c) of control and 1 mM SA-treated grape berries during 45 days of storage at 2 °C. Values are the mean ± SD of three biological replicates. In the case of flesh firmness estimation, determinations were carried out independently using 15 different fruits. Different letters within each parameter indicate statistically significant differences ($p$ < 0.05).

(Figure 1b), for which SA-treated fruit exhibited significantly ($p$ < 0.05) higher flesh firmness (1.1 ± 0.1 N) after 45 days of storage as compared to the control (0.8 ± 0.1 N). In addition, as expected, chilling injury evaluated by ion leakage increased during storage, although it was affected by treatment (Figure 1c). At the end of storage, relative membrane leakage of SA-treated grape berries was 41.3 ± 3.2%, which was significantly ($p$ < 0.05) lower than that of control fruit (57.3 ± 4.0%).

**Changes in Protein Expression Profiles of Grape Berries after SA Treatment.** Our preliminary study indicated that phenol extraction procedure produced a better protein extraction and fewer interfering compounds as compared with the TCA/acetone extraction method. A similar conclusion was reported in an analysis of the proteome of grape and orange tissues.[26,27] 2-DE analysis was conducted using pH 4−7 strips and 12% SDS-PAGE, and about 500 protein spots were reproducibly detected in CBB-stained gel (Figure 2). After normalization for the total density of all spots on the corresponding gel, quantitative analysis indicated that 91 protein spots showed a fold change >1.5 at least at one time point as compared between the control and SA-treated samples.

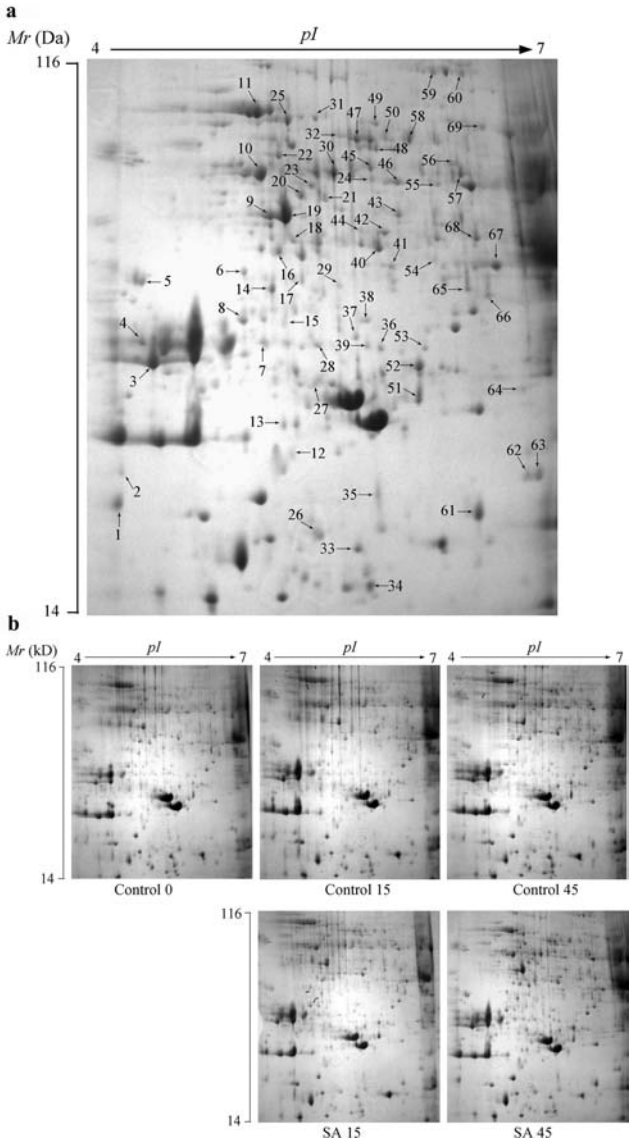


**Figure 2.** Two-dimensional gel electrophoresis of total proteins from grape berries during postharvest storage: (a) 69 differentially expressed protein spots subjected to SA treatment; (b) representative 2-DE profiles of proteins from SA-treated grape berries and respective control at different time points during postharvest storage.

MALDI-TOF MS analysis was carried out for the differentially expressed proteins, and 69 proteins were unambiguously identified by searching against the NCBInr viridiplantae protein database using the PMF data (Table 1), representing an identification rate of 75.8%.

These 69 proteins were classified into 8 functional groups on the basis of their putative roles in biological processes, including carbohydrate and energy metabolism, response to storage environmental stimuli, protein biosynthesis and degradation, amino acid and fatty acid metabolism, signal transduction, cytoskeleton, secondary metabolism, and unclassified (Figure 3). Accordingly, the major categories found to be affected by SA treatment were carbohydrate and energy metabolism and response to storage environmental stimuli, which might provide a clue to understanding the effectiveness of SA treatment to protect against environmental stresses while maintaining fruit quality.

**Table 1. Identification of SA-Regulated Proteins in Grape Berries during Postharvest Storage at 2 °C for 45 Days**

| | | | observed | | theoretical | | | | | ratio[a] | |
|---|---|---|---|---|---|---|---|---|---|---|---|
| spot | protein name | accession no. | $M_r$ | p$I$ | $M_r$ | p$I$ | score | matched peptides | sequence coverage (%) | 15 days | 45 days |
| | | | | | **Response to Storage Environmental Stimuli** | | | | | | |
| 1 | translationally controlled tumor protein homologue | gil225432249 | 24.8 | 4.5 | 19.0 | 4.5 | 103 | 8 | 55 | 0.98 ± 0.14 | 1.90 ± 0.23 |
| 11 | heat shock cognate 70 kDa protein | gil359486799 | 71.9 | 5.5 | 71.5 | 5.2 | 213 | 18 | 40 | 0.75 ± 0.09 | 1.60 ± 0.11 |
| 15 | L-ascorbate peroxidase 2 | gil225435177 | 33.6 | 5.6 | 27.7 | 5.7 | 129 | 9 | 44 | 3.67 ± 0.87 | 1.78 ± 0.33 |
| 25 | heat shock protein 60 kDa | gil225433375 | 61.0 | 5.7 | 61.7 | 5.9 | 152 | 16 | 40 | 1.02 ± 0.20 | 2.03 ± 0.37 |
| 31 | heat shock protein 71 kDa | gil225429229 | 69.8 | 5.9 | 72.9 | 5.8 | 135 | 15 | 28 | 2.11 ± 0.27 | 0.53 ± 0.09 |
| 33 | heat shock protein 18.2 kDa | gil225449292 | 22.3 | 5.8 | 17.1 | 5.5 | 61 | 7 | 37 | 0.64 ± 0.10 | 0.45 ± 0.07 |
| 34 | glycine-rich RNA-binding protein | gil359475330 | 19.7 | 5.8 | 16.4 | 6.3 | 144 | 13 | 82 | 0.91 ± 0.12 | 0.50 ± 0.10 |
| 37 | oxidoreductase | gil298204534 | 32.6 | 6.0 | 28.7 | 8.4 | 134 | 11 | 57 | 1.64 ± 0.15 | 1.23 ± 0.06 |
| 51 | probable glutathione *S*-transferase | gil225462612 | 26.6 | 6.4 | 25.7 | 6.1 | 98 | 8 | 35 | 1.26 ± 0.22 | 2.53 ± 0.47 |
| 52 | L-ascorbate peroxidase 2 | gil225435177 | 33.8 | 6.1 | 27.7 | 5.7 | 181 | 16 | 65 | 2.18 ± 0.33 | 1.47 ± 0.29 |
| 61 | major allergen Pruav 1 | gil225431844 | 24.1 | 6.4 | 17.3 | 6.0 | 112 | 10 | 59 | 1.25 ± 0.17 | 3.50 ± 0.72 |
| 62 | temperature-induced lipocalin | gil526117984 | 25.6 | 6.6 | 21.6 | 6.6 | 129 | 14 | 60 | 5.45 ± 0.80 | 0.84 ± 0.07 |
| 63 | temperature-induced lipocalin | gil77744883 | 21.9 | 7.1 | 21.6 | 6.6 | 113 | 8 | 49 | 4.97 ± 0.94 | 1.34 ± 0.17 |
| 69 | heat shock protein STI-like | gill359497489 | 64.6 | 6.9 | 36.3 | 5.8 | 80 | 6 | 25 | 1.71 ± 0.11 | 1.45 ± 0.10 |
| | | | | | **Carbohydrate and Energy Metabolism** | | | | | | |
| 6 | pyruvate dehydrogenase E1 | gil225425166 | 40.9 | 5.8 | 39.7 | 5.5 | 135 | 12 | 35 | 0.91 ± 0.12 | 2.66 ± 0.37 |
| 8 | oxygen-evolving enhancer protein 1 | gil147791852 | 33.4 | 5.4 | 33.4 | 5.9 | 159 | 12 | 51 | 1.12 ± 0.06 | 1.70 ± 0.12 |
| 10 | ATP synthase subunit $\beta$ | gil225456079 | 45.7 | 5.5 | 59.3 | 5.9 | 303 | 25 | 64 | 0.84 ± 0.10 | 0.61 ± 0.08 |
| 22 | ATP synthase CF1 $\alpha$ subunit | gil456061643 | 62.1 | 5.6 | 56.2 | 5.4 | 162 | 14 | 29 | 1.70 ± 0.19 | 1.14 ± 0.17 |
| 24 | V-type proton ATPase | gil225443399 | 64.8 | 5.7 | 69.0 | 5.2 | 275 | 22 | 47 | 0.64 ± 0.16 | 1.37 ± 0.09 |
| 27 | soluble inorganic pyrophosphatase | gil359476682 | 32.5 | 5.6 | 24.5 | 5.6 | 92 | 6 | 35 | 0.36 ± 0.05 | 0.29 ± 0.7 |
| 30 | enolase | gil225455555 | 54.7 | 5.7 | 48.3 | 6.2 | 278 | 28 | 71 | 1.96 ± 0.14 | 0.36 ± 0.04 |
| 32 | 2,3-bisphosphoglycerate-independent phosphoglycerate mutase | gil225439064 | 64.4 | 5.6 | 61.3 | 5.6 | 189 | 21 | 47 | 2.24 ± 0.27 | 0.32 ± 0.08 |
| 38 | phosphomannomutase | gil147856872 | 35.2 | 5.8 | 28.3 | 5.6 | 154 | 16 | 52 | 4.45 ± 1.06 | 0.90 ± 0.05 |
| 41 | aldose 1-epimerase | gil225456177 | 41.3 | 5.9 | 37.2 | 5.9 | 91 | 10 | 33 | 2.59 ± 0.44 | 1.33 ± 0.26 |
| 42 | fumarylacetoacetase-like | gil147771009 | 44.3 | 6.2 | 45.9 | 5.7 | 116 | 9 | 30 | 1.73 ± 0.20 | 0.79 ± 0.07 |
| 44 | phosphoglycerate kinase | gil225464999 | 44.2 | 5.8 | 42.5 | 6.3 | 68 | 7 | 22 | 0.82 ± 0.05 | 2.08 ± 0.39 |
| 46 | enolase | gil225455555 | 54.5 | 5.8 | 48.3 | 6.2 | 158 | 15 | 48 | 1.15 ± 0.13 | 0.58 ± 0.06 |
| 48 | pyruvate decarboxylase isozyme 1 | gil225443847 | 43.1 | 5.8 | 63.2 | 5.6 | 210 | 18 | 33 | 1.59 ± 0.19 | 1.23 ± 0.09 |
| 49 | succinate dehydrogenase | gil225430776 | 65.1 | 6.2 | 74.3 | 6.1 | 149 | 13 | 30 | 1.26 ± 0.05 | 2.17 ± 0.28 |
| 50 | pyruvate decarboxylase 1 | gil10732644 | 64.0 | 5.9 | 63.5 | 6.1 | 172 | 15 | 34 | 3.55 ± 0.96 | 0.78 ± 0.03 |
| 54 | enolase | gil225455555 | 53.9 | 6.3 | 48.3 | 6.2 | 78 | 8 | 27 | 1.15 ± 0.03 | 1.57 ± 0.09 |
| 55 | enolase | gil225455555 | 53.2 | 6.5 | 48.3 | 6.2 | 134 | 9 | 33 | 1.61 ± 0.13 | 0.92 ± 0.19 |
| 57 | enolase | gil225455555 | 52.8 | 6.7 | 48.3 | 6.2 | 138 | 11 | 39 | 0.91 ± 0.05 | 2.10 ± 0.09 |
| 58 | pyruvate decarboxylase 1 | gil10732644 | 63.5 | 6.0 | 63.5 | 6.1 | 192 | 16 | 37 | 2.83 ± 0.13 | 1.44 ± 0.08 |
| 59 | aconitate hydratase 2 | gil225460961 | 111.0 | 6.1 | 110.7 | 6.7 | 146 | 17 | 16 | 4.11 ± 0.93 | 2.17 ± 0.35 |
| 64 | triosephosphate isomerase | gil225449541 | 27.8 | 7.3 | 27.4 | 6.3 | 126 | 9 | 48 | 0.90 ± 0.14 | 1.87 ± 0.11 |
| 67 | malate dehydrogenase | gil225438145 | 39.8 | 6.9 | 35.9 | 6.2 | 183 | 15 | 59 | 7.36 ± 1.51 | 1.45 ± 0.30 |
| 68 | phosphoglycerate kinase | gil225464999 | 43.1 | 6.8 | 42.5 | 6.3 | 105 | 9 | 29 | 0.81 ± 0.04 | 1.60 ± 0.09 |
| | | | | | **Protein Biosynthesis and Degradation** | | | | | | |
| 2 | elongation factor 1-$\delta$-like | gil225456295 | 38.7 | 4.6 | 25.1 | 4.5 | 136 | 13 | 40 | 0.76 ± 0.09 | 2.25 ± 0.33 |
| 7 | metacaspase-5-like | gil526117457 | 35.6 | 5.3 | 46.7 | 5.1 | 90 | 10 | 31 | 2.23 ± 0.38 | 2.81 ± 0.24 |
| 13 | proteasome subunit $\beta$ type-3-A | gil225459609 | 30.7 | 5.3 | 23.2 | 5.3 | 111 | 9 | 53 | 2.22 ± 0.46 | 2.25 ± 0.19 |
| 20 | eukaryotic initiation factor 4A-15-like | gil297738640 | 51.8 | 5.8 | 47.1 | 5.4 | 264 | 21 | 61 | 4.01 ± 0.81 | 3.40 ± 0.10 |
| 23 | 26S protease regulatory subunit 6B | gil359478860 | 53.9 | 5.8 | 47.2 | 5.4 | 229 | 18 | 50 | 1.00 ± 0.03 | 3.37 ± 0.62 |
| 26 | translation initiation factor 5A-2 | gil359491680 | 23.0 | 5.6 | 17.6 | 5.6 | 105 | 7 | 40 | 1.22 ± 0.07 | 1.88 ± 0.25 |
| 45 | leucine aminopeptidase 2 | gil297743644 | 56.6 | 6.2 | 55.4 | 5.7 | 134 | 12 | 30 | 0.40 ± 0.05 | 2.16 ± 0.28 |
| 56 | mitochondrial-processing peptidase subunit $\beta$ | gil225452974 | 56.6 | 6.7 | 58.6 | 6.4 | 184 | 18 | 46 | 0.47 ± 0.07 | 0.69 ± 0.04 |
| 60 | elongation factor 2-like isoform 1 | gil225462164 | 109.8 | 6.2 | 94.9 | 5.8 | 68 | 7 | 12 | 6.51 ± 1.03 | 1.36 ± 0.22 |
| | | | | | **Secondary Metabolism** | | | | | | |
| 43 | leucoanthocyanidin dioxygenase | gil224038270 | 46.4 | 6.0 | 40.5 | 5.5 | 187 | 16 | 48 | 1.92 ± 0.20 | 1.20 ± 0.25 |
| 65 | isoflavone reductase-like protein 6 | gil76559896 | 36.9 | 6.7 | 33.9 | 6.0 | 111 | 9 | 36 | 0.76 ± 0.07 | 4.05 ± 0.80 |
| 66 | isoflavone reductase | gil225428436 | 36.0 | 6.8 | 33.9 | 6.1 | 186 | 12 | 56 | 0.84 ± 0.21 | 3.51 ± 0.66 |

**Table 1. continued**

| spot | protein name | accession no. | observed $M_r$ | observed pI | theoretical $M_r$ | theoretical pI | score | matched peptides | sequence coverage (%) | ratio[a] 15 days | ratio[a] 45 days |
|---|---|---|---|---|---|---|---|---|---|---|---|
| | | | **Amino Acid and Fatty Acid Metabolism** | | | | | | | | |
| 12 | lactoylglutathione lyase isoform 1 | gil225436504 | 45.6 | 5.5 | 26.6 | 7.7 | 171 | 15 | 59 | 2.79 ± 0.30 | 1.46 ± 0.23 |
| 14 | kynurenine formamidase-like | gil147838052 | 36.9 | 5.6 | 30.1 | 5.2 | 112 | 8 | 34 | 1.18 ± 0.19 | 2.41 ± 0.53 |
| 16 | adenosine kinase 2 | gil296086001 | 41.2 | 5.6 | 37.4 | 5.4 | 194 | 13 | 46 | 3.00 ± 0.89 | 0.94 ± 0.16 |
| 17 | cysteine synthase isoform 2 | gil225451235 | 40.4 | 5.5 | 34.5 | 5.4 | 145 | 12 | 41 | 1.29 ± 0.05 | 3.64 ± 0.55 |
| 18 | glutamine synthetase | gil14161136 | 43.1 | 5.7 | 39.2 | 5.4 | 74 | 7 | 28 | 0.99 ± 0.06 | 2.58 ± 0.67 |
| 29 | enoyl-[acyl-carrier-protein] reductase [NADH] | gil225441423 | 37.9 | 6.0 | 41.6 | 8.9 | 159 | 13 | 47 | 1.03 ± 0.12 | 2.07 ± 0.10 |
| 39 | 3-ketoacyl-CoA synthase 7-like | gil470131245 | 33.4 | 6.2 | 51.1 | 8.8 | 74 | 8 | 25 | 0.20 ± 0.06 | 0.37 ± 0.04 |
| 40 | glutamine synthetase | gil225451379 | 42.4 | 6.2 | 39.5 | 5.7 | 50 | 5 | 17 | 0.81 ± 0.15 | 0.29 ± 0.07 |
| | | | **Cytoskeleton** | | | | | | | | |
| 9 | putative actin 1 | gil225431585 | 41.2 | 5.5 | 41.9 | 5.5 | 110 | 14 | 37 | 2.58 ± 0.81 | 2.12 ± 0.29 |
| 19 | actin 7 | gil225431585 | 46.4 | 5.7 | 41.9 | 5.3 | 145 | 13 | 49 | 2.25 ± 0.31 | 1.29 ± 0.26 |
| 21 | actin 7 | gil225431585 | 47.1 | 5.8 | 41.9 | 5.3 | 119 | 11 | 45 | 2.19 ± 0.19 | 1.79 ± 0.22 |
| 35 | actin-depolymerizing factor 2-like isoform 1 | gil297746121 | 25.3 | 5.8 | 15.6 | 5.9 | 67 | 5 | 54 | 3.49 ± 0.91 | 1.43 ± 0.27 |
| | | | **Signal Transduction** | | | | | | | | |
| 4 | 14-3-3 protein | gil526117762 | 35.6 | 4.7 | 29.5 | 4.8 | 123 | 18 | 46 | 0.53 ± 0.14 | 1.59 ± 0.10 |
| | | | **Unclassified** | | | | | | | | |
| 3 | unnamed protein product | gil297736664 | 33.8 | 4.7 | 18.0 | 8.9 | 41 | 3 | 19 | 1.17 ± 0.11 | 1.60 ± 0.08 |
| 5 | uncharacterized protein | gil225434253 | 40.2 | 4.7 | 34.7 | 4.7 | 79 | 10 | 34 | 1.03 ± 0.05 | 2.29 ± 0.27 |
| 28 | hypothetical protein | gil147805616 | 35.3 | 5.5 | 27.4 | 5.6 | 113 | 9 | 34 | 1.51 ± 0.21 | 1.41 ± 0.13 |
| 36 | hypothetical protein | gil147805616 | 31.6 | 6.2 | 27.4 | 5.6 | 127 | 11 | 29 | 1.43 ± 0.11 | 1.70 ± 0.15 |
| 47 | uncharacterized protein | gil356540988 | 63.7 | 6.1 | 115.6 | 6.1 | 74 | 7 | 10 | 1.87 ± 0.08 | 1.03 ± 0.12 |
| 53 | uncharacterized protein | gil225458237 | 30.9 | 6.5 | 29.8 | 5.9 | 169 | 11 | 50 | 1.91 ± 0.20 | 1.04 ± 0.08 |

[a]Ratio of relative abundance of corresponding spot in samples treated by SA versus the control. Data are the mean values ± SD of three replicates.

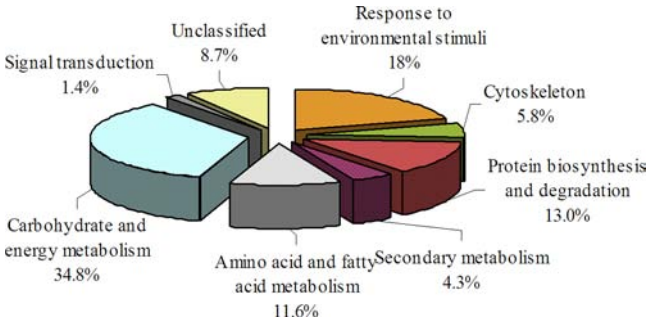


**Figure 3.** Pie chart showing functional classes of identified proteins. This classification is based on MIPS functional catalogue database (http://mips.helmholtz-muenchen.de/proj/funcatDB/) and related literature data.

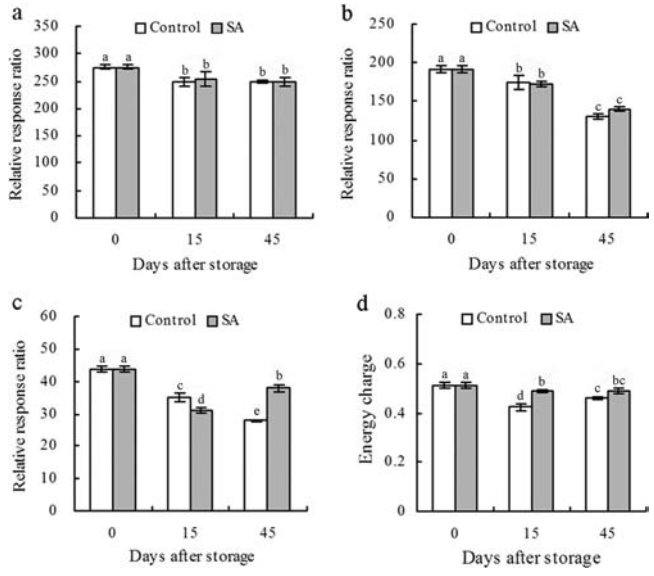


**Figure 4.** Changes of fructose (a), glucose (b), sucrose (c), and energy charge (d) in control and 1 mM SA-treated grape berries during 45 days of storage at 2 °C. Variation of levels of sugars are expressed as the relative response ratio with respect to the ribitol internal standard and normalized to the fresh weight of the sample. Data are the mean ± SD of three biological replicates. Different letters within each parameter indicate statistically significant differences ($p < 0.05$).

**Changes of Sugars Contents and Energy Charge.** Both the control and SA-treated grape berries showed a continual decline in fructose and glucose levels during the full experiment period, and no significant difference was observed between SA-treated and control samples (Figure 4a,b). However, the contents of sucrose in SA-treated grape berries decreased dramatically after 15 days of storage and exhibited a lower sucrose level as compared to that in the control (Figure 4c). At the later storage, fruits treated with SA showed pronounced higher levels of sucrose than in the control.

Distinct changes of energy charge were also observed in SA-treated and the control grape berries during storage (Figure 4d). The energy charge in control fruit decreased significantly after 15 days of storage and increased slightly at the later storage stage. SA treatment maintained the obvious higher energy charge in comparison with the control fruit.

## DISCUSSION

In the present study, SA treatment effectively reduced postharvest loss and chilling injury of grape berries during subsequent cold storage, which was manifested by decreased weight loss, softening, and membrane damage as compared to control fruit. The effect of SA on increasing resistance to environmental stress and preserving fruit quality has been reported for other fruit such as pomegranate,[11] sweet cherry,[7,28] and peach.[12,29] However, little information related to SA treatment is available at a systemic biological level. Further proteomic analyses allowed for a total of 69 SA-responsive proteins to be identified by MS. Functional analysis revealed that the major categories found to be affected by SA treatment were carbohydrate and energy metabolism and response to storage environmental stimuli, which accounted for 34.8 and 18.0% of the total identified proteins, respectively, and were higher than the 22.5 and 11.5% predicted for the whole genome of plant species.[30] For harvested grape berries, storage conditions and natural maturation were the primary factors affecting fruit quality and, therefore, it can be expected that carbohydrate metabolism and response to storage environmental stimuli may dominate the cellular processes and participate in combination or separately in regulating the responses to SA treatment.

In terms of fruit under postharvest conditions, carbohydrate metabolism and energy supply not only affect fruit quality but also are closely related to chilling tolerance during cold storage.[31,32] On the basis of proteomic analysis, a number of proteins with known roles in glycolysis and tricarboxylic acid cycle, such as pyruvate dehydrogenase (spot 6), enolase (spots 30, 46, 54, 55, and 57), 2,3-bisphosphoglycerate-independent phosphoglycerate mutase (spot 32), phosphoglycerate kinase (spots 44 and 68), succinate dehydrogenase (spot 49), aconitate hydratase (spot 59), trisphosphate isomerase (spot 64), and malate dehydrogenase (spot 67), and four proteins associated with energy metabolism, including ATP synthase subunit $\beta$ (spot 10), ATP synthase CF1 $\alpha$ subunit (spot 22), V-type proton ATPase (spot 24), and soluble inorganic pyrophosphatase (spot 27), were found to be up-regulated in stored grape berries after SA treatment. Enhanced expression of these enzymes may result in activation of carbohydrate catabolism and increasing energy supply. As a result, increased sucrose consumption and energy charge were observed in SA-treated fruit in comparison with the control, especially during the first 15 days of cold storage. Recently, increasing evidence has shown that development of chilling injury in several types of fruit is partially attributed to limited availability of energy or low energy production, whereas maintenance of higher levels of energy status alleviates chilling damage. For example, pretreatments with methyl jasmonate[25] and oxalic acid[33,34] enhance chilling tolerance of peach and mango fruit by inducing enzyme activities related to energy metabolism and maintaining high levels of ATP and energy charge. Therefore, increased expression of these enzymes associated with carbohydrate metabolism and energy production could provide sufficient energy supply, thereby reducing chilling injury of grape berries during cold storage.

There is evidence that chilling may impose oxidative stress on plant tissues,[35] and the alleviation of chilling damaging in resistant plants may be related to their ability to reduce and to scavenge free radicals through activated antioxidant system.[36] In this study, SA treatment increased the abundances of several antioxidant enzymes, such as ascorbate peroxidase (spots 15 and 52), glutathione *S*-transferase (spot 51), and oxidoreductase (spot 37). Other studies have also indicated that the activities of antioxidant enzymes appear to be increased by SA treatment and, as a result, may play a major role in responses to chilling damage-induced oxidative stress.[7,12,29]

Heat shock proteins (HSPs) are one of the major classes of chaperone molecules in higher plants and play a crucial role in protecting plants against stresses by re-establishing normal protein configuration and thus helping to maintain cellular homostasis.[37] Abiotic stresses usually caused protein dysfunction, so maintaining proteins in their functional configuration and preventing the aggregation of non-native proteins are particularly important for cell survival under chilling stress conditions.[38] In the present study, several HSPs including HSP 18.2 (spot 33), HSP 60 (spot 25), HSP 70 (spots 11 and 31), and HSP STI-like (spot 69) as well as translationally controlled tumor protein (spot 1), which was recently designated a novel heat shock protein,[39] were also up-regulated in SA-treated grape berries compared to the control during postharvest cold storage. Similarly, treatments with SA or methyl salicylate prior to cold storage increase the synthesis of HSPs and, at the same time, prevent chilling injury in tomato[40] and peach.[28] Moreover, spots 62 and 63 exhibited increased expression after SA treatment and were identified as temperature-induced lipocalin; this protein has been supposed to be associated with abiotic stress response and is correlated with the plant's capacity to develop chilling tolerance.[41,42]

The present work profiles the biochemical and proteomic changes in postharvest grape berries subjected to SA treatment and provides an overview regarding the crucial response components and subsequent processes during the subsequent cold storage. In SA-treated grape berries, fruit quality loss is reduced and chilling damage is inhibited, with decreased flesh firmness and weight loss and membrane leakage. Comparative proteomic analysis reveals that the induction of HSPs, antioxidant enzymes, and proteins involved in carbohydrate catabolism and energy production in SA-treated fruit may constitute the molecular basis for the protection against chilling injury and reduced postharvest loss. Many areas of research remain open after all of these findings, for instance, the elucidation of the changes in specific enzymes involved in carbohydrate metabolism as well as metabolomic studies during postharvest storage and how these are affected by SA treatment.

## AUTHOR INFORMATION

### Corresponding Author

*(Y.W.) E-mail: wangy1974@ujs.edu.cn. Phone: 86-511-88797059. Fax: 86-511-88797201. Mail: School of Food and Biological Engineering, Jiangsu University, 301 Xuefu Road, Zhenjiang 212013, China.

### Author Contributions

‖H.C. and X.Y. made equal contributions to this study.

### Funding

This project was cosupported by the Natural Science Foundation of Jiangsu Province, China (BK2008242), and Priority Academic Program Development of Jiangsu Higher Education Institutions (PAPD).

### Notes

The authors declare no competing financial interest.

## REFERENCES


(1) Sabir, F. K.; Sabir, A. Quality response of table grapes (*Vitis vinifera* L.) during cold storage to postharvest cap stem excision and hot water treatments. *Int. J. Food Sci. Technol.* **2013**, *48*, 999−1006.

(2) Lurie, S.; Crisosto, C. H. Chilling injury in peach and nectarine. *Postharvest Biol. Technol.* **2005**, *37*, 195−208.

(3) Sharma, R. R.; Singh, D.; Singh, R. Biological control of postharvest diseases of fruits and vegetables by microbial antagonists: a review. *Biol. Control* **2009**, *50*, 205−221.

(4) Schirra, M.; D'Aquino, S.; Cabras, P.; Angioni, A. Control of postharvest diseases of fruit by heat and fungicides: efficacy, residue levels, and residue persistence. A review. *J. Agric. Food Chem.* **2011**, *59*, 8531−8542.

(5) Asghari, M.; Aghdam, M. S. Impact of salicylic acid on post-harvest physiology of horticultural crops. *Trends Food Sci. Technol.* **2010**, *21*, 502−509.

(6) Raskin, I. Role of salicylic acid in plants. *Annu. Rev. Plant Physiol. Plant Mol. Biol.* **1992**, *43*, 439−463.

(7) Valero, D.; Díaz-Mula, H. M.; Zapata, P. J.; Castillo, S.; Guillén, F.; Martínez-Romero, D.; Serrano, M. Postharvest treatments with salicylic acid, acetylsalicylic acid or oxalic acid delayed ripening and enhanced bioactive compounds and antioxidant capacity in sweet cherry. *J. Agric. Food Chem.* **2011**, *59*, 5483−5489.

(8) Yang, Z.; Cao, S.; Zheng, Y.; Jiang, Y. Combined salicyclic acid and ultrasound treatments for reducing the chilling injury on peach fruit. *J. Agric. Food Chem.* **2012**, *60*, 1209−1212.

(9) Zhang, H. Y.; Ma, L. C.; Wang, L.; Jiang, S.; Dong, Y.; Zheng, X. D. Biocontrol of gray mold decay in peach fruit by integration of antagonistic yeast with salicylic acid and their effects on postharvest quality parameters. *Biol. Control* **2008**, *47*, 60−65.

(10) Abbasi, N. A.; Hafeez, S.; Tareen, M. J. Salicylic acid prolongs shelf life and improves quality of 'Maria Delicia' peach fruit. *Acta Hortic.* **2010**, *880*, 191−197.

(11) Sayyari, M.; Castillo, S.; Valero, D.; Díaz-Mula, H. D.; Serrano, M. Acetyl salicylic acid alleviates chilling injury and maintains nutritive and bioactive compounds and antioxidant activity during postharvest storage of pomegranates. *Postharvest Biol. Technol.* **2011**, *60*, 136−142.

(12) Tareen, M. J.; Abbasi, N. A.; Hafiz, I. A. Postharvest application of salicylic acid enhanced antioxidant enzyme activity and maintained quality of peach cv. 'Flordaking' fruit during storage. *Sci. Hortic.* **2012**, *142*, 221−228.

(13) Hertog, M. L. A. T. M.; Rudell, D. R.; Pedreschi, R.; Schaffer, R. J.; Geeraerd, A. H.; Nicolaï, B. M.; Ferguson, I. Where systems biology meets postharvest. *Postharvest Biol. Technol.* **2011**, *62*, 223−237.

(14) Pedreschi, R.; Lurie, S.; Hertog, M.; Nicolaï, B.; Mes, J.; Woltering, E. Post-harvest proteomics and food security. *Proteomics* **2013**, *13*, 1772−1783.

(15) Huerta-Ocampo, J. Á.; Osuna-Castro, J. A.; Lino-López, G. J.; Barrera-Pacheco, A.; Mendoza-Hernández, G.; De León-Rodríguez, A.; Barba de la Rosa, A. P. Proteomic analysis of differentially accumulated proteins during ripening and in response to 1-MCP in papaya fruit. *J. Proteomics* **2012**, *75*, 2160−2169.

(16) Martínez-Esteso, M. J.; Sellés-Marchart, S.; Lijavetzky, D.; Pedrenõ, M. A.; Bru-Martínez, R. A DIGE-based quantitative proteomic analysis of grape berry flesh development and ripening reveals key events in sugar and organic acid metabolism. *J. Exp. Bot.* **2011**, *62*, 2521−2569.

(17) Pedreschi, R.; Vanstreels, E.; Carpentier, S.; Hertog, M.; Lammertyn, J.; Robben, J.; Noben, J. P.; Swennen, R.; Vanderleyden, J.; Nicolaï, B. M. Proteomic analysis of core breakdown disorder in Conference pears (*Pyrus communis* L.). *Proteomics* **2007**, *7*, 2083−2099.

(18) Sánchez-Bel, P.; Egea, I.; Sánchez-Ballesta, M. T.; Martinez-Madrid, C.; Fernandez-Garcia, N.; Romojaro, F.; Olmos, E.; Estrella, E.; Bolarín, M. C.; Flores, F. B. Understanding the mechanisms of chilling injury in bell pepper fruits using the proteomic approach. *J. Proteomics* **2012**, *75*, 5463−5478.

(19) Lara, M. V.; Borsani, J.; Budde, C. O.; Lauxmann, M. A.; Lombardo, V. A.; Murray, R.; Andreo, C. S.; Drincovich, M. F. Biochemical and proteomic analysis of 'Dixiland' peach fruit (*Prunus persica*) upon heat treatment. *J. Exp. Bot.* **2009**, *60*, 4315−4333.

(20) Giraldo, E.; Díaz, A.; Corral, J. M.; García, A. Applicability of 2-DE to assess differences in the protein profile between cold storage and not cold storage in nectarine fruits. *J. Proteomics* **2012**, *75*, 5774−5782.

(21) Luo, Z.; Chen, C.; Xie, J. Effect of salicylic acid treatment on alleviating postharvest chilling injury of 'Qingnai' plum fruit. *Postharvest Biol. Technol.* **2011**, *62*, 115−120.

(22) Yuan, X.; Wu, Z.; Li, H.; Wang, Y.; Liu, F.; Cai, H.; Newlove, A. A.; Wang, Y. Biochemical and proteomic analysis of 'Kyoho' grape (*Vitis labruscana*) berries during cold storage. *Postharvest Biol. Technol.* **2014**, *88*, 79−87.

(23) Wang, Y.; Kroon, J. K. M.; Slabas, A. R.; Chivasa, S. Proteomics reveals new insights into the role of light in cadmium response in *Arabidopsis* cell suspension cultures. *Proteomics* **2013**, *13*, 1145−1158.

(24) Yun, Z.; Gao, H.; Liu, P.; Liu, S.; Luo, T.; Jin, S.; Xu, Q.; Xu, J.; Cheng, Y.; Deng, X. Comparative proteomic and metabolomic profiling of citrus fruit with enhancement of disease resistance by postharvest heat treatment. *BMC Plant Biol.* **2013**, *13*, 44.

(25) Jin, P.; Zhu, H.; Wang, J.; Chen, J. J.; Wang, X. L.; Zheng, Y. H. Effect of methyl jasmonate on energy metabolism in peach fruit during chilling stress. *J. Sci. Food Agric.* **2013**, *93*, 1827−1832.

(26) Perotti, V. E.; Del Vecchio, H. A.; Sansevich, A.; Meier, G.; Bello, F.; Cocco, M.; Garrán, S. M.; Anderson, C.; Vazquez, D.; Podesta, F. E. Proteomic, metabolomic, and biochemical analysis of heat treated Valencia oranges during storage. *Postharvest Biol. Technol.* **2011**, *62*, 97−114.

(27) Marsoni, M.; Vannini, C.; Campa, M.; Cucchi, U.; Espen, L.; Bracale, M. Protein extraction from grape tissues by two-dimensional electrophoresis. *Vitis* **2005**, *44*, 181−186.

(28) Giménez, M. J.; Valverde, J. M.; Valero, D.; Guillén, F.; Martínez-Romero, D.; Serrano, M.; Castillo, S. Quality and antioxidant properties on sweet cherries as affected by preharvest salicylic and acetylsalicylic acids treatments. *Food Chem.* **2014**, *160*, 226−232.

(29) Wang, L.; Chen, S.; Kong, W.; Li, S.; Archbold, D. D. Salicylic acid pretreatment alleviates chilling injury and affects the antioxidant system and heat shock proteins of peaches during cold storage. *Postharvest Biol. Technol.* **2006**, *41*, 244−251.

(30) The Arabidopsis Genome Initiative. Analysis of the genome sequence of the flowering plant *Arabidopsis thaliana*. *Nature* **2000**, *408*, 796−815.

(31) Agopian, D.; Ghedini, R.; Peroni-Okita, F. H. G.; Soares, C. A.; Mainardi, J. A.; do Nasci-mento, J. R. O.; Cordenunsi, B. R.; Lajolo, F. M.; Purgatto, E. Low temperature induced changes in activity and protein levels of the enzymes associated to conversion of starch to sucrose in banana fruit. *Postharvest Biol. Technol.* **2011**, *62*, 133−140.

(32) Cao, S.; Yang, Z.; Zheng, Y. Sugar metabolism in relation to chilling tolerance of loquat fruit. *Food Chem.* **2013**, *136*, 139−143.

(33) Jin, P.; Zhu, H.; Wang, L.; Shan, T.; Zheng, Y. Oxalic acid alleviates chilling injury in peach fruit by regulating energy metabolism and fatty acid contents. *Food Chem.* **2014**, *161*, 87−93.

(34) Li, P.; Zheng, X.; Liu, Y.; Zhu, Y. Pre-storage application of oxalic acid alleviates chilling injury in mango fruit by modulating proline metabolism and energy status under chilling stress. *Food Chem.* **2014**, *142*, 72−78.

(35) Imahori, Y.; Takemura, M.; Bai, J. Chilling-induced oxidative stress and antioxidant responses in mume (*Prunus mume*) fruit during low temperature storage. *Postharvest Biol. Technol.* **2008**, *49*, 54−60.

(36) Aghdam, M. S.; Bodbodak, S. Physiological and biochemical mechanisms regulating chilling tolerance in fruits and vegetables under postharvest salicylates and jasmonates treatments. *Sci. Hortic.* **2013**, *156*, 73−85.

(37) Aghdam, M. S.; Sevillano, L.; Flores, F. B.; Bodbodak, S. Heat shock proteins as biochemical markers for postharvest chilling stress in fruits and vegetables. *Sci. Hortic.* **2013**, *160*, 54−64.

(38) Wang, W.; Vinocur, B.; Shoseyov, O.; Altman, A. Role of plant heat-shock proteins and molecular chaperones in the abiotic stress response. *Trends Plant Sci.* **2004**, *9*, 244−252.

(39) Gnanasekar, M.; Dakshinamoorthy, G.; Ramaswamy, K. Translationally controlled tumor protein is a novel heat shock protein with chaperone-like activity. *Biochem. Biophys. Res. Commun.* **2009**, *386*, 333−337.
(40) Ding, C. K.; Wang, C. Y.; Gross, K. C.; Smith, D. L. Reduction of chilling injury and transcript accumulation of heat shock protein genes in tomatoes by methyl jasmonate and methyl salicylate. *Plant Sci.* **2001**, *161*, 1153−1159.
(41) Charron, J. B.; Ouellet, F.; Pelletier, M.; Danyluk, J.; Chauve, C.; Sarhan, F. Identification, expression, and evolutionary analyses of plant lipocalins. *Plant Physiol.* **2005**, *139*, 2017−2028.
(42) Chi, W. T.; Fung, R. W.; Liu, H. C.; Hsu, C. C.; Charng, Y. Y. Temperature-induced lipocalin is required for basal and acquired thermotolerance in *Arabidopsis*. *Plant Cell Environ.* **2009**, *32*, 917−927.

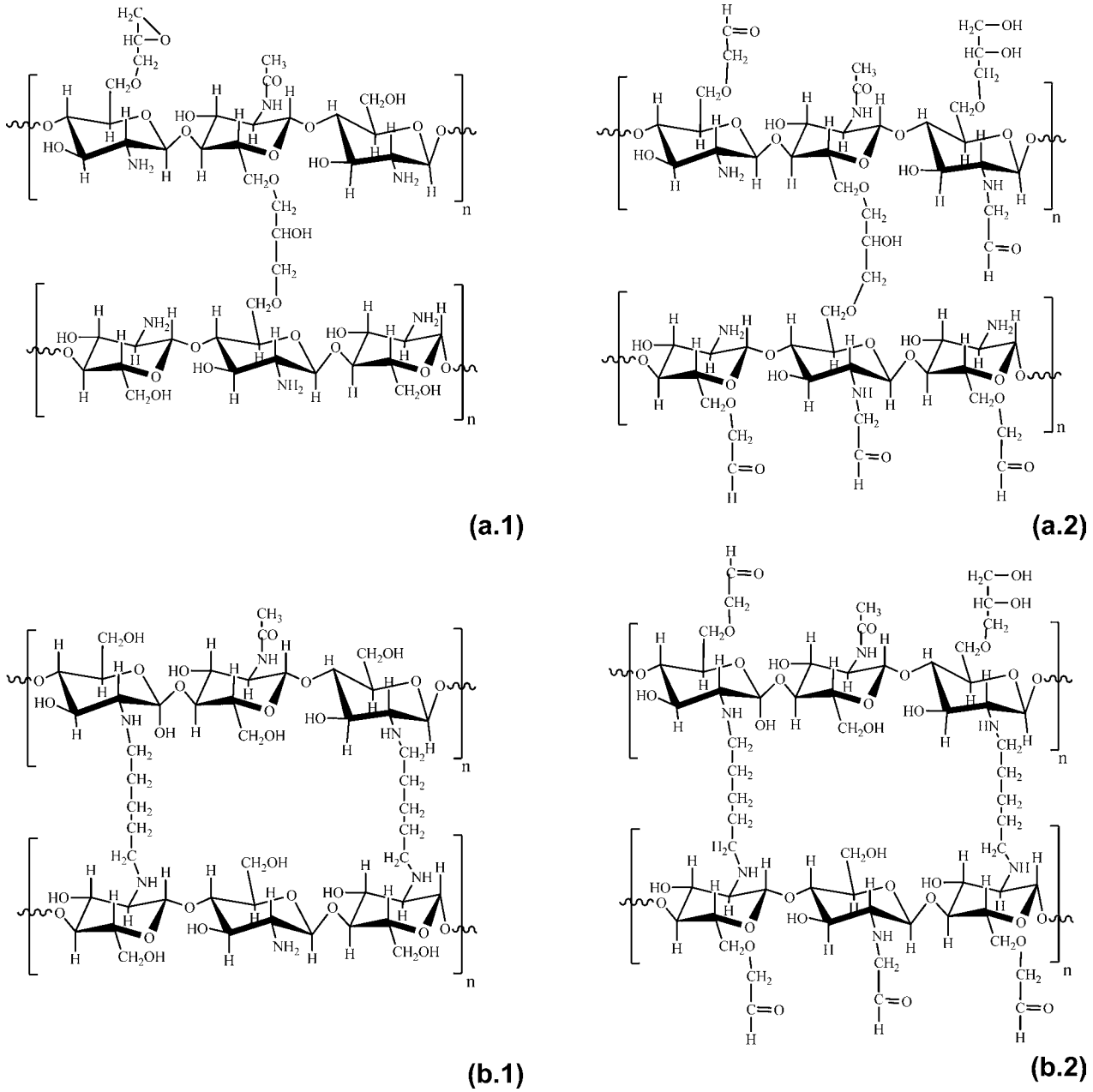


**Figure 1.** Possible structures after cross-linking (1) and activation (2) of C-EPI-EPI (a) and C-GA-EPI (b).

usually offers the highest degree of rigidification[25] and, consequently, enzyme stabilization, being normally selected when the objective is to improve the enzyme stability and/or when the immobilized biocatalyst will be used in an aqueous media where immobilization by adsorption is in most cases precluded.[26] However, the strength of the enzyme−support linkage makes it difficult or impossible to recover the support after enzyme inactivation; therefore, support cost may have a high impact on the economics of the process employing the immobilized biocatalyst.

Chitosan is a natural biopolymer outstanding for its relatively low cost, innocuousness, biocompatibility, antimicrobial activity, and the presence of functional groups that may be chemically modified.[27,28] It is a linear polysaccharide composed of $\beta$-(1−4)-linked D-glucosamine and *N*-acetyl-D-glucosamine units, which is produced by partial deacetylation of chitin that is obtained from the exoskeletons of crustaceans, particularly from wastes of the seafood-processing industry.[29] The use of chitosan as a carrier for the covalent immobilization of enzymes requires the introduction of functional groups that can react with the amino acid residues of the protein surface. Additionally, polymer chains must be cross-linked to improve the support mechanical resistance and avoid its solubilization in aqueous acidic media due to its cationic nature ($pK_a$ of the amino groups $\sim$ 6.5).[27] One typical derivatization method is the cross-linking and activation of chitosan with the bifunctional reagent glutaraldehyde (GA). The chemistry of the reaction between GA and amino groups is not fully understood, and according to the pH, the reaction mechanism may involve Schiff bases, nucleophilic substitution of amino groups, and Michael addition.[30,31] The reaction of GA with chitosan allows the cross-linking of different polymer chains and the activation of the support with aldehyde groups that may react with the enzyme through its amino groups (lysine residues and terminal


dx.doi.org/10.1021/jf500351j | J. Agric. Food Chem. 2014, 62, 10126−10135

amino group)[32,33] and eventually with other surface functional groups (thiols, phenols, and imidazoles).[30] Epichlorohydrin (EPI) has been also utilized in the derivatization of chitosan because it may react with amino and hydroxyl groups of the polymer, cross-linking different chitosan chains and activating the support with epoxide groups. The reaction occurs mainly through the chitosan hydroxyl groups when high temperature and alkaline media are utilized.[34,35] Because part of the residual epoxy groups may be spontaneously hydrolyzed, a heterofunctional support is obtained, presenting epoxide, diols, and amino groups. The residual epoxy groups may be also hydrolyzed, and diols could be then oxidized with periodate to aldehyde groups that form Schiff bases with the $\varepsilon$-amino group of protein lysine residues. To avoid the opening of the chitosan pyranosidic rings due to the oxidation of vicinal diols with periodate,[36] a limited quantity of periodate should be added and chitosan chains should be previously cross-linked. This final step of support modification presents the advantage of obtaining a more homogeneous support, and aldehydes may favor a more intense multipoint covalent attachment than when epoxy groups are utilized because the instability of Schiff bases should favor immobilization through the enzyme surface area with the highest density of lysine residues.[37]

It has been reported that according to the methodology utilized for chitosan derivatization, the immobilization yield and thermal stability of the biocatalyst may be modified.[33,38,39] These results may be related to the modification of chitosan functional groups, the activation degree, and/or the modification of the structure of the support by varying the cross-linking process. The objective of this investigation was to design a methodology for chitosan derivatization that offers the best compromise of expressed activity and thermal stability of an immobilized biocatalyst of *B. circulans* $\beta$-galactosidase for its further application in GOS synthesis in repeated batch operation.

## MATERIALS AND METHODS

**Materials.** A commercial preparation of $\beta$-galactosidase from *B. circulans* (Biolactasa-NTL CONC X2) in the form of a liquid solution was purchased from BIOCON (Barcelona, Spain), presenting 31.3 ± 0.5 mg of protein per mL and 1353 ± 11 IU per mL (determination of enzyme activity is in section Analysis). *o*-Nitrophenyl-$\beta$-D-galactopyranoside (*o*-NPG) was from Carbosynth Limited (Bershire, UK). Lactose monohydrate was from Quimatic S.A. (Santiago, Chile). Sodium metaperiodate and glycerol were purchased from Merck (Darmstadt, Germany). EPI, GA, sodium borohydride, *o*-nitrophenol (*o*-NP), and chitosan (≥75% deacetylated; MW 190,000−375,000; batch 061M0046 V) were from Sigma-Aldrich (St. Louis, MO, USA). All other reagents were of the highest available purity and used as purchased.

**Analysis.** Enzymatic activity of $\beta$-galactosidase was assessed spectrophotometrically by measuring the production of *o*-NP at 420 nm. The reaction was initiated by adding 50 $\mu$L of $\beta$-galactosidase solution or suspension to 2 mL of 45 mM *o*-NPG solution, using a temperature-controlled cell with constant magnetic stirring. One international unit of $\beta$-galactosidase activity (IU) was defined as the amount of enzyme producing 1 $\mu$mol of *o*-NP per minute from a 45 mM *o*-NPG solution in 0.1 M citrate−phosphate buffer, pH 6, at 25 °C. The extinction molar coefficient of *o*-NP under the assay conditions was 560 $M^{-1}$ $cm^{-1}$.

Protein concentration was determined according to the Bradford methodology, using bovine serum albumin as standard.[40]

Lactose and products of GOS synthesis (galactose, glucose, and GOS) were measured as previously reported, using a Jasco RI 2031 HPLC delivery system, provided with a refractive index detector, an isocratic pump (Jasco PU2080), an autosampler (Jasco AS 2055), and BP-100 Ag columns (300 mm × 7.8 mm) for carbohydrate analysis (Benson Polymerics, Reno, NV, USA).[41]

**Support Preparation.** Chitosan particles were produced as previously reported.[39] Chitosan was solubilized in acetic acid solution (3% v/v) to achieve a concentration of 1.5% (w/v) and stirred for 12 h. This solution was fed by gravity and sprayed into 1 M NaOH in 40% (v/v) ethanol solution under stirring. The particles were recovered and washed with distilled water and phosphate buffer (0.05 M, pH 7.0). The particles were derivatized by two different methodologies, and the possible chemistry involved after cross-linking and activation of chitosan is presented in Figure 1.

*Cross-Linking with Glutaraldehyde and Activation with Epichlorohydrin (C-GA-EPI).* Chitosan particles were cross-linked with GA as previously reported,[39,42] modifying the quantity of GA utilized. To favor the polymer cross-linking, 1 mol of GA was added per 4 equiv mol of chitosan amino groups, assuming 75% deacetylation. The imines formed by the reaction of GA with the amino groups of chitosan were reduced to secondary amines with $NaBH_4$ to form stable bonds. Finally, the cross-linked chitosan was activated with excess EPI to favor chitosan activation. A typical cross-linking and activation process was performed as follows: 1 g of chitosan particles was suspended in 10 mL of a solution of 0.78 g/L of GA prepared in 5 mM phosphate buffer, pH 7, and maintained under stirring for 30 min at 4 °C. The cross-linked particles were washed with distilled water. For the reduction of imines, 1 g of cross-linked particles was suspended in 10 mL of a solution of 3.8 g/L of $NaBH_4$ in 0.1 M bicarbonate buffer, pH 10, and maintained under stirring for 2 h at 25 °C. Afterward, the particles were washed with distilled water. The support was activated by suspending 1 g of support in 6 mL of an aqueous solution containing 40 g/L of NaOH, 37% (v/v) acetone, and 3.8 g/L of $NaBH_4$ at 4 °C. Then, EPI was added to reach a final concentration of 185 g/L. The mixture was stirred at 25 °C for 18 h, and the support was carefully washed with 20% (v/v) aqueous acetone solution, with distilled water, and finally with 50 mM phosphate buffer, pH 7.0. The support was finally contacted with a 0.5 M $H_2SO_4$ solution during 1 h to hydrolyze all unreacted epoxy groups, and then the diol groups were oxidized during 2 h with an aqueous solution containing $NaIO_4$ (a ratio of 1 g of support per 10 mL of solution was used in both steps). Because 1 mol of $NaIO_4$ oxidizes 1 equiv mol of diol, the activation degree (moles of aldehyde groups per gram of support) was modified by varying the concentration of $NaIO_4$ utilized during the oxidation step (10−25 mM).

*Cross-Linking and Activation with Epichlorohydrin (C-EPI-EPI).* Chitosan particles were derivatized in a two-step process with EPI as previously reported.[24] For support cross-linking, 1 mol of EPI was contacted per 4 equiv mol of primary hydroxyl groups of chitosan, assuming a 75% deacetylation. For this process, the chitosan particles (1 g) were resuspended in 2 mL of mixture with 4.8 g/L of EPI and 2.7 g/L of NaOH at 45 °C during 2 h. The cross-linked support was then activated with EPI following the same procedure as the activation of C-GA-EPI. For both supports the quantification of aldehyde groups was done spectrophotometrically by back-titration with $NaHCO_3$/KI.[38]

**Enzyme Immobilization.** The enzyme was immobilized in C-GA-EPI and C-EPI-EPI contacting 10 mL of the enzyme solution per 1 g of support at 25 °C. The $\beta$-galactosidase solution was prepared in 0.1 M bicarbonate buffer, pH 10, with 20% (v/v) of glycerol, which was used to avoid enzyme inactivation during immobilization. Finally, to obtain stable bonds between the enzyme and the support, the Schiff bases formed were reduced by adding $NaBH_4$ to reach a final concentration of 1 mg/mL. The suspension was maintained under stirring during 30 min at 25 °C, and the biocatalyst was thoroughly washed with distilled water.

Immobilization was followed by measuring the enzyme activity in the suspension and in the supernatant. The activity of the suspension was determined according to the same methodology utilized for the soluble enzyme. Immobilization yield in terms of the bound protein ($IY_P$) was defined as the mass ratio of immobilized protein (difference between contacted protein and unbound protein in the supernatant) to contacted protein. Immobilization yield in terms of expressed

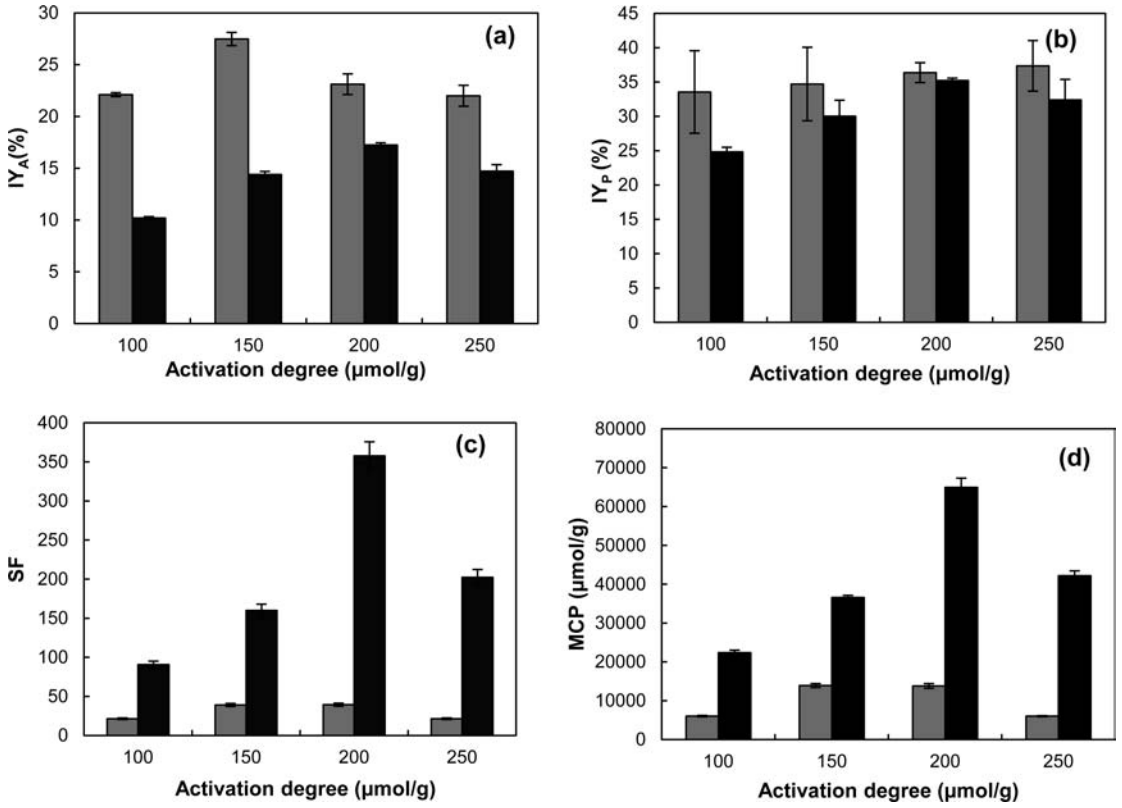


**Figure 2.** Effect of the activation degree of C-GA-EPI (gray bars) and C-EPI-EPI (black bars) on the performance of immobilized *B. circulans* β-galactosidase: (a) immobilization yield in terms of expressed activity ($IY_A$); (b) immobilization yield in terms of protein ($IY_P$); (c) stability factor (SF); (d) maximum catalytic potential (MCP). Immobilization conditions: 0.1 M citrate−phosphate buffer, pH 10, 20% glycerol, and 25 °C. Inactivation conditions: 60 °C and 0.1 M citrate−phosphate buffer, pH 6.

activity ($IY_A$) was defined as the ratio of the activity expressed by the immobilized biocatalyst to the contacted activity.

**Selection of the Methodology of Chitosan Derivatization and Optimization of Immobilization Conditions.** To select a methodology of chitosan derivatization, an enzymatic solution of 1.3 mg protein/mL was immobilized in C-GA-EPI and C-EPI-EPI with different activation degrees for 10 h, under the conditions previously mentioned. The performance of the biocatalysts was evaluated in terms of their immobilization yield and thermal stability. The thermal stability was evaluated through the stability factor (SF), defined as the ratio of the half-lives of immobilized and soluble biocatalyst at 60 °C and pH 6 (0.1 M citrate−phosphate buffer). Half-life was calculated after modeling biocatalyst inactivation kinetics by a biphasic mechanism:

$$\frac{A_I}{A_{I0}} = \left[1 + \alpha \times \frac{k_1}{k_2 - k_1}\right] \times \exp(-k_1 \times t) - \left[\alpha \times \frac{k_1}{k_2 - k_1}\right] \times \exp(-k_2 \times t) \quad (1)$$

$A_I/A_{I0}$ represents the residual activity at time $t$, $\alpha$ is the specific activity ratio of the intermediate species with respect to the native enzyme species, and $k_1$ and $k_2$ are the transition rate constants from the native to the intermediate and from the intermediate to the final enzyme species, respectively.

To consider both the activity of the immobilized biocatalyst and its thermal stability, the lumped parameter maximum catalytic potential (MCP) was also utilized for selecting a chitosan derivatization methodology.[39,41] MCP integrates the variation of expressed activity ($A_I$) along biocatalyst inactivation (eq 2), considering the time of biocatalyst utilization ($t_f$) as the one at which residual activity is 35%.

$$\mathrm{MCP} = \int_0^{t_f} A_I \, dt \quad (2)$$

After selecting the chitosan derivatization methodology, the contacted protein and immobilization time were optimized using a central composite rotatable design of two variables at two levels with five replicas at the central point.

**Galacto-oligosaccharide Synthesis.** GOS synthesis with the soluble and immobilized β-galactosidase was carried out using 50% (w/w) lactose solution at pH 6 (0.1 M citrate−phosphate buffer) and 60 °C. β-Galactosidase activity in the reaction mixture was adjusted to 40 IU/g lactose, as previously reported.[41] To evaluate the impact of reusing the immobilized enzyme on GOS synthesis and measure the biocatalyst thermal stability under reactive conditions, sequential batches of GOS synthesis were carried out. In this case, the ratio of biocatalyst mass to lactose mass was maintained constant and equal to the one used in the first batch.

The following parameters were used for evaluating GOS synthesis:

Yield ($Y_{GOS}$): maximum GOS mass ($M_{GOS}$) per unit mass of initial lactose mass ($M_{L0}$)

$$Y_{GOS} = \frac{M_{GOS}}{M_{L0}} \times 100 \quad (3)$$

Volumetric productivity ($\pi$): total GOS mass per unit of reaction volume ($V$) and unit of reaction time ($t$). For the purposes of this work, $\pi$ was evaluated at the time when maximum GOS concentration was achieved.

$$\pi = \frac{M_{GOS}}{V \times t} \quad (4)$$

Cumulative specific productivity ($\pi_C$): total GOS mass obtained over the whole operation of sequential batches ($n$ batches) per unit mass of biocatalyst protein ($M_{BP}$) and unit of reaction time. For the purposes of this work, total GOS mass of each batch was evaluated at the moment when maximum GOS concentration was achieved.


dx.doi.org/10.1021/jf500351j | J. Agric. Food Chem. 2014, 62, 10126−10135

$$\pi_C = \frac{\sum_{batch1}^{batchn} M_{GOS}}{M_{BP} \times \sum_{batch1}^{batchn} t} \quad (5)$$

In the case of the immobilized enzyme, $\pi_C$ is expressed in terms of the mass of protein that was contacted with the support for biocatalyst immobilization. $M_B$ represents the mass of biocatalyst utilized in the first batch of GOS synthesis.

$$\pi_C = \frac{\sum_{batch1}^{batchn} M_{GOS}}{M_B \times P_c \times \sum_{batch1}^{batchn} t} \quad (6)$$

## RESULTS AND DISCUSSION

**Selection of Chitosan Derivatization Method.** Chitosan particles were derivatized either using glutaraldehyde for cross-linking and epichlorohydrin for support activation (C-GA-EPI) or else using epichlorohydrin for both cross-linking and activation (C-EPI-EPI). The derivatization of chitosan with epichlorohydrin was done in a two-step process because it was previously reported[39] that this methodology allows a higher degree of activation than when chitosan is derivatized in just one step.[38] This difference may be related to the fact that the first step of cross-linking should produce some steric hindrances that limit the additional cross-linking of chitosan chains when a high concentration of epichlorohydrin is contacted during the second step of derivatization, favoring the support activation. The characterization of C-GA-EPI is presented as Supporting Information. In the case of C-EPI-EPI, its physical and chemical characterization was reported previously,[39] showing that the used methodology allows the modification of the amino and hydroxyl groups of chitosan. In the case of C-GA-EPI, the modification was tested with FTIR, showing that the GA and EPI groups have reacted with the chitosan matrix and new aldehyde groups were introduced as reflected by the best resolution bands related with the vibration of C—N of amine and C═O of aldehydes (1570 and 1650 $cm^{-1}$, respectively) (Figure SM3, Supporting Information).

The concentration of aldehyde groups of C-GA-EPI and C-EPI-EPI was modified by varying the concentration of $NaIO_4$ utilized for the oxidation of the support. After oxidation, all $NaIO_4$ was reacted, obtaining supports with activation degrees in the range from 100 to 250 $\mu$mol of aldehyde per gram. The effect of chitosan derivatization method over $IY_A$, $IY_P$, SF, and MCP of the immobilized enzyme is presented in Figure 2. The inactivation kinetics of each biocatalyst was modeled by a biphasic mechanism (eq 1), and the values of the corresponding inactivation parameters are summarized in Table 1.

The activation degree of both supports affected the biocatalysts' expressed activity; however, immobilized protein varied significantly only in the case of C-EPI-EPI. In general, C-GA-EPI produced the higher values of $IY_A$ and $IY_P$ independent of the aldehyde concentration in the support. With both supports $IY_P$ was higher than $IY_A$, which is explained by the immobilization of proteins different from the $\beta$-galactosidase (the commercial enzyme preparation is not pure) and also by the presence of diffusional restrictions and/or inactivation of the catalyst due to the immobilization process. The stability (SF) of the biocatalysts immobilized in both supports also varied according to the activation degree. The maximum values of $IY_A$ and SF were obtained when the C-GA-EPI and C-EPI-EPI were activated with 150 and 200 $\mu$mol of aldehyde per gram of support, respectively. The increase in the concentration of aldehyde groups in the support should allow the immobilization of a higher proportion of the contacted enzyme and favor multipoint interaction between the protein and the support, which may explain the increase of expressed activity and stability until 150 and 200 $\mu$mol of aldehyde per gram of C-GA-EPI and C-EPI-EPI, respectively. On the other hand, the decrease of $IY_A$ in the supports with a higher activation degree may be explained by the formation of covalent bonds close to the active site or by an excessive stiffening of the protein, reducing mobility below the minimum level required for catalysis. In the case of SF, an excessive stiffening of the protein may expose areas more prone to denaturation, explaining the lower thermal stability of the biocatalysts. In general, independent of the activation degree, best results were obtained with C-GA-EPI in terms of $IY_A$: in the case of C-GA-$EPI_{150}$ $IY_A$ was almost twice that obtained with C-EPI-$EPI_{150}$. The opposite effect was observed for SF, a better performance being obtained with the $\beta$-galactosidase immobilized in C-EPI-EPI, irrespective of the activation degree. The highest stability was obtained with C-EPI-$EPI_{200}$, for which the SF was 4 times the value reported for the biocatalyst of *B. circulans* $\beta$-galactosidase immobilized in glyoxyl-agarose under optimized conditions and 7 times the value reported for the enzyme immobilized in silica support.[41,43] Because C-GA-EPI and C-EPI-EPI were activated using the same methodology, the different performance obtained with both supports may be explained by a difference in support structure as a consequence of their cross-linking process. When the combined effect of activity and stability was assessed using MCP as lumped parameter, the support C-EPI-$EPI_{200}$ offered the best performance due to the prevalence of the effect of thermal stabilization. This support was selected for the further optimization of protein loading and immobilization time.

**Table 1. Inactivation Parameters of *B. circulans* $\beta$-Galactosidase Immobilized in Different Chitosan Supports, Determined According to a Series Biphasic Model (Equation 1)[a]**

| support | $k_1$ ($h^{-1}$) | $k_2$ ($h^{-1}$) | $\alpha$ | $R^2$ |
|---|---|---|---|---|
| C-GA-$EPI_{100}$ | 1.35 | 0.03 | 0.28 | 0.998 |
| C-GA-$EPI_{150}$ | 0.77 | 0.02 | 0.29 | 0.988 |
| C-GA-$EPI_{200}$ | 0.94 | 0.03 | 0.37 | 0.999 |
| C-GA-$EPI_{250}$ | 1.37 | 0.05 | 0.28 | 0.996 |
| C-EPI-$EPI_{100}$ | 1.14 | 0.03 | 0.53 | 0.996 |
| C-EPI-$EPI_{150}$ | 1.83 | 0.03 | 0.60 | 0.999 |
| C-EPI-$EPI_{200}$ | 0.63 | 0.02 | 0.58 | 0.996 |
| C-EPI-$EPI_{250}$ | 2.54 | 0.03 | 0.63 | 0.993 |

[a] $R^2$, coefficient of determination.

The leaching of $\beta$-galactosidase from the derivatized supports was not evaluated in this work because Bernal et al.[44] showed that the covalent immobilization of this enzyme in a support activated with aldehyde groups avoids the leaching of the enzyme.

**Optimization of Immobilization Conditions.** Biocatalyst specific activity and thermal stability are important parameters for the industrial application of immobilized enzymes because the first one will define the quantity of catalyst required for a specific reaction and the latter will determine its lifespan. Biocatalyst specific activity varies according to the quantity of enzyme contacted during the immobilization process, whereas it has been reported that the thermal stability of an immobilized enzyme may be improved through the increase of immobiliza-

tion time.[45] To set the range of contacted protein to be considered in the optimization of immobilization conditions, the maximum protein loading capacity of C-EPI-EPI was assessed (Figure 3), obtaining a maximum of 23.8 mg of

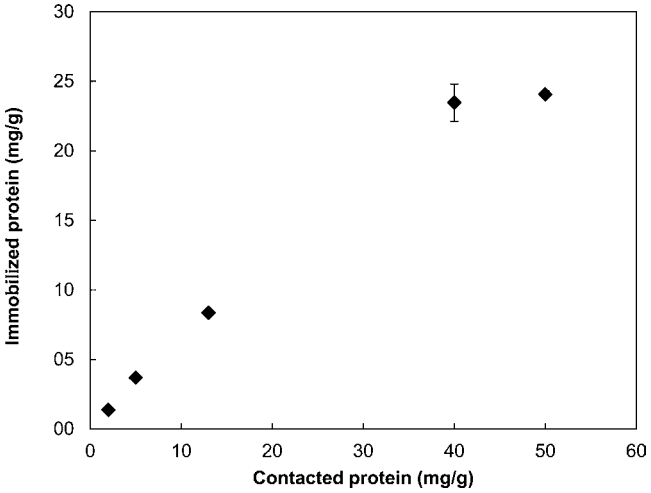


**Figure 3.** Loading capacity of C-EPI-EPI$_{200}$ expressed in terms of *B. circulans* $\beta$-galactosidase protein content.

immobilized protein per gram of support. This maximum loading capacity was 45 and 20% lower than the values reported for the immobilization of *B. circulans* $\beta$-galactosidase in glyoxyl-agarose[41] and acrylic resins,[46] respectively. Such a difference may be due to the lower total surface area. The range of immobilization time considered for the optimization of the immobilization process was established after evaluating the stability of the biocatalysts at maximum protein loading and at 10% of that maximum. Two different immobilization times were considered: the minimum time required for obtaining a constant activity in the supernatant ($t_{min}$) and $t_{min}$ plus 24 h. As shown in Figure 4, thermal stability of the biocatalyst loaded with the maximum quantity of protein was independent of immobilization time, in contrast to the biocatalyst loaded with a lower quantity of protein. This effect may be explained by a difference in the multipoint interaction between the enzyme and support due to the nonhomogeneous surface of the support, obtaining higher interaction intensity when the enzyme is first linked to the most reactive areas and a lower interaction intensity when the enzyme is immobilized in the less reactive areas. This effect was also reported for glyoxyl-agarose.[41]

Considering the interaction observed between the quantity of protein contacted and the immobilization time, both variables were optimized by a central composite design, using MCP as response parameter (Figure 5). The response surface was modeled by a second-order polynomial equation (eq 7), obtaining the maximum value of MPC when 25.8 mg/g was contacted for $t_{min}$ plus 14.1 h (total immobilization time = 38.1 h).

$$\mathrm{MCP} = P_c \times 35010.8 + t_{add} \times 17136.5 - t_{add} \times P_c \times 127.9 - P_c^2 \times 640.5 - t_{add}^2 \times 491.4 - 190011 \quad (7)$$

The ANOVA test was performed, obtaining a $p$ value of 0.0005, an $R^2$ value of 0.9366, and an adjusted $R$ value of 0.8913. The optimized conditions were validated experimentally, obtaining a MCP of 367,032 $\mu$mol/g (4.5% lower than the predicted value). The optimized biocatalyst expressed 280 ± 7 IU/g, with an IY$_A$ of 17.3 ± 0.4% and an IY$_P$ of 61.5 ± 3.9%. The expressed activity was 53% lower than the value reported for the enzyme immobilized under optimized conditions in glyoxyl-agarose.[41] However, the SF obtained with the enzyme immobilized in chitosan was 450% higher than the corresponding value obtained with the agarose biocatalyst.[41] Additionally, the use of chitosan presents an economic advantage, because one of the limiting factors in the use of agarose is its high cost.[47]

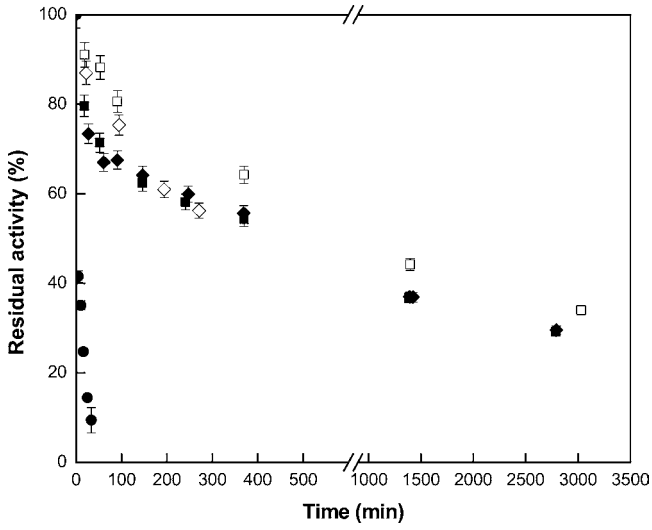


**Figure 4.** Thermal inactivation at 60 °C and pH 6 (0.1 M citrate–phosphate buffer) of the soluble enzyme (closed circles) and derivatives of $\beta$-galactosidase immobilized in C-EPI-EPI$_{200}$ at maximum protein loading capacity (solid symbols) and at 10% of that maximum (open symbols) at different immobilization times: (rhombuses) $t_{min}$; (squares) $t_{min}$ + 48 h. $t_{min}$ is the minimum time required to obtain a constant activity in the supernatant.

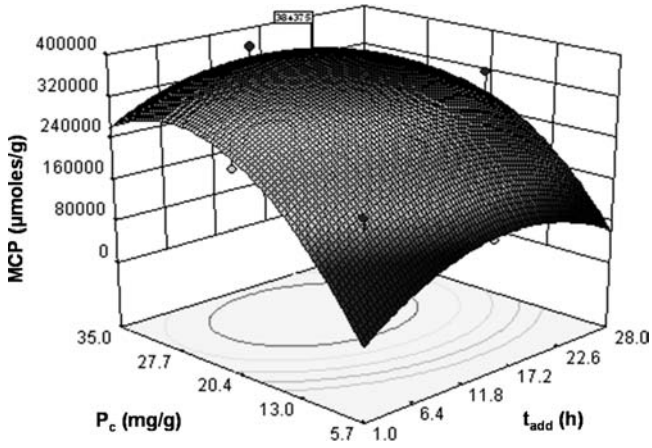


**Figure 5.** Optimization of *B. circulans* $\beta$-galactosidase immobilization in C-EPI-EPI$_{200}$, considering additional immobilization time ($t_{add}$) and contacted protein as variables and maximum catalytic potential (MCP) as objective function. Immobilization conditions: 0.1 M citrate–phosphate buffer, pH 10, 20% glycerol, and 25 °C.

**Galacto-oligosaccharide Synthesis.** The optimized biocatalyst was utilized in the synthesis of GOS in repeated batch operation. A comparison of Y$_{GOS}$ and $\pi$ values obtained in one batch of GOS synthesis catalyzed by the soluble and immobilized $\beta$-galactosidase is presented in Table 2. The


dx.doi.org/10.1021/jf500351j | J. Agric. Food Chem. 2014, 62, 10126–10135

**Table 2. Comparison of Synthesis of GOS with Soluble β-Galactosidase and β-Galactosidase Immobilized in C-EPI-EPI$_{200}$[a]**

| parameter | soluble β-gal | β-gal/C-EPI-EPI$_{200}$ |
|---|---|---|
| $Y_{GOS}$ (%) | 38.3 | 39.1 |
| $\pi$ ($g_{GOS}$/h·L) | 462.2 | 473.7 |

[a] $Y_{GOS}$, GOS yield; $\pi$, volumetric productivity.

production of GOS was not affected by the immobilization of the enzyme, as reflected by the lack of a significant variation in $Y_{GOS}$ and $\pi$. These results indicate that diffusional restrictions in the immobilized enzyme are not significant and the immobilization process did not produce conformational changes or steric hindrances that affect the activity of the biocatalyst. In contrast, Huerta et al.[42] and Sheu et al.[48] reported that the synthesis of GOS with *Aspergillus oryzae* β-galactosidase immobilized in chitosan derivatized with glutaraldehyde resulted in a lower $Y_{GOS}$ than the one obtained with the soluble enzyme, a result explained by the presence of diffusional restrictions. The insignificant effect of diffusional restrictions in the biocatalyst of *B. circulans* β-galactosidase immobilized in C-EPI-EPI$_{200}$ may be explained by the use of a lower enzyme loading and/or by differences in the support size and structure. Considering that several isoenzymes of *B. circulans* β-galactosidase have been identified in the commercial soluble enzyme preparation,[18−20] the absence of variation in $Y_{GOS}$ and $\pi$ also indicates that the relative activity of each isoform was not significantly altered upon immobilization. The profile of GOS obtained with β-galactosidase immobilized in C-EPI-EPI$_{200}$ was similar to the one obtained with the soluble enzyme (Figure 6). This pattern remained unchanged along 10 repeated batches, as may be observed in Figure 7.

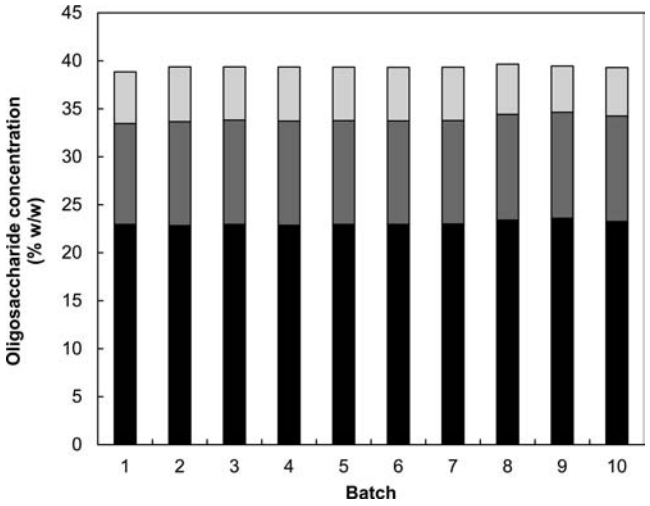


**Figure 7.** Product distribution of GOS synthesized by the β-galactosidase from *B. circulans* immobilized in C-EPI-EPI$_{200}$ along batches in repeated batch operation: (black bars) trisaccharides; (gray bars) tetrasaccharides; (white bars) penta- and hexasaccharides. Reaction conditions: 50% (w/w) initial lactose concentration, 0.1 M citrate−phosphate buffer, pH 6, and 60 °C. Biocatalyst added in the first batch was adjusted to 40 IU/g initial lactose, and for the subsequent batches the ratio of biocatalyst mass to lactose mass was maintained constant and equal to the one used in the first batch.

To make a fair comparison between the soluble and immobilized β-galactosidase, the parameters cumulative specific productivity ($\pi_c$) and total mass of GOS per mass of contacted protein ($R_{GOS}$) were evaluated. The expression of each parameter in terms of the contacted protein takes into consideration the immobilization yield; therefore, both the soluble and immobilized enzymes are compared considering

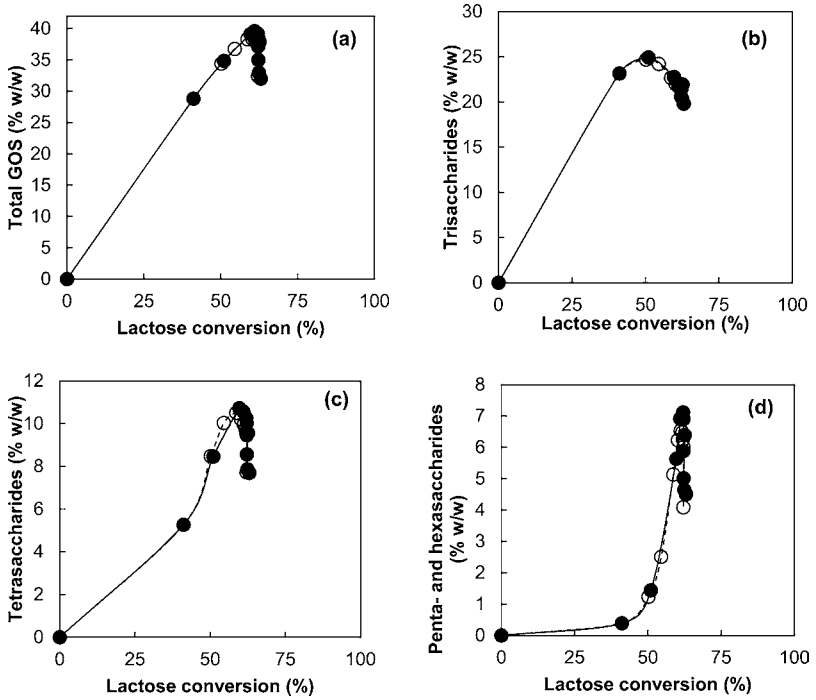


**Figure 6.** Profiles of GOS synthesized by *B. circulans* β-galactosidase: (a) total GOS; (b) trisaccharides; (c) tetrasaccharides; (d) penta- and hexasaccharides; (solid symbols) soluble enzyme; (open symbols) enzyme immobilized under optimized conditions in C-EPI-EPI$_{200}$. Reaction conditions: 50% (w/w) initial lactose concentration, 0.1 M citrate−phosphate buffer, pH 6, 60 °C, and 40 IU/g initial lactose.

the total mass of protein expended for the production of GOS. The values of $\pi_c$ along 10 successive batches are presented in Figure 8a. The $\pi_C$ of the first batch of synthesis was lower for the immobilized enzyme due to the loss of activity during immobilization; however, the reutilization of the biocatalyst compensates for the loss of activity, requiring only four sequential batches to surpass the $\pi_C$ of the soluble enzyme. After 10 successive batches, the $\pi_C$ of the immobilized enzyme was 2.9 times the value obtained with the soluble enzyme. This value is lower than the $\pi_C$ reported for the enzyme immobilized in glyoxyl-agarose[41] due to the lower expressed activity of the biocatalyst. The advantage associated with the high thermal stability of the enzyme immobilized in C-EPI-EPI$_{200}$ should be observed with a higher number of batches or extending the time of each batch. Values of $R_{GOS}$ are presented in Figure 8b, observing that after 10 batches almost 1 kg of GOS per gram of contacted protein is produced when the immobilized biocatalyst is utilized. The thermal stability of the immobilized enzyme was compared under reactive and nonreactive conditions (Figure 9), observing a positive modulation by the reaction media. Under reactive conditions, <10% of the initial biocatalyst hydrolytic activity was lost after 10 successive batches.

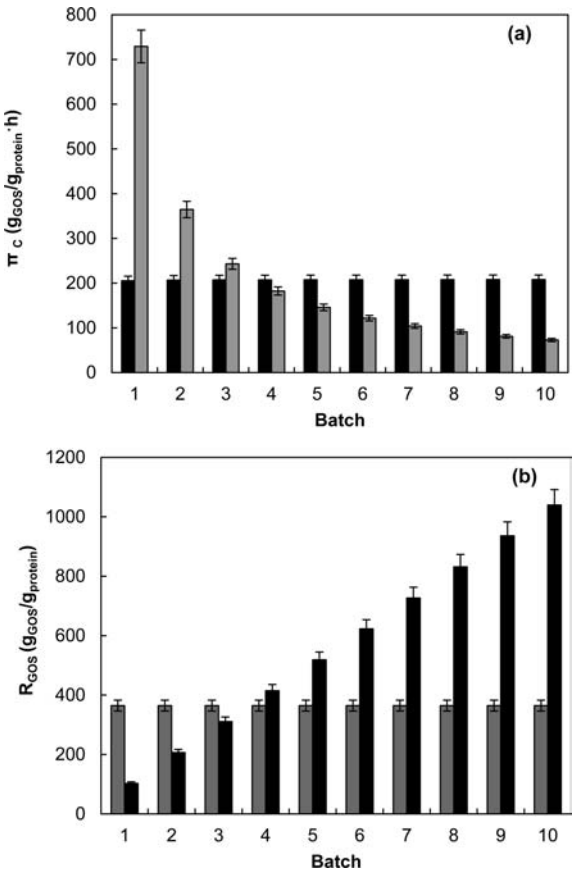


**Figure 8.** Comparison of soluble $\beta$-galactosidase (gray bars) and $\beta$-galactosidase immobilized under optimized conditions in C-EPI-EPI$_{200}$ (black bars): (a) cumulative GOS productivity in terms of contacted protein ($\pi_c$); (b) accumulated mass of GOS per unit mass of contacted protein ($R_{GOS}$). Reaction conditions: 50% (w/w) initial lactose concentration, 0.1 M citrate−phosphate buffer, pH 6, and 60 °C. Biocatalyst added in the first batch was adjusted to 40 IU/g initial lactose, and for the subsequent batches the ratio of biocatalyst mass to lactose mass was maintained constant and equal to the one used in the first batch.

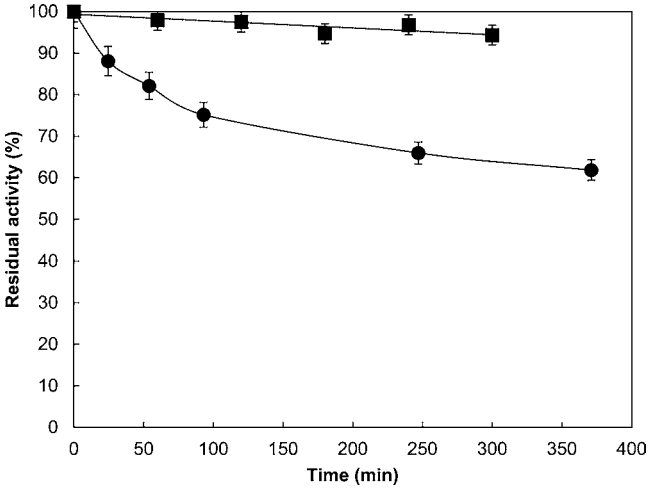


**Figure 9.** Comparison of thermal stability of $\beta$-galactosidase immobilized under optimized conditions in C-EPI-EPI$_{200}$ under nonreactive (circles) and reactive (squares) conditions. Nonreactive conditions: 0.1 M citrate−phosphate buffer, pH 6, 60 °C. Reactive conditions: 50% (w/w) initial lactose concentration, 0.1 M citrate−phosphate buffer, pH 6, 60 °C.

In conclusion, the cross-linking agent utilized for chitosan derivatization and the activation degree of the support had a high impact on the performance of the immobilized *B. circulans* $\beta$-galactosidase. The best compromise between expressed activity and thermal stability was obtained with the enzyme immobilized in cross-linked chitosan and activated with epichlorohydrin at a degree of activation of 200 $\mu$mol of aldehydes per gram of support. The optimization of immobilization conditions (protein load and immobilization time) increased biocatalyst expressed activity and thermal stability. The optimized biocatalyst was applied to the synthesis of GOS, without affecting the product profile obtained with the soluble enzyme. Four successive batches were required for obtaining a cumulative specific productivity higher than the one obtained with the soluble enzyme. The appropriate design of a low-cost support, such as chitosan, is a good strategy for the development of a highly stable biocatalyst adequate for GOS synthesis.

## ■ ASSOCIATED CONTENT

### Supporting Information

Physical and chemical characterization of chitosan cross-linked with glutaraldehyde and activated with epichlorohydrin (C-GA-EPI). This material is available free of charge via the Internet at http://pubs.acs.org.

## ■ AUTHOR INFORMATION

### Corresponding Author

*(A.I.) E-mail: aillanes@ucv.cl.

### Funding

Work financed by Chilean Fondecyt Grant 1100050. Doctoral fellowship to P.U. from Conicyt-Chile is acknowledged.

### Notes

The authors declare no competing financial interest.

## REFERENCES


(1) Adam, A. C.; Rubio-Texeira, M.; Polaina, J. Lactose: the milk sugar from a biotechnological perspective. *Crit. Rev. Food Sci. Nutr.* **2004**, *44*, 553−557.

(2) Playne, M. J.; Crittenden, R. G. Galacto-oligosaccharides and other products derived from lactose. In *Advanced Dairy Chemistry*; McSweeney, P. L. H., Fox, P. F., Eds.; Springer Science&Business Media: New York, 2009; pp 121−201.

(3) Guerrero, C.; Vera, C.; Illanes, A. Optimisation of synthesis of oligosaccharides derived from lactulose (fructosyl-galacto-oligosaccharides) with β-galactosidases of different origin. *Food Chem.* **2013**, *138*, 2225−2232.

(4) Irazoqui, G.; Giacomini, C.; Batista-Viera, F.; Brena, B. M.; Cardelle-Cobas, A.; Corzo, N.; Jimeno, M. L. Characterization of galactosyl derivatives obtained by transgalactosylation of lactose and different polyols using immobilized β-galactosidase from *Aspergillus oryzae*. *J. Agric. Food Chem.* **2009**, *57*, 11302−11307.

(5) Roberfroid, M. Prebiotics: the concept revisited. *J. Nutr.* **2007**, *137*, 830−837S.

(6) Tzortzis, G.; Vulevic, J. Galacto-oligosaccharide prebiotics. In *Prebiotic and Probiotic Science and Technology*; Charalampopoulos, D., Rastall, R. A., Eds.; Springer Science&Bussiness Media: New York, 2009; pp 207−244.

(7) Boon, M. A.; Janssen, A. E. M.; van't Riet, K. Effect of temperature and enzyme origin on the enzymatic synthesis of galactooligosaccharides. *Enzyme Microb. Technol.* **2000**, *26*, 271−281.

(8) Guerrero, C.; Vera, C.; Plou, F.; Illanes, A. Influence of reaction conditions on the selectivity of the synthesis of lactulose with microbial β-galactosidases. *J. Mol. Catal. B: Enzym.* **2011**, *72*, 206−212.

(9) Huber, R. E.; Kurz, G.; Wallenfels, K. A. A quantitation of the factors which affect the hydrolase and transgalactosylase activities of β-galactosidase (*E. coli*) on lactose. *Biochemistry* **1976**, *15*, 1994−2001.

(10) Splechtna, B.; Nguyen, T. H.; Steinbo, M.; Kulbe, K. D.; Lorenz, W.; Haltrich, D. Production of prebiotic galacto-oligosaccharides from lactose using β-galactosidases from *Lactobacillus reuteri*. *J. Agric. Food Chem.* **2006**, *54*, 4999−5006.

(11) Gosling, A.; Stevens, G. W.; Barber, A. R.; Kentish, S. E.; Gras, S. L. Effect of the substrate concentration and water activity on the yield and rate of the transfer reaction of β-galactosidase from *Bacillus circulans*. *J. Agric. Food Chem.* **2011**, *59*, 3366−3372.

(12) Chen, S. X.; Wei, D. Z.; Hu, Z. H. Synthesis of galacto-oligosaccharides in AOT/isooctane reverse micelles by β-galactosidase. *J. Mol. Catal. B−Enzym.* **2001**, *16*, 109−114.

(13) Gaur, R.; Pant, H.; Jain, R.; Khare, S. K. Galacto-oligosaccharide synthesis by immobilized *Aspergillus oryzae* β-galactosidase. *Food Chem.* **2006**, *97*, 426−430.

(14) Pessela, B. C. C.; Dellamora-Ortiz, G.; Betancor, L.; Fuentes, M.; Guisán, J. M.; Fernandez-Lafuente, R. Modulation of the catalytic properties of multimeric β-galactosidase from *E. coli* by using different immobilization protocols. *Enzyme Microb. Technol.* **2007**, *40*, 310−315.

(15) Boon, M. A.; Janssen, A. E. M.; van't Riet, K. Effect of temperature and enzyme origin on the enzymatic synthesis of galactooligosaccharides. *Enzyme Microb. Technol.* **2000**, *26*, 271−281.

(16) Urrutia, P.; Rodríguez-Colinas, B.; Fernández-Arrojo, L.; Ballesteros, A.; Wilson, L.; Illanes, A.; Plou, F. A detailed analysis of galactooligosaccharides synthesis with β-galactosidase from *Aspergillus oryzae*. *J. Agric. Food Chem.* **2013**, *61*, 1081−1087.

(17) Mozaffar, Z.; Nakanishi, K.; Matsuno, R.; Kamikuba, T. Production and properties of β-galactosidases from *Bacillus circulans*. *Agric. Biol. Chem.* **1984**, *48*, 3053−3061.

(18) Vetere, A.; Paoletti, S. Separation and characterization of three β-galactosidases from *Bacillus circulans*. *Biochim. Biophys. Acta* **1998**, *1380*, 223−232.

(19) Song, J.; Abe, K.; Imanaka, H.; Imamura, K.; Minoda, M.; Yamaguchi, S.; Nakanishi, K. Causes of the production of multiple forms of β-galactosidase by *Bacillus circulans*. *Biosci., Biotechnol., Biochem.* **2011**, *75*, 268−271.

(20) Warmerdam, A.; Paudel, E.; Jia, W.; Boom, R. M.; Janssen, A. E. M. Characterization of β-galactosidase isoforms from *Bacillus circulans* and their contribution to GOS production. *Appl. Biochem. Biotechnol.* **2013**, *170*, 340−358.

(21) Stepankova, V.; Bidmanova, S.; Koudelakova, T.; Prokop, Z.; Chaloupkova, R.; Damborsky, J. Strategies for stabilization of enzymes in organic solvents. *ACS Catal.* **2013**, *3*, 2823−2836.

(22) Verma, M. L.; Barrow, C. J.; Puri, M. Nanobiotechnology as a novel paradigm for enzyme immobilisation and stabilisation with potential applications in biodiesel production. *Appl. Microbiol. Biotechnol.* **2013**, *97*, 23−39.

(23) Rodrigues, R. C.; Ortiz, C.; Berenguer-Murcia, A.; Torres, R.; Fernández-Lafuente, R. Modifying enzyme activity and selectivity by immobilization. *Chem. Soc. Rev.* **2013**, *42*, 6290−6307.

(24) Hernandez, K.; Fernandez-Lafuente, R. Control of protein immobilization: coupling immobilization and site-directed mutagenesis to improve biocatalyst or biosensor performance. *Enzyme Microb. Technol.* **2011**, *48*, 107−122.

(25) Garcia-Galan, C.; Berenguer-Murcia, A.; Fernandez-Lafuente, R.; Rodrigues, R. C. Potential of different enzyme immobilization strategies to improve enzyme performance. *Adv. Synth. Catal.* **2011**, *353*, 2885−2904.

(26) Hanefeld, U.; Gardossi, L.; Magner, E. Understanding enzyme immobilisation. *Chem. Soc. Rev.* **2008**, *38*, 453−468.

(27) Krajewska, B. Application of chitin- and chitosan-based materials for enzyme immobilization: a review. *Enzyme Microb. Technol.* **2004**, *35*, 126−139.

(28) Wang, K. Enzyme immobilization on chitosan-based supports. In *Chitosan-Based Hydrogels*; Yao, K., Yao, J., Li, F., Yin, Y., Eds.; Functions and Applications; CRC Press: Boca Raton, FL, USA, 2012; pp 339−406.

(29) Górecka, E.; Jastrzębska, M. Immobilization techniques and biopolymer carriers. *Food Sci.* **2011**, *75*, 65−68.

(30) Barbosa, O.; Ortiz, C.; Berenguer-Murcia, A.; Torres, R.; Rodrigues, R. C.; Fernandez-Lafuente, R. Glutaraldehyde in bio-catalysts design: a useful crosslinker and a versatile tool in enzyme immobilization. *RSC Adv.* **2014**, *4*, 1583−1600.

(31) Migneault, I.; Dartiguenave, C.; Bertrand, M. J.; Waldron, K. C. Glutaraldehyde: behavior in aqueous solution, reaction with proteins, and application to enzyme crosslinking. *BioTechniques* **2004**, *37*, 790−802.

(32) Singh, A. N.; Singh, S.; Suthar, N.; Dubey, V. K. Glutaraldehyde-activated chitosan matrix for immobilization of a novel cysteine protease, procerain B. *J. Agric. Food Chem.* **2011**, *59*, 6256−6262.

(33) Manrich, A.; Galvão, C. M. A.; Jesus, C. D. F.; Giordano, R. C.; Giordano, R. L. C. Immobilization of trypsin on chitosan gels: use of different activation protocols and comparison with other supports. *J. Biol. Macromol.* **2008**, *43*, 54−61.

(34) Cestari, A. R.; Vieira, E. F.; Mota, J. A. The removal of an anionic red dye from aqueous solutions using chitosan beads − the role of experimental factors on adsorption using a full factorial design. *J. Hazard. Mater.* **2008**, *160*, 337−343.

(35) Vieira, R. S.; Beppu, M. M. Chitosan as adsorbent for heavy metal ions: performance and adsorption mechanism. In *Water Resources Research Progress*; Robinson, L. N., Ed.; Nova Science Publishers: New York, 2008; pp 149−175.

(36) Feng, Y.; Yang, L.; Li, F. A novel sensing platform based on periodate-oxidized chitosan. *Anal. Methods.* **2010**, 2011−2016.

(37) Mateo, C.; Palomo, J. M.; Fernandez-Lorente, G.; Guisan, J. M.; Fernandez-Lafuente, R. Improvement of enzyme activity, stability and selectivity via immobilization techniques. *Enzyme Microb. Technol.* **2007**, *40*, 1451−1463.

(38) Rodrigues, D. S.; Mendes, A. A.; Adriano, W. S.; Gonçalves, L. R. B.; Giordano, R. L. C. Multipoint covalent immobilization of microbial lipase on chitosan and agarose activated by different methods. *J. Mol. Catal. B−Enzym.* **2008**, *51*, 100−109.

(39) Urrutia, P.; Bernal, C.; Escobar, S.; Santa, C.; Mesa, M.; Wilson, L.; Illanes, A. Influence of chitosan derivatization on its physicochemical characteristics and its use as enzyme support. *J. Appl. Polym. Sci.* **2014**, DOI: 10.1002/APP.40701.

(40) Bradford, M. M. A rapid and sensitive method for the quantitation of microgram quantities of protein utilizing the principle of protein-dye binding. *Anal. Biochem.* **1976**, *72*, 248−254.
(41) Urrutia, P.; Mateo, C.; Guisan, J. M.; Wilson, L.; Illanes, A. Immobilization of *Bacillus circulans* β-galactosidase and its application in the synthesis of galacto-oligosaccharides under repeated-batch operation. *Biochem. Eng. J.* **2013**, *77*, 41−48.
(42) Huerta, L. M.; Vera, C.; Guerrero, C.; Wilson, L.; Illanes, A. Synthesis of galacto-oligosaccharides at very high lactose concentrations with immobilized β-galactosidases from *Aspergillus oryzae*. *Process Biochem.* **2011**, *46*, 245−252.
(43) Bernal, C.; Sierra, L.; Mesa, M. Improvement of thermal stability of β-galactosidase from *Bacillus circulans* by multipoint covalent immobilization in hierarchical macro-mesoporous silica. *J. Mol. Catal. B−Enzym.* **2012**, *84*, 166−172.
(44) Bernal, C.; Mesa, M.; Sierra, L. Design of β-galactosidase/silica biocatalysts: impact of the enzyme properties and immobilization pathways on their catalytic performance. *Eng. Life Sci.* **2014**, *14*, 85−94.
(45) Pedroche, J.; Yust, M.; Mateo, C.; Fernández-Lafuente, R.; Girón-Calle, J.; Alaiz, M.; Vioque, J.; Guisán, J. M.; Millán, F. Effect of support and experimental conditions in the intensity of the multipoint covalent attachment of proteins on glyoxyl-agarose supports: correlation between enzyme-support linkages and thermal stability. *Enzyme Microb. Technol.* **2007**, *40*, 1160−1166.
(46) Torres, P.; Batista-Viera, F. Improved biocatalysts based on *Bacillus circulans* β-galactosidase immobilized onto epoxy-activated acrylic supports: applications in whey processing. *J. Mol. Catal. B−Enzym.* **2012**, *83*, 57−64.
(47) Brena, B.; Batista-Viera, F. Immobilization of cnzymes: a literature survey. In *Immobilization of Enzymes and Cells*; Guisan, J. M., Ed.; Humana Press: Totowa, NJ, USA, 2006; pp 15−30.
(48) Sheu, D. C.; Li, S. Y.; Duan, K. J.; Chen, C. W. Production of galactooligosaccharides by β-galactosidase immobilized on glutaraldehyde-treated chitosan beads. *Biotechnol. Technol.* **1998**, *12*, 273−276.

The geographical origin[26,27] and the manufacturing process, including fermentation,[28] need to be highlighted as key factors that might greatly influence polyphenolic distribution.

To develop an efficient calibration model using NIRS, a solid database representative of the chemical variability of the product[29,30] and a reliable reference analysis were prerequisites. To achieve this goal, we first built a large database of samples (with different geographical origins, phenotypes, and fermentation conditions). Second, different flavan-3-ol extraction procedures were studied to choose the one allowing a quick and reliable analysis to be applied on a large cocoa sample for NIRS calibration purposes. In addition to the already known extraction techniques involving sonication or Ultra-Turax homogenization,[10,17,18,31,32] a Fast-Prep (FP) device was used for the first time for cocoa flavan-3-ol extraction.

With the large and robust database we generated and with the optimized extraction protocols, we set out to build a quantitative and efficient model for predicting flavan-3-ol content. The changes occurring within the beans were correlated with the sum of temperatures (ST)[33] during fermentation for different cocoa origins, and the changes in flavan-3-ols monitored by NIRS were studied.

## MATERIALS AND METHODS

**Chemicals.** Hexane, acetone, methanol, and acetonitrile were of HPLC grade, purchased from Carlo Erba (Val de Reuil, France). Formic acid was also purchased from Carlo Erba. The reference compounds (−)-epicatechin and proanthocyanidin dimers $B_1$ and $B_2$ were obtained from Sigma Chemical Co. (St. Louis, MO, USA).

**Cocoa Bean Sampling.** Thirty microfermentation trials were carried out in three different countries (Ecuador, Madagascar, and Dominican Republic), in line with producers' usual practices. A microfermented sample was composed of about 700 g of fresh cocoa beans placed in nets and positioned in fermentation boxes at three different defined levels (close to the top, in the middle, close to the bottom).[34] The temperature of each microfermented sample was recorded every 15 min by sensors (Thermo-boutons IP65 40/+85 +/−0.5, Laboratoires Humeau, France) placed in the nets. The nets were surrounded by the mass of fresh cocoa beans to ensure a sufficient volume of cocoa for fermentation to proceed. Fermentation was carried out for 6 days with mixing every 2 days (48 and 96 h). One sample per position and per fermentation was taken each day and then sun-dried to a final moisture content close to 7%. In addition, the cocoa mass was sampled every 2 days during mixing for each fermentation trial and then sun-dried like the microfermented samples.

The experimental design led to 635 samples: 524 microfermented samples and 111 cocoa mass samples. This sampling was completed with 83 samples from Cameroon, Ghana, Indonesia, and Trinidad and Tobago. Those samples, used in other projects, were prepared and handled in the same way as the others, but no survey of the temperature was carried out. The total number of samples used for this study was 718. In addition to that, for the 524 microfermented samples, the ST was calculated by using the integral of the curve of temperatures from the beginning of fermentation to the time of sampling with a baseline fixed at 20 °C, as described previously.[33]

About 100 g of unshelled dried cocoa was ground in a "Valentin" blender (SEB, France) under liquid nitrogen, sifted to 0.5 mm, and stored at −20 °C prior to analysis.

**Flavan-3-ol Extraction and Quantification.** To investigate the phenolic content, and for NIR calibration, wet chemistry was carried out on 193 samples selected from the set of 718 samples. The 193 samples were randomly selected under the constraint of having the same sample percentage per class (fermentation time, origin, position in the box). The 193 samples were analyzed in the laboratory and were used for NIR model development.

*Fast-Prep Extraction (FPE).* A Fast-Prep-24 device (MP Biomedicals, Eschwege, Germany) at 6.5 m $s^{-1}$ was used with a garnet matrix and 1/4 ceramic sphere as the lysing matrix. Cocoa powder (100.0 ± 0.1 mg) was defatted two times for 1 min with 1 mL of hexane. Following centrifugation (5 min, 21400*g*, 4 °C), the upper organic phase was discarded to remove lipids. The solid phase (defatted cocoa powder) was then extracted for 1 min with 1 mL of acetone/water/formic acid (70:30:0.1, v/v/v). After centrifugation (21400*g*, 5 min, 4 °C), the upper phase was collected and the solid phase was re-extracted using the same conditions. The two fractions were then gathered, and the solvent was eliminated by a rotavapor (50 °C). Flavan-3-ols were thereafter extracted with methanol/water (50:50 v/v) and injected into HPLC. The analysis was carried out in duplicate. Replicates were consolidated using the Student *t* test at 95%, based on the standard deviation of samples.

*Ultra-Turax Extraction.* One gram of cocoa powder was added to 20 mL of hexane and finely ground for 2 min at 2000 rpm with an Ultra-Turax T25 digital (Staufen, Germany). After centrifugation (10 min, 21400*g*, 4 °C), the hexane phase was discarded. The defatted powder was then extracted with the blender for 2 min with 20 mL of acetone/water/formic acid (70:30:0.1, v/v/v). The organic phase was then recovered by evaporation (same conditions as above) and injected into HPLC.

*Pressurized Liquid Extraction (PLE).* PLEs were carried out on an ASE350 automated sample extractor (Dionex, Idstein, Germany) using 10 mL stainless steel extraction cells. One gram of cocoa powder was mixed with 5 g of diatomaceous earth. The mixture was loaded into the cartridge. The remaining free space of the cell was filled with diatomaceous earth. Cocoa powder was first defatted with four cycles of hexane for 5 min each (60 °C, 1500 psi). The hexane phase was eliminated by a rotavapor (50 °C). Flavan-3-ols were thereafter extracted with one cycle (5 min) of an acetone/water/formic acid (70:30:0.1, v/v/v) mixture at 70 °C and 1451 psi. The organic phase was then recovered by evaporation (same conditions as above) and injected into HPLC. The volume flush was 20 mL of acetone/water/formic acid (70:30:0.1 v/v/v).

*HPLC-DAD Analysis.* Prior to injection, all of the samples were filtered through a 0.45 μm syringe filter. The HPLC analysis was performed on an HPLC system from the Agilent Technologies 1200 series (Agilent Technologies, Santa Clara, CA, USA). Separation was achieved at 30 °C using a 250 mm × 4.6 mm i.d., 5 μm, end-capped reversed-phase Lichrospher ODS-2 (Interchim, Montluçon, France). The mobile phase was water/acetonitrile/formic acid (99:0.8:0.2, v/v/v) (solvent A) and acetonitrile (solvent B). Proanthocyanidins were eluted using the following gradient: 5% of B for 4 min, then from 5 to 35% B in 41 min and from 35 to 100% B in 15 min. At the end, the column was equilibrated to its initial state. The injection volume was 20 μL, and detection was carried out between 200 and 600 nm.

*Quantification.* Quantification of flavan-3-ols was achieved through external calibration curves established at 280 nm with epicatechin, proanthocyanidin $B_1$, and proanthocyanidin $B_2$ standards (0−120 mg/L), leading to $R^2$ = 0.93, 0.92, and 0.99, respectively.

*HPLC-MS Analysis.* After passing through the flow cell of the diode array detector, the column eluate was split and at 0.25 mL/min was directed to an LCQ ion trap mass spectrometer fitted with an electrospray interface (Thermo Finnigan, San Jose, CA, USA). Experiments were performed in both negative and positive ion modes. The scan range was 100−2000 and scan rate, 1 scan/s. The desolvation temperatures were 250 and 300 °C in the positive and negative ion modes, respectively. The high spray voltage was set at 5000 V. Nitrogen was used as the dry gas at a flow rate of 75 mL/min. Identification was achieved on the basis of the ion molecular mass, MS, and UV−visible spectra. The identifications of catechin, epicatechin, proanthocyanidin $B_1$, and proanthocyanidin $B_2$ were confirmed by direct injection of authentic standards. Total flavan-3-ols were quantified as the sum of individual compounds.

**NIRS Prediction.** NIRS acquisitions were obtained on a Foss 6500 monochromator (Foss, Silver Spring, MD, USA) using a spin cell sample module. About 3 g of cocoa powder was analyzed by diffuse reflectance from 400 to 2500 nm in 2 nm steps. Data were saved as the average of 32 scans and stored as $\log(1/R)$, where $R$ was the

Table 1. Statistical Parameters of the NIR Equation for Each Phenolic Constituent[a]

| Calibration | | | | | | | | |
|---|---|---|---|---|---|---|---|---|
| constituent | $N$ | mean (mg/g) | SD (mg/g) | SEC (mg/g) | $R^2$ | SECV (mg/g) | terms ($n$) | outliers[b] ($n$) | RPD = SECV/SD |
| (−)-epicatechin | 158 | 9.23 | 6.30 | 1.04 | 0.97 | 1.46 | 9 | 5 | 4.32 |
| proanthocyanidin $B_1$ | 157 | 2,18 | 1.45 | 0.31 | 0.96 | 0.41 | 8 | 6 | 3.54 |
| proanthocyanidin $B_2$ | 156 | 1,82 | 1.03 | 0.24 | 0.95 | 0.29 | 6 | 7 | 3.55 |
| total flavan-3-ols | 155 | 18.28 | 11.59 | 1.61 | 0.98 | 2.30 | 10 | 8 | 5.03 |
| **Validation** | | | | | | | | | |
| constituent | $N$ | mean (mg/g) | SD (mg/g) | SEP (mg/g) | slope | bias | SEPc (mg/g) | $R^2$p | RPDp = SEP/SD |
| (−)-epicatechin | 30 | 10.54 | 6.19 | 1.81 | 0.97 | −0.78 | 1.67 | 0.93 | 3.41 |
| proanthocyanidin $B_1$ | 30 | 2.38 | 1.43 | 0.29 | 1.02 | 0.06 | 0.29 | 0.96 | 4.85 |
| proanthocyanidin $B_2$ | 30 | 1.96 | 0.97 | 0.24 | 0.98 | 0.02 | 0.24 | 0.94 | 4.12 |
| total flavan-3-ols | 30 | 20.82 | 11.48 | 2.33 | 0.98 | −0.62 | 2.28 | 0.96 | 4.93 |

[a]$N$, number of samples; SD, standard deviation; SEC, standard error of calibration; $R^2$, coefficient of multiple determination; SECV, standard error of cross-validation; RPD, ratio of performance to deviation; SEP, standard error of prediction; SEPc, standard error of prediction bias-corrected; $R^2$p, coefficient of multiple determination for prediction; RPDp, ratio of performance to deviation for prediction. [b]Student's $t$ test.

reflectance at each wavelength. Spectra were acquired in a random order.

Statistical analyses were performed using Win-ISI II software (Infrasoft International, Port Matilda, PA, USA) and XLstat software (Addinsoft, Paris, France).

*Spectrum Pretreatment.* Different pretreatments were tested. The one adopted was a mathematical correction for light scattering, using the standard normal variate and detrend correction.[35] Then, the second derivative was calculated on five data points and smoothed using Savitzky and Golay polynomial smoothing on five data points on the whole data set including visible and near-infrared wavelengths.

*Principal Component Analysis (PCA).* Prior to calibration development, a PCA was used to extract relevant information from the spectral matrix ($n$ = 193). The generalized Mahalanobis distance ($H$) was calculated on the extracted PCs for each sample. This statistical distance is useful for defining boundaries of the population and a similarity index between spectra. No sample displayed a Mahalanobis distance greater than the distance limit (3), so all of the samples were kept in the database.

*NIR Calibration Development.* To optimize the model parameters and assess the performance of the predictive model, the 193 samples analyzed in the laboratory were separated into two groups, one for calibration and one for validation. The validation subset comprised 30 samples: 14 samples corresponding to two independent geographical origins (Ghana and Indonesia) and 16 randomly selected samples. The calibration subset comprised the remaining 163 samples. The calibration equations for the phenolic content were constructed with the calibration subset using the modified partial least-squares regression (mPLS) algorithm of WinISI software.[30] Calibration statistics included the following parameters: standard deviation (SD), coefficient of determination ($R^2$), standard error of calibration (SEC), and standard error of cross-validation (SECV).

Cross-validation was used during calibration development to select the optimum number of latent variables and to minimize overfitting of the equations. For SECV estimation, 25% of the samples were predicted using a calibration model developed with the other 75%. SECV estimation was repeated four times and the average calculated. In addition to $R^2$, the ratio of performance to deviation (RPD = SD/SECV) was used to evaluate the general quality of the fit obtained for each equation. Unlike SEC and SECV, RPD has no units and can therefore be compared between parameters.[36] The Student $t$ test was used to identify $t$-outlier samples during calibration development. Outlier detection was based on the standardized residuals (= error/SECV) with a cutoff of 2.5. Two passes of outlier elimination were used.[37] The standard error of prediction (SEP), corresponding to the standard deviation of residuals, was estimated by predicting the validation subset using a model developed on the calibration subset. The ratio of performance to deviation of prediction (RPDp) was also calculated as RPDp = SDval/SEP (where SDval was the standard deviation of validation samples). The quality of the fit between flavan-3-ol values from HPLC-DAD analysis and flavan-3-ol NIRS-predicted values was evaluated from the linear regression slope, the $R^2$p, and the bias.

On the basis of these results, the final NIRS calibration was developed using the 193 samples and applied to the 635 samples for which the ST was calculated to predict the polyphenolic content. The predicted values were studied as a function of fermentation time and the ST.

## RESULTS AND DISCUSSION

**Comparison of Flavan-3-ol Extraction Techniques.** The three extraction methods were compared for their flavan-3-ol extraction yield and their relative repeatability. It clearly appeared that epicatechin required two cycles to be extracted at >95% using Fast-Prep, whereas only one cycle was needed for PLE proanthocyanidin extraction (>95%) (results not shown).

A three-way ANOVA was performed on the total flavan-3-ol content with fermentation time, repetition, and extraction type as factors. A strong effect of fermentation time ($F$ = 1773.4; $p$ < 0.0001) and a lesser effect of extraction type ($F$ = 14.5; $p$ = 0.001) appeared. The Newman−Keuls test ($\alpha$ = 5%) showed that Fast-Prep enabled the extraction of a significantly higher content (21.3 mg/g of dried cocoa) than PLE (20.5 mg/g of dried cocoa). The lowest level of flavan-3-ols was obtained with the Ultra-Turax technique (19.7 mg/g of dried cocoa).

Seven samples covering the range of flavan-3-ol contents were extracted twice with the three different extraction methods to express the repeatability of (−)-epicatechin extraction yield. For total flavan-3-ol quantification, the smallest coefficient of variation was obtained with Fast-Prep extraction (0.75%); it was close to that achieved with PLE (1.27%), with the highest being for the Ultra-Turax method (2.67%), but remained very low whatever extraction device was used. The coefficients of variation were not significantly different for proanthocyanidin $B_1$ and proanthocyanidin $B_2$ (results not shown).

The Fast-Prep extraction procedure was preferred considering that the repeatability of this device was greater than for the other devices, with the advantage of its rapidity and easy-handling.

**Determination of Polyphenolic Content.** For the 193 samples selected, the flavan-3-ols were extracted by Fast-Prep and quantified by HPLC-DAD.

The most abundant component was (−)-epicatechin, with an average of 9.4 mg/g of cocoa powder and a standard deviation of 6.3 mg/g. The values were regularly distributed between the

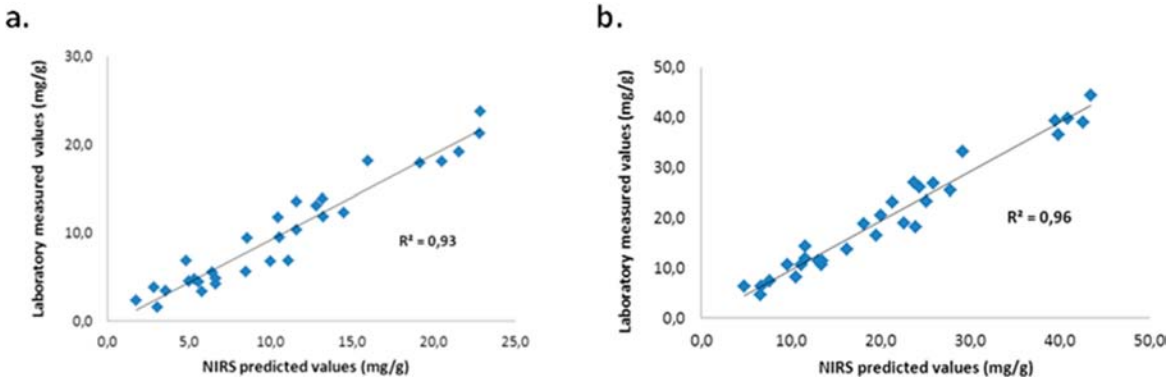


**Figure 1.** Scatter plot of NIRS-predicted values versus laboratory values for the validation set: (a) (−)-epicatechin; (b) total flavan-3-ols.

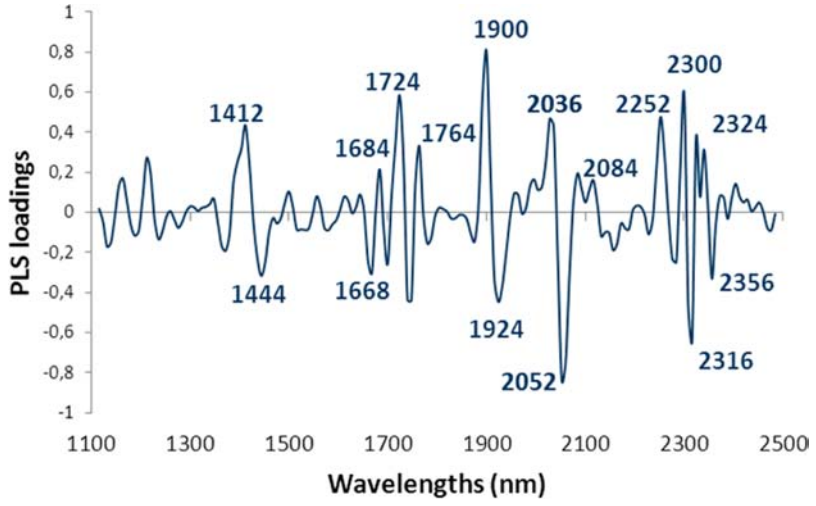


**Figure 2.** First PLS loadings as a function of the wavelengths observed for (−)-epicatechin calibration.

minimum and maximum values. This distribution reflected the experimental design assuming the hypothesis that flavan-3-ol content is linked to the fermentation time. The distribution was then considered optimum for developing NIR calibration.[30]

**NIRS Models and Validation.** The models developed for each individual component were efficient; the number of latent variables (PLS terms) introduced in the models ranged from 6 to 10 (Table 1). The $R^2$ values were between 0.95 and 0.98, and five to eight outliers ($t$ test) were removed during calibration.

These models were applied to estimate the SEP by predicting the validation set. The SEP values were between 0.24 mg/g (for proanthocyanidin $B_2$) and 2.33 mg/g (for total flavan-3-ols). The regression between predicted values and laboratory values led to $R^2$p values between 0.93 and 0.96 with nonsignificant bias and slope. The RPDp values were >3, reflecting the efficiency and the robustness of the models.

The scatter plot of NIRS-predicted values versus laboratory (Figure 1) values for the validation set highlighted the quality of the calibration for the whole range of the component concentration.

This accuracy was not expected due to NIR sensitivity, which is known to be around 0.1% for quantification. We put forward the hypothesis that NIRS was mainly calibrated on an indirect strong correlation due to the changes occurring during fermentation and the interactions of flavan-3-ols with some major components such as proteins. The amount of proteins in cocoa (10−15% of dry bean weight),[38] their hydrolysis, and their complexation with flavan-3-ols during fermentation, probably by surface contact and hydrogen-bonding,[39] lead to regression models computed on a correlation between proteins and flavan-3-ols. Those kinds of correlations make it difficult to interpret the size and the sign of the regression coefficients.[40] The contribution of flavan-3-ols in NIR spectra patterns is difficult to interpret, even on pure components. As an example, some of the absorption bands of pure (−)-epicatechin (data not shown) could also be assigned to N−H bond vibrations from proteins, polypeptides, amino acids, and amides: 1458, 1986, 2014, 2062, 2302, and 2474 nm.[41] However, the interpretation of PLS loadings (generated from raw or derivative spectra) could efficiently help to bring out such correlations. The observation of the loadings associated with the first PLS term (Figure 2) for (−)-epicatechin calibration revealed high coefficients[41] in the NIR region associated with (1) NH bonds at 2052 nm (proteins) and 2300 nm (amino acids); (2) C═O bonds at 1900 nm (second overtone stretching) from $-CO_2H-$ (acids), at 2036 nm (C═O stretching second overtone of $CONH_2$), and at 1924 nm (stretching, second overtone of CONH); (3) CH bond of aromatics at 1444 nm (and phenolic group) and 1684 nm; and (4) O−H bonds at 1412 nm, 2084 nm (R−OH), and 2252 nm (starch).

The remaining coefficients were associated with CH bonds from $CH_2$ and $CH_3$; a coefficient at 1668 nm could be assigned to CH from *cis*-RCH═CHR[1].

These patterns in PLS loadings were similar for proanthocyanidins and total flavan-3-ols. The relationship between bands related to proteins and bands related to O−H and

aromatic groups confirmed the close and strong relationship between proteins and flavan-3-ols. The evolution of these two compounds is dependent on fermentation conditions and follows similar kinetics. The accuracy of the model, despite low concentration levels, was directly linked to this strong relationship between proteins and flavan-3-ol compounds that occurs during fermentation and drastically changes spectrum profiles.

**Changes in Phenolic Compounds during Fermentation.** The phenolic compounds of the 718 samples were predicted by NIRS using the model developed. The values ranged from 0 to 46.6 mg/g for total flavan-3-ols, 5.4 mg/g for proanthocyanidin $B_1$, 4.3 mg/g for proanthocyanidin $B_2$, and 25.5 mg/g for (−)-epicatechin, with standard deviations of 10.6, 1.3, 1.0, and 5.7 mg/g, respectively. As expected, and whatever the origin, the phenolic content decreased significantly with fermentation time: total flavan-3-ol concentration fell from an average of 33.3 mg/g for unfermented samples to an average of 6.2 mg/g at the end of fermentation (Figure 3). A similar decrease was observed in previous studies.[12,15,42,43]

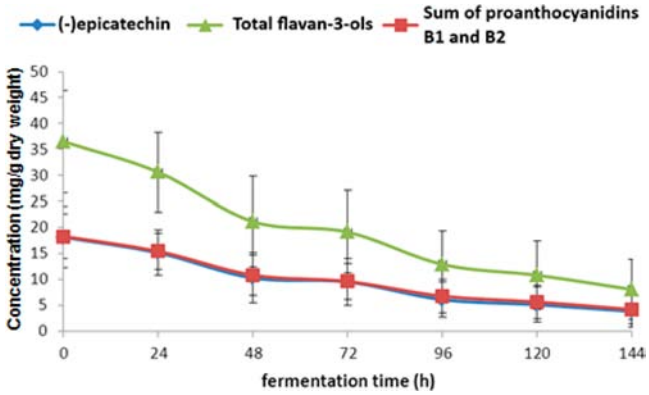


**Figure 3.** Evolution of (−)-epicatechin, sum of proanthocyanidins $B_1$ and $B_2$, and total flavan-3-ol concentration during fermentation.

Each compound was highly correlated to the others, enabling us to focus only on the evolution of the total flavan-3-ol content during fermentation.

A two-way ANOVA was performed to test the influence of cocoa origins and fermentation time on the total flavan-3-ol content. The ANOVA highlighted the strongest significant effect of the fermentation time ($F$ = 96.3; $p$ < 0.0001) compared to the origin ($F$ = 52.5; $p$ < 0.0001). According to the ANOVA-SNK (Newman−Keuls) test ($\alpha$ = 5%), for the fermentation time, the total flavan-3-ol concentration values were not significantly different for 120 and 144 h only.

As for the origin, the Dominican Republic, Madagascar, and Indonesia samples had significantly lower flavan-3-ol content values than those from Trinidad and Tobago, Ecuador, and Ghana. Samples from Cameroon were not significantly different from Ghana, but different from the others. Those variations could be explained by differences in the cocoa varieties used, endogenous microflora, fermentation conditions (size and material of boxes, harvest and pod opening delays, etc.), environmental conditions, etc.

The interaction between origin and fermentation time was also significant (Figure 4) and was due to differences in the kinetics of flavan-3-ol degradation depending on the origin. Samples from Indonesia displayed particular kinetics because no variation in flavan-3-ol content was observed after 48 h. This

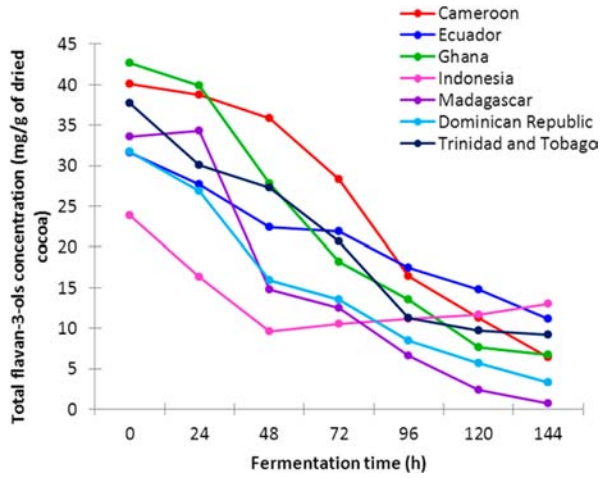


**Figure 4.** Total flavan-3-ol content predicted values versus fermentation times per geographical origin.

behavior was similar for other constituents measured on those samples, such as ammonia nitrogen or free amino acids (data not shown). One hypothesis is that no fermentation occurred after 48 h, probably due to poor fermentation conditions.

**Fermentation Monitoring and Relationship with Phenolic Content.** Temperatures were recorded at the exact place where samples in the net were located. The temperature profiles measured for the 30 microfermentations were similar to those in the literature with an average of 33 °C after 24 h, a rise to 40 °C at 96 h, and ending up close to 44 °C at the end of fermentation.

To better understand the effect of temperature on cocoa fermentation, the ST was calculated for each microfermented sample. For the 524 microfermented samples, the calculated values of the ST ranged from 0 to 3662 °C. They were regularly distributed. At 24 h the ST was relatively uniform with an average value equal to 265 ± 51 °C. The dispersion increased after 72 h, whereas at 144 h, the average ST was close to 2811 ± 387 °C. Unsurprisingly, the dispersion of ST was greater with the progression of fermentation and reflected the high heterogeneity of the batches. On this basis, we investigated the usefulness of ST for keeping track of flavan-3-ol changes (Figure 5).

There was a significant correlation ($r$ = 0.80) between both parameters, which could be described as a logarithmic equation. Each fermentation batch analyzed separately led to a high correlation between total flavan-3-ol concentration and the ST (e.g., $R^2$ = 0.87 for a particular batch randomly selected from the whole set). The minimum $R^2$ observed per batch was 0.44 and the highest, 0.92, for an average value of 0.74. This result was expected and confirmed the correlation between ST and flavan-3-ol concentration.

The ST factor explained changes occurring in the flavan-3-ol content more accurately than the fermentation time, whatever the geographical origin, phenotype, or position in the box studied. Flavan-3-ol derivatives and ST could be used by farmers and chocolate manufacturers to check fermentation levels.

In conclusion, this study, based on a large collection of samples and a robust experimental design, confirmed the effect of fermentation on the polyphenolic content of cocoa beans and the feasibility of using it as a marker of fermentation time. The Fast-Prep technique, a repeatable, easy-to-use, and quick

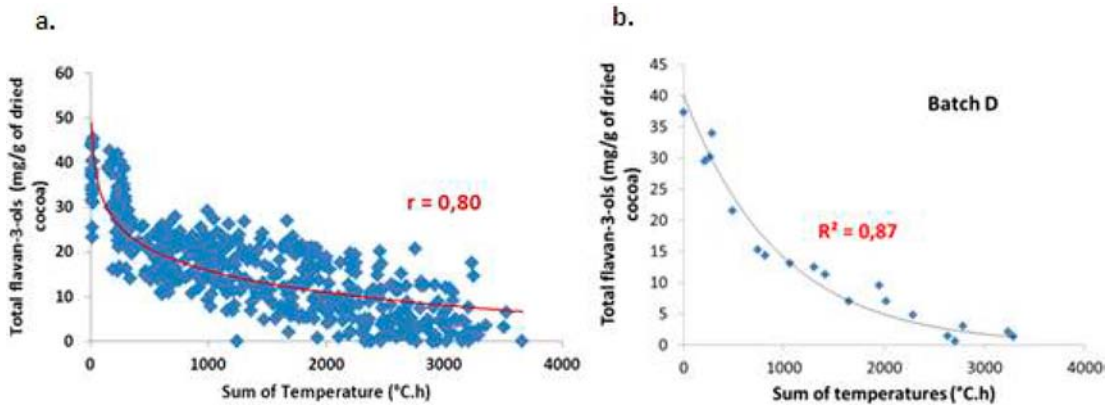


**Figure 5.** Scatter plot of total flavan-3-ol concentration versus the sum of temperatures for the whole database (a) and for a particular batch (b).

extraction method, was tested and used to calibrate the NIRS. This made it possible to effectively enlarge the database. Chocolate manufacturers could use the NIRS model on dry cocoa sample to predict fermentation levels by estimating the polyphenolic content. To complete this study, a specific study on tanning occurring with flavan-3-ols and proteins would give more information on reactions taking place during fermentation and on the specificity of the NIRS response. In addition, samples from other geographical origins (such as Ivory Coast or Brazil) need to be analyzed to enhance the robustness of the model.

## AUTHOR INFORMATION

### Corresponding Author

*(F.D.) Centre de Coopération Internationale en Recherche Agronomique pour le Développement (CIRAD) Département PERSYST, UMR Qualisud TA 80/16, 34398 Montpellier Cedex 5, France. Phone: +33 4 67 61 44 32. Fax: +33 4 67 61 44 33. E-mail: fabrice.davrieux@cirad.fr.

### Notes

The authors declare no competing financial interest.

## ACKNOWLEDGMENTS

We gratefully acknowledge Valrhona and their partner, the Cocoa Research Unit of the University of the West Indies, for providing cocoa and Gerard Fourny for preparing samples in Trinidad and Tobago. We also thank Peter Biggins, from CIRAD, for revising the English.

## REFERENCES

(1) de Brito, E. S.; García, N. H. P.; Gallão, M. I.; Cortelazzo, A. L.; Fevereiro, P. S.; Braga, M. R. Structural and chemical changes in cocoa (*Theobroma cacao* L) during fermentation, drying and roasting. *J. Sci. Food Agric.* **2001**, *81*, 281−288.

(2) Sukha, D. *The influence of processing location, growing environment and polen donor effects on the flavour and quality of selected cacao (Theobroma cacao L.) genotypes.* University of the West Indies, St. Augustine, 2008.

(3) Aculey, P. C.; Snitkjaer, P.; Owusu, M.; Bassompiere, M.; Takrama, J.; Norgaard, L.; Petersen, M. A.; Nielsen, D. S. Ghanaian cocoa bean fermentation characterized by spectroscopic and chromatographic methods and chemometrics. *J. Food Sci.* **2010**, *75*, 300−307.

(4) Voigt, J.; Heinrichs, H.; Voigt, G.; Biehl, B. Cocoa-specific aroma precursors are generated by proteolytic digestion of the vicilin-like globulin of cocoa seeds. *Food Chem.* **1994**, *50*, 177−184.

(5) Senanayake, M.; Jansz, E. R.; Buckle, K. A. Effect of different mixing intervals on the fermentation of cocoa beans. *J. Sci. Food Agric.* **1997**, *74*, 42−48.

(6) Vincent, J. C. Influence de différents traitements technologiques sur la fermentation du cacao et le goût du chocolat. *Cafe Cacao The* **1970**, *XIV*, 303−322.

(7) Lima, L. J. R.; Almeida, M. H.; Nout, M. J. R.; Zwietering, M. H. *Theobroma cacao* L., "The Food of the Gods": equality determinants of commercial cocoa beans, with particular reference to the impact of fermentation. *Crit. Rev. Food Sci.* **2011**, *51*, 731−761.

(8) Lopez, A. S.; Dimick, P. S. Cocoa fermentation. In *Biotechnology: Enzymes, Biomass, Food and Feed*; Wiley-VCH Publisher: New York, 1995; pp 561−577.

(9) Quesnel, V. C. Agents inducing the death of cacao seeds during fermentation. *J. Sci. Food Agric.* **1965**, *16*, 441−447.

(10) Forsyth, W. G. C. Cacao polyphenolic substances. II. Changes during fermentation. *Biochem. J.* **1952**, *51*, 516−520.

(11) Hansen, C. E.; del Olmo, M.; Burri, C. Enzyme activities in cocoa beans during fermentation. *J. Sci. Food Agric.* **1998**, *77*, 273−281.

(12) Wollgast, J.; Anklam, E. Review on polyphenols in *Theobroma cacao*: changes in composition during the manufacture of chocolate and methodology for identification and quantification. *Food Res. Int.* **2000**, *33*, 423−447.

(13) Buyukpamukcu, E.; Goodall, D. M.; Hansen, C. E.; Keely, B. J.; Kochhar, S.; Wille, H. Characterization of peptides formed during fermentation of cocoa bean. *J. Agric. Food Chem.* **2001**, *49*, 5822−5827.

(14) Lerceteau, E.; Rogers, J.; Petiard, V.; Crouzillat, D. Evolution of cacao bean proteins during fermentation: a study by two-dimensional electrophoresis. *J. Sci. Food Agric.* **1999**, *79*, 619−625.

(15) Kim, H.; Keeney, P. G. (−)-Epicatechin content in fermented and unfermented cocoa beans. *J. Food Sci.* **1984**, *49*, 1090−1092.

(16) Hammerstone, J. F.; Lazarus, S. A.; Mitchell, A. E.; Rucker, R.; Schmitz, H. H. Identification of procyanidins in cocoa (*Theobroma cacao*) and chocolate using high-performance liquid chromatography/mass spectrometry. *J. Agric. Food Chem.* **1999**, *47*, 490−496.

(17) Adamson, G. E.; Lazarus, S. A.; Mitchell, A. E.; Prior, R. L.; Cao, G.; Jacobs, P. H.; Kremers, B. G.; Hammerstone, J. F.; Rucker, R. B.; Ritter, K. A.; Schmitz, H. H. HPLC method for the quantification of procyanidins in cocoa and chocolate samples and correlation to total antioxidant capacity. *J. Agric. Food Chem.* **1999**, *47*, 4184−4188.

(18) Belščak, A.; Komes, D.; Horžić, D.; Ganić, K. K.; Karlović, D. Comparative study of commercially available cocoa products in terms of their bioactive composition. *Food Res. Int.* **2009**, *42*, 707−716.

(19) Sánchez-Rabaneda, F.; Jáuregui, O.; Casals, I.; Andrés-Lacueva, C.; Izquierdo-Pulido, M.; Lamuela-Raventós, R. M. Liquid chromatographic/electrospray ionization tandem mass spectrometric study of the phenolic composition of cocoa (*Theobroma cacao*). *J. Mass Spectrom.* **2003**, *38*, 35−42.

(20) Zak, D. L.; Keeney, P. G. Changes in cocoa proteins during ripening of fruit, fermentation, and further processing of cocoa beans. *J. Agric. Food Chem.* **1976**, *24*, 483−486.

(21) Jumnongpon, R.; Chaiseri, S.; Hongsprabhas, P.; Healy, J. P.; Meade, S. J.; Gerrard, J. A. Cocoa protein crosslinking using Maillard chemistry. *Food Chem.* **2012**, *134*, 375−380.
(22) Niemenak, N.; Rohsius, C.; Elwers, S.; Omokolo Ndoumou, D.; Lieberei, R. Comparative study of different cocoa (*Theobroma cacao* L.) clones in terms of their phenolics and anthocyanins contents. *J. Food Compos. Anal.* **2006**, *19*, 612−619.
(23) Mayer, A. M. Polyphenol oxidases in plants and fungi: going places? A review. *Phytochemistry* **2006**, *67*, 2318−2330.
(24) Whitacre, E.; Oliver, J.; van den Broek, R.; van Engelen, P.; Kremers, B.; van der Horst, B.; Stewart, M.; Jansen-Beuvink, A. Predictive analysis of cocoa procyanidins using near-infrared spectroscopy techniques. *J. Food Sci.* **2003**, *68*, 2618−2622.
(25) Alvarez, C.; Perez, E.; Cros, E.; Lares, M.; Assemat, S.; Boulanger, R.; Davrieux, F. The use of near infrared spectroscopy to determine the fat, caffeine, theobromine and (−)-epicatechin contents in unfermented and sun-dried beans of Criollo cocoa. *J. Near Infrared Spectrosc.* **2012**, *20*, 307−315.
(26) Caligiani, A.; Acquotti, D.; Cirlini, M.; Palla, G. $^{1}$H NMR study of fermented cocoa (*Theobroma cacao* L.) beans. *J. Agric. Food Chem.* **2010**, *58*, 12105−12111.
(27) Counet, C.; Ouwerx, C.; Rosoux, D.; Collin, S. Relationship between procyanidin and flavor contents of cocoa liquors from different origins. *J. Agric. Food Chem.* **2004**, *52*, 6243−6249.
(28) Cooper, K. A.; Campos-Giménez, E.; Jiménez Alvarez, D.; Nagy, K.; Donovan, J. L.; Williamson, G. Rapid reversed phase ultra-performance liquid chromatography analysis of the major cocoa polyphenols and inter-relationships of their concentrations in chocolate. *J. Agric. Food Chem.* **2007**, *55*, 2841−2847.
(29) Davrieux, F.; Allal, F.; Piombo, G.; Kelly, B.; Okulo, J. B.; Thiam, M.; Diallo, O. B.; Bouvet, J. M. Near infrared spectroscopy for high-throughput characterization of shea tree (*Vitellaria paradoxa*) nut fat profiles. *J. Agric. Food Chem.* **2010**, *58*, 7811−7819.
(30) Shenk, J.; Westerhaus, M. Population definition, sample selection, and calibration procedures for near infrared reflectance spectroscopy. *Crop Sci.* **1991**, *31*.
(31) Kelm, M. A.; Johnson, J. C.; Robbins, R. J.; Hammerstone, J. F.; Schmitz, H. H. High-performance liquid chromatography separation and purification of cacao (*Theobroma cacao* L.) procyanidins according to degree of polymerization using a diol stationary phase. *J. Agric. Food Chem.* **2006**, *54*, 1571−1576.
(32) Camu, N.; González, Á.; De Winter, T.; Van Schoor, A.; De Bruyne, K.; Vandamme, P.; Takrama, J. S.; Addo, S. K.; De Vuyst, L. Influence of turning and environemental contamination on the dynamics of populations of lactic acid and acetic acid bacteria involved in spontaneous cocoa bean heap fermentation in Ghana. *Appl. Environ. Microbiol.* **2008**, *74*, 86−98.
(33) Hue, C.; Gunata, Z.; Bergounhou, A.; Assemat, S.; Boulanger, R.; Sauvage, F. X.; Davrieux, F. Near infrared spectroscopy as a new tool to determine cocoa fermentation levels through ammonia nitrogen quantification. *Food Chem.* **2014**, *148*, 240−245.
(34) Sukha, D. A.; Butler, D. R.; Umaharan, P.; Boult, E. The use of an optimized organoleptic assessment protocol to describe and quantify different flavour attributes of cocoa liquors made from Ghana and Trinitario beans. *Eur. Food Res. Technol.* **2008**, *226*, 405−413.
(35) Barnes, R. J.; Dhanoa, M. S.; Lister, S. J. Standard normal variate transformation and de-trending of near-infrared diffuse reflectance spectra. *Appl. Spectrosc.* **1989**, *43*, 772−777.
(36) Williams, P. What does the raw material have to say? *NIR News* **1993**, *4*, 13.
(37) Burns, D. A.; Ciurczak, E. W. *Handbook of near-Infrared Analysis*; Dekker: New York, 1992.
(38) Bertazzo, A.; Comai, S.; Brunato, I.; Zancato, M.; Costa, C. V. L The content of protein and non-protein (free and protein-bound) tryptophan in *Theobroma cacao* beans. *Food Chem.* **2011**, *124*, 93−96.
(39) Baxter, N. J.; Lilley, T. H.; Haslam, E.; Williamson, M. P. Multiple interactions between polyphenols and a salivary proline-rich protein. *Biochem. J.* **1997**, *36*, 5566−5577.
(40) Westad, F.; Schmidt, A.; Kermit, M. Incorporating chemical band-assignment in near infrared spectroscopy regression models. *J. Near Infrared Spectrosc.* **2008**, *16*, 265−273.
(41) Osborne, B. G.; Fearn, T.; Hindle, P. H. *Practical NIR Spectroscopy with Applications in Food and Beverage Analysis*; Longman Group: Harlow, Essex, UK, 1993.
(42) Davrieux, F.; Boulanger, R.; Assemat, S.; Portillo, E.; Cros, E. Détermination du niveau de fermentation et des teneurs en flavan-3-ols du cacao marchand par spectrométrie proche infrarouge. In *15th International Cocoa Research Conference*, San Jose, Costa Rica, 2006.
(43) Payne, M. J.; Hurst, W. J.; Miller, K. B.; Rank, C.; Stuart, D. A. Impact of fermentation, drying, roasting, and Dutch processing on epicatechin and catechin content of cacao beans and cocoa ingredients. *J. Agric. Food Chem.* **2010**, *58*, 10518−10527.

In the present study, we aim to use various microscopy techniques to characterize the structure of morphologically different starch granules isolated from TRS mature kernels. The mature kernels will be mapped in situ using light microscopy to identify the spatial distribution of morphologically different granules in the endosperm. This study could increase our understanding of heterogeneous starch granules from high-amylose cereal and would provide important information on the formation of heterogeneous starch granules resulting from kernel development.

## MATERIALS AND METHODS

**Plant Materials.** An *indica* rice cultivar Te-qing (TQ) and its transgenic line (TRS) with high amylose and RS contents were used in this study. TRS was generated from TQ after transgenic inhibition of both SBE I and SBE IIb through an antisense RNA technique and was homozygous for the transgene.[6] TQ and TRS were cultivated in the transgenic close experiment field of Yangzhou University, Yangzhou, China.

**Starch Isolation.** Starches were isolated from TQ and TRS mature kernels according to the method of Wei et al.[16] with some modifications. Brown rice seeds were steeped in distilled water at 4 °C overnight and homogenized with ice-cold water in a home blender. The homogenate was squeezed through five layers of cotton cloth. The residue was homogenized and squeezed twice more in a mortar with a pestle to facilitate the release of starch granules. The combined extract was filtered with 100-, 200-, and 400-mesh sieves and centrifuged at 3000*g* for 10 min. The yellow gel-like layer on top of the packed white starch granule pellet was carefully scraped off and discarded. The process of centrifugation separation was repeated several times until no dirty material existed. The precipitated starch was further washed with anhydrous ethanol two times, dried at 40 °C, ground into powders, and passed through a 100-mesh sieve.

**Light Microscopy.** A starch suspension (1%, w/v) was prepared with 50% glycerol. 10 $\mu$L of starch suspension was placed on the microscope slide and covered with a coverslip. The starch granule shape and Maltese cross were viewed with an Olympus BX53 polarized light microscope equipped with a CCD camera under normal and polarized light. Iodine-stained starches were prepared and observed according to the method of Evans et al.[18] with some modifications. 5 mg of starch was stained in 0.5 mL of iodine solution (0.5% NaAc buffer, pH4.5, 25% glycerol, 0.04% $I_2$, 0.06% KI) for 30 min in darkness. 10 $\mu$L of iodine-stained starch suspension was first viewed under normal light, and then the same field was viewed under polarized light. All the iodine-stained starch granules were photographed under the same conditions in order to compare the polarization colors. Iodine-stained starches had four kinds of polarization colors: blue, fuchsia, red, and interior dark blue and exterior brown. For one type of heterogeneous starch granules, 50 granules were randomly chosen to be analyzed for polarization color for one experiment. The experiments were performed in triplicate.

**Confocal Laser Scanning Microscopy.** Starch granules were stained with the fluorophore APTS (8-amino-1,3,6-pyrenetrisulfonic acid) and prepared for confocal laser scanning microscope (CLSM) essentially as previously described by Blennow et al.[19] Images were recorded on a CLSM (LSM 710, Carl Zeiss MicroImaging GmbH) using a 488 nm laser line for excitation, and light was detected in the interval from 500 to 535 nm. For morphology observation, laser power capacity and master gain were adjusted to maximum saturation. To compare the fluorescence intensity, the laser power was kept constant at 1%, and images were recorded at the master gain of 620 for all starch granules. The conditions allowed all granules to have no saturation of the detector for every dot in all granules. For every type of heterogeneous starch granules, 60 granules were randomly chosen to be recorded. Image analysis was performed using the Carl Zeiss ZEN 2010 software.

**Hot Stage Microscopy.** Starch suspension was prepared by suspending about 10 mg of starch in 1.0 mL of double distilled water by using a vortex mixer. The suspension was transferred onto a slide, covered with a coverslip, and sealed with nail polish to prevent moisture loss during heating. The sealed specimen was then mounted on a Kitazato hot stage apparatus and observed under a long focus M Plan Semi Apochromat objective (50× magnification) using an Olympus polarized microscope during heating. The hot stage was heated from 25 to 50 °C at a heating rate of 5 °C/min and from 50 to 100 °C at a heating rate of 1 °C/min.

The gelatinization temperatures were measured according to the method of Konik-Rose et al.[20] with some modifications. The starch slurry was photographed under polarized light using an Olympus DP72 CCD camera during heating from 50 to 100 °C at 1 °C intervals. Three group experiments were carried out for every type of starch granule. For every group experiment, more than 100 granules of every type of heterogeneous starch granules were analyzed from 10 to 30 photographs. For every granule, the temperature at which the granule lost birefringence was recorded. The granule number was counted at the lost birefringence temperature. Plotting the granule number percentage of birefringence loss against the temperature produced a gelatinization curve. The initial, middle, and end gelatinization temperatures were obtained from the gelatinization curve when 5%, 50%, and 95% of granules had lost their birefringence.

The swelling of starch granule during heating was viewed under normal light and photographed using an Olympus DP72 CCD camera from 40 to 95 °C at 5 °C intervals. The area of starch granule was analyzed from the micrograph with a JEDA 801D morphological image analysis system (Jiangsu JEDA Science-Technology Development Co., Ltd., Nanjing, China). Fifty starch granules were measured for every type of heterogeneous starch granule. The starch granule swelling was presented as area swelling percentage (ASP) from ungelatinized granule at 40 °C and calculated by the equation ASP (%) = $A_t/A_i \times 100$, where $A_i$ and $A_t$ represented the area of starch granule at initial (40 °C) and specific testing temperature, respectively.

**Kernel Sections for Light Microscopy.** In order to soften the kernels, mature kernels were first fixed in a fixation solution (2.5% glutaraldehyde and 4% paraformaldehyde in 0.1 M phosphate buffer at pH 7.2) for 2 h at room temperature and then held overnight at 4 °C. The softened kernels were transversely cut with a razor blade at the midregion of the kernel to obtain thin tissue blocks. The tissue blocks were then fixed in the same fixation solution again for 48 h at 4 °C. After fixation, the blocks were washed 3 times with phosphate buffer, successively dehydrated in gradient ethanol, and embedded in LR White Resin. The semithin sections of 2 $\mu$m thickness were cut with a glass knife on a Leica Ultrathin Microtome (EM UC7), stained with iodine solution (25% glycerol, 0.07% $I_2$, 0.14% KI) for 10 min in darkness, and observed with an Olympus BX53 light microscope equipped with a CCD camera.

**Statistical Analysis.** One-way analysis of variance (ANOVA) and Tukey's test ($p < 0.05$) were used for statistical analysis of the difference of properties of TQ starch granule, TRS starch individual granule, TRS starch aggregate granule, TRS starch elongated granule, and TRS starch interior hollow granule using the SPSS 16.0 Statistical Software Program. All the replications were technical replicates.

## RESULTS AND DISCUSSION

**Morphology of Heterogeneous Starch Granules.** Starch granules isolated from TQ and TRS mature kernels were observed under normal and polarized light (Figure 1). Most TQ starch granules were regular and polygonal (Figure 1A,C) with all of them showing one central hilum and one typical Maltese cross (Figure 1a,c). Therefore, TQ starch granules were morphologically homogeneous. TQ starch is a compound starch that separates during isolation into many subgranules.[17] In the present study, the TQ starch granules isolated were the subgranules of compound starch that appeared as individual granules.

As found previously,[17] TRS starch granules showed significantly different morphologies (Figure 1B,b). These

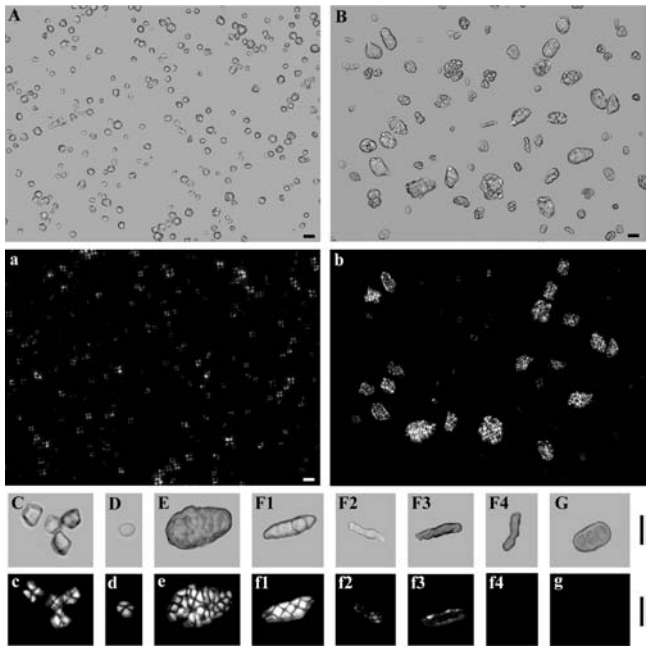


**Figure 1.** Microphotographs of starch granules under normal (A−G) and polarized (a−g) light. (A, C, a, c) TQ starch, (B, D−G, b, d−g) TRS starch, (C, D, c, d) individual granule, (E, e) aggregate granule, (F, f) elongated granule, (G, g) interior hollow granule. Scale bar = 10 $\mu$m.

granules could be divided into four types: individual, aggregate, elongated, and interior hollow granules according to their morphologies and Maltese crosses (Figure 1D−G,d−g). The individual granules of TRS and TQ starches all had the central hila and one typical Maltese cross on one granule, but there were significant differences in morphology and size. The TRS individual granules were spherical and smaller than the polygonal-shaped TQ individual granules (Figure 1D,d). The TRS aggregate granules were large and voluminous with nonangular rounded bodies and numerous bright Maltese crosses within granules (Figure 1E,e). Under transmission electron microscopy, the large voluminous and nonangular rounded body was observed to consist of many small subgranules. Some of these subgranules at the periphery of the starch fuse together and form a thick band or wall encircling the entire exterior of the starch granule, which prevents the release of subgranules during starch isolation.[17] Therefore, the large voluminous and nonangular rounded bodies were called aggregate granules, which were observed to have numerous Maltese crosses (Figure 1e). This agrees with the findings of Wei and his colleagues that the aggregate granule consisted of many subgranules and each subgranule contained a hilum and a Maltese cross.[17] The TRS elongated granules displayed different shapes including rods and filaments and could be further classified into three types: full birefringence, partial birefringence, and no birefringence according to their birefringence patterns (Figure 1F,f). The elongated granules with full birefringence patterns had three or more clear Maltese crosses within granules (Figure 1f1). Some of the elongated granules with partial birefringence showed only weak birefringence along the edge of the granules, while others displayed a birefringence pattern consisting of combinations of one or more Maltese crosses and weak to no birefringence on other parts of the granule (Figure 1f2,f3). The third type of elongated granule exhibited no birefringence (Figure 1f4). This phenomenon has also been reported elsewhere in high-amylose maize starch granules.[15,21] The percentage of elongated starch granules increases with the increasing amylose content in high-amylose maize.[10] The TRS interior hollow granules were mostly irregular and deformed, and exhibited extremely weak to no birefringence (Figure 1g), which was the same as interior hollow starch granules from high-amylose SGP-1 null wheat.[22]

Aggregate, elongated, and interior hollow starch granules have been observed in high-amylose rice,[12,17] maize,[10,15] wheat,[5,9] and barley.[11] However, the mode of formation of interior hollow granules is not clear at present. Birefringence patterns are the result of orderly aligned polymers or crystallites. Different birefringence patterns show various radial orientations and alignments of the crystallites' regions within the granules.[23,24] In the present study, the TQ and TRS individual starch granules and the subgranules of TRS aggregate starch granule had a typical Maltese cross in the hilum, indicating that the starch molecules were aligned in a radial order centered at the hilum and perpendicular to the granule surface.[21] In high-amylose maize, about 36% and 55% of elongated granules have partial birefringence and no birefringence, respectively.[15] In high-amylose wheat and barley, over 90% of interior hollow starch granules are not birefringent.[5,11] In the present study, the TRS elongated and interior hollow starch granules had weak or no birefringence, indicating that the starch molecules of granules were not radially aligned, which might result from the high amylose concentrations in these granules. The amylose molecules of granules are not expected to be specifically uniformly oriented.[19] The significantly different birefringence patterns of TRS starch granules indicated that the arrangement of starch molecules varied between heterogeneous granules and within the same granule.

**Polarization Colors of Iodine-Stained Heterogeneous Starch Granules.** Iodine staining in combination with polarized light microscopy has been used to reveal the structural heterogeneity of starch granules.[15,18] The color of iodine-stained starch under polarized light is termed the polarization color.[25] TQ and TRS starch granules stained with iodine solution (0.04% $I_2$ and 0.06% KI) were viewed under normal and polarized light (Figure 2). The TQ starch showed a homogeneous blue polarization color at the Maltese cross (Figure 2a,c), while the TRS starch granules exhibited significantly heterogeneous polarization colors. There were three types of polarization colors for TRS individual granules: blue (Figure 2d1), dark red (Figure 2d2), and a dark blue interior with brown exterior (Figure 2d3). The TRS aggregate granules displayed four types of polarization colors: blue (Figure 2e1), fuchsia (Figure 2e2), dark red (Figure 2e3), and a dark blue interior with brown exterior (Figure 2e4). Both the TRS elongated and interior hollow granules exhibited two types of polarization colors: dark red (Figure 2f1,g1) and a dark blue interior with brown exterior (Figure 2f2,g2). Table 1 summarizes the percentages of iodine-stained starch granules with different polarization colors. The TRS starch granules showed significant heterogeneity in polarization color between heterogeneous granules and within the same granule. Most of the TRS individual granules showed a blue polarization color, aggregate granules a dark red polarization color, and elongated and interior hollow granules a dark blue interior with brown exterior polarization color. The present results agree with previous reports that the polarization color of iodine-stained

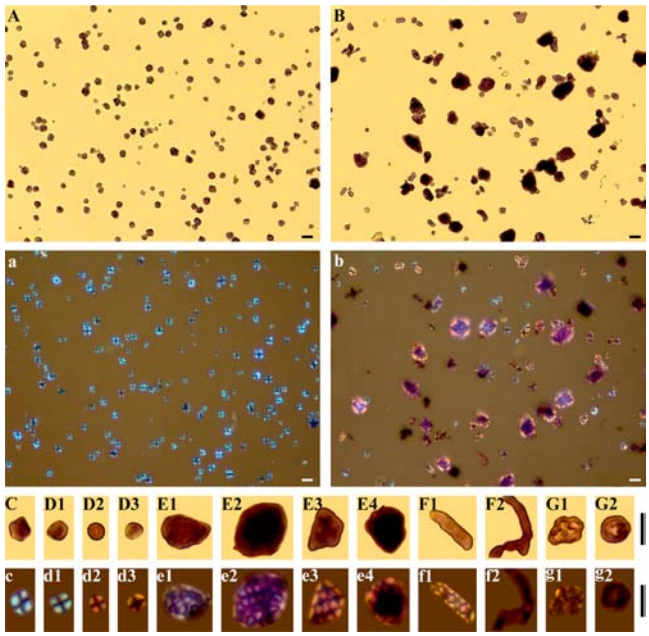


**Figure 2.** Microphotographs of iodine-stained starch granules under normal (A–G) and polarized (a–g) light. (A, C, a, c) TQ starch, (B, D–G, b, d–g) TRS starch, (C, D, c, d) individual granule, (E, e) aggregate granule, (F, f) elongated granule, (G, g) interior hollow granule, (c, d1, e1) showing the blue color, (e2) showing the fuchsia color, (d2, e3, f1, g1) showing the dark red color, (d3, e4, f2, g2) showing the dark blue interior with brown exterior. Scale bar = 10 $\mu$m.

starch is similar to that observed under normal light for waxy and normal starch and different from that observed under normal light for high-amylose starch. The *ae* single mutant high-amylose maize starch appears blue under normal light and pink under polarized light.[18,25]

The explanation of polarization color is based on absorption effects in combination with birefringence.[26] It is generally known that the amylose–iodine complex normally shows blue under normal light, but, in fact, the color of the complex depends on the degree of polymerization (DP) of the amylose helix. The color of the amylose–iodine complex changes from brown (DP 21–24) to red (DP 25–29), red–violet (DP 30–38), blue–violet (DP 37–46), and finally blue (DP > 47).[27] In the same manner as amylose, the linear branches of amylopectin, which form a helix, can also develop a red or orange amylopectin–iodine complex. The external chain length is equally important for iodine staining of amylopectin.[27−29] It is believed that the radially ordered alignment of starch molecules results in birefringence and the random orientation in no birefringence.[30] The intensity of birefringence is not in proportion to the amylopectin content but is positively correlated with the proportion of symmetrically and radially oriented amylopectin molecules.[18] When starch molecules (amylose and amylopectin) are completely radially oriented, iodine-stained starch granules will exhibit a blue polarization color because the amylose–iodine complex generates a stronger color than the amylopectin–iodine complex. When only the amylopectin is oriented radially, the intensity of birefringence will be slightly reduced and iodine-stained starch granules will display a pink polarization color resulting from the amylopectin–iodine complex. When only the amylose is oriented radially, the intensity of birefringence will be markedly diminished and iodine-stained starch granules will display a blue polarization color resulting from the amylose–iodine complex.[18] In the present study, all TQ starch granules and most of the TRS individual granules showed a blue polarization color, indicating that these granules contained radially oriented starch molecules. Some TRS aggregate granules exhibited a fuchsia polarization color, indicating that both the amylopectin and amylose were partly radially oriented. As a result of the less symmetrical radial orientation of amylopectin and the randomly oriented amylose, a dark red polarization color was observed in some TRS individual, aggregate, elongated, and interior hollow granules. The dark reddish polarization color has also been observed in some maize amylose-extender (*ae*) mutant starch granules.[18] The polarization colors of a dark blue interior with brown exterior were also observed in TRS starch granules (Figure 2d3,e4,f2,g2). The different colors within a granule indicated that its structure was heterogeneous. This structural heterogeneity within a granule has been also reported in high-amylose maize starches.[13−15,18] The significantly different polarization colors of the TRS starch granules indicated that heterogeneity in the orientations of amylose and amylopectin existed between heterogeneous granules and within the same granule.

**Fluorescence Intensities of APTS-Stained Heterogeneous Starch Granules.** CLSM photographs of APTS-stained starch granules provide information about the internal structure of starch granules.[31] The reducing end of the starch molecule is reacted specifically with APTS leading to a 1:1 stoichiometric ratio for starch molecule labeling. Owing to its smaller size, amylose contains a much higher molar ratio of reducing ends per glucose residue than amylopectin, which leads to a higher by-weight labeling of amylose when constructing a detailed map of the distribution of amylose and amylopectin within starch granules.[19] The distribution of amylose and amylopectin within the TQ and TRS starch granules stained with APTS are shown in Figure 3. TQ starch granules showed a strong fluorescent dot in the central hilum (Figure 3A), indicating a high density of amylose in the center of the granule. This phenomenon has also been reported in normal cereal starch granules.[17,31] Because of the high content of amylose, the TRS starch granules exhibited a fluorescence too strong for observing the

**Table 1. Percentages (%) of Iodine-Stained Starch Granules with Different Polarization Colors[a]**

| starches | blue | fuchsia | dark red | dark blue interior with brown exterior |
|---|---|---|---|---|
| TQ individual granule | 100.0 ± 0.0 c | –[b] | – | – |
| TRS | | | | |
| individual granule | 46.4 ± 1.8 b | – | 37.6 ± 0.9 b | 16.0 ± 2.5 a |
| aggregate granule | 0.3 ± 0.5 a | 23.9 ± 1.4 | 38.2 ± 0.5 b | 37.6 ± 0.6 b |
| elongated granule | – | – | 39.9 ± 2.2 b | 60.1 ± 2.2 c |
| interior hollow granule | – | – | 3.0 ± 0.5 a | 97.0 ± 0.5 d |

[a]Data (mean ± SD) in the same column with different lowercase letters were significantly different ($p < 0.05$, $n = 3$). [b]Data were not detected.

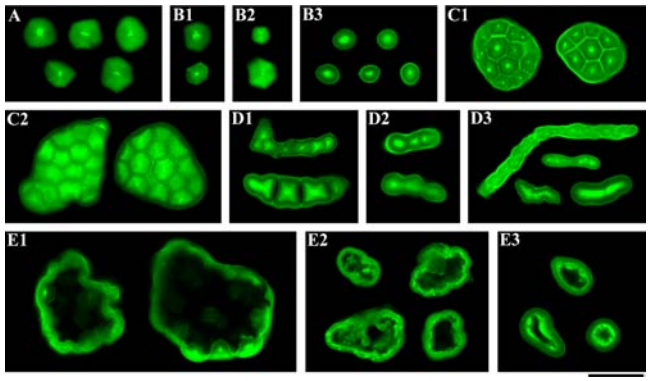


**Figure 3.** CLSM optical sections of starch granules stained with APTS. (A) TQ starch, (B–E) TRS starch, (A, B) individual granule, (C) aggregate granule, (D) elongated granule, (E) interior hollow granule. Scale bar = 10 $\mu$m.

microstructure under the same conditions of laser power and master gain as the TQ starch (data not shown). Figure 3B–E shows the microstructure and fluorescence distribution of TRS starch granules at a lower laser power. For the TRS individual granules, there were three types of amylose distribution pattern (Figure 3B). For the first type, some TRS individual granules had a slightly smaller size than the TQ starch granules with a bright fluorescent dot in the hilum (Figure 3B1). This type of amylose distribution was similar to that of the individual TQ granule. Starch granules with this type of amylose distribution might display a blue polarization color (Figure 2d1). The second type of TRS individual granule exhibited strong fluorescence evenly over the whole granule (Figure 3B2), indicating a high level of amylose distribution in the whole granule, and might display a dark blue interior with brown exterior polarization colors (Figure 2d3). The third type of TRS individual granule had a significantly smaller size and a larger central strongly fluorescent dot compared with the individual TQ granules. This type of starch also had an intense fluorescence around the granule's circumference (Figure 3B3), indicating that the amylose was concentrated mainly around the central hilum and the circumference of granule and might result in the dark red polarization color (Figure 2d2).

For TRS aggregate granules, the CLSM optical sections clearly revealed that the large voluminous and nonangular rounded bodies consisted of many subgranules and a band encircled the entire circumference of the granule (Figure 3C). There were two types of amylose distribution patterns in the TRS aggregate granules. The first type, consisting of most of the aggregate granules, showed intense fluorescent dots in the hila of subgranules and a bright fluorescence around the circumference of the granules and the subgranules (Figure 3C1), indicating that the amylose was distributed mainly in the central hilum regions of the subgranules and the circumference of the granules and subgranules. This type of aggregate granule might display the blue and fuchsia polarization colors (Figure 2e1,e2). The second type of aggregate granule had such strong fluorescence on the subgranules that the microstructure of the granule could not be clearly viewed under the same viewing conditions as the first type of aggregate granule (data not shown). Figure 3C2 shows the amylose distribution of the second type of aggregate granule using a lower laser power than the first type of aggregate granule. The interior of the subgranules exhibited a uniformly intense fluorescence and the band encircling the entire circumference of granules a weak fluorescence. This result suggests that the amylose content, which was largely distributed in the subgranules, was very high in the second type of aggregate granule and would result in a dark red polarization color (Figure 2e3) or a dark blue interior with brown exterior polarization colors (Figure 2e4). The internal structure and amylose distribution of TRS aggregate granules agreed with previous reports on high-amylose rice and maize starch aggregate granules.[15,17]

For TRS elongated granules, there were three types of amylose distribution (Figure 3D). The first type consisted of three or more regular and polyhedral subgranules. These subgranules were arranged in a line and encircled by a band with the hila of subgranules showing strong fluorescence (Figure 3D1). This type of elongated granule had many clear Maltese crosses (Figure 1f1) and showed a dark red polarization color (Figure 2f1). The second type had no clear subgranule inside, but three or more highly fluorescent clear round dots were arranged in a line inside the granule, which might result from the aberrant formation of subgranules (Figure 3D2). This type of elongated granule had some Maltese crosses (Figure 1f1) and might display a dark red polarization color (Figure 2f1). The third type had an intensely fluorescent interior (Figure 3D3). This type of elongated granule might have only a weak birefringence along the edge of the granule or no birefringence (Figure 1f2–f4) and resulted in a dark blue interior with brown exterior polarization colors (Figure 2f2). The different amylose distribution patterns in elongated starch granules have been reported in high-amylose maize.[15,21]

For TRS interior hollow granules, irregular granule shapes could be observed and there were three types of amylose distribution (Figure 3E). Some TRS interior hollow granules had a few subgranules adjacent to the encircling band. These subgranules were polyhedral and had central hila. The hila of subgranules and the encircling band of the granule displayed highly strong fluorescence (Figure 3E1). The second type of interior hollow granule showed a brightly fluorescent band encircling the entire circumference and a weakly fluorescent interior that consisted of very small starch molecules (Figure 3E2). The third type of interior hollow granule exhibited a weakly fluorescent band encircling the entire circumference, but the interior of the band displayed very strong fluorescence (Figure 3E3). These results revealed that the formation of the subgranules inside the TRS interior hollow granules was aberrant, which resulted in no birefringence or very weak birefringence in the encircling band (Figure 1g). The strongly fluorescent band indicated a very high amylose content, which resulted in a dark red polarization color (Figure 2g1) or a dark blue interior with brown exterior polarization colors (Figure 2g2).

These amylose and amylopectin distributions within the TQ and TRS starch granules (Figure 3) indicate that heterogeneity in amylose and amylopectin distribution existed in all starch granules, which agreed with previous reports.[17,19,31] The distribution patterns of amylose and amylopectin (Figure 3) showed that the TQ starch granules were homogeneous, and the TRS starch granules were highly heterogeneous, which agreed with results on high-amylose maize starch.[15]

As previously reported, the fluorescence intensity of APTS-stained starch granules as imaged by CLSM was positively correlated with amylose content.[19,32] To compare the difference in amylose content between heterogeneous starch granules, the fluorescence intensities of the optical sections

**Table 2. Fluorescence Intensities and Gelatinization Temperatures of Starch Granules[a]**

| starches | fluorescence int (arbitrary units)[b] | gelatinization temp (°C)[c] | | |
|---|---|---|---|---|
| | | $T_i$ | $T_m$ | $T_e$ |
| TQ individual granule | 17.3 ± 6.6 a | 64.5 ± 0.5 a | 72.1 ± 0.2 a | 76.3 ± 0.3 a |
| TRS | | | | |
| individual granule | 26.7 ± 15.0 b | 68.9 ± 0.1 b | 75.1 ± 1.1 b | 79.2 ± 1.0 b |
| aggregate granule | 44.4 ± 14.7 c | 72.2 ± 1.1 c | 77.4 ± 1.0 c | 82.3 ± 0.5 c |
| elongated granule | 43.7 ± 18.2 c | 76.5 ± 0.7 d | 80.0 ± 0.1 d | 84.6 ± 0.1 d |
| interior hollow granule | 63.1 ± 16.2 d | –[d] | – | – |

[a]Data (mean ± SD) in the same column with different lowercase letters were significantly different ($p < 0.05$, $n = 60$ for fluorescence intensity and 3 for gelatinization temperature). [b]The intensity of fluorescence was measured in CLSM optical sections of starch granules. [c]Gelatinization temperatures ($T_i$, initial temperature; $T_m$, middle temperature; $T_e$, end temperature) were measured by hot stage microscopy. [d]Data were not detected.

were analyzed under the same photographic conditions, which provided no saturation of the detector for every dot in all starch granules in the present study (Table 2). Compared with the TQ starches, TRS starches showed a significantly higher fluorescence intensity, which corresponded with a higher amylose content.[6,16] For the TRS heterogeneous starch granules, interior hollow granules and individual granules had the highest and lowest fluorescence intensity, respectively. These results indicated that a significant heterogeneity in amylose content existed between TRS heterogeneous starch granules and that the interior hollow granule and individual granule had the highest and lowest amylose content, respectively.

**Gelatinization Properties of Heterogeneous Starch Granules.** Hot stage microscopy is a sensitive in situ method to investigate the simultaneous behaviors of granule swelling, gelatinization temperature, and crystallinity disruption.[20,33,34] The behaviors during TQ and TRS starch gelatinization were investigated using hot-stage microscopy in the present study, and the results are presented in Figure 4. Before gelatinization, the starch granule retained its intact morphology as observed under normal light and showed a bright and clear Maltese cross pattern under polarized light. During gelatinization, the birefringence intensity of the granule faded away when the heating temperature rose above the initial gelatinization temperature, and this loss of birefringence was accompanied by granule swelling. Although TQ and TRS starches had different morphologies, their crystallinity disruption patterns were similar. During heating, the crystallinity disruption started in the hilum region and was accompanied by a small amount of swelling. With increasing heating temperature, the crystallinity disruption and swelling propagated from the inner hilum to the outer region of the starch granule. At this stage, the crystal structure of the outer area of the granule was still undisrupted. During the last stage of the gelatinization process, the crystallinity of the outer region of the granule was disrupted. These crystallinity disruption patterns for TQ and TRS starches were similar to those of various starches with central hila.[34]

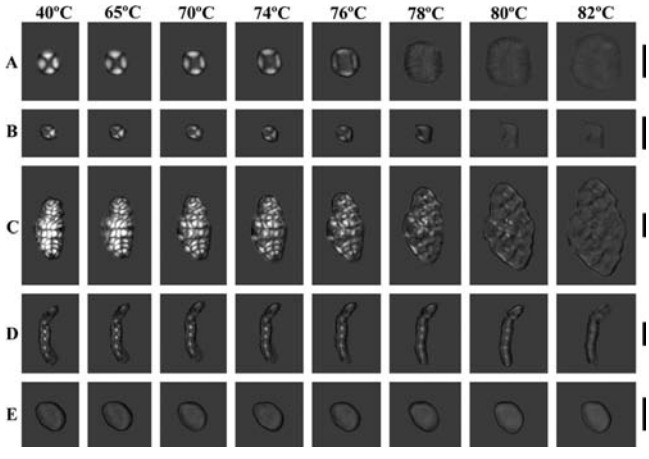


**Figure 4.** Gelatinization of starch granules under polarized light at different temperatures. (A) TQ individual starch granule; (B, C, D, E) TRS individual, aggregate, elongated, and interior hollow starch granule, respectively. Scale bar = 10 μm.

The gelatinization temperatures of TQ and TRS starch granules with the associated changes in birefringence are presented in Table 2.[20] The TRS starches showed significantly higher gelatinization temperatures than the TQ starch. Among the TRS heterogeneous starches, the individual and elongated starch granules had the lowest and highest gelatinization temperatures, respectively. The TRS interior hollow granules exhibited extremely weak or no birefringence, therefore their gelatinization temperature could not be detected in the present study. The gelatinization temperature of starch is related to a variety of factors including granule morphology and size, amylose content, amylopectin structure, and crystallinity type.[35,36] In high-amylose starches, the amylose double helices and the amylose–lipid complex require a high temperature and energy to disrupt and therefore give rise to a high gelatinization temperature.[37] High-amylose maize starch consists of aggregate and elongated granules. The amylose molecules interact and form antiparallel double helices between the adjacent two subgranules, and the continuous outer layer of these fused granules is composed of more amylose.[21] In the present study, the TRS elongated and aggregate granules had higher gelatinization temperatures than the TRS individual granules, indicating that the elongated and aggregate granules had a higher amylose content and gelatinization resistance than the TRS individual granules. These results agreed with the fluorescence intensity of APTS-stained starch granules (Table 2).

The swelling of granules was investigated continuously in situ at 5 °C intervals from 40 to 85 °C during heating (Figure 4) and was calculated as the sectional area swelling percentage compared with ungelatinized granules at 40 °C in Table 3. Compared with that at 40 °C, the granule size of TQ and TRS starch did not significantly change at 50 °C and the size started to increase above 55 °C. Below 75 °C, the granule swelling was not significantly different between TQ and TRS starches. The swelling of TQ starch granules increased markedly above 75 °C

Table 3. Area Swelling Percentages (%) of Starch Granules Measured by Hot Stage Microscopy at Different Temperatures[a]

| | | TRS | | | |
|---|---|---|---|---|---|
| temp (°C) | TQ individual granule | individual granule | aggregate granule | elongated granule | interior hollow granule |
| 45 | 100.3 ± 0.5 aA | 100.2 ± 0.3 aA | 100.2 ± 0.2 aA | 100.1 ± 0.3 aA | 100.2 ± 0.2 aA |
| 50 | 100.5 ± 0.5 aA | 100.3 ± 0.4 aA | 100.3 ± 0.3 aA | 100.4 ± 0.3 aA | 100.4 ± 0.4 aA |
| 55 | 101.0 ± 1.2 aA | 101.0 ± 0.8 aA | 100.6 ± 0.5 aA | 100.9 ± 0.5 aA | 100.7 ± 1.6 aA |
| 60 | 102.2 ± 1.8 aA | 103.0 ± 3.1 aA | 102.0 ± 1.2 aA | 102.6 ± 1.8 aA | 102.3 ± 2.2 aA |
| 65 | 104.8 ± 2.9 aA | 106.3 ± 5.5 aA | 105.0 ± 4.6 aA | 105.5 ± 2.9 aA | 103.9 ± 3.0 aA |
| 70 | 115.1 ± 17.8 aA | 112.5 ± 11.2 aA | 114.7 ± 8.4 aA | 110.0 ± 3.8 aA | 108.3 ± 3.5 bA |
| 75 | 183.0 ± 38.9 bC | 136.7 ± 25.4 bB | 131.3 ± 14.0 bAB | 121.5 ± 9.0 bAB | 111.7 ± 4.4 bA |
| 80 | 396.1 ± 42.0 cE | 230.3 ± 51.2 cD | 179.6 ± 38.9 cC | 140.0 ± 20.2 cB | 117.8 ± 6.4 cA |
| 85 | –[b] | – | 231.6 ± 62.8 dC | 157.5 ± 30.3 dB | 127.7 ± 11.4 dA |

[a]Data (mean ± SD) in the same column with different lowercase letters and in the same line with different capital letters were significantly different ($p < 0.05$, $n = 50$). [b]Data were not detected.

and was significantly higher than that of the TRS starches. Above 75 °C, the swelling of TRS starch granules exhibited significant differences between heterogeneous granules at the same temperature. The swelling of individual and interior hollow granules was the highest and lowest, respectively. Swelling was not measured above 80 °C for TQ starch and TRS individual starch granules and above 85 °C for TRS aggregate, elongated, and interior hollow starch granules because of the deformation, folding, and disruption of the swollen granules at high temperatures. Amylose is considered to contribute to the inhibition of the water absorption and swelling of starch, whereas amylopectin tends to promote these processes. Owing to the decrease of amylopectin content, in high-amylose starch granules, a small quantity of amylose forms the double helical structure through self-interactions. Furthermore, the amylose double helices and the amylose–lipid complex, which only disrupt at high temperature, will strongly inhibit the swelling of high-amylose starch.[37] During gelatinization, the starch chains interact in the crystalline and amorphous regions of the high-amylose starch granule. The interactions of amylose chains (involving amylose–lipid and amylose–amylose) may result in the formation of new crystallites with varying stability in the amorphous and crystalline regions of the granule. In contrast, the interactions of amylopectin chains do not lead to the formation of new crystallites.[38] It has been reported that swelling power is significantly negatively correlated with the amylose content.[39,40] In the present study, TRS starch had a significantly lower level of granule swelling than TQ starch above 75 °C, which might result from the high amylose content, the high level of amylose–lipid complex chains, and the interactions of amylose chains that formed the most stable new crystallites in TRS starch. The granule swelling showed significant differences between TRS heterogeneous starch granules. The individual and interior hollow granules had the highest and lowest granule swelling, respectively, which might have resulted from significantly different morphology, amylose content, and amylose distribution.

**Spatial Distribution of Heterogeneous Starch Granules in Endosperm.** The combined use of resin semithin sections in which starch is retained within cells and KI/$I_2$ staining is a powerful in situ technique to observe the kernel shape, starch morphology, and spatial distribution of granules in the endosperm. On the basis of the visual examination of transverse sections at the midregion of 10 mature kernels of TQ and TRS, there was a clear difference in the kernel shape, starch granule morphology, and spatial distribution of starch granules in the endosperm between TQ and TRS (Figures 5 and 6). For kernel shape, the thickness of kernel was significantly lower in TRS than in TQ, which agreed with the mature kernel appearance.[6] The sections were stained with iodine so that starch granules were specifically stained blue. The degree of filling of the starch was significantly higher in the TQ endosperm than in the TRS endosperm, resulting in the decrease of kernel weight of TRS.[6]

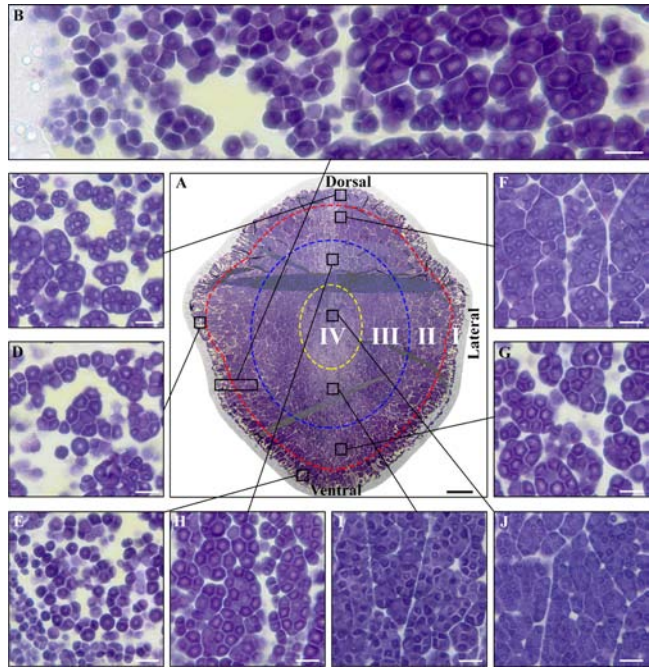


**Figure 5.** Microphotographs of iodine-stained transverse sections at the midregion of TQ mature kernel. (B–J) Showing starch granule morphology in different regions of endosperm. Scale bar = 200 μm for A and 10 μm for B–J.

Regarding the starch granule morphology, TQ showed typical compound starch structure and was homogeneous. The compound starch was composed of many separate subgranules, formed simultaneously within a single amyloplast, but each separate granule had a central hilum (Figure 5). During grain isolation, the compound starch can be ground into separate individual granules. TRS starch showed significant heterogeneity in its morphology as compound, aggregate, elongated, and interior hollow starches. The compound starch can be broken up into individual starch granules, while aggregate granules can remain intact with the surrounding band (Figure 6).

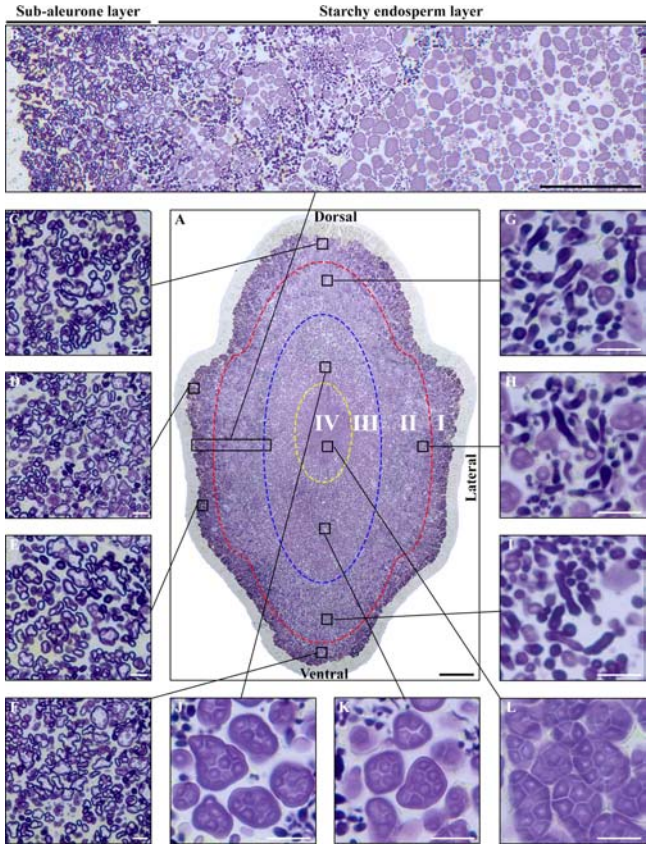


**Figure 6.** Microphotographs of iodine-stained transverse sections at the midregion of TRS mature kernel. (B) Showing the distribution of heterogeneous starch granules in subaleurone layer and starchy endosperm cells, (C–F) showing interior hollow starch granule in region I of endosperm, (G–I) showing elongated starch granule in region II of endosperm, (J, K) showing aggregate starch granule in region III of endosperm, (L) showing individual starch granule in region IV of endosperm. Scale bar = 200 $\mu$m for A, 100 $\mu$m for B, and 10 $\mu$m for C–L.

Regarding the spatial distribution of starch, the compound starch was homogeneously distributed in the whole TQ endosperm, except that the central endosperm cells were packed more tightly than the surrounding endosperm cells (Figure 5). TRS heterogeneous starch granules had a significant regional distribution in the endosperm (Figure 6). The interior hollow starch granules (Figure 6C–F) were mainly distributed in the subaleurone layer (Figure 6, region I), the elongated granules (Figure 6G–I) in the peripheral starchy endosperm cells adjacent to the subaleurone layer (Figure 6, region II), the aggregate granules (Figure 6J,K) in the starchy endosperm cells between the subaleurone layer and the central region of kernel (Figure 6, regions II and III), and the compound starch (Figure 6L) in the central regional of the kernel (Figure 6, region IV).

The spatial distribution of starch granules was mapped within the kernel. The present study suggests that the level of heterogeneity of the TRS starch granules in the endosperm varied remarkably between different regions of the endosperm and became more heterogeneous from the inner to the outer endosperm. The highest level of heterogeneity was observed in the peripheral starchy endosperm adjacent to the subaleurone layer (Figure 6, region II). It is necessary to explain the reason for this spatial distribution of heterogeneous starch granules in the endosperm. In rice, the formation of starch granules starts at the central region of the endosperm and propagates outward to the outer endosperm cells. Consequently, the peripheral endosperm cells are the final parts of the endosperm to be filled with starch granules. This process is completed about 1 month after the initiation of starch granule formation in the central region of the endosperm.[41] This would imply that the greatest level of heterogeneity occurred in TRS starch granules that were deposited late during the development of the kernel, and that the level of heterogeneity was less in granules formed during the early development of the kernel. Cereal storage starches are semicrystalline granules consisting of the two main components: amylose and amylopectin. Their biosynthesis is a complex system involving four classes of enzyme: ADP-glucose pyrophosphorylase, starch synthase, SBE, and starch debranching enzyme. The granule-bound starch synthase is essential for amylose biosynthesis, while amylopectin is synthesized by the combined actions of several isoforms of starch synthase, SBE, and starch debranching enzyme.[42] The SBEs play a pivotal role in amylopectin biosynthesis and occur in cereals in three classes: SBE I, IIa, and IIb.[8] SBE I plays a role in the formation of long chains of amylopectin, SBE IIb generates short chains, and SBE IIa partially, but not fully, supports the functions of SBE I and IIb.[6] The expression of starch-related enzymes varies dramatically between the early and late stages of endosperm development.[43] The granule-bound starch synthase I (GBSS I) is the most important enzyme for amylose biosynthesis in the endosperm. The mRNA of GBSS I increases with the development of rice endosperm,[44] and the activities of both SBE I and IIb are inhibited in the middle and late stages of TRS kernel development.[6] The inhibition of SBE I/IIb not only increases amylose content but also changes the structure of starch granules, leading to a broad population of morphological types. The spatial distribution of heterogeneous starch granules has suggested that the individual granule (compound starch) was synthesized at the early stage of endosperm development, the aggregate and elongated granules at the middle stage, and the interior hollow granules at the late stage. The formation and spatial distribution of these heterogeneous starch granules result from changes in the activities of SBEs during kernel development.

In conclusion, a range of microscopic techniques have been used to observe and characterize the morphology and structure of starch granules isolated from the mature kernels of high-amylose rice (TRS) and its wild-type rice (TQ). The mature kernels have been mapped in situ using light microscopy to identify the spatial distribution of starch granules in the endosperm. These studies have revealed that TQ starch granules were homogeneous in their morphology, structure, and spatial distribution in the endosperm. In contrast, TRS starch showed significant heterogeneity in morphology consisting of individual, aggregate, elongated, and interior hollow granules. The polarization colors of iodine-stained starch granules and fluorescence intensities of APTS-stained starch granules indicated that the individual and interior hollow granules had the lowest and highest amylose contents, respectively, among the TRS heterogeneous starch granules. The results of hot-stage microscopy showed that the individual and interior hollow granules had the lowest and highest resistance to heating, respectively. The kernel sections revealed that the individual granules existed mainly in the middle of the endosperm, the interior hollow granules in the subaleurone layer cells, the elongated granules in the peripheral starchy endosperm cells adjacent to the subaleurone layer, and the

aggregate granules in the starchy endosperm cells between the subaleurone layer and the middle of the endosperm. These results suggest that the morphology and structure of TRS starch granules and their spatial distribution in endosperm were all heterogeneous. This heterogeneity might have resulted during kernel development.

## AUTHOR INFORMATION


### Corresponding Author

*College of Bioscience and Biotechnology, Yangzhou University, Yangzhou 225009, China. Tel: +86 514 87997217. E-mail: cxwei@yzu.edu.cn.



### Funding

This study was financially supported by grants from the Ministry of Science and Technology of China (2012CB944803), the National Natural Science Foundation of China (31270221), the Qing Lan Project of Jiangsu Province, the Talent Project of Yangzhou University, the Innovation Program for Graduates of Jiangsu Province (CXZZ13_0895), and the Priority Academic Program Development of Jiangsu Higher Education Institutions.


### Notes

The authors declare no competing financial interest.

## ABBREVIATIONS USED

APTS, 8-amino-1,3,6-pyrenetrisulfonic acid; CLSM, confocal laser scanning microscope; RS, resistant starch; SBE, starch branching enzyme; TQ, Te-qing (wild type rice cultivar); TRS, transgenic RS rice line

## REFERENCES


(1) Englyst, H. N.; Kingman, S. M.; Cummings, J. H. Classification and measurement of nutritionally important starch fractions. *Eur. J. Clin. Nutr.* **1992**, *46*, S33−S50.

(2) Sang, Y. J.; Bean, S.; Seib, P. A.; Pedersen, J.; Shi, Y. C. Structure and fuctional properties of sorghum starches differing in amylose content. *J. Agric. Food Chem.* **2008**, *56*, 6680−6685.

(3) Nugent, A. P. Health properties of resistant starch. *Nutr. Bull.* **2005**, *30*, 27−54.

(4) Li, L.; Jiang, H. X.; Campbell, M.; Blanco, M.; Jane, J. L. Characterization of maize amylose-extender (*ae*) mutant starches. Part I: relationship between resistant starch contents and molecular structures. *Carbohydr. Polym.* **2008**, *74*, 396−404.

(5) Regina, A.; Bird, A.; Topping, D.; Bowden, S.; Freeman, J.; Barsby, T.; Kosar-Hashemi, B.; Li, Z. Y.; Rahman, S.; Morell, M. High-amylose wheat generated by RNA interference improves indices of large-bowel health in rats. *Proc. Natl. Acad. Sci. U.S.A.* **2006**, *103*, 3546−3551.

(6) Zhu, L. J.; Gu, M. H.; Meng, X. L.; Cheung, S. C. K.; Yu, H. X.; Huang, J.; Sun, Y.; Shi, Y. C.; Liu, Q. Q. High-amylose rice improves indices of animal health in normal and diabetic rats. *Plant Biotechnol. J.* **2012**, *10*, 353−362.

(7) Kang, H. J.; Hwang, I. K.; Kim, K. S.; Choi, H. C. Comparative structure and physicochemical properties of Ilpumbyeo, a high-quality japonica rice, and its mutant, Suweon 464. *J. Agric. Food Chem.* **2003**, *51*, 6598−6603.

(8) Carciofi, M.; Blennow, A.; Jensen, S. L.; Shaik, S. S.; Henriksen, A.; Buléon, A.; Holm, P. B.; Hebelstrup, K. H. Concerted suppression of all starch branching enzyme genes in barley produces amylose-only starch granules. *BMC Plant Biol.* **2012**, *12*, 223.

(9) Slade, A. J.; McGuire, C.; Loeffler, D.; Mullenberg, J.; Skinner, W.; Fazio, G.; Holm, A.; Brandt, K. M.; Steine, M. N.; Goodstal, J. F.; Knauf, V. Development of high amylose wheat through TILLING. *BMC Plant Biol.* **2012**, *12*, 69.

(10) Jiang, H. X.; Campbell, M.; Blanco, M.; Jane, J. L. Characterization of maize amylose-extender (*ae*) mutant starches: Part II. structures and properties of starch residues remaining after enzymatic hydrolysis at boiling-water temperature. *Carbohydr. Polym.* **2010**, *80*, 1−12.

(11) Regina, A.; Kosar-Hashemi, B.; Ling, S.; Li, Z. Y.; Rahman, S.; Morell, M. Control of starch branching in barley defined through differential RNAi suppression of starch branching enzyme IIa and IIb. *J. Exp. Bot.* **2010**, *61*, 1469−1482.

(12) Kim, K. S.; Hwang, H. G.; Kang, H. J.; Hwang, I. K.; Lee, Y. T.; Choi, H. C. Ultrastructure of individual and compound starch granules in isolation preparation from a high-quality, low-amylose rice, Ilpumbyeo, and its mutant, G2, a high-dietary fiber, high-amylose rice. *J. Agric. Food Chem.* **2005**, *53*, 8745−8751.

(13) Wellner, N.; Georget, D. M. R.; Parker, M. L.; Morris, V. J. In situ Raman microscopy of starch granule structures in wild type and *ae* mutant maize kernels. *Starch/Stärke* **2011**, *63*, 128−138.

(14) Liu, D.; Parker, M. L.; Wellner, N.; Kirby, A. R.; Cross, K.; Morris, V. J.; Cheng, F. Structural variability between starch granules in wild type and in *ae* high-amylose mutant maize kernels. *Carbohydr. Polym.* **2013**, *97*, 458−468.

(15) Cai, C. H.; Zhao, L. X.; Huang, J.; Chen, Y. F.; Wei, C. X. Morphology, structure and gelatinization properties of heterogeneous starch granules from high-amylose maize. *Carbohydr. Polym.* **2014**, *102*, 606−614.

(16) Wei, C. X.; Xu, B.; Qin, F. L.; Yu, H. G.; Chen, C.; Meng, X. L.; Zhu, L. J.; Wang, Y. P.; Gu, M. H.; Liu, Q. Q. C-type starch from high-amylose rice resistant starch granules modified by antisense RNA inhibition of starch branching enzyme. *J. Agric. Food Chem.* **2010**, *58*, 7383−7388.

(17) Wei, C. X.; Qin, F. L.; Zhu, L. J.; Zhou, W. D.; Chen, Y. F.; Wang, Y. P.; Gu, M. H.; Liu, Q. Q. Microstructure and ultrastructure of high-amylose rice resistant starch granules modified by antisense RNA inhibition of starch branching enzyme. *J. Agric. Food Chem.* **2010**, *58*, 1224−1232.

(18) Evans, A.; McNish, N.; Thompson, D. B. Polarization colors of lightly iodine-stained maize starches for amylose-extender and related genotypes in the W64A inbred line. *Starch/Stärke* **2003**, *55*, 250−257.

(19) Blennow, A.; Hansen, M.; Schulz, A.; Jørgensen, K.; Donald, A. M.; Sanderson, J. The molecular deposition of transgenically modified starch in the starch granule as imaged by functional microscopy. *J. Struct. Biol.* **2003**, *143*, 229−241.

(20) Konik-Rose, C. M.; Moss, R.; Rahman, S.; Appels, R.; Stoddard, F.; McMaster, G. Evaluation of the 40 mg swelling test for measuring starch functionality. *Starch/Stärke* **2001**, *53*, 14−20.

(21) Jiang, H. X.; Horner, H. T.; Pepper, T. M.; Blanco, M.; Campbell, M.; Jane, J. L. Formation of elongated starch granules in high-amylose maize. *Carbohydr. Polym.* **2010**, *80*, 533−538.

(22) Yamamori, M.; Quynh, N. T. Differential effects of Wx-A1,-B1 and-D1 protein deficiencies on apparent amylose content and starch pasting properties in common wheat. *Theor. Appl. Genet.* **2000**, *100*, 32−38.

(23) Gallant, D. J.; Bouchet, B.; Baldwin, P. M. Microscopy of starch: evidence of a new level of granule organization. *Carbohydr. Polym.* **1997**, *32*, 177−191.

(24) Pérez, S.; Bertoft, E. The molecular structures of starch components and their contribution to the architecture of starch granules: a comprehensive review. *Starch/Stärke* **2010**, *62*, 389−420.

(25) Seckinger, H. L.; Wolf, M. J. Polarization colors of maize starches varying in amylose content and genetic background. *Starch/Stärke* **1966**, *18*, 1−5.

(26) Evans, A.; Thompson, D. B. Resistance to $\alpha$-amylase digestion in four native high-amylose maize starches. *Cereal Chem.* **2004**, *81*, 31−37.

(27) John, M.; Schmidt, J.; Kneifel, H. Iodine-maltosaccharide complexes: relation between chain-length and colour. *Carbohydr. Res.* **1983**, *119*, 254−257.

(28) Knutson, C. A. Evaluation of variations in amylose-iodine absorbance spectra. *Carbohydr. Polym.* **1999**, *42*, 65−72.

(29) Saibene, D.; Seetharaman, K. Segmental mobility of polymers in starch granules at low moisture contents. *Carbohydr. Polym.* **2006**, *64*, 539−547.
(30) French, D. Organization of starch granules. In *Starch: Chemistry and Technology*; Whistler, R. L., Bemiller, J. N., Paschall, E. F., Eds.; Academic Press: New York, 1984; pp 183−247.
(31) Glaring, M. A.; Koch, C. B.; Blennow, A. Genotype-specific spatial distribution of starch molecules in the starch granule: a combined CLSM and SEM approach. *Biomacromolecules* **2006**, *7*, 2310−2320.
(32) Chen, P.; Yu, L.; Simon, G.; Petinakis, E.; Dean, K.; Chen, L. Morphologies and microstructures of corn starches with different amylose-amylopectin ratios studied by confocal laser scanning microscope. *J. Cereal Sci.* **2009**, *50*, 241−247.
(33) Cai, C. H.; Cai, J. W.; Zhao, L. X.; Wei, C. X. *In situ* gelatinization of starch using hot stage microscopy. *Food Sci. Biotechnol.* **2014**, *23*, 15−22.
(34) Cai, C. H.; Wei, C. X. In situ observation of crystallinity disruption patterns during starch gelatinization. *Carbohydr. Polym.* **2013**, *92*, 469−478.
(35) Richardson, P. H.; Jeffcoat, R.; Shi, Y. C. High-amylose starches: from biosynthesis to their use as food ingredients. *MRS Bull.* **2000**, *25*, 20−24.
(36) Lindeboom, N.; Chang, P. R.; Tyler, R. T. Analytical, biochemical and physicochemical aspects of starch granule size, with emphasis on small granule starches: a review. *Starch/Stärke* **2004**, *56*, 89−99.
(37) Shi, Y. C.; Capitani, T.; Trzasko, P.; Jeffcoat, R. Molecular structure of a low-amylopectin starch and other high-amylose maize starches. *J. Cereal Sci.* **1998**, *27*, 289−299.
(38) Hoover, R.; Manuel, H. The effect of heat−moisture treatment on the structure and physicochemical properties of normal maize, waxy maize, dull waxy maize and amylomaize V starches. *J. Cereal Sci.* **1996**, *23*, 153−162.
(39) Hermansson, A. M.; Svegmark, K. Developments in the understanding of starch functionality. *Trends Food Sci. Technol.* **1996**, *7*, 345−353.
(40) Tester, R. F.; Morrison, W. R. Swelling and gelatinization of cereal starches. I. Effects of amylopectin, amylose, and lipids. *Cereal Chem.* **1990**, *67*, 551−557.
(41) Hoshikawa, K. Anthesis, fertilization and development of caryopsis. In *Science of the Rice Plant. Vol. 1 Morphology*; Matsuo, T., Hoshikawa, K., Eds.; Food and Agriculture Policy Research Center: Tokyo, 1993; pp 339−376.
(42) Tian, Z. X.; Qian, Q.; Liu, Q. Q.; Yan, M. X.; Liu, X. F.; Yan, C. J.; Liu, G. F.; Gao, Z. Y.; Tang, S. Z.; Zeng, D. L.; Wang, Y. H.; Yu, J. M.; Gu, M. H.; Li, J. Y. Allelic diversities in rice starch biosynthesis lead to a diverse array of rice eating and cooking qualities. *Proc. Natl. Acad. Sci. U.S.A.* **2009**, *106*, 21760−21765.
(43) Ohdan, T.; Francisco, P. B.; Sawada, T.; Hirose, T.; Terao, T.; Satoh, H.; Nakamura, Y. Expression profiling of genes involved in starch synthesis in sink and source organs of rice. *J. Exp. Bot.* **2005**, *56*, 3229−3244.
(44) Dian, W.; Jiang, H.; Wu, P. Evolution and expression analysis of starch synthase III and IV in rice. *J. Exp. Bot.* **2005**, *56*, 623−632.

erythrocytes and lower plasma α-tocopherol contents with LC-PUFA enriched formulas.[7,11] Preterm infants are most likely more susceptible to peroxidation, therefore these findings cannot be extrapolated to term infants. Moreover, other studies in preterm infants showed no effect of LC-PUFA enrichment on vitamin E levels or markers of oxidative stress (i.e., total plasma antioxidant capacity (PAC), serum malondialdehyde (MDA), total peroxides and total antioxidant capacity (TAC)).[9,10] Interestingly, even antioxidant effects of n-3 fatty acids or LC-PUFA were reported in preterm infants receiving parenteral nutrition enriched with n-3 LC-PUFA plus added vitamin E, compared to a standard soybean-oil-based lipid emulsion or getting LC-PUFA enriched compared to not-enriched formulas.[8,14]

The aim of this study was to assess the ratio of vitamin E content to estimated need. Our findings were based on the unsatured fatty acid content in a large sample of commercially available formulas on the German market ($n$ = 31 LC-PUFA enriched; $n$ = 29 not LC-PUFA enriched). This ratio was then set as a risk indicator for oxidative damage primarily in the formulas themselves and which, theoretically, might have consequences for the antioxidant status of the infants. For risk assessment, we deemed the whole spectrum of vitamin E as an important antioxidant with respect to the prevention of lipid peroxidation. The whole spectrum of fatty acids (the potential oxidants) was weighed with regard to the number of double bonds, and this represented the estimated vitamin E need.

In addition, to figure out potential differences between LC-PUFA enriched formulas and not enriched formulas, we used breast milk and its ratio of vitamin E content to vitamin E need as a reference.

The present analysis was conducted in the context of the nutritional intervention trial on complementary feeding (i.e., PINGU), which is entitled "Poly unsaturated fatty acids in child nutrition—A German multimodal optimization study".

## MATERIALS AND METHODS

**PINGU Study Design and Milk Sampling.** The current investigation is part of the PINGU-study, a double-blinded randomized controlled intervention trial conducted in 2010—2013 in the region of Dortmund, Germany. The primary objective of PINGU was to examine the effects of an optimization of the n-3 PUFA supply in commercial complementary food via rapeseed oil rich in ALA, the precursor of endogenous DHA synthesis, or DHA-rich fish (salmon) on infant DHA status and functional outcomes in the second 6 months of life. The PINGU study was partially double blinded; that is, in the corn oil (control) and rapeseed oil group, the affiliation was blinded, whereas the ingredient fish can be identified olfactorily.[15]

In total, 214 women (median age: 33 yrs) and their infants were enrolled, of which 205 kept the first study appointment (T0) at the end of the child's eighth week of life. The aim was to mirror the early period of exclusively milk feeding. T0 appointments took place from June 2011 to January 2013. From the age of 8 weeks onward, infants' nutrition was assessed by daily weighed dietary records kept by mothers who also collected formula packages. Nine formula brands were reported to be used. Upon request, producers provided product samples of almost their entire assortments of formulas for term infants offered on the German market. A total of $n$ = 60 different formula were supplied, of which $n$ = 31 were LC-PUFA enriched (FM(+)) and $n$ = 29 were not LC-PUFA enriched (FM(−)).

Exclusively and partially breastfeeding mothers ($n$ = 150) were instructed to take three milk samples during one nursing (at the beginning, in the middle, and at the end; 2—3 mL at each point) on the day before the T0 appointment. They then stored the samples in their household freezer overnight before transporting them on ice to the FKE. Samples were stored at −80 °C and shipped on dry ice for further analyses (fatty acids: Dr. von Hauner'sches Kinderspital, Ludwig-Maximilians-University Munich, Germany; vitamin E: Institute of Nutrition, Friedrich Schiller University Jena, Jena, Germany). Valid analyses of both fatty acids and vitamin E were available in 118 breast milk (BM) samples.

**Chemicals.** For fatty acid analysis: The standard mixture of fatty acid methyl esters was provided by GLC569, Nuchek (Elysian, U.S.A.). Methanolic hydrogen chloride (HCl) was purchased from Sigma-Aldrich (Deisenhofen, Germany) and diluted with methanol from J.T Baker (via CLN, Freising, Germany) (0.6 M). Hexan was also provided by J.T. Baker (via CLN, Freising, Germany). Butylated hydroxytoluene was purchased from Fluka (Deisenhofen, Germany) and tripentadecanoin was provided by Avanti Polar Lipids (Alabaster, U.S.A.).

For vitamin E analysis: Stock solutions of α-, β-, γ-, δ-tocopherol were obtained from Calbiochem, Merck (Darmstadt, Germany) ($c$ = 1 mg/mL), α-, β-, γ-, δ-tocotrienol were from Davos Life Sciences (Singapore, Singapore) ($c$ = 1 mg/mL) and α-tocopherol acetate was from Sigma-Aldrich (Taufkirchen, Germany) ($c$ = 2 mg/mL). Absolute ethanol was purchased from Merck KGaA (Darmstadt, Germany) and $n$-hexane from VWR International GmbH (Darmstadt, Germany). Methyl-*tert*-butyl ether was provided by Th. Geyer GmbH & Co KG (Renningen, Germany).

**Fatty Acid Analysis.** The procedure for milk fatty acid analysis was adapted from the method described by Lepage and Roy for various matrices.[16] Mixtures of BM (a combination of equal measures of fore milk and hind milk) as well as ready-to-feed solutions of formulas were prepared by shaking at room temperature. Twenty microliters of the prepared samples was then transferred into a 4 mL brown glass vial and dissolved in a mixture of 1.9 mL methanolic HCl (0.6 M) and 0.3 mL hexane (containing 200 mg/L butylated hydroxytoluene and 104 mg/L tripentadecanoin as radical scavenger and internal standard, respectively).

The closed vial was heated to 100 °C for 60 min to transfer fatty acids into their methyl esters. After cooling, 0.5 mL water was added, and after mixing, the reaction vial was centrifuged (5 min, 1500 g) to achieve separation between a lower methanol/water phase and an upper hexane phase containing the methyl esters. A 0.1 mL aliquot of the hexane phase was diluted with 0.5 mL hexane and stored at −20 °C until gas chromatographic analysis. For gas chromatography (GC), an Agilent 7890 GC (Agilent, Waldbronn, Germany) equipped with a programmable temperature vaporizer (Gerstel, Mühlhein, Germany), a BPX-70 column (length 50 m, inner diameter 0.25 mm, SGE, Milton Keynes, U.K.), and a flame ionization detector was used. The gas chromatograph was operated under Agilent ChemStation Rev B.04 software, which was also used for chromatographic data evaluation. The injection volume and injector temperature were set to 3 μL and 30 °C, respectively. The sample was vaporized by increasing the injector temperature to 300 °C at a rate of 12°/s. The temperature program of the gas

Table 1. $\alpha$-D-Tocopherol Equivalent Calculation[13,15]

| | | milk type | | |
|---|---|---|---|---|
| | | formulas | | breast milk |
| vitamin E | factor | scenario 1 | scenario 2 | |
| $\alpha$-D-tocopherol acetate[a] | 0.91 | x | - | n. c. |
| $\alpha$-D,L tocopherol acetate[a] | 0.67 | - | x | n. c. |
| $\alpha$-D,L-tocopherol[a] | 0.74 | - | x | n. c. |
| $\alpha$-D-tocopherol[a] | 1 | x | - | x |
| $\beta$-tocopherol | 0.5 | x | x | x |
| $\gamma$-tocopherol | 0.25 | x | x | x |
| $\delta$-tocopherol | 0.01 | x | x | <d. l. |
| $\alpha$-tocotrienol | 0.303 | x | x | <d. l. |
| $\beta$-, $\gamma$-, $\delta$-tocotrienol | not considered | x | x | <d. l. |

x = included, n. c. = not contained, d. l. = detection limit. [a]Allowed vitamin E isomers in formulas.

chromatography started at 50 °C and increased after a 0.5 min delay with a rate of 40°/min to 150 °C, 6°/min to 180 °C, and 1.8°/min to 215 °C. The initial flow of the carrier gas, helium, was set to 1.5 mL/min. After 23 min of chromatography, the flow was increased to 1.7 mL/min.

Fatty acid methyl esters were identified by comparing retention times of sample peaks with the retention times of a methyl ester standard mixture. This standard was also used to determine response factors of individual fatty acids relative to pentadecanoic acid methyl ester. The experimental setup enabled estimation of the fat content (weight/volume) by summation of the analyzed fatty acids and determination of percentage contributions (% weight/weight) of fatty acids with chain lengths from 8 to 24 carbon atoms to total milk fatty acids.

**Vitamin E Analysis.** Simultaneously, we determined $\alpha$-tocopherol acetate, tocopherols, and tocotrienols from breast milk and infant formulas. The second human milk sample collected (in the middle of one nursing) was used for vitamin E analyses by HPLC (high-performance liquid chromatography) according to the modified method reported by Moltó-Puigmartí et al.[17] After thawing the breast milk samples in a water bath at 30 °C and homogenization in an ultrasonic bath for 1 min, 100 $\mu$L of ethanolic solution containing $\alpha$-tocopherol acetate (0.1 mg/mL) was added as internal standard to 500 $\mu$L of milk. Absolute ethanol (1000 $\mu$L) was added for deproteinization. After vortexing for 1 min, samples were left to rest for 10 min and then mixed with 1000 $\mu$L of *n*-hexane, followed by another 5 min incubation, and again 1 min of vortex-mixing. After centrifugation for 5 min (3700g) at room temperature, the hexanoic layer was removed. The remaining lower layer was extracted again twice. The combined extracts were evaporated under nitrogen at 30 °C until dry. The residue was then resuspended in 500 $\mu$L *n*-hexane/methyl-*tert*-butyl ether (98 + 2 v/m), vortex-mixed for 30 s, and centrifuged (14 000 rpm) at room temperature 2 min. An aliquot of this solution (150 $\mu$L) was transferred into an amber vial, and 20 $\mu$L was injected into the HPLC system.

For infant formula analysis, 500 $\mu$L of the formula prepared as ready-to-feed was used following the analogous procedure as for breast milk. The following steps were different to the breast milk preparation: the extraction was conducted only once; the residue was redissolved in 1000 $\mu$L *n*-hexane/methyl-*tert*-butyl ether (98 + 2 v/m). As the internal standard $\alpha$-tocopherol acetate (used for breast milk) is a common food additive in formulas, in these cases, $\alpha$-tocopherol acetate was measured separately assuming a loss of 3% and then used as an additive internal standard in the main measurement.

HPLC was performed according to a procedure modified from that of Balz et al. with a normal phase HPLC column, Eurospher 100 DIOL; 250 × 4.0 mm; 5 $\mu$m (Knauer, Berlin, Germany), and *n*-hexane/methyl-*tert*-butyl ether (98 + 2 v/m) as mobile phase (isocratic).[18] The vitamin E forms are eluted in the order: $\alpha$-tocopherol acetate, $\alpha$-tocopherol, $\alpha$-tocotrienol, $\beta$-tocopherol, $\gamma$-tocopherol, $\beta$-tocotrienol, $\gamma$-tocotrienol, $\delta$-tocopherol, and $\delta$-tocotrienol. The temperature and flow were set at 35 °C and 1.5 mL/min, respectively. The whole separation procedure took 45 min. For fluorescence detection (Merck-Hitachi, Darmstadt, Germany), the wavelengths $\lambda_{EX}$ = 292 nm and $\lambda_{EM}$ = 330 nm were used. A triple determination was conducted.

For vitamin E quantification, five dilutions of stock solutions of $\alpha$-, $\beta$-, $\gamma$-, $\delta$-tocopherol, $\alpha$-, $\beta$-, $\gamma$-, $\delta$-tocotrienol ($c$ = 1 mg/mL) and $\alpha$-tocopherol acetate (c = 2 mg/mL) were prepared to obtain the calibration curves. Dilutions ranged from 1:100 for $\alpha$-tocopherol acetate to 1:20 000 for $\delta$-tocotrienol. The mean recovery rate was 87% in breast milk and 92% in formulas.

The limits of detection (LOD) ranged from 0.28 $\mu$g of $\alpha$-tocopherol in 100 mL of breast milk to 6.01 $\mu$g of $\alpha$-tocopherol acetate in 100 mL of formula. The limit of quantification (LOQ) amounted to 3.3-fold of the respective LOD values.

**Pentaenoic Fatty Acid Equivalents (PE) and Arachidonic Acid Equivalents (AE).** It is suggested that the vitamin E demand to protect fatty acids from oxidation is related to their degree of unsaturation, that is, 0.06, 0.4, 0.6, 0.8, 1.0, 1.2 mg of $\alpha$-D-tocopherol equivalents ($\alpha$-TE) per gram of monoenoic, dienoic, trienoic, tetraenoic, pentaenoic, and hexaenoic fatty acids, respectively.[19,20] As 1 mg $\alpha$-TE is required for 1 g pentaenoic fatty acids, we calculated "pentaenoic fatty acid equivalents" (PE) on the basis of the whole analyzed fatty acid spectrum to express the individual oxidative potential of formula and breast milk samples.

The Commission Directive 2006/141/EC on infant formulas and follow-on formulas and amending Directive 1999/21/EC stated a calculation for an optimal $\alpha$-TE/unsaturated fatty acid ratio based on the main polyunsaturated fatty acids: 0.5, 0.75, 1.0, 1.25, and 1.5 mg $\alpha$-TE per g linoleic (18:2 n-6), $\alpha$-linolenic (18:3 n-3), arachidonic (20:4 n-6), eicosapentaenoic (20:5 n-3), and docosahexaenoic acid (22:6 n-3) respectively.[2] We refer to the results of this approach to calculating vitamin E needs as "arachidonic acid equivalents (AE)".

**α-D-Tocopherol Equivalents (α-TE).** In accordance with the conversion factors of the German Nutrition Society (DGE), we expressed vitamin E activity of the vitamin E isomers as α-D-tocopherol equivalent (α-TE).[19] Each of the analyzed formulas contained added vitamin E. Four forms are allowed by law: 2 α-tocopherol forms (α-**D**-tocopherol—also naturally occurring, e.g., in plant oils—and α-**D,L**-(= *all-rac)* tocopherol) and 2 α-tocopherol **acetate** forms (α-**D**-tocopherol acetate and α-**D,L**-(= *all-rac)* tocopherol acetate).[2] As the list of ingredients provided no information about the exact vitamin E variants and our method of vitamin E analysis allowed no distinction between D- and D,L-isomers, we calculated two scenarios on the basis of the different antioxidant activities of the vitamin E isomers. The naturally occurring α-D-forms (RRR) have higher biological activity than the *all-rac* forms. This is because gut absorption of naturally occurring α-D-forms is highest among all eight possible isomers resulting from the three chiralic C-atoms. In contrast, the *all-rac* forms are a racemic mixture of all eight possible isomers in equimolar concentrations.[21,22] Scenario 1 (best antioxidant scenario) included α-D-tocopherol acetate and α-D-tocopherol, scenario 2 (worst antioxidant scenario) included the *all-rac* forms (α-D,L-tocopherol acetate and α-D,L-tocopherol) (see Table 1). Conversion factors of the *all-rac* forms were taken from Belitz et al. 2001.[23]

**Statistical Analysis.** All statistical tests were performed using SAS procedures (version 9.2, Statistical Analysis Systems, Cary, NC, U.S.A.). As most variables were not normally distributed, Wilcoxon tests were generally used to identify differences between LC-PUFA-enriched formulas (FM(+)) and standard formulas (FM(−)), between FM(+) and breast milk (BM) and between FM(−) and BM concerning the three topics: fatty acid composition, vitamin E content, and α-TE/unsaturated fatty acid index ratios.

## RESULTS AND DISCUSSION

**Formulas and Mothers' Characteristics.** The formulas tested comprised a balanced proportion of infant formulas and follow-on formulas, and of LC-PUFA enriched ($n$ = 31) and not enriched ($n$ = 29) formulas (Figure 1). Infant formulas were more often LC-PUFA enriched than follow-on formulas, using fish oil and, in 8 cases, also fungal oil (*Mortierella alpine*).

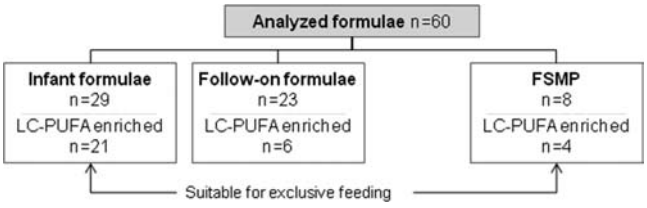


**Figure 1.** Specification of the analyzed formulas ($n$ = 60), LC-PUFA = long chain polyunsaturated fatty acids, FSMP = foods for special medical purposes (e.g., in the case of diarrhea).

Maternal characteristics of PINGU participants, of which breast milk samples were available and analyzed ($n$ = 118), are shown in Table 2.

**Unsaturated Fatty Acid Equivalents (PE, AE) and Fatty Acids Profile.** Interestingly, our results showed that PE and AE (i.e., the calculated relative vitamin E need) did not differ between FM(+) and FM(−) (Table 3), although one might assume higher values resulting from use of fish and fungal oil in the recipes for FM(+) by the producers. This finding can be explained by our consideration of the whole fatty acid profile. In fact, n-3 LC-PUFA (i.e., EPA and DHA) were markedly higher in FM(+), but total n-3 PUFA was only moderately higher, because ALA, the main n-3 fatty acid, was similar in both kinds of formulas. Similarly applicable for n-6 fatty acids, FM(+) showed higher values of n-6 LC-PUFA (AA in particular (Table 3)) but lower total n-6 PUFA values as a result of lower LA values (the main n-6 fatty acid in formulas). Thus, total PUFA tends to be higher in FM(−) (which is significant for percentage values). Total fatty acids, SFA, and MUFA contents, indeed, did not differ between FM(+) and FM(−).

**Table 2. Maternal Characteristics of PINGU Participants of Which Breast Milk Samples Were Available and Analyzed ($n$ = 118)**

| maternal characteristic | mean | SD |
|---|---|---|
| age (years) | 33 | 5 |
| gestational age (weeks) | 40 | 4 |
| body mass index ($n$ = 117, 2 months *pp*) | 26 | 5 |
| primiparous (%, yes/no) | 57/43 | |
| university entrance diploma (%, yes/no) | 59/41 | |
| SES (%, low/medium/high, $n$ = 113)[a] | 3/34/64 | |
| smoker (%, yes/no)[b] | 5/95 | |

[a]SES = Socioeconomic status, defined according to maternal level of school education, maternal level of professional education, and household income before pregnancy. [b]At least 1 cigarette/d.

In BM, higher values for SFA and lower values for both n-6 and n-3 PUFA, LA, and ALA were found than in FM(+) or FM(−) (Table 3). In contrast, the sums of n-6 LC-PUFA and n-3 LC-PUFA were markedly higher in BM, which was only partly explained by differences in AA and EPA. DHA values were similar in FM(+) and BM. Main reason for differences in LC-PUFA was the contribution of further LC-PUFA in BM, for example, 20:3 n-6 LC-PUFA and 22:5 n-3 LC-PUFA (data not shown). Ratios of LA/ALA were lower in both types of formulas compared with BM, the ratio of n-6/n-3 PUFA of BM was located in between the two types of formulas, and n-6/n-3 LC-PUFA ratio was similar in FM(−) and BM, and about twice as high as in FM(+). PE and AE were generally higher in both of the FM types than in BM (Table 3).

**α-Tocopherol Equivalents (α-TE) and Vitamin E Profile.** FM(−) showed higher α-TE and total vitamin E (sum of all vitamers) values than FM(+) in both vitamin E scenarios (Table 4), that is, even when assuming exclusively the *all-rac* vitamin E forms were used for supplementation. Obviously, and in contrast to what could be expected, producers used less α-tocopherol acetate on average in their recipes for FM(+) than for FM(−). However, the amounts of vitamin E content in all formulas were in accordance with the European legislation. Nonetheless, most analyzed values were below the values indicated by label declaration.[2]

Formulas contained the whole spectrum of naturally occurring vitamin E forms (Table 4) (predominantly α- and γ-tocopherol), without differences between FM(+) and FM(−). In BM, only tocopherols were detected—mainly α-tocopherol—in similar proportions as in FM. Compared to BM, both formulas showed markedly higher vitamin E contents caused by the supplementation with the synthetic α-tocopherol acetate.

In fact, BM as a natural "product" is individually composed and depends on the mother's diet. Although no clear

**Table 3. Fatty Acid Composition (in mg/100 mL and in % of Total Fatty Acids) of Enriched Formulae (FM(+), $n$ = 31), Not Enriched Formulae (FM(−), $n$ = 29) and Breast Milk (BM, $n$ = 118)**

| | | FM (+) | SD | FM(−) | SD | BM | SD |
|---|---|---|---|---|---|---|---|
| total fatty acids | g/100 mL | 2.69 | ±0.39 | 2.81 | ±0.67 | 2.72 | ±0.79 |
| FA | | | | | | | |
| SFA | mg | 1006.71 | ±217.46 | 986.18 | ±213.65 | 1186. 87[b,c] | ±347.15 |
| | % | 37.45 | ±5.85 | 35.42 | ±3.75 | 43.87[b,c] | ±4.84 |
| MUFA | mg | 1162.12 | ±198.43 | 1242.30 | ±332.4 | 1152.05 | ±371.92 |
| | % | 43.31 | ±4.29 | 43.99 | ±3.32 | 42.07 | ±3.88 |
| PUFA | | | | | | | |
| total PUFA | mg | 516.67 | ±102.00 | 581.67[p = 0.07] | ±161.18 | 384.60[b,c] | ±138.46 |
| | % | 19.24 | ±2.57 | 20.59[a] | ±1.53 | 14.07[b,c] | ±2.66 |
| n-6 PUFA | mg | 449.08 | ±97.13 | 521.77[a] | ±148 | 335.75[b,c] | ±123.09 |
| | % | 16.72 | ±2.7 | 18.46[a] | ±1.55 | 12.28[b,c] | ±2.45 |
| n-6 LC-PUFA | mg | 9.38 | ±2.23 | 1.05[a] | ±1.18 | 29.81[b,c] | ±9.07 |
| | % | 0.35 | ±0.08 | 0.04[a] | ±0.05 | 1.26[b,c] | ±0.19 |
| 18:2 (LA) | mg | 438.50 | ±97.13 | 519.85[a] | ±147 | 301.82[b,c] | ±114.47 |
| | % | 16.32 | ±2.74 | 18.39[a] | ±1.52 | 11.02[b,c] | ±2.36 |
| 20:4 (AA) | mg | 7.69 | ±2.00 | 0.46[a] | ±0.53 | 11.39[b,c] | ±3.73 |
| | % | 0.29 | ±0.07 | 0.02[a] | ±0.02 | 0.42[b,c] | ±0.08 |
| n-3 PUFA | mg | 67.02 | ±12.49 | 59.49[a] | ±15.77 | 44.84[b,c] | ±19.56 |
| | % | 2.49 | ±0.29 | 2.12[a] | ±0.3 | 1.64[b,c] | ±0.49 |
| n-3 LC-PUFA | mg | 8.40 | ±1.69 | 0.53[a] | ±1.05 | 14.06[b,c] | ±8.24 |
| | % | 0.31 | ±0.05 | 0.02[a] | ±0.04 | 0.52[b,c] | ±0.22 |
| 18:3 (ALA) | mg | 58.62 | ±11.52 | 58.96 | ±15.64 | 30.78[b,c] | ±14.77 |
| | % | 2.18 | ±0.28 | 2.10 | ±0.29 | 1.13[b,c] | ±0.41 |
| 20:5 (EPA) | mg | 1.43 | ±0.33 | 0.23[a] | ±0.35 | 2.14[b,c] | ±1.93 |
| | % | 0.05 | ±0.01 | <0.01[a] | ±0.01 | 0.08[b,c] | ±0.05 |
| 22:6 (DHA) | mg | 6.22 | ±1.38 | 0.17[a] | ±0.41 | 6.35[c] | ±4.59 |
| | % | 0.23 | ±0.04 | <0.01[a] | ±0.02 | 0.23[c] | ±0.13 |
| ratios | | | | | | | |
| LA/ALA | | 7.66 | ±1.86 | 8.92[a] | ±1.53 | 10.74[b,c] | ±3.76 |
| n-6/n-3 PUFA | | 6.84 | ±1.6 | 8.88[a] | ±1.52 | 7.93[b,c] | ±2.26 |
| n-6/n-3 LC-PUFA | | 1.13 | ±1.60 | 2.27[a] | ±1.6 | 2.34[b] | ±0.63 |
| FA unsaturation index | | | | | | | |
| PE | mg based | 298.33 | ±52.36 | 319.88 | ±86.15 | 247.13[b,c] | ±82.22 |
| | % based | 11.11 | ±1.12 | 11.33 | ±0.67 | 9.04[b,c] | ±1.21 |
| AE | mg based | 282.02 | ±53.46 | 305.15 | ±83.52 | 197.59[b,c] | ±72.4 |
| | % based | 10.50 | ±1.26 | 10.81 | ±0.77 | 7.22[b,c] | ±1.41 |

[a]Significant difference between FM(+) and FM(−). [b]Significant difference between BM and FM(+). [c]Significant difference between BM and FM(−), SD = standard deviation, FA = fatty acids, SFA = short chain fatty acids, MUFA = monounsaturated fatty acids, PUFA = polyunsaturated fatty acids, LC-PUFA = long chain polyunsaturated fatty acids, LA = linoleic acid, AA = arachidonic acid, ALA = $\alpha$-linolenic acid, EPA = eicosapentaenoic acid, DHA = docosahexaenoic acid, PE = pentaenoic fatty acid equivalent, AE = arachidonic acid equivalent.

**Table 4. Vitamin E Content ($\mu$g/100 mL) of Enriched Formulae (FM(+), $n$ = 31), Not Enriched Formulae (FM(−), $n$ = 29), and Breast Milk (BM, $n$ = 118)**

| | FM (+) | SD | FM(−) | SD | BM | SD |
|---|---|---|---|---|---|---|
| $\alpha$-tocopherol | 479.0 | ±113.76 | 494.9 | ±118.7 | 569.3 | ±322.3 |
| $\beta$-tocopherol | 8.7 | ±4.2 | 9.5 | ±5.5 | 11.3[b,c] | ±7.0 |
| $\gamma$-tocopherol | 190.5 | ±26.8 | 247.3 | ±194.1 | 59.3[b,c] | ±33.9 |
| $\delta$-tocopherol | 24.3 | ±9.2 | 37.3 | ±51.7 | n.d. | |
| total tocotrienol | 311.1 | ±174.4 | 389.6 | ±1.7 | n.d. | |
| $\alpha$-tocopherol acetate | 274.0 | ±131.2 | 442.5[a] | ±255.7 | n.d. | |
| total vitamin E[d] | 1287.6 | ±180.3 | 1621.0[a] | ±509.8 | 640.0[b,c] | ±354.3 |
| $\alpha$-TE[e] | | | | | | |
| scenario 1 | 810.0 | ±121.6 | 1001.1[a] | ±299.3 | 589.9[b,c] | ±331.6 |
| scenario 2 | 615.1 | ±88.3 | 761.7[a] | ±229.2 | 589.9[b,c] | ±331.6 |

[a]Significant difference between FM(+) and FM(−). [b]Significant difference between BM and FM(+). [c]Significant difference between BM and FM(−). [d]Total vitamin E = sum of all vitamers. [e]$\alpha$-TE = sum of all vitamers except of $\beta$-, $\gamma$-, $\delta$-tocotrienol corrected by a factor according to their biological activity (see Materials and Methods), Table; n.d. = not detected, SD = standard deviation, $\alpha$-TE = $\alpha$-tocopherol equivalent.

**Table 5. α-Tocopherol Equivalent Concentration in Formula and Breast Milk (Marked Grey) From Different Countries**

| reference | location | *n* | α-TE calculation/analyzed vitamin E forms | α-TE range (mean) in μg/100 mL |
|---|---|---|---|---|
| Balz et al. 1993 | Germany | 5 infant formulas (no specification) | α-TE (α-TA × 0.67 + α-toc × 1 +β-toc × 0.4 + γ-toc × 0.1 + δ-toc × 0.01 + α-t3 × 0.3 + β-t3 × 0.05 + γ-t3 × 0.01) | 835−1187 |
| | | 2 breast milk samples (no specification) | only α-, β-, γ- tocopherol detectable | 390−780 |
| Chávez-Servín et al. 2008 | Spain | 20 initial formulas from the local market in Barcelona | α-TE (α-TA × 0.7 + α-toc × 1 + γ-toc × 0.2 + δ-toc × 0.1) | 658−2780 μg/100 g |
| Haro-Vicente et al. 2013 | Spain | 1 formula extra produced in a pilot plant | | 1780 |
| Kaempf-Rotzoll et al. 2003 | Germany | 2 preterm formulas, LCP-enriched (FM(+)) or not (FM(−) | α-TE (α-toc × 1+ γ-toc × 0.25)[b] | FM (+): 1614<br>FM(−): 1876 |
| | | 29 breast milk samples of 11 mothers 15−42 d *pp* | | − (419) |
| Martysiak-Żurowska et al. 2012 | Poland | 5 initial and 5 follow-on formulas from 5 most frequently purchased brands | α-TE (α-toc × 1+ γ-toc × 0.25) | IF's: 309−714 (495)<br>FF's: 471−731 (582) |
| | | 19 breast milk samples, 90 d *pp* | | − (213) |
| Miquel et al. 2004 | Spain | 4 formulas extra produced in a pilot plant (2 enriched with α-tocopherol, 2 with α-tocopherol acetate) | α-TE (α-TA × 0.7 + α-toc × 1 + γ-toc × 0.2 + δ-toc × 0.1) | 1079−1477 μg/13 g milk powder, the amount we assumed is corresponding to 100 mL ready to feed milk |
| Sziklai-Lásló et al. 2009 | Hungary | 26 formulas (6 IF, 15 FF, 5 SF) commercially available | α-TE (α-toc × 1, γ-toc × 0.25) | IF: 16−475 (198)<br>FF: 61−331 (177)<br>SF: 44−196 (103) |
| | | 18 breast milk samples 0.5−5 months *pp* | | 211−518 (330) |

[a]α-TE = α-tocopherol equivalent, IF = initial formula, FF = follow-on formula, SF = special milk, α-TA = α-tocopherol acetate, α-toc = α-tocoherol, β-toc = β-tocopherol, γ-toc = γ-tocopherol, δ-toc = δ-tocopherol, α-t3 = α-tocotrienol, β-t3 = β-tocotrienol, γ-t3 = γ-tocotrienol. [b]We calculated α-TE on the basis of the given α- and γ-tocopheryl values.



dx.doi.org/10.1021/jf502469b | J. Agric. Food Chem. 2014, 62, 10153−10161

Table 6. α-Tocopherol Equivalent/Unsaturated Fatty Acid Index Ratios of LC-PUFA Enriched Formulae (FM(+), $n = 31$), Not Enriched Formulae (FM(−), $n = 29$) and Breast Milk (BM, $n = 118$)

| | | FM (+) | SD | FM(−) | SD | BM | SD |
|---|---|---|---|---|---|---|---|
| α-TE/PE | | | | | | | |
| scenario 1 | mg based | 2.8 | ±0.7 | 3.3 | ±1.3 | 2.5[b,c] | ±1.4 |
| | % based | 73.4 | ±12.1 | 88.6[p = 0.06] | ±27.3 | 66.1[b,c] | ±37.2 |
| scenario 2 | mg based | 2.1 | ±0.5 | 2.5 | ±1.0 | 2.5 | ±1.4 |
| | % based | 55.8 | ±8.8 | 67.4[p=0.06] | ±20.8 | 66.1 | ±37.2 |
| α-TE/AE | | | | | | | |
| scenario 1 | mg based | 3.0 | ±0.8 | 3.5 | ±1.4 | 3.2 | ±1.9 |
| | % based | 78.1 | ±14.3 | 92.9[p=0.08] | ±28.7 | 84.2[c] | ±47.9 |
| scenario 2 | mg based | 2.3 | ±0.6 | 2.7 | ±1.0 | 3.2[b] | ±1.9 |
| | % based | 59.3 | ±10.4 | 70.7[p=0.09] | ±21.9 | 84.2[b] | ±47.9 |

[a]Significant difference between FM(+) and FM(−). [b]Significant difference between BM and FM(+). [c]Significant difference between BM and FM(−), α-TE = α-tocopherol equivalent, PE = pentaenoic fatty acid equivalent, AE = arachidonic acid equivalent.

association exists between the vitamin E content of maternal nutrition and vitamin E content of BM, there is at least evidence for the roles of fat quantity and quality of mothers' diets on BM.[24−27]

Published data on analyzed vitamin E contents in commercially available infant formulas in Europe are scarce, and reported values differ between studies (Table 5).[26,28,29] Our results were in the range reported by Balz et al., Martysiak-Zurowska et al., Chavez-Servin et al., and Miquel et al.[18,26,28,30] Lower values reported by Sziklai-Lásló et al. 2009 might have resulted from not considering the added α-tocopherol acetate.[29] Kaempf-Rotzoll et al. observed higher values of vitamin E in preterm formulas.[14] In agreement with our results, all studies except one (Sziklai-Lásló et al. 2009) found higher α-TE in formulas than in human milk (Table 5).

**α-Tocopherol Equivalent/Unsaturated Fatty Acids Index Ratios (α-TE/PE, α-TE/AE).** According to absolute fatty acid concentration analysis (mg/100 mL), α-TE/PE and α-TE/AE (i.e., the ratios between vitamin E content and need of individual products) ranged from 1.6 to 4.3 (mean value of 2.8 in Table 6) and 1.6 to 4.7 (mean value of 3.0 in Table 6), respectively, in FM(+) in scenario 1 (assuming the high vitamin E values). Similar values were calculated for FM(−), excluding one upper outlier (α-TE/PE: 7.6, α-TE/AE: 8.0). As expected, the ratios were lower in scenario 2 (Table 6), but still above 1. In other words, vitamin E content was higher than the estimated relative vitamin E need in all formulas, and as such, were in accordance with legal regulations.[2] Based on absolute FA amounts, α-TE/PE and α-TE/AE did not differ between FM(+) and FM(−). However, using relative (%-) values for the unsaturated fatty acids, α-TE/PE and α-TE/AE tended to be higher in FM(−) ($0.1 > p > 0.05$) (Table 6).

In BM, α-TE/PE and α-TE/AE showed a wider interindividual variability, ranging from 0.7 to 11.32 (mean value of 2.5 in Table 5) and 0.9 to 14.5 (mean value of 3.5 in Table 6) respectively, including five upper outliers. However, the highest values within the normal range (i.e., within the whiskers) were 5.0 and 6.4.

The comparison of FM with BM showed inconsistent results. When BM was used as the reference, FM(−) showed (in both vitamin E scenarios) similar or higher vitamin E need to vitamin E content ratios than BM. This applied also for FM(+) compared to BM, except for the calculation with arachidonic acid equivalents (AE) in scenario 2 where BM showed higher vitamin E need to vitamin E content ratios than FM(+).

There are no generally agreed upon approaches to calculate an adequate ratio of α-tocopherol equivalents relative to unsaturated fatty acid contents in infant formulas. A simplified parameter to assess antioxidant protection is the vitamin E/PUFA ratio, irrespective of PUFA composition.[6] Based on manufacturers' data, values of 6.6 and 3.92 mg vitamin E/g PUFA in LC-PUFA enriched and not-enriched formulas, respectively, and in another study, 2.8 mg vitamin E/g PUFA for both kinds of formulas were stated.[11,12] Calculation of this ratio (i.e., vitamin E as α-tocopherol equivalents, see "α-TE" in Table 4; and PUFA as sum of all PUFA without consideration of the degree of unsaturation, see "total PUFA" in Table 3) in our formulas samples resulted in mean values of 1.24 (range 0.67−1.92) in FM(+) and 1.39 (0.57−3.21), in FM(−), when the worst α-TE calculation was used (scenario 2). However, excepting 4 formulas in scenario 2 (2 formulas in scenario 1 with higher vitamin E values), all samples were in line with the ESPGHAN recommendation of at least 0.9 mg vitamin E/g PUFA.[6] Kaempf-Rotzoll et al. observed that the ratio of total tocopherol to fatty acid double bonds did not differ between LC-PUFA enriched and not-enriched formulas but were markedly higher than in BM.[14]

**Strengths and Limitations.** Our study analyzed the vitamin E and unsaturated fatty acid content in a large sample of commercial infant and follow-on formulas. The relative vitamin E need to prevent lipid peroxidation could only be calculated based on two models proposed by the current European food legislation (AE) or the whole fatty acid spectrum (PE).[2,19] A further limitation is the lack of consensus with respect to conversion factors for calculation of alpha tocopherol equivalents.[19,23,31] Moreover, the label declaration on formula packages did not reveal which one of the four vitamin E forms permitted by EU legislation was added, and in which proportions. Therefore, we calculated a lowest and a highest value scenario to reflect a possible range.

Regarding our analytical methods, the calculation of total fat contents from fatty acid analysis is expected to underestimate fat content by about 5% because glycerol and other lipid components such as cholesterol are not included. This may contribute to the observed lower mean fat contents calculated from our analyses (2.7 g/100 mL) as compared to label declarations (3.3 g/100 mL).

Breast milk analysis was based on a mixed sample of fore and hind milk, while vitamin E was analyzed in a milk sample from the midpoint of nursing. We assume that the fat content of the mixture of fore and hind milk would be representative of the

midpoint milk sample given that milk fat content increases from fore to hind milk.[32] However, a certain range of variation needs to be considered.

Our results indicate an adequate vitamin E content relative to unsaturated fatty acid content in present-day commercial infant and follow-on formulas. On average, the vitamin E content was more than twice as high as the estimated vitamin E need (based on absolute fatty acid values). Our findings show that breast milk tends to contain higher ratios of vitamin E to unsaturated fatty acids than LC-PUFA-enriched formulas (at least in a worst-case scenario). Therefore, the potential effects of increasing vitamin E content in LC-PUFA enriched formulas should be explored in further investigations concerning composition of relevant ingredients in infant formulas.

## AUTHOR INFORMATION


### Corresponding Author

*E-mail: stimming@fke-do.de. Fax: +49(0) 231 71 15 81. Phone: +49 (0) 231 79 22 10 32.



### Funding

The PINGU project was financially supported by the German federal ministry of education and research (Study code 01EA1335).

### Notes

The authors declare no competing financial interest.


## ACKNOWLEDGMENTS

All authors participated in manuscript preparation and critical revision, L.L. and M.S. conducted the statistical analyses and data interpretation, and M.S. wrote the manuscript. J.D. and B.K. conducted and supervised the fatty acid analysis. A.S. conducted vitamin E analysis under supervision of V.B. M.K. supervised the study. M.K. had full access to all the data in the study and takes responsibility for the integrity of the data and the accuracy of the data analysis.

## ABBREVIATIONS USED

$\alpha$-TE,$\alpha$-tocopherol equivalent; AA,arachidonic acid; AE,arachidonic acid equivalent; BM,breast milkz; ALA,$\alpha$-linolenic acid; DGE,German Nutrition Society; DHA,docosahexaenoic acid; EFSA,European Food Safety Authority; EPA,eicosapentaenoic acid; ESPGHAN,European Society of Pediatric Gastroenterology, Hepatology and Nutrition; FA,fatty acids; FM,formulas; FM(+),LC-PUFA-enriched formulas; FM(−),standard formulas, i.e. not LC-PUFA-enriched formulas; FKE,Forschungsinstitut für Kinderernährung, Research Institute of Child Nutrition; GC,gas chromatography; HCl,hydrogen chloride; HPLC,high-performance liquid chromatography; LDL,low density lipoprotein; LA,linoleic acid; LC-PUFA,long-chain polyunsaturated fatty acids; MUFA,monounsaturated fatty acids; PE,pentaenoic fatty acid equivalent; PUFA,polyunsaturated fatty acids; SFA,short chain fatty acids

## REFERENCES


(1) Koletzko, B.; Bauer, C. P.; Bung, P.; Cremer, M.; Flothkotter, M.; Hellmers, C.; Kersting, M.; Krawinkel, M.; Przyrembel, H.; Rasenack, R.; Schafer, T.; Vetter, K.; Wahn, U.; Weissenborn, A.; Wockel, A. German national consensus recommendations on nutrition and lifestyle in pregnancy by the 'Healthy Start - Young Family Network. *Ann. Nutr. Metab.* **2013**, *63*, 311−322.

(2) COMMISSION DIRECTIVE 2006/141/EC of 22 December 2006 on infant formulae and follow-on formulae and amending Directive 1999/21/EC, 2006. EUR-Lex. Access to European Law. http://eur-lex.europa.eu/browse/summaries.html.

(3) Schwartz, J.; Drossard, C.; Dube, K.; Kannenberg, F.; Kunz, C.; Kalhoff, H.; Kersting, M. Dietary intake and plasma concentrations of PUFA and LC-PUFA in breastfed and formula fed infants under real-life conditions. *Eur. J. Nutr.* **2010**, *49*, 189−195.

(4) Qawasmi, A.; Landeros-Weisenberger, A.; Bloch, M. H. Meta-analysis of LCPUFA supplementation of infant formula and visual acuity. *Pediatrics* **2013**, *131*, 262−272.

(5) Simmer, K.; Patole, S. K.; Rao, S. C. Long-chain polyunsaturated fatty acid supplementation in infants born at term. *Cochrane Database Syst. Rev.* **2011**, 10.1002/14651858.CD000376.pub3.

(6) Aggett, P.; Bresson, J. L.; Hernell, O.; Koletzko, B.; Lafeber, H.; Michaelson, K. F.; Micheli, J. L.; Ormisson, A.; de Sousa, J. S.; Weaver, L. Comment on the vitamin E content in infant formulas, follow-on formulas, and formulas for low birth weight infants. ESPGHAN Committee on Nutrition. European Society of Pediatric Gastroenterology, Hepatology and Nutrition. *J. Pediatr. Gastroenterol. Nutr.* **1998**, *26*, 351−352.

(7) Koletzko, B.; Decsi, T.; Sawatzki, G. Vitamin E status of low birthweight infants fed formula enriched with long-chain polyunsaturated fatty acids. *Int. J. Vitam. Nutr. Res.* **1995**, *65*, 101−104.

(8) Skouroliakou, M.; Konstantinou, D.; Koutri, K.; Kakavelaki, C.; Stathopoulou, M.; Antoniadi, M.; Xemelidis, N.; Kona, V.; Markantonis, S. A double-blind, randomized clinical trial of the effect of omega-3 fatty acids on the oxidative stress of preterm neonates fed through parenteral nutrition. *Eur. J. Clin. Nutr.* **2010**, *64*, 940−947.

(9) Siahanidou, T.; Lazaropoulou, C.; Michalakakou, K.; Papassotiriou, I.; Bacoula, C.; Mandyla, H. Oxidative stress in preterm infants fed a formula containing long-chain polyunsaturated fatty acids (LCPUFA). *Am. J. Perinatol.* **2007**, *24*, 475−479.

(10) Ramirez, M.; Gallardo, E. M.; Souto, A. S.; Weissheimer, C.; Gil, A. Plasma fatty-acid composition and antioxidant capacity in low birthweight infants fed formula enriched with n-6 and n-3 long-chain polyunsaturated fatty acids from purified phospholipids. *Clin. Nutr.* **2001**, *20*, 69−76.

(11) Koletzko, B.; Sauerwald, U.; Keicher, U.; Saule, H.; Wawatschek, S.; Bohles, H.; Bervoets, K.; Fleith, M.; Crozier-Willi, G. Fatty acid profiles, antioxidant status, and growth of preterm infants fed diets without or with long-chain polyunsaturated fatty acids. A randomized clinical trial. *Eur. J. Nutr.* **2003**, *42*, 243−253.

(12) Gonzalez-Corbella, M. J.; Lopez-Sabater, M. C.; Castellote-Bargallo, A. I.; Campoy-Folgoso, C.; Rivero-Urgell, M. Plasma and erythrocyte alpha-tocopherol and plasma retinol concentrations in term infants fed formula enriched with long-chain polyunsaturated fatty acids. *Eur. J. Clin. Nutr.* **1998**, *52*, 813−8.

(13) Decsi, T.; Koletzko, B. Growth, fatty acid composition of plasma lipid classes, and plasma retinol and alpha-tocopherol concentrations in full-term infants fed formula enriched with omega-6 and omega-3 long-chain polyunsaturated fatty acids. *Acta Paediatr.* **1995**, *84*, 725−732.

(14) Kaempf-Rotzoll, D. E.; Hellstern, G.; Linderkamp, O. Influence of long-chain polyunsaturated fatty acid formula feeds on vitamin E status in preterm infants. *Int. J. Vitam. Nutr. Res.* **2003**, *73*, 377−387.

(15) Mesch, C. M.; Stimming, M.; Wagner, A.; Libuda, L.; Kersting, M. Recruitment of mothers with infants in an intervention trial − initial findings from the PINGU-study. *Ernaehrungs Umschau international* **2013**, *7*, 110−115.

(16) Lepage, G.; Roy, C. C. Direct transesterification of all classes of lipids in a one-step reaction. *J. Lipid Res.* **1986**, *27*, 114−120.

(17) Molto-Puigmarti, C.; Castellote, A. I.; Lopez-Sabater, M. C. Ultra-High-Pressure Liquid Chromatographic method for the analysis of tocopherols in human colostrum and milk. *J. Chromatogr. A* **2009**, *1216*, 4388−4394.

(18) Balz, M. K.; Schulte, E.; Thier, H.-P. Simultaneous Determination of a-Tocopheryl Acetate, Tocopherols and Tocotrienols by HPLC with Fluorescence Detection in Foods. *Fat Sci. Technol.* **1993**, *95*, 215−220.

(19) German Nutrition Society (DGE); Austrian Nutrition Society (ÖGE); Swiss Society for Nutrition Research (SGE); and Swiss Nutrition Association (SVE); *Reference values for nutrient intake*. Umschau/Braus: Frankfurt/Main, 2000.
(20) Horwitt, M. K. Status of human requirements for vitamin E. *Am. J. Clin. Nutr.* **1974**, *27*, 1182−1193.
(21) Weiss, W. P.; Hogan, J. S.; Wyatt, D. J. Relative bioavailability of all-rac and RRR vitamin E based on neutrophil function and total alpha-tocopherol and isomer concentrations in periparturient dairy cows and their calves. *J. Dairy Sci.* **2009**, *92*, 720−731.
(22) Vagni, S.; Saccone, F.; Pinotti, L.; Baldi, A. Vitamin E Bioavailability: Past and Present Insights. *Food Nutr. Sci.* **2011**, *2*, 1088−1096.
(23) Belitz, H.-D.; Grosch, W.; Schieberle, P. *Lehrbuch der Lebensmittelchemie*; Springer Verlag: Berlin, 2001; Vol. *5*.
(24) Antonakou, A.; Chiou, A.; Andrikopoulos, N. K.; Bakoula, C.; Matalas, A. L. Breast milk tocopherol content during the first six months in exclusively breastfeeding Greek women. *Eur. J. Nutr* **2011**, *50*, 195−202.
(25) Dimenstein, R.; Medeiros, A. C.; Cunha, L. R.; Araujo, K. F.; Dantas, J. C.; Macedo, T. M.; Stamford, T. L. Vitamin E in human serum and colostrum under fasting and postprandial conditions. *J.. Pediatr.* **2010**, *86*, 345−348.
(26) Martysiak-Zurowska, D.; Szlagatys-Sidorkiewicz, A.; Zagierski, M. Concentrations of alpha- and gamma-tocopherols in human breast milk during the first months of lactation and in infant formulas. *Matern. Child Nutr.* **2012**, *9*, 473−482.
(27) Tokusoglu, O.; Tansug, N.; Aksit, S.; Dinc, G.; Kasirga, E.; Ozcan, C. Retinol and alpha-tocopherol concentrations in breast milk of Turkish lactating mothers under different socio-economic status. *Int. J. Food Sci. Nutr.* **2008**, *59*, 166−174.
(28) Chavez-Servin, J. L.; Castellote, A. I.; Lopez-Sabater, M. C. Simultaneous analysis of Vitamins A and E in infant milk-based formulae by normal-phase high-performance liquid chromatography-diode array detection using a short narrow-bore column. *J. Chromatogr. A* **2006**, *1122*, 138−143.
(29) Sziklai-László, I.; Majchrzak, D.; Elmadfa, I.; Cser, M. Á. Selenium and vitamin E concentrations in human milk and formula milk from Hungary. *J. Radioanal. Nucl. Chem.* **2009**, *279*, 585−590.
(30) Miquel, E.; Alegría, A.; Barberá, R.; Farré, R.; Clemente, G. Stability of tocopherols in adapted milk-based infant formulas during storage. *Int. Dairy J.* **2004**, *14*, 1003−1011.
(31) McLaughlin, P. J.; Weihrauch, J. L. Vitamin E content of foods. *J. Am. Diet. Assoc.* **1979**, *75*, 647.
(32) Emery, W. B., III; Canolty, N. L.; Aitchison, J. M.; Dunkley, W. L. Influence of sampling on fatty acid composition of human milk. *Am. J. Clin. Nutr.* **1978**, *31*, 1127−1130.

a prototype designed in the Lima University laboratories, which consists of a cylinder with holes of 1/16 in. in which the seeds were loaded and then pressed by a piston actuated by a hydraulic system assisted by a motor of 1 horsepower (HP). An average amount of 2 kg of shelled seeds was used for each sample in order to obtain enough oil for complete characterization. After the extraction the oil was filtered with a centrifugal filter (30 min, 3600 rpm). Crude oil samples were stored in dark bottles at 4 °C until analysis.

**Reagents and Solutions.** Acetone, diethyl ether, hexane, propionitrile, and THF were supplied by VWR International (West Chester, PA, USA). The Si-SPE cartridges were from Varian (EA Middelburg, The Netherlands). Standards of 5-$\alpha$-cholestan-3$\beta$-ol and trilinolenin (LnLnLn) were from Sigma-Adrich Co. (St. Louis, MO, USA). Hexamethyldisilazane, pyridine, trimethylchloroxilane, and standards of eicosane and tocopherols were from Merck-España (Merck Group, Darmstadt, Germany). All chemical reagents were analytical grade.

**Physical−Chemical Determinations.** The physical−chemical parameters included in the current legislation for Sacha inchi oils and other regulations for other edible oils were determined in the crude oils.[10]

*Free Fatty Acids and Peroxide Values.* AOCS Official Methods were followed to determine FFA and peroxide indexes.[15,16]

*UV Evaluation.* Specific extinction at 270 nm (K270) was evaluated according to the European Union Standard Methods.[17]

*Oxidative Stability.* The induction time was evaluated using a Rancimat equipment (743 Rancimat Metrohm Co., Basel, Switzerland), following the standard Official Method Cd 12-b-92,[18,19] with an air flow of 20 L·h$^{-1}$ and 100 ± 1 °C.

*Other Physical Parameters.* Parameters such as viscosity and density were measured using a Stabinger SVM 3000 viscometer (Anton Paar GmbH Graz, Austria). The refractive index was determined with a temperature-controlled Abbe refractometer (Hilger & Watts Ltd., London, U.K.).[3,20]

**Major Components.** *Triacylglycerol Composition.* The TG composition was obtained as follows: oil samples at a concentration of 50 mg·mL$^{-1}$ in acetone were analyzed by RP-HPLC. The separations were done on a Merck Li-Chrospher 100 RP-18 column (250 mm × 4 mm i.d.; 4 $\mu$m particle size) thermostated at 20 °C. The liquid chromatograph (Beckman-Coulter, Fullerton, CA, USA) was equipped with a pumping unit (118 solvent module) and used propionitrile as the mobile phase at a flow rate of 0.6 mL·min$^{-1}$. Oil solutions in acetone (10 $\mu$L) were injected using an autosampler (508 system). Detection was done with a PerkinElmer 200 RI detector.[21]

*Polar Glyceridic Compounds.* PC were assessed with small modifications of the already published method, by separating the oils in two fractions by Si-SPE using 1 g cartridges.[22,23] Thus, 200 mg of oil samples were weighed in 10 mL volumetric flasks and dissolved in hexane. On each case an aliquot of this solution (2 mL) was introduced into the cartridge and then eluted with 15 mL of the hexane:diethyl ether 87:13 (v/v) admixture. The fraction containing the nonaltered TG was rejected. A second fraction was collected eluting with 15 mL of diethyl ether. The latter fraction was evaporated until dryness, re-dissolved in 1 mL of THF and injected onto the HPLC (Hewlett-Packard 1050 series). The HPSEC system is equipped with an Agilent PL gel of 5 $\mu$m, a 100 Å column, and a Merck La Chrom RI Detector L-7490. THF was used as eluent at a flow rate of 0.7 mL·min$^{-1}$. The injection volume was 20 $\mu$L. The compounds eluted from the columns according to their molecular size, so those with the largest molecular sizes were eluted earlier and were quantified as individual percentages of the total eluted compounds and also as absolute quantities using an external standard of pure TG in THF at concentrations of 5−10 mg·mL$^{-1}$.

*Fatty Acid Composition.* The FFA composition was determined as the composition of FAME by GC after transesterification of the oils with 2 N KOH in methanol, according to the IUPAC Standard Method.[20,24] The chromatographic analysis was done using an Agilent 5890 GC system (Palo Alto, CA, USA) equipped with a split injector (1:50 split ratio), a polar capillary column (poly(90% biscyanopropyl−10% cyanopropylphenyl)siloxane, 60 m × 0.25 mm i.d.; 0.20 $\mu$m film thickness) and a FID. Hydrogen was used as the carrier gas at a flow rate of 1.0 mL·min$^{-1}$. The detector and injector temperatures were 225 and 250 °C, respectively. The initial oven temperature was 180 °C, and a temperature gradient from 180 to 220 °C at 3 °C min$^{-1}$ was applied. Injections of 1 $\mu$L each were performed automatically.

**Minor Unsaponifiable Compounds.** The percentage of the total unsaponifiable fraction was calculated gravimetrically after subjecting the oil samples to a saponification procedure carried out according to the IUPAC 2401 Official Method.[25]

*Tocopherols.* Tocopherols were determined according to the IUPAC Standard Method 2432.[26] An oil solution in hexane at a concentration of 10 mg·mL$^{-1}$ was prepared and analyzed by HPLC fitted with a Si-column (250 mm × 4 mm i.d.; 4 $\mu$m particle size). The elution solvent was a hexane:2-propanol (99:1, v/v) mixture at a flow rate of 1 mL·min$^{-1}$. Detection was done by fluorescence (RF-10AXL Shimadzu fluorescence detector), setting excitation and emission at $\lambda$ = 290 and $\lambda$ = 330 nm, respectively. For quantitative determinations standards of tocopherols in hexane at concentrations of 4−6 $\mu$g·mL$^{-1}$ were prepared and injected.

*Sterol Composition.* The sterol fraction was isolated from the unsaponifiable matter by silica TLC using plates impregnated with potassium hydroxide with the purpose of retaining the remaining saponified compounds. The plate was developed twice with a mixture of petroleum ether:diethyl ether (87:13, v/v). The isolated fraction was scratched off and extracted with hot chloroform and diethyl ether. The solution was evaporated until dryness, derivatized with 500 $\mu$L of the 1:3:9 (v/v/v) trimethylchloroxilane:hexamethyldisilazane:pyridine admixture and analyzed by GC. The gas chromatograph (Agilent 6890N) was equipped with a fused silica low-polarity capillary column (poly(5% diphenyl−95% dimethyl)siloxane, 30 m × 0.25 mm i.d. × 0.25 $\mu$m film thickness), and FID. The oven program was isothermal at 260 °C with a split ratio of 1:50. Hydrogen was used as carrier gas at a flow rate of 1 mL·min$^{-1}$. The temperatures of the injector and detector were 300 °C. The quantitative determination was done using $\alpha$-cholestanol as internal standard.

*Aliphatic Saturated Hydrocarbons.* HC were isolated by low-pressure column chromatography filled with 15 g of silica gel (Si-60) impregnated with $AgNO_3$.[27] A sample of 0.5 g of oil was introduced into the column, and the fraction containing the aliphatic hydrocarbons was eluted with 80 mL of petroleum ether. This fraction was evaporated until dryness, re-dissolved in 0.5 mL of hexane, and analyzed by GC. The gas chromatograph was equipped with a low-polarity capillary column (poly-5% diphenyl−95% dimethylsiloxane, 12 m × 0.32 mm i.d. × 0.1 $\mu$m film thickness) and an on-column injection

Table 1. Physical−Chemical Parameters of the Sacha Inchi (*P. Huayllabambana* L.) Oils[a]

| | harvest 1 | | harvest 2 | |
|---|---|---|---|---|
| | $M(n=14)$ (%) | range | $M(n=14)$ (%) | range |
| acidity value | 1.8a ± 0.1 | 0.5−4.7 | 1.6b ± 0.1 | 0.5−3.7 |
| peroxide value (meq $O_2 \cdot kg^{-1}$) | 8.4a ± 0.2 | 1.5−19.1 | 3.3b ± 0.2 | 2.1−5.6 |
| $K_{270}$ | 0.14b ± 0.01 | 0.10−0.28 | 0.19a ± 0.01 | 0.14−0.23 |
| stability (h) | 2.8a ± 0.1 | 2.0−3.4 | 3.0a ± 1.2 | 1.8 ± 5.5 |
| density (25 °C) ($g \cdot cm^{-3}$) | 0.927a ± 0.001 | 0.926−0.930 | 0.925a ± 0.002 | 0.920−0.930 |
| refractive index | 1.480a ± 0.0001 | 1.480−1.481 | 1.482a ± 0.0004 | 1.481−1.482 |
| viscosity (20 °C) ($mm^2 \cdot s^{-1}$) | 42.8a ± 0.9 | 41.2−44.0 | 41.1a ± 2.2 | 38.9−43.8 |

[a]Data are the average of 14 samples and are expressed as the mean ± SD. Different letters (a, b) represent significant differences.

Table 2. Major Compounds of Sacha Inchi (*P. huayllabambana* L.) Oils: Triglyceride, Polar Glyceridic Compounds and Fatty Acid Methyl Esters[a]

| | samples | | | |
|---|---|---|---|---|
| | harvest 1 | | harvest 2 | |
| | $M(n=14)$ | range | $M(n=14)$ | range |
| | Triglycerides (wt % on total) | | | |
| ECN 36 (LnLnLn) | 20.0 ± 1.18 | 17.7−22.5 | 20.0 ± 1.84 | 18.0−23.0 |
| ECN 38 (LnLnL) | 26.3 ± 0.7 | 25.3−27.5 | 26.0 ± 1.21 | 22.6−27.7 |
| ECN 40 (LnLL + LnLnP + LnLnO) | 20.6 ± 0.79 | 19.2−21.8 | 20.9 ± 0.86 | 19.4−23.1 |
| ECN 42 (LLL + OOLn + LLP + POLn) | 20.7 ± 1.20 | 19.4−22.8 | 22.5 ± 1.10 | 19.0−24.0 |
| ECN 44 (LLO + OOLn + LLP + POLn) | 7.0 ± 0.70 | 6.0−8.3 | 7.6 ± 0.94 | 6.0−10.5 |
| ECN 46 (OOL + LnPP + PLO) | 2.5 ± 0.48 | 1.8−3.4 | 2.4 ± 0.79 | 1.39−5.0 |
| ECN 48 (OOO + POO) | 1.3 ± 0.75 | 0.5−2.7 | 0.5 ± 0.28 | 0.1−1.0 |
| ECN 50 (SSO) | 0.7 ± 0.7 | 0.0−2.5 | <0.01 | |
| | Polar Compounds (wt % on Total) | | | |
| oxTG | 31.4 ± 3.0 | 27.7−37.1 | 21.6 ± 5.9 | 13.6−29.9 |
| DG | 41.6 ± 3.0 | 37.8−45.4 | 42.7 ± 5.1 | 33.5−52.5 |
| MG | 2.1 ± 0.7 | 0.6−3.3 | 2.5 ± 1.1 | 1.2−4.5 |
| FA | 24.9 ± 3.0 | 20.8−32.2 | 33.1 ± 6.2 | 26.4−47.0 |
| total (% on oil) | 3.4a ± 0.7 | | 4.0a ± 1.5 | |
| | Fatty Acids (wt % on Total) | | | |
| C16:0 | 4.6 ± 0.2 | 4.3−4.9 | 4.9 ± 0.38 | 4.4−5.7 |
| C16:1 | 0.07 ± 0.0 | 0.06−0.09 | 0.08 ± 0.02 | 0.05−0.15 |
| C17:0 | 0.08 ± 0.0 | 0.07−0.10 | 0.08 ± 0.02 | 0.05−0.21 |
| C18:0 | 1.6 ± 0.1 | 1.5−2.0 | 1.7 ± 0.2 | 1.3−2.1 |
| ω9-C18:1 | 8.0 ± 0.6 | 8.2−10.4 | 7.8 ± 0.56 | 6.8−8.8 |
| ω7-C18:1 | 1.0 ± 0.01 | 0.9−1.0 | 0.93 ± 0.06 | 0.80−1.10 |
| ω6-C18:2 | 26.2 ± 0.7 | 25.0−27.3 | 25.8 ± 0.6 | 24.5−26.9 |
| C20:0 | 0.30 ± 0.1 | 0.20−0.30 | 0.25 ± 0.05 | 0.21−0.44 |
| ω3-C18:3 | 58.1 ± 1.4 | 55.5−60.4 | 58.2 ± 1.5 | 55.9−60.4 |

[a]Data are the average of 14 samples and are expressed as the mean ± SD. The same letter (a) represents no significant differences.

system. The initial oven temperature was set at 80 °C for 2 min, and the rate was established at 12 °C·min$^{-1}$ up to 280 °C, then at 7 °C·min$^{-1}$, and then up to 340 °C. The injector temperature was 80 °C and was allowed to follow the oven temperature program. The FID temperature was 350 °C. Eicosane (C20:0) at a concentration of 0.05 mg·mL$^{-1}$ was used as internal standard.

*Statistical Analysis.* Each sample was analyzed in triplicate, and data were presented as the average of the 14 data obtained in each crop. The statistical analyses were run using the GraphPad Prism version 5.01 for Windows software. The crops were compared by ANOVA. When significance was observed, the Tukey test was applied. Significant differences ($p > 0.05$) are specified with different letters.

## RESULTS AND DISCUSSION

**Oil Yield.** Compared to Sacha inchi *P. volubilis*, currently the most widely used cultivar for oil extraction and commercialization, the *P. huayllabambana* species is almost twice its size (1.7−4.1 cm$^3$ vs 4.1−8.0 cm$^3$) and weight, having an oil yield after pressing and filtration in the range of 30.3−41.2% with respect to the shelled seeds.

**Analytical Indexes and Oxidative Stability.** The values of the indexes commonly used to evaluate the initial quality of vegetable oils, i.e., FA, PV, and $K_{270}$, were found within the expected ranges for crude oils of good quality, with some remarkable exceptions. Regulation for extra virgin and virgin Sacha inchi oils establishes a maximum of 1.0 and 2.0 (expressed as a percent of oleic acid) of FA, respectively. Table 1 shows the results of the quality parameters, and it can be observed that the average value obtained for the 28 oil


dx.doi.org/10.1021/jf5028697 | J. Agric. Food Chem. 2014, 62, 10162−10169

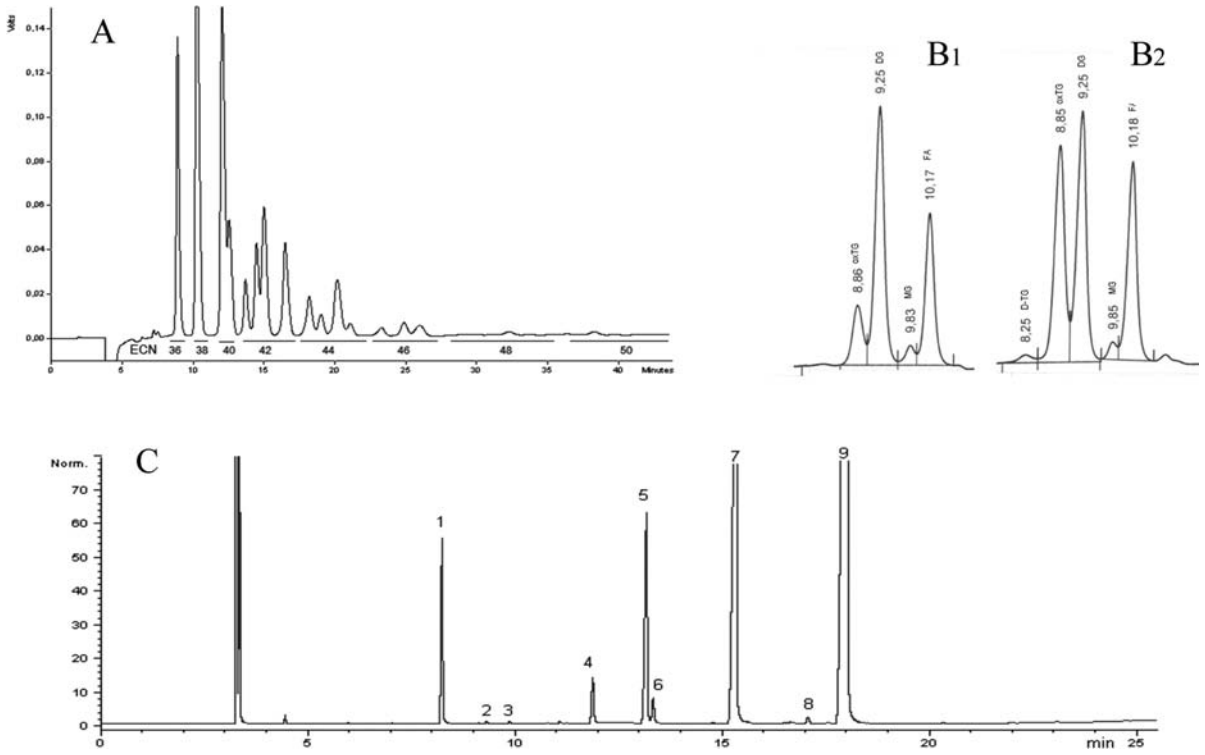


**Figure 1.** Chromatogram profiles of the major compounds of Sacha inchi *P. huayllabambana* oils, where panels are described as follows: (A) HPLC-RI of triglycerides with ECN 36−50; (B1 and B2) HPSEC-RI of polar compounds and dimers of tryglicerides (D-TG), oxidized triglycerides (oxTG), diglycerides (DG), monoglycerides (MG), free fatty acids (FFA); (C) HRGC of FA for (1) palmitic C16:0, (2) palmitoleic C16:1, (3) margaric C17:0, (4) estearic C18:0; (5) oleic $\omega$9-C18:1, (6) vacenic $\omega$7-C18:1, (7) linoleic $\omega$6-C18:2, (8) arachidic C20:0, and (9) linolenic $\omega$3-C18:3 acids.

samples from the two harvests under study is within the established ranges for virgin oils. Half of the samples can be classified as extra virgin, 29% as virgin, and 21% are neither extra virgin nor virgin oils. These results are indicating that Sacha inchi *P. huayllabambana* seeds are highly susceptible to hydrolysis, yielding oils with acidity over the established limits. The high hydrolyzation level showed is not an exclusive characteristic of *P. huayllabambana* oil samples. Actually some published data on *P. volubilis* also present acidity values over the limits established in the regulations.[28,29]

Regarding the oxidation state of the oils, the mean values were shown to be within the limits included in the regulations, although three of the samples overpassed the 10 meq $O_2 \cdot kg^{-1}$ maximum established in the NTP.

Concerning the absorbance at 270 nm, there is not a limit established in the NTP Regulation. Olive oil regulation includes a limit of 0.22 for extra virgin and 0.25 for virgin olive oils. The results on the analyzed Sacha inchi oils drove us to categorize a high number of samples (24) as extra virgin, and 3 as virgin, whereas only one dropped out of both categories.

Most of the PV data reported for *P. huayllabambana* were within the limits established by the regulations. It can be observed that some of the samples from the first harvest yielded oils with PV over the limit, but that the oils obtained from the second harvest showed a significantly lower value, which means lower oxidation level, undoubtedly due to a more suitable storage period in the second repetition of the study. Nevertheless their absorbance at 270 nm is higher, although with no meaningful differences.

The oxidative stability determined by Rancimat gave IP of 2.0−3.4 h, at 100 °C. These values are rather low compared to those of other edible oils such as olive or sunflower oils, but they are similar or even higher than those of oils with similar unsaturation level, such as safflower or flax oils.[30] No significant differences are found between the two harvests under study.

We have to consider that these oils were obtained from raw seeds. In the case of carrying out a previous seed roasted process, an increase of the oil stability is to be expected, as occurred with argan seeds.[2,3] These kinds of processes have been recently carried out with Sacha inchi (*P. volubilis*).[31]

Density, refractive index, and viscosity are physical parameters determined to differentiate and to characterize the oils and mainly are used for commercial purposes. The density values at 20 °C were in the 0.920−0.930 $g \cdot cm^{-3}$ range and were within the requirements of the NTP. These values are slightly higher than those reported at the same temperature for other vegetable oils such as sunflower or olive (0.898−0.906).[3]

The refractive index at 20 °C for the first harvest ranged from 1.480 to 1.482 and is within the ranges set in the NTP. For the second harvest the average of the 14 samples under study was over the limit established in the NTP. These results were also higher than those reported for other vegetable oils (1.461 to 1.474).[32]

The kinematic viscosity data at 20 °C were in the 38.9−44.0 $mm^2 \cdot s^{-1}$ range, the averages being 42.8 and 41.1 $mm^2 \cdot s^{-1}$ for the first and second harvests, respectively. These values are higher than those reported at the same temperature for *P. volubilis*.[8]

**Major Saponifiable Compounds.** *Triglyceride Molecular Species.* A detailed study of the TG was carried out by means of RP-HPLC-RI, and it is summarized in Table 2. The eluting order of each TG molecular species can be determined using

Table 3. Main Unsaponifiable Components, Sterols, Tocopherols, and Aliphatic Hydrocarbons, Determined by Split-GC, FL-HPLC, and on-Column-GC, Respectively, of Sacha Inchi (*P. huayllabambana* L.) Seed Oils[a]

| | Samples | | | |
|---|---|---|---|---|
| | harvest 1 | | harvest 2 | |
| | M (n=14) | Range | M (n=14) | Range |
| **UNSAPONIFIABLE MATTER (%)** | $1.30^{a(*)} \pm 0.50$ | 0.70 - 2.20 | $0.83^{b(*)} \pm 0.24$ | 0.70 – 1.35 |
| **TOCOPHEROLS** (wt% on total) | | | | |
| α | n.c. | - | n.c. | - |
| β | n.d. | - | n.d. | - |
| γ | 68.9 | 65.2-70.0 | 63.5 | 53.6-67.1 |
| δ | 31.1 | 30.0-34.8 | 36.5 | 32.9-46.4 |
| Total ($mg \cdot kg^{-1}$) | $2820.6^{a} \pm 379.4$ | 1810.8-2977.9 | $2329.0^{b} \pm 361.5$ | 1973.1-2692.8 |
| **STEROLS** (wt% on total) | | | | |
| Cholesterol | 0.3 ± 0.06 | 0.2 – 0.4 | 0.3 ± 0.04 | 0.2 – 0.4 |
| Campesterol | 5.0 ± 0.30 | 4.5 – 5.6 | 4.8 ± 0.18 | 4.6 – 5.1 |
| Stigmasterol | 29.7 ± 1.60 | 26.5 – 32.3 | 30.5 ± 1.14 | 29.2 – 32.3 |
| Δ7-Campesterol | 0.5 ± 0.39 | 0.1 – 1.0 | 0.5 ± 0.10 | 0.1 – 1.1 |
| Clerosterol | 0.7 ± 0.09 | 0.6 – 0.8 | 0.8 ± 0.04 | 0.8 – 0.9 |
| β-sitosterol | 60.1 ± 1.57 | 57.9 – 63.1 | 59.2 ± 1.52 | 57.1 – 61.5 |
| Sitostanol | 0.6 ± 0.09 | 0.5 – 0.8 | 0.6 ± 0.06 | 0.5 – 0.7 |
| Δ5-Avenasterol | 1.6 ± 0.18 | 1.2 – 2.0 | 1.7 ± 0.07 | 1.6 – 1.8 |
| Δ5,24-Stigmastadienol | 0.3 ± 0.09 | 0.2 – 0.4 | 0.4 ± 0.04 | 0.3 – 0.4 |
| Δ7-Stigmastenol | 0.6 ± 0.09 | 0.5 – 0.8 | 0.7 ± 0.13 | 0.6 – 0.9 |
| Δ7-Avenasterol | 2.3 ± 1.57 | 0.2 – 3.4 | 0.3 ± 0.04 | 0.3 – 0.3 |
| Total ($mg \cdot kg^{-1}$) | $1931.2^{a} \pm 143.2$ | 1652.9 – 2236.0 | $1877.7^{a} \pm 92.2$ | 1788.4 – 2013.3 |
| **ALIPHATIC HYDROCARBONS** (wt% on total) | | | | |
| $H_{21:0}$ | 10.6± 1.55 | 10.2-14.0 | 10.4± 0.44 | 10.2-10.7 |
| $H_{22:0}$ | 10.3± 1.07 | 10.0-12.6 | 11.0± 0.10 | 10.9-11.1 |
| $H_{23:0}$ | 38.5± 1.16 | 37.8-41.8 | 37.3± 1.00 | 36.4-38.6 |
| $H_{24:0}$ | 18.8± 1.00 | 17.9-19.7 | 18.7± 0.55 | 17.9-19.3 |
| $H_{25:0}$ | 14.0± 1.57 | 13.7-16.3 | 14.2± 0.48 | 13.8-14.7 |
| $H_{26:0}$ | 2.6± 0.15 | 2.3-2.8 | 2.5± 0.12 | 2.4-2.6 |
| $H_{27:0}$ | 1.8± 0.10 | 1.5-2.0 | 2.0± 0.15 | 1.1-2.6 |
| $H_{28:0}$ | 1.9± 0.38 | 1.4-2.2 | 2.1± 0.22 | 1.5-2.7 |
| $H_{29:0}$ | 1.5± 0.78 | 0.5-2.0 | 1.8± 0.98 | 0.5-2.7 |
| Total ($mg \cdot kg^{-1}$) | $137.5^{a} \pm 16.7$ | 114.8-170.7 | $139.6^{a} \pm 4.89$ | 134.8-144.6 |
| Odd/Even Ratio | 2.0±0.2 | | 1.9±0.2 | |

[a]Data are the average of 14 samples and are expressed as the mean ± SD. Different letters (a, b) represent significant differences. n.c., not quantified, <1%; n.d.: not detected.

the standard of LnLnLn, which elutes as the first TG peak. One should take into account that under the isocratic conditions used in this work the retention times for TG are directly proportional to the number of carbon atoms and inversely proportional to the total number of double bonds in the three fatty acyl chains. TG molecular species can be grouped according to their ECN, defined as the total acyl-carbon number in the molecule minus twice the total number of double bonds of the fatty acids comprising the TG.[21]

As one can observe in Figure 1A the ECN of the main TG identified are within the range from 36 to 42, normally with combinations of Ln and L. Thus, the four main TG are LnLnLn, LnLnL, LnLL, and LLL (ECN 36, 38, 40, and 42, respectively). Also TG with ECN 44, 46, 48, and 50 are found, but in minor proportions. Fanali and co-workers[6] reported the TG composition of Sacha inchi *P. volubilis* oils from Peruvian producers for the first time. Remarkable differences can be found with the *P. huayllabambana* species presently studied. Thus, although in both species LnLnL (ECN 38) is the major TG, for *P. huayllabambana* this TG is higher than the whole group of TG with ECN 40 (26% vs 21%), which is the main TG group reported for *P. volubilis* (28.7%).[6]

*Glyceridic Polar Compounds.* The quantitative determination of glyceridic polar compounds gives a direct evaluation of all the compounds having polarity higher than that of the TG, the major compounds in edible fats and oils. The composition and profile of the PC is the most valuable and common methodology utilized for evaluating the alteration in heated oils. The fraction isolated by Si-SPE was quantified using HPSEC, separating the compounds according to their molecular size: D-TG, oxTG, DG, MG, and FFA (Figure 1B1 and 1B2). Quantitative PC data (Table 2), which include values between 2.3 and 7.5% for Sacha inchi *P. huayllabambana* oils, show percentages below 5−6% in most of the samples studied, which is indicative of good quality oils.[34] No comparison can be done with other Sacha inchi species since no PC data have been reported. As can be observed, the PC fraction is mainly composed of DG and FFA in a ratio of 2:1 approximately. It is noteworthy the presence of MG in proportions around 0.6−3.3% in all analyzed samples, confirming that the susceptibility of the seed to hydrolization goes beyond the DG formation. Some of the evaluated samples exhibited a high level of compounds related to hydrolization such as DG and FA, and also important quantities of oxTG and D-TG (Figure 1B2).

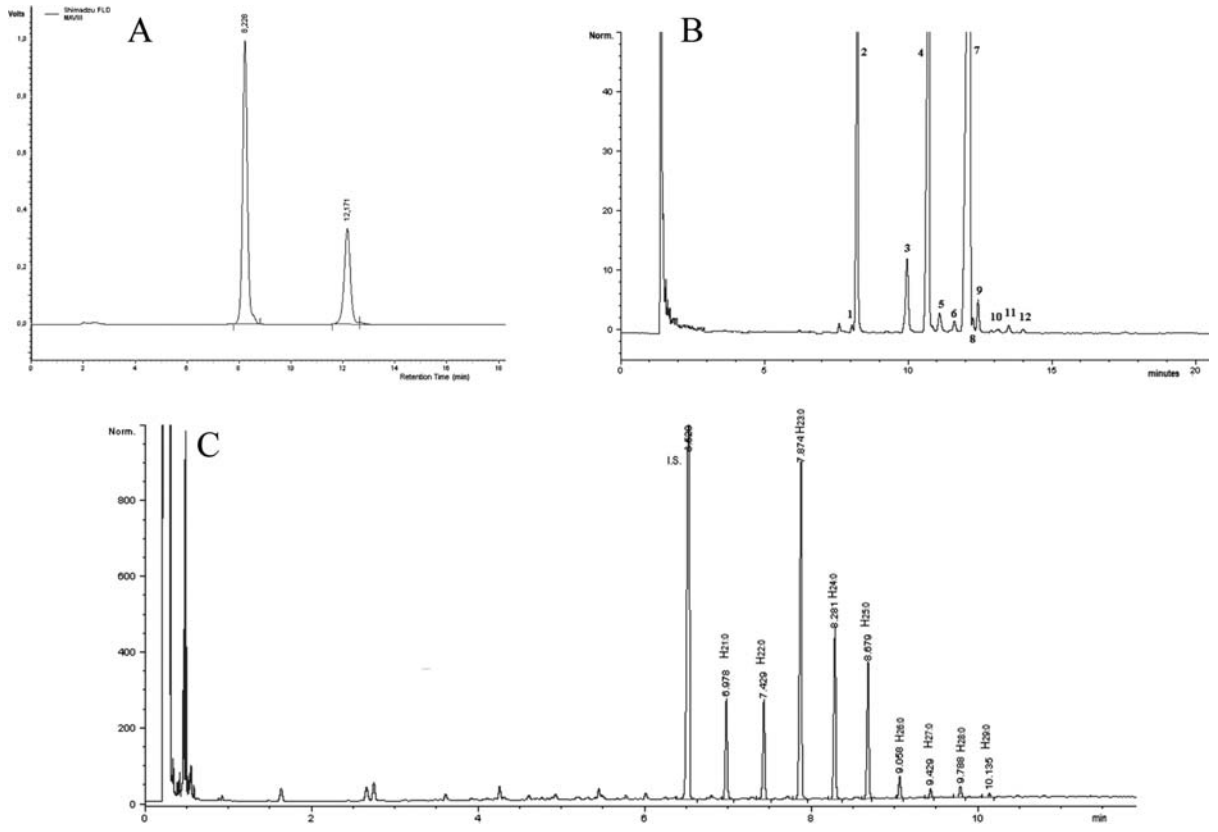


**Figure 2.** Chromatogram profiles of the main unsaponifiable compounds of the Sacha inchi *P. huayllabambana* oils: (A) tocopherols HPLC-FL profile (Rt 8.22, $\gamma$-tocopherol; Rt 12.17, $\delta$-tocopherol); (B) sterol GC profile for (1) cholesterol, (2) I.S (Internal Standard: $\alpha$-cholestanol), (3) campesterol, (4) stigmasterol, (5) Δ7-campesterol, (6) clerosterol, (7) $\beta$-sitosterol, (8) sitostanol, (9) Δ5-avenasterol, (10) Δ5,24-stigmastadienol, (11) Δ7-stigmastenol, and (12) Δ7-avenasterol; (C) aliphatic saturated hydrocarbon on-column GC profile. I.S: Internal Standard, H20.

The PC method, designed in the beginning for oils subjected to frying processes, gives us valuable information on the alteration of the Sacha inchi seeds due to hydrolysis. Moreover, all oil samples contain oxTG as has been seen in other edible oils but an important number of them also have high quantities of minor glyceridic components, which indicates the facility of Sacha inchi oils to oxidative alteration, which is expected due to their high unsaturation degree.

*Fatty Acid Composition.* A representative chromatogram of the FAME of Sacha inchi *P. huayllabambana* oil is presented in Figure 1C. There we can observe the high percentage of Ln, as well as the presence of $\omega$7-C18:1 and the absence of C20:1. The results (Table 2) indicate no significant differences between the two studied harvests. The high contents of Ln (55.5−60.7%) and L (25.0−27.3%) stand out. These values are slightly different from those reported for Sacha inchi *P. volubilis*.[28,35] The $\omega$6:$\omega$3 ratio determined in this work for Sacha inchi *P. huayllabambana* is 0.45:1, which is lower than those reported for Sacha inchi *P. volubilis* (0.75:1), since for the commercial species the Ln content is low (47−50%).

**Main Unsaponifiable Components.** We have studied the total quantity of the unsaponifiable matter as well as the sterol, tocopherols, and aliphatic hydrocarbons profiles and contents.

The total unsaponifiable matter (Table 3) differs for both harvests and in some samples is out of the limits established in the regulations (0.36%). At this point it is important to highlight that the limit established in the regulation is not really reasonable since just the addition of the values regarding valuable unsaponifiable components such as sterols and tocopherols exceeds it.

Figure 2 represents the chromatograms of the main unsaponifiable compounds of Sacha inchi *P. huayllabambana* oils studied here.

*Tocopherols.* $\gamma$-Tocopherol and $\delta$-tocopherol are the main species that can be directly separated and quantified by HPLC using fluorescence detector (Figure 2A). In a few number of samples also $\alpha$-tocopherol is present, but with percentages lower than 0.1. $\gamma$-Tocopherol was the major tocopherol with percentages above 65% in most of the samples. High variability is found in their total quantities not only between harvests but also among samples within the same harvest (Table 3). This fact can be explained by taking into account that these compounds, specially $\delta$-tocopherol, are powerful antioxidants and protect the highly unsaturated TG of Sacha inchi oils against oxidation, resulting in their degradation. The results obtained regarding the tocopherol content of the Sacha inchi *P. huayllabambana* are slightly higher than data published for *P. volubilis* species.[6,28] However, they are above the maximum limit established in the most recent Peruvian Regulations for Sacha inchi *P. volubilis* oils.[36] This recent regulation concerning only *P. volubilis* species establishes a maximum limit of 0.7, 0.29, 136.7, and 85.6 mg·kg$^{-1}$ for $\alpha$, $\beta$, $\gamma$, and $\delta$, respectively, which is at the least strange.

*Sterols.* Related to the sterols GC profile (Figure 2B), 12 peaks can be separated including $\alpha$-cholestanol, which is added as an internal standard for quantitation purposes. The major peak corresponds to $\beta$-sitosterol (peak 7), as in the majority of


dx.doi.org/10.1021/jf5028697 | J. Agric. Food Chem. 2014, 62, 10162−10169

vegetable oils, with percentages above 60%. Stigmasterol (peak 4) is the second most important sterol in Sacha inchi oils, which is in agreement with recent data reported by Muñoz Jáuregui and co-workers[13] where sterols were determined by HPLC. In rare cases, as occur in Sacha inchi oils, including the *P. volubilis* species, the stigmasterol content is higher than the campesterol concentration.[5] For most edible oils, the ratio campesterol/stigmasterol is higher than 1.[37] This is the case of olive oil, where its regulation establishes explicitly that the stigmasterol content must be lower than that of campesterol.[17] The campesterol/stigmasterol ratios calculated in this work are within the 0.14−0.21 range, the stigmasterol concentration being six times that of campesterol. This high stigmasterol content can provide interesting properties to Sacha inchi oils since this phytosterol plays an important role in reducing the inflammatory processes.

*Aliphatic Saturated Hydrocarbons.* HC form a remarkable group of minor unsaponifiable compounds present in edible fats and oils. At present, they are considered as intermediate metabolites in the formation of other minor compounds, such as aliphatic alcohols, with specific roles. Figure 2C shows an on-column gas chromatogram corresponding to the aliphatic saturated hydrocabons of Sacha inchi *P. huayllabambana* oil. The main peaks correspond to H21 heneicosane; H22 docosane; H23 tricosane; H24 tetracosane, and H25 pentacosane. A minor amount of H19 nonadecane; H26 hexacosane, H27 heptacosane, H28 octacosane, and H29 nonacosane are also present. Surprisingly both the odd and even series were present. The procedure was applied using impregnated silver nitrate silica to ensure that only saturated hydrocarbons eluted from the silica column. Results of the mean concentrations of the main aliphatic saturated hydrocarbons and also their total quantities evaluated using as standard a solution of heneicosane (*n*-H20:0) at concentration of 0.05 $mg \cdot mL^{-1}$ are included in Table 3. The high concentrations of the H23:0 hydrocarbon with values of 36−38%, followed by those of H24 (17−19%) and H25 (13−15%), are remarkable. As can be observed, the area relation between hydrocarbons with even and odd carbon-atom number is around 2, although the odd series is the most abundant one, as in the main edible vegetable oils. However, the even carbon number series is present in important concentrations. This fact must be pointed out as distinctive of Sacha inchi oils when compared with other vegetable oils.[37] Data on hydrocarbons and their relative concentrations in edible oils have been scarcely studied with regard to their usefulness. In this sense it has been proposed as a good parameter for beeswaxes authentication, allowing one to discriminate in the adulterations with paraffin[33] and also to distinguish among olive oil varieties.[38]

To summarize, we will conclude as follows: The concentration ranges of minor and major components of cold-pressing Sacha inchi *P. huayllabambana* oils studied can serve as a valuable guide in forthcoming enlargement of the regulations. Changes and extension in the normative are necessary as it would ensure better control of these oils avoiding the presence of adulteration with other seeds of lower prices. It also serves to encompass analytical parameters of other Sacha inchi species since there are almost no studies concerning this. It should be pointed out that some objective analytical determinations can help to characterize Sacha inchi oils both *P. volubilis* and *P. huayllabambana*. Such is the case of their characteristic sterol profile with its particular campesterol/stigmasterol ratio. Determinations of FAME and TG compositions indicate that *P. huayllabambana* oils are more unsaturated than *P. volubilis*, which affects to the presence of TG molecular species with lower ECN for the first of the species. Results demonstrate that the studied species have a seasonal stable composition, not influenced by the harvest year significantly.

Finally, their high susceptibility to oxidative and hydrolytic alterations is another common characteristic of these valuable oils. At this point it is convenient to emphasize the need to protect the product from the time of seed harvest, passing by the oil extraction up to their marketing, in order to guarantee their unique and valuable properties.

## AUTHOR INFORMATION

### Corresponding Author

*Tel.: +34-9546115550 (ext 299). Fax: +34954611550. E-mail: mcperezcamino@ig.csic.es.

### Funding

The Spanish AECID funded the project AP/036672/11 and the Scientific Institute of Investigation of Lima University (IDIC)- Perú, funded part of this work.

### Notes

The authors declare no competing financial interest.

## ACKNOWLEDGMENTS

We thank Diana Gómez Castillo for her assistance in the laboratory.

## ABBREVIATIONS USED

DG, diglycerides; ECN, equivalent carbon number; FA, free acidity; FAME, fatty acid methyl esters; FFA, free fatty acids; FID, flame ionization detector; GC, gas chromatography; HC, hydrocarbons; RP-HPLC, reverse phase−high-performance liquid chromatography; HPSEC, high performance size exclusion chromatography; i.d., internal diameter; IP, induction periods; I.S., internal standard; L, linoleic acid; Ln, linolenic acid; MG, monoglycerides; oxTG, oxidized triglycerides; PC, glyceridic polar compounds; PV, peroxide value; RI, refractive index; Rt, retention time; Si-SPE, silica solid phase extraction; TG, triglycerides; THF, tetrahydrofuran; TLC, thin layer chromatography; UC, unsaponifiable compounds

## REFERENCES

(1) Hamaker, B. R.; Valles, C.; Gilman, R.; Hardmeier, R. M.; Clark, D.; Garcia, H. H.; Gonzales, A. E.; Kohlstad, I.; Castro, M. Amino acid and fatty acid profiles of the Inca peanut (Plukenetia volubilis). *Cereal Chem.* **1992**, *69*, 461−463.

(2) Cayuela, J. A.; Rada, M.; Pérez-Camino, M. C.; Benaissa, M.; Abdelaziz, E.; Guinda, A. Characterization of artisanally and semi-automatically extracted argan oils from Morocco. *Eur. J. Lipid Sci. Technol.* **2008**, *110*, 1159−1166.

(3) Ourrach, I.; Rada, M.; Pérez-Camino, M. C.; Benaissa, M.; Guinda, A. Detection of argan oil adulterated with vegetable oils: new markers. *Grasas Aceites* **2012**, *63*, 355−364.

(4) Bondioli, P.; Della Bella, L.; Rettke, P. Alpha linolenic acid rich oils. Composition of Plukenetia volubilis (Sacha Inchi) oil from Peru. *Riv. Ital. Sostanze Grasse.* **2006**, *83*, 120−123.

(5) Chasquibol, N.; Moreda, W.; Yácono, J. C.; Pérez-Camino, M. C. Preliminary characterization studies on sacha inchi (*Plukenetia volubilis L.*) seeds and oils grown in San Martín, Perú. *20th International symposium on plant lipids (ISPL)*, Sevilla, Spain; CSIC: Madrid, Spain, 2012; p 167.

(6) Fanali, C.; Dugo, L.; Cacciola, F.; Beccaria, M.; Grasso, S.; Dacha, M.; Dugo, P.; Mondello, L. Chemical characterization of sacha inchi

(*Plukenetia volubilis* L.) oil. *J. Agric. Food Chem.* **2011**, *59*, 13043−13049.
(7) Guillén, M. D.; Ruiz, A.; Cabo, N.; Chirinos, R.; Pascual, G. Characterization of sacha inchi (*Plukenetia volubilis* L.) oil by FTIR spectroscopy and $^{1}$H NMR. Comparison with linseed oil. *J. Am. Oil Chem. Soc.* **2003**, *80*, 755−762.
(8) Gutierrez, L. F.; Rosada, L. M.; Jimenez, A. Chemical composition of sacha inchi (*Plukenetia volubilis* L.) seeds and characteristics of their lipid fraction. *Grasas Aceites* **2011**, *62*, 76−83.
(9) Maurer, N. E.; Hatta-Sakoda, B.; Pascual-Chagman, G.; Rodriguez-Saona, L. E. Characterization and authentication of a novel vegetable source of omega-3 fatty acids, sacha inchi (*Plukenetia volubilis* L.) oil. *Food Chem.* **2012**, *134*, 1173−1180.
(10) NTP. Norma Técnica Peruana 151.400. *Requisitos aceite sacha inchi*, INDECOPI: Lima, Peru, 2009.
(11) Bussmann, R.; Téllez, C.; Glenn, A. *Plukentia huayllambambana* sp.nov (Euphorbiaceae) from upper Amazon of Perú. *Nord. J. Bot.* **2009**, *27*, 313−315.
(12) Rodríguez, A.; Corazon-Guivin, M.; Cachique, D.; Mejia, K.; Del Castillo, D.; Renno, J.; García Dávila, D. Diferenciación morfológica y por ISSR (inter simple sequence repeats) de especies del género plukentia (Euphorbiaceae) de la amazonía peruana: Propuesta de una nueva especie. *Rev. Peru. Biol.* **2010**, *17*, 325−330.
(13) Muñoz Jauregui, A.; Alvarado-Ortíz, C.; Castañeda, B.; Lizaraso, F.; Barnett, E.; Cárdenas, L.; Manco, E. Estudio nutricional de *Plukentia huayllabambana* sp.nov. *Rev. Soc. Quim. Perú* **2013**, *79*, 47−56.
(14) Ruíz, C.; Díaz, C.; Anaya, J.; Rojas, R. Análisis proximal, antinutrientes, perfil de ácidos grasos y de aminoácidos de semillas y tortas de 2 especies de sacha inchi (*Plukenetia volubilis* y *Plukenetia huayllabambana*). *Rev. Soc. Quim. Perú* **2013**, *79*, 29−36.
(15) AOCS Official methods of analysis. Method Ca 5a-40. Determination of free fatty acids. *Official methods and recommended practices of the AOCS.*; American Oil Chemists' Society: Champaign, IL, USA, 2012.
(16) AOCS Official methods of analysis. Method Ja 8-87. Determination of peroxide value. *Official methods and recommended practices of the AOCS*; American Oil Chemists' Society: Champaign, IL, USA, 2013.
(17) *Commission Regulation (EEC) No. 61/2011. Amending regulation (EEC) No. 2568/91 on the characteristics of olive oil and olive-residue oil and on the relevant methods of analysis*; European Economic Community: Brussels, Belgium, 2011; pp 1−14.
(18) AOCS Official methods of analysis. Method Cd 12b-92. Sampling and analysis of commercial fats and oils: Oil stability index. *Official methods and recommended practices of the AOCS*; American Oil Chemists' Society: Champaign, IL, USA, 1997.
(19) Gutiérrez-Rosales, F. Determinación de la estabilidad oxidativa de aceites de oliva vírgenes: Comparación entre el método del oxígeno activo (A.O.M.) y el método rancimat. *Grasas Aceites* **1989**, *40*, 1−5.
(20) IUPAC Standard Method 2.301. *Standard methods for the analysis of oils, fats and derivatives.* Preparation of fatty acid methyl ester.Blackwell Scientific: Oxford, Great Britain, 1987.
(21) Moreda, W.; Pérez-Camino, M. C.; Cert, A. Improved method for the determination of triacylglycerols in olive oils by high performance liquid chromatography. *Grasas Aceites* **2003**, *54*, 175−179.
(22) IUPAC Standard Method 2.507. *Standard methods for the analysis of oils, fats and derivatives*. Determination of polar fats in frying fats. Blackwell Scientific: Oxford, Great Britain, 1987.
(23) Schoenfelder, W. Determination of monoglycerides, diglycerides, triglycerides and glycerol in fats by means of gel permeation chromatography [C-VI 5b(02)]. *Eur. J. Lipid Sci. Technol.* **2003**, *105*, 45−48.
(24) IUPAC Standard Method 2.302. *Standard methods for the analysis of oils, fats and derivatives*. Determination of FAMES by capillary GC. Blackwell Scientific: Oxford, Great Britain, 1987.
(25) IUPAC Standard Method 2.401. *Standard methods for the analysis of oils, fats and derivatives*.Determination of the unsaponifiable matter. Blackwell Scientific: Oxford, Great Britain, 1987.
(26) IUPAC Standard Method 2.432. *Standard methods for the analysis of oils, fats and derivatives*. Determination of tocopherol and tocotrienols in vegetable oils and fats by HPLC. Blackwell Scientific: Oxford, Great Britain, 1987.
(27) Moreda, W.; Pérez-Camino, M. C.; Cert, A. Gas and liquid chromatography of hydrocarbons in edible vegetable oils. *J. Chromatogr. A* **2001**, *936*, 159−171.
(28) Follegatti-Romero, L.; Follegatti-Romero, C. R.; Piantino, R.; Grimaldi, F.; Cabral, L. Supercritical $CO_2$ extraction of omega-3 rich oil from Sacha inchi (Plukenetia volubilis L.) seeds. *J. Supercrit. Fluids* **2009**, *49*, 323−329.
(29) Liua, Q.; Xua, Y.; Zhanga, P.; Naa, Z.; Tanga, T.; Shia, Y. Chemical composition and oxidative evolution of Sacha Inchi (Pluketia volubilis L.) oil from Xishuangbanna (China). *Grasas Aceites* **2014**, *65*, e012 DOI: http://dx.doi.org/10.3989/gya.075713.
(30) Bozan, B.; Temelli, F. Chemical composition and oxidative stability of flax, safflower and poppy seed and seed oils. *Bioresour. Technol.* **2008**, *99*, 6354−6359.
(31) Cisneros, F. H.; Paredes, D.; Arana, A.; Cisneros-Zevallos, L. Chemical composition, oxidative stability and antioxidant capacity of oil extrated from roasted seeds of sacha inchi (*Plukenetia volubilis* L). *J. Agric. Food Chem.* **2014**, *62*, 5191−5197.
(32) *Norma del CODEX (STAN 210-1999) para aceites vegetales especificados*; Food and Agriculture Organization of the United Nations: Rome, Italy, 1999; pp 1−14).
(33) Jiménez, J.; Bernal, M.; del Nozal, L.; Toribio, J.; Bernal, J. Detection of beeswax adulterations using concentration guide-values. *Eur. J. Lipid Sci. Technol.* **2007**, *109*, 682−690.
(34) Santos, M. F. G.; Marmesat, S.; Brito, E. S.; Alves, R. E.; Dobarganes, M. C.; Santos, M. Major components in oils obtained from Amazonian palm fruits. *Grasas Aceites* **2013**, *64*, 328−334.
(35) Prado, I.; Prado, W. M.; Giufrida, V.; Alvarez, V.; Cabral, S.; Quispe-Condori, M. D. A.; Saldaña, L.; Cardozo Filho, I. Phase Equilibrium Measurements of Sacha Inchi Oil (Plukenetia volubilis) and $CO_2$ at High Pressures. *J. Am. Oil Chem. Soc.* **2011**, *88*, 1263−1269.
(36) NTP. Norma Técnica Peruana 151.400, amendment to NTP 151.400, 2009. *Requisitos Aceite Sacha Inchi*, INDECOPI: Lima, Peru, 2014.
(37) Moreda, W.; Pérez-Camino, M. C.; Cert, A. Neutral lipids: Unsaponifiable matter. In *Handbook of Food Analysis*, 2nd ed., Revised and Expanded; Marcel Dekker: New York, 2004; pp 313−347.
(38) Guinda, A.; Lanzón, A.; Albi, T. Differences in Hydrocarbons of virgin olive oils obtained from several olive varieties. *J. Agric. Food Chem.* **1996**, *44*, 1723−1726.

**Table 1. Film Formulations**

| formulation | PLA (wt %) | PHB (wt %) | ATBC (wt %) | I168 (wt %) | CAT (wt %) |
|---|---|---|---|---|---|
| PLA (control) | 99.8 | | | 0.2 | |
| PLA−ATBC | 84.8 | | 15 | 0.2 | |
| PLA−CAT | 94.8 | | | 0.2 | 5 |
| PLA−ATBC−CAT | 79.8 | | 15 | 0.2 | 5 |
| PLA−PHB | 74.85 | 24.95 | | 0.2 | |
| PLA−PHB−ATBC | 63.6 | 21.2 | 15 | 0.2 | |
| PLA−PHB−CAT | 71.1 | 23.7 | | 0.2 | 5 |
| PLA−PHB−ATBC−CAT | 59.85 | 19.95 | 15 | 0.2 | 5 |

On the other hand, current worldwide trends to reduce the use of food additives have given way to investigations of incorporating additives, such as antimicrobial or antioxidant compounds, into food packaging. These systems are known as active food packaging and offer the opportunity to provide continuous release of active compound from packaging material to the foodstuffs, having an important effect on the shelf life extension without the need of direct incorporation of additives into the final food product. However, active agents could show higher affinity for the polymer matrix than the foodstuffs. Consequently, the design of active packaging systems is aimed to obtain an effective release capacity of active agent from the polymer matrix. It is known that the plasticizer presence increases the polymer chain mobility in PLA−PHB blends,[7,8] and for this reason it is expected that the mass transport of the active agent should be modified,[16] resulting in an effective way to improve the release of the active substance from the polymer matrix.[17] One of the main drawbacks of polymer modifiers is the negative effect of the additives on the thermal stability. Thermal degradation is responsible for serious damage to many polymeric materials during processing.[11] In this sense, antioxidants are chosen as active substances not only to protect food deterioration and extend its shelf life[17,18] but also to protect the polymer matrices from thermo-oxidative degradation during processing[18,19] because antioxidants are able to act with the free radicals formed during thermo-oxidation, blocking further polymer degradation.[20]

Currently, synthetic additives are being replaced by natural preservatives due to safety[16] and environmental concern. Most of the common natural antioxidants are phenolic compounds derived from flavonoids,[18,20] which are sourced primarily from renewable resources and have been in use for centuries. For instance, catechins are flavonoids with multiple biological effects[18] that have gained considerable attention due to their potential benefits on human health[21] related to antimutagenic, antidiabetic, anti-inflammatory, and prevention activities against several kinds of cancer.[22] From a technological aspect, catechins have been suggested as effective natural antioxidants in many polyolefins for active food-packaging applications.[16,18,21] Catechin, one of the major active constituents of green tea, represents a natural food-grade additive that inhibits lipid oxidation, increasing the shelf life of foods,[23] and has a positive acceptance among consumers owing its well-known healthy properties. With regard to the polymers' transformation, the extrusion process is one of the most widely used processing technologies in the packaging industry.[24] Because PLA−PHB blends should be processed in the region from at least 160 °C to below 200 °C,[3] catechin, which is a nonvolatile compound, is optimal for melt processing to avoid or reduce its loss during polymer processing.[18]

The main objective of this work was to develop a biodegradable active packaging based on PLA−PHB blends with added catechin, as antioxidant agent, intended for fatty food-packaging application. These systems were plasticized with ATBC with the dual objective of overcoming ductility required for film manufacturing and uses as well as improving the kinetics of release of catechin from the polymer matrix to the foodstuff. The developed materials were characterized with regard to their structure and nanomechanical and thermal properties. The release capacity of catechin into a fatty food simulant after the release process was tested, as well as its antioxidant effectiveness, and the morphological, structural, and nanomechanical properties were also followed during the material exposure to the selected food simulant.

## MATERIALS AND METHODS

**Materials and Chemicals.** Poly(lactic acid) (PLA 2003D, $M_n$ = 98000 g mol$^{-1}$, 4 wt % D-isomer) was supplied by NatureWorks (USA), and poly(hydroxybutyrate) (PHB, under the trade name PHI) was acquired from NaturePlast (France). Catechin dehydrate (CAT), (−)-epicatechin (EC), Irgafos 168 [tris(2,4-di*tert*-butylphenyl)-phosphate] (I168), acetyl tri-*n*-butyl citrate (ATBC) ($M$ = 402 g mol$^{-1}$, $T_m$ = −80 °C, 98% purity), and 2,2-diphenyl-1-picrylhydrazyl (DPPH) 95% free radical were purchased from Sigma-Aldrich (Madrid, Spain). Methanol (MeOH) and ethanol (EtOH) of HPLC grade were supplied by Merck (Darmstadt, Germany). Water was purified by means of a Milli-Q ultrapure water purification system (Millipore, Bedford, MA, USA).

**Sample Preparation.** Samples were prepared by melt-blending the materials in a microextruder equipped with twin conical corotating screws (MiniLab Haake Rheomex CTW5, Thermo Scientific) with a capacity of 7 cm$^3$. A screw rotation rate of 40 rpm, temperature of 190 °C, and residence time of 1 min were used. Irgafos 168 was incorporated in all cases at 0.2% to protect the polymer during processing steps. The concentration ratios of the obtained films are summarized in Table 1.

**Sample Characterization.** *Field Emission Scanning Electron Microscopy (FESEM).* The film cross sections performed in liquid nitrogen were coated with a thin palladium−gold layer to be observed by FESEM (Supra 25-Zeiss).

*Thermogravimetric Analysis (TGA).* TGA was performed with a thermogravimetric analyzer TGA/SDTA-851e Mettler Toledo (Schwarzenbach, Switzerland). Tests were run under dynamic mode from 30 to 600 °C at 10 °C min$^{-1}$ in air (50 mL min$^{-1}$). The initial degradation temperatures ($T_0$) were determined at 5% mass loss, whereas temperatures at the maximum degradation rate ($T_{max}$) were calculated from the first derivative of the TGA curves (DTG).

*Differential Scanning Calorimetry (DSC).* Dynamic DSC experiments were performed in a Mettler Toledo calorimeter by using two different atmospheres of air (250 mL/min) and nitrogen (50 mL/min) with sample weight about 4 mg in hermetic aluminum pans.

Samples analyzed under air conditions were heated from 30 to 350 °C at a heating rate of 10 °C min$^{-1}$ to determine the maximum temperature at which the polymers degrade (onset oxidation temperature, OOT). OOT values were calculated as the intersection

point between the baseline and the tangent to the degradation peak. Meanwhile, samples analyzed under nitrogen conditions were subjected to a cycle program consisting of a first heating stage from 30 to 180 °C at a heating rate of 10 °C $min^{-1}$, followed by a cooling process to 30 °C at 30 °C $min^{-1}$ and subsequent heating to 250 °C to erase the materials' thermal history. The glass transition temperature ($T_g$) was taken at the midpoint of heat capacity changes. The melting temperature ($T_m$) and cold crystallization temperature ($T_{cc}$) were obtained from the second heating, and the degree of crystallinity ($\chi_c$) was calculated through eq 1

$$\chi_c = 100\% \times \left[\frac{\Delta H_m - \Delta H_c}{\Delta H_m^c}\right] \times \frac{1}{W_{PLA}} \quad (1)$$

where $\Delta H_m$ is the melting enthalpy, $\Delta H_{cc}$ is the cold crystallization enthalpy, and $\Delta H_m^c$ is the melting heat associated with pure crystalline PLA (93 J $g^{-1}$) and WPLA is the proportion of PLA in the blend.[25]

*X-ray Diffraction (XRD).* The crystalline phases of the nanocomposite films were studied by using XRD equipment (Bruker AXS D5005, SCSIE Universitat de València).

Scanning was performed on square film surfaces (15 mm × 15 mm) mounted in an appropriate sample holder. The patterns for profile fitting were obtained from a diffractometer using Cu K$\alpha$ radiation with a scanning step of 0.02° between 2.5° and 40° in 2$\theta$ with a collection time of 10 s per step, and the voltage was held at 40 kV.

*Wettability.* The surface wettability of films was evaluated by measuring the water contact angle with an Easy-Drop Standard goniometer FM140 (Krüss GmbH, Hamburg, Germany) equipped with a camera and analysis software (Drop Shape Analysis SW21; DSA1). Samples for wettability measurements were prepared as disk films with an average thickness between 180 and 230 $\mu$m by a compression molding process at 180 °C in a hot press (Mini C 3850, Caver, Inc., Wabash, IN, USA). The contact angle was calculated by randomly adding 5 drops of distilled water (2 $\mu$L) with a syringe onto the film surface at room temperature, and the average values of 10 measurements for each drop were used.

*Release Studies.* Release studies of the antioxidant flavonoid catechin were conducted by the determination of the specific migration into a solution of 50% ethanol as a fatty food simulant (simulant D1)[26] at 40 °C.

Release tests were performed by total immersion of preweighed rectangular strip film pieces (80 ± 0.099 mm × 3.40 ± 0.26 mm × 1.20 ± 0.14 mm) in 10 mL of food simulant contained in glass-stoppered tubes with PTFE closures at 40 °C. For fatty food products that will be stored at ambient conditions (temperatures between 20 and 40 °C) during not more than 30 days, legislation orders that food packaging materials should be assayed at contact temperature in worst foreseeable use of 40 °C for 10 days. In this work, the release test was conducted during 20 days. Thus, samples were taken at 1, 5, 10, and 20 days. Working standard catechin solution in the food simulant and pure simulant were run simultaneously with the release test to check for interferences, and all samples were performed in triplicate.

*Measurement of Released Antioxidant.* The released catechin was measured after the contact period; an aliquot of each simulant was filtered through an Acrodisc PTFE CR 13 mm, 0.2 $\mu$m filter (Waters, Milford, MA, USA) and quantified by HPLC-PDA-FL. A Waters 2695 HPLC system with a gradient pump and automatic injector was used for high-performance liquid chromatography (HPLC) analysis equipped with a stainless steel column packed with SunFire C18 (150 mm × 3.0 mm, 3.5 $\mu$m) (Waters) kept at 35 °C following the methodology described by Castro López et al.[16] The method consisted of a two-solvent gradient elution at a flow rate of 0.5 mL $min^{-1}$. Mobile phase was composed by water (A) and methanol (B). The following gradient elution profile was used: Mobile phase composition started at 25% B and was maintained for 0.5 min. Then, it was linearly increased to 40% B in 4.5 min, to 60% B in 1 min, and to 100% B in 2 min. Finally, it was maintained for 3 min and brought back to recover the initial chromatographic conditions. Detection was performed on a photodiode array detector (PDA, model 996 UV) set in the range of 200−400 nm (277 nm output signal as a quantification wavelength) coupled in series with a fluorescence detector (FL, model 2475, Waters) with an excitation wavelength of 280 nm and an emission wavelength of 310 nm.[21] Output signals were monitored and processed with a personal computer operated under Empower software (Waters). Catechin and epicatechin were identified by means of retention time and UV spectrum. Release data were expressed as the percentage of catechin released into the food simulant after the contact period: amount of catechin released per kilogram of film with reference to the initial amount of catechin loaded per kilogram of film formulation.

The stability of catechin was also evaluated in the simulant under selected exposure conditions by storing a solution of the additive in the simulant in parallel with the release tests and quantified using the same procedure as for the samples.[17]

The release process is normally described by the kinetics of the diffusion of the antioxidant in the film and is expressed by the diffusion coefficient ($D$). $D$ is usually estimated using the Fickian diffusion law.[16,17] When the release of antioxidant reached equilibrium, a rigorous model for describing the migration controlled by Fickian diffusion in a packaging film is used as explained in eq 2:

$$\frac{M_t}{M_{F,\infty}} = 1 - \sum_{n=0}^{\infty} \frac{8}{(2n+1)^2\pi^2} \exp\left[\frac{-D(2n+1)^2\pi^2 t}{L_p^2}\right] \quad (2)$$

$M_t$ is the mass of the migrant in the food simulant at a particular time $t$ (s), $M_{F,\infty}$ is the mass of the migrant in the food at equilibrium, $L_p$ is the film thickness (cm), $D$ is the diffusion coefficient ($cm^2$ $s^{-1}$), and $t$ (s) is time.

Nevertheless, when release is slow and equilibrium is not reached at the end of the experiment, with the boundary condition of $M_t/M_p < 0.6$, eq 3 can be used:

$$\frac{M_t}{M_p} = \frac{4}{L_p}\left(\frac{Dt}{\pi}\right)^{1/2} \quad (3)$$

$M_p$ is the initial loading of antioxidants in the film, $D$ is estimated from the slope of the plot of $M_t/M_p$ versus $t^{1/2}$, and the intersection with the $x$-axis represents the time lag.

*Antioxidant Activity.* The antioxidant effectiveness of development materials was measured according to the DPPH method by determining the absorbance of release medium at different times by means of a UV−vis spectrophotometer at 517 nm. The antioxidant activity was obtained according to eq 4

$$I\ (\%) = \left(\frac{Abs_{control} - Abs_{sample}}{Abs_{control}}\right) \times 100\% \quad (4)$$

where $I$ (%) is the percentage of inhibition. The results were calculated in percent of inhibition as the mean of three replicates, and they were expressed as the equivalent of gallic acid (GA) concentration (ppm) by using a calibrated curve of gallic acid concentration versus $I$ (%).

*Nanomechanical Analysis.* The mechanical hardness ($H$) and elastic modulus ($E$) properties of films before release studies and after 10 days of contact with food simulant D1 were determined by a nanoindenter machine G-200 (Agilent Technologies, Santa Clara, CA, USA). All samples were indented in the same experiment. All samples before release studies and those after 10 days in food simulant were indented during the same test. Indentations were performed at maximum 2000 nm constant depth using a Berkovich diamond tip. An array of 16 indentations was performed for each sample. The area function that is used to estimate the contact area at low depths was previously calibrated in fused silica. The stiffness required to calculate the contact area beyond indenter and elastic modulus was obtained by means of the continuous stiffness measurement (CSM) technique.[27,28] The CSM technique provides in-depth profiles of the stiffness response and, subsequently, in-depth profiles of $H$ and $E$.

*Statistical Analysis.* Experimental data were statistically analyzed with OriginPro 8 software. One-way analysis of variance (ANOVA) was carried out, and significant differences among formulations were

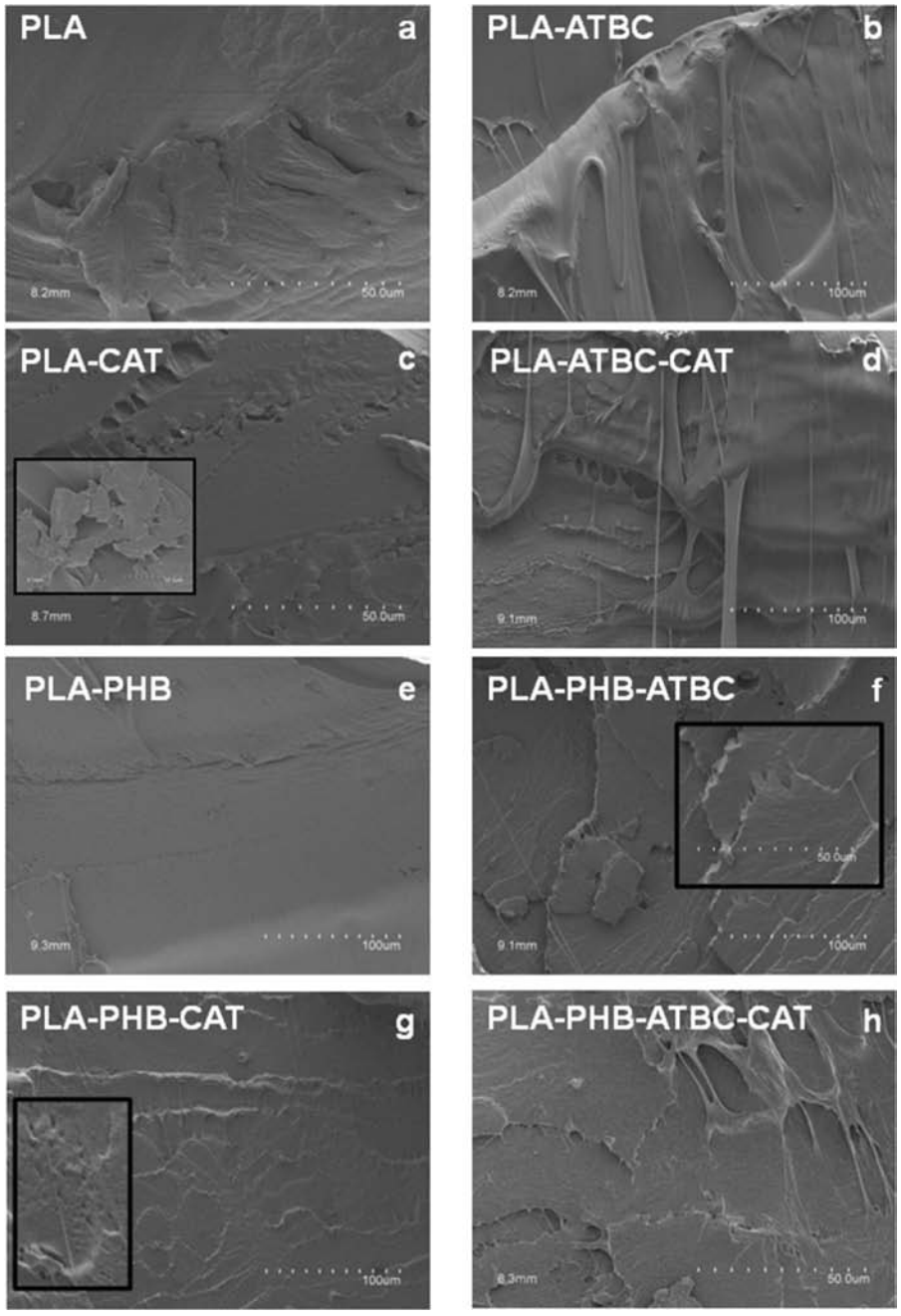


**Figure 1.** Microstructure of fracture surface of unplasticized (left side) and plasticized films (right side).

recorded at the 95% confidence level according to Tukey's post hoc test.

## RESULTS AND DISCUSSION

**Morphological Characterization.** Figure 1 shows FESEM images of cryofractured surfaces of unplasticized (left side) and plasticized films (right side). Whereas unplasticized films showed a smooth fracture, plasticized samples showed a clear plastic behavior with no apparent phase separation. These results show that ATBC is well incorporated into the PLA and PLA−PHB matrices in agreement with previous observations.[8] The characteristic plastic behavior was more evident in PLA−ATBC (Figure 1b) and PLA−ATBC−CAT (Figure 1d) than in plasticized PLA−PHB counterparts (Figure 1f ,h). The PLA and PLA−PHB films incorporated with CAT appear to be more porous without a plain smoothness (Figure 1c,g).

**Thermal Characterization.** *Thermogravimetric Analysis.* The thermal decomposition was studied by TGA and DTG (Figure 2). Stabilized with catechin and unstabilized PLA and plasticized PLA materials decomposed in a one-step process (Figure 2a), whereas PLA−PHB blend counterparts decomposition took place in two well-separated steps. In the first degradation process the total weight loss is close to 25% and corresponds to the degradation of PHB, and the second stage is related with the degradation of PLA. Figure 2b shows that PHB decreases the thermal stability of the final formulation in accordance with previous results.[7,8]

Table 2 also summarizes the main thermal parameters obtained by TGA and DTG. Whereas ATBC shifted the $T_0$ to


dx.doi.org/10.1021/jf5029812 | J. Agric. Food Chem. 2014, 62, 10170−10180

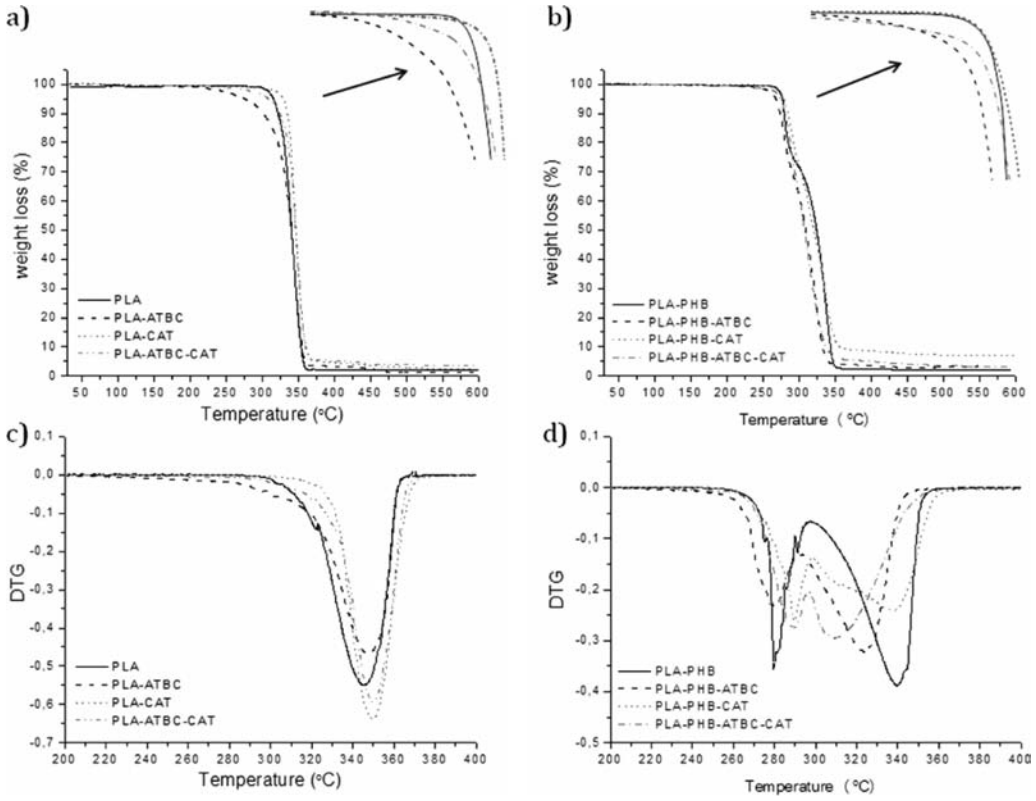


**Figure 2.** TGA and DTG of PLA-based (a, c) and PLA−PHB-based (b, d) films.

**Table 2. TGA and DSC Thermal Parameters of PLA and PLA−PHB Samples**

| | $T_0$ (°C) | $T_{max}$ PHB (°C) | $T_{max}$ PLA (°C) | OOT (°C) | $T_g$ (°C) | $T_{cc}$ (°C) | $T_m$ (°C) | $\Delta H_{cc}$ (J/g) | $\Delta H_m$ (J/g) | $\chi_c$ (%) |
|---|---|---|---|---|---|---|---|---|---|---|
| PLA | 315.7 | | 345.5 | 265.7 | 63.8 | 118.1 | 153.4 | 24.5 | 27.9 | 3.6 |
| PLA−ATBC | 276.0 | | 346.5 | 232.0 | 45.81 | 95.9 | 153.8 | 22.3 | 25.0 | 3.5 |
| PLA−CAT | 329.3 | | 349.6 | 320.2 | 64.7 | 129.6 | 154.1 | 12.6 | 15.3 | 3.1 |
| PLA−ATBC−CAT | 308.8 | | 350.1 | 299.3 | 54.4 | 115.8 | 145.0 | 24.5 | 27.1 | 3.4 |
| PLA−PHB | 275.0 | 279.3 | 339.7 | 267.7 | 63.2 | 130.0 | 158.6 | 8.5 | 11.9 | 4.8 |
| PLA−PHB−ATBC | 268.4 | 279.4 | 323.8 | 271.8 | 60.6 | 106.3 | 157.0 | 19.0 | 22.4 | 5.7 |
| PLA−PHB−CAT | 279.3 | 289.5 | 337.8 | 280.0 | 62.1 | 150.0 | 155.4 | 0.1 | 7.2 | 4.9 |
| PLA−PHB−ATBC−CAT | 275.1 | 289.5 | 309.6 | 281.2 | 57.7 | 126.0 | 152.5 | 5.3 | 8.1 | 5.1 |

lower degradation temperatures, catechin led to an increment in $T_0$, delaying the beginning of the thermal decomposition process in all cases indicative of an effective stabilizing effect. As well, catechin presence leads to a displacement of the $T_{max}$ of PLA toward slightly higher values in PLA and plasticized PLA samples (PLA−CAT and PLA−ATBC−CAT). However, in PLA−PHB blends at the same time as the $T_{max}$ corresponding to the degradation of PHB showed a considerable increment of about 10 °C with catechin addition, the $T_{max}$ of PLA was shifted to lower values, and this behavior was particularly noticeable in PLA−PHB−ATBC−CAT, where the reduction was about 14 °C. The antioxidant capacity of catechin protects the polymer thermal degradation at the first stage leading the $T_{max}$ of the blends to higher values, and then the degradation at higher temperatures is accelerated.

*Differential Scanning Calorimetry.* The OOT was used to evaluate the effectiveness of catechin to increase the polymer stability under oxidative atmosphere, and results are summarized in Table 2. OOT values clearly increased with the addition of catechin in all cases, showing its effectiveness to protect PLA, PLA−PHB, plasticized PLA, and plasticized PLA−PHB against oxidation, as was already commented for TGA results above. However, PLA-based materials stabilized with catechin showed higher values of OOT than PLA−PHB counterparts, in good accordance with $T_0$ values. It must be noted that whereas ATBC decreases the thermal stability of PLA, it slightly increases the thermal stability of PLA−PHB blend due to the fact ATBC improves the interaction between both polymers.[8] Consequently, catechin could be considered as a natural stabilizer for PLA, PLA−PHB, and their plasticized systems.

Panels a and b of Figure 3 show the thermograms for the DSC second heating where it is possible to observe the glass transition temperature ($T_g$), the cold crystallization exotherm ($T_{cc}$), and the melting endotherm ($T_m$) of the PLA-based (Figure 3a) and PLA−PHB-based (Figure 3b) films, showing that the cooling conditions applied did not produce the crystallization of PLA. DSC thermal properties are also summarized in Table 2. ATBC induced the depression in $T_g$ of all samples, confirming its plasticizing effect also reported and discussed in a previous study.[8] Moreover, the lowest $T_g$ values were presented by PLA−ATBC followed by PLA−ATBC−CAT due to their higher plastic behavior, in good

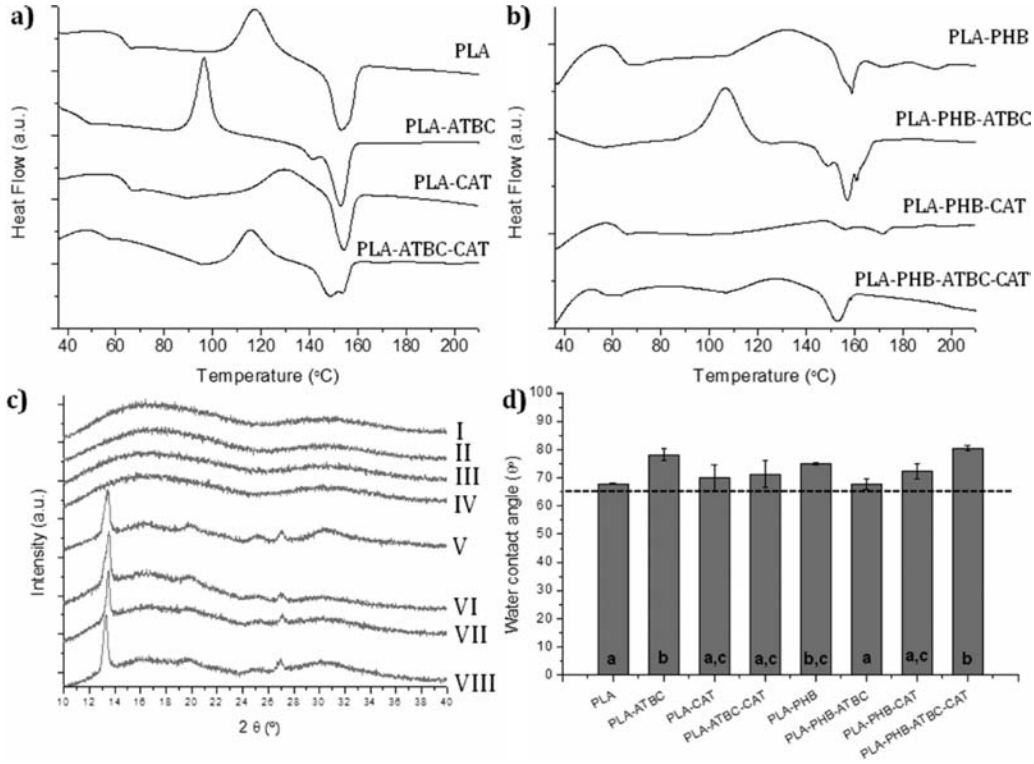


**Figure 3.** DSC second heating scan of (a) PLA-based films and (b) PLA−PHB-based films. (c) X-ray diffraction patterns of (I) PLA, (II) PLA−ATBC, (III) PLA−CAT, (VI) PLA−ATBC−CAT, ( V) PLA−PHB, (VI) PLA−PHB−CAT, and (VII) PLA−PHB−ATBC−CAT. (d) Contact angle measurements of PLA-based and PLA−PHB-based films. Different letters on the bars indicate significant differences between formulations ($p < 0.05$).

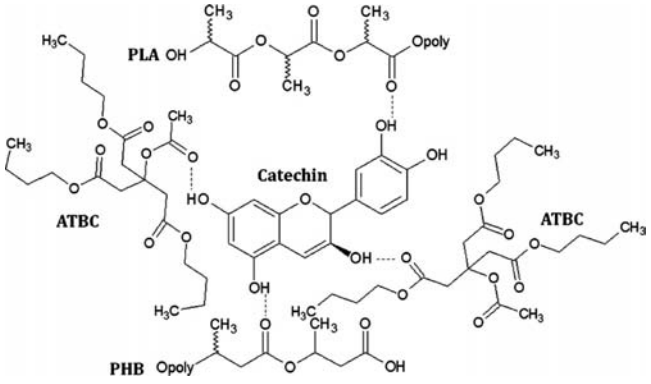


**Figure 4.** Proposed molecular interaction between PLA, PHB, ATBC, and catechin.

accordance with FESEM micrographs. ATBC also shifted the $T_{cc}$ to lower values, whereas catechin shifted the $T_{cc}$ to higher temperatures probably as a result of increased crystal nuclei density, which requires more thermal energy to crystallize PLA. Catechin presence also promoted faster crystallization of PLA and PLA−PHB and the plasticized systems, most likely due to hydrogen-bonding interactions between catechin hydroxyl groups and carbonyl groups of PLA and PHB. Figure 4 shows the proposed molecular interaction. Similar findings were previously reported by López de Dicastillo et al., who found an induction effect of catechin on the crystal nucleation of maleic anhydride modified poly(propylene) (MAPP) and also the formation of intermolecular hydrogen bonds between catechin and poly(propylene) (PP).[18]

PHB slightly increased $T_m$ temperature with respect to the neat PLA,[7] suggesting miscibility between both polymers ascribed to a transesterification reaction between PLA and PHB chains during melt blending.[4] Although PLA can crystallize showing different polymorphisms, namely, the alpha ($\alpha$), beta ($\beta$), and gamma ($\gamma$) forms, from the melt PLA crystallizes in the $\alpha$ form.[29] Neat PLA showed the $T_m$ corresponding to the melt of stable $\alpha$ homocrystals developed during the heating process. Meanwhile, plasticized PLA systems (PLA−ATBC and PLA−ATBC−CAT) showed a multimelting behavior ascribed to the presence of different PLA crystals. Disordered $\alpha'$ crystals are formed when the $T_{cc}$ is below 110 °C.[30] PLA is known for its slow crystallization rate.[31,32] However, the crystallization rate of PLA is higher at temperatures between 100 and 118 °C,[33] at which disorder-to-order phase transition ($\alpha'$ to $\alpha$) takes place.[30] Similar findings were observed in PLA plasticized with oligomeric lactic acid (OLA).[34] On the other hand, the presence of multimelting temperatures in PLA−PHB blends, after the PLA melting peak, at around 175 and 185 °C corresponds to the as-formed PHB crystals during blending process and recrystallized PHB crystals formed during DSC heating, respectively.[3,5] Different behavior was observed in plasticized PLA−PHB blends (PLA−PHB−ATBC and PLA−PHB−ATBC−CAT). PLA−PHB−ATBC showed the $T_{cc}$ below 110 °C and as a consequence the multimelting PLA peak as well as the as-formed and recrystallized PHB crystals, whereas the multimelting behavior was not detected for PLA−PHB−ATBC−CAT. The CAT presence considerably shifted the $T_{cc}$ from 106.3 °C in PLA−PHB−ATBC to 126.0 °C in PLA−PHB−ATBC−CAT, avoiding the formation of disordered PLA $\alpha'$ crystals. The nonappearance of as-formed and recrystallized PHB crystals

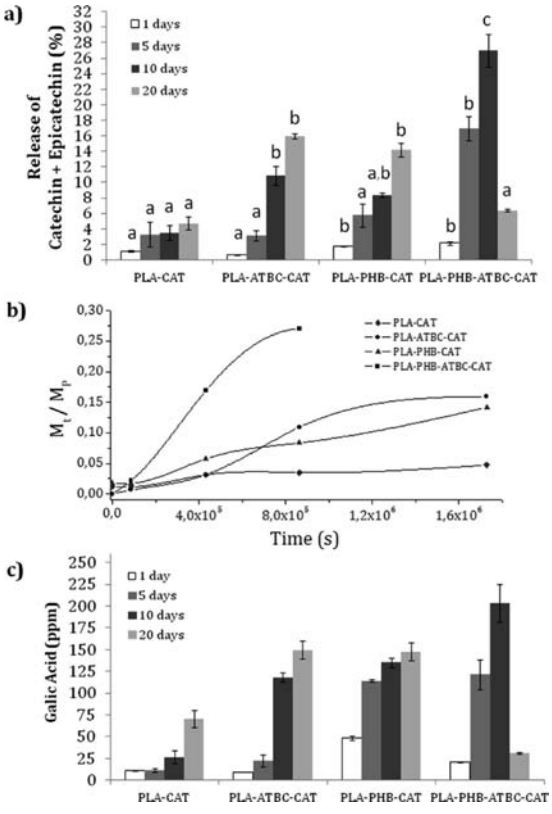


**Figure 5.** (a) Catechin (%) released from PLA-based and PLA−PHB-based materials calculated by means of HPLC-PDA. (b) Diffusion kinetics of catechin from PLA-based and PLA−PHB-based materials. (c) Antioxidant activity of catechin expressed as gallic acid concentration (ppm) measured by DPPH radical scavengers. Different letters on the bars within the same day indicate significant differences between formulations ($p < 0.05$).

could be related with an improvement in the interfacial adhesion between PLA, PHB, and ATBC due to CAT presence.

*X-ray Diffraction.* Figure 3c shows a comparative plot of the crystalline profiles of films. PLA had one broad diffraction peak centered at $2\theta = 15°$ and a smaller one centered at $2\theta = 31°$. The X-ray patterns of PLA−ATBC, PLA−CAT, and PLA−ATBC−CAT are very similar to that of neat PLA. The presence of crystalline PHB showed an increase in the crystallinity of PLA in the PLA−PHB blend, in good accordance with the increase of the degree of crystallinity calculated by DSC (Table 2). The characteristic reflection peaks of PHB at $2\theta = 13.5°$ and $2\theta = 16.9°$, as well as the weak peaks at higher $2\theta$, are observed because the crystal growth rate of PHB is higher and faster than that of PLA.[35]

*Wettability.* The surface hydrophobicity is an important issue in materials intended for food-packaging applications because they are required to protect foodstuffs from humidity during transport, handling, and storage.[9] Thus, water contact angle measurements were conducted to study the water absorption of these material surfaces (Figure 3d). The line at 65 $\theta°$ represents the limit value between a hydrophilic surface ($\theta° < 65°$) and a hydrophobic surface ($\theta° > 65°$). All studied formulations showed values higher than 65°, showing a poor affinity of the water to the material surfaces and highlighting their potential use for packaging applications. The addition of 15 wt % ATBC and 25 wt % of PHB significantly increased the water resistance of PLA ($p < 0.05$). Meanwhile, the wettability of PLA and PLA−PHB remained practically unchanged ($p > 0.05$) with the addition of 5 wt % of catechin in PLA−CAT and PLA−PHB−CAT.

PLA−PHB−ATBC−CAT film resulted in material with a surface hydrophobicity increased ($p < 0.05$) with respect of those of PLA−PHB−ATBC and PLA−PHB−CAT. One possible explanation for this behavior could be that there is a strong interaction of catechin hydroxyl groups with PLA and PHB chains and the interaction is also improved with the presence of ATBC. As a consequence, catechin hydroxyl groups did not show surface orientation affecting the surface chemical properties, leading to an increase in the surface hydrophobicity.

*Catechin Release.* The release of the catechin from PLA-based and PLA−PHB-based developed materials expressed as the percentage of catechin and epicatechin released into food simulant D1 at 1, 5, 10, and 20 days and their diffusion kinetics obtained by HPLC-PDA are shown in Figure 5, panels a and b, respectively. The incorporation of ATBC showed a significant increase of the release capacity from PLA and PLA−PHB matrices. After 10 contact days, levels of released catechin increased about 3 times in both PLA and PLA−PHB with respect to the corresponding films without plasticizer. Castro-Lopez et al. also showed an improvement in the release of antioxidants from a polypropylene matrix due to the use of plasticizers in the formulations with increased diffusion coefficients between 1 and 2 orders of magnitude.[16] Diffusion coefficients were estimated from Figure 5b and from the slope of the curve obtained by eq 3, and they also showed the positive effect of the presence of plasticizer on the release of catechin from PLA-based and PLA−PHB-based materials. Increased values from $1.9 \times 10^{-12}$ cm$^2$ s$^{-1}$ in PLA−CAT to $8.3 \times 10^{-11}$ cm$^2$ s$^{-1}$ in PLA−CAT−ATBC and from $2.6 \times 10^{-11}$ cm$^2$ s$^{-1}$ in PLA−PHB−CAT to $3.5 \times 10^{-10}$ cm$^2$ s$^{-1}$ in PLA−PHB−CAT−ATBC were observed due to the ability of plasticizer to increase the polymer chain mobility and, thus, the release of catechin.

It is expected that the higher amount of crystalline regions of PLA−PHB blends slowed the diffusion of catechin. However, the addition of PHB showed somewhat an increment in the release of active compound in comparison with those formulations without PHB, particularly noticeable in PLA−PHB−ATBC−CAT film (Figure 5a). The incorporation of PHB produced only an induction period in the diffusion process, due to the limited polymer chain mobility in PLA−PHB-based blends, leading to an increase in time lag from 30 s in PLA−CAT to 209 s and to 252 s in PLA−PHB−CAT and PLA−PHB−ATBC−CAT, respectively. This increase in the time lag can be justified by the increase of interactions between catechin and the PLA−PHB blend matrix. However, once the diffusion process started, the release of catechin became faster in PHB-added samples as shown by the increment in 1 order of magnitude of the diffusion coefficient with respect to PLA-based material counterparts. This behavior could be ascribed to the higher affinity of the simulant D1 with less polar catechin-added PLA−PHB blends in comparison with catechin-added PLA equivalents, as was already commented for the wettability test. Thus, the higher penetration capacity of simulant D1 in the PLA−PHB matrix than in PLA matrix, after the required time lag, accelerated the catechin release process as a function of time.

Additionally, after the 10 contact days, enhanced crystallinity of all tested materials was observed by XRD (Figure 6). The diffraction patterns clearly show an increased intensity of the

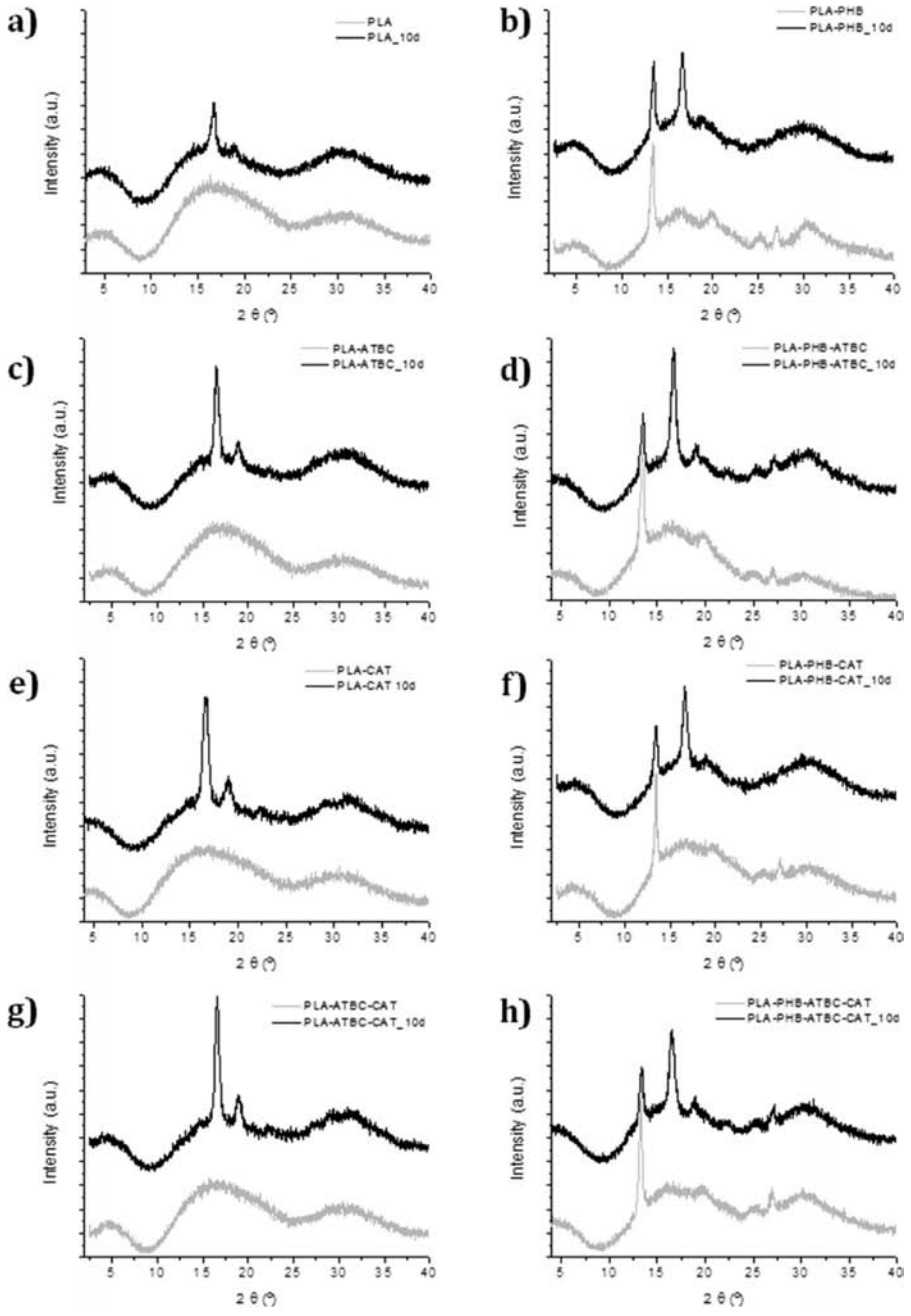


**Figure 6.** X-ray diffraction patterns of PLA-based and PLA−PHB-based films before and after 10 days of contact with simulant D1.

peak at $2\theta = 16.5°$ for all formulations, attributed to the typical $\alpha$ crystal form of the crystalline phase of PLA,[34] showing the highest intensity in plasticized samples. Thus, the higher penetration capacity of simulant D1 in PLA−PHB blends at the same time as the increase of crystallinity of amorphous PLA based materials led to comparable catechin release profiles for PLA−ATBC−CAT and PLA−PHB−CAT at 5, 10, and 20 contact days in simulant D1.

The highest diffusion process was observed for PLA−PHB−ATBC−CAT samples between 0 and 10 days. However, at the highest period of contact time studied here of 20 days, a reduction of catechin concentration occurred, showing the not possible lower value than those obtained at 5 and 10 days. This unexpected result could be explained by the feasible interaction between the free catechin molecules in the food simulant, possible forming dimers or oligomers, which cannot be quantified by the experimental methodology used here. In fact, in a food simulant the released compound is dispersed in the food simulant where no oxidation processes are happening, as can occur in a real packaged food environment. The molecules of catechin released from the packaging are expected to interact with food components, jamming oxidation processes.

It should be taken into account that the inherent biodegradability of PLA-based materials could be a drawback in food packaging, where the material structure needs to be guaranteed at least during the food's shelf life.[36] For this reason, the morphology of cross sections of the films after 10 and 20 days exposed to simulant D1 was also studied by FESEM (Figure 7). PLA-based and PLA−PHB-based materials preserved their structure at 10 days of the migration test. Meanwhile, PLA, PLA−ATBC (Figure 7a), and PLA−PHB and


dx.doi.org/10.1021/jf5029812 | J. Agric. Food Chem. 2014, 62, 10170−10180

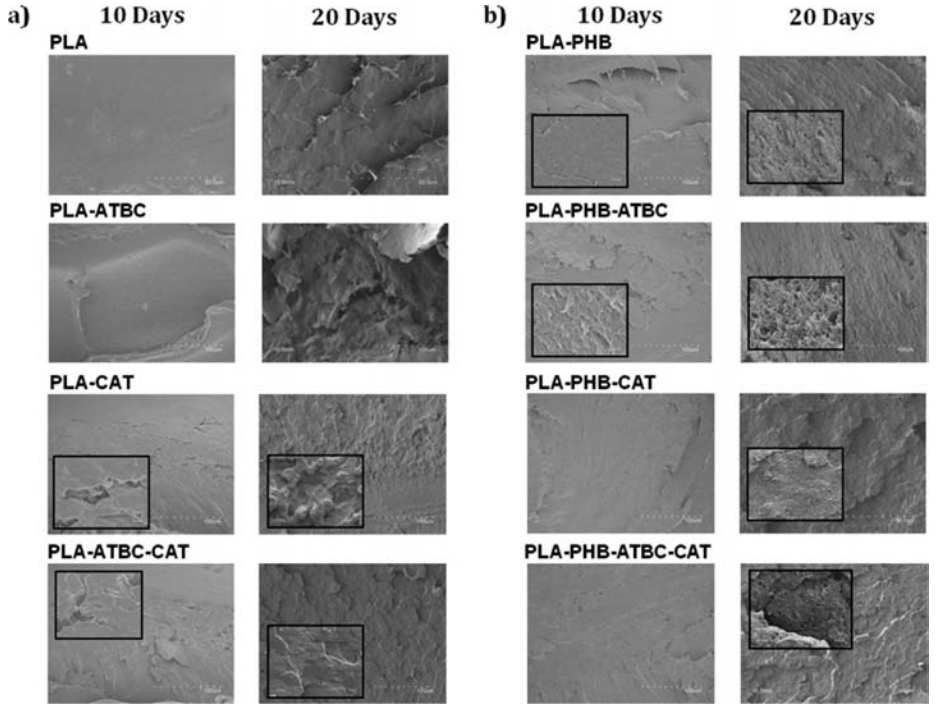


**Figure 7.** FESEM images of (a) PLA-based materials and (b) PLA−PHB-based materials after 10 and 20 days of exposure to simulant D1.

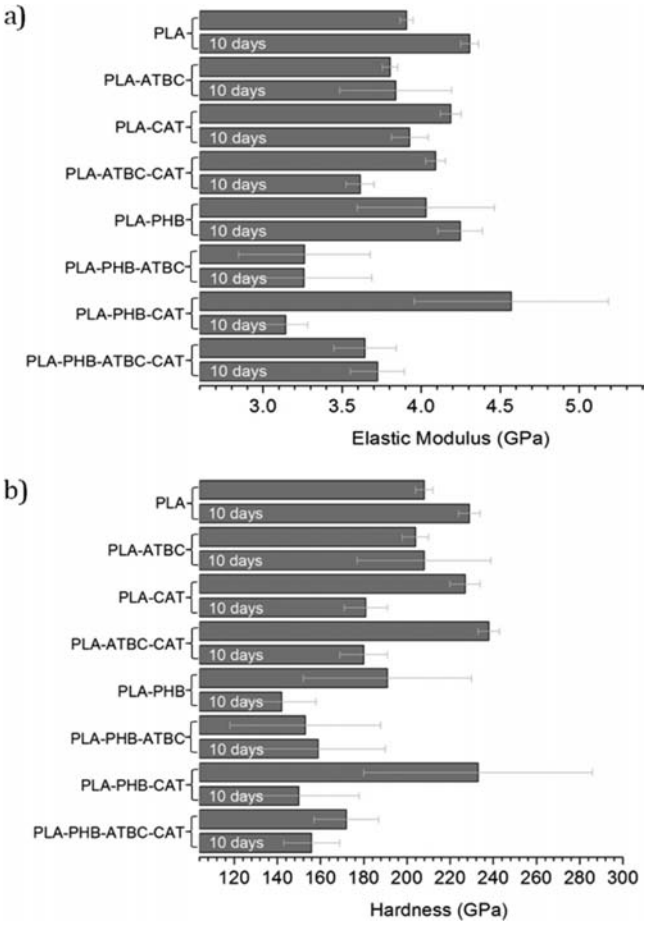


**Figure 8.** Nanomechanical results of materials essayed before and after 10 days in contact with simulant D1: (a) elastic modulus ($E$); (b) nanohardness ($H$).

PLA−PHB−ATBC (Figure 7b) showed increased plastic behavior at 20 days caused by the plasticization effect produced by the simulant dispersion into the polymer matrix. In most cases, the materials become rougher with increasing time in contact with food simulant. As well, at 20 days some cavities were formed in PLA catechin-incorporated samples (Figure 7a), whereas many cavities were observed in PLA−PHB catechin incorporated samples (Figure 7b) as a result of the higher loss of catechin in those samples. This observation supported our conclusion that higher levels of catechin than those obtained here should be released from PLA−PHB−ATBC−CAT sample after 20 days in contact with food simulant.

All catechin-incorporated materials showed an effective release of catechin in worst foreseeable use conditions between 0 and 10 days as indicated by current legislation for fatty food intended to be transported, handled, and stored at ambient conditions.

*Antioxidant Activity.* The effectiveness of the developed materials as antioxidant packaging systems was demonstrated by the reduction of stable free radical DPPH caused by catechin presence in the food simulant, and the obtained results are expressed as gallic acid (GA) concentration (Figure 5c). As expected, the antioxidant activity shows comparative tendency to the catechin release. It is known that the solubility characteristics of the antioxidant can determine its effectiveness.[37] Catechin shows high solubility in ethanol (50 g $L^{-1}$),[18] and consequently catechin-incorporated materials usually show high activity in ethanol-containing simulants.[16,18,22,38,39] Thus, the high affinity of catechin for fatty food simulants and its high antioxidant activity give good reasons for its addition in plasticized PLA and PLA−PHB materials for fatty foodstuff.

*Mechanical Features of the Films.* The mechanical behavior of all samples before and after 10 days in contact with food simulant D1 was assayed by means of a nanoindenter test. The mean of elastic modulus ($E$) and hardness ($H$) values for each

sample was calculated in the range from 500 to 1000 nm. The obtained values are shown in Figure 8. As expected, plasticized samples before release studies showed lower $H$ and $E$ values than unplasticized ones, showing the effectiveness of ATBC to plasticize PLA and PLA−PHB systems.[8,10] On the other hand, catechin-added samples showed increased $H$ and $E$ values with respect to their counterparts without catechin. This result confirms that catechin produced a somewhat reinforcing effect blocking the elastic and plastic deformation mechanisms owing to the enhancement of the materials' interfacial adhesion in the blend, in accordance with DSC experiments (see Differential Scanning Calorimetry). An increase in PLA and PLA−PHB modulus was also observed in PLA−PHB blends reinforced with cellulose nanocrystals[9] ascribed to an enhancement in the interface interaction between PLA and PHB due to nanocellulose presence.[3]

The nanomechanical results of assayed samples after release studies showed scattered values, probably due to residues of simulant D1 and/or released components from the polymer matrices on their surfaces. This activated surface is able to affect the short distance forces between the surface and nanoindenter tip. After 10 days in contact with simulant D1, catechin-added materials revealed in general a drastic diminution of $E$ and $H$ values as a result of the release of catechin to the food simulant, with the exception of PLA−PHB−ATBC−CAT, which mainly maintained the mechanical properties without significant changes. This result highlights an additional positive effect of catechin incorporation to plasticized PLA−PHB systems.

## AUTHOR INFORMATION


### Corresponding Author

*(M.P.A.) E-mail: marina.arrieta@gmail.com.



### Funding

This work has been supported by the Spanish Ministry of Economy and Competitiveness (MAT2011-28648-C02-01 and MAT2011-28468-C02-02). M.P.A. is a recipient of a Santiago Grisolía Fellowship (Generalitat Valenciana) (GRISOLIA/2011/007).


### Notes

The authors declare no competing financial interest.

## ACKNOWLEDGMENTS


We gratefully acknowledge Prof. M. Dolores Salvador (Polytechnic University of Valencia) for her assistance with nanomechanical analysis.


## ABBREVIATIONS USED

PLA, poly(lactic acid); PHB, poly(hydroxybutyrate); ATBC, acetyl(tributyl citrate); CAT, catechin dehydrate; EC, (−)-epicatechin; I168, Irgafos 168 [tris(2,4-di*tert*-butylphenyl)-phosphate]; DPPH, 2,2-diphenyl-1-picrylhydrazyl; MeOH, methanol; EtOH, ethanol; FESEM, field emission scanning electron microscopy; TGA, thermogravimetric analysis; DTG, first derivative of the TGA curve; DSC, differential scanning calorimetry; $T_g$, glass transition temperature; $T_m$, melting temperature; $T_{cc}$, crystallization temperature; $\chi_c$, degree of crystallinity; $\Delta H_m$, melting enthalpy; $\Delta H_{cc}$, cold crystallization enthalpy; $\Delta H_m^c$, melting heat of pure crystalline PLA; XRD, X-ray diffraction; HPLC, high-performance liquid chromatography; PDA, photodiode array detector; FL, fluorescence detector; $D$, diffusion coefficient; $M_t$, mass of the migrant in the food simulant at time $t$; $t$, time; $M_{F,\infty}$, mass of the migrant in the food at equilibrium; $L_p$, film thickness; $I$ (%), percentage of inhibition; GA, gallic acid; $H$, hardness; $E$, elastic modulus; CSM, continuous stiffness measurement; OOT, oxidation onset temperature; MAPP, maleic anhydride grafted into polypropylene; PP, polypropylene; OLA, oligomeric lactic acid

## REFERENCES


(1) Auras, R.; Harte, B.; Selke, S. An overview of polylactides as packaging materials. *Macromol. Biosci.* **2004**, *4*, 835−864.

(2) Armentano, I.; Bitinis, N.; Fortunati, E.; Mattioli, S.; Rescignano, N.; Verdejo, R.; Lopez-Manchado, M. A.; Kenny, J. M. Multifunctional nanostructured PLA materials for packaging and tissue engineering. *Prog. Polym. Sci.* **2013**, *38*, 1720−1747.

(3) Arrieta, M. P.; Fortunati, E.; Dominici, F.; Rayón, E.; López, J.; Kenny, J. M. Multifunctional PLA−PHB/cellulose nanocrystal films: processing, structural and thermal properties. *Carbohydr. Polym.* **2014**, *107*, 16−24.

(4) Zhang, L.; Xiong, C.; Deng, X. Miscibility, crystallization and morphology of poly(β-hydroxybutyrate)/poly(D,L-lactide) blends. *Polymer* **1996**, *37*, 235−241.

(5) Zhang, M.; Thomas, N. L. Blending polylactic acid with polyhydroxybutyrate: the effect on thermal, mechanical, and biodegradation properties. *Adv. Polym. Technol.* **2011**, *30*, 67−79.

(6) Ni, C.; Luo, R.; Xu, K.; Chen, G. Q. Thermal and crystallinity property studies of poly(L-lactic acid) blended with oligomers of 3-hydroxybutyrate or dendrimers of hydroxyalkanoic acids. *J. Appl. Polym. Sci.* **2009**, *111*, 1720−1727.

(7) Arrieta, M. P.; López, J.; Hernández, A.; Rayón, E. Ternary PLA−PHB−limonene blends intended for biodegradable food packaging applications. *Eur. Polym. J.* **2014**, *50*, 255−270.

(8) Arrieta, M. P.; Samper, M. D.; López, J.; Jiménez, A. Combined effect of poly(hydroxybutyrate) and plasticizers on polylactic acid properties for film Intended for food packaging. *J. Polym. Environ.* **2014**, DOI: 10.1007/s10924-014-0654-y.

(9) Arrieta, M. P.; Fortunati, E.; Dominici, F.; Rayón, E.; López, J.; Kenny, J. M. PLA-PHB/cellulose based films: mechanical, barrier and disintegration properties. *Polym. Degrad. Stab.* **2014**, *107*, 139−149.

(10) Arrieta, M. P.; López, J.; Rayón, E.; Jiménez, A. Disintegrability under composting conditions of plasticized PLA-PHB blends. *Polym. Degrad. Stab.* **2014**, *108*, 307−318.

(11) Arrieta, M. P.; López, J.; Ferrándiz, S.; Peltzer, M. A. Characterization of PLA-limonene blends for food packaging applications. *Polym. Test.* **2013**, *32*, 760−768.

(12) Martino, V. P.; Jiménez, A.; Ruseckaite, R. A.; Avérous, L. Structure and properties of clay nano-biocomposites based on poly(lactic acid) plasticized with polyadipates. *Polym. Adv. Technol.* **2011**, *22*, 2206−2213.

(13) Pillin, I.; Montrelay, N.; Grohens, Y. Thermo-mechanical characterization of plasticized PLA: is the miscibility the only significant factor? *Polymer* **2006**, *47*, 4676−4682.

(14) Jamshidian, M.; Arab Tehrany, E.; Cleymand, F.; Leconte, S.; Falher, T.; Desobry, S. Effects of synthetic phenolic antioxidants on physical, structural, mechanical and barrier properties of poly lactic acid film. *Carbohydr. Polym.* **2012**, *87*, 1763−1773.

(15) European Food Safety Authority. Scientific Opinion on Flavouring Group Evaluation 10, Revision 3 (FGE.10Rev3): Aliphatic primary and secondary saturated and unsaturated alcohols, aldehydes, acetals, carboxylic acids and esters containing an additional oxygenated functional group and lactones from chemical groups 9, 13 and 30. *EFSA J.* **2012**, *10*, 25−63.

(16) Castro López, M. M.; López de Dicastillo, C.; López-Vilariño, J. M.; González-Rodríguez, M. V. Improving the capacity of polypropylene to be used in antioxidant active films: incorporation of plasticizer and natural antioxidants. *J. Agric. Food Chem.* **2013**, *61*, 8462−8470.

(17) Castro López, M. M.; Dopico García, S.; Ares Pernas, A.; López Vilariño, J. M.; González Rodríguez, M. V. Effect of PPG-PEG-PPG on

the tocopherol-controlled release from films intended for food-packaging applications. *J. Agric. Food Chem.* **2012**, *60*, 8163−8170.
(18) López De Dicastillo, C.; Castro-López, M. M.; Lasagabaster, A.; López-Vilariño, J. M.; González-Rodríguez, M. V. Interaction and release of catechin from anhydride maleic-grafted polypropylene films. *ACS Appl. Mater. Interfaces* **2013**, *5*, 3281−3289.
(19) Peltzer, M.; Navarro, R.; López, J.; Jiménez, A. Evaluation of the melt stabilization performance of hydroxytyrosol (3,4-dihydroxyphenylethanol) in polypropylene. *Polym. Degrad. Stab.* **2010**, *95*, 1636−1641.
(20) Samper, M. D.; Fages, E.; Fenollar, O.; Boronat, T.; Balart, R. The potential of flavonoids as natural antioxidants and UV light stabilizers for polypropylene. *J. Appl. Polym. Sci.* **2013**, *129*, 1707−1716.
(21) López de Dicastillo, C.; Castro-López, M. M.; López-Vilarino, J. M.; González-Rodríguez, M. V. Immobilization of green tea extract on polypropylene films to control the antioxidant activity in food packaging. *Food Res. Int.* **2013**, *53*, 522−528.
(22) Castro-López, M. M.; López-Vilariño, J. M.; González-Rodríguez, M. V. Analytical determination of flavonoids aimed to analysis of natural samples and active packaging applications. *Food Chem.* **2014**, *150*, 119−127.
(23) Lante, A.; Friso, D. Oxidative stability and rheological properties of nanoemulsions with ultrasonic extracted green tea infusion. *Food Res. Int.* **2013**, *54*, 269−276.
(24) Torres, A.; Romero, J.; Macan, A.; Guarda, A.; Galotto, M. J. Near critical and supercritical impregnation and kinetic release of thymol in LLDPE films used for food packaging. *J. Supercrit. Fluids* **2014**, *85*, 41−48.
(25) Turner, J. F.; Riga, A.; O'Connor, A.; Zhang, J.; Collis, J. Characterization of drawn and undrawn poly-L-lactide films by differential scanning calorimetry. *J. Therm. Anal. Calorim.* **2004**, *75*, 257−268.
(26) European Commission.. No. 10/2011 of 14 January 2011 on plastic materials and articles intended to come into contact with food. *Off. J. Eur. Union* **2011**, *L12*, 1−89.
(27) Rayón, E.; López, J.; Arrieta, M. P. Mechanical characterization of microlaminar structures extracted from cellulosic materials using nanoindentation technique. *Cell Chem. Technol.* **2013**, *47*, 345−351.
(28) Rayón, E.; Ferrandiz, S.; Rico, M. I.; López, J.; Arrieta, M. P. Microstructure, mechanical and thermogravimetric characterization of cellulosic by-products obtained from the biomass seeds. *Int. J. Food Prop.* **2014**, DOI: 10.1080/10942912.2014.884578.
(29) Navarro-Baena, I.; Kenny, J. M.; Peponi, L. Crystallization and thermal characterization of biodegradable tri-block copolymers and poly(ester-urethane)s based on PCL and PLLA. *Polym. Degrad. Stab.* **2014**, *108*, 140−150.
(30) Zhang, J.; Tashiro, K.; Tsuji, H.; Domb, A. J. Disorder-to-order phase transition and multiple melting behavior of poly(L-lactide) investigated by simultaneous measurements of WAXD and DSC. *Macromolecules* **2008**, *41*, 1352−1357.
(31) Rodríguez, C.; Arencón, D.; Belzunce, J.; Maspoch, M. L. Small punch test on the analysis of fracture behaviour of PLA-nanocomposite films. *Polym. Test.* **2014**, *33*, 21−29.
(32) Courgneau, C.; Ducruet, V.; Avérous, L.; Grenet, J.; Domenek, S. Nonisothermal crystallization kinetics of poly(lactide) − effect of plasticizers and nucleating agent. *Polym. Eng. Sci.* **2013**, *53*, 1085−1098.
(33) Jamshidian, M.; Tehrany, E. A.; Imran, M.; Jacquot, M.; Desobry, S. Poly-lactic acid: production, applications, nanocomposites, and release studies. *Compr. Rev. Food Sci. Food Saf.* **2010**, *9*, 552−571.
(34) Burgos, N.; Martino, V. P.; Jiménez, A. Characterization and ageing study of poly(lactic acid) films plasticized with oligomeric lactic acid. *Polym. Degrad. Stab.* **2013**, *98*, 651−658.
(35) Abdelwahab, M. A.; Flynn, A.; Chiou, B. S.; Imam, S.; Orts, W.; Chiellini, E. Thermal, mechanical and morphological characterization of plasticized PLA-PHB blends. *Polym. Degrad. Stab.* **2012**, *97*, 1822−1828.
(36) Dopico-García, M. S.; Ares-Pernas, A.; González-Rodríguez, M. V.; López-Vilariño, J. M.; Abad-López, M. J. Commercial biodegradable material for food contact: methodology for assessment of service life. *Polym. Int.* **2012**, *61*, 1648−1654.
(37) Gómez-Estaca, J.; López-de-Dicastillo, C.; Hernández-Muñoz, P.; Catalá, R.; Gavara, R. Advances in antioxidant active food packaging. *Trends Food Sci. Technol.* **2014**, *35*, 42−51.
(38) López-De-Dicastillo, C.; Alonso, J. M.; Catalá, R.; Gavara, R.; Hernández-Munoz, P. Improving the antioxidant protection of packaged food by incorporating natural flavonoids into ethylene-vinyl alcohol copolymer (EVOH) films. *J. Agric. Food Chem.* **2010**, *58*, 10958−10964.
(39) López De Dicastillo, C.; Nerín, C.; Alfaro, P.; Catalá, R.; Gavara, R.; Hernández-Muñoz, P. Development of new antioxidant active packaging films based on ethylene vinyl alcohol copolymer (EVOH) and green tea extract. *J. Agric. Food Chem.* **2011**, *59*, 7832−7840.

expression of the small-intestinal glucose transporter SGLT1.[16] Our group has shown that oligomeric cocoa procyanidins offer improved protective effects against obesity, insulin resistance, and impaired glucose tolerance than monomeric and polymeric cocoa procyanidins during high-fat feeding in mice.[17]

Cider production volume continues to increase across the U.S. and has become a viable value-added processing option in regions such as Virginia that have traditionally been large apple producers but only recently have become major cider producers. As the cider industry expands into new regions, so does demand for apple cultivars with relatively high concentrations of endogenous phenolic compounds. Polyphenol composition and concentration is highly variable across apple cultivar, growing locations, and harvest year.[18] This variability has also been observed in many other fruits, including grape-derived products,[19] and can be exacerbated when the oxidation products of the native polyphenols that may be formed during storage and processing are taken into consideration.[20]

While cider apple polyphenols have been the subject of ongoing research programs in Europe, most notably in Spain,[18,21] the U.K.,[8,22] and France,[23] only a few studies on cider apples have been conducted in the U.S. in apple growing regions of New York[24,25] and Michigan.[26] To date, no work has been published regarding polyphenol composition of cider apples grown in Mid-Atlantic or Southeastern states in the U.S., despite the rapid increase of cider production in this region.

Currently, the U.S. apple industry is dominated by culinary apples that contain lower malic acid and polyphenol levels[27] than preferred for cider production. In order to utilize widely available cultivars, commercial production practice often involves addition of food-grade acids and polyphenols to obtain the target sensory character for cider. Exogenous polyphenols can be added to improve astringency, bitterness, and mouthfeel. In red grape wines, exogenous polyphenol-based products added at the manufacturers' recommended rates may actually have negative sensory impacts,[28] suggesting the practical limitations of this common production strategy.

In order to support the burgeoning cider industry in Virginia by identifying apple cultivars for cider production, we selected widely grown dessert (e.g., Fuji, Golden Delicious, Granny Smith, Jonagold, Pink Lady, and Red Delicious) cultivars, generally consumed fresh, and processing (e.g., Enterprise, GoldRush, Idared Rome, and York) cultivars, generally processed into juice or sauce, for this study. A few cultivars in our study (e.g., Arkansas Black, Black Twig, Stayman, and Winesap) are found in older orchards throughout the Mid-Atlantic region, while others (e.g., Harrison, Newtown Pippin, Suncrisp, and Virginia Gold) are currently preferred for cider production in Virginia.

In the current study, we quantified the chemical composition, including 21 individual phenolic compounds of interest from 20 apple cultivars with the aim of identifying suitable cultivars for cider production. The purposes for this analysis was to compare apple cultivars and identify cultivars grown in Virginia that contain sufficient endogenous polyphenols to meet consumer sensory expectation, thus precluding or reducing the need for additions of commercial polyphenol adjuncts. In addition, we aim to inform cultivar selection for future studies involving apple polyphenols and human health.

## MATERIALS AND METHODS

**Chemicals and Standards.** Catechin monomers [(+)-catechin (C), (−)-epicatechin (EC), (−)-epicatechin gallate (ECG), (−)-epigallocatechin (EGC), and (−)-epigallocatechin gallate (EGCG)], chlorogenic acid (3-caffeoylquinic acid), phloretin, phloridzin (phloretin 2′-$\beta$-D-glucoside), quercetin, isoquercitrin (quercetin-3-$\beta$-D-glucoside), hyperin (quercetin-3-D-galactoside), and ascorbic acid were purchased from Sigma-Aldrich (St. Louis, MO, U.S.A.). Procyanidin (PC) dimer $B_2$ and trimer $C_1$ were obtained from ChromaDex (Irvine, CA, U.S.A.). Purified procyanidin dimer $B_1$, dimer $B_2$-gallate, dimer $B_5$, trimer $T_2$, tetramer cinnamtannin $A_2$ ($CinnA_2$), and procyanidin pentamer and hexamer fractions were obtained from Planta Analytica (Danbury, CT, U.S.A.). Solvents for sample preparation and extraction were ACS grade or better (Fisher, Pittsburgh, PA, U.S.A. or VWR, Radnor, PA, U.S.A.). Solvents for UPLC-MS/MS were LC-MS grade (VWR).

**Apple Cultivars.** A total of 600 apple samples belonging to 20 cultivars [Black Twig, Enterprise, Fuji (BC2), Golden Delicious, GoldRush, Granny Smith, Idared, Jonagold, Newtown Pippin, Pilot, Cripps Pink (Pink Lady), Red Delicious (Bisbee), Rome (Taylor), Stayman, Suncrisp, Virginia Gold, Winesap, and York (Red Yorking)] were harvested from the Alson H. Smith, Jr. Agricultural Research and Extension Center (AREC, Winchester, VA, U.S.A.) and (Arkansas Black and Harrison) from Albermarle CiderWorks (North Garden, VA, U.S.A.) in September and October 2013. Fruit were harvested from the exterior part of the tree canopy from a height between 1 to 1.5 m from the ground, placed into cardboard bushel (80 fruit) boxes, and brought to the AREC, where they were stored for 1 to 3 weeks at 4 °C until the time of analysis. Photographs of the 20 cultivars are shown in Supporting Information, Figure S1. These cultivars were selected from 40+ potential Virginia-grown cultivars and represent those of greatest interest to the Virginia cider industry based on current availability in Virginia, desirability as historically significant cider apples, and acceptable horticultural performance.

**Fruit Chemistry and Maturity Parameters.** Fruit weight, peel color, flesh firmness, starch index, pH, soluble solid content (SSC), and titratable acidity (TA) were measured at the AREC in Winchester, VA. Juice samples for total polyphenol concentration measurement by the Folin−Ciocalteu (FC) method were also collected from these apple samples. The remaining fruit were brought to a commercial storage facility in Winchester, VA and stored at 1 °C, 90% relative humidity, under ambient atmospheric gases (i.e., no active adjustments were made to the oxygen, carbon dioxide, nitrogen, or other gas concentrations) for 1−3 weeks before fruit maturity analysis (conducted at the AREC in Winchester, VA) and 4−6 weeks until transferred to the Virginia Tech main campus (Blacksburg, VA) for UPLC-MS/MS analysis.

Fifteen apples from each cultivar were weighed and visually assessed for percent red blush (0−100%) or green background color (1 = green, 2 = light green, 3 = yellowish green, 4 = yellow). Flesh firmness was measured on the same 15 samples, after removing part of the peel at two locations along the equator of each apple, with a Fruit Texture Analyzer penetrometer [Güss Manufacturing (Pty) Ltd.; Strand, S.A.] fitted with a cylindrical 11.1 mm diameter Effegi tip. Starch index was determined by staining the stem-side of an equatorial cross-section of the apples with iodine solution (0.22% w/v iodine, 0.88% w/v potassium iodine) and visual rating, where 1

Table 1. MRM[a] Settings for Detecting and Quantifying Phenolic Compounds by ESI-MS/MS[b] in Twenty Cultivars of Apples Grown in Virginia

| compound | detection window (min) | molecular weight (g/mol) | parent ion[c] $[M - H]^-$ ($m/z$) | daughter ion ($m/z$) | cone voltage (V) | collision energy (eV) |
|---|---|---|---|---|---|---|
| C | 2.3−3.2 | 290.092 | 289.09 | 245.05 | 36 | 14 |
| EC | 2.4−2.9 | 290.092 | 289.09 | 245.05 | 42 | 12 |
| ECG | 2.5−3.6 | 442.076 | 440.92 | 169 | 38 | 16 |
| EGC | 2.6−3.5 | 306.038 | 305.03 | 124.97 | 40 | 22 |
| PC $B_1$ | 2.78−3.28 | 578.07 | 577.13 | 289.1 | 38 | 24 |
| unknown dimer 1[d] | 2.85−3.25 | 578.136 | 577.14 | 425.1 | 34 | 16 |
| PC $T_2$ | 3.00−3.45 | 866.218 | 865.21 | 289.1 | 36 | 48 |
| chlorogenic acid | 3.10−3.60 | 354.31 | 353.06 | 191.09 | 28 | 20 |
| unknown dimer 2[d] | 3.40−3.90 | 578.136 | 577.13 | 425.1 | 34 | 16 |
| PC $B_2$ | 3.42−3.92 | 578.04 | 577.13 | 425.1 | 36 | 16 |
| PC $C_1$ | 3.70−4.20 | 866.218 | 865.21 | 287.08 | 46 | 32 |
| $CinA_2$ | 3.71−4.21 | 1154.808 | 576.4 | 125.01 | 26 | 34 |
| unknown dimer 3[d] | 3.83−4.33 | 578.136 | 577.13 | 425.1 | 34 | 16 |
| PC pentamers | 4.00−4.50 | 1442.820 | 720.4 | 125.02 | 26 | 44 |
| PC hexamers | 4.34−4.84 | 731.038 | 864.51 | 125.01 | 32 | 56 |
| PC $B_5$ | 4.40−4.90 | 578.136 | 577.13 | 289.1 | 30 | 26 |
| hyperin | 4.50−4.90 | 464.38 | 463.06 | 300.19 | 52 | 26 |
| isoquercitrin | 4.55−4.90 | 464.38 | 463.06 | 300.19 | 50 | 30 |
| phloridzin | 5.45−5.85 | 436.41 | 435.1 | 273.13 | 40 | 16 |
| quercetin | 6.30−6.80 | 302.23 | 301.01 | 151.02 | 40 | 22 |
| phloretin | 7.15−7.55 | 274.26 | 273.05 | 167.03 | 42 | 18 |

[a]MRM: multireaction monitoring. [b]ESI-MS/MS: electrospray ionization tandem mass spectrometry. [c]$[M - H]^-$: deprotonated, negatively charged pseudomolecular parent (precursor) ion; MRMs employed singly charged parent ions except for cinnamtannin tetramer $A_2$, pentamers, hexamers, heptamers, octamers, which were doubly charged ($[M - 2H]^{2-}$). [d]Likely procyanidin dimers B3, B4, B6, B7, or B8.

= 100% staining and 8 = 0% staining[29] Three pooled samples each containing five apples were used to measure SSC, TA, pH, and total polyphenols by FC. The calyx half of each apple was juiced in a Champion Juicer (Lodi, CA), and SSC was measured using a digital PAL-1 refractometer (Atago U.S.A., Inc., Bellevue, WA) and reported as °Brix. TA was measured by titrating a 5 mL juice aliquot against a standardized 0.1 N NaOH solution to an end-point of pH 8.1 with a 848 Titrino Plus autotitrator (Herisau, CH). A 50 mL aliquot of the juiced apples was shipped overnight in a Styrofoam cooler with ice packs to the Virginia Tech Enology Service Lab (Blacksburg, VA) for total polyphenol concentration analysis.

**Total Polyphenols.** All chemical reagents were from Fisher Scientific (Suwanne, GA) unless otherwise noted. Absorbance measurements were made using a BioTek Epoch Microplate Spectrophotometer (Winooski, VT) and Corning Costar UV-Transparent Microplates (Corning, NY). Juice samples were centrifuged for 15 min at 3500*g* to remove nonsoluble solids. The supernatant fraction was diluted 10:1 in 10% glucose solution, and the 280 nm absorbance was read. Using the obtained absorbance value fresh supernatant was diluted with water to yield an approximate $OD_{280\ nm}$ of 1 AU. The diluted supernatants were analyzed for total polyphenols by the FC method.[30] Standards for the total polyphenols were generated using gallic acid from 0 mg/L to 500 mg/L in steps of 50 mg/L. The reaction was carried out in a 96-well, 2.2 mL storage block (Thermo Fisher, Suwanee, GA). The reaction mixture consists of 10 $\mu$L of standard or sample, 790 $\mu$L of water, and 50 $\mu$L of FC reagent (MP Biomedicals, Solon, OH). Three min after the addition of the FC reagent, 150 $\mu$L of 2 M sodium carbonate solution was added. The reaction mixture was incubated for 2 h at 21 °C. The 765 nm absorbance was measured by transferring 300 $\mu$L of the reaction mix to a 96-well microplate. Total polyphenol content was determined by linear regression from the standard curve plot and multiplying by the dilution factor.

**Sample Storage and Preparation for UPLC-MS/MS Analysis.** Immediately before analysis, apples to be analyzed by UPLC-MS/MS were transferred from the commercial cold storage facility to the Virginia Tech Main Campus (Blacksburg, VA), where they were stored in a walk-in cooler at 4 °C for 2−4 weeks prior to sample preparation. For each apple variety, peel and flesh samples from 15 individual apples were prepared. A consumer-grade apple peeler was used to remove the peel from each apple. Peel samples (1−2 g) were immediately weighed and placed and into a preservative solution (0.83 M acetic acid and 0.02% w/v ascorbic acid) to inhibit polyphenol oxidation. Flesh samples (~1 g) were immediately weighed and placed and into preservative solution. Peel and flesh samples were stored at −80 °C until extraction and analysis. Samples were thawed at 25 °C prior to extraction, and the preservative solution was decanted and discarded. Peel and flesh samples from five individual apples were pooled, resulting in $n = 3$ pooled replicates for each cultivar. Pooled samples were homogenized in 100 mL of acetone/water/acetic acid (70:28:2 v/v/v), sonicated (5 min), and centrifuged (10 min, 4 °C, 8000*g*). An aliquot of the supernatant was filtered (13 mm nylon syringe filter, 0.22 $\mu$m, VWR). Samples were prepared for UPLC-MS/MS analysis by combining 25 $\mu$L of filtered sample with 500 $\mu$L of 95:5 phase A/phase B (see UPLC-MS/MS Analysis Section, to follow, for phase compositions) in certified LCMS vials (Waters, Milford, MA).

**UPLC-MS/MS Analysis.** The polyphenolic composition of the apple cultivars was quantified by UPLC-MS/MS. UPLC was performed on a Waters Acquity H-class UPLC module with an Acquity UPLC HSS T3 column (2.1 mm × 100 mm, 1.8 $\mu$m particle size) maintained at 40 °C. Binary gradient

**Table 2. Fruit Weight, Peel Color, Firmness, Starch Index, pH, Soluble Sugar Content, Titratable Acidity (TA), and Total Polyphenol Concentration from 20 Apple Cultivars[a] Harvested in Virginia in 2013**

| cultivar | fruit weight (g) | red color (0−100%) | green background color (1−4) | fruit firmness (N) | starch (1−8) | soluble solids (°Brix) | pH | TA[b] (g/L) | total polyphenols[c] (mg GAE/L) |
|---|---|---|---|---|---|---|---|---|---|
| Arkansas Black | 227 (10.7) | 96.3 (1.1) | | 97.2 (1.6) | 6.5 (0.2) | 12.8 (0.2) | 3.64 (0.0) | 7.52 (0.6) | 241 (21.1) |
| Black Twig | 243 (12.8) | 63.5 (5.8) | | 96.3 (2.9) | 5.5 (0.4) | 14.8 (0.3) | 3.47 (0.0) | 12.13 (0.1) | 415 (19.0) |
| Enterprise | 248 (16.7) | 96.8 (1.0) | | 65.0 (1.5) | 7.3 (0.2) | 13.0 (0.1) | 3.76 (0.0) | 9.35 (0.1) | 398 (10.5) |
| Fuji | 235 (10.4) | 89.8 (1.5) | | 67.3 (1.6) | 8.0 (0.0) | 14.6 (1.0) | 4.11 (0.0) | 4.59 (0.1) | 238 (10.4) |
| Golden Delicious | 189 (9.2) | | 2.5 (0.1) | 59.1 (1.1) | 7.6 (0.1) | 13.1 (1.0) | 3.84 (0.0) | 5.71 (0.6) | 218 (4.4) |
| GoldRush | 161 (4.3) | | 3.1 (0.1) | 83.4 (1.3) | 6.0 (0.3) | 15.0 (1.0) | 3.49 (0.0) | 11.09 (0.5) | 359 (74.5) |
| Granny Smith | 201 (7.6) | | 1.3 (0.1) | 74.9 (0.9) | 5.4 (0.1) | 11.8 (0.4) | 3.51 (0.0) | 9.95 (0.2) | 361 (21.3) |
| Harrison | 91 (5.4) | | 3.8 (0.1) | 98.4 (1.1) | 5.0 (0.0) | 16.1 (0.2) | 3.51 (0.0) | 11.06 (0.2) | 926 (9.1) |
| Idared | 222 (7.4) | 81.1 (4.5) | | 56.6 (1.1) | 5.7 (0.1) | 12.3 (0.5) | 3.54 (0.0) | 8.31 (0.7) | 229 (13.7) |
| Jonagold | 240 (12.8) | 86.5 (4.2) | | 44.7 (1.4) | 8.0 (0.0) | 12.4 (0.7) | 3.92 (0.0) | 4.20 (0.2) | 301 (60.4) |
| Newtown Pippin | 186 (10.4) | | 2.0 (0.0) | 99.7 (1.5) | 2.2 (0.4) | 13.4 (0.2) | 3.51 (0.0) | 11.25 (0.3) | 267 (33.2) |
| Pilot | 250 (12.3) | 55.7 (6.5) | | 81.9 (1.3) | 6.1 (0.2) | 15.6 (0.8) | 3.75 (0.0) | 7.62 (0.3) | 336 (37.4) |
| Pink Lady | 172 (4.6) | 57.0 (4.8) | | 84.7 (0.8) | 5.6 (0.1) | 13.0 (0.4) | 3.55 (0.0) | 9.35 (0.2) | 211 (5.0) |
| Red Delicious | 196 (10.2) | 98.2 (0.2) | | 68.7 (1.3) | 7.5 (0.1) | 13.0 (0.6) | 4.32 (0.0) | 2.58 (0.1) | 300 (67.8) |
| Rome | 199 (7.5) | 66.0 (6.1) | | 66.3 (1.4) | 7.7 (0.1) | 12.2 (0.3) | 3.68 (0.0) | 4.94 (0.2) | 288 (6.4) |
| Stayman | 171 (5.1) | 94.6 (1.6) | | 67.5 (1.9) | 4.9 (0.3) | 13.3 (0.2) | 3.62 (0.0) | 7.37 (0.3) | 253 (30.0) |
| Suncrisp | 204 (8.7) | | 3.1 (0.1) | 69.7 (0.8) | 7.0 (0.2) | 13.7 (0.9) | 3.72 (0.0) | 6.64 (0.3) | 313 (23.5) |
| Virginia Gold | 198 (7.0) | | 2.3 (0.1) | 70.6 (1.4) | 7.0 (0.2) | 11.4 (0.1) | 3.54 (0.0) | 7.74 (0.9) | 236 (8.9) |
| Winesap | 189 (9.2) | 84.5 (3.7) | | 67.9 (1.7) | 6.6 (0.2) | 13.2 (0.8) | 3.69 (0.0) | 7.89 (0.5) | 373 (127.9) |
| York | 212 (9.8) | 91.9 (1.6) | | 91.1 (2.7) | 3.8 (0.1) | 13.6 (0.5) | 3.67 (0.0) | 7.01 (0.3) | 215 (12.1) |

[a]Measurements were made on uncut whole fruit for fruit weight, red color, green background color, fruit firmness; bottom half of fruits were used for starch; pressed juice was used for soluble solids, pH, TA, and total polyphenols. Values are means, followed by standard errors in parentheses. [b]TA: titratable acidity, expressed as malic acid equivalents. [c]FC method was used.



dx.doi.org/10.1021/jf503379t | J. Agric. Food Chem. 2014, 62, 10181−10191

elution was carried out with 0.1% formic acid in water (phase A) and 0.1% formic acid in acetonitrile (ACN, phase B). Linear gradient elution was performed at a flow rate of 0.6 mL/min as follows: 95% A (0−0.5 min), 65% A (6.5 min), 20% A (7.5−8.6 min), 95% A (8.7−10.5 min). Sample temperature was maintained at 10 °C. UPLC effluent was analyzed by (−)-electrospray ionization (ESI) coupled to tandem mass spectrometry (MS/MS) on a Waters Acquity triple quadrupole (TQD) MS. Ionization was performed in (−) mode to generate pseudomolecular parent ions $[M - H]^-$ of compounds to be quantified (with the exception of cinnamtannin $A_2$, pentamers and hexamers, for which $[M - 2H]^{2-}$ was the most abundant pseudomolecular parent ion). ESI was performed with a capillary voltage of −4.25 kV, cone voltage of 30.0 V, extractor voltage of 3.0 V, and source and desolvation temperatures of 150 and 400 °C, respectively. Cone and desolvation gases were $N_2$ at flow rates 75 and 900 L/h, respectively. MS/MS was performed using Ar as the collision gas at 0.25 mL/min in the collision cell. Multireaction monitoring (MRM) was performed on pseudomolecular parent (precursor) ions and signature daughter (product) ions following collision-induced dissociation (CID). MS data collection was set to 10 points/peak with an average peak width of 6 s. The autodwell setting was used to automatically calculate dwell time based on an interscan delay time of 0.02 s for each transition. The TQD was operated in quantitation mode, with the mass resolution of the first and second quadrupoles set at 1.0 and 0.75, respectively. The Intellistart function of MassLynx was used to develop and optimize MRM parameters for each compound of interest. Compound solutions were directly infused into the ESI source in combination with a background flow of 50% phase A/50% phase B at 0.6 mL min. Intellistart automatically generated a single MRM transition for each compound centered on the exact monoisotopic mass of the parent (precursor) and daughter (product) ions, with a mass window of 0.2 amu (i.e., exact monoisotopic mass determined by Intellistart ±0.1). Refer to Table 1 for MRM parameters for each compound of interest. Refer to Supporting Information, Figure S2 for structures of quantified compounds. All compound peaks were processed and quantified using the QuanLynx function of MassLynx software. Peaks were smoothed using a mean smoothing method with 2−3 smoothing iterations and a smoothing width of 1. Compounds were quantified based on external standard curves of authentic standards in 0.1% formic acid in water: 0.1% formic acid in ACN (95:5 v/v). Calibration and method validation parameters are presented in Supporting Information, Table S1.

**Statistical Analysis.** Data were expressed as mean ± SEM for $n = 3$ replicate sets of five apples for UPLC-MS/MS analyses, pH, SSC, TA, and FC, and $n = 15$ replicates for fruit size, peel color, flesh firmness, and starch data. Statistical analyses were performed using Prism v6.0e (GraphPad Software, Inc., La Jolla, CA). Data for total catechin, total PC, total flavan-3-ol, total quercetin derivatives, total phloretin derivatives, chlorogenic acid, and total of measured polyphenols in both peel and flesh were analyzed by one-way ANOVA followed by all possible pairwise comparisons using Tukey's HSD posthoc test. Significance was defined as $P < 0.05$.

**Safety.** We report no unique safety considerations for the present research.

## RESULTS

Fruit size, peel color, and flesh firmness varied among cultivars, but all were within commercially acceptable ranges[31] (Table 2). With the exception of some of the later-maturing cultivars (Newtown Pippin, Stayman, and York), the apples had starch indices greater than 5, indicating that most of the stored starch had converted to sugar. GoldRush, Harrison, and Pilot all had SSC values greater than 15°Brix, which would result in a higher than average alcohol content in the resulting cider. Starch and SSC contents were not significantly correlated ($r^2 = 0.471$, $P = 0.3583$). Fuji, Golden Delicious, Jonagold, and Red Delicious had pH values greater than 3.8 (a threshold above which microbial control becomes more difficult in the fermentation process). Above pH 3.8, the standard recommendation is to add exogenous organic acid to the juice to bring the pH below 3.8. Black Twig, GoldRush, Harrison, and Newtown Pippin had the highest concentrations of titratable acidity, whereas Red Delicious had the lowest titratable acidity. For most cultivars in this study, total polyphenol content in juice pressed from whole fruits during the maturity assessment ranged from 211 and 415 mg GAE/L. With a total polyphenol content of 926 mg GAE/L in juice pressed from whole fruits, Harrison had more than twice the total polyphenol concentration in juice pressed from whole fruits as determined by FC than any other apple cultivar in this study.

Peel and flesh concentrations (mean ± SEM) for all individual polyphenols measured in apple cultivars are presented in Supporting Information, Tables S2−S5. Summary data for total catechins, total procyanidins (PCs), and total flavan-3-ols (catechins + procyanidins) in peel and flesh of apple cultivars are shown in Figure 1. There were extreme variations in the levels of catechins, PCs, and total flavan-3-ols between cultivars. Mean levels of total catechins varied from 0.000381 to 1.22 μg/g and 0.0530 to 4.17 μg/g for flesh and peel, respectively. In all cases, mean total catechin levels in peel were greater than those in flesh. The predominant catechins in both peel and flesh were EC followed by C (Supporting Information, Tables S2, S4). Mean levels of total PCs varied from 0.805 to 65.2 and 3.34 to 122 μg/g for flesh and peel, respectively. Similar to total catechins, mean total PC levels in peel were greater than those in flesh. PC $B_1$ was by far the predominant PC in both peel and flesh (Supporting Information, Tables S2, S4). Mean levels of total flavan-3-ols (catechins + PCs) ranged from 0.806 to 66.5 and 3.60 to 124 μg/g for flesh and peel, respectively. The majority of the flavan-3-ols in both peel and flesh were PCs; catechins made up just 0.0474 to 4.28 and 0.814 to 7.05% of the total flavanols by weight in flesh and peel, respectively. As the mean total PC and catechin levels were both greater in peel than those in flesh for all cultivars, this was also reflected in total flavan-3-ol levels.

Summary data for chlorogenic acid, total quercetin derivatives, and total phloretin derivatives in peel and flesh of apple cultivars are shown in Figure 2. Mean levels of total quercetin derivatives ranged from 0.00131 to 0.0186 and 0.144 to 3.24 μg/g for flesh and peel, respectively. Mean levels of total quercetin derivatives were higher in peel compared to flesh for all cultivars. Hyperin and isoquercitrin were the predominant quercetin derivatives in both flesh and peel; quercitin aglycone was much less abundant (Supporting Information, Tables S3, S5). Mean levels of total phloretin derivatives ranged from ND (not detected) to 63.5 and ND to 414 μg/g for flesh and peel, respectively (refer to Supporting Information, Table 1 for lower

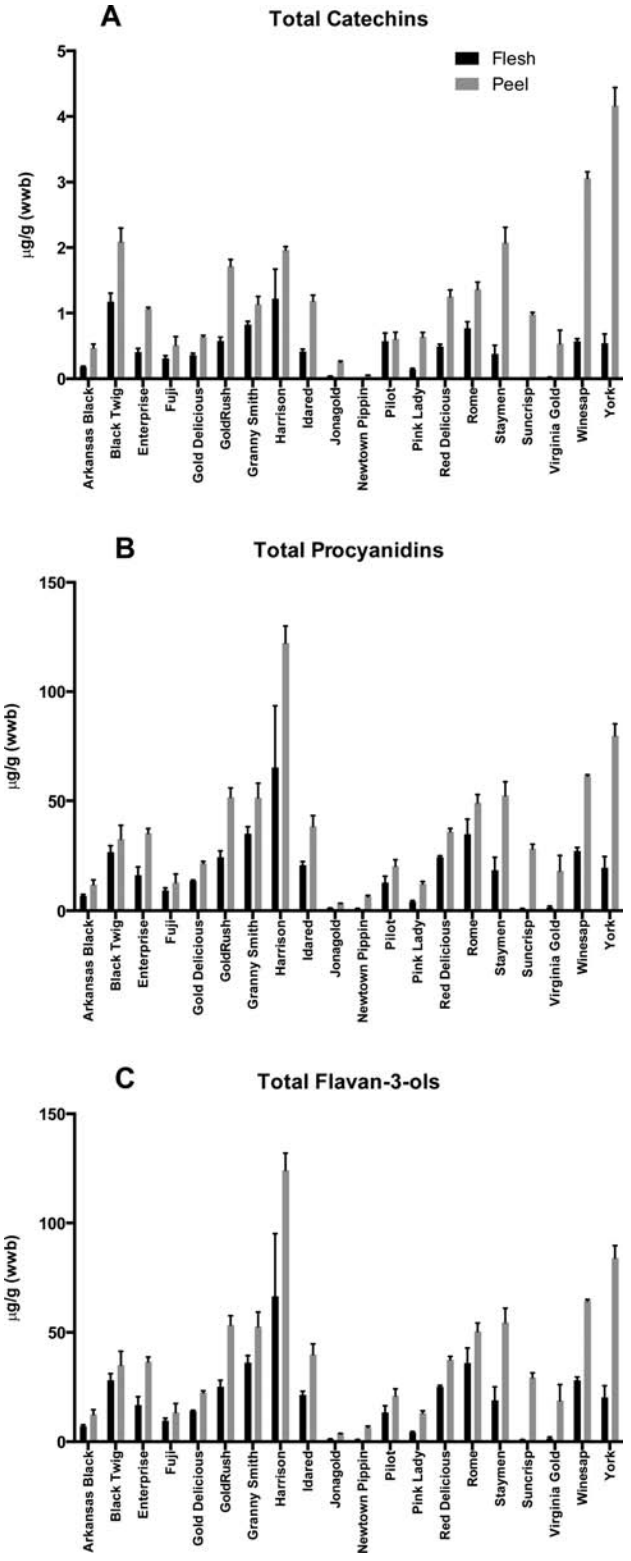


**Figure 1.** Peel and flesh concentrations of total measured catechins (A), total measured procyanidins (B), and total measured flavan-3-ols (C) in apple cultivars. Values are expressed on a wet weight basis (wwb). Values represent the mean ± SEM for $n = 3$ replicates (except for Harrison, flesh where $n = 2$). Total catechins = Σ[(−)-EGC, (+)-C, (−)-EC, (−) ECG], total procyanidins = Σ[PC $B_1$, PC $B_2$, PC $B_5$, 3 unidentified PC dimers, PC $C_1$, PC $T_2$, Cin$A_2$, PC pentamers, PC hexamers], total flavan-3-ols = total catechins + total procyanidins. Note that not all possible flavonoid glycosides were quantified by this analysis.

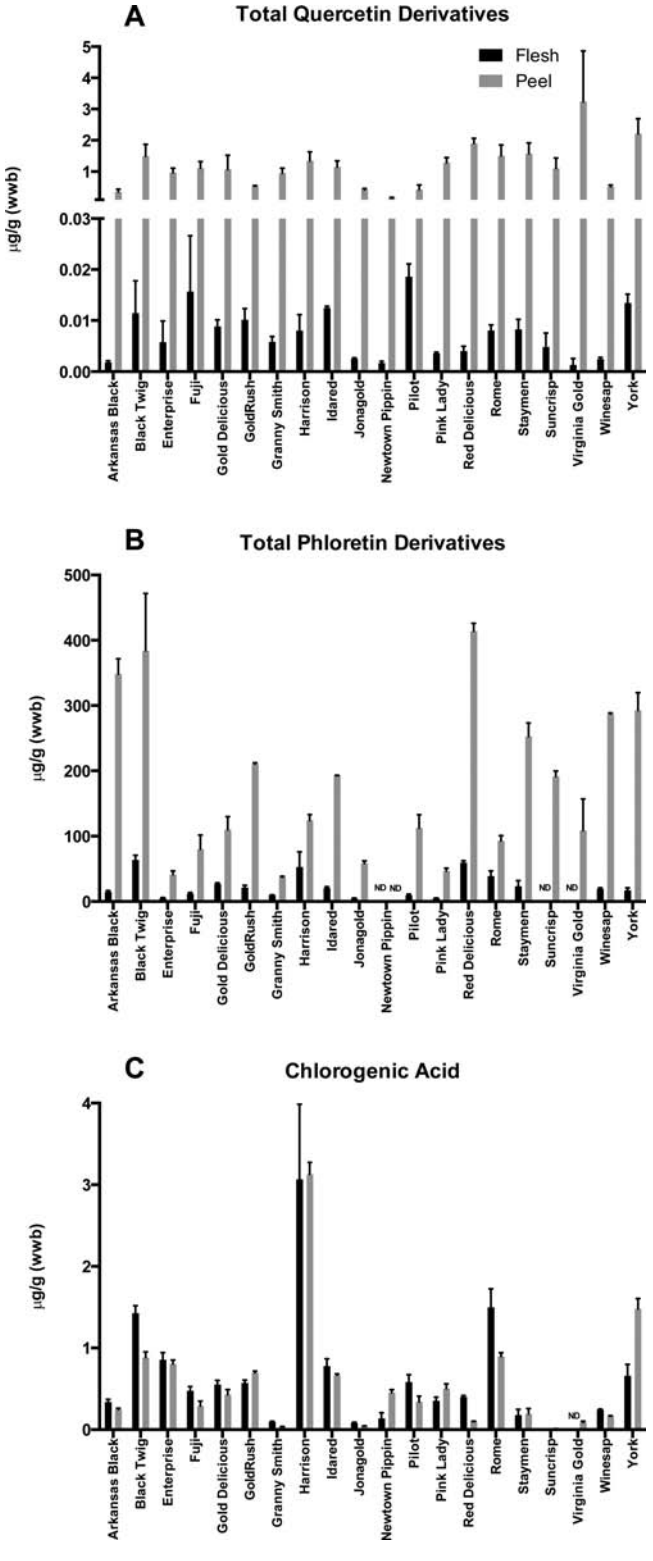


**Figure 2.** Peel and flesh concentrations of total measured quercetin derivatives (A), total measured phloretin derivatives (B), and chlorogenic acid (C) in apple cultivars. Values are expressed on a wet weight basis (wwb). Values represent the mean ± SEM for $n = 3$ replicates (except for Harrison, flesh where $n = 2$). ND = not detected. Total quercetin derivatives = Σ[hyperin, isoquercitrin, quercetin] and total phloretin derivatives= Σ[phloridzin, phloretin]. Note that not all possible flavonoid glycosides were quantified by this analysis.

limits of quantification and detection). Mean levels of total phloretin derivatives were higher in peel compared to flesh for all cultivars. No phloretin derivatives were detected in flesh or peel of Newtown Pippin, flesh of Suncrisp, or flesh of Virginia Gold. Phloridzin was by far the predominant phloretin derivative in peel; phloretin aglycone was only present in trace amount (5−7 orders of magnitude lower than phloridzin) (Supporting Information, Tables S3, S5). In flesh, phloridzin was the only phloretin derivative detected; no phloretin aglycone was detected in any flesh sample (Supporting Information, Tables S3, S5).

Mean chlorogenic acid levels ranged from ND to 3.07 and 0.00661 to 3.13 μg/g for flesh and peel, respectively. In contrast to values for all other measured compounds, mean chlorogenic acid levels were higher in flesh than peel for many cultivars (Arkansas Black, Black Twig, Enterprise, Fuji, Gold Delicious, Granny Smith, Ida Red, Jonagold, Pilot, Red Delicious, Rome, and Winesap).

The differences between peel and flesh concentrations of total quercetin and phloretin derivatives (Figure 2A,B) were much more pronounced than for total catechins, total PCs, or total flavan-3-ols (Figure 1), whereas the concentrations of chlorogenic acid in peel and flesh were very similar (Figure 2C). Overall, PC $B_1$ and phloridzin were clearly the most abundant individual compounds in both peel and flesh for most cultivars, although individual variations did occur (Supporting Information, Tables S2−S5). As mentioned previously, Newtown Pippin had no phloridzin in peel or flesh. Newtown Pippin also had little PC $B_1$ in either peel or flesh. VA Gold had no PC $B_1$ in flesh. Neither Virginia Gold nor Suncrisp had detectable phloridzin in flesh, as mentioned previously.

The sums of all individual compounds (catechins, PCs, chlorogenic acid, quercetin derivatives, and phloretin derivatives) in peel and flesh of apple cultivars are shown in Figure 3. Mean levels of all compounds measured varied from 0.943 to 122 and 7.11 to 453 μg/g for flesh and peel, respectively. For all cultivars, the total concentration of all individual compounds was greater in peel than flesh. However, extreme variation was observed in the ratio of total compounds in peel versus flesh: the concentration of total compounds in peel ranged from 1.9-fold to 222-fold greater than the concentration in flesh. The majority of the cultivars had a 1.9−7.9 fold difference between peel and flesh. York, Jonagold, and Arkansas Black had differences of 10.0, 10.8, and 16.2-fold, respectively. VA Gold and Suncrisp were extreme outliers, with differences of 87.3 and 222-fold, respectively.

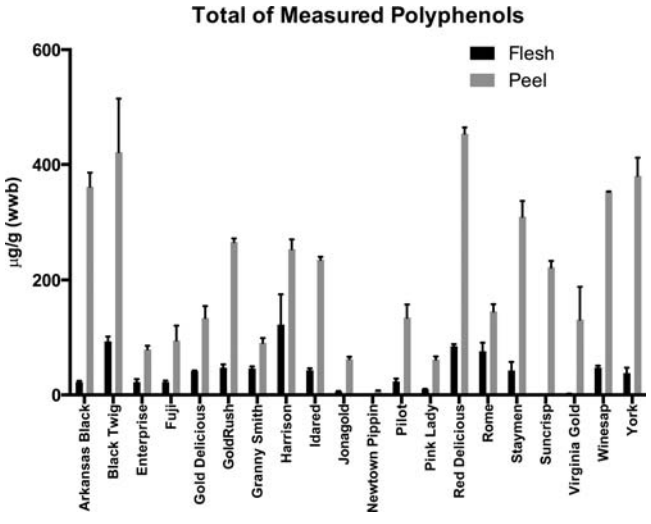


**Figure 3.** Peel and flesh concentrations of total measured polyphenols in apple cultivars. Values are expressed on a wet weight basis (wwb). Values represent the mean ± SEM for $n$ = 3 replicates (except for Harrison, flesh where $n$ = 2). Total measured polyphenols = Σ[total measured catechins, total measured procyanidins, total measured quercetin derivatives, total measured phloretin derivatives, chlorogenic acid]. Note that not all possible flavonoid glycosides were quantified by this analysis.

Linear regression analyses relating the sums of all individual compounds in peel with the sums of all individual compounds in flesh of apple cultivars are shown in Figure 4A. There appeared to be a moderate linear relationship between the sums of all individual compounds in flesh and peel ($r^2$ = 0.306, 95% CI for slope: 0.0347−0.238, slope is significantly different from 0, $P$ = 0.0114). Linear regression analyses relating the sums of all individual compounds in peel and flesh with the total polyphenol concentration in pressed juice (measured by the FC assay) of apple cultivars are shown in Figure 4B,C. There appeared to be no linear relationship between the sum of all individual compounds in peel and the total polyphenol levels in pressed juice ($r^2$ = 0.01667, 95% CI for slope: −0.419−0.718, slope is not significantly different from 0, $P$ = 0.59). There was a moderate linear relationship between the sum of all individual compounds in flesh and the total polyphenol concentration in pressed juice ($r^2$ = 0.430, 95% CI for slope: 1.33−4.83, slope is significantly different from 0, $P$ = 0.0017).

The overall effect of cultivar on the quantitative profile of the various classes of polyphenols measured is presented in Table 3. For all classes of compounds, cultivar had a statistically significant effect ($P$ < 0.05) on the amounts present in both flesh and peel, and this effect was highly significant ($P$ < 0.0001 for all compounds except total quercetin derivatives in both peel and flesh). Pairwise comparisons between all cultivars for each class of polyphenol measured in flesh and peel are shown in Supporting Information.

## DISCUSSION

Qualitative and quantitative polyphenol profiles vary widely across apple cultivars grown in Virginia. We observed significant differences across cultivar for concentration in both peel and flesh for catechins, procyanidins, total flavan-3-ols, total quercetin derivatives, total phloretin derivatives, and chlorogenic acid, as well as total measured polyphenols. Differences in fruit chemistry across cultivars were previously reported for cider apples grown in Spain, France, the U.K., New York, and other regions.[18,21,23,24,32] The total concentration of polyphenols measured by UPLC observed in fruit from Virginia (ranging from 7 μg/g wwb in peel for Newtown Pippin to 453 μg/g wwb in peel for Red Delicious) is low compared to similar surveys conducted in other cider-producing regions. This may be due to the fact that only select flavonoid aglycones were quantified in this study, and thus our total level of polyphenols does not account for some glycosides which may make up a significant fraction of the total flavonoids in apple. This study was designed to profile differences in select compounds rather than quantify all major flavonoid glycosides in apples. This may also be due to the fact that flesh and peel samples were stored in a preservative solution, which was decanted and discarded prior to extraction. Therefore, some polyphenols, particularly the most water-soluble compounds, may have leached into the solution and been discarded prior to extraction. However, it

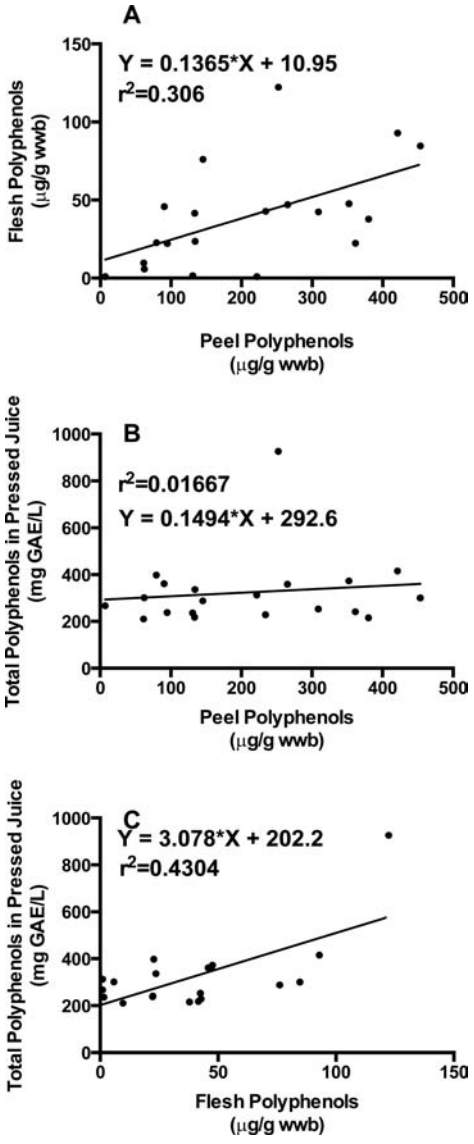


**Figure 4.** Linear regression analysis of peel and flesh concentrations of total polyphenols measured by UPLC-MS/MS (A), peel concentrations of total measured polyphenols measured by UPLC-MS/MS and total polyphenolic content of juice pressed from whole apples (B), and peel concentrations of total measured polyphenols measured by UPLC-MS/MS and total polyphenolic content of juice pressed from whole apples (C). The polyphenolic concentrations of juice pressed from whole apples were measured using the FC assay, and are expressed as mg gallic acid equivalents (GAE)/L juice. Data points represent the mean for $n = 3$ replicates (except for Harrison flesh, where $n = 2$). Note that not all possible flavonoid glycosides were quantified by this analysis.

should be noted that samples were frozen at −80 °C immediately following immersion in the preservative, and the preservative was immediately decanted after thawing. Therefore, the exposure time of the samples to the liquid preservative was minimal. Furthermore, all samples were treated equally, and thus this approach does not affect our primary objective of comparing differences in polyphenol levels between cultivars. Furthermore, a search of the literature and Phenol-Explorer reveal extreme variation in all compounds, including some reports of undetected flavonols, including quercetin and its derivatives.[33] In addition to analytical methodological differences, variations in genotype, climate, orchard management practices, and fruit maturity are expected to result in tremendous variation in polyphenol content. English cider apples contained 546 to 6306 μg/g fresh weight total polyphenols in peel, and 485 to 4920 μg/g in flesh.[32] Juice pressed from milled Spanish cider apples contained 67 to 927 mg/L total polyphenols, expressed as tannic acid equivalents. This may reflect the desired characteristics for cider in each of these regions.

**Table 3. Overall Statistical Significance of the Effect of Cultivar on Various Classes of Polyphenols in Both Apple Flesh and Peel**

| | *P*-values[a] | |
|---|---|---|
| measure | flesh | peel |
| catechins | <0.0001 | <0.0001 |
| procyanidins | <0.0001 | <0.0001 |
| total flavan-3-ols | <0.0001 | <0.0001 |
| total quercetin derivatives | 0.0154 | 0.0035 |
| total phloretin derivatives | <0.0001 | <0.0001 |
| chlorogenic acid | <0.0001 | <0.0001 |
| total of measured polyphenols | <0.0001 | <0.0001 |

[a] *P*-values from one-way ANOVA analysis.

It should be noted that no standardized conditions exist for extraction of polyphenols from apples. Recently reported conditions include a wide array of extraction solvent, including: methanol (MeOH)/0.1% formic acid, MeOH/water/acetic acid (70:29:1), MeOH/water (70:30), acetone/water (80:20), ethanol (EtOH)/water/formic acid (80:20:1), and aqueous buffer solutions (or no extraction, i.e., direct analysis of pressed and filtered juice).[34−39] The observed qualitative and quantitative profiles of polyphenols likely differ greatly depending upon the chosen extraction conditions. Our conditions were chosen to maximize extraction of the flavan-3-ols, particularly the PCs, due to our interest in the sensory implications of monomeric catechins and oligomerized PCs (the "hard" vs "soft" tannins) as well as the chemistry and health benefits of these compounds.[40] Furthermore, flavonoids such as quercetin, kaempferol, and phloretin are typically present in various glucoside forms, which complicate accurate determination of the total levels of these compounds. Although we have measured the aglycones and a few glycosides, the compounds measured in this study do not fully represent the compendium of glycosides of compounds such as quercetin, kaempferol, and phloretin. Therefore, these data should not be interpreted as exhaustive, rather as representative of the differences in flavonoid compositions between these cultivars. Analytical strategies to better quantify these compounds have included measurement of as many glycosides as possible,[41] as well as hydrolysis of the glycosides to yield the aglycone form.[36] We plan to employ glycoside hydrolysis in future studies to more accurately quantify total flavonoid levels. As with extraction conditions, the chosen analytical strategy likely influences the observed results. For example, for total polyphenol concentration in pressed juice from whole fruits presented with maturity parameters in Table 2, Harrison showed the highest total polyphenol concentration by the FC method, whereas Harrison showed intermediate values for total polyphenol concentration in peel in Figure 3, compared to other cultivars in the study. These differences are due to differences in both sample processing methods and analytical methods employed for maturity assessment, wherein juice was

pressed from whole fruit and analyzed by the FC method, and the individual polyphenol determination wherein peel and flesh were analyzed separately via UPLC-MS. Although the results are certainly influenced by the sample preparation and analytical methods, the results of this study indicate that there is a correlation between total polyphenols in flesh by UPLC-MS and total polyphenols in juice pressed from whole fruits (such as is used in cider production) by FC. In Figure 4B,C, the correlation coefficient for total polyphenols in pressed juice by FC with total polyphenols in peel, $r^2 = 0.02$, is much lower than the correlation coefficient of total polyphenols in pressed juice by FC with total polyphenols in flesh by UPLC-MS at $r^2 = 0.43$. Despite the variability imparted by differences in analytical approach, advancements in food analytical chemistry over the past decade have provided new perspectives on the extent of diversity in polyphenol composition across plant materials. Coupled with the increasingly sophisticated understanding of the impact of specific classes of polyphenols on physiology and health outcomes,[10,17,40,42] information on polyphenol composition observed across fruit genotypes and growing conditions[21,23,24,32,43−45] can be utilized to make informed selections of sources of fruit juice, extracts, and byproducts for use in future investigations of bioactivity and bioavailability of polyphenols. Phenol-Explorer is a useful online database which compiles results from thousands of studies on polyphenol content in a wide range of foods.[46]

Our results are consistent with previous studies showing that polyphenols are concentrated in the peel compared to the flesh of apples on a $\mu$g/g basis.[41,47] However, the much larger total mass of flesh than peel per fruit may result in larger total masses of specific compounds in the flesh versus peel.[38] The sum of the concentrations of compounds measured by UPLC ranged from 1.9- to 222-fold greater in peel versus flesh with high variability across cultivars. This variability is expected to impact extraction efficiency of polyphenols from milled apples into juice during processing.[48] For example, mechanical pressing parameters could be adjusted to allow for increased extraction of polyphenols from the peel in cultivars with very high peel/flesh polyphenol concentration ratios like Virginia Gold and Suncrisp, whereas these techniques would be less useful in cultivars like Harrison and Rome where flesh polyphenol concentration is relatively high. Future work is needed to examine the impact of processing parameters on the fate of polyphenols through the cider production process, from fruit to juice to fermented finished product.

In Virginia, the cultivars Harrison, Granny Smith, Rome, Winesap, and Black Twig had the highest concentration of total flavan-3-ols in flesh, indicating the highest potential for imparting desired sensory character from polyphenols to cider under current processing conditions where extraction of polyphenols from peel is minimal.[48] The highest concentrations of total flavan-3-ols in peel were found in Harrison, York, Winesap, Staymen, and GoldRush. These results indicate that further experimental work on improvement of polyphenol extraction from peel to pressed juice could increase total flavan-3-ol concentration in juice from cultivars such as York.

Phloridzin, a compound with a bittersweet taste, was found in highest concentration in the flesh of Black Twig, Red Delicious, Harrison, Rome, and Golden Delicious, and in the peel of Red Delicious, Black Twig, Arkansas Black, York, and Winesap. Phloretin, which can mask bitter taste,[49] was found in only very low concentrations of <0.01 $\mu$g/g wwb across cultivars and tissues in our study. Highest total polyphenol concentrations in flesh were found in Harrison, Black Twig, Red Delicious, Rome, and Winesap, and in the peel of Red Delicious, Black Twig, York, Arkansas Black, and Winesap. The sensory impact of phloridzin and flavan-3-ols would be expected to vary depending on sugar, alcohol, and acid concentration in cider; therefore, it is useful to consider the concentration of these categories of polyphenols in addition to total polyphenol concentration when selecting cultivars for cider production.

In addition to variation across cultivars, cultural practices and orchard maturity have been demonstrated to impact polyphenol concentration in cider apples.[44] Understanding how polyphenol composition and concentration change as orchards mature and respond to different climates and cultural practices will be important in achieving consistent production of fruit with optimal polyphenol concentration and composition to support the growth of the cider industry in Virginia. Based on the results of this study, the cultivars Harrison, Granny Smith, Rome, Winesap, and Black Twig show the highest potential for imparting desired polyphenol character to cider under current growing and processing conditions.

## ■ ASSOCIATED CONTENT

### Supporting Information

Structures of quantified compounds, images of all apple cultivars; peel and flesh concentrations of individual polyphenol compounds in apple cultivars measured by UPLC-MS/MS: (−)-EGC, (+)-C, (−)-EC, (−) ECG, PC $B_1$, PC $B_2$, PC $B_5$, three unidentified PC dimers, PC $C_1$, PC $T_2$, Cin$A_2$, PC pentamers, PC hexamers, hyperin, isoquercitrin, quercetin, phloridzin, and phloretin; pairwise comparisons between all apple cultivars for each class of polyphenol measured. This material is available free of charge via the Internet at http://pubs.acs.org.

## ■ AUTHOR INFORMATION

### Corresponding Author

*E-mail: amanda.stewart@vt.edu. Fax: 1 (540) 231-9293. Phone: 1 (540) 231-0868.

### Present Address

§United States Department of Agriculture (USDA) Agricultural Research Service (ARS) Nutrient Data Laboratory, Beltsville, MD.

### Funding

This study was supported by a grant from the Virginia Department of Agriculture and Consumer Services (VDACS)-USDA Specialty Crop Block Grant program to evaluate cider apple varieties, salary support for Drs. Peck, Stewart, and Neilson from Virginia Agricultural Experiment Station (VAES), and research funding support for Neilson and Stewart from the Department of Food Science and Technology and the College of Agriculture and Life Sciences at the Virginia Polytechnic Institute and State University.

### Notes

The authors declare no competing financial interest.

## ■ ACKNOWLEDGMENTS

The authors acknowledge the contributions of David Carbaugh, Abby Kowalski, and Taylor Mackintosh from the Peck Lab. We also thank the Shelton family for donating fruit for this

experiment. We would also like to thank Ann Sandbrook, Virginia Tech Enology Service Lab.

## ABBREVIATIONS USED

acetonitrile, ACN; Agricultural Research and Extension Center, AREC; (+)-catechin, C; cinnamtannin $A_2$, Cinn$A_2$; collision-induced dissociation, CID; degree of polymerization, DP; electrospray ionization, ESI; (−)-epicatechin, EC; (−)-epicatechin gallate, ECG; (−)-epigallocatechin, EGC; (−)-epigallocatechin gallate, EGCG; ethanol, EtOH; Folin-Ciocalteu, FC; gallic acid equivalents, GAE; methanol, MeOH; multireaction monitoring, MRM; not detected, ND; procyanidin, PC; pseudomolecular parent ion, $[M-H]^-$; sodium-glucose linked transporter 1, SGLT1; soluble solid content, SSC; tandem mass spectrometry, MS/MS; titratable acidity, TA

## REFERENCES

(1) *Report of Wine Premises Operations 2007−2012*; Alcohol Tobacco and Trade Bureau. U.S. Department of the Treasury: Washington, DC, 2013. http://www.ttb.gov/statistics/reports.shtml.

(2) Tandon, K.; Worobo, R. W.; Churey, J. J.; Padilla-Zakour, O. I. Storage quality of pasteurized and UV treated apple cider. *J. Food Process. Preserv.* **2003**, *27*, 21−35.

(3) Soares, S.; Kohl, S.; Thalmann, S.; Mateus, N.; Meyerhof, W.; De Freitas, V. Different Phenolic Compounds Activate Distinct Human Bitter Taste Receptors. *J. Agric. Food Chem.* **2013**, *61*, 1525−1533.

(4) Lesschaeve, I.; Noble, A. C. Polyphenols: factors influencing their sensory properties and their effects on food and beverage preferences. *Am. J. Clin. Nutr.* **2005**, *81*, 330S−335S.

(5) Kallithraka, S.; Bakker, J.; Clifford, M. N. Evaluation of bitterness and astringency of (+)-catechin and (−)-epicatechin in red wine and in model solution. *J. Sens. Stud.* **1997**, *12*, 25−37.

(6) Bordenave, N.; Hamaker, B. R.; Ferruzzi, M. G. Nature and consequences of non-covalent interactions between flavonoids and macronutrients in foods. *Food Funct.* **2014**, *5*, 18−34.

(7) Lowenthal, J. Ueber die Bestimmung des Gerbstoffs. *Z. Anal. Chem. Freseniu.* **1877**, *16*, 33−48.

(8) Lea, A. G. H. Cidermaking. In *Fermented Beverage Production*; Lea, A. G. H., Piggot, J. R., Eds.; Blackie Academic and Professional: Glasgow, 1996; p 29.

(9) Tomas-Barberan, F. A.; Andres-Lacueva, C. Polyphenols and Health: Current State and Progress. *J. Agric. Food Chem.* **2012**, *60*, 8773−8775.

(10) Gu, Y.; Hurst, W. J.; Stuart, D. A.; Lambert, J. D. Inhibition of Key Digestive Enzymes by Cocoa Extracts and Procyanidins. *J. Agric. Food Chem.* **2011**, *59*, 5305−5311.

(11) Etxeberria, U.; Fernandez-Quintela, A.; Milagro, F. I.; Aguirre, L.; Alfredo Martinez, J.; Portillo, M. P. Impact of Polyphenols and Polyphenol-Rich Dietary Sources on Gut Microbiota Composition. *J. Agric. Food Chem.* **2013**, *61*, 9517−9533.

(12) Tomas-Barberan, F. A.; Mine, Y. A Key to Understanding the Effects of Food Bioactives in Health, Gut Microbiota. *J. Agric. Food Chem.* **2013**, *61*, 9755−9757.

(13) Kim, Y.; Choi, Y.; Ham, H.; Jeong, H.-S.; Lee, J. Polymeric procyanidin fraction from defatted grape seeds protects HepG2 cells against oxidative stress by inducing phase II enzymes via Nrf2 activation. *Food Sci. Biotechnol.* **2013**, *22*, 485−491.

(14) Scapagnini, G.; Vasto, S.; Abraham, N. G.; Caruso, C.; Zella, D.; Galvano, F. Modulation of Nrf2/ARE Pathway by Food Polyphenols: A Nutritional Neuroprotective Strategy for Cognitive and Neurodegenerative Disorders. *Mol. Neurobiol.* **2011**, *44*, 192−201.

(15) Manzano, S.; Williamson, G. Polyphenols and phenolic acids from strawberry and apple decrease glucose uptake and transport by human intestinal Caco-2 cells. *Mol. Nutr. Food Res.* **2010**, *54*, 1773−1780.

(16) Masumoto, S.; Akimoto, Y.; Oike, H.; Kobori, M. Dietary Phloridzin Reduces Blood Glucose Levels and Reverses Sglt1 Expression in the Small Intestine in Streptozotocin-Induced Diabetic Mice. *J. Agric. Food Chem.* **2009**, *57*, 4651−4656.

(17) Dorenkott, M. R.; Griffin, L. E.; Goodrich, K. M.; Thompson-Witrick, K. A.; Fundaro, G.; Ye, L.; Stevens, J. R.; Ali, M.; O'Keefe, S. F.; Hulver, M. W.; Neilson, A. P. Oligomeric Cocoa Procyanidins Possess Enhanced Bioactivity Compared to Monomeric and Polymeric Cocoa Procyanidins for Preventing the Development of Obesity, Insulin Resistance, and Impaired Glucose Tolerance during High-Fat Feeding. *J. Agric. Food Chem.* **2014**, *62*, 2216−2227.

(18) Alonso-Salces, R. M.; Herrero, C.; Barranco, A.; Lopez-Marquez, D. M.; Berrueta, L. A.; Gallo, B.; Vicente, F. Polyphenolic compositions of Basque natural ciders: A chemometric study. *Food Chem.* **2006**, *97*, 438−446.

(19) Xu, Y.; Simon, J. E.; Welch, C.; Wightman, J. D.; Ferruzzi, M. G.; Ho, L.; Passinetti, G. M.; Wu, Q. Survey of Polyphenol Constituents in Grapes and Grape-Derived Products. *J. Agric. Food Chem.* **2011**, *59*, 10586−10593.

(20) Guyot, S.; Bernillon, S.; Poupard, P.; Renard, C.. Multiplicity of Phenolic Oxidation Products in Apple Juices and Ciders, from Synthetic Medium to Commercial Products. In *Recent Advances in Polyphenol Research*; Daayf, F., Lattanzio, V., Eds.; Wiley-Blackwell: Oxford, U.K., 2008; Vol. *1*, pp 278−292.

(21) Alonso-Salces, R. M.; Guyot, S.; Herrero, C.; Berrueta, L. A.; Drilleau, J. F.; Gallo, B.; Vicente, F. Chemometric characterisation of Basque and French ciders according to their polyphenolic profiles. *Anal. Bioanal. Chem.* **2004**, *379*, 464−475.

(22) Lea, A. G. H.; Arnold, G. M. Phenolics of Ciders - Bitterness and Astringency. *J. Sci. Food Agric.* **1978**, *29*, 478−483.

(23) Guyot, S.; Marnet, N.; Sanoner, P.; Drilleau, J. F. Direct thiolysis on crude apple materials for high-performance liquid chromatography characterization and quantification of polyphenols in cider apple tissues and juices. *Methods Enzymol.* **2001**, *335*, 57−70.

(24) Valois, S.; Merwin, I. A.; Padilla-Zakour, O. I. Characterization of fermented cider apple cultivars grown in upstate New York. *J. Am. Pomol. Soc.* **2006**, *60*, 113−128.

(25) Merwin, I. A.; Valois, S.; Padilla-Zakour, O. I. Cider Apples and Cider-Making Techniques in Europe and North America. In *Horticultural Reviews*; Janick, J., Ed. **2008**; Vol. *34*, pp 365−415.

(26) Kelkar, S.; Dolan, K. Modeling the effects of initial nitrogen content and temperature on fermentation kinetics of hard cider. *J. Food Eng.* **2012**, *109*, 588−596.

(27) *Production and Utilization Analysis for 2013*; U.S. Apple Assocation: Vienna, VA, 2013; p 41.

(28) Harbertson, J. F.; Parpinello, G. P.; Heymann, H.; Downey, M. O. Impact of exogenous tannin additions on wine chemistry and wine sensory character. *Food Chem.* **2012**, *131*, 999−1008.

(29) Blanpied, G. D.; Silsby, K. J. Predicting Harvest Date Windows for Apples. In *Cornell Cooperative Extension Bulletin*, **1992**; Information Bulletin Vol. *221*, p 18.

(30) Waterhouse, A. Determination of Total Phenolics. *Current Protocols in Food Analytical Chemistry* **2002**, DOI: 10.1002/0471142913.faa0101s06.

(31) Hampson, C. R.; Kemp, H. Characteristics of Important Commercial Apple Cultivars. In *Apples: Botany, Production, and Uses*; Ferree, D. C., Warrington, I. J., Eds.; CABI Publishing: Cambridge, MA, 2003.

(32) Marks, S. C.; Mullen, W.; Crozier, A. Flavonoid and chlorogenic acid profiles of English cider apples. *J. Sci. Food Agric.* **2007**, *87*, 719−728.

(33) Guyot, S.; Le Bourvellee, C.; Marnet, N.; Drilleau, J. F. Procyanidins are the most abundant polyphenols in dessert apples at maturity. *Lebensm.-Wiss. Technol.* **2002**, *35*, 289−291.

(34) Ceymann, M.; Arrigoni, E.; Schärer, H.; Bozzi Nising, A.; Hurrell, R. F. Identification of apples rich in health-promoting flavan-3-ols and phenolic acids by measuring the polyphenol profile. *J. Food Compos. Anal.* **2012**, *26*, 128−135.

(35) Goulas, V.; Kourdoulas, P.; Makris, F.; Theodorou, M.; Fellman, J. K.; Manganaris, G. A. Comparative polyphenolic antioxidant profile

and quality of traditional apple cultivars as affected by cold storage. *Int. J. Food Sci. Technol.* **2014**, *49*, 2037−2044.
(36) Karaman, Ş.; Tütem, E.; Başkan, K. S.; Apak, R. Comparison of antioxidant capacity and phenolic composition of peel and flesh of some apple varieties. *J. Sci. Food Agric.* **2013**, *93*, 867−875.
(37) Matthes, A.; Schmitz-Eiberger, M. Polyphenol content and antioxidant capacity of apple fruit: effect of cultivar and storage conditions. *J. Appl. Bot. Food Qual.* **2012**, *82*, 152−157.
(38) McGhie, T. K.; Hunt, M.; Barnett, L. E. Cultivar and growing region determine the antioxidant polyphenolic concentration and composition of apples grown in New Zealand. *J. Agric. Food Chem.* **2005**, *53*, 3065−3070.
(39) Volz, R. K.; McGhie, T. K. Genetic variability in apple fruit polyphenol composition in Malus× domestica and Malus sieversii germplasm grown in New Zealand. *J. Agric. Food Chem.* **2011**, *59*, 11509−11521.
(40) Goodrich, K. M.; Neilson, A. P. Simultaneous UPLC−MS/MS analysis of native catechins and procyanidins and their microbial metabolites in intestinal contents and tissues of male Wistar Furth inbred rats. *J. Chromatogr. B* **2014**, *958*, 63−74.
(41) Jakobek, L.; García-Villalba, R.; Tomás-Barberán, F. A. Polyphenolic characterisation of old local apple varieties from Southeastern European region. *J. Food Compos. Anal.* **2013**, *31*, 199−211.
(42) Goodrich, K. M.; Fundaro, G.; Griffin, L. E.; Grant, A. Q.; Hulver, M. W.; Ponder, M. A.; Neilson, A. P. Chronic administration of dietary grape seed extract increases colonic expression of gut tight junction protein occludin and reduces fecal calprotectin: a secondary analysis of healthy Wistar Furth rats. *Nutr. Res. (N.Y.)* **2012**, *32*, 787−794.
(43) Peck, G. M.; Merwin, I. A.; Watkins, C. B.; Chapman, K. W.; Padilla-Zakour, O. I. Maturity and Quality of 'Liberty' Apple Fruit Under Integrated and Organic Fruit Production Systems Are Similar. *Hortscience* **2009**, *44*, 1382−1389.
(44) Lea, A. G. H.; Beech, F. W. Phenolics of ciders - effect of cultural conditions. *J. Sci. Food Agric.* **1978**, *29*, 493−496.
(45) del Campo, G.; Berregi, I.; Iturriza, N.; Santos, J. I. Ripening and changes in chemical composition of seven cider apple varieties. *Food Sci. Technol. Int.* **2006**, *12*, 477−487.
(46) Neveu, V.; Perez-Jimenez, J.; Vos, F.; Crespy, V.; du Chaffaut, L.; Mennen, L.; Knox, C.; Eisner, R.; Cruz, J.; Wishart, D.; Scalbert, A. Phenol-Explorer: an online comprehensive database on polyphenol contents in foods. *Database* **2010**, DOI: 10.1093/database/bap024.
(47) Vieira, F. G. K.; Borges, G. D. S. C.; Copetti, C.; Di Pietro, P. F.; Nunes, E. D. C.; Fett, R. Phenolic compounds and antioxidant activity of the apple flesh and peel of eleven cultivars grown in Brazil. *Sci. Hortic.* **2011**, *128*, 261−266.
(48) Renard, C. M. G. C.; Le Quere, J. M.; Bauduin, R.; Symoneaux, R.; Le Bourvellec, C.; Baron, A. Modulating polyphenolic composition and organoleptic properties of apple juices by manipulating the pressing conditions. *Food Chem.* **2011**, *124*, 117−125.
(49) Ley, J. P.; Paetz, S.; Blings, M.; Hoffmann-Lucke, P.; Riess, T.; Krammer, G. E. Structural analogues of hispolon as flavor modifiers. In *Expression of Multidisciplinary Flavour Science*, Proceedings of the 12th Querman Symposium, Interlaken, Switzerland, 2008; Blank, I., Wuest, M., Yeretzian, C., Eds.; Zuercher Hochschule fuer Angewandte Wissenschaften, Institut fuer Chemie und Biologische Chemie: Waedenswil, Germany, 2010; pp 402−405.

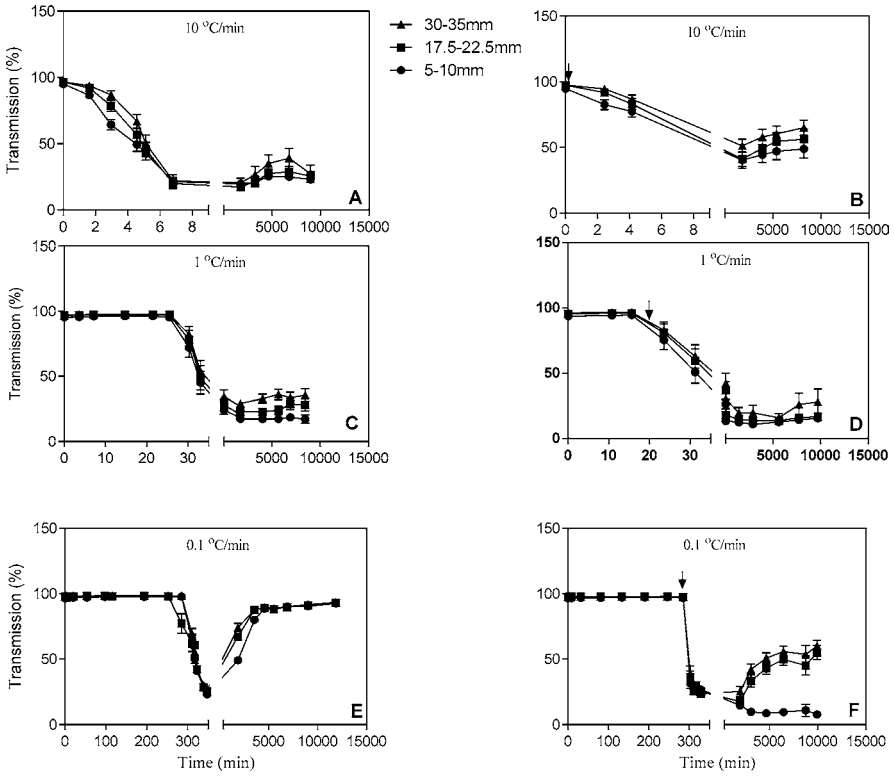


**Figure 1.** Transmission measurements of 0.5% BW in soybean oil crystallized at 25 °C for 7 days using different cooling rates (0.1, 1, and 10 °C/min) without (left column) and with (right column) HIU: (A, B) 10 °C/min; (C, D) 1 °C/min; (E, F) 0.1 °C/min. Transmission measurements were performed at the bottom of the tube (5−10 mm from the bottom, solid circles), at the middle of the tube (17.5−22.5 mm, solid squares), and at the top of the tube (30−35 mm, solid triangles). The arrow (right column) indicates the moment at which HIU was applied. One hundred percent transmission of light indicates there is no turbidity, and 0% transmission indicates that the contents of the assay tubes are completely turbid.

pure corn oil, Great Value pure olive oil, high-oleic All Natural Louana pure safflower oil, high-oleic Antoine & Muse imported pure sunflower oil, and Pure Wesson soybean oil were used in our experiments. Beeswax was supplied by Koster Keunen, Inc. BW is composed of wax esters (35%, mainly C50), hydroxyl esters (24%, mainly ester of 15-hydroxypalmitic acid and C24−C34 alcohols), hydrocarbon (14%), diesters (12%), free acids (12%), and unidentified compounds (6%).[14] Samples of 0.5 and 1% BW in vegetable oils were used. Three different cooling rates were evaluated (0.1, 1, and 10 °C/min) to represent slow, medium, and fast cooling rates. BW was mixed with the oils and heated to 100 °C in an oven to allow for complete melting and dissolution of the wax in the oil. Samples were kept at 100 °C for at least 30 min, and then 5 g of the melted samples was placed in customized tubes for transmission measurements (see section below) and placed again in the oven to ensure that no wax crystallized during the filling of the tubes.

**Fatty Acid Compositions in Different Oils.** Fatty acid compositions of the oils were determined as described by Ye et al.[20] using a gas chromatograph (Shimadzu 2010) equipped with a flame ionization detector (Shimadzu, Columbia, MD, USA).

**Cooling Rate Measurement.** After the samples had bee kept in the oven for 30 min, samples were cooled from 60 to 25 °C using the three different cooling rates previously mentioned. Slower cooling rates (0.1 and 1 °C/min) were achieved using a programmable water bath (Lauda Ecoline Staredition (Delran, NJ, USA). The fast cooling rate (10 °C/min) was achieved by placing the hot samples in a water bath (VWR, model 1160S (Buffalo Grove, IL, USA), that was preset at the crystallization temperature (25 °C).

**High-Intensity Ultrasound (HIU).** HIU operating at a frequency of 20 kHz was applied to the samples using a 2 mm probe (part 4423, Qsonica Sonicators, Newtown, CT, USA) with a vibration amplitude of 180 $\mu$m for 10 s, which resulted in a power level of 10 W. To achieve maximum efficiency of the ultrasound waves, HIU was applied in the presence of crystals;[20] therefore, HIU was applied at 300, 20, and 1.5 min for the 0.5% BW samples cooled at 0.1, 1, and 10 °C/min cooling rates, respectively. HIU was applied at 300, 15, and 1.5 min for 1% BW cooled at 0.1, 1, and 10 °C/min cooling rates, respectively.

**Transmission Measurement.** The crystallization behavior of the samples was followed by measuring the transmission of light through the samples. When samples crystallize, they create a certain amount of turbidity, showing a decrease in the transmission of light. Transmission of light through the samples was taken with TurbiScan equipment (Turbiscan Classic, MA2000, L'Union, France), and data were analyzed using computer software (Turbisoft version 1.2.1). Melted samples (5 g) were placed in the TurbiScan tubes reaching a height of 40 ± 0.5 mm, and transmission was measured as a function of time. Transmission of the tubes was measured at three different levels, 5−10 mm (bottom), 17.5−22.5 mm (middle), and 30−35 mm (top), respectively, from the bottom of the tubes. TurbiScan data were taken on a daily basis for 7 days, from the start of the experiment. Details regarding the operation of TurbiScan can be found in Martini and Tippetts.[21]

**Crystal Morphology.** After 1 week of storage in an incubator at 25 °C, crystals present in the samples were evaluated. Samples were taken from the middle of the tube when no phase separation was observed and from the bottom when phase separation was observed. Crystal morphology was analyzed at different cooling rates at different concentrations of BW in different oils crystallized with and without the use of HIU. The crystals were observed using a polarized light microscope (Olympus BX41, Olympus Optical Co., Tokyo, Japan). A small amount of sample containing crystals was placed on a glass microscope slide and covered gently with a glass cover slip. Digital images of the polarized specimens were captured using Lumenera's Infinity 2 (Lumenera Corp., Nepean, Canada). Approximately 10 pictures of each sample and crystallization run were taken to obtain approximately 200 crystals. These pictures were used to measure crystal sizes using ImageJ 1.42q (Wayne Rasband, National Institutes of Health, USA).

**Differential Scanning Calorimetry (DSC).** The melting profile of the different samples crystallized at 25 °C for 7 days was measured using DSC (TA Instruments DSC model Q20 1963 with RCS cooling system, New Castle, DE, USA). Samples were centrifuged at 25 °C at 3000*g* for 30 min to separate the crystals from the oil and achieve higher resolution in the DSC. The DSC baseline and temperature were calibrated with a pure indium standard. Approximately 10 mg of crystals was placed in Tzero aluminum pans, covered and sealed with Tzero aluminum lids. The samples were heated from 25 to 100 °C with a ramp of 5 °C/min to analyze the melting profile of the samples. TA Universal Analysis software was used to analyze the onset and peak temperatures.

**Statistics.** Samples were crystallized in triplicate. From each crystallization run, transmission measurements were taken in quintuplicate and DSC measurements were taken in duplicate. TurbiScan data were reported using GraphPad Prism6 software (Graphpad Software, San Diego, CA, USA). Crystal sizes were analyzed using Microsoft Office Excel 2010 (Microsoft Corp., Redmond, WA, USA). Statistical analysis was performed using two-way ANOVA test using GraphPad Prism6 software.

## RESULTS AND DISCUSSION

**Effect of Cooling Rate, Wax Concentration, and HIU on BW Crystallization.** Figure 1 shows transmission measurements of 0.5% BW in soybean oil crystallized to 25 °C for 7 days using three different cooling rates (0.1, 1, and 10 °C/min). The *x*-axis denotes time of storage at 25 °C, and the *y*-axis is the percentage of transmission through the wax/oil sample. Transmission counts were taken at the bottom, middle, and top of the tube to evaluate if crystallization occurs in a homogeneous manner throughout the tube. As expected, samples crystallized more quickly when cooled at the fast cooling rate (10 °C/min) and reached a minimum value of approximately 25% transmission after 7 h (Figure 1A) at 25 °C. When samples were crystallized at 1 °C/min (Figure 1C), values of transmission similar to the ones observed for the sample crystallized at 10 °C/min were obtained. However, when the sample was crystallized at 1 °C/min, slighter higher values of transmission were observed after 1 day (1440 min) at 25 °C at the middle and top of the tube compared to the transmission values obtained at the bottom of the tube. This indicates that some degree of phase separation occurs under these conditions when the sample gets less turbid over time due to crystal sedimentation. This effect is even more significant when samples are cooled at 0.1 °C/min (Figure 1E), when a significant phase separation is observed after the first day of storage at 25 °C (note the significant increase in transmission in Figure 1E), and a high transmission value (∼100%) is observed after 3 days (4320 min), suggesting that the tube is completely clear after 3 days of storage and that the crystals have sedimented at the bottom of the tube (lower than 5 mm from the bottom). Therefore, it is evident that the cooling rate has a direct influence on the phase separation of the wax in oil mixture.

HIU was used in these samples to evaluate if this processing tool could help in stabilizing crystal networks and therefore delay phase separation. When HIU was applied in samples crystallized at the fast cooling rate, higher transmission values (27 ± 7 and 65 ± 6% for samples crystallized without and with HIU, respectively) were observed (Figure 1B), suggesting that HIU delays wax crystallization under these conditions. Figure 1D shows that HIU slightly delays phase separation when samples were cooled at 1 °C/min because transmission values obtained at the bottom, middle, and top of the tube are similar. This can be observed by comparing transmission values reported in panels C and D of Figure 1 at 30−35 mm (35 ± 5 and 28 ± 10%, respectively). A significant delay in phase separation is observed for samples crystallized at the slow cooling rate and with HIU application. No phase separation was observed at the bottom of the tube, and significantly lower transmission values were observed in the middle and top of the tubes (Figure 1F) compared to the same sample crystallized without the use of HIU (Figure 1E). These data suggest that HIU can help in the stabilization of a crystalline network to avoid phase separation, especially when samples are processed using slow cooling rates.

To understand the results reported in Figure 1, the morphology of the crystals was evaluated using polarized light microscopy after storage. Figure 2 shows the morphology

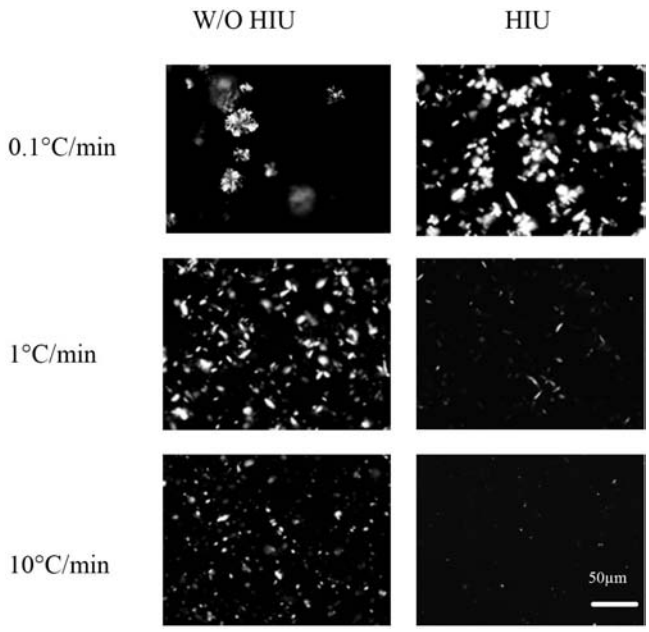


**Figure 2.** Morphology of crystals obtained when 0.5% BW in SBO is crystallized at 25 °C for 7 days at different cooling rates (0.1, 1, and 10 °C/min) without (left column) and with (right column) HIU. Crystal pictures were taken at 20× magnification under polarized light microscopy. The white bar corresponds to 50 μm.

of crystals obtained for the 0.5% BW samples crystallized in soybean oil at different cooling rates (0.1, 1, and 10 °C/min) with and without the use of HIU. As expected, bigger crystals where obtained when samples were crystallized at slow cooling rates. Previous research has reported the increase in crystal size when lipids are crystallized using slow cooling rates.[22] In addition, this figure shows that HIU reduced crystal sizes and morphologies, especially for the BW crystallized at slow cooling rates: big spherulites are observed in the sample crystallized without the use of HIU, and smaller crystals are observed when HIU was used.

The experiments performed in Figures 1 and 2 were repeated using a BW concentration of 1% to evaluate the effect of cooling rate and sonication when a higher wax concentration is used. Figure 3 shows the transmission measurements for these samples. All of the crystallization conditions remained constant except the timing of the ultrasound application. HIU was applied at 5 h, 15 min, and 1.5 min for 0.1, 1, and 10 °C/min, respectively. This change was performed so that HIU could be applied at the moment when the first crystals appeared. The

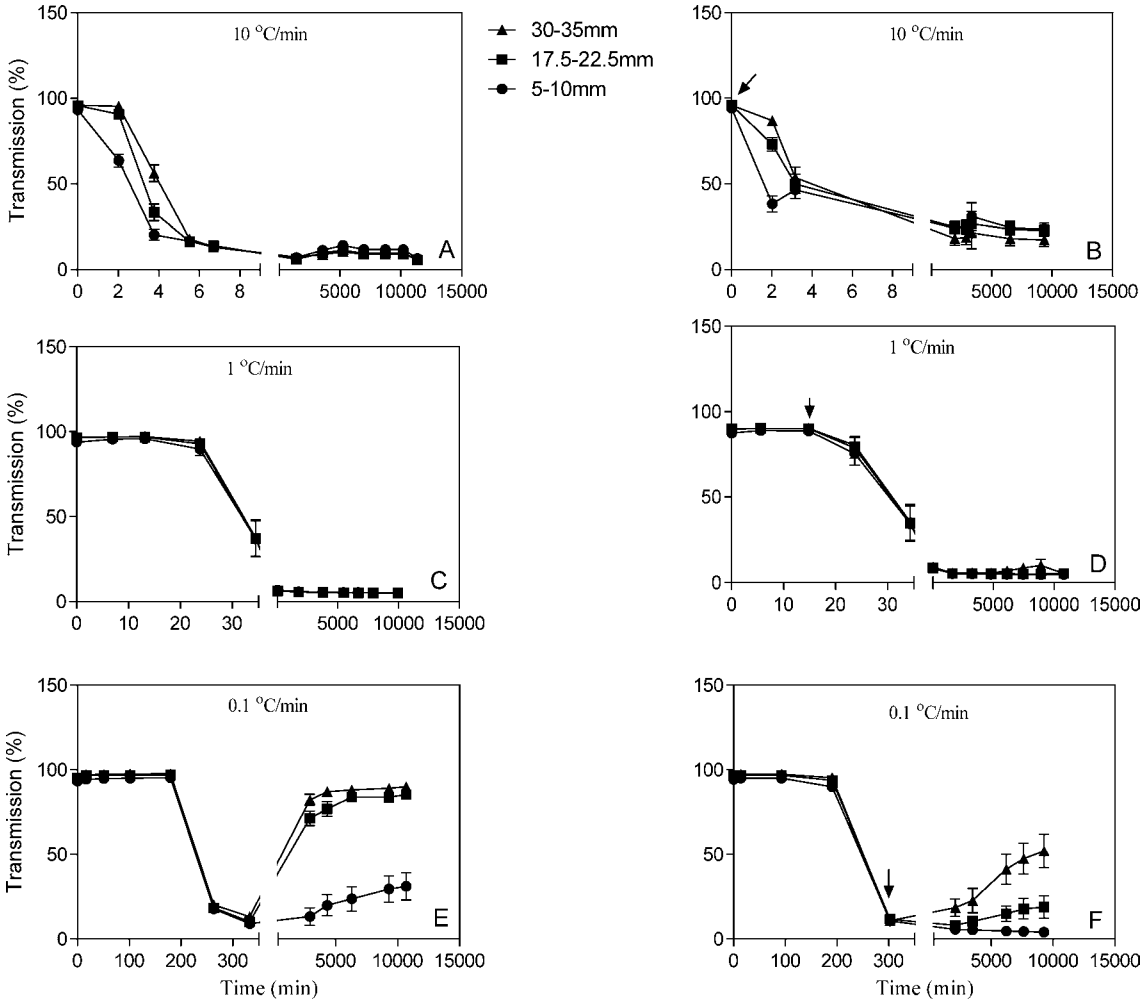


**Figure 3.** Transmission measurements of 1% BW in soybean oil crystallized at 25 °C for 7 days using different cooling rates (0.1, 1, and 10 °C/min) without (left column) and with (right column) HIU: (A, B) 10 °C/min; (C, D) 1 °C/min; (E, F) 0.1 °C/min. Transmission measurements were performed at the bottom of the tube (5−10 mm from the bottom, solid circles), at the middle of the tube (17.5−22.5 mm, solid squares), and at the top of the tube (30−35 mm, solid triangles). The arrow (right column) indicates the moment at which HIU was applied. One hundred percent transmission of light indicates there is no turbidity, and 0% transmission indicates that the contents of the assay tubes are completely turbid.

higher concentration of BW (1 vs 0.5%) induced crystallization, and therefore HIU was applied sooner. Figure 3 shows that no phase separation was observed in the samples crystallized at intermediate (1 °C/min) and fast cooling rates (10 °C/min) with transmission values of 5 ± 0 and 7 ± 2%, respectively (Figure 3, panels A and C, respectively). Some degree of phase separation was observed in samples crystallized at the slow cooling rate with transmission values of 90 ± 2% at the top of the tube and 31 ± 8% at the bottom of the tube (Figure 3F). The use of HIU did not affect the final transmission value of the samples crystallized at 1 and 10 °C/min (Figure 3B,D) but significantly affected transmission values and therefore phase separation of samples crystallized at slow cooling rates (Figure 3F). The transmission values for these samples decreased to 52 ± 10% at the top of the tube and 19 ± 7% at the bottom of the tube. Similarly to the results reported for the 0.5% samples, these results show that HIU delayed phase separation during storage.

Figure 4 shows the morphology of crystals obtained for the samples discussed in Figure 3 after 7 days of storage at 25 °C. Even though a slight decrease in the crystal size is observed as a consequence of sonication, the effects are not as evident as the ones observed for the 0.5% BW in soybean oil samples (Figure 2). Figure 4 shows that the morphology of the BW crystals cooled at 0.1 °C/min is not changed as a consequence of sonication as reported for the 0.5% BW samples.

Results reported in Figures 1−4 suggest that a significant phase separation occurs when 0.5 and 1% of BW is crystallized at the slow cooling rate (0.1 °C/min) in soybean oil and that this phase separation can be delayed using HIU. Previous research on natural waxes with soybean oil was done by Hwang et al.[14,15] and suggested that sunflower wax works best toward crystallization and cooling rate in a concentration range of 0.5−10%. Dassanayake et al.[12] evaluated the crystallization behavior of rice bran, carnauba, and candelilla wax in olive oil and salad oil (50% canola + 50% soybean oil) and suggested that the long, thin, needle-shaped crystal structures formed by rice bran wax in the above oils might be responsible for the good gelling properties of this wax. Similar to our data, Toro-Vazquez et al.[5] showed that 1% candelilla wax crystallized in safflower oil showed phase separation during storage for 3 months. Even though some wax/oil combinations have been studied as discussed above, it is not clear how the type of oil affects the crystallization of waxes. However, the existing literature and our

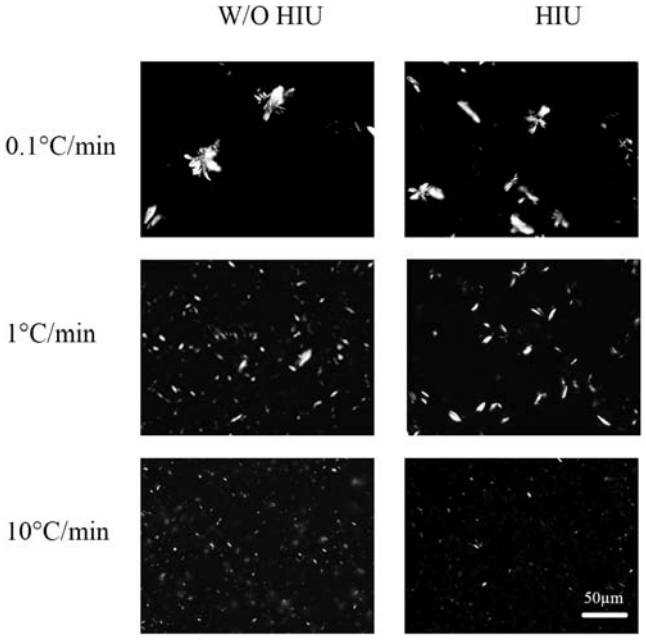


**Figure 4.** Morphology of crystals obtained when 1% BW in SBO is crystallized at 25 °C for 7 days at different cooling rates (0.1, 1, and 10 °C/min) without (left column) and with (right column) HIU. Crystal pictures were taken at 20× magnification under polarized light microscopy. The white bar corresponds to 50 $\mu$m.

data agree on the fact that wax concentration and cooling rate have a direct impact on wax crystallization. Therefore, the next step in our research is to evaluate if the crystallization of BW is affected by the type of oil used when crystallized at 0.1 °C/min.

**Effect of Oil Type and Sonication on BW Crystallization.** Table 1 shows the fatty acid composition of the oils used in this research. These oils were chosen to include different and typical chemical compositions found in vegetable oils. For example, canola and sunflower oils have approximately 62% of oleic acid (C18:1), whereas olive and safflower oils have higher contents of oleic acid (approximately 73 and 76%, respectively). On the other hand, corn and soybean oils have lower contents of oleic acid with values of approximately 29 and 23%, respectively.

Figure 5 shows the crystallization behavior of 0.5% BW in different vegetable oils cooled at 0.1 °C/min. Phase separation was observed in 0.5% BW samples crystallized in all of the oils tested (canola, corn, olive, safflower, and sunflower) when stored. It is interesting to note that the crystallization behavior of the 0.5% BW solutions is significantly affected by the type of oils used. For example, when BW is crystallized in soybean oil, the sample starts crystallizing at approximately 300 min (Figure 1E). The onset of crystallization is lower for canola, corn, olive, safflower, and sunflower with an onset of crystallization of approximately 200 min for canola and sunflower and 250 min for corn, olive, and safflower (Figure 5A,C,E,G,I). As previously discussed, phase separation was very marked when 0.5% BW was crystallized in soybean oil (Figure 1E). Phase separation was observed in all the other samples but to a lower degree. When 0.5% BW was crystallized in canola oil (Figure 5A), the sample remained turbid at the bottom of the tube even after 5000 min (~3.5 days) of storage with transmission values of 22 ± 1%. However, some degree of phase separation is present after the first day of storage, which is evidenced by higher transmission values observed at the top of the tube (50 ± 4%). This phase separation becomes more evident at approximately 3500 min (~2.5 days), when the transmission increased to 61 ± 5% at the top of the tube and to 33 ± 3% in the middle of the tube. The use of HIU in this sample inhibited crystallization, and lower values of transmission were observed (60 ± 15% at the bottom of the tube at 1500 min). These transmission values remained constant during storage, indicating that phase separation was delayed due to the use of HIU. When 0.5% BW was crystallized in corn oil (Figure 5C), the sample shows more turbidity (24 ± 7%) at the bottom after 5000 min of storage compared to the middle (39.6 ± 5.3%) and top (51 ± 7%) of the tube. HIU application (Figure 5D) made the transmission values approximately similar at the bottom (29 ± 10%), middle (32 ± 11%), and top (32 ± 11%) of the tube, suggesting the lack of phase separation. The transmission at the bottom part of 0.5% olive oil (Figure 5E) was low (42 ± 7%) up to 4200 min and then increased over time. Similar results were observed at the middle (65 ± 5%) and top (73 ± 2%) of the tube. When HIU was used (Figure 5F), transmission levels were lower at the bottom (22 ± 6%), middle (45 ± 9%), and top (46 ± 8%) part of the tube after 4700 min. When 0.5% BW was crystallized in safflower oil (Figure 5G), the contents at the bottom part (38 ± 2%) of the tube were more turbid than the middle (53 ± 2%) and top (60 ± 2%), but no changes in transmission values were observed when HIU was applied (Figure 5H) with approximately the same turbidity obtained throughout all levels of the tube (transmission at bottom, 63 ±

**Table 1. Fatty Acid Compositions of the Oils Used in This Research**[a]

| fatty acid | canola | corn | olive | soybean | sunflower | safflower |
|---|---|---|---|---|---|---|
| C16:0 | 4.4 ± 0.0 | 11.9 ± 0.3 | 11.8 ± 0.1 | 11.1 ± 0.1 | 4.4 ± 0.6 | 4.9 ± 0.2 |
| C18:0 | 2.0 ± 0.1 | 1.8 ± 0.2 | 2.5 ± 0.0 | 4.4 ± 0.0 | 3.4 ± 0.1 | 1.4 ± 0.7 |
| C18:1 | 63.9 ± 5.4 | 29.9 ± 2.7 | 73.8 ± 1.1 | 23.9 ± 2.7 | 63.6 ± 2.0 | 80.4 ± 3.3 |
| C18:2c9 c12 | 19.8 ± 0.0 | 55.4 ± 1.8 | 11.2 ± 0.8 | 53.6 ± 0.2 | 28.3 ± 0.2 | 12.6 ± 0.2 |
| C18:3c9 c12 c15 | 9.8 ± 0.7 | 0.9 ± 0.2 | 0.6 ± 0.2 | 7.0 ± 0.3 | 0.3 ± 0.0 | 0.6 ± 0.3 |
| SFA | 6.5 | 13.7 | 14.3 | 15.5 | 7.8 | 6.4 |
| UFA | 93.5 | 86.2 | 85.6 | 84.5 | 92.2 | 93.6 |
| MUFA | 63.9 | 29.9 | 73.8 | 23.9 | 63.6 | 80.4 |
| PUFA | 29.5 | 56.4 | 11.8 | 60.6 | 28.6 | 13.2 |
| total | 100.0 | 100.0 | 100.0 | 100.0 | 100.0 | 100.0 |

[a]Mean values and standard deviation of two replicates are reported. Fatty acids present at levels below 0.5% are not reported.

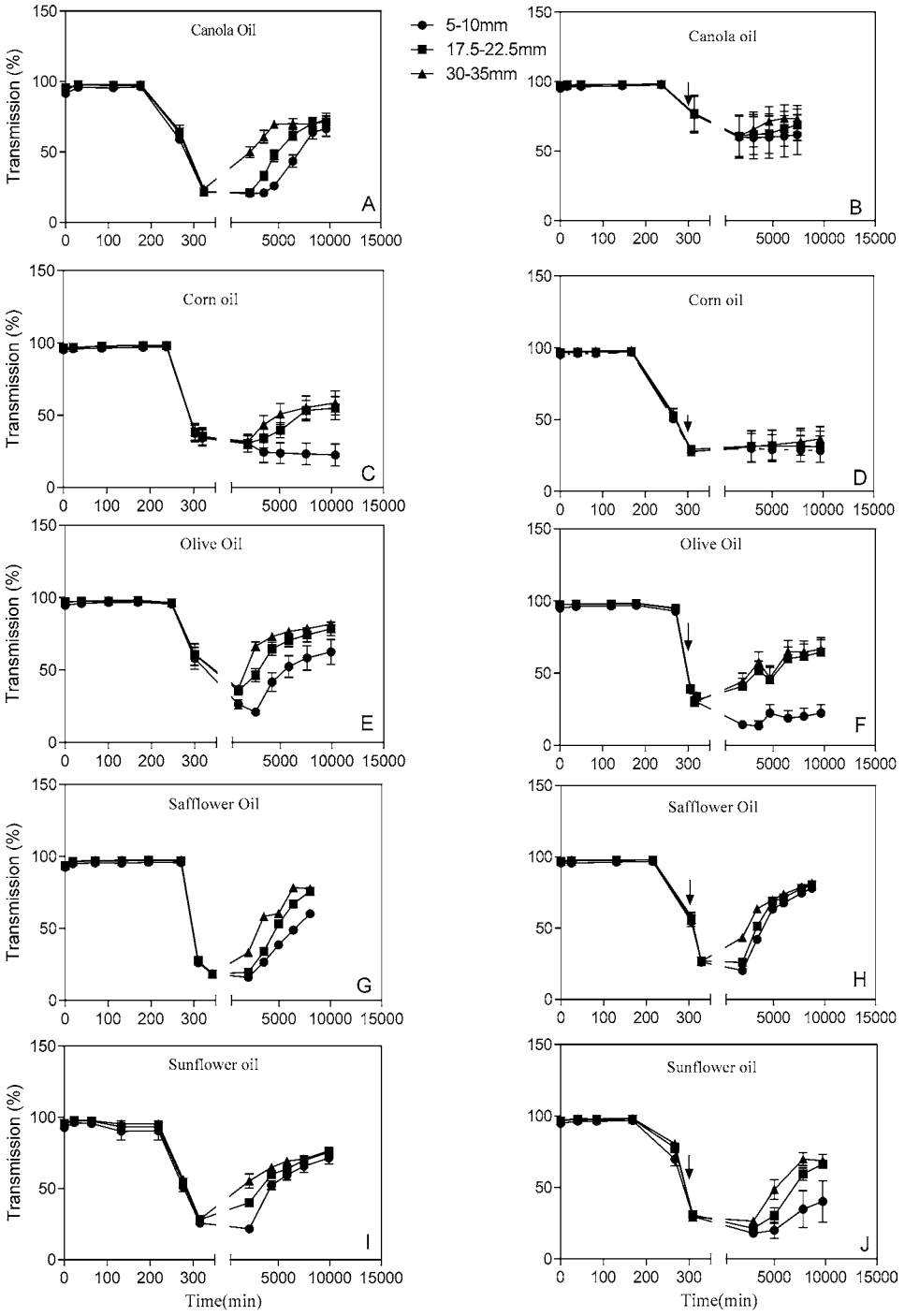


**Figure 5.** Transmission measurements of 0.5% BW in different edible oils crystallized at 25 °C for 7 days using a slow cooling rate of 0.1 °C/min without (left column) and with (right column) HIU: (A, B) canola oil; (C, D) corn oil; (E, F) olive oil; (G, H) safflower oil; (I, J) sunflower oil. The arrow shows the time of HIU application, that is, 300 min after the start of the experiment.

2%; middle, 69 ± 1%; and top, 70 ± 1.6%) after 5000 min. When 0.5% BW was crystallized in sunflower oil, the transmission at the bottom after 5000 min was 59 ± 3% and the transmissions in the middle and top portions were 64 ± 3 and 69 ± 3%, respectively. The transmission through sunflower oil (Figure 5J) shows more turbidity with HIU application after 5000 min at all levels of the tube. The bottom part reached a transmission value of 20 ± 6%, and the middle and top reached 30 ± 6 and 49 ± 7%, respectively. Overall, the stability toward phase separation increased in the order soybean oil < olive oil < sunflower oil < canola oil < safflower oil < corn oil. These results suggest that (a) for the same type and amount of wax, the type of oil used affects the degree of phase separation and (b) HIU can help in the delay of phase separation to different degrees depending on the oil used. However, it is not clear how the type of oil affects BW crystallization. For example, corn oil and soybean oil have both very similar fatty acid compositions (Table 1, 29.9 vs 23.9% of oleic acid), and the crystallization behavior of BW and phase separation observed are significantly different (Figures 1E and 5C) where more phase separation is observed in the soybean oil samples and a greater effect of sonication is observed in the corn oil samples (Figures 1F and


dx.doi.org/10.1021/jf503393h | J. Agric. Food Chem. 2014, 62, 10192−10202

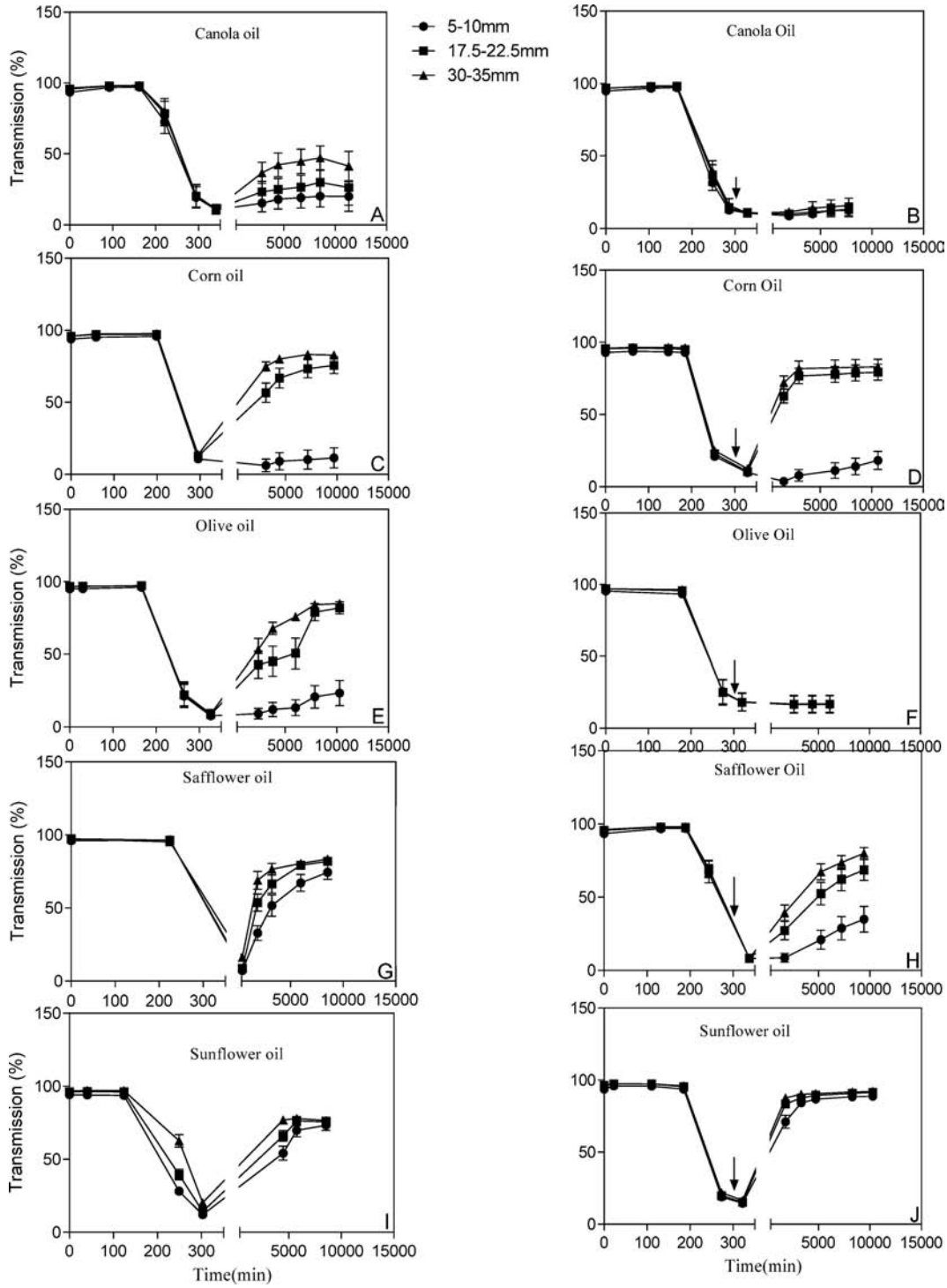


**Figure 6.** Transmission measurements of 1% BW in different edible oils crystallized at 25 °C for 7 days using a slow cooling rate of 0.1 °C/min without (left column) and with (right column) HIU: (A, B) canola oil; (C, D) corn oil; (E, F) olive oil; (G, H) safflower oil; (I, J) sunflower oil. The arrow shows the time of HIU application, that is, 300 min after the start of the experiment.

5D). It is possible that the differences observed are a consequence of the C18:3 content because the value observed in soybean oil is approximately 87% higher than in corn oil.

Similarly, Figure 6 shows the crystallization behavior of 1% BW in different vegetable oils cooled at 0.1 °C/min. Phase separation was observed in 1% BW samples crystallized in all of the oils tested (canola, corn, olive, safflower, and sunflower) when stored and was affected by the type of oil used. When 1% BW samples were crystallized in canola oil (Figure 6A), the sample remains more turbid at the bottom (18 ± 7%) after 5000 min and the transmissions at the middle and top parts were 25 ± 8 and 42 ± 8%, respectively. At 340 min the transmissions in all three levels were the same for 1% BW samples in canola oil (almost 11%). When HIU (Figure 6B) was applied in 1% BW in canola oil sample, the transmission at the top level after 6000 min was 15 ± 5% and the transmissions at bottom and middle of the tube after 6000 min were 12 ± 4 and 12 ± 4%, respectively. This low value of transmission


dx.doi.org/10.1021/jf503393h | J. Agric. Food Chem. 2014, 62, 10192−10202

suggests that HIU decreases phase separation of 1% BW in canola oil. When 1% BW samples were crystallized in corn oil (Figure 6C), the contents at the top (80 ± 3%) and middle (67 ± 7%) of the tube were more transparent than that at the bottom part after 4500 min kept at 25 °C. Data collected from 1% BW sample with HIU application (Figure 6D) show no different transmission pattern (top level, 82 ± 5%; middle, 78 ± 6%; and bottom, 11 ± 5.4%) in all levels of transmission after 6500 min of storage at 25 °C compared to the sample crystallized without HIU (Figure 6C). Previous research in our laboratory in anhydrous milk fat showed that the effect of HIU is less effective in samples crystallized under high driving forces.[19] In this case, the higher concentration of wax (1 vs 0.5%) might create a high enough driving force that inhibits the effect of sonication to some degree. When 1% BW is crystallized in olive oil (Figure 6E), more turbidity at the bottom of the tube (13 ± 6%) is observed compared to the turbidity at the middle and top (50 ± 10.5 and 76 ± 3%, respectively). The transmissions obtained for 1% BW samples crystallized with HIU (Figure 6F) were similar for the entire tube length. The bottom part shows 17 ± 6% transmission, the middle part shows 17 ± 6% transmission, and the top part shows 17 ± 6% transmission. Similar to the results shown for 1% BW crystallized in canola oil, HIU inhibited phase separation for a period of 7 days. When 1% BW samples were crystallized in safflower oil (Figure 6G), phase separation was observed with transmission values of 80 ± 2% at the top, 79 ± 3% in the middle, and 67 ± 6% at the bottom after 6000 min of storage. When HIU was applied (Figure 6H), the transmission after 5200 min at the bottom was 21 ± 6.5%. Lower transmission values were also obtained in sonicated samples in the middle (52 ± 8%) and in the top (67 ± 6%) sections of the tube. These results suggest that HIU helped delay phase separation in 1% BW crystallized in safflower oil. When 1% BW was crystallized in sunflower oil (Figure 6I), there was a difference in transmission in the three sections of the tube after 4500 min; the contents in the bottom section are more turbid (54 ± 5% transmission) than those in the middle (66 ± 4%) and top (77 ± 3%) sections. When HIU was applied in that sample (Figure 6J), transmission values through all sections of the tubes remained almost similar to the ones obtained without the use of HIU. Transmission values were 87 ± 2% at the bottom, 90 ± 2% in the middle, and 91 ± 1% at the top.

Figures 5 and 6 show that the degree of phase separation is not related to wax concentration and that the effect of HIU toward the delay of phase separation at both wax concentrations (0.5 and 1%) highly depends on the type of oil used. The stability toward phase separation observed at 0.5% BW does not correlate with stability observed at 1% BW. For example, BW/corn oil samples are the most stable toward phase separation when used at a 0.5% level, whereas BW/canola oil is the most stable when used at 1%. Data reported in Figure 6 show that the stability toward phase separation increases in the following order: safflower oil < sunflower oil < soybean oil < corn oil < olive oil < canola oil. These data suggest that phase separation is probably related to the content of saturated fatty acids (SFA), where a higher content of SFA in the vegetable oil results in less phase separation. Table 1 shows that soybean, corn, and olive oils have a higher amount of SFA (15.5, 13.7, and 14.3%, respectively), and these oils show the least phase separation (Figures 1 and 6). On the other hand, sunflower and safflower oils have lower SFA contents of 7.8 and 6.4%, respectively, and show more phase separation (Figure 6). The mixture of canola oil/BW seems to be an exception to this hypothesis because this sample is the most stable toward phase separation and has a low content of SFA (Figure 6; Table 1). It is possible that for a similar content of SFA a higher content of PUFA contributes to the higher stability toward phase separation. This could explain the different behaviors observed for canola oil and safflower oil samples and also for olive oil and corn oil (Table 1).

As suggested by Dassanayake et al.,[12,13] it is likely that the physical characteristics (oleogel formation, phase separation) of the crystallized material are affected by the type of crystalline network formed. Therefore, to better understand the different crystallization behaviors observed in BW samples crystallized in different oils with and without HIU, we analyzed the morphology of the crystals obtained after 7 days of storage. Figures 7 and 8 show the morphology of crystals obtained in 0.5 and 1% BW, respectively, crystallized in different oils with and without HIU at 0.1 °C/min and stored at 25 °C for 7 days. Crystal morphology significantly changed depending on the type of oil used. When 0.5% BW was crystallized in canola oil without the use of HIU, big spherulites similar to the ones found in soybean oil were observed (Figures 2 and 7). This

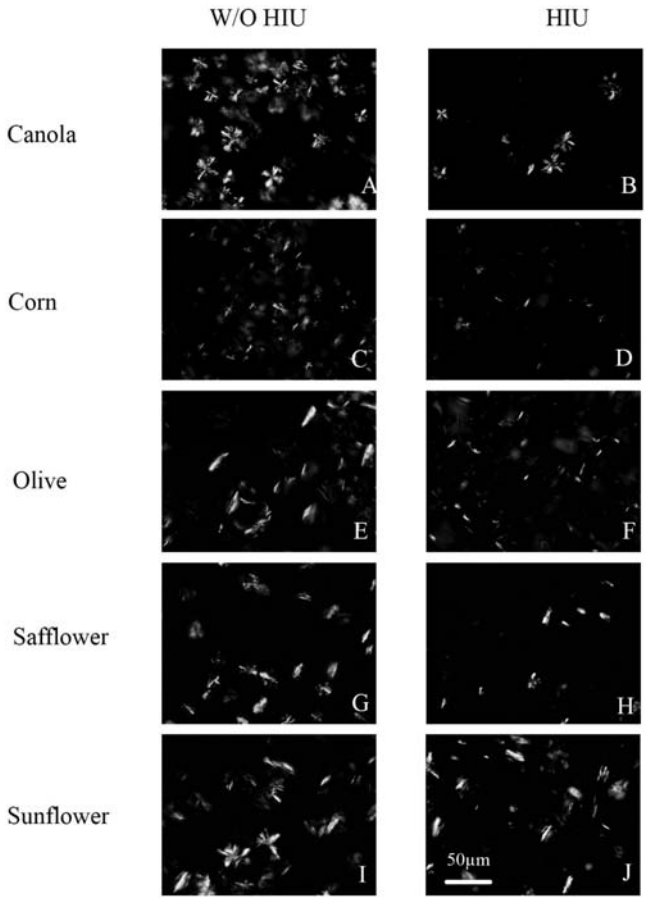


**Figure 7.** Morphology of crystals obtained when 0.5% BW is crystallized in different edible oils at a slow cooling rate (0.1 °C/min) without (left column) and with (right column) HIU after 7 days of storage at 25 °C: (A, B) canola oil; (C, D) corn oil; (E, F) olive oil; (G, H) safflower oil; (I, J) sunflower oil. Crystal pictures were taken at 20× magnification under polarized light microscopy. The white bar corresponds to 50 $\mu$m.

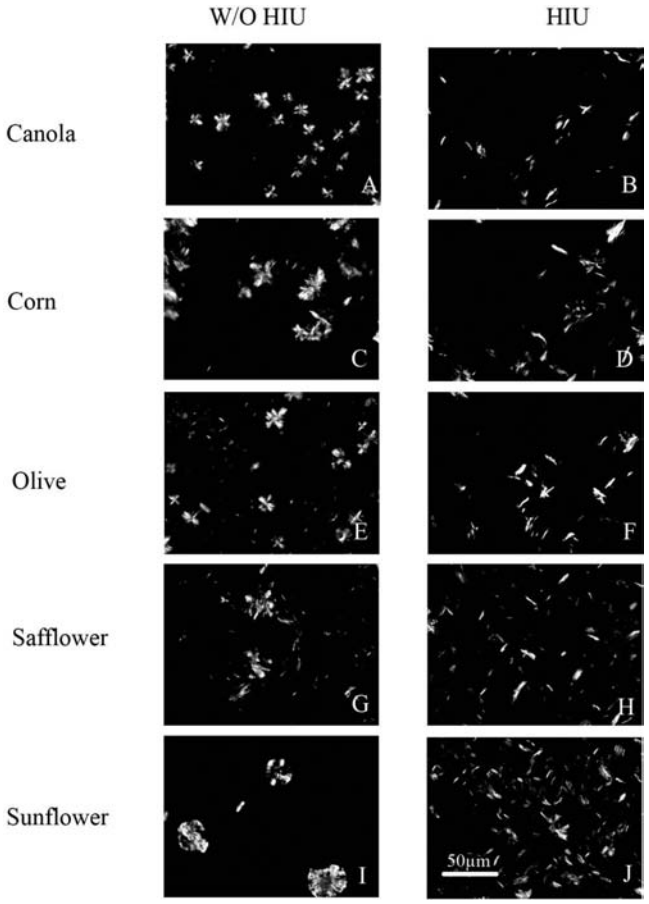


**Figure 8.** Morphology of crystals obtained when 1% BW is crystallized in different edible oils at a slow cooling rate (0.1 °C/min) without (left column) and with (right column) HIU after 7 days of storage at 25 °C: (A, B ) canola oil; (C, D) corn oil; (E, F) olive oil; (G, H) safflower oil; (I, J) sunflower oil. Crystal pictures were taken at 20× magnification under polarized light microscopy. The white bar corresponds to 50 $\mu$m.

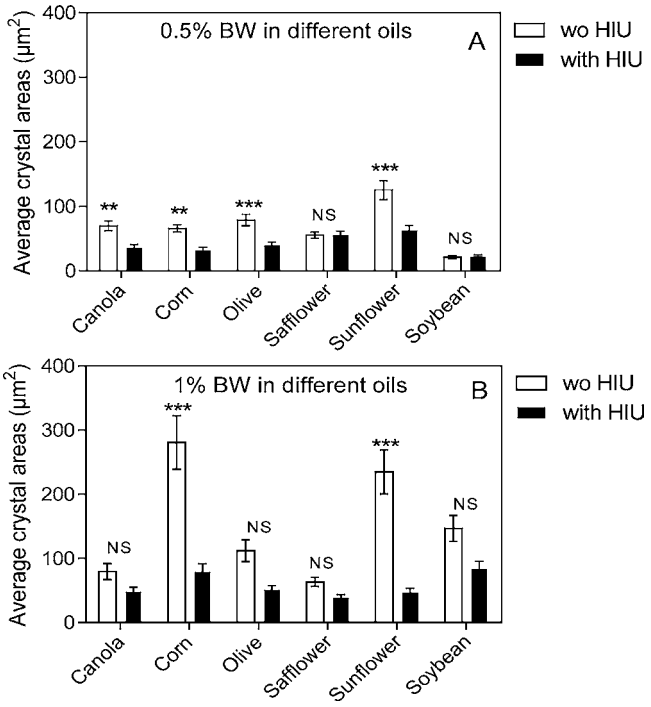


**Figure 9.** Mean crystal area ($\mu$m$^2$) of crystals obtained when 0.5% (A) or 1% (B) BW is crystallized in different vegetable oils (canola, corn, olive, safflower, sunflower, and soybean) at 0.1 °C/min after 7 days of storage at 25 °C. Mean values and standard errors are reported. (*) $p < 0.05$, (**) $p < 0.01$, (***) $p < 0.001$; NS means nonsignificant ($\alpha = 0.05$). Minimum count of the crystals taken was 200 in all cases.

type of morphology was also observed in the BW crystallized in sunflower oil, although the spherulites were not as well formed as the ones observed in canola and soybean oils. Spherulite morphologies were maintained in BW crystallized in canola oil with the use of HIU but were not observed in BW crystallized in soybean and sunflower oils with HIU. Spherulites were also observed when 1% BW was crystallized in all of the vegetable oils but were not present when BW was crystallized in the presence of HIU. Crystal morphology does not seem to explain the differences found in phase separation as a function of type of oil used; however, spherulites seem to be more often associated with phase separation. In general, HIU breaks down the spherulites, and small needle-like crystals are observed. We hypothesize that these needle-like crystals can interact more readily with each other, allowing for more oil entrapment and therefore delaying phase separation.

Figure 9 shows crystal average areas of samples crystallized with and without the use of HIU. It can be observed that HIU generated significantly smaller ($\alpha = 0.05$) crystals in 0.5% BW in all oils with the exception of safflower and soybean oils (Figure 9A). These two oils were the ones on which HIU had the least effects on decreasing the degree of phase separation (Figure 5G–J). The effect of HIU in reducing crystal size in the 1% BW solutions was not as evident as the one observed in the 0.5% BW solutions. HIU reduced crystal areas in 1% BW in corn and sunflower oils ($p < 0.05$), whereas no significant effect was observed in the other oils (Figure 9B). It is interesting to note that even though no significant differences were found in crystal areas in some of these samples, HIU was still effective at delaying phase separation. These results suggest that the effect of crystal area is less important in stabilizing the crystalline network at higher concentrations.

Further analysis on the characteristics of the crystals formed in BW/vegetable oil systems was performed using DSC. Table 2 illustrates onset and peak temperatures of crystals obtained from 0.5 and 1% BW crystallized in different oils (canola, corn, olive, safflower, sunflower, and soybean) at 0.1 °C/min with and without HIU application after 7 days of storage. The melting behavior of the wax crystals obtained from the different wax/oil combinations was very similar to $T_{on}$ values between 38 and 41 °C for the 0.5% samples and between 38 and 45 °C for the 1% samples. In general, the use of HIU resulted in a narrower melting profile as evidenced by either higher $T_{on}$ values or lower $T_p$ values in the sonicated samples. It is likely that the effect of HIU in delaying phase separation is related to the generation of a less fractionated crystalline network where similar molecules can interact strongly among them, entrapping more oil.

Overall, this study shows that several processing conditions can affect phase separation in wax/oil systems. Cooling rate, wax concentration, and type of oil play important roles in the crystallization behavior of waxes, which can also be controlled by using HIU. It is still not clear how the different types of oils affect the crystallization of waxes, but this research suggests that crystal morphology might play an important role in phase separation. Other factors such as the presence of minor

Table 2. Onset ($T_{on}$) and Peak ($T_p$) Temperatures of Crystals Obtained from 0.5 and 1% BW Crystallized in Different Edible Oils (Canola, Corn, Olive, Safflower, Sunflower, And Soybean) at 0.1 °C/min without and with HIU after 7 Days at 25 °C[a]

| | | 0.5% BW | | | 1% BW | | |
|---|---|---|---|---|---|---|---|
| | | W/O HIU | HIU | signif | W/O HIU | HIU | signif |
| BW in canola | $T_{on}$ (°C) | 41.2 ± 0.0 | 40.7 ± 0.5 | NS | 38.0 ± 0.4 | 40.6 ± 1.4 | NS |
| | $T_p$ (°C) | 53.8 ± 0.0 | 51.3 ± 0.5 | *** | 50.3 ± 1.9 | 52.2 ± 1.9 | NS |
| BW in corn | $T_{on}$ (°C) | 39.9 ± 0.3 | 39.2 ± 0.6 | NS | 41.3 ± 0.1 | 40.9 ± 0.9 | NS |
| | $T_p$ (°C) | 50.4 ± 0.5 | 47.0 ± 0.4 | *** | 50.8 ± 0.5 | 51.8 ± 0.5 | NS |
| BW in olive | $T_{on}$ (°C) | 39.1 ± 0.3 | 40.7 ± 0.1 | NS | 37.9 ± 0.4 | 43.1 ± 0.9 | * |
| | $T_p$ (°C) | 50.1 ± 0.5 | 52.1 ± 0.2 | ** | 47.4 ± 0.0 | 54.1 ± 0.7 | * |
| BW in safflower | $T_{on}$ (°C) | 40.3 ± 0.1 | 42.2 ± 0.4 | * | 44.0 ± 1.0 | 44.1 ± 1.1 | NS |
| | $T_p$ (°C) | 52.2 ± 0.7 | 54.6 ± 0.6 | ** | 57.8 ± 0.8 | 54.1 ± 2.0 | * |
| BW in sunflower | $T_{on}$ (°C) | 41.0 ± 0.9 | 41.5 ± 0.7 | NS | 47.0 ± 0.1 | 48.9 ± 2.2 | NS |
| | $T_p$ (°C) | 52.4 ± 0.5 | 53.2 ± 0.6 | NS | 57.4 ± 0.9 | 58.7 ± 0.9 | NS |
| BW in soybean | $T_{on}$ (°C) | 38.8 ± 1.1 | 40.5 ± 0.1 | * | 42.5 ± 0.1 | 38.3 ± 1.4 | * |
| | $T_p$ (°C) | 50.9 ± 0.2 | 51.8 ± 0.5 | NS | 53.8 ± 0.4 | 51.7 ± 0.0 | NS |

[a]Mean values and standard deviation of two independent runs are reported. NS means that $T_{on}$ or $T_p$ within each BW/oil samples is not significantly different ($\alpha = 0.05$). (*) $p < 0.05$; (**) $p < 0.01$; (***) $p < 0.001$.

components and the solubility of wax in the different oils might also play an important role in the crystallization behavior of these molecular entities and therefore on the phase separation observed during storage. Results presented in this study suggest that HIU can be used to delay phase separation in wax/oil systems that have the potential to be used as *trans*-fat replacements in food products.

## AUTHOR INFORMATION


### Corresponding Author

*(S.M.) Phone: (435) 797-8136. Fax: (435) 797-2179. E-mail: silvana.martini@usu.edu.



### Funding

This work was supported by the Utah Agricultural Experiment Station, Utah State University, and approved as Journal Paper 8693.


### Notes

The authors declare no competing financial interest.

## ACKNOWLEDGMENTS

We thank Dr. Robert Ward for GC analysis.

## ABBREVIATIONS USED

BW, beeswax; HIU, high-intensity ultrasound; PLM, polarized light microscopy; DSC, differential scanning calorimetry

## REFERENCES


(1) Shi, R.; Zhang, Q.; Vrieskoop, F.; Yuan, Q.; Liang, H. Preparation of organogel with tea polyphenols complex for enhancing the antioxidation properties of edible oil. *J. Agric. Food Chem.* **2014**, *62*, 8379−8384.

(2) Sawalha, H.; den Adel, R.; Venema, P.; Bot, A.; Flöter, E.; van der Linden, E. Organogel-emulsions with mixtures of β-sitosterol and γ-oryzanol: influence of water activity and type of oil phase on gelling capability. *J. Agric. Food Chem.* **2012**, *60*, 3462−3470.

(3) Jadhav, S. R.; Hwang, H.; Huang, Q.; John, G. Medium-chain sugar amphiphiles: a new family of healthy vegetable oil structuring agents. *J. Agric. Food Chem.* **2013**, *61*, 12005−12011.

(4) Kerr, R. M.; Tombokan, X.; Ghosh, S.; Martini, S. Crystallization behavior of anhydrous milk fat-sunflower oil wax blends. *J. Agric. Food Chem.* **2011**, *59*, 2689−2695.

(5) Toro-Vazquez, J. F.; Morales-Rueda, J. A.; Dibildox-Alvarado, E.; Charo-Alonso, M.; Alonzo-Macias, M.; Gonzalez-Chavez, M. M. Thermal and textural properties of organogels developed by candelilla wax in safflower oil. *J. Am. Oil Chem. Soc.* **2007**, *84*, 989−1000.

(6) Morales-Rueda, J. A.; Dibilidox-Alvarado, E.; Charo-Alonso, M. A.; Toro-Vazquez, J. F. Rheological properties of candelilla wax and dotriacontane organogels measured with a true-gap system. *J. Am. Oil Chem. Soc.* **2009**, *86*, 765−772.

(7) Morales-Rueda, J. A.; Dibilidox-Alvarado, E.; Charo-Alonso, M. A.; Weiss, R. G.; Toro-Vazquez, J. F. Thermo-mechanical properties of candelilla wax and dotriacontane organogels in safflower oil. *Eur. J. Lipid Sci. Technol.* **2009**, *111*, 207−215.

(8) Toro-Vazquez, J. F.; Alonzo-Macias, M.; Dibilidox-Alvarado, E.; Charo-Alsonso, M. A. The effect of tripalmitin crystallization on the thermomechanical properties of candelilla wax organogels. *Food Biophys.* **2009**, *4*, 199−212.

(9) Toro-Vazquez, J. F.; Morales-Rueda, J.; Mallia, V. A.; Weiss, R. G. Relationship between molecular structure and thermo-mechanical properties of candelilla wax abd amides derived from (*R*)-12-hydroxystearic acid as gelators of safflower oil. *Food Biophys.* **2010**, *5*, 193−202.

(10) Chopin-Doroteo, M.; Morales-Rueda, J. A.; Dibilidox-Alvarado, E.; Charo-Alonso, M. A.; de la Peña-Gil, A.; Toro-Vazquez, J. F. The effect of shearing in the thermo-mechanical properties of candelilla wax and candelilla wax-tripalmitin organogels. *Food Biophys.* **2011**, *6*, 359−376.

(11) Alvarez-Mitre, F. M.; Morales-Rueda, J. A.; Dibilidox-Alvarado, E.; Charo-Alonso, M. A.; Toro-Vazquez, J. F. Shearing as a variable to engineer the rheology of candelilla wax organogels. *Food Res. Int.* **2012**, *49*, 580−587.

(12) Dassanayake, L. S. K.; Kodali, D. R.; Ueno, S.; Sato, K. Physical properties of ricebran wax in bulk and organogels. *J. Am. Oil Chem. Soc.* **2009**, *86*, 1163−1173.

(13) Dassanayake, L. S.; Kodali, D. R.; Ueno, S.; Sato, K. Crystallization kinetics of organogels prepared by rice bran wax and vegetable oils. *J. Oleo Sci.* **2012**, *61*, 1−9.

(14) Hwang, H. S.; Kim, S.; Singh, M.; Winkler-Moser, J. K.; Liu, S. X. Organogel formation of soybean oil with waxes. *J. Am. Oil Chem. Soc.* **2012**, *89*, 639−647.

(15) Hwang, H. S.; Singh, M.; Bakota, E. L.; Winkler-Moser, J. K.; Kim, S.; Liu, S. X. Margarine from Organogels of plant wax and soybean oil. *J. Am. Oil Chem. Soc.* **2013**, *90*, 1705−1712.
(16) Blake, A. I.; Co, E. D.; Marangoni, A. G. Structure and physical properties of plan wax crystal networks and their relationship to oil binding capacity. *J. Am. Oil Chem. Soc.* **2014**, *91*, 885−903.
(17) Yilmaz, E.; Öğütcü, M. Properties and stability of hazelnut oil organogels with beeswax and monoglyceride. *J. Am. Oil Chem. Soc.* **2014**, *91*, 1007−1017.
(18) Dassanayake, L. S.; Kodali, D. R.; Ueno, S. Formation of oleogels based on edible lipid materials. *Curr. Opin. Colloid Interface Sci.* **2011**, *16*, 432−439.
(19) U.S. Food and Drug Administration. Food Additive Status List, http://www.fda.gov/Food/IngredientsPackagingLabeling/FoodAdditivesIngredients/ucm091048.htm (accessed June 2014).
(20) Ye, Y.; Wagh, A.; Martini, S. Using high intensity ultrasound as a tool to change the functional properties of interesterified soybean oil. *J. Agric. Food Chem.* **2011**, *59*, 10712−10722.
(21) Martini, S.; Tippetts, M. Effect of processing conditions on the crystallization behavior and destabilization kinetics of oil-in-water emulsions. *J. Am. Oil Chem. Soc.* **2008**, *85*, 119−128.
(22) Martini, S.; Herrera, M. L.; Hartel, R. W. Effect of cooling rate on crystallization behavior of milk fat fraction/sunflower oil blends. *J. Am. Oil Chem. Soc.* **2002**, *79*, 1055−1062.

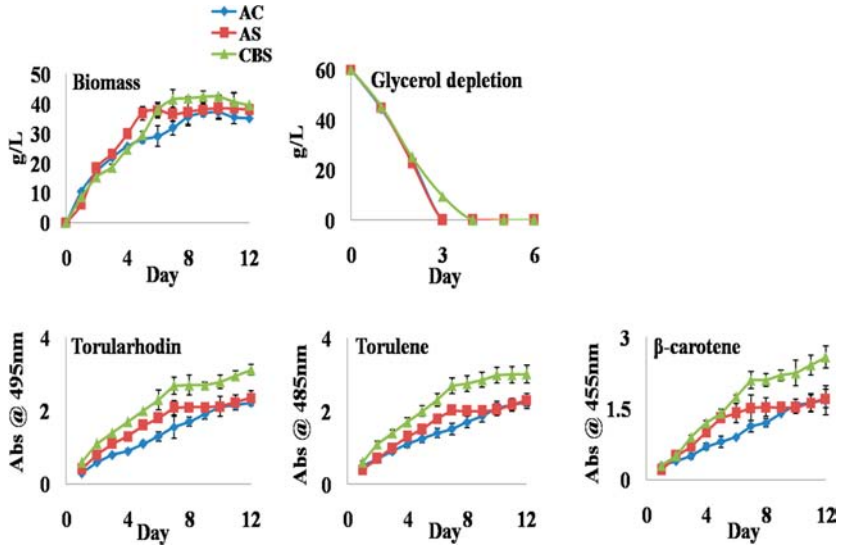


**Figure 2.** Biomass concentration, extracellular glycerol levels, and spectrophotometric quantitation of carotenoids torularhodin (**1**), torulene (**2**), and $\beta$-carotene (**3**) of all three strains. The error bar indicates the SD.

may be a more potent singlet oxygen quencher than $\beta$-carotene, due to its longer polyene chain.

The emerging foodomics trend uses a mass spectrophotometry (MS) based approach to advance food science and nutrition, for its fast and high-throughput nature.[18] Under the foodomics field, untargeted metabolomics is an analytical strategy to identify all metabolites in an organism under a given set of conditions.[19] This use of metabolomics ranges from analyzing wine profiles for the development of a predictive model to aid wine development by nontargeted GC-MS[20] to studying microbial metabolism[21] and is also used to identify the main compound in strawberry responsible for its anti-inflammatory benefits.[22]

The ability of *R. toruloides* to use glycerol as a substrate for fermentation has been well explored.[6,23,24] Its proteomic profile has also been studied in lipid-accumulating conditions using LC-MS-based metabolomic technology.[11] However, studies on the metabolism of this unique yeast on glycerol, and its mechanism to convert glycerol into carotenoids are lacking. In this study we analyze the potential of carotenoid production from three strains grown on glycerol using HPLC and their metabolic changes at four different growth phases via GC-MS. The differential metabolite profile would also be useful to understand the differences in carotenoid production between the strains.

## MATERIALS AND METHODS

**Fermentation of *R. toruloides*.** Over the past years, many studies have shown that the yeast *R. toruloides* can use glycerol as the sole carbon source for fermentation. From over a decade of work on this species, we have chosen three strains: *R. toruloides* ATCC 10788 (AC) is from the American Type Culture Collection ane was one of the first strains to be investigated for its lipid-producing ability.[25] AS 2.1389 (AS) is from the China General Microbiological Culture Collection Center and its genome was recently sequenced, which enables future genetic work.[11] To both of these strains we added CBS 5490 (CBS), which was purchased from the largest fungal culture collection worldwide (Central Bureau voor Schimmelcultures, Utrecht, The Netherlands); it is a novel strain that has not yet been studied. All strains were maintained on YPG agar plates containing (per liter) 20 g of glycerol, 20 g of peptone, 10 g of yeast extract, and 20 g of agar. Overnight culture was used to inoculate each 250 mL Erlenmeyer flask at an optical density (OD) of 0.2 containing 50 mL of fermentation media. Fermentation media contained (per liter) 20 g of peptone, 10 g of yeast extract, and 60 g of glycerol, purity = 99% (Sigma, St. Louis, MO, USA). Fermentation was carried out in an incubator for 12 days in 250 mL Erlenmeyer flasks at 30 °C, with shaking at 250 rpm. Three biological replicates were carried out for each strain.

**Growth and Carotenoid Extraction.** To measure the growth of the yeasts, the OD of the culture media was measured at a wavelength of 600 nm, using a Nano Drop 2000 UV spectrophotometer (Thermo Scientific, Waltham, MA, USA). Dry cell weight was quantitated by drying 1 mL of washed culture supernatant in an oven set at 70 °C until constant dry cell weight (DCW). Biomass was quantitated by using a standard curve correlating OD at 600 nm to dry cell weight. To analyze the intracellular carotenoid content of the cells, 1 mL of culture media was taken. The cells were centrifuged at 10000*g*, washed with Milli-Q water, and broken with glass beads using a Fast Prep bead grinder (MP Biomedicals, Solon, OH, USA). Carotenoids were extracted with acetone until the cell pellet was colorless. Carotenoids were measured and quantitated using standards from CaroteNature (Ostermundigen, Switzerland). The spectrophotometric measurement of carotenoids was according to their absorption maxima peak ($\lambda_{max}$), which is the middle maximum of their UV−vis spectra in acetone. They were measured as follows: torularhodin, **1**, at 495 nm; torulene, **2**, at 485 nm; and $\beta$-carotene, **3**, at 455 nm.

**Carotenoid Characterization and Quantitation.** To confirm the quantitation and characterization of carotenoids extracted in acetone in each strain, high-performance liquid chromatography (HPLC) equipped with a photodiode array detector was used as it is a validated method.[26] The carotenoids torularhodin (**1**), torulene (**2**), and $\beta$-carotene (**3**) were identified on the basis of their retention times using standards from CaroteNature. An Agilent 1100 series instrument was employed, and the column used was a 250 mm × 4.6 mm i.d., 5 $\mu$m, Li-Chrospher 100 RP-18, with a 4 mm × 4 mm i.d. guard column of the same material (Merck, Rahway, NJ, USA). A gradient from 70 to 100% acetone in Milli-Q water at a flow rate of 0.5 mL/min was used as the mobile phase. Detection was performed at 450 nm, and the UV−vis absorption spectra were recorded online with the photodiode array detection system.

**Extracellular Glycerol Analysis.** To analyze extracellular glycerol levels in the culture media, 1 mL of culture medium was taken every 24 h and filtered. Glycerol was quantitated using HPLC equipped with a refractive index detector using a standard of purity of 99% (Sigma). The column used was an Aminex HPX-87H column (Bio-Rad, Hercules, CA, USA). Milli-Q water was used as the mobile phase at a

flow rate of 0.6 mL/min, with temperature controlled at 65 °C, and detection was performed at 210 nm.

**Metabolic Profile of Each Strain at Different Growth Phases and GC-MS Analysis.** The intracellular metabolites were extracted from all three strains at four different time points: early log growth phase on day 1, middle of log growth phase on day 4, as cells enter stationary phase on day 7, and during death phase at the end of fermentation on day 12. Cell suspensions with an OD of 10 were lysed and quenched in 800 μL of ice-cold methanol using glass beads and a bead grinder. Ten microliters of 2 mg/mL ribitol dissolved in Milli-Q water was added to each sample as an internal standard to correct for any loss of metabolite during the extraction process. The supernatant was extracted and then air-dried using a heat block set at 30 °C overnight. Next, 50 μL of 20 mg/mL solution of methoxyamine hydrochloride in pyridine was added to protect the carbonyl groups and incubated at 37 °C for 1 h. Silylation was then carried out by adding 99 μL of *N*-methyl-*N*-(trimethylsilyl)trifluoroacetamide (MSTFA) with 1 μL of trimethylchlorosilane (TMCS) and incubated for 30 min at 70 °C.

Samples were then shaken vigorously for 2 h at room temperature before they were transferred to sample vials and covered with Parafilm to prevent evaporation. Metabolite analysis was carried out using gas chromatography coupled with a mass spectrophotometer (GC-MS). All samples for GC-MS were run within 24 h. One microliter of sample was injected using a Shimadzu QP 2010 Plus GC-MS system. The oven temperature was kept at 75 °C for 4 min, raised at 4 °C/min to a final temperature of 280 °C, and held for 2 min. Mass spectra were recorded from $m/z$ 35 to 600 with a scan time of 0.2 s.[27] The total elution time for mass spectra collected for each sample was 58 min. Data processing and metabolite identification were carried out accordingly.[28]

## RESULTS AND DISCUSSION

**Growth of Three *R. toruloides* Strains on Glycerol.** We have found 60 g/L to be the optimized glycerol concentration to ensure growth and carotenoid production in the three strains (data not shown). Glycerol is able to enter the cell through diffusion and/or active transport.[29] Extracellular glycerol in the culture media was depleted from the culture media by day 3 for strains AC and AS and by day 4 for strain CBS. This showed that the three strains could assimilate glycerol and grew comparatively well (Figure 2). From the biomass curve of the three strains in Figure 2, we define that all three strains were in the logarithmic (log) phase of growth from days 1 and 6, entered stationary phase on day 7, and were in the death phase by day 12. Cells underwent division and replication by obtaining energy from glycerol through glycolysis. The best strain to use glycerol as a substrate for cell growth was CBS. The cells produced the highest concentration of biomass (42.3 g/L) during late stationary phase, as compared to 37.2 g/L by AC and 38.4 g/L by AS (Figure 2).

**Carotenoid Quantitation by UV Spectrophotometer.** *Rhodosporidium* yeasts are known to produce the carotenoids torularhodin, **1**; torulene, **2**; and β-carotene, **3**.[14] In the three strains, carotenoid concentration reached a plateau during stationary growth phase (Figure 2). The strain CBS was the highest carotenoid producer of all strains for the three types of carotenoids: torularhodin, **1**; torulene, **2**; and β-carotene, **3**.

**Characterization and Quantitation of Carotenoids by HPLC.** To our knowledge, there has been no report of the characterization of carotenoids in these strains. It was found that the carotenoid values obtained by spectrophotometry and HPLC greatly differed, so the values quantitated by HPLC were taken as it is a more accurate method.[30] The milli-absorbance units (mAU) obtained from the HPLC profile were quantitated using carotene standards. Our analysis showed that all strains produced torularhodin (**1**), torulene (**2**), and β-carotene (**3**) in different percentages (Figure 3), although torularhodin (**1**) was

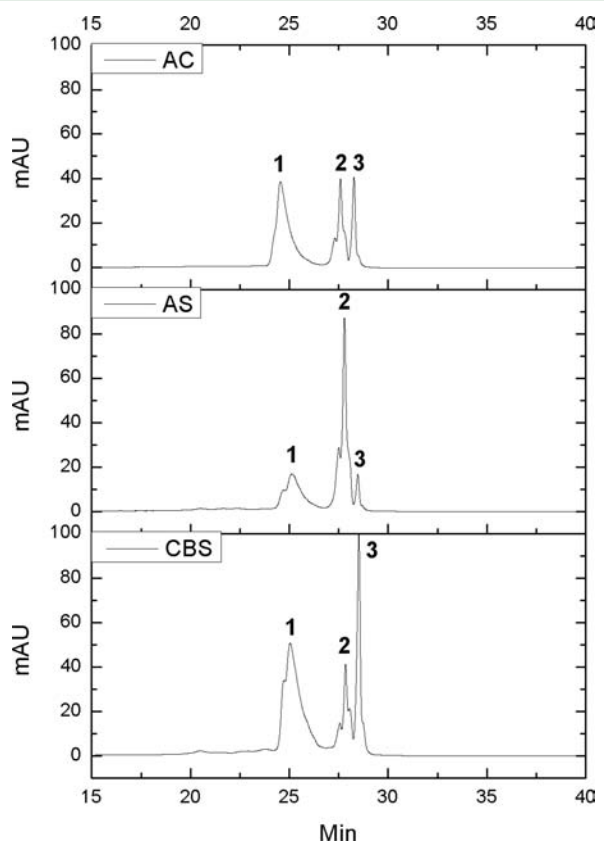


**Figure 3.** Representative HPLC profile of carotenoids in the three strains, AC, AS, and CBS. In each HPLC profile the following carotenoids were identified: torularhodin, **1**; torulene, **2**; β-carotene, **3**.

the most abundant carotenoid in all three strains. All of the carotenoids eluted within 24−28 min as shown in Table 1. The HPLC results confirmed the UV spectrophotometer findings that CBS was the highest carotenoid producer. As quantitated from HPLC, at the end of fermentation on day 12, it produced 28.5 mg/L, as compared to 18 mg/L by AC and 19.3 mg/L by AS. It also produced the highest amount of the industrially relevant compound β-carotene, **3** (Figure 3).

**Comparison of the Metabolite Profiles during Different Growth Phases.** Metabolomics was used to investigate and shed light onto the differences in carotenoid accumulation in the three strains on a metabolic level. The changes in intermediates would help to explain the cellular metabolism accounting for the different carotenoid productions in the three strains. In total, 13 important differential metabolites were identified, and the changes in their levels are shown in Figures 5 and 6. The metabolites could be classified into carbohydrates, TCA cycle intermediates, fatty acids, and amino acids. To apply the knowledge of metabolomic changes seen in the cell, we have mapped the changes in relation to biochemical pathways, as depicted in Figure 4. This gives a view of the metabolite changes in comparison to the other strains AC and AS, which could help us to understand the reason for higher carotenoid accumulation in strain CBS.

**Carbohydrate Metabolites.** Glycerol was used as the sole carbon source in this study. In the cell, glycolysis is the pathway that supplies the cells with energy, by breaking down sugars

**Table 1. Production of Carotenoids by the Three Strains Quantitated by HPLC**

| | | strain | | | | | |
|---|---|---|---|---|---|---|---|
| | | AC | | AS | | CBS | |
| carotenoid | ret time (min) | mg/L | % of total carotenoids | mg/L | % of total carotenoids | mg/L | % of total carotenoids |
| torularhodin, **1** | 24.5−25.1 | 7.4 | 41 | 12.5 | 65 | 19.7 | 69 |
| torulene, **2** | 27.3−27.9 | 7 | 39 | 2.5 | 13 | 2.0 | 7 |
| $\beta$-carotene, **3** | 28.0−28.5 | 3.6 | 20 | 4.3 | 22 | 6.8 | 24 |
| total | | 18 | | 19.3 | | 28.5 | |

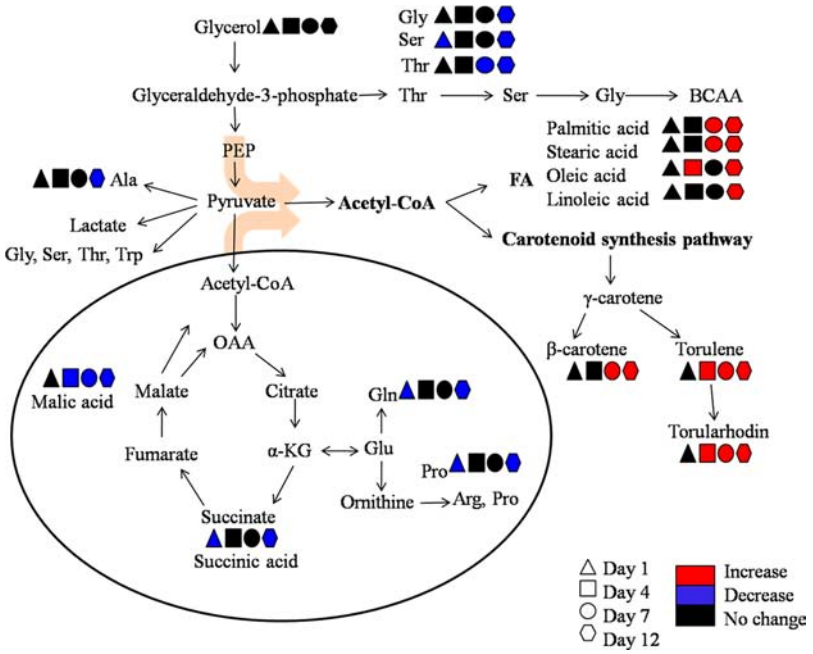


**Figure 4.** Metabolic changes in strain CBS mapped onto metabolic pathways during the four different growth phases on days 1, 4, 7, and 12. Colored symbols represent an increase, decrease, or no change in the level of the metabolite at each time point, as compared to the other strains AC and AS. Orange arrows represent the general flow of metabolic flux in strain CBS.

such as glycerol, to form the final pyruvate molecule. During glycolysis, glycerol is converted into glyceraldehyde-3-phosphate, transformed into phosphoenolpyruvate (PEP), and finally into pyruvate (Figure 4). Pyruvate may enter the mitochondria and is converted into acetyl-CoA, which enters the citric acid cycle (TCA). Acetyl-CoA is an important molecule as it is the precursor of the fatty acid and carotenoid synthesis pathway.[31] In Figure 5, the intracellular metabolite glycerol was found to decrease in all three strains in comparatively the same manner as glycolysis took place.

**Amino Acid Metabolites.** Amino acids can be synthesized from compounds in the glycolysis pathway and TCA cycle. The glycolysis pathway provides the substrate glyceraldehyde-3-phosphate for the synthesis of threonine, serine, and glycine, which are used to form branched-chain amino acids (Figure 4). The amino acid alanine is synthesized from the pyruvate molecule provided by the glycolysis pathway. Glutamate and proline are synthesized from the intermediate of the TCA cycle, $\alpha$-ketoglutarate ($\alpha$-KG).

Interestingly, we observe that the strain CBS demonstrated a unique amino acid metabolic profile. In comparison to AC and AS strains, all of the amino acids were generally synthesized in lower amounts (Figure 5). This might suggest that the cellular mechanism of the CBS strain preferably synthesized less amino acids, which resulted in more available acetyl-CoA to enter the carotenoid and fatty acid synthesis pathways. This could contribute to the higher levels of carotenoids and total intracellular fatty acids observed in strain CBS.

**TCA Cycle Intermediate Metabolites.** The TCA cycle is a key metabolic pathway in all cells. After glycolysis, pyruvate enters the mitochondria and is converted into acetyl-CoA, which undergoes oxidative phosphorylation to provide energy for the cell in the form of NADH and NADPH. The TCA cycle contains intermediates such as succinic acid and malic acid.

In strain CBS we also observed a general down-regulation in production of the TCA cycle intermediates, malic acid and succinic acid, as compared to strains AC and AS (Figure 6). Therefore, we propose that the TCA cycle was down-regulated to enable more acetyl-CoA from glycolysis to enter the carotenoids and fatty acid synthesis pathway. This contributes to higher carotenoid production in strain CBS. This is also seen in a previous study in which the decrease of the TCA cycle intermediate malic acid enhanced $\beta$-carotene production in the yeast *Blakeslea trispora*.[32]

**Fatty Acid Metabolites.** *R. toruloides* is an oleaginous yeast that has been studied for its ability to accumulate high amounts of lipids. The total intracellular fatty acids synthesized by all three strains was palmitic acid, oleic acid, linoleic acid, and stearic acid, which is in accordance with previous results.[23] The highest carotenoid-producing strain, CBS, was also the highest

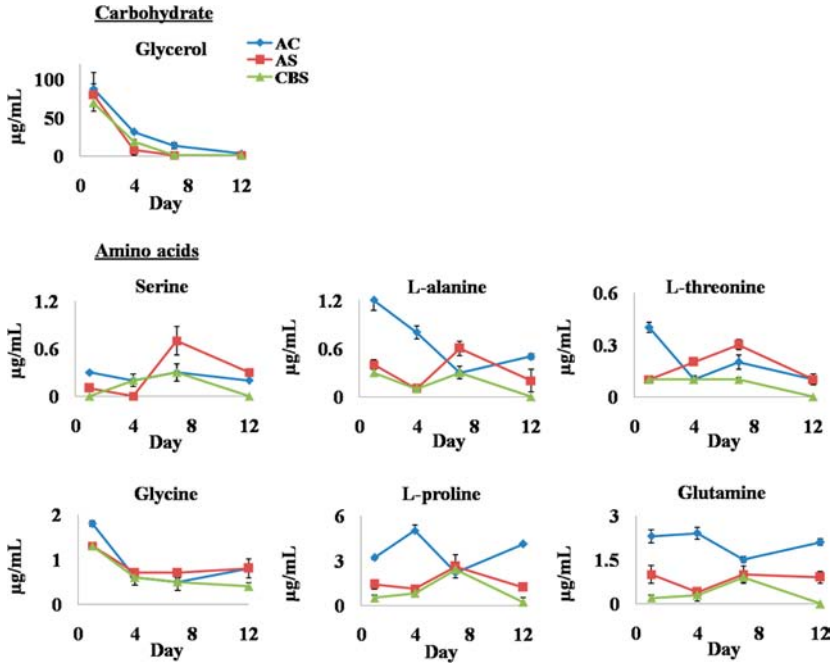


**Figure 5.** Quantitated metabolite profiling in the three strains AC, AS, and CBS during different growth phases by GC-MS: changes in the carbohydrate metabolite glycerol and amino acid levels of serine, glycine, threonine, alanine, glutamine, and proline. The error bar indicates the SD of three biological replicates.

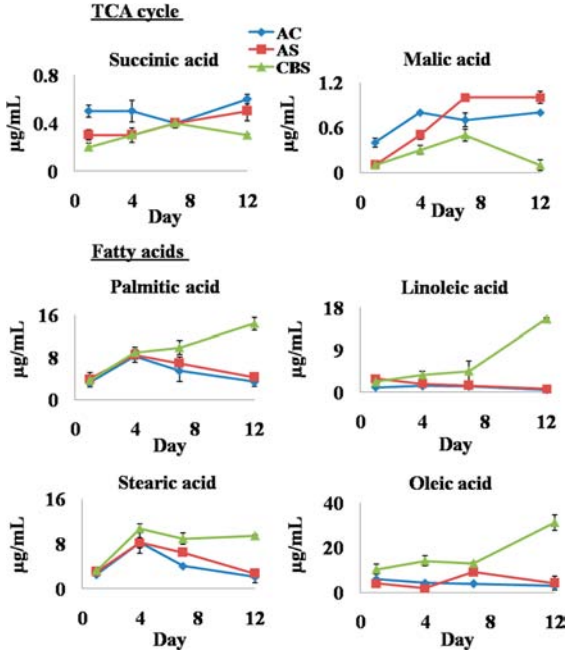


**Figure 6.** Quantitated metabolite profiling in the three strains AC, AS, and CBS during different growth phases by GC-MS: changes in the TCA cycle intermediate metabolites malic acid and succinic acid, and levels of the total intracellular fatty acids metabolites (oleic acid, stearic acid, linoleic acid, and palmitic acid). The error bar indicates the SD of three biological replicates.

fatty acid producer, especially the unsaturated oleic acid and linoleic acid (Figure 6).

The cell membrane is made up of a phospholipid bilayer where many biochemical processes take place. Both fatty acids and carotenoids are localized in the lipid bilayer membrane. Carotenoid–lipid interactions play a role in the regulation of membrane fluidity and integrity. $\beta$-Carotene molecules are randomly integrated in the hydrophobic interior of the lipid bilayer. Its ability to penetrate deeper into the membrane is dependent on the fluidity of the membrane. Higher amounts of unsaturated fatty acids in the bilayer result in increased membrane fluidity, thereby allowing more $\beta$-carotene to accumulate deeper into the interior of the bilayer.[33] Therefore, the high content of the unsaturated fatty acids, oleic acid and linoleic acid, in strain CBS may have served not to increase the membrane stability but to improve the cell membrane fluidity to enhance the accumulation of all three carotenoids. In support of this, a study by Li et al.[34] has also shown that oleic acid could help increase membrane fluidity to overcome ethanol stress in *Saccharomyces cerevisiae*.

In addition, intracellular fatty acids form TAG and sterol esters, which are stored inside lipid bodies.[35] The increased synthesis of total intracellular fatty acid metabolites observed in strain CBS means more lipid bodies can be formed. Oleic acid has been suggested to be the main constituent in the formation of lipid bodies in *Dunaliella*.[36] It has been proposed that formation of lipid bodies was the driving force of $\beta$-carotene synthesis. This is because lipid bodies have the ability to sequester $\beta$-carotene molecules, stimulating more $\beta$-carotene production.[37] In light of our results it is possible that the higher production of fatty acids, especially the oleic acid levels in strain CBS, resulted in more lipid bodies formed, which can sequester all three carotenoids including torularhodin, **1**; torulene, **2**; and $\beta$-carotene, **3**. The sequestering by lipid bodies thus promoted an increase for overall total carotenoid accumulation which was not reported previously. Therefore, our study found a strong correlation between fatty acid production and carotenoid biosynthesis, especially in the unsaturated fatty acids oleic acid, which could help increase membrane fluidity and lipid body formation.

**Carotenoid Synthesis Pathway.** Isoprenoids such as carotenoids are secondary metabolites produced at highest

levels during late log phase to early stationary phase,[38] which is consistent with our observations. As seen in Figure 4, in the carotenoid synthesis pathway, γ-carotene is the metabolic branch point for β-carotene and the torulene/torularhodin pathway. From γ-carotene, cyclization forms the dicyclic carotenoid β-carotene, whereas oxidation takes place to form the monocyclic carotenoid torulene, **2**, and further oxidation into torularhodin, **1**.[39] In all strains the highly oxidized end product torularhodin, **1**, was the major carotenoid formed (Table 1). The regulatory mechanisms controlling the carotenoid synthesis pathways are not well understood, and further studies are required.

In summary, the use of a metabolomics strategy to study the metabolic profile at different time points has allowed us to gain insight into the metabolism and biochemical pathways of *R. toruloides*. Also, it helped us understand the underlying differences in carotenoid-producing ability between strains. The results suggested that fatty acid synthesis was beneficial to increase carotenoid production. However, more studies on the relationship between fatty acids and carotenoid synthesis is needed. Knowledge from this study could aid future work to increase carotenoid yields by metabolic engineering in microorganisms, for example, to down-regulate the TCA cycle and amino acid synthesis and increase the unsaturated fatty acid production such as oleic acid.

## ■ ASSOCIATED CONTENT

### Supporting Information

Supplementary Table S1 lists the retention times of all differential metabolites identified using the NIST library. Figure S1 shows the total ion chromatogram from GC-MS analysis of all three strains on d 12. Figure S2 shows the neutral lipid content in each strain at the end of fermentation by Nile red staining. Figure S3 shows the analysis of total nitrogen in the culture media during fermentation. This material is available free of charge via the Internet at http://pubs.acs.org.

## ■ AUTHOR INFORMATION

### Corresponding Author

*(W.-N.C.) Phone: +65 63162870. Fax: +65 67947553. E-mail: WNChen@ntu.edu.sg.

### Notes

The authors declare no competing financial interest.

## ■ ACKNOWLEDGMENTS

Strain AS 2.1389 was a kind gift from Professor Zongbao (Kent) Zhao from Dalian Institute of Chemical Physics in China. We thank NEWRI for support.

## ■ ABBREVIATIONS USED

strain ATCC, 10788 strain AC; strain AS, 2.1389 strain AS; strain CBS, 5490 strain CBS; BCAA, branched-chain amino acid; α-KG, α-ketoglutarate; OAA, oxaloacetate; PEP, phosphoenolpyruvate

## ■ REFERENCES

(1) Yang, F.; Hanna, M.; Sun, R. Value-added uses for crude glycerol – a byproduct of biodiesel production. *Biotechnol. Biofuels* **2012**, *5*, 13 DOI: 10.1186/1754-6834-5-13.

(2) Dobson, R.; Gray, V.; Rumbold, K. Microbial utilization of crude glycerol for the production of value-added products. *J. Ind. Microbiol. Biotechnol.* **2012**, *39*, 217–226.

(3) Zhao, X.; Peng, F.; Du, W.; Liu, C.; Liu, D. Effects of some inhibitors on the growth and lipid accumulation of oleaginous yeast *Rhodosporidium toruloides* and preparation of biodiesel by enzymatic transesterification of the lipid. *Bioprocess Biosyst. Eng.* **2012**, *35*, 993–1004.

(4) Wang, Q.; Guo, F. J.; Rong, Y. J.; Chi, Z. M. Lipid production from hydrolysate of cassava starch by *Rhodosporidium toruloides* 21167 for biodiesel making. *Renewable Energy* **2012**, *46*, 164–168.

(5) Zhao, X.; Wu, S.; Hu, C.; Wang, Q.; Hua, Y.; Zhao, Z. K. Lipid production from Jerusalem artichoke by *Rhodosporidium toruloides* Y4. *J. Ind. Microbiol. Biotechnol.* **2010**, *37*, 581–585.

(6) Saenge, C.; Cheirsilp, B.; Suksaroge, T. T.; Bourtoom, T. Potential use of oleaginous red yeast *Rhodotorula glutinis* for the bioconversion of crude glycerol from biodiesel plant to lipids and carotenoids. *Process Biochem.* **2011**, *46*, 210–218.

(7) Politino, M.; Tonzi, S. M.; Burnett, W. V.; Romancik, G.; Usher, J. J. Purification and characterization of a cephalosporin esterase from *Rhodosporidium toruloides*. *Appl. Environ. Microbiol.* **1997**, *63*, 4807–4811.

(8) Zhu, L.; Cui, W.; Fang, Y.; Liu, Y.; Gao, X.; Zhou, Z. Cloning, expression and characterization of phenylalanine ammonia-lyase from *Rhodotorula glutinis*. *Biotechnol. Lett.* **2013**, *35*, 751–756.

(9) Botes, A. L. Affinity purification and characterization of a yeast epoxide hydrolase. *Biotechnol. Lett.* **1999**, *21*, 511–517.

(10) Li, Y.; Zhao, Z.; Bai, F. High-density cultivation of oleaginous yeast *Rhodosporidium toruloides* Y4 in fed-batch culture. *Enzyme Microb. Technol.* **2007**, *41*, 312–317.

(11) Zhu, Z.; Zhang, S.; Liu, H.; Shen, H.; Lin, X.; Yang, F.; Zhou, Y. J.; Jin, G.; Ye, M.; Zou, H.; Zhao, Z. K. A multi-omic map of the lipid-producing yeast *Rhodosporidium toruloides*. *Nat. Commun.* **2012**, *3*, DOI: 10.1038/ncomms2112.

(12) Ribeiro, B. D.; Barreto, D. W.; Coelho, M. A. Z. Technological aspects of β-carotene production. *Food Bioprocess Technol.* **2011**, *4*, 693–701.

(13) Guedes, A. C.; Amaro, H. M.; Malcata, F. X. Microalgae as sources of carotenoids. *Mar. Drugs* **2011**, *9*, 625–644.

(14) Buzzini, P.; Innocenti, M.; Turchetti, B.; Libkind, D.; van Broock, M.; Mulinacci, N. Carotenoid profiles of yeasts belonging to the genera *Rhodotorula*, *Rhodosporidium*, *Sporobolomyces*, and *Sporidiobolus*. *Can. J. Microbiol.* **2007**, *53*, 1024–1031.

(15) Buzzini, P. Production of yeast carotenoids by using agro-industrial by-products. *Agro Food Ind. Hi-Tech* **2001**, *12*, 7–10.

(16) Sakaki, H.; Nakanishi, T.; Tada, A.; Miki, W.; Komemushi, S. Activation of torularhodin production by *Rhodotorula glutinis* using weak white light irradiation. *J. Biosci. Bioeng.* **2001**, *92*, 294–297.

(17) Sakaki, H.; Nochide, H.; Komemushi, S.; Miki, W. Effect of active oxygen species on the productivity of torularhodin by *Rhodotorula glutinis* no. 21. *J. Biosci. Bioeng.* **2002**, *93*, 338–340.

(18) Capozzi, F.; Bordoni, A. Foodomics: a new comprehensive approach to food and nutrition. *Genes Nutr.* **2013**, *8*, 1–4.

(19) Herrero, M.; Simõ, C.; García-Cañas, V.; Ibáñez, E.; Cifuentes, A. Foodomics: MS-based strategies in modern food science and nutrition. *Mass Spectrom. Rev.* **2012**, *31*, 49–69.

(20) Schmidtke, L. M.; Blackman, J. W.; Clark, A. C.; Grant-Preece, P. Wine metabolomics: objective measures of sensory properties of Semillon from GC-MS profiles. *J. Agric. Food Chem.* **2013**, *61*, 11957–11967.

(21) Cevallos-Cevallos, J. M.; Reyes-De-Corcuera, J. I.; Etxeberria, E.; Danyluk, M. D.; Rodrick, G. E. Metabolomic analysis in food science: a review. *Trends Food Sci. Technol.* **2009**, *20*, 557–566.

(22) Lee, J.; Kim, S.; Namgung, H.; Jo, Y.-H.; Bao, C.; Choi, H.-K.; Auh, J.-H.; Lee, H. J. Ellagic acid identified through metabolomic analysis is an active metabolite in strawberry ('seolhyang') regulating lipopolysaccharide-induced inflammation. *J. Agric. Food Chem.* **2013**, *62*, 3954–3962.

(23) Xu, J.; Zhao, X.; Wang, W.; Du, W.; Liu, D. Microbial conversion of biodiesel byproduct glycerol to triacylglycerols by oleaginous yeast *Rhodosporidium toruloides* and the individual effect of some impurities on lipid production. *Biochem. Eng. J.* **2012**, *65*, 30–36.

(24) Uckun Kiran, E.; Trzcinski, A.; Webb, C. Microbial oil produced from biodiesel by-products could enhance overall production. *Bioresour. Technol.* **2013**, *129*, 650−654.
(25) Turcotte, G.; Kosaric, N. The effect of C/N ratio on lipid production by *Rhodosporidium toruloides* ATCC 10788. *Biotechnol. Lett.* **1989**, *11*, 637−642.
(26) Kimura, M.; Kobori, C. N.; Rodriguez-Amaya, D. B.; Nestel, P. Screening and HPLC methods for carotenoids in sweetpotato, cassava and maize for plant breeding trials. *Food Chem.* **2007**, *100*, 1734−1746.
(27) Wang, M.; Bai, J.; Chen, W. N.; Ching, C. B. Metabolomic profiling of cellular responses to carvedilol enantiomers in vascular smooth muscle cells. *PLoS One* **2010**, DOI: 10.1371/journal.-pone.0015441.
(28) Seiber, J. N.; Molyneux, R. J.; Schieberle, P. Targeted metabolomics: a new section in the journal of agricultural and food chemistry. *J. Agric. Food Chem.* **2013**, *62*, 22−23.
(29) Chatzifragkou, A.; Dietz, D.; Komaitis, M.; Zeng, A. P.; Papanikolaou, S. Effect of biodiesel-derived waste glycerol impurities on biomass and 1,3-propanediol production of *Clostridium butyricum* VPI 1718. *Biotechnol. Bioeng.* **2010**, *107*, 76−84.
(30) Rodriguez-Amaya, D. B.; Kimura, M. *HarvestPlus Handbook for Carotenoid Analysis*; International Food Policy Research Institute (IFPRI): Washington, DC, USA, 2004.
(31) Fakas, S.; Makri, A.; Bellou, S.; Aggelis, G. Pathways to aerobic glycerol catabolism and their regulation. In *Microbial Conversions of Raw Glycerol*; Nova Science Publishers: New York, 2009; pp 9−18.
(32) Hu, X.; Li, H.; Tang, P.; Sun, J.; Yuan, Q.; Li, C. GC-MS-based metabolomics study of the responses to arachidonic acid in *Blakeslea trispora*. *Fungal Gen. Biol.* **2013**, *57*, 33−41.
(33) Popova, A. V.; Andreeva, A. S. Carotenoid-lipid interactions. *Adv. Planar Lipid Bilayers Liposomes* **2013**, *17*, 215−236.
(34) Li, Z.; Ma, X.; Li, A.; Zhang, C. A novel potential source of *β*-carotene: *Eustigmatos cf. polyphem* (Eustigmatophyceae) and pilot *β*-carotene production in bubble column and flat panel photobioreactors. *Bioresour. Technol.* **2012**, *117*, 257−263.
(35) Fujimoto, T.; Ohsaki, Y.; Cheng, J.; Suzuki, M.; Shinohara, Y. Lipid droplets: a classic organelle with new outfits. *Histochem. Cell Biol.* **2008**, *130*, 263−279.
(36) Lamers, P. P.; Janssen, M.; De Vos, R. C. H.; Bino, R. J.; Wijffels, R. H. Carotenoid and fatty acid metabolism in nitrogen-starved *Dunaliella salina*, a unicellular green microalga. *J. Biotechnol.* **2012**, *162*, 21−27.
(37) Rabbani, S.; Beyer, P.; Lintig, J. V.; Hugueney, P.; Kleinig, H. Induced *β*-carotene synthesis driven by triacylglycerol deposition in the unicellular alga *Dunaliella bardawil*. *Plant Physiol.* **1998**, *116*, 1239−1248.
(38) Siddiqui, M. S.; Thodey, K.; Trenchard, I.; Smolke, C. D. Advancing secondary metabolite biosynthesis in yeast with synthetic biology tools. *FEMS Yeast Res.* **2012**, *12*, 144−170.
(39) Sperstad, S.; Lutnaes, B. F.; Stormo, S. K.; Liaaen-Jensen, S.; Landfald, B. Torularhodin and torulene are the major contributors to the carotenoid pool of marine *Rhodosporidium babjevae* (Golubev). *J. Ind. Microbiol. Biotechnol.* **2006**, *33*, 269−273.

means of a coulimetric electrode array detection. *J. Agric. Food Chem.* **2000**, *48*, 5178−5183.
(5) International Olive Council (IOC). *Determination of biophenols in olive oil by HPLC*; COI/T.20/Doc. No. 29, November 2009.
(6) European Community Council Regulation No. 432/2012 of 16 May 2012 establishing a list of permitted health claims made on foods, other than those referring to the reduction of disease risk and to children's development and health. *Off. J. Eur. Communities L.* **2012**, *136*, 1−40.

## AUTHOR INFORMATION

### Corresponding Author

*(M.Z.T.) E-mail: tsimidou@chem.auth.gr. Phone: + 30 2310 997796. Fax: + 30 2310 997847.

### Notes

The authors declare no competing financial interest.

## REFERENCES

(1) Mastralexi, A.; Nenadis, N.; Tsimidou, M. Z. Addressing analytical requirements to support health claims on "olive oil polyphenols" (EC Regulation 432/2012). *J. Agric. Food Chem.* **2014**, *62*, 2459−2461.

(2) Romero, C.; Brenes, M. Analysis of total contents of hydroxytyrosol and tyrosol in olive oils. *J. Agric. Food Chem.* **2012**, *60*, 9017−9022.

(3) http://www.internationaloliveoil.org/news/view/666-year-2014-news/483-new-procedure-for-presenting-proposals-for-the-revision-of-ioc-standards (accessed July 17, 2014).

(4) Purcaro, G.; Codony, R.; Pizzale, R.; Mariani, C.; Conte, L. Evaluation of total hydroxytyrosol and tyrosol in extra virgin olive oils. *Eur. J. Lipid Sci. Technol.* **2014**, *116*, 805−811.

for foods, only a few studies have focused on feed-processing effects on pesticide persistence.

The pellet feeds that originate from cereals are the most frequently used feedstuffs for ducks and other poultry.[19] Therefore, chlorpyrifos residual behaviors in field crops (i.e., rice, maize, and soybean) were determined according to the "Guideline on Pesticide Residue Trials" of China, and in the results of field trials, processing steps of duck pellet feed were mimicked to investigate chlorpyrifos persistence in these steps. Finally, the potential exposure risks of chlorpyrifos in duck feeding were evaluated, under the conditions of domestic ducks fed processed pellet feeds that originated from the heaviest contaminated raw materials of this study.

## MATERIALS AND METHODS

**Materials.** Commercial seeds of rice, maize, and soybean for field trials were purchased from Zhejiang Wuwangnong Seeds Co., Ltd. (Hangzhou, China). Stock solution of chlorpyrifos (100 μg/mL in acetonitrile) was obtained from the Agro-Environmental Protection Institute, Ministry of Agriculture (Beijing, China). Commercial 40% chlorpyrifos emulsifiable concentrate (EC, w/v) was the product of Zhejiang Xinnong Chemical Co., Ltd. (Hangzhou, China). *N*-Propylethylenediamine (PSA) and graphitized carbon black (GCB) were provided by Bonna-Agela Technologies, Inc. (Tianjin, China). Analytical grade acetonitrile, ethyl acetate, $MgSO_4$, and NaCl were obtained from East China Pharmaceutical Group Co., Ltd. (Hangzhou, China). Chromatography grade acetonitrile and methanol were products of Honeywell International Inc. (Morris Plains, NJ, USA). Ultrapure water was the product of a Milli-Q system (Bedford, MA, USA). A paddy husker machine and a cereal grain milling machine were products of Tianyang Co., Ltd. (Shangdong, China). A poultry pellet miller was purchased from Gemco Machinery Co., Ltd. (Henan, China). A screw oil press machine was the product of Weichang Machinery Co., Ltd. (Rizhao, China).

**Field Trials.** The field trials for chlorpyrifos residual behaviors on rice, maize, and soybean were performed in Danzhou (109.5 E, 19.5 N), Hangzhou (102.1 E, 30.2 N), and Haerbin (126.3 E, 45.5 N), and the field trials strictly complied with the "Guideline on Pesticide Residue Trials" (NY/T788-2004) in China.[20] Each field trial consisted of triplicate test plots and a control plot (30 $m^2$ for each plot), and each plot was separated by a buffer area. Chlorpyrifos 40% EC (w/v) was selected as the tested formulation in field residue trials. The recommended dosages (0.864 kg ai $ha^{-1}$ for rice, 0.720 kg ai $ha^{-1}$ for maize, and 0.240 kg ai $ha^{-1}$ for soybean) and 1.5 times recommended dosages (1.296 kg ai $ha^{-1}$ for rice, 1.080 kg ai $ha^{-1}$ for maize, and 0.360 kg ai $ha^{-1}$ for soybean) were chosen for field trials. The pesticide was sprayed on fields of mid- and late-planting periods two or three times at intervals of 7−14 days (7 days for rice, 10 days for maize, and 14 days for soybean) for each time during 2011 and 2012. Pesticide was sprayed on fields by a knap-sack hand sprayer (product of Shandong Shenglu machine works, Shandong, China), and there was no precipitation during the spraying period. Field samples were collected from each plot on days 7 and 14 for rice, days 10 and 20 for maize, and days 14 and 28 for soybean after the last chlorpyrifos spraying. After harvest, all samples were dried in the shade under ambient conditions. Afterward, the samples were transported at 4 °C in darkness by labeled polyethylene bags to the laboratory and stored at −20 °C until analysis.

**Feed Processing for Chlorpyrifos Persistent.** As we know, pellet feeds are the most used feedstuff for poultry (e.g., ducks and goose) feeding.[19] Generally, pellet feed processing steps include paddy rice hulling, milling, grinding, shelled corn grinding, soybean seed squashing, and granulating (Figure 1). In this study, the raw crop materials (paddy rice, shelled corn, and soybean seed) with the highest chlorpyrifos residues obtained from field trials were selected for pellet feed processing works to evaluate the chlorpyrifos persistent. Rice grain was hulled to yield brown rice and hull, and the brown rice was further milled to polishing rice and rice bran. The soybean seed was roasted at 120 °C for 0.5 h to remove moisture. The dried soybean seed was squashed to produce soybean meal and soybean oil by screw press. As ingredients of duck pellet feeds, brown rice, rice bran, shelled corn, and soybean meal were further ground to powder, mixed, and granulated to pellet feeds. During the feed processing, raw materials and intermediate products (i.e., rice grain, rice hulls, rice bran, brown rice powder, rice bran powder, maize seed, maize powder, soybean seed, soybean meal, and soybean meal powder) in each step were collected, and the chlorpyrifos residues were determined. On the basis of the residual results of each step, chlorpyrifos persistence in feed processing works was evaluated, and final residues in different duck pellet feeds were calculated on the basis of two typical duck feed formulas in southern China (Table 1).

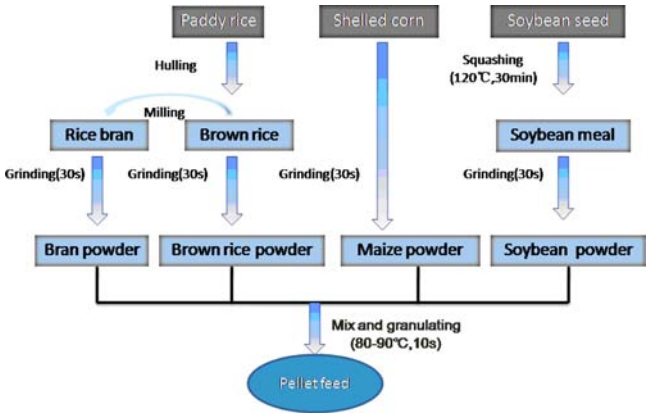


**Figure 1.** Flowchart of duck pellet feed processing in southern China.

**Table 1. Formula Ingredients of Two Typical Duck Pellet Feeds in Southern China**

| feed A | | feed B | |
|---|---|---|---|
| ingredient | content (%) | ingredient | content (%) |
| maize | 59.50 | brown rice | 60.00 |
| rice bran | 10.00 | rice bran | 5.00 |
| soybean meal | 21.30 | soybean meal | 25.00 |
| fish meal | 7.20 | fish meal | 8.00 |
| tricalcium phospahte | 0.35 | tricalcium phospahte | 0.35 |
| limestone | 0.40 | limestone | 0.40 |
| salt | 0.25 | salt | 0.25 |
| DL-methionine | 0.07 | DL-methionine | 0.07 |
| trace mineral premix | 0.50 | trace mineral premix | 0.50 |
| vitamin premix | 0.43 | vitamin premix | 0.43 |

**Sample Preparation and Chlorpyrifos Determination.** Extraction and cleaning procedures of chlorpyrifos from raw materials and the intermediate products were performed according to the methods of Qu et al. with minor modifications.[21] An aliquot of 5.0 g of homogenized sample was transferred to a 50 mL Teflon centrifuge tube with 10 mL of ultrapure water and immersed for 30 min. Afterward, 25 mL of acetonitrile acidified with 1 M HCl (99:1, v/v) was added and shaken for 15 min by an oscillator, followed by centrifugation for 5 min at 966*g* (room temperature). The supernatant was transferred into a 100 mL glass measuring cylinder with a graduated stopper. The extraction steps were repeated again, the extracts were pooled, and then 8 g of NaCl was added. The extracted mixture was shaken vigorously for 1 min and left to stand for 30 min. An aliquot of 10 mL of organic extract was concentrated using a rotary vacuum evaporator at 40 °C and dried with a gentle stream of nitrogen. The residue was redissolved with 1.0 mL of ethyl acetate in a 2.5 mL microcentrifuge tube with a mixture of 150 mg of $MgSO_4$, 25 mg of GCB, and 50 mg of PSA. The tube was shaken vigorously for 1 min and centrifuged for 5 min at 9030*g* (room temperature). The

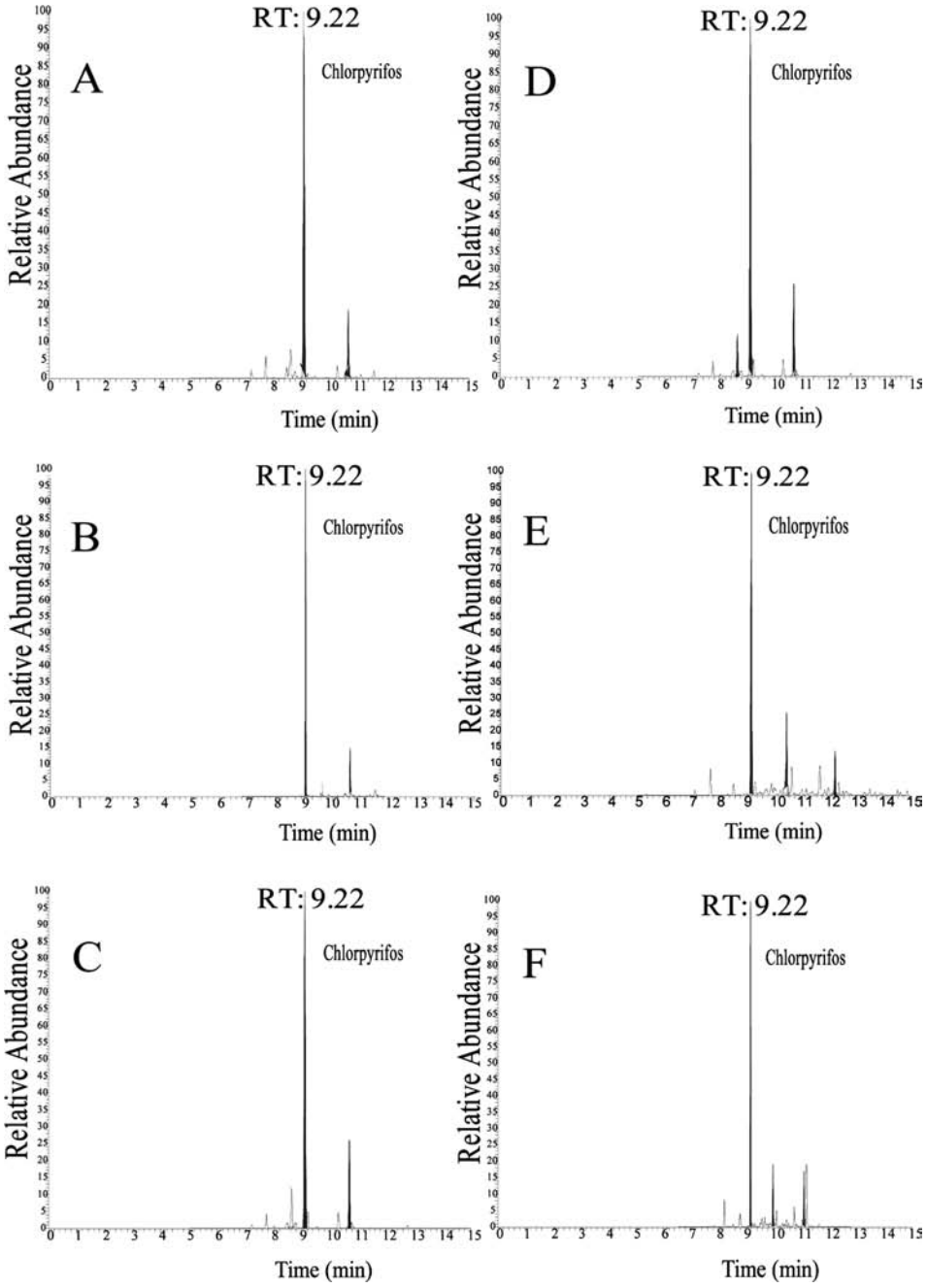


**Figure 2.** Total ion chromatograms obtained from fortified samples of paddy rice (A), brown rice (B), rice bran (C), shelled corn (D), soybean seed (E), and soybean meal (F).

extract was filtered through a 0.22 $\mu$m PVDF filter before analysis. Chlorpyrifos determination by GC-MS/MS was performed following the method of Zhao et al.[15] TSQ Quantum gas chromatography (GC, Thermo Fisher Scientific, USA) with a GC system TRACE GC Ultra and a triple-quadrupole mass spectrometer Quantum (mass range from $m/z$ 10 to 3000) was used throughout the determination. Samples were injected with an AS3000 autosampler into a split/splitless injector. The Zebron ZB-MultiResidue-2 capillary column (30 m × 0.25 mm i.d, 0.25 $\mu$m film thickness, Guangzhou FLM Scientific Instrument Co., Ltd., Guangzhou, China) was applied for analyte separation. The precursor ion was selected by analyzing the 20 $\mu$g/L chlorpyrifos standard solution under the full scan mode in the GC-MS system, and the highest intensity ion ($m/z$ 314) was used for subsequent fragmentation to create product ions ($m/z$ 286 and 258). The retention time of chlorpyrifos was approximately 9.22 min.

Recoveries of the analytical method were evaluated by spiked blank samples at three chlorpyrifos concentrations with six replicates. The spiked samples were kept at room temperature for 2 h to allow solvent evaporation before analysis. Matrix effects were evaluated by comparing the slopes of solvent and matrix calibration sets. Series 1 was prepared by diluting the stock standard solution in solvent at three concentrations of 5, 50, and 500 $\mu$g/kg and series 2 by diluting the stock standard solution in matrix extract that was obtained from pesticide-free sample.

**Statistical Analysis.** Unless otherwise indicated, all tests were performed in three replicates, and the values are presented as means ± standard deviation (SD). Data were statistically evaluated by one-way ANOVA analysis with SPSS base 11.0 software. Once a significant difference was observed, the least significant difference (LSD) test was applied to validate the differences among means.

## RESULTS AND DISSUSSION

**Analytical Method Validation.** The GC-MS analytical results of chlorpyrifos extracted from fortified samples indicated that no interference peak was observed that might affect the analysis accuracy of the pesticide (Figure 2). At three fortified concentrations (0.01, 0.1, and 0.5 mg/kg), the chlorpyrifos recoveries ranged from 81.8 to 110.7% in different raw materials and intermediate products, and the relative standard deviations (RSDs) were from 3.2 to 11.6% (Table 2). The

**Table 2. Chlorpyrifos Analytical Recoveries and RSDs in Different Fortification Samples**

| matrix | fortification level (mg/kg) | mean recovery (%) | RSD (%) |
|---|---|---|---|
| rice grain | 0.5 | 93.6 | 4.6 |
| | 0.1 | 94.2 | 5.3 |
| | 0.01 | 89.3 | 6.8 |
| brown rice | 0.5 | 95.8 | 4.3 |
| | 0.1 | 93.6 | 5.6 |
| | 0.01 | 81.8 | 7.9 |
| rice bran | 0.5 | 90.8 | 3.2 |
| | 0.1 | 83.5 | 4.6 |
| | 0.01 | 90.2 | 8.8 |
| shelled corn | 0.5 | 91.5 | 3.5 |
| | 0.1 | 86.4 | 6.5 |
| | 0.01 | 82.6 | 4.9 |
| soybean seed | 0.5 | 85.3 | 4.8 |
| | 0.1 | 108.6 | 5.6 |
| | 0.01 | 93.2 | 9.5 |
| soybean meal | 0.5 | 91.2 | 4.6 |
| | 0.1 | 96.4 | 10.5 |
| | 0.01 | 110.7 | 11.6 |

LODs and LOQs of the determination were calculated on the basis of signal-to-noise ratios (S/N) of 3 (3:1) and 10 times (10:1) the background chromatographic noise, respectively. The LOD and LOQ were estimated to be 0.0006 and 0.002 mg/kg for paddy rice, brown rice, rice bran, and shelled corn, respectively. For the substrates of soybean seed and soybean meal, the LOD and LOQ were estimated to be 0.0009 and 0.003 mg/kg, respectively. Recoveries slightly greater than 100% were observed for some substrates (i.e., soybean seed and soybean meal), and this result indicated that the matrices may affect the pesticide recovery.[22] Matrix effects of chlorpyrifos ranged from 92 to 118%, which indicated that the matrix effect was acceptable for quantitative analysis.

**Chlorpyrifos Final Residues in Field Trials.** In China, chlorpyrifos is registered for rice at the recommended dosage of 0.864 kg ai $ha^{-1}$ with a preharvest interval (PHI) of at least 7 days, followed by good agricultural practice (GAP) conditions. In the six field trials, which were performed following the "Guideline on Pesticide Residue Trials" in China at 1× (0.864 kg ai $ha^{-1}$) and 1.5× (1.296 kg ai $ha^{-1}$) the recommended dosage, the chlorpyrifos residues of harvest paddy rice treated two or three times with chlorpyrifos all exceed the MRL of rice grain in China (0.5 mg/kg, GB 2763-2012).[23] (Figure 3A,B), and the results are consistent with the previous study.[10] The highest chlorpyrifos residue in paddy rice is 12.0 mg/kg, which was much higher than the MRL on corn forage and fodder set by the U.S. Environment Protection Agency (8.0 mg/kg).[24] The chlorpyrifos residues of paddy rice showed positive correlations to the pesticide applied dosage and spraying times. The results indicated that chlorpyrifos residues were relatively high if the rice crops were treated at the recommended dosage more than two times, and the residues of this study definitely pose serious health risks in foods for human consumption and even as feed material for animal production. The chlorpyrifos residues based on "Guideline on Pesticide Residue Trials" in rice suggest that the pesticide (chlorpyrifos EC, 40%) should be applied fewer than two times at the recommended dosage (≤0.864 kg ai $ha^{-1}$), and the harvest interval (from the last spraying to crop harvest) should be >14 days.

Unlike rice, chlorpyrifos is not officially registered for maize and soybean by means of spraying in China, but dosages of 0.720 kg ai $ha^{-1}$ with a PHI of 10 days for maize and 0.240 kg ai $ha^{-1}$ with a PHI of 14 days for soybeans are recommended by the product (chlorpyrifos EC, 40%) handling instructions. In the 1.5× dosage trials, chlorpyrifos residues in shelled corn with three treatments and 10 days PHI all exceed the maize MRL of China (0.05 mg/kg, GB 2763-2012)[23] (Figure 3C,D). About half of the shelled corn in two years' field trials exceed the maize MRL of China, and the highest residue is 0.605 mg/kg. Similarly to paddy rice, chlorpyrifos residues of shelled corn showed positive correlations to pesticide applied dosage and spraying times. The field trial results by means of spraying indicated that the recommended dosage of 0.720 kg ai $ha^{-1}$ (chlorpyrifos EC, 40%) should be applied on maize crop fewer than two times or with a PHI of longer than 20 days. In soybean trials, five soybean seeds (about 20.8%) exceed the soybean MRL of China (0.1 mg/kg, GB 2763-2012),[23] and the highest residue was 0.220 mg/kg (Figure 3E,F). The residual results of soybean trials were obviously better than those of rice and maize crops, but under the recommended spraying conditions of this study, some residues still exceeded the soybean MRL of China. Field trials of soybean by means of spraying indicated that the recommended dosage of 0.240 kg ai $ha^{-1}$ (chlorpyrifos EC, 40%) applied on soybean crops under the conditions of this study was slightly high, fewer treatments or a longer PHI being obligatory. Field trials of three crops indicated that the chlorpyrifos recommended dosages appeared to be high for rice, maize, and soybean application, and a revised GAP is required for crop production. For each crop, residual levels were moderately different from location to location and from year to year. These results were consistent with the previous study that pesticide residues were affected significantly by various environmental factors (e.g., temperature, humidity, soil characteristics, and climate), which are always diverse from different locations or years.[25]

**Chlorpyrifos Transfers during Pellet Feed Processing.** Chlorpyrifos residue of the raw rice grain selected for pellet feed processing was 12.0 mg/kg. After hulling, the chlorpyrifos residue in brown rice was 7.42 mg/kg and the transfer rate from rice grain to brown rice was 61.8%. Chlorpyrifos residue in rice bran was 12.7 mg/kg after milling processing (Figure 4A,B). The processing results showed that a considerable proportion of chlorpyrifos deposited on the skin of the rice grain, and the finding was similar to chlorpyrifos residual behaviors on vegetables and fruits.[13,26] Brown rice and rice bran were manufactured to powder by grinding for approximately 30 s under a temperature lower than 50 °C, and the chlorpyrifos

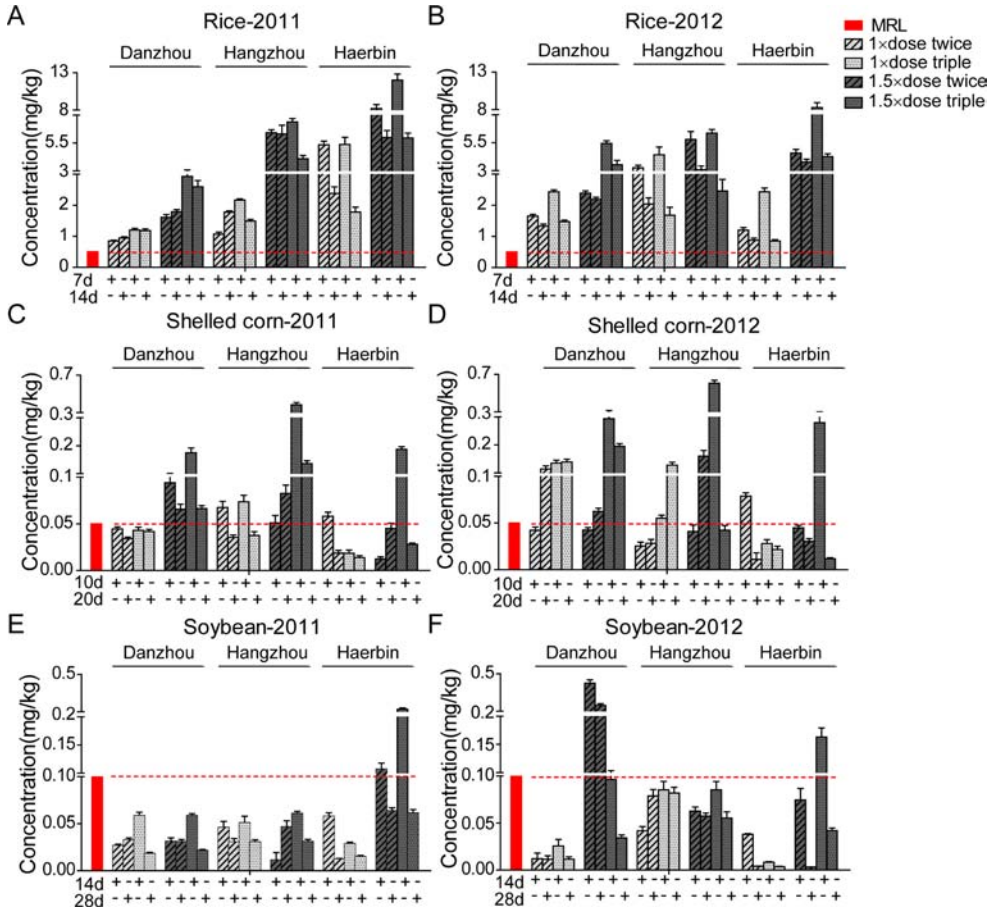


**Figure 3.** Chlorpyrifos residues of rice grain, shelled corn, and soybean seed produced from six field trials.

removal by grinding step was <10%. The grinding process showed only limited influence on chlorpyrifos removal for intermediate product of rice, and the result was consistent with the study of the grinding process during honey production.[27] After granulating, chlorpyrifos residue in rice bran pellet feed reduced to 7.58 mg/kg and the transfer rate was similar to the process step from wheat flour to baking bread.[28] In the granulating step, high temperature is considered as the most important factor for chlorpyrifos breakdown, and the pesticide loss is normally ascribed to physicochemical processes (e.g., evaporation, codistillation, and thermal degradation). During the rice processing steps, chlorpyrifos residues in the processed products of brown rice, rice bran, and pellet feeds ranged from 4.68 to 12.7 mg/kg, which were much higher than the American regulation limit (3.0 mg/kg) on alfalfa forage used as animal feed commodities set by the U.S. Environment Protection Agency.[24] After the processing steps, rice intermediate products and pellet feeds were unsafe as animal feed if the raw rice grain was contaminated by chlorpyrifos at 12.0 mg/kg.

Grinding and granulating are the main steps of shelled corn processing. After grinding, the mean loss of chlorpyrifos was 4.13%, which also proved that chlorpyrifos was stable at low temperature. After granulating, chlorpyrifos residue was 0.0414 mg/kg with a removal rate of 28.6% (Figure 4A,B). The final chlorpyrifos residue in processed maize pellet feed was much lower than that of rice pellet feeds, but the transfer rate from shelled corn to maize pellet feed (68.4%) was higher than those of rice grain to rice pellet feeds (63.2% for pellet feed of rice bran; 39.0% for pellet feed of brown rice).

The chlorpyrifos reduction in soybean meal was 73.8% during the squashing process, indicating that hot squashing led to a significant chlorpyrifos removal. In the grinding process, the loss of chlorpyrifos in soybean meal was 7.12%. The chlorpyrifos reduction of soybean pellet feed is 81.5% after several conventional processing steps. This might be attributed to the physical−chemical properties of chlorpyrifos including the solubility in oils. The high fat-soluble characteristic of chlorpyrifos (logarithm of partition coefficient $P$ is 5.1) makes the pesticide transfer from soybean to the oil layer easy during the squashing processing.[29] Chlorpyrifos residue was 0.0408 mg/kg after soybean meal manufactured to pellet feed by granulating, and the reduction was 23.7%, which was slightly lower than that of processed products of brown rice (30.9%) and maize (28.6%). Similar to the previous study, reduction of chlorpyrifos was significantly enhanced if the processing steps involved heat treatment.[30] Chlorpyrifos residues in soybean intermediate product and pellet feed were reduced more significantly than those of rice and maize because the soybean processing steps involved two heating procedures (soybean roasting and pellet feed granulating) and oil pressing.

**Processing Factors and Feed Safety Assessment.** Processing factors (PFs, pesticide concentration in processed product/pesticide concentration in preprocessing material) are usually adopted to assist dietary assessment of pesticide intake from processed commodities.[31] On the basis of the residues and processing transfer rates in three cereal products in this

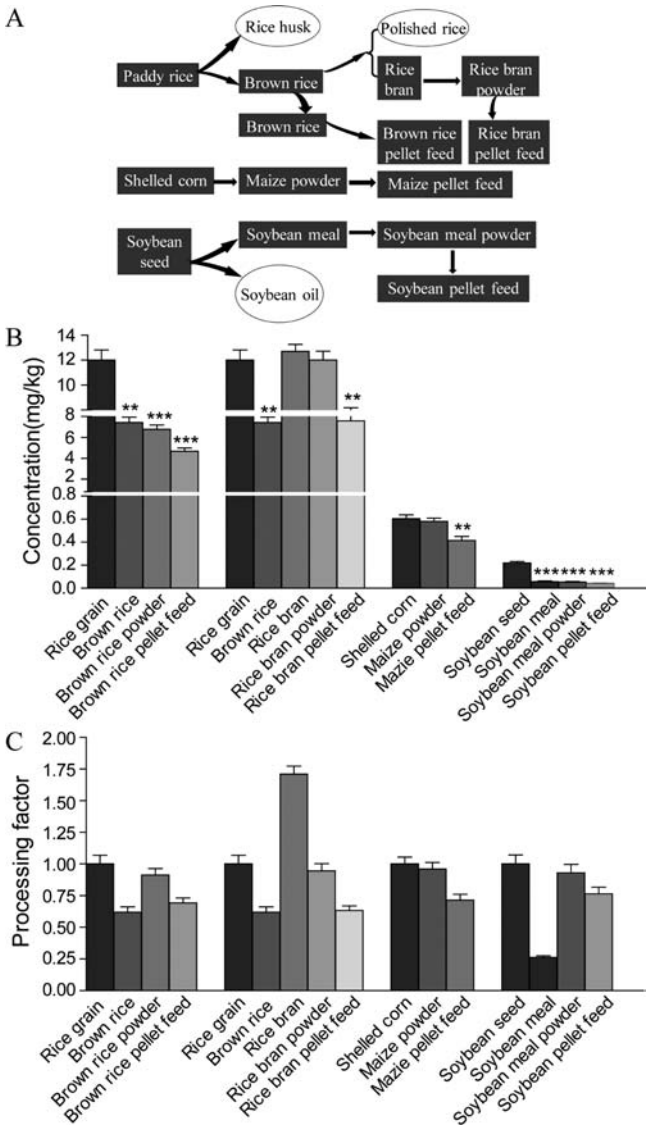


**Figure 4.** Three cereal-processing products, chlorpyrifos residues, and processing factors during duck pellet feed manufacture: (A) intermediate and processing products; (B) chlorpyrifos residues; (C) processing factors. (**) $P < 0.01$; (***) $P < 0.001$.

study, PFs were calculated and evaluated according to Joint Meeting on Pesticide Residues (JMPR).[32] PF values <1.0 indicate a chemical residue reduction in the processed commodity, whereas a value >1.0 indicates a chemical residue rise in the processed products.[33] Results of this study showed that the three cereals' PF values in each processing step were generally <1.0, except for the milling process of brown rice (Figure 4C), and these results were consistent with previous studies.[13,34] The grinding process exhibited only a slight effect on chlorpyrifos reduction (PFs, 0.912−0.959). Compared to other processing steps (e.g., hulling, milling, and granulating), chlorpyrifos was stable in grinding processing at low temperature. The PF value of soybean squashing showed a dramatic chlorpyrifos reduction from soybean seed to soybean meals (PF, 0.262), and the result was also supported by the transfer rate discussed above (a great amount of chlorpyrifos was transferred to soybean oil). This finding was similar to the study of Holland et al.,[30] in which the lipophilic pesticides used for postharvest pests led to serious residues in oil products. High-temperature processing was involved in pellet feeds, for final pellet forming, and this was one of the most important factors contributing to pesticide reduction in each feed material (PFs, 0.632−0.763).

Two duck pellet feeds (feeds A and B) in southern China were consistent for final chlorpyrifos residues based on the feed formula ingredients in Table 1 and the chlorpyrifos concentrations of processed products (Figure 4B). On the basis of the raw material residues, the processing PFs, and the duck pellet feed ingredients, the final residues in two duck pellet feeds were 1.01 mg/kg for feed A and 3.20 mg/kg for feed B. Obviously, the feed using rice as energy resource was more seriously contaminated than that using maize as energy resource. The residues calculated here should be a little higher than those of industrial productions, because material storage was not considered, although previous study indicated that postharvest storage showed only limited effects on pesticide removal.[1] Generally, animal toxicological testing is not obligatory as part of chlorpyrifos official registration, but is intensively recommended when the residue of animal diet is >0.1 mg/kg.[3] For healthy aquaculture and food safety, the duck pellet feeds (feeds A and B) of this study definitely required further toxicological evaluation.

## AUTHOR INFORMATION

### Corresponding Author

*(Y.Z. and Q.W.) Fax: 86-571-86401834. E-mail: microbesyu@yahoo.com.

### Funding

This work was supported by grants from Zhejiang Provincial Science and Technology Project (2011C12024), International Cooperation Project of Ministry of Science and Technology (2013DFA31450), and International Cooperation Project of Zhejiang Province (2013C24021).

### Notes

The authors declare no competing financial interest.

## REFERENCES

(1) Salas, J. H.; Gonzalez, M. M.; Noa, M.; Perez, N. A.; Diaz, G.; Gutierrez, R.; Zazueta, H.; Osuna, I. Organophosphorus pesticide residues in Mexican commercial pasteurized milk. *J. Agric. Food Chem.* **2003**, *51*, 4468−4471.

(2) Tsiplakou, E.; Anagnostopoulos, C. J.; Liapis, K.; Haroutounian, S. A.; Zervas, G. Pesticides residues in milks and feedstuff of farm animals drawn from Greece. *Chemosphere* **2010**, *80*, 504−512.

(3) MacLachlan, D. J.; Bhula, R. Estimating the residue transfer of pesticides in animal feedstuffs to livestock tissues, milk and eggs: a review. *Aust. J. Exp. Agric.* **2008**, *48*, 589−598.

(4) Adzitey, F.; Adzitey, S. P. Duck production: has a potential to reduce poverty among rural households in Asian communities − a review. *J. World's Poult. Res.* **2011**, *1*, 7−10.

(5) Kan, C. A.; Meijer, G. The risk of contamination of food with toxic substances present in animal feed. *Anim. Feed Sci. Technol.* **2007**, *133*, 84−108.

(6) Chen, C.; Qian, Y.; Liu, X.; Tao, C.; Liang, Y.; Li, Y. Risk assessment of chlorpyrifos on rice and cabbage in China. *Regul. Toxicol. Pharmacol.* **2012**, *62*, 125−130.

(7) Oliver, G. R.; Bolles, H. G.; Shurdut, B. A. Chlorpyrifos: probabilistic assessment of exposure and risk. *Neurotoxicology* **2000**, *21*, 203−208.

(8) Marino, D.; Ronco, A. Cypermethrin and chlorpyrifos concentration levels in surface water bodies of the Pampa Ondulada, Argentina. *Bull. Environ. Contam. Toxicol.* **2005**, *75*, 820−826.

(9) Wang, L.; Liang, Y.; Jiang, X. Analysis of eight organophosphorus pesticide residues in fresh vegetables retailed in agricultural product

markets of Nanjing, China. *Bull. Environ. Contam. Toxicol.* **2008**, *81*, 377−382.
(10) Zhang, C. Z.; Zhang, X. M.; Tian, Z. H.; He, D. J.; Liu, X. J. Degradation of chlorpyrifos and fipronil in rice from farm to fork and risk assessment. *Agric. Sci. China* **2010**, *9*, 754−763.
(11) Fan, S.; Zhang, F.; Deng, K.; Yu, C.; Liu, S.; Zhao, P.; Pan, C. Spinach or amaranth contains highest residue of metalaxyl, fluazifop-P-butyl, chlorpyrifos, and λ-cyhalothrin on six leaf vegetables upon open field application. *J. Agric. Food Chem.* **2013**, *61*, 2039−2044.
(12) Uygun, U.; Senoz, B.; Öztürk, S.; Koksel, H. Degradation of organophosphorus pesticides in wheat during cookie processing. *Food Chem.* **2009**, *117*, 261−264.
(13) Han, Y. T.; Li, W.; Dong, F. S.; Xu, J.; Liu, X. G.; Li, Y. B.; Kong, Z. Q.; Liang, X. Y.; Zheng, Y. Q. The behavior of chlorpyrifos and its metabolite 3,5,6-trichloro-2-pyridinol in tomatoes during home canning. *Food Control* **2013**, *31*, 560−565.
(14) Cogburn, R. R.; Simonaitis, R. A.; Webb, B. D. Fate of malathion and chlorpyrifos methyl in rough rice and milling fractions before and after parboiling and cooking. *J. Econ. Entomol.* **1990**, *83*, 1636−1639.
(15) Zhao, L.; Ge, J.; Liu, F.; Jiang, N. Effects of storage and processing on residue levels of chlorpyrifos in soybeans. *Food Chem.* **2014**, *150*, 182−186.
(16) Zabik, M. J.; El-Hadidi, M. F.; Cash, J. N.; Zabik, M. E.; Jones, A. L. Reduction of azinphos-methyl, chlorpyrifos, esfenvalerate, and methomyl residues in processed apples. *J. Agric. Food Chem.* **2000**, *48*, 4199−4203.
(17) Randhawa, M. A.; Anjum, F. M.; Ahmed, A.; Randhawa, M. S. Field incurred chlorpyrifos and 3,5,6-trichloro-2-pyridinol residues in fresh and processed vegetables. *Food Chem.* **2007**, *103*, 1016−1023.
(18) Ling, Y.; Wang, H.; Yong, W.; Zhang, F.; Sun, L.; Yang, M. L.; Wu, Y. N.; Chu, X. G. The effects of washing and cooking on chlorpyrifos and its toxic metabolites in vegetables. *Food Control* **2011**, *22*, 54−58.
(19) Calet, C. The relative value of pellets versus mash and grain in poultry nutrition. *World's Poult. Sci. J.* **1965**, *21*, 23−52.
(20) *Guideline for Pesticide Residue Testing*; China Agriculture Press: Beijing, China, 2004; NY/T788-2004.
(21) Qu, L. J.; Zhang, H.; Zhu, J. H.; Yang, G. S.; Aboul-Enein, H. Y. Rapid determination of organophosphorous pesticides in leeks by gas chromatography-triple quadrupole mass spectrometry. *Food Chem.* **2010**, *122*, 327−332.
(22) Kumar, A.; Nadda, G.; Shanker, A. Determination of chlorpyrifos 20% EC (Dursban 20 EC) in scented rose and its products. *J. Chromatogr., A* **2004**, *1050*, 193−199.
(23) *National Food Safety Standard Maximum Residue Limits for Pesticides in Food*; National Standards of the People's Republic of China: Beijing, China, 2012; GB 2763-2012, pp 29−30.
(24) U.S. EPA. *Chlorpyrifos; Tolerances for Residues*; Washington, DC, USA, 1991; pp 363−364.
(25) Li, W. X.; Chen, M.; Chen, W. T.; Qiao, C. K.; Li, M. H.; Han, L. J. Determination of mepiquat chloride in cotton crops and soil and its dissipation rates. *Ecotoxicol. Environ. Saf* **2012**, *85*, 137−143.
(26) Chavarri, M. J.; Herrera, A.; Arino, A. The decrease in pesticides in fruit and vegetables during commercial processing. *Int. J. Food Sci. Technol.* **2005**, *40*, 205−211.
(27) Zhu, Q.; Cao, W.; Chen, N.; Wang, B.; Yu, S. Effects of the processing steps on chlorpyrifos levels during honey production. *Food Control* **2010**, *21*, 1497−1499.
(28) Sharma, J.; Satya, S.; Kumar, V.; Tewary, D. K. Dissipation of pesticides during bread making. *J. Chem. Health Food Saf.* **2005**, *12*, 504−512.
(29) Eddleston, M.; Mohamed, F.; Davies, J. O.; Eyer, P.; Worek, F.; Sheriff, M. H.; Buckley, N. A. Respiratory failure in acute organophosphorus pesticide self-poisoning. *QJM* **2006**, *99*, 513−522.
(30) Holland, P.; Hamilton, D.; Ohlin, B.; Skidmore, M. Effects of storage and processing on pesticide residues in plant products. *Pure App. Chem.* **1994**, *66*, 335−356.
(31) Amvrazi, E. G.; Albanis, T. A. Multiclass pesticide determination in olives and their processing factors in olive oil: comparison of different olive oil extraction systems. *J. Agric. Food Chem.* **2008**, *56*, 5700−5709.
(32) FAO/WHO. *Condex Maximum Limits for Pesticides Residues*; Codex Alimentarious Commission FAO and WHO: Rome, Italy, 2006.
(33) Timme, G.; Walz-Tylla, B. Chapter 4. Effects of food preparation and processing on pesticide residues in commodities of plant origin. *Pesticide Residues in Food and Drinking Water: Human Exposure and Risks*; Hamilton, D., Crossley, S., Eds.; Wiley: Hoboken, NJ, USA, 2004; pp 121−148
(34) Balinova, A.; Mladenova, R.; Obretenchev, D. Effect of grain storage and processing on chlorpyrifos-methyl and pirimiphos-methyl residues in post-harvest-treated wheat with regard to baby food safety requirements. *Food Addit. Contam.* **2006**, *23*, 391−397.

sampled). We will apply headspace SPME for the sampling and concentration of surface volatiles followed by GCMS for separation, detection, and identification. Principal component analysis (PCA) will be applied to the chromatograms to characterize surface volatile peak patterns that differentiate PTD from non-PTD coffee. This study is the first both to characterize the volatile organics *on the surface* of green coffee beans and to utilize SPME−GCMS for the study of potato taste defect. Parts of this research were presented at the Coffee Research Symposium, convened by the Rwandan Ministry of Agriculture[24] and the Global Knowledge Initiative,[25] March 17−18, 2014, Kigali, Rwanda.

## MATERIALS AND METHODS

**Chemicals.** Standard compounds were obtained from Fisher Scientific Co. or Sigma/Aldrich Co., U.S.A. ($C_{11}$−$C_{18}$ standard alkane mixture, hexanal, 2-pentylfuran, nonanal, 1-octen-3-ol, 2-ethyl-1-hexanol, benzaldehyde, 3-methylbutanoic acid, heptanal, 2-*E*-hexenal, pentanol, octanal, 6-methyl-5-hepten-2-one, decanal, hexanoic acid, 2-isopropyl-3-methoxypyrazine, 2-isobutyl-3-methoxypyrazine, 1-hexanol, limonene, octanoic acid, phenol, octyl acetate, 1-dodecene, 2,6-dimethylpyridine, methylsalicylate, 1-tetradecene). Note that 1-methoxy-4-propylbenzene, phenylethylalcohol, 2,6,10,14-tetramethylpentadecane, hexadecanoic acid, and dodecanal were identified by mass spectral match but not confirmed by standard.

**Samples and Characterization.** Fifty-two samples (Arabica coffee, varietal Bourbon) were sent directly from the coffee growing regions of Rwanda in the 2012 and 2013 harvest seasons to the Rogers Family Company laboratory in Lincoln, California, where they were characterized by physical and sensorial analysis. All samples were conventionally grown in the sun at 5000−8000 feet elevation on small farms. Physical characteristics included moisture content (%), screen size distribution, sorting, and counting defects. Sensorial analysis consisted of standard cupping of a medium roasted sample by four experienced cuppers, which for our purposes classified the samples as either "PTD" or "non-PTD". PTD samples tested positive at rates from 1 in 6 cups to 1 in 20 cups. Green coffee samples from each batch were forwarded to Seattle University along with the characterization data. For the purpose of this study, the detailed origins of the samples were not included. The samples varied in size from 100 to 400 g and were stored as received in plastic bags at room temperature until analyzed.

**Sample Preparation.** The SPME sampling conditions used here were previously validated and applied in studies of green and roasted coffee.[12−15] Whole bean green coffee (70.0 g, approximately 400 beans, randomly selected) was placed in a headspace bottle (125 mL) with a PFTE/silicone septum cap (Supelco, U.S.A., 27236). The SPME fiber used was triple phase 50/30 $\mu$m DVB/Carboxen/PDMS coated (Supelco, U.S.A., 57328-U). Prior to first use, the fiber was preconditioned at 250 °C in the injection port of the GCMS for 30 min. The fiber was exposed in the headspace above the coffee beans for 60 min while the assembly was immersed in a 60 °C water bath. The headspace-to-volume ratio was approximately 1:10. The fiber was desorbed in the GC injection port for 5 min at 250 °C in the splitless mode using a Supelco specific SPME injection insert of 0.75 mm i.d.

**Organization of Study.** Samples selected randomly were subjected to GCMS analysis in batches of three to five per day. Blank samples were run once per day under the bean analysis conditions and provided negligible response. One to four replicates of each sample were analyzed, depending on size of coffee sample received. Usually, replicates were not run on the same day. In all there were 52 samples that resulted in 115 GCMS runs.

**Gas Chromatographic and Mass Spectrometric Analysis.** The GCMS conditions here were previously validated in several studies of green and roasted coffee.[16,17] An Agilent 5890 gas chromatograph was used as equipped with a 60 m × 0.25 mm i.d., 0.25 $\mu$m film thickness Stabilwax capillary column (Restek, 10641, Supelco, U.S.A.), an Agilent 5972 mass-selective detector, and Agilent ChemStation software. Analyses were done in the splitless mode using helium gas carrier at 1.0 mL/min flow. Column temperature was maintained at 40 °C for 11 min, then raised to 190 °C at 3 °C/min, held at 190 °C for 10 min, and finally raised from 190 to 250 °C at 15 °C/min. Mass spectra were recorded following electronic impact ionization at 70 eV. The mass range for data collection was 40−400 Da with 0.3 s scan interval. The data were collected and analyzed by GCMS Agilent ChemStation software (GCMSD1 operating software with Enhanced Data Analysis) using the NIST-05 and Wiley FFNSC-2 mass spectral databases. Peak assignments were made using dual criteria of mass spectral database and linear retention index[26,27] match. Retention indices of the eluted compounds were calculated on the basis of the standard alkane mixture ($C_{11}$−$C_{18}$). By comparing the retention indices and unique mass spectra with the reference library matches and literature retention indices,[28] tentative assignments were obtained, and they were confirmed by running known standards under the bean analysis conditions.

**Chromatographic Analysis of Ground Bean Samples.** Green coffee samples were frozen to −70 °C and then ground in a blender (Waring Commercial, model 51BL30, Fisher Sci., U.S.A.), with the size fraction less than 2 mm (U.S.A. Standard Test Sieve, No. 10, 2 mm, Fisher Sci., U.S.A.) being considered representative of the interior of the beans and analyzed for volatiles. A 3.5 g ground sample in a 40 mL sample vial was heated to 60 °C, sampled by SPME, and analyzed chromatographically by the procedure as described above in the Chromatographic and Mass Spectrometric Analysis section.

**Statistical Analyses.** Principal component analysis (PCA) allows comparison and classification of complex samples using their entire gas chromatographic (GC) profiles, avoiding selection and identification of individual peaks and peak-area integrations, while taking into account the large number of minor peaks and peak shape information. Due to minor drifts in retention times, data alignment is required prior to applying PCA to GC data. This approach, utilizing the entire instrument output, has been applied successfully to chromatographic[29,30] and spectral[31] analysis of complex systems. The PCA was accomplished using software within the PLS Toolbox v. 7.5.2[32] running on the Matlab platform v.R2013b.[33] See Chapter 4 of Brereton[34] for a general discussion of PCA in the chemometric context.

The GC/MS signal, total ion current (TIC) as a function of time, was collected every 0.4 s, yielding approximately 11 132 observations for each 75 min run. Visual inspection revealed that all useful data had retention times in the range 17.2−70.9 min, and the GC data sets were truncated accordingly, yielding data objects of 7951 variables corresponding to points in the chromatogram. Prior to analysis, the GC data objects were aligned using correlation-optimized warping (COW) according to the procedures of Tomasi et al.[35] The reference chromatogram (pt 61a) was selected as having the maximum cumulative product of correlation coefficients for a subset of 52 chromatograms collected in midstudy.[36] Parameters used in the alignment (segment = 100, slack = 15) were determined by their systematic variation with graphical assessment of the resulting aligned chromatograms. After alignment, further preprocessing included baseline correction using the Eilers and Boelens[37] method with Whittaker[38] filter ($p$ = 0.001, lambda = 100), followed by mean-centering.

The resulting principal component model was then subjected to the VARIMAX rotation[39] in order to facilitate the interpretation of the potato taste samples in terms of the loadings on a single factor.

## RESULTS AND DISCUSSION

**Chromatograms of Whole Bean Samples.** In all, 115 chromatographic runs of surface volatiles were performed on 52 characterized whole bean samples. One to four replicates were collected, depending on availability of sample, and in all cases they were reproducible. Six of the samples in the study were confirmed with PTD by the taste testers. Visual inspection of the chromatograms revealed obvious differences between the potato taste (PTD) and nonpotato taste (non-PTD) samples. Typical non-PTD and PTD surface volatile chromatograms are

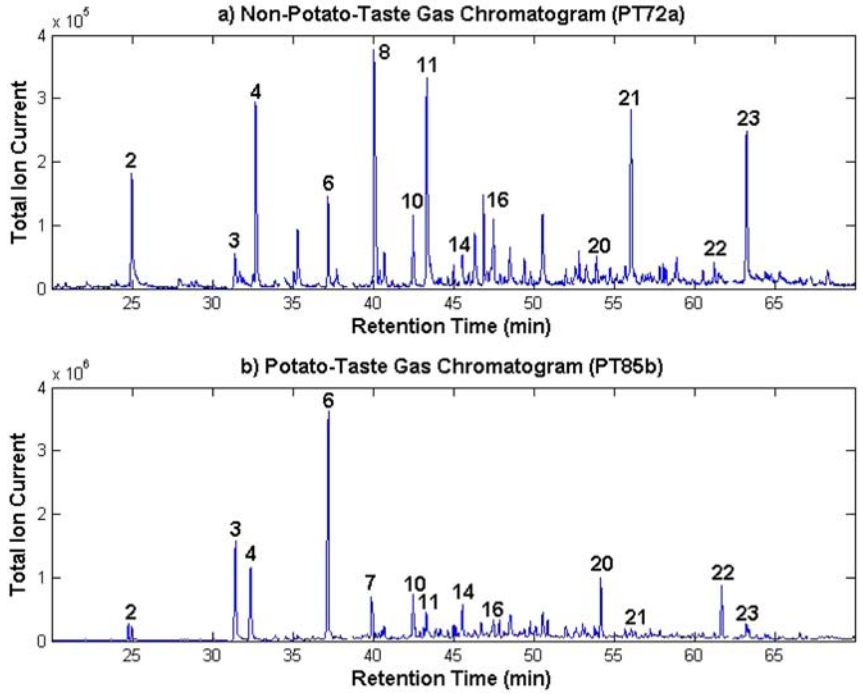


**Figure 1.** Gas chromatograms for whole bean green coffee samples: (a) non-potato-taste (Pt 72a) and (b) potato-taste (Pt 85b). Compounds are labeled according to Table 1.

shown in Figures 1a and 1b, respectively. The sample analyses are labeled in the figures with a number designating their index in our laboratory records and a letter indicating the replication. For example, "Pt 85b" refers to second analysis ("b") of the sample designated "85". Note the difference in scale for the ordinate axes: the total ion current scale is 10 times greater (to $4.0 \times 10^6$) in the PTD chromatogram as compared to the non-PTD chromatogram ($4.0 \times 10^5$) The retention times and compound identifications for the major peaks are given in Table 1.

Peaks occurring at 31.1, 38.5, 45.4, 62.2, and 67.2 min corresponded to silyl esters originating from the SPME sampling conditions and were eliminated from further analysis. These assignments were confirmed through a blank sampling experiment. A peak of widely varying intensity at 34.3 min was identified as 1-dodecene. The intensity of this peak correlated strongly with the elapsed time between processing of the coffee beans in the field and their analysis in the lab. This is consistent with 1-dodecene being a product of on-the-shelf oxidation of unsaturated plant oils, and the development of a cardboard-like odor.[40] Having no significance in the present context, the 1-dodecene peak was eliminated from further analysis. The peaks labeled "8" at 40.1 min (Figure 1a) and "7" at 39.9 min (Figure 1b) are "unidentified" by the MS analysis.

Peaks corresponding to tridecane (6), dodecane (3), tetradecane (10), and methylsalicylate (22) are observed to have much larger intensities in the PTD chromatograms than in the non-PTD ones (note the different ordinate scales). Peak "20" at 54.3 min corresponding to 1-methoxy-4-propylbenzene is variable among the PTD chromatograms and observed only at reduced intensity in the non-PTD chromatograms. This pattern of relatively intense alkane peaks in PTD samples is denoted in this study as a "PTD profile."

Two samples (Pts 77a and 80a) that were characterized as "non-PTD" by the taste testers were found to have the PTD profile (i.e., high alkane concentrations) in their surface volatile chromatograms. The PCA (see below) also characterized them as "PTD." These samples were from farms adjacent to those

**Table 1. Selected Observed Peaks for Whole Bean and Ground Samples (non-PTD and PTD)**

| label | retention time (min) | linear retention index | compound |
|---|---|---|---|
| 1 | 24.8 | 1100 | undecane |
| 2 | 25.1 | 1104 | hexanal |
| 3 | 31.5 | 1200 | dodecane |
| 4 | 32.5 | 1216 | limonene |
| – | 34.3 | 1247 | 1-dodecene |
| 5 | 35.4 | 1266 | 2,6-dimethylpyridine |
| 6 | 37.3 | 1300 | tridecane |
| 7 | 39.9 | 1348 | unidentified |
| 8 | 40.1 | 1352 | unidentified |
| 9 | 40.7 | 1363 | 1-hexanol |
| 10 | 42.6 | 1400 | tetradecane |
| 11 | 43.4 | 1416 | nonanal |
| 12 | 45.1 | 1450 | 1-tetradecene |
| 13 | 45.2 | 1452 | 2-isopropyl-3-methoxypyrazine |
| 14 | 45.7 | 1463 | 1-octen-3-ol |
| 15 | 47.0 | 1490 | octylacetate |
| 16 | 47.6 | 1502 | 2-ethyl-1-hexanol |
| 17 | 48.5 | 1522 | decanal |
| 18 | 49.7 | 1547 | 2-isobutyl-3-methoxypyrazine |
| 19 | 50.7 | 1569 | benzaldehyde |
| 20 | 54.3 | 1651 | 1-methoxy-4-propylbenzene[a] |
| 21 | 56.1 | 1693 | 3-methylbutanoic acid |
| 22 | 61.8 | 1832 | methylsalicylate |
| 23 | 63.4 | 1873 | hexanoic acid |
| 24 | 67.3 | 1976 | phenylethylalcohol[a] |
| 25 | 72.0 | 2106 | phenol |
| 26 | 73.4 | 2146 | octanoic acid |

[a]Identified by mass spectral match, but not confirmed by standard.

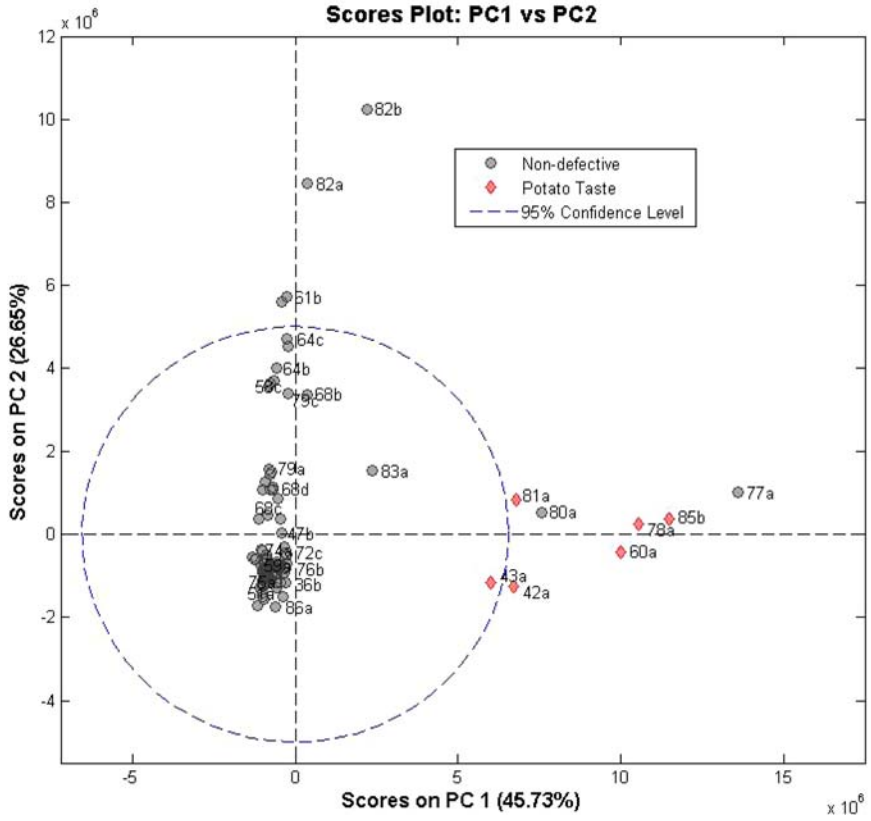


**Figure 2.** PCA scores biplot (PC1 vs PC2) for 115 whole bean green coffee samples (after VARIMAX rotation).

that had PTD, which suggested PTD could possibly be verified by further taste testing of these samples. However, due to limited sample availability, further testing was not possible.

Surprisingly, neither IPMP nor IBMP was observed in any of the PTD or the non-PTD chromatograms of surface volatiles when the samples were heated at 60 °C. Standards of IPMP and IBMP showed them to be found at 45.2 and 49.7 min, respectively. To determine if a higher temperature would release these pyrazines, PTD and non-PTD samples were heated to 90 or 100 °C, but still no IPMP or IBMP was observed among the surface volatiles. Samples could not be heated over 100 °C because roasting chemistry begins above 100 °C, producing new compounds.

**PCA of Chromatograms.** Principal component analysis (PCA) was utilized to classify the 115 samples as either PTD or non-PTD. In general, a model with two principal components was found to be satisfactory, accounting for 72% of the variance in the data sets. In Figure 2 is the scores biplot (PC1 versus PC2) for the 115 data objects. A VARIMAX rotation has been applied to the component axes to bring the cluster of PTD samples into good alignment with the PC1 axis, facilitating interpretation in terms of the PC1 loadings. Note first that all samples identified as PTD by the taste testers (red diamonds) appear in a cluster well separated from the much larger number of non-PTD samples (black circles). As already noted above from the visual inspection of the chromatograms, Pts 77a and 80a appear firmly within the PTD cluster, strongly suggesting that they would be likely to reveal PTD character upon further sensorial testing. The remaining 107 non-PTD points exhibit very little spread along the PC1 axis as would be indicative of PTD chromatograms.

In Figure 3 is presented a plot of the loadings for PC1. Since the PTD cluster of data lies close to the positive PC1 axis in the scores biplot, we can interpret the loadings as characteristic of the chemical "profile" that classifies these points as PTD and separates them from the other samples. This indicates that compared to the non-PTD samples, PTD samples have strongly increased levels of dodecane and tridecane; moderately increased levels of tetradecane, 1-octene-3-ol, 2-ethyl-1-hexanol, and limonene; slightly increased levels of 1-methoxy-4-propylbenzene and methylsalicylate, and *decreased* levels of 3-methylbutanoic acid. The strongest features of this PTD profile are increased levels of several alkanes and a decreased level of 3-methylbutanoic acid. Of interest is the observation of increased methylsalicylate (oil of wintergreen) in the PTD profile. Methylsalicylate is derived from salicylic acid, a plant hormone, and is known to increase in response to insect attacks.[41] This compound has not been reported among the volatiles of "normal" green coffee[15,17,19] but has been reported among the volatiles in defective moldy/earthy coffee.[8] Consistent with the previous visual observations, no evidence of IPMP or IBMP is found in the loadings for PC1.

In Figure 2, the spread within the non-PTD samples is along PC2, with the two replicates of Pt 82 having the largest displacements. Examination of the PC2 loadings and the GC's for Pt 82 indicates that those samples have relatively large concentrations of nonanal ("11") and an unidentified compound ("7").

**Chromatograms of Ground Samples.** The surface volatiles observed in chromatograms of whole bean samples (above) revealed differences between PTD and non-PTD coffees that serve to classify the coffees but were not the same as the reported differences in the literature[1] in that the whole bean chromatograms did not include IPMP or IBMP. However, the previous observations[1] were based on finely ground samples that were solvent-extracted and put through a multistep process

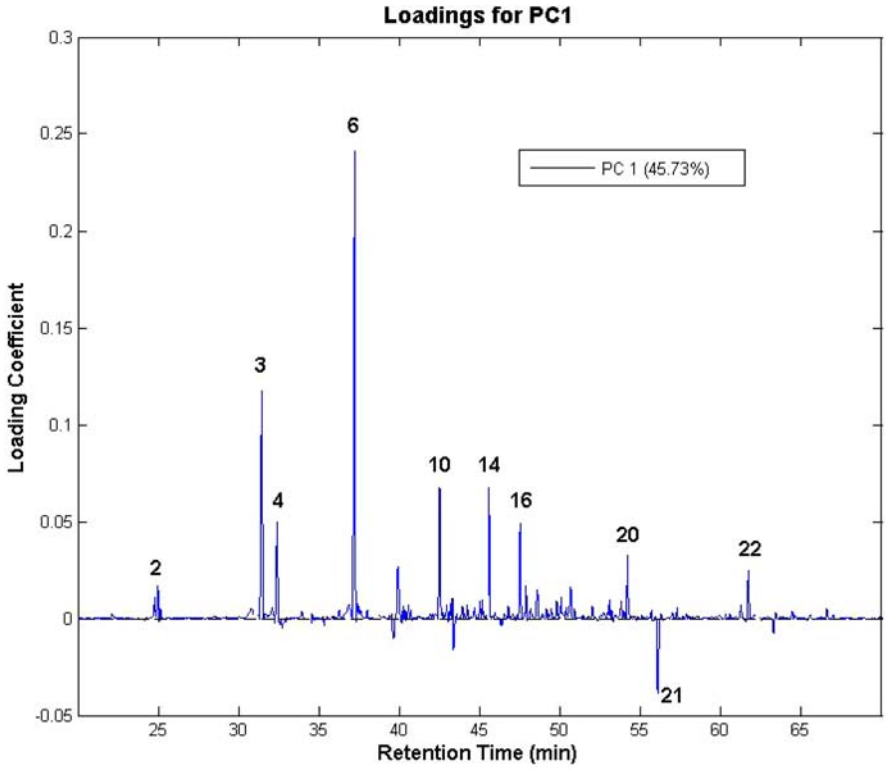


**Figure 3.** PCA loadings plot for PC1. Compounds are labeled according to Table 1.

before chromatography. When using ground samples previously, the volatiles were extracted from the interior of the coffee beans and the concentration of surface volatiles would be insignificant in the mixture. Since in our research (above), IPMP and IBMP, which were assumed to bring about PTD, were not observed in the surface volatiles of PTD coffee, they must have been in the interior of the PTD beans. Thus, further experiments were designed to measure the interior volatiles of the beans. PTD and non-PTD green coffee samples were frozen to −70 °C, ground in a blender with the size fraction less than 2 mm being considered representative of the interior of the beans, and analyzed for volatiles. A 3.5 g ground sample was sampled and analyzed chromatographically by the PSPME−GCMS procedure as described above in the Materials and Methods Section.

Due to limited quantity of samples, two non-PTD and four PTD samples were used to collect nine chromatograms of ground samples (two non-PTD and seven PTD). In addition to these samples a large Burundian sample (see section below) was used to collect 13 more chromatograms. In contrast to the surface volatile case, the intense PTD profile (mainly alkanes) was not observed in the interior of either PTD or non-PTD samples. Among the interior volatiles, hexanal, hexanol, nonanal, 3-methylbutanoic acid, and hexanoic acid were prominent and similar in intensity in both the PTD and non-PTD chromatograms. These compounds have been previously observed in studies of ground green coffee beans.[14−16,19,20] IBMP was found in both types of sample at approximately the same amount, but IPMP was detected *only* in the PTD sample, in agreement with the previous findings of Becker[1] that IPMP was found at increased levels in PTD coffee. Further, the lack of IPMP or IBMP among the surface volatiles shows that these compounds are found only inside the beans. Our results are consistent with a hypothesis that the IPMP was produced *in the seeds* and not deposited on the seed surface by a bacterial growth in the fruit, as had been suggested by Bouyjou.[4]

**Chromatograms of Insect Damaged PT Coffee Beans.** Given that the IPMP occurs inside the beans, it would be illustrative to determine if its level is the same throughout a PTD sample or is concentrated in specific beans, for example, those exhibiting visible signs of insect damage. Further, if the elevated IPMP level is associated with *antestia* activity, then coffee with known *antestia* damage should exhibit the PTD profile in the whole beans and the PTD-associated pyrazines in the ground coffee. To test these hypotheses, a large (several kilogram) sample of PTD coffee was needed so that it could be sorted into the defect categories. None of the Rwandan samples was large enough, but we were fortunate to receive a large donated sample of Burundian coffee that had very weak PTD (1 cup in 120 confirmed by a tasting panel). This sample was sorted into the following fractions: insect-damaged (brown spots indicative of *antestia* activity), UV fluorescent (presumably from the presence of a fluorescent microbe on the bean surface), broken (during removal of the parchment and silverskin), withered (characteristic of poor cultivation conditions), and bulk (no defects, after the other fractions were removed).

SPME−GCMS analysis of the bulk fraction gave results indicative of non-PTD coffee, i.e., no prominent alkane PTD profile in the whole bean chromatogram and IBMP with only a trace of IPMP in the ground bulk chromatogram. In contrast, the chromatogram of the whole bean insect-damaged fraction did feature a prominent tridecane peak with accompanying dodecane and tetradecane peaks, similar to the profile that characterized PTD whole bean coffee. The chromatogram of the whole-bean insect-damaged fraction (Figure 4a) did not have peaks attributed to IPMP or IBMP, whereas chromatogram of the ground-bean insect-damaged fraction (Figure 4b) exhibited both. Comparing the chromatograms of the sorted fractions

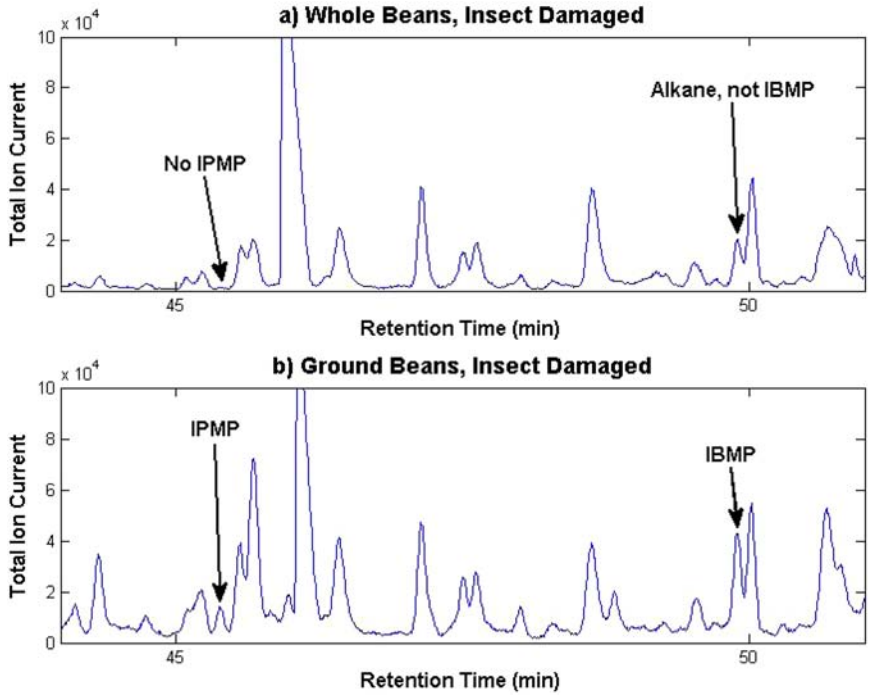


**Figure 4.** Expanded GC region from insect damaged sample: (a) whole beans and (b) ground beans.

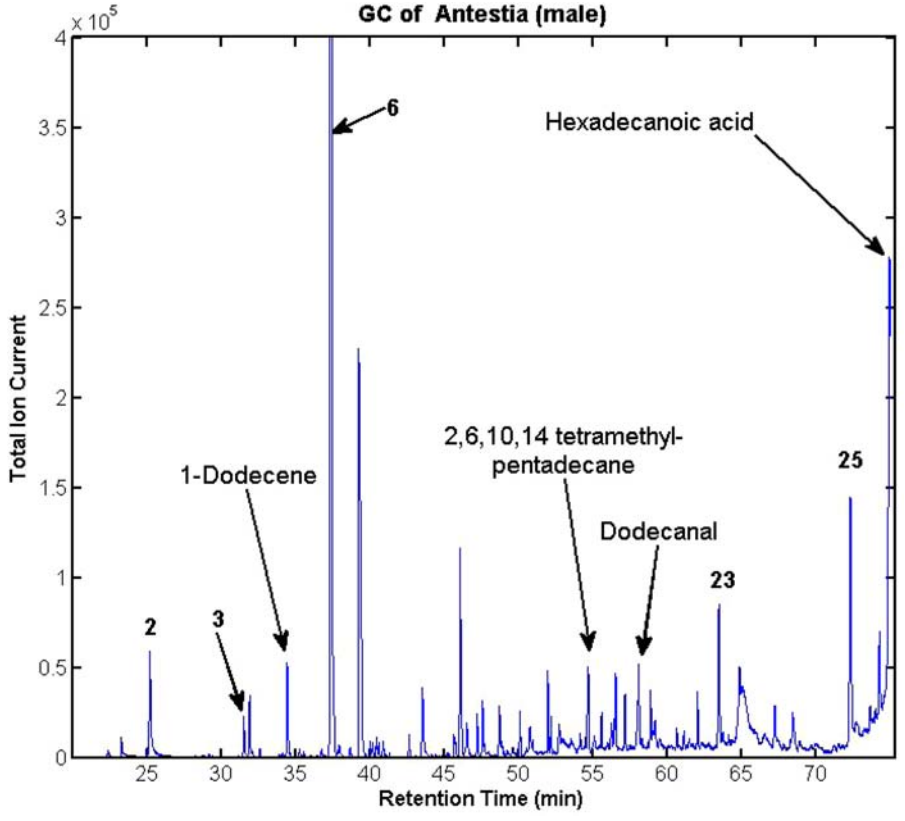


**Figure 5.** GC analysis of a whole, male *Antestia* bug. Peaks without labels are unidentified.

revealed that the IBMP peak was about the same size in all the fractions whereas the IPMP/IBMP peak ratio varied from 0 in the bulk fraction to 0.08, 0.11, and 0.32 in the broken, UV fluorescent, and insect-damaged fractions, respectively. The presence of the PTD profile in the whole-bean insect-damaged fraction, along with the IPMP and IBMP presence in the ground-bean insect-damaged fraction (and only trace IPMP in the bulk sample), is the first direct evidence observed to date for the association of *antestia* activity with both the surface alkane and interior pyrazine PTD profiles. Lower levels of IPMP were observed in the UV fluorescent and broken bean samples. Future experiments will focus on establishing a more

quantitative relationship between interior IPMP level and surface alkane levels.

**Chromatograms of Whole Desiccated *Antestia* Bugs.** In order to test the hypothesis that the PTD surface profile, consisting mainly of tridecane, dodecane, and tetradecane, is associated with volatile compounds possibly deposited by the *antestia* bug, specimens of *antestia* were obtained from Rwanda and chromatograms of whole bug volatiles were collected. Male and female *antestia* were collected, kept separately, killed by freezing, and then dried before transport to the U.S. The specimens were frozen at −15 °C immediately upon arrival, and when needed, a single whole bug was transferred to a 40 mL sample vial, sealed with a septum cap, heated to 60 °C, and then sampled by headspace SPME for 5 min and subjected to chromatographic analysis by the same procedure described in the Materials and Methods section.

Male and female specimens each were analyzed in triplicate and gave very similar chromatograms with the same set of volatiles, including hexanal, dodecane, 1-dodecene, tridecane, 2,6,10,14-tetramethylpentadecane, hexanoic acid, and phenol (see Figure 5). The three major compounds of the *antestia* chromatograms, tridecane (largest), dodecane, and tetradecane, were also detected as the three major compounds in the PTD profile of the surface volatiles of green coffee. The pheromones of *antestia orbitalis* have not been studied; however, in the literature, tridecane, dodecane, and tetradecane are prominent among the pheromones identified as defensive compounds in pentadomidae species related to *antestia*, such as *Agroecus griseus,*[42] *Cosmopepla bimaculata,*[43] and *Nezara viridula*.[44]

In summary, the results of the analysis of surface volatile compounds on green coffee indicate a clear pattern of distinction between PTD and non-PTD coffees. The four prominent identifiable compounds found at higher levels in PTD coffee surface were dodecane, tridecane, tetradecane, and 2-ethyl-1-hexanol, while 3-methylbutanoic acid was found at decreased levels. Long-chain alkanes have not previously been associated with volatile compounds of ground green coffee.[6−9,20,23] However, long-chain alkyl compounds are frequently found as constituents of plants and insects, for example, on leaf surfaces and seed surfaces, and are used as pheromones by insects. Several studies include alkanes such as tridecane, dodecane, tetradecane, and undecane on lists of defensive pheromones secreted by stink bugs related to *antestia*.[42−44] These results support the hypotheses that PTD is associated with *antestia* feeding activity and that IPMP, which imparts potato taste in roasted coffee, is produced inside the coffee beans, possibly in response to the stress of *antestia* damage.

## AUTHOR INFORMATION


### Corresponding Author

*E-mail: sjackels@seattleu.edu.



### Funding

E.E.M. and A.G.O. acknowledge research support from Rogers Family Company, the Peach Foundation, and Seattle University Center for Environmental Justice and Sustainability. This research was partially supported by the Seattle University Chemistry Department.


### Notes

The authors declare no competing financial interest.

## ACKNOWLEDGMENTS


We thank the Rogers Family Company for characterized green coffee samples and Dr. Mario Serracin for collecting the *antestia* bugs and for the photo. Mr. Andrew Gerard of Global Knowledge Initiative (http://globalknowledgeinitiative.org) is acknowledged for his critical role in facilitating the communication essential to the accomplishment of this research project.


## REFERENCES


(1) Becker, R.; Dohla, B.; Nitz, S.; Vitzthum, O. G. Identification of the "Peasy" Off-Flavour Note in Central African Coffees. In *Proceedings of the 12th International Scientific Colloquim of Coffee*, Montreaux, Switzerland, 29 June−3 July 1987; Association for Science and Information on Coffee (ASIC): Paris, France, 1987; pp 203 − 215.

(2) Bouyjou, B.; Fourny, G.; Perreaux, D. Le Goût de Pomme de Terre du Café Arabica au Burundi. In *Proceedings of the 15th International Scientific Colloquim on Coffee*, Montpellier, France, 6−11 June 1993; Association for Science and Information on Coffee (ASIC): Paris, France, 1993; pp 357−369.

(3) Cilas, C.; Bouyjou, B.; Decazy, B. Frequency and distribution of *Antestiopsis orbitalis* Westwood (Hem., Pentatomidae) in coffee plantations in Burundi: Implications for sampling techniques. *J. Appl. Entomol.* **1998**, *122*, 601−606.

(4) Bouyjou, B.; Decazy, B.; Fourny, G. L'élimination du "goût de Pomme de Terre" dans le Café Arabica du Burundi. *Plant., Rech., Dev.* **1999**, *6*, 107−115.

(5) Matsuura, Y.; Hosokawa, T.; Takema, F.; Serracin, M.; Tulgetske, G. M.; Miller, T. A.; Fukatsu, T. Bacterial symbionts of a devastating coffee pest, the stinkbug *Antestiopsis thunbergii* (Hemiptera: Pentatomidae). *Appl. Environ. Microbiol.* **2014**, *80*, 3769−3775.

(6) Holscher, W.; Steinhart, H. Aroma compounds in green coffee. In *Food Flavors: Generation, Analysis and Process Influence*; Charalambous, G., Ed.; Developments in Food Science 37A; Elsevier Science: Amsterdam The Netherlands, 1995; pp 785−803.

(7) Czerny, M.; Grosch, W. Potent odorants of raw arabica coffee. Their changes during roasting. *J. Agric. Food Chem.* **2000**, *48*, 868−872.

(8) Cantergiani, E.; Brevard, H.; Krebs, Y.; Feria-Morales, A.; Amado, R.; Yeretzian, C. Characterisation of the aroma of green Mexican coffee and identification of mouldy/earthy defect. *Eur. Food Res. Technol.* **2001**, *212*, 648−657.

(9) Lee, K.-G.; Shibamoto, T. Analysis of volatile components isolated from Hawaiian green coffee beans (Coffea Arabica L.). *Flavour Fragrance J.* **2002**, *17*, 349−351.

(10) Variyar, P. S.; Ahmad, R.; Bhat, A.; Niyas, Z.; Sharma, A. Flavoring components of raw monsooned arabica coffee and their changes during radiation processing. *J. Agric. Food Chem.* **2003**, *51*, 7945−7950.

(11) Scheidig, C.; Czerny, M.; Schieberle, P. Changes in key odorants of raw coffee beans during storage under defined conditions. *J. Agric. Food Chem.* **2007**, *55*, 5768−5775.

(12) Bicchi, C. P.; Panero, O. M.; Pellegrino, G. M.; Vanni, A. C. Characterization of roasted coffee and coffee beverages by solid phase microextraction—Gas chromatography and principal component analysis. *J. Agric. Food Chem.* **1997**, *45*, 4680−4686.

(13) Roberts, D. D.; Pollien, P.; Milo, C. Solid-phase microextraction method development for headspace analysis of volatile flavor compounds. *J. Agric. Food Chem.* **2000**, *48*, 2430−2437.

(14) Rocha, S.; Maeztu, L.; Barros, A.; Cid, C.; Coimbra, M. A. Screening and distinction of coffee brews based on headspace solid phase microextraction/gas chromatography/principal component analysis. *J. Sci. Food Agric.* **2003**, *84*, 43−51.

(15) Mondello, L.; Costa, R.; Tranchida, P. Q.; Dugo, P.; Lo Presti, M.; Festa, S.; Fazio, A.; Dugo, G. Reliable characterization of coffee bean aroma profiles by automated headspace solid phase microextraction−gas chromatography−mass spectrometry with the support of a dual-filter mass spectra library. *J. Sep. Sci.* **2005**, *28*, 1101−1109.

(16) Zambonin, C. G.; Balest, L.; De Benedetto, G. E.; Palmisano, F. Solid-phase microextraction−gas chromatography mass spectrometry and multivariate analysis for the characterization of roasted coffees. *Talanta* **2005**, *66*, 261−265.

(17) Lopez-Galilea, I.; Fournier, N.; Cid, C.; Guichard, E. Changes in headspace volatile concentrations of coffee brews caused by the roasting process and brewing procedure. *J. Agric. Food Chem.* **2006**, *54*, 8560−8566.
(18) Baggenstoss, J.; Poisson, L.; Kaegi, R.; Perren, R.; Escher, F. Coffee roasting and aroma formation: Application of different time-temperature conditions. *J. Agric. Food Chem.* **2008**, *56*, 5836−5846.
(19) Toci, A. T.; Farah, A. Volatile compounds as potential defective coffee beans' markers. *Food Chem.* **2008**, *108*, 1133−1141.
(20) Gonzalez-Rios, O.; Suarez-Quiroz, M. L.; Boulanger, R.; Barel, M.; Guyot, B.; Guiraud, J-.P.; Schorr-Galindo, S. Impact of "ecological" post-harvest processing on the volatile fraction of coffee beans. I. Green coffee. *J. Food Compos. Anal.* **2007**, *20*, 289−296.
(21) Agresti, P. D. C. M.; Franca, A. S.; Oliveira, L. S.; Augusti, R. Discrimination between defective and non-defective Brazilian coffee beans by their volatile profile. *Food Chem.* **2008**, *106*, 787−796.
(22) Ribeiro, J. S.; Teofilo, R. F.; Salva, T.; Augusto, F.; Ferreira, M. M. C. Exploratory and discriminative studies of commercial processed Brazilian coffees with different degrees of roasting and decaffeinated. *Braz. J. Food Technol.* **2013**, *16*, 198−206.
(23) Bertrand, B.; Boulanger, R.; Dussert, S.; Ribeyre, F.; Berthiot, L.; Descroix, F.; Joet, T. Climatic factors directly impact the volatile organic compound fingerprint in green Arabica coffee bean as well as coffee beverage quality. *Food Chem.* **2012**, *135*, 2575−2583.
(24) Coffee Research Symposium Tentative Progam. http://www.naeb.gov.rw/fileadmin/documents/AGENDA.pdf (accessed Sep 12, 2014).
(25) Global Knowledge Initiative: International Convening. http://www.globalknowledgeinitiative.org/news/eliminate-coffee-potato-taste-defect-east-africa.html (accessed Sep 12, 2014).
(26) Van den Dool, H.; Kratz, P. D. A generalization of the retention index system including linear temperature programmed gas−liquid partition chromatography. *J. Chromatogr.* **1963**, *11*, 463−471.
(27) Martos, P. A.; Saraullo, A.; Pawliszyn, J. Estimation of air/coating distribution coefficients for solid phase microextraction using retention indexes from linear temperature-programmed capillary gas chromatography: Application to the sampling and analysis of total petroleum hydrocarbons in air. *Anal. Chem.* **1997**, *69*, 402−408.
(28) Goodner, K. L. Practical retention index models of OV-101, DB-1, DB-5, and DB-Wax for flavor and fragrance compounds. *LWT—Food Sci. Technol.* **2008**, *41*, 951−958.
(29) Nielsen, N-P.V.; Carstensen, J. M.; Smedsgaard, J. Aligning of single and multiple wavelength chromatographic profiles for chemometric data analysis using correlation optimized warping. *J. Chromatogr. A* **1998**, *805*, 17−35.
(30) Pierce, K.; Hope, J. L.; Johnson, K. J.; Wright, B. W.; Synovec, R. E. Classification of gasoline data obtained by gas chromatography using a piecewise alignment algorithm combined with feature selection and principal component analysis. *J. Chromatogr. A* **2005**, *1096*, 101−110.
(31) Indahl, U. G.; Sahni, N. S.; Kirkus, B.; Naes, T. Multivariate strategies for classification based on NIR-spectra with application to mayonnaise. *Chemometr. Intell. Lab.* **1999**, *49*, 19−31.
(32) *PLS Toolbox*, V 7.5.2. Software for chemometric multivariate analysis. Eigenvector Research, Inc: Wenatchee, WA, 2014.
(33) *Matlab*, V R2013b. Software for numerical computation, visualization, and programming. Mathworks, Inc: Natick, MA, 2013.
(34) Brereton, R. G. Chapter 4: Pattern Recognition. In *Chemometrics: Data Analysis for the Laboratory and Chemical Plant*; Wiley: Chichester, England, 2003; pp 183−270.
(35) Tomasi, G.; van den Berg, F.; Andersson, C. Correlation optimized warping and dynamic time warping as preprocessing methods for chromatographic data. *J. Chemometr.* **2004**, *18*, 231−241.
(36) Skov, T.; van den Berg, F.; Tomasi, G.; Bro, R. Automated alignment of chromatographic data. *J. Chemometr.* **2006**, *20*, 484−497.
(37) Eilers, P.H.C.; Boelens, H. F. M. *Baseline correction with asymmetric least squares smoothing*. October 21, 2005, Amazon Web Services. http://zanran_storage.s3.amazonaws.com/www.science.uva.nl/ContentPages/443199618.pdf (accessed Jul 10, 2014).
(38) Whittaker, E. T. On a new method of graduation. *P. Edinburgh Math. Soc.* **1922**, *41*, 63−75.
(39) Kaiser, H. F. The varimax criterion for analytic rotation in factor analysis. *Psychometrika* **1958**, *23*, 187−200.
(40) Osawa, C. C.; Goncalves, L. A. G.; Da Silva, M. A. A. P. Odor significance of the volatiles formed during deep-frying with palm olein. *J. Am. Oil Chem. Soc.* **2013**, *90*, 183−189.
(41) James, D. G.; Price, T. S. Field-testing of methyl salicylate for recruitment and retention of beneficial insects in grapes and hops. *J. Chem. Ecol.* **2004**, *30*, 1613−28.
(42) Favaro, C. F.; Santos, T. B.; Zarbin, P. H. G. Defensive compounds and male-produced sex pheromone of the stink bug *Agroecus griseus*. *J. Chem. Ecol.* **2012**, *38*, 1124−1132.
(43) Krall, B. S.; Bartelt, R. J.; Lewis, C. J.; Whitman, D. W. Chemical defense in the stink bug *Cosmopepla bimaculata*. *J. Chem. Ecol.* **1999**, *25*, 2477−2494.
(44) Borges, M.; Jepson, P. C.; Howse, P. E. Long-range mate location and close-range courtship behavior of the green stink bug, *Nezara viridula*, and its mediation by sex pheromones. *Entomol. Exp. Appl.* **1987**, *44*, 205−212.

different cleavage sites that can be used as substrate. In addition, each cleavage site can be present in different peptides formed during hydrolysis. For this reason, the selectivity has recently been defined as the relative rate at which the enzyme cleaves each individual cleavage site compared to the total rate of hydrolysis of all cleavage sites in the protein.[9]

Furthermore, it has already been shown that there were large differences in terms of selectivity toward cleavage sites after the same type of amino acid for the hydrolysis by *Bacillus licheniformis* protease (BLP) of a 1% (w/v) WPI solution.[9] In the present study, the same specific enzyme (BLP) was used for the hydrolysis of 0.1−10% (w/v) whey protein isolate (WPI) at constant enzyme/substrate ratio. The molar concentration of most of the peptides (i.e., >90% of the total $UV_{214}$ signal) in the hydrolysates was determined at different points during the hydrolysis. From the kinetics of formation of the peptides, the influence of substrate concentration on the selectivity of the enzyme was determined.

## MATERIALS AND METHODS

**Materials.** Bipro, a commercial whey protein isolate (WPI), was obtained from Davisco Foods International Inc. (Le Sueur, MN, USA). It contained (by weight) 74.0% $\beta$-lactoglobulin, 12.5% $\alpha$-lactalbumin, 5.5% bovine serum albumin, and 5.5% immunoglobulin, according to specifications of the supplier. The protein content (N × 6.32)[4] of the powder was 93.4% (w/w) as determined by Dumas.[10] BLP, specific for Glu−X bonds and for Asp−X bonds,[11] was obtained from Novozymes (NS-37005) (Bagsvaerd, Denmark). BLP (4.5% protein, N × 6.25, 0.3 AU/mg/min as determined by the azocasein assay[12]) was partly insoluble and was fractionated as described before.[9] The freeze-dried material was found to contain 60% protein (N × 6.25) from which 78% is the enzyme BLP (23.6 kDa) and 14% is the pro-peptide (6.9 kDa) based on $UV_{214}$, as determined by RP-UPLC-MS.[9] An activity of 3.9 AU/mg/min was determined by the azocasein assay. All other chemicals were of analytical grade and purchased from Sigma or Merck.

**Hydrolysis.** Protein solutions were prepared by dispersing WPI powder at a concentration of 45% (w/v) in Milli-Q water (18.2 MΩ·cm), followed by stirring overnight at 4 °C. Insoluble parts were removed by centrifugation (30 min, 4000*g*, 20 °C), and the supernatant obtained (30% (w/v)) was diluted to the required final concentrations 0.1−10% (w/v) as determined by $UV_{280}$.[4] Hydrolyses were performed using a pH-stat at pH 8, which is described to be the optimum pH for the enzyme BLP.[13] Solutions of WPI at 0.1, 0.25, 0.5, 1, 5, and 10% (w/v) were hydrolyzed at 40 °C and pH 8 using NaOH at concentrations of 0.02, 0.05, 0.1, 0.2, 1, and 2 M, respectively, to keep the pH constant. Protein solutions (10 mL) were equilibrated for at least 15 min at 40 °C and adjusted to pH 8.0 before addition of BLP dissolved at 5% (w/v) in Milli-Q water (0.30 $\mu$L of enzyme/mg of protein). The DH was calculated on the basis of the added volume of NaOH with $\alpha$, the average degree of dissociation of the $\alpha$-NH groups ($1/\alpha$ = 1.20 at 40 °C and pH 8.0) and $h_{total}$, the total number of peptide bonds per gram protein substrate ($h_{total}$(WPI) = 8.5) as described before.[4,14]

The overall rate of hydrolysis $k_{hydr}$ was calculated using eq 1

$$\mathrm{DH} = \frac{1}{a}\ln(1 + k_{hydr}t) \quad (1)$$

in which $k_{hydr}$ and $a$ are fitting parameters for the overall hydrolysis rate ($s^{-1}$) and an inactivation parameter, respectively, and $t$ is the time in seconds.[15] The overall relative rate of hydrolysis was determined using the highest value of overall hydrolysis rate as 100%. The overall hydrolysis rates of BLP were compared with previous results obtained with Alcalase.[4]

Samples were taken during the hydrolysis of 0.1, 0.5, 1, 5, and 10% (w/v) protein solutions at different degrees of hydrolysis (1.5, 3, 4.5, 6, and 7%). These samples were then centrifuged (5 min, 19000*g*, 15 °C). Supernatant and pellet were separated, and the supernatants were inactivated by adjusting the pH to 2 with 5 M HCl. The pH was set back to 8.0 after at least 10 min of inactivation before storage of the samples at −20 °C. Centrifugation was performed before the pH adjustment to 2, to avoid losses of material resulting from the pH adjustment. It has indeed been noted that there was formation of insoluble aggregates at pH 2. These aggregates were resolubilized at pH 8.

Separate experiments were performed to confirm that no inactivation of enzyme took place during hydrolysis and that the inactivation at low pH was irreversible.

To confirm that the enzyme does not autohydrolyze under these conditions, 30 $\mu$L of BLP dissolved to a concentration of 5% (w/v) was added to 9 mL of Milli-Q water and incubated at 40 °C and pH 8 for 1 h. After this incubation, a concentrated solution of WPI (10% (w/v)) was added to the enzyme at a final concentration of 1% (w/v) WPI. The hydrolysis was followed with the pH-stat for 1 h. The same experiment was performed with fresh enzyme, and it was concluded that no significant enzyme inactivation occurs.

As previously described for Alcalase,[4] the inactivation was verified by hydrolyzing a sample of 1% WPI for 10 min using the pH-stat. The pH was brought to pH 2 to inactivate the enzyme and readjusted to pH 8 after 10 min. After readjustment of the pH to 8, the pH remained constant (for 1 h), indicating that the enzyme had indeed lost its activity.

Samples obtained during the hydrolysis of 0.1 and 0.5% (w/v) WPI were freeze-dried after the pH was readjusted to pH 8.0 and redissolved to a concentration of 1% (w/v) to have the same concentration for all samples for analysis on RP-UPLC-ESI-MS.

**Solubility.** The protein and peptide contents in the supernatants of the samples taken at different DH values were determined using Dumas (N × 6.32)[4] using a Flash EA 1112 NC Analyzer (Thermo Fisher Scientific, Waltham, MA, USA). The proportion of soluble protein was calculated by dividing the concentration of protein of the supernatants by the concentration of protein in the solution before centrifugation (5 min, 19000*g*, 15 °C) at DH = 0.

**Reverse Phase Ultrahigh-Performance Liquid Chromatography (RP-UHPLC).** Samples obtained during hydrolysis were analyzed on an Acquity UPLC System (Waters, Milford, MA, USA) using an Acquity UPLC BEH 300 C18 column (2.1 × 150 mm, 1.7 $\mu$m particle size) with an Acquity BEH C18 Vanguard precolumn (2.1 × 50 mm, 1.7 $\mu$m particle size). Eluent A was 1% (v/v) acetonitrile (ACN) containing 0.1% (v/v) trifluoroacetic acid (TFA) in Milli-Q water, and eluent B was 100% ACN containing 0.1% (v/v) TFA. To reduce disulfide bridges and to facilitate peptide annotation, samples were first incubated for 2 h with 100 mM dithiothreitol (DTT) in 50 mM Tris·HCl, pH 8.0, at a concentration of 0.5% (w/v). After incubation, samples were further diluted in eluent A to a final concentration of 0.1% (w/v) and centrifuged (10 min, 19000*g*, 20 °C). Samples (4 $\mu$L) were injected into the column thermostated at 40 °C.[9]

The amount of remaining intact proteins ($\beta$-lactoglobulins A and B and $\alpha$-lactalbumin) was determined using the following elution profile: 0−2 min, isocratic on 30% B; 2−12 min, linear gradient from 30 to 50% B; 12−15 min, linear gradient from 50 to 100% B; 15−20 min, isocratic on 100% B; 20−21 min, from 100 to 30% B; and 21−30 min, isocratic on 30% B. The flow rate was 350 $\mu$L $min^{-1}$. The proportion of remaining intact $\alpha$-lactalbumin and $\beta$-lactoglobulin was determined by dividing the area of the $UV_{214}$ peak obtained for each protein at different DH values by the peak area obtained for each intact protein before hydrolysis. The proportion of $\beta$-lactoglobulin takes into account the proportions of both A and B variants.

For separation of the peptides a different elution profile was used: 0−2 min, isocratic on 3% B; 2−10 min, linear gradient from 3 to 22% B; 10−16 min, linear gradient from 22 to 30% B; 16−19 min, linear gradient from 30 to 100% B; 19−24 min, isocratic on 100% B; 24−26 min, linear gradient from 100 to 3% B; and 26−30 min, isocratic on 3% B. The flow rate was 350 $\mu$L $min^{-1}$. Detection was performed using a PDA, which scanned the absorbance from 200 to 400 nm at a 1.2 nm resolution with 20 points per second.

**Electron Spray Ionization Time-of-Flight Mass Spectrometry (ESI-Q-TOF-MS).** The mass spectra of the hydrolysates were determined with an online Synapt high-definition mass spectrometer (Waters), coupled to the RP-UPLC system, equipped with a z-spray electrospray ionization (ESI) source, a hybrid quadrupole, and an orthogonal time-of-flight (Q-TOF). The system was calibrated using the peptide Glu-1-Fibrinopeptide B ($m/z$ 1570.6 in positive mode). The capillary voltage was set to 3 kV with the source operation in positive ion mode and the source temperature at 120 °C. The sample cone was operated at 35 V. Nitrogen was used as desolvation gas (250 °C, 800 L/h) and cone gas (200 L/h). The trap gas was set at 1.5 mL/min. MS and MS/MS (MSe method) were performed between $m/z$ 100 and 2000 with a scan time of 0.3 s. The trap collision energy was set at 6 V in single MS mode and ramped from 20 to 30 V in MSe mode. The transfer collision energy was set at 4 V in MS and switched between 4 and 10 V in the MSe mode. UV and MS data were acquired using MassLynx v4.1 (Waters).

**Peptide Identification and Quantification.** For peptide identification, internal lock mass was applied on every chromatogram for MS and MS/MS data with two previously identified masses chosen among the most abundant masses, of which the sequences were identified manually. The identification of MS and MSe ion peaks was done by Biopharmalynx software (v 1.3) with the parameters described before.[9] The annotation was first done using a method to identify peptides cleaved after Glu and Asp residues. Next, a generic method was used in which no enzyme specificity was selected. For UV peaks where the automatic annotation did not yield a peptide sequence, a manual analysis of the MS and MS/MS data was used to assign the peptide sequence. For the total peptide quantification, peaks in the $UV_{214}$ chromatogram were included until 90−95% of the total $UV_{214}$ area was included. Peptides from $\beta$-lactoglobulin and $\alpha$-lactalbumin as well as the intact protein were quantified using the $UV_{214}$. In the case of coeluting peptides, the UV peak area was divided over the coeluting peptides based on the MS intensity (based on the assumption that coeluting peptides have comparable overall properties, i.e., charge, size, and hydrophobicity). For the further determination of the selectivity, only peptides from $\beta$-lactoglobulin were considered.

The quantification of the peptides was based on the UV signal at 214 nm, using eq 2

$$C_{\text{peptide}} = 1 \times 10^6 \left( \frac{A_{214}}{\varepsilon_{214} l V_{\text{inj}} k_{\text{cell}}} \right) Q \tag{2}$$

in which $C_{\text{peptide}}$ ($\mu$M) is the concentration of peptide, $A_{214}$ (AU·min) is the UV peak area at 214 nm, $V_{\text{inj}}$ ($\mu$L) is the volume of sample injected, $Q$ is the flow rate in $\mu$L min$^{-1}$, and $l$ is the path length of the UV cell, which is 1 cm according to the manufacturer. The value for the cell constant $k_{\text{cell}}$ was previously determined to be 0.66 using pure peptides, but depends on the geometry of the UV detector used.[16] The molar extinction coefficient at 214 nm of each peptide ($\varepsilon_{214}$) was calculated as described before.[17] Peak areas were annotated up to 150,000 $\mu$AU·min, and the linearity range of detection has been established for peak areas up to 350,000 $\mu$AU·min.

**Quality of the Annotation and Quantification.** For each hydrolysate, the quality of the peptide identification and of the quantification was described by three different parameters. First, the amino sequence coverage was determined by calculating the number (#) of unique annotated amino acids divided by the total number (#) of amino acids present in the parental protein sequence.[18]

$$\text{amino acid sequence coverage} = \frac{\text{\# of unique annotated amino acids}}{\text{\# of amino acids in protein sequence}} \times 100 \tag{3}$$

The amino acid sequence coverage was 100% for most samples. Only for samples DH 6 and 7% at 5 and 10% (w/v) WPI was an amino acid sequence coverage of 95% obtained. To take into account the fact that each part of the sequence was covered by several peptides, the peptide sequence coverage was determined as a second quality parameter on the peptide annotation.[9] It is defined as the number of amino acids (# AA) in annotated peptides divided by the total number of amino acids (# AA) present in all peptides (annotated peptides and missing peptides) as in eq 4:

$$\text{peptide sequence coverage} = \frac{\text{\# AA (annotated peptides)}}{\text{\# AA (annotated peptides)} + \text{\# AA (missing peptides)}} \times 100 \tag{4}$$

The peptide sequence coverage was found to be on average 95 ± 3% for all hydrolysates. No distinction between variants can be made for the calculation of the peptide sequence coverage. It was indeed not possible to assign the peptides to a variant, except for the peptides containing the mutant amino acids (positions 64 and 118).

To determine the completeness of the quantification, the molar sequence coverage was calculated. For that, the concentration of each amino acid $C_n$ ($\mu$M) was calculated using the molar concentration of each individual (annotated) peptide $C_{\text{peptide}}$ ($\mu$M). With this, each individual amino acid of the primary sequence of $\beta$-lactoglobulin has been quantified in the hydrolysate. The molar sequence coverage was calculated using eq 5

$$\text{molar sequence coverage} = \left( 1 - \frac{\sqrt{\frac{\sum (C_n - C_0)^2}{(\text{\# AA} - 1)}}}{C_0} \right) \times 100 \tag{5}$$

where $C_n$ is the concentration ($\mu$M) of each amino acid $n$ in the protein and $C_0$ is the initial concentration of the protein ($\mu$M). # AA is the number of amino acid residues in the sequence.

**Determination of Enzyme Selectivity.** To describe the selectivity of the enzyme, the rate at which individual peptide bonds are hydrolyzed (e.g., between Glu-45 and Leu-46) was determined. To do this, first, the concentrations of all peptides originating from hydrolysis of the same peptide bond ($C_{i,t}$) in the parent molecule were calculated using eq 6:

$$C_{i,t} = \sum \{ C_{\text{peptide}}[x - y]_t | i = x - 1 \cup i = y \} \tag{6}$$

In other words, the concentration of cleavage products formed at each time point $t$, after hydrolyzing peptide bond $i$, equals the sum of all peptides of the sequence $[x{-}y]$, for which $i = (x - 1)$ (i.e., starts on position P1′) or $i = y$ (i.e., ends on position P1). This means that the number of cleaved bonds is equal to the concentration of cleavage site products $C_{i,t}$ divided by 2. This also means the peptides that are formed from hydrolysis after the amino acid $i$ or which end by the amino acid $i$.

For each cleavage site the apparent cleavage rate ($k_{i,\text{app}}$ in s$^{-1}$) was then calculated by fitting eq 7 to the experimental data

$$C_{i,t} = 2(C_0 - C_0 \, e^{-k_{i,\text{app}} t}) \tag{7}$$

in which $C_{i,t}$ ($\mu$M) is the concentration of cleavage products determined for each time point $t$ and $C_0$ is the initial concentration of protein ($\mu$M).

Because one peptide can be formed through different pathways during the hydrolysis, there is no definite mechanistic equation (at the current moment) that can be used to fit the curves of the concentration of cleavage site products as a function of time. For most of the curves (e.g., 85 of 95) the first-order fit was satisfactory (e.g., $R^2 > 0.8$). However, the fit was not as good for cleavage sites hydrolyzed at a later stage of the hydrolysis. Still, using a different fit would only introduce more fitting parameters and inaccuracies. Hence, the first-order kinetics fit was the most efficient.

The rate of selective hydrolysis $k_i$ (s$^{-1}$ mg$^{-1}_{\text{enzyme}}$) was defined as

$$k_i = \frac{k_{i,\text{app}}}{m_{\text{E}}} \tag{8}$$

in which $m_{\text{E}}$ is the mass of enzyme added for the hydrolysis (in mg). Subsequently, the selectivity$_{\beta\text{-lg}}$ (%) was calculated by dividing the rate of selective hydrolysis ($k_i$) of each individual cleavage site by the sum

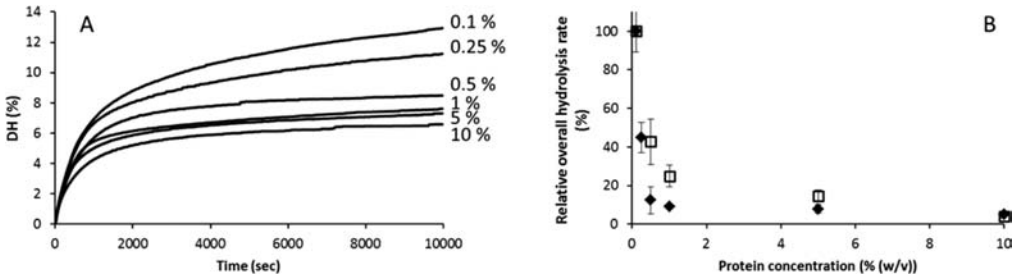


**Figure 1.** (A) DH curves of 0.1−10% (w/v) WPI hydrolyzed by BLP at constant E/S and (B) relative overall hydrolysis rate $k_{hydr}$ for hydrolysis of WPI by BLP (◆) and by Alcalase (□) as a function of the initial WPI concentration at constant E/S.

of the rate of selective hydrolysis of all cleavage sites at each protein concentration as in eq 9:

$$\text{selectivity}_{\beta\text{-lg}}\,(\%) = \frac{k_i}{\sum k_j} \times 100 \tag{9}$$

It should be noted that in this definition of selectivity, the final value depends on the total number of cleavage sites. As such, it may be difficult to compare this value with values determined for different substrates. The benefit of the current definition is that the total selectivity (in one experiment) adds up to 100%. Therefore, the value represents which fraction of the enzyme total activity corresponds to the cleavage of a particular site. In addition, all cleavage sites, even those with low selectivity, were hydrolyzed, which indicates that the enzyme tries all possible locations. Therefore, we assumed that the number of times the enzyme attacks a certain cleavage site (per unit time) does not depend on the rate of cleavage of other cleavage sites. It should only be considered that the attack of the enzyme on a cleavage site does not directly lead to hydrolysis or that for some cleavage sites the hydrolysis takes more time. Consequently, the rate of cleavage of site $i$ does not depend on the rate of cleavage of all sites $j$ ($j \neq (i)$.

**Reproducibility of the Analysis.** The relative overall hydrolysis was calculated from three repeated hydrolysis experiments, and the standard deviation was calculated for each condition.

To test the reproducibility of the UPLC-$UV_{214}$ quantification method, one sample (1% WPI, DH 4.5%) was injected three times. The concentration determined for individual peptides showed a typical standard error of 6%. In addition, the reproducibility of the complete analysis was tested. For this, two separate hydrolysis experiments were performed at the same protein concentration (0.5% (w/v) WPI). During each hydrolysis, samples were taken at DH 1.5, 3, and 6%. Peptides were annotated (i.e., assigned to a sequence) and quantified for all hydrolysates. The error of peptide sequence coverage and molar sequence coverage was calculated for the hydrolysate at each DH. The values of standard errors (standard deviation/mean × 100) were averaged to determine the analysis error. The quality of the annotation as described by the peptide sequence coverage showed a standard error of 2.5%. The molar sequence coverage showed a standard error of 18%. Finally, the determined selectivity showed a typical standard error of 15%.

## RESULTS AND DISCUSSION

**Protein Hydrolysis at Different Substrate Concentrations.** The DH of WPI hydrolyzed by BLP at constant enzyme/substrate ratio reached after 10000 s decreases with increasing initial protein concentration from DH = 14% for 0.1% (w/v) WPI to DH = 6% for 10% (w/v) WPI (Figure 1A). The effect of concentration observed here for WPI hydrolyzed by BLP was compared to previous results obtained for hydrolysis of WPI by Alcalase, an enzyme mixture that mostly contains the a-specific enzyme subtilisin.[4] In both cases the rate of hydrolysis as seen, for instance, in the initial slope of the DH versus time curve and quantified by the overall hydrolysis rate $k_{hydr}$, decreased with increasing substrate concentration (Figure 1B).

The solubility of all the hydrolysates was determined to be 96 ± 5%. This result shows that the effect of the initial substrate concentration on the overall hydrolysis rate is not due to the formation of insoluble aggregates. It also indicates that the peptides identified represent the complete sample. On this basis, the pellet was not analyzed for peptides. The hydrolysates obtained at different concentrations can thus be compared for detailed analysis of the hydrolysates and peptides formed as a function of initial protein concentration. It has also been shown that even at high protein concentrations, such as 30% (w/v) WPI, no aggregation or oligomerization was measured by size exclusion chromatography.[4] In addition, it was previously shown that the increase in protein concentration does not result in a significant increase in viscosity (2.0 mPa·s at 10% (w/v) WPI and 27 mPa·s at 30% (w/v) WPI).[4] Moreover, as described in a previous study,[14] the substrate concentrations used here (0.1−10% (w/v) WPI equivalent to 36 μM−3.6 mM) are above the reported threshold for substrate inhibition (<350 μM). Above the reported threshold, the substrate inhibition curve tends to reach a plateau. In that study,[14] it was concluded that substrate inhibition could not explain the decrease in hydrolysis rate with increasing substrate concentration.

The hydrolysis was also characterized by the decrease of intact proteins as a function of the DH. Changes in this curve indicate changes in the preference for the hydrolysis of intact protein versus the hydrolysis of intermediate peptides formed. These curves are found to be similar for all initial protein concentrations (0.1−10% (w/v) WPI), with no remaining intact β-lactoglobulin above DH 4.5% (Figure 2). In other words, the accessibility toward the intact protein relative to the accessibility toward the peptides was not affected by the initial

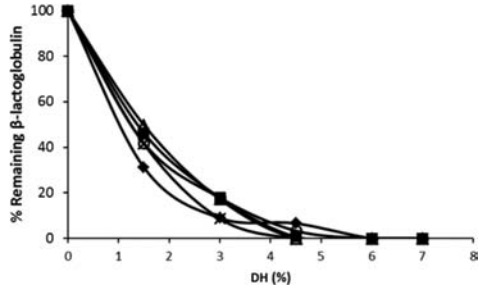


**Figure 2.** Remaining intact β-lactoglobulin as a function of DH for different initial substrate concentrations of (◆) 0.1%, (■) 0.5%, (△) 1%, (×) 5%, and (○) 10% (w/v) WPI (0.1% WPI corresponds to a concentration of 37 μM β-lactoglobulin).

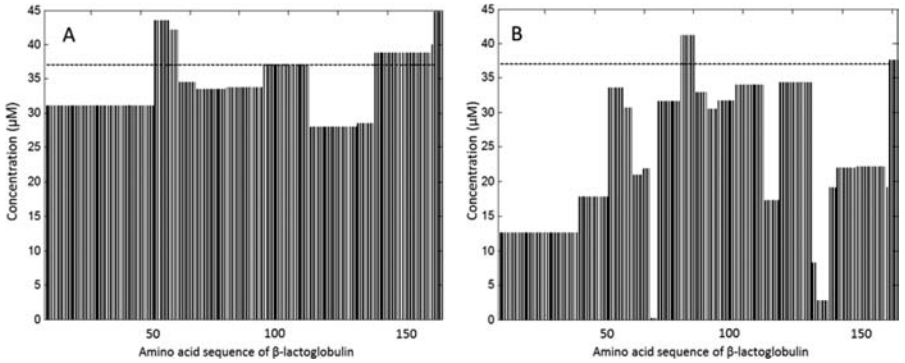


**Figure 3.** Concentration of all amino acids ($C_n$) for (A) 1% (w/v) WPI at DH 1.5% and (B) 5% (w/v) WPI at DH 6%. The dotted line (···) indicates the initial protein concentration. Hydrolysates were diluted to 0.1% (w/v) prior to analysis.

**Table 1. A-specific Peptides Annotated during Enzymatic Protein Hydrolysis of 0.1−10% (w/v) WPI by BLP and the Parental Peptides**

| parental peptide | sequence | a-specific peptides annotated |
|---|---|---|
| [56−62] | ILLQ−KWE | [56−59]−[60−62] |
| [75−89] | KTKIP −VFKIDALNE | [75−80]−[81−89] |
| [135−157] | KFDKALK−ALPMHIRLSFNPTQLE | [135−141]−[142−157] |
| [135−158] | KFDKALK−ALPMHIRLSFNPTQLEE | [135−141]−[142−158] |
| [138−157] | KALKALPM−HIRLS−FNPTQLE | [138−145]−[146−157] and [146−150]−[151−157] |
| [138−158] | KALKALPM−HIRLS−FNPTQLEE | [138−145]−[146−158] and [146−150]−[151−158] |

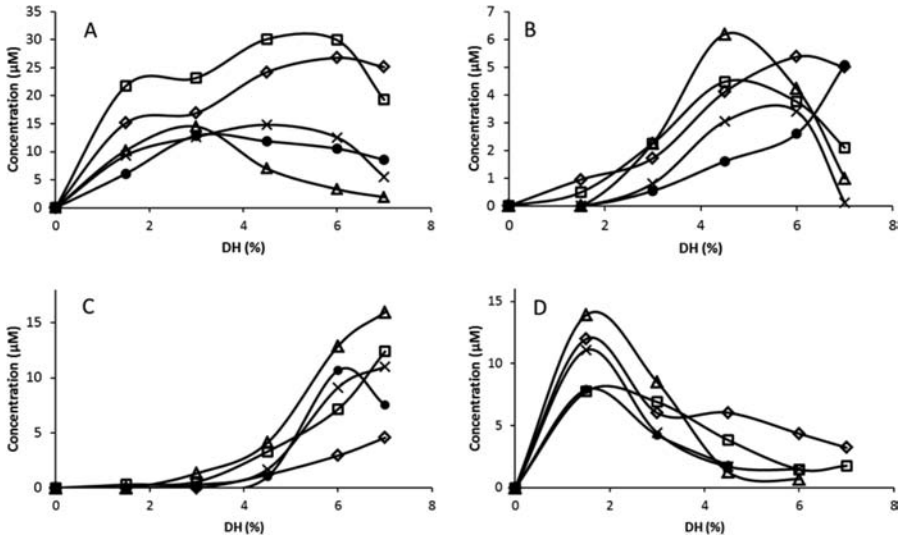


**Figure 4.** Concentration ($\mu$M) of different peptides as a function of DH for different initial protein concentrations (◇) 0.1%, (□) 0.5%, (△) 1%, (×) 5%, and (●) 10% (w/v) WPI. All hydrolysates were diluted to 0.1% (w/v) prior to analysis.

substrate concentration. The onset temperature of denaturation of $\beta$-lactoglobulin, as determined by DSC, is 60 °C, and the midpoint of unfolding is at 77 °C.[19] In addition, no intact $\beta$-lactoglobulin was present at DH 4.5%, which corresponds to a maximum incubation time of 30 min (at the highest protein concentration). On this basis, it was assumed that there is no significant effect of denaturation of the intact $\beta$-lactoglobulin on the observed behavior.

Both the solubility of the hydrolysates and the difference in accessibility of the intact protein relative to that of peptides are independent of the initial protein concentration, whereas the overall hydrolysis rate is affected by the initial protein concentration at constant enzyme/substrate ratio. To determine if the mechanism of hydrolysis depends on the initial substrate concentration, the peptides formed during the hydrolysis were identified.

**Identification and Quantification of the Peptides.** For all samples at different DH and different initial substrate concentrations, a total of 77 peptides were identified and quantified. The quality of the quantification was determined by calculating the molar sequence coverage. The molar sequence coverage provides an indication of the concentration of each amino acid of the parental protein sequence found in the peptides identified compared to the initial protein concentration (eq 5). The molar sequence coverage was 70 ± 10%, indicating a quite complete annotation and quantification. Still, for some amino acids, a concentration higher than expected is obtained and for others a concentration lower than expected is

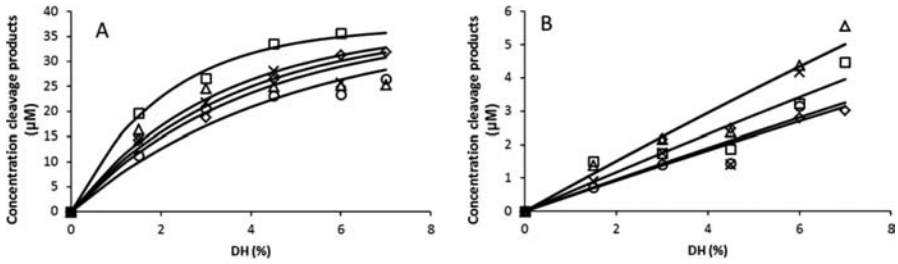


**Figure 5.** Concentration of cleavage products as a function of DH for (A) cleavage site 45 and (B) cleavage site 157 for different initial protein concentrations of (◇) 0.1%, (□) 0.5%, (△) 1%, (×) 5%, and (○) 10% (w/v) WPI. Symbols indicate experimental data, and solid lines show the fits from eq 7.

determined (Figure 3). At increasing DH, in some parts of the sequence not all amino acids were present at the expected concentration. Some amino acids were not annotated at all (Figure 3B). This finding is most likely due to the formation of free amino acids or short peptides, which are not annotated in RP-UPLC. In total, 5 free amino acids can theoretically be obtained during hydrolysis of $\beta$-lactoglobulin by BLP (45-E, 65-E, 130-D, 131-E, 158-E). Over all hydrolysates, 13 of the 77 peptides annotated are so-called a-specific peptides. These peptides were the result of cleavage of previously formed (specific) peptides. For instance, the formation of $\beta$-lg[56−59] and $\beta$-lg[60−62] results from the cleavage of the specific peptide $\beta$-lg[56−62] (Table 1). The formation of a-specific peptides was actually increased with increasing substrate concentration and DH, whereas the overall hydrolysis rate decreased (data not shown). It was assumed that certain peptides formed as a result of the enzyme action are not stable in solution. These peptides autohydrolyze to form the a-specific peptides mentioned (Table 1). Similar instability of peptides has been described for several isolated cases such as the vasoactive intestinal peptide[20] or for RNA splicing.[21]

The formation and further breakdown of all peptides were monitored as a function of the DH for the different initial protein concentrations. Different types of peptide release kinetics were observed as a function of the initial protein concentration (Figure 4). For some peptides no clear effect (i.e., larger than the experimental error) of substrate concentration on their formation and subsequent hydrolysis was observed, for example, peptide $\beta$-lg[135−162] (Figure 4D). For this peptide, at each DH, there was no clear trend of the peptide concentration as a function of initial substrate concentration. Others, such as peptide $\beta$-lg[1−45], showed two types of kinetics for low (0.1−0.5% (w/v) WPI) and for high initial substrate concentrations (1−10% (w/v) WPI) (Figure 4A). For peptides such as $\beta$-lg[1−45], a higher peptide concentration (25−30 $\mu$M) was reached at low substrate concentrations (<1% WPI) than at high substrate concentrations (12 $\mu$M). This fact indicated a faster rate of formation than degradation at low substrate concentrations and a comparable rate of formation and degradation at high substrate concentrations. In other words, the maximum concentration of peptide reached during hydrolysis was lower at high initial substrate concentrations (Figure 4A). Peptide $\beta$-lg(A)[90−127] is an intermediate peptide formed from at least two cleavages on the intact protein (Figure 4B). For this peptide different formation and further hydrolysis behavior were observed for the different initial concentrations. For the final peptide $\beta$-lg(A)[115−127], no large effect of initial substrate concentration on its formation was observed up to DH 4.5% (Figure 4C), and large effects were observed at DH 7% with concentration varying from 4 to 15 $\mu$M.

**Influence of Substrate Concentration on Selectivity.** *Kinetics of Hydrolysis.* On the basis of the peptide identification and quantification, the concentration of cleavage products $C_{i,t}$ was determined (eq 6). The concentration of cleavage products, for example, for residues 45 and 157, as a function of DH can be compared for the different initial substrate concentrations (Figure 5). The concentration of cleavage products was comparable for all initial substrate concentrations. The concentration was higher for cleavage site 45 than for cleavage site 157. The apparent cleavage rate $k_{i,\mathrm{app}}$ (Supporting Information) and rate of selective hydrolysis $k_i$ of each cleavage site were determined on the basis of the concentration of cleavage products as a function of time (eqs 7 and 8). Large differences in the rate of selective hydrolysis were observed for all cleavage sites for all protein concentrations with rates varying from $2.5 \times 10^{-2}$ to $1.0 \times 10^{-7}$ $s^{-1}$ $mg^{-1}{}_{enzyme}$ and even 0 for some of the cleavage sites (Figure 6).

On the basis of the rate of selective hydrolysis of 1% (w/v) WPI, the cleavage sites were divided into five groups. The first group consists of four Glu residues with a rate of selective hydrolysis of $6.5 \times 10^{-3}$ $s^{-1}$ $mg^{-1}{}_{enzyme}$. The second group consists of five Glu residues with a rate of selective hydrolysis of $2.4 \times 10^{-3}$ $s^{-1}$ $mg^{-1}{}_{enzyme}$ (Figure 6A). The third group consists of four Glu residues for which the rate of selective hydrolysis is 10 times lower than that for the first two groups, $4.3 \times 10^{-4}$ $s^{-1}$ $mg^{-1}{}_{enzyme}$ (Figure 6B). Two Glu residues have a rate comparable to that of the Asp residues ($9.5 \times 10^{-6}$ $s^{-1}$ $mg^{-1}{}_{enzyme}$), forming a fourth group (Figure 6C). Finally, one Glu residue (44) and four Asp residues (53, (A)-64, 98, and 130) are not hydrolyzed at all, constituting the fifth group.

Whereas the overall division of the cleavage sites into five groups was comparable for all initial substrate concentrations, for a few of these cleavage sites a clear effect of initial substrate concentration was observed. For the nine Glu residues for which the enzyme had a high or intermediate rate of selective hydrolysis, a decrease in the rate of selective hydrolysis was observed with increasing substrate concentration (from $1.3 \times 10^{-3}$ $s^{-1}$ $mg^{-1}{}_{enzyme}$ for 0.1% (w/v) WPI to $2.3 \times 10^{-4}$ $s^{-1}$ $mg^{-1}{}_{enzyme}$ for 10% (w/v) WPI (Figure 6A). This was expected because the overall hydrolysis rate determined from the DH versus time curves was decreased (Figure 1B).

*Nonannotated Cleavage Sites.* For 5 of 27 potential cleavage sites, no rate of hydrolysis was determined, because no peptides were annotated starting or ending at these cleavage sites. There are two reasons for this. First, cleavage sites 53-D and 130-D are surrounded by other cleavage sites (51-E and 55-E and 129-D and 131-E, respectively), for which cleavages were observed. The cleavages occurring on 53-D and 130-D

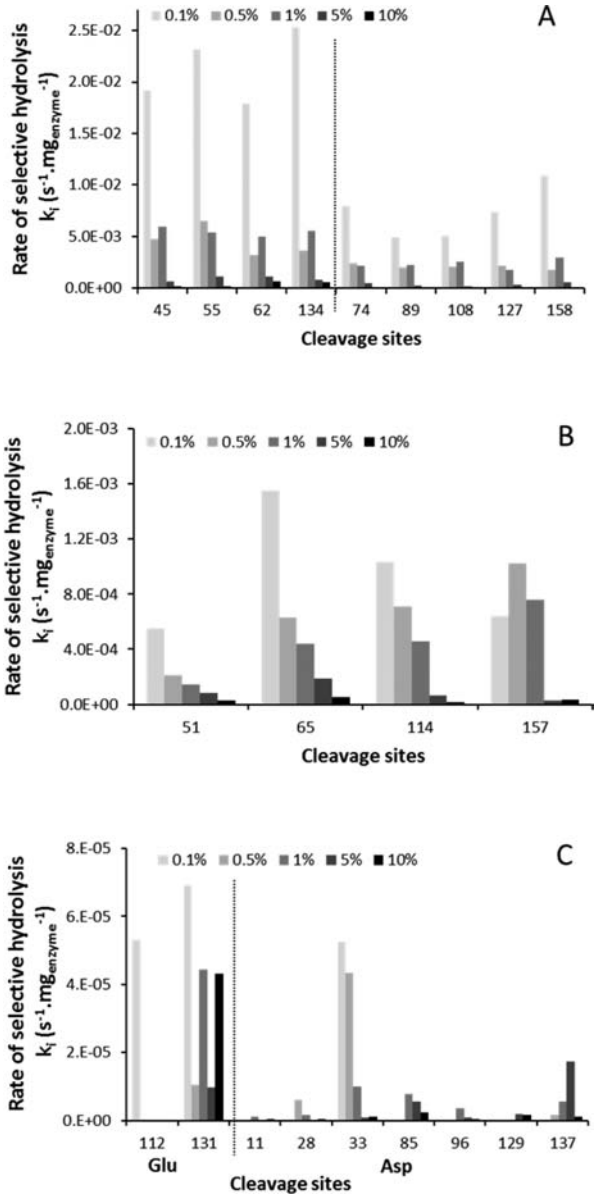


**Figure 6.** Rate of selective hydrolysis $k_i$ of the enzyme toward glutamic acid and aspartic acid residues divided in three groups with (A) Glu with high and intermediate rates of selective hydrolysis, (B) Glu with low rate of selective hydrolysis, and (C) Glu with very low rate of selective hydrolysis and Asp for the different initial protein concentrations (0.1−10% (w/v) WPI).

might lead to the formation of single amino acids or dipeptides. The short peptides and free amino acids are generally not detected during LC-MS analysis. The difficulty of annotating short peptides and free amino acids in RP-HPLC has been mentioned before.[22] This could be solved by analyzing the free amino acids, using a different gradient or a different type of column than reversed phase. Second, for cleavage sites 44-E and 64-E, a glutamic acid on the P1′ position is found: 45-E and 65-E. It has been previously suggested that the presence of a negative charge on position P1′ hinders the hydrolysis by BLP.[11]

*Determination of the Selectivity.* The selectivity was determined for all cleavage sites identified for all protein concentrations (0.1−10% (w/v) WPI). The selectivity is determined as the rate of selective hydrolysis of each cleavage site divided by the rate of selective hydrolysis of all cleavage sites for each substrate concentration (eq 9; Table 2). The selectivity showed a typical standard error (standard deviation/mean × 100) of 15%. Large differences are observed over all cleavage sites for each initial substrate concentration from 17 to 0.001%. The cleavage sites are divided into five groups, based on the groups defined for the rate of selective hydrolysis (Figure 6). The enzyme selectivity toward the first four Glu residues is on average ∼16%. The selectivity toward the second group (five Glu) is ∼6%, and toward the third group (four Glu) the average selectivity is ∼1.4%. The fourth group contains two Glu and seven Asp, for which the enzyme has a selectivity of ∼0.027%. The fifth group contains the cleavage sites for which no hydrolysis was observed (Table 2). Enzyme selectivity has never been studied in this way. There are no studies describing the kinetics of formation of all peptides present in the hydrolysates. Peptide annotation and quantification have been done at a single DH point, for example, for $\beta$-lactoglobulin hydrolyzed by BLP.[16] In that study, cleavage sites 44, 53, and 98 were, for example, observed not to be cleaved by BLP. This corresponds to the same cleavage sites as in the current study. The observation that not all cleavage sites are used was made for $\beta$-casein hydrolyzed by the same enzyme, for which the peptides were annotated at different time points. In that study, 5 (of 19) Glu residues were found not to be hydrolyzed by the enzyme.[23]

*Influence of Substrate Concentration.* The large differences in selectivity toward all cleavage sites are quite similar for all substrate concentrations. Still, two main effects of protein concentration are observed on the selectivity, first in the group with the highest selectivity and second on the group with aspartic acid residues. First, in the group of cleavage sites for which the enzyme has the highest selectivity, the selectivity toward cleavage sites 62 and 134 is 2 times higher at 10% (w/v) WPI than at the other protein concentrations (Figure 7). The selectivity toward cleavage sites 45 and 55, on the other hand, is 2 times lower at 10% (w/v) WPI than at the other concentrations (Figure 7). As shown in Figure 3, especially in the N-terminal part of the sequence, there are amino acids that were not annotated/quantified to the expected concentration. Over the total UV area, at higher DH values only 50−70% of the total (at DH = 0) UV signal is recovered. However, this effect is similar for all concentrations. Therefore, it was concluded that a change in selectivity as a function of original substrate concentration can still be identified as a significant effect. It may be expected that at higher concentrations differences occur as a result of peptide aggregation, or shuffling of disulfide bridges. Aggregation was shown to increase with DH,[24] and disulfide shuffling was shown to occur during hydrolysis at pH 8.[25] However, the difference in selectivity between 45/55 and 62/134 is already apparent from an early point in the hydrolysis and thus cannot be attributed to differences in these effects.

Reasons for the changes in selectivity for these four cleavage sites can be sought in the primary, secondary, tertiary, and quaternary structures of the protein. Different amino acids were found on the neighboring positions of the four cleavage sites for which the largest effects of the substrate concentration were observed (45, 55, 62, and 134). Therefore, it was concluded that there is no clear indication that neighboring amino acids had a specific influence on the enzyme selectivity. In addition, all four cleavage sites are present at the solvent-exposed surface of the protein (Figure 8). Therefore, the cleavage sites would

**Table 2. Selectivity$_{\beta\text{-lg}}$ (Percent) of the Enzyme toward All Cleavage Sites for the Different Initial Protein Concentrations (0.1−10% (w/v) WPI)[a]**

| | | cleavage site | 0.10% | 0.50% | 1% | 5% | 10% |
|---|---|---|---|---|---|---|---|
| Glu with high selectivity | | 45 | 15 | 15 | 17 | 11 | 7 |
| | | 55 | 18 | 21 | 15 | 18 | 9 |
| | | 62 | 14 | 10 | 14 | 19 | 30 |
| | | 134 | 20 | 12 | 16 | 13 | 26 |
| Glu with intermediate selectivity | | 74 | 6 | 8 | 6 | 9 | 5 |
| | | 89 | 4 | 6 | 6 | 5 | 5 |
| | | 108 | 4 | 7 | 7 | 3 | 1 |
| | | 127 | 6 | 7 | 5 | 5 | 3 |
| | | 158 | 9 | 6 | 8[b] | 9 | 5 |
| Glu with low selectivity | | 51 | 0.44 | 0.68 | 0.4 | 1.4 | 1.1 |
| | | 65 | 1.2 | 2 | 1.2 | 3.1 | 2.3 |
| | | 114 | 0.82 | 2.3 | 1.3[b] | 1.1 | 0.7 |
| | | 157 | 0.51[b] | 3.3 | 2.1[b] | 0.5 | 1.6 |
| cleavages sites with very low selectivity | Glu | 112 | 0.042[b] | nd[c] | nd | nd | nd |
| | | 131 | 0.055[b] | 0.0083 | 0.035 | 0.0077 | 0.034 |
| | Asp | 11 | nd | nd | 0.0031[b] | 0.0036 | 0.018 |
| | | 28 | nd | 0.019 | 0.0044 | 0.0017 | 0.019 |
| | | 33 | 0.042[b] | 0.14[b] | 0.028 | 0.016 | 0.048 |
| | | 85 | nd | nd | 0.022 | 0.09 | 0.1 |
| | | 96 | nd | nd | 0.0099 | 0.013 | 0.015 |
| | | 129 | nd | nd | nd | 0.032 | 0.071 |
| | | 137 | nd | 0.0054[b] | 0.016 | 0.29 | 0.047 |
| nonhydrolyzed residues | Glu | 44 | nd | nd | nd | nd | nd |
| | Asp | 53 | nd | nd | nd | nd | nd |
| | | $\beta$-lg(A)-64 | nd | nd | nd | nd | nd |
| | | 98 | nd | nd | nd | nd | nd |
| | | 130 | nd | nd | nd | nd | nd |
| sum apparent cleavage rate | | | 0.125 | 0.031 | 0.036 | 0.0061 | 0.0023 |

[a]Typical standard errors (standard deviation/mean × 100) < 15%. The sum of selectivities of all cleavage sites at each substrate concentration is 100%. To allow recalculation of absolute values of rates (eqs 6 and 7), the sum of apparent cleavage rate is indicated for each substrate concentration. [b]Cleavage sites for which the $R^2$ of the first-order fit (eq 7) was <0.8. [c]Peptides were analyzed until a DH of 7%; for certain cleavage sites no corresponding peptides were found, indicating that the selectivity is <0.001% (nd).

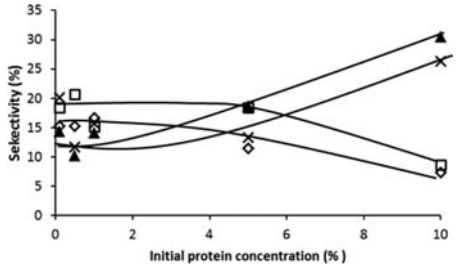


**Figure 7.** Enzyme selectivity toward four cleavage sites, (◇) 45, (□) 55, (▲) 62, and (×) (134), as a function of the initial substrate concentration.

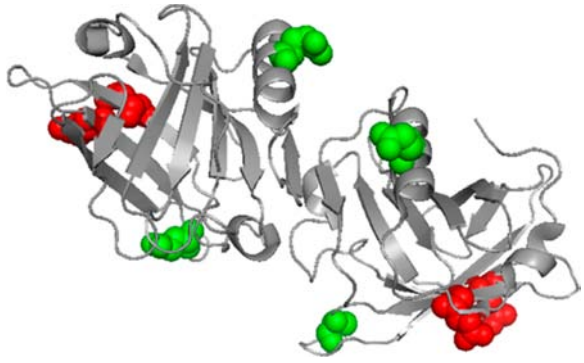

**Figure 8.** Three-dimensional structure of $\beta$-lactoglobulin as dimer (pdb entry 2q39). Cleavage sites 45 and 55 are highlighted in red, and cleavage sites 62 and 134 are highlighted in green.

be expected to be equally accessible for the enzyme. The accessibility may be influenced by the fact that the protein occurs as a dimer at pH 8. Moreover, the fraction of $\beta$-lactoglobulin dimers increases with increasing concentration.[26] This was expected to reduce the accessibility of cleavage sites 62 and 134, because they are in close proximity to the dimer interface (Figure 8). In contrast to expectation, the enzyme has an increased selectivity for these cleavage sites at increased substrate concentration. With respect to secondary structure, it has been described for trypsin that $\alpha$-helices hinder the physical approach of the enzyme,[27] but for BLP such information is not available. However, cleavage sites 45 and 55 are both found on $\beta$-sheets, whereas cleavage sites 62 and 134 are not. This might


dx.doi.org/10.1021/jf503151f | J. Agric. Food Chem. 2014, 62, 10230−10239

be an indication that β-sheets are more difficult for the enzyme to approach. Currently there is no clear argument to explain the significant change in selectivity toward these four cleavages sites as a function of protein concentration.

For other cleavage sites after Glu residues, some influence of the concentration is observed. For instance, cleavage site 51 has a higher selectivity at high initial substrate concentrations (5 and 10% (w/v) WPI) than at low substrate concentrations (0.1−1% (w/v) WPI). Cleavage sites such as 51 have a lower selectivity than cleavage sites 45, 55, 62, and 134. Consequently, their influence on the composition of the hydrolysates is smaller.

Second, the enzyme selectivity toward the cleavage sites after Asp residues is higher at high initial substrate concentrations (>1% (w/v)) than at the low concentrations (0.1−1% (w/v) WPI). The average selectivity toward Asp residues is 0.01% for low concentrations (0.1−1% (w/v) WPI) and 0.06% for high concentrations (5 and 10% (w/v) WPI) (Table 2).

By increasing the substrate concentration at constant enzyme/substrate ratio during enzymatic protein hydrolysis, the overall hydrolysis rate is decreased and a lower DH is reached. For the cleavage sites Glu-62 and Glu-134 and Glu-45 and Glu-55, for which the enzyme has a very high selectivity, a 2 times higher or lower selectivity, respectively, is observed at 10% (w/v) WPI than at the other substrate concentrations. In addition, the enzyme selectivity toward Asp residues is higher at high initial substrate concentrations (≥5% (w/v) WPI) than at low substrate concentrations. This finding shows that changing the substrate concentration influences both the overall hydrolysis rate and the mechanism of hydrolysis.

## ■ ASSOCIATED CONTENT

### Supporting Information

Table containing values for the apparent cleavage rate of the enzyme toward all cleavage sites, determined from hydrolysis at different initial protein concentrations (0.1−10% (w/v) WPI), which were used to calculate the rates of selective hydrolysis shown in Figure 6. This material is available free of charge via the Internet at http://pubs.acs.org.

## ■ AUTHOR INFORMATION

### Corresponding Author

*(P.A.W.) Phone: +31-317 483786. E-mail: peter.wierenga@wur.nl.

### Funding

The research leading to these results was conducted within the EU-ITN LEANGREENFOOD network, funded by the European Community's Seventh Framework Program [FP7/2007-2013] under Grant Agreement 238084.

### Notes

The authors declare no competing financial interest.

## ■ REFERENCES

(1) Hardt, N. A.; van der Goot, A. J.; Boom, R. M. Influence of high solid concentrations on enzymatic wheat gluten hydrolysis and resulting functional properties. *J. Cereal Sci.* **2013**, *57*, 531−536.

(2) Chabanon, G.; Chevalot, I.; Framboisier, X.; Chenu, S.; Marc, I. Hydrolysis of rapeseed protein isolates: kinetics, characterization and functional properties of hydrolysates. *Process Biochem.* **2007**, *42*, 1419−1428.

(3) Camacho Rubio, F.; González Tello, P.; Fernández Cuadrado, V.; Páez Dueñas, M.; Márquez Moreno, M. C. Hydrolysis of casein by Alcalase. *Rev. Esp. Cienc. Tecnol. Aliment.* **1993**, *33*, 59−70.

(4) Butré, C. I.; Wierenga, P. A.; Gruppen, H. Effects of ionic strength on the enzymatic hydrolysis of diluted and concentrated whey protein isolate. *J. Agric. Food Chem.* **2012**, *60*, 5644−5651.

(5) Ng, K.; Rosenberg, A. Possible coupling of chemical to structural dynamics in subtilisin BPN′ catalyzed hydrolysis. *Biophys. Chem.* **1991**, *39*, 57−68.

(6) Qi, X. L.; Brownlow, S.; Holt, C.; Sellers, P. Thermal denaturation of β-lactoglobulin: effect of protein concentration at pH 6.75 and 8.05. *Biochim. Biophys. Acta: Protein Struct. Mol. Enzymol.* **1995**, *1248*, 43−49.

(7) Silvestre, M. P. C.; Afonso, W. O.; Lopes Junior, C. O.; Silva, V. D. M.; Morais, H. A.; de Souza, M. W. S.; Silva, M. R. Use of subtilisin and pancreatin for hydrolyzing whey protein concentrate. *Am. J. Food Technol.* **2011**, *6*, 647−660.

(8) Spellman, D.; O'Cuinn, G.; FitzGerald, R. J. Physicochemical and sensory characteristics of whey protein hydrolysates generated at different total solids levels. *J. Dairy Res.* **2005**, *72*, 138−143.

(9) Butré, C. I.; Sforza, S.; Gruppen, H.; Wierenga, P. A. Introducing enzyme selectivity: a quantitative parameter to describe enzymatic protein hydrolysis. *Anal. Bioanal. Chem.* **2014**, *406*, 5827−5841.

(10) Kosters, H. A.; Wierenga, P. A.; Gruppen, H. SELDI-TOF-MS as a rapid tool to study food related protein-peptide interactions. *Food Hydrocolloids* **2010**, *24*, 667−673.

(11) Breddam, K.; Meldal, M. Substrate preferences of glutamic-acid-specific endopeptidases assessed by synthetic peptide substrates based on intramolecular fluorescence quenching. *Eur. J. Biochem.* **1992**, *206*, 103−107.

(12) Akpinar, O.; Penner, M. H. Peptidase activity assays using protein substrates. In *Current Protocols in Food Analytical Chemistry*; Wiley: Corvallis, OR, USA, 2001.

(13) Svendsen, I.; Breddam, K. Isolation and amino acid sequence of a glutamic acid specific endopeptidase from *Bacillus licheniformis*. *Eur. J. Biochem.* **1992**, *204*, 165−171.

(14) Butré, C. I.; Wierenga, P. A.; Gruppen, H. Influence of water availability on the enzymatic hydrolysis of proteins. *Process Biochem.* **2014**, DOI: 10.1016/j.procbio.2014.08.009.

(15) Martínez-Araiza, G.; Castaño-Tostado, E.; Amaya-Llano, S. L.; Regalado-González, C.; Martínez-Vera, C.; Ozimek, L. Modeling of enzymatic hydrolysis of whey proteins. *Food Bioprocess Technol.* **2012**, *5*, 2596−2601.

(16) Kosters, H. A.; Wierenga, P. A.; De Vries, R.; Gruppen, H. Characteristics and effects of specific peptides on heat-induced aggregation of β-lactoglobulin. *Biomacromolecules* **2011**, *12*, 2159−2170.

(17) Kuipers, B. J. H.; Gruppen, H. Prediction of molar extinction coefficients of proteins and peptides using UV absorption of the constituent amino acids at 214 nm to enable quantitative reverse phase high-performance liquid chromatography−mass spectrometry analysis. *J. Agric. Food Chem.* **2007**, *55*, 5445−5451.

(18) Wa, C.; Cerny, R.; Hage, D. S. Obtaining high sequence coverage in matrix-assisted laser desorption time-of-flight mass spectrometry for studies of protein modification: analysis of human serum albumin as a model. *Anal. Biochem.* **2006**, *349*, 229−241.

(19) Van Teeffelen, A. M. M.; Broersen, K.; De Jongh, H. H. J. Glucosylation of β-lactoglobulin lowers the heat capacity change of unfolding; a unique way to affect protein thermodynamics. *Protein Sci.* **2005**, *14*, 2187−2194.

(20) Mody, R.; Tramontano, A.; Paul, S. Spontaneous hydrolysis of vasoactive intestinal peptide in neutral aqueous solution. *Int. J. Pept. Protein Res.* **1994**, *44*, 441−447.

(21) Perler, F. B.; Davis, E. O.; Dean, G. E.; Gimble, F. S.; Jack, W. E.; Neff, N.; Noren, C. J.; Thorner, J.; Belfort, M. Protein splicing elements: inteins and exteins − a definition of terms and recommended nomenclature. *Nucleic Acids Res.* **1994**, *22*, 1125−1127.

(22) Schlichtherle-Cerny, H.; Affolter, M.; Cerny, C. Hydrophilic interaction liquid chromatography coupled to electrospray mass spectrometry of small polar compounds in food analysis. *Anal. Chem.* **2003**, *75*, 2349−2354.

(23) Kalyankar, P.; Zhu, Y.; O'Cuinn, G.; FitzGerald, R. J. Investigation of the substrate specificity of glutamyl endopeptidase using purified bovine β-casein and synthetic peptides. *J. Agric. Food Chem.* **2013**, *61*, 3193−3204.
(24) Creusot, N.; Gruppen, H.; van Koningsveld, G. A.; de Kruif, C. G.; Voragen, A. G. J. Peptide-peptide and protein-peptide interactions in mixtures of whey protein isolate and whey protein isolate hydrolysates. *Int. Dairy J.* **2006**, *16*, 840−849.
(25) Caessens, P. W. J. R.; Daamen, W. F.; Gruppen, H.; Visser, S.; Voragen, A. G. J. β-Lactoglobulin hydrolysis. 2. Peptide identification, SH/SS exchange, and functional properties of hydrolysate fractions formed by the action of plasmin. *J. Agric. Food Chem.* **1999**, *47*, 2980−2990.
(26) Owusu Apenten, R. K.; Galani, D. Thermodynamic parameters for beta-lactoglobulin dissociation over a broad temperature range at pH 2.6 and 7.0. *Thermochim. Acta* **2000**, *359*, 181−188.
(27) Fernández, A.; Riera, F. β-Lactoglobulin tryptic digestion: a model approach for peptide release. *Biochem. Eng. J.* **2013**, *70*, 88−96.

Table 1. Analytical Characteristics for the HSH-GC-MS Determination of Halogenated VOCs and Mass Values Used for MS Detection

| compound | LOD (ng/L) | linear range (μg/L) | precision RSD (%)[a] intraday | precision RSD (%)[a] interday | $m/z$[b] |
|---|---|---|---|---|---|
| dichloromethane (DCM) | 50 | 0.17−100 | 5.1 | 5.9 | **49**, 84, 86 |
| 1,2-dichloroethane (1,2-DCE) | 50 | 0.17−100 | 5.2 | 6.2 | 49, **62**, 64 |
| carbon tetrachloride (CTC) | 8 | 0.03−50 | 4.6 | 5.4 | 82, **117**, 119 |
| 1,2-dibromoethane (1,2-DBE) | 35 | 0.12−100 | 4.8 | 5.6 | 27, **107**, 109 |
| trichloromethane (TCM) | 10 | 0.03−50 | 4.7 | 5.5 | 47, **83**, 85 |
| bromodichloromethane (BDCM) | 10 | 0.03−50 | 4.9 | 5.7 | **83**, 85, 129 |
| dibromochloromethane (DBCM) | 15 | 0.05−50 | 5.1 | 6.1 | 91, 127, **129** |
| dichloroiodomethane (DCIM) | 20 | 0.07−50 | 5.2 | 6.0 | **83**, 85, 175 |
| tribromomethane (TBM) | 20 | 0.07−50 | 4.9 | 5.7 | 171, **173**, 252 |
| bromochloroiodomethane (BCIM) | 35 | 0.12−100 | 5.0 | 6.1 | **127**, 129, 131 |
| dibromoiodomethane (DBIM) | 50 | 0.17−100 | 5.2 | 6.1 | **173**, 175, 127 |
| chlorodiiodomethane (CDIM) | 50 | 0.17−100 | 5.0 | 6.0 | 127, **175**, 177 |
| bromodiiodomethane (BDIM) | 100 | 0.30−100 | 5.2 | 6.0 | 127, **219**, 221 |
| triiodomethane (TIM) | 100 | 0.30−100 | 5.3 | 6.2 | 127, 140, **267** |

[a]RSD, relative standard deviation ($n$ = 11) for 5 μg/L. [b]$m/z$ values (base peaks for quantification are boldfaced).

(1 h in a 90 °C water bath). Other HS−solid phase microextraction (SPME)[20] or purge-and-trap[21] GC methods require the dilution or centrifugation of beverages, which produces a loss of the species through volatilization. More recently, an HS-SPME method has been applied to determine four THMs in soft drinks[22] and beer.[23] In general, these methods require manual sample manipulation with low sensitivity because they are adapted from water methodologies.

The aims of this work were (i) to develop a solventless SHS-GC−mass spectrometric method with enough sensitivity to determine target analytes at nanogram per liter levels in beverages; (ii) to include six emerging iodinated THMs for the first time, in addition to the four common THMs and four VOCs regulated in treated water; and (iii) to discriminate the source of these species through treated water employed for beverage preparation or by contamination through the industrial process (i.e., washing, bottling line, etc.).

## MATERIALS AND METHODS

**Chemicals and Standards.** The 14 species included in this study with their corresponding acronyms are indicated in Table 1. The majority of standards and the internal standard, 1,2-dibromopropane, were supplied from Sigma-Aldrich (Madrid, Spain). Iodinated THM (DCIM, BCIM, DBIM, CDIM, and BDIM) standards were supplied by Cansyn (Toronto, Canada). Methanol, sulfuric acid, and salts were supplied from Merck (Darmstadt, Germany). Stock standard solutions containing 1 g/L of each compound were prepared in methanol and stored in amber glass vials at −20 °C. Working-standard solutions were prepared on a daily basis by dilution at the microgram per liter level in mineral water (untreated water and free of DBPs).

**Static Headspace and Gas Chromatographic Conditions.** The experimental setup for the SHS-GC-MS determination of VOCs and THMs consisted of an SHS autosampler G1888 and an HP 6890N gas chromatograph (Agilent Technologies, Palo Alto, CA, USA) equipped with an HP 5973N mass selective detector. The operating conditions for the HS autosampler were as follows: vial equilibration time, 15 min; oven temperature, 80 °C; vial pressurization time, 30 s; loop fill time, 3 s; valve/loop temperature, 100 °C. Helium (6.0 grade purity, Air Liquid, Seville, Spain) was used both to pressurize vials and to drive the headspace formed to the injection port of the chromatograph via a transfer line at 110 °C. Injection was done in the split mode (split ratio 1:20) for 1 min with an inlet temperature of 250 °C; flow rate of carrier gas (He) was fixed at 1 mL/min. The gas chromatographic separation was achieved on an HP-5MS UI fused silica capillary column (30 m × 0.25 mm × 0.25 μm film thickness) coated with a stationary phase consisting of 5% phenyl−95% methylpolysiloxane supplied by Agilent. Oven temperature was programmed as follows: 40 °C for 5 min, raised to 100 °C at 25 °C/min, held for 2 min, ramped at 30 °C/min to 250 °C, and finally held for 3 min. The MS was operated in the electron impact ionization mode at 70 eV, and ion source and quadrupole temperatures were set at 250 and 150 °C, respectively. Optimization experiments were conducted in total ion chromatography mode between $m/z$ 25 and 400 at 3.5 scans/s. The ions selected for identification and quantification of VOCs and THMs (SIM mode) are listed in Table 1; $m/z$ values for 1,2-dibromopropane (IS) were 42, 121 (base peak), 123.

**Sample Preparation.** The commercial beverages (soft drinks and juices) used in this study were purchased at local markets in Spain (one of the largest producers of fruits and derivatives in Europe). Several brands with different packaging types and different flavors were selected. In the laboratory, samples were stored refrigerated or at room temperature, depending on the manufacturer's instructions, and the seal of each bottle was broken right before its analysis. Freshly squeezed orange juice (blank) was used to optimize the analytical parameters of the method. For the preparation of the blank, fresh oranges were hand-peeled and homogenized with a laboratory squeezer. Food utensils were always washed with mineral water to ensure the prevention of DBP contamination.

**Analytical Procedure.** Beverages were mixed in their own container for 1 min by manual shaking. Ten milliliters of beverage or standard solution containing between 0.03 and 100 μg/L of each target analytes and 5 μg/L of 1,2-dibromopropane (IS) was placed in a 20 mL glass vial containing 4 g of NaCl. For carbonated soft drink analyses, 300 μL of a 6 mol/L NaOH solution was also added to eliminate the carbonic acid present. Then, the vial was immediately sealed and vortexed for 1 min for mixing purposes and placed in the autosampler carousel. Samples were analyzed by SHS-GC-MS, using the operating conditions mentioned above.

## RESULTS AND DISCUSSION

**Evaluation of Chemical Parameters.** First, the SHS variables were studied using 10 mL of freshly squeezed orange juice containing 10 μg/L of each VOC and THM, 5 μg/L of the IS, and 3 g of NaCl in a 20 mL glass vial. The most relevant parameters were oven temperature (60−80 °C) and vial equilibration time (5−20 min), providing the best results at 80 °C and 15 min, respectively. Other instrumental parameters did not present significant changes in the abundance signals for the

compounds, and a pressurization time of 30 s and a venting time of 12 s were selected as the working values.

Salting-out increases the ionic strength of the aqueous solution; this can decrease the solubility of organic species, improving their distribution from the aqueous solution to the headspace. Hence, the addition of NaCl was studied between 0 and 5 g. The analytical signal of the compounds increased with increases in the amounts of salt up to 4 g; therefore, this amount was selected per 10 mL of sample. The effect of the sample pH on the extraction of the 14 species was studied in the 2.5−9.0 range by adjusting the fortified juice with diluted $H_2SO_4$ or NaOH as required. As the peak area ratio of all species remained constant throughout this range, beverage samples were analyzed without pH adjustment. Fruit juices did not present any problem for their analyses by SHS, but carbonated soft drinks can have certain problems due to the presence of $CO_2$. When a soft drink bottle is opened, the pressure is reduced to atmospheric pressure, causing decomposition of the carbonic acid, releasing $CO_2$. This loss of $CO_2$ originates a sweep of the most volatile compounds into the atmosphere. Moreover, the $CO_2$ could be competing with the analytes for the headspace in the vial. To solve this problem, different procedures have been proposed, such as nitrogen bubbling, agitation, or ultrasonication.[24] However, these decarbonation methods can remove the volatile compounds from the matrix, so the best alternative can be the addition of NaOH to eliminate carbonic acid, which does not involve the volatilization of the analytes. With the wide pH range of the proposed method (2.5−9.0) taken into account, the addition of NaOH up to pH 8−9 is possible. For this purpose, the recovery of the 14 species was studied by adding various volumes (0−350 $\mu$L) of a 6 mol/L NaOH solution to 10 mL of a representative carbonated soda. As can be seen in Figure 1 (for nine representative analytes),

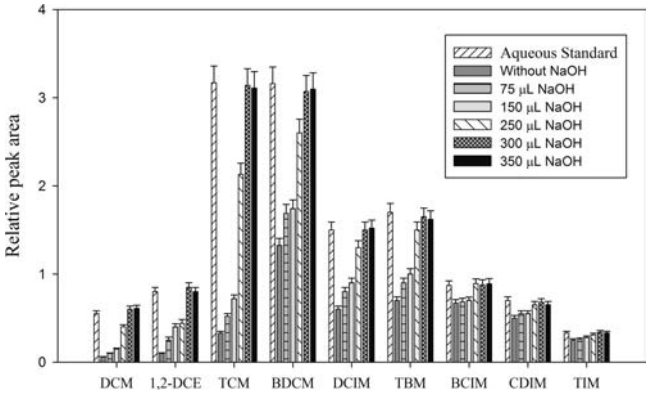


**Figure 1.** Influence of the addition of variable volumes of a 6 mol/L NaOH solution to 10 mL of fortified natural orange juice on the recoveries of nine representative analytes versus an aqueous standard. Concentration: 10 $\mu$g/L of each compound. Error bars are the standard deviation for five measurements.

the relative peak areas were extremely low for the most volatile compounds (DCM, 1,2-DCE, CTC, and TCM) without NaOH, whereas the addition of NaOH solution to the carbonated sample reduced the loss of these compounds. The recovery (versus an aqueous standard solution) for all analytes improved as the volume of NaOH increased to 300 $\mu$L (pH ∼8.4). This improvement was more noticeable for the most volatile analytes, which underwent an increase of ∼90% as compared to the aqueous standard. For 1,2-DBE, BDCM, DBCM, DCIM, and TBM, recoveries increased ∼40−50%, whereas for the majority of iodinated THMs (BCIM, CDIM, DBIM, BDIM, and TIM), this increase was only ∼10−20%. The final volume selected was 300 $\mu$L of a 6 mol/L NaOH solution added to 10 mL of carbonated soft drink because it provided a sample pH of ∼8.4 (the prevalent species is $HCO_3^-$; $pK_a$ = 6.1).

Finally, the efficiency percentage of the whole process for the 14 compounds in a fresh orange juice (blank) was calculated in quintuplicate by a second SHS extraction of the remaining liquid phase to check the absence of any compound. For this purpose, 10 mL of the blank was fortified with 10 $\mu$g/L of each compound and salt according to the procedure. The average yield of the whole analytical process was ≥95% for all analytes, showing that the method is adequate for the determination of these species.

**Sensitivity and Validation of the Method.** Linear range, analyte detectability, and precision of the proposed method were studied under optimal experimental conditions (see Table 1). Calibration curves were constructed by using fresh orange juice fortified with 0.03−100 $\mu$g/L of each compound and processed as described under Analytical Procedure. The equations for the standard curves were obtained by plotting the analyte to internal standard peak area ratios against the amount of the analytes. Regression coefficients were >0.995 in all cases. Limits of detection (LODs) were determined as the analyte concentration that provides a chromatographic peak equal to 3 times the regression standard deviation, $S_{y/x}$, divided by the slope of each calibration graph. The lower limit of the linear range corresponds to the limit of quantification, which is 3.3 × LOD.[25] The precision was calculated by measuring 11 fresh orange juices on the same day and different days. The results obtained were satisfactory, with average RSD values ranging from 5.0 ± 0.2 to 5.9 ± 0.3% for intra- and interdays, respectively, which indicates that the method is absolutely repeatable and reproducible.

In the bibliography, different solventless techniques have been employed for the determination of several VOCs and THMs in beverages and foods. All of these methodologies have been proposed only for the four common THMs and do not reach the sensitivity of the proposed method.[4,17−23] In addition, some of these methodologies involve the manipulation of the beverages by dilution[20]/centrifugation[21]/heating in water baths,[4] etc., with the consequent loss of volatile compounds. More recently, the four THMs have been determined in soft drinks[21] and beers,[22] but the method is ca. 10 times less sensitive than the present alternative.

To validate the proposed method, a recovery study was conducted by analyzing several representative soft drinks and fruit juices fortified with 5 and 20 $\mu$g/L of each compound ($n$ = 5). The analytical responses (taking into account the genuine concentration of the analytes) from all samples were compared to similar standard additions to mineral water. Good recoveries (93−95% for apple, 94−96% for pineapple, 92−96% for orange, and 90−92% for peach juices; 94−96% for tonic; and 95−97% for soda) were obtained for all compounds.

**Analysis of Beverage Samples.** VOCs and THMs can occur in beverages through multiple pathways, namely, (i) inclusion of drinking water as an ingredient in the production of the beverages; (ii) accumulation and sorption from retained water in beverage packaging and wrapping that had been disinfected/washed with chlorinated sanitizers; (iii) contamination by contact with cleaners/disinfectants used in beverage processing equipment, rinses with water in beverage processing, storage, and/or marketing; and (iv) formation during beverage preparation due to reactions between residual chlorine and

Table 2. Concentrations[a] of THMs (Micrograms per Liter) Found in Soft Drinks

| sample | flavor | TCM | BDCM | DBCM | DCIM | TBM | TTHMs[b] |
|---|---|---|---|---|---|---|---|
| tea 1 | lemon | 1.1 ± 0.1 | 0.51 ± 0.03 | 0.23 ± 0.01 | ND[c] | <0.07[d] | 1.8 ± 0.1 |
| tea 2 | peach | 27 ± 2 | 3.1 ± 0.2 | 0.24 ± 0.01 | ND | ND | 30 ± 2 |
| tea 3 | passion fruit | 14 ± 1 | 3.5 ± 0.2 | 0.73 ± 0.04 | ND | <0.07 | 18 ± 1 |
| isotonic 1 | lemon | 23 ± 1 | 4.6 ± 0.3 | 0.76 ± 0.04 | ND | ND | 28 ± 2 |
| isotonic 2 | lemon | 1.8 ± 0.1 | 0.18 ± 0.01 | 0.08 ± 0.01 | ND | <0.07 | 2.1 ± 0.1 |
| isotonic 3 | | 27 ± 2 | 3.4 ± 0.2 | 0.27 ± 0.02 | ND | <0.07 | 31 ± 2 |
| isotonic 4 | | 31 ± 2 | 3.4 ± 0.2 | 0.26 ± 0.02 | <0.07 | <0.07 | 35 ± 2 |
| fruit beverage 1 | lemon | 7.1 ± 0.4 | 0.70 ± 0.04 | 0.11 ± 0.01 | ND | ND | 7.9 ± 0.5 |
| fruit beverage 2 | apple | 21 ± 1 | 1.3 ± 0.1 | 0.10 ± 0.01 | ND | ND | 22 ± 1 |
| fruit beverage 3 | lemon | 5.1 ± 0.3 | 0.44 ± 0.03 | <0.05 | ND | ND | 5.5 ± 0.3 |
| fruit beverage 4 | orange | 6.8 ± 0.4 | 1.1 ± 0.1 | 0.11 ± 0.01 | ND | <0.07 | 8.0 ± 0.5 |
| fruit beverage 5 | orange | 14 ± 1 | 1.2 ± 0.1 | 0.13 ± 0.01 | ND | ND | 15 ± 1 |
| fruit beverage 6 | pineapple | 23 ± 1 | 1.4 ± 0.1 | 0.20 ± 0.01 | ND | ND | 25 ± 1 |
| tonic 1 | | 20 ± 1 | 1.2 ± 0.1 | 0.18 ± 0.01 | ND | ND | 21 ± 1 |
| tonic 2 | | 3.8 ± 0.2 | 0.39 ± 0.02 | <0.05 | ND | ND | 4.2 ± 0.2 |
| tonic 3 | | 16 ± 1 | 2.1 ± 0.1 | 0.32 ± 0.02 | ND | ND | 18 ± 1 |
| soda 1 | | 35 ± 2 | 2.0 ± 0.1 | 0.25 ± 0.01 | ND | ND | 37 ± 2 |
| soda 2 | lemon | 20 ± 1 | 4.5 ± 0.3 | 0.82 ± 0.05 | 0.11 ± 0.01 | <0.07 | 25 ± 1 |
| soda 3 | lemon | 7.6 ± 0.4 | 0.62 ± 0.04 | 0.07 ± 0.01 | ND | ND | 8.3 ± 0.5 |
| soda 4 | lemon | 9.6 ± 0.6 | 0.70 ± 0.04 | <0.05 | ND | ND | 10 ± 1 |
| soda 5 | lemon | 31 ± 2 | 1.5 ± 0.1 | 0.12 ± 0.01 | ND | ND | 33 ± 2 |
| soda 6 | lemon | 28 ± 2 | 1.4 ± 0.1 | 0.19 ± 0.01 | ND | ND | 30 ± 2 |
| soda 7 | orange | 1.0 ± 0.1 | 0.22 ± 0.01 | 0.13 ± 0.01 | ND | <0.07 | 1.4 ± 0.1 |
| soda 8 | orange | 22 ± 1 | 3.4 ± 0.2 | 0.55 ± 0.03 | ND | <0.07 | 26 ± 2 |
| soda 9 | orange | 3.9 ± 0.2 | 0.31 ± 0.02 | <0.05 | ND | <0.07 | 4.2 ± 0.2 |
| soda 10 | orange | 31 ± 2 | 1.5 ± 0.1 | 0.12 ± 0.01 | ND | ND | 33 ± 2 |
| soda 11 | orange | 24 ± 1 | 1.3 ± 0.1 | 0.10 ± 0.01 | ND | ND | 25 ± 1 |
| soda 12 | cola | 6.5 ± 0.4 | 0.68 ± 0.04 | 0.08 ± 0.01 | ND | ND | 7.3 ± 0.4 |
| soda 13 | cola | 5.4 ± 0.3 | 0.45 ± 0.03 | 0.06 ± 0.01 | ND | ND | 5.9 ± 0.3 |
| soda 14 | cola | 5.7 ± 0.3 | 0.44 ± 0.03 | <0.05 | ND | ND | 6.1 ± 0.4 |
| soda 15 | cola | 27 ± 2 | 4.5 ± 0.3 | 0.80 ± 0.05 | 0.10 ± 0.01 | <0.07 | 32 ± 2 |
| soda 16 | cola | 7.4 ± 0.4 | 0.63 ± 0.04 | 0.07 ± 0.01 | ND | <0.07 | 8.1 ± 0.5 |
| soda 17 | cola | 28 ± 2 | 4.9 ± 0.3 | 0.92 ± 0.05 | <0.07 | <0.07 | 34 ± 2 |
| soda 18 | cola | 43 ± 3 | 7.8 ± 0.5 | 1.3 ± 0.1 | 0.13 ± 0.01 | 0.17 ± 0.01 | 52 ± 3 |
| soda 19 | cola | 16 ± 1 | 1.0 ± 0.1 | 0.08 ± 0.01 | ND | ND | 17 ± 1 |
| soda 20 | cola | 28 ± 2 | 6.3 ± 0.4 | 1.3 ± 0.1 | 0.13 ± 0.01 | <0.07 | 36 ± 2 |
| soda 21 | cola | 1.6 ± 0.1 | 0.09 ± 0.01 | 0.06 ± 0.01 | ND | ND | 1.8 ± 0.1 |
| soda 22 | cola | 31 ± 2 | 6.4 ± 0.4 | 1.2 ± 0.1 | <0.07 | <0.07 | 39 ± 2 |
| soda 23 | cola | 14 ± 1 | 0.90 ± 0.05 | 0.08 ± 0.01 | ND | <0.07 | 15 ± 1 |
| soda 24 | cola | 34 ± 2 | 7.1 ± 0.4 | 0.52 ± 0.03 | <0.07 | <0.07 | 42 ± 2 |

[a] ± standard deviation, $n = 5$. [b] Total THMs. [c] Not detected. [d] <LOQ.

precursors present in food, for example, carbohydrates, lipids, and proteins. The samples selected for analysis, soft drinks and fruit juices, are products that contain water as an ingredient and that are frequently consumed every day.

The proposed SHS-GC-MS method was applied to determine 4 VOCs and 10 THMs in 100 types of samples: 40 soft drinks (teas, isotonics, fruit beverages, tonics, and sodas) and 60 fruit juices (natural juices 100%, reconstituted juices, and nectars). All samples gave positive results containing up to five THMs including DCIM, in different distributions and levels; none of the four VOCs studied were present in these beverages. Tables 2 and 3 list the concentrations of the THMs found at detectable concentrations in soft drinks (ca. 90% water) and fruit juices (up to 70% water), respectively. The analytes not shown were either not contained or present at levels below their LODs. The species TCM, BDCM, and DBCM were present in practically all samples and at higher concentrations, whereas TBM and DCIM were found in lower proportions. This could be explained because the water used in food applications is frequently disinfected with chlorine due to its economic impact and simple use.

Table 2 lists the levels of each THM found in soft drinks as well as the total concentration of trihalomethanes (TTHMs). There are two levels of TTHM concentrations: soft drinks A for concentrations <15 μg/L ($n = 15$; average value of 5.5 ± 2.8 μg/L) and soft drinks B containing ≥15 μg/L ($n = 25$; average value of 28.8 ± 9.1 μg/L). From Table 2 it can be concluded that (i) there were no significant differences in either TTHM concentrations in each kind of soft drink (tea, tonic, soda, etc.) or in the species of THMs; (ii) there were no differences between flavors (lemon, orange, cola, etc.) in the same kind of soft drinks; and (iii) the presence of THMs in these beverages should be ascribed to the type of treated water employed in their preparation. One factor that influenced the TTHM concentrations was the factory that bottled the samples. Each factory has a different source of water, and the levels of

Table 3. Concentrations[a] of THMs (Micrograms per Liter) Found in Fruit Juices

| sample | fruit | factory | TCM | BDCM | DBCM | TBM | TTHMs[b] |
|---|---|---|---|---|---|---|---|
| natural juice 1 | apple | A | 0.20 ± 0.01 | ND[c] | ND | ND | 0.20 ± 0.01 |
| natural juice 2 | pineapple | A | 0.39 ± 0.02 | 0.22 ± 0.01 | ND | ND | 0.61 ± 0.03 |
| natural juice 3 | orange | A | 0.27 ± 0.02 | ND | ND | ND | 0.27 ± 0.02 |
| natural juice 4 | orange | B | 0.48 ± 0.03 | 0.11 ± 0.01 | ND | ND | 0.59 ± 0.03 |
| natural juice 5 | orange | C | 0.60 ± 0.03 | 0.23 ± 0.01 | ND | ND | 0.83 ± 0.05 |
| natural juice 6 | orange | D | 0.33 ± 0.02 | ND | ND | ND | 0.33 ± 0.02 |
| natural juice 7 | orange | E | 0.52 ± 0.03 | ND | ND | ND | 0.52 ± 0.03 |
| reconstituted juice 1 | apple | F | 0.36 ± 0.02 | 0.06 ± 0.01 | 0.06 ± 0.01 | <0.07[d] | 0.48 ± 0.03 |
| reconstituted juice 2 | apple | G | 0.92 ± 0.05 | 1.6 ± 0.1 | 1.4 ± 0.1 | 0.26 ± 0.02 | 4.2 ± 0.2 |
| reconstituted juice 3 | pineapple | H | 3.6 ± 0.2 | 3.3 ± 0.2 | 2.9 ± 0.2 | 0.40 ± 0.02 | 10 ± 1 |
| reconstituted juice 4 | orange | D | ND | ND | 0.07 ± 0.01 | 0.12 ± 0.01 | 0.19 ± 0.01 |
| reconstituted juice 5 | orange | H | 3.0 ± 0.2 | 3.7 ± 0.2 | 3.3 ± 0.2 | 0.50 ± 0.03 | 11 ± 1 |
| reconstituted juice 6 | orange | I | 0.45 ± 0.03 | ND | 0.08 ± 0.01 | 0.13 ± 0.01 | 0.66 ± 0.04 |
| reconstituted juice 7 | peach | H | 1.8 ± 0.1 | 1.6 ± 0.1 | 1.5 ± 0.1 | 0.22 ± 0.01 | 5.1 ± 0.3 |
| reconstituted juice 8 | peach | J | 3.1 ± 0.2 | 0.27 ± 0.02 | ND | ND | 3.4 ± 0.2 |
| reconstituted juice 9 | grape | D | 0.56 ± 0.03 | 0.18 ± 0.01 | <0.05 | ND | 0.74 ± 0.04 |
| reconstituted juice 10 | cranberry | A | 0.32 ± 0.02 | 0.25 ± 0.01 | 0.21 ± 0.01 | ND | 0.78 ± 0.04 |
| reconstituted juice 11 | mix | A | 0.38 ± 0.02 | 0.05 ± 0.01 | <0.05 | ND | 0.43 ± 0.03 |
| reconstituted juice 12 | mix | A | 0.37 ± 0.02 | ND | 0.16 ± 0.01 | 0.29 ± 0.02 | 0.82 ± 0.05 |
| reconstituted juice 13 | mix | A | 0.72 ± 0.04 | 3.7 ± 0.2 | ND | ND | 4.4 ± 0.3 |
| reconstituted juice 14 | mix | C | 0.39 ± 0.02 | 0.08 ± 0.01 | 0.05 ± 0.01 | <0.07 | 0.52 ± 0.03 |
| reconstituted juice 15 | mix | C | 0.27 ± 0.02 | <0.03 | <0.05 | <0.07 | 0.27 ± 0.02 |
| reconstituted juice 16 | mix | D | 10 ± 1 | 2.2 ± 0.1 | 0.62 ± 0.04 | ND | 13 ± 1 |
| reconstituted juice 17 | mix | D | 0.23 ± 0.01 | ND | <0.05 | ND | 0.23 ± 0.01 |
| reconstituted juice 18 | mix | D | 2.2 ± 0.1 | ND | ND | ND | 2.2 ± 0.1 |
| reconstituted juice 19 | mix | H | 2.0 ± 0.1 | 1.5 ± 0.1 | 1.3 ± 0.1 | 0.10 ± 0.01 | 4.9 ± 0.3 |
| reconstituted juice 20 | mix | J | 6.0 ± 0.3 | 0.92 ± 0.05 | 0.16 ± 0.01 | ND | 7.1 ± 0.4 |
| reconstituted juice 21 | mix | K | 1.9 ± 0.1 | 0.30 ± 0.02 | 0.15 ± 0.01 | 0.11 ± 0.01 | 2.5 ± 0.1 |
| nectar 1 | apple | A | 0.93 ± 0.05 | 0.30 ± 0.02 | 0.16 ± 0.01 | 0.10 ± 0.01 | 1.5 ± 0.1 |
| nectar 2 | apple | C | 0.35 ± 0.02 | 0.24 ± 0.01 | 0.18 ± 0.01 | 0.13 ± 0.01 | 0.90 ± 0.05 |
| nectar 3 | apple | C | 6.3 ± 0.4 | 2.1 ± 0.1 | 0.52 ± 0.03 | 0.18 ± 0.01 | 9.1 ± 0.5 |
| nectar 4 | apple | J | 4.5 ± 0.3 | 1.1 ± 0.1 | 0.19 ± 0.01 | 0.10 ± 0.01 | 5.9 ± 0.3 |
| nectar 5 | pineapple | A | 3.2 ± 0.2 | 2.6 ± 0.2 | 2.8 ± 0.2 | 0.51 ± 0.03 | 9.1 ± 0.5 |
| nectar 6 | pineapple | B | 2.2 ± 0.1 | 0.21 ± 0.01 | ND | ND | 2.4 ± 0.1 |
| nectar 7 | pineapple | F | 0.38 ± 0.02 | ND | ND | ND | 0.38 ± 0.02 |
| nectar 8 | pineapple | J | 12 ± 1 | 1.6 ± 0.1 | 0.24 ± 0.01 | ND | 14 ± 1 |
| nectar 9 | pineapple | J | 8.5 ± 0.5 | 1.0 ± 0.1 | 0.12 ± 0.01 | ND | 9.6 ± 0.6 |
| nectar 10 | pineapple | L | 32 ± 2 | 5.3 ± 0.3 | 0.96 ± 0.06 | ND | 38 ± 2 |
| nectar 11 | pineapple | L | 16 ± 1 | 3.3 ± 0.2 | 0.60 ± 0.03 | ND | 20 ± 1 |
| nectar 12 | orange | B | 5.8 ± 0.3 | 0.86 ± 0.05 | 0.12 ± 0.01 | ND | 6.8 ± 0.4 |
| nectar 13 | orange | B | 2.1 ± 0.1 | 0.43 ± 0.03 | 0.11 ± 0.01 | ND | 2.6 ± 0.2 |
| nectar 14 | orange | C | 0.26 ± 0.02 | 0.12 ± 0.01 | 0.17 ± 0.01 | 0.39 ± 0.02 | 0.94 ± 0.05 |
| nectar 15 | orange | C | 18 ± 1 | 4.8 ± 0.3 | 0.86 ± 0.05 | ND | 24 ± 1 |
| nectar 16 | orange | D | 0.22 ± 0.01 | 0.19 ± 0.01 | 0.25 ± 0.01 | 0.36 ± 0.02 | 1.0 ± 0.1 |
| nectar 17 | orange | G | 5.9 ± 0.3 | 4.6 ± 0.3 | 2.9 ± 0.2 | 0.31 ± 0.02 | 14 ± 1 |
| nectar 18 | orange | I | 1.3 ± 0.1 | 0.82 ± 0.05 | 0.89 ± 0.05 | 0.46 ± 0.03 | 3.5 ± 0.2 |
| nectar 19 | orange | J | 4.0 ± 0.2 | 0.93 ± 0.05 | 0.17 ± 0.01 | 0.12 ± 0.01 | 5.2 ± 0.3 |
| nectar 20 | orange | K | 3.3 ± 0.2 | 0.41 ± 0.02 | ND | ND | 3.7 ± 0.2 |
| nectar 21 | orange | L | 17 ± 1 | 3.8 ± 0.2 | 0.78 ± 0.04 | ND | 22 ± 1 |
| nectar 22 | peach | G | 1.5 ± 0.1 | 1.3 ± 0.1 | 1.1 ± 0.1 | <0.07 | 3.9 ± 0.2 |
| nectar 23 | peach | L | 16 ± 1 | 2.9 ± 0.2 | 0.61 ± 0.03 | ND | 20 ± 1 |
| nectar 24 | peach | L | 9.6 ± 0.6 | 2.0 ± 0.1 | 0.45 ± 0.03 | ND | 12 ± 1 |
| nectar 25 | pear | G | 2.6 ± 0.2 | 2.5 ± 0.1 | 1.9 ± 0.1 | 0.27 ± 0.02 | 7.3 ± 0.4 |
| nectar 26 | grapefruit | G | 2.4 ± 0.1 | 2.2 ± 0.1 | 1.7 ± 0.1 | 0.20 ± 0.01 | 6.5 ± 0.4 |
| nectar 27 | grapefruit | J | 3.9 ± 0.2 | 0.64 ± 0.04 | 0.19 ± 0.01 | ND | 4.7 ± 0.3 |
| nectar 28 | guava | A | 2.9 ± 0.2 | 1.5 ± 0.1 | 0.97 ± 0.06 | 0.14 ± 0.01 | 5.5 ± 0.3 |
| nectar 29 | mango | C | 0.67 ± 0.04 | 0.25 ± 0.01 | 0.24 ± 0.01 | 0.20 ± 0.01 | 1.4 ± 0.1 |
| nectar 30 | passion fruit | A | 4.8 ± 0.3 | 2.3 ± 0.1 | 1.1 ± 0.1 | 0.16 ± 0.01 | 8.4 ± 0.5 |
| nectar 31 | mix | C | 0.12 ± 0.01 | 0.17 ± 0.01 | 0.25 ± 0.01 | 0.38 ± 0.02 | 0.92 ± 0.05 |
| nectar 32 | mix | D | ND | ND | 0.16 ± 0.01 | 0.29 ± 0.02 | 0.45 ± 0.03 |

[a] ± standard deviation, $n = 5$. [b] Total THMs. [c] Not detected. [d] <LOQ.

THMs depend on the disinfection process. However, in this case, no differences were found between TTHM concentrations, presumably because the samples manufactured came from only four different factories, so there was not great variability. By way of example, tea 2 and soda 7 contain 30 and 1.4 μg/L, respectively, and both were manufactured in the same factory. Thus, the differences between the two groups of soft drinks (A and B) could be associated with the type of treated water used in their manufacturing at each moment. No sample exceeded the limits established for the concentration of TTHMs, so the soft drinks were prepared with water from the distribution network or treated water prepared in the same factory following EU normatives.[10] This has been corroborated by analyzing five soft drinks elaborated with mineral water (free of DBPs), which was negative for the species studied or contained chloroform only at very low levels (<1 μg/L). Figure 2 shows the chromatogram for

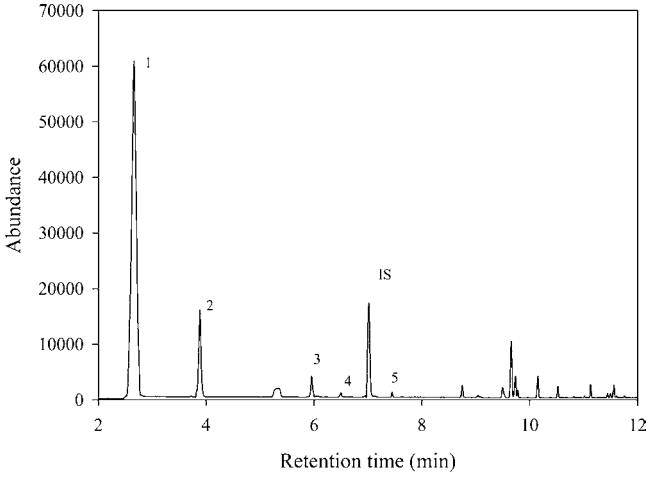


**Figure 2.** GC-MS chromatogram in SIM mode obtained in the analysis of soda 18. Peaks: (1) TCM; (2) BDCM; (3) DBCM; (4) DCIM; (5) TBM; (IS) internal standard. For compound abbreviations, see Table 1.

soda 18, which shows the peaks corresponding to the five species of THMs detected. After a retention time of 9 min, some peaks appeared in the chromatogram that correspond to flavors or other volatile compounds present in the beverage; these compounds did not interfere with the target analytes, so there was no matrix interference.

Table 3 shows the results obtained in the analysis of 60 fruit juices and nectars. In this case, only the four common THMs were found in these samples. DCIM was not detected because its level is associated with the amount of treated water in the beverage, and fruit juices contain a lower volume of water than soft drinks. The average TTHM concentrations in 100% natural juices were always <1 μg/L, and the predominant species was chloroform (TCM) followed by BDCM. As these juices do not contain treated water, the presence of these species at such a low level can be ascribed to contamination from the use of chlorinated sanitizers in the industry. In contrast, reconstituted juices can contain up to four THMs, and there are two distinctive groups as in soft drinks; reconstituted juices A with TTHM concentrations <1 μg/L and reconstituted juices B containing >2 μg/L. The average value for groups A and B were 0.5 ± 0.2 ($n$ = 10) and 6.2 ± 3.6 ($n$ = 11) μg/L, respectively. Moreover, the kind of fruit was not a relevant parameter because the same fruit was present in both groups. On the other hand, the average values of reconstituted juices A were similar to those of natural juice, but there was a significant difference because brominated species were present in reconstituted juices due only to the addition of treated water. With regard to nectar (ca. 50−75% of water), the average TTHM concentration was higher than that obtained in reconstituted juices, depending on the higher water volume.[26] Hence, there were noticeable variations in concentrations of TTHMs for natural juices, 100%, reconstituted juices, nectars, and soft drinks with average values of 0.47, 3.5, 8.3, and 20 μg/L, respectively, according to the volume of treated water included.

Figure 3 shows the distribution of the total trihalomethane concentrations as box plots in the beverages studied. The

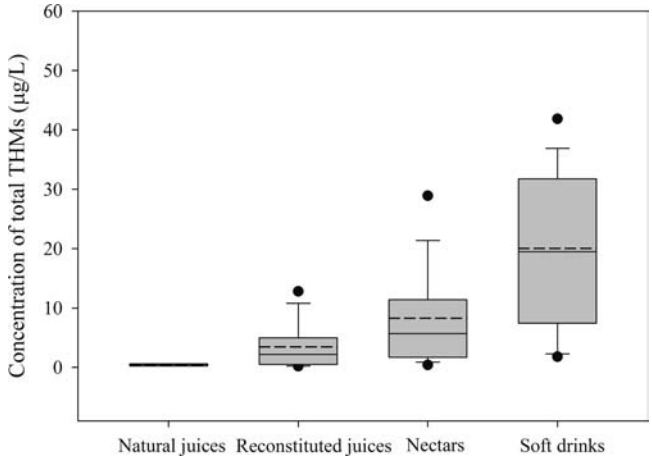


**Figure 3.** Representation of the total trihalomethane concentrations distributed as box plots in the beverages. The box plots indicate the mean concentration (dashed line) and the 10th, 25th, 50th, 75th, and 90th percentiles (points denote the 5th and 95th percentiles).

bottom and top of the box correspond to the 25th and 75th percentiles, whereas the band (median) inside the box is related to the 50th. The ends of the whiskers represent the lowest and highest observations, and the spacing between the different parts of the box give an indication of the degree of spread and skewedness in the data. There are again two different groups, nectars A with TTHM concentrations <6 μg/L ($n$ = 17; average value of 2.6 ± 1.9 μg/L) and nectars B with concentrations >6 μg/L ($n$ = 15; average value of 14.7 ± 8.7 μg/L). As occurred in the previous case, these variations cannot be attributed to the kind of fruit but rather to the difference between the qualities of the treated water used in their production. Moreover, this deduction was consolidated by comparison to the same product (nectar) manufactured in different bottling factories ($n$ = 12) shown in Table 3 following a word code. Thus, the average TTHM concentrations in nectars produced by A (nectars 1, 5, 28, and 30) or L (nectars 10, 11, 21, 23, and 24) bottling factories were 6.1 or 22.2 μg/L, respectively. Thus, in our study, the juices from factory L always provided the highest concentrations of THMs. These variations in the concentration of THMs in the same product can be explained on the basis of the type of treated water employed at each moment. Figure 4 shows the chromatograms obtained from the analysis of natural juice 7 (A), reconstituted juice 2 (B), and nectar 21 (C). Finally, for comparison purposes, several reconstituted juices of various flavors were analyzed from different European countries. As can be seen in Table 4, no sample presented TTHM concentrations above the levels allowed by EPA or EU for drinking water (80 or 100 μg/L).[9,10] Once again, two differentiated groups existed: one

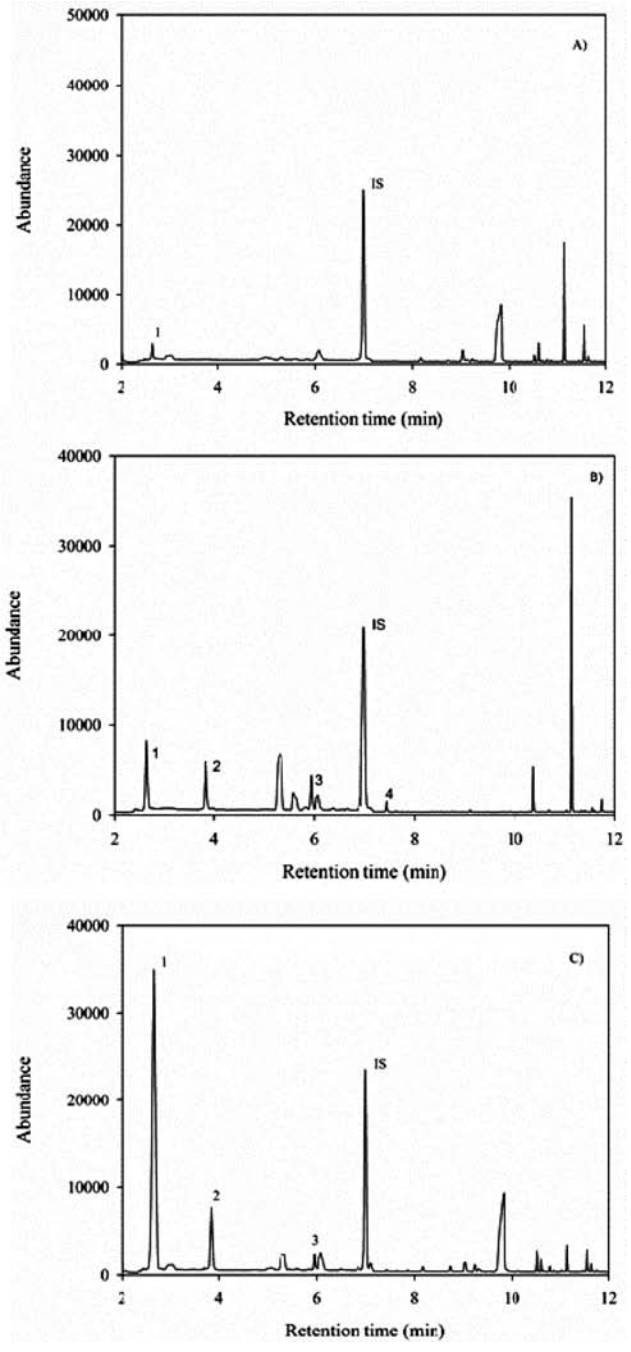


**Figure 4.** GC-MS chromatograms in SIM mode obtained in the analysis of natural juice 7 (A), reconstituted juice 2 (B), and nectar 21 (C) samples. Peaks: (1) TCM; (2) BDCM; (3) DBCM; (4) TBM; (IS) internal standard. For compound abbreviations, see Table 1.

for TTHM concentrations of 0.4 ± 0.2 μg/L ($n$ = 8) and the other for 9.9 ± 8.2 μg/L ($n$ = 6), similar to Spanish juices.

This study has revealed that chloroform can appear at concentrations <1 μg/L in beverages without treated water as a consequence of contamination due to the chlorinated sanitizers usually employed in the food industry. The treated water included as an ingredient is the main source of the presence of THMs, and the concentration and speciation of these compounds depend on the volume of treated water as well as the water-quality employed. Moreover, brominated THMs and one iodinated one (DCIM) appeared in these samples, which can be used as an indicator of the presence of treated water.

**Table 4. THMs Found in Reconstituted Fruit Juices from Several European Countries (±SD, Micrograms per Liter, $n$ = 5)**

| | country (flavor) | | | | | | | | | | | | | |
|---|---|---|---|---|---|---|---|---|---|---|---|---|---|---|
| compd | France (apple) | France (orange) | Poland (orange) | Poland (orange) | Belgium (orange) | Belgium (orange) | Belgium (orange) | Belgium (mix) | Belgium (mix) | Belgium (cranberry) | Portugal (apple) | Portugal (mix) | Portugal (mix) | Portugal (peach) |
| TCM | ND[a] | 0.77 ± 0.04 | 0.36 ± 0.02 | 0.25 ± 0.01 | 0.35 ± 0.02 | 0.90 ± 0.05 | 18 ± 1 | 17 ± 1 | 0.61 ± 0.03 | 14 ± 1 | 3.6 ± 0.2 | 0.26 ± 0.02 | 1.8 ± 0.1 | 0.45 ± 0.03 |
| DCBM | ND | ND | ND | ND | ND | 0.21 ± 0.01 | 0.14 ± 0.01 | 1.3 ± 0.1 | ND | 1.1 ± 0.1 | 1.1 ± 0.1 | 0.12 ± 0.01 | ND | 0.18 ± 0.01 |
| DBCM | 0.13 ± 0.01 | ND | ND | ND | ND | ND | 0.08 ± 0.01 | 0.09 ± 0.01 | ND | 0.44 ± 0.03 | ND | <0.05[b] | ND | ND |
| TBM | 0.09 ± 0.01 | ND | ND | ND | ND | ND | <0.07 | ND | ND | <0.07 | ND | ND | ND | ND |
| TTHMs[c] | 0.22 ± 0.01 | 0.77 ± 0.04 | 0.36 ± 0.02 | 0.25 ± 0.02 | 0.35 ± 0.02 | 1.1 ± 0.1 | 18 ± 1 | 18 ± 1 | 0.61 ± 0.03 | 16 ± 1 | 4.7 ± 0.3 | 0.38 ± 0.02 | 1.8 ± 0.1 | 0.63 ± 0.04 |

[a]Not detected. [b]<LOQ. [c]Total THMs.


dx.doi.org/10.1021/jf503431q | J. Agric. Food Chem. 2014, 62, 10240−10247

The proposed method could be adopted by public laboratories to perform routine controls of VOCs and THMs in beverages.

On the other hand, if it is estimated that a person can consume 2 L per day of drinking water (this includes drinking water consumed in the form of juices and other beverages containing tap water)[27] and taking into account that the most contaminated sample (soda 18 in Table 2) contained 52 $\mu$g/L of total THMs, a person could ingest >100 $\mu$g/L of THMs each day (MCL 80−100 $\mu$g/L).[9,10] This problem is aggravated because the default assumption of 2 L per day is not always appropriate or conservative with respect to populations, climates, and physical activity; thus, variations between 3.8 and 4.8 L have been referenced.[28] On the other hand, although chlorinated THMs were the common THMs present in beverages, some samples contained high concentrations of brominated compounds (reconstituted juice 5 and nectar 5 in Table 3) and one iodinated compound (sodas 18 and 20 in Table 2), these compounds being more cytotoxic and genotoxic when compared to their chlorinated analogues. In our opinion, the contribution of human exposure through beverages such as fruit juices and soft drinks per day is significant, taking into account that there are other sources of exposure through foods during the day. Thus, it is deemed acceptable to include these compounds as emergent pollutants in beverages because they have been already established as such for drinking water in several countries.

## AUTHOR INFORMATION


### Corresponding Author

*(M.G.) Phone/fax: +34-957-218-614. E-mail: mercedes.gallego@uco.es.



### Funding

This work was funded within the frameworks of Projects CTQ2013-42701 (Spain's Ministry of Education) and P09-FQM-4732DGI (Andalusian Regional Government). FEDER provided additional funding. I.M. is grateful for the award of a predoctoral grant from Project P09-FQM-4732DGI.


### Notes

The authors declare no competing financial interest.

## REFERENCES


(1) Richardson, S. D.; Ternes, T. A. Water analysis: emerging contaminants and current issues. *Anal. Chem.* **2011**, *83*, 4614−4648.

(2) Fleming-Jones, M. E.; Smith, R. E. Volatile organic compounds in foods: a five year study. *J. Agric. Food Chem.* **2003**, *51*, 8120−8127.

(3) Heikes, D. L.; Jensen, S. R.; Fleming-Jones, M. E. Purge and trap extraction with GC−MS determination of volatile organic compounds in table-ready foods. *J. Agric. Food Chem.* **1995**, *43*, 2869−2875.

(4) Entz, R. C.; Thomas, K. W.; Diachenko, G. W. Residues of volatile halocarbons in foods using headspace gas chromatography. *J. Agric. Food Chem.* **1982**, *30*, 846−849.

(5) Hrudey, S. E; Charrois, J. W. *Dinsinfection By-products and Human Health*, 1st ed.; IWA Publishing: London, UK, 2012.

(6) Richardson, S. D.; Fasano, F.; Ellington, J. J.; Crumley, F. G.; Buettner, K. M.; Evans, J. J.; Blount, B. C.; Silva, L. K.; Waite, T. J.; Luther, G. W.; McKague, A. B.; Miltner, R. J.; Wagner, E. D.; Plewa, M. J. Occurrence and mammalian cell toxicity of iodinated disinfection byproducts in drinking water. *Environ. Sci. Technol.* **2008**, *42*, 8330−8338.

(7) Irwin, R. J.; VanMouwerik, M.; Stevens, L.; Seese, M. D.; Basham, W. *Environmental Contaminants Encyclopedia*; National Park Service, Water Resources Division: Fort Collins, CO, USA, 1998.

(8) Aggazzotti, G.; Righi, E.; Fantuzzi, G.; Biasotti, B.; Ravera, G.; Kanitz, S.; Barbone, F.; Sansebastiano, G.; Battaglia, M. A.; Leoni, V.; Fabiani, L.; Triassi, M.; Sciacca, S. Collaborative Group for the Study of Chlorinated Drinking Waters and Pregnancy. Chlorination by-products (CBPs) in drinking water and adverse pregnancy outcomes in Italy. *J. Water Health* **2004**, *2*, 233−247.

(9) U.S. Environmental Protection Agency: National Primary Drinking Water Standards, 2003; http://www.epa.gov/safewater/mcl (accessed May 15, 2014).

(10) Directive 98/83/EC of the Council of 3 November 1998. *Off. J. Eur. Communities* **1998**, *L330*, 32−54.

(11) *Guidelines for Drinking-Water Quality*, 4th ed.; World Health Organization: Geneva, Switzerland, 2011.

(12) Jones, D. B.; Song, H.; Karanfil, T. The effects of selected preoxidation strategies on I-THM formation and speciation. *Water Res.* **2012**, *46*, 5491−5498.

(13) Bichsel, Y.; Gunten, U. V. Formation of iodo-trihalomethanes during disinfection and oxidation of iodide-containing waters. *Environ. Sci. Technol.* **2000**, *34*, 2784−2791.

(14) Richardson, S. D.; Thruston, A. D., Jr.; Caughran, T. V.; Chen, P. H.; Collette, T. W.; Schenck, K. M.; Lykins, B. W., Jr.; Rav-Acha, C.; Glezer, V. Identification of new drinking water disinfection by-products from ozone, chlorine dioxide, chloramine, and chlorine. *Water, Air, Soil Pollut.* **2000**, *123*, 95−102.

(15) *Exposure Factors Handbook, General Factors, Vol. 1*; U.S. Environmental Protection Agency, Office of Research and Development: Washington, DC, USA, 1997; EPA /600/P-95/002Fa.

(16) Food and Agriculture Organization of the United Nations/World Health Organization. *Benefits and Risks of the Use of Chlorine-Containing Disinfectants in Food Production and Food Processing*; Rome, Italy, 2008.

(17) Huang, A. T.; Batterman, S. Formation of trihalomethanes in foods and beverages. *Food Addit. Contam.* **2009**, *26*, 947−957.

(18) Graham, R. C.; Robertson, J. K. Analysis of trihalomethanes in soft drinks. *J. Chem. Educ.* **1988**, *65*, 735−737.

(19) Miyahara, M.; Toyoda, M.; Ushijima, K.; Nose, N.; Saito, Y. Volatile halogenated hydrocarbons in foods. *J. Agric. Food Chem.* **1995**, *43*, 320−326.

(20) Page, B. D.; Lacroix, G. Application of solid-phase micro-extraction to the headspace gas chromatographic analysis of halogenated volatiles in selected foods. *J. Chromatogr.* **1993**, *648*, 199−211.

(21) Campillo, N.; Viñas, P.; López-García, I.; Aguinaga, N.; Hernández-Córdoba, M. Purgue-and-trap capillary gas chromatography with atomic emission detection for volatile halogenated organic compounds determination in waters and beverages. *J. Chromatogr., A* **2004**, *1035*, 1−8.

(22) Dos Santos, M. S.; Martendal, E.; Carasek, E. Determination of THMs in soft drink by solid-phase microextraction and gas chromatography. *Food Chem.* **2011**, *127*, 290−295.

(23) Dos Santos, M. S.; Carasek, E. Development of a simple analytical method for determining trihalomethanes in beer using a headspace solid-phase microextraction technique. *Quim. Nova* **2013**, *36*, 1052−1056.

(24) Pizarro, C.; Pérez-del-Notario, N.; González-Sáiz, J. M. Optimisation of a simple and reliable method based on headspace solid-phase microextraction for the determination of volatile phenols in beer. *J. Chromatogr., A* **2010**, *1217*, 6013−6021.

(25) Miller, N. J.; Miller, J. C. *Statistics and Chemometrics for Analytical Chemistry*, 5th ed.; Prentice Hall: Englewood Cliffs, NJ, USA, 2005.

(26) Directive 2001/112/CE of the Council of 20 December 2001. *Off. J. Eur. Communities* **2001**, *L10*, 58−66.

(27) World Health Organization. *Guidelines for Drinking-Water Quality, Vol. 1, Recommendation*, 3rd ed.; Geneva, Switzerland, 2008.

(28) World Health Organization. *Domestic Water Quantity, Service Level and Health*; Geneva, Switzerland, 2003.

on GCE modified with AFc/CB/PVB has not been reported so far.

Additionally, to differentiate free and total sulfite, different sample pretreatment procedures are used. Kim[7] reported that free and total sulfite in three dehydrated foods were analyzed by extraction of the sulfite at pH 2.0 and 8.9, respectively, and ion chromatography (IC) with electrochemical detection was used. Warner[23] found that the rate of dissociation of the reversibly bound sulfite in wine and other foods was relatively slow at pH 3.0 but very rapid at pH 7.0. This difference in kinetics was exploited to develop a procedure to detect free and reversibly bound sulfite in food. Koch[24] investigated the influence of the pH on the efficiency of bound sulfite release. Hydroxymethylsulfonate (HMS) was chosen as a model substance for bound sulfite and was spiked in blank wine. It was found that at pH 6.0 only <20% of bound sulfite was recovered, while in alkaline solution (pH 11.0) an average recovery of about 90% was yielded. From the above publications, we can see that it still is a controversial issue as to how to extract sulfite from foods, and some of the current extraction methods might not be suitable for electrochemical analysis because they detect sulfite in the form of sulfate[24] or HMS,[23] which do not respond on the electrode via the above proposed eletrocatalytic oxidation process. Therefore, the second aim of this work was to examine appropriate extraction pH to differentiate free and total sulfite, matching the following measurement by the above-mentioned electrochemical method using an AFc/CB/PVB modified electrode, and to apply this method in muscle foods.

## 2. MATERIALS AND METHODS

**Chemicals and Reagents.** Chemical standards including sodium sulfite (Acros, Belgium), sodium metabisulfite (Aladdin, China), HMS (Aladdin, China), and AFc (J&K Scientific Ltd., China) were used as purchased without further purification. Reagents including pyrophosphate, tripolyphosphate, sodium chloride, citric acid, nitrate, phosphate, sulfuric acid, hydrochloric acid, sodium hydroxide, anhydrous ethanol, propyl alcohol, and PVB, poly(vinylidene fluoride) (PVDF) were of analytical grade and obtained from Aladdin, China. Nafion perfluorinated ion-exchange resin (5 wt %) was purchased from Sigma-Aldrich Chemical Co. (U.S.A.). Carbon black (Super-P-Li) was obtained from Timcal, Belgium. The supporting electrolyte used for all experiments was a 0.2 mol $L^{-1}$ sodium chloride solution. The working standard solutions of sodium sulfite and sodium metabisulfite were prepared daily in supporting electrolyte.

**Apparatus.** All cyclic voltammetric experiments were performed on a computer-controlled LK2005A Electrochemistry Workstation (Lanlike, China) with a conventional three-electrode configuration. A platinum electrode served as the counter electrode, and the saturated calomel electrode (SCE) was used as a reference in all electrochemical experiments. The working electrode (3 mm diameter) was GCE or GCE modified with appropriate chemicals including PVB, PVB/CB, PVB/AFc, PVB/CB/AFc, AFc/Nafion, and CB/AFc/Nafion. The working electrode for cyclic voltammogram scanning was operated within a potential range of 0−0.8 V (vs SCE) at scan rate of 50 mV $s^{-1}$. All tests were conducted at room temperature. The pH was measured using a Sartorius pH meter, model PB-10, employing a combined glass electrode with a SCE as external reference electrode.

**Preparation of Working Electrodes.** The GCE was polished with metallographic sandpaper polishing (5 $\mu$m) and then with 0.3 $\mu$m alumina powders ($\alpha$-$Al_2O_3$) on a wet polishing cloth to a mirror finish. Afterward, the electrode was successively cleaned using 1:1 (v/v) nitrate solution and anhydrous ethanol and rinsed with distilled water (4−5 min) with the aid of ultrasonic leaching. The freshly polished GCE was pretreated by cycling the potential several times between −0.2 and 1.2 V vs SCE, at a scan rate of 50 mV $s^{-1}$ in 0.5 mol $L^{-1}$ sulfuric acid solution until a steady signal was obtained (about 10−13 cycles). To prepare the modified electrode, a well-dispersed suspension was first prepared by perfect hand mixing of 5.0 mg of AFc and 100.0 mg of PVB; for AFc to be well dissolved, 5 mL of anhydrous ethanol was added. Subsequently, 125.0 mg of CB was added to the mixture, which was then diluted to 10 mL with anhydrous ethanol. For modifying GCE, 3.0 $\mu$L of the suspension was carefully dropped on the clean surface of the GCE using a micropipette, and it was left to dry at room temperature. Other modified electrodes (GCE/PVB, GCE/CB/PVB, GCE/CB/AFc, and GCE/CB/AFc/PVB) were prepared according the same procedure described above by dropping their corresponding chemical suspensions on the surface of GCE. The GCE/AFc/Nafion and GCE/CB/AFc/Nafion electrodes were made using Nafion instead of PVB.

**Sample Preparation.** Raw iced shrimps were purchased from the local markets and delivered to the lab in half an hour. Once delivered to the lab, the shell of the shrimps was peeled and homogenized using a JYL-350 food processor (Joyoung, China) and kept in a refrigerator for further use. Prior to analysis, muscle food was weighed accurately (10 g) into a 50 mL centrifuge tube, and 35 mL of propyl alcohol (2%, v/v) solution was added to stabilize sulfite inhibiting oxidation to their sulfate constituents.[25] Afterward, the sample was adjusted to the appropriate pH values using 0.5 mol $L^{-1}$ hydrochloric acid or 0.5 mol $L^{-1}$ sodium hydroxide (pH 8.4 for the extraction of free sulfite, pH 11.0 for the total sulfite) and then extracted with the aid of ultrasonic leaching for 10 min and centrifuged (3K15 model, Sigma, Gemany) at 8000 g for 15 min at 4 °C. The suspension was vacuumed filtered and transferred to a volumetric flask and then diluted to 50 mL with 2% (v/v) propyl alcohol for the following electrochemical measurement. The quantification of sulfite was carried out by using an external standard calibration curve based on the cyclic voltammograms.

For comparison study, an IC method was used for the determination of splitting samples, and the detailed description of sample preparation procedure has already been reported elsewhere.[8] In the current work, for the extraction of total sulfite the same procedure was followed, and for the extraction of free sulfite pH 8.4 was used.

## 3. RESULTS AND DISCUSSION

**Electrochemical Behavior of Sulfite at GCE/CB/AFc/PVB.** Figure 1A shows the typical cyclic voltammograms of 2.0 mmol $L^{-1}$ sulfite (0.2 mol $L^{-1}$ sodium chloride as supporting solution, pH 8.0 without adjustment) at bare GCE (a), GCE/PVB (b), GCE/PVB/AFc (c), GCE/PVB/CB (d), and GCE/CB/AFc/PVB (e). As seen in Figure 1A-a, the use of a bare GCE yielded a cyclic voltammogram with one anodic peak at 0.601 V, showing a small current value around 6.0 $\mu$A. When PVB was coated on the surface of GCE (Figure 1A-b), it was observed that the anodic peak disappeared, indicating that the electron transfer may be cut off by PVB film due its insulating property. When CB was coated within PVB membrane (Figure 1A-d), it was observed that the peak showed up at around 0.60 V with a small current value of about 7.0 $\mu$A, a little bit higher than that at bare electrode (Figure 1A-a), indicating that CB can effectively improve the electron-transfer kinetics, which can be attributed to its excellent electric conductivity. To improve this result in terms of sensitivity and selectivity, a modified GCE with PVB/CB/AFc was evaluated (Figure 1A-e). As seen in Figure 1A-e, a much improved and sharp electrochemical peak of sulfite was observed at the GCE/CB/AFc/PVB occurring at a much lower potential of about 0.50 V with much higher current of 14.5 $\mu$A, which shifted negatively by about 0.1 V. At a given level of AFc concentration, the anodic peak current increased with the increase of the sulfite concentration, and when the concentration of AFc changed, the concentration range of sulfite changed accordingly, indicating a typical electrochemical behavior for electrocatalytic oxidation by a mediator. Furthermore, it was observed that the

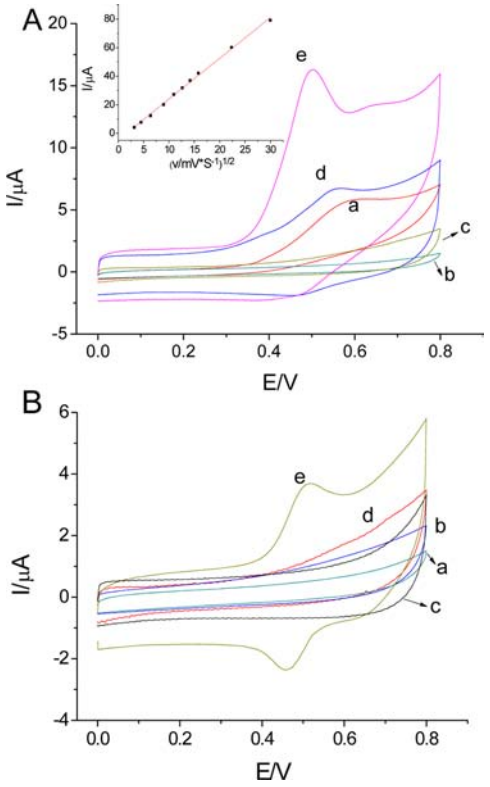


**Figure 1.** Cyclic voltammograms of 2.0 mmol $L^{-1}$ sulfite (A) (0.2 mol $L^{-1}$ NaCl as supporting solution) and 0.2 mol $L^{-1}$ NaCl (B) at bare GCE (a), GCE/PVB (b), GCE/AFc/PVB (c), GCE/CB/PVB (d), and GCE/CB/AFc/PVB (e). Inset of (A): the linear relationship between the oxidation peak currents and the square root of the scan rate. All tests were conducted at a scan rate of 50 mV $s^{-1}$.

sulfite oxidation peak current was proportional to the square root of the scan rate in the range of 10−900 mV $s^{-1}$ (Figure 1A, inset), which suggested that the reaction system of sulfite was controlled by diffusion. Similar results were found at bare electrode with the presence of AFc in sulfite aqueous solution.[15] However, the electrocatalysis of AFc could not take effect with the absence of CB at the GCE/PVB/AFc (Figure 1A-c), which further proved that CB improved the electron-transfer kinetics.

Figure 1B shows the typical cyclic voltammograms of supporting solution of 0.2 mol $L^{-1}$ sodium chloride (pH 8.0) at the corresponding electrodes the same as used in Figure 1A. As seen in Figure 1B, no peak showed up when using bare GCE, GCE/PVB, GCE/PVB/AFc, and GCE/PVB/CB. When GCE/CB/AFc/PVB (Figure 1B-e) was used, a quasi-reversible redox peak appeared at the potential of 0.511 V (anodic) and 0.447 V (cathodic) with $\Delta E_p \sim 64$ mV and $I_{pa}/I_{pc} \sim 1$, which was attributed to the AFc itself, indicating the electrode itself responded in the sodium chloride supporting solution. Fortunately, the peak current was much lower compared to that in sulfite solution, indicating that the interface caused by AFc was acceptable.

**Optimization Studies for Modification of GCE.** As a solid powder mediator, AFc is difficult to be modified on the smooth surface of GCE as to be mounted in a tube toward fabrication of a carbon paste electrode. In this work, several polymer films such as Nafion, PVDF, and PVB were tried to immobilize AFc onto the surface of the GCE. Nafion, as a sulfonated tetrafluoroethylene based fluoropolymer-copolymer, is widely used in the chemical modified electrodes because of its excellent film-forming, dissolving dispersing ability, stability, and ion-exchange properties.[26] The responses of both 2.0 mmol $L^{-1}$ sulfite and 0.2 mol $L^{-1}$ sodium chloride solution at GCE/CB/AFc/Nafion and GCE/AFc/Nafion were investigated. A pair of reversible redox peaks was observed in aqueous 0.2 mol $L^{-1}$ sodium chloride solution at GCE/CB/AFc/Nafion at potentials of 0.420 V (anodic) and 0.370 V (cathodic) with $\Delta E_p \sim 15$ mV and $I_{pa}/I_{pc} \sim 1$, which was apparently the redox peak of AFc. Another pair of almost equally high redox peaks at nearly the same potential was observed in aqueous 0.2 mmol $L^{-1}$ sulfite solution using the same electrode, which was also thought to be the redox peaks of AFc itself, showing that the anodic peak generated by the AFc catalytic oxidation of sulfite was absent. The same phenomena were observed at GCE/AFc/Nafion. This could be explained by the fact that the surface of GCE/CB/AFc/Nafion was electronegative charged and accordingly electrostatic repulsion of $SO_3^{2-}$ was generated, which made it hard for sulfite to approach the surface of the electrode. Also, when PVDF was used, film coating was difficult to be formed on the surface of GCE. As for PVB, it worked well in terms of stability and film-forming performance; moreover, no electrostatic repulsion of $SO_3^{2-}$ was observed, so PVB was chosen as the membrane matrix of the modified electrode.

The effects of the content of CB in the range of 3−60 $\mu$g on the detection of the aqueous 2.0 mmol $L^{-1}$ sulfite at GCE/CB/AFc/PVB were studied and are shown in Figure 2A. As seen, the sulfite oxidation peak increased with the increase of the content of CB from 3 to 35 $\mu$g. For content higher than 35 $\mu$g, the anodic peak current did not change much anymore, probably due to a saturation of the conductive area at the surface of the electrode. It was thought that CB in the

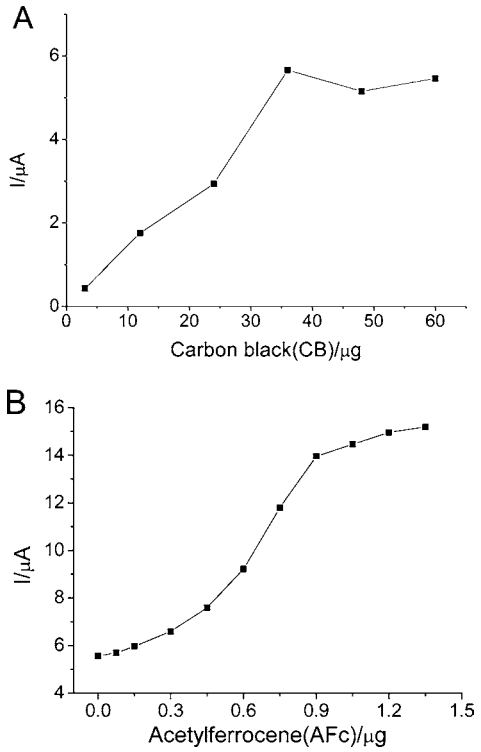


**Figure 2.** Effects of the content of CB (A) and AFc (B) on the current generated by the oxidation of 2.0 mmol $L^{-1}$ sulfite at GCE/CB/AFc/PVB.


dx.doi.org/10.1021/jf503339v | J. Agric. Food Chem. 2014, 62, 10248−10253

membrane structure of modified electrodes can affect electron transfer in the process of electrode reaction. Moreover, CB might create plenty of electroactive sites for analytes by increasing the effective area of modified electrode surface. In this way, 35 $\mu$g of CB was selected when modifying the CGE.

Figure 2B shows the effects of the content of AFc in the range of 0−1.3 $\mu$g on the current generated by the oxidation of 2.0 mmol $L^{-1}$ sulfite in 0.2 mol $L^{-1}$ sodium chloride solution at GCE/CB/AFc/PVB. As seen, the response of sulfite increased with increase of AFc; when the content was higher than 0.9 $\mu$g, the response current of sulfite became almost constant, suggesting that the sulfite response at a given concentration could not keep increasing by the sustained increase of the amount of catalyst. Therefore, AFc content at about 0.9 $\mu$g was chosen as optimal for the determination of sulfite.

**Electrochemical Responses of Sulfites under Different pH Conditions.** The proposed electrochemical method measures the current generated by direct oxidation of sulfite at electrodes. Moreover, the relative concentration of oxosulfur species is determined by the pH of the sample solution. At basic pH, $SO_3^{2-}$ is the predominant sulfur oxoanion, and at acidic pH, $HSO_3^-$ and $SO_3^{2-}$ exist in equilibrium.[7,27] It is necessary to optimize the extraction pH for the differentiation purpose of free and total sulfite as well as for the optimization of electrochemical signal of $SO_3^{2-}$. In this work, the electrochemical responses of sodium metabisulfite and HMS in aqueous solutions under different pH values were investigated. For comparison study, sodium sulfite was used as a contrast (Figure 3). Sodium metabisulfite and HMS were chosen to be studied because the former one is the most commonly used source of sulfur dioxide for seafood applications,[28,29] and the latter one can be regarded as a model substance for bound sulfite and can resolve into bisulfite and formaldehyde at basic conditions.[24] As shown in Figure 3A, no significant sulfite current was detected when pH < 6.0 in 2.0 mmol $L^{-1}$ sodium metabisulfite solution, possibly due to the absence of $SO_3^{2-}$, while $HSO_3^-$ was the predominant ion. With the increase of pH from 6.0 to 8.4, the sulfite oxidation peak response increased dramatically. When pH was higher than 8.4, the response approached constant. This phenomenon could be explained by the fact that the concentration of $SO_3^{2-}$ increased with the increase of pH in aqueous sodium metabisulfite. When pH > 8.4, the concentration of $SO_3^{2-}$ no longer increased. When it comes to sodium sulfite, the current response has a similar change trend as sodium metabisulfite with the change of pH (Figure 3C). As for HMS shown in Figure 3B, no significant peak current was detected at pH < 11.0, and a much improved and significant sulfite oxidation peak current response at the pH > 11.0 was detected. When pH > 11.0, the response leveled out, indicating that HMS no longer released sulfite at pH > 11.0. However, even at pH > 11.0, the response of HMS was about 60−70% of those signals of the same molar concentration of both sodium sulfite and sodium metabisulfite, probably because the HMS may present partly as irreversible bound form under this condition. As for the potential, it was hardly affected by the pH and was in the range of 0.45−0.5 V throughout the whole studied pH ranges for both HMS and sodium metabisulfite. Figure 3A−C may also indicate that pH above 11.0 is the optimum pH for the extraction of total sulfite, while pH around 8.4 is suitable to extract free sulfite, which well matches the electrochemical detection.

**Calibration Curve, Limit of Detection, and Repeatability of GCE/CB/AFc/PVB.** The optimized cyclic voltammetric (CV) experimental parameters were employed to acquire the analytical curve for sulfite. Cyclic voltammograms obtained after successive additions of the sulfite standard solution at GCE/CB/AFc/PVB are shown in Figure 4 with the concentration ranging from 0.03 to 4.0 mmol $L^{-1}$ in 0.2 mol $L^{-1}$ sodium chloride solution (pH 8.4). The inset in this figure depicted the analytical curve obtained for sulfite with the corresponding regression equation $I_{ap}$ ($\mu$A) = 2.899 + 6.935 × $10^{-3}$ C $SO_3^{2-}$ (mol $L^{-1}$) and correlation coefficient ($R^2$) 0.9994. The limit of detection (LOD), based on a signal-to-noise ratio of three (S/N = 3), was found to be 15 $\mu$M (calculated as $SO_2$), which is comparable to the previous reports using AFc modified carbon paste electrode to detect sulfite,[30] and was in the approximate order of magnitude compared with other electrochemical sensors modified with sensing material such as copper-salen[31] and iron-hexacyanoferrate.[32]

The intraday repeatability of the peak current was determined by successive measurements ($n$ = 7) of a 2.0 mmol $L^{-1}$ sulfite solution, and the relative standard deviation

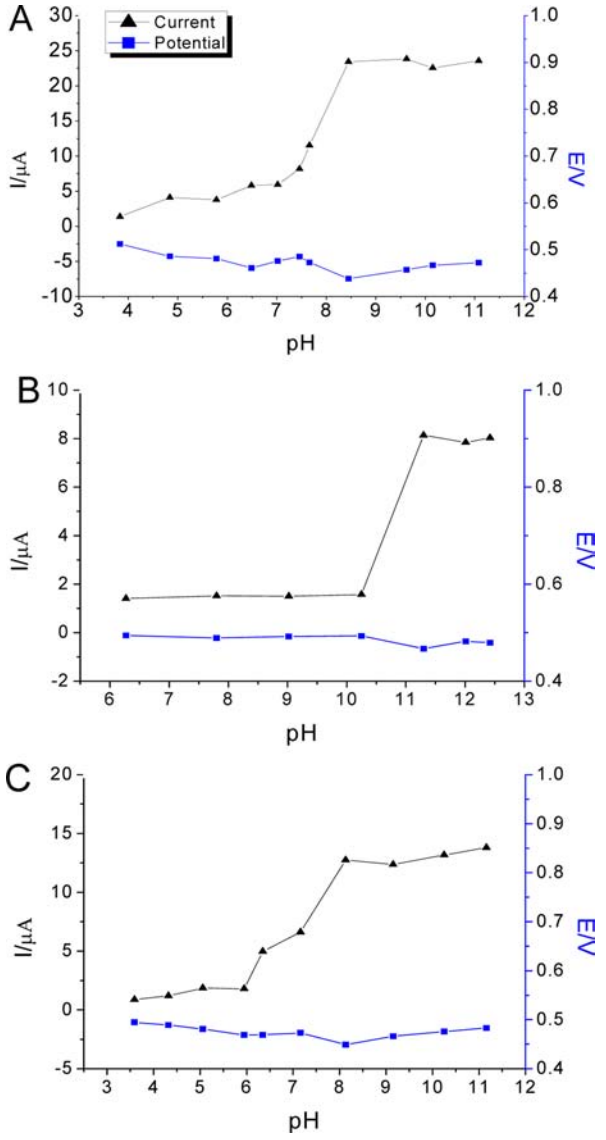


**Figure 3.** Electrochemical responses of 2.0 mmol $L^{-1}$ sodium sulfite (A), sodium metabisulfite (B), and HMS (C) at GCE/CB/AFc/PVB under different pH conditions.


dx.doi.org/10.1021/jf503339v | J. Agric. Food Chem. 2014, 62, 10248−10253

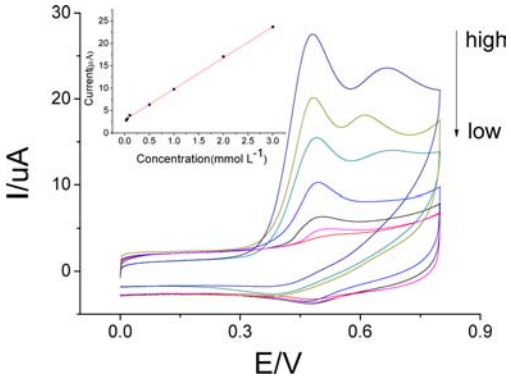


**Figure 4.** Cyclic voltammograms of sulfite concentration ranging from 0.03 to 4.0 mmol $L^{-1}$ at GCE/CB/AFc/PVB in 0.2 mol $L^{-1}$ NaCl (pH 8.4) as electrolyte with a scan rate of 50 mV $s^{-1}$; the inset is the calibration curve constructed by plotting current response vs sulfite concentration.

(RSD) of 2.4% was obtained. After a total of 15 successive measurements, compared with the first run, the peak current decreased around 5.0%, suggesting it is better to reprepare the electrode. In addition, five GCE/CB/AFc/PVB electrodes made in three successive days exhibited very stable responses (RSD = 7.2%, $n$ = 5) in the same 2.0 mmol $L^{-1}$ sulfite solution, showing thus the good repeatability of the electrode.

**Interference Study.** The suitability of the developed electrochemical sensor mainly depends on the influence of interfering species presented in real samples along with sulfite.[33] In order to apply the developed sensor for real sample analysis, the influence of interferences presented in seafood samples was studied by spiking these species in their proper forms in the muscle food matrices. No interferences could be found when including up to 100-fold of $Na^+$, $K^+$, $SO_4^{2-}$, and $Cl^-$, and 25-fold of pyrophosphate, tripolyphosphate, citric acid, nitrate, and phosphate in the standard solution of 2.0 mmol $L^{-1}$ sulfite. The largest tolerance yielded an error of less than ±5% of the analytical signal of sulfite.

**Sample Analysis and Comparison with IC Method.** Homogenized raw shrimp muscle foods spiked with sulfite at three levels (10, 30, and 100 mg $kg^{-1}$, calculated as $SO_2$) were used to evaluate the precision and recovery of the proposed method, at the same time, compared with a modified IC method using the splitting samples. Free or total sulfite was selectively extracted from matrix using pH 8.4 for extracting free sulfite and pH 11.0 for total sulfite as described above, and the results are summarized in Table 1. As shown, recovery values of 90.8, 88.6, and 88.1% were obtained at three fortified levels of 10, 30, and 100 mg $kg^{-1}$, respectively, with corresponding RSD of 2.2, 6.4, and 2.8% using the proposed method. When IC method was used, recovery values of 86.0, 83.0, and 87.7% were achieved respectively with corresponding RSD of 5.8, 3.2, and 1.5%. Moreover, Table 1 also demonstrates that free sulfite is the major form of sulfite in shrimp muscle foods with free/total ratio varying from 0.75 to 0.85 at three fortified levels using the proposed method and from 0.80 to 0.88 using the IC method, which is in accordance with other reports.[34] Additionally, the deviations between the two methods were in the range of −2.8−2.9 for free sulfite and 0.4−6.8 for total sulfite. Overall, no significant differences were observed between the two methods in terms of recovery, RSD, and free/total ratio.

## AUTHOR INFORMATION


### Corresponding Author

*E-mail: liwang-wh@hotmail.com. Tel.: 86-571-56975563. Fax: 86-571-56975801-9098.


### Notes

The authors declare no competing financial interest.

## ACKNOWLEDGMENTS

Financial supports from Zhejiang Provincial Natural Science Foundation of China (LY12C20013), National Natural Science Foundation of China (30800916) and National Science & Technology Pillar Program (2012BAD29B06) are gratefully acknowledged. The authors thank Mr. Feng Guo for providing the chemical material of carbon black for this study.

## ABBREVIATIONS USED

GCE, glassy carbon electrode; AFc, acetylferrocene; CB, carbon black; PVB, poly(vinyl butyral); HMS, hydroxymethylsulfonate; PVDF, poly(vinylidene fluoride); SCE, saturated calomel electrode; IC, ion chromatography

## REFERENCES


(1) Martins, S. I.; Jongen, W. M.; Van Boekel, M. A. A review of Maillard reaction in food and implications to kinetic modelling. *Trends Food Sci. Technol.* **2000**, *11*, 364−373.

(2) Manzocco, L.; Calligaris, S.; Mastrocola, D.; Nicoli, M. C.; Lerici, C. R. Review of non-enzymatic browning and antioxidant capacity in processed foods. *Trends Food Sci. Technol.* **2000**, *11*, 340−346.

(3) Lock, J.; Davis, J. The determination of disulphide species within physiological fluids. *TrAC, Trends Anal. Chem.* **2002**, *21*, 807−815.

(4) Gunnison, A. F.; Jacobsen, D. W. Sulfite hypersensitivity. A critical review. *CRC Crit. Rev. Toxicol.* **1987**, *17*, 185−214.

(5) Monier-Williams, G. W. *The Determination of Sulphur Dioxide in Foods*; HM Stationery Office: London, U.K., 1927.


**Table 1. Comparison of the Proposed Method with Reference Method (IC) in the Determination of Sulfite in Fortified Shrimp Muscle Samples**

| | proposed method | | | | | reference method (IC) | | | | | relative error (%)[d] | |
|---|---|---|---|---|---|---|---|---|---|---|---|---|
| | mean value ± SD ($n$ = 3) (mg $kg^{-1}$) | | | | | mean value ± SD ($n$ = 3) (mg $kg^{-1}$) | | | | | | |
| fortified level[a] (mg $kg^{-1}$) | free $SO_2$ | total $SO_2$ | recovery (%)[b] | RSD (%)[c] | free/total | free $SO_2$ | total $SO_2$ | recovery (%)[b] | RSD (%)[c] | free/total | free $SO_2$ | total $SO_2$ |
| 10 | 7.1 ± 0.3 | 9.1 ± 0.2 | 90.8 | 2.2 | 0.78 | 6.9 ± 0.2 | 8.6 ± 0.5 | 86.0 | 5.8 | 0.80 | 2.9 | 5.8 |
| 30 | 21.1 ± 1.2 | 26.6 ± 1.7 | 88.6 | 6.4 | 0.79 | 21.7 ± 1.9 | 24.9 ± 0.8 | 83.0 | 3.2 | 0.87 | 2.7 | 6.8 |
| 100 | 75.4 ± 1.7 | 88.0 ± 2.5 | 88.1 | 2.8 | 0.85 | 77.6 ± 2.6 | 87.7 ± 1.3 | 87.7 | 1.5 | 0.88 | −2.8 | 0.4 |

[a]Expressed as mg $kg^{-1}$ of $SO_2$. [b]Recovery calculated as the determined total sulfite divided by fortified level. [c]RSD calculated as standard deviation (SD) divided by total sulfite. [d](100 × (proposed method − reference method))/reference method.

(6) Li, Y.; Zhao, M. Simple methods for rapid determination of sulfite in food products. *Food Control* **2006**, *17*, 975−980.
(7) Kim, H. J.; Kim, Y. K. Analysis of free and total sulfites in food by ion chromatography with electrochemical detection. *J. Food Sci.* **1986**, *51*, 1360−1361.
(8) Iammarino, M.; Di Taranto, A.; Muscarella, M.; Nardiello, D.; Palermo, C.; Centonze, D. Development of a new analytical method for the determination of sulfites in fresh meats and shrimps by ion-exchange chromatography with conductivity detection. *Anal. Chim. Acta* **2010**, *672*, 61−65.
(9) Trenerry, V. C. The determination of the sulphite content of some foods and beverages by capillary electrophoresis. *Food Chem.* **1996**, *55*, 299−303.
(10) Isaac, A.; Davis, J.; Livingstone, C.; et al. Electroanalytical methods for the determination of sulfite in food and beverages. *TrAC, Trends Anal. Chem.* **2006**, *25* (6), 589−598.
(11) Paixão, T. R.; Bertotti, M. Ruthenium oxide hexacyanoferrate modified electrode for hydrogen peroxide detection. *Electroanalysis* **2008**, *20*, 1671−1677.
(12) Alamo, L. S. T.; Tangkuaram, T.; Satienperakul, S. Determination of sulfite by pervaporation-flow injection with amperometric detection using copper hexacyanoferrate-carbon nanotube modified carbon paste electrode. *Talanta* **2010**, *81*, 1793−1799.
(13) Ramírez, G.; Goya, M. C.; Mendoza, L.; Matsuhiro, B.; Isaacs, M.; Yo-Ying, C.; Arévalo, M. C.; Henríquez, J.; Cheuquepán, W.; Aguirre, M. J. Iron porphyrin-modified electrodes: Influence of the method of modification on the stability and electroactivity in oxidation of sulfite or hydrogensulfite in ethanol−water solutions. *J. Coord. Chem.* **2009**, *62*, 2782−2791.
(14) Lucero, M.; Ramírez, G.; Riquelme, A.; Azocar, I.; Isaacs, M.; Armijo, F.; Förster, J. E.; Trollund, E.; Aguirre, M. J.; Lexa, D. Electrocatalytic oxidation of sulfite at polymeric iron tetra(4-aminophenyl)porphyrin-modified electrode. *J. Mol. Catal. A: Chem.* **2004**, *221*, 71−76.
(15) Gao, Z. N.; Ma, J. F.; Liu, W. Y. Electrocatalytic oxidation of sulfite by acetylferrocene at glassy carbon electrode. *Appl. Organomet. Chem.* **2005**, *19*, 1149−1154.
(16) Kumar, S. S.; Narayanan, S. S. Electrocatalytic oxidation of sulfite on a nickel aquapentacyanoferrate modified electrode: Application for simple and selective determination. *Electroanalysis* **2008**, *20*, 1427−1433.
(17) Sartori, E. R.; Takeda, H. H.; Fatibello-Filho, O. Glassy carbon electrode modified with functionalized carbon nanotubes within a poly(allylamine hydrochloride) film for the voltammetric determination of sulfite in foods. *Electroanalysis* **2011**, *23*, 2526−2533.
(18) Kim, J.-M.; Rhee, S.-W. Electrochemical properties of porous carbon black layer as an electron injector into iodide redox couple. *Electrochim. Acta* **2012**, *83*, 264−270.
(19) Terasawa, N.; Yamato, K. Comparison of electrochemical and electromechanical properties of a high performance carbon black polymer actuator and a single-walled carbon nanotube polymer actuator. *Sens. Actuators, B* **2013**, *176*, 1103−1109.
(20) Tang, D.; Yuan, R.; Chai, Y.; Zhang, L.; Zhong, X.; Dai, J.; Liu, Y. Novel potentiometry immunoassay with amplified sensitivity for diphtheria antigen based on Nafion, colloidal Ag, and polyvinyl butyral as matrixes. *J. Biochem. Biophys. Methods* **2004**, *61*, 299−311.
(21) Guinovart, T.; Crespo, G. A.; Rius, F. X.; Andrade, F. J. A reference electrode based on polyvinyl butyral (PVB) polymer for decentralized chemical measurements. *Anal. Chim. Acta* **2014**, *821*, 72−80.
(22) Ghosh, A. K.; Ramachandhran, V.; Hanra, M. S.; et al. Studies on fouling and gel polarisation aspects of polyvinyl butyral blended cellulose acetate ultrafiltration membrane by resistance model approach. *Indian J. Chem. Technol.* **2000**, *7* (2), 55−60.
(23) Warner, C. R.; Daniels, D. H.; Fitzgerald, M. C.; Joe, F. L.; Diachenko, G. W. Determination of free and reversibly bound sulphite in foods by reverse-phase, ion-pairing high-performance liquid chromatography. *Food Addit. Contam.* **1990**, *7*, 575−581.
(24) Koch, M.; Köppen, R.; Siegel, D.; Witt, A.; Nehls, I. Determination of total sulfite in wine by ion chromatography after in-sample oxidation. *J. Agric. Food Chem.* **2010**, *58*, 9463−9467.
(25) De-Carvalho, L. M.; Schwedt, G. Sulfur speciation by capillary zone electrophoresis: Conditions for sulfite stabilization and determination in the presence of sulfate, thiosulfate, and peroxodisulfate. *Fresenius J. Anal. Chem.* **2000**, *368*, 208−213.
(26) Mauritz, K. A.; Moore, R. B. State of understanding of nafion. *Chem. Rev.* **2004**, *104*, 4535−4585.
(27) Barbe, J. C.; de Revel, G.; Joyeux, A.; Lonvaud-Funel, A.; Bertrand, A. Role of carbonyl compounds in SO(2) binding phenomena in musts and wines from botrytized grapes. *J. Agric. Food Chem.* **2000**, *48*, 3413−3419.
(28) Da Costa Machado Matos Carvalho, I. M.; Cavalcante, A. A. M.; Dantas, A. F.; Pereira, D. L. A.; Rocha, F. C. C.; Oliveira, F. M. d.; Da Silva, J. Environmental mutagenicity and toxicity caused by sodium metabisulfite in sea shrimp harvesting in Piauí, Brazil. *Chemosphere* **2011**, *82*, 1056−1061.
(29) Corte, L.; Roscini, L.; Zadra, C.; Antonielli, L.; Tancini, B.; Magini, A.; Emiliani, C.; Cardinali, G. Effect of pH on potassium metabisulphite biocidic activity against yeast and human cell cultures. *Food Chem.* **2012**, *134*, 1327−1336.
(30) Bai, L.; Gao, Z. N. Electrocatalytic oxidation of an sulfite at acetylferrocene modified carbon paste electrode and its electrochemical kinetics. *Chin. J. Anal Lab* **2008**, *27* (5), 80−83.
(31) Dadamos, T. R. L.; Teixeira, M. F. S. Electrochemical sensor for sulfite determination based on a nanostructured copper-salen film modified electrode. *Electrochim. Acta* **2009**, *54*, 4552−4558.
(32) García, T.; Casero, E.; Lorenzo, E.; Pariente, F. Electrochemical sensor for sulfite determination based on iron hexacyanoferrate film modified electrodes. *Sens. Actuators, B* **2005**, *106*, 803−809.
(33) Devaramani, S.; Malingappa, P. Synthesis and characterization of cobalt nitroprusside nano particles: Application to sulfite sensing in food and water samples. *Electrochim. Acta* **2012**, *85*, 579−587.
(34) Armentia-Alvarez, A.; Garcia-Moreno, C.; Peña-Egido, M. J. Residual levels of sulfite in raw and boiled frozen shrimp: Variability, distribution, and losses. *J. Food Prot.* **1994**, *57*, 66−69.

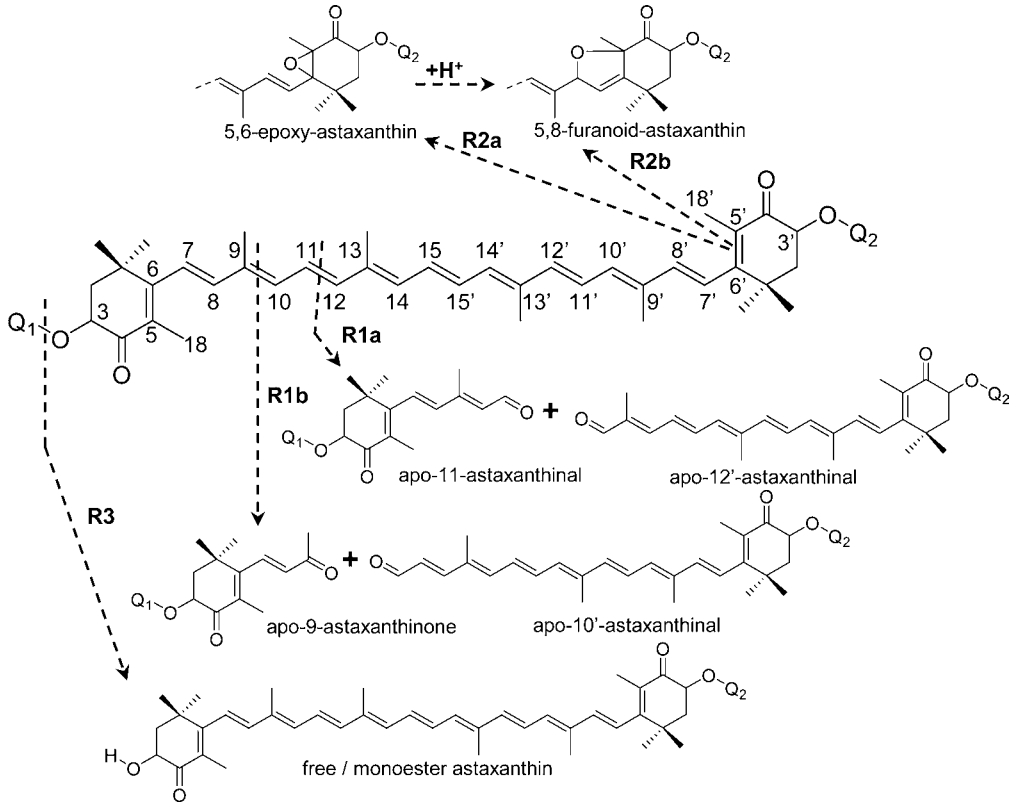


**Figure 1.** Chemical structures of astaxanthin and examples of degradation reactions and products. Reaction 1 (R1a and R1b) CDB cleavage; reaction 2 (R2a and R2b), 5,6-epoxide and 5,8-furanoid formation; reaction 3 (R3), de-esterification. Free astaxanthin, $Q_1 = Q_2 = H$; astaxanthin monopalmitate, $Q_1 = (C{=}O){-}C_{15}H_{31}$ and $Q_2 = H$; astaxanthin dipalmitate, $Q_1 = Q_2 = (C{=}O){-}C_{15}H_{31}$.

hypochlorite. The reaction products formed from *β,β*-carotene by hypochlorite bleaching were *β*-apo-13-carotenone, *β*-apo-15-carotenal, and *β*-apo-14′-carotenal. Furthermore, smaller volatiles derived from C7−C8 (e.g., *β*-cyclocitral) and C9−10 (e.g., *β*-ionone, dihydroactinidiolide) cleavages were found.[17,18]

Unlike *β,β*-carotene, xanthophylls (oxygenated carotenoids), comprising, among others, astaxanthin, canthaxanthin, lutein, and zeaxanthin, have not gained much attention, with respect to neither autoxidation nor hypochlorite bleaching. Furthermore, the fate of the fatty acid ester has not been assessed. For hypochlorite bleaching, it has been reported that the xanthophylls lutein, zeaxanthin, *α*-cryptoxanthin, (*β*-)-cryptoxanthin, and anhydrolutein were degraded, but no reaction products were described.[19] Upon oxidation of canthaxanthin by nickel peroxide, mainly apo-canthaxanthinals and canthaxanthinones were found.[20] It was also shown that upon autoxidation of free astaxanthin a series of apo-astaxanthinals and -astaxanthinones were found with apo-13-astaxanthinone as the main reaction product.[21] Treatment by peroxynitrite resulted in a mixture of apo-astaxanthins and nitro-astaxanthins.[22] The stability of the ester bond connecting astaxanthin and a fatty acid has never been assessed using light-accelerated autoxidation or hypochlorite bleaching, although the deliberate removal of the fatty acid by means of methanolic saponification and lipases has been reported.[23,24]

As a consequence of esterfication with fatty acids, the number of potential xanthophyll oxidative degradation products is expected to be larger than that for nonesterified xanthophylls. Therefore, this study reports on the analysis of apo-astaxanthin mixtures using a new method comprising reversed phase ultrahigh-performance liquid chromatography (RP-UHPLC) in combination with in-line electrospray ionization mass spectrometry (ESI-MS). For triggering the formation of reaction products through the various routes R1a, R1b, R2a, R2b and R3, light-accelerated autoxidation and hypochlorite bleaching were performed on astaxanthin, astaxanthin monopalmitate ester, and astaxanthin dipalmitate ester. The experiments were performed in pure solvent to minimize matrix effects.

## MATERIALS AND METHODS

**Materials.** (3*RS*)-Apo-12′-astaxanthinal (>98% w/w), (3*RS*,3′*RS*)-astaxanthin (97% w/w), (3*RS*,3′*RS*)-astaxanthin monopalmitate (97% w/w), and (3*RS*,3′*RS*)-astaxanthin dipalmitate (98% w/w) were purchased from CaroteNature (Lupsingen, Switzerland). ULC-MS grade methanol absolute (≥99.9% w/w), acetonitrile (≥99.9% w/w), water and formic acid (99% w/w), AR grade ethyl acetate (99.8% w/w), and HPLC grade chloroform (≥99.9% v/v, corrected for stabilizer, stabilized by 0.5−1.5% (w/v) ethanol) were purchased from Biosolve (Valkenswaard, The Netherlands). Sodium hypochlorite solution (active Cl 12.3−14.9% w/v) in $H_2O$ was purchased from Carl Roth (Karlsruhe, Germany).

**Preparation of Carotenoid Stock Solutions.** Apo-12′-astaxanthinal, free astaxanthin, astaxanthin monopalmitate, and astaxanthin dipalmitate were separately dissolved in chloroform. All stock solution concentrations were determined spectrophotometrically in hexane/chloroform (minimum 98% (v/v) *n*-hexane). Astaxanthin concentrations were determined at 470 nm using the absorption coefficient $A^{1\%}_{1\ cm}$ of 2100 L $g^{-1}$ $cm^{-1}$.[25] For astaxanthin monopalmitate and dipalmitate, concentrations were subsequently corrected for the difference in molecular weight, assuming that the fatty acid moiety did not contribute to absorption, yielding values of $A^{1\%}_{1\ cm}$ of 1501 and 1167 L $g^{-1}$ $cm^{-1}$, respectively. For apo-12′-astaxanthinal, concentrations were determined at 421 nm using $A^{1\%}_{1\ cm}$ of 2276 L $g^{-1}$ $cm^{-1}$.[26]

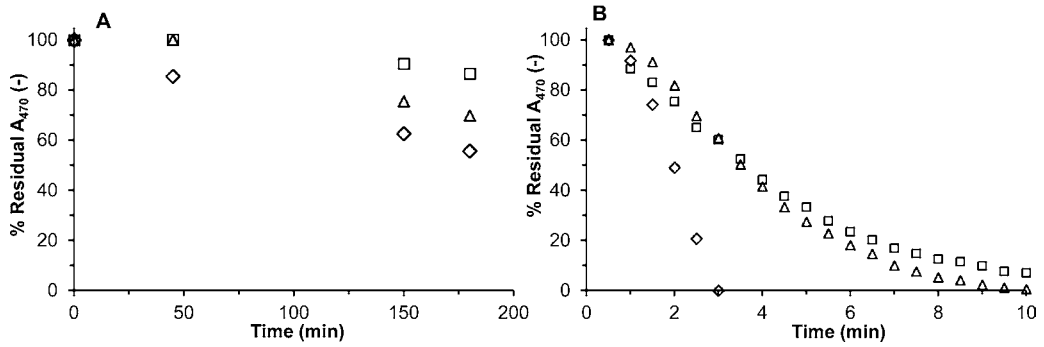


**Figure 2.** Decrease in visible absorption of various astaxanthins subjected to (A) light-accelerated autoxidation and (B) hypochlorite bleaching over time at 470 nm followed by spectrophotometry: free astaxanthin (□); astaxanthin monopalmitate (△); astaxanthin dipalmitate (◇).

**Light-Accelerated Autoxidation.** Free astaxanthin, astaxanthin monopalmitate, and astaxanthin dipalmitate were separately diluted in methanol to concentrations of 18.0, 19.6, and 24.0 $\mu$M, respectively. Aliquots (1.5 mL) were transferred to quartz cuvettes (type 114-QS, Hellma Analytics, Müllheim, Germany) closed with stoppers. A headspace of approximately 50 $\mu$L was left, filled with atmospheric air. Three cuvettes for each type of astaxanthin were irradiated for 3 h in a Suntest XLS+ (Atlas MTS, Chicago, IL, USA) equipped with a 1700 W xenon arc lamp and window glass filter. Irradiation energy was set to 30 W $m^{-2}$, and black standard temperature was maintained at 79 °C, which corresponded to a methanol sample temperature of 55 °C. The triplicates were pooled per type of astaxanthin and evaporated to dryness under a stream of nitrogen. Next, samples were redissolved in ethyl acetate and subsequently supplemented with acetonitrile to reach a ratio of ethyl acetate/acetonitrile 1:3 (v/v). Prior to UHPLC injection, samples were filtered using Whatman Rezist 13 0.45 $\mu$m PTFE syringe filters (GE Life Sciences, Fairfield, CT, USA).

**Hypochlorite Bleaching.** Bleaching of astaxanthin with hypochlorite was adapted from ref 15. Free astaxanthin, astaxanthin monopalmitate, and astaxanthin dipalmitate were diluted in 900 $\mu$L of methanol to concentrations of 30.3, 32.9, and 40.4 $\mu$M, respectively. Subsequently, degradation was carried out by the addition of 65 $\mu$L of approximately 12% (w/v) NaOCl solution and incubation for 10 min at room temperature in daylight. Estimation of the decrease in absorbance at 470 nm in time was made by comparison with a methanol/hypochlorite blank. Subsequently, the methanol layer was extracted three times using 900 $\mu$L of *n*-hexane each time. The *n*-hexane layers were pooled and evaporated to dryness under a stream of nitrogen in the dark. Rearrangement of 5,6-epoxides into 5,8-furanoids was performed by dissolving the evaporated hexane layer in 2.0 mL of 100% (v/v) ethanol. Eight hundred microliters of the ethanol-resolved degradation products was acidified with 50 $\mu$L of 0.1 M HCl.[27,28] Prior to UHPLC analysis, samples were prepared as for light-accelerated autoxidation.

**RP-UHPLC-PDA-ESI-MS Analysis of Degradation Products.** Separation and identification of carotenoid degradation products were carried out using a Thermo Accela UHPLC system (Thermo Scientific, San Jose, CA, USA) equipped with a pump, degasser, autosampler, and photodiode array (PDA) detector and coupled in-line to a LTQ-Velos double ion trap mass spectrometer equipped with a heated ESI probe (Thermo Scientific). Samples were injected onto an Acquity UPLC BEH Shield RP18 column (2.1 × 150 mm, 1.7 $\mu$m particle size; Waters, Milford, MA, USA) fitted to a Vanguard precolumn (2.1 × 5 mm, 1.7 $\mu$m particle size; Waters). The flow rate was 300 $\mu$L $min^{-1}$, operated at 23 °C. The eluents used were the following: 1% (v/v) acetonitrile in Millipore water (A), acetonitrile (B), and ethyl acetate (C), all containing 0.10% (v/v) formic acid as a mobile phase modifier. The elution program was started from 95% (v/v) A/5% (v/v) B and followed by 0−20 min linear gradient to 100% (v/v) B, 20−25 min isocratic at 100% (v/v) B, 25−32 min linear gradient to 100% (v/v) C, and 32−35 min isocratic at 100% (v/v) C. The eluent was adjusted to its initial composition in 10 min, followed by equilibration for 5 min. Detection wavelengths for UV−vis were set at 280 ± 0.5, 370 ± 0.5, and 450 ± 0.5 nm. Data were recorded at 10 Hz.

Mass spectrometric data were recorded in positive ion mode. Nitrogen was used as both sheath (30 arbitrary units) and auxiliary gas (10 arbitrary units). Settings of the mass spectrometer were tuned by 3 $\mu$L $min^{-1}$ direct injection of apo-12′-astaxanthinal in a mixture of ethyl acetate/acetonitrile 1:3 (v/v). Most settings were optimized via automatic tuning by using LTQ Tune Plus 2.7 (Thermo Scientific). The temperature of the ion transfer tube was 450 °C and the source voltage, 3.5 kV. Data were recorded over the $m/z$ segments 150−350 (0.50−10.00 min), 250−500 (10.00−15.40 min), 350−500 (15.40−19.00 min), 420−680 (19.00−23.00 min), 400−575 (23.00−24.40 min), 400−590 (24.40−24.95 min), 542−650 (24.95−26.80 min), 615−720 (26.80−29.30 min), and 615−1250 (29.30−37.00 min). Within these segments dynamic data-dependent $MS^2$ fragmentation was performed on the most intense parent ion ($x$ = 1) and subsequently on the second most intense parent ($x$ = 2). Dynamic exclusion was used to identify coeluting apo-astaxanthins. Also, it served the purpose of fragmenting both $[M + H]^+$ and $[M + Na]^+$ spectra within one chromatographic peak. A repeat count of two $MS^2$ spectra per parent ion and a maximum of $x$ = 25 or within a time frame of 5.0 s were used as settings. The collision-induced dissociation was set to 35%. Data acquisition and reprocessing were done with Xcalibur 2.2 (Thermo Scientific).

## RESULTS AND DISCUSSION

**Time Course of Color Loss of Various Astaxanthins.** The astaxanthin degradation was performed by light-accelerated autoxidation via exposure to high-intensity light conditions and elevated temperatures. Conventional autoxidation in darkness at lower temperatures could take up to several weeks.[29] Exposure of the parental *all-trans* forms of the three types of astaxanthin to light-accelerated autoxidation decreased the absorption at 470 nm (Figure 2A). After 180 min of exposure, a decrease of 13% for the free astaxanthin was observed, 30% of the monoester, and 44% of the diester. Subsequently, UHPLC-PDA-ESI-MS was used to assess the degradation products formed. As it is known that $\beta,\beta$-carotene forms small volatile compounds upon extensive degradation,[8,9] our degradation experiments were terminated with a high proportion of residual parent material, so that an overview of intermediate degradation products would be obtained. After 45 min, the absorption of the free astaxanthin and monoester was not reduced (Figure 2A). Their absorption spectra showed only a hypsochromic shift of 3−5 nm (data not shown). In contrast, the diester already showed a decrease in $A_{470}$ of 14% within 45 min. This indicated that esterification can influence color stability, which has also been reported before.[30,31]

The three types of astaxanthin were also exposed to bleaching with astaxanthin/HOCl ratios in the range of 1:3.5

and 1:5.0 (mol/mol). These ratios were reported to occur (locally) in inflamed tissues in the body.[18] The three types of astaxanthins all showed a ~100% decrease in $A_{470}$ upon bleaching, within 10 min (Figure 2B). This indicated that the reaction approached the end-point. No noticeable differences in stability between the free and monopalmitate astaxanthin degradation were observed, whereas the dipalmitate astaxanthin showed a more rapid degradation, as was also observed with light-accelerated autoxidation. No plausible explanation for this difference could be provided. Due to the different nature of the light-accelerated autoxidation and hypochlorite bleaching, they resulted in different sets of degradation products, which were used to design the LC-MS analysis method.

**Free Apo-astaxanthinals and Apo-astaxanthinones (R1a, R1b).** The absorbance maxima of the various degradation products of astaxanthin (esters) are expected to be related to the number of CDBs present in the molecules. To detect the widest array of apo-astaxanthins possible by PDA, detection wavelengths were set at 450, 370, and 280 nm. Using these three wavelengths, upon light-accelerated autoxidation a plethora of peaks was found, of which 44 could be tentatively annotated (Figure 3 and Table 1). Free apo-astaxanthinals and -astaxanthinones were found at different detection wavelengths and eluted between approximately 7.0 and 18.0 min. For the astaxanthin dipalmitate samples no PDA response was observed, indicating that no free apo-astaxanthinals and -astaxanthinones were formed. A first ascertainment of the apo-astaxanthinals and -astaxanthinones was done by locating their predicted $m/z$ values with the full scan MS data accompanying a chromatographic peak (Table 1). Using this approach, the matching protonated parent masses ($[M + H]^+$) for apo-9- and apo-13-astaxanthinone and apo-11-, apo-15-, apo-14′-, apo-12′-, and apo-10′-astaxanthinal were found upon treatment of both free and monopalmitate astaxanthin. The accompanying absorption spectra of these apo-astaxanthins had increasing $\lambda_{max}$ values from apo-9-astaxanthinone (260−270 nm) to apo-10′-astaxanthinal (452 nm). The smallest aldehyde, apo-7-astaxanthinal, was probably also formed. However, our approach will not visualize this compound due to its limited conjugated system or likely volatile properties. Nevertheless, the MS trace showed $[M + H]^+$ ($m/z$ 183) values that could potentially be associated with apo-7-astaxanthinal, but no diagnostic $MS^2$ fragments could be obtained for a reliable annotation.

The identification was further verified by analyzing $MS^2$ fragmentation of all $[M + H]^+$ parents annotated and comparison with the $MS^2$ spectrum of the apo-12′-astaxanthinal standard, which had retention time, parent mass, and $MS^2$ fragmentation similar to those of the apo-12′-astaxanthinal formed (peak 12) in our degradation study. The $MS^2$ spectra of the apo-astaxanthinals and -astaxanthinones all showed similar fragmentation behavior upon CID fragmentation (Supporting Information Table S1). In Figure 4A fragmentation of apo-12′-astaxanthinal is displayed as an example. The most intense neutral loss in the $MS^2$ spectra of the free apo-astaxanthinals and -astaxanthinones was 18 Da, yielding the fragment $m/z$ 363.2. The loss originates from the hydroxyl group at C3, analogous to water neutral loss with the (native) astaxanthin molecule.[32] The second water loss, yielding the fragment with $m/z$ 345.1, might have originated from the loss of the aldehyde group at C12′. An exception to this dominant water loss was found for apo-11-astaxanthinal, which showed a neutral loss of 42 Da ($m/z$ 205) as the main fragment. This preference for

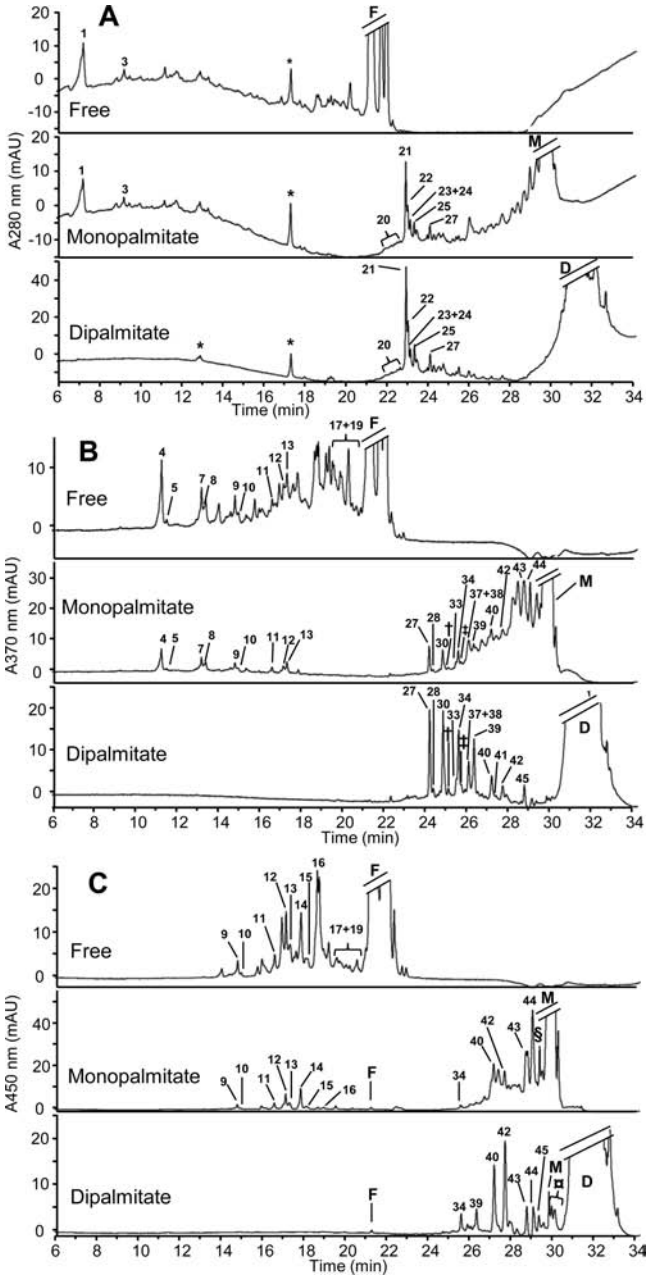


**Figure 3.** RP-UHPLC-UV chromatograms of free astaxanthin, its monoester, and its diester in methanol after 3 h of light-accelerated degradation: (A) 280 nm; (B) 370 nm; (C) 450 nm. F, free *all-trans*- and *cis*-astaxanthin; M, *all-trans*- and *cis*-astaxanthin monoester palmitate; D, *all-trans*- and *cis*-astaxanthin diester palmitate; ∗, ghost peak; †, peak 29; ‡, peak 34; §, peaks 46, 47, and 48; ¤, peaks 49, 50, and 51.

ejecting 42 Da instead of 18 Da could not be explained. CID fragmentation of $[M + H]^+$ apo-12′-astaxanthinal, and all of the other free apo-astaxanthin aldehydes and ketones described, resulted in a multitude of smaller fragments, typical for carotenoids.[7] In our study, these smaller mass fragments at, for example, $m/z$ 201, 187, 185, 173, 161, 157, 147, 145, 135, 133, and 119 could be interpreted similarly as for apo-carotenals and -carotenones derived from $\beta,\beta$-carotene upon EI-MS, in which a saturated carbon−carbon bond is fragmented and the molecular ion is rearranged. A series of polyene fragmentations and tandem rearrangements resulted in multiple

**Table 1. Apo-astaxanthins and Epoxy-astaxanthins Formed during Light-Accelerated Autoxidation and Hypochlorite Degradation of Free Astaxanthin, Astaxanthin Monopalmitate, and Astaxanthin Dipalmitate Tentatively Assigned by UHPLC-ESI-MS[a]**

| no. | Rt (min) | identification[b] | method[c] | UV−vis$_{max}$ (nm) | $[M + H]^+$, $[M + Na]^{\pm}$ ($m/z$) |
|---|---|---|---|---|---|
| | | **Apo-astaxanthin Ketones** | | | |
| **1** | 7.30 | apo-9-astaxanthinone | L | 260−270 | 223.1 |
| **22** | 22.98 | apo-9-astaxanthinone PE | L | 260−270[d] | 461.3, 483.3 |
| **23** | 23.10 | apo-9-astaxanthinone PE | L, H | 260−270[d] | 461.3, 483.3 |
| **4** | 11.24 | apo-13-astaxanthinone | L, H | 345 | 289.1 |
| **5** | 11.49 | apo-13-astaxanthinone | L | 345 | 289.2 |
| **27** | 24.05 | apo-13-astaxanthinone PE | L, H | 340 | 527.4, 549.4 |
| **28** | 24.22 | apo-13-astaxanthinone PE | L | 330 | 527.4, 549.4 |
| | | **Apo-astaxanthin Aldehydes** | | | |
| **20** | 21.81−22.39[e] | apo-7-astaxanthinal PE | L | <260 | 421.2, 443.1 |
| **3** | 9.27 | apo-11-astaxanthinal | L, H | 300−305 | 249.1 |
| **24** | 23.10 | apo-11-astaxanthinal PE | L, H | 260−270[d] | 487.3, 509.3 |
| **25** | 23.29 | apo-11-astaxanthinal PE | L, H | 313 | 487.3, 509.3 |
| **7** | 13.15 | apo-15-astaxanthinal | L, H | 381 | 315.2 |
| **8** | 13.27 | apo-15-astaxanthinal | L, H | 363 | 315.2 |
| **30** | 24.69 | apo-15-astaxanthinal PE | L, H | 377 | 553.4, 575.4 |
| **31** | 24.94 | apo-15-astaxanthinal PE | L, H | 380−390[d] | 553.4, 575.4 |
| **9** | 14.75 | apo-14′-astaxanthinal | L, H | 414 | 341.2 |
| **10** | 14.92 | apo-14′-astaxanthinal | L, H | 403 | 341.2 |
| **34** | 25.43 | apo-14′-astaxanthinal PE | L, H | 398[d] | 579.4, 601.4 |
| **35** | 25.54 | apo-14′-astaxanthinal PE | H | 397 | 579.4, 601.4 |
| **37** | 25.91 | apo-14′-astaxanthinal PE | L | 342[d] | 579.4, 601.4 |
| **12** | 17.07 | apo-12′-astaxanthinal | L, H | 429 | 381.2 |
| **40** | 27.01 | apo-12′-astaxanthinal PE | L, H | 430 | 619.4, 641.4 |
| **41** | 27.23 | apo-12′-astaxanthinal PE | H | 412 | 619.4, 641.4 |
| **14** | 17.78 | apo-10′-astaxanthinal | L | 452 | 407.2 |
| **15** | 18.05 | apo-10′-astaxanthinal | L | 410 | 407.2 |
| **42** | 27.54 | apo-10′-astaxanthinal PE | L | 449 | 645.4, 667.5 |
| **44** | 28.88 | apo-8′-astaxanthinal PE | L | 450 | 685.4 |
| **45** | 29.15 | apo-8′-astaxanthinal PE | L | 440 | 685.4 |
| **2** | 8.71 | **Epoxy-apo-astaxanthin Ketones** epoxy-apo-9-astaxanthinone | H | 268−271 | 239.1 |
| **21** | 22.89 | epoxy-apo-9-astaxanthinone PE | L, H | 260−270[d] | 477.2 |
| **26** | 23.37 | epoxy-apo-9-astaxanthinone PE | H | 260−270[d] | 477.3 |
| **6** | 12.83 | epoxy-apo-13-astaxanthinone | H | 336 | 305.1 |
| **29** | 24.67 | epoxy-apo-13-astaxanthinone PE | H | 335 | 543.4, 565.3 |
| | | **Epoxy-apo-astaxanthin Aldehydes** | | | |
| **32** | 25.31 | epoxy-apo-15-astaxanthinal PE | H | 393 | 569.4 |
| **36** | 25.56 | epoxy-apo-15-astaxanthinal PE | L | 401[d] | 569.4 |
| **38** | 25.91 | epoxy-apo-15-astaxanthinal PE | L | 342[d] | 569.4 |
| **13** | 17.24 | epoxy-apo-12′-astaxanthinal | L | 409 | 397.2 |
| **39** | 26.15 | epoxy-apo-12′-astaxanthinal PE | L | 394 | 635.4 |
| **43** | 28.58 | epoxy-apo-12′-astaxanthinal PE | L | 420 | 635.4, 657.4 |
| | | **Epoxy-astaxanthins** | | | |
| **17** | 18.00−20.50[e] | epoxy-astaxanthin | L | ND[f] | 613.3 |
| **18** | 18.00−20.50[e] | diepoxy-astaxanthin | L | ND[f] | 629.3 |
| **19** | 18.00−20.50[e] | triepoxy-astaxanthin | L | ND[f] | 645.3 |
| **46** | 29.30−29.60[e] | epoxy-astaxanthin PE | L | 400 | 851.6, 873.7 |
| **47** | 29.30−29.60[e] | diepoxy-astaxanthin PE | L | ND[f] | 889.5 |
| **48** | 29.30−29.60[e] | triepoxy-astaxanthin PE | L | ND[f] | 905.5 |
| **49** | 30.60−31.10[e] | epoxy-astaxanthin diPE | L | ND[f] | 1089.8 |
| **50** | 30.60−31.10[e] | diepoxy-astaxanthin diPE | L | ND[f] | 1106.7 |
| **51** | 30.60−31.10[e] | triepoxy-astaxanthin diPE | L | ND[f] | 1143.8 |
| | | **Other Apo-astaxanthins** | | | |
| **33** | 25.34 | epoxy-apo-15-astaxanthinoic acid PE | L | 400[d] | 585.4, 607.4 |
| **11** | 16.53 | apo-12′-astaxanthinoic acid | L | 414 | 397.2 |
| **16** | 18.65 | apo-8′-astaxanthinol | L | 425 | 449.2 |

[a]Degradation products are divided into classes and sorted from smallest carotenoid backbone upward. Underlined parent masses were in the $[M + Na]^+$ ionization state. Peak numbers refer to Figures 3 and 6. Additional $MS^2$ fragmentation data are given in Tables S1 and S2 of the Supporting Information. [b]Epoxides can be either in the 5,6 or 5,8 configuration. PE, palmitate ester; diPE, dipalmitate ester. [c]L, light-accelerated autoxidation; H, hypochlorite bleaching. [d]Mixture of visible spectra due to coelution. [e]No accurate retention time could be determined. [f]ND, not determined.



dx.doi.org/10.1021/jf503520q | J. Agric. Food Chem. 2014, 62, 10254−10263

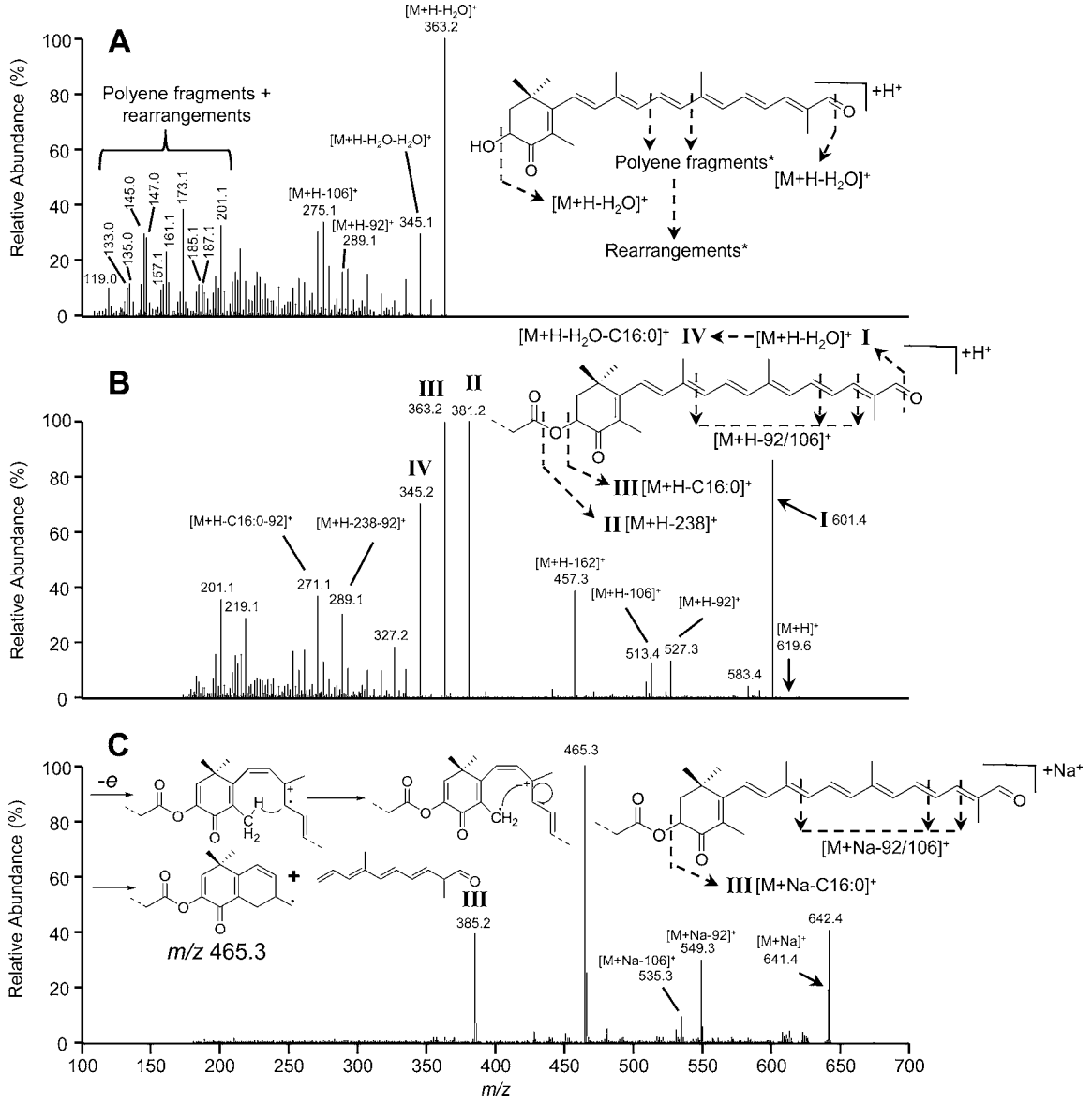


**Figure 4.** (A) $MS^2$ spectrum of $[M + H]^+$ apo-12′-astaxanthinal; (B) $MS^2$ spectrum of $[M + H]^+$ apo-12′-astaxanthinal palmitate ester; (C) $MS^2$ spectrum of $[M + Na]^+$ apo-12′-astaxanthinal palmitate ester. ∗, examples; fragmentation can occur at multiple C−C bonds in the polyene moiety. Roman numerals refer to $MS^2$ fragments in Supporting Information Table S2.

ejections of $CH_4$ and $CH_2$, giving rise to this wide array of smaller $MS^2$ fragment ions.[7] Fragments resulting from toluene and xylene polyene elimination products were low in abundance and could in the case of apo-12′ astaxanthinal be annotated to $m/z$ 289.1 and 275.1. Other fragment ions could not be rerouted to a fragmentation of the parent ion.

**Apo-astaxanthinal and Apo-astaxanthinone Palmitate Esters (R1a, R1b).** When astaxanthin monopalmitate and dipalmitate were subjected to light-accelerated autoxidation, additional peaks appeared in the hydrophobic region of the chromatogram (21.5−30 min) (Figure 3). Again, a first annotation was performed by tracing their respective parent masses (Table 1). Upon assessment of the UV−vis absorption spectra of the peaks, a similar trend was observed as for the free apo-astaxanthinals and -astaxanthinones (Figure 5). The absorption maxima slightly deviated from previously reported $\lambda_{max}$ values of purified free apo-astaxanthinals and -astaxanthinones (1−14 nm), possibly due to the use of the different LC solvents and coelution with other reaction products.[21] This led to the conclusion that a series of apo-9- to apo-8′-astaxanthinals and -astaxanthinones palmitate esters were formed.

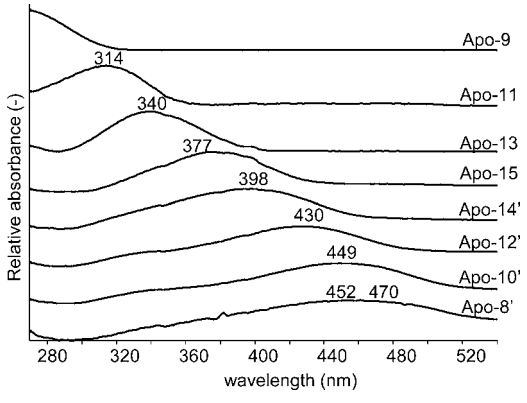


**Figure 5.** Overlay of UV−vis absorbance spectra of several apo-astaxanthin palmitate ester ketones and aldehydes.


dx.doi.org/10.1021/jf503520q | J. Agric. Food Chem. 2014, 62, 10254−10263

Similar to the astaxanthin esters, $MS^2$ spectra were used to identify the apo-astaxanthin backbone and the esterified fatty acid (Supporting Information Table S2).[32] As an example, the fragmentation of $[M + H]^+$ apo-12′-astaxanthinal palmitate (peak 40) is explained (Figure 4B). Again, water loss, yielding fragment $m/z$ 601.4 (**I**) was observed, but this time resulting from the aldehyde or ketone group. Most abundant were the fragments at $m/z$ 381.2 (**II**), representing the apo-12′-astaxanthinal backbone, and $m/z$ 363.2 (**III**), which represented the apo-astaxanthin that ejected C16:0. The typical polyene elimination products toluene (92 Da) and xylene (106 Da) were found at $m/z$ 527.3 and 513.4, respectively, albeit in low intensities. Toluene and xylene neutral losses were formed only for apo-12′-astaxanthins and larger apo-astaxanthins and not for the smaller ones. Furthermore, tandem losses of water and palmitate yielded the fragment at $m/z$ 345.2 (**IV**). Also, tandem losses of palmitate ketene and toluene (yielding $m/z$ 289.1) and palmitate and toluene (yielding $m/z$ 271.1) were observed. Contrary to the free apo-7-astaxanthinal, molecular ions of the palmitate ester of apo-7-astaxanthinal (peak 20) could be detected between Rt values of 21.8 and 22.4 min. Upon fragmentation of both the $[M + H]^+$ and $[M + Na]^+$ parents ($m/z$ 421.2 and 443.1, respectively), diagnostic fragments **I**, **II**, and **III** could be annotated (Supporting Information Table S2).

As an additional confirmation of the apo-astaxanthinal and -astaxanthinone palmitoyl structures, esterified astaxanthin sodium adducts $[M + Na]^+$ were analyzed. It has been shown that upon fragmentation, the $MS^2$ of sodiated ions strongly deviated from the protonated $MS^2$ fragmentation.[32,33] This was also the case for apo-astaxanthin palmitate esters as shown in Figure 4C. No fragments similar to **II** were found in this case; only the palmitate loss **III** is visible at $m/z$ 385.2 (for apo-7-astaxanthinal and apo-9-astaxanthinone a neutral loss of 238 Da was visible). The main fragment at $m/z$ 465.3 represented a sodiated benzonium ion and could be explained, similarly as for astaxanthin esters, by ring closure at C18 to C9 after electron rearrangement at C5−C6 (Figure 4C inset).[33,34] Remarkably, the formation of this benzonium ion was dominant over the other fragments and could already be observed with apo-9-astaxanthinone. As the sodiated parent mass of apo-9-astaxanthinone is $m/z$ 483.3, one might argue that the $m/z$ 465.4 fragment represents a simple water loss.

**Other Apo-astaxanthins and *cis*-Apo-astaxanthins (R1a, R1b).** Besides aldehyde and keto functional groups, we also screened for apo-astaxanthinols and apo-astaxanthinoic acids. Only one apo-astaxanthinol could be annotated. Instead of the parent mass of apo-8′-astaxanthinal, an $m/z$ of 449.2 was detected, suggestive for apo-8′-astaxanthinol (peak 16, Table 1 and Figure 3C). The presence of a C7−C8 CDB apo-8′-degradation product indicated that probably the corresponding apo-7-astaxanthin was also formed.

In Table 1, it can be observed that similar apo-astaxanthinal or -astaxanthinone structures were annotated to multiple chromatographic peaks (e.g., peaks 4/5, 7/8, 9/10, 14/15, and 39/43). Probably these represented different *cis*-apo-astaxanthin geometrical isomers. As also *cis*-isomers were formed from *all-trans*-astaxanthin (results not shown), this conclusion seems plausible. Assignment of the geometrical isomers using blue shifts in $\lambda_{max}$ compared to the *all-trans* isomer is common practice. As these compounds were present in trace amounts, and because it was not always possible to baseline separate degradation products to obtain a spectrum representing a single compound, *cis* and *all-trans* annotations were not pursued.

**Epoxy-astaxanthins (R2a, R2b).** The formation of epoxides was observed for intact astaxanthin (esters) upon light-accelerated degradation (Table 1). For the free astaxanthin, parent masses associated with mono-, di-, and triepoxides (e.g., epoxides on the C5−C6, C5′-C6′, and C15−C15′ positions) were found (peaks 17−19), eluting together with a plethora of other components just before the free astaxanthin peak F at 370 nm (Figure 3B). Presumably, the astaxanthin epoxides were also visible at 450 nm (Figure 3C), because epoxides normally show a small hypsochromic shift compared to astaxanthin, as will be elaborated later. Fragmentation of the epoxides showed two consecutive water losses and again a multitude of smaller fragments, the most intense of which were annotated in Tables S1 and S2 of the Supporting Information. Most likely, the epoxide groups were in the 5,6-epoxide or the 5,8-furanoid position, reported predominant in autoxidation of $\beta,\beta$-carotene.[5,9] When the carotenoid's C5−C6 and C5′-C6′ positions are occupied with epoxides, a third epoxide group might, for example, be located at the 15−15′ position.[9] Similarly, mono-, di-, and triepoxides were found for astaxanthin monopalmitate (peaks 46−48) and dipalmitate (peaks 49−51) (Table 1; Figure 3B,C). Also for the monopalmitate, the formation of intact astaxanthin epoxides upon autoxidation was observed as a large hump, which made it difficult to pinpoint exact retention times.

**Epoxy-apo-astaxanthinones and -astaxanthinals (R1a, R1b, R2a, R2b).** Two abundant free apo-astaxanthins, which were found upon hypochlorite degradation of free astaxanthin, its monopalmitate, and its dipalmitate, had parent masses of $m/z$ 239.1 and 305.1. These corresponded to the masses of epoxy-apo-9-astaxanthinone (peak 2) and epoxy-apo-13-astaxanthinone (peak 6), respectively (Table 1; Figure 6). Furthermore, for the astaxanthin monopalmitate and dipalmitate, the esterified forms of the epoxy-apo-9-astaxanthinone with $m/z$ 477.3 (peak 26) and epoxy-apo-13-astaxanthinone with $m/z$ 543.4 (peak 29) were annotated. Following the identification strategy used throughout this study, the epoxy palmitate ester species were identified by fragments **II** and **III** (Figure 4B), similar to apo-12′-astaxanthinal palmitate.

$MS^2$ fragmentation could not clarify the position of the epoxide groups, as both parent ions would result in similar fragment ions.[5,35] Therefore, further evidence for the identification of the apo-9 and apo-13 epoxide ketones was provided by the UV−vis absorption spectra. First, the epoxy-apo-13-astaxanthinone (peak 6) and its palmitate ester (peak 29) showed a blue shift of approximately 5 nm in the UV−vis absorption spectrum compared to apo-13-astaxanthinone (palmitate ester) (Figure 7A). This indicated that the conjugated system was only slightly shortened. The magnitude of the hypsochromic shift is dependent on the position of the epoxide group. Typically, a 5,6-epoxide group shortens the conjugated system with only a single double bond, whereas with a 5,8-furanoid group two double bonds are sacrificed. For intact carotenoids, epoxidation results in blue shifts of 4−13 nm for 5,6-epoxides (e.g., zeaxanthin−antheraxanthin) and blue shifts of 23−28 nm for 5,8-furanoids (e.g., zeaxanthin−mutatoxanthin).[36] For the apo-9 epoxide ketones a blue shift could not be detected due to the detection limits of the PDA detector. Although the influence of a shortened carbon skeleton of apo-astaxanthins on the magnitude of the hypsochromic shift has never been reported, the observed blue shift indicated the

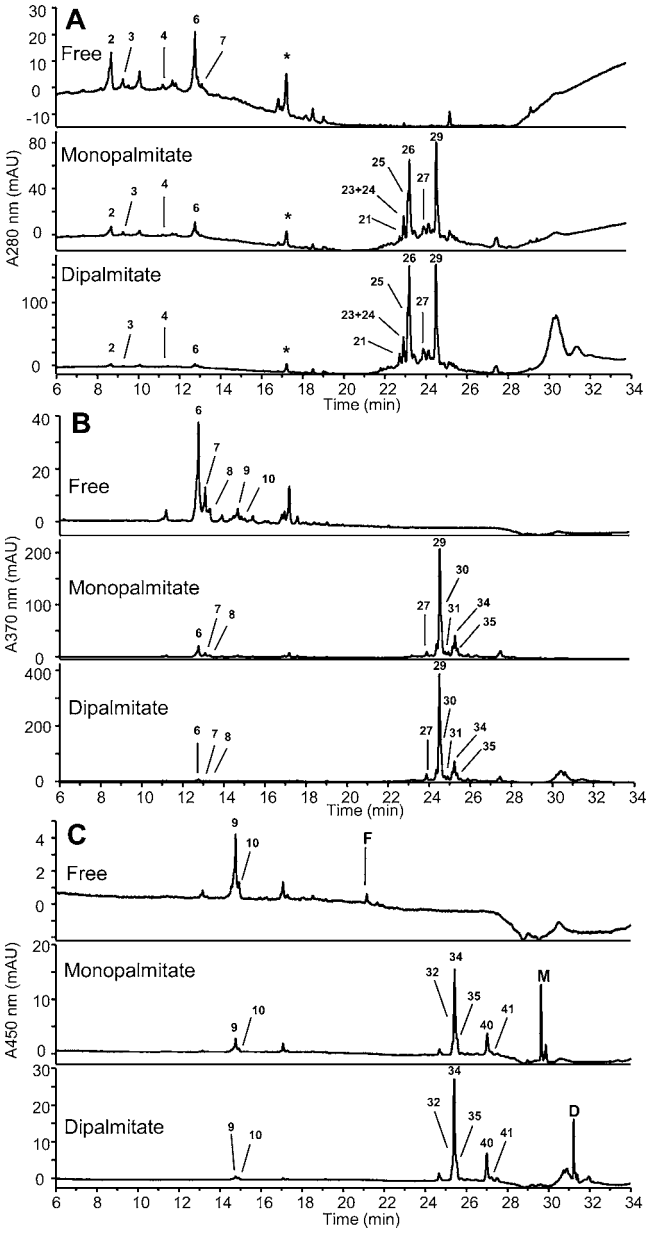


**Figure 6.** RP-UHPLC-UV profiles of hypochlorite-degraded free, monoester, and diester astaxanthin in methanol: (A) 280 nm; (B) 370 nm; (C) 450 nm. F, free *all-trans-* and *cis*-astaxanthin; M, *all-trans-* and *cis*-astaxanthin monoester palmitate; D, *all-trans-* and *cis*-astaxanthin diester palmitate; ∗, ghost peak.

presence of a 5,6-epoxide rather than a 5,8-furanoid group for the apo-13 epoxide (peak 29).

Acidification of the apo-astaxanthin degradation products in ethanol with 0.1 M hydrochloric acid, followed by RP-UHPLC analysis, did not lead to unambiguous annotation of the 5,6 or 5,8 configuration of the epoxide group (Figure 7B).[28] Peaks 21 and 26 (apo-9) remained intact, hinting at a 5,8-configuration. Peak 29 (apo-13) only partially disappeared, and no ketone-related new peaks appeared, hinting at either a 5,6-epoxide or a 5,8-furanoid configuration. However, for peak 29 the hypsochromic shift after acidification was only 9 nm, which might be attributed to the disappearance of apo-15-astaxanthinal palmitate (peak 30) (Figure 7B). This small hypsochromic shift would argue in favor of the 5,6-epoxide. The acidification protocol was originally designed for intact carotenoids, thus without the presence of reactive aldehyde and ketone groups as in apo-astaxanthins. All apo-astaxanthin aldehydes disappeared upon acidification, whereas the less reactive ketones partially remained. Therefore, acidification seems less suitable for distinguishing 5,6-epoxides and 5,8-furanoids in the more reactive apocarotenoids.

Epoxidation of carotenoids with HOCl might proceed as has been described for unsaturated fatty acids and cholesterol.[37] In Figure 7C this reaction is visualized as follows: the electrophilic addition of HOCl to the 5−6 CDB results in intermediate **1**. The remaining $OH^-$ is added to either C5 or C6, resulting in chlorohydrin carotenoids (**2**). The 5,6-epoxide (**3**) or 5,8-furanoid (**4**) is subsequently formed by dehydrochlorination of **2**.[38] Additionally, the released HCl from **2** might trigger the conversion of **3** into **4**. Chlorohydrins might also be an end-point in this type of reaction,[37] but this was not the case here, as indicated by the isotope ratio of parent mass $m/z$ 305.1 (Figure 7D). The presence of a chlorohydrin structure would have resulted in a relative intensity of 32% for the third parent mass isotope ($m/z$ 307.1), for which only a relative intensity of 3.8% was found. This supported the formation of 5,6-epoxides or 5,8-furanoids and excluded the presence of a chlorohydrin structure.

Epoxy-apo-astaxanthinals and -astaxanthinones were also found in conjunction with reaction 1 upon light-accelerated degradation. For free astaxanthin and astaxanthin monopalmitate epoxy-apo-12′-astaxanthinal (peak 13) was annotated (Table 1). The absorbance maximum of the epoxy-apo-12′-astaxanthinal had a hypsochromic shift of approximately 20 nm compared to apo-12′-astaxanthinal. Besides apo-astaxanthins esterified with palmitate, also their epoxidized forms were found upon degradation of astaxanthin monopalmitate and dipalmitate. The palmitoyl esters of epoxy-apo-9-astaxanthinone (peak 21), epoxy-apo-15-astaxanthinal (peaks 32, 36, and 38), epoxy-apo-12′-astaxanthinal (peaks 39 and 43), and epoxy-apo-15-astaxanthinoic acid (peak 33) were all traced. The occurrence of multiple epoxides can be explained by either isomerization of the polyene backbone (*all-trans* to *cis* conversion), or the variation in 5,6-epoxide or 5,8-furanoid, or a combination thereof.

**Degradation of the Fatty Acid Ester (R3).** Upon examination of the diester chromatograms (Figures 3C and 6C), de-esterification was observed with especially the hypochlorite bleaching treatment, as free apo-astaxanthins (e.g., peaks 2−4 and 6−10) were formed. The de-esterification did not lead to the annotation of any new compounds and proceeded in conjunction with reaction 1 and, occasionally, reaction 2. Most probably, the de-esterification proceeded via a base-induced hydrolysis with the apo-astaxanthin as the leaving group. The reactive nucleophile in this case is likely a hypochlorite anion ($OCl^-$) or a hydroxide ($OH^-$) resulting from the HOCl. As the degradation was performed in methanol, also a methoxide anion ($MeO^-$) might have served as nucleophile, resulting in a fatty acid methyl ester.

For light-accelerated autoxidation, trace amounts of free astaxanthin (peak F) and astaxanthin monopalmitate (peak M) were found (Figure 3C). When the degradation was continued to 7 h, also no accumulation of free astaxanthin and astaxanthin monopalmitate was observed (data not shown). Observation of the trace amounts of de-esterification products upon light-accelerated autoxidation (e.g., a system that does not favor de-esterification) underscores the sensitivity of the analysis method employed.

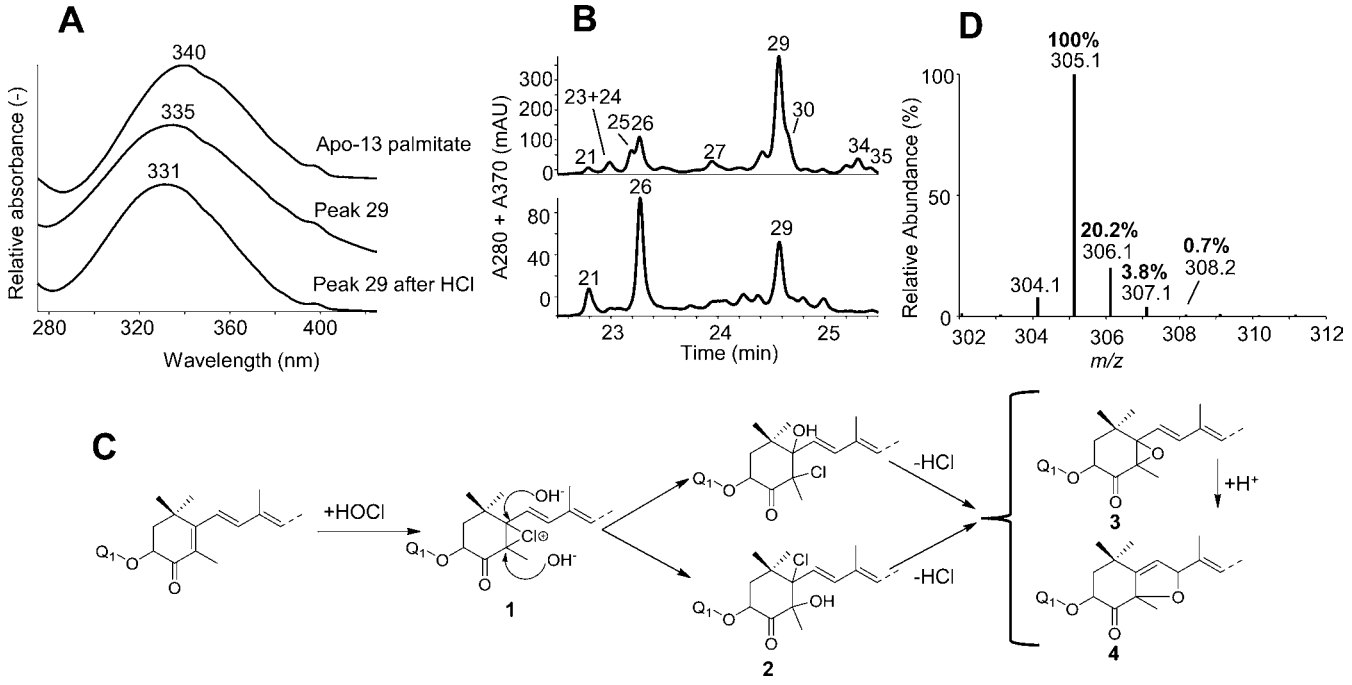


**Figure 7.** (A) Overlay of UV−vis absorption spectra of apo-13-astaxanthinone palmitate ester (top), epoxy-apo-13-astaxanthinone palmitate ester (middle), and epoxy-apo-13-astaxanthinone palmitate ester after acidification with HCl (bottom); (B) RP-UHPLC-UV profiles (sum of detection wavelengths 280 and 370 nm) of hypochlorite-degraded astaxanthin dipalmitate (top) and 0.1 M HCl acidified hypochlorite degraded astaxanthin dipalmitate (bottom) Numbers refer to Table 1. (C) Reaction scheme for the formation of chlorohydrins (**2**) via intermediate cloronium ion **1** and conversion to 5,6-epoxy-apo-astaxanthin (**3**) or 5,8-furanoid-apo-astaxanthin (**4**) by dehydrochlorination. $Q_1$ is either H or (C═O)-$C_{15}H_{31}$, (D) Full MS spectrum of epoxy-apo-13-astaxanthinone (peak 6), average of 31 spectra.

## ■ ASSOCIATED CONTENT

### Ⓢ Supporting Information

Additional $MS^2$ fragmentation data of nonesterified apo-astaxanthins (Table S1) and palmitoyl apo-astaxanthins (Table S2). This material is available free of charge via the Internet at http://pubs.acs.org.

## ■ AUTHOR INFORMATION

### Corresponding Author

*(J.-P.V.) Mail: Laboratory of Food Chemistry, Wageningen University, P.O. Box 8129, 6700 EV Wageningen, The Netherlands. Phone: +31 (0)317 482234. E-mail: jean-paul.vincken@wur.nl.

### Funding

This work was supported by FeyeCon D&I and by grants from NL Agency and the Ministry of Education, Culture and Science (Project FND09014).

### Notes

The authors declare no competing financial interest.

## ■ ABBREVIATIONS USED

HOCL, hypochlorous acid; $OCl^-$, hypochlorite; RP-UHPLC-PDA-ESI-MS, reversed phase ultrahigh-performance liquid chromatography with photo diode array and in-line electrospray ionization mass spectrometric detection; CDB, conjugated double bond; $[M + H]^+$, protonated parent ion; $[M + Na]^+$, sodiated parent ion

## ■ REFERENCES

(1) Guedes, A. C.; Amaro, H. M.; Malcata, F. X. Microalgae as sources of carotenoids. *Mar. Drugs* **2011**, *9*, 625−644.

(2) Hussein, G.; Sankawa, U.; Goto, H.; Matsumoto, K.; Watanabe, H. Astaxanthin, a carotenoid with potential in human health and nutrition. *J. Nat. Prod.* **2006**, *69*, 443−449.

(3) Miao, F.; Lu, D.; Li, Y.; Zeng, M. Characterization of astaxanthin esters in *Haematococcus pluvialis* by liquid chromatography-atmospheric pressure chemical ionization mass spectrometry. *Anal. Biochem.* **2006**, *352*, 176−81.

(4) Boon, C. S.; McClements, D. J.; Weiss, J.; Decker, E. A. Factors influencing the chemical stability of carotenoids in foods. *Crit. Rev. Food Sci. Nutr.* **2010**, *50*, 515−532.

(5) Rodriguez, E. B.; Rodriguez-Amaya, D. B. Formation of apocarotenals and epoxycarotenoids from *β*-carotene by chemical reactions and by autoxidation in model systems and processed foods. *Food Chem.* **2007**, *101*, 563−572.

(6) Stratton, S. P.; Schaefer, W. H.; Liebler, D. C. Isolation and identification of singlet oxygen oxidation products of *β*-carotene. *Chem. Res. Toxicol.* **1993**, *6*, 542−547.

(7) Marty, C.; Berset, C. Degradation products of *trans-β*-carotene produced during extrusion cooking. *J. Food Sci.* **1988**, *53*, 1880−1886.

(8) Kanasawud, P.; Crouzet, J. C. Mechanism of formation of volatile compounds by thermal degradation of carotenoids in aqueous medium. 1. *β*-Carotene degradation. *J. Agric. Food Chem.* **1990**, *38*, 237−243.

(9) Mordi, R. C.; Walton, J. C.; Burton, G. W.; Hughes, L.; Ingold, K. U.; Lindsay, D. A.; Moffatt, D. J. Oxidative degradation of *β*-carotene and *β*-apo-8′-carotenal. *Tetrahedron* **1993**, *49*, 911−928.

(10) Albrich, J. M.; McCarthy, C. A.; Hurst, J. K. Biological reactivity of hypochlorous acid: implications for microbicidal mechanisms of leukocyte myeloperoxidase. *Proc. Natl. Acad. Sci. U.S.A.* **1981**, *78*, 210−214.

(11) Hazen, S. L.; Hsu, F. F.; Gaut, J. P.; Crowley, J. R.; Heinecke, J. W. Modification of proteins and lipids by myeloperoxidase. In *Methods in Enzymology*; Lester, P., Ed.; Academic Press: New York, 1999; Vol. 300, pp 88−105.

(12) Panasenko, O. M.; Gorudko, I. V.; Sokolov, A. V. Hypochlorous acid as a precursor of free radicals in living systems. *Biochemistry (Moscow)* **2013**, *78*, 1466−1489.
(13) Norkus, E. P.; Norkus, K. L.; Dharmarajan, T. S.; Schierle, J.; Schalch, W. Serum lutein response is greater from free lutein than from esterified lutein during 4 weeks of supplementation in healthy adults. *J. Am. Coll. Nutr.* **2010**, *29*, 575−585.
(14) Granado, F.; Olmedilla, B.; Gil-Martinez, E.; Blanco, I. Lutein ester in serum after lutein supplementation in human subjects. *Br. J. Nutr.* **1998**, *80*, 445−449.
(15) Alija, A. J.; Bresgen, N.; Sommerburg, O.; Siems, W.; Eckl, P. M. Cytotoxic and genotoxic effects of $\beta$-carotene breakdown products on primary rat hepatocytes. *Carcinogenesis* **2004**, *25*, 827−831.
(16) Siems, W.; Salerno, C.; Crifo, C.; Sommerburg, O.; Wiswedel, I. $\beta$-Carotene degradation products − formation, toxicity and prevention of toxicity. In *Food Factors for Health Promotion*; Yoshikawa, T., Ed.; Karger: Basel, Switzerland, 2009; Vol. 61, pp 75−86.
(17) Handelman, G. J.; Vankuijk, F. J. G. M.; Chatterjee, A.; Krinsky, N. I. Characterization of products formed during the autoxidation of $\beta$-carotene. *Free Radical Biol. Med.* **1991**, *10*, 427−437.
(18) Sommerburg, O.; Langhans, C. D.; Arnhold, J.; Leichsenring, M.; Salerno, C.; Crifò, C.; Hoffmann, G. F.; Debatin, K. M.; Siems, W. G. $\beta$-Carotene cleavage products after oxidation mediated by hypochlorous acid − a model for neutrophil-derived degradation. *Free Radical Biol. Med.* **2003**, *35*, 1480−1490.
(19) Panasenko, O. M.; Panasenko, O. O.; Briviba, K.; Sies, H. Hypochlorite destroys carotenoids in low density lipoproteins thus decreasing their resistance to peroxidative modification. *Biochemistry (Moscow)* **1997**, *62*, 1140−1145.
(20) Lutz-Roder, A.; Jezussek, M.; Winterhalter, P. Nickel peroxide induced oxidation of canthaxanthin. *J. Agric. Food Chem.* **1999**, *47*, 1887−1891.
(21) Etoh, H.; Suhara, M.; Tokuyama, S.; Kato, H.; Nakahigashi, R.; Maejima, Y.; Ishikura, M.; Terada, Y.; Maoka, T. Auto-oxidation products of astaxanthin. *J. Oleo Sci.* **2012**, *61*, 17−21.
(22) Hayakawa, T.; Kulkarni, A.; Terada, Y.; Maoka, T.; Etoh, H. Reaction of astaxanthin with peroxynitrite. *Biosci., Biotechnol., Biochem.* **2008**, *72*, 2716−2722.
(23) Yuan, J. P.; Chen, F. Purification of *trans*-astaxanthin from a high-yielding astaxanthin ester-producing strain of the microalga *Haematococcus pluvialis*. *Food Chem.* **2000**, *68*, 443−448.
(24) Halldorsson, A.; Haraldsson, G. G. Fatty acid selectivity of microbial lipase and lipolytic enzymes from salmonid fish intestines toward astaxanthin diesters. *J. Am. Oil Chem. Soc.* **2004**, *81*, 347−353.
(25) Britton, G. Chapter 2: UV/visible spectroscopy. In *Carotenoids, Vol. 1B, Spectroscopy*; Britton, G., Liaaen-Jensen, S., Pfander, H., Eds.; Birkhäuser Verlag: Basel, Switzerland, 1995; pp 13−62.
(26) CaroteNature GmbH, Lupsingen, Switzerland, data sheet (*rac*)-12′-apo-astaxanthinal.
(27) Rivera, S. M.; Canela-Garayoa, R. Analytical tools for the analysis of carotenoids in diverse materials. *J. Chromatogr., A* **2012**, *1224*, 1−10.
(28) Eugster, C. H. Chapter 4. Chemical derivatization: microscale tests for the presence of common functional groups in carotenoids. In *Carotenoids, Vol. 1A, Isolation and Analysis*; Britton, G., Liaaen-Jensen, S., Pfander, H., Eds.; Birkhäuser Verlag: Basel, Switzerland, 1995; pp 71−80.
(29) Ghidouche, S.; Rey, B.; Michel, M.; Galaffu, N. A rapid tool for the stability assessment of natural food colours. *Food Chem.* **2013**, *139*, 978−985.
(30) Minguez-Mosquera, M. I.; Jaren-Galan, M. Kinetics of the decolouring of carotenoid-pigments. *J. Sci. Food Agric.* **1995**, *67*, 153−161.
(31) Subagio, A.; Wakaki, H.; Morita, N. Stability of lutein and its myristate esters. *Biosci., Biotechnol., Biochem.* **1999**, *63*, 1784−1786.
(32) Frassanito, R.; Cantonati, M.; Flaim, G.; Mancini, I.; Guella, G. A new method for the identification and the structural characterisation of carotenoid esters in freshwater microorganisms by liquid chromatography/electrospray ionisation tandem mass spectrometry. *Rapid Commun. Mass Spectrom.* **2008**, *22*, 3531−3539.
(33) Weesepoel, Y.; Vincken, J.-P.; Pop, R. M.; Liu, K.; Gruppen, H. Sodiation as a tool for enhancing the diagnostic value of MALDI-TOF/TOF-MS spectra of complex astaxanthin ester mixtures from *Haematococcus pluvialis*. *J. Mass Spectrom.* **2013**, *48*, 862−874.
(34) Baldas, J.; Porter, Q. N.; Leftwick, A. P.; Holzel, R.; Weedon, B. C. L.; Szabolcs, J. Mass spectrometry of carotenoid ketones. *J. Chem. Soc. D* **1969**, 415−416.
(35) Enzell, C. R.; Back, S. Chapter 7: Mass spectrometry. In *Carotenoids, Vol. 1B, Spectroscopy*; Britton, G., Liaaen-Jensen, S., Pfander, H., Eds.; Birkhäuser Verlag: Basel, Switzerland, 1995; pp 261−320.
(36) Egeland, E. S. Part VII: Data sheets aiding identification of phytoplankton carotenoids and chlorophylls. In *Phytoplankton Pigments: Characterization, Chemotaxonomy, and Applications in Oceanography*; Roy, S., Llewellyn, C. A., Egeland, E. S., Johnsen, G., Eds.; Cambridge University Press: New York, 2011; pp 665−822.
(37) Spickett, C. M.; Jerlich, A.; Panasenko, O. M.; Arnhold, J.; Pitt, A. R.; Stelmaszynska, T.; Schaur, R. J. The reactions of hypochlorous acid, the reactive oxygen species produced by myeloperoxidase, with lipids. *Acta Biochim. Polym. (Engl. Transl.)* **2000**, *47*, 889−899.
(38) Panasenko, O. M. The mechanism of the hypochlorite-induced lipid peroxidation. *BioFactors* **1997**, *6*, 181−190.

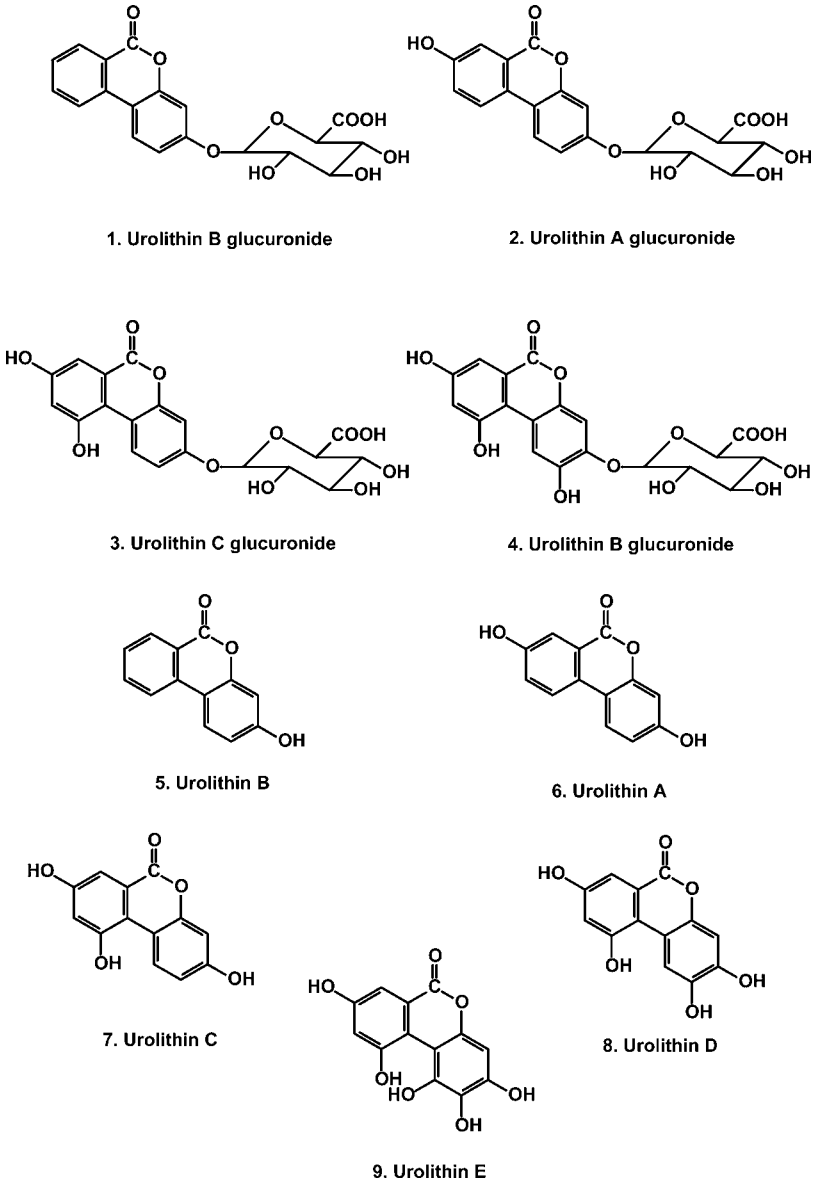


**Figure 1.** Structures of the urolithin glucuronides and free urolithins: urolithin B glucuronide, **1**; urolithin A glucuronide, **2**; urolithin C glucuronide, **3**; urolithin D glucuronide, **4**; urolithin B, **5**; urolithin A, **6**; urolithin C, 7; urolithin D, **8**; urolithin E, **9**.

and AnaeroGen sachets for generating $CO_2$ and BR55 anaerobic indicators were obtained from Oxoid Ltd. (Basingstoke, UK).

**Source of Walnuts.** California walnuts (Sweet Valley brand) were purchased from a local supermarket.

**Study Design.** Four healthy volunteers were entered into the study. No restriction with regard to general diet was enforced, only ingestion of supplements or medication and walnuts was forbidden for 3 weeks prior to the study. The volunteers consumed peeled walnuts (200 g) starting at 9:00 a.m. on day 1 and completed ingestion within 4 h. Morning urine samples were collected 1 day later.

On the basis of urine urolithin excretion data, one volunteer (V-1) displaying the most dynamic profile of ellagitannin metabolites was selected for a further in-depth study of blood, feces, and urine.

V-1 was female, aged 43, a nonsmoker and nonvegetarian, without a history of gastrointestinal or any other chronic diseases, and was not involved in a weight-reducing dietary regimen. On day 1, 24 h urine and fecal samples were collected. On day 2 of the study, 200 g of commercially available peeled walnuts was consumed over the course of the morning between 9:00 a.m. and 12:00 p.m. Successive urine and fecal samples were collected separately over the following 7 days. Additionally, plasma samples were collected on days 2, 3, and 4 of the study in 2−4 h periods. On day 8, the ingestion of 200 g of peeled walnuts was repeated, and successive urine and fecal samples were again collected up to day 13 of the study.

**Collection and Storage of Urine, Blood, and Fecal Samples for V-1.** *Urine.* Following ingestion of a further 200 g of walnuts by V-1, all subsequent urine samples were collected in measuring cylinders, noting the time and volume. Aliquots of 2 and 10 mL were pipetted into plastic test tubes (15 mL), and the rest was discarded. During the day, samples were placed immediately at −80 °C, whereas outside working hours, samples were placed at −20 °C overnight before transport to the laboratory and subsequent storage at −80 °C.

*Feces.* For V-1, all fecal samples were collected throughout the two intervention phases, in preweighed round plastic containers of 10 cm diameter. The plastic containers plus feces were reweighed for wet weight calculations. During the day, samples were placed immediately at −80 °C, whereas after working hours samples were placed at −20 °C overnight before transport to the laboratory and subsequent storage at −80 °C. The samples were freeze-dried within 8 days of collection to obtain dry weights and were pulverized to a fine homogeneous powder prior to Soxhlet extraction.


dx.doi.org/10.1021/jf5040652 | J. Agric. Food Chem. 2014, 62, 10264−10273

*Plasma.* During the first intervention period of the two-stage intervention study with V-1, blood samples (4−5 mL) were taken from the basilic vein into heparin prepared tubes at different time points; five samples on day 2 (ingestion of walnuts), five samples on days 3 and, and four samples on day 4 of the study. The blood samples were centrifuged (13000 rpm) at 5 °C for 10 min, and plasma was frozen at −80 °C.

**Column Chromatography on Sephadex LH-20.** Dried urine extraction residues, after suspension in absolute ethanol, were adsorbed on Sephadex LH-20 by freeze-drying, prior to addition to the free volume at the head of glass columns (38 cm × 4.5 cm i.d.) filled to ca. 5 cm from the top with Sephadex LH-20 in ethanol. After bedding down of the gel material, fractionation was conducted by successive elution with ethanol followed by increasing concentrations of methanol (5−50%) in ethanol followed by 100% methanol (250 mL of each solvent). Fractions (250 mL) were collected, and the solvent was removed by rotary evaporation in vacuo at 40 °C.

**Column Chromatography on C18.** The dried fractions obtained by Sephadex LH-20 chromatography were dissolved in 2% acetic acid (2.0 mL) and applied to C18 columns for subfractionation. The columns were preconditioned with methanol (4.0 mL) and 2% acetic acid (4.0 mL) and were not allowed to dry. Elution was performed with solvent mixtures containing increasing concentrations of methanol (5−50%) in 2% acetic acid followed by 100% methanol. The solvent was removed on a SpeedVac (Bachhofer, Reutlingen, Germany). Individual phenolic compounds, in relevant fractions, were purified by semipreparative HPLC for structure elucidation by spectroscopic analysis.

**Isolation of Urolithin Glucuronides from Urine.** A week later, three of the healthy volunteers again consumed 200 g of walnuts, acccording to the same protocol as before. The following morning, first-pass urine was collected, and the volume of urine was reduced in vacuo on a rotary evaporator. The samples were all worked up separately. Sephadex LH-20 was added, and the remaining urine was adsorbed on this substrate by freeze-drying prior to addition to the free volume at the head of individual glass columns (38 cm × 4.5 cm i.d.), filled to ca. 5 cm from the top, with Sephadex LH-20 in ethanol and fractionated as described above. The dried fractions were dissolved in methanol (5.0 mL) prior to analyses by analytical reverse-phase HPLC and HPLC-ESI-MS. The fractions obtained from the Sephadex column were subfractionated on C18 columns as described above. Dried subfractions were suspended in methanol (2 mL) and diluted when necessary prior to reverse-phase analytical HPLC and HPLC-ESI-MS. Phenolic compounds were purified by semipreparative HPLC for spectroscopic analysis.

**Generation of Free Urolithins by Fermentation of Ellagic Acid in Vitro.** Reference-free urolithins were unavailable commercially and therefore were produced by bacterial fermentation according to the following protocol. Urolithins were produced by adding ellagic acid (50.0 mg) in ethanol (5.0 mL) to BHI broth (100 mL) in Duran bottles (100 mL) fortified with the reducing agents, sodium formaldehyde sulfoxylate (300 mg/L) and L-cysteine HCl (500 mg/L), to a final concentration of 1 mg/mL. After previous sterilization at 120 °C for 20 min, the medium was steamed for 30 min, immediately prior to use, to remove residual oxygen, and allowed to cool before inoculation with freshly voided fecal matrix (100 mg) from three of the volunteers. The bottles with open caps were placed in an anaerobic churn (neoLAB, Heidelberg, Germany) containing an indicator of anaerobiosis (Anaerobic indicator, BR55), which turned from pink to white on generation of an anaerobic atmostphere, by two freshly opened sachets of ascorbic acid (AnaeroGen).

The fermentation broths were centrifuged and metabolites extracted on two C18 (5 g) (octadecyl-modified silica, Chromabond) columns. The columns were preconditioned with methanol (50 mL) and 2% acetic acid (50 mL). The fermentation solutions were eluted, and the columns were washed twice with distilled water (50 mL). The columns were allowed to dry and eluted with methanol (50 mL). Solvent from the combined eluants was removed by rotary evaporation, and the dried extracts were dissolved in methanol (2.0 mL). The metabolites were analyzed by analytical HPLC and HPLC-ESI-MS and purified by semipreparative HPLC prior to spectroscopic analyses.

**Semipreparative HPLC.** Semipreparative HPLC was conducted on a HP 1100 liquid chromatograph (Agilent Technologies, Waldbronn, Germany) fitted with a C18 column (10 mm i.d.) similar to that used for analytical HPLC. For the separation of individual compounds in the extracts, the mobile phase (3 mL/min) consisted of 0.2% acetic acid in distilled water (solvent A) and acetonitrile (solvent B), utilizing the following solvent gradient profile over a total run time of 50 min: initially 95% A for 1 min; reduced to 90% A over 9 min; to 85% A over 10 min; to 80% A over 10 min; to 0% A over 5 min; and continuing at 0% A until completion of the run. Peaks eluting from the column were collected on a HP 220 microplate sampler and subsequently lyophilized.

**Electrospray Ionization Mass Spectrometry (ESI-MS).** HPLC-ESI-MS was conducted on an Agilent 1100 HPLC, coupled to a HP 1101 single-quadrupole, mass-selective detector (Agilent Technologies). The column used was a 250 mm × 4.5 mm i.d., 5 μm, RP-18 with a 4 mm × 4 mm i.d. guard column of the same material (Latek, Eppelheim, Germany). The mobile phase consisted of 2% acetic acid in water (solvent A) and acetonitrile (solvent B) with the following gradient profile: initially 95% A for 10 min; reduced to 90% A over 1 min; to 60% A over 9 min; to 80% A over 10 min; to 60% A over 10 min; to 0% A over 5 min; and continuing at 0% A until completion of the run. Volumes (10 μL) were injected into the HPLC, and phenolic compounds in the eluant were detected at 278 and 340 nm with a diode array UV detector (HP 1040M). Mass spectra in negative-ion selected ion monitoring (SIM) mode were generated under the following conditions: fragmentor voltage, 100 V; capillary voltage, 2500 V; nebulizer pressure, 30 psi; drying gas temperature, 350 °C; mass range, 100−1500 Da. The ions used for the detection of glucuronidated and free urolithins are listed in Table 1. Instrument control and data handling were performed with the same software as for analytical HPLC.

**Table 1. Details of the Parameters Used for Detection of the Urolithins by HPLC-ESI-MS in Negative Ion Selected Ion Monitoring Mode**

| | phenolic compound | formula | exact mass *M* (calcd) | selected $[M-H]^-$ ion | HPLC-MS ret time (min) |
|---|---|---|---|---|---|
| 1 | urolithin B glucuronide | $C_{19}H_{16}O_9$ | 388.079 | 387 | 33.74 |
| 2 | urolithin A glucuronide | $C_{19}H_{16}O_{10}$ | 404.074 | 403 | 25.82, 26.18, 27.11, 27.42 |
| 3 | urolithin C glucuronide | $C_{19}H_{16}O_{11}$ | 420.069 | 419 | 27.77 |
| 4 | urolithin D glucuronide | $C_{19}H_{16}O_{12}$ | 436.064 | 435 | 23.37, 25.57, 29.34, 33.64 |
| 5 | urolithin B | $C_{13}H_8O_3$ | 212.047 | 211 | 42.68 |
| 6 | urolithin A | $C_{13}H_8O_4$ | 228.042 | 227 | 41.94 |
| 7 | urolithin C | $C_{13}H_8O_5$ | 244.037 | 243 | 37.84, 39.67 |
| 8 | urolithin D | $C_{13}H_8O_6$ | 260.032 | 259 | 36.24, 37.74 |
| 9 | urolithin E | $C_{13}H_8O_7$ | 276.027 | 275 | 27.98 |

**Total Polyphenol Content of Walnuts Evaluated by the Folin−Ciocalteu Assay.** Preparation of a cold walnut extract was conducted according to the method of Anderson et al.,[14] whereby 50 g of powdered walnuts (frozen for 24 h) was incubated in a solution of 75% aqueous acetone containing sodium metabisulfite (10 mg/L) at 4 °C for 4 days. The acetone was decanted and evaporated under reduced pressure, and methanol (50% aqueous, v/v) was added. The solution was extracted three times with *n*-hexane. The defatted solution was freeze-dried and dissolved in 100 mL of 10% aqueous dimethyl sulfoxide and used for the analysis of total polyphenols.

To evaluate the total polyphenol content of walnuts, 20 μL of gallic acid standard solution or walnut extract was mixed with 1.58 mL of double-distilled water and 100 μL of Folin−Ciocalteu phenol reagent

N2 (Sigma-Aldrich, Deisenhof, Germany) in a 2 mL cuvette. After 8.5 min, 300 μL of sodium carbonate solution (200 g/L) was added, and the solution was stirred and incubated for 30 min at 40 °C, following the procedure of Waterhouse.[15] The absorbance was measured at 765 nm on a spectrophotometer (Pharmacia Biotech, Ultraspec 3000) against a blank. Different concentrations of gallic acid (0.5−10 mM) in 10% aqueous dimethyl sulfoxide were used to generate a standard curve with a slope of 0.1534 (SD = 0.00329, $P < 0.0001$). The total polyphenol content was calculated as gallic acid equivalents (GAE).

**Total and Individual Content of Phenolic Compounds in Walnuts As Evaluated by Soxhlet Extraction and HPLC-ESI-MS.** Freeze-dried walnuts (5 g) were delipidated by extraction with hexane (3 × 150 mL) for 3 h. The walnut cake was dried under a stream of nitrogen and further extracted with methanol (3 × 150 mL) for 3 h. The methanol extracts were combined, and solvent was removed by rotary evaporation. The dried residue was immobilized on Sephadex LH-20 and fractionated by successive elution with increasing concentrations of methanol in ethanol as described. Phenolic compounds in the fractions were identified by HPLC-ESI-MS and quantitated against standard curves of the purified metabolites.

**Sample Analyses.** *Urine.* Urine samples (20 μL) were analyzed for urolithin metabolites of ellagitannins by HPLC-ESI-MS operating in negative ion SIM mode, using the ions listed in Table 1. Calculation of the amounts of individual metabolites were conducted with the relevant standard curves listed in Table 2.

**Table 2. Standard Curves of Purified Glucuronidated Urolithins, Free Urolithins, and Uric Acid Generated by HPLC-ESI-MS in Selected Ion Monitoring Negative Ion Mode**

| substance with mass | slope | *R* | *P* |
|---|---|---|---|
| urolithin B glucuronide | 5791 | 0.999 | <0.0001 |
| urolithin A glucuronide | 9101 | 0.999 | <0.0001 |
| urolithin C glucuronide | 738 | 0.999 | <0.0001 |
| urolithin D glucuronide | 7418 | 0.998 | <0.001 |
| urolithin B | 4318 | 0.999 | <0.0001 |
| urolithin A | 12035 | 0.996 | <0.0001 |
| urolithin C | 657 | 0.997 | <0.001 |
| urolithin D | 9618 | 0.999 | <0.0001 |
| uric acid | 7.710 | 0.999 | <0.0001 |

*Plasma.* Prior to analysis, blood samples were defrosted and centrifuged. To plasma samples (500 μL) were added 0.2 M hydrochloric acid (100 μL) and ethanol (2.0 mL), and the mixture was vortexed vigorously for 2 min and centrifuged at 13000 rpm for 15 min. The ethanol layer was aspirated and the procedure repeated twice. The combined ethanol extracts (6.0 mL) were evaporated to dryness under a stream of nitrogen and suspended in 200 μL of phosphate buffer (pH 6.6) prior to analysis (20 μL) by HPLC-ESI-MS under the conditions described for the analysis of urine samples. Calculations of the amounts of individual metabolites were conducted with the relevant standard curves listed in Table 2.

*Feces.* Homogenized dried fecal powders (2.5 g) were extracted in a Soxhlet apparatus with *n*-hexane for 3 h to remove lipids. Residual powders, after drying under a stream of nitrogen, were extracted with methanol (3 h), and solvent was removed by rotary evaporation at 35 °C.

The extracts were dried, weighed, and suspended in 10 mL of methanol. Of the homogenized solutions, 1.0 mL was transferred to an Eppendorf microfuge tube and centrifuged at 3500*g* for 5 min. The upper methanol layer was aspirated and analyzed (20 μL) by HPLC-ESI-MS, operating in the SIM mode using the ions listed in Table 1. The residue was dissolved in DMSO (1.0 mL) and likewise analyzed (20 μL) by HPLC-ESI-MS. Calculation of the amount of metabolites was conducted using the relevant standard curves listed in Table 2.

**Antioxidant Assays.** *DPPH Assay.* The DPPH assay was conducted as previously described.[16] Raw urine and fecal extracts were diluted 1:10 and 1:100 with methanol, respectively. Plasma samples (100 μL) were added to 100 μL of perchloric acid. The samples were centrifuged at 13000 rpm for 5 min, and the supernatants (150 μL) were neutralized with 10 M sodium hydroxide (5 μL), and 20 μL of this solution was used in the assay. Each batch of samples was measured simultaneously with Trolox at concentrations of 50−1000 μM. Using the percentage degradation of DPPH, at the different Trolox concentrations, a standard curve was constructed, which was always exponential. To obtain linear regression curves, the data points were subdivided into two parts. With Trolox concentrations of 250−1000 μM, a linear regression curve was calculated and used for the calulation of all Trolox equivalents for all data points ≥10% DPPH value. With Trolox concentrations of 50−250 μM a linear regression curve was calculated and used for the calulation of all Trolox equivalents for all data points ≤10% DDPH. The Trolox equivalents calculated were corrected for dilution factors and, in the case of urine and feces, calculated in relation to the amount of urine or fecal extracts.

*FRAP Assay.* The FRAP assay was conducted as previously described.[16] Raw urine and fecal extracts were diluted 1:10 and 1:100 with acetate buffer (300 mM sodium acetate, pH, 3.6). Plasma samples were prepared as described for the DPPH assay. Each batch of samples was measured simultaneously with Trolox at concentrations of 50−1000 μM to obtain a linear regression curve. Using this linear regression curve, the Trolox equivalents for each sample of fecal extracts, plasma, and urine were calculated and corrected for dilution factors.

*ORAC Assay.* The ORAC assay was conducted as described previously.[16] To precipitate proteins, plasma samples (100 μL) were mixed with 0.5 M perchloric acid (100 μL) and centrifuged. Of the upper layer, 100 μL was mixed with 10 M sodium hydroxide solution (2 μL). The plasma extracts, diluted 1:100 or 1:200 with ORAC buffer, and aliquots (10 μL) were placed in quadruplicate in a 96-well plate to measure peroxy radical scavenging capacity. Raw urine and fecal extracts were diluted 1:50 and 1:200, respectively, with ORAC buffer prior to analysis.

**Statistics.** The Trolox equivalent values of pure compounds and biospecimens in the DPPH assay were correlated with the Tablecurve program (Jandel Scientific, Chicago, IL, USA). Correlations between urolithin and uric acid concentrations and antioxidant capacity in the biospecimens were evaluated by linear regression using the Origin program (version 7.5).

## RESULTS AND DISCUSSION

**Concentration of Total Phenolic Compounds in Walnuts.** On the basis of the Folin−Ciocalteu assay, the total amount of polyphenol compounds ingested after intervention with 200 g of walnuts equated to 3.11 g calculated as gallic acid equivalents. This is almost identical to that reported by Anderson et al.,[14] at 3.2 g pf polyphenol/200 g of walnuts. However, the total amount of polyphenolic compounds detected in the same batch of walnuts following Soxhlet extraction, column chomatography, and identification[17] and quantitation by HPLC-ESI-MS equated to 5.013 g of ellagitannins alone, of which 3.228 g was ellagic acid moieties (Table 3).

**Identification of Urolithin Glucuronides and Free Urolithins Isolated and Purified from Urine and Fermentation Experiments, Respectively.** A range of glucuronidated urolithins were isolated and purified from large-scale extractions of urine samples from the volunteers. The basic structures were elucidated by HPLC-ESI-MS (Table 1). These (Figure 1) were urolithin B glucuronide, **1**; urolithin A glucuronide (four isomers), **2**; urolithin C glucuronide (two isomers), **3**; and urolithin D glucuronide (four isomers), **4**. From the fecal extracts and fermentation experiments the following free urolithins were characterized (Figure 1), namely,

**Table 3. Content of Ellagitannins Detected in Walnuts Following Soxhlet Extraction and Identification by HPLC-ESI-MS and Nano-ESI-MS-MS**

| phenolic compound | mg/200 g | ellagic acid moieties (mg/200 g) |
|---|---|---|
| ellagic acid | 167 | 167 |
| pedunculagin | 1657 | 1276 |
| isostrictinin | 163 | 78 |
| strictinin | 369 | 177 |
| ellagic acid xyloside | 142 | 99 |
| methyl valoneate dilactone | 54 | 33 |
| valoneate dilactone | 122 | 78 |
| tellimagrandin I | 253 | 96 |
| tellimagrandin II | 257 | 82 |
| 2,3-*O*-(*S*)-hexahydroxydiphenoyl-D-glucose | 296 | 186 |
| eugeniin | 57 | 18 |
| casuarictin | 163 | 106 |
| casuarinin | 313 | 203 |
| praecoxin A | 300 | 189 |
| methyl praecoxin A | 700 | 440 |
| total (g) | 5.013 | 3.228 |

urolithin B, **5**; urolithin A, **6**; urolithin C (two isomers), **7**; urolithin D (two isomers), **8**; and urolithin E, **9**.

**Concentration of Glucuronidated Urolithins in Urine of the Volunteers.** A wide interindividual variation (Figure 2) in gastrointestinal ellagitannin metabolism was apparent among the four volunteers, as judged by the profiles in urine 1 day after ingestion: volunteer 1, excreted mainly urolithin A, C, and D glucuronides (5.67 mM); volunteer 2, mainly urolithin A and B glucuronides (1.75 mM); volunteer 3, mainly urolithin A, B, and C glucuronides (0.72 mM); and volunteer 4, only urolithin A glucuronides (4.0 mM).

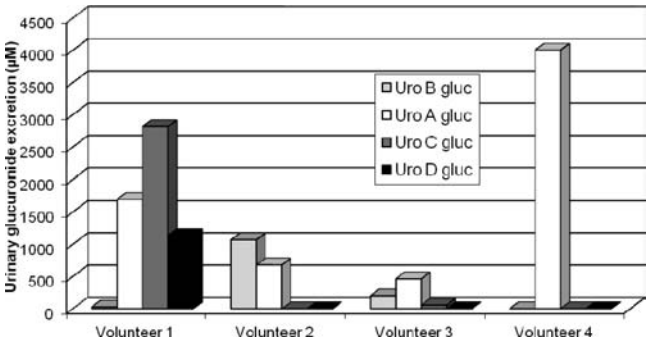


**Figure 2.** Profile of glucuronidated urolithins in the urine of the four volunteers following intervention with walnuts (200 g).

**Concentration of Urolithins in Sequential Urine, Plasma, and Fecal Samples in Volunteer 1.** *Urine.* The concentration of total glucuronidated urolithins in successive urine samples of V-1 is depicted in Figure 3A, whereas the contribution by the major individual glucuronides is shown in Figure 4A.

As shown in Figure 3A, maximal excretion (4.6 mM) of glucuronidated urolithins in urine, during intervention phase 1, was attained 2 days after ingestion of walnuts, whereas during phase 2, it attained 8.0 mM somewhat earlier at 1 day after ingestion. Appreciable levels were also detected for as long as 4 days after ingestion. Overall, the ingestion of 200 g of walnuts by V-1 (equivalent to 3.228 g of ellagic acid moieties) led to total excretions of 2.02 and 2.24 g of urolithin glucuronides in

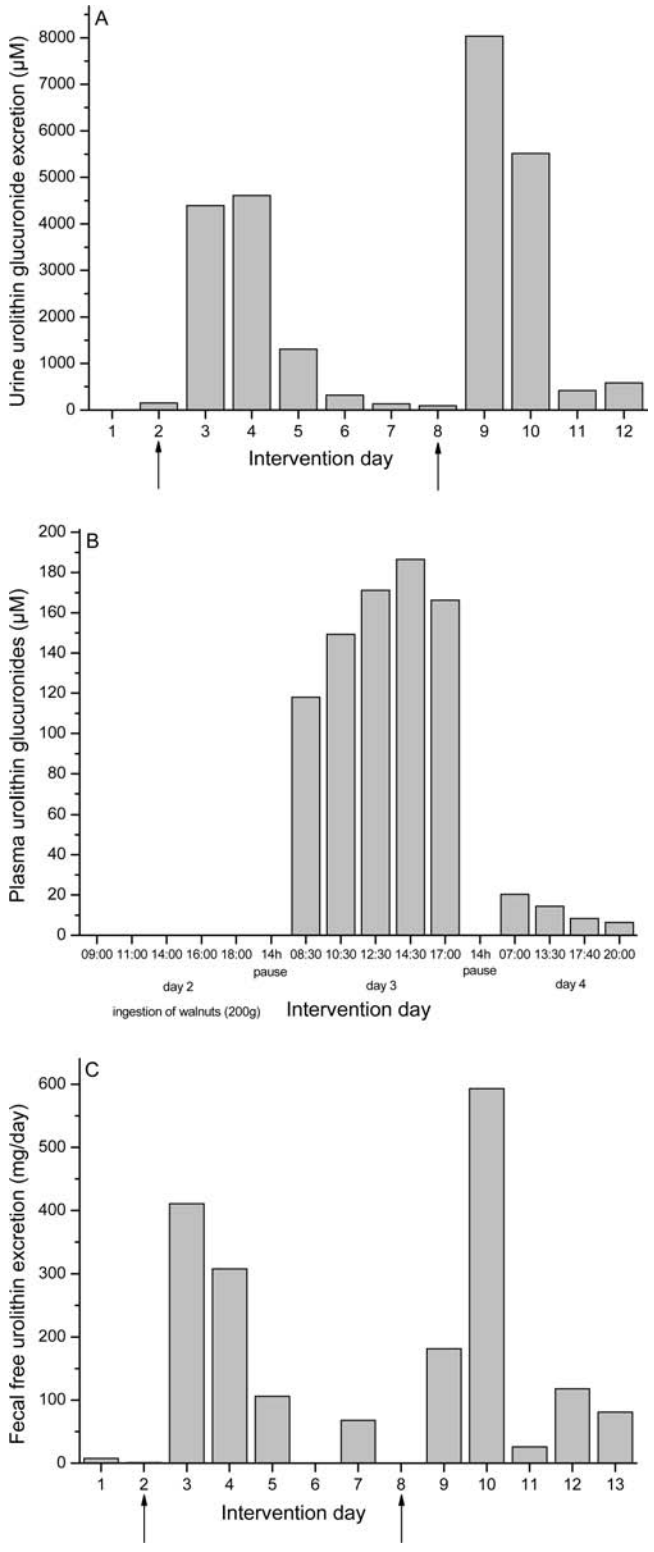


**Figure 3.** (A) Total glucuronidated urolithins in urine of volunteer 1 following intervention with walnuts (200 g), on days 2 and 8 as indicated by the arrows. (B) Total glucuronidated urolithins in plasma of volunteer 1 following intervention with walnuts (200 g) during phase 1 of the study. (C) Total free urolithins in feces of volunteer 1 following intervention with walnuts on days 2 and 8 as indicated by the arrows.

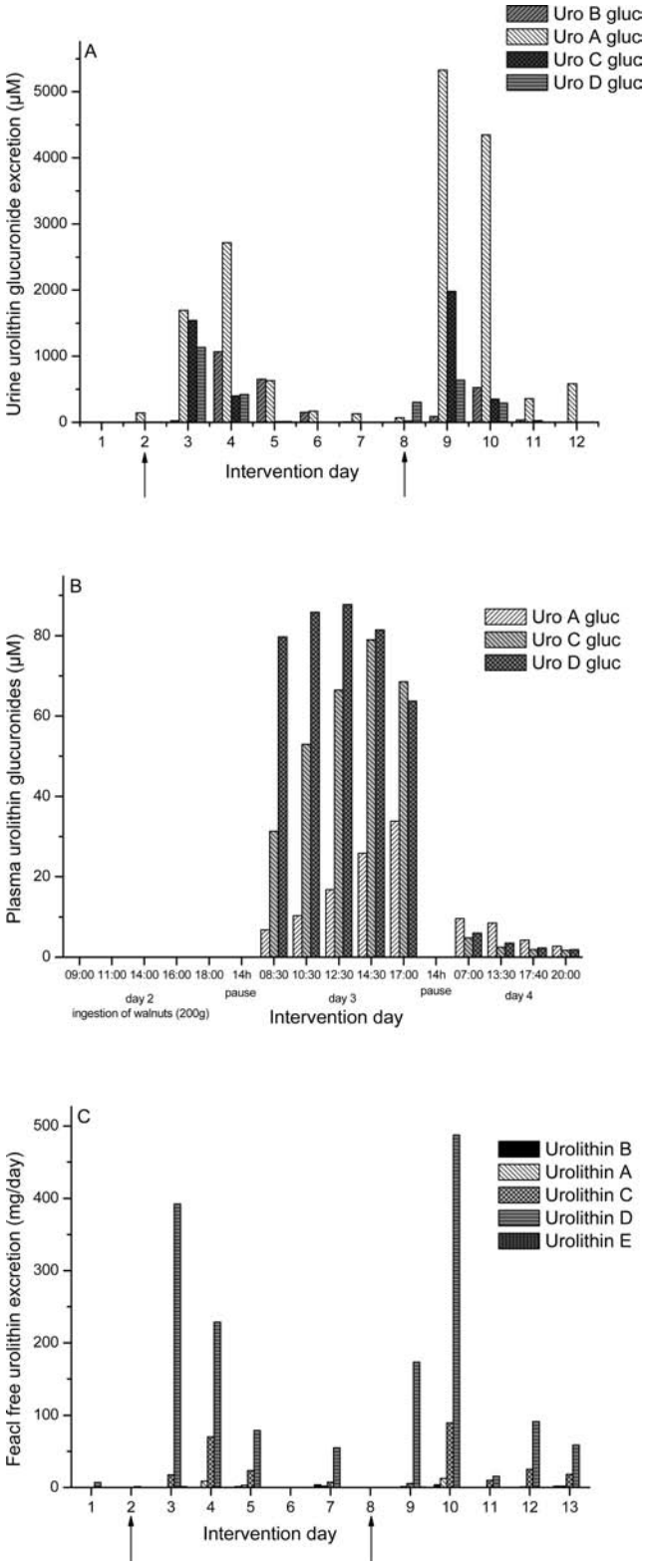


**Figure 4.** (A) Distribution of individual glucuronidated urolithins in the urine of volunteer 1 following intervention with walnuts (200 g) on days 2 and 8 as indicated by the arrows. (B) Distribution of individual glucuronidated urolithins in the plasma of volunteer1 following intervention with walnuts (200 g) during phase 1 of the study. (C) Distribution of free urolithins in the feces of volunteer1 following intervention with walnuts on days 2 and 8 as indicated by the arrows.

urine after phases 1 and 2, respectively, which means that 63 and 69% were excreted via this route. The major metabolites identified in the urine of V-1, during intervention phase 1, were urolithin A glucuronides at 2.72 mM on day 3 (2 days later) and during phase 2 also urolithin A glucuronides at 5.33 mM on day 9 (1 day later). Appreciable levels of urolithin B glucuronide appeared in the urine 2 days later (Figure 4B) after ingestion, during both intervention phases, confirming that metabolism proceeds from polyhydroxylated to monohydroxylated metabolites.[15,17]

*Plasma.* Consecutive 2−4 h plasma samples, over 3 days, were analyzed, showing that the concentration of total urolithin glucuronides rose over 32 h in plasma to a maximum of 185 $\mu$M following walnut ingestion and declined rapidly over the next 12 h. The distribution in plasma displayed a Gaussian curve taking into account the 14 h breaks during nonworking hours. The concentration of total glucuronidated urolithins in successive plasma samples of V-1 is depicted in Figure 3B, whereas the contribution by the major individual glucuronides is shown in Figure 4B. Three major glucuronidated urolithins were detected in plasma samples, namely, urolithin A, C, and D glucuronides. Because the degradation of ellagitannins proceeds from higher to lower hydroxylated forms,[18] the concentration of urolithin D glucuronide (up to 87 $\mu$M) and urolithin C glucuronide (up to 79 $\mu$M) in blood rose in the first 14 h after ingestion and represented the highest concentrations detected in plasma. Maximal levels of urolithin A glucuronide (35 $\mu$M) were apparent 6 h later, 20 h after ingestion.

*Feces.* The number of fecal samples produced per day was variable; for example, on day 2 of the study, fecal samples were not produced (days 6 and 8), sometimes two or more, so on day 9 and 12 two samples and three on day 7. The excretion of total free urolithins in successive fecal extracts of V-1 is depicted in Figure 3C, whereas the contribution by the major individual urolithins (mg/day) is shown in Figure 4C. The urolithins detected were mainly urolithins A, B, C, and D along with minor amounts of urolithin E. After phase 1 ingestion of 200 g of walnuts by V-1, 893 mg of urolithins was excreted in feces over 6 days, and after phase 2 ingestion, a similar amount of 919 mg was excreted in 5 days. This indicates that, on average, 28% of ingested ellagitannins was excreted via this route after the intervention phases. The major urolithins excreted in feces were urolithin D isomers, with the highest excretion at 392 mg/day on day 3 during phase 1 and 488 mg/day on day 10 during phase 2, respectively. Urolithin C was excreted at concentrations of 70 mg/day on day 4 (2 days after ingestion) and 89 mg/day on day 10 (again 2 days after ingestion) during phase 2.

**Antioxidant Capacity of Pure Urolithin Glucuronides and Free Urolithins.** Urolithin glucuronides (Table 4), purified by semipreparative HPLC and examined in the DPPH assay, were very ineffective. The highest concentration of the three urolithin glucuronides tested (1.0 mM) led to a reduction of the DPPH radical of between 5 and 22% only. Free monohydroxylated (urolithin B) and dihydroxylated (urolithin A) urolithins (Table 4) also displayed negligible activity in the DPPH assay, with reductions of the DPPH radical, at a concentration of 1.0 mM, of only 13 and 25%, respectively. The other free urolithins examined, urolithins C and D, displayed much higher activity, with $IC_{50}$ values of 142 and 57 $\mu$M, respectively.

The urolithin glucuronides and free urolithins were also very weak in the FRAP assay (Table 4), with concentrations in the

**Table 4. Antioxidant Capacity of Purified Glucuronidated and Free Urolithins and Reference Compounds**

| | DPPH assay ($IC_{50}$)[a] or $M_1$[b] at 1.0 mM | FRAP ($EC_1$)[c] ($\mu$M) | ORAC units[d] |
|---|---|---|---|
| urolithin B glucuronide | 5%* | 6340 | 0.33 ± 0.02 |
| urolithin A glucuronide | 22%* | 2483 | 1.89 ± 0.08 |
| urolithin C glucuronide | 7%* | 7138 | 1.48 ± 0.01 |
| urolithin B | 15%* | 7922 | 0.65 ± 0.04 |
| urolithin A | 13%* | 1291 | 1.84 ± 0.03 |
| urolithin C | 141.6 $\mu$M | 2683 | 1.23 ± 0.05 |
| urolithin D | 56.7 $\mu$M | 1803 | 0.57 ± 0.07 |
| Trolox | 65.96 $\mu$M | 527 | 1.0 |
| gallic acid | 19.06 $\mu$M | 170 | 2.50 ± 0.10 |
| uric acid | 11.38 $\mu$M | 379 | 1.19 ± 0.01 |
| ellagic acid | 13.11 $\mu$M | 139 | 1.85 ± 0.05 |

[a]$IC_{50}$, concentration of substance ($\mu$M) at which 50% of the DPPH radical is scavenged. [b]Percent reduction of DPPH at a concentration of 1.0 mM. [c]$EC_1$, concentration of substance ($\mu$M) giving an absorbance increase equivalent to 1 mM Fe $2^+$ solution. [d]One ORAC unit equals the inhibition of the declining fluorescence produced by 1 $\mu$M Trolox.

ranges of 2.5−7.1 and 1.3−7.9 mM, respectively, required to reduce 1 mM $Fe_3^+$ as compared to the standard compounds tested, namely, ellagic acid, gallic acid, uric acid, and Trolox with $EC_1$ values of 139, 170, 379, and 527 $\mu$M.

In contrast to the FRAP and DPPH assays, both glucuronidated and free urolithins A and C show much higher activity in the ORAC assay (Table 4). Of the pure urolithins tested, activity increases in the order urolithin B glucuronide (0.33 ± 0.02) < urolithin C glucuronide (1.48 ± 0.01) < urolithin A glucuronide (1.89 ± 0.08), whereas of the free urolithins tested, activity increases in the order urolithin D (0.57 ± 0.07) < urolithin B (0.65 ± 0.04) < urolithin C (1.23 ± 0.05) < urolithin A (1.84 ± 0.03) in comparison to Trolox were evident.

**Antioxidant Capacity of Raw Urine, Plasma, and Fecal Methanol Extracts in the DPPH, FRAP, and ORAC Assays.** *Raw Urine.* As shown in Table 5, the antioxidant capacity of raw urine samples did not correlate with the concentration of total glucuronidated urolithins (mean, 555 ± 92 $\mu$M; range, 6−2761 $\mu$M) as determined by HPLC-ESI-MS across the assays. However, strong positive correlations between the concentration of uric acid (mean, 3.01 ± 0.19 mM; range, 0.87−7.89 mM) in the raw urine were evident in all of the assays (DPPH, $R = 0.61$, $P < 0.0001$; FRAP, $R = 0.62$, $P < 0.0001$; ORAC, $R = 0.53$, $P < 0.0001$).

**Table 5. Antioxidant Capacity of Total Urolithin Glucuronides and Uric Acid in Urine Samples of Volunteer 1**

| | correlation | slope | *P* | *R* | *n* |
|---|---|---|---|---|---|
| DPPH | total urolithin glucuronides ($\mu$M) | 0.03562 | 0.50 | 0.09 | 56[a] |
| | uric acid ($\mu$M) | 0.52273 | <0.0001 | 0.61 | 67[b] |
| FRAP | total urolithin glucuronides ($\mu$M) | 0.008 | 0.79 | −0.04 | 56 |
| | uric acid ($\mu$M) | 0.5202 | <0.0001 | 0.62 | 67 |
| ORAC | total urolithin glucuronides ($\mu$M) | 0.22778 | 0.80 | 0.03 | 56 |
| | uric acid ($\mu$M) | 0.94501 | <0.0001 | 0.53 | 67 |

[a]Correlation based on urine samples that contained urolithin glucuronides ($n = 56$); urine samples on day 1 of ingestion did not contain urolithins. [b]Correlation based on all urine samples ($n = 67$).

*Plasma.* As shown in Table 6, the antioxidant capacity of protein-free plasma was negatively correlated with the concentration of both total glucuronidated urolithins and uric acid, respectively, in all assays. Possibly, the urolithin data are compromised by dilution (inherent in the assay) and matrix effects, but with the relatively constant levels of uric acid (317 ± 10 $\mu$M; range, 283−393 $\mu$M) a positive correlation would not be expected.

**Table 6. Antioxidant Capacity of Total Urolithin Glucuronides and Uric Acid in Plasma Samples of Volunteer 1**

| | correlation | slope | *P* | *R* | *n* |
|---|---|---|---|---|---|
| DPPH | total urolithin glucuronides ($\mu$M) | −1.012 | 0.13 | −0.54 | 9[a] |
| | uric acid ($\mu$M) | −0.176 | 0.28 | −0.31 | 14[b] |
| FRAP | total urolithin glucuronides ($\mu$M) | −0.69442 | 0.02 | −0.74 | 9 |
| | uric acid ($\mu$M) | 0.11387 | 0.23 | 0.34 | 14 |
| ORAC | total urolithin glucuronides ($\mu$M) | −1.36116 | 0.004 | −0.85 | 9 |
| | uric acid ($\mu$M) | 0.11531 | 0.58 | 0.16 | 14 |

[a]Correlation based on urine samples that contained urolithin glucuronides ($n = 9$); plasma samples on day 1 of ingestion did not contain urolithins. [b]Correlation based on all plasma samples ($n = 14$).

*Fecal Extracts.* As shown in Table 7, the antioxidant capacity of fecal extracts correlated positively with the concentration of total urolithins as determined by HPLC-ESI-MS in both the DPPH ($R = 0.81$, $P < 0.01$) and FRAP ($R = 0.80$, $P < 0.01$) assays. However, the association in the ORAC assay was negative ($R = -0.40$, $P > 0.05$). The positive correlation in the DPPH and FRAP assays can be mainly attributed to the high concentrations of urolithin D ($R = 0.67$, $P < 0.05$; $R = 0.76$, $P < 0.05$, respectively) in the fecal extracts, which supports the data for the pure compound (Table 4). The negative correlation in the ORAC assay is readily explained by the low antioxidant capacity of pure urolithin D in this assay (Table 4).

**Table 7. Antioxidant Capacity of Total Free Urolithins and Urolithin D in Fecal Extracts of Volunteer 1**

| | correlation | slope | *P* | *R* | *n* |
|---|---|---|---|---|---|
| DPPH | total free urolithins ($\mu$M) | 3461.2 | <0.01 | 0.81 | 10 |
| | urolithin D ($\mu$M) | 985.73 | <0.05 | 0.67 | 10 |
| FRAP | total free urolithins ($\mu$M) | 2315.9 | <0.01 | 0.80 | 10 |
| | urolithin D ($\mu$M) | 751.7 | <0.05 | 0.76 | 10 |
| ORAC | total free urolithins ($\mu$M) | 23.37 | 0.23 | −0.40 | 10 |
| | urolithin D ($\mu$M) | 4.99 | 0.51 | 0.24 | 10 |

The urolithin glucuronides present in the urine of the four volunteers, intervened with walnuts, were very different in terms of their profiles and concentrations and reflect the

variable capacity of the human intestinal flora to metabolize ellagitannins as shown previously.[19]

In the detailed two-stage walnut (200 g; equivalent to 3.228 g of ellagic acid moieties) intervention study with V-1, a very high proportion of the ellagitannins they contain was metabolized to urolithins, as demonstrated by excretions, on average, of 66% in urine and 28% in feces, which attained a maximum of 11% in blood during phase 1 of the study. Over the two intervention phases, 94% of ellagitannins (based on ellagic acid moieties) ingested was detected in urine and feces. This indicates highly efficient degradation of ellagitannins to urolithins by the gastrointestinal flora in this subject. Excretion of 66% urolithins in urine also reflects the high bioavailability of urolithins in humans. Maximal excretion during phases 1 and 2 attained 4.6 and 8.0 mM, respectively.

In addition, walnut ingestion led to maximal plasma concentrations of up to 35 $\mu$M urolithin A glucuronides, up to 79 $\mu$M urolithin C glucuronides, and up to 87 $\mu$M urolithin D glucuronides. Calculating the maximal value of urolithin glucuronides in this volunteer shows that 25% of the ingested ellagitannins from walnuts is present in blood in the form of urolithins within the first 24 h after ingestion.

The urine excretion data are fairly consistent with those of Cerda et al.,[20] who reported a mean total excretion of 11.17 mM (urolithin A + urolithin B) in 15 patients after a daily intake of pomegranate juice (400 mL) equivalent to 2.66 g of ellagitannin precursors. In addition, Gonzalez-Barrio et al.[21] reported maximal values of 44 $\mu$M urolithin glucuronides in urine after a challenge in humans with raspberries (300 g) containing much lower levels of ellagitannins and ellagic acid, at a combined concentration of 140 $\mu$M. This represents an excretion rate of 31% in urine based on ellagitannins ingested.

With regard to urolithin concentration in blood samples, our data, however, are in stark contrast to other reports. Surprisingly, Gonzalez-Barrio et al.[21] were unable to detect urolithins in plasma samples. In another study by Gonzalez-Sarrias et al.,[22] walnuts were fed (3 × 35 g) to human volunteers and led to a concentration of only 0.11 ± 0.05 $\mu$M urolithin A glucuronide in blood.

The negative antioxidant capacity of purified urolithin glucuronides in the DPPH and FRAP assays is in agreement with previous studies.[3] By contrast, they were far more effective in the ORAC assay, urolithin A glucuronide (1.89 ± 0.08) > urolithin C glucuronide (1.48 ± 0.01) > urolithin B glucuronide (0.33 ± 0.02), in comparison to Trolox. Sufficient urolithin D glucuronide isomer could not be purified for comparison.

The free compounds urolithins A and B were not very effective in the DPPH and FRAP assays, as was also the case for urolithins C and D in the FRAP assay. By contrast, urolithin C and, especially, urolithin D were effective antioxidants in the DPPH assay. In the ORAC assay, the data mirrored strongly the data for the glucuronidated metabolites, urolithin A (1.84 ± 0.03) > urolithin C (1.23 ± 0.05) > urolithin B (0.65 ± 0.04) > urolithin D (0.57 ± 0.07).

These data contradict several reported studies[3,23] which have shown that free urolithins do not display antioxidant activity in a range of assays. However, this represents the first report of antioxidant capacity by pure urolithins tested in the ORAC assay and underscores the need to evaluate compounds in a minimum of three assays.

With regard to the content of metabolites in urine, urolithin glucuronide concentration was negative, whereas uric acid concentration was positive across the antioxidant assays ($P < 0.0001$). A correlation between urolithin glucuronide concentration and antioxidant capacity in plasma was also not observed. By contrast, the data pertaining to the free urolithins in the fecal extracts closely reflected the data for the purified compounds. A strong association ($P < 0.01$) for total urolithin concentration was observed in both the DPPH and FRAP assays, with the major contribution from urolithin D ($P < 0.05$). However, the very weak associations in the ORAC assay with regard to total urolithins ($P > 0.2$) and urolithin D ($P > 0.5$) concentration reflect the data obtained with pure urolithin D (ORAC value, 0.57 ± 0.07), which was the major metabolite in fecal extracts.

The strong association between the high levels of uric acid detected in urine and antioxidant capacity is consistent with previous reports.[24−26] However, with regard to the ORAC assay, it is difficult to explain the discrepancy between urine urolithin levels given that the majority of the final concentrations of the urolithins in the assay were far above the effective concentrations of the pure compounds (Table 4). For plasma biospecimens, perhaps this is not the case because levels were close to, or below, the effective concentrations of the pure compounds (Table 4). Nevertheless, the plasma data are consistent with the ORAC and FRAP data of McKay et al.,[27] who also demonstrated nonsignificant changes, following intervention with albeit lower doses of either 21 or 42 g of walnuts per day. It is interesting to note that in contrast to our data and those of McKay et al.[27] with regard to plasma antioxidant capacity over the long term, short-term studies indicate rapid increases in plasma antioxidant capacity following walnut ingestion.[28] We are of the opinion that this has little relevance to the urolithins, which are produced only by bacterial metabolism of ellagitannins in the large intestine.

With regard to urolithins (in terms of comparing pure compounds with biospecimen concentration), consistent data were obtained for urolithin D in the fecal biospecimen extracts and the pure compound. Possibly, this is due to semi-purification and concentration of urolithin D in the Soxhlet extraction step. The inconsistencies in the correlations with regard to urolithin glucuronide concentration in urine and plasma biospecimens (the latter may be due to dilution effects), compared to the data generated with pure compounds, need to be clarified in the future by solid/liquid phase extraction methods to exclude possible matrix effects. In this sudy, although the data for the antioxidant capacity of urolithins in urine and possibly plasma biospecimens, in comparison to pure compounds, are equivocal, the results for the fecal extracts are not. The positive antioxidant capacities of the fecal extracts, rich in urolithin D, in the DPPH and FRAP assays, but negative in the ORAC assay, mirror exactly the data for the purified compounds and confirm the cell-based assay of Bialonska et al.[6] This points to a potential chemopreventive effect, with regard to colorectal cancer, given that urolithins also inhibit cell proliferation and induce apoptosis in HT-29 cells,[29] exhibit anti-inflammatory effects,[30] and inhibit Wnt signaling[31] in a human 293T cell line. Finally, although the number of subjects entered into the study was low ($n = 4$), they served the purpose of this pilot study to a certain extent. However, given the data generated from successive biospecimens from V-1, it would have been helpful had a similar protocol been possible for the other three volunteers. Unfortunately, due to logistic problems, this was not the case.

In summary, the data in this pilot study show that the metabolism of ellagitannins in four volunteers gave rise to a diverse profile and a highly variable concentration of urolithins in urine. The concentration of glucuronidated urolithins in urine, surprisingly, did not correlate with antioxidant capacity, in contrast to data generated with purified individual urolithins. This discrepancy warrants further investigation. However, the antioxidant capacity of urine biospecimens was highly correlated with uric acid concentration. The antioxidant capacity of fecal extracts correlated positively with the concentration of urolithin D, in both the DPPH and FRAP assays, but not in the ORAC assay, which was entirely consistent with the in vitro assays for pure urolithin D.

## AUTHOR INFORMATION

### Corresponding Author

*(R.W.O.) Phone: +49-6221-42-3317. Fax: +49-6221-42-3375. E-mail: robert.owen@nct-heidelberg.de.

### Notes

The authors declare no competing financial interest.

## REFERENCES

(1) Cerda, B.; Llorach, R.; Ceron, J. J.; Espin, J. C.; Tomas-Barberan, F. A. Evaluation of the bioavailability and metabolism in the rat of punicalagin, an antioxidant polyphenol from pomegranate juice. *Eur. J. Nutr.* **2003**, *42* (1), 18−28.

(2) Espin, J. C.; Gonzalez-Barrio, R.; Cerda, B.; Lopez-Bote, C.; Rey, A. I.; Tomas-Barberan, F. A. Iberian pig as a model to clarify obscure points in the bioavailability and metabolism of ellagitannins in humans. *J. Agric. Food Chem.* **2007**, *55* (25), 10476−10485.

(3) Cerda, B.; Espin, J. C.; Parra, S.; Martinez, P.; Tomas-Barberan, F. A. The potent in vitro antioxidant ellagitannins from pomegranate juice are metabolised into bioavailable but poor antioxidant hydroxy-6*H*-dibenzopyran-6-one derivatives by the colonic microflora of healthy humans. *Eur. J. Nutr.* **2004**, *43* (4), 205−220.

(4) Seeram, N. P.; Henning, S. M.; Zhang, Y.; Suchard, M.; Li, Z.; Heber, D. Pomegranate juice ellagitannin metabolites are present in human plasma and some persist in urine for up to 48 h. *J. Nutr.* **2006**, *136* (10), 2481−2485.

(5) Larrosa, M.; Gonzalez-Sarrias, A.; Yanez-Gascon, M. J.; Selma, M. V.; Azorin-Ortuno, M.; Toti, S.; Tomas-Barberan, F.; Dolara, P.; Espin, J. C. Anti-inflammatory properties of a pomegranate extract and its metabolite urolithin-A in a colitis rat model and the effect of colon inflammation on phenolic metabolism. *J. Nutr. Biochem.* **2010**, *21* (8), 717−725.

(6) Bialonska, D.; Kasimsetty, S. G.; Khan, S. I.; Ferreira, D. Urolithins, intestinal microbial metabolites of pomegranate ellagitannins, exhibit potent antioxidant activity in a cell-based assay. *J. Agric. Food Chem.* **2009**, *57* (21), 10181−10186.

(7) Adams, L. S.; Zhang, Y.; Seeram, N. P.; Heber, D.; Chen, S. Pomegranate ellagitannin-derived compounds exhibit antiproliferative and antiaromatase activity in breast cancer cells in vitro. *Cancer Prev. Res. (Phila.)* **2010**, *3* (1), 108−113.

(8) Hardman, W. E.; Ion, G. Suppression of implanted MDA-MB 231 human breast cancer growth in nude mice by dietary walnut. *Nutr. Cancer* **2008**, *60* (5), 666−674.

(9) Seeram, N. P.; Aronson, W. J.; Zhang, Y.; Henning, S. M.; Moro, A.; Lee, R. P.; Sartippour, M.; Harris, D. M.; Rettig, M.; Suchard, M. A.; Pantuck, A. J.; Belldegrun, A.; Heber, D. Pomegranate ellagitannin-derived metabolites inhibit prostate cancer growth and localize to the mouse prostate gland. *J. Agric. Food Chem.* **2007**, *55* (19), 7732−7737.

(10) Espin, J. C.; Larrosa, M.; Garcia-Conesa, M. T.; Tomas-Barberan, F. Biological significance of urolithins, the gut microbial ellagic acid-derived metabolites: the evidence so far. *Evidence-Based Complement. Altern. Med.* **2013**, 270−418.

(11) Owen, R. W.; Giacosa, A.; Hull, W. E.; Haubner, R.; Wurtele, G.; Spiegelhalder, B.; Bartsch, H. Olive-oil consumption and health: the possible role of antioxidants. *Lancet Oncol.* **2000**, *1*, 107−112.

(12) Bartsch, H.; Nair, J.; Owen, R. W. Exocyclic DNA adducts as oxidative stress markers in colon carcinogenesis: potential role of lipid peroxidation, dietary fat and antioxidants. *Biol. Chem.* **2002**, *383* (6), 915−921.

(13) Khan, N.; Afaq, F.; Mukhtar, H. Cancer chemoprevention through dietary antioxidants: progress and promise. *Antioxid. Redox Signal.* **2008**, *10* (3), 475−510.

(14) Anderson, K. J.; Teuber, S. S.; Gobeille, A.; Cremin, P.; Waterhouse, A. L.; Steinberg, F. M. Walnut polyphenolics inhibit in vitro human plasma and LDL oxidation. *J. Nutr.* **2001**, *131* (11), 2837−2842.

(15) Waterhouse, A. L. Determination of total phenolics. In *Current Protocols in Food Analytical Chemistry*; Wrolstad, R. E., Ed.; Wiley: Hoboken, NJ, USA, 2001.

(16) Pfundstein, B.; El Desouky, S. K.; Hull, W. E.; Haubner, R.; Erben, G.; Owen, R. W. Polyphenolic compounds in the fruits of Egyptian medicinal plants (*Terminalia bellerica*, *Terminalia chebula* and *Terminalia horrida*): characterization, quantitation and determination of antioxidant capacities. *Phytochemistry* **2010**, *71* (10), 1132−1148.

(17) Fukuda, T.; Ito, H.; Yoshida, T. Antioxidative polyphenols from walnuts (*Juglans regia* L.). *Phytochemistry* **2003**, *63* (7), 795−801.

(18) Garcia-Villalba, R.; Beltran, D.; Espin, J. C.; Selma, M. V.; Tomas-Barberan, F. A. Time course production of urolithins from ellagic acid by human gut microbiota. *J. Agric. Food Chem.* **2013**, *61* (37), 8797−8806.

(19) Cerda, B.; Tomas-Barberan, F. A.; Espin, J. C. Metabolism of antioxidant and chemopreventive ellagitannins from strawberries, raspberries, walnuts, and oak-aged wine in humans: identification of biomarkers and individual variability. *J. Agric. Food Chem.* **2005**, *53* (2), 227−235.

(20) Cerda, B.; Soto, C.; Albaladejo, M. D.; Martinez, P.; Sanchez-Gascon, F.; Tomas-Barberan, F.; Espin, J. C. Pomegranate juice supplementation in chronic obstructive pulmonary disease: a 5-week randomized, double-blind, placebo-controlled trial. *Eur. J. Clin. Nutr.* **2006**, *60* (2), 245−253.

(21) Gonzalez-Barrio, R.; Borges, G.; Mullen, W.; Crozier, A. Bioavailability of anthocyanins and ellagitannins following consumption of raspberries by healthy humans and subjects with an ileostomy. *J. Agric. Food Chem.* **2010**, *58* (7), 3933−3939.

(22) Gonzalez-Sarrias, A.; Gimenez-Bastida, J. A.; Garcia-Conesa, M. T.; Gomez-Sanchez, M. B.; Garcia-Talavera, N. V.; Gil-Izquierdo, A.; Sanchez-Alvarez, C.; Fontana-Compiano, L. O.; Morga-Egea, J. P.; Pastor-Quirante, F. A.; Martinez-Diaz, F.; Tomas-Barberan, F. A.; Espin, J. C. Occurrence of urolithins, gut microbiota ellagic acid metabolites and proliferation markers expression response in the human prostate gland upon consumption of walnuts and pomegranate juice. *Mol. Nutr. Food Res.* **2010**, *54* (3), 311−322.

(23) Gonzalez-Sarrias, A.; Zorin-Ortuno, M.; Yanez-Gascon, M. J.; Tomas-Barberan, F. A.; Garcia-Conesa, M. T.; Espin, J. C. Dissimilar in vitro and in vivo effects of ellagic acid and its microbiota-derived metabolites, urolithins, on the cytochrome P450 1A1. *J. Agric. Food Chem.* **2009**, *57* (12), 5623−5632.

(24) Atawodi, S. E.; Pfundstein, B.; Haubner, R.; Spiegelhalder, B.; Bartsch, H.; Owen, R. W. Content of polyphenolic compounds in the Nigerian stimulants *Cola nitida* ssp. alba, *Cola nitida* ssp. *rubra* A. Chev, and *Cola acuminata* Schott & Endl and their antioxidant capacity. *J. Agric. Food Chem.* **2007**, *55* (24), 9824−9828.

(25) Godycki-Cwirko, M.; Krol, M.; Krol, B.; Zwolinska, A.; Kolodziejczyk, K.; Kasielski, M.; Padula, G.; Grebowski, J.; Kazmierska, P.; Miatkowski, M.; Markowski, J.; Nowak, D. Uric acid but not apple polyphenols is responsible for the rise of plasma antioxidant activity after apple juice consumption in healthy subjects. *J. Am. Coll. Nutr.* **2010**, *29* (4), 397−406.

(26) Lotito, S. B.; Frei, B. The increase in human plasma antioxidant capacity after apple consumption is due to the metabolic effect of

fructose on urate, not apple-derived antioxidant flavonoids. *Free Radical Biol. Med.* **2004**, *37* (2), 251−258.
(27) McKay, D. L.; Chen, C. Y.; Yeum, K. J.; Matthan, N. R.; Lichtenstein, A. H.; Blumberg, J. B. Chronic and acute effects of walnuts on antioxidant capacity and nutritional status in humans: a randomized, cross-over pilot study. *Nutr. J.* **2010**, *9*, 21.
(28) Torabian, S.; Haddad, E.; Rajaram, S.; Banta, J.; Sabate, J. Acute effect of nut consumption on plasma total polyphenols, antioxidant capacity and lipid peroxidation. *J. Hum. Nutr. Diet.* **2009**, *22* (1), 64−71.
(29) Kasimsetty, S. G.; Bialonska, D.; Reddy, M. K.; Ma, G.; Khan, S. I.; Ferreira, D. Colon cancer chemopreventive activities of pomegranate ellagitannins and urolithins. *J. Agric. Food Chem.* **2010**, *58* (4), 2180−2187.
(30) Larrosa, M.; Gonzalez-Sarrias, A.; Yanez-Gascon, M. J.; Selma, M. V.; Zorin-Ortuno, M.; Toti, S.; Tomas-Barberan, F.; Dolara, P.; Espin, J. C. Anti-inflammatory properties of a pomegranate extract and its metabolite urolithin-A in a colitis rat model and the effect of colon inflammation on phenolic metabolism. *J. Nutr. Biochem.* **2010**, *21* (8), 717−725.
(31) Sharma, M.; Li, L.; Celver, J.; Killian, C.; Kovoor, A.; Seeram, N. P. Effects of fruit ellagitannin extracts, ellagic acid, and their colonic metabolite, urolithin A, on Wnt signaling. *J. Agric. Food Chem.* **2010**, *58* (7), 3965−3969.

activity of calcium-binding peptides may be used as one kind of food additive that prevents bone disorders.

## MATERIALS AND METHODS

**Materials.** Whey protein (WPC80, containing 80.5% protein) was kindly provided by Hilmar Corporation (Batch 20111107, Hilmar, CA). The commercial proteases, Flavourzyme (EC. 3.4.11.1, $2 \times 10^6$ units/g) and Protamex (EC. 3.4.24.28, $1.5 \times 10^6$ units/g), were purchased from Novo (Novozymes, Denmark). Toyopearl DEAE-650M and Sephadex G-25 were offered by Amersham Pharmacia (Amersham Pharmacia Co., Uppsala, Sweden). All of the other chemicals and solvents were of analytical grade.

**Hydrolysis of Whey Protein.** A total of 5% (w/v) whey protein solution was denatured in 80 °C for 20 min, and the pH was adjusted to 7.0. The sample was hydrolyzed using Flavourzyme and Protamex (2:1, w/w) with a substrate/enzyme ratio of 25:1 (w/w) at 49 °C for 7 h. Hydrolysate was heated at boiling water for 10 min to inactive the enzyme and cooled to room temperature. The mixture was subsequently centrifuged at 16000*g* for 20 min, and then the supernatant named whey protein hydrolysate (WPH) was lyophilized and stored at −20 °C for subsequent investigation.

**Purification and Identification of Calcium-Binding Peptide.** *Ion-Exchange Chromatography on Diethylaminoethyl (DEAE).* The peptide that could bind with calcium and form peptide−calcium chelate was defined as the calcium-binding peptide. The slurry of Toyopearl DEAE-650M was packed in a column (20 × 2.5 cm) and then equilibrated at 5 column volume (CV) of 20 mM Tris-HCl buffer (pH 9.0) as the equilibrating buffer. Afterward, 100 mg of the lyophilized hydrolysates that had been through 0.45 μm filter film was dissolved in 10 mL of the same buffer (pH 9.0) and loaded on the column. Then, after washing with the equilibrating buffer, the collected peak was labeled as the non-absorbed fraction. The bond peptides were eluted by a gradient elution with the same buffer containing 0−0.5 M NaCl. The flow rate was 0.5 mL/min; fraction volume was 5 mL/tube; elution was monitored at 214 nm; all peaks were collected; and calcium-binding capacities of the fractions were determined.

*Gel Filtration on Sephadex G-25.* The fraction with the highest calcium-binding capacity was pooled and lyophilized; 200 mg of the sample was dissolved in 5 mL of deionized water and loaded onto a Sephadex G-25 column (100 × 2.0 cm), which had previously been equilibrated with deionized water, and then eluted with deionized water at a flow rate of 0.3 mL/min. The eluate was monitored by measuring the absorbance at 214 nm. After calcium-binding capacity was determined, the fraction with the highest activity was pooled and lyophilized.

*High-Performance Liquid Chromatography (HPLC) on C18.* The lyophilized sample collected from G-25 was dissolved in distilled water approximately equivalent to 30 mg/mL and purified by semi-preparative reversed-phase high-performance liquid chromatography (RP-HPLC) on C18 reversed silica gel chromatography (Gemini 5 μm C18, 250 × 10 mm, Phenomenex, Inc., Torrance, CA). Elution was performed on solution A [0.05% trifluoroacetic acid (TFA) in water] and solution B (0.05% TFA in acetonitrile) with a gradient of 0−30% B at 1.0 mL/min for 50 min. The elution was monitored at 214 nm, and the absorption peaks were fractionated for measuring the calcium-binding activity. The injection volume was generally 200 μL.

*Identification of the Purified Calcium-Binding Peptide.* The molecular mass and amino acid sequence of the purified calcium-binding peptide were determined using liquid chromatography−electrospray ionization/mass spectrometry (LC−ESI/MS, Delta Prep 4000, Waters Co., Milford, MA) over the $m/z$ range of 300−3000.

*Calcium-Binding Capacity Assay.* The calcium-binding capacity was defined as the content of calcium (μg) bound with peptide (mg) after the chelating reaction. Lyophilized whey protein hydrolysate was dissolved in deionized water to be 1.0 mg/mL and mixed with 5 mM $CaCl_2$ in 0.2 M sodium phosphate buffer (pH 8.0). The solution was stirred at 37 °C for 2 h, and pH was maintained at 8.0 with a pH meter. The reaction mixture was centrifuged at 10000*g* at room temperature for 10 min to remove insoluble calcium phosphate salts. Sodium phosphate was used as the calcium-binding buffer, which could react with calcium ion and peptide, separately, and show obviously different reactions. Calcium ion could combine with phosphate to form calcium phosphate precipitation, while peptide could take calcium ion from precipitation. As a result, peptide−Ca chelate was a water-soluble substance, and a soluble calcium content in the supernatant represented the calcium content associated with the peptide.[16] The calcium contents in the supernatant were determined using a colorimetric method with *ortho*-cresolphthalein complexone reagent.[17] The absorbance at 570 nm was determined after adding the working solution to the sample. The experiments were performed in triplicate, and values were expressed as the mean ± standard deviation (SD).

**Characterization of the Purified Calcium-Binding Peptide.** *Formation of the Peptide−Calcium Chelate.* Peptide−calcium chelate was the chelating component of the reaction between dipeptide Gly-Tyr and calcium ion. The calcium-binding chelate was prepared by adding 5 mL of 1% (w/v) $CaCl_2$ into 20 mL of 2.5% (w/v) calcium-binding peptide solution. The reaction was placed in a controlled water bath with constant agitation (100 rpm) at 37 °C for 2 h after the pH of the solution was adjusted to 7.0 by the addition of 0.1 M NaOH. Then, the mixture was added with absolute ethanol (9 times of solution volume) to remove free calcium and centrifuged at 10000*g* for 10 min, and the precipitates was lyophilized for analysis.

*Ultraviolet (UV) Absorption Spectroscopy Assay.* The UV spectra of the calcium-binding peptide and peptide−calcium chelate were recorded over the wavelength range from 190 to 400 nm by a UV−vis spectrophotometer (UV-2600, UNICO Instrument Co., Ltd., Shanghai, China) as the method described by Chen et al.[18] The calcium-binding peptide of 0.2 mg/mL was prepared. The peptide−calcium chelate was prepared by adding 0, 2, 4, 6, 8, and 10 μM $CaCl_2$ to 0.2 mg/mL calcium-binding peptide solution, separately. The mixed solution reacted at room temperature for 30 min.

*Fluorescence Spectra Analysis.* Fluorescence spectra were measured to monitor conformational changes in the peptide induced by calcium chelation using the F-4600 fluorescence spectrophotometer (Hitachi Co., Japan). The excitation wavelength was 280 nm, and emission wavelengths between 290 and 360 nm were recorded.

*Fourier Transform Infrared Spectroscopy (FTIR) Measurement.* A total of 1 mg of calcium-binding peptide powder or peptide−calcium chelate was ground evenly with 100 mg of dry KBr under infrared light to the size below 2.5 μm. Then, the transparent KBr piece was made at 60 MPa. To examine whether the variation in pellet thickness causes significant interference in the measured spectra, three different pellets were prepared from the same sample and their FTIR spectra were compared. The average of these three spectra was then used for analysis. The FTIR spectra were recorded using an infrared spectrophotometer (360 Intelligent, Thermo Nicolet Co., Waltham, MA) over a wavenumber region between 4000 and 400 $cm^{-1}$ at a resolution of 4 $cm^{-1}$, and the sample spectra were background-subtracted using a spectrum collected in the absence of a peptide−calcium chelate sample. Therefore, the physical variation in the FTIR spectra caused by the KBr technique had been removed prior to the FTIR spectra analysis. A total of 64 scans were recorded per sample in the FTIR spectra, and the peak signals in the spectra were analyzed using OMNIC 8.2 software (Thermo Nicolet Co., Madison, WI).

*$^1$H Nuclear Magnetic Resonance (NMR) Spectroscopy Assay.* The peptide−calcium chelate and calcium-binding peptide (0.5 mg) were dissolved in 500 μL of deionized water, separately. A total of 50 μL of deuterium oxide ($D_2O$) was added after the pH of the solution was adjusted to 6.5. The samples were transferred into 5 mm NMR tubes and subjected to NMR analysis with a Bruker Avance III spectrometer (Bruker Biospin, Rheinstetten, Germany).

*Differential Scanning Calorimetry (DSC) Analysis.* Thermogravimetry (TG)−DSC simultaneous thermal analyzer (STA449C, NETZSCH, Germany) was employed to measure the thermal property. Hermetic pans with lyophilized powder samples (5 mg) were heated from 50 to 600 °C at a programmed heating rate of 10 °C/min in a argon atmosphere. An empty pan was used as a reference.

*ζ Potential Measurement.* A Malvern Nano ZS Zetasizer based on dynamic light scattering was employed to measure the ζ potential. The system works according to the phase analysis light scattering (PALS) principle. The volume of all samples (3 mg) was 15 mL with autotitration by 0.25 M NaOH or HCl. The samples were equilibrated for 30 s before titration.

*Calcium-Releasing Percentage Experiment.* The calcium-releasing percentage determination of peptide−calcium chelate and $CaCl_2$ was examined according to the method described by Wang et al.[19] Peptide−calcium chelate and $CaCl_2$ were dissolved in deionized water, separately, equivalent to 10 μg/mL. The pH of these solutions was adjusted to 2.0, 3.0, 4.0, 5.0, 6.0, 7.0, and 8.0. After incubation in a shaking water bath for 2 h at 37 °C, the solutions were centrifuged in a refrigerated centrifuge at 10000*g* for 10 min. The calcium amount in the supernatant and the total calcium in the whole solution were determined by the colorimetric method with an *ortho*-cresolphthalein complexone reagent. The calcium releasing percentage was calculated as follows:

$$\text{calcium-releasing percentage (\%)} = \text{Ca amount in supernatant (g)/total Ca in solution (g)} \times 100$$

**Statistical Analyses.** All data were presented as means (SDs) conducted with three replicates. The statistical analysis was performed using SPSS 16.0 software (SPSS, Inc., Chicago, IL). Analysis of variance (ANOVA) was performed to determine the significance of the main effects. A value of $p < 0.05$ was considered statistically significant.

## RESULTS AND DISCUSSION

**Purification and Identification of the Calcium-Binding Peptide.** Bioactive peptides are usually purified using a combination of chromatographic techniques.[20] Throughout the purification process, calcium-binding activity of WPH was assessed using the colorimetric method with an *ortho*-cresolphthalein complexone reagent.[17] Three fractions (F1, F2, and F3) of the WPHs were divided on a DEAE anion-exchange chromatography column (Figure 1). The calcium-binding capacity was noticeably higher in F2 and F3 compared to F1 (Figure 1). Moreover, in comparison to WPH (33.92 μg/mg), the calcium-binding capacity of F2 was significantly improved (57.02 μg/mg).

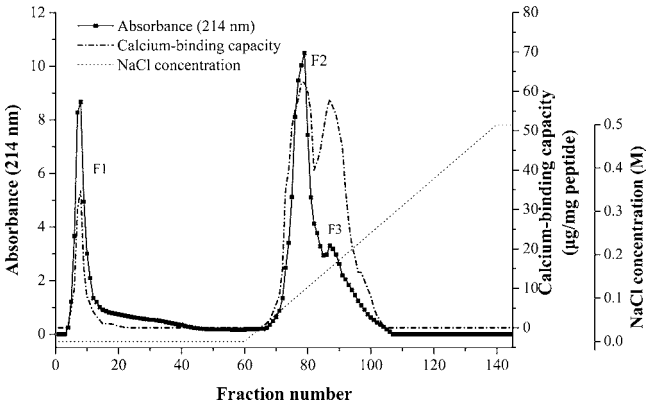


**Figure 1.** Fractionation on a DEAE anion-exchange chromatography column and the calcium-binding capacity of the three fractions separated from the DEAE column. The peptide was washed with the binding buffer (0.02 M Tris−HCl buffer at pH 9.0) and eluted with a linear gradient of 0−0.5 M NaCl in the same buffer.

Fraction F2 with the highest calcium-binding capacity was further separated using size-dependent Sephadex G-25 gel filtration chromatography resulting in four major fractions, named F21, F22, F23, and F24 (Figure 2). F23 exerted the most excellent calcium-binding capacity (Figure 2). The result was consistent with some previous reports, which showed that a lower molecular mass peptide exhibited a tendency to combine with calcium ion.[21,23] It is reported that the lowest molecular weight peptide fraction (<1 kDa) had the higher calcium-binding activity through ultrafiltration and small molecular peptide fractions purified on a G-25 column possessed higher calcium-binding capacity.[21,22]

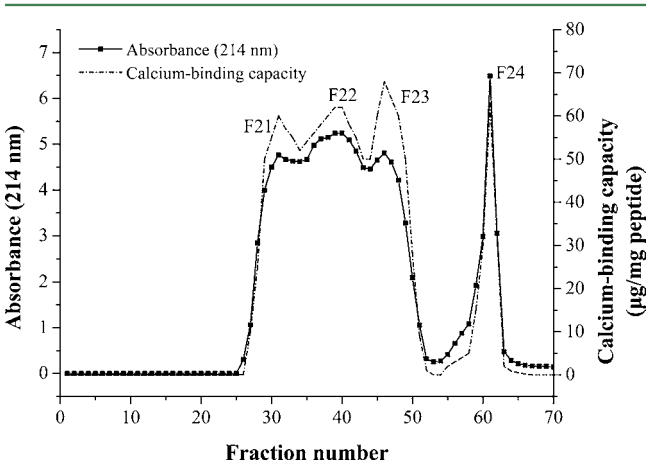


**Figure 2.** Fractionation of the fraction F2 with the highest calcium-binding activity from DEAE chromatography on a Sephadex G-25 gel filtration chromatography column and the calcium-binding capacity of the fractions F21−F24 separated from a Sephadex G-25 column.

The active peak F23 was pooled, dissolved in distilled water, and loaded onto semi-preparative C18 RP-HPLC. The fraction F23 was separated into 13 major distinct fractions (Figure 3A). Each fraction was pooled, and calcium-binding capacity was determined subsequently (Figure 3B). Among 13 distinct fractions, fraction 7 showed the highest calcium-binding ability, and then it was further fractionated by RP-HPLC on a C18 column. The elution profile showed that fraction 7 was composed of five peaks, and fraction 2 (Figure 4A), one of the eluted peaks, was the purifed peptide. The calcium-binding capacity of fraction 2 reached 75.38 μg/mg (Figure 4B). The chromatographic profile of fraction 2 on analytic C18 RP-HPLC (Figure 5) showed only a single peak called WPH-A, indicating the high purity of the isolated peptide.

The amino acid sequence of WPH-A eluted from RP-HPLC chromatography was identified by LC−ESI/MS (Figure 6). According to the mass/charge ratio ($m/z$) of 238.99 Da of the molecular ion peak ($[M + H]^+$), the molecular mass of WPH-A was confirmed to be 237.99 Da. The $m/z$ of fragment ion y1 was 181.99 Da, which resulted from the relative molecular mass of tyrosine in addition with one hydrogen atom. On the basis of calculation in ESI ion molecular mass, one residue in WPH-A was Tyr and the other one was Gly. Therefore, the animo acid sequence was determined to be Gly-Tyr. The result was confirmed by comparison to data from the National Center for Biotechnology Information (NCBI) database.

Not only could the differences in the net charge and length of peptides influence the extent of chelate formation with metal ion, but also the different amino acid residues of peptides affected their activities,[14,24] including the amino acid composition and sequence of the peptides.[25] Chaud et al.[14] reported that tyrosine seemed to bind with divalent metal

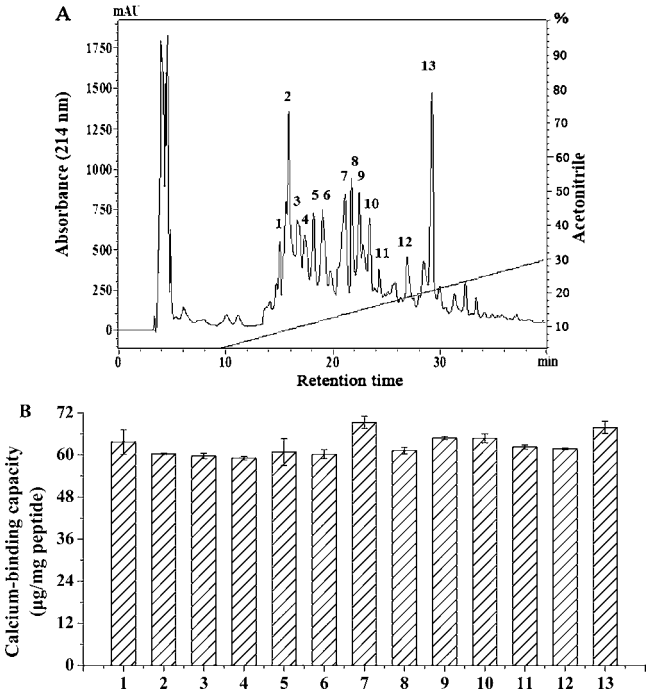


**Figure 3.** (A) Fraction F23 from a Sephadex G-25 column and then applied to a semi-preparative C18 RP-HPLC column. The column was then washed with a linear gradient of 0−30% acetonitrile containing 0.05% TFA. (B) Calcium-binding capacity for the fractions 1−13 of F23 separated from semi-preparative HPLC.

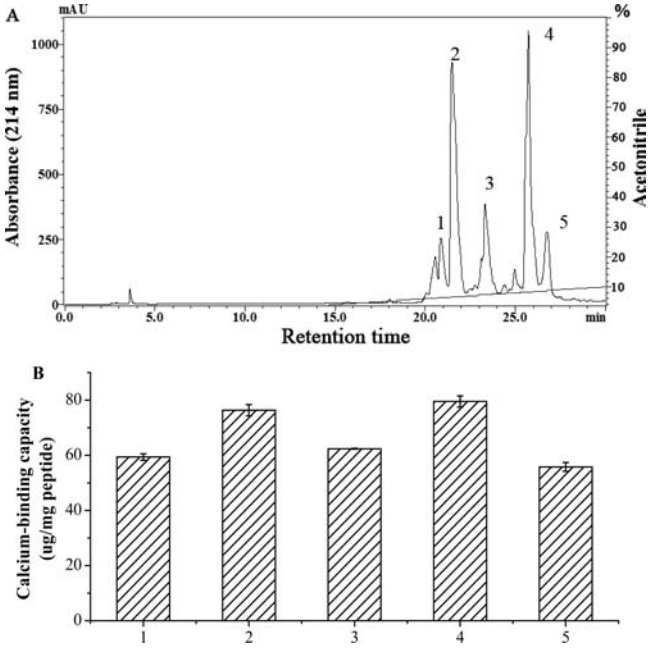


**Figure 4.** (A) RP-HPLC of fraction 7 derived from preparative HPLC. The column was then washed with a linear gradient of 0−10% acetonitrile containing 0.05% TFA. (B) Calcium-binding capacity of fractions 1−5 from RP-HPLC.

cations through oxygen of the phenolic hydroxyl group. The phosphorylation of tyrosine and serine residues could provided suitable binding sites for positively charged metals, such as calcium, iron, or zinc.[26] Moreover, the animo acid glycine was considered as an organic ligand having the metal ion binding function. Jung et al.[27] purified a calcium-binding peptide from

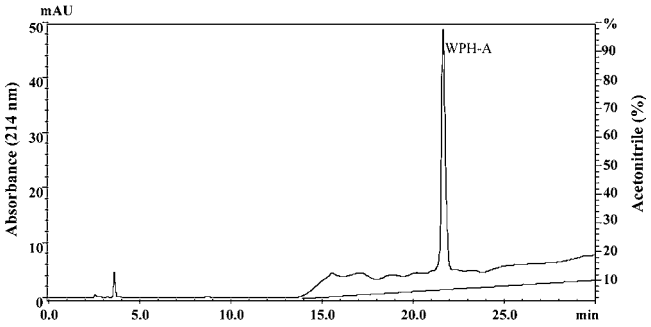


**Figure 5.** Analytic RP-HPLC of the peak WPH-A for purify identification. The column was washed with a linear gradient of 0−10% acetonitrile containing 0.05% TFA.

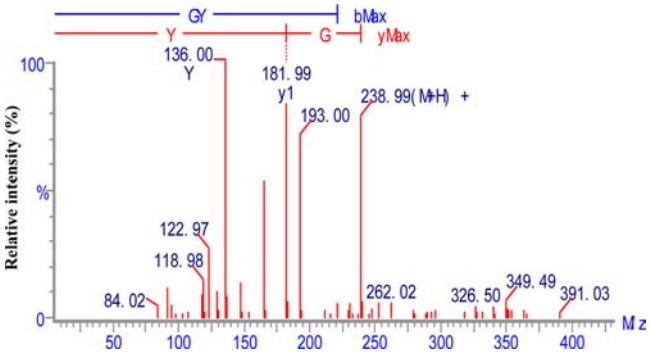


**Figure 6.** Identification of the amino acid sequence of the calcium-binding peptide using LC−ESI/MS.

Alaska pollack containing Gly, Ser, and Val. Hoki bone hydrolysates had a high affinity to calcium, and the major animo acid composition of the peptide included Gly, Asp, and Glu.[28] An iron-chelating peptide with multi-glycine residues was also purified from anchovy muscle protein.[29] In this study, a calcium-binding peptide was identified to contain Gly and Tyr residues; both of them contributed to combine with divalent minerals.

**Characterization of the Purified Calcium-Binding Peptide.** *UV Absorption Spectroscopy Assay.* The UV spectra of calcium-binding peptide Gly-Tyr showed an obvious difference from that of the Gly-Tyr−Ca chelate (Figure 7). A strong absorption band was observed at about 200 nm, which could be regarded as the characteristics of the amide bond in peptide. Another absorption peak at around 280 nm appeared in both Gly-Tyr and Gly-Tyr−Ca chelate, resulting from the characteristic UV absorption of Tyr. With the addition of calcium ion to dipeptide Gly-Tyr, the intensity of the absorption band of the amide bond became higher than that of dipeptide alone. In the magnified UV spectra image, the red shifts of the band, such as the red curve in Figure 7, could be clearly observed and a small peak arose in the dipeptide−calcium chelate.

Through observing the shifts and intensity changes of UV bands, the UV absorption situation of the amide bond in peptide and the side group in Tyr could be analyzed. The UV spectra phenomenon was consistent with some other studies, which demonstrated that the spatial structure with the chirality of the chromospheres (C═O and −COOH) and auxochromes (−OH and $-NH_2$) of peptides changed after incorporating with the calcium ion.[30,31] The main reason for the intensity changes of the band indicated that the oxygen atom of the


dx.doi.org/10.1021/jf502412f | J. Agric. Food Chem. 2014, 62, 10274−10282

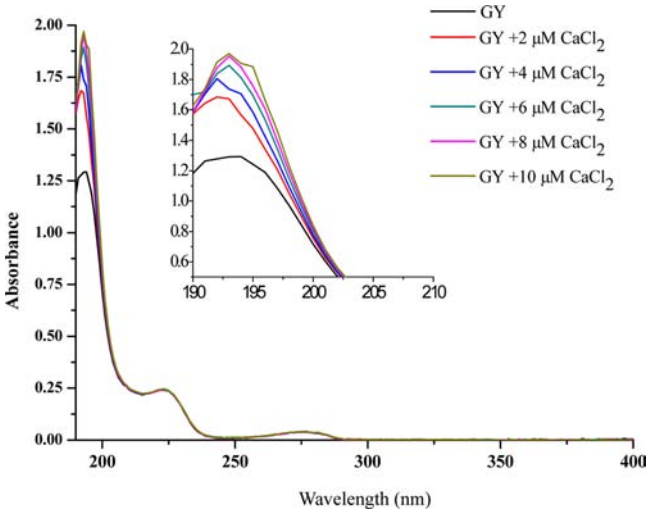


**Figure 7.** UV spectra of Gly-Tyr and Gly-Tyr−Ca chelate over the wavelength range from 190 to 400 nm.

carbonyl group and nitrogen of the amino group in the peptide bond with calcium.[32] The appearance of a small peak reflected the difference of relevant valence electron transition when more calcium ion reacted with Gly-Tyr. All of these band changes suggest that Gly-Tyr could bind with calcium ion and form the Gly-Tyr−Ca chelate.

*Fluorescence Spectra Analysis.* The purified calcium-binding dipeptide Gly-Tyr contained aromatic amino acid Tyr, which could generate endogenous fluorescent at a proper excitation wavelength. The fluorescence emission spectra of Gly-Tyr was examined to monitor its structural modification with $CaCl_2$ treatment. Through fluorescence quenching, the calcium binding sites could be speculated. The fluorescence spectra of Gly-Tyr and Gly-Tyr−Ca chelate are shown in Figure 8. When excited at 280 nm, Tyr in Gly-Tyr exhibited an intrinsic fluorescence emission maximum at 310 nm. With the increased calcium ion concentration, the endogenous fluorescence decreased dramatically, which meant that calcium ion had a significant effect on the Gly-Tyr structure. Especially, apparent folding and conformation modification of Gly-Tyr happened at the beginning of the addition with 5 $\mu$M $CaCl_2$.

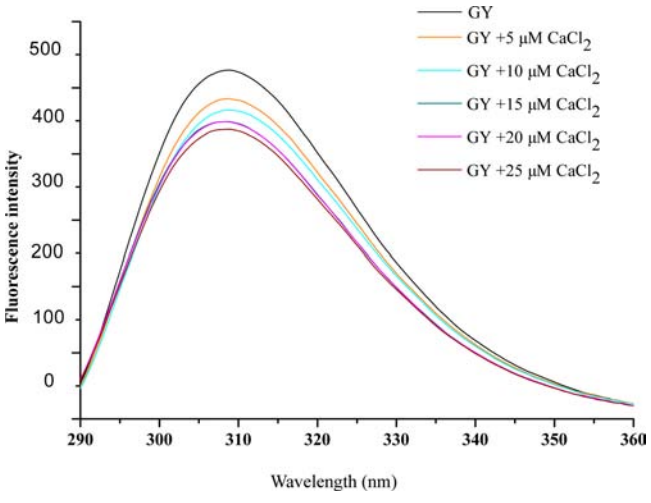


**Figure 8.** Fluorescence emission spectra of the peptide Gly-Tyr at various concentrations of $Ca^{2+}$.

This result is consistent with that of the iron-chelating peptides from anchovy (*Engraulis japonicus*) muscle protein.[29] Reddi et al.[33] demonstrated that the $Zn^{II}$ binding energy was used to fold the peptide in the zinc-binding reaction of a zinc-finger peptide. As the concentration of $CaCl_2$ increased, fluorescence quenching became weaker than before. It meant that there were not any spared binding sites in Gly-Tyr for the calcium ion. This experimental evidence suggested that the structure of functional binding sites in Gly-Tyr changed, resulting in the formation of the Gly-Tyr−Ca chelate when $CaCl_2$ reacted with Gly-Tyr. The addition of metal ion induced the intrinsic fluorescence quenching of protein or peptide, especially for the oligo-peptide without thermodynamic structure stability.[34] Generally, the calcium ion could cause fluorescence quenching of the calcium-binding peptide, which likely contributed to the decrease in the fluorescence intensity.[19]

*FTIR Measurement.* Changes in the characteristic FTIR absorption peaks of some functional binding sites in peptide could reflect the interaction of metal ion with organic ligand groups in the peptide. To analyze calcium-ion-induced changes in the structure of the calcium-binding peptide Gly-Tyr, the FTIR technique was employed.

Figure 9 depicted the infrared spectrum of Gly-Tyr in the absence and presence of calcium. There were significant

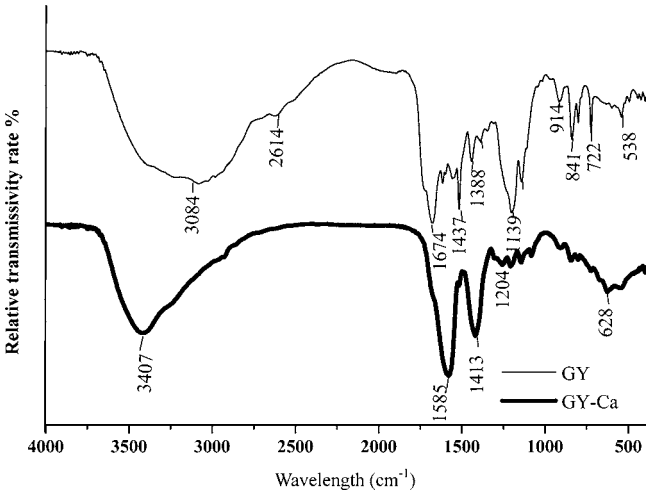


**Figure 9.** FTIR spectra of Gly-Tyr and Gly-Tyr−Ca chelate in the regions from 4000 to 400 $cm^{-1}$.

differences between Gly-Tyr and Gly-Tyr−Ca chelate. The results implied that the wavenumbers (1674 and 1437 $cm^{-1}$) of the amide I band were shifted to lower frequencies (1585 and 1413 $cm^{-1}$) after the addition of calcium, which stood for infrared absorption of the carbanyl group caused by the antisymmetric stretching vibration $\upsilon_{as}$ ($COO^-$) and the symmetric stretching vibration $\upsilon_s$ ($COO^-$) of carboxylic acid ions. Upon coordination with the Gly-Tyr−Ca chelate, the C bands corresponding to the carboxyl groups at 1204 and 1139 $cm^{-1}$ exhibited two weaker peaks in the fingerprint region. It is reported that ferric chloride could bind with casein enzymatic hydrolysates to form the $Fe^{3+}$−peptide complex, and the chief iron-binding site relates to the amide and carboxylate groups.[14] When metal ions combined with ligand atoms, such as O, N, and S, of organic compounds to form the chelate, the absorption peaks because of vibration of the coordinate bonds were typically located in the far-infrared region. The

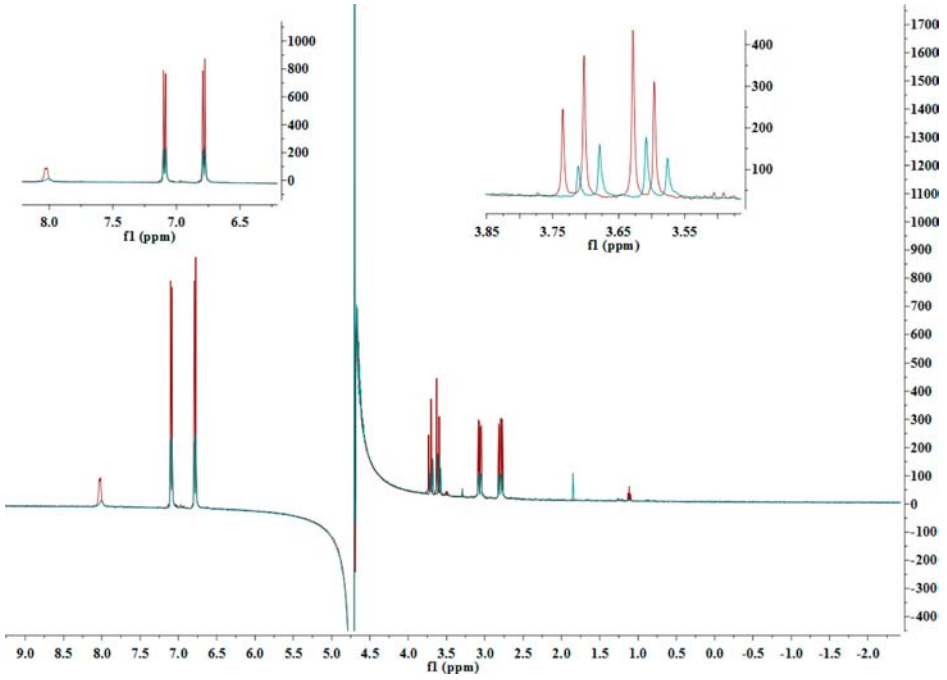


**Figure 10.** [1]H NMR spectral region from −0.30 to 10.00 ppm of Gly-Tyr and Gly-Tyr−Ca chelate (the red line means Gly-Tyr, and the green line means Gly-Tyr−Ca).

Ca−O vibration band was located between 500 and 800 $cm^{-1}$, while the interaction between the peptide and calcium ion resulted in a broadening and decreased intensity of the peaks; even some band absorptions disappeared, which was in agreement with the report by Chen et al.[18] Absorption of a high frequency at 3084 $cm^{-1}$ referred to the antisymmetric stretching vibration $\upsilon_{as}$ (N−H) and the symmetric stretching vibration $\upsilon_{s}$ (N−H) of the N−H bond in the Gly-Tyr spectrum. Absorption of a high frequency at 3200−3600 $cm^{-1}$ referred to the possible Ph−O-H strech and H bonds of hydration in the Gly-Tyr spectrum. With the coordination of the calcium−peptide complex, the waveform and the absorbance values had greatly changed. After the addition of calcium, the chelation reaction resulted in a shift to a higher wavenumber (3407 $cm^{-1}$), which indicated that the electron cloud density of N−H in Gly-Tyr became stronger because of the inductive effect or dipole field effect.

These phenomena indicated that the interaction between Gly-Tyr and calcium occurred via the carboxyl oxygen atoms and amino group nitrogen atoms in the peptide, which were similar to the calcium-binding peptides derived from soybean protein hydrolysates.[35]

*[1]H NMR Spectroscopy Assay.* The low-field region, from 6.75 to 8.00 ppm, of the Gly-Tyr and Gly-Tyr−Ca NMR spectrum (Figure 10) contained signals from aromatic group tyrosine (6.75 and 7.10 ppm) and N−H of the amide bond (8.00 ppm). The symmetric doublet in the region of 3.55−3.75 ppm corresponded to H spin coupling cracking in $\alpha$-H of Gly and Tyr. The signals at 3.00 and 2.75 ppm arose from two $\beta$-H atoms of tyrosine. With the addition of the calcium ion, the symmetric doublet signals of $\alpha$-H in Gly-Tyr shifted to lower parts per million (ppm) values, whose chemical shift was approximately 0.025 ppm. The change in hydrogen atom spin coupling cracking resonance signal peaks was caused by the combination of Gly-Tyr and calcium, thereby the electron density around the hydrogen nucleus in Gly-Tyr was affected.

The chemical shift information on [1]H NMR could explain the distribution of the electron cloud density around the hydrogen nucleus among different substances; consequently, the reaction situation between the purified calcium-binding dipeptide Gly-Tyr and calcium ion could be revealed. A declined electron cloud density along with a decreased shielding effect and intensive resonant frequency led to the movement of resonance signal peaks to a lower field region.

*TG−DSC Analysis.* The thermostability of samples was investigated through DSC and TG thermal analysis. There were remarkable differences of peak temperatures between dipeptide Gly-Tyr and Gly-Tyr−Ca chelate (Figure 11). The TG−DSC curve of Figure 11A showed that the thermal decomposition reaction of Gly-Tyr was not single in the whole process of weight loss. The thermal transitions at 179.40, 269.15, 359.99, and 530.51 °C were accompanied by weight loss of 25.74, 14.23, 15.15, and 14.32%, respectively. These endothermic peaks were caused by the C−N bond in Gly-Tyr. Whereas, obviously high shift endothermic peaks were observed at 428.77, 462.05, 504.07, and 550.93 °C after calcium ion treatment (Figure 11B). Meanwhile, TG of Gly-Tyr−Ca showed a flat and decline curve with a mass loss of 80%, which demonstrated that calcium-ion-processed Gly-Tyr resulted in a great increase in the DSC peak temperature accompanied by less and reduced weight loss, indicating that the Gly-Tyr−Ca chelate exhibited distinct thermal stability. This result suggested that Ca-processed dipeptide Gly-Tyr was less sensitive to heat denaturation with a higher peak temperature because of the formation of the Gly-Tyr−Ca chelate compound and the thermal stability of Gly-Tyr−Ca chelate was higher than that of Gly-Tyr alone.

*$\zeta$ Potential.* The principal of $\zeta$ potential was polarization of the water that occurred in the interface of two phases and then inducing that potential difference that existed in the phases. Figure 12 presented the $\zeta$ potential values of the Gly-Tyr−Ca chelate compared to Gly-Tyr without the calcium ion. The


dx.doi.org/10.1021/jf502412f | J. Agric. Food Chem. 2014, 62, 10274−10282

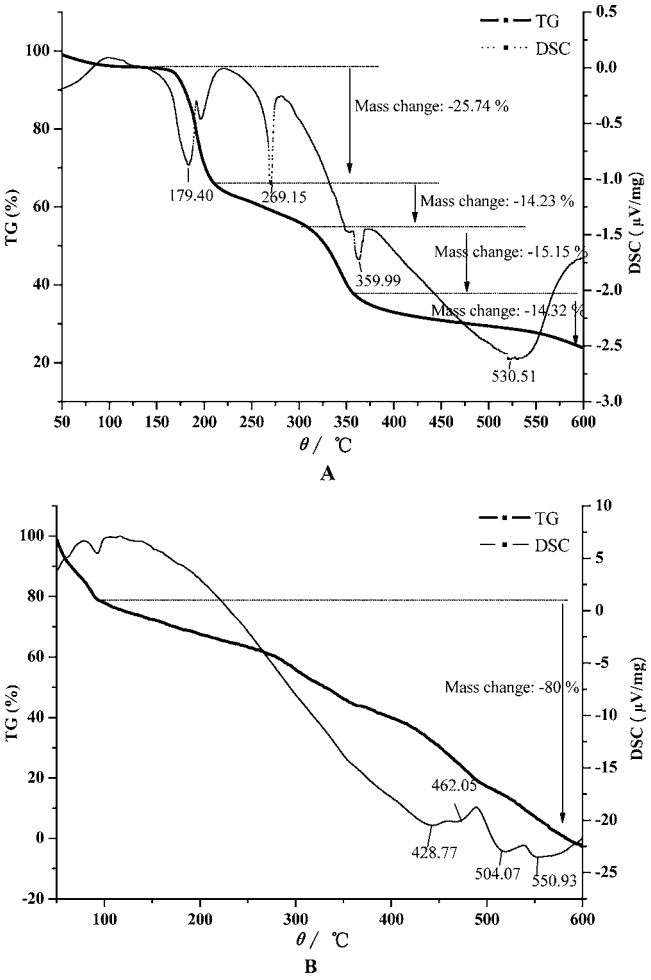


**Figure 11.** Typical DSC thermograms of (A) Gly-Tyr and (B) Gly-Tyr−Ca chelate.

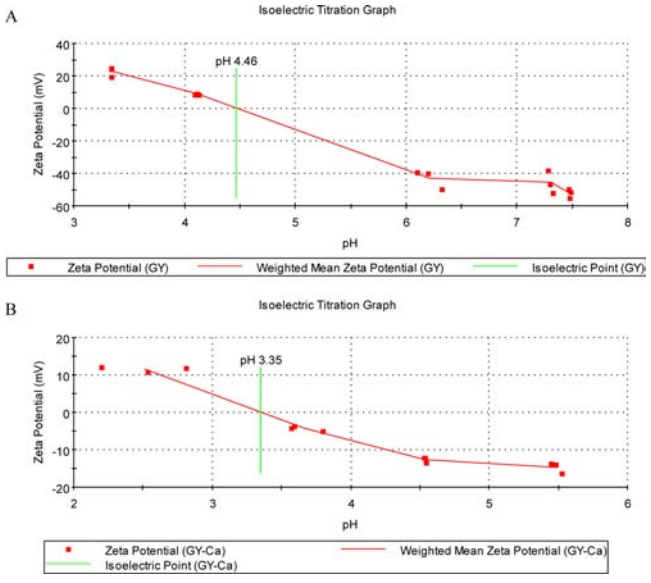


**Figure 12.** ζ potential of (A) Gly-Tyr and (B) Gly-Tyr−Ca chelate.

initial pH of Gly-Tyr in aqueous solution was measured to be 3.34 (Figure 12A). It meant that dipeptide Gly-Tyr in aqueous solution exhibited acid property. While in the Gly-Tyr−Ca chelate, the initial pH 5.45 approached neutral pH 7.0, which indicated that the addition of calcium improved the pH value of Gly-Tyr, inducing a weaker charge, and made it prone to be an neutral molecule (Figure 12B). Besides, the ζ potential ranged from positive charge (19.3 mV) to negative charge (−13.8 mV) when the calcium ion was added to dipeptide Gly-Tyr. Figure 12A also showed that the pI of Gly-Tyr was 4.46, while that of Gly-Tyr−Ca was 3.35. The pI decreased with the calcium ion treated on Gly-Tyr. In addition, the pH 3.34 of Gly-Tyr in aqueous solution was closer to its pI 4.46 than that of Gly-Tyr−Ca, which suggested that Gly-Tyr−Ca was more stable than Gly-Tyr alone. In the same pH value range, the changes of the ζ potential absolute value of Gly-Tyr−Ca were less than those of Gly-Tyr and Gly-Tyr−Ca possessed a lower ζ potential absolute value. The result indicated that Gly-Tyr−Ca existed as a molecular structure in aqueous solution without two different phases or double electrode layers. Through this experimental evidence, it could be speculated that the calcium ion was surrounded by the functional binding sites, such as the carboxyl and amino groups, of Gly-Tyr by a coordinate bond exhibiting an neutral molecule without being a form of inorganic calcium, to enhance its stability in the gastrointestinal tract.

*Calcium-Releasing Percentage Assay.* The calcium-releasing percentage of the Gly-Tyr−Ca chelate and $CaCl_2$ at different pH values is shown in Figure 13. The solubility

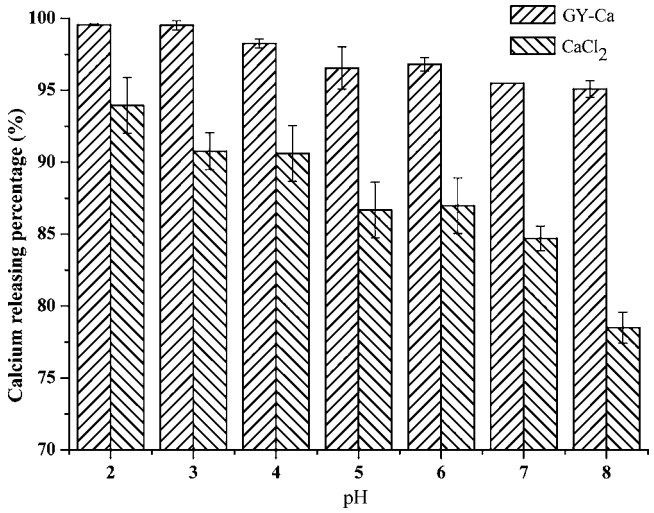


**Figure 13.** Calcium-releasing percentage of the Gly-Tyr−Ca chelate and $CaCl_2$ at pH values of 2.0, 3.0, 4.0, 5.0, 6.0, 7.0, and 8.0, separately.

between Gly-Tyr−Ca and $CaCl_2$ was apparently different. For both of them, the calcium-releasing percentage reduced with the increase of pH. While at any pH value, the calcium-releasing percentage of Gly-Tyr−Ca was obviously higher than that of $CaCl_2$. The calcium-releasing amount in the Gly-Tyr−Ca chelate was relatively stable in the pH that ranged from 2.0 to 8.0, maintaining above 95%, whereas that of $CaCl_2$ decreased significantly from 93.94% at pH 2.0 to 78.48% at pH 8.0. The result implied that calcium in Gly-Tyr−Ca had good solubility whether at pH 2.0 or 8.0, which was similar to the pH values of the human stomach or gastric environment; consequently, precipitation could not form.[36]

It is essential to discuss the dissolved status of the peptide−calcium chelate in the human gastrointestinal tract because the calcium ion probably reacted with phytic or oxalic acid to become insoluble in the stomach and form $Ca(OH)_2$ in the


dx.doi.org/10.1021/jf502412f | J. Agric. Food Chem. 2014, 62, 10274−10282

intestinal tract. The finding of our study suggested that the purified dipeptide Gly-Tyr contributed to improve the solubility of Ca under gastrointestinal tract pH values and was effectively absorbed by intestinal epithelial cells. The result suggests that it is feasible to produce natural calcium-chelating peptide as functional food additives.

*Hypothetical Molecular Structural Formula of the Gly-Tyr−Ca Chelate.* According to the results of frontal structural characterizations, including UV absorption spectroscopy, FTIR, fluorescence spectra, and $^1$H NMR spectroscopy, the functional binding sites of Gly-Tyr contained an oxygen atom of the carbonyl group and nitrogen of the amino or imino group in the peptide bond. Futhermore, the $\zeta$ potential experiment indicated that the calcium ion was surrounded by these functional binding bonds in Gly-Tyr through a coordinate bond. Therefore, the molecular structural formula of the Gly-Tyr−Ca chelate was speculated in Figure 14.

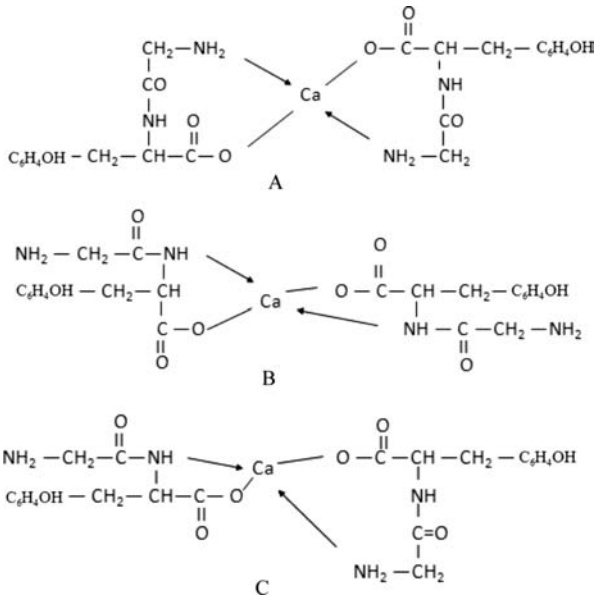


**Figure 14.** Hypothetical molecular structural formula of the Gly-Tyr−Ca chelate.

## AUTHOR INFORMATION

### Corresponding Author

*Telephone: +86-591-22866375. Fax: +86-591-22866278. E-mail: shywang@fzu.edu.cn.

### Funding

This work was supported by the National Marine Public Welfare Projects (201305022), the Fujian Natural Science Foundation of China (2013J01132), the open funding of Fujian Provincial Key Laboratory of Photocatalysis−State Key Laboratory Breeding Base of China (038018), Natural Science Foundation of China (31471623).

### Notes

The authors declare no competing financial interest.

## REFERENCES

(1) O'Keeffe, M. B.; FitzGerald, R. J. Antioxidant effects of enzymatic hydrolysates of whey protein concentrate on cultured human endothelial cells. *Int. Dairy J.* **2014**, *36*, 128−135.

(2) O'Loughlin, I. B.; Murray, B. A.; Brodkorb, A.; FitzGerald, R. J.; Kelly, P. M. Production of whey protein isolate hydrolysate fractions with enriched ACE-inhibitory activity. *Int. Dairy J.* **2014**, *38*, 101−103.

(3) Zhao, L. N.; Huang, S. L.; Cai, X. X.; Hong, J.; Wang, S. Y. A specific peptide with calcium chelating capacity isolated from whey protein hydrolysate. *J. Funct. Foods* **2014**, *10*, 46−53.

(4) Xu, R. Calcium binding of peptides derived from enzymatic hydrolysates of whey protein concentrate. *Int. J. Dairy Technol.* **2009**, *62*, 170−173.

(5) Bennett, T.; Desmond, A.; Harrington, M.; McDonagh, D.; FitzGerald, R.; Flynn, A.; Cashman, K. D. The effect of high intakes of casein and casein phosphopeptide on calcium absorption in the rat. *Br. J. Nutr.* **2000**, *83*, 673−680.

(6) Kim, S.; Shin, H.; Lim, J. Separation of calcium-binding protein derived from enzymatic hydrolysates of cheese whey protein. *Asian-Australas. J. Anim. Sci.* **2004**, *17*, 712−718.

(7) Singh, G.; Muthukumarappan, K. Influence of calcium fortification on sensory, physical and rheological characteristics of fruit yogurt. *LWT—Food Sci. Technol.* **2008**, *41*, 1145−1152.

(8) Guéguen, L.; Pointillart, A. The bioavailability of dietary calcium. *J. Am. Coll. Nutr.* **2000**, *19*, 119S−136S.

(9) Cilla, A.; Lagarda, M. J.; Alegría, A.; de Ancos, B.; Cano, M. P.; Sánchez-Moreno, C.; Plaza, L.; Barberá, R. Effect of processing and food matrix on calcium and phosphorous bioavailability from milk-based fruit beverages in Caco-2 cells. *Food Res. Int.* **2011**, *44*, 3030−3038.

(10) Kim, S.; Lim, J. Calcium-binding peptides derived from tryptic hydrolysates of cheese whey protein. *Asian-Australas. J. Anim. Sci.* **2004**, *17*, 1459−1464.

(11) Lee, S. H.; Song, K. B. Isolation of a calcium-binding peptide from enzymatic hydrolysates of porcine blood plasma protein. *J. Korean Soc. Appl. Biol. Chem.* **2009**, *52*, 290−294.

(12) Bronner, F.; Pansu, D. Nutritional aspects of calcium absorption. *J. Nutr.* **1999**, *129*, 9−12.

(13) Rerat, A.; Nunes, C. S.; Mendy, F.; Roger, L. Amino acid absorption and production of pancreatic hormones in non-anaesthetized pigs after duodenal infusions of a milk enzymic hydrolysate or free amino acids. *Br. J. Nutr.* **1988**, *60*, 121−136.

(14) Chaud, M. V.; Izumi, C.; Nahaal, Z.; Shuhama, T.; Bianchi, M. D. L. P.; Freitas, O. D. Iron derivatives from casein hydrolysates as a potential source in the treatment of iron deficiency. *J. Agric. Food Chem.* **2002**, *50*, 871−877.

(15) Kim, S.; Seo, I.; Khan, M.; Ki, K.; Lee, W.; Lee, H.; Shin, H.; Kim, H. Enzymatic hydrolysis of heated whey: Iron-binding ability of peptides and antigenic protein fractions. *J. Dairy Sci.* **2007**, *90*, 4033−4042.

(16) Sato, R.; Shindo, M.; Gunshin, H.; Noguchi, T.; Naito, H. Characterization of phosphopeptide derived from bovine $\beta$-casein: An inhibitor to intraintestinal precipitation of calcium phosphate. *Biochim. Biophys. Acta* **1991**, *1077*, 413−415.

(17) Gitelman, H. J. An improved automated procedure for the determination of calcium in biological specimens. *Anal. Biochem.* **1967**, *18*, 521−531.

(18) Chen, D.; Liu, Z.; Huang, W.; Zhao, Y.; Dong, S.; Zeng, M. Purification and characterisation of a zinc-binding peptide from oyster protein hydrolysate. *J. Funct. Foods* **2013**, *5*, 689−697.

(19) Zhou, J.; Wang, X.; Ai, T.; Cheng, X.; Guo, H.; Teng, G.; Mao, X. Preparation and characterization of $\beta$-lactoglobulin hydrolysate−iron complexes. *J. Dairy Sci.* **2012**, *95*, 4230−4236.

(20) Megías, C.; Pedroche, J.; Yust, M. M.; Girón-Calle, J.; Alaiz, M.; Millán, F.; Vioque, J. Affinity purification of copper-chelating peptides from sunflower protein hydrolysates. *J. Agric. Food Chem.* **2007**, *55*, 6509−6514.

(21) Huang, G. R.; Ren, Z. Y.; Jiang, J. X.; Chen, W. W. Purification of a hepta-peptide with iron binding activity from shrimp processing by-products hydrolysates. *Adv. J. Food Sci. Technol.* **2012**, *4*, 207−212.

(22) Huang, G.; Ren, L.; Jiang, J. Purification of a histidine-containing peptide with calcium binding activity from shrimp

processing byproducts hydrolysate. *Eur. Food Res. Technol.* **2011**, *232*, 281−287.
(23) Huang, G.; Ren, Z.; Jiang, J. Separation of iron-binding peptides from shrimp processing by-products hydrolysates. *Food Bioprocess Technol.* **2011**, *4*, 1527−1532.
(24) Reddy, I. M.; Mahoney, A. W. Solution visible difference spectral properties of $Fe^{3+}$−L-amino acid complexes at pH 6.60. *J. Agric. Food Chem.* **1995**, *43*, 1436−1443.
(25) Lv, Y.; Liu, Q.; Bao, X.; Tang, W.; Yang, B.; Guo, S. Identification and characteristics of iron-chelating peptides from soybean protein hydrolysates using IMAC-$Fe^{3+}$. *J. Agric. Food Chem.* **2009**, *57*, 4593−4597.
(26) Miquel, E.; Farré, R. Effects and future trends of casein phosphopeptides on zinc bioavailability. *Trends Food Sci. Technol.* **2007**, *18*, 139−143.
(27) Jung, W. K.; Karawita, R.; Heo, S. J.; Lee, B. J.; Kim, S. K.; Jeon, Y. J. Recovery of a novel Ca-binding peptide from Alaska Pollack (*Theragra chalcogramma*) backbone by pepsinolytic hydrolysis. *Process Biochem.* **2006**, *41*, 2097−2100.
(28) Jung, W. K.; Park, P. J.; Byun, H. G.; Moon, S. H.; Kim, S. K. Preparation of hoki (*Johnius belengerii*) bone oligophosphopeptide with a high affinity to calcium by carnivorous intestine crude proteinase. *Food Chem.* **2005**, *91*, 333−340.
(29) Wu, H. H.; Liu, Z. Y.; Zhao, Y. H.; Zeng, M. Y. Enzymatic preparation and characterization of iron-chelating peptides from anchovy (*Engraulis japonicus*) muscle protein. *Food Res. Int.* **2012**, *48*, 435−441.
(30) Houser, R. P.; Fitzsimons, M. P.; Barton, J. K. Metal-dependent intramolecular chiral induction: The $Zn^{2+}$ complex of an ethidium−peptide conjugate. *Inorg. Chem.* **1999**, *38*, 1368−1370.
(31) Armas, A.; Sonois, V.; Mothes, E.; Mazarguil, H.; Faller, P. Zinc(II) binds to the neuroprotective peptide humanin. *J. Inorg. Biochem.* **2006**, *100*, 1672−1678.
(32) Blindauer, C. A.; Harvey, I.; Bunyan, K. E.; Stewart, A. J.; Sleep, D.; Harrison, D. J.; Berezenko, S.; Sadler, P. J. Structure, properties, and engineering of the major zinc binding site on human albumin. *J. Biol. Chem.* **2009**, *284*, 23116−23124.
(33) Reddi, A. R.; Guzman, T. R.; Breece, R. M.; Tierney, D. L.; Gibney, B. R. Deducing the energetic cost of protein folding in zinc finger proteins using designed metallopeptides. *J. Am. Chem. Soc.* **2007**, *129*, 12815−12827.
(34) Beyer, R. L.; Hoang, H. N.; Appleton, T. G.; Fairlie, D. P. Metal clips induce folding of a short unstructured peptide into an $\alpha$-helix via turn conformations in water. Kinetic versus thermodynamic products. *J. Am. Chem. Soc.* **2004**, *126*, 15096−15105.
(35) Bao, X. L.; Lv, Y.; Yang, B. C.; Ren, C. G.; Guo, S. T. A study of the soluble complexes formed during calcium binding by soybean protein hydrolysates. *J. Food Sci.* **2008**, *73*, C117−C121.
(36) Wang, X.; Zhou, J.; Tong, P.; Mao, X. Zinc-binding capacity of yak casein hydrolysate and the zinc-releasing characteristics of casein hydrolysate−zinc complexes. *J. Dairy Sci.* **2011**, *94*, 2731−2740.

the chemical composition, instrumental taste profile measured by an electronic tongue, and antioxidant and metal chelating activities of mixtures of green, yellow, and red teas. Furthermore, a simultaneous optimization of the tea mixture was carried out to render the best combination of teas with maximized in vitro antioxidant activities as well as instrumental taste profile.

## MATERIAL AND METHODS

**Chemicals.** Gallic acid, (−)-epicatechin, (+)-catechin, chlorogenic acid, caffeine, epigallocatechin gallate, Folin−Ciocalteu reagent, 6-hydroxy-2,5,7,8-tetramethylchroman-2-carboxylic acid (Trolox), 2,4,6-tripyridyl-*s*-triazine (TPTZ), ferrozine (3-(2-pyridyl)-5,6-di(2-furyl)-1,2,4-triazine-5′,5″-disulfonic acid disodium salt), 2,2-diphenyl-1-picrylhydrazyl (DPPH), neocuproine (2,9-dimethyl-1,10-phenanthroline), sodium molybdate dihydrate, and pyrocatechol violet (3,3′,4′-trihydroxyfuchsone-2″-sulfonic acid) were purchased from Sigma-Aldrich (Zwijndrecht, The Netherlands). Procyanidin primer A2 was obtained from Extrasynthese (Genay, France). Butanol, ammonium acetate, copper(II) chloride, copper sulfate pentahydrate, hydrochloric acid, methanol, phosphoric acid, ethanol, acetic acid, aluminum chloride hexahydrate, sodium acetate anhydrous, iron(II) chloride tetrahydrate, iron(II) sulfate heptahydrate, and sodium carbonate were purchased from Merck (Darmstadt, Germany).

**Tea Samples.** Authentic dried leaves of red, green, and yellow teas, all from *C. sinensis* var. *sinensis*, cultivated and manufactured in China, were kindly donated by Herbaflora (São Paulo, Brazil). The particle sizes of samples were between 20 and 40 mesh. A certificate of botanical authenticity of these vegetable materials can be obtained directly from the producer and authors.

**Experimental Design and Tea Preparation.** To assess the effects of binary and ternary mixtures of green, yellow, and red teas on chemical composition, instrumental taste profile, and antioxidant/metal chelating activities, a three-component simplex-centroid mixture design composed of 10 experimental assays was employed, in which the independent variables (factors) were green, yellow, and red teas. All batches of tea infusions were prepared according to the mixture design layout presented in Table 1. The sequence of experiments was performed randomly.

To prepare the tea samples, tea leaves were ground using a pestle and mortar to obtain a homogeneous fine powder. Then, each tea infusion was prepared by pouring 100 mL of ultrapure water at 80 °C on a flask containing 2.0 g of leaves and brewed for 8.5 min under magnetic stirring and covered with a lid. Brewed tea samples were then filtered through Whatman no. 1 qualitative paper and centrifuged for 10 min at 2000 rpm, and the supernatant was aliquoted into eppendorfs and stored at −25 °C until analysis. Part of each infusion ($v$ = 70 mL) was allowed to cool until 25 °C, and teas were immediately used for assessing the instrumental taste profile.

**Instrumental Taste Profile (e-Tongue).** The instrumental taste profile of tea samples was assessed by measuring the sourness, bitterness, umami, richness (aftertaste umami), astringency, saltiness, and the aftertaste due to astringency using a commercial taste sensing system (model SA402B, Intelligent Sensor Technology Inc., Atsugi-shi, Japan). Artificial lipid-based membranes (similar to that of the human tongue) that detect the signs via potential measurements were used in the measurements. The taste sensor unit approximates and translates molecular information into simple and understandable human information (taste quality traits). Briefly, an aliquot of about 30 mL of each sample was placed in 50 mL plastic glasses for electronic tongue (e-tongue) detection, and analyses were conducted at 20 °C. The measuring time was set to 30 s for each sample, and the sensors were rinsed lightly for 6 s using a standard solution (30 mM KCl + 0.30 mM tartaric acid; conductivity between 4.0 and 4.2 mS/cm and pH in the range of 3.5−3.6) to measure the aftertaste. After that, sensors were rinsed in an alcoholic solution (28.5 mL/100 mL ethanol) for 90 s to remove adsorbed compounds from the lipid membrane, and sensors were again rinsed in the cleaning solution (30 mM KCl + 0.30 mM tartaric acid) for another 240 s to remove the

**Table 1. Chemical Composition of *C. sinensis* Tea Samples As Measured by UV−Vis Spectrometry and High-Performance Liquid Chromatography[a]**

| green tea | red tea | yellow tea | assay | flavan-3-ols (mg PCY/L) | total phenolic compounds (mg GAE/L) | *o*-diphenols (mg CAE/L) | chlorogenic acid (mg/L) | (+)-catechin (mg/L) | (−)-epicatechin (mg/L) | epigallocatechin gallate (mg/L) | caffeine (mg/L) | gallic acid (mg/L) |
|---|---|---|---|---|---|---|---|---|---|---|---|---|
| 1 | 0 | 0 | 1 | 154.59 ± 0.26a | 525.87 ± 4.90bc | 540.77 ± 21.10b | 2.41 ± 0.22 | 12.47 ± 0.96 | 95.50 ± 0.09 | 253.78 ± 0.11 | 245.02 ± 2.44 | 33.21 ± 0.14 |
| 0 | 1 | 0 | 2 | 146.57 ± 10.05ab | 668.49 ± 52.91a | 336.11 ± 14.67f | 0.36 ± 0.02 | 2.19 ± 0.00 | 14.12 ± 0.03 | 0.15 ± 0.04 | 622.00 ± 1.12 | 73.92 ± 0.08 |
| 0 | 0 | 1 | 3 | 104.46 ± 7.18d | 374.11 ± 7.07e | 557.76 ± 9.54ab | 0.85 ± 0.00 | 10.89 ± 0.01 | 88.83 ± 0.07 | 403.84 ± 0.38 | 600.43 ± 0.24 | 33.44 ± 0.26 |
| 0.5 | 0.5 | 0 | 4 | 152.04 ± 15.92a | 634.30 ± 13.86a | 428.53 ± 24.92cde | 0.22 ± 0.00 | 9.24 ± 0.03 | 84.93 ± 0.05 | 4.46 ± 0.01 | 438.76 ± 0.44 | 136.32 ± 0.18 |
| 0 | 0.5 | 0.5 | 5 | 123.60 ± 9.81bcd | 538.28 ± 10.58b | 456.44 ± 19.07cd | 0.93 ± 0.15 | 6.52 ± 0.00 | 87.36 ± 0.00 | 30.16 ± 0.27 | 603.55 ± 0.19 | 169.29 ± 0.10 |
| 0.5 | 0 | 0.5 | 6 | 132.90 ± 24.48abc | 460.34 ± 7.92d | 586.27 ± 30.17a | 1.27 ± 0.21 | 15.39 ± 0.08 | 89.91 ± 0.11 | 314.70 ± 0.52 | 412.07 ± 0.57 | 32.13 ± 1.99 |
| 0.666 | 0.167 | 0.167 | 7 | 147.67 ± 15.41ab | 552.65 ± 41.97b | 469.59 ± 6.20c | 1.58 ± 0.01 | 15.34 ± 0.30 | 102.21 ± 0.08 | 150.61 ± 0.44 | 352.82 ± 1.59 | 91.64 ± 0.51 |
| 0.167 | 0.666 | 0.167 | 8 | 140.01 ± 20.70abc | 630.17 ± 52.84a | 406.08 ± 23.68e | 0.53 ± 0.03 | 5.45 ± 0.07 | 63.03 ± 0.04 | 0.79 ± 0.22 | 553.09 ± 4.22 | 130.96 ± 5.19 |
| 0.167 | 0.167 | 0.666 | 9 | 113.76 ± 25.72cd | 478.84 ± 30.54cd | 566.66 ± 45.04ab | 0.61 ± 0.01 | 11.65 ± 0.22 | 98.51 ± 0.06 | 266.48 ± 0.77 | 537.55 ± 2.16 | 82.52 ± 12.84 |
| 0.333 | 0.333 | 0.333 | 10 | 136.91 ± 24.56abc | 557.23 ± 14.57b | 424.49 ± 18.94de | 1.01 ± 0.07 | 11.07 ± 0.02 | 104.09 ± 0.12 | 84.36 ± 0.55 | 481.41 ± 0.40 | 146.94 ± 0.07 |
| *p* value (normality) | | | | 0.75 | 0.85 | 0.57 | 0.16 | 0.68 | 0.003 | 0.16 | 0.34 | 0.22 |
| *p* value (homoscedasticity) | | | | 0.37 | 0.59 | 0.94 | 0.25 | 0.69 | 0.87 | 0.33 | 0.49 | 0.16 |
| *p* value (one-way ANOVA) | | | | 0.0003 | <0.0001 | <0.0001 | <0.0001 | <0.0001 | <0.0001 | <0.0001 | <0.0001 | <0.0001 |

[a]Different letters in the same column represent statistically different results according to Duncan's multiple-comparison test ($p < 0.05$).


dx.doi.org/10.1021/jf504480f | J. Agric. Food Chem. 2014, 62, 10283−10296

alcohol and re-establish the sensors. The rinsing procedure is important to reach stable potential readings before analysis of the next sample. A total of four replicated measurements were run on each sample, whereas the first cycle was discarded due to instability, and the other three responses were averaged. The sensor outputs of the samples (electric potential) were converted into taste intensity values on a scale where one unit is the sensor output difference corresponding to a 20% concentration difference in the standard substance solution.[15] In the current research, these taste intensities are designated estimated intensity of taste (EIT) values.

**Chemical Composition.** The Folin−Ciocalteu reducing power (total phenolic compounds) of teas was assessed in triplicate using the method proposed by Singleton and Rossi[16] with modifications. For this purpose, a standard curve of gallic acid (0−150 mg/L) was built, and absorbance was read at $\lambda$ = 725 nm. Results were expressed as milligrams of gallic acid equivalents per liter of tea (mg GAE/L).

The content of flavan-3-ols (tannins) of teas was assessed in triplicate by oxidative depolymerization in HCl/*n*-butanol at 90 °C for 20 min.[17] A calibration curve was built using procyanidin primer A2 (0−125 mg/L), and absorbance was read at $\lambda$ = 540 nm. The results were expressed as milligrams of procyanidin primer A2 equivalents per liter of tea (mg PCY/L).

The *o*-diphenols content was estimated by using the sodium molybdate method,[18] with modifications to microplates. Briefly, a 50 $\mu$L aliquot of tea (1:5) was mixed with 200 $\mu$L of a 5 g/100 mL sodium molybdate dihydrate solution (ethanol in water at a proportion of 1:1 v/v) and allowed to react for 25 min. The absorbance was recorded at $\lambda$ = 370 nm against a blank (EtOH/water 1:1 v/v). A standard curve of chlorogenic acid (0−160 mg/L) was plotted, and results were expressed as milligrams of chlorogenic acid equivalents per liter of tea (mg CAE/L).

Gallic acid, (+)-catechin, caffeine, (−)-epicatechin, chlorogenic acid, and epigallocatechin gallate (EGCG) were quantified by high-performance liquid chromatography by means of a chromatograph (HPLC) coupled with a diode array detector (DAD) from Agilent Technologies 1100 series equipment containing a quaternary pump and an automated injector. The chromatographic separation was carried out on a Luna $C_{18}$ column (250 × 4.6 mm, 5 $\mu$m; Phenomenex, Torrance, CA, USA) maintained at 35 °C. The DAD was set up at 210 nm for all compounds except for chlorogenic acid that was monitored at 320 nm. A volume of 20 $\mu$L was injected after filtration of tea using a 0.45 $\mu$m pore size polyvinylidene difluoride membrane (Millipore, Tullagreen, Ireland). The mobile phase was composed of solvent A (acetonitrile) and solvent B (0.05% v/v phosphoric acid solution) with a gradient program as follows: 0−8 min, linear gradient 5−8% A; 8−28 min, linear gradient 8−10% A; 28−40 min, 10% A isocratic elution; 40−55 min, linear gradient 10−14% A; 55−80 min, linear gradient 14−24% A; and 80−90 min, 24% A isocratic elution at a flow rate of 1 mL/min, as described elsewhere.[10] The quantification of each compound was performed by comparing the peak area with calibration curves ($n$ = 5 evenly spaced concentrations) of chemical standards. The limit of detection (LOD) and limit of quantification (LOQ) were calculated as the concentration giving signals equal to 3 and 10 times, respectively, the signal-to-noise ratio. The regression parameters, retention time, LOD, and LOQ of all compounds measured are presented in Table 1 of the Supporting Information, and typical chromatograms of standards are presented in Figure 1 of the Supporting Information.

**Antioxidant and Metal Chelation Activities.** The cupric reducing antioxidant activity (CUPRAC) of teas measures the ability of an extract to reduce substances by electron transfer, at a physiological pH. CUPRAC was evaluated in triplicate by the colorimetric method employing neocuproine as outlined by Apak et al.[19] Trolox standard solutions were prepared at a concentration ranging from 90 to 3000 $\mu$mol/L, and absorbance was read at $\lambda$ = 450 nm. The results were expressed as millimoles of trolox equivalents per liter of tea (mmol TE/L).

The ferric reducing antioxidant power (FRAP) of teas is a direct test that measures the total antioxidant levels in a given sample as no activity-changing interactions between antioxidants occur in the system. FRAP was measured four times according to the method by Benzie and Strains,[20] with modifications to microplates. An aliquot of 300 $\mu$L of the freshly prepared FRAP reagent and 10 $\mu$L of diluted tea (1:25) were added to each well, and the absorbance was recorded at $\lambda$ = 593 nm after 30 min of reaction. The FRAP reagent was prepared by mixing sodium acetate buffer (300 mM, pH 3.6), a solution of TPTZ (10 mM) in 40 mM HCl, and 20 mM $FeCl_3{\cdot}6H_2O$ using the proportion 10:1:1 (v/v/v). A standard curve of trolox (100−1000 $\mu$mol/L) was plotted to quantify the reducing power of teas. The results were expressed in millimoles of trolox equivalents per liter (mmol TE/L).

The free radical scavenging activity toward 2, 2-diphenyl-1-picrylhydrazyl (DPPH) of each tea measures the sequential proton loss electron transfer from the antioxidants to the DPPH radical. DPPH was performed four times according to a method reported elsewhere,[21] with modifications to microplates. An aliquot of 5 $\mu$L of dilute tea (1:11) or methanol (blank) was mixed with 195 $\mu$L of a 125 $\mu$mol/L methanolic solution of DPPH and left to react for 30 min at room temperature, and the absorbance was read at $\lambda$ = 517 nm. The antioxidant activity (% of inhibition) was calculated as $[1 - (A_{517}\ \text{sample}/A_{517}\ \text{blank})] \times 100$.

Ferrous ion chelating ability was determined in triplicate by measuring the formation of the $Fe^{2+}$−ferrozine complex according to the method proposed by Carter,[22] with modifications to microplates. For this purpose, to an aliquot of 50 $\mu$L of diluted tea (1:5), 160 $\mu$L of ultrapure water and 15 $\mu$L of a 0.30 mM $FeCl_2{\cdot}4H_2O$ solution were added in a microtiter plate. After 5 min of incubation, the reaction was initiated by adding 30 $\mu$L of a 0.80 mM ferrozine solution, and the final mixture was incubated for 15 min at room temperature. Distilled water (30 $\mu$L) instead of ferrozine solution was used as a blank, which was used to correct for unequal color of the sample solutions. The formed magenta complex was measured at $\lambda$ = 562 nm. Water was used as a negative control. The percentage of $Fe^{2+}$−ferrozine complex formation was calculated as $Fe^{2+}$ chelating rate (%) = $[1 - (\text{Abs}_{\text{sample}} - A_{\text{solution without ferrozine}})/A_{\text{control}}] \times 100$.

Copper ion-chelating activity of tea mixtures was determined using a previous method.[23] Briefly, an aliquot of 200 $\mu$L of sodium acetate buffer at 50 mM, pH 5.7, was mixed with 8.5 $\mu$L of a 2 mM pyrocatechol violet solution and 25 $\mu$L of a 0.1 mg/mL (w/v) $CuSo_4{\cdot}5H_2O$ solution and 30 $\mu$L of diluted tea (1:5) or water (blank). The 96 wells were shaken for 15 s and allowed to react for 20 min at room temperature. Then, absorbance at $\lambda$ = 632 nm was measured using a microplate reader (Synergy-BIOTEK, Winooski, VT, USA). The percentage of inhibition of pyrocatechol violet−$Cu^{2+}$ complex formation was calculated as $Cu^{2+}$ chelating activity (%) = $[(\text{Abs}_{\text{control}} - \text{Abs}_{\text{sample}})/\text{Abs}_{\text{control}}] \times 100$.

**Statistical Analysis and Response Surface Methodology.** Data are presented as means and standard deviations. To apply RSM, significant statistical differences were investigated by one-way analysis of variances (ANOVA) for parametric and homoscedastic data or Welch-ANOVA for parametric nonhomoscedastic data. For this purpose, normality of data was checked by Shapiro−Wilk's test and homoscedasticity was tested by Brown−Forsythe's test. When data did not conform to a normal distribution, results were transformed using the Box−Cox approach. Differences among means were analyzed by Duncan's multiple-comparison test taking on $p < 0.05$. Linear correlation analysis was performed to verify the degree of association between responses, and regression analysis, based on the ordinary least-squares regression, was applied to some of the responses to explain the correlation through a mathematical function.[24] The instrumental taste profile and the chemical compounds quantified by HPLC and UV−vis spectrophotometry were also correlated by using principal component analysis aiming at a more comprehensive and broader understanding of experimental data.[25]

When differences among tea samples were verified by one-way ANOVA ($p < 0.05$), RSM was applied to model the analytical measurements as a function of the factors (tea types).[26] The regression model equation of three-component mixtures to estimate the coefficients is presented in eq 1

Table 2. Antioxidant and Metal Chelating Activities of *C. sinensis* Teas[a]

| assay | copper chelating activity (%) | FRAP (mmol TE/L) | DPPH (% inhibition) | CUPRAC (mmol TE/L) | iron chelating activity (%) |
|---|---|---|---|---|---|
| 1 | 43.27 ± 2.04d | 14.78 ± 0.30e | 42.34 ± 1.18d | 9.22 ± 0.15c | 38.89 ± 2.12b |
| 2 | 55.39 ± 1.05a | 25.02 ± 0.33a | 56.40 ± 0.67a | 11.42 ± 0.22a | 35.54 ± 1.02e |
| 3 | 53.20 ± 1.91ab | 10.16 ± 0.17g | 22.93 ± 0.95g | 5.55 ± 0.11f | 28.68 ± 0.75f |
| 4 | 49.83 ± 1.54bc | 20.76 ± 0.44b | 46.57 ± 0.23b | 10.52 ± 0.12b | 41.93 ± 1.29a |
| 5 | 54.55 ± 1.34ab | 16.60 ± 0.38c | 45.76 ± 1.13bc | 8.72 ± 0.12d | 36.01 ± 1.77e |
| 6 | 51.85 ± 2.78abc | 13.92 ± 0.39f | 32.87 ± 0.65f | 7.74 ± 0.11e | 29.46 ± 0.93f |
| 7 | 52.36 ± 3.25abc | 15.99 ± 0.25d | 43.51 ± 0.60cd | 9.31 ± 0.24c | 38.50 ± 1.64bc |
| 8 | 53.05 ± 1.69ab | 20.91 ± 0.33b | 47.24 ± 0.84b | 10.47 ± 0.26b | 36.24 ± 0.46cd |
| 9 | 50.17 ± 4.53bc | 14.02 ± 0.25f | 32.18 ± 0.18f | 7.48 ± 0.10e | 34.53 ± 0.82e |
| 10 | 47.64 ± 4.30cd | 14.79 ± 0.07e | 43.39 ± 4.59cd | 9.09 ± 0.16c | 36.79 ± 1.05bcd |
| *p* value (normality) | 0.48 | 0.46 | 0.10 | 0.79 | 0.39 |
| *p* value (homoscedasticity) | 0.96 | 0.90 | <0.001 | 0.96 | 0.82 |
| *p* value (one-way ANOVA/Welch test) | 0.0009 | <0.0001 | <0.0001 | <0.0001 | <0.0001 |

[a]Different letters in the same column represent statistically different results according to Duncan's multiple-comparison test ($p < 0.05$).

Table 3. Instrumental Taste Profile of Tea Samples As Measured by an Electronic Tongue[a]

| assay | sourness (EIT) | bitterness (EIT) | astringency (EIT) | aftertaste[b] (EIT) | umami (EIT) | richness (EIT) | saltiness (EIT) |
|---|---|---|---|---|---|---|---|
| 1 | 41.00 ± 0.00f | −6.94 ± 0.00d | −2.18 ± 0.00f | 4.68 ± 0.00b | −16.44 ± 0.00b | 7.23 ± 0.00d | 0.60 ± 0.00e |
| 2 | 41.20 ± 0.04de | −5.12 ± 0.07a | 0.13 ± 0.07c | 5.29 ± 0.20a | −17.61 ± 0.07f | 9.10 ± 0.24a | 4.24 ± 0.11a |
| 3 | 40.59 ± 0.21g | −10.41 ± 0.16i | −1.61 ± 0.92e | 1.31 ± 0.55g | −16.05 ± 0.22a | 2.40 ± 0.36g | −2.51 ± 0.47h |
| 4 | 41.77 ± 0.04b | −6.00 ± 0.05b | −0.94 ± 0.12d | 5.37 ± 0.16a | −17.23 ± 0.04de | 8.20 ± 0.06c | 2.84 ± 0.05b |
| 5 | 41.38 ± 0.03c | −7.52 ± 0.04f | −1.59 ± 0.15e | 4.28 ± 0.05c | −17.06 ± 0.09cd | 5.82 ± 0.13e | 1.82 ± 0.15d |
| 6 | 41.05 ± 0.12ef | −8.62 ± 0.05g | −2.88 ± 0.25g | 3.89 ± 0.08d | −16.60 ± 0.05b | 5.01 ± 0.16f | −0.24 ± 0.16f |
| 7 | 42.11 ± 0.04a | −7.07 ± 0.02e | −1.99 ± 0.20ef | 4.80 ± 0.09b | −17.02 ± 0.07c | 7.05 ± 0.10d | 1.60 ± 0.02d |
| 8 | 41.33 ± 0.00cd | −6.45 ± 0.00c | 2.86 ± 0.00a | 2.90 ± 0.00e | −17.59 ± 0.00f | 8.61 ± 0.00b | 2.34 ± 0.00c |
| 9 | 39.42 ± 0.10h | −9.06 ± 0.03h | 0.59 ± 0.04c | 1.66 ± 0.12f | −16.62 ± 0.18b | 4.99 ± 0.20f | −1.40 ± 0.11g |
| 10 | 41.09 ± 0.12ef | −7.56 ± 0.03f | 1.61 ± 0.06b | 2.60 ± 0.08e | −17.30 ± 0.11e | 7.20 ± 0.21d | 0.75 ± 0.08e |
| *p* value (normality) | 0.19 | 0.95 | 0.45 | 0.31 | 0.69 | 0.51 | 0.99 |
| *p* value (homoscedasticity) | 0.35 | 0.26 | 0.05 | 0.07 | 0.66 | 0.57 | 0.10 |
| *p* value (one-way ANOVA) | <0.0001 | <0.0001 | <0.0001 | <0.0001 | <0.0001 | <0.0001 | <0.0001 |

[a]Different letters in the same column represent statistically different results according to Duncan's multiple-comparison test ($p < 0.05$). [b]Aftertaste due to astringency.

$$Y = b_1x_1 + b_2x_2 + b_3x_3 + b_{12}x_1x_2 + b_{13}x_1x_3 + b_{23}x_2x_3 + b_{123}x_1x_2x_3 \quad (1)$$

where $Y$ is the predicted response; $b_1$, $b_2$, and $b_3$ are the regression coefficients for linear effects; $b_{12}$, $b_{13}$, and $b_{23}$ represent the binary interaction coefficients; and $b_{123}$ is the ternary regression coefficient. In the same sense, $x_1$, $x_2$, and $x_3$ represent the fractions of green, red, and yellow teas, respectively.

The analysis of variance of the above equation was calculated, and the effects and regression coefficients of individual linear, quadratic, and cubic terms were determined. Nonsignificant regression coefficients ($p < 0.10$) were discarded, and data were refitted to obtain the final model for each parameter. Then, the regression coefficients were used to generate two-dimensional contour plots for each response variable. The adequacy and goodness of fitting were assessed by calculating the coefficient of determination ($R^2$) and adjusted $R^2$.[27] For all regression models, the residuals plots were examined for obvious patterns (predicted vs experimental data) and formally tested for normality using Shapiro−Wilk's test.

After modeling of the responses, the following variables were used to optimize the extraction of antioxidants and instrumental taste profile of the *C. sinensis* tea mixtures: the main objective was to maximize the CUPRAC, iron-chelating activity, and DPPH activities and the flavan-3-ols content and to balance the instrumental bitterness of the tea, about which consumers often complain. For this purpose, the desirability function proposed by Derringer and Suich[28] was employed, and the $d$ value, which is a measure of how much the proposed formulation conforms to the main objective of optimization, was obtained. All statistical analysis was performed by Action v. 2.6 (Statcamp, Brazil) and Statistica v. 7 (StatSoft, Tulsa, OK, USA) software.

## RESULTS AND DISCUSSION

**Chemical Composition, Instrumental Taste Profile, and Antioxidant/Metal Chelating Activities.** The chemical composition data are listed in Table 1, whereas the antioxidant/metal chelating activities and the instrumental taste profile of tea mixtures are presented in Tables 2, and 3, respectively. The contents of flavan-3-ols and total phenolic substances varied from 104.46 to 154.59 mg/L (median = 138.46 mg/L) and from 374.11 to 668.49 mg/L (median = 545.47 mg/L), whereas the content of *o*-diphenols varied from 336.11 to 586.27 mg/L (median = 463.01 mg/L). The antioxidant activity presented a higher variation: although DPPH data were comprehended between 22.93 and 56.40% inhibition (median = 43.45% inhibition), FRAP and CUPRAC were in the ranges of 5.55−11.42 mmol TE/L (median = 9.16 mmol TE/L) and 10.16−25.02 mmol TE/L (median =15.39 mmol TE/L). The

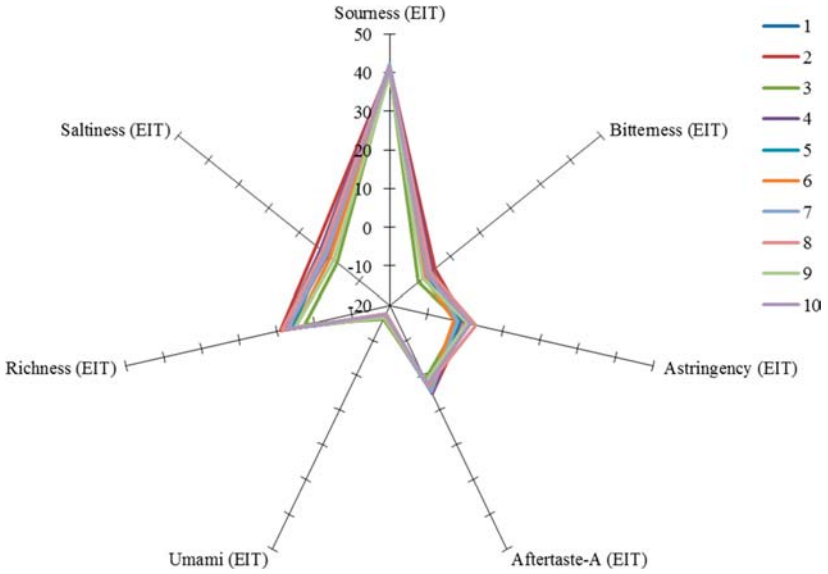


**Figure 1.** Instrumental taste profile of *Camellia sinensis* teas obtained by an electronic tongue. See Table 1 for sample codes.

iron chelating activity ranged from 28.68 to 41.93% of complex formation (median = 36.13% of complex formation), and copper chelating activity ranged from 43.27 to 55.39% inhibition (median = 52.10% inhibition). Overall, when Duncan's multiple comparison of means was performed, red tea presented the highest content of total phenolic compounds, caffeine, and gallic acid, the lowest content of chlorogenic acid, (+)-catechin, (−)-epicatechin, and epigallocatechin gallate, and the highest antioxidant power as measured by FRAP, CUPRAC, DPPH, and copper chelating activity. Green tea presented the highest content of flavan-3-ols, (+)-catechin, and (−)-epicatechin and the lowest caffeine content (Tables 1 and 2). On the other hand, yellow tea presented higher levels of epigallocatechin gallate and *o*-diphenols, the lowest levels of flavan-3-ols and total phenolic compounds, and intermediate levels of other phenolic compounds as measured by HPLC. All of these results are in accordance with those obtained by Zhang et al.[10,11] Likewise, Wang et al.[29] evaluated 87 *C. sinensis* teas marketed in China and verified that the (+)-catechin, epigallocatechin gallate, and (−)-epicatechin contents decreased in the following order: green tea > oolong tea > white tea > black tea. The results observed in the current study corroborate the idea that fermentation and oxidation processes used to manufacture different types of teas lead to a decrease in the content of catechin components.

With regard to the chemical composition and antioxidant effects of *C. sinensis* teas, many studies have shown contradictory results: Some authors state that green tea presents the best chemical profile and antioxidant power as compared to other *C. sinensis* teas. Fernàndez et al.[30] verified that the content of catechins in nonfermented *C. sinensis* teas (green and white) is higher than in fermented teas (black, oolong, red). Likewise, Karori et al.[31] concluded that the antioxidant activities of green and white teas, measured by the DPPH assay, are comparable and higher than the values observed for black tea. Carloni et al.[14] evaluated the phenolic compounds and antioxidant activity (ABTS, ORAC, LDL-oxidation) and iron chelating activity of white, black, and green teas and verified that green tea presented the highest antioxidant power and lowest iron-chelating activity. Conversely, in our study, green tea also presented the lowest inhibition of pyrocatechol violet−$Cu^{2+}$ complex formation and the highest percentage of $Fe^{2+}$−ferrozine complex formation. Once no phenolic compound was correlated with copper and iron chelating activities, it is hypothesized that the presence of compounds that present hydroxyl and carbonyl functions may play a role in copper ion chelating activity rather than only phenolic compounds.[14]

The taste of teas is the most important sensory factor for assessing their quality, and although it is common practice to evaluate the taste profile and acceptance by means of a taste panel (trained or not), the use of electronic tongues is advantageous over human responses as their use eliminates the subjectivity and individual preferences. In this regard, red tea presented the highest instrumental bitterness, aftertaste due to astringency, saltiness, and richness (umami aftertaste), whereas yellow tea showed the opposite behavior (Figure 1 and Table 3). Indeed, bitterness, aftertaste, and astringency are limitation factors of tea consumption in Western countries. Binary and ternary mixtures of *C. sinensis* teas presented higher astringency and sourness as compared to green, red, or yellow teas alone (Table 3). Astringency is a tactile sensation perceived as drying of the epithelium of the oral cavity due to the content of tannins (flavan-3-ols) and other phenolic compounds in the matrix. Sourness, which is related to the content of acidic compounds in tea, presented statistical differences among teas, but a low variation was observed. Herein, sourness was correlated to the total content of flavan-3-ols ($r$ = 0.669, $p$ = 0.034). According to Kim et al.,[32] the teas are available in many different fermentation levels for consumption ranging from green to black, and during the oxidative process the flavan-3-ols are transformed to theaflavin, thearubigin, and other high molecular mass pigments; decreased bitterness, astringency, and flavor are derived during the fermentation process.

**Correlation Analysis.** When multiple analytical variables are analyzed, it is often interesting to analyze how they are interconnected with each other. From a chemical standpoint, the correlation between sensory properties and chemical composition with antioxidant and metal chelating activity can be used by food companies to develop potentially functional products as well as to monitor the quality of *C. sinensis* teas. In the current study, Pearson's correlation coefficient was used to express the degree of association between variables, and results

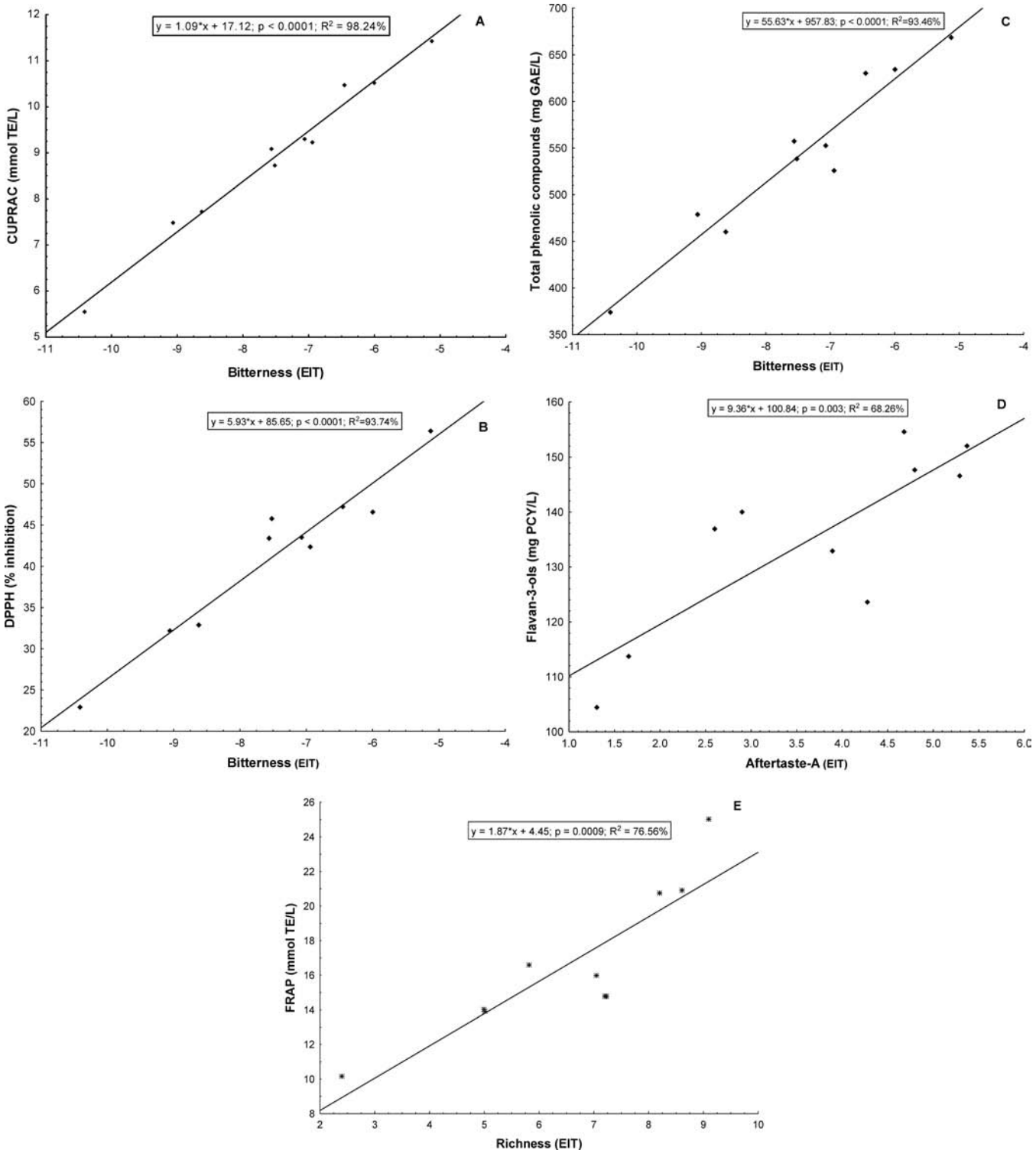


**Figure 2.** Regression analysis coupled to analysis of variances to explain the relationship between bitterness and CUPRAC (A), between bitterness and DPPH (B), between bitterness and total phenolic compounds (C), between aftertaste due to astringency and flavan-3-ols content (D), and between richness and FRAP (E) of *C. sinensis* teas.

showed that CUPRAC, DPPH, and FRAP were significantly ($p < 0.05$) correlated to the content of flavan-3-ols ($r = 0.829$, $r = 0.747$, $r = 0.613$), total phenolic compounds ($r = 0.989$, $r = 0.955$, $r = 0.944$), bitterness ($r = 0.991$, $r = 0.968$, $r = 0.915$), aftertaste due to astringency ($r = 0.732$, $r = 0.735$, $r = 0.636$), richness ($r = 0.988$, $r = 0.936$, $r = 0.875$), and saltiness ($r = 0.960$, $r = 0.971$, $r = 0.937$). In the same sense, iron chelating activity was correlated to the content of flavan-3-ols ($r = 0.747$, $p = 0.013$), total phenolic compounds ($r = 0.724$, $p = 0.018$), bitterness ($r = 0.737$, $p = 0.015$), richness ($r = 0.750$, $p = 0.012$), and saltiness ($r = 0.642$, $p = 0.045$). It is important to note this is the first report in the literature that correlates the intensity of instrumental taste attributes with chemical

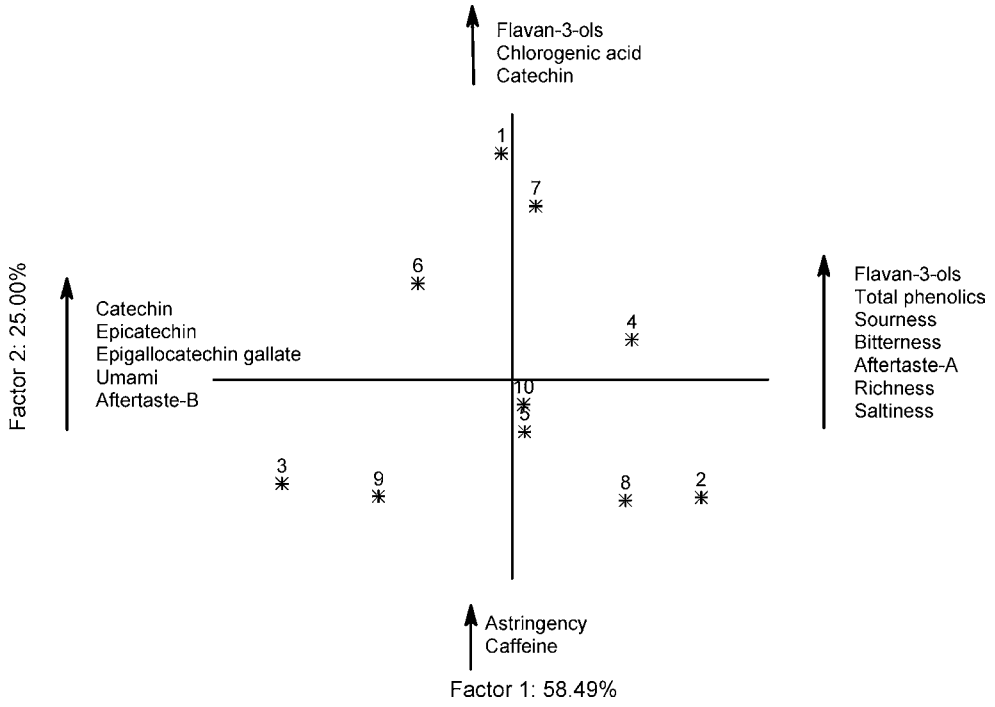


**Figure 3.** Principal component analysis showing the correlation between instrumental taste profile and chemical composition of mixtures of green, red, and yellow teas. See Table 1 for sample codes.

composition and antioxidant activity of *C. sinensis* tea mixtures (Figure 2).

Although green and yellow teas undergo very similar technological production operations, the flavan-3-ols, total phenolic compounds, and *o*-diphenols varied significantly between them. From a chemical standpoint, red tea (fully oxidized and partially fermented) presented the lowest *o*-diphenols content besides having the highest total phenolic compounds, whereas yellow tea (less processed as compared to red teas) had the highest *o*-diphenols content besides presenting the lowest total phenolic compounds content, corroborating the results obtained by Cabrera et al.[33] Indeed, it is plausible that the during fermentation of leaves, mono-, di-, and some trihydroxy phenolic compounds are either polymerized or oxidized to theaflavins and thearubigins and, therefore, the higher the oxidation and fermentation time that *C. sinensis* leaves undergo, the lower the *o*-diphenols content is. This trend can also be observed by linear correlation analysis: total phenolic compounds were inversely correlated to *o*-diphenols ($r = -0.884$, $p < 0.001$) and by the lower concentration of gallic acid in red tea (Table 2). In addition, it is known that total phenolic compounds and, specifically, *o*-diphenols display a high and significant correlation with in vitro antioxidant activity assays in many food and beverage matrices. The total phenolic compounds content was higher in fermented and fully oxidized tea (red tea), with consequently lower *o*-diphenols content, and a significant and strong correlation was observed between *o*-diphenols and DPPH ($r = -0.877$, $p = 0.001$), FRAP ($r = -0.858$, $p = 0.001$), and CUPRAC ($r = -0.835$, $p = 0.003$), whereas a low-intensity and nonsignificant correlation was observed with copper chelating activity ($r = -0.342$, $p = 0.334$) and iron chelating activity ($r = -0.516$, $p = 0.126$). These results indicate that *o*-diphenols alone do not play an important role in chelating transition metal ions, and perhaps interactions among all reducing materials are responsible for the metal chelating effect of tea.

With regard to the individual phenolic compounds measured by HPLC, correlation analysis revealed that chlorogenic acid was correlated to copper chelating activity ($r = 0.617$, $p = 0.050$), whereas gallic acid was not correlated to any antioxidant activity assay. Similarly to what was observed for *o*-diphenols, red tea (fully oxidized and fermented) presented the lowest content of chlorogenic acid, (+)-catechin, (−)-epicatechin, and epigallocatechin, and an inverse correlation was observed for these compounds and the antioxidant activity: (+)-catechin versus CUPRAC ($r = -0.548$), DPPH ($r = -0.618$), and FRAP ($r = -0.741$); (−)-epicatechin versus CUPRAC ($r = -0.573$), DPPH ($r = -0.583$), and FRAP ($r = -0.792$); and epigallocatechin gallate versus CUPRAC ($r = -0.876$), DPPH ($r = -0.908$), iron chelating activity ($r = -0.676$), and FRAP ($r = -0.852$). These results also clearly indicated that the oxidation and fermentation processes that *C. sinensis* undergo influence the antioxidant power of teas. Additionally, future works should focus on the quantification of theaflavins and thearubigins and how these substances (alone and in combination to other phenolic compounds) affect the bioactivity of tea mixtures. Our data corroborate the findings of Cao et al.,[34] who concluded that phenolic compounds with higher numbers of −OH substitutions on the B ring display considerably more effectiveness against free radicals and by binding transition metals, which means that epigallocatechin gallate presents a higher antioxidant power as compared to (+)-catechin and (−)-epicatechin. In the same way, Zhang et al.[10] analyzed different *C. sinensis* teas (white, oolong, and green teas) and verified that epigallocatechin gallate contributed between 67 and 79% of the total antioxidant activity as measured by the DPPH assay.

To facilitate the interpretation of correlation analysis between phenolic composition determined by HPLC, UV−vis

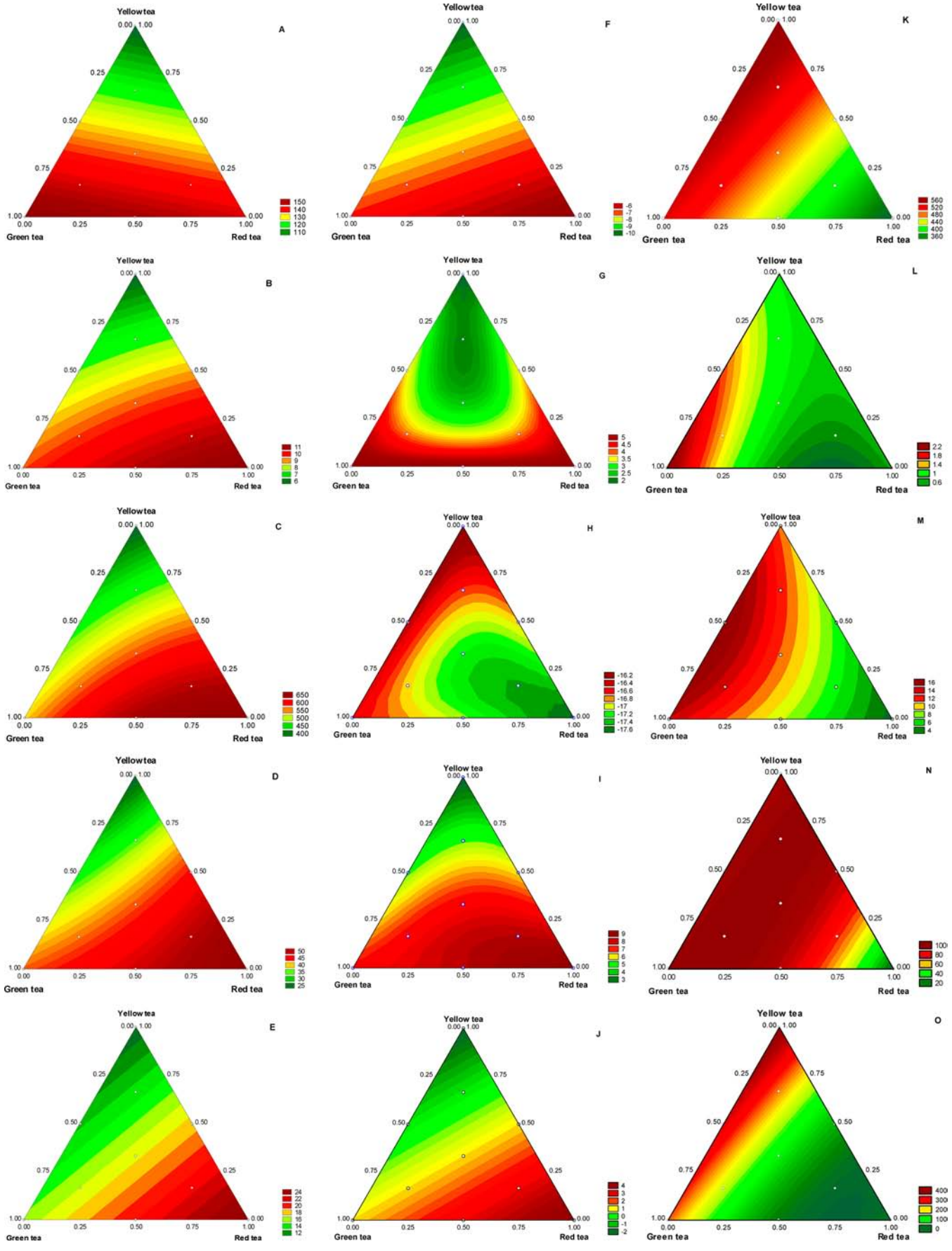


**Figure 4.** continued


dx.doi.org/10.1021/jf504480f | J. Agric. Food Chem. 2014, 62, 10283−10296

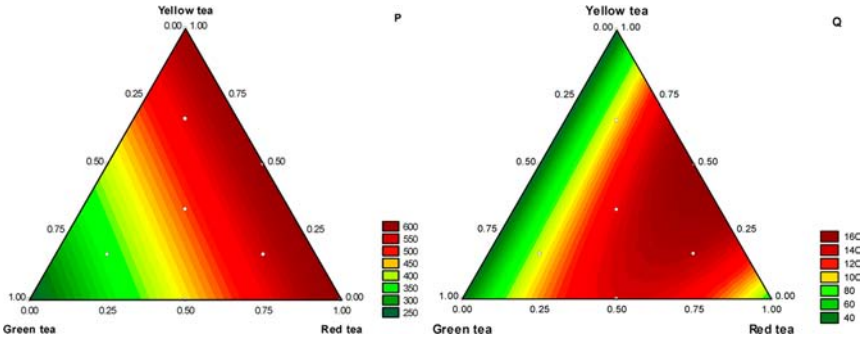


**Figure 4.** Response surface plots to show the effects of green, red, and yellow teas on the content of flavan-3-ols (mg PCY/L) (A), cupric ion reducing antioxidant power (mmol TE/L) (B), total phenolic compounds (mg GAE/L) (C), free radical scavenging activity toward DPPH (% inhibition) (D), ferric reducing antioxidant power (mmol TE/L) (E), bitterness (EIT) (F), aftertaste due to astringency (EIT) (G), umami (EIT) (H), richness (EIT) (I), saltiness (EIT) (J), *o*-diphenols (mg CAE/L) (K), chlorogenic acid (L), (+)-catechin (M), (−)-epicatechin (N), epigallocatechin gallate (O), caffeine (P), and gallic acid (Q) of *C. sinensis* tea mixtures.

spectrophotometry, and instrumental taste profile, a two-dimensional projection of samples was made using principal component analysis, and results are presented in Figure 3. Data showed that samples 2 (red tea), 3 (yellow tea), 8 (67% red + 17% green + 17% yellow), and 9 (17% red + 17% green + 67% yellow) presented the highest EIT for astringency, whereas samples 3, 6 (50% green + 50% yellow), and 9, which presented the highest content of (+)-catechin, (−)-epicatechin, and epigallocatechin gallate, had the highest EIT values for umami and aftertaste due to bitterness. Samples 2, 4 (50% red + 50% green), and 8, which have the highest values of flavan-3-ols and total phenolic materials, seemed to be more sour, bitter, rich, and salty and had a stronger aftertaste due to astringency as compared to the other teas. This two-dimensional projection (principal component 1 vs principal component 2) explained up to 83.5% of data variability.

**Response Surface Methodology and Optimization.** The effects of green, red, and yellow teas and their binary and ternary mixtures on chemical composition, objective taste profile, and antioxidant and metal chelation activities of teas as well as the mathematical models obtained by RSM and the statistical parameters of such models are presented in Figure 4 and Table 4. Astringency and sourness could not be modeled using RSM as the $R^2$ values (parameter that indicates how well experimental data fit a statistical model) were much lower than 30% (data not shown) and no significant effect of factors was observed, which means that the cubic model was not effective in representing the experimental data suitably.

It is possible to observe that there was a significant ($p < 0.05$) effect of each type of tea on all response variables measured in the study. However, binary mixtures of either green/red, green/yellow, or red/yellow teas were only statistically significant for CUPRAC, total phenolic compounds, DPPH, and extraction of all compounds measured by HPLC. In these cases, binary mixtures of teas enhanced the extraction of phenolic compounds and antioxidant capacity of tea. Ternary mixtures of green, red, and yellow teas seemed to have a significant effect on aftertaste due to astringency, umami taste, and tea sensory richness. For example, the binary combination of green/red, green/yellow, and red/yellow teas had a positive and significant effect on CUPRAC, whereas the mixture of green and red teas enhanced the extraction of total phenolic compounds, and the mixture of red and yellow teas increased the free radical scavenging activity toward DPPH.

Using ANOVA, the significance and suitability of the RSM models (Table 4) could be evaluated, and for all cases $p$ values below 0.05 were attained, indicating that the mathematical equation proposed to explain each response variable was satisfactory. Additionally, the $R^2$ values were >60%, which means that most of the variability in experimental data could be explained by the second-order mathematical models. For the iron and copper chelating activities, the $R^2$ values were slightly lower (63.95 and 61.71%, respectively) than the ones obtained for the instrumental taste profile, antioxidant activity, and phenolic composition of tea samples. From a practical standpoint, high $R^2$ values are not always easy to be obtained when a biochemical reaction needs to be fit into a mathematical equation, once a more robust model is required or even no modeling is possible for certain responses. The main idea of multiple regression obtained by RSM is to compress the data into an equation relating the independent factors (tea type, for example) in a way to comprehensively explain the phenomena under investigation, to try to explain as much information as possible and test the suitability of these models in predicting future observations.

When a RSM model is proposed, not only do the equation and $R^2$ values need to be taken into consideration to make inferences about the statistical quality (goodness of fitting) of the model but the residues (alignment between observed and predicted values) and adjusted $R^2$ (calculates the proportion of the variation in the dependent variable accounted by the explanatory variables) also need to be calculated and discussed. In the current study, in addition to the significance ($p$ value) and $R^2$ values, the normality of residues was formally evaluated by Shapiro−Wilk's test, which revealed that for all models the observed versus the expected (predicted) values were closely related and the residues followed a normal distribution ($p_{\text{Shapiro−Wilk}} > 0.05$). The adjusted $R^2$ was also provided, and results evidence the closeness between adjusted and "raw" $R^2$ values, indicating the models could describe satisfactorily the instrumental taste profile, chemical composition, antioxidant, and metal chelating activity of *C. sinensis* tea samples.

The simultaneous optimization of the tea mixture using the CUPRAC, DPPH, and iron chelating activities, flavan-3-ols content, and instrumental bitterness led to a formulation containing 14.81% green tea, 28.33% red tea, and 56.86% yellow tea, with a desirability function of 0.9441, which means that this formulation is, theoretically, the best option to obtain a mixture with maximized antioxidant capacity (DPPH and

**Table 4. Effects of Green (A), Red (B), and Yellow (C) Teas and Their Binary and Ternary Mixtures on Chemical Composition, Instrumental Taste Profile, and Antioxidant and Metal Chelation Activities of *C. sinensis* Teas**

| response variable | factor | regression coefficient | standard error | *t* value | *p* value | −95% confidence | 95% confidence |
|---|---|---|---|---|---|---|---|
| flavan-3-ols | (A) green tea | 156.99 | 2.02 | 77.60 | <0.001 | 152.21 | 161.78 |
| | (B) red tea | 145.99 | 2.02 | 72.16 | <0.001 | 141.21 | 150.78 |
| | (C) yellow tea | 102.78 | 2.02 | 50.81 | <0.001 | 97.99 | 107.56 |
| | $R^2$ | 0.9791 | | | | | |
| | adjusted $R^2$ | 0.9731 | | | | | |
| | *p* value (model) | <0.001 | | | | | |
| | *p* value (normality of residues) | 0.26 | | | | | |
| total phenolic compounds | (A) green tea | 524.75 | 6.24 | 84.11 | <0.001 | 507.42 | 542.07 |
| | (B) red tea | 668.49 | 6.24 | 107.15 | <0.001 | 651.16 | 685.81 |
| | (C) yellow tea | 375.33 | 6.24 | 60.16 | <0.001 | 358.01 | 392.66 |
| | AB | 164.79 | 28.75 | 5.73 | <0.001 | 84.97 | 244.60 |
| | $R^2$ | 0.9896 | | | | | |
| | adjusted $R^2$ | 0.9844 | | | | | |
| | *p* value (model) | <0.001 | | | | | |
| | *p* value (normality of residues) | 0.76 | | | | | |
| *o*-diphenols | (A) green tea | 526.61 | 23.73 | 22.19 | <0.001 | 470.49 | 582.74 |
| | (B) red tea | 325.64 | 23.73 | 13.72 | <0.001 | 269.51 | 381.76 |
| | (C) yellow tea | 579.53 | 23.73 | 24.42 | <0.001 | 523.42 | 635.65 |
| | $R^2$ | 0.8814 | | | | | |
| | adjusted $R^2$ | 0.8475 | | | | | |
| | *p* value (model) | <0.001 | | | | | |
| | *p* value (normality of residues) | 0.59 | | | | | |
| chlorogenic acid | (A) green tea | 1.179 | 0.12 | 10.07 | <0.001 | 0.89 | 1.47 |
| | (B) red tea | 0.264 | 0.12 | 2.25 | 0.07 | −0.02 | 0.55 |
| | (C) yellow tea | 0.391 | 0.10 | 3.87 | 0.01 | 0.14 | 0.64 |
| | AB | −1.001 | 0.30 | −3.30 | 0.02 | −1.74 | −0.26 |
| | $R^2$ | 0.8828 | | | | | |
| | adjusted $R^2$ | 0.8243 | | | | | |
| | *p* value (model) | 0.003 | | | | | |
| | *p* value (normality of residues) | 0.15 | | | | | |
| (+)-catechin | (A) green tea | 6.92 | 0.53 | 13.08 | <0.001 | 5.63 | 8.22 |
| | (B) red tea | 1.28 | 0.46 | 2.79 | 0.03 | 0.16 | 2.40 |
| | (C) yellow tea | 5.33 | 0.53 | 10.07 | <0.001 | 4.04 | 6.63 |
| | AC | 4.07 | 1.37 | 2.97 | 0.03 | 0.72 | 7.43 |
| | $R^2$ | 0.9437 | | | | | |
| | adjusted $R^2$ | 0.9156 | | | | | |
| | *p* value (model) | <0.001 | | | | | |
| | *p* value (normality of residues) | 0.64 | | | | | |
| (−)-epicatechin | (A) green tea | 48.22 | 2.14 | 22.52 | <0.001 | 42.72 | 53.73 |
| | (B) red tea | 5.73 | 2.40 | 2.38 | 0.06 | −0.45 | 11.90 |
| | (C) yellow tea | 44.58 | 2.14 | 20.81 | <0.001 | 39.07 | 50.08 |
| | AB | 32.36 | 5.54 | 5.84 | <0.001 | 18.12 | 46.60 |
| | BC | 37.82 | 5.54 | 6.83 | <0.001 | 23.58 | 52.06 |
| | $R^2$ | 0.9808 | | | | | |
| | adjusted $R^2$ | 0.9654 | | | | | |
| | *p* value (model) | <0.001 | | | | | |
| | *p* value (normality of residues) | 0.80 | | | | | |
| epigallocatechin gallate | (A) green tea | 122.32 | 9.22 | 13.26 | <0.001 | 98.61 | 146.03 |

**Table 4. continued**

| response variable | factor | regression coefficient | standard error | *t* value | *p* value | −95% confidence | 95% confidence |
|---|---|---|---|---|---|---|---|
| | (C) yellow tea | 205.16 | 9.22 | 22.24 | <0.001 | 181.45 | 228.88 |
| | AB | −118.19 | 23.86 | −4.95 | <0.001 | −179.53 | −56.85 |
| | BC | −159.67 | 23.86 | −6.69 | <0.001 | −220.99 | −98.35 |
| | $R^2$ | 0.9885 | | | | | |
| | adjusted $R^2$ | 0.9793 | | | | | |
| | *p* value (model) | <0.001 | | | | | |
| | *p* value (normality of residues) | 0.05 | | | | | |
| caffeine | (A) green tea | 122.25 | 2.18 | 56.10 | <0.001 | 116.92 | 127.59 |
| | (B) red tea | 310.41 | 1.88 | 164.97 | <0.001 | 305.81 | 315.02 |
| | (C) yellow tea | 299.03 | 2.18 | 137.22 | <0.001 | 293.70 | 304.37 |
| | AC | −12.83 | 5.65 | −2.27 | 0.06 | −26.65 | 0.98 |
| | $R^2$ | 0.9989 | | | | | |
| | adjusted $R^2$ | 0.9983 | | | | | |
| | *p* value (model) | <0.001 | | | | | |
| | *p* value (normality of residues) | 0.33 | | | | | |
| gallic acid | (A) green tea | 17.43 | 5.06 | 3.44 | 0.02 | 4.42 | 30.45 |
| | (B) red tea | 35.27 | 5.67 | 6.21 | 0.001 | 20.67 | 49.86 |
| | (C) yellow tea | 14.81 | 5.06 | 2.92 | 0.03 | 1.79 | 27.82 |
| | AB | 83.13 | 13.09 | 6.35 | 0.001 | 49.47 | 116.80 |
| | BC | 113.24 | 13.09 | 8.65 | 0.003 | 79.59 | 146.90 |
| | $R^2$ | 0.9703 | | | | | |
| | adjusted $R^2$ | 0.9465 | | | | | |
| | *p* value (model) | 0.005 | | | | | |
| | *p* value (normality of residues) | 0.23 | | | | | |
| iron chelating activity | (A) green tea | 39.30 | 2.04 | 19.28 | <0.001 | 34.48 | 44.12 |
| | (B) red tea | 38.49 | 2.04 | 18.89 | <0.001 | 33.67 | 43.31 |
| | (C) yellow tea | 29.19 | 2.04 | 14.33 | <0.001 | 24.37 | 34.01 |
| | $R^2$ | 0.6395 | | | | | |
| | adjusted $R^2$ | 0.5365 | | | | | |
| | *p* value (model) | 0.03 | | | | | |
| | *p* value (normality of residues) | 0.48 | | | | | |
| copper chelating activity | (A) green tea | 45.57 | 1.86 | 24.47 | <0.001 | 41.16 | 49.97 |
| | (B) red tea | 54.78 | 1.86 | 29.42 | <0.001 | 50.38 | 59.19 |
| | (C) yellow tea | 53.04 | 1.86 | 28.48 | <0.001 | 48.63 | 57.44 |
| | $R^2$ | 0.6171 | | | | | |
| | adjusted $R^2$ | 0.5077 | | | | | |
| | *p* value (model) | 0.03 | | | | | |
| | *p* value (normality of residues) | 0.84 | | | | | |
| DPPH | (A) green tea | 42.31 | 1.42 | 29.70 | <0.001 | 38.82 | 45.79 |
| | (B) red tea | 54.68 | 1.65 | 33.15 | <0.001 | 50.65 | 58.72 |
| | (C) yellow tea | 22.77 | 1.65 | 13.80 | <0.001 | 18.73 | 26.81 |
| | BC | 22.90 | 8.55 | 2.68 | 0.04 | 1.98 | 43.82 |
| | $R^2$ | 0.9727 | | | | | |
| | adjusted $R^2$ | 0.9590 | | | | | |
| | *p* value (model) | <0.001 | | | | | |
| | *p* value (normality of residues) | 0.21 | | | | | |
| ferric reducing antioxidant power (FRAP) | (A) green tea | 15.28 | 0.74 | 20.55 | <0.001 | 13.52 | 17.04 |
| | (B) red tea | 24.65 | 0.74 | 33.14 | <0.001 | 22.89 | 26.4 |
| | (C) yellow tea | 10.16 | 0.74 | 13.66 | <0.001 | 8.4 | 11.92 |

**Table 4. continued**

| response variable | factor | regression coefficient | standard error | *t* value | *p* value | −95% confidence | 95% confidence |
|---|---|---|---|---|---|---|---|
| | $R^2$ | 0.9579 | | | | | |
| | adjusted $R^2$ | 0.9459 | | | | | |
| | *p* value (model) | <0.001 | | | | | |
| | *p* value (normality of residues) | 0.60 | | | | | |
| cupric reducing antioxidant power (CUPRAC) | (A) green tea | 9.22 | 0.07 | 134.16 | <0.001 | 9.03 | 9.41 |
| | (B) red tea | 11.45 | 0.07 | 166.61 | <0.001 | 11.26 | 11.64 |
| | (C) yellow tea | 5.54 | 0.07 | 80.7 | <0.001 | 5.35 | 5.73 |
| | AB | 0.97 | 0.32 | 3.05 | <0.001 | 0.09 | 1.83 |
| | AC | 1.51 | 0.32 | 4.77 | <0.001 | 0.63 | 2.38 |
| | BC | 1.08 | 0.32 | 3.42 | <0.001 | 0.2 | 1.96 |
| | $R^2$ | 0.9992 | | | | | |
| | adjusted $R^2$ | 0.9983 | | | | | |
| | *p* value (model) | <0.001 | | | | | |
| | *p* value (normality of residues) | 0.12 | | | | | |
| bitterness | (A) green tea | −6.91 | 0.10 | −71.79 | <0.001 | −7.14 | −6.68 |
| | (B) red tea | −5.12 | 0.10 | −53.23 | <0.001 | −5.35 | −4.89 |
| | (C) yellow tea | −10.39 | 0.10 | −108.03 | <0.001 | −10.62 | −10.17 |
| | $R^2$ | 0.9945 | | | | | |
| | adjusted $R^2$ | 0.9929 | | | | | |
| | *p* value (model) | <0.001 | | | | | |
| | *p* value (normality of residues) | 0.57 | | | | | |
| aftertaste due to astringency | (A) green tea | 5.36 | 0.57 | 9.34 | <0.001 | 3.95 | 6.76 |
| | (B) red tea | 5.26 | 0.57 | 9.17 | <0.001 | 3.86 | 6.66 |
| | (C) yellow tea | 1.70 | 0.57 | 2.95 | 0.03 | 0.29 | 3.10 |
| | ABC | −45.91 | 18.83 | −2.44 | 0.05 | −91.98 | 0.17 |
| | $R^2$ | 0.8322 | | | | | |
| | adjusted $R^2$ | 0.7483 | | | | | |
| | *p* value (model) | <0.001 | | | | | |
| | *p* value (normality of residues) | 0.85 | | | | | |
| umami | (A) green tea | −16.61 | 0.12 | −140.30 | <0.001 | −16.90 | −16.32 |
| | (B) red tea | −17.73 | 0.12 | −149.79 | <0.001 | −18.02 | −17.44 |
| | (C) yellow tea | −16.16 | 0.12 | −136.47 | <0.001 | −16.45 | −15.87 |
| | ABC | −12.86 | 3.89 | −3.31 | 0.02 | −22.37 | −3.35 |
| | $R^2$ | 0.9409 | | | | | |
| | adjusted $R^2$ | 0.9113 | | | | | |
| | *p* value (model) | <0.001 | | | | | |
| | *p* value (normality of residues) | 0.48 | | | | | |
| richness | (A) green tea | 7.20 | 0.15 | 46.99 | <0.001 | 6.82 | 7.57 |
| | (B) red tea | 9.23 | 0.15 | 60.28 | <0.001 | 8.86 | 9.61 |
| | (C) yellow tea | 2.50 | 0.15 | 16.30 | <0.001 | 2.12 | 2.87 |
| | ABC | 27.09 | 5.03 | 5.39 | <0.001 | 14.79 | 39.39 |
| | $R^2$ | 0.9937 | | | | | |
| | adjusted $R^2$ | 0.9905 | | | | | |
| | *p* value (model) | <0.001 | | | | | |
| | *p* value (normality of residues) | 0.58 | | | | | |
| saltiness | (A) green tea | 1.02 | 0.41 | 2.50 | 0.04 | 0.06 | 1.99 |
| | (B) red tea | 4.38 | 0.41 | 10.71 | <0.001 | 3.41 | 5.35 |
| | (C) yellow tea | −2.39 | 0.41 | −5.85 | <0.001 | −3.36 | −1.42 |
| | $R^2$ | 0.9412 | | | | | |

**Table 4. continued**

| response variable | factor | regression coefficient | standard error | *t* value | *p* value | −95% confidence | 95% confidence |
|---|---|---|---|---|---|---|---|
| | adjusted $R^2$ | 0.9243 | | | | | |
| | *p* value (model) | <0.001 | | | | | |
| | *p* value (normality of residues) | 0.74 | | | | | |

**Table 5. Predicted and Experimental Values for the Optimized Ternary Mixture of Green (14.81%), Yellow (56.86%), and Red Teas (28.33%)**

| response variable | goal | predicted mean value | −95% prediction | +95% prediction | experimental value | relative absolute error[a] (%) |
|---|---|---|---|---|---|---|
| bitterness (EIT) | intermediate value | −8.38 | −8.72 | −8.05 | −8.30 ± 0.00 | 0.95 |
| flavan-3-ols content (mg PCY/L) | maximize | 122.88 | 114.64 | 131.12 | 125.90 ± 4.38 | 2.46 |
| cupric ion reducing antioxidant power (mmol TE/L) | maximize | 8.10 | 7.68 | 8.52 | 7.96 ± 0.06 | 1.74 |
| iron-chelating activity (%) | maximize | 34.12 | 26.17 | 42.07 | 41.89 ± 0.64 | 22.77 |
| free radical scavenging activity (% inhibition) | maximize | 37.12 | 29.35 | 44.89 | 42.26 ± 0.13 | 13.84 |

[a]Relative absolute error (RAE) was calculated as RAE (%) = [(experimental mean value − predicted mean value)/predicted mean value] × 100 as outlined by Granato et al.[27]

CUPRAC), iron chelating activity, and flavan-3-ols and a balanced bitterness. This formulation was prepared and analyzed using the same experimental assays, and the obtained results were compared with the values predicted by each final regression model (Table 5). All experimental data were within the ±95% prediction interval, meaning the regression models can be regarded as significant and predictive. Therefore, to obtain a maximized antioxidant/metal chelating power, higher content of flavan-3-ols, and mild bitterness, a sample containing 14.81% green tea, 28.33% red tea, and 56.86% yellow tea should be produced. This sample presented 0.44 ± 0.02 mg/L chlorogenic acid, 50.66 ± 6.66 mg/L gallic acid, 251.90 ± 0.06 mg/L epigallocatechin gallate, 9.65 ± 0.01 mg/L (+)-catechin, 73.84 ± 0.18 mg/L (−)-epicatechin, and 533.18 ± 0.15 mg/L caffeine.

In conclusion, response surface methodology was successful in modeling the extraction of phenolic compounds, instrumental taste profile, and antioxidant and metal chelating properties of mixtures of green, yellow, and red *C. sinensis* teas, and the regression equations developed can be used for prediction purposes. The system was subjected to a multiresponse optimization, and the best formulation to obtain a tea with intermediate level of bitterness and maximized antioxidant activity is by mixing 14.81% green tea, 28.33% red tea, and 56.86% yellow tea. Overall, our results clearly corroborate the fact that the oxidation and fermentation processes that *C. sinensis* undergoes highly influence the chemical composition and antioxidant capacity of teas.

## ■ ASSOCIATED CONTENT

### Ⓢ Supporting Information

Figure 1 and Table 1 are typical chromatograms of the HPLC analysis and regression analysis of the chemical compounds measured by HPLC, respectively. This material is available free of charge via the Internet at http://pubs.acs.org.

## ■ AUTHOR INFORMATION

### Corresponding Author

*(D.G.) Phone: +55 42 3220-3268. Fax: +55 42 3220-3072. E-mail: granatod@gmail.com.

### Funding

We thank CNPq for one Researcher Grant (D. S. Nunes, Process 307329/2013-5) and CAPES (CAPES/PNPD, and CAPES − Science Without Borders scholarship − D. Granato − Process 8771-13-8) for financial support to conduct this research.

### Notes

The authors declare no competing financial interest.

## ■ REFERENCES

(1) Chattopadhyay, C.; Chakrabarti, N.; Chatterjee, M.; Mukherjee, S.; Sarkar, K.; Chaudhuri, A. R. Black tea (*Camellia sinensis*) decoction shows immunomodulatory properties on an experimental animal model and in human peripheral mononuclear cells. *Pharm. Res.* **2012**, *4*, 15−21.

(2) Ramirez-Mares, M. V.; Chandra, S.; de Mejia, E. G. *In vitro* chemopreventive activity of *Camellia sinensis*, *Ilex paraguariensis* and *Ardisia compressa* tea extracts and selected polyphenols. *Mutat. Res.* **2004**, *554*, 53−65.

(3) Tenore, G. C.; Stiuso, P.; Campiglia, P.; Novellino, E. *In vitro* hypoglycaemic and hypolipidemic potential of white tea polyphenols. *Food Chem.* **2013**, *141*, 2379−2384.

(4) Chatterjee, P.; Chandra, S.; Dey, P.; Bhattacharya, S. Evaluation of anti-inflammatory effects of green tea and black tea: a comparative *in vitro* study. *J. Adv. Pharm. Technol. Res.* **2012**, *3*, 136−138.

(5) Chauhan, D. S.; Bhattacharya, S.; Ahmed, K. K. M. Comparative *in vitro* antioxidant evaluation of different extracts of *Camellia sinensis* leaves form different geographical locations in India. *Pharmacog. J.* **2012**, *4*, 46−49.

(6) Granato, D.; Bassani, D. C.; Nunes, D. S. Quality control of *Camellia sinensis* and *Ilex paraguariensis* teas marketed in Brazil based on total phenolics, flavonoids and free-radical scavenging activity using chemometrics. In *Mathematical and Statistical Approaches in Food Science and Technology*, 1st ed.; Granato, D., Ares, G., Organizers; Wiley Blackwell: Oxford, UK, 2014; Vol. 1, pp 219−230.

(7) Zielinski, A. A. F.; Haminiuk, C. W. I.; Alberti, A.; Nogueira, A.; Demiate, I. M.; Granato, D. A comparative study of the phenolic compounds and the *in vitro* antioxidant activity of different Brazilian teas using multivariate statistical techniques. *Food Res. Int.* **2014**, *60*, 246−254.

(8) Kumar, A. S.; Mazumder, A.; Saravanan, V. S. Antihyperlipidemic activity of *Camellia sinensis* leaves in Triton WR-1339 induced albino rats. *Pharm. Mag.* **2008**, *4*, 60−64.

(9) Rains, T. M.; Agarwal, S.; Maki, K. C. Antiobesity effects of green tea catechins: a mechanistic review. *J. Nutr. Biochem.* **2011**, *22* (1), 1−7.
(10) Zhang, Y.; Li, Q.; Xing, H.; Lu, X.; Zhao, L.; Qu, K.; Bi, K. Evaluation of antioxidant activity of ten compounds in different tea samples by means of an on-line HPLC−DPPH assay. *Food Res. Int.* **2013**, *53*, 847−856.
(11) Zhang, L.; Zhang, Z.; Ling, T.; Wan, X. Chinese dark teas: post fermentation, chemistry and biological activities. *Food Res. Int.* **2013**, *53*, 600−607.
(12) Alcázar, A.; Ballesteros, O.; Jurado, J. M.; Pablos, F.; Martín, M. J.; Vilches, J. L.; Navalón, A. Differentiation of green, white, black, oolong, and pu-erh teas according to their free amino acids content. *J. Agric. Food Chem.* **2007**, *55*, 5960−5965.
(13) Rusak, G.; Komes, D.; Likić, S.; Horžić, D.; Kovač, M. Phenolic content and antioxidative capacity of green and white tea extracts depending on extraction conditions and the solvent used. *Food Chem.* **2008**, *110*, 852−858.
(14) Carloni, P.; Tiano, L.; Padella, L.; Bacchetti, T.; Customu, C.; Kay, A.; Damiani, E. Antioxidant activity of white, green and black tea obtained from the same tea cultivar. *Food Res. Int.* **2013**, *53*, 900−908.
(15) Habara, M.; Toko, K. Taste sensor. In *Encyclopedia of Sensors*; Grimes, C. A., Dickey, E. C., Pishko, M. V., Eds.; American Scientific Publishers: Stevenson Ranch, CA, USA, 2006; Vol. 10, pp 107−119.
(16) Singleton, V. L.; Rossi, J. A., Jr. Colorimetry of total phenolics with phosphomolybdic−phosphotungstic acid reagent. *Am. J. Enol. Vitic.* **1965**, *16*, 144−158.
(17) Porter, L. J. Tannins. In *Methods in Plant Biochemistry. Plant Phenolics*; Harborne, J. B., Ed.; Academic Press: New York, 1989; pp 389−419.
(18) Durán, R. M.; Padilla, R. B.; Martín, A. M.; Ursinos, J. A. F.; Mendoza, J. A. Biodegradación de los compuestos fenólicos presentes en el alpechín. *Grasas Aceites* **1991**, *42*, 271−276.
(19) Apak, R.; Güçlü, K.; Özyürek, M.; Çelik, S. E. Mechanism of antioxidant capacity assays and the CUPRAC (cupric ion reducing antioxidant capacity) assay. *Microchim. Acta* **2008**, *160*, 413−419.
(20) Benzie, I. F. F.; Strain, J. J. The ferric reducing ability of plasma (FRAP) as a measure of "antioxidant power": the FRAP assay. *Anal. Biochem.* **1996**, *239*, 70−76.
(21) Brand-Williams, W.; Cuvelier, M. E.; Berset, C. Use of free-radical method to evaluate antioxidant activity. *LWT−Food Sci. Technol.* **1995**, *28*, 25−30.
(22) Carter, P. Spectrophotometric determination of serum iron at the submicrogram level with a new reagent (ferrozine). *Anal. Biochem.* **1971**, *40*, 450−458.
(23) Saiga, A.; Tanabe, S.; Nishimura, T. Antioxidant activity of peptides obtained from porcine myofibrillar proteins by protease treatment. *J. Agric. Food Chem.* **2003**, *51*, 3661−3667.
(24) Granato, D.; Calado, V. M. A.; Jarvis, B. Observations on the use of statistical methods in food science and technology. *Food Res. Int.* **2014**, *55*, 137−149.
(25) Zielinski, A. A. F.; Haminiuk, C. W. I.; Nunes, C. A.; Schnitzler, E.; van Ruth, S. M.; Granato, D. Chemical composition, sensory properties, provenance, and bioactivity of fruit juices as assessed by chemometrics: a critical review and guideline. *Compr. Rev. Food Sci. F* **2014**, *13*, 300−316.
(26) Bassani, D. C.; Nunes, D. S.; Granato, D. Optimization of phenolics and flavonoids extraction conditions and antioxidant activity of roasted yerba-mate leaves (*Ilex paraguariensis* A. St.-Hil., Aquifoliaceae) using response surface methodology. *An. Acad. Bras. Cienc.* **2014**, *86*, 923−934.
(27) Granato, D.; de Castro, I. A.; Ellendersen, L. S. N.; Masson, M. L. Physical stability assessment and sensory optimization of a dairy-free emulsion using response surface methodology. *J. Food Sci.* **2010**, *75*, S149−S155.
(28) Derringer, G.; Suich, R. Simultaneous optimization of several response variables. *J. Qual. Technol.* **1980**, *12*, 214−219.
(29) Wang, K.; Liu, F.; Liu, Z.; Huang, J.; Xu, Z.; Li, Y.; Chen, J.; Gong, Y.; Yang, X. Comparison of catechins and volatile compounds among different types of tea using high performance liquid chromatograph and gas chromatograph mass spectrometer. *Int. J. Food Sci. Technol.* **2011**, *46*, 1406−1412.
(30) Fernández, P. L.; Pablos, F.; Martin, M. J.; Gonzalez, A. G. Study of catechin and xanthine tea profiles as geographical tracers. *J. Agric. Food Chem.* **2002**, *50*, 1833−1839.
(31) Karori, S. M.; Wachira, F. N.; Wanyoko, J. K.; Ngure, R. M. Antioxidant capacity of different types of tea products. *Afr. J. Biotechnol.* **2007**, *6*, 2287−2296.
(32) Kim, Y.; Goodner, K. L.; Park, J. D.; Choi, J.; Talcott, S. T. Changes in antioxidant phytochemicals and volatile compositions of *Camellia sinensis* by oxidation during tea fermentation. *Food Chem.* **2011**, *129*, 1331−1342.
(33) Cabrera, C.; Gimenez, R.; López, M. C. Determination of tea components with antioxidant activity. *J. Agric. Food Chem.* **2003**, *51*, 4427−4435.
(34) Cao, G.; Sofic, E.; Prior, R. L. Antioxidant and prooxidant behavior of flavonoids: structure-activity relationships. *Free Radical Biol. Med.* **1997**, *22*, 749−60.

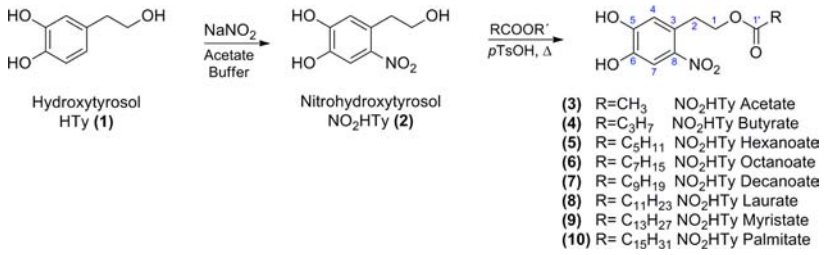


**Figure 1.** Chemical structures of hydroxytyrosol (**1**), nitrohydroxytyrosol (**2**), and nitrohydroxytyrosyl esters (acetate (**3**), butyrate (**4**), hexanoate (**5**), octanoate (**6**), decanoate (**7**), laurate (**8**), myristate (**9**), and palmitate (**10**)).

methanol, acetone, sodium nitrite, hydrogen chloride, iron(III) chloride hexahydrate, sodium hydrogen phosphate, potassium dihydrogen phosphate, acetic acid, sodium acetate trihydrate, hexadeuterated dimethyl sulfoxide (DMSO-$d_6$), ethyl acetate, and methyl esters (butyrate, hexanoate, octanoate, decanoate, laurate, myristate, and palmitate) were from Aldrich (Madrid, Spain).

Fluorescein, methylated $\beta$-cyclodextrin (RMCD), 2,2′-azinobis(3-ethylbenzothiazoline-6-sulfonic acid) diammonium salt (98%) (ABTS), 2,2′-azobis(2-amidinopropane) dihydrochloride (AAPH), and 2,4,6-tri-(2-pyridyl)-1,3,5-triazine (TPTZ) were from Sigma (Madrid, Spain).

HTy was recovered with 95% purity from olive oil wastewaters[16] and further purified by column chromatography.

NMR spectra were recorded on a Bruker AVANCE 500 spectrophotometer operating at 500.13 MHz ($^1$H) and 125.75 MHz ($^{13}$C). Chemical shifts are given in parts per million, with the residual solvent signals (2.49 ppm for $^1$H and 39.5 ppm for $^{13}$C) as references. Samples were dissolved (10−20 mg/mL) in DMSO-$d_6$, and spectra were recorded at 303 K. High-resolution CI or FAB mass spectra (HRMS) were obtained on a Micromass AUTOSPECQ spectrometer.

**Synthesis Procedures.** *Synthesis of Nitrohydroxytyrosol (2).* HTy (**1**, 154 mg, 1 mmol) was added to 0.1 M acetate buffer (pH 3.8) (200 mL) followed by sodium nitrite (138 mg, 2 mmol). After 30 min at room temperature, the mixture was extracted with ethyl acetate (6 × 50 mL), and the combined organic layers were dried over anhydrous sodium sulfate and taken to dryness to give a yellow residue (180 mg). The resulting residue was purified by column chromatography (ethyl acetate/hexane 3:1) to obtain pure nitrohydroxytyrosol (**2**) (160.2 mg, 80.5% yield) as a yellow solid, previously described by Napolitano et al.:[17] mp 197 °C (dec); $^1$H NMR (500 MHz, DMSO-$d_6$) $\delta$ 10.05 (bs, 2H, phenolic OHs), 7.43 (s, 1H, $H_7$), 6.75 (s, 1H, $H_4$), 4.65 (bs, 1H, alcoholic OH), 3.56 (t, $J$ = 6.8 Hz, 2H, $H_1$), 2.90 (t, 2H, $H_2$); $^{13}$C NMR (125 MHz, DMSO-$d_6$) $\delta$ 150.9 ($C_5$), 143.7 ($C_6$), 139.7 ($C_8$), 127.8 ($C_3$), 118.5 ($C_4$), 112.0 ($C_7$), 61.0 ($C_1$), 36.0 ($C_2$); HRMS (CI) $m/z$ calcd for $C_8H_{10}NO_5$ $[M + H]^+$ 200.0559, found 200.0566 (3.5 ppm).

*General Method for Esterification.* $p$-Toluenesulfonic acid (10 mg) was added to a solution of nitrohydroxytyrosol (**2**, 199 mg, 1 mmol) in 16 mL of a 1:1 mixture of THF and the corresponding alkyl ester (acetate, butyrate, hexanoate, octanoate, decanoate, laurate, myristate, or palmitate). The resulting mixture was stirred at 60−65 °C until completion of the reaction (TLC). The solvent was evaporated, and the resulting residue was purified by column chromatography using silica gel as stationary phase and different hexane/diethyl ether mixtures as eluent to yield pure nitrohydroxytyrosyl ester derivatives (**3**−**10**), the chemical structures of which are depicted in Figure 1.

*Data for Nitrohydroxytyrosyl Acetate (3):* 96% yield; obtained as a white solid; mp 107−109 °C; $^1$H NMR (500 MHz, DMSO-$d_6$) $\delta$ 10.11 (bs, 2H, phenolic OHs), 7.46 (s, 1H, $H_7$), 6.74 (s, 1H, $H_4$), 4.18 (t, $J$ = 6.6 Hz, 2H, $H_1$), 3.06 (t, 2H, $H_2$), 1.94 (s, 3H, $H_{2'}$);$^{13}$C NMR (125 MHz, DMSO-$d_6$) $\delta$ 170.2 ($C_{1'}$), 151.2 ($C_5$), 144.2 ($C_6$), 139.8 ($C_8$), 126.2 ($C_3$), 118.4 ($C_4$), 112.2 ($C_7$), 63.4 ($C_1$), 31.8 ($C_2$), 20.6 ($C_{2'}$); HRMS (CI) $m/z$ calcd for $C_{10}H_{11}NO_6$ $[M]^{\bullet+}$ 241.0586, found 241.0591 (1.9 ppm).

*Data for Nitrohydroxytyrosyl Butyrate (4):* 70% yield; obtained as a syrup; $^1$H NMR (500 MHz, DMSO-$d_6$) $\delta$ 10.34 and 9.85 (2 bs, 2H, phenolic OHs), 7.46 (s, 1H, $H_7$), 6.73 (s, 1H, $H_4$), 4.20 (t, $J$ = 6.5 Hz, 2H, $H_1$), 3.07 (t, 2H, $H_2$), 2.20 (t, $J$ = 7.2 Hz, 2H, $H_{2'}$), 1.48 (m, 2H, $H_{3'}$), 0.81 (t, $J$ = 7.4 Hz, 3H, $H_{4'}$); $^{13}$C NMR (125 MHz, DMSO-$d_6$) $\delta$ 172.5 ($C_{1'}$), 151.2 ($C_5$), 144.2 ($C_6$), 139.7 ($C_8$), 126.3 ($C_3$), 118.5 ($C_4$), 112.2 ($C_7$), 63.2 ($C_1$), 35.3 ($C_{2'}$), 31.9 ($C_2$), 17.8 ($C_{3'}$), 13.3 ($C_{4'}$); HRMS (FAB) $m/z$ calcd for $C_{12}H_{15}NO_6Na$ $[M + Na]^+$ 292.0797, found 292.0796 (0.4 ppm).

*Data for Nitrohydroxytyrosyl Hexanoate (5):* 80% yield; obtained as a syrup; $^1$H NMR (500 MHz, DMSO-$d_6$) $\delta$ 10.10 (bs, 2H, phenolic OHs), 7.46 (s, 1H, $H_7$), 6.73 (s, 1H, $H_4$), 4.20 (t, $J$ = 6.5 Hz, 2H, $H_1$), 3.07 (t, 2H, $H_2$), 2.20 (t, $J$ = 7.4 Hz, 2H, $H_{2'}$), 1.45 (m, 2H, $H_{3'}$), 1.21 (m, 4H, $H_{4'}$ and $H_{5'}$), 0.82 (t, $J$ = 7.4 Hz, 3H, $H_{6'}$); $^{13}$C NMR (125 MHz, DMSO-$d_6$) $\delta$ 172.7 ($C_{1'}$), 151.2 ($C_5$), 144.1 ($C_6$), 139.7 ($C_8$), 126.2 ($C_3$), 118.4 ($C_4$), 112.2 ($C_7$), 63.2 ($C_1$), 33.4 ($C_{2'}$), 31.8 ($C_2$), 30.5 ($C_{4'}$), 24.0 ($C_{3'}$), 21.7 ($C_{5'}$), 13.7 ($C_{6'}$); HRMS (FAB) $m/z$ calcd for $C_{14}H_{19}NO_6Na$ $[M + Na]^+$ 320.1110, found 320.1107 (1.0 ppm).

*Data for Nitrohydroxytyrosyl Octanoate (6):* 72% yield; obtained as a colorless liquid; $^1$H NMR (500 MHz, DMSO-$d_6$) $\delta$ 10.10 (bs, 2H, phenolic OHs), 7.47 (s, 1H, $H_7$), 6.73 (s, 1H, $H_4$), 4.20 (t, $J$ = 6.5 Hz, 2H, $H_1$), 3.07 (t, 2H, $H_2$), 2.20 (t, $J$ = 7.4 Hz, 2H, $H_{2'}$), 1.44 (m, 2H, $H_{3'}$), 1.21 (m, 8H, $H_{4'}$−$H_{7'}$), 0.82 (t, $J$ = 7.4 Hz, 3H, $H_{8'}$); $^{13}$C NMR (125 MHz, DMSO-$d_6$) $\delta$ 172.7 ($C_{1'}$), 151.2 ($C_5$), 144.2 ($C_6$), 139.7 ($C_8$), 126.3 ($C_3$), 118.4 ($C_4$), 112.2 ($C_7$), 63.2 ($C_1$), 33.5 ($C_{2'}$), 31.9 ($C_2$), 31.1 ($C_{6'}$), 28.4−28.3 ($C_{4'}$ and $C_{5'}$), 24.4 ($C_{3'}$), 22.0 ($C_{7'}$), 13.9 ($C_{8'}$); HRMS (CI) $m/z$ calcd for $C_{16}H_{24}NO_6$ $[M + H]^+$ 326.1604, found 326.1601 (0.8 ppm).

*Data for Nitrohydroxytyrosyl Decanoate (7):* 81% yield; obtained as a white solid; mp 65−66 °C; $^1$H NMR (500 MHz, DMSO-$d_6$) $\delta$ 10.33 and 9.84 (2 bs, 2H, phenolic OHs), 7.47 (s, 1H, $H_7$), 6.74 (s, 1H, $H_4$), 4.20 (t, $J$ = 6.5 Hz, 2H, $H_1$), 3.07 (t, 2H, $H_2$), 2.21 (t, $J$ = 7.4 Hz, 2H, $H_{2'}$), 1.45 (m, 2H, $H_{3'}$), 1.22 (m, 12H, $H_{4'}$−$H_{9'}$), 0.84 (t, $J$ = 6.9 Hz, 3H, $H_{10'}$); $^{13}$C NMR (125 MHz, DMSO-$d_6$) $\delta$ 172.6 ($C_{1'}$), 151.1 ($C_5$), 144.1 ($C_6$), 139.7 ($C_8$), 126.2 ($C_3$), 118.4 ($C_4$), 112.2 ($C_7$), 63.2 ($C_1$), 33.4 ($C_{2'}$), 31.8 ($C_2$), 31.2 ($C_{8'}$), 28.7−28.3 ($C_{4'}$−$C_{7'}$), 24.2 ($C_{3'}$), 22.0 ($C_{9'}$), 13.8 ($C_{10'}$); HRMS (FAB) $m/z$ calcd for $C_{18}H_{27}NO_6Na$ $[M + Na]^+$ 376.1736, found 376.1736 (0.0 ppm).

*Data for Nitrohydroxytyrosyl Laurate (8):* 58% yield; obtained as a white solid; mp 76−77 °C; $^1$H NMR (500 MHz, DMSO-$d_6$) $\delta$ 10.10 (bs, 2H, phenolic OHs), 7.47 (s, 1H, $H_7$), 6.73 (s, 1H, $H_4$), 4.20 (t, $J$ = 6.5 Hz, 2H, $H_1$), 3.07 (t, 2H, $H_2$), 2.21 (t, $J$ = 7.4 Hz, 2H, $H_{2'}$), 1.44 (m, 2H, $H_{3'}$), 1.22 (m, 16H, $H_{4'}$−$H_{11'}$), 0.84 (t, $J$ = 6.9 Hz, 3H, $H_{12'}$); $^{13}$C NMR (125 MHz, DMSO-$d_6$) $\delta$ 172.6 ($C_{1'}$), 151.2 ($C_5$), 144.1 ($C_6$), 139.7 ($C_8$), 126.2 ($C_3$), 118.4 ($C_4$), 112.2 ($C_7$), 63.2 ($C_1$), 33.4 ($C_{2'}$), 31.8 ($C_2$), 31.2 ($C_{10'}$), 28.9−28.3 ($C_{4'}$−$C_{9'}$), 24.3 ($C_{3'}$), 22.0 ($C_{11'}$), 13.9 ($C_{12'}$); HRMS (FAB) $m/z$ calcd for $C_{20}H_{31}NO_6Na$ $[M + Na]^+$ 404.2049, found 404.2045 (1.0 ppm).

*Data for Nitrohydroxytyrosyl Myristate (9).* 60% yield; obtained as a white solid; mp 84−85 °C; $^1$H NMR (500 MHz, DMSO-$d_6$) $\delta$ 10.11 (bs, 2H, phenolic OHs), 7.46 (s, 1H, $H_7$), 6.73 (s, 1H, $H_4$), 4.20 (t, $J$ = 6.6 Hz, 2H, $H_1$), 3.07 (t, 2H, $H_2$), 2.20 (t, $J$ = 7.4 Hz, 2H, $H_{2'}$), 1.44 (m, 2H, $H_{3'}$), 1.22 (m, 20H, $H_{4'}$−$H_{13'}$), 0.84 (t, $J$ = 6.9 Hz, 3H, $H_{14'}$); $^{13}$C NMR (125 MHz, DMSO-$d_6$) $\delta$ 172.7 ($C_{1'}$), 151.2 ($C_5$), 144.1 ($C_6$), 139.7 ($C_8$), 126.2 ($C_3$), 118.4 ($C_4$), 112.2 ($C_7$), 63.2 ($C_1$), 33.4 ($C_{2'}$), 31.8 ($C_2$), 31.2 ($C_{12'}$), 29.0−28.3 ($C_{4'}$−$C_{11'}$), 24.3 ($C_{3'}$), 22.0 ($C_{13'}$), 13.9 ($C_{14'}$); HRMS (FAB) $m/z$ calcd for $C_{22}H_{35}NO_6Na$ $[M + Na]^+$ 432.2362, found 432.2361 (0.2 ppm).

Table 1. $^1$H NMR Data (500.13 MHz, DMSO-$d_6$, 303 K) for Compounds 1−10[a]

| | 1 | 2 | 3 | 4 | 5 | 6 | 7 | 8 | 9 | 10 |
|---|---|---|---|---|---|---|---|---|---|---|
| phenethyl unit | | | | | | | | | | |
| 1 | 3.49 (t) ($J_{1',2'}$ = 7.2) | 3.56 (t) ($J_{1',2'}$ = 6.8) | 4.18 (t) ($J_{1',2'}$ = 6.6) | 4.20 (t) ($J_{1',2'}$ = 6.5) | 4.20 (t) ($J_{1',2'}$ = 6.5) | 4.20 (t) ($J_{1',2'}$ = 6.5) | 4.20 (t) ($J_{1',2'}$ = 6.5) | 4.20 (t) ($J_{1',2'}$ = 6.5) | 4.20 (t) ($J_{1',2'}$ = 6.6) | 4.20 (t) ($J_{1',2'}$ = 6.5) |
| 2 | 2.52 (t) | 2.90 (t) | 3.06 (t) | 3.07 (t) | 3.07 (t) | 3.07 (t) | 3.07 (t) | 3.07 (t) | 3.07 (t) | 3.07 (t) |
| 4 | 6.57 (d) ($J_{4',8'}$ = 2.0) | 6.75 (s) | 6.74 (s) | 6.73 (s) | 6.73 (s) | 6.73 (s) | 6.74 (s) | 6.73 (s) | 6.73 (s) | 6.73 (s) |
| 7 | 6.60 (d) ($J_{7',8'}$ =8.0) | 7.43 (s) | 7.46 (s) | 7.46 (s) | 7.46 (s) | 7.47 (s) | 7.47 (s) | 7.47 (s) | 7.46 (s) | 7.47 (s) |
| 8 | 6.42 (dd) | | | | | | | | | |
| acyl chain | | | | | | | | | | |
| 2′ | | | 1.94 (s) | 2.20 (t) ($^3J$ = 7.2) | 2.20 (t) ($^3J$ = 7.4) | 2.20 (t) ($^3J$ = 7.4) | 2.21 (t) ($^3J$ = 7.4) | 2.21 (t) ($^3J$ = 7.4) | 2.20 (t) ($^3J$ = 7.4) | 2.20 (t) ($^3J$ = 7.4) |
| 3′ | | | | 1.48 (m) | 1.45 (m) | 1.45 (m) | 1.45 (m) | 1.44 (m) | 1.44 (m) | 1.44 (m) |
| 4′ | | | | 0.81 (t) ($^3J$ = 7.4) | 1.21 (m) | 1.21 (m) | 1.22 (m) | 1.22 (m) | 1.22 (m) | 1.22 (m) |
| 5′ | | | | | 1.21 (m) | 1.21 (m) | 1.22 (m) | 1.22 (m) | 1.22 (m) | 1.22 (m) |
| 6′ | | | | | 0.82 (t) ($^3J$ = 7.4) | 1.21 (m) | 1.22 (m) | 1.22 (m) | 1.22 (m) | 1.22 (m) |
| 7′ | | | | | | 1.21 (m) | 1.22 (m) | 1.22 (m) | 1.22 (m) | 1.22 (m) |
| 8′ | | | | | | 0.82 (t) ($^3$J = 7.4) | 1.22 (m) | 1.22 (m) | 1.22 (m) | 1.22 (m) |
| 9′ | | | | | | | 1.22 (m) | 1.22 (m) | 1.22 (m) | 1.22 (m) |
| 10′ | | | | | | | 0.84 (t) ($^3J$ = 6.9) | 1.22 (m) | 1.22 (m) | 1.22 (m) |
| 11′ | | | | | | | | 1.22 (m) | 1.22 (m) | 1.22 (m) |
| 12′ | | | | | | | | 0.84 (t) ($^3J$ = 6.9) | 1.22 (m) | 1.22 (m) |
| 13′ | | | | | | | | | 1.22 (m) | 1.22 (m) |
| 14′ | | | | | | | | | 0.84 (t) ($^3J$ = 6.9) | 1.22 (m) |
| 15′ | | | | | | | | | | 1.22 (m) |
| 16′ | | | | | | | | | | 0.84 (t) ($^3J$ = 6.9) |

[a]Chemical shifts ($\delta$ in parts per million) and coupling constants ($J$ in hertz).

*Data for Nitrohydroxytyrosyl Palmitate (**10**):* 55% yield; obtained as a white solid; mp 90−91 °C; $^1$H NMR (500 MHz, DMSO-$d_6$) $\delta$ 10.12 (bs, 2H, phenolic OHs), 7.47 (s, 1H, $H_7$), 6.73 (s, 1H, $H_4$), 4.20 (t, $J$ = 6.5 Hz, 2H, $H_1$), 3.07 (t, 2H, $H_2$), 2.20 (t, $J$ = 7.4 Hz, 2H, $H_{2'}$), 1.44 (m, 2H, $H_{3'}$), 1.22 (m, 24H, $H_{4'}$−$H_{15'}$), 0.84 (t, $J$ = 6.9 Hz, 3H, $H_{16'}$); $^{13}$C NMR (125 MHz, DMSO-$d_6$) $\delta$ 172.6 ($C_{1'}$), 151.2 ($C_5$), 144.1 ($C_6$), 139.7 ($C_8$), 126.2 ($C_3$), 118.4 ($C_4$), 112.2 ($C_7$), 63.2 ($C_1$), 33.4 ($C_{2'}$), 31.8 ($C_2$), 31.2 ($C_{14'}$), 29.0−28.3 ($C_{4'}$−$C_{13'}$), 24.3 ($C_{3'}$), 22.0 ($C_{15'}$), 13.9 ($C_{16'}$); HRMS (FAB) $m/z$ calcd for $C_{24}H_{39}NO_6Na$ $[M + Na]^+$ 460.2675, found 460.2689 (3.0 ppm).

**Ferric Reducing Antioxidant Power (FRAP) Assay.** The FRAP assay was carried out according to the procedure described by Pulido et al.[18] The antioxidant potential of the synthesized compounds was estimated from their ability to reduce the ferric tripyridyltriazine (TPTZ−Fe(III)) complex to its stable ferrous form (TPTZ−Fe(II)). Briefly, the FRAP reagent contained 2.5 mL of a 10 mM TPTZ solution in 40 mM HCl, plus 2.5 mL of 20 mM $FeCl_3{\cdot}6H_2O$ and 25 mL of 0.3 M acetate buffer to a final pH of 3.6. This reagent was freshly prepared and warmed to 37 °C prior to use. Nine hundred microliters of FRAP reagent was mixed with 90 $\mu$L of distilled water and 30 $\mu$L of either a standard, methanol (as appropriate reagent blank), or a test sample (ranging from 50 to 400 $\mu$M for esters with shorter acyl chain (≤6) and from 100 to 1000 $\mu$M for esters with longer acyl chain (≥8)). All compounds were dissolved in methanol. Once the mixture was shaken, readings at the absorption maximum at 595 nm were taken every 20 s, and the reaction was monitored up to 30 min at 37 °C, using a UV−visible Varian (Cary 50 BIO) spectrophotometer equipped with a thermostated autocell-holder. The reading at 30 min was selected in each case for the calculation of FRAP values. Methanolic solutions of Trolox were used for calibration. The FRAP values are expressed as millimolar TEAC (Trolox equivalent). All analyses were run in triplicate.

**ABTS Assay.** The free radical scavenging capacity was measured using the ABTS decoloration method[19] with some modifications. The method is based on the capacity of different components to scavenge the ABTS radical cation ($ABTS^{\bullet+}$) compared to a standard antioxidant (Trolox). Briefly, ABTS was dissolved in a 2.45 mM potassium persulfate solution and stored in the dark at room temperature for 12−16 h, to set a 7 mM concentration of ABTS radical cation ($ABTS^{\bullet+}$) solution. The $ABTS^{\bullet+}$ stock solution was diluted with methanol to get an absorbance of 0.70 ± 0.02 at 730 nm. After the addition of 0.1 mL of sample dissolved in methanol (ranging from 50 to 400 $\mu$M for esters up to butyrate and from 100 to 500 $\mu$M for the rest of the compounds), methanol as a blank, or Trolox standard to 3.9 mL of diluted $ABTS^{\bullet+}$ solution, absorbance readings were taken every 20 s at 30 °C over 6 min, using a UV−visible spectrophotometer. The percentage inhibition of absorbance was plotted against time, and the area under the curve (0−360 s) was calculated. Methanolic solutions of known concentrations of Trolox were used for calibration. Results are expressed in millimolar TEAC (Trolox equivalent). Each value is the average of three determinations.

**Oxygen Radical Scavenging Capacity (ORAC) Assay.** The oxygen radical scavenging capacity was measured by the lipophilic ORAC assay according to the method developed by Huang et al.[20] with some modifications. The assay is based on the fluorescence decay of a reference substance (fluorescein) after the addition of a peroxyl radical (AAPH), which acts as an initiator of the oxidative reaction. Nitrohydroxytyrosol (**2**) and its derivatives (**3**−**10**) from 5 to 25 $\mu$M

Table 2. $^{13}C$ NMR Chemical Shifts (Parts per Million; 125.76 MHz, DMSO-$d_6$, 303 K) for Compounds 1−10

| | 1 | 2 | 3 | 4 | 5 | 6 | 7 | 8 | 9 | 10 |
|---|---|---|---|---|---|---|---|---|---|---|
| phenethyl unit | | | | | | | | | | |
| 1 | 62.5 | 61.0 | 63.4 | 63.2 | 63.2 | 63.2 | 63.2 | 63.2 | 63.2 | 63.2 |
| 2 | 38.4 | 36.0 | 31.8 | 31.9 | 31.8 | 31.9 | 31.8 | 31.8 | 31.8 | 31.8 |
| 3 | 130.1 | 127.8 | 126.2 | 126.3 | 126.2 | 126.3 | 126.2 | 126.2 | 126.2 | 126.2 |
| 4 | 116.2 | 118.5 | 118.4 | 118.5 | 118.4 | 118.4 | 118.4 | 118.4 | 118.4 | 118.4 |
| 5 | 144.8 | 150.9 | 151.2 | 151.2 | 151.2 | 151.2 | 151.1 | 151.2 | 151.2 | 151.2 |
| 6 | 143.2 | 143.7 | 144.2 | 144.2 | 144.1 | 144.2 | 144.1 | 144.1 | 144.1 | 144.1 |
| 7 | 115.3 | 112.0 | 112.2 | 112.2 | 112.2 | 112.2 | 112.2 | 112.2 | 112.2 | 112.2 |
| 8 | 119.3 | 139.7 | 139.8 | 139.7 | 139.7 | 139.7 | 139.7 | 139.7 | 139.7 | 139.7 |
| acyl chain | | | | | | | | | | |
| 1′ | | | 170.2 | 172.5 | 172.7 | 172.7 | 172.6 | 172.6 | 172.7 | 172.6 |
| 2′ | | | 20.6 | 35.3 | 33.4 | 33.5 | 33.4 | 33.4 | 33.4 | 33.4 |
| 3′ | | | | 17.8 | 24.0 | 24.4 | 24.2 | 24.3 | 24.3 | 24.3 |
| 4′ | | | | 13.3 | 30.5 | 28.4−28.3 | 28.7−28.3 | 28.9−28.3 | 29.0−28.3 | 29.0−28.3 |
| 5′ | | | | | 21.7 | 28.4−28.3 | 28.7−28.3 | 28.9−28.3 | 29.0−28.3 | 29.0−28.3 |
| 6′ | | | | | 13.7 | 31.1 | 28.7−28.3 | 28.9−28.3 | 29.0−28.3 | 29.0−28.3 |
| 7′ | | | | | | 22.0 | 28.7−28.3 | 28.9−28.3 | 29.0−28.3 | 29.0−28.3 |
| 8′ | | | | | | 13.9 | 31.2 | 28.9−28.3 | 29.0−28.3 | 29.0−28.3 |
| 9′ | | | | | | | 22.0 | 28.9−28.3 | 29.0−28.3 | 29.0−28.3 |
| 10′ | | | | | | | 13.8 | 31.2 | 29.0−28.3 | 29.0−28.3 |
| 11′ | | | | | | | | 22.0 | 29.0−28.3 | 29.0−28.3 |
| 12′ | | | | | | | | 13.9 | 31.2 | 29.0−28.3 |
| 13′ | | | | | | | | | 22.0 | 29.0−28.3 |
| 14′ | | | | | | | | | 13.9 | 31.2 |
| 15′ | | | | | | | | | | 22.0 |
| 16′ | | | | | | | | | | 13.9 |

and Trolox standard (6.25, 12.5, 25, 50, 75, and 100 $\mu$M) were dissolved in 7% methylated $\beta$-cyclodextrin (RMCD) in acetone/water (1:1, v/v) solution. Then, 25 $\mu$L of either Trolox, test sample, or solvent as blank was added to a 96-well microplate followed by the addition of 150 $\mu$L of fluorescein work solution ($8.5 \times 10^{-5}$ mM) prepared in 75 mM phosphate buffer (pH 7.4). The microplate reader (Bio-Tek, Winooski, VT, USA) was programmed to record every 2 min for 120 min at 485 and 528 nm excitation and emission wavelengths, respectively, the fluorescence after the addition of 30 $\mu$L of AAPH (153 mM) as peroxyl radical generator, which was also prepared in 75 mM phosphate buffer (pH 7.4). Trolox was used for calibration, and values are expressed as millimolar TEAC (Trolox equivalent). All analyses were run in quadruplicate.

**Statistical Analysis.** Results are expressed as means ± standard deviation (SD) of three measurements for the ABTS and FRAP assays and of four measurements for the ORAC assay. The data were subjected to a one-way analysis of variance (ANOVA) using the program SPSS 19.0. The level of significance was set at $p < 0.05$.

## RESULTS

**Preparation and Characterization of Nitrohydroxytyrosyl Esters (3−10).** Hydroxytyrosol recovered from olive oil wastewaters (OOWW) was used as starting material for the synthesis of new compounds. Slight modifications to the procedure described by Napolitano et al.[17] allowed increased yield of nitrohydroxytyrosol (**2**) formation from 60 to 80%. These modifications consisted in the use of a higher concentration of reactants and a shorter reaction time. Nitrohydroxytyrosol (**2**) was obtained as a yellow solid and further esterified following the procedure described by our research group[21,22] to directly obtain the nitroester derivatives **3−10** (Figure 1) with moderate to excellent yields. Synthetic nitrohydroxytyrosyl esters (**3−10**) were characterized by NMR and HR-MS spectroscopy. $^1H$ and $^{13}C$ NMR chemical shifts (Tables 1 and 2, respectively) were unequivocally assigned for each derivative by 2D heteronuclear correlation experiments (HSQC and HMBC spectra) and were in good agreement with the proposed structures. In addition, the study by HRMS spectrometry of the molecular ion for compounds **3−10** confirmed their calculated molecular masses and elemental compositions, with a mass deviation ranging between 0.0 and 3.0 ppm (see Materials and Methods).

**Antioxidant Activity Evaluation of Nitrohydroxytyrosol (2) and Its Acyl Derivatives (3−10).** Results of the reducing power by the FRAP assay and the radical scavenging activity using ABTS and ORAC assays of nitrohydroxytyrosol (**2**) and its acyl derivatives (**3−10**) are summarized in Figure 2 and Table 3, expressed as millimolar TEAC (Trolox equivalent).

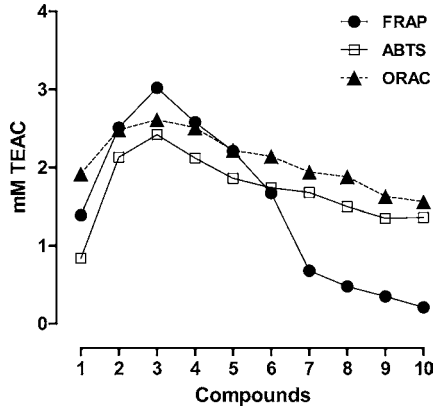


**Figure 2.** Graphical representation of data from FRAP, ABTS, and ORAC assays of hydroxytyrosol (**1**), nitrohydroxytyrosol (**2**), and nitrohydroxytyrosyl esters (**3−10**).

Table 3. Reducing Power Evaluated Using the FRAP Assay and Radical Scavenging Activity Assessed Using ABTS and ORAC Assays of Hydroxytyrosol (1), Nitrohydroxytyrosol (2), and Nitrohydroxytyrosyl Esters (3−10)[a]

| compd | FRAP assay (mM) | ABTS assay (mM) | ORAC assay (mM) |
|---|---|---|---|
| 1[b] | 1.39 ± 0.05e | 0.84 ± 0.02g | 1.92 ± 0.04d |
| 2 | 2.51 ± 0.04b | 2.13 ± 0.07b | 2.48 ± 0.04b |
| 3 | 3.02 ± 0.05a | 2.42 ± 0.08a | 2.61 ± 0.05a |
| 4 | 2.58 ± 0.03b | 2.12 ± 0.06b | 2.51 ± 0.04b |
| 5 | 2.21 ± 0.03c | 1.86 ± 0.05c | 2.22 ± 0.06c |
| 6 | 1.67 ± 0.02d | 1.74 ± 0.05d | 2.14 ± 0.04c |
| 7 | 0.68 ± 0.06f | 1.68 ± 0.06d | 1.94 ± 0.05d |
| 8 | 0.48 ± 0.05g | 1.50 ± 0.05e | 1.88 ± 0.04d |
| 9 | 0.35 ± 0.02h | 1.35 ± 0.04f | 1.63 ± 0.04e |
| 10 | 0.21 ± 0.03i | 1.36 ± 0.06f | 1.56 ± 0.05e |

[a]The data represent the mean ± standard deviation of three determinations for FRAP and ABTS assays and four determinations for ORAC assay. Results are expressed as mM Trolox equivalent (TEAC, mM). All values within a column with different letters are significantly different, $p < 0.05$. [b]FRAP and ABTS values of HTy (1) have been previously published by Mateos et al.[8] and are included for comparative purposes.

**FRAP Assay.** Nitrohydroxytyrosol (2) exhibited higher reducing activity than HTy (1). The antioxidant activity of the new nitrohydroxytyrosyl esters (3−10) in comparison with their precursor nitrohydroxytyrosol (2) varied depending on the length of the acyl side chain. Thus, nitrohydroxytyrosyl acetate (3) presented significantly higher antioxidant activity than nitrohydroxytryrosol (2), whereas nitrohydroxytyrosyl butyrate (4) showed similar activity, but the more lipophilic compounds hexanoate (5) and octanoate (6) presented lower activity and decanoate, laurate, myristate, and palmitate (7−10) presented activity even lower than that of HTy (1).

**ABTS Assay.** The radical scavenging activities of nitrohydroxytyrosol (2) and its acyl derivatives, nitrohydroxytyrosyl esters (3−10), showed a tendency similar to the reducing activity. The nitro functional group induced a positive effect on antioxidant activity because nitrohydroxytyrosol (2) as its acyl derivatives (3−10) showed higher antioxidant activity than their precursor HTy (1). Within the nitro derivatives, nitrohydroxytyrosol (2) showed lower activity than nitrohydroxytyrosyl acetate (3), similar to that of butyrate derivative (4) and higher than the rest of the tested ester derivatives (5−10).

**ORAC Assay.** The oxygen radical scavenging capacities of nitrohydroxytyrosyl esters (3−10) and their precursors, nitrohydroxytyrosol (2) and HTy (1), were in agreement with the results from the FRAP and ABTS analyses. Nitrohydroxytyrosol (2) showed higher antioxidant capacity than HTy (1), whereas its acyl derivatives (3−10) showed different behaviors related to the side-chain length; that is, the shorter chain of nitrohydroxytyrosyl acetate (3) and butyrate (4) was associated with higher and similar activity, respectively, whereas the longer acyl chains (5−10) were related with significantly lower antioxidant capacities with respect to the nitro derivative precursor (2). Almost all nitro derivatives (2−7) showed potency higher than or equal to that of HTy (1) except laurate (8), myristate (9), and palmitate (10) derivatives.

## DISCUSSION

Natural dietary antioxidants have the potential to be therapeutic and/or preventative agents against free radicals by combating oxidative stress. Reactive oxygen species accumulation in cellular components is the major factor causing molecular injury, which ultimately leads to cell aging as well as other age-related degenerative diseases.[23] Phenolic compounds in virgin olive oil have been widely studied, focusing on their antioxidant activity.[24] Among these compounds, there is evidence that HTy (1) presents relevant bioactivity, which highlights its potential preventing oxidative stress.[25] Recently, another compound also naturally present in virgin olive oil, hydroxytyrosyl acetate, is gaining interest due to its higher bioavailability,[6,7] biological activity, and particularly antioxidant activity compared to HTy.[8−12] Olive oil phenols have also shown neuroprotective properties,[1,4,12] which prompted the hypothesis that nitrocatechol derivatives of HTy might present interesting biological activities with potential as effective and safer therapeutic alternatives to the nitrocatechols currently used in the treatment of Parkinson's disease.[13−15] In the present work, the synthesis of nitrohydroxytyrosol and up to eight derivatives is presented together with the characterization of their antioxidant activity.

After nitrohydroxytyrosol (2) was obtained, a chemoselective transesterification procedure[21,22] was applied to esterify it, yielding nitrohydroxytyrosyl acetate (3) as well as other more lipophilic nitrohydroxytyrosyl ester derivatives such as butyrate, hexanoate, octanoate, decanoate, laurate, myristate, and palmitate, labeled 4, 5, 6, 7, 8, 9, and 10, respectively (Figure 1). Subsequently, in the present work the antioxidant activity characterization of nitrohydroxytyrosol (2) and its acyl derivatives (3−10) was evaluated using complementary methods (FRAP, ABTS, and ORAC) and comparatively studied against results previously published for free HTy.[8]

As expected, the synthesis of nitroester derivatives (3−10) took place in good to excellent yield. The esterification reaction used to obtain the nitroester derivatives (3−10) had been previously set up[21,22] and presented significant advantages with respect to other methods used to synthesize lipophilic ester phenolic derivatives.[26,27]

According to the results obtained, the antioxidant activity of nitro derivatives of HTy (2−10) depended on the length of the acyl side chain. The addition of a nitro functional group to the HTy chemical structure, yielding nitrohydroxytyrosol (2), induced a positive, significant increase in the antioxidant activity (Table 3). The enhanced antioxidant capacity of nitrohydroxytyrosol (2) is in accordance with the stabilization of the phenoxyl radical by ortho substitutions with electron-donating groups described by other authors.[28,29]

As mentioned, the length of the linear acyl side chain of nitroester derivatives (3−10) induced variable effects on antioxidant activity. The shorter acyl side chains (from two to four carbon atoms) stabilized the phenoxyl radical, thus enhancing or maintaining the antioxidant activity of their precursor (2), whereas longer acyl side chains (six or more carbon atoms) induced a negative effect on the antioxidant activity, probably due to steric hindrance. These results disagree with the polar paradox that assumes that there is a linear relationship between the hydrophobic character and antioxidant capacity of a compound.[30] Nevertheless, they are in accordance with results previously reported for hydroxytyrosyl esters,[8] homovanillyl esters,[31] chlorogenate esters,[32] rosmarinate

esters,[33] and other lipophilic HTy derivatives such as alkyl hydroxytyrosyl ethers.[34] In fact, this nonlinear phenomenon called the *cutoff effect*, coined by Laguerre et al.,[32] has been observed in both biological and physicochemical systems.[35] Three possible mechanisms of actions have been proposed to explain this effect: the *reduced mobility*, *internalization*, and *self-aggregation* hypotheses,[36] but no definitive conclusions have been yet reached.[37]

Moreover, a nonlinear association between biological activity and the lipophilic nature of homologous series of molecules has already been described. Ester derivatives of gallic acid were cytotoxic to L1210 leukemia cells,[38] whereas hydroxytyrosyl ethers showed antiplatelet effects in blood from healthy human volunteers[39] and after oral administration to rats.[40] Additionally, cytotoxic activity of hydroxytyrosol alkyl ether derivatives against A549 lung cancer cells and MRC5 nonmalignant lung fibroblasts was recently described.[41] In all of the aforementioned studies, biological activity increased up to medium length of the acyl or alkyl side chain, whereas the most lipophilic compounds showed lower biological activities.

In conclusion, a series of nitroderivatives has been synthesized from natural olive oil phenols to increase the assortment of compounds with a putative effect against Parkinson's disease. Compounds with shorter acyl side lengths showed higher antioxidant activities compared to HTy, whereas this activity progressively decreased further with the length of the acyl side chain in good accordance with the cutoff theory. Experiments to test their neuroprotective potential will follow.

## AUTHOR INFORMATION


### Corresponding Authors

*(R.M.) Mail: Department of Metabolism and Nutrition, Instituto de Ciencia y Tecnología de Alimentos y Nutrición (ICTAN-CSIC), C/José Antonio Nováis 10, Ciudad Universitaria, Madrid, Spain. E-mail: raquel.mateos@ictan.csic.es.

*(J.L.E.) Mail: Department of Organic and Pharmaceutical Chemistry, Faculty of Pharmacy, University of Seville, C/Prof. Garcia Gonzalez 2, E41012 Seville, Spain. E-mail: jles@us.es.

### Author Contributions

‖M.T. and E.G. contributed equally to this work.



### Funding

This work was supported by Grant P09-AGR-5098 from Junta de Andalucía (Spain). E.G. thanks Junta de Andalucía for a predoctoral fellowship.


### Notes

The authors declare no competing financial interest.

## REFERENCES


(1) Martin-Pelaez, S.; Covas, M. I.; Fito, M.; Kusar, A.; Pravst, I. Health effects of olive oil polyphenols: recent advances and possibilities for the use of health claims. *Mol. Nutr. Food Res.* **2013**, *57*, 760−771.

(2) EFSA Panel on Dietetic Products, Nutrition and Allergies. *EFSA J.* **2011**, *9*, 2033−2058.

(3) Guasch-Ferre, M.; Hu, F. B.; Martinez-Gonzalez, M. A.; Fito, M.; Bullo, M.; Estruch, R.; Ros, E.; Corella, D.; Recondo, J.; Gomez-Gracia, E.; Fiol, M.; Lapetra, J.; Serra-Majem, L.; Munoz, M. A.; Pinto, X.; Lamuela-Raventos, R. M.; Basora, J.; Buil-Cosiales, P.; Sorli, J. V.; Ruiz-Gutierrez, V.; Martinez, J. A.; Salas-Salvado, J. Olive oil intake and risk of cardiovascular disease and mortality in the PREDIMED Study. *BMC Med.* **2014**, *12*, 78 DOI: 10.1186/1741-7015-12-78.

(4) Khalatbary, A. R. Olive oil phenols and neuroprotection. *Nutr. Neurosci.* **2013**, *16*, 243−249.

(5) Mateos, R.; Espartero, J. L.; Trujillo, M.; Rios, J. J.; Leon-Camacho, M.; Alcudia, F.; Cert, A. Determination of phenols, flavones, and lignans in virgin olive oils by solid-phase extraction and high-performance liquid chromatography with diode array ultraviolet detection. *J. Agric. Food Chem.* **2001**, *49*, 2185−2192.

(6) Mateos, R.; Pereira-Caro, G.; Saha, S.; Cert, R.; Redondo-Horcajo, M.; Bravo, L.; Kroon, P. A. Acetylation of hydroxytyrosol enhances its transport across differentiated CaCo-2 cell monolayers. *Food Chem.* **2011**, *125*, 865−872.

(7) Mateos, R.; Goya, L.; Bravo, L. Metabolism of olive oil phenols hydroxytyrosol, tyrosol, and hydroxytyrosyl acetate by human hepatoma HepG2 cells. *J. Agric. Food Chem.* **2005**, *53*, 9897−9905.

(8) Mateos, R.; Trujillo, M.; Pereira-Caro, G.; Madrona, A.; Cert, A.; Espartero, J. L. New lipophilic tyrosyl esters. Comparative antioxidant evaluation with hydroxytyrosyl esters. *J. Agric. Food Chem.* **2008**, *56*, 10960−10966.

(9) Pereira-Caro, G.; Mateos, R.; Sarria, B.; Cert, R.; Goya, L.; Bravo, L. Hydroxytyrosyl acetate contributes to the protective effects against oxidative stress of virgin olive oil. *Food Chem.* **2012**, *131*, 869−878.

(10) Grasso, S.; Siracusa, L.; Spatafora, C.; Renis, M.; Tringali, C. Hydroxytyrosol lipophilic analogues: enzymatic synthesis, radical scavenging activity and DNA oxidative damage protection. *Bioorg. Chem.* **2007**, *35*, 137−152.

(11) Bouallagui, Z.; Bouaziz, M.; Lassoued, S.; Engasser, J. M.; Ghoul, M.; Sayadi, S. Hydroxytyrosol acyl esters: biosynthesis and activities. *Appl. Biochem. Biotechnol.* **2011**, *163*, 592−599.

(12) Gonzalez-Correa, J. A.; Navas, M. D.; Lopez-Villodres, J. A.; Trujillo, M.; Espartero, J. L.; De La Cruz, J. P. Neuroprotective effect of hydroxytyrosol and hydroxytyrosol acetate in rat brain slices subjected to hypoxia-reoxygenation. *Neurosci. Lett.* **2008**, *446*, 143−146.

(13) Gordin, A.; Kaakkola, S.; Teravainen, H. Clinical advantages of COMT inhibition with entacapone − a review. *J. Neural Transm.* **2004**, *111*, 1343−1363.

(14) Bonifacio, M. J.; Palma, P. N.; Almeida, L.; Soares-da-Silva, P. Cathecol-*O*-methyltransferase and its inhibitors in Parkinson diseases. *CNS Drugs* **2007**, *13*, 352−379.

(15) Lautala, P.; Kivimaa, M.; Salomies, H. Glucuronidation of entacapone, nitecapone, tolcapone and some other nitrocatechols by rat liver microsomes. *Pharm. Res.* **1997**, *14*, 1444−1448.

(16) Fernández-Bolaños, J.; Heredia, A.; Rodríguez, G.; Rodríguez, R.; Jiménez, A.; Gillen, R. Methods for obtaining purified hydroxytyrosol from products and byproducts derived from the olive tree. U.S. 6849,770 B2, 2005.

(17) Napolitano, A.; Panzella, L.; Savarese, M.; Sacchi, R.; Giudicianni, I.; Paolillo, L.; d'Ischia, M. Acid-induced structural modifications of unsaturated fatty acids and phenolic olive oil constituents by nitrite ions: a chemical assessment. *Chem. Res. Toxicol.* **2004**, *17*, 1329−1337.

(18) Pulido, R.; Bravo, L.; Saura-Calixto, F. Antioxidant activity of dietary polyphenols as determined by a modified ferric reducing/antioxidant power assay. *J. Agric. Food Chem.* **2000**, *48*, 3396−3402.

(19) Re, R.; Pellegrini, N.; Proteffente, A.; Pannala, A.; Yang, M.; Rice-Evans, C. Antioxidant activity applying an improved ABTS radical cation decolouration assay. *Free Radical Biol. Med.* **1999**, *26*, 1231−1237.

(20) Huang, D.; Ou, B.; Hampsch-Woodill, M.; Flanagan, J. A.; Deemer, E. K. Development and validation of oxygen radical absorbance capacity assay for lipophilic antioxidants using randomly methylated $\beta$-cyclodextrin as the solubility enhancer. *J. Agric. Food Chem.* **2002**, *50*, 1815−1821.

(21) Alcudia, F.; Cert, A.; Espartero, J. L.; Mateos, R.; Trujillo, M. Method of preparing hydroxytyrosyl esters, esters thus obtained and use of same. PCT WO 2004/005237, 2004.

(22) Trujillo, M.; Mateos, R.; Collantes de Teran, L.; Espartero, J. L.; Cert, R.; Jover, M.; Alcudia, F.; Bautista, J.; Cert, A.; Parrado, A. Lipophilic hydroxytyrosyl esters. Antioxidant activity in lipid matrices and biological systems. *J. Agric. Food Chem.* **2006**, *54*, 3779−3785.

(23) Balsano, C.; Alisi, A. Antioxidant effects of natural bioactive compounds. *Curt. Pharm. Des.* **2009**, *15*, 3063−3073.
(24) Visioli, F.; Bernardini, E. Extra virgin olive oil's polyphenols: biological activities. *Curr. Pharm. Design.* **2011**, *17*, 786−804.
(25) Ting, H.; Xiao-Wei, H.; Jian-Guo, J.; Xin-Lin, X. Hydroxytyrosol and its potential therapeutic effects. *J. Agric. Food Chem.* **2014**, *62*, 1449−1455.
(26) Fernandez-Bolaños, J. G.; Lopez, O.; Fernandez-Bolaños, J.; Rodriguez-Gutierrez, G. Hydroxytyrosol and derivatives: isolation, synthesis and biological properties. *Curr. Org. Chem.* **2008**, *12*, 442−463.
(27) Chillemi, R.; Sciuto, S.; Spatafora, C.; Tringali, C. Hydroxytyrosol lipophilic analogues: synthesis, radical scavenging activity and human cell oxidative damage protection. In *Olives and Olive Oil in Health and Disease Prevention*; Preedy, V. R., Watson, R. R., Eds.; Academic Press: New York, 2010; pp 1233−1243.
(28) Pokorny, J. Major factors affecting the antioxidant of lipids. In *Autoxidation of Unsaturated Lipids*; Chan, H., Ed.; Academic Press: London, UK, 1987; pp 141−206.
(29) Chimi, H.; Cillard, J.; Cillard, P.; Rahmani, M. Peroxyl radical scavenging activity of some natural phenolic antioxidants. *J. Am. Oil Chem. Soc.* **1991**, *68*, 307−312.
(30) Porter, W.; Black, E. D.; Drolet, A. M. Use of a polyamide oxidative fluorescence test on lipid emulsions: contrast in relative effectiveness of antioxidant in bulk versus dispersed systems. *J. Agric. Food Chem.* **1989**, *37*, 615−624.
(31) Madrona, A.; Pereira-Caro, G.; Bravo, L.; Mateos, R.; Espartero, J. L. Preparation and antioxidant activity of tyrosyl and homovanillyl ethers. *Food Chem.* **2011**, *129*, 1169−1178.
(32) Laguerre, M.; Giraldo, L. J.; Lecomte, J.; Figueroa-Espinoza, M. C.; Barea, B.; Weiss, J. Chain length affects antioxidant properties of chlorogenate esters in emulsion: the cutoff theory behind the polar paradox. *J. Agric. Food Chem.* **2009**, *57*, 11335−11342.
(33) Laguerre, M.; Lopez-Giraldo, L. J.; Lecomte, J.; Figueroa-Espinoza, M. C.; Barea, B.; Weiss, J.; Decker, E. A.; Villeneuve, P. Relationship between hydrophobicity and antioxidant ability of "phenolipids" in emulsion: a parabolic effect of the chain length of rosmarinate esters. *J. Agric. Food Chem.* **2010**, *58*, 2869−2876.
(34) Pereira-Caro, G.; Madrona, A.; Bravo, L.; Espartero, J. L.; Alcudia, F.; Cert, A.; Mateos, R. Antioxidant activity evaluation of alkyl hydroxytyrosyl ethers, a new class of hydroxytyrosol derivatives. *Food Chem.* **2009**, *115*, 86−91.
(35) Laguerre, M.; Bayrasy, C.; Lecomte, J.; Chabi, B.; Decker, E. A.; Wrutniak-Cabello, C.; Cabello, G.; Villeneuve, P. How to boost antioxidants by lipophilization? *Biochimie* **2013**, *95*, 20−26.
(36) Laguerre, M.; Lecomte, J.; Villeneuve, P. The physico-chemical basis of phenolic antioxidant activity. *Lipid Technol.* **2014**, *26*, 59−62.
(37) Laguerre, M.; Bayrasy, C.; Panya, A.; Weiss, J.; McClements, D. J.; Lecomte, J.; Decker, E. A.; Villeneuve, P. What makes good antioxidants in lipid-based systems? The next theories beyond the polar paradox. *Crit. Rev. Food Sci. Nutr.* **2015**, *55*, 183−201.
(38) Locatelli, C.; Rosso, R.; Santos-Silva, M. C.; De Souza, C. A.; Licínio, M. A.; Leal, P.; Bazzo, M. L.; Yunes, R. A.; Creczynski-Pasa, T. B. Ester derivatives of gallic acid with potential toxicity toward L1210 leukemia cells. *Bioorg. Med. Chem.* **2008**, *16*, 3791−3799.
(39) Reyes, J. J.; De la Cruz, J. P.; Munoz-Marin, J.; Guerrero, A.; Lopez-Villodres, J. A.; Madrona, A.; Espartero, J. L.; Gonzalez-Correa, J. A. Antiplatelet effect of new lipophilic hydroxytyrosol alkyl ether derivatives in human blood. *Eur. J. Nutr.* **2013**, *52*, 591−599.
(40) Muñoz-Marin, J.; De La Cruz, J. P.; Reyes, J. J.; López-Villodres, J. A.; Guerrero, A.; López-Leiva, I.; Espartero, J. L.; Labajos, M. T.; González-Correa, J. A. Hydroxytyrosyl alkyl ether derivatives inhibit platelet activation after oral administration to rats. *Food Chem. Toxicol.* **2013**, *58*, 295−300.
(41) Calderon-Montano, J. M.; Madrona, A.; Burgos-Moron, E.; Orta, M. L.; Mateos, R.; Espartero, J. L.; Lopez-Lazaro, M. Selective cytotoxic activity of new lipophilic hydroxytyrosol alkyl ether derivatives. *J. Agric. Food Chem.* **2013**, *61*, 5046−5053.

Table 1. $^{1}H$ and $^{13}C$ NMR Data of Pyrenophoric Acids B and C (1 and 2)[a]

| | 1 | | | 2 | | |
|---|---|---|---|---|---|---|
| position | $\delta_C$[b] | $\delta_H$ ($J$ in Hz) | HMBC | $\delta_C$ | $\delta_H$ ($J$ in Hz) | HMBC |
| 1 | 169.1 C | | | 169.0 C | | |
| 2 | 116.0 CH | 5.72 (1H) s[c] | Me-6 | 114.9 CH | 5.58 (1H) s[c] | Me-6 |
| 3 | 152.1 C | | Me-6 | 153.2 C | | Me-6 |
| 4 | 128.7 CH | 7.78 (1H) d (15.9) | H-2, H-12, Me-6 | 132.0 CH | 7.55 (1H) d (15.7) | Me-6 |
| 5 | 138.0 CH | 6.32 (1H) d (15.9) | | 136.7 CH | 6.34 (1H) dd (15.7, 9.9) | |
| 6 | 21.6 $CH_3$ | 2.04 (3H) s[c] | | 21.4 $CH_3$ | 2.06 (3H) s[c,d] | |
| 7 | 79.6 C | | H-5, Me-13, Me-14 | 53.4 CH | 2.20 (1H) dd (9.9, 5.1) | Me-15 |
| 8 | 38.7 C | | Me-14, Me-15 | 38.9 C | | Me-15 |
| 9 | 44.7 $CH_2$ | 1.73 (2H) m | | 69.2 CH | 4.38 (1H) m | |
| 10 | 66.9 CH | 4.13 (1H) quint (3.2) | | 69.0 CH | 3.77 (1H) quint (4.4) | |
| 11 | 30.4 $CH_2$ | 1.76 (1H) br d (15.1) 1.51 (1H) ddd (15.1, 13.0, 3.2) | | 38.5 $CH_2$ | 1.91 (1H) dt (12.7, 4.4) 1.71 (1H) quint (7.0) | |
| 12 | 20.6 CH | 2.36 (1H) m | | 21.4 CH | 2.06 (1H) m[d] | |
| 13 | 25.1 $CH_3$ | 1.27 (3H) s | | 29.4 $CH_3$ | 1.25 (3H) s[d] | H-7 |
| 14 | 29.1 $CH_3$ | 1.25 (3H) s | | 29.4 $CH_3$ | 1.25 (3H) s[d] | H-7 |
| 15 | 15.6 $CH_3$ | 0.84 (3H) d (6.8) | | 18.5 $CH_3$ | 1.05 d (3H) (7.6) | H-12 |

[a]The chemical shifts are in $\delta$ values (ppm) from TMS. 2D $^{1}H,^{1}H$ (COSY) and 2D $^{13}C,^{1}H$ (HSQC) NMR experiments delineated the correlations of all protons and the corresponding carbons. [b]Multiplicities were assigned by DEPT spectra. [c]These signals are allylic coupled. [d]These signals are overlapped.

(HMBC), and nuclear Overhauser enhancement spectroscopy (NOESY) experiments[11] were performed using Varian microprograms. HRESI MS were recorded on an Agilent Technologies 6120 quadrupole LC/MS (Santa Clara, CA, USA) instrument. Analytical and preparative TLC were performed on silica gel (Kieselgel 60, $F_{254}$ plates, 0.25 and 0.5 mm) (Merck, Darmstadt, Germany). The spots were visualized by exposure to UV radiation (254 nm) and/or by spraying first with 10% $H_2SO_4$ in MeOH and then with 5% phosphomolybdic acid in EtOH, followed by heating at 110 °C for 10 min. Column chromatography was performed on a silica gel column (Kieselgel 60, 0.063−0.200 mm) (Merck).

**Fungal Strain.** The *P. semeniperda* strain WRK10-22 used in this study was obtained from a *B. tectorum* seed bank sample collected from the Whiterocks exclosure (−112.7780 longitude 40.3282 latitude, 1446 m elevation) in Skull Valley, Tooele County, Utah, USA, in November 2010. For details see Masi et al.[8]

**Production, Extraction, and Purification of Phytotoxins.** To produce solid culture on *B. tectorum* seeds, 6.6 mg of WRK10-22 conidia suspended in sterile $H_2O$ were added to 200 g of soaked, autoclaved *B. tectorum* seeds, and the mixture was placed in a sterile 1 L Erlenmeyer flask with an aluminum foil cap at 22 °C. The flask was hand-shaken periodically during the 4-week incubation period to prevent caking together of the grains. The culture was then spread in pans and air-dried for at least several weeks prior to extraction. The dried material was then minced using a laboratory mill and extracted with 500 mL of MeOH/$H_2O$ (1% NaCl) (55:45, v/v). The mixture was centrifuged for 1 h at 10,000 rpm. The pellet was extracted again with the same solvent mixture in the same conditions, and the two supernatants were then pooled (pH 5.5), defatted by *n*-hexane (2 × 500 mL), and extracted with $CH_2Cl_2$ (3 × 500 mL). The resulting aqueous phase was acidified to pH 2 with formic acid and extracted with EtOAc (3 × 500 mL).

The EtOAc organic extracts were combined, dried ($Na_2SO_4$), and evaporated under reduced pressure to yield a brown solid residue (193.4 mg) that showed significant phytotoxic activity in a *B. tectorum* coleoptile bioassay. It was then subjected to bioassay-guided fractionation through column chromatography (750 mm × 30 mm) on silica gel, eluted with 1 L of EtOAc/MeOH/$H_2O$ (75:20:5, v/v/v), affording six groups of homogeneous fractions. The residue (16.4 mg) of the second fraction was further purified by TLC on silica gel, eluted with $CH_2Cl_2$/MeOH (9:1, v/v), yielding pyrenophoric acid, **3** ($R_f$ 0.36, 10.2 mg), as a homogeneous amorphous solid. The residue (14.6 mg) of the third fraction was further purified by TLC on silica gel, eluted with $CH_2Cl_2$/MeOH (9:1, v/v), yielding abscisic acid, **4** ($R_f$ 0.30, 3.2 mg, 16 mg/kg), as a white crystal powder and a mixture of two compounds. The mixture was further purified by TLC on silica gel, eluted with EtOAc/MeOH/$H_2O$ (9.5:0.3:0.2, v/v/v), yielding pyrenophoric acid B, **1** ($R_f$ 0.62, 1.8 mg, 9 mg/kg), and pyrenophoric acid C, **2** ($R_f$ 0.72, 1.6 mg, 8 mg/kg), both as homogeneous amorphous solids.

The $CH_2Cl_2$ organic extracts were combined, dried ($Na_2SO_4$), and evaporated under reduced pressure to yield a brown solid residue (694.4 mg), which essentially contained cytochalasin B (**7**) as shown by TLC analysis carried out in comparison with an authentic sample of the toxin. The mixture was washed with small aliquots (5 × 1 mL) of MeOH, and **7** was crystallized twice from EtOAc−*n*-hexane (1:5, v/v), giving white needles (223.2 mg). The mother liquors of cytochalasin B crystallization (155.3 mg) were combined with the initial MeOH washing (for a residual total extract of 470.1 mg) and fractionated by different steps of column chromatography and TLC on silica gel, affording a further amount of **7** (118.6 mg, for a total of 341.8 mg, 1025.4 mg/kg) and pyrenophoric acid (**3**, 6.3 mg, for a total of 16.5 mg, 82.5 mg/kg) as well as cytochalasin A (**5**, 12.3 mg, 61.5 mg/kg), cytochalasin F (**9**, 7.9 mg, 23.7 mg/kg), cytochalasin Z3 (**8**, 0.8 mg, 4.0 mg/kg), and deoxaphomin (**6**, 18.3 mg, 91.5 mg/kg).

*Pyrenophoric Acid B (**1**).* $[\alpha]_D^{25}$: +21.3 ($c$ = 0.18); IR $\nu_{max}$ 3394, 1727, 1670, 1554, 1260 $cm^{-1}$; UV $\lambda_{max}$ nm (log $\varepsilon$) 256 (4.75); $^{1}H$ and $^{13}C$ NMR spectra, see Table 1; HRESI MS (+) spectrum $m/z$ 286.1979 [$C_{15}H_{28}NO_4$, calcd 286.2018, M + $NH_4$]$^+$; HRESI MS (−) spectrum $m/z$ 267.5917 [$C_{15}H_{23}O_4$, calcd 267.1596, M − H]$^-$.

*Pyrenophoric Acid C (**2**).* $[\alpha]_D^{25}$: +67.7 ($c$ = 0.16); IR $\nu_{max}$ 3412, 1731, 1668, 1556, 1260 $cm^{1}$; UV $\lambda_{max}$ nm (log $\varepsilon$) 257 (4.68); $^{1}H$ and $^{13}C$ NMR spectra, see Table 1; HRESI MS (+) spectrum $m/z$ 286.2026 [$C_{15}H_{28}NO_4$, calcd 286.2018, M + $NH_4$]$^+$; HRESI MS (−) spectrum $m/z$ 267.6075 [$C_{15}H_{23}O_4$, calcd 267.1596, M − H]$^-$.

*Pyrenophoric Acid (**3**).* $^{1}H$ NMR spectrum was very similar to that previously reported.[9] HRESI MS (+) spectrum $m/z$ 286.2011 [$C_{15}H_{28}NO_4$, calcd 286.2018, M + $NH_4$]$^+$.

*(+)-Abscisic Acid (**4**).* $[\alpha]_D^{25}$: +270.2 ($c$ = 0.22 MeOH) [lit.[12] $[\alpha]_D^{23}$: +278.3 ($c$ = 0.21, MeOH)]; IR $\nu_{max}$ 3378, 1648, 1625, 1601, 1261 $cm^{-1}$ [lit.[13] $\nu_{max}$ (solid) 3394, 1646, 1622, 1597, 1248 $cm^{-1}$]; $^{1}H$ NMR spectrum was very similar to that previously reported;[13] HRESI MS (+) spectrum $m/z$ 265.1495 [$C_{15}H_{21}O_4$, calcd 265.1505, M + H]$^+$.

**Cheatgrass Seedling Bioassay.** Pyrenophoric acids B, **1**, and C, **2**, pyrenophoric acid, **3**, abscisic acid, **4**, cytochalasin A, **5**, deoxaphomin, **6**, cytochalasin B, **7**, and cytochalasin F, **9**, were first

dissolved in DMSO, and then brought up to the assay concentration of $10^{-3}$ M or $10^{-4}$ M with distilled water (the final content of DMSO was 2%). Pyrenophoric acid, **3**, and cytochalasins **5**, **6**, **7**, and **9** were also assayed in mixture (1:1 molar ratio) at $10^{-4}$ M with the same procedure. For each sample and concentration, 1.33 mL of the solution was pipetted into each of three 6 cm Petri dishes onto the surface of one filter paper. Seeds were incubated in 2% DMSO in the control treatment.

Six host seeds were arranged onto the surface of each filter paper in a pattern that made it possible to track individual seeds. Petri dishes were sealed with Parafilm to retard moisture loss and incubated at 20 °C with a 12/12 light/dark photoperiod. Germination was scored each day, and germination day was tracked individually for each seed. Five days after germination, the coleoptile and radicle length of each seedling was measured and recorded using electronic calipers. Most seeds germinated within 3 days. Seeds that did not germinate within 7 days (<5%) were excluded from analysis, while seeds that produced a radicle but no coleoptile were scored with a coleoptile length of zero. Cytochalasin Z3, **8**, was not tested because of the small amount obtained.

**Statistical Analysis.** Three separate experiments were performed, each with its own control. The first included the four cytochalasins, **5**, **6**, **7**, and **9**, at two concentrations ($10^{-3}$ and $10^{-4}$ M), while the second included the three pyrenophoric acids, **1**, **2**, and **3**, and abscisic acid, **4**, at the same two concentrations. The third experiment included each additive pairwise combination of cytochalasins **5**, **6**, **7**, and **9** (6 pairs) and pairwise combinations of each cytochalasin with pyrenophoric acid, **3**, at $10^{-4}$ M (4 pairs). Pyrenophoric acids B, **1**, and C, **2**, could not be included in this last experiment because of the small amounts obtained. The objective of the pairwise tests was to determine whether the combined effects of the different toxins were additive, less than additive, or synergistic.

Data from the first two experiments were analyzed using two-way analysis of variance (ANOVA; SAS Proc GLM) with compound and concentration as fixed effects and day-5 coleoptile length, day-5 radicle length, and germination time as the response variables. Data from the third experiment were combined with data from the pure compound bioassays at $10^{-4}$ M to permit comparisons between pure compounds and pairs of compounds and were then subjected to a similar analysis. LSMeans comparisons from the ANOVAs were used to test the statistical significance of differences between treatment means ($P < 0.05$). Coleoptile and radicle length data were log-transformed to improve homogeneity of variance prior to analysis. Germination percentage was also included in the data presentation but was not analyzed statistically because of inadequate replication.

Coleoptile and radicle length data are presented as reductions relative to the control, i.e., 1 − (treatment/control), while germination time data are presented as germination delay, i.e., treatment germination time − control germination time, in order to make the data comparable across experiments with different control treatments. A separate test confirmed that the DMSO controls did not differ significantly across experiments for any response variable.

## RESULTS AND DISCUSSION

When a *P. semeniperda* strain (WRK10-22) was cultured for the first time on host cheatgrass seeds (*B. tectorum*) and the culture was extracted, pyrenophoric acid, **3** (Figure 1), and a large quantity of cytochalasin B (**7**, Figure 1) were isolated from the $CH_2Cl_2$ extract, together with cytochalasin A, **5**, deoxaphomin, **6**, cytochalasin Z3, **8**, and cytochalasin F, **9** (Figure 1). The physical and spectroscopic properties of these compounds were identical to those previously reported,[7,9] confirming that the fungus is able to produce these metabolites when grown on host seeds (*B. tectorum*).[8,9]

The aqueous phase remaining after $CH_2Cl_2$ extraction was acidified (pH 2) and extracted with EtOAc. From the purification of this organic extract two additional polar metabolites were isolated together with the known abscisic

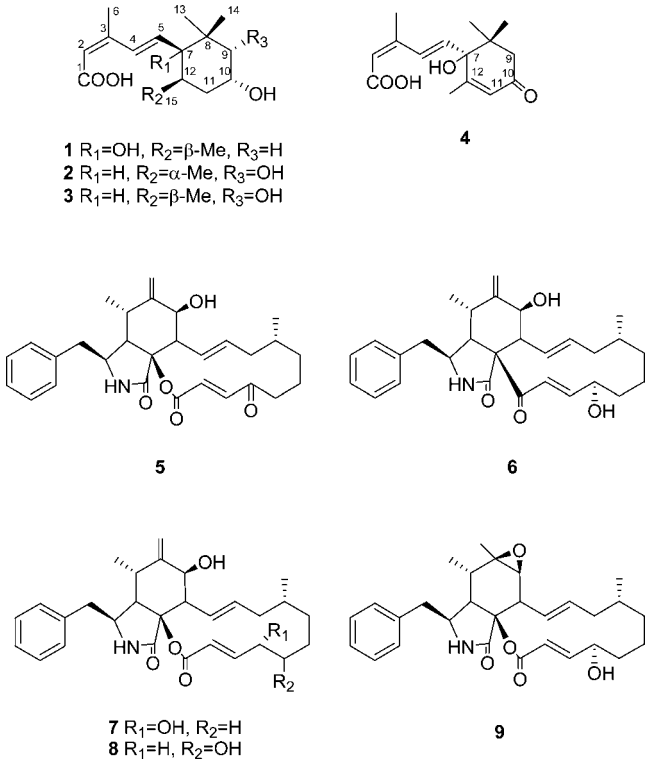


**Figure 1.** Structures of pyrenophoric acid B, **1**, pyrenophoric acid C, **2**, pyrenophoric acid, **3**, abscisic acid, **4**, cytochalasin A, **5**, deoxaphomin, **6**, cytochalasin B, **7**, cytochalasin Z3, **8**, and cytochalasin F, **9**.

acid, **4** (Figure 1), and a further amount of pyrenophoric acid, **3** (Figure 1). Both polar metabolites showed a molecular formula of $C_{15}H_{24}O_4$ as deduced from their HRESI MS, consistent with four hydrogen deficiencies. The preliminary investigation of their $^1H$ and $^{13}C$ NMR spectra, carried out in comparison with those of pyrenophoric acid, **3**,[9] showed that they are very closely related to **3**, and, being new, they were named pyrenophoric acids B, **1**, and C, **2** (Figure 1).

The $^1H$ and $^{13}C$ NMR spectra of **1** and **2** showed the signal pattern of a 3-methylpenta-2,4-dienoic acid, linked at C-7 with the same stereochemistry as in **3**, also confirmed on the basis of the couplings observed in their COSY, HSQC, and HMBC spectra.[11] However, they differed significantly for the cyclohexyl moiety system.

The $^1H$ NMR of **1** (Table 1) differed from that of **3** essentially by the absence of the double doublet of H-7 while H-5 was a doublet ($J$ = 15.9 Hz) at $\delta$ 6.32 instead of the expected double doublet as in **3**. H-5 in the COSY spectrum[11] was *trans* coupled with H-4, which showed a doublet ($J$ = 15.9 Hz) at $\delta$ 7.78. As expected, the COSY spectrum also showed the absence of the coupling between H-7 with H-12, which appeared as a multiplet at $\delta$ 2.36. These results and the molecular formula suggested the presence of a tertiary hydroxy group bonded at C-7. This was confirmed by the corresponding signal observed in the $^{13}C$ NMR spectrum (Table 1) at the typical chemical shift value of $\delta$ 79.6.[14] This carbon (C-7) significantly coupled in the HMBC spectrum with H-5 and both Me-13 and Me-14. A further significant difference, observed comparing the $^1H$ and $^{13}C$ NMR spectra of **1** to those of **3**, was the absence of the signals due to the hydroxylated secondary carbon C-9 and the presence of the signals of a further methylene group ($H_2C$-9) at $\delta$ 1.73 (2H)


dx.doi.org/10.1021/jf5035515 | J. Agric. Food Chem. 2014, 62, 10304−10311

m/44.7 $CH_2$.[14,15] $H_2$-9, in the COSY spectrum, coupled with the proton of the adjacent secondary hydroxylated carbon (CH-10), which resonated as a quintet ($J$ = 3.2 Hz) at $\delta$ 4.13, being also coupled with both protons of the other adjacent methylene group ($H_2$C-11) appearing as a broad doublet ($J$ = 15.1) and a doublet of double doublets ($J$ = 15.1, 13.0, and 3.2 Hz) at $\delta$ 1.76 and 1.51. The latter protons ($H_2$-11) were also coupled with the multiplet of H-12, and this was coupled in turn with the geminal methyl group (Me-15) appearing as a doublet ($J$ = 6.8 Hz) at $\delta$ 0.84. The other two methyl groups resonated as singlets at $\delta$ 1.27 and 1.25 (Me-13 and Me-14). The couplings observed in the HSQC spectrum allowed us to assign the chemical shifts at $\delta$ 138.0, 128.7, 116.0, 66.9, 30.4, 29.1, 25.1, 20.6, and 15.6 to C-5, C-4, C-2, C-10, C-11, C-14, C-13, C-12 and C-15. Those observed in the HMBC spectrum between C-3 with Me-6 and C-8 with Me-13 and Me-15 allowed us to attribute to these two quaternary carbons the chemical shifts of $\delta$ 152.1 and 38.7. The remaining signal at the typical chemical shift value for a carboxylic group at $\delta$ 169.1 was assigned to C-1.[14] Thus, the chemical shifts were assigned to all the protons and corresponding carbons as reported in Table 1, and **1** could be formulated as 5-(1,4-dihydroxy-2,2,6-trimethylcyclohexyl)-3-methylpenta-2,4-dienoic acid.

This structure was confirmed by the other couplings observed in the HMBC spectrum (Table 1) and by the HRESI MS data, which showed the ammonium cluster $[M + NH_4]^+$ at $m/z$ 286.1979. When the same spectrum was recorded in negative ion mode, the pseudomolecular ion $[M - H]^-$ was recorded at $m/z$ 267.5917.

The relative stereochemistry of **1**, as depicted in Figure 1, was deduced from the coupling constants measured in the $^1$H NMR spectrum. In particular, also by comparison with the value observed in **3**, the values measured for the coupling constants between H-12 and both protons of $H_2$-11 and those for the coupling of H-10 and $H_2$-11 and H-9 allowed us to locate H-10 and H-12 as $\beta$-equatorial and $\alpha$-axial as in **3**. The comparison of the chemical shifts of protons and carbons (essentially HC-5, C-8 and HC-12) surrounding C-7 with those of **3** allowed us to locate its hydroxy group $\alpha$-equatorial. The relative stereochemistry of **1** was also confirmed by the inspection of its Drieding model.

Therefore, **1** could be formulated as (2*Z*,4*E*)-5-[(1*R**,4*R**,6*R**)-1,4-dihydroxy-2,2,6-trimethylcyclohexyl]-3-methylpenta-2,4-dienoic acid. Comparing the $^1$H and $^{13}$C NMR spectra (Table 1) of **2** with those of **3,** the cyclohexyl moiety present in both compounds appeared very similar. In fact, H-7 was observed in the $^1$H NMR spectrum as a double doublet ($J$ = 9.9 and 5.1 Hz) at $\delta$ 2.20 and was coupled in the COSY spectrum with H-5 and H-12. H-12, a multiplet at $\delta$ 2.06 (overlapped to the signal of Me-6), coupled with its geminal methyl group (Me-15) and with both protons of the adjacent methylene group $H_2$C-11, which resonated, respectively, as a doublet ($J$ = 7.6 Hz), a double triplet ($J$ = 12.7 and 4.4 Hz), and a quintet ($J$ = 7.0 Hz) at $\delta$ 1.05, 1.91, and 1.71. The latter two protons ($H_2$-11) coupled with the proton of the adjacent hydroxylated secondary carbon (HC-10) resonating as a quintet ($J$ = 4.4 Hz) at $\delta$ 3.77, and this latter (H-10) was also coupled with the proton of the other hydroxylated secondary carbon (HC-9), appearing as multiplet at $\delta$ 4.38. The two methyl groups (Me-13 and Me-14) gave an overlapped signal integrating for six protons at $\delta$ 1.25. The couplings observed in the HSQC spectrum allowed us to assign the signals at $\delta$ 136.7, 132.0, 114.9, 69.2, 69.0, 53.4, 38.5, 29.4, 21.4, and 18.5 to C-5, C-4, C-2, C-9, C-10, C-7, C-11, Me-13 and Me-14 (overlapped signals), C-12 and Me-6 (overlapped signals), and Me-15. The couplings observed in the HMBC spectrum between C-3 with Me-6 and C-8 with Me-15 allowed the signal at $\delta$ 153.2 and 38.9 to be assigned to these two quaternary carbons. Thus, the remaining signal present at the typical chemical shift for a carboxylic group at $\delta$ 169.0 was assigned to C-1.[14]

On the basis of these results pyrenophoric acid C (**2**) could be formulated as 5-(3,4-dihydroxy-2,2,6-trimethylcyclohexyl)-3-methylpenta-2,4-dienoic acid, the same structural formula obtained for **3**. This structure was confirmed by the other couplings observed in the HMBC spectrum (Table 1) and by the data of the HRESI MS spectra. These latter recorded in positive ion mode showed the ammonium cluster $[M + NH_4]^+$ at $m/z$, 286.2026, while in negative ion mode they showed the pseudomolecular ion $[M - H]^-$ at $m/z$ 267.6075.

The only difference between **2** and **3** is in the stereochemistry of the cyclohexyl ring. H-12 was located $\beta$-equatorial (opposite that in **3**), and H-11a and H-11b were located $\beta$-axial and $\alpha$-equatorial as in **3**. This was deduced by measuring the values of the coupling constants in the $^1$H NMR spectrum, between H-12 and H-7 and also between H-12 and both $H_2$-11 and comparing these to the coupling constant values of **3**. Similarly the values recorded for the coupling of H-10 with both $H_2$-11 and H-9 allowed us to locate this proton (H-10) as $\beta$-equatorial and H-9 as $\beta$-axial as in **3**. The correlation observed between H-9 and H-10 in the NOESY spectrum allowed us to confirm this last proton (H-9) as $\beta$-axial. The comparison of the chemical shifts of protons and carbons (essentially HC-5, C-8, and HC-12) surrounding C-7 with those of **3** allowed us to locate its hydrogen group $\alpha$-equatorial. The relative stereochemistry of **2** as depicted in Figure 1 was also confirmed by the inspection of its Drieding model.

Thus, pyrenophoric acid C (**2**) could be formulated as (2*Z*,4*E*)-5-[(1*S**,3*S**,4*R**,6*S**)-3,4-dihydroxy-2,2,6-trimethylcyclohexyl]-3-methylpenta-2,4-dienoic acid. Both **1** and **2**, as well as **3**, are sesquiterpenoids closely related to the well-known (+)-abscisic acid (**4**). This latter is a plant hormone with roles in environmental stress response, stomatal control of plant water balance, leaf senescence promotion, and growth inhibition. **4** also regulates other important physiological processes in plants including seed development, storage product deposition, and dormancy.[16] The biosynthesis and the metabolism of **4** have been extensively studied,[17−19] and several abscisic acid derivatives have been synthesized.[20,21] However, **4** is not a plant-specific compound but one found in organisms across kingdoms from bacteria to animals, suggesting that it is a ubiquitous and versatile substance that can modulate the physiological functions of various organisms.[22] **4** has also been previously reported as a fungal metabolite.[23,24] Natural abscisic acid analogues have also been isolated from fungi during recent years.[9,25]

The compound **1** was previously reported, in racemic mixture, as a synthetic product (named PBI-175) in a patent regarding the use of abscisic acid derivatives to enhance synchrony of germination and emergence in plants.[21] This racemic mixture was prepared starting from the compound (±)-(8*R**,10*S**)-8-acetoxymethyl-1,5-dioxaspiro[5,5]undecan-9-one, following the procedure previously reported.[26] Only the $^1$H NMR and HRMS data were shown, and no results of biological activity were highlighted. In this paper **1** is described for the first time as a phytotoxic natural product isolated in its

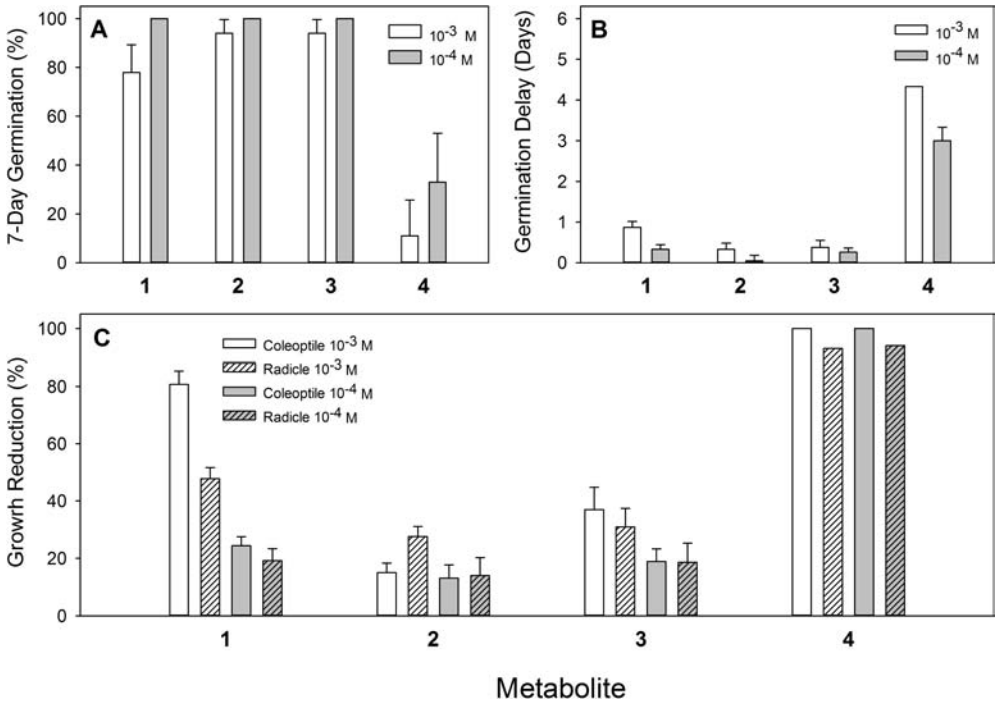


**Figure 2.** Results of host (*Bromus tectorum*) seedling bioassays with abscisic acid, **4**, and the related compounds pyrenophoric acid, **3**, pyrenophoric acid B, **1**, and pyrenophoric acid C, **2**, produced by the seed pathogen *Pyrenophora semeniperda*, at two concentrations ($10^{-3}$ and $10^{-4}$ M) (A) Seed germination percentage after 7 days. (B) Seed germination delay relative to the 2% DMSO control. (C) % coleoptile and radicle 5-day length reduction relative to the 2% DMSO control. Error bars represent standard error of the mean.

pure enantiomeric form from the cheatgrass seed culture of the fungus *P. semeniperda*. Other synthetic analogues related to pyrenophoric acid B were reported in the previously cited patent and in a related paper on the metabolism of biologically active abscisic acid analogues.[21,27]

Seedling bioassays with pyrenophoric acid (**3**), absisic acid (**4**) produced by the fungus, and the two new related compounds pyrenophoric acids B and C (**1** and **2**) demonstrated a hierarchical order of toxicity. All four compounds caused significant 5-day coleoptile and radicle length reductions relative to the control even at the lower concentration, demonstrating their potential role as phytotoxins (Figures 2 and 3). Not surprisingly, **4** was by far the most active compound, and was able to suppress most germination, delay the germination of seeds which did germinate, completely suppress coleoptile elongation, and greatly reduce radicle length relative to the control (Figures 2A, 2B, and 2C). We obtained a similar result in an earlier study with a synthetically produced (±)-abscisic acid, which completely suppressed germination of *B. tectorum* seeds.[9]

Among pyrenophoric acid analogs (**1** and **2**), only pyrenophoric acid B (**1**) was able to reduce 7-day germination and cause significant germination delay relative to the control (Figures 2A and2B). It also caused significantly more coleoptile and radicle growth reduction than the other two compounds at $10^{-3}$ M (Figure 2C). None of these effects were significant at the lower concentration. Pyrenophoric acid (**3**) caused more coleoptile growth suppression than pyrenophoric acid C (**2**), but only at the higher concentration. The relative toxicity ranking of the four compounds was therefore abscisic acid ≫ pyrenophoric acid B > pyrenophoric acid > pyrenophoric acid C (**4** ≫ **1** > **3** > **2**). These results allow us to consider structure−activity relationships between abscisic acid (**4**) and the related pyrenophoric acids (**1**−**3**). The presence at C-10 of

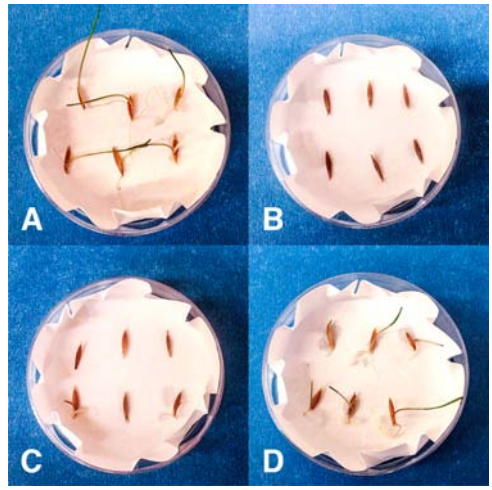


**Figure 3.** Host (*Bromus tectorum*) seedlings 5 days after germination for (A) the 2% DMSO control treatment, (B) abscisic acid, **4**, at $10^{-4}$ M (showing lack of germination), (C) pyrenophoric acid B, **1**, at $10^{-4}$ M, and (D) pyrenophoric acid, **3**, at $10^{-4}$ M.

the $\alpha,\beta$-unsaturated ketone in **4** seems to play a central role in the strong germination-inhibiting activity of this compound. The absence of this moiety in **1**, **2**, and **3** causes a noticeable activity reduction. The hydroxy group at C-7 in **4** and **1** also seems to be involved, as it is absent in the less active **2** and **3**. Furthermore, the stereochemistry of the chiral C-7 in **4**, compared with that of **1**−**3**, could be important in increasing activity, while the difference between **2** and **3** at C-12 should be unimportant. To better understand the potential mode of action of pyrenophoric acids and which structural features are involved, suitable semisynthetic derivatives should be prepared from **1**−**3** and tested in seedling bioassays.


dx.doi.org/10.1021/jf5035515 | *J. Agric. Food Chem.* 2014, 62, 10304−10311

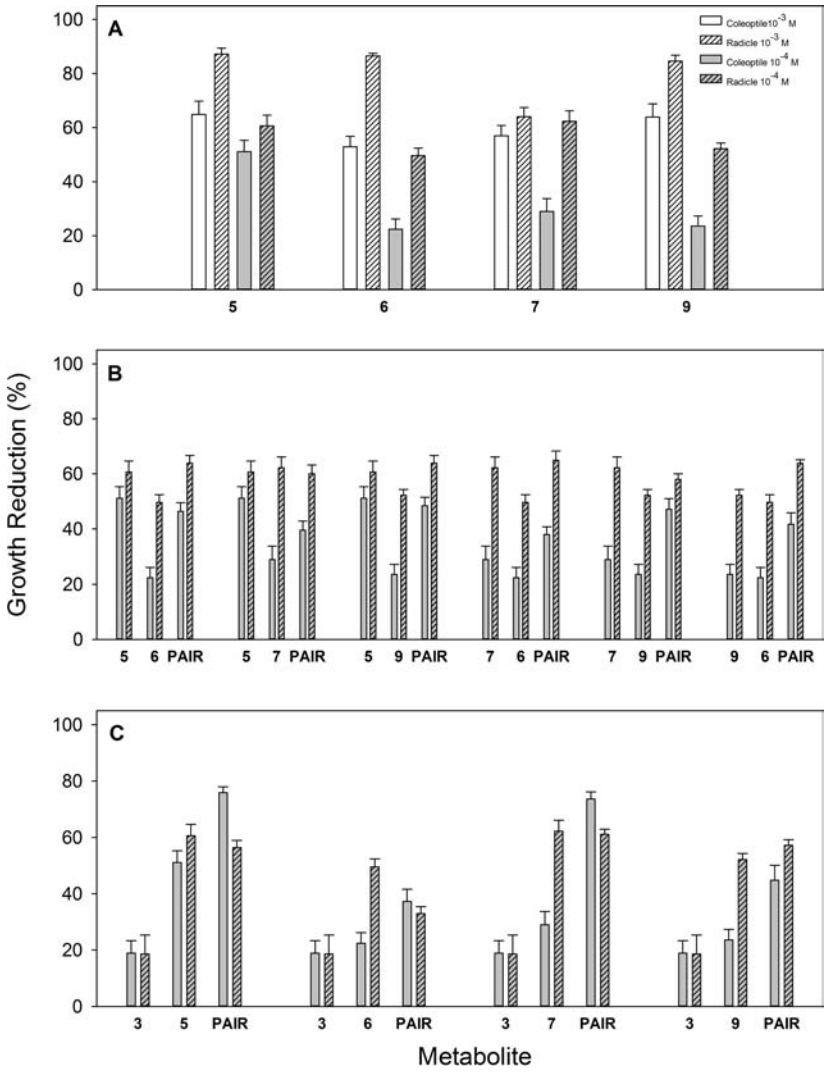


**Figure 4.** Results of host (*Bromus tectorum*) seedling bioassays showing the reduction in 5-day radicle and coleoptile length relative to the 2% DMSO control for four cytochalasins [cytochalasin A, **5**, cytochalasin B, **7**, cytochalasin F, **9**, and deoxaphomin, **6**] produced by the seed pathogen *Pyrenophora semeniperda*: (A) applied singly at two concentrations ($10^{-3}$ and $10^{-4}$ M), (B) applied in pairwise additive combination with each other at $10^{-4}$ M, and (C) applied in pairwise additive combination with pyrenophoric acid, **3**, at $10^{-4}$ M. Error bars represent standard error of the mean.

In the bioassay with pure cytochalasins, all four compounds significantly reduced 5-day coleoptile and radicle length at both concentrations relative to the control, clearly demonstrating their toxicity on this host (Figure 4A). Toxicity was consistently higher at $10^{-3}$ concentration (except for the effect of **7** on radicle growth, which was similar at the two concentrations). The growth-suppressive effect was far from additive, however, suggesting some form of saturation at higher concentrations. The negative effect on radicle growth was generally greater than the effect on coleoptile growth. There was little difference among the compounds in their impact on seedling growth at high concentration, but at low concentration, **5** caused significantly more coleoptile growth reduction than the other three compounds. In contrast with their strong toxicity to seedlings, cytochalasins had no significant effect on germination time or percentage (data not shown).

When the cytochalasins were combined additively in pairwise combinations at $10^{-4}$ M, there was no sign of an additive effect on radicle growth suppression in five of six pairs, with suppression caused by the most toxic compound (**5** or **7**) not significantly less than the effect of the combined compounds (Figure 4B). Only the combination of cytochalasin F and deoxyphomin (**9** and **6**) resulted in a significant radicle growth suppression increase relative to either compound alone. For coleoptile growth suppression, combinations that included **5** resulted in no significant increase in suppression relative to this compound applied singly. Combinations that included **7** but not **5** resulted in increased suppression relative to the pure compounds, while the combination of **9** and **6** resulted in a nearly additive effect. These results suggest that when more toxic cytochalasins are included in the pairwise combination, the apparent saturation effect observed at higher concentrations of pure compounds is also evident.

When cytochalasins were combined in pairwise combinations with pyrenophoric acid, there was again little indication of an additive effect on radicle growth suppression, with no significant increase in suppression beyond that achieved by cytochalasins applied as pure compounds (Figure 4C). There was actually a significant decrease in toxicity to radicles when pyrenophoric acid (**3**) was combined with deoxaphomin (**6**). In contrast to the effect on radicles, the effect of pyrenophoric acid−cytochalasin combinations on coleoptile growth suppres-

sion was at least additive or nearly so. When **7** was combined with **3**, the toxicity effect on coleoptiles was clearly synergistic, with a growth reduction of 74%, or 1.54 times the reduction predicted by a strictly additive effect (19% + 29% = 48%).

In conclusion, the structures of two new sesquiterpenoids, named pyrenophoric acids B and C and isolated from *B. tectorum* culture of *P. semeniperda*, were reported. They are closely related to pyrenophoric acid, previously isolated from the same fungus, being the 7-dehydro-7-hydroxy and the 12-epimer of this acid. They are structurally related to abscisic acid, which was also isolated from the fungus in this study.

As is true for most of the secondary metabolites produced by fungi, the biological functions of phytotoxic metabolites produced by *P. semeniperda* in pathogenesis on *B. tectorum* seeds are still largely unknown. We have demonstrated here that these metabolites are produced by the fungus on seeds of the host of origin and not just in standard wheat seed culture. This makes it more likely that they have some function in pathogenesis. As cytochalasin B is produced in quantities orders of magnitude greater than other secondary metabolites known to be produced by this fungus, it seems likely that it is important in terms of pathogenesis. The detection of a series of closely related cytochalasins could suggest that they represent sequential steps in biosynthesis of the principal compound or possibly degradation products.[28] Cytochalasin B is well-known to interfere with cytokinesis through its action on the actin skeleton of cells, making it a logical candidate as a compound that could facilitate pathogenesis on seeds by interfering with germinant development. Similarly, abscisic acid is the most likely of the sesquiterpenoid group of compounds produced by *P. semeniperda* to play a direct role in pathogenesis on seeds because of its ability to delay or halt germination. This compound and related pyrenophoric acids were detected in very small quantities, however. The failure to detect abscisic acid and related compounds in biologically significant amounts could be an artifact of cultural conditions on autoclaved seeds. The synergistic effect of pyrenophoric acid and cytochalasin B on coleoptile growth suppression suggests that they may play complementary roles in pathogenesis, especially if the effect of cytochalasin B is saturating at relatively low concentrations, making the large disparity in production levels less important. However, this begs the question of why the fungus produces such large quantities of cytochalasin B.

An annotated genome assembly for *P. semeniperda* is now available, and the putative gene cluster for cytochalasin biosynthesis in this fungus has been identified.[29] Gene silencing studies to directly determine how cytochalasin B and other phytotoxins produced by *P. semeniperda* function in pathogenesis provide the most promising approach for understanding the activities in vivo of the diverse array of phytotoxic metabolites produced.

## ■ ASSOCIATED CONTENT

### Supporting Information

NMR and HRESI MS spectra of **1** and **2**. This material is available free of charge via the Internet at http://pubs.acs.org.

## ■ AUTHOR INFORMATION

### Corresponding Author

* Tel: +39 081 2539178. E-mail: evidente@unina.it.

### Funding

This research was funded in part by Grant JFSP-11-S-2-6 to S.M. from the Joint Fire Sciences Program of the U.S. Departments of Agriculture and Interior and in part by Programme STAR financially supported by UniNA and Compagnia di San Paolo.

### Notes

The authors declare no competing financial interest.

## ■ ACKNOWLEDGMENTS

Logistical support at Brigham Young University was provided to M.M. by Dr. Paul Savage of the Chemistry Department. A.E. is associated with Istituto di Chimica Biomolecolare del CNR, Pozzuoli, Italy.

## ■ REFERENCES

(1) Stahlman, P. W.; Miller, S. D. Downy brome (*Bromus tectorum*) interference and economic thresholds in winter wheat (*Triticum aestivum*). *Weed Sci.* **1990**, *38*, 224−228.

(2) Ostlie, M. H.; Howatt, K. A. Downy brome (*Bromus tectorum*) competition and control in no-till spring wheat. *Weed Technol.* **2013**, *27*, 502−508.

(3) Brooks, M. L.; D'Antonio, C. M.; Richardson, D. M.; Grace, J. B.; Keeley, J. E.; Di Tomaso, J. M.; Hobbs, R. J.; Pellant, M.; Pyke, D. Effects of invasive alien plants on fire regimes. *Bioscience* **2004**, *54*, 677−688.

(4) Meyer, S. E.; Clement, S.; Beckstead, J. US Patent Application Number US20130035231, 2013.

(5) Medd, R. H. A review of the world distribution and host range of *Pyrenophora semeniperda*. *Rev. Plant Pathol.* **1992**, *71*, 891−901.

(6) Stewart, T. E.; Allen, P. S.; Meyer, S. E. First report of *Pyrenophora semeniperda* in Turkey and Greece. *Plant Dis.* **2009**, *93*, 1351−1351.

(7) Evidente, A.; Andolfi, A.; Vurro, M.; Zonno, M. C.; Motta, A. Cytochalasins Z1, Z2 and Z3, three 24-oxa[14]cytochalasans produced by *Pyrenophora semeniperda*. *Phytochemistry* **2002**, *60*, 45−53.

(8) Masi, M.; Evidente, A.; Meyer, S.; Nicholson, J.; Muñoz, A. Effect of strain and cultural conditions on the production of cytochalasin B by the potential mycoherbicide *Pyrenophora semeniperda* (Pleosporaceae, Pleosporales). *Biocontrol Sci. Technol.* **2013**, *24*, 53−64.

(9) Masi, M.; Meyer, S.; Cimmino, A.; Andolfi, A.; Evidente, A. Pyrenophoric acid, a phytotoxic sesquiterpenoid penta-2,4-dienoic acid produced by a potential mycoherbicide, *Pyrenophora semeniperda*. *J. Nat. Prod.* **2014**, *77*, 925−930.

(10) Masi, M.; Meyer, S.; Clement, S.; Andolfi, A.; Cimmino, A.; Evidente, A. Spirostaphylotrichina W, a spirocyclic γ-lactam isolated from liquid culture of *Pyrenophora semeniperda*, a potential mycoherbicide for cheatgrass (*Bromus tectorum*) biocontrol. *Tetrahedron* **2014**, *70*, 1497−1501.

(11) Berger, S.; Braun, S. *200 and More Basic NMR Experiments: a Practical Course*, 1st ed.; Wiley-VCH: Weinheim, Germany, 2004.

(12) Kikuzaki, H.; Kayano, S.-I.; Fukutsuka, N.; Aoki, A.; Kasamatsu, K.; Yamasaki, Y.; Mitani, T.; Nakatani, N. Abscisic acid related compounds and lignans in prunes (*Prunus domestica* L.) and their oxygen radical absorbance capacity (ORAC). *J. Agric. Food Chem.* **2004**, *52*, 344−349.

(13) Smith, T. R.; Clark, A. J.; Clarkson, G. J.; Taylor, P. C.; Marsh, A. Concise enantioselective synthesis of abscisic acid and a new analogue. *Org. Biomol. Chem.* **2006**, *22*, 4186−4192.

(14) Breitmaier, E.; Voelter, W. *Carbon-13 NMR Spectroscopy*; VCH: Weinheim, Germany, 1987; pp 183−280.

(15) Pretsch, E.; Bühlmann, P.; Affolter, C. *Structure Determination of Organic Compounds—Tables of Spectral Data*, 3rd ed.; Springer-Verlag: Berlin, Germany, 2000; pp 161−243.

(16) Oritani, T.; Kiyota, H. Biosynthesis and metabolism of abscisic acid and related compounds. *Nat. Prod. Rep.* **2003**, *20*, 414−425.

(17) Inomata, M.; Hirai, N.; Yoshida, R.; Ohigashi, H. Biosynthesis of abscisic acid by the direct pathway via ionylideneethane in a fungus, *Cercospora cruenta*. *Biosci., Biotechnol., Biochem.* **2004**, *68*, 2571−2580.
(18) Zaharia, L. I.; Walker-Simmon, M. K.; Rodriguez, C. N.; Abrams, S. R. Chemistry of abscisic acid, abscisic acid catabolites and analogs. *J. Plant Growth Regul.* **2005**, *24*, 274−284.
(19) Kitahata, N.; Asami, T. Chemical biology of abscisic acid. *J. Plant Res.* **2011**, *124*, 549−557.
(20) Sondheimer, E.; Walton, D. C. Structure-activity correlations with compounds related to abscisic acid. *Plant Physiol.* **1970**, *45*, 244−248.
(21) Abrams, S. R.; Gusta, L. V.; Reany, M. J. T.; Ewan, B. E. US Patent Application Number US005518995A, 1996.
(22) Takezawa, D.; Komatsu, K.; Sakata, Y. ABA in bryophytes: how a universal growth regulator in life became a plant hormone? *J. Plant Res.* **2011**, *124*, 437−453.
(23) Tudzynsky, B.; Sharon, A. In *The Mycota X: Industrial Applications*; Osiewacz, H., Ed.; Springer-Verlag: Berlin, Germany, 2002; pp 183−211.
(24) Hartung, W. The evolution of abscisic acid (ABA) and ABA function in lower plants, fungi and lichens. *Funct. Plant Biol.* **2010**, *37*, 806−812.
(25) Zheng, Y. B.; Lu, C. H.; Shen, Y. M. New abscisic acid-related metabolites from *Phellinus vaninii*. *J. Asian Nat. Prod. Res.* **2012**, *14*, 613−617.
(26) Lamb, N.; Abrams, S. R. Synthesis of optically active cyclohexanone analogs of the plant hormone abscisic acid. *Can. J. Chem.* **1990**, *68*, 1151−1162.
(27) Lamb, N.; Shaw, A. C.; Abrams, S. R.; Reaney, M. J.; Ewan, B.; Robertson, A. J.; Gusta, L. V. Oxidation of the 8′-position of a biologically active abscisic acid analogue. *Phytochemistry* **1993**, *34*, 905−917.
(28) Scherlach, K.; Boettger, D.; Remme, N.; Hertweck, C. The chemistry and biology of cytochalasans. *Nat. Prod. Rep.* **2010**, *27*, 869−886.
(29) Soliai, M. M.; Meyer, S. E.; Udall, J. A.; Elzinga, D. E.; Hermansen, R. A.; Bodily, P. M.; Hart, A. A.; Coleman, C. E. *De novo* genome assembly of the fungal plant pathogen *Pyrenophora semeniperda*. *PLoS One* **2014**, *9*, e87045.

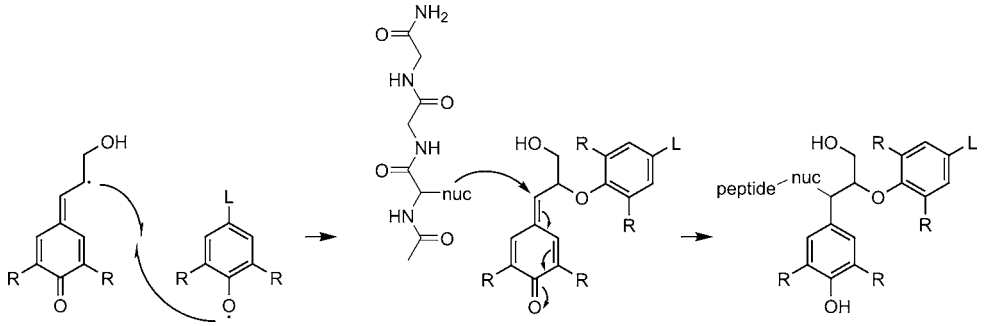


**Figure 1.** Lignin−peptide cross-linking pathway. Lignin−peptide cross-links form when nucleophilic side chains of amino acids react with quinone methides formed during lignin $\beta$-ether coupling. R = H or OMe, L = lignin.

To investigate the propensity for lignin−peptide cross-linking under biomimetic conditions, lignin dehydrogenation polymer (DHP) was prepared in aqueous solutions containing tripeptides. Each tripeptide had the general structure X−glycine−glycine (XGG), with X being cysteine (C), lysine (K), histidine (H), aspartic acid (D), glutamic acid (E), serine (S), tyrosine (Y), threonine (T), or hydroxyproline (Hyp). These amino acids were previously identified as being reactive (or potentially reactive in the case of T and Hyp) toward lignin QMs.[17] The general peptide structure and predicted mode of lignin−peptide cross-linking are shown in Figure 1. The C-termini and N-termini of the peptides were blocked via amidation and acetylation, respectively, to ensure that the amino acid of interest (i.e., residue X) contained the only nucleophilic moiety. Glycine was chosen as the "place holder" residue due to its expected lack of reactivity toward lignin. The lengths of the peptides were limited to three residues because in vitro reactions of large peptides with DHPs result in the formation of lignin−peptide complexes that are insoluble and thus difficult to characterize (e.g., liquid state NMR becomes impractical) (results not shown). Tripeptides were added in 25% mol/mol ratio to the lignin monomer (coniferyl alcohol) because it was previously reported that lignin DHPs contain between 20 and 30% $\beta$-ether linkages.[19] Thus, the ratio of nucleophilic amino acids to lignin $\beta$-ether QMs was expected to be approximately 1:1 over the course of the polymerization reaction.

Fourier-transform infrared spectroscopy (FT-IR), scanning electron microscopy (SEM), energy dispersive X-ray spectroscopy (EDS), and nuclear magnetic resonance spectroscopy (NMR) were used to characterize the lignin−peptide adducts. FT-IR and, more recently, NMR, have become staples of lignin characterization.[20−22] Multidimensional NMR techniques (e.g., heteronuclear single quantum coherence (HSQC)) are particularly useful because the shift degeneracies observed in 1D spectra are largely eliminated. Furthermore, diagnostic NMR shifts of lignin−peptide model compounds have previously been assigned.[17] SEM imaging of synthetic and native lignins has not garnered much research attention,[23,24] but the technique was employed here to visualize morphological differences between neat DHP and the lignin−peptide adducts. It was useful to also collect EDS elemental analysis data while the lignin−peptide samples were in the SEM instrument, with the presence of nitrogen suggesting peptide incorporation. Through the use of these techniques this study provides new insights into the propensities and mechanisms of lignin−peptide linkage formation. It is expected that this will be useful toward the continued study of lignin formation in both native and mutant plant lines.

## MATERIALS AND METHODS

**Materials.** All chemicals necessary for DHP preparation were purchased from Sigma with the exception of the peptides (>95% purity), which were purchased from Peptide 2.0 (www.peptide2.com). The peptides acquired were of the sequence XGG, where X represents one of the following: cysteine (C), lysine (K), histidine (H), aspartic acid (D), glutamic acid (E), serine (S), tyrosine (Y), threonine (T), or hydroxyproline (Hyp).

**Synthesis of Lignin DHP and Lignin−Peptide Adducts.** Guaiacyl-based DHP was synthesized in sodium phosphate buffer (pH 6.5) using coniferyl alcohol as the sole lignin monomer.[18] The DHP crude product was centrifuged (10000*g*, 20 min, 4 °C) and the pellet washed four times with distilled water. The DHP product was then lyophilized to yield dry DHP (typical yields 60−70%), which was characterized via NMR as described below and was found to contain shifts typical of G−DHP.[20,22]

Lignin−peptide adducts were prepared as above, with the exception that 25% peptide to coniferyl alcohol (mol/mol basis, all tripeptides were freely water-soluble at the concentrations employed) was added to the flask containing coniferyl alcohol prior to the start of the reaction. The crude reaction products were centrifuged, washed four times, and lyophilized as described above to yield tan powders. Products were stored at −40 °C and characterized using FT-IR, SEM, EDS, and NMR.

**Scanning Electron Microscopy and Energy Dispersive X-ray Spectroscopy.** SEM images were collected on a field emission SEM (FESEM-FEI NanoSEM 630) at 2 or 3 kV under high vacuum ($1.7 \times 10^{-6}$ Torr). Samples were not sputter-coated prior to imaging. Characteristic X-rays were collected with an X-Max silicon drift detector (Oxford Instruments) at 10 kV under low-vacuum conditions (0.6 Torr) to prevent sample charging. Elements were selected and quantified using Aztec Energy Analyzer Software (Oxford Instruments). Three locations were analyzed per adduct, and average atomic percentages and standard deviations are reported under Results and Discussion.

**Nuclear Magnetic Resonance Spectroscopy.** The neat peptides (25 mg) were dissolved in DMSO-$d_6$/pyridine-$d_5$ (4:1 v/v, 500 $\mu$L), and proton (16 scans), carbon (4000 scans), HMQC (64 scans), and HMBC (32 scans) spectra were collected using standard Bruker pulse programs on a Bruker DRX-400 (400 MHz $^1$H resonance frequency) using the central solvent peak [$\delta_H/\delta_C$, dimethyl sulfoxide (DMSO), 2.50/39.50 ppm] as internal standard. In the case of DHP and the lignin−peptide adducts, NMR spectra were acquired on a Bruker Biospin (Billerica, MA, USA) AVANCE 500 (500 MHz $^1$H resonance frequency) spectrometer fitted with a cryogenically cooled gradient probe having inverse geometry, that is, with the proton coils closest to the sample. Spectra were processed with Bruker's Topspin 3.1 software, using the central solvent peak as internal reference [$\delta_H/\delta_C$, dimethyl sulfoxide (DMSO), 2.50/39.5 ppm]. The DHP or lignin−peptide adducts (~45 mg) were placed in an NMR tube (i.d. =

4.1 mm), dissolved in DMSO-$d_6$/pyridine-$d_5$ (4:1 v/v, 500 $\mu$L), and subjected to adiabatic HSQC ('hsqcetgpsisp2.2') experiment. In the case of DHP−YGG, HMBC ("hmbcgpndqf"), COSY ("cosygpqf"), and NOESY ("noesyesgpph") experiments were also conducted to attempt to determine the lignin−tyrosine cross-linking mechanism. Processing used typical matched Gaussian apodization in F2 (LB = −0.3, GB = 0.001), squared cosine-bell, and one level of linear prediction (32 coefficients) in F1.[25] For an estimation of the various interunit linkage types in DHP and lignin−peptide adducts, the well-resolved $C_\alpha$−$H_\alpha$ contours were integrated; no correction factors were used.

**Fourier-Transform Infrared Spectroscopy.** Lignin DHP, neat peptides, and lignin−peptide adducts were analyzed using a Bruker Vertex V70 spectrometer (Bruker Optics) equipped with an MVP-Pro diamond single reflection ATR accessory (Harrick Scientific), and 100 scans at 6 $cm^{-1}$ resolution were averaged for each sample using a DTGS detector and a scan frequency of 5 kHz. In all cases, the spectrum of the clean diamond crystal was used as the reference spectrum. All spectral manipulations were performed using OPUS 6.0 (Bruker Optics).

## RESULTS AND DISCUSSION

**Preparation and Yields of the Lignin−Peptide Adducts.** Lignin DHP was prepared in aqueous solutions containing water-soluble tripeptides (25% peptide/coniferyl alcohol mol/mol basis). Each tripeptide contained one nucleophilic amino acid and blocked N- and C-termini to mimic inclusion within a larger protein and to prohibit potential side reactions. The lignin−peptide adducts were collected via centrifugation, washed, and characterized via FT-IR, SEM, EDS, and NMR. Water-soluble residues that remained in the supernatants following centrifugation and adduct collection were not analyzed. The results, detailed below, indicate covalent incorporation of CGG and YGG peptides into the lignin polymer, whereas other peptides did not show significant reactivity.

Yields for the DHP and lignin−peptide adducts are shown in Table 1. Yields were determined by dividing the mass of recovered solids by the total starting mass (i.e., combined mass of lignin monomer and peptide). The yield of the DHP control was typical.[18] In the cases of CGG and YGG (which we show below to be considerably reactive toward lignin), the yields of recoverable DHP were depressed. In these cases, the authors perceived that a portion of the lignin−peptide adducts may have been aqueous soluble and thus held in solution during the centrifugation process. Characterizations of these aqueous-soluble fractions was not carried out.

**Table 1. Yield Data for the DHP and Lignin−Peptide Adducts**

| | CA[a] (mg) | peptide (mg) | yield (mg) | yield (%) |
|---|---|---|---|---|
| DHP | 200.0 | 0.0 | 130.0 | 65.0 |
| DHP−CGG | 200.0 | 88.4 | 100.0 | 34.7 |
| DHP−KGG | 200.0 | 83.6 | 174.5 | 61.5 |
| DHP−HGG | 200.0 | 86.1 | 176.0 | 61.5 |
| DHP−DGG | 200.0 | 80.0 | 180.0 | 64.3 |
| DHP−EGG | 200.0 | 83.9 | 197.9 | 69.7 |
| DHP−SGG | 200.0 | 72.2 | 172.8 | 63.5 |
| DHP−YGG | 200.0 | 93.3 | 114.2 | 38.9 |
| DHP−TGG | 200.0 | 76.1 | 179.1 | 64.9 |
| DHP−HypGG | 200.0 | 79.4 | 177.4 | 63.5 |

[a]CA, coniferyl alcohol

**Lignin−Peptide Morphology.** SEM was used to compare the morphologies of neat DHP and the lignin−peptide coproducts (Figure 2). The neat DHP particles clumped together to form nearly perfect spheres, as reported previously.[23,26] Comparatively, spheres of lignin−peptide adducts tended to form large, aggregate domains. This alteration of morphology was observed regardless of whether the peptide in question was covalently incorporated into the lignin (e.g., see DHP−DGG in Figure 2 and in Figure S2 in the Supporting Information). This change in morphology was most likely the result of favorable interactions with water; that is, the more hydrophilic tripeptides surrounded the more hydrophobic lignin particles, as would be expected in a heterogeneous polymerization. Further research is necessary to determine the influence of noncovalent interpolymer interactions during lignin polymerization.

**Lignin−Peptide Linkage Identification.** Figure 3 shows the heteronuclear single-quantum coherence (HSQC) spectrum of DHP−CGG. This 2D NMR technique is particularly useful for lignin analysis because the shift degeneracy observed in 1D NMR spectra is largely avoided. Novel shifts are shown in green, red, and blue, whereas standard lignin shifts are shown in black.[20,21] Reference shifts of neat CGG (purple) were added to the spectrum during processing; these shifts were not observed in the DHP−CGG spectrum. Some peptide shifts migrated as a result of DHP−CGG cross-linking. For example, the cys-$^{13}C/^{1}H_\alpha$ shift (originally at 4.5/56.0 ppm in neat CGG) migrated to 4.6/52.8 ppm and the cys-$^{13}C/^{1}H_\beta$ shift (originally at 2.8/26.6 ppm in neat CGG) migrated to 2.8/32.9 ppm in the DHP−CGG adduct. These shifts migrated upon lignin−peptide cross-linking due to their proximity to the thiol group, which is the reactive center of the CGG peptide. Shifts of proton and carbon atoms located far from the reactive thiol were largely unaffected by cross-linking (e.g., shifts at 3.9/42.8 and 3.8/42.5 ppm).

Two novel lignin shifts, found at 4.4/50.1 ppm (Figure 4, red peak) and 4.8/81.3 ppm (Figure 4, blue peak), confirmed covalent cross-linking of DHP with CGG. Similar lignin $\alpha$-shifts (4.3/50.4 ppm) and $\beta$-shifts (4.7/81.7 ppm) were previously reported in a model compound study wherein a single cysteine residue was reacted with a lignin model quinone methide.[17] The minute differences in shift locations can be attributed to changes in chemical environment between a small lignin model compound and a high molecular weight lignin. Volume integration of the HSQC contours showed that approximately 33% of the $\beta$-ether linkages in DHP−CGG exhibited cysteine functionality at the $\alpha$-carbon, whereas the remaining $\beta$-ether linkages exhibited typical $\alpha$-hydroxyl functionality and a minor fraction of $\alpha$-aryl ether ($\alpha$-*O*-aryl) moieties. This indicated that cysteine was an efficient trapper of lignin QMs under biomimetic conditions.

Figure 4 shows the HSQC spectrum of DHP−YGG. As with the DHP−CGG adduct, incorporation of YGG peptide into lignin was evidenced by the appearance of diagnostic chemical shifts (Figure 4, green and orange contours). Reference shifts of neat YGG (purple, solid yellow, and solid orange contours) were added during processing.

Several factors confound evidence for cross-linking between tyrosine-based peptide (YGG) with lignin. The structural similarity of tyrosine and the lignin monomer, coniferyl alcohol, led to substantial degeneracy in the NMR spectra, as discussed in greater detail below. In addition, the cross-linking of YGG with DHP may have occurred via two mechanisms. The first

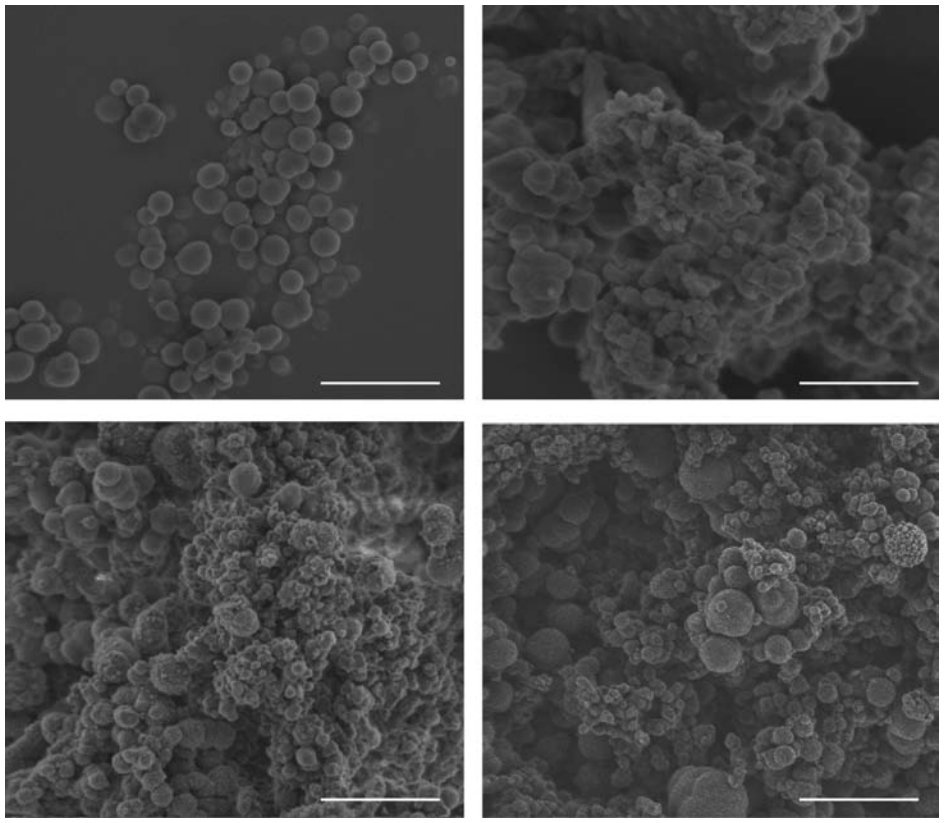

**Figure 2.** SEM images of DHP (top left), DHP−CGG (top right), DHP−YGG (bottom left), and DHP−DGG (bottom right). Scale bar = 2 $\mu$m. Refer to the Supporting Information for SEM images of other lignin−peptide adducts, which displayed morphologies similar to those of the DHP−DGG adduct.

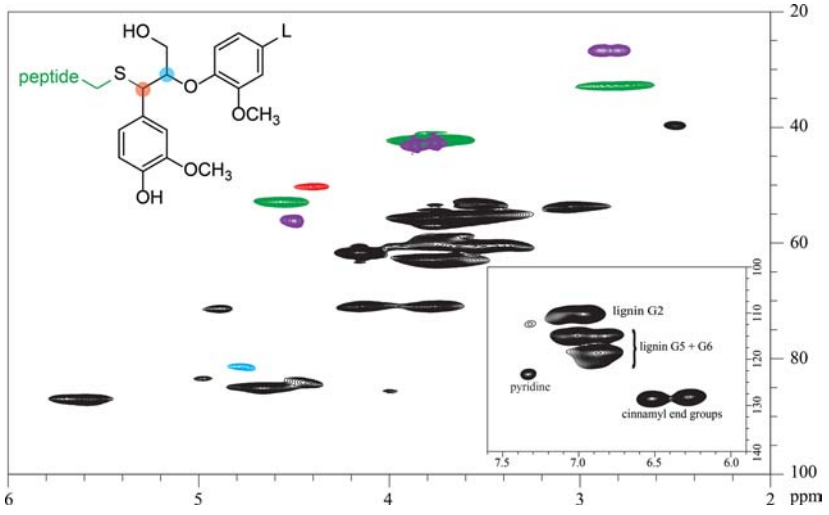


**Figure 3.** Side-chain and aromatic regions (inset) of the HSQC NMR spectrum of DHP−CGG. Black shifts are typical of G−DHPs, green shifts correspond to peptide $\alpha$- and $\beta$-signals, and red and blue shifts correspond to lignin $\alpha$- and $\beta$-signals in $\beta$-ether/$\alpha$-cysteine structures (top left). Purple shifts were added during processing to indicate shifts of neat CGG peptide.

potential mechanism involves oxidation of the phenolic hydroxyl of tyrosine by horseradish peroxidase, followed by recombination of the tyrosine radical with a radical on the lignin polymer. Previous work relied upon stop-flow kinetics to show that this mechanism is probably unfavorable.[16] Still, we investigated the possibility of this compound forming by conducting heteronuclear multiple bond correlation (HMBC), correlation spectroscopy (COSY), and nuclear Overhauser effect spectroscopy (NOESY) (data not shown). However, we were unable to conclusively assign NMR shifts of lignin−tyrosine linkages formed in this manner. Either the mechanism is not valid under our experimental conditions and/or the shift degeneracy between lignin−tyrosine linkages and typical lignin shifts is too great to allow necessary spectral resolution.

A second cross-linking mechanism between lignin and tyrosine is also possible if the phenolic hydroxyl of tyrosine quenches the lignin quinone methide to form the $\alpha$-aryl ether structure shown in Figure 4. Importantly, phenolic hydroxyls of

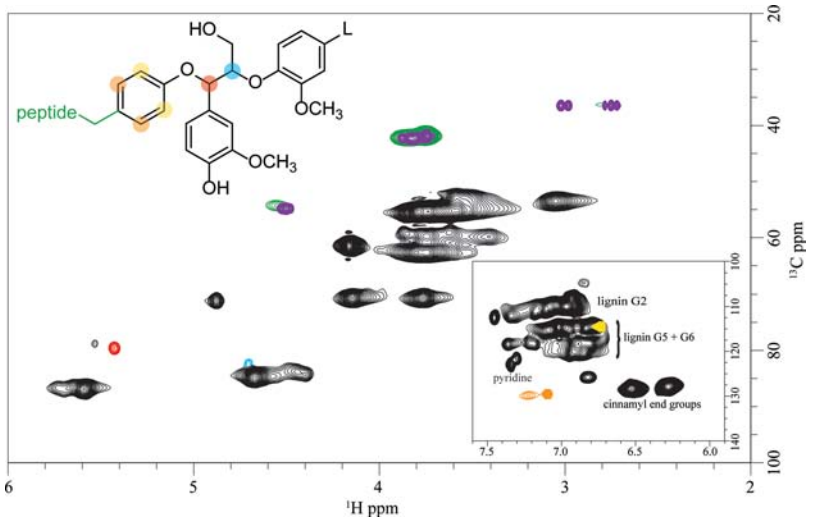


**Figure 4.** Side-chain and aromatic regions (inset) of the HSQC NMR spectrum of DHP−YGG. Black shifts are typical of G−DHPs, green shifts correspond to peptide $\alpha$- and $\beta$-signals, and red and blue shifts correspond to lignin $\alpha$- and $\beta$-signals in $\beta$-ether/$\alpha$-tyrosine structures (top left) and/or lignin−lignin $\alpha$-*O*-aryl structures. Purple shifts were added during processing to indicate shifts of neat YGG peptide. Within the aromatic region, solid yellow and orange shifts (added during processing) were assigned to the aromatic ring of tyrosine in neat YGG.

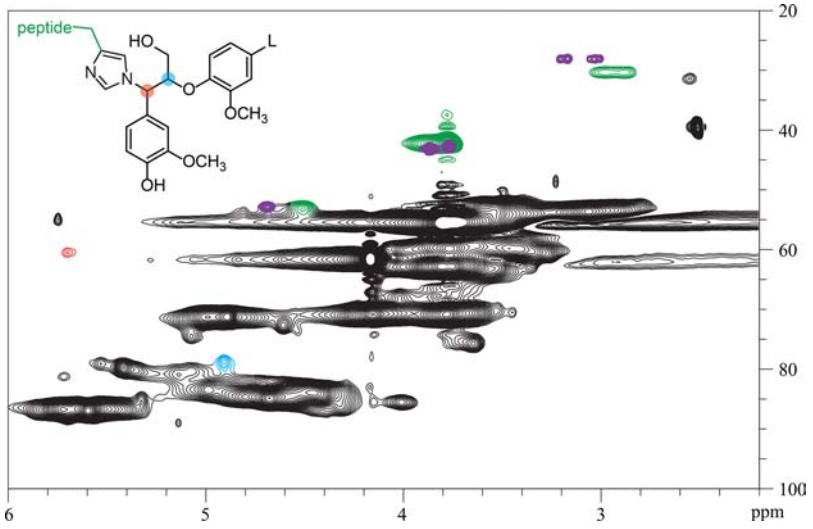


**Figure 5.** Side-chain region of the HSQC NMR spectrum of DHP−HGG. Black shifts are typical of G−DHPs, green shifts correspond to peptide $\alpha$- and $\beta$-signals, and red and blue shifts correspond to lignin $\alpha$- and $\beta$-signals in $\beta$-ether/$\alpha$-histidine structures (top left). Purple shifts were added during processing to indicate shifts of neat HGG peptide.

the monolignols could participate in the same reaction. Given the similarity of these structures, shift degeneracy again complicates the investigation of the mechanism, as a lignin−tyrosine model compound exhibited similar NMR shifts ($\alpha$-$^{1}$H/$^{13}$C, 5.5/78.3 ppm in DMSO/pyridine) to $\alpha$-aryl ether linkages known to occur in neat coniferyl alcohol-based DHPs ($\alpha$-$^{13}$C, 79.01 ppm in DMSO).[17,27]

In an attempt to overcome this issue, the well-resolved HSQC $\alpha$-signals of neat DHP and DHP−YGG adduct were integrated. It was observed that $\alpha$-aryl ether shifts comprised approximately 4.2% of the total $\alpha$-signal in DHP−YGG but only 1.9% in neat DHP synthesized under similar conditions. This increase could be due to cross-linking, but other factors exist as well, such as imprecision in the HSQC volume integration or random variation among DHP syntheses (other lignin−peptide adducts displayed similarly high $\alpha$-aryl ether signals), making it unclear if the structure shown in Figure 4 formed in the DHP−YGG adduct. In summary, previous work,[16] as well as the NMR, IR, and EDS data (shown below), strongly suggests that the YGG peptide cross-linked with lignin DHP via quenching the quinone methide; however, diagnostic evidence supporting this remains elusive.

Peptide peaks could always be observed when the HSQC contours were viewed quite low (i.e., near the signal-to-noise limit), even for lignin−peptide adducts other than DHP−CGG and DHP−YGG. Figure 5 shows the HSQC spectrum of DHP−HGG. This sample showed the highest concentration of peptide after DHP−CGG and DHP−YGG. A putative lignin−$\alpha$-histidine cross-link was observed at 5.7/60.4 ppm, in good agreement with the $\alpha$-shift of a lignin−histidine model compound (5.7/60.2 ppm).[17] Volume integration showed that the lignin−$\alpha$-histidine shift accounted for only ∼0.1% of the total lignin $\alpha$-signal. It is noteworthy that this low abundance of peptide was detected by HSQC NMR but not readily detected by IR or EDS, thus illustrating the sensitivity of multidimensional NMR toward investigating lignin−protein linkages.

**Table 2. Interunit Linkage Ratios of the DHP and Lignin−Peptide Adducts[a]**

| | HSQC signal ratios | | | | | |
|---|---|---|---|---|---|---|
| | $\beta$-ether/$\alpha$-OH | $\beta$-ether/$\alpha$-$O$-aryl | $\beta$-ether/$\alpha$-peptide | $\beta$-5 | $\beta$-$\beta$ | dibenz |
| DHP | 27.3 | 1.9 | | 50.3 | 19.2 | 1.2 |
| DHP−CGG | 8.6 | 1.5 | 5.1 | 50.8 | 32.4 | 1.6 |
| DHP−DGG | 10.1 | 5.5 | 0.1 | 54.1 | 30.2 | tr |
| DHP−EGG | 13.1 | 4.6 | 0.1 | 54.1 | 27.2 | 0.9 |
| DHP−KGG | 4.7 | 3.1 | tr | 62.3 | 29.9 | tr |
| DHP−HGG | 20.4 | 0.9 | 0.1 | 57.7 | 20.3 | 0.6 |
| DHP−SGG | 11.1 | 2.3 | tr | 52.5 | 34.1 | tr |
| DHP−YGG | 11.5 | | 4.2 | 51.7 | 32.5 | tr |
| DHP−TGG | 21.8 | 0.9 | tr | 54.1 | 22.2 | 1.0 |
| DHP−HypGG | 17.7 | 2.7 | tr | 53.2 | 26.2 | 0.2 |

[a]The table shows lignin interunit linkage ratios (as percentage of total $\alpha$-signal) for DHP and lignin−peptide adducts. In the case of DHP−YGG the DHP−$\alpha$-peptide shift was degenerate with standard lignin $\alpha$-$O$-aryl shifts; thus, the $\beta$-ether/$\alpha$-$O$-aryl and $\beta$-ether/$\alpha$-peptide quantities were combined. tr, trace (<0.1%).

Other lignin−peptide adducts exhibited less abundant (<0.1%) NMR peptide shifts than DHP−HGG.

Volume integration of the HSQC contour signals allowed for comparison of the various lignin interunit linkages among DHP and lignin−peptide adducts (Table 2). The column "$\beta$-ether/$\alpha$-peptide" documents the evidence for those tripeptides that covalently reacted. The neat DHP contained typical linkage ratios.[18,19,28] Linkage ratios varied among the lignin−peptide adducts, but decreased $\beta$-ether content with increased pinoresinol ($\beta$-$\beta$) content was generally observed. This occurred regardless of covalent reactivity toward the lignin DHP, demonstrating the ability of a matrix material (in this case peptides) to influence lignin structure during polymerization.

**Supporting Techniques for Lignin−Peptide Characterization.** In addition to NMR, which can provide direct evidence of covalent cross-linking, other techniques were used to show peptide incorporation into lignin. Figure 6 shows FT-IR spectra of DHP−CGG, DHP−YGG, and neat DHP. Infrared spectra of other lignin−peptide adducts can be found in the Supporting Information (Figure S1). The DHP IR spectrum exhibited bands typical of lignin DHPs.[22] The DHP−CGG and DHP−YGG spectra exhibited three peaks indicative of peptide incorporation into the lignin. The shoulder near 3200 $cm^{-1}$ was attributed to N−H stretching in amide functional groups, the peak at 1658 $cm^{-1}$ increased dramatically and was attributed to increased C═O stretching due to the incorporation of amide functional groups, and the shoulder at 1540 $cm^{-1}$ was attributed to N−H deformation with C−N stretching, again indicating incorporation of amide functionalities.[29] It is notable that these shifts displayed greater intensity in the DHP−CGG adduct compared to the DHP−YGG adduct, suggesting greater incorporation of CGG peptide over YGG peptide. These peaks were not observed in the IR spectra of other lignin−peptide adducts, suggesting a lack of peptide incorporation (see Figure S1). In the case of DHP−CGG and DHP−YGG, incorporation of peptide into the lignin polymer caused an increase in the band at 1505 $cm^{-1}$, which was previously assigned to aromatic skeletal vibrations.[22] This increase in peak height was not observed in other lignin−peptide products, and the origin of this increased peak intensity is unclear. Although the IR results suggested incorporation of CGG and YGG peptides into lignin DHP, peaks directly attributable to lignin−peptide linkages were not identified.

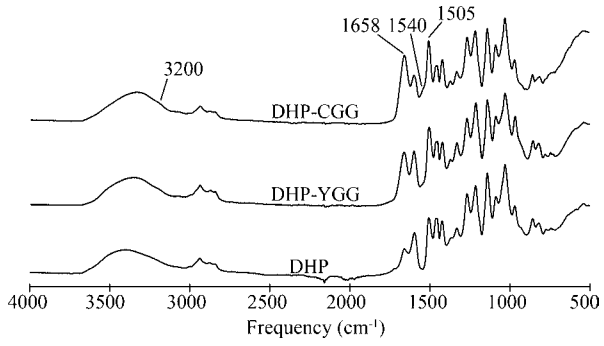


**Figure 6.** FT-IR spectra of (top to bottom) DHP−CGG, DHP−YGG, and neat DHP.

EDS was used to determine elemental compositions of neat DHP and the lignin−peptide adducts. The DHP and most lignin−peptide adducts contained 0% nitrogen (Table 3), indicating no detectable incorporation of peptide into the lignin. In comparison, DHP−CGG and DHP−YGG contained 3.5 and 2.0% nitrogen, respectively. This provided compelling evidence for incorporation of cysteine- and tyrosine-containing peptides into the lignin DHP and suggested that cysteine reacted more readily with lignin compared to tyrosine, in agreement with the IR data.

**Table 3. EDS Elemental Analysis Data for DHP and the Lignin−Peptide Adducts[a]**

| | average atomic % (SD) | | | |
|---|---|---|---|---|
| | carbon | oxygen | nitrogen | sulfur |
| DHP | 78.8 (2.8) | 21.2 (2.9) | 0.0 (0.0) | 0.0 (0.0) |
| DHP−CGG | 76.5 (2.0) | 18.9 (1.2) | 3.5 (0.7) | 1.2 (0.3) |
| DHP−KGG | 86.8 (2.5) | 13.2 (2.5) | 0.0 (0.0) | 0.0 (0.0) |
| DHP−HGG | 90.5 (2.1) | 9.5 (2.5) | 0.0 (0.0) | 0.0 (0.1) |
| DHP−DGG | 82.8 (3.8) | 17.2 (3.8) | 0.0 (0.0) | 0.0 (0.0) |
| DHP−EGG | 83.7 (2.0) | 15.4 (1.1) | 0.0 (0.0) | 0.6 (0.8) |
| DHP−SGG | 86.3 (2.9) | 13.7 (2.9) | 0.0 (0.0) | 0.0 (0.0) |
| DHP−YGG | 84.0 (2.7) | 14.0 (1.1) | 2.0 (1.7) | 0.0 (0.0) |
| DHP−TGG | 85.8 (1.1) | 14.2 (1.1) | 0.0 (0.0) | 0.0 (0.0) |
| DHP−HypGG | 84.4 (0.2) | 15.6 (0.2) | 0.0 (0.0) | 0.0 (0.0) |

[a]Atomic percentages are reported as averages of three sampling locations. Standard deviations are shown in parentheses. Trace levels of calcium account for the balance in the case of DHP−EGG.

**Conclusions.** Individual amino acids bearing nucleophilic side chains were previously shown to react with a lignin model quinone methide in dichloromethane, yielding adducts at the lignin $\alpha$-position.[17] In the present study, we extended this work by introducing nucleophilic tripeptides during lignin DHP synthesis under biomimetic conditions.

Lignin DHP was prepared using coniferyl alcohol as the sole lignin monomer, and peptides were added having the general structure XGG, in which X was an amino acid residue with a nucleophilic side chain (i.e., C, K, H, D, E, S, Y, T, and Hyp). The lignin was precipitated via centrifugation and washed to yield lignin−peptide adducts. Analysis using FT-IR, EDS, and NMR showed that CGG and YGG were reactive toward lignin, whereas other peptides were not. In the case of DHP−CGG, HSQC NMR showed that cross-linking occurred at the lignin $\alpha$-position (Figures 3 and 4). The cross-linking pathway of DHP with YGG could not be conclusively elucidated. SEM imaging showed that lignin−peptide adducts exhibited a unique morphology compared to neat DHP, regardless of peptide incorporation into the lignin. With regard to lignin interunit linkage ratios, the quantity of $\beta$-ether linkages was typically depressed in DHPs synthesized in the presence of peptides, whereas the quantity of pinoresinol structures increased. The yields of DHP−CGG and DHP−YGG were depressed compared to neat DHP yields.

We have shown that cysteine cross-links with lignin under biomimetic conditions and that tyrosine most likely follows a similar cross-linking pathway. This suggests that cross-linking may occur in the cell walls of both native and transgenic plant lines. Further research is needed to investigate whether this cross-linking does occur and to discover how the plant might control and benefit from such cross-linking (i.e., does it help stiffen the wall, assist water conduction, provide protection from pathogens, etc.). In addition, a better understanding of lignin−protein linkages could lead to novel strategies for manipulating lignin biosynthesis and improving lignin extractability, as previously explored.[14,15] This could reduce lignin recalcitrance, which is currently a barrier to using lignocellulosic materials in developing industries such as biofuels. It is anticipated that this work will lead to future studies of lignin−protein linkages in planta and a more thorough understanding of how such linkages could be tailored and modified.

## ■ ASSOCIATED CONTENT

### Supporting Information

Supplemental SEM, FT-IR, and NMR data. This material is available free of charge via the Internet at http://pubs.acs.org.

## ■ AUTHOR INFORMATION


### Corresponding Author

**(B.G.D.) Phone: 484-629-5636. Email: brett.g.diehl@gmail.com.

### Author Contributions

Both authors contributed equally to this work.



### Funding

This material is based upon work supported as part of The Center for LignoCellulose Structure and Formation, an Energy Frontier Research Center funded by the U.S. Department of Energy, Office of Basic Energy Sciences, under Award DE-SC0001090. Student fellowships were provided by the USDA National Needs Program and the National Science Foundation via the CarbonEARTH program.

### Notes

The authors declare no competing financial interest.

## ■ ACKNOWLEDGMENTS

Many thanks to Julie Anderson and Melisa Yashinski (PSU MRI) for acquisition of SEM/EDS data and for valuable discussions. Thanks also to Dr. John Ralph, Yuki Tobimatsu, and Matt Regner for valuable discussions regarding multidimensional NMR of lignin.


## ■ REFERENCES


(1) Boerjan, W.; Ralph, J.; Baucher, M. Lignin biosynthesis. *Annu. Rev. Plant Biol.* **2003**, *54*, 519−546.

(2) Stewart, J. J.; Kadla, J. F.; Mansfield, S. D. The influence of lignin chemistry and ultrastructure on the pulping efficiency of clonal aspen (*Populus termuloides* Michx). *Holzforschung* **2006**, *60*, 111−122.

(3) Chen, F.; Dixon, R. A. Genetic manipulation of lignin biosynthesis to improve biomass characteristics for agro-industrial processes. *In Vitro Cell. Dev. Biol.−Anim.* **2008**, *44*, S28−S29.

(4) Li, X.; Weng, J. K.; Chapple, C. Improvement of biomass through lignin modification. *Plant J.* **2008**, *54*, 569−581.

(5) Chapple, C.; Ladisch, M.; Meilan, R. Loosening lignin's grip on biofuel production. *Nat. Biotechnol.* **2007**, *25*, 746−748.

(6) Jung, H. G. Forage lignins and their effects on fiber digestibility. *Agron. J.* **1989**, *81*, 33−38.

(7) Jung, H. G.; Allen, M. S. Characteristics of plant cell walls affecting intake and digestibility of forages by ruminants. *J. Anim. Sci.* **1995**, *73*, 2774−2790.

(8) Balakshin, M.; Capanema, E.; Gracz, H.; Chang, H.; Jameel, H. Quantification of lignin-carbohydrate linkages with high-resolution NMR spectroscopy. *Planta* **2011**, *233*, 1097−1110.

(9) Miyagawa, Y.; Takemoto, O.; Takano, T.; Kamitakahara, H.; Nakatsubo, F. Fractionation and characterization of lignin carbohydrate complexes (LCCs) of *Eucalyptus globulus* in residues left after MWL isolation. Part I: Analyses of hemicellulose-lignin fractionation (HC-L). *Holzforschung* **2012**, *66*, 459−465.

(10) Toikka, M.; Sipilä, J.; Teleman, A.; Brunow, G. Lignin-carbohydrate model compounds. Formation of lignin-methyl arabinoside and lignin-methyl galactoside benzyl ethers via quinone methide intermediates. *J. Chem. Soc., Perkin Trans. 1* **1998**, *1*, 3813−3818.

(11) Yuan, T.; Sun, S.; Xu, F.; Sun, R. Charcterization of lignin structures and lignin-carbohydrate complex (LCC) linkages by quantitative $^{13}$C and 2D HSQC NMR spectroscopy. *J. Agric. Food Chem.* **2011**, *59*, 10604−10614.

(12) Leary, G. J. Quinone methides and the structure of lignin. *Wood Sci. Technol.* **1980**, *14*, 21−34.

(13) Ralph, J.; Schatz, P. F.; Lu, F.; Kim, H.; Akiyama, T.; Nelsen, S. F. Quinone methides in lignification. In *Quinone Methides*; Rokita, S. E., Ed.; Wiley: Hoboken, NJ, USA, 2009; pp 385−420.

(14) Liang, H.; Frost, C. J.; Wei, X.; Brown, N. R.; Carlson, J. E.; Tien, M. Improved sugar release from lignocellulosic material by introducing a tyrosine-rich cell wall peptide gene in poplar. *Clean* **2008**, *36*, 662−668.

(15) Xu, Y.; Chen, C.; Thomas, T. P.; Azadi, P.; Diehl, B.; Tsai, C.; Brown, N.; Carlson, J. E.; Tien, M.; Liang, H. *Plant Cell Rep.* **2013**, *32*, 1827−1841.

(16) Cong, F.; Diehl, B. G.; Hill, J. L.; Brown, N. R.; Tien, M. Covalent bond formation between amino acids and lignin: cross-coupling between proteins and lignin. *Phytochemistry* **2013**, *96*, 449−456.

(17) Diehl, B. G.; Watts, H. D.; Kubicki, J. D.; Regner, M. R.; Ralph, J.; Brown, N. R. Towards lignin-protein crosslinking: amino acid adducts of a lignin model quinone methide. *Cellulose* **2014**, *21*, 1395−1407.

(18) Terashima, N.; Atalla, R. H.; Ralph, S. A.; Landucci, L. L.; Lapierre, C.; Monties, B. New preparations of lignin polymer models under conditions that approximate cell wall lignification. *Holzforschung* **1995**, *49*, 521−527.
(19) Tobimatsu, Y.; Elumalai, S.; Grabber, J. H.; Davidson, C. L.; Pan, X.; Ralph, J. Hydroxycinnamate conjugates as potential monolignol replacements: in vitro lignification and cell wall studies with rosmarinic acid. *ChemSusChem* **2012**, *5*, 676−686.
(20) Capanema, E. A.; Balakshin, M. Y.; Kadla, J. F. A comprehensive approach for quantitative lignin characterization by NMR spectroscopy. *J. Agric. Food Chem.* **2004**, *52*, 1850−1860.
(21) Kim, H.; Ralph, J. Solution-state 2D NMR of ball-milled plant cell wall gels in DMSO-$d_6$/pyridine-$d_5$. *Org. Biomol. Chem.* **2010**, *8*, 576−591.
(22) Faix, O.; Beinhoff, O. FTIR spectra of milled wood lignins and lignin polymer models with enhanced resolution obtained by deconvolution. *J. Wood Chem. Technol.* **1988**, *8*, 505−522.
(23) Micic, M.; Radotic, K.; Jeremic, M.; Djikanovic, D.; Kammer, S. B. Study of the lignin model compound supramolecular structure by combination of near-field scanning optical microscopy and atomic force microscopy. *Colloids Surf., B* **2004**, *34*, 33−40.
(24) Terashima, N.; Awano, T.; Takabe, K.; Yoshida, M. Formation of macromolecular lignin in gingko xylem cell walls as observed by FESEM. *C. R. Biol.* **2004**, *327*, 903−910.
(25) Mansfield, S. D.; Kim, H.; Lu, F.; Ralph, J. Whole plant cell wall characterization using solution-state 2D NMR. *Nat. Protoc.* **2012**, *7*, 1579−1589.
(26) Micic, M.; Radotic, K.; Jeremic, M.; Leblanc, R. M. Study of the self-assembly of the lignin model compound on cellulose model substrate. *Macromol. Biosci.* **2003**, *3*, 100−106.
(27) Ralph, S. A.; Ralph, J.; Landucci, L. L. *NMR Database of Lignin and Cell Wall Model Compounds*, available at URL http://ars.usda.gov/Services/docs.htm?docid=10491 (November 2004).
(28) Terashima, N.; Akiyama, T.; Ralph, S.; Evtuguin, D.; Neto, C. P.; Parkas, J.; Paulsson, M.; Westermark, U.; Ralph, J. 2D-NMR (HSQC) difference spectra between specifically $^{13}$C-enriched and unenriched protolignin of *Ginkgo biloba* obtained in the solution state of whole cell wall material. *Holzforschung* **2009**, *63*, 379−384.
(29) Socrates, G. *Infrared and Raman Characteristic Group Frequencies*, 3rd ed.; Wiley: West Sussex, UK, 2001.

white flour fraction in Rialto and Riband, respectively. In the whole grain, Fe-NA/DMA accounted for 5.3 and 7.3% of the total iron in Rialto and Riband, respectively. Our method did not allow a separation of Fe−NA from Fe−DMA as the two complexes are very similar. Therefore, increasing NA and/or DMA is another strategy for increasing bioavailable iron in plant foods, but this requires the use of transgenic technologies.

The aim of this research was to investigate whether there are differences in iron availability between unleavened bread made from wholegrain and white flours from two commercial wheat cultivars differing in the total iron concentration (Rialto, a hard wheat used for bread, which is high in iron; and Riband, a soft wheat used for biscuits and cakes, which is low in iron). Caco-2 cells are widely used as an in vitro model to study iron bioavailability,[25−27] and previous studies have shown good agreement between in vitro results (using this particular cell line) and in vivo determination of iron bioavailability from food in the presence of enhancers and inhibitors[28,29] (e.g., ascorbic acid (AA) and calcium[30,31]). We have therefore used Caco-2 cells, in combination with simulated gastrointestinal digestion of unleavened bread, to determine the availability of iron from MFP, iron(II) chloride, and iron(II) sulfate and the effects of NA, DMA, and AA on iron uptake into the cells.

## MATERIALS AND METHODS

**Preparation of Grain Materials and Unleavened Bread.** Two commercial wheat cultivars (Rialto and Riband) that accumulate different levels of iron in their grain[10] were grown in field trials at Rothamsted Research in 2010, as described by Shewry et al.[32] Grains were milled in a Buhler mill (MLU-202) at Campden BRI, Gloucestershire, UK, to obtain whole wheat (100% extraction) and white flour (Riband, 38 ± 2.1% extraction; Rialto, 41 ± 3.4% extraction). Unleavened bread was made on a small scale: 20 g of flour was placed in a silica crucible, 5.76 mL of deionized water and 0.4 g of salt were added, and the mixture was kneaded into dough. The dough was left to proof at 30 °C for 30 min before being baked at 200 °C for 15 min. The breads were then broken up by hand into smaller pieces, approximately 0.5 $cm^3$, before flash freezing in liquid nitrogen and freeze-drying for 72 h. Samples were then homogenized and ground to a fine flour in an agate ball mill (Retsch PM400, Düsseldorf, Germany). The characteristics of the flours and unleavened bread samples are summarized in Table 1.

**Table 1. Iron and Phytate Content of Rialto and Riband Flours and Unleavened Breads**

| flour type | iron (mg/kg) in flour[a] | phytate (g/kg dry wt) in unleavened bread[b] | phytic acid/iron molar ratio |
|---|---|---|---|
| Rialto white | 11.9 ± 0.8 | 1.0 ± 0.1 | 7.13 |
| Rialto wholegrain | 46.7 ± 4.3 | 6.4 ± 0.2 | 11.60 |
| Riband white | 6.7 ± 0.5 | 0.4 ± 0.01 | 5.08 |
| Riband wholegrain | 30.3 ± 1.7 | 4.5 ± 0.2 | 12.57 |

[a]Total Fe (±SE, $n$ = 3) determined by ICP-MS. [b]Analysis of phytate was performed using a commercially available kit (K-PHYT 12/12 Megazyme, Ireland), as per the manufacturer's instructions. Eiither 0.5 of 1.0 g of sample was extracted with 10 mL of HCl followed by an enzymatic dephosphorylation step with phytase and alkaline phosphatase and precipitation using a color reagent prepared from AA in sulfuric and ammonium molybdate. The absorbance (655 nm) of free phosphorus and total phosphorus (±SE, $n$ = 3) was compared to phosphorus standards using a Varioskan spectrometer (Thermo, Finland).

**Solutions of Ascorbic Acid, Monoferric Phytate, Nicotianamine, and 2′-Deoxymugineic Acid for Caco-2 Cell Studies.** In Caco-2 cell studies, it is common practice to add AA to give an AA/Fe molar ratio in the range of 10−20:1, the amount being calculated on the basis of the concentration of iron in the samples.[26,33] However, as there was wide variation in total iron in the unleavened bread samples, ranging from 6.65 to 46.7 mg/kg, a standard amount of AA (880 μM, AA dissolved in Milli-Q water) was added to each gram of unleavened bread. Although this meant that some samples had a higher AA/Fe ratio than others (Table 2), the amount of AA added was high enough to ensure that it achieved maximal effect on iron uptake into Caco-2 cells, as observed in previous studies.[34]

**Table 2. Iron and Ascorbic Acid (AA) Concentrations of Unleavened Bread Digests**

| unleavened bread (1 g) | Fe content (μg) | Fe content (μmol/L) | AA (μmol/L) | Fe/AA molar ratio |
|---|---|---|---|---|
| Riband white | 6.7 | 8.0 | 880 | 1:110 |
| Rialto white | 11.9 | 14.2 | 880 | 1:62 |
| Riband wholegrain | 30.3 | 36.2 | 880 | 1:24 |
| Rialto wholegrain | 46.7 | 55.7 | 880 | 1:16 |
| Riband white fortified | 36.7 | 43.8 | 880 | 1:20 |
| Rialto white fortified | 41.9 | 50.0 | 880 | 1:18 |
| Riband wholegrain fortified | 60.3 | 72.0 | 880 | 1:12 |
| Rialto wholegrain fortified | 76.7 | 91.6 | 880 | 1:10 |

Monoferric phytate (MFP) was prepared from a solution of 100 mL of 0.5 M acetic acid, 10 g of sodium phytate, and 1 g of ferric chloride. The mixture was stirred for 2 h until all of the sodium phytate was completely dissolved, 100 mL of 95% (v/v) ethanol was added, and the solution was left overnight. The precipitate was then collected by centrifugation (5000$g$ for 10 min) (Medowrose Scientific Ltd., Oxford, UK), washed three times with acetone, allowed to air-dry, and stored in a desiccator.[35] The final product was analyzed by inductively coupled plasma atomic emission spectroscopy after digestion in ultrapure $HNO_3$ and $HClO_4$ (87:13% v/v).

Commercial sources of DMA and NA, with certified chemical composition (see TOC graphic), were purchased from Toronto Research Chemicals Inc. (Toronto, Canada). Both DMA and NA form 1:1 molar complexes with Fe. The F (II)−NA solution was prepared from ferrous sulphate (Sigma-Aldrich, Vienna, Austria), and Fe(III)−DMA was prepared from ferric chloride (Sigma-Aldrich). Each of the compounds was dissolved separately in Milli-Q water, and appropriate solutions were then mixed immediately to avoid oxidation. The molar concentrations are given in the captions of the figures.

**Cell Culture Procedures.** Caco-2 cells were grown in collagen-coated six-well plates (Greiner, Dungannon, UK) at a density of 4.75 × $10^4$ in 2 mL of Dulbecco's modified Eagle's medium (DMEM) (LGC, Teddington, UK) supplemented with 10% fetal bovine serum, 2 mM L-glutamine, 5 mL of 5000 u/mL penicillin/streptomycillin solution (Gibco, Paisley, UK), and 5 mL of 100× nonessential amino acids (Sigma, Dorset, UK). Media were replaced every 2 days. Cells between passages 27 and 34 were used for experiments at 13 days post seeding, and 24 h prior to experimentation, cells were switched to serum-free medium (minimum essential medium, MEM)[37] supplemented as above with the exception of fetal bovine serum. Experiments without a simulated digestion phase were initiated by the addition of fresh serum-free medium containing the appropriate treatment. After 24 h, the treatment medium was aspirated from the six-well plates, and the cells were washed twice with 2 mL of PBS. Deionized water was then applied to each well, and the Caco-2 cells were scraped off using an inverted 10 μL pipet tip. The cell suspension from each well was sonicated on ice, three times for 5 s, using a probe sonicator and stored at −20 °C.

Initially, the simulated digestion procedures were identical to those reported by Glahn et al.[27,38] However, due to the low iron content of the flour samples, the sample volume was increased from 0.5 to 1 g and subsequently to 3 g, which produced a thick digestate, so the duodenal phase of the simulated digestion was performed in a test tube for 2 h and not above the Caco-2 monolayer (the usual procedure in Glahn's assay). Experiments with unleavened bread were initiated with iron deprivation of the cells by switching from supplemented DMEM to MEM. Twenty-four hours of simulated digestion[27,37] was then carried out with the following modification: the duodenal phase of digestion was continued for 2 h in test tubes (rather than over the cells) at 37 °C on a rotating table, and once completed all samples were centrifuged at 21000*g* for 10 min to remove any sample residue, which could have resulted in physical blockage of the dialysis membrane. After centrifugation, 10% of the resulting supernatant from each treatment was applied to the dialysis membranes and placed over the appropriate wells. Cells were incubated for 1 h with the supernatant at 37 °C on a rotating table at a speed of 20 oscillations per minute, after which time the digests were removed and the cells were incubated for a further 23 h. Then they were harvested, sonicated, and frozen at −20 °C. For the analysis sonicated cell lysates were defrosted at room temperature and kept on ice, and a spectroferritin ELISA assay (Ramco Laboratories, Stafford, TX, USA) was carried out 24 h post sonication, according to the manufacturer's instructions. Total protein was quantified using a BCA protein assay (Pierce, Rockford, IL, USA), and iron availability assessed from the ferritin content (expressed as ng/mg protein), a surrogate measure of iron bioavailability.[38,39]

**Experiments Using Ascorbic Acid, Monoferric Phytate, Nicotianamine, and 2-Deoxymugineic Acid.** A series of experiments were also performed without a simulated digestion. Solutions containing NA, DMA, and MFP were prepared in Milli-Q water. When appropriate, AA was added either at 1:9 molar ratio (Figure 4) or various ratios (Figure 5). The pH was adjusted to 2, and the samples were incubated for 1 h at 37 °C. The samples were diluted with MEM to the desired iron concentrations (1.6 or 3.11 $\mu$g Fe/mL) and incubated in a water bath at 37 °C for 1 h. Because small concentrated volumes of NA, DMA, or MFP solutions were used (600 $\mu$L were diluted in 6 mL), they did not markedly affect the pH of the treatment solutions (the final pH was 6.9−7.0). Before addition to the cell monolayers, all treatment solutions were filtered with 0.22 $\mu$m syringe filters (Merck Millipore, Watford, UK). The cells were incubated for 24 h and then harvested, sonicated, and analyzed as described above.

**Statistical Analysis.** Unless otherwise stated, all statistical analyses were performed using SPSS Inc. (Chicago, IL, USA; version 16.0.0). One-way ANOVA with Tukey's post hoc was used to examine pairwise differences on power-transformed data. Data are presented as the mean ± SD. Differences were considered significant at $p < 0.05$.

## RESULTS

**Caco-2 Ferritin Response to Unleavened Flat Bread Samples: Simulated Digestion Experiments.** Data obtained from 1 g samples of unleavened breads (Figure 1) showed that significantly more ferritin was produced with white Riband flour than with wholegrain Riband and Rialto flours, in the presence of AA ($p < 0.005$ and $p = 0.004$, respectively). There were no significant differences in ferritin formation between the wholegrain and white flour breads from the two cultivars. When 3 g samples were used (Figure 2), the cells exposed to white unleavened bread (Rialto and Riband) produced significantly more ferritin protein than cells exposed to wholegrain breads ($p < 0.0005$ in both cases). Cells exposed to white bread from Riband produced significantly more ferritin than cells exposed to the other breads ($p < 0.0005$ in all comparisons).

To increase the cell response further, all flour samples were supplemented with ferrous sulfate with 30 mg Fe/kg prior to the production of the bread (Figure 3). There was a significantly higher cell ferritin response to unleavened bread made from white than from wholegrain flour, for both Rialto and Riband ($p < 0.0005$ for all comparisons). Cells exposed to Riband wholegrain bread produced significantly more ferritin than cells exposed to Rialto wholegrain bread ($p = 0.001$). The cell ferritin response to the positive control (53.54 $\mu$M $FeSO_4$) was not significantly different from the cell response to Riband white bread, but was significantly higher than the response to Rialto white and wholegrain and to Riband wholegrain breads ($p = 0.049$, $p < 0.0005$, and $p < 0.0005$, respectively). The cell response to unleavened bread made from Rialto wholegrain flour was not significantly different from the blank (17.7 ± 2.5 ng/mg total protein).

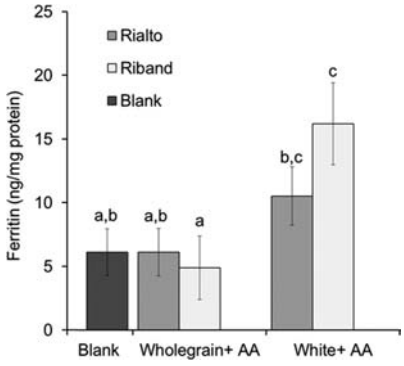


**Figure 1.** Ferritin concentration in Caco-2 cells exposed to digests prepared from 1 g of unleavened bread made from Rialto and Riband white and wholegrain flours in the presence of 880 $\mu$mol/L ascorbic acid (AA), expressed as ferritin concentration (ng/mg total protein). Data represent the mean ± SD ($n = 6$). Bars without a common letter (a−c) are significantly different, $p < 0.05$.

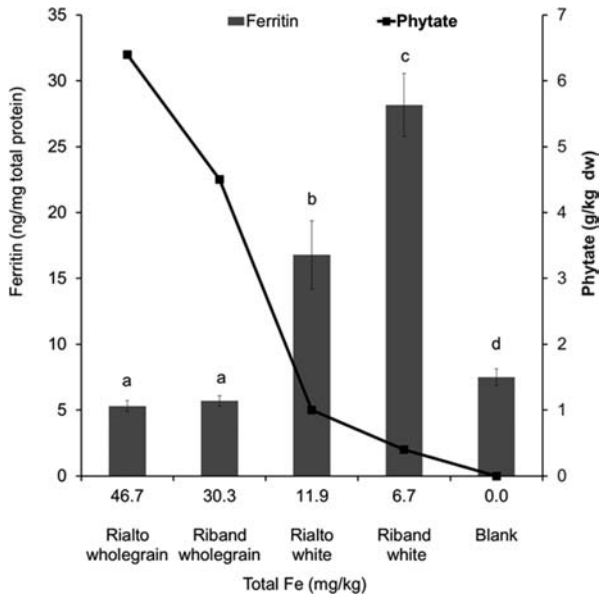


**Figure 2.** Ferritin concentration in Caco-2 cells exposed to digests prepared from 3 g of unleavened bread made from Rialto and Riband white and wholegrain flours in the presence of 880 $\mu$mol/L ascorbic acid (AA) expressed as ferritin concentration (ng/mg total protein, gray bars, *y*-axis). The phytate content (g/kg dry weight) of the unleavened bread is shown on the second *y*-axis and the iron content (mg/kg) on the *x*-axis. Data represent the mean ± SD ($n = 6$). Bars without a common letter (a−c) are significantly different, $p < 0.05$.

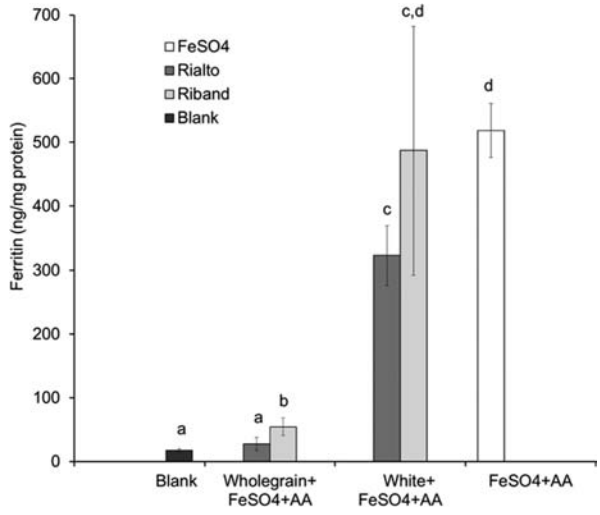


**Figure 3.** Ferritin concentration (ng/mg protein) in Caco-2 cells exposed to digests prepared from unleavened bread made from Rialto and Riband white and wholegrain flours in the presence of 880 $\mu$mol/L ascorbic acid (AA) and 53.54 $\mu$M ferrous sulfate ($FeSO_4$). Data represent the mean ± SD ($n$ = 6). Bars without a common letter (a–d) are significantly different, $p < 0.05$.

**Cell Ferritin Response to Iron(II), Iron(III), or MFP Treatments with Nicotianamine, Ascorbic Acid, 2-Deoxymugineic Acid, or Nicotianamine plus Ascorbic Acid.** AA was present in the treatments (Figure 4) at a ratio of approximately 1:9 (Fe/AA), whereas DMA or NA was present at a ratio of 1:1 (Fe/NA or DMA). The cell ferritin response to iron with NA (Figure 4) was significantly higher than to iron with DMA ($p < 0.0005$), suggesting that NA is a more potent enhancer of iron uptake than DMA (at the tested molar ratio). The response was also significantly increased when AA was added to the iron with DMA ($p < 0.0005$), but further addition of NA had no extra effect.

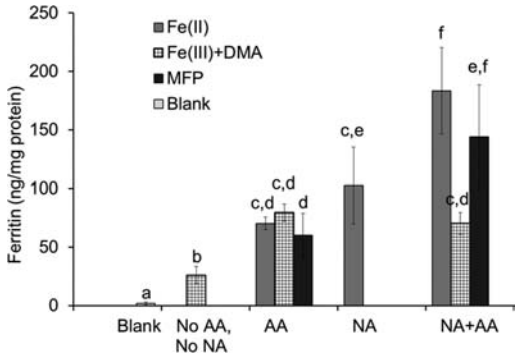


**Figure 4.** Ferritin concentration (ng/mg protein) in Caco-2 cells exposed to 1.6 $\mu$g of ferrous chloride (Fe(II)), ferric chloride (Fe(III))–DMA, or MFP in the presence of NA (at 1:1 Fe to NA ratio) or AA (at 1:9 Fe to AA ratio). Cell response is expressed as ferritin concentration (ng/mg total protein). Data represent the mean ± SD ($n$ = 6). Bars without a common letter (a–d) are significantly different, $p < 0.05$.

The cell ferritin responses to MFP plus AA and iron(II) chloride plus AA were not significantly different, suggesting that the availabilities are similar. Also, further addition of NA to MFP plus AA or to iron(II) chloride plus AA significantly increased ferritin formation in cells ($p < 0.0005$ in both comparisons).

An experiment (Figure 5) was also designed to determine whether there was a dose–response effect of NA and to compare it with AA, the most potent known enhancer of iron uptake. Cells exposed to iron in the presence of increasing NA concentrations (from 1:0.25 Fe/NA molar ratio through 1:0.5 to 1:1 molar ratio) produced significantly more ferritin with increasing NA ($p < 0.0005$, $p = 0.001$, and $p = 0.004$, respectively). When a higher Fe/NA molar ratio of 1:4 was used, the ferritin levels were not significantly different from those in cells exposed to a 1:0.5 Fe/NA molar ratio. The cell ferritin response was positively related to AA concentration (from 1:0.25 Fe/AA molar ratio through 1:4 and 1:10 molar ratio; $p = 0.002$, $p < 0.0005$, and $p < 0.0005$, respectively). Cells exposed to the highest molar ratio of Fe to AA (1:10) produced ferritin at similar levels to cells exposed to the lowest molar ratio of Fe to NA (1:0.25), indicating that NA is a more potent enhancer of iron bioavailability than AA and evoked the highest ferritin response.

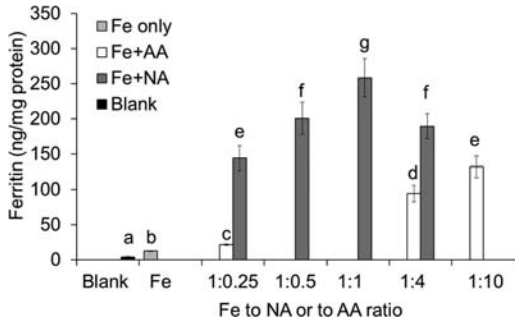


**Figure 5.** Ferritin concentration in Caco-2 cells exposed to 3.11 $\mu$g (13.88 $\mu$M) of ferrous sulfate ($FeSO_4$) with or without NA at Fe/NA ratios of 1:0.25, 1:0.5, 1:1, and 1:4 or AA at Fe/AA ratios of 1:0.25, 1:4, or 1:10. Cell response is expressed as ferritin concentration (ng/mg total protein). Data represent the mean ± SD ($n$ = 6). Bars without a common letter (a–f) are significantly different, $p < 0.05$.

## DISCUSSION

Unleavened bread made with white flour from the wheat cultivar Riband contained more available iron (when in the presence of AA) than the other breads tested, despite having the lowest iron content of all samples. A likely explanation for this is that it contained the lowest phytate content and lowest phytic acid/iron molar ratio (Table 1); there was an inverse relationship between cell ferritin response and phytate content (Figure 2). When unleavened bread was supplemented with iron (30 $\mu$g/g), together with AA (Figure 3), the same trend was observed.

Another contributory factor to the difference in iron availability between bread made from white and wholegrain flour may be the content of phenolic acids. Although not analyzed in our samples, limited data in the literature suggest that white flour has a much lower concentration of phenolic acids[40] as they are found primarily in the bran fraction.[41] Nevertheless, the difference observed between bread made from Riband and Rialto white flour is unlikely to be explained by their content of phenolic acids. Fernandez-Orozco et al.[42] analyzed flour from a number of locations and years and found no differences in the content of free phenolic acids between Riband and Rialto wholegrain flours (both contained 12 ± 7

μg/g), but Riband (990 ± 87 μg/g) had a significantly higher total phenolic acids content ($p = 0.026$) than Rialto (833 ± 118 μg/g). As the ferritin response was higher in Riband, assuming typical phenolic acids concentrations in the wheat samples used in these experiments, this indicates that phytate is the main determinant of iron bioavailability.

The cell ferritin response was inversely proportional to the concentrations of phytate and iron in the breads tested. However, because the iron contents of the samples were not the same, the AA/Fe molar ratios in the samples differed (Table 2), with the highest AA/Fe ratio being present in the sample with the lowest iron content (Riband white unleavened bread). The rationale for using the same amount of AA for all samples is that when AA is used in excess/ it should have a similar effect across all iron concentrations.[34]

Since 1953, it has been mandatory in the United Kingdom to add iron to white and brown flours to restore the content to the levels found in wholegrain flour (16.5 mg $kg^{-1}$).[43,44] The iron present in wholegrain products is not bioavailable due to the presence of inositol phophates $IP_6$, $IP_5$, $IP_4$, and $IP_3$, which bind iron tightly. However, iron present in monoferric phytate, found in wheat,[35] appears to be more bioavailable (Figure 4). In dogs, monoferric phytate has been shown to be about 50% as available as ferrous sulfate at a low dose of iron (1.5 mg), although only one-seventh as available at a higher dose of iron (15 mg).[36]

NA had a clear enhancing effect on iron availability, being a more potent enhancer of iron uptake than DMA (Figure 4) and AA (Figure 5) (as also reported by Zheng et al.[21] for rice flour). The lowest molar ratio of Fe/NA that was tested (1:0.25) had an effect similar to that of AA at a 1:10 Fe/AA molar ratio (Figure 5).The most effective Fe/NA molar ratios observed in this study were 1:1 to 1:4 (Figure 5). Zheng et al.[21] also reported that a 1:1 Fe/NA molar ratio was the most effective for wild type rice and that a 1:4 Fe/NA molar ratio was most effective for a transgenic rice grain expressing an additional nicotianamine synthase (*NAS*) gene. However, these results cannot be directly compared with those presented here as the iron compounds were examined in the absence of a food matrix and the test materials were not subjected to a simulated digestion procedure.

In the samples studied the phytate levels had more influence on iron bioavailability than total iron, a finding that should be taken into account in the development of biofortification strategies to reduce iron deficiency anemia. Our results also demonstrated that MFP with AA provoked a similar cell ferritin response to iron(II) chloride plus AA, whereas endogenous phytate (mainly $IP_6$ and $IP_5$) in wheat flour prevented iron from being taken up into Caco-2 cells.

## AUTHOR INFORMATION


### Corresponding Author

*(S.F.-T.) E-mail: s.fairweather-tait@uea.ac.uk. Phone: +44 1603 591304. Fax: +44 1603 593752.



### Funding

Rothamsted Research is funded by the Biotechnology and Biological Sciences Research Council (BBSRC) of the United Kingdom, and T.E. and A.A.W. were supported by BBSRC Ph.D. studentships. T.E. and P.R.S. received additional support from HarvestPlus Project 8055 "Optimising the quality, species and availability of Fe in modern bread wheat cultivars in order to prevent global Fe deficiencies" and A.A.W. from the Kellogg Co. (BBSRC CASE studentship).


### Notes

The authors declare no competing financial interest.

[‖]T.E. and A.A.W. are joint first authors.

## ABBREVIATIONS USED

AA, ascorbic acid; MFP, monoferric phytate; NA, nicotianamine; DMA, 2′-deoxymugineic acid; DMEM, Dulbecco's modified Eagle's medium; MEM, minimum essential medium

## REFERENCES


(1) McLean, E.; Egli, I.; Cogswell, M.; De Benoist, B.; Wojdyla, D. Worldwide prevalence of anaemia in preschool aged children, pregnant women and non-pregnant women of reporductive age. In *Nutritional Anaemia*; Kraemer, K., Zimmermann, M. B., Eds.;Sight and Life Press: Basel, Switzerland, 2007; pp 1−12.

(2) Scientific Advisory Committee on Nutrition. *Iron and Health*; TSO: London, UK, 2010.

(3) Thavarajah, D.; Thavarajah, P.; Wejesuriya, A.; Rutzke, M.; Glahn, R. P.; Combs, G. F.; Vandenberg, A. The potential of lentil (*Lens culinaris* L.) as a whole food for increased selenium, iron, and zinc intake: preliminary results from a 3 year study. *Euphytica* **2011**, *180*, 123−128.

(4) Velu, G.; Velu, G.; Rai, K. N.; Muralidharan, V.; Kulkarni, V. N.; Longvah, T.; Raveendran, T. S. Prospects of breeding biofortified pearl millet with high grain iron and zinc content. *Plant Breed.* **2007**, *126*, 182−185.

(5) Haas, J. D.; Beard, J. L.; Murray-Kolb, L. E.; del Mundo, A. M.; Felix, A.; Gregorio, G. B. Iron-biofortified rice improves the iron stores of nonanemic Filipino women. *J. Nutr.* **2006**, *135*, 2823−2830.

(6) Ortiz-Monasterio, J. I.; Palacios-Rojas, N.; Meng, E.; Pixley, K.; Trethowan, R.; Peña, R. J. Enhancing the mineral and vitamin content of wheat and maize through plant breeding. *J. Cereal Sci.* **2007**, *46*, 293−307.

(7) Bouis, H. E.; Hotz, C.; McClafferty, B.; Meenakshi, J. V.; Pfeiffer, W. H. Biofortification: a new tool to reduce micronutrient malnutrition. *Food Nutr. Bull.* **2011**, *32*, S31−S40.

(8) Qureshi, I. M.; Khattak, T. N.; Akhtar, J. Determination of iron in different types of wheat flours. *Int. J. Agric. Biol.* **2002**, *4*, 297−299.

(9) Oury, F.-X.; Leenhardt, F.; Rémésy, C.; Chanliaud, E.; Duperrier, B.; Balfourier, F.; Charmet, G. Genetic variability and stability of grain magnesium, zinc and iron concentrations in bread wheat. *Eur. J. Agron.* **2006**, *25*, 177−185.

(10) Zhao, F. J.; Su, Y. H.; Dunham, S. J.; Rakszegi, M.; Bedo, Z.; McGrath, S. P.; Shewry, P. R. Variation in mineral micronutrient concentrations in grain of wheat lines of diverse origin. *J. Cereal Sci.* **2009**, *49*, 290−295.

(11) Eagling, T.; Neal, A. L.; McGrath, S. P.; Fairweather-Tait, S.; Shewry, P. R.; Zhao, F. J. Distribution and speciation of iron and zinc in grain of two wheat genotypes. *J. Agric. Food Chem.* **2014**, *62*, 708−716.

(12) Cakmak, I.; Kalayci, M.; Kaya, Y.; Torun, A. A.; Aydin, N.; Wang, Y.; Arisoy, Z.; Erdem, H.; Yazici, A.; Gokmen, O.; Ozturk, L.; Horst, W. J. Biofortification and localization of zinc in wheat grain. *J. Agric. Food Chem.* **2010**, *58*, 9092−9102.

(13) Zhang, Y.; Shi, R.; Rezaul, K. M.; Zhang, F.; Zou, C. Iron and zinc concentrations in grain and flour of winter wheat as affected by foliar application. *J. Agric. Food Chem.* **2010**, *58*, 12268−12274.

(14) White, P. J.; Broadley, M. R. Biofortifying crops with essential mineral elements. *Trends Plant Sci.* **2005**, *10*, 586−593.

(15) Persson, D. P.; Hansen, T. H.; Laursen, K. H.; Schjoerring, J. K.; Husted, S. Simultaneous iron, zinc, sulfur and phosphorus speciation analysis of barley grain tissues using SEC-ICP-MS and IP-ICP-MS. *Metallomics* **2009**, *1*, 418−426.

(16) Schlemmer, U.; Frølich, W.; Prieto, R. M.; Grases, F. Phytate in foods and significance for humans: food sources, intake, processing, bioavailability, protective role and analysis. *Mol. Nutr. Food Res.* **2009**, *53* (Suppl. 2), S330−S375.

(17) Sandberg, A. S.; Brune, M.; Carlsson, N. G.; Hallberg, L.; Skoglund, E.; Rossander-Hulthén, L. Inositol phosphates with different numbers of phosphate groups influence iron absorption in humans. *Am. J. Clin. Nutr.* **1999**, *70*, 240−246.
(18) Engle-Stone, R.; Yeung, A.; Welch, R.; Glahn, R. Meat and ascorbic acid can promote Fe availability from Fe-phytate but not from Fe-tannic acid complexes. *J. Agric. Food Chem.* **2005**, *53*, 10276−10284.
(19) Lee, S.; Jeon, U. S.; Lee, S. J.; Kim, Y. K.; Persson, D. P.; Husted, S.; Schjørring, J. K.; Kakei, Y.; Masuda, H.; Nishizawa, N. K.; An, G. Iron fortification of rice seeds through activation of the nicotianamine synthase gene. *Proc. Natl. Acad. Sci. U.S.A.* **2009**, *106*, 22014−22019.
(20) Higuchi, K.; Watanabe, S.; Takahashi, M.; Kawasaki, S.; Nakanishi, H.; Nishizawa, N. K.; Mori, S. Nicotianamine synthase gene expression differs in barley and rice under Fe-deficient conditions. *Plant J.* **2001**, *25*, 159−167.
(21) Zheng, L.; Cheng, Z.; Ai, C.; Jiang, X.; Bei, X.; Zheng, Y.; Glahn, R. P.; Welch, R. M.; Miller, D. D.; Lei, X. G.; Shou, H. Nicotianamine, a novel enhancer of rice iron bioavailability to humans. *PLoS One* **2010**, *5*, No. e10190.
(22) Cheng, L.; Wang, F.; Shou, H.; Huang, F.; Zheng, L.; He, F.; Li, J.; Zhao, F.-J.; Ueno, D.; Ma, J. F.; Wu, P. Mutation in nicotianamine aminotransferase stimulated the Fe(II) acquisition system and led to iron accumulation in rice. *Plant Physiol.* **2007**, *145*, 1647−1657.
(23) Shojima, S.; Nishizawa, N.-K.; Fushiya, S.; Nozoe, S.; Irifune, T.; Mori, S. Biosynthesis of phytosiderophores. In vitro biosynthesis of 2′-deoxymugineic acid from L-methionine and nicotianamine. *Plant Physiol.* **1990**, *93*, 1497−1503.
(24) Mino, Y.; Ishida, T.; Ota, N.; Inoue, M.; Kyosuke, N.; Tsunematsu, T.; Tanaka, H.; Sugiura, Y. Mugineic acid-iron (III) complex and its structurally analogous cobalt(III) complex: characterization and implication for absorption and transport of iron in gramineous plants. *J. Am. Chem. Soc.* **1983**, *105*, 4671−4676.
(25) Glahn, R. P.; Wortley, G. M.; South, P. K.; Miller, D. D. Inhibition of iron uptake by phytic acid, tannic acid, and ZnCl 2: studies using an in vitro digestion/Caco-2 cell model. *J. Agric. Food Chem.* **2002**, *50*, 390−395.
(26) Glahn, R. P.; Cheng, Z.; Welch, R. M.; Gregorio, G. B. Comparison of iron bioavailability from 15 rice genotypes: studies using an in vitro digestion/Caco-2 cell culture model. *J. Agric. Food Chem.* **2002**, *50*, 3586−3591.
(27) Glahn, R. P.; Lee, O. A.; Yeung, A.; Goldman, M. I.; Miller, D. D. Caco-2 cell ferritin formation predicts nonradiolabeled food iron availability in an in vitro digestion/Caco-2 cell culture model. *J. Nutr.* **1998**, *128*, 1555−1561.
(28) Yun, S.; Habicht, J.-P.; Miller, D. D.; Glahn, R. P. An in vitro digestion/Caco-2 cell culture system accurately predicts the effects of ascorbic acid and polyphenolic compounds on iron bioavailability in humans. *J. Nutr.* **2004**, *134*, 2717−2721.
(29) Garcia, M. N.; Flowers, C.; Cook, J. D. The Caco-2 cell culture system can be used as a model to study food iron availability. *J. Nutr.* **1996**, *126*, 251−258.
(30) Thompson, B. A. V.; Sharp, P. A.; Elliott, R.; Fairweather-Tait, S. J. Inhibitory effect of calcium on non-heme iron absorption may be related to translocation of DMT-1 at the apical membrane of enterocytes. *J. Agric. Food Chem.* **2010**, *58*, 8414−8417.
(31) Kalgaonkar, S.; Lönnerdal, B. Effects of dietary factors on iron uptake from ferritin by Caco-2 cells. *J. Nutr. Biochem.* **2008**, *19*, 33−39.
(32) Shewry, P. R.; Piironen, V.; Lampi, A. M.; Edelmann, M.; Kariluoto, S.; Nurmi, T.; Fernandez-Orozco, R.; Ravel, C.; Charmet, G.; Andersson, A. A.; Aman, P.; Boros, D.; Gebruers, K.; Dornez, E.; Courtin, C. M.; Delcour, J. A.; Rakszegi, M.; Bedo, Z.; Ward, J. L. The HEALTHGRAIN wheat diversity screen: effects of genotype and environment on phytochemicals and dietary fiber components. *J. Agric. Food Chem.* **2010**, *58*, 9291−9298.
(33) Ariza-Nieto, M.; Blair, M. W.; Welch, R. M.; Glahn, R. P. Screening of iron bioavailability patterns in eight bean (*Phaseolus vulgaris* L.) genotypes using the Caco-2 cell in vitro model. *J. Agric. Food Chem.* **2007**, *55*, 7950−7956.
(34) Glahn, R. P.; Lee, O. A.; Miller, D. D. In vitro digestion/Caco-2 cell culture model to determine optimal ascorbic acid to Fe ratio in rice cereal. *J. Food Sci.* **2008**, *64*, 925−928.
(35) Morris, E. R.; Ellis, A. Isolation of monoferric phytate from wheat bran and its biological value as an iron source to the rat. *J. Nutr.* **1976**, *106*, 753−760.
(36) Lipschitz, D. A.; Simpson, K. M.; Cook, J. D.; Morris, E. R. Absorption of monoferric phytate by dogs. *J. Nutr.* **1979**, *109*, 1154−1160.
(37) Thompson, B.; Sharp, P.; Elliott, R.; Al-Mutairi, S.; Fairweather-Tait, S. J. Development of a modified Caco-2 cell model system for studying iron availability in eggs. *J. Agric. Food Chem.* **2010**, *58*, 3833−3839.
(38) Glahn, R. P.; Wien, E. M.; van Campen, D. R. V.; Miller, D. D. Caco-2 Cell iron uptake from meat and casein digests parallels in vivo studies: use of a novel in vitro method for rapid estimation of iron bioavailability. *J. Nutr.* **1996**, *126*, 332−339.
(39) Wawer, A. A.; Sharp, P. A.; Perez-Moral, N.; Fairweather-Tait, S. J. Evidence for an enhancing effect of alginate on iron availability in Caco-2 cells. *J. Agric. Food Chem.* **2012**, *60*, 11318−11322.
(40) Mattila, P.; Pihlava, J.-M.; Hellstrom, J. Contents of phenolic acids, alkyl- and alkenylresorcinols, and avenanthramides in commercial grain products. *J. Agric. Food Chem.* **2005**, *53*, 8290−8295.
(41) Beta, T.; Nam, S.; Dexter, J. E.; Sapirstein, H. D. Phenolic content and antioxidant activity of pearled wheat and roller-milled fractions. *Cereal Chem.* **2005**, *82*, 390−393.
(42) Fernandez-Orozco, R.; Harflett, L. L. C.; Shewry, P. R.; Ward, J. L. Effects of environment and genotype on phenolic acids in wheat in the HEALTHGRAIN diversity screen. *J. Agric. Food Chem.* **2010**, *58*, 9341−9352.
(43) Statutory instruments. *The Bread and Flour Regulations*; Food Standards Agency: London, UK, 1998; p 141.
(44) Hurrell, R.; Bothwell, T.; Cook, J. D.; Dary, O.; Davidsson, L.; Fairweather-Tait, S.; Hallberg, L.; Lynch, S.; Rosado, J.; Walter, T.; Whittaker, P. SUSTAIN Task Force. The usefulness of elemental iron for cereal flour fortification: a SUSTAIN Task Force Report. *Nutr. Rev.* **2002**, *60*, 391−406.

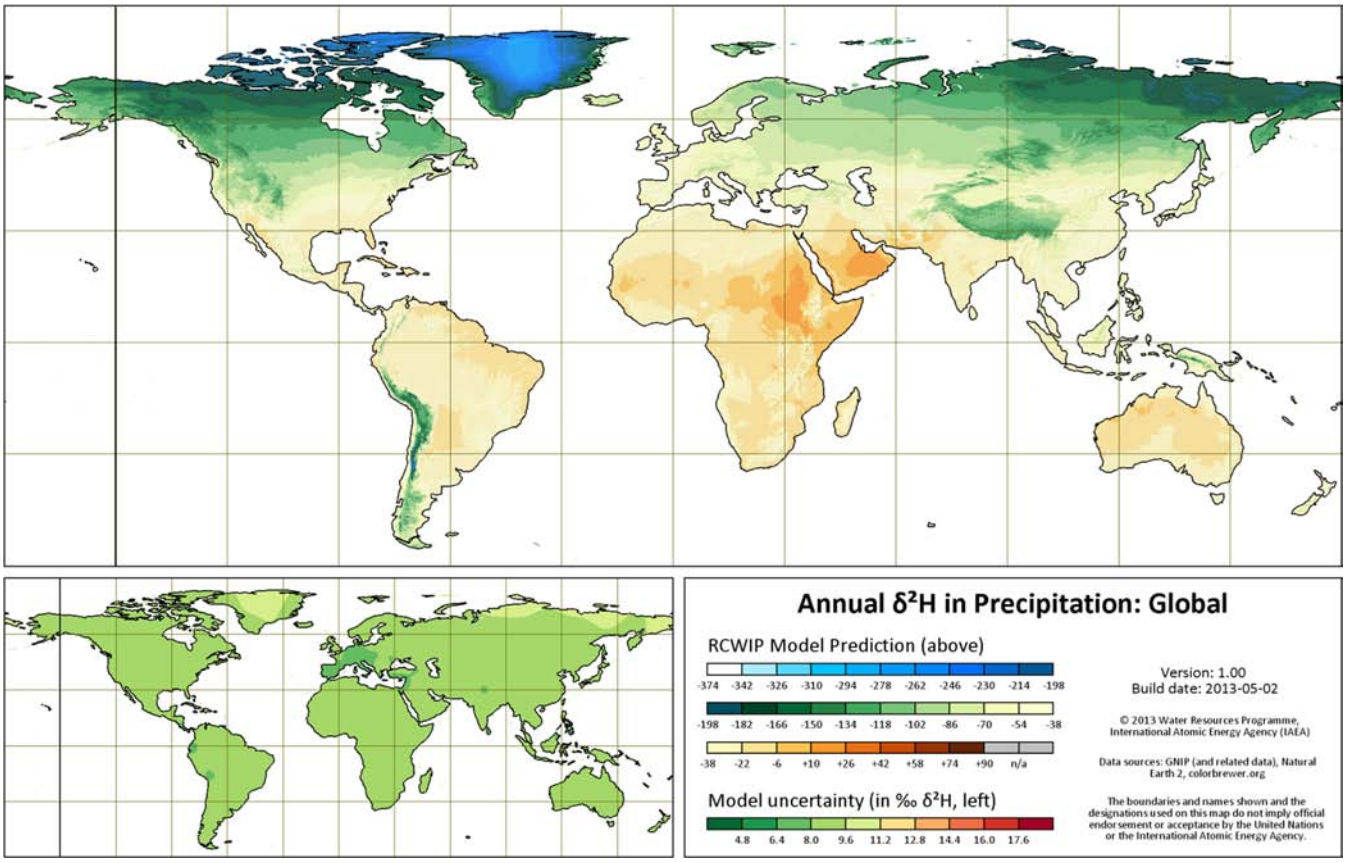


**Figure 1.** Regionalized cluster-based water isotope prediction model of $\delta^2$H in precipitation, developed by the International Atomic Energy Agency (IAEA).[22−24]

the location of its habitat. Because the plant absorbs water and uses it for biosynthesis of metabolites, the values of $\delta^2$H in the local precipitation will be reflected in these secondary metabolites, for example, vanillin from the vanilla orchid.[11−13]

The values of $\delta^{13}$C and $\delta^2$H can be measured by isotope ratio mass spectrometry (IRMS). IRMS is capable of measuring the natural abundance of stable isotopes.[14] Previous studies have investigated the authenticity of vanilla flavor using either elemental analyzer−IRMS (EA−IRMS) or gas chromatography−IRMS (GC−IRMS).[15−17] In these studies, it was shown that GC can be used to separate vanillin from the other components of a vanilla extract and that compound-specific data can be measured.

In this study, three types of vanillin were analyzed by gas chromatography−combustion−isotope ratio mass spectrometry (GC−C−IRMS) to investigate if the $\delta^{13}$C values differed enough to assign each group with a specific $\delta^{13}$C interval. In this way, an unknown sample of vanillin can be categorized by measuring its $\delta^{13}$C value. Additionally, gas chromatography pyrolysis isotope ratio mass spectrometry (GC−P−IRMS) was used for determining $\delta^2$H of vanillin from vanilla pods from various locations to test if it is possible to assign a $\delta^2$H interval to a specific geographic area. To the knowledge of the authors, this is the first time measurements of $\delta^2$H of vanilla pods from more than three different geographical origins have been characterized.

## MATERIALS AND METHODS

**Samples.** A total of 82 vanilla flavors of different origin were analyzed: 2 produced synthetically by Sigma-Aldrich (Brondby, Denmark), 1 sample produced by fermentation of natural eugenol by Rhodia (www.rhodia.com), and 79 natural vanilla pods of different types and geographical origin: 54 pods of the type *V. planifolia*, 15 pods of *V. tahitensis*, and 10 pods of unknown species. The geographical origin was known for 71 of the vanilla pods. The vanilla pods analyzed, originated from Madagascar, French Polynesia, India, New Caledonia, Tonga, Vanuatu, Mexico, Africa (Congo and Uganda), Indonesia, and New Guinea (including Papua New Guinea).

**Chemicals.** Ethanol used for extraction was of 96% purity and purchased from CCS Healthcare AB (Borlänge, Sweden). Ethyl acetate and cyclohexane used for extraction were purchased from Rathburn Chemicals, Ltd. (Walkerburn, U.K.), and anhydrous sodium sulfate was purchased from Merck (Darmstadt, Germany). A mixture of $C_{11}$, $C_{15}$, and $C_{20}$ alkanes (Chiron, Trondheim, Norway) with known values of $\delta^{13}$C (−26.11, −30.02, and −33.06‰) were used for sample calibration against the reference standard: Vienna-Pee Dee Belemnite (V-PDB). Two samples of caffeine (1 and 2) with different $\delta$ values (91.4 and −152.8‰), purchased from Arndt Schimmelmann (Indiana University, Bloomington, IN), were used for $\delta^2$H calibration against the reference standard: Vienna-Standard Mean Ocean Water (V-SMOW).

**Sample Preparation.** Vanilla pods were cut lengthwise; the seeds were scraped out; and the rest of the pod was cut in pieces less than 5 mm. Vanilla seeds and pods were placed in a closed flask, and for every 15 g of vanilla, 46 g of water and 54 g of 96% ethanol were added and macerated at ambient temperature for approximately 72 h during constant stirring with a stir bar (500 rpm). The flask was protected against sunlight. Afterward, the mixture was filtered, and the filter cake was pressed. This method extracted most of the vanillin because a second extraction resulted in less than 10% vanillin content compared to the first extraction. A total of 3 mL of the ethanol/water extract was further extracted with 3 mL of ethyl acetate/cyclohexane (1:1) and dried with anhydrous sodium sulfate. Samples were diluted 4 times

with ethyl acetate/cyclohexane (1:1) prior to GC−C−IRMS analyses, while no dilution was used before GC−P−IRMS analyses. One extraction was made for each vanilla pod. Synthetic vanillin and vanillin from eugenol were dissolved in ethyl acetate/cyclohexane (1:1). Each sample was analyzed 3 times by GC−C−IRMS and GC−P−IRMS, and results are given as a mean of the 3 determinations.

**GC Analyses.** Separation of the samples was performed on a Trace GC Ultra (Thermo Scientific, Bremen, Germany) fitted with a DB-5 capillary column (Agilent Technologies, Böblingen, Germany) (30 m × 0.250 mm inner diameter, with $d_f$ of 0.25 $\mu$m). The following GC conditions were employed: splitless injection, injector temperature of 230 °C, initial oven temperature of 40 °C, ramp at 4 °C/min to 150 °C, and ramp at 7 °C/min to 260 °C for 1 min. Helium was used as the carrier gas at 1.4 mL/min for GC−C−IRMS analysis and 1.2 mL/min for GC−P−IRMS; otherwise, the GC parameters were the same for the determination of $\delta^{13}$C and $\delta^{2}$H.

**IRMS Analysis.** For the determination of $\delta^{13}$C, compounds eluting from GC were combusted in an oxidation reactor (NiO tube with NiO/CuO/Pt) operated at 1000 °C, purchased from Thermo Scientific (Bremen, Germany). For $\delta^{2}$H determinations, compounds eluting from GC were converted in a high-temperature pyrolysis reactor (HTC reactor), consisting of a ceramic tube with no catalyst and operated at 1420 °C. The HTC reactor was purchased from Thermo Scientific (Bremen, Germany). The converted compounds from either the combustion reactor or the HTC reactor were analyzed on a Delta V Advantage isotope ratio mass spectrometer from Thermo Scientific (Bremen, Germany).

**Standardization against Primary Standards.** The standards of known isotopic values were analyzed in every sequence together with vanilla samples. The measured isotopic values for the standards were used to create an isotopic calibration of the samples, to express the final results in delta notation with the unit "per mille" versus V-SMOW and V-PDB, separately: $\delta = (R_{sample} - R_{standard})/R_{standard} \times 1000‰$, where $R$ is the ratio of the heavy/light isotopes.

**Statistical Analysis.** $t$ tests have been used for comparison of means between two groups. Variance homogeneity have been established preliminary using $F$ tests. One-way analysis of variation (ANOVA) has been used when more than two groups are compared. Afterward, Tukey's test is used to establish the correlation between the groups.

## RESULTS AND DISCUSSION

Vanillin is the main contributing compound to the vanilla flavor. The molecule is identical in its elemental composition regardless of the production method: natural, synthetic, or biovanillin. We determined the ratios of stable carbon isotopes by GC−C−IRMS of 82 vanillin samples to test if these results could be used to differentiate between the three production methods. A total of 2 samples of synthetic vanillin, 1 sample of biovanillin, and vanillin extracted from 79 vanilla pods were analyzed. Figure 2 shows a partial GC−C−IRMS chromatogram of mass 44 for a vanilla extract.

**Authenticity of Vanillin: Plant Species.** There was a significant difference in the $\delta^{13}$C between vanillin extracted from *V. planifolia* compared to vanillin from *V. tahitensis* (Figure 3) ($t$ test; $p < 0.001$). The range of $\delta^{13}$C values was from −21.8 to −17.8‰ for *V. planifolia* ($n$ = 54) and from −19.1 to −15.5‰ for *V. tahitensis* ($n$ = 15). The results show that *V. tahitensis* is more enriched in the heavy carbon isotope than *V. planifolia*. These findings are consistent with the results obtained by Scharrer et al. and Greule et al.[16,18]

**Authenticity of Vanillin: Production Method.** Synthetic vanillin from two different productions was found to have values of $\delta^{13}$C at −27.4 and −31.7‰, while biovanillin was measured to −30.9‰ (Figure 3). Because the $\delta^{13}$C value of biovanillin is within the range found for synthetic vanillin, the stable isotope analysis of carbon is not sufficient to differentiate

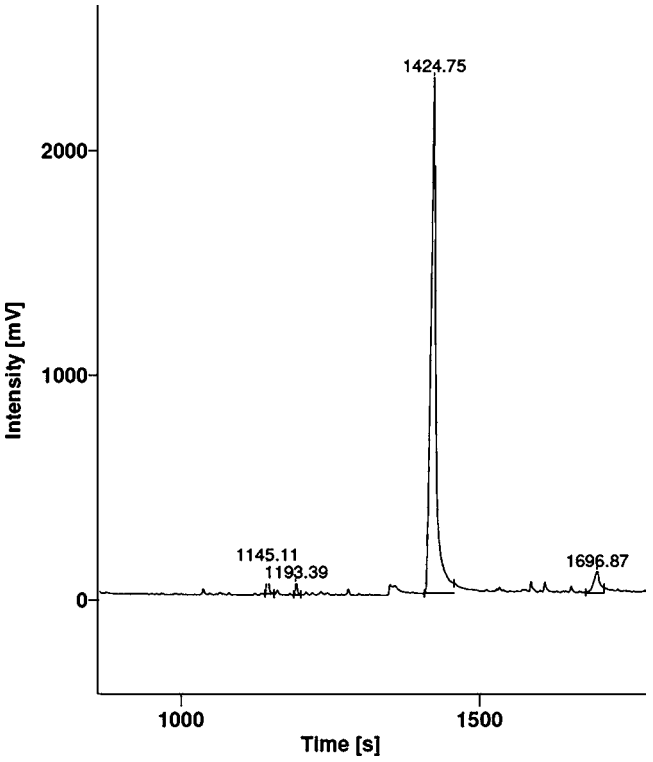


**Figure 2.** Partial GC−C−IRMS chromatogram showing the ion current of mass 44. The large peak with the retention time at 1424 is vanillin.

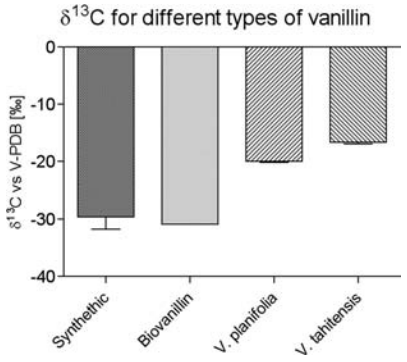


**Figure 3.** $\delta^{13}$C versus V-PDB for vanillin of known authenticity: obtained from chemical synthesis ($n$ = 2), fermentation of eugenol ($n$ = 1), and vanilla pods of the types *V. planifolia* ($n$ = 54) and *V. tahitensis* ($n$ = 15). Error bars equal standard errors of the means within the sample group.

the two groups and other methods have to be considered for authentification, i.e., measurements of site-specific isotopic ratios.[19] The $\delta^{13}$C value of the sample of biovanillin was −30.9‰, which is within the interval for $C_3$ plant material. Stable isotope analyses of synthetic and natural eugenol showed values of $\delta^{13}$C similar to biovanillin from eugenol (results not shown) and indicate that the isotope ratio of carbon does not change significantly when converted from eugenol to vanillin during fermentation.

Precursors used for the production of synthetic vanillin are generally derived from petrochemicals, with a $\delta^{13}$C similar or lower than $C_3$ plants.[20] In the case of biovanillin made by the fermentation of eugenol, the $\delta^{13}$C values found are similar to the values of synthetic vanillin in this study. However, Scharrer

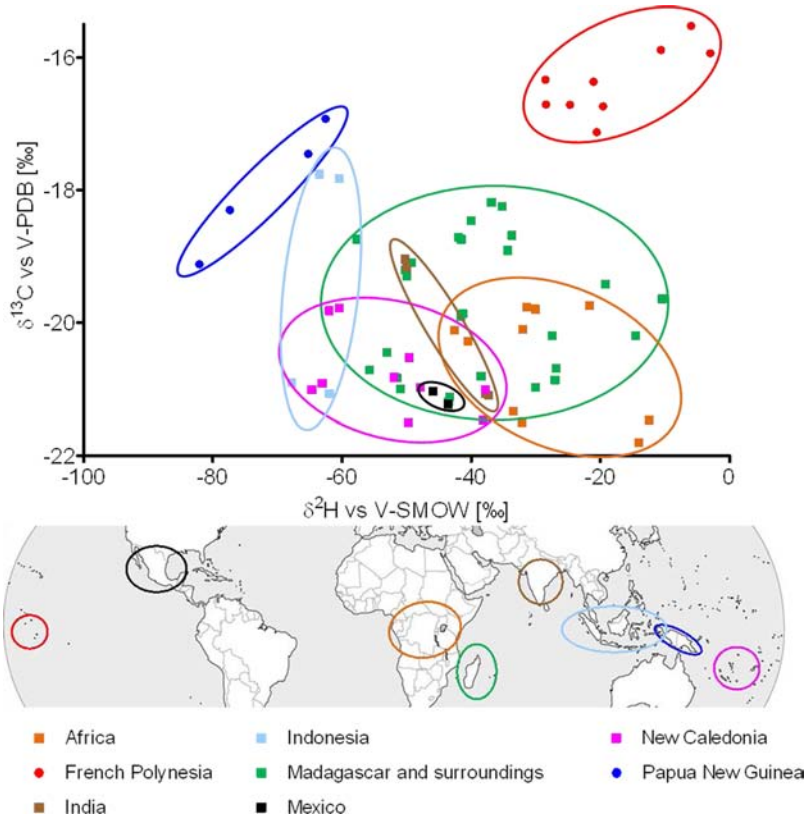


**Figure 4.** Results of $\delta^2$H versus V-SMOW and $\delta^{13}$C versus V-PDB for vanillin extracted from vanilla pods. Points are labeled with geographic origin. The geographical origins are separated by colors, with *V. tahitensis* represented by circles and *V. planifolia* represented by squares. The large circles in the scatter plot are color-correlated to the circles in the world map, showing the regions from where the samples originate.

**Table 1. Measured Values of $\delta^{13}$C versus V-PDB and $\delta^2$H versus V-SMOW for Vanilla Pods Originating from New Caledonia, French Polynesia, Mexico, Africa, Madagascar, India, Indonesia, and New Guinea**

| | | $\delta^{13}$C versus V-PDB (‰) | | | | $\delta^2$H versus V-SMOW (‰) | | | |
|---|---|---|---|---|---|---|---|---|---|
| | *n* | $\bar{x}$ | *s* | minimum | maximum | $\bar{x}$ | *s* | minimum | maximum |
| New Caledonia, Tonga, and Vanuatu | 10 | −20.8 | 0.6 | −21.5 | −19.8 | −52.5 | 9.8 | −64.6 | −37.8 |
| French Polynesia | 9 | −16.4 | 0.5 | −17.1 | −15.5 | −18.0 | 9.4 | −28.5 | −3.0 |
| Mexico | 2 | −21.1 | 0.1 | −21.2 | −21.0 | −44.7 | 1.6 | −45.9 | −43.6 |
| Africa (Congo and Uganda) | 10 | −20.6 | 0.8 | −21.8 | −19.7 | −29.0 | 10.1 | −42.6 | −12.4 |
| Madagascar | 28 | −19.8 | 1.0 | −21.3 | −18.2 | −38.9 | 12.1 | −57.7 | −10.4 |
| India | 4 | −20.1 | 1.2 | −21.1 | −19.0 | −43.8 | 7.3 | −50.2 | −37.3 |
| Indonesia | 4 | −19.4 | 1.9 | −21.1 | −17.8 | −63.4 | 3.2 | −67.8 | −60.4 |
| New Guinea | 4 | −18.0 | 1.0 | −19.1 | −16.9 | −71.8 | 9.4 | −82.1 | −62.5 |

et al. found that biovanillin could be differentiated from synthetic vanillin using GC−C−IRMS. The precursor for the biovanillin used by Scharrer et al. was not specified.[18] Therefore, it might be possible to authenticate biovanillin made from $C_3$ plant material other than eugenol using the measurement of $\delta^{13}$C.

Values of $\delta^{13}$C for natural vanillin extracted from vanilla pods were in the range from −21.8 to −15.5‰, while vanillin from other sources had values of $\delta^{13}$C between −31.7 and −27.4‰. Thus, natural vanillin is more enriched in the heavy carbon isotope compared to vanillin originating from fermentations or chemical synthesis. This difference was expected because natural vanillin is extracted from CAM plants, which have higher values of $\delta^{13}$C than $C_3$ plant materials used for the production of biovanillin by fermentations. O'Leary found that CAM plants often have values of $\delta^{13}$C between −20 and −10‰, while $\delta^{13}$C for molecules from $C_3$ plants have values between −33 and −24‰.[9] The results from this study are consistent with the findings by O'Leary.

To differentiate between vanillin from vanilla pods and vanillin made otherwise, the values of synthetic vanillin and biovanillin are tested against values of $\delta^{13}$C for vanillin extracted from vanilla pods. Because the two species of vanilla pods are found to have significant different means, the non-natural vanillin has to be tested against both species separately. This results in three groups: one containing synthetic and biovanillin, a second containing all vanillin results for *V. planifolia*, and a third group with vanillin results for *V. tahitensis*. A one-way ANOVA followed by a Tukey's test showed significant difference between the three groups ($p < 0.001$). Values of $\delta^{13}$C versus V-PDB can therefore be used to determine if vanillin originates from a vanilla pod or is produced otherwise.

**Traceability of Vanillin.** Ratios of the heavy/light stable isotopes of hydrogen differ around the world primarily as a result of longitudinal, altitudinal, and continental effects. Because plants take up water from their surroundings, the ratio of stable hydrogen isotopes in plants will resemble the ratio of their specific geographic location.[13] In this study, natural vanillin was analyzed for $\delta^2$H by GC−P−IRMS to investigate whether the differences in $\delta^2$H values are large enough to differentiate between the geographic origins of growth.

Figure 4 shows results of $\delta^{13}$C plotted against results of $\delta^2$H for vanillin extracted from vanilla pods. The average, standard deviation, maximum, and minimum values of $\delta^{13}$C and $\delta^2$H for each geographic origin are shown in Table 1. Samples from French Polynesia and New Guinea are all of the species *V. tahitensis*, while the rest of the vanilla samples are *V. planifolia*. Samples of *V. tahitensis* from New Guinea are more depleted in the heavy carbon isotope than samples of *V. tahitensis* from French Polynesia. Growth conditions may be a possible explanation for the differences in values of $\delta^{13}$C between these two countries. West et al. describes how marijuana grown in an indoor environment has significant lower values of $\delta^{13}$C than plants grown outdoors. The respired $CO_2$ has lower values of $\delta^{13}$C than atmospheric $CO_2$. Therefore, in a closed environment, with poor ventilation, the respired $CO_2$ will not mix well with the atmosphere and, thereby, decrease the values of $\delta^{13}$C.[21] In places with intensive sunlight, it is necessary to protect the vanilla orchid, either in the form of support trees or by covering the plants.[5] In the last-mentioned case, the cover could cause poor ventilation and, consequently, lower the values of $\delta^{13}$C in the vanilla plants.

Figure 4 shows results of $\delta^{13}$C versus $\delta^2$H for natural vanillin, and it is seen that adjacent geographic locations are grouped together. Vanillin extracted from vanilla pods originating from French Polynesia differ from the other samples. Because vanilla pods from French Polynesia are solely of the species *V. tahitensis*, which are more enriched in the heavy carbon atom than *V. planifolia*, they can be separated from other geographic origins growing *V. planifolia* based on their values of $\delta^{13}$C. Even within samples of *V. tahitensis*, the two different locations, French Polynesia and New Guinea, are easily separated ($p < 0.001$) because their values of $\delta^2$H differ by more than 30‰.

The lowest $\delta^2$H values were found for vanillin extracted from vanilla pods from New Guinea and Indonesia, with mean values of $-71.8 \pm 9.4$ and $-63.4 \pm 3.2$‰, respectively. India and New Caledonia samples are more enriched in deuterium than New Guinea and Indonesia. $\delta^2$H mean values are $-43.8 \pm 7.3$‰ for India and $-52.5 \pm 9.8$‰ for New Caledonia. Values of $\delta^2$H for vanillin from Madagascar and surrounding islands show more variation than the other origins analyzed (Figure 4). The mean $\delta^2$H value of vanillin samples from Madagascar is $-38.9 \pm 12.1$‰. The highest values of $\delta^2$H are found for French Polynesia and Africa, with a mean value of $-18.0 \pm 9.4$ and $-29.0 \pm 10.1$‰, respectively.

One of the highest values of $\delta^2$H is found for vanilla grown in Africa (Uganda and Congo). From Africa, there is a tendency toward decreasing values of $\delta^2$H moving east. This trend can also be seen in the regionalized cluster-based water isotope prediction (RCWIP) model developed by IAEA,[22−24] which shows the predicted annual $\delta^2$H in precipitation (Figure 1). The agreement between the measured $\delta^2$H values of vanillin and the RCWIP model supports that the plants incorporate water from its surroundings without significant isotopic fractionation.[13]

Tests showed that values of $\delta^{13}$C versus V-PDB for *V. planifolia* are significantly different from those of *V. tahitensis*, To use this knowledge about vanilla species, the geographical origins are separated into two groups: one group for origins growing only *V. planifolia* (Madagascar, Mexico, India, Africa, Indonesia, and New Caledonia) and a second group growing only *V. tahitensis* (French Polynesia and New Guinea). Values of $\delta^2$H versus V-SMOW for the geographical origins in the group of *V. planifolia* are tested using one-way ANOVA followed by a Tukey's post-test. This test shows that values of $\delta^2$H for vanillin originating from Indonesia can be separated from vanillin from Africa ($p < 0.001$) and Madagascar ($p < 0.01$). Furthermore, vanillin from New Caledonia can be separated from vanillin originating from Africa ($p < 0.001$) and Madagascar ($p < 0.05$). Values of $\delta^2$H versus V-SMOW for vanilla pods originating from French Polynesia and New Guinea are tested using a $t$ test and found to be significantly different ($p < 0.001$).

The combined use of results of $\delta^{13}$C and $\delta^2$H analyses for vanillin, extracted from vanilla pods, shows a relatively close clustering pending upon species as well as geographic location of growth. Analysis of $\delta$ values of carbon and hydrogen by compound-specific IRMS is a useful tool in the verification of the authenticity and traceability of vanilla pods.

## AUTHOR INFORMATION


### Corresponding Author

*Telephone: +45-35-88-71-23. Fax: +45-35-88-74-48. E-mail: asoha@food.dtu.dk.



### Funding

The authors thank A/S Einar Willumsen for supporting the project and partially providing the sample material.

### Notes

The authors declare no competing financial interest.


## REFERENCES


(1) Van Rijswijk, W.; Frewer, L. J. Consumer needs and requirements for food and ingredient traceability information. *Int. J. Consum. Stud.* **2012**, *36*, 282−290.

(2) Korthou, H.; Verpoorte, R. Vanilla. In *Flavours and Fragrances: Chemistry, Bioprocessing and Sustainability*; Berger, R. G., Ed.; Springer: Hannover, Germany, 2007; pp 203−217.

(3) European Parliament, Council of the European Union. *Regulation (EU) No 1169/2011 of the European Parliament and of the Council of 25 October 2011 on the Provision of Food Information to Consumers, Amending Regulations (EC) No 1924/2006 and (EC) No 1925/2006 of the European Parliament and of the Council, and Repealing Commission Directive 87/250/EEC, Council Directive 90/496/EEC, Commission Directive 1999/10/EC, Directive 2000/13/EC of the European Parliament and of the Council, Commission Directives 2002/67/EC and 2008/5/EC and Commission Regulation (EC) No 608/2004 Text with EEA Relevance*; European Parliament, Council of the European Union: Brussels, Belgium, 2011.

(4) Rao, S. R.; Ravishankar, G. A. Vanilla flavour: Production by conventional and biotechnological routes. *J. Sci. Food Agric.* **2000**, *80*, 289−304.

(5) Lubinsky, P. Cultivation systems. In *Vanilla*; Odoux, E., Grisoni, M., Eds.; CRC Press: Boca Raton, FL, 2010; pp 75−95.

(6) European Parliament, Council of the European Union. *Regulation (EC) No 1334/2008 of the European Parliament and of the Council of 16 December 2008 on Flavourings and Certain Food Ingredients with Flavouring Properties for Use in and on Foods and Amending Regulation (EC) No 1601/91 of the Council, Regulations (EC) No 2232/96 and*

*(EC) No 110/2008 and Directive 2000/13/EC*; European Parliament, Council of the European Union: Brussels, Belgium, 2008.
(7) Zamzuri, N. A.; Abd-Aziz, S. Biovanillin from agro wastes as an alternative food flavour. *J. Sci. Food Agric.* **2013**, *93*, 429−438.
(8) Hilmer, J.; Hammerschmidt, F.; Losing, G. Authentication of vanilla. In *Vanilla*; Odoux, E., Grisoni, M., Eds.; CRC Press: Boca Raton, FL, 2010; pp 237−249.
(9) O'Leary, M. H. Carbon isotopes in photosynthesis. *Bioscience* **1988**, *38*, 328−336.
(10) Lamprecht, G.; Pichlmayer, F.; Schmid, E. R. Determination of the authenticity of vanilla extracts by stable-isotope ratio analysis and component analysis by HPLC. *J. Agric. Food Chem.* **1994**, *42*, 1722−1727.
(11) Primrose, S.; Woolfe, M.; Rollinson, S. Food forensics: Methods for determining the authenticity of foodstuffs. *Trends Food Sci. Technol.* **2010**, *21*, 582−590.
(12) Kelly, S.; Heaton, K.; Hoogewerff, J. Tracing the geographical origin of food: The application of multi-element and multi-isotope analysis. *Food Feed Chem.* **2005**, *16*, 555−567.
(13) Ehleringer, J. R.; Dawson, T. E. Water uptake by plants: Perspectives from stable isotope composition. *Plant, Cell Environ.* **1992**, *15*, 1073−1082.
(14) Sessions, A. L. Isotope-ratio detection for gas chromatography. *J. Sep. Sci.* **2006**, *29*, 1946−1961.
(15) Bensaid, F. F.; Wietzerbin, K.; Martin, G. J. Authentication of natural vanilla flavorings: Isotopic characterization using degradation of vanillin into guaiacol. *J. Agric. Food Chem.* **2002**, *50*, 6271−6275.
(16) Greule, M.; Tumino, L. D.; Kronewald, T.; Hener, U.; Schleucher, J.; Mosandl, A.; Keppler, F. Improved rapid authentication of vanillin using $\delta^{13}C$ and $\delta^{2}H$ values. *Eur. Food Res. Technol.* **2010**, *231*, 933−941.
(17) Kaunzinger, A.; Juchelka, D.; Mosandl, A. Progress in the authenticity assessment of vanilla. 1. Initiation of authenticity profiles. *J. Agric. Food Chem.* **1997**, *45*, 1752−1757.
(18) Scharrer, A.; Mosandl, A. Progress in the authenticity assessment of vanilla. 2. $\delta^{13}C_{V\text{-}PDB}$ correlations and methodical optimisations. *Dtsch. Lebensm.-Rundsch.* **2002**, *98*, 117−121.
(19) Tenailleau, E. J.; Lancelin, P.; Robins, R. J.; Akoka, S. Authentication of the origin of vanillin using quantitative natural abundance $^{13}C$ NMR. *J. Agric. Food Chem.* **2004**, *52*, 7782−7787.
(20) Hoefs, J. Isotope fractionation processes of selected elements. In *Stable Isotope Geochemistry*; Hoefs, J., Ed.; Springer-Verlag: Göttingen, Germany, 2009.
(21) West, J. B.; Hurley, J. M.; Ehleringer, J. R. Stable isotope ratios of marijuana. I. Carbon and nitrogen stable isotopes describe growth conditions. *J. Forensic Sci.* **2009**, *54*, 84−89.
(22) Terzer, S.; Wassenaar, L. I.; Araguás-Araguás, L. J.; Aggarwal, P. K. Global isoscapes for $\delta^{18}O$ and $\delta^{2}H$ in precipitation: Improved prediction using regionalized climatic regression models. *Hydrol. Earth Syst. Sci.* **2013**, *17*, 4713−4728.
(23) International Atomic Energy Agency (IAEA). *Regionalized Cluster-Based Water Isotope Prediction (RCWIP) Model—Gridded Precipitation $\delta^{18}O|\delta^{2}H|\delta^{18}O$ and $\delta^{2}H$ Isoscape Data*; IAEA: Vienna, Austria, 2014; http://www.iaea.org/water (accessed June 25, 2014).
(24) International Atomic Energy Agency (IAEA)/World Meteorological Organization (WMO). *Global Network of Isotopes in Precipitation*; IAEA/WMO: Vienna, Austria, 2014; http://www.iaea.org/water (accessed June 25, 2014).

## MATERIALS AND METHODS

**Flower Collection Sites.** Flower collection sites were selected with the assistance of local beekeepers. The sites were spread across New Zealand between latitudes 34° and 41° S and between longitudes 171° and 179° E. The sites recommended by beekeepers were those regarded as yielding mānuka honey with measurable NPA; the Whanganui site was chosen to provide contrast as it yielded "bush" honey rather than mānuka honey with measurable NPA, and the Northland survey was undertaken because the variety of *L. scoparium* in Northland differs from the rest of New Zealand. The range of sites also afforded the opportunity for comparison with the study of honeys by Stephens.[12] Sampling at the Coromandel, East Cape, Waikato, Wairarapa, Whanganui, and Nelson sites was carried out during the flowering seasons (November−December) in 2009 and 2010 and for the East Cape and Waikato sites also in 2011. A separate collection of samples from the Northland region was made in 2010 and 2011. Most site visits in remote locations occurred once each year, and only specimens that were flowering on the day of the visit were sampled; this was an unavoidable bias. More accessible cultivated trees around the University of Waikato campus were used for testing of the effect of sampling methods, floral gender, and age on nectar quality.

**Sampling Protocol.** The trees sampled in 2009 were resampled in 2010 except for those that had died in the interim. In 2011 additional trees located within 50 m of the existing test trees at the East Cape sites were sampled. Further samples were collected in the Auckland and Waikato regions in 2012, both cultivars and wild accessions. The trees were sampled, whenever possible, on a fine day. Entire flowers were picked off individually or scraped off between two fingers drawn from the base toward the apex of the shoot. In addition to collection of flower samples in 2009, soil was collected (with a small trowel at 2 m from the trunk of each tree, samples approximately 15 × 10 × 20 cm in dimension), and foliage was collected for leaf oil analyses. All samples were stored in airtight bags and chilled with ice while transported, until they could be transferred to a freezer (−20 °C) for storage until analysis.

**Herbarium Depository.** Accessions collected from the wild were assigned to one of the two varieties recognized for *L. scoparium*: either var. *scoparium* or var. *incanum*.[13] Voucher specimens for each tree were deposited in the University of Waikato Herbarium (WAIK).

**Materials.** *o*-(2,3,4,5,6-Pentafluorobenzyl)hydroxylamine hydrochloride (PFBHA) (derivatization grade) and methylglyoxal (43.2%) were obtained from Fluka Analytical (Buchs, Germany). Dihydroxyacetone (97%), hydroxyacetone (technical grade 90%), sucrose (99+%), D-(−)-fructose (99+%), D-mannitol (98+%), and citric acid (99.5%) were obtained from Sigma-Aldrich (Sydney, Australia). 1-(Trimethylsilyl)imidazole (TMSI) was obtained from Thermo Scientific (Scoresby, Australia). D-(+)-Glucose (AR) grade was obtained from BDH Laboratory (Murarrie, Australia). Deionized water was obtained from a Barnstead Epure water system at 17.9 MΩ. Dichloromethane (analytical grade) was obtained from Ajax Finechem (Sydney Australia) or purified using a Pure Solv solvent purification system model PS-SD-5 (Innovative Technology, Amesbury, MA, USA).

**Extraction of Nectar.** The methodology was based upon that of Morrant et al.[14] Frozen flowers were removed from the sample bag, giving preference whenever possible to open flowers in good condition. Either 20 (20F), 10 (10F), or 1 (1F) flower(s) was placed in 4, 2, or 1 mL of water, respectively, and kept for 20 min. After standing, the flowers were removed and the nectar/water solution was frozen if analysis was not performed immediately. Ten replicates of the 20F or 10F method were carried out for each bag/tree when there was sufficient material.

**Single-Flower Test.** Some of the trees, especially the Northland and East Cape samples collected in 2011, yielded insufficient flowers for the 10F or 20F test. Comparison of the 1F and 20F tests was carried out using replicates ($n$ = 10) from three *L. scoparium* 'Martinii' (*L.* 'Martinii') trees sampled on the University of Waikato campus.

**Preparation of Nectar for Dihydroxyacetone Detection.** To a vial containing hydroxyacetone (internal standard, 10 μL, 0.5 mg/mL) and nectar extract (20F, 200 μL; 10F, 200 μL; 1F, 400 μL) was added and mixed PFBHA (50 μL, 20 mg/mL in a pH 4 citric buffer), and the mixture was kept for 1 h. Dichloromethane (20F, 2 mL; 10F, 2 mL; 1F, 1 mL) was added and mixed. The vial was then placed in a freezer (0 °C) until the aqueous layer froze to aid extraction. An aliquot (1 mL) of the dichloromethane layer was withdrawn into a GC vial (1.5 mL). TMSI (50 μL) was added, mixed, and allowed to stand (1 h) before analysis by GC-FID.

**Preparation of Nectar for Sugar Detection.** To a vial containing mannitol (internal standard, 5 μL, 5 mg/mL) was added nectar extract (20F, 20 μL; 10F, 20 μL; 1F, 50 μL), and the vial contents were freeze-dried. To the dry sample was added and mixed TMSI (50 μL), and the mixture was kept at room temperature. Heptane (1 mL) was added with mixing before analysis by GC-FID.

**GC-FID Parameters.** The column used was a 0.32 mm × 0.25 μm i.d., 30 m, Zebron ZB-5 capillary GC column (Agilent Technologies, Santa Clara, CA, USA). For all methods a 2 μL injection into a splitless inlet with a 2 mL/min purge flow was used, with the FID held at 300 °C. $H_2$ flow was 30 mL/min; air flow, 400 mL/min; and $N_2$ makeup flow, 10 mL/min.

For the detection of dihydroxyacetone, the inlet was set to 250 °C and used a $H_2$ carrier gas flow of 2 mL/min. The temperature program was 130 °C held for 5 min, increased at 10 °C/min to 250 °C, and then held at that temperature for 6 min. Dihydroxyacetone was quantitated against hydroxyacetone as an internal standard and used a calibration curve constructed over the range of 0.003−0.015 mg/mL. The limits of detection for dihydroxyacetone and methylglyoxal were $3.00 \times 10^{-8}$ and $4.58 \times 10^{-7}$ g/mL, respectively. The limits of quantitation for dihydroxyacetone and methylglyoxal were $1.00 \times 10^{-7}$ and $1.53 \times 10^{-6}$ g/mL, respectively.

For the detection of sugars, the inlet was set to 280 °C with a $H_2$ carrier gas flow of 4 mL/min. The temperature program was 100 °C held for 1 min, increased at 30 °C/min to 200 °C, increased at 10 °C/min to 250 °C, and finally increased at 30 °C/min to 300 °C. The sugars were quantitated against D-mannitol as an internal standard with a response factor found for each sugar. The response was measured over the range of 50−150 mg/mL and gave fructose, 0.5335; glucose, 0.8217; and sucrose, 0.7126. Fructose, glucose, and sucrose were summed to give total sugars.

**Expression of Results for Dihydroxyacetone Content.** Dihydroxyacetone content is expressed as a ratio of DHA/total nectar sugar (Tsugar). The assumption was made that all of the sugars in honey derive ultimately from the nectar and that the ratio for dihydroxyacetone to total sugar would be indicative of the expected ratio in the early honey before maturation because dihydroxyacetone might be expected to have volatility similar to that of the sugars. Ten replicates for each tree were assayed and after outliers were determined (single outlier and largest/smallest or two largest/smallest tests);[17] results are expressed as the mean and 95% standard error.

**Measurement of Nectar DHA/Tsugar in Australian Species.** The nectars of some Australian species (*L. juniperinum* Sm., *L. liversidgei* R.T.Baker & H.G.Sm., *L. laevigatum* (Gaertn.) F.Muell.) were analyzed at the University of the Sunshine Coast in southern Queensland. Sampling from wild populations occurred principally in the coastal region of northern New South Wales. Sample preparation was as above, but GC-MS was utilized.

**GC-MS Parameters.** The column used was a 30 m × 0.25 mm × 0.25 μm i.d. Elite 5MS gas capillary column (PerkinElmer, Melbourne, Australia). Analyses were carried out using a PerkinElmer Clarus 580 gas chromatograph coupled to a PerkinElmer Clarus SQ85 mass spectrometer (all PerkinElmer instruments were supplied by PerkinElmer, Melbourne, Australia). The carrier gas (helium) flow was set to 1 mL/min for both the sugar and dihydroxyacetone analyses. For the sugar analysis the inlet was configured to shut the split from 0.20 to 1.00 min and open with a 50:1 ratio; it was maintained at 280 °C. The oven program was the same as described for the New Zealand samples. Compound ionization was at 70 eV electron impact, analyzing $m/z$ 70−440 over 4.50−11.00 min. For the dihydroxyacetone analysis, the inlet was configured as for the sugar analysis except the temperature was maintained at 250 °C. The oven

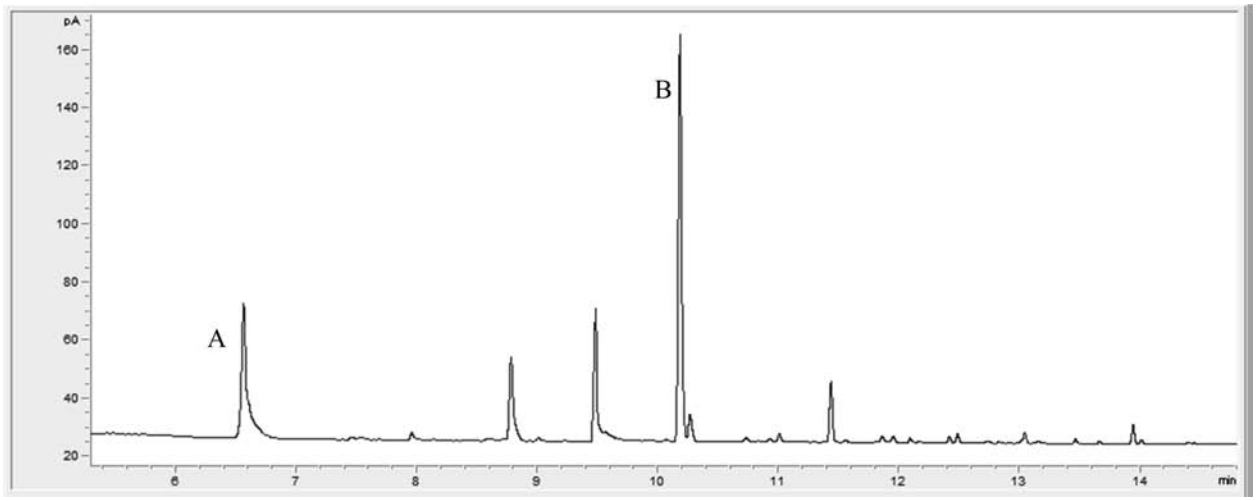


**Figure 1.** GC-FID chromatogram of a nectar sample used for dihydroxyacetone quantitation: (A) hydroxyacetone used as internal standard; (B) dihydroxyacetone.

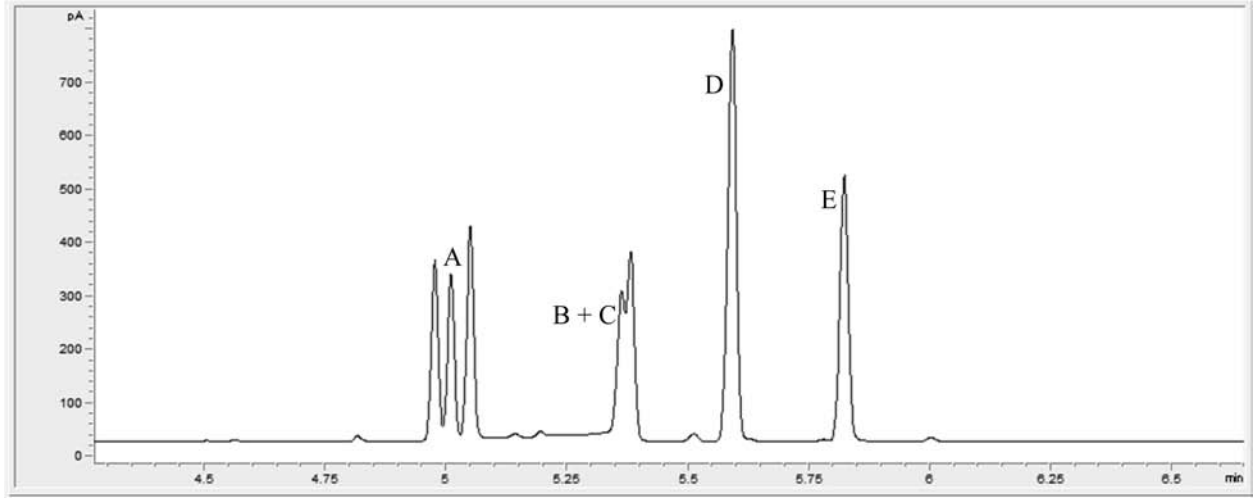


**Figure 2.** GC-FID chromatogram of a nectar sample used for sugar quantitation. The peaks at (A) are fructose, those at (C) and (E) are glucose, and that at (D) is mannitol used as an internal standard. (B) arises from an organic acid and was not included in the glucose peak area.

program was the same as that outlined for the New Zealand specimens. Compound ionization was at 70 eV electron impact, analyzing $m/z$ 45−440 over 4.50−23.00 min.

**Statistical Analyses.** Statistical analyses were carried out using Microsoft Excel or Minitab 16.

## RESULTS AND DISCUSSION

To simplify discussion, nectar DHA/Tsugar has been divided into three classifications: low (<0.001 mg/mg), moderate (0.001−0.002 mg/mg), and high (>0.002 mg/mg).

**Choice of Methodology for Nectar Sampling and Extraction.** Stephens et al.[15] analyzed nectar of *L. scoparium* ($n$ = 6) for phenolics and for methylglyoxal; the methodology employed by those authors was to use direct sampling by pipet.[15] For the current study this method was considered, but it was decided that it was far too time-consuming for this broad-based preliminary survey, which was often carried out in isolated areas, accessed only with difficulty and often under inclement conditions. This view is supported by the conclusions of Morrant et al.,[14] who have reviewed methods of nectar collection.

Two methods of extracting nectar from the previously collected flowers were compared: washing (20 min) and individual dipping (three times). Each method was repeated eight times using 20 flowers per sample for flowers from the same tree, and the absolute dihydroxyacetone content was analyzed; mean and %RSD were respectively 0.0056 mg (26%) and 0.00020 mg (90%). Washing was therefore used in this survey. Morrant et al.[14] also recommended washing of cut flowers as the most practical method and, indeed, found this to be preferable to and more reproducible than the use of micropipets.[14]

Stephens et al.[15] did not assay dihydroxyacetone; methylglyoxal was assayed but only reported as a trace, so no numerical comparison between methods in that study and the current study is possible.

**Method Validation.** *Gas Chromatography Methodology for Analysis of Dihydroxyacetone and Methylglyoxal with PFBHA Derivatization.* PFBHA derivatization with analysis by reversed phase HPLC has been used previously to assay dihydroxyacetone and methylglyoxal simultaneously in honey;[4] it was decided that GC-FID would supply the requisite sensitivity for nectar samples. The derivatization and GC-FID

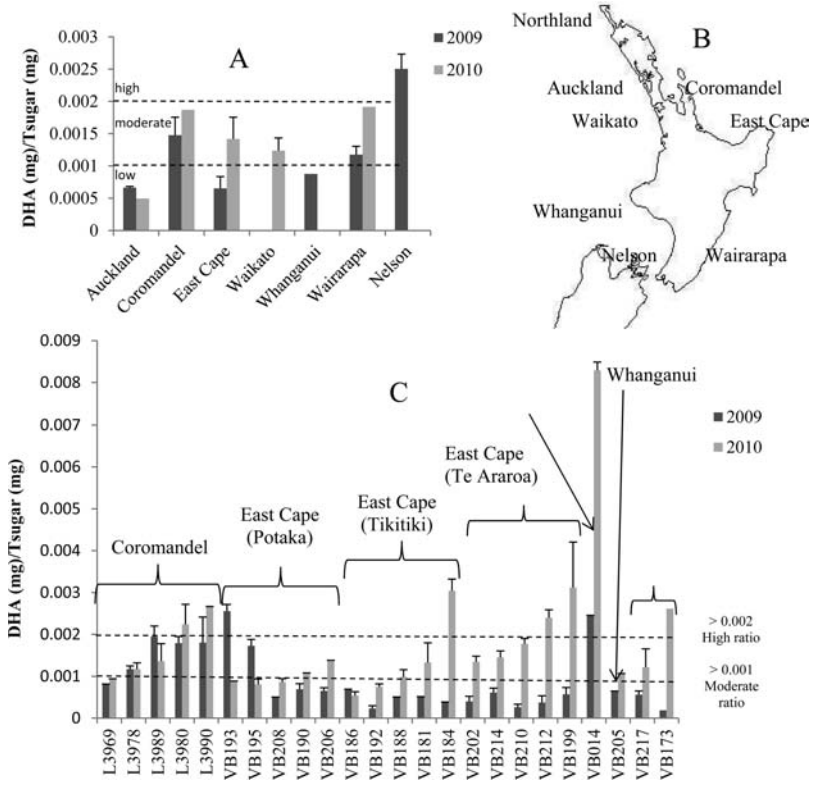


**Figure 3.** (A) Plot of the mean nectar DHA/Tsugar of all wild trees for each region for the two flowering seasons 2009 and 2010 (error bars are standard error values). (B) Map of locations across the North Island and upper South Island of New Zealand. (C) Plot of nectar DHA/Tsugar values for all trees that were sampled in both 2009 and 2010, grouped into regions and then ascending order of 2010 value. The only tree from Waikato that was tested in both years was a cultivar growing in a suburban garden (not included in panel A; error bars are standard error values).

analysis of samples was optimized using standards of hydroxyacetone, dihydroxyacetone, and methylglyoxal. Nectar samples spiked with these standards were used to ensure that the derivatizing agent PFBHA was present in sufficient excess. Under the conditions used, hydroxyacetone (internal standard), dihydroxyacetone, and methylglyoxal eluted at 6.6, 10.1, and 13.1 min, respectively. Responses for dihydroxyacetone and methylglyoxal (measured as analyte/internal standard versus analyte) were linear from 0 to 0.0016 mg ($R^2$ = 0.9998) and from 0 to 0.015 mg ($R^2$ = 0.9815), respectively. The LOQ for dihydroxyacetone corresponded to a minimum detectable mass of 20.5 ng and that for methylglyoxal to 313 ng. The LODs were respectively 6.16 and 93.8 ng. Methylglyoxal was never detected at a level that allowed quantitation in any nectar samples in this study (Figure 1); the presence of methylglyoxal in nectar samples assayed by others[15] might be because the methodology employed was more sensitive than that used here or might indicate that the flowers or nectar samples had been exposed to elevated temperatures or stored for prolonged periods at room temperature prior to analysis.[16]

*Gas Chromatography Methodology for Analysis of Sugars with TMS Derivatization.* Response factors of sucrose, glucose, and fructose relative to the internal standard mannitol were ascertained by varying weight ratios and comparing area ratios and were 0.7126, 0.8217, and 0.5335, respectively. Varying the quantity of derivatization agent from 50 to 200 μL demonstrated that 50 μL was sufficient excess. As sugars were always readily observed, LOD and LOQ were not required. Under the chromatographic conditions used for the analysis, fructose (multiple furanose and pyranose anomers) eluted at 4.9−5.1 min, glucose (pyranose anomers) at 5.6 and 5.8 min, and mannitol at 5.7 min (Figure 2).

*Duration of Washing for Nectar Extraction.* The duration of washing was based upon the method of Morrant et al.,[14] who found no difference between 1 and 20 min but a significant difference between 20 and 60 min. In this study extended washing of the flowers (230 min) resulted in a ∼25% decrease in DHA/Tsugar, presumably because sugar was leaching from other parts of the flower.

*Reproducibility Tests.* To ascertain day-to-day reproducibility of the method, samples from eight trees were assayed (20F, $n$ = 10) on two different days. Statistically, three of the trees gave significantly different results between days ($p$ = 0.0010, 0.0007, and 0.000), whereas five did not ($p$ = 0.1597, 0.8899, 1.000, 1.000, and 1.000), but in only one case did a tree change its DHA/Tsugar classification. The weather conditions on each day of sampling may have had an influence on these results as rain and wind can remove nectar from the open bowl of the mānuka flower, as can visits by pollinators.

*Stability of Nectar Extract.* The stability of the nectar extract was ascertained for samples from three trees in which replicates ($n$ = 10) were stored frozen and others ($n$ = 5) were left to stand at room temperature overnight before analysis. The samples that were left to stand darkened in color overnight, but a $z$ test for two sample means showed that there was no change in the DHA/Tsugar ratio. To test the stability of the derivatized samples, duplicates from one tree were prepared for both dihydroxyacetone and sugar assays and injected into the GC at the beginning and the end of the sequence; the time lapse for the sugar assay was ∼315 min and for the dihydroxyacetone

assay, ~702 min. The results for DHA/Tsugar were identical to two significant figures.

*Comparison of 10-Flower (10F) and 20-Flower (20F) Tests.* The 10F test was compared with the 20F test using replicates ($n$ = 10) from three different trees; the difference between the two tests was insignificant at the 95% confidence level. The percentage relative standard deviation was higher for the 10F than for the 20F test but did not exceed 25%.

*Comparison of the Single-Flower Test (1F) and the 20F Test.* Some of the trees, especially the Northland samples and the East Cape samples collected in 2011, yielded insufficient flowers for the 20 or 10 flower test. Comparison of the 1F and 20F tests was carried out using replicates ($n$ = 10) from three trees. The ranges of percentage difference between the two tests for the two ratios, DHA/Tsugar and fructose/glucose, were 5.52−20.21 and 1.83−17.44, respectively. The percentage relative standard deviation for the 1F test was much higher than for the 20F test and also much higher than the percentage difference between the two methods. This indicates, as might be expected, that there is variability between individual flowers on the same tree. To confirm that biological variation exceeded experimental variation, replicates ($n$ = 5) of a single extraction (20F) were compared to multiple extractions (20F, $n$ = 10) for three different trees. For the single extraction percentage relative standard deviations were 1.20, 2.54, and 3.13 for the three trees, and the corresponding values for the multiple extractions were 14.36, 9.06, and 25.80. This confirms that the greatest source of variation is that within a single tree, the cause of which is not yet established but may include active removal by pollinators and variation related to the different stages of flower maturity.

*Transference of Nectar.* The residue from an empty sample bag was rinsed out and assayed, and dihydroxyacetone equivalent to about half that found in 20 flowers was measured (a bag typically contained ~500 flowers). This confirms that transfer of nectar between flowers and the bag and presumably also between flowers is occurring; this may partially account for the variation observed in the single-flower test.

**Variation of Nectar DHA/Tsugar between Regions and Years and within Regions.** *Variation of Nectar DHA/Tsugar between Regions and Years.* Regional and annual variation in nectar DHA/Tsugar was observed (Figure 3). Only the Coromandel and East Cape regions had sufficient samples in both years for a statistical test of the effect of sampling year. A balanced ANOVA showed that the mean DHA/Tsugar for the East Cape region was significantly different ($p$ = 0.02) between 2009 and 2010, whereas the Coromandel region did not differ between years ($p$ = 0.5). The change observed in the East Cape samples was sufficient to alter the classification from low in 2009 to moderate in 2010.

Only the Coromandel, East Cape, and Wairarapa regions had sufficient samples for a test of effect of region on DHA/Tsugar. A one-way ANOVA test followed by mean separation using Tukey's method detected an overall region effect ($p$ = 0.05). Mean nectar DHA/Tsugar did not differ between the Coromandel and Wairarapa samples, but the East Cape values were lower in both 2009 and 2010.

*Variation within Regions.* Significant differences in nectar DHA/Tsugar were observed between trees within the Coromandel sampling site (Figure 3). All trees were located within a radius of 100 m, but a range of classifications from low to high was observed. There were three soil orders present at this Coromandel site, but no relationship between soil order and DHA/Tsugar could be found. To further investigate variation within a region, an additional collection was made in the East Cape region in 2011. From eight sites, one or more trees of various classifications (low−high), which had been sampled previously, were selected, and other trees within a 50 m radius were also sampled. Even within a narrow radius individual trees differed significantly in their nectar DHA/Tsugar (Table 1), in some cases ranging from high to low classifications.

The Northland/Auckland region was surveyed in 2010 and 2011 (Figure 4). For this survey the region was divided into two zones: Northland, encompassing the area from Cape Reinga to 36.3° S (zone 1) and the Auckland/Coromandel regions south of 36.3° S (zone 2). In zone 1 *L. scoparium* var. *incanum* Cockayne predominates,[18] whereas in zone 2 and the rest of New Zealand most wild mānuka honeys are considered to be *L. scoparium* var. *scoparium*. The individual tree returning an exceptionally high value belonged to *L. scoparium* var. *incanum* located in a maintained area. The individual with a midmoderate result was also from *L. scoparium* var. *incanum*. The only other individual demonstrating a high classification belonged to *L. scoparium* var. *scoparium* as did the two specimens with low−moderate results. The remaining individuals consisted of a mixture of var. *scoparium* ($n$ = 23) and var. *incanum* ($n$ = 16), all of which scored in the low classification. No apparent trend exists relating either of these varieties to high nectar DHA/Tsugar.

Stephens[12] grouped 463 mānuka honey samples (from a single season, 2001−2002 and supplied by apiarists) by region and by mean "unique mānuka factor" (UMF), a measure of nonperoxide antibacterial activity. Waikato ($n$ = 6) and Coromandel ($n$ = 23) returned high values of activity (>14 UMF), although other Coromandel honeys returned intermediate levels ($n$ = 16; 12.6 UMF) and low levels ($n$ = 63; 10.5 UMF). Some East Coast honeys returned intermediate levels of activity ($n$ = 22, 12.5 UMF), whereas others returned lower levels ($n$ = 17; 10.9 UMF). Wairarapa honeys returned low levels of activity ($n$ = 12; 9.4 UMF) as did samples from the northern South Island ($n$ = 41; 9.1 UMF), whereas Northland demonstrated high levels of activity ($n$ = 35; 14.8 UMF). These findings concur with the variability observed in the current study in both the Coromandel region and the East Cape and, to some extent, the finding that the East Cape values were lower than those for the Coromandel. However, the Wairarapa, Northland, and northern South Island results are in contrast. The Waikato result, with the exclusion of the garden cultivar, is somewhat lower than expected from Stephens's results, which relate to honeys originating from wild mānuka in swamplands, but in the current study the trees were sampled from drier locations, which might possibly account for the observed difference.

Caution should be exercised when these two studies are compared because variability of classification of dihydroxyacetone content between seasons was observed in the current study at one location, and further work (unpublished data) indicated that the conditions of storage by the apiarist strongly influence the efficiency of conversion of dihydroxyacetone to methylglyoxal in maturing mānuka honey and hence the final UMF value.

**Nectar DHA/Tsugar in Commercial New Zealand Originated Cultivars.** The specimen used to first illustrate the presence of dihydroxyacetone in nectar was a red-pink-flowered cultivar *L.* 'Martinii', which is widely available from

**Table 1. Comparison of DHA/Tsugar in Trees Sampled in 2011**

| site | specimen ID | DHA/Tsugar (mg/mg) |
|---|---|---|
| 1 | **VB184**[a] | **0.00032** |
| | VB052 | 0.00049[b] |
| | VB074 | NQ[c] |
| | VB107 | 0.00082[c] |
| 2 | **VB192** | **0.00086** |
| | VB050[b] | 0.00039[c] |
| 3 | **VB197** | **0.00095** |
| | VB088[b] | 0.00141[c] |
| | VB090 | 0.00071[c] |
| | VB131[b] | 0.00261[c] |
| | VB146[b] | 0.00271[c] |
| 4 | **VB193** | **0.00088** |
| | VB002[b] | 0.00079 |
| | VB010 | 0.00104[c] |
| | VB089[b] | 0.00066 |
| 5 | **VB195** | **0.00081** |
| | VB053 | 0.00080 |
| | VB054 | 0.00032[c] |
| | VB140[b] | 0.00063 |
| 6 | **VB181** | **0.00133** |
| | VB051 | 0.00053[c] |
| | VB083 | 0.00064[c] |
| | VB099 | 0.00186[c] |
| | VB100 | 0.00109 |
| | VB105[b] | 0.00088[c] |
| | VB142 | 0.00107[c] |
| 7 | **VB183** | **0.00034** |
| | VB093 | 0.00242[c] |
| | VB114 | 0.00248[c] |
| | VB115 | 0.00091[c] |
| | VB145 | 0.00095[c] |
| 8 | **VB199** | **0.00312** |
| | **VB202** | **0.00130** |
| | **VB214** | **0.00145** |
| | VB137 | 0.00421[c] |
| | VB070 | 0.00200 |
| | VB067 | 0.00195 |
| | VB071 | 0.00168 |
| | VB102 | 0.00044[c] |

[a]The trees (and the corresponding DHA/Tsugar value) originally sampled in 2010 are shown in bold. [b]Tree with a significantly different DHA/Tsugar from the original tree at that site. [c]Dihydroxyacetone was below the level of quantitation.

plant nurseries and which was growing in a suburban garden in Hamilton. This cultivar consistently gave substantially higher nectar DHA/Tsugar values than any of the wild specimens tested (Figure 3).

*L.* 'Martinii' is believed to be a cross between the pink-flowered, *L. scoparium* 'Keatleyi' and the red-flowered *L. scoparium* 'Nichollsii' (*L.* 'Nichollsii'),[19] which is no longer found in New Zealand, but *L. scoparium* 'Red Ensign' (*L.* 'Red Ensign') is thought to be a newer name for *L.* 'Nichollsii Improved'.[19] The nectar DHA/Tsugar for several *L.* 'Martinii' and *L.* 'Red Ensign' plants from which flowers were collected in 2011 and 2012 (including VB014 from the original survey) was classified as high or very high (Table 2). When compared to regional variation between wild plants, only the Nelson region had a mean DHA/Tsugar approaching that of *L.* 'Martinii' and *L.* 'Red Ensign' (between 0.002 and 0.003 in 2009); all other regions had means <0.002 (Figure 3).

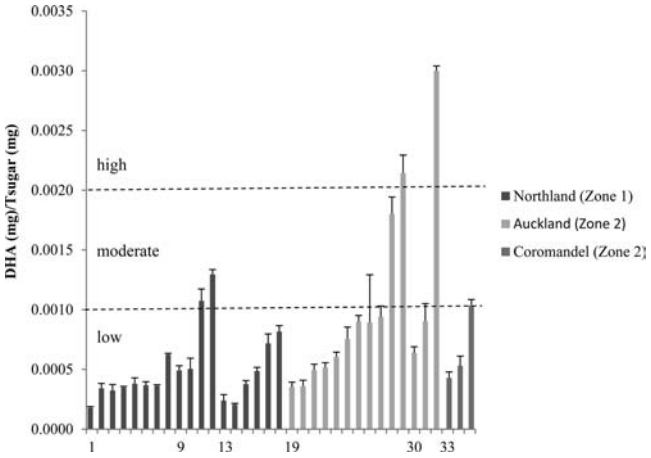


**Figure 4.** Nectar DHA/Tsugar values for Northland, Auckland, and Coromandel trees sampled between 2010 and 2011 (error bars are standard error values). The numbers on the *x*-axis indicate the first tree in each zone of sampling. Trees 1–8 were from upper Northland, trees 9–12 from upper East Northland, trees 13–18 from lower East Northland, trees 19–29 from North Auckland, trees 30–32 from South Auckland, and trees 33–35 from the Coromandel region.

**Table 2. DHA/Tsugar Values for *L.* 'Martinii' and *L.* 'Red Ensign' Collected in 2011–2012**

| sample | variety | year | DHA/Tsugar (mg/mg) |
|---|---|---|---|
| VB014 | *L.* 'Martinii' | 2011 | 0.00435 |
| 1 | *L.* 'Martinii' | 2011 | 0.00353 |
| 2 | *L.* 'Martinii' | 2011 | 0.00374 |
| 3 | *L.* 'Martinii' | 2012 | 0.00287 |
| 4 | *L.* 'Martinii' | 2012 | 0.00402 |
| 5 | *L.* 'Martinii' | 2012 | 0.00379 |
| 6 | *L.* 'Martinii' | 2012 | 0.00304 |
| 7 | *L.* 'Red Ensign' | 2012 | 0.00318 |
| 8 | *L.* 'Red Ensign' | 2012 | 0.00429 |
| 9 | *L.* 'Red Ensign' | 2012 | 0.00511 |
| 10 | *L.* 'Martinii' | 2012 | 0.00171 |

In addition to the aforementioned pink- and red-flowered garden cultivars, >150 cultivars have been named. These have been obtained from the wild and also selected in cultivation.[5,19−21]

To further examine the possibility that some garden cultivars may exhibit unusually high nectar DHA/Tsugar, a collection of cultivars was made at the Auckland Botanic Gardens in a single day (10F, 10 replicates) (Table 3). All cultivars with levels of dihydroxyacetone below the limit of quantitation were still producing nectar sugars; that is, the Tsugar values were readily measured. From this small, preliminary survey it would appear that red or pink coloration in a cultivar is often associated with high nectar DHA/Tsugar but that this is also often suppressed to moderate or low when a double flower is present; the only


dx.doi.org/10.1021/jf5045958 | J. Agric. Food Chem. 2014, 62, 10332−10340

**Table 3. Comparison of Nectar DHA/Tsugar Values of Mānuka Cultivars at the Auckland Botanic Gardens in 2012**

| cultivar[a] | description | DHA/Tsugar |
|---|---|---|
| ***L.* 'Nanum'** | pink single-flowered dwarf | NT[b] |
| *L.* 'Tui' | pink-centered single-flowered dwarf | 0.00435 mg/mg **HIGH** |
| *L.* 'Kea' | pink single-flowered dwarf | 0.00105 mg/mg **HIGH** |
| *L.* 'Wiri Shelley' (*L.* 'Kea' × *L.* 'Wiri Sandra') | pink single-flowered | 0.00452 mg/mg **HIGH** |
| ***L.* 'Sherryl Lee'** | pink single-flowered | NT[a] |
| *L.* 'Wiri Sandra' | pink single-flowered | 0.00312 mg/mg **HIGH** |
| ***L.* 'Pink Pearl'** (seed parent = *L.* 'Album Flore-pleno') | white double-flowered | NT[a] |
| *L.* 'Sunraysia' | white and red double-flowered | NQ[c] **LOW** |
| *L.* 'Rose Glory' | pink double-flowered | NT[a] |
| *L.* 'Wiri Joan' (seed parent = *L.* 'Rose Glory') | red double-flowered | NQ **LOW** |
| *L.* 'Rose Queen' | pink double-flowered | 0.00079 mg/mg **LOW** |
| *L.* 'Wiri Linda' (seed parent = *L.* 'Rose Queen') | white double flowered | 0.00079 mg/mg **LOW** |
| *L.* 'Crimson Glory' | red double-flowered | 0.00099 mg/mg **LOW** |
| *L.* 'Blossom' | pink double-flowered | 0.00103 mg/mg **MODERATE** |
| *L.* 'Autumn Glory' | pink double-flowered | 0.00144 mg/mg **MODERATE** |
| *L.* 'Rosy Morn' | pink double-flowered | 0.00152 mg/mg **MODERATE** |
| *L.* 'Burgundy Queen' | red double-flowered | 0.00208 mg/mg **HIGH** |
| *L.* 'Wiri Donna' | red single-flowered | 0.00414 mg/mg **HIGH** |
| ***L.* 'Flore-pleno'** | pink double-flowered | NT[a] |
| *L.* 'Snow Flurry' | white double-flowered | NQ[b] **LOW** |
| *L.* 'Red Damask' | red double-flowered | NQ[b] **LOW** |
| ***L.* 'Nichollsii'** | red double-flowered | NT[a] |
| *L.* 'Red Ensign' | red single-flowered | NT[a] |
| *L.* 'Wiri Amy' (seed parent = *L.* 'Red Ensign') | red single-flowered | 0.00694 mg/mg **HIGH** |
| *L.* 'Wiri Kerry' (seed parent = *L.* 'Wiri Amy') | red double-flowered dwarf | NQ[b] **LOW** |
| **unconfirmed parentage** | | |
| *L.* 'Black Robin' | red single-flowered | 0.00598 mg/mg **HIGH** |
| *L.* 'Elizabeth Jane' | red single-flowered dwarf | 0.00742 mg/mg **HIGH** |

[a]Cultivars are presented in groups, with the putative original seed parents of each group in bold.[4,19] [b]Cultivars not available for testing in this survey, but known to belong within the same group. [c]Dihydroxyacetone was below the level of quantitation.

exception to this is *L. scoparium* 'Burgundy Queen', a red double that was classified as high. High nectar DHA/Tsugar values are observed in *L. scoparium* 'Nanum Tui' (*L.* 'Nanum Tui'), a single-flowered dwarf ,and in pink single-flowered cultivars also derived from *L. scoparium* 'Nanum'.

**Nectar DHA/Tsugar in Australian Species of *Leptospermum*.** Australia has 87 species of *Leptospermum* inhabiting various ranges.[21] Honey from *L. polygalifolium* has also been shown to contain dihydroxyacetone and methylglyoxal,[4] indicating that production of dihydroxyacetone in the nectar is found elsewhere in the genus. To confirm this, a limited survey of Australian species was carried out in southern Queensland at the University of the Sunshine Coast. Samples were obtained from wild populations in southern Queensland or northern New South Wales, which abuts southern Queensland. *Leptospermum scoparium* 'Merinda' (*L.* 'Merinda'), which is a complex cross between two interspecific hybrids of Australian species, was also included in this survey, but the plant sampled was growing in New Zealand. Some of the Australian *Leptospermum* species contained dihydroxyacetone (in two cases being nonquantatible), and DHA/Tsugar differed both between and within species (Table 4). This confirms that

**Table 4. DHA/Tsugar Ratios in Australian Species of *Leptospermum***

| species | sample | DHA/Tsugar (mg/mg) |
|---|---|---|
| *L. liversidgei* | 1 | 0.00273 |
| | 2 | 0.00084 |
| *L. juniperinum* | 1 | NQ[a] |
| | 2 | 0.00386 |
| | 3 | 0.00159 |
| *L. laevigatum* | 1 | NQ[a] |
| *L.* 'Merinda' | 1 | 0.00069 |

[a]Dihydroxyacetone was below the level of quantitation.

production of high levels of dihydroxyacetone in the nectar is a characteristic of the genus *Leptospermum* and that the same degree of variation in DHA/Tsugar seen in *L. scoparium* probably occurs in other *Leptospermum* species as well.

**Other Factors That Might Relate to DHA/Tsugar.** *Composition of Leaf Oil.* Some degree of correlation occurred between leaf oil and nectar DHA/Tsugar in some regions (East Cape and Wairarapa regions; adjusted $R^2$ values of 80.7 and 88.9%, respectively) with multivariate analysis of different leaf oils in different areas. This agrees with recently published findings[22] that FT-Raman spectroscopy of leaf material can be used as a predictive model for dihydroxyacetone levels in floral nectar of mānuka.

*Sex of the Flower.* *L. scoparium* is andromonecious, that is, it bears both hermaphrodite and male-only flowers.[23] A significant difference was observed between flowers of different sexes with male flowers having higher DHA/Tsugar due to elevated levels of dihydroxyacetone.

*Age of the Flower.* The hypanthium is initially green in new flowers and as a general rule turns dark red with age. Both dihydroxyacetone and Tsugar values were higher in flowers with red hypanthia.

*Soil Composition.* No correlation could be found with soil order or soil quantifiable components. This is similar to the observation that soil properties had no discernible effect upon leaf oil[10] or the activity of honey derived from a certain area.[12]

*Coverage with Sooty Mold.* Sooty mold indicates a scale insect infestation, which is a potential stressor for the plant and which might affect dihydroxyacetone production, but no correlation was found between DHA/Tsugar and coverage with sooty mold.

**Nectar Sugars.** Dihydroxyacetone in nectar could be produced by the plant or by microbes present in the flower.[24,25] Sucrose was not detected in any of the *L. scoparium* nectars

assayed, indicating a hexose-dominant nectar of the type associated with pollination by small, unspecialized insects.[26] This concurs with classification of the dish-shaped mānuka flower as open-access and visited by a variety of insect feeders/pollinators.[27] The ratio of fructose to glucose in the 2009 and 2010 North Island nectar samples was 1.65:1 ($R^2$ = 0.9164), clearly differing from the 1:1 ratio expected if the nectar was solely derived from the hydrolysis of sucrose. The predominance of fructose found in the nectars of *L. scoparium* in the field may indicate the effect of a microorganism, specifically yeast, transported by visiting insects such as ants.[24,25]

An ongoing study of fructose/glucose ratios in mānuka honeys of various NPA found a mean of 1.29 and a range from 0.98 to 1.67 ($n$ = 1483, $s$ = 0.10) (P. Bray, personal communication). There is no obvious explanation for the difference between the honeys and the nectar as it seems unlikely that the nectar extraction procedure utilized here is selective for fructose. Given that visitation by insects and colonization by microbes are essentially random, it is possible that this particular set of trees simply fell to the high end of the range expressed by the honeys.

This method was developed and validated for assaying DHA/Tsugar in floral nectar from cut flowers and was applied to a survey of wild *L. scoparium* and also for a survey of cultivars and a limited survey of Australian species. Within the wild populations, variation in DHA/Tsugar within and between regions and, in some cases, between seasons was observed although no relationship to soil composition could be elucidated. Results were partially aligned with a previous survey of honeys from these regions[12] with the reservation that levels of dihydroxyacetone in nectar do not always accurately reflect methylglyoxal in honey because of the effects of storage conditions. In some regions leaf oil composition could be correlated to DHA/Tsugar, and this is corroborated by a study demonstrating that spectroscopy of leaf material can be used to predict dihydroxyacetone content of nectar.[22] Nectar sugars indicate that the flower is pollinated by small nonspecialized insects and that sugar composition is likely to be affected by microbial species transferred from a variety of pollinators. Horticultural cultivars frequently exhibited very high nectar DHA/Tsugar, and this is likely to indicate a genetic predisposition. Australian species also exhibited elevated nectar DHA/Tsugar, and variation within and between species was observed; this confirms that the phenomenon operates at the genus level. This was, however, a limited survey, and a larger survey needs to be undertaken of further species and cultivars in Australia and extended to other wild populations in New Zealand. There were indications that the age and the sex of the flower may influence DHA/Tsugar, and more detailed studies under controlled conditions will be reported separately.

## ■ ASSOCIATED CONTENT

### Supporting Information

Complete information on location and type of trees sampled, details of experimental procedures, and results for investigation of other factors that might influence DHA/Tsugar (Tables S1 and S2 and Figures S1-S6 as well as additional text and experimental details). This material is available free of charge via the Internet at http://pubs.acs.org.

## ■ AUTHOR INFORMATION

### Corresponding Author

*(M.R.) E-mail: mtr9@students.waikato.ac.nz.

### Funding

S.W. and J.K. were supported by TechNZ M.Sc. Scholarships during the course of this work.

### Notes

The authors declare no competing financial interest.

## ■ ACKNOWLEDGMENTS

We thank Steens New Zealand Ltd., Nature's Country Gold Ltd., Evan Rarere, and Lochinver Station for organizing access to sites for collection and/or providing honey samples. We also thank Graeme Platt, Noel Porter, and Michael Howes for collecting flower samples in Northland/Auckland, the Nelson region, and Northern New South Wales, respectively, and Jack Hobbs and the staff of Auckland Botanic Gardens for allowing access to their collection of cultivars and for assistance with identification of *L.* 'Martinii' and other cultivars.

## ■ ABBREVIATIONS USED

PFBHA, *O*-(2,3,4,5,6-pentafluorobenzyl) hydroxylamine hydrochloride; TMSI, 1-(trimethylsilyl)imidazole; Tsugar, total sugar in the nectar sample; 20F, 20-flower extraction; 10F, 10-flower extraction; 1F, single-flower extraction

## ■ REFERENCES

(1) Adams, C. J.; Boult, C. H.; Beadman, B. J.; Farr, J. M.; Grainger, M. N. C.; Manley-Harris, M.; Snow, M. J. Isolation by HPLC and characterisation of the bioactive fraction of New Zealand manuka (*Leptospermum scoparium*) honey. *Carbohydr. Res.* **2008**, *343*, 651−659.

(2) Atrott, J.; Henle, T. Methylglyoxal in manuka honey- correlation with antibacterial properties. *Czech J. Food Sci.* **2009**, *27*, S163−S165.

(3) Adams, C. J.; Manley-Harris, M.; Molan, P. C. The origin of methylglyoxal in New Zealand manuka (*Leptospermum scoparium*) honey. *Carbohydr. Res.* **2009**, *344*, 1050−1053.

(4) Windsor, S.; Pappalardo, M.; Brooks, P.; Williams, S.; Manley-Harris, M. A convenient analysis for dihydroxyacetone and methylglyoxal in Australian honeys. *J. Pharmacogn. Phytother.* **2012**, *4*, 6−11.

(5) Dawson, M. A history of *Leptospermum scoparium* in cultivation: discoveries from the wild. *N. Z. Garden J.* **2009**, *12*, 21−25.

(6) Ronghua, Y.; Mark, A.; Wilson, J. Aspects of the ecology of the indigenous shrub *Leptospermum scoparium* (Myrtaceae) in New Zealand. *N. Z. J. Bot.* **1984**, *22*, 483−507.

(7) Cook, J. M.; Mark, A.; Shore, B. F. Responses of *Leptospermum scoparium* and *L. ericoides* (Myrtaceae) to water logging. *N. Z. J. Bot.* **1980**, *18*, 233−246.

(8) Greer, D. H.; Robinson, L. A. Temperature control of the development of frost hardiness in two populations of *Leptospermum scoparium*. *Tree Physiol. (Oxford, U.K.)* **1995**, *15*, 399−404.

(9) Harris, W.; Decourtye, L. Winter climate comparison between France and New Zealand: effect of frost damage on populations of *Leptospermum scoparium* JR et G Forst grown at three locations in France. *Agronomie* **1991**, *11*, 847−861.

(10) Douglas, M. H.; van Klink, J. W.; Smallfield, B. M.; Perry, N. B.; Anderson, R. E.; Johnstone, P.; Weavers, R. T. Essential oils from New Zealand manuka: triketone and other chemotypes of *Leptospermum scoparium*. *Phytochemistry* **2004**, *65*, 1255−1264.

(11) Stephens, J. M.; Molan, P. C.; Clarkson, B. D. A review of *Leptospermum scoparium* (Myrtaceae) in New Zealand. *N. Z. J. Bot.* **2005**, *43*, 431−449.

(12) Stephens, J. M. *The Factors Responsible for the Varying Levels of UMF in Manuka (Leptospermum scoparium) Honey*; University of Waikato: Hamilton, New Zealand, 2006.

(13) Allan, H. H. *Flora of New Zealand*; Government Printer: Wellington, New Zealand, 1961; Vol. I.

(14) Morrant, D.; Schumann, R.; Petit, S. Field methods for sampling and storing nectar from flowers with low nectar volumes. *Ann. Bot. (Oxford, U.K.)* **2009**, *103*, 533−542.
(15) Stephens, J. M.; Schlothauer, R. C.; Morris, B. D.; Yang, D.; Fearnley, L.; Greenwood, D. R.; Loomes, K. M. Phenolic compunds and methylglyoxal in some New Zealand manuka and kanuka honeys. *Food Chem.* **2010**, *120*, 78−86.
(16) Popoff, T.; Theander, O.; Westerlund, E. Formation of aromatic compounds from carbohydrates. VI. Reaction of dihydroxyacetone in slightly acidic aqueous solution. *Acta Chem. Scand. B* **1978**, *B32*, 1−7.
(17) Burke, S. Missing values, outliers, robust statistics and non-parametric methods. Scientific Data Management. *LC-GC Eur. Online Suppl.* **2001**, 19−24.
(18) Douglas, M. H.; Anderson, R.; van Klink, J.; Perry, N.; Smallfield, B. *Defining North Island Manuka Chemotype Resources*; Crop and Food Research Report 447; Ministry of Agriculture and Forestry Sustainable Farming Fund: Wellington, New Zealand, 2001.
(19) Dawson, M. A history of *Leptospermum scoparium* in cultivation: garden selections. *N. Z. Garden J.* **2010**, *13*, 2−9.
(20) Metcalf, L. *The Cultivation of New Zealand Trees and Shrubs*; Reed: Auckland, New Zealand, 1987; p 184.
(21) Dawson, M. Australian *Leptospermum* in cultivation: species and cultivars. *N. Z. Garden J.* **2012**, *15*, 14−22.
(22) Nickless, E. M.; Holroyd, S. E.; Stephens, J. M.; Gordon, K. C.; Wargent, J. J. Analytical FT-Raman spectroscopy to chemotype *Leptospermum scoparium* and generate predictive models for screening for dihydroxyacetone levels in floral nectar. *J. Raman Spectrosc.* **2014**, DOI: 10.1002/jrs.4576.
(23) Bennick, R. M. *The Effects of Honeybees (Apis mellifera) on the bBiodiversity of Manuka (Leptospermum scoparium) Patches*; Massey University: Palmerston North, New Zealand, 2009.
(24) De Vega, C.; Herrera, C. M. Microorganisms transported by ants induce changes in floral nectar composition of an ant-pollinated plant. *Am. J. Bot.* **2013**, *100*, 792−800.
(25) Herrera, C. M.; de Vega, C.; Pozo, M. I. Invisible floral larcenies: microbial communities degrade floral nectar of bumble bee-pollinated plants. *Ecology* **2008**, *89*, 2369−2376.
(26) Heil, M. Nectar: generation, regulation and ecological functions. *Trends Plant Sci.* **2011**, *16*, 191−200.
(27) Newstrom, L.; Robertson, A. Progress in understanding pollination systems in New Zealand. *N. Z. J. Bot.* **2005**, *43*, 1−59.

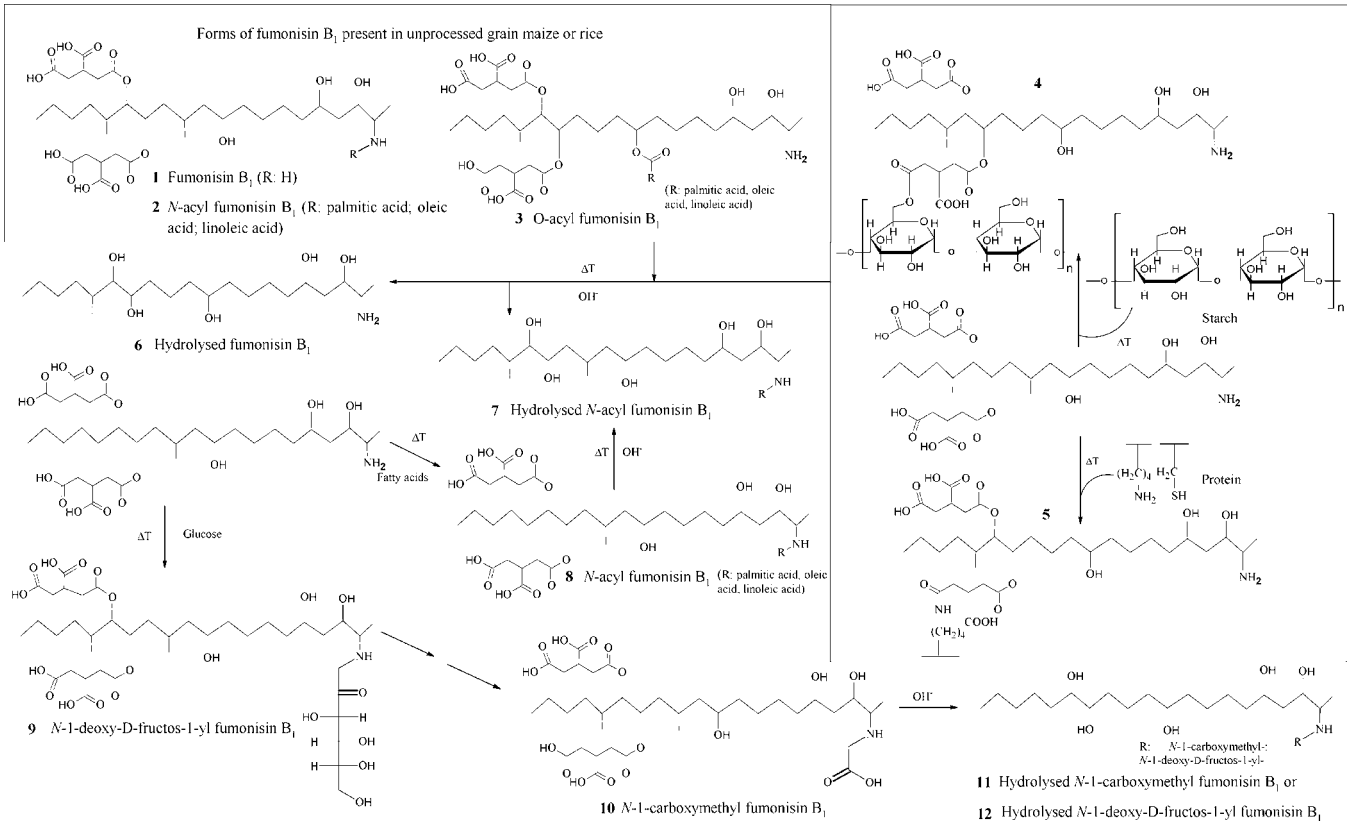


**Figure 1.** Various forms of fumonisins and their transformation paths during technological processes.[8,10,16,19,20]

tolerance to gluten are particularly vulnerable to fumonisins because maize products are the basis of a gluten-free diet in developed countries.[22,23] Free, hidden, and fumonisins esterified with fatty acids hydrolyze in alkaline medium into hydrolyzed fumonisin molecules, for example, **6** (Figure 1).[10,21] The concentrations of fumonisin $B_1$ in the total bound form and in the protein form detected in alkali-processed corn-based foods were higher by about 1.3 and 0.9 times, respectively, than fumonisin $B_1$ concentrations determined by traditional methods.[22] There has been some indirect evidence reported in the literature that formation of selected types of masked fumonisins with corn constituents might be promoted in the alkaline medium during grain nixtamalization.[24]

Due to the lack of literature data concerning thermal stability of the hidden fumonisins, in this work an attempt was made to assess the influence of the baking process on the reduction of the content of free and hidden fumonisins in gluten-free bread.

## MATERIALS AND METHODS

**Chemicals.** Both native and $^{13}C$-labeled fumonisin $B_1$, $B_2$, and $B_3$ analytical standards used in this study were supplied by Biopure (Tulln, Austria). The concentration of all native standards was 50 $\mu$g/mL; those of $^{13}C_{34}$-fumonisin $B_1/B_2/B_3$ standards were 25, 10, and 10 $\mu$g/mL, respectively. The purities of the used labeled fumonisin standards were as follows: $^{13}C$-fumonisin $B_1$ ($^{13}C_{34}$-fumonisin $B_1$), 76.2%; $^{13}C_{33}$-fumonisin $B_1$, 19.8%; $^{13}C_{32}$-fumonisin $B_1$, 4%); $^{13}C$-fumonisin $B_2$ ($^{13}C_{34}$-fumonisin $B_2$, 85.6%; $^{13}C_{33}$-fumonisin $B_2$, 13%; $^{13}C_{32}$-fumonisin $B_2$, 1.3%); $^{13}C$-fumonisin $B_3$ ($^{13}C_{34}$-fumonisin $B_3$, 78.2%; $^{13}C_{33}$-fumonisin $B_3$, 16.8%; $^{13}C_{32}$-fumonisin $B_3$, 3.3%; and $^{13}C_{31}$-fumonisin $B_3$, 1.8%). All of the HPLC grade solvents were supplied by Rathburn Chemicals (Walkerburn, UK). Formic acid, acetic acid, and potassium hydroxide of p.a. grade were supplied by POCH (Gliwice, Poland). The FumoZON AFFINIMIP molecularly imprinted polymeric (MIPs) solid phase extraction cartridges were supplied by Polyintell (Val de Reuil, France).

**Samples.** Gluten-free maize flour of particle size <1 mm naturally contaminated with fumonisins (a courtesy of Silesian Grain, Ziębice, Poland) was used to prepare dough by the direct method and by the sourdough-based method. The flour was produced from grain that was not approved for marketing or use as food/feed. The breads were produced with two methods in two parallel series for each method. In each series three loaves of bread were produced. Two samples from each bread were taken and analyzed in triplicate.

**Dough Processing: Direct Method.** All of the ingredients listed (see the Supporting Information), except sourdough and oil, were mixed and kneaded using a KitchenAid kneader (Benton Harbor, MI, USA) set to a low speed for 6 min. Subsequently, oil was added to the trough and the dough was kneaded for another 4 min. The dough temperature after kneading was 32 °C. In a preliminary experiment several dough pieces containing different amounts of added water were baked in parallel to find the optimum dough yield (mass of dough obtained from 100 g of flour) and the dough producing the highest quality bread. The bread for analyses was baked from the optimal dough in triplicates.

**Dough Processing: Sourdough Method.** Sourdough was prepared from corn flour (600 g) and water (900 mL) with an addition of a starter culture Saf Levain LV2 (Cérences, France) (3 g) and subsequently fermented at 30 °C for 20 h. Saf Levain LV2 fermentation starter supplied by Lesafree was used. That composition of lyophilized lactic acid bacteria and yeast allows bakery sourdough yo be produced in a single-step process in <20 h. The used LV2 starter contains strains of *Lactobacillus brevis* and heterofermentative lactic acid bacteria that produce organic acids (including high quantities of acetic acid) during the fermentation process. The LV2 starter features a higher acetic acid/lactic acid concentration ratio than another fermentation starter offered by the same supplier (LV1). The produced maize bread has a clear and rich flavor.

The dough was prepared from matured sourdough plus ingredients given in the Supporting Information and kneaded as described in the

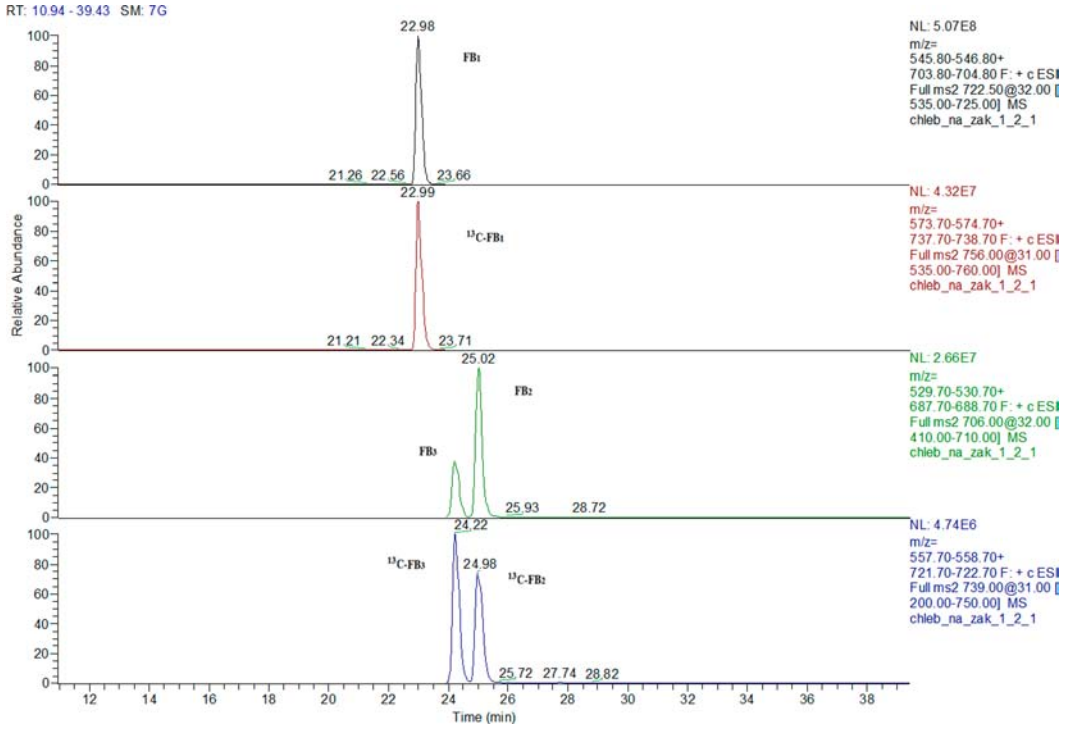


**Figure 2.** CID-MS/MS chromatograms of free fumonisins extracted from maize bread (prepared with sourdough).

previous section until the mixture became homogeneous. The optimum dough yield was evaluated as described above. Immediately after the preparation, the dough pieces were loaded into molds each holding 150 g and grown inside a fermentation chamber at 40 °C and 75% relative air humidity.

The dough grown to an optimal volume was then baked inside a Piccolo Wachtel Winkler shelf oven for 38 min at 260 °C lowered to 210 °C. Baking was initially carried out with steaming.

**Preparation of Samples for Analysis of Free Fumonisins.** The sample preparation procedure previously proposed by Bryła et al.[25] with some major modifications was used to assess levels of free fumonisins. Briefly, 2.5 g of sample (flour or bread) was placed in a 50 mL glass beaker and spiked with 10 $\mu$L of internal standard mixture ($^{13}C_{34}$-fumonisins $B_1$, $B_2$, and $B_3$). The sample was subsequently homogenized with 10 mL of a methanol/acetonitrile/water (25:25:50 v/v/v) mixture for 3 min. The mixture was centrifuged at 10730*g* for 10 min. Five milliliters of the supernatant was diluted with 5 mL of water. Eight milliliters (4 mL × 2) of the diluted solution was loaded on a MIP cartridge previously conditioned with acetonitrile and water (2 mL each). The flow rate was 3−4 drops/s. The cartridge was washed with 6 mL of an acetonitrile/water mixture (40:60 v/v) and subsequently eluted with 4 mL of formic acid/methanol mixture (2:98 v/v). The eluate was evaporated to dryness using a rotary evaporator operated at 40 °C and then redissolved in 1 mL of methanol/water/formic acid mixture (10:89.9:0.1 v/v/v). Each sample was sonicated for 13 s in an ultrasonic bath to ensure complete dissolution of analytes, filtered through a PTFE 0.2 $\mu$m syringe filter into an autosampler vial, and injected into the LC-MS/MS system. Calibration curves were plotted using matrix-matched calibration standards prepared in the same way as the samples. Dry residues were dissolved in standard solution instead of pure solvent mixture.

**Preparation of Samples for Analysis of Total Fumonisins.** The total concentration of free and hidden/bound fumonisins was determined in alkaline-digested samples, in which free, hidden, and some bound fumonisins undergo hydrolysis to hydrolyzed fumonisins. Briefly, 0.5 g of a well-ground sample (flour or bread) was placed in a 50 mL Falcon-type PP centrifuge tube and spiked with 10 $\mu$L of fumonisin $B_1$, $B_2$, and $B_3$ $^{13}C_{34}$-labeled internal standard solutions. Subsequently, 10 mL of 2 M KOH was added. The hydrolysis was conducted for 24 h at room temperature. The analytes were extracted into 12.5 mL of dichloromethane by shaking. The samples were centrifuged at 10730*g*. Five milliliters of supernatant was transferred into a round-bottom flask and evaporated using a rotary evaporator operated at 40 °C. The dry residues were redissolved in 1 mL of 30:69.9:0.1 methanol/water/acetic acid mixture, filtered through a 0.2 $\mu$m nylon syringe filter, and transferred into autosampler vials.

The labeled internal standards were used to monitor analyte recovery rates, to adjust the analyte concentrations by the rates calculated for the corresponding internal standards, and to eliminate the errors resulting from incomplete hydrolysis. The accuracy of the analytical procedure was thus substantially improved.

The quotient of molar masses was used as a conversion factor for calculation of analyte concentration before the hydrolysis. The results were expressed as concentration of free fumonisins. The calibration solutions of hydrolyzed fumonisins $B_1$, $B_2$, and $B_3$ were prepared from fumonisin $B_1$, $B_2$, and $B_3$ standards, each of 5 $\mu$g/mL concentration. Matrix-matched calibration was applied. To prepare the solutions, 0.5 g portions of fumonisin-free flour were spiked with 10 $\mu$L of each labeled internal standard (of analyte concentration like in the samples) and with an appropriate amount of native standard and then processed as for samples. The spiked samples, the calibration standards, and the QA/QC samples were prepared and processed simultaneously to maintain identical hydrolysis conditions (time and temperature).

**Hidden Fumonisin Assessment.** The hidden fumonisin concentration was calculated by subtraction of two measured values: suitably corrected concentration of sum of free plus hidden forms after hydrolysis minus concentration of free forms before hydrolysis. It was assumed that the concentrations of all fumonisins in the analyzed samples were proportional to the determined concentrations of hydrolyzed forms with the quotient of molar masses of compounds present before the hydrolysis and after it as the proportionality factor.

**Analytical Method Performance.** The basic statistical parameters of the analytical method (including analyte recovery and recovery repeatability) were assessed using some laboratory-made spiked samples prepared from fumonisin-free maize grain. The samples were prepared at three different concentration levels and analyzed in triplicate. The developed method performed satisfactorily. Average recovery rates of free fumonisins from samples spiked at 200 ($n$ = 4),

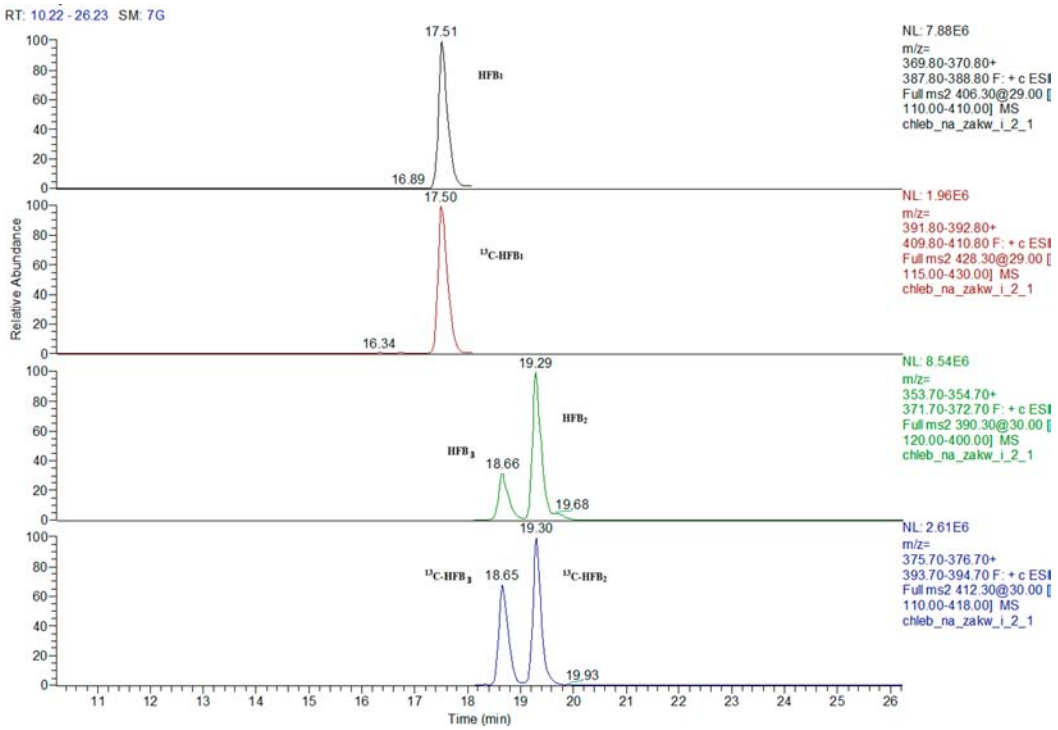


**Figure 3.** CID-MS/MS chromatograms of fumonisins extracted from maize bread (prepared with sourdough) hydrolyzed under alkaline medium.

500 ($n$ = 4), and 800 $\mu$g/kg ($n$ = 4) were 102 ± 11.5, 106 ± 12.3, and 97 ± 11.5% for fumonisins $B_1$, $B_2$, and $B_3$, respectively (mean recovery values calculated for three fortification levels). The average recovery rates of hydrolyzed fumonisins from the samples spiked at 280 ($n$ = 5), 560 ($n$ = 5), and 1120 $\mu$g/kg ($n$ = 5) for hydrolyzed fumonisin $B_1$ or at 275 ($n$ = 5), 550 ($n$ = 5), and 1100 $\mu$g/kg ($n$ = 5) for hydrolyzed fumonisins $B_2$ and fumonisin $B_3$ were 94 ± 10.9, 99 ± 11.5, and 98 ± 12% for hydrolyzed fumonisins $B_1$, $B_2$, and $B_3$, respectively. The calibration curves plotted against matrix-matched calibration standards were linear (coefficient of determination $R^2 > 0.99$) within the 13−1200 $\mu$g/kg range for fumonisins $B_1$, $B_2$, and $B_3$, within the 22−5040 $\mu$g/kg range for hydrolyzed fumonisin $B_1$, and within the 22−4950 $\mu$g/kg range for hydrolyzed fumonisins $B_2$ and $B_3$. The lowest points of calibration curves, 13 $\mu$g/kg for fumonisins $B_1$, $B_2$, and $B_3$ and 22 $\mu$g/kg for hydrolyzed fumonisins $B_1$, $B_2$, and $B_3$, were taken as the limit of quantification (LOQ). The signal-to-noise ratio at these concentrations was not less than 10:1.

The method was also validated within the framework of an interlaboratory proficiency test performed between September and November 2013 on a test sample provided under the FAPAS program (Food Analysis Performance Assessment Scheme), Report 2297. The concentration of free fumonisins $B_1$ and $B_2$ in maize was evaluated. The results expressed as $Z$ score were 0.3 and 0.6, respectively, for fumonisins $B_1$ and $B_2$. They were considered satisfactory.

**LC-MS/MS Analysis.** A high-performance liquid chromatograph, coupled to an LTQ ion trap mass spectrometer (Thermo Finnigan, Austin, TX, USA), was used for this study. The chromatographic system was equipped with an autosampler, a column thermostat, a degasser, and a quaternary gradient pump. The chromatographic separations were performed on pentafluorophenyl (PFP) and octadecyl (C18) silica-based reversed-phase columns. The free fumonisins were separated on a 100 mm × 2.1 mm, 2.6 $\mu$m pore size, PFP Kinetex core−shell column, whereas the hydrolyzed fumonisins were separated on a 150 mm × 2.0 mm, 3 $\mu$m pore size, C18 Luna column (both supplied by Phenomenex, Torrance, CA, USA). The mobile phase flow rate was in all cases set at 0.15 mL/min. The following mobile phase gradient was used in analyses of free fumonisins (A = water, B = methanol, C = 2% acetic acid/water mixture): 0−4 min (initial), 60% A + 30% B + 10% C; 14−28 min, 10% A + 80% B + 10% C; 32−55 min, back to the initial conditions. A representative chromatogram of fumonisins extracted from maize bread prepared with sourdough is shown in Figure 2. The following mobile phase gradient was used in the analyses of hydrolyzed fumonisins (A = water, B = methanol; both phases contained 0.1% acetic acid): initial 0−3 min, 70% A; 7−20 min, 35% A; 21−31 min, 100% B; 33−48 min, 70% A. A chromatogram of fumonisins extracted from maize bread prepared with sourdough and hydrolyzed under alkaline medium is shown in Figure 3.

The compounds were analyzed charged in an electrospray ionization (ESI) source. The nebulizing/auxiliary gas ($N_2$) flow rates were set constant at 20/10 AU, respectively. Helium was used as the dumping gas. Values ($m/z$) corresponding to pseudo molecular ions $[M + H]^+$ of fumonisins $B_1$, $B_2$, and $B_3$ and hydrolyzed fumonisins $B_1$, $B_2$, and $B_3$ were used as precursors in all CID experiments. The mass spectrometer scanning windows in the CID mode were set according to the main produced daughter ions from the selected precursor: 722 (fumonisin $B_1$) − 535 − 725; 706 (fumonisins $B_2$ and $B_3$) − 410 − 710; 406 (hydrolyzed fumonisin $B_1$) − 120 − 410; and 390 (hydrolyzed fumonisins $B_2$ and $B_3$) − 120 − 400. The data were acquired and analyzed using Xcalibur 1.2 software. The optimized CID parameters are given in the Supporting Information.

**Statistical Analysis.** Statistical evaluations of the data were performed using Statgraphics 4.1. (Graphics Software System, STCC, Inc., Rockville, MD, USA) computer software. The significance of the differences between determined concentrations were assessed using a one-way ANOVA statistical test. To evaluate the significance of the differences between the only two variables (concentrations), a Tukey's test at $\alpha$ = 0.05 was applied.

## RESULTS AND DISCUSSION

Because hidden fumonisins in food products could not be directly determined in this study, their concentration was assessed on the basis of the concentration of hydrolyzed fumonisins formed during alkaline digestion of samples. A strong basic medium can break noncovalent interactions that prevent extraction of fumonisins bound as inclusion complexes, degrade spatial structure of macromolecules, denaturize

proteins, and cause starch swelling and saponification of lipids in cereals. In effect, free, hidden, and O-acylated fumonisins are all hydrolyzed into hydrolyzed fumonisins $B_1$, $B_2$, and $B_3$.

The concentrations of both free and hidden fumonisins found in the studied bread samples are listed in Table 1 and shown in Figure 4. The concentrations in bread have been calculated on the basis of flour mass used for baking.

**Measured Concentrations (Free and Freeplus Hidden Fumonisins).** The single-factor analysis of variance of data shown in Table 1 and charted in Figure 4 revealed statistically significant ($p$ value $\leq 0.05$) differences between concentrations of free fumonisins in flour and bread: the sum of fumonisins dropped from 5101 ± 564 μg/kg in flour to 3569 ± 184 μg/kg in bread prepared with sourdough (i.e., by 30%) and to 3470 ± 325 μg/kg in bread prepared without sourdough (i.e., by 32%). The differences between both bread values are too small to be statistically significant. The sourdough addition did not influence the concentration of free fumonisins in baked breads.

The literature data on fumonisin behavior during baking are scarce. Jackson et al.[26] reported a 16−28% decrease in fumonisin $B_1$ concentration (initial = 5 mg/kg) during baking of maize muffins at 175 and 200 °C for 20 min. The highest drop was observed in near-surface layers of the muffins, whereas the reduction was lower in the crumb. Castelo et al.[27] did not find any significant drop in the initial 5 mg/kg fumonisin $B_1$ concentration during baking of maize muffins at 204 °C for 20 min, but found that the toxin concentration dropped by 48% during baking at 232 °C. Avantaggiato et al.[28] baked maize muffins spiked with native and $^{14}$C-labeled fumonisin $B_1$ (15 μg per muffin) at 210 °C for 25 min and observed a 52−57% decrease in fumonisin $B_1$ concentration. The same authors repeated their experiments using maize flour spiked with $^{14}$C-labeled fumonisin $B_1$, synthesized by fungi from $^{14}$C-labeled sodium acetate, at 1.56 μg per muffin and observed a 51% reduction. Such diversity of results might have different roots: different baking conditions (temperature, time of the process), different sizes of the used dough portions, different dough pH values. Jackson et al.[29] reported that the thermal stability of fumonisins is pH-dependent. Their model studies on buffered solutions showed that <27% of fumonisin $B_1$ should degrade at temperatures ≤125 °C applied for 60 min, whereas an 18−90% degradation level (depending on pH of the reaction medium) is to be expected at a temperature of 150 °C applied for 60 min. The highest degradations were observed at pH 4 and 10. More than 90% of fumonisin $B_1$ degraded at temperatures above 175 °C regardless of pH. In this context it must be pointed out that distribution of temperature inside a baking bread is usually not uniform, temperatures in the crumb being significantly lower than those in the crust. Normally, the temperature in the crumb center does not exceed 100 °C. In this study the dough prepared with sourdough had pH 4.6, whereas dough prepared without sourdough had pH 5.5. Despite this, that no statistically significant difference between the fumonisin concentrations in breads baked from both types of dough was observed.

Thus, several studies proved that fumonisins may undergo degradation as a result of heat treatment. Some of the results indicate also that fumonisin $B_1$ might be present in thermally processed complex food matrix in various forms bound to proteins (**5**, Figure 1), sugars (**9**, **10**), including starch (**4**) or fatty acids (**8**).[8,20,22] Dough additives such as monohydrates (glucose, fructose) or milk (containing lactose) might increase the rate of nonenzymatic browning reaction occurring between

**Table 1. Mean Determined Concentration of Individual, Total, Free, and Hidden Fumonisins in Maize Flour and Bread**

| | | mean concentration ± SD (μg/kg) | | | | | | | | | | | |
|---|---|---|---|---|---|---|---|---|---|---|---|---|---|
| | | free (F) | | | free + hidden (F + H) | | | total concentration | | | | flour-to-bread reduction level (%) | | |
| product | $n$ | fumonisin $B_1$ | fumonisin $B_2$ | fumonisin $B_3$ | fumonisin $B_1$ | fumonisin $B_2$ | fumonisin $B_3$ | F | F + H | H | H/F ratio | F | F + H | H |
| flour | 4 | 3845 ± 373 | 832 ± 68 | 424 ± 79 | 6660 ± 499 | 1214 ± 37 | 882 ± 86 | 5101 ± 564 | 8756 ± 913 | 3655 | 0.72 | | | |
| bread (indirect method) | 6 | 1539 ± 73$^a$ | 263 ± 31$^a$ | 80 ± 3$^a$ | 2542 ± 92$^a$ | 612 ± 36$^a$ | 290 ± 19$^a$ | 1882 ± 98$^a$ | 3444 ± 84$^a$ | 1562$^a$ | 0.83 | | | |
| | | 2918 ± 138$^b$ | 499 ± 59$^b$ | 151 ± 6$^b$ | 4820 ± 178$^b$ | 1160 ± 67$^b$ | 550 ± 36$^b$ | 3569 ± 184$^b$ | 6531 ± 161$^b$ | 2962$^b$ | | 30 | 25 | 19 |
| bread (direct method) | 6 | 1496 ± 132$^a$ | 205 ± 32$^a$ | 77 ± 6$^a$ | 2593 ± 178$^a$ | 583 ± 20$^a$ | 285 ± 28$^a$ | 1778 ± 167$^a$ | 3461 ± 202$^a$ | 1683$^a$ | 0.95 | | | |
| | | 2920 ± 257$^b$ | 400 ± 62$^b$ | 150 ± 12$^b$ | 5062 ± 347$^b$ | 1138 ± 43$^b$ | 556 ± 52$^b$ | 3470 ± 325$^b$ | 6756 ± 392$^b$ | 3286$^b$ | | 32 | 23 | 10 |

$^a$Directly after baking. $^b$Directly after baking, concentration calculated on the flour mass basis.


dx.doi.org/10.1021/jf504077m | J. Agric. Food Chem. 2014, 62, 10341−10347

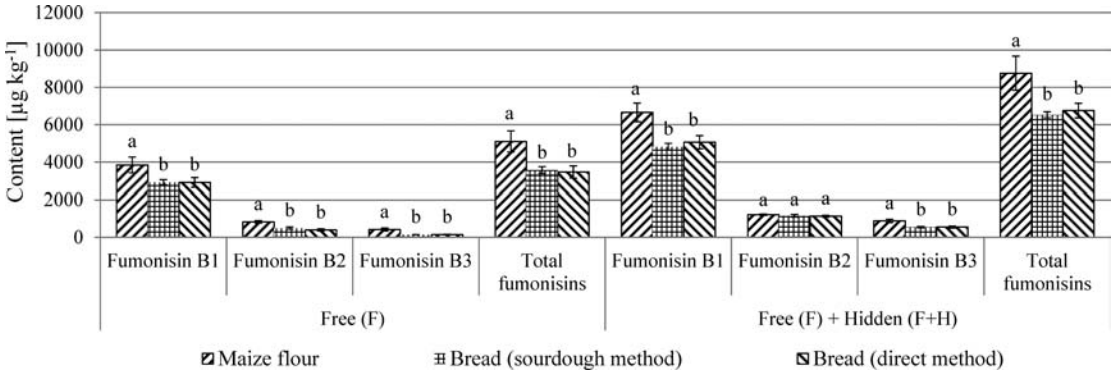


**Figure 4.** Determined mean (±SD) concentrations of free and free plus hidden fumonisins in maize flour and bread (related to mass of flour used to prepare dough). Statistically homologous groups have been marked with identical letters.

the fumonisin amine group and the carbohydrate carbonyl group. In effect, they could reduce fumonisin concentration.[26,30] Due to the structural changes resulting from reactions of fumonisin molecules with food components,[8,22] in such a way that functional groups in the fumonisin molecule necessary for its identification are blocked or unavailable, it is in fact impossible to apply conventional analytical methods for its analysis. In this respect bound fumonisins will be considered degraded. In this study an indirect method based on alkaline digestion of samples was utilized to quantitate masked fumonisins. In such a case the analytical procedure involved quantification of fumonisin degradation products formed during hydrolysis. However, some N-acylated (**7**, Figure 1) and N-alkylated (**11**, **12**) derivatives are not quantified because such bonds are not susceptible to the alkaline-catalyzed hydrolysis.[10,20] The resulting total fumonisin contents is a sum of free fumonisins and fumonisins both covalently[8] and noncovalently bonded to biopolymers[24] as well as *O*-esters of fatty acids. The latter were identified in small quantities in *F. verticllioides* cultures grown in vitro on rice or corn.[16−19] Therefore, it is expected that the group of masked fumonisins quantified in the unprocessed corn covers mainly the hidden forms that covalently or noncovalently interact with macroconstitutive food compounds.[31]

The baking process reduced the sum of free plus hidden fumonisins from 8756 ± 913 μg/kg in flour to 6531 ± 161 μg/kg in bread made with sourdough (by 25%) and to 6756 ± 392 μg/kg in bread made without sourdough (by 23%) (Table 1). The performed statistical assessment using the single-factor analysis of variance technique did not reveal any significant differences between type breads (Figure 4).

**Calculated Concentrations (Hidden Fumonisins).** The concentrations of hidden fumonisins were calculated as the differences between free plus hidden and free fumonisins. The baking process reduced hidden fumonisin contents from 3655 μg/kg in flour to 2962 μg/kg in bread made with sourdough (by 19%) and to 3286 μg/kg in bread made without sourdough (by 10%) (Table 1).

The observed lower degradation rate of the masked fumonisins compared to their free forms during baking of bread might be explained by the co-occurrence of the opposite types of reactions. It is possible that simultaneously covalent bonds between fumonisins and biopolymers are being formed or degraded. Nonetheless, the rates of the hidden fumonisin synthesis and degradation might be significantly different. The results of some studies performed in model systems indicate the formation of covalent bounds between carboxyl groups of fumonisins and a hydroxyl group present in the starch molecule or amine groups of proteins.[8] Burns et al.[24] introduced some indirect evidence indicating the possible interactions of fumonisins with corn components during cooking in the nixtamalization process. The authors suggest that the alkaline medium might promote such types of reactions.

It might be also concluded that the observed lower reduction levels of hidden forms than of free forms mean that hidden fumonisins in maize flour are simply more thermally stable than free fumonisins. The average hidden/free ratio increased as a result of the baking process from an initial 0.72 in flour to 0.83 in bread produced with sourdough and to 0.95 in bread made without sourdough. Literature data on the thermal stability of free fumonisins are scarce, and data on the stability of hidden forms are practically unavailable. Therefore, it is difficult to compare the results of this study with other reports.

The results of this study revealed that hidden fumonisins may have a higher thermal stability compared to their native forms. Natural biopolymers (such as starch or proteins) capable of noncovalently interacting with fumonisins can stabilize their structure and consequently increase their thermal stability. Assuming that concentrations of both hidden and native fumonisins in maize and maize milling products are comparable, thermal processing would increase a relative share of hidden forms in total concentration. Considering other published reports that hidden fumonisins (covalently or noncovalently bound) might be released to form free (native) molecules in the digestive tract,[10,31] it seems that further studies on the stability of hidden fumonisins during thermal processing at different pH values are needed to assess toxicological hazards for consumers.

## ■ ASSOCIATED CONTENT

### Ⓢ Supporting Information

Tables of raw materials used to prepare dough and optimal ionization and ion trap scanning parameters operated in ESI-CID-MS/MS mode. This material is available free of charge via the Internet at http://pubs.acs.org.

## ■ AUTHOR INFORMATION

### Corresponding Author

*(M.B.) Phone:+48 22 606 38 34. Fax: +48 22 849 91 67. E-mail: marcin.bryla@ibprs.pl.

### Funding

This study was financially supported by the 2012/05/N/NZ9/01316 National Science Centre grant.

## Notes

The authors declare no competing financial interest.

## REFERENCES


(1) Gelderblom, W. C.; Jaśkiewicz, K.; Marasas, W. F.; Thiel, P. G.; Horak, R. M.; Vleggaar, R.; Kriek, N. P. Fumonisins − novel mycotoxins with cancer-promoting activity produced by *Fusarium moniliforme*. *Appl. Environ. Microbiol.* **1988**, *54*, 1806−1811.

(2) Scott, P. M. Recent research on fumonisins: a review. *Food Addit. Contam. Part A* **2012**, *29*, 242−248.

(3) Bryła, M.; Roszko, M.; Szymczyk, K.; Jędrzejczak, R.; Obiedziński, M. W.; Sękul, J. Fumonisins in plant-origin food and fodder − a review. *Food Addit. Contam. Part A* **2013**, *30*, 1626−1640.

(4) Waśkiewicz, A.; Beszterda, M.; Goliński, P. Occurrence of fumonisins in food − an interdisciplinary approach to the problem. *Food Control* **2012**, *26*, 491−499.

(5) Pagliuca, G.; Zironi, E.; Ceccolini, A.; Matera, R.; Serrazanetti, G. P.; Pivac, A. Simple method for the simultaneous isolation and determination of fumonisin $B_1$ and its metabolite aminopentol-1 in swine liver by liquid chromatography−fluorescence detection. *J. Chromatogr., B* **2005**, *819*, 97−103.

(6) Wan Norhasima, W. M.; Abdulamir, A. S.; Abu Bakar, F.; Son, R.; Norhafniza, A. The health and toxic adverse effects of *Fusarium* fungal mycotoxin, fumonisins, on human population. *Am. J. Infect. Dis.* **2009**, *5*, 273−281.

(7) Gazzotti, T.; Zironi, E.; Lugoboni, B.; Barbarossa, A.; Piva, A.; Pagliuca, G. Analysis of fumonisins $B_1$, $B_2$ and their hydrolysed metabolites in pig liver by LC−MS/MS. *Food Chem.* **2011**, *125*, 1379−1384.

(8) Seefelder, W.; Knecht, A.; Humpf, H. U. Bound fumonisin B1: analysis of fumonisin-B1 glyco and amino acid conjugates by liquid chromatography−electrospray ionization−tandem mass spectrometry. *J. Agric. Food Chem.* **2003**, *51*, 5567−5573.

(9) Berthiller, F.; Schuhmacher, R.; Adam, G.; Krska, R. Formation, determination and significance of masked and other conjugated mycotoxins. *Anal. Bioanal. Chem.* **2009**, *395*, 1243−1252.

(10) Falavigna, C.; Cirlini, M.; Galaverna, G.; Dall'Asta, C. Masked fumonisins in processed food: co-occurrence of hidden and bound forms and their stability under digestive conditions. *World Mycotox. J.* **2012**, *5*, 325−334.

(11) Berthiller, F.; Crews, C.; Dall'Asta, Ch.; De Saeger, S.; Haesaert, G.; Karlovsky, P.; Oswald, I. P.; Seefelder, W.; Speijers, G.; Stroka, J. Masked mycotoxins: a review. *Mol. Nutr. Food Res.* **2013**, *57*, 165−186.

(12) Lu, Y.; Clifford, L.; Hauck, C. C.; Hendrich, S.; Osweiler, G.; Murphy, P. A. Characterization of fumonisin $B_1$-glucose reaction kinetics and products. *J. Agric. Food Chem.* **2002**, *50*, 4726−4733.

(13) Poling, S. M.; Plattner, R. D.; Weisleder, D. *N*-(1-Deoxy-D-fructos-1-yl) fumonisin $B_1$, the initial reaction product of fumonisin $B_1$ and D-glucose. *J. Agric. Food Chem.* **2002**, *50*, 1318−1324.

(14) Howard, P. C.; Couch, L. H.; Patton, R. E.; Eppley, R. M.; Doerge, D. M.; Churchwell, M. I.; Marques, M. M.; Okerberg, C. V. Comparison of the toxicity of several fumonisin derivatives in a 28-day feeding study with female B6C3F 1 mice. *Toxicol. Appl. Pharmacol.* **2002**, *185*, 153−165.

(15) Voss, K. A.; Riley, R. T.; Jackson, L. S.; Jabłoński, J. E.; Bianchini, A.; Bullerman, L. B.; Hanna, M. A.; Ryu, D. Extrusion cooking with glucose supplementation of fumonisin-contaminated corn grits protects against nephrotoxicity and disrupted sphingolipid metabolism in rats. *Mol. Nutr. Food Res.* **2011**, *55*, S312−S320.

(16) Bartók, T.; Tölgyesi, L.; Mesterházy, Á.; Bartók, M.; Szécsi, Á. Identification of the first fumonisin mycotoxins with three acyl groups by ESI-ITMS and ESI-TOFMS following RP HPLC separation: palmitoyl, linoleoyl and oleoyl $EFB_1$ fumonisin isomers from a solid culture of *Fusarium verticillioides*. *Food Addit. Contam. Part A* **2010**, *27*, 1714−1723.

(17) Bartók, T.; Szécsi, Á.; Juhász, K.; Bartók, M.; Mesterházy, Á. ESI-MS and MS/MS identification of the first ceramide analogues of fumonisin $B_1$ mycotoxin from a *Fusarium verticillioides* culture following RP-HPLC separation. *Food Addit. Contam. Part A* **2013**, *30*, 1651−1659.

(18) Falavigna, C.; Cirlini, M.; Galaverna, G.; Sforza, S.; Dossena, A.; Dall'Asta, Ch. LC/ESI-MS/MS analysis outlines the different fumonisin patterns produced by *F. verticillioides* in culture media and in maize kernels. *J. Mass Spectrom.* **2012**, *47*, 1170−1176.

(19) Falavigna, C.; Lazzaro, I.; Galaverna, G.; Battilani, P.; Dall'Asta, Ch. Fatty acid esters of fumonisins: first evidence of their presence in maize. *Food Addit. Contam. Part A* **2013**, *30*, 1606−1613.

(20) Park, J. W.; Scott, P. M.; Lau, B.-Y. Analysis of *N*-fatty acyl fumonisins in alkali-processed corn foods. *Food Sci. Biol.* **2013**, *22*, 147−152.

(21) Dall'Asta, C.; Mangia, M.; Berthiller, F.; Molinelli, A.; Sulyok, M.; Schuhmacher, R.; Krska, R.; Galaverna, G.; Dossena, A.; Marchelli, R. Difficulties in fumonisin determination: the issue of hidden fumonisins. *Anal. Bioanal. Chem.* **2009**, *395*, 1335−1345.

(22) Dall'Asta, C.; Galaverna, G.; Mangia, M.; Sforza, S.; Dossena, A.; Marchelli, R. Free and bound fumonisins in gluten-free food products. *Mol. Nutr. Food Res.* **2009**, *53*, 492−499.

(23) Dall'Asta, C.; Scarlato, P. A.; Galaverna, G.; Brighenti, F.; Pellegrini, N. Dietary exposure to fumonisins and evaluation of nutrient intake in a group of adult celiac patient on a gluten-free diet. *Mol. Nutr. Food Res.* **2012**, *56*, 632−640.

(24) Burns, T. D.; Snook, M. E.; Riley, R. T.; Voss, K. A. Fumonisin concentrations and *in vivo* toxicity of nixtamilized *Fusarium verticilloides* culture material: evidence for fumonisin-matrix interactions. *Food Chem. Toxicol.* **2008**, *46*, 2841−2848.

(25) Bryła, M.; Jędrzejczak, R.; Roszko, M.; Szymczyk, K.; Obiedziński, M. W.; Sękul, J.; Rzepkowska, M. Application of molecularly imprinted polymers to determine $B_1$, $B_2$, and $B_3$ fumonisins in cereal products. *J. Sep. Sci.* **2013**, *36*, 578−584.

(26) Jackson, L. S.; Katta, S. K.; Fingerhut, D. D.; DeVries, J. W.; Bullerman, L. B. Effects of baking and frying on the fumonisin $B_1$ content of corn-based foods. *J. Agric. Food Chem.* **1997**, *45*, 4800−4805.

(27) Castelo, M. M.; Sumner, S. S.; Bullerman, L. B. Stability of fumonisins in thermally processed corn products. *J. Food Prot.* **1998**, *61*, 1030−1033.

(28) Avantaggiato, G.; De La Campa, R.; Miller, J. D.; Visconti, A. Effects of muffin processing on fumonisins from $^{14}C$ labeled toxins produced in cultured corn kernels. *J. Food Prot.* **2003**, *66*, 1873−1878.

(29) Jackson, L. S.; Hlywka, J. J.; Senthil, K. R.; Bullerman, L. B.; Musser, S. M. Effects of time, temperature, and pH on the stability of fumonisin $B_1$ in an aqueous model system. *J. Agric. Food Chem.* **1996**, *44*, 906−912.

(30) Murphy, P. A.; Hendrich, S.; Hopmans, E. C.; Hauck, C. C.; Lu, Z., Buseman, G.; Munkvold, G. Effect of processing on fumonisin content of corn. In *Fumonisins in Food*; Jackson, L. S., DeVries, J. W., Bullerman, L. B., Eds.; Plenum Publishing: New York, 1996; pp 223−234.

(31) Dall Asta, C.; Falavigna, C.; Galaverna, G.; Dossena, A.; Marchelli, R. In vitro digestion assay for determination of hidden fumonisins in maize. *J. Agric. Food Chem.* **2010**, *58*, 12042−12047.

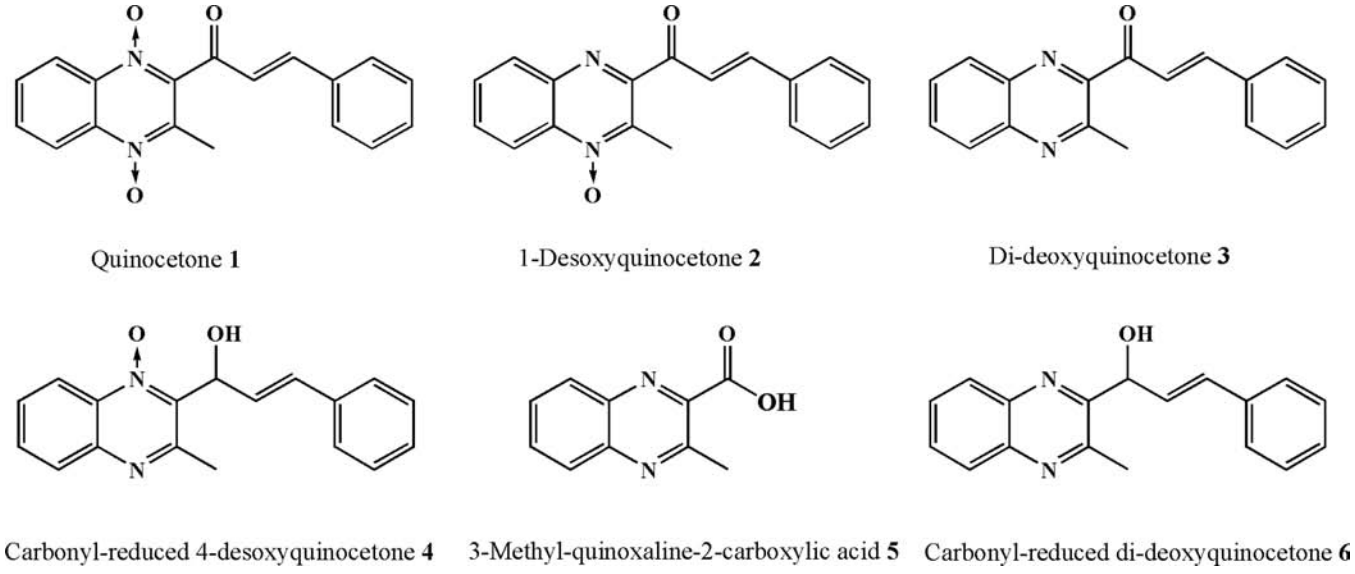


**Figure 1.** Molecular structures of quinocetone, **1**, and its main metabolites, **2**−**6**.

## MATERIALS AND METHODS

**Chemicals and Reagents.** The analytical standards of **1**−**6** (98% purity) were obtained from the Institute of Veterinary Pharmaceuticals (Huazhong Agricultural University, Wuhan, People's Republic of China). Individual stock standard solutions (1000 μg/mL) of all analytes were prepared by dissolving each pure standard in methanol (MeOH). A mixed standard fortification solution [20 μg/mL (10 μg/mL for **1** and **2**)] was prepared by combining 2.0 mL (1.0 mL for **1** and **2**) of each stock standard and diluting with MeOH to obtain a final volume of 100 mL. The stock solutions were stored in amber vials at −20 °C and stabilized for 3 months. The mixed fortification solution was also stored in an amber vial at −20 °C and then stabilized for 1 month. Distilled water was further purified by passing it through a Milli-Q Plus apparatus (Millipore, Bedford, MA, USA). HPLC grade MeOH and acetonitrile (MeCN) were purchased from Tedia (Fairfield, OH, USA). Other chemicals, including formic acid, metaphosphoric acid, and zinc acetate, were of analytical reagent grade.

**Feed.** The feed used in this study was purchased from Wuhan Lvhong Bioscience and Technology Co., Ltd. (Wuhan, People's Republic of China). The feed formula was strictly in accordance with the recommended formula of the U.S. National Research Council. Premix (4%; 2.5 g/kg quinocetone concentration) and complete feed (100 mg/kg quinocetone concentration) were initially prepared. The blank feed and the medicated feed were analyzed using the HPLC method described by Wu et al.[17] to determine drug content. The results indicated that no quinoxaline compound was detected in the blank feed, and only quinocetone (98 ± 6 mg/kg feed, $n$ = 9) was found in the medicated feed.

**Animals and Sampling.** The study was performed in accordance with the guidelines of the Committee on the Care and Use of Laboratory Animals of China (permit SYXK 2007-0044). Thirty healthy castrated crossbred (large white × landrace) pigs (50−65 kg) were purchased from the Breeding Pig Testing Center (Wuhan, People's Republic of China); these pigs were housed in six 8 m × 10 m pigpens, which were cleaned daily. Thirty-six 1-day-old healthy Cobb500 broilers were purchased from Charoen Pokphand Group (Wuhan, People's Republic of China); these broilers were kept in stainless steel cages. Sixty healthy carp (400−600 g) were purchased from the Wuhan Fish Breeding Farm (Wuhan, People's Republic of China); these carp were placed in a fish tank with circulating water. The animal houses were maintained at 25 ± 2 °C room temperature with 45−65% relative humidity. All of the animals were allowed a 7 day acclimation period before our experiments were conducted; a standard ration based on corn and soybean was fed twice a day and tap water was available ad libitum. The animals were randomly divided into a control group ($n$ = 5, 6, and 10 for pigs, broilers, and carp, respectively) and a test group ($n$ = 25, 30, and 50 for pigs, broilers, and carp, respectively). The control groups were fed the standard ration without quinoxaline compounds. The test groups were provided with medicated feed for 90, 42, and 60 consecutive days for pigs, broilers, and carp, respectively. The medicated feed contained a standard ration premixed with quinocetone at a level of 100 mg/kg diet, which was slightly higher than the recommended level of quinocetone preparations.[1]

At different time points [6 h, 1, 3, 7, and 14 days (6 h, 1, 3, 5, and 7 days for broilers, and 6 h, 1, 3, 5, and 10 days for carp)], 1 control and 5 medicated pigs (6 medicated broilers and 10 medicated carp) were anesthetized and sacrificed. The pigs and broilers were slaughtered using captive bolt stunning equipment and exsanguinated in accordance with the guidelines provided by the American Veterinary Medical Association for euthanasia,[23] the carp were euthanized in a MS-222/water (1:10000) bath. Liver, kidney, muscle, and fat (skin) specimens were collected. All of the samples were placed in labeled plastic bags in an ice bath, immediately homogenized, and frozen at −20 °C until these samples were analyzed.

**Analysis of Analytes.** *Sample Preparation.* Samples (2 ± 0.1 g) were transferred into a 50 mL centrifuge tube, and 8 mL of 1% metaphosphoric acid in MeOH/MeCN/water (50:20:30, v/v/v) was added to the sample. The mixtures were shaken using a vortex system for 5 min, ultrasonicated for 10 min at room temperature, and centrifuged at 2160$g$ for 10 min. The supernatant was then transferred into a 50 mL centrifuge tube. The same extraction procedure was repeated. The two supernatants were combined, and 1 mL of 10% aqueous zinc acetate was added to the extracts. These extracts were mixed by vortexing for 2 min and centrifuged at 13500$g$ for 10 min; afterward, the supernatant was transferred and diluted with 1% metaphosphoric acid to obtain a final volume of 64 mL, which was ready for the cleanup procedure.

The HLB cartridge (60 mg, 3 mL) (Waters Corp., Milford, MA, USA) was preconditioned with 3 mL of MeOH and 3 mL of water. Flow rates for conditioning and washing were set at 3 mL/min. The entire extracts were loaded onto the SPE column at a flow rate of 1 mL/min. The column was washed with 3 mL of water and 3 mL of 10% MeOH and dried by purging air at a rate of 10 mL/min for 5 min. The analytes were eluted with 3 mL of MeCN at a flow rate of 1.0 mL/min into a 10 mL tube and evaporated to dryness under a stream of nitrogen at 45 °C. The dry residue was dissolved in 1 mL of 20% MeCN, vortexed for 1 min, and centrifuged at 16600$g$ for 10 min. The resulting solution was then filtered using a 0.22 μm nylon Millipore chromatographic filter, and a 20 μL aliquot was analyzed by HPLC.

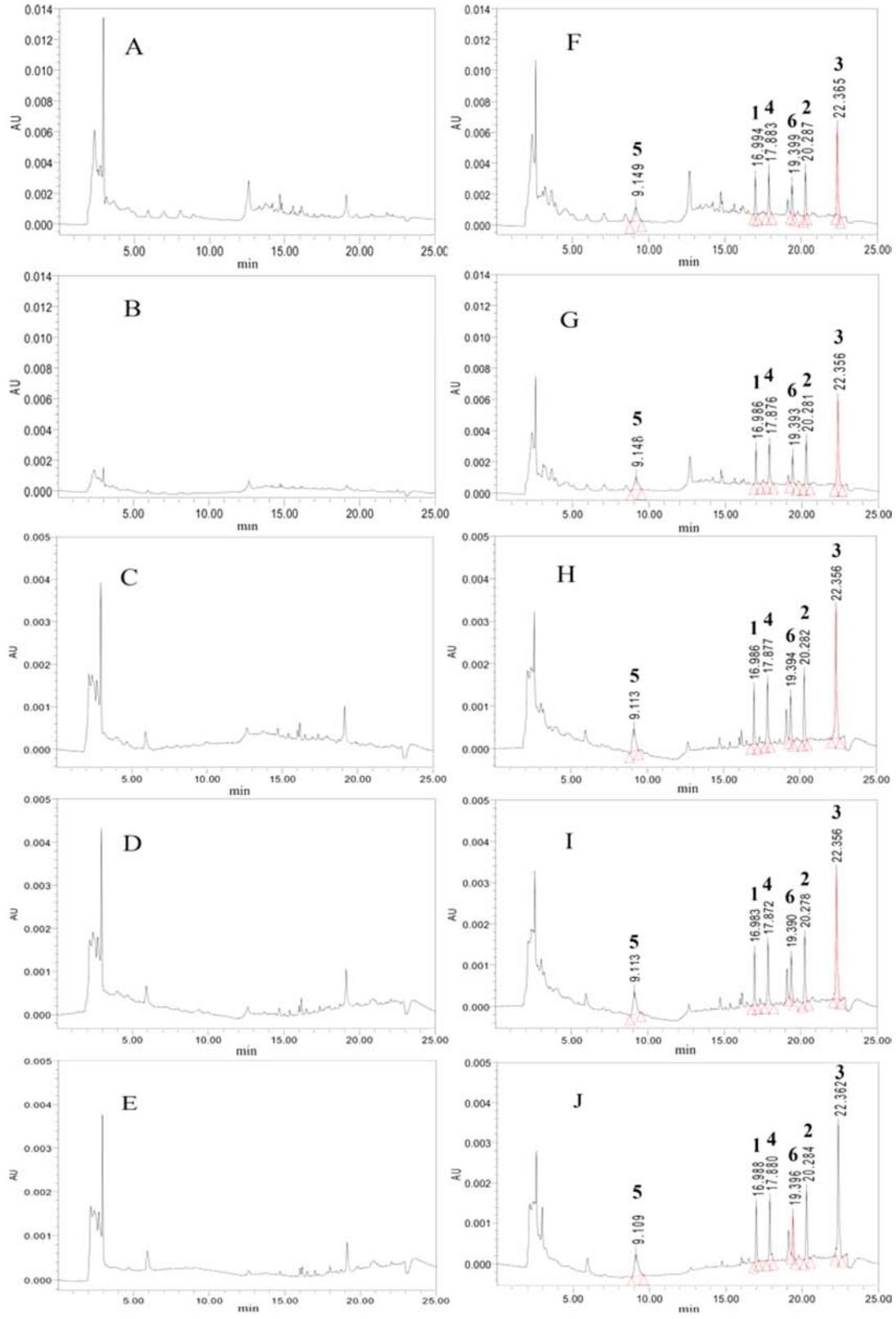


**Figure 2.** Chromatograms of (A) blank pig liver, (B) kidney, (C) broiler muscle, (D) sebum, and (E) carp skin sample, (F) blank pig liver, (G) kidney, (H) broiler muscle, (I) sebum, and (J) carp skin sample spiked with quinocetone and its main metabolites.

The other tested cartridges were an Oasis MAX (60 mg, 3 mL) (Waters Corp.) and an SCX (500 mg, 3 mL) (Agilent, Santa Clara, CA, USA).

*HPLC Analysis.* HPLC analysis was performed using a Waters 2695 HPLC system coupled with a UV detector. Chromatographic separation was conducted using a ZORBAX SB-$C_{18}$ column (250 mm × 4.6 mm i.d., 5 $\mu$m; Agilent Technology, USA) coupled with a 2 mm $C_{18}$ guard column at a flow rate of 1.0 mL/min at 30 °C in a column oven. Mobile phase component A was 1% formic acid, and component B was MeCN. The mobile phase gradient profile was as


dx.doi.org/10.1021/jf5042867 | J. Agric. Food Chem. 2014, 62, 10348−10356

follows: 0 min, 80% A; 8 min, 80% A; 15 min, 35% A; 20 min, 10% A; 20.1 min, 80% A; 25 min, 80% A. The UV detector was set at a wavelength of 320 nm for all of the compounds. The developed method was validated with reference to the implemented validation procedure for residues in food animal products, as described in EU Commission Decision 2002/657/EC under Council Directive 96/23/EC.[24]

*Calibration Curve and Linearity.* The standard mixture calibration curves were generated on five different days at seven concentration levels from 2 to 500 μg/L for **1** and **2** and from 4 to 500 μg/L for **3**−**6**. The analyses were performed in triplicate. The method was further tested by matrix-matched calibration curves, which were obtained by fortification with the six compounds at each of the six concentrations from 2 to 200 μg/kg. The calibration curves constructed on five separate days were analyzed to evaluate the linearity of each curve. Slope, intercept, and correlation coefficient were calculated for each standard curve. Unknown concentrations were calculated from the equation of the calibration curve.

*Limits of Detection (LOD) and Limits of Quantification (LOQ).* LOD was calculated by comparing the 3-fold variation of signal-to-noise ratio (S/N = 3:1) obtained from the extract analysis of the blank samples; LOQ was calculated using S/N = 10:1.

*Accuracy and Precision.* Blank samples were fortified at three different levels (1, 2, and 4 times the LOQ). For the intraday experiment, six sets of each concentration were run. Six replicates of the three concentrations were analyzed on five different days for the interday experiment. Accuracy was defined by the mean absolute recovery, which was calculated by comparing the peak area of the extracted sample with that of the standard working solution. Precision was defined by relative standard deviation (RSD).

*Specificity.* Method specificity was verified by analyzing blank samples and observing residue-interfering peaks. The results were evaluated by the presence of interfering substances at the specified retention time.

*Stability.* Stability experiments were conducted to investigate the stability of quinocetone and its metabolites in incurred samples stored at −20 °C within 6 months. The incurred samples were extracted, thawed, and analyzed every week. The measured values were compared with those in freshly incurred samples in triplicate. The results indicated that quinocetone and its metabolites were stable for 4 months in the incurred samples during storage at −20 °C.

**Data Analysis.** To determine the tissue depletion profile, we analyzed the concentrations of quinocetone and its metabolites by using a linear regression model of natural log-transformed average concentration of quinocetone and its metabolites (ln *C*) against time. The last three time-point data were fit to the first-order rate equation $C = C_0\ e^{-kt}$, where *C* is the concentration of quinocetone and its metabolites on day *t*, $C_0$ is the initial concentration, elimination rate constant ($k$) is the slope of the linear regression equation for the log-transformed residue concentration (ln *C*) against time, and the half-life of elimination ($t_{1/2k}$) is calculated from the equation $t_{1/2k} = \ln 2/k$ for each tissue.

The withdrawal time (WDT) was estimated by the Statistical Tool for Data Analysis of Draft Maximum Residue Limits for Veterinary Drugs (MRLVDs) in Edible Tissues.[25] The approach is primarily based on linear regression analysis and statistical estimation of one-sided upper tolerance limits for the marker residue depletion in the individual target tissues. An iterative procedure is then used to calculate for different time points on the depletion curve the intake of residues of concern in the food basket. The calculated intake of residues is compared with the acceptable daily intake (ADI), and the time point of depletion below the ADI is selected to determine the MRLs.

The estimated daily intake (EDI) was adopted to calculate the quantity of residues of toxic concern for a food basket that includes 300 g of muscle, 100 g of liver, 50 g of kidney, and 50 g of fat. The concentration of residues was calculated using the median of the residue distribution, expressed as the marker residue **3**, with inclusion of factors (when required) to convert the marker residue concentration to total residues. For each food commodity, the highest species-specific median residue value is used in the calculation. The global estimated chronic dietary exposure (GECDE) to quinocetone residue for the population group of interest is "the highest exposure calculated using the 97.5th percentile consumption figure for a single food selected from all the foods plus the mean dietary exposure from all the other relevant foods" and is calculated as

$$\text{GECDE} = \text{highest exposure from one animal product} + \text{total mean exposure from all other products}$$

Descriptive statistical parameters, such as mean, standard deviation (SD), and coefficient of variation (CV), were calculated. Data were statistically analyzed using Microsoft Excel 2007.

## RESULTS AND DISCUSSION

**Sample Pretreatment.** Low recoveries of all six analytes were obtained when MeOH or MeCN was used alone as an extraction solvent. However, almost all of the analytes were extracted when 30% water was added to MeOH and MeCN, but the recovery of **5** was low. All of the compounds were extracted with recoveries of >80% when 1% metaphosphoric was added to MeOH/MeCN/water (50:20:30, v/v/v). On the basis of the properties of the six compounds and the sample/matrix composition, we used the following test cartridges: Oasis HLB, Oasis MAX, and SCX cartridges. With SCX, the recovery was low, and interferences were observed at the same retention time as **5**. Sin et al.[26] recommended the SPE cleanup on Oasis MAX for **5**, but the method was not suitable for other compounds. Comparative studies indicated that Oasis HLB was superior to the other cartridges in terms of good recovery (>90%) and low matrix interference. During the elution steps of Oasis HLB, MeCN and MeOH were selected because of their good extraction efficiencies. MeCN showed high elution power to acquire high recoveries and low interference. The techniques were improved, thereby reducing the total time of sample pretreatment to <2 h.

**HPLC Method Validation.** *Linearity.* The linearity of the standard mixtures was good for all of the analytes at tested concentrations, as indicated by correlation coefficients >0.9999 for all of the curves. Matrix-matched calibration standard curves were used to quantitate the target analytes in animal tissues and to ensure that the method was as accurate as possible. The correlation coefficient values of the analytes within the range from 2 to 200 μg/kg were >0.99.

*Specificity.* On the basis of the comparison of background noise with various matrices, our results showed that no interference peak was detected at the retention time of the tested compounds (Figure 2).

*LOD and LOQ.* The LODs of **1** and **2** were 5 μg/kg in liver and kidney tissues and 3 μg/kg in muscle and fat tissues. The LODs of **3**−**6** were 10 μg/kg in liver and kidney tissues and 6 μg/kg in muscle and fat tissues. The LOQs of **1** and **2** were 20 μg/kg in liver and kidney tissues and 10 μg/kg in muscle and fat tissues. The LOQs of **3**−**6** were 40 μg/kg in liver and kidney tissues and 20 μg/kg in muscle and fat tissues.

*Accuracy and Precision.* The results of recovery and reproducibility of the method at the specified concentration range on five separate days were calculated. The mean recoveries ranged from 61.5 to 81.5%. The interday values were <11.7%, indicating that the proposed method could precisely and accurately determine quinocetone and its metabolites in animal tissues.

**Characteristics of Quinocetone Residues in Food-Producing Animals.** The concentrations of quinocetone and

**Table 1. Concentrations of Quinocetone and Its Metabolites in Tissues of Pigs, Broilers, and Carp at Different Days after the Administration of Quinocetone**

| | | compound ($\mu$g/kg) | | | | | |
|---|---|---|---|---|---|---|---|
| tissue | time (days) | **1** | **2** | **3** | **4** | **5** | **6** |
| | | | | **Pigs** | | | |
| liver | 0.25 | 62.5 ± 5.0 | 83.0 ± 7.8 | 173.5 ± 10.6 | 83.3 ± 7.4 | 63.8 ± 5.7 | 42.2 ± 2.6 |
| | 1 | 33.1 ± 3.4 | ND[a] | 161.6 ± 15.9 | 67.4 ± 7.7 | 43.8 ± 4.3 | ND |
| | 3 | ND | ND | 103.2 ± 8.4 | 40.1 ± 3.9 | ND | ND |
| | 7 | ND | ND | 40.1 ± 3.7 | ND | ND | ND |
| kidney | 0.25 | 50.9 ± 5.2 | 81.8 ± 8.1 | 167.5 ± 7.7 | ND | 41.5 ± 2.9 | ND |
| | 1 | ND | ND | 164.3 ± 4.3 | ND | ND | ND |
| | 3 | ND | ND | 131.3 ± 10.4 | ND | ND | ND |
| | 7 | ND | ND | 40.1 ± 3.62 | ND | ND | ND |
| muscle | 0.25 | 19.5 ± 1.2 | 22.3 ± 1.7 | 40.4 ± 2.3 | ND | 28.5 ± 2.0 | ND |
| | 1 | 17.8 ± 1.4 | 14.9 ± 1.3 | 32.8 ± 2.8 | ND | ND | ND |
| | 3 | ND | ND | 20.2 ± 1.7 | ND | ND | ND |
| fat | 0.25 | 11.6 ± 1.1 | 20.2 ± 1.7 | ND | ND | 33.0 ± 2.9 | ND |
| | 1 | 10.2 ± 0.4 | ND | ND | ND | ND | ND |
| | | | | **Broilers** | | | |
| liver | 0.25 | ND | 101.1 ± 7.1 | 142.7 ± 7.5 | 52.8 ± 3.5 | 41.4 ± 2.3 | ND |
| | 1 | ND | 45.5 ± 3.4 | 112.4 ± 10.3 | 40.5 ± 3.2 | ND | ND |
| | 3 | ND | ND | 52.5 ± 2.4 | ND | ND | ND |
| | 5 | ND | ND | 40.6 ± 1.2 | ND | ND | ND |
| kidney | 0.25 | 56.6 ± 3.4 | 83.2 ± 7.6 | 130.6 ± 10.2 | ND | 49.1 ± 3.3 | ND |
| | 1 | ND | 32.1 ± 1.5 | 121.1 ± 9.6 | ND | 40.1 ± 0.9 | ND |
| | 3 | ND | ND | 44.7 ± 3.3 | ND | ND | ND |
| | 5 | ND | ND | 40.4 ± 1.2 | ND | ND | ND |
| muscle | 0.25 | 29.6 ± 2.5 | ND | 44.8 ± 3.5 | ND | ND | ND |
| | 1 | 10.3 ± 0.5 | ND | 33.6 ± 3.9 | ND | ND | ND |
| | 3 | ND | ND | 20.5 ± 1.0 | ND | ND | ND |
| fat | 0.25 | 26.9 ± 2.5 | 26.6 ± 1.9 | 30.6 ± 2.0 | 29.7 ± 1.2 | ND | ND |
| | 1 | 17.3 ± 1.0 | ND | 20.3 ± 0.4 | ND | ND | ND |
| | | | | **Carp** | | | |
| liver | 0.25 | 29.6 ± 3.0 | 38.0 ± 4.5 | 74.9 ± 5.8 | ND | ND | ND |
| | 1 | 20.8 ± 0.6 | 20.6 ± 0.5 | 41.3 ± 0.8 | ND | ND | ND |
| | 3 | ND | ND | 40.3 ± 0.1 | ND | ND | ND |
| kidney | 0.25 | 27.9 ± 2.4 | 35.2 ± 3.2 | 77.6 ± 5.3 | 43.1 ± 1.6 | ND | ND |
| | 1 | ND | 24.4 ± 1.9 | 62.2 ± 5.6 | ND | ND | ND |
| | 3 | ND | ND | 40.1 ± 0.1 | ND | ND | ND |
| muscle | 0.25 | 22.3 ± 4.2 | ND | 39.4 ± 2.9 | 26.8 ± 2.4 | ND | ND |
| | 1 | ND | ND | 21.6 ± 0.9 | ND | ND | ND |
| skin | 0.25 | 15.0 ± 1.6 | ND | 26.1 ± 1.7 | ND | ND | ND |
| | 1 | ND | ND | 20.2 ± 0.1 | ND | ND | ND |

[a]Samples were below the LOQ of analysis method.

its metabolites in pig, broiler, and carp edible tissues for each time point were averaged, and the SD of each was calculated (Table 1). The highest concentrations of all of the related compounds in all of the edible tissues were obtained at 6 h after the last dosing. At all time points, the highest concentrations were detected in the liver, and the lowest concentrations were measured in the muscle or fat (skin).

*Pigs.* After the drugs were consecutively administered for 3 months, **1**−**6** were detected in the liver at 6 h postmedication, and the residual concentrations ranged between 42.2 and 173.5 $\mu$g/kg. **1**−**3** and **5** were detected in the kidney and muscle at


dx.doi.org/10.1021/jf5042867 | J. Agric. Food Chem. 2014, 62, 10348−10356

**Table 2. Comparison of Chronic Dietary Exposure Assessments for Quinocetone for the General Population**

| | food consumption (g/day) | | | | | | | exposure from each food (μg/day) | | |
|---|---|---|---|---|---|---|---|---|---|---|
| food category | model diet | mean chronic | high chronic | median residue (μg/kg) | M:T | analytical method recovery (%) | EDI (μg/day) | high consumers | mean total population | ADI (%) |
| pork muscle[a] | 300 | 114 | 415 | 40 | 0.30 | 62.1 | **64.4** | 89.1 | **24.5** | |
| mammalian trimmed fat, skin, and added fat | 50 | 14 | 125 | 10 | 0.31 | 64.3 | 2.5 | 6.3 | **0.7** | |
| mammalian liver | 100 | 2 | 237 | 173 | 0.29 | 62.3 | **95.8** | **226.9** | 1.9 | |
| mammalian kidney | 50 | 0.5 | 166 | 164 | 0.29 | 68.5 | **41.3** | 137.0 | **0.4** | |
| poultry muscle | 300 | 118 | 352 | 45 | 0.34 | 68.4 | 58.0 | 68.1 | **22.8** | |
| poultry fat and skin | 50 | 1 | 23 | 30 | 0.36 | 64.4 | **6.5** | 3.0 | **0.1** | |
| poultry offal (kidney) | 150 | 5 | 188 | 134 | 0.31 | 62.8 | 103.2 | 129.4 | **3.4** | |
| fish | 300 | 27 | 655 | 39 | 0.38 | 64.8 | 47.5 | 103.7 | **4.3** | |
| EDI | | | | | | | 208[b] | | | 69 |
| mean exposure from all foods | | | | | | | | | 58 μg/day | |
| mean exposure for adult of 60 kg body weight | | | | | | | | | 1.0 μg/kg bw/day | 19 |
| GECDE | | | | | | | | | 283[c] μg/day | |
| GECDE for adult of 60 kg body weight | | | | | | | | | 4.7 μg/kg bw/day | 94 |

[a]Total residue = marker residue/ratio (M:T)/analytical method recovery. [b]For each food commodity, the highest species-specific median residue value is used in the calculation of EDI. [c]The GECDE is the sum of the bold values for high consumer exposure and mean total population exposure.

the withdrawal time of 6 h, and the residual concentrations ranged between 19.5 and 167.5 μg/kg. **1** and **3**−**5** were detected in the liver after 1 day. **3** was detected in the liver and kidney after 7 days and in the muscle after 3 days. Low amounts of **1**, **2**, and **5** were detected in the fat at the withdrawal time of 6 h, and the residual concentrations ranged between 11.6 and 33.0 μg/kg; residues were found at values approximately equal to the LOQ of the method after a withdrawal time of 1 day. The linear regression analysis results between the natural log of the concentration of **3** and the withdrawal time in the liver, kidney, and muscle are listed as follows: $C_{\text{liver-3}} = 205.0\ e^{-0.232t}$, $C_{\text{kidney-3}} = 233.2\ e^{-0.244t}$, $C_{\text{muscle-3}} = 42.2\ e^{-0.248t}$. Hence, $t_{1/2ke}$ values of **3** in the liver, kidney, and muscle of pigs were 2.99, 2.84, and 2.79 days, respectively.

*Broilers.* **2**−**5** were detected in the liver at the withdrawal time of 6 h, and the residual concentrations ranged between 41.4 and 142.7 μg/kg. **2** and **4** were detected in the liver after 1 day. **1**−**3** were detected in the kidney and fat at the withdrawal time of 6 h, and the residual concentrations were between 26.6 and 130.6 μg/kg. **2** and **5** were detected for 1 day in the kidney. Quinocetone was detected in the muscle and fat at 1 day at very low concentrations of 10.3 and 17.3 μg/kg, respectively, slightly higher than the LOQ of the method. **3** was detected in the liver and kidney for 5 days, in the muscle for 3 days, and in the fat for 1 day. The elimination equations of **3** in the liver, kidney, and muscle of broiler were calculated using the regression curves, which were $C_{\text{liver-3}} = 133.9\ e^{-0.257t}$, $C_{\text{kidney-3}} = 137.7\ e^{-0.276t}$, and $C_{\text{muscle-3}} = 46.6\ e^{-0.285t}$. Hence, the $t_{1/2ke}$ values of **3** in the liver, kidney, and muscle of the broiler were 2.70, 2.51, and 2.43 days, respectively.

*Carp.* **5** and **6** were not detected in the tissues of carp. **1**−**3** were detected in the liver at withdrawal times of 6 h and 1 days, and the residual concentrations ranged between 20.6 and 74.9 μg/kg. **1**−**4** were detected in the kidney at the withdrawal time of 6 h, and the residual concentrations ranged between 27.9 and 77.6 μg/kg. **1** was detected in the kidney for 1 day. **1** and **3** were detected in the muscle and skin at the withdrawal time of 6 h, **4** was detected in the muscle at the withdrawal time of 6 h, and the residual concentration was 26.8 μg/kg. **3** was detected in the liver and kidney for 3 days and in the muscle and skin for 1 day. The linear regression analysis results between the natural log of the concentration of **3** and the withdrawal time in the liver and the kidney are listed as follows: $C_{\text{liver-3}} = 64.6\ e^{-0.181t}$ and $C_{\text{kidney-3}} = 80.7\ e^{-0.235t}$. The elimination half-lives of **3** in the liver and kidney of carp calculated from the elimination equations were 3.83 days for liver and 2.95 days for kidney.

In this study, depletion of quinocetone residues in three food animals was investigated. The results showed that quinocetone was eliminated rapidly in pigs, broilers, and carp; no metabolites could be detected after the withdrawal time of 7 days.

The present residue depletion study showed the same residual marker, the same target tissue, and the same tendency in elimination rate as the radioactive tracer studies,[12] but these results differed from those in previous studies, suggesting that **5** is the marker residue.[13,21] **5** likely conjugates with glycine in vivo. In previous studies, sodium hydroxide or hydrochloric acid is applied to hydrolyze the samples, showing that **5** is released from **5**-glycine; other compounds are also degraded to **5**; thus, the concentration of **5** is very high and can be detected for a long time.[13,21] In our study, a method previously reported[18,22] was modified using 1% metaphosphoric acid in MeOH/MeCN/water (50:20:30, v/v/v) to ensure the stability of the compounds in tissues. In this case, the real **5** (free **5** and **5** released from **5**-glycine) was extracted; hence, the results were different from those in previous reports.

The depletion rate of quinocetone-related residues in pig, broiler, and carp tissues was found in the following order: fat (skin) > muscle > kidney > liver. This result indicated that the liver is the key organ of quinocetone residues. According to the principle of pharmacokinetics, the distributions of compounds in the body depend on organ blood flow and compound affinity to tissues. Blood supply to the liver and kidney is higher than that to muscle and fat. Therefore, a comparatively higher level of **3** was found in the liver and kidney than in other organs or tissues.

The depletion rate of the six compounds in the liver was observed in the order **6** > **2** > **1** > **5** > **4** > **3**. This result

indicated that **3** is the main compound that produces residues in pigs, broilers, and carp for the longest time when quinocetone was administered consecutively to these animals. Therefore, **3** could be the key compound for quinocetone residue monitoring compared with other compounds. The long half-lives of **3** in tissues may be attributed to the following reasons. **3** (didesoxyquinocetone) is one of the reduced metabolites of quinocetone. The polarity of **3** is much lower than that of other metabolites. As a result, **3** may be easily retained in organs and tissues.

Although the residue marker of quinocetone in the three animals was possibly **3**, certain differences were found in the residue characteristics of different animals. **6** could be detected only in pig liver. **5** could not be detected in carp tissues. Our results showed that the differences in metabolic processes could be accounted for the differences in distribution. In addition, $t_{1/2\ ke\text{-}3}$ in the liver was detected in the following order: carp > pigs > broilers. This result could be attributed to the differences in the metabolic absorption and metabolic enzymes of different animals.

**Acceptable Daily Intake (ADI).** On the basis of the toxicology results, the no observed effect level (NOEL) of quinocetone is 5 mg/kg bw/day.[27] The safety factor usually chosen is 100 in the situation where a NOEL is derived from a long-term animal study on the assumption that humans are 10 times as sensitive as the test animals used in such studies and that a 10-fold range of sensitivity within the human population may exist, but genotoxicity of quinocetone was noted in previous studies,[2] so a higher safety factor of 1000 was employed.[28] Then the ADI is 5 μg/kg bw/day.

**Dietary Exposure Assessment.** *Estimated Daily Intake (EDI).* Results below the LOQ are assigned a value of half of the LOQ when the median residue concentration is calculated. On the basis of the established model diet, the exposure to quinocetone expressed as the EDI, and calculated from the M:T and analytical method recovery adjusted median residue, was 208 μg/person/day. Dietary exposure was estimated to be 69% of the ADI (Table 2).

*Assumptions for Dietary Exposure Assessment.* The following assumptions were used in dietary exposure estimates: residues are found in pork, poultry, and fish; residues are found in muscle, liver, kidney, skin, and fat; all poultry offal is assumed to be kidney (worst-case scenario).

*Global Estimated Chronic Dietary Exposure (GECDE).* For the general population group, mammalian liver was the major contributor to estimated exposure from quinocetone residue (Table 2). Mammalian fat and kidney and poultry fat and skin contributed only negligible amounts to overall exposure estimates. Using the median residue as input, GECDE was 4.7 μg/kg bw/day, 94% of the ADI of 5 μg/kg bw/day (Table 2), and did not exceed the ADI.

*Comparison to EDI Estimates.* The calculations based on the model diet found that the median residue resulted in exposure estimated below the ADI for the general population. Similarly, the GECDE calculations found that exposure estimates were below the ADI for the general population, but they were higher than the EDI. Mammalian liver was the major contributor to chronic exposure estimates. In summary, none of the chronic exposure estimates resulted in exceeding the ADI.

**Withdrawal Time (WDT).** The EDI chart reveals that the EDI was below the ADI at zero withdrawal intervals in pigs and carp and at the withdrawal time of 72 h in broilers (Figure 3); therefore, it is recommended that the WDT of quinocetone is 0 days in pigs and carp and 3 days in broilers.

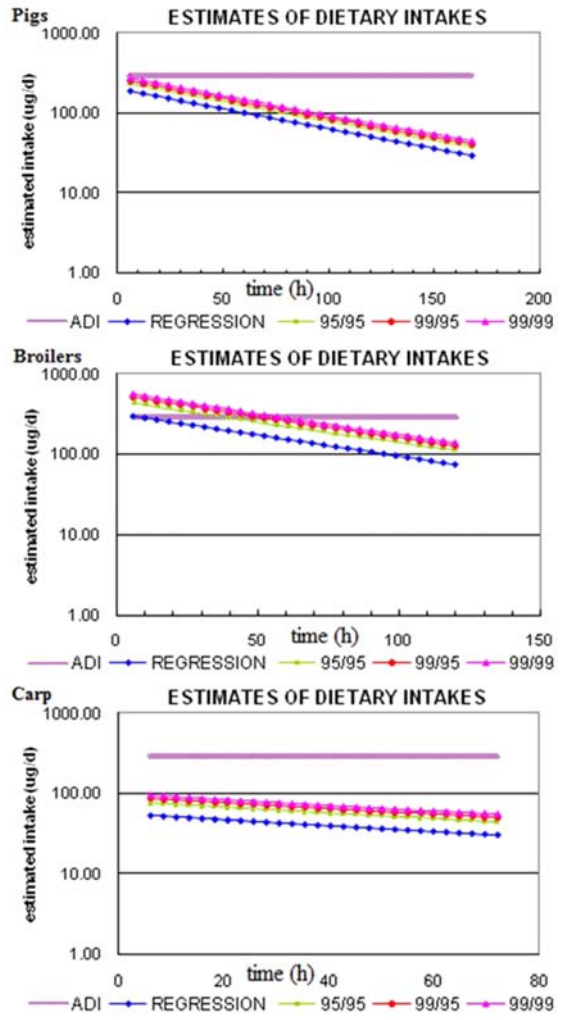


**Figure 3.** Estimated intakes (μg/person/day) versus time in pigs, broilers, and carp.

The prolonged presence of quinocetone-related residues in edible tissues is a potential risk for consumers. Considering that the established WDT was based on dietary exposure assessment, we could use the proposed WDT for residue monitoring of quinocetone in food-producing animals. In contrast to LC-MS/MS, HPLC-UV is probably more suitable for routine quinocetone residue monitoring analyses. HPLC-UV could be efficiently applied in a quinocetone monitoring program. The application of this technology could significantly improve the monitoring procedures for the illegal use of quinocetone to ensure food safety.

Our results provided the residue profile of quinocetone and its metabolites in edible tissues. On the basis of these residue data in edible tissues, our conclusion is that the liver is the target tissue and **3** is the residual marker of quinocetone in food animals. A withdrawal period of 0 days was estimated for quinocetone in pigs and carp, and 3 days was the estimated WDT in broilers. In addition, an HPLC-UV method was established to simultaneously and quantitatively determine quinocetone and its five major metabolites in edible tissues of pig, broiler, and carp. The recoveries in edible tissues spiked at

10−160 μg/kg ranged from 61.5 to 81.5% with interday RSD < 11.7%. These results also provided scientific evidence for the routine residue monitoring of quinocetone in food-producing animals.

## AUTHOR INFORMATION


### Corresponding Author

*(Z.Y.) Phone: 0086-27-87287186. Fax: 0086-27-87672232. E-mail: yuan5802@mail.hzau.edu.cn.



### Funding

This work was supported by grants from the National Natural Science Foundation of China (31272614), the National Basic Research Program of China (2009CB118800), the Special Fund for Agro-scientific Research in the Public Interest (201203040), and the Recommend international advanced agricultural science and technology plan (2011-G4).


### Notes

The authors declare no competing financial interest.

## ABBREVIATIONS USED

ADI, acceptable daily intake; WDT, withdrawal time; MRL, maximum residue limit; EMEA, European Medical Evaluation Agency; AVMA, American Veterinary Medical Association; EDI, estimates of dietary intake; GECDE, global estimated chronic dietary exposure

## REFERENCES


(1) Ministry of Agriculture, People's Republic of China, 2003; Notice 295.

(2) Ihsan, A.; Wang, X.; Zhang, W.; Tu, H.; Wang, Y.; Huang, L.; Iqbal, Z.; Cheng, G.; Pan, Y.; Liu, Z.; Tan, Z.; Zhang, Y.; Yuan, Z. Genotoxicity of quinocetone, cyadox and olaquindox in vitro and in vivo. *Food Chem. Toxicol.* **2013**, *59*, 207−214.

(3) Yang, W.; Fu, J.; Xiao, X.; Yan, H.; Bao, W.; Wang, D.; Hao, L.; Nussler, A. K.; Yao, P.; Liu, L. Quinocetone triggers oxidative stress and induces cytotoxicity and genotoxicity in human peripheral lymphocytes of both genders. *J. Sci. Food Agric.* **2013**, *93*, 1317−1325.

(4) Wang, X.; Zhang, W.; Wang, Y. L.; Ihsan, A.; Dai, M. H.; Huang, L. L.; Chen, D. M.; Tao, Y. F.; Peng, D. P.; Liu, Z. L.; Yuan, Z. H. Two generation reproduction and teratogenicity studies of feeding quinocetone fed to Wistar rats. *Food Chem. Toxicol.* **2012**, *50* (5), 1600−1609.

(5) Wang, X.; Zhang, W.; Wang, Y.; Peng, D.; Ihsan, A.; Huang, X.; Huang, L.; Liu, Z.; Dai, M.; Zhou, W.; Yuan, Z. H. Acute and sub-chronic oral toxicological evaluations of quinocetone in Wistar rats. *Regul. Toxicol. Pharmacol.* **2010**, *58*, 421−427.

(6) Wang, D.; Luo, X.; Zhong, Y.; Yang, W.; Xu, M.; Liu, Y.; Meng, J.; Yao, P.; Yan, H.; Liu, L. Pu-erh black tea extract supplementation attenuates the oxidative DNA damage and oxidative stress in Sprague−Dawley rats with renal dysfunction induced by subchronic 3-methyl-2-quinoxalin benzenevinylketo-1,4-dioxide exposure. *Food Chem. Toxicol.* **2012**, *50*, 147−154.

(7) Wang, D.; Zhong, Y.; Luo, X.; Wu, S.; Xiao, R.; Bao, W.; Yang, W.; Yan, H.; Yao, P.; Liu, L. Pu-erh black tea supplementation decreases quinocetone-induced ROS generation and oxidative DNA damage in Balb/c mice. *Food Chem. Toxicol.* **2011**, *49*, 477−484.

(8) Yu, M.; Xu, M.; Liu, Y.; Yang, W.; Rong, Y.; Yao, P.; Yan, H.; Wang, D.; Liu, L. Nrf2/ARE is the potential pathway to protect Sprague−Dawley rats against oxidative stress induced by quinocetone. *Regul. Toxicol. Pharmacol.* **2013**, *66*, 279−285.

(9) Liu, Z. Y.; Huang, L. L.; Chen, D. M.; Dai, M. H.; Tao, Y. F.; Wang, Y. L.; Yuan, Z. H. Application of electrospray ionization hybrid ion trap/time-of-flight mass spectrometry in the rapid characterization of quinocetone metabolites formed in vitro. *Anal. Bioanal. Chem.* **2010**, *396* (3), 1259−1271.

(10) Shen, J.; Yang, C.; Wu, C.; Feng, P.; Wang, Z.; Li, Y.; Li, Y.; Zhang, S. Identification of the major metabolites of quinocetone in swine urine using ultra-performance liquid chromatography/electrospray ionization quadrupole time-of-flight tandem mass spectrometry. *Rapid Commun. Mass Spectrom.* **2010**, *24*, 375−383.

(11) Wu, H.; Yang, C.; Wang, Z.; Shen, J.; Zhang, S.; Feng, P.; Li, L.; Cheng, L. Metabolism profile of quinocetone in pig by ultra-performance liquid chromatography quadrupole time-of-flight mass spectrometry. *Eur. J. Drug Metab. Pharmacokinet.* **2012**, *37* (2), 141−154.

(12) Li, J.; Huang, L.; Wang, X.; Pan, Y.; Liu, Z.; Chen, D.; Tao, Y.; Yuan, Z. Metabolic disposition and excretion of quinocetone in rats, pigs, broilers, and carp. *Food Chem. Toxicol.* **2014**, *69*, 109−119.

(13) Huang, L.; Xiao, A.; Fan, S.; Yin, J.; Liu, D.; Qiu, Y.; Yuan, Z. Development of liquid chromatographic methods for determination quinocetone and its main metabolites in edible tissues of swine and chicken. *J. AOAC Int.* **2005**, *88* (2), 472−478.

(14) Hu, G. M.; Huang, L. L.; Yuan, Z. H. Pharmacokineties and residue depletion of quinocetone in carp. Master's dissertation, Huazhong Agricultural University, Hubei, China, 2008 (in Chinese).

(15) Li, J. Y.; Li, J. S.; Xu, Z. Z.; Zhao, R. C.; Miao, X. L.; Zhang, J. Y.; Lu, R. H. The determination and residues of quinocetone in swines. *Prog. Vet. Med.* **2004**, *25* (4), 117−120.

(16) Li, J. Y.; Li, J. S.; Zhao, R. C.; Miao, X. L.; Zhang, J. Y.; Zhou, X. Z. Study on residues of quinocetone in edible chicken tissues. *Prog. Vet. Med.* **2008**, *29* (4), 34−37.

(17) Wu, Y.; Wang, Y.; Huang, L.; Tao, Y.; Yuan, Z.; Chen, D. Simultaneous determination of five quinoxaline-1,4-dioxides in animal feeds using ultrasonic solvent extraction and high-performance liquid chromatography. *Anal. Chim. Acta* **2006**, *569*, 97−102.

(18) Wu, Y.; Yu, H.; Wang, Y.; Huang, L.; Tao, Y.; Chen, D.; Peng, D.; Liu, Z.; Yuan, Z. Development of a high-performance liquid chromatography method for the simultaneous quantification of quinoxline-2-carboxylic acid and methyl-3-quinoxaline-2-carboxylic acid in animal tissues. *J. Chromatogr., A* **2007**, *1146*, 1−7.

(19) Zhang, J.; Li, M.; Li, L.; Li, Y.; Peng, B.; Zhang, S.; Gao, H.; Zhou, W. Investigation of the ultrasound effect and target analyte selectivity of dispersive liquid−liquid microextraction and its application to a quinocetone pharmacokinetic study. *J. Chromatogr., A* **2012**, *1268*, 1−8.

(20) Fang, J.; Li, Y.; Wu, S.; Ma, K.; Li, H.; Gao, Z.; Dong, F. Determination of quinocetone and its two major metabolites in chicken liver and muscle tissues by liquid chromatography-tandem mass spectrometry. *Anal. Methods* **2012**, *4*, 1149−1154.

(21) Yong, Y.; Liu, Y.; He, L.; Xu, L.; Zhang, Y.; Fang, B. Simultaneous determination of quinocetone and its major metabolites in chicken tissues by high-performance liquid chromatography tandem mass spectrometry. *J. Chromatogr., B* **2013**, *919−920*, 30−37.

(22) Li, Y.; Liu, K.; Beier, R. C.; Cao, X.; Shen, J.; Zhang, S. Simultaneous determination of mequindox, quinocetone and their major metabolites in chicken and pork by UPLC−MS/MS. *Food Chem.* **2014**, *160*, 171−179.

(23) AVMA. Panel on Euthanasia 2000 Report of the AVMA panel on euthanasia. *J. Am. Vet. Med. Assoc.* **2001**, *218*, 669.

(24) Commission Decision of 12 August 2002 implementing Council Directive 96/23/EC concerning the performance of analytical methods and the interpretation of results (2002/657/EC). *Off. J. Eur. Communities* **2002**, *L221*, 8.

(25) 62nd meeting of FAO/WHO Joint Expert Committee on Food Additives, 2003; http://www.fao.org/fileadmin/user_upload/agns/zip/tool_1.1551.zip (accessed June 2, 2013).

(26) Sin, D. W. M.; Chung, L. P. K.; Lai, M. M. C.; Siu, S. M. P.; Tang, H. P. O. Determination of quinoxaline-2-carboxylic acid, the major metabolite of carbadox, in porcine liver by isotope dilution gas chromatography-electron capture negative ionization mass spectrometry. *Anal. Chim. Acta* **2004**, *508* (2), 147−158.

(27) Zhang, W.; Huang, L. L.; Wang, Y. L.; Yuan, Z. H. Preclinical toxicity of quinocetone. Master's dissertation, Huazhong Agricultural University, Hubei, China, 2007 (in Chinese).

(28) WHO (World Health Organization). Evaluation of certain veterinary drug residues in food. *Fortieth Report of the Joint FAO/WHO Expert Committee on Food Additives*; WHO Technical Report Series 815; Geneva, Switzerland, 1991.

JOURNAL OF AGRICULTURAL AND FOOD CHEMISTRY

ARTICLE

pubs.acs.org/JAFC

# Monitoring of Quality and Stability Characteristics and Fatty Acid Compositions of Refined Olive and Seed Oils during Repeated Pan- and Deep-Frying Using GC, FT-NIRS, and Chemometrics

Akram Zribi,[†] Hazem Jabeur,[†] Felix Aladedunye,[§] Ahmed Rebai,[#] Bertrand Matthäus,[§] and Mohamed Bouaziz*[,†,⊥]

[†]Laboratoire d'Électrochimie et Environnement, École Nationale d'Ingénieurs de Sfax, Université de Sfax, B.P. 1173, 3038 Sfax, Tunisia

[§]Department for Safety and Quality of Cereals, Working Group for Lipid Research, Max Rubner-Institut (MRI), , Schützenberg 12, D-32756 Detmold, Germany

[#]Laboratoire de Microorganismes et Biomolécules, Équipe des Procédés de Criblage Moléculaires et Cellulaires, Centre de Biotechnologie de Sfax, B.P. 1177, 3018, Sfax, Tunisia

[⊥]Institut Supérieur de Biotechnologie de Sfax, Université de Sfax, B.P. 1175, 3038, Sfax, Tunisia

**ABSTRACT:** Refined olive, corn, soybean, and sunflower oils were used as cooking oils for deep-frying at two different temperatures, 160 and 190 °C, and for pan-frying of potatoes at 180 °C for 10 successive sessions under the usual domestic practice. Several chemical parameters were assayed during frying operations to evaluate the status of the frying oils. Refined olive oil, as frying oil, was found to be more stable than the refined seed oils. In fact, this oil has proven the greatest resistance to oxidative deterioration, and its *trans*-fatty acid contents and percentages of total polar compounds were found to be lower at 160 °C during deep-frying. Finally, chemometric analysis has demonstrated that the lowest deterioration of the quality of all refined oils occurred in the refined olive oil during deep-frying at 160 °C and the highest deterioration occurred in the refined sunflower oil during pan-frying at 180 °C.

**KEYWORDS:** refined oils, deep-frying, pan-frying, frying temperatures, oil quality, Fourier-transformed near-infrared spectroscopy

## INTRODUCTION

Frying is one of the most popular methods of food processing, in which a foodstuff is submerged into heated oil exposed to atmospheric oxygen, moisture from the foodstuff, and high temperature with simultaneous heat and mass transfer.[1]

The selection of new industrial frying oils should satisfy many requirements. First of all, the product should be easy to use and keep good quality standards during prolonged exposure to high temperatures. Stability to oxidation during a prolonged exposure to high temperatures is one of the main characteristics that an industrial frying oil should possess, as its physical, chemical, and nutritional properties may undergo significant modifications during thermoxidation.[2] When lipids are subjected to a frying process, a wide range of complex chemical reactions such as oxidation, hydrolysis, isomerization, cyclization, and polymerization take place, which can degrade the oil. Undesirable constituents and off-flavors are developed in frying oil due to these chemical reactions.[3] Indeed, these reactions are influenced by the type and quality of the oil, the food properties, and the food/oil ratio, among other parameters,[4] altogether determining the frying oil performance.[5] Each vegetable oil is characterized by a typical stability against oxidation, which is dependent on the fatty acid composition, particularly the unsaturation degree and the content and composition of minor compounds. As a consequence, there is a need to define the point at which the fat or oil ought to be replaced. This is linked to the percentage of total polar compounds (TPC) formed during fryings. Today, it is well-known that when its TPC percentage is >25%, a fat or an oil for frying purposes must be discarded.[6]

A previous method described by Waltking and Wessels[7] was based on the separation by column chromatography on silica gel of two fractions. In fact, the first fraction contains the unaltered part or nonpolar compounds of the fat, which are unaltered triglycerides, and the second is composed of the altered products or polar compounds of frying fats. These decomposition products, also known as polar contaminant materials (PCM), tend to remain liquid and cannot be filtered out of the oil. They are also deposited on the surfaces of the fryer and absorbed by food. The PCM fraction is thought to include most of the potential toxic products produced in frying oils. In the biological tests conducted by López-Varela et al.,[8] rats fed used frying oil were found to exhibit liver damage. According to Andrikopoulos et al.,[9] the presence of byproducts of lipid peroxidation in food is undesirable because the nutritional value of food decreases with the destruction of unsaturated fatty acids (UFAs) and other essential food constituents with an unsaturated lipid structure such as vitamin E during the deep- and pan-frying of potatoes.

To obtain further information about polymerization changes that occur during frying, polar fractions that were previously obtained by column chromatography were analyzed by high-performance size exclusion chromatography (HPSEC).[10] These traditional chemical methods of oil analysis are commonly time-consuming and/or need substantial amounts of solvents.

Received: July 2, 2014
Revised: September 23, 2014
Accepted: September 29, 2014
Published: September 29, 2014

ACS Publications © 2014 American Chemical Society

**Table 1. Characteristics of Fresh Refined Oil Samples[a]**

| | ROO | RCO | RSO | RSfO |
|---|---|---|---|---|
| free acidity (%) | 0.06 ± 0.00a | 0.09 ± 0.00b | 0.11 ± 0.00c | 0.13 ± 0.00d |
| peroxide value (mequiv $O_2$/kg) | 2.13 ± 0.05a | 2.49 ± 0.07b | 4.43 ± 0.11c | 4.60 ± 0.10c |
| $K_{232}$ | 2.26 ± 0.04a | 2.37 ± 0.06b | 3.66 ± 0.10c | 4.57 ± 0.13d |
| $K_{270}$ | 0.48 ± 0.01a | 1.41 ± 0.03b | 2.03 ± 0.06c | 3.53 ± 0.11d |
| total phenols (mg/kg) | 85.09 ± 1.48a | 30.77 ± 0.47b | 23.41 ± 0.51c | 14.55 ± 0.29d |
| induction time (h) | 4.39 ± 0.03a | 3.55 ± 0.04b | 3.34 ± 0.03c | 2.18 ± 0.02d |

[a] ROO, refined olive oil; RCO, refined corn oil; RSO, refined soybean oil; RSfO, refined sunflower oil; $K_{232}$ and $K_{270}$, spectrophotometric indices. Each value represents the mean of three determinations ($n = 3$) ± standard deviation. Different lower case letters (a, b, c, and d) within the same row indicate significant differences ($p < 0.05$) between the fresh and refined oil sample groups.

The development of a simple and rapid test is needed to proficiently monitor oil quality.

Fourier-transformed near-infrared spectroscopy (FT-NIRS) is an important tool used for quality control and process monitoring in the food industry because it is s less expensive, relatively fast, and nondestructive technique to analyze fats and oils. It is also considered as the optimal tool to describe all aspects of fat degradation.[11] FT-NIRS is used for quantitative and qualitative measurements of edible oils and fats as a result of the development of instrumental macroprogramming for automated routine operations and the application of chemometrical techniques for multicomponent analysis.[12−14]

The purpose of the present research study is to investigate and compare the deterioration effect of successive deep-fryings at two different temperatures, 160 and 190 °C, and pan-frying sessions of potatoes at 180 °C on the quality of four refined vegetable oils, namely, refined olive, corn, soybean, and sunflower oils, under the real household practice of frying. Indeed, after frying, each sample of refined oil was examined for free acidity (FA), absorption coefficients $K_{232}$ and $K_{270}$, TPC, dimeric and polymeric triacylglycerols (DPTG), anisidine value (AnV), fatty acid compositions, and *trans*-fatty acid (TFA) contents as well as oxidative stability (through a Rancimat apparatus).

## MATERIALS AND METHODS

**Chemicals and Reagents.** Ethanol (≥99.9%) and *n*-heptane (99.0%) were obtained from Riedel-de Haën (Steinheim, Germany). Cyclohexane (99.5%), *n*-hexane (99.0%), and diethyl ether (≥99.7%) were purchased from Merck KGaA (Darmstadt, Germany). Potassium hydroxide (85.0%) was obtained from CDM (Karlsruhe, Germany), and potassium iodide (>99.0%) was purchased from Chem-Lab (Zedelgem, Belgium). Sodium hydroxide (>99.0%) was supplied by Scharlau Chemie S.A. (Barcelona, Spain). Acetic acid (100.0%) and chloroform (>99.1%) were obtained from AnalaR NORMAPUR (La Chapelle-sur-Erdre cedex, France). Folin−Ciocalteu reagent was obtained from Fluka (Buchs, Switzerland). FAMEs multistandards (>99.0%) were purchased from Sigma Chemical Co. (St. Louis, MO, USA).

**Oil Samples.** The studied oils during the successive pan- and deep-frying sessions were refined olive oil (ROO), refined corn oil (RCO), refined soybean oil (RSO), and refined sunflower oil (RSfO). These oil samples were obtained from the National Oil Office of Sfax, Tunisia.

**Frying Process.** Spunta variety potatoes from Tunisia were peeled, cut uniformly (0.5 cm thick, 2 cm × 5 cm pieces, on average), washed, and wiped before the frying experiments, which were conducted in the same manner as the actual household cooking process.[15]

Pan-frying was performed in an uncovered stainless steel pan fryer (5.5 cm in height, 20.5 cm in diameter). Five hundred grams of potatoes was pan-fried each time in 0.3 L of refined oil, at 180 °C for 6 min, using an electric plate of a conventional electric kitchen cooker equipped with a thermostat. The oil temperature was monitored with a digital thermometer attached to a steel probe.

For deep-frying, a common domestic-type electric fryer was used. It is equipped with a thermostat (160 and 190 °C) and supplied with an inert cross-linked steel wire mesh that allows the food to be dipped into the oil without coming in contact with the fryer's inner surface. In every frying session, 400 g of potatoes was deep-fried for 8−9 and 11−12 min at 190 and 160 °C, respectively, in 2.0 L of refined oil, without replenishment. For the deep-frying experiments, the fryer's lid was closed when the cooling started. The same thing applied to the pan-frying experiments. It is to be noted that the stainless steel pan fryer was completely covered when cooling. After cooling (≈30 min), the frying process was repeated 10 times using new potatoes in the same oil. Samples of the fresh refined oils together with those sampled after each two successive pan- and deep-frying sessions were stored in sealed dark glass bottles at −20 °C until examination.

**Determination of Standard Quality and Composition Parameters.** Free acidity (FA) was determined according to International Norm ISO 660 "Determination of acid value and acidity",[16] peroxide value (PV) was determined according to International Norm ISO 3690 "Determination of peroxide value",[17] and the coefficients of specific extinction at 232 and 270 nm ($K_{232}$ and $K_{270}$) were determined according to the COI "Spectrophotometric investigation in the ultraviolet".[18] FA, given as a percentage of major fatty acid (% of oleic acid for the ROO and % of linoleic acid for the refined seed oils), was determined by the titration of a solution of oil dissolved in ethanol/diethyl ether (1:1, v/v) with ethanolic potash (0.1 N). PV, expressed in milliequivalents of active oxygen per kilogram of oil (mequiv $O_2$/kg of oil), was determined as follows: a mixture of oil and chloroform/acetic acid (2:3, v/v) was left to react with a saturated solution of potassium iodide in the dark; the free iodine was then titrated with a sodium thiosulfate solution (0.01 N). $K_{232}$ and $K_{270}$ were calculated from absorption at 232 and 270 nm, respectively, with a spectrophotometer (UNICO, SQ-2800, USA), using pure cyclohexane as a blank. The total phenols were evaluated colorimetrically at 725 nm with the Folin−Ciocalteu reagent.[15]

**Determination of Total Polar Compounds, Dimeric and Polymeric Triacylglycerols, and Anisidine Value.** TPC, DPTG, and AnV were determined by FT-NIRS following the DGF standard method C-VI 21a (13).[11] An MPA multipurpose FT-NIR analyzer equipped with an OPUS LAB spectroscopy software interface (Bruker Optik GmbH, Ettlingen, Germany) was used for data acquisition and analysis.

**Determination of Fatty Acids Composition.** The methyl esters for the determination of the *cis*- and *trans*-fatty acids by the use of capillary column gas chromatography (GC) were prepared according to a standard protocol (vigorous shaking of the solution of oil in *n*-heptane (0.1 g in 2 mL) with 0.2 mL of 2 N methanolic potassium hydroxide).[19,20] The GC analysis of FAMEs was performed on an

AutoSystem gas chromatograph equipped with a flame ionization detector (FID) (HP 6890N, Agilent, Palo Alto, CA, USA). The column used was a capillary Agilent CP-Sil88 (length = 50 m, i.d. = 0.25 mm, and film thickness = 0.20 $\mu$m), and the analysis conditions were as follows: the initial column temperature was settled at 165 °C for 25 min, then raised at a gradient of 5 °C/min to 195 °C; the temperature of the injector and detector was set at 250 °C; helium was used as the carrier gas at a flow rate of 1 mL/min and 1:100 split ratio; the injection volume was 1 $\mu$L.

*cis*- and *trans*-FAMEs were identified through a comparison of their retention times versus pure standards analyzed under the same conditions. They were quantified according to their percentage area, obtained by the integration of the peaks. The results were expressed as the percentages of individual fatty acids in the lipid fraction. The 10 fatty acids (*cis*) considered in this study were palmitic (C16:0), hypogeic (C16:1n-9) + palmitoleic (C16:1n-7), margaric (C17:0), margaroleic (C17:1), stearic (C18:0), oleic (C18:1n-9) + *Z*-vaccenic (C18:1n-7), linoleic (C18:2), linolenic (C18:3), arachidic (C20:0), and gondoic (C20:1n-9) acids. The TFAs considered in this study included *trans*-octadecenoic (tC18:1), *trans*,*trans*-octadecadienoic (tt C18:2), *cis*,*trans*- and *trans*,*cis*-octadecadienoic [(ct + tc) C18:2], and *trans*,*cis*,*trans*-, *cis*,*cis*,*trans*-, *cis*,*trans*,*cis*-, and *trans*,*cis*,*cis*-octadecatrienoic [(tct + cct + ctc + tcc) C18:3] acids expressed as percentages of fatty acid methyl esters.

**Determination of Oxidative Stability by Rancimat Apparatus.** The oxidative stability was evaluated by a Metrohm Rancimat model 743 (Herisau, Switzerland) following AOCS Official Method Cd 12b-92.[21] The oil samples (5.0 g) were heated at 120 °C, with a continuous air flow of 20 L/h passing through the samples. The conductivity cells were filled with 60 mL of deionized water. The time needed for the appearance of a sudden water conductivity rise, caused by the adsorption of volatiles derived from oil oxidation, was registered as the induction time in hours.

**Statistical Analysis.** The results were expressed as the mean ± standard deviation (SD) of three measurements for the analytical determination. Significant differences between the values of all parameters were determined at $p < 0.05$ according to the one-way ANOVA: post hoc comparisons (Student−Newman−Keuls test).

Nonstandardized principal component analysis (PCA) was applied to characterize the effect of the frying method and distinct temperatures on the quality and stability characteristics and compositions of ROO, RCO, RSO, and RSfO before and after 10 successive frying sessions according to all of the parameters investigated without any rotation type. The PCA type was Pearson ($n$), the biplot type was correlation biplot, and the coefficient was automatic. The Pearson correlation matrix and the PCA plots were performed using XLSTAT software for Windows (v. 2014.1.08, Addinsoft, New York, NY, USA).

The estimated marginal means are the means for each factor, adjusted for any other factor or covariate in the model. These means can be obtained by SPSS (general linear model, GLM) which corresponds to the means of $Y$ for each level of the factor at the mean value of the covariate. If the factor is independent, the marginal means are equal to the means of levels for each factor considered alone. The repeated measures analysis of variance (ANOVA) was applied to confirm the PCA results according to all of the parameters investigated during both frying methods at distinct temperatures. The Student−Newman−Keuls test and the repeated measures analysis were performed using SPSS Statistics 17.0 for Windows (SPSS Inc., 2008).

## RESULTS AND DISCUSSION

The results of the analytical indices based on the chemical changes obtained from the studied fresh oils and their corresponding ones after different fryings are given in Tables 1 and 2.

**Changes in Free Acidity during Frying.** The free fatty acids (FFAs) content results from the hydrolysis of triacylglycerol (TAG) as well as the further decomposition of hydroperoxides. The released fatty acids are more susceptible to thermal oxidation under frying temperatures. The oxidized products of fatty acids give the off-flavors and odors (hydrolytic rancidity) to the frying medium and fried foods.[22,23] Therefore, controlling the level of FFA within a reasonable range would prevent the breakdown of fats.

During titration, it is not possible to differentiate between acids formed by hydrolysis and those formed by oxidation or thermal oxidation. Therefore, the effect of heating on FA cannot be exactly described. Furthermore, the volatility of FFAs and their degradation to more volatile products affect the FFA levels obtained as the sum of the FFAs initially present and those formed by treatments.

The changes in the FFA percentages of the studied oils during 10 successive frying sessions with both frying methods at distinct temperatures are given in Table 2. Slow but significant ($p < 0.05$) increases of FFAs were shown for all refined oils. Besides, the highest percentage of FFAs was detected after pan-frying at 180 °C, followed by deep-frying at 190 and 160 °C, in decreasing order.

Indeed, the pan-fried refined sunflower oil at 180 °C (RSfO P-F) and deep-fried refined olive oil at 160 °C (ROO 160 °C) show the highest and lowest susceptibilities to the hydrolysis of fatty acids, respectively. Our previous study[15] has shown that the ROO has the lowest content in FFAs when compared with the RSO after five successive pan-frying sessions at 180 °C. Generally, low amounts of FFA were formed during frying, and this parameter is not suitable to be used as a quality indicator for frying oils.[15,24,25] Newly developed frying oils usually form smaller amounts of FFA than frying fats used commonly for this process.[26]

**Changes in the Specific Extinction Coefficients during Frying.** The lower solubility of oxygen at high frying temperatures promotes thermal reactions. The main products of thermal degradation are isomerization products such as *trans*-isomers, cyclization products such as cyclic monomeric TAGs, and polymerization products such as nonpolar dimeric and oligomeric TAGs.[27]

Cooling from 180 °C to room temperature slightly increased the oxygen content of oil in a short period. During the next frying session, the decrease in oxygen content was observed again.[28] It is important to note that both the oxygen absorbed in oil during cooling and the high temperature play an important role in the deterioration of the oil during frying.[28−30] Under ambient conditions, autoxidation occurs by free radical mechanism where hydroperoxides play a primary role.[31] Hydroperoxides do not accumulate due to their instability at frying temperature, but rather spontaneously decompose to form dimers and volatile products.[32]

The oxidation of polyunsaturated fatty acids (PUFAs) is accompanied by the increase in ultraviolet (UV) absorption. In fact, the UV absorption at 232 and 270 increases with the formation of the conjugated dienes and trienes. The resulting conjugated dienes exhibit an intense absorption at 232 nm; similarly, the conjugated trienes absorb at 270 nm.

The changes in $K_{232}$ and $K_{270}$ of the studied oils during 10 successive frying sessions with both frying methods at distinct temperatures are shown in Table 2. In this study, the ROO had the lowest level of conjugated dienes and trienes compared with

**Table 2. Quality Characteristics of Refined Oils before and after Each Two Successive Frying Sessions[a]**

| | ROO | | | | RCO | | | |
|---|---|---|---|---|---|---|---|---|
| | fresh | 160 °C | 190 °C | P-F | fresh | 160 °C | 190 °C | P-F |
| **free acidity (%)** | | | | | | | | |
| session 2 | 0.06 ± 0.00Aa | 0.07 ± 0.00ABa | 0.07 ± 0.00ABa | 0.08 ± 0.00Ba | 0.09 ± 0.00Ab | 0.09 ± 0.00Ab | 0.09 ± 0.00Ab | 0.10 ± 0.00Ab |
| session 4 | 0.06 ± 0.00Aa | 0.07 ± 0.00ABa | 0.08 ± 0.00BCa | 0.09 ± 0.00Ca | 0.09 ± 0.00Ab | 0.09 ± 0.00Ab | 0.10 ± 0.00Ab | 0.13 ± 0.00Bb |
| session 6 | 0.06 ± 0.00Aa | 0.08 ± 0.00Ba | 0.08 ± 0.00Ba | 0.11 ± 0.00Ca | 0.09 ± 0.00Ab | 0.10 ± 0.00Ab | 0.10 ± 0.00Ab | 0.14 ± 0.00Bb |
| session 8 | 0.06 ± 0.00Aa | 0.09 ± 0.00Ba | 0.09 ± 0.00Ba | 0.11 ± 0.00Ca | 0.09 ± 0.00Ab | 0.11 ± 0.00Bb | 0.11 ± 0.00Bb | 0.16 ± 0.00Cb |
| session 10 | 0.06 ± 0.00Aa | 0.09 ± 0.00Ba | 0.11 ± 0.00Ca | 0.13 ± 0.00 Da | 0.09 ± 0.00Ab | 0.11 ± 0.00Bb | 0.13 ± 0.00Cb | 0.20 ± 0.00Db |
| $K_{232}$ | | | | | | | | |
| session 2 | 2.26 ± 0.04Aa | 2.58 ± 0.06Ba | 2.79 ± 0.07Ca | 2.98 ± 0.09 Da | 2.37 ± 0.06Ab | 2.64 ± 0.05Ba | 3.29 ± 0.06Cb | 4.41 ± 0.07Db |
| session 4 | 2.26 ± 0.04Aa | 2.71 ± 0.09Ba | 2.96 ± 0.04Ca | 3.34 ± 0.07 Da | 2.37 ± 0.06Ab | 3.21 ± 0.06Bb | 4.26 ± 0.07Cb | 6.85 ± 0.09Db |
| session 6 | 2.26 ± 0.04Aa | 3.09 ± 0.07Ba | 3.38 ± 0.10Ca | 4.07 ± 0.13 Da | 2.37 ± 0.06Ab | 4.06 ± 0.08Bb | 4.74 ± 0.05Cb | 7.10 ± 0.11Db |
| session 8 | 2.26 ± 0.04Aa | 4.28 ± 0.11Ba | 4.44 ± 0.09Ba | 5.82 ± 0.18Ca | 2.37 ± 0.06Ab | 5.04 ± 0.07Bb | 6.09 ± 0.08Cb | 8.09 ± 0.06Db |
| session 10 | 2.26 ± 0.04Aa | 4.78 ± 0.08Ba | 5.25 ± 0.17Ca | 6.97 ± 0.04 Da | 2.37 ± 0.06Ab | 5.95 ± 0.11Bb | 6.34 ± 0.10Cb | 9.64 ± 0.07Db |
| $K_{270}$ | | | | | | | | |
| session 2 | 0.48 ± 0.01Aa | 0.67 ± 0.00Ba | 0.88 ± 0.01Ca | 1.11 ± 0.01 Da | 1.41 ± 0.03Ab | 1.56 ± 0.01Bb | 1.67 ± 0.02Cb | 1.95 ± 0.04Db |
| session 4 | 0.48 ± 0.01Aa | 0.89 ± 0.01Ba | 1.15 ± 0.00Ca | 1.35 ± 0.01 Da | 1.41 ± 0.03Ab | 1.60 ± 0.02Bb | 1.98 ± 0.05Cb | 2.20 ± 0.03Db |
| session 6 | 0.48 ± 0.01Aa | 0.96 ± 0.00Ba | 1.51 ± 0.02Ca | 1.58 ± 0.02 Da | 1.41 ± 0.03Ab | 1.74 ± 0.01Bb | 2.14 ± 0.06Cb | 2.46 ± 0.02Db |
| session 8 | 0.48 ± 0.01Aa | 1.15 ± 0.00Ba | 1.55 ± 0.01Ca | 1.76 ± 0.02 Da | 1.41 ± 0.03Ab | 2.07 ± 0.01Bb | 2.32 ± 0.03Cb | 2.55 ± 0.01Db |
| session 10 | 0.48 ± 0.01Aa | 1.18 ± 0.01Ba | 1.56 ± 0.02Ca | 1.89 ± 0.04 Da | 1.41 ± 0.03Ab | 2.35 ± 0.04Bb | 2.67 ± 0.05Cb | 2.89 ± 0.07Db |

[a] ROO, refined olive oil; RCO, refined corn oil; RSO, refined soybean oil; RSfO, refined sunflower oil; P-F, pan-frying; $K_{232}$ and $K_{270}$, spectrophotometric indices. Each value represents the mean of three determinations ($n$ = 3) ± standard deviation. Different upper case letters (A, B, C, and D) within the same row indicate significant differences ($p < 0.05$) for the same refined oil at distinct temperatures and different frying methods. Different lower case letters (a, b, c, and d) within the same row indicate significant differences ($p < 0.05$) between refined oil sample groups at the same temperature and the same frying method.

**Table 3. *cis*- and *trans*-Fatty Acid Compositions of Refined Oils before and after 10 Successive Frying Sessions[a]**

| | ROO | | | | RCO | | | |
|---|---|---|---|---|---|---|---|---|
| fatty acid (%) | fresh | 160 °C | 190 °C | P-F | fresh | 160 °C | 190 °C | P-F |
| C16:0 | 17.53 ± 0.09Aa | 17.56 ± 0.13Aa | 17.60 ± 0.11Aa | 17.65 ± 0.15Aa | 12.39 ± 0.12Ab | 12.44 ± 0.06Ab | 12.51 ± 0.07Ab | 12.59 ± 0.13Ab |
| C16:(1n-9) + (1n-7) | 2.45 ± 0.03Aa | 2.44 ± 0.02Aa | 2.43 ± 0.02Aa | 2.41 ± 0.02Aa | 0.16 ± 0.00Ab | 0.15 ± 0.00ABb | 0.14 ± 0.00Bb | 0.14 ± 0.00Bb |
| C17:0 | 0.04 ± 0.00Aa | 0.04 ± 0.00Aa | 0.04 ± 0.00Aa | 0.05 ± 0.00Aa | 0.07 ± 0.00Ab | 0.07 ± 0.00Ab | 0.07 ± 0.00Ab | 0.07 ± 0.00Ab |
| C17:1 | 0.07 ± 0.00Aa | 0.08 ± 0.00ABa | 0.08 ± 0.00ABa | 0.09 ± 0.00Ba | 0.03 ± 0.00Ab | 0.03 ± 0.00Ab | 0.03 ± 0.00Ab | 0.04 ± 0.00Ab |
| C18:0 | 2.30 ± 0.01Aa | 2.31 ± 0.02Aa | 2.31 ± 0.01Aa | 2.32 ± 0.02Aa | 1.95 ± 0.03Ab | 1.96 ± 0.02Ab | 1.96 ± 0.03Ab | 1.99 ± 0.03Ab |
| C18:(1n-9) + (1n-7) | 58.29 ± 0.25Aa | 58.39 ± 0.28Aa | 58.50 ± 0.26Aa | 58.64 ± 0.31Aa | 28.42 ± 0.19Ab | 28.53 ± 0.13Ab | 28.65 ± 0.17ABb | 28.90 ± 0.20Bb |
| C18:2 | 18.09 ± 0.10Aa | 17.98 ± 0.09ABa | 17.84 ± 0.11BCa | 17.70 ± 0.12Ca | 55.37 ± 0.28Ab | 55.23 ± 0.29ABb | 55.12 ± 0.28ABb | 54.84 ± 0.30Bb |
| C18:3 | 0.67 ± 0.00Aa | 0.63 ± 0.00Ba | 0.61 ± 0.00Ca | 0.54 ± 0.00 Da | 0.93 ± 0.01Ab | 0.91 ± 0.00Bb | 0.84 ± 0.00Cb | 0.75 ± 0.00Db |
| C20:0 | 0.38 ± 0.00Aa | 0.38 ± 0.00Aa | 0.39 ± 0.00ABa | 0.40 ± 0.00Ba | 0.44 ± 0.00Ab | 0.45 ± 0.00ABb | 0.45 ± 0.00ABb | 0.46 ± 0.00Bb |
| C20:(1n-9) | 0.18 ± 0.00Aa | 0.19 ± 0.00ABa | 0.20 ± 0.00Ba | 0.20 ± 0.00Ba | 0.24 ± 0.00Ab | 0.23 ± 0.00ABb | 0.23 ± 0.00ABb | 0.22 ± 0.00Bb |
| TC18:1 | 0.03 ± 0.00Aa | 0.06 ± 0.00Ba | 0.08 ± 0.00Ca | 0.14 ± 0.00 Da | 0.02 ± 0.00Aa | 0.04 ± 0.00Bb | 0.04 ± 0.00Bb | 0.07 ± 0.00Cb |
| Σ(TC18:2 +TC18:3) | 0.12 ± 0.00Aa | 0.17 ± 0.00Ba | 0.19 ± 0.00Ca | 0.23 ± 0.00 Da | 0.17 ± 0.00Ab | 0.23 ± 0.00Bb | 0.27 ± 0.00Cb | 0.79 ± 0.01Db |
| Σ SFA (*cis*) | 20.25 ± 0.10Aa | 20.29 ± 0.15Aa | 20.34 ± 0.12Aa | 20.42 ± 0.17Aa | 14.85 ± 0.15Ab | 14.92 ± 0.08Ab | 14.99 ± 0.10Ab | 15.11 ± 0.16Ab |
| Σ MUFA (*cis*) | 60.99 ± 0.28Aa | 61.10 ± 0.30Aa | 61.21 ± 0.28Aa | 61.34 ± 0.33Aa | 28.85 ± 0.19Ab | 28.94 ± 0.13Ab | 29.05 ± 0.17ABb | 29.30 ± 0.20Bb |
| Σ PUFA (*cis*) | 18.76 ± 0.10Aa | 18.61 ± 0.09ABa | 18.45 ± 0.11Ba | 18.24 ± 0.12Ca | 56.30 ± 0.29Ab | 56.14 ± 0.29Ab | 55.96 ± 0.28ABb | 55.59 ± 0.30Bb |
| Σ UFA (*cis*) | 79.75 ± 0.38Aa | 79.71 ± 0.39Aa | 79.66 ± 0.39Aa | 79.58 ± 0.45Aa | 85.15 ± 0.48Ab | 85.08 ± 0.42Ab | 85.01 ± 0.45Ab | 84.89 ± 0.50Ab |
| C18:2/C16:0 | 1.03 | 1.02 | 1.01 | 1.00 | 4.46 | 4.43 | 4.40 | 4.35 |

[a] ROO, refined olive oil; RCO, refined corn oil; RSO, refined soybean oil; RSfO, refined sunflower oil; SFA, saturated fatty acids; PUFA, polyunsaturated fatty acids; MUFA, monounsaturated fatty acids; UFA, unsaturated fatty acids; P-F, pan-frying. Each value represents the mean of three determinations ($n$ = 3) and three independent experiments. Different upper case letters (A, B, C, and D) within the same row indicate significant differences ($p < 0.05$) for the same refined oil at distinct temperatures and different frying methods. Different lower case letters (a, b, c, and d) within the same row indicate significant differences ($p < 0.05$) between refined oil sample groups at the same temperature with the same frying method.

**Table 2. Continued**

| RSO | | | | RSfO | | | |
|---|---|---|---|---|---|---|---|
| fresh | 160 °C | 190 °C | P-F | fresh | 160 °C | 190 °C | P-F |
| 0.11 ± 0.00Ac | 0.11 ± 0.00Ac | 0.11 ± 0.00Ac | 0.13 ± 0.00Bc | 0.13 ± 0.00Ad | 0.14 ± 0.00ABd | 0.14 ± 0.00ABd | 0.15 ± 0.00Bd |
| 0.11 ± 0.00Ac | 0.12 ± 0.00Ac | 0.14 ± 0.00Bc | 0.16 ± 0.00Cc | 0.13 ± 0.00Ad | 0.14 ± 0.00Ad | 0.16 ± 0.00Bd | 0.17 ± 0.00Bc |
| 0.11 ± 0.00Ac | 0.14 ± 0.00Bc | 0.14 ± 0.00Bc | 0.20 ± 0.00Cc | 0.13 ± 0.00Ad | 0.15 ± 0.00Bc | 0.18 ± 0.00Cd | 0.20 ± 0.00Dc |
| 0.11 ± 0.00Ac | 0.14 ± 0.00Bc | 0.17 ± 0.00Cc | 0.22 ± 0.00Dc | 0.13 ± 0.00Ad | 0.17 ± 0.00Bd | 0.20 ± 0.00Cd | 0.22 ± 0.00Dc |
| 0.11 ± 0.00Ac | 0.15 ± 0.00Bc | 0.21 ± 0.00Cc | 0.23 ± 0.00Dc | 0.13 ± 0.00Ad | 0.18 ± 0.00Bd | 0.21 ± 0.00Cc | 0.26 ± 0.00Dd |
| 3.66 ± 0.10Ac | 4.12 ± 0.08Bb | 4.54 ± 0.03Cc | 5.32 ± 0.06Dc | 4.57 ± 0.13Ad | 6.18 ± 0.09Bc | 6.30 ± 0.14Bd | 6.84 ± 0.17Cd |
| 3.66 ± 0.10Ac | 4.70 ± 0.06Bc | 5.08 ± 0.07Cc | 7.18 ± 0.10Dc | 4.57 ± 0.13Ad | 6.36 ± 0.18Bd | 7.17 ± 0.12Cd | 8.45 ± 0.23Dd |
| 3.66 ± 0.10Ac | 5.28 ± 0.07Bc | 5.40 ± 0.08Bc | 7.86 ± 0.13Cc | 4.57 ± 0.13Ad | 7.93 ± 0.21Bd | 8.60 ± 0.27Cd | 9.89 ± 0.22Dd |
| 3.66 ± 0.10Ac | 6.18 ± 0.11Bc | 6.36 ± 0.06Cc | 8.27 ± 0.09Dc | 4.57 ± 0.13Ad | 9.74 ± 0.18Bd | 11.10 ± 0.35Cd | 13.80 ± 0.37Dd |
| 3.66 ± 0.10Ac | 6.56 ± 0.09Bc | 6.73 ± 0.11Bc | 10.27 ± 0.06Cc | 4.57 ± 0.13Ad | 11.76 ± 0.24Bd | 14.90 ± 0.43Cd | 17.69 ± 0.54Dd |
| 2.03 ± 0.06Ac | 2.18 ± 0.03Bc | 2.25 ± 0.04Cc | 2.59 ± 0.06Dc | 3.53 ± 0.11Ad | 3.65 ± 0.07Ad | 3.68 ± 0.06Ad | 3.83 ± 0.06Bd |
| 2.03 ± 0.06Ac | 2.28 ± 0.01Bc | 2.51 ± 0.05Cc | 2.75 ± 0.03Dc | 3.53 ± 0.10Ad | 3.76 ± 0.03Bd | 3.79 ± 0.04Bd | 4.03 ± 0.07Cd |
| 2.03 ± 0.06Ac | 2.36 ± 0.07Bc | 2.52 ± 0.03Cc | 2.94 ± 0.08Dc | 3.53 ± 0.10Ad | 3.91 ± 0.08Bd | 4.05 ± 0.03Cd | 4.21 ± 0.05Dd |
| 2.03 ± 0.06Ac | 2.53 ± 0.02Bc | 2.86 ± 0.04Cc | 3.08 ± 0.07Dc | 3.53 ± 0.10Ad | 4.20 ± 0.11Bd | 4.26 ± 0.07Bd | 4.41 ± 0.08Cd |
| 2.03 ± 0.06Ac | 2.77 ± 0.03Bc | 2.97 ± 0.06Cc | 3.22 ± 0.10Dc | 3.53 ± 0.10Ad | 4.35 ± 0.09Bd | 4.55 ± 0.03Cd | 4.89 ± 0.10Dd |

**Table 3. Continued**

| RSO | | | | RSfO | | | |
|---|---|---|---|---|---|---|---|
| fresh | 160 °C | 190 °C | P-F | fresh | 160 °C | 190 °C | P-F |
| 10.28 ± 0.15Ac | 10.36 ± 0.10Ac | 10.42 ± 0.12Ac | 10.54 ± 0.16Ac | 6.78 ± 0.10Ad | 6.86 ± 0.08Ad | 6.91 ± 0.11Ad | 6.98 ± 0.13Ad |
| 0.12 ± 0.00Ac | 0.12 ± 0.00Ac | 0.11 ± 0.00ABc | 0.10 ± 0.00Bc | 0.14 ± 0.00Ad | 0.14 ± 0.00Ab | 0.13 ± 0.00ABb | 0.12 ± 0.00Bd |
| 0.09 ± 0.00Ac | 0.09 ± 0.00Ac | 0.09 ± 0.00Ac | 0.09 ± 0.00Ac | 0.04 ± 0.00Aa | 0.04 ± 0.00Aa | 0.04 ± 0.00Aa | 0.04 ± 0.00Aa |
| 0.05 ± 0.00Ac | 0.05 ± 0.00Ac | 0.06 ± 0.00Ac | 0.06 ± 0.00Ac | 0.04 ± 0.00Abc | 0.04 ± 0.00Abc | 0.05 ± 0.00Ac | 0.05 ± 0.00Abc |
| 3.70 ± 0.05Ac | 3.71 ± 0.03Ac | 3.71 ± 0.04Ac | 3.73 ± 0.04Ac | 3.35 ± 0.04Ad | 3.36 ± 0.04Ad | 3.38 ± 0.05Ad | 3.41 ± 0.05Ad |
| 26.76 ± 0.22Ac | 27.06 ± 0.18ABc | 27.28 ± 0.21Bc | 27.80 ± 0.23Cc | 25.84 ± 0.21Ad | 26.19 ± 0.19Bd | 26.50 ± 0.22Bd | 26.91 ± 0.24Cd |
| 52.40 ± 0.32Ac | 52.26 ± 0.24Ac | 52.14 ± 0.30ABc | 51.76 ± 0.28Bc | 63.21 ± 0.45Ad | 62.79 ± 0.38ABd | 62.43 ± 0.36BCd | 61.98 ± 0.39Cd |
| 6.07 ± 0.08Ac | 5.81 ± 0.06Bc | 5.62 ± 0.07Cc | 5.33 ± 0.06Dc | 0.22 ± 0.00Ad | 0.19 ± 0.00Bd | 0.17 ± 0.00Cd | 0.10 ± 0.00Dd |
| 0.33 ± 0.00Ac | 0.33 ± 0.00Ac | 0.34 ± 0.00Ac | 0.34 ± 0.00Ac | 0.23 ± 0.00Ad | 0.23 ± 0.00Ad | 0.23 ± 0.00Ad | 0.24 ± 0.00Ad |
| 0.20 ± 0.00Ac | 0.21 ± 0.00Ac | 0.23 ± 0.00Bb | 0.25 ± 0.00Cc | 0.15 ± 0.00Ad | 0.16 ± 0.00ABd | 0.16 ± 0.00ABc | 0.17 ± 0.00Bd |
| 0.03 ± 0.00Aa | 0.05 ± 0.00Bab | 0.06 ± 0.00Bc | 0.09 ± 0.00Cc | 0.02 ± 0.00Aa | 0.06 ± 0.00Ba | 0.07 ± 0.00Bac | 0.09 ± 0.00Cc |
| 0.28 ± 0.00Ac | 0.43 ± 0.00Bc | 0.46 ± 0.00Cc | 1.13 ± 0.01Dc | 0.54 ± 0.00Ad | 0.65 ± 0.01Bd | 0.70 ± 0.01Cd | 1.18 ± 0.02Dd |
| 14.40 ± 0.20Ac | 14.49 ± 0.13Ac | 14.56 ± 0.16Ac | 14.70 ± 0.20Ac | 10.40 ± 0.14Ad | 10.49 ± 0.12Ad | 10.56 ± 0.16Ad | 10.67 ± 0.18Ad |
| 27.13 ± 0.22Ac | 27.44 ± 0.18ABc | 27.68 ± 0.21Bc | 28.21 ± 0.23Cc | 26.17 ± 0.21Ad | 26.53 ± 0.19Bd | 26.84 ± 0.22Bd | 27.25 ± 0.24Cd |
| 58.47 ± 0.40Ac | 58.07 ± 0.30ABc | 57.76 ± 0.37Bc | 57.09 ± 0.34Cc | 63.43 ± 0.45Ad | 62.98 ± 0.38ABd | 62.60 ± 0.36BCd | 62.08 ± 0.39Cd |
| 85.60 ± 0.62Ab | 85.51 ± 0.48Ab | 85.44 ± 0.58Ab | 85.30 ± 0.57Ab | 89.60 ± 0.66Ac | 89.51 ± 0.57Ac | 89.44 ± 0.58Ac | 89.33 ± 0.63Ac |
| 5.09 | 5.04 | 5.00 | 4.91 | 9.32 | 9.15 | 9.03 | 8.87 |

the other frying oils, followed by the RCO after deep-frying at 160 and 190 °C. However, the RSO and RSfO frying oils showed high levels in the absorption coefficient recorded at 232 and 270 nm in increasing order, especially after 10 pan-frying sessions at 180 °C. In this context, $K_{232}$ increased highly and significantly ($p < 0.05$) from 3.66 and 4.57 to 10.27 and 17.69 and $K_{270}$ augmented significantly ($p < 0.05$) from 2.03 and 3.53 to 3.22 and 4.89 for RSO and RSfO, respectively. This indicates that higher amounts of conjugated dienes and trienes are formed during frying (Table 2). Like dienes, the trienes could also form polymers during the frying process.[30]

These results are in good agreement with those reported by Marinova et al.[33] In fact, with respect to the conjugated diene and triene accumulations, ROO is the most stable oil. Moreover, for the polyunsaturated oils, although RCO is less stable than ROO, it is more stable than RSO.

**Changes in Total Polar Compounds during Frying.** The measurement of TPC is recognized as one of the most accurate assessments of the oxidative degradation of frying oils.[34−36] Many countries have established regulatory limits for TPC in frying oils and considered 25% as a limit.[26,28]

The changes in the TPC percentages of the studied oils after 10 frying sessions with both frying methods at distinct temperatures are shown in Figure 1a. High and significant ($p < 0.05$) increases of TPC were illustrated especially after pan-frying at 180 °C for the polyunsaturated oils from 4.39, 5.54, and 7.52% to 17.19, 17.08, and 17.75% for RCO, RSO, and RSfO, respectively, whereas small but significant increases ($p < 0.05$) were observed for the ROO after deep-frying at 160 and 190 °C from 3.45 to 5.11 and 5.74%, respectively, followed by RCO, RSO, and RSfO in increasing order. These results show that the oils containing higher percentages of UFAs provide more polar compounds compared to the more saturated ones. As can be seen from Figure 1a, whereas the RSfO P-F proves the highest TPC percentage at 180 °C, ROO D-F at 160 °C showed the lowest level of TPC at the end of the frying process. This indicates that the high stability of ROO to changes in TAGs that occurred during the frying experiments can be explained by considering that the ROO is rich in monounsaturated fatty acids (MUFAs), especially in oleic acid.[37]

In a related study, Matthäus[38] has determined the frying stability of high-oleic rapeseed oils and found that high-oleic rapeseed oils have lower TPC levels after 72 h of frying when compared with other commonly used edible oils. Warner and Knowlton[39] reported that genetically modified corn oils, which contain 65% oleic acid, have remarkably lower TPC levels after 20 h of frying at 190 °C as compared with normal corn oils. Similar findings were also seen in Abdulkarim's work, which has demonstrated that high-oleic *Moringa oleifera* seed oils show a lower TPC level after 30 h of frying at 185 °C as compared with other vegetable oils.[40]

The TPC results of this research study are in good agreement with those reported by Marinova et al.,[33] which have proven that ROO contains the lowest level of TPC followed by RCO, RSO, and RSfO in increasing order.

**Changes in Dimeric and Polymeric Triacylglycerols during Frying.** As a consequence of prolonged oxidation, ether, peroxy, or carbon−carbon bridged dimers and oligomers of TAG are formed. Because of their high molecular weight, these components remain in the oil and can provide reliable indications of the performance of oils/fats under frying conditions.[41]

The changes in the DPTG of the studied oils after 10 frying sessions with both frying methods at distinct temperatures are shown in Figure 1b. Indeed, high and significant ($p < 0.05$) increases of DPTG were illustrated especially after pan-frying at 180 °C for the polyunsaturated oils from 0.54, 0.65, and 0.82% to 8.40, 10.57, and 9.34% for RCO, RSO, and RSfO, respectively, whereas after pan-frying at 180 °C, ROO showed the lowest DPTG percentage ranging from 0.69 to 6.37%.

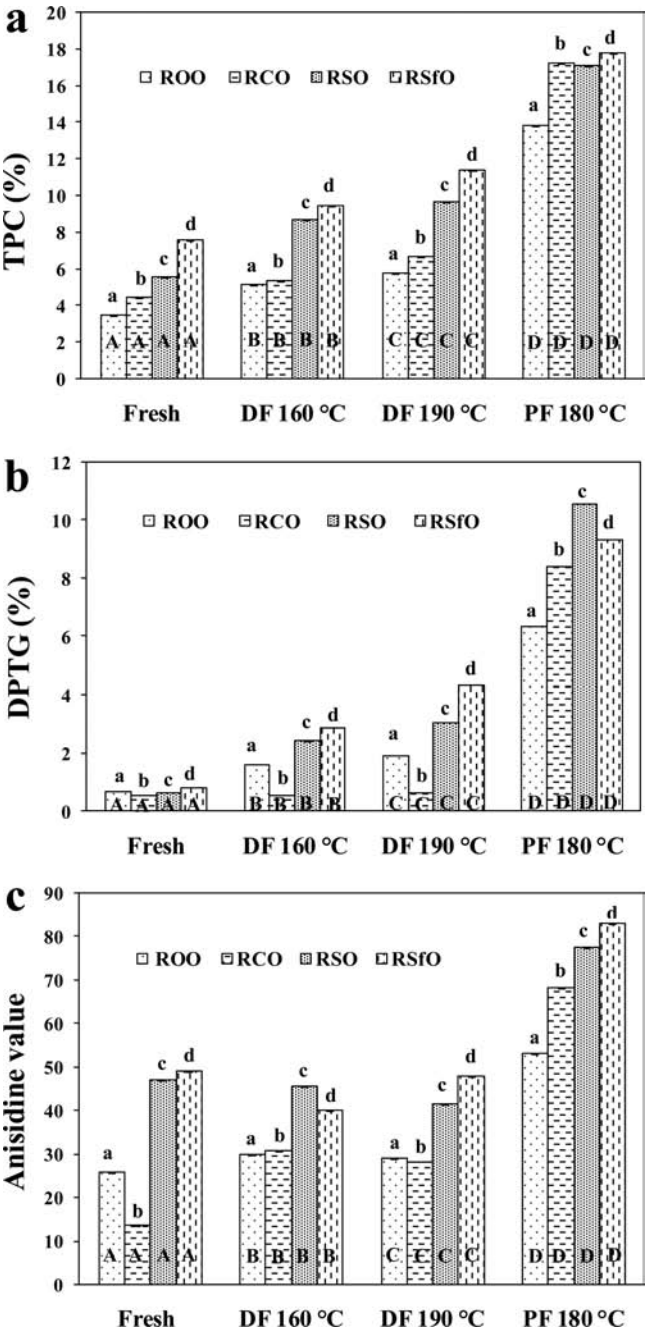


**Figure 1.** Changes in the composition of total polar compounds (a), dimeric and polymeric triacylglycerols (b), and anisidine value (c) before and after 10 pan- and deep-frying sessions at distinct temperatures (each value represents the mean of three determinations ($n = 3$); standard deviation <0.10%). Different upper case letters (A, B, C, and D) indicate significant differences ($p < 0.05$) for the same refined oil at distinct temperatures with different frying methods. Different lower case letters (a, b, c, and d) indicate significant differences ($p < 0.05$) between refined oil sample groups at the same temperature with the same frying method.

Slow but significant ($p < 0.05$) increases of DPTG were shown after deep-frying at 160 and 190 °C, especially for RCO and ROO from 0.54 and 0.69% to 0.57 and 1.62%, and to 0.66 and 1.93%. Yet RSO and RSfO revealed the highest levels of DPTG, which varied from 0.65 and 0.82% to 2.43 and 2.88% and to 3.05 and 4.35% after deep-frying at 160 and 190 °C, respectively. Thus, the highest percentage of DPTG was observed after pan-frying at 180 °C, followed by the deep-frying at 190 and 160 °C, in decreasing order.

The increase in DPTG is due to the formation of higher molecular weight substances by polymerization occurring at elevated frying temperature.[42] The oil containing a higher percentage of PUFAs exhibits a great tendency to form polymeric compounds rather than a highly saturated fatty acid-containing oil.

**Changes in Anisidine Value (AnV) during Frying.** The *p*-anisidine value is a measurement of nonvolatile aldehyde content in an oil, principally 2-alkenals and 2,4-dienals, formed as secondary degradation products from fatty acid hydroperoxides.[43] A *p*-anisidine value is, therefore, a measure of the oxidative state of an oil. A lower *p*-anisidine value in an oil indicates a lower oxidation level in that oil.

The changes in the AnV of the studied refined oils after 10 frying sessions with both frying methods at distinct temperatures are shown in Figure 1c. A clear variation was observed during deep-frying at both temperatures, 160 and 190 °C. Significant ($p < 0.05$) increases of AnV for ROO and RCO ranged from 25.71 and 13.52 to 29.63 and 30.47 and to 28.98 and 28.13 after frying at 160 and 190 °C, respectively. Nevertheless, significant ($p < 0.05$) decreases of AnV for RSO and RSfO were observed from 46.78 and 48.94 to 45.39 and 39.81 and to 41.31 and 47.87 after frying at 160 and 190 °C, respectively. This is presumably due to the participation of the target carbonyls in the further deteriorative reactions, principally, polymerization. It is noteworthy that these two oils (RSO and RSfO) contain the highest level of initial AnV (Figure 1c).

High and significant ($p < 0.05$) increases in the AnV of all refined oils were observed after 10 pan-frying sessions at 180 °C, especially for the RSfO with 82.92, followed by the RSO with 77.29, RCO with 68.15, and ROO with 53.10 in decreasing order compared to that of fresh oils: 48.94 for RSfO, 46.78 for RSO, 13.52 for RCO, and 25.71 for ROO. The highest values were found for RSfO and RSO, indicating extensive degradation of oxidized UFAs. These results have confirmed that RSfO and RSO are more susceptible to oxidation at high frying temperature than the other frying oils during pan-frying. This could be due to the presence of a high concentration of PUFAs, especially in RSfO followed by RSO. The latter are found to be more susceptible to oxidation when compared to the other frying oils, especially the monounsaturated oil as ROO.

The higher *p*-anisidine levels in the polyunsaturated oils, especially RSfO and RSO after 10 deep- and pan-frying sessions, being related with the formation of oxidation products, can also give some insight into the higher TPC observed in these samples. These results have proven that these vegetable oils present minor resistance to oxidation under frying conditions when compared to ROO, which is in good agreement with those reported by Casal et al.[44]

**Changes in Fatty Acid Compositions during Frying.** Being the main oils constituent, and by nature, the most important factor determining the oxidative stability, fatty acids are evaluated in detail in the current study. Olive oil, as expected, is characterized by a high degree of MUFAs, particularly oleic acid, thus contributing to the beneficial cardiovascular health effects.[45]

The fatty acid compositions of the studied oils are shown in Table 3. For all fresh frying oils, the most predominant fatty acids are palmitic (6.78−17.53%), oleic (25.84−58.29%), and linoleic (18.09−63.21%) acids.

RSfO is characterized by a dominant polyunsaturated fraction, particularly linoleic acid (63.21%), and a comparatively low amount of oleic acid (25.84%). When the relative percentages of fatty acids of all studied oils were compared after 10 frying sessions, a slight decrease (not significant, $p > 0.05$) of UFAs was observed, with the consequent increase (not significant, $p > 0.05$) in the percentages of saturated fatty acids (SFAs) (Table 3). The decrease is particularly noticeable ($p < 0.05$) in the PUFAs, presumably by oxidation, with the linoleic and linolenic acids. Despite the remarkable amount of PUFAs in RSfO, the lowest reduction in the amount of PUFAs was observed in ROO during the frying process. Indeed, the amount of C16:0 slightly increased but not significantly ($p > 0.05$) for all of the oils under investigation. As shown in Table 3, the amount of C18:1 is found to slightly increase in all studied oils during frying. These results are in accordance with those of Enríquez-Fernández et al.[46] and Romero et al.,[47] which suggest that the increase in oleic acid might be attributed to the linoleic and linolenic acid degradation.

The ratios of C18:2/C16:0 are shown in Table 3. For all studied oils, these ratios highly declined after 10 successive frying sessions, especially for RSfO followed by RSO, RCO, and ROO, and during pan-frying at 180 °C, deep-frying at 190 °C, and deep-frying at 160 °C, in decreasing order. Indeed, linoleic and palmitic acids are usually used as indicators of the extent of fat deterioration because linoleic acid is more susceptible to oxidation, whereas palmitic acid is more stable against oxidation. Therefore, the ratio of C18:2/C16:0 is also used to indicate the degree of oxidative deterioration of frying oil.[15,33,36,42]

**Changes in *trans*-Fatty Acid Compositions during Frying.** Elaidic acid, a *trans*-fatty acid from oleic acid, was present in all studied oils in small amounts even after 10 successive frying sessions. A high temperature (190 °C) can increase the amount of *trans*-isomers during deep-frying (Figure 2; Table 3). For all refined seed oils, the *trans* PUFA contents showed significant increases ($p < 0.05$) after 10 successive pan- and deep-frying sessions (Table 3). Indeed, the high increase of the *trans* PUFA contents was detected in RSfO followed by RSO and RCO, in decreasing order. However, a very small increase of these compounds was detected in ROO. In all studied oils and especially the seed oils, the higher deteriorations occurred during pan-frying at 180 °C, followed by deep-frying at 190 and 160 °C, in decreasing order. Published results reported by Zribi et al.[15] showed that a high increase of the *trans* PUFA contents was detected in RSO and a very small increase was detected in ROO after five successive pan-frying sessions.

Moreno et al.[48] reported that the intensive heating of oils caused an increase in the *trans* PUFA contents. For instance, the TFA content increased from 0.23 to 1.10% when sunflower oil was heated at 200 °C for 40 min and increased to 3.20% when heated at 250 °C for the same duration.

**Changes in Oxidative Stability during Frying.** The Rancimat method is frequently used for evaluating or predicting oxidative stabilities under heating conditions, known as induction time. Despite being an important tool for comparison of

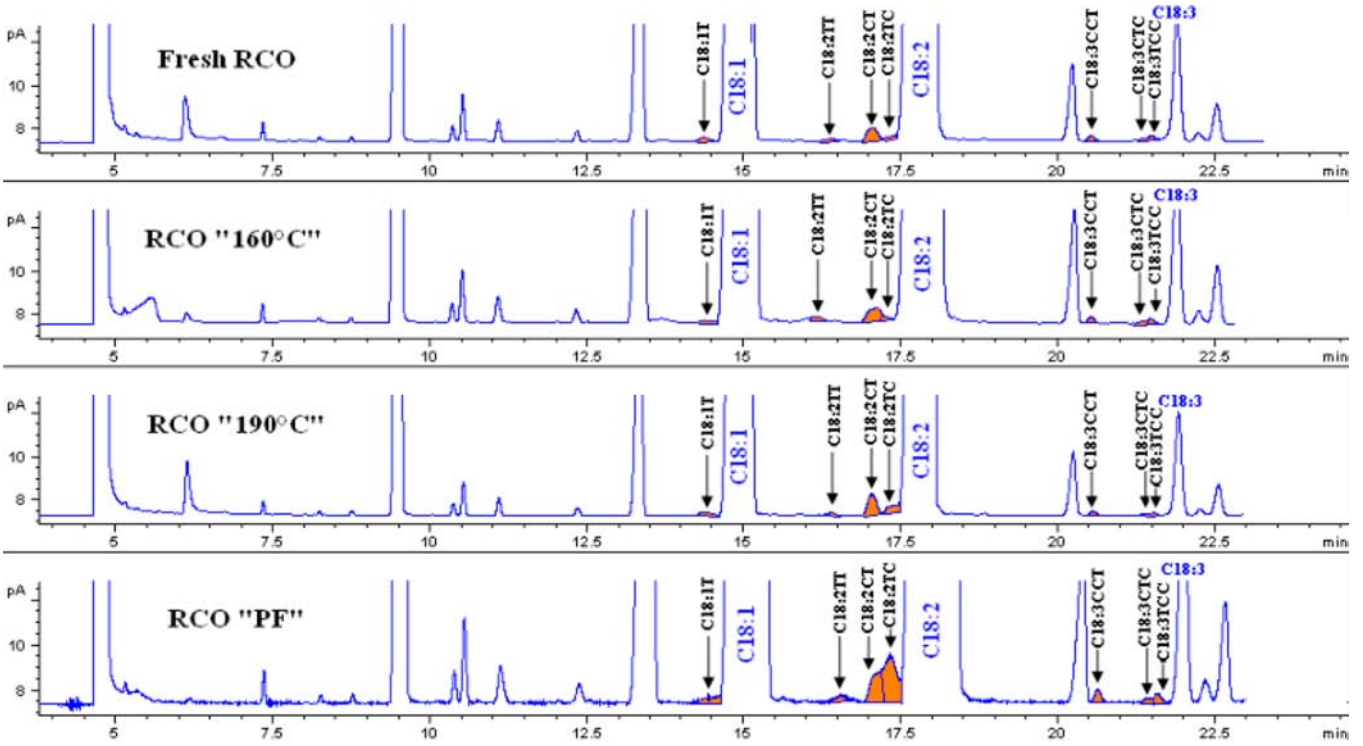


**Figure 2.** Gas chromatograms of *cis*/*trans* refined corn oil (RCO) before and after 10 successive pan- and deep-frying sessions at distinct temperatures. PF, pan-frying.

**Table 4. Oxidative Stability Measured by Rancimat Apparatus of Studied Refined Oils**[a]

| | ROO | RCO | RSO | RSfO |
|---|---|---|---|---|
| IT of fresh oil (h) | 4.39 ± 0.03Aa | 3.55 ± 0.04Ab | 3.34 ± 0.03Ac | 2.18 ± 0.02Ad |
| IT of 5 fryings at 160 °C (h) | 1.93 ± 0.04Ba | 1.59 ± 0.03Bb | 1.25 ± 0.03Bc | 0.88 ± 0.01Bd |
| IT of 5 fryings at 190 °C (h) | 0.98 ± 0.02Ca | 0.77 ± 0.03Cb | 0.65 ± 0.02Cc | 0.49 ± 0.00Cd |
| IT of 5 fryings P-F (h) | 0.25 ± 0.00 Da | 0.17 ± 0.00Db | 0.13 ± 0.00Dc | 0.06 ± 0.00Dd |
| IT of 10 fryings at 160 °C (h) | 0.00 ± 0.00Ea | 0.00 ± 0.00Ea | 0.00 ± 0.00Ea | 0.00 ± 0.00Ea |
| IT of 10 fryings at 190 °C (h) | 0.00 ± 0.00Ea | 0.00 ± 0.00Ea | 0.00 ± 0.00Ea | 0.00 ± 0.00Ea |
| IT of 10 fryings P-F (h) | 0.00 ± 0.00Ea | 0.00 ± 0.00Ea | 0.00 ± 0.00Ea | 0.00 ± 0.00Ea |

[a] ROO, refined olive oil; RCO, refined corn oil; RSO, refined soybean oil; RSfO, refined sunflower oil; IT, induction time; P-F, pan-frying. Each value represents the mean of three determinations ($n = 3$) ± standard deviation. Different upper case letters (A, B, C, D, and E) within the same column indicate significant differences ($p < 0.05$) for the same refined oil at distinct temperatures and different frying methods. Different lower case letters (a, b, c, and d) within the same row indicate significant differences ($p < 0.05$) between refined oil sample groups at the same temperature with the same frying method.

different vegetable oils, the results are not directly transposable to real frying conditions.

Clearly distinct results are observed for all oil samples (Table 4). The highest oxidative stability is depicted for ROO at 4.39 h, followed by RCO at 3.55 h and RSO at 3.34 h. The RSfO presents a clearly reduced stability at only 2.18 h.

The oxidative resistance of all studied refined oils decreased significantly ($p < 0.05$) after 5 deep-frying sessions and then declined to 0 h after 10 deep-frying sessions. The most resistant oil during deep-frying at 160 and 190 °C was ROO at 1.93 and 0.98 h, respectively, which had the lowest percentage of TPC after deep-frying at both temperatures, followed by RCO at 1.59 and 0.77 h and RSO at 1.25 and 0.65 h. However, the less resistant oil during deep-frying at 160 and 190 °C was the RSfO with 0.88 and 0.49 h, respectively, which had the highest percentage of TPC after deep-frying at both temperatures. Furthermore, as already mentioned above, the high stability of the ROO can be explained by its richness in MUFAs, especially in oleic acid.

With regard to the pan-fried refined oils, their oxidative resistance still decreased significantly ($p < 0.05$) after 5 pan-frying sessions at 180 °C and then declined to 0 h after 10 pan-frying sessions. The highest stability value was registered for ROO at 0.25 h, which had the lowest percentage of TPC after pan-frying, followed by RCO at 0.17 h and RSO at 0.13 h, whereas the lowest stability value was registered for RSfO at 0.06 h, which had the highest percentage of TPC after pan-frying.

Similar results reported by Casal et al.[44] showed that for the refined oils, ROO presented a high oxidative resistance during deep-frying when compared with a refined seed oil such as RSfO, which presented the lowest resistance to oxidation.

**Chemometric Analysis.** PCA was applied to the data set of all analyses performed for ROO, RCO, RSO, and RSfO before and

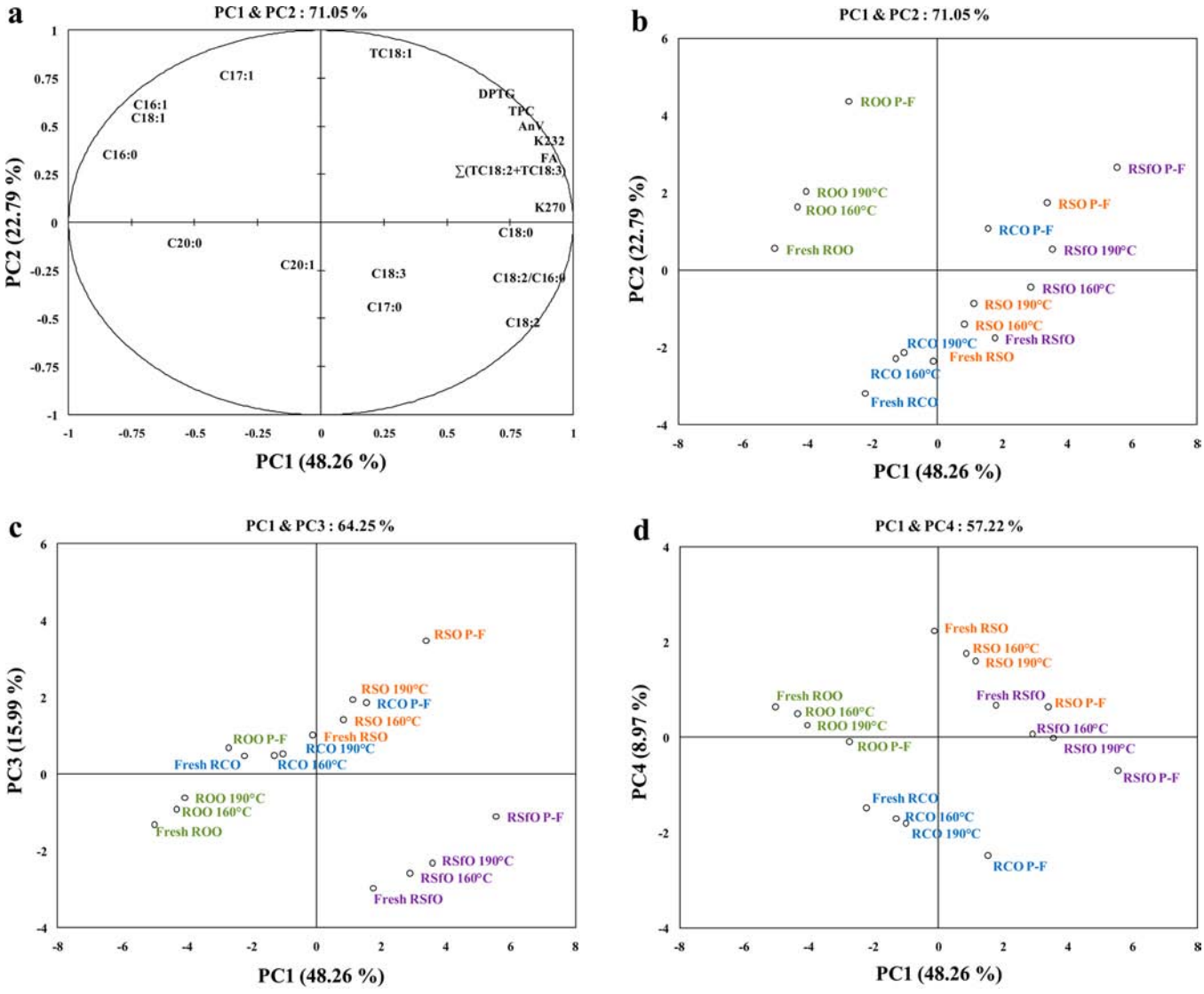


**Figure 3.** Principal component analysis applied to all samples analyzed before and after 10 pan- and deep-frying sessions at distinct temperatures considering 19 variables presented in the loading plot (a) and 16 observations shown in the score plots (b, c, and d). FA, free acidity; $K_{232}$ and $K_{270}$, spectrophotometric indices; TPC, total polar compounds; DPTG, dimeric and polymeric triacylglycerols; AnV, anisidine value; ROO, refined olive oil; RCO, refined corn oil; RSO, refined soybean oil; RSfO, refined sunflower oil.

after 10 successive pan- and deep-frying sessions at distinct temperatures, and four factors were selected justifying 96.01% of total variance (PC1, 48.26%; PC2, 22.79%; PC3, 15.99%; and PC4, 8.97%). With regard to these factors, all fresh and frying oils could be differentiated on the PCA diagram (Figure 3).

First, the first principal component (PC1) was mainly correlated by the following parameters: free acidity, $K_{232}$, $K_{270}$, ∑(TC18:2 + TC18:3), C16:0, C16:1, C18:1, C18:2, C20:0, C18:2/C16:0, TPC, and AnV. It can therefore be considered as a stability axis. Second, the second principal component (PC2) was dominated by the following parameters: TC18:1, C17:1, and DPTG (Figure 3a). The third and fourth principal components (PC3) and (PC4) were mainly correlated to C17:0, C18:3, and C20:1 and to C18:0, respectively.

PC1 clearly separates the most stable frying oil ROO from the other oils (RCO, RSO, and RSfO), with the least stable frying oil being RSfO. PC2 has proven that deep-frying at 160 °C is the best frying method for all refined oils, followed by deep-frying at 190 °C, and the worst is pan-frying at 180 °C (Figure 3b). More precisely, PC1 opposes ROO (in the negative side) to RSfO (in the positive side), whereas PC2 separates each fresh oil, deep-frying oil at 160 and 190 °C, and pan-frying oil at 180 °C. Besides, PC3 further separates RSfO (in the negative side) from all other oils and mainly RSO and RCO (Figure 3c). The two groups RCO and RSO are well separated by PC4, where RSO was found in the positive side and RCO in the negative side (Figure 3d).

According to the PCA, the least deteriorated oil is ROO during deep-frying, especially at 160 °C, and the highest is RSfO during pan-frying at 180 °C. Indeed, fresh ROO, ROO at 160 °C, and ROO at 190 °C are highly and negatively related to PC1, which are characterized by their highest C18:1 and C16:0 percentages and very lowest TC18:1 contents, whereas ROO P-F is related positively to PC2, which is correlated with the increase in TC18:1. Moreover, RSfO P-F is highly related to PC1, which is correlated positively with the slight increase of the free acidity

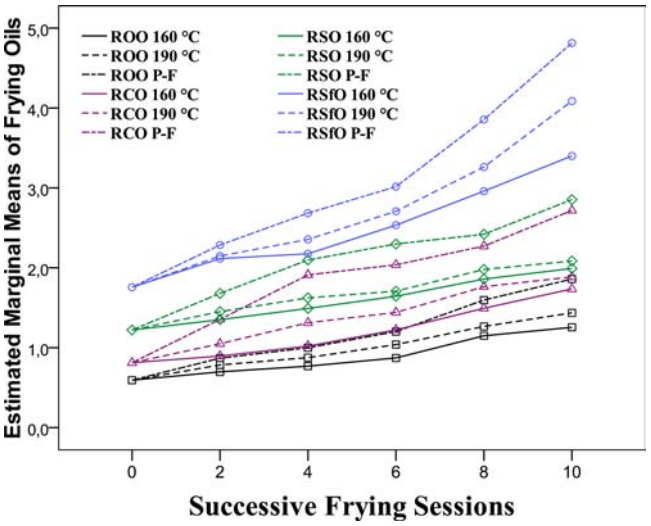


**Figure 4.** Repeated measures analysis of variance (ANOVA) of some parameters [free acidity, $K_{232}$, $K_{270}$, TC18:1, and Σ(TC18:2 + TC18:3)] analyzed after each two successive pan- and deep-frying sessions. ROO, refined olive oil (□); RCO, refined corn oil (△); RSO, refined soybean oil (◇); RSfO, refined sunflower oil (○); P-F, pan-frying.

and significant increases of the $K_{232}$, $K_{270}$, AnV, TPC, and Σ(TC18:2 + TC18:3) percentages.

The analysis of variance of some parameters of the refined oils such as free acidity, $K_{232}$, $K_{270}$, TC18:1, and Σ(TC18:2 + TC18:3) obtained after each two successive pan- and deep-frying sessions at distinct temperatures is shown in Figure 4. Indeed, the repeated measures analysis of variance indicates that the quality of ROO, followed by RCO, shows better chemical characteristics than those of RSO and RSfO after 10 successive frying sessions, especially during deep-frying at 160 °C.

In conclusion, changes in the characteristics and compositions of the studied oils have shown that ROO is the most stable oil during deep-frying at 160 °C, whereas RSfO is the least stable during pan-frying at 180 °C. Therefore, ROO appears to be a good substitute for the refined seed oils in domestic frying applications. Thus, the choice of a stable frying oil having a good quality and adequate frying temperature and frying method is of great importance to maintain a low deterioration during frying operations and hence obtain high-quality fried foods.

## AUTHOR INFORMATION

### Corresponding Author

*(M.B.) Phone: +216 98 667 581. Fax: +216 74 674 364. E-mail: mohamed.bouaziz@fsg.rnu.tn.

### Funding Sources

We thank the Ministère de l'Enseignement Supérieur et de la Recherche Scientifique and the Ministère de l'Agriculture (ONH-Sfax), Tunisia, for support of this research work.

### Notes

The authors declare no competing financial interest.

## ACKNOWLEDGMENT

We thank Leila Mahfoudhi, teacher of English at the Sfax Faculty of Science, for having proofread the manuscript.

## ABBREVIATIONS USED

ANOVA, analysis of variance; AnV, anisidine value; DPTG, dimeric and polymeric triacylglycerols; D-F, deep-frying; FA, free acidity; FAMEs, fatty acid methyl esters; FFAs, free fatty acids; FT-NIR, Fourier transformed near-infrared; FT-NIRS, Fourier transformed near-infrared spectroscopy; GC, gas chromatography; HPSEC, high-performance size exclusion chromatography; IT, induction time; $K_{232}$ and $K_{270}$, spectrophotometric indices; MUFA, monounsaturated fatty acids; PC, principal component; PCA, principal component analysis; PCM, polar contaminant materials; PUFA, polyunsaturated fatty acids; PV, peroxide value; P-F, pan-frying; RCO, refined corn oil; ROO, refined olive oil; RSfO, refined sunflower oil; RSO, refined soybean oil; SFA, saturated fatty acids; TAG, triacylglycerol; TPC, total polar compounds; TFA, *trans*-fatty acid; UFA, unsaturated fatty acids; UV, ultraviolet

## REFERENCES

(1) Warner, K. Chemistry of frying oils. In *Food Lipids: Chemistry, Nutrition, and Biotechnology*; Akoh, C. C., Min, D. B., Eds.; CRC Press: Boca Raton, FL, USA, 2008; pp 189−202.

(2) Goburdhun, D.; Jhurree, B. Effect of deep-fat frying on fat oxidation in soybean oil. *Int. J. Food Sci. Nutr.* **1995**, *46*, 363–371.

(3) Innawong, B.; Mallikarjunan, P.; Irudayaraj, J.; Marcy, J. E. The determination of frying oil quality using Fourier transform infrared attenuated total reflectance. *Lebensm.-Wiss. Technol.* **2004**, *37*, 23–28.

(4) Saguy, I. S.; Dana, D. Integrated approach to deep fat frying: engineering, nutrition, health and consumer aspects. *J. Food Eng.* **2003**, *56*, 143–152.

(5) Andrikopoulos, N. K.; Kalogeropoulos, N.; Falirea, A.; Barbagianni, M. N. Performance of virgin olive oil and vegetable shortening during domestic deep-frying and pan-frying of potatoes. *Int. J. Food Sci. Technol.* **2002**, *37*, 177–190.

(6) Blumenthal, M. M. A new look at the chemistry and physics of deep fat frying. *Food Technol.* **1991**, *45*, 68–71.

(7) Waltking, A. E.; Wessels, H. Chromatographic separation of polar and nonpolar components of frying fats. *J. Assoc. Off. Anal. Chem.* **1981**, *64*, 1329–1330.

(8) López-Varela, S.; Sánchez-Muniz, F. J.; Cuesta, C. Decreased food efficiency ratio, growth retardation and changes in liver fatty acid composition in rats consuming thermally oxidized and polymerized sunflower oil used for frying. *Food Chem. Toxicol.* **1995**, *33*, 181–189.

(9) Andrikopoulos, N. K.; Dedoussis, G. V. Z.; Falirea, A.; Kalogeropoulos, N.; Hatzinikola, H. S. Deterioration of natural antioxidant species of the vegetable edible oils during the domestic deep-frying and pan-frying of potatoes. *Int. J. Food Sci. Nutr.* **2002**, *53*, 351–363.

(10) Dobarganes, M. C.; Pérez-Camino, M. C.; Márquez-Ruiz, G. High performance size exclusion chromatography of polar compounds in heated and non-heated fats. *Fat Sci. Technol.* **1988**, *90*, 308–311.

(11) Gertz, C.; Fiebig, H. J.; Hancock, J. N. S. FT-near infrared (NIR) spectroscopy − screening analysis of used frying fats and oils for rapid determination of polar compounds, polymerized triacylglycerols, acid value and anisidine value [DGF C-VI 21a (13)]. *Eur. J. Lipid Sci. Technol.* **2013**, *115*, 1193–1197.

(12) Gerde, J. A.; Hardy, C. L.; Hurburgh, C. R., Jr.; White, P. J. Rapid determination of degradation in frying oils with near-infrared spectroscopy. *J. Am. Oil Chem. Soc.* **2007**, *84*, 519–522.

(13) Du, R.; Lai, K.; Xiao, Z.; Shen, Y.; Wang, X.; Huang, Y. Evaluation of the quality of deep frying oils with fourier transform near-infrared and mid-infrared spectroscopy. *J. Food Sci.* **2012**, *77*, C261–C266.

(14) Gertz, C.; Behmer, D. Application of FT-NIR spectroscopy in assessment of used frying fats and oils. *Eur. J. Lipid Sci. Technol.* **2014**, *116*, 756–762.

(15) Zribi, A.; Gargouri, B.; Jabeur, H.; Rebaï, A.; Abdelhedi, R.; Bouaziz, M. Enrichment of pan-frying refined oils with olive leaf phenolic-rich extract to extend the usage life. *Eur. J. Lipid Sci.Technol.* **2013**, *115*, 1443–1453.

(16) International Norm. Animal and vegetable fats and oils, determination of acid value and acidity, ISO 660, 3rd ed.; 2009.

(17) International Norm. Animal and vegetable fats and oils, determination of peroxide value, ISO 3690, 3rd ed.; 2001.

(18) International Olive Council. COI/T, 20/Doc. No. 19 Rev. 3. Spectrophotometric investigation in the ultraviolet, 2010.

(19) International Olive Council. COI/T, 20/Doc. No. 24. Preparation of the fatty acid methyl esters from olive oil and olive pomace oil, 2001.

(20) International Olive Council. COI/T, 20/Doc. No. 17 Rev. 1. Determination of trans unsaturated fatty acids by capillary column gas chromatography, 2001.

(21) American Oil Chemists' Society. *Official Methods and Recommended Practices of the American Oil Chemists' Society*; Champaign, IL, USA, 1992; AOCS Official Method Cd 12b-92: oxidative stability index.

(22) Lin, S.; Akoh, C. C.; Reynolds, A. E. The recovery of used frying oils with various adsorbents. *J. Food Lipid* **1998**, *5*, 1–16.

(23) Nawar, W. W. Lipids. In *Food Chemistry*, 3rd ed.; Fennema, O. R., Ed.; Dekker: New York, 1996; pp 225−319.

(24) Romano, R.; Giordano, A.; Vitiello, S.; Le Grottaglie, L.; Musso, S. S. Comparison of the frying performance of olive oil and palm superolein. *J. Food Sci.* **2012**, *77*, C519–C531.

(25) Przybylski, R.; Gruczynska, E.; Aladedunye, F. Performance of regular and modified canola and soybean oils in rotational frying. *J. Am. Oil Chem. Soc.* **2013**, *90*, 1271–1280.

(26) Firestone, D.; Stier, R. F.; Blumenthal, M. M. Regulation of frying fats and oils. *Food Technol.* **1991**, *45*, 90–94.

(27) Velasco, J.; Marmesat, S.; Dobarganes, M. C. Chemistry of frying. In *Advances in Deep-Fat Frying of Foods*; Sumnu, G., Sahin, S., Eds.; Taylor & Francis: Boca Raton, FL, USA, 2008; pp 33−56.

(28) Totani, N.; Yawata, M.; Mori, T.; Hammond, E. G. Oxygen content and oxidation in frying oil. *J. Oleo Sci.* **2013**, *62*, 989–995.

(29) Clark, W. L.; Serbia, G. W. Safety aspects of frying fats and oils. *Food Technol.* **1991**, *45*, 84–89.

(30) Choe, E.; Min, D. B. Chemistry of deep-fat frying oils. *J. Food Sci.* **2007**, *72*, R77–R86.

(31) Dobarganes, M. C.; Velasco, J. Analysis of lipid hydroperoxides. *Eur. J. Lipid Sci. Technol.* **2002**, *104*, 420–428.

(32) Frankel, E. N. Oxidation in multiphase systems. In *Lipid Oxidation*; Frankel, E. N., Ed.; Oily Press: Dundee, UK, 1998; pp 161−186.

(33) Marinova, E. M.; Seizova, K. A.; Totseva, I. R.; Panayotova, S. S.; Marekov, I. N.; Momchilova, S. M. Oxidative changes in some vegetable oils during heating at frying temperature. *Bulg. Chem. Commun.* **2012**, *44*, 57–63.

(34) Velasco, J.; Marmesat, S.; Berdeaux, O.; Márquez-Ruiz, G.; Dobarganes, M. C. Formation of short-chain glycerol-bound oxidation products and oxidised monomeric triacylglycerols during deep-frying and occurrence in used frying fats. *Eur. J. Lipid Sci. Technol.* **2004**, *106*, 728–735.

(35) Blumenthal, M. M. Frying technology. In *Bailey's Industrial Oil and Fat Products*, 5th ed.; Hui, Y. H., Ed.; Wiley: New York, 1996; Vol. 3, pp 429−482.

(36) Serjouie, A.; Tan, C. P.; Mirhosseini, H.; Che Man, Y. B. Effect of vegetable-based oil blends on physicochemical properties of oils during deep-fat frying. *Am. J. Food Technol.* **2010**, *5*, 310–323.

(37) Tabee, E.; Jagerstad, M.; Dutta, P. C. Frying quality characteristics of French fries prepared in refined olive oil and palm olein. *J. Am. Oil Chem. Soc.* **2009**, *86*, 885–893.

(38) Matthäus, B. Utilization of high-oleic rapeseed oil for deep-fat frying of French fries compared to other commonly used edible oils. *Eur. J. Lipid Sci. Technol.* **2006**, *108*, 200–211.

(39) Warner, K.; Knowlton, S. Frying quality and oxidative stability of high-oleic corn oils. *J. Am. Oil Chem. Soc.* **1997**, *74*, 1317–1322.

(40) Abdulkarim, S. M.; Long, K.; Lai, O. M.; Muhammad, S. K. S.; Ghazali, H. M. Frying quality and stability of high-oleic *Moringa oleifera* seed oil in comparison with other vegetable oils. *Food Chem.* **2007**, *105*, 1382–1389.

(41) Aladedunye, F. A.; Przybylski, R. Performance of palm olein and modified rapeseed, sunflower, and soybean oils in intermittent deep-frying. *Eur. J. Lipid Sci. Technol.* **2014**, *116*, 144–152.

(42) Aladedunye, F. A.; Przybylski, R. Degradation and nutritional quality changes of oil during frying. *J. Am. Oil Chem. Soc.* **2009**, *86*, 149–156.

(43) O'Keefe, S. F.; Pike, O. A. Fat characterization. In *Food Analysis*, 4th ed.; Nielsen, S. S., Ed.; Springer: New York, 2010; pp 239−260.

(44) Casal, S.; Malheiro, R.; Sendas, A.; Oliveira, B. P.; Pereira, J. A. Olive oil stability under deep-frying conditions. *Food Chem. Toxicol.* **2010**, *48*, 2972–2979.

(45) Kuna, A.; Achinna, P. Mono unsaturated fatty acids for CVD and diabetes: a healthy choice. *Int. J. Nutr. Pharmacol. Neurol. Dis.* **2013**, *3*, 236–248.

(46) Enríquez-Fernández, B. E.; Álvarez de la Cadena y Yañez, L.; Sosa-Morales, M. E. Comparison of the stability of palm olein and a palm olein/canola oil blend during deep-fat frying of chicken nuggets and French fries. *Int. J. Food Sci. Technol.* **2011**, *46*, 1231–1237.

(47) Romero, A.; Cuesta, C.; Sánchez-Muniz, F. J. Effect of replenishment during deep-fat frying of frozen foods in a sunflower oil and high-oleic acid sunflower oil. *J. Am. Oil Chem. Soc.* **1998**, *75*, 161–167.

(48) Moreno, M. C. M. M.; Olivares, D. M.; López, F. J. A.; Adelantado, J. V. G.; Reig, F. B. Determination of unsaturation grade and trans isomers generated during thermal oxidation of edible oils and fats by FTIR. *J. Mol. Struct.* **1999**, *482*−*483*, 551–556.

involve complex chemical reactions to immobilize the targets and their analogues onto the matrixes but also alter the inherent structure of the target molecules, possibly leading to a reduction in aptamer affinity toward their original targets. Although Yang and Bowser reported that they screened aptamers for *N*-methyl mesoporphyrin IX (MW = 580 g/mol) by capillary electrophoresis (CE)−SELEX, allowing for the binding and separation steps to occur in free solution without steric hindrance,[22] CE−SELEX employs expensive capillary electrophoresis as an instrumental platform for SELEX, which limits its application in aptamer selection. Recently, Park et al. reported an immobilization-free method for screening aptamers against insulin assisted by graphene oxide (GO)[23] as well as against whole bovine viral diarrhea virus type 1 via a similar method.[24] GO is a well-known graphene derivative; one of its important properties is that ssDNA can be strongly adsorbed on its surface because of hydrophobic and $\pi-\pi$ stacking interactions between the nucleobases and GO, whereas dsDNA adsorption on GO is very weak because of the shielding of nucleobases by the phosphate backbone.[25,26]

In the present study, we used GO for screening aptamers against the small-molecule target T-2. Measures were taken during SELEX to generate high-quality aptamers for T-2. The incubation system throughout the selection process contained 1.0% (volume ratio) of methanol to increase the compatibility of T-2 and the oligonucleotides. Because T-2 is relatively insoluble in water,[6] the toxin was dissolved in methanol, a common extraction solvent used in current detection, which enabled T-2 to gain full access to the ssDNAs in free solution. In addition, common mycotoxins that are potentially found in combination with T-2 were added, starting at the sixth round of SELEX to increase the specificity of the generated aptamers for T-2. The presented methodology eliminates the necessity of solid-phase attachment, avoids structural changes in the target molecule, reduces the potential for non-specific interactions, and does not rely on expensive instrumentation. Therefore, our proposed method is believed to be a more versatile technique than previously reported methods to a certain extent.

## MATERIALS AND METHODS

**Chemicals and Reagents.** The initial ssDNA library and primers for amplification were synthesized by Integrated DNA Technologies (Coralville, IA). T-2, fumonisin $B_1$ ($FB_1$), and ochratoxin A (OTA) were obtained from Fermentek, Ltd. (Jerusalem, Israel); zearalenone (ZEN), aflatoxin $B_1$ ($AFB_1$), and acrylamide/bis-acrylamide (30% solution) were purchased from Sigma-Aldrich (St. Louis, MO). The operators were required to wear gloves and masks to avoid exposure to the above toxins. GO was prepared from graphite powder using a modified Hummer's method,[27] as described previously by our group.[28] A homogeneous suspension of GO (approximately 5.0 mg/mL) was prepared by ultrasonic vibration and used throughout the experiment. The reagents for polymerase chain reaction (PCR) amplification and 5′-carboxyfluorescein (FAM)-labeled aptamers were obtained from Sangon Biotech. Co., Ltd. (Shanghai, China). Lambda exonuclease enzyme (5000 units/mL) and 10× lambda exonuclease reaction buffer were purchased from New England BioLabs (Ipswich, MA). Chromatographically pure methanol and other unspecified chemicals and reagents of analytical grade were purchased from Sinopharm Chemical Reagent Co., Ltd. (Shanghai, China). Solutions were prepared with ultrapure water processed with a Millipore Direct-Q3 ultrapure water system (Billerica, MA).

**Apparatus.** All PCRs were performed in a C1000 thermocycler (Hercules, CA). The observation of polyacrylamide gel was carried out using a Chemi Doc XRS+ imaging system with Image Lab software (Hercules, CA). A ND-1000 spectrophotometer (Wilmington, DE) was used to measure the nucleic acid concentration. Fluorescent detection was performed using a F-7000 fluorescence spectrophotometer (Tokyo, Japan). Circular dichroism (CD) spectroscopy was performed on a MOS-450/AF-CD (Claix, France) spectropolarimeter interfaced with a computer with Biokine V4.51 software installed.

**Generation of ssDNA Library.** An 80 nucleotide oligonucleotide ssDNA library consisting of a central 40 nucleotide randomized region flanked by two 20 nucleotide primer binding sites was used as the initial library (5′-CAGCTCAGAAGCTTGATCCT-N40-GACTC-GAAGTCGTGCATCTG-3′) on the basis of the study by Tang et al.[29] The ssDNA library and subsequent aptamer pools were amplified by symmetric PCR with a forward primer (5′-CAGCTCAGAAGCTT-GATCCT-3′) and phosphorylated reverse primer (5′-P-CAGATG-CACGACTTCGAGTC-3′) under the following conditions: 5 min at 94 °C, repeated cycles of 30 s at 94 °C, 30 s at 53 °C, and 30 s at 72 °C, followed by 5 min at 72 °C. The PCR cycles were optimized in each round of SELEX to obtain the intended 80 base pair products. The PCR products were analyzed using 8% native PAGE and purified by a PCR Product Purification Kit (Generay Biotech. Co., Ltd., Shanghai, China). Subsequently, the concentrations of recovered products were measured using a ND-1000 spectrophotometer to estimate the amount of lambda exonuclease needed. The phosphorylated antisense strands were digested by lambda exonuclease according to the instructions of the supplier (New England BioLabs). After identification using 8% denaturing PAGE with 7 M urea, the digestion products were purified, precipitated, and subsequently used as the ssDNA library.

***In Vitro* Selection.** The GO−SELEX process is illustrated in Scheme 1. Prior to being mixed with target mycotoxin T-2, the ssDNA library dissolved in binding buffer (BB; 10 mM Tris-HCl, 150 mM NaCl, 10 mM KCl, and 2.5 mM $MgCl_2$ at pH 7.4)[30] was heated at 94 °C for 5 min, immediately cooled on ice for 15 min, and placed at 25 °C for 10 min. In the first round, folded ssDNA (1 nmol) was incubated with T-2 (100 nmol) in 400 $\mu$L of special binding buffer, which contained 1.0% methanol, for 2 h at 25 °C with tilting and rotation. Subsequently, 10.0 mg of GO (mass ratio of GO/ssDNA is 400:1) from the above-mentioned GO suspension by centrifugation were added to the mixture of potential aptamers and unbound ssDNA, and the solution was incubated at 25 °C for 40 min. This mixture containing GO was centrifuged at 13 000 rpm/min for 10 min, and the supernatant containing ssDNAs bound to T-2 was collected, while the deposit with unbound ssDNAs adsorbed onto GO was discarded. The collected potential aptamer pool was amplified by PCR, and the ssDNA products were generated by lambda exonuclease digestion of the phosphorylated strands from dsDNA products. The subsequent round of GO−SELEX was performed with the purified library.

Counter GO−SELEX was performed starting from the sixth round to improve the specificity of the aptamers against T-2. The ssDNA library (200 pmol) was first incubated with a mixture of $FB_1$, ZEN, $AFB_1$, or OTA (5 nmol, individually) in 400 $\mu$L of incubation buffer for 60 min, and then GO (2.0 mg) was added and incubated for 40 min. During this process, the oligonucleotides that did not bind to the counter-targets were adsorbed onto the GO surface by $\pi-\pi$ stacking

**Scheme 1. Schematic Illustration of the Aptamer Selection Procedure**

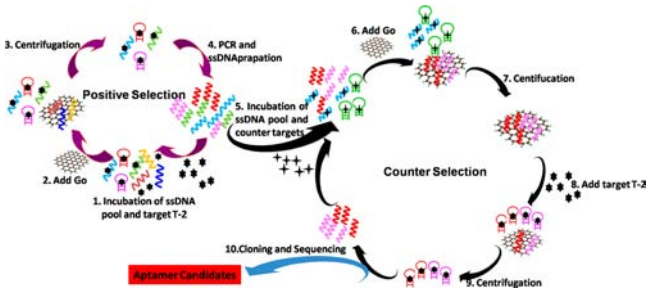

Table 1. Total of 27 Sequences (Primers Omitted) Obtained after Cloning and Sequencing[a]

| family | code number | variable $N_{40}$ sequences from the 21st to 60th position (5′−3′) | nucleotide | $\Delta G$ | occurrence |
|---|---|---|---|---|---|
| | Seq.1 | TATTCGTCAAGTCCTCTGCCACATTACGCTCTTAACGCTG | 40 | −7.0 | 1 |
| F1 | Seq.2 | TAGCACACAACCCTTTGATTGGGATATCTCATCCCTCG | 38 | −11.5 | 20 |
| | Seq.19 | GTCTTAGATTAGATTAAAAAACTTATATTGCTAAAACCCG | 40 | −5.7 | 1 |
| F2 | Seq.6 | ACCACAGCCAGTAAGTCCCGTAGGCCCTGGTTGGGCTGTT | 40 | −14.5 | 1 |
| | Seq.9 | ATGTCATATTACACTACTCATTCGTGCTTTCTTCGTTTT | 39 | −9.9 | 1 |
| F3 | Seq.12 | GTAGCTTAAAATTTATGGAGGTATGTTTCACTTTTCATTT | 40 | −4.9 | 1 |
| | Seq.16 | GTATATCAAGCATCGCGTGTTTACACATGCGAGAGGTGAA | 40 | −17.3 | 2 |

[a]The affinity and $K_d$ of the underlined sequences were characterized using binding assays.

interactions, while those bound to the counter-targets remained suspended in the buffer. After separation by centrifugation, GO on which oligonucleotides were adsorbed was resuspended and washed with BB 5 times for harsher conditions. Subsequently, target T-2 (20 nmol) was mixed with the GO−ssDNAs and incubated further for 2 h in 400 μL of buffer, to recover the aptamers from the GO surface. The mixture solution was centrifuged, and the supernatant containing potential aptamers was collected. This obtained library pool was amplified by PCR, and ssDNA was again generated by lambda exonuclease digestion and purification.

**Cloning and Sequencing of the Enriched Pool.** Following 10 rounds of selection, the enriched ssDNA pool was amplified by unmodified primers. The purified PCR product was cloned using the pMD-19T cloning vector (Takara Biotech.Co., Ltd., Dalian, China) and transformed into *Escherichia coli* DH5α. Through blue−white spot screening, 30 white positive clones were randomly selected and cultured in LB medium containing 50 μg/mL ampicillin, followed by plasmid DNA extraction using a Plasmid MiniPrep Kit (Generay Biotech. Co., Ltd., Shanghai, China). Finally, the extracted plasmid DNA with inserted aptamer candidates were sequenced by Sangon Biotech. Co., Ltd. (Shanghai, China). Multiple sequence alignment of the obtained sequences was analyzed using DNAMAN software,[31] and the secondary structure of each sequence was predicted using RNAstructure 4.6 software (http://rna.urmc.rochester.edu/RNAstructure.html) with paraments of maximum percent energy difference of 10 and maximum number of structures of 20.

**Binding Assays.** The aptamers were heat-denatured and cooled on ice, using the same procedure as for the *in vitro* selection, prior to use. To identify individual aptamer candidates, binding assays for each FAM-labeled representative sequence and its truncated sequence (without the primer-binding regions) were conducted by incubating a fixed amount of T-2 (1 μM) with various concentrations of the synthetic sequences, ranging from 5 to 200 nM, in 500 μL of BB in the dark for 2 h. Then, GO proportional to the amount of ssDNA present was added to each tube, and the mixture was incubated in the dark for 40 min. After centrifugation, the fluorescence intensity of the T-2/aptamer complexes in the supernatant was measured using a F-7000 fluorescence spectrophotometer with excitation at 490 nm. Negative controls without T-2 added were used to determine non-specific binding. All of the binding assay experiments were repeated 3 times. The equilibrium dissociation constant ($K_d$) of aptamer/T-2 binding was determined using GraphPad Prism 5.0 software based on a nonlinear fit of the T-2/aptamer complex fluorescence intensities for a range of aptamer concentrations.

**Evaluation of Specificity.** Three sequences with lower $K_d$ values were selected to evaluate the specificity of the aptamers against T-2 based on the binding assay results. The specificity test was performed as follows: GO (0.3 mg/mL) in the special binding buffer was incubated with the aptamers (100 nM), along with T-2 or $FB_1$, ZEN, $AFB_1$, or OTA (10 μM, individually), for 2 h in the dark. The negative control for each sequence was mixed with BB instead of any mycotoxin targets. Subsequently, each of the mixtures was centrifuged at 13 000 revolutions per minute (rpm) for 10 min, and the supernatant was collected and kept in the dark. Finally, the fluorescence of each supernatant was measured using a F-7000 fluorescence spectrophotometer with excitation at 490 nm.

**CD Spectroscopy Assay.** To further investigate the mechanism of binding between the preferred aptamer Seq.16 and target T-2, CD spectroscopy was used to study the conformation of the ssDNA aptamer before and after binding with free T-2 in free solution. Aptamer Seq.16 (1 μM) was incubated with or without target T-2 (20 μM) for 2 h in special binding buffer as well as a tube of pure T-2 (20 μM) in the vibration oven (total volume of each was 400 μL). Subsequently, these samples were analyzed on a MOS-450/AF-CD (France) spectropolarimeter with recording of the CD spectra from 230 to 320 nm.

**Aptamer-Based Fluorescent Bioassay.** The potential application of aptamer Seq.16 for the detection of T-2 in beer was explored by a fluorescent bioassay. Canned beer purchased from a local supermarket (50 mL) was completely degassed by sonication, and then the $CO_2$-free beer was filtered through a 13 mm, 0.22 μm nylon syringe filter. Prior to being used in the study, the beer sample was analyzed by mass spectrometry to make sure that T-2 was undetectable. The beer was spiked with the stock solution of T-2 to obtain a final concentration of 1 mM T-2. From this spiked sample, several dilutions from 0.05 to 500 μM T-2 were prepared with non-spiked beer. Then, 400 μL of folded 5′-FAM-labeled Seq.16 (125 nM) in 5× BB was mixed with 100 μL of beer sample at a final concentration of T-2 ranging from 0.01 to 100.0 μM, along with GO (150 μg). The control group was set similarly but without T-2 added. The mixtures (500 μL) were incubated in the dark for 2 h with gentle shaking. Subsequently, each of the mixtures was centrifuged at 14 000 rpm for 10 min, and the fluorescent intensity of the supernatant collected was measured using a F-7000 fluorescence spectrophotometer with excitation at 490 nm.

## RESULTS AND DISCUSSION

**Screening of Aptamers against T-2.** Several preliminary experiments were conducted before the screening of aptamers against T-2. The critical point at which approximately 500 μg of GO could adsorb 100 pmol of the ssDNA pool was first determined by an adsorption test using the initial library pool. The double ratio of GO/ssDNA was maintained throughout the selection process to ensure that the ssDNAs not bound to T-2 were completely adsorbed. Next, a series of PCRs containing 0, 0.1, 1.0, or 10.0% (volume ratio) methanol in the PCR system was performed to study the effect of the methanol content in the special binding buffer on PCR amplification (see the Supporting Information). Finally, 1.0% methanol was selected for use in the incubation system during *in vitro* selection, enabling the T-2 toxin full access to ssDNAs in free solution. A balance was achieved between control of the selection conditions and PCR amplification, which greatly contributed to the screening of aptamers against T-2.

During the formal SELEX process, T-2 was used as the target, and several common mycotoxins, including $FB_1$, ZEN, $AFB_1$, and OTA, were treated as counter-targets. The counter-targets are known to be produced by the same fungus species or to likely coexist with the target mycotoxin in a heterogeneous environment. Five rounds of counter selection following five

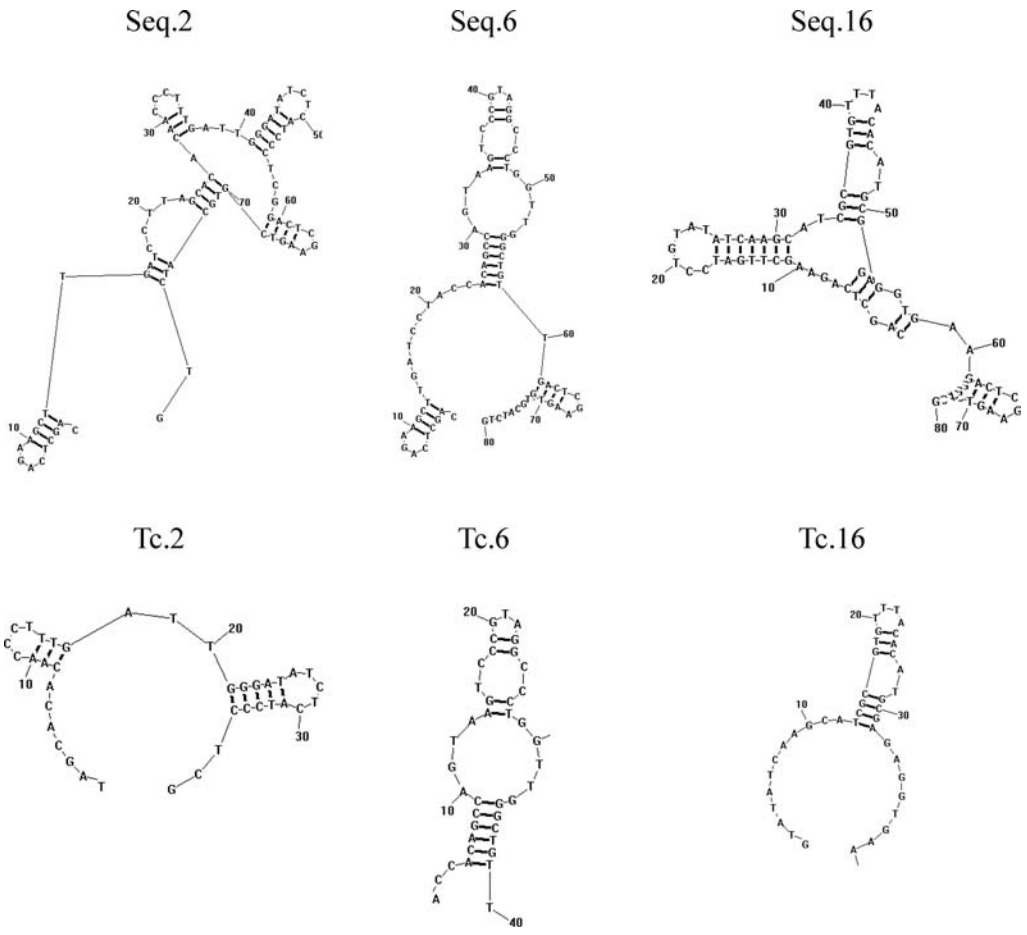


**Figure 1.** Secondary structure models of representative aptamers and their truncated sequences predicted by software RNAstructure 4.6.

rounds of positive selection increased the specificity of aptamers by the efficient removal of non-specific sequences in each round. The recovery amount of ssDNA bound to T-2 was measured by a ND-1000 spectrophotometer, and selection was finished in the 10th round when we observed that the recovery ratio of it was much higher than that of the first round. The above-mentioned GO−SELEX procedure eliminated the necessity for solid-phase attachment, thus avoiding structural changes in the target molecule, reducing the potential for non-specific interactions, and not relying on expensive instrumentation.

**Preliminary Identification of Aptamers.** After the 10th round of immobilization-free SELEX, a total 30 recombinant plasmids were sent for sequencing. Finally, 27 sequences of aptamer candidates were successfully obtained from Sangon Biotech. Co., Ltd., and they were grouped into three families, as presented in Table 1. The aptamer candidate termed Seq.2 was the sequence with the highest abundance in the enriched library, but two bases were missing in the variable N40 region. As Viswanathan et al. reported, GC-rich regions in the templates can cause the formation of stem-loop secondary structures that have been known to promote polymerase jumping during PCR amplification.[32] This polymerase jumping produces smaller PCR products with missing sequences for the template stem-loop region.[33] Similar cases have been reported for the study by McKeague et al. of fumonisin $B_1$ aptamers[34] and the study by Kiani et al. of digoxin aptamers.[35] However, these missing bases would not matter if Seq.2 exhibited high affinity and specificity toward target T-2.

Representative aptamers from each family were selected on the basis of DNA homology, as analyzed using DNAMAN software, and the lowest predicted free energy of formation $\Delta G$, as calculated using RNAstructure 4.6 software. The sequences that occurred twice or more in the cloning results were chosen because these sequences may be present in higher abundance. Meanwhile, aptamers with lower $\Delta G$ were also chosen, because these sequences should possess more stable secondary structures, which help to maintain the stability of the target/aptamer complexes. The secondary structures of the representative aptamers Seq.2, Seq.6, and Seq.16 and their truncated sequences Tc.2, Tc.6, and Tc.16 predicted by RNAstructure 4.6 software are shown in Figure 1. Unique stems, loops, bulges, hairpins, triplexes, and pseudo-knots assembled in the aptamers may have contributed to the specific binding of these aptamers to target T-2.

**Affinity of DNA Aptamers to T-2.** The binding saturation curves of the measured fluorescence intensity of the T-2/aptamer complexes (after deduction of the blank background) plotted against the aptamer concentration (5, 10, 25, 50, 100, or 200 nM) were generated, and the $K_d$ values for the aptamer sequences were calculated by nonlinear regression analysis using GraphPad Prism 5.0 (Figure 2). Among the tested sequences, the $K_d$ values of Seq.2 (62.4 ± 12.1 nM), Seq.6 (37.2 ± 8.4 nM), and Seq.16 (20.8 ± 3.1 nM) were relatively lower than that of Tc.6 (81.3 ± 21.7 nM), indicating higher affinities to T-2. The binding of the aptamers to their targets typically resulted from structure compatibility, stacking of aromatic rings, electrostatic interactions, van der Waals forces,

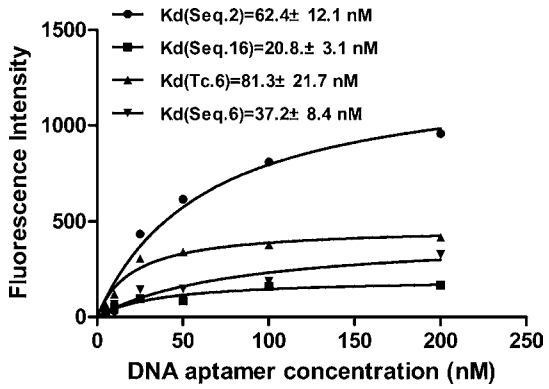


**Figure 2.** Binding saturation curves and determination of the dissociation constants ($K_d$) of aptamers against T-2 by nonlinear regression analysis using GraphPad Prism 5.0.

and hydrogen-bond interactions or a combination of these effects.[36] As seen in Figure 1, the secondary structure of the short sequence Tc.6 is similar to that of Seq.6 but the secondary structures of Tc.2 and Tc.16 remarkably differed from those of their full-length sequences. This difference might be the reason for the lack of affinity of sequence Tc.2 and Tc.16 to target T-2, which was most likely caused by the truncation of primer-binding regions that resulted in a failure to form the three-dimensional structures essential for binding.

**Specificity of Aptamers.** On the basis of the results of the affinity assays, three aptamers (Seq.2, Seq.6, and Seq.16) with lower $K_d$ values for T-2 were selected for specificity testing. The specificity tests were performed using a competitive binding method inspired by the report by Lu et al.[37] GO was mixed with each FAM-labeled aptamer, along with the target molecule T-2 or with $FB_1$, ZEN, $AFB_1$, or OTA. In the presence of T-2, the binding between the FAM-labeled DNA and target molecules should alter the conformation of the FAM-labeled DNA and disturb the interaction between the ssDNA and GO, thus shifting the FAM-labeled DNA into the supernatant.[37] From Figure 3, all of the three aptamer candidates (Seq.2, Seq.6, and Seq.16) exhibited obviously higher corrected

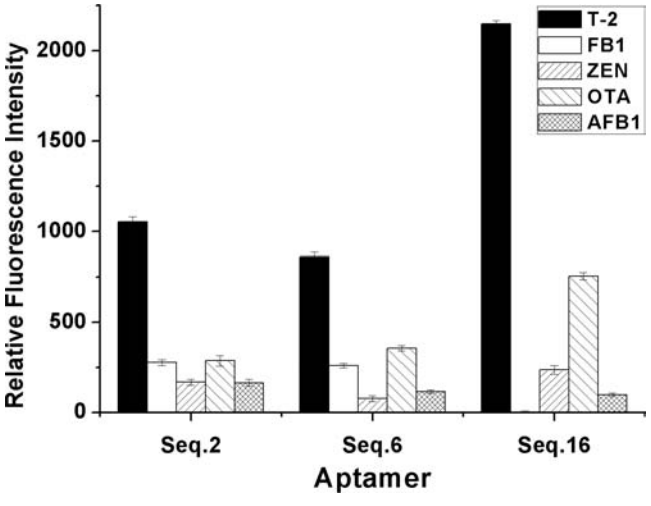


**Figure 3.** Characterization of the specificity of aptamers Seq.2, Seq.6, and Seq.16 by a competitive binding assay. The data shown are corrected values with the negative control signal value deducted. Each data point represents the mean ± standard deviation of three replicates.

fluorescence intensities in the presence of T-2, in comparison to incubation with the counter-targets, and aptamer Seq.16 was found to be significantly more specific to target T-2.

**Study of the Interaction Mode between T-2 and Aptamer.** The CD spectroscopy assay is a powerful and sensitive technology to study the interaction mode between small molecules and DNA aptamers. For further study of conformational information on Seq.16, CD spectra were recorded before and after binding with T-2 in special binding solution. As shown in Figure 4, the CD spectrum of pure T-2 is

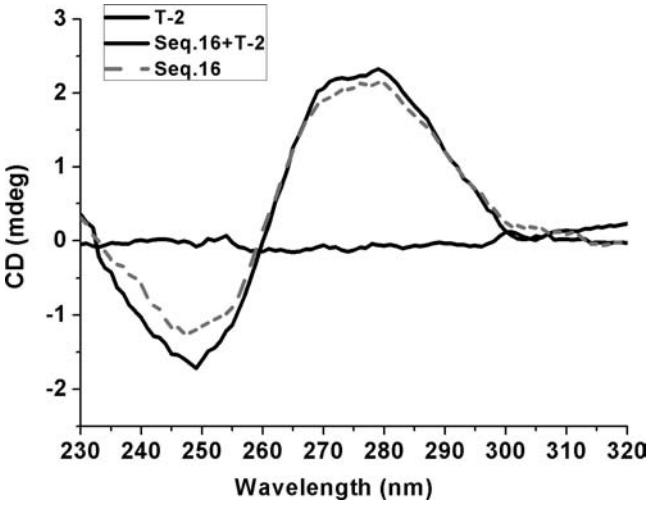


**Figure 4.** CD spectra of T-2 and aptamer Seq.16 in the absence or presence of T-2. The final concentration of T-2 is 20 $\mu$M, and that of the aptamer is 1 $\mu$M.

near the baseline, almost zero signal. The CD spectrum of pure aptamer Seq.16 displays a negative band at 249 nm and a positive band at 280 nm, indicating that the aptamer may have an A-form duplex of the hairpin structure.[38] The addition of T-2 caused a slight increase of the positive band around 280 nm and an apparent decrease of the negative band around 250 nm, suggesting that the binding of T-2 to Seq.16 could promote the formation of the A-form duplex of the hairpin structure.

**Application of Aptamer Seq.16.** To demonstrate the potential application of aptamer Seq.16, we performed a fluorescent bioassay for the detection of T-2 in beer samples. Matrix background interference from beer was reduced by diluting the sample 5 times with BB. Because of the high affinity and specificity of Seq.16 against the target T-2, the binding events between the aptamers and targets disturb the interaction between the ssDNA and GO, thus reserving the FAM-labeled aptamers in the supernatant. In the absence of T-2, the fluorescent intensity of the diluted beer sample was at a minimum; in the presence of different concentrations of T-2, the fluorescent intensity varied. A calibration curve of aptamer-based detection of T-2 in beer was created by plotting the relative fluorescence intensity ($\Delta I$) against the T-2 concentration of undiluted beer (Figure 5), in which $\Delta I$ represents the difference of fluorescence intensity in the presence and absence of T-2. A linear correlation ($R^2$ = 0.988) was obtained between 0.5 and 37.5 $\mu$M (0.1 and 7.5 $\mu$M in the diluted beer sample). The sensitivity of the developed bioasssay was investigated, and the limit of detection (LOD) for T-2 was found to be 0.4 $\mu$M in the real beer sample. Recovery tests were performed for evaluation of the accuracy of the developed method for T-2

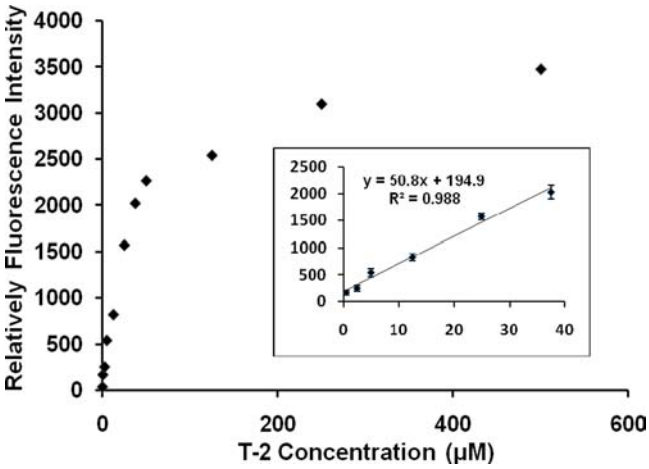


**Figure 5.** Calibration curve for T-2 in beer measured by the aptamer-based fluorescent bioassay.

determination in beer. A good assay recovery for spiked real beer samples was obtained, as listed in Table 2. The preliminary study in the work shows potential application of the selected aptamer in the detection of T-2 in real samples. A further study is ongoing in our laboratory to develop advanced biosensors for T-2 detection, with an increased sensitivity and a decreased detection limit, by means of the signal amplification technique.

**Table 2. Recovery of T-2 in Spiked Beer by the Aptamer-Based Fluorescent Bioassay**

| T-2 added ($\mu$M) | T-2 detected ($\mu$M) ($n$ = 3) | recovery (%) |
|---|---|---|
| 2.5 | 2.34 ± 0.14 | 93.6 |
| 12.5 | 12.6 ± 0.12 | 100.8 |
| 25.0 | 26.5 ± 0.12 | 106.0 |

## ■ ASSOCIATED CONTENT

### Ⓢ Supporting Information

Impact of methanol on PCR amplification. This material is available free of charge via the Internet at http://pubs.acs.org.

## ■ AUTHOR INFORMATION

### Corresponding Authors

*Telephone/Fax: +86-510-85917023. E-mail: wusj@jiangnan.edu.cn.

*Telephone/Fax: +86-510-85917023. E-mail: wangzp@jiangnan.edu.cn.

### Funding

This work was partly supported by the National Science and Technology Support Program of China (2012BAK08B01), the Science and Technology Supporting Project of Jiangsu Province (BE2011621 and BE2012614), the National Natural Science Foundation of China (NSFC) (21375049), JSCI-Q_2012IK166, the Research Fund for the Doctoral Program of Higher Education (20110093110002), NCET-11-0663, and JUSRP51309A.

### Notes

The authors declare no competing financial interest.

## ■ REFERENCES

(1) Li, Y.; Wang, Z.; Beier, R.; Shen, J.; De Smet, D.; De Saeger, S.; Zhang, S. T-2 toxin, a trichothecene mycotoxin: Review of toxicity, metabolism, and analytical methods. *J. Agric. Food Chem.* **2011**, *59*, 3441−3453.

(2) Pascale, M.; Panzarini, G.; Visconti, A. Determination of HT-2 and T-2 toxins in oats and wheat by ultra-performance liquid chromatography with photodiode array detection. *Talanta* **2012**, *89*, 231−236.

(3) Sibanda, L.; De Saeger, S.; Peteghem, C.; Grabarkiewicz-Szczesna, J.; Tomczak, M. Detection of T-2 toxin in different cereals by flow-through enzyme immunoassay with a simultaneous internal reference. *J. Agric. Food Chem.* **2000**, *48*, 5864−5867.

(4) European Food Safety Authority (EFSA). *Occurrence Data of Trichothecene Mycotoxins T-2 Toxin and HT-2 Toxin in Food and Feed*; EFSA: Parma, Italy, 2010; http://www.efsa.europa.eu/en/supporting/pub/66e.htm (accessed May 31, 2011).

(5) Wannemacher, R. W.; Wiener, S. L. Trichothecene mycotoxins. In *Textbook of Military Medicine*; Bellamy, R. F., Ed.; Borden Institute, Office of The Surgeon General, Department of the Army: Washington, D.C., 1997, Chapter 34, pp 655−676.

(6) Duffy, M. J.; Reid, R. S. Measurement of the stability of T-2 toxin in aqueous solution. *Chem. Res. Toxicol.* **1993**, *6*, 524−529.

(7) Raisbeck, M. F.; Rottinghaus, G. E.; Kendall, J. D. In *Effects of Naturally Occurring Mycotoxins on Ruminants*; Smith, J. E., Henderson, R. S., Eds.; CRC Press: Boca Raton, FL, 1991; Vol. *241*, pp 647−677.

(8) Li, Y.; Luo, X.; Yang, S.; Cao, X.; Wang, Z.; Shi, W.; Zhang, S. High specific monoclonal antibody production and development of an ELISA method for monitoring T-2 toxin in rice. *J. Agric. Food Chem.* **2014**, *62*, 1492−1497.

(9) Sun, Y.; Zhang, Y.; Zhao, H.; Zheng, J.; Hu, F.; Fang, B. Liquid chromatography−tandem mass spectrometry method for toxicokinetics, tissue distribution, and excretion studies of T-2 toxin and its major metabolites in pigs. *J. Chromatogr. B: Anal. Technol. Biomed. Life Sci.* **2014**, *958*, 75−82.

(10) Pal, A.; Acharya, D.; Saha, D.; Dhar, D. K. Development of a membrane-based immunofiltration assay for the detection of T-2 toxin. *Anal. Chem.* **2004**, *76*, 4237−4240.

(11) Soleimany, F.; Jinap, S.; Faridah, A.; Khatib, A. A UPLC−MS/MS for simultaneous determination of aflatoxins, ochratoxin A, zearalenone, DON, fumonisins, T-2 toxin and HT-2 toxin, in cereals. *Food Control* **2012**, *25*, 647−653.

(12) Kong, W.; Zhang, X.; Shen, H.; Yang, Z.; Yang, M. Validation of a gas chromatography−electron capture detection of T-2 and HT-2 toxins in Chinese herbal medicines and related products after immunoaffinity column clean-up and pre-column derivatization. *Food Chem.* **2012**, *132*, 574−581.

(13) Barna-vetro, I.; Gyongyosi, A.; Solti, L. Monoclonal antibody-based enzyme-linked immunosorbent assay of fusarium T-2 and zearalenone toxins in cereals. *Appl. Environ. Microbiol.* **1994**, *60*, 729−731.

(14) Molinelli, A.; Grossalbe, K.; Führer, M.; Baumgartner, S.; Sulyok, M.; Krska, R. Development of qualitative and semiquantitative immunoassay-based rapid strip tests for the detection of T-2 toxin in wheat and oat. *J. Agric. Food Chem.* **2008**, *8*, 2589−2594.

(15) Ellington, A. D.; Szostak, J. W. In vitro selection of RNA molecules that bind specific ligands. *Nature* **1990**, *346*, 818−822.

(16) Tuerk, C.; Gold, L. Systematic evolution of ligands by exponential enrichment: RNA ligands to bacteriophage T4 DNA polymerase. *Science* **1990**, *249*, 505−510.

(17) Niazi, J. H.; Lee, S. J.; Gu, M. B. Single-stranded DNA aptamers specific for antibiotics tetracyclines. *Bioorg. Med. Chem.* **2008**, *16*, 7245−7253.

(18) Cruz-Aguado, J. A.; Penner, G. Determination of ochratoxin A with a DNA aptamer. *J. Agric. Food Chem.* **2008**, *56*, 10456−10461.

(19) Song, K. M.; Cho, M.; Jo, H.; Min, K.; Jeon, S. H.; Kim, T.; Han, M. S.; Ku, J. K.; Ban, C. Gold nanoparticle-based colorimetric detection of kanamycin using a DNA aptamer. *Anal. Biochem.* **2011**, *415*, 175−181.

(20) Mehta, J.; Van Dorst, B.; Rouah-Martin, E.; Herrebout, H.; Scippod, M. L. In vitro selection and characterization of DNA

aptamers recognizing chloramphenicol. *J. Biotechnol.* **2011**, *155*, 361−369.
(21) Song, K. M.; Jeong, E.; Jeon, W.; Jo, H.; Ban, C. A coordination polymer nanobelt (CPNB)-based aptasensor for sulfadimethoxine. *Biosens. Bioelectron.* **2012**, *33*, 113−119.
(22) Yang, J.; Bowser, M. T. Capillary electrophoresis−SELEX selection of catalytic DNA aptamers for a small-molecule porphyrin target. *Anal. Chem.* **2013**, *85*, 1525−1530.
(23) Park, J. W.; Tatavarty, R.; Kim, D. W.; Jung, H. T.; Gu, M. B. Immobilization-free screening of aptamers assisted by graphene oxide. *Chem. Commun.* **2012**, *48*, 2071−2073.
(24) Park, J. W.; Lee, S. J.; Cho, E. J.; Kim, J.; Song, J. Y.; Gu, M. B. An ultra-sensitive detection of a whole virus using dual aptamers developed by immobilization-free screening. *Biosens. Bioelectron.* **2014**, *51*, 324−329.
(25) Wu, M.; Kempaiah, R.; Huang, P.; Maheshwari, V.; Liu, J. Adsorption and desorption of DNA on graphene oxide studied by fluorescently labeled oligonucleotides. *Langmuir.* **2011**, *27*, 2731−2738.
(26) Chen, C.; Zhao, J.; Jiang, J.; Yu, R. A novel exonuclease III-aided amplification assay for lysozyme based on graphene oxide platform. *Talanta* **2012**, *101*, 357−361.
(27) Hummers, W. S.; Offeman, R. E. Preparation of graphitic oxide. *J. Am. Chem. Soc.* **1958**, *80*, 1339.
(28) Wu, S.; Duan, N.; Ma, X.; Xia, Y.; Wang, H.; Wang, Z.; Zhang, Q. Multiplexed fluorescence resonance energy transfer aptasensor between upconversion nanoparticles and graphene oxide for the simultaneous determination of mycotoxins. *Anal. Chem.* **2012**, *84*, 6263−6270.
(29) Tang, J.; Yu, T.; Guo, L.; Xie, J.; Shao, N.; He, Z. *In vitro* selection of DNA aptamer against abrin toxin and aptamer-based abrin direct detection. *Biosens. Bioelectron.* **2007**, *22*, 2456−2463.
(30) Qi, C.; Bing, T.; Mei, H.; Yang, X.; Liu, X.; Shangguan, D. G-quadruplex DNA aptamers for zeatin recognizing. *Biosens. Bioelectron.* **2013**, *41*, 157−162.
(31) Duan, N.; Ding, X.; He, L.; Wu, S.; Wei, Y.; Wang, Z. Selection, identification and application of a DNA aptamer against *Listeria monocytogenes*. *Food Control* **2013**, *33*, 239−243.
(32) Viswanathan, V. K.; Krcmarik, K.; Cianciotto, N. P. Template secondary structure promotes polymerase jumping during PCR amplification. *BioTechniques* **1999**, *27*, 508−11.
(33) Kang, J.; Lee, M. S.; Gorenstein, D. G. The enhancement of PCR amplification of a random sequence DNA library by DMSO and betaine: Application to in vitro combinatorial selection of aptamers. *J. Biochem. Biophys. Methods* **2005**, *64*, 147−151.
(34) McKeague, M.; Bradley, C. R.; Girolamo, A. D.; Visconti, A.; Miller, J. D.; DeRosa, M. C. Screening and initial binding assessment of fumonisin B1 aptamers. *J. Mol. Sci.* **2010**, *11*, 4864−4881.
(35) Kiani, Z.; Shafiei, M.; Rahimi-Moghaddama, P.; Karkhaneb, A. A.; Ebrahimi, S. A. In vitro selection and characterization of deoxyribonucleic acid aptamers for digoxin. *Anal. Chim. Acta* **2012**, *748*, 67−72.
(36) Ruff, K. M.; Snyder, T. M.; Liu, D. R. Enhanced functional potential of nucleic acid aptamer libraries patterned to increase secondary structure. *J. Am. Chem. Soc.* **2010**, *132*, 9453−9464.
(37) Lu, C. H.; Yang, H. H.; Zhu, C. L.; Chen, X.; Chen, G. N. A graphene platform for sensing biomolecules. *Angew. Chem., Int. Ed.* **2009**, *48*, 4785−4787.
(38) Bozza, M.; Sheardy, R. D.; Dilone, E.; Scypinski, S.; Galazka, M. Characterization of the secondary structure and stability of an RNA aptamer that binds vascular endothelial growth factor. *Biochemistry* **2006**, *45*, 7639−7643.

**Table 1. Pesticides, Exact Mass, and UHPLC Retention Time for Data Processing and Quantification and UHPLC/ESI Q-Orbitrap MS Method Performance Results**

| Pesticides | Molecular formula | Precursor Exact mass[a] | | | Fragements or ions used for quantification[b] | Retention Time | Fruits[f] | | | Vegetables[f] | | |
|---|---|---|---|---|---|---|---|---|---|---|---|---|
| | | $[M+H]^+$ | $[M+NH_4]^+$ | $[M+Na]^+$ | | | Overall recovery[c] (%) | Intermediate precision[d] (%) | Measurement uncertainty[e] (%) | Overall recovery[c] (%) | Intermediate precision[d] (%) | Measurement uncertainty[e] (%) |
| 1[g] | 2 | 3 | 4 | 5 | 7 | 8 | 9 | 10 | 11 | 12 | 13 | 14 |
| Abamectin B1a | C48H72O14 | 873.49948 | 890.52603 | **895.48143** | | 10.01 | 101.4 | 5.6 | 13.8 | 94.7 | 4.9 | 15.2 |
| Acephate | C4H10NO3PS | **184.01918** | 201.04573 | 206.00112 | | 1.88 | 93.5 | 3.9 | 8.1 | 92.0 | 6.5 | 17.7 |
| Acetamiprid | C10H11ClN4 | **223.07450** | 240.10105 | 245.05645 | | 4.47 | 98.5 | 3.8 | 8.4 | 96.3 | 4.0 | 9.2 |
| Acetochlor | C14H20ClNO2 | **270.12553** | 287.15208 | 292.10748 | | 8.24 | 98.3 | 3.9 | 8.6 | 94.2 | 4.3 | 11.6 |
| Acibenzolar-S-methyl | C8H6N2OS2 | **210.99943** | 228.02598 | 232.98138 | | 7.48 | 92.3 | 3.6 | 22.4 | 88.5 | 5.2 | 14.5 |
| Aclonifen | C12H9ClN2O3 | **265.03745** | 282.06400 | 287.01939 | | 8.30 | 97.1 | 10.0 | 21.4 | 90.6 | 11.8 | 26.9 |
| Acrinathrin | C26H21F6NO5 | 542.13967 | 559.16622 | **564.12161** | | 9.91 | 92.1 | 5.9 | 18.6 | 83.3 | 6.1 | 19.7 |
| Akton | C12H14Cl3O3PS | **374.95396** | 391.98051 | 396.93591 | | 9.39 | 97.0 | 4.2 | 10.9 | 90.2 | 6.2 | 15.4 |
| Alachlor | C14H20ClNO2 | **270.12553** | 287.15208 | 292.10748 | | 8.27 | 98.3 | 3.9 | 8.6 | 94.2 | 4.3 | 11.6 |
| Aldicarb | C7H14N2O2S | 191.08488 | 208.11142 | 213.06682 | **116.05285** | 5.32 | 99.8 | 4.0 | 8.0 | 95.4 | 6.9 | 16.3 |
| Allethrin | C19H26O3 | **303.19547** | 320.22202 | 325.17742 | | 9.33 | 97.3 | 4.6 | 10.3 | 87.9 | 8.8 | 20.6 |
| Allidochlor | C8H12ClNO | **174.06802** | 191.09457 | 196.04996 | | 5.50 | 97.7 | 4.0 | 8.6 | 95.6 | 4.2 | 9.8 |
| Ametryn | C9H17N5S | **228.12774** | 245.15429 | 250.10969 | | 7.00 | 96.6 | 3.8 | 7.9 | 91.6 | 4.4 | 12.1 |
| Amicarbazone | C10H19N5O2 | 242.16115 | 259.18770 | **264.14310** | | 6.00 | 98.4 | 5.2 | 11.8 | 95.1 | 5.5 | 12.8 |
| Aminocarb | C11H16N2O2 | **209.12845** | 226.15500 | 231.11040 | | 2.20 | 97.4 | 4.0 | 9.0 | 92.8 | 5.7 | 17.6 |
| Ancymidol | C15H16N2O2 | **257.12845** | 274.15500 | 279.11040 | | 6.16 | 98.5 | 3.4 | 8.8 | 93.2 | 3.9 | 8.6 |
| Anilofos | C13H19ClNO3PS2 | **368.03053** | 385.05707 | 390.01247 | | 8.50 | 98.0 | 3.8 | 8.5 | 91.9 | 4.2 | 11.9 |
| Aramite | C15H23ClO4S | 335.10783 | **352.13438** | 357.08978 | | 9.30 | 97.3 | 4.3 | 11.8 | 90.2 | 4.8 | 12.3 |
| Aspon | C12H28O5P2S2 | **379.09262** | 396.11916 | 401.07456 | | 9.60 | 95.6 | 4.1 | 10.0 | 90.1 | 3.9 | 12.8 |
| Asulam | C8H10N2O4S | 231.04340 | 248.06995 | **253.02535** | | 2.28 | 84.5 | 6.6 | 24.7 | **68.1** | 13.9 | **89.9** |
| Atrazine | C8H14ClN5 | **216.10105** | 233.12760 | 238.08299 | | 6.81 | 96.4 | 3.5 | 8.1 | 92.4 | 3.8 | 10.6 |
| Azaconazole | C12H11Cl2N3O2 | **300.03011** | 317.05666 | 322.01205 | | 7.08 | 98.0 | 4.0 | 8.2 | 93.7 | 4.3 | 9.2 |
| Azadirachtin | C35H44O16 | 721.27021 | 738.29676 | **743.25216** | | 6.52 | 100.5 | 4.6 | 13.1 | 96.4 | 11.5 | 23.2 |
| Azamethiphos | C9H10ClN2O5PS | **324.98093** | 342.00748 | 346.96288 | | 5.84 | 98.7 | 3.8 | 11.2 | 97.9 | 3.3 | 19.1 |
| Azinphos-ethyl | C12H16N3O3PS2 | 346.04435 | 363.07089 | **368.02629** | | 7.92 | 103.4 | 4.1 | 11.8 | 90.7 | 7.0 | 35.3 |
| Azinphos-methyl | C10H12N3O3PS2 | 318.01305 | 335.03959 | **339.99499** | | 7.15 | 101.1 | 4.1 | 12.0 | 92.7 | 4.6 | 14.5 |
| Azoxystrobin | C22H17N3O5 | **404.12410** | 421.15065 | 426.10604 | | 7.35 | 97.5 | 4.0 | 8.8 | 93.1 | 4.0 | 10.2 |
| Barban | C11H9Cl2NO2 | **258.00831** | 275.03486 | 279.99026 | | 7.74 | 99.1 | 4.5 | 10.5 | 89.2 | 10.6 | 21.7 |
| Benalaxyl | C20H23NO3 | **326.17507** | 343.20162 | 348.15701 | | 8.50 | 96.8 | 4.2 | 9.1 | 91.0 | 4.3 | 11.8 |
| Benazolin | C9H6ClNO3S | **243.98297** | 261.00952 | 265.96491 | | 5.64 | **31.4** | 14.4 | **59.7** | **35.5** | 14.6 | **72.4** |
| Bendiocarb | C11H13NO4 | **224.09173** | 241.11828 | 246.07368 | | 6.07 | 99.2 | 3.7 | 7.6 | 95.1 | 4.1 | 10.6 |
| Benfluralin | C13H16F3N3O4 | **336.11657** | 353.14312 | 358.09851 | | 9.63 | 93.3 | 5.9 | 14.2 | 86.8 | 7.7 | 20.5 |
| Benfuracarb | C20H30N2O5S | 411.19482 | **428.22137** | 433.17676 | | 9.06 | **79.4** | 11.9 | 24.0 | **74.8** | 15.3 | 30.7 |
| Benodanil | C13H10INO | **323.98798** | 341.01453 | 345.96993 | | 6.71 | 98.0 | 3.4 | 7.9 | 92.7 | 3.8 | 9.0 |
| Benoxacor | C11H11Cl2NO2 | **260.02396** | 277.05051 | 282.00591 | | 7.25 | 99.1 | 4.0 | 9.1 | 88.7 | 5.4 | 18.6 |
| Bensulide | C14H24NO4PS3 | 398.06778 | 415.09433 | **420.04973** | | 8.24 | 100.2 | 5.2 | 12.9 | 94.2 | 4.4 | 16.6 |
| Benzoximate | C18H18ClNO5 | **364.09463** | 381.12118 | 386.07657 | | 8.69 | 95.2 | 5.5 | 15.0 | | | |
| Bifenox | C14H9Cl2NO5 | 341.99305 | 359.01960 | **363.97500** | | 8.80 | 101.7 | 7.9 | 25.9 | 89.4 | 9.7 | 21.7 |
| Bifenthrin | C23H22ClF3O2 | 423.13332 | **440.15987** | 445.11526 | | 10.38 | 87.4 | 8.1 | 18.2 | 80.7 | 7.5 | 19.7 |
| Bispyribac | C19H18N4O8 | **431.11974** | 448.14629 | 453.10168 | | 7.63 | **72.1** | 6.9 | 22.0 | **70.2** | 8.1 | 27.8 |
| Bitertanol | C20H23N3O2 | **338.18630** | 355.21285 | 360.16825 | | 8.67 | 96.6 | 6.2 | 16.0 | 97.2 | 10.5 | 26.9 |
| Boscalid | C18H12Cl2N2O | **343.03995** | 360.06649 | 365.02189 | | 7.60 | 100.6 | 8.2 | 17.7 | 90.4 | 7.7 | 19.2 |
| Brodifacoum | C31H23BrO3 | **523.09033** | 540.11688 | 545.07228 | | 10.00 | 93.2 | 6.4 | 14.3 | 86.3 | 5.8 | 16.0 |
| Bromadiolone | C30H23BrO4 | 527.08525 | 544.11180 | **549.06719** | | 9.08 | 94.5 | 5.8 | 18.3 | 84.2 | 6.7 | 19.3 |
| Bromuconazole, cis- | C13H12BrCl2N3O | **375.96136** | 392.98791 | 397.94330 | | 8.38 | 97.3 | 4.7 | 11.7 | 90.7 | 6.4 | 13.9 |
| Bromuconazole, trans- | C13H12BrCl2N3O | **375.96136** | 392.98791 | 397.94330 | | 7.88 | 97.2 | 5.2 | 10.4 | 91.2 | 6.5 | 14.2 |
| Bupirimate | C13H24N4O3S | **317.16419** | 334.19074 | 339.14613 | | 8.03 | 96.2 | 3.7 | 8.3 | 91.0 | 4.5 | 12.8 |
| Buprofezin | C16H23N3OS | **306.16346** | 323.19001 | 328.14540 | | 9.20 | 93.5 | 4.0 | 10.0 | 87.9 | 3.9 | 12.9 |
| Butachlor | C17H26ClNO2 | **312.17248** | 329.19903 | 334.15443 | | 9.33 | 96.1 | 14.3 | 28.7 | 89.0 | 11.0 | 22.9 |
| Butafenacil | C20H18ClF3N2O6 | 475.08783 | **492.11437** | 497.06977 | | 7.93 | 99.6 | 4.7 | 11.0 | 95.4 | 4.9 | 11.5 |
| Butralin | C14H21N3O4 | **296.16048** | 313.18703 | 318.14243 | | 9.70 | 94.3 | 4.2 | 11.1 | 89.1 | 5.6 | 16.6 |
| Butylate | C11H23NOS | **218.15731** | 235.18386 | 240.13926 | | 9.11 | 93.5 | 4.6 | 10.9 | 86.9 | 6.1 | 14.3 |
| Cadusafos | C10H23O2PS2 | **271.09498** | 288.12153 | 293.07693 | | 8.86 | 97.3 | 3.4 | 8.2 | 91.4 | 3.9 | 13.3 |
| Carbaryl | C12H11NO2 | 202.08626 | 219.11280 | 224.06820 | **145.06479** | 6.34 | 99.8 | 3.2 | 7.8 | 96.7 | 3.3 | 8.1 |
| Carbendazim | C9H9N3O2 | **192.07675** | 209.10330 | 214.05870 | | 3.20 | 100.0 | 3.3 | 7.4 | 95.9 | 2.9 | 6.7 |
| Carbetamide | C12H16N2O3 | **237.12337** | 254.14992 | 259.10531 | | 5.65 | 98.2 | 4.0 | 8.3 | 95.4 | 4.4 | 10.3 |
| Carbofuran | C12H15NO3 | **222.11247** | 239.13902 | 244.09441 | | 6.11 | 103.2 | 3.4 | 7.3 | 98.6 | 3.3 | 8.9 |
| Carbofuran-3-hydroxy | C12H15NO4 | 238.10738 | 255.13393 | 260.08933 | **220.09682** | 4.44 | 99.4 | 3.4 | 8.0 | 97.4 | 4.0 | 9.4 |
| Carbophenothion | C11H16ClO2PS3 | **342.98113** | 360.00768 | 364.96308 | | 9.57 | 93.3 | 5.0 | 11.4 | 86.8 | 6.4 | 21.3 |
| Carboxin | C12H13NO2S | **236.07398** | 253.10053 | 258.05592 | | 6.24 | 96.1 | 3.4 | 6.9 | 87.1 | 4.5 | 20.7 |
| Carfentrazone-ethyl | C15H14Cl2F3N3O3 | **412.04371** | 429.07026 | 434.02565 | | 8.33 | 97.4 | 3.8 | 9.1 | 85.4 | 6.3 | 18.4 |
| Carpropamid | C15H18Cl3NO | **334.05267** | 351.07922 | 356.03462 | | 8.50 | 98.4 | 4.3 | 10.5 | 91.7 | 4.3 | 12.4 |
| Chlorbromuron | C9H10BrClN2O2 | **292.96869** | 309.99524 | 314.95064 | | 7.60 | 99.5 | 5.8 | 11.6 | 90.1 | 4.9 | 13.4 |
| Chlorbufam | C11H10ClNO2 | **224.04728** | 241.07383 | 246.02923 | | 7.50 | 98.0 | 6.8 | 14.3 | 87.9 | 9.3 | 27.4 |
| Chlordimeform | C10H13ClN2 | **197.08400** | 214.11055 | 219.06595 | | 3.81 | 93.7 | 3.7 | 8.6 | 104.4 | 3.2 | 15.1 |
| Chlorfenvinphos | C12H14Cl3O4P | **358.97681** | 376.00335 | 380.95875 | | 8.55 | 103.9 | 4.0 | 10.7 | 95.0 | 4.5 | 9.5 |
| Chlorfluazuron | C20H9Cl3F5N3O3 | **539.97024** | 556.99679 | 561.95219 | | 9.74 | 93.6 | 4.6 | 18.1 | 91.7 | 4.3 | 11.4 |
| Chloridazon | C10H8ClN3O | **222.04287** | 239.06942 | 244.02481 | | 4.36 | 95.6 | 4.2 | 8.9 | 94.6 | 3.5 | 8.3 |
| Chlorimuron-ethyl | C15H15ClN4O6S | **415.04736** | 432.07391 | 437.02930 | | 7.60 | 81.5 | 8.2 | 23.2 | 80.5 | 18.1 | 39.9 |
| Chlorotoluron | C10H13ClN2O | **213.07892** | 230.10547 | 235.06086 | | 6.63 | 98.5 | 3.2 | 6.7 | 94.7 | 3.6 | 8.4 |
| Chloroxuron | C15H15ClN2O2 | **291.08948** | 308.11603 | 313.07143 | | 7.91 | 97.7 | 4.3 | 8.6 | 89.4 | 4.2 | 15.0 |
| Chlorpropham | C10H12ClNO2 | 214.06293 | 231.08948 | 236.04488 | **172.0164** | 7.75 | 97.9 | 6.5 | 15.1 | 89.0 | 12.0 | 24.2 |
| Chlorpyrifos | C9H11Cl3NO3PS | **349.93356** | 366.96011 | 371.91550 | | 9.74 | 96.3 | 3.9 | 10.5 | 89.9 | 4.8 | 13.4 |
| Chlorpyrifos-methyl | C7H7Cl3NO3PS | **321.90226** | 338.92881 | 343.88420 | | 8.83 | 95.9 | 4.9 | 12.8 | 88.4 | 6.8 | 16.6 |
| Chlorpyrifos-oxon | C9H11Cl3NO4P | **333.95640** | 350.98295 | 355.93835 | | 8.21 | 90.7 | 3.1 | 10.9 | **65.1** | 4.4 | **106.0** |


dx.doi.org/10.1021/jf503778c | J. Agric. Food Chem. 2014, 62, 10375−10391

**Table 1. continued**

| Pesticides | Molecular formula | Precursor Exact mass[a] | | | Fragements or ions used for quantification[b] | Retention Time | Fruits[f] | | | Vegetables[f] | | |
|---|---|---|---|---|---|---|---|---|---|---|---|---|
| | | [M + H]$^+$ | [M + $NH_4$]$^+$ | [M + Na]$^+$ | | | Overall recovery[c] (%) | Intermediate precision[d] (%) | Measurement uncertainty[e] (%) | Overall recovery[c] (%) | Intermediate precision[d] (%) | Measurement uncertainty[e] (%) |
| 1[g] | 2 | 3 | 4 | 5 | 7 | 8 | 9 | 10 | 11 | 12 | 13 | 14 |
| Clethodim | C17H26ClNO3S | 360.13947 | 377.16602 | 382.12141 | | 8.97 | 100.0 | 4.3 | 9.5 | 87.9 | 8.1 | 18.2 |
| Clodinafop-propargyl | C17H13ClFNO4 | 350.05899 | 367.08554 | 372.04094 | | 8.31 | 94.2 | 3.6 | 12.5 | | | |
| Clofentezine | C14H8Cl2N4 | 303.01988 | 320.04643 | 325.00182 | | 8.65 | 92.3 | 16.1 | 41.2 | 85.2 | 9.5 | 21.1 |
| Cloquintocet-mexyl | C18H22ClNO3 | 336.13610 | 353.16265 | 358.11804 | | 9.28 | 96.7 | 4.4 | 9.2 | 89.1 | 4.3 | 13.8 |
| Clothianidin | C6H8ClN5O2S | 250.01600 | 267.04255 | 271.99794 | | 4.01 | 100.9 | 4.5 | 11.7 | 98.6 | 3.5 | 11.1 |
| Coumaphos | C14H16ClO5PS | 363.02174 | 380.04828 | 385.00368 | | 8.46 | 97.7 | 4.4 | 9.7 | 92.2 | 4.6 | 13.7 |
| Coumaphos-oxon | C14H16ClO6P | 347.04458 | 364.07113 | 369.02652 | | 7.20 | 99.1 | 3.2 | 8.3 | 92.3 | 4.4 | 16.0 |
| Crotoxyphos | C14H19O6P | 315.09920 | 332.12575 | 337.08115 | | 7.62 | 98.0 | 4.2 | 10.2 | 87.9 | 8.6 | 21.6 |
| Crufomate | C12H19ClNO3P | 292.08638 | 309.11293 | 314.06833 | | 8.29 | 97.6 | 4.0 | 8.0 | 91.4 | 4.0 | 9.7 |
| Cumyluron | C17H19ClN2O | 303.12587 | 320.15242 | 325.10781 | | 7.84 | 97.4 | 4.4 | 9.6 | 91.6 | 4.8 | 12.1 |
| Cyanazine | C9H13ClN6 | 241.09630 | 258.12285 | 263.07824 | | 5.72 | 98.0 | 5.0 | 11.9 | 97.0 | 9.0 | 21.8 |
| Cyanofenphos | C15H14NO2PS | 304.05556 | 321.08211 | 326.03751 | | 8.43 | 101.3 | 8.0 | 19.1 | 88.6 | 14.1 | 32.8 |
| Cyazofamid | C13H13ClN4O2S | 325.05205 | 342.07860 | 347.03400 | | 8.13 | 95.7 | 4.3 | 10.2 | 90.2 | 5.0 | 11.6 |
| Cyclanilide | C11H9Cl2NO3 | 274.00323 | 291.02977 | 295.98517 | | 8.00 | 68.9 | 7.3 | 26.4 | 67.6 | 9.8 | 29.7 |
| Cycloate | C11H21NOS | 216.14166 | 233.16821 | 238.12361 | | 8.88 | 94.3 | 4.2 | 10.0 | 87.5 | 4.0 | 11.7 |
| Cyclohexamide | C15H23NO4 | 282.16998 | 299.19653 | 304.15193 | | 5.57 | 95.8 | 7.1 | 16.9 | 92.4 | 4.7 | 15.2 |
| Cycloxydim | C17H27NO3S | 326.17844 | 343.20499 | 348.16039 | | 8.92 | 90.3 | 4.0 | 14.8 | 78.2 | 7.9 | 23.1 |
| Cycluron | C11H22N2O | 199.18049 | 216.20704 | 221.16243 | | 7.08 | 97.9 | 4.2 | 8.7 | 94.7 | 3.4 | 9.0 |
| Cyflufenamid | C20H17F5N2O2 | 413.12830 | 430.15484 | 435.11024 | | 8.67 | 99.1 | 3.5 | 9.4 | 90.8 | 5.9 | 14.7 |
| Cyfluthrin | C22H18Cl2FNO3 | 434.07205 | 451.09860 | 456.05400 | | 9.74 | 94.5 | 7.5 | 15.4 | 87.6 | 8.4 | 17.6 |
| Cymoxanil | C7H10N4O3 | 199.08257 | 216.10912 | 221.06451 | | 3.81 | 98.8 | 4.5 | 9.9 | 96.6 | 5.0 | 12.9 |
| Cypermethrin | C22H19Cl2NO3 | 416.08148 | 433.10802 | 438.06342 | | 9.84 | 95.7 | 6.6 | 15.3 | 89.4 | 8.9 | 19.4 |
| Cyphenothrin | C24H25NO3 | 376.19072 | 393.21727 | 398.17266 | | 9.94 | 93.2 | 8.4 | 17.4 | 82.1 | 5.3 | 34.0 |
| Cyproconazole | C15H18ClN3O | 292.12112 | 309.14767 | 314.10306 | | 7.79 | 97.2 | 3.8 | 8.4 | 91.3 | 5.1 | 11.4 |
| Cyprodinil | C14H15N3 | 226.13387 | 243.16042 | 248.11582 | | 8.15 | 94.7 | 4.1 | 9.1 | 88.3 | 4.2 | 13.2 |
| Cyprosulfamide | C18H18N2O5S | 375.10092 | 392.12747 | 397.08286 | | 5.81 | 98.1 | 5.2 | 14.4 | 91.9 | 4.7 | 10.5 |
| Cyromazine | C6H10N6 | 167.10397 | 184.13052 | 189.08592 | | 1.32 | 75.4 | 5.4 | 18.8 | 76.4 | 4.4 | 13.3 |
| Daimuron | C17H20N2O | 269.16484 | 286.19139 | 291.14678 | | 7.75 | 98.5 | 4.1 | 8.6 | 92.3 | 3.6 | 9.4 |
| Deltamethrin | C22H19Br2NO3 | 503.98045 | 521.00700 | 525.96239 | | 9.82 | 96.7 | 4.5 | 9.8 | 95.2 | 5.1 | 16.3 |
| Demeton-S | C8H19O3PS2 | 259.05860 | 276.08515 | 281.04054 | | 7.33 | 92.8 | 6.6 | 14.8 | 89.7 | 5.5 | 14.7 |
| Demeton-S-methylsulphon | C6H15O5PS2 | 263.01713 | 280.04368 | 284.99907 | | 3.28 | 99.3 | 3.4 | 7.8 | 97.0 | 4.3 | 10.4 |
| Desmedipham | C16H16N2O4 | 301.11828 | 318.14483 | 323.10023 | | 7.12 | 98.4 | 5.3 | 11.9 | 92.3 | 7.8 | 17.0 |
| Dialifos | C14H17ClNO4PS2 | 394.00979 | 411.03634 | 415.99173 | 208.01598 | 8.75 | 101.7 | 3.6 | 15.2 | 99.4 | 3.4 | 26.9 |
| Di-allate | C10H17Cl2NOS | 270.04807 | 287.07462 | 292.03001 | | 9.00 | 95.3 | 4.8 | 11.7 | 85.9 | 6.8 | 15.9 |
| Diazinon | C12H21N2O3PS | 305.10833 | 322.13488 | 327.09027 | | 8.55 | 96.6 | 4.1 | 9.8 | 90.7 | 3.9 | 12.1 |
| Dichlofenthion | C10H13Cl2O3PS | 314.97728 | 332.00383 | 336.95923 | | 9.38 | 95.5 | 7.1 | 16.4 | 85.3 | 9.8 | 29.8 |
| Dichlormid | C8H11Cl2NO | 208.02905 | 225.05560 | 230.01099 | | 6.18 | 98.5 | 4.1 | 8.4 | 95.9 | 4.3 | 9.5 |
| Dichlorvos | C4H7Cl2O4P | 220.95318 | 237.97973 | 242.93512 | | 6.03 | 83.1 | 5.5 | 39.8 | 70.8 | 6.1 | 49.0 |
| Diclobutrazol | C15H19Cl2N3O | 328.09779 | 345.12434 | 350.07974 | | 8.39 | 97.1 | 4.2 | 9.4 | 91.0 | 5.2 | 13.2 |
| Diclocymet | C15H18Cl2N2O | 313.08690 | 330.11344 | 335.06884 | | 8.11 | 100.3 | 4.5 | 10.2 | 95.1 | 5.1 | 11.5 |
| Dicrotophos | C8H16NO5P | 238.08389 | 255.11043 | 260.06583 | | 3.88 | 96.5 | 3.8 | 9.0 | 94.1 | 5.0 | 11.7 |
| Diethofencarb | C14H21NO4 | 268.15433 | 285.18088 | 290.13628 | 226.10739 | 7.36 | 99.9 | 3.5 | 7.8 | 95.0 | 4.2 | 9.7 |
| Difenacoum | C31H24O3 | 445.17982 | 462.20637 | 467.16177 | | 9.59 | 94.1 | 5.6 | 11.8 | 87.8 | 6.1 | 14.3 |
| Difenoconazole | C19H17Cl2N3O3 | 406.07197 | 423.09852 | 428.05392 | | 8.86 | 96.8 | 4.2 | 9.0 | 90.2 | 5.5 | 14.5 |
| Diflubenzuron | C14H9ClF2N2O2 | 311.03934 | 328.06589 | 333.02128 | | 8.22 | 98.7 | 4.2 | 9.4 | 93.1 | 4.6 | 12.6 |
| Dimepiperate | C15H21NOS | 264.14166 | 281.16821 | 286.12361 | | 8.94 | 90.5 | 6.3 | 12.8 | 85.3 | 4.8 | 17.2 |
| Dimethachlor | C13H18ClNO2 | 256.10988 | 273.13643 | 278.09183 | | 7.16 | 98.0 | 5.5 | 11.3 | 94.5 | 4.2 | 10.9 |
| Dimethametryn | C11H21N5S | 256.15904 | 273.18559 | 278.14099 | | 8.11 | 96.8 | 4.2 | 9.1 | 90.3 | 4.2 | 12.5 |
| Dimethenamid | C12H18ClNO2S | 276.08195 | 293.10850 | 298.06390 | | 7.58 | 98.8 | 3.7 | 8.1 | 87.9 | 10.7 | 26.2 |
| Dimethoate | C5H12NO3PS2 | 230.00690 | 247.03345 | 251.98884 | | 4.36 | 97.6 | 3.6 | 7.8 | 96.4 | 3.7 | 9.5 |
| Dimethomorph | C21H22ClNO4 | 388.13101 | 405.15756 | 410.11296 | | 7.75 | 97.3 | 5.3 | 11.0 | 92.7 | 5.8 | 13.5 |
| Dimethylvinphos | C10H10Cl3O4P | 330.94551 | 347.97205 | 352.92745 | | 7.91 | 99.5 | 3.7 | 9.0 | 94.3 | 4.2 | 10.7 |
| Dimetilan | C10H16N4O3 | 241.12952 | 258.15607 | 263.11146 | | 4.72 | 97.2 | 4.0 | 9.0 | 94.2 | 4.0 | 12.3 |
| Dimoxystrobin | C19H22N2O3 | 327.17032 | 344.19687 | 349.15226 | | 8.34 | 96.7 | 4.3 | 8.9 | 92.3 | 4.8 | 12.8 |
| Diniconazole | C15H17Cl2N3O | 326.08214 | 343.10869 | 348.06409 | | 8.84 | 97.2 | 3.6 | 8.9 | 91.9 | 5.2 | 12.8 |
| Dinotefuran | C7H14N4O3 | 203.11387 | 220.14042 | 225.09581 | | 2.30 | 94.3 | 4.2 | 9.2 | 92.8 | 4.6 | 11.8 |
| Dioxacarb | C11H13NO4 | 224.09173 | 241.11828 | 246.07368 | 167.07027 | 4.38 | 92.8 | 4.7 | 19.9 | 95.1 | 5.1 | 10.9 |
| Dioxathion | C12H26O6P2S4 | 457.01602 | 474.04257 | 478.99797 | | 9.18 | 99.9 | 7.8 | 16.6 | 90.0 | 7.9 | 18.8 |
| Diphenamid | C16H17NO | 240.13829 | 257.16484 | 262.12024 | | 7.16 | 98.1 | 3.7 | 7.7 | 94.0 | 4.0 | 8.7 |
| Diphenylamine | C12H11N | 170.09643 | 187.12298 | 192.07837 | | 7.92 | 71.1 | 6.0 | 113.5 | 55.3 | 17.6 | 96.9 |
| Dipropetryn | C11H21N5S | 256.15904 | 273.18559 | 278.14099 | | 8.11 | 96.8 | 4.2 | 9.1 | 90.3 | 4.2 | 12.5 |
| Disulfoton | C8H19O2PS3 | 275.03576 | 292.06230 | 297.01770 | | 8.75 | 102.0 | 5.5 | 16.0 | 98.6 | 5.4 | 11.5 |
| Ditalimfos | C12H14NO4PS | 300.04539 | 317.07194 | 322.02734 | | 7.99 | 88.4 | 5.4 | 13.4 | 80.0 | 4.7 | 16.1 |
| Dithiopyr | C15H16F5NO2S2 | 402.06154 | 419.08809 | 424.04348 | | 9.01 | 98.0 | 4.2 | 9.5 | 90.5 | 7.6 | 17.9 |
| Diuron | C9H10Cl2N2O | 233.02429 | 250.05084 | 255.00624 | | 7.24 | 99.7 | 3.7 | 7.4 | 94.6 | 5.5 | 13.9 |
| Dodemorph | C18H35NO | 282.27914 | 299.30569 | 304.26109 | | 7.11 | 80.6 | 5.9 | 11.9 | 75.2 | 5.6 | 16.2 |
| Edifenphos | C14H15O2PS2 | 311.03238 | 328.05893 | 333.01433 | | 8.44 | 97.1 | 3.5 | 7.8 | 89.9 | 4.1 | 10.2 |
| Emamectin B1a | C49H75NO13 | 886.53112 | 903.55767 | 908.51306 | | 9.47 | 92.0 | 6.1 | 12.2 | 87.8 | 6.0 | 13.9 |
| EPN | C14H14NO4PS | 324.04539 | 341.07194 | 346.02734 | | 8.86 | 95.6 | 9.3 | 19.7 | 86.2 | 13.5 | 31.4 |
| Epoxiconazole | C17H13ClFN3O | 330.08039 | 347.10694 | 352.06234 | | 8.08 | 98.8 | 4.1 | 9.9 | 91.9 | 4.5 | 10.9 |
| Eprinomectin B1a | C50H75NO14 | 914.52603 | 931.55258 | 936.50798 | | 9.81 | 102.6 | 6.3 | 15.1 | 94.2 | 6.2 | 20.9 |
| EPTC | C9H19NOS | 190.12601 | 207.15256 | 212.10796 | | 8.34 | 95.7 | 4.7 | 10.8 | 91.2 | 5.0 | 13.2 |
| Esprocarb | C15H23NOS | 266.15731 | 283.18386 | 288.13926 | | 9.24 | 95.2 | 3.8 | 10.1 | 87.8 | 3.7 | 11.4 |
| Ethidimuron | C7H12N4O3S2 | 265.04236 | 282.06891 | 287.02430 | | 3.96 | 98.6 | 5.3 | 13.2 | 96.8 | 4.4 | 10.8 |
| Ethiofencarb | C11H15NO2S | 226.08963 | 243.11618 | 248.07157 | 107.04914 | 6.52 | 114.2 | 69.0 | 138.6 | 87.2 | 26.8 | 53.8 |
| Ethiofencarb-sulfone | C11H15NO4S | 258.07946 | 275.10600 | 280.06140 | | 4.00 | 99.8 | 3.7 | 8.4 | 98.3 | 4.5 | 11.3 |


dx.doi.org/10.1021/jf503778c | J. Agric. Food Chem. 2014, 62, 10375−10391

**Table 1. continued**

| Pesticides | Molecular formula | Precursor | | | Fragements or ions used for quantification[b] | Retention Time | Fruits[f] | | | Vegetables[f] | | |
|---|---|---|---|---|---|---|---|---|---|---|---|---|
| | | Exact mass[a] | | | | | Overall recovery[c] (%) | Intermediate precision[d] (%) | Measurement uncertainty[e] (%) | Overall recovery[c] (%) | Intermediate precision[d] (%) | Measurement uncertainty[e] (%) |
| | | $[M + H]^+$ | $[M + NH_4]^+$ | $[M + Na]^+$ | | | | | | | | |
| 1[g] | 2 | 3 | 4 | 5 | 7 | 8 | 9 | 10 | 11 | 12 | 13 | 14 |
| Ethiofencarb-sulfoxide | C11H15NO3S | **242.08454** | 259.11109 | 264.06649 | | 3.85 | 95.9 | 6.0 | 12.3 | 99.1 | 4.9 | 11.7 |
| Ethiolate | C7H15NOS | **162.09471** | 179.12126 | 184.07666 | | 7.10 | 95.6 | 6.3 | 14.1 | 95.9 | 11.4 | 25.2 |
| Ethion | C9H22O4P2S4 | **384.99489** | 402.02144 | 406.97684 | | 9.31 | 96.3 | 4.5 | 9.2 | 88.1 | 10.9 | 25.3 |
| Ethiprole | C13H9Cl2F3N4OS | **396.98990** | 414.01645 | 418.97184 | | 7.58 | 100.4 | 4.4 | 10.1 | 89.9 | 9.0 | 27.2 |
| Ethirimol | C11H19N3O | **210.16009** | 227.18664 | 232.14203 | | 5.39 | 91.6 | 3.8 | 9.3 | 87.0 | 4.0 | 14.6 |
| Ethofumesate | C13H18O5S | **287.09477** | 304.12132 | 309.07672 | | 7.45 | 99.5 | 3.6 | 9.1 | 93.1 | 5.3 | 11.9 |
| Ethoprophos | C8H19O2PS2 | **243.06368** | 260.09023 | 265.04563 | | 8.11 | 99.2 | 3.6 | 7.4 | 95.3 | 3.6 | 9.0 |
| Etobenzanid | C16H15Cl2NO3 | **340.05018** | 357.07672 | 362.03212 | | 8.44 | 97.2 | 4.5 | 10.0 | 90.9 | 4.6 | 13.7 |
| Etofenprox | C25H28O3 | 377.21112 | **394.23767** | 399.19307 | | 10.26 | 93.4 | 4.9 | 15.4 | 86.6 | 7.6 | 16.8 |
| Etoxazole | C21H23F2NO2 | **360.17696** | 377.20351 | 382.15891 | | 9.57 | 95.7 | 4.5 | 11.0 | 90.5 | 4.6 | 11.8 |
| Etrimfos | C10H17N2O4PS | **293.07194** | 310.09849 | 315.05389 | | 8.44 | 96.5 | 3.9 | 8.9 | 90.5 | 4.2 | 11.9 |
| Famoxadone | C22H18N2O4 | 375.13393 | 392.16048 | **397.11588** | | 8.53 | 98.5 | 6.7 | 16.6 | 92.3 | 7.2 | 17.5 |
| Famphur | C10H16NO5PS2 | **326.02803** | 343.05458 | 348.00997 | | 6.74 | 98.8 | 3.9 | 8.2 | 93.1 | 3.8 | 10.3 |
| Fenamidone | C17H17N3OS | **312.11651** | 329.14306 | 334.09845 | | 7.56 | 97.7 | 4.0 | 8.7 | 85.1 | 10.6 | 23.1 |
| Fenamiphos | C13H22NO3PS | **304.11308** | 321.13963 | 326.09502 | | 8.23 | 96.0 | 3.7 | 8.0 | 90.2 | 4.4 | 13.0 |
| Fenamiphos-sulfone | C13H22NO5PS | **336.10291** | 353.12946 | 358.08485 | | 6.29 | 100.2 | 3.6 | 8.3 | 96.3 | 4.2 | 9.7 |
| Fenamiphos-sulfoxide | C13H22NO4PS | **320.10799** | 337.13454 | 342.08994 | | 6.18 | 98.6 | 4.1 | 8.8 | 95.7 | 3.4 | 7.6 |
| Fenarimol | C17H12Cl2N2O | **331.03995** | 348.06649 | 353.02189 | | 8.00 | 96.5 | 5.3 | 11.5 | 89.6 | 6.3 | 14.1 |
| Fenazaquin | C20H22N2O | **307.18049** | 324.20704 | 329.16243 | | 9.91 | 92.3 | 4.7 | 11.6 | 85.8 | 4.4 | 12.6 |
| Fenbuconazole | C19H17ClN4 | **337.12145** | 354.14800 | 359.10340 | | 8.14 | 99.4 | 4.6 | 10.5 | 93.1 | 4.8 | 12.5 |
| Fenhexamid | C14H17Cl2NO2 | **302.07091** | 319.09746 | 324.05286 | | 7.98 | 94.7 | 4.2 | 9.4 | 83.0 | 10.6 | 28.6 |
| Fenoxanil | C15H18Cl2N2O2 | **329.08181** | 346.10836 | 351.06375 | | 8.23 | 99.1 | 3.6 | 8.6 | 94.0 | 4.2 | 12.1 |
| Fenoxycarb | C17H19NO4 | **302.13868** | 319.16523 | 324.12063 | | 8.24 | 98.2 | 3.8 | 8.4 | 88.2 | 4.0 | 18.4 |
| Fenpiclonil | C11H6Cl2N2 | **236.99808** | 254.02463 | 258.98002 | | 7.29 | 99.0 | 3.0 | 7.0 | 91.8 | 4.6 | 10.9 |
| Fenpropathrin | C22H23NO3 | **350.17507** | 367.20162 | 372.15701 | | 9.62 | 94.4 | 6.0 | 12.5 | 89.9 | 6.2 | 14.8 |
| Fenpropidin | C19H31N | **274.25293** | 291.27948 | 296.23487 | | 7.26 | 86.9 | 6.0 | 14.3 | **78.9** | 7.2 | 17.5 |
| Fenpropimorph | C20H33NO | **304.26349** | 321.29004 | 326.24544 | | 7.42 | 85.9 | 5.1 | 10.7 | 80.0 | 4.4 | 12.8 |
| Fenpyroximate | C24H27N3O4 | **422.20743** | 439.23398 | 444.18938 | | 9.63 | 96.4 | 4.5 | 10.0 | 92.3 | 6.5 | 15.0 |
| Fensulfothion | C11H17O4PS2 | **309.03786** | 326.06441 | 331.01981 | | 6.93 | 98.6 | 3.6 | 7.8 | 94.7 | 4.7 | 10.5 |
| Fenthion | C10H15O3PS2 | **279.02730** | 296.05385 | 301.00924 | | 8.41 | 93.5 | 3.9 | 14.4 | 85.4 | 8.1 | 17.7 |
| Fenthion-sulfone | C10H15O5PS2 | **311.01713** | 328.04368 | 332.99907 | | 6.42 | 99.7 | 3.8 | 8.7 | 95.0 | 4.9 | 10.0 |
| Fenthion-sulfoxide | C10H15O4PS2 | **295.02221** | 312.04876 | 317.00416 | | 6.26 | 102.6 | 4.5 | 14.1 | 99.0 | 5.0 | 10.5 |
| Fentrazamide | C16H20ClN5O2 | 350.13783 | 367.16438 | 372.11977 | **197.12845** | 8.42 | 98.9 | 3.8 | 8.3 | 92.0 | 4.1 | 11.0 |
| Fenuron | C9H12N2O | **165.10224** | 182.12879 | 187.08418 | | 4.18 | 96.3 | 3.3 | 8.2 | 95.3 | 4.1 | 9.5 |
| Fenvalerate | C25H22ClNO3 | 420.13610 | **437.16265** | 442.11804 | | 9.86 | 93.0 | 5.1 | 11.6 | 86.8 | 7.8 | 18.0 |
| Fipronil | C12H4Cl2F6N4OS | 436.94598 | **453.97253** | 458.92793 | | 8.26 | 99.6 | 5.3 | 13.5 | 93.2 | 7.3 | 19.8 |
| Flonicamid | C9H6F3N3O | **230.05357** | 247.08012 | 252.03552 | | 3.24 | 100.0 | 3.8 | 8.6 | 94.7 | 6.4 | 14.7 |
| Fluazifop-butyl | C19H20F3NO4 | **384.14172** | 401.16827 | 406.12366 | | 9.10 | 97.4 | 3.7 | 9.5 | 84.0 | 6.5 | 21.1 |
| Flubendiamide | C23H22F7IN2O4S | 683.03059 | 700.05714 | 705.01254 | **407.97611** | 8.30 | 98.5 | 4.5 | 10.6 | 94.4 | 4.9 | 11.5 |
| Flucarbazone | C12H11F3N4O6S | **397.04242** | 414.06897 | 419.02436 | | 5.18 | **77.4** | 8.8 | 32.2 | **73.3** | 9.0 | 27.0 |
| Flucythrinate | C26H23F2NO4 | 452.16679 | **469.19334** | 474.14874 | | 9.47 | 95.2 | 4.4 | 11.2 | 88.7 | 6.7 | 15.9 |
| Fludioxonil | C12H6F2N2O2 | **249.04701** | 266.07356 | 271.02896 | | 7.60 | 101.0 | **22.1** | 48.8 | | | |
| Flufenacet | C14H13F4N3O2S | **364.07374** | 381.10029 | 386.05568 | | 8.03 | 98.2 | 4.3 | 10.4 | 93.5 | 4.5 | 11.5 |
| Flufenoxuron | C21H11ClF6N2O3 | **489.04352** | 506.07006 | 511.02546 | | 9.52 | 94.8 | 5.0 | 15.7 | 92.3 | 5.2 | 13.3 |
| Flumetralin | C16H12ClF4N3O4 | **422.05252** | 439.07907 | 444.03447 | | 9.60 | 92.4 | 5.2 | 13.1 | 88.5 | 6.5 | 19.4 |
| Flumetsulam | C12H9F2N5O2S | **326.05178** | 343.07833 | 348.03372 | | 4.16 | 90.8 | 6.8 | 17.6 | 85.7 | 7.0 | 23.6 |
| Flumioxazin | C19H15FN2O4 | 355.10886 | 372.13541 | **377.09081** | | 7.15 | 99.0 | 7.1 | 18.6 | | | |
| Fluometuron | C10H11F3N2O | **233.08962** | 250.11617 | 255.07157 | | 6.55 | 99.2 | 3.5 | 7.0 | 95.3 | 3.6 | 8.8 |
| Fluopicolide | C14H8Cl3F3N2O | **382.97271** | 399.99926 | 404.95465 | | 7.70 | 97.7 | 4.8 | 10.6 | 92.6 | 4.2 | 10.9 |
| Fluorochloridone | C12H10Cl2F3NO | **312.01643** | 329.04298 | 333.99838 | | 7.81 | 98.9 | 4.0 | 9.4 | 91.7 | 6.9 | 15.6 |
| Fluoxastrobin | C21H16ClFN4O5 | **459.08660** | 476.11315 | 481.06855 | | 7.90 | 97.2 | 4.3 | 9.7 | 92.1 | 4.3 | 11.8 |
| Fluquinconazole | C16H8Cl2FN5O | **376.01627** | 393.04282 | 397.99821 | | 7.88 | 99.0 | 4.7 | 10.1 | 93.4 | 4.7 | 12.6 |
| Fluroxypyr | C7H5Cl2FN2O3 | **254.97340** | 271.99995 | 276.95535 | | 5.54 | **46.9** | 10.0 | 42.8 | **46.5** | 11.7 | **55.3** |
| Flusilazole | C16H15F2N3Si | **316.10761** | 333.13416 | 338.08955 | | 8.24 | 97.4 | 3.9 | 9.1 | 91.5 | 4.5 | 12.2 |
| Flutolanil | C17H16F3NO2 | **324.12059** | 341.14714 | 346.10253 | | 7.67 | 100.6 | 4.0 | 9.4 | 94.4 | 3.9 | 9.9 |
| Flutriafol | C16H13F2N3O | **302.10995** | 319.13649 | 324.09189 | | 6.81 | 99.5 | 4.0 | 9.6 | 93.6 | 4.3 | 9.3 |
| Fomesafen | C15H10ClF3N2O6S | 438.99730 | **456.02384** | 460.97924 | | 7.51 | 89.3 | 6.4 | 16.6 | 83.3 | 12.1 | 25.0 |
| Fonofos | C10H15OPS2 | **247.03747** | 264.06402 | 269.01941 | | 8.48 | 96.4 | 4.8 | 10.8 | 90.6 | 3.9 | 11.3 |
| Forchlorfenuron | C12H10ClN3O | **248.05852** | 265.08507 | 270.04046 | | 6.84 | 95.6 | 4.2 | 8.9 | 90.4 | 4.2 | 9.9 |
| Fosthiazate | C9H18NO3PS2 | **284.05385** | 301.08040 | 306.03579 | | 6.58 | 98.2 | 3.6 | 7.8 | 95.5 | 4.3 | 9.7 |
| Fuberidazole | C11H8N2O | **185.07094** | 202.09749 | 207.05288 | | 3.97 | 94.5 | 8.0 | 18.3 | 90.2 | 7.3 | 19.4 |
| Furalaxyl | C17H19NO4 | **302.13868** | 319.16523 | 324.12063 | | 7.43 | 98.0 | 3.4 | 7.5 | 93.6 | 3.7 | 10.1 |
| Furathiocarb | C18H26N2O5S | **383.16352** | 400.19007 | 405.14546 | | 9.11 | 97.9 | 3.8 | 9.9 | 90.6 | 4.4 | 12.6 |
| Griseofulvin | C17H17ClO6 | **353.07864** | 370.10519 | 375.06059 | | 6.78 | 98.1 | 3.9 | 8.4 | 94.0 | 3.8 | 9.7 |
| Halofenozide | C18H19ClN2O2 | 331.12078 | 348.14733 | **353.10273** | | 7.49 | 101.2 | 6.9 | 15.4 | **77.7** | **28.5** | **58.6** |
| Haloxyfop | C15H11ClF3NO4 | **362.04015** | 379.06670 | 384.02209 | | 8.34 | **69.4** | 8.4 | 24.2 | **65.9** | 10.1 | 30.9 |
| Heptenophos | C9H12ClO4P | **251.02345** | 268.05000 | 273.00539 | | 7.07 | 97.9 | 4.1 | 8.5 | 90.7 | 4.4 | 17.1 |
| Hexaconazole | C14H17Cl2N3O | **314.08214** | 331.10869 | 336.06409 | | 8.65 | 97.2 | 3.6 | 8.8 | 90.8 | 6.4 | 13.1 |
| Hexaflumuron | C16H8Cl2F6N2O3 | 460.98889 | 478.01544 | **482.97084** | | 8.87 | 98.9 | 6.9 | 19.0 | 90.9 | 7.9 | 19.6 |
| Hexazinone | C12H20N4O2 | **253.16590** | 270.19245 | 275.14785 | | 6.09 | 96.9 | 4.0 | 8.1 | 92.6 | 3.5 | 9.8 |
| Hexythiazox | C17H21ClN2O2S | **353.10850** | 370.13505 | 375.09045 | | 9.42 | 96.2 | 4.7 | 10.5 | 89.3 | 4.8 | 15.2 |
| Imazalil | C14H14Cl2N2O | **297.05560** | 314.08214 | 319.03754 | | 6.74 | 87.8 | 4.0 | 9.2 | **76.9** | 5.7 | 20.9 |
| Imazamethabenz-methyl | C16H20N2O3 | **289.15467** | 306.18122 | 311.13661 | | 6.02 | 97.0 | 3.9 | 7.8 | 95.8 | 6.9 | 13.9 |
| Imazamox | C15H19N3O4 | **306.14483** | 323.17138 | 328.12678 | | 4.73 | **51.7** | 6.7 | 34.8 | **49.6** | 6.2 | 38.7 |
| Imazapyr | C13H15N3O3 | **262.11862** | 279.14517 | 284.10056 | | 4.12 | **30.9** | 9.0 | **51.9** | **30.0** | 8.3 | **56.1** |


dx.doi.org/10.1021/jf503778c | J. Agric. Food Chem. 2014, 62, 10375−10391

**Table 1. continued**

| Pesticides | Molecular formula | Precursor Exact mass[a] | | | Fragements or ions used for quantification[b] | Retention Time | Fruits[f] | | | Vegetables[f] | | |
|---|---|---|---|---|---|---|---|---|---|---|---|---|
| | | [M + H]$^+$ | [M + $NH_4$]$^+$ | [M + Na]$^+$ | | | Overall recovery[c] (%) | Intermediate precision[d] (%) | Measurement uncertainty[e] (%) | Overall recovery[c] (%) | Intermediate precision[d] (%) | Measurement uncertainty[e] (%) |
| 1[g] | 2 | 3 | 4 | 5 | 7 | 8 | 9 | 10 | 11 | 12 | 13 | 14 |
| Imazaquin | C17H17N3O3 | 312.13427 | 329.16082 | 334.11621 | | 6.00 | 63.1 | 6.1 | 25.0 | 60.0 | 6.2 | 34.9 |
| Imibenconazole | C17H13Cl3N4S | 410.99993 | 428.02648 | 432.98187 | | 9.26 | 94.3 | 5.9 | 13.7 | 89.0 | 6.1 | 15.2 |
| Imidacloprid | C9H10ClN5O2 | 256.05958 | 273.08613 | 278.04152 | | 3.96 | 98.9 | 4.5 | 15.2 | 98.5 | 4.1 | 10.7 |
| Imiprothrin | C17H22N2O4 | 319.16523 | 336.19178 | 341.14718 | | 7.96 | 103.3 | 4.3 | 11.1 | 79.6 | 8.0 | 69.1 |
| Inabenfide | C19H15ClN2O2 | 339.08948 | 356.11603 | 361.07143 | | 7.40 | 91.9 | 5.0 | 14.0 | 88.2 | 6.3 | 14.3 |
| Indanofan | C20H17ClO3 | 341.09390 | 358.12045 | 363.07584 | | 8.04 | 98.2 | 6.9 | 14.2 | 90.1 | 6.3 | 13.6 |
| Indoxacarb | C22H17ClF3N3O7 | 528.07799 | 545.10454 | 550.05993 | | 8.83 | 97.7 | 4.2 | 8.9 | 94.6 | 6.4 | 14.8 |
| Ipconazole | C18H24ClN3O | 334.16807 | 351.19462 | 356.15001 | | 8.94 | 95.8 | 3.9 | 8.9 | 89.6 | 4.2 | 11.9 |
| Iprobenfos | C13H21O3PS | 289.10218 | 306.12873 | 311.08412 | | 8.33 | 96.9 | 4.3 | 9.3 | 91.3 | 4.9 | 12.8 |
| Iprovalicarb | C18H28N2O3 | 321.21727 | 338.24382 | 343.19921 | | 7.94 | 98.3 | 4.1 | 8.4 | 94.9 | 4.2 | 10.3 |
| Isazophos | C9H17ClN3O3PS | 314.04895 | 331.07550 | 336.03090 | | 7.87 | 97.9 | 4.1 | 9.0 | 93.2 | 4.2 | 10.4 |
| Isocarbamid | C8H15N3O2 | 186.12370 | 203.15025 | 208.10565 | | 4.90 | 95.3 | 3.5 | 10.4 | 94.6 | 3.9 | 9.2 |
| Isocarbophos | C11H16NO4PS | 290.06104 | 307.08759 | 312.04299 | | 6.96 | 100.2 | 4.9 | 14.6 | 93.5 | 5.4 | 15.3 |
| Isofenphos | C15H24NO4PS | 346.12364 | 363.15019 | 368.10559 | | 8.66 | 100.9 | 5.0 | 14.7 | 94.5 | 10.2 | 20.5 |
| Isofenphos-oxon | C15H24NO5P | 330.14649 | 347.17304 | 352.12843 | | 7.89 | 97.4 | 4.1 | 8.9 | 94.7 | 4.7 | 12.1 |
| Isoprocarb | C11H15NO2 | 194.11756 | 211.14410 | 216.09950 | 137.09609 | 6.96 | 99.5 | 6.6 | 14.6 | 98.3 | 6.6 | 17.3 |
| Isopropalin | C15H23N3O4 | 310.17613 | 327.20268 | 332.15808 | | 9.82 | 91.7 | 5.6 | 11.8 | 87.0 | 5.1 | 15.5 |
| Isoprothiolane | C12H18O4S2 | 291.07193 | 308.09848 | 313.05387 | | 7.68 | 97.8 | 4.1 | 8.9 | 92.6 | 4.0 | 10.5 |
| Isoproturon | C12H18N2O | 207.14919 | 224.17574 | 229.13113 | | 6.90 | 98.0 | 3.7 | 7.5 | 94.1 | 3.8 | 8.3 |
| Isoxaben | C18H24N2O4 | 333.18088 | 350.20743 | 355.16283 | | 7.66 | 97.8 | 4.2 | 8.9 | 92.8 | 4.1 | 9.9 |
| Isoxadifen-ethyl | C18H17NO3 | 296.12812 | 313.15467 | 318.11006 | | 8.31 | 99.0 | 4.0 | 8.9 | 90.5 | 5.0 | 14.1 |
| Isoxaflutole | C15H12F3NO4S | 360.05119 | 377.07774 | 382.03313 | | 6.91 | 94.0 | 4.4 | 10.3 | 87.4 | 7.3 | 17.1 |
| Isoxathion | C13H16NO4PS | 314.06104 | 331.08759 | 336.04299 | | 8.59 | 97.5 | 4.0 | 9.2 | 91.5 | 3.7 | 11.4 |
| Ivermectin B1a | C48H74O14 | 875.51513 | 892.54168 | 897.49708 | | 10.50 | 96.3 | 5.5 | 12.2 | 88.2 | 19.6 | 39.3 |
| Kresoxim-methyl | C18H19NO4 | 314.13868 | 331.16523 | 336.12063 | | 8.33 | 97.8 | 5.6 | 12.0 | 92.4 | 7.2 | 17.2 |
| Lactofen | C19H15ClF3NO7 | 462.05619 | 479.08274 | 484.03814 | | 9.17 | 95.2 | 4.6 | 10.0 | 88.9 | 4.3 | 12.6 |
| Lambda-cyhalothrin | C23H19ClF3NO3 | 450.10783 | 467.13438 | 472.08978 | | 9.70 | 95.5 | 6.4 | 19.3 | 90.6 | 7.1 | 26.8 |
| Linuron | C9H10Cl2N2O2 | 249.01921 | 266.04576 | 271.00115 | | 7.41 | 98.9 | 3.5 | 8.1 | 93.2 | 3.7 | 10.2 |
| Lufenuron | C17H8Cl2F8N2O3 | 510.98570 | 528.01225 | 532.96764 | | 9.24 | 96.3 | 7.4 | 29.4 | 86.1 | 12.2 | 37.3 |
| Malathion | C10H19O6PS2 | 331.04334 | 348.06989 | 353.02529 | | 7.66 | 100.0 | 4.2 | 9.3 | 93.7 | 4.8 | 9.7 |
| Malathion O-analog | C10H19O7PS | 315.06619 | 332.09274 | 337.04813 | | 6.15 | 98.4 | 3.9 | 7.9 | 94.9 | 3.5 | 7.5 |
| Mandipropamid | C23H22ClNO4 | 412.13101 | 429.15756 | 434.11296 | | 7.58 | 99.3 | 4.1 | 9.3 | 90.5 | 6.1 | 14.6 |
| Mefenacet | C16H14N2O2S | 299.08488 | 316.11142 | 321.06682 | | 7.81 | 96.9 | 4.0 | 8.1 | 91.8 | 4.1 | 10.5 |
| Mefluidide | C11H13F3N2O3S | 311.06717 | 328.09372 | 333.04912 | | 6.12 | 95.8 | 4.4 | 9.9 | 90.4 | 3.8 | 9.9 |
| Mepanipyrim | C14H13N3 | 224.11822 | 241.14477 | 246.10017 | | 7.87 | 97.2 | 4.1 | 8.4 | 91.1 | 4.1 | 11.7 |
| Mephosfolan | C8H16NO3PS2 | 270.03820 | 287.06475 | 292.02014 | | 5.96 | 98.2 | 3.7 | 8.0 | 95.6 | 3.8 | 8.6 |
| Mepronil | C17H19NO2 | 270.14886 | 287.17540 | 292.13080 | | 7.67 | 98.7 | 4.2 | 9.2 | 93.0 | 4.2 | 11.1 |
| Mesotrione | C14H13NO7S | 340.04855 | 357.07510 | 362.03049 | | 4.94 | 64.0 | 7.5 | 25.1 | 66.2 | 8.5 | 32.9 |
| Metaflumizone | C24H16F6N4O2 | 507.12502 | 524.15157 | 529.10697 | | 9.18 | 99.1 | 6.4 | 15.5 | 93.9 | 6.3 | 16.6 |
| Metalaxyl | C15H21NO4 | 280.15433 | 297.18088 | 302.13628 | | 6.95 | 97.9 | 3.8 | 8.0 | 94.9 | 4.1 | 10.3 |
| Metazachlor | C14H16ClN3O | 278.10547 | 295.13202 | 300.08741 | | 6.85 | 97.0 | 3.9 | 8.4 | 94.2 | 3.8 | 9.5 |
| Metconazole | C17H22ClN3O | 320.15242 | 337.17897 | 342.13436 | | 8.63 | 96.7 | 4.1 | 8.9 | 88.5 | 5.3 | 13.8 |
| Methabenzthiazuron | C10H11N3OS | 222.06956 | 239.09611 | 244.05150 | | 6.75 | 97.1 | 3.5 | 7.2 | 93.8 | 3.3 | 8.8 |
| Methacrifos | C7H13O5PS | 241.02941 | 258.05596 | 263.01135 | | 6.75 | 98.2 | 4.6 | 9.6 | 96.8 | 5.6 | 12.5 |
| Methamidophos | C2H8NO2PS | 142.00861 | 159.03516 | 163.99056 | | 1.51 | 90.7 | 4.2 | 9.2 | 88.0 | 3.5 | 10.0 |
| Methidathion | C6H11N2O4PS3 | 302.96913 | 319.99568 | 324.95108 | 145.00663 | 7.03 | 99.2 | 4.1 | 9.5 | 95.0 | 5.0 | 11.6 |
| Methiocarb | C11H15NO2S | 226.08963 | 243.11618 | 248.07157 | 169.06816 | 7.51 | 99.8 | 3.7 | 7.5 | 86.8 | 11.3 | 26.9 |
| Methiocarb-sulfone | C11H15NO4S | 258.07946 | 275.10600 | 280.06140 | | 4.63 | 98.9 | 3.5 | 7.0 | 96.3 | 4.2 | 10.6 |
| Methiocarb-sulfoxide | C11H15NO3S | 242.08454 | 259.11109 | 264.06649 | | 4.26 | 99.4 | 3.1 | 13.1 | 100.7 | 3.6 | 22.9 |
| Methomyl | C5H10N2O2S | 163.05357 | 180.08012 | 185.03552 | 88.02209 | 3.11 | 106.5 | 5.0 | 10.3 | 106.2 | 6.0 | 13.4 |
| Methoprotryne | C11H21N5OS | 272.15396 | 289.18051 | 294.13590 | | 7.00 | 96.4 | 3.9 | 8.3 | 92.0 | 4.8 | 13.2 |
| Methoxyfenozide | C22H28N2O3 | 369.21727 | 386.24382 | 391.19921 | 313.15467 | 7.72 | 98.7 | 4.3 | 9.5 | 94.1 | 3.5 | 8.2 |
| Metobromuron | C9H11BrN2O2 | 259.00767 | 276.03422 | 280.98961 | | 6.67 | 97.8 | 3.5 | 8.0 | 94.1 | 3.4 | 8.6 |
| Metolachlor | C15H22ClNO2 | 284.14118 | 301.16773 | 306.12313 | | 8.30 | 97.1 | 3.7 | 8.1 | 92.7 | 3.6 | 11.6 |
| Metolcarb | C9H11NO2 | 166.08626 | 183.11280 | 188.06820 | | 5.64 | 99.8 | 4.2 | 8.9 | 97.7 | 6.0 | 12.8 |
| Metominostrobin | C16H16N2O3 | 285.12337 | 302.14992 | 307.10531 | | 7.11 | 99.3 | 4.0 | 8.3 | 94.9 | 4.0 | 10.0 |
| Metosulam | C14H13Cl2N5O4S | 418.01381 | 435.04036 | 439.99575 | | 6.14 | 94.8 | 4.7 | 11.4 | 89.5 | 5.4 | 14.1 |
| Metoxuron | C10H13ClN2O2 | 229.07383 | 246.10038 | 251.05578 | | 5.26 | 98.2 | 3.9 | 7.9 | 95.4 | 3.6 | 8.5 |
| Metrafenone | C19H21BrO5 | 409.06451 | 426.09106 | 431.04646 | | 8.69 | 96.5 | 4.0 | 9.2 | 91.0 | 4.8 | 13.9 |
| Metribuzin | C8H14N4OS | 215.09611 | 232.12266 | 237.07805 | | 5.92 | 96.2 | 4.4 | 10.6 | 91.5 | 7.8 | 17.5 |
| Mevinphos, cis- | C7H13O6P | 225.05225 | 242.07880 | 247.03420 | | 5.06 | 92.9 | 6.7 | 20.8 | 93.4 | 4.6 | 13.0 |
| Mexacarbate | C12H18N2O2 | 223.14410 | 240.17065 | 245.12605 | | 4.31 | 96.8 | 3.4 | 7.9 | 77.8 | 12.5 | 82.4 |
| Molinate | C9H17NOS | 188.11036 | 205.13691 | 210.09231 | | 7.80 | 96.5 | 3.7 | 8.1 | 92.8 | 3.7 | 9.0 |
| Monocrotophos | C7H14NO5P | 224.06824 | 241.09478 | 246.05018 | | 3.52 | 96.0 | 4.3 | 9.2 | 94.8 | 4.8 | 11.7 |
| Monolinuron | C9H11ClN2O2 | 215.05818 | 232.08473 | 237.04013 | | 6.40 | 97.8 | 3.5 | 8.6 | 94.9 | 4.2 | 9.3 |
| Moxidectin | C37H53NO8 | 640.38439 | 657.41094 | 662.36634 | | 10.33 | 97.4 | 7.3 | 16.7 | 93.3 | 6.3 | 14.6 |
| Myclobutanil | C15H17ClN4 | 289.12145 | 306.14800 | 311.10340 | | 7.84 | 97.8 | 4.3 | 9.5 | 93.2 | 4.4 | 10.5 |
| Naled | C4H7Br2Cl2O4P | 378.78985 | 395.81640 | 400.77180 | | 7.20 | 40.1 | 11.9 | 104.3 | | | |
| Napropamide | C17H21NO2 | 272.16451 | 289.19105 | 294.14645 | | 8.15 | 98.2 | 3.8 | 8.4 | 93.1 | 4.2 | 11.3 |
| Naptalam | C18H13NO3 | 292.09682 | 309.12337 | 314.07876 | 144.08078 | 6.13 | 54.0 | 12.5 | 35.1 | 54.8 | 9.8 | 42.6 |
| Neburon | C12H16Cl2N2O | 275.07125 | 292.09779 | 297.05319 | | 8.39 | 98.3 | 3.9 | 9.0 | 91.4 | 4.2 | 11.6 |
| Nitenpyram | C11H15ClN4O2 | 271.09563 | 288.12218 | 293.07757 | | 3.02 | 45.8 | 5.8 | 201.3 | | | |
| Nitralin | C13H19N3O6S | 346.10673 | 363.13328 | 368.08868 | | 8.32 | 97.5 | 5.6 | 11.9 | 91.6 | 5.5 | 13.9 |
| Norflurazon | C12H9ClF3N3O | 304.04590 | 321.07245 | 326.02785 | | 7.08 | 97.7 | 3.5 | 7.9 | 93.9 | 5.8 | 15.2 |
| Novaluron | C17H9ClF8N2O4 | 493.01959 | 510.04614 | 515.00153 | | 9.02 | 97.8 | 4.0 | 17.1 | 88.9 | 7.2 | 18.1 |


dx.doi.org/10.1021/jf503778c | J. Agric. Food Chem. 2014, 62, 10375−10391

**Table 1. continued**

| Pesticides | Molecular formula | Precursor Exact mass[a] [M + H]+ | [M + NH4]+ | [M + Na]+ | Fragements or ions used for quantification[b] | Retention Time | Fruits[f] Overall recovery[c] (%) | Intermediate precision[d] (%) | Measurement uncertainty[e] (%) | Vegetables[f] Overall recovery[c] (%) | Intermediate precision[d] (%) | Measurement uncertainty[e] (%) |
|---|---|---|---|---|---|---|---|---|---|---|---|---|
| 1[g] | 2 | 3 | 4 | 5 | 7 | 8 | 9 | 10 | 11 | 12 | 13 | 14 |
| Noviflumuron | C17H7Cl2F9N2O3 | 528.97628 | 546.00283 | 550.95822 | | 9.47 | 100.5 | 7.3 | 16.6 | 93.3 | 5.7 | 17.1 |
| Nuarimol | C17H12ClFN2O | 315.06950 | 332.09604 | 337.05144 | | 7.57 | 97.2 | 4.0 | 8.8 | 92.4 | 5.3 | 13.9 |
| Octhilinone | C11H19NOS | 214.12601 | 231.15256 | 236.10796 | | 8.23 | 73.0 | 9.6 | 57.4 | 62.7 | 14.1 | 56.6 |
| Ofurace | C14H16ClNO3 | 282.08915 | 299.11570 | 304.07109 | | 6.19 | 99.7 | 3.8 | 7.6 | 93.7 | 2.8 | 10.2 |
| Omethoate | C5H12NO4PS | 214.02974 | 231.05629 | 236.01169 | | 2.20 | 103.3 | 7.4 | 15.4 | 104.6 | 24.4 | 50.5 |
| Orbencarb | C12H16ClNOS | 258.07139 | 275.09794 | 280.05333 | | 8.75 | 96.6 | 3.6 | 9.8 | 87.3 | 5.4 | 11.4 |
| Oryzalin | C12H18N4O6S | 347.10198 | 364.12853 | 369.08393 | | 8.16 | 97.5 | 7.9 | 15.8 | 93.2 | 9.3 | 18.6 |
| Oxadiazon | C15H18Cl2N2O3 | 345.07672 | 362.10327 | 367.05867 | | 9.38 | 97.4 | 3.8 | 8.6 | 87.1 | 8.8 | 24.8 |
| Oxadixyl | C14H18N2O4 | 279.13393 | 296.16048 | 301.11588 | | 5.68 | 98.6 | 3.6 | 8.2 | 95.8 | 4.8 | 10.4 |
| Oxamyl | C7H13N3O3S | 220.07504 | 237.10159 | 242.05698 | | 3.00 | 98.5 | 4.7 | 9.5 | 98.9 | 5.5 | 14.7 |
| Oxamyl-oxime | C5H10N2O2S | 163.05357 | 180.08012 | 185.03552 | | 2.24 | 96.6 | 4.2 | 9.2 | 94.2 | 3.5 | 11.2 |
| Oxycarboxin | C12H13NO4S | 268.06381 | 285.09035 | 290.04575 | | 4.85 | 97.9 | 4.3 | 10.5 | 97.0 | 3.7 | 8.8 |
| Oxydemeton-methyl | C6H15O4PS2 | 247.02221 | 264.04876 | 269.00416 | | 3.21 | 95.6 | 4.2 | 9.6 | 94.6 | 4.6 | 10.4 |
| Paclobutrazol | C15H20ClN3O | 294.13677 | 311.16332 | 316.11871 | | 7.77 | 98.8 | 4.3 | 9.2 | 94.0 | 4.6 | 11.6 |
| Pebulate | C10H21NOS | 204.14166 | 221.16821 | 226.12361 | | 8.81 | 95.4 | 4.0 | 10.4 | 89.4 | 4.3 | 10.7 |
| Penconazole | C13H15Cl2N3 | 284.07158 | 301.09813 | 306.05352 | | 8.54 | 96.2 | 3.9 | 8.1 | 89.8 | 4.3 | 11.4 |
| Pencycuron | C19H21ClN2O | 329.14152 | 346.16807 | 351.12346 | | 8.82 | 96.3 | 3.7 | 8.4 | 90.1 | 4.0 | 12.4 |
| Pendimethalin | C13H19N3O4 | 282.14483 | 299.17138 | 304.12678 | | 9.57 | 97.1 | 4.9 | 12.7 | 88.8 | 8.5 | 19.0 |
| Penoxsulam | C16H14F5N5O5S | 484.07086 | 501.09741 | 506.05280 | | 6.48 | 99.3 | 5.7 | 18.0 | 94.4 | 6.0 | 12.1 |
| Permethrin, cis- | C21H20Cl2O3 | 391.08623 | 408.11278 | 413.06817 | | 10.24 | 89.2 | 8.8 | 18.5 | 81.8 | 9.0 | 21.2 |
| Permethrin, trans | C21H20Cl2O3 | 391.08623 | 408.11278 | 413.06817 | | 10.06 | 90.2 | 5.7 | 17.1 | 77.0 | 5.8 | 36.3 |
| Phenmedipham | C16H16N2O4 | 301.11828 | 318.14483 | 323.10023 | | 7.20 | 97.6 | 10.2 | 21.3 | 91.9 | 5.8 | 12.7 |
| Phenothrin | C23H26O3 | 351.19547 | 368.22202 | 373.17742 | | 10.22 | 89.3 | 5.9 | 15.6 | 79.2 | 9.8 | 30.9 |
| Phenthoate | C12H17O4PS2 | 321.03786 | 338.06441 | 343.01981 | | 8.39 | 99.5 | 7.4 | 14.8 | 93.2 | 7.0 | 18.0 |
| Phorate | C7H17O2PS3 | 261.02010 | 278.04665 | 283.00205 | | 8.73 | 95.7 | 7.0 | 15.0 | 85.5 | 10.0 | 24.4 |
| Phorate-sulfone | C7H17O4PS3 | 293.00993 | 310.03648 | 314.99188 | | 6.85 | 99.3 | 3.7 | 8.2 | 96.3 | 3.9 | 10.4 |
| Phosalone | C12H15ClNO4PS2 | 367.99414 | 385.02069 | 389.97608 | | 8.72 | 99.0 | 3.4 | 8.8 | 90.3 | 5.7 | 15.0 |
| Phosmet | C11H12NO4PS2 | 318.00181 | 335.02836 | 339.98376 | | 7.27 | 98.5 | 3.3 | 7.3 | 95.3 | 4.7 | 13.3 |
| Phosphamidon | C10H19ClNO5P | 300.07621 | 317.10276 | 322.05816 | | 5.75 | 98.2 | 4.0 | 8.8 | 94.6 | 4.7 | 10.7 |
| Phoxim | C12H15N2O3PS | 299.06138 | 316.08793 | 321.04332 | | 8.39 | 96.9 | 14.7 | 29.5 | | | |
| Picolinafen | C19H12F4N2O2 | 377.09077 | 394.11732 | 399.07271 | | 9.29 | 96.1 | 3.9 | 11.3 | 91.6 | 3.8 | 12.3 |
| Picoxystrobin | C18H16F3NO4 | 368.11042 | 385.13697 | 390.09236 | 205.08592 | 8.35 | 99.0 | 5.7 | 11.8 | 93.0 | 4.5 | 12.3 |
| Pinoxaden | C23H32N2O4 | 401.24348 | 418.27003 | 423.22543 | | 8.84 | 56.9 | 6.6 | 106.2 | | | |
| Piperonyl butoxide | C19H30O5 | 339.21660 | 356.24315 | 361.19855 | | 9.34 | 96.7 | 4.8 | 10.0 | 88.8 | 4.9 | 14.0 |
| Piperophos | C14H28NO3PS2 | 354.13210 | 371.15865 | 376.11404 | | 8.93 | 97.4 | 4.3 | 9.3 | 91.1 | 4.7 | 12.9 |
| Pirimicarb | C11H18N4O2 | 239.15025 | 256.17680 | 261.13220 | | 5.59 | 96.9 | 3.8 | 8.5 | 94.4 | 4.1 | 10.3 |
| Pirimiphos-ethyl | C13H24N3O3PS | 334.13488 | 351.16142 | 356.11682 | | 9.27 | 95.0 | 4.2 | 9.5 | 89.8 | 4.0 | 12.7 |
| Pirimiphos-methyl | C11H20N3O3PS | 306.10358 | 323.13012 | 328.08552 | | 8.70 | 95.6 | 4.3 | 9.8 | 89.7 | 4.1 | 12.2 |
| Pretilachlor | C17H26ClNO2 | 312.17248 | 329.19903 | 334.15443 | | 9.07 | 97.1 | 3.7 | 8.1 | 91.0 | 4.1 | 12.3 |
| Probenazole | C10H9NO3S | 224.03759 | 241.06414 | 246.01954 | | 5.77 | 96.8 | 3.8 | 25.7 | 87.0 | 3.8 | 9.8 |
| Prochloraz | C15H16Cl3N3O2 | 376.03809 | 393.06464 | 398.02003 | | 8.68 | 93.6 | 4.3 | 9.2 | 86.6 | 5.4 | 15.8 |
| Prodiamine | C13H17F3N4O4 | 351.12747 | 368.15402 | 373.10941 | | 9.42 | 97.2 | 5.2 | 11.7 | 91.0 | 6.4 | 15.9 |
| Profenophos | C11H15BrClO3PS | 372.94242 | 389.96897 | 394.92436 | | 9.21 | 96.2 | 4.5 | 10.3 | 88.1 | 4.6 | 13.2 |
| Promecarb | C12H17NO2 | 208.13321 | 225.15975 | 230.11515 | | 7.78 | 99.9 | 4.1 | 8.1 | 95.2 | 4.1 | 10.7 |
| Prometon | C10H19N5O | 226.16624 | 243.19279 | 248.14818 | | 6.50 | 96.9 | 4.4 | 8.8 | 92.8 | 4.6 | 10.7 |
| Prometryn | C10H19N5S | 242.14339 | 259.16994 | 264.12534 | | 7.61 | 95.5 | 8.6 | 18.1 | 88.2 | 7.2 | 15.6 |
| Propachlor | C11H14ClNO | 212.08367 | 229.11022 | 234.06561 | | 6.92 | 98.0 | 3.5 | 7.6 | 95.5 | 3.6 | 8.7 |
| Propamocarb | C9H20N2O2 | 189.15975 | 206.18630 | 211.14170 | | 2.50 | 86.5 | 4.1 | 12.5 | 87.4 | 4.6 | 11.5 |
| Propanil | C9H9Cl2NO | 218.01340 | 235.03995 | 239.99534 | | 7.46 | 98.3 | 4.2 | 9.3 | 89.2 | 6.2 | 20.5 |
| Propargite | C19H26O4S | 351.16246 | 368.18901 | 373.14440 | | 9.54 | 96.7 | 5.1 | 10.2 | 92.0 | 5.7 | 14.0 |
| Propazine | C9H16ClN5 | 230.11670 | 247.14325 | 252.09864 | | 7.44 | 98.1 | 3.6 | 7.3 | 92.2 | 4.0 | 10.9 |
| Propetamphos | C10H20NO4PS | 282.09234 | 299.11889 | 304.07429 | | 7.82 | 98.1 | 5.9 | 13.9 | 94.2 | 8.4 | 19.1 |
| Propiconazole | C15H17Cl2N3O2 | 342.07706 | 359.10361 | 364.05900 | | 8.52 | 96.5 | 7.6 | 15.3 | 90.3 | 6.8 | 16.3 |
| Propisochlor | C15H22ClNO2 | 284.14118 | 301.16773 | 306.12313 | | 8.55 | 98.3 | 4.5 | 9.0 | 91.2 | 5.0 | 14.3 |
| Propoxur | C11H15NO3 | 210.11247 | 227.13902 | 232.09441 | 168.06552 | 6.02 | 99.5 | 3.1 | 8.5 | 96.8 | 4.1 | 8.3 |
| Pymetrozine | C10H11N5O | 218.10364 | 235.13019 | 240.08558 | | 1.86 | 83.5 | 3.8 | 22.9 | 86.6 | 5.4 | 21.6 |
| Pyracarbolid | C13H15NO2 | 218.11756 | 235.14410 | 240.09950 | | 6.08 | 97.1 | 4.0 | 8.6 | 92.5 | 3.3 | 8.6 |
| Pyraclofos | C14H18ClN2O3PS | 361.05370 | 378.08025 | 383.03565 | | 8.59 | 97.3 | 3.6 | 8.8 | 91.2 | 5.1 | 14.0 |
| Pyraclostrobin | C19H18ClN3O4 | 388.10586 | 405.13241 | 410.08781 | | 8.54 | 97.8 | 4.0 | 8.8 | 92.1 | 4.1 | 13.0 |
| Pyraflufen-ethyl | C15H13Cl2F3N2O4 | 413.02772 | 430.05427 | 435.00967 | | 8.45 | 96.8 | 3.4 | 11.1 | 74.2 | 5.0 | 97.3 |
| Pyrasulfotole | C14H13F3N2O4S | 363.06209 | 380.08864 | 385.04403 | | 5.30 | 71.9 | 15.5 | 33.2 | 74.3 | 6.5 | 22.9 |
| Pyrazophos | C14H20N3O5PS | 374.09340 | 391.11995 | 396.07535 | | 8.57 | 97.5 | 3.7 | 10.9 | 91.8 | 5.8 | 17.1 |
| Pyridaben | C19H25ClN2OS | 365.14489 | 382.17144 | 387.12683 | | 9.87 | 93.3 | 4.5 | 10.3 | 88.4 | 4.8 | 14.7 |
| Pyridalyl | C18H14Cl4F3NO3 | 489.97527 | 507.00181 | 511.95721 | | 10.56 | 80.9 | 7.1 | 22.4 | 71.8 | 7.7 | 18.7 |
| Pyridaphenthion | C14H17N2O4PS | 341.07194 | 358.09849 | 363.05389 | | 7.79 | 97.6 | 4.4 | 8.9 | 93.5 | 4.3 | 10.8 |
| Pyridate | C19H23ClN2O2S | 379.12415 | 396.15070 | 401.10610 | | 10.10 | 51.6 | 7.5 | 140.8 | | | |
| Pyrifenox | C14H12Cl2N2O | 295.03995 | 312.06649 | 317.02189 | | 7.87 | 84.7 | 4.3 | 45.7 | 78.2 | 8.5 | 38.0 |
| Pyrimethanil | C12H13N3 | 200.11822 | 217.14477 | 222.10017 | | 7.10 | 96.6 | 3.9 | 7.8 | 91.1 | 4.1 | 11.7 |
| Pyriproxyfen | C20H19NO3 | 322.14377 | 339.17032 | 344.12571 | | 9.27 | 95.5 | 4.1 | 9.3 | 86.0 | 8.1 | 18.6 |
| Pyroquilon | C11H11NO | 174.09134 | 191.11789 | 196.07329 | | 5.89 | 95.6 | 3.6 | 8.1 | 94.2 | 3.8 | 8.5 |
| Pyroxsulam | C14H13F3N6O5S | 435.06930 | 452.09585 | 457.05124 | | 5.94 | 92.6 | 4.6 | 10.0 | 90.9 | 5.6 | 12.2 |
| Quinalphos | C12H15N2O3PS | 299.06138 | 316.08793 | 321.04332 | | 8.28 | 97.8 | 3.9 | 8.7 | 91.9 | 4.8 | 12.8 |
| Quinoclamine | C10H6ClNO2 | 208.01598 | 225.04253 | 229.99793 | | 5.63 | 97.3 | 3.3 | 9.1 | 93.6 | 3.5 | 9.9 |
| Quinoxyfen | C15H8Cl2FNO | 308.00397 | 325.03052 | 329.98592 | | 9.41 | 95.1 | 3.9 | 10.5 | 87.9 | 4.1 | 13.3 |
| Quizalofop | C17H13ClN2O4 | 345.06366 | 362.09021 | 367.04561 | | 8.19 | 62.3 | 9.7 | 26.3 | 66.4 | 9.9 | 37.2 |


dx.doi.org/10.1021/jf503778c | J. Agric. Food Chem. 2014, 62, 10375−10391

**Table 1. continued**

| Pesticides | Molecular formula | Precursor Exact mass[a] | | | Fragements or ions used for quantification[b] | Retention Time | Fruits[f] | | | Vegetables[f] | | |
|---|---|---|---|---|---|---|---|---|---|---|---|---|
| | | $[M+H]^+$ | $[M+NH_4]^+$ | $[M+Na]^+$ | | | Overall recovery[c] (%) | Intermediate precision[d] (%) | Measurement uncertainty[e] (%) | Overall recovery[c] (%) | Intermediate precision[d] (%) | Measurement uncertainty[e] (%) |
| 1[g] | 2 | 3 | 4 | 5 | 7 | 8 | 9 | 10 | 11 | 12 | 13 | 14 |
| Quizalofop-ethyl | C19H17ClN2O4 | 373.09496 | 390.12151 | 395.07691 | | 9.05 | 97.2 | 3.5 | 7.8 | 78.5 | 5.0 | 50.4 |
| Resmethrin | C22H26O3 | 339.19547 | 356.22202 | 361.17742 | | 10.02 | 91.6 | 4.9 | 15.1 | 77.3 | 6.7 | 39.5 |
| Rotenone | C23H22O6 | 395.14892 | 412.17546 | 417.13086 | | 8.15 | 95.3 | 4.2 | 8.7 | 90.0 | 4.2 | 11.0 |
| Saflufenacil | C17H17ClF4N4O5S | 501.06171 | 518.08826 | 523.04365 | | 7.21 | 100.0 | 7.0 | 15.2 | 94.8 | 11.3 | 24.4 |
| Schradan | C8H24N4O3P2 | 287.13964 | 304.16619 | 309.12158 | | 4.98 | 93.2 | 3.8 | 8.6 | 90.7 | 3.9 | 10.5 |
| Secbumeton | C10H19N5O | 226.16624 | 243.19279 | 248.14818 | | 6.54 | 97.5 | 4.2 | 8.4 | 92.5 | 4.6 | 10.9 |
| Sethoxydim | C17H29NO3S | 328.19409 | 345.22064 | 350.17604 | | 9.14 | 93.5 | 4.4 | 8.8 | 83.6 | 6.2 | 15.2 |
| Siduron | C14H20N2O | 233.16484 | 250.19139 | 255.14678 | | 7.44 | 97.5 | 3.6 | 7.3 | 92.2 | 4.3 | 9.6 |
| Simazine | C7H12ClN5 | 202.08540 | 219.11195 | 224.06734 | | 6.00 | 97.3 | 3.9 | 10.0 | 94.8 | 3.4 | 8.3 |
| Simeconazole | C14H20FN3OSi | 294.14324 | 311.16979 | 316.12519 | | 8.08 | 98.1 | 4.6 | 9.7 | 92.2 | 4.3 | 10.9 |
| Spinetoram | C42H69NO10 | 748.49942 | 765.52597 | 770.48137 | | 8.90 | 85.5 | 4.9 | 14.5 | 81.9 | 5.5 | 15.4 |
| Spinosyn A | C41H65NO10 | 732.46812 | 749.49467 | 754.45007 | | 8.62 | 89.5 | 5.2 | 11.2 | 84.7 | 4.8 | 11.6 |
| Spinosyn D | C42H67NO10 | 746.48377 | 763.51032 | 768.46572 | | 8.88 | 88.3 | 6.4 | 12.8 | 83.8 | 6.3 | 14.2 |
| Spirodiclofen | C21H24Cl2O4 | 411.11244 | 428.13899 | 433.09439 | | 9.69 | 84.6 | 5.8 | 24.7 | 73.5 | 6.8 | 27.7 |
| Spiromesifen | C23H30O4 | 371.22169 | 388.24824 | 393.20363 | 273.14852 | 9.53 | 80.7 | 5.1 | 39.8 | 69.1 | 5.3 | 54.0 |
| Spirotetramat | C21H27NO5 | 374.19620 | 391.22275 | 396.17814 | | 7.94 | 93.8 | 4.4 | 8.9 | 84.8 | 7.5 | 19.9 |
| Spiroxamine | C18H35NO2 | 298.27406 | 315.30061 | 320.25600 | | 7.68 | 83.9 | 5.5 | 11.9 | 76.9 | 6.0 | 13.3 |
| Sulcotrione | C14H13ClO5S | 329.02450 | 346.05105 | 351.00644 | | 5.60 | 56.8 | 9.7 | 30.0 | 53.3 | 11.8 | 42.3 |
| Sulfentrazone | C11H10Cl2F2N4O3S | 386.98915 | 404.01570 | 408.97109 | | 6.28 | 102.8 | 5.6 | 15.3 | 96.4 | 5.8 | 13.2 |
| Sulfotep | C8H20O5P2S2 | 323.03001 | 340.05656 | 345.01196 | | 8.39 | 97.3 | 4.0 | 9.0 | 91.1 | 3.6 | 12.3 |
| Sulprofos | C12H19O2PS3 | 323.03576 | 340.06230 | 345.01770 | | 9.45 | 90.7 | 3.5 | 13.5 | 83.7 | 6.3 | 17.1 |
| Tau-fluvalinate | C26H22ClF3N2O3 | 503.13438 | 520.16093 | 525.11633 | | 10.00 | 90.7 | 7.0 | 14.7 | 84.3 | 6.6 | 16.4 |
| Tebuconazole | C16H22ClN3O | 308.15242 | 325.17897 | 330.13436 | | 8.46 | 97.0 | 4.1 | 8.3 | 91.4 | 4.8 | 11.8 |
| Tebufenozide | C22H28N2O2 | 353.22235 | 370.24890 | 375.20430 | | 8.26 | 95.7 | 5.1 | 10.5 | 89.2 | 7.2 | 25.0 |
| Tebufenpyrad | C18H24ClN3O | 334.16807 | 351.19462 | 356.15001 | | 9.18 | 97.9 | 5.3 | 11.8 | 90.8 | 4.1 | 12.1 |
| Tebupirimfos | C13H23N2O3PS | 319.12398 | 336.15053 | 341.10592 | | 9.25 | 96.7 | 4.3 | 9.4 | 89.7 | 3.5 | 12.4 |
| Tebuthiuron | C9H16N4OS | 229.11176 | 246.13831 | 251.09370 | | 6.18 | 96.5 | 3.9 | 7.8 | 92.5 | 3.2 | 7.7 |
| Teflubenzuron | C14H6Cl2F4N2O2 | 380.98152 | 398.00807 | 402.96347 | | 9.34 | 100.5 | 6.9 | 18.1 | 85.6 | 12.7 | 40.2 |
| Tembotrione | C17H16ClF3O6S | 441.03810 | 458.06465 | 463.02004 | | 7.02 | 73.8 | 7.5 | 18.2 | 72.6 | 8.8 | 26.0 |
| Temephos | C16H20O6P2S3 | 466.99700 | 484.02355 | 488.97894 | | 9.20 | 93.5 | 4.2 | 11.4 | 90.7 | 4.9 | 13.7 |
| Tepraloxydim | C17H24ClNO4 | 342.14666 | 359.17321 | 364.12861 | | 7.89 | 105.9 | 5.1 | 12.7 | 101.6 | 4.6 | 12.8 |
| Terbacil | C9H13ClN2O2 | 217.07383 | 234.10038 | 239.05578 | | 6.19 | 97.6 | 7.7 | 19.5 | 93.6 | 10.3 | 21.8 |
| Terbufos | C9H21O2PS3 | 289.05141 | 306.07795 | 311.03335 | | 8.43 | 95.7 | 24.9 | 50.8 | 89.9 | 4.1 | 10.2 |
| Terbufos-sulfone | C9H21O4PS3 | 321.04123 | 338.06778 | 343.02318 | | 7.37 | 98.3 | 3.8 | 8.3 | 94.6 | 3.6 | 9.0 |
| Terbumeton | C10H19N5O | 226.16624 | 243.19279 | 248.14818 | | 6.63 | 97.2 | 3.9 | 8.1 | 92.1 | 3.9 | 11.1 |
| Terbuthylazine | C9H16ClN5 | 230.11670 | 247.14325 | 252.09864 | | 7.58 | 96.9 | 8.0 | 16.3 | 85.7 | 8.7 | 23.1 |
| Terbutryn | C10H19N5S | 242.14339 | 259.16994 | 264.12534 | | 7.68 | 97.4 | 3.9 | 9.8 | 89.9 | 3.7 | 10.6 |
| Tetrachlorvinphos | C10H9Cl4O4P | 364.90653 | 381.93308 | 386.88848 | | 8.31 | 98.9 | 4.0 | 9.1 | 90.9 | 4.8 | 10.0 |
| Tetraconazole | C13H11Cl2F4N3O | 372.02881 | 389.05536 | 394.01075 | | 8.08 | 99.4 | 5.3 | 11.0 | 93.3 | 4.6 | 12.3 |
| Tetramethrin | C19H25NO4 | 332.18563 | 349.21218 | 354.16758 | | 9.16 | 97.7 | 3.9 | 9.6 | 88.5 | 5.0 | 17.3 |
| Thiabendazole | C10H7N3S | 202.04334 | 219.06989 | 224.02529 | | 3.70 | 99.6 | 3.9 | 7.8 | 95.7 | 2.9 | 6.4 |
| Thiacloprid | C10H9ClN4S | 253.03092 | 270.05747 | 275.01287 | | 4.90 | 97.2 | 4.0 | 9.8 | 96.4 | 3.9 | 8.5 |
| Thiamethoxam | C8H10ClN5O3S | 292.02656 | 309.05311 | 314.00851 | | 3.31 | 94.6 | 4.6 | 10.5 | 95.1 | 4.0 | 10.0 |
| Thiazopyr | C16H17F5N2O2S | 397.10037 | 414.12692 | 419.08231 | | 8.41 | 99.0 | 4.0 | 9.2 | 93.2 | 4.3 | 12.9 |
| Thidiazuron | C9H8N4OS | 221.04916 | 238.07571 | 243.03110 | | 5.95 | 90.8 | 4.6 | 11.6 | 87.4 | 5.2 | 13.4 |
| Thiodicarb | C10H18N4O4S3 | 355.05629 | 372.08284 | 377.03824 | | 6.42 | 79.5 | 6.7 | 30.6 | | | |
| Thiofanox-sulfone | C9H18N2O4S | 251.10600 | 268.13255 | 273.08795 | | 4.06 | 98.4 | 4.4 | 9.1 | 96.9 | 5.5 | 13.1 |
| Thiofanox-sulfoxide | C9H18N2O3S | 235.11109 | 252.13764 | 257.09303 | | 4.28 | 96.0 | 4.7 | 9.5 | 96.1 | 7.6 | 16.6 |
| Thionazin | C8H13N2O3PS | 249.04573 | 266.07228 | 271.02767 | | 6.90 | 98.5 | 3.7 | 8.1 | 95.7 | 3.4 | 8.3 |
| Tolclofos-methyl | C9H11Cl2O3PS | 300.96163 | 317.98818 | 322.94358 | | 8.67 | 97.6 | 4.4 | 12.3 | 87.6 | 6.1 | 18.7 |
| Tolfenpyrad | C21H22ClN3O2 | 384.14733 | 401.17388 | 406.12928 | | 9.21 | 95.0 | 4.1 | 11.8 | 90.8 | 4.6 | 13.8 |
| Tralkoxydim | C20H27NO3 | 330.20637 | 347.23292 | 352.18832 | | 9.39 | 96.3 | 5.0 | 12.2 | 87.7 | 4.8 | 13.6 |
| Tralomethrin | C22H19Br4NO3 | 661.81712 | 678.84367 | 683.79907 | 682.83959 | 10.08 | 83.4 | 4.9 | 29.1 | 73.4 | 9.5 | 25.8 |
| Triadimefon | C14H16ClN3O2 | 294.10038 | 311.12693 | 316.08233 | | 7.81 | 98.3 | 4.1 | 8.3 | 93.5 | 4.6 | 10.3 |
| Triadimenol | C14H18ClN3O2 | 296.11603 | 313.14258 | 318.09798 | | 7.93 | 97.6 | 5.3 | 13.4 | 96.6 | 5.2 | 13.2 |
| Tri-allate | C10H16Cl3NOS | 304.00909 | 321.03564 | 325.99104 | | 9.52 | 94.1 | 4.7 | 11.1 | 85.5 | 5.3 | 13.8 |
| Triazophos | C12H16N3O3PS | 314.07228 | 331.09882 | 336.05422 | | 7.84 | 98.9 | 4.6 | 9.2 | 93.4 | 3.9 | 10.8 |
| Tribufos | C12H27OPS3 | 315.10344 | 332.12999 | 337.08539 | | 9.91 | 94.0 | 4.5 | 10.1 | 87.1 | 4.7 | 15.5 |
| Trichlorfon | C4H8Cl3O4P | 256.92985 | 273.95640 | 278.91180 | | 4.38 | 101.9 | 3.9 | 13.1 | 102.1 | 3.2 | 23.7 |
| Tricyclazole | C9H7N3S | 190.04334 | 207.06989 | 212.02529 | | 5.15 | 94.0 | 4.1 | 9.1 | 93.6 | 3.8 | 9.6 |
| Trietazine | C9H16ClN5 | 230.11670 | 247.14325 | 252.09864 | | 8.01 | 97.7 | 4.0 | 8.0 | 92.1 | 3.8 | 11.6 |
| Trifloxystrobin | C20H19F3N2O4 | 409.13697 | 426.16352 | 431.11891 | | 8.90 | 97.3 | 4.3 | 9.1 | 91.7 | 4.1 | 12.6 |
| Trifloxysulfuron | C14H14F3N5O6S | 438.06897 | 455.09551 | 460.05091 | | 6.78 | 91.5 | 4.7 | 11.8 | 86.3 | 6.5 | 15.2 |
| Triflumizole | C15H15ClF3N3O | 346.09285 | 363.11940 | 368.07480 | | 9.01 | 93.0 | 4.1 | 8.9 | 86.4 | 8.0 | 18.9 |
| Triflumuron | C15H10ClF3N2O3 | 359.04048 | 376.06703 | 381.02243 | | 8.60 | 99.9 | 4.0 | 9.6 | 92.9 | 3.9 | 11.6 |
| Trifluralin | C13H16F3N3O4 | 336.11657 | 353.14312 | 358.09851 | | 9.61 | 93.1 | 6.2 | 14.0 | 86.8 | 7.7 | 20.5 |
| Triforine | C10H14Cl6N4O2 | 432.93207 | 449.95862 | 454.91401 | | 7.30 | 97.2 | 6.3 | 17.3 | 83.2 | 15.8 | 43.6 |
| Trimethacarb | C11H15NO2 | 194.11756 | 211.14410 | 216.09950 | 137.09609 | 7.09 | 99.8 | 3.5 | 7.6 | 97.3 | 4.5 | 11.1 |
| Trinexapac-ethyl | C13H16O5 | 253.10705 | 270.13360 | 275.08899 | | 7.00 | 83.4 | 12.4 | 29.7 | 84.6 | 23.5 | 57.4 |
| Triticonazole | C17H20ClN3O | 318.13677 | 335.16332 | 340.11871 | | 8.00 | 96.6 | 5.5 | 11.1 | 90.7 | 5.5 | 12.2 |
| Uniconazole | C15H18ClN3O | 292.12112 | 309.14767 | 314.10306 | | 8.25 | 96.9 | 5.1 | 10.6 | 90.2 | 5.0 | 12.3 |
| Vamidothion | C8H18NO4PS2 | 288.04876 | 305.07531 | 310.03071 | | 4.41 | 96.4 | 3.9 | 8.4 | 94.4 | 4.0 | 10.5 |


dx.doi.org/10.1021/jf503778c | J. Agric. Food Chem. 2014, 62, 10375−10391

**Table 1. continued**

| Pesticides | Molecular formula | Precursor Exact mass[a] [M + H]+ | [M + NH4]+ | [M + Na]+ | Fragements or ions used for quantification[b] | Retention Time | Fruits[f] Overall recovery[c] (%) | Intermediate precision[d] (%) | Measurement uncertainty[e] (%) | Vegetables[f] Overall recovery[c] (%) | Intermediate precision[d] (%) | Measurement uncertainty[e] (%) |
|---|---|---|---|---|---|---|---|---|---|---|---|---|
| 1[g] | 2 | 3 | 4 | 5 | 7 | 8 | 9 | 10 | 11 | 12 | 13 | 14 |
| Warfarin | C19H16O4 | **309.11214** | 326.13868 | 331.09408 | | 7.54 | 96.4 | 4.5 | 8.9 | 84.5 | 10.5 | 24.4 |
| Zoxamide | C14H16Cl3NO2 | **336.03194** | 353.05849 | 358.01388 | | 8.53 | 97.6 | 3.8 | 9.5 | 92.1 | 4.6 | 13.1 |
| **Internal standards** | | | | | | | | | | | | |
| Carbendazim d4 (IS) | C9H5D4N3O2 | **196.10186** | 213.12841 | 218.08381 | | 3.20 | | | | | | |
| Carbofuran d3 (IS) | C12H12D3NO3 | **225.13130** | 242.15785 | 247.11325 | | 6.11 | | | | | | |
| Thiabendazole d4 (IS) | C10H3D4N3S | **206.06845** | 223.09500 | 228.05040 | | 3.70 | | | | | | |

[a]Numbers or text in bold font and underlined indicates ionization form or charge state for data processing or quantification. [b]Exact mass or measured accurate mass was used for quantification. The electron mass (0.000549 amu) is subtracted when exact mass is calculated. [c]Bold and underlined indicate pesticides with recoveries not in the range of 81−110%. [d]Bold and underlined indicate pesticides with intermediate precision >20%. [e]Bold and underlined indicate pesticides MU > 50%. [f]For data in red font, the method performance was based on three spike levels, i.e., 90.0, 240.0, and 400.0 μg/kg, due to its poor sensitivity. For data in blue font, the method performance was based on two spike levels, i.e., 240.0 and 400.0 μg/kg, due to its poor sensitivity. [g]Column number.

problem is liquid chromatography−mass spectrometry (LC-MS), which has been widely used to quantify LC-amenable (or thermally labile) pesticides and to confirm their identities in fruits and vegetables at low parts-per-billion (ppb) concentration levels.[7,8]

Liquid chromatography coupled with quadrupole tandem mass spectrometry with electrospray ionization (LC/ESI-MS/MS) as an interface is the most commonly used LC-MS system for pesticide residue analysis. This system configuration allows for increased selectivity and sensitivity when operated in multiple-reaction monitoring (MRM) mode. Current advances in mass spectrometers have made it possible to determine hundreds of targeted pesticides in a single analysis. However, LC-MS/MS requires extensive compound-dependent parameter optimization. Alternatively, an LC can be coupled to full scan mass spectrometers such as Orbitrap and time-of-flight (TOF) mass spectrometers. These types of MS have been increasingly used for quantification, identification, characterization, and structural elucidation of pharmaceuticals, pesticides, veterinary drugs, unknown contaminants, and their transformation or degradation products in foods and environmental samples.[9−12] The Orbitrap and TOF mass spectrometers (recently advanced models) offer high resolution (>20000 fwhm), accurate mass measurement (<5 ppm), excellent full MS scan sensitivity, and complete mass spectral information. The full MS scan data allow for the screening of targeted analytes, quantification of selected compounds, confirmation of positive findings, identification of unknowns or metabolites, and retrospective analysis even when appropriate standards are not available at the time of analysis.[13,14] Currently, a quadrupole Orbitrap (Q-Orbitrap) can easily achieve a resolving power >70000 fwhm for routine practice and still be sensitive enough to quantify at trace ppb concentration levels. The resolving power and accurate mass measurement capability of the Q-Orbitrap (<5 ppm) provide confidence in differentiating analytes of interest from coeluting compounds in complex matrices for both quantification and identification. Moreover, Q-Orbitrap MS/MS and QqTOF MS/MS, which have their quadruople filter function and collision cell enabled, can provide product-ion spectra with accurate mass measurements that permit unequivocal identification for compounds of interest. In routine practice, Orbitrap and TOF mass spectrometers operated in full MS scan mode have been favored for multiresidue screening purposes. If any incurred analytes are found, they are further identified using Q-Orbitrap MS/MS and QqTOF MS/MS.

This paper discusses the development and validation of a method that can rapidly quantify and accurately identify 451 pesticides in fruits and vegetables at low (∼10) ppb concentration levels using an UHPLC/ESI Q-Orbitrap along with the QuEChERs extraction procedure. The UHPLC/ESI Q-Orbitrap MS operated in full MS scan mode for screening and quantification was evaluated, and the UHPLC/ESI Q-Orbitrap Full MS/dd-$MS^2$ (i.e., data-dependent scan) mode for identification was demonstrated. The UHPLC/ESI Q-Orbitrap mass spectrometer proved to be a very promising and powerful tool for the determination of pesticide residues in fruits and vegetables. This is the first validated UHPLC/ESI Q-Orbitrap method to quantify 451 pesticide residues in fruits and vegetables. The method proved to be robust and sensitive enough to determine pesticide residues at low ppb concentration levels. The sample extraction was also quick and simple enough to allow for high-throughput testing of routine samples, which will greatly benefit monitoring programs while satisfying regulatory purposes.

## MATERIALS AND METHODS

**Materials and Reagents.** Five fruit and five vegetable blank samples were obtained from either local markets or previous years' sample monitoring program. Fruits included apple, banana, grape, orange, and strawberry. Vegetables included carrot, potato, tomato, broccoli, and lettuce. All samples were homogenized using a food processor, and 2 kg of each sample was prepared and kept in −20 °C. Pierce LTQ ESI positive ion calibration solution (10 mL) was purchased from ThermoFisher Scientific (Rockford, IL, USA). The calibration solution, which includes *n*-butylamine (*m*/*z* 74), caffeine (*m*/*z* 195 and its fragment *m*/*z* 138), Ultramark 1621 (*m*/*z* 1022, 1122, 1222, 1322, 1422, 1522, 1622, 1722, and 1822), and MRFA (*m*/*z* 524), was used to tune and calibrate the Q-Orbitrap. Ammonium acetate (reagent grade), formic acid (LC-MS grade, ∼98%), ammonium formate (for mass spectrometry, >99.0%), and LC-MS acetonitrile (Chromasolv, 2.5 L) were purchased from Sigma-Aldrich Corp (Canada). ENVIRO CLEAN MYLAR pouches (6.0 g of anhydrous magnesium sulfate ($MgSO_4$) and 1.5 g of anhydrous sodium acetate) and ENVIRO CLEAN extraction columns (900 mg of $MgSO_4$, 150 mg of $C_{18}$, and 300 mg of primary−secondary amine (PSA), 15 mL centrifuge tubes) were purchased from United Chemical Technologies, Inc. (Bristol, PA, USA). Acetic acid (glacial acetic acid, reagent grade, 99.7%), acetonitrile (distilled in glass), and methanol (distilled in glass) were obtained from Caledon Laboratories

Ltd. (Canada). Water (18.2 MΩ·cm) used for reagent and sample preparation was obtained from a Barnstead Nanopure system (Thermo Scientific, USA). Pesticide standards (Table 1, column 1) were obtained from EQ Laboratories Inc. (USA), Riedel-de Haen AG (Germany), or Chem Service (USA). Internal standards carbendazim-$d_4$ and carbofuran-$d_3$ were purchased from EQ Laboratories Inc. (USA), and thiabendazole-$d_4$ was from Chemical Synthesis Services (Northern Ireland). LC vials were Mini-UniPrep syringeless filter devices with polypropylene housing and PVDF 0.45 μm membrane (Whatman Inc., USA).

**Preparation of Standard Solutions.** Individual pesticide standard stock solutions were generally prepared at a concentration of 4000.0 μg/mL in methanol/acetonitrile (50 + 50, v/v). Due to their poor solubility in methanol, carbendazim was prepared at 200.0 μg/mL, and some pesticides were prepared at 1000.0 or 2000.0 μg/mL. Intermediate pesticide standard mix working solutions were prepared at 10.0 or 15.0 μg/mL in methanol/acetonitrile (50 + 50, v/v), from stock solutions. Because of the large number of pesticides (>450), intermediate solutions were prepared in separate 200 mL (15 μg/mL, including 210 stocks) and 250 mL (10 μg/mL, including 241 stocks) volumetric flasks. Stock and intermediate solutions were stored at −20 °C. A six-level pesticide standard mix working solution was prepared by transferring 0.15, 0.75, 3.0, 6.0, 9.0, and 15.0 mL of 10.0 μg/mL and 0.1, 0.5, 2.0, 4.0, 6.0, and 10.0 mL of 15.0 μg/mL intermediate working solution into six separate 50 mL volumetric flasks for their respective concentration levels and then making up to volume with methanol. The resulting concentrations were 0.03, 0.15, 0.60, 1.20, 1.80, and 3.00 μg/mL, which were used to construct the matrix-matched standard calibration curves. Four-level sample spike pesticide standard working solutions were prepared by transferring 1.5, 13.5, 36.0, and 60.0 mL of 10.0 μg/mL and 1.0, 9.0, 24.0, and 40.0 mL of 15.0 μg/mL intermediate working solution into four separate 100 mL volumetric flasks and making up to volume with methanol for their respective concentration levels. The resulting concentrations were 0.15, 1.35, 3.60, and 6.00 μg/mL, which were used for sample fortification. Internal standard working solutions (5.0 and 0.5 μg/mL) including carbofuran-$d_3$, carbendazim-$d_4$, and thiabendazole-$d_4$ were prepared in a mixture of methanol/acetonitrile (50 + 50, v/v). All working solutions were stored at 4 °C.

**Preparation of Reagent Solutions.** Acetonitrile/acetic acid (99 + 1, v/v) was prepared by mixing 990 mL of acetonitrile with 10 mL of acetic acid. Ammonium acetate (0.1 M) was prepared by weighing 7.7 g of ammonium acetate and dissolving it in 800 mL of water. After transfer into a 1000 mL volumetric flask, the solution was made up to volume with water. Solvent buffer was a mixture of 0.1 M ammonium acetate and methanol (50 + 50, v/v).

**UHPLC/ESI Q-Orbitrap Parameters.** The UHPLC/ESI Q-Orbitrap system consisted of an Accela 1250 LC pump and an Accela open autosampler coupled with a Q Exactive mass spectrometer (ThermoFisher Scientific, Germany). The system was controlled by Xcalibur 2.2 software.

*(a). UHPLC.* UHPLC mobile phase A was 4 mM ammonium formate and 0.10% formic acid in water, and mobile phase B was 4 mM ammonium formate and 0.10% formic acid in methanol. The UHPLC column utilized was a Hypersil Gold, 100 mm × 2.1 mm, 1.9 μm column (Thermo Scientific, USA). The UHPLC guard column was an Accucore aQ 10 × 2.1 mm, 2.6 μm Defender cartridge (Thermo Scientific, USA). The UHPLC gradient profile and flow rate are shown in Figure 1. The column oven temperature was set at 45 °C, and the autosampler temperature was set at 5 °C. The injection volume was 5 μL, and the total run time was 14 min.

*(b). Q-Orbitrap Parameters.* The Q-Exactive ion source was equipped with a heated electrospray ionization (HESI) probe, and the Q-Orbitrap was tuned and calibrated using positive LTQ calibration solution once a week. The Q-Exactive was operated in either full MS-SIM or full MS/dd-MS$^2$ positive mode. In full MS-SIM, the Q-Oritrap performed full MS scan without high-energy collision dissociation (HCD) fragmentation. The full MS scan range was set from $m/z$ 80 to 1100 (0−12.0 min). The mass resolution was set to 70000 fwhm at $m/z$ 200, and the instrument was tuned for maximum ion throughput.

A

**UHPLC Gradient Profile**

| | Time | A% | B% | μL/min |
|---|---|---|---|---|
| 0 | 0.00 | 88.0 | 12.0 | 300 |
| 1 | 8.00 | 5.0 | 95.0 | 300 |
| 2 | 9.00 | 0.0 | 100.0 | 300 |
| 3 | 11.00 | 0.0 | 100.0 | 300 |
| 4 | 11.10 | 88.0 | 12.0 | 300 |
| 5 | 14.00 | 88.0 | 12.0 | 300 |

B

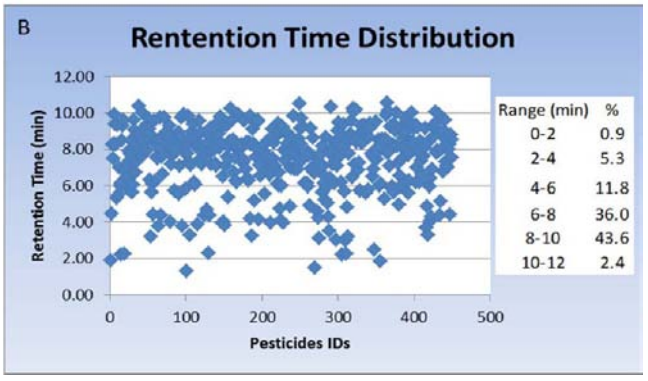


**Figure 1.** UHPLC gradient profile and 451 pesticides elution distribution.

AGC (automatic gain control) target or the number of ions to fill C-Trap was set at 1.0 × 10$^6$ with a maximum injection time (IT) of 250 ms. All quantitative data in this study were acquired using full MS-SIM mode.

Targeted identification was achieved by full scan MS, and if a targeted pesticide was present, its precursor ion scan, provided by an inclusion list, triggered a data-dependent MS$^2$ (dd-MS$^2$) scan. During full MS scan, the mass resolution was set at 70000 fwhm, AGC target at 1.0 × 10$^6$, maximum IT 250 ms, and scan range from $m/z$ 80 to 1100. If the targeted compound was detected within the 10 ppm mass error window and achieved by a designated intensity threshold (i.e., setting of 1.7 × 10$^5$), the precursor ion in the inclusion list was then isolated by the quadrupole and sent to the HCD collision cell for fragmentation via the C-trap. The inclusion list consists of precursor ions that are of interest for targeted identification and is provided in Table 1, columns 3−5. The precursor ion was fragmented with stepped normalized collision energy (NCE) to generate the resulting dd-MS$^2$ product ion spectrum. At this stage, the mass resolution of the Orbitrap analyzer was set at 35000 fwhm, AGC target at 2 × 10$^5$, maximum IT at 120 ms, and isolation window at 1.0 $m/z$, NCE at 40 ± 50%, underfill ratio at 10%, intensity threshold at 1.7 × 10$^5$, apex trigger at 2−4 s, and dynamic exclusion at 10.0 s. Other Q-Exactive generic parameters were sheath gas flow rate set at 60, Aux gas flow rate at 30, sweep gas flow rate at 2, spray voltage (kV) at 3.50, capillary temperature (°C) at 350, S-lens level at 55.0, and heater temperature (°C) at 350.

**Sample Preparation and Extraction Procedure.** Sample extraction and cleanup procedures followed the buffered QuEChERS[14] or AOAC Official Method 2007.01[15] with a slight modification. For the fortification experiment, fruit and vegetable samples (15.0 g/sample) were weighed into individual 50 mL polypropylene centrifuge tubes (VWR International, Canada). One milliliter per four-level sample spike pesticide standard working solution(s) was added into four centrifuge tubes to provide 10.0, 90.0, 240.0, and 400.0 μg/kg of pesticide equivalent in samples, followed by the addition of 300 μL of 5.0 μg/mL internal calibration standard working solution (100.0 μg/kg equivalent in samples). The centrifuge tubes were capped, mixed, and left to stand for 15 min at room temperature. Then, 14 mL of acetonitrile/acetic acid (99 + 1, v/v) mixture was added to individual samples and mixed for 45 s, followed by adding 1.5 g of anhydrous sodium acetate and 6.0 g of anhydrous magnesium sulfate from an ENVIRO CLEAN MYLAR pouch. One milliliter of organic solvent (methanol/acetonitrile, 50 + 50, v/v), resulting from the addition of the pesticide standard working solutions, was accounted for and added

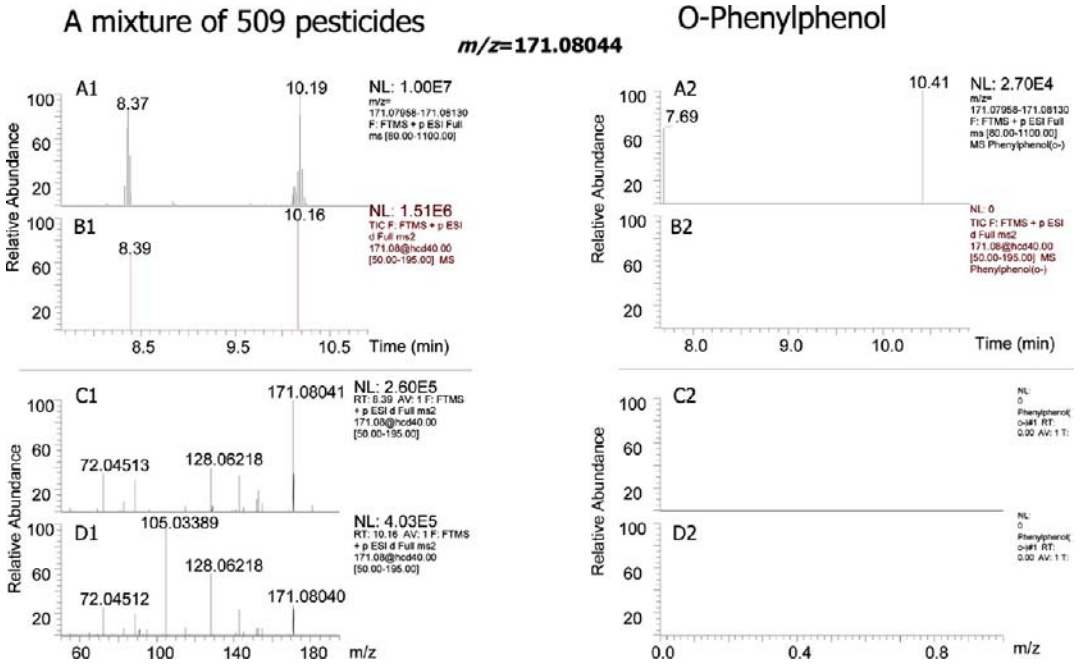


**Figure 2.** UHPLC/ESI Q-Orbitrap Full MS/dd-MS$^2$ chromatograms and product ion spectra. A mixture of 509 pesticides (50 $\mu$g/L in solvent buffer) and single O-Phenylphenol (50 $\mu$g/L in solvent buffer) were injected and analyzed: (left) Mixture of 509 pesticides; (right) O-Phenylphenol; (A1, A2) extracted ion chromatograms of $m/z$ 171.08044 with a mass tolerance of 5 ppm, if detected; (B1, B2) dd-MS$^2$ chromatograms of $m/z$ 171.08044, if detected; (C1, C2) dd-MS$^2$ product ion spectra of $m/z$ 171.08044, if triggered at 8.39 min; (D1, D2) dd-MS$^2$ product ion spectra of $m/z$ 171.08044, if triggered at 10.16 min.

up to a total of 15 mL organic solvent for extraction. The centrifuge tubes were capped, shaken at 1500 rpm using a Geno/Grinder 2010 (SPEX SamplePrep, USA) for 1 min, and then centrifuged at 3000 rpm (~2100$g$) for 3 min using an Allegra 6 centrifuge (Beckman Coulter Inc., USA). Supernatants were transferred (7 mL/sample) into individual 15 mL polypropylene centrifuge tubes or ENVIRO CLEAN extraction columns that contain 900 mg of $MgSO_4$, 150 mg of $C_{18}$, and 300 mg of PSA for cleanup. The centrifuge tubes were capped, shaken by hand for 45 s, and centrifuged at 3000 rpm (~2100$g$) for 3 min. Ninety microliters of each sample extract and 410 $\mu$L of solvent buffer were transferred into separate Mini-UniPrep vials (Whatman Inc., USA). The vials were capped, vortexed for 30 s, and pressed to filter the solution. Sample extracts were ready for UHPLC/ESI Q-Orbitrap injection.

**Preparation of Matrix-Matched Calibration Standards and Calculation.** Matrix-matched calibration standards were prepared by adding standards and internal standards to blank sample extracts after sample extraction and cleanup. A blank fruit or vegetable sample (15.0 g/sample) was weighed into a 50 mL centrifuge tube, and the sample was processed through the extraction procedure as described above (but using 15 mL of acetonitrile/acetic acid (99 + 1, v/v) mixture for extraction). After 90 $\mu$L of blank sample extracts and 377 $\mu$L of solvent buffer had been transferred into each of six Mini-UniPrep vials (Whatman Inc., USA), 15 $\mu$L of each six-level pesticide standard mix working solution and 18 $\mu$L of 0.50 $\mu$g/mL internal calibration working solution were added to the individual vials, providing 5.0, 25.0, 100.0, 200.0, 300.0, and 500.0 $\mu$g/kg per standard and 100.0 $\mu$g/kg per internal standard equivalent in samples. The vials were capped, vortexed for 30 s, and pressed to filter the solution. Sample extracts were ready for UHPLC/ESI Q-Orbitrap injection.

Matrix-matched standard calibration curves for each individual pesticide were constructed using TraceFinder 3.1 (optimized for Environmental and Food Safety) software. Concentration ($\mu$g/kg (ppb)) versus the ratio (analyte area/IS area) of each individual pesticide was plotted. Deuterium-labeled standards carbendazim-$d_4$, carbofuran-$d_3$, and thiabendazole-$d_4$ were used as internal standards for their respective native compounds for quantification. Other pesticides used carbofuran-$d_3$ as an internal standard for quantification. In general, a quadratic function was applied to the calibration curves based on the line of best fit. Occasionally, linear regression may be used for quantification. The $1/x$ weighting was used to improve the accuracy for quantification of pesticides at low concentrations. Responses for the unknown concentration or fortified samples were compared to the curves to calculate the amount of pesticide residues ($\mu$g/kg (ppb)) in samples. Matrix-matched calibration standards were prepared fresh for each batch of samples.

**Experimental Design and Method Validation.** The method was validated according to the nested experimental design, which was described elsewhere.[16] The main factors of variances associated with the method performance or measurement uncertainties of an in-house validated method were concentrations or spiked levels of analytes, matrix effects, day-to-day variation, and within-day variation of the method. The last two factors are designated the intermediate precision. In this study, there were a total of five fruits (i.e., apple, banana, grape, orange, and strawberry) and five vegetables (i.e., carrot, potato, tomato, broccoli, and lettuce). For each matrix, samples were spiked at 10.0, 90.0, 240.0, and 400.0 $\mu$g/kg, in triplicate. Spike experiments were repeated on two different days or by two analysts. Overall recovery, intermediate precision, and measurement uncertainty were calculated using a combined computer program that consisted of SAS codes (SAS Software release 9.3, SAS Institute Inc., USA) along with a Microsoft Excel (Microsoft Office 2010) workbook.

## RESULTS AND DISCUSSION

**QuEChERs.** Pesticides were extracted from fruits and vegetables (15 g/sample) following the buffered QuEChERS method[14] or AOAC Official Method 2007.01.[15] The whole procedure consisted of two steps including (1) extraction with acetonitrile containing 1% acetic acid, $MgSO_4$, and sodium acetate or (2) cleanup by dispersive solid-phase extraction (d-SPE) using $MgSO_4$, PSA, and $C_{18}$. Previous methods used ChloroFiltr, a polymeric-based sorbent used in the cleanup of chlorophyll-rich matrices such as lettuce and broccoli.[14] To simplify the method and avoid confusion, the d-SPE that

**Table 2. Isobaric Pesticides and Their Exact Mass, UHPLC Retention Time, and UHPLC/ESI Q-Orbitrap MS Method Performance**

| Pesticides | Molecular formula | Precursor Exact mass[a] $[M+H]^+$ | Precursor Exact mass[a] $[M+NH_4]^+$ | Precursor Exact mass[a] $[M+Na]^+$ | Fragements or ions used for quantification[b] | Retention Time | Fruits[f] Overall recovery[c] (%) | Fruits[f] Intermediate precision[d] (%) | Fruits[f] Measurement uncertainty[e] (%) | Vegetables[f] Overall recovery[c] (%) | Vegetables[f] Intermediate precision[d] (%) | Vegetables[f] Measurement uncertainty[e] (%) |
|---|---|---|---|---|---|---|---|---|---|---|---|---|
| 1[g] | 2 | 3 | 4 | 5 | 7 | 8 | 9 | 10 | 11 | 12 | 13 | 14 |
| Methomyl | C5H10N2O2S | 163.05357 | 180.08012 | 185.03552 | **88.02209** | 3.11 | 106.5 | 5.0 | 10.3 | 106.2 | 6.0 | 13.4 |
| Oxamyl-oxime | C5H10N2O2S | **163.05357** | 180.08012 | 185.03552 | | 2.24 | 96.6 | 4.2 | 9.2 | 94.2 | 3.5 | 11.2 |
| Isoprocarb | C11H15NO2 | 194.11756 | 211.14410 | 216.09950 | **137.09609** | 6.96 | 99.5 | 6.6 | 14.6 | 98.3 | 6.6 | 17.3 |
| Trimethacarb | C11H15NO2 | 194.11756 | 211.14410 | 216.09950 | **137.09609** | 7.09 | 99.8 | 3.5 | 7.6 | 97.3 | 4.5 | 11.1 |
| **Pebulate** | C10H21NOS | **204.14166** | 221.16821 | 226.12361 | | **8.81** | 95.4 | 4.0 | 10.4 | 89.4 | 4.3 | 10.7 |
| **Vernolate** | C10H21NOS | **204.14166** | 221.16821 | 226.12361 | | **8.81** | 95.5 | 4.3 | 11.1 | 89.4 | 4.3 | 10.7 |
| Bendiocarb | C11H13NO4 | **224.09173** | 241.11828 | 246.07368 | | 6.07 | 99.2 | 3.7 | 7.6 | 95.1 | 4.1 | 10.6 |
| Dioxacarb | C11H13NO4 | 224.09173 | 241.11828 | 246.07368 | **167.07027** | 4.38 | 92.8 | 4.7 | 19.9 | 95.1 | 5.1 | 10.9 |
| Ethiofencarb | C11H15NO2S | 226.08963 | 243.11618 | 248.07157 | **107.04914** | 6.52 | **114.2** | **69.0** | **138.6** | 87.2 | **26.8** | **53.8** |
| Methiocarb | C11H15NO2S | 226.08963 | 243.11618 | 248.07157 | **169.06816** | 7.51 | 99.8 | 3.7 | 7.5 | 86.8 | 11.3 | 26.9 |
| **Prometon** | C10H19N5O | **226.16624** | 243.19279 | 248.14818 | | 6.50 | 96.9 | 4.4 | 8.8 | 92.8 | 4.6 | 10.7 |
| **Secbumeton** | C10H19N5O | **226.16624** | 243.19279 | 248.14818 | | 6.54 | 97.5 | 4.2 | 8.4 | 92.5 | 4.6 | 10.9 |
| Terbumeton | C10H19N5O | **226.16624** | 243.19279 | 248.14818 | | 6.63 | 97.2 | 3.9 | 8.1 | 92.1 | 3.9 | 11.1 |
| Propazine | C9H16ClN5 | **230.11670** | 247.14325 | 252.09864 | | 7.44 | 98.1 | 3.6 | 7.3 | 92.2 | 4.0 | 10.9 |
| Terbuthylazine | C9H16ClN5 | **230.11670** | 247.14325 | 252.09864 | | 7.58 | 96.9 | 8.0 | 16.3 | 85.7 | 8.7 | 23.1 |
| Trietazine | C9H16ClN5 | **230.11670** | 247.14325 | 252.09864 | | 8.01 | 97.7 | 4.0 | 8.0 | 92.1 | 3.8 | 11.6 |
| Ethiofencarb-sulfoxide | C11H15NO3S | **242.08454** | 259.11109 | 264.06649 | | 3.85 | 95.9 | 6.0 | 12.3 | 99.1 | 4.9 | 11.7 |
| Methiocarb-sulfoxide | C11H15NO3S | **242.08454** | 259.11109 | 264.06649 | | 4.26 | 99.4 | 3.1 | 13.1 | 100.7 | 3.6 | 22.9 |
| Prometryn | C10H19N5S | 242.14339 | 259.16994 | 264.12534 | | 7.61 | 95.5 | 8.6 | 18.1 | 88.2 | 7.2 | 15.6 |
| Terbutryn | C10H19N5S | 242.14339 | 259.16994 | 264.12534 | | 7.68 | 97.4 | 3.9 | 9.8 | 89.9 | 3.7 | 10.6 |
| **Dimethametryn** | C11H21N5S | **256.15904** | 273.18559 | 278.14099 | | **8.11** | 96.8 | 4.2 | 9.1 | 90.3 | 4.2 | 12.5 |
| **Dipropetryn** | C11H21N5S | **256.15904** | 273.18559 | 278.14099 | | **8.11** | 96.8 | 4.2 | 9.1 | 90.3 | 4.2 | 12.5 |
| Ethiofencarb-sulfone | C11H15NO4S | **258.07946** | 275.10600 | 280.06140 | | 4.00 | 99.8 | 3.7 | 8.4 | 98.3 | 4.5 | 11.3 |
| Methiocarb-sulfone | C11H15NO4S | **258.07946** | 275.10600 | 280.06140 | | 4.63 | 98.9 | 3.5 | 7.0 | 96.3 | 4.2 | 10.6 |
| **Acetochlor** | C14H20ClNO2 | **270.12553** | 287.15208 | 292.10748 | | 8.24 | 98.3 | 3.9 | 8.6 | 94.2 | 4.3 | 11.6 |
| **Alachlor** | C14H20ClNO2 | **270.12553** | 287.15208 | 292.10748 | | 8.27 | 98.3 | 3.9 | 8.6 | 94.2 | 4.3 | 11.6 |
| Metolachlor | C15H22ClNO2 | **284.14118** | 301.16773 | 306.12313 | | **8.30** | 97.1 | 3.7 | 8.1 | 92.7 | 3.6 | 11.6 |
| Propisochlor | C15H22ClNO2 | **284.14118** | 301.16773 | 306.12313 | | **8.55** | 98.3 | 4.5 | 9.0 | 91.2 | 5.0 | 14.3 |
| Cyproconazole | C15H18ClN3O | **292.12112** | 309.14767 | 314.10306 | | 7.79 | 97.2 | 3.8 | 8.4 | 91.3 | 5.1 | 11.4 |
| Uniconazole | C15H18ClN3O | **292.12112** | 309.14767 | 314.10306 | | 8.25 | 96.9 | 5.1 | 10.6 | 90.2 | 5.0 | 12.3 |
| Phoxim | C12H15N2O3PS | **299.06138** | 316.08793 | 321.04332 | | 8.39 | 96.9 | 14.7 | 29.5 | | | |
| Quinalphos | C12H15N2O3PS | **299.06138** | 316.08793 | 321.04332 | | 8.28 | 97.8 | 3.9 | 8.7 | 91.9 | 4.8 | 12.8 |
| Desmedipham | C16H16N2O4 | **301.11828** | 318.14483 | 323.10023 | | 7.12 | 98.4 | 5.3 | 11.9 | 92.3 | 7.8 | 17.0 |
| Phenmedipham | C16H16N2O4 | **301.11828** | 318.14483 | 323.10023 | | 7.20 | 97.6 | 10.2 | 21.3 | 91.9 | 5.8 | 12.7 |
| Fenoxycarb | C17H19NO4 | **302.13868** | 319.16523 | 324.12063 | | 8.24 | 98.2 | 3.8 | 8.4 | 88.2 | 4.0 | 18.4 |
| Furalaxyl | C17H19NO4 | **302.13868** | 319.16523 | 324.12063 | | 7.43 | 98.0 | 3.4 | 7.5 | 93.6 | 3.7 | 10.1 |
| Butachlor | C17H26ClNO2 | **312.17248** | 329.19903 | 334.15443 | | 9.33 | 96.1 | 14.3 | 28.7 | 89.0 | 11.0 | 22.9 |
| Pretilachlor | C17H26ClNO2 | **312.17248** | 329.19903 | 334.15443 | | 9.07 | 97.1 | 3.7 | 8.1 | 91.0 | 4.1 | 12.3 |
| Ipconazole | C18H24ClN3O | **334.16807** | 351.19462 | 356.15001 | | 8.94 | 95.8 | 3.9 | 8.9 | 89.6 | 4.2 | 11.9 |
| Tebufenpyrad | C18H24ClN3O | **334.16807** | 351.19462 | 356.15001 | | 9.18 | 97.9 | 5.3 | 11.8 | 90.8 | 4.1 | 12.1 |
| **Benfluralin** | C13H16F3N3O4 | **336.11657** | 353.14312 | 358.09851 | | 9.63 | 93.3 | 5.9 | 14.2 | 86.8 | 7.7 | 20.5 |
| **Trifluralin** | C13H16F3N3O4 | **336.11657** | 353.14312 | 358.09851 | | 9.61 | 93.1 | 6.2 | 14.0 | 86.8 | 7.7 | 20.5 |
| Bromuconazole, cis- | C13H12BrCl2N3O | **375.96136** | 392.98791 | 397.94330 | | 8.38 | 97.3 | 4.7 | 11.7 | 90.7 | 6.4 | 13.9 |
| Bromuconazole, trans- | C13H12BrCl2N3O | **375.96136** | 392.98791 | 397.94330 | | 7.88 | 97.2 | 5.2 | 10.4 | 91.2 | 6.5 | 14.2 |
| Permethrin, cis- | C21H20Cl2O3 | 391.08623 | **408.11278** | 413.06817 | | 10.24 | 89.2 | 8.8 | 18.5 | 81.8 | 9.0 | 21.2 |
| Permethrin, trans | C21H20Cl2O3 | 391.08623 | **408.11278** | 413.06817 | | 10.06 | 90.2 | 5.7 | 17.1 | **77.0** | 5.8 | 36.3 |

[a]Number or text in bold font and unerlined indicates ionization form or charge state for data processing or quantification. [b]Exact mass or measured accurate mass was used for quantification. The electron mass (0.000549 amu) is subtracted when exact mass is calculated. [c]Bold and underlined indicate pesticides with recoveries not in the range of 81−110%. [d]Bold and underlined indicate pesticides intermediate precision >20%. [e]Bold and underlined indicate pesticides MU > 50%. [f]For data in red font, the method performance was based on three spike levels, i.e., 90.0, 240.0, and 400.0 μg/kg, due to its poor sensitivity. For data in blue font, the method performance was based on two spike levels, i.e., 240.0 and 400.0 μg/kg, due to its poor sensitivity. [g]Column number.

contained 900 mg of $MgSO_4$, 150 mg of $C_{18}$, and 300 mg of PSA was used for all matrices in the cleanup step for this method. An experiment (data not shown) proved that no obvious differences regarding matrix effects were observed between d-SPEs with or without ChloroFiltr. In addition, sample extracts were diluted 5.56 times (90 μL of extracts + 410 μL of solvent buffer). The Mini-UniPrep vials, consisting of a polyvinylidene difluoride (PVDF) membrane, filtered some of the light green coextractives or precipitates in the final extracts after sample extract dilution prior to UHPLC/ESI Q-Orbitrap injection. Therefore, the QuEChERS method without ChloroFiltr proved to be a simple, practical, and fast extraction procedure to achieve UHPLC/ESI Q-Orbitrap quantification of pesticide residues at trace level in fruits and vegetables.

**UHPLC.** Four hundred and fifty-one pesticides and three isotopically labeled standards (Table 1, column 1) were chromatographically separated within 12 min under a gradient profile (Figure 1A) using a Hypersil Gold (100 mm × 2.1 mm, 1.9 μm) column with methanol and water, each containing 4 mM ammonium formate and 0.10% formic acid, as mobile phases. Initially, a Waters Acquity UPLC BEH $C_{18}$ (100 mm × 2.1 mm, 1.7 μm) column with acetonitrile and water (10 mM ammonium acetate)[14] was chosen for the study. However, higher detection limits were observed for some of the compounds. To improve sensitivity, different LC methods were compared, and then an UHPLC method, which used Hypersil Gold (100 mm × 2.1 mm, 1.9 μm) column, was adopted.[17] The Hypersil Gold (100 mm × 2.1 mm, 1.9 μm) column generally provided better chromatographic resolution

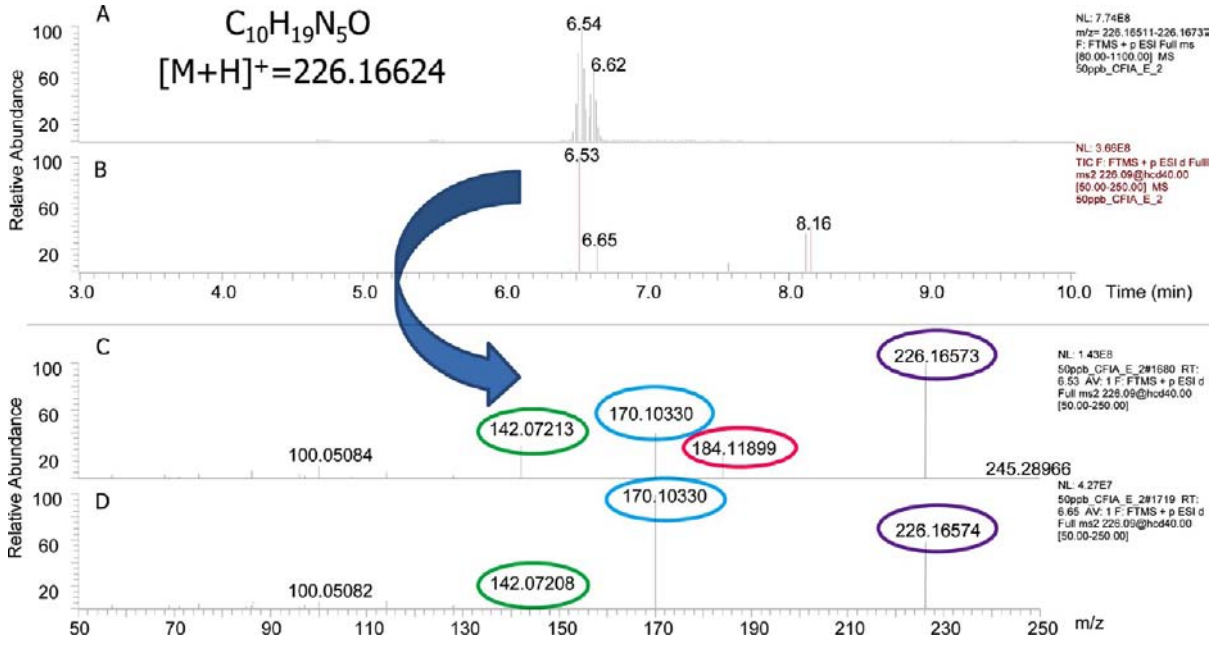


**Figure 3.** UHPLC/ESI Q-Orbitrap Full MS/dd-MS$^2$ chromatograms and product ion spectra. A mixture of 451 pesticides (50 $\mu$g/L in solvent buffer) was injected and analyzed: (A) extracted ion chromatogram of $m/z$ 226.16624 with a mass tolerance of 5 ppm; (B) dd-MS$^2$ chromatogram of $m/z$ 226.16624; (C) dd-MS$^2$ product ion spectrum of $m/z$ 226.16624 at 6.53 min; (D) dd-MS$^2$ product ion spectrum of $m/z$ 226.16624 at 6.65 min.

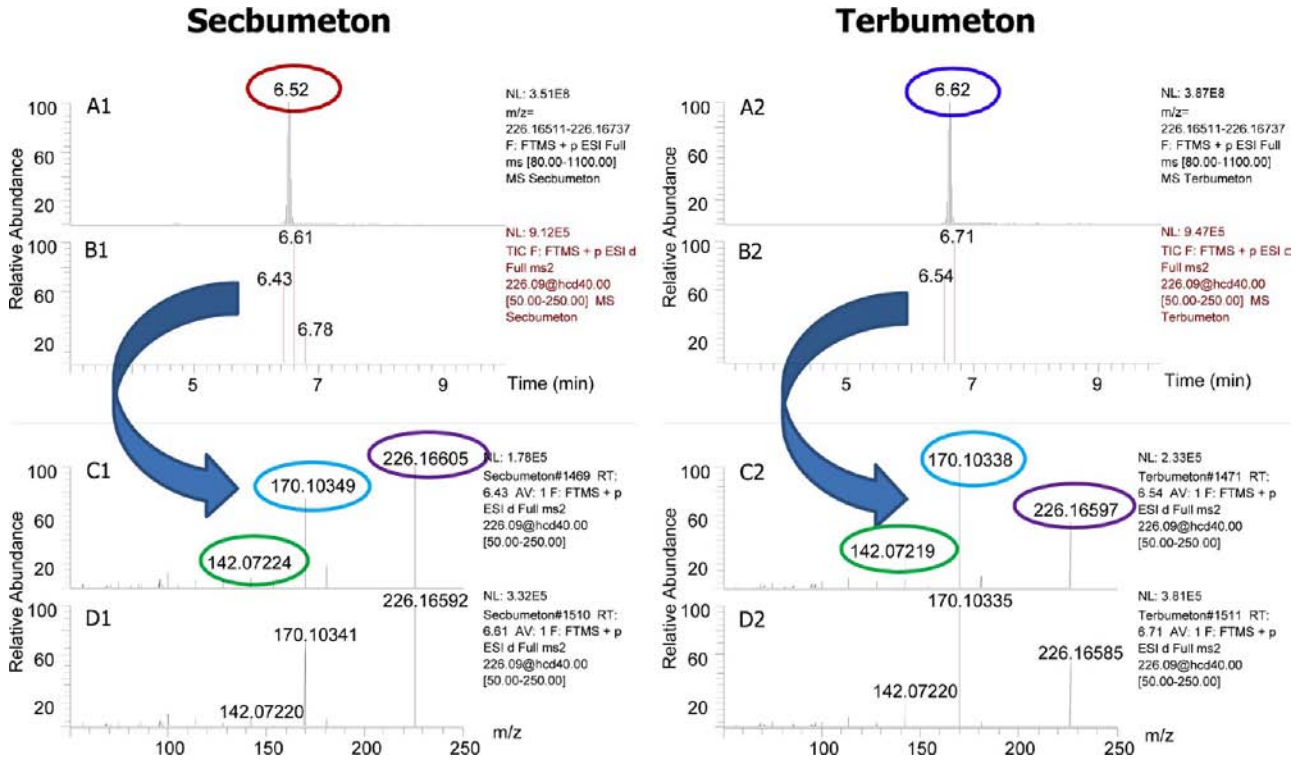


**Figure 4.** UHPLC/ESI Q-Orbitrap Full MS/dd-MS$^2$ chromatograms and product ion spectra. Individual secbumeton or terbumeton (50 $\mu$g/L in solvent buffer) was injected and analyzed: (left) secbumeton; (right) terbumeton; (A1, A2) extracted ion chromatogram of $m/z$ 226.16624 with a mass tolerance of 5 ppm; (B1, B2) dd-MS$^2$ chromatogram of $m/z$ 226.16624; (C1, C2) dd-MS$^2$ product ion spectra of $m/z$ 226.16624 at 6.43 and 6.54 min, respectively; (D1, D2) dd-MS$^2$ product ion spectra of $m/z$ 226.16624 at 6.61 and 6.71 min, respectively.

and higher responses compared to an Acquity UPLC BEH $C_{18}$ column for improved sensitivity. The gradient profile also was modified so that the elution of pesticides was optimized over the 12 min run time (Figure 1B). Under the modified gradient profile, 79.6% of pesticides were eluted between 6 and 10 min or 91.4% between 4 and 10 min. The span of the retention time distribution reduced the number of concurrent pesticides and provided sufficient time for the dd-MS$^2$ experiment between full MS scans.

Under most circumstances, an extracted ion presented as a single LC peak or baseline separation from other peaks, which was a result of superior resolving power of both UHPLC and

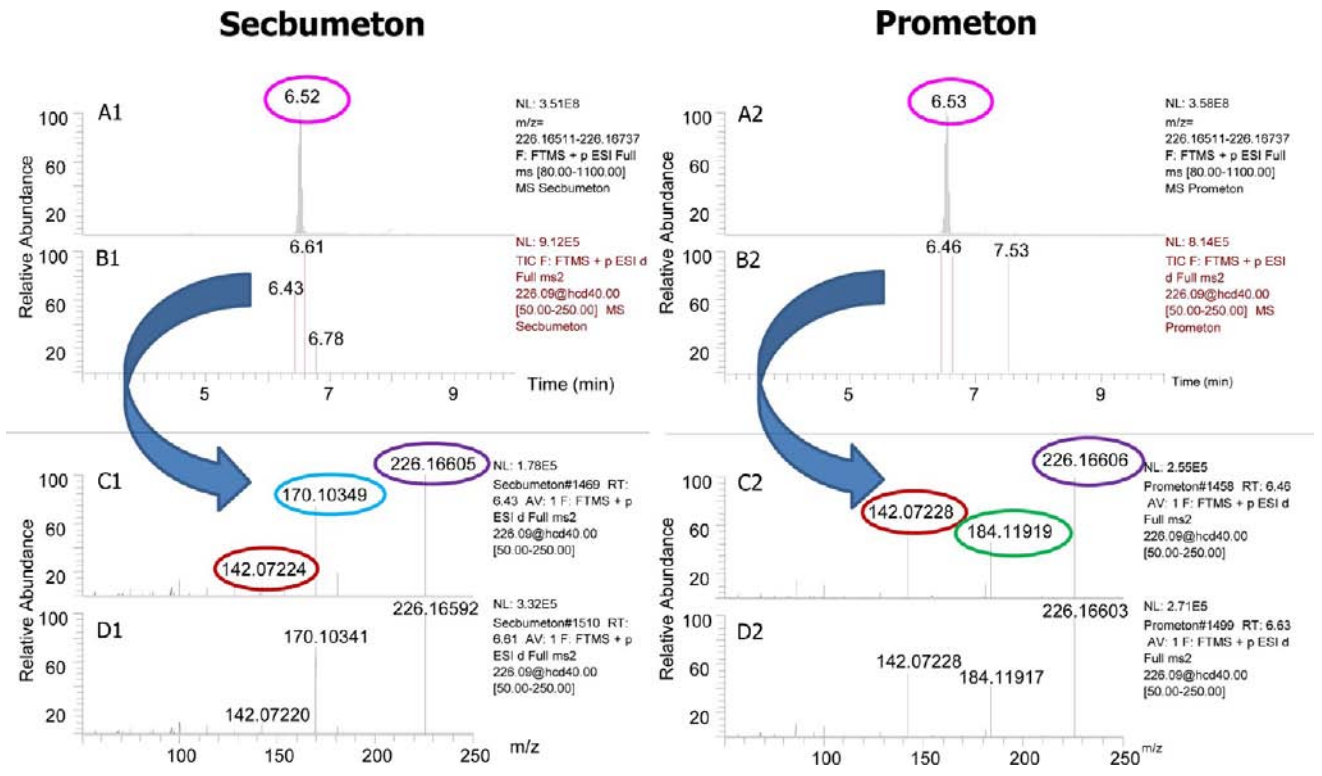


**Figure 5.** UHPLC/ESI Q-Orbitrap Full MS/dd-MS$^2$ chromatograms and product ion spectra. Individual secbumeton or prometon (50 $\mu$g/L in solvent buffer) was injected and analyzed: (left) secbumeton; (right) prometon; (A1, A2) extracted ion chromatograms of $m/z$ 226.16624 with a mass tolerance of 5 ppm; (B1, B2) dd-MS$^2$ chromatograms of $m/z$ 226.16624; (C1, C2) dd-MS$^2$ product ion spectra of $m/z$ 226.16624 at 6.43 and 6.46 min, respectively; (D1, D2) dd-MS$^2$ product ion spectra of $m/z$ 226.16624 at 6.61 and 6.63 min, respectively.

Q-Orbitrap MS, with the exception of coeluting isomeric compounds. Pesticides were eluted between 1.0 and 11.0 min, and their peak shapes were of Gaussian distribution with a baseline peak width of 5−10 s. The retention times were reproducible under ±0.2 min within and between batches for most of the pesticides. The scan rate of 3 Hz with the resolution, set at 70000 fwhm at $m/z$ 200, is more than adequate to generate sufficient data points for quantification. For example, at least 18 data points across the chromatographic peak were generated with a 6 s (0.1 min) baseline peak width.

**Q-Orbitrap MS.** When operated in its full MS-SIM mode in a range from $m/z$ 80.0 to 1100.0 with 70000 fwhm at $m/z$ 200, the Q-Orbitrap acquired full MS scan data for the screening and quantitation of the 451 pesticides listed in Table 1. When operated in full MS/dd-MS$^2$ mode, the Q-Orbitrap acquired product ion spectra with accurate mass measurement for identification according to a list of targeted exact masses (Table 1, columns 3−5). In the current study, "stepped" normalized collision energy (NCE) was used for dd-MS$^2$ fragmentation. The Q-Orbitrap performed a three-step 40 ± 50% NCE (i.e., the center energy 40 NCE; plus one above, 60 NCE; and one below, 20 NCE) fragmentation on the precursor ion. All fragments created in the three steps were collected sequentially in the HCD and sent together to the Orbitrap analyzer for single-scan detection. Stepped NCE worked for most but not all of the pesticides because some pesticides are not optimally fragmented in the 40 ± 50% NCE range.

At the initial stage of method development, we prepared a mixture of 509 pesticides and injected it into the system. It was thought that individual pesticides in the mixture would have been identified simply on the basis of high mass-resolving power and accurate mass measurement in conjunction with UHPLC chromatographic resolution. However, this assumption did not account for impurities present in the mixture, which possibly led to false identification, and therefore the injection of each individual pesticide became necessary. Figure 2 showed an example of potential misidentifications when a mixture of pesticides was injected into the system during the method development stage. O-Phenylphenol has a $m/z$ 171.08044, if protonated. In full MS scan, two peaks were found at 8.37 and 10.19 min (Figure 2A1), respectively, for $m/z$ 171.08044 with a mass tolerance of 5 ppm, and dd-MS$^2$ was triggered twice at 8.39 and 10.16 min (Figure 2B1), resulting in product ion spectra as shown in Figure 2C1,D1. To identify the O-Phenylphenol peak, its neat standard (50 ppb in solvent) was injected into the system. No peaks were detected to trigger dd-MS$^2$ for O-Phenylphenol (Figure 2A2,B2,C2,D2), indicating the peaks were results of chemical impurities. Therefore, it was required that individual pesticide standards were injected in full MS/dd-MS$^2$ mode to obtain both retention times and product ion spectra during the method development stage. This step proved to be critical because it provided data for the identification of individual pesticides in a mixture or sample matrices and for generating exact mass spectral library in future.

Another challenge was to identify or differentiate isomeric compounds in the mixture of pesticides. Table 2 lists 22 pairs or groups of isomers among 451 pesticides that required both LC retention times (LC resolution) and dd-MS$^2$ product ion spectra (MS fragmentation) for identification and differentiation. For example, secbumeton, terbumeton, and prometon are isomers and share the same precursor ion ($[M + H]^+$) with $m/z$ 226.16624. When a mixture of standards was injected, the three compounds eluted at 6.54 and 6.62 min (Figure 3A), and dd-MS$^2$ was triggered twice at 6.53 and 6.65 min,

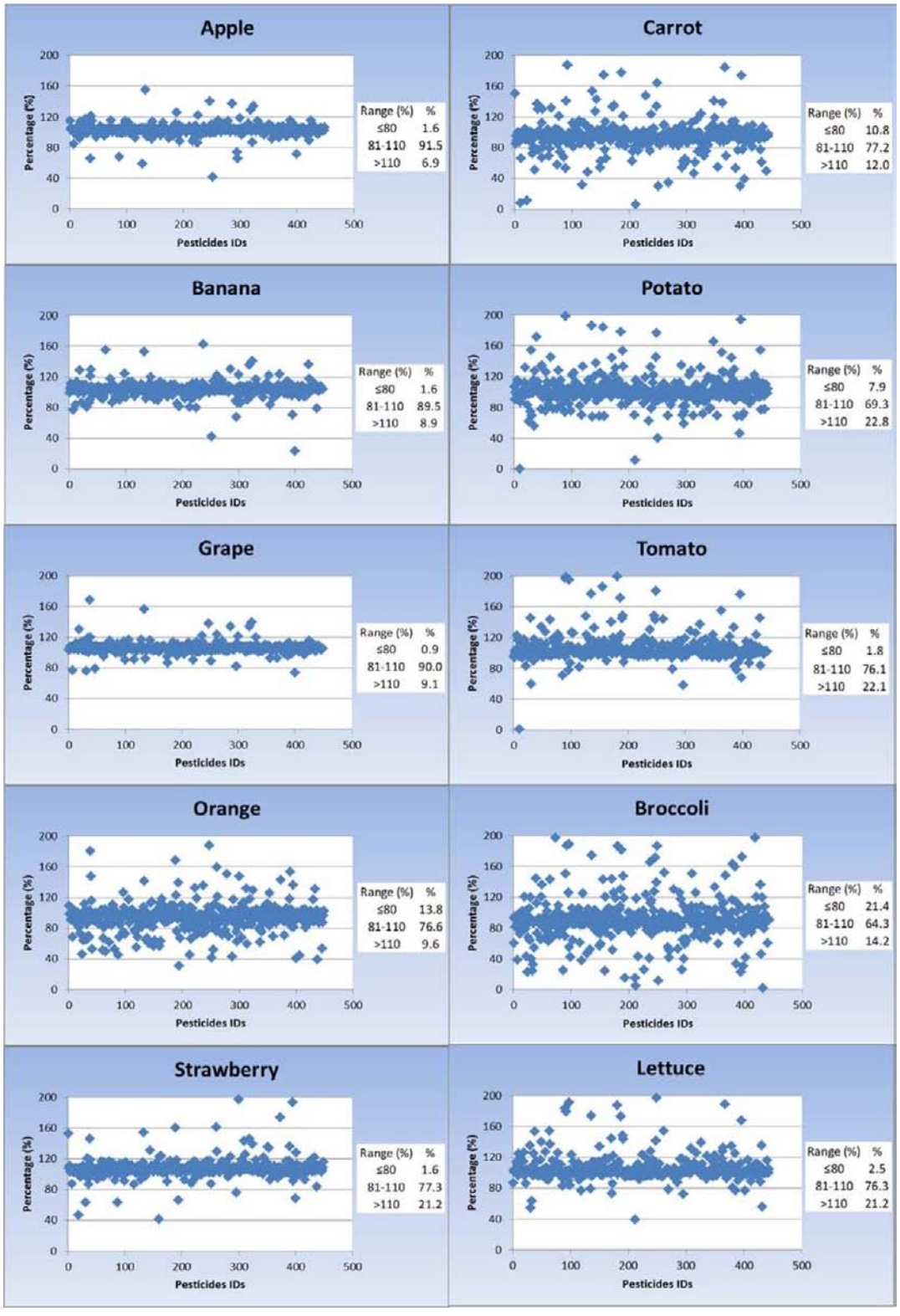


**Figure 6.** UHPLC/ESI Q-Orbitrap MS matrix effects. The 451 pesticides were prepared in sample extracts (a total of 10 matrices) and solvent buffer at a concentration of 100 $\mu$g/kg equivalent in sample: (left) fruits; (right) vegetables.

respectively (Figure 3B). The corresponding product ion spectra are shown in Figure 3C,D, and the observed differences revealed a product ion at $m/z$ 184.11899 and relative ion intensities. To identify and differentiate the three compounds, individual standards were injected, and chromatograms and mass spectra are shown in Figures 4 and 5. Secbumeton (6.52 min) and terbumeton (6.62 min) were chromatography resolved (Figure 4A1,A2) but shared the same major fragment ions with different relative intensities (Figure 4C1,D1,C2,D2). Secbumeton (6.52 min) and prometon (6.53 min) coeluted (Figure 5A1,A2) but possessed different fragment ions ($m/z$ 170.10349 and 184.11919, Figure 5, panels C1 and D1 and C2


dx.doi.org/10.1021/jf503778c | J. Agric. Food Chem. 2014, 62, 10375−10391

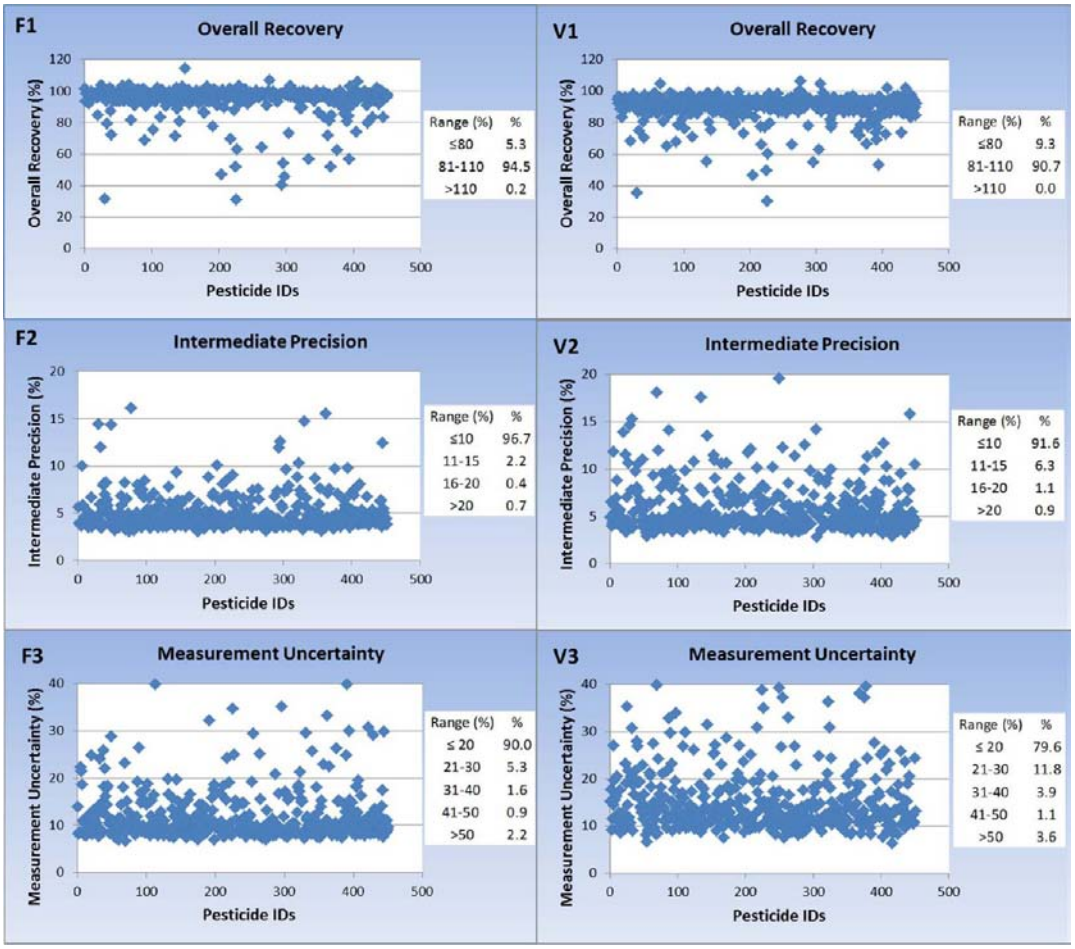


**Figure 7.** UHPLC/ESI Q-Orbitrap MS method performance for analysis of 451 pesticides in fruits and vegetables: (left) fruits; (right) vegetables; (A) overall recovery; (B) intermediate precision; (C) measurement uncertainty.

and D2, respectively). Prometon (6.53 min) and terbumeton (6.62 min) were chromatographically resolved (Figures 4A2 and 5A2) and possessed different fragment ions ($m/z$ 184.11919 and 170.10338, Figures 5C2,D2 and 4C2,D2, respectively). Therefore, dd-$MS^2$ was required to differentiate between secbumeton and prometon. Among the 22 pairs or groups of isomers, only 5 pairs were not chromatographically resolved, and dd-$MS^2$ was necessary for identification when detected in full MS mode.

**Matrix Effects.** Sample matrix could either enhance or suppress the ionization of pesticides; its effects might vary from sample to sample and ultimately affect the UHPLC/ESI Q-Orbitrap MS quantitative results. To evaluate matrix effects, the responses of pesticides in sample extracts were compared to those pesticide standards prepared in solvent buffer at 100 $\mu$g/kg equivalent in sample. In fruit matrices (Figure 6), pesticides experienced fewer matrix effects in apple, banana, and grape than in orange and strawberry. About 90% pesticides had ion suppression <20% or ion enhancement ≤10% in apple, banana, and grape, but only 77% of pesticides fell into the same range in orange and strawberry. More pesticides were subjected to ion suppression in orange or ion enhancement in strawberry. In vegetable matrices (Figure 6), pesticides generally experienced both ion suppression and enhancement. For example, >20% of pesticides in potato, tomato, and lettuce were subjected to ion enhancement (≥10%), whereas >10% of pesticides in carrot and broccoli experienced ion suppression (>20%).

Matrix-matched standard calibration curves along with isotopically labeled standards were required to compensate for matrix effects and were used to assess the UPLC/ESI Q-Orbitrap MS quantitative accuracy. Three commercially available deuterium-labeled standards, that is, carbendazim-$d_4$, carbofuran-$d_3$, and thiabendazole-$d_4$, were used as internal standards for quantifying their respective native compounds, and carbofuran-$d_3$ was utilized for all other pesticides. The calibration curves were observed to be linear or quadratic with coefficient of determinations ($R^2$) ≥ 0.97. Because of matrix effects, ion source contamination, or other unidentified factors, the responses of some pesticides either decreased or increased slightly over time. To average out the response changes during the course, the matrix-matched standard calibration curves were constructed on the basis of the two injections, that is, before and after spike samples, so as to improve the method performance.

**Quantification and Method Performance.** The UHPLC/ESI Q-Orbitrap MS method was validated according to a nested design, reported elsewhere, to evaluate the method performance characteristics including accuracy expressed as overall recovery, intermediate precision, and measurement uncertainty (MU).[16] Four factors, concentrations or spiked levels of pesticides, matrix effects, day-to-day variation, and within-day variation, were considered for the evaluation, and the experimental details were described under Materials and Methods. Data were grouped into two sets, that is, fruits and

vegetables, so that statistics were valid. The method performance results are summarized in Tables 1 and 2 and are illustrated in Figure 7. Depending on the type of sample matrices, about 94.5% of the pesticides in fruits or 90.7% in vegetables had recoveries between 81 and 110%; 99.3% of the pesticides in fruits and 99.1% of the pesticides in vegetables had an intermediate precision ≤20%; and 97.8% of the pesticides in fruits or 96.4% of the pesticides in vegetables showed measurement uncertainty ≤50%, which was a recommended default value in EU Document No. SANCO/12495/2011 for pesticide analysis and enforcement decisions (MRL exceedances).[18] Although five pairs of isomeric compounds that were not chromatographically resolved (Table 2) had very good method performance, they needed to be quantified separately when found in samples. Overall, the UHPLC/ESI Q-Orbitrap MS can serve as a liable and practical tool for quantification.

**Pesticide Identification.** The identification of any pesticides using UHPLC/ESI Q-Orbitrap mass spectrometry was based on mass accuracy and chromatographic retention time. SANCO/12495/2011[18] required ≥2 diagnostic ions (preferably the precursor ion and its product ion) with mass accuracy <5 ppm along with retention time tolerance of ±0.2 min for identification. The UHPLC/ESI Q-Orbitrap provided a measured mass accuracy <5 ppm and retention time tolerance within ±0.2 min. Full MS/dd-MS$^2$ was able to obtain product ion spectra that included both precursor and product ions with accurate masses. Currently, this identification was achieved using the system software. Further study will be to expand existing or develop new software to build a searchable exact mass spectral library or chemical compound database that can be used for efficient screening and identification.

**Method Sensitivity.** The lowest concentration levels (LCL) of individual pesticides, which indicated the method sensitivity, were determined according to the recommended default LC peak height value, that is, $1.0 \times 10^4$, reported elsewhere for Orbitrap.[19,20] To ensure the peaks were real, the peak areas were taken into account by calculating a ratio of peak height and peak area. If the ratio were >1.5, then the condition was satisfied and LCL by peak height can be determined. The signal-to-noise (S/N) ratio approach was not used because it was not practical as a result of a lack of background present in high mass resolution chromatograms. Approximately 85% of the pesticides could be detected and quantified at ≤5 μg/kg. The method proved to be sensitive enough to quantify most of the pesticides at 10 μg/kg, which is a default concentration for pesticides with no MRLs.

In conclusion, UHPLC/ESI Q-Orbitrap proved to be a powerful tool for the determination of up to 451 pesticide residues in fruits and vegetables. The UHPLC/ESI Q-Orbitrap MS, that is, full MS scan, provided superior method accuracy, repeatability, and sensitivity for quantification. Generally, about 94.5% of the pesticides in fruits or 90.7% in vegetables had recoveries between 81 and 110%; 99.3% of the pesticides in fruits and 99.1% of the pesticides in vegetables had an intermediate precision ≤20%; and 97.8% of the pesticides in fruits or 96.4% of the pesticides in vegetables showed measurement uncertainty ≤50%. UHPLC/ESI Q-Orbitrap dd-MS$^2$ provided product ion spectra with accurate mass measurement that allowed identification of pesticides. Overall, UHPLC/ESI Q-Orbitrap along with QuEChERs offers a practical tool for pesticide residue analysis in routine monitoring programs for food safety.

## AUTHOR INFORMATION


### Corresponding Author

*(J. Wang) Phone: (403) 338-5273. Fax: (403) 338-5299. E-mail: jian.wang@inspection.gc.ca.


### Notes

The authors declare no competing financial interest.

## ACKNOWLEDGMENTS

We are grateful to Daniel Leung and Wendy Cheung, Calgary Laboratory, Canadian Food Inspection Agency, for the purchase and preparation of pesticide standards for the study.

## REFERENCES


(1) Regulation (EC) No. 396/2005 of the European Parliament and of the Council of 23 February 2005 on maximum residue levels of pesticides in or on food and feed of plant and animal origin and amending Council Directive 91/414/EEC. *Off. J. Eur. Union* **2005**, *L 70*, 1−16.

(2) EU Pesticides MRLs; maximum pesticide levels for food products for human consumption and animal feedingstuffs; http://ec.europa.eu/sanco_pesticides/public/index.cfm?event=homepage&CFID=1404859&CFTOKEN=69040180&jsessionid=2405714dcd661a78e106TR# (accessed May 23, 2014).

(3) Codex Pesticides MRLs; pesticide residues in food and feed; maximum residue limits; http://www.codexalimentarius.net/pestres/data/pesticides/index.html?lang=en (accessed June 2, 2014).

(4) Health Canada. Maximum Residue Limits for Pesticides; http://www.hc-sc.gc.ca/cps-spc/pest/part/protect-proteger/food-nourriture/mrl-lmr-eng.php (accessed May 23, 2014).

(5) CFIA, Canadian Food Inspection Agency. http://www.inspection.gc.ca/ (accessed May 23, 2014).

(6) Soriano, J. M.; Jimenez, B.; Font, G.; Molto, J. C. Analysis of carbamate pesticides and their metabolites in water by solid phase extraction and liquid chromatography: a review. *Crit. Rev. Anal. Chem.* **2001**, *31*, 19−52.

(7) Kuster, M.; Lopez de Alda, M.; Barcelo, D. Liquid chromatography-tandem mass spectrometric analysis and regulatory issues of polar pesticides in natural and treated waters. *J. Chromatogr., A* **2008**, *1216*, 520−529.

(8) Alder, L.; Greulich, K.; Kempe, G.; Vieth, B. Residue analysis of 500 high priority pesticides: better by GC-MS or LC-MS/MS? *Mass Spectrom. Rev.* **2006**, *25*, 838−865.

(9) Wang, J. Analysis of macrolide antibiotics, using liquid chromatography-mass spectrometry, in food, biological and environmental matrices. *Mass Spectrom. Rev.* **2009**, *28*, 50−92.

(10) Kaufmann, A.; Butcher, P.; Maden, K.; Walker, S.; Widmer, M. Multi-residue quantification of veterinary drugs in milk with a novel extraction and cleanup technique: salting out supported liquid extraction (SOSLE). *Anal. Chim. Acta* **2014**, *820*, 56−68.

(11) Hernández, F.; Sancho, J.; Ibáñez, M.; Abad, E.; Portolés, T.; Mattioli, L. Current use of high-resolution mass spectrometry in the environmental sciences. *Anal. Bioanal. Chem.* **2012**, *403*, 1251−1264.

(12) Meyer, M.; Maurer, H. Current applications of high-resolution mass spectrometry in drug metabolism studies. *Anal. Bioanal. Chem.* **2012**, *403*, 1221−1231.

(13) Wang, J.; Chow, W.; Leung, D. Applications of LC/ESI-MS/MS and UHPLC QqTOF MS for the determination of 148 pesticides in fruits and vegetables. *Anal. Bioanal. Chem.* **2010**, *396*, 1513−1538.

(14) Wang, J.; Chow, W.; Leung, D.; Chang, J. Application of ultrahigh-performance liquid chromatography and electrospray ionization quadrupole orbitrap high-resolution mass spectrometry for determination of 166 pesticides in fruits and vegetables. *J. Agric. Food Chem.* **2012**, *60*, 12088−12104.

(15) AOAC Official Method 2007.01. Pesticide residues in foods by acetonitrile extraction and partitioning with magnesium sulfate gas chromatography/mass spectrometry and liquid chromatography/tandem mass spectrometry. First Action, 2007.

(16) Wang, J.; Wotherspoon, D. Determination of pesticides in apples by liquid chromatography with electrospray ionization tandem mass spectrometry and estimation of measurement uncertainty. *J. AOAC Int.* **2007**, *90*, 550−567.
(17) Non-targeted screening and accurate mass confirmation of 510 pesticides on the high resolution Exactive Benchtop LC/MS Orbitrap mass spectromter. Application Note: 51878; http://www.thermoscientific.fr/eThermo/CMA/PDFs/Articles/articlesFile_54153.pdf (accessed June 17, 2014).
(18) Method validation and quality control procedures for pesticide residues analysis in food and feed. Document No. SANCO/12495/2011 Supersedes Document No. SANCO/10684/2009 Implemented by 01/01/2012; http://ec.europa.eu/food/plant/protection/pesticides/docs/qualcontrol_en.pdf (accessed June 17, 2014).
(19) Thomas, A.; Geyer, H.; Schänzer, W.; Crone, C.; Kellmann, M.; Moehring, T.; Thevis, M. Sensitive determination of prohibited drugs in dried blood spots (DBS) for doping controls by means of a benchtop quadrupole/Orbitrap mass spectrometer. *Anal. Bioanal. Chem.* **2012**, *403*, 1279−1289.
(20) Hurtaud-Pessel, D.; Jagadeshwar-Reddy, T.; Verdon, E. Development of a new screening method for the detection of antibiotic residues in muscle tissues using liquid chromatography and high resolution mass spectrometry with a LC-LTQ-Orbitrap instrument. *Food Addit. Contam. Part A* **2011**, *28*, 1340−1351.

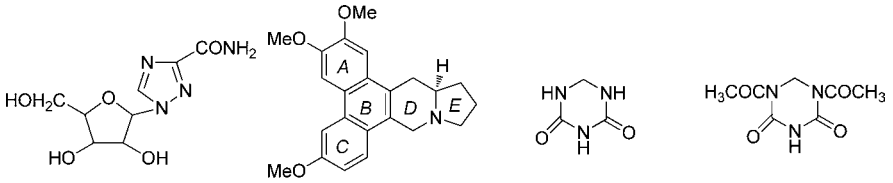


**Figure 1.** Chemical structures of ribavirin, antofine, DHT, and DADHT.

$GF_{254}$ with detection by UV. Melting points were determined using an X-4 binocular microscope melting point apparatus (Beijing Tech Instruments Co., Beijing, China), and the thermometer was uncorrected. $^1$H NMR spectra were obtained by using Bruker AV 400 and Varian Mercury plus 400 MHz spectrometers with $CDCl_3$ or DMSO-$d_6$ as solvent. Chemical shifts ($\delta$) were given in parts per million (ppm) and were measured downfield from internal tetramethylsilane. $^{13}$C NMR spectra were recorded by using a Bruker AV 400 (100 MHz) with $CDCl_3$ or DMSO-$d_6$ as solvent. Chemical shifts ($\delta$) were reported in parts per million using the solvent peak. High-resolution mass spectra were obtained with an FT-ICR MS spectrometer (Ionspec, 7.0 T).

**General Synthetic Procedure for Alcohols 45−47.** To a mixture of $LiAlH_4$ (0.03 mol) in 150 mL of THF at 0 °C was added corresponding acids **42−44** (0.02 mol) in portions. The solution was refluxed for an additional 2 h, then brought back to 0 °C, at which point 10 mL of EtOAc was added dropwise, followed by 10 mL of 2 N HCl. The solution was stirred and filtered, and the solvent was removed by rotary evaporation to give corresponding alcohols **45−47**.

*(2,3,6,7-Tetramethoxyphenanthren-9-yl)methanol (**45**):* yield, 95%; white powder; mp, 183−185 °C (lit.[25] mp, 181−182 °C); $^1$H NMR (400 MHz, $CDCl_3$) $\delta$ 7.83 (s, 1H), 7.78 (s, 1H), 7.59 (s, 1H), 7.55 (s, 1H), 7.21 (s, 1H), 5.13 (s, 2H), 4.13 (s, 3H), 4.13 (s, 3H), 4.07 (s, 3H), 4.03 (s, 3H), 1.75 (s, 1H); $^{13}$C NMR (100 MHz, $CDCl_3$) $\delta$ 148.8, 148.6, 148.4, 148.3, 131.9, 125.6, 124.7, 124.3, 124.1, 123.3, 108.1, 104.5, 102.9, 102.4, 64.1, 55.8, 55.8, 55.7, 55.6.

*(2,3,6-Trimethoxyphenanthren-9-yl)methanol (**46**):* yield, 93%; white powder; mp, 183−184 °C (lit.[26] mp, 187 °C); $^1$H NMR (400 MHz, $CDCl_3$) $\delta$ 8.05 (d, $J$ = 9.0 Hz, 1H), 7.83 (s, 1H), 7.77 (s, 1H), 7.45 (s, 1H), 7.21 (d, $J$ = 9.0 Hz, 1H), 7.09 (s, 1H), 5.07 (s, 2H), 4.06 (s, 3H), 4.00 (s, 3H), 3.96 (s, 3H), 2.02 (s, 1H); $^{13}$C NMR (100 MHz, $CDCl_3$) $\delta$ 158.0, 149.4, 149.1, 132.8, 131.7, 127.0, 126.1, 124.3, 124.1, 123.1, 115.1, 108.3, 104.6, 103.3, 64.2, 56.0, 55.8, 55.5.

*(3,6,7-Trimethoxyphenanthren-9-yl)methanol (**47**):* yield, 94%; white powder; mp, 161−162 °C (lit.[25] mp, 157−158 °C); $^1$H NMR (400 MHz, $CDCl_3$) $\delta$ 7.85 (s, 1H), 7.79 (s, 1H), 7.74 (d, $J$ = 8.7 Hz, 1H), 7.56 (s, 1H), 7.50 (s, 1H), 7.17 (d, $J$ = 8.7 Hz, 1H), 5.06 (s, 2H), 4.09 (s, 3H), 4.04 (s, 3H), 4.00 (s, 3H), 1.78 (s, 1H); $^{13}$C NMR (100 MHz, $CDCl_3$) $\delta$ 158.4, 149.4, 148.8, 131.4, 131.2, 130.2, 125.8, 125.5, 124.8, 124.6, 115.4, 104.8, 103.9, 103.7, 64.7, 56.0, 55.9, 55.5.

**Synthetic Procedure for 1.** Alcohol **45** (10 mmol) was dissolved in 200 mL of $CHCl_3$ and cooled to 0 °C. A solution of $PBr_3$ (15 mmol) in 40 mL of $CHCl_3$ was added dropwise under nitrogen. The solution was then stirred at room temperature for 4 h and poured over ice, and the two layers were separated. The organic phase was dried over anhydrous $Na_2SO_4$, filtered, and concentrated in vacuo to afford **48** as a white solid. Bromide **48** was then redissolved in 120 mL of DMF.

To the solution of $Me_2NH$ (14.2 mmol) in DMF (80 mL) was added $(i\text{-Pr})_2$NEt (15.6 mmol), and the mixture was stirred for 10 min. Then the above solution of bromide **48** was added. The mixture was stirred at 90 °C for 3 h and then cooled to room temperature. Then 300 mL of $H_2O$ was added, followed by 300 mL of $CH_2Cl_2$. The product was partitioned between $CH_2Cl_2$ and $H_2O$. The organic layer was dried over anhydrous $Na_2SO_4$, filtered, and concentrated to obtain a crude product. The crude product was purified by flash column chromatography to give compound **1** (2.8 g, 80%) as a white powder: mp, 157−159 °C; $^1$H NMR (400 MHz, DMSO-$d_6$) $\delta$ 8.01 (s, 1H), 7.98 (s, 1H), 7.68 (s, 1H), 7.52 (s, 1H), 7.37 (s, 1H), 4.02 (s, 3H), 4.02 (s, 3H), 3.90 (s, 3H), 3.90 (s, 3H), 3.76 (s, 2H), 2.24 (s, 6H); $^{13}$C NMR (100 MHz, DMSO-$d_6$) $\delta$ 149.0, 148.7, 148.6, 148.0, 130.1, 125.4, 125.2, 125.0, 124.6, 123.9, 108.4, 106.1, 103.9, 103.7, 62.7, 55.9, 55.8, 55.3, 55.1, 45.1; ESI-HRMS ($m/z$), calcd for $C_{21}H_{26}NO_4$ $[M + H]^+$ 356.1856, found 356.1853.

**General Synthetic Procedure for Compounds 24, 27, 30, 33, 36, 39, and 40.** Corresponding alcohols **45−47** (10 mmol) were dissolved in 200 mL of $CHCl_3$ and cooled to 0 °C. A solution of $PBr_3$ (15 mmol) in 40 mL of $CHCl_3$ was added dropwise under nitrogen. The solution was then stirred at room temperature for 4 h and poured over ice, and the two layers were separated. The organic phase was dried over anhydrous $Na_2SO_4$, filtered, and concentrated in vacuo to afford corresponding bromides **48−50**, which were then redissolved in 120 mL of DMF.

To the solution of corresponding alkylamines (3 mmol) in DMF (80 mL) was added $(i\text{-Pr})_2$NEt (12 mmol), and the mixture was stirred for 10 min. Then the above solution of bromide **48** was added. The mixture was stirred at 90 °C for 3 h and then cooled to room temperature. Then 300 mL of $H_2O$ was added, followed by 300 mL of $CH_2Cl_2$. The product was partitioned between $CH_2Cl_2$ and $H_2O$. The organic layer was dried over anhydrous $Na_2SO_4$, filtered, and concentrated to obtain a crude product. The crude product was purified by flash column chromatography to give compounds **24**, **27**, **30**, **33**, **36**, **39**, and **40**.

*Methyl 6-(bis((2,3,6,7-tetramethoxyphenanthren-9-yl)methyl)-amino)hexanoate (**24**):* yield, 60%; white powder; mp, 191−192 °C; $^1$H NMR (400 MHz, $CDCl_3$) $\delta$ 7.74 (s, 2H), 7.74 (s, 2H), 7.56 (s, 2H), 7.48 (s, 2H), 7.17 (s, 2H), 4.11 (s, 6H), 4.07 (s, 6H), 4.06 (s, 4H), 4.03 (s, 6H), 3.58 (s, 3H), 3.49 (s, 6H), 2.61 (t, $J$ = 8.0 Hz, 2H), 2.10 (t, $J$ = 8.0 Hz, 2H), 1.78−1.69 (m, 2H), 1.48−1.39 (m, 2H), 1.22−1.16 (m, 2H); $^{13}$C NMR (100 MHz, $CDCl_3$) $\delta$ 174.0, 149.1, 148.9, 148.8, 148.4, 130.6, 126.9, 126.1, 125.9, 124.9, 124.3, 108.1, 106.1, 103.0, 102.8, 59.6, 56.1, 56.0, 55.9, 55.4, 54.5, 51.4, 33.9, 27.1, 27.0, 24.7; ESI-HRMS ($m/z$), calcd for $C_{45}H_{51}NO_{10}Na$ $[M + Na]^+$ 788.3405, found 788.3405.

*Methyl 5-(bis((2,3,6,7-tetramethoxyphenanthren-9-yl)methyl)-amino)pentanoate (**27**):* yield, 50%; white powder; mp, 202−204 °C; $^1$H NMR (400 MHz, $CDCl_3$) $\delta$ 7.72 (s, 4H), 7.53 (s, 2H), 7.44 (s, 2H), 7.15 (s, 2H), 4.09 (s, 6H), 4.06 (s, 6H), 4.02 (s, 10H), 3.57 (s, 3H), 3.48 (s, 6H), 2.59 (t, $J$ = 8.0 Hz, 2H), 2.10 (t, $J$ = 8.0 Hz, 2H), 1.75−1.68 (m, 2H), 1.58−1.48 (m, 2H); $^{13}$C NMR (100 MHz, $CDCl_3$) $\delta$ 173.8, 149.2, 148.9, 148.8, 148.5, 130.5, 126.8, 126.1, 125.9, 125.0, 124.3, 108.2, 106.1, 103.0, 102.8, 59.5, 56.1, 56.0, 55.9, 55.5, 54.4, 51.4, 33.7, 26.7, 22.9; ESI-HRMS ($m/z$), calcd for $C_{44}H_{49}NO_{10}Na$ $[M + Na]^+$ 744.3249, found 744.3246.

*Methyl 4-(bis((2,3,6,7-tetramethoxyphenanthren-9-yl)methyl)-amino)butanoate (**30**):* yield, 67%, white powder; mp, 125−127 °C; $^1$H NMR (400 MHz, $CDCl_3$) $\delta$ 7.75 (s, 2H), 7.74 (s, 2H), 7.57 (s, 2H), 7.46 (s, 2H), 7.17 (s, 2H), 4.11 (s, 6H), 4.08 (s, 10H), 4.03 (s, 6H), 3.49 (s, 6H), 3.45 (s, 3H), 2.65 (t, $J$ = 8.0 Hz, 2H), 2.17 (t, $J$ = 8.0 Hz, 2H), 2.07−2.02 (m, 2H); $^{13}$C NMR (100 MHz, $CDCl_3$) $\delta$ 172.6, 148.2, 147.9, 147.8, 147.5, 129.3, 126.05, 124.9, 124.8, 123.9, 123.3, 107.2, 104.9, 102.0, 101.8, 58.4, 55.1, 55.0, 54.8, 54.4, 52.8, 50.3, 30.9, 21.6; ESI-HRMS ($m/z$), calcd for $C_{43}H_{47}NO_{10}Na$ $[M + Na]^+$ 760.3092, found 760.3099.

*Methyl 3-(bis((2,3,6,7-tetramethoxyphenanthren-9-yl)methyl)-amino)propanoate (**33**):* yield, 79%; white powder; mp, 145−147 °C; $^1$H NMR (400 MHz, $CDCl_3$) $\delta$ 7.74 (s, 2H), 7.73 (s, 2H), 7.57 (s,

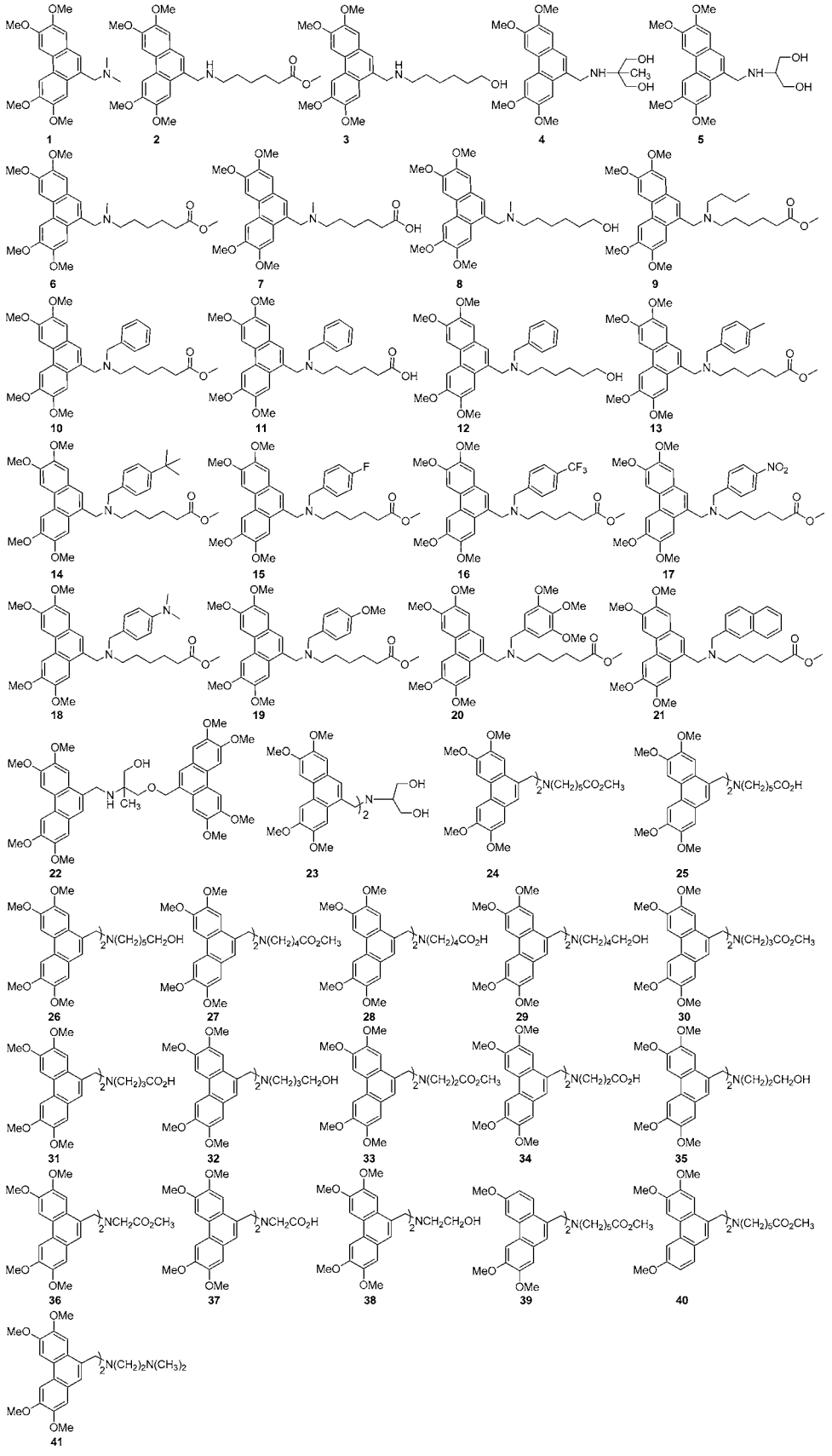

**Figure 2.** Chemical structures of antofine derivatives **1**−**41**.

2H), 7.43 (s, 2H), 7.16 (s, 2H), 4.10 (s, 6H), 4.09 (s, 4H), 4.07 (s, 6H), 4.03 (s, 6H), 3.53 (s, 6H), 3.41 (s, 3H), 3.05 (t, $J$ = 8.0 Hz, 2H), 2.62 (t, $J$ = 8.0 Hz, 2H); $^{13}$C NMR (100 MHz, $CDCl_3$) $\delta$ 172.9, 149.3, 148.9, 148.8, 148.6, 130.0, 126.9, 126.0, 125.8, 125.0, 124.4, 108.2,


dx.doi.org/10.1021/jf5028894 | J. Agric. Food Chem. 2014, 62, 10393−10404

106.0, 103.1, 102.8, 59.2, 56.1, 56.0, 55.9, 55.5, 51.4, 50.4, 32.1; ESI-HRMS ($m/z$), calcd for $C_{42}H_{45}NO_{10}Na$ $[M + Na]^+$ 746.2936, found, 746.2935.

*Methyl 2-(bis((2,3,6,7-tetramethoxyphenanthren-9-yl)methyl)-amino)acetate (**36**):* yield, 68%; white powder; mp, 126−128 °C; $^1$H NMR (400 MHz, DMSO-$d_6$) $\delta$ 7.96 (s, 2H), 7.95 (s, 2H), 7.63 (s, 2H), 7.52 (s, 2H), 7.34 (s, 2H), 4.20 (s, 4H), 4.01 (s, 6H), 3.99 (s, 6H), 3.90 (s, 6H), 3.57 (s, 3H), 3.43 (s, 2H), 3.38 (s, 6H); $^{13}$C NMR (100 MHz, $CDCl_3$) $\delta$ 171.8, 149.3, 149.0, 148.8, 148.7, 129.8, 127.0, 126.0, 125.8, 125.0, 124.5, 108.2, 106.4, 103.0, 102.9, 77.5, 77.1, 76.8, 58.8, 56.1, 56.0, 55.9, 55.7, 54.8, 51.2; ESI-HRMS ($m/z$), calcd for $C_{41}H_{43}NO_{10}Na$ $[M + Na]^+$ 732.2779, found 732.2774.

*Methyl 6-(bis((2,3,6-trimethoxyphenanthren-9-yl)methyl)-amino)hexanoate (**39**):* yield, 66%; white powder; mp, 189−190 °C; $^1$H NMR (400 MHz, $CDCl_3$) $\delta$ 8.04 (d, $J$ = 8.0 Hz, 2H), 7.82 (d, $J$ = 4.0 Hz, 4H), 7.47 (s, 2H), 7.16 (s, 2H), 6.92 (dd, $J$ = 12.0, 4.0 Hz, 2H), 4.09 (s, 6H), 4.03 (s, 6H), 4.00 (s, 10H), 3.59 (s, 3H), 2.56 (t, $J$ = 8.0 Hz, 2H), 2.09 (t, $J$ = 8.0 Hz, 2H), 1.68−1.61 (m, 2H), 1.46−1.39 (m, 2H), 1.18−1.10 (m, 2H); $^{13}$C NMR (100 MHz, $CDCl_3$) $\delta$ 173.1, 156.7, 148.3, 147.8, 130.7, 130.5, 127.0, 126.0, 124.7, 124.4, 123.2, 113.4, 107.1, 102.8, 102.3, 57.7, 55.0, 54.8, 54.4, 53.0, 50.3, 32.9, 26.0, 25.0, 23.6; ESI-HRMS ($m/z$), calcd for $C_{43}H_{47}NO_8Na$ $[M + Na]^+$ 728.3194, found 728.3196.

*Methyl 6-(bis((3,6,7-trimethoxyphenanthren-9-yl)methyl)-amino)hexanoate (**40**):* yield, 63%; white powder; mp, 111−113 °C; $^1$H NMR (400 MHz, $CDCl_3$) $\delta$ 7.85 (s, 2H), 7.82 (s, 2H), 7.75 (d, $J$ = 8.8 Hz, 2H), 7.61 (s, 2H), 7.48 (s, 2H), 7.18 (d, $J$ = 8.8 Hz, 2H), 4.07 (s, 6H), 4.05 (s, 4H), 4.01 (s, 6H), 3.58 (s, 3H), 3.47 (s, 6H), 2.60 (t, $J$ = 8.0 Hz, 2H), 2.09 (t, $J$ = 8.0 Hz, 2H), 1.77−1.69 (m, 2H), 1.46−1.38 (m, 2H), 1.22−1.13 (m, 2H); $^{13}$C NMR (100 MHz, $CDCl_3$) $\delta$ 173.9, 158.2, 149.2, 148.7, 131.0, 129.9, 127.4, 127.3, 125.7, 124.8, 115.4, 106.2, 103. 9, 103.5, 59.4, 56.0, 55.6, 55.4, 54.4, 51.4, 33.9, 27.1, 26.9, 24.7; ESI-HRMS ($m/z$), calcd for $C_{43}H_{47}NO_8Na$ $[M + Na]^+$ 728.3194, found 728.3192.

**General Synthetic Procedure for Compounds 25, 28, 31, 34, and 37.** The mixture of corresponding esters **24**, **27**, **30**, **33**, and **36** (0.34 mmol), 4 M NaOH (15 mL), and 1,4-dioxane (15 mL) was refluxed for 4 h and concentrated to 15 mL. The mixture was acidified (pH 6) with diluted hydrochloric acid and filtered to afford corresponding acids **25**, **28**, **31**, **34**, and **37**.

*6-(Bis((2,3,6,7-tetramethoxyphenanthren-9-yl)methyl)amino)-hexanoic acid (**25**):* yield, 92%; white powder; mp, 235 °C (dec); $^1$H NMR (400 MHz, DMSO-$d_6$) $\delta$ 7.95 (s, 2H), 7.94 (s, 2H), 7.62 (s, 2H), 7.39 (s, 2H), 7.32 (s, 2H), 4.00 (s, 6H), 3.98 (s, 10H), 3.89 (s, 6H), 3.33 (s, 6H), 2.45 (t, $J$ = 8.0 Hz, 2H), 1.82 (t, $J$ = 8.0 Hz, 2H), 1.72−1.63 (m, 2H), 1.34−1.25 (m, 2H), 1.15−1.05 (m, 2H); $^{13}$C NMR (100 MHz, DMSO-$d_6$) $\delta$ 177.0, 149.0, 148.7, 148.5, 148.0, 129.9, 126.5, 125.3, 125.2, 124.7, 123.9, 108.2, 105.8, 103.9, 103.6, 58.7, 55.8, 55.8, 55.3, 54.7, 54.3, 36.5, 27.3, 26.8, 25.6; ESI-HRMS ($m/z$), calcd for $C_{44}H_{49}NO_{10}Na$ $[M + Na]^+$ 774.3249, found 774.3247.

*5-(Bis((2,3,6,7-tetramethoxyphenanthren-9-yl)methyl)amino)-pentanoic acid (**28**):* yield, 82%; white powder; mp, >300 °C; $^1$H NMR (400 MHz, DMSO-$d_6$) $\delta$ 7.91 (s, 4H), 7.53 (s, 2H), 7.33 (s, 2H), 7.29 (s, 2H), 3.98 (s, 6H), 3.96 (s, 6H), 3.88 (s, 10H), 3.28 (s, 6H), 2.44 (t, $J$ = 8.0 Hz, 2H), 1.84 (t, $J$ = 8.0 Hz, 2H), 1.71−1.57 (m, 2H), 1.37−1.25 (m, 2H); $^{13}$C NMR (100 MHz, DMSO-$d_6$) $\delta$ 178.1, 149.0, 148.6, 148.5, 148.0, 129.9, 126.5, 125.3, 125.3, 124.6, 123.9, 108.2, 105.7, 103.9, 103.6, 58.5, 55.8, 55.7, 55.3, 54.7, 54.4, 36.7, 26.8, 24.0; ESI-HRMS ($m/z$), calcd for $C_{43}H_{47}NO_{10}Na$ $[M + Na]^+$ 760.3092, found 760.3088.

*4-(Bis((2,3,6,7-tetramethoxyphenanthren-9-yl)methyl)amino)-butanoic acid (**31**):* yield, 95%; white powder; mp, 224−226 °C; $^1$H NMR (400 MHz, DMSO-$d_6$) $\delta$ 7.95 (s, 2H), 7.94 (s, 2H), 7.63 (s, 2H), 7.43 (s, 2H), 7.32 (s, 2H), 4.00 (s, 10H), 3.98 (s, 6H), 3.89 (s, 6H), 3.35 (s, 6H), 2.55 (t, $J$ = 4.0 Hz, 2H), 1.95−1.88 (m, 2H), 1.86−1.79 (m, 2H); $^{13}$C NMR (100 MHz, DMSO-$d_6$) $\delta$ 176.7, 149.0, 148.6, 148.1, 130.0, 126.5, 125.4, 125.3, 124.7, 123.9, 108.3, 105.8, 104.0, 103.7, 58.7, 55.9, 55.8, 55.3, 54.9, 54.6, 35.3, 23.8; ESI-HRMS ($m/z$), calcd for $C_{42}H_{45}NO_{10}Na$ $[M + Na]^+$ 746.2936, found 746.2938.

*3-(Bis((2,3,6,7-tetramethoxyphenanthren-9-yl)methyl)amino)-propanoic acid (**34**):* yield, 97%; yellow powder; mp, 234−236 °C; $^1$H NMR (400 MHz, DMSO-$d_6$) $\delta$ 7.95 (s, 2H), 7.94 (s, 2H), 7.63 (s, 2H), 7.43 (s, 2H), 7.33 (s, 2H), 4.00 (s, 6H), 3.98 (s, 10H), 3.89 (s, 6H), 3.35 (s, 6H), 2.76 (t, $J$ = 8.0 Hz, 2H), 2.40−2.34 (t, $J$ = 8.0 Hz, 2H); $^{13}$C NMR (100 MHz, DMSO-$d_6$) $\delta$ 176.4, 149.0, 148.7, 148.5, 148.0, 130.1, 126.4, 125.4, 125.3, 124.7, 123.8, 108.2, 106.0, 103.9, 103.7, 58.5, 55.9, 55.8, 55.3, 54.8, 51.8, 35.6; ESI-HRMS ($m/z$), calcd for $C_{41}H_{43}NO_{10}Na$ $[M + Na]^+$ 732.2779, found 732.2772.

*2-(Bis((2,3,6,7-tetramethoxyphenanthren-9-yl)methyl)amino)-acetic acid (**37**):* yield, 96%; white powder; mp, >300 °C; $^1$H NMR (400 MHz, DMSO-$d_6$) $\delta$ 7.97 (s, 2H), 7.95 (s, 2H), 7.94 (s, 2H), 7.62 (s, 2H), 7.32 (s, 2H), 4.09 (s, 4H), 4.00 (s, 6H), 3.98 (s, 6H), 3.90 (s, 6H), 3.41 (s, 6H), 2.99 (s, 2H); $^{13}$C NMR (100 MHz, DMSO-$d_6$) $\delta$ 174.7, 148.9, 148.8, 148.5, 148.3, 130.7, 126.4, 125.8, 125.4, 124.6, 123.9, 108.3, 107.2, 103.8, 103.7, 58.7, 55.9, 55.8, 55.3, 55.3; ESI-HRMS ($m/z$), calcd for $C_{40}H_{41}NO_{10}Na$ $[M + Na]^+$ 718.2623, found 718.2616.

**General Synthetic Procedure for Compounds 26, 29, 32, 35, and 38.** To a mixture of $LiAlH_4$ (1.17 mmol) in 30 mL of THF at 0 °C were added corresponding esters **24**, **27**, **30**, **33**, and **36** (0.39 mmol) in portions. The solution was stirred for 8 h at room temperature and then brought back to 0 °C, at which point 30 mL of $CH_2Cl_2$ was added, followed by 30 mL of 2 M NaOH. The product was partitioned between $CH_2Cl_2$ and $H_2O$. The organic layer was dried over anhydrous $Na_2SO_4$, filtered, and concentrated to obtain a crude product. The crude product was purified by flash column chromatography to give compounds **26**, **29**, **32**, **35**, and **38**.

*6-(Bis((2,3,6,7-tetramethoxyphenanthren-9-yl)methyl)amino)-hexan-1-ol (**26**):* yield, 86%; white powder; mp, 163−165 °C; $^1$H NMR (400 MHz, $CDCl_3$) $\delta$ 7.75 (s, 4H), 7.57 (s, 2H), 7.50 (s, 2H), 7.17 (s, 2H), 4.11 (s, 6H), 4.08 (s, 6H), 4.06 (s, 4H), 4.03 (s, 6H), 3.72 (s, 1H), 3.48 (s, 6H), 3.44−3.39 (m, 2H), 2.60 (t, $J$ = 8.0 Hz, 2H), 1.77−1.68 (m, 2H), 1.36−1.29 (m, 2H), 1.23−1.17 (m, 2H), 1.14−1.09 (m, 2H); $^{13}$C NMR (100 MHz, $CDCl_3$) $\delta$ 148.1, 147.8, 147.8, 147.4, 129.6, 125.9, 125.1, 124.8, 123.9, 123.2, 107.1, 105.2, 101.9, 101.7, 61.7, 58.6, 55.1, 55.0, 54.8, 54.4, 53.4, 31.6, 26.2, 24.4; ESI-HRMS ($m/z$), calcd for $C_{44}H_{51}NO_9Na$ $[M + Na]^+$ 760.3456, found 760.3449.

*5-(Bis((2,3,6,7-tetramethoxyphenanthren-9-yl)methyl)amino)-pentan-1-ol (**29**):* yield, 91%; white powder; mp, 156−158 °C; $^1$H NMR (400 MHz, $CDCl_3$) $\delta$ 7.75 (s, 2H), 7.74 (s, 2H), 7.57 (s, 2H), 7.48 (s, 2H), 7.17 (s, 2H), 4.11 (s, 6H), 4.08 (s, 6H), 4.06 (s, 4H), 4.03 (s, 6H), 3.47 (s, 6H), 3.38 (t, $J$ = 4.0 Hz, 2H), 2.62 (t, $J$ = 8.0 Hz, 2H), 1.79−1.72 (m, 2H), 1.53 (s, 1H), 1.32−1.20 (m, 4H); $^{13}$C NMR (100 MHz, $CDCl_3$) $\delta$ 149.2, 148.9, 148.9, 148.5, 130.7, 126.9, 126.1, 125.9, 125.0, 124.3, 108.2, 106.2, 103.0, 102.9, 62.8, 59.7, 56.1, 56.1, 55.9, 55.5, 54.6, 32.5, 27.2, 23.7; ESI-HRMS ($m/z$), calcd for $C_{43}H_{49}NO_9Na$ $[M + Na]^+$ 746.3300, found 746.3297.

*4-(Bis((2,3,6,7-tetramethoxyphenanthren-9-yl)methyl)amino)-butan-1-ol (**32**):* yield, 91%; white powder; mp, 134−136 °C; $^1$H NMR (400 MHz, $CDCl_3$) $\delta$ 7.70 (s, 4H), 7.53 (s, 2H), 7.42 (s, 2H), 7.14 (s, 2H), 4.09 (s, 6H), 4.05 (s, 6H), 4.01 (s, 10H), 3.46 (s, 6H), 3.38 (t, $J$ = 4.0 Hz, 2H), 2.60 (t, $J$ = 4.0 Hz, 2H), 1.80−1.71 (m, 2H), 1.47−1.38 (m, 2H); $^{13}$C NMR (100 MHz, $CDCl_3$) $\delta$ 148.1, 147.8, 147.7, 147.4, 129.4, 125.8, 125.0, 124.8, 123.9, 123.2, 107.1, 105.1, 101.9, 101.7, 61.3, 58.4, 55.0, 55.0, 54.8, 54.4, 53.5, 29.6, 22.5; ESI-HRMS ($m/z$), calcd for $C_{42}H_{47}NO_9Na$ $[M + Na]^+$ 732.3143, found 732.3148.

*3-(Bis((2,3,6,7-tetramethoxyphenanthren-9-yl)methyl)amino)-propan-1-ol (**35**):* yield, 97%; white powder; mp, 214−216 °C; $^1$H NMR (400 MHz, $CDCl_3$) $\delta$ 7.74 (s, 4H), 7.60 (s, 2H), 7.35 (s, 2H), 7.17 (s, 2H), 4.11 (s, 6H), 4.09 (s, 4H), 4.06 (s, 6H), 4.02 (s, 6H), 3.48 (s, 6H), 3.42 (t, $J$ = 4.0 Hz, 2H), 2.89−2.81 (m, 2H), 1.94−1.86 (m, 2H), 1.43 (s, 1H); $^{13}$C NMR (100 MHz, $CDCl_3$) $\delta$ 148.3, 147.9, 147.8, 147.7, 128.6, 126.5, 124.7, 123.9, 123.4, 107.1, 104.5, 102.1, 101.8, 61.7, 58.4, 55.1, 54.9, 54.9, 54.3, 52.5, 28.1; ESI-HRMS ($m/z$), calcd for $C_{41}H_{45}NO_9Na$ $[M + Na]^+$ 718.2987, found 718.2986.

*2-(Bis((2,3,6,7-tetramethoxyphenanthren-9-yl)methyl)amino)-ethanol (**38**):* yield, 58%; white powder; mp, 246−248 °C; $^1$H NMR (400 MHz, $CDCl_3$) $\delta$ 7.76 (s, 2H), 7.74 (s, 2H), 7.58 (s, 2H), 7.29 (s, 2H), 7.18 (s, 2H), 4.16 (s, 4H), 4.11 (s, 6H), 4.06 (s, 6H), 4.03 (s,

6H), 3.64 (s, 2H), 3.41 (s, 6H), 2.86 (s, 2H); $^{13}$C NMR (100 MHz, $CDCl_3$) $\delta$ 148.4, 148.0, 147.9, 147.9, 128.5, 126.7, 124.7, 124.1, 123.6, 107.2, 104.0, 102.3, 101.8, 58.6, 57.9, 55.1, 55.0, 54.9, 54.6, 54.2; ESI-HRMS ($m/z$), calcd for $C_{40}H_{43}NO_9Na$ $[M + Na]^+$ 704.2830, found 704.2823.

**Synthetic Procedure for 2,3,6,7-Tetramethoxyphenanthrene-9-carbaldehyde (51).** A mixture of alcohol **45** (5 g, 15.23 mmol), silica (10 g), and pyridinium chlorochromate (PCC, 9.85 g, 45.69 mmol) in $CH_2Cl_2$ (150 mL) was stirred at room temperature for 10 h and then filtered. The filtrate was concentrated by rotary evaporation and purified by flash column chromatography to give compound **51** (4.02 g, 80%) as a yellow powder: mp, 227−228 °C (lit.[27] mp, 210−214 °C); $^1$H NMR (400 MHz, $CDCl_3$) $\delta$ 10.27 (s, 1H), 8.98 (s, 1H), 8.07 (s, 1H), 7.80 (s, 1H), 7.78 (s, 1H), 7.35 (s, 1H), 4.17 (s, 3H), 4.14 (s, 3H), 4.11 (s, 3H), 4.07 (s, 3H).

**Synthetic Procedure for Methyl 6-(((2,3,6,7-Tetramethoxyphenanthren-9-yl)methyl)amino)hexanoate (2).** A mixture of aldehyde **51** (1.2 g, 3.68 mmol), $Et_3N$ (0.42 g, 4.12 mmol), AcOH (5 drops), and methyl 6-aminohexanoate hydrochloride (0.74 g, 4.05 mmol) in $CH_2Cl_2$ (40 mL) was refluxed for 6 h. The solution was cooled to room temperature and concentrated in vacuo. The resulting solid was dissolved in MeOH (30 mL), followed by the addition of AcOH (5 drops) and $NaBH_3CN$ (0.47 g, 7.40 mmol). The solution was stirred at room temperature for 3 h and concentrated in vacuo. To the resulting mixture were added $CH_2Cl_2$ (30 mL), $H_2O$ (20 mL), and saturated $NaHCO_3$ solution (10 mL), and the two layers were separated. The organic phase was dried over anhydrous $Na_2SO_4$, filtered, concentrated, and purified by flash column chromatography to give compound **2** (1.14 g, 68%) as a yellow powder: mp, 104−106 °C; $^1$H NMR (400 MHz, $CDCl_3$) $\delta$ 7.75 (s, 1H), 7.67 (s, 1H), 7.58 (s, 1H), 7.42 (s, 1H), 7.18 (s, 1H), 4.16 (s, 2H), 4.08 (s, 3H), 4.07 (s, 3H), 4.06 (s, 3H), 4.02 (s, 3H), 3.64 (s, 3H), 2.79 (t, $J$ = 8.0 Hz, 2H), 2.28 (t, $J$ = 8.0 Hz, 2H), 1.71−1.65 (m, 2H), 1.64−1.57 (m, 2H), 1.40−1.33 (m, 2H); $^{13}$C NMR (100 MHz, $CDCl_3$) $\delta$ 174.1, 149.3, 149.0, 148.9, 148.8, 130.1, 126.0, 125.1, 125.0, 124.8, 124.3, 108.3, 104.7, 103.4, 102.8, 56.1, 56.0, 56.0, 55.9, 51.7, 51.5, 49.2, 33.9, 29.2, 26.8, 24.7; ESI-HRMS ($m/z$), calcd for $C_{26}H_{33}NO_6Na$ $[M + Na]^+$ 478.2200, found 478.2208.

**Synthetic Procedure for 6-(((2,3,6,7-Tetramethoxyphenanthren-9-yl)methyl)amino)hexan-1-ol (3).** A procedure similar to that used for the preparation of compounds **26**, **29**, **32**, **35**, and **38** was used: yield, 89%; white powder; mp, 83−85 °C; $^1$H NMR (400 MHz, DMSO-$d_6$) $\delta$ 8.02 (s, 1H), 7.98 (s, 1H), 7.60 (s, 1H), 7.58 (s, 1H), 7.34 (s, 1H), 4.34 (s, 1H), 4.13 (s, 2H), 4.03 (s, 3H), 4.02 (s, 3H), 3.92 (s, 3H), 3.90 (s, 3H), 3.40−3.36 (m, 2H), 2.67 (t, $J$ = 6.8 Hz, 2H), 1.56−1.47 (m, 2H), 1.44−1.39 (m, 2H), 1.35−1.28 (m, 4H); $^{13}$C NMR (100 MHz, $CDCl_3$) $\delta$ 149.1, 148.9, 148.8, 148.6, 130.8, 126.0, 125.1, 125.0, 124.3, 124.1, 108.2, 104.6, 103.3, 102.7, 62.7, 56.0, 56.0, 55.9, 52.1, 49.7, 32.7, 29.8, 27.1, 25.7; ESI-HRMS ($m/z$), calcd for $C_{25}H_{34}NO_5$ $[M + H]^+$ 428.2431, found 428.2440.

**General Synthetic Procedure for Compounds 6, 9, 10, and 13−21.** A mixture of compound **3** (0.18 g, 0.40 mmol) and NaH (0.03 g, 1.20 mmol) was stirred at room temperature for 30 min, and then corresponding bromides or iodides (0.60 mmol) were added. The solution was stirred for a further 3 h, followed by the addition of $H_2O$ (150 mL) and $CH_2Cl_2$ (100 mL), and the two layers were separated. The organic phase was dried over anhydrous $Na_2SO_4$, filtered, concentrated, and purified by flash column chromatography to give corresponding compounds **6**, **9**, **10**, and **13−21**.

*Methyl 6-(methyl((2,3,6,7-tetramethoxyphenanthren-9-yl)methyl)amino)hexanoate (**6**):* reaction with $CH_3I$, yield, 89%; yellow powder; mp, 128−129 °C; $^1$H NMR (400 MHz, DMSO-$d_6$) $\delta$ 8.00 (s, 1H), 7.98 (s, 1H), 7.77 (s, 1H), 7.51 (s, 1H), 7.36 (s, 1H), 4.02 (s, 3H), 4.02 (s, 3H), 3.90 (s, 6H), 3.81 (s, 2H), 3.55 (s, 3H), 2.43 (t, $J$ = 8.0 Hz, 2H), 2.22 (t, $J$ = 8.0 Hz, 2H), 2.13 (s, 3H), 1.56−1.52 (m, 2H), 1.48−1.41 (m, 2H), 1.31−1.26 (m, 2H); $^{13}$C NMR (100 MHz, $CDCl_3$) $\delta$ 173.1, 148.1, 147.9, 147.8, 147.4, 124.9, 124.0, 123.3, 107.2, 104.9, 102.0, 101.8, 56.7, 55.1, 55.0, 54.9, 54.8, 50.5, 40.9, 32.9, 26.1, 26.0, 23.8; ESI-HRMS ($m/z$), calcd for $C_{27}H_{35}NO_6$ $[M + Na]^+$ 492.2357, found 492.2361.

*Methyl 6-(butyl((2,3,6,7-tetramethoxyphenanthren-9-yl)methyl)amino)hexanoate (**9**):* reaction with BuI, yield, 80%; yellow powder; mp, 96−98 °C; $^1$H NMR (400 MHz, $CDCl_3$) $\delta$ 7.97 (s, 1H), 7.81 (s, 1H), 7.79 (s, 1H), 7.50 (s, 1H), 7.20 (s, 1H), 4.13 (s, 6H), 4.04 (s, 6H), 3.94 (s, 2H), 3.62 (s, 3H), 2.52−2.42 (m, 4H), 2.18 (t, $J$ = 7.2 Hz, 2H), 1.56−1.46 (m, 6H), 1.31−1.20 (m, 4H), 0.84 (t, $J$ = 7.2 Hz, 3H); $^{13}$C NMR (100 MHz, $CDCl_3$) $\delta$ 174.1, 149.0, 148.8, 148.7, 148.2, 131.4, 126.1, 126.1, 125.7, 124.9, 124.2, 108.2, 106.5, 102.9, 102.8, 59.3, 56.1, 56.0, 55.9, 53.9, 53.5, 51.4, 34.0, 29.4, 27.0, 26.7, 24.8, 20.7, 14.1; ESI-HRMS ($m/z$), calcd for $C_{30}H_{42}NO_6$ $[M + H]^+$ 512.3007, found 512.3012.

*Methyl 6-(benzyl((2,3,6,7-tetramethoxyphenanthren-9-yl)methyl)amino)hexanoate (**10**):* reaction with BnBr, yield, 95%; yellow powder; mp, 90−92 °C; $^1$H NMR (400 MHz, DMSO-$d_6$) $\delta$ 7.99 (s, 1H), 7.97 (s, 1H), 7.74 (s, 1H), 7.60 (s, 1H), 7.36 (s, 1H), 7.33−7.27 (m, 4H), 7.23−7.20 (m, 1H), 4.02 (s, 3H), 4.01 (s, 3H), 3.93 (s, 2H), 3.90 (s, 3H), 3.83 (s, 3H), 3.56 (s, 2H), 3.52 (s, 3H), 2.38 (t, $J$ = 8.0 Hz, 2H), 2.10 (t, $J$ = 8.0 Hz, 2H), 1.56−1.47 (m, 2H), 1.34−1.25 (m, 2H), 1.17−1.09 (m, 2H); $^{13}$C NMR (100 MHz, $CDCl_3$) $\delta$ 173.0, 148.1, 147.8, 147.8, 147.2, 138.9, 129.9, 128.1, 127.1, 125.8, 125.2, 125.0, 124.0, 123.3, 107.2, 105.5, 101.9, 101.9, 58.2, 58.0, 55.1, 55.0, 55.0, 54.9, 52.6, 50.4, 32.9, 25.9, 25.6, 23.7; ESI-HRMS ($m/z$), calcd for $C_{33}H_{39}NO_6Na$ $[M + Na]^+$ 568.2670, found 568.2674.

*Methyl 6-((4-methylbenzyl)((2,3,6,7-tetramethoxyphenanthren-9-yl)methyl)amino)hexanoate (**13**):* reaction with *p*-methylbenzyl bromide, yield, 70%; white powder; mp, 88−90 °C; $^1$H NMR (400 MHz, $CDCl_3$) $\delta$ 7.85 (s, 1H), 7.80 (s, 1H), 7.78 (s, 1H), 7.53 (s, 1H), 7.20−7.18 (m, 3H), 7.07 (d, $J$ = 7.6 Hz, 2H), 4.12 (s, 3H), 4.11 (s, 3H), 4.04 (s, 3H), 3.96 (s, 5H), 3.61 (s, 3H), 3.54 (s, 2H), 2.44 (t, $J$ = 7.2 Hz, 2H), 2.31 (s, 3H), 2.15 (t, $J$ = 7.6 Hz, 2H), 1.61−1.55 (m, 2H), 1.50−1.42 (m, 2H), 1.24−1.17 (m, 2H); $^{13}$C NMR (100 MHz, $CDCl_3$) $\delta$ 174.2, 149.2, 149.0, 148.9, 148.4, 136.9, 136.5, 131.2, 129.3, 128.9, 126.3, 126.2, 126.2, 125.1, 124.4, 108.3, 106.7, 103.1, 103.0, 59.3, 58.8, 56.3, 56.1, 56.0, 53.6, 51.5, 34.1, 27.1, 26.8, 24.9, 21.2; ESI-HRMS ($m/z$), calcd for $C_{34}H_{42}NO_6$ $[M + H]^+$ 560.3007, found 560.3010.

*Methyl 6-((4-(tert-butyl)benzyl)((2,3,6,7-tetramethoxyphenanthren-9-yl)methyl)amino)hexanoate (**14**):* reaction with 4-*tert*-butylbenzyl bromide, yield, 92%; yellow powder; mp, 84−86 °C; $^1$H NMR (400 MHz, $CDCl_3$) $\delta$ 7.80 (s, 1H), 7.79 (s, 1H), 7.77 (s, 1H), 7.54 (s, 1H), 7.28 (d, $J$ = 8.0 Hz, 2H), 7.24 (d, $J$ = 8.0 Hz, 2H), 7.20 (s, 1H), 4.12 (s, 3H), 4.11 (s, 3H), 4.04 (s, 3H), 3.96 (s, 2H), 3.93 (s, 3H), 3.61 (s, 3H), 3.56 (s, 2H), 2.46 (t, $J$ = 7.2 Hz, 2H), 2.15 (t, $J$ = 7.6 Hz, 2H), 1.61−1.56 (m, 2H), 1.48−1.42 (m, 2H), 1.29 (s, 9H), 1.24−1.19 (m, 2H); $^{13}$C NMR (100 MHz, $CDCl_3$) $\delta$ 174.1, 149.7, 149.1, 148.8, 148.8, 148.2, 136.8, 131.1, 128.9, 126.9, 126.2, 126.0, 125.0, 125.0, 124.3, 108.2, 106.6, 102.9, 59.2, 58.7, 56.1, 56.1, 56.0, 55.9, 53.7, 51.4, 34.4, 34.0, 31.4, 26.9, 26.7, 24.7; ESI-HRMS ($m/z$), calcd for $C_{37}H_{48}NO_6$ $[M + H]^+$ 602.3476, found 602.3481.

*Methyl 6-((4-fluorobenzyl)((2,3,6,7-tetramethoxyphenanthren-9-yl)methyl)amino)hexanoate (**15**):* reaction with 4-fluorobenzyl bromide, yield, 94%; white powder; mp, 116−118 °C; $^1$H NMR (400 MHz, $CDCl_3$) $\delta$ 7.85 (s, 1H), 7.81 (s, 1H), 7.78 (s, 1H), 7.54 (s, 1H), 7.23−7.20 (m, 3H), 6.93 (t, $J$ = 8.8 Hz, 2H), 4.13 (s, 3H), 4.12 (s, 3H), 4.04 (s, 3H), 3.98 (s, 3H), 3.98 (s, 2H), 3.62 (s, 3H), 3.52 (s, 2H), 2.45 (t, $J$ = 7.6 Hz, 2H), 2.18 (t, $J$ = 7.6 Hz, 2H), 1.64−1.57 (m, 2H), 1.53−1.45 (m, 2H), 1.27−1.20 (m, 2H); $^{13}$C NMR (100 MHz, $CDCl_3$) $\delta$ 174.0, 149.2, 148.9, 148.8, 148.3, 144.3, 130.5, 129.4, 129.1, 128.8, 128.5, 128.3, 126.3, 125.9, 125.8, 125.6, 125.1, 125.0, 125.0, 124.9, 124.9, 124.4, 122.9, 120.2, 108.1, 106.3, 102.9, 102.8, 59.3, 58.3, 56.1, 56.0, 55.9, 55.9, 54.3, 51.5, 33.9, 27.0, 26.8, 24.7.

*Methyl 6-(((2,3,6,7-tetramethoxyphenanthren-9-yl)methyl)(4-(trifluoromethyl)benzyl)amino)hexanoate (**16**):* reaction with 4-(trifluoromethyl)benzyl bromide, yield, 88%; white powder; mp, 127−129 °C; $^1$H NMR (400 MHz, DMSO-$d_6$) $\delta$ 7.99 (s, 1H), 7.96 (s, 1H), 7.71 (s, 1H), 7.63 (d, $J$ = 8.0 Hz, 2H), 7.61 (s, 1H), 7.49 (d, $J$ = 8.0 Hz, 2H), 7.36 (s, 1H), 4.02 (s, 3H), 4.01 (s, 3H), 3.97 (s, 2H), 3.90 (s, 3H), 3.84 (s, 3H), 3.64 (s, 2H), 3.52 (s, 3H), 2.41 (t, $J$ = 7.2 Hz, 2H), 2.12 (t, $J$ = 7.2 Hz, 2H), 1.58−1.51 (m, 2H), 1.35−1.28 (m, 2H), 1.18−1.13 (m, 2H); $^{13}$C NMR (100 MHz, $CDCl_3$) $\delta$ 174.0,

149.2, 148.9, 148.8, 148.3, 144.3, 130.5, 129.1, 128.9 (q, $J$ = 31.9 Hz, 1C), 126.3, 125.9, 125.8, 125.1, 124.9 (q, $J$ = 3.6 Hz, 1C), 124.4, 124.2 (q, $J$ = 270.1 Hz, 1C), 120.2, 108.1, 106.3, 102.9, 102.8, 59.3, 58.3, 56.1, 56.0, 55.9, 55.9, 54.3, 51.5, 33.9, 27.0, 26.8, 24.7; ESI-HRMS ($m/z$), calcd for $C_{34}H_{39}F_3NO_6$ $[M + H]^+$ 614.2724, found 614.2725.

*Methyl 6-((4-nitrobenzyl)((2,3,6,7-tetramethoxyphenanthren-9-yl)methyl)amino)hexanoate (**17**):* reaction with 4-nitrobenzyl bromide, yield, 96%; yellow powder; mp, 132−134 °C; $^1$H NMR (400 MHz, $CDCl_3$) $\delta$ 8.01 (d, $J$ = 8.4 Hz, 2H), 7.85 (s, 1H), 7.79 (s, 1H), 7.76 (s, 1H), 7.54 (s, 1H), 7.33 (d, $J$ = 8.4 Hz, 2H), 7.19 (s, 1H), 4.14 (s, 3H), 4.12 (s, 3H), 4.04 (s, 8H), 3.64 (s, 3H), 3.62 (s, 2H), 2.52 (t, $J$ = 7.2 Hz, 2H), 2.23 (t, $J$ = 7.2 Hz, 2H), 1.71−1.64 (m, 2H), 1.59−1.53 (m, 2H), 1.33−1.25 (m, 2H); $^{13}$C NMR (100 MHz, $CDCl_3$) $\delta$ 174.0, 149.3, 149.0, 148.9, 148.3, 148.2, 146.8, 130.2, 129.3, 126.4, 125.9, 125.7, 125.1, 124.5, 123.2, 108.1, 106.2, 103.0, 102.8, 59.5, 58.0, 56.1, 56.0, 55.9, 54.9, 51.5, 33.9, 27.0, 27.0, 24.8; ESI-HRMS ($m/z$) calcd for $C_{33}H_{39}N_2O_8$ $[M + H]^+$ 591.2701, found 591.2711.

*Methyl 6-((4-(dimethylamino)benzyl)((2,3,6,7-tetramethoxyphenanthren-9-yl)methyl)amino)hexanoate (**18**):* reaction with 4-(dimethylamino)benzyl bromide, yield, 37%; yellow powder; mp, 44−46 °C; $^1$H NMR (400 MHz, $CDCl_3$) $\delta$ 7.86 (s, 1H), 7.79 (s, 1H), 7.78 (s, 1H), 7.53 (s, 1H), 7.20 (s, 1H), 7.18 (d, $J$ = 8.0 Hz, 2H), 6.66 (d, $J$ = 8.0 Hz, 2H), 4.12 (s, 6H), 4.04 (s, 3H), 3.95 (s, 3H), 3.94 (s, 2H), 3.61 (s, 3H), 3.50 (s, 2H), 2.91 (s, 6H), 2.43 (t, $J$ = 6.8 Hz, 2H), 2.15 (t, $J$ = 7.6 Hz, 2H), 1.60−1.52 (m, 2H), 1.47−1.42 (m, 2H), 1.23−1.17 (m, 2H); $^{13}$C NMR (100 MHz, $CDCl_3$) $\delta$ 174.1, 149.7, 149.0, 148.8, 148.7, 148.2, 131.3, 130.1, 127.6, 126.1, 126.0, 124.9, 124.2, 112.5, 108.2, 106.7, 102.9, 102.8, 77.4, 77.3, 77.1, 76.7, 59.0, 58.3, 56.1, 56.1, 56.0, 55.9, 53.2, 51.4, 40.8, 34.0, 26.9, 26.6, 24.7; ESI-HRMS ($m/z$), calcd for $C_{35}H_{45}N_2O_6$ $[M + H]^+$ 589.3272, found 589.3278.

*Methyl 6-((4-methoxybenzyl)((2,3,6,7-tetramethoxyphenanthren-9-yl)methyl)amino)hexanoate (**19**):* reaction with 4-methoxybenzyl bromide, yield, 83%; white powder; mp, 92−94 °C; $^1$H NMR (400 MHz, $CDCl_3$) $\delta$ 7.86 (s, 1H), 7.80 (s, 1H), 7.78 (s, 1H), 7.53 (s, 1H), 7.21−7.20 (m, 3H), 6.80 (d, $J$ = 8.0 Hz, 2H), 4.12 (s, 3H), 4.12 (s, 3H), 4.04 (s, 3H), 3.97 (s, 3H), 3.96 (s, 2H), 3.77 (s, 3H), 3.61 (s, 3H), 3.51 (s, 2H), 2.44 (t, $J$ = 7.2 Hz, 2H), 2.16 (t, $J$ = 7.2 Hz, 2H), 1.63−1.56 (m, 2H), 1.49−1.43 (m, 2H), 1.26−1.19 (m, 2H); $^{13}$C NMR (100 MHz, $CDCl_3$) $\delta$ 174.1, 158.5, 149.1, 148.8, 148.7, 148.2, 131.9, 131.1, 130.3, 128.7, 126.2, 126.0, 125.0, 124.3, 113.5, 108.2, 106.6, 102.9, 102.8, 59.1, 58.2, 56.1, 56.0, 56.0, 55.9, 55.3, 53.4, 51.4, 34.0, 26.9, 26.7, 24.7; ESI-HRMS ($m/z$), calcd for $C_{34}H_{42}NO_7$ $[M + H]^+$ 576.2956, found 576.2952.

*Methyl 6-(((2,3,6,7-tetramethoxyphenanthren-9-yl)methyl)(3,4,5-trimethoxybenzyl)amino)hexanoate (**20**):* reaction with 4-(3,4,5-trimethoxy)benzyl bromide, yield, 54%; white powder; mp, 129−131 °C; $^1$H NMR (400 MHz, $CDCl_3$) $\delta$ 7.89 (s, 1H), 7.81 (s, 1H), 7.77 (s, 1H), 7.55 (s, 1H), 7.19 (s, 1H), 6.42 (s, 2H), 4.12 (s, 3H), 4.11 (s, 3H), 4.03 (s, 5H), 3.99 (s, 3H), 3.76 (s, 3H), 3.71 (s, 6H), 3.63 (s, 3H), 3.48 (s, 2H), 2.56 (t, $J$ = 7.6 Hz, 2H), 2.22 (t, $J$ = 7.2 Hz, 2H), 1.70−1.63 (m, 2H), 1.59−1.52 (m, 2H), 1.34−1.28 (m, 2H); $^{13}$C NMR (100 MHz, $CDCl_3$) $\delta$ 174.0, 152.8, 149.2, 148.9, 148.8, 148.3, 136.5, 136.0, 130.9, 126.2, 126.0, 125.9, 125.1, 124.3, 108.1, 106.6, 105.5, 103.0, 102.9, 60.8, 59.1, 58.7, 56.1, 56.0, 55.9, 54.6, 51.5, 34.0, 27.1, 26.9, 24.8; ESI-HRMS ($m/z$), calcd for $C_{36}H_{46}NO_9$ $[M + H]^+$ 636.3167, found 636.3172.

*Methyl 6-((naphthalen-2-ylmethyl)((2,3,6,7-tetramethoxyphenanthren-9-yl)methyl)amino)hexanoate (**21**):* reaction with 2-(bromomethyl)naphthalene, yield, 69%; yellow viscous oil; $^1$H NMR (400 MHz, DMSO-$d_6$) $\delta$ 7.99 (s, 1H), 7.97 (s, 1H), 7.88−7.82 (m, 4H), 7.79 (s, 1H), 7.63 (s, 1H), 7.50−7.37 (m, 3H), 7.37 (s, 1H), 4.02 (s, 3H), 4.01 (s, 5H), 3.91 (s, 3H), 3.81 (s, 3H), 3.72 (s, 2H), 3.50 (s, 3H), 2.44 (t, $J$ = 8.0 Hz, 2H), 2.09 (t, $J$ = 8.0 Hz, 2H), 1.59−1.52 (m, 2H), 1.32−1.26 (m, 2H), 1.18−1.12 (m, 2H); $^{13}$C NMR (100 MHz, $CDCl_3$) $\delta$ 174.0, 149.2, 148.9, 148.8, 148.3, 137.5, 133.3, 132.6, 130.9, 127.7, 127.6, 127.6, 126.3, 126.0, 125.9, 125.5, 125.0, 124.4, 108.2, 106.6, 102.9, 59.4, 59.1, 56.1, 56.0, 55.9, 53.8, 51.4, 33.9, 27.0, 26.7, 24.8; ESI-HRMS ($m/z$), calcd for $C_{37}H_{41}NO_6Na$ $[M + Na]^+$ 618.2826, found 618.2832.

*6-(Methyl((2,3,6,7-tetramethoxyphenanthren-9-yl)methyl)amino)hexanoic acid (**7**):* a procedure similar to that used for the preparation of compound **25** was used; yield, 60%; yellow powder; mp, 168−170 °C; $^1$H NMR (400 MHz, MeOD) $\delta$ 7.84 (s, 1H), 7.77 (s, 1H), 7.59 (s, 1H), 7.29 (s, 1H), 7.18 (s, 1H), 4.50 (s, 2H), 3.89 (s, 6H), 3.86 (s, 3H), 3.79 (s, 3H), 3.05−2.97 (m, 2H), 2.57 (s, 3H), 2.05 (t, $J$ = 6.4 Hz, 2H), 1.70−1.62 (m, 2H), 1.48−1.40 (m, 2H), 1.26−1.19 (m, 2H); $^{13}$C NMR (100 MHz, DMSO-$d_6$) $\delta$ 174.4, 149.3, 148.8, 148.6, 148.1, 125.2, 125.0, 124.6, 124.1, 108.4, 106.0, 104.0, 103.7, 62.8, 56.8, 55.9, 55.9, 55.4, 55.3, 40.9, 33.6, 26.3, 24.3; ESI-HRMS ($m/z$), calcd for $C_{26}H_{34}NO_6$ $[M + H]^+$ 456.2381, found 456.2387.

*6-(Benzyl((2,3,6,7-tetramethoxyphenanthren-9-yl)methyl)amino)hexanoic acid (**11**):* a procedure similar to that used for the preparation of compound **25** was used;yield, 73%; white powder; mp, 148−150 °C; $^1$H NMR (400 MHz, DMSO-$d_6$) $\delta$ 11.60 (s, 1H), 7.99 (s, 1H), 7.97 (s, 1H), 7.76 (s, 1H), 7.60 (s, 1H), 7.36 (s, 1H), 7.32−7.25 (m, 4H), 7.22−7.19 (m, 1H), 4.02 (s, 3H), 4.01 (s, 3H), 3.94 (s, 2H), 3.90 (s, 3H), 3.84 (s, 3H), 3.54 (s, 2H), 2.38 (t, $J$ = 6.8 Hz, 2H), 2.05 (t, $J$ = 7.2 Hz, 2H), 1.58−1.50 (m, 2H), 1.35−1.27 (m, 2H), 1.18−1.10 (m, 2H); $^{13}$C NMR (100 MHz, DMSO-$d_6$) $\delta$ 174.4, 149.0, 148.7, 148.6, 147.9, 139.6, 130.1, 128.7, 128.1, 126.7, 125.9, 125.4, 125.2, 124.7, 123.9, 108.3, 106.1, 103.8, 103.7, 58.4, 58.0, 55.9, 55.7, 55.4, 55.3, 53.1, 33.5, 26.4, 25.9, 24.2; ESI-HRMS ($m/z$), calcd for $C_{32}H_{38}NO_6$ $[M + H]^+$ 532.2694, found 532.2699.

*6-(Methyl((2,3,6,7-tetramethoxyphenanthren-9-yl)methyl)amino)hexan-1-ol (**8**):* a procedure similar to that used for the preparation of compound **26** was used; yield, 90%; white powder; mp, 101−103 °C; $^1$H NMR (400 MHz, DMSO-$d_6$) $\delta$ 8.00 (s, 1H), 7.98 (s, 1H), 7.78 (s, 1H), 7.51 (s, 1H), 7.36 (s, 1H), 4.31 (t, $J$ = 4.8 Hz, 1H), 4.02 (s, 6H), 3.90 (s, 6H), 3.80 (s, 2H), 3.33−3.27 (m, 2H), 2.43 (t, $J$ = 6.8 Hz, 2H), 2.12 (s, 3H), 1.57−1.49 (m, 2H), 1.35−1.33 (m, 2H), 1.30−1.25 (m, 2H), 1.23−1.18 (m, 2H); $^{13}$C NMR (100 MHz, $CDCl_3$) $\delta$ 149.1, 148.8, 148.7, 148.3, 130.7, 126.0, 126.0, 125.7, 125.0, 124.3, 108.2, 106.2, 102.9, 102.8, 62.9, 62.3, 57.8, 56.1, 56.0, 55.9, 55.8, 42.1, 32.7, 30.3, 29.7, 27.5, 27.3, 25.6; ESI-HRMS ($m/z$), calcd for $C_{26}H_{36}NO_5$ $[M + H]^+$ 442.2588, found 442.2596.

*6-(Benzyl((2,3,6,7-tetramethoxyphenanthren-9-yl)methyl)amino)hexan-1-ol (**12**):* a procedure similar to that used for the preparation of compound **26** was used; yield, 86%; yellow powder; mp, 99−101 °C; $^1$H NMR (400 MHz, DMSO-$d_6$) $\delta$ 7.99 (s, 1H), 7.97 (s, 1H), 7.77 (s, 1H), 7.59 (s, 1H), 7.36 (s, 1H), 7.30−7.27 (m, 4H), 7.22−7.17 (m, 1H), 4.25 (s, 1H), 4.02 (s, 3H), 4.01 (s, 3H), 3.94 (s, 2H), 3.90 (s, 3H), 3.84 (s, 3H), 3.54 (s, 2H), 3.27−3.20 (m, 2H), 2.38 (t, $J$ = 6.4 Hz, 2H), 1.59−1.52 (m, 2H), 1.26−1.23 (m, 2H), 1.17−1.12 (m, 2H), 1.09−1.03 (m, 2H); $^{13}$C NMR (100 MHz, $CDCl_3$) $\delta$ 148.1, 147.8, 147.7, 147.1, 138.9, 130.0, 128.2, 127.1, 125.8, 125.2, 125.0, 125.0, 123.9, 123.3, 107.1, 105.6, 101.8, 101.7, 61.8, 58.3, 58.0, 55.1, 55.0, 54.9, 54.9, 52.5, 31.7, 29.3, 26.0, 25.9, 24.4; ESI-HRMS ($m/z$), calcd for $C_{32}H_{40}NO_5$ $[M + H]^+$ 518.2901, found 518.2909.

**Synthetic Procedure for 2-Methyl-2-(((2,3,6,7-tetramethoxyphenanthren-9-yl)methyl)amino)propane-1,3-diol (4).** A mixture of 2-amino-2-methyl-1,3-propanediol (0.98 mmol), $Et_3N$ (1.34 mmol), and bromide **48** (0.89 mmol) in DMF (20 mL) was stirred at room temperature for 4 h, followed by the addition of $H_2O$ (150 mL) and $CH_2Cl_2$ (100 mL), and the two layers were separated. The organic phase was dried over anhydrous $Na_2SO_4$, filtered, concentrated, and purified by flash column chromatography to give compound **4** (0.24 g, 64%) as a white powder: mp, 108−110 °C; $^1$H NMR (400 MHz, $CDCl_3$) $\delta$ 7.78 (s, 1H), 7.72 (s, 1H), 7.70 (s, 1H), 7.58 (s, 1H), 7.20 (s, 1H), 4.23 (s, 2H), 4.09 (s, 6H), 4.04 (s, 3H), 4.02 (s, 3H), 3.59−3.50 (m, 4H), 1.16 (s, 3H); $^{13}$C NMR (100 MHz, $CDCl_3$) $\delta$ 149.30, 148.96, 148.93, 148.87, 130.59, 126.05, 125.48, 125.11, 125.02, 124.38, 108.23, 104.75, 103.37, 102.74, 67.22, 57.68, 56.04, 56.02, 55.99, 55.90, 44.48, 18.20; ESI-HRMS ($m/z$), calcd for $C_{23}H_{29}NO_6Na$ $[M + Na]^+$ 438.1887, found 438.1884.

*2-(((2,3,6,7-Tetramethoxyphenanthren-9-yl)methyl)amino)-propane-1,3-diol (**5**):* a procedure similar to that used for the preparation of compound **4** was used; yield, 51%; white powder; mp, 182−184 °C; $^1$H NMR (400 MHz, DMSO-$d_6$) $\delta$ 8.02 (s, 1H), 7.98 (s, 1H), 7.62 (s, 2H), 7.35 (s, 1H), 4.52 (s, 2H), 4.20 (s, 2H), 4.03 (s,

**Scheme 1. Synthesis of Compounds 1 and 24−40**

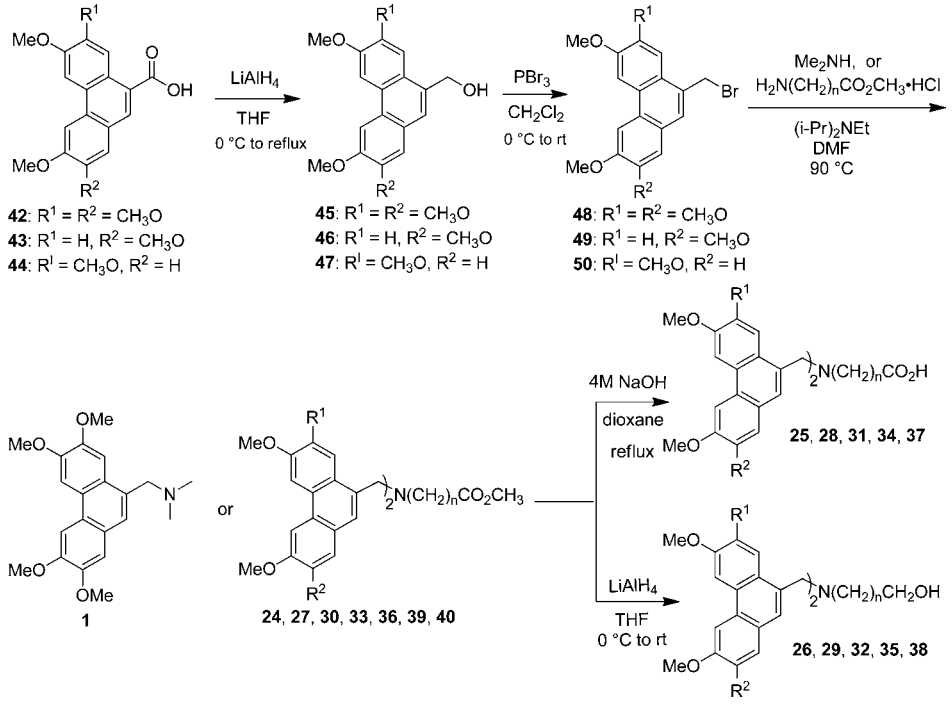


3H), 4.02 (s, 3H), 3.93 (s, 3H), 3.90 (s, 3H), 3.56−3.52 (m, 2H), 3.48−3.44 (m, 2H), 3.32 (s, 1H), 2.81−2.76 (m, 1H); $^{13}$C NMR (100 MHz, DMSO-$d_6$) $\delta$ 148.9, 148.7, 148.6, 148.3, 125.6, 124.8, 124.5, 123.9, 123.7, 108.4, 105.5, 104.1, 103.8, 61.2, 61.1, 55.9, 55.9, 55.4, 55.3, 49.9; ESI-HRMS ($m/z$), calcd for $C_{22}H_{27}NO_6Na$ [M + Na]$^+$ 424.1731, found 424.1739.

*2-Methyl-3-((2,3,6,7-tetramethoxyphenanthren-9-yl)methoxy)-2-(((2,3,6,7-tetramethoxyphenanthren-9-yl)methyl)amino)propan-1-ol (**22**):* a procedure similar to that used for the preparation of compound **24** was used; yield, 31%; white powder; mp, 161−163 °C; $^1$H NMR (400 MHz, DMSO-$d_6$) $\delta$ 8.02 (s, 1H), 7.99 (s, 1H), 7.97 (s, 1H), 7.95 (s, 1H), 7.65 (s, 1H), 7.55 (s, 2H), 7.35 (s, 2H), 7.26 (s, 1H), 4.96 (dd, $J$ = 28.0, 12.0 Hz, 2H), 4.64−4.61 (m, 1H), 4.02−4.01 (m, 14H), 3.89 (s, 3H), 3.88 (s, 3H), 3.81 (s, 3H), 3.74 (s, 3H), 3.54 (s, 2H), 3.47−3.44 (m, 2H), 1.15 (s, 3H); $^{13}$C NMR (100 MHz, DMSO-$d_6$) $\delta$ 149.2, 148.8, 148.8, 148.6, 148.5, 148.4, 148.3, 148.0, 132.4, 129.3, 125.6, 125.2, 125.0, 124.9, 124.6, 124.5, 124.2, 123.7, 123.6, 108.5, 108.2, 105.5, 105.2, 104.0, 103.9, 103.7, 103.6, 72.8, 72.1, 65.0, 56.6, 55.9, 55.8, 55.8, 55.3, 55.3, 55.1, 55.0, 44.4, 19.2; ESI-HRMS ($m/z$), calcd for $C_{42}H_{48}NO_{10}Na$ [M + Na]$^+$ 748.3092, found 748.3095.

*2-(Bis((2,3,6,7-tetramethoxyphenanthren-9-yl)methyl)amino)-propane-1,3-diol (**23**):* a procedure similar to that used for the preparation of compound **24** was used; yield, 69%; yellow powder; mp, 152−154 °C; $^1$H NMR (400 MHz, $CDCl_3$) $\delta$ 7.75 (s, 2H), 7.73 (s, 2H), 7.59 (s, 2H), 7.23 (s, 2H), 7.16 (s, 2H), 4.40 (s, 4H), 4.12 (s, 4H), 4.11 (s, 6H), 4.06 (s, 6H), 4.02 (s, 6H), 3.42 (s, 6H), 3.30−3.23 (m, 1H), 2.36 (s, 2H); $^{13}$C NMR (100 MHz, $CDCl_3$) $\delta$ 149.4, 149.0, 149.0, 148.9, 129.5, 128.1, 125.7, 125.7, 125.14, 124.5, 108.2, 104.8, 103.4, 102.8, 59.7, 56.1, 56.0, 55.9, 55.1, 54.6, 45.7; ESI-HRMS ($m/z$), calcd for $C_{41}H_{45}NO_8Na$ [M + Na]$^+$ 734.2936, found 734.2941.

**Synthetic Procedure for $N^1$,$N^1$-Dimethyl-$N^2$,$N^2$-bis((2,3,6,7-tetramethoxyphenanthren-9-yl)methyl)ethane-1,2-diamine (41).** A mixture of aldehyde **51** (0.38 g, 1.17 mmol), *N*,*N*-dimethylethylenediamine (0.049 g, 0.55 mmol), $NaBH_3CN$ (0.11 g, 1.65 mmol), AcOH (5 drops) in MeOH (30 mL), and $CH_2Cl_2$ (15 mL) was refluxed for 6 h. Then the mixture was cooled to room temperature, concentrated, and purified by flash column chromatography to give compound **41** (0.15 g, 39%) as a yellow powder: mp, 138−140 °C; $^1$H NMR (400 MHz, $CDCl_3$) $\delta$ 7.73 (s, 2H), 7.72 (s, 2H), 7.58 (s, 2H), 7.45 (s, 2H), 7.17 (s, 2H), 4.10 (s, 6H), 4.07 (s, 10H), 4.03 (s, 6H), 3.52 (s, 6H), 2.85 (t, $J$ = 6.8 Hz, 2H), 2.62 (t, $J$ = 6.8 Hz, 2H), 2.13 (s, 6H); $^{13}$C NMR (100 MHz, $CDCl_3$) $\delta$ 148.2, 147.9, 147.8, 147.5, 129.1, 125.9, 124.9, 124.8, 123.9, 123.3, 107.1, 105.0, 102.0, 101.7, 58.9, 56.2, 55.1, 55.0, 54.9, 54.5, 51.2, 44.3; ESI-HRMS ($m/z$), calcd for $C_{42}H_{49}N_2O_8$ [M + H]$^+$ 709.3483, found 709.3482.

**Antiviral Biological Assay.** *Phytotoxic Activity.* Growing 5−6-leaf stage tobaccos (*Nicotiana tabacum* var. Xanthi nc) were selected. The compound solution (500 $\mu$g/mL) was smeared on the leaves. The local lesion numbers were then counted and recorded 3−4 days later.

*Purification of Tobacco Mosaic Virus.* Using Gooding's method,[21] the upper leaves of *N. tabacum* L. inoculated with TMV were selected and ground in phosphate buffer and then filtered through a double-layer pledget. The filtrate was centrifuged at 10000*g* for 15 min, treated with polyethylene glycol (PEG) twice, and centrifuged again. The whole experiment was processed at 4 °C. Absorbance value was estimated at 260 nm by ultraviolet spectrophotometer.

$$\text{virus concn} = (A_{260} \times \text{dilution ratio})E^{0.1\%,260\text{nm}}_{1\text{cm}}$$

*Antiviral Activity of Compounds against TMV in Vitro.* The in vitro activity of the synthesized compounds against TMV was evaluated by using the conventional half-leaf method.[22] Fresh leaf of the growing 5−6-leaf stage tobacco (*N. tabacum* var. Xanthi nc) mechanically inoculated (concentration of TMV = 10 $\mu$g/mL) was cut into halves along the main vein. The halves were immersed into the solution of 500 $\mu$g/mL of the compounds and double-distilled water for 20 min, respectively, and then kept still at 25 °C for 72 h. Each compound was replicated at least three times.

*Protective Effect of Compounds against TMV in Vivo.*[23] Growing 5−6-leaf stage tobaccos (*N. tabacum* var. Xanthi nc) were selected. The compound solution was smeared on the left side, and the solvent serving as control was smeared on the right side of growing tobacco (*N. tabacum* var. Xanthi nc) leaves of the same ages. The leaves were then inoculated with the virus after 12 h. A brush was dipped in TMV of 10 $\mu$g/mL to inoculate the leaves, which were previously scattered with silicon carbide. The leaves were then washed with water and rubbed softly along the nervature once or twice. The local lesion numbers appearing 3−4 days after inoculation were counted. There are three replicates for each compound.


dx.doi.org/10.1021/jf5028894 | J. Agric. Food Chem. 2014, 62, 10393−10404

**Scheme 2. Synthesis of Compounds 2, 3, and 6−21**

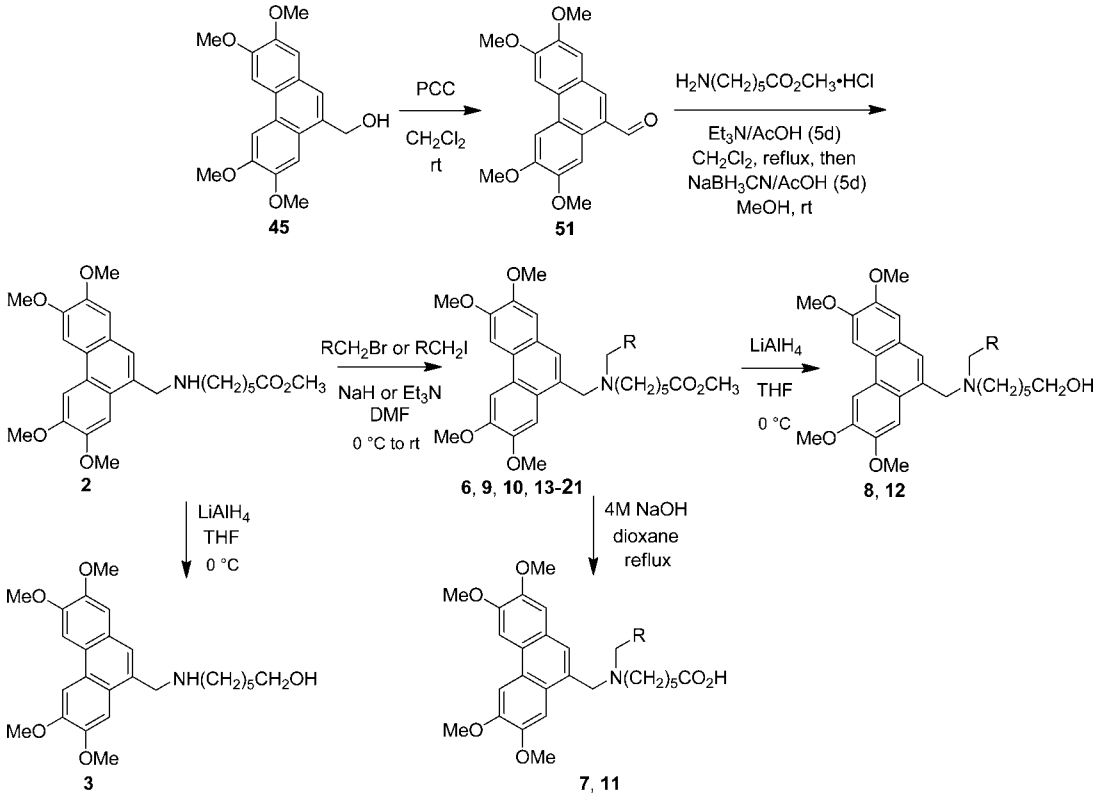


**Scheme 3. Synthesis of Compounds 4, 5, 22, and 23**

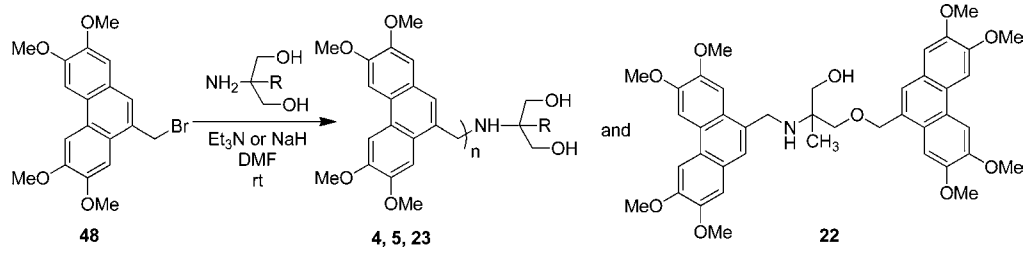


*Inactivation Effect of Compounds against TMV in Vivo.*[23] Growing 5−6-leaf stage tobaccos (*N. tabacum* var. Xanthi nc) were selected. The virus of 10 μg/mL was inhibited by mixing with the compound solution at the same volume for 30 min. The mixture was then inoculated on the left sides of the leaves, whereas the right sides of the leaves were inoculated with the mixture of solvent and the virus for control. The local lesion numbers were recorded 3−4 days after inoculation. There were three replicates for each compound.

*Curative Effect of Compounds against TMV in Vivo.*[23] Growing 5−6-leaf stage tobaccos (*N. tabacum* var. Xanthi nc) were selected. TMV (concentration = 10 μg/mL) was dipped and inoculated on the whole leaves. Then the leaves were washed with water and dried. The compound solution was smeared on the left side, and the solvent was smeared on the right side for control. The local lesion numbers were then counted and recorded 3−4 days after inoculation. There were three replicates for each compound.

The in vitro and in vivo inhibition rates of the compound were then calculated according to the following formula ("av" means average, and controls were not treated with compound):

$$\text{inhibition rate (\%)} = [(\text{av local lesion no. of control} - \text{av local lesion no. of drug-treated}) / \text{av local lesion no. of control}] \times 100\%$$

## RESULTS AND DISCUSSION

**Chemistry.** Reduction of acids **42**−**44**[24] with $LiAlH_4$ gave alcohols **45**−**47**, which were treated with $PBr_3$ to afford bromides **48**−**50**. Coupling of **48**−**50** with corresponding amines gave the antofine derivatives **1**, **24**, **27**, **30**, **33**, **36**, **39**, and **40**. Treatment of **24**, **27**, **30**, **33**, and **36** with 4 M NaOH solution gave acids **25**, **28**, **31**, **34**, and **37**. Reduction of **24**, **27**, **30**, **33**, and **36** with $LiAlH_4$ afforded alcohols **26**, **28**, **32**, **35**, and **38** (Scheme 1).

**Scheme 4. Synthesis of Compound 41**

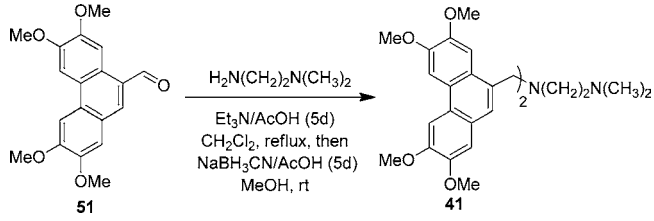


As shown in Scheme 2, oxidation of alcohol **45** with pyridiniumchlorochromate (PCC) gave aldehyde **51**, which was


dx.doi.org/10.1021/jf5028894 | J. Agric. Food Chem. 2014, 62, 10393−10404

Table 1. Antiviral Activity of Compounds 1−41 against TMV[a]

| | | | in vivo | | |
|---|---|---|---|---|---|
| compd | concn (μg/mL) | in vitro inhibition rate (%) | inactivation effect (%) | curative effect (%) | protection effect (%) |
| **1** | 500 | 43.0 ± 1.8 | 47.8 ± 2.3 | 46.9 ± 1.5 | 42.6 ± 3.1 |
| | 100 | 22.3 ± 2.0 | 9.7 ± 3.4 | 14.2 ± 2.1 | 18.3 ± 2.7 |
| **2** | 500 | 43.6 ± 1.6 | 37.5 ± 2.4 | 40.3 ± 3.5 | 39.2 ± 2.1 |
| | 100 | 18.1 ± 1.3 | 20.1 ± 2.3 | 16.5 ± 2.1 | 15.8 ± 3.0 |
| **3** | 500 | 32.6 ± 1.4 | 35.4 ± 2.2 | 38.7 ± 1.8 | 28.9 ± 1.7 |
| | 100 | 0 | 5.9 ± 2.3 | 10.3 ± 2.2 | 0 |
| **4** | 500 | 9.8 ± 1.5 | 0 | 10.4 ± 3.1 | 15.2 ± 3.3 |
| **5** | 500 | 12.7 ± 2.0 | 15.7 ± 3.1 | 26.3 ± 4.0 | 23.4 ± 3.8 |
| **6** | 500 | 51.3 ± 1.2 | 42.2 ± 1.6 | 43.4 ± 1.3 | 50.8 ± 2.0 |
| | 100 | 20.0 ± 2.1 | 26.4 ± 2.3 | 21.5 ± 2.5 | 18.2 ± 1.9 |
| **7** | 500 | 35.4 ± 1.3 | 18.9 ± 2.8 | 32.0 ± 2.3 | 28.2 ± 2.7 |
| **8** | 500 | 24.3 ± 1.7 | 29.5 ± 1.9 | 36.7 ± 3.2 | 34.1 ± 2.0 |
| | 100 | 0 | 0 | 0 | 0 |
| **9** | 500 | 40.6 ± 1.5 | 49.3 ± 3.6 | 45.8 ± 3.2 | 44.5 ± 2.5 |
| | 100 | 25.0 ± 2.1 | 29.6 ± 3.0 | 20.0 ± 1.7 | 17.6 ± 1.2 |
| **10** | 500 | 57.6 ± 1.1 | 52.6 ± 1.3 | 49.4 ± 1.7 | 55.3 ± 1.4 |
| | 100 | 19.5 ± 1.6 | 29.8 ± 1.2 | 20.2 ± 1.6 | 27.1 ± 1.7 |
| **11** | 500 | 27.7 ± 2.3 | 18.3 ± 1.9 | 23.6 ± 2.8 | 17.4 ± 2.1 |
| **12** | 500 | 31.1 ± 1.8 | 21.4 ± 1.1 | 28.5 ± 1.2 | 26.9 ± 1.9 |
| **13** | 500 | 30.0 ± 1.3 | 32.4 ± 1.2 | 34.1 ± 1.4 | 31.8 ± 1.5 |
| | 100 | 0 | 0 | 0 | 0 |
| **14** | 500 | 40.7 ± 1.1 | 38.4 ± 1.5 | 38.3 ± 1.8 | 30.2 ± 1.8 |
| | 100 | 12.5 ± 1.2 | 10.6 ± 1.5 | 15.4 ± 1.3 | 0 |
| **15** | 500 | 42.2 ± 1.9 | 39.5 ± 1.2 | 33.5 ± 1.2 | 37.6 ± 1.7 |
| | 100 | 0 | 10.0 ± 1.6 | 7.9 ± 1.2 | 12.4 ± 1.4 |
| **16** | 500 | 29.6 ± 1.6 | 28.5 ± 1.3 | 34.6 ± 1.3 | 31.8 ± 1.8 |
| **17** | 500 | 27.8 ± 3.0 | 30.0 ± 4.1 | 32.2 ± 3.2 | 23.6 ± 4.7 |
| **18** | 500 | 55.3 ± 2.3 | 45.8 ± 3.1 | 50.9 ± 2.1 | 46.3 ± 1.9 |
| | 100 | 23.9 ± 1.1 | 20.5 ± 2.3 | 26.5 ± 1.8 | 21.7 ± 1.5 |
| **19** | 500 | 50.0 ± 1.2 | 45.8 ± 1.4 | 46.9 ± 1.2 | 46.2 ± 2.1 |
| | 100 | 27.6 ± 1.7 | 21.4 ± 1.6 | 23.1 ± 1.6 | 24.7 ± 2.0 |
| **20** | 500 | 38.2 ± 1.2 | 43.2 ± 2.1 | 40.0 ± 2.4 | 38.9 ± 1.5 |
| | 100 | 0 | 17.3 ± 1.3 | 10.6 ± 1.9 | 11.1 ± 1.4 |
| **21** | 500 | 32.2 ± 2.1 | 30.3 ± 2.6 | 40.9 ± 2.3 | 37.1 ± 2.5 |
| | 100 | 0 | 0 | 12.7 ± 1.6 | 8.2 ± 1.5 |
| **22** | 500 | 42.5 ± 2.1 | 44.3 ± 2.0 | 45.8 ± 2.3 | 52.1 ± 1.3 |
| | 100 | 19.3 ± 2.2 | 18.9 ± 1.7 | 18.4 ± 2.1 | 22.7 ± 2.1 |


dx.doi.org/10.1021/jf5028894 | J. Agric. Food Chem. 2014, 62, 10393−10404

**Table 1. continued**

| | | | in vivo | | |
|---|---|---|---|---|---|
| compd | concn ($\mu$g/mL) | in vitro inhibition rate (%) | inactivation effect (%) | curative effect (%) | protection effect (%) |
| **23** | 500 | 0 | 28.5 ± 1.9 | 17.7 ± 1.9 | 22.7 ± 2.1 |
| **24** | 500 | 30.0 ± 2.4 | 24.6 ± 2.4 | 22.3 ± 3.2 | 28.9 ± 2.6 |
| **25** | 500 | 38.6 ± 3.1 | 40.3 ± 3.2 | 32.0 ± 1.7 | 37.5 ± 2.3 |
| | 100 | 17.2 ± 1.3 | 12.2 ± 1.9 | 8.3 ± 1.5 | 10.6 ± 1.2 |
| **26** | 500 | 32.7 ± 2.1 | 36.3 ± 3.1 | 28.6 ± 2.5 | 30.5 ± 2.1 |
| | 100 | 0 | 0 | 0 | 5.4 ± 1.4 |
| **27** | 500 | 27.5 ± 3.4 | 20.0 ± 2.1 | 26.7 ± 2.7 | 23.6 ± 2.3 |
| **28** | 500 | 36.1 ± 2.3 | 30.0 ± 2.8 | 27.5 ± 2.6 | 34.1 ± 2.8 |
| | 100 | 10.9 ± 3.1 | 0 | 0 | 11.8 ± 1.9 |
| **29** | 500 | 30.6 ± 1.3 | 28.3 ± 3.2 | 25.9 ± 1.7 | 21.7 ± 1.6 |
| **30** | 500 | 38.3 ± 2.1 | 39.5 ± 2.0 | 32.9 ± 1.8 | 34.2 ± 1.7 |
| | 100 | 18.2 ± 2.5 | 11.5 ± 2.6 | 12.4 ± 2.3 | 15.8 ± 2.7 |
| **31** | 500 | 28.8 ± 2.1 | 30.5 ± 2.0 | 24.1 ± 2.0 | 28.2 ± 2.4 |
| **32** | 500 | 33.3 ± 3.2 | 21.5 ± 2.6 | 27.4 ± 2.1 | 31.3 ± 2.4 |
| **33** | 500 | 47.3 ± 3.1 | 44.7 ± 2.3 | 37.6 ± 2.6 | 42.5 ± 4.2 |
| | 100 | 12.8 ± 1.8 | 23.2 ± 3.2 | 14.3 ± 1.7 | 19.5 ± 2.1 |
| **34** | 500 | 30.0 ± 2.1 | 27.2 ± 1.4 | 20.9 ± 2.6 | 27.4 ± 3.2 |
| **35** | 500 | 39.8 ± 1.3 | 37.4 ± 1.5 | 33.2 ± 2.1 | 36.0 ± 2.4 |
| | 100 | 19.8 ± 2.5 | 16.2 ± 1.6 | 10.3 ± 2.4 | 17.1 ± 1.7 |
| **36** | 500 | 25.1 ± 3.1 | 35.2 ± 1.7 | 29.4 ± 2.3 | 27.9 ± 2.7 |
| **37** | 500 | 15.9 ± 1.4 | 23.4 ± 3.2 | 23.6 ± 2.8 | 18.8 ± 1.6 |
| **38** | 500 | 47.8 ± 2.1 | 45.6 ± 2.6 | 41.7 ± 2.2 | 49.3 ± 1.7 |
| | 100 | 22.5 ± 2.7 | 18.6 ± 2.1 | 12.0 ± 1.7 | 20.6 ± 1.2 |
| **39** | 500 | 20.7 ± 1.3 | 31.5 ± 4.2 | 24.2 ± 2.1 | 27.0 ± 2.5 |
| **40** | 500 | 50.1 ± 3.0 | 41.9 ± 2.8 | 44.1 ± 2.3 | 44.9 ± 2.2 |
| | 100 | 23.7 ± 3.1 | 18.3 ± 2.7 | 13.2 ± 2.3 | 17.0 ± 1.3 |
| **41** | 500 | 30.0 ± 1.4 | 22.2 ± 1.6 | 20.9 ± 1.8 | 28.5 ± 1.6 |
| antofine | 500 | 52.8 ± 1.3 | 42.7 ± 1.8 | 46.0 ± 2.1 | 45.5 ± 1.5 |
| | 100 | 27.4 ± 1.5 | 15.3 ± 1.8 | 19.4 ± 1.8 | 20.4 ± 1.5 |
| ribavirin | 500 | 40.4 ± 2.0 | 34.7 ± 1.8 | 35.9 ± 1.2 | 38.2 ± 1.9 |
| | 100 | 12.5 ± 2.1 | 14.4 ± 2.5 | 10.5 ± 3.1 | 15.2 ± 2.7 |

[a]All results are expressed as means ± SD.

coupled with methyl 6-aminohexanoate hydrochloride to give compound **2**. Reduction of **2** with $LiAlH_4$ afforded alcohol **3**. Coupling of **2** with corresponding bromides or iodides gave the antofine derivatives **6**, **9**, **10**, and **13**−**21**. Treatment of **6** and **10** with 4 M NaOH solution gave acids **7** and **11**. Reduction of **6** and **10** with $LiAlH_4$ afforded alcohols **8** and **12**.

Coupling of bromide **48** with corresponding alkamines gave the antofine derivatives **4**, **5**, **22**, and **23** (Scheme 3). It is worth mentioning that reaction of **48** with excess alkamine gave only N,O-dialkylation compound **22**. Using a similar procedure for the preparation of derivatives **1**, **24**, **27**, **30**, **33**, **36**, **39**, and **40** could not afford **41** due to the presence of *N*,*N*-dimethyl. As an

alterative method, compound **41** was prepared by coupling of **51** with excess amine (Scheme 4).

**Bioactivities and the Structure−Activity Relationship.** *Phytotoxic Activity.* The antofine derivatives **1**−**41** were first tested for their phytotoxic activity against *N. tabacum* var. Xanthi nc, and the results indicated that these natural product-based compounds showed no phytotoxic activity at 500 μg/mL.

*Antiviral Activity in Vitro and in Vivo.* To make a judgment of the antiviral potency of the antofine derivatives **1**−**41**, the precursor antofine and commercial plant virucide vibavirin were used as controls.

The first in vitro anti-TMV bioassay indicated that all of the tested compounds displayed good antiviral activity, of which compounds **1**, **2**, **6**, **10**, **18**, **19**, **33**, **38**, and **40** exhibited higher inhibition than ribavirin (Table 1). Therefore, these compounds were bioassayed further to investigate their antiviral activity in vivo.

As shown in Table 1, the antofine derivatives **1**−**41** also exhibited good to excellent in vivo anti-TMV activity; especially compounds **10**, **18**, and **19** displayed higher antiviral activity than the precursor antofine and commercial plant virucide ribavirin, thus emerging as new lead compounds.

Among the phenanthrenyl methyl amines **2**−**5**, long-chain containing compounds **2** and **3** exhibited better antiviral activity, and the ester group is favorable for activity (antiviral effect, **2** > **3**). It is worth mentioning that dimethyl amine compound **1** showed a higher antiviral effect than compounds **2**−**5**, and compound **6** displayed better activity than **2**, which indicated that the hydrogen on the N atom is unfavorable for antiviral activity. To further investigate the substituents on the long chain, compounds **6**−**8** and **10**−**12** were prepared. The bioassay results indicated that the ester group is more suitable than acid and hydroxy groups (antiviral effect, **6** > **7**, **8**; antiviral effect, **10** > **11**, **12**). The main difference between compounds **6**, **9**, and **10** lies in the substituents on the N atom. Compounds **6** and **9** displayed similar good antiviral activities, which are lower than that of compound **10**. The results indicated that the replacement of methyl with *n*-butyl is tolerant, and benzyl is more suitable for antiviral activity than an alkyl group. To investigate the substituents on benzyl, compounds **13**−**21** were prepared. Only compounds **18** and **19** maintained good antiviral activity (antiviral effect, **10** ≈ **18** ≈ **19**). The results indicated that the benzyl lies in a sensitive area for antiviral activity.

In previous work, we have found that the presence of nitrogen in the tertiary amine and the phenanthrene ring are essential for high antiviral activity.[18,19] The increase of phenanthrene ring may raise the interaction between small molecular compound and TMV RNA. On the basis of the above hypothesis, a series of two phenanthrene rings containing compounds **22**−**41** were synthesized and evaluated for their antiviral activity. Unfortunately, most of these compounds exhibited only moderate antiviral activity. Only compounds **22**, **38**, and **40** maintained good antiviral activity (antiviral effect, **22** ≈ **38** ≈ **40** ≈ **6**). The results indicated that phenanthrene is important for these compounds, but not the more the better.

In summary, on the basis of our previous structure−activity relationship and antiviral mechanism studies, a series of phenanthrene and alkylamine chain containing antofine derivatives **1**−**41** were prepared and systematically evaluated for their antiviral activity against TMV. The bioassay results indicated that most of these compounds exhibited good to excellent anti-TMV activity, of which compounds **10**, **18**, and **19** displayed higher activity than the precursor antofine and commercial ribavirin, thus emerging as potential inhibitors of plant virus. The D and E rings of antofine were proved to be not indispensable. Phenanthrene is important for these compounds, but not the more the better. The novel concise structure provides another new template for antiviral studies, which may have different mechanisms of action. Further studies on structural optimization and mode of action are currently underway in our laboratories.

## ■ ASSOCIATED CONTENT

### Ⓢ Supporting Information

$^{1}$H NMR, $^{13}$C NMR, and HRMS spectra of compounds **1**−**41**. This material is available free of charge via the Internet at http://pubs.acs.org.

## ■ AUTHOR INFORMATION


### Corresponding Author

*(Q.W.) E-mail: wangqm@nankai.edu.cn. Phone: 0086-22-23503952. Fax: 0086-22-23503952.

### Author Contributions

‖Z.W. and P.W. contributed equally to this paper.



### Funding

This work was supported by the National Key Project for Basic Research (2010CB126106), the National Natural Science Foundation of China (21132003, 21121002, 21372131, 21402142), and the Specialized Research Fund for the Doctoral Program of Higher Education (20130031110017).


### Notes

The authors declare no competing financial interest.

## ■ REFERENCES


(1) Hari, V.; Das, P. Ultra microscopic detection of plant viruses and their gene products. In *Plant Disease Virus Control*; Hadidi, A., Khetarpal, R. K., Koganezawa, H., Eds.; APS Press: St. Paul, MN, 1998; pp 417−427.

(2) Ritzenthaler, C. Resistance to plant viruses: old issue, new answer. *Curr. Opin. Biotechnol.* **2005**, *16*, 118−122.

(3) Wei, L. Z.; Meng, F. S. Antiviral composition containing fucoidan and ribavirin for preventing and treating plant viral diseases. CN 101869111A, 20101027, CAN 153:573294, 2010.

(4) Song, B. A.; Yang, S.; Jin, L. H.; Bhadury, P. S. *Environment-Friendly Anti-plant Viral Agents*; Chemical Industry Press and Springer Press: Beijing, China, 2009; pp 1−305.

(5) Xue, W.; Song, B. A.; Wang, H.; He, W.; Yang, S.; Jin, L. H.; Hu, D. Y.; Liu, G.; Lu, P. Synthesis and anti-TMV activity of 2-[5-(3,4,5-trimethoxyphenyl)-1,3,4-thiadiazole-2-ylthiomethyl]-1-(2,3,4-trimethoxy)phenyl ketoxime ether derivatives. *Chin. J. Org. Chem.* **2006**, *26*, 702−706.

(6) Ouyang, G. P.; Chen, Z.; Cai, X. J.; Song, B. A.; Bhadury, P. S.; Yang, S.; Jin, L. H.; Xue, W.; Hu, D. Y.; Zeng, S. Synthesis and antiviral activity of novel pyrazole derivatives containing oxime esters group. *Bioorg. Med. Chem.* **2008**, *16*, 9699−9707.

(7) Chen, M. H.; Chen, Z.; Song, B. A.; Bhadury, P. S.; Yang, S.; Cai, X. J.; Hu, D. Y.; Xue, W.; Zeng, S. Synthesis and antiviral activities of chiral thiourea derivatives containing an α-aminophosphonate moiety. *J. Agric. Food Chem.* **2009**, *57*, 1383−1388.

(8) Ouyang, M. A.; Wein, Y. S.; Zhang, Z. K.; Kuo, Y. H. Inhibitory activity against tobacco mosaic virus (TMV) replication of pinoresinol and syringaresinol lignans and their glycosides from the root of *Rhus javanica* var. *roxburghiana*. *J. Agric. Food Chem.* **2007**, *55*, 6460−6465.

(9) Chen, J.; Yan, X. H.; Dong, J. H.; Sang, P.; Fang, X.; Di, Y. T.; Zhang, Z. K.; Hao, X. J. Tobacco mosaic virus (TMV) inhibitors from *Picrasma quassioides* Benn. *J. Agric. Food Chem.* **2009**, *57*, 6590−6595.

(10) Lu, M.; Han, Z. Q.; Xu, Y.; Yao, L. *In vitro* and *in vivo* anti-tobacco mosaic virus activities of essential oils and individual compounds. *J. Microbiol. Biotechnol.* **2013**, *23*, 771−778.
(11) Hu, Q. F.; Zhou, B.; Huang, J. M.; Gao, X. M.; Shu, L. D.; Yang, G. Y.; Che, C. T. Antiviral phenolic compounds from *Arundina gramnifolia*. *J. Nat. Prod.* **2013**, *76*, 292−296.
(12) Hansen, A. J. Antiviral chemicals for plant disease control. *Crit. Rev. Plant Sci.* **1989**, *8*, 45−88.
(13) Qian, X. H.; Lee, P. W.; Cao, S. China: Forward to the green pesticides via a basic research program. *J. Agric. Food Chem.* **2010**, *58*, 2613−2623.
(14) Seiber, J. N. Sustainability and agricultural and food chemistry. *J. Agric. Food Chem.* **2011**, *59*, 1−21.
(15) An, T. Y.; Huang, R. Q.; Yang, Z.; Zhang, D. K.; Li, G. R.; Yao, Y. C.; Gao, J. Alkaloids from *Cyanachum komarovii* with inhibitory activity against the tobacco mosaic virus. *Phytochemistry* **2001**, *58*, 1267−1269.
(16) Huang, Z. Q.; Liu, Y. X.; Fan, Z. J.; Wang, Q. M.; Li, G. R.; Yao, Y. C.; Yu, X. S.; Huang, R. Q. Antiviral activity of alkaloids from *Cynanchum komarovii*. *Fine Chem. Intermediates* **2007**, *37* (20−24), 46.
(17) Wang, Q. M.; Yao, Y. C.; Huang, R. Q.; Fan, Z. J.; Li, G. R.; Yu, X. S. Antiviral activity of antofine from *Cynanchum komarovii*. *Agrochemicals* **2007**, *46*, 425−427.
(18) Wang, Q. M.; Wang, K. L.; Huang, Z. Q.; Liu, Y. X.; Li, H.; Hu, T. S.; Jin, Z.; Fan, Z. J.; Huang, R. Q. Derivatives and salts of phenanthro indolizidine and phenanthro quinolizidine, and their application as agricultural virucides. CN 101189968A, 20080604, CAN 149:97630, 2008.
(19) Cui, M. B.; Wang, K. L.; Wang, Q. M.; Huang, R. Q. Concise synthesis of benzoindolizidine derivatives and bioactivity evaluation. *Lett. Org. Chem.* **2008**, *5*, 98−102.
(20) Gao, S.; Zhang, R. Y.; Yu, Z. H.; Xi, Z. Antofine analogues can inhibit tobacco mosaic virus assembly through small-molecule−RNA interactions. *ChemBioChem* **2012**, *13*, 1622−1627.
(21) Gooding, G. V. J.; Hebert, T. T. A simple technique for purification of tobacco mosaic virus in large quantities. *Phytopathology* **1967**, *57*, 1285−1290.
(22) Chen, N. C. *Pesticide's Bioassay Technique*; Beijing Agriculture University: Beijing, People's Republic of China, 1990; p 194.
(23) Li, S. Z.; Wang, D. M.; Jiao, S. M. In *Pesticide Experiment Methods-Fungicide Sector*; Li, S. Z., Ed.; Agriculture Press of China: Beijing, China, 1991; pp 93−94.
(24) Wang, K. L.; Lü, M. Y.; Wang, Q. M.; Huang, R. Q. Iron(III) chloride-based mild synthesis of phenanthrene and its application to total synthesis of phenanthroindolizidine alkaloids. *Tetrahedron* **2008**, *64*, 7504−7510.
(25) Yamashita, S.; Kurono, N.; Senboku, H.; Tokuda, M.; Orito, K. Synthesis of phenanthro[9,10-*b*]indolizidin-9-ones, phenanthro[9,10-*b*]quinolizidin-9-one, and related benzolactams by $Pd(OAc)_2$-catalyzed direct aromatic carbonylation. *Eur. J. Org. Chem.* **2009**, *8*, 1173−1180.
(26) Buckley, T. F., III; Rapoport, H. Amino acids as chiral educts for asymmetric products. Chirally specific syntheses of tylophorine and cryptopleurine. *J. Org. Chem.* **1983**, *48*, 4222−4232.
(27) Rozwadowska, M. D.; Tomczak, A. The synthesis of (4*S*,5*S*)-(−)-isocytoxazone. *Tetrahedron: Asymmetry* **2009**, *20*, 2048−2051.

**Table 1. Sequences of Primers and Probes Used in This Study**

| primer name | primer sequence (5′−3′) | amplicon (bp) | purpose |
|---|---|---|---|
| RPL21-1F | CCTAGCCCGTTTCATCTAATGTGTCCTA | 161 | taxon-specific detection |
| RPL21-1R | TACTACCAACGAGAACCATTAGAGAGC | | |
| RPL21-P | TGGATGCATTTCATGGCTCATCTTTGT | | |
| RPL21-2F | TCCGCAAGAAGGGGTACAT | 441 | probe for southern blotting |
| RPL21-2R | GAAGAGTTCATCACAGGCACAC | | |
| RPL21-*Kpn*I | GGGGTACCGGTATGCCGCACAAGTT | 1242 | sequencing |
| RPL21-*Sac*I | TCCGAGCTCACTCCTCGTTGCACCTGGAT | | |
| NPR1-1F | GAGAAGACGACACTGCTGAGAAACGACTACA | 148 | detection of GM wheat |
| NPR1-1R | GTTGATTTCGATGTGGAAGAAGTCGAATCT | | |
| NPR1-P | AAGAAGGCCTTTAGTGAGGACAATTTGGA | | |

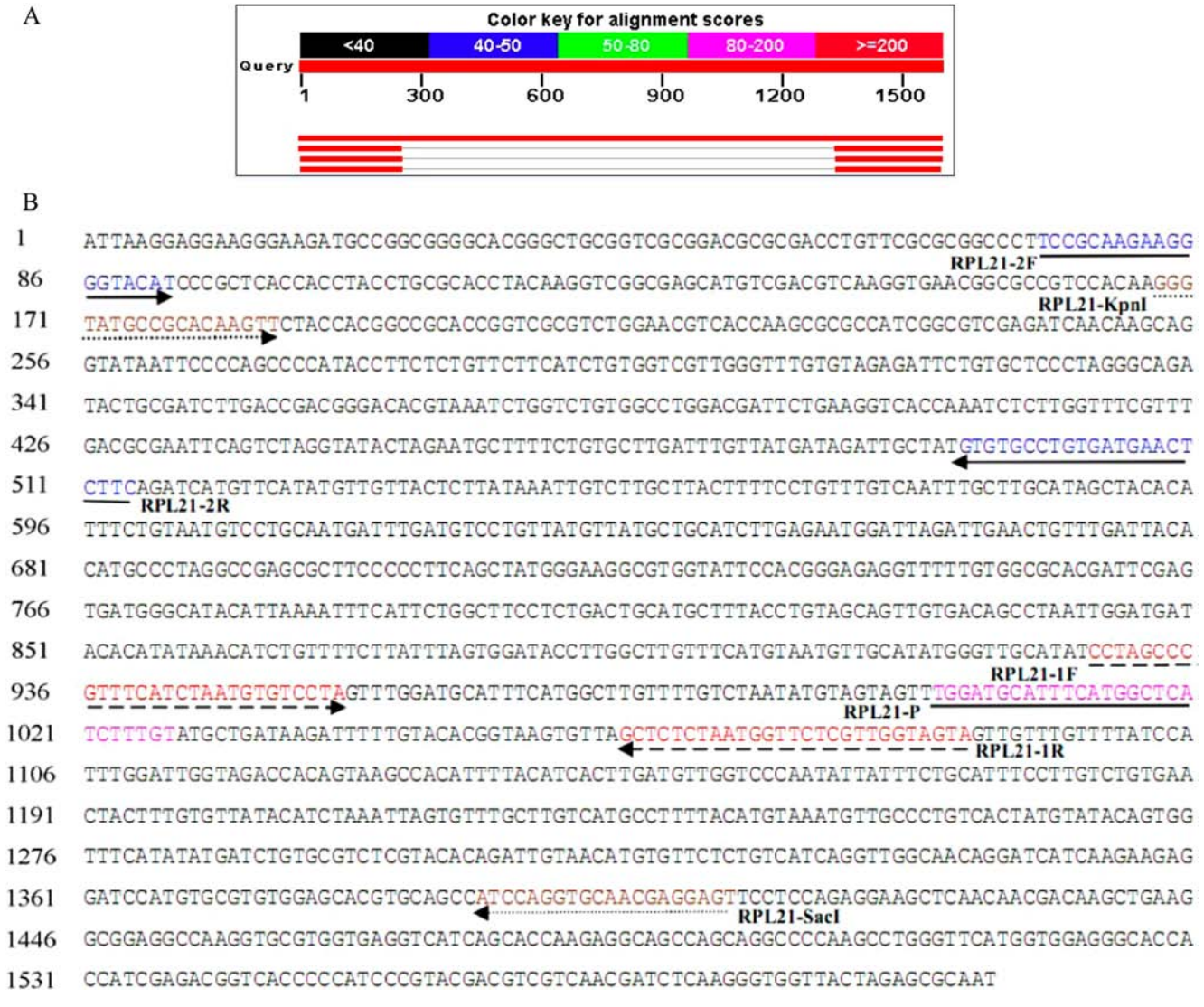


**Figure 1.** Homology analyses of the wheat *RPL21* gene and its sequence and positions for annealing by primers. (A) BLAST analysis of wheat *RPL21* based on the nucleotide collection database. (B) Primers and their annealing positions are indicated by underlines and labels.

lines, and the *Waxy-D1* gene assay was validated to be useful in establishing qualitative and quantitative PCR analyses of GM wheat.[26] However, some Chinese wheat landraces were null *Waxy-D1* mutants.[27,28] Moreover, none of these endogenous reference genes was verified for detecting GM wheat contents with GM wheat materials.

In the present work, we investigated whether the wheat *ribosomal protein L21* (*RPL21*) gene encoding 60S ribosomal protein L21 was a good candidate to serve as a wheat endogenous reference gene for a GM wheat assay. *RPL21* was found by searching database sequences. We designed species-specific primers based on this gene and developed conventional and quantitative real-time PCR systems. Furthermore, we developed the construct-specific real-time PCR method using *NPR1* GM wheat, and seven mixed *NPR1* GM wheat samples

of known content were also quantitatively analyzed using the developed real-time PCR method.

## MATERIALS AND METHODS

**Plant Materials.** A total of 17 plant species were used for the specificity test of the designated primers: barley (*Hordeum vulgare* L.), maize (*Zea mays* L.), rye (*Secale cereale* L.), tomato (*Lycopersicon esculentum* Mill.), common bean (*Phaseolus vulgaris* L.), rapeseed (*Brassica napus* L.), Chinese cabbage (*Brassica campestris* L. ssp. *pekinensis*), cotton (*Gossypium hirsutum* L.), soybean (*Glycine max* L. Merr.), mung bean (*Phaseolus vulgaris* L.), *Arabidopsis* [*Arabidopsis thaliana* (L.) Heynh.], cucumber (*Cucumis sativus* L.), sweet potato [*Ipomoea batatas* (L.) Lam.], pea (*Pisum sativum* L.), rice (*Oryza sativa* L.), sunflower (*Helianthus annuus* L.), and sorghum (*Sorghum bicolor* L. Moench). All samples were obtained from local stores.

A total of 18 common wheat (AABBDD) varieties from different ecological regions in China, including hard winter wheat, hard spring wheat, soft winter wheat, and soft spring wheat, were stored in our laboratory or kindly provided by Professor Jun Yin from Henan Agricultural University (Zhengzhou, Henan, China). *Triticum urartu* (AA), *Aegilops speltoides* (BB), and *Aegilops tauschii* (DD) were kindly provided by Professor Jizeng Jia from the Institute of Crop Science, the Chinese Academy of Agriculture Sciences, China. The *NPR1* (non-expressor of PR genes) GM wheat line R4 was developed in our laboratory.[29]

**DNA Extraction.** Total genomic DNA from seedlings of the 17 plant species, 18 common wheat varieties, 3 diploid wheat species, and dry flour of common wheat was extracted using the cetyltrimethylammonium bromide (CTAB) protocol.[30] The concentration and quality of the purified DNA samples were measured and evaluated using a Shimadzu UV-1800 spectrophotometer (Shimadzu Corporation, Kyoto, Japan), and the DNA quality was further checked by 1% (w/v) agarose gel electrophoresis in 0.5× TBE with ethidium bromide staining.

**Oligonucleotide Primers and Probes.** Oligonucleotide primers and probes used in this study were designed with Primer Premier 5 (PREMIER Biosoft, Palo Alto, CA) and are listed in Table 1. Primers RPL21-1F/1R, RPL21-2F/2R, and RPL21-*Kpn*I/*Sac*I were designed on the basis of the wheat *RPL21* gene sequence (GenBank HM138481.1). The annealing sites of these primers are shown in Figure 1. The primer pair NPR1-1F/1R was designed according to the sequence of the *A. thaliana NPR1* gene (GenBank NM_105102.2), which was integrated into an elite wheat cultivar Yangmai11.[29] The TaqMan probes were labeled on the 5′ end with the 6-carboxyfluorescein (FAM) reporter dye, and 6-carboxytetramethylrhodamine (TAMRA) quencher dye was attached to the 3′ end. All of the primers and probes were synthesized by Sangon (Shanghai, China). The probe for southern blot was a fragment derived from 74 to 514 of the wheat *RPL21* sequence (Figure 1B) amplified with primer pair PRPL21-2F/2R (Table 1) using a Takara random primer DNA labeling kit, version 2 (TaKaRa, Dalian, China).

**Southern Blot Analysis.** Aliquots of 15 μg of DNA from young leaves of common wheat culture Yangmai11 were digested with 60 units of restriction enzymes *Hind*III and *Nde*I (TaKaRa) overnight and electrophoresed on 0.8% agarose gels. DNA fragments were transferred onto a nylon membrane (Hybond-$N^+$, Amersham, Buckinghamshire, U.K.) and hybridized with an $\alpha$-[$^{32}$P]-dCTP-labeled DNA fragment derived from the *RPL21* sequence amplified with primer pair RPL21-2F/2R (Figure 1). Autoradiography was conducted using a Fujifilm imaging plate and cassette, which was analyzed with a Fuji BAS1800-II system (Fujifilm, Tokyo, Japan).

**Sequencing Analysis of the *RPL21* Gene.** The specific DNA fragments were amplified with the primer pair RPL21-*Kpn*I/*Sac*I from the common wheat variety Yangmai11 and three diploid ancestral species, *T. urartu* (AA), *A. speltoides* (BB), and *A. tauschii* (DD), employing the KOD Plus DNA polymerase PCR kit (TaKaRa). The amplified DNA fragments were cloned into pBluescript SK(−) vector and analyzed with the ABI Prism 3730 genetic analyzer (Invitrogen Co., Ltd., Shanghai, China). The sequences obtained were aligned using DNAMAN software (Lynnon Biosoft, Quebec, Canada).

**Conventional PCR Conditions.** Conventional PCR assays were carried out in a 25 μL final volume on a thermal cycling instrument (MyCycler, Bio-Rad, Hercules, CA). Each reaction mixture contained the following reagents: 10× EasyTaq buffer (TransGen Biotech, Beijing, China), 2 units of EasyTaq polymerase (TransGen), 120 μM dNTPs (TaKaRa), 1 μL of template (about 50 ng), 0.5 μM of each primer, and double-distilled water (dd$H_2O$). Conventional PCR programs were as follows: 5 min of predenaturation at 94 °C, followed by 35 cycles of 30 s at 94 °C, 30 s at 60 °C, and 30 s at 72 °C, and a final extension of 10 min at 72 °C. The PCR-amplified products were analyzed by 1% (w/v) agarose electrophoresis in 0.5× TBE with ethidium bromide staining. As for PCRs used to test the limit of detection (LOD), wheat genomic DNA was serially diluted to 6250, 1250, 250, 50, 10, 2, and 1 initial template copies of the haploid genome based on the DNA content of 17.3 pg/haploid genome in common wheat;[24] these dilutions were used in PCRs with the primer pair RPL21-1F/1R under the conditions described above.

**Quantitative Real-Time PCR.** Quantitative real-time PCR reactions were performed in a 20 μL final volume containing 50 ng of sample DNA, 10 μL of FastStart Universal Probe Master (Roche Applied Science, Indianapolis, IN), 0.5 μM each of the forward and reverse primers, and 0.2 μM FAM/TAMRA-labeled oligonucleotide probe. Real-time PCR reactions were run on a Roche LightCycler 480 (Roche, Mannheim, Germany) using the following program: 95 °C for 10 min, 40 cycles of denaturation at 95 °C for 20 s each, followed by annealing at 60 °C for 40 s. For the generation of standard curves of the two genes *RPL21* and *NPR1*, extracted genomic DNA from GM wheat line R4 was diluted 5-fold to final copy numbers of 5000, 1000, 200, 40, and 8 per reaction. All of the quantitative PCRs were repeated 3 times, each with three replicates. The resulting data were analyzed, and standard curves were constructed with the LightCycler 480 software release 1.5.0 (Roche).

## RESULTS AND DISCUSSION

**Selection of Wheat Endogenous Reference Gene.** The application of an endogenous reference gene makes the detection of plant species more practical and precise. Reference genes must be species-specific and have a low and consistent copy number in different varieties of the same species.[11] To choose a suitable reference gene in common wheat, large amounts of gene information were collected from GenBank and several candidates were evaluated. After BLAST and homology analyses, the 60S ribosomal protein L21 (RPL21) in the common wheat genome (accession number HM138481.1) was found to have low homology with the sequences from other non-wheat species. The homologue in *Arabidopsis* to this chloroplast ribosomal protein L21 is required for chloroplast development and embryogenesis,[31] whereas the exact biological function of the *RPL21* gene in wheat is not yet known.

Sequence alignment analyses indicated that a region of the wheat *RPL21* sequence from 257 to 1322 nucleotides displayed no homology with other known sequences in the database (Figure 1A). Subsequently, primers specific to this region were designed, and a specificity analysis for each primer was performed by a BLAST search for each primer against several public and genetically modified organism (GMO) DNA sequence databases, such as NCBI. Any primer showing homology with non-relevant DNA sequences was discarded. Finally, we designed the primer pair RPL21-1F/1R, which spanned a sequence of 161 base pairs (bp) within the region of 257−1322 nucleotides and was wheat-specific (Table 1 and Figure 1B). The specificity of the primers was further tested in both qualitative and quantitative assays.

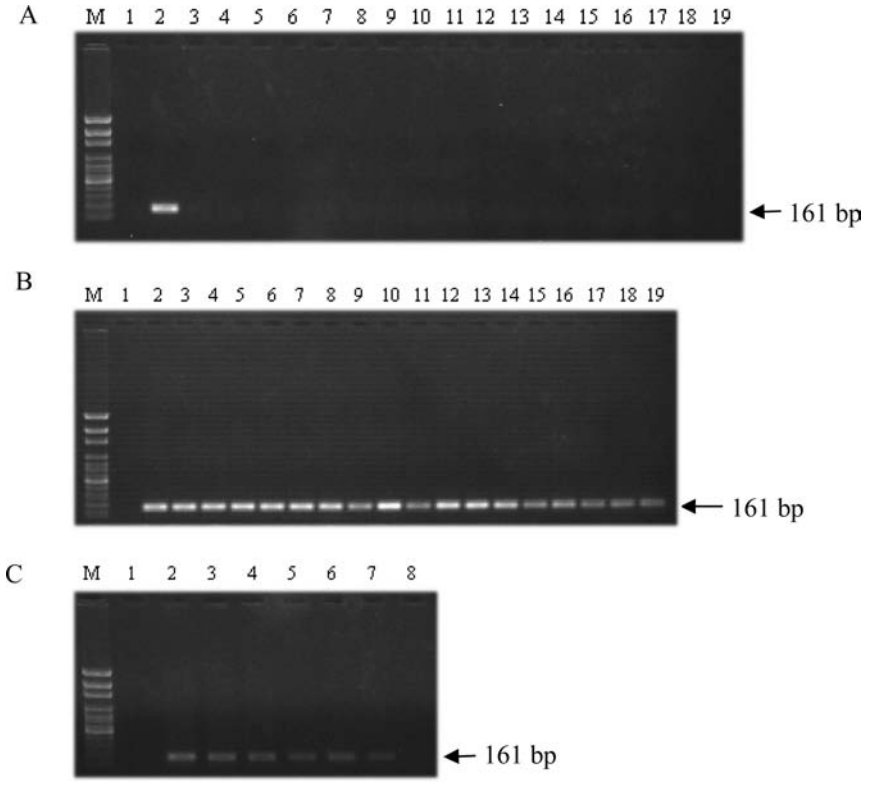


**Figure 2.** Agarose gel electrophoresis of conventional PCR products amplified with the RPL21-1F/1R primer pair. (A) PCR-amplified products with DNA from wheat and other plant species: (1) no DNA template control, (2) common wheat, (3) barley, (4) maize, (5) rye, (6) tomato, (7) bean, (8) rapeseed, (9) Chinese cabbage, (10) cotton, (11) soybean, (12) mung bean, (13) *Arabidopsis*, (14) cucumber, (15) sweet potato, (16) pea, (17) rice, (18) sunflower, (19) sorghum and (M) 100 bp ladder size standard. (B) PCR-amplified products with DNA from (2−19) 18 different varieties of common wheat, (1) no DNA template control, and (M) 100 bp ladder size marker. (C) PCR-amplified products with serial dilutions of common wheat DNA: (1) no DNA template control, (2) 6250 copies, (3) 1250 copies, (4) 250 copies, (5) 50 copies, (6) 10 copies, (7) 2 copies, (8) 1 copy, and (M) 100 bp ladder size standard.

**Specificity, Allelic Stability, and Sensitivity of *RPL21* Systems in Conventional Qualitative PCR.** To assess the specificity of the *RPL21* gene-based PCR system using the primer pair RPL21-1F/1R, qualitative PCRs were performed using 50 ng of genomic DNA extracted from 17 plant species that are either closely related to common wheat or frequently consumed plant materials. A single 161 bp DNA fragment was amplified only from wheat, whereas no product was amplified from any of the other 16 plant species (Figure 2A), demonstrating that the *RPL21* gene is wheat-specific.

To examine whether an allelic variation of the *RPL21* gene is present in wheat, genomic DNA isolated from 18 common wheat varieties collected from different ecological regions in China was tested by PCR with the primer pair RPL21-1F/1R. As shown in Figure 2B, all of the varieties contained one DNA fragment of identical size (161 bp) and similar intensity, indicating the presence of the same amplicon in those wheat genotypes. Thus, the RPL21 fragment has no allelic variation among the wheat varieties.

To further evaluate the sensitivity of the primer pair, known amounts of wheat genomic DNA isolated from Yangmai11 were assayed by conventional PCR. A series of wheat genomic DNA dilutions containing approximately 6250, 1250, 250, 50, 10, 2, and 1 initial template copies of the haploid genome was used in PCRs with the primer pair RPL21-1F/1R to test its LOD. The expected 161 bp amplicon was obtained in all of the dilutions, except for the level of 1 copy and water (Figure 2C), indicating that the LOD of the primer pair RPL21-1F/1R was as low as about 2 copies of common wheat haploid genome. This level of sensitivity was similar to that of a wheat *ALMT1* system (2.3 copies) and better than that of *Waxy-D1* system (7 copies).[24,25]

**Copy and Amplicon Number of the Wheat *RPL21* Gene.** The copy number of an endogenous reference gene is critical for GMO quantification. Targeting a gene sequence with a single or stably low copy number should result in stable real-time PCR assays.[25] To estimate the copy number of the *RPL21* gene in the common wheat genome, we designed another primer pair RPL21-2F/2R to amplify a 441 bp DNA fragment used as a probe for southern blot analysis. Wheat genomic DNA from Yangmai11 digested with *Hind*III and *Nde*I was hybridized with the 441 bp DNA fragment derived from the *RPL21* gene (Figure 1B), revealing three hybridizing bands in both enzyme-digested DNA samples (Figure 3). Among the three bands, one had stronger signal intensity than the other two bands, which had similar intensities in both digests. These results suggest that the stronger band was the sequence from the AA genome nearly identical (about 98% identity) to the probe, whereas the weak bands were the sequences from the BB and DD genomes, respectively, which have low similarity to the probe (see Figure S1 of the Supporting Information). Therefore, the *RPL21* gene may have 3 copies or 1 copy in the common wheat genome. In the *Waxy-D* system, two hybridizing bands were detected in southern blots, suggesting the presence of 1 or 2 copies,[25] whereas the copy numbers of

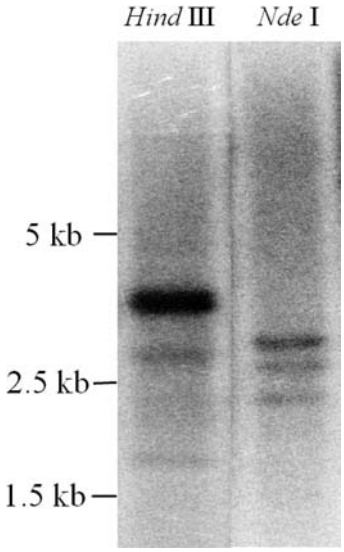


**Figure 3.** Estimation of the copy number of a wheat *RPL21* gene as illustrated by genomic southern blot of common wheat (Yangmai11) genomic DNA digested with *Hind*III and *Nde*I, separately, and hybridized to a 441 bp probe of the *RPL21* gene amplified with primer pair RPL21-2F/2R.

other endogenous reference genes from wheat have not been confirmed.[12,18,24]

Common wheat is a hexaploid species with the genome constitution of AABBDD originating from three diploid ancestral species: *T. urartu* (AA), *A. speltoides* (BB), and *A. tauschii* (DD).[32] Allopolyploidization leads to the generation of duplicated homeologous genes (homeologs). Therefore, most genes in hexaploid wheat are present as triplicate homeologs.[33]

To obtain information on the amplicon number generated by the primer pair RPL21-1F/1R from ancestral wheat species, the primer pair RPL21-*Kpn*I/*Sac*I was used to amplify fragments (about 1242 bp) from *T. urartu*, *A. speltoides*, and *A. tauschii*. The alignment of the four amplified sequences (see Figure S1 of the Supporting Information) showed that the annealing sites of the primer pair RPL21-1F/1R were only present in the A genome but not in the B or D genomes, thus generating only one amplicon in common wheat (Figure 4). Conventional PCRs with the primer pair RPL21-1F/1R confirmed that one expected 161 bp DNA fragment was amplified from *T. urartu* (AA) and common wheat (AABBDD), but no amplicon was obtained from *A. speltoides* (BB) or *A. tauschii* (DD) (data not shown). Thus, the *RPL21* gene was apparently evolutionarily derived from diploid *T. urartu*, and the primer pair RPL21-1F/1R generated only one amplicon from the A genome of common wheat.

**Quantitative Assay Based on LOD and Limit of Quantification (LOQ).** When quantifying a nucleotide sequence by real-time PCR, LOD and LOQ are the most important parameters, referring to the lowest quantity of target that can be reliably detected and quantified with a probability of ≥95%.[34,35] The absolute limit is the lowest number of initial template copies that can be detected and quantified. To determine LOD and LOQ of the established method based on the primer pair RPL21-1F/1R by real-time PCR, six serial dilutions of common wheat DNA containing approximately 5000, 1000, 200, 40, 8, and 1.6 haploid genomes were prepared and tested in seven replicates per dilution. As shown in Table 2,

**Table 2. Amplification Data Used To Determine the Absolute LOD and LOQ**

| estimated template copies | signal rate (number of positive signals) | mean $C_p$ values | SD | RSD (%) |
|---|---|---|---|---|
| 5000 | 7/7 | 24.27 | 0.14 | 0.57 |
| 1000 | 7/7 | 26.68 | 0.14 | 0.53 |
| 200 | 7/7 | 28.89 | 0.16 | 0.56 |
| 40 | 7/7 | 31.12 | 0.25 | 0.83 |
| 8 | 7/7 | 33.45 | 0.37 | 1.12 |
| 1.6 | 4/7 | 35.81 | ND | ND |
| 0 | 0/7 | >45 | ND | ND |

the ability to detect *RPL21* decreased with the reduction of genomic DNA copy number, and 1.6 copies of wheat genomic DNA were detected 3 times in the seven replicates, indicating that the LOD value was about 2 copies. This value is in accordance with that determined by the conventional PCRs. A LOD of 2 haploid genome copies was reported for the wheat *Waxy-D1*, *acc1*, and *ALMT1* systems,[12,24,25] and a LOD of 5 genome copies was reported for the *PKABA1* system.[18]

The LOQ values were calculated on the basis of the crossing point ($C_p$) values and confidence intervals.[12] The results showed that approximately 8 initial template copies were required to obtain reliable quantification results with 95% confidence under ideal conditions (Table 2), indicating that the LOQ of the RPL21-1F/1R-based real-time PCR assay was about 8 copies of haploid genome.[36,37] This value is 2.5−4-fold lower than that of the *ALMT1* (20 copies) and *acc1* (30 copies) systems, respectively.[12,24] No such information is available for the *Waxy-D* and *PKABA1* systems.

**Construct-Specific Qualitative PCR Detection of *NPR1* in Transgenic Wheat.** To validate the applicability and sensitivity of the developed *RPL21* system with transgenic

**Figure 4.** Sequence alignment of a portion of the wheat *RPL21* gene containing the region amplified with the primer pair RPL21-1F/1R with DNA from *T. aestivum* (AABBDD, GenBank accession number HM138481.1), *T. urartu* (AA), *A. speltoides* (BB), and *A. tauschii* (DD). The sequences in the red boxes were the region annealed with the primer pair RPL21-1F/1R.

wheat materials, we selected a stably transgenic wheat line R4 that contained a *NPR1* gene from *A. thaliana*.[29] To detect the content of *NPR1* in wheat line R4 through quantitative real-time PCR, the sensitivity and specificity of the construct-specific sequence of *NPR1* were first evaluated using qualitative PCR. The construct-specific primer pair NPR1-1F/1R (Table 1) was designed on the basis of the *NPR1* sequence to establish the construct-specific conventional PCR assay. As shown in Figure 5A, a 148 bp DNA fragment was amplified only from

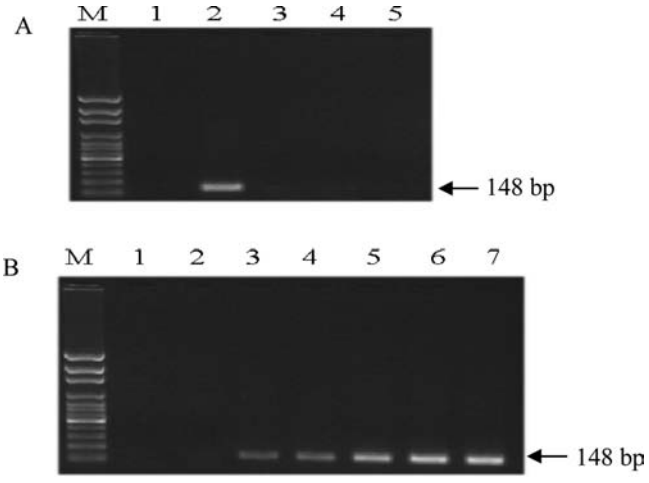


**Figure 5.** Agarose gel electrophoresis of conventional PCR products with the primer pair NPR1-1F/1R. (A) PCR-amplified products from *NPR1* transgenic wheat line R4 and some non-GM wheat varieties: (1) no DNA template control, (2) transgenic wheat line R4, (3) Yangmai11, (4) Zhenmai9023, (5) Yangmai158, and (M) 100 bp ladder size standard. (B) PCR-amplified products with DNA from a non-GM wheat mixed with serial dilutions with GM wheat line R4: (1) no DNA template control, (2) 0%, (3) 0.2%, (4) 1%, (5) 0.5%, (6) 2.0%, (7) 5.0%, and (M) 100 bp ladder size standard.

*NPR1* transgenic wheat and not from other non-GM wheat varieties and no template control, indicating a high specificity of this primer pair.

To test the LOD of the established construct-specific PCR assay, pure dried wheat flour from transgenic line R4 was mixed at proportions of 0, 0.2, 0.5, 1.0, 2.0, and 5.0% with flour from non-transgenic wheat variety Yangmai11 and subjected to DNA isolation and PCR analyses. In conventional PCR assays, an aliquot of 50 ng of genomic DNA was used as the template per reaction. The results showed that the expected 148 bp target DNA fragment of *NPR1* gene was generated from all levels of transgenic wheat flour, except for 0% and no template control, indicating that the LOD of the conventional PCR assay is at least 0.2%. This level corresponds to about 6 copies of wheat haploid genome (AABBDD = 6; Figure 5B), confirming that the construct-specific PCR assay is highly specific and sensitive for practical detection of *NPR1* transgenic wheat samples.

**Establishment of Standard Curves.** To establish a method to estimate the contents of transgenic wheat, two standard curves (one for endogenous gene *RPL21* and the other for transgenic gene *NPR1*) through five 5-fold serial dilutions (corresponding to 5000, 1000, 200, 40, and 8 copies of the wheat haploid genome per reaction) were performed in transgenic wheat line R4, in which an *A. thaliana NPR1* gene was integrated into wheat variety Yangmai11.[29] The calculated $C_p$ values were plotted versus the log copies of total DNA of each starting quantity. The correlation coefficients ($R^2$) of the standard curves were 0.993 and 0.997, respectively (Figure 6), indicating a good linearity for both assays. On the basis of the equation $E = 10^{-(1/\text{slope})} - 1$, the PCR efficiency can be calculated and the ideal slope should be −3.32 for 100% PCR efficiency.[38] Slopes in the range from −3.1 to −3.6 are acceptable, indicating PCR efficiency from 90 to 110%. The two efficiencies were 101.3% for endogenous *RLP21* and 97.4% for *NPR1* in the standard dilutions, indicating that the PCR efficiencies were acceptable. The acceptable PCR reaction efficiencies and the good linearity between the logarithm of initial DNA quantities and $C_p$ indicated that the established real-time PCR systems of *RLP21* and *NPR1* are suitable for quantitative analysis.

**Quantification of the Samples with Known Transgenic Wheat Content.** Seven samples with 0.5, 1, 2, 5, 20, 50, or 100% of GM wheat contents were prepared by mixing pure dried wheat flour of transgenic line R4 with non-GM dried wheat flour on a w/w basis, from which DNA was extracted. An aliquot of 50 ng of DNA from each sample was used as a template in each reaction, and GM contents were calculated on the basis of the standard curves using the relative quantification method. The quantitative results of these seven samples were 0.45, 0.85, 1.90, 4.56, 17.37, 48.17, and 108.26%, respectively (Table 3). The quantified biases (mean tested value versus true value) of tested samples ranged from 4.88 to 15.22%, and the relative standard deviation (RSD) values ranged from 5.19 to 10.63%. All variations from the samples were below 25%, the accepted level for GMO quantification.[38] These findings suggest that the *RPL21* gene can be used as the wheat endogenous reference gene for quantifying GM wheat food contents, and the established construct-specific PCR systems are suitable for the quantification of practical samples derived from *NPR1* transgenic wheat. A previous study used a *PKABA1*-based system to test 10 samples of food and feed and showed that 8 of the analyzed samples presumably contained wheat contents, and on the basis of that, the authors stated that *PKABA1* could be used for the detection of GM wheat.[18] However, no previous study has quantified genuine GM wheat contents using an endogenous reference gene system. The *RPL21* system developed in this study can quantify GM wheat contents as little as 0.5%, satisfying the labeling regulations in the European Union and many other countries.[5−7] To our knowledge, this is the first study to detect the contents of GM wheat using a reference gene system with quantitative real-time PCR.

In conclusion, the wheat *RPL21* gene used as an endogenous reference gene was validated for GM wheat detection and quantification with qualitative and real-time quantitative PCR assays. Southern blot with common wheat DNA and sequence analyses of common wheat together with its three diploid ancestral species congruently indicated that the primer pair RPL21-1F/1R had only one amplicon in common wheat. The LOD of conventional PCR was 2 copies of wheat haploid genome. The LOD and LOQ of real-time PCR were 2 and 8 copies of wheat haploid genome, respectively. Furthermore, two standard curves of *RPL21* and *NPR1* were established using *NPR1* transgenic wheat, and seven mixed samples with known content of *NPR1* GM wheat were relatively accurately quantified using the established real-time PCR method. All of these results demonstrate that the *RPL21* gene is a suitable endogenous reference gene for GM wheat detection, and the developed *RPL21* system will facilitate the enforcement of GMO labeling for wheat in the near future.

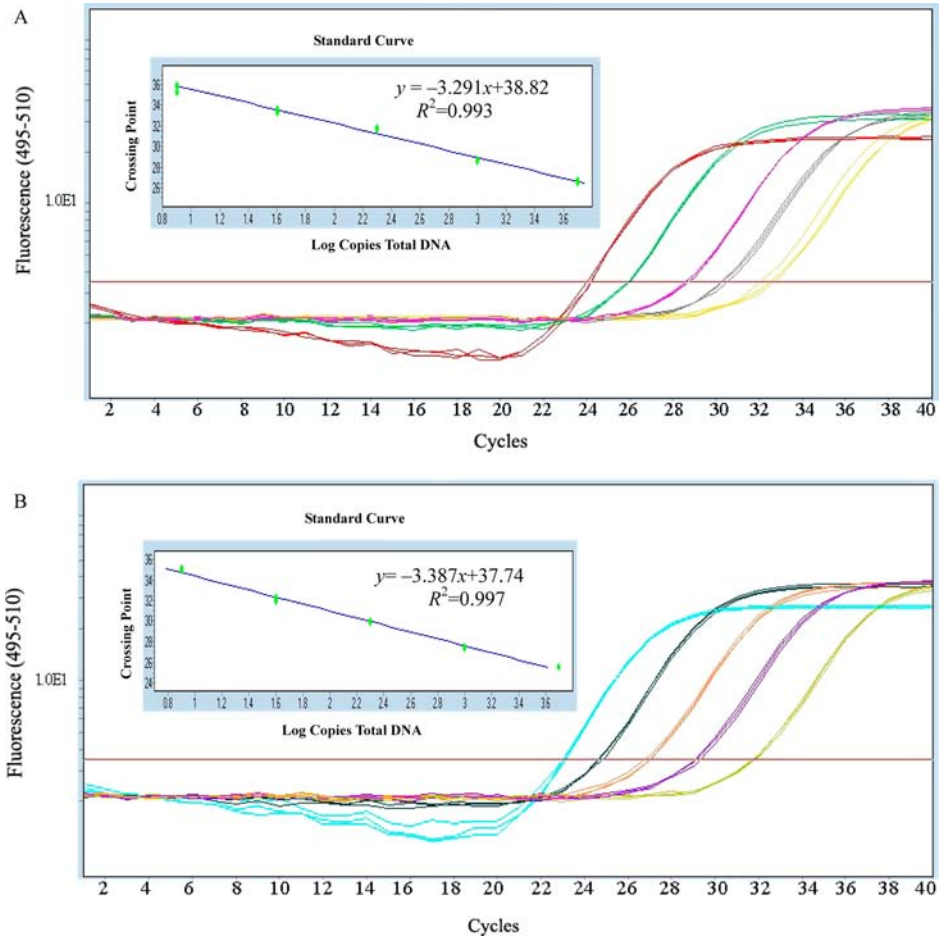


**Figure 6.** Real-time PCR assay of the logarithmic plots resulting from the amplification of five 5-fold serial dilutions (corresponding to 5000, 1000, 200, 40, and 8 copies of the wheat haploid genome per reaction) of DNA from GM wheat line R4 and its relative standard curve obtained with the crossing point ($C_p$) value versus the log of each initial total DNA for (A) *RPL21* gene and (B) *NPR1* gene.

**Table 3. Quantification of *NPR1* Transgenic Wheat Content in Seven Mixed Samples**

| | construct amounts × 100/endogenous amounts | | | accuracy | | precision | |
|---|---|---|---|---|---|---|---|
| true value (%) | mean 1 | mean 2 | mean 3 | mean (%) | bias (%) | SD | RSD (%) |
| 0.50 | 0.49 | 0.46 | 0.40 | 0.45 | 10.19 | 0.00043 | 8.76 |
| 1.0 | 0.80 | 0.86 | 0.88 | 0.85 | 15.22 | 0.00042 | 5.19 |
| 2.0 | 1.74 | 1.99 | 1.97 | 1.90 | 4.88 | 0.0014 | 8.14 |
| 5.0 | 4.57 | 5.20 | 3.92 | 4.56 | 8.77 | 0.0064 | 13.99 |
| 20 | 16.85 | 15.35 | 19.90 | 17.37 | 13.15 | 0.023 | 13.76 |
| 50 | 41.67 | 48.56 | 54.28 | 48.17 | 3.66 | 0.063 | 15.16 |
| 100 | 100.59 | 103.69 | 120.49 | 108.26 | 8.26 | 0.11 | 10.64 |

## ■ ASSOCIATED CONTENT

### Supporting Information

Sequence alignment of the *RPL21* gene from *T. aestivum* (AABBDD, accession number HM138481.1), *T. urartu* (AA), *A. speltoides* (BB), and *A. tauschii* (DD), with the latter three amplified by the primer pair RPL21-*Kpn*I/*Sac*I (Figure S1). This material is available free of charge via the Internet at http://pubs.acs.org.

## ■ AUTHOR INFORMATION

### Corresponding Authors

*E-mail: hepingli@mail.hzau.edu.cn.
*E-mail: yucailiao@mail.hzau.edu.cn.

### Funding

This work was supported by the Ministry of Agriculture of China (2011ZX08002-001 and 2014ZX0800202B-001) and the National Natural Science Foundation of China (31271717).

### Notes

The authors declare no competing financial interest.

## ■ ACKNOWLEDGMENTS

The authors thank Prof. Jizeng Jia for diploid wheat materials, Prof. Jun Yin for common wheat materials, and Mr. Hong-Jie Du for assistance of PCR.

## ABBREVIATIONS USED

PCR, polymerase chain reaction; GMO, genetically modified organism; GM, genetically modified; LOD, limit of detection; LOQ, limit of quantification; FAM, 6-carboxyfluorescein; TAMRA, 6-carboxytetramethylrhodamine; CTAB, cetyltrimethylammonium bromide; $C_p$, crossing point; SD, standard deviation; RSD, relative standard deviation

## REFERENCES


(1) James, C. *Global Status of Commercialized Biotech/GM Crops: 2012*; International Service for the Acquisition of Agri-biotech Applications: Ithaca, NY, 2013; Brief 44.

(2) Hellmich, R.; Hellmich, K. Use and impact of Bt maize. *Nat. Educ. Knowl.* **2012**, *3*, 4.

(3) Lu, C. The first approved transgenic rice in China. *GM Crops* **2010**, *1*, 113−115.

(4) Wei, J.; Li, F.; Guo, J.; Li, X.; Xu, J.; Wu, G.; Zhang, D.; Yang, L. Collaborative ring trial of the papaya endogenous reference gene and its polymerase chain reaction assays for genetically modified organism analysis. *J. Agric. Food Chem.* **2013**, *61*, 11363−11370.

(5) European Communities (EC).. European Commission Regulation (EC) 1829/2003 and 1830/2003. *Off. J. Eur. Communities: Legis.* **2003**, *268*, 1−28.

(6) Ministry of Agriculture and Forestry of Korea. *Notification 2000-31*; Ministry of Agriculture and Forestry of Korea: Seoul, South Korea, 2000.

(7) Food and Marketing Bureau, Ministry of Agriculture, Forestry, and Fisheries. *Notification 1775*; Food and Marketing Bureau, Ministry of Agriculture, Forestry, and Fisheries: Tokyo, Japan, 2000.

(8) Ministry of Agriculture of the People's Republic of China. *Order 10*; Ministry of Agriculture of the People's Republic of China: Beijing, China, 2002.

(9) Valasek, M.; Repa, J. The power of real-time PCR. *Adv. Physiol. Educ.* **2005**, *29*, 151−159.

(10) Zhang, D.; Guo, J. The development and standardization of testing methods for genetically modified organisms and their derived products. *J. Integr. Plant Biol.* **2011**, *53*, 539−551.

(11) Chaouachi, M.; El Malki, R.; Berard, A.; Romaniuk, M.; Laval, V.; Brunel, D.; Bertheau, Y. Development of a real-time PCR method for the differential detection and quantification of four Solanaceae in GMO analysis: potato (*Solanum tuberosum*), tomato (*Solanum lycopersicum*), eggplant (*Solanum melongena*), and pepper (*Capsicum annuum*). *J. Agric. Food Chem.* **2008**, *56*, 1818−1828.

(12) Hernández, M.; Esteve, T.; Pla, M. Real-time polymerase chain reaction based assays for quantitative detection of barley, rice, sunflower, and wheat. *J. Agric. Food Chem.* **2005**, *53*, 7003−7009.

(13) Ding, J.; Jia, J.; Yang, L.; Wen, H.; Zhang, C.; Liu, W.; Zhang, D. Validation of a rice specific gene, *sucrose phosphate synthase*, used as the endogenous reference gene for qualitative and real-time quantitative PCR detection of transgenes. *J. Agric. Food Chem.* **2004**, *52*, 3372−3377.

(14) Jiang, L.; Yang, L.; Zhang, H.; Guo, J.; Mazzara, M.; Van den Eede, G.; Zhang, D. International collaborative study of the endogenous reference gene, *sucrose phosphate synthase* (*SPS*), used for qualitative and quantitative analysis of genetically modified rice. *J. Agric. Food Chem.* **2009**, *57*, 3525−3532.

(15) Yang, L.; Zhang, H.; Guo, J.; Pan, L.; Zhang, D. International collaborative study of the endogenous reference gene *LAT52* used for qualitative and quantitative analyses of genetically modified tomato. *J. Agric. Food Chem.* **2008**, *56*, 3438−3443.

(16) Hernández, M.; Río, A.; Esteve, T.; Prat, S.; Pla, M. A rapeseed-specific gene, *acetyl-CoA carboxylase*, can be used as a reference for qualitative and real-time quantitative PCR detection of transgenes from mixed food samples. *J. Agric. Food Chem.* **2001**, *49*, 3622−3627.

(17) Guo, J.; Yang, L.; Liu, X.; Zhang, H.; Qian, B.; Zhang, D. Applicability of the *chymopapain* gene used as endogenous reference gene for transgenic Huanong No. 1 papaya detection. *J. Agric. Food Chem.* **2009**, *57*, 6502−6509.

(18) Rønning, S.; Berdal, K.; Andersen, C.; Holst-Jensen, A. Novel reference gene, *PKABA1*, used in a duplex real-time polymerase chain reaction for detection and quantitation of wheat- and barley-derived DNA. *J. Agric. Food Chem.* **2006**, *54*, 682−687.

(19) James, D.; Schmidt, A.; Wall, E.; Green, M.; Masri, S. Reliable detection and identification of genetically modified maize, soybean, and canola by multiplex PCR analysis. *J. Agric. Food Chem.* **2003**, *51*, 5829−5834.

(20) Shang, Y.; Zhu, P.; Huang, K.; Liu, W.; Tian, W.; Luo, Y.; Xu, W. A peach (*Prunus persica*)-specific gene, *Lhcb2*, used as an endogenous reference gene for qualitative and real-time quantitative PCR to detect fruit products. *LWT—Food Sci. Technol.* **2014**, *55*, 218−223.

(21) Hernández, M.; Duplan, M.; Berthier, G.; Vaïtilingom, M.; Hauser, W.; Freyer, R.; Pla, M.; Bertheau, Y. Development and comparison of four real-time polymerase chain reaction systems for specific detection and quantification of *Zea mays* L. *J. Agric. Food Chem.* **2004**, *52*, 4632−4637.

(22) Brenchley, R.; Spannagl, M.; Pfeifer, M.; Barker, G.; D'Amore, R.; Allen, A.; McKenzie, N.; Kramer, M.; Kerhornou, A.; Bolser, D.; Kay, S.; Waite, D.; Trick, M.; Bancroft, I.; Gu, Y.; Huo, N.; Luo, M.; Sehgal, S.; Gill, B.; Kianian, S.; Anderson, O.; Kersey, P.; Dvorak, J.; McCombie, W.; Hall, A.; Mayer, K.; Edwards, K.; Bevan, M.; Hall, N. Analysis of the bread wheat genome using whole-genome shotgun sequencing. *Nature* **2012**, *491*, 705−710.

(23) Xia, L.; Ma, Y.; He, Y.; Jones, H. GM wheat development in China: Current status and challenges to commercialization. *J. Exp. Bot.* **2012**, *63*, 1785−1790.

(24) Vautrin, S.; Zhang, D. Real-time polymerase chain reaction assay for endogenous reference gene for specific detection and quantification of common wheat-derived DNA (*Triticum aestivum* L.). *J. AOAC Int.* **2007**, *90*, 794−801.

(25) Iida, M.; Yamashiro, S.; Yamakawa, H.; Hayakawa, K.; Kuribara, H.; Kodama, T.; Furui, S.; Akiyams, H.; Maitani, T.; Hino, A. Development of taxon-specific sequences of common wheat for the detection of genetically modified wheat. *J. Agric. Food Chem.* **2005**, *53*, 6294−6300.

(26) Huang, H.; Cheng, F.; Wang, R.; Zhang, D.; Yang, L. Evaluation of four endogenous reference genes and their real-time PCR assays for common wheat quantification in GMOs detection. *PloS One* **2013**, *8*, No. e75850.

(27) Du, X.; Hao, C.; Zhang, X.; Ma, Z.; You, G.; Wang, L.; Dong, Y. Genetic diversity of *Waxy* gene in Chinese wheat landraces. *Acta Agron. Sin.* **2007**, *33*, 503−506.

(28) Yamamori, M.; Nakamura, T.; Endo, T. R.; Nagamine, T. Waxy protein deficiency and chromosomal location of coding genes in common wheat. *Theor. Appl. Genet.* **1994**, *89*, 179−184.

(29) Gao, C.; Kou, X.; Li, H.; Zhang, J.; Saad, A.; Liao, Y. Inverse effects of *Arabidopsis NPR1* gene on fusarium seedling blight and fusarium head blight in transgenic wheat. *Plant Pathol.* **2013**, *62*, 383−392.

(30) Li, H.; Zhang, J.; Shi, R.; Huang, T.; Fischer, R.; Liao, Y. Engineering fusarium head blight resistance in wheat by expression of a fusion protein containing a *Fusarium*-specific antibody and an antifungal peptide. *Mol. Plant-Microbe Interact.* **2008**, *21*, 1242−1248.

(31) Yin, T.; Pan, G.; Liu, H.; Wu, J.; Li, Y.; Zhao, Z.; Fu, T.; Zhou, Y. The chloroplast ribosomal protein L21 gene is essential for plastid development and embryogenesis in *Arabidopsis*. *Planta* **2012**, *235*, 907−921.

(32) Feldman, M.; Levy, A. Allopolyploidy: A shaping force in the evolution of wheat genomes. *Cytogenet. Genome Res.* **2005**, *109*, 250−258.

(33) Hu, Z.; Han, Z.; Song, N.; Chai, L.; Yao, Y.; Peng, H.; Ni, Z.; Sun, Q. Epigenetic modification contributes to the expression divergence of three *TaEXPA1* homeologs in hexaploid wheat (*Triticum aestivum*). *New Phytol.* **2013**, *197*, 1344−1352.

(34) Berdal, K.; Holst-Jensen, A. Roundup ready soybean event specific real-time quantitative PCR assay and estimation of the

practical detection and quantification limits in GMO analyses. *Eur. Food Res. Technol.* **2001**, *213*, 432−438.
(35) Bonfini, L.; Heinze, P.; Kay, S.; Van den Eede, G. *Review of GMO Detection and Quantification Techniques*; Institute for Health and Consumer Protection, Food Products and Consumer Goods Unit: Ispra, Italy, 2002.
(36) Jiang, L.; Yang, L.; Rao, J.; Guo, J.; Wang, S.; Liu, J.; Lee, S.; Zhang, D. Development and in-house validation of the event-specific qualitative and quantitative PCR detection methods for genetically modified cotton MON15985. *J. Sci. Food Agric.* **2010**, *90*, 402−408.
(37) Yang, L.; Xu, S.; Pan, A.; Yin, C.; Zhang, K.; Wang, Z.; Zhou, Z.; Zhang, D. Event specific qualitative and quantitative polymerase chain reaction detection of genetically modified MON863 maize based on the 5′-transgene integration sequence. *J. Agric. Food Chem.* **2005**, *53*, 9312−9318.
(38) Ginzinger, D. Gene quantification using real-time quantitative PCR: An emerging technology hits the mainstream. *Exp. Hematol.* **2002**, *30*, 503−512.

development of heterogeneous catalysts for the interesterification reaction in an environmentally friendly manner has become an area of great importance particularly from the green chemistry point of view.

The interesterification reaction involves as least two oils with different FA compositions. Due to the complex compositions in the oils, it is hard to evaluate quantitatively the interesterification process. For the optimization of the catalyst preparation conditions, in the current study, soybean oil and methyl stearate were used as reactants, and the incorporation of stearoyl groups into TAGs was determined by gas chromatography (GC) techniques.[22] Besides, the interesterification reaction between soybean oil and lard was also carried out to investigate the properties of the interesterified products.

Alumina has attracted much interest as a heterogeneous catalyst support, due to its high surface area, simple structure and availability.[23] Thus, in the present study, $KNO_3/Al_2O_3$ catalysts with different $KNO_3$ loadings were prepared using alumina as a catalyst support, and then were tested in the interesterification reaction. The prepared solid catalysts were characterized by using Hammett titration method, power X-ray diffraction (XRD), scanning electron microscopy (SEM), and nitrogen adsorption−desorption techniques. The effect of calcination temperature and $KNO_3$ loading was investigated with the interesterification of soybean oil with methyl stearate in terms of stearoyl incorporation into the TAGs. By using this solid base catalyst, the interesterification reactions of soybean oil and lard blends were carried out in a batch reactor, and the properties of the interesterified products were investigated by gas chromatography (GC), high-performance liquid chromatography (HPLC), and confocal laser scanning microscopy.

## MATERIALS AND METHODS

**Materials.** Refined soybean oil and lard used in this study were purchased from the local supermarket. Methyl stearate (≥98%) was obtained from Sinopharm Chemical Reagent Corporation (Shanghai, China). The alumina used as a support, with a surface area of 123 $m^3/g$, was obtained from Tianjin Chemical Reagent Factory. Porcine pancreatic lipase (EC 3.1.1.3, Type II; PPL) used for the analysis of FA profiles at the *sn*-2 position of the interesterified TAGs, was purchased from Sigma-Aldrich Corporation (St. Louis, U.S.A.). All the other materials used were of analytical or chromatographical grades.

**Catalyst Preparation.** The potassium-doped alumina catalysts ($KNO_3/Al_2O_3$), with different loadings of $KNO_3$ over the alumina support, were prepared by the conventional incipient-wetness impregnation method with an aqueous solution of $KNO_3$ using commercial alumina as a support. In a typical preparation, the required amount of alumina was placed into the aqueous $KNO_3$ solution. The resulting suspensions were stirred for 24 h at room temperature, and water was then evaporated at 80 °C under reduced pressure. The concentration of initial $KNO_3$ solution was changed to prepare the solid catalyst with different $KNO_3$ loadings. After impregnation the white solid obtained hereby was dried overnight and was finally calcined under an air flow at 500−900 °C for 6 h prior to the catalytic tests. The solid catalysts prepared with various $KNO_3$ loadings of 30, 35, 40, and 45 wt %, were expressed as $30\%KNO_3/Al_2O_3$,$35\%KNO_3/Al_2O_3$, $40\%KNO_3/Al_2O_3$, and $45\%KNO_3/Al_2O_3$, respectively.

**Catalyst Characterization.** Powder X-ray diffraction (XRD) patterns of selected samples were obtained with a Bruker-AXS NanoSTAR instrument. Nickel filtered K$\alpha$ radiation of copper was used at 40 kV and 30 mA. The data were analyzed with the DiffracPlus software, and the phases were identified using the powder diffraction file database (JCPDS, International Centre for Diffraction Data)

Basic strengths of the solid catalyst (H_) were determined by using various Hammett indicators. For this purpose, about 300 mg of the sample was placed into 1 mL Hammett indicator solution diluted with 10 mL of methanol and allowed to equilibrate for 2 h. The basic strength is quoted as being stronger than the weakest indictor that shows a color change, and weaker than the strongest indicator, which exhibits no color change. The basicity of the solid catalyst was measured by the method of Hammett indicator involving the benzene carboxylic acid (0.02 mol/L methanol solution).[17]

Scanning electron microscope (SEM) measurements were performed with a field-emission microscope (JEOL, JSM-6390LV) using an accelerating voltage of 15 kV. The nitrogen adsorption−desorption isotherms at −196 °C were measured using a Quantachrome NOVA 1000e instrument. The Brunauer−Emmett−Teller (BET) method was used to calculate the specific surface area. The total pore volume and pore size distribution were estimated according to the Barrett−Joyner−Halenda (BJH) method based on the adsorption isotherm.

**Interesterification Procedures.** The interesterification of soybean oil and methyl stearate was carried out in a 50 mL round-bottom flask. Prior to each reaction, a mixture of 20 g of soybean oil and 41 g of methyl stearate was dried in the reactor under reduced pressure at 80 °C. By adding 10 wt % of the solid catalyst, the heterogeneous reaction mixture was allowed to proceed under reduced pressure at 200 °C. Constant stirring at 750 rpm was used to minimize mass transfer limitations. After 4 h of reaction time, the reactor was cooled to room temperature. Thereafter, the catalyst was recovered from the reaction mixture by simple filtration, and the filtrate was then used for subsequent analysis.

Soybean oil and lard were blended in different proportions of 80:20, 60:40, 40:60, 20:80 ratios (w/w), and then the binary blends were interesterified in batch reactors. In order to avoid oil oxidation, the interesterifications were carried out in a nitrogen atmosphere. Portions (100 g) of the blends were initially heated under vacuum at 80 °C to remove air and moisture. When the reaction mixture had reached a reaction temperature of 100 °C, 5 wt % of the solid catalyst was added in a batch reactor, and the blends were stirred vigorously. The interesterification reaction of different blends of soybean oil and lard was performed under reduced pressure at 100 °C in a 150 mL stoppered flask with magnetic stirring (∼750 rpm) for a time frame of 5 h. At the end of the reaction, the interesterified product was filtered, and then employed for subsequent analysis.

**Analytical Methods.** The FA compositions of triacylglycerols were analyzed by a gas chromatography (GC) according to AOAC method.[24] After complete conversion of FA residues into fatty acid methyl esters (FAMEs), the methylated FA residues were determined using an Agilent 6890 N gas chromatograph (Santa Clara, CA. U.S.A.) equipped with a flame-ionization detector, an auto injector and a fused silica capillary column (60 m × 0.25 mm) coated with 0.25 $\mu$m of BPX-70 (SGE, Australia). Nitrogen was used as a carrier gas at flow rate of 1.2 mL/min with a split ratio of 1:20. The temperatures of injector and detector were set at 260 and 300 °C, respectively. The initial temperature of the program was increased to 160 °C and then held for 5 min. This temperature was finally increased to 200 °C at a rate of 5 °C/min, and held isothermally for another 42 min at the final temperature. The FAME composition was identified by comparison with the relative retention time of FAME standards. The FAME content was obtained by area normalization and expressed as mass percentage.[25]

For the interesterification of soybean oil with methyl stearate, the triacylglycerol was separated from the reaction mixtures by thin-layer chromatography (TLC) on a silica gel 60G plate. The interesterified blends were spotted on TLC silica gel plates, and then developed with petroleum ether/ethyl ether/acetic acid (90:10:1,v/v/v). The developed TLC plates were sprayed with 2% 2,7-dichlorofluorescein in methanol. Bands corresponding to triacylglycerols, which were identified using triolein as the standard, were scraped from the silica plates, extracted with *n*-hexane, and subsequently analyzed for the FA profiles. The progress of the interesterification reaction was followed by the determination of stearoyl incorporation into the TAGs.

The FA profiles at the *sn*-2 position of triacylglycerols were measured by using pancreatic lipase according to the method described in the literature.[25] The pancreatic lipase can be applied to

hydrolyze selectively FAs at sn-1,3 positions of TAGs, producing 2-monoacylglycerol and FAs. The formed 2-monoacylglycerol was separated by TLC plates, and the *sn*-2 positional analysis of FA residues in the TAGs was carried out by GC techniques after 2-monoacylglycerol was totally converted to FAMEs as described previously.

For the interesterification of soybean oil with lard, the variation of TAG compositions occurred during the reaction was assessed using high-performance liquid chromatography (HPLC) fitted with commercially packed Genesis C18 column (150 mm × 4.6 $mm^2$).[25] Each sample was dissolved in chloroform (10 mg/mL), and 20 $\mu$L of the dissolved sample was injected into the HPLC system. The elution solvent consisted of dichloromethane and acetonitrile (HPLC grade) at a gradient composition from 35% acetonitrile increasing to 55% dichloromethane in 45 min. The column temperature was held at 40 °C. The TAG species were detected by an evaporative light scattering detector (Alltech 500). Individual TAG species were identified tentatively by comparing the relative retention time with those of TAG standards and according to the literature.[26,27]

The iodine value (IV) for the interesterified product was measured according to the AOCS Official Method Cd 1c-85 (AOCS, 2009).[25]

Slip melting point (SMP) was determined according to the AOCS Official Method *Cc* 3−25 (AOCS, 2009) using the open capillary tube method,[25] The capillary tubes filled with 1 cm high column of the samples were stored in a refrigerator for 16 h prior to the measurements in a beaker of cold water. Thereafter, the sample tube was heated gradually, and the temperature at which the sold fat in the tube began to rise, was considered to be the SMP. This measurement was performed in triplicate, and the reported SMPs were the average of the determinations.

The crystal morphology of the interesterified product was observed using a XP-203 polarized light microscopy fitted with a digital video camera. The samples were first heated at 70 °C in a water bath and maintained at this temperature for 30 min to eliminate all crystal nuclei. Afterward, about 10 mg of melted sample was placed on a preheated microscope slide, cooled to 25 °C and then held for 20 h. The crystal morphology was taken at room temperature.

## RESULTS AND DISCUSSION

**Catalyst Characterization.** A Hammett indicator method was employed to evaluate the basic properties.[17] The alumina support was acidic and could change the color of dimethylaminoazobenzene (H_= 3.3) from yellow to red, and in consistent with this, the transesterification did not proceed when the alumina support was acted as a catalyst. However, as the $KNO_3$ was loaded and subsequently calcined at 700 °C, the thus-obtained solid base catalyst showed the basic strength values (H_) of 15 < H_18.4, and the basicity of 35% $KNO_3/Al_2O_3$ catalyst was determined to be 6.97 mmol/g. Owing to the basicity, the solid catalyst displayed comparable activities to the reaction as expected.

Figure 1 gives the XRD patterns of the $KNO_3/Al_2O_3$ catalysts prepared at different conditions. As can be seen, the XRD pattern of uncalcinated $KNO_3/Al_2O_3$ sample exhibited the characteristic peaks of $Al_2O_3$ and $KNO_3$ (curve a in Figure 1).[28] Besides, there were other minor peaks, which could not be unequivocally identified. In the XRD pattern of 35%$KNO_3/Al_2O_3$ catalyst calcined at 500 °C, in addition to the XRD peaks associated with alumina, only three peaks of $KNO_3$ was observed (curve c in Figure 1). As the calcination temperature increased beyond 700 °C, the number of the XRD peak corresponding to $KNO_3$ phase was found to further decrease, indicating the decomposition of loaded $KNO_3$ during the calcination processes. In the case of 30% $KNO_3/Al_2O_3$ catalysts calcined at 700 °C (curve b in Figure 1), the diffraction lines of $Al_2O_3$ were visible; however the $KNO_3$ phases were decreased

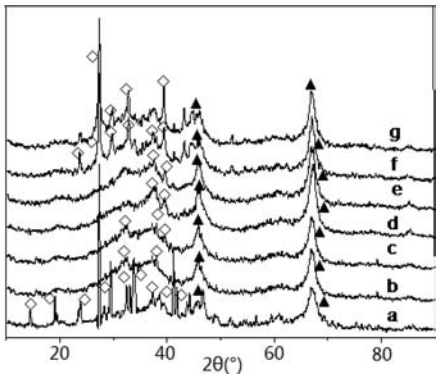


**Figure 1.** Power X-ray diffraction patterns for samples: (a) uncalcined 35%$KNO_3/Al_2O_3$; (b) 30%$KNO_3/Al_2O_3$ calcined at 700 °C; (c) 35% $KNO_3/Al_2O_3$ calcined at 500 °C; (d) 35%$KNO_3/Al_2O_3$ calcined at 700 °C; (e) 35%$KNO_3/Al_2O_3$ calcined at 800 °C; (f) 40%$KNO_3/Al_2O_3$ calcined at 700 °C; and (g) 45%$KNO_3/Al_2O_3$ calcined at 700 °C. (◇),$KNO_3$; (▲), $Al_2O_3$.

in number when compared with the uncalcined sample. With increasing the $KNO_3$ loading beyond 35%, the diffraction peaks attributed to $KNO_3$ phases were observed to increase both in intensity and in number, mostly due to the overloading of $KNO_3$ that saturated the alumina surface. At these $KNO_3$ loadings, the dispersion of excess potassium compound could mask the active base sites that serve as active sites for the interesterification reaction. However, no obvious peak for $K_2O$ phase was clearly registered in the XRD patterns. The catalytically active phase such as $K_2O$ might have been present in an amorphous state, which was not detected by XRD techniques. By drawing on the results, it is reasonable to state that the surface basicity and the subsequent catalytic activity are resulted from the decomposition of impregnated $KNO_3$ and the formation of $K_2O$ and Al—O—K groups that can act as active sites for the interesterification reactions.[18,20]

SEM techniques can be used to investigate the morphology feature of the solid catalyst. The typical SEM micrograph of alumina support and solid catalyst is illustrated in Figure 2. As can be seen, the support was presented as irregular shaped agglomerations of alumina particles with clear edges, with particle size ranging from approximately 2−5 $\mu$m. As evidenced in Figure 2, no significant morphological change was found between the alumina support and the solid base catalyst. After loading with the potassium compounds, the alumina cluster or agglomeration with clear demarcation into regions could also be observed. This observation suggested that the alumina retained its structure during the catalyst preparation process, and there was a homogeneous distribution of potassium compounds on alumina supports, which were important for catalysis.

The nitrogen adsorption−desorption isotherms of the alumina support and the prepared catalyst are presented in Figure 3. The two samples exhibited the type IV isotherm according the IUPAC classification with a obvious hysteresis loop of type H4, implying the existence of micropores with narrow pore size distributions. Clearly, a significant reduction in the adsorbed volume was observed after impregnation of alumina support with potassium compounds, mostly likely owing to the pores obstruction of the active sites in the support, evidencing the incorporation of potassium compounds into the alumina support.

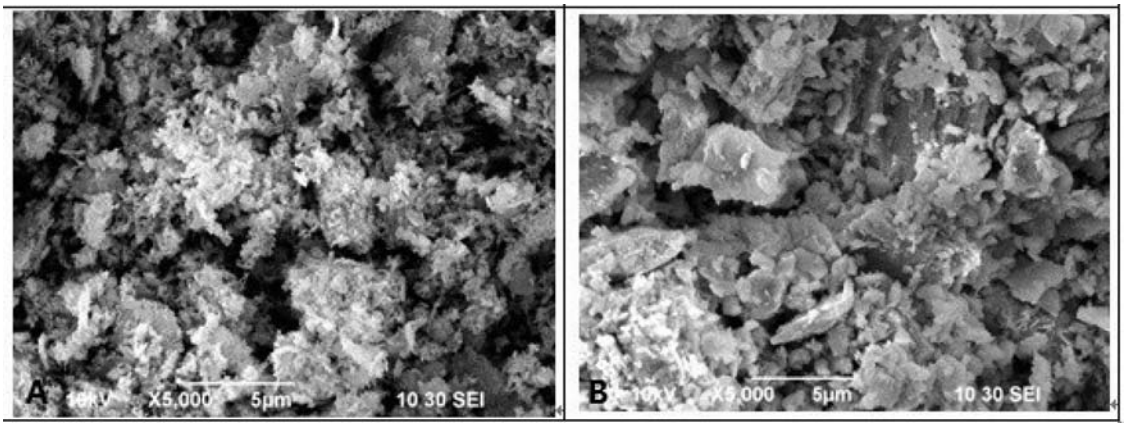


**Figure 2.** Scanning electron micrographs of samples: (a) $Al_2O_3$ and (b) 35%$KNO_3$/$Al_2O_3$ catalyst.

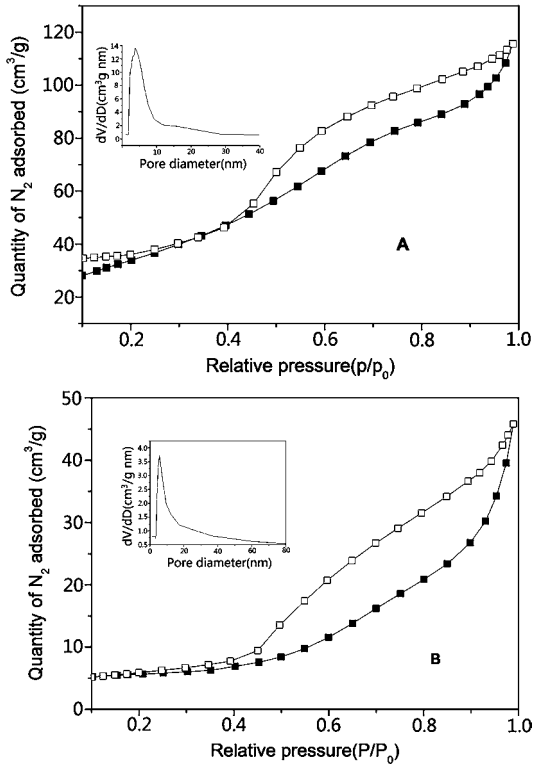


**Figure 3.** Nitrogen adsorption/desorption isotherms and pore size distribution profiles of samples: (a) $Al_2O_3$ and (b) 35%$KNO_3$/$Al_2O_3$ catalyst.

The textural properties of the solid base catalyst are shown in Table 1. The alumina support gave a surface area of 123 $m^2$/g, and an mean pore size of 5.8 nm, In the case of the solid catalyst, the surface area calculated from the $N_2$ adsorption−desorption isotherm was decreased to 19 $m^2$/g, while the pore size was decreased to 3.8 nm. Anyway, an obvious decrease of the surface area occurred after $KNO_3$ was impregnated and calcined at a higher temperature. Moreover, a decrease in the pore size and pore volume was also observed. Such results further demonstrated the potassium compounds on the alumina support were formed by the decomposition of potassium nitrates at a higher calcination temperature.

**Table 1. Textual Characteristics of $Al_2O_3$ and 35%$KNO_3$/$Al_2O_3$ Catalyst**

| sample | $S_{BET}$[a] ($m^2$/g) | $V_p$[b] ($cm^3$/g) | $D_{BJH}$[c] (nm) |
|---|---|---|---|
| $Al_2O_3$ | 123 | 0.17 | 5.8 |
| $KNO_3/Al_2O_3$ | 19 | 0.07 | 3.8 |

[a]BET surface area. [b]Pore volume. [c]Average pore diameter from BJH desorption.

**Influence of Catalyst Preparation Conditions on the Catalytic Activities.** In the current study, the interesterification of soybean oil and methyl stearate was chosen to investigate the effect of catalyst preparation conditions on the catalytic activity. To optimize the $KNO_3$ loading, different loading amounts of $KNO_3$ were employed for the preparation of the catalyst. Table 2 shows the evolution of stearoyl incorporation on the solid catalyst with different $KNO_3$ loadings. As can be seen, the stearoyl incorporation achieved at the $KNO_3$ loading of 20% was 30.8%, and then increased to the maximum value of 50.6% with increasing the $KNO_3$ loading up to 35%. However, with subsequent increase in the $KNO_3$ loading, the stearoyl incorporation remained nearly unchanged. In light of the results, the suitable $KNO_3$ loading is determined to be 35%.

**Table 2. Different Catalyst Preparation Conditions and the Results of the Interesterification between Soybean Oil and Methyl Stearate Catalyzed by the Heterogeneous Catalyst**

| entry | loading amount of $KNO_3$ (h) | calcination temperature (°C) | stearoyl incorporation (%) |
|---|---|---|---|
| 1 | 35 | 500 | 0 |
| 2 | 35 | 600 | 0 |
| 3 | 35 | 650 | 0 |
| 4 | 35 | 700 | 50.6 |
| 5 | 35 | 750 | 46.1 |
| 6 | 35 | 800 | 38.2 |
| 7 | 20 | 700 | 30.8 |
| 8 | 25 | 700 | 37.6 |
| 9 | 30 | 700 | 46.7 |
| 10 | 40 | 700 | 48.2 |
| 11 | 45 | 700 | 45.3 |

In order to assess the effect of calcination temperature on the catalytic activity of the solid catalyst, the calcination temperature was set from 500 to 800 °C. The experimental results are also included in Table 2. As observed, the catalyst did not exhibit any activity in the transesterification reaction as the calcination temperature was below 700 °C. The maximum


dx.doi.org/10.1021/jf503726a | J. Agric. Food Chem. 2014, 62, 10414−10421

**Table 3. Fatty Acid Composition (Percent) and Iodine Values of Lard, Soybean Oil and Their Blends in Different Ratios before and after Interesterification Reaction**

| LA/SO ratio | myristic | palmitic | palmtoleic | stearic | oleic | linoleic | linolenic | IV |
|---|---|---|---|---|---|---|---|---|
| LA | 14:0 | 16:0 | 16:1 | 18:0 | 18:1 | 18:2 | 18:3 | |
| | 1.8 ± 0.1 | 26.5 ± 0.1 | 2.5 ± 0.2 | 12.3 ± 0.2 | 38.7 ± 0.2 | 17.2 ± 0.1 | 0.7 ± 0.1 | 67.2 |
| 80:20 before | 1.3 ± 0.2 | 23.8 ± 0.1 | 2.1 ± 0.2 | 11.7 ± 0.1 | 39.6 ± 0.1 | 17.5 ± 0.2 | 1.6 ± 0.1 | 42.8 |
| 80:20 after | 1.4 ± 0.0 | 25.1 ± 0.2 | 2.6 ± 0.2 | 12.2 ± 0.1 | 39.6 ± 0.2 | 17.5 ± 0.2 | 1.6 ± 0.5 | 41.9 |
| 60:40 before | 1.4 ± 0.1 | 23.9 ± 0.2 | 2.0 ± 0.1 | 8.9 ± 0.5 | 33.4 ± 0.1 | 27.5 ± 0.1 | 2.8 ± 0.1 | 57.1 |
| 60:40 after | 1.2 ± 0.0 | 23.6 ± 0.1 | 1.7 ± 0.2 | 11.2 ± 0.2 | 33.9 ± 0.2 | 27.3 ± 0.0 | 2.1 ± 0.1 | 58.0 |
| 40:60 before | 1.0 ± 0.2 | 19.6 ± 0.0 | 1.5 ± 0.0 | 7.3 ± 0.2 | 36.7 ± 0.2 | 29.8 ± 0.1 | 3.9 ± 0.1 | 74.1 |
| 40:60 after | 1.1 ± 0.2 | 20.4 ± 0.5 | 1.4 ± 0.0 | 7.8 ± 0.1 | 35.4 ± 0.1 | 29.8 ± 0.0 | 3.9 ± 0.0 | 74.8 |
| 20:80 before | 0.4 ± 0.1 | 14.8 ± 0.1 | 0.6 ± 0.1 | 6.3 ± 0.2 | 28.1 ± 0.0 | 44.2 ± 0.3 | 5.6 ± 0.1 | 84.0 |
| 20:80 after | 0.5 ± 0.1 | 15.8 ± 0.4 | 0.8 ± 0.2 | 7.0 ± 0.0 | 28.1 ± 0.0 | 42.3 ± 0.2 | 5.0 ± 0.2 | 83.7 |
| SO | 0.0 ± 0.0 | 11.9 ± 0.2 | 0.0 ± 0.0 | 3.4 ± 0.2 | 22.2 ± 0.5 | 55.0 ± 0.4 | 7.6 ± 0.1 | 134.5 |

**Table 4. Triacylglycerol Composition (Percent) of Lard, Soybean Oil, and Their Blends in Different Ratios before and after Interesterification Reaction**

| TAG | LA | 80:20 | | 60:40 | | 40:60 | | 20:80 | | SO |
|---|---|---|---|---|---|---|---|---|---|---|
| | | before | after | before | after | before | after | before | after | |
| LLnLn | 0.0 | 0.0 | 0.0 | 0.3 | 0.7 | 0.2 | 0.6 | 0.5 | 0.8 | 1.2 |
| LLLn | 0.0 | 0.0 | 0.0 | 0.5 | 0.3 | 0.5 | 0.2 | 0.8 | 0.5 | 1.1 |
| LLL | 0.0 | 3.8 | 3.2 | 7.6 | 6.4 | 10.4 | 9.4 | 15.3 | 12.5 | 17.2 |
| 0LL | 0.7 | 5.2 | 4.3 | 8.7 | 5.6 | 11.8 | 7.9 | 14.1 | 12.8 | 16.3 |
| OOL | 1.8 | 3.7 | 5.5 | 6.6 | 4.8 | 10.9 | 8.6 | 12.3 | 10.7 | 14.5 |
| OOO | 3.3 | 2.6 | 1.8 | 1.7 | 1.5 | 0.9 | 0.8 | 0.3 | 0.2 | 0.0 |
| StOO | 3.6 | 2.8 | 2.3 | 2.6 | 1.9 | 2.8 | 2.5 | 2.4 | 2.1 | 2.1 |
| StOL | 4.7 | 3.7 | 2.5 | 3.5 | 2.8 | 3.1 | 2.7 | 2.7 | 1.8 | 1.2 |
| PLnLn | 0.0 | 0.3 | 0.2 | 0.5 | 0.4 | 0.7 | 0.6 | 0.9 | 0.8 | 1.1 |
| PLLn | 0.4 | 0.5 | 0.4 | 0.4 | 0.3 | 0.2 | 0.6 | 1.6 | 1.5 | 1.7 |
| POL | 8.9 | 9.6 | 6.7 | 10.5 | 7.6 | 10.8 | 8.6 | 11.7 | 9.2 | 12.4 |
| PLL | 13.7 | 13.5 | 16.5 | 15.3 | 18.7 | 15.8 | 19.2 | 16.1 | 21.6 | 20.8 |
| POO | 22.8 | 19.7 | 15.4 | 16.5 | 13.2 | 12.4 | 10.6 | 9.2 | 8.2 | 4.7 |
| PStO | 12.8 | 11.7 | 14.8 | 9.5 | 12.8 | 7.2 | 10.5 | 4.8 | 6.1 | 1.2 |
| PStSt | 3.2 | 2.8 | 1.9 | 1.6 | 1.3 | 0.7 | 0.4 | 0.0 | 0.0 | 0.0 |
| MOL | 1.5 | 1.3 | 1.6 | 0.7 | 0.9 | 0.7 | 0.9 | 0.2 | 0.3 | 0.0 |
| PPL | 8.6 | 6.8 | 7.8 | 5.2 | 7.8 | 4.2 | 6.7 | 3.1 | 4.6 | 2.4 |
| PPO | 9.7 | 8.7 | 9.8 | 6.3 | 8.7 | 4.4 | 6.8 | 3.2 | 4.8 | 1.5 |
| PPSt | 1.8 | 1.3 | 2.8 | 0.8 | 1.8 | 0.8 | 1.2 | 0.5 | 0.7 | 0.0 |
| MPO | 1.3 | 1.2 | 1.8 | 0.7 | 1.6 | 0.5 | 0.8 | 0.0 | 0.0 | 0.0 |

stearoyl incorporation of 50.6% was achieved at a calcination temperature of 700 °C. However, when the calcination temperature was further increased beyond 700 °C, there was an obvious decline trend in stearoyl incorporation to be observed. Accordingly, the best calcination temperature is 700 °C.

**Fatty Acid Composition and Iodine Value.** The interesterification of lard and soybean oil was carried out using the solid catalyst prepared at a calcination temperature of 700 °C with a $KNO_3$ loading of 35%. Table 3 shows the total FA compositions and the iodine values (IV) of lard, soybean oil and their binary blends before and after the interesterification. The total FA profile of lard was oleic acid (38.7%), palmitic acid (26.5%), linoleic acid (17.2%), stearic acid (12.3%) and palmitoleic acid (2.5%), with the IV of 67.2. The predominant FAs in the lard were accounted to be about 40% of long-chain saturated FAs, and accordingly at room temperature the lard was usually in solid state. As shown in Table 3, soybean oil had predominantly the following FA profiles: linoleic acid (55%), oleic acid (22.2%) and palmitic acid (11.9%), with small amounts of linolenic acid (7.6%) and stearic acid (3.4%). The IV of the soybean oil was determined to be 134.5. Owing to large amounts of mono- and polyunsaturated FAs, soybean oil always exhibited a liquid state at room temperatures. The total FA profile and IV of lard and soybean oil are in agreement with those reported in the literature.[29]

As indicated in Table 3, there was no significant change in the total FA profile to be observed for the different blends of lard and soybean oil after the interesterification reaction. Moreover, the IV of the binary blends before and after the CIE reaction remained almost constant, implying that the interesterification did not affect the degree of saturation. Besides, the *trans* FAs were not detected in the interesterified blends catalyzed by the solid base catalyst, and the interesterification did not cause conjugation during the interesterification process. These results revealed that the total FA compositions of the binary blends were not significantly altered between the initial blend and the interesterified product. In spite of this, at the present study, the distribution pattern of FAs in the TAGs can influence the physicochemical and nutritional properties.

The FA compositions at *sn*-2 position for the 60:40 blend, before and after the CIE catalyzed using the solid catalyst, were investigated. The interesterification reaction did not occur without catalyst under the reaction conditions employed here. It was shown that palmitic acid, stearic acid, oleic acid, linoleic acid at *sn*-2 position for the 60:40 blend of lard and soybean oil were varied from 29.5%, 21.6%, 25.5% and 22.8% to 33.9%, 16.1%, 20.3% and 29.1%, respectively, after the CIE reaction. As a consequence, the FA compositions on the glycerol backbone were changed obviously after the interesterification reaction, and thus the solid catalyst was demonstrated to be active for the interesterification of soybean oil with lard.

**Triacylglycerol Composition.** The TAG compositions of lard, soybean oil as well as their blends before and after the interesterification, are presented in Table 4. As observed, the main TAG compositions of lard were POO (22.8%), PLL (13.7%), PStO (12.8%), PPO (9.7%), POL(8.9%), PPL (8.6%), and StOL (4.7%). The soybean oil contained a wide range of unsaturated TAG species such as PLL (20.8%), LLL (17.2%), OLL (16.3%), OOL (14.5%), POL (12.4%), and POO (4.7%). As illustrated in Table 4, for different mass ratios of lard to soybean oil, different TAG species of the reaction mixtures were obtained. Moreover, the interesterification of the blends could result in a noticeable change in the TAG species as compared to their physical blends. For example, when the 60:40 blend of lard and soybean oil was interesterified, the interesterified product showed a reduced amount on POO, POL, OLL, LLL, OOL, and StOL from 16.5%, 10.5%, 8.7%, 7.6%, 6.6%, and 3.5% to 13.2%,7.6%,5.6%,6.4%, 4.8%, and 2.8%, respectively, but an increased amount of PLL, PStO, PPO,PPL, StOL, and PPSt from 15.3%, 9.5%, 6.3%,5.2%, and 0.8% to 18.7%,12.8%,8.7%,7.8%, and 1.8% was observed as a result of the CIE reaction. Similar phenomena were also reported previously.[27] Indeed, it is difficult to evaluate quantitatively the progression of the interesterification process due to the complex compositions in the reaction mixture. According to the method described by De Clercq et al.,[30] the degree of interesterification (DI) could be evaluated on the basis of TAG composition in the interesterified product. For the 80:20, 60:40, 40:60, and 20:80 blends of lard and soybean oil, the DI for the interesterification reaction was calculated to be 47.4%,76.8%, 81.4% and 43.6%, respectively. These obtained results suggested that the solid catalyst could efficiently catalyze the interesterification reaction.

In the present investigation, to avoid hydrolysis reaction, free water was totally removed from the reaction mixture under reduced pressure prior to the interesterification process. Moreover, the acid value (AV) of the feedstocks was lowered below 0.1 mg KOH/g, since the free fatty acid could result in the deactivation of the solid base catalyst. Therefore, after the interesterification reaction, the undesirable byproducts, such as free fatty acids, monoglycerides, and diglycerides formed by the hydrolysis reaction, were not detected by TLC techniques. However, in the enzymatic interesterification catalyzed by immobilized lipase, such byproducts were formed during the reaction as water is essential to maintain the activity of enzyme.[31]

**Slip Melting Point.** In general, the melting properties vary with the TAG composition in the interesterified product, and the slip melting points (SMPs) of the samples are associated with their TAG compositions. The interesterification reactions between solid fat and liquid oil were conducted to obtain fat mixtures with better melting behavior. The SMP was determined by the open capillary tube method, and the results are presented in Table 5. It was shown that the SMPs of the physical blends and the interesterified blends were significantly different, and the proportion of lard to soybean oil had significant effect on the SMP. As observed, these physical blends showed SMPs ranging from 26.2 to 44.1 °C, and the SMP was decreased with an increase in the proportion of soybean oil in the blends mostly due to the increase of the unsaturated FAs. Notably, the interesterified blends possessed lower SMPs for all samples when compared with their physical blends, which could be regarded as another evidence for the catalyst activity. The interesterified fat had an SMP below 37 °C, showing that it could melt almost completely at body temperature. This observation has demonstrated that the heterogeneous interesterification could give an attractive method for producing new tailored-fats with desired melting profiles that meet consumer preferences.

**Table 5. Slip Melting Point of Binary Soybean Oil and Lard Blends before and after Interesterification Reaction**

| LA/SO | SMP (°C) | |
|---|---|---|
| | before CIE | after CIE |
| 80:20 | 44.1 ± 0.1 | 38.6 ± 0.1 |
| 60:40 | 39.3 ± 0.1 | 34.5 ± 0.1 |
| 40:60 | 33.4 ± 0.1 | 30.4 ± 0.0 |
| 20:80 | 26.2 ± 0.0 | 23.1 ± 0.1 |

**Crystal Structure and Crystal Morphology.** Crystal properties can greatly influence the consistency and acceptability of the final product. Small crystals result in firmer products, whereas large crystals yield a sandy mouthfeel.[32] Figure 4 shows the crystal microstructures of the selected samples. As can be seen, soybean oil displayed no any distinct crystal at a temperature of 25 °C, while lard contained a dense network of nearly globular collections of clustered crystals. For the physical blend of lard and soybean oil, the sample exhibited small spherulite and needle-shaped like structure with no evident regular pattern, which was probably resulted from a dilution of the lard microstructure. Compared with the physical blend, the interesterified sample showed a very small crystal size, less aggregation, no large crystals, and a more homogeneous distribution of the crystals. As a result, the interesterification of soybean oil with lard led to not only a decrease in the size of the crystal, but also a change in the morphology with a network of small crystal. Small crystals are necessary for margarine fats and shortenings, owing to their stabilization of air bubbles to food products. The change in textural properties can be explained by the variation in TAG compositions observed for the interesterification. The TAG composition can be responsible for arrangement of different kinds of crystals, which strongly influences the product texture.

In conclusion, an environmentally friendly catalyst based on alumina impregnated with potassium was prepared by the conventional incipient-wetness impregnation method. The prepared solid catalyst was demonstrated to be an efficient solid base catalyst for the interesterification reactions. The HPLC analysis of the TAGs and analysis of the *sn*-2 positional FA compositions showed that the CIE reaction could lead to the rearrangement of FAs in the TAGs. After the interesterification, the SMPs and crystal morphology of the interesterificated products were varied substantially. The solid catalyst has several advantages of green or sustainable chemistry for

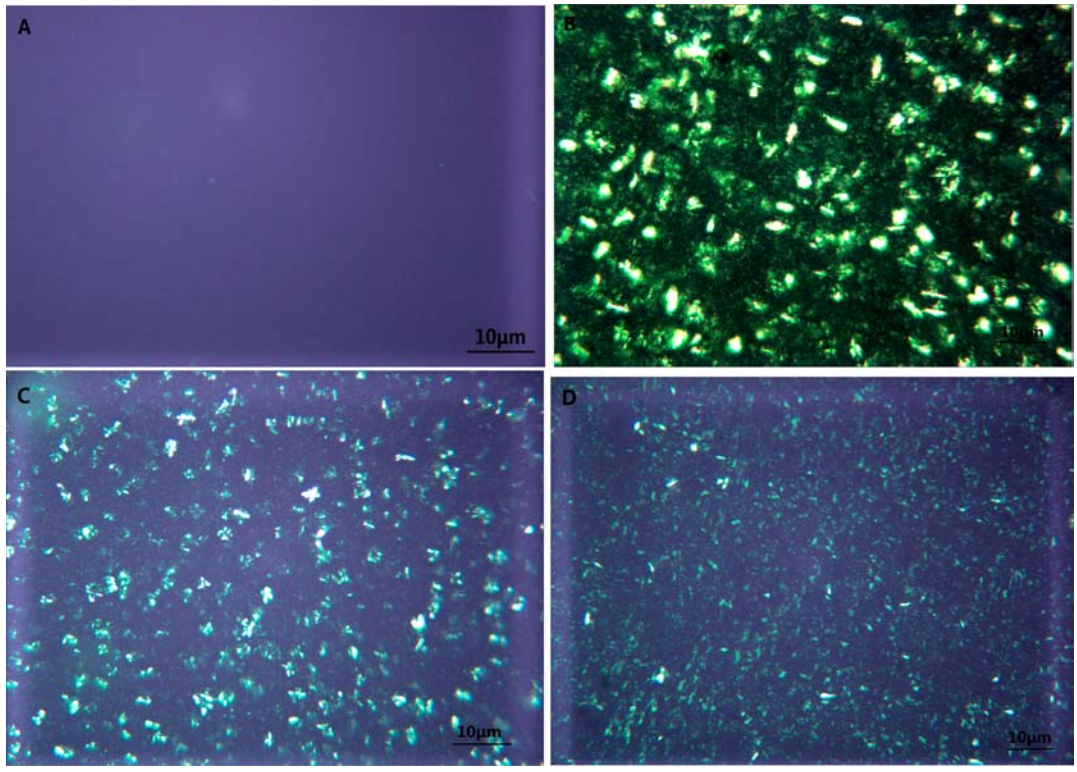


**Figure 4.** Crystal morphology of samples: (a) soybean oil; (b) lard; (c) physical 60:40 blend of lard and soybean oil; and (d) interesterificated 60:40 blend of lard and soybean oil.

catalyst recovery, high catalytic activity, and recyclability of the solid catalyst.

## AUTHOR INFORMATION

### Corresponding Author

*Tel.: +86 371 67756302; fax: +86 371 67756718; e-mail: xwenlei@163.com.

### Funding

This work was financially supported by research grants from the National Natural Science Foundation of China (Project No. 21276066, 21476062), the Plan for Scientific Innovation Talent of Henan Province (144200510006) and the Program for Innovative Research Team in Universities of Henan Province in China (2012IRTSTHN009).

### Notes

The authors declare no competing financial interest.

## ABBREVIATIONS USED

AOCS, American Oil Chemists' Society; BET, Brunauer−Emmett−Teller; BJH, Barrett−Joyner−Halenda; CIE, chemical interesterification; EIE, enzymatic interesterification; FA, fatty acid; FAME, fatty acid methyl ester; FT-IR, Fourier transform infrared; GC, gas chromatography; HPLC, high-performance liquid chromatography; IV, iodine value; L, linoleic acid; LA, lard; Ln, linolenic acid; 2-MAG, 2-monoacylglycerol; O, oleic acid; P, palmitic acid; SEM, scanning electron microscopy; PPL, porcine pancreatic lipase; SMP, slip melting point; SO, soybean oil; St, stearic acid; TAG, triacylglycerol; TLC, thin-layer chromatography; XRD, power X-ray diffraction

## REFERENCES

(1) Philippaerts, A.; Breesch, A.; De Cremer, G.; Kayaert, P.; Hofkens, J.; Van den Mooter, G.; Sels, B. Physical properties of nutritive shortenings produced from regioselective hardening of soybean oil with Pt containing zeolite. *J. Am. Oil Chem. Soc.* **2011**, *88*, 2023−2034.

(2) Xu, X. Production of specific-structured triacylglycerols by lipase-catalyzed reactions: A review. *Eur. J. Lipid. Sci. Techol.* **2000**, *102*, 287−303.

(3) Lee, J. H.; Akoh, C. C.; Himmelsbach, D. S.; Lee, K. T. Preparation of interesterified plastic fats from fats and oils free of trans fatty acid. *J. Agric. Food Chem.* **2008**, *56*, 4039−4046.

(4) Etherton, P. K. Trans fatty acid and coronary heart diseases risk. *Am. J. Clin. Nutr.* **1995**, *62*, 655S−708S.

(5) Dhaka, V.; Gulia, N.; Ahlawat, K. S.; Khatkar, B. S. Trans fats-sources, health risks and alternative approach: a review. *J. Food Sci. Technol.* **2011**, *48*, 534−541.

(6) Ferrari, R. A.; Esteves, W.; Mukherjee, K. D. Alteration of steroyl ester content and positional distribution of fatty acids in triacylglycerols by chemical and enzymatic interesterification of plant oils. *J. Am. Oil Chem. Soc.* **1997**, *74*, 93−96.

(7) Pacheco, C.; Palla, C.; Crapiste, G. H.; Carrín, M. E. Optimization of reaction conditions in the enzymatic interesterification of soybean oil and fully hydrogenated soybean oil to produce plastic fats. *J. Am. Oil Chem. Soc.* **2013**, *90*, 391−400.

(8) Ribeiro, A. P. B.; Grimaldi, R.; Gioielli, L. A.; Goncalves, L. A. G. Zero *trans* fats from soybean oil and fully hydrogenated soybean oil: physico-chemical properties and food applications. *Food Res.Int.* **2009**, *42*, 401−410.

(9) Jeyarani, T.; Reddy, S. Y. Effect of enzymatic interesterification on physicochemical properties of mahua oil and kokum fat blend. *Food Chem.* **2010**, *123*, 249−253.

(10) Xu, X.; Skands, A. R. H.; Høy, C. E.; Mu, H.; Balchen, S.; Adler-Nissen, J. Production of specific-structured lipids by enzymatic interesterification: elucidation of acyl migration by response surface design. *J. Am. Oil Chem. Soc.* **1988**, *75*, 1179−1186.

(11) Yang, T.; Fruekilde, M. B.; Xu, X. Applications of immobilized *Thermomyces lanuginosa* lipase in interesterification. *J. Am. Oil Chem. Soc.* **2003**, *80*, 881−887.

(12) Rousseau, D.; Marangoni, A. G.; Jeffrey, K. R. The influence of chemical interesterification on the physicochemical properties of complex fat systems. 2. morphology and polymorphism. *J. Am. Oil Chem. Soc.* **1998**, *75*, 1833−1839.
(13) Meng, Z.; Liu, Y.; Shan, L.; Jin, Q.; Wang, X. Reduction of graininess formation in beef tallow-based plastic fats by chemical interesterification of beef tallow and canola oil. *J. Am. Oil Chem. Soc.* **2010**, *87*, 1435−1442.
(14) Raquel, C.; Véronique, G.; Roland, V.; Wim, D. G. Chemical and enzymatic interesterification of a blend of palm stearin: soybean oil for low trans-margarine formulation. *J. Am. Oil Chem. Soc.* **2009**, *86*, 681−697.
(15) Soares, F.A.S.D.M.; da Silva, R. C.; da Silva, C. G.; Lourenco, M. B.; Soares, D. F.; Gioielli, L. A. Effects of chemical interesterification on physicochemical properties of blends of palm stearin and palm olein. *Food Res. Int.* **2009**, *42*, 1287−1294.
(16) Semwal, S.; Arora, A. K.; Badoni, R. P.; Tuli, D. K. Biodiesel production using heterogeneous catalysts. *Bioresour. Technol.* **2011**, *102*, 2151−2161.
(17) Yang, Z.; Xie, W. Soybean oil transesterification over zinc oxide modified with alkali earth metals. *Fuel Process. Technol.* **2007**, *88*, 631−638.
(18) Xie, W.; Li, H. Alumina-supported potassium iodide as a heterogeneous catalyst for biodiesel production from soybean oil. *J. Mol. Catal. A-Chem.* **2006**, *155*, 1−9.
(19) Kim, Y. K.; Hao, L. F.; Park, J. I.; Miyawaki, J.; Mochida, I.; Yoon, S. H. Catalytic activity and activation mechanism of potassium carbonate supported on perovskite oxide for coal char combustion. *Fuel* **2012**, *94*, 516−522.
(20) Calvino-Casilda, V.; Martín-Aranda, R. M.; López-Peinado, A. J.; Sobczak, I.; Ziolek, M. Catalytic properties of alkali metal-modified oxide supports for the Knoevenagel condensation: kinetic aspects. *Catal. Today* **2009**, *142*, 278−282.
(21) Xie, W.; Qi, C. Interesterification of soybean oil and lard blends catalyzed by SBA-15-*pr*-$NR_3OH$ as a heterogeneous base catalyst. *J. Agric. Food Chem.* **2013**, *61*, 3373−3381.
(22) Konishi, H.; Neff, W. E.; Mounts, T. L. Chemical interesterification with regioselectivity for edible oils. *J. Am. Oil Chem. Soc.* **1993**, *70*, 411−415.
(23) Montanari, T.; Castoldi, L.; Lietti, L.; Busca, G. Basic catalysis and catalysis assisted by basicity: FT-IR and TPD characterization of potassium-doped alumina. *Appl. Catal. A-Gen.* **2011**, *400*, 61−69.
(24) Hartman, L.; Lago, R. C. Rapid preparation of fatty acid methyl esters from lipids. *Lab. Pract.* **1973**, *22*, 475−494.
(25) AOCS. Official Methods and Recommended Practices of the American Oil Chemists' Society, 5th ed.; AOCS Press: Champaign, IL, 2009; Methods Ce 1−62; Ce 5b-89;Cc 3−25; Cd 1c-85; Cj 1−94.
(26) Adhikari, P.; Shin, J. A.; Lee, J. H.; Hu, J. N.; Zhu, X. M.; Akoh, C. C.; Lee, K. T. Production of trans-free margarine stock by enzymatic interesterification of rice bran oil, palm stearin and coconut oil. *J. Sci. Food Agric.* **2010**, *90*, 703−711.
(27) Silva, R. C.; Cotting, L. N.; Poltronieri, T. P.; Balcão, V. M.; de Almeida, D. B.; Goncalves, L. A.G.; Grimaldi, R.; Gioielli, L. A. The effects of enzymatic interesterification on the physical-chemical properties of blends of lard and soybean oil. *LWT - Food Sci.Technol.* **2009**, *42*, 1275−1282.
(28) Islama, A.; Taufiq-Yap, Y. H.; Chu, C. M.; Ravindra, P.; Chan, E. S. Transesterification of palm oil using KF and $NaNO_3$ catalysts supported on spherical millimetric $\gamma$-$Al_2O_3$. *Renew. Energy* **2013**, *59*, 23−29.
(29) da Silva, R. C.; Soares, F. A. S. D. M.; Fernandes, T. G.; Castells, A. L. D.; da Silva, K. C. G.; Gonçalves, M. I. A.; Ming, C. C.; Gonçalves, L.A.G.; Gioielli, L. A. Interesterification of lard and soybean oil blends catalyzed by immobilized lipase in a continuous packed bed reactor. *J. Am. Oil Chem. Soc.* **2011**, *88*, 1925−1933.
(30) De Clercq, N.; Danthine, S.; Nguyen, M. T.; Gibon, V.; Dewettinck, K. Enzymatic interesterification of palm oil and fractions: Monitoring the degree of interesterification using different methods. *J. Am. Oil Chem. Soc.* **2012**, *89*, 219−229.
(31) Rønne, T. H.; Yang, T.; Mu, H.; Jacobsen, C.; Xu, X. Enzymatic interesterification of butterfat with rapeseed oil in a continuous packed bed reactor. *J. Agric. Food Chem.* **2005**, *53*, 5617−5624.
(32) Norizzah, R.; Chong, C. L.; Cheow, C. S.; Zaliha, O. Effects of chemical interesterification on physicochemical properties of palm stearin and palm kernel olein blends. *Food Chem.* **2004**, *86*, 229−235.

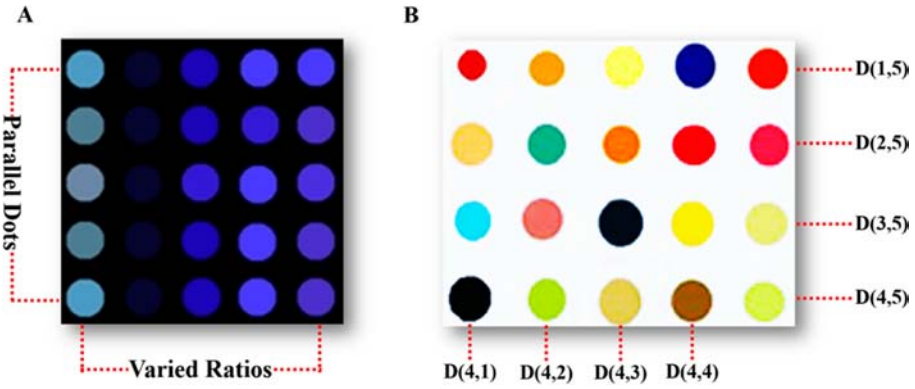


**Figure 1.** (A) Difference map of a selection-oriented sensor array with five parallel dots. (B) Actual map of the detection-oriented sensor array and arrangement of the sensing dots.

to distinguish liquors belonging to similar flavor types or forged liquors produced by diluting industrial alcohol with water.[13] In view of reliability, accuracy, and reproducibility, the most efficient analytical methods undoubtedly depend on large equipment, including headspace solid-phase microextraction gas chromatography,[14] ambient glow discharge ionization mass spectrometry,[15] headspace solid phase microextraction−mass spectrometry,[3,16] gas chromatography−mass spectrometry (GC-MS),[1,6] and infrared spectroscopy.[17−19] However, unavoidable drawbacks such as complicated pretreatment, time-consuming procedures, requirement for professional operation, and also high cost,greatly hinder their application for in situ real-time measurements.[7,15,20] Furthermore, due to the complicated composition of ingredients in the liquor, it is rather difficult to realize an accurate recognition of the overall characteristics of hundreds of Chinese liquors through component-by-component analysis of individual sample. Hence, it is of great significance to develop a rapid and reliable method to realize convenient evaluation of the authenticity of Chinese liquor as well as easy characterization of the unique personality of each liquor sample.

Analysis methods based on sensory techniques, commonly referred to as electronic nose or electronic tongue, have offered a powerful alternative to analyze foodstuffs in the recent years.[20,21] Treating the complicated mixed sample as a single analyte, they are able to give a combined sensor response to the target and thus achieve fast yet efficient discrimination of those mixtures.[13,22] The challenge is that those sensors require relatively complicated post pattern recognition methods to collect feature information and can hardly avoid signal overlap of closely similar samples because they usually lack chemical discrimination.[22−24] In view of those shortcomings, the colorimetric sensor array stands out as a good candidate to address the above-mentioned problems.[25] Inspired by the mammalian gustatory and olfactory systems, such a sensor can give unique visible fingerprints to the complex analytes in either the liquid phase or the headgas.[26,27] Successful application of colorimetric sensor arrays has been reported to distinguish drinks including beers,[28] soft drinks,[26] coffees,[29] and also Chinese liquors.[12,23] However, the high concentration of ethanol and water in high-alcoholic Chinese liquors might not only mask the response of other compounds, which contain more individual information on the liquor rather than alcoholic strength, but also shorten the sensor life.[30] Besides, as most of the sensitive dots in the sensor array rely on nonspecific interactions such as van der Waals interaction, Lewis acid−base interaction, $\pi-\pi$ interaction, and physical adsorption, efficient discrimination of liquor samples that are similar in flavor and composition remains a big challenge.

In the present study, we fabricated a new colorimetric sensor array based on volatile markers determined by GC-MS to characterize Chinese liquor. In total 17 volatile markers were selected by applying factor analysis to fabricate a 4 × 5 sensor array sensitive to different groups of markers. Data analysis was performed by principal component analysis (PCA) and hierarchical clustering analysis (HCA) to distinguish 12 base liquor samples and 15 commercial liquors. The main focus of this study is to develop a reliable sensor to discriminate high-alcoholic liquors and to identify different commercial Chinese liquors of different brands and flavor types. This effort develops a simple method that may prove to be useful for the quality control of Chinese liquors in the market and even in mass production.

## MATERIALS AND METHODS

**Chemicals and Stock Solution Preparation.** All 12 base Chinese liquors (listed in Table S1 of the Supporting Information (SI)) were kindly provided by Luzhou laojiao Co. Ltd. (Luzhou, China), and 15 commercially available Chinese liquors (listed in SI Table S2) were purchased from a local supermarket in Chongqing city, China. 5,10,15,20-Tetraphenylporphine, 5,10,15,20-tetraphenylporphine indium, 5,10,15,20-tetrakis(pentafluorophenyl)porphyrin iron(III) chloride, and 5,10,15,20-tetraphenylporphine zinc were obtained from Frontier Scientific (Logan, UT, USA). All other indicator dyes (see SI Table S3) were supplied by Sigma-Aldrich (St. Louis, MO, USA). 2,4-Dinitrophenylhydrazine (DNPH) and ammonium ceric nitrate were purchased from Aladin Reagent (Shanghai, China). Hydrochloric acid (HCl), sulfuric acid ($H_2SO_4$), NaOH, potassium persulfate, nitric acid, absolute ethanol, and other reagents of analytical purity were all obtained from Chuandong Reagent (Chengdu, China). Porous hydrophilic membrane used for dye staining was bought from Shanghai Minglie Chemical Engineering Science Co. Ltd. (Shanghai, China). Ultrapure water was generated by a Millipore Direct-Q Water system (Molsheim, France). A PHS-3C pH detector (Shanghai Jingke Equipment, Shanghai, China), ultrasonic atomizer apparatus (Shanghai Yuyue Medical Equipment Co., Shanghai, China), and Media microwave oven were used in the study.

DNPH solution was prepared according to our previous study.[31] To be specific, 0.4 g of DNPH was added to a mixed solution of 3 mL of water and 10 mL of ethanol, and then 2 mL of concentrated sulfuric acid was added dropwise. The solution was stirred for 10 min and then went through filter paper to obtain a yellow DNPH store solution. The prophyrin solutions were prepared using DMF solution and stored in a dark place before use. Marker solutions used for sensitive dot selection were freshly prepared using a mixed solution of absolute ethanol and deionized water (60:40) upon detection. All other solutions without specification were prepared using deionized water.

**Table 1. Concentrations (Grams per Liter) of Principal Volatile Components in Different Raw Liquors**

| volatile compound | liquor | | | | | | | | | | | |
|---|---|---|---|---|---|---|---|---|---|---|---|---|
| | 1 | 2 | 3 | 4 | 5 | 6 | 7 | 8 | 9 | 10 | 11 | 12 |
| acetaldehyde | 0.0921 ± 0.0004 | 0.0729 ± 0.0002 | 0.0613 ± 0.0010 | 0.0345 ± 0.0016 | 0.0238 ± 0.0013 | 0.0098 ± 0.0004 | 0.0693 ± 0.0022 | 0.1928 ± 0.0014 | 0.0872 ± 0.0065 | 0.0479 ± 0.0034 | 0.0486 ± 0.0020 | 0.0098 ± 0.0007 |
| furfural | 0.0325 ± 0.0004 | 0.0441 ± 0.0017 | 0.0397 ± 0.0014 | 0.0290 ± 0.0006 | 0.0297 ± 0.0018 | 0.0867 ± 0.0030 | 0.0335 ± 0.0011 | 0.0447 ± 0.0009 | 0.0327 ± 0.0020 | 0.0353 ± 0.0016 | 0.0444 ± 0.0016 | 0.0632 ± 0.0016 |
| acetal | 0.2500 ± 0.008 | 0.2028 ± 0.0771 | 0.1692 ± 0.0013 | 0.0870 ± 0.0013 | 0.1272 ± 0.0011 | 0.0246 ± 0.0011 | 0.1749 ± 0.0013 | 0.4617 ± 0.0020 | 0.1586 ± 0.0013 | 0.0965 ± 0.0012 | 0.1264 ± 0.0019 | 0.0226 ± 0.0013 |
| methanol | 0.0866 ± 0.002 | 0.0812 ± 0.0023 | 0.0688 ± 0.0022 | 0.0512 ± 0.0009 | 0.0519 ± 0.0021 | 0.0180 ± 0.0016 | 0.0618 ± 0.0011 | 0.1136 ± 0.0015 | 0.0628 ± 0.0011 | 0.0542 ± 0.0021 | 0.0569 ± 0.0017 | 0.0250 ± 0.0012 |
| isoamylol | 0.0128 ± 0.0005 | 0.0105 ± 0.0021 | 0.0100 ± 0.0007 | 0.0430 ± 0.0007 | 0.0475 ± 0.0030 | 0.0027 ± 0.0006 | 0.0094 ± 0.0008 | 0.0182 ± 0.0007 | 0.0102 ± 0.0008 | 0.0429 ± 0.0017 | 0.0474 ± 0.0008 | 0.0062 ± 0.0007 |
| *sec*-butyl alcohol | 0.0209 ± 0.009 | 0.0165 ± 0.0011 | 0.0067 ± 0.0005 | 0.0114 ± 0.0011 | 0.0158 ± 0.0014 | 0 | 0.0378 ± 0.0009 | 0.0561 ± 0.0013 | 0.0135 ± 0.0005 | 0.0357 ± 0.0015 | 0.0592 ± 0.0014 | 0.0021 ± 0.0003 |
| *n*-propyl alcohol | 0.0719 ± 0.0006 | 0.0887 ± 0.0014 | 0.0536 ± 0.0011 | 0.0268 ± 0.0017 | 0.0284 ± 0.0017 | 0.0124 ± 0.0013 | 0.0695 ± 0.0020 | 0.1016 ± 0.0006 | 0.0613 ± 0.0012 | 0.0364 ± 0.0014 | 0.0470 ± 0.0007 | 0.0120 ± 0.0009 |
| isobutanol | 0.0607 ± 0.0004 | 0.0642 ± 0.0029 | 0.0510 ± 0.0015 | 0.0112 ± 0.0008 | 0.0133 ± 0.0007 | 0 | 0.0615 ± 0.0007 | 0.0828 ± 0.0017 | 0.0525 ± 0.0011 | 0.0117 ± 0.0008 | 0.0163 ± 0.0005 | 0 |
| 2-pentanol | 0.0153 ± 0.0004 | 0.0142 ± 0.0022 | 0.0064 ± 0.0008 | 0.0102 ± 0.0004 | 0.0116 ± 0.0009 | 0 | 0.0100 ± 0.0002 | 0.0216 ± 0.0011 | 0.0076 ± 0.0004 | 0.0151 ± 0.0013 | 0.0216 ± 0.0009 | 0 |
| *n*-butanol | 0.0454 ± 0.0006 | 0.0551 ± 0.0018 | 0.0272 ± 0.0012 | 0.0409 ± 0.0014 | 0.0396 ± 0.0022 | 0 | 0.0494 ± 0.0011 | 0.1001 ± 0.0008 | 0.0355 ± 0.0007 | 0.0622 ± 0.0018 | 0.0689 ± 0.0016 | 0.0073 ± 0.0004 |
| 2-methylbutanol | 0.2616 ± 0.0008 | 0.2782 ± 0.0014 | 0.2799 ± 0.0033 | 0.0430 ± 0.0008 | 0.0475 ± 0.0015 | 0.0027 ± 0.0008 | 0.2704 ± 0.0013 | 0.3083 ± 0.0014 | 0.3598 ± 0.0016 | 0.0429 ± 0.0012 | 0.0474 ± 0.0010 | 0.0062 ± 0.0006 |
| hexanol | 0.0427 ± 0.0003 | 0.0487 ± 0.0020 | 0.0379 ± 0.0016 | 0.0294 ± 0.0013 | 0.0273 ± 0.0024 | 0.0074 ± 0.0005 | 0.0365 ± 0.0018 | 0.0563 ± 0.0007 | 0.0356 ± 0.0013 | 0.0320 ± 0.0010 | 0.0344 ± 0.0014 | 0.0148 ± 0.0013 |
| *n*-amyl alcohol | 0.0176 ± 0.0005 | 0.0178 ± 0.0010 | 0.0166 ± 0.0015 | 0.0160 ± 0.0012 | 0.0160 ± 0.0008 | 0.0139 ± 0.0007 | 0.0167 ± 0.0010 | 0.0203 ± 0.0013 | 0.0162 ± 0.0006 | 0.0163 ± 0.0009 | 0.0174 ± 0.0006 | 0.0143 ± 0.0009 |
| acetic acid | 0.4167 ± 0.0009 | 0.4166 ± 0.0101 | 0.3307 ± 0.0026 | 0.4423 ± 0.0020 | 0.4279 ± 0.0028 | 0.4563 ± 0.0027 | 0.3417 ± 0.0015 | 0.3484 ± 0.0020 | 0.2296 ± 0.0041 | 0.2936 ± 0.0065 | 0.4109 ± 0.0037 | 0.5795 ± 0.0024 |
| propanoic acid | 0.0185 ± 0.0005 | 0.0145 ± 0.0011 | 0.0188 ± 0.0010 | 0.0133 ± 0.0009 | 0.0127 ± 0.0011 | 0.0169 ± 0.0018 | 0.0142 ± 0.0008 | 0.0194 ± 0.0007 | 0.0164 ± 0.0014 | 0.0095 ± 0.0007 | 0.0104 ± 0.0005 | 0.0161 ± 0.0014 |
| butyric acid | 0.1534 ± 0.0044 | 0.2459 ± 0.0018 | 0.01202 ± 0.0033 | 0.1851 ± 0.0024 | 0.1637 ± 0.0021 | 0.2098 ± 0.0014 | 0.1307 ± 0.0021 | 0.1779 ± 0.0010 | 0.1041 ± 0.0036 | 0.2997 ± 0.0022 | 0.2588 ± 0.0030 | 0.3484 ± 0.0015 |
| isopropylacetic acid | 0.0221 ± 0.0012 | 0.0327 ± 0.0030 | 0.0176 ± 0.0009 | 0.0154 ± 0.0017 | 0.0132 ± 0.0006 | 0.0195 ± 0.0015 | 0.0161 ± 0.0013 | 0.0285 ± 0.0013 | 0.0122 ± 0.0009 | 0.0335 ± 0.0015 | 0.0307 ± 0.0013 | 0.0333 ± 0.0012 |
| valeric acid | 0.0175 ± 0.0006 | 0.0260 ± 0.0012 | 0.0134 ± 0.0007 | 0.0180 ± 0.0012 | 0.0139 ± 0.0004 | 0.0186 ± 0.0013 | 0.0116 ± 0.0009 | 0.0218 ± 0.0008 | 0.1809 ± 0.0027 | 0.0304 ± 0.0013 | 0.0265 ± 0.0011 | 0.0329 ± 0.0021 |
| caproic acid | 0.2578 ± 0.0010 | 0.3768 ± 0.0089 | 0.2361 ± 0.0013 | 0.2547 ± 0.0031 | 0.1899 ± 0.0017 | 0.2504 ± 0.0028 | 0.1913 ± 0.0016 | 0.2957 ± 0.0016 | 0.0107 ± 0.0007 | 0.4618 ± 0.0030 | 0.3868 ± 0.0024 | 0.6080 ± 0.0037 |
| ethyl formate | 0.03921 ± 0.0005 | 0.3227 ± 0.0051 | 0.2374 ± 0.0019 | 0.2592 ± 0.0021 | 0.3453 ± 0.0036 | 0.1492 ± 0.0010 | 0.344 ± 0.0014 | 0.3100 ± 0.0013 | 0.3087 ± 0.0019 | 0.2362 ± 0.0017 | 0.4744 ± 0.0018 | 0.1782 ± 0.0020 |
| ethyl acetate | 0.9094 ± 0.0004 | 0.7104 ± 0.0083 | 0.6508 ± 0.0036 | 1.4858 ± 0.0015 | 2.2313 ± 0.0190 | 0.0502 ± 0.0014 | 1.0874 ± 0.0102 | 1.2526 ± 0.0033 | 0.8323 ± 0.0030 | 2.1080 ± 0.0405 | 1.1516 ± 0.0031 | 0.0656 ± 0.0011 |
| propionic ether | 0.0826 ± 0.0044 | 0.0899 ± 0.0014 | 0 | 0.0621 ± 0.0005 | 0.0689 ± 0.0018 | 0 | 0.0714 ± 0.0011 | 0.0953 ± 0.0009 | 0.0381 ± 0.00011 | 0.0886 ± 0.0032 | 0.0937 ± 0.0011 | 0 |
| ethyl butyrate | 0.2013 ± 0.0017 | 0.1848 ± 0.0020 | 0.1483 ± 0.0018 | 0.6704 ± 0.0042 | 0.8816 ± 0.0035 | 0.0156 ± 0.0017 | 0.2444 ± 0.0014 | 0.2313 ± 0.0014 | 0.2195 ± 0.0007 | 0.8740 ± 0.0024 | 0.4356 ± 0.0020 | 0.0231 ± 0.0010 |
| isoamyl acetate | 0.0607 ± 0.0084 | 0.0538 ± 0.0010 | 0.0449 ± 0.0013 | 0.0203 ± 0.0015 | 0.0219 ± 0.0014 | 0.0180 ± 0.0019 | 0.0385 ± 0.0012 | 0.0883 ± 0.0014 | 0.0366 ± 0.0014 | 0.0236 ± 0.0011 | 0.0274 ± 0.0006 | 0.0188 ± 0.0006 |
| ethyl valerate | 0.0349 ± 0.0012 | 0.0402 ± 0.0025 | 0.0220 ± 0.0009 | 0.0708 ± 0.0017 | 0.0848 ± 0.0013 | 0.0025 ± 0.0004 | 0.0290 ± 0.0015 | 0.0519 ± 0.0015 | 0.0244 ± 0.0009 | 0.0949 ± 0.0026 | 0.0637 ± 0.0013 | 0.0038 ± 0.0004 |
| ethyl hexanoate | 1.4568 ± 0.0017 | 1.203 ± 0.0410 | 1.5631 ± 0.0064 | 8.0944 ± 0.164 | 8.6231 ± 0.0274 | 0.4086 ± 0.0023 | 1.8658 ± 0.0369 | 0.8848 ± 0.0023 | 2.8279 ± 0.0023 | 9.2601 ± 0.0713 | 4.3751 ± 0.0241 | 0.5728 ± 0.0015 |
| ethyl heptylate | 0.0168 ± 0.0001 | 0.0168 ± 0.0021 | 0.0151 ± 0.0006 | 0.0468 ± 0.0007 | 0.0472 ± 0.0025 | 0.0046 ± 0.0003 | 0.0160 ± 0.0014 | 0.0165 ± 0.0019 | 0.0150 ± 0.0005 | 0.0599 ± 0.0011 | 0.0373 ± 0.0015 | 0.0066 ± 0.0004 |
| ethyl lactate | 3.2531 ± 0.0264 | 3.2648 ± 0.1260 | 2.9841 ± 0.0141 | 1.4161 ± 0.0402 | 1.4302 ± 0.0260 | 1.8266 ± 0.0106 | 2.7088 ± 0.0121 | 3.2366 ± 0.0471 | 2.6423 ± 0.0277 | 1.2717 ± 0.0121 | 1.3765 ± 0.0180 | 2.3821 ± 0.0035 |
| ethyl palmitate | 0.0172 ± 0.0005 | 0.0205 ± 0.0065 | 0.0212 ± 0.0007 | 0.0504 ± 0.0014 | 0.0450 ± 0.0014 | 0.0429 ± 0.0017 | 0.0182 ± 0.0006 | 0.0175 ± 0.0005 | 0.0279 ± 0.0018 | 0.0162 ± 0.0014 | 0.0158 ± 0.0009 | 0.0401 ± 0.0019 |
| ethyl oleate | 0.0138 ± 0.0010 | 0.0144 ± 0.0076 | 0.0147 ± 0.0011 | 0.0119 ± 0.0007 | 0.0122 ± 0.0007 | 0.0108 ± 0.0006 | 0.0134 ± 0.0012 | 0.0148 ± 0.0013 | 0.0125 ± 0.0008 | 0.0125 ± 0.0006 | 0.0093 ± 0.0003 | 0.0125 ± 0.0008 |
| 3-hydroxy-2-butanone | 0.0730 ± 0.0008 | 0.1067 ± 0.0030 | 0.0443 ± 0.0037 | 0.0184 ± 0.0010 | 0.0213 ± 0.0005 | 0.0176 ± 0.0011 | 0.0477 ± 0.0021 | 0.1350 ± 0.0016 | 0.0442 ± 0.0011 | 0.0194 ± 0.0007 | 0.0274 ± 0.0014 | 0.0201 ± 0.0007 |



dx.doi.org/10.1021/jf503345z | J. Agric. Food Chem. 2014, 62, 10422−10430

**Analysis of Volatile Components in Base Liquors Using GC-MS.** An Agilent 5975I GC-MS with a 7683B automatic sampler was coupled with a FID detector to analyze the volatile components in the 12 base Chinese liquors. Using a cross-linked silica capillary column (30 mm length, 0.25 mm inside diameter, and 0.25 $\mu$m coating thickness), the initial column temperature was set at 40 °C, held for 2 min, and then heated to 80 °C at a rate of 5 °C/min; this temperature was held for 2 min and then raised to 260 °C at a heating rate of 10 °C/min and held for 10 min. High-purity nitrogen was applied as eluant gas using split sampling with a split ratio of 30:1. The sample volume for GC was 1 $\mu$L and 2−5 $\mu$L for MS. Resultant data about the volatile components were analyzed using SPSS (version 18.0) software.

**Fabrication of the Sensor Array.** After determination of the volatile markers, sensitive dyes were subsequently selected for each group of markers. A virtual library of possible combinations for different markers was first constructed according to former studies and our previous study. Practically, taking the selection of sensitive dots for acidic markers as an example, acetic acid solutions with a concentration of 0.4 g/L (average concentration of 12 base liquor samples) were prepared using 60% ethanol (in deionized water) as standard simulated samples. Because the pH of all the base liquors was detected between 3.1 and 4.1, Congo red and bromophenol blue were selected as responsive dyes. The mixture of dyes was kept in ultrasonic agitation for 10 s, and then a quartz capillary was used to deliver approximately 0.1 $\mu$L of solution onto the surface of a porous hydrophilic membrane to fabricate a selection-oriented sensor array (Figure 1A). Once printed, the arrays were placed in a 500 mL beaker saturated in nitrogen atmosphere for 30 min and subsequently dried in a 60 °C oven for 24 h, after which the oven temperature was reduced to 35 °C and the arrays were left for another 24 h.

The image of the sensor array was captured before detection; 5 mL of standard simulated sample atomized with an ultrasonic atomizer apparatus was then sprayed upon the array sealed with preservative film in Petri plate (8 cm in diameter) and held for at least 5 min before its image was taken finally. Comparing the images of the array before and after exposure to the sample, color change profiles were automatically obtained. The detailed working principle of the sensory system and data process can be found in our former study.[32] By analyzing resultant color change (RGB) and the relative standard error of parallel dots, the combination and concentration of the dyes in the sensitive dots were subsequently optimized. After optimization of all the sensitive dots, the 4 × 5 sensor array (see Figure 1B) was fabricated finally. The sensor arrays were subjected to the above-mentioned preparing procedure, and the arrays were stored in a nitrogen-flushed dark environment before use.

**Discrimination of the Liquor Samples.** After fabrication of the sensor array, 12 base liquor samples and 15 commercial Chinese liquors were analyzed subsequently. Briefly, 5 mL of liquor sample was atomized with an ultrasonic atomizer apparatus and then sprayed upon the array sealed with preservative film in a Petri plate (8 cm in diameter) and then held for 1 min. Then, it was placed in the microwave oven and treated for 2 min (400 W, 60 °C). Data acquisition was performed with a routine procedure mentioned in our previous experiments and finally analyzed using the SPSS software. It should be noted that the detection of each sample, both liquor samples and simulated ones, was performed repeatedly at least five times, and the average images were used for follow-up data analysis.

## RESULTS AND DISCUSSION

**Selection of Markers.** The composition of the volatile components analyzed by GC-MS of 12 base liquors is listed in Table 1. There were more than 30 volatile compounds in those liquors, and their concentrations varied significantly in different samples. To simplify data analysis, factor analysis method was first applied to find the principal components (PCs). Table 2 summarizes the eigen values of the correlation matrices. As can be seen from the table, the first 10 components covered >99.8% of accumulative contribution rate dominated by the first three

**Table 2. Results of Factor Analysis Using the Concentrations of Principal Volatile Components**

| component | eigen value | contribution rate (%) | accumulative contribution rate (%) |
|---|---|---|---|
| **1** | 12.918 | 40.369 | 40.369 |
| **2** | 9.217 | 28.804 | 69.173 |
| **3** | 6.213 | 19.415 | 88.589 |
| **4** | 1.262 | 3.945 | 92.534 |
| **5** | 0.876 | 2.737 | 95.271 |
| **6** | 0.758 | 2.368 | 97.639 |
| **7** | 0.283 | 0.883 | 98.522 |
| **8** | 0.195 | 0.608 | 99.131 |
| **9** | 0.158 | 0.495 | 99.626 |
| **10** | 0.064 | 0.199 | 99.852 |

PCs. Then maximum orthogonal rotation of the factor loading matrices was performed using a varimax method to find the relationship between the volatile compounds and the first three principal components. It was found that the first PC had a closer positive relationship with acetaldehyde, furfural, acetal, isoamylol, 2-butyl alcohol, *n*-propyl alcohol, isobutanol, *n*-butanol, and isoamyl acetate. Those compounds were normally regarded as the origin of taste (or mouthfeel) of Chinese liquors. Because ester compounds (ethyl acetate, ethyl butyrate, ethyl valerate, ethyl hexanoate, and ethyl lactate), which are important substances constituting the flavor of Chinese liquors,[33,34] exhibited a higher contribution rate to the second PC than other compounds, we can assume that the second component mainly depends on the flavor composition. For the third principal component, organic acids including acetic acid, butyric acid, isopropylacetic acid, and caproic acid dominated its cumulative load value (Table 3). As a result, in total 17 kinds of compounds were selected to serve as markers in the base liquors, those being acetaldehyde, furfural, acetal, isoamylol, 2-butyl alcohol, *n*-propyl alcohol, isobutanol, *n*-butanol, acetic acid, butyric acid, isopropylacetic acid, caproic acid, ethyl acetate, ethyl butyrate, ethyl valerate, ethyl hexanoate, and ethyl lactate. We subsequently reanalyzed the 12 base liquors (each with 5 control samples) using only the concentration information on the selected markers to confirm whether it can discriminate the 60 base liquor samples. As expected, PCA and HCA all showed correct discrimination of the liquors directly using the concentration information on the selected 17 markers (Figure 2B,C). Most importantly, the factor analysis result resembles closely that obtained from all of the volatile compounds, which again demonstrated the feasibility of the selected 17 volatile compounds to distinguish the base liquor samples.

**Fabrication of the Sensor Array.** Successful discrimination of Chinese liquors using sensory techniques has been reported by our group and other groups previously.[7,12,20] Because those studies rely on either complex post data analysis or nonspecific interaction between sensing materials and liquor samples, it remains a big challenge to realize in-depth recognition of each kind of Chinese liquor with respect to raw materials in production, brewing techniques, and even storage methods. In view of these problems, we endeavored to develop an easy yet efficient sensor to discriminate Chinese liquor using volatile makers selected for the base liquors. Despite the complexity of the selected 17 markers, they can be classified into 4 groups, including alcohol, acid, ester, and aldehyde, so it is not unreasonable to discriminate those liquors on the basis of

Table 3. Cumulative Load Values of the Compounds for the First Three Principal Components (PC)

| variance | PC 1 | PC 2 | PC 3 | variance | PC 1 | PC 2 | PC 3 |
|---|---|---|---|---|---|---|---|
| **acetaldehyde** | 0.928 | −0.134 | −0.107 | **isopropylacetic acid** | 0.231 | −0.050 | 0.957 |
| **furfural** | 0.810 | −0.584 | 0.427 | valeric acid | −0.080 | −0.087 | −0.904 |
| **acetal** | 0.916 | −0.058 | −0.126 | **caproic acid** | −0.124 | 0.022 | 0.915 |
| methanol | 0.030 | 0.008 | −0.223 | ethyl formate | 0.639 | 0.232 | −0.174 |
| **isoamylol** | 0.914 | 0.905 | 0.047 | **ethyl acetate** | 0.253 | 0.937 | −0.128 |
| **2-butyl alcohol** | 0.945 | 0.275 | 0.246 | propionic ether | 0.730 | 0.523 | 0.127 |
| ***n*-propyl alcohol** | 0.931 | −0.183 | −0.097 | **ethyl butyrate** | −0.035 | 0.991 | −0.044 |
| **isobutanol** | 0.844 | −0.296 | −0.261 | isoamyl acetate | 0.892 | −0.294 | −0.082 |
| 2-pentanol | 0.638 | 0.428 | 0.127 | **ethyl valerate** | 0.248 | 0.952 | 0.069 |
| ***n*-butanol** | 0.881 | 0.380 | 0.144 | **ethyl hexanoate** | −0.198 | 0.975 | −0.059 |
| 2-methylbutanol | 0.669 | −0.345 | −0.382 | ethyl heptylate | −0.023 | −0.780 | 0.084 |
| hexanol | 0.738 | 0.092 | −0.074 | **ethyl lactate** | 0.562 | 0.929 | −0.120 |
| *n*-amyl alcohol | 0.771 | 0.107 | −0.029 | ethyl palmitate | −0.732 | 0.115 | −0.307 |
| **acetic acid** | −0.397 | −0.220 | 0.893 | ethyl oleate | 0.508 | −0.191 | −0.117 |
| **butyric acid** | −0.277 | 0.106 | 0.913 | 3-hydroxy-2-butanone | −0.376 | 0.535 | 0.212 |

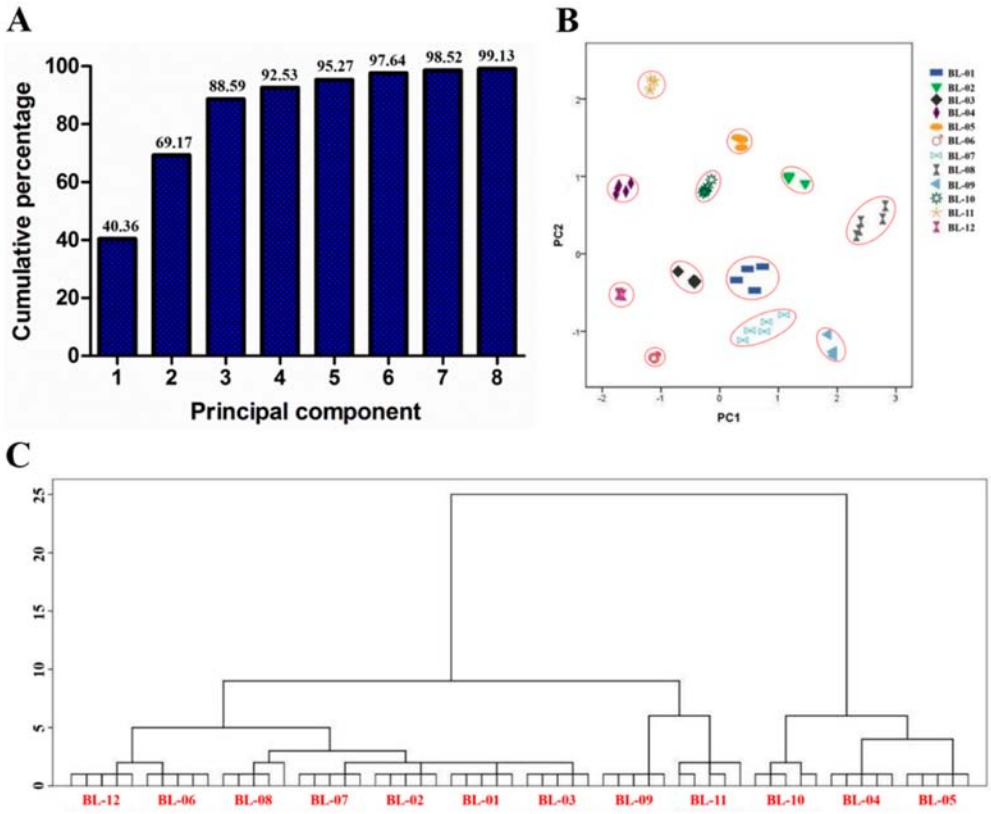


**Figure 2.** (A) Cumulative percentage of the first three principal components. (B) Plot of the first two principal components by PCA with data obtained from GC-MS. (C) HCA dendrogram of 12 base liquors with 5 controls.

responsive materials sensitive to organic alcohol, acid, ester, and aldehyde. Considering that all of the sensitive dots are selected and fabricated in a similar way, we here choose dot, D12 (specific to alcohol), to illustrate the procedure to fabricate individual sensitive dots. Typically, when certain combinations of the dyes were selected, it was used to make a selection-oriented sensor array, which was then used to test simulated standard samples. We use Euclidean distance change (root of the sum of $\Delta R^2$, $\Delta G^2$, and $\Delta B^2$ of each sensor dot) to measure the response. As can be seen from Figure S1A (SI), different combinations of the dyes showed varied responses, and higher responses were observed when the ratios were set at 4:1 and 3:1. We finally chose 3:1 as the optimized ratio to obtain high stability of the resultant sensitive dot because it showed the lowest RSD (SI Figure S1B). Finally, in total 20 combinations were selected as sensor dots (see Table S3 (SI) for detailed information). Specifically, D11−D15 were specific to organic alcohols, D21−D23 were specific to esters (catalyzed by microwave), D24, D25, and D31 were specific to acid via acid−base reactions (see Figure S2 (SI)), and the rest were specific to aldehydes, the detection mechanism of which was explained in detail in our former study.[31]

**Discrimination of the Base Liquors with High Alcoholic Strength.** Sixty base wine samples (5 controls for each kind of

base Chinese liquor) were then selected to test the recognition ability of the newly developed colorimetric sensor array. We first studied the time-dependent response of the sensor after its interaction with the liquor samples. Figure 3 shows that the

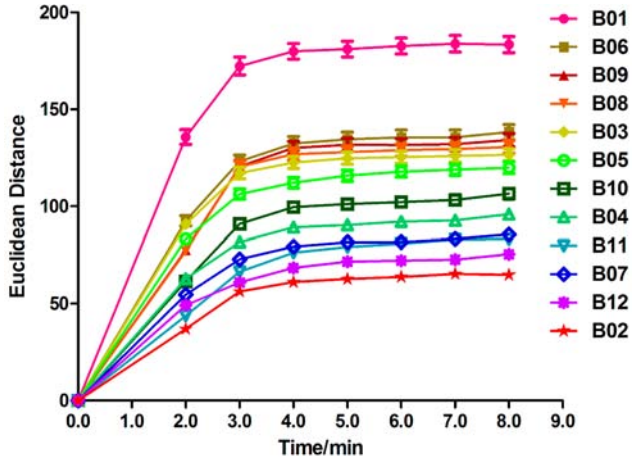


**Figure 3.** Time-dependent responses of the sensor array upon interaction with 12 base liquor samples.

Euclidean distance of all the samples increased until they reached equilibrium in 4 min. This indicates that 4 min is long enough for the interaction to establish an equilibrium. The colorful profiles of the base liquors in Figure 4A demonstrated that different base liquors showed significant difference, which can even be differentiated by the naked eye. When analyzing individual sensor dots, we found that samples BL-4 (72% in alcoholic strength) and BL-5 (72.1% in alcoholic strength) exhibited similar colorimetric responses in D11 and D12, specific to alcohols with low molecular weight (mostly ethanol), but completely different responses in other sensitive dots. This suggested that a difference in alcoholic strength did not conceal the colorimetric response of the sensor array. Besides, the responses of D11 and D12 in BL-4 and BL-5 were clearly different from other samples (even BL-10 with an alcoholic strength of 71.4%), indicating that the sensor had fine discrimination of alcoholic strength.

Statistical analysis of the data was applied to get a further understanding of the interaction between the sensor and the base liquors. The cumulative load values of individual dots for the first three principal components, which cover >70% of the cumulative contribution rate, are listed in Table S4 in the SI. The results suggested that the first one mainly relied on the discrimination of esters, the second relied on aldehydes, and the third relied greatly on organic acids, which is partly consistent with analysis by GC-MS. Results of the first two principal components are plotted in Figure 4B; the successful classification of different base liquor samples is indicative of the good discrimination ability of the sensor array. Moreover, correct clustering of the 60 samples by HCA further proved the sensor to have excellent performance in screening among different base liquors (Figure 4C), and it also realized almost the same grouping of the samples as that by GC-MS analysis (Figure 2C), demonstrating its discriminating ability comparable with that of GC-MS to some extent. Therefore, we can conclude that the colorimetric sensor developed in the present study has good performance in distinguishing different base Chinese liquors and that the recognition is based on the combination of specific affinity of individual sensitive dots to volatile markers, which constitute the specificity of different liquors, including alcohols, esters, acids, and aldehydes.

**Discrimination of 15 Commercial Liquors.** Lastly, the colorimetric sensor was applied to common Chinese liquors

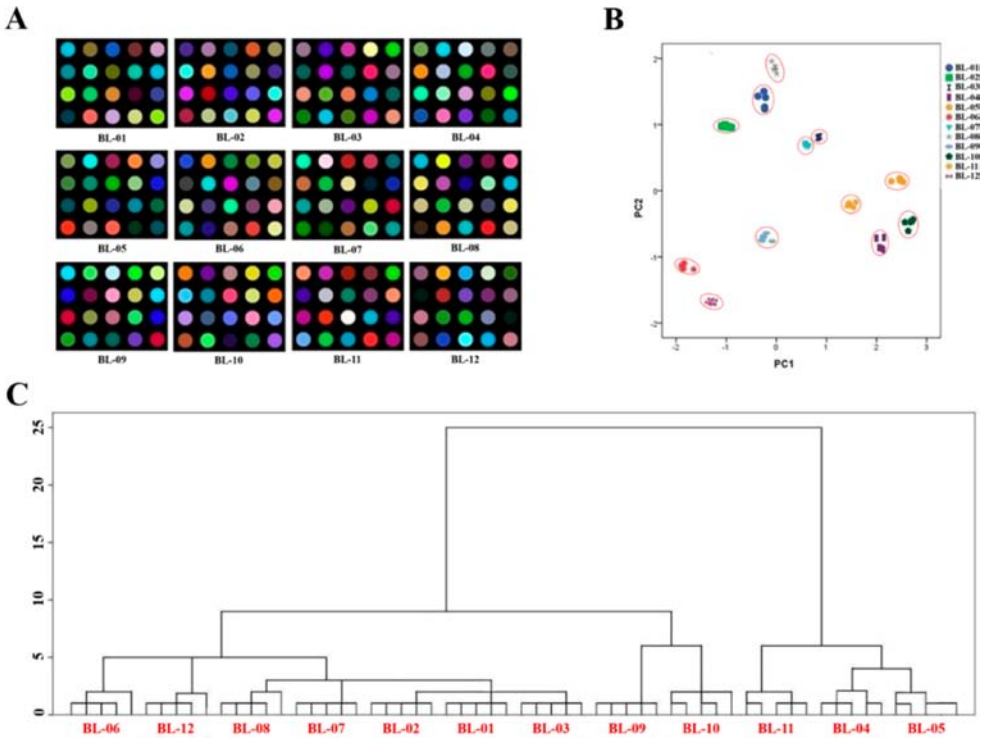


**Figure 4.** (A) Colorimetric maps of 12 base liquors. (B) Plot of the first two principal components by PCA with data obtained from the colorimetric sensor. (C) HCA dendrogram of 12 base liquors with 5 controls.

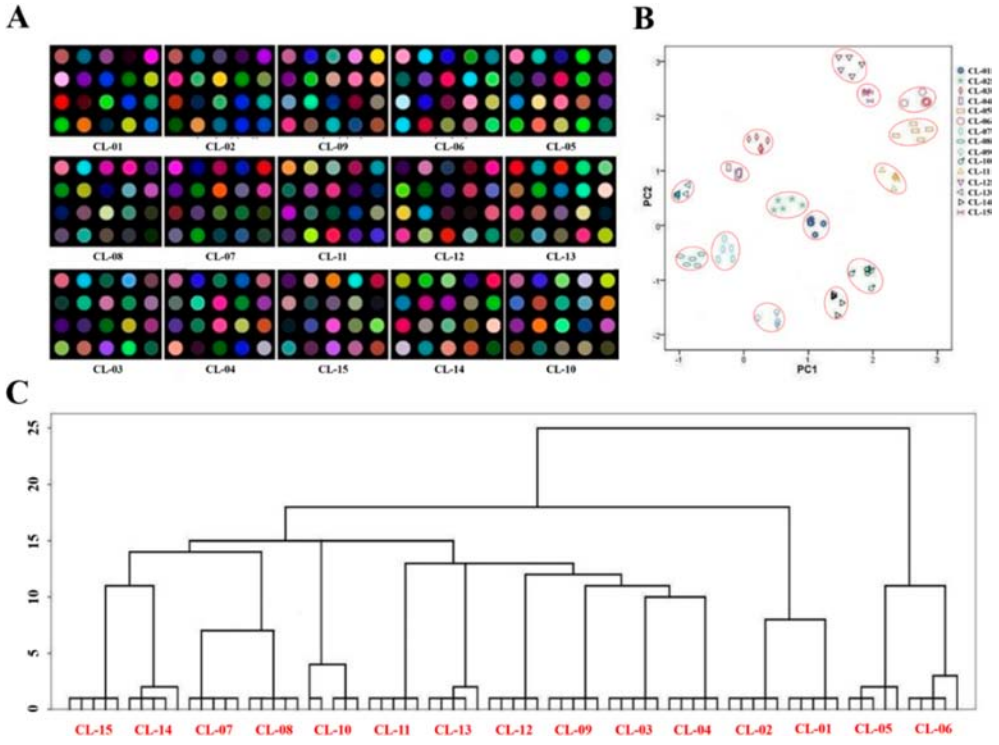


**Figure 5.** (A) Colorimetric maps of 15 Chinese liquors. (B) Plot of the first two principal components by PCA with data obtained from the colorimetric sensor. (C) HCA dendrogram of 15 Chinese liquors with 5 controls.

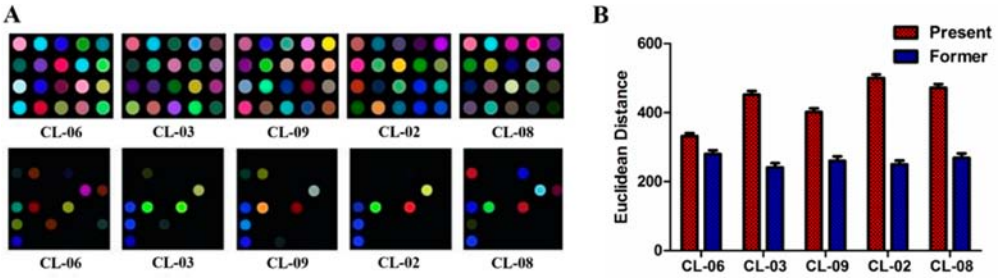


**Figure 6.** (A) Difference map of a selection-oriented sensor array with five parallel dots. (B) Actual map of the detection-oriented sensor array and arrangement of the sensing dot.

that are commercially available in the supermarket. The colorimetric maps of 15 selected kinds of Chinese liquors are shown in Figure 5A. It can be seen from the figure that different brands of Chinese liquors exhibited different responses in the sensor array and the differences can also be distinguished by the naked eye. Similar to the base liquors, liquor samples of the same alcoholic strength showed analogous colorimetric responses in D11 and D12 and were hardly alike in other dots, which is again verified that it is immune to high ethanol interfering. A plot of the first two principal components is shown in Figure 5A, demonstrating again the good recognition of the commercial Chinese liquors. PCA study also suggested that the first PC mostly relied on discrimination of esters and aldehydes. The second one mainly relied on organic acids and the third greatly on alcohols, which is slight different from base liquors. Moreover, the cumulative contribution rate (65.6%) of the first three principal components for the commercial liquor was lower than that of the base liquors. This might result from the change of marker compounds in liquor aging process of the commercial Chinese liquor by base liquor as well as its storage.[35]

A HCA study was also used to analyze the data (R, G, and B valued of each dot and Euclidean distance) obtained from colorimetric reaction. It was found that control samples of the same brand clustered together without any misclassification, and different liquors of the same flavor type grouped together first, then with others. However, samples of the same alcoholic strength did not cluster close with each other in the dendrogram. Those results suggested that discrimination of the Chinese liquors by the sensor array was dominated by the flavor types, relying on esters and aldehydes, instead of alcoholic strength. Moreover, we also compared the colorimetric response of the present sensor with that depending on cross-responsive mechanism by non-specific interactions in former studies (Figure 6). This showed that the present one exhibited significantly better response to selected Chinese liquor samples, and the Euclidean distances were much higher than in the former, despite the former having more sensitive dots.

In summary, facile discrimination of 12 high-alcoholic Chinese base liquors from Luzhou Co., Ltd., and 15 commercial Chinese liquors of different brands and flavor types was achieved with a freshly developed colorimetric sensor array. On the basis of 17

volatile markers determined by GC-MS analysis and subsequent factor analysis including acetaldehyde, furfural, acetal, isoamylol, 2-butyl alcohol, *n*-propyl alcohol, isobutanol, *n*-butanol, acetic acid, butyric acid, isopropylacetic acid, caproic acid, ethyl acetate, ethyl butyrate, ethyl valerate, ethyl hexanoate, and ethyl lactate, the sensor realized correct identification of both base liquors with high alcoholic volume and commercial liquors within the same flavor type just by comparison of the color change profiles. Statistical analysis including PCA and HCA suggested that no misclassification was observed for both liquor samples, and the discrimination had a close relationship with the characteristic flavor compounds (esters, aldehydes, and acids) and alcoholic strength in the liquors. Because the response of the sensor array improved significantly in comparison with those that rely on nonspecific interactions and its discrimination ability was partly comparable with GC-MS, we can envisage its potential application for quality surveillance of Chinese liquors in the market and even in mass production.

## ■ ASSOCIATED CONTENT

### Supporting Information

Detailed information about 12 base Chinese liquors and 15 commercial Chinese liquors, composition of each sensor dot, and other information. This material is available free of charge via the Internet at http://pubs.acs.org.

## ■ AUTHOR INFORMATION


### Corresponding Author

*(D.H.) Phone: +86 23 65112673. Fax: +86 23 65102507. E-mail: houcj@cqu.edu.cn.



### Funding

We acknowledge financial support from the National Natural Science Foundation (No. 81171414, 81271930, and 31171684), Key Technologies R&D Program of Sichuan Province of China (2013FZ0043 and 2010NZ0093), Key Technologies R&D Program of China (2012BAI19B03), and Sharing fund of Chongqing University's large equipment.


### Notes

The authors declare no competing financial interest.

## ■ REFERENCES


(1) Xiao, Z.; Yu, D.; Niu, Y.; Chen, F.; Song, S.; Zhu, J.; Zhu, G. Characterization of aroma compounds of Chinese famous liquors by gas chromatography−mass spectrometry and flash GC electronic-nose. *J. Chromatogr., B* **2014**, *945*−*946*, 92−100.

(2) Du, H.; Fan, W.; Xu, Y. Characterization of geosmin as source of earthy odor in different aroma type Chinese liquors. *J. Agric. Food Chem.* **2011**, *59* (15), 8331−8337.

(3) Cheng, P.; Fan, W.; Xu, Y. Determination of Chinese liquors from different geographic origins by combination of mass spectrometry and chemometric technique. *Food Control* **2014**, *35* (1), 153−158.

(4) Du, H.; Lu, H.; Xu, Y.; Du, X. Community of environmental streptomyces related to geosmin development in Chinese liquors. *J. Agric. Food Chem.* **2013**, *61* (6), 1343−1348.

(5) Fan, W.; Qian, M. C. Headspace solid phase microextraction and gas chromatography−olfactometry dilution analysis of young and aged Chinese "Yanghe Daqu" liquors. *J. Agric. Food Chem.* **2005**, *53* (20), 7931−7938.

(6) Zheng, J.; Liang, R.; Wu, C.; Zhou, R.; Liao, X. Discrimination of different kinds of Luzhou-flavor raw liquors based on their volatile features. *Food Res. Int.* **2014**, *56*, 77−84.

(7) Liu, M.; Han, X.; Tu, K.; Pan, L.; Tu, J.; Tang, L.; Liu, P.; Zhan, G.; Zhong, Q.; Xiong, Z. Application of electronic nose in Chinese spirits quality control and flavour assessment. *Food Control* **2012**, *26* (2), 564−570.

(8) Wang, C.; Shi, D.; Gong, G. Microorganisms in Daqu: a starter culture of Chinese Maotai-flavor liquor. *World J. Microbiol. Biotechnol.* **2008**, *24* (10), 2183−2190.

(9) Wu, X.; Zheng, X.; Han, B.; Vervoort, J.; Nout, M. J. R. Characterization of Chinese liquor starter, "Daqu", by flavor type with $^{1}$H NMR-based nontargeted analysis. *J. Agric. Food Chem.* **2009**, *57* (23), 11354−11359.

(10) Du, H.; Xu, Y. Determination of the microbial origin of geosmin in Chinese liquor. *J. Agric. Food Chem.* **2012**, *60* (9), 2288−2292.

(11) Kireeva, I. How to register geographical indications in the European Community. *World Patent Inf.* **2011**, *33* (1), 72−77.

(12) Qin, H.; Huo, D.; Zhang, L.; Yang, L.; Zhang, S.; Yang, M.; Shen, C.; Hou, C. Colorimetric artificial nose for identification of Chinese liquor with different geographic origins. *Food Res. Int.* **2012**, *45* (1), 45−51.

(13) Zhang, Q.; Xie, C.; Zhang, S.; Wang, A.; Zhu, B.; Wang, L.; Yang, Z. Identification and pattern recognition analysis of Chinese liquors by doped nano ZnO gas sensor array. *Sens. Actuators, B* **2005**, *110* (2), 370−376.

(14) Zhang, J.; Li, L.; Gao, N.; Wang, D.; Gao, Q.; Jiang, S. Feature extraction and selection from volatile compounds for analytical classification of Chinese red wines from different varieties. *Anal. Chim. Acta* **2010**, *662* (2), 137−142.

(15) Zhen, C.; Zhou, Y.; Zhang, N.; Wang, J.; Xiong, C.; Chen, S.; Nie, Z. Differentiation of Chinese liquors by using ambient glow discharge ionization mass spectrometry. *Analyst* **2013**, *138*, 3830−3835.

(16) Cheng, P.; Fan, W.; Xu, Y. Quality grade discrimination of Chinese strong aroma type liquors using mass spectrometry and multivariate analysis. *Food Res. Int.* **2013**, *54* (2), 1753−1760.

(17) Dong, D.; Zheng, W.; Wang, W.; Zhao, X.; Jiao, L.; Zhao, C. A new volatiles-based differentiation method of Chinese spirits using longpath gas-phase infrared spectroscopy. *Food Chem.* **2014**, *155*, 45−49.

(18) Chen, H.; Tan, C.; Wu, T.; Wang, L.; Zhu, W. Discrimination between authentic and adulterated liquors by near-infrared spectroscopy and ensemble classification. *Spectrochim. Acta Part A: Mol. Biomol. Spectrosc.* **2014**, *130* (0), 245−249.

(19) Li, Z.; Wang, P.; Huang, C.; Shang, H.; Pan, S.; Li, X. Application of Vis/NIR spectroscopy for Chinese liquor discrimination. *Food Anal. Methods* **2014**, *7* (6), 1337−1344.

(20) Jing, Y.; Meng, Q.; Qi, P.; Zeng, M.; Li, W.; Ma, S. Electronic nose with a new feature reduction method and a multi-linear classifier for Chinese liquor classification. *Rev. Sci. Instrum.* **2014**, *85* (5), 1−11.

(21) Li, Z.; Wang, N.; Raghavan, G. S. V.; Vigneault, C. Volatiles evaluation and dielectric properties measurements of Chinese spirits for quality assessment. *Food Bioprocess Technol.* **2011**, *4* (2), 247−253.

(22) Zhou, Q.; Zhang, S.; Li, Y.; Xie, C.; Li, H.; Ding, X. A Chinese liquor classification method based on liquid evaporation with one unmodulated metal oxide gas sensor. *Sens. Actuators, B* **2011**, *160* (1), 483−489.

(23) Ya, Z.; He, K.; Lu, Z.; Yi, B.; Hou, C.; Shan, S.; Huo, D.; Luo, X. Colorimetric artificial nose for baijiu identification. *Flavour Fragrance J.* **2012**, *27* (2), 165−170.

(24) Janzen, M. C.; Ponder, J. B.; Bailey, D. P.; Ingison, C. K.; Suslick, K. S. Colorimetric sensor arrays for volatile organic compounds. *Anal. Chem.* **2006**, *78* (11), 3591−3600.

(25) Rakow, N. A.; Suslick, K. S. A colorimetric sensor array for odour visualization. *Nature* **2000**, *406* (6797), 710−713.

(26) Zhang, C.; Suslick, K. S. Colorimetric sensor array for soft drink analysis. *J. Agric. Food Chem.* **2007**, *55* (2), 237−242.

(27) Feng, L.; Musto, C. J.; Suslick, K. S. A simple and highly sensitive colorimetric detection method for gaseous formaldehyde. *J. Am. Chem. Soc.* **2010**, *132* (12), 4046−4047.

(28) Zhang, C.; Bailey, D. P.; Suslick, K. S. Colorimetric sensor arrays for the analysis of beers: a feasibility study. *J. Agric. Food Chem.* **2006**, *54* (14), 4925−4931.

(29) Suslick, B. A.; Feng, L.; Suslick, K. S. Discrimination of complex mixtures by a colorimetric sensor array: coffee aromas. *Anal. Chem.* **2010**, *82* (5), 2067−2073.
(30) García, M.; Fernández, M. J.; Fontecha, J. L.; Lozano, J.; Santos, J. P.; Aleixandre, M.; Sayago, I.; Gutiérrez, J.; Horrillo, M. C. Differentiation of red wines using an electronic nose based on surface acoustic wave devices. *Talanta* **2006**, *68* (4), 1162−1165.
(31) Li, J.; Hou, C.; Huo, D.; Yang, M.; Fa, H.; Yang, P. Development of a colorimetric sensor array for the discrimination of aldehydes. *Sens. Actuators, B* **2014**, *196*, 10−17.
(32) Hou, C.; Dong, J.; Zhang, G.; Lei, Y.; Yang, M.; Zhang, Y.; Liu, Z.; Zhang, S.; Huo, D. Colorimetric artificial tongue for protein identification. *Biosens. Bioelectron.* **2011**, *26* (10), 3981−3986.
(33) Zhu, S.; Lu, X.; Ji, K.; Guo, K.; Li, Y.; Wu, C.; Xu, G. Characterization of flavor compounds in Chinese liquor Moutai by comprehensive two-dimensional gas chromatography/time-of-flight mass spectrometry. *Anal. Chim. Acta* **2007**, *597* (2), 340−348.
(34) Fan, W.; Qian, M. C. Identification of aroma compounds in Chinese 'Yanghe Daqu' liquor by normal phase chromatography fractionation followed by gas chromatography−olfactometry. *Flavour Fragrance J.* **2006**, *21* (2), 333−342.
(35) Mo, X.; Fan, W.; Xu, Y. Changes in volatile compounds of Chinese rice wine wheat Qu during fermentation and storage. *J. Inst. Brew.* **2009**, *115* (4), 300−307.

Two of the most commonly used methods for the determination of phenolic acids are (1) a total phenolic acids method in which the substrate is subjected directly to base hydrolysis in the presence of EDTA and ascorbic acid[9] and (2) extraction and separation of soluble (free, conjugated) and insoluble bound phenolic acids followed by hydrolysis in the absence of absorbate and EDTA.[10] In the present study, we carried out a direct comparison of these two methods in refined and whole wheat flours of three wheat varieties. We subsequently investigated the effects of the major processes in refined and whole wheat breadmaking by evaluating the phenolic acid and composition in each of the three wheat varieties utilizing the total phenolic acids method. Phytochemicals were analyzed in flour (F), mixed dough (MD), proofed dough (PD), bottom crust (BCT), crumb (CM), and upper crust (UCT) fractions of all wheat varieties.

## MATERIALS AND METHODS

**Wheat and Bread Samples.** Three spring wheat cultivars representing three wheat classes, 'Westbred 936' (hard red), 'Alpowa' (soft white), and 'Blanca Grande' (hard white), were grown as previously described.[11] Grain was tempered and milled to approximately 70% extraction (refined white flour) on a Bühler MLU-202 flour mill. The particle size of bran and shorts mill streams was reduced with a pin mill so that ≥70% passed through a 180 μm sieve; reduced fractions were then blended with the refined wheat flour to produce whole wheat flour. Flour samples were stored at −20 °C prior to processing.

Bread was prepared from refined and whole wheat flours of each variety following the 100 g straight-dough pan bread test (90 min fermentation and 33 min proof are used, then doughs are baked for 21 min at 218 °C).[12,13] Dough and bread fractions were made as follows: a dough sample was frozen immediately after mixing, referred to as "mixed dough", and another dough sample was frozen after proofing, referred to as "proofed dough". After baking, the loaves were divided into the following three components: "upper crust", which represented that part of the loaf exposed directly to oven temperatures; "bottom crust", representing that part of the crust in contact with the loaf pan; and "crumb", which was everything except crust fractions. The crust components were scraped to remove the adhering crumb component. Each fraction was lyophilized and stored at −20 °C. Each flour sample was also tested as the "starting point". Dried samples were broken up with a mortar and pestle and ground in a Tecator Cemotec 1090 burr mill set at the finest setting and stored at −20 °C. Prior to analysis, each fraction was further ground to a particle size of 40 mesh using a Micromill manufactured by Bel Art Products (Pequannock, NJ, USA).

**Chemicals and Reagents.** Phenolic acid (vanillic, caffeic, syringic, *p*-coumaric, ferulic, and sinapic acids) standards and ascorbic acid were purchased from Sigma-Aldrich (St. Louis, MO, USA). Sodium hydroxide and all solvents (ethyl ether, ethyl acetate, and methanol) were obtained from Fisher Chemicals (Fair Lawn, NJ, USA). All chemicals and solvents were of either analytical grade or HPLC grade and were used directly without further purification. Ethylenediaminetetraacetic acid (EDTA) was purchased from EMD Chemicals (Gibbstown, NJ, USA). Polyvinylidene difluoride (PVDF) syringe filters with a pore size of 0.45 μm were purchased from National Scientific Co. (Duluth, GA, USA).

**Comparison of Two Phenolic Acid Methods.** Flour samples from the three wheat varieties were hydrolyzed separately by two common methods. Method A allowed separation of soluble (free and conjugated) and bound insoluble phenolic acids,[10] and method B involved direct hydrolysis of the total phenolic acids in the sample in the presence of EDTA and ascorbic acid.[14] Briefly, the ground sample was extracted with acetone/methanol/water (7:7:6, v/v/v) first to obtain the soluble supernatant and residue. Soluble free and conjugated phenolics were first acidified (pH 2) by hydrochloric acid; free phenolics were extracted by ethyl ether and ethyl acetate (1:1, v/v), and then conjugated phenolics were hydrolyzed with 2 N sodium hydroxide and acidified with 6 N HCl. Free phenolic acids were extracted with diethyl ether and ethyl acetate (1:1, v/v). The residue was stored overnight at room temperature and hydrolyzed with 2 N sodium hydroxide, acidified by hydrochloric acid, and then extracted with ethyl ether and ethyl acetate (1:1, v/v) for analysis of insoluble bound phenolic acid. After evaporation of the organic phase under nitrogen, the residue was redissolved in methanol/water (75:25, v/v) and filtered through a 0.45 μm membrane filter. The filtered extract was analyzed for phenolic acid quantification by HPLC. In method B, the ground flour sample was mixed with 2 N NaOH containing 10 mM EDTA and 1% ascorbic acid for 30 min at 40−45 °C.[15] The reaction mixture was acidified with 6 N HCl and then extracted with ethyl acetate. The organic phase was dried, and the residue was redissolved in methanol/water (75:25, v/v). Then, the extract was filtered through a 0.45 μm membrane filter and analyzed by HPLC. Four replicate base hydrolyses, extractions, and analyses of each fraction were carried out.

**Analysis of Phenolic Acids by HPLC-ESI-MS.** Quantification of phenolic acids from all samples was carried out using an Agilent 1290 Infinity LC system coupled to diode array (DA) and mass spectrometry (MS) detectors from Agilent Technologies (Palo Alto, CA, USA). Identification of phenolic acids was achieved by comparison of mass and ultraviolet spectral data as previously reported and by comparison of retention time with authentic commercial phenolic acid standards.[9,14] Briefly, separation of phenolic acids was achieved using a reversed phase C18 Luna column (150 × 4.6 mm; particle size = 5 μm) from Phenomenex (Torrance, CA, USA) at ambient temperature (between 22 and 27 °C) as previously described.[9] Separation was achieved using a binary gradient with two solvents. Solvent A was 0.1% (v/v) formic acid in water, and solvent B was 0.1% (v/v) formic acid in methanol. The flow rate was set to 1 mL $min^{-1}$. Twenty microliters was used for injection. The linear gradient consisted of 5−30% B for 25 min, followed by 30% B for 35 min, then ramped from 30 to 100% B for 10 min, and held at 100% B for 5 min. The mobile phase concentration was returned to 5% B and held for 10 min before the next injection. The mass spectral data were collected in both positive and negative ion modes at low and high fragment voltages (70 and 250 V). The instrument was set to scan from 100 to 750 mass units. The temperature of the drying gas was 300 °C at a flow rate of 12 L $min^{-1}$; the capillary voltage for both positive and negative ion modes was adjusted at 3000 V and a nebulizer pressure of 50 psi. The LC system was directly connected to a mass spectrometer with no stream splitting.

**Statistical Analysis.** Data were reported as means ± standard deviations (SD) for four replicate treatments. One-way analysis of variance (ANOVA) and Tukey's tests were performed using SPSS (SPSS for Windows, version 10.0.5, SPSS Inc., Chicago, IL, USA). Correlation analyses were performed using a two-tailed Pearson correlation test. Statistical significance was declared at $P < 0.05$.

## RESULTS AND DISCUSSION

**Comparison of Two Methods for Phenolic Acid Hydrolysis and Extraction.** There are two chemical methods commonly used for extraction of phenolic acids. Method A allowed the separation of soluble (free and conjugated) and insoluble bound phenolic acids, whereas method B directly extracted phenolic acids after base hydrolysis of the plant matrix in the presence of EDTA and ascorbic acid.[15] The results using method A (Figure 1A,B) showed that most (>82%) of the phenolic acids in all three varieties exist in insoluble bound form. These results were similar to those previously published in a study from our group and by other researchers.[10,11,16] Ferulic acid was the most abundant phenolic acid present in soluble and insoluble bound forms for all three wheat varieties. It accounted for about 64.1−67.9% of total soluble phenolic acids and for between 84.4 and 85.6% of total insoluble bound phenolic acids (Figure 1C,D). Whent et al.[11] also found that ferulic and *p*-coumaric acids were primarily in the insoluble

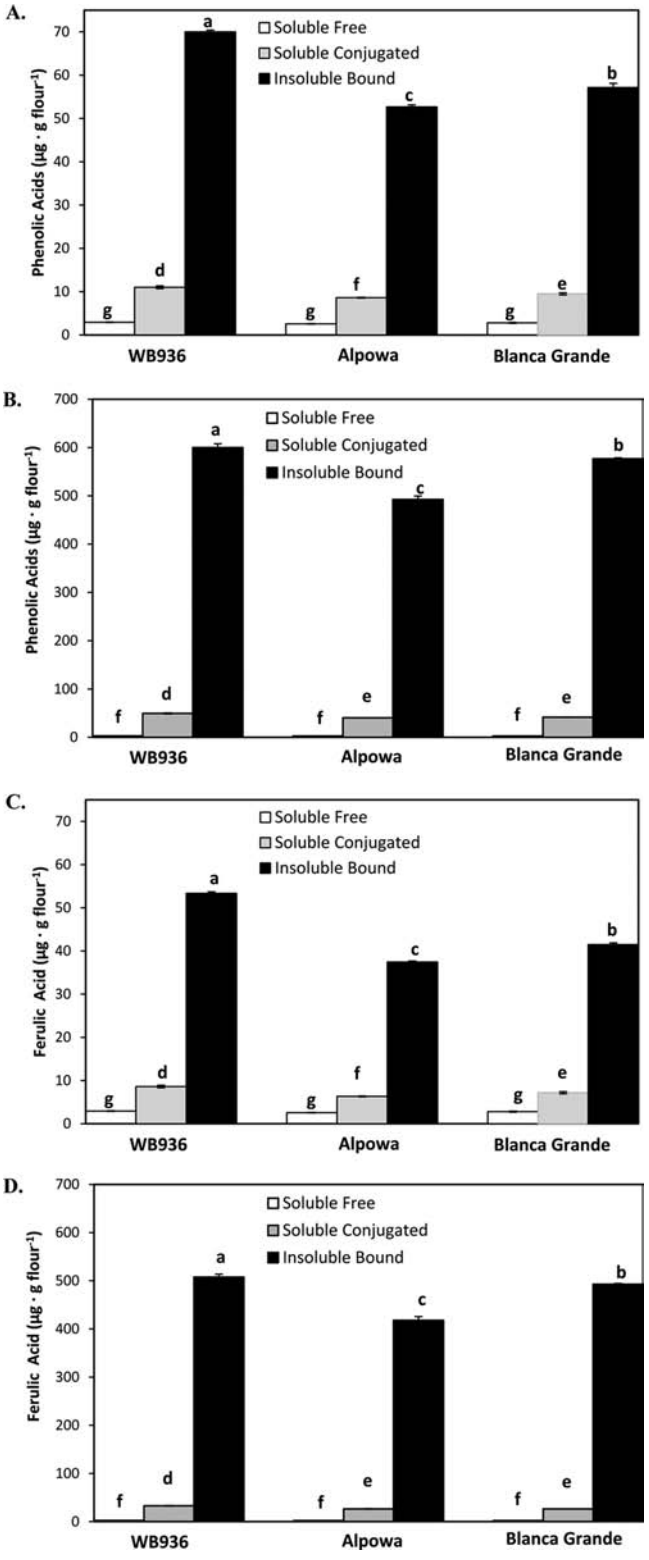


**Figure 1.** Soluble (free and conjugated) and insoluble bound phenolic acids of (A) refined wheat (RF) and (B) whole wheat (WW) flours of three wheat varieties. Soluble (free and conjugated) and insoluble bound ferulic acid of (C) refined wheat (RF) and (D) whole wheat (WW) flours of three wheat varieties. The same letter indicates no statistical difference, whereas different letters stand for significant statistical difference ($P > 0.05$).

bound form in flour samples from five wheat varieties. A similar high concentration (89.2−94.6%) of the insoluble bound form of ferulic acid has been reported in a previous study by Moore et al.[10]

The amounts of total phenolic acids quantified in all three wheat varieties using method B hydrolysis and extraction were significantly higher than those of method A ($P < 0.05$). This is primarily due to the presence of additional antioxidant ascorbic acid and chelating agent EDTA. However, method A provided useful information on the soluble and insoluble bound phenolic acids that may also have importance in the determination of the bioavailability of the bioactive phenolic acids. In the present study, method B (base hydrolysis in the presence of EDTA and ascorbic acid) was used for comparison of phenolic acids content in refined and whole wheat fractions.

**Comparison of Phenolic Acids in Refined versus Whole Wheat Fractions.** The quantities of total phenolic acids extracted from the refined flour samples were significantly lower than those from the whole wheat flour samples (Figure 2). This is in agreement with previously published papers in

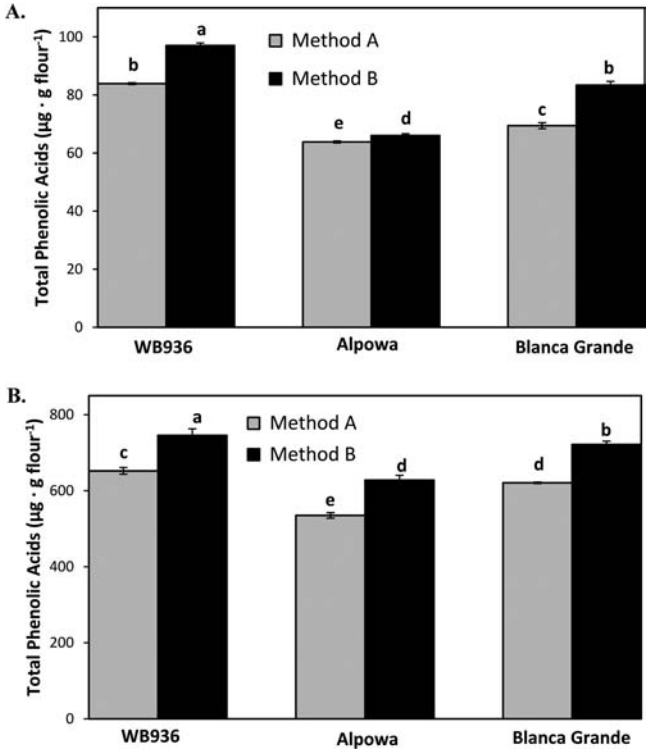


**Figure 2.** Total phenolic acids of (A) refined wheat (RF) and (B) whole wheat (WW) flours of three wheat varieties by using two extraction methods. Method A involves separation of soluble (free and conjugated) and insoluble bound phenolic acids, whereas method B allows only determination of total phenolic acids in the presence of EDTA and ascorbic acid. The same letter indicates no statistical difference, whereas different letters stand for significant statistical difference ($P > 0.05$).

which authors observed only about $^{1}/_{10}$ of the total phenolic acids content in wheat flour as compared to the whole grain flour.[17−19]

The phenolic acid composition and content in refined (RF) and whole wheat (WW) flour (F), mixed dough, proofed dough, bottom crust, crumb, and upper crust are presented in Tables 1, 2, and 3. In terms of overall abundance, FA was the most abundant phenolic acid, accounting for a mean of 59% (range from 51 to 68%) of TPA among RF fractions and a


dx.doi.org/10.1021/jf501941r | J. Agric. Food Chem. 2014, 62, 10431−10436

Table 1. Total Phenolic Acids (TPA) of the Flour, Dough, and Bread Fractions from 'WB936' (Hard Red Wheat) Variety[a]

| type | fraction | VA | CA | SyA | *p*-CA | SiA | FA | total |
|---|---|---|---|---|---|---|---|---|
| RF | flour | 1.0 ± 0.0f | 8.3 ± 0.0c | 2.6 ± 0.1e | 4.5 ± 0.0d | 15.0 ± 0.1b | 65.6 ± 0.9b | 97.0 ± 0.9b |
| RF | MD | 1.5 ± 0.1e | 8.8 ± 0.1b | 5.2 ± 0.6d | 4.5 ± 0.3d | 14.3 ± 1.0b | 55.0 ± 4.9c | 89.3 ± 6.5c |
| RF | PD | 1.7 ± 0.1d | 8.8 ± 0.0b | 6.7 ± 0.3ab | 4.4 ± 0.3d | 14.1 ± 0.3b | 52.7 ± 3.2c | 88.6 ± 2.2c |
| RF | CM | 4.4 ± 0.2b | 8.9 ± 0.1b | 6.3 ± 0.4bc | 6.4 ± 0.1b | 14.8 ± 0.1b | 68.7 ± 1.1ab | 109.6 ± 3.5a |
| RF | BCT | 7.4 ± 0.1a | 9.4 ± 0.3a | 7.6 ± 0.9a | 5.6 ± 0.2c | 14.1 ± 0.3b | 66.3 ± 1.4b | 110.5 ± 1.3a |
| RF | UCT | 4.2 ± 0.1c | 8.9 ± 0.6b | 6.0 ± 0.5cd | 7.0 ± 0.5a | 17.1 ± 0.8a | 70.6 ± 2.5a | 113.8 ± 1.4a |
| WW | flour | 24.7 ± 1.7a | 12.5 ± 0.4e | 27.5 ± 0.4ab | 21.0 ± 0.4b | 57.7 ± 2.4a | 602.2 ± 11.3a | 745.6 ± 20.1a |
| WW | MD | 18.2 ± 1.5b | 17.6 ± 0.5bc | 21.1 ± 0.5c | 17.5 ± 0.1 cd | 56.2 ± 4.1ab | 563.6 ± 33.6ab | 694.3 ± 29.0ab |
| WW | PD | 13.7 ± 0.1c | 15.9 ± 0.7cd | 25.7 ± 0.5b | 15.5 ± 1.1d | 49.0 ± 6.5c | 534.7 ± 43.4bc | 654.4 ± 50.2bc |
| WW | CM | 10.9 ± 0.4d | 15.1 ± 2.5d | 22.9 ± 0.8c | 18.5 ± 3.6bcd | 52.0 ± 3.2bc | 534.4 ± 48.9bc | 650.5 ± 51.1bc |
| WW | BCT | 23.5 ± 0.2a | 19.4 ± 0.7a | 29.1 ± 1.8a | 24.9 ± 0.6a | 42.7 ± 5.4d | 569.8 ± 8.9ab | 709.5 ± 12.0ab |
| WW | UCT | 11.6 ± 0.4d | 17.9 ± 1.7ab | 17.4 ± 1.9d | 20.2 ± 3.3bc | 37.8 ± 2.8d | 631.9 ± 94.1a | 736.9 ± 97.0a |

[a]RF, refined wheat; WW, whole wheat; CM, crumb; UCT, upper crust; BCT, bottom crust; MD, mixed dough; PD, proofed dough. VA, CA, SyA, *p*-CA, FA, and SiA stand for vanillic, caffeic, syringic, *p*-coumaric, ferulic, and sinapic acids, respectively. Results are expressed as $\mu g\ g^{-1}$ of flour (F), dough (MD or PD), or bread (BCT, CM, or UCT) on a dry sample weight basis. The results are expressed as the mean ± SD of four replicate extractions and analysis followed by a letter. The same letter indicates no statistical difference, whereas different letters stand for significant statistical difference ($P > 0.05$).

Table 2. Total Phenolic Acids (TPA) of the Flour, Dough, and Bread Fractions from 'Alpowa' (Soft White Wheat) Variety[a]

| type | fraction | VA | CA | SyA | *p*-CA | SiA | FA | total |
|---|---|---|---|---|---|---|---|---|
| RF | flour | 3.8 ± 0.2d | 2.8 ± 0.2d | 6.3 ± 0.2c | 5.1 ± 0.1d | 10.0 ± 0.1b | 38.1 ± 0.6bc | 66.0 ± 0.6c |
| RF | MD | 4.5 ± 0.2bc | 2.9 ± 0.0d | 6.8 ± 0.2c | 5.7 ± 0.1b | 9.1 ± 0.1bc | 35.6 ± 0.4cd | 64.9 ± 0.4c |
| RF | PD | 4.2 ± 0.4cd | 3.3 ± 0.2c | 9.6 ± 0.5b | 5.6 ± 0.1c | 8.9 ± 0.1c | 33.3 ± 1.9d | 64.9 ± 2.2c |
| RF | CM | 5.2 ± 0.5b | 3.3 ± 0.1c | 13.0 ± 1.6a | 5.9 ± 0.1a | 9.2 ± 1.0bc | 39.2 ± 2.5ab | 75.7 ± 1.8b |
| RF | BCT | 5.1 ± 0.7b | 3.5 ± 0.0b | 7.4 ± 1.0c | 5.6 ± 0.1c | 7.7 ± 1.0d | 38.2 ± 3.6bc | 67.5 ± 5.19c |
| RF | UCT | 9.0 ± 0.5a | 3.8 ± 0.2a | 9.6 ± 1.4b | 5.8 ± 0.1b | 11.2 ± 0.2a | 41.7 ± 1.2a | 81.0 ± 6.0a |
| WW | flour | 38.3 ± 1.3a | 9.3 ± 0.4c | 14.1 ± 0.2b | 13.3 ± 0.5b | 63.1 ± 1.1b | 489.8 ± 13.9cd | 627.8 ± 12.8b |
| WW | MD | 10.0 ± 0.8d | 9.2 ± 0.1c | 13.3 ± 2.2b | 14.0 ± 1.4ab | 60.2 ± 3.0b | 462.8 ± 11.7de | 569.5 ± 18.0c |
| WW | PD | 40.0 ± 1.5a | 4.8 ± 0.1e | 14.1 ± 1.5b | 14.6 ± 0.7a | 75.2 ± 3.0a | 458.7 ± 8.4e | 607.3 ± 7.3b |
| WW | CM | 13.8 ± 2.0c | 7.4 ± 0.7d | 15.8 ± 2.3b | 14.3 ± 0.3ab | 35.0 ± 2.1d | 521.6 ± 10.2ab | 607.9 ± 13.5b |
| WW | BCT | 13.8 ± 2.3c | 11.0 ± 0.2b | 19.7 ± 0.4a | 14.3 ± 0.6ab | 49.7 ± 3.0c | 504.4 ± 40.1bc | 608.1 ± 25.2b |
| WW | UCT | 20.3 ± 1.1b | 12.7 ± 0.2a | 14.9 ± 2.2b | 13.3 ± 0.4b | 70.7 ± 3.3a | 547.8 ± 3.9a | 679.9 ± 4.3a |

[a]RF, refined wheat; WW, whole wheat; CM, crumb; UCT, upper crust; BCT, bottom crust; MD, mixed dough; PD, proofed dough. VA, CA, SyA, *p*-CA, FA, and SiA stand for vanillic, caffeic, syringic, *p*-coumaric, ferulic, and sinapic acids, respectively. Results are expressed as $\mu g\ g^{-1}$ of flour (F), dough (MD or PD), or bread (BCT, CM, or UCT) on a dry sample weight basis. The results are expressed as the mean ± SD of four replicate extractions and analysis followed by a letter. The same letter indicates no statistical difference, whereas different letters stand for significant statistical difference ($P > 0.05$).

mean of 81% (range from 76 to 86%) among WW fractions. Sinapic acid was the second most abundant phenolic acid, accounting for means of 13 and 8.5% of TPA in RF and WW fractions, respectively. Among the fractions evaluated, TPA ranged from 5.5- to 9.8-fold greater in WW fractions than in RF fractions (Tables 1−3). All individual phenolic acids were also higher in WW than in RF fractions (Tables 1−3). The greatest increases came from FA and sinapic acid, which had 11.5- and 5.5-fold increases, respectively, in WW compared to RF when averaged across fractions and varieties. Our results are consistent with previous studies demonstrating that total phenoilc acids were around 10-fold greater in whole wheat than in refined wheat products and are also consistent with our additional work on two other varieties.[19,20] In addition, Baublis et al.[21] reported that antioxidant activity was better in whole wheat than in refined wheat products.

The dramatic increase in FA in WW compared to RF fractions was correlated with previously demonstrated higher levels (8.4−15.5-fold) of FA in rye bran than in RF flour.[22] Ferulates were also far more abundant (ca. 100-fold) in the outer tissues of the wheat kernel, including aleurone and pericarp, compared to the starchy endosperm tissue; ferulate ester and ether cross-linkages were most abundant in the outer pericarp.[4] The latter observations indicate that FA is far lower in the endosperm, consistent with our observation that FA is far lower in RF compared to WW fractions.

**Comparison of Processing Fractions within Each Variety.** In comparison of the phenolic acid compositions among the six RF fractions, the upper crust fraction had the highest TPA of all fractions in all three varieties. RF upper crust also had the highest FA content in 'WB936' and 'Alpowa' (Tables 1−3). However, in 'Blanca Grande', FA content in the upper crust did not stand out among the fractions. Among the three RF bread fractions, the crumb fraction had the lowest TPA levels in 'WB936' and 'Blanca Grande', but in 'Alpowa' the bottom crust TPA was lower than that of the crumb. Both mixed and proofed dough fractions generally had slightly lower TPA and FA than bread fractions. However, the two dough fractions were similar, suggesting that fermentation had little effect on FA and TPA contents. When the effect of processing

Table 3. Total Phenolic Acids (TPA) of the Flour, Dough, and Bread Fractions from 'Blanca Grande' (Hard White Wheat) Variety[a]

| type | fraction | VA | CA | SyA | *p*-CA | SiA | FA | total |
|---|---|---|---|---|---|---|---|---|
| RF | flour | 3.8 ± 0.3d | 2.8 ± 0.0d | 12.9 ± 0.2a | 5.0 ± 0.1c | 8.7 ± 0.5b | 50.2 ± 0.6a | 83.4 ± 1.3bc |
| RF | MD | 7.3 ± 0.7c | 3.4 ± 0.1b | 6.8 ± 0.7b | 5.8 ± 0.1ab | 7.1 ± 0.7c | 42.2 ± 2.4c | 72.6 ± 3.0e |
| RF | PD | 6.7 ± 0.4c | 3.3 ± 0.1b | 5.6 ± 0.3c | 5.9 ± 0.1a | 11.7 ± 0.4a | 47.9 ± 1.4b | 81.2 ± 2.0 cd |
| RF | CM | 4.5 ± 0.2d | 3.3 ± 0.1b | 7.2 ± 1.2b | 5.9 ± 0.1a | 9.3 ± 0.6b | 48.3 ± 0.6b | 78.6 ± 1.8d |
| RF | BCT | 11.2 ± 0.8b | 3.2 ± 0.0c | 5.8 ± 0.2c | 5.8 ± 0.0b | 9.1 ± 0.3b | 49.6 ± 0.6ab | 84.5 ± 1.0b |
| RF | UCT | 15.2 ± 1.0a | 4.1 ± 0.1a | 6.7 ± 0.2b | 5.8 ± 0.0b | 9.2 ± 0.1b | 48.6 ± 1.1ab | 89.6 ± 2.2a |
| WW | flour | 26.8 ± 0.7c | 5.8 ± 0.7c | 11.9 ± 2.1b | 17.4 ± 0.4b | 66.2 ± 1.7b | 593.8 ± 11.4ab | 721.8 ± 8.6ab |
| WW | MD | 36.5 ± 1.4a | 7.3 ± 0.4b | 18.7 ± 3.2a | 17.6 ± 0.2b | 49.8 ± 2.7c | 580.5 ± 16.7bc | 710.6 ± 15.6bc |
| WW | PD | 18.6 ± 1.2d | 8.9 ± 0.2a | 18.8 ± 1.1a | 18.6 ± 0.4a | 84.6 ± 3.2a | 598.4 ± 20.9ab | 747.9 ± 26.3a |
| WW | CM | 12.4 ± 1.7e | 8.7 ± 0.1a | 18.3 ± 0.7a | 18.5 ± 0.4a | 84.7 ± 1.5a | 566.0 ± 12.2c | 708.6 ± 15.5bc |
| WW | BCT | 30.1 ± 4.4b | 8.9 ± 0.5a | 17.6 ± 1.6a | 17.2 ± 0.5b | 49.9 ± 4.1c | 567.0 ± 18.1c | 690.8 ± 20.3c |
| WW | UCT | 31.9 ± 3.9b | 9.3 ± 0.9a | 18.8 ± 1.1a | 18.7 ± 0.6a | 49.9 ± 1.5c | 619.4 ± 13.9a | 748.0 ± 19.0a |

[a]RF, refined wheat; WW, whole wheat; CM, crumb; UCT, upper crust; BCT, bottom crust; MD, mixed dough; PD, proofed dough. VA, CA, SyA, *p*-CA, FA, and SiA stand for vanillic, caffeic, syringic, *p*-coumaric, ferulic, and sinapic acids, respectively. Results are expressed as $\mu g\ g^{-1}$ of flour (F), dough (MD or PD), or bread (BCT, CM, or UCT) on a dry sample weight basis. The results are expressed as the mean ± SD of four replicate extractions and analysis followed by a letter. The same letter indicates no statistical difference, whereas different letters stand for significant statistical difference ($P > 0.05$).

of RF fractions on the minor phenolic acids, that is, those other than FA, was examined, some trends were noted. In two of three varieties, the highest levels of vanillic, caffeic, and sinapic acids were seen in the RF upper crust, similar to the trends noted above for FA and TPA. Also, the lowest levels of vanillic, caffeic, and *p*-coumaric acids were seen in the RF flour of all three varieties, suggesting the possibility that the availability to hydrolysis or chemistry of these phenolic acids may be altered during processing.

The TPA trends among WW and RF fractions were similar as the upper crust, bottom crust, and flour fractions were generally higher than crumb, mixed dough, and proof dough fractions. TPA and FA in the dough fractions were, on average, similar to those in the crumb fraction. As in RF fractions, the TPA and FA levels were generally similar in the two WW dough fractions. No consistent trends were observed in examination of the effect of processing on the minor phenolic acids of WW fractions.

It is a safe generalization that, in our study, the total process of preparing bread did not decrease TPA, FA, and other phenolic acids. Similarly, Mattila et al.[19] found that baking did not significantly reduce the concentration of phenolic acids. In both RF and WW fractions we generally observed a slight decrease in TPA and FA in preparing dough fractions from flour. Accordingly, decreases in individual insoluble bound phenolic acids during dough preparation have also been reported by Abdel-Aal and Rabalski.[8] Similarly, Han and Koh[23] found an approximately 40% decrease in antioxidant activity in dough compared to flour samples.

The decrease generally observed in dough preparation was more than compensated for by an increase in TPA and FA in baked bread fractions. The increase during baking appeared to be correlated with temperature, because the upper crust (highest temperature) most often had the highest TPA and FA levels. It is possible that intense heat rendered phenolic acids more physically accessible or chemically more susceptible to the hydrolysis process. Similar increases in phenolic acid levels and antioxidant activity during baking were reported in two other studies[8,22] and in our own evaluations in two other wheat varieties.[20]

**Comparison of Wheat Varieties.** When RF fractions for the three varieties were compared, TPA and FA contents were always highest in 'WB936', intermediate in 'Blanca Grande', and lowest in 'Alpowa' (Tables 1−3). In the WW fractions, TPA and FA contents for 'Alpowa' were consistently lowest as expected, but there was no consistent trend in the relative levels of TPA or FA when 'WB936' and 'Blanca Grande' were compared. Specifically for the WW flour fraction, however, FA content was greatest in 'WB936', intermediate in 'Blanca Grande', and lowest in 'Alpowa' (Tables 1−3), as previously reported.[11]

**Conclusions.** We investigated the effect of the breadmaking process and wheat varieties on the quantities of phenolic acids of refined and whole wheat fractions. Two commonly used base hydrolysis methods for the analysis of phenolic acids were tested. Method A provided information on the soluble (free and conjugated) and insoluble bound phenolic acids, which may have significantly different bioavailabilities and nutritional properties. Using method A, insoluble phenolics were far more abundant than soluble formsm but both soluble and insoluble phenolics were several times more abundant in WW flour than in RF flour (Figure 1A,B). Using both methods A and B, FA was the predominant phenolic acid present in both soluble and bound insoluble forms for all three wheat varieties. In method B, the whole sample was directly hydrolyzed in the presence of ascorbic acid and EDTA and showed 5−17% higher yields of TPA than method A (Figure 2).

The effects of processing and varieties on phenolic composition in RF and WW fractions were evaluated using method B. FA was the most abundant phenolic acid, accounting for means of 59 and 81% of TPA among all RF and WW fractions, respectively. All phenolic acids measured were more abundant in WW than in RF fractions (Tables 1−3). The greatest increase came from FA, which had an 11.5-fold increase in WW compared to RF when averaged across fractions and varieties.

Evaluation of the effects of the processing steps revealed that TPA and FA tended to decrease slightly in both RF and WW doughs compared to flour. However, the two dough fractions generally had similar TPA and FA levels, indicating that

fermentation had little effect. The decrease generally observed in preparing dough was more than compensated for by an increase in TPA and FA in both RF and WW bread fractions. The increase during baking appeared to be related to temperature, because the upper crust, exposed to the greatest heat, generally had the highest TPA and FA levels. It is possible that intense heat rendered phenolic acids more physically accessible or chemically more susceptible to the hydrolysis process.

When RF fractions for the three varieties were compared, TPA and FA contents were always highest in 'WB936', intermediate in 'Blanca Grande', and lowest in 'Alpowa' (Tables 1−3). In the WW fractions, TPA and FA contents for 'Alpowa' were consistently lowest as expected, but there was no consistent trend in the relative levels of TPA or FA when 'WB936' and 'Blanca Grande' were compared.

In summary, we observed slightly higher TPA yields when samples were directly hydrolyzed in the presence of ascorbate and EDTA (method B) than when a procedure that omitted these reagents (method A) was used. Among the three varieties evaluated, 'WB936' and 'Blanca Grande' consistently had higher TPA levels than 'Alpowa'. The effects of processing on phenolic acid composition were evaluated using direct hydrolysis (method B). TPA generally decreased slightly in dough compared to flour, but increased during baking, which was especially notable in the upper crust fraction, which was exposed to the most intense heat. Results clearly indicated that the phenolic acids measured do not decrease, and may even increase slightly, when bread is prepared from RF and WW flour.

## AUTHOR INFORMATION

### Corresponding Author

*(D.L.) Phone: (301) 504-7247. Fax: (301) 504-8314. E-mail: Dave.Luthria@ars.usda.gov.

### Funding

This project was supported by Agriculture and Food Research Initiative Grant 2009-02347 from the USDA National Institute of Food and Agriculture.

### Notes

The authors declare no competing financial interest.

## ACKNOWLEDGMENTS

We acknowledge Samina Shami of USDA-ARS for her assistance in carrying out experimentation.

## REFERENCES

(1) Jones, J. M. Grain-based foods and health. *Cereal Foods World* **2006**, *51*, 108−113.

(2) Fardet, A. New hypotheses for the health-protective mechanisms of whole-grain cereals: what is beyond fibre? *Nutr. Res. Rev.* **2010**, *23*, 65−134.

(3) USDA. Dietary guidelines for Americans 2010, http://www.health.gov/dietaryguidelines/dga2010/document/pdf/DGA2010.pdf (accessed July 24, 2013).

(4) Barron, C.; Surget, A.; Rouau, X. Relative amounts of tissue in mature wheat (*Triticum aestivum* L.) grain and their carbohydrate and phenolic acid composition. *J. Cereal Sci.* **2007**, *45*, 88−96.

(5) Hansen, H. B.; Andreasen, M. F.; Nielsen, M. M.; Larsen, L. M.; Knudsen, K. E. B.; Meyer, A. S.; Christensen, L. P.; Hansen, A. Changes in dietary fibre, phenolic acids and activity of endogenous enzymes during rye bread-making. *Eur. Food Res.Technol.* **2002**, *214*, 33−42.

(6) Michalska, A.; Amigo-Benavent, M.; Zielinski, H.; Del Castillo, M. D. Effect of bread making on formation of Maillard reaction products contributing to the overall antioxidant activity of rye bread. *J. Cereal Sci.* **2008**, *48*, 123−132.

(7) Moore, J.; Luther, M.; Cheng, Z.; Yu, L. Effects of baking conditions, dough fermentation, and bran particle size on antioxidant properties of whole-wheat pizza crusts. *J. Agric. Food Chem.* **2009**, *57*, 832−839.

(8) Abdel-Aal, E. S. M.; Rabalski, I. Effect of baking on free and bound phenolic acids in whole grain bakery products. *J. Cereal Sci.* **2013**, *57*, 312−318.

(9) Luthria, D. L.; Liu, K.; Memon, A. A. Phenolic acids and antioxidant capacity of distillers dried grains with solubles (DDGS) as compared with corn. *J. Am. Oil Chem. Soc.* **2012**, *89*, 1297−1304.

(10) Moore, J.; Hao, Z.; Zhou, K.; Luther, M.; Costa, J.; Yu, L. Carotenoid, tocopherol, phenolic acid, and antioxidant properties of Maryland-grown soft wheat. *J. Agric. Food Chem.* **2005**, *53*, 6649−6657.

(11) Whent, M.; Huang, H.; Xie, Z.; Lutterodt, H.; Yu, L.; Fuerst, E.; Morris, C.; Yu, L.; Luthria, D. Phytochemical composition, anti-inflammatory, and antiproliferative activity of whole wheat flour. *J. Agric. Food Chem.* **2012**, *60*, 2129−2135.

(12) AACC. Methods 10-10B and 46-30. In *Approved Methods of the American Association of Cereal Chemists*, 10th ed.; AACC: St. Paul, MN, USA, 2000.

(13) Yu, L.; Haley, S.; Perret, J.; Harris, M. Antioxidant properties of hard winter wheat extracts. *Food Chem.* **2002**, *78*, 457−461.

(14) Luthria, D. L.; Mukhopadhyay, S.; Krizek, D. T. Content of total phenolics and phenolic acids in tomato (*Lycopersicon esculentum* Mill.) fruits as influenced by cultivar and solar UV radiation. *J. Food Compos. Anal.* **2006**, *19*, 771−777.

(15) Nardini, M.; Cirillo, E.; Natella, F.; Mencarelli, D.; Comisso, A.; Scaccini, C. Detection of bound phenolic acids: prevention by ascorbic acid and ethylenediaminetetraacetic acid of degradation of phenolic acids during alkaline hydrolysis. *Food Chem.* **2002**, *79*, 119−124.

(16) Adom, K.; Sorrells, M.; Liu, R. Phytochemical profiles and antioxidant activity of wheat varieties. *J. Agric. Food Chem.* **2003**, *51*, 7825−7834.

(17) Beta, T.; Shin, N.; Dexter, J. E.; Sapirstein, H. D. Phenolic content and antioxidant activity of pearled wheat and roller-milled fractions. *Cereal Chem.* **2005**, *82*, 390−393.

(18) Hatcher, D. W.; Kruger, J. E. Simple phenol acids in flours prepared from Canadian wheat: relationship to ash content, color, and polyphenol oxidase activity. *Cereal Chem.* **1997**, *74*, 337−343.

(19) Mattila, P.; Pihlava, J.; Hellström, J. Contents of phenolic acids, alkyl-and alkenylresorcinols, and avenanthramides in commercial grain products. *J. Agric. Food Chem.* **2005**, *53*, 8290−8295.

(20) Lu, Y.; Lv, J.; Bayard, A.; Yu, L.; Fuerst, E. P.; Morris, C. F.; Yu, L.; Luthria, D. Effect of processing on phytochemical profile and antiproliferative activity of dough and bread fractions made from refined and whole wheat flours. *J. Food Sci.* (submitted for publication).

(21) Baublis, A.; Decker, E. A.; Clydesdale, F. M. Antioxidant effect of aqueous extracts from wheat based read-to-eat breakfast cereals. *Food Chem.* **2000**, *68*, 1−6.

(22) Andreasen, M. F.; Christensen, L. P.; Meyer, A. S.; Hansen, Å. Ferulic acid dehydrodimers in rye (*Secale cereal* L.). *J. Cereal Sci.* **2000**, *31*, 303−307.

(23) Han, H.; Koh, B. Antioxidant activity of hard wheat flour, dough and bread prepared using various processes with the addition of different phenolic acids. *J. Sci. Food Agric.* **2011**, *91*, 604−608.

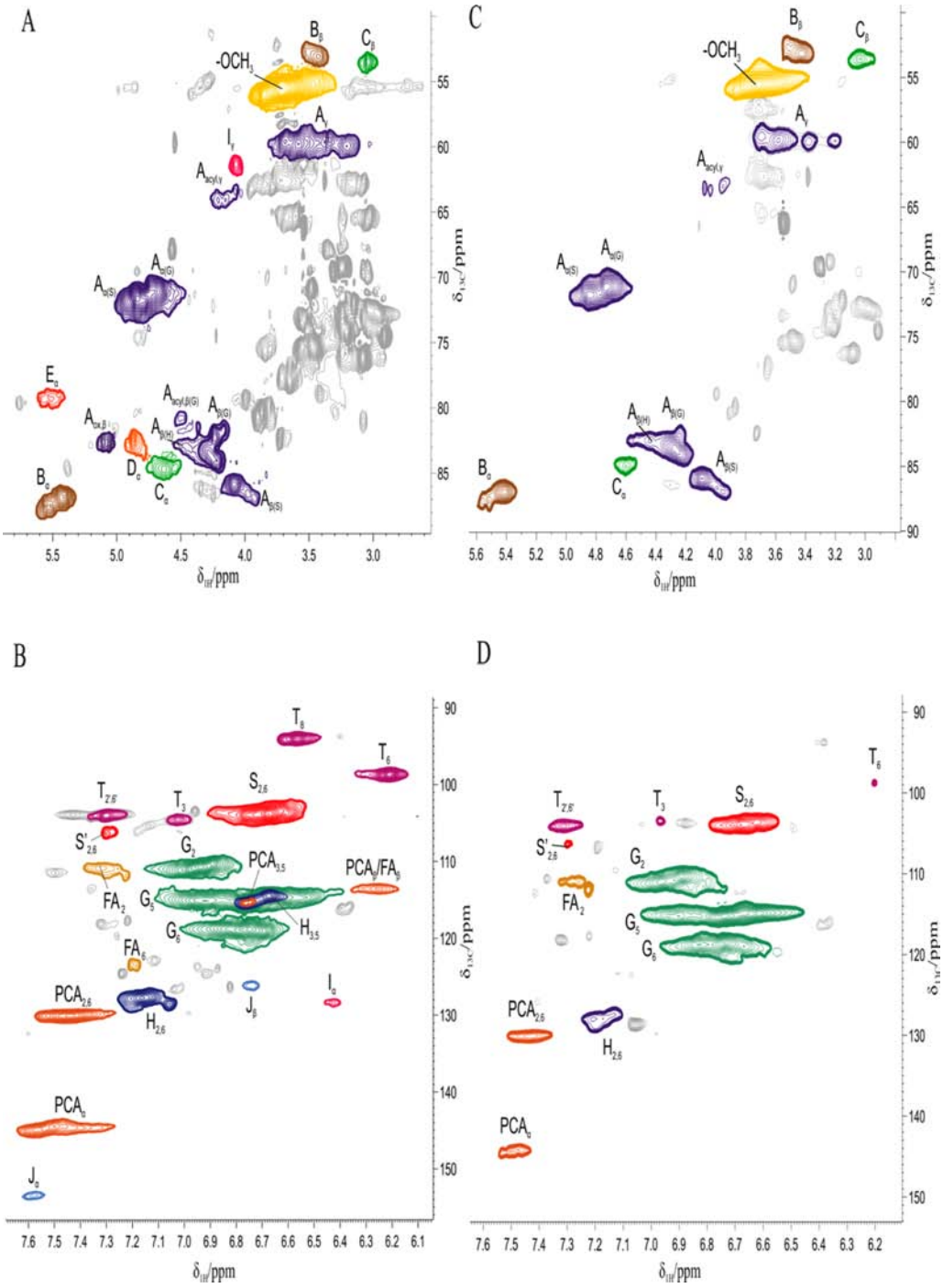


**Figure 1.** (A) Side-chain region ($\delta_C/\delta_H$, 50−90/2.5−5.7 ppm) on contour-plotted $^1$H−$^{13}$C HSQC NMR spectrum of wheat straw EMAL, (B) aromatic/unsaturated region ($\delta_C/\delta_H$, 88−160/6.05−7.65 ppm) on contour-plotted $^1$H−$^{13}$C HSQC NMR spectrum of wheat straw EMAL, (C) side-chain region ($\delta_C/\delta_H$, 50−90/2.5−5.7 ppm) on contour-plotted $^1$H−$^{13}$C HSQC NMR spectrum of SE-treated wheat straw EMAL, and (D) aromatic/unsaturated region ($\delta_C/\delta_H$, 88−160/6.05−7.65 ppm) on contour-plotted $^1$H−$^{13}$C HSQC NMR spectrum of SE-treated wheat straw EMAL.

straw bound more of the hydrolytic enzymes (*Trichoderma reesei* Cel7A and Cel7A-core) compared to the non-pretreated analogues.[16] This indicates that chemical changes that are detrimental to the saccharification process take place within the lignin structure during the SE process. Several studies regarding the impact of SE on the lignin structure have been reported. The major effects are the decrease in the level of $\beta$-O-4′ units and an increase in the level of C−C condensed structures and other interunit linkages ($\beta$-1′ and $\beta$-5′) formed via radical coupling reactions.[17−19] Dependent upon the SE conditions, the formation of higher molecular weight lignins has been observed, explained by competing depolymerization and repolymerization reactions.[19]

The aim of the present study was to elucidate the chemical changes within the enzymatic mild acidolysis lignin of wheat straw structure, caused by the SE process. NMR techniques using state-of-the-art pulse variations [quantitative 2D $^1$H−$^{13}$C HSQC, 2D $^1$H−$^{13}$C HMBC, and one-dimensional (1D) $^{31}$P NMR]


dx.doi.org/10.1021/jf504622j | J. Agric. Food Chem. 2014, 62, 10437−10444

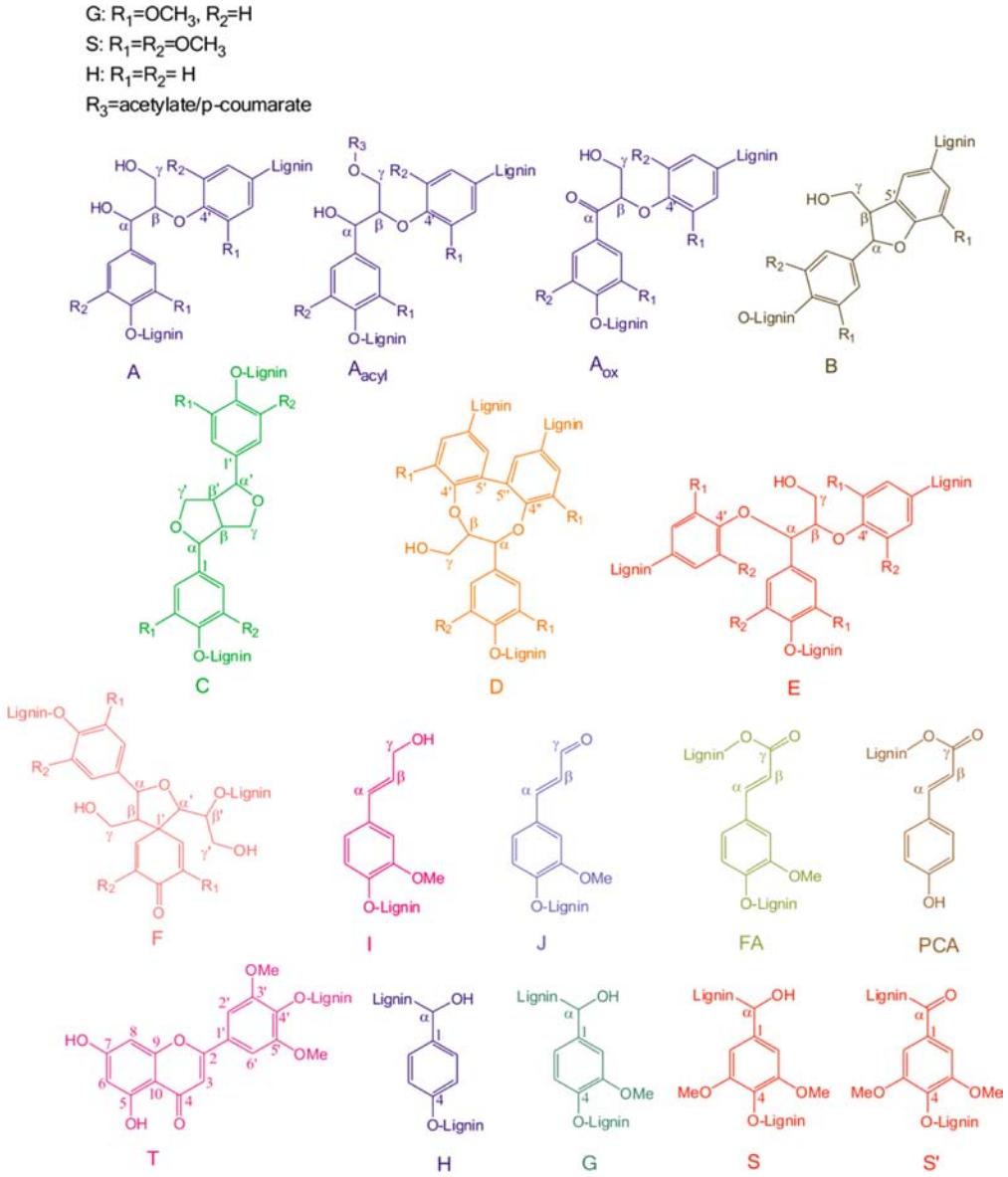


**Figure 2.** Main lignin structures detected: (A) $\beta$-O-4′, ($A_{acyl}$) $\beta$-O-4′ alkyl-aryl ethers with acylated $\gamma$-OH, ($A_{ox}$) $C_\alpha$-oxidized $\beta$-O-4′ structure, (B) phenylcoumaran ($\beta$-5′), (C) resinol $\beta$-$\beta$′, (D) dibenzodioxocin (5-5′-O-4′), (E) $\alpha$,$\beta$-diarylether, (F) spirodienone ($\beta$-1), (I) cinnamyl alcohol, (J) cinnamyl aldehyde, (PCA) *p*-coumarate, (FA) ferulate, (H) *p*-hydroxyphenyl unit, (G) guaiacyl unit, (S) syringyl unit, and (S′) $C_\alpha$-oxidized S unit.

have been applied for the structural characterization of the lignins. Density functional theory calculations have been used to support the proposed routes in which coupling reactions are followed by homolytic cleavage of the $\beta$-O-4′ linkages. The structure of lignin in wheat straw has been elucidated previously. Also, the incorporation of tricin in the lignin via $\beta$-O-4 in G units has been reported.[3] In this study, quantitative data about the removal of tricin during SE were obtained by a novel $^{31}$P NMR method. Homolytic cleavage of $\beta$-O-4 substructures in the lignin during SE was also elucidated using theoretical calculations, and a comparison was carried out using model systems (G−O−G, G−O−S, and G−O−T).

## MATERIALS AND METHODS

**Lignins and Lignin Model Compounds.** Lignins were isolated from raw wheat straw (MTT Agrifood Research, Jokioinen, Finland) before and after SE treatment, employing the enzymatic mild acidolysis lignin (EMAL) isolation method.[20,21] The milled wheat straw sample was pretreated with steam at 200 °C using a 10 min residence time, and the treatment was terminated by fast release of pressure. Isolation of EMAL lignin from non-treated and SE treated wheat straw involved the following four main steps: extraction of acetone-soluble material, ball milling, enzymatic hydrolysis of cell wall carbohydrates, and lignin extraction with a mildly acidic dioxane/water mixture. The lignin isolation procedure is explained in more detail in the literature.[16] 4′,5,7-Trihydroxy-3′,5′-dimethoxyflavone (tricin) was purchased from SelectLab Chemicals GmbH (Bönen, Germany) and used as received.

**2D $^1$H−$^{13}$C HSQC and HMBC NMR Measurements.** For the 2D $^1$H−$^{13}$C HSQC and HMBC experiments, 50 mg of the lignin sample was dissolved in 1 mL of dimethyl sulfoxide (DMSO)-$d_6$, and the experiments were carried out at 30 °C on a 600 MHz Bruker Avance III NMR spectrometer equipped with a CPQCI cryoprobe. The quantitative HSQC spectra were acquired using echo/anti-echo time proportional phase incrementation (TPPI) selection, and matched sweep adiabatic pulses optimized for $^{13}$C sweep width of 200−50 ppm were used for all 180° $^{13}$C pulses to compensate for the differences in the $^1J_{CH}$ coupling constants.[22] The HMBC experiments were optimized for 8 Hz (62.5 ms) long-range couplings. Matrices of 2048 × 256 (HSQC) or 2048 × 512 (HMBC) data points were collected and


dx.doi.org/10.1021/jf504622j | J. Agric. Food Chem. 2014, 62, 10437−10444

**Table 1. Assignment of Selected $^{13}C/^{1}H$ Chemical Shifts Observed in HSQC NMR Spectra of Wheat Straw Lignin[a]**

| $\delta_C/\delta_H$ (ppm) | assignment |
|---|---|
| 52.9/3.43 | $C_\beta$–$H_\beta$ in phenylcoumaran substructures ($B_\beta$) |
| 53.4/3.03 | $C_\beta$–$H_\beta$ in $\beta$-$\beta'$ resinol substructures ($C_\beta$) |
| 55.4/3.71 | C–H in metoxyl group ($-OCH_3$) |
| 59.4/3.7 and 59.7/3.6 | $C_\gamma$–$H_\gamma$ in $\beta$-O-4′ substructures ($A_\gamma$) |
| 61.3/4.07 | $C_\gamma$–$H_\gamma$ in cinnamyl alcohol end groups ($I_\gamma$) |
| 62.7/3.77 | $C_\gamma$–$H_\gamma$ in phenylcoumaran substructures ($B_\gamma$) |
| 63.9/4.15 and 4.21 | $C_\gamma$–$H_\gamma$ in $\gamma$-acylated $\beta$-O-4′ substructures ($A_{acyl}$) |
| 70.9/4.71 | $C_\alpha$–$H_\alpha$ in $\beta$-O-4′ linked to a G unit ($A_{\alpha(G)}$) |
| 70.9/3.8 and 4.1 | $C_\gamma$–$H_\gamma$ in $\beta$-$\beta'$ resinol substructures ($C_\gamma$) |
| 71.6/4.83 | $C_\alpha$–$H_\alpha$ in $\beta$-O-4′ linked to a S unit ($A_{\alpha(S)}$) |
| 79.1/5.54 | $C_\alpha$–$H_\alpha$ in $\alpha$-O-4′-linked substructures ($E_\alpha$) |
| 80.7/4.50 | $C_\beta$–$H_\beta$ in $\gamma$-acylated $\beta$-O-4′ structures linked to a G unit ($A_{acyl\beta}$) |
| 82.5/4.87 | $C_\alpha$–$H_\alpha$ in dibenzodioxocin substructures ($D_\alpha$) |
| 82.6/5.11 | $C_\beta$–$H_\beta$ in $\alpha$-oxidized $\beta$-O-4′ substructures ($A_{ox\beta}$) |
| 82.9/4.45 | $C_\beta$–$H_\beta$ in $\beta$-O-4′ linked to a H unit ($A_{\beta(H)}$) |
| 83.8/4.26 | $C_\beta$–$H_\beta$ in $\beta$-O-4′ linked to a G unit ($A_{\beta(G)}$) |
| 84.6/4.62 | $C_\alpha$–$H_\alpha$ in $\beta$-$\beta'$ resinol substructures ($C_\alpha$) |
| 84.8/7.46 | $C_{\alpha'}$–$H_{\alpha'}$ in spirodienone substructures ($F_{\alpha'}$) |
| 85.4/3.84 | $C_\beta$–$H_\beta$ in dibenzodioxocin substructures ($D_\beta$) |
| 85.9/4.09 | $C_\beta$–$H_\beta$ in $\beta$-O-4′ linked to a S unit ($A_{\beta(S)}$) |
| 86.7/5.42 | $C_\alpha$–$H_\alpha$ in phenylcoumaran substructures ($B_\alpha$) |
| 94.1/6.56 | $C_8$–$H_8$ in tricin ($T_8$) |
| 98.7/6.21 | $C_6$–$H_6$ in tricin ($T_6$) |
| 103.7/6.67 | $C_2$–$H_2$ and $C_6$–$H_6$ in etherified S units ($S_{2,6}$) |
| 103.9/7.29 | $C_{2'}$–$H_{2'}$ and $C_{6'}$–$H_{6'}$ in tricin ($T_{2',6'}$) |
| 104.5/7.02 | $C_3$–$H_3$ in tricin ($T_3$) |
| 106.3/7.30 | $C_2$–$H_2$ and $C_6$–$H_6$ in $\alpha$-oxidized S units ($S'_{2,6}$) |
| 110.8/6.96 | $C_2$–$H_2$ in G units ($G_2$) |
| 113.6/6.25 | $C_\beta$–$H_\beta$ in $p$-coumarate ($PCA_\beta$) and ferulate ($FA_\beta$) |
| 114.4/6.67 and 115.4/6.76 | $C_5$–$H_5$ in G units ($G_5$) |
| 118.8/6.75 | $C_6$–$H_6$ in G units ($G_6$) |
| 123.5/7.18 | $C_6$–$H_6$ in ferulate ($FA_6$) |
| 126.2/6.74 | $C_\beta$–$H_\beta$ in cinnamyl aldehyde end groups ($J_\beta$) |
| 127.7/7.16 | $C_2$–$H_2$ and $C_6$–$H_6$ in H units ($H_{2,6}$) |
| 128.4/6.20 | $C_\beta$–$H_\beta$ in cinnamyl alcohol end groups ($I_\beta$) |
| 128.4/6.42 | $C_\alpha$–$H_\alpha$ in cinnamyl alcohol end groups ($I_\alpha$) |
| 130.0/7.44 | $C_2$–$H_2$ and $C_6$–$H_6$ in $p$-coumarate ($PCA_{2,6}$) |
| 144.9/7.56 | $C_\alpha$–$H_\alpha$ in $p$-coumarate ($PCA_\alpha$) and ferulate ($FA_\alpha$) |
| 153.3/7.58 | $C_\alpha$–$H_\alpha$ cinnamyl aldehyde end groups ($J_\alpha$) |
| 191.1/9.78 | $C_\alpha$–$H_\alpha$ in Ar–$C_\alpha H_\alpha$=O (ArCHO) |
| 194.1/9.57 | $C_\gamma$–$H_\gamma$ in cinnamyl aldehyde end groups ($J_\gamma$) |

[a]Signal identification was carried out according to the literature.[3,25]

zero-filled once in F1, and a $\pi/2$-shifted squared sine bell weighting function was applied in both dimensions prior to the Fourier transformation.

**$^{31}$P NMR Measurements and Size-Exclusion Chromatography (SEC) Analyses.** For $^{31}$P NMR analyses, the lignin samples and tricin were phosphorylated and the freshly prepared samples were measured with $^{31}$P NMR at room temperature. The experimental procedure has been explained in detail previously.[23] A 500 MHz Bruker Avance III NMR spectrometer equipped with 5.0 mm broadband observe (BBO) probe was used for the measurements. Chemical shifts are relative to the reaction product of water with tetramethyldioxaphospholane, which gives a sharp signal in pyridine/$CDCl_3$ at 132.2 ppm. The following NMR parameters were used: scans, 512; pulse delay, 5 s; Lorentzian line broadening, 4 Hz.

SEC analyses were carried out using a HPLC system (Waters Corp., Milford, MA) equipped with 8 × 3000 mm MCX 1000 and 100 000 Å columns (Polymer Standard Services, Mainz, Germany) and a Waters 2998 UV detector (Waters Corp., Milford, MA) set at 280 nm using 0.1 M NaOH eluent (0.5 mL/min flow rate). For the SEC analysis, lignins were dissolved in 0.1 M NaOH (1 mg/mL) solutions overnight, followed by filtration through a 0.45 $\mu$m polytetrafluoroethylene (PTFE) syringe filter. Results were calculated relative to polystyrenesulfonate sodium salt standard using Waters Empower 3 software.

**Table 2. Amount of Main Interunit Linkages and Structural Characteristics Detected in Wheat Straw before (EMAL) and after the SE Treatment from the Integration of $^{1}H-^{13}C$ Correlation Signals in HSQC NMR Spectra**

| | wheat straw | |
|---|---|---|
| interunit linkage[a] | EMAL | SE |
| $\beta$-O-4′ (G + S) | 66 | 51 |
| $\beta$-O-4′ (S) | 41 | 26 |
| $\beta$-O-4′ (G) | 25 | 25 |
| $\beta$-5 | 10 | 16 |
| $\beta$-$\beta$ | 5 | 3 |
| 5-5′-O-4′ | 8 | 2 |
| $\beta$-1 (including SD) | trace | trace |
| $\alpha$-oxidized $\beta$-O-4′[b] | 6 | 2 |
| $\alpha$,$\beta$-diaryl ethers | 3 | 1 |
| cinnamyl alcohol | 0.7 | 0.6 |
| cinnamyl aldehyde | 1.4 | 1.5 |
| aromatic units[a] | | |
| S/G ratio | 0.6 | 0.4 |
| PCA | 11 | 5 |
| FA | 2.7 | 1.9 |
| PCA/FA ratio | 4.0 | 2.6 |
| tricin | 13 | 2 |

[a]Expressed as the number per 100 $C_9$ units ($0.5S_{2,6} + G_2$). [b]$H_\beta$–$C_\beta$ correlation signal integral.

**Density Functional Calculations.** All calculations were performed with Gaussian 09, C.01 using the facilities of the Alabama Supercomputer Center in Huntsville, AL. All structures were optimized at the M06-2X level of theory, using the 6-311++G(d,p) basis set and the fine grid consisting of 75 radial shells and 302 angular points per shell. Frequency calculations were performed on the stationary points identified. Bond dissociation enthalpies were determined as the difference between the enthalpy of the reactant and products.

## RESULTS AND DISCUSSION

The amounts of the lignin units and the detected interunit linkages in wheat straw EMALs before and after steam explosion treatment were determined by 2D $^{1}H-^{13}C$ HSQC NMR experiments (Figure 1). The lignin subunits detected are presented in Figure 2, and the spectroscopic assignments based on the literature are presented in Table 1.

The quantitation was based on the assumption that the $C_2$ position in G units and the $C_2$ and $C_6$ positions in the S units are not substituted. Thus, ($G_2 + S_{2,6}/2$) was used as an internal standard. The interunit linkages were determined by careful integration of the $H_\alpha$–$C_\alpha$ correlation signals in the HSQC NMR spectra (with the exception of $H_\beta$–$C_\beta$ in the $\alpha$-oxidized $\beta$-O-4′ structure) and comparing to the total $C_9$ unit integral. $H_\gamma$–$C_\gamma$ correlation signals originating from resinol structures were shown only as a trace in the HSQC NMR spectra. Calculated amounts of the main interunit linkages and structural characteristics are shown in Table 2. It was observed that the S-type $\beta$-O-4′ interunit linkages were cleaved preferentially (36% decrease), whereas no cleavage on $\beta$-O-4′ in the G type was observed. Recently, incorporation of tricin into the wheat straw lignin via $\beta$-O-4′ in the G unit has been reported.[3] Accordingly, also, these linkages were cleaved during the SE treatment, leading to significant loss of tricin

(85% decrease). The result is in accordance with the literature,[19] where the cleavage of $\beta$-O-4′ structures during SE is depicted as one of the most predominant depolymerization reactions in lignin. Our results show that various $\beta$-O-4′ substructures differ in the tendency to cleave.

The SE treatment also caused an increase in the average lignin molar mass ($M_w$) from 3600 to 6100 as measured with SEC (Figure 3).[16] This was contradictory with the observed rather high degree of cleavage of the aryl ethers but can be explained by competing repolymerization reactions.

From Table 2, it can be seen that SE alters the lignin structure in several ways. Besides the decrease in the content of $\beta$-O-4′, an increase in the amount of phenylcoumaran ($\beta$-5′) interunit linkages after the SE treatment was also detected. Upon heating lignin with water, rearrangement from alkyl-aryl ether ($\beta$-O-4′) to phenylcoumaran ($\beta$-5′) has been previously reported.[24] It has been proposed that this rearrangement is initiated by the homolytic cleavage of $\beta$-O-4′, followed by the formation of the new linkage. To evaluate if the conclusions made based on the NMR analyses are sound from the theoretical point of view, calculations were performed to elucidate the thermodynamic feasibility of the rearrangement reaction.

The results also indicated that the SE treatment of wheat straw caused a substantial decrease of cinnamic acids, particularly *p*-coumaric acid, which acylates a portion of $\gamma$-OH of the lignin side chain in grasses, and may thus be hydrolytically cleaved during the autocatalytic SE treatment. The higher levels of the *p*-coumarates (11 per $C_9$) in comparison to the value presented in the literature [4% in milled wood lignin (MWL) wheat straw] may be explained by the milder hydrolytic conditions applied in the EMAL process compared to MWL isolation.

The wheat straw lignin samples were analyzed by $^{31}$P NMR to obtain more information on the hydroxyl groups on lignin. Because the lignin was known to contain tricin, it was necessary to apply a model compound for signal verification in the $^{31}$P NMR spectrum. As a consequence, a novel quantitative

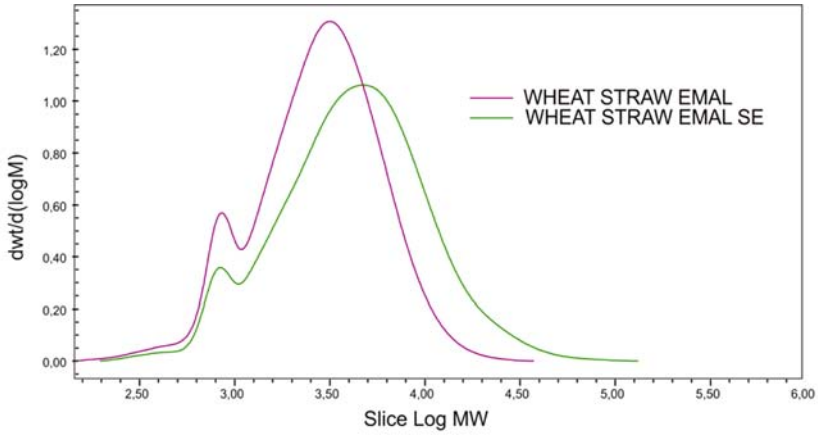


| Sample | Mn | Mw | PD |
|---|---|---|---|
| WHEAT STRAW EMAL | 2 100 | 3 600 | 1.7 |
| WHEAT STRAW EMAL SE | 2 700 | 6 100 | 2.2 |

**Figure 3.** Calculated SEC results of wheat straw lignins before (purple) and after (green) the SE treatment. Both $M_n$ and $M_w$ of the wheat straw lignin increased after the SE treatment, alongside with the polymerization degree (PD).

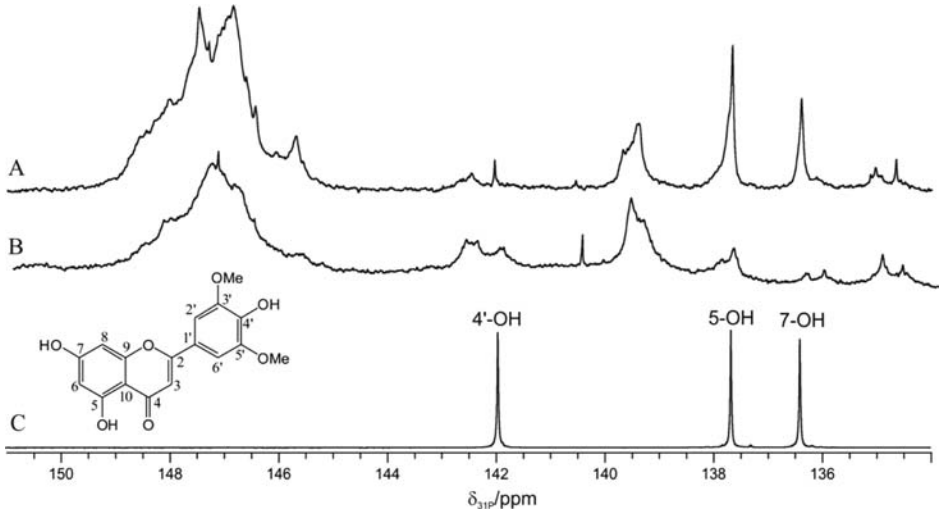


**Figure 4.** (A) $^{31}$P NMR spectrum of wheat straw EMAL, (B) $^{31}$P NMR of SE-treated wheat straw EMAL, and (C) structure of tricin with $^{31}$P NMR showing three different −OH groups in the molecule.


dx.doi.org/10.1021/jf504622j | J. Agric. Food Chem. 2014, 62, 10437−10444

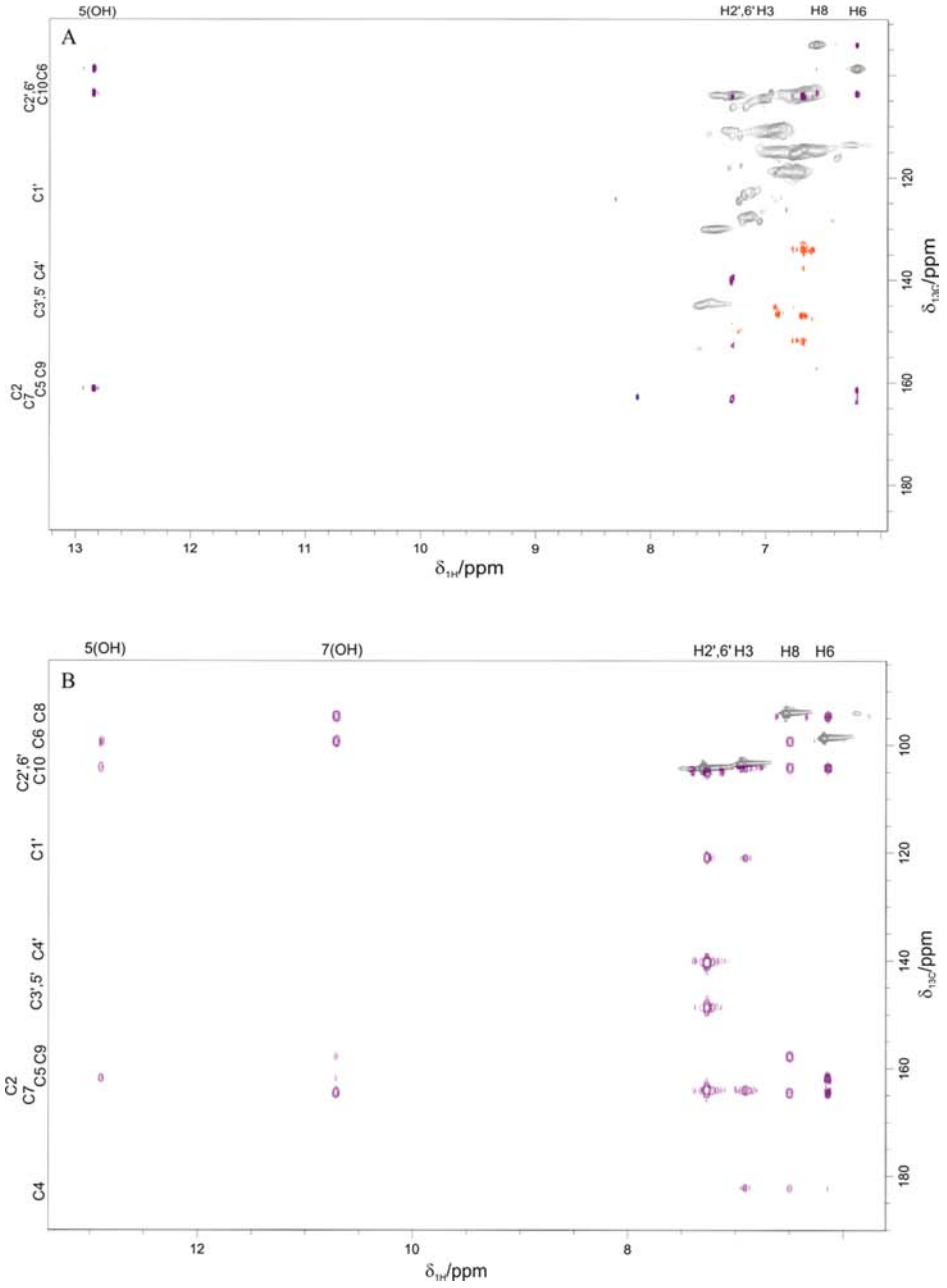


**Figure 5.** (A) Stacked HSQC (gray) and HMBC (violet) NMR spectra of wheat straw EMAL and (B) stacked HSQC (gray) and HMBC (violet) NMR spectra of the tricin model compound, showing the main long-range correlations recorded with Δ = 62.5 ms. Long-range correlation signals not originating from tricin are shown in orange.

method for tricin was developed. In addition, a comparison of the model compound and the wheat straw lignin showed evidence of 4′-OH of tricin being the linking site to lignin. The $^{31}$P NMR spectra of the phosphitylated lignins before and after SE pretreatment along with a pure tricin model compound sample are shown in Figure 4.

As seen from the $^{31}$P NMR spectrum (Figure 4C), the pure tricin (4′,5,7-trihydroxy-3′,5′-dimethoxyflavone) molecule shows three distinct chemical shifts at 136.40, 137.67, and 141.96 ppm. We have tentatively assigned these to 7-OH, 5-OH, and 4′-OH hydroxyl groups, respectively. In the literature, the chemical shift at 136.40 ppm has been previously detected and reported as phenol hydroxyl in unknown structures.[25]

The tricin signals found in the wheat straw EMAL lignin $^{31}$P NMR spectrum (Figure 4A) are much more intense in the sample before the SE treatment, confirming the presence of tricin in wheat straw lignin and its partial cleavage in the SE pretreatment. The quantitative results of tricin contents prior to and after the SE treatment are 0.15 and 0.02 mmol/g of lignin, respectively, determined using the tricin peak of $C_7$−OH for quantitation. Furthermore, the signal of the 4′-OH group was significantly less intense than the two others, indicative of its role in linking to lignin. Tricin incorporation into the lignin network through $\beta$-O-4′ ether linkages was thus confirmed both by $^{31}$P NMR and based on the tricin $C_{4'}$ carbon chemical shift ($\delta_{^{13}C}$, 139.6 ppm).

Figure 5 presents the long-range $^{13}$C−$^{1}$H correlations of the tricin moiety between the wheat straw EMAL sample and the tricin model compound. Interestingly, $C_7$−OH correlation ($\delta_{^{1}H}$, 10.7 ppm in model compound) is missing in the wheat straw


dx.doi.org/10.1021/jf504622j | J. Agric. Food Chem. 2014, 62, 10437−10444

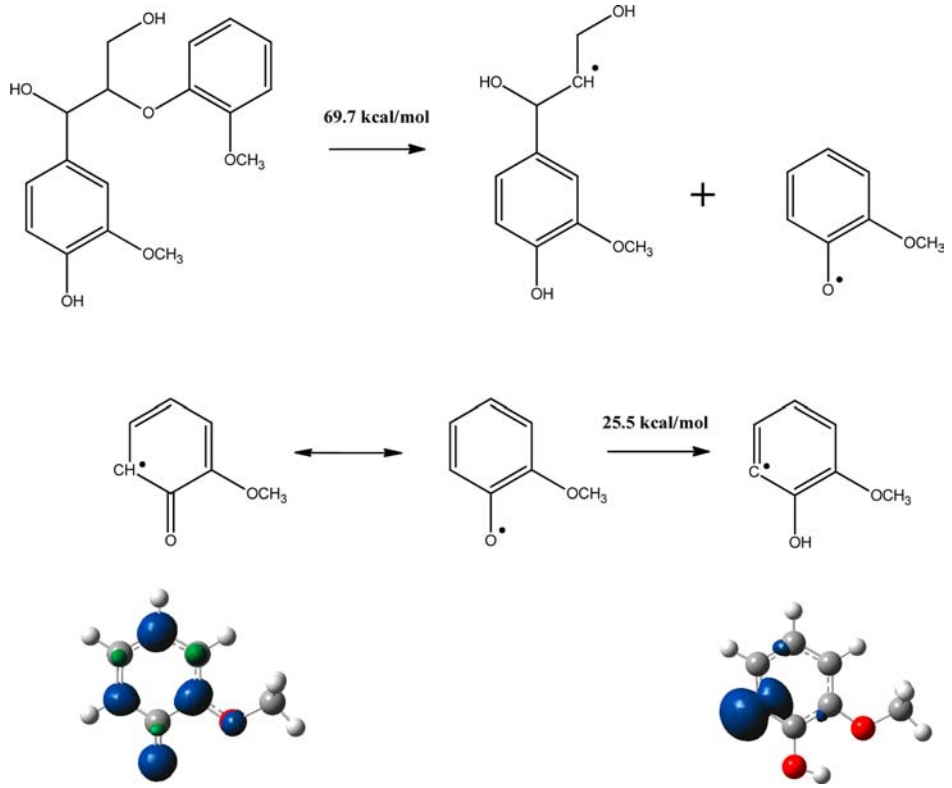


**Figure 6.** Homolytic $\beta$-O-4 cleavage reaction in G−O−G with formed phenoxy radical tautomers. The illustrations represent spin densities.

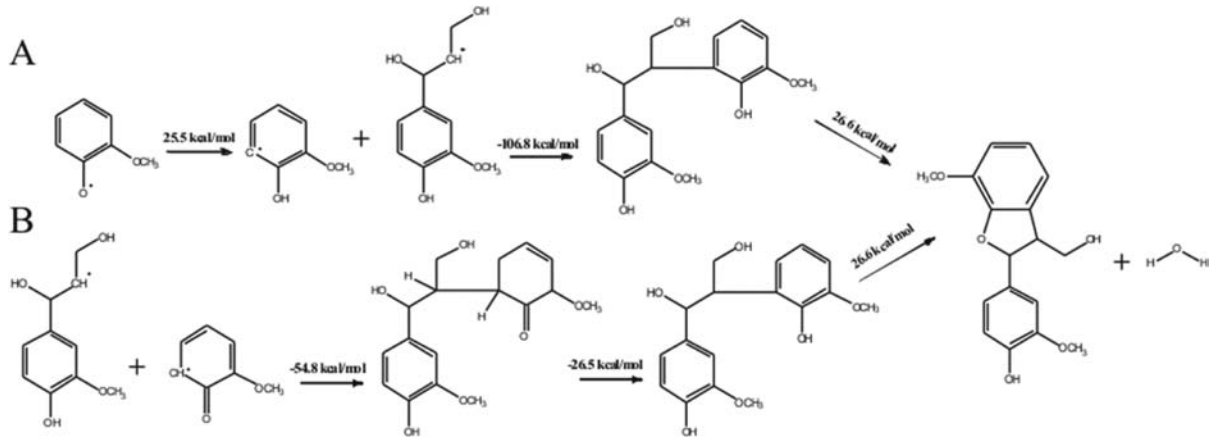


**Figure 7.** Schematic presentation of two routes (A and B) for the $\beta$-O-4 to $\beta$-5 transformation.

EMAL spectrum, even though $C_5$−OH ($\delta^1_H$, 12.9 ppm in wheat straw and model compound) is easily detectable. This may be due to higher acidity of $C_7$−OH. Some of the long-range correlations of the tricin are also missing from the wheat straw EMAL spectrum, indicating the impact of the presence of lignin and carbohydrates toward the visibility of long-range correlations. We also noticed that the tricin T8 $^1H-^{13}C$ correlation signal ($\delta_C/\delta_H$, 94.1/6.56) shows a small shift upfield ($\delta_C/\delta_H$, 93.8/6.38) after SE treatment, whereas the T6 signal was not shifted.

The feasibility of the postulated lignin reactions during the SE treatment were evaluated by comparing the bond dissociation energies. The $\beta$-O-4 bond dissociation energies for the homolytic cleavage reactions were calculated for G−O−G-, G−O−S-, and G−O−T-type $\beta$-O-4 structures. G−O−G showed the highest dissociation energy (69.7 kcal/mol); G−O−S showed intermediate dissociation energy (68.4 kcal/mol); and G−O−T showed the lowest dissociation energy (67.9 kcal/mol). These values are in accordance with the 2D NMR data (Table 2), which indicated the order of stability of $\beta$-O-4′ structures to be G−O−G > G−O−S > G−O−T.

Figure 6 presents an example of the homolytic $\beta$-O-4 cleavage, including G−O−G moieties with relevant tautomerization of the phenoxy radical and including the spin densities of the alternative radical forms.

The feasibility of possible reaction routes leading to the homolytic $\beta$-O-4 cleavage was evaluated on the basis of their energetic requirements. Two possible reaction routes (A and B) for the cleavage, followed by transformation to the $\beta$-5 substructure are presented in Figure 7.

The first route (A) requires and includes the formation of a tautomer from the phenoxy radical, while the second route (B)


dx.doi.org/10.1021/jf504622j | J. Agric. Food Chem. 2014, 62, 10437−10444

couples the phenoxy radical and β-O-4 radical without the need for tautomerization. Altogether, the transformation from β-O-4 to β-5 (+water) substructure requires energy of around 15 kcal/mol, which could be adequately provided by the SE process. It is worth pointing out that the β-5 dilignol is actually a more stable form than the original β-O-4 dimer by 11.6 kcal/mol.

In conclusion, homolytic cleavage of the β-O-4 linkages and recoupling to β-5 linkages were identified as the main reaction types of lignin in SE treatment. The β-O-4 bond dissociation energies for the homolytic cleavage reactions were calculated for G−O−G (69.7 kcal/mol), G−O−S (68.4 kcal/mol), and G−O−T (67.9 kcal/mol) type β-O-4 structures. This was confirmed by 2D $^{1}H-^{13}C$ HSQC and $^{1}H-^{13}C$ HMBC NMR data, indicating nearly complete removal of tricin and significant reduction of G−O−S units. We also postulated means to identify and measure the amount of tricin in the lignin sample with the aid of a 1D $^{31}P$ NMR experiment.

The development of biomass pretreatment methods in the field of biorefinery is of vital importance for generating value-added biomaterials and chemicals. The presence of tricin as part of the lignin structure may generate more diversity in the use of lignin as a feedstock for value-added products. The cleavage of tricin from lignin may also enhance saccharification, even if the mechanism for this cannot be explained on the basis of the present results.

## AUTHOR INFORMATION


### Corresponding Author

*Telephone: +358400156497. Fax: +358207227026. E-mail: harri.heikkinen@vtt.fi.


### Notes

The authors declare no competing financial interest.

## REFERENCES


(1) Vanholme, R.; Demedts, B.; Morreel, K.; Ralph, J.; Boerjan, W. Lignin biosynthesis and structure. *Plant Physiol.* **2010**, *153*, 895−905.

(2) Hatfield, R.; Vermerris, W. Lignin formation in plants: The dilemma of linkage specificity. *Plant Physiol.* **2001**, *126*, 1351−1357.

(3) del Río, J.; Rencoret, J.; Prinsen, P.; Martínez, Á.T.; Ralph, J.; Gutiérrez, A. Structural characterization of wheat straw lignin as revealed by analytical pyrolysis, 2D-NMR, and reductive cleavage methods. *J. Agric. Food Chem.* **2012**, *60*, 5922−5935.

(4) Yuan, T.-Q.; Xu, S.-N.; Sun, R.-C. Characterization of lignin structures and lignin−carbohydrate complex (LCC) linkages by quantitative $^{13}C$ and 2D HSQC NMR spectroscopy. *J. Agric. Food Chem.* **2011**, *59*, 10604−10614.

(5) Rencoret, J.; Marques, G.; Gutiérrez, A.; Nieto, L.; Santos, J. I.; Jiménez-Barbero, J.; Martínez, Á.T.; del Río, J. HSQC-NMR analysis of lignin in woody (*Eucalyptus globulus* and *Picea abies*) and non-woody (*Agave sisalana*) ball-milled plant materials at the gel state. *Holzforschung* **2008**, *63*, 691−698.

(6) Karhunen, P.; Rummakko, P.; Sipila, J.; Brunow, G.; Kilpelainen, I. Dibenzodioxocins. A novel type of linkage in softwoods lignins. *Tetrahedron Lett.* **1995**, *36*, 167−170.

(7) Zhang, L.; Gellerstedt, G. NMR observation of a new lignin structure, a spiro-dienone. *Chem. Commun.* **2001**, 2744−2745.

(8) Setala, H.; Pajunen, A.; Rummakko, P.; Sipila, J.; Brunow, G. A novel type of spiro compound formed by oxidative cross coupling of methyl sinapate with a syringyl lignin model compound. A model system for the β-1 pathway in lignin biosynthesis. *J. Chem. Soc., Perkin Trans. 1* **1999**, 461−464.

(9) Ohra-aho, T.; Tenkanen, M.; Tamminen, T. Direct analysis of lignin and lignin-like components from softwood kraft pulp by Py−GC/MS. *J. Anal. Appl. Pyrolysis* **2005**, *74*, 123−128.

(10) Evtuguin, D.; Neto, C. P.; Silva, A. M. S.; Domingues, P. M.; Amado, F. M. L.; Robert, D.; Faix, O. Comprehensive study on the chemical structure of dioxane lignin from plantation *Eucalyptus globulus* wood. *J. Agric. Food Chem.* **2001**, *49*, 4252−4261.

(11) Heikkinen, S.; Toikka, M.; Karhunen, P.; Kilpeläinen, I. Quantitative 2D HSQC (Q-HSQC) via suppression of *J*-dependence of polarization transfer in NMR spectroscopy: Application to wood lignin. *J. Am. Chem. Soc.* **2003**, *125*, 4362−4367.

(12) Zhang, L.; Gellerstedt, G. Quantitative 2D HSQC NMR determination of polymer structures by selecting suitable internal standard references. *Magn. Reson. Chem.* **2007**, *45*, 37−45.

(13) Sette, M.; Wechselberger, R.; Crestini, C. Elucidation of lignin structure by quantitative 2D NMR. *Chem.—Eur. J.* **2011**, *17*, 9529−9535.

(14) Ramos, L. P.; Breuil, C.; Kuschner, D. J.; Saddler, J. N. Steam pre-treatment conditions for effective enzymatic hydrolysis and recovery yields of *Eucalyptus viminalls* wood chips. *Holzforschung* **1992**, *46*, 149−154.

(15) Jakobsons, J.; Hortling, B.; Erins, P.; Sundquist, J. Characterization of alkali soluble fraction of steam exploded birch wood. *Holzforschung* **1995**, *49*, 51−59.

(16) Rahikainen, J. L.; Martin-Sampedro, R.; Heikkinen, H.; Rovio, S.; Marjamaa, K.; Tamminen, T.; Rojas, O. J.; Kruus, K. Inhibitory effect of lignin during cellulose bioconversion: The effect of lignin chemistry on non-productive enzyme adsorption. *Bioresour. Technol.* **2013**, *133*, 270−278.

(17) Li, S.; Lundquist, K. Cleavage of arylglycerol β-aryl ethers under neutral and acid conditions. *Nord. Pulp Pap. Res. J.* **2000**, *15*, 292−299.

(18) Robert, D.; Bardet, M.; Lapierre, C. Structural changes in aspen lignin during steam explosion treatment. *Cell. Chem. Technol.* **1988**, *22*, 221−230.

(19) Li, J.; Henriksson, G.; Gellerstedt, G. Lignin depolymerization/repolymerization and its critical role for delignification of aspen wood by steam explosion. *Bioresour. Technol.* **2007**, *98*, 3061−3068.

(20) Guerra, A.; Filpponen, I.; Lucia, L. A.; Saquing, C.; Baumberger, S.; Argyropoulos, D. S. Toward a better understanding of the lignin isolation process from wood. *J. Agric. Food Chem.* **2006**, *54*, 5939−5947.

(21) Wu, S.; Argyropoulos, D. S. An improved method for isolating lignin in high yield and purity. *J. Pulp Pap. Sci.* **2003**, *29*, 235−240.

(22) Zwahlen, C.; Legault, P.; Vincent, S. J. F.; Greenblatt, J.; Konrat, R.; Kay, L. E. Methods for measurements of intermolecular NOEs by multinuclear NMR spectroscopy: Application to a bacteriophage λ N-peptide/*boxB* RNA complex. *J. Am. Chem. Soc.* **1997**, *119*, 6711−6721.

(23) Granata, A.; Argyropoulos, D. S. 2-Chloro-4,4,5,5-tetramethyl-1,3,2-dioxaphospholane, a reagent for the accurate determination of the uncondensed and condensed phenolic moieties in lignins. *J. Agric. Food Chem.* **1995**, *43*, 1538−1544.

(24) Nimz, H. A new type of rearrangement in the lignin field. *Angew. Chem.* **1966**, *5*, 843.

(25) Yang, Q.; Wu, S.; Lou, R.; Gaojin, L. V. Structural characterization of lignin from wheat straw. *Wood Sci. Technol.* **2011**, *45*, 419−431.

In this study, we aimed to develop new types of substrates consisting of monolayer graphene, gold film, and/or AuNRs structures. The performance of these substrates was evaluated in SERS measurement for the detection of three types of pesticides. Multivariate statistical analysis such as partial least-squares (PLS) was used in data analysis for the quantification of the analytes, and the detection limits of the target analytes were obtained and evaluated.

## MATERIALS AND METHODS

**Preparation of Chemicals.** Cetyltrimethylammonium bromide (CTAB), silver nitrate, ascorbic acid, and $HAuCl_4$ were purchased from Sigma-Aldrich (St. Louis, MO, USA). Silicon wafers were purchased from Ted Pella (Redding, CA, USA). Two OP pesticides (azinphos-methyl and phosmet) and one CB pesticide (carbaryl) were purchased from Fisher Scientific (Pittsburgh, PA, USA). All of the glassware was carefully washed with aqua regia freshly prepared before experiments.

Pure pesticide solutions of 100 ppm (w/v) stock solutions of azinphos-methyl, phosmet, and carbaryl were prepared in volumetric flasks using a mixed solvent system (acetonitrile/$H_2O$ = 1:1, v/v). Solutions of 0.01, 0.1, 0.5, 1, 10, and 50 ppm pesticides were prepared by serial dilutions from the 100 ppm solution. The solvent without pesticides was used as the control.

**Gold Film Silicon Substrate.** A thin layer of gold was deposited on a silicon wafer or monolayer graphene substrate (Graphene Supermarket, NY, USA) in a desktop sputter coater (Quorum Technologies K650X, UK). Samples were grown with an argon pressure of 0.06−0.09 mbar. The thickness of gold film was measured by a quartz crystal microbalancer.

**Synthesis of Gold Nanorods.** AuNRs were synthesized using a seed-mediated method. Seed solution was prepared by adding 120 $\mu$L of a freshly prepared ice-cold solution of 10 mM sodium borohydride into 0.1 mL of 0.1 M CTAB and 0.1 mL of 5 mM $HAuCl_4$ aqueous solution at 25 °C. The resulting pale brown solution was vortexed for 2 min and then stored at 25 °C for 1 h in the dark. Growth solution was prepared by mixing 42.5 mL of 0.1 M CTAB, 1.35 mL of 10 mM $HAuCl_4$, 0.27 mL of 10 mM silver nitrate, and 0.65 mL of 0.1 M ascorbic acid. The solution was homogenized by gentle stirring, and to the resulting colorless solution was added 0.075 mL of freshly prepared seed solution followed by gentle stirring for 20 s. The reaction mixture was set aside in the dark at 28 °C for 24 h. The solution turned from colorless to greenish brown or reddish brown. Finally, the AuNR solution was centrifuged at 4293*g* for 10 min (Eppendorf MiniSpin) to remove excess CTAB and redispersed in Milli-Q water (18.2 MΩ cm). The centrifugation procedure was repeated at 1073*g* for 10 min to obtain purified AuNRs. The purified AuNRs were dispersed in 100 $\mu$L of Milli-Q water and sonicated (45 kHz) for 30 min.

**Fabrication of SERS Substrates.** Purified AuNRs were dispersed in Milli-Q water (1 mL of AuNR solution pellet in 20 $\mu$L of water). Then 10 $\mu$L of AuNR solution was cast on (1) a monolayer graphene silicon slide (G-AuNR), (2) a gold film (40 nm thickness)−monolayer graphene−silicon slide (G-Au-AuNR), and (3) a gold film (40 nm thickness)−silicon (Au-AuNR). All of the prepared substrates were placed in Petri dishes that were sealed by adhesive tape and put in a humidity chamber (humidity of ∼30%) at 25 °C. The drops on the silicon surface were finally dried after 3 h of evaporation. Figure 1 describes the structure of each type of substrate.

**SERS Measurements.** A volume of 0.2 $\mu$L of the pure pesticide solution was transferred onto the surface of a substrate using a micropipet. The substrate, which was fixed on a glass slide, was then placed on a hot plate and heated at 40 °C until the solvent completely evaporated. A Renishaw RM1000 Raman spectrometer system (Gloucestershire, UK) equipped with a Leica DMLB microscope (Wetzlar, Germany) was used in this study. This system is equipped with a 785 nm near-infrared diode laser source. During the measurement, light from the high-power (maximum at 300 mW) diode laser was directed and focused onto the sample on a microscope

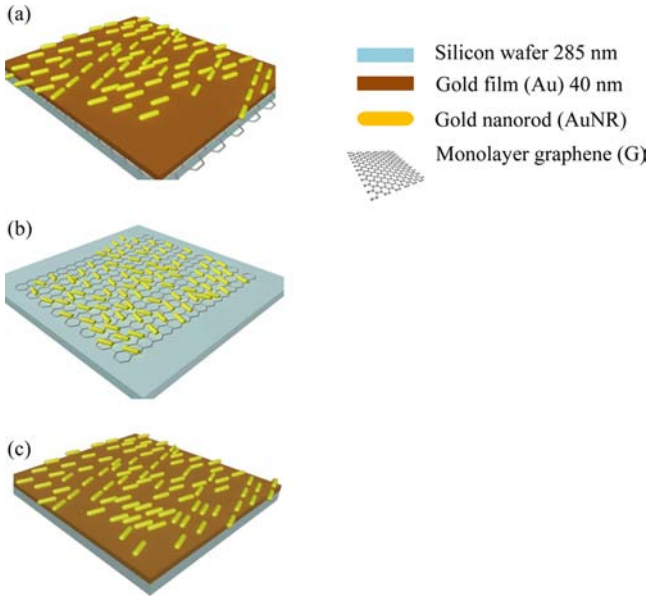


**Figure 1.** Structures of substrates: (a) graphene−AuNR (G-AuNR); (b) graphene−Au−AuNR (G-Au-AuNR); (c) Au-AuNR.

stage through a ×50 objective. Raman scattering signals were detected by a 578 × 385 pixel charge-coupled device array detector. The size of each pixel was 22 × 22 $\mu$m. Spectral data were collected by WiRE 3.2 software (Gloucestershire, UK). In this study, the spectra of samples were collected using a ×50 objective with 10 s exposure time, 0% focus, and ∼20 mW laser power in the extended mode. Detection ranges for each pesticide were 500−1800 $cm^{-1}$ for all of the pesticides. The detection range was determined in a way that the range was as narrow as possible, but no obvious signals were missed.

**Data Analysis.** The software Delight version 3.2.1 (D-Squared Inc., LaGrande, OR, USA) was used for data analysis. SERS spectral data were analyzed following our previously published methods.[2] Briefly, data preprocessing algorithms including polynomial subtract were employed to adjust the baseline shift. The PLS model, a multivariate statistical regression model, was constructed to predict analyte concentrations in tested samples. The number of PLS latent variables was optimized on the basis of the lowest root-mean-square error of prediction (RMSEP) values to avoid overfitting of spectral data. In this study, spectral data were smoothed with a Gaussian function at 4 $cm^{-1}$ followed by a second-derivative transformation with a 12 $cm^{-1}$ gap before PLS was conducted.

$$\mathrm{RMSEP} = \sqrt{\frac{\sum_i^n (\hat{c}_i - c_i)^2}{n}} \quad (1)$$

In this equation, $n$ is the number of samples, $\hat{c}_i$ is the predicted pesticide concentration (ppm), and $c_i$ is the actual pesticide concentration (ppm). The correlation coefficient ($R$) and RMSEP were used to evaluate the model. The higher the $R$ value or the lower the RMSEP value is, the better predictability the model has.

The limit of detection (LOD) with 99.86% confidence interval can be calculated from the PLS calibration curve based on characteristic peaks in SERS spectra using the formula

$$\mathrm{LOD} = 3\sigma/m \quad (2)$$

in which $\sigma$ is the standard error of predicted concentration and $m$ is the slope of the calibration curve. In a PLS model, $\sigma$ equals RMSEP.

## RESULTS AND DISCUSSION

The SPR of synthesized AuNRs displays two adsorption features as shown in Figure 2. This result is in agreement with several previous paper[23−25] that showed a strong feature at 778 nm of AuNRs due to the resonant propagation of surface

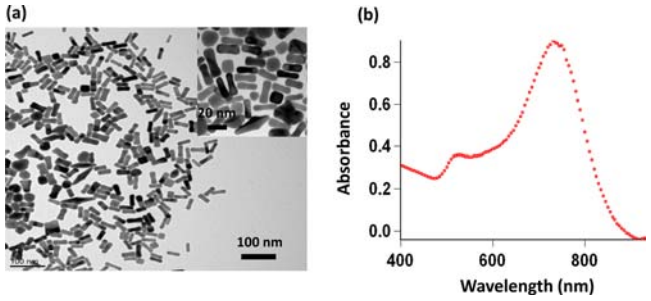


**Figure 2.** TEM image of AuNRs (a) and UV−vis spectrum of purified AuNRs (b).

plasmons along the longitudinal axis. A weak peak at 540 nm is a characteristic peak of the impurities of spherical gold nanoparticles. Overall, the long AuNRs are dominant in the purified AuNR solution, which can be used for SERS measurement with a 785 nm excitation source. In addition, the UV−vis absorption spectrum in Figure 2b shows a narrow absorption band, indicating a highly monodispersed substrate morphology. TEM imaging demonstrates that AuNRs are rod shaped with a width and length of 119.87 and 50.69 nm, respectively. The aspect ratio (length/width) of AuNRs is ~2.36 (Figure 2a). The TEM image also shows that there was a small amount of cubic and spherical nanoparticles on the TEM grids.

To investigate whether G-Au-AuNR, G-AuNR, and Au-AuNR substrates can be used as effective SERS substrates in the detection of pesticides, a droplet of each pesticide solution was deposited on the surface of the substrate. As shown in Figure 3a, no visible Raman signals of azinphos-methyl were observed on the G-AuNR substrate, whereas obvious SERS peaks of azinphos-methyl were obtained on the G-Au-AuNR and Au-AuNR substrates. The same results were also obtained for carbaryl (Figure 3b) and phosmet (data not shown). The band assignments of the peaks are consistent with previous studies.[2] A strong peak at 1380 $cm^{-1}$ is due to symmetric vibration of the naphthalene ring, and a peak at 1440 $cm^{-1}$ arises from an unspecified vibration of this ring. Interestingly, we found that Raman signals of all three types of pesticides on G-Au-AuNR substrate are much stronger than those on G-AuNR and Au-AuNR substrates. To calculate the contribution of enhancement from graphene, we chose the SERS intensity of carbaryl on these three substrates at two selected characteristic peaks (1380 and 1440 $cm^{-1}$). As shown in Figure 3c, the SERS intensity of these two peaks of carbaryl on G-Au-AuNR substrate are 2 times higher than that of Au-AuNR and hundreds of times higher than that of G-AuNR substrate.

There are two widely accepted mechanisms for SERS enhancement: electromagnetic mechanism (EM) and chemical mechanism (CM). EM is considered the main enhancement, resulting from the large increase of the local electric field caused by SPR on roughened metal surface, such as gold or silver. Several recent studies suggested that SERS enhancement can be not only from the gold nanostructure (AuNR and Au film) but also from the monolayer graphene.[20,26−29] The enhancement mechanism of graphene is believed to be from the partial contribution of high thermal conductivity of graphene. Xu et al. observed that the morphology of the metal film changed after a relatively large laser power exposure if there was no graphene layer present, whereas it remained stable for the G-Au film

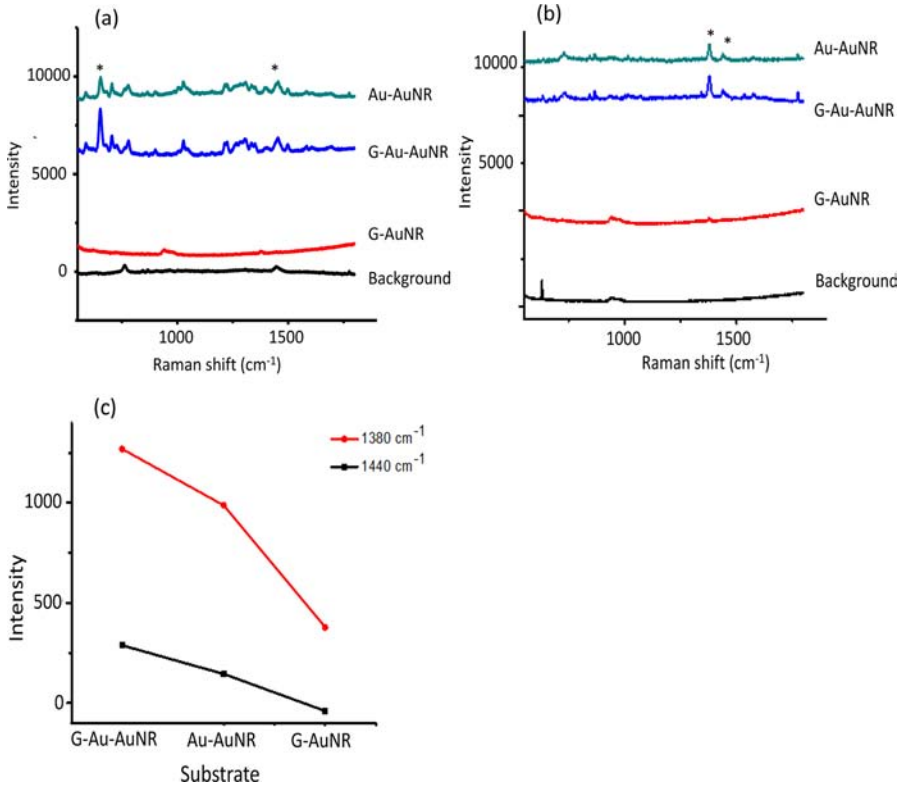


**Figure 3.** Raman spectra of (a) 100 ppm of azinphos-methyl and (b) 100 ppm of carbaryl on Au-AuNR, G-Au-AuNR, and G-AuNR substrate. The peaks marked by an asterisk (*) are the characteristic band of pesticides. (c) Intensity of two characteristic peaks of carbaryl on three kinds of substrate.

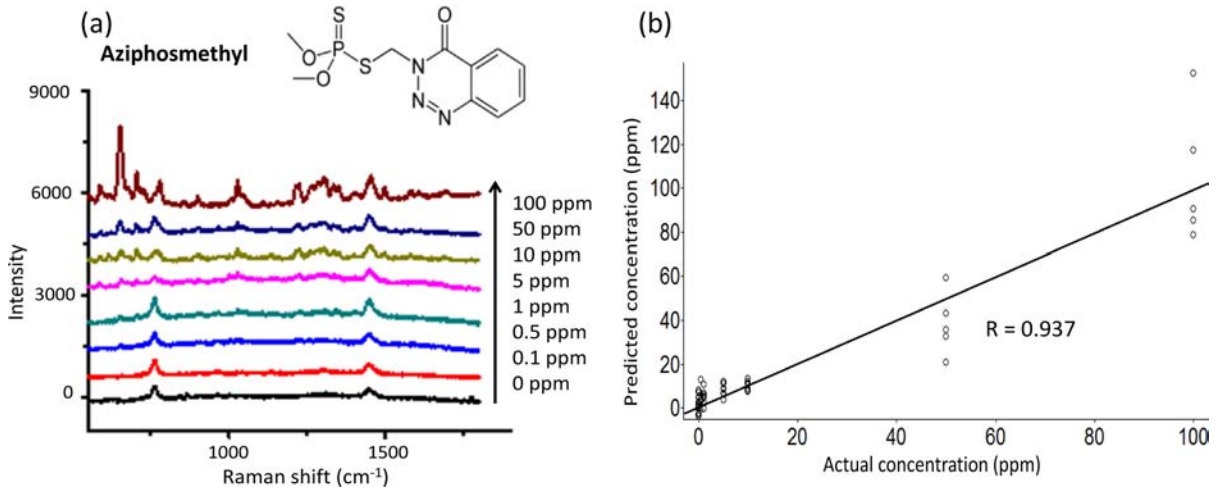


**Figure 4.** (a) SERS spectra of azinphos-methyl on G-Au-AuNR substrate. (b) Calibration curve of predicted azinphos-methyl concentration (ppm) versus actual concentration (ppm) using the PLS models: smoothing at 4 $cm^{-1}$, baseline adjustment by subtracting a first-order polynomial function; six latent variables; spectral region, 500−1800 $cm^{-1}$; spectral number ($n$ = 58).

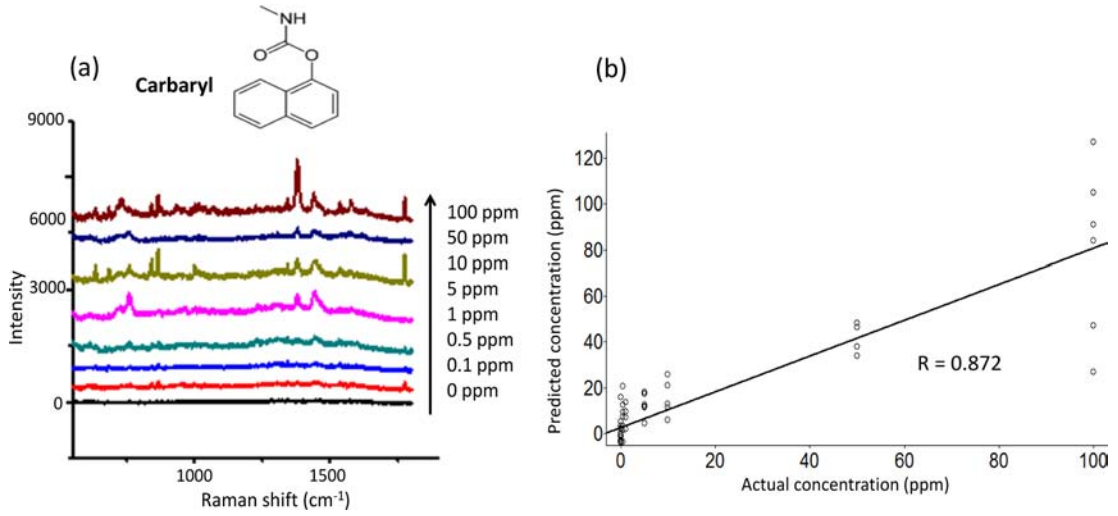


**Figure 5.** (a) SERS spectra of carbaryl on G-Au-AuNR substrate. (b) Calibration curve of predicted carbaryl concentration (ppm) versus actual concentration (ppm) using the PLS models: smoothing at 4 $cm^{-1}$, baseline adjustment by subtracting a first order polynomial function; three latent variables; spectral region 500−1800 $cm^{-1}$; spectral number ($n$ = 52).

substrate.[22] Although SERS signals on Au-AuNR substrate were much stronger than those on G-AuNR, the Raman intensity of characteristic peaks of azinphos-methyl was slightly weaker than that of G-Au-AuNR.

Schedin et al. studied SERS measurement using graphene patterned with a square array of Au nanodisks on $SiO_2$(300 nm)/Si and implied that both G and 2D bands of graphene at 633 nm were significantly enhanced.[27] The authors found that the graphene scales combined with the nanoparticle cross section, the 4th power of the Mie enhancement, are inversely proportional to the 10th power of the separation between graphene and the nanoparticle. The grown AuNRs significantly enhanced Raman signals of reduced graphene oxide (rGO) by 34-fold at the tip of the long AuNRs, which is the highest Raman enhancement of rGO by gold nanostructures ever reported.[27] Ling et al. used graphene as a substrate for Raman enhancement.[26] By coupling or not coupling with gold nanoparticles (AuNPs) or silver nanoparticles (AgNPs), the Raman signals of the molecules on monolayer graphene are clearer, stronger, and more reproducible than that on the $SiO_2$/Si substrate, indicating a clear SERS effect on the atomically flat surface of monolayer graphene. Additionally, the authors also found that graphene makes the SERS system more stable and that the graphene−SERS (G-SERS) process does not require special sample preparation. Their results showed that the enhancement factor of G-SERS was even slightly higher than those of normal SERS for most of bands and that the presence of the graphene layer did not cause the localized EM field to decay observably in its vicinity and possibly led to additional chemical enhancement.[26]

Kim et al. obtained Raman spectra of a single-layer graphene sheet placed in different gold substrates in the context of SERS. The difference in the enhancement factors among various gold substrates is explained with a model based on the spatial distribution and polarization of the local field and the orientation of inserted graphene sheet.[29] Besides graphene, its other two derivatives, graphene oxide (GO) and rGO, have also been studied as promising substrates for SERS. A study used GO-based SERS substrate to acquire Raman spectra of rodamine, melamine, and cephalexin,[21] but the results showed

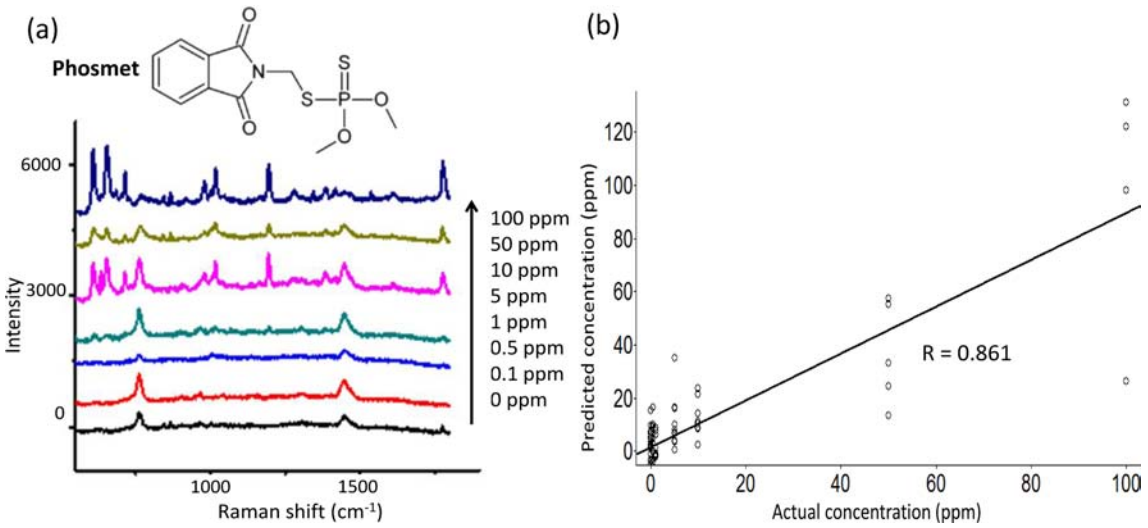


**Figure 6.** (a) SERS spectra of phosmet. (b) Calibration curve of predicted phosmet concentration (ppm) versus actual concentration (ppm) using the PLS models: smoothing at 4 $cm^{-1}$; baseline adjustment by subtracting a first-order polynomial function; five latent variables; spectral region, 500−1800 $cm^{-1}$; spectral number ($n$ = 75).

a weak enhancement of SERS due to CM of graphene.[21] This same conclusion was also reached in another study by Yu et al.[28] In our study, we observed that the main SERS enhancer still relied on the EM of noble metal nanostructures. This is consistent with another study[30] using fabricated Ag or AuNPs-decorated rGO on Si substrate as an efficient SERS substrate to detect aromatic molecules with a low detection limit at the nanomolar level. Due to the combination of AuNPs and graphene, the Raman signals of the dye were dramatically enhanced by this novel substrate.[30] In summary, this line of studies demonstrates that G-Au-AuNR substrate is a promising SERS substrate for the detection of various analytes.

Most commercial SERS substrates either are in the form of a colloidal solution containing metal nanoparticles or are silicon chip-based flat substrates with a thin layer of metal deposited on top. The main drawback of colloidal SERS substrates is that a surfactant is needed to stabilize the solution and prevent or reduce the aggregation and precipitation of metallic nanoparticles. The surfactant may affect the SERS measurement, and the reproducibility of colloidal SERS substrates is low.[31,32] In addition, target molecules have to be mixed with colloidal SERS nanoparticles, which complicates the sample preparation step and limits the application of colloidal SERS substrates. In contrast, chip-based SERS substrates are more stable and have good reproducibility. Sample solution can be easily transferred onto a substrate using a micropipet.

In addition, we studied the reliability of G-Au-AuNR substrate in the characterization and quantification of pesticides. Figure 4 shows the average SERS spectra of different concentrations of azinphos-methyl, and a linear calibration curve was constructed by monitoring the intensity of the peaks in a selected region (500−1800 $cm^{-1}$). Similar results were provided for carbaryl (Figure 5) and phosmet (Figure 6). The band assignments are shown in Table 1. PLS analysis was conducted to obtain the RMSEP values from the PLS models of each pesticide. The lowest RMSEP value was achieved and used to construct the PLS prediction model. Figure 4b illustrates the plot between the predicted concentration and actual concentration of pesticides ($R$ = 0.87; RMSEP = 15.87 × $10^{-5}$). For carbaryl (Figure 5) and phosmet (Figure 6), $R$ values are 0.87 and 0.84 and RMSEP values are 16.08 × $10^{-5}$ and 21.21 × $10^{-5}$, respectively. These results demonstrate that the SERS method coupled with PLS can be used as a reliable method to quantify pesticides.

**Table 1. Band Assignment of the Major Peak in SER Spectra from Three Pesticides**[a]

| band ($cm^{-1}$) | assignment |
|---|---|
| | **Azinphos-methyl** |
| 585 | (C═O) deformation vibration |
| 703 | benzene ring breathing |
| 778, 899 | 1,2,3-triazine ring breathing |
| 1026 | ssymmetric P—O—C deformation vibration |
| 1224 | (C—H) in P—O—$CH_3$ |
| 1260 | (C—N) in S—$CH_2$—N |
| 1283 | (C—N) in S—$CH_2$—N |
| 1334 | 1,2,3-triazine ring breathing |
| 1364 | O—H stretching |
| 1450 | (N≡N) stretching |
| 1497 | 1,2,3-triazine ring breathing |
| | **Carbaryl** |
| 868 | $CH_2$ out of plane deformation vibration |
| 1340 | $NO_2$ symmetric stretching mode |
| 1380 | symmetric ring vibration |
| 1575 | (C═C) phenyl stretch |
| | **Phosmet** |
| 607, 653 | (P═S) stretch |
| 714 | benzene ring breathing |
| 1018 | asymmetric P—O—C deformation vibration |
| 1196 | (C—H) in P—O—$CH_3$ |
| 1410 | (C—H) in S-$CH_3$—N |
| 1535 | N═N stretching |

[a]References 2 and 26−28.

The LODs of azinphos-methyl, phosmet, and carbaryl of G-Au-AuNRs substrate were calculated by using eq 2. The calibration curve of azinphos-methyl is shown in Figure 7. As compared to the maximum residue limits of the three pesticides in fruits (apples) of FAO/WHO and English standard (Table 2), the LOD of the SERS method coupled with this substrate meets the requirement for carbaryl and phosmet. However,


dx.doi.org/10.1021/jf5036417 | J. Agric. Food Chem. 2014, 62, 10445−10451

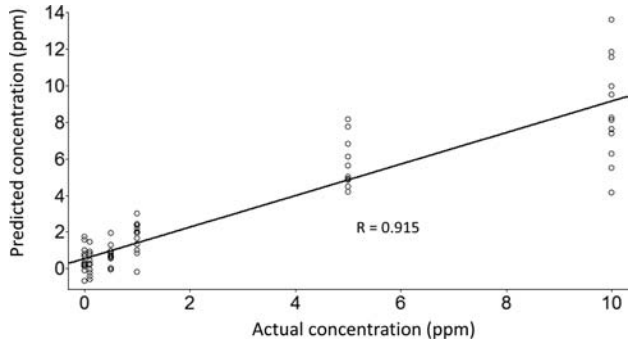


**Figure 7.** Calibration curve of predicted azinphos-methyl concentration (ppm) versus actual concentration (ppm) using the PLS models: smoothing at 4 $cm^{-1}$; baseline adjustment by subtracting a first-order polynomial function; five latent variables; spectral region, 500−1800 $cm^{-1}$; spectral number ($n$ = 74).

**Table 2. Limit of Detection of Using G-Au-AuNR Substrate for Detection of Azinphos-methyl, Carbaryl, and Phosmet**

| pesticide | $R$ | LOD (ppm) | 70% recovery | MRL[a] (ppm) | MRL[b] (ppm) |
|---|---|---|---|---|---|
| carbaryl | 0.915 | 5 | 3.647 | 6−10 | 5 |
| phosmet | 0.800 | 9 | 6.125 | 10 | 10[c] |
| azinphos-methyl | 0.914 | 5 | 3.598 | 1 | 1 |

[a]Maximum residue limits in apple of FAO/WHO. [b]Maximum residue limits in apple of England. [c]Codex Alimentarius Commission.

more studies are needed to improve the results of this method for testing azinphos-methyl.

In summary, a simple, fast, and efficient method was developed to fabricate new SERS substrates by coating an AuNR-decorated graphene sheet on Si substrate. This substrate exhibits strong Raman enhancement due to the unique properties of graphene and the deposited AuNRs. The performance of this G-Au-AuNRs substrate was evaluated using three types of pesticides (azinphos-methyl, carbaryl, and phosmet). The LODs of carbaryl and phosmet meet the maximum residue limits set by the FAO/WHO and the European Union. These results demonstrate that there is a great potential to use graphene and gold materials for food safety applications. More research is needed to improve the performance of SERS substrates using different materials and use them to test real food products.

## AUTHOR INFORMATION

### Corresponding Author

*(M.L.) Phone: (573) 884-6718. Fax: (573) 884-7964. E-mail: linme@missouri.edu.

### Funding

This research was supported by the University of Missouri Research Board.

### Notes

The authors declare no competing financial interest.

## ACKNOWLEDGMENTS

We acknowledge assistance from the Electron Microscopy Core facility at the University of Missouri in electron microscopy analysis.

## REFERENCES

(1) Cairns, T.; Sherma, J. *Emerging Strategies for Pesticide Analysis*; CRC Press: Boca Raton, FL, USA, 1992; Vol. 1.

(2) Liu, B.; Zhou, P.; Liu, X.; Sun, X.; Li, H.; Lin, M. Detection of pesticides in fruits by surface-enhanced Raman spectroscopy coupled with gold nanostructures. *Food Bioprocess Technol.* **2012**, 1−9.

(3) Lin, M. The application of surface-enhanced Raman spectroscopy to identify and quantify chemical adulterants or contaminants in foods. *Handbook of Vibrational Spectroscopy*; Wiley: Chichester, UK, 2010

(4) Du, X.; Chu, H.; Huang, Y.; Zhao, Y. Qualitative and quantitative determination of melamine by surface-enhanced Raman spectroscopy using silver nanorod array substrates. *Appl. Spectrosc.* **2010**, *64*, 781−785.

(5) Fan, C.; Hu, Z.; Mustapha, A.; Lin, M. Rapid detection of food- and waterborne bacteria using surface-enhanced Raman spectroscopy coupled with silver nanosubstrates. *Appl. Microbiol. Biotechnol.* **2011**, 1−9.

(6) He, L.; Lin, M.; Li, H.; Kim, N. J. Surface-enhanced Raman spectroscopy coupled with dendritic silver nanosubstrate for detection of restricted antibiotics. *J. Raman Spectrosc.* **2009**, *41*, 739−744.

(7) Lin, M.; He, L.; Awika, J.; Yang, L.; Ledoux, D.; Li, H.; Mustapha, A. Detection of melamine in gluten, chicken feed, and processed foods using surface enhanced Raman spectroscopy and HPLC. *J. Food Sci.* **2008**, *73*, T129−T134.

(8) Shende, C.; Gift, A.; Inscore, F.; Maksymiuk, P.; Farquharson, S. Inspection of pesticide residues on food by surface-enhanced Raman spectroscopy. *Proc. SPIE−Int. Soc. Opt. Eng.* **2004**, 29, DOI: 10.1117/12.511941.

(9) Shende, C.; Inscore, F.; Sengupta, A.; Stuart, J.; Farquharson, S. Rapid extraction and detection of trace chlorpyrifos-methyl in orange juice by surface-enhanced Raman spectroscopy. *Sens. Instrum. Food Qual. Saf.* **2010**, *4*, 101−107.

(10) Yakes, B. J.; Lipert, R. J.; Bannantine, J. P.; Porter, M. D. Detection of *Mycobacterium avium* subsp. *paratuberculosis* by a sonicate immunoassay based on surface-enhanced Raman scattering. *Clin. Vaccine Immunol.* **2008**, *15*, 227−234.

(11) Murphy, C. J.; Sau, T. K.; Gole, A. M.; Orendorff, C. J.; Gao, J.; Gou, L.; Hunyadi, S. E.; Li, T. Anisotropic metal nanoparticles: synthesis, assembly, and optical applications. *J. Phys. Chem. B* **2005**, *109*, 13857−13870.

(12) Grzelczak, M.; Vermant, J.; Furst, E. M.; Liz-Marzán, L. M. Directed self-assembly of nanoparticles. *ACS Nano* **2010**, *4*, 3591−3605.

(13) Rycenga, M.; Cobley, C. M.; Zeng, J.; Li, W.; Moran, C. H.; Zhang, Q.; Qin, D.; Xia, Y. Controlling the synthesis and assembly of silver nanostructures for plasmonic applications. *Chem. Rev.* **2011**, *111*, 3669−3712.

(14) Nanova Q-SERS, www.q-sers.com (accessed Aug 1, 2014).

(15) Silmeco SERS, http://www.silmeco.com/ (accessed Aug 1, 2014).

(16) Chen, H.; Müller, M. B.; Gilmore, K. J.; Wallace, G. G.; Li, D. Mechanically strong, electrically conductive, and biocompatible graphene paper. *Adv. Mater.* **2008**, *20*, 3557−3561.

(17) Geim, A. K.; Novoselov, K. S. The rise of graphene. *Nat. Mater.* **2007**, *6*, 9.

(18) Kuila, T.; Bose, S.; Khanra, P.; Mishra, A. K.; Kim, N. H.; Lee, J. H. Recent advances in graphene-based biosensors. *Biosens. Bioelectron.* **2011**, *26*, 4637−4648.

(19) Lee, C.; Wei, X.; Kysar, J. W.; Hone, J. Measurement of the elastic properties and intrinsic strength of monolayer graphene. *Science* **2008**, *321*, 385−388.

(20) He, S.; Liu, K. K.; Su, S.; Yan, J.; Mao, X.; Wang, D.; He, Y.; Li, L. J.; Song, S.; Fan, C. Graphene-based high-efficiency surface-enhanced Raman scattering-active platform for sensitive and multiplex DNA detection. *Anal. Chem.* **2012**, *84*, 4622−4627.

(21) Liang, W.; Chen, X.; Sa, Y.; Feng, Y.; Wang, Y.; Lin, W. Graphene oxide as a substrate for Raman enhancement. *Appl. Phys. A: Mater. Sci. Process.* **2012**, 1−5.

(22) Xu, W.; Ling, X.; Xiao, J.; Dresselhaus, M. S.; Kong, J.; Xu, H.; Liu, Z.; Zhang, J. Surface enhanced Raman spectroscopy on a flat graphene surface. *Proc. Natl. Acad. Sci. U.S.A.* **2012**, *109*, 9281−9286.
(23) Murphy, C. J.; Thompson, L. B.; Chernak, D. J.; Yang, J. A.; Sivapalan, S. T.; Boulos, S. P.; Huang, J.; Alkilany, A. M.; Sisco, P. N. Gold nanorod crystal growth: from seed-mediated synthesis to nanoscale sculpting. *Curr. Opin. Colloid Interface Sci.* **2011**, *16*, 128−134.
(24) Saute, B.; Premasiri, R.; Ziegler, L.; Narayanan, R. Gold nanorods as surface enhanced Raman spectroscopy substrates for sensitive and selective detection of ultra-low levels of dithiocarbamate pesticides. *Analyst* **2012**, *137*, 5082−5087.
(25) Tong, L.; Wei, Q.; Wei, A.; Cheng, J. X. Gold nanorods as contrast agents for biological imaging: optical properties, surface conjugation and photothermal effects. *Photochem. Photobiol.* **2009**, *85*, 21−32.
(26) Ling, X.; Xie, L.; Fang, Y.; Xu, H.; Zhang, H.; Kong, J.; Dresselhaus, M. S.; Zhang, J.; Liu, Z. Can graphene be used as a substrate for Raman enhancement? *Nano Lett.* **2009**, *10*, 553−561.
(27) Schedin, F.; Lidorikis, E.; Lombardo, A.; Kravets, V. G.; Geim, A. K.; Grigorenko, A. N.; Novoselov, K. S.; Ferrari, A. C. Surface enhanced Raman spectroscopy of graphene. *ACS Nano* **2010**, *4*, 5617−5626.
(28) Yu, X.; Lin, K.; Qiu, K.; Cai, H.; Li, X.; Liu, J.; Pan, N.; Fu, S.; Luo, Y.; Wang, X. Increased chemical enhancement of Raman spectra for molecules adsorbed on fluorinated reduced graphene oxide. *Carbon* **2012**, *50*, 4512−4517.
(29) Kim, N.; Oh, M. K.; Park, S.; Kim, S. K.; Hong, B. H. Effect of gold substrates on the Raman spectra of graphene. *Bull. Korean Chem. Soc.* **2010**, *31*, 999.
(30) Lu, G.; Li, H.; Liusman, C.; Yin, Z.; Wu, S.; Zhang, H. Surface enhanced Raman scattering of Ag or Au nanoparticle-decorated reduced graphene oxide for detection of aromatic molecules. *Chem. Sci.* **2011**, *2*, 1817−1821.
(31) Aroca, R. F.; Alvarez-Puebla, R. A.; Pieczonka, N.; Sanchez-Cortez, S.; Garcia-Ramos, J. V. Surface-enhanced Raman scattering on colloidal nanostructures. *Adv. Colloid Interface Sci.* **2005**, *116*, 45−61.
(32) Fan, M.; Andrade, G. F. S.; Brolo, A. G. A review on the fabrication of substrates for surface enhanced Raman spectroscopy and their applications in analytical chemistry. *Anal. Chim. Acta* **2011**, *693*, 7−25.

**Table 1. Primer Sequences Used for RT-PCR**

| gene (accession no.) | forward | reverse |
|---|---|---|
| COX-2 (NM_011198) | 5′-TGGTGCCTGGTCTGATGATG-3′ | 5′-GTGGTAACCGCTCAGGTGTTG-3′ |
| iNos2 (XM_147149) | 5′-CCCTCCTGATCTTGTGTTGGA-3 | 5′-TCAACCCGAGCTCCTGGAA-3′ |
| IL1$\beta$ (NM_008361) | 5′-CAACCA ACAAGTGATATTCTCCATG-3′ | 5′-GATCCACACTCTCCA GCTGCA-3′ |
| TNF-$\alpha$ (NM_013693) | 5′-CATCTTCTCAAAATTCGAGTGACAA-3′ | 5′-TGGGAGTAGACAAGGTACAACCC-3′ |
| IL6 (NM_031168) | 5′-TAGTCCTTCCTACCCCAATTTCC-3′ | 5′-TTGGTCCTTAGCCACTCCTTC-3′ |
| actin (NM_007393) | 5′-AACCGTGAAAAGATGACCCAGAT-3′ | 5′-CACAGCCTGGATGGCTACGT-3′ |

deposited at the Chrysler Herbarium, Rutgers University, New Brusnwick, NJ, USA.

**Preparation of the Extract.** Dry seeds were ground into powder, and the seed powder (2 g) was extracted in 95% ethanol (20 mL) for 24 h at room temperature with continuous agitation provided by a platform shaker. After extraction, the sample was filtered and the solvent removed by rotary evaporation, yielding 40.25 mg (2%). The extract was dissolved in 95% ethanol to appropriate concentrations for in vitro assays, chemical characterization, and bioactivity-guided fractionation.

**COX-2 in Vitro Assay.** Grains of paradise extract was dissolved in 95% ethanol at a concentration of 1 mg/mL. The activity of the extract was tested with a colorimetric COX (ovine) inhibitor screening assay (catalog no. 760111, Cayman Chemical, Ann Arbor, MI, USA). The screening assay measures the peroxidase activity of cyclooxygenase by monitoring the appearance of oxidized *N*,*N*,*N*′,*N*′-tetramethyl-*p*-phenylenediamine (TMPD) at 590 nm as previously described.[12] A relatively higher TMPD concentration corresponds to a greater absorbance at 590 nm, a greater peroxidase activity, and a greater COX-2 activity (i.e., less inhibition of COX-2 activity). The assays were performed according to the manufacturer's instructions.

**Bioassay-Guided Purification of the Extract.** Purification and isolation of compounds were carried out using a preparatory HPLC from Waters Corp. (Milford, MA, USA) consisting of a W717 plus autosampler, a W600E multisolvent delivery system, a W600 controller, a W490E multiwavelength detector, and a Waters fraction collector. A Waters liquid chromatography−mass spectrometry (LC-MS) Integrity system consisting of a solvent delivery system with a W616 pump and a W600S controller, a W717 plus autosampler, a W996 PDA detector, and a Waters TMD Thermabeam electron impact (EI) single-quadrupole mass detector with fixed ionization energy of 70 eV was used for analysis. Data were collected and analyzed with the Waters Millennium v. 3.2 software, linked with the sixth edition of the Wiley Registry of Mass Spectral Data, containing 229,119 EI spectra of 200,500 compounds.

**Gene Expression: Macrophage Cell Culture.** The mouse monocyte/macrophage cell line RAW 264.7 (ATCC TIB-71 obtained from American Type Culture Collection, Manassas, VA, USA) was maintained in Dulbecco's modified Eagle medium (DMEM; Invitrogen Inc., Carlsbad, CA, USA) supplemented with 100 U/mL penicillin, 100 $\mu$g/mL streptomycin, and 10% heat-inactivated fetal bovine serum (Sigma-Aldrich Co.). The cells were kept in a 37 °C incubator with 5% $CO_2$. Cells were subcultured by scraping when plates reached 90% confluence with a 1:5 ratio in fresh medium.

Cells were seeded at a density of $4 \times 10^5$ cells per well (viable cell counts were carried out by trypan blue staining using a hemocytometer) in 24-well plates 12 h prior to treatment. The cells were then treated with test compounds dissolved in dimethyl sulfoxide (DMSO) at predetermined doses (based on MTS assays) for 2 h before elicitation with bacterial endotoxin lipopolysaccharide from *Escherichia coli* serotype 055:B5 (LPS) (Sigma-Aldrich Co.) at 1 $\mu$g/mL for an additional 6 h. For every experiment one positive control (cells treated only with LPS and vehicle) and one negative control (cells treated with vehicle only) were included. Three replicates were made for both treatments and the controls. Final concentration of DMSO in cells was 1%. The same concentration was used as vehicle control. At the end of the treatment period, cells were harvested in Trizol reagent for subsequent cellular RNA extraction.

**Gene Expression: Cell Viability Assay and Dose Range Determination.** A Cell Titer 96 MTS assay kit (Promega Corp., Madison, WI, USA) was used to determine the relative number of viable cells remaining after incubation with treatments. The assay has been performed according to the manufacturer's protocol and a previously described method.[18]. In short, the assay was performed by treating cells with different extract concentrations, followed by adding 20 $\mu$L of reagent 3-4,5-(dimethylthiazol-2-yl)-5-(3-carboxymethoxyphenyl)-2-(4-sulfophenyl)-2*H*-tetrazolium/phenazine methosulfate (MTS/PMS) directly to culture wells and incubating for 3 h at 37 °C. Plates were read using a microplate reader (Molecular Devices, Sunnyvale, CA, USA) at 490 nm. For dose range studies, the highest nontoxic concentrations for respective compound/extract were selected.

**Gene Expression: Quantitative Polymerase Chain Reaction (qPCR) and Data Analysis.** The synthesized cDNAs were diluted 4-fold. Two microliters of each diluted sample was added to 0.5 $\mu$L of gene-specific primers (6 $\mu$M, oligos synthesized by IDT Inc., Coralville, IA, USA) and 12.5 $\mu$L of Brilliant SYBR green PCR master mix (2×) (Stratagene, La Jolla, CA, USA) containing green jump-start Taq ready mix, and the final volume was brought to 25 $\mu$L by adding sterile distilled water. Carboxy-X-rhodamine (ROX) was used as an internal dye. To avoid interference due to genomic DNA contamination, only intron-overlapping primers were selected using Primer Express vers. 2.0 software (Applied Biosystems, Foster City, CA, USA) as shown in Table 1. PCR amplifications were performed on a MX3000p system (Stratagene, La Jolla, CA, USA) as described in ref 19. RNA expressions for genes of interest, normalized with respect to the expression of housekeeping $\beta$-actin gene, were analyzed using the $\Delta\Delta$Ct method.[19]

**Carrageenan-Induced Rat Paw Edema.** Groups of Long Evans-derived male rats with body weights of 150 ± 10 g were housed six animals per cage in a room kept at 22−23 °C with 60−70% humidity and a 12 h light/dark cycle for 1 week prior to the start of the study. Access to standard laboratory chow and water was ad libitum. All aspects of this work including housing, experimentation, and disposal of animals were performed in general accordance with the International Guiding Principles for Biomedical Research Involving Animals (CIOMS Publication ISBN 9290360194, 1985), and the protocol was approved by MDS Pharma (King of Prussia, PA, USA). The animals were fasted overnight prior to use.

Grains of paradise extract and pure compounds ([6]-paradol, [6]-shogaol, [6]-gingerol) were administered per os (extract at 1000 and 500 mg/kg and pure compounds at 150 mg/kg) suspended in 0.2% Tween-80/10% ethanol 1 h before right hind paw injection of carrageenan (0.1 mL of 1% suspension intraplantar, TCI, Tokyo, Japan). Aspirin (150 mg/kg, Sigma-Aldrich Co.) was used as a reference compound (positive control). The severity of the hind paw edema as a measure of inflammation was recorded 3 h after carrageenan administration using a plethysmometer (Ugo Basile, Comerio, VA, Italy) with water cell (25 mm diameter). Reduction of edema was calculated by comparison with vehicle control. The anti-inflammatory activity is expressed as a percentage of edema reduction.

**Statistical Analysis.** Statistical comparisons were performed between the vehicle control and treated groups. For the in vitro and in vivo assays, the results are presented as the mean ± standard deviation (SD) The statistical analysis was calculated by using the analysis of variance (ANOVA) test and followed by post hoc analysis using Tukey's multiple-comparison test.

## RESULTS AND DISCUSSION

In a search for novel anti-inflammatory compounds we evaluated ethanolic extract of grains of paradise (*A. melegueta*) for inhibition of COX-2 enzyme activity, inhibition of pro-inflammatory genes expression (in vitro), and anti-inflammatory activity in rat paw edema assay (in vivo), and the active compounds from the extract were characterized.

**COX-2 Enzyme Inhibitory Activity and Active Compound Characterization.** At an initial concentration of 1 mg/mL, the ethanolic extract demonstrated inhibitory activity against COX-2, similar to the drug Vioxx that was used as a positive control. The level of inhibition for the extract was 76% compared to 87% for Vioxx (Table 2). Biochemical analytical data indicated that the extract is a complex mixture of compounds. In order to identify compounds responsible for the observed activity, the extract was subjected to bioactivity guided fractionation with concurrent LC-MS analysis. Bioactivity guided fractionation was performed in the following manner:

Grains of paradise extract (1 g, obtained from a large-scale extraction) was dissolved in 95% ethanol (20 mL) and fractionated using a preparatory HPLC. For the initial purification, a Waters 19 × 300 mm symmetry preparative C8 reverse phase column was used. The mobile phases consisted of 100% acetonitrile ($CH_3CN$) and 0.5% of acetic acid in water (v/v). For the initial separation, a gradient from 5% $CH_3CN$ to 95% $CH_3CN$ over 35 min was used with a flow rate of 8 mL/min. Ten fractions (volume of 40 mL each) at 5 min intervals were collected and tested for COX-2 inhibitory activity. Fraction 8 (F8; yield = 360 mg) had the highest activity and was further purified using similar conditions as before except the gradient was run over 70 min. Four fractions were collected from F8, and they were subjected to the COX-2 assay. The most active fraction, F8-2 (4 mL volume, eluted at 59.2 min at 282 nm; yield = 90 mg), was then purified using a 10 × 250 mm Curacil-PFP column and an isocratic run with a mobile phase consisting of 0.5% acetic acid in water/methanol/$CH_3CN$ (2:3:5) at a flow rate 3 mL/min. Four fractions were collected from F8-2, and F8-2-3 (1.45 mL volume, eluted at 8.67 min, at 282 nm; yield = 49.5 mg) was found to have the highest inhibitory activity on COX-2 enzyme. This fraction was refractionated using the conditions described previously, with the exception of the flow rate, which was reduced to 1 mL/min. Three fractions were collected from F8-2-3, and F8-2-3-2 (1.48 mL volume, eluted at 25.29 min, at 282 nm; yield = 32.2 mg) had the highest inhibitory activity. This fraction was identified as [6]-paradol (95% purity) using LC-MS and $^1H$, $^{13}C$, and 2D

**Table 2. In Vitro COX-2 Enzyme Inhibition by the Ethanolic Extract of Grains of Paradise and Its Anti-inflammatory Components**[a]

| treatment | inhibition (%) ± SD |
|---|---|
| control[b] | 2 ± 2 |
| *A. melegueta* extract | 76 ± 6.7*** |
| [6]-gingerol | 7 ± 11.7 |
| [6]-shogaol | 68 ± 6.4*** |
| [6]-paradol | 91 ± 3.6*** |
| Vioxx | 87 ± 1.5*** |

[a]Data are shown as mean inhibition ± SD in %. Significance: ***, 0.1%. [b]All samples were tested at the concentration of 1 mg/mL. Control, celery extract at 1 mg/mL; whole extract, grains of paradise (*A. melegueta*) extract at 1 mg/mL; Vioxx (MW 314.36) at 1 mg/mL, 3.18 mM; [6]-gingerol (MW 294.38) at 1 mg/mL, 3.39 mM; [6]-shogaol (MW 276.37) at 1 mg/mL, 3. 62 mM; [6]-paradol (MW 278) at 1 mg/mL, 3.60 mM.

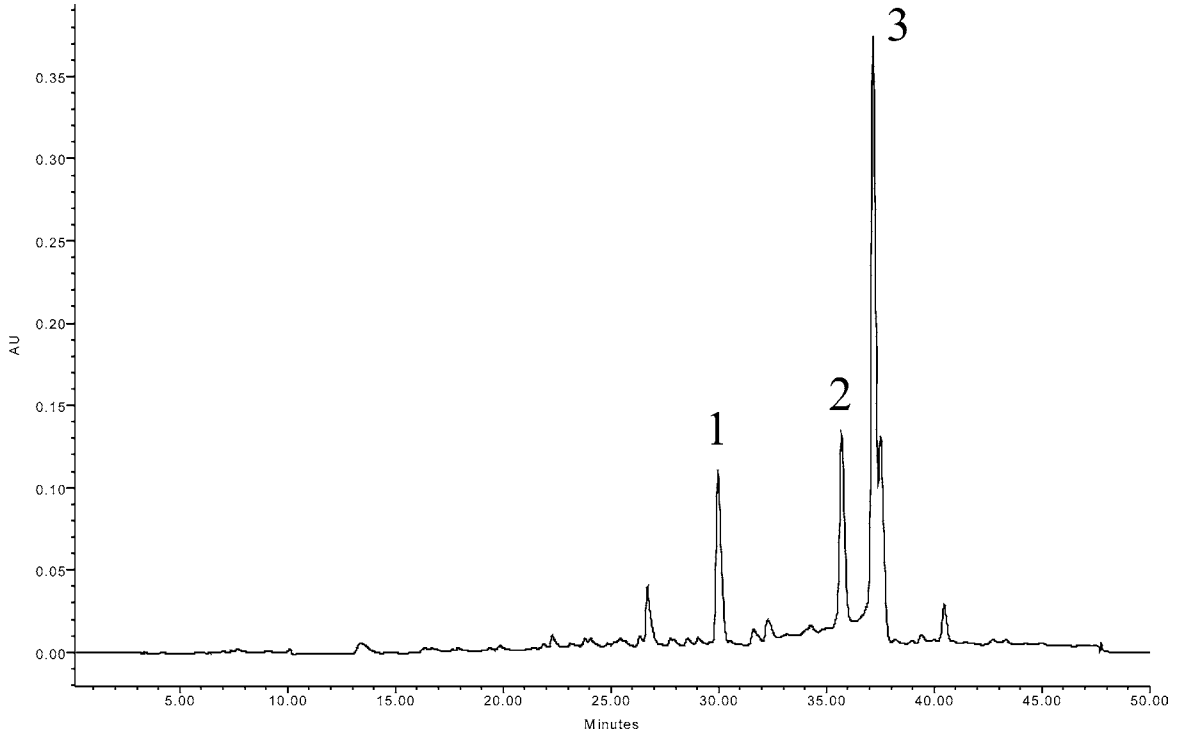


**Figure 1.** HPLC chromatogram of grains of paradise (*A. melegueta*) extract showing putative compounds. Peaks: 1, [6]-gingerol; 2, [6]-shogaol; 3, [6]-paradol.

NMR data.[20,21] The purification procedure was repeated multiple times to obtain sufficient amounts of [6]-paradol for in vitro and in vivo experiments.

Chemical analysis of the extract revealed three major peaks (Figure 1). The UV spectra and mass fragmentation patterns of these peaks matched the compounds of the gingerol family previously identified in *A. melegueta*[22] and in other members of Zingiberaceae.[23] The most abundant were putatively identified as [6]-gingerol, [6]-shogaol, and [6]-paradol at 1.0 mg/g [6]-gingerol, 0.53 mg/g [6]-shogaol, and 1.2 mg/g [6]-paradol per gram of the extract. All three compounds were assayed for COX-2 enzyme inhibitory activity at the same concentration (1 mg/mL) as the whole extract and Vioxx. [6]-Paradol was the most active with 91% inhibition, followed by [6]-shogaol (68%), and [6]-gingerol (7%) (Table 2). Paradol inhibitory activity was higher than those of Vioxx (87%) and the whole extract (76%), confirming it as the most active compound as found in the bioactivity-guided fractionation assay. [6]-Gingerol and [6]-shogaol were commercially purchased, and [6]-paradol was isolated by bioactivity-guided fractionation (as described above).

**Inhibition of Expression of Pro-inflammatory Genes (in Vitro).** In addition to inhibiting the pro-inflammatory COX-2 enzyme, the extract of grains of paradise was also tested for inhibition of pro-inflammatory genes. The genes tested were tumor necrosis factor alpha (TNF$\alpha$), interleukin-1beta (IL-1$\beta$), interleukin-6 (IL-6), COX-2, and inducible nitric oxide synthase (iNOS).

The in vitro experiments were designed to quantify the relative amount of transcripts for target genes (COX2, iNOS, TNF$\alpha$, IL6, and IL1$\beta$) within the total RNA in individual cell batches following treatments with the extract or its three major gingerols. All experiments were started with an equal number of cells for each treatment. For each assay, two control sets were monitored (Figure 2). The in vitro experiments showed that both ethanolic extract of grains of paradise extract and [6]-shogaol were inhibitory in a dose-dependent manner ($p < 0.05$ by ANOVA) on IL1$\beta$ (Figure 2) but not on other genes tested. The extract was significantly cytotoxic to macrophages at concentrations >20 $\mu$g/mL and hence could not be tested for gene expression inhibition beyond that concentration. [6]-Shogaol did not affect the transcription of other genes at 5 $\mu$g/mL, its highest nontoxic concentration. [6]-Paradol and [6]-gingerol did not show any significant inhibitory activities at the noncytotoxic concentration range up to 30 and 50 $\mu$g/mL, respectively (data not shown).

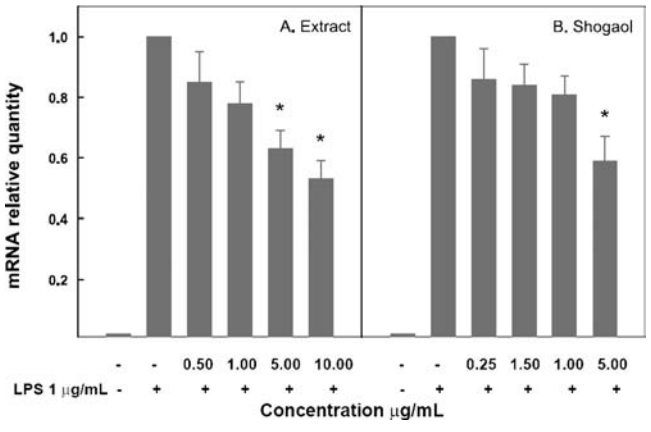


**Figure 2.** Effect of grains of paradise extract (A) and [6]-shogaol (B) on IL1$\beta$ gene expression in LPS-activated RAW macrophages measured by the mRNA quantity relative to the response to LPS activation only (positive control) that is normalized to a value of 1.00. Lower values represent greater inhibitory effects with 0.00 corresponding to a complete inhibition of the induced gene expression. Values are the mean ± SD. (*) $p < 0.05$ (compared with positive control).

**Anti-inflammatory Activity in Rat Paw Edema Assay (in Vivo).** To investigate whether the observed in vitro COX-2 enzyme and gene expression inhibitory properties translate into in vivo anti-inflammatory activity, we tested the extract in a rat paw carrageenan edema assay, which is commonly used for testing anti-inflammatory agents. Initially, two doses of the whole extract were given per os (orally) to the animals, 1000 and 500 mg/kg. Aspirin was used as a positive control at a 150 mg/kg dose. At 1000 mg/kg, the extract demonstrated anti-inflammatory effect, reducing edema by 49% (Table 3). At the lower dose (500 mg/kg) the extract exhibited a reduced anti-inflammatory effect (11% edema reduction). At the same time, aspirin reduced edema by 43% at 150 mg/kg. Therefore, grains of paradise extract does have in vivo anti-inflammatory activity, but it was not as effective as aspirin.

**Table 3. Inhibition of Carrageenan-Induced Rat Paw Edema by Grains of Paradise Ethanolic Extract and Its Main Components, [6]-Gingerol, [6]-Shogaol, and [6]-Paradol, with Aspirin as a Positive Control[a]**

| | treatment | dose | average paw difference ± SD | inhibition (%) |
|---|---|---|---|---|
| I | | | | |
| | vehicle | 10 mL/kg | 90 ± 3.5 | |
| | *A. melegueta* extract | 500 mg/kg | 80 ± 13.7 | 11 |
| | | 1000 mg/kg | 46 ± 4.2** | 49 |
| | aspirin | 150 mg/kg | 51 ± 5.1** | 43 |
| II | | | | |
| | vehicle | 10 mL/kg | 85 ± 3.3 | |
| | [6]-paradol | 150 mg/kg | 68 ± 6.7* | 20 |
| | aspirin | 150 mg/kg | 54 ± 8.5*** | 36 |
| III | | | | |
| | vehicle | 10 mL/kg | 79 ± 3.4 | |
| | [6]-shogaol | 150 mg/kg | 49 ± 5.4*** | 38 |
| | [6]-gingerol | 150 mg/kg | 59 ± 8.5** | 25 |
| | aspirin | 150 mg/kg | 50 ± 8.6*** | 37 |

[a]Test substances were administered orally 60 min before the right hind paw received an injection of carrageenan (0.1 mL of 1% suspension intraplantar). Hind paw edema was measured 3 h later; paw sizes were compared, and average paw difference (expressed in mL) established and inhibition were calculated relative to the vehicle-treated animals in the control group. Data are shown as the mean ± SD and percentages of inhibition. Significance levels: *, 5%; **, 1%; ***, 0.1%.

To analyze the anti-inflammatory activity of single compounds, the most active compound in the COX-2 enzymatic assay, [6]-paradol, has been isolated from the extract and tested in in vivo assay at the same dose level as aspirin (150 mg/kg), which was used as a positive control. At this dose it inhibited the rat paw edema by 20% and aspirin by 36%, respectively. Two other compounds from the extract, [6]-gingerol and [6]-shogaol, given at 150 mg/kg, inhibited edema by 25 and 38%, respectively. In the same assay aspirin given at 150 mg/kg inhibited the edema by 37%. Therefore, [6]-shogaol, the most active compound in the gene expression

assays, was also the most active compound in vivo and demonstrated anti-inflammatory activity similar to that of aspirin (Table 3).

Results of our study demonstrated the inhibitory activity of grains of paradise ethanolic extract in COX-2 in vitro enzymatic assay. The bioactivity-guided fractionation revealed that the [6]-paradol present in the extract is the most effective inhibitor of COX-2 enzymatic activity. [6]-Paradol and two other major compounds present in the extract, [6]-gingerol and [6]-shogaol, belong to the gingerol family of compounds. The results for the enzymatic inhibition support previous reports on gingerols as inhibitors of the arachidonic acid biosynthetic pathway. In one study, ginger rhizome extract (*Zingiber officinale* Roscoe, Zingiberaceae) was investigated for inhibition of COX-1 enzyme and antiplatelet aggregation activity. [8]-Paradol, a natural constituent of ginger, was the most active inhibitor and stronger than aspirin.[24] Similar studies on COX-2 enzyme inhibitory activity revealed that ginger constituents [8]-paradol and [8]-shogaol had strong inhibitory activity.[25] Additionally, structure−activity study on gingerols and COX-2 inhibition has shown that the paradols showed the highest affinity for COX-2 followed by the shogaols and then the gingerols.[26] Our data, together with the above-mentioned studies on compounds from ginger, suggest that compounds from the gingerol family are cyclooxygenase inhibitors. When the gingerols from the extract were tested for the inhibition of expression of pro-inflammatory genes (COX2, iNOS, TNF$\alpha$, IL6, and IL1$\beta$), the whole extract and [6]-shogaol exhibited inhibitory activity on IL1$\beta$ gene expression, whereas other genes have not been affected.

To evaluate how these in vitro activities at enzyme and gene level transpond into in vivo activity, we used the cyclo-oxygenase-dependent carrageenan-induced paw edema assay,[27] a standard model to reproduce acute inflammation in vivo. The ethanolic extract of grains of paradise exhibited anti-inflammatory activity in this assay. This also confirmed the anti-inflammatory activity reported earlier for the aqueous extract of grains of paradise.[5,12] Additionally, the three major gingerols present in the extract were also effective in reducing the inflammation with [6]-shogaol at a level comparable to that of aspirin.

Because grains of paradise ethanolic extract and major gingerols present in it showed in vitro inhibition of COX-2 enzyme activity and ethanolic extract and [6]-shogaol reduction in expression of pro-inflammatory IL1$\beta$ gene, we could hypothesize that the extract may have a dual mode of action, at the gene and enzyme levels. Inhibition by [6]-paradol and other gingerols present in the extract of COX-2 enzyme activity and inhibition by [6]-shogaol of pro-inflammatory gene expression could impair prostaglandin (the end product of the cyclooxygenase pathway) production, thereby reducing the inflammatory process in vivo. Gingerols from ginger (*Z. officinale*) have been previously reported to inhibit prostaglandin biosynthesis.[28] However, to put more light on this, our extract and its compounds require further studies, especially on how the whole ethanolic extract and its three major isolated gingerols affect prostaglandin levels. In conclusion, this study with in vitro and in vivo assays has demonstrated that the ethanolic extract of grains of paradise and its major compounds have anti-inflammatory potential at the enzyme and in vivo levels, but they need to be further evaluated.

## AUTHOR INFORMATION


### Corresponding Author

*Phone: +381 21 485 3824. E-mail: nebojsa.ilic@fins.uns.ac.rs.



### Funding

Research supported by Phytomedics Inc. (Jamesburg NJ, USA); NIH Center for Dietary Supplements Research on Botanicals and Metabolic Syndrome, Grant 1-P50 AT002776-01; Fogarty International Center of the NIH under U01 TW006674 for the International Cooperative Biodiversity Groups; and Rutgers University. Additional support came from the National Center for Complementary and Alternative Medicine of NIH under 1-K99 AT004245-01.


### Notes

The authors declare no competing financial interest.

## ACKNOWLEDGMENTS


Excellent technical assistance was provided by Reneta Pouleva and Ruth Dorn. We thank Cheryl Lyn Dybas for a critical reading of the manuscript.


## REFERENCES


(1) Gallin, J. I.; Snyderman, R. *Inflammation: Basic Principles and Clinical Correlates*, 3rd ed.; Lippincott Williams & Wilkins: Philadelphia, PA, USA, 1999; pp 1−3.

(2) Dannenberg, A. J.; Altorki, N. K.; Boyle, J. O.; Dang, C.; Howe, L. R.; Weksler, B. B.; Subbaramaiah, K. Cyclo-oxygenase 2: a pharmacological target for the prevention of cancer. *Lancet Oncol.* **2001**, *2*, 544−551.

(3) Huss, U.; Ringbom, T.; Perera, P.; Bohlin, L.; Vasaenge, M. Screening of ubiquitous plant constituents for COX-2 inhibition with a scintillation proximity based assay. *J. Natl. Prod.* **2002**, *65*, 1517−1521.

(4) Surh, Y. J. Anti-tumor promoting potential of selected spice ingredients with antioxidative and anti-inflammatory activities: a short review. *Food Chem. Toxicol.* **2002**, *40*, 1091−1097.

(5) Umukoro, S.; Ashorobi, R. B. Further studies on the antinociceptive action of aqueous seed extract of *Aframomum melegueta*. *J. Ethnopharmacol.* **2007**, *109*, 501−504.

(6) Akendengue, B.; Louis, A. M. Medicinal plants used by the Masango people in Gabon. *J. Ethnopharmacol.* **1994**, *41*, 193−200.

(7) Galal, A. M. Anti-microbial activity of 6-paradol and related compounds. *Int. J. Pharmacog.* **1996**, *31*, 64−69.

(8) Kamtchouing, P.; Mbongue, G. Y. F.; Dimo, T.; Watcho, P.; Jatsa, H. B.; Sokeng, S. D. Effects of *Aframomum melegueta* and *Piper guineense* on sexual behaviour of male rats. *Behav. Pharmacol.* **2002**, *13*, 243−247.

(9) Alo, M. N.; Anyim, C.; Igwe, J. C.; Elom, M.; Uchenna, D. S. Antibacterial activity of water, ethanol and methanol extracts of *Ocimum gratissimum*, *Vernonia amygdalina* and *Aframomum melegueta*. *Adv. Appl. Sci. Res.* **2012**, *3*, 844−848.

(10) Chiejina, N. V.; Ukeh, J. A. Antimicrobial properties and phytochemical analysis of methanolic extracts of *Aframomum melegueta* and *Zingiber officinale* on fungal diseases of tomato fruit. *J. Nat. Sci. Res.* **2012**, *2*, 10−15.

(11) Mbongue, G. Y. F.; Kamtchouing, P.; Dimo, T. Effects of the aqueous extract of dry seeds of *Aframomum melegueta* on some parameters of the reproductive function of mature male rats. *Andrologia* **2012**, *44*, 53−58.

(12) Umukoro, S.; Ashorobi, R. B. Effect of *Aframomum melegueta* seed extract on thermal pain and on carrageenin-induced edema. *Nig. Q. J. Hosp. Med.* **2001**, *11*, 220−225.

(13) Umukoro, S.; Ashorobi, R. B. Further pharmacological studies on aqueous seed extract of *Aframomum melegueta* in rats. *J. Ethnopharmacol.* **2008**, *115*, 489−493.

(14) Lawal, B. A. S.; Aderibigbe, A. O.; Essiet, G. A.; Essien, A. D. Hypotensive and antihypertensive effects of *Aframomum melegueta* seeds in humans. *Int. J. Pharmacol.* **2007**, *3*, 311−318.

(15) Sugita, J.; Yoneshiro, T.; Hatano, T.; Sayuri, A.; Takeshi, I.; Hideyo, U.; Toshihiko, I.; Toshimitsu, K.; Yuko, K.; Masayuki, S. Grains of paradise (*Aframomum melegueta*) extract activates brown adipose tissue and increases whole-body energy expenditure in men. *Br. J. Nutr.* **2013**, *110*, 733−738.
(16) Sugita, J.; Yoneshiro, T.; Sugishima, Y.; Ikemoto, T.; Uchiwa, H.; Suzuki, I.; Masayuki, S. Daily ingestion of grains of paradise (*Aframomum melegueta*) extract increases whole-body energy expenditure and decreases visceral fat in humans. *J. Nutr. Sci. Vitaminol.* **2014**, *60*, 22−27.
(17) Kulmacz, R. J.; Lands, W. E. M. Requirements for hydroperoxide by the cyclooxygenase and peroxidase activities of prostaglandin H synthase. *Prostaglandins* **1983**, *25*, 531−540.
(18) Liu, Y.; Chakravarty, S.; Dey, M. Phenethylisothiocyanate alters site- and promoter-specific histone tail modifications in cancer cells. *PLoS One* **2013**, *8*, 1−13.
(19) Dey, M.; Ribnicky, D.; Kurmukov, A. G.; Raskin, I. Transcriptional modulation and *in vivo* anti-inflammatory activity of a seed preparation containing phenethylisothiocyanate. *J. Pharmacol. Exp. Ther.* **2006**, *317*, 326−333.
(20) Gröblacher, B.; Maier, V.; Kunert, O.; Bucar, F. Putative mycobacterial efflux inhibitors from the seeds of *Aframomum melegueta*. *J. Nat. Prod.* **2012**, *75*, 1393−1399.
(21) Wu, Q.; Cho, J.; Yoo, K.; Jeong, T.; Park, J.; Kim, S.; Kang, J.; Chung, I.; Choi, M.; Lee, K.; Chung, H.; Bang, M.; Baek, N. A new phenanthrene derivative and two diarylheptanoids from the roots of *Brassica rapa* ssp. *campestris* inhibit the growth of cancer cell lines and LDL-oxidation. *Arch. Pharm. Res.* **2013**, *36*, 423−429.
(22) Escoubas, P.; Lajide, L.; Mizutani, J. Part 2. Termite antifeedant activity in *Aframomum melegueta*. *Phytochemistry* **1995**, *40*, 1097−1099.
(23) Connell, D. W. Natural pungent compounds. III. Paradols and associated compounds. *Aust. J. Chem.* **1970**, *23*, 369−376.
(24) Nurtjahja-Tjendraputra, E.; Ammit, A. J.; Roufogalis, B. D.; Tran, V. H.; Duke, C. C. Effective anti-platelet and COX-1 enzyme inhibitors from pungent constituents of ginger. *Thromb. Res.* **2003**, *111*, 259−265.
(25) Tjendraputra, E.; Tran, V. H.; Liu-Brennan, D.; Roufogalis, B. D.; Duke, C. C. Effect of ginger constituents and synthetic analogues on cyclooxygenase-2 enzyme in intact cells. *Bioorg. Chem.* **2001**, *29*, 156−163.
(26) van Breemen, R. B.; Tao, Y.; Li, W. Cyclooxygenase-2 inhibitors in ginger (*Zingiber officinale*). *Fitoterapia* **2011**, *82*, 38−43.
(27) Gamache, D. A.; Povlishock, J. T.; Ellis, E. F. Carrageenan-induced brain inflammation. Characterization of the model. *J. Neurosurg.* **1986**, *65*, 679−685.
(28) Kiuchi, F.; Iwakem, S.; Shibuya, M.; Hanaoka, A.; Sankawa, U. Inhibition of prostaglandin and leukotriene biosynthesis by gingerols and diarylheptaniods. *Chem. Pharm. Bull.* **1992**, *40*, 387−391.

precise role of autophagy in the death of tumor cells, especially TMZ-treated glioblastoma cells, is not yet entirely clear.

Because previous studies have shown the potential anticancer effects of pine needle extracts, we performed this study to investigate the anti-glioblastoma effects as well as the bioactive compounds present in pine needle extracts. In particular, chrysin (5,7-dihydroxyflavone), a major phenolic compound in pine needle extract, may be responsible for the anticancer properties of pine needle extracts.[11] Chrysin exhibits antioxidant and antiviral activities, reduces blood lipids, and prevents mutagenesis. In one study, chrysin showed antitumor activities by suppressing tumor cell proliferation and inducing apoptosis.[12] However, studies on the effects of chrysin on human glioblastoma are rare. In this study, we showed that chrysin was the most active ingredient in pine needle extract that induced apoptosis and suppressed the migration and invasion of glioblastoma cell line GBM8901. Furthermore, chrysin markedly inhibited autophagy and reduced MGMT expression, which may contribute to TMZ chemoresistance. Taken together, our results suggested that pine needle extracts containing chrysin might provide potential beneficial effects against glioblastoma and attenuate resistance to TMZ in a synergistic behavior. This may help in developing anti-proliferative and anti-recurrence strategies by sensitizing glioblastoma cells resistant to TMZ.

## MATERIALS AND METHODS

**Materials.** Chrysin, TMZ, 4′,6-diamidino-2-phenylindole (DAPI), 3-(4,5-dimethylthiazol-2-yl)-2,5-diphenyltetrazolium bromide (MTT), propidium iodide (PI), 3-methyladenine (3-MA), chloroquine (CQ), and rapamycin were purchased from Sigma-Aldrich (München, Germany). Caspase inhibitor zVAD-fmk was obtained from R&D Systems (Minneapolis, MN). Antibodies to β-actin, anti-pmTOR, anti-mTOR, beclin1, p62, and MGMT were obtained from Santa Cruz Biotechnology (Santa Cruz, CA). Cleaved PARP, cleaved caspase 3, anti-pAkt, and anti-Akt antibodies were obtained from Millipore (Bedford, MA). Anti-LC3, Atg5-Atg12, and Atg7 antibodies were purchased from Novus Biologicals (Littleton, CO). Acridine orange was obtained from Life Technologies (Rockville, MD).

**Sample Preparation.** Fresh leaves (pine needles) of *P. morrisonicola* Hayata were collected from Taiwanese mountains in Nantou county at elevations of 300−2300 m. The preparation of pine needle extracts for this study was modified from a previous report.[13] Briefly, pine needles were air-dried, homogenized, and ground. The obtained powder (200 g) was extracted with water, methanol, or ethanol at room temperature for 48 h. Next, the respective solutions were filtered and dried by evaporation of the filtrates in vacuum at 40 °C. The pine needle extracts of water, methanol, and ethanol were named pine water extract (PWE), pine methanol extract (PME), and pine ethanol extract (PEE), respectively. The dried samples were stored at −20 °C until further use.

**Cell Culture and Viability Assay.** GBM8901 human glioblastoma cells, EOC 13.31 glia cells, and Detroit 551 and NIH3T3 fibroblast cells were obtained from Bioresources Collection and Research Center (Hsinchu, Taiwan). GBM8901 cells were maintained in RPMI-1640 medium; Detroit 551 cells were maintained in minimum essential medium (MEM); and EOC 13.31 and NIH3T3 cells were maintained in Dulbecco's modified Eagle's medium (DMEM) (Gibco). Primary mixed glial cell cultures were established from neonatal rat brain tissue according to a previous protocol.[14] All cultures were supplemented with 10% fetal calf serum, 100 units/mL penicillin, 100 μg/mL streptomycin, and 2 mM L-glutamine and incubated at 37 °C in a humidified atmosphere of 5% $CO_2$. In the viability assay, the cells were seeded in 96-well plates at a density of $1 \times 10^4$ cells/well and were incubated overnight. Next, the cells were treated with indicated conditions. After 24 h, the tetrazolium salt MTT was added to the medium according to the instructions of the manufacturer. Only viable cells metabolized MTT to a purple product formazan, which was quantified spectrophotometrically at 550 nm. The cell viability was determined as the percentage of control cells treated with the vehicle alone.

**High-Performance Liquid Chromatography (HPLC) and Tandem Mass Spectrometry (MS/MS) Analyses.** Sample separation was performed using a HPLC system (JASCO model PU-2080, Tokyo, Japan). Isocratic chromatography was performed using separate reversed-phase (RP)-HPLC by employing the following conditions: fractionation in a LUNA C18 analytical column packed with 5 μm particles (250 × 4.6 mm, Phenomenex, Torrance, CA) and elution with a mobile phase (deionized water/methanol/formic acid = 79.1:20:0.1) at a flow rate of 1.0 mL/min that was monitored at a wavelength of 280 nm [SPD-10 AV ultraviolet−visible (UV−vis) detector, Shimadzu, Kyoto, Japan]. MS was performed using an API 3000 triple quadruple mass spectrometer equipped with a Turbo IonSpray interface operated in negative electrospray ionization (ESI, AB SCIEX, Framingham, MA). All quantitative and qualitative analyses were performed in a multiple reaction monitoring (MRM) scan.

**Western Blot Analysis.** GBM8901 cells were harvested and homogenized in lysis buffer [50 mM Tris−HCl at pH 8.0, 5 mM ethylenediaminetetraacetic acid (EDTA), 150 mM NaCl, 0.5% Nonidet P-40, 0.5 mM phenylmethylsulfonyl fluoride, and 0.5 mM dithiothreitol] for 30 min at 4 °C. Equal amounts of total cellular proteins (50 μg) were resolved by sodium dodecyl sulfate−polyacrylamide gel electrophoresis (SDS−PAGE), transferred onto polyvinylidene difluoride membranes (Millipore), and probed using primary antibodies, followed by horseradish-peroxidase-conjugated secondary antibodies. The immunocomplexes were visualized using enhanced chemiluminescence kits (Millipore).

**Nucleus Morphology.** Changes in cell nuclei morphology that were characteristic of apoptosis were examined using a fluorescence microscope (AXioskop 2, Zeiss) on cells grown on coverslips. For this, cells were fixed in 4% paraformaldehyde after 24 h of treatment with the indicated compound, permeabilized in ice-cold methanol, and incubated with 1 ng/mL 4′,6-diamidino-2-phenylindole (DAPI) staining under the fluorescence microscope for 15 min at room temperature.

**Apoptosis by Flow Cytometry.** Cells were cultured as described above. The percentage of sub-G1 apoptotic cells was examined by the propidium iodide (PI) technique using flow cytometry. Briefly, GBM8901 cells ($1 \times 10^6$/mL) were fixed in 70% methanol, resuspended in phosphate-buffered saline (PBS) incubated with 50 μg/mL PI for 0.5 h, and analyzed by FACScan (Becton Dickinson, San Jose, CA).

**Cell Migration and Invasion Assay.** The cell migration and invasion assays were performed in a 24-well Boyden chamber with an 8 μm pore size polycarbonate membrane (Corning, NY). For the migration assay, $1 \times 10^5$ cells in 200 μL serum-free medium were added to the upper compartment of the chamber; the lower compartment was filled with 600 μL of RPMI 1640 supplemented with 10% fetal bovine serum (FBS). After incubation at 37 °C for 24 h, GBM8901 cells remaining in the upper chamber were removed using swabs. The cells on the lower surface of the membrane were fixed with methanol, stained with 0.1% crystal violet, photographed, and counted using a light microscope. The invasion assay was performed using the same procedure, except that the membrane was coated with Matrigel (BD Biosciences) to form a matrix barrier and $3 \times 10^4$ GBM8901 cells were added to the upper compartment of the chamber.

**Acridine Orange Staining.** Acridine orange is a dye that specifically labels intracellular acidic vesicles. GBM8901 cells were treated with the indicated compounds for 24 h. The cells were then stained with 1 μg/mL acridine orange for 15 min, washed with RPMI 1640 medium, and examined under the fluorescence microscope.

**Protein Expression Knockdown by siRNA Technology.** The beclin1 and Atg7 siRNA gene silencer (human) dsRNA was obtained from Santa Cruz Biotechnology (sc-44286 and sc-41448). Neuroblastoma cells were transfected with dsRNAs using siRNA transfection reagent (Santa Cruz) and incubated for 6 h. Afterward, the cells were analyzed by immunoblot for protein expression.

**Statistical Analysis.** All data were obtained from at least three separate experiments and were expressed as the mean ± standard error of the mean (SEM). Statistical comparison of the differences among multiple groups was performed using one-way analysis of variation

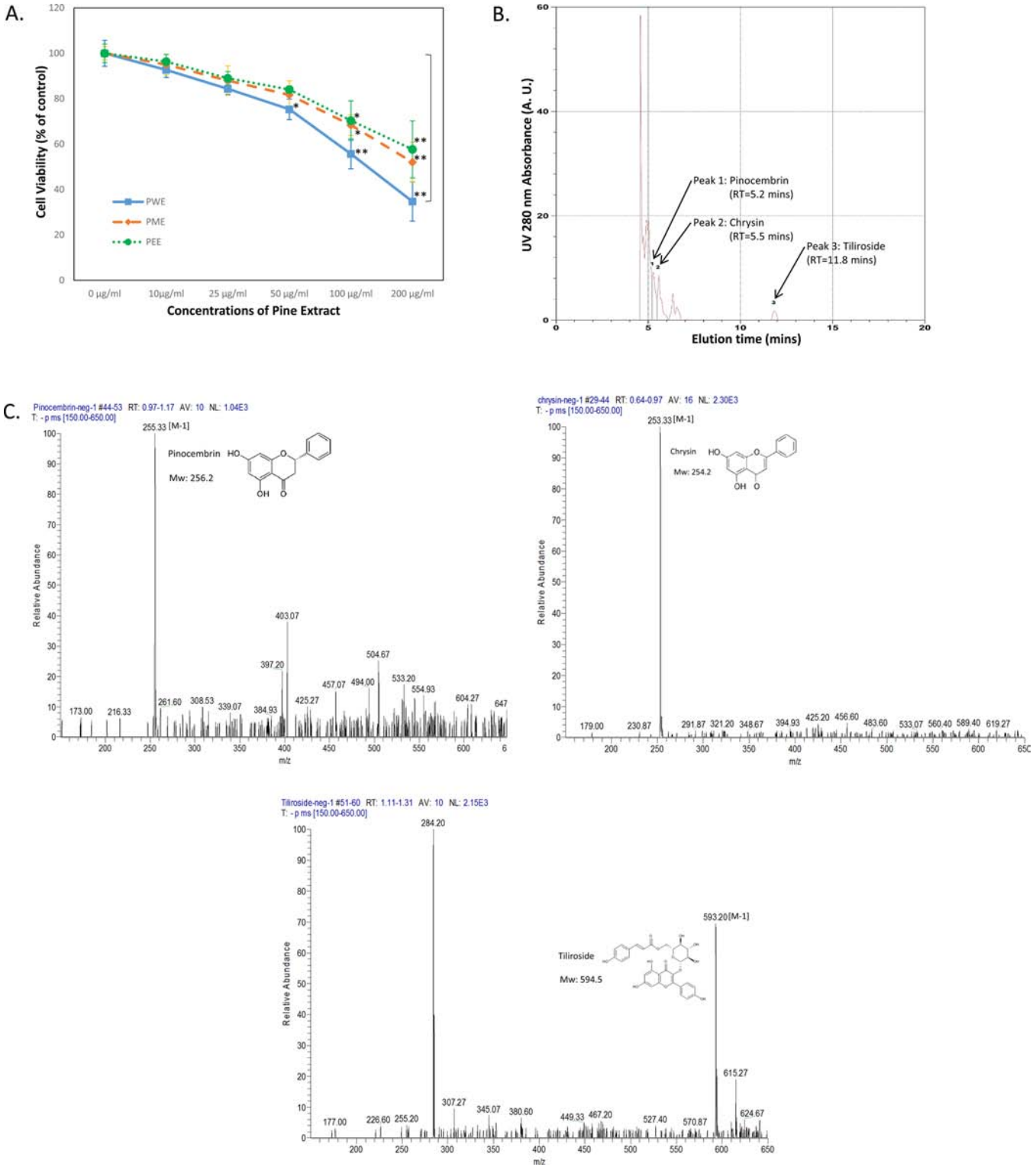


**Figure 1.** *P. morrisonicola* Hayata needle extracts have cytotoxic effects on GBM8901 cells. (A) Cytotoxic potential of the three solvent extracts. GBM8901 cells were incubated with 0−200 $\mu$g/mL pine extracts for 24 h. Cytotoxicity was measured using the MTT method, and the values are represented as the mean ± SEM of triplicates. PME, pine methanol extract; PEE, pine ethanol extract; PWE, pine water extract. (B) Major ingredients of PWE were identified by HPLC. Three compounds, pinocembrin [retention time (RT) = 5.2 min], chrysin (RT = 5.5 min), and tiliroside (RT = 11.8 min), were identified in the extracts. (C) MS/MS product ion profiles of pinocembrin, chrysin, and tiliroside. (∗) $p < 0.05$ and (∗∗) $p < 0.01$ when compared to non-treated cells using the one-way ANOVA test.

(ANOVA) tests, and differences between pairs of groups were compared using Student's $t$ test. Statistical significance was assumed when the $p$ value was ≤0.05. All of the statistical analyses were performed using the SPSS statistical software (SPSS, Inc., Chicago, IL).

## RESULTS

### Cytotoxic Effects of Various Solvent Extracts of *P. morrisonicola* (Hayata) on the GBM8901 Cell Line.


dx.doi.org/10.1021/jf501234b | J. Agric. Food Chem. 2014, 62, 10458−10467

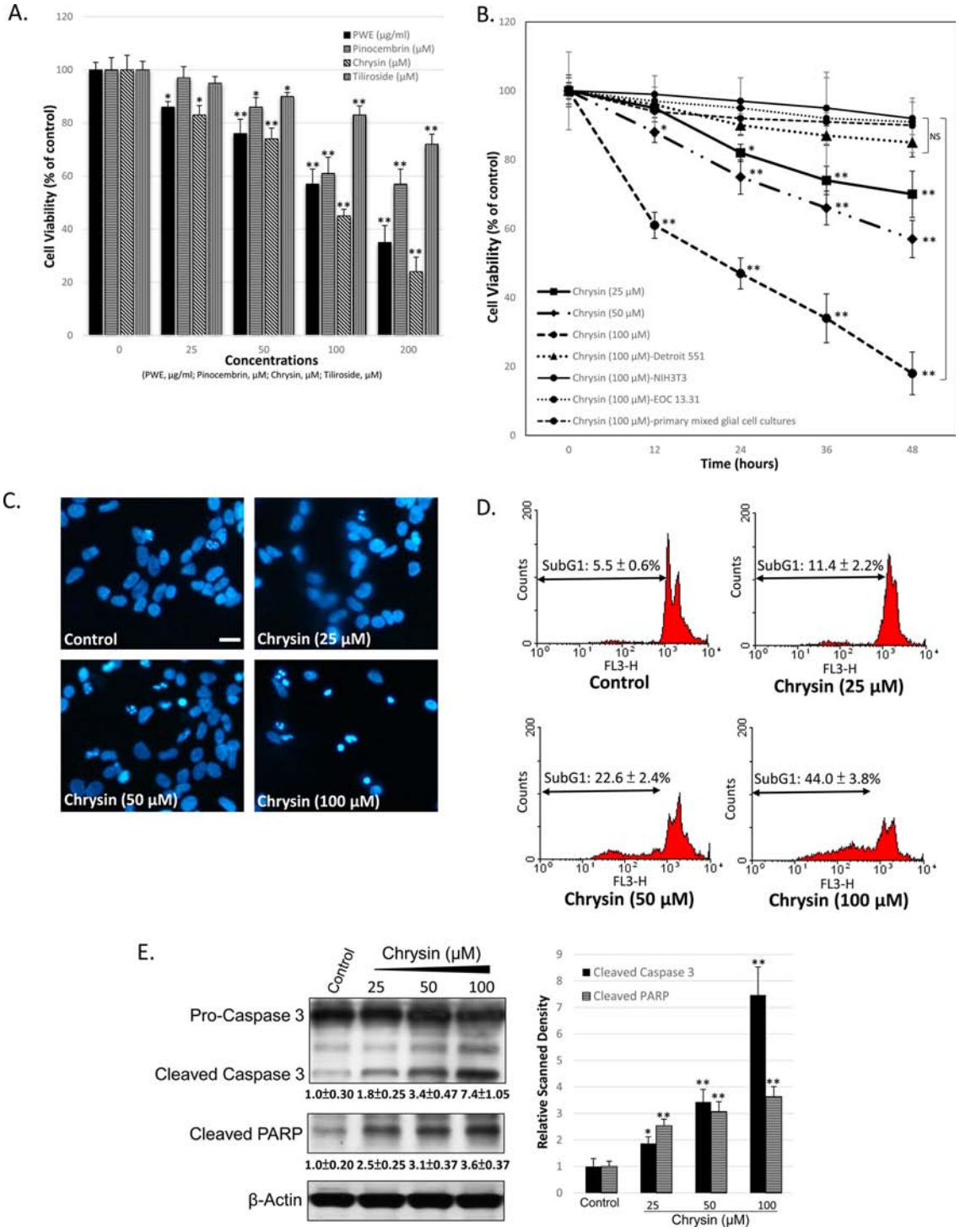


**Figure 2.** Chrysin-induced apoptosis in GBM8901 cells. (A) Effects of PWE, pinocembrin, chrysin, and tiliroside against GBM8901 cells after 24 h of treatment. Among these compounds, chrysin showed the most powerful anti-glioblastoma activity by reducing cell viability. (B) Chrysin exerted cytotoxicity in GBM8901 cells in a dose-dependent manner but only limited the effect in Detroit 551 human normal skin fibroblasts at a concentration of 100 $\mu$M. Measuring apoptosis by (C) fragmented nuclei stained and (D) flow cytometry analysis. (E) Caspase 3 and PARP activation were determined by immunoblotting and evaluated in chrysin-treated GBM8901 cells. Results are expressed as the mean ± SEM of three independent experiments performed in triplicates. (*) $p < 0.05$ and (**) $p < 0.01$ when compared to non-treated cells using the one-way ANOVA test. Proteins from three independent western blot experiments were quantified using densitometry and normalized to actin band intensity. The scale bar represents 50 $\mu$m.

Phenolic compounds are commonly present in pine and are reported to have multiple biological effects, such as growth suppression and death induction. To determine whether pine needle extracts have antiproliferative effects on glioblastoma cells, the ability of crude pine needle extracts to inhibit the viability of GBM8901 cells was examined. Figure 1A shows the cytotoxic effect of various solvent extracts of pine needles, including PME, PEE, and PWE. The $IC_{50}$ values of PWE, PME, and PEE were 121.0, 208.5, and 243.7 $\mu$g/mL, respectively. Of these different solvent extracts, the inhibitory effect of PME was


dx.doi.org/10.1021/jf501234b | J. Agric. Food Chem. 2014, 62, 10458−10467

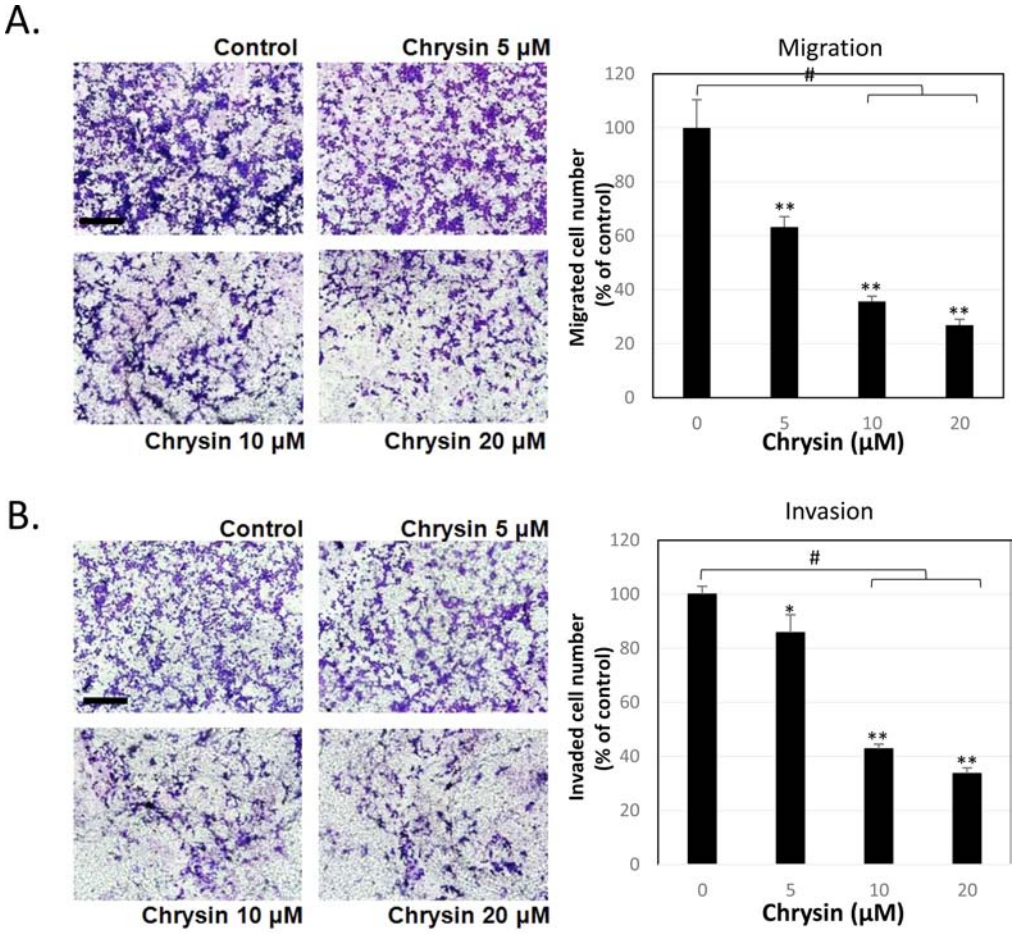


**Figure 3.** Chrysin inhibits the migration and invasion of GBM8901 cells. Transwell migration and Matrigel invasion assays showed that chrysin treatment resulted in a significant inhibition of (A) 74% in migration and (B) 68% in invasion. Experiments were performed in triplicates, and values are presented as the mean ± SEM. (#) $p < 0.05$ for one-way ANOVA or (∗) $p < 0.05$ and (∗∗) $p < 0.01$ for Student's $t$ test.

similar to that of PEE at a higher concentration. However, the $IC_{50}$ value of PWE on GBM8901 cell viability was the lowest. To determine the active ingredients on pine needle extracts that act against GBM8901 cells, the PWE was further analyzed using HPLC (Figure 1B). Using C18 column material and an acidic mobile phase, all of the major constituents of PWE were well-resolved within 20 min. HPLC signals were assigned by standard comparison of UV spectra and were then used directly for MS/MS studies to identify the specific compounds. Using these methods, three compounds were identified from the extract: pinocembrin, chrysin, and tiliroside. These results indicate that the three phenolic compounds were predominantly present in PWE and represented approximately 29% of the total flavonoid content.

**Chrysin Reduces the Proliferation and Induces Apoptosis in GBM8901 Cells.** To determine the most active component of PWE, the cytotoxicity of these pure individual compounds was examined. As shown in Figure 2A, all of the compounds inhibited the proliferation of GBM8901 cells significantly. However, chrysin showed the highest inhibitory activity against GBM8901 cells, indicating that chrysin has a greater anti-glioblastoma activity in PWE. Figure 2B shows that chrysin concentrations ranging from 25 to 100 $\mu$M inhibited the growth of GBM8901 cells in a time-dependent manner. The growth inhibition was approximately 50% at a concentration of 100 $\mu$M after 24 h. However, exposure of several normal cell lines, including Detroit 551, NIH3T3, EOC 13.31, and rat primary mixed glial cells, to 100 $\mu$M chrysin did not induce significant growth inhibition. These results confirmed that chrysin might inhibit the growth of glioblastoma cancer cells without significantly affecting normal cells. To determine further the relationship between growth inhibition and apoptosis, cells were stained with the nuclear staining cytochemistry dye DAPI to analyze the morphology of the nuclei. As shown in Figure 2C, observation of stained fragmented nuclei confirmed that chrysin induced apoptosis in GBM8901 cells. Apoptotic cells were simultaneously quantified by flow cytometry, and there was a significant increase in the percentage of cells in the sub-G1 phase after treatments of chrysin (Figure 2D). Apoptosis induction by chrysin was further examined by western blotting. Figure 2E shows a dose-dependent cleavage of caspase 3 and poly(ADP-ribose)-polymerase (PARP) in GBM8901 cells treated with chrysin. Thus, a higher concentration of chrysin (100 $\mu$M) induced apoptosis after 24 h of treatment.

**Chrysin Inhibits Migration and Invasion by GBM8901 Cells.** The above results showed that chrysin induced apoptosis in glioblastoma cells through caspase 3 and PARP pathways. However, a low concentration of chrysin (25 $\mu$M) did not show this strong apoptosis-inducing effect. Most studies have reported that glioblastoma is the most migratory and invasive brain tumor and is invariably fatal for affected patients.[15] Therefore, GBM8901 cells were treated with chrysin to determine their


dx.doi.org/10.1021/jf501234b | J. Agric. Food Chem. 2014, 62, 10458−10467

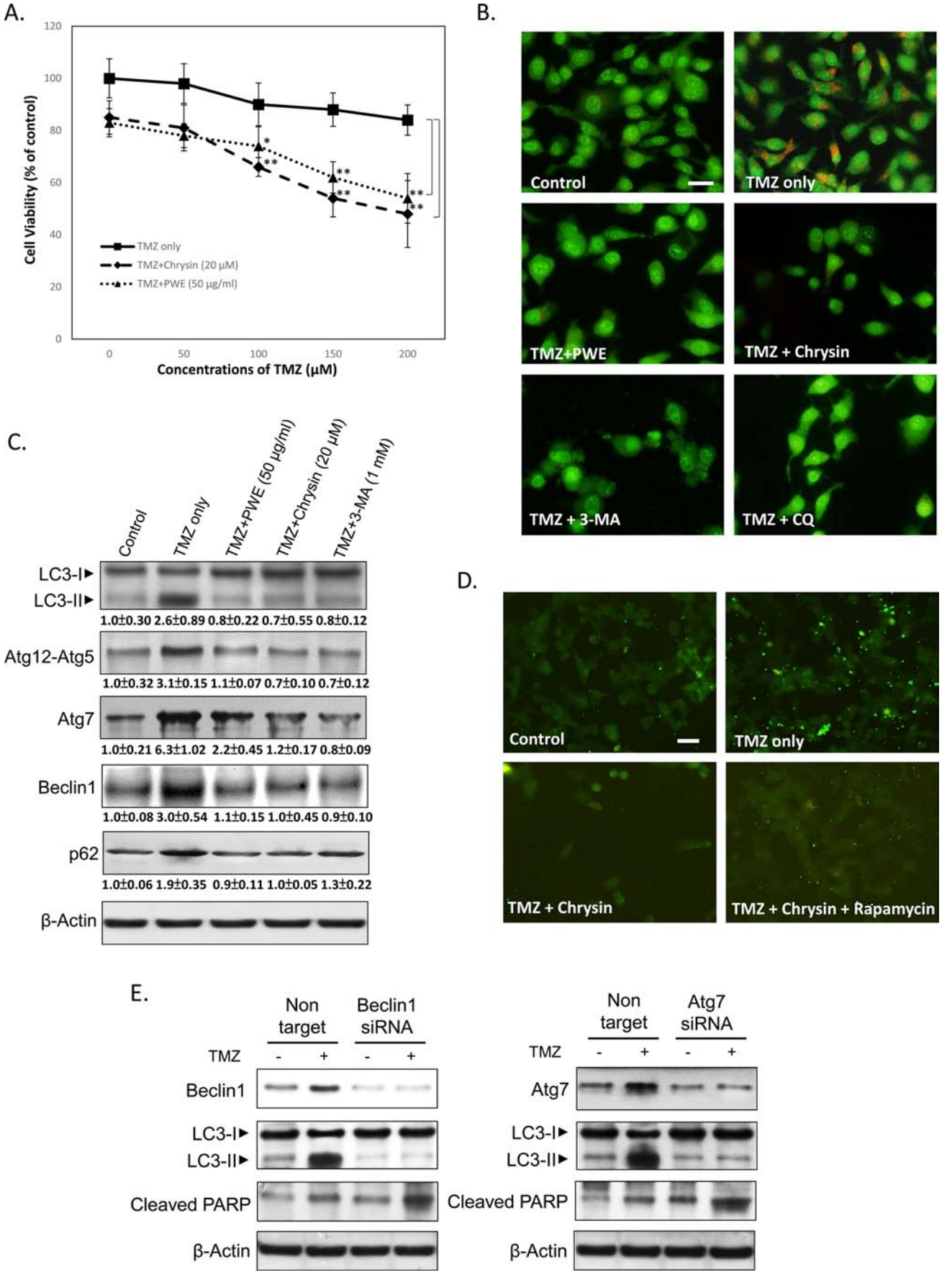


**Figure 4.** continued


dx.doi.org/10.1021/jf501234b | J. Agric. Food Chem. 2014, 62, 10458−10467

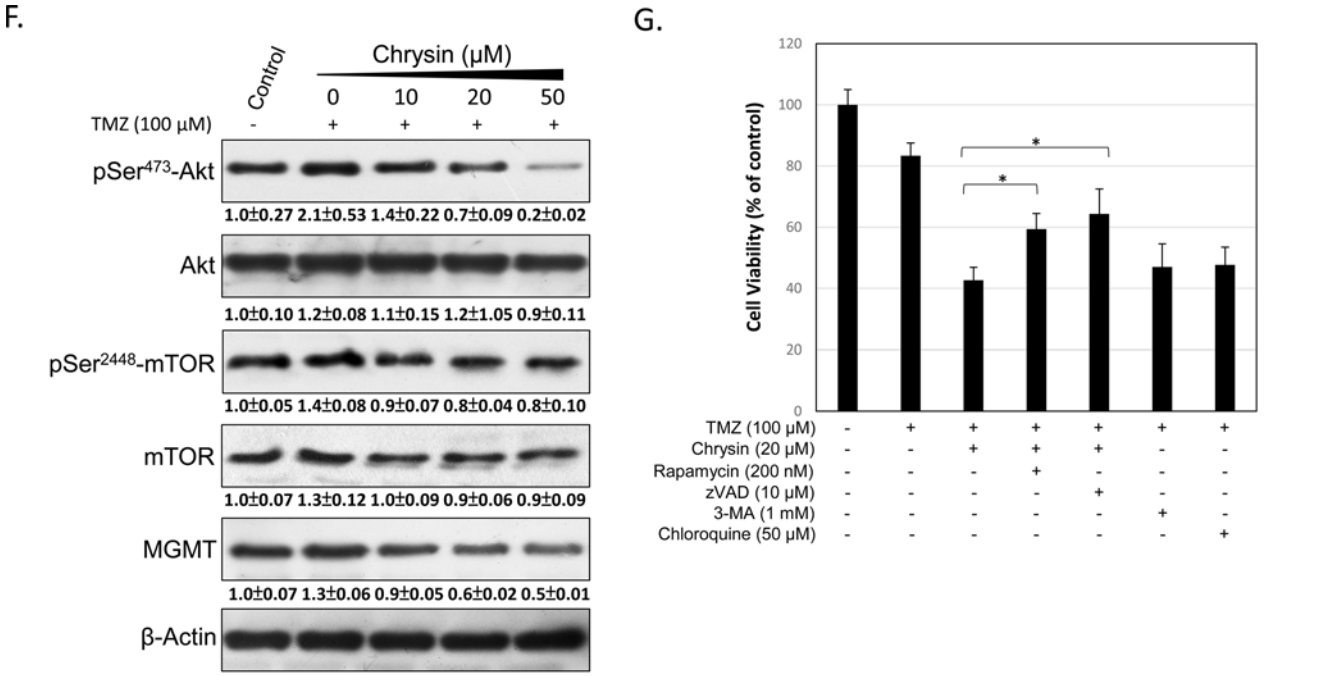


**Figure 4.** Chrysin sensitizes GBM8901 cells to TMZ-induced cytotoxicity. (A) Cells were treated for 24 h with the indicated concentrations of TMZ and chrysin (20 $\mu$M) or PWE (50 $\mu$g/mL). (*) $p < 0.05$ and (**) $p < 0.01$ when compared to TMZ-treated cells for the one-way ANOVA test. (B) Fluorescence microscopy analysis of GBM8901 cells treated with TMZ and chrysin (20 $\mu$M), PWE (50 $\mu$g/mL), 3-MA (1 mM), or CQ (50 $\mu$M) for 24 h, followed by acridine orange staining. The formation of acridine-orange-accumulating acidic vacuoles (orange−red fluorescence) in TMZ-treated cells was significantly suppressed by chrysin, PWE, and autophagic inhibitors 3-MA or CQ treatments. (C) Western blots showing autophagy induction by monitoring LC3, Atg12−Atg5 conjugate, Atg7, beclin1, and p62 levels in GBM8901 cells treated or not treated with TMZ (100 $\mu$M) alone or in combination with PWE (50 $\mu$g/mL), chrysin (20 $\mu$M), or 3-MA (1 mM) for 24 h. (D) Fluorescent microscopy analysis of cells LC3 treated with TMZ (100 $\mu$M) alone or combined with chrysin (20 $\mu$M) or rapamycin (200 nM) co-treatments for 24 h. (E) Beclin1 and Atg7 siRNA (20 nmol/L pool) knockdown was confirmed via western blot, and autophagy blockade was validated using LC3-II western blot. Enhanced apoptosis in response to TMZ (100 $\mu$M) was determined via PARP cleavage. (F) Western blot analysis showed p-Akt/Akt, p-mTOR/mTOR, and MGMT in GBM8901 cells alone or treated with increasing concentrations of chrysin in combination with TMZ (100 $\mu$M). (G) Both rapamycin (200 nM) and zVAD-fmk (10 $\mu$M) treatments for 24 h blocked chrysin-induced cell death significantly. However, 3-MA or CQ treatments enhance cell death similar to that in chrysin-treated groups. (*) $p < 0.05$ and (**) $p < 0.01$ when compared to cells treated with TMZ + chrysin for Student's $t$ test. The mean ± SEM of three independent experiments performed in triplicates is shown. Proteins from three independent western blot experiments were quantified using densitometry and normalized to actin band intensity. The scale bar represents 50 $\mu$m.

migratory and invasive capacities, which are the two most important features of malignant cells. As shown in Figure 3A, chrysin treatment remarkably suppressed the migration of GBM8901 cells by approximately 40−70% in a dose-dependent manner compared to that in control groups. Because cell migration is believed to be a fundamental step in tumor invasion, we next examined the effect of chrysin on the invasive capacity of GBM8901 cells. Treatment of Matrigel-coated wells with chrysin reduced cell invasion significantly in a dose-dependent manner. Because we used a lower dose of chrysin, the above anti-metastatic effects of chrysin were not mainly attributed to its cytotoxicity, as shown in Figure 2B. Our findings suggest that low levels of chrysin effectively inhibited cell migration and invasion by GBM8901 cells.

**Chrysin Sensitizes GBM8901 Cells to TMZ by Inhibiting Autophagy and Attenuating MGMT Expression.** Because TMZ therapy is the current standard of care for patients with malignant glioblastoma, we next examined whether TMZ can decrease cell growth of the GBM8901 cell line. As shown in Figure 4A, TMZ was unable to decrease the growth of GBM8901 cells even at concentrations of up to 200 $\mu$M. These results are consistent with the results of previous studies, which showed that GBM8901 cells are grade-IV GBM cells with an inherent tendency of drug resistance and recurrence.[16] In contrast, a combination of PWE (50 $\mu$g/mL) or chrysin (20 $\mu$M) with TMZ had synergistic cytotoxic effects on GBM8901 cells. This suggested that PWE or chrysin might be effective TMZ-sensitizing agents. Studies have been reported that therapeutic resistance of glioblastoma is attributed to the activation of drug-induced autophagy. Therefore, we first used acridine orange staining to examine whether acidic vacuoles were induced in GBM8901 cells after treatment with TMZ. After exposure to TMZ (100 $\mu$M) for 24 h, cells showed an increase in orange fluorescence, indicating the accumulation of acridine orange in the acidic compartments of TMZ-treated cells. However, co-treatment with PWE or chrysin significantly decreased the orange fluorescence (Figure 4B). Similar to PWE or chrysin, treated cells with the autophagy inhibitors 3-methyladenine (3-MA) and chloroquine (CQ) can both significantly reduce the number of detected orange acidic vesicles. To verify the obtained results, western immunoblotting was performed to probe the autophagy hallmark LC3. TMZ-induced autophagy was determined by the shift in the molecular weight of LC3 from LC3-I to LC3-II. On the other hand, PWE or chrysin markedly inhibited TMZ-induced LC3-II formation. Similar reduction was observed in Atg7, Atg12−Atg5 conjugate, beclin1, and p62. Besides, autophagy inhibition was accomplished using 3-MA, which caused similar effects compared to chrysin groups (Figure

4C). Furthermore, an increase of LC3 punctate dots was observed in TMZ-only groups but abolished by co-treating of chrysin (Figure 4D). In contrast, chrysin-induced autophagy blockade returned to levels similar to those of control for the rapamycin-treated cells. Thus, these independent approaches suggested that TMZ-induced autophagy in GBM8901 cells was inhibited by the co-administration of PWE or chrysin. To further confirm the observations, knockdown of the autophagy constituent, beclin1 and Atg7, was conducted using target-specific siRNAs and cells were treated with or without TMZ, as shown in Figure 4E. Both beclin1 and Atg7 knockdown resulted in pronounced GBM8901 cell apoptosis in response to TMZ treatment. One study reported that TMZ-induced autophagy in glioblastoma cells is dependent upon MGMT.[17] Because MGMT overexpression is a principle mechanisms contributing to TMZ resistance in glioblastoma cells, we examined whether chrysin regulated MGMT expression to increase sensitivity to TMZ. Immunoblotting results shown in Figure 4F indicated that GBM8901 cells expressed higher levels of MGMT, irrespective of TMZ treatment. However, application of chrysin markedly suppressed MGMT expression by inhibiting AKT signaling in a dose-dependent manner. Besides, the expression of phospho-mTOR ($Ser^{2448}$) was unaltered by chrysin, indicating chrysin-inhibited autophagy through a mTOR signaling-independent pathway. To further elucidate the impact of autophagy on chrysin-mediated cell death, GBM8901 cells were treated with autophagy inducers or inhibitors to determine cell viability. As shown in Figure 4G, 3-MA or CQ enhanced glioblastoma cell death similar to that in chrysin-treated groups. However, both rapamycin and zVAD-fmk treatments blocked chrysin-induced cell death, indicating that autophagy supported the viability of GBM8901 cells against chrysin-induced apoptosis. Taken together, these data showed that chrysin might sensitize GBM8901 cells to TMZ by attenuating MGMT expression and TMZ-induced autophagy simultaneously.

## DISCUSSION

Glioblastoma is the most malignant human brain tumor, characterized by increased growth and invasion. The standard therapy for glioblastoma is maximal resection, followed by radiotherapy and concurrent chemotherapy with drugs, such as TMZ. However, glioblastoma is still associated with poor prognosis because of high recurrence after TMZ chemotherapy. To enhance the benefit of TMZ in the treatment of aggressive glioblastoma, effective combination strategies that sensitize glioblastoma cells to TMZ are important to prevent the recurrence of these tumors. In this regard, natural products, such as flavonoids, have received considerable attention because of their lower side effects.[18] In this study, we evaluated the inhibitory effects of pine needle extracts on a malignant glioblastoma cell line GBM8901. Our results showed that chrysin, a major biologically active component in pine needle extracts, inhibited the growth and invasiveness of the glioblastoma cell line. We further observed that chrysin also suppressed TMZ-induced autophagy, which protects glioblastoma cells against chronic TMZ treatment. Signaling through both the Akt pathway and autophagy is frequently activated in glioblastoma cells.[19] Because autophagy is a prosurvival response that makes glioblastoma cells resistant to chemotherapy, our results suggested that use of the nutraceutical chrysin for inhibiting Akt activation and stress-induced autophagy may be a potential therapeutic approach for treating glioblastoma, especially in cases of TMZ-resistant tumor recurrence.

The therapeutic benefit of TMZ also depends upon its ability to alkylate/methylate the DNA in tumor cells. MGMT expression in glioblastoma cells is the most critical determinant of TMZ resistance.[20] MGMT counteracts the effects of TMZ by removing DNA methyl adducts, suggesting that downregulation of MGMT is effective for the management of TMZ-resistant glioblastoma.[21] To date, many clinical trials have aimed to modulate MGMT expression for increasing TMZ efficiency. In this regard, our present study showed that chrysin administration suppressed MGMT expression. Previous studies have suggested that Akt activation contributes to MGMT overexpression in glioblastoma.[22] These findings indicated that chrysin-inhibited Akt signaling may be a strong and selective approach against TMZ-resistant glioblastoma.[23] Logically, activation of Akt-mTOR signaling inhibits autophagy. However, our data indicated that mTOR phosphorylation was unaltered but phosphorylation of Akt at $Ser^{473}$ was significantly inactivated by chrysin treatment. This indicates chrysin-inhibited autophagy through an Akt-mTOR signaling-independent pathway. Interestingly, accumulating studies indicated that autophagy is mediated in many circumstances by negative modulation of apoptosis.[24] Moreover the autophagy-associated protein, LC3, and Akt were maintained during the treatment with TMZ, suggesting that glioblastoma cells escape from TMZ-induced cell death because of Akt signaling pathways.[25] Our results demonstrated that chrysin induces apoptosis and downregulates Akt of GBM8901 cells significantly, suggesting that chrysin-induced apoptotic signaling serves to inhibit autophagy. This result is consistent with those of previous studies, which have shown that pharmacologic inhibition of stress-induced autophagy was reported to promote chemotherapeutic response.[26] However, the mechanisms mediating the counter-regulation of apoptosis and autophagy are not yet fully understood. In addition, recent studies have reported that chrysin inhibits nuclear factor E2-related factor 2 (Nrf2) by downregulating the PI3K/Akt/Nrf2 pathway.[27] The Nrf2 signaling is known to activate autophagy-related genes independent of mTOR.[28] Thus, our data indicated that chrysin decreased the expression of Akt, which may have contribute to the inhibition of autophagy by a similar pathway in GBM8901 cells. However, these ideas remain to be examined further.

Chrysin, a natural, biologically active dietary flavonoid extracted from propolis and other plants, has various beneficial health effects. Chrysin exerts an anticancer effect through various mechanisms, including inhibition of the PI3K/Akt pathway and activation of mitogen/stress-activated kinase 1 (MSK1) signaling.[29,30] Chrysin also selectively sensitizes cancer cells to apoptosis via tumor necrosis factor-related apoptosis-inducing ligand (TRAIL) by inhibiting STAT3 and Mcl-1.[31] Moreover, chrysin decreases the expression of vimentin, suggesting that it attenuates epithelial−mesenchymal transition and suppresses metastases.[29] This results indicate the potential of chrysin in treating cancer and overcoming therapeutic resistance. In this study, we reported that chrysin is an active compound in pine needle extracts and potentially inhibits autophagy and MGMT expression, thus sensitizing glioblastoma cells to TMZ. Similar results were obtained by Markiewicz-Żukowska et al., who showed antiproliferative properties of chrysin-rich ethanolic extract of propolis in glioblastoma and its synergistic action with TMZ.[32] On the basis of these results, we proposed that chrysin may be a useful monotherapy to enhance brain tumor apoptosis and inhibit tumor migration/invasion or a component of combination therapy to overcome TMZ resistance and prolong

the survival of patients with malignant glioblastoma. Pine needle extracts and chrysin are reported to have various effects on the central nervous system (CNS),[13,33] suggesting that chrysin may have the ability to cross the blood−brain barrier (BBB). In fact, most flavonoids are amphipathic molecules that appears to be capable of passing the BBB and reaching the CNS.[34] However, further studies, especially in *in vivo* models, are needed to elucidate the efficacy of the anti-glioblastoma effects of chrysin.

In conclusion, we identified an efficient method to extract chrysin from pine needles and evaluated the anti-glioblastoma effects of chrysin, which could be potentially used as an efficacious component in functional food products. Our study also showed a novel role of chrysin in sensitizing glioblastoma cells to TMZ. These findings are consistent with those obtained from a model that simultaneously suppresses TMZ-induced autophagy and MGMT expression in TMZ-resistant glioblastoma, suggesting that modulation of the autophagic pathway may be a novel way to modify resistance to TMZ. Therefore, chrysin in combination with TMZ chemotherapeutic agent warrants further examination.

## AUTHOR INFORMATION

### Corresponding Author

*Telephone: +886-4-2473-0022, ext. 12405. Fax: +886-4-2472-3229. E-mail: dll@csmu.edu.tw.

### Funding

This work was supported by grants from the Chung Shan Medical University−Jen-Ai Hospital (CSMU-JAH-101-002), the Changhua Christian Hospital (101-CCH-IRP-23), and the Ministry of Science and Technology (98-2320-B-040-015-MY3 and 101-2320-B-040-015-MY3). The fluorescence microscope and imaging analyzer were performed in the Instrument Center of Chung Shan Medical University, which is supported by the Ministry of Science and Technology, Ministry of Education, and Chung Shan Medical University.

### Notes

The authors declare no competing financial interest.

## REFERENCES

(1) Yen, G. C.; Duh, P. D.; Huang, D. W.; Hsu, C. L.; Fu, T. Y. Protective effect of pine (*Pinus morrisonicola* Hay.) needle on LDL oxidation and its anti-inflammatory action by modulation of iNOS and COX-2 expression in LPS-stimulated RAW 264.7 macrophages. *Food Chem. Toxicol.* **2008**, *46*, 175−185.

(2) Hsu, T. Y.; Sheu, S. C.; Liaw, E. T.; Wang, T. C.; Lin, C. C. Antioxidant activity and effect of *Pinus morrisonicola* Hay. on the survival of leukemia cell line U937. *Phytomedicine* **2005**, *12*, 663−669.

(3) Park, Y. S.; Jeon, M. H.; Hwang, H. J.; Park, M. R.; Lee, S. H.; Kim, S. G.; Kim, M. Antioxidant activity and analysis of proanthocyanidins from pine (*Pinus densiflora*) needles. *Nutr. Res. Pract.* **2011**, *5*, 281−287.

(4) Vehlow, A.; Cordes, N. Invasion as target for therapy of glioblastoma multiforme. *Biochim. Biophys. Acta* **2013**, *1836*, 236−244.

(5) Omuro, A.; DeAngelis, L. M. Glioblastoma and other malignant gliomas: A clinical review. *J. Am. Med. Assoc.* **2013**, *310*, 1842−1850.

(6) Hart, M. G.; Garside, R.; Rogers, G.; Stein, K.; Grant, R. Temozolomide for high grade glioma. *Cochrane Database Syst. Rev.* **2013**, *4*, No. CD007415.

(7) Johannessen, T. C.; Bjerkvig, R. Molecular mechanisms of temozolomide resistance in glioblastoma multiforme. *Expert Rev. Anticancer Ther.* **2012**, *12*, 635−642.

(8) Silber, J. R.; Bobola, M. S.; Blank, A.; Chamberlain, M. C. $O^6$-Methylguanine-DNA methyltransferase in glioma therapy: Promise and problems. *Biochim. Biophys. Acta* **2012**, *1826*, 71−82.

(9) Lin, C. J.; Lee, C. C.; Shih, Y. L.; Lin, T. Y.; Wang, S. H.; Lin, Y. F.; Shih, C. M. Resveratrol enhances the therapeutic effect of temozolomide against malignant glioma in vitro and in vivo by inhibiting autophagy. *Free Radical Biol. Med.* **2012**, *52*, 377−391.

(10) Lefranc, F.; Kiss, R. Autophagy, the Trojan horse to combat glioblastomas. *Neurosurg. Focus* **2006**, *20*, No. E7.

(11) Nuopponen, M.; Willfor, S.; Jaaskelainen, A. S.; Vuorinen, T. A UV resonance Raman (UVRR) spectroscopic study on the extractable compounds in Scots pine (*Pinus sylvestris*) wood. Part II. Hydrophilic compounds. *Spectrochim. Acta, Part A* **2004**, *60*, 2963−2968.

(12) Khoo, B. Y.; Chua, S. L.; Balaram, P. Apoptotic effects of chrysin in human cancer cell lines. *Int. J. Mol. Sci.* **2010**, *11*, 2188−2199.

(13) Bolandghamat, S.; Moghimi, A.; Iranshahi, M. Effects of ethanolic extract of pine needles (*Pinus eldarica* Medw.) on reserpine-induced depression-like behavior in male Wistar rats. *Pharmacogn. Mag.* **2011**, *7*, 248−253.

(14) Tamashiro, T. T.; Dalgard, C. L.; Byrnes, K. R. Primary microglia isolation from mixed glial cell cultures of neonatal rat brain tissue. *J. Visualized Exp.* **2012**, No. e3814.

(15) Alves, T. R.; Lima, F. R.; Kahn, S. A.; Lobo, D.; Dubois, L. G.; Soletti, R.; Borges, H.; Neto, V. M. Glioblastoma cells: A heterogeneous and fatal tumor interacting with the parenchyma. *Life Sci.* **2011**, *89*, 532−539.

(16) Lee, P. Y.; Chen, C. L.; Lin, Z. Z.; Cheng, A. L.; Chen, E. I.; Whang-Peng, J.; Huang, C. Y. The Aurora kinases inhibitor VE-465 is a novel treatment for glioblastoma multiforme. *Oncology* **2013**, *84*, 326−335.

(17) Knizhnik, A. V.; Roos, W. P.; Nikolova, T.; Quiros, S.; Tomaszowski, K. H.; Christmann, M.; Kaina, B. Survival and death strategies in glioma cells: Autophagy, senescence and apoptosis triggered by a single type of temozolomide-induced DNA damage. *PloS One* **2013**, *8*, No. e55665.

(18) Haar, C. P.; Hebbar, P.; Wallace, G. C., IV; Das, A.; Vandergrift, W. A., III; Smith, J. A.; Giglio, P.; Patel, S. J.; Ray, S. K.; Banik, N. L. Drug resistance in glioblastoma: A mini review. *Neurochem. Res.* **2012**, *37*, 1192−1200.

(19) Fan, Q. W.; Weiss, W. A. Autophagy and Akt promote survival in glioma. *Autophagy* **2011**, *7*, 536−538.

(20) Jiang, G.; Li, L. T.; Xin, Y.; Zhang, L.; Liu, Y. Q.; Zheng, J. N. Strategies to improve the killing of tumors using temozolomide: Targeting the DNA repair protein MGMT. *Curr. Med. Chem.* **2012**, *19*, 3886−3892.

(21) Fukushima, T.; Takeshima, H.; Kataoka, H. Anti-glioma therapy with temozolomide and status of the DNA-repair gene MGMT. *Anticancer Res.* **2009**, *29*, 4845−4854.

(22) Zhang, L. H.; Yin, A. A.; Cheng, J. X.; Huang, H. Y.; Li, X. M.; Zhang, Y. Q.; Han, N.; Zhang, X. TRIM24 promotes glioma progression and enhances chemoresistance through activation of the PI3K/Akt signaling pathway. *Oncogene* **2014**, DOI: 10.1038/onc.2013.593.

(23) Sami, A.; Karsy, M. Targeting the PI3K/AKT/mTOR signaling pathway in glioblastoma: Novel therapeutic agents and advances in understanding. *Tumor Biol.* **2013**, *34*, 1991−2002.

(24) Gordy, C.; He, Y. W. The crosstalk between autophagy and apoptosis: Where does this lead? *Protein Cell* **2012**, *3*, 17−27.

(25) Carmo, A.; Carvalheiro, H.; Crespo, I.; Nunes, I.; Lopes, M. C. Effect of temozolomide on the U-118 glioma cell line. *Oncol. Lett.* **2011**, *2*, 1165−1170.

(26) Zou, Y.; Wang, Q.; Li, B.; Xie, B.; Wang, W. Temozolomide induces autophagy via ATMAMPKULK1 pathways in glioma. *Mol. Med. Rep.* **2014**, *10*, 411−416.

(27) Gao, A. M.; Ke, Z. P.; Shi, F.; Sun, G. C.; Chen, H. Chrysin enhances sensitivity of BEL-7402/ADM cells to doxorubicin by suppressing PI3K/Akt/Nrf2 and ERK/Nrf2 pathway. *Chem.-Biol. Interact.* **2013**, *206*, 100−108.

(28) Mizushima, N.; Levine, B. Autophagy in mammalian development and differentiation. *Nat. Cell Biol.* **2010**, *12*, 823−830.

(29) Yang, B.; Huang, J.; Xiang, T.; Yin, X.; Luo, X.; Huang, J.; Luo, F.; Li, H.; Li, H.; Ren, G. Chrysin inhibits metastatic potential of human triple-negative breast cancer cells by modulating matrix metalloproteinase-10, epithelial to mesenchymal transition, and PI3K/Akt signaling pathway. *J. Appl. Toxicol.* **2014**, *34*, 105−112.

(30) Liu, H.; Hwang, J.; Li, W.; Choi, T. W.; Liu, K.; Huang, Z.; Jang, J. H.; Thimmegowda, N. R.; Lee, K. W.; Ryoo, I. J.; Ahn, J. S.; Bode, A. M.; Zhou, X.; Yang, Y.; Erikson, R. L.; Kim, B. Y.; Dong, Z. A derivative of chrysin suppresses two-stage skin carcinogenesis by inhibiting mitogen- and stress-activated kinase 1. *Cancer Prev. Res.* **2014**, *7*, 74−85.
(31) Lirdprapamongkol, K.; Sakurai, H.; Abdelhamed, S.; Yokoyama, S.; Athikomkulchai, S.; Viriyaroj, A.; Awale, S.; Ruchirawat, S.; Svasti, J.; Saiki, I. Chrysin overcomes TRAIL resistance of cancer cells through Mcl-1 downregulation by inhibiting STAT3 phosphorylation. *Int. J. Oncol.* **2013**, *43*, 329−337.
(32) Markiewicz-Żukowska, R.; Borawska, M. H.; Fiedorowicz, A.; Naliwajko, S. K.; Sawicka, D.; Car, H. Propolis changes the anticancer activity of temozolomide in U87MG human glioblastoma cell line. *BMC Complementary Altern. Med.* **2013**, *13*, 50.
(33) Jager, A. K.; Saaby, L. Flavonoids and the CNS. *Molecules* **2011**, *16*, 1471−1485.
(34) Faria, A.; Meireles, M.; Fernandes, I.; Santos-Buelga, C.; Gonzalez-Manzano, S.; Duenas, M.; de Freitas, V.; Mateus, N.; Calhau, C. Flavonoid metabolites transport across a human BBB model. *Food Chem.* **2014**, *149*, 190−196.

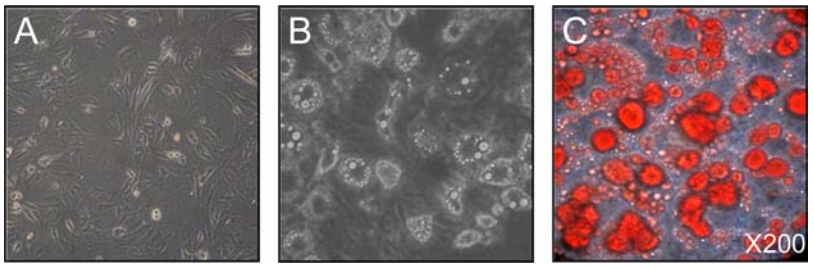


**Figure 1.** Morphology and oil red O staining of differentiated 3T3-L1 cells: (A) morphology of 3T3-L1 preadipocytes before differentiation; (B) morphology of differentiated 3T3-L1 cells at 10 day. (C) On 10 day after differentiation, the cells were stained with oil red O and viewed under a microscope.

kinase 1 (S6K1) and the mammalian target of rapamycin complex 1 (mTORC1) signaling pathway in adipose tissue, suggesting that this compound regulates diet-induced obesity.[19]

However, there has been no study on the effect of fisetin on the regulation of adipokines, particularly adiponectin, in terms of obesity and adiposity. Therefore, this study aimed to investigate the effect of fisetin on the regulation of adiponectin expression in association with other related regulators such as SIRT1 and PPARs using 3T3-L1 preadipocyte cells, which finally differentiate to mature adipocytes.

## MATERIALS AND METHODS

**Materials.** Fisetin, dexamethasone, 3-isobutyl-1-methylxanthine (IBMX), insulin, oil red O, and sirtinol were obtained from Sigma-Aldrich (St. Louis, MO, USA). PPAR$\alpha$ antagonist GW6471 was purchased from Tocris (Ellisville, MO, USA). PPAR$\gamma$ antagonist T0070907 was purchased from Cayman (Ann Arbor, MI, USA). Anti-adiponectin, anti-PPAR$\alpha$, anti-PPAR$\gamma$, anti-PGC-1, anti-acetyl-lysine, anti-AMPK, anti-phospho-AMPK (T172), and anti-$\beta$-actin antibodies were obtained from Santa Cruz Biotechnology (Santa Cruz, CA, USA). SIRT1 siRNA and scrambled control siRNA-A were also purchased from Santa Cruz Biotechnology. Anti-rabbit IgG light chain was purchased from Aviva Systems Biology (San Diego, CA, USA). A mouse adiponectin Quantikine ELISA kit was purchased from R&D Systems (Minneapolis, MN, USA).

**Cell Culture and Differentiation.** 3T3-L1 mouse preadipocytes were obtained from American Type Culture Collection (ATCC, Rockville, MD, USA). Preadipocytes were maintained under Dulbecco's modified Eagle's medium (DMEM) supplemented with 10% bovine calf serum (BCS) in a 37 °C humidified atmosphere containing 5% $CO_2$. Passage numbers of cells used were between 10 and 20. Two days after full confluence, cells were induced to differentiate by exposure to 1 $\mu$M dexamethasone, 0.5 mM IBMX, and 10 $\mu$g/mL insulin in DMEM with 10% FBS for 72 h. Cells were replaced with DMEM supplemented with 10% FBS and 10 $\mu$g/mL insulin. Another 2 days later, the medium was changed to DMEM with 10% FBS. Thereafter, cells were maintained by exchanging media every 2 days with DMEM with 10% FBS until used in the experiments 10−14 days after initiation of the differentiation protocol. The cells were used for experiments whenever 80−90% of the cells exhibited the adipocyte phenotype by accumulation of lipid droplets.

**Oil Red O Staining.** Cell medium was discarded from fully differentiated 3T3-L1 adipocytes. Cells were prefixed with 10% formalin for 5 min at room temperature. After prefix, formalin was discarded and the same volume of fresh formalin was added. Cells were incubated at room temperature for at least 1 h or more. The parafilm was wrapped over the plate to prevent drying. After fixing of the cells, formalin was discarded, and the cells were washed with 60% isopropanol. After cells were completely dried, oil red O staining working solution (Sigma-Aldrich) filtered at 0.2 $\mu$m pore size was added, and the cells were stained for 10−20 min. After staining, oil red O solution was removed and $dH_2O$ was added immediately. Cells were washed with distilled water four times. Cells were observed and photographed by using an Olympus CKX41 microscope (Olympus, Japan).

**Immunoblot Analysis.** Fisetin-treated differentiated cells were harvested and washed twice in ice-cold PBS. Samples were placed in ice-cold lysis buffer containing 40 mM HEPES (pH 7.5), 120 mM NaCl, 1 mM EDTA, 1% Triton, and EDTA-free protease inhibitor cocktail (Roche Diagnostics, Mannheim, Germany) for 30 min. Cell lysates were clarified by centrifugation (13000 rpm for 30 min). Protein concentrations were determined using a Bicinchoninic Acid Protein Assay Kit (Sigma-Aldrich). Proteins were separated in 8% or 12.5% SDS-PAGE and transferred onto polyvinylidene difluoride (PVDF) membrane (Millipore, Bedford, MA, USA). The membrane was blocked in 5% nonfat dry milk dissolved in Tris-buffered saline (TBS) for 1 h. After washing with TBS with 0.05% Tween-20, the membrane was incubated with primary antibodies and then incubated with horseradish peroxidase (HRP)-conjugated secondary antibodies. The bands were detected using the enhanced chemiluminescence (ECL) reagent (Santa Cruz Biotechnology).

**Immunoprecipitation.** After cell lysis, cell lysates were clarified by centrifugation. Cell extract (200−500 $\mu$g) was precleared with protein A/G agarose (Santa Cruz Biotechnology) on a rotating platform plate at 4 °C for 1 h. Then sample was incubated with antibody on a rotation platform plate at 4 °C for 2 h. After a washing with PBS, the sample was subjected to SDS-PAGE and immunoblot analysis.

**SIRT1 Activity Assay.** SIRT1 activity assay proceeded with a Deacetylase Fluorometric Activity Assay Kit (Enzo Life Sciences, Farmingdale, NY, USA), according to the manufacturer's instructions. Briefly, differentiated 3T3-L1 cells were treated with different concentrations of fisetin. Cells were extracted as described above, and then the protein concentration in the cell lysate was quantified with deacetylase buffer. Reactions with cell lysate were performed in the presence of 200 $\mu$M Fluor-de-Lys substrate. Then Fluor-de-Lys developer was treated for 30 min. Finally, the fluorescence was read using a fluorometric reader (Victor 3 Multilabel Plate Readers, PerkinElmer, Waltham, MA, USA) with excitation of 360 nm and emission at 460 nm. Negative controls were also included for normalization.

**RT-PCR Analysis.** Cells were harvested, and total RNA was isolated using QIAzol-Regent (Qiagen, Germany). An equal quantity of total RNA was reverse transcribed using Omniscript Reverse Transcriptase (Qiagen) and Oligo-dT primer. The cDNA was amplified using *Taq* DNA polymerase (Cosmo Genetech, Korea) and primer sets. The primer sequences were as follows: adiponectin primers, 5′-TGGAGAGAAGGGAGAGAAAGG-3′ and 5′-TGGTCG-TAGGTGA AGAGAACG-3′; GAPDH primers, 5′-CATGGCCTT-CCGTGTTCCTAT-3′ and 5′-CCTGCTTCACCACCTTCTTGA-3′. PCR products were separated by electrophoresis in agarose gel containing ethidium bromide.

**PPAR Activity Assay.** A PPAR Transcription Factor Assay Kit (Cayman) was used for the determination of PPAR$\alpha$ and PPAR$\gamma$ DNA binding and transcription activity. Briefly, cells were harvested and placed in hypotonic buffer on ice for 15 min. Nonidet P-40 (10%) was added and gently mixed. The turbid lysate were clarified by centrifugation at 4 °C. The supernatant was transferred to a new tube as cytosolic fraction. The pellet was also resuspended with ice-

cold complete nuclear extraction buffer and rocked vigorously for 45 min. The lysate was clarified by centrifugation at 4 °C, and the supernatant was collected as nuclear fraction. The nuclear fractions were added to consensus dsDNA-coated 96-wells as a quantitatively equal amount. After primary antibody (anti-PPAR$\alpha$ antibody or anti-PPAR$\gamma$ antibody) incubation, horseradish peroxidase-conjugated secondary antibody was added, and the optical density of each well was measured using a Multiskan plate reader (Thermo Scientific, Waltham, MA, USA) with 450 nm wavelength.

**Small Interfering RNA (siRNA).** For SIRT1 siRNA transfections, 3T3-L1 adipocytes, 2−3 days post differentiation, were transfected with Lipofectamine RNAiMAX (Invitrogen, Carlsbad, CA, USA), according to the manufacturer's protocol. Following 24 h of transfection with 40 nM siRNA, the protein level of SIRT1 was analyzed with anti-SIRT1 antibody.

**Statistical Analysis.** Data are expressed as means ± SE. Statistical comparisons were performed by using one-way analysis of variance and Student's $t$ test. Differences were considered significant at $p < 0.05$.

## RESULTS

**Fisetin Up-regulates Adiponectin Expression in Differentiated 3T3-L1 Cells.** Mouse 3T3-L1 preadipocytes were differentiated to mature adipocytes as described under Materials and Methods. Cell morphology showed that differentiated 3T3-L1 cells had many lipid droplets indicating lipid accumulation, whereas these were not observed in undifferentiated preadipocytes (Figure 1A,B). The oil red O staining was executed to confirm differentiation and lipid droplet formation with red pigments (Figure 1C). Differentiated 3T3-L1 cells were exposed to fisetin with range of concentration from 1 nM to 10 $\mu$M for 24 h. The culture media were collected and subjected to ELISA. Adiponectin was secreted from 3T3-L1 adipocyte cells in response to fisetin treatment in a concentration-dependent manner (Figure 2A). The adiponectin expression levels in fisetin-treated 3T3-L1 cells were also determined by immunoblot analysis. As shown in Figure 2B, protein expression levels of adiponectin were up-regulated upon the addition of fisetin in a similar pattern to adiponectin secretion. The mRNA levels of adiponectin were also up-regulated upon treatment with fisetin (Figure 2C).

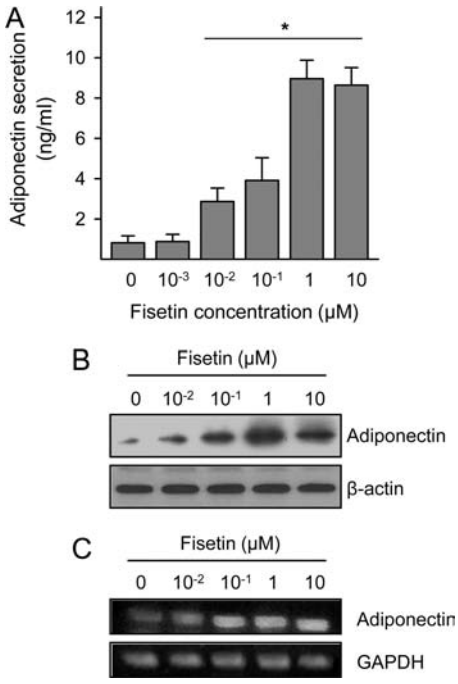


**Figure 2.** Effect of fisetin on adiponectin expression and secretion in 3T3-L1 adipocytes. Differentiated 3T3-L1 cells were treated with the indicated concentration of fisetin for 24 h. (A) Adiponectin levels released from 3T3-L1 cells were determined using adiponectin ELISA kit. (B) Protein levels of adiponectin in 3T3-L1 cell lysate were analyzed by immunoblot assay using anti-adiponectin antibody. (C) Total RNA was purified from 3T3-L1 cells and subjected to RT-PCR analyses using primers specific for adiponectin. (*) $p < 0.05$ by Student's $t$ test.

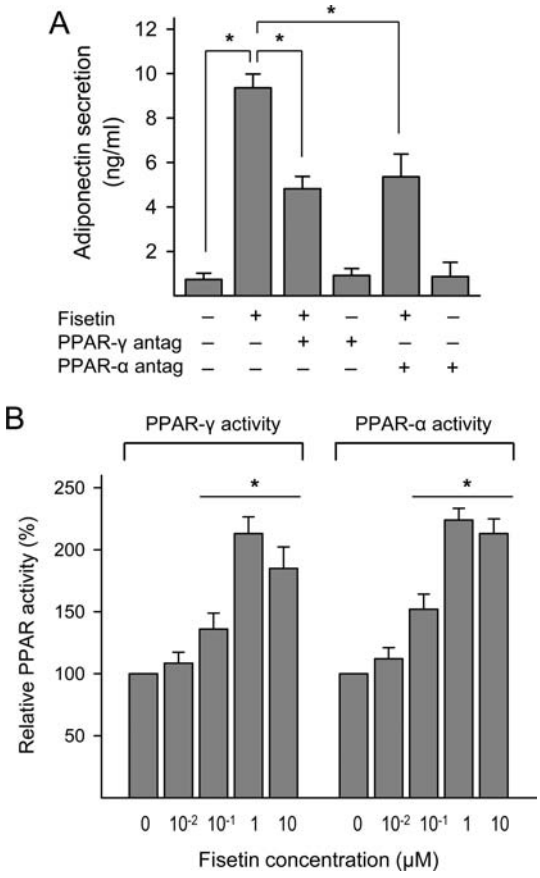


**Figure 3.** Effect of PPARs on fisetin-induced adiponectin up-regulation. (A) Differentiated 3T3-L1 cells were pretreated with PPAR-$\gamma$ antagonist (20 $\mu$M T0070907) or PPAR-$\alpha$ antagonist (20 $\mu$M GW6471) for 1 h and then treated with 1 $\mu$M fisetin for 24 h. Adiponectin levels released from cells were determined using adiponectin ELISA kit. (B) Differentiated 3T3-L1 cells were treated with the indicated concentration of fisetin for 24 h. PPARs activity was determined in nuclear extracts using a PPAR transcription factor assay kit. (*) $p < 0.05$ by Student's $t$ test.

**Fisetin Activates PPARs, Which Up-regulates Adiponectin Expression.** To assess the effects of PPARs on the adiponectin production induced by fisetin treatment in 3T3-L1 cells, we used two selective antagonists, T0070907, a PPAR-$\gamma$ antagonist, and GW6471, a PPAR-$\alpha$ antagonist. Differentiated 3T3-L1 cells were pretreated with T0070907 or GW6471 for 1 h and then treated with 1 $\mu$M fisetin for 24 h. As shown in Figure 3A, fisetin-induced adiponectin production was significantly inhibited by both antagonists. In addition, fisetin induced the activation of the PPARs in a concentration-dependent manner, reaching a maximum at 1 $\mu$M (Figure 3B).

**Fisetin Induces SIRT1 Activation.** To determine whether SIRT1 is involved in fisetin-induced adiponectin production,

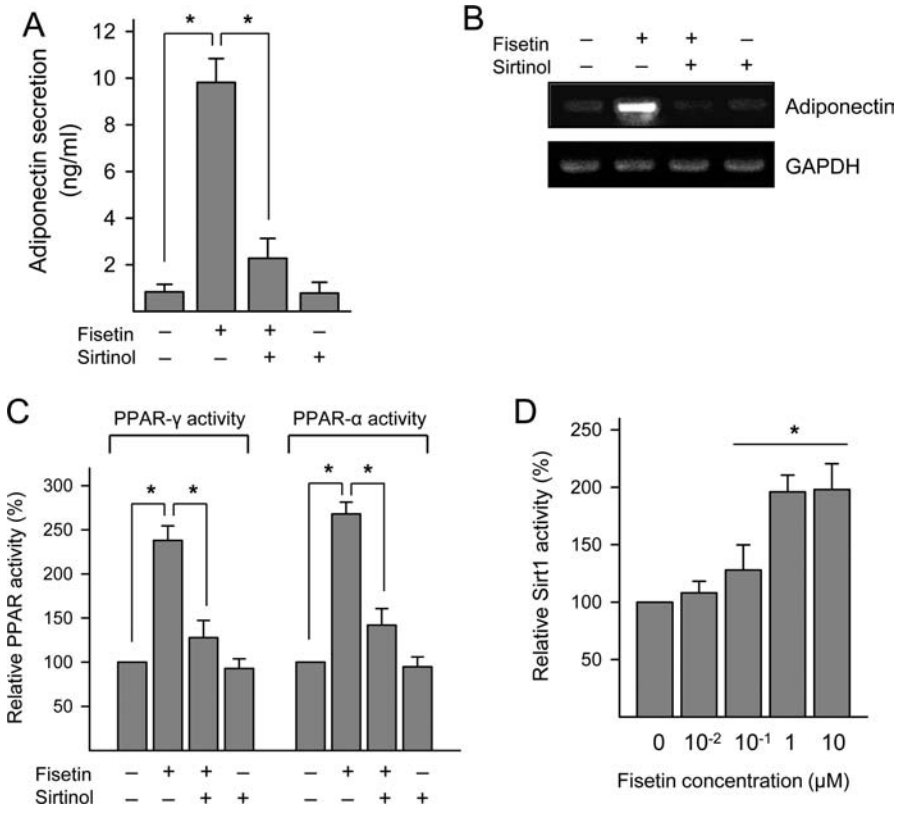


**Figure 4.** Effect of SIRT1 on fisetin-induced adiponectin up-regulation. Differentiated 3T3-L1 cells were pretreated with SIRT1 inhibitor (60 $\mu$M sirtinol) for 1 h and then treated with 1 $\mu$M fisetin for 24 h. (A) Adiponectin levels released from 3T3-L1 cells were determined using adiponectin ELISA kit. (B) Total RNA was purified from 3T3-L1 cells and subjected to RT-PCR analyses using primers specific for adiponectin. (C) PPAR-$\gamma$ and PPAR-$\alpha$ activities were determined in nuclear extracts using PPAR transcription factor assay kit. (D) Differentiated 3T3-L1 cells were treated with the indicated concentration of fisetin for 24 h. SIRT1 activity was determined with a deacetylase fluorometric activity assay kit. (*) $p < 0.05$ by Student's $t$ test.

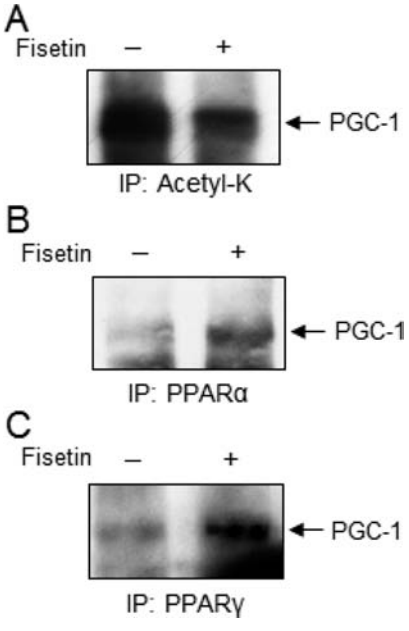


**Figure 5.** Interaction between PPARs and PGC-1. Differentiated 3T3-L1 cells were treated with 1 $\mu$M fisetin for 24 h. Cell lysate was immunoprecipitated with antiacetyl-lysine antibody (A), anti-PPAR-$\alpha$ antibody (B), or anti-PPAR-$\gamma$ antibody (C). Then immunoprecipitant samples were analyzed by immunoblot assay with anti-PGC-1 antibody.

we examined the effect of treatment with a SIRT1 inhibitor, sirtinol, on fisetin-induced adiponectin expression and secretion in 3T3-L1 cells. Fisetin-induced adiponectin release was significantly suppressed by treatment with sirtinol (Figure 4A). RT-PCR data also showed that inhibition of SIRT1 leads to a significant decrease in expression level of adiponectin induced by fisetin (Figure 4B). Moreover, the SIRT1 inhibitor suppressed fisetin-induced PPAR activation (Figure 4C). To check whether fisetin affected SIRT1 activity, we measured the intracellular SIRT1 activity in fisetin-treated adipocytes. It was found that fisetin increased the SIRT1 activity in a concentration-dependent manner (Figure 4D).

**Fisetin Promotes PPARs–PGC-1 Interaction.** We examined whether fisetin treatment alters the acetylation level of PGC-1 and the interaction between PPARs and PGC-1 in 3T3-L1 cells. Fisetin-treated cell lysates were immunoprecipitated with anti-acetyl lysine antibody and immunoblotted with anti-PGC-1 antibody. As shown in Figure 5A, fisetin reduced the acetylation level of PGC-1. Also, an immunoprecipitation study using anti-PPAR antibodies showed that the interaction of PPARs and PGC-1 was significantly elevated in fisetin-treated cells (Figure 5B,C).

**Effects of SIRT1 Knock-Down on PPARs and PGC-1 in Fisetin-Treated Adipocytes.** To confirm the molecular mechanisms of SIRT1-mediated adiponectin expression in fisetin-treated adipocytes, we used siRNA to silence SIRT1 gene expression. The SIRT1 protein level was significantly decreased in the cells transfected with SIRT siRNA compared


dx.doi.org/10.1021/jf502849j | J. Agric. Food Chem. 2014, 62, 10468–10474

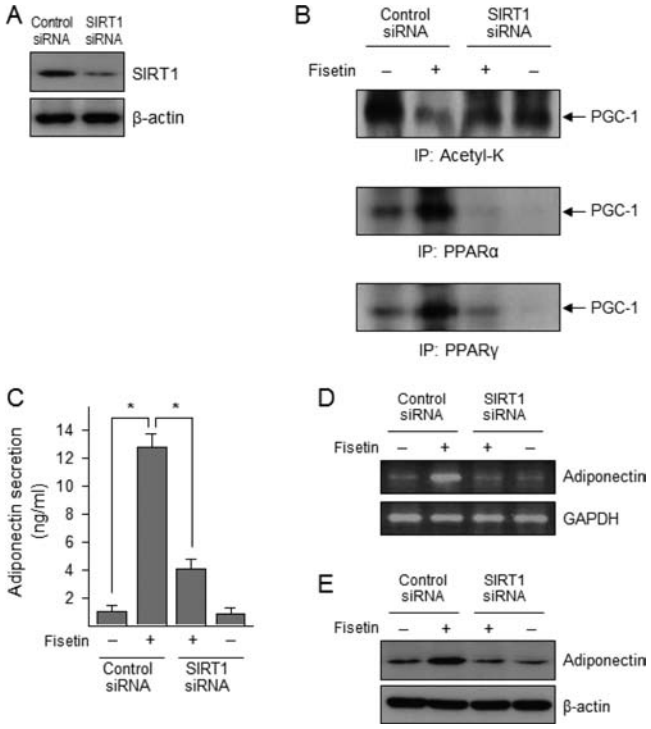


**Figure 6.** Effects of SIRT1 knock-down on PPARs−PGC-1 interaction and adiponectin production. (A) Differentiated 3T3-L1 cells were transfected with SIRT1 siRNA or control siRNA. After 24 h, SIRT1 levels were analyzed by immunoblot assay using anti-SIRT1 antibody. (B) After 24 h of transfection with SIRT1 siRNA, 3T3-L1 cells were incubated with 1 $\mu$M fisetin for 24 h. Cell lysate was immunoprecipitated with antiacetyl-lysine antibody, anti-PPAR-$\alpha$ antibody, or anti-PPAR-$\gamma$ antibody. Then immunoprecipitant samples were analyzed by immunoblot assay with anti-PGC-1 antibody. (C) Differentiated 3T3-L1 cells transfected with SIRT1 siRNA were treated with 1 $\mu$M fisetin for 24 h. Adiponectin levels released from cells were determined using an adiponectin ELISA kit. (D) Expression of adiponectin was determined by RT-PCR analysis. (E) Protein levels of adiponectin in cell lysate were analyzed by immunoblot assay using anti-adiponectin antibody. (*) $p < 0.05$ by Student's $t$ test.

to control siRNA (Figure 6A). We found that SIRT1 knockdown led to a decrease in deacetylation of PGC-1 in fisetin-treated cells (Figure 6B). Knockdown of SIRT1 also largely decreased fisetin-induced interaction of PPARs and PGC-1 (Figure 6B). To check the changes of adiponectin production by SIRT1 knockdown, we measured the secreted adiponectin in the culture medium. Fisetin-stimulated adiponectin production was significantly blocked by SIRT1 knockdown (Figure 6C), and there was a high correlation with mRNA expression and protein level in the cells (Figure 6D,E).

## ■ DISCUSSION

This study shows that fisetin, a dietary flavonoid, significantly promoted the expression of adiponectin through the activation of SIRT1-deacetylase and PPARs in adipocytes. In this study, we found increased expression and secretion of adiponectin in 3T3-L1 cells upon treatment with fisetin in a concentration-dependent manner. The activities of PPARs and SIRT1 were also increased by the stimulation of fisetin. In addition, fisetin-induced adiponectin secretion was inhibited by PPARs antagonists. The up-regulation of adiponectin and the activation of PPARs by fisetin were also prevented by SIRT1 inhibitor and knockdown with SIRT1 siRNA. Furthermore, fisetin promoted the deacetylation of PGC-1 and its interaction with PPARs. We also confirmed an important role of SIRT1-mediated deacetylation in regulating the PPARs−PGC-1 interaction and adiponectin production induced by fisetin. This is the first study showing the beneficial effect of fisetin on the adipokine regulation in adipocytes, thereby being considered to contribute to the modulation of the pathogenesis of obesity-linked metabolic disorders and vascular diseases.

Previous studies demonstrated that several polyphenols and bioactive natural products promoted the expression and secretion of adiponectin in adipocytes.[12−14] According to Yen et al., polyphenolic compounds (i.e., resveratrol, quercetin, and *p*-coumaric acid) increased the levels of secreted adiponectin and antioxidant enzymes and inhibited the production of cytokines and intracellular reactive oxygen species in the tumor necrosis factor receptor-stimulated 3T3-L1 adipocytes.[12] In this study, we also found that fisetin, one of flavonoids, increased adiponectin gene expression and its secretion in 3T3-L1 cells. Fisetin is a naturally occurring flavonoid, commonly found in strawberries and other fruits, that belongs to the flavonoid groups of plant polyphenols.[17−20] Fisetin was reported to exert a wide range of biological activities such as anti-inflammatory,[21] antioxidant,[22] and anticancer activities.[23] Also, Lee and Bae reported an antiadiposity effect of fisetin, which suppressed preadipocyte proliferation at early stages of differentiation, partly mediated by cell cycle arrest during adipogenesis.[24] We also tested several fisetin analogues for adiponectin production using ELISA in differentiated 3T3-L1 cells. However, the other compounds including apigenin did not exhibit considerable adiponectin production (data not shown).

Adiponectin is the most abundantly secreted adipokine, particularly derived from the adipocytes, which is involved in a variety of pathophysiological processes such as obesity, diabetes, and CVDs and exerts various beneficial effects as an antidiabetic, antiatherogenic, and anti-inflammatory.[6−9] Various studies reported that PPAR$\alpha$ and PPAR$\gamma$ are important transcription factors involved in adipogenesis and adipokine expression.[25−27] The initiation of adiponectin gene promotion was known to require the formation of PPAR$\gamma$ and retinoid X receptor (RXR) or PPAR$\alpha$−RXR complex,[28] thereby the complex binding with adiponectin promoter region for the activation. As an essential initiation condition for its activity, PPAR−RXR complexes were reported to require PGC-1 to bind with the complex itself to invoke transcriptional activation, which up-regulates adiponectin gene expression.[28,29] In addition, the deacetylation of SIRT1, a family of sirtuins that are characterized as its deacetylase activity against nonhistone protein, was reported to participate in the regulation of various transcription factors, for example, PGC-1, forkhead box-type O transcription factors, liver X receptor, RXR p53, mammalian target of rapamycin complex 1, and insulin receptor substrate 2.[30−34] According to recent studies, SIRT1 binds with PGC-1 and deacetylases PGC-1 to restore its activity to work as a PPAR coactivator, thereby binding with the PPAR$\gamma$−RXR or PPAR$\alpha$−RXR complex.[35−37]

In our study, PPARs and SIRT1 were significantly activated by fisetin treatment in 3T3-L1 cells, and fisetin-induced adiponectin secretions were inhibited by PPAR antagonists and SIRT1 inhibitor. Fisetin-induced PPAR activations were also prevented by SIRT1 inhibition and knockdown, and the deacetylation of PGC-1 and its interaction with PPARs were promoted by fisetin. Therefore, our data suggested that fisetin can up-regulate adiponectin expression by increasing SIRT1-

deacetylase activity, which catalyzes PGC-1 deacetylation, leading to an increase in the interaction with PPAR complex and ultimately to transcriptional activation. Our findings may have clinical importance given that adiponectin has multiple beneficial effects on obesity-related medical complications.[38] Moreover, fisetin is thought to prevent adipocyte differentiation, thereby maintaining preadipocytes in an undifferentiated state,[24] whereas in certain conditions such as differentiated state, cells can encounter the different responses that are activated to promote adiponectin production with another physiological signal under fisetin treatment. Hence, fisetin could have potential applications in the prevention and treatment of diseases, alternative medicine, and other therapeutic approaches by modulating the concentration or improving the bioavailability.

In summary, this study showed that fisetin, a dietary flavonoid, increased adiponectin gene transcription by inducing SIRT1-deacetylase activity. The activation of SIRT1 by fisetin may be connected to PGC-1 deacetylation, which increases its interaction with PPAR complex, which triggers up-regulation of adiponectin promoters. This is the first report of the beneficial effect of fisetin on the regulation of adipokine derived from adipocytes. The discovery of fisetin as an up-regulator of adiponectin expression that functions to enhance insulin sensitivity, suppress inflammation, and increase energy expenditure may exert its beneficial biofunction, thereby fisetin being considered as a contributor for modulating the pathogenesis of obesity-linked metabolic disorders.

## AUTHOR INFORMATION

### Corresponding Author

*(J.H.C.) Fax: +82-31-881-7077. E-mail: jhchung@cha.ac.kr.

### Funding

Basic Science Research Program (Grant 2006-2005303) through the National Research Foundation of Korea (NRF) funded by the Ministry of Education, Science and Technology.

### Notes

The authors declare no competing financial interest.

## ABBREVIATIONS USED

PPARs, peroxisome proliferator-activated receptors; SIRT1, silent mating type information regulation 2 homologue 1; CVDs, cardiovascular diseases; C/EBPs, CCAAT/enhancer-binding proteins; AMPK, AMP-activated protein kinase; S6K1, p70 ribosomal S6 kinase 1; mTORC1, mammalian target of rapamycin complex 1; RXR, retinoid X receptor; IBMX, 3-isobutyl-1-methylxanthine

## REFERENCES

(1) Mello, M. M.; Studdert, D. M.; Brennan, T. A. Obesity — the new frontier of public health law. *N. Engl. J. Med.* **2006**, *354*, 2601−2610.

(2) Hossain, P.; Kawar, B.; El Nahas, M. Obesity and diabetes in the developing world — a growing challenge. *N. Engl. J. Med.* **2007**, *356*, 213−215.

(3) Baillargeon, J.; Rose, D. P. Obesity, adipokines, and prostate cancer. *Int. J. Oncol.* **2006**, *28*, 737−745.

(4) de Ferranti, S.; Mozaffarian, D. The perfect storm: obesity, adipocyte dysfunction, and metabolic consequences. *Clin. Chem.* **2008**, *54*, 945−955.

(5) Gu, P.; Xu, A. Interplay between adipose tissue and blood vessels in obesity and vascular dysfunction. *Rev. Endocr. Metab. Disord.* **2013**, *14*, 49−58.

(6) Yamauchi, T.; Kamon, J.; Waki, H.; Terauchi, Y.; Kubota, N.; Hara, K.; Mori, Y.; Ide, T.; Murakami, K.; Tsuboyama-Kasaoka, N.; Ezaki, O.; Akanuma, Y.; Gavrilova, O.; Vinson, C.; Reitman, M. L.; Kagechika, H.; Shudo, K.; Yoda, M.; Nakano, Y.; Tobe, K.; Nagai, R.; Kimura, S.; Tomita, M.; Froguel, P.; Kadowaki, T. The fat-derived hormone adiponectin reverses insulin resistance associated with both lipoatrophy and obesity. *Nat. Med.* **2001**, *7*, 941−946.

(7) Weyer, C.; Funahashi, T.; Tanaka, S.; Hotta, K.; Matsuzawa, Y.; Pratley, R. E.; Tataranni, P. A. Hypoadiponectinemia in obesity and type 2 diabetes: close association with insulin resistance and hyperinsulinemia. *J. Clin. Endocrinol. Metab.* **2001**, *86*, 1930−1935.

(8) Hotta, K.; Funahashi, T.; Arita, Y.; Takahashi, M.; Matsuda, M.; Okamoto, Y.; Iwahashi, H.; Kuriyama, H.; Ouchi, N.; Maeda, K.; Nishida, M.; Kihara, S.; Sakai, N.; Nakajima, T.; Hasegawa, K.; Muraguchi, M.; Ohmoto, Y.; Nakamura, T.; Yamashita, S.; Hanafusa, T.; Matsuzawa, Y. Plasma concentrations of a novel, adiposespecific protein, adiponectin, in type 2 diabetic patients. *Arterioscler. Thromb. Vasc. Biol.* **2000**, *20*, 1595−1599.

(9) Iwashima, Y.; Katsuya, T.; Ishikawa, K.; Ouchi, N.; Ohishi, M.; Sugimoto, K.; Fu, Y.; Motone, M.; Yamamoto, K.; Matsuo, A.; Ohashi, K.; Kihara, S.; Funahashi, T.; Rakugi, H.; Matsuzawa, Y.; Ogihara, T. Hypoadiponectinemia is an independent risk factor for hypertension. *Hypertension* **2004**, *43*, 1318−1323.

(10) Yim, M. J.; Hosokawa, M.; Mizushina, Y.; Yoshida, H.; Saito, Y.; Miyashita, K. Suppressive effects of amarouciaxanthin A on 3T3-L1 adipocyte differentiation through down-regulation of PPARγ and C/EBPα mRNA Expression. *J. Agric. Food Chem.* **2011**, *59*, 1646−1652.

(11) Huang, B.; Yuan, H. D.; Kim, D. Y.; Quan, H. Y.; Chung, S. H. Cinnamaldehyde prevents adipocyte differentiation and adipogenesis via regulation of peroxisome proliferator-activated receptor-γ (PPARγ) and AMP-activated protein kinase (AMPK) pathways. *J. Agric. Food Chem.* **2011**, *59*, 3666−3673.

(12) Yen, G. C.; Chen, Y. C.; Chang, W. T.; Hsu, C. L. Effects of polyphenolic compounds on tumor necrosis factor-α (TNF-α)-induced changes of adipokines and oxidative stress in 3T3-L1 adipocytes. *J. Agric. Food Chem.* **2011**, *59*, 546−551.

(13) Kim, O. Y.; Lee, S. M.; Do, H.; Moon, J.; Lee, K. H.; Cha, Y. J.; Shin, M. J. Influence of quercetin-rich onion peel extracts on adipokine expression in the visceral adipose tissue of rats. *Phytother. Res.* **2012**, *26*, 432−437.

(14) Wang, A.; Liu, M.; Liu, X.; Dong, L. Q.; Glickman, R. D.; Slaga, T. J.; Zhou, Z.; Liu, F. Up-regulation of adiponectin by resveratrol: the essential roles of the Akt/FOXO1 and AMP-activated protein kinase signaling pathways and DsbA-L. *J. Biol. Chem.* **2011**, *286*, 60−66.

(15) Hertog, M. G. L.; Feskens, E. J. M.; Hollman, P. C. H.; Katan, M. B.; Kromhout, D. Dietary antioxidant flavonoids and risk of coronary heart disease: the Zutphen Elderly Study. *Lancet* **1993**, *342*, 1007−1011.

(16) Moon, J.; Do, H. J.; Kim, O. Y.; Shin, M. J. Antiobesity effects of quercetin-rich onion peel extract on the differentiation of 3T3-L1 preadipocytes and the adipogenesis in high fat-fed rats. *Food Chem. Toxicol.* **2013**, *58*, 347−354.

(17) Khan, N.; Syed, D. N.; Ahmad, N.; Mukhtar, H. Fisetin: a dietary antioxidant for health promotion. *Antioxid. Redox Signal.* **2013**, *19*, 151−162.

(18) Wood, J. G.; Rogina, B.; Lavu, S.; Howitz, K.; Helfand, S. L.; Tatar, M.; Sinclair, D. Sirtuin activators mimic caloric restriction and delay ageing in metazoans. *Nature* **2004**, *430*, 686−689.

(19) Jung, C. H.; Kim, H.; Ahn, J.; Jeon, T. I.; Lee, D. H.; Ha, T. Y. Fisetin regulates obesity by targeting mTORC1 signaling. *J. Nutr. Biochem.* **2013**, *24*, 1547−1554.

(20) Adhami, V. M.; Syed, D. N.; Khan, N.; Mukhtar, H. Dietary flavonoid fisetin: a novel dual inhibitor of PI3K/Akt and mTOR for prostate cancer management. *Biochem. Pharmacol.* **2012**, *84*, 1277−1281.

(21) Wu, M. Y.; Hung, S. K.; Fu, S. L. Immunosuppressive effects of fisetin in ovalbumin-induced asthma through inhibition of NF-κB activity. *J. Agric. Food Chem.* **2011**, *59*, 10496−10504.

(22) Woodman, O. L.; Chan, E. Ch. Vascular and anti-oxidant actions of flavonols and flavones. *Clin. Exp. Pharmacol. Physiol.* **2004**, *31*, 786−790.
(23) Ying, T. H.; Yang, S. F.; Tsai, S. J.; Hsieh, S. C.; Huang, Y. C.; Bau, D. T.; Hsieh, Y. H. Fisetin induces apoptosis in human cervical cancer HeLa cells through ERK1/2-mediated activation of caspase-8-/caspase-3-dependent pathway. *Arch. Toxicol.* **2012**, *86*, 263−273.
(24) Lee, Y.; Bae, E. J. Inhibition of mitotic clonal expansion mediates fisetin-exerted prevention of adipocyte differentiation in 3T3-L1 cells. *Arch. Parm. Res.* **2013**, *36*, 1377−1384.
(25) Tan, J. T.; McLennan, S. V.; Song, W. W.; Lo, L. W.; Bonner, J. G.; Williams, P. F.; Twigg, S. M. Connective tissue growth factor inhibits adipocyte differentiation. *Am. J. Physiol. Cell Physiol.* **2008**, *295*, C740−C751.
(26) Ikeda, D.; Sakaue, S.; Kamigaki, M.; Ohira, H.; Itoh, N.; Ohtsuka, Y.; Tsujino, I.; Nishimura, M. Knockdown of macrophage migration inhibitory factor disrupts adipogenesis in 3T3-L1 cells. *Endocrinology* **2008**, *149*, 6037−6042.
(27) Wang, M.; Wang, J. J.; Li, J.; Park, K.; Qian, X.; Ma, J. X.; Zhang, S. X. Pigment epithelium-derived factor suppresses adipogenesis via inhibition of the MAPK/ERK pathway in 3T3-L1 preadipocytes. *Am. J. Physiol. Endocrinol. Metab.* **2009**, *297*, E1378−E1387.
(28) Plutzky, J. The PPAR-RXR transcriptional complex in the vasculature: energy in the balance. *Circ. Res.* **2011**, *108*, 1002−1016.
(29) Rowe, G. C.; Jiang, A.; Arany, Z. PGC-1 coactivators in cardiac development and disease. *Circ. Res.* **2010**, *107*, 825−838.
(30) Chau, M. D.; Gao, J.; Yang, Q.; Wu, Z.; Gromada, J. Fibroblast growth factor 21 regulates energy metabolism by activating the AMPK-SIRT1-PGC-1alpha pathway. *Proc. Natl. Acad. Sci. U.S.A.* **2010**, *107*, 12553−12558.
(31) An, B. S.; Tavera-Mendoza, L. E.; Dimitrov, V.; Wang, X.; Calderon, M. R.; Wang, H. J.; White, J. H. Stimulation of Sirt1-regulated FoxO protein function by the ligand-bound vitamin D receptor. *Mol. Cell. Biol.* **2010**, *30*, 4890−4900.
(32) Li, X.; Zhang, S.; Blander, G.; Tse, J. G.; Krieger, M.; Guarente, L. SIRT1 deacetylates and positively regulates the nuclear receptor LXR. *Mol. Cell* **2007**, *28*, 91−106.
(33) Yuan, F.; Xie, Q.; Wu, J.; Bai, Y.; Mao, B.; Dong, Y.; Bi, W.; Ji, G.; Tao, W.; Wang, Y.; Yuan, Z. MST1 promotes apoptosis through regulating Sirt1-dependent p53 deacetylation. *J. Biol. Chem.* **2011**, *286*, 6940−6945.
(34) Gagarina, V.; Gabay, O.; Dvir-Ginzberg, M.; Lee, E. J.; Brady, J. K.; Quon, M. J.; Hall, D. J. SirT1 enhances survival of human osteoarthritic chondrocytes by repressing protein tyrosine phosphatase 1B and activating the insulin-like growth factor receptor pathway. *Arthritis Rheum.* **2010**, *62*, 1383−1392.
(35) Sugden, M. C.; Caton, P. W.; Holness, M. J. PPAR control: it's SIRTainly as easy as PGC. *J. Endocrinol.* **2010**, *204*, 93−104.
(36) Fuentes, E.; Guzmán-Jofre, L.; Moore-Carrasco, R.; Palomo, I. Role of PPARs in inflammatory processes associated with metabolic syndrome. *Mol. Med. Rep.* **2013**, *8*, 1611−1616.
(37) Tontonoz, P.; Spiegelman, B. M. Fat and beyond: the diverse biology of PPARγ. *Annu. Rev. Biochem.* **2008**, *77*, 289−312.
(38) Antoniades, C.; Antonopoulos, A. S.; Tousoulis, D.; Stefanadis, C. Adiponectin: from obesity to cardiovascular disease. *Obes. Rev.* **2009**, *10*, 269−279.

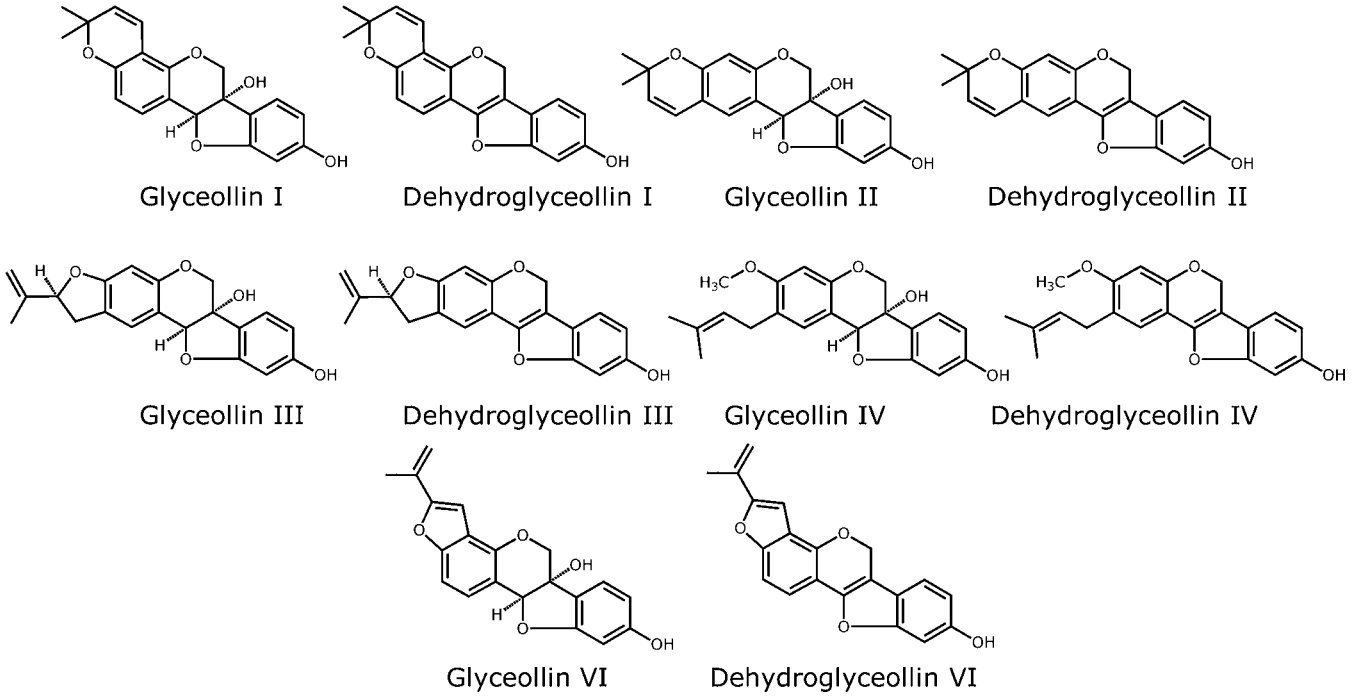


**Figure 1.** Structures of glyceollins and dehydroglyceollins assigned in soy extracts.

## MATERIALS AND METHODS

**Materials.** Soybeans, *Glycine max* (L.) Merrill, were provided by Frutarom (Londerzeel, Belgium). Acetic acid (HOAc) (HPLC grade), daidzein, genistein, coumestrol, L-leucine, L-histidine, sodium hydroxide (NaOH) pellets, and 17$\beta$-estradiol ($E_2$) were purchased from Sigma-Aldrich (St. Louis, MO, U.S.A.). Ethanol (100%, analytical grade), D-(+)-glucose (dextrose), ammonium sulfate and dimethyl sulfoxide (DMSO) were purchased from Merck (Darmstadt, Germany) and yeast nitrogen base without amino acids and without ammonium sulfate, and agar were obtained from Becton-Dickinson (Franklin Lakes, NJ U.S.A.). HOAc (ULC/MS grade), acetonitrile (ACN) (ULC/MS and HPLC-R grade), silica gel (60 Å, 70−230 mesh), water (ULC/MS grade), ethyl acetate (LC-MS grade), and methanol (ULC/MS grade) were purchased from Biosolve BV (Valkenswaard, The Netherlands). Water for other purposes than UHPLC was prepared using a Milli-Q water purification system (Millipore, Molsheim, France). The reporter yeast strain was provided by RIKILT (Wageningen, The Netherlands).

***Rhizopus*-Challenged Germination and Extraction of Soybean Seedlings.** Soybeans, *Glycine max* (L.) Merril, were germinated and challenged with the fungus *Rhizopus microsporus var. oryzae* (LU581) as previously described.[7] After germination and challenging, the soybean sprouts were freeze-dried and milled with a Retsch Ultra centrifugal mill ZM (Haan, Germany), using a 0.5 mm sieve. Soybeans were defatted by hexane. Next, isoflavonoids were extracted with ethanol and subsequent drying was performed as described elsewhere.[7] The dried extract containing the isoflavonoids is referred to as soy extract.

**Heat Treatment of Soy Extract.** The soy extract was suspended in either 0.56 M HOAc or water to a concentration of 10.7 mg/mL. The suspension was heated in a water bath of 100 °C, during three independent experiments. Samples were taken after 20, 30, 40, 50, 60, and 70 min in experiment 1; after 10, 30, 60, and 120 min in experiment 2; after 1, 5, 30, 60, 180, and 240 min in experiment 3. After the heat treatment, ethanol (EtOH) was added to obtain a 70% (v/v) EtOH concentration. Solubilisation was enhanced in a water bath of 40 °C for 5 min followed by sonification at 25 °C for 10 min. Finally, the samples were centrifuged (18.500*g*; 5 min; RT) and the supernatant was stored at −20 °C.

**RP Flash Chromatography.** For Flash chromatography, the untreated soya extract and a modified soy extract (0.56 M HOAc, 70 min at 100 °C) were used. Solvents were evaporated under vacuum, frozen and lyophilized. A Grace Reveleris Flash system was used to obtain fractions enriched in glyceollins or dehydroglyceollins. The untreated and treated soy extract (52.2 mg DW) were solubilized in methanol acidified with 0.1% (v/v) HOAc to a concentration of 5 mg/mL (5 min in a water bath of 40 °C, followed by 10 min sonication at 25 °C). This solution was added to 3 g silica and the soy extract was coated onto silica particles by using a rotary evaporator. The soy extract-coated silica was transferred into an empty 5 g cartridge and closed with a plunger. The cartridge was placed upstream of a 12 g Reveleris C18 RP column (particle size 38.6 $\mu$m) (Grace Davison Discovery Science, Columbia, MD, U.S.A.). Water (Milli-Q) acidified with 0.1% (v/v) HOAc (HPLC grade) + 1% (v/v) ACN (HPLC-grade), eluent A, and ACN (HPLC-grade) acidified with 0.1% (v/v) HOAc (HPLC grade), eluent B, were used as eluents. The flow rate was 30 mL/min and the experiment was performed at room temperature. The following elution profile was used: 0−5 min, linear gradient from 0 to 40% B; 5−9 min, linear gradient from 40 to 50% B; 9−14 min, isocratic on 50% B; 14−19 min, linear gradient from 50 to 60% B; 19−24 min, linear gradient from 60 to 70% B; 24−27 min, linear gradient from 70 to 80% B; 27−28 min, linear gradient from 80 to 84% B; 28−33 min, linear gradient from 84 to 96% B; 33−35 min, linear gradient from 96 to 100% B. Absorption was measured at 280 nm. During the entire run, fractions of 10 mL were collected. All fractions were analyzed with UHPLC-MS. Fractions containing similar glyceollins or dehydroglyceollins were pooled. Solvents from pools containing dehydroglyceollins were evaporated under vacuum, frozen, and lyophilized. Ethyl acetate was added to the pools containing glyceollins in a ratio 3:1 (v/v). This liquid−liquid partitioning was performed three times. The pooled ethyl acetate fractions were evaporated under vacuum, frozen, and lyophilized. The pools were resolubilized in 70% (v/v) ethanol for analysis with UHPLC-MS and resolubilized in DMSO to determine the estrogenicity.

**RP-UHPLC-ESI-MS Analysis.** Samples were analyzed on an Accela ultra high performance liquid chromatography (RP-UHPLC) system (Thermo Scientific, San Jose, CA, U.S.A.) equipped with a pump, autosampler and PDA detector. Samples (5 $\mu$L for the soy extract and 1 $\mu$L for isoflavonoid-enriched pools) were injected on an Acquity UPLC BEH Shield RP18 column (2.1 × 5 mm$^2$, 1.7 $\mu$m particle size)

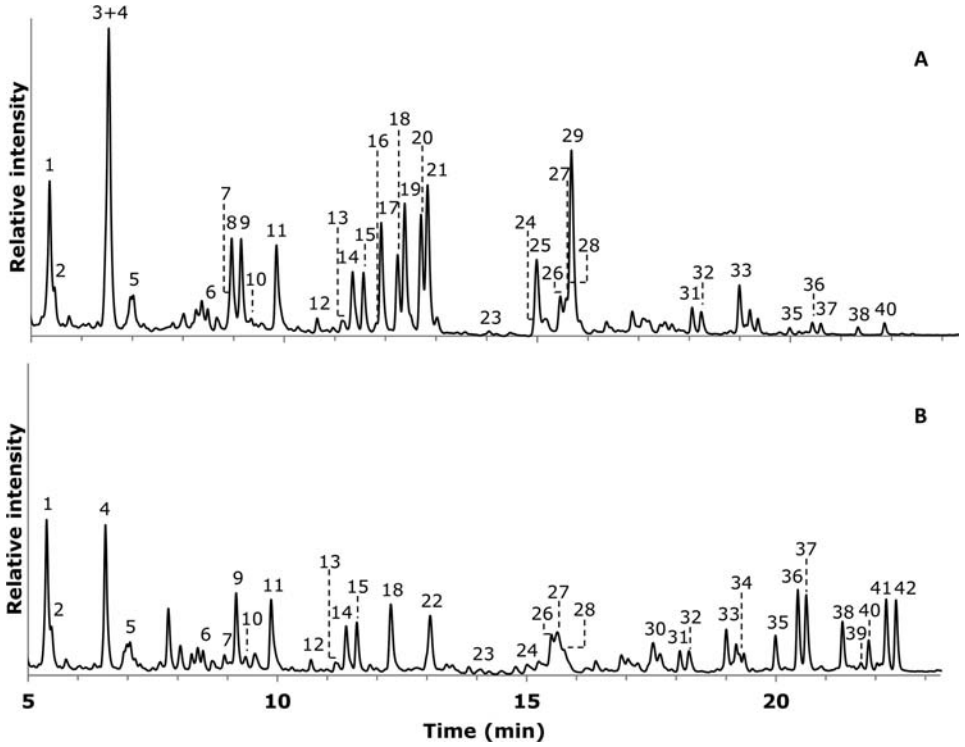


**Figure 2.** RP-UHPLC-UV profile of untreated (A) and heat (60 min)/acid treated (B) soy extract. Peak numbers refer to compounds in Table 1.

with an Acquity UPLC Shield RP18 Vanguard guard-column (2.1 × 5 $mm^2$, 1.7 $\mu$m particle size; Waters, Milford, MA, U.S.A.). Water acidified with 0.1% (v/v) HOAc + 1% (v/v) ACN, eluent A, and ACN acidified with 0.1% (v/v) HOAc, eluent B, were used as eluents. The flow rate was 300 $\mu$L/min, the column temperature was controlled at 35 °C, and the PDA detector was set to measure 200−400 nm. The following elution profile was used: 0−1 min, isocratic on 9% B; 1−3 min, linear gradient from 9 to 25% B; 3−10 min, linear gradient from 25 to 50% B; 10−13 min, isocratic on 50% B; 13−23 min, linear gradient from 50 to 100% B; 23−25 min, isocratic on 100% B; 25−26 min, linear gradient from 100 to 9% B; 26−31 min, isocratic on 9% B.

Mass spectrometric (MS) data were obtained by analyzing samples on a LTQ-Velos (Thermo Scientific) equipped with a heated ESI-MS probe coupled to the RP-UHPLC. Nitrogen gas was used as sheath and auxiliary gas. Data were collected over a $m/z$ range of 150−1500 in both positive (PI) and negative (NI) mode. Data-dependent $MS^2$ analysis was performed with a normalized collision energy of 35%. Most settings were optimized via automatic tuning using "Tune Plus" (Xcaliber 2.1, Thermo Scientific). The system was tuned with genistein in both PI and NI mode. For the PI an NI mode, the source voltage were 4.50 kV and 3.50 kV, respectively. In both ionization modes the ion transfer tube (ITT) temperature and the probe temperature were 400 and 50 °C, respectively.

The identification of isoflavonoids was based on UV and MS spectra using the approach reported earlier.[6,7,12] The quantification of isoflavonoids was performed based on their absorption at 280 nm by means of Xcalibur (version 2.1.0, Thermo Scientific). As for many compounds no commercial standards were available, the amounts of isoflavonoid were expressed as mg daidzein equivalents per gram challenged soybean seedling extract, in which daidzein was used as a generic standard to make a calibration curve with five data points (0.001−0.01 mg/mL, $R^2$ = 0.996).

**Determination of Molecular Characteristics.** Molecular structures were evaluated using the software program ChemBio3D Ultra 12 (Cambridgesoft, Waltham, MA, U.S.A.) after MM2 molecule minimization.

**Determination of Estrogenic Activity.** Estrogenicity was determined as described elsewhere[13] with slight modifications. Cultures of the yeast estrogen biosensor with either ER$\alpha$ or ER$\beta$ were grown overnight at 30 °C and 200 rpm. At the late log phase, both cultures were diluted in minimal medium supplemented with either L-leucine (ER$\alpha$) or L-histidine (ER$\beta$) to an optical density value at 630 nm ($OD_{630}$) of 0.045 ± 0.005 and 0.200 ± 0.005 for ER$\alpha$ and ER$\beta$, respectively. For determination of ER agonism, 200 $\mu$L aliquots of diluted yeast cultures were combined with 2 $\mu$L of test compound or isoflavonoid fraction in a 96-well plate. Dilution series of each sample were prepared in DMSO ranging from 0.0001−10 $\mu$g/mL. The final concentration of DMSO in the assay did not exceed 1% (v/v). Each sample concentration was assayed in triplicate. Exposure was performed for 6 or 24 h for the ER$\beta$ or ER$\alpha$ assay, respectively, at 30 °C and orbital shaking at 200 rpm. Fluorescence and OD were measured at 0 and 24 h for the ER$\alpha$ and at 0 and 6 h for the ER$\beta$ in a Tecan Infinite F500 (Männedorf, Switzerland), using an excitation filter of 485 nm (bandwidth, 20 nm) and an emission filter of 535 nm (bandwidth, 35 nm). The fluorescence signals of the samples were corrected with the signal obtained with the diluted yeast suspension at $t$ = 0. In order to verify the viability of the yeast in each well, the absorbance was measured at 630 nm. Cytotoxicity occurred when the yeast growth was inhibited for more than 30% during the incubation and these incubations were not further considered. DMSO (blank) and control samples containing 17$\beta$-estradiol (E2) dissolved in DMSO were included in each experiment. The $EC_{50}$ values for 17$\beta$-estradiol in the ER$\alpha$ and ER$\beta$ bioassay were 0.66 nM and 0.18 nM, respectively, and were in line with those reported previously.[13] $EC_{50}$ calculations were performed in Sigma Plot (8.02, SPSS Inc., Chicago, IL, U.S.A.). The relative estrogen potency (REP) of a compound was determined by dividing the $EC_{50}$ of E2 by the $EC_{50}$ of the compound. The $EC_{50}$ values could not be calculated in all cases, due to toxicity of the compounds toward the yeast. To be consistent for all compounds, the REP was determined by thresholds, i.e., the threshold of $E_2$ divided by the threshold of the compound. The threshold value was defined as the value where the slope was >0.4 units relative absorbance per log difference in concentration. The threshold values for 17$\beta$-estradiol in the ER$\alpha$ and ER$\beta$ bioassay were 5.44 × $10^{-8}$ and 2.45 × $10^{-8}$ mg/mL, respectively. For the determination of ER antagonism, the yeast cells were exposed to 2 $\mu$L of $EC_{70}$ (ER$\alpha$) or $EC_{90}$ (ER$\beta$) of 17$\beta$-estradiol in combination with 2 $\mu$L of different dilutions of test compound or

fraction (measured in triplicates). For antagonism, the decrease of the maximal response in percentages was determined.

## RESULTS

**Identification of Isoflavonoids in Untreated and Heated Soy Extracts.** Comparison of the chromatograms of the 60 min acid/heat treated and untreated soy extract showed that a number of compounds were acid/heat unstable (Figure 2). In total, 42 peaks were distinguished using UV, MS, and $MS^2$ in negative and positive mode (Table 1), many of which were annotated in our previous studies.[6,7] Peaks 22, 30, 34−38, and 40 were new. They seemed to be formed upon acid/heat treatment at the expense of peaks 3, 8, 17, 19−21, 25, and 29, which all represented 6a-hydroxy-pterocarpans. The newly formed compounds had molecular masses minus 18 Da compared to the original 6a-hydroxy-pterocarpans. Moreover, the newly formed compounds showed a second absorption maximum between 330 and 364 nm, besides the one at around 280 nm (Table 1). This indicated that these newly formed compounds have a larger conjugated system than the 6a-hydroxy-pterocarpans. Taken together, this might suggest that the 6a-hydroxy-pterocarpans were converted into 6a,11a-pterocarpenes. Formation of 6a,6-pterocarpenes seems unlikely as these compounds have a less extensive conjugated system, consistent with their lower $\lambda_{max}$ of 302 nm.[14] For 6a,11a-pterocarpenes, other than those from soybean, absorption maxima between 330 and 350 nm have been reported, similar to those observed in the present study.[15]

*MS and $MS^2$ NI Mode.* Compound **22** with an $m/z$ value of 253 in NI mode produced fragment ions $m/z$ 209 $[M - H - CO_2]^-$, 225 $[M - H - CO]^-$, and 235 $[M - H - H_2O]^-$. It was tentatively assigned as dehydroglycinol. Compound **30** was tentatively assigned as dehydroglyceofuran based on a $m/z$ of 335 in NI mode and fragment ions with a $m/z$ of 291 $[M - H - CO_2]^-$, and 307 $[M - H - CO]^-$. Compound **34** was tentatively identified as dehydroglyceollidin II with a $m/z$ of 321 in NI mode. In NI $MS^2$ mode fragment ions $m/z$ 265 $[M - H - 2CO]^-$, 277 $[M - H - CO_2]^-$, and 306 $[M - H - CH_3]^-$ were formed. Compounds **35**−**37** were tentatively assigned as dehydroglyceollin I, II, and III, as these compounds have a $m/z$ of 319 in NI mode. They produced the fragment ions $m/z$ 291 $[M - H - CO]^-$ and 275 $[M - H - CO_2]^-$ in NI $MS^2$ mode. Assuming that compounds **35**−**37** had the same elution order as their corresponding glyceollins, peak **35** was tentatively annotated as dehydroglyceollin III, peak **36** as dehydroglyceollin II, and peak **37** as dehydroglyceollin I. Compound **38** was tentatively annotated as dehydroglyceollin IV with a $m/z$ of 335 in NI mode. In NI, $MS^2$ a loss of a methyl radical was observed. This is indicative for the presence of a methoxy group.[16] Compound **40** had a $m/z$ of 317 in NI mode and was tentatively identified as dehydroglyceollin VI, with neutral losses of CO (28 Da) and $CO_2$ (44 Da). In this study, only traces of *retro*-Diels−Alder fragments were observed in NI $MS^n$ for the compounds described above. Such MS behavior was also found in other studies performed with pterocarpenes and coumestans.[15,17] Both these subclasses of isoflavonoids have a relatively large conjugated system. This results in small neutral losses and no apparent A-ring or B-ring fragment ions, due to the resistance against cleavage of the C-ring or D-ring.

*MS and $MS^2$ PI Mode.* Additional data for confirmation that the prenylated compounds after the treatment were formed at the expense of the 6a-hydroxy-pterocarpans came from PI MS analysis, which allowed prediction of the type of prenylation.[18] For compounds **34**−**38** and **40** neutral losses of 42 and 56 Da were observed in PI $MS^2$. The ratio (42:56) was <1 for compound **34** and **38**, which suggested that these compounds had a prenyl chain. This ratio was >1 for compounds **35** and **36**, indicative for a pyran ring. Compounds with a furan ring are known to show a different behavior.[17] Glyceollin III has a 2″-isopropenyl-dihydrofuran-group and the ratio (42:56) is >1. However, glyceollin VI has a 2″-isopropenyl-furano-group and the ratio is <1. Upon fragmentation of compounds **35** and **40**, which were probably formed from glyceollin III and glyceollin VI, respectively, it was observed that the ratio for compound **35** was >1 and that for compound **40** was <1. This is in line with the corresponding 6a-hydroxy-pterocarpans. On the basis of UV data, $MS^n$ data in negative and positive mode the compounds were tentatively annotated as 6a,11a-pterocarpenes. It seems that the 6a-hydroxyl group of the original 6a-hydroxy-pterocarpans was first protonated, followed by dehydration and formation of a double bond during the heat treatment. This resulted in a more extensive conjugated system than the original 6a-hydroxy-pterocarpan. These findings are in accordance with previous data.[11] They suggest that the 6a-hydroxy-pterocarpan glyceollin I forms the thermodynamically more stable 6a,11a-pterocarpene dehydroglyceollin I upon water loss.[11] Structures of the main prenylated 6a-hydroxy-pterocarpans and 6a,11a-pterocarpenes are shown in Figure 1. Note that the nomenclature of glyceollins and dehydroglyceollins is ambiguous in literature, as elaborated in the footnote of Table 1.

Peaks **39**, **41**, and **42** appeared only after 20 min of acid/heat treatment. They all had a $m/z$ value in NI mode of 277.2169, corresponding to the molecular formula of $C_{18}H_{30}O_2$. Similar $m/z$ values suggest that compounds **39**, **41**, and **42** were isomers. Despite the fact that the amount of these compounds increases and the amount of dehydroglyceollin I, II, and III decreases after longer duration of incubation, it is unlikely that there is a relationship between these compound groups, considering the molecular formulas of dehydroglyceollins ($C_{20}H_{16}O_4$) and compounds **39**, **41**, and **42**.

**Stability of 6a-Hydroxy-Pterocarpans Compared to Other Soy Isoflavonoids.** The soy extract contained different subclasses of isoflavonoids (Table 1). Before heating, 6a-hydroxy-pterocarpans comprised 45% of the total area at 280 nm of all isoflavonoids, coumestans 10%, isoflavones 43%, and pterocarpenes 1%. After a 60 min combined heat/acid treatment all 6a-hydroxy-pterocarpans were converted. Now, 29% of the total area of isoflavonoids belonged to the subclass of pterocarpenes, 20% corresponded to coumestans, and 51% to isoflavones. The compositions were expressed as percentages of the total peak area, as molecular extinction coefficients were not known for all compounds. Comparing the total peak area of the untreated soy extract and the treated soy extract (60 min 100 °C + 0.56 M HOAc), it can be calculated that a loss of 45% of the total isoflavonoids occurred during acid/heat treatment (Figure 2). When only heat was applied a loss of 19% was observed (data not shown). Considering the scope of this study, this loss of isoflavonoids was not further elaborated. The conversion of isoflavonoids when heated with and without acid at different time points can be seen in Figure 3. The 6a-hydroxy-pterocarpans were converted for 23% after 5 min, and for 53% after 20 min; within 180 min at 100 °C all 6a-hydroxy-pterocarpans were converted. This transition was accelerated with acid: after 5 min 32% was converted and within 20 min all 6a-hydroxy-pterocarpans were converted. This is in agreement

**Table 1. Compounds Tentatively Assigned In The Soy Extracts By UHPLC-ESI-MS[a]**

| no. | rt. (min) | $UV_{max}$ (nm) | identification | subclass | molecular formula | $[M - H]^-$ | $MS^2$ product ions (relative intensity)[b] | $[M + H]^+$ | $MS^2$ product ions (relative intensity)[b] |
|---|---|---|---|---|---|---|---|---|---|
| 1 | 5.56 | 250 | Daidzin | Isoflavone | $C_{21}H_{20}O_9$ | 415 | 253(100) | 417 | 255(100) |
| 2 | 5.66 | 257 | Glycitin | Isoflavone | $C_{22}H_{22}O_{10}$ | 445 | 283(100) | 447 | 285(100) |
| 3 | 6.73 | 283 | Glycinol | Pterocarpan | $C_{15}H_{12}O_5$ | 271 | 161(100), 227(25) | 255[c] | 199(100), 227(66), 237(11) |
| 4 | 6.74 | 260 | Genistin | Isoflavone | $C_{21}H_{20}O_{10}$ | 431 | 296(100), 311(8) | 433 | 271(100) |
| 5 | 7.22 | 257 | Biochanin A | Isoflavone | $C_{16}H_{12}O_5$ | 283 | 268(100) | 285 | 270(100) |
| 6 | 8.69 | 260 | Acetyl-genistin | Isoflavone | $C_{27}H_{30}O_{15}$ | 473 | 269(100) | 475 | 271(100) |
| 7 | 9.14 | 256 | Glycitein | Isoflavone | $C_{16}H_{12}O_5$ | 283 | 268(100) | 285 | 257(14), 270(100) |
| 8 | 9.16 | 257, 291 | Glyceofuran | Pterocarpan | $C_{20}H_{18}O_6$ | 353 | 335(100), 149(13) | 337[c] | 188(39), 309(100), 319(76) |
| 9 | 9.35 | 248 | Daidzein | Isoflavone | $C_{15}H_{10}O_4$ | 253 | 209(58), 225(100), 253(45) | 255 | 199(100), 227(61), 237(25) |
| 10 | 9.55 | 286 | 2′-hydroxygenistein | Isoflavone | $C_{15}H_{10}O_6$ | 285 | 199(10), 217(100), 241(10) | 287 | 217(100), 259(49), 269(20) |
| 11 | 10.05 | 286, 353 | C-methyl-coumestrol | Coumestan | $C_{16}H_{10}O_5$ | 281 | 253(100) | 283 | 255(100) |
| 12 | 10.85 | 286 | Naringenin | Flavanone | $C_{15}H_{12}O_5$ | 271 | 151(100), 177(22) | 273 | 153(100) |
| 13 | 11.35 | 257 | Prunetin | Isoflavone | $C_{16}H_{12}O_5$ | 283 | 240(24), 255(100), 268(11) | 285 | 229(7), 257(100), 267(2) |
| 14 | 11.55 | 350 | Isotrifoliol | Coumestan | $C_{16}H_{10}O_6$ | 297 | 282(100) | 299 | 267(8), 271(100), 284(20) |
| 15 | 11.77 | 260 | Genistein | Isoflavone | $C_{15}H_{10}O_5$ | 269 | 201(63), 225(100), 241(34) | 271 | 153(100), 215(74), 243(65), 253(35) |
| 16 | 12.01 | 285 | Glyceollidin I | Pterocarpan | $C_{20}H_{20}O_5$ | 339 | 161(100), 324(54) | 323[c] | 267(100) |
| 17 | 12.12 | 285 | Glyceollidin II | Pterocarpan | $C_{20}H_{20}O_5$ | 339 | 161(100), 324(45) | 323[c] | 267(100) |
| 18 | 12.44 | 304, 343 | Coumestrol | Coumestan | $C_{15}H_8O_5$ | 267 | 211(11), 239(100), 267(24) | 269 | 197(26), 225(30), 241(100) |
| 19 | 12.58 | 289 | Glyceollin III | Pterocarpan | $C_{20}H_{18}O_5$ | 337 | 149(14), 293(6), 319(100) | 321[c] | 251(98), 279(100), 306(73) |
| 20 | 12.90 | 283 | Glyceollin II | Pterocarpan | $C_{20}H_{18}O_5$ | 337 | 149(37), 293(22), 319(100) | 321[c] | 251(81), 279(100), 306(79) |
| 21 | 13.03 | 283 | Glyceollin I | Pterocarpan | $C_{20}H_{18}O_5$ | 337 | 149(78), 293(34), 319(100) | 321[c] | 293(38), 303(100), 306(84) |
| 22 | 13.26 | 284, 352, 357 | Dehydroglycinol | Pterocarpene | $C_{15}H_{10}O_4$ | 253 | 209(61), 225(100), 235(36) | 255 | 199(30), 213(22), 227(100) |
| 23 | 14.25 | 288 | A-ring prenylated 2′-hydroxydaidzein | Isoflavone | $C_{20}H_{20}O_5$ | 337 | 282(88), 293(100), 337(37) | 339 | 283(100) |
| 24 | 15.17 | 257 | B-ring prenylated glycitein | Isoflavone | $C_{21}H_{20}O_5$ | 351 | 336(100) | 353 | 285(9), 297(100) |
| 25 | 15.19 | 287, 308 | Glyceollin VI | Pterocarpan | $C_{20}H_{16}O_5$ | 335 | 149(16), 317(100) | 319[c] | 263(100), 291(72), 319(11) |
| 26 | 15.65 | 252 | A-ring prenylated daidzein | Isoflavone | $C_{20}H_{18}O_4$ | 321 | 266(100) | 323 | 267(100) |
| 27 | 15.77 | 262 | A-ring prenylated 2′-hydroxygenistein | Isoflavone | $C_{20}H_{18}O_6$ | 353 | 267(38), 284(93), 285(100) | 355 | 299(100) |
| 28 | 15.84 | 257 | B-ring prenylated daidzein | Isoflavone | $C_{20}H_{18}O_4$ | 321 | 265(100), 252(4) | 323 | 255(11), 267(100) |
| 29 | 15.87 | 285 | Glyceollin IV | Pterocarpan | $C_{21}H_{22}O_5$ | 353 | 148(5), 149(14), 335(100) | 337[c] | 281(100), 269(50) |
| 30 | 17.78 | 273, 331 | Dehydroglyceofuran | Pterocarpene | $C_{20}H_{16}O_5$ | 335 | 280(100), 291(14), 307(30) | 337 | 281(100), 309(8) |
| 31 | 18.26 | 264 | A-ring prenylated genistein | Isoflavone | $C_{20}H_{18}O_5$ | 337 | 282(100), 283(8), 309(4) | 339 | 283(100) |
| 32 | 18.44 | 261 | B-ring prenylated genistein | Isoflavone | $C_{20}H_{18}O_5$ | 337 | 281(100), 282(19), 337(65), 293(13) | 339 | 271(18), 283(100) |
| 33 | 19.19 | 307, 343 | 4-prenyl-coumestrol | Coumestan | $C_{20}H_{16}O_5$ | 335 | 280(100), 281(12) | 337 | 281(100) |
| 34 | 19.46 | 286, 340, 355 | Dehydroglyceollidin II | Pterocarpene | $C_{20}H_{18}O_4$ | 321 | 265(100), 277(12), 306(12) | 323 | 267(100), 281(20) |
| 35 | 20.19 | 296, 344, 359 | Dehydroglyceollin III | Pterocarpene | $C_{20}H_{16}O_4$ | 319 | 275(24), 277(100), 291(22) | 321 | 253(53), 279(48), 293(75), 306(100) |
| 36 | 20.64 | 273, 349, 364 | Dehydroglyceollin II | Pterocarpene | $C_{20}H_{16}O_4$ | 319 | 275(38), 277(100), 291(90), 304(85) | 321 | 253(19), 279(33) 293(100), 306(52) |



dx.doi.org/10.1021/jf503127c | J. Agric. Food Chem. 2014, 62, 10475−10484

**Table 1. continued**

| no. | rt. (min) | $UV_{max}$ (nm) | identification | subclass | molecular formula | $[M - H]^-$ | $MS^2$ product ions (relative intensity)[b] | $[M + H]^+$ | $MS^2$ product ions (relative intensity)[b] |
|---|---|---|---|---|---|---|---|---|---|
| 37 | 20.81 | 288, 332 | Dehydroglyceollin I | Pterocarpene | $C_{20}H_{16}O_4$ | 319 | 275(32), 291(100), 304(38) | 321 | 279(28), 293(100), 306(74) |
| 38 | 21.54 | 292, 340, 356 | Dehydroglyceollin IV | Pterocarpene | $C_{21}H_{20}O_4$ | 335 | 320(100) | 337 | 281(30), 295(15), 321(100) |
| 39 | 21.91 | 273, 290 | unknown degradation product | | $C_{18}H_{30}O_2$ | 277 | 179(10), 233(100), 259(38) | 279 | 123(69), 137(48), 223(50), 261(100) |
| 40 | 22.06 | 280, 355 | Dehydroglyceollin VI | Pterocarpene | $C_{20}H_{14}O_4$ | 317 | 273(20), 289(100) | 319 | 275(50), 291(52), 304(100) |
| 41 | 22.41 | 262, 271, 282 | unknown degradation product | | $C_{18}H_{30}O_2$ | 277 | 179(9), 233 (100), 259(28) | 279 | 123(39), 137(41), 223(42), 261(100) |
| 42 | 22.61 | 259, 268, 279 | unknown degradation product | | $C_{18}H_{30}O_2$ | 277 | 179(10), 233 (100), 259(24) | 279 | 123(40), 137(40), 223(42), 261(100) |

[a]The nomenclature of glyceollins and dehydroglyceollins is ambiguous. The nomenclature in this article is based on Simons et al. and Aisyah et al.[6,7] Glyceollin VI in this article is sometimes also referred to as clandestacarpin in the literature. Dehydroglyceollin III in this article is also referred to as glyceollin VI in the literature. In the current work, "glyceollin" always refers to prenylated 6a-hydroxy-pterocarpans, whereas "dehydroglyceollin" always refers to prenylated 6a,11a-pterocarpenes. [b]Only peaks with a relative intensity of 4% or higher were considered, with a maximum of the four most abundant product ions. [c]The $[M + H - H_2O]^+$ dominated in the $MS^1$ compared to the $[M + H]^+$.




**Figure 3.** Conversion of 6a-hydroxy-pterocarpans in time with (○) or without acid (●) and the conversion of other isoflavonoids in time with (□) or (■) without acid.

with a previous study, showing that glyceollin I was unstable at temperatures above 40 °C and at pH values below 4.[11] The other three subclasses of isoflavonoids showed little conversion (~15%) and acid did not accelerate this conversion. This suggests that the 6a-hydroxyl group of 6a-hydroxy-pterocarpans in particular is susceptible to acid. This is in line with a thermal degradation study, in which daidzein and genistein did not degrade after 3 h of heating at 150 °C, whereas a minimal degradation of glycitein was seen after 1 h of heating.[19] In contrast, it has also been shown[20] that degradation of daidzein and genistein, occurred at 120 °C and pH 7 and 9.

**Preparative Enrichment of Prenylated 6a-Hydroxy-Pterocarpans and 6a,11a-Pterocarpenes.** In order to compare the estrogenic properties of glyceollins and dehydro-glyceollins, the (treated) soy extracts were fractionated using Flash chromatography, with a fairly good separation considering the particle size of the column material (Figure 4). All fractions were analyzed by RP-UHPLC-MS, and it was seen that the first 20 fractions contained unprenylated isoflavonoids (data not shown). The subsequent fractions contained prenylated isoflavonoids and the compositional analysis of these fractions is shown in Figure 5. Different prenylated isoflavonoids could be separated and different pools were made based on this compositional analysis (Figure 4). Fractions 28−29 and 33−36 contained the prenylated 6a-hydroxy-pterocarpans, mainly present before the treatment. Fractions 28 and 29 were combined to obtain pool 1, and 97% of this pool comprised of the 6a-hydroxy-pterocarpans glyceollin I, II, and III. Pool 2 (fractions 33−36) contained 74% glyceollin IV and VI. Fractions 58−66 and 71−75 contained the prenylated 6a,11a-pterocarpenes, obtained in high quantities after the heat/acid treatment. Fractions 58−66 were combined to obtain pool 3, which consisted of 88% dehydroglyceollin I, II, and III. Pool 4 (fractions 71−75) contained 89% dehydroglyceollin IV and VI (Table 2 and Supporting Information (SI) Figure S1). It should be noted that the sample used for Flash chromatography was dried at slightly elevated temperatures, which resulted in a larger proportion of 6a,11a-pterocarpenes than in the untreated sample shown in Figure 2A. This sample is further referred to as "mildly treated". The treated sample used for Flash chromatography had a further increased proportion of 6a,11a-pterocarpenes (pool 3 and 4) compared to the untreated sample, at the expense of 6a-hydroxy-pterocarpans (pool 1 and 2) (data not shown).

**Change in Estrogenic Activities upon Heating.** The different pools were tested for their estrogenic activities (Figure 6). Agonistic activities were expressed as relative estrogen

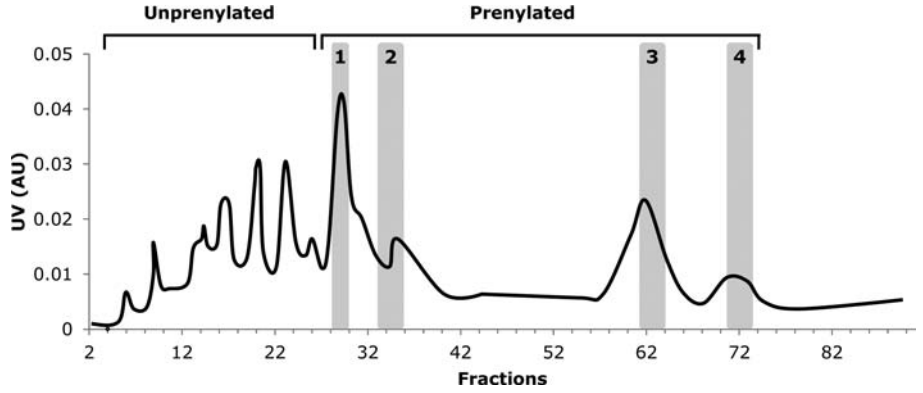


**Figure 4.** Flash chromatography UV profile of the mildly treated soy extract. Gray areas refer to the four different pools collected.

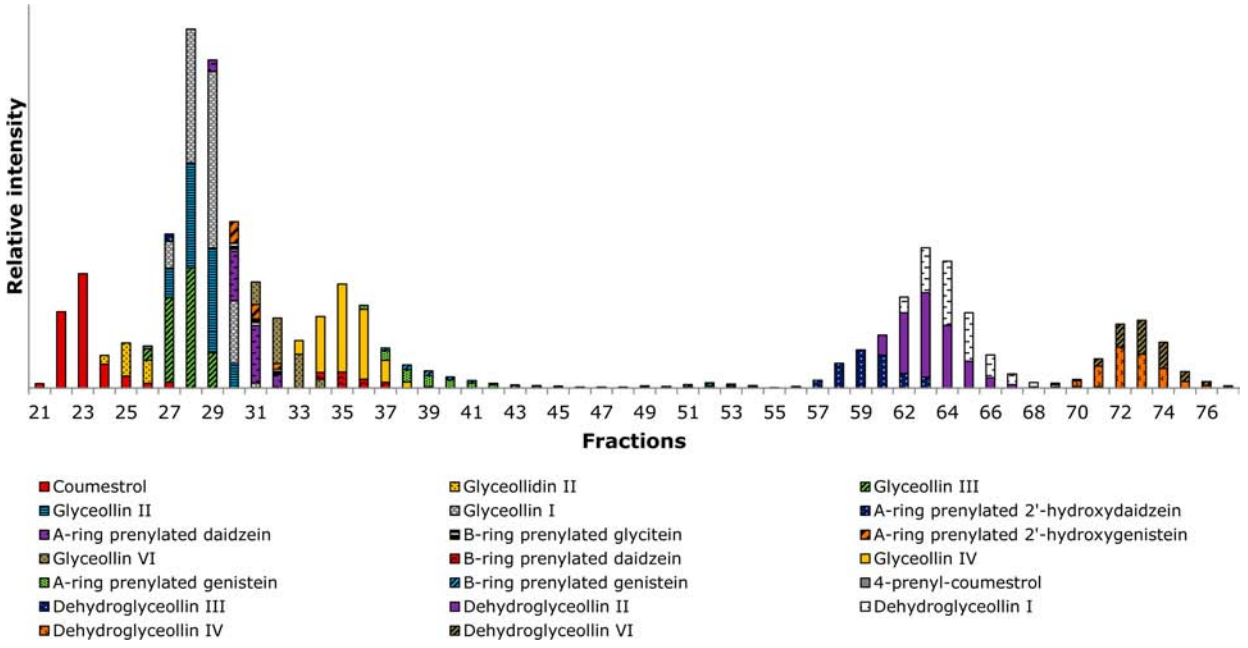


**Figure 5.** Content of Flash chromatography fractions of the mildly treated soy extract determined by RP-UHPLC-MS.

**Table 2. Quantitative Analysis Of Prenylated Isoflavonoids In The Enriched Pools**

| pool | identification | area 280 nm (%) |
|---|---|---|
| 1 | Glyceollin III | 15.3 |
| | Glyceollin II | 31.1 |
| | Glyceollin I | 51.0 |
| | Other | 2.6 |
| 2 | Glyceollin VI | 0.9 |
| | Glyceollin IV | 72.6 |
| | Other | 26.5 |
| 3 | Dehydroglyceollin III | 10.3 |
| | Dehydroglyceollin II | 38.1 |
| | Dehydroglyceollin I | 39.3 |
| | Other | 12.3 |
| 4 | Dehydroglyceollin IV | 81.2 |
| | Dehydroglyceollin VI | 7.9 |
| | Other | 10.9 |

potencies (REPs) based on the threshold values, and antagonistic activities were expressed as the decrease of the maximal response in percentages. Pool 1 (glyceollin I–III) showed a slight ER agonistic activity toward ER$\alpha$ (REP 1.1 × $10^{-5}$) and a clear agonistic activity toward ER$\beta$ (REP 1.2 × $10^{-4}$). No antagonistic properties of pool 1 could be established toward both receptors (Figure 6A,C). Estrogenic activity of glyceollin I–III seemed ambiguous, as it was previously shown that glyceollin I, II, and III could act as agonist and antagonist toward estrogen receptors.[8−10] Taken together, the present results and those from previous studies[8−10] indicated that glyceollin I, II, and III might act as SERMs. Pool 2, containing glyceollin IV and VI, showed a slight agonistic activity toward ER$\alpha$ (REP 1.1 × $10^{-5}$), a clear agonistic activity toward ER$\beta$ (REP 1.0 × $10^{-4}$), and slight antagonistic activities toward ER$\alpha$ and ER$\beta$ (34% and 24%, respectively) (Figure 6A,C), indicating that glyceollin IV and VI are partial agonists or can act as SERMs.[21] Other assays, e.g., proliferation assays based on human breast cells or U2-OS based ER-CALUX bioassays, are needed to conclude on the exact estrogenic classification. Figure 6B,D shows the estrogenic activities of the corresponding dehydroglyceollins (pools 3 and 4). Figure 6B showed that the dehydroglyceollins had clear antagonistic properties toward ER$\alpha$, i.e., 78% decrease with pool 3 (dehydroglyceollin I, II, and III) and 26% decrease with pool 4 (dehydroglyceollin IV and VI), whereas no ER$\alpha$ agonistic activity was observed (Figure 6B). Toward ER$\beta$, dehydrogly-

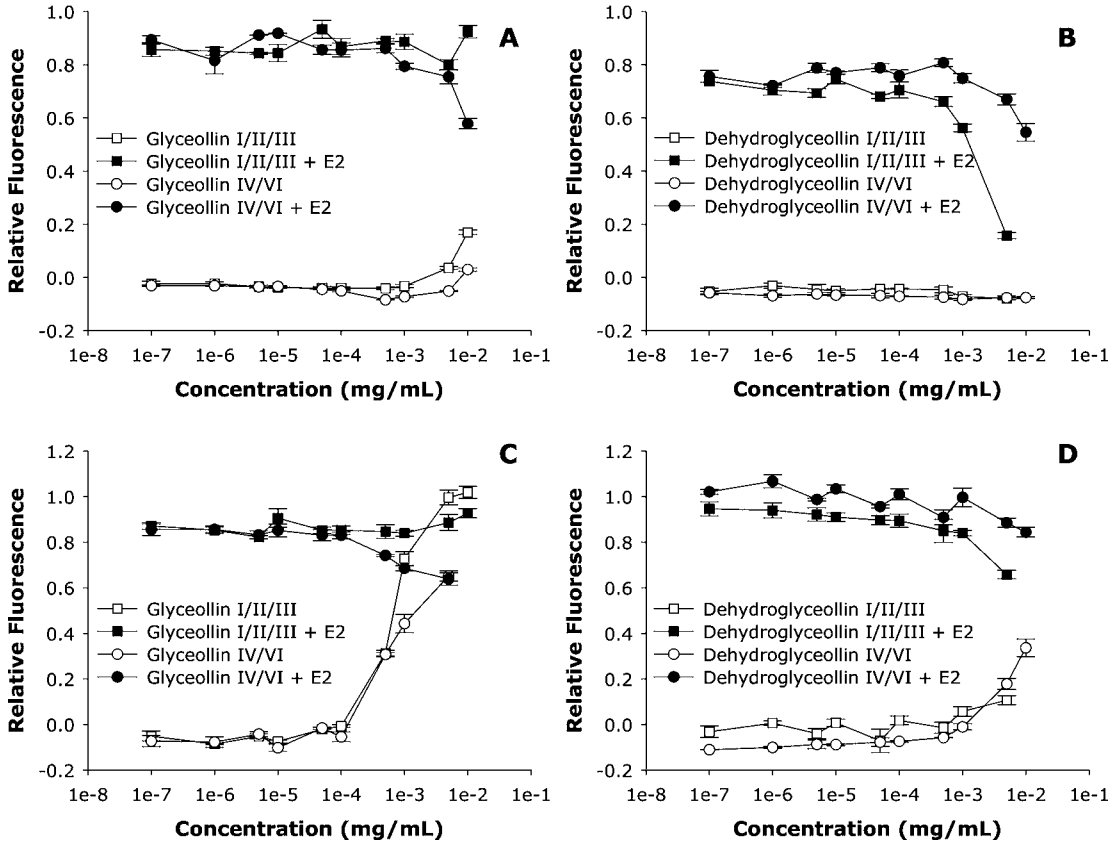


**Figure 6.** Transcriptional activation by ER$\alpha$ (A and B) and ER$\beta$ (C and D) in response to pools 1−4.

ceollins seemed to have both agonistic and antagonistic properties (Figure 6D), indicating that these compounds could act as partial agonists or as SERMs. No agonistic response was detected for dehydroglyceollin I−III, whereas the REP value of dehydroglyceollin IV/VI was $9.8 \times 10^{-5}$. The antagonistic effects resulted in a 28% decrease in estrogenic activity for dehydroglyceollin I−III and 15% for dehydroglyceollin IV/VI. In summary, glyceollins showed higher agonistic activity toward ER$\beta$ than toward ER$\alpha$, which is in line with literature.[2] In particular, the response toward ER$\alpha$ changed from agonistic for glyceollin I−III to full antagonistic for dehydroglyceollins I−III. Toward ER$\beta$ a decrease in agonistic activity was observed after heating.

## DISCUSSION

Compounds are considered estrogenic when they activate the ER at concentrations below $10^4$ times that of estradiol.[22] Thus, REP values $\geq 1 \times 10^{-4}$ indicate that compounds (or pools) have clear estrogenic properties, which was not always the case with the pools tested in the present study. Intriguingly, the estrogenic properties of glyceollins and their corresponding dehydroglyceollins were different.

After heat/acid treatment, the dehydroglyceollins that were formed from 6a-hydroxy-pterocarpans showed full antagonistic properties toward ER$\alpha$ and lower agonistic activities toward ER$\beta$. It has been suggested[23] that the removal of the 6a-hydroxyl group with the concomitant extra planarity of the dehydroglyceollins might increase the binding to the estrogen receptor. This was not observed in the present study. Nevertheless, our results clearly showed that dehydroglyceollins had different mode of action toward both receptor types compared to the 6a-hydroxy-pterocarpans. The natural ligand 17$\beta$-estradiol has two hydroxyl groups, each on one side of the molecule. These are required for binding to the estrogen receptor, the distance of which is important for binding. When the geometry of glyceollins and dehydroglyceollins is compared (Figure 7), it is apparent that the length of the two compounds

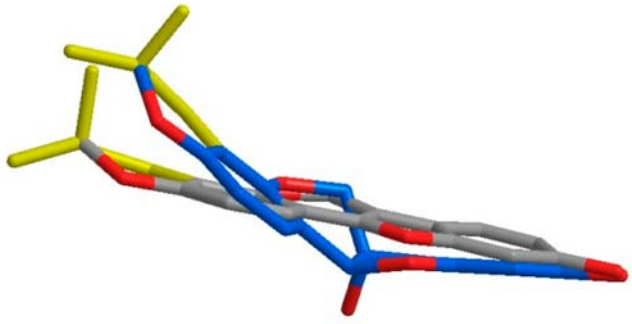

**Figure 7.** Molecular structures of glyceollin I (blue) and dehydroglyceollin I (gray). Prenyl group is indicated in yellow.

is different. With the increased planarity of the dehydroglyceollins, the distance between the two hydroxyl groups of dehydroglyceollins becomes larger than that in glyceollins. Furthermore, the orientation of the prenyl group changes between the two compounds as a result of the planarity. This might affect binding in the ligand-binding domain of the receptor, turning the agonistic response observed for glyceollins into the antagonistic response observed for dehydroglyceollins in case of ER$\alpha$, and into a decreased agonistic response observed for dehydroglyceollins in case of ER$\beta$.

Glyceollins showed agonistic activities to both estrogen receptors. This gives the opportunity to use these glyceollins of elicited soy sprouts in food supplements to prevent menopausal complaints. It is known that dietary agonistic estrogens, like soy isoflavones, are helpful to counteract the drop in endogenous estrogen levels in postmenopausal women.[4,24] The present results show that care should be taken during processing (e.g., when soy glyceollins are processed into food supplements) or isolation, because 6a-hydroxy-pterocarpans are prone to transformation upon which estrogenic characteristics can change, i.e., drop in estrogenic activity or switch from agonistic to antagonistic behavior.

Alternatively, heat and acid might be used to modulate estrogenicity of elicited soy sprouts in a relatively simple way. After the treatment, the dehydroglyceollins showed full antagonistic activity toward ER$\alpha$. Full antagonistic compounds, like fulvestrant and RU 58668, are well-known molecules in treatment of patients with breast cancer.[21,25,26] Full antagonists are rare, and dehydroglyceollins might represent a new class of ER$\alpha$ antagonists, although further verification of their in vitro antiestrogenic potency by other bioassays and their in vivo activity remain to be established.

## ■ ASSOCIATED CONTENT

### Supporting Information

RP-UHPLC-UV profiles of the untreated soy extract and the different enriched pools. This material is available free of charge via the Internet at http://pubs.acs.org.

## ■ AUTHOR INFORMATION


### Corresponding Author

*Phone: +31 317 483211; fax: +31 317 484893; e-mail: harry.gruppen@wur.nl.


### Notes

The authors declare no competing financial interest.

## ■ ACKNOWLEDGMENTS

We would like to thank Dr. Tina Ritschel (Computational Discovery and Design Group, Center for Molecular and Biomolecular Informatics, Radboudumc, The Netherlands) for providing insights on molecular dimensions of pterocarpans and pterocarpenes, and Hugo Cardoso (Laboratory of Food Chemistry, Wageningen University, The Netherlands) for his technical assistance.

## ■ REFERENCES


(1) Veitch, N. C. Isoflavonoids of the leguminosae. *Nat. Prod. Rep.* **2013**, *30*, 988−1027.

(2) Simons, R.; Gruppen, H.; Bovee, T. F. H.; Verbruggen, M. A.; Vincken, J.-P. Prenylated isoflavonoids from plants as selective estrogen receptor modulators (phytoSERMs). *Food Funct.* **2012**, *3*, 810−827.

(3) Snyder, R. D.; Gillies, P. J. Reduction of genistein clastogenicity in Chinese hamster V79 cells by daidzein and other flavonoids. *Food Chem. Toxicol.* **2003**, *41*, 1291−1298.

(4) Setchell, K. D. Phytoestrogens: The biochemistry, physiology, and implications for human health of soy isoflavones. *Am. J. Clin. Nutr.* **1998**, *68*, 1333S−1346S.

(5) Boue, S. M.; Cleveland, T. E.; Carter-Wientjes, C.; Shih, B. Y.; Bhatnagar, D.; McLachlan, J. M.; Burow, M. E. Phytoalexin-enriched functional foods. *J. Agric. Food Chem.* **2009**, *57*, 2614−2622.

(6) Aisyah, S.; Gruppen, H.; Madzora, B.; Vincken, J.-P. Modulation of isoflavonoid composition of *Rhizopus oryzae* elicited soybean (*Glycine max*) seedlings by light and wounding. *J. Agric. Food Chem.* **2013**, *61*, 8657−8667.

(7) Simons, R.; Vincken, J.-P.; Roidos, N.; Bovee, T. F. H.; van Iersel, M.; Verbruggen, M. A.; Gruppen, H. Increasing soy isoflavonoid content and diversity by simultaneous malting and challenging by a fungus to modulate estrogenicity. *J. Agric. Food Chem.* **2011**, *59*, 6748−6758.

(8) Zimmermann, M. C.; Tilghman, S. L.; Boué, S. M.; Salvo, V. A.; Elliott, S.; Williams, K. Y.; Skripnikova, E. V.; Ashe, H.; Payton-Stewart, F.; Vanhoy-Rhodes, L.; Fonseca, J. P.; Corbitt, C.; Collins-Burow, B. M.; Howell, M. H.; Lacey, M.; Shih, B. Y.; Carter-Wientjes, C.; Cleveland, T. E.; McLachlan, J. A.; Wiese, T. E.; Beckman, B. S.; Burow, M. E. Glyceollin I, a novel antiestrogenic phytoalexin isolated from activated soy. *J. Pharmacol. Exp. Ther.* **2010**, *332*, 35−45.

(9) Payton-Stewart, F.; Khupse, R. S.; Boué, S. M.; Elliott, S.; Zimmermann, M. C.; Skripnikova, E. V.; Ashe, H.; Tilghman, S. L.; Beckman, B. S.; Cleveland, T. E.; McLachlan, J. A.; Bhatnagar, D.; Wiese, T. E.; Erhardt, P.; Burow, M. E. Glyceollin I enantiomers distinctly regulate ER-mediated gene expression. *Steroids* **2010**, *75*, 870−878.

(10) Kim, H. J.; Suh, H. J.; Kim, J. H.; Kang, S. C.; Park, S.; Lee, C. H.; Kim, J. S. Estrogenic activity of glyceollins isolated from soybean elicited with *Aspergillus sojae*. *J. Med. Food* **2010**, *13*, 382−390.

(11) Luniwal, A.; Khupse, R.; Reese, M.; Liu, J.; El-Dakdouki, M.; Malik, N.; Fang, L.; Erhardt, P. Multigram synthesis of glyceollin I. *Org. Process Res. Dev.* **2011**, *15*, 1149−1162.

(12) Simons, R.; Vincken, J.-P.; Bohin, M. C.; Kuijpers, T. F. M.; Verbruggen, M. A.; Gruppen, H. Identification of prenylated pterocarpans and other isoflavonoids in *Rhizopus* spp. elicited soya bean seedlings by electrospray ionisation mass spectrometry. *Rapid Commun. Mass Spectrom.* **2011**, *25*, 55−65.

(13) Bovee, T. F. H.; Helsdingen, R. J. R.; Rietjens, I. M. C. M.; Keijer, J.; Hoogenboom, R. L. A. P. Rapid yeast estrogen bioassays stably expressing human estrogen receptors [alpha] and [beta], and green fluorescent protein: A comparison of different compounds with both receptor types. *J. Steroid Biochem. Mol. Biol.* **2004**, *91*, 99−109.

(14) Fedoreyev, S. A.; Bulgakov, V. P.; Grishchenko, O. V.; Veselova, M. V.; Krivoschekova, O. E.; Kulesh, N. I.; Denisenko, V. A.; Tchernoded, G. K.; Zhuravlev, Y. N. Isoflavonoid Composition of a Callus Culture of the Relict Tree *Maackia amurensis* Rupr. et Maxim. *J. Agric. Food Chem.* **2008**, *56*, 7023−7031.

(15) Yang, M.; Wang, W.; Sun, J.; Zhao, Y.; Liu, Y.; Liang, H.; Guo, D.-a. Characterization of phenolic compounds in the crude extract of *Hedysarum multijugum* by high-performance liquid chromatography with electrospray ionization tandem mass spectrometry. *Rapid Commun. Mass Spectrom.* **2007**, *21*, 3833−3841.

(16) Ma, Y. L.; Li, Q. M.; Van den Heuvel, H.; Claeys, M. Characterization of flavone and flavonol aglycones by collision-induced dissociation tandem mass spectrometry. *Rapid Commun. Mass Spectrom.* **1997**, *11*, 1357−1364.

(17) Simons, R. *Prenylated isoflavonoids from soya and licorice*; Ph.D. thesis Wageningen University, Wageningen, the Netherlands, 2011.

(18) Simons, R.; Vincken, J.-P.; Bakx, E. J.; Verbruggen, M. A.; Gruppen, H. A rapid screening method for prenylated flavonoids with ultra-high-performance liquid chromatography/electrospray ionisation mass spectrometry in licorice root extracts. *Rapid Commun. Mass Spectrom.* **2009**, *23*, 3083−3093.

(19) Stintzing, F. C.; Hoffmann, M.; Carle, R. Thermal degradation kinetics of isoflavone aglycones from soy and red clover. *Mol. Nutr. Food Res.* **2006**, *50*, 373−377.

(20) Ungar, Y.; Osundahunsi, O. F.; Shimoni, E. Thermal stability of genistein and daidzein and its effect on their antioxidant activity. *J. Agric. Food Chem.* **2003**, *51*, 4394−4399.

(21) Bovee, T. F. H.; Thevis, M.; Hamers, A. R. M.; Peijnenburg, A. A. C. M.; Nielen, M. W. F.; Schoonen, W. G. E. J. SERMs and SARMs: Detection of their activities with yeast based bioassays. *J. Steroid Biochem. Mol. Biol.* **2010**, *118*, 85−92.

(22) Glazier, M.; Bowman, M. A. A review of the evidence for the use of phytoestrogens as a replacement for traditional estrogen replacement therapy. *Arch. Int. Med.* **2001**, *161*, 1161−1172.
(23) De-Eknamkul, W.; Umehara, K.; Monthakantirat, O.; Toth, R.; Frecer, V.; Knapic, L.; Braiuca, P.; Noguchi, H.; Miertus, S. QSAR study of natural estrogen-like isoflavonoids and diphenolics from Thai medicinal plants. *J. Mol. Graphics Model.* **2011**, *29*, 784−794.
(24) Usui, T. Pharmaceutical prospects of phytoestrogens. *Endocr. J.* **2006**, *53*, 7−20.
(25) Bovee, T.; Schoonen, W.; Hamers, A.; Bento, M.; Peijnenburg, A. Screening of synthetic and plant-derived compounds for (anti)-estrogenic and (anti)androgenic activities. *Anal. Bioanal. Chem.* **2008**, *390*, 1111−1119.
(26) Cardoso, F.; Bischoff, J.; Brain, E.; Zotano, Á. G.; Lück, H.-J.; Tjan-Heijnen, V. C.; Tanner, M.; Aapro, M. A review of the treatment of endocrine responsive metastatic breast cancer in postmenopausal women. *Cancer Treat. Rev.* **2013**, *39*, 457−465.

chemical structures isolated from fungal pathogens belonging to *Diplodia*, *Didymella*, *Phoma*, *Pyrenophora*, and *Seiridium* genera on the seed germination and radicle growth of four major broomrape species. This work was designed to investigate the ability of metabolites isolated from the above cited plant and fungi to either stimulate suicidal seed germination or inhibit germination induced by a germination-inducing factor on four broomrape species *Orobanche crenata*, *Orobanche cumana*, *Orobanche minor*, and *Phelipanche ramosa*. Their effect on the radicle growth and their potential as lead compounds to develop new classes of bioherbicides was also evaluated and discussed.

## MATERIALS AND METHODS

**Fungal Sources and Tested Metabolites.** Sphaeropsidin A, **4**, sphaerospidone, **5**, and *epi*-sphaeropsidone, **3**; cyclopaldic acid, **1**; and *epi*-epoformin, **2** (Figure 1), were purified,

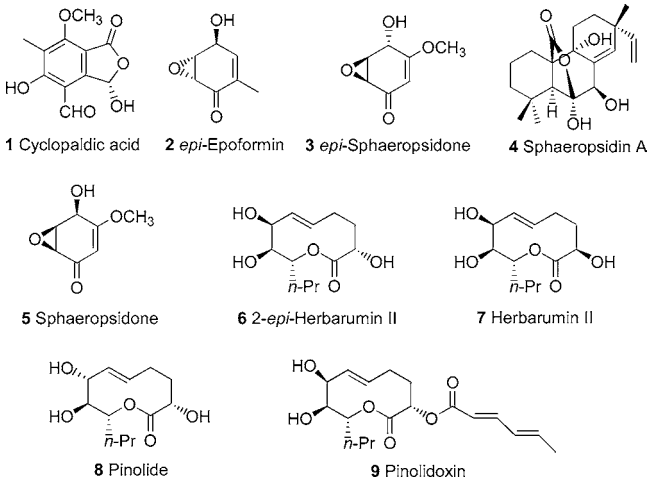


**Figure 1.** Phytotoxins isolated from *Seiridium cupressi* and *Diplodia* spp.—cyclopaldic acid, *epi*-epoformin, *epi*-sphaeropsidone, sphaeropsidin A, and sphaeropsidone (**1**–**5**)—and from *Didymella pinodes*—*epi*-herbarumin II, herbarumin II, pinolide, and pinolidoxin (**6**–**9**).

respectively, all as white needles from the culture filtrates of *Diplodia cupressi*,[17,18] *Seiridium cupressi*,[19] and *Diplodia quercivora*.[20] Pinolidoxin, **9**; pinolide, **8**; herbarumin II, **7**; and *epi*-herbarumin II, **6** (Figure 1), were isolated from the culture filtrates of *Didymella pinodes*.[21] Cavoxin, **10**, and cavoxone, **11**, and chenopodolin, **12**; chenopodolan C, **13**; and 6-hydroxymellein, **14** (Figure 2), were isolated, respectively, from the culture filtrates of *Phoma cava*[22] and *Phoma chenopodiicola*.[23,24] Cytochalasins A, **15**, and B, **16**, and deoxaphomin, **17** (Figure 2), were isolated from the solid culture of *Pyrenophora seminiperda*.[25] All the above cited fungal metabolites were freshly isolated from the fungal cultures according to the protocols reported in the literature and were identified by $^1$H NMR and electrospray ionization mass spectrometry (ESI MS), comparing these data with those previously described. Finally, fusaric acid, **21** (Figure 3), was purchased from Sigma (St. Louis, MO).

**Plant Source and Tested Metabolites.** Inuloxins A, **19**, and C, **20**, and $\alpha$-costic acid, **18** (Figure 3), were freshly isolated from the aerial part of *Inula viscosa* according to the previously reported protocol[16] and were identified by $^1$H NMR and ESI MS, comparing these data with those previously described.

**Induction of *Orobanche* Seed Germination by Fungal and Plant Metabolites.** The biological activity of the metabolites (Figures 1–3) isolated from *Diplodia* spp., *Didymella pinodes*,

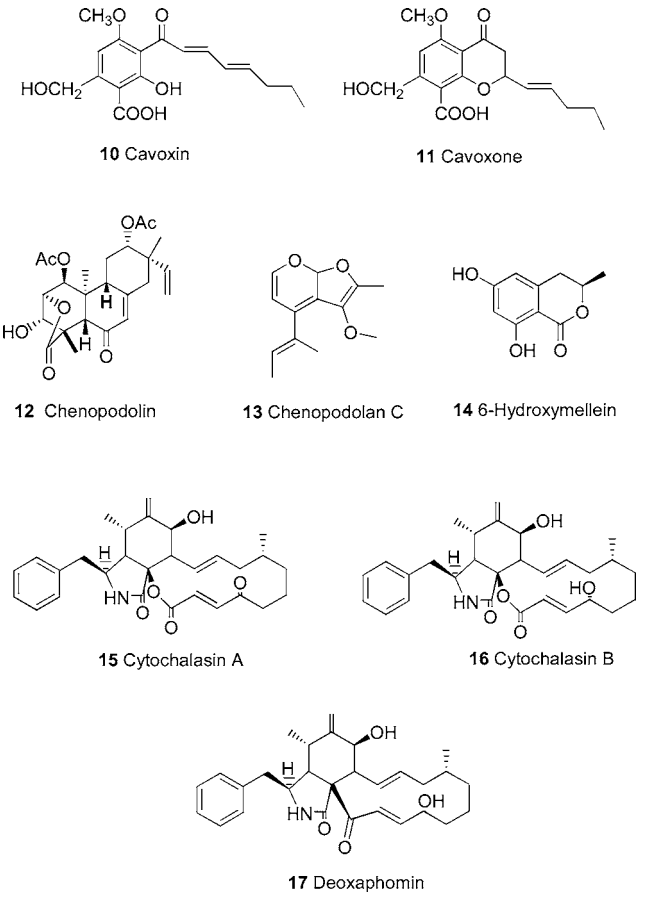


**Figure 2.** Phytotoxins isolated from *Phoma* spp.—cavoxin, cavoxone, chenopodolin, chenopodolan C, and 6-hydroxymellein (**10**–**14**)—and from *Pyrenophora seminiperda*—cytochalasins A and B and deoxaphomin (**15**–**17**).

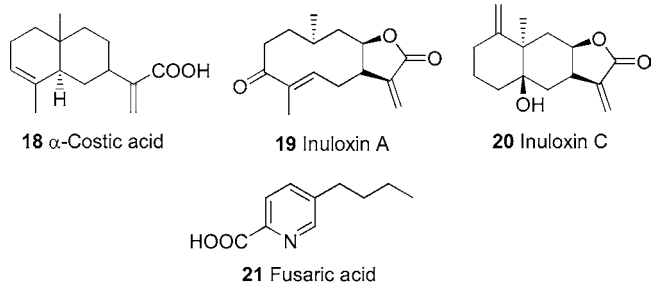


**Figure 3.** Phytotoxins isolated from *Inula viscosa*, $\alpha$-costic acid and inuloxins A and C (**18**–**20**). Fusaric acid (**21**).

*Phoma* spp., *P. seminiperda*, *S. cupressi*, and *I. viscosa* was assayed on *O. crenata*, *O. cumana*, *O. minor*, and *P. ramosa* seeds. For this purpose, seeds were surface sterilized by immersion in 0.5% (w/v) NaOCl and 0.02% (v/v) Tween 20, were sonicated for 2 min, were rinsed thoroughly with sterile distilled water, and were dried in a laminar air flow cabinet. Approximately 100 seeds of each broomrape species were placed separately on 9 mm diameter glass fiber filter paper disks (GFFP) moistened with 50 $\mu$L of sterile distilled water. Subsequently, GFFP disks were placed inside sterile 10 cm Petri dishes, were sealed with parafilm, and were kept for 10 days in the dark at 22 °C to allow seed conditioning. GFFP disks were transferred inside laminar flow cabinet to sterile filter paper to remove excess water, and then they were transferred to a new 10 cm sterile Petri dish.


dx.doi.org/10.1021/jf504609w | J. Agric. Food Chem. 2014, 62, 10485–10492

Tested samples, dissolved in methanol, were diluted with sterilized distilled water to a final concentration of $10^{-4}$ M. The final concentration of methanol was adjusted to 0.70% (v/v). Each disk containing conditioned seeds was treated with 50 $\mu$L aliquot of the respective test solution. Each treatment was replicated three times. Seeds treated with distilled water (containing 0.70% methanol) or the synthetic strigolactone GR24[26,27] at 0.6 and 0.06 mM were included as controls for comparison. The seeds were incubated in the dark at 22 °C for 7 days prior to examination for germination. Seeds with an emerged radicle were scored as germinated using a stereoscopic microscope at 30 × magnification, and the percentage of germination was established for each dish.

**Inhibition of *Orobanche* Seed Germination and Radicle Growth by Fungal and Plant Metabolites.** The inhibitory activity of the various above metabolites (Figures 1−3) on seed germination and radicle growth of *O. crenata, O. cumana, O. minor,* and *P. ramosa* was assayed as reported previously.[28] A solution of the GR24 ($10^{-6}$ M) was prepared in sterile distilled water. Immediately before use, stock solutions of each toxin prepared in methanol were diluted in the GR24 solution to $10^{-4}$ M of each toxin while keeping constant the GR24 concentrations and methanol in order to allow comparisons. Broomrape seeds were surface sterilized and conditioned as described above. GFFP disks containing conditioned broomrape seeds were transferred inside a flow laminar cabinet to a sterile sheet of filter paper to remove excess moisture and were transferred to a 10 cm diameter Petri dish. Fifty microliter aliquots of each toxin-GR24 were applied to each GFFP disk containing the seeds. Petri dishes were sealed with Parafilm and were stored in the dark at 22 °C for 7 days to promote germination and radicle growth. Then, seeds were observed under stereoscopic microscope in order to score levels of allelopathic-mediated inhibition of broomrape seed germination and radicle growth.

**Statistical Analysis.** All the bioassays were performed twice with at least three replicates. Percentage data were approximated to normal frequency distribution by means of angular transformation $\{180/\pi \times \text{arcsine}(\text{sqrt}[\%/100])\}$ and were subjected to analysis of variance (ANOVA) using SPSS software for Windows, version 21.0 (SPSS Inc., Chicago, Illinois, U.S.A.). The significance of mean differences between each treatment against its respective control was evaluated by the two-sided Dunnett test. Null hypothesis was rejected at the level of 0.05.

## RESULTS AND DISCUSSION

Phytotoxins isolated from plant pathogenic fungi as well as those produced by an allelopathic plant were used in a bioactivity screening on seed germination and radicle growth of *O. crenata, O. cumana, O. minor*, and *P. ramosa*, four major broomrape species constraining production of major agricultural crops worldwide.

The phytotoxins belong to different classes of natural compounds as sphaeropsidin A, **4** (Figure 1), and chenopodolin, **12** (Figure 2), which are tetracyclic pimarane diterpenes, and as *epi*-epoformin, **2**; *epi*-sphaeropsidone, **3**; and sphaeropsidone, **5** (Figure 1), which are cyclohexene epoxide. *epi*-Herbarumin II, **6**; herbarumin II, **7**; pinolide, **8**; and pinolidoxin, **9** (Figure 1), are nonenolides, while cytochalasins A, **15**, and B, **16**, and deoxaphomin, **17** (Figure 2), are 24-oxa[14] and [13] cytochalasans, respectively. Cavoxin, **10**; cavoxone, **11**; chenopodolan C, **13**; and 6-hydroxymellein, **14** (Figure 2), are a chalcone, a chromanone, a furopyran and a hydroxymellein. $\alpha$-Costic acid, **18**, and inuloxins A, **19**, and C, **20** (Figure 3), are bi- and tricyclic sesquiterpenes. Finally, cyclopaldic, **1** (Figure 1), and fusaric acid, **21** (Figure 3), are a substituted benzofuranone and a substituted pyridinic acid, respectively.

**Phytotoxin Activity as Stimulators of Broomrape Suicidal Germination.** The stimulation activity of these metabolites on broomrape seed germination was tested on four broomrape species—*O. crenata, O. cumana, O. minor,* and *P. ramosa*. All metabolites belonging to bi- and tricyclic sesquiterpenes class (inuloxins A and C and $\alpha$-costic acid) induced significant germination on seeds of *O. cumana* (Figure 4A). The effect of inuloxin A, **19**, and $\alpha$-costic acid, **18** (Figure 3), was stronger than inuloxin C, **20** (Figure 3). Interestingly, *O. cumana* seeds that germinated with inuloxin C showed short radicles with light brown patches, symptoms that were not observed in seedlings germinated with inuloxin A and $\alpha$-costic acid. In addition to bi- and tricyclic sesquiterpenes, cyclopaldic acid, **1** (Figure 1), a substituted benzofuranone, induced significant germination of *O. cumana* seeds (Figure 4A). The rest of the metabolites tested did not induce any germination in *O. cumana* seeds except for the positive control. *P. ramosa* seeds were induced to germinate when exposed to inuloxin A and $\alpha$-costic acid but not when exposed to inuloxin C or cyclopaldic acid (Figure 4B). In addition, *epi*-sphaeropsidone, **3** (Figure 1), a cyclohexene epoxide, induced significant germination on *P. ramosa* but not in the rest of the broomrape species tested (Figure 4B). *O. crenata* and *O. minor* seeds did not germinate when exposed to any of the compounds tested except for the positive control (data not shown).

**Phytotoxin Activity as Inhibitors of Broomrape Germination and Radicle Growth.** In addition to germination-inducing activity, each compound was also tested as potential inhibitor for broomrape development by inhibiting its germination (Figure 5) and its radicle growth (Figure 6). Each metabolite was mixed with the germination factor GR24 and was applied to conditioned seeds of *O. crenata, O. cumana, O. minor,* and *P. ramosa*. *epi*-Epoformin, **2**, and sphaeropsidin A, **4** (Figure 1), significantly inhibited germination of *O. crenata* and *O. cumana* seeds (Figure 5A and B). Inhibition of *O. minor* and *P. ramosa* seed germination was induced by sphaeropsidin A but not by *epi*-epoformin (Figure 5C and D). All cytochalasans, **15**−**17** (Figure 2), inhibited the germination of *P. ramosa* seeds (Figure 5D), but germination of *Orobanche* species was not inhibited by this class of compounds except that deoxaphomin, **17** (Figure 2), induced inhibition of *O. crenata* germination (Figure 5A).

Regarding inhibition of radicle growth, all cyclohexene oxides (**2**, **3**, and **5**, Figure 1) and cytochalasans (**15**−**17**, Figure 2) induced a strong and significant reduction on broomrape radicle length when compared with control radicles (i.e., radicles emerged from seeds induced only with GR24, Figures 6 and 7). This is very significant from a parasitic weed control point of view, as broomrape radicles have limited growth length and constitute the organ that establishes host contact and carries the attachment and penetration organ in its tip. Despite the similar effect on radicle growth inhibition performed by cyclohexene oxides and cytochalasans, there were important differences in the appearance of the radicles treated with each class of compound. While radicles of all broomrape species exposed to cytochalasans quickly turned brown and necrotic (Figure 7B), radicles exposed to cyclohexene oxides although much shorter than the control radicles had a healthy appearance (Figure 7C). In addition, *O. crenata* and *O. cumana* radicles exposed to cyclohexene epoxides developed a dense layer of papilla-like structures at the tip of the radicle

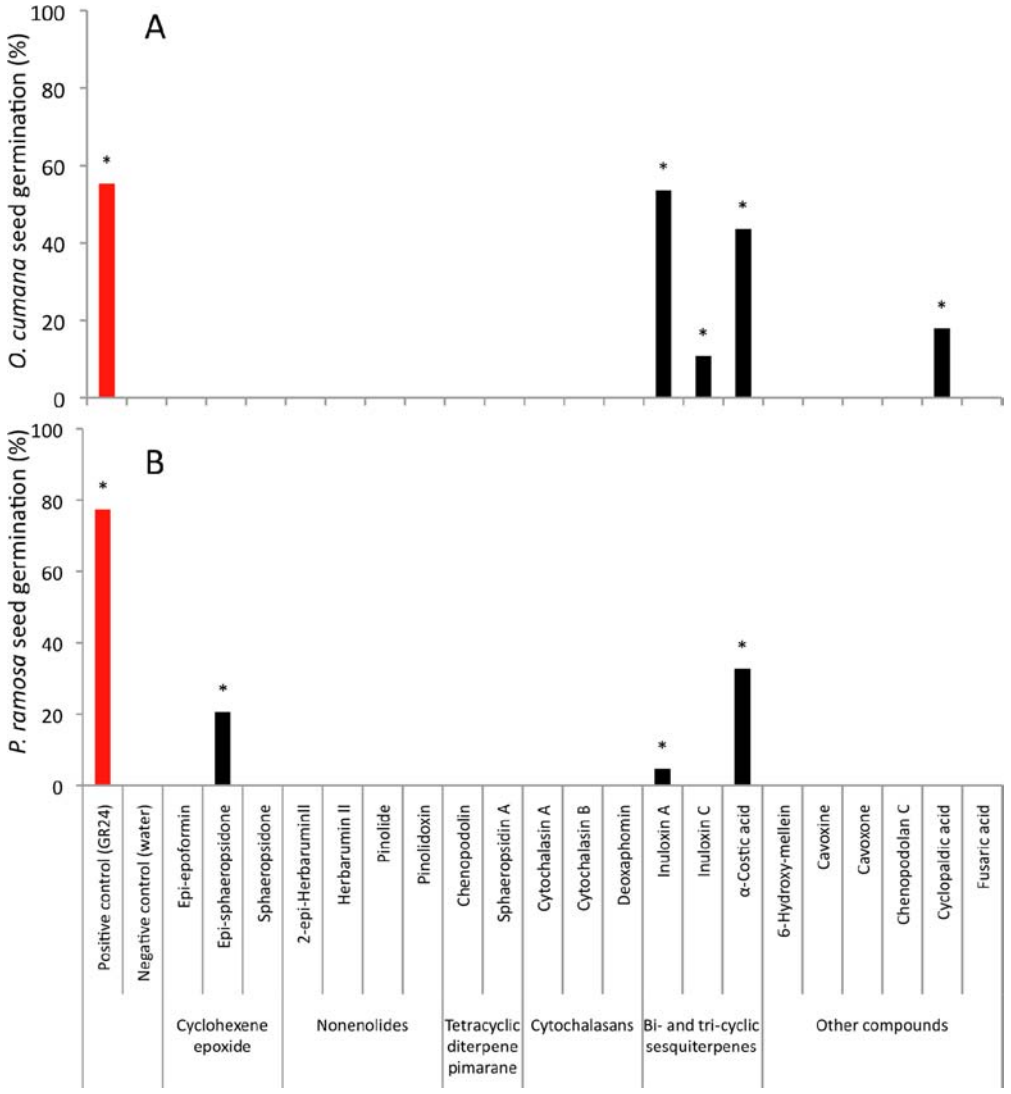


**Figure 4.** Stimulatory effect on (A) *O. cumana* and (B) *Phelipanche ramosa* seed germination of the tested phytotoxins. The asterisk (*) indicates differences at the 0.05 level compared with the negative control (seeds treated with water).

(Figure 7C). The papilla layer was not observed in radicles exposed to any other compound in this work.

The tetracyclic pimarane diterpene, sphaeropsidin A, **4** (Figure 1), showed a strong phytotoxic effect on all broomrapes species tested inducing inhibition of both germination and radicle growth. Radicles of broomrape exposed to sphaeropsidin A quickly turned brown and necrotic.

Inuloxin C, **20** (Figure 3), did not significantly inhibit broomrape germination, and its inducing effect on suicidal germination, in absence of germination-inducing factor GR24, was low and restricted to *O. cumana* (Figure 4A). Despite this stimulatory activity observed in *O. cumana*, when broomrape seeds were exposed to a mixture of GR24 and inuloxin C, germinated seedlings developed radicles that were shorter than those in the controls, and this effect was observed in seeds of all the broomrape species tested. In addition, *O. crenata* and *O. cumana* radicles exposed to inuloxin C showed light brown patches (Figure 7D), which could point to a cytotoxic effect although this fact needs further investigation. This combined activity allows differentiating inuloxin C from the other sesquiterpenes tested regarding its potential for agronomical use. Inuloxin C, rather than being a good candidate for suicidal germination-based herbicide, like inuloxin A and $\alpha$-costic acid, would be a better candidate for broomrapes post-germination herbicide reducing the parasitic capability of attacking the host crop by reducing the attachment organ length.

Some structure−activity relationships could be evaluated within the same class of the natural compounds. The different activity showed on broomrape germination by *epi*-epoformin, **2** (Figure 1, strong inhibitor of *O. cumana* seed germination), and *epi*-sphaeropsidone, **3** (Figure 1, stimulant of *P. ramosa* seed germination), and sphaeropsidone, **5** (Figure 1, practically inactive), which have the same carbon skeleton, should be due to the different stereochemistry of the epoxy ring and that of the hydroxy group at C-5. On the other hand, common structural features such as the 5-hydroxycyclohexenone-1,6-oxide group in these three compounds induced radicle growth cessation in all broomrapes tested and induced the differentiation of a papillae layer in the radicle tip of *O. crenata* and *O. cumana*. No reports have been previously published on these effects on broomrape development mediated by these chemical structures.

Sphaeropsidin A, **4** (Figure 1), showed a strong phytotoxic effect by inhibiting both germination and radicle growth on all the broomrapes species tested while chenopodolin, **12** (Figure 2),

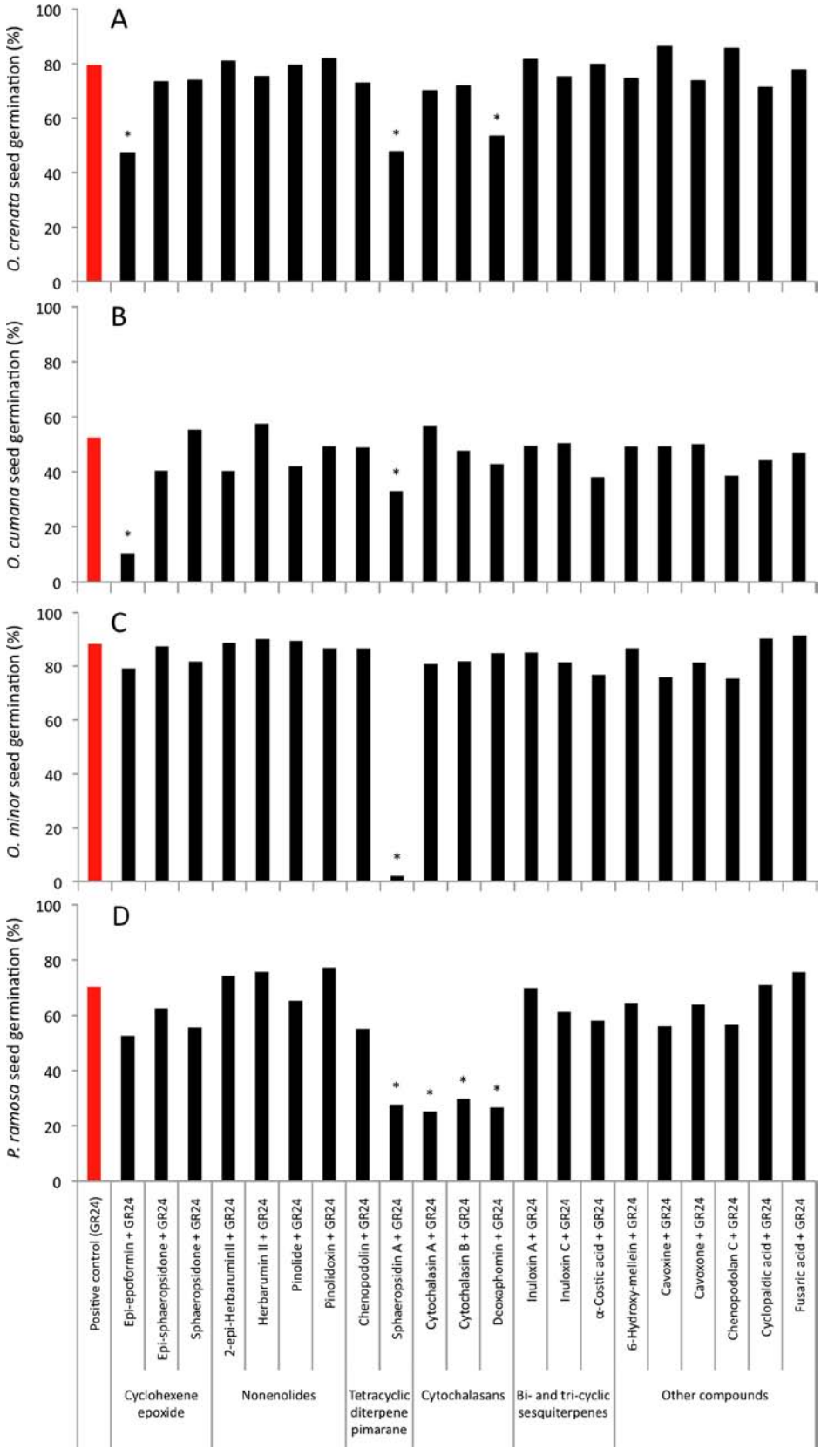


**Figure 5.** Inhibitory effect on (A) *Orobanche crenata*, (B) *O. cumana*, (C) *O. minor*, and (D) *Phelipanche ramosa* seed germination of the tested phytotoxins. The asterisk (*) indicates differences at the 0.05 level compared with the positive control (seeds induced to germinate with GR24).

is inactive. Both are tetracyclic pimarane diterpenes but strongly differ in the junction between γ-lactone ring and phenanthrene ring system and in the functionalities of the latter.

The different biological activity observed between the three sesquiterpenes tested, with α-costic acid and inuloxins A inducing *O. cumana* and *P. ramosa* germination and inuloxin C displaying


dx.doi.org/10.1021/jf504609w | J. Agric. Food Chem. 2014, 62, 10485−10492

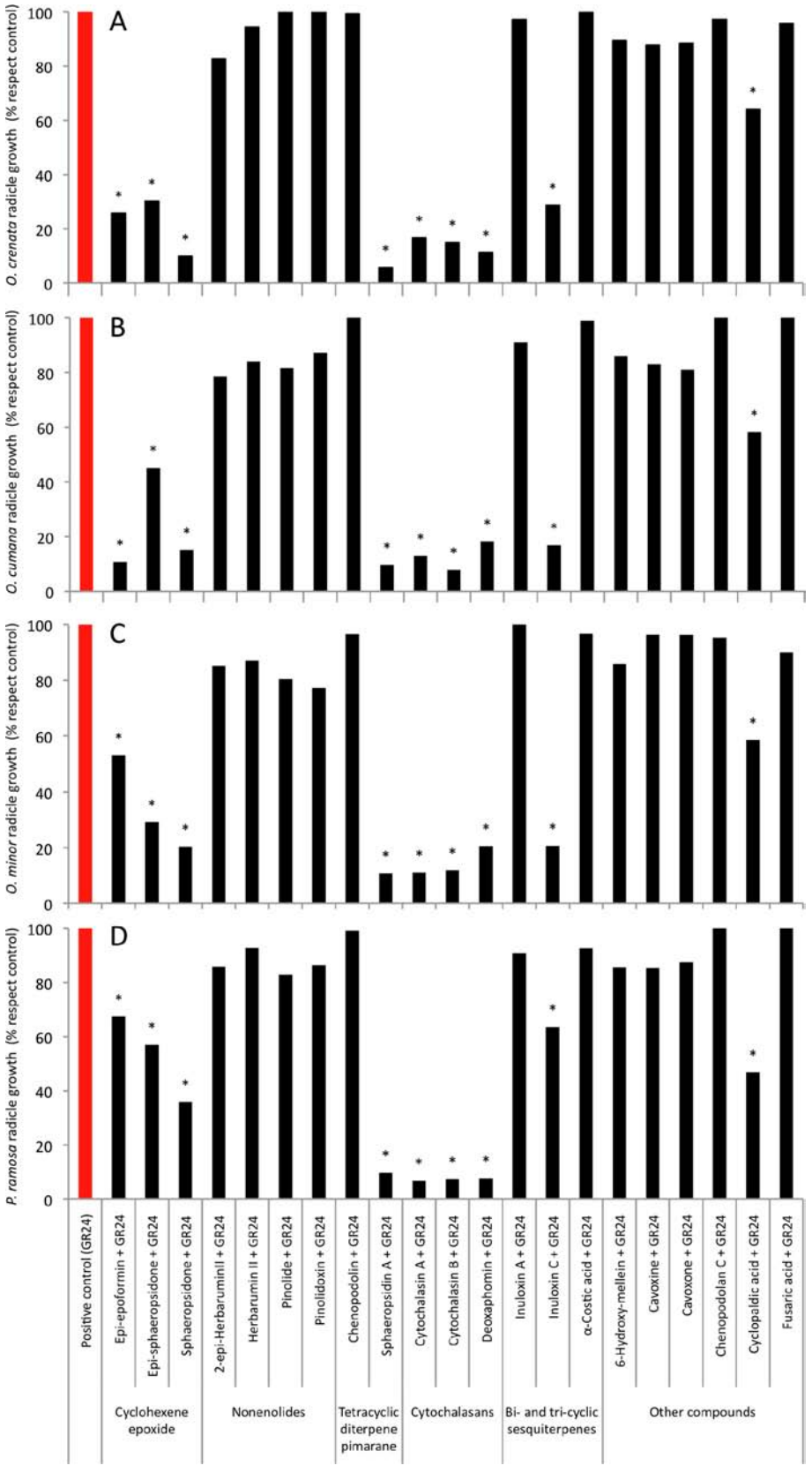


**Figure 6.** Inhibition of broomrape radicle growth induced by the tested phytotoxins. The broomrape species tested were (A) *Orobanche crenata*, (B) *O. cumana*, (C) *O. minor*, and (D) *Phelipanche ramosa*. The asterisk (*) indicates differences at the 0.05 level compared with the positive control (seeds induced to germinate with GR24).

mainly a phytotoxic effect, was due to the different organization of the carbon skeleton and also to their different functionalities and stereochemistry. These results were in agreement with those reported previously testing the same compounds on *O. crenata*.[16]


dx.doi.org/10.1021/jf504609w | J. Agric. Food Chem. 2014, 62, 10485−10492

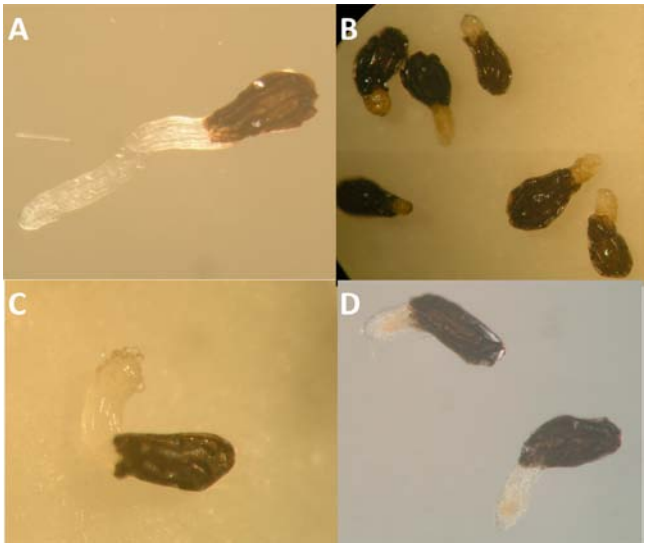


**Figure 7.** Radicle growth modification by fungal and plant toxins observed at 7 days after GR24 aplication. (A) *Orobanche* control radicle, (B) cytochalasin-treated *Orobanche* radicle, (C) cyclohexene epoxide-treated *Orobanche* radicle, and (D) inuloxin C-treated *Orobanche* radicle.

The structural differences between the three cytochalasans tested did not lead to differences in biological activities for broomrape germination and radicle growth. All of them similarly induced phytotoxic effects on broomrape by inhibiting seed germination and radicle growth inhibition and toxicity in radicles. Herbicidal effects mediated by deoxaphomin, cytochalasin A, and cytochalasin B inducing necrosis in tissues of other weeds have been previously reported,[29] but this effect was never tested in broomrape germination and radicle growth. Previously, cytochalasins E and B were tested on *Striga* seed germination, and of them, only cytochalasin E inhibited *Striga* germination by 50%, cytochalasin B being noninhibitory.[30] Unfortunately, these authors did not evaluate the effect of the toxic effects in *Striga* radicles. We have found that cytochalasans inhibit germination only in the *Phelipanche* species but not in the *Orobanche* species. In addition, we observed a strong toxic effect in radicles of all broomrape species tested by inhibiting their growth and inducing darkening in the radicle. The germination bioassays widely conducted on broomrape research are based on the quantification of seeds with emerged radicle through the seed coat. A seed with emerged radicle is counted as germinated. However, in bioassays where the herbicide tested is inducing such a strong reduction on seedling development as that in this work by cytochalasans, it is difficult to discern between inhibition of the strict germination process and inhibition of initial seedling development. Seed germination is a complex physiological process where the seed transforms from dormant to metabolically active, and this process begins with perception of dormancy breaking/germination inducing signals and ends with the beginning of radicle emergence through the seed coat. In the present study, lack of visible radicle in *P. ramosa* induced by cytochalasans does not mean strictly germination inhibition as the toxins could have allowed germination triggered by GR24, but the seedling development could be inhibited so strongly that the radicle did not make it through the seed coat. Cytochalasan-treated *P. ramosa* seeds showed either no radicle visible or such a short radicle that it was extending in length very little from the seed cover. Inhibitory effect of cytochalasans on *P. ramosa* germination may be confounded with strong inhibition of initial seedling development because of the radicle remaining inside the seed coat.

In conclusion, 21 phytotoxins belonging to different classes of natural compounds isolated from different pathogenic fungi and an allelophatic plant were tested on four different broomrape species. The discovery of the negative effect on radicle growth exerted by sphaeropsidin A and compounds belonging to cyclohexene epoxides and cytochalasans is the first step that paves the way for the development of herbicides promoting the interruption of parasitic life cycle before host attachment and crop resource withdrawal by the parasite. Further studies on these compounds could lead to the development of a new and unexplored strategy for broomrape control. In addition to radical growth inhibition, some compounds induced the inhibition of germination in the presence of parasitic plant germination-factor GR24. *epi*-Epoformin, **2**; sphaeropsidin A, **4** (Figure 1); and cytochalasans caused the strongest inhibition of seed germination, and this effect adds to the effect of radicle growth inhibition to strengthen the potential of these substances as candidates for broomrape seedbank management in agricultural soils cultivated with susceptible crop species. Interesting species-specific activity was discovered for some of the compounds tested inducing broomrape seed germination. *P. ramosa* seed germination was induced by *epi*-sphaeropsidone, **3**, and cyclopaldic acid, **1** (Figure 1), and inuloxin A, **19** (Figure 3), while germination of *O. cumana* was only induced by sesquiterpenes. Seeds from the *O. crenata* and *O. minor* species did not germinate in the presence of any of the compounds tested except for the positive control. This specificity is important from a point of view of parasitic plant germination biology because the unresponsive broomrape species and particularly *O. minor* are broomrape species with high sensitivity to a broad range of compounds and root exudates.[31,32] The strong effect induced by inuloxin A and $\alpha$-costic acid on *O. cumana* opens new research addressing broomrape control through a suicidal germination strategy for this broomrape species. Among the rest of the active compounds as broomrape germination inductors, *epi*-sphaeropsidone and cyclopaldic acid are probably too weak in their current structural form to have practical applications for field delivery as suicidal germination-inducing herbicides; however, as described before, the report of this activity is important because of the special evolutionary strategy of parasitic plants that allows them to germinate in the presence of host-derived factors. The germination biology of parasitic plants is far from completely elucidated, and it has been suggested that combination of compounds may confer specific host recognition patterns. Metabolites promoting low germination inducing activity may have a role on modulation of host recognition in a species-specific manner. In addition, those compounds that showed activities can be subjected to structural modifications in order to increase the intensity of germination-inducing activities. The results represent important findings for further studies on new compounds as tools to be used in the design of new approaches for parasitic weed control such as nature-inspired herbicides or engineering resistant crops by enhancing expression of allelochemicals or phytotoxins against parasitic weed germination and development.[33]

## AUTHOR INFORMATION

### Corresponding Author

*Tel: +39 081 2539178. Fax: +39 081 674330. E-mail: evidente@unina.it.

## Funding

The research was carried out in part in the frame of Programme STAR, financially supported by UniNA and Compagnia di San Paolo, and in part in the frame of project FP7-ARIMNet-MEDILEG. This work was carried out within the COST ACTION FA1206 Strigolactones: biological roles and applications. Monica Fernández-Aparicio has received support from the European Union, in the framework of the Marie-Curie FP7 COFUND People Programme, through the award of an AgreenSkills' fellowship (under grant agreement n° PCOFUND-GA-2010−267196). A. E. is associated with the Istituto di Chimica Biomolecolare del CNR, Pozzuoli, Italy.

## Notes

The authors declare no competing financial interest.

## REFERENCES

(1) Parker, C. Observations on the current status of *Orobanche* and *Striga* problems worldwide. *Pest Manage. Sci.* **2009**, *65*, 453−459.

(2) Rubiales, D.; Fernández-Aparicio, M. Innovations in parasitic weeds management in legume crops. *Agron. Sustain. Dev.* **2012**, *32*, 433−449.

(3) Joel, D. M.; Hershenhorn, J.; Eizenberg, H.; Aly, R.; Ejeta, G.; Rich, P. J.; Ransom, J. K.; Sauerborn, J.; Rubiales, D. Biology and management of weedy root parasites. *Hortic. Rev.* **2007**, *33*, 267−349.

(4) Rubiales, D.; Fernández-Aparicio, M.; Wegmann, K.; Joel, D. Revisiting strategies for reducing the seedbank of *Orobanche* and *Phelipanche* spp. *Weed Res.* **2009**, *49*, 23−33.

(5) Hershenhorn, J.; Eizenberg, H.; Dor, E.; Kapulnik, Y.; Goldwasser, Y. *Phelipanche aegyptiaca* management in tomato. *Weed Res.* **2009**, *49*, 34−47.

(6) Pérez-de-Luque, A.; Eizenberg, H.; Grenz, J. H.; Sillero, J. C.; Ávila, C. M.; Sauerborn, J.; Rubiales, D. Broomrape management in faba bean. *Field Crops Res.* **2010**, *115*, 319−328.

(7) Rimando, A. M.; Duke, S. O. In *Natural Products for Pest Management*; Rimando, A. M., Duke, S. O., Eds.; ACS Symposium Series No. 927; American Chemical Society: Washington, DC, U.S.A., 2006; p 388.

(8) Vurro, M.; Boari, A.; Evidente, A.; Andolfi, A.; Zermane, N. Natural metabolites for parasitic weed management. *Pest Manag. Sci.* **2009**, *65*, 566−571.

(9) Yoneyama, K.; Awad, A. A.; Xie, X.; Yoneyama, K.; Takeuchi, Y. Strigolactones as germination stimulants for root parasitic plants. *Plant Cell Physiol.* **2010**, *51*, 1095−1103.

(10) Evidente, A.; Fernández-Aparicio, M.; Cimmino, A.; Rubiales, D.; Andolfi, A.; Motta, A. Peagol and peagoldione, two new strigolactone like metabolites isolated from pea root exudates. *Tetrahedron Lett.* **2009**, *50*, 6955−6958.

(11) Evidente, A.; Cimmino, A.; Fernández-Aparicio, M.; Andolfi, A.; Rubiales, D.; Motta, A. Polyphenols, including the new peapolyphenols A-C, from root exudates stimulate *Orobanche foetida* seed germination. *J. Agric. Food Chem.* **2010**, *58*, 2902−2907.

(12) Evidente, A.; Cimmino, A.; Fernández-Aparicio, M.; Rubiales, D.; Andolfi, A.; Melck, D. Soyasapogenol B and *trans*-22-dehydrocampesterol from common vetch (*Vicia sativa* L.) root exudates stimulate broomrape seed germination. *Pest Manage. Sci.* **2011**, *67*, 1015−1022.

(13) Yoneyama, K.; Takeuchi, Y.; Ogasawara, M.; Kannai, M.; Sugimoto, Y.; Sassa, T. Cotilenins and fusicoccins stimulate seed germination of *Striga hermonthica* (Del.) Beth and *Orobanche minor* Smith. *J. Agric. Food Chem.* **1998**, *46*, 1583−1586.

(14) Evidente, A.; Andolfi, A.; Fiore, M.; Boari, A.; Vurro, M. Stimulation of *Orobanche ramosa* seed germination by fusicoccin derivatives: a structure-activity relationships study. *Phytochemistry* **2006**, *67*, 19−26.

(15) Fernández-Aparicio, M.; Andolfi, A.; Cimmino, A.; Rubiales, D.; Evidente, A. Stimulation of seed germination of *Orobanche* species by ophiobolin A and fusicoccin derivatives. *J. Agric. Food Chem.* **2008**, *56*, 8343−8347.

(16) Andolfi, A.; Zermane, N.; Cimmino, A.; Avolio, F.; Boari, A.; Evidente, A. Inuloxins A-D, phytotoxic bi- and tri-cyclic sesquiterpene lactones produced by *Inula viscosa*: potential for broomrapes and field dodder management. *Phytochemistry* **2013**, *86*, 112−120.

(17) Evidente, A.; Sparapano, L.; Motta, A.; Giordano, F.; Fierro, O.; Frisullo, S. A phytotoxic pimarane diterpene of *Sphaeropsis sapinea* f. sp. *cupressi*, the pathogen of a canker disease of cypress. *Phytochemistry* **1996**, *42*, 1541−1546.

(18) Evidente, A.; Sparapano, L.; Fierro, O.; Bruno, G.; Giordano, F.; Motta, A. Sphaeropsidone and epishaeropsidone, two phytotoxic dimedone methyl ethers produced by *Sphaeropsis sapinea* f. sp. *cupressi* grown in liquid cultures. *Phytochemistry* **1998**, *48*, 1139−1143.

(19) Graniti, A.; Sparapano, L.; Evidente, A. Cyclopaldic acid, a major phytotoxic metabolite of *Seiridium cupressi*, the pathogen of a canker disease of cypress. *Plant Pathol.* **1992**, *41*, 563−568.

(20) Andolfi, A.; Maddau, L.; Basso, S.; Linaldeddu, B. T.; Cimmino, A.; Scanu, B.; Deidda, A.; Tuzi, A.; Evidente, A. Diplopimarane, a phytotoxic 20-*nor*-*ent*-pimarane produced by the oak pathogen *Diplodia quercivora*. *J. Nat. Prod.* **2014**, accepted.

(21) Cimmino, A.; Andolfi, A.; Fondevilla, S.; Abouzeid, M. A.; Rubiales, D.; Evidente, A. Pinolide, a new nonenolide produced by *Didymella pinodes*, the causal agent of *Ascochyta* blight on *Pisum sativum*. *J. Agric. Food Chem.* **2012**, *60*, 5273−5278.

(22) Evidente, A.; Randazzo, G.; Iacobellis, N. S.; Bottalico, A. Structure of cavoxin, a new phytotoxin from *Phoma cava* and cavoxone, its related chroman-4-one. *J. Nat. Prod.* **1985**, *48*, 916−923.

(23) Cimmino, A.; Andofi, A.; Zonno, M. C.; Avolio, F.; Santini, A.; Tuzi, A.; Berestetskiy, A.; Vurro, M.; Evidente, A. Chenopodolin: a phytotoxic unrearranged *ent*-pimaradiene diterpene produced by *Phoma chenopodicola*, a fungal pathogen for *Chenopodium album* biocontrol. *J. Nat. Prod.* **2013**, *76*, 1291−1297.

(24) Cimmino, A.; Andofi, A.; Zonno, M. C.; Avolio, F.; Berestetskiy, A.; Vurro, M.; Evidente, A. Chenopodolans A-C: phytotoxic furopyrans produced by *Phoma chenopodiicola*, a fungal pathogen of *Chenopodium album*. *Phytochemistry* **2013**, *96*, 208−213.

(25) Evidente, A.; Andolfi, A.; Vurro, M.; Zonno, M. C.; Motta, A. Cytochalasins Z1, Z2 and Z3, three 24-oxa[14]cytochalasans produced by *Pyrenophora seminiperda*. *Phytochemistry* **2002**, *60*, 45−53.

(26) Johnson, A.; Rosebery, G.; Parker, C. A. A novel approach to *Striga* and *Orobanche* control using synthetic germination stimulant. *Weed Res.* **1976**, *16*, 223−227.

(27) Zwanenburg, B.; Mwakaboko, A. S.; Reizelman, A.; Anikumar, G.; Sethumadhavan, D. Structure and function of natural and synthetic signalling molecules in parasitic weed germination. *Pest Manage. Sci.* **2009**, *65*, 478−491.

(28) Fernández-Aparicio, M.; Cimmino, A.; Evidente, A.; Rubiales, D. Inhibition of *Orobanche crenata* seed germination and radicle growth by allelochemicals identified in cereals. *J. Agric. Food Chem.* **2013**, *61*, 9797−9803.

(29) Berestetskiy, A.; Dmitriev, A.; Mitina, G.; Lisker, I.; Andolfi, A.; Evidente, A. Nonenolides and cytochalasins with phytotoxic activity against *Cirsium arvense* and *Sonchus arvensis*: a structure-activity relationship study. *Phytochemistry* **2008**, *69*, 953−960.

(30) Zonno, M. C.; Vurro, M. Effect of fungal toxins on germination of *Striga hermonthica* seeds. *Weed Res.* **1999**, *39*, 15−20.

(31) Fernández-Aparicio, M.; Yoneyama, K.; Rubiales, D. The role of strigolactones in host specificity of *Orobanche* and *Phelipanche* seed germination. *Seed Sci. Res.* **2011**, *21*, 55−61.

(32) Fernández-Aparicio, M.; Flores, F.; Rubiales, D. Recognition of root exudates by seeds of broomrape (*Orobanche* and *Phelipanche*) species. *Ann. Bot.* **2009**, *103*, 423−431.

(33) Fernández-Aparicio, M.; Westwood, J. H.; Rubiales, D. Agronomic, breeding, and biotechnological approaches to parasitic plant management through manipulation of germination stimulant levels in agricultural soils. *Botany* **2011**, *89*, 813−826.

potential molecular protein networks. To the best of our knowledge, this is the first proteomics study to report the antidepressive mechanism of WGE.

## MATERIALS AND METHODS

**Material Extraction and Composition Determination.** WGE was provided by Koda Pharmaceutical Company (Taoyuan, Taiwan). To obtain WGE, 700 g of dried rhizome of GE was boiled twice with 6 and 4.8 L of water for 1 h, respectively. Then, the extract was filtered, freeze-dried, and stored until utilization. Fluoxetine was obtained from Eli Lilly Company (Taiwan).

An LC-NET II/ADC (JASCO, Easton, MD, USA) high-performance liquid chromatography (HPLC) system, which consisted of a pump (PU-2089-PLUS) and a UV detector (UV-2075-PLUS), with a Phenomenex Luna $C_{18}$ column (250 × 4.6 mm, 5 $\mu$m, Torrance, CA, USA) and Chrompass analyzing program, was used for analyzing the composition of WGE. An acetonitrile−water solution (10:90, v/v) was used as the mobile phase at 1 mL/min flow rate. The mobile phase was filtered using 0.45 $\mu$m Millipore filters, the UV detector was set at 220 nm, and the oven was set at 35 °C to maintain the column temperature. The injected sample volume was 20 $\mu$L.

**Animal and Treatments.** Male Sprague−Dawley rats (4 weeks old) were purchased from BioLasco Taiwan Company (Taipei, Taiwan) and housed individually at controlled day/night cycle (12 h light/dark), temperature (23 ± 2 °C), and humidity (60 ± 10%). Free access to food and water was provided and recorded every day. Rats were randomly separated into three groups (7 rats/group): control (CTL), WGE, and fluoxetine (FLX). After 2 weeks of habituation, oral administration was initiated and continued for 21 days with ultrapure water, fluoxetine (20 mg/kg body weight), and WGE (500 mg/kg body weight) to CTL, FLX, and WGE groups, respectively. The dosage was based our preliminary studies. Animal protocol was reviewed and approved by the Institutional Animal Care and Use Committee of National Taiwan University, Taiwan (Approval Number: NTU-IACUC-96-56). The protocol complied with guidelines described in the "Animal Protection Law", amended on June 29, 2011, Hua-Zong-(1)-Yi-Tzi-10000136211, Council of Agriculture, Executive Yuan, Taiwan.

**Forced Swimming Test.** The protocol of the FST was described previously.[12] This method followed the procedure developed by Porsolt et al.[14] The behavior of rats during the FST was video recorded. Films were analyzed by ForcedSwimScan software (CleverSys, Reson, VA, USA) for calculating the duration of immobility.

**Sacrifice and Protein Extraction.** After the FST, rats were deeply anesthetized by $CO_2$ and decapitated, and the frontal cortex and hippocampus were dissected from the brain immediately. The dissected tissues were frozen at −80 °C until further analysis. The frozen tissues were ground into a powder with liquid nitrogen and dissolved with lysis buffer containing 7 M urea, 2 M thiourea, 65 mM DTT, 4% CHAPS, and a cocktail of proteinase and phosphatase inhibitors (Roche, Rotkreuz, Switzerland). The samples were centrifuged at 12000$g$ for 2 h, and the precipitates were discarded. Protein extracts were quantified by the Bradford protein assay (Bio-Rad, Hercules, CA, USA).

**Proteomics and Bioinformatics Analysis.** Due to the limitations in the sampling of the 2-DE system, three replicates from CTL and WGE, which had the most opposite duration of immobility in the FST, were further analyzed by 2-DE. Protein extracts were loaded onto the Immobiline DryStrip 18 cm pH 3−10 nonlinear gel strips (GE Healthcare, Pittsburgh, PA, USA) with 350 $\mu$L of rehydration buffer (lysis buffer plus 0.5% IPG buffer). The voltage−time program of isoelectric focusing was set at 50 V for 12 h and 100, 250, 500, 1000, 3000, and 5000 V for 1 h, respectively, and 8000 V for a total of 56 000 V × h. Prior to the second dimension, strips were equilibrated for 15 min in buffer (6 M urea, 30% glycerol, 2% SDS, 50 mM Tris-HCl, 0.002% bromophenol blue, and 0.02% w/v DTT), then soaked for 15 min in the same buffer (replacing DTT with 0.025% IAA). Then the second dimension separation was performed using 10 mA/gel electrophoresis for 18 h on 10−18% polyacrylamide gels at 4 °C by using the PROTEAN II xi Multi-Cell 2-D electrophoresis system (Bio-Rad). The gels were fixed (10% methanol, 7% acetic acid solution for 30 min) and stained with Sypro Ruby dye (Life Technologies, Grand Island, NY, USA). After the destaining process, a Typhoon scanner 9200 (GE Healthcare) was used to scan the gels (100 $\mu$m). PDQuest Basic 2-D analysis software version 8.0 (Bio-Rad) was used for protein spot analysis. The spots on the gel were automatched by PDQuest and manually corrected based on their relative location. Only the significantly expressed spots were selected and subjected to in-gel tryptic digestion.

**In-Gel Tryptic Digestion.** The protein spots that differed significantly were picked up from 2-D gels manually using a UV light box. Then, the gels of the spots were washed with 50% acetonitrile (ACN)−25 mM $NH_4HCO_3$ at room temperature for 20 min, and the solution was replaced by 100% ACN. After washing, gel pieces were dried by a SpeedVac concentrator (Savant, Holbrook, NY, USA). Then, the dried gel plugs were crushed and incubated with 1% trypsin (Promega, Madison, WI, USA) in 25 mM $NH_4HCO_3$ at 37 °C for 16 h. Peptides were extracted subsequently by 50% ACN−5% trifluoroacetic acid (TFA) from gel crushes and then dried with a SpeedVac concentrator. The dried pellets were rehydrated, resuspended with 0.1% TFA, and then concentrated with a C18 ZipTip (Millipore). After washing the C18 ZipTip with 0.1% formic acid (FA), the peptides were eluted with 75% ACN−0.1% FA.

**Peptide Sequence Analyses.** The matched protein spots of the frontal cortex (loading protein: 400 $\mu$g) and hippocampus (loading protein: 400 $\mu$g) were subjected to concerted matrix-assisted laser desorption ionization (MALDI) with time-of-flight (TOF) to operate peptide mass fingerprinting (PMF) and CID MS/MS mass spectrometry. In order to catch more possible proteins, the proteins of the hippocampus were loaded as 450 $\mu$g into the 2-DE system again, and the spots were submitted to a liquid chromatography electronic spray ionization (LC-ESI)-quantitative-TOF Ultima API (Micromass) instrument. The peptide sequencing analyses were performed by the Core Facilities for Protein Structural Analysis located at the Institute of Biological Chemistry, Academia Sinica, Taiwan. The protocols of LC-ESI-Q-TOF and MALDI-TOF were announced on the Web site of the Core Facilities (http://cfpsa.sinica.edu.tw/eng_04_filedownload.php#F3, material and method of mass analysis section). MS and MS/MS data were submitted to the Mascot protein online search program (Matrix Science, Boston, MA, USA) based on Swissprot and the NCBI database to identify proteins by PMF and MS/MS ion search.

**Bioinformatics Analysis.** Metacore (Thomas Reuters, New York, NY, USA), a systemic bioinformatics software, was employed to evaluate the function of proteins, relationship and interactions between proteins, and the potential signaling maps, based on a huge database. In Metacore, the "GeneGo Process Network" shows the cooperative relationships between identified proteins and the "GeneGo Pathway Maps" provides related signaling cascades. All of the candidates in the lists were ranked by −log($p$ value) table. A higher −log($p$ value) indicated by Metacore suggested a higher possibility for its occurrence.

**Western Blot (WB).** The protein extracts were solubilized individually in sample buffer (62.5 mM Tris-HCl, 10% glycerol, 2% SDS, and 0.01% bromophenol blue), heated at 95 °C for 10 min, and subjected to one-dimensional SDS polyacrylamide gel electrophoresis (SDS-PAGE). Following SDS-PAGE, proteins were transferred onto a polyvinylidene fluoride membrane (Millipore, Billerica, MA, USA). Following transfer, 5% bovine serum albumin (BSA) in Tris-buffered saline with 0.1% Tween-20 (TBS-T) was used to block the membranes. Then, the membranes were incubated with TBS-T-diluted primary antibodies. The primary antibodies were Slit1 and Slit2 (Genetex, Irvine, CA, USA), Robo1 and Robo2 (Genetex), RhoA (Cell Signaling, Danvers, MA, USA), PFN1 (Cell Signaling), CRMP2 (Cell Signaling), and GAPDH (Genetex). The corresponding secondary antibodies (Cell Signaling) were added for 1 h at room temperature. Membranes were soaked in ECL solution (PerkinElmer, Santa Clara, CA, USA), and the images were obtained using a UVP Autochemi system. Finally, ImageJ software (National Institutes of Health, USA) was utilized for quantification.

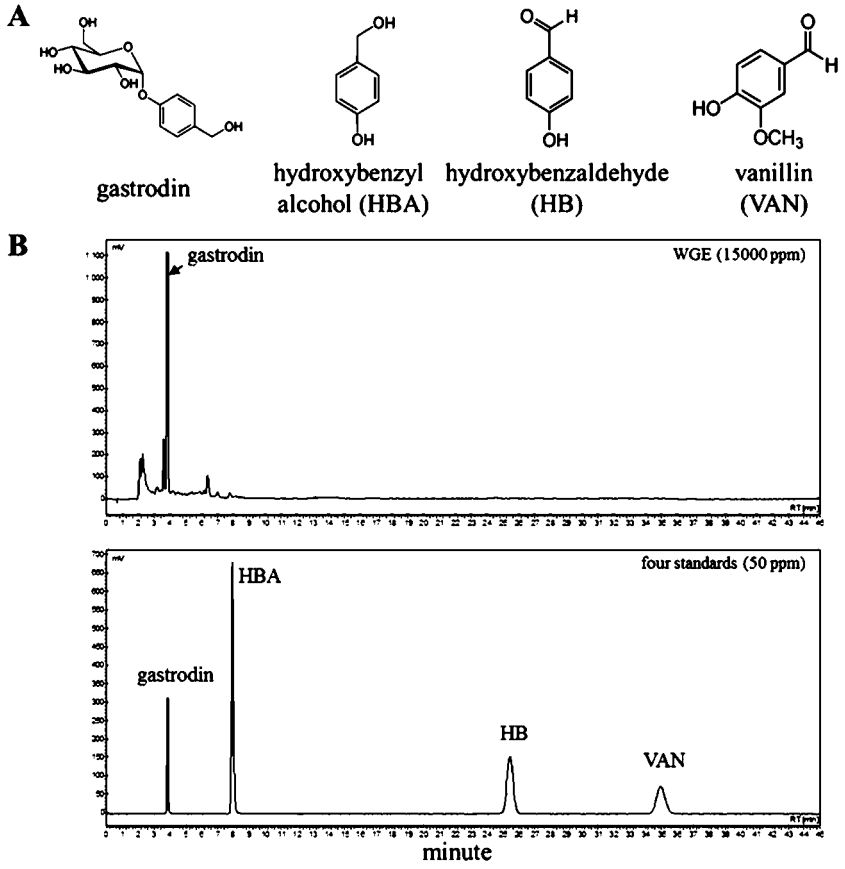


**Figure 1.** (A) Chemical structure of four major active compounds in *Gastrodia elata* Blume. (B) Chromatogram of the water extract of *G. elata* Blume (WGE). Different concentrations of WGE and standard were analyzed by HPLC: WGE (top, 15 000 ppm), standards (bottom, 50 ppm).

**Statistical Analysis.** The results are represented as mean ± SD. Student's unpaired *t* test (2-DE spots comparison and WB) and one-way ANOVA with Duncan's multiple test (body weight, daily intakes, and FST) were employed. $p < 0.05$ (body weight, daily intakes, FST, bioinformatics analysis, and WB) and at least $p < 0.1$ (2-DE spots comparison) were considered statistically different.

## RESULTS

**Active Compounds in WGE.** We determined gastrodin, HBA, HB, and VAN, which are considered to be the major active compounds in GE, by HPLC using a $C_{18}$ column. Similar to gastrodin standard, a signal appeared at 4 min after injection. This peak was further confirmed as gastrodin by MS/MS analysis (data not shown). After quantification, WGE composed with 2.48% gastrodin. However, three other compounds could not be detected in WGE by the HPLC system (Figure 1).

**Animal Behavior and Daily Intakes.** Figure 2 shows the significant difference after FST between each group. CTL demonstrated a higher duration (100.4 ± 23.3 s) of immobility behavior than that of WGE (63.2 ± 19.1 s) and FLX (32.8 ± 5.8 s). In addition, FLX and WGE significantly increased the duration of swimming in comparison to CTL (CTL: 97.04 ± 27.4 s, WGE: 134.2 ± 19.7 s, FLX: 128.2 ± 20.4 s). The duration of struggling behavior was elevated after administration with WGE but was not significant compared to CTL. During experiment, FLX influenced food and water intake and hindered body weight gain. In contrast, WGE administration did not interfere with body weight gain and water intake; even food intake was only slightly affected (Table 1).

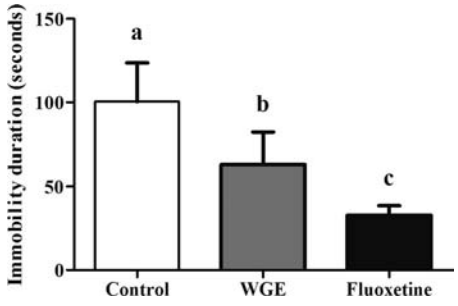


**Figure 2.** Effect of water extract of *Gastrodia elata* Blume on the immobility behavior in rats in the forced swimming test. [abc] indicate significant differences between one another in each group ($p < 0.05$) analyzed by ANOVA and Duncan's multiple range test.

**2-DE and Protein Identification.** Forty-six spots had significant differences out of the 316 matched spots in the frontal cortex (loading protein 400 μg, fold change ≥2, at least $p < 0.1$). Among 46 spots, 30 proteins were identified by MALDI-TOF. In the hippocampus, 29 spots were significantly different in similar conditions to that of the frontal cortex, and 17 proteins were identified. However, 17 protein identities may not be adequate for bioinformatics analyses. To address this issue, we further loaded more proteins (450 μg) for the hippocampus into the 2-DE system and switched to a higher sensitivity MS system (LC-ESI). Finally, 25 proteins, which were not included in the list of 17 proteins from the initial matching, were identified from the 39 differentially expressed spots in the second separation (fold change ≥2, at least $p < 0.1$). Thus,


dx.doi.org/10.1021/jf503132c | J. Agric. Food Chem. 2014, 62, 10493−10503

Table 1. Body Weight and Daily Intake[a]

| parameter | week[b] | CTL | WGE | FLX |
|---|---|---|---|---|
| body weight (g) | W0 | 227.2 ± 7.4 D | 221.5 ± 12.8 d | 223.1 ± 5.5 D |
| | W1 | 280.8 ± 13.8 Ca | 270.5 ± 18.3 Cab | 257.7 ± 9.3 Cb |
| | W2 | 341.6 ± 16.6 Ba | 329.8 ± 10.6 Ba | 299.3 ± 14.8 Bb |
| | W3 | 384.0 ± 18.5 Aa | 370.6 ± 11.4 Aa | 321.9 ± 18.4 Aab |
| food intake (g) | W0 | 23.8 ± 2.8 C | 21.3 ± 1.9 C | 22.6 ± 2.4 B |
| | W1 | 27.4 ± 1.0 Ba | 25.4 ± 2.3 Bb | 21.3 ± 1.6 Bc |
| | W2 | 29.0 ± 1.3 Ba | 26.8 ± 2.8 Bb | 23.0 ± 0.9 Bc |
| | W3 | 32.3 ± 2.3 Aa | 31.1 ± 2.3 Aa | 26.5 ± 2.3 Ab |
| water intake (g) | W0 | 39.9 ± 2.0 | 38.6 ± 2.8 | 39.6 ± 2.8 A |
| | W1 | 39.7 ± 3.0 a | 38.6 ± 5.4 a | 31.9 ± 4.7 Bb |
| | W2 | 40.7 ± 2.6 a | 41.7 ± 5.0 a | 32.7 ± 2.9 Bb |
| | W3 | 42.0 ± 3.6 a | 44.1 ± 5.4 a | 32.1 ± 2.1 Bb |

[a]The capital letters represent the significant differences in the specific group in different weeks. The lower case letters symbolize the significant differences between different treatment groups in the same week. All of the results were subjected to ANOVA with Duncan's post hoc analysis ($p < 0.05$). [b]W0: the habituation period, W1−3: the first to the third week.

42 total proteins were identified from the hippocampus. The information on identified proteins such as protein name, peptide matching percentage, and fold change is shown in Tables 2 and 3 for the frontal cortex and hippocampus, respectively. The zoom-in spot images on 2-DE gel and quantitative charts of specific identified proteins are shown in Figure 3.

**Bioinformatics Analysis.** To elucidate the mechanism underlying the antidepressive-like activity of WGE, the identified proteins were uploaded to Metacore. A cytoskeleton-related process emerged with a high ranking in the analysis of functional classifications based on the GeneGo Process Network (Figure 4A). Furthermore, Slit−Robo signaling emerged with the highest score in the predicted pathways analyzed by the GeneGo Pathway Map of Metacore (Figure 4B). The gel images of these identified proteins related to cytoskeleton remodeling and the Slit−Robo pathway are shown in Figure 3. Besides, we found similar results when the two regions were assessed individually (data not shown). Therefore, the Slit−Robo pathway probably mediates the antidepressive-like activity of WGE. The proteins shown on the Slit−Robo signaling map were built using the Metacore database (Figure 5). The tubulin and actin subunits, actin-related protein 3 (ARP3), dihydropyrimidinase-related protein 2 (DPYL2; also named CRMP2), and profilin1 (PFN1), which were identified in 2-DE, are presented with a "ratio bar (WGE compared to CTL)" on the upper right corner of the symbols.

**Western Blot.** WB was employed to validate the expression of the proteins associated with Slit−Robo signaling, which emerged with the highest score for the predicted pathways. In addition to CRMP2 and PFN1 identified in 2-DE, Slit1, Slit2, Robo1, Robo2, and RhoA were also analyzed (Figure 6). The result showed that Slit1 was markedly down-regulated in both regions after WGE administration. However, the expression of Slit2 was not equally down-regulated. WGE did not influence the expression of Robo1 and Robo2, the receptors of Slits. The down-regulation of the negative regulator RhoA was discovered in the WGE group. In contrast, incremental changes in the expression of CRMP2 and PFN1 were observed.

## DISCUSSION

Previously, we found that *G. elata* Blume reduced depressive-like behavior and influenced the monoaminergic neurotransmitters of the frontal cortex, hippocampus, amygdala, and striatum of rats subjected to FST, a common behavior model for evaluating the antidepressive activity of medicine. To exclude the influence on animal locomotion of treatments, an open field test was performed. During a 5 min observation for the open field test, the travel distance and velocity of rats were not affected by administrations (data not shown). This result indicates that the influence of the behaviors in the FST was not coming from the change of locomotion.

In the present study, we detected the composition of WGE in order to realize the active components that could be responsible for the antidepressive effect of WGE. The HPLC fingerprint indicated that among the four candidates only gastrodin could be detected in the WGE (Figure 1). This profile was similar to Zhang's study.[15] In contrast, HBA, HB, and VAN could be detected in the diethyl ether fraction of a methanolic extract of GE.[16] Zhang's research indicated that gastrodin ameliorated depressive-like behavior and up-regulated the expression of brain-derived neurotrophic factor (BDNF).[17] In addition, the reduction of glutamate-induced apoptosis in differentiated PC12 cells via regulating CaMKII/ASK-1/p38 and MAPK/p53 signals by gastrodin had been noticed.[18] However, the blood brain barrier hinders compounds acting on the central nervous system (CNS), which is the difficulty in drug development for mood disorders. Pharmacokinetic studies showed that gastrodin could be detected in plasma after gavage with WGE[15] and quickly appeared in brain microdialysates after gastrodin administration in rats.[19,20] Furthermore, gastrodin could be absorbed via glucose transporters 1 (GLUT1) that are distributed in the brain and intestine, on the basis of its glycoside structure.[21] These findings suggested that WGE could be absorbed and directly act on the CNS, implying that gastrodin is the major active compound of WGE. Thus, gastrodin was surmised to be the major potential active component for the antidepressive-like effect of WGE.

The relationship between neurocytoskeletal remodeling, neuroplasticity, and depression has been discovered.[22,23] In addition to the original pharmaceutical designs, many antidepressants not only influenced the level of neurotransmitters but also stimulated neurocytoskeletal rearrangement and elevated neuroplasticity.[24−26] In the present study, many cytoskeleton-related proteins were up-regulated by 2−5-fold after chronic administration with WGE. According to the network analysis, the detection of cytoskeleton rearrangement with the highest score in bioinformatics analysis indicated the potential interaction between identified proteins (Figure 4A). Hence, WGE could enhance neurocytoskeletal rearrangement and be associated with

**Table 2. List of Differentially Expressed Proteins in the Frontal Cortex[a]**

| SSP[b] | accession no. | protein name | theoretical M/W | theoretical pI | identified by[d] | mascot score (MS, MS/MS) | no. of peptides identified (MS, MS/MS) | sequence coverage rate (%) (MS, MS/MS)[c] | fold change (WGE/CTL)[f] |
|---|---|---|---|---|---|---|---|---|---|
| | | | | Up-regulation | | | | | |
| 0206 | P62260 | 14-3-3 protein epsilon (1433E) | 29 174 | 4.63 | MS, MS/MS | 58, 85 | 10, 2 | 36%, 11% | 2.01** |
| 1203 | Q5XI54 | leucine-rich repeat-containing protein 48 (LRC48) | 60 798 | 4.66 | MS | 62, N/D | 6, N/D | 20%, N/D | 2.47** |
| 1302 | B2RYG6 | ubiquitin thioesterase (OTUB1) | 31 270 | 4.85 | MS, MS/MS | 63, 49 | 6, 1 | 38%, 5% | 3.58** |
| 1612[e] | P85108 | tubulin $\beta$-2A chain (TBB2A) | 49 907 | 4.78 | MS/MS | N/D, 74 | N/D, 2 | N/D, 7% | 3.16** |
| | Q3KRE8 | tubulin $\beta$-2B (TBB2B) | 49 953 | 4.78 | MS/MS | N/D, 74 | N/D, 2 | N/D, 7% | |
| 1616 | P68370 | tubulin $\alpha$-1A chain (TBA1A) | 50 136 | 4.94 | MS/MS | 81, 148 | 12, 4 | 38%, 14% | 8.48** |
| 1619 | P50398 | Rab GDP dissociation inhibitor alpha (GDIA) | 50 537 | 5.00 | MS, MS/MS | 75, 207 | 10, 4 | 31%, 13% | 2.92* |
| 1711[e] | P85108 | tubulin $\beta$-2A chain (TBB2A) | 49 907 | 4.78 | MS, MS/MS | 73, 94 | 11, 2 | 34%, 7% | 2.47* |
| | Q3KRE8 | tubulin $\beta$-2B chain (TBB2B) | 49 953 | 4.78 | MS, MS/MS | 73, 94 | 11, 2 | 34%, 7% | |
| | Q6P9T8 | tubulin $\beta$-4B chain (TBB4B) | 49 801 | 4.79 | MS/MS | N/D, 94 | N/D, 2 | N/D, 7% | |
| | Q4QRB4 | tubulin $\beta$-3 chain (TBB3) | 50 419 | 4.82 | MS | 60, N/D | 9, N/D | 25%, N/D | |
| | P69897 | tubulin $\beta$-5 chain (TBB5) | 49 671 | 4.78 | MS, MS/MS | 63, 94 | 10, 2 | 31%, 7% | |
| 2203 | Q8VD52 | pyridoxal phosphate phosphatase (PLPP) | 33 115 | 5.44 | MS, MS/MS | 54, 70 | 7, 1 | 32%, 3% | 2.14** |
| 2205 | O35920 | calpain-9 (CAN9) | 78 989 | 5.14 | MS/MS | N/D, 59 | N/D, 9 | N/D, 19% | 4.46*** |
| 2312 | P85969 | $\beta$-soluble NSF attachment protein (SNAB) | 33 470 | 5.32 | MS, MS/MS | 56, 68 | 7, 2 | 34%, 12% | 2.41** |
| 2411 | P59215 | guanine nucleotide-binding protein G (o) subunit alpha (GNAO) | 40 069 | 5.34 | MS/MS | N/D, 102 | N/D, 2 | N/D, 9% | 4.70*** |
| 2509 | Q5RKI1 | eukaryotic initiation factor 4A-II (IF4A2) | 46 125 | 5.33 | MS/MS | N/D, 89 | N/D, 2 | N/D, 8% | 2.72* |
| 2613[e] | P60711 | actin, cytoplasmic 1 (ACTB) | 41 737 | 5.26 | MS/MS | N/D, 79 | N/D, 2 | N/D, 9% | 2.53* |
| | P63259 | actin, cytoplasmic2 (ACTG) | 41 793 | 5.31 | MS/MS | N/D, 79 | N/D, 2 | N/D, 9% | |
| 3507 | Q9WTT6 | guanine deaminase (GUAD) | 51 016 | 5.56 | MS | 65, N/D | 6, N/D | 20%, N/D | 3.27* |
| 3619 | P47942 | dihydropyrimidinase-related protein 2 (DPYL2) | 62 278 | 5.95 | MS/MS | 75, 109 | 9, 3 | 29%, 9% | 2.49* |
| 3710 | P62815 | V-type proton ATPase subunit B, brain isoform (VATB2) | 56 551 | 5.57 | MS/MS | 120, 178 | 16, 4 | 42%, 11% | 3.55*** |
| 3810 | D4A133 | V-type proton ATPase catalytic subunit A (VATA) | 68 265 | 5.42 | MS/MS | N/D, 194 | N/D, 4 | N/D, 11% | 2.88* |
| 4203 | D3ZG43 | NADH dehydrogenase [ubiquinone] iron–sulfur protein 3, mitochondrial (NADU3) | 30 226 | 6.67 | MS/MS | N/D, 64 | N/D, 2 | N/D, 9% | 3.58*** |
| 4309 | P42123 | L-lactate dehydrogenase B chain (LDHB) | 36 612 | 5.70 | MS/MS | 60, 58 | 8, 1 | 33%, 5% | 2.11** |
| 4313 | D4ACB8 | chaperonin subunit 8 Theta (CCT8) | 59 589 | 5.44 | MS | 57, N/D | 8, N/D | 19%, N/D | >100*** |
| 4405 | Q4 V8E4 | coiled-coil domain- containing protein 104 (CC104) | 39 590 | 4.93 | MS | 48, N/D | 6, N/D | 29%, N/D | 2.51* |
| 4506 | Q4 V7C7 | actin-related protein 3 (ARP3) | 47 357 | 5.61 | MS, MS/MS | 57, 71 | 7, 2 | 27%, 8% | 2.61*** |
| 4609 | P62815 | V-type proton ATPase subunit B, brain isoform (VATB 2) | 56 551 | 5.57 | MS, MS/MS | 110, 103 | 15, 2 | 39%, 6% | 2.69*** |
| 8108 | P62963 | profilin 1 (PFN1) | 14 957 | 8.08 | MS/MS | N/D, 40 | N/D, 1 | N/D, 12% | 4.03* |
| 8209 | Q9Z2L0 | voltage-dependent anion-selective channel protein 1 (Vdac) | 30 756 | 8.62 | MS/MS | N/S, 106 | N/D, 2 | N/D, 14% | 2.22* |
| 8216 | P04905 | glutathione S-transferase Mu 1 (GSTM1) | 25 914 | 8.27 | MS/MS | N/D, 68 | N/D, 2 | N/D, 13% | 2.73* |
| | | | | Down-regulation | | | | | |
| 1303 | P14668 | annexin A5 (ANXA5) | 35 745 | 4.93 | MS, MS/MS | 68, 52 | 7, 1 | 34%, 5% | −4.16*** |
| 3203 | P85971 | 6-phosphogluconolactonase (6PGL) | 27 234 | 5.54 | MS/MS | N/D, 64 | N/D, 8 | N/D, 41% | −3.23* |
| 5105 | Q9Z0 V6 | thioredoxin-dependent peroxide reductase (PRDX3) | 28 295 | 7.14 | MS/MS | N/D, 82 | N/D, 2 | N/D, 9% | −2.17* |
| 7416 | P16617 | phosphoglycerate kinase 1 (PGK1) | 44 538 | 8.02 | MS, MS/MS | 73, 52 | 9, 3 | 39%, 11% | −2.38** |

[a]These proteins were differentially expressed in the water extract of *Gastrodia elata* Blume (WGE) and control (CTL) groups and were detected by MALDI-TOF mass spectrometry. [b]The SSP is the serial number assigned by the gel image analysis software. [c]N/D means that the spot was not detected by MS or MS/MS. [d]The protein identities were identified from MS and/or MS/MS method in the Mascot protein online search program. [e]All the protein identities that were matched successfully from the Mascot protein online search program are presented (more than one protein was identified from one spot). [f]Asterisk represents the significance of the spot comparing between WGE and CTL (***$p < 0.01$, **$p < 0.05$, *$p < 0.1$).

neuroplasticity and an antidepressive-like effect. On the basis of the bioinformatics analysis, the identified proteins that were associated with actin filament, microtubule, and neurofilament processes will be discussed in the following section.

Actin remodeling is facilitated by dendritic branching and synaptogenesis during neuronal growth. We discovered that actin, actin-related protein 3 (APR3), cyclase-associated protein 2 (CAP2), and profilin1 (PFN1), which were related to actin

**Table 3. List of Differentially Expressed Proteins in the Hippocampus[a]**

| SSP[b] | accession no. | protein name | theoretical M/W | theoretical pI | identified by[f] | mascot score (MS, MS/MS) | no. of peptide identification (MS, MS/MS) | sequence coverage rate (%) (MS, MS/MS)[c] | fold change (WGE/CTL)[g] |
|---|---|---|---|---|---|---|---|---|---|
| | | | | Up-regulation | | | | | |
| 3517[d] | P07335 | creatine kinase B-type (KCRB) | 42 725 | 5.39 | MS, MS/MS | 130, 121 | 14, 3 | 48%, 12% | 2.04** |
| 3808[d] | D4A133 | V-type proton ATPase catalytic subunit A (VATA) | 68 265 | 5.42 | MS | 105, N/D | 14, N/D | 32%, N/D | 6.42* |
| 5216[d] | P31399 | ATP synthase subunit d (ATP5H) | 18 763 | 6.17 | MS, MS/MS | 82, 40 | 6, 3 | 49%, 34% | 2.44** |
| 6718[d] | Q5RKI0 | WD repeat-containing protein 1 (WDR1) | 66 181 | 6.15 | MS | 62, N/D | 10, N/D | 30%, N/D | 2.44** |
| 8146[d] | P10111 | peptidyl-prolyl cis−trans isomerase A (PPIA) | 17 863 | 8.34 | MS/MS | N/D, 98 | N/D, 2 | N/D, 20% | 2.34* |
| 8148[d] | P62963 | profilin 1 (PFN1) | 14 957 | 8.48 | MS, MS/MS | 67, 29 | 5, 2 | 53%, 21% | 3.01* |
| 8233[d] | P04905 | glutathione S-transferase Mu 1 (GSTM1) | 25 914 | 8.27 | MS/MS | N/D, 72 | N/D, 2 | N/D, 13% | 5.87* |
| 9316[d] | A7VJC2 | heterogeneous nuclear ribonucleoproteins A2/B1 (ROA2) | 37 478 | 8.97 | MS, MS/MS | 80, 158 | 9, 3 | 37%, 15% | 2.07* |
| 1107[e,h] | P11240 | cytochourome *c* oxidase subunit 5A (COX5A) | 16 130 | 6.08 | MS/MS | 170 | 6 | 26% | 3.01* |
| | P55051 | fatty acid-binding protein, brain (FABP7) | 14 864 | 5.46 | MS/MS | 104 | 2 | 19% | |
| 1109[e] | Q6PEC4 | S-phase kinase-associated protein 1 (SKP1) | 18 672 | 4.44 | MS/MS | 197 | 7 | 32% | 4.05*** |
| 1113[e] | P62870 | transcription elongation factor B polypeptide 2 (ELOB) | 13 170 | 4.87 | MS/MS | 50 | 2 | 12% | 2.11* |
| 1307[e] | Q5M7T6 | ATPase, H+ transporting, lysosomal 38 kDa, V0 subunit d1 (protein Atp6v0d1) | 40 301 | 4.89 | MS/MS | 436 | 13 | 33% | 2.25* |
| 1615[e,h], | Q6P9 V9 | tubulin $\alpha$-1B chain (TBA1B) | 50 152 | 4.94 | MS/MS | 253 | 6 | 14% | 3.04*** |
| 1616[e,h,] | P10719 | ATP synthase subunit $\beta$ (ATPB) | 56 318 | 5.19 | MS/MS | 2076 | 29 | 53% | 2.75*** |
| | Q6P9T8 | tubulin $\beta$-2C chain (TBB2C) | 49 799 | 4.79 | MS/MS | 4574 | 75 | 71% | |
| | P85108 | tubulin $\beta$-2A chain (TBB2A) | 49 875 | 4.78 | MS/MS | 4564 | 81 | 75% | |
| | P69897 | tubulin $\beta$-5 chain (TBB5) | 49 671 | 4.78 | MS/MS | 4472 | 76 | 71% | |
| | Q3KRE8 | tubulin $\beta$-2B chain (TBB2B) | 49 921 | 4.78 | MS/MS | 4468 | 80 | 74% | |
| | B4F7C2 | tubulin $\beta$-4 chain (TBB4B) | 49 586 | 4.78 | MS/MS | 4176 | 68 | 75% | |
| | Q4QRB4 | tubulin $\beta$-3 chain (TBB3) | 50 386 | 4.82 | MS/MS | 2962 | 59 | 64% | |
| | Q5XIF6 | tubulin $\alpha$-4A chain (TBA4A) | 49 924 | 4.95 | MS/MS | 277 | 6 | 16% | |
| 1703[e] | P18418 | calreticulin (CALR) | 47 995 | 4.33 | MS/MS | 687 | 18 | 37% | 2.43** |
| 1705[e] | P19527 | neurofilament light polypeptide (NFL) | 61 471 | 4.62 | MS/MS | 1826 | 36 | 49% | 4.34** |
| 2410[e] | P60711 | actin, cytoplasmic 1 (ACTB) | 41 737 | 5.29 | MS/MS | 1820 | 30 | 60% | 2.19** |
| 2413[e] | O35179 | endophilin-A1 (SH3G2) | 39 874 | 5.26 | MS/MS | 466 | 10 | 39% | 2.60*** |
| 2519[e] | | | | | | | | | 3.42** |
| 2610[e,h] | Q6P9 V9 | tubulin $\alpha$-1B chain (TBA1B) | 50 120 | 4.94 | MS/MS | 3348 | 61 | 71% | 4.05*** |
| | P68370 | tubulin $\alpha$-1A chain (TBA1A) | 50 136 | 4.94 | MS/MS | 3184 | 58 | 71% | |
| | Q5XIF6 | tubulin $\alpha$-4A chain (TBA4A) | 49 924 | 4.95 | MS/MS | 3075 | 54 | 63% | |
| | Q68FR8 | tubulin $\alpha$-3 chain (TBA3) | 49 960 | 4.97 | MS/MS | 2619 | 47 | 58% | |
| | Q4QRB4 | tubulin $\beta$-3 chain (TBB3) | 50 386 | 4.82 | MS/MS | 1778 | 47 | 55% | |
| | P69897 | tubulin $\beta$-5 chain (TBB5) | 49 671 | 4.78 | MS/MS | 1543 | 30 | 55% | |
| 2520[e] | Q68FY0 | cytochourome *b*-*c*1 complex subunit 1, mitochondrial (QCR1) | 52 849 | 5.57 | MS/MS | 2940 | 40 | 55% | 2.14** |
| 2715[e] | P50398 | Rab GDP dissociation inhibitor $\alpha$ (GDIA) | 50 537 | 5.00 | MS/MS | 62 | 2 | 2% | 2.54* |
| 2720[e] | Q68FY0 | cytochourome *b*-*c*1 complex subunit 1, mitochondrial (QCR1) | 52 849 | 5.57 | MS/MS | 72 | 1 | 2% | 2.35** |
| 2723[e] | P63018 | heat shock protein 71 kDa protein (HSP7C) | 70 871 | 5.37 | MS/MS | 140 | 2 | 4% | 2.94*** |
| 3632[e] | P47942 | dihydropyrimidinase- related protein 2 (DPYL2) | 62 278 | 5.95 | MS/MS | 94 | 2 | 5% | 3.65** |
| 6525[e] | P04764 | $\alpha$-enolase (ENOA) | 47 128 | 6.16 | MS/MS | 121 | 1 | 4% | 2.09* |
| 6617[e] | P52481 | adenylyl cyclase-associated protein 2 (CAP2) | 52 879 | 6.69 | MS/MS | 63 | 2 | 4% | 2.26** |
| 6620[e] | Q62950 | dihydropyrimidinase- related protein 1 (DPYL1) | 62 196 | 6.64 | MS/MS | 88 | 2 | 2% | 2.01* |
| 7432[e] | P51635 | alcohol dehydrogenase (AK1A1) | 36 506 | 6.84 | MS/MS | 54 | 2 | 8% | 2.23* |
| 7617[e] | P10860 | glutamate dehydrogenase 1, mitochondrial (DHE3) | 61 416 | 8.05 | MS/MS | 83 | 2 | 2% | 2.18** |
| 7621[e] | | | | | MS/MS | 59 | 2 | 2% | 7.1** |
| 7622[e] | P62630 | elongation factor 1-$\alpha$1 (EF1A1) | 50 114 | 9.10 | MS/MS | 65 | 2 | 2% | 2.49** |


dx.doi.org/10.1021/jf503132c | J. Agric. Food Chem. 2014, 62, 10493−10503

**Table 3. continued**

| SSP[b] | accession no. | protein name | theoretical M/W | theoretical pI | identified by[f] | mascot score (MS, MS/MS) | no. of peptide identification (MS, MS/MS) | sequence coverage rate (%) (MS, MS/MS)[c] | fold change (WGE/CTL)[g] |
|---|---|---|---|---|---|---|---|---|---|
| | | | | Up-regulation | | | | | |
| 8608[e] | P15999 | ATP synthase subunit $\alpha$, mitochondrial (ATPA) | 59 754 | 9.22 | MS/MS | 121 | 1 | 2% | 2.93** |
| | | | | Down-regulation | | | | | |
| 2817[d] | Q66HF1 | NADH-ubiquinone oxido- reductase 75 kDa subunit, mitochondrial (NDUS1) | 79 412 | 6.65 | MS, MS/MS | 93, 68 | 14, 3 | 30%, 6% | −2.17*** |
| 2820[d] | P46462 | transitional endoplasmic reticulum ATPase (TERA) | 89 349 | 5.14 | MS | 75, N/D | 11, N/D | 23%, N/D | −2.08** |
| 3210[d] | P85971 | 6-phosphogluconolactonase (6PGL) | 27 234 | 5.54 | MS | 64, N/D | 8, N/D | 41%, N/D | −4.17** |
| 3809[d] | P48721 | stress-70 protein (GRP75) | 73 858 | 5.81 | MS, MS/MS | 54, 181 | 10, 4 | 21%, 7% | −2.56** |
| 4608[d] | P11598 | protein disulfide-isomerase A3 (PDIA3) | 56 588 | 5.88 | MS/MS | N/D, 84 | N/D, 3 | N/D, 7% | −2.32*** |
| 5224[d] | Q9Z0 V6 | thioredoxin-dependent peroxide reductase (PRDX3) | 28 295 | 7.14 | MS/MS | N/D, 55 | N/D, 1 | N/D, 5% | −2.08*** |
| 6826[d] | P21575 | dynamin 1 (DYN1) | 97 295 | 6.44 | MS, MS/MS | 72, N/D | 13, N/D | 23%, N/D | −3.33** |
| 6827[d] | | | | | MS, MS/MS | 125, 47 | 17, 1 | 29%, 1% | −2.08** |
| 7717[d] | P11980 | pyruvate kinase isozymes M1/M2 (KPYM) | 57 818 | 6.63 | MS, MS/MS | 96, 127 | 13, 4 | 34%, 11% | −2.12** |

[a]These proteins were differentially expressed between the water extract of *Gastrodia elata* Blume (WGE) and control (CTL) groups. [b]The SSP is the serial number assigned by the gel image analysis software. [c]N/D means that the spot was not detected by MS or MS/MS. [d]Total loading protein was 400 $\mu$g, and the spots were analyzed by MALDI-TOF mass spectrometry. [e]Total loading protein was 450 $\mu$g, and the spots were analyzed by LC-ESI mass spectrometry. [f]The protein identities were identified from MS and/or MS/MS method in the Mascot protein online search program. [g]Asterisk represents the significance from spot comparing between WGE and CTL (***$p < 0.01$, **$p < 0.05$, *$p < 0.1$). [h]All the protein identities that were matched successfully from the Mascot protein online search program are presented (more than one protein was identified from one spot; more than one spot was identified as the same protein).

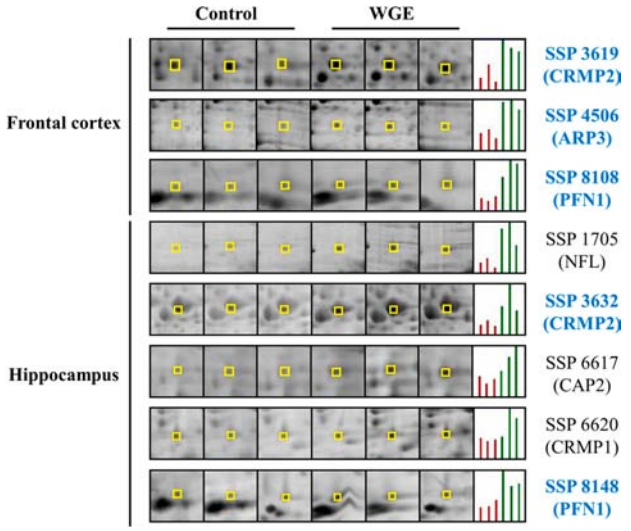


**Figure 3.** Magnified gel images and quantification of differentially expressed proteins related to cytoskeleton remodeling in the frontal cortex and hippocampus. The matched spots are located in the center of each zoom-in gel image with yellow squares. The charts beside the gel images show the quantification results. The red and green bars represent respectively the expressed density of the matched spots for each of three replications of the control and WGE. The protein name in blue signifies that protein is involved in the Slit−Robo pathway. CRMP2, dihydropyrimidinase-related protein-2; ARP3, actin-related protein 3; PFN1, profilin-1; NFL, neurofilament light chain; CAP2, adenylyl cyclase-associated protein 2; CRMP1, dihydropyrimidinase-related protein-1.

processes, were up-regulated in the WGE group. ARP2 and ARP3 form an ARP 2/3 complex and control the dependent branch function of actin filaments in rapidly developed neuronal regions such as lamellipodia and filopodia. These molecular effects have also been reported in pharmacological studies of antidepressants such as nortriptyline in rats.[24] Actin dynamic programs include the CAP family. According to Peche et al., CAP1 abundantly exists in many tissues, but CAP2 is specifically highly expressed in brain, heart, and skeletal muscle.[27] The cooperative model between CAP, actin, and cofilin in the promotion of actin dynamics and synaptogenesis was established.[28] In the same study, Moriyama et al. also noted that the functions of CAP1 and CAP2 are analogous. However, research indicated that a defect in CAP is correlated with mood disorders.[29] Similar to CAP and ARP, the expression of PFN1 was also increased in the WGE group. PFN1 regulates the mechanisms related to fixing actins on the phosphoinositide of the plasma membrane and assists in the formation of actin filaments during neuronal growth. Thus, PFN1 was shown to be an essential factor for neuronal differentiation, synaptic plasticity, and stabilizing the dendritic spine morphology.[30] In contrast, actin-related genes were down-regulated in the mice that are sensitive to depression and the post-mortem cerebrum of mood disorder victims.[29] In our study, we showed that WGE stimulates the expression of proteins associated with actin processes (Tables 2 and 3), which in turn facilitates its antidepressive-like effect.

Like the roles of actin during neuronal growth, microtubules are polymerized to elongate the axon and dendritic trunk. In the present study, we found that the essential factor, CRMP2, was up-regulated in both the frontal cortex and hippocampus. However, dysfunction of CRMP2 has a strong correlation with psychiatric disorders. Recent proteomics data indicated that CRMP2 is down-regulated severely in rats with depressive-like behavior induced by UCMS.[31] Post-mortem research also noted a reduction in the expression of CRMP2 in the frontal cortex of patients with MDD and bipolar disorder.[32] Hence, CRMP2 is considered to be a potential biomarker for MDD. Another CRMP protein, CRMP1, was also up-regulated in the

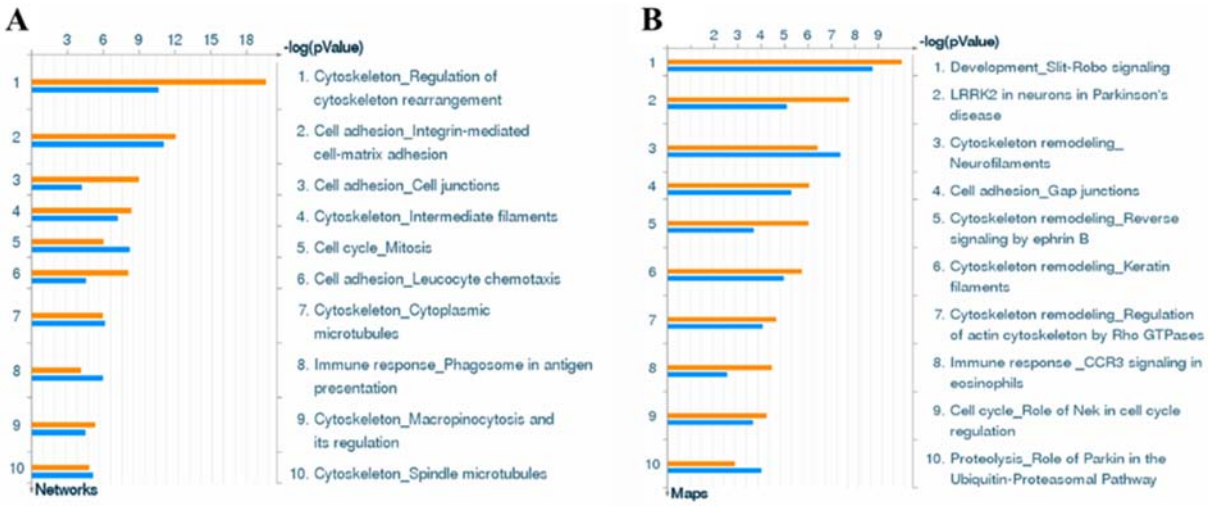


**Figure 4.** Metacore-analyzed results presented as −log($p$ value) chart of matched protein identities for potential molecular networks and pathways. A higher value in the chart represents a higher correlation and possibility. (A) GeneGo Process Network; (B) GeneGo Pathway Maps (orange chart: frontal cortex; blue chart: hippocampus).

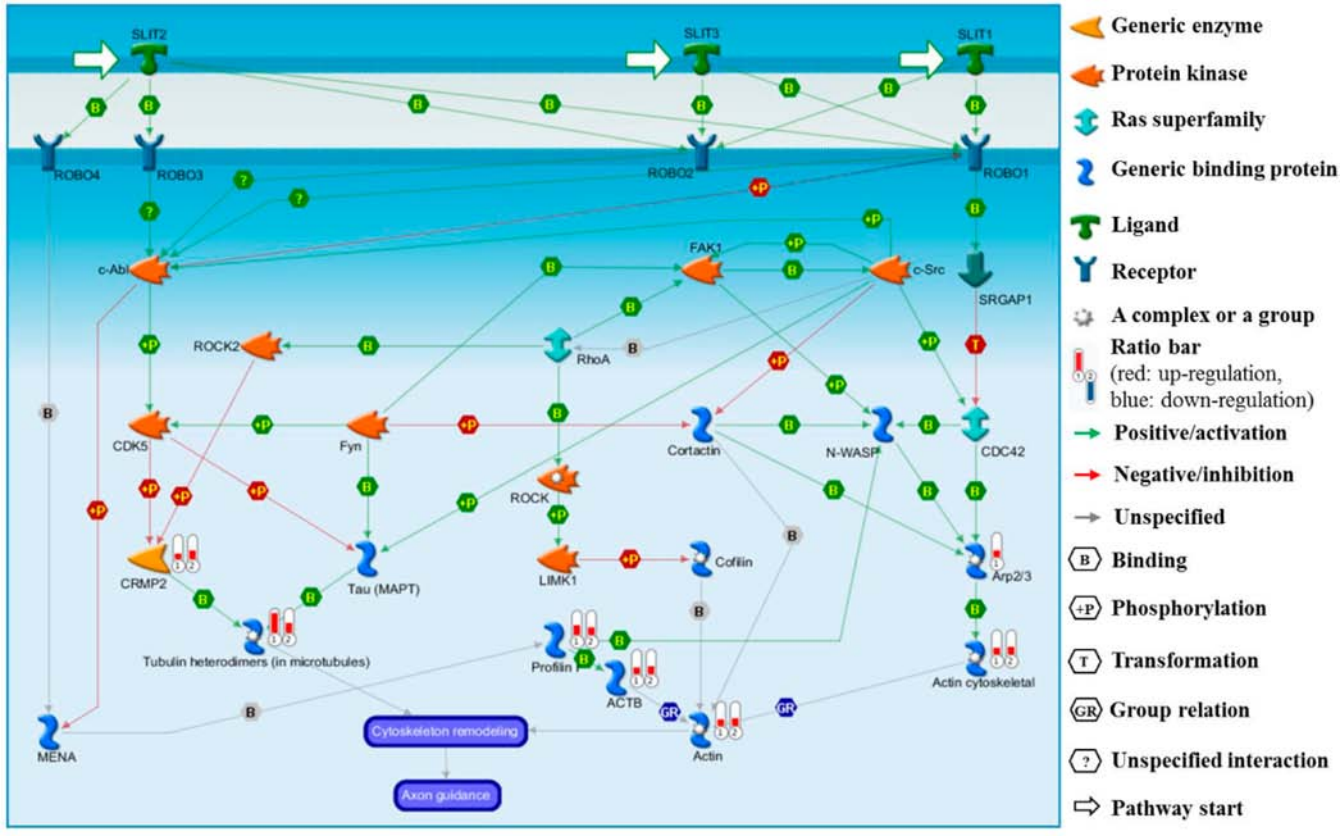


**Figure 5.** Pathway map for Slit−Robo signaling and the downstream factors. Proteins labeled with "1" and "2" represent the proteins identified from 2-DE of the frontal cortex and hippocampus, respectively. The ratio bars on the upper right corner of the symbols represent the expression ratio between the water extract of *Gastrodia elata* Blume (WGE) and the control (CTL) (WGE/CTL). c-Abl, c-Abl nonreceptor tyrosine kinase; CDK5, cyclin-dependent kinase 5; ROCK, Rho-associated protein kinase; CRMP2, dihydropyrimidinase-related protein-2; Arp 2/3, actin-related protein 2/3 complex; RhoA, Ras homologous member A; c-Src, Proto-oncogene tyrosine-protein kinase Src; CDC42, cell division cycle 42; N-WASP, neural Wiskott−Aldrich syndrome protein; FAK1, focal adhesion kinase 1.

hippocampus. The function of CRMP1 is similar to CRMP2, which stimulates neuronal pathfinding and axon elongation. Research has proved that a deficiency of CRMP1 also leads to a defect in neuronal development.[33] In contrast, antidepressants up-regulate the expression of CRMP proteins and tubulin-based processes.[34] Hence, up-regulation of CRMP1 and -2 reflect the activation of microtubule-dependent activity in the brain after WGE administration.

Neurofilament light chain (NFL), which forms intermediate filaments and composes the axon structure with medium


dx.doi.org/10.1021/jf503132c | J. Agric. Food Chem. 2014, 62, 10493−10503

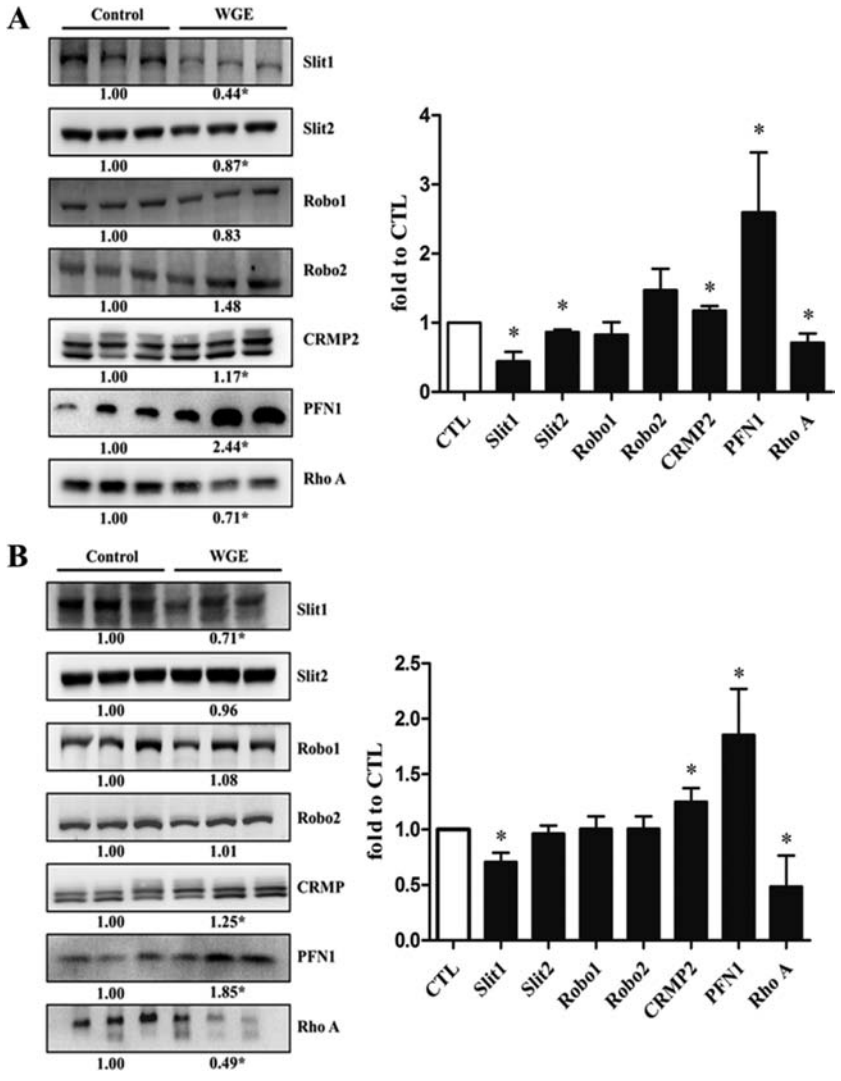


**Figure 6.** Western blot analysis of the regulators in the Slit−Robo pathway in the (A) frontal cortex and (B) hippocampus. The value on the bottom of each group and the chart images represent the ratio of expressed levels, which were normalized with the expression of GAPDH and relative to the control group. * indicates significant difference between control and WGE ($p < 0.05$) analyzed by Student's unpaired $t$ test.

(NFM) and heavy chains (NFH), was highly up-regulated after WGE administration (Table 3). Studies have showed that, similar to other cytoskeletal units, negative regulation of neurofilaments is possibly related to neurodegenerative diseases.[35] Foot-shock-induced depressive-like behavior in rats presented with lower expression of NFL but not NFM and NFH in the hippocampus.[36] Moreover, antidepressants enhanced the expression of NFL and synaptic remodeling.[37] Thus, incremental increase in the expression of NFL may be related to cytoskeleton remodeling and a neuroplasticity-stimulating effect of WGE.

The Slit−Robo pathway emerged with the highest score in the bioinformatics analysis of the predicted mechanisms for the antidepressive-like effects of WGE (Figure 4B). During neuronal growth, the axon is elongated and guided to another target neuron by the attractive and repulsive activities of Netrin and Slits, respectively. These actions involve excited cytoskeletal remodeling. The repulsive property of Slits includes the deactivation or down-regulation of positive regulators such as CRMP2 and PFN1 and activation of negative factors such as Ras homologous member A (RhoA). This program operates especially in the embryo, so that axons grow and allow the neural plate to construct the networks. Thus, the Slit−Robo signal is generally regarded as an essential process for embryonic neuronal development. Interestingly, *slit* and *robo* are not only expressed in the embryonic developmental phase but maintain a high level in postnatal stages and adults.[38] Marillat et al. also demonstrated that the expression of *slit1* and *robo2* changes in the hippocampus from postnatal day 10, the stage when synapses are rapidly generated. It seems that Slit−Robo signaling has some other activities in addition to mediating embryonic neuronal development. In fact, some research revealed that Slit−Robo may suppress neuroplasticity. Lin et al. discovered that dopaminergic neuronal extension and neurite growth are restricted by Slits and stimulated by Netrin.[39,40] Furthermore, this phenomenon was also validated in a stem cell-derived neuron mode.[40] In addition, a negative regulator, RhoA, is also involved in the Slit−Robo pathway. Down-regulation of RhoA correlates to neuronal growth. Cheng et al. observed that BDNF down-regulated the expression of RhoA, which stimulated neuronal growth.[41] Besides, L-glutamate (L-Glu), an excitatory transmitter, promotes and stabilizes dendritic growth and spine formation, results in neuroplasticity, and is correlated with Rac1/Cdc42 activation


dx.doi.org/10.1021/jf503132c | J. Agric. Food Chem. 2014, 62, 10493−10503

and reduction of RhoA activity.[42] According to these studies, down-regulation of the Slit−Robo pathway plays a potential role in neuroplasticity.

The WB results validated the expression of mediators involved in Slit−Robo signaling, which was matched by Metacore (Figure 6). To the best of our knowledge, there was no study indicating the potential relationship between the Slit−Robo pathway, pathology, and pharmacology for depression. In this study, based on the bioinformatics analyses and validation processes, stimulating neurocytosekeletal remodeling and enhancing neuroplasticity due to down-regulation of the Slit−Robo pathway might be one of the mechanisms to achieve the antidepressive-like activity of WGE.

## AUTHOR INFORMATION


### Corresponding Author

*Tel: 886-2-3366-4129. Fax: 886-2-2362-0849. E-mail: lysheen@ntu.edu.tw.

### Author Contributions

#Shui-Tein Chen and Lee-Yan Sheen have contributed equally.



### Funding

This research work was partially funded by the National Science Council (NSC97-2313-B-002-014-MY3) and National Taiwan University (aim for top university program, number 102R-7620), Taiwan. Proteomic mass spectrometry analyses were performed by Core Facilities for Protein Structural Analysis, Institute of Biological Chemistry, Academia Sinica, Taiwan, supported by a grant from National Science Council (NSC100-2325-B-001-029).


### Notes

The authors declare no competing financial interest.

## ABBREVIATIONS USED

FST, forced swimming test; WGE, water extract of *Gastrodia elata* Blume; CTL, control; FLX, fluoxetine; 2-DE, two-dimensional electrophoresis

## REFERENCES


(1) Mathers, C.; Fat, D. M.; Boerma, J. T. *Global Burden of Disease 2004 Update*. World Health Organization: Switzerland, 2008; Vol. *20*.

(2) Castren, E. Is mood chemistry? *Nat. Rev. Neurosci.* **2005**, *6*, 241−246.

(3) Pittenger, C.; Duman, R. S. Stress, depression, and neuroplasticity: a convergence of mechanisms. *Neuropsychopharmacology* **2008**, *33*, 88−109.

(4) Lin, E. H.; Von Korff, M.; Katon, W.; Bush, T.; Simon, G. E.; Walker, E.; Robinson, P. The role of the primary care physician in patients' adherence to antidepressant therapy. *Med. Care* **1995**, *33*, 67−74.

(5) Gonzalez, J.; Williams, J. W., Jr.; Noel, P. H.; Lee, S. Adherence to mental health treatment in a primary care clinic. *J. Am. Board Fam. Pract.* **2005**, *18*, 87−96.

(6) Li, H. X.; Ding, M. y.; Lv, K.; Wei, Y.; Yu, J. Y. Identification and determination of the active compounds in *Gastrodia elata* Blume by HPLC. *J. Liq. Chromatogr. Relat. Technol.* **2001**, *24*, 579−588.

(7) Yu, S. J.; Kim, J. R.; Lee, C. K.; Han, J. E.; Lee, J. H.; Kim, H. S.; Hong, J. H.; Kang, S. G. *Gastrodia elata* Blume and an active component, p-hydroxybenzyl alcohol reduce focal ischemic brain injury through antioxidant related gene expressions. *Biol. Pharm. Bull.* **2005**, *28*, 1016−1020.

(8) Hsieh, C. L.; Lin, J. J.; Chiang, S. Y.; Su, S. Y.; Tang, N. Y.; Lin, G. G.; Lin, I. H.; Liu, C. H.; Hsiang, C. Y.; Chen, J. C.; Ho, T. Y. *Gastrodia elata* modulated activator protein 1 via c-Jun N-terminal kinase signaling pathway in kainic acid-induced epilepsy in rats. *J. Ethnopharmacol.* **2007**, *109*, 241−247.

(9) Tsai, C. F.; Huang, C. L.; Lin, Y. L.; Lee, Y. C.; Yang, Y. C.; Huang, N. K. The neuroprotective effects of an extract of *Gastrodia elata*. *J. Ethnopharmacol.* **2011**, *138*, 119−125.

(10) Manavalan, A.; Feng, L.; Sze, S. K.; Hu, J. M.; Heese, K. New insights into the brain protein metabolism of *Gastrodia elata*-treated rats by quantitative proteomics. *J. Proteomics* **2012**, *75*, 2468−2479.

(11) Zhou, B. H.; Li, X. J.; Liu, M.; Wu, Z.; Ming, H. X. Antidepressant-like activity of the *Gastrodia elata* ethanol extract in mice. *Fitoterapia* **2006**, *77*, 592−594.

(12) Chen, P. J.; Hsieh, C. L.; Su, K. P.; Hou, Y. C.; Chiang, H. M.; Lin, I. H.; Sheen, L. Y. The antidepressant effect of *Gastrodia elata* Bl. on the forced swimming test in rats. *Am. J. Chin. Med.* **2008**, *36*, 95−106.

(13) Chen, P. J.; Hsieh, C. L.; Su, K. P.; Hou, Y. C.; Chiang, H. M.; Sheen, L. Y. Rhizomes of *Gastrodia elata* B(L) possess antidepressant-like effect via monoamine modulation in subchronic animal model. *Am. J. Chin. Med.* **2009**, *37*, 1113−1124.

(14) Porsolt, R. D.; Bertin, A.; Blavet, N.; Deniel, M.; Jalfre, M. Immobility induced by forced swimming in rats: effects of agents which modify central catecholamine and serotonin activity. *Eur. J. Pharmacol.* **1979**, *57*, 201−210.

(15) Zhang, W.; Sheng, Y. X.; Zhang, J. L. Determination and pharmacokinetics of gastrodin and p-hydroxybenzylalcohol after oral administration of *Gastrodia elata* Bl. extract in rats by high-performance liquid chromatography-electrospray ionization mass spectrometric method. *Phytomedicine* **2008**, *15*, 844−850.

(16) Kim, H. J.; Hwang, I. K.; Won, M. H. Vanillin, 4-hydroxybenzyl aldehyde and 4-hydroxybenzyl alcohol prevent hippocampal CA1 cell death following global ischemia. *Brain Res.* **2007**, *1181*, 130−141.

(17) Zhang, R.; Peng, Z.; Wang, H.; Xue, F.; Chen, Y.; Wang, Y.; Tan, Q. Gastrodin ameliorates depressive-like behaviors and up-regulates the expression of BDNF in the hippocampus and hippocampal-derived astrocyte of rats. *Neurochem. Res.* **2014**, *39*, 172−179.

(18) Jiang, G.; Wu, H.; Hu, Y.; Li, J.; Li, Q. Gastrodin inhibits glutamate-induced apoptosis of PC12 cells via inhibition of CaMKII/ASK-1/p38 MAPK/p53 signaling cascade. *Cell Mol. Neurobiol.* **2014**, *34*, 591−602.

(19) Lin, L. C.; Chen, Y. F.; Lee, W. C.; Wu, Y. T.; Tsai, T. H. Pharmacokinetics of gastrodin and its metabolite p-hydroxybenzyl alcohol in rat blood, brain and bile by microdialysis coupled to LC-MS/MS. *J. Pharm. Biomed. Anal.* **2008**, *48*, 909−917.

(20) Wang, Q.; Chen, G.; Zeng, S. Distribution and metabolism of gastrodin in rat brain. *J. Pharm. Biomed. Anal.* **2008**, *46*, 399−404.

(21) Cai, Z.; Huang, J.; Luo, H.; Lei, X.; Yang, Z.; Mai, Y.; Liu, Z. Role of glucose transporters in the intestinal absorption of gastrodin, a highly water-soluble drug with good oral bioavailability. *J. Drug Targetting* **2013**, *21*, 574−580.

(22) Luo, L. Actin cytoskeleton regulation in neuronal morphogenesis and structural plasticity. *Annu. Rev. Cell Dev. Biol.* **2002**, *18*, 601−635.

(23) Svitkina, T.; Lin, W. H.; Webb, D. J.; Yasuda, R.; Wayman, G. A.; Van Aelst, L.; Soderling, S. H. Regulation of the postsynaptic cytoskeleton: roles in development, plasticity, and disorders. *J. Neurosci.* **2010**, *30*, 14937−14942.

(24) Piubelli, C.; Gruber, S.; El Khoury, A.; Mathe, A. A.; Domenici, E.; Carboni, L. Nortriptyline influences protein pathways involved in carbohydrate metabolism and actin-related processes in a rat gene-environment model of depression. *Eur. Neuropsychopharmacol.* **2011**, *21*, 545−562.

(25) Piubelli, C.; Vighini, M.; Mathe, A. A.; Domenici, E.; Carboni, L. Escitalopram affects cytoskeleton and synaptic plasticity pathways in a rat gene-environment interaction model of depression as revealed by proteomics. Part II: environmental challenge. *Int. J. Neuropsychopharmacol.* **2011**, *14*, 834−855.

(26) Ladurelle, N.; Gabriel, C.; Viggiano, A.; Mocaer, E.; Baulieu, E. E.; Bianchi, M. Agomelatine (S20098) modulates the expression of

cytoskeletal microtubular proteins, synaptic markers and BDNF in the rat hippocampus, amygdala and PFC. *Psychopharmacology (Berlin, Ger.)* **2012**, *221*, 493−509.
(27) Peche, V.; Shekar, S.; Leichter, M.; Korte, H.; Schroder, R.; Schleicher, M.; Holak, T. A.; Clemen, C. S.; Ramanath, Y. B.; Pfitzer, G.; Karakesisoglou, I.; Noegel, A. A. CAP2, cyclase-associated protein 2, is a dual compartment protein. *Cell. Mol. Life Sci.* **2007**, *64*, 2702−2715.
(28) Moriyama, K.; Yahara, I. Human CAP1 is a key factor in the recycling of cofilin and actin for rapid actin turnover. *J. Cell Sci.* **2002**, *115*, 1591−1601.
(29) Nakatani, N.; Ohnishi, T.; Iwamoto, K.; Watanabe, A.; Iwayama, Y.; Yamashita, S.; Ishitsuka, Y.; Moriyama, K.; Nakajima, M.; Tatebayashi, Y.; Akiyama, H.; Higuchi, T.; Kato, T.; Yoshikawa, T. Expression analysis of actin-related genes as an underlying mechanism for mood disorders. *Biochem. Biophys. Res. Commun.* **2007**, *352*, 780−786.
(30) Birbach, A. Profilin, a multi-modal regulator of neuronal plasticity. *BioEssays* **2008**, *30*, 994−1002.
(31) Yang, Y.; Yang, D.; Tang, G.; Zhou, C.; Cheng, K.; Zhou, J.; Wu, B.; Peng, Y.; Liu, C.; Zhan, Y.; Chen, J.; Chen, G.; Xie, P. Proteomics reveals energy and glutathione metabolic dysregulation in the prefrontal cortex of a rat model of depression. *Neuroscience* **2013**, *247*, 191−200.
(32) Johnston-Wilson, N. L.; Sims, C. D.; Hofmann, J. P.; Anderson, L.; Shore, A. D.; Torrey, E. F.; Yolken, R. H. Disease-specific alterations in frontal cortex brain proteins in schizophrenia, bipolar disorder, and major depressive disorder. The Stanley Neuropathology Consortium. *Mol. Psychiatry* **2000**, *5*, 142−149.
(33) Su, K. Y.; Chien, W. L.; Fu, W. M.; Yu, I. S.; Huang, H. P.; Huang, P. H.; Lin, S. R.; Shih, J. Y.; Lin, Y. L.; Hsueh, Y. P.; Yang, P. C.; Lin, S. W. Mice deficient in collapsin response mediator protein-1 exhibit impaired long-term potentiation and impaired spatial learning and memory. *J. Neurosci.* **2007**, *27*, 2513−2524.
(34) Marais, L.; Hattingh, S. M.; Stein, D. J.; Daniels, W. M. A proteomic analysis of the ventral hippocampus of rats subjected to maternal separation and escitalopram treatment. *Metab. Brain Dis.* **2009**, *24*, 569−586.
(35) Al-Chalabi, A.; Miller, C. C. Neurofilaments and neurological disease. *BioEssays* **2003**, *25*, 346−355.
(36) Reines, A.; Cereseto, M.; Ferrero, A.; Bonavita, C.; Wikinski, S. Neuronal cytoskeletal alterations in an experimental model of depression. *Neuroscience* **2004**, *129*, 529−538.
(37) Guest, P. C.; Knowles, M. R.; Molon-Noblot, S.; Salim, K.; Smith, D.; Murray, F.; Laroque, P.; Hunt, S. P.; De Felipe, C.; Rupniak, N. M.; McAllister, G. Mechanisms of action of the antidepressants fluoxetine and the substance P antagonist L-000760735 are associated with altered neurofilaments and synaptic remodeling. *Brain Res.* **2004**, *1002*, 1−10.
(38) Marillat, V.; Cases, O.; Nguyen-Ba-Charvet, K. T.; Tessier-Lavigne, M.; Sotelo, C.; Chedotal, A. Spatiotemporal expression patterns of slit and robo genes in the rat brain. *J. Comp. Neurol.* **2002**, *442*, 130−155.
(39) Lin, L.; Rao, Y.; Isacson, O. Netrin-1 and slit-2 regulate and direct neurite growth of ventral midbrain dopaminergic neurons. *Mol. Cell Neurosci.* **2005**, *28*, 547−555.
(40) Lin, L.; Isacson, O. Axonal growth regulation of fetal and embryonic stem cell-derived dopaminergic neurons by Netrin-1 and Slits. *Stem Cells* **2006**, *24*, 2504−2513.
(41) Cheng, P. L.; Lu, H.; Shelly, M.; Gao, H.; Poo, M. M. Phosphorylation of E3 ligase Smurf1 switches its substrate preference in support of axon development. *Neuron* **2011**, *69*, 231−243.
(42) Sin, W. C.; Haas, K.; Ruthazer, E. S.; Cline, H. T. Dendrite growth increased by visual activity requires NMDA receptor and Rho GTPases. *Nature* **2002**, *419*, 475−480.

**Table 1. Eggplant Scion and Rootstock Varieties Included in the Experiments**

| plant material | code | fruit shape or characteristics | seed company | country of origin |
|---|---|---|---|---|
| commercial varieties | | | | |
| Blackbell F1 | BB | elongated oval | Petoseed | USA |
| Epic F1 | EC | cylindrical | Petoseed | USA |
| Galine F1 | GA | round oval | Clause | France |
| landrace | | | | |
| Domači srednje dolgi | DSD | round flask | Semenarna Ljubljana | Slovenia |
| rootstock | | | | |
| Beaufort F1 (*S. lycopersicum* L. × *S. habrochaites*) | BE | cold tolerant root system with strong branching, resulting in a very strong plant | De Ruiter | Holland |

**Table 2. Monthly Meteorological Data from May to September of 2010 and 2011 from Ljubljana Meteorological Station on the Experimental Field of the Biotechnical Faculty, University of Ljubljana[a]**

| | year 2010 | | | | | year 2011 | | | | | |
|---|---|---|---|---|---|---|---|---|---|---|---|
| month | TS | TOD | TX | TM | MSR | TS | TOD | TX | TM | MSR | MRS |
| May | 15.3 | 0.7 | 19.8 | 11.2 | 14.5 | 17.0 | 2.4 | 23.6 | 9.5 | 22.6 | 19.1 |
| June | 20.3 | 2.5 | 25.5 | 14.5 | 19.4 | 20.0 | 1.1 | 25.5 | 14.7 | 20.2 | 20.3 |
| July | 22.9 | 3.0 | 28.9 | 17.3 | 20.6 | 21.1 | 1.2 | 26.9 | 15.3 | 20.9 | 20.1 |
| August | 20.3 | 1.2 | 26.0 | 15.5 | 16.9 | 22.8 | 3.7 | 29.5 | 16.2 | 21.0 | 17.3 |
| September | 14.7 | −0.8 | 19.2 | 11.3 | 10.5 | 19.4 | 3.9 | 26.4 | 13.7 | 15.4 | 13.0 |

[a]TS, mean monthly air temperature (°C); TOD, temperature deviation from the 1961−1990 average (°C); TX, mean maximum air temperature for the month (°C); TM, mean minimum air temperature for the month (°C); MSR, mean daily solar radiation (MJ $m^{-2}$); MSR, average of the mean daily solar radiation (MJ $m^{-2}$) for the period 1961−1990.

growing season are reported. All phenolic compounds were confirmed using a mass spectrometer with an electrospray interface (ESI) operating in negative ion mode. The results provide information on the advantages of grafted eggplant fruit, which are recognized in the outer and inner quality parameters and are important from the point of view of the consumer as well as the vegetable producer. Knowing the effect of grafting on important fruit quality traits, especially changes in the phenolic profile, could also be very helpful for rootstock breeders, who have stressed the market value of fruits of grafted plants as a focus of most rootstock breeding efforts.[7]

## MATERIALS AND METHODS

**Plant Material.** Fruits were collected from three commercial varieties of eggplant, Blackbell F1 (BB), Epic F1 (EC), Galine F1 (GA), and landrace Domači srednje dolgi (DSD), which had been grafted onto tomato rootstock Beaufort F1 (BE) (and self-grafted plants were used as a control) using the cleft procedure described by Lee[30] and were grown in experiments from May until September in 2010 and 2011, on the experimental field (latitude 46°2′, longitude 14°28′, 298 m asl) of the Biotechnical Faculty in Ljubljana, Slovenia. The main characteristics of each of the varieties are presented in Table 1.

Successfully grafted plants were transplanted on May 24 in both years at a planting density of 0.8 × 0.8 $m^2$ (plant density of 12 500 plants $ha^{-1}$) in an unheated three-span greenhouse with flap ventilation at the ridge and roll-up ventilation at the side walls. Each span was 6 m wide and 25 m long and covered with a transparent polycarbonate Lexan corrugated sheet (LCS100, SABIC Innovative Plastics, Netherlands), with 89% visible light transmittance and <3% UV transmission. On the side walls, polyethylene film was used for roll-up ventilation. In both years, a completely randomized block design was used, with four eggplant varieties and two rootstocks (BE and self-grafted), four replicates per each grafted combination and 6 plants per replicate, making a total of 24 plants per treatment (scion/rootstock combination) and 192 plants for each experiment.

The soil of the experimental site is classified as gleyic fluvisol and endogenic fluvisol containing 24 g $kg^{-1}$ soil organic matter in the 0−0.3 m soil layer. At the beginning of the season, the average initial soil nitrate content was 5.2 mg $kg^{-1}$ for the same depth, soil assimilable P and K was 22 and 28 mg $kg^{-1}$, respectively, on the basis of which application rates of macronutrients were calculated according to the Regulations on Integrated Production of Vegetables. One day before transplanting, granulated mineral fertilizers were incorporated on the plots at a rate of 70 kg N $ha^{-1}$, 50 kg P $ha^{-1}$ and 235 kg K $ha^{-1}$, and 20 kg Ca $ha^{-1}$ as calcium ammonium nitrate, super phosphate, and potassium sulfate, respectively. The remaining N and Ca (150 and 184 kg $ha^{-1}$) were applied via fertigation with the water-soluble fertilizer (WSF) calcium nitrate (Multi-Cal, Haifa Chemicals, Israel). Irrigation was applied as required through a drip tape (T-tape TSX 500 model, T-systems International) beneath the plastic mulch. Diseases were managed with applications of Vertimec (Syngenta Agro d.o.o., Ljubljana, Slovenia) (0.05% on July 11, 2010 and on July 4, 2011) and Calipso SC 480 (Bayer Ag., Leverkusen, Germany) (0.03% on July 27, 2011).

**Weather Conditions.** Average daily temperature and total daily solar irradiation (presented in Table 2) during the experimental period from May to September of 2010 and 2011 were taken from the meteorological station on the experimental field of the Biotechnical Faculty in Ljubljana, Slovenia. It can be assumed that the environmental conditions in the greenhouse were very similar to those in the open field but, on the basis of experience from previous years, 3−4 °C higher. The weather during the experimental period in 2010 was comparable to the long-term average, but the average daily temperatures were slightly above the long-term average, with the highest positive deviation in June (by 2.5 °C) and in July (by 3 °C), while the average daily temperature in September fell below the long-term average daily temperature by 0.8 °C. The year 2011 was comparable to the long-term average in terms of temperature. Higher temperatures compared to the long-term average (more than 3 °C higher) were measured in May, August, and September.

More solar radiation compared to the long-term average was measured in all months during the experimental period in both years. The highest monthly averages of total daily solar radiation in 2010 were in June and July, 27 and 15% above the long-term average, respectively. Higher than average solar radiation was recorded in 2011, being highest in May (58%), August (45%), and September (55%).

**Fruit Sampling.** Fruit harvesting began 56 days after transplanting in 2010 and 60 days in 2011. Commercially mature fruit were harvested weekly; in the first year there were 12 pickings altogether and 11 in the second year of trials. Carpometric characteristics were measured in fruits of all scion/rootstock combinations, which were harvested in the middle of the harvesting period, 86 and 94 days after transplanting in the first and second year, respectively. For each scion/rootstock combination and each of four replications, six eggplant fruits were randomly selected from among marketable and undamaged fruits. Variation of carpometric characteristics [fruit weight (g), fruit length (cm), fruit width (cm), fruit length/width, and calyx prickles (0 = none; 9 = very many) (>30)], as well as color measurement and polyphenolic content, was studied on these samples.

**Color Measurements.** Skin color measurements were conducted to confirm skin color uniformity within individual varieties and among them in order to eliminate the effect of skin color as a factor that could influence the chemical composition of anthocyanins. Skin color was measured on the equatorial region of the fruits using a Minolta CR 300 Chroma portable colorimeter (Minolta Co., Osaka, Japan) with C illuminant for each fruit, and an average for individual varieties was calculated. Fruit chromaticity was expressed in $L^*$, $a^*$, $b^*$ color space coordinates (CIELAB). Color was described by the CIRG index, specifically intended for the evaluation of the external color of violet-colored fruits[31] and calculated as $(180 - h)/[L^* + \sqrt{(a^2 + b^2)}]$, where $h$ represents the hue angle.

**Determination of Browning.** Fruit flesh color was measured using the same colorimeter (Minolta CR 300) to determine the lightness of fruit pulp by measuring the $L^*$ value (0 = black, 100 = white). Fruit was cut transversally at the midpoint between the blossom and stem ends, and measurements were made on the surface immediately after being cut, 10 min later, and after 30 min, when maximum browning was achieved.

The oxidation potential was estimated using the method of Larrigaudiere et al.[32] with a slight modification as suggested by Concellon et al.[25,33] A colorimeter was used to measure the color parameter $L^*$ on the section obtained, as described earlier. Measurements obtained immediately after cutting were marked $L_0$, those obtained after 10 min were marked $L_{10}$, and those after 30 min were marked $L_{30}$. The browning potential was expressed as $\Delta L_{10} = (L_0 - L_{10})$ and $\Delta L_{30} = (L_{30} - L_0)$.

**Chemicals.** The standards used to determine the phenolic compounds in samples were chlorogenic acid (5-caffeoylquinic acid) and quercetin 3-O-rutinoside from Sigma-Aldrich and (−)-epicatechin, (+)-catechin, delphinidine, quercetin 3-*O*-rhamnoside, quercetin-3-*O*-galactoside, and quercetin 3-*O*-glucoside from Fluka Chemie (Buchs, Switzerland). Methanol for extraction of phenolics was acquired from Sigma-Aldrich. The chemicals for the mobile phases were HPLC−MS-grade acetonitrile and formic acid from Fluka. Water for the mobile phase was double distilled and purified with the Milli-Q system (Millipore, Bedford, MA)

**Extraction and HPLC−MS/MS Identification of Phenolic Compound.** The eggplant fruits were peeled with a mechanical peeler and the peel was separated from the pulp. The extraction of fruit samples (peel and pulp separately) was done as described by Mikulic-Petkovsek et al.[34] with some modification. Fresh eggplant samples were ground to a fine powder in a mortar chilled with liquid nitrogen. The samples of 10 g of pulp or 5 g of peel were extracted with 10 mL of methanol containing 3% (v/v) formic acid and 3% (w/v) 2,6-di-*tert*-butyl-4-methylphenol (BHT) in a cooled ultrasonic bath for 1 h. BHT was added to the samples in order to prevent oxidation. After extraction, the fruit extracts were centrifuged for 7 min at 10 000 rpm. The supernatant was filtered through a Chromafil AO-45/25 polyamide filter produced by Macherey-Nagel and transferred to a vial prior to injection into the HPLC system. The individual phenolic compounds were analyzed using the Thermo Finnigan Surveyor HPLC system (Thermo Scientific, San Jose, CA) with a diode array detector at 280 nm (flavanols, cinnamic acid derivatives), 350 nm (flavonols), and 530 nm (anthocyanins). A Phenomenex (Torrance, CA) HPLC column C18 (150 × 4.6 mm, Gemini 3 $\mu$m) protected with a Phenomenex Security guard column and operated at 25 °C was used for the separation of phenolic compounds. The injection volume was 20 $\mu$L and the flow rate was maintained at 1 mL min$^{-1}$. The elution solvents were aqueous 1% formic acid and 5% acetonitrile (A) and 100% acetonitrile (B). The samples were eluted according to the linear gradient described by Marks et al.:[35] 0−5 min, 3−9% B; 5−15 min, 9−16% B; 15−45 min, 16−50% B; 45−50 min, 50% isocratic mixture. This step was followed by washing and reconditioning of the column. Compound identification was achieved by comparing the retention times and their UV−vis spectra from 200 to 600 nm, as well as by the addition of an external standard.

The identity of the phenolic compounds was confirmed using a mass spectrometer (Thermo Scientific, LCQ Deca XP MAX) with electrospray ionization (ESI) operating in positive (for anthocyanins) and negative (other phenolic groups) ion modes.

Full-scan data-dependent MS scanning from $m/z$ 115 to 2000 was used for the analyses. Quantification was achieved on the basis of the concentrations of the corresponding external standard. For compounds lacking reference compounds, related compounds were used as standards for quantification. Delphinidin 3-rutinoside-5-galactoside, delphinidin 3-rutinoside-5-glucoside, and delphinidin 3-rutinoside were therefore quantified in equivalents of delphinidin. The concentrations of phenolic compounds were expressed in mg kg$^{-1}$ of fresh weight (FW).

**Statistical Evaluation.** The experiment was treated as a two-factorial experiment in four randomized replications. The first factor (eggplant variety) had four levels: BB, EC, GA, and DSD, while the second factor (rootstock) had two levels (BE, self-grafted plants). Results were analyzed using the Statgraphics Plus 4.0 program (Manugistics. Inc., Rockville, MD). Prior to the Anova test, Levene's test for equality of variances was performed. Data from all of the analyses were tested for any differences among scion/rootstock combinations within each year using two-way analysis of variance (ANOVA). The differences were tested using the Duncan test with a significance level of 0.05. The means and the standard errors for variety, treatment, and the interaction V × T, which were taken from the ANOVA table, are presented.

The average three-part composition of anthocyanins expressed by absolute amounts was analyzed using multivariate analysis of variance (MANOVA) and a further separate ANOVA test for three variables (D-3-rutinoside, D-3-rutinoside-5-galactoside, and D-3-rutinoside-5-glucoside).

## RESULTS

Data for yield, expressed as the number of fruits per plant, and other visible fruit traits, such as fruit weight, color, and shape, as well as fruit calyx prickles, for the eggplant varieties grafted onto tomato rootstock are presented in Table 3. For the number of fruits per plant, both main effects (rootstock and variety) were significant ($p = 0.001$) in both years, while the interaction between them ($p = 0.01$) was significant only in 2011. In 2010, grafting significantly increased the number of fruits per plant for all varieties, while in 2011 the same effect of grafting was found with two varieties and landrace but not with GA. The significant effect of variety on fruit yield was also confirmed by ANOVA ($p = 0.001$), with a significantly higher number of fruits per plant for all commercial varieties compared to landrace DSD.

For the average fruit weight, ANOVA showed a significant impact of variety ($p = 0.001$) in 2010, while in 2011 both main effects were significant, as was also their interaction. In the first year, heavier fruits were recorded with BB and DSD compared to EC and GA, while between them no significant differences were found (Table 2). In the second year, grafting increased the average fruit weight with GA, EC, and DSD compared to self-grafted plants, but the differences were significant only with landrace DSD ($p = 0.01$).

For the color index CIRG, ANOVA showed a significant impact of varieties in both years, and in 2011 the V × T

Table 3. Visible Quality Traits of Three Commercial Eggplant Varieties (BB, EC, GA) and One Eggplant Landrace (DSD) Grafted onto Tomato Rootstock (Rs) and Self-Grafted (Sg)[a]

| year | variety | treatment | number of fruit per plant | fruit weight (g) | CIRG | fruit length/width ratio | fruit calyx prickles (scale 0−9) |
|---|---|---|---|---|---|---|---|
| 2010 | BB | Rs | 8.5 | 238.2 | 6.8 | 1.62 | 2.33 |
| | | Sg | 6.4 | 236.4 | 6.6 | 1.72 | 3.00 |
| | DSD | Rs | 5.8 | 246.8 | 6.7 | 1.29 | 1.17 |
| | | Sg | 4.1 | 239.4 | 6.5 | 1.36 | 3.67 |
| | EC | Rs | 8.6 | 208.6 | 7.1 | 2.08 | 1.00 |
| | | Sg | 7.1 | 202.4 | 7.0 | 2.14 | 2.00 |
| | GA | Rs | 9.2 | 224.7 | 6.9 | 1.70 | 1.67 |
| | | Sg | 6.8 | 196.8 | 6.5 | 1.80 | 2.67 |
| | sign.[b] | V (SE[c]) | *** (0.39) | *** (9.47) | ** (0.08) | *** (0.05) | ** (0.23) |
| | | T (SE) | *** (0.27) | NS | NS | NS | *** (0.16) |
| | | V × T (SE) | NS | NS | NS | NS | NS |
| | | BB | 7.4 ab | 237.2 a | 6.7 b | 1.67 ab | 2.67 a |
| | | DSD | 4.9 b | 243.0 a | 6.6 b | 1.32 b | 2.42 a |
| | | EC | 7.8 a | 205.1 b | 7.0 a | 2.11 a | 1.51 b |
| | | GA | 8.0 a | 210.2 b | 6.7 b | 1.75 ab | 2.17 ab |
| | | Rs | 8.1 a | 177.7 | 6.8 | 1.67 | 1.54 a |
| | | Sg | 6.1 b | 217.5 | 6.7 | 1.75 | 2.83 b |
| 2011 | BB | Rs | 7.9 bc | 276.7 ab | 8.6 a | 1.97 a | 1.20 |
| | | Sg | 3.3 e | 299.3 a | 6.5 bc | 1.76 bc | 3.33 |
| | DSD | Rs | 9.4 ab | 256.9 bc | 5.3 c | 1.53 bc | 1.17 |
| | | Sg | 4.8 d | 197.1 e | 6.1 bc | 1.37 d | 3.67 |
| | EC | Rs | 10.1 a | 249.4 bc | 5.5 c | 1.54 bc | 1.00 |
| | | Sg | 7.1 c | 231.9 cd | 7.1 b | 1.83 ab | 2.00 |
| | GA | Rs | 7.3 c | 245.2 cd | 6.5 bc | 1.48 b | 1.67 |
| | | Sg | 6.9 c | 218.8 de | 5.6 c | 1.79 a | 2.67 |
| | sign. | V (SE) | *** (0.44) | *** (17.08) | * (0.39) | *** (0.05) | *** (0.12) |
| | | T (SE) | *** (0.31) | ** (12.36) | NS | NS | *** (0.17) |
| | | V × T (SE) | ** (0.62) | ** (21.35) | ** (0.49) | *** (0.08) | NS |
| | | BB | 5.6 | 287.2 | 7.5 | 1.8 | 2.3 ab |
| | | DSD | 7.1 | 226.6 | 5.7 | 1.5 | 2.4 a |
| | | EC | 8.6 | 241.5 | 6.3 | 1.7 | 1.5 c |
| | | GA | 7.1 | 231.3 | 6.1 | 1.6 | 2.2 b |
| | | Rs | 8.7 | 256.1 | 6.4 | 1.6 | 1.3 b |
| | | Sg | 5.5 | 236.6 | 6.3 | 1.7 | 2.9 a |

[a]Different letters in rows denote significant differences in treatment (Duncan test, $p < 0.05$). [b]The significance is designated by asterisks as follows: *statistically significant differences at *P*-value below 0.05; **statistically significant differences at *P*-value below 0.01; ***statistically significant differences at *P*-value below 0.001. [c]SE = standard error for significant term.

interaction was also significant ($p = 0.01$). The CIRG index ranged from 6.5 to 7.1 in 2010 and from 5.3 to 8.6 in 2011, which indicated a very dark-violet skin of the eggplant fruit. According to Carreño et al.,[36] a CIRG index of 5 indicates red-dark violet skin, 5.7 indicates red-black fruit skin, and higher than 6 indicates blue-black fruit skin. In 2010, the darkest fruit skin was recorded with variety EC, with a CIRG index of 7.0, while the CIRG indexes of other varieties were lower than 6.9. In 2011, grafting significantly increased the darkness of the fruit peel with indexes for BB from 6.5 (self-grafted plants) to 8.6 (plants grafted onto BE), while with EC darkness decreased from 7.1 (self-grafted plants) to 5.5 (plants grafted onto BE).

The length/width ratio of fruit was significantly influenced by variety ($p = 0.001$) in 2010. Although ANOVA did not confirm a significant effect of grafting on fruit shape in 2010, we found more elongated shapes with self-grafted plants of all varieties, with a higher length/width ratio compared to fruits from plants grafted onto rootstock. A significant effect of varieties on fruit shape was expected, since fruit shape is highly genetically controlled.[37] EC had the most elongated fruits among all tested varieties. In 2011, the significant impact of the V × T interaction ($p = 0.001$) indicated that fruits of BB and landrace DSD plants grafted onto BE were more elongated than the fruits of self-grafted plants; with EC and GA, the opposite effect was recorded.

Finally, an important visible trait of eggplant fruit is calyx prickles, which is an undesirable trait for handling eggplant fruits. In both years, ANOVA confirmed the significant impact of grafting on decreasing the amount of calyx prickles, since the scores of this trait for fruits from grafted plants were lower than those from self-grafted plants. A significant effect of variety on calyx prickles was reflected in the highest scores for it in fruits from landrace DSD, in both years, compared to those of other commercial varieties.

The lightness of the fruit pulp immediately after cutting ($L_0$) was similar in grafted and self-grafted plants, with values

between 80 and 82.0 and with no significant impact of grafting in either the central or lateral parts of the pulp surface (Table 4). Differences were significant among varieties, in both years. DSD and GA showed whiter pulp, both laterally and centrally, while fruits from BB had the darkest pulp. The effect of grafting combination on the browning potential was assessed by measurements of the lightness of the fruit pulp 10 min ($L_{10}$) and 30 min ($L_{30}$) after slicing, and the difference with $L_0$ was calculated as the index of browning potential.[38] ANOVA showed a significant effect of rootstock ($p$ = 0.01) on the browning potential only 10 min after cutting ($L_{10}$) in 2010 and of varieties ($p$ = 0.001) in both years. Browning was more evident in the peripheral part of the fruit section, both 10 and 30 min after cutting. In 2010, the effect of grafting on changes of browning pulp tissues was recorded in lower browning potential ($\Delta L_{10}$ was 2.8) on the lateral part of the pulp of grafted fruit compared to the fruits of self-grafted plants ($\Delta L_{10}$ was 4.8). After 30 min no significant differences regarding the grafting effect on browning potential were found, and the same effects were also recorded in 2011. In 2011 grafting did not affect the browning potential of eggplant pulp 10 and 30 min after cutting. In relation to varieties, a higher browning potential after 30 min was found in the lateral section of BB in 2010 and DSD and GA in 2011. The variety with the lowest browning potential in the lateral section after 30 min was DSD in 2010 and BB and EC in 2011.

In the four eggplant varieties that were grafted onto BE tomato rootstock, we identified and quantified 13 phenolics (Tables 5−7) belonging to four groups: hydroxycinnamic acids, flavonols, flavanols, and anthocyanins. Compounds of the first three groups were identified in eggplant pulp, while anthocyanins were identified in the eggplant peel. Great differences in relation to variety and grafting treatment were found in the individual phenolic groups between the years. These results are in accordance with data reported by Lata et al.,[39] who observed up to 70% differences in phenolics between seasons.

In the fruit pulp we found the following hydroxycinnamic acids: chlorogenic, caffeic, *p*-coumaric, and ferulic acids. Hydroxycinnamic acids were the highest represented group of phenolics in the eggplant fruit of all four varieties, ranging from 25 to 45% in 2010 and from 34 to 51% in 2011. For total hydroxycinnamic acids, ANOVA showed a statistically significant effect of variety ($p$ = 0.001) in 2010 and the interaction V × T in both years. In 2010, fruits of BB (from grafted and self-grafted plants) had the highest total hydroxycinnamic acid contentration, and no significant differences were found between them. The effect of grafting on hydroxycinnamic acid content was recorded with DSD, where grafting onto BE caused their increase in comparison with the fruits from self-grafted plants and with GA and EC, where the opposite effect was found. In 2011, grafting had no effect on changes in total hydroxycinnamic acid content in fruits of commercial varieties while for DSD a significant decrease was found (Tables 6 and 7).

In terms of quantity, quercetins are a minor phenol group in eggplant fruits, ranging from 1 to 4% of the total analyzed phenolic concentration. The analysis of flavonols covered four types of quercetin glycoside: quercetin 3-rhamnoside accounted for approximately 75−90% of total flavonol concentration, followed by quercetin 3-rutinoside (4−17%), quercetin 3-glucoside (2−8%) and quercetin 3-galactoside (1−2%). Total flavonols were significantly influenced by variety and interaction of V × T in 2010 and by both main factors and their interaction in 2011. In 2010, grafting on rootstock significantly increased the total

**Table 4. Changes in Browing of Pulp Tissue Measured Rapidly after Cutting ($L_0$) and Browning Potential ($\Delta L_{10}$ after 10 min, $\Delta L_{30}$ after 30 min) in Central and Lateral Sections of Eggplant As Affected by Grafting and Varieties[a]**

| | | year 2010 | | | | | | year 2011 | | | | | |
|---|---|---|---|---|---|---|---|---|---|---|---|---|---|
| | | $L_0$ | | $\Delta L_{10}$ | | $\Delta L_{30}$ | | $L_0$ | | $\Delta L_{10}$ | | $\Delta L_{30}$ | |
| | | central | lateral | central | lateral | central | lateral | central | lateral | central | lateral | central | lateral |
| T | Rs | 81.8 | 80.4 | 1.4 | 2.8 b | 2.0 | 7.6 | 80.8 | 80.6 | 1.9 | 3.3 | 2.2 | 6.7 |
| | Sg | 80.9 | 80.9 | 1.9 | 4.8 a | 2.7 | 8.2 | 81.6 | 81.2 | 2.9 | 3.5 | 3.7 | 7.8 |
| sign.[b] | | NS[c] | NS | NS | ** (0.22)[d] | NS | NS | NS | NS | NS | NS | NS | NS |
| V | BB | 78.2 | 78.6 | 1.6 b | 4.8 b | 3.9 a | 8.3 a | 78.9 ab | 77.8 b | 2.1 a | 4.2 b | 2.8 a | 6.8 b |
| | DSD | 80.7 | 80.4 | 2.4 a | 3.7 a | 3.9 a | 5.8 b | 80.9 a | 80.4 a | 2.1 a | 5.8 a | 2.9 a | 8.6 a |
| | EC | 79.3 | 79.2 | 2.2 ab | 3.4 b | 2.8 b | 7.2 ab | 79.3 ab | 79.2 ab | 1.8 b | 5.4 ab | 2.1 b | 7.2 b |
| | GA | 80.2 | 80.6 | 2.8 a | 3.5 b | 3.3ab | 6.3 b | 80.2 a | 80.6 a | 1.9 b | 4.5 b | 2.2 b | 8.2 a |
| sign. | | NS | NS | ** (0.216) | ** (0.19) | * (0.38) | * (0.22) | * (0.78) | * (0.86) | ** (0.05) | ** (0.12) | * (0.02) | ** (0.31) |
| V × T | | NS | NS | NS | NS | NS | NS | NS | NS | NS | NS | NS | NS |

[a]Different letters in rows denote significant differences in treatment (Duncan test, $p < 0.05$). [b]The significance is designated by asterisks as follows: *statistically significant differences at *P*-value below 0.05; **statistically significant differences at *P*-value below 0.01; ***statistically significant differences at *P*-value below 0.001. [c]NS = not significant. [d]Standard errors are in the parentheses.


dx.doi.org/10.1021/jf503338m | J. Agric. Food Chem. 2014, 62, 10504−10514

Table 5. Identification of Phenolic Compounds in the Peel and Pulp of Eggplant Fruit in Negative and Positive Ions with HPLC−MS and $MS^2$

| phenolic group | $\lambda_{max}$ (nm) | $M^+$ or $[M - H]^-$ ($m/z$)[a] | $MS^2$ ($m/z$) | tentative identification |
|---|---|---|---|---|
| hydroxycinnamic acids | 328, 234 | 353 | 191, 179 | chlorogenic acid |
| | 241, 323 | 179 | 135, 161 | caffeic acid |
| | 310, 225 | 163 | 119 | *p*-coumaric acid |
| | 295, 322 | 193 | 134, 178, 149 | ferulic acid |
| flavanols | 279, 234 | 289 | 245 | catechin |
| | 279, 234 | 289 | 245 | epicatechin |
| flavonols | 354, 234 | 609 | 301 | quercetin 3-rutinoside |
| | 356, 256, 234 | 463 | 301 | quercetin 3-galactoside |
| | 356, 254, 234 | 463 | 301 | quercetin 3-glucoside |
| | 353, 268, 255 | 447 | 301 | quercetin 3-rhamnoside |
| anthocyanins | 280, 525 | 611 | 465/303 | delphinidin 3-rutinoside |
| | 279, 526 | 773 | 611/465/303 | delphinidin 3-rutinoside-5-galactoside |
| | 281, 525 | 773 | 611/465/303 | delphinidin 3-rutinoside-5-glucoside |

[a]Anthocyanins were obtained in positive ion mode and other phenolics in negative ion mode.

flavonols in fruits of the landrace DSD and decreased in GA. A more consistent impact of grafting on total flavonol concentrations was observed in 2011, where grafting increased their concentration in fruits of EC and GA (Tables 6 and 7).

Within flavanols, monomeric catechin and epicatechin were analyzed in eggplant pulp. Catechin was a more abundant individual flavanol in the eggplant fruits than epicatechin, representing 50−80% of the total flavanol concentration. Their concentrations ranged from 30 to 45% in 2010 and from 25 to 40% in 2011 of the total phenolic concentration. Significant changes in total flavanols were observed only in 2010, for which ANOVA showed a significant impact of variety and interaction V × T. Fruits of grafted EC and GA had significantly lower total flavanol concentrations than fruits from self-grafted plants. The opposite effect, with significantly higher total flavanol concentration was found in grafted fruits from DSD compared to self-grafted fruits.

In terms of quantity, anthocyanins were the third most represented phenolic group in eggplant fruits after hydroxycinnamic acids and flavanols. Their concentration ranged from 15 to 30% of the total analyzed phenolic concentration. In the fruit peel we identified and quantified the following anthocyanins: delphinidin 3-rutinoside, delphinidin 3-rutinoside-5-galactoside, and delphinidin 3-rutinoside-5-glucoside. Delphinidin 3-rutinoside was found in the highest mean concentrations in all the samples and represented 90−95% in 2010 and 83−92% in 2011 of the total anthocyanin concentration. Delphinidin 3-rutinoside-5-galactoside was the second most represented, ranging from 2 to 7% in 2010 and from 7 to 13% in 2011. Delphinidin 3-rutinoside-5-glucoside was found in the lowest mean concentrations, ranging from 1 to 3% in both years. ANOVA confirmed a significant effect of grafting ($p = 0.01$) on total anthocyanin concentration only in 2010, when grafting decreased the total anthocyanin concentration in the peel of eggplant fruits with all tested varieties.

## DISCUSSION

In recent years, a high quality of vegetable fruits is even more important than total fruit yield, due to the benificial role of vegetables in the human diet.[11] External quality described by visual traits such as fruit size, shape, color, and calyxs prickles are important criterion in making purchasing decisions of eggplant fruits.[1] Among many strategies, such as genetic selection, optimization of the environmental conditions, and agricultural practices, grafting represents an efficient technological tool where a scion/rootstock combination plays an important role in the achievement of the established tasks.[5,7,10] It is well-known that scion variety mainly affects the final yield and quality traits of fruit in grafted plants,[40] but rootstock effects can alter these characteristics,[1,3,4] possibly due to changes in vigor and concentration of growth regulators induced by the rootstocks.[8] Further, differences in the requirements for assimilating mineral nutrients between tomato (rootstock) and eggplant (scion) also altered the quality of fruit yield.[41] In our study, higher yield and the changes of visual characteristics of fruits from grafted and self-grafted plants could be explained by the successful adoption by the scion of the main rootstock's characteristics, already described in Table 1. The lower presence of calyx prickles, observed in fruits from grafted plants, may indicate more vigorous and balanced growth[41] of grafted plants than self-grafted ones, since the prickles in the eggplant calyx are probably caused by biotic or abiotic stresses.[17]

Eggplant has a high antioxidant capacity, mainly attributed to its high content of phenolic compounds.[14] First evaluations of phenolic acid constituents in eggplant fruit from different accessions and varieties were reported by Stommel and Whitaker[12] latter in phytochemical investigations, and the impact of different cultivation systems, grafting techniques, and methods of sample preparation on phenolic constituents were examined.[3,8,28,42] In accordance with the above-mentioned studies, the analyzed composition, and the content of the main phenolic groups (hydroxycinnamic acids, flavonols, flavanols, and anthocyanins) in eggplant pulp and peel showed high dependence not only on variety but also on rootstock, as well as on environmental conditions, since the phenolic profile varied during the two growing periods. In 2010, less solar radiation and lower mean daily temperatures (Table 2) led to less favorable environmental conditions for growth and development of eggplant fruits. It seems that higher vigor of grafted plants of commercial varieties is more expressed under such temperate environmental conditions, where rootstock hastened plant growth and development, which resulted in higher yield. We picked a significantly higher number of fruits per plant (7.5−8) from plants of grafted commercial varieties compared to the grafted landrace (Table 3).

On the other hand, it could be expected that fruits from grafted commercial varieties had not reached physiological maturity at harvesting, because they grew faster than self-grafted plants and we picked them at a younger maturity stage. At physiological maturity, the contents of sugars, ascorbic acid,

**Table 6. Significance for Varieties (V), Treatment (T), and Interaction (V × T), with Standard Error in Parentheses; Means of Individual Phenolic Compounds (in mg kg$^{-1}$ FW); and Results of Duncan's Multiple Comparison Test for Significant Terms, for the Year 2010**[a]

| | significance (SE)[b] | | | V | | | | T | | V × T | | | | | | | |
|---|---|---|---|---|---|---|---|---|---|---|---|---|---|---|---|---|---|
| | V | T | V × G | BB | DSD | EC | GA | Sg | Rs | BB × Sg | BB × Rs | DSD × Sg | DSD × Rs | EC × Sg | EC × Rs | GA × Sg | GA × Rs |
| chlorogenic acid | *** (19.3)[c] | NS[d] | *** (27.3) | 389.4 | 279.1 | 213.7 | 262.7 | 297.1 | 275.4 | 480.9 a | 413.0 ab | 169.4 de | 348.5 bc | 215.5 d | 120.9 e | 307.4 c | 184.1 de |
| caffeic acid | *** (2.7) | NS | ***(3.6) | 31.1 | 26.3 | 27.3 | 12.9 | 26.1 | 22.8 | 38.5 ab | 36.0 b | 19.8 c | 38.8 ab | 47.5 a | 20.3 c | 17.7 c | 6.3 d |
| *p*-coumaric acid | *** (0.9) | **(0.7) | *** (1.4) | 3.5 | 3.0c | 12.5 | 6.9 | 8.7 | 4.2 | 3.1 bcd | 3.3 bc | 2.2 d | 5.3 bc | 15.7 a | 5.4 b | 15.7 a | 1.4 cd |
| ferulic acid | NS | NS | NS | 3.5 | 4.1 | 3.7 | 3.7 | 4.2 | 3.3 | 4.6 | 2.1 | 3.6 | 0.8 | 3.6 | 2.1 | 5.6 | 1.6 |
| **tot. hydroxycinnamic acids** | ***** (21.4)** | **NS** | ***** (30.3)** | **427.6** | **312.5** | **257.3** | **286.8** | **336.3** | 305.8 | **527.2 a** | **454.4 a** | **231.5 ef** | **393.4 bc** | **282.3 de** | **148.8 f** | **346.4 cd** | **193.3 ef** |
| q 3-rut | ** (0.21) | NS | NS | 0.97 b | 0.64 b | 1.61 a | 1.85 a | 1.11 | 1.43 | 0.7 | 1.2 | 0.5 | 0.8 | 1.1 | 2.1 | 1.8 | 1.9 |
| q 3-gal | NS | NS | NS | 0.28 | 0.28 | 0.32 | 0.45 | 0.33 | 0.31 | 0.3 | 0.2 | 0.2 | 0.3 | 0.2 | 0.4 | 0.5 | 0.5 |
| q 3-gluc | *** (0.05) | NS | NS | 0.49 a | 0.14 b | 0.13 b | 0.45 a | 0.35 | 0.26 | 0.5 | 0.5 | 0.1 | 0.2 | 0.1 | 0.1 | 0.6 | 0.3 |
| q 3-rham | *** (1.48) | NS | *** (2.1) | 19.6 | 16. | 14.8 | 24.6 | 21.8 | 16.0 | 20.1 b | 19.1 bc | 14.7 d | 22.4 b | 16.4 bc | 13.3 cd | 28.5 a | 20.8 b |
| **tot. flavonol** | ***** (1.59)** | **NS** | ***** (2.2)** | **21.3** | **17.7** | **16.9** | **27.4** | **23.7** | **18.5** | **21.7 b** | **20.9 b** | **15.7 d** | **23.7 b** | **17.8 bc** | **15.9 d** | **31.3 a** | **23.5 b** |
| catechin | NS | NS | NS | 270.0 | 150.2 | 235.6 | 224.1 | 187.4 | 253.4 | 260.1 | 280.8 | 136.5 | 175.9 | 288.1 | 183.5 | 288.9 | 160.2 |
| epicatechin | *** (11.29) | *** (7.9) | *** (16.0) | 153.1 | 103.3 | 139.1 | 49.3 | 147.1 | 76.1 | 159.0 ab | 148.6 b | 81.8 cd | 160.2 ab | 195.8 a | 83.8 c | 72.9 c | 26.1 d |
| **tot. flavanol** | ***** (41.41)** | ***** (29.1)** | ***** (58.2)** | **424.2** | **253.1** | **375.6** | **274.1** | **400.2** | **263.2** | **419.2 ab** | **429.4 a** | **218.3 c** | **336.1 abc** | **483.9 a** | **267.3 bc** | **361.9 ab** | **186.3 c** |
| del 3-rut | NS | *** (14.2) | NS | 181.2 | 132.1 | 194.1 | 163.8 | 201.5 a | 134.1 b | 187.6 | 174.8 | 162.1 | 102.3 | 236.2 | 151.9 | 220.2 | 107.5 |
| del 3-rut-5-gal | *** (1.17) | * (0.8) | *** (1.6) | 14.7 | 4.8 | 9.6 | 7.0 | 10.5 | 7.5 | 15.9 b | 13.6 ab | 0.9 f | 8.6 de | 14.5 ab | 4.6 ef | 10.7 f | 3.4 bc |
| del 3-rut-5-glu | *** (0.42) | NS | NS | 5.9 a | 3.6 b | 2.7 b | 2.6 b | 3.9 | 3.5 | 6.4 | 5.5 | 2.9 | 4.2 | 3.3 | 2.0 | 2.8 | 2.4 |
| **tot. anthocianins** | **NS** | **** (15.0)** | **NS** | **201.9** | **140.5** | **206.3** | **173.5** | **215.9 a** | **145.2 b** | **210.0** | **193.9** | **165.9** | **115.1** | **254.0** | **158.6** | **233.7** | **113.2** |
| **tot. phenolics** | **** (46.83)** | **NS** | **** (64.7)** | **789.4** | **583.4** | **631.9** | **565.8** | **666.5** | **618.8** | **1178.2 b** | **1098.6 ab** | **540.1 bc** | **868.8 e** | **1038.0 a** | **590.6 cd** | **973.2 bc** | **516.3 de** |

[a]Different letters in rows denote significant differences in treatment (Duncan test, $p < 0.05$). [b]Se = standard error for the significant term. [c]The significance is designated by asterisks as follows: *statistically significant differences at *P*-value below 0.05; **statistically significant differences at *P*-value below 0.01; ***statistically significant differences at *P*-value below 0.001. [d]NS = not significant.



dx.doi.org/10.1021/jf503338m | J. Agric. Food Chem. 2014, 62, 10504−10514

**Table 7. Significance for Varieties (V), Treatment (T), and Interaction (V × T), with Standard Error in Parentheses; Means of Individual Phenolic Compounds (in mg kg$^{-1}$ FW); and Results of Duncan's Multiple Comparison Test for Significant Terms, for the Year 2011**[a]

| | significance (SE)[b] | | | V | | | | T[c] | | V × T | | | | | | | |
|---|---|---|---|---|---|---|---|---|---|---|---|---|---|---|---|---|---|
| | V | T | V × G | BB | DSD | EC | GA | Sg | Rs | BB × Sg | BB × Rs | DSD × Sg | DSD × Rs | EC × Sg | EC × Rs | GA × Sg | GA × Rs |
| chlorogenic acid | NS | NS[d] | ** (27.2)[e] | 326.6 | 299.2 | 259.2 | 279.7 | 300.7 | 281.7 | 353.6 ab | 299.8 abc | 372.4 a | 226.1 c | 238.3 c | 280.3 b | 238.8 c | 320.8 ab |
| caffeic acid | NS | NS | * (4.7) | 24.8 | 23.0 | 20.8 | 13.8 | 21.1 | 20.1 | 18.6 abc | 31.0 a | 29.5 ab | 16.6 bcd | 27.4 abc | 14.3 c | 9.0 d | 18.6 abcd |
| *p*-coumaric acid | ** (1.6) | * (1.2) | NS | 3.7 b | 2.8 b | 14.4 a | 5.3 b | 8.5 a | 4.6 b | 6.0 | 1.6 | 2.7 | 3.0 | 17.3 | 11.5 | 8.3 | 2.3 |
| ferulic acid | * (0.7) | NS | NS | 3.8 b | 6.7 a | 4.6 b | 4.7 ab | 4.9 | 5.03 | 3.4 | 4.2 | 6.6 | 6.9 | 4.7 | 4.5 | 5.0 | 4.5 |
| **tot. hydroxycinnamic acids** | **NS** | **NS** | ** (31.1) | **359.0** | **331.8** | **299.1** | **303.7** | **335.3** | **311.4** | **381.5 ab** | **336.6 abc** | **411.2 a** | **252.5 d** | **287.7 cd** | **310.5 b** | **261.1c** | **346.3 abc** |
| q 3-rut | NS | NS | * (0.5) | 1.6 | 1.3 | 1.8 | 0.8 | 1.3 | 1.4 | 2.2 ab | 1.0 bc | 1.4 bc | 1.3 bc | 0.9 c | 2.8 a | 0.9 b | 0.8 c |
| q 3-gal | NS | NS | ** (0.1) | 0.2 | 0.3 | 0.2 | 0.3 | 0.3 | 0.2 | 0.3 bc | 0.2 bc | 0.6 a | 0.2 bc | 0.1 c | 0.4 a | 0.3 b | 0.3 bc |
| q 3-gluc | NS | ** (0.1) | ** (0.2) | 0.8 | 0.8 | 0.7 | 0.5 | 0.9 | 0.5 | 1.5 a | 0.3 c | 1.0 ab | 0.7 bc | 0.7 bc | 0.8 b | 0.7 b | 0.4 c |
| q 3-rham | ** (1.7) | ** (1.3) | * (2.5) | 16.5 | 17.8 | 9.6 | 16.4 | 12.4 | 17.7 | 13.4 bcd | 19.6 ab | 19.4 abc | 16.3 abcd | 6.9 e | 12.3 c | 10.2 d | 22.6 a |
| **tot. flavonol** | * (1.9) | * (1.4) | * (2.7) | **19.8** | **20.4** | **12.4** | **18.1** | **15.1** | **19.9** | **17.4 abc** | **21.2 ab** | **22.4 ab** | **18.5 abcd** | **8.6 e** | **16.2 abc** | **12.2 de** | **24.2 a** |
| catechin | * (24.2) | NS | NS | 151.4 b | 155.3 b | 258.4 | 181.31 | 178.5 | 194.7 | 110.1 | 192.8 | 158.3 | 152.3 | 237.8 | 279.0 | 207.9 | 154.7 |
| epicatechin | NS | NS | * (19.6) | 102.8 | 95.1 | 85.9 | 57.0 | 87.2 | 82.9 | 76.7 abc | 127.9 a | 121.8 ab | 68.4 cd | 113.1 abc | 58.8 c | 37.2 d | 76.9 abcd |
| **tot. flavanol** | **NS** | **NS** | **NS** | **253.7** | **250. 5** | **344.8** | **238.3** | **256.7** | **277.7** | **186.8** | **320.7** | **280.2** | **220.7** | **351.0** | **337.8** | **245.1** | **231.6** |
| del 3-rut | NS | NS | NS | 167.2 | 128.4 | 171.2 | 138.0 | 138.5 | 164.0 | 137.9 | 196.7 | 111.6 | 145.4 | 185.4 | 157.1 | 119.1 | 156.9 |
| del 3-rut-5-gal | ** (2.0) | NS | NS | 20.9 a | 18.9 a | 17.3 a | 10.6 b | 15.0 | 18.8 | 19.6 | 22.2 | 14.3 | 23.6 | 16.8 | 17.9 | 9.4 | 11.9 |
| del 3-rut-5-glu | ** (0.5) | NS | NS | 5.2 a | 4.4 a | 4.6 a | 2.6 b | 3.7 | 4.6 | 4.8 | 5.7 | 3.1 | 5.7 | 4.4 | 4.9 | 2.8 | 2.5 |
| **tot. anthocianins** | **NS** | **NS** | **NS** | **193.4** | **151.8** | **193.2** | **151.3** | **157.3** | **187.6** | **162.3** | **224.5** | **129.0** | **174.7** | **206.6** | **179.9** | **131.4** | **171.2** |
| **tot. phenolics** | **NS** | **NS** | ** (68.8) | **632.0** | **602.7** | **655.9** | **560.2** | **616.2** | **609.1** | **747.9 bcd** | **903.0 a** | **842.7 ab** | **666.5 cde** | **853.9 ab** | **844.4 a** | **649.8 c** | **773.3 bc** |

[a]Different letters in rows denote significant differences in treatment (Duncan test, $p < 0.05$). [b]SE = standard error for significant term. [c]Sg = self-grafted. Rs = rootstock. [d]NS = not significant. [e]The significance is designated by asterisks as follows: *statistically significant differences at *P*-value below 0.05; **statistically significant differences at *P*-value below 0.01; ***statistically significant differences at *P*-value below 0.001.



dx.doi.org/10.1021/jf503338m | J. Agric. Food Chem. 2014, 62, 10504−10514

and polyphenols are the highest in eggplant fruits and then significantly decreased.[48] Our assumption was partly confirmed by the chemical analysis of phenolic constituents in eggplant fruits, which showed a lower concentrations of all phenolic constituents in grafted fruits in comparison with the fruits from self-grafted plants. The opposite effect was found for the landrace/rootstock combination, where we harvested only five fruits per plant in that year, which indicates that fruits from the landrace grew more slowly; thus, they could reach their physiological maturity by harvest date, which was confirmed also with an increase of the phenolic contents in grafted plants compared to self-grafted ones.

Anthocyanins are the most important group within flavonoids for the production of a dark red or purple color of the eggplant peel.[21] The composition of anthocyanins in fruits from our study was relatively similar to those observed by Sadilova et al.[21] and Wu and Prior.[43] On the other hand, the composition of anthocyanins is largely conditioned by eggplant variety and growth conditions.[2,23,38,44] This could be one of the reasons why our results differed from the data reported by Azuma et al.,[45] who identified an acylated anthocyanin, known as nasunin, as the prevailing anthocyanin in Japanese eggplant varieties. In our study, the concentrations of anthocyanins, which were analyzed in eggplant peel in 2010, showed high dependence on grafting. Their concentration significantly decreased in fruits from grafted plants compared to the fruits from self-grafted plants. This response was probably a consequence of more shaded fruits, since grafted plants had a higher habitus with much bigger leaves (data not shown), with which the fruits were covered. Since accumulation of anthocyanins is strongly light-exposure-dependent,[29,46] it could be additionally suggested that, in order to produce fruits with a higher anthocyanin concentration and thus with higher nutritional value, grafted eggplant plants should properly be pruned and illuminated.

As eggplant is ranked among the top 10 vegetables in terms of antioxidant activity, mainly due to the fruit phenolic constituents, the high browning potential of the fruit pulp could be expected.[1,28,18] Browning appears on cutting, when disruption of cellular structures leads to release of the enzyme polyphenol oxidase (PPO), which oxidizes phenolics, and in the presence of oxygen, *o*-quinones are polymerized, causing brown-colored pigments.[18] Eggplant varieties differed in their extents of postcut browning, which could be due to variations in the PPO activity or level of soluble phenolics.[7,17,18] In contrast to the findings of Gisbert et al.[8] and Moncada et al.,[3] who reported that little or no effect of grafting on fruit phenolics content was found, in our study grafting decreased the phenolics concentration in fruits of commercial varieties in 2010, while the landrace/rootstock combination gave a significant increase (in 2010) and decrease (in 2011) of phenolics concentration. Higher phenolic concentration in grafted DSD eggplant pulp in 2010, in addition to the lowest fruit yield among the grafted treatments (Table 3), may be an additional indicator of the stress in this scion/rootstock combination, since stress conditions induce an accumulation of phenolics.[1,47] An inverse effect of grafting in DSD in the next year of the study probably indicated a higher diversity among landrace plants compared to the plants of the other commercial hybrid varieties, for which a very similar pattern of phenolic concentration changes were observed in both years. An interesting result of our study is that the fruits from the same landrace/rootstock grafted combination behaved differently during the two growing season, which could be explain with findings reported by Hanson,[2] who suggest that environmental factors, above all light, temperature and water management, influenced the types or levels of phenolic compounds in eggplant fruits. During the growing seasons in our study, weather conditions were very similar, with temperatures slightly above the long-term average in both years, but with a little lower solar radiation in 2010 than in 2011, which contributed to less suitable growing conditions for eggplants in that year.

In accordance with the studies on the impact of different factors on browning potential of eggplant fruit pulp,[17,18,33] the browning potential in our study showed high dependence on variety and partly on grafting combination. As regards the different correlations between phenolic contents and browning potential (positive for EC and GA and negative for the landrace DSD), the importance of other main antioxidants, such as reduced ascorbate, could be evidenced.[18,38] The content of ascorbic acid, which has antibrowning properties because it reduces enzymatically formed *o*-quinones to their precursor diphenols, is also genetically, developmentally, and environmentally dependent;[17] therefore, variations of its content in fruits from our treatments could be expected. The syntheses of sugars, ascorbic acid, and polyphenols are developmentally conditioned and reached their maximum values about 6 weeks from eggplant fruit set. This fact emphasizes the importance of considering this point for determination of the physiological maturation stage of the fruit,[48] in order to harvest eggplant fruits with higher nutritional value. There are also some other variety-dependent factors, like intracellular pH, which affects the activity of the polyphenol oxidase enzyme, or cellular factors, such as cell size, which may have a role in browning and color evaluation of the fruit pulp.[25]

In conclusion, the impact of grafting commercial eggplant varieties and landrace onto tomato rootstock on internal and external eggplant fruit characteristics is not equal and is largely conditioned by scion/rootstock combination and environmental conditions. For all tested varieties data indicated a positive effect of grafting on yield and visual traits of eggplant fruits. Grafted plants were more vigorous than self-grafted plants and gave higher yield. For some varieties grafting influenced also fruit shape and size and for all varieties decreased the presence of calyx prickles. Higher vigor of grafted plants negatively influenced the concentration of anthocyanins; therefore, pruning of grafted plants to improve the color and phenolics concentration in eggplants peel should be performed during the growing period. For some of the commercial varieties grafted onto tomato rootstock, a decrease of the phenolic content in eggplant pulp was found, compared to self-grafted plants. The effect of grafting eggplant landrace onto tomato rootstock showed an inconsistent trend in the phenolics content of eggplant samples, which indicated that the synthesis of phenolics in landrace fruit is probably dependent also on environmental factors, especially on light conditions. With additional analysis with which a higher presence of reducing antioxidants in eggplant fruits could be confirmed, our results would become more promising and useful, especially when grafted varieties showed better characteristics and as such deserve more attention by rootstock breeders. Further research work should focus on the evaluation of the complete chemical profile of eggplant fruits picked from the different scion/roostock combinations and on the observation of their growth and development. With this knowledge, appropriate criteria for the determination of the physiological maturity stage of fruits can be define in order to get

the eggplant with higher content of substances responsible for flavor, nutritional value, and sensorial characteristics of eggplant fruits.

## AUTHOR INFORMATION


### Corresponding Author

*E-mail: nina.kacjan.marsic@bf.uni-lj.si. Fax: +386 1 423 10 88. Tel: +386 1 320 31 13.


### Notes

The authors declare no competing financial interest.

## ABBREVIATIONS USED

BB, Blackbell; DSD, Domači srednje dolgi; EC, Epic; GA, Galine; BE, Beaufort; V, variety (commercial varieties and landrace); T, treatment (self-grafted plants and plants grafted onto rootstock); Rs, rootstock; Sg, self-grafted plants; sign., significance.

## REFERENCES


(1) Gisbert, C.; Prohens, J.; Nuez, F. Performance of eggplant grafted onto cultivated, wild, and hybrid materials of eggplant and tomato. *Int. J. Plant Prod.* **2011**, *5*, 367−380.

(2) Hanson, P. M.; Yang, R. Y.; Tsou, S. C. S.; Ledesma, D.; Engle, L.; Lee, T. C. Diversity in eggplant (*Solanum melongena*) for superoxide scavenging activity, total phenolics, and ascorbic acid. *J. Food Compos. Anal.* **2006**, *19*, 594−600.

(3) Moncada, A.; Miceli, A.; Vetrano, F.; Mineo, V.; Planeta, D.; D'Anna, F. Effect of grafting on yield and quality of eggplant (*Solanum melongena* L.). *Sci. Hortic.* **2013**, *149*, 108−114.

(4) Passam, H. C.; Stylianou, M.; Kotsiras, A. Performance of eggplant grafted on tomato and eggplant rootstocks. *Eur. J. Hortic. Sci.* **2005**, *70*, 130−134.

(5) Lee, J. M.; Oda, M., Grafting of herbaceous vegetable and ornamental crops. *Hortic. Rev.* **2003**, *28*.

(6) Bletsos, F.; Thanassoulopoulos, C.; Roupakias, D. Effect of grafting on growth, yield, and Verticillium wilt of eggplant. *HortScience* **2003**, *38*, 183−186.

(7) King, S. R.; Davis, A. R.; Zhang, X. P.; Crosby, K. Genetics, breeding and selection of rootstocks for Solanaceae and Cucurbitaceae. *Sci. Hortic.* **2010**, *127*, 106−111.

(8) Gisbert, C.; Prohens, J.; Raigon, M. D.; Stommel, J. R.; Nuez, F. Eggplant relatives as sources of variation for developing new rootstocks: Effects of grafting on eggplant yield and fruit apparent quality and composition. *Sci. Hortic.* **2011**, *128*, 14−22.

(9) Schwarz, D.; Rouphael, Y.; Colla, G.; Venema, J. H. Grafting as a tool to improve tolerance of vegetables to abiotic stresses: Thermal stress, water stress and organic pollutants. *Sci. Hortic.* **2010**, *127*, 162−171.

(10) Davis, A. R.; Perkins-Veazie, P.; Hassell, R.; Levi, A.; King, S. R.; Zhang, X. P. Grafting effects on vegetable quality. *HortScience* **2008**, *43*, 1670−1672.

(11) Rouphael, Y.; Schwarz, D.; Krumbein, A.; Colla, G. Impact of grafting on product quality of fruit vegetables. *Sci. Hortic.* **2010**, *127*, 172−179.

(12) Stommell, J. R.; Whitaker, B. D. Phenolic acid content and composition of eggplant fruit in a germplasm core subset. *J. Am. Soc. Hortic. Sci.* **2003**, *128*, 704−710.

(13) Akanitapichat, P.; Phraibung, K.; Nuchklang, K.; Prompitakkul, S. Antioxidant and hepatoprotective activities of five eggplant varieties. *Food Chem. Toxicol.* **2010**, *48*, 3017−3021.

(14) Cao, G. H.; Sofic, E.; Prior, R. L. Antioxidant capacity of tea and common vegetables. *J. Agric. Food Chem.* **1996**, *44*, 3426−3431.

(15) Matsubara, K.; Kaneyuki, T.; Miyake, T.; Mori, M. Antiangiogenic activity of nasunin, an antioxidant anthocyanin, in eggplant peels. *J. Agric. Food Chem.* **2005**, *53*, 6272−6275.

(16) Han, S. W.; Tae, J.; Kim, J. A.; Kim, D. K.; Seo, G. S.; Yun, K. J.; Choi, S. C.; Kim, T. H.; Nah, Y. H.; Lee, Y. M. The aqueous extract of *Solanum melongena* inhibits PAR2 agonist-induced inflammation. *Clin. Chim. Acta* **2003**, *328*, 39−44.

(17) Prohens, J.; Rodriguez-Burruezo, A.; Raigon, M. D.; Nuez, F. Total phenolic concentration and browning susceptibility in a collection of different varietal types and hybrids of eggplant: Implications for breeding for higher nutritional quality and reduced browning. *J. Am. Soc. Hortic. Sci.* **2007**, *132*, 638−646.

(18) Mishra, B. B.; Gautam, S.; Sharma, A. Free phenolics and polyphenol oxidase (PPO): The factors affecting post-cut browning in eggplant (*Solanum melongena*). *Food Chem.* **2013**, *139*, 105−114.

(19) Huang, H. Y.; Chang, C. K.; Tso, T. K.; Huang, J. J.; Chang, W. W.; Tsai, Y. C. Antioxidant activities of various fruits and vegetables produced in Taiwan. *Int. J. Food Sci. Nutr.* **2004**, *55*, 423−429.

(20) Ichiyanagi, T.; Kashiwada, Y.; Shida, Y.; Ikeshiro, Y.; Kaneyuki, T.; Konishi, T. Nasunin from eggplant consists of cis−trans isomers of delphinidin 3-[4-(*p*-coumaroyl)-L-rhamnosyl (1→6)glucopyranoside]-5-glucopyranoside. *J. Agric. Food Chem.* **2005**, *53*, 9472−9477.

(21) Sadilova, E.; Stintzing, F. C.; Carle, R. Anthocyanins, colour and antioxidant properties of eggplant (*Solanum melongena* L.) and violet pepper (*Capsicum annuum* L.) peel extracts. *Z. Naturforsch. C* **2006**, *61*, 527−535.

(22) Okmen, B.; Sigva, H. O.; Mutlu, S.; Doganlar, S.; Yemenicioglu, A.; Frary, A. Total antioxidant activity and total phenolic contents in different turkish eggplant (*Solanum melongena* L.) cultivars. *Int. J. Food Prop.* **2009**, *12*, 616−624.

(23) Raigon, M. D.; Prohens, J.; Munoz-Falcon, J. E.; Nuez, F. Comparison of eggplant landraces and commercial varieties for fruit content of phenolics, minerals, dry matter and protein. *J. Food Compos. Anal.* **2008**, *21*, 370−376.

(24) Savvas, D.; Lenz, F. Influence of NaCl concentration in the nutrient solution on mineral composition of eggplants grown in sand culture. *J. Appl. Bot.* **1996**, *70*, 124−127.

(25) Concellon, A.; Anon, M. C.; Chaves, A. R. Characterization and changes in polyphenol oxidase from eggplant fruit (*Solanum melongena* L.) during storage at low temperature. *Food Chem.* **2004**, *88*, 17−24.

(26) Raigon, M. D.; Rodriguez-Burruezo, A.; Prohens, J. Effects of organic and conventional cultivation methods on composition of eggplant fruits. *J. Agric. Food Chem.* **2010**, *58*, 6833−6840.

(27) Luthria, D.; Singh, A. P.; Wilson, T.; Vorsa, N.; Banuelos, G. S.; Vinyard, B. T. Influence of conventional and organic agricultural practices on the phenolic content in eggplant pulp: Plant-to-plant variation. *Food Chem.* **2010**, *121*, 406−411.

(28) Singh, A. P.; Luthria, D.; Wilson, T.; Vorsa, N.; Singh, V.; Banuelos, G. S.; Pasakdee, S. Polyphenols content and antioxidant capacity of eggplant pulp. *Food Chem.* **2009**, *114*, 955−961.

(29) Manach, C.; Scalbert, A.; Morand, C.; Remesy, C.; Jimenez, L. Polyphenols: Food sources and bioavailability. *Am. J. Clin. Nutr.* **2004**, *79*, 727−747.

(30) Lee, J. M. Cultivation of grafted vegetables. 1. Current status, grafting methods, and benefits. *HortScience* **1994**, *29*, 235−239.

(31) Fernandez-Lopez, J. A.; Almela, L.; Munoz, J. A.; Hidalgo, V.; Carreno, J. Dependence between colour and individual anthocyanin content in ripening grapes. *Food Res. Int.* **1998**, *31*, 667−672.

(32) Larrigaudiere, C.; Lentheric, I.; Vendrell, M. Relationship between enzymatic browning and internal disorders in controlled-atmosphere stored pears. *J. Sci. Food Agric.* **1998**, *78*, 232−236.

(33) Concellon, A.; Anon, M. C.; Chaves, A. R. Effect of low temperature storage on physical and physiological characteristics of eggplant fruit (*Solanum melongena* L.). *Lebensm.-Wiss. Technol.* **2007**, *40*, 389−396.

(34) Mikulic-Petkovsek, M.; Slatnar, A.; Stampar, F.; Veberic, R. The influence of organic/integrated production on the content of phenolic compounds in apple leaves and fruits in four different varieties over a 2-year period. *J. Sci. Food Agric.* **2010**, *90*, 2366−2378.

(35) Marks, S. C.; Mullen, W.; Crozier, A. Flavonoid and chlorogenic acid profiles of English cider apples. *J. Sci. Food Agric.* **2007**, *87*, 719−728.

(36) Carreño, J.; Martínez, A.; Almela, L.; Fernández-López, A. Proposal of a index for the objective evaluation of the color of red table grapes. *Food Res. Int.* **1995**, *28*, 5.
(37) Chen, N. C.; Li, H. M. Cultivation and breeding of eggplant. *AVRDC, Shanuan, Tainan, Taiwan* **2003**, *1*, 6.
(38) Prohens, J.; Blanca, J. M.; Nuez, F. Morphological and molecular variation in a collection of eggplants from a secondary center of diversity: Implications for conservation and breeding. *J. Am. Soc. Hortic. Sci.* **2005**, *130*, 54−63.
(39) Lata, B.; Przeradzka, M.; Binkowska, M. Great differences in antioxidant properties exist between 56 apple cultivars and vegetation seasons. *J. Agric. Food Chem.* **2005**, *53*, 8970−8978.
(40) Munoz-Falcon, J. E.; Prohens, J.; Rodriguez-Burruezo, A.; Nuez, F. Potential of local varieties and their hybrids for the improvement of eggplant production in the open field and greenhouse cultivation. *Int. J. Food Agric Environ.* **2008**, *6*, 83−88.
(41) Kawaguchi, M.; Taji, A.; Backhouse, D.; Oda, M. Anatomy and physiology of graft incompatibility in solanaceous plants. *J. Hortic. Sci. Biotechnol.* **2008**, *83*, 581−588.
(42) Luthria, D. L.; Mukhopadhyay, S. Influence of sample preparation on assay of phenolic acids from eggplant. *J. Agric. Food Chem.* **2006**, *54*, 41−47.
(43) Wu, X. L.; Prior, R. L. Identification and characterization of anthocyanins by high-performance liquid chromatography−electrospray ionization-tandem mass spectrometry in common foods in the United States: Vegetables, nuts, and grains. *J. Agric. Food Chem.* **2005**, *53*, 3101−3113.
(44) Whitaker, B. D.; Stommel, J. R. Distribution of hydroxycinnamic acid conjugates in fruit of commercial eggplant (*Solanum melongena* L.) cultivars. *J. Agric. Food Chem.* **2003**, *51*, 3448−3454.
(45) Azuma, K.; Ohyama, A.; Ippoushi, K.; Ichiyanagi, T.; Takeuchi, A.; Saito, T.; Fukuoka, H. Structures and antioxidant activity of anthocyanins in many accessions of eggplant and its related species. *J. Agric. Food Chem.* **2008**, *56*, 10154−10159.
(46) Awad, M. A.; de Jager, A.; van der Plas, L. H. W.; van der Krol, A. R. Flavonoid and chlorogenic acid changes in skin of 'Elstar' and 'Jonagold' apples during development and ripening. *Sci. Hortic.* **2001**, *90*, 69−83.
(47) Dixon, R. A.; Paiva, N. L. Stress-induced phenylpropanoid metabolism. *Plant Cell* **1995**, *7*, 1085−1097.
(48) Esteban, R. M.; Molla, E. M.; Robredo, L. M.; Lopezandreu, F. J. Changes in the chemical-composition of eggplant fruits during development and ripening. *J. Agric. Food Chem.* **1992**, *40*, 998−1000.

extract (GSE) could reduce plasma TC, with focus on the interaction of dietary GSE with the gene expressions of hepatic SREBP2, LXR$\alpha$, HMG-CoA-R, LDL-R, and CYP7A1 as well as intestinal NPC1L1, ACAT2, MTP, and ABCG5/8.

## MATERIALS AND METHODS

**Diet.** Three diets were prepared as previously described with minor modifications.[14] The control diet (CTL) was prepared by mixing the following powdered ingredients (g/kg): cornstarch, 507; casein, 242; lard, 50; sucrose, 119; mineral mix, 40; vitamin mix, 20; gelatin, 20; DL-methionine, 1; and cholesterol, 1. Two GSE diets were similarly prepared by adding 0.5% GSE (L-GSE) or 1.0% GSE (H-GSE) into the control diet. All three diets contained 0.1% cholesterol by weight and had 68.2, 26.4, and 5.4% energy from carbohydrate, protein, and fat, respectively. A 0.1% cholesterol diet in this study could induce plasma cholesterol concentration to about 240 mg/dL or 6.2 mM, which is borderline for the diagnosis of human hypercholesterolemia. The rationale for adding 0.5 and 1.0% GSE into diet was that the recommended dose of dietary supplements, for example, phytosterols, is 2−3 g per day to decrease plasma LDL-cholesterol, translating to a dose of 0.8−1.2 g plant sterol esters/1000 kcal provided that humans daily consume about 2500 kcal of energy. In the present study, GSE was added in diets at two doses of 0.5 and 1.0%, which were equivalent to 0.8 and 1.6 g per 1000 kcal for humans, respectively.

**Hamsters.** Thirty male Golden Syrian hamsters (aged 2.5 months) were randomly divided into three groups ($n$ = 10 each) and fed one of the three diets for 6 weeks. Hamsters were housed in an animal room at 23 °C with a 12/12 h light−dark cycle. Food consumption was measured daily, and the fecal outputs from each hamster were collected weekly. Blood samples were collected from the retro-orbital sinus under light anesthesia using a mixture of ketamine, xylazine, and saline (v/v/v; 4:1:5) at weeks 0, 3, and 6 after overnight fasting. At the end of week 6, hamsters were sacrificed under carbon dioxide anesthesia. Organs were removed, washed with saline, weighed, and frozen in liquid nitrogen. The first 5 cm of duodenum was discarded, and the remaining 30 cm of the small intestine was kept. All samples were stored in a −80 °C freezer before analysis. The whole experimental protocol was approved and performed under the guidelines of the Animal Experimental Ethical Committee, The Chinese University of Hong Kong.

**HPLC Analysis of Gingerols and Shogaols.** GSE was obtained from Sabinsa Corp. (Piscataway, NJ, USA). Individual gingerols and shogaols were separated and quantified using an HPLC-ECD system (ESA, Chelmsford, MA, USA), which consists of an ESA model 584 HPLC pump, an ESA model 542 autosampler, an ESA organizer, and an ESA electrochemical detector (ECD) coupled with two ESA model 6210 four sensor cells.[15,16] A Gemini C18 column (150 mm × 4.6 mm, 5 $\mu$m; Phenomenex, Torrance, CA, USA) was used for chromatographic analysis at a flow rate of 1.0 mL/min. The mobile phases consisted of solvent A (30 mM sodium phosphate buffer containing 1.75% acetonitrile and 0.125% tetrahydrofuran, pH 3.35) and solvent B (15 mM sodium phosphate buffer containing 58.5% acetonitrile and 12.5% tetrahydrofuran, pH 3.45). The gradient elution had the following profile: 20% B from 0 to 3 min; 20−55% B from 3 to 11 min; 55−60% B from 11 to 12 min; 60−65% B from 12 to 13 min; 65−100% B from 13 to 40 min; 100% B from 40 to 45 min; and then 20% B from 45.1 to 50 min. The cells were then cleaned at a potential of 1000 mV for 1 min. The injection volume of the sample was 10 $\mu$L. The eluent was monitored by the Coulochem electrode array system (CEAS) with potential settings at −100, 0, 100, 200, 300, 400, and 500 mV. Data for Figure 1 were from the channel set at 300 mV of the CEAS. Individual gingerols and shogaols were identified by comparing the retention times of authentic standards. HPLC analysis found that GSE mainly consisted of 29.4% 6-gingerol, 4.5% 8-gingerol, 5.3% 10-gingerol, 4.3% 6-shogaol, 0.5% 8-shogaol, and 1.8% 10-shogaol (Figure 1).

**Analysis of Plasma Lipids.** Commercial enzymatic kits from Infinity (Waltham, MA, USA.) and Stanbio Laboratories (Boerne, TX, USA) were used to determine the plasma TC, HDL-C, and TG, respectively. Non-HDL-C was calculated by deducting HDL-C from TC.

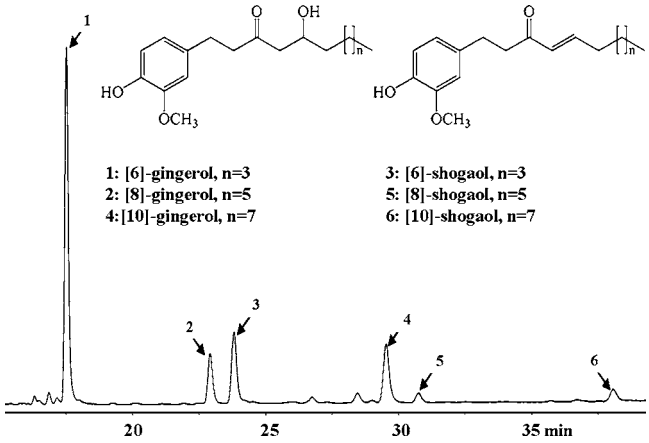


**Figure 1.** HPLC chromatogram of gingerol- and shogaol-enriched ginger extract (GSE). Peaks: 1, 6-gingerol; 2, 8-gingerol; 3, 6-shogaol; 4, 10-gingerol; 5, 8-shogaol; 6, 10-shogaol.

**Analysis of Hepatic Cholesterol.** Total cholesterol in the liver was determined using a gas chromatograph (GC) method as we previously described.[14] In brief, total lipids were extracted from the liver into a solvent mixture of chloroform/methanol (2:1, v/v) with the addition of 5$\alpha$-cholestane (1.0 mg) as an internal standard. The total lipids were saponified, followed by the conversion of cholesterol to its trimethylsilyl ether (TMS) derivative. Cholesterol-TMS derivative was determined using a Shimadzu GC-14B gas chromatograph equipped with a fused silica capillary column (SAC-5, 30 m × 0.25 mm, i.d.; Supelco, Inc., Bellefonte, PA, USA) and a flame ionization detector.

**Analysis of Atherosclerotic Plaque.** The severity of atherosclerosis in the endothelial layer of the aorta was measured as previously described.[17] In brief, aortas were cut open vertically, stained with saturated oil red for 30 min, and washed with 2-propanol three times and then distilled water twice before scanning with a table scanner (Epson 1220 perfection, Epson Co., Tokyo, Japan). The area of atherosclerotic plaque was analyzed by a computer images analyzing program (Sigma Scan Pro 5.0, SPSS, Inc., Chicago, IL, USA).

**Analysis of Hepatic and Fecal Lipids.** In brief, total lipids from 100 mg of liver or 300 mg of feces were extracted with the addition of heptadecanoic acid (0.9 mg) as an internal standard by chloroform/methanol (2:1, v/v). The solvents were evaporated under a gentle stream of nitrogen, and the lipids were then methylated with 14% BF3 in methanol. The resultant total fatty acid methyl esters (FAME) were analyzed on a Shimadzu GC 2010 equipped with a flame ionization detector and a HP Innowax capillary column (30 m × 0.5 $\mu$m, i.d. = 0.32 mm). The temperature was increased from 150 to 200 °C at a rate of 15 °C/min, further increased to 25 °C at a rate of 2 °C/min, and finally kept at 250 °C for 15 min. Injector and detector temperatures were set at 250 and 270 °C, respectively. Helium was used as a carrier gas at a rate of 1.5 mL/min.[18]

**Analysis of Fecal Sterols.** Total fecal outputs from each hamster at weeks 1 and 6 were freeze-dried, ground, and thoroughly mixed before analysis. Both fecal neutral and acidic sterols were measured according to the previous method.[19] In brief, 300 mg fecal samples were weighed with the addition of 5$\alpha$-cholestane (0.5 mg) as an internal standard for neutral sterols and hyodeoxycholic acid (0.3 mg) as an internal standard for acidic sterols. The fecal samples were first saponified, followed by extraction of the total neutral sterols with cyclohexane. The fecal neutral sterols were then converted to their TMS derivatives before GC analysis. Similarly, the acidic sterols in the aqueous phase were extracted, converted to their corresponding TMS derivatives, and subjected to GC analysis.

**Real-Time PCR.** mRNA of intestinal NPC1L1, ACAT2, MTP, and ABCG5/8 and hepatic SREBP2, HMG-CoA-R, LDL-R, LXR$\alpha$, and

**Table 1. Changes in Plasma Total Cholesterol (TC), Triacylglycerols (TG), HDL-Cholesterol (HDL-C), Non-HDL-Cholesterol (Non-HDL-C), Liver Cholesterol, and Atherosclerotic Plaque in Hamsters Fed the Control (CTL) and the Two Experimental Diets Containing 0.5% GSE (L-GSE) and 1.0% GSE (H-GSE) for 0, 3, and 6 Weeks[a]**

| | CTL | L-GSE | H-GSE | regression ($R$) | $P$ value |
|---|---|---|---|---|---|
| week 0 | | | | | |
| TC (mg/dL) | 125.7 ± 11.1 | 126.2 ± 16.2 | 125.8 ± 11.7 | −0.009 | 0.961 |
| TG (mg/dL) | 69.6 ± 15.0 | 62.2 ± 10.0 | 63.6 ± 8.5 | −0.329 | 0.082 |
| HDL-C (mg/dL) | 92.8 ± 16.9 | 90.6 ± 11.7 | 89.9 ± 10.9 | −0.046 | 0.812 |
| non-HDL-C (mg/dL) | 33.9 ± 14.7 | 35.6 ± 20.5 | 35.9 ± 13.4 | 0.029 | 0.880 |
| non-HDL-C/HDL-C | 0.39 ± 0.24 | 0.41 ± 0.27 | 0.41 ± 0.17 | −0.002 | 0.994 |
| HDL-C/TC | 0.74 ± 0.11 | 0.73 ± 0.13 | 0.72 ± 0.09 | −0.018 | 0.926 |
| week 3 | | | | | |
| TC (mg/dL) | 268.9 ± 31.7a | 230.3 ± 46.5b | 195.5 ± 20.4c | −0.670 | 0.001 |
| TG (mg/dL) | 156.3 ± 83.7.9 | 116.8 ± 41.3 | 107.5 ± 23.7 | −0.289 | 0.128 |
| HDL-C (mg/dL) | 147.4 ± 11.5a | 136.7 ± 21.1a | 118.4 ± 16.5b | −0.588 | 0.001 |
| non-HDL-C (mg/dL) | 121.5 ± 34.8a | 93.6 ± 34.3ab | 77.1 ± 22.4b | −0.520 | 0.004 |
| non-HDL-C/HDL-C | 0.84 ± 0.30 | 0.69 ± 0.24 | 0.67 ± 0.24 | −0.255 | 0.183 |
| HDL-C/TC | 0.55 ± 0.07 | 0.60 ± 0.08 | 0.61 ± 0.09 | 0.258 | 0.176 |
| week 6 | | | | | |
| TC (mg/dL) | 259.4 ± 32.5a | 240.6 ± 18.3a | 209.1 ± 24.3b | −0.645 | 0.001 |
| TG (mg/dL) | 140.5 ± 48.1 | 144.7 ± 42.2 | 124.5 ± 41.4 | −0.074 | 0.703 |
| HDL-C (mg/dL) | 132.8 ± 22.5a | 117.6 ± 18.9ab | 102.7 ± 14.8b | −0.564 | 0.001 |
| non-HDL-C (mg/dL) | 126.6 ± 34.2 | 122.9 ± 21.8 | 106.4 ± 27.8 | −0.295 | 0.120 |
| non-HDL-C/HDL-C | 0.99 ± 0.35 | 1.08 ± 0.31 | 1.07 ± 0.33 | 0.074 | 0.635 |
| HDL-C/TC | 0.51 ± 0.09 | 0.49 ± 0.07 | 0.50 ± 0.09 | −0.093 | 0.630 |
| liver cholesterol (mg/g) | 48.2 ± 8.3a | 38.8 ± 7.9b | 38.7 ± 5.8b | −0.472 | 0.023 |
| atherosclerotic plaque (%) | 17.1 ± 10.8a | 7.4 ± 1.6b | 7.2 ± 3.9b | −0.524 | 0.010 |

[a]Data are expressed as the mean ± SD. Mean values in a row with different letters differ significantly ($p < 0.05$). $R$ is the coefficient of correlation for the regression analysis on the dose-dependent effect of GSE on target lipoproteins.

**Table 2. Changes in Major Liver Fatty Acids and Daily Excretion of Fecal Fatty Acids in Hamsters Fed the Control (CTL) and the Two Experimental Diets Containing 0.5% GSE (L-GSE) and 1.0% (H-GSE) for 6 Weeks[a]**

| FA | CTL | L-GSE | H-GSE | regression ($R$) | $P$ value |
|---|---|---|---|---|---|
| liver (mg/g) | | | | | |
| 16:0 | 7.71 ± 1.25a | 6.49 ± 0.31b | 6.57 ± 0.80b | −0.461 | 0.012 |
| 18:0 | 5.72 ± 1.24 | 4.61 ± 0.48 | 4.95 ± 0.68 | −0.326 | 0.084 |
| total SFAs | 14.18 ± 2.56a | 11.74 ± 0.72b | 12.17 ± 1.33b | −0.417 | 0.024 |
| 18:1n-9 | 28.85 ± 5.99a | 24.83 ± 2.31b | 24.56 ± 1.66b | −0.426 | 0.021 |
| 18:1n-7 | 1.31 ± 0.24a | 1.18 ± 0.10ab | 1.10 ± 0.11b | −0.492 | 0.007 |
| total MUFAs | 33.72 ± 6.76a | 29.30 ± 2.61b | 28.63 ± 2.01b | −0.445 | 0.016 |
| 18:2n-6 | 3.65 ± 0.80 | 3.19 ± 0.36 | 3.21 ± 0.39 | −0.315 | 0.096 |
| 20:4n-6 | 2.03 ± 0.45 | 1.62 ± 0.19 | 1.73 ± 0.30 | −0.337 | 0.074 |
| 22:6n-3 | 1.10 ± 0.22 | 0.84 ± 0.11 | 0.95 ± 0.20 | −0.286 | 0.133 |
| total PUFAs | 7.51 ± 1.58 | 6.25 ± 0.65 | 6.53 ± 0.91 | −0.327 | 0.084 |
| total FAs | 55.41 ± 10.64a | 47.29 ± 3.41b | 47.33 ± 3.20b | −0.444 | 0.016 |
| feces (mg/day) | | | | | |
| 16:0 | 1.90 ± 0.66b | 2.37 ± 0.51b | 2.91 ± 0.49a | 0.615 | <0.001 |
| 18:0 | 1.30 ± 0.45b | 1.49 ± 0.47b | 1.99 ± 0.54a | 0.515 | 0.004 |
| total SFAs | 4.19 ± 1.28b | 5.02 ± 1.13b | 6.17 ± 1.10a | 0.586 | 0.001 |
| 18:1n-9 | 0.81 ± 0.24b | 1.12 ± 0.35a | 1.29 ± 0.19a | 0.605 | 0.001 |
| 18:1n-7 | 0.63 ± 0.28b | 0.85 ± 0.17a | 0.92 ± 0.21a | 0.472 | 0.010 |
| total MUFAs | 2.35 ± 0.79b | 3.17 ± 0.61a | 3.43 ± 0.47a | 0.579 | 0.001 |
| 18:2n-6 | 0.12 ± 0.04c | 0.18 ± 0.06b | 0.22 ± 0.04a | 0.697 | <0.001 |
| total PUFAs | 0.17 ± 0.06c | 0.24 ± 0.07b | 0.31 ± 0.05a | 0.705 | <0.001 |
| total FAs | 6.71 ± 2.08b | 8.43 ± 1.78a | 9.91 ± 1.54a | 0.603 | 0.001 |

[a]Data are expressed as the mean ± SD. Mean values in a row with different letters differ significantly ($p < 0.05$). FA, fatty acid; SFAs, saturated fatty acids; MUFAs, monounsaturated fatty acids; PUFAs, polyunsaturated fatty acids. $R$ is the coefficient of correlation for the regression analysis on the dose-dependent effect of GSE on target fatty acids.

CYP7A1 was quantified as previously described.[14] Total RNA was extracted by Trizol reagent (Invitrogen, Carslbad, CA, USA), followed by conversion to complementary DNA (cDNA) with a high-capacity cDNA reverse transcription kit (Applied Biosystems, Foster City, CA,

Table 3. Daily Fecal Excretion of Neutral and Acidic Sterols as well as Sterol Balance in Hamsters Fed the Control (CTL) and the Experimental Diets Containing 0.5% GSE (L-GSE) and 1.0% GSE (H-GSE) for 6 Weeks[a]

| | CTL | L-GSE | H-GSE | regression ($R$) | $P$ value |
|---|---|---|---|---|---|
| neutral sterols (mg/day) | | | | | |
| coprostanol | 0.57 ± 0.36b | 1.21 ± 0.78a | 1.69 ± 0.71a | 0.588 | 0.001 |
| coprostanone | 0.19 ± 0.05 | 0.25 ± 0.06 | 0.21 ± 0.10 | 0.138 | 0.466 |
| cholesterol | 0.89 ± 0.49b | 0.90 ± 0.28b | 1.47 ± 0.39a | 0.398 | 0.029 |
| dihydrocholesterol | 0.29 ± 0.08c | 0.47 ± 0.25b | 0.65 ± 0.21a | 0.606 | <0.001 |
| total | 2.04 ± 0.43b | 2.82 ± 1.14b | 4.02 ± 1.08a | 0.622 | <0.001 |
| acidic sterols (mg/day) | | | | | |
| lithocholic acid | 0.97 ± 0.58b | 1.74 ± 1.20ab | 2.31 ± 1.21a | 0.494 | 0.032 |
| deoxycholic acid | 0.39 ± 0.12b | 0.47 ± 0.16b | 0.85 ± 0.24a | 0.708 | 0.001 |
| chenodeoxycholic acid + cholic acid | 0.40 ± 0.25b | 0.66 ± 0.42ab | 1.21 ± 0.70a | 0.588 | 0.008 |
| total | 1.76 ± 0.88b | 2.86 ± 1.70ab | 4.36 ± 1.98a | 0.584 | 0.009 |
| cholesterol intake (mg/day) | 11.25 ± 0.36 | 12.09 ± 0.27 | 12.06 ± 1.00 | 0.460 | 0.084 |
| net sterol retention (mg/day) | 8.01 ± 0.52a | 6.79 ± 1.86a | 4.10 ± 0.81b | −0.793 | 0.001 |
| apparent cholesterol absorption (%) | 73.20 ± 5.33a | 56.21 ± 16.10ab | 33.28 ± 8.33b | −0.829 | <0.001 |

[a]Data are expressed as the mean ± SD. Mean values in a row with different letters differ significantly ($p < 0.05$). Net sterol retention = [cholesterol intake − total neutral sterols − total acidic sterols]. Apparent cholesterol absorption = [net sterol retention ÷ cholesterol intake] × 100. $R$ is the coefficient of correlation for the regression analysis on the dose-dependent effect of GSE on target sterol.

USA). Reverse transcription was conducted in a thermocycler (Gene Amp PCR system 9700, Applied Biosystems), and the synthesized cDNA was stored at −20 °C. A fast real-time PCR system 7500 (Applied Biosystems) was used to analyze RT-PCR of small intestinal and hepatic genes. SYBR green was used as a fluorophore for RT-PCR analysis of small intestinal NPC1L1, ACAT2, MTP, ABCG5/8, and cyclophilin, whereas primers and TaqMan probes were used for RT-PCR analysis of liver SREBP2, HMG-CoA-R, LDL-R, LXR$\alpha$, CYP7A1, and GAPDH. Data were analyzed using Sequence Detection software version 1.3.1.21 (Applied Biosystems).

**Western Blotting.** Total liver proteins were extracted and separated on a 7% sodium dodecyl sulfate polyacrylamide gel, followed by transfer to polyvinylidene difluoride membranes according to the previous method with modifications.[14] The membranes were blocked in 3% nonfat milk (dissolved in Tris-buffered saline with Tween-20) for 1 h, followed by incubation overnight at 4 °C in the same solution consisting of anti-SREBP2 antibody (Santa Cruz Biotechnology, Santa Cruz, CA, USA), anti-HMG-CoA-R (Upstate USA, Lake Placid, NY, USA), anti-LDL-R antibody (Santa Cruz Biotechnology), anti-LXR$\alpha$ (Santa Cruz Biotechnology), or anti-CYP7A1 (Santa Cruz Biotechnology). After incubation at 4 °C for another hour in diluted horseradish peroxidase-linked goat anti-rabbit IgG, donkey anti-rabbit IgG, or goat anti-mouse IgG, membranes developed with ECL enhanced chemiluminescence agent were subjected to autoradiography on SuperRX medical X-ray film. Densitometry was analyzed by using Bio-Rad Quantity One (Bio-Rad Laboratories, Hercules, CA, USA), and protein concentrations of SREBP2, HMG-CoA-R, LDL-R, LXR$\alpha$, and CYP7A1 were normalized with $\beta$-actin (Santa Cruz Biotechnology).

**Statistical Analysis.** Values from each measurement were expressed as the mean ± standard deviation (SD), $n = 10$. All data were analyzed using one-way analysis of variance (ANOVA) followed by Fisher's LSD test. A simple linear regression analysis was carried out in SPSS to assess the dose-dependent activity of GSE.

## RESULTS

**Food Intake and Body and Organ Weights.** All three groups had a similar daily food intake of 11−12 g with similar body weight gain during the experimental period. No differences in relative organ weights of heart, kidney, testes, and perirenal fat pad were seen among the three groups (data not shown).

**Plasma TC, TG, HDL-C, and Non-HDL-C, Liver Cholesterol, and Aortic Atherosclerotic Plaque.** Plasma lipoprotein cholesterol was measured at weeks 1, 3, and 6. At week 0, similar levels of plasma TC, TG, HDL-C, and non-HDL-C were observed in the three groups of hamsters (Table 1). In response to the switch from the chow diet to the high-cholesterol diets, plasma TC in all three groups increased at week 3 compared with that in week 0. When the experiment approached the end of week 3, hamsters fed the two GSE diets began to show a marked decline in plasma TC compared with the control group. At the end of week 6, plasma TC concentrations in the control, L-GSE, and H-GSE groups were 259.4, 240.6, and 209.1 mg/dL, respectively, demonstrating that GSE decreased plasma TC in a dose-dependent manner ($P < 0.01$). However, dietary GSE had no effect on plasma TG. Like its effect on plasma TC, dietary GSE could decrease hepatic cholesterol concentration and atherosclerotic plaque (Table 1).

**Hepatic and Fecal Lipids.** Dietary GSE significantly affected the fatty acid profile of liver and fecal lipids (Table 2). To be specific, it decreased total fatty acids in the liver by 15%. This was characterized by a proportional decrease in saturated fatty acids (SFAs), monounsaturated fatty acids (MUFAs), and polyunsaturated fatty acids (PUFAs). In contrast, dietary GSE increased the excretion of fecal total fatty acids by 26−48% in a dose-dependent manner. Similarly, dietary GSE could increase the excretion of all individual fecal fatty acids by 15−83%.

**Fecal Sterols and Apparent Cholesterol Absorption.** Some cholesterol in the liver is metabolized to primary bile acids mainly as cholic and chenodeoxycholic acids and secreted via the bile duct into the intestinal lumen, where they emulsify and help absorb fats or are excreted into the large intestine. In the intestine, cholesterol is converted to it metabolites by microbial bioconversion, with coprostanol and dihydrocholesterol as the main products. Dietary GSE increased the excretion of primary bile acids by 65−200%, whereas it increased the excretion of secondary bile acids (lithocholic and deoxycholic acids) by 20−138%. Dietary GSE at a high dose increased the excretion of fecal cholesterol by 65%. As a whole, dietary GSE could decrease the excretion of total neutral sterols by 38−97% (Table 3). By using the equation described previously,[14] apparent cholesterol absorption (%) = [(cholesterol intake −

total fecal neutral sterols − total fecal acidic sterols) ÷ cholesterol intake] × 100, it was found that dietary GSE could dose-dependently decrease cholesterol absorption (CTL group, 73.20%; L-GSE group, 56.21%; H-GSE group, 33.28%, $p < 0.001$, Table 3).

**Results of Real-Time PCR and Western Blot Analyses.** Real-time PCR results showed that dietary GSE down-regulated mRNA of intestinal NPC1L1, ACAT2, MTP, and ABCG5 in a dose-dependent manner; however, it had no significant effect on mRNA of ABCG8 (Figure 2). We were not able to measure the protein mass of intestinal NPC1L1, ACAT2, MTP, and ABCG5/8 because they are commercially unavailable. With regard to its effect on the target genes in the liver, dietary GSE up-regulated the gene level of hepatic SREBP2; however, it had no effect on the protein mass of SREBP2 (Figures 3 and 4). Similarly, dietary GSE down-regulated the mRNA LXR$\alpha$ with its protein mass being unaffected. In contrast, dietary GSE caused a nearly 2.0-fold increase in not only the mRNA but also the protein level of hepatic CYP7A1 (Figures 3 and 4).

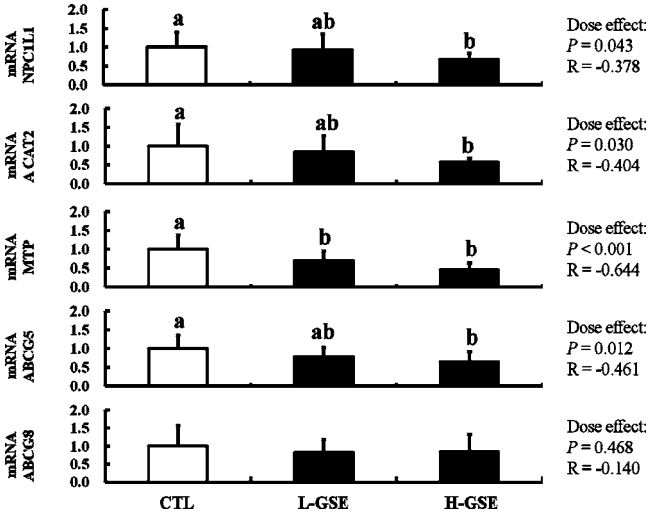


**Figure 2.** Effect of gingerol- and shogaol-enriched ginger extract (GSE) on mRNA levels of intestinal Niemann−Pick C1-like 1 (NPC1L1), acyl coenzyme A:cholesterol acyltransferase 2 (ACAT2), microsomal triacylglycerol transport protein (MTP), and ATP binding cassette transporters (ABCG5 and ABCG8) in hamsters fed the control (CTL) and the two experimental diets containing 0.5% GSE (L-GSE) and 1.0% GSE (H-GSE). *R* is the coefficient of correlation for the regression analysis on the dose-dependent effect of GSE on target sterols. Bars with different letters differ significantly, $p < 0.05$.

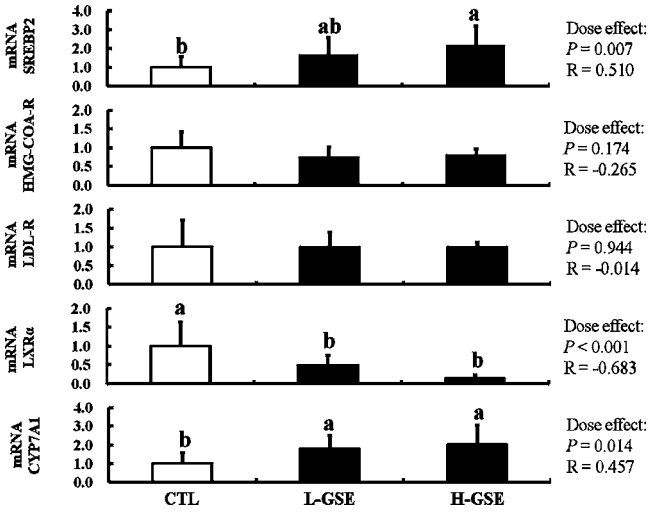


**Figure 3.** Effect of gingerol- and shogaol-enriched ginger extract (GSE) on mRNA levels of hepatic sterol regulatory element-binding protein 2 (SREBP2), 3-hydroxy-3-methylglutaryl-CoA reductase (HMG-CoA-R), LDL receptor (LDL-R), liver X receptor-alpha (LXR$\alpha$), and cholesterol-7$\alpha$-hydroxylase (CYP7A1) in hamsters fed the control (CTL) and the two experimental diets containing 0.5% GSE (L-GSE) and 1.0% GSE (H-GSE). *R* is the coefficient of correlation for the regression analysis on the dose-dependent effect of GSE on target sterols. Bars with different letters differ significantly, $p < 0.05$.

## DISCUSSION

The present study examined the hypocholesterolemic activity of dietary GSE and the underlying mechanism using hamsters as an animal model. In general, results regarding the effect of GSE on plasma TC were consistent with published data in rats,[6] mice,[10] rabbits,[8,9] and broilers.[20] The major observations in the present study were that dietary GSE could reduce plasma TC by 6−18%, atherosclerotic plaque by 57%, hepatic cholesterol by 20%, and total liver lipids by 15%, confirming dietary GSE was effective in treating not only hypercholesterolemia but also non-alcohol-induced fatty liver disease.[21] The present study was the first to systematically investigate the underlying mechanisms by which dietary GSE reduced plasma TC concentration.

Two possible mechanisms associated with the cholesterol-lowering activity of dietary GSE were explored. The first mechanism was that that dietary GSE reduced plasma TC by increasing the excretion of fecal neutral sterols via inhibiting cholesterol absorption with the following supportive evidence. First, fecal sterol analysis found that dietary GSE increased the excretion of fecal cholesterol by 65% and total fecal neutral sterols by 38−97%. Second, real-time PCR analysis affirmed that dietary GSE down-regulated the gene expression of transporters and enzymes involved in cholesterol absorption. Intestinal NPC1L1 is a sterol transporter responsible for taking the cholesterol from the intestinal lumen to enterocytes, whereas ACAT2 in the enterocytes catalyzes an essential reaction that esterifies free cholesterol to cholesteryl ester (CE) before it can be packed into chylomicrons. At the final step of cholesterol absorption, MTP assembles CE into chylomicrons, which are transported into the blood vial the lymph system. ABCG5/8 are also sterol transporters that shuttle the unabsorbed cholesterol in the enterocytes back to the intestinal lumen for excretion. The present study clearly demonstrated that dietary GSE could down-regulate the mRNA of intestinal NPC1L1, ACAT2, MTP, and ABCG5 (Figure 2). At a molecular level, dietary GSE favorably modulated the plasma lipoprotein profile, largely mediated by increasing cholesterol excretion via down-regulation of the target proteins involved in cholesterol absorption.

Excessive cholesterol in the liver is eliminated by converting cholesterol to bile acids. The second mechanism underlying GSE's cholesterol-lowering activity was that it could modulate the cholesterol homeostasis in a way enhancing the bile acid synthesis. This mechanism was supported by the observation that dietary GSE significantly enhanced the excretion of bile acids, leading to 63−147% increases in the excretion of fecal total acidic sterols (Table 3). This was accompanied by up-regulation of hepatic CYP7A1, a key enzyme in bile acid

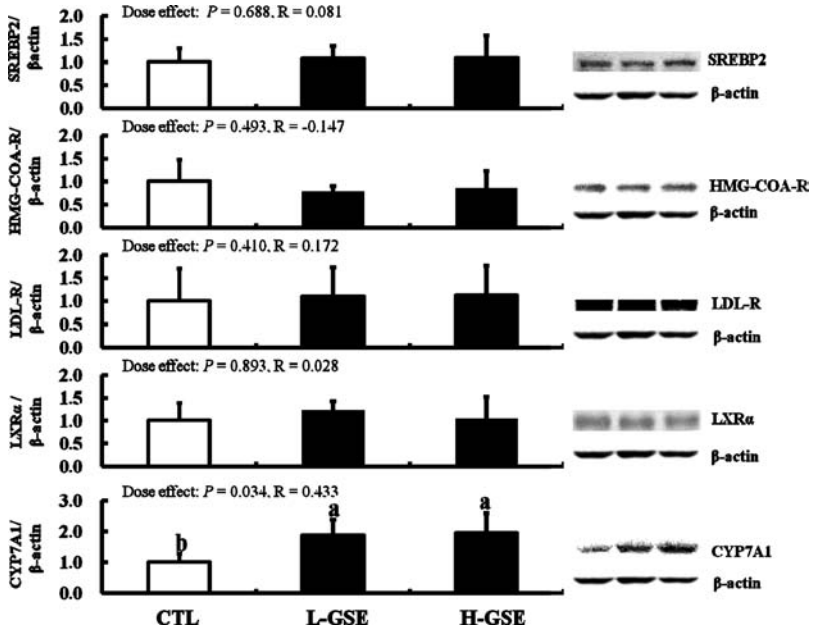


**Figure 4.** Effect of gingerol- and shogaol-enriched ginger extract (GSE) on protein mass of hepatic sterol regulatory element-binding protein 2 (SREBP2), 3-hydroxy-3-methylglutaryl-CoA reductase (HMG-CoA-R), LDL receptor (LDL-R), liver X receptor-alpha (LXR$\alpha$), and cholesterol-7$\alpha$-hydroxylase (CYP7A1) in hamsters fed the control (CTL) and the two experimental diets containing 0.5% GSE (L-GSE) and 1.0% GSE (H-GSE). *R* is the coefficient of correlation for the regression analysis on the dose-dependent effect of GSE on target sterols. Bars with different letters differ significantly, $p < 0.05$.

synthesis in the liver, and down-regulation of hepatic LXR$\alpha$, a cholesterol sensor in the liver (Figures 3 and 4). When CYP7A1 was up-regulated, cholesterol in the liver was subsequently converted to bile acids, leading to a reduction of cholesterol concentration in the liver and consequently a reduction in plasma TC. In fact, the present study found that dietary GSE was able to decrease hepatic cholesterol by 20% and plasma TC by 19%. As a cholesterol sensor in the liver, down-regulation of mRNA LXR$\alpha$ was expected (Figure 3). The present study clearly demonstrated the cholesterol-lowering activity of dietary GSE was mediated not only by inhibition on cholesterol absorption but also by enhancing the production of bile acids in the liver and their excretion in the intestine. HMG-CoA-R is a regulating enzyme in cholesterol synthesis in the liver, whereas LDL-R is responsible for the removal of plasma LDL cholesterol from circulation into the liver. Although dietary GSE could up-regulate mRNA of SREBP2, it had no effect on mRNA and protein mass of hepatic HMG-CoA-R and LDL-R, suggesting that plasma TC-lowering activity of GSE was unlikely mediated by modulating cholesterol removal and synthesis.

In summary, we systematically studied the effect of dietary GSE on plasma TC and gene expression of intestinal NPC1L1, ACAT2, MTP, and ABCG5/8 as well as hepatic SREBP2, HMG-CoA-R, LDL-R, LXR$\alpha$, and CYP7A1 in hamsters fed a high-cholesterol diet. It was clear that GSE could decrease plasma TC concentration via the combination of two mechanisms, inhibition of cholesterol absorption and enhancement of bile acid excretion, leading to substantial reductions in the apparent cholesterol absorption from 73.20% in the control to 56.21 and 33.28% in the L-GSE and H-GSSE groups, respectively. This was accompanied by up-regulation of hepatic CYP7A1 and down-regulation on the genes of intestinal NPC1L1, ACAT2, and MTP.

## AUTHOR INFORMATION


### Corresponding Author

*(Z.-Y.C.) Phone: (852) 3943-6382. Fax: (852) 2603-7246. E-mail: zhenyuchen@cuhk.edu.hk.



### Funding

This project was supported by a grant from the Hong Kong Research Grant Council (CUHK 462813).

### Notes

The authors declare no competing financial interest.


## REFERENCES


(1) Shukla, Y.; Singh, M. Cancer preventive properties of ginger: a brief review. *Food Chem. Toxicol.* **2007**, *45*, 683−690.

(2) Surh, Y. J. Anti-tumor promoting potential of selected spice ingredients with antioxidative and anti-inflammatory activities: a short review. *Food Chem. Toxicol.* **2002**, *40*, 1091−1097.

(3) Govindarajan, V.; Connell, D. Ginger − chemistry, technology, and quality evaluation: part 1. *Crit. Rev. Food Sci. Nutr.* **1983**, *17*, 1−96.

(4) Sang, S.; Hong, J.; Wu, H.; Liu, J.; Yang, C. S.; Pan, M. H.; Badmaev, V.; Ho, C. T. Increased growth inhibitory effects on human cancer cells and anti-inflammatory potency of shogaols from Zingiber officinale relative to gingerols. *J. Agric. Food Chem.* **2009**, *57*, 10645−10650.

(5) Nammi, S.; Kim, M. S.; Gavande, N. S.; Li, G. Q.; Roufogalis, B. D. Regulation of low-density lipoprotein receptor and 3-hydroxy-3-methylglutaryl coenzyme A reductase expression by zingiber officinale in the liver of high-fat diet-red rats. *Basic Clin. Pharmacol. Toxicol.* **2010**, *106*, 389−395.

(6) ElRokh, E.-S. M.; Yassin, N. A.; El-Shenawy, S. M.; Ibrahim, B. M. Antihypercholesterolaemic effect of ginger rhizome (*Zingiber officinale*) in rats. *Inflammopharmacology* **2010**, *18*, 309−315.

(7) Srinivasan, K.; Sambaiah, K. The effect of spices on cholesterol 7$\alpha$-hydroxylase activity and on serum and hepatic cholesterol levels in the rat. *Int. J. Vitam. Nutr. Res.* **1990**, *61*, 364−369.

(8) Verma, S.; Singh, M.; Jain, P.; Bordia, A. Protective effect of ginger, *Zingiber officinale* Rose on experimental atherosclerosis in rabbits. *Indian J. Exp. Biol.* **2004**, *42*, 736−738.

(9) Bhandari, U.; Sharma, J.; Zafar, R. The protective action of ethanolic ginger (*Zingiber officinale*) extract in cholesterol fed rabbits. *J. Ethnopharmacol.* **1998**, *61*, 167−171.
(10) Fuhrman, B.; Rosenblat, M.; Hayek, T.; Coleman, R.; Aviram, M. Ginger extract consumption reduces plasma cholesterol, inhibits LDL oxidation and attenuates development of atherosclerosis in atherosclerotic, apolipoprotein E-deficient mice. *J. Nutr.* **2000**, *130*, 1124−1131.
(11) Alizadeh-Navaei, R.; Roozbeh, F.; Saravi, M.; Pouramir, M.; Jalali, F.; Moghadamnia, A. A. Investigation of the effect of ginger on the lipid levels. A double blind controlled clinical trial. *Saudi Med. J.* **2008**, *29*, 1280−1284.
(12) Chen, Z. Y.; Ma, K. Y.; Liang, Y.; Peng, C.; Zuo, Y. Role and classification of cholesterol-lowering functional foods. *J. Funct. Foods* **2011**, *3*, 61−69.
(13) Chen, Z. Y.; Jiao, R.; Ma, K. Y. Cholesterol-lowering nutraceuticals and functional foods. *J. Agric. Food Chem.* **2008**, *56*, 8761−8773.
(14) Ma, K. Y.; Yang, N.; Jiao, R.; Peng, C.; Guan, L.; Huang, Y.; Chen, Z. Y. Dietary calcium decreases plasma cholesterol by down-regulation of intestinal NPC1L1 and MTP and up-regulation of CYP7A1 and ABCG5/8 in hamsters. *Mol. Nutr. Food Res.* **2011**, *55*, 247−258.
(15) Chen, H.; Lv, L.; Soroka, D.; Warin, R. F.; Parks, T. A.; Hu, Y.; Zhu, Y.; Chen, X.; Sang, S. Metabolism of [6]-shogaol in mice and in cancer cells. *Drug Metab. Dispos.* **2012**, *40*, 742−753.
(16) Shao, X.; Lv, L.; Parks, T.; Wu, H.; Ho, C. T.; Sang, S. Quantitative analysis of ginger components in commercial products using liquid chromatography with electrochemical array detection. *J. Agric. Food Chem.* **2010**, *58*, 12608−12614.
(17) Ng, C. H.; Qiang Yao, X.; Huang, Y.; Chen, Z. Y. Oxidised cholesterol is more hypercholesterolaemic and atherogenic than non-oxidised cholesterol in hamsters. *Br. J. Nutr.* **2008**, *99*, 749−755.
(18) Si, W.; Liang, Y.; Ma, K. Y.; Chung, H. Y.; Chen, Z. Y. Antioxidant activity of capsaicinoid in canola oil. *J. Agric. Food Chem.* **2012**, *60*, 6230−6234.
(19) Jiao, R.; Zhang, Z.; Yu, H.; Huang, Y.; Chen, Z. Y. Hypocholesterolemic activity of grape seed proanthocyanidin is mediated by enhancement of bile acid excretion and up-regulation of CYP7A1. *J. Nutr. Biochem.* **2010**, *21*, 1134−1139.
(20) Saeid, J. M.; Mohamed, A. B.; Al-Baddy, M. A. Effect of aqueous extract of ginger (*Zingiber officinale*) on blood biochemistry parameters of broiler. Int. *J. Poult. Sci.* **2010**, *9*, 944−947.
(21) Chang, C. J.; Liou, S. S.; Tzeng, T. F.; Liu, I. M. The ethanol extract of *Zingiber zerumbet* Smith attenuates non-alcoholic fatty liver disease in hamsters fed on high-fat diet. *Food Chem. Toxicol.* **2014**, *65*, 33−42.

**Table 1. Primers Used for Gene Expression Analysis**

| gene | accession no. | forward primer (5′ to 3′) | reverse primer (5′ to 3′) | product size (bp) |
|---|---|---|---|---|
| *MrCHS* | GQ340759 | AGTTCAAGAGCATGTGTGAC | TGGCAGCTTCTTTGCCTAGT | 167 |
| *MrCHI* | GQ340760 | GCCATCGGGGTGTACTTAGA | GTTACCCGATAACGGCAAGA | 210 |
| *MrF3H* | GQ340761 | GTCGACATGGACCAGAAGGT | GGAGCAAGAGGGTGATGGTA | 112 |
| *MrF3′H* | GQ340762 | GGATTGCTGCCTGAGAAG | CAGATAACCGTGTGGAGAC | 155 |
| *MrDFR1* | GQ340763 | GACAATCAACGGGTTGTTAG | GACTGGCTTTTGGTGCTCTTC | 118 |
| *MrDFR2* | GQ340764 | AACGGTGAACGGGGTGTTGA | TACTTTCCTTTGGTGCTCAGA | 118 |
| *MrANS* | GQ340765 | CTAGTGGGAAGCTCGAGTGG | GCTAGCGCTCTCAGTTGCTT | 142 |
| *MrUFGT* | GQ340766 | TTTCCTCGACCAAACCAGAC | CTTACCTCCCTCCCATCTC | 186 |
| *MrMYB1* | GQ340767 | GACTGAGGTGGCTGAATTATC | CATCGTTCGCTGTTCTTCC | 150 |
| *MrINV1* | JR053938 | GTTGAAAGCTTCGCTCAAGG | ACTGAGGAAGTGATAGTGGC | 134 |
| *MrINV2* | JR053939 | TCCCGTGCTTGAAGGTGAAA | AAGAACAATCGTGCTGCTCC | 144 |
| *MrINV3* | JR053940 | TACACGACCGCTCCTATCC | TCTATGGGCTGTTGGCTTTG | 127 |
| *MrSPS1* | JR053941 | TGTGATCCTGAAGGGTGTGG | CGAAGCTCGAATGTCGTTGC | 139 |
| *MrSPS2* | JR053942 | CATTGTCCAAGGGTGTTATAGG | ACTTCCTCCTTCTCAATACTGG | 105 |
| *MrSPS3* | JR053943 | AGGGAGAGGAAGCTCAGCAT | AGGGAGAGGAAGCTCAGCAT | 132 |
| *MrACT* | GQ340770 | AATGGAACTGGAATGGTCAAGG | CCCGACATAGGCATCTTTCTG | 132 |

## MATERIALS AND METHODS

**Plant Materials.** Five 5-year-old Chinese bayberry (*Myrica rubra* Sieb. and Zucc.) trees were chosen for these experiments from commercial orchards in Zhejiang Province, China. Two types of varieties, 'Biqi' (BQ) and 'Dongkui' (DK), were obtained from the Cixi (30°12′N, 121°24′ E) and Xianju (28°85′N, 120°61′E), respectively. Fruit were collected at five developmental stages from 57 to 113 days after flower bloom (DAFB) with an interval of 14 days from May 1 to July 31 in 2013. At each stage, 10 fruit on each branch and 2 fruiting branches from each bayberry trees were selected. All of the samples were healthy and uniformly distributed around the tree. There were 10 fruit on each tree used to measure fruit diameter during different developmental stages (see Supporting Information S1). After transportation to laboratory in 2 h, 20 fruit from each variety were selected for color measurement. All samples were immediately frozen in liquid nitrogen, and then stored at −81 °C until use.

**Total Anthocyanin Content Determination.** To prepare the fruit extract, 1 g samples from each replicate were homogenized with 5 mL of precooled acidified water (3% formic acid), and after centrifugation at 10 000*g* for 15 min (4 °C), another 5 mL of precooled acidified water was used to extract the residue again. The supernatant was combined to make the final volume of 25 mL for analysis. Total anthocyanin content of bayberry extract was measured using the pH differential method.[9] Absorbance was measured at 510 and 700 nm, respectively, in different buffers at pH 1.0 and 4.5, using $A = [(A510 - A700)\ \mathrm{pH1.0} - (A510 - A700)\ \mathrm{pH4.5}]$ with a molar extinction coefficient of cyanidin 3-glucoside (Cy-3-Glu) of 29 600. Results were expressed as milligrams of Cy-3-Glu equivalents per gram of fresh weight. All analysis was repeated three times using three biological replicates

**Sugars Extraction and HPLC Determination.** The extraction of sugars from bayberries was modified from a method described by Eyéghé-Bickong et al.[10] Briefly, 80 mg of frozen homogenized bayberry tissue from each replicate was weighed off into 800 μL of $dH_2O$ containing 5% (w/v) insoluble PVPP and vortexed for 5 min to homogenize. An equal volume of chloroform was added to the mixture, and the biphasic solvent was vortexed for 5 min to mix and incubated at 50 °C for 30 min with continuous shaking. After incubation, the microfuge tube was centrifuged at 12 000*g* for 10 min at room temperature to recover the upper aqueous phase containing the sugars. The supernatant was passed through a 0.22 μm membrane filter (Millipore Corp., Bedford, MA) for HPLC analysis. All analysis was repeated three times using three biological replicates

Chromatographic analysis of sugars was carried out on a Waters 2695-series HPLC system (Waters Corp., Milford, MA) equipped with a refractive index detector and Empower 3 software. A COSMOSIL Sugar-D column (4.6 mm i.d. × 250 mm) and COSMOSIL Sugar-D guard column (4.6 mm i.d. × 10 mm) both from NacalaiTesque Inc. (Kyoto, Japan) were used. The mobile phase was HPLC grade acetonitrile/water (65:35, v/v) with a flow rate of 1.0 mL/min at 35 °C, and sample volume injected was 20 μL. A refractive index detector maintained at 35 °C was used for detection purposes. The column was equilibrated for 10 min at the starting conditions before each injection. The sugars were identified on the basis of comparison of their retention times with those of pure standards and quantified using standard calibration curves.

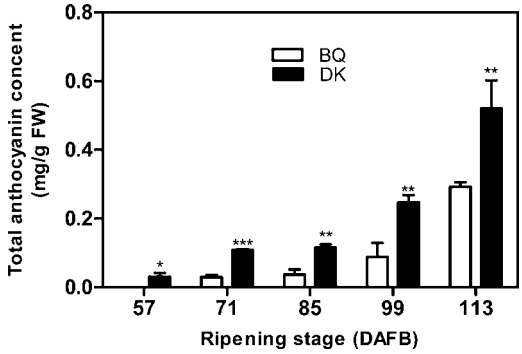


**Figure 1.** Changes of total anthocyanin content in Chinese bayberries during fruit development. Values are the means ±SE. Vertical bars represent the standard errors of the means. Asterisks indicate significant differences between 'Dongkui' and 'Biqi' samples (Duncan's multiple range test; $^*P < 0.05$, $^{**}P < 0.01$, and $^{***}P < 0.001$).

**Total RNA Extraction and cDNA Synthesis.** Total RNA was isolated using a Plant Total RNA Extraction Kit (Genotheramics, Suzhou, China) according to the manufacturer's instructions. Extracted RNA was purified with amplification grade RNase-free DNase I (Omega, Norcross, GA) to remove any DNA contamination prior to cDNA synthesis. Reverse transcription (RT) was carried out using 2 μg of total RNA and the SuperRT First Strand cDNA Synthesis Kit (CWBIO, Beijing, China), following the manufacturer's instructions.

**Quantitative Real-Time PCR (qPCR).** qRT-PCR was conducted using a total volume of 12.5 μL reaction containing 0.5 μL of the synthesized cDNA, 0.25 μL of 10 μM each forward and reverse primers, 6.5 μL of the SYBR Green PCR Master Mix (Thermo Scientific, Pittsburgh, PA), and 5 μL of RNase-free water. Amplifications were performed using Mx3000P qRT-PCR System (Agilent Stratagene, Santa Clara, CA). The amplification program consisted of an initial denaturation step of 95 °C for 7 min, followed by 40 cycles of 15 s at 95 °C, and combined with each primer specific annealing temperature ranged from 50 to 60 °C for 30 s. Melting curve analysis was performed at the end of 40 cycles to ensure proper amplification of target fragments. *MrACT* (GenBank accession no. GQ340770) was used to

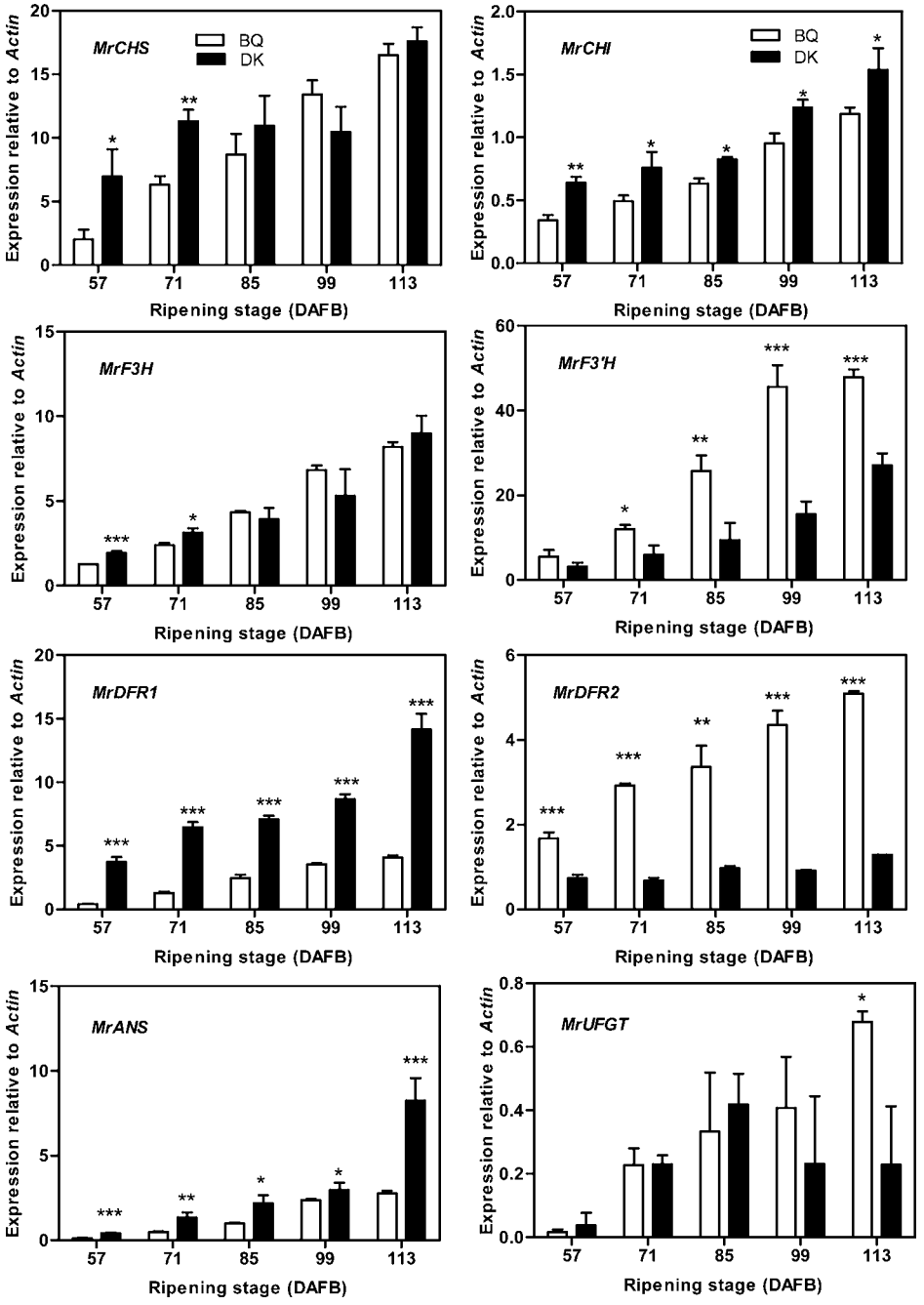


**Figure 2.** Expression of anthocyanin biosynthetic genes in Chinese bayberries during fruit development. Values are the means ±SE. Vertical bars represent the standard errors of the means. Asterisks indicate significant differences between 'Dongkui' and 'Biqi' samples (Duncan's multiple range test; $*P < 0.05$, $**$ $P < 0.01$, and $***P < 0.001$).

normalize as endogenous reference, and transcripts were quantified using the standard curve method. All analysis was repeated three times using three biological replicates, and primer sequences used for real time PCR are listed in Table 1.

**Statistical Analysis.** All values are shown as the mean ±SE. Statistical analysis was performed using the SPSS package program version 16.0 (SPSS Inc., Chicago, IL). Student's unpaired *t* test was used to compare the means at $P < 0.05$.

## RESULTS

**Changes of Total Anthocyanin Content During Fruit Development.** The total anthocyanin content in 'DK' and 'BQ' bayberries increased continuously during fruit development (Figure 1). Generally, 'DK' fruit had higher levels of anthocyanins than 'BQ' fruit, and the content in 'DK' fruit was nearly 2 times that in 'BQ' fruit at 113 DAFB. No anthocyanin was detected in 'BQ' fruit at 57 DAFB.

**Expression of Anthocyanin Biosynthetic Genes During Fruit Development.** As shown in Figure 2, transcript levels of biosynthetic genes *MrCHS*, *MrCHI*, *MrF3H*, *MrF3′H*, *MrDFR1*, and *MrANS* increased throughout fruit development in both bayberry cultivars. Expression of *MrDFR2* and *MrUFGT* in 'DK' fruit showed a gradual increase with ripening, but no significant change was observed in *MrDFR2* transcript level in 'BQ' fruit. Transcript abundance of *MrUFGT* in 'BQ' fruit increased with fruit development from 57 to 85 DAFB and then declined toward to maturity. As compared to 'BQ' fruit, 'DK' fruit experienced


dx.doi.org/10.1021/jf503317k | J. Agric. Food Chem. 2014, 62, 10522−10528

higher expression of *MrCHI*, *MrDFR1*, and *MrANS*, whereas the transcript levels of *MrF3′H* and *MrDFR2* were significantly lower during fruit development. Higher expression levels of *MrCHS* and *MrF3H* were found in 'DK' fruit from 57 to 71 DAFB, but there was no significant difference between the two cultivars from 85 to 113 DAFB. Meanwhile, a significant higher *MrUFGT* was observed in 'DK' fruit at the end of fruit development.

**Expression of *MrMYB1* During Fruit Development.** Transcript abundance of *MrMYB1* increased gradually during bayberry fruit development. Expression of *MrMYB1* was higher in 'DK' fruit than that in 'BQ' fruit (Figure 3).

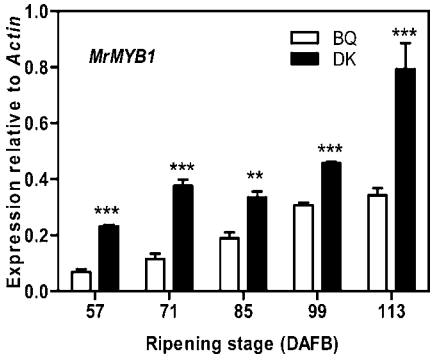


**Figure 3.** Expression of *MrMYB1* in Chinese bayberries during fruit development. Values are the means ±SE. Vertical bars represent the standard errors of the means. Asterisks indicate significant differences between 'Dongkui' and 'Biqi' samples (Duncan's multiple range test; $*P < 0.05$, $** P < 0.01$, and $***P < 0.001$).

**Changes of Glucose, Fructose, and Sucrose During Fruit Development.** The changes of glucose, fructose, and sucrose differed from the two bayberry cultivars (Figure 4). In 'DK' fruit, levels of glucose and fructose accumulated at early development stage and showed the first peak at 71 DAFB, followed by the second peak at 99 DAFB (Figure 4A,B), whereas sucrose content increased with fruit development from 57 to 99 DAFB, and then decreased slightly toward maturity (Figure 4C). However, all of the three soluble sugars in 'BQ' fruit accumulated throughout fruit development. Significantly higher levels of glucose, fructose, and sucrose were observed in 'DK' fruit compared with that in 'BQ' fruit (Figure 4).

**Expression of Sucrose Phosphate Synthase and Sucrose Invertase Genes During Fruit Development.** Both of the bayberry cultivars experienced a similar expression patterns in SPS genes during fruit ripening (Figure 5). No significant change in expression level was observed for *MrSPS1*, whereas the transcript abundance of *MrSPS2* showed a slight increase during fruit development. The transcript level of *MrSPS3* increased with fruit development from 57 to 85 DAFB and then decreased slightly toward maturity. A significantly higher expression level of these three SPS genes was observed in 'DK' fruit than 'BQ' during fruit development.

Three INV genes, *MrINV1*, *MrINV2*, and *MrINV3*, showed similar expression patterns in 'DK' fruit (Figure 5). Transcript levels of these three INV genes decreased with fruit development from 57 to 71 DAFB, and then increased gradually from 71 to 99 DAFB followed by a decline toward maturity. In 'BQ' fruit, the expression levels of *MrINV2* and *MrINV3* were detected only at an early stage of fruit development from 57 to 71 DAFB. Moreover, no expression of *MrINV1* was detected in this cultivar. 'DK' fruit showed remarkably higher expression of these

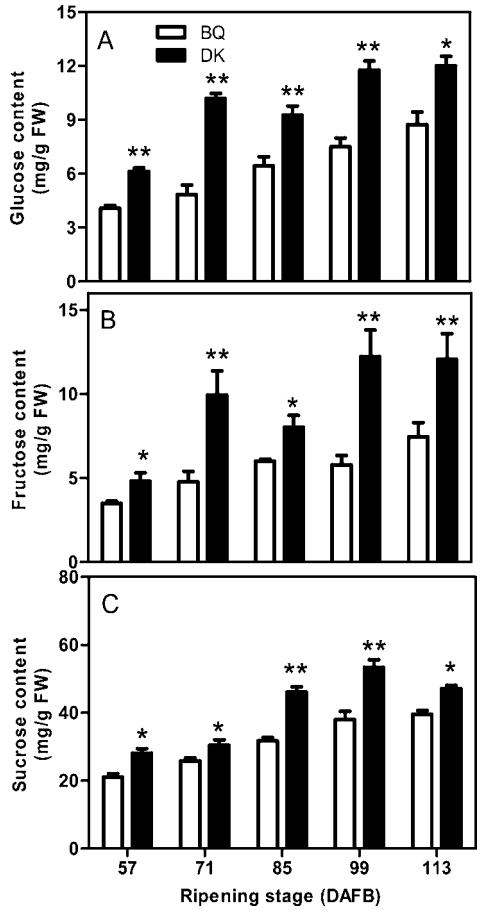


**Figure 4.** Changes of glucose (A), fructose (B), and sucrose (C) in Chinese bayberries during fruit development. Values are the means ±SE. Vertical bars represent the standard errors of the means. Asterisks indicate significant differences between 'Dongkui' and 'Biqi' samples (Duncan's multiple range test; $*P < 0.05$, $** P < 0.01$, and $***P < 0.001$).

three INV genes compared to 'BQ' fruit throughout the fruit development.

**Correlation between Total Anthocyanins and Levels of Glucose, Fructose, and Sucrose.** A common positive linear correlation was observed between anthocyanin and soluble sugars such as glucose, fructose, and sucrose in Chinese bayberry fruit. The corresponding correlation coefficients were 0.79, 0.79, and 0.72, respectively (Figure 6). From this linear function, threshold values of glucose, fructose, and sucrose (3.64, 2.74, and 18.5 mg/g FW, respectively), above which bayberries were stimulated to accumulate anthocyanins, could be obtained.

## DISCUSSION

In Chinese bayberry fruit, changes in the levels of anthocyanin accumulation have been well-known to occur during fruit ripening.[8,11] The results of our study indicated a progressive increase of anthocyanin accumulation as the bayberry fruit developed which was in agreement with the previous report.[12] However, fruit pigmentation differed significantly between the two tested cultivars. The maturation led to a more favorable red color in 'DK' fruit, in which higher anthocyanin content was observed compared to that in 'BQ' fruit. However, according to Niu et al.,[8] 'DK' fruit was red whereas 'BQ' was dark red-purple which was due to a higher content of anthocyanins than 'DK'. In our study, we observed that 'BQ' presented a 2-fold reduction


dx.doi.org/10.1021/jf503317k | J. Agric. Food Chem. 2014, 62, 10522−10528

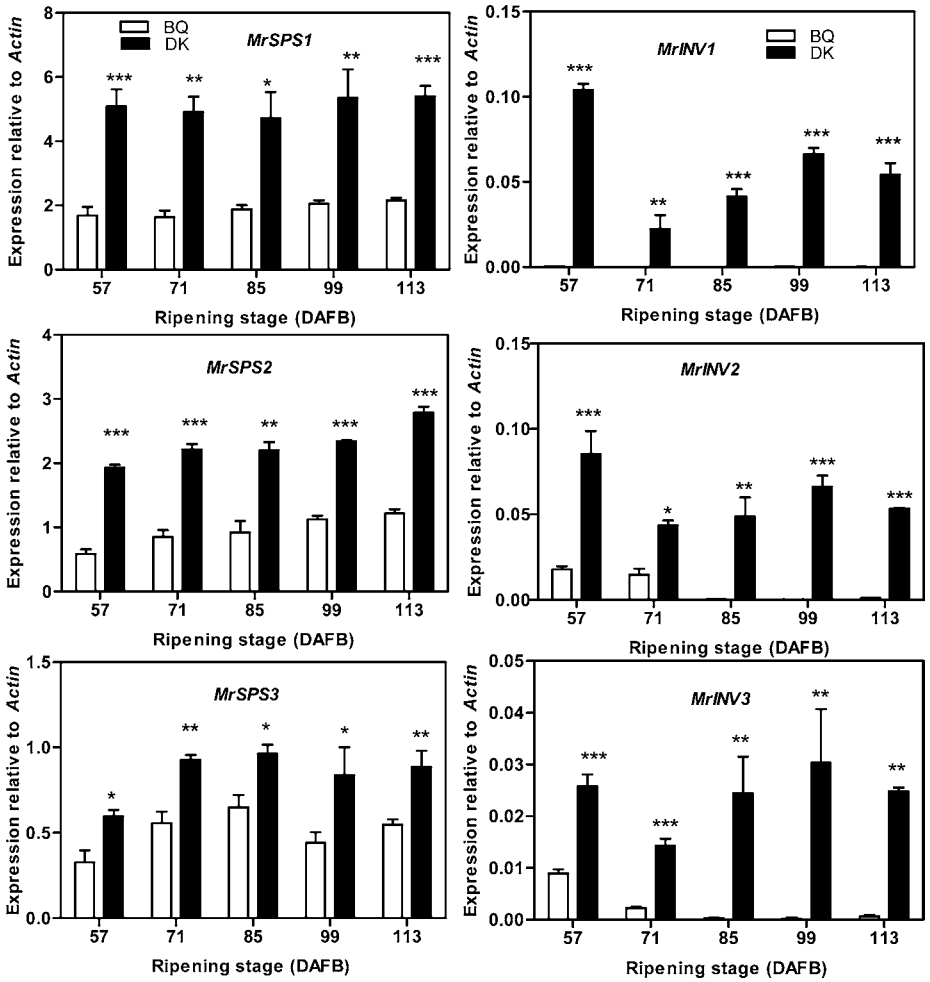


**Figure 5.** Expression of sucrose phosphate synthase and sucrose invertase genes in Chinese bayberries during fruit development. Values are the means ±SE. Vertical bars represent the standard errors of the means. Asterisks indicate significant differences between 'Dongkui' and 'Biqi' samples (Duncan's multiple range test; $^{*}P < 0.05$, $^{**}P < 0.01$, and $^{***}P < 0.001$).

in anthocyanins when compared to 'DK'. The difference in terms of anthocyanins in the two varieties between the published paper and our studies was associated with the temperature difference in the two different places where the fruit was picked (see Supporting Information S2).

Expression of flavonoid genes has been shown to be correlated with anthocyanin accumulation during fruit development in apple, grape, pear, and Chinese bayberry.[8,11,13,14] Therefore, the transcription of genes in the anthocyanin biosynthesis pathway was investigated by qPCR in present study. All of the biosynthetic genes studied were expressed in all the samples from the two cultivars taken at the different developmental stages. Expression of these genes in bayberry fruit increased during ripening, regardless of the cultivars. In particular, the higher transcript levels of *MrCHI*, *MrDFR1*, and *MrANS* in 'DK' fruit was in parallel to its higher anthocyanin concentration during fruit development. These data suggested that these three genes might be the key regulatory genes in the process of anthocyanin biosynthesis in Chinese bayberries. However, inconsistent with its anthocyanin content, 'BQ' fruit also exhibited higher expression of *MrF3′H* and *MrDFR2* at each fruit development stage in comparison with 'DK' fruit. In grapes, Boss et al.[13] reported that samples without anthocyanins expressed all major anthocyanin biosynthesis genes except *UFGT*, and they suggested that these genes were associated with the other biosynthesis pathways, notably those involved in the biosynthesis of aurones, flavones, flavonols, iosflavonoids, and proanthocyanindins. These specific expression patterns of *MrF3′H* and *MrDFR2* in Chinese bayberries were likely related to these other pathways, because phenolic compounds such as catechin and epicatechin, present in bayberries, are synthesized by proanthocyanindin biosynthesis pathway. *MrMYB1* is a known activator of the bayberry anthocyanin pathway.[8] In accord with anthocyanin content, 'DK' fruit was associated with higher *MrMYB1* transcription than 'BQ'. Overall, anthocyanin and transcript quantifications in Chinese bayberry fruit performed in this study suggested a possible mechanism controlling pigment patterns in bayberry fruit. We have found that less red-colored fruit 'BQ' were related to lower anthocyanin accumulation, which was explained by reduced transcript levels of several antho cyanin pathway genes evaluated, including the structural genes in the pathway, and *MrMYB1*, a transcription factor which regulates them.

Sugar is a common regulator for the expression of genes encoding metabolic enzymes and proteins involved in photosynthesis, carbohydrate metabolism, pathogenesis,[15] and anthocyanin biosynthesis.[16,17] Glucose and fructose are primarily derived from the hydrolysis of the imported sucrose via invertase. Our data clearly suggested that the metabolism of sugars in bayberries varied from different cultivars and development stages.


dx.doi.org/10.1021/jf503317k | J. Agric. Food Chem. 2014, 62, 10522−10528

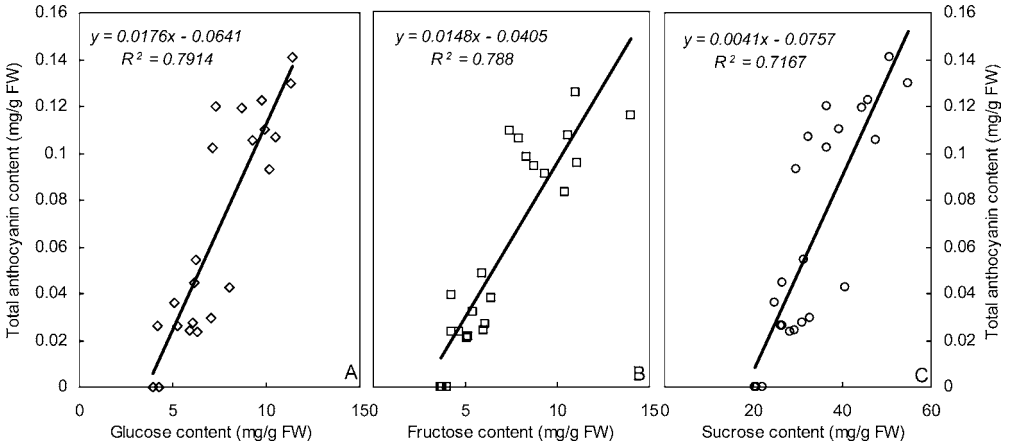


**Figure 6.** Correlation between total anthocyanins and levels of glucose (A), fructose (B), and sucrose (C) in both cultivars.

'DK' fruit experienced significantly higher expression of INV genes than 'BQ', indicating more glucose and fructose were produced and available for accumulation. However, it must be pointed that, being different from 'BQ', contents of glucose and fructose in 'DK' showed two peaks in relation to the expression pattern of INV genes. At the early stage of fruit development (57 DAFB), relatively higher expression of INV genes found in this study matched the first peak of glucose and fructose accumulation at 71 DAFB. Subsequently, the increased expression of these three INV genes from 71 to 99 DAFB indicated that the generation of glucose and fructose increased toward maturity. There are two sources of sucrose for accumulation: the imported sucrose that has not been metabolized and newly synthesized sucrose. In our present study, sucrose content in bayberries accumulated during fruit ripening regardless of the cultivars. However, the high transcript levels of SPS genes and very low expression of INV genes suggested that newly synthesized sucrose via SPS contributed significantly to the total sucrose level. The higher expression levels of SPS genes in 'DK' fruit toward maturity were consistent with faster accumulation of sucrose during this period. Therefore, taking into account all the expression studies involved in sugar metabolism, sucrose accumulation in bayberry fruit during ripening is of SPS type according to the categorization of mechanisms controlling sugar accumulation in fruit by Yamaki,[18] as in strawberry, apple, and melon.[19−21] A direct correlation between sucrose accumulation and SPS transcript levels has also been demonstrated in banana, melon, and apple fruit.[20−22]

Many studies have revealed the stimulatory effects of sugars on anthocyanin accumulation in a variety of plant species, of which sugars seem to not only be general carbohydrate sources, but also act as signal molecule to activate/repress the reactions.[2,17] For example, in flowers, sugar levels increase during petal development. Corollas cultured *in vitro* without sucrose do not elongate or show color.[2] Anthocyanin accumulation in grape berries commenced at veraison and sugar accumulating began, and continued throughout berry ripening,[4] which can be promoted by sucrose in grape cell suspensions and intact detached grape.[23,24] Similarly, sugars enhanced anthocyanin biosynthesis in radish hypocotyls.[5] In our experiment, during bayberry development, anthocyanin accumulation was consistent with the levels of glucose, fructose, and sucrose. Also, the correlation analysis revealed a significant relationship between levels of anthocyanin and sugars. A few studies demonstrated that this regulation is mediated by the expression of genes involved in anthocyanin synthesis.[6,25,26] In an *Arabidopsis* mutant impaired in phloem unloading and thereby having an accumulation of high sugar levels, anthocyanin accumulated in the leaves as a result of sucrose-induced expression of anthocyanin biosynthesis-related genes.[25] In sliced grape berries, sucrose up-regulated *VvF3H* expression, coinciding with enhanced anthocyanin levels.[6] In our study, increased expression of anthocyanin biosynthetic and regulatory genes has been observed with the accumulation of glucose, fructose, and sucrose during bayberry ripening regardless of the cultivars. In addition, the transcripts of *MrF3H*, *MrANS*, and *MrMYB1* in 'DK' fruit were dramatically higher than that in 'BQ', which was in compliance with the higher sugar levels. These results suggested that the accumulated sugars in Chinese bayberry fruit may play an important role in inducing expression of anthocyanin biosynthetic and regulatory genes, which was largely responsible for the pigmentation in bayberries.

In conclusion, we demonstrated a close correlation between the production of anthocyanins and the amount of sugars such as glucose, fructose, and sucrose during fruit ripening in Chinese bayberry fruit. The data presented confirm a specific role of high sugar levels in the promotion of the synthesis of specific secondary metabolites. However, the direct evidence that sugars enhance anthocyanin accumulation is still unknown because the study of the effects of sugars on bayberries still attached to intact plants is very challenging due to the large size of plant, interplant, intercluster, and interberry variability. Recently, an *in vitro* culture system that enabled long-term culture covering the whole ripening processes was developed in grapes in order to reveal the synthesis of anthocyanin in response to sugar levels.[23] A similar model system that enables easy modulation of the sugar status in Chinese bayberry fruit is therefore desirable to decipher the biochemical and molecular mechanisms of this regulation, which needs further investigation.

## ■ ASSOCIATED CONTENT

### Ⓢ Supporting Information

Additional information as noted in the text. This material is available free of charge via the Internet at http://pubs.acs.org.

## ■ AUTHOR INFORMATION

### Corresponding Author

*E-mail: yangzf@zwu.edu.cn. Phone: +86-574-88222229. Fax: +86-574-88222991.

### Author Contributions

⊥These authors contributed equally to this work.

### Notes

The authors declare no competing financial interest.

## ■ ACKNOWLEDGMENTS

This study was supported by the National Natural Science Foundations of China (31101356).

## ■ ABBREVIATIONS USED

ANS, anthocyanidin synthase; BQ, Biqi; CHS, chalcone synthase; CHI, chalcone isomerase; DAFB, day after flower bloom; DFR, dihydroflavonol 4-reductase; DK, Dongkui; F3H, flavanone 3-hydroxylase; F3′H, flavonoid 3′-hydroxylase; INV, sucrose invertase; qPCR, quantitative real-time PCR; SPS, sucrose phosphate synthase; UFGT, UDP glucose-flavonoid 3-*O*-glucosyl transferase

## ■ REFERENCES

(1) Winkel-Shirley, B. Flavonoid biosynthesis: A colourful model for genetics, biochemistry, cell biology, and biotechnology. *Plant Physiol.* **2001**, *126*, 485−493.

(2) Weiss, D. Regulation of flower pigmentation and growth: Multiple signaling pathways control anthocyanin synthesis in expanding petals. *Physiol. Plant* **2000**, *110*, 152−157.

(3) Ohto, M.; Onai, K.; Furukawa, Y.; Aoki, E.; Araki, T.; Nakamura, K. Effects of sugar on vegetative development and floral transition in *Arabidopsis*. *Plant Physiol.* **2001**, *127*, 252−261.

(4) Gonzalez-SanJose, M. L. Relationship between anthocyanins and sugars during the ripening of grape berries. *Food Chem.* **1992**, *43*, 193−197.

(5) Hara, M.; Oki, K.; Hoshino, K.; Kuboi, T. Enhancement of anthocyanin biosynthesis by sugar in radish (*Raphanus sativus*) hypocotyls. *Plant Sci.* **2003**, *164*, 259−265.

(6) Zheng, Y.; Tian, L.; Liu, H.; Pan, Q.; Zhan, J.; Huang, W. Sugars induce anthocyanin accumulation and flavanone 3-hydroxylase expression in grape berries. *Plant Growth Regul.* **2009**, *58*, 251−260.

(7) Yang, Z. F.; Zheng, Y. H.; Cao, S. F. Effect of high oxygen atmosphere storage on quality, antioxidant enzymes, and DPPH radical scavenging activity of Chinese bayberry fruit. *J. Agric. Food Chem.* **2009**, *57*, 176−181.

(8) Niu, S. S.; Xu, C. J.; Zhang, W. S.; Zhang, B.; Li, X.; Wang, K. L.; Ferguson, I. B.; Allan, A. C.; Chen, K. S. Coordinated regulation of anthocyanin biosynthesis in Chinese bayberry (*Myrica rubra*) fruit by a R2R3MYB transcription factor. *Planta* **2010**, *231*, 887−899.

(9) Cheng, G. W.; Breen, P. J. Activity of phenylalanine ammonialyase (PAL) and concentration of anthocyanins and phenolics in developing strawberry fruit. *J. Am. Soc. Hortic. Sci.* **1991**, *116*, 865−869.

(10) Eyéghé-Bickong, H. A.; Alexandersson, E. O.; Gouws, L. M.; Young, P. R.; Vivier, M. A. Optimization of an HPLC method for the simultaneous quantification of the major sugars and organic acids in grapevine berries. *J. Chromatogr., B* **2012**, *885*−*886*, 43−49.

(11) Feng, S. Q.; Wang, Y. L.; Yang, S.; Xu, Y. T.; Chen, X. S. Anthocyanin biosynthesis in pears is regulated by a R2R3-MYB transcription factor PyMYB10. *Planta* **2010**, *232*, 245−255.

(12) Feng, C.; Chen, M.; Xu, C. J.; Bai, L.; Yin, X. R.; Li, X.; Allan, A. C.; Ferguson, I. B.; Chen, K. S. Transcriptomic analysis of Chinese bayberry (*Myrica rubra*) fruit development and ripening using RNA-Seq. *BMC Genomics* **2012**, *13*, 19.

(13) Boss, P. K.; Davies, C.; Robinson, S. P. Analysis of the expression of anthocyanin pathway genes in developing *Vitis vinifera* L. cv shiraz grape berries and the implications for pathway regulation. *Plant Physiol.* **1996**, *111*, 1059−1066.

(14) Honda, C.; Kotoda, N.; Wada, M.; Kondo, S.; Kobayashi, S.; Soejima, J.; Zhang, Z.; Tsuda, T.; Moriguchi, T. Anthocyanin biosynthetic genes are coordinately expressed during red colouration in apple skin. *Plant Physiol. Biochem.* **2002**, *40*, 955−962.

(15) Rolland, F.; Baena-Gonzalez, E.; Sheen, J. Sugar sensing and signaling in plants: Conserved and novel mechanisms. *Annu. Rev. Plant Biol.* **2006**, *57*, 675−709.

(16) Baier, M.; Hemmann, G.; Holman, R.; Corke, F.; Card, R.; Smith, C.; Rook, F.; Bevan, M. W. Characterization of mutants in *Arabidopsis* showing increased sugar-specific gene expression, growth, and developmental responses. *Plant Physiol.* **2004**, *134*, 81−91.

(17) Mita, S.; Hirano, H.; Nakamura, K. Negative regulation in the expression of a sugar-inducible gene in *Arabidopsis thaliana*. *Plant Physiol.* **1997**, *114*, 575−582.

(18) Yamaki, S. Physiology and metabolism of fruit development: biochemistry of sugar metabolism and compartmentation in fruits. *Acta Hortic.* **1995**, *398*, 109−120.

(19) Dai, N.; Cohen, S.; Portnoy, V.; Tzuri, G.; Harel-Beja, R.; Pompan-Lotan, M.; Carmi, N.; Zhang, G.; Diber, A.; Pollock, S.; Karchi, H.; Yeselson, Y.; Petreikov, M.; Shen, S.; Sahar, U.; Hovav, R.; Lewinsohn, E.; Tadmor, Y.; Granot, D.; Ophir, R.; Sherman, A.; Fei, Z.; Giovannoni, J.; Burger, Y.; Katzir, N.; Schaffer, A. A. Metabolism of soluble sugars in developing melon fruit: a global transcriptional view of the metabolic transition to sucrose accumulation. *Plant Mol. Biol.* **2011**, *76*, 1−18.

(20) Hubbard, N. L.; Pharr, D. M.; Huber, S. C. Sucrose phosphate synthase and other sucrose metabolizing enzymes in fruits of various species. *Physiol. Plant* **1991**, *82*, 191−196.

(21) Li, M. J.; Feng, F. J.; Cheng, L. L. Expression patterns of genes involved in sugar metabolism and accumulation during apple fruit development. *PLoS One* **2012**, *7*, e33055 DOI: 10.1371/journal.-pone.0033055.

(22) Choudhury, R. S.; Roy, S.; Sengupta, D. N. A comparative study of cultivar differences in sucrose phosphate synthase gene expression and sucrose formation during banana fruit ripening. *Postharvest Biol. Technol.* **2009**, *54*, 15−24.

(23) Dai, Z. W.; Meddar, M.; Renaud, C.; Merlin, I.; Hilbert, G.; Delrot, S.; Gomès, E. Long-term in vitro culture of grape berries and its application to assess the effects of sugar supply on anthocyanin accumulation. *J. Exp. Bot.* **2014**, DOI: 10.1093/jxb/ert489.

(24) Larronde, F.; Krisa, S.; Decendit, A.; Chèze, C.; Deffieux, G.; Mérillon, M. Regulation of polyphenols production in *Vitis vinifera* cell suspension cultures by sugars. *Plant Cell Rep.* **1998**, *17*, 946−950.

(25) Loreti, E.; Povero, G.; Novi, G.; Solfanelli, C.; Alpi, A.; Perata, P. Gibberellins, jasmonate and abscisic acid modulate the sucrose induced expression of anthocyanin biosynthetic genes in *Arabidopsis*. *New Phytol.* **2008**, *4*, 1−13.

(26) Solfanelli, C.; Poggi, A.; Loreti, E.; Alpi, A.; Perata, P. Sucrose-specific induction of the anthocyanin biosynthetic pathway in *Arabidopsis*. *Plant Physiol.* **2006**, *140*, 637−646.

working volume of 3 L of the production liquid medium including (g/L) 80.0 g of sucrose, 6.0 g of $K_2HPO_4$, 0.9 g of yeast extract, 0.5 g of $MgSO_4$, 4.0 g of NaCl, and different concentrations of $(NH_4)_2SO_4$. The fermentor loaded with 3 L of the production culture medium was autoclaved at 121 °C for 15 min. A total of 150 mL of the seed culture medium was transferred to the production culture medium. The pullulan fermentation was performed at 28 °C and 300 rpm with an aeration rate of 3 L/min. The pH was maintained at 6.5 by the addition of either 2 M NaOH or 2 M HCl.

**Determination of Pullulan Production and Biomass.** Properly distilled water was added to the fermentation liquor to dilute. The broth was heated at 80 °C in a water bath for 30 min and then centrifuged at 10000*g* for 20 min to separate the biomass and insoluble debris. Two volumes of precooling 95% (v/v) ethanol was added to the supernatant and stirred and placed at 4 °C for 24 h to deposit the exopolysaccharide thoroughly. The sediment was isolated by centrifugation at 15000*g* for 20 min, washed with ethanol again, and dried at 80 °C until the weight was constant. The biomass sediment from the initial centrifugation was washed three times with distilled water by centrifugation at 10000*g* for 5 min and dried at 80 °C until the dry cell weight (DCW) was constant. Pullulan production and DCW were expressed as grams per liter.

**$(NH_4)_2SO_4$ Concentration.** For residual $(NH_4)_2SO_4$ concentration determination, a revised indophenol method was used.[13] The fermentation liquor (2 mL) was centrifuged at 4000*g* to separate microorganisms and other precipitates. Hundred-fold distilled water was added to the supernatant to dilute and then adjusted to pH 7.0. Next, 25 mL of sample was mixed with 10 mL of phenol nitroprusside buffer. To this mixture was added 15 mL of hypochlorite reagent, and the mixture was held at room temperature for 45 min for color development. The absorbance of the solution was measured at 290 nm.

**Protein Preparation for 2-DE.** Cells were harvested by centrifugation at 15000*g* for 20 min at 4 °C and washed three times with ultrapure water by centrifugation at 10000*g* for 5 min. Cells were ground in liquid nitrogen after freeze-drying. The fine powder was suspended in acetone including 0.07% (w/v) dithiothreitol (DTT) and 10% (w/v) trichloroacetic acid (TCA) and incubated at −20 °C overnight. The suspension was centrifuged at 15000*g* for 15 min at 4 °C, and the sediment was washed three times with precooling acetone including 0.07% (w/v) DTT. The sediment was dried and redissolved in rehydration solution [7 M urea, 2 M thiourea, 2% (w/v) CHAPS, 1.8 mM DTT, 0.5% (w/v) Pharmalyte 3−10] and then centrifuged at 15000*g* for 20 min at 4 °C. The limpid supernatant including the soluble proteins was stored in aliquots at −80 °C. The method of Bradford was used to determine protein concentration with bull serum albumin as standard.[14]

**2-DE.** The protein extracts (250 μg/gel) were loaded for 2-DE as follows. The 24 cm strips (Immobiline Drystrip) covering a nonlinear pH 3−11 (GE Healthcare) were rehydrated in 450 μL of rehydration solution for 16 h at room temperature. Isoelectric focusing was operated by the Ettan IPGphor (GE Healthcare) with a ceramic tray manifold at 20 °C. Each strip was limited to a maximum current of 50 μA. The isoelectric focusing electrophoresis program followed the protocol rehydration at 50 V for 12 h (step), 500 V for 1 h (step), 1000 V for 1 h (step), 10000 V for 1 h (gradient), and 11000 V for 10 h (step).

The strip is taken from the strip holder. The redundant oil and protein solutions were absorbed by filter paper. The IPG gel strips were respectively incubated in an equilibration solution [50 mM Tris-HCl, pH 8.8, 6 M urea, 30% (v/v) glycerol, 2% (w/v) SDS, and 0.002% bromophenol blue] with 1% DTT and 2.5% iodoacetamide for 15 min. Then the equilibrated gel strips were put on a 1.5 mm 12.5% polyacrylamide gel and sealed with agarose sealing solution [25 mM Tris-base, 192 mM glycine, 0.1% (w/v) SDS, 0.5% agarose, and 0.002% (w/v) bromophenol blue]. The second-dimensional separation was performed by the ETTAN DALTsix (GE Healthcare) in a cold chamber at 15 °C. SDS-PAGE was operated at a constant voltage of 100 V for 45 min and at 200 V for 6−8 h until the bromophenol blue arrived at the bottom of the gel. After SDS-PAGE, the separated proteins were visualized by silver staining as previously described.[15]

**Image Analysis.** Silver-stained gels were scanned using an Image Scanner (Amersham Biosciences). Date analysis was carried out utilizing Image Master 2D Platinum 5.0 software (Amersham Biosciences). For each treatment, three gels from three independent treatments were studied. Gel spots were automatically tested and manually edited and deleted when necessary. Evidently spots were marked by calibrating and matching the gel. Next, the three replicate gels were compared to each other and merged into a master gel, containing the spots distributed on the three gels for every independent experiment. To quantify and contradistinguish the protein spots, standardization of the volume ratio was performed. The significantly changed spots were chosen with at lowest a 0.2-fold decrease and a 5.0-fold increase in the normalized volume ratio.

**In-Gel Digestion.** The differentially expressed protein spots were excised for digestion. The gel spot was washed and the destained solution removed. Fifty percent acetonitrile (ACN) and 100% ACN were successively added for 5 min. The samples were rehydrated in 2−4 μL of mass spectroscopy grade gold trypsin (Promega, Madison, WI, USA) solution (20 μg/mL in 25 mM $NH_4HCO_3$) for 30 min. Then, 20 μL of cover solution (25 mM $NH_4HCO_3$, 10% ACN) was added for digestion for 16 h at 37 °C. The supernatant was shifted to another tube, and the gel was extracted with 50 μL of extraction buffer [67% ACN and 5% trifluoroacetic acid (TFA)]. The supernatant of the gel spot and the peptide extracts were combined and freeze-dried for mass spectrometry.

**Mass Spectrometry Analysis.** The freeze-dried power was suspended with 5 μL of 0.1% TFA and then mixed with a saturated solution of α-cyano-4-hydroxy-*trans*-cinnamic acid in 50% ACN and 0.1% TFA, at the ratio of 1:1. One microliter of the mixture was spotted on a stainless steel sample target board. Peptide MS and MS/MS were performed on an ABI 5800 MALDI-TOF/TOF Plus mass spectrometer (Applied Biosystems, Foster City, CA, USA). Data were obtained in a positive MS reflector using a CalMix5 standard to adjust the instrument (ABI5800 Calibration Mixture). The integrated MS and MS/MS data were disposed by the GPS Explorer V3.6 software (Applied Biosystems, USA) with default parameters. On the basis of the combination of MS and MS/MS spectra, proteins were successfully identified in the standard of 95% or higher confidence interval of their scores in the Mascot V2.3 search engine (Matrix Science Ltd., London, UK), using the search parameters as follows: NCBInr-Funji database; trypsin as the digestion enzyme; one missed cleavage site; fixed modifications, carbamidomethyl (C); partial modifications, acetyl (protein N-term), deamidated (NQ), dioxidation (W), oxidation (M); 100 ppm for precursor ion tolerance and 0.5 Da for fragment ion tolerance.

## RESULTS AND DISCUSSION

**Effect of Different $(NH_4)_2SO_4$ Concentrations on Pullulan Fermentation.** The effect of various concentrations of $(NH_4)_2SO_4$ on cell growth and pullulan production by *A. pullulans* CGMCC1234 is shown in Figure 1. The results acquired at different $(NH_4)_2SO_4$ concentrations proved that the $(NH_4)_2SO_4$ played a vital role on pullulan formation. The carbon flux from merging into fungal cell material to pullulan synthesis was dependent on $(NH_4)_2SO_4$ concentration. When 0.6 g/L of $(NH_4)_2SO_4$ was added into the medium, pullulan concentration achieved the maximum and the production was 37.72 g/L. A higher concentration of $(NH_4)_2SO_4$ brought about the higher level of biomass but reduced the pullulan production. Just 9.45 g/L of pullulan was obtained when 1.5 g/L $(NH_4)_2SO_4$ was added; meanwhile, 12.31g/L DCW was obtained. The possible reason was that excess $(NH_4)_2SO_4$ could not be entirely expended until the end of the fermentation stage, which led to the growth of cell biomass and reduced pullulan production. However, insufficient nitro-

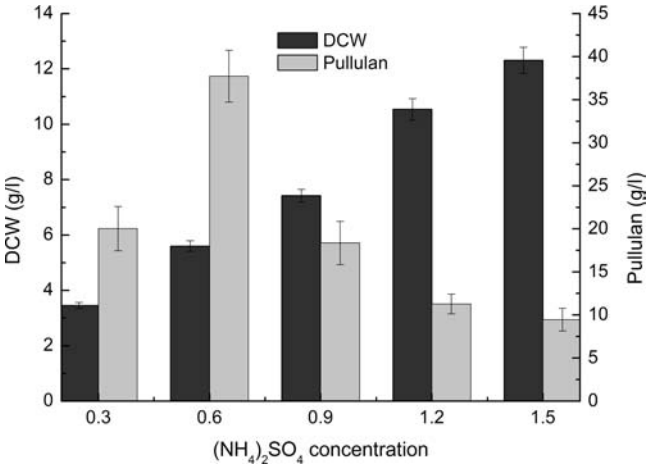


**Figure 1.** Effect of $(NH_4)_2SO_4$ concentration on DCW and pullulan production of *A. pullulans* CGMCC1234 during culture development in a 5 L stirred tank fermentor. Values are given as means ± standard deviation ($n$ = 3).

gen source sparked off the reduction of both biomass and pullulan. When 0.3 g/L $(NH_4)_2SO_4$ was added to the culture medium, just 20.03 g/L pullulan was obtained.

Comparison of the fermentation parameters of *A. pullulans* CGMCC1234 with 0.6 and 1.2 g/L $(NH_4)_2SO_4$ is shown in Figure 2. With 0.6 g/L $(NH_4)_2SO_4$ addition, the biomass growth was apparently inhibited after 36 h. In the meantime, $(NH_4)_2SO_4$ was consumed almost at 36 h. Nevertheless, 1.2 g/L $(NH_4)_2SO_4$ was exhausted until 84 h and the biomass constantly increased through the end of the fermentation. Interestingly, compared to the 1.2 g/L $(NH_4)_2SO_4$ group, the pullulan formation of the 0.6 g/L $(NH_4)_2SO_4$ group was more quickly increased during the 4 days of cultivation. The production of pullulan under nitrogen limit was 3.3-fold as compared to the nitrogen-replete group. Providing excess nitrogen could induce the promotion of cell biomass, but not increase pullulan production.[16]

Nitrogen metabolism was a strictly conducted process in fungi; therefore, fungi had the capacity to exploit finite nitrogen source for cell growth. Effective supervision of the nitrogen metabolism process possibly endowed fungi with the ability to utilize varieties of ecological niches.[17] For *A. pullulans* CGMCC1234 in the nitrogen-limited condition, the medium with 0.6 g/L $(NH_4)_2SO_4$ group displayed sensitivity to pullulan formation. Excess nitrogen source would impel carbon flux flow toward biomass production. The depletion of nitrogen induced exopolysaccharide accumulation of *A. pullulans* fermentation.

**Protein Identification.** In previous studies, we found that exopolysaccharide accumulation was not tightly related to cell growth. When *A. pullulans* cells reached a stationary phase and the cell growth was limited, pullulan could be synthesized more as a secondary metabolite.[18] To search for differences in physiological metabolism and its administration between the cell biomass growth and secondary metabolite pullulan biosynthesis in *A. pullulans* CGMCC1234 cells in the presence of high and low levels of nitrogen source, proteins extracted from the cells of culture medium with 0.6 and 1.2 g/L $(NH_4)_2SO_4$ group at 60 h were subjected to proteome analysis. The representational gel maps of the proteins separated from the *A. pullulans* cells cultivated in the nitrogen-limited medium and the nitrogen-replete medium are shown in Figure 3. As

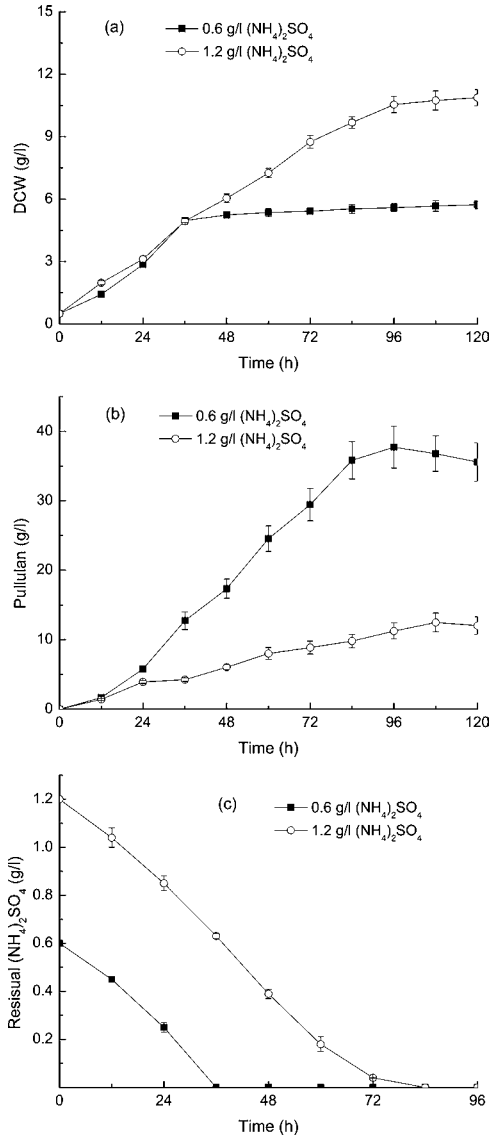


**Figure 2.** Effect of nitrogen-limited cultivation with 0.6 g/L $(NH_4)_2SO_4$ and nitrogen-replete cultivation with 1.2 g/L $(NH_4)_2SO_4$ on the DCW (a), pullulan production (b), and residual $(NH_4)_2SO_4$ concentration (c) of *A. pullulans* CGMCC1234 during culture development in a 5 L stirred tank fermentor. Values are given as means ± standard deviation ($n$ = 3).

analyzed through Image Master, approximately 1100 visualized spots were found on the gels.

After comparison and analysis the gel images, altogether 19 protein spots from the whole cell protein gels were excised and subjected to MALDI-TOF/TOF. The successfully identified proteins were marked on the 2-DE gel maps (Figure 3), and more detailed information about identified proteins is shown in Table 1. Among the 19 protein spots cut for MALDI-TOF/TOF analysis, 12 protein spots were successfully identified, achieving a 63% identification rate. Meanwhile, the identified proteins were matched to known proteins from the fungus species and other microorganisms. Of the 12 protein spots identified, 7 were up-regulated under the nitrogen repletion and 5 were up-regulated under the nitrogen limitation (Table 1). The up-regulated proteins in the nitrogen-replete sample contained nascent polypeptide-associated complex subunit $\beta$, peroxiredoxin-6, $\alpha$-glucan branching enzyme, fructose-bisphos-


dx.doi.org/10.1021/jf503390f | J. Agric. Food Chem. 2014, 62, 10529−10534

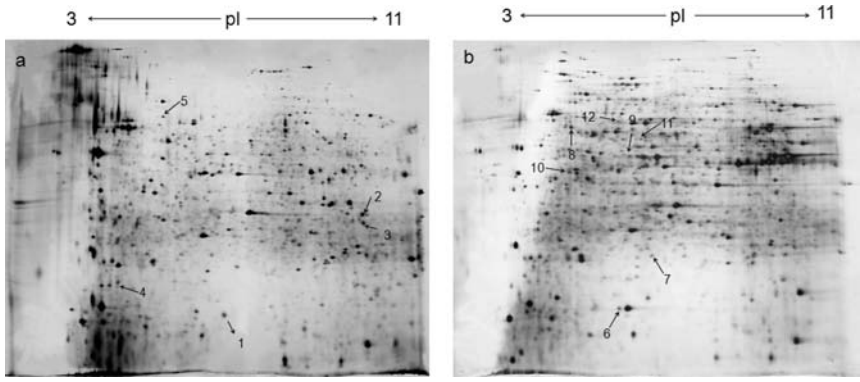


**Figure 3.** Comparative 2-DE gel analyses of cellular proteins of *A. pullulans* CGMCC1234 cultivated in the nitrogen-limited medium (a) and the nitrogen-replete medium (b). Protein spots marked on the maps with arrows and numbers represent the 12 identified proteins analyzed with MALDI-TOF/TOF.

**Table 1. Identification of Differentially Expressed Protein Spots from *A. pullulans* CGMCC1234 Cells Produced with the Addition of 0.6 and 1.2 g/L $(NH_4)_2SO_4$ by Proteomic Analysis with 2D-GE and MALDI-TOF/TOF MS[a]**

| spot no. | accession no. | protein name | organism | mascot score | coverage (%) | theor $M_w$ | theor pI |
|---|---|---|---|---|---|---|---|
| 1 | gil485919582 | putative cyanate hydratase protein | *Neofusicoccum parvum* UCRNP2 | 115 | 8 | 17443 | 5.96 |
| 2 | gil334683219 | mitochondrial peroxiredoxin-1 | *Diplodia seriata* | 247 | 21 | 25596 | 8.59 |
| 3 | gil336260705 | hypothetical protein SMAC_07435 | *Sordaria macrospora* k-hell | 56 | 13 | 25156 | 5.97 |
| 4 | gil145249406 | ATP synthase subunit $\beta$ | *Aspergillus niger* CBS 513.88 | 56 | 9 | 19969 | 4.75 |
| 5 | gil225681491 | Hsp70-like protein | *Paracoccidioides brasiliensis* Pb03 | 163 | 4 | 73805 | 5.91 |
| 6 | gil302420083 | nascent polypeptide-associated complex subunit $\beta$ | *Verticillium alfalfae* VaMs.102 | 94 | 7 | 17253 | 4.96 |
| 7 | gil189202520 | peroxiredoxin-6 | *Pyrenophora tritici-repentis* Pt-1C-BFP | 157 | 9 | 25367 | 5.88 |
| 8 | gil320586098 | $\alpha$-glucan branching enzyme | *Grosmannia clavigera* kw1407 | 278 | 5 | 133585 | 5.65 |
| 9 | gil398408315 | fructose-bisphosphate aldolase | *Zymoseptoria tritici* IPO323 | 80 | 4 | 39652 | 5.63 |
| 10 | gil225681690 | arginase | *Paracoccidioides brasiliensis* Pb03 | 118 | 6 | 31748 | 5.46 |
| 11 | gil154323902 | enolase | *Botryotinia fuckeliana* B05.10 | 97 | 3 | 47196 | 5.26 |
| 12 | gil302501588 | hypothetical protein ARB_01037 | *Arthroderma benhamiae* CBS 112371 | 103 | 4 | 45451 | 5.18 |

[a]The 19 chosen protein spots showed significant difference in expression level between the nitrogen-limited and the nitrogen-replete conditions of culture as analyzed by 2D eletrophoresis. Of the 19 protein spots excised for MALDI-TOF/TOF analysis, 12 proteins were identified.

phate aldolase, arginase, enolase, and hypothetical protein ARB_01037. In comparison, five identified proteins, including putative cyanate hydratase protein, mitochondrial peroxiredoxin-1, hypothetical protein SMAC_07435, ATP synthase subunit $\beta$, and Hsp70-like protein, revealed up-regulation in the nitrogen-limited sample.

**Proteome Changes.** Fructose-bisphosphate aldolase (spot 9 in Figure 3 and Table 1) and enolase (spot 11 in Figure 3 and Table 1) were two proteins involved in the glycolytic pathway. Fructose-bisphosphate aldolase, generally referred to as aldolase, was an enzyme responsible for the catalysis of fructose 1,6-bisphosphate to glyceraldehyde 3-phosphate (G3P) and dihydroxyacetone phosphate (DHAP). Aldolase could also catalyze sedoheptulose 1,7-bisphosphate and fructose 1-phosphate to generate DHAP.[19] Glycolysis, a catabolic pathway, used the forward reaction. Enolase, also called phosphopyruvate hydratase, was a metalloenzyme catalyzing a reversible reaction of the conversion of phosphoenolpyruvate (PEP) to 2-phosphoglycerate (2-PG), the penultimate step of glycolytic pathway. Aldolase and enolase both belonged to the class lyase. These two enzymes could catalyze the reverse reaction, according to the environmental concentrations of substrates.[20] Increasing evidence has revealed that enolase had mutiple capabilities and played an important part in the transcriptional regulation of glycolysis flux. For instance, enolase participated in adjusting and controlling glycolysis flux through induction of the expression of Rag1 glucose permease in *Kluyveromyces lactis*.[21] It was obvious that more $(NH_4)_2SO_4$ up-regulated fructose-bisphosphate aldolase and enolase protein, leading to the carbon flux toward glycolic pathway for the growth of biomass.

$\alpha$-Glucan branching enzyme (spot 8 in Figure 3 and Table 1) was an essential enzyme that catalyzed the development of the $\alpha$-1,6-glucosidic linkages in glucan chains by scission of an $\alpha$-1,4-linked oligosaccharide from growing $\alpha$-1,4-glucan chains and the subsequent attachment of the oligosaccharide to the $\alpha$-1,6 position. It was involved in the biosynthesis of both glycogen and capsular $\alpha$-D-glucan.[22] Excess nitrogen source might accelerate the biosynthesis of intracellular glycogen but reduce the pullulan production. Simon et al. found that pullulan synthesis was increasing while glycogen production was decreasing during growth, so it should be possible that the kinetics of production of these two kinds of polysaccharides were inversely correlated.[23]

Arginase (spot 10 in Figure 3 and Table 1) was a manganese-containing enzyme and ubiquitous to all domains of life. Arginase catalyzed the hydrolysis of L-arginine into L-ornithine and urea. This reaction was the initial step in catabolism of

arginine and the terminal step in anabolism of urea.[24] Excess nitrogen source stimulated amino acid biosynthesis and metabolism in *A. pullulans* CGMCC1234 cells.

Nascent polypeptide-associated complex subunit $\beta$ (spot 6 in Figure 3 and Table 1) was part of the nascent polypeptide-associated complex (NAC). A component of the NAC was a dynamic ribosomal transport corridor. It protected the newly formed polypeptides from interaction with other cytoplasmic proteins to guarantee suitable nascent protein targeting. Furthermore, the NAC could effectively enhance the interaction of ribosome and the membrane of mitochondria and also prevent improper interaction of nonsecretory nascent polypeptides translated from ribosome and translocation sites in the endoplasmic reticulum membrane. Hence, the NAC could efficiently improve the import of mitochondrial protein.[25−27] Numerous proteins were synthesized when *A. pullulan* cells rapidly multiplied in sufficient nitrogen source. The up-regulation of nascent polypeptide-associated complex was conducive to protein transport and transcription regulation.

The 70 kDa heat shock proteins (Hsp70) (spot 5 in Figure 3 and Table 1) belonged to a family of widespread heat shock proteins. Proteins with similar structures were found in almost all organisms. Hsp70 played a crucial role in protein folding in the cells and meanwhile helped to protect the cells from environmental pressure. Hsp70 seemed to be involved in treating defective and damaged proteins. Hsp70 could be able to protect protein from aggregating through close connection to fractional synthesized peptide sequences.[28] As the nitrogen source was consumed, the environment outside the cells became rigorous; the expression of more Hsp70 could protect *A. pullulans* cells from oxidative stress, which generally hurts proteins, leading to aggregation and partial unfolding.

ATP synthases (spot 4 in Figure 3 and Table 1) were membrane-bound enzymes existing in mitochondrial inner membrane and vacuoles. The basic function of ATP synthases was to synthesize ATP using an electrochemical ion gradient. Some ATP synthases worked in reverse, using the energy from the hydrolysis of ATP to create a proton gradient. Studies suggested that pullulan synthesis involved UDP-glucose, required ATP, and proceeded through lipid intermediates.[29] It was obvious that nitrogen-limited cells generated more ATP necessary for metabolism including polymerization of precursor to form pullulan and excretion of pullulan to the culture broth.

In this work, the fermentation results obtained showed that proper concentration (0.6 g/L) of $(NH_4)_2SO_4$ was important for pullulan biosynthesis. Excess nitrogen source would enhance the accumulation of biomass, but decreased the pullulan production. Nitrogen limitation in *A. pullulans* CGMCC1234 seemed to influence the flux change of carbon flux flow toward exopolysaccharide accumulation. The proteomic results revealed that the expression of antioxidant-related enzymes and energy-generating enzymes and the depression of the enzymes concerning amino acid biosynthesis, glycogen biosynthesis, glycolysis, protein transport, and transcriptional regulation under nitrogen limitation, caused a conversion of metabolic flux from the glycolysis pathway to the pullulan biosynthesis pathway. This research supplies a new perspective into the understanding of the mechanism of pullulan biosynthesis and will apply practical significance for the improvement of pullulan production from *A. pullulans*.

## AUTHOR INFORMATION


### Corresponding Author

*(Q.T.) Phone/fax: +86 510 85919170. E-mail: qytong@263.net.



### Funding

This work was supported by the National Natural Science Foundation of China (31401657), the Priority Academic Program Development of Jiangsu Higher Education Institutions.


### Notes

The authors declare no competing financial interest.

## REFERENCES


(1) Cheng, K. C.; Demirci, A.; Catchmark, J. M. Pullulan: biosynthesis, production, and applications. *Appl. Microbiol. Biotechnol.* **2011**, *92*, 29−44.

(2) Singh, R. S.; Saini, G. K.; Kennedy, J. F. Pullulan: microbial sources, production and applications. *Carbohydr. Polym.* **2008**, *73*, 515−531.

(3) Shingel, K. I. Current knowledge on biosynthesis, biological activity, and chemical modification of the exopolysaccharide, pullulan. *Carbohydr. Res.* **2004**, *339*, 447−460.

(4) Bulmer, M. A.; Catley, B. J.; Kelly, P. J. The effect of ammonium ions and pH on the elaboration of the fungal extracellular polysaccharide, pullulan, by *Aureobasidium pullulans*. *Appl. Microbiol. Biotechnol.* **1987**, *25*, 362−365.

(5) Gibbs, P. A.; Seviour, R. J. Does the agitation rate and/or oxygen saturation influence exopolysaccharide production by *Aureobasidium pullulans* in batch culture? *Appl. Microbiol. Biotechnol.* **1996**, *46*, 503−510.

(6) Sang, Y. L. Bacterial polyhydroxyalkanoates. *Biotechnol. Bioeng.* **1996**, *49*, 1−14.

(7) Wu, J. R.; Yu, L. J.; Zhan, X. B.; Zheng, Z. Y.; Lu, J.; Lin, C. C. NtrC-dependent regulatory network for curdlan biosynthesis in response to nitrogen limitation in *Agrobacterium* sp. ATCC 31749. *Process Biochem.* **2012**, *47*, 1552−1558.

(8) Jiang, L.; Wu, S.; Kim, J. M. Effect of different nitrogen sources on activities of UDPG-pyrophosphorylase involved in pullulan synthesis and pullulan production by *Aureobasidium pullulans*. *Carbohydr. Polym.* **2011**, *86*, 1085−1088.

(9) Bhadauria, V.; Banniza, S.; Wang, L. X.; Wei, Y. D.; Peng, Y. L. Proteomics studies of phytopathogenic fungi, oomycetes and their interactions with hosts. *Eur. J. Plant Pathol.* **2010**, *126*, 81−95.

(10) Böhmer, M.; Colby, T.; Böhmer, C.; Bräutigam, A.; Schmidt, J.; Bölker, M. Proteomic analysis of dimorphic transition in the phytopathogenic fungus *Ustilago maydis*. *Proteomics* **2007**, *7*, 675−685.

(11) Wittmann-Liebold, B.; Graack, H. R.; Pohl, T. Two-dimensional gel electrophoresis as toll for proteomics studies in combination with protein identification by mass spectrometry. *Proteomics* **2006**, *6*, 4688−4703.

(12) Kim, Y.; Nandakumar, M. P.; Marten, M. R. Proteomics of filamentous fungi. *Trends Biotechnol.* **2007**, *25*, 395−400.

(13) Scheiner, D. Determination of ammonia and Kjeldahl nitrogen by indophenols method. *Water Res.* **1976**, *10*, 31−36.

(14) Bradford, M. A rapid sensitive method for the quantitation of microgram quantities utilizing the principle of protein-dye binding. *Anal. Biochem.* **1976**, *72*, 248−254.

(15) Shevchenko, A.; Wilm, M.; Vorm, O.; Mann, M. Mass spectrometric sequencing of proteins from silver-stained polyacrylamide gels. *Anal. Chem.* **1996**, *68*, 850−858.

(16) Orr, D.; Zheng, W.; Campbell, B. S.; McDougall, B. M.; Seviour, R. J. Culture conditions affect the chemical composition of the exopolysaccharide synthesized by the fungus *Aureobasidium pullulans*. *J. Appl. Microbiol.* **2009**, *107*, 691−698.

(17) Donofrio, N. M.; Oh, Y.; Lundy, R.; Pan, H.; Brown, D. E.; Jeong, J. S.; Coughlan, S.; Mitchell, T. K.; Dean, R. A. Global gene

expression during nitrogen starvation in the rice blast fungus *Magnaporthe grisea*. *Fungal Genet. Biol.* **2006**, *43*, 605−617.
(18) Sheng, L.; Zhu, Gui.; Tong, Q. Effect of uracil on pullulan production by *Aureobasidium pullulans* CGMCC1234. *Carbohydr. Polym.* **2014**, *101*, 435−437.
(19) Merkulova, M.; Hurtado-Lorenzo, A.; Hosokawa, H.; Zhuang, Z.; Brown, D.; Ausiello, D. A.; Marshansky, V. Aldolase directly interacts with ARNO and modulates cell morphology and acidic vesicle distribution. *Am. J. Physiol.* **2011**, *300*, C1442−C1455.
(20) Díaz-Ramos, A.; Roig-Borrellas, A.; García-Melero, A.; López-Alemany, R. α-Enolase, a multifunctional protein: its role on pathophysiological situations. *J. Biomed. Biotechnol.* **2012**, *2012*, No. 156795.
(21) Lemaire, M.; Wesolowski-Louvel, M. Enolase and glycolytic flux play a role in the regulation of the glucose permease gene RAG1 of *Kluyveromyces lactis*. *Genetics* **2004**, *168*, 723−731.
(22) Sambou, T.; Dinadayala, P.; Stadthagen, G.; Barilone, N.; Bordat, Y.; Constant, P.; Levillain, F.; Neyrolles, O.; Gicquel, B.; Lemassu, A.; Daffé, M.; Jackson, M. Capsular glucan and intracellular glycogen of *Mycobacterium tuberculosis*: biosynthesis and impact on the persistence in mice. *Mol. Microbiol.* **2008**, *70*, 762−774.
(23) Simon, L.; Bremond, K.; Gallant, D. J.; Bouchonneau, M.; Bouchet, B. Studies on pullulan extracellular production and glycogen intracellular content in *Aureobasidium pullulans*. *Can. J. Microbiol.* **1998**, *44*, 1193−1199.
(24) Quintero, M. J.; MuroPastor, A. M.; Herrero, A.; Flores, E. Arginine catabolism in the cyanobacterium *Synechocystis* sp. strain PCC 6803 involves the urea cycle and arginase pathway. *J. Bacteriol.* **2000**, *182*, 1008−1015.
(25) Fünfschilling, U.; Rospert, S. Nascent polypeptide-associated complex stimulates protein import into yeast mitochondria. *Mol. Cell. Biol.* **1999**, *10*, 3289−3299.
(26) Reimann, B.; Bradsher, J.; Franke, J.; Hartmann, E.; Wiedmann, M.; Prehn, S. Initial characterization of the nascent polypeptide-associated complex in yeast. *Yeast* **1999**, *15*, 397−407.
(27) Franke, J.; Reimann, B.; Hartmann, E.; Köhlerl, M.; Wiedmann, B. Evidence for a nuclear passage of nascent polypeptide-associated complex subunits in yeast. *J. Cell Sci.* **2001**, *114*, 2641−2648.
(28) Morano, K. A. New tricks for an old dog: the evolving world of Hsp70. *Ann. N.Y. Acad. Sci.* **2007**, *1113*, 1−14.
(29) Leathers, T. D. Biotechnological production and applications of pullulan. *Appl. Microbiol. Biotechnol.* **2003**, *62*, 468−473.

storage protein diversity and of the relationships between the considerable numbers of inbred lines should aid in the development of breeding programs that efficiently utilize the available rye germplasm. The high resolution and separation efficiency of the presented CZE method facilitated the rapid identification of the rye HMW-SS compositions in the lines. The qualitative compositions of the rye HMW-SS in the inbred lines determined by CZE in this study were then compared with SDS-PAGE data.

## MATERIALS AND METHODS

**Plant Materials.** The experiment was performed on 68 inbred lines of winter rye (*S. cereale* L.) from generation $S_{20}$, which were obtained by self-pollination and from the selection of 14 rye cultivars and two inbred forms (Table 1). Simultaneously grains from six rye cultivars (cv., accession number, origin country (Everest, 30206, FRA; Buriatskaya, 30308, RUS; Lekkeroggen, 30660, GER; Ponsi, 31004, SWE; Radosinska Record, 30143, SVK; Stel, 31032, SWE)) obtained from the National Centre for Plant Genetic Resources, Radzików, Poland and three standard triticale cultivars Binova (2*/13 + 16/5.1r + 6.4r), Eldorado (1/7 + 8/2r + 5.3r), and Titan (2*/7 + 18/1.2r + 6.5r) were analyzed.

The inbred rye lines were obtained by self-pollination of the individual plants and of the sisters bred within the cultivars and the bred forms for 11 years. For this purpose, two ears from each plant and one ear from each of the two plants of a given variety or form were placed under a tomophane isolator. In the wax maturity phase, the isolators containing ears were cut off and the grains from the ears were manually collected. In the subsequent year, the seeds from the isolated plants from a given variety and a bred form were sown separately. This cycle was repeated for 5 years to obtain phenotypically equalized inbred lines of winter rye, which were subjected to self-pollination and selection for the subsequent 5 years. Using this approach, we obtained individual inbred lines of winter rye of genetically defined morphological features. Then, sets of 100 kernels from each of the selected inbred lines were sown every second year in plots of 1 $m^2$.

Prior to flowering, the plants were protected with canvas sheets that were spread on metal frames, which were then removed from plants representing a given line after flowering. The ears were manually cut at full maturity and were threshed in a laboratory threshing machine. Then, the seed germination energies and abilities were evaluated on the basis of observations of 100 kernels from each line sown in three batches. If the ability of the kernels to germinate was greater than 80% for a given inbred line, the seeds were dried to a moisture content of 7−8% in a chamber containing air with approximately 20% relative humidity and at 20 °C. Finally, the seeds from a given line were cleaned and sealed under a vacuum in laminated foil sheets. The samples of seeds representing the studied lines were stored in this form at −25 °C.

**Reagents and Chemical Materials.** Iminodiacetic acid (IDA), (hydroxylpropyl)methylcellulose (HPMC), acetonitrile (AcN), poly(vinylpyrrolidone) (PVP; $M_r \sim 360{,}000$), dithiothreitol (DTT), urea, and *N*-dodecyl-*N*,*N*-dimethyl-3-ammonio-1-propanesulfonate (lauryl sulphobetaine, SB3-12) were purchased from Sigma (St. Louis, MO, USA). Poly(ethylene oxide) (PEO) with a molecular weight of 8,000,000 Da and acrylamide were acquired from Aldrich (Milwaukee, WI, USA). Sodium phosphate monobasic and dibasic, potassium phosphate monobasic, and sodium hydroxide were the products of J. T. Baker (Phillipsburg, NJ, USA). All chemicals were of electrophoresis or analytical grade.

All solutions were prepared in deionized 18 MΩ·m water using a Milli-Q system (Millipore, Bedford, MA, USA). The solutions were filtered through a 0.5 μm Millipore membrane filter before being injected into the capillary.

**Apparatus.** The CZE experiments were performed on a Beckman Coulter P/ACE system MDQ capillary electrophoresis instrument. The system was equipped with a high-voltage power supply, diode array detector, and 32 Karate ver. 8.0 software (Beckman Coulter) for system control and data handling. The separations were performed using uncoated fused-silica capillaries (Polymicro Technologies, Phoenix, AZ, USA) with internal diameter of 50 μm and 31.2 cm in total length (detection at 10.2 cm from the capillary outlet). The temperature was maintained at 40 °C during all runs.

**Table 1. Sixty-eight Rye Inbred Lines Used in This Study with Determined HMW-SS Compositions**

| cultivar/variety | no. of inbred lines | HMW-SS compositions | description of inbred lines |
|---|---|---|---|
| Pancerne | 6 | 5.1r + 6.4r | L4, L420/97, D855/1, Mbj/4, H9/3, L96/4, |
| | 2 | 5.2*r + 6.5r | L428/97w, L428/97n |
| | 2 | 5.1r | L228, L318/2 |
| | 1 | 1.9r + 5.4r | L427 |
| | 2 | heterozygosity | L520, L140/3/7 |
| Dankowskie Selekcyjne | 8 | 5.1r + 6.4r | L305, L230/2/9, L103, L18/1, L410/04, L147/1, L305/2, Ll1/94 |
| | 1 | 5.2*r + 6.5r | L298/97, |
| | 1 | 2r + 7r | L169/1/10 |
| | 2 | heterozygosity | BcL148bp/10, L9/99/8 |
| Forms short-stem from Jeleniec | 6 | 5.1r + 6.4r | L299, L310, L522, Mns/1, L518, L517, |
| | 3 | 2r + 6.6r | L299/L1, J74/3, L237/94/1 |
| | 1 | 5.3*r +7r | H32 |
| | 1 | heterozygosity | kz/2 |
| Smolickie | 5 | 5.1r + 6.4r | Bj1, L186/2/2, bj/98, chlp/n, L185/2/1 |
| | 2 | 2r + 7r | L145, Nsegr/1/11/12 |
| | 1 | 2.1r + 5.4r | L68/7/8 |
| Dankowskie Zlote | 1 | 5.3*r + 7r | L59 |
| | 1 | 5.2*r + 6.5r | L176/1 |
| | 1 | 6.1r + 7.2r | lo segr |
| | 1 | heterozygosity | L29/3/2 |
| Chrobre | 2 | 5.1r + 6.4r | L208, kpl/2/18 |
| | 2 | 5.2*r + 6.5r | L338, L155 |
| | 1 | 5.3*r + 7 r | M15/3 |
| | 1 | heterozygosity | L154/6 |
| Wojcieszyckie | 1 | 5.1r + 6.4r | L267/2/25 |
| | 1 | 2r + 7r | CH7/99 |
| | 1 | heterozygosity | S67p/94/4 |
| Omka | 1 | 2r + 7r | 127 |
| | 1 | heterozygosity | sl/2/1 |
| Zelandzkie | 1 | 5.1r + 6.4r | Ch5/99 |
| | 1 | 2r + 7r | Ch2/99 |
| Uniwersalne | 2 | 2r + 6.6r | L233, L260/94 |
| Garczynskie | 1 | 2r + 7r | 8/segr/5 |
| Karlik | 1 | 5.1r + 6.4r | L128 |
| Mikulickie | 1 | 5.2*r + 6.5r | L245 |
| Kamalinskaja4 | 1 | 2.1r + 5.4r | L127bk/97 |
| Vjatka | 1 | 2r + 6.6r | pc-wch/95 |

**Extraction of HMW Secalin Subunits from Rye Flour.** HMW secalin subunits were extracted from 50 mg of rye flour. First, twice preextraction was performed with 0.5 mL of 0.4 M NaCl and 0.067 M $HKNaPO_4$ (pH 7.6) at room temperature to remove the albumins and globulins (mixing each time on a vortex mixer for 10 min and centrifuging for 5 min at 12500*g*). The 40 kDa γ- and ω-secalins were removed by two 10 min extractions using 70% (v/v) ethanol, followed by centrifugation at 15000*g* for 10 min. Then, the HMW-SS and 75 kDa γ-secalins were isolated from the sediment by an extraction for 30 min with 0.05 M Tris buffer (titrated by HCl to pH 7.5) containing 50% (v/v) 1-propanol, 2 M urea, and 1% (w/v) DTT at 60 °C under


dx.doi.org/10.1021/jf502926q | J. Agric. Food Chem. 2014, 62, 10535−10541

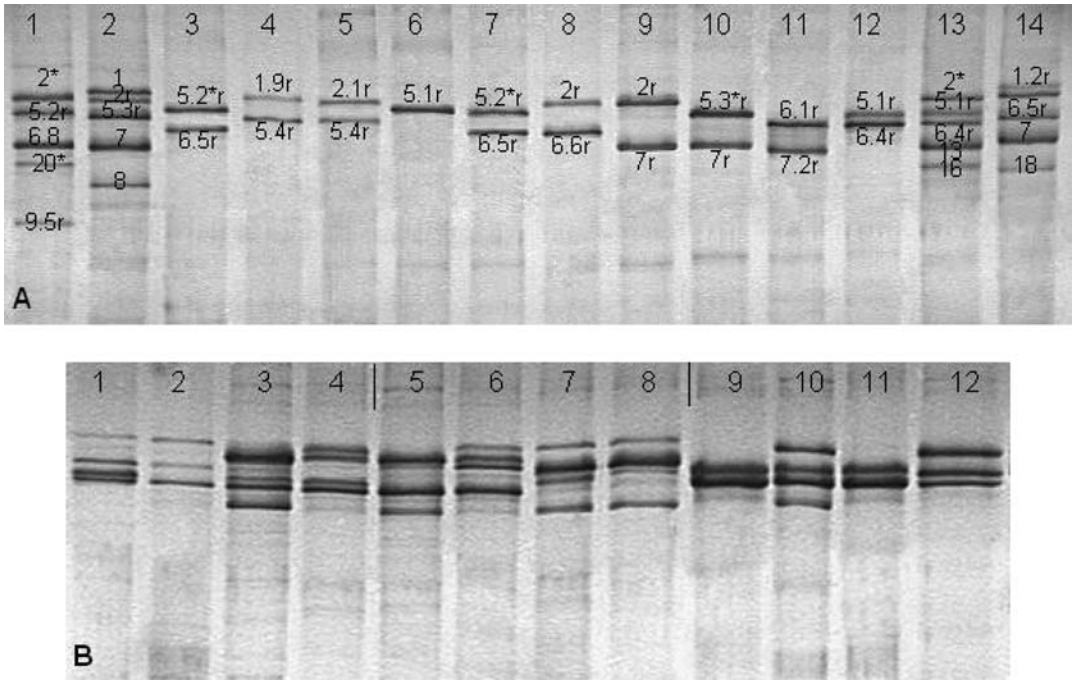


**Figure 1.** SDS-PAGE patterns of rye high-molecular-weight secalin subunits (HMW-SS) from analyzed inbred lines (A) and cultivars (B). Panel A: lane 1, standard triticale cv. Vision (2*/6.8 + 20*/5.2r + 9.5r); lane 2, standard triticale cv. Eldorado (1/7 + 8/2r + 5.3r); lane 3, L428/97n (5.2*r + 6.5r); lane 4, L427 (1.9r + 5.4r); lane 5, L127bk/97 (2.1r + 5.4r); lane 6, L228 (5.1r); lane 7, L298/97 (5.2*r + 6.5r); lane 8, L260/94 (2r + 6.6r); lane 9, Ch2/99 (2r + 7r); lane 10, L59 (5.3*r + 7r); lane 11, lo segr (6.1r + 7.2r); lane 12, H9/3 (5.1r + 6.4r); lane 13, standard triticale cv. Binova (2*/13 + 16/5.1r + 6.4r); lane 14, standard triticale cv. Titan (2*/7 + 18/1.2r + 6.5r). Panel B: lanes 1−4, rye cv. Ponsi; lanes 5−8, rye cv. Stel; lanes 9−12, rye cv. Everest.

nitrogen. This mixture was then centrifuged at 13000*g* for 15 min. The obtained supernatant was aliquoted between two tubes, and half of the volume of the reduced proteins was alkylated with 4-vinylpyridine at 60 °C for 30 min. Then, the alkylated and nonalkylated HMW proteins were precipitated by the addition of 1-propanol to a final concentration of 60% (v/v), and the samples were stored at 4 °C overnight. The precipitated HMW-SS were collected after centrifugation for 8 min at 15000*g*. Next, the HMW-SS precipitates were redissolved in 75 μL of a solution containing 40% (v/v) AcN + 0.1% (v/v) trifluoroacetic acid (TFA) and 2 M urea, vortexed for 30 min at 60 °C, and centrifuged again for 10 min at 15000*g*. All samples were used for SDS-PAGE and CZE analyses within 24 h of extraction.

**Separation of Rye HMW-SS by SDS-PAGE.** The alkylated HMW secalin subunits that were obtained from the rye samples and the triticale cultivars (as protein standards) were separated by electrophoresis on a vertical SDS-PAGE gel using a Protean II xi cell unit (Bio-Rad, Hercules, CA, USA) and the discontinuous Tris-HCl−glycine buffer system of Laemmli.[27] A 10 μL aliquot of a protein sample was loaded onto the upper 4.5% gel, and separation was performed on 12.0% (m/v; 1.35% C) polyacrylamide in resolving solution at 240 V for 45 min after the tracking dye migrated off the gel. The gels were stained overnight with Coomassie Brilliant Blue G-250. The designation of the rye HMW-GS in the inbred lines was performed according to McIntosh et al.[28]

**Separation of Rye HMW-SS by CZE.** The HMW protein separations were conducted according to Salmanowicz[29] with some modifications. A solution containing 75 mM IDA (pH 2.7), 0.15% PEO with a molecular weight of 8,000,000 Da, 26 mM SB3-12, and 15% (v/v) AcN was used as the separation buffer. A buffer containing 0.1 M IDA, 0.2% (m/v) PVP with a $M_w$ of $0.36 \times 10^6$, 0.05% (m/v) HPMC, and 20% (v/v) ACN was used to dynamically coat the capillary wall. Conditioning comprised a rinsing sequence of 1.0 M NaOH, ultrapure water, 0.1 M HCl, ultrapure water, and buffer (all at 275.7 kPa and for 2 min). For the first use on a day, the capillary was additionally flushed with 1 M HCl for 20 min, followed by a 5 min rinse with Milli-Q water and 15 min with separation buffer. The separations were performed with a constant voltage of 10 kV at 40 °C. The samples were injected hydrodynamically under low pressure (3.45 Pa) for 10 s into the anodic end. The separation buffer and dynamic coating of the capillary wall solution were stored in a refrigerator at 4 °C after being degassed with a vacuum system in an ultrasonic tank. Proteins were detected by UV absorbance measurements at 200 nm. The HMW-SS extracts were filtered through a 0.20 μm PVDF syringe filter prior to CZE analysis. The particular HMW-SS were identified through comparisons of single and mixed samples and the results obtained from the SDS-PAGE separations. Three protein separations were performed by CZE for each analytical assay.

**Statistical Analysis.** The resolution was calculated using the half-width method. The mean differences were compared using an unpaired Student's *t* test. All statistical analyses were performed using Statistica software (version 10.0 PL, StatSoft Polska).

## RESULTS AND DISCUSSION

**SDS-PAGE Analysis of Rye HMW-SS.** Alkylated rye HMW protein extracts from 68 inbred lines were used for the identification of allelic variation of HMW-SS compositions by one-dimensional SDS-PAGE. Figure 1A shows the electrophoretic patterns of the rye HMW secalin subunits detected in the selected inbred lines and two standard triticale cultivars. The presented patterns revealed wide variability in the qualitative composition of these subunits. Also earlier conducted analysis of storage proteins in 11 inbred lines showed a difference in the number of bands and their molecular masses.[30]

The SDS-PAGE gel patterns for the particular inbred lines showed two major protein bands for the rye HMW-SS: a more slowly moving x-subunit and a more quickly moving y-subunit. A total of 59 analyzed lines appeared to show genetic homogeneity, while the remaining 9 lines were found to be heterogeneous. It was difficult to make exact identifications of

the subunits because of the very similar electrophoretic mobilities of the rye HMW-SS in the SDS-PAGE gel. The nomenclature commonly used for wheat was used to mark the protein bands in the separating gels: numeration of the bands in the order of their migration in the gel in reference to the bands of the standard wheat HMW glutenin subunits using Arabic numerals with the letter "r" at the end. In the analyzed lines, 9 tentative HMW-SS compositions were detected. Six rye HMW-SS isoforms have similar electrophoretic mobilities, as previously described isoforms from triticale cultivars,[29] and four of them were marked as x-type (2r, 5.1r, 5.2r, and 5.3r), and two as y-type (6.4r and 6.5r). Moreover, three new x-type (1.9r, 2.1r and 6.1r) rye HMW-SS isoforms and four new y-type (5.4r, 6.6r, 7r, and 7.2r) subunits were detected in the gels. In 30 analyzed rye inbred lines, the triticale HMW-SS composition 5.1r + 6.4r was identified (Table 1). A majority of these lines (25 lines) had been selected from the 4 initial rye cultivars (cvs Pancerne, Dańkowskie Selekcyjne, Jeleniec, and Smolickie).

**Optimization of CZE Separation Conditions.** The HMW fraction from the inbred line D855/1 containing the composition 5.1r + 6.4r was used as a model protein mixture for the development of the CZE separation method. Until now, an isoelectric buffer system composed of IDA in conjunction with 0.3 M PEO, 26 mM SB3-12, and 30% AcN has been applied as the running buffer for the separation of the triticale HMW-SS together with wheat HMW glutenin subunits in uncoated fused-silica capillaries.[30] Good solubility of rye HMW-SS in low-concentration 15% (v/v) AcN in conjunction with 2 M urea in comparison with 40% AcN used earlier for redissolution of the mixture of the wheat and rye HMW proteins in triticale cultivars[29] enabled the development of a more efficient method of separation of these classes of proteins. The resolution was determined to be optimum at a concentration of 80 mM IDA in the running buffer containing 0.15% PEO, 26 mM SB3-12, and 15% AcN. This modified procedure maintained satisfactory peak shapes and separation efficiencies for the major peaks of wheat HMW-GS at $(4.6-6.8) \times 10^5$ plates/m. The alkylated rye HMW-SS isoforms migrated in the capillary faster than the nonalkylated isoforms ($t_m$ of major x-type peaks, 10.8 and 12.5 min, respectively), but the reproducibilities and separation efficiencies of the individual protein peaks were less satisfactory (not presented). The relative standard deviation (RSD) values for the migration times ($t_m$) of peaks representing the major x-type and y-type peaks of the alkylated subunits ranged from 1.04% to 1.66%, whereas those of the nonalkylated subunits ranged from 0.49% to 0.84%.

**Detection of Rye HMW Secalin Subunits in Inbred Lines by CZE.** In contrast to the challenging rye HMW-SS identifications on the SDS-PAGE gels due to the very similar electrophoretic mobilities and molecular masses of the particular subunits, the CZE separation of these subunits enabled the correct identification of the specific subunits on the basis of their peak migration times within 16 min. The CZE profiles of nine selected inbred rye lines with detected various HMW-SS compositions are presented in Figure 2A–I. The presented electropherograms of the nonalkylated proteins indicated satisfactory separation of all rye HMW-SS isoforms. The HMW-SS that were isolated from the homogeneity inbred lines were separated into two individual peaks representing x- and y-type subunits, with the exception of two lines that contained only an x-type subunit (Figure 2E). In most cases, a

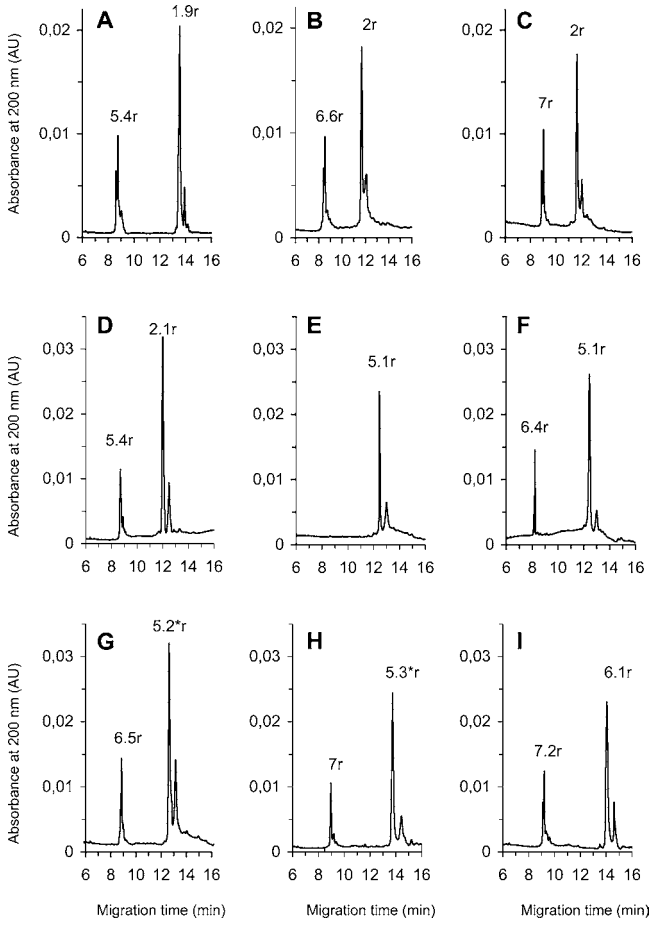


**Figure 2.** CZE electropherograms of nonalkylated rye HMW-SS from selected inbread lines with different subunits compositions: (A) L427 (1.9r + 5.4r), (B) L260/94 (2r + 6.6r), (C) Ch2/99 (2r + 7r), (D) L127bk/97 (2.1r + 5.4r), (E) L228 (5.1r), (F) H9/3 (5.1r + 6.4r), (G) L298/97 (5.2*r + 6.5r), (H) L59 (5.3*r + 7r), and (I) lo segr (6.1r + 7.2r). Proteins were separated at 10.0 kV and 40 °C with a 75 mM isoelectric IDA buffer, containing of 0.15 M PEO, 26 mM SB3-12, and 15% AcN. Prior to the separation, the capillary was rinsed with 0.1 M IDA solution containing 0.2% PVP, 0.05% HPMC, and 20% AcN.

major peak and one or two minor peaks for each HMW-SS were observed. The multiple detected CZE peaks for individual HMW-SS indicated various posttranslational modifications of these subunits. Additionally, the multiple peaks for wheat HMW-GS and triticale HMW-SS have previously been detected via CZE[25,26,29,31] and capillary isoelectric focusing.[32] The migration order of the rye HMW-SS in the capillaries differed from the relative electrophoretic mobilities in the SDS-PAGE gels. The differences in the identifications of the HMW-SS compositions determined by SDS-PAGE and CZE methods could be caused by the various intensities following the staining of the individual HMW secalin bands in SDS-PAGE gels, owing to considerable quantitative differences in these subunits revealed by CZE analysis. Moreover, rye HMW-SS possess similar molecular masses, which makes the identification of particular subunits on the basis of SDS-PAGE patterns in comparison with CZE profiles very difficult. In total, seven x-type and six y-type HMW-SS were designated via the CZE method (Table 1). The rye HMW-SS were separated in the capillary within two time ranges, namely, the y-type subunits with shorter migration times (8.21–9.18 min) and the x-type subunits with longer migration times (11.68–14.06 min)

**Table 2. Means of Migration Times ($t_m$) of Individual x- and y-Type HMW Secalin Subunits in Rye Inbred Lines Determined by CZE Method**

| x-type | 1.9r | 2r | 2.1r | 5.1r | 5.2*r | 5.3*r | 6.1r |
|---|---|---|---|---|---|---|---|
| *n* | 1 | 13 | 2 | 32 | 7 | 3 | 1 |
| $t_m$ (min) | 13.53 ± 0.15 | 11.64 ± 0.12 | 12.01 ± 0.11 | 12.33 ± 0.13 | 12.63 ± 0.10 | 13.74 ± 0.16 | 14.06 ± 0.18 |

| y-type | 5.4r | 6.4r | 6.5r | 6.6r | 7r | 7.2r |
|---|---|---|---|---|---|---|
| *n* | 3 | 30 | 7 | 6 | 10 | 1 |
| $t_m$ (min) | 8.74 ± 0.10 | 8.21 ± 0.08 | 8.84 ± 0.09 | 8.46 ± 0.06 | 8.98 ± 0.06 | 9.18 ± 0.09 |

(Table 2). Both the detected rye x-type and y-type HMW-SS migrated in the capillary with time ranges similar to those of the triticale HMW glutenin subunits (HMW-GS), whereas the typical rye HMW-SS exhibited a wider range of migration times than the triticale HMW-SS.[26,29] The lack of considerable distinction between the rye HMW-SS migration times from the European triticale cultivars,[33] from which they earlier were obtained, can only be demonstrated based on the limited utilization of rye germplasm for the creation of this synthetic species.

Generally, the x-type rye HMW-SS in the analyzed lines were more abundant than the y-type subunits. Seven x-type HMW-SS were distinguished on the basis of their CZE migration times (Table 1). Using the SDS-PAGE electrophoretic mobilities of wheat HMW-GS bands as points of reference,[26] the following names were assigned to the rye HMW-SS: 1.9r, 2r, 2.1r, 5.1r, 5.2*r, 5.3*r, and 6.1r. Only two x-type subunits earlier identified in the triticale rye cultivars, 2r and 5.1r, were also detected in the presented CZE study. However, the remaining five rye subunits were new and had not been described before. New subunits 5.2*r and 5.3*r possessed SDS-PAGE electrophoretic mobilities that were similar to those of the earlier detected triticale subunits 5.2r and 5.3r,[29] respectively, but they had considerably different migration times using CZE analysis. The relative migration order of the x-type rye HMW-SS encoded by genes on the *Glu-R1* locus was 6.1r > 5.3*r > 1.9r > 5.2*r > 5.1r > 2.1r > 2r (from the slowest to the fastest). In summary, the presented CZE data did not fully confirm the classification of the specific encoded HMW-SS alleles based on the SDS-PAGE analysis.

Six rye y-type HMW-SS were distinguished in the analyzed material based on their migration times via the CZE method, of which four were new and had not been previously described (Table 1). According to their relative electrophoretic mobilities in the SDS-PAGE gels, the following names were assigned to these subunits: 5.4r, 6.4r, 6.5r, 6.6r, 7r, and 7.2r. The y-type subunits 7r and 7.2r, the smallest of the subunits as determined by SDS-PAGE, exhibited the longest migration times, 8.98 and 9.18 min, respectively (Table 2). Additionally, most analyzed rye samples contained y-type subunit 6.4r, which possessed the shortest $t_m$ of 8.21 min. The relative migration order of the y-type rye HMW-SS encoded by genes on the *Glu-R1* locus was 7.2r > 7r > 6.5r > 5.4r > 6.6r > 6.4r (from the slowest to the fastest).

The following eight new HMW secalin subunit pairs 1.9r + 5.4r (*Glu-R1h*), 2r + 6.6r (*Glu-R1i*), 2r + 7r (*Glu-R1j*), 2.1r + 5.4r (*Glu-R1k*), 5.1r + Null (*Glu-R1l*), 5.2*r + 6.5r (*Glu-R1m*), 5.3*r + 7r (*Glu-R1n*), and 6.1r + 7.2r (*Glu-R1p*) were identified on the basis of the CZE analysis performed in this study and after regarding the nomenclature for rye allelic variants (pairs of x + y). The rye HMW-SS allelic compositions 5.1r + 6.4r and 2r + 7r were the most frequently identified (41.1% and 10.3%, respectively) in the analyzed inbred lines, whereas the compositions 1.9r + 5.4r and 6.1r + 7.2r occurred very rarely (at 1.5%).

**Detection of HMW Secalin Subunits in Rye Cultivars.** The separation of rye HMW secalin subunits from six cultivars was performed using SDS-PAGE and CZE methods. The SDS-PAGE patterns of the rye HMW-SS obtained from four selected single grains descending from three cultivars are shown in Figure 1B. The obtained SDS-PAGE electropherograms revealed considerable genetic variations in the rye HMW-SS and resulted in highly diverse subunit band patterns. The majority of the lanes in the SDS gel showed four protein bands (two x-type and two y-type subunits) with different protein staining intensities. The correct identification of particular x + y HMW-SS subunit pairs was therefore not possible. The presence of two x-type and two y-type HMW-SS on SDS-PAGE gels for the individual rye cultivars has also been presented before in other works.[10,17,25,34] The occurrence of two to four inbred lines that were selected earlier from individual initial rye cultivars differing in their HMW-SS compositions confirmed the high level of rye polymorphism (Table 1).

The CZE analysis of the rye HMW secalin fraction from single grains of six cultivars fully confirmed the works of other authors[11,23,24] who identified the multilines (mixtures of genotypes) of most rye cultivars. Generally, the HMW-SS fractions from the analyzed rye cultivars were separated into four major peaks representing two x- and two y-type subunits (Figure 3A,B). Moreover, there often occurred considerable quantitative differences in the peak areas for the particular x + y subunit pairs. Although certain single seeds of the rye cultivars presented very characteristic CZE profiles of the HMW-SS, generally the high levels of heterogeneity and heterozygosity made cultivar identification very difficult, which is in contrast to

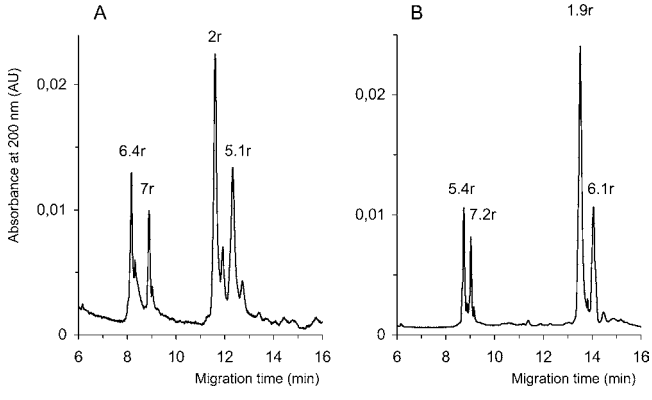


**Figure 3.** CZE electropherograms of rye HMW-SS from two selected cultivars: (A) cv. Lekkeroggen (5.1r + 6.4r and 2r + 7r) and (B) cv. Buriatskaya (1.9r + 5.4r and 6.1r + 7.2r). Separation conditions were as described in Figure 2.

the case of identifying cultivars of wheat, triticale, and barley.[35,36]

In conclusion, it has been proven that HMW secalin subunits from rye inbred lines can be rapidly (below 15 min) separated via CZE method with both high resolution and good reproducibility. Using selective preparation of HMW proteins precipitated by addition of 1-propanol to a final concentration of 60% (v/v), 75 kDa γ-secalins from HMW protein extract were eliminated, which have migration times similar to those of HMW-SS during the CZE separation. The HMW-SS were separated into two major peaks (x-type and y-type subunits), with the exception of two lines that contained only the x-type subunit. The CZE analysis of rye HMW secalin fraction fully confirmed the occurrence of the mixture of genotypes in single grains of rye cultivars. A knowledge of the HMW secalin subunit composition of the particular rye samples enables breeders the utilization of rye germplasm in a wider range for the creation of new genotypes of triticale and wheat species with desirable properties. Fast and more accurate characterization of rye HMW-SS by CZE is an efficient alternative to identification of these proteins by the standard SDS-PAGE analysis.

## AUTHOR INFORMATION


### Corresponding Author

*E-mail: bsal@igr.poznan.pl.

### Author Contributions

[§]B.P.S. and M.L. contributed equally to this work.


### Notes

The authors declare no competing financial interest.

## ABBEVIATIONS USED

HMW-SS, high molecular weight secalin subunit; CZE, capillary zone electrophoresis; HPMC, hydroxypropylmethylcellulose; IDA, iminodiacetic acid; PEO, poly(ethylene oxide); PVP, poly(vinylpyrrolidone); AcN, acetonitrile; SB3-12, *N*-dodecyl-*N*,*N*-dimethyl-3-ammonio-1-propanesulfonate

## REFERENCES


(1) Tang, Z. X.; Ross, K.; Ren, Z. L.; Yang, Z. J.; Zhang, H. Y.; Chikmawati, T.; Miftahudin; Gustafson, J. P. Secale. In *Wild Crop Relatives: Genomic and Breeding Resources: Cereals*; Kole, C., Ed.; Springer: Berlin, 2011; pp 367−396.

(2) Bushuk, W. Rye production and uses worldwide. *Cereal Foods World* **2001**, *46*, 70−73.

(3) *Agricultural Production, Supply, and Distribution*; http://www.indexmundi.com/agriculture/.

(4) Radzyminska, M.; Garbowska, B.; Jakubowska, D. Health quality and nutritional value of rye bread produced on a small and large scale in Poland. *Ital. J. Food Sci.* **2013**, *25*, 126−132.

(5) Isaksson, H.; Fredriksson, H.; Andersson, R.; Olsson, J.; Åman, P. Effect of rye bread breakfasts on subjective hunger and satiety: A randomized controlled trial. *Nutr. J.* **2009**, *8*, 39.

(6) Horszwald, A.; Troszyńska, A.; Dolores del Castillo, M.; Zieliński, H. Protein profile and sensorial properties of rye breads. *Eur. Food Res. Technol.* **2009**, *229*, 875−886.

(7) Kipp, B.; Belitz, H. D.; Seilmeier, W.; Wieser, H. Comparative studies of high Mr subunits of rye and wheat. I. Isolation and biochemical characterization and effects on gluten extensibility. *J. Cereal Sci.* **1996**, *23*, 227−234.

(8) Ragaee, S. M.; Campbell, G. L.; Scoles, G. J.; Mc Leod, J. G.; Tyler, R. T. Studies on rye (*Secale cereale* L.) lines exhibiting a range of extract viscosities. 2. Rheological and baking characteristics of rye and rye/wheat blends and feeding value for chicks of whole meals and breads. *J. Agric. Food Chem.* **2001**, *49*, 2446−2453.

(9) Branlard, G.; Dardevet, M.; Amiour, N.; Igrejas, G. Allelic diversity of HMW and LMW glutenin subunits and omega-gliadins in French bread wheat (*Triticum aestivum* L.). *Genet. Resour. Crop Evol.* **2003**, *50*, 669−679.

(10) Ribeiro, M.; Seabra, L.; Ramos, A.; Santos, S.; Pinto-Carnide, O.; Carvalho, C.; Igrejas, G. Polymorphism of the storage proteins in Portuguese rye (*Secale cereale* L.) populations. *Hereditas* **2012**, *149*, 72−74.

(11) Shewry, P. R.; Parmar, S.; Miflin, B. J. Extraction, separation and polymorphism of the prolamin storage proteins (secalins) of rye. *Cereal Chem.* **1983**, *60*, 1−6.

(12) Shewry, P. R.; Kreis, M.; Burgess, S. R.; Parmar, S.; Miflin, B. J. The synthesis and deposition of the prolamin storage proteins (secalins) of rye. *Planta* **1983**, *159*, 439−445.

(13) Gellrich, C.; Schieberle, P.; Wieser, H. Biochemical characterization and quantification of the storage protein (secalin) types in rye flour. *Cereal Chem.* **2003**, *80*, 102−109.

(14) Shewry, P. R.; Field, J. M.; Lew, E. J.-L.; Kasadra, D. D. The purification and characterization of two groups of storage proteins (secalins) from rye (*Secale cereale* L.). *J. Exp. Bot.* **1982**, *33*, 261−268.

(15) Lawrence, G. J.; Shepherd, R. W. Inheritance of glutenin protein subunits of wheat. Mapping the nucleolus organiser region, seed protein loci and isozyme loci on chromosome 1R in rye. *Theor. Appl. Genet.* **1981**, *60*, 333−337.

(16) Singh, N. K.; Shepherd, K. W. Mapping of the genes controlling high-molecular-weight glutenin subunits of rye on the long arm of chromosome 1R. *Genet. Res.* **1984**, *44*, 117−123.

(17) De Bustos, A.; Jouve, N. Characterisation and analysis of new HMW-glutenin alleles encoded by the *Glu-R1* locus of *Secale cereale*. *Theor. Appl. Genet.* **2003**, *107*, 74−83.

(18) Koehler, P.; Wieser, H. Comparative studies of high Mr subunits of rye and wheat. III. Localisation of cysteine residues. *J. Cereal Sci.* **2000**, *32*, 189−197.

(19) Shewry, P. R.; Bechtel, D. B. Morphology and chemistry of the rye grain. In *Rye: Production, chemistry and technology*, 2nd ed.; Bushuk, W., Ed.; AACC: St. Paul, MN, USA, 2001; pp 69−121.

(20) Lukaszewski, A. Cytogenetically engineered rye chromosomes 1R to improve bread-making quality of hexaploid triticale. *Crop Sci.* **2006**, *46*, 2183−2194.

(21) Hansen, H. B.; Møller, B.; Andersen, S. B.; Jørgensen, J. R.; Hansen, Å. Grain characteristics, chemical composition, and functional properties, of rye (*Secale cereale* L.) as influenced by genotype and harvest year. *J. Agric. Food Chem.* **2004**, *52*, 2282−2291.

(22) Hansen, H. B.; Rasmussen, C. V.; Knudsen, K. E. B.; Hansen, Å. Effects of genotype and harvest year on content and composition of dietary fibre in rye (*Secale cereale* L.) grain. *J. Sci. Food Agric.* **2003**, *83*, 76−85.

(23) Kubiczek, R. P.; Huebner, F. R.; Bietz, J. A. Reversed-phase high performance liquid chromatography of secalins: Application to rye cultivar identification. *J. Cereal Sci.* **1993**, *17*, 191−201.

(24) Petrovičová, L.; Gálová, Z.; Chňapek, M.; Kečkešová, M. Protein polymorphism in genetic resources of rye using SDS-PAGE. *J. Microbiol. Biotechnol. Food Sci.* **2013**, *2*, 1531−1539.

(25) Yan, Y.; Yu, J.; Jiang, Y.; Hu, Y.; Cai, M.; Hsam, S. L. K.; Zeller, F. J. Capillary electrophoresis separation of high molecular weight glutenin subunits in bread wheat (*Triticum aestivum* L.) and related species with phosphate-based buffers. *Electrophoresis* **2003**, *24*, 1429−1436.

(26) Salmanowicz, B. P. Detection of high molecular weight glutenin subunits in triticale (× *Triticosecale* Wittm.) cultivars by capillary zone electrophoresis. *J. Agric. Food Chem.* **2008**, *56*, 9355−9361.

(27) Laemmli, U. K. Cleavage of structural proteins during the assembly of the head of bacteriophage T4. *Nature* **1970**, *227*, 680−685.

(28) McIntosh, R. A.; Yamazaki, Y.; Devos, K. M.; Dubcovsky, J.; Rogers, W. J.; Appels, R. Catalogue of gene symbols for wheat. *Annu. Wheat Newsl.* **2003**, *49*, 246−282.

(29) Salmanowicz, B. P. Identification and characterization of high molecular-weight secalins from triticale seeds by capillary zone electrophoresis. *Electrophoresis* **2010**, *31*, 2226−2235.
(30) Kubicka, H.; Carrillo, J. M.; Benito, C. Zmienność morfologiczna i polimorfizm białek zapasowych w liniach wsobnych żyta ozimego (*Secale cereale* L.) (Morphological variability and storage proteins polymorhism in inbred lines of winter rye *Secale cereale* L.; in Polish). *Zeszyty Naukowe Politechniki Białostockiej* **2005**, *10*, 257−265.
(31) Yan, Y.; Jiang, Y.; Sun, M.; Yu, J.; Xiao, Y.; Zheng, J.; Hu, Y.; Cai, M.; Li, Y.; Hsam, S. L. K.; Zeller, F. J. Rapid identification of HMW glutenin subunits from different hexaploid wheat species by acid capillary electrophoresis. *Cereal Chem.* **2004**, *81*, 561−566.
(32) Salmanowicz, B. P.; Langner, M.; Franaszek, S. Charge-based characterisation of high-molecular-weight glutenin subunits from common wheat by capillary isoelectric focusing. *Talanta* **2014**, *129*, 9−14.
(33) Amiour, N.; Bouguennec, A.; Marcoz, C.; Sourdille, P.; Bourgoin, M.; Khelifi, D.; Branlard, G. Diversity of seven glutenin and secalin loci within triticale cultivars grown in Europe. *Euphytica* **2002**, *123*, 295−305.
(34) Rzepka-Plevneš, D.; Smolik, M.; Lebecka, K. Polimorfizm białek zapasowych wybranych form żyta (*Secale* sp.) określony techniką SDS-PAGE (Polymorphism of seed protein in some rye (*Secale* sp.) forms determined by SDS-PAGE electrophoresis; in Polish). *Biuletyn Instytutu Hodowli i Aklimatyzacji Roślin* **2004**, *231*, 247−253.
(35) Vandeweghe, I. Comparative study of electrophoretic methods for cultivar identification of wheat and triticale. *Seed Sci. Technol.* **1991**, *19*, 41−50.
(36) Dimova, D.; Mihova, G.; Vulcheva, D.; Vulchev, D.; Ivanova, I. Using polymorphism of grain storage proteins for identification of feed barley varieties. *Bulg. J. Agric. Sci.* **2010**, *16*, 436−442.

**Table 1. UV−Vis and MS Characteristics (LC-MS and -MS$^E$ in Negative Ionization Mode) of Phenolic Compounds Identified in Freeze-Dried Aqueous Extracts of Green and Fermented *Cyclopia maculata***

| peak[a] | $t_R$ (min)[b] | $\lambda_{max}$[c] (nm) | accurate mass[d] | error (ppm) | proposed molecular formula | fragments | phenolic compound |
|---|---|---|---|---|---|---|---|
| 1 | 3.38 | 235, 280, 316 | 423.0927 | 0.0 | $C_{19}H_{19}O_{11}$ | 423 (32), 333 (16), 303 (100), 223 (7), 193 (27), 165 (6), 125 (5), 109 (5) | maclurin-3-*C*-*β*-glucoside |
| 2 | 5.75 | 293 | 407.0978 | −0.2 | $C_{19}H_{19}O_{10}$ | 407 (48), 317 (24), 287 (100), 245 (10), 193 (5) | iriflophenone-3-*C*-*β*-glucoside |
| 3 | 6.26 | 263, 276, 317, 366 | 871.1915 | 2.1 | $C_{40}H_{39}O_{22}$ | 871 (100), 751 (17), 691 (13), 557 (24), 539 (5), 421 (53), 403 (5), 331 (8), 301 (13), 269 (7)[e] | unidentified |
| 4 | 8.55 | 239, 257, 317, 366 | 421.0768 | −0.7 | $C_{19}H_{17}O_{11}$ | 421 (100), 331 (19), 301 (27), 271 (5), 259(5) | mangiferin |
| 5 | 8.84 | 237, 259, 327 | 437.0716 | −0.9 | $C_{19}H_{17}O_{12}$ | 437(100), 347 (54), 317 (83), 288 (23), 274 (9) | hydroxymangiferin |
| 6 | 9.05 | 239, 255, 316, 365 | 421.0767 | −0.9 | $C_{19}H_{17}O_{11}$ | 421 (100), 331 (35), 301 (50), 271 (7), 258 (9) | isomangiferin |
| 7 | 9.24 | 235, 271, 329 | 593.1498 | −1.3 | $C_{27}H_{29}O_{15}$ | 593 (100), 503 (5), 473 (14), 383 (17), 353 (24), 297 (7) | apigenin-6,8-di-*C*-glucoside (vicenin-2) |
| 8 | 9.61 | 281[f] | 449.1080 | 0.9 | $C_{21}H_{21}O_{11}$ | 449 (83), 287 (100), 151 (89), 135 (48) | eriodictyol-*O*-hexoside |
| 9 | 10.20 | 236, 255, 272, 323 | 437.0727 | −1.6 | $C_{19}H_{17}O_{12}$ | 437 (100), 347 (6), 317 (43), 289 (15) | hydroxyisomangiferin |
| 10 | 10.39 | 282[f] | 449.1087 | 0.7 | $C_{21}H_{21}O_{11}$ | 449 (67), 287 (100), 151 (84), 135 (41), 107 (10) | eriodictyol-*O*-hexoside |
| 11 | 11.78 | 279 | 613.1779 | 1.6 | $C_{27}H_{33}O_{16}$ | 613 (100), 595 (34), 493 (29), 475 (6), 433 (66), 403 (36), 373 (65), 331 (8), 297 (19), 269 (17), 209 (14), 135 (16) | 3-hydroxyphloretin-3′,5′-di-*C*-hexoside |
| 12 | 12.70 | 281, 330sh | 595.1660 | −0.5 | $C_{27}H_{31}O_{15}$ | 595 (89), 287 (100), 151 (70), 135 (20), 107 (6) | eriodictyol-7-*O*-rutinoside (eriocitrin) |
| 13 | 13.76 | 256, 264, 350 | 593.1519 | 2.2 | $C_{27}H_{29}O_{15}$ | 593 (100), 285 (87) | luteolin-7-*O*-rutinoside (scolymoside) |
| 14 | 14.18 | 280 | 597.1826 | 1.2 | $C_{27}H_{33}O_{15}$ | 597 (100), 477 (21), 459 (5), 417 (9), 387 (45), 357 (62), 345 (7), 315 (22), 285 (13), 209 (11) | phloretin-3′,5′-di-*C*-glucoside |
| 15 | 16.73 | 283, 328sh | 609.1814 | −0.8 | $C_{28}H_{33}O_{15}$ | 609 (56), 301 (100) | hesperetin-7-*O*-rutinoside (hesperidin) |

[a]Peak numbers correspond to peaks in Figure 1. [b]Recorded during LC-DAD-MS analysis using a Waters Acquity UPLC instrument. [c]sh, shoulder. [d]Accurate mass determined experimentally. [e]Data acquired in MS/MS mode. [f]Typical flavanone shoulder at ca. 330 nm not detected due to low concentration.

and problematic integration due to background absorption. The same problems were observed for *C. subternata* analyzed using the "generic" HPLC method.[18]

The present paper therefore describes the development and application of a validated HPLC method using diode array detection (DAD) suitable for the qualitative and quantitative analysis of *C. maculata* aqueous extracts. Mass spectrometry (MS) was applied to confirm peak purity and the identity of known compounds and to tentatively identify additional compounds. Extracts were prepared from the unfermented plant material of a large number of wild-harvested and cultivated seedling plants to understand the extent of batch-to-batch variation that could be expected when using this species for the production of nutraceutical extracts. Variation in extract composition was assessed in terms of the content of individual phenolic compounds and chemometric analysis of the chromatographic fingerprints, using similarity analysis and principal component analysis (PCA). The major compounds present in extracts of fermented *C. maculata* plant material were also analyzed to assess changes in quantitative composition with "fermentation" as this type of extract is also used by the food industry as an ingredient.

## MATERIALS AND METHODS

**Chemicals.** All chemicals were of analytical grade and sourced from either Sigma-Aldrich (St. Louis, MO, USA) or Merck Chemicals (Darmstadt, Germany); HPLC gradient grade acetonitrile was purchased from Merck. Authentic reference standards with purity >95% were obtained from Sigma-Aldrich (hesperidin and scolymoside), Extrasynthese (Genay, France; mangiferin, eriocitrin, and eriodictyol-7-*O*-glucoside), Phytolab (Vestenbergsgreuth, Germany; vicenin-2), and Chemos (Regenstauf, Germany; isomangiferin). Iriflophenone-3-*C*-glucoside (purity ≥94%), isolated from *Cyclopia genistoides*,[19] was obtained from the Post-Harvest and Wine Technology Division, ARC Infruitec-Nietvoorbij (Stellenbosch, South Africa). Deionized water, prepared using an Elix water purification system (Millipore, Milford, MA, USA), was further purified to HPLC grade using a Milli-Q Academic water purification system (Millipore).

**Plant Material and Extract Preparation.** Two sets of plant material were used in the present study. All plants were identified by M. Joubert, a honeybush cultivation expert from the ARC Honeybush Breeding Program (Cultivar Development Division, ARC Infruitec-Nietvoorbij, Stellenbosch, South Africa) on the basis of the classification of Schutte.[20] Plant material for sample set 1 comprised nine batches of plant material, harvested during summer (December 2009) from bushes forming part of the same natural population growing in marsh land on Welgedacht farm (Riversdale, South Africa). The shoots from two to three bushes made up a batch. Each plant material batch ($n$ = 9) was processed as follows: Thick stems with little or no side stems were removed, and the plant material was mechanically shredded (≤3 mm), mixed, and divided into two sub-batches for preparation of unfermented and fermented plant material ($n$ = 9 each). The unfermented plant material was prepared by drying one sub-batch without delay in a cross-flow drying tunnel at 40 °C for 6 h (<10% moisture content). The dried plant material was then sieved for 90 s to obtain the fraction <1.4 mm (12 mesh) using a SMC Mini-sifter (JM Quality Services, Cape Town, South Africa). Sifting removed mostly coarse pieces of stems. The other sub-batch was "fermented" (oxidized) by adding tap water to the cut plant material to

achieve a moisture content of ca. 60−65%, followed by heating at 90 °C for 16 h. Drying and sieving were performed as described above.

Plant material for sample set 2 comprised shoots of individual seedlings ($n$ = 40; 2 years old) grown in pots at ARC Infruitec-Nietvoorbij (Stellenbosch, South Africa) and harvested during winter (June 2011). The seeds for the pot trial were collected from a natural population, also growing in marsh land on Welgedacht farm. Thick stems were removed, and the remaining plant material was dried intact at 40 °C in a drying tunnel to ca. 8−10% moisture content. The dried plant material was ground to a powder with a Retsch mill (1 mm sieve; Retsch GmbH, Haan, Germany).

A freeze-dried extract of each plant material sample was prepared as described by de Beer et al.[21] Extracts were reconstituted by dissolving them in deionized water (ca. 6 mg/mL), and aliquots were frozen at −20 °C until analysis.

**HPLC-DAD Method Development and Validation.** All HPLC-DAD analyses were performed on an Agilent 1200 series HPLC instrument, consisting of an in-line degasser, quaternary pump, autosampler, column oven, and DAD, controlled by Chemstation software (Agilent Technologies Inc., Santa Clara, CA, USA). The following columns were evaluated using the solvent gradient as reported by de Beer and Joubert:[18] a Zorbax SB-C18 (100 × 4.6 mm; 1.8 μm; 80 Å) and a Zorbax Eclipse XDB-C18 (150 × 4.6 mm; 5 μm; 80 Å) from Agilent Technologies (Waldbronn, Germany); a Kinetex C18 (150 × 4.6 mm; 2.6 μm; 100 Å) with core−shell technology and a Gemini-NX C18 (150 × 4.6 mm; 3 μm; 110 Å) from Phenomenex (Santa Clara, CA, USA). A randomly selected pair of unfermented and fermented extracts were employed for method development to allow for expected profile differences introduced by fermentation. For optimization of separation conditions on the selected column, acetic acid and formic acid as aqueous phases (solvent A) and acetonitrile and methanol as organic modifiers (solvent B) were evaluated as mobile phases. Furthermore, scouting gradients, using 2% acetic acid (A) and acetonitrile (B), were evaluated at different temperatures. The final method, subjected to validation, entailed separation on the Gemini-NX C18 column at 30 °C and 1 mL/min flow rate using 2% acetic acid (A) and acetonitrile (B). The mobile phase gradient profile was as follows: 0−2 min, 8% B; 2−31 min, 8−38% B; 31−32 min, 38−50% B; 32−33 min, 50% B; 33−34 min, 50−8% B; 34−44 min, 8% B. The extracts used for method development and a standard calibration mixture were used for method validation. This entailed determination of the linearity of response, compound stability over a 24 h period, and intra- and interday precision, as previously described.[18] The specificity of the method was evaluated by assessing the purity of peaks based on UV−vis and MS spectra.

**Identification of Phenolic Compounds.** LC-MS analyses were conducted on a Waters Acquity UPLC equipped with a binary pump, in-line degasser, autosampler, column oven, and DAD (Waters, Milford, MA, USA), which was coupled to a Synapt G2 Q-TOF mass spectrometer (Waters) with an electrospray ionization (ESI) source. Data acquisition and analysis were performed using MassLynx v.4.1 (Waters). The LC method used was the same as described for the validated HPLC-DAD method except for the following modifications: gradient time delayed by 0.2 min (each step); percentage of solvent B increased by 0.5% at each time interval; and temperature increased by 2 °C. These alterations were necessary to obtain similar separations on the Waters UPLC as on the Agilent HPLC instrument.

UV−vis spectra were recorded from 235 to 450 nm. Prior to introduction into the ionization chamber, the eluent was split in a ratio of 3:2. MS and $MS^E$ data were attained in both positive and negative ESI modes using a 3 μL injection volume. Mass ranges of 200−1500 and 50−1500 Da were used for MS and $MS^E$ acquisition modes, respectively. A collision energy ramp from 25 to 60 V was used for $MS^E$. Leucine enkephalin was used as lock mass, and the instrument was calibrated using a sodium formate solution. The MS ionization parameters were as follows: desolvation temperature, 275 °C; source temperature, 120 °C; nitrogen flow rate, 650 L/h; capillary voltage, 2500 V; cone voltage, 15 V. In the case of LC-MS/MS analysis (for compound **3**), a scan range of 50−875 Da was used with a collision trap energy of 30 V.

**Quantification of Phenolic Compounds using HPLC-DAD.** UV−vis spectra were recorded from 200 to 550 nm for all samples. The xanthones (mangiferin and isomangiferin) and the flavone (vicenin-2) were quantified using peak areas at 320 nm, whereas the flavanones (eriocitrin, an eriodictyol-*O*-hexoside (**8**; Table 1) and hesperidin) and benzophenones (iriflophenone-3-*C*-glucoside and maclurin-3-C-glucoside) were quantified using peak areas at 288 nm. Seven-point calibration curves were constructed with the available authentic standards by dilution of the stock solutions in water. Due to the small quantity available, iriflophenone-3-*C*-glucoside was not included in the calibration series and was quantified using a response factor (1.1511) previously determined relative to hesperidin. Furthermore, maclurin-3-*C*-glucoside and eriodictyol-*O*-hexoside were quantified as iriflophenone-3-*C*-glucoside and eriocitrin equivalents, respectively, due to the unavailability of authentic reference standards. Calibration curves were developed to accommodate the expected concentration range (μg injected) of the compounds in the extracts, namely, mangiferin (0.02−4.9 μg), isomangiferin (0.005−1.3 μg), eriocitrin (0.007−1.8 μg), hesperidin (0.009−2.3 μg), and vicenin-2 (0.01−1.0 μg).

**Data Analysis.** *Analyis of Variance (ANOVA).* Quantitative data were subjected to univariate ANOVA using SAS, version 9.2 (SAS Institute, Cary, NC, USA). The Shapiro−Wilk test was performed to test for normality. Student's $t$ test was used to calculate the least significant difference (LSD) at the 5% level to facilitate a comparison of mean values.

*Pretreatment of Chromatograms for Fingerprint Analysis.* The recorded absorbance matrices for the duplicate injections of each extract (wavelengths × time) of *C. maculata* ($n$ = 98) were exported from ChemStation software (Agilent) as *.csv files for the wavelength range from 220 to 500 nm (2 nm bandwidth) and from 0 to 40 min using a ChemStation macro, export3D (available in the Agilent user contribution library). The *.csv files were each changed to comma delimited format in Microsoft Excel (2010) and then imported into MATLAB R2012b (The MathWorks, Natick, MA, USA). All matrices contained 12000 time (data) points and were averaged to individual absorbance vectors (absorbance × time). These new vectors were arranged into a new matrix, with dimensions of 98 × 12000 (duplicate extracts × time). Peak alignment was conducted by means of correlation-optimized warping (COW)[22] using MATLAB code freely available from www.models.life.ku.dk/DTW_COW, followed by background elimination by means of the penalized asymmetric least-squares (PALS) method.[23] Normalization[24] to a constant sum was then performed by dividing each signal value for each sample by the sum of all signal values for that specific sample. The time axis of the matrix was shortened to remove irrelevant data. The final dimensions of the new matrix were 98 × 5381.

*Similarity Analysis.* Similarity analysis of the extracts was conducted by determining the correlation coefficients between fingerprints of the extracts. The similarity analysis conducted in this study was based on the Pearson product-moment correlation coefficient, $r$.[25]

$$r(\mathbf{x}_1, \mathbf{x}_2) = \frac{\mathrm{cov}(\mathbf{x}_1\mathbf{x}_2)}{s_{x1}s_{x2}} = \frac{\sum_{j=1}^{q}(x_{1j} - \bar{x}_1)(x_{2j} - \bar{x}_2)}{\sqrt{\sum_{j=1}^{q}(x_{1j} - \bar{x}_1)^2 \sum_{j=1}^{q}(x_{2j} - \bar{x}_2)^2}} = \frac{(\mathbf{x}_1 - \bar{x}_1)(\mathbf{x}_2 - \bar{x}_2)}{\|\mathbf{x}_1 - \bar{x}_1\| \|\mathbf{x}_2 - \bar{x}_2\|} \quad (1)$$

This coefficient was calculated between each pair of fingerprints, $\mathbf{x}_i$, where $i$ = 1, 2, ..., $p$ are the samples evaluated, and each fingerprint comprises absorbance measurements at $j$ = 1, 2, ..., $q$ time points. In each case $\mathbf{x}_1$ and $\mathbf{x}_2$ are the individual fingerprints or vectors that were considered; $x_{1j}$ and $x_{2j}$ are the absorbances that were measured for each fingerprint at the specific $j$th time point, and $x_1$ and $x_2$ are the mean values of the respective absorbances of each fingerprint. Furthermore, cov is the covariance of the fingerprints and $s_{xi}$ is the standard deviation of the fingerprints.

*Principal Component Analysis.* PCA was conducted on the same data as for similarity analysis after mean centering to determine whether any relevant information could be extracted from the data.

$$X = TP^t + E \quad (2)$$

The data matrix was decomposed into a product of two matrices where **T** is the score matrix, **P** is the loading matrix, $\mathbf{P}^t$ is the transpose of **P**, and **E** is the matrix of residuals.

## RESULTS AND DISCUSSION

**HPLC-DAD Method Development and Validation.** The method described in de Beer et al.[21] was not suitable for the analysis of *C. maculata* extracts, due to minor unidentified compounds, which were not present in *C. subternata*, coeluting with mangiferin and isomangiferin. Column performance was therefore assessed with regard to the separation of mangiferin and isomangiferin from the unidentified coeluting compounds. Of the four columns evaluated, the Gemini-NX C18 column provided the best separation, as observed for *C. subternata*.[21] However, the gradient differed from that used for *C. subternata* to allow adequate resolution in this case. Separation at 30 °C provided the lowest degree of coelution for hesperidin, eriocitrin, and iriflophenone-3-*C*-glucoside, while also maintaining optimal resolution for mangiferin and isomangiferin. The HPLC-DAD chromatograms of green and fermented *C. maculata* extracts using the optimized conditions are illustrated in Figure 1.

To determine the suitability of the developed method for the routine analysis of the major phenolic compounds in green and fermented *C. maculata* extracts, method validation was conducted (data summarized in Supporting Information Tables S1–S3). The linearity of the standard calibration curves was excellent ($r^2$ = 1.000) (Table S1). The stability (Table S2) of the compounds in the standard calibration mixture and extracts and the intra- and interday precision (Table S3) of the method were good (%RSD values <4 and <5%, respectively, except for vicenin-2, which had a +5.9% change over 24 h).

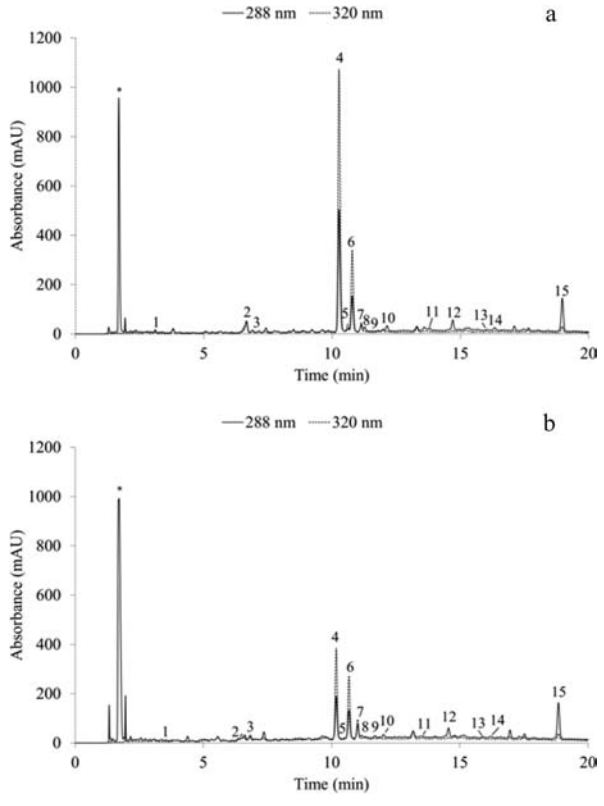


**Figure 1.** HPLC-DAD chromatograms (Agilent 1200 HPLC system) of aqueous extracts prepared from (a) green and (b) fermented *Cyclopia maculata* plant material using the optimized method (∗, ascorbic acid peak; see Table 1 for identity of numbered peaks).

**Identification of Phenolic Compounds.** LC-MS analysis was conducted on paired green and fermented *C. maculata* aqueous extracts ($n$ = 1 each) in both positive and negative ESI modes. LC-MS and -$MS^E$ data of each peak in negative ionization mode were used in combination with comparison of the relative retention times and UV–vis spectra with those of the authentic reference standards, where available, to identify the compounds (Table 1). LC-MS and -$MS^E$ data obtained in positive ionization mode are presented in the Supporting Information (Table S4) as further evidence of compound identification. The presence of iriflophenone-3-*C*-glucoside (**2**), mangiferin (**4**), isomangiferin (**6**), vicenin-2 (**7**), eriocitrin (**12**), scolymoside (**13**), and hesperidin (**15**) was confirmed in both the green and fermented extracts using authentic reference standards. Of these, vicenin-2 (**7**) was identified for the first time in *C. maculata*. Additional compounds were tentatively identified by comparison to published data (Table 1); these will be discussed in more detail in the sections below with respect to their MS fragmentation patterns, retention behavior, and UV–vis spectra. Compound structures, including proposed structures for tentatively identified compounds, are shown in Figure 2.

*Xanthones.* Two additional xanthones (**5** and **9**), with UV–vis spectra similar to those of mangiferin and isomangiferin, were detected at retention times 8.84 and 10.20 min, respectively. Both compounds displayed pseudomolecular ions at $m/z$ 437 ($[M - H]^-$), and a molecular formula of $C_{19}H_{18}O_{12}$ ($[M - H]^-$) is proposed. Both compounds also displayed major fragment ions at $m/z$ 317 ($[M - H - 120]^-$) and $m/z$ 347 ($[M - H - 90]^-$), indicating C-glycosidic structures.[26] Furthermore, compounds **5** and **9** differ from isomers **4** and **6** by 16 amu. These data suggest possible hydroxylated derivatives of mangiferin and isomangiferin. The principal $MS^E$ fragments confirm that the additional hydroxyl group is attached to the aglycone moiety in both cases. According to their relative elution order, compounds **5** and **9** are presumably the hydroxylated derivatives of mangiferin (**4**) and isomangiferin (**6**), respectively. They eluted slightly later than compounds **4** and **6**, respectively, which was somewhat surprising in view of the additional OH group. Hydroxylation most likely occurs at position 5 or 8 (indicated by $R_3$ or $R_4$) on the B ring (Figure 2), although this could not be confirmed on the basis of the available MS data. These compounds have not been reported previously in *Cyclopia* species.

Compound **3**, with the proposed molecular formula of $C_{40}H_{39}O_{22}$ ($[M - H]^-$), had a retention time of 6.26 min and a molecular ion at $m/z$ 871 $[M - H]^-$. This compound seems to be a derivative of mangiferin (**4**) or isomangiferin (**6**), because it contains fragments identical to these compounds at $m/z$ 421 ((iso)mangiferin molecular ion), $m/z$ 331 ($[M - H - 90]^-$), and $m/z$ 301 ($[M - H - 120]^-$). The much higher molecular weight of compound **3** appears to indicate a dimeric derivative of (iso)mangiferin,[27,28] although the lower retention time is not consistent with this and rather points to a highly glycosylated derivative. High molecular weight fragments also indicate the presence of more than one *C*-glycosidic group, for example $m/z$


dx.doi.org/10.1021/jf5028735 | J. Agric. Food Chem. 2014, 62, 10542–10551

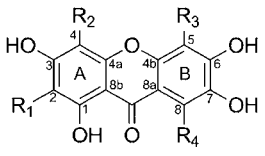

*Xanthones*
Mangiferin (**4**): $R_1$ = glucosyl; $R_2$, $R_3$, $R_4$ = H
Isomangiferin (**6**): $R_2$ = glucosyl; $R_1$, $R_3$, $R_4$ = H
Hydroxymangiferin (**5**) *: $R_1$ = glucosyl; $R_2$ = H; $R_3$ or $R_4$ = OH or H
Hydroxyisomangiferin (**9**) *: $R_2$ = glucosyl; $R_1$ = H; $R_3$ or $R_4$ = OH or H

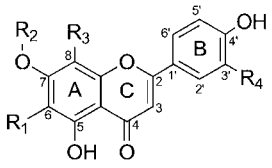

*Flavones*
Apigenin-6,8-di-*C*-glucoside (Vicenin-2) (**7**): $R_1$, $R_3$ = glucosyl; $R_2$, $R_4$ = H
Scolymoside (**13**): $R_1$, $R_3$ = H; $R_2$ = rutinosyl; $R_4$ = OH

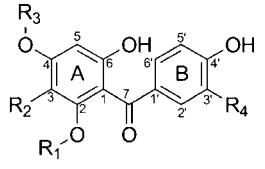

*Benzophenones*
Maclurin-3-*C*-*β*-glucoside (**1**): $R_1$, $R_3$ = H; $R_2$ = glucosyl; $R_4$ = OH
Iriflophenone-3-*C*-*β*-glucoside (**2**): $R_1$, $R_3$, $R_4$ = H; $R_2$ = glucosyl

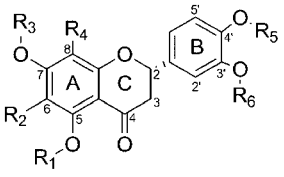

*Flavanones*
Eriodictyol-*O*-hexoside (**8**, **10**) *: $R_1$ or $R_3$ = hexosyl or H; $R_2$, $R_4$, $R_5$, $R_6$ = H
Eriocitrin (**12**): $R_3$ = rutinosyl; $R_1$, $R_2$, $R_4$, $R_5$, $R_6$ = H
Hesperidin (**15**): $R_3$ = rutinosyl; $R_5$ = $CH_3$; $R_1$, $R_2$, $R_4$, $R_6$ = H

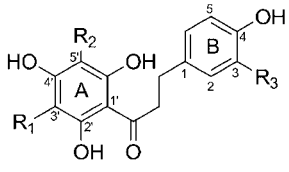

*Dihydrochalcones*
3-Hydroxyphloretin-3′,5′-di-*C*-hexoside (**11**): $R_1$, $R_2$ = hexosyl; $R_3$ = OH
Phloretin-3′,5′-di-*C*-glucoside (**14**): $R_1$, $R_2$ = glucosyl; $R_3$ = H

**Figure 2.** Structures of phenolic compounds identified in freeze-dried aqueous extracts of green and fermented *Cyclopia maculata* (∗ indicates that the positions of hexosyl or hydroxyl moieties are not certain).

751 ($[M - H - 120]^-$), *m/z* 691 ($[M - H - 2 \times 90]^-$), *m/z* 601 ($[M - H - 120 - 150]^-$), and *m/z* 571 ($[M - H - 2 \times 150]^-$) (Supporting Information, Figure S2). This compound needs to be investigated further, as no structure could be proposed with certainty on the basis of currently available data.

*Benzophenones.* Compound **1**, with a retention time of 3.38 min, had a pseudomolecular ion at *m/z* 423 ($[M - H]^-$), and a molecular formula of $C_{19}H_{19}O_{11}$ $[M - H]^-$ is proposed on the basis of accurate mass data. Its relative retention, UV−vis spectrum, and MS fragmentation pattern are consistent with those of maclurin-3-*C*-*β*-glucoside, a compound present in the leaves of *Mangifera indica* L.[29,30] and *C. genistoides*.[31] Maclurin-3-*C*-*β*-glucoside has not been reported previously in *C. maculata*.

*Dihydrochalcones.* Compounds **14** and **11** had retention times of 14.18 and 11.78 min, respectively. Molecular formulas of $C_{27}H_{33}O_{15}$ ($[M - H]^-$) and $C_{27}H_{33}O_{16}$ ($[M - H]^-$) are proposed for compounds **14** and **11**, respectively. The UV−vis spectra, retention behavior, and $MS^E$ fragments of the two compounds correspond to phloretin-3′,5′-di-*C*-glucoside (**14**)[32] and its hydroxylated derivative, 3-hydroxyphloretin-3′,5′-di-*C*-hexoside (**11**), as discussed in de Beer et al.[21] Phloretin-3′,5′-di-*C*-glucoside has previously been identified in an aqueous extract of green *C. maculata* using LC-MS.[6] 3-Hydroxyphloretin-3′,5′-di-*C*-hexoside is identified here for the first time in *C. maculata*.

*Flavanone O-glycosides.* Compounds **8** and **10**, with similar pseudomolecular ions at *m/z* 449 ($[M - H]^-$) and fragments at *m/z* 287 ($[M - H - 162]^-$) and *m/z* 151, eluted at retention times of 9.61 and 10.39 min, respectively. Their UV−vis spectra were characteristic of flavanones. On the basis of these data and the major fragment ion corresponding to eriodictyol, compounds **8** and **10** were tentatively identified as eriodictyol-*O*-hexosides. An eriodictyol-5-*O*-glucoside and eriodictyol-7-*O*-glucoside were previously isolated from *C. intermedia* and identified by means of nuclear magnetic resonance (NMR).[10] However, both compounds **8** and **10** showed earlier retention times compared to an authentic reference standard of eriodictyol-7-*O*-glucoside. Similar retention behavior has been noted for the 5-*O*-glucosides of quercetin and apigenin compared to their 7-*O*-glucoside counterparts.[33] Consequently, these compounds may be the (*R*)- and (*S*)-diastereomers of eriodictyol-5-*O*-glucoside, which can be separated by reversed phase LC.[34] No eriodictyol-hexosides have been reported previously in *C. maculata*.

**Quantitative Phenolic Composition of Green and Fermented *C. maculata* Extracts.** Fermentation conditions employed in the current study were based on those used by industry. The validated HPLC-DAD method was used to quantify the major xanthones (mangiferin and isomangiferin), flavanones (hesperidin, eriocitrin, and an eriodictyol-*O*-hexoside), benzophenones (iriflophenone-3-*C*-*β*-glucoside and maclurin-3-*C*-*β*-glucoside), and a flavone (vicenin-2) (Table 2). Maclurin-3-*C*-*β*-glucoside, iriflophenone-3-*C*-*β*-glucoside, and the eriodictyol-*O*-hexoside could not be quantified in fermented extracts due to their substantially lower levels


dx.doi.org/10.1021/jf5028735 | J. Agric. Food Chem. 2014, 62, 10542−10551

**Table 2. Quantitative Data from Aqueous Extracts of Unfermented (Green) and Fermented *C. maculata* (Wild-Harvested) ($n$ = 9; Set 1)**

| compound | content (g/100 g soluble solids) | | | | |
|---|---|---|---|---|---|
| | mean | min | max | SD[a] | %RSD[b] |
| **Green** | | | | | |
| maclurin-3-*C*-glucoside | 0.08 | 0.06 | 0.10 | 0.01 | 17.75 |
| iriflophenone-3-*C*-glucoside | 0.38 | 0.32 | 0.47 | 0.05 | 13.32 |
| mangiferin | 5.18 a[c] | 4.29 | 6.04 | 0.50 | 9.70 |
| isomangiferin | 1.48 a | 1.3 | 1.71 | 0.12 | 8.04 |
| vicenin-2 | 0.20 a | 0.16 | 0.24 | 0.02 | 10.12 |
| eriodictyol-*O*-hexoside | 0.14 | 0.11 | 0.17 | 0.02 | 14.27 |
| eriocitrin | 0.33 a | 0.31 | 0.38 | 0.02 | 7.04 |
| hesperidin | 0.89 a | 0.75 | 0.99 | 0.09 | 10.13 |
| **Fermented** | | | | | |
| mangiferin | 1.04 b | 0.69 | 1.40 | 0.26 | 25.23 |
| isomangiferin | 0.62 b | 0.50 | 0.74 | 0.10 | 15.76 |
| vicenin-2 | 0.21 a | 0.18 | 0.25 | 0.02 | 10.93 |
| eriocitrin | 0.16 b | 0.12 | 0.20 | 0.03 | 16.10 |
| hesperidin | 0.51 b | 0.39 | 0.51 | 0.07 | 13.74 |

[a]Standard deviation. [b]Relative standard deviation as percentage of mean. [c]Different letters indicate significant ($p$ < 0.05) differences between green and fermented extracts.

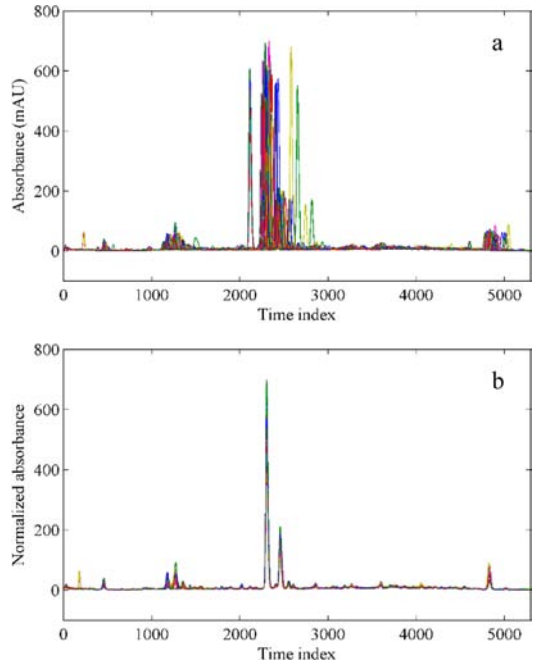


**Figure 3.** Overlay of *Cyclopia maculata* chromatographic fingerprints ($n$ = 49) (a) before and (b) after pretreatment.

compared to green extracts and poor resolution with other minor compounds. Mangiferin, isomangiferin, eriocitrin, and hesperidin levels decreased by 80, 57, 52, and 42%, respectively, following fermentation. Positioning of the sugar moiety on the dibenzo-$\gamma$-pirone structure clearly affects stability as exemplified by the difference in the stabilities of mangiferin and isomangiferin. Hesperidin has been shown to be more thermally stable than other flavanones, such as narirutin, during pasteurization treatments of citrus juice.[35−37] Vicenin-2 remained stable during fermentation.

*C. maculata*, compared to other species analyzed to date, including *C. subternata*, *C. sessiliflora*, *C. intermedia*, and *C. genistoides*,[18,21] appears to have a less complex chromatographic profile, where only a few compounds are present in significant amounts for quantification purposes. Mangiferin and isomangiferin contents of extracts from green *C. maculata* were lower than those of *C. genistoides*, which to date had the highest mangiferin content of the species analyzed.[12,17,33] *C. maculata* extracts, however, contain more mangiferin than those of *C. subternata*, *C. intermedia*, and *C. sessiliflora*[18,21,38] and thus have potential for further development as a food ingredient extract with high mangiferin content, considering the interest in mangiferin as a nutraceutical compound.[13]

**Assessment of Genotypic Variation Using Chemometric Analysis.** To investigate the genotypic variation of *C. maculata*, the quantitative data for individual phenolic compounds and the complete chromatographic fingerprints of aqueous extracts were analyzed. The data from unfermented extracts of sample set 1 (wild-harvested; $n$ = 9) were combined with those of sample set 2 (cultivated; $n$ = 40) to provide a larger sample set.

*Data Pretreatment for Development of Fingerprints.* Before chemometric analysis of chromatographic fingerprints could be performed, a number of pretreatment steps were essential. The chromatograms of the *C. maculata* extracts before any pretreatment are shown in Figure 3a. From this figure it is clear that peak alignment was needed due to extreme shifts in peak retention times. These shifts could be due to column aging and general experimental variation,[17] as analyses were performed over a period of 4 months. Pretreatment, therefore, started with peak alignment, which was achieved by means of COW. This method was chosen because it is an efficient and popular method among chemometricians[15,25,39] and MATLAB code is freely available. COW consists of piecewise linear alignment of chromatograms toward a target chromatogram by means of stretching and compressing of segments using dynamic programming.[22] Peak alignment entails a trial-and-error-based selection of the best input parameters to obtain the optimal alignment toward a target chromatogram.[22] The latter chromatogram was selected as the one showing the highest correlation with all of the chromatograms in the sample set.[40] The optimal number of segments for alignment of the data set was between 60 and 100, whereas the optimal slack size was between 20 and 30 data points.

After peak alignment, the background was removed from the data set to further improve the relevance of the data for analysis.[23] A value of $10^4$ for the lambda ($\lambda$) input parameter for smoothing (usually between $10^2$ and $10^9$) was deemed optimal after visual inspection of the results.[41] The first derivatives of the signals were used to determine the signal smoothness. To account for differing HPLC injection volumes due to inevitable small instrumental variations and experimental weighing errors, normalization was applied to each vector (injection) to scale them to the same unit. Figure 3b shows the chromatograms after acceptable pretreatment was achieved. The chromatograms were shortened after pretreatment of the data, by removing the elution time representing the dead volume and the ascorbic acid peak from the start, and the time required for the re-equilibration of the column from the end of the chromatogram. The removal of these chromatogram sections was necessary to exclude all information that would not represent relevant data. Consequently, the dimensions of the new matrix were 98 × 5381.

*Comparison of Chromatographic Fingerprints and Quantitative Data.* The similarity of the fingerprint of each

sample extract to those of all other extracts was evaluated by calculating the Pearson product-moment correlation coefficients ($r$). For similar fingerprints, the correlation is high when $r$ is close to 1.[17] The results are presented in the form of a heat map indicating $r$ values for each pair of fingerprints by means of colors (Figure 4). Fingerprints for duplicate injections were

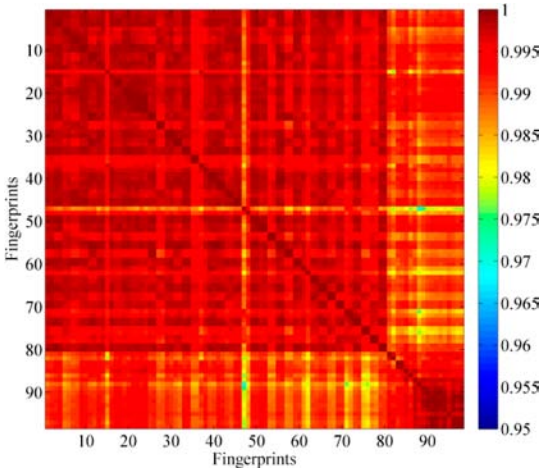


**Figure 4.** Heat map of correlation coefficients between fingerprints of *Cyclopia maculata* ($n$ = 98) after pretreatment (duplicate injections are shown as separate measurements).

extremely similar, confirming that pretreatment was effective. The similarity analysis showed that all of the extracts were surprisingly similar, with $r$ values ranging between ca. 0.97 and 1.00 (Figure 4). These high correlation values may, in part, be attributed to the simplicity of the chromatogram, which comprises only two large- and three medium-intensity peaks and many minor peaks. The high level of mangiferin in the samples, relative to the other compounds, limits the quantities injected so that detector response for the minor peaks is low. The fingerprints of the extracts prepared from wild-harvested (set 1) and cultivated (set 2) plants were very similar with regard to $r$ values. The wild-harvested plants were from the same wild population that provided the seeds for cultivated plants.

PCA was also performed on the combined data matrix of sample sets 1 and 2 after mean centering of the fingerprints to further explore the genotypic variation of the phenolic profile of *C. maculata*. On the basis of the first two principal components (PCs), the wild-harvested samples (set 1; $n$ = 9; no. 81−98) were clearly separated from the rest of the samples (set 2; $n$ = 40; no. 1−80) in the bottom right quadrant (Figure 5a). As indicated by the loadings (Figure 5b,c), this clustering of the wild-harvested samples is associated to a large extent with mangiferin and isomangiferin contents, whereas the samples from set 2 are associated with the remaining compounds. Quantitative data (Tables 2 and 3) showed that the mangiferin and isomangiferin contents of wild-harvested samples were slightly lower than those of the cultivated samples. On the other hand, the extracts of the wild-harvested samples contained only about half of the levels of hesperidin, maclurin-3-C-glucoside, and iriflophenone-3-C-glucoside compared to the extracts of set 2; this is likely the reason for the differentiation of the samples observed in Figure 5a. The lower hesperidin content for set 1 samples is attributed to the sieving process that removed the coarse pieces of stem. Analysis of *C.*

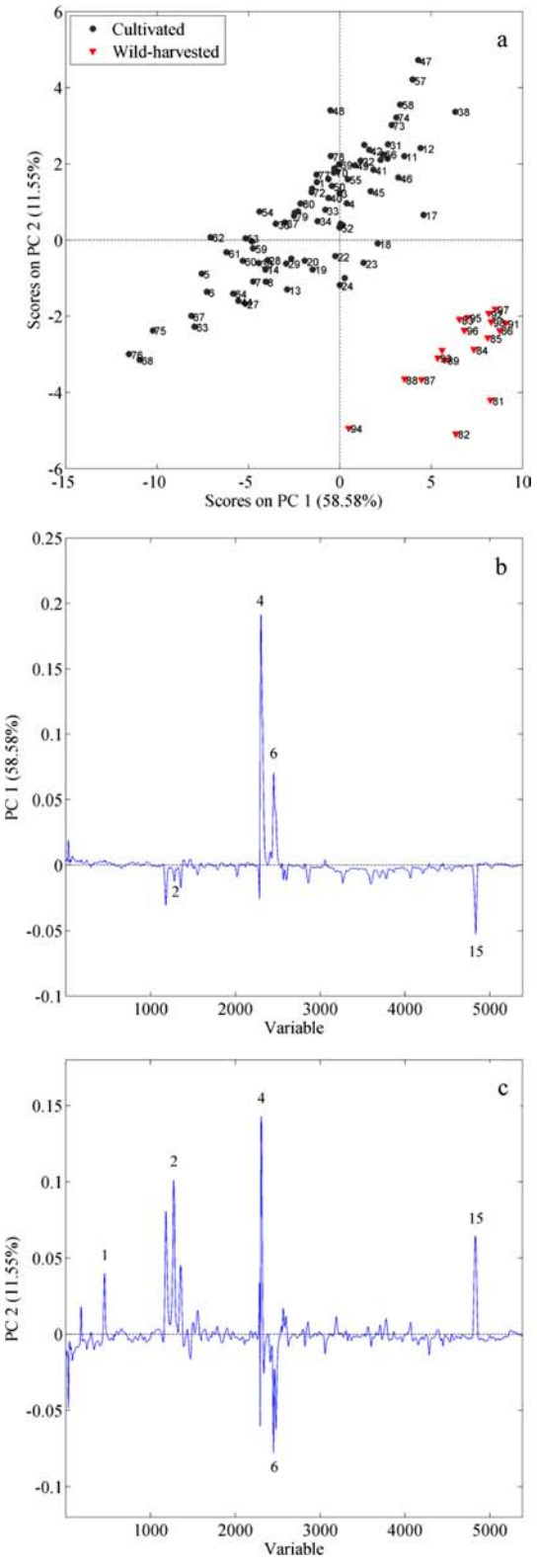


**Figure 5.** (a) PCA scores plot of PC1 versus PC2 for fingerprints of *Cyclopia maculata* samples ($n$ = 98) and loadings plots of (b) PC1 and (c) PC2.

*maculata*[42] and *C. subternata*[21] leaf and stem plant material showed that hesperidin is mostly concentrated in the stems. However, this does not explain the lower iriflophenone-3-C-glucoside and maclurin-3-C-glucoside concentrations in the wild-harvested samples. Other differences between the sample

**Table 3. Quantitative Data from Aqueous Extracts of Unfermented (Green) *C. maculata* (Cultivated) ($n$ = 40; Set 2)**

| compound | content (g/100 g soluble solids) | | | | |
|---|---|---|---|---|---|
| | mean | min | max | SD[a] | %RSD[b] |
| maclurin-3-*C*-glucoside | 0.15 | 0.07 | 0.35 | 0.06 | 40.29 |
| iriflophenone-3-*C*-glucoside | 0.62 | 0.25 | 1.47 | 0.23 | 37.64 |
| mangiferin | 5.87 | 4.02 | 8.09 | 0.96 | 16.33 |
| isomangiferin | 1.65 | 1.23 | 2.13 | 0.21 | 12.49 |
| vicenin-2 | 0.29 | 0.15 | 0.35 | 0.04 | 14.47 |
| eriodictyol-*O*-hexoside | 0.28 | 0.15 | 0.47 | 0.07 | 23.02 |
| eriocitrin | 0.44 | 0.25 | 0.69 | 0.11 | 24.01 |
| hesperidin | 1.78 | 1.44 | 2.69 | 0.23 | 12.90 |

[a]Standard deviation. [b]Relative standard deviation as percentage of mean.

sets include growing conditions and harvest season: wild-harvested plants grew in marshy conditions and were harvested in summer, whereas the cultivated plants were irrigated and harvested in winter. Joubert et al.,[43] investigating *C. genistoides*, showed that environmental factors could affect levels of these compounds.

For PC3 of the fingerprint data ($n$ = 98) of the extracts, more information was revealed and sample duplicates 47 and 48 were separated from the other samples (Figure 6a). Upon further investigation (Figure 6b), it was determined that the chromatograms of this sample contained a peak (peak a) that none of the other samples contained (Supporting Information, Figure S3). According to the quantitative data this "atypical" sample also had the highest quantity of hesperidin (data not shown). The loadings of PC3 also indicate that hesperidin contributes to this differentiation (Figure 6b). PC4 and PC5 did not reveal any further information of interest.

If similarity analysis were performed using a fixed cutoff of 0.95 for $r$, the "atypical" sample would still be considered as similar to the other samples, despite its having the lowest overall correlation with the other samples. Additional exploratory analysis (PCA) was useful to identify a unique feature while indicating some basis for differentiation from the other samples. It is therefore advisible that similarity analysis should not be used in isolation. Overall, the variation between the fingerprints of the different *C. maculata* extracts was relatively small, except for the clear differences in hesperidin content based on the stem-to-leaf ratio and the presence of an "atypical" extract. Quantitative data for selected compounds in the cultivated seedlings (Table 3) indicated relatively low variation, with %RSD values ranging from 12.5 to 16.3% for mangiferin, isomangiferin, vicenin-2, and hesperidin. The other compounds varied substantially more (%RSD values between 23.0 and 40.3%). Variation of the latter compounds in the wild-harvested seedlings was less than observed for the cultivated seedlings. In the case of wild-harvested seedlings, shoots of two to three bushes comprised a batch (i.e., sample) to obtain sufficient plant material for processing into paired unfermented and fermented plant material. The low variation in the xanthone content of *C. maculata* extracts would simplify production of extracts standardized on xanthone content. Previous research demonstrated large variation in the levels of the xanthones in *C. subternata* seedlings (%RSD > 30%),[21] one of the *Cyclopia* species used to prepare honeybush food ingredient extract that is standardized on mangiferin content.[2]

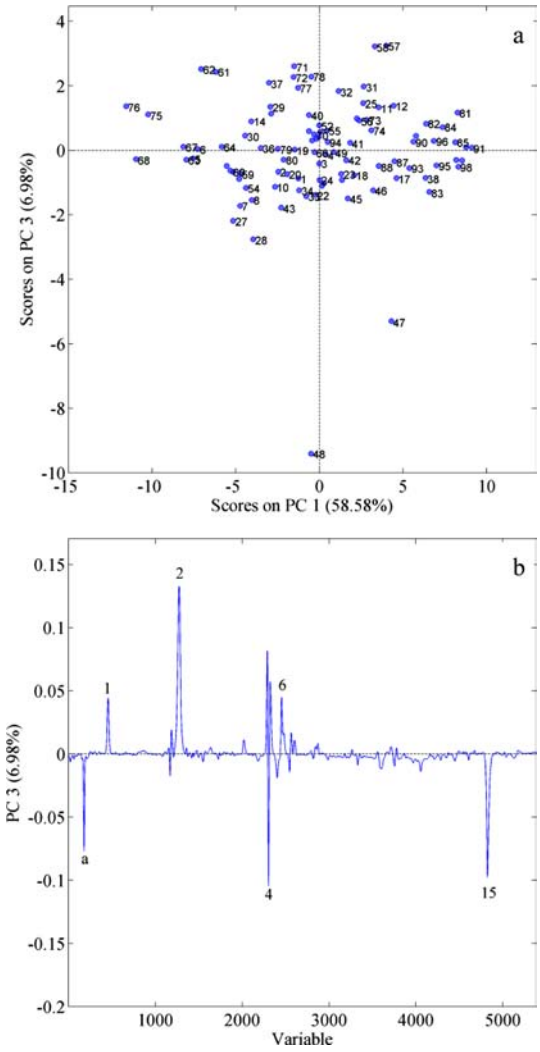


**Figure 6.** (a) PCA scores plot of PC1 versus PC3 for fingerprints of *Cyclopia maculata* samples ($n$ = 98) and (b) loadings plot of PC3.

In conclusion, the validated HPLC-DAD method proved suitable for the quantification of the major phenolic compounds present in aqueous *C. maculata* extracts and construction of chromatographic fingerprints. Several new compounds were tentatively identified for the first time in *C. maculata,* as well as in *Cyclopia* species, by means of LC-DAD hyphenated with high-resolution MS. The fermentation process decreased the concentrations of the phenolic compounds (except for vicenin-2), with the most notable effect on the xanthones mangiferin and isomangiferin. Quantitative data for individual phenolic compounds and fingerprint analysis of the complete chromatogram revealed that *C. maculata* shows very low genotypic variation, making this *Cyclopia* species ideal for the production of standardized food ingredient extracts.

## ■ ASSOCIATED CONTENT

### Ⓢ Supporting Information

Figures S1−S3 and Tables S1−S4. This material is available free of charge via the Internet at http://pubs.acs.org.

## ■ AUTHOR INFORMATION

### Corresponding Author

*(D.B.) Phone: +27 21 809 3449. Fax: +27 21 809 3430. E-mail: DBeerD@arc.agric.za.

**Present Address**

[#](A.E.S.) Post-Harvest and Wine Technology Division, Agricultural Research Council (ARC), Infruitec-Nietvoorbij, Private Bag X5026, Stellenbosch 7599, South Africa.

**Notes**

The authors declare no competing financial interest.

## ■ ACKNOWLEDGMENTS

E. L. Willenburg, Department of Science and Technology, Professional Development Program (DST-PDP) postdoctoral fellow (NRF Grant 78992), is hereby acknowledged for isolation of iriflophenone-3-C-glucoside.

## ■ REFERENCES

(1) du Toit, J.; Joubert, E.; Britz, T. J. Honeybush tea − a rediscovered indigenous South African herbal tea. *J. Sustainable Agric.* **1998**, *12*, 67−84.

(2) Joubert, E.; Joubert, M. E.; Bester, C.; de Beer, D.; de Lange, J. H. Honeybush (*Cyclopia* spp.): From local cottage industry to global markets − the catalytic and supporting role of research. *S. Afr. J. Bot.* **2011**, *77*, 887−907.

(3) Joubert, E.; Gelderblom, W. C. A.; Louw, A.; de Beer, D. South African herbal teas: *Aspalathus linearis*, *Cyclopia* spp. and *Athrixia phylicoides* − a review. *J. Ethnopharmacol.* **2008**, *119*, 376−412.

(4) Mose Larsen, P.; Fey, S. J.; Louw, J.; Joubert, L. *An anti-diabetic extract of honeybush*. World Intellectual Property Organization, WO 2008/110552A2, 2008.

(5) Muller, C. J. F.; Joubert, E.; Gabuza, K.; de Beer, D.; Fey, S. J.; Louw, J. Assessment of the antidiabetic potential of an aqueous extract of honeybush (*Cyclopia intermedia*) in streptozotocin and obese insulin resistant Wistar rats. In *Phytochemicals − Bioactivities and Impact on Health*;, Rasooli, I., Ed.; InTech: Rijeka, Croatia, 2011; DOI: 10.5772/28574.

(6) Dudhia, Z.; Louw, J.; Muller, C.; Joubert, E.; de Beer, D.; Kinnear, C.; Pheiffer, C. *Cyclopia maculata* and *Cyclopia subternata* (honeybush tea) inhibits adipogenesis in 3T3-L1 pre-adipocytes. *Phytomedicine* **2013**, *20*, 401−408.

(7) Pheiffer, C.; Dudhia, Z.; Louw, J.; Muller, C.; Joubert, E. *Cyclopia maculata* (honeybush tea) stimulates lipolysis in 3T3-L1 adipocytes. *Phytomedicine* **2013**, *20*, 1168−1171.

(8) Ferreira, D.; Kamara, B. I.; Brandt, E. V.; Joubert, E. Phenolic compounds from *Cyclopia intermedia* (honeybush tea). 1. *J. Agric. Food Chem.* **1998**, *46*, 3406−3410.

(9) Kamara, B. I.; Brand, D. J.; Brandt, E. V.; Joubert, E. Phenolic metabolites from honeybush tea (*Cyclopia subternata*). *J. Agric. Food Chem.* **2004**, *52*, 5391−5395.

(10) Kamara, B. I.; Brandt, E. V.; Ferreira, D.; Joubert, E. Polyphenols from honeybush tea (*Cyclopia intermedia*). *J. Agric. Food Chem.* **2003**, *51*, 3874−3879.

(11) Kokotkiewicz, A.; Luczkiewicz, M.; Sowinski, P.; Glod, D.; Gorynski, K.; Bucinski, A. Isolation and structure elucidation of phenolic compounds from *Cyclopia subternata* Vogel (honeybush) intact plant and *in vitro* cultures. *Food Chem.* **2012**, *133*, 1373−1382.

(12) Chellan, N.; Joubert, E.; Strijdom, H.; Roux, C.; Louw, J.; Muller, C. J. F. Aqueous extract of unfermented honeybush (*Cyclopia maculata*) attenuates STZ-induced diabetes and *β*-cell cytotoxicity. *Planta Med.* **2014**, *80*, 622−629.

(13) Vyas, A.; Syeda, K.; Ahmad, A.; Padhye, S.; Sarkar, F. H. Perspectives on medicinal properties of mangiferin. *Mini-Rev. Med. Chem.* **2012**, *12*, 412−425.

(14) Joubert, E.; Otto, F.; Grüner, S.; Weinreich, B. Reversed-phase HPLC determination of mangiferin, isomangiferin and hesperidin in *Cyclopia* and the effect of harvesting date on the phenolic composition of *C. genistoides*. *Eur. Food Res. Technol.* **2003**, *216*, 270−273.

(15) Tistaert, C.; Dejaegher, B.; Heyden, Y. V. Chromatographic separation techniques and data handling methods for herbal fingerprints: a review. *Anal. Chim. Acta* **2011**, *690*, 148−161.

(16) *Guidelines for the Assessment of Herbal Medicines*; World Health Organisation: Geneva, Switzerland, 1991; accessible at http://whqlibdoc.who.int/hq/1991/WHO_TRM_91.4.pdf (accessed May 20, 2014).

(17) Alaerts, G.; Dejaegher, B.; Smeyers-Verbeke, J.; Vander Heyden, Y. Recent developments in chromatographic fingerprints from herbal products: set-up and data analysis. *Comb. Chem. High Throughput Screening* **2010**, *13*, 900−922.

(18) de Beer, D.; Joubert, E. Development of HPLC method for *Cyclopia subternata* phenolic compound analysis and application to other *Cyclopia* spp. *J. Food Compos. Anal.* **2010**, *23*, 289−297.

(19) Malherbe, C. J.; Willenburg, E.; de Beer, D.; Bonnet, S. L.; van der Westhuizen, J. H.; Joubert, E. Iriflophenone-3-*C*-glucoside from *Cyclopia genistoides*: isolation and quantitative comparison of antioxidant capacity with mangiferin and isomangiferin using on-line HPLC antioxidant assays. *J. Chromatogr., B* **2014**, *951−952C*, 164−171.

(20) Schutte, A. L. Systematics of the genus *Cyclopia* Vent. (Fabaceae, Podalyrieae). *Edinburgh J. Bot.* **1997**, *54*, 125−170.

(21) de Beer, D.; Schulze, A. E.; Joubert, E.; de Villiers, A.; Malherbe, C. J.; Stander, M. A. Food ingredient extracts of *Cyclopia subternata* (honeybush): variation in phenolic composition and antioxidant capacity. *Molecules* **2012**, *17*, 14602−14624.

(22) Tomasi, G.; van den Berg, F.; Andersson, C. Correlation optimized warping and dynamic time warping as preprocessing methods for chromatographic data. *J. Chemom.* **2004**, *18*, 231−241.

(23) Eilers, P. H. C. Parametric time warping. *Anal. Chem.* **2004**, *76*, 404−411.

(24) Hendriks, M. M. W. B.; Cruz-Juarez, L.; Bont, D. D.; Hall, R. D. Preprocessing and exploratory analysis of chromatographic profiles of plant extracts. *Anal. Chim. Acta* **2005**, *545*, 53−64.

(25) Alaerts, G.; Van Erps, J.; Pieters, S.; Dumarey, M.; van Nederkassel, A. M.; Goodarzi, M.; Smeyers-Verbeke, J.; Vander Heyden, Y. Similarity analyses of chromatographic fingerprints as tools for identification and quality control of green tea. *J. Chromatogr., B* **2012**, *910*, 61−70.

(26) Abad-García, B.; Garmón-Lobato, S.; Berrueta, L. A.; Gallo, B.; Vicente, F. New features on the fragmentation and differentiation of *C*-glycosidic flavone isomers by positive electrospray ionization and triple quadrupole mass spectrometry. *Rapid Commun. Mass Spectrom.* **2008**, *22*, 1834−1842.

(27) Isaka, M.; Palasarn, S.; Kocharin, K.; Saenboonrueng, J. A cytotoxic xanthone dimer from the entomopathogenic fungus *Aschersonia* sp. BCC 8401. *J. Nat. Prod.* **2005**, *68*, 945−946.

(28) Wang, J.-N.; Hou, C.-Y.; Liu, Y.-L.; Lin, L.-Z.; Gil, R. R.; Cordell, G. A. Swertifrancheside, an HIV-reverse transcriptase inhibitor and the first flavone-xanthone dimer, from *Swertia franchetiana*. *J. Nat. Prod.* **1994**, *57*, 211−217.

(29) Tanaka, T.; Sueyasu, T.; Nonaka, G.; Nishioka, I. Tannins and related compounds. XXI. Isolation and characterization of galloyl and *p*-hydroxybenzoyl esters of benzophenone and xanthone *C*-glucosides from *Mangifera indica* L. *Chem. Pharm. Bull.* **1984**, *32*, 2676−2686.

(30) Zhang, Y.; Han, L.; Ge, D.; Liu, X.; Liu, E.; Wu, C.; Gao, X.; Wang, T. Isolation, structural elucidation, MS profiling, and evaluation of triglyceride accumulation inhibitory effects of benzophenone *C*-glucosides from leaves of *Mangifera indica* L. *J. Agric. Food Chem.* **2013**, *61*, 1884−1895.

(31) Kokotkiewicz, A.; Luczkiewicz, M.; Pawlowska, J.; Luczkiewicz, P.; Sowinski, P.; Witkowski, J.; Bryl, E.; Bucinski, A. Isolation of xanthone and benzophenone derivatives from *Cyclopia genistoides* (L.) Vent. (honeybush) and their pro-apoptotic activity on synoviocytes from patients with rheumatoid arthritis. *Fitoterapia* **2013**, *90*, 199−208.

(32) Roowi, S.; Crozier, A. Flavonoids in tropical citrus species. *J. Agric. Food Chem.* **2011**, *59*, 12217−12225.

(33) Grayer, R. J.; Kite, G. C.; Veitch, N. C.; Eckert, M. R.; Marin, P. D.; Senanayake, P.; Paton, A. J. Leaf flavonoid glycosides as chemosystematic characters in *Ocimum*. *Biochem. Syst. Ecol.* **2002**, *30*, 327−342.

(34) Pan, J.; Zhang, S.; Yan, L.; Tai, J.; Xiao, Q.; Zou, K.; Zhou, Y.; Wu, J. Separation of flavanone enantiomers and flavanone glucoside diastereomers from *Balanophora involucrata* Hook. f. by capillary electrophoresis and reversed-phase high-performance liquid chromatography on a C18 column. *J. Chromatogr., A* **2008**, *1185*, 117−129.
(35) Dhuique-Mayer, C.; Tbatou, M.; Carail, M.; Caris-Veyrat, C.; Dornier, M.; Amiot, M. J. Thermal degradation of antioxidant micronutrients in citrus juice: kinetics and newly formed compounds. *J. Agric. Food Chem.* **2007**, *55*, 4209−4216.
(36) Gil-Izquierdo, A.; Gil, M. I.; Ferreres, F. Effect of processing techniques at industrial scale on orange juice antioxidant and beneficial health compounds. *J. Agric. Food Chem.* **2002**, *50*, 5107−5114.
(37) Sánchez-Moreno, C.; Plaza, L.; Elez-Martínez, P.; De Ancos, B.; Martín-Belloso, O.; Cano, M. P. Impact of high pressure and pulsed electric fields on bioactive compounds and antioxidant activity of orange juice in comparison with traditional thermal processing. *J. Agric. Food Chem.* **2005**, *53*, 4403−4409.
(38) Joubert, E.; Richards, E. S.; van der Merwe, J. D.; de Beer, D.; Manley, M.; Gelderblom, W. C. A. Effect of species variation and processing on phenolic composition and in vitro antioxidant activity of aqueous extracts of *Cyclopia* spp. (honeybush tea). *J. Agric. Food Chem.* **2008**, *56*, 954−963.
(39) Lucio-Gutiérrez, J. R.; Garza-Juárez, A.; Coello, J.; Maspoch, S.; Salazar-Cavazos, M. L.; Salazar-Aranda, R.; Waksman de Torres, N. Multi-wavelength high-performance liquid chromatographic fingerprints and chemometrics to predict the antioxidant activity of *Turnera diffusa* as part of its quality control. *J. Chromatogr., A* **2012**, *1235*, 68−76.
(40) Daszykowski, M.; Walczak, B. Target selection for alignment of chromatographic signals obtained using monochannel detectors. *J. Chromatogr., A* **2007**, *1176*, 1−11.
(41) Eilers, P. H. C.; Boelens, H. F. M. Baseline correction with asymmetric least squares smoothing, 2005; accessible at http://www.science.uva.nl/~hboelens/publications/draftpub/Eilers_2005.pdf (accessed May 20, 2014).
(42) Du Preez, B. V. P. *Cyclopia maculata − Source of Flavanone Glycosides as Precursors of Taste-Modulating Aglycones*; Stellenbosch University, Stellenbosch, South Africa, 2014.
(43) Joubert, E.; de Beer, D.; Hernández, I.; Munné-Bosch, S. Accummulation of mangiferin, isomangiferin, iriflophenone-3-*C*-*β*-glucoside and hesperidin in honeybush leaves (*Cyclopia genistoides* Vent.) in response to harvest time, harvest interval and seed source. *Ind. Crops Prod.* **2014**, *56*, 74−82.

sugared water at 37 °C for 20 min and added to the remaining six containers at a concentration of 25 g of yeast/hL, as suggested by the manufacturer. In both cases, the yeast inoculum was mixed with marc and spread at the bottom, middle, and top of the containers to ensure its homogeneous distribution in the pomace. Then the containers were hermetically closed and the fermentation and storage were performed at room temperature until distillation.

**Distillation.** Each 50 kg fermentation tank was divided in two equal portions, which were distilled separately by one method or the other. Six distillations per yeast were performed in both distillation systems.

*Alembic Distillations.* Fermented Albariño grape pomace (22−23 kg) was distilled in a 50 L copper charentais alembic. The base of the boiler was heated by direct fire, with natural gas as a heating source, and tap water was used to cool the total condenser. The heating power was set to obtain an initial average distillation rate in the range 1.3−1.8 L/h. On the basis of sensorial analysis, distillation products were separated into three fractions: head, heart, and tail. The head fractions were defined as the first 220 mL; the following 2320 and 1740 mL were collected as heart fraction for L1 and L2 distillates, respectively; and the following 600 and 880 mL were collected as tail fraction for L1 and L2 distillates, respectively.

*Packed-Column Distillations.* Fermented grape pomace of Albariño variety (22−23 kg) was distilled in a packed column with a 50 L copper boiler, previously described by Garcia-Llobodanin et al.[23] The base of the boiler was heated by direct fire, and the heating and partial condenser cooling rates of the distillation column were adjusted to obtain a distillate flow rate of 1.03 L/h. The first 240 and 280 mL was collected as head fraction for L1 and L2 distillates, respectively; the heart fraction was defined as the following 2320 and 2290 mL for L1 and L2 distillates, respectively; and the tail fraction was defined as the following 210 and 310 mL for L1 and L2 distillates, respectively.

**Microbiological Control.** Samples from grape pomace before fermentation and from each container before distillation were taken for yeast isolation. Twenty grams of marc was randomly collected from each container, dispersed in 100 mL of YEPD, and incubated in a rotary shaker at 28 °C for 2 h. Then the appropriate decimal dilutions in sterile water were spread on WL nutrient agar (Scharlau Microbiology, Barcelona, Spain) supplemented with 100 μg/mL chloramphenicol to inhibit bacterial growth. The plates were incubated at 28 °C until visible colonies appeared. After counting, 20 colonies from each sample were randomly selected, isolated as pure cultures on fresh YEPD plates, and stored in the same medium with 15% (v/v) glycerol at −70 °C for further characterization. All isolated colonies were plated on lysine agar medium (Scharlau Microbiology, Barcelona, Spain) to distinguish between *Saccharomyces* and non-*Saccharomyces* yeasts. *Saccharomyces* yeasts do not grow in this medium.

Yeast isolates were characterized at species level by polymerase chain reaction (PCR) amplification of the 5.8S rRNA gene and the two ribosomal internal transcribed spacers (ITS) and subsequent restriction analysis with the endonucleases *Hin*fI, *Hae*III, and *Cfo*I.[29] PCR products and their corresponding restriction fragments were separated on 2% and 3% agarose gels in 1× Tris−acetate−ethylenediaminetetraacetic acid (TAE) buffer, respectively. After staining with ethidium bromide (0.5 μg/mL), the DNA pattern bands were visualized under UV light and photographed with a Gelprinter Plus system (TDI).

Additionally, PCR amplification and sequencing of D1/D2 region of 26S rDNA gene were used to confirm yeast identification. The D1 and D2 domains were amplified by use of the primers NL-1 and NL-4 as described by Kurtzman and Robnett.[30] PCR products were purified by use of the PCR Extract Mini kit (5PRIME) according to the supplier's instructions. The same primers were used for sequencing with a BigDye Terminator v3.1 cycle sequencing kit (Applied Biosystems) and a 3130xl genetic analyzer (Applied Biosystems). Sequence similarities were obtained by use of GenBank BLASTN search facilities.[31] The identification was considered as correct when the identity of gene sequences was 98% or higher.

Those yeasts identified as *S. cerevisiae* were characterized at strain level by analysis of mitochondrial DNA restriction fragment length polymorphism (mtDNA-RFLP). Total DNA was obtained as described by Querol et al.[32] DNA samples were digested with the restriction endonuclease *Hin*fI (Promega) and the fragments obtained were separated by electrophoresis on 0.8% (w/v) agarose gels and visualized as described above.

**Chemical Analysis of Distillates.** Ethanol content (%, v/v) was measured by electronic densimetry according to the official method.[33]

Chemical composition of heart fractions was determined by gas chromatography coupled with flame ionization detector (GC-FID), with direct injection of the distillate, previously adjusted to 40% (v/v). Analyses were carried out on two different columns. Macroconstituents (methanol, higher alcohols, acetaldehyde, 1,1-diethoxyethane, ethyl acetate, ethyl lactate, 1-hexanol, isobutyraldehyde, ethyl formate, methyl acetate, 2-propenal, 2-butanol, and allylic alcohol) were determined on a capillary column CP WAX-57 CB (Varian) (50 m × 0.32 mm i.d. × 0.2 μm film thickness) on an Agilent 6890 chromatograph (Agilent Technologies, Waldbronn, Germany) equipped with a split/splitless injector following the methodology reported by López-Vázquez et al.[9] Separation of the remaining compounds was done on a Supelcowax 10 capillary column (30 m × 0.32 mm × 0.25 μm film thickness; Supelco Inc., Bellefonte, PA) in a Varian CP3900 GC chromatograph as described by López-Vázquez et al.[34] Samples were analyzed in triplicate.

**Sensory Analysis.** Evaluation of the distillates was carried out in two steps: first a ranking preference test and then a descriptive analysis. All distillates (heart fractions) were diluted with Milli-Q-treated water (Millipore Corp., Bedford, MA) to an ethanol content of 40% (v/v). The samples were served at room temperature in Association Française de Normalisation (AFNOR) glasses labeled with random numbers.

The first evaluation was carried out by a group of 10 females and 27 males, 18−60 years old (potential consumers) but not trained in specific evaluation of distillates. They were asked to rank by preference the distillates, evaluating separately aroma and taste of the spirits. The results were analyzed by the Friedman statistical test.

The second evaluation was a descriptive sensory analysis performed by a trained panel (five people) with experience in distillates assessment. Previously, the most representative descriptive attributes of the distillates were defined in an initial tasting session according to the method described in the ISO 13299:2003 standard.[35] The chosen attributes were aroma and taste descriptors. This test consisted of a preliminary round-table discussion, where the panelists defined the terms: 11 aroma descriptors (floral, fruity, vegetal/herbaceous, spicy, positive general impression, solvent, rancid, oxidized, pungent, burnt/smoky, negative general impression) and eight taste descriptors (astringency, mellowness, sweet, harmony, alcoholic, persistence, prickling, and general quality in mouth). Then an individual smelling and tasting of the samples was carried out by the panelists in order to qualify the distillates. The intensities of the descriptors were rated on a discontinuous scale from 0 to 5. A score of 0 indicated that a descriptor was not perceived, and a score of 5 indicated the highest intensity.

**Statistical Analysis.** One-way analysis of variance (ANOVA) was applied to the data obtained from the GC analysis. The aim was to ascertain whether the distillation system and/or yeast strain led to any significant differences (at 5% level) in volatile composition of the spirits. The variables that showed significant differences were used for principal component analysis (PCA). All statistical analyses were performed with the SPSS statistical package (version 17.0).

## RESULTS AND DISCUSSION

**Microbiological Control.** Albariño grape pomace presented a yeast population of $2.3 \times 10^5$ colony-forming units (cfu)/mL before inoculation and fermentation. This value was similar to that described by Bovo et al.[14] for Italian marcs but lower than the counts reported in more recent studies.[12,15] The distribution of yeast species is the following: *Metschnikowia pulcherrima* and *Hanseniaspora uvarum* were the predominant species found, at 43.5% and 52.2%, respectively, whereas *S.*

**Table 1. Alcohol Balances in Both Distillation Systems for Albariño Grape Pomace Spirit[a]**

| | copper charentais alembic | | packed column | |
|---|---|---|---|---|
| units | L1 ($n$ = 5) | L2 ($n$ = 6) | L1 ($n$ = 5) | L2 ($n$ = 6) |
| | Heart-Fraction Ethanol Alcoholic Strength | | | |
| % (v/v) | 61.92 ± 4.50 a,a | 50.68 ± 3.14 a,b | 75.80 ± 3.86 b,a | 75.2 ± 4.55 b,a |
| | Heart-Fraction Ethanol Yield | | | |
| % | 81.2 ± 8.33 a,a | 65.66 ± 6.5 a,b | 86.7 ± 2.91 a,a | 83.91 ± 2.6 b,a |
| L p.a./100 kg of grape pomace[b] | 7.89 ± 0.59 a,a | 5.87 ± 0.61 a,b | 8.28 ± 0.60 a,a | 8.93 ± 0.46 b,a |
| | Total Higher Alcohols Recovered | | | |
| g/100 L of real distillate | 469.3 ± 48.3 a,a | 367.2 ± 61.8 a,b | 409.7 ± 51.4 a,a | 397.1 ± 60.4 a,a |
| g/100 kg of grape pomace | 40.46 ± 2.9 a,a | 32.8 ± 7.19 a,b | 37.4 ± 7.03 a,a | 42.2 ± 5.18 a,a |
| | Total Linear Alcohols Recovered | | | |
| g/100 L of real distillate | 0.30 ± 0.75 a,a | 0.23 ± 0.04 a,b | 0.21 ± 0.04 b,a | 0.21 ± 0.03 a,a |
| mg/100 kg of grape pomace | 29.2 ± 10.1 a,a | 20.55 ± 8.2 a,b | 19.97 ± 9.04 b,a | 22.33 ± 5.11 a,a |
| | Total Monoterpenols Recovered | | | |
| g/100 L of real distillate | 1.35 ± 0.24 a,a | 1.05 ± 0.16 a,b | 1.0 ± 0.12 b,a | 1.16 ± 0.20 a,b |
| mg/100 kg of grape pomace | 131.7 ± 18.29 a,a | 93.92 ± 13.04 a,b | 100.2 ± 13.85 b,a | 124.13 ± 19.2 b,b |
| | Total 1-Linalool Recovered | | | |
| g/100 L of real distillate | 0.45 ± 0.04 a,a | 0.39 ± 0.06 a,a | 0.37 ± 0.02 b,a | 0.40 ± 0.04 a,a |
| mg/100 kg of grape pomace | 43.4 ± 2.26 a,a | 35.2 ± 5.45 a,b | 37.6 ± 4.45 b,a | 42.9 ± 4.6 b,b |

[a]Different letters before the comma in the same row indicate a significant difference ($p \leq 0.05$) with respect to the distillation system (within the same yeast strain). Different letters after the comma in the same row indicate a significant difference ($p \leq 0.05$) with respect to the yeast strain (within the same distillation system). [b]p.a.:pure alcohol.

**Table 2. Macroconstituent Composition of Distillates (Heart Fraction) Obtained from Albariño Grape Pomace Fermented with Different Yeast Strains[a]**

| | macroconstituent (g/hL p.a.) | | | |
|---|---|---|---|---|
| | copper charentais alembic | | packed column | |
| compd | L1 ($n$ = 5) | L2 ($n$ = 6) | L1 ($n$ = 5) | L2 ($n$ = 6) |
| methanol | 432.87 ± 30.04 a,a | 579.99 ± 33.03 a,b | 438.15 ± 35.88 a,a | 616.15 ± 83.9 a,b |
| ethyl acetate | 221.00 ± 58.60 a,a | 126.43 ± 63.41 a,b | 109.44 ± 91.5 b,a | 105.10 ± 78.7 a,a |
| acetaldehyde | 31.96 ± 10.54 a,a | 23.76 ± 5.84 a,a | 21.73 ± 9.54 b,a | 21.21 ± 4.74 a,a |
| 1,1-diethoxyethane | 30.95 ± 14.05 a,a | 12.84 ± 4.64 a,b | 34.39 ± 22.06 a,a | 30.86 ± 7.79 b,a |
| $\sum$ acetaldehyde + 1,1-diethoxyethane | 62.92 ± 24.41 a,a | 36.61 ± 10.47 a,b | 56.12 ± 31.5 a,a | 52.07 ± 11.82 b,a |
| 1-propanol | 63.26 ± 4.72 a,a | 77.43 ± 4.93 a,b | 57.24 ± 8.09 a,a | 72.89 ± 5.96 a,b |
| 2-methyl-1-propanol | 134.56 ± 4.01 a,a | 152.03 ± 23.15 a,a | 104.09 ± 25.01 b,a | 129.50 ± 28.0 a,a |
| 1-butanol | 1.06 ± 1.27 a,a | 0.14 ± 0.04 a,a | 0.34 ± 0.13 b,a | 0.60 ± 1.01 a,a |
| 2-butanol | 0.33 ± 0.02 a,a | 0.32 ± 0.04 a,a | 0.24 ± 0.06 a,a | 0.26 ± 0.06 a,a |
| allylic alcohol | 0.11 ± 0.05 a,a | 0.03 ± 0.02 a,b | 0.05 ± 0.05 b,a | 0.03 ± 0.02 a,a |
| 2-methyl-1-butanol | 95.75 ± 4.89 a,a | 84.93 ± 22.92 a,a | 72.02 ± 14.79 b,a | 69.57 ± 18.1 a,a |
| 3-methyl-1-butanol | 282.90 ± 12.19 a,a | 244.5 ± 71.44 a,a | 218.64 ± 36.89 b,a | 200.4 ± 53.2 a,a |
| $\sum$ total higher alcohols[b] | 577.98 ± 18.75 a,a | 559.3 ± 117.5 a,a | 452.62 ± 91.2 a,a | 473.2 ± 101.3 a,a |
| ethyl lactate | 33.28 ± 7.89a,a | 53.89 ± 12.26a,b | 19.74 ± 9.44b,a | 19.53 ± 8.45b,a |
| 1-hexanol | 7.47 ± 0.47 a,a | 7.68 ± 1.10 a,a | 5.58 ± 0.88 b,a | 6.22 ± 0.84 b,a |
| isobutyraldehyde | 0.79 ± 0.66 a,a | 0.27 ± 0.09 a,b | 0.27 ± 0.14 b,a | 0.25 ± 0.08 a,a |
| ethyl formate | 2.17 ± 1.22 a,a | 0.93 ± 0.36 a,b | 1.36 ± 0.35 b,a | 1.033 ± 0.33 a,a |
| methyl acetate | 2.15 ± 0.58 a,a | 1.62 ± 0.76 a,a | 1.15 ± 0.96 b,a | 1.30 ± 0.86 a,a |
| 2-propenal | 0.62 ± 0.30 a,a | 0.32 ± 0.10 a,a | 0.61 ± 0.35 a,a | 0.67 ± 0.16 b,a |

[a]Different letters before the comma in the same row indicate a significant difference ($p \leq 0.05$) with respect to the distillation system (within the same yeast strain). Different letters after the comma in the same row indicate a significant difference ($p \leq 0.05$) with respect to the yeast strain (within the same distillation system). [b]$\sum$ 1-propanol, 2-Methyl-1-propanol, 1-butanol, 2-butanol, allylic alcohol, 2-methyl-1-butanol, and 3-methyl-1-butanol.

*cerevisiae* was not detected. An isolate of *Pichia kluyveri* was also identified at 4.3%. These results partially agree with those reported by Bovo et al.[14] for Italian marcs. They found that *Hanseniaspora* sp. and *M. pulcherrima* were the main yeasts, although their distribution was different, with dominance of the apiculate yeasts, and *S. cerevisiae* was present below the detection limits. Other yeast species have been reported in Prosecco marcs[14] and marcs from Portugal.[13]

**Table 3. Microconstituent Ester Content of Distillates (Heart Fraction) Obtained from Albariño Grape Pomace Fermented with Different Yeast Strains[a]**

| | esters (g/hL p.a.) | | | |
|---|---|---|---|---|
| | copper charentais alembic | | packed column | |
| compd | L1 ($n$ = 5) | L2 ($n$ = 6) | L1 ($n$ = 5) | L2 ($n$ = 6) |
| isobutyl acetate | 0.18 ± 0.04 a,a | 0.13 ± 0.04 a,a | 0.12 ± 0.05 b,a | 0.09 ± 0.05 a,a |
| butyl acetate | <LOD[b] | 0.06 ± 0.02 a,a | 0.39 ± 0.23 b,a | 0.26 ± 0.08 b,a |
| isoamyl acetate | 1.28 ± 0.25 a,a | 0.73 ± 0.32 a,a | 1.25 ± 0.64 a,a | 0.98 ± 0.62 a,a |
| hexyl acetate | 0.05 ± 0.03 a,a | 0.03 ± 0.02 a,a | 0.04 ± 0.02 a,a | 0.07 ± 0.06 a,a |
| 2-phenylethyl acetate | 0.14 ± 0.09 a,a | 0.13 ± 0.04 a,a | 0.11 ± 0.08 b,a | 0.14 ± 0.07 a,a |
| ∑ acetates of higher alcohols | 1.65 ± 0.48 a,a | 1.08 ± 0.44 a,b | 1.91 ± 1.02 a,a | 1.54 ± 0.86 a,b |
| ethyl butyrate | 0.46 ± 0.10 a,a | 0.29 ± 0.13 a,a | 0.28 ± 0.09 a,a | 0.38 ± 0.26 a,a |
| ethyl hexanoate | 2.72 ± 0.32 a,a | 1.16 ± 0.42 a,b | 2.16 ± 0.61 b,a | 1.14 ± 0.57 a,b |
| ethyl octanoate | 2.92 ± 0.38 a,a | 1.14 ± 0.39 a,b | 3.90 ± 0.50 b,a | 2.06 ± 0.13 b,b |
| ethyl decanoate | 4.19 ± 0.50 a,a | 1.93 ± 0.51 a,b | 5.53 ± 0.31 b,a | 3.10 ± 0.46 b,b |
| ethyl dodecanoate | 1.58 ± 0.19 a,a | 0.82 ± 0.12 | 1.94 ± 0.16 b,a | 1.23 ± 0.17 b,b |
| ∑ ethyl esters C6−C12[c] | 11.87 ± 1.39 a,a | 5.05 ± 1.44 a,b | 13.53 ± 1.60 b,a | 7.54 ± 1.33 b,b |
| ethyl tetradecanoate | 0.33 ± 0.06 a,a | 0.17 ± 0.22 a,b | 0.38 ± 0.03 a,a | 0.39 ± 0.08 b,a |
| ethyl hexadecanoate | 2.42 ± 0.83 a,a | 0.90 ± 0.29 a,b | 3.63 ± 0.46 b,a | 4.38 ± 0.77 b,a |
| ethyl octadecanoate | <LOD | <LOD | <LOD | 0.07 ± 0.02 |
| ethyl 9-octadecenoate | 0.37 ± 0.16 a,a | 0.12 ± 0.07 a,b | 0.40 ± 0.07 a,a | 0.43 ± 0.07 b,a |
| ethyl 9,12-octadecadienonate | 2.26 ± 0.77 a,a | 1.45 ± 0.43 a,b | 1.88 ± 0.55 a,a | 2.16 ± 0.41 b,a |
| ethyl 9,12,15-octadecatrienoate | 1.01 ± 0.43 a,a | 0.86 ± 0.17 a,a | 0.69 ± 0.26 | 0.87 ± 0.22 a,a |
| ∑ ethyl esters C14−C18 | 6.39 ± 2.64 a,a | 3.51 ± 1.0 a,b | 6.98 ± 1.38 a,a | 8.30 ± 1.57 b,a |
| isoamyl hexanoate | 0.07 ± 0.03 a,a | 0.03 ± 0.02 | 0.04 ± 0.01 b,a | 0.01 ± 0.02 a,a |
| isoamyl octanoate | 0.04 ± 0.01 a,a | 0.01 ± 0.0 a,b | 0.05 ± 0.02 a,a | 0.01 ± 0.01 a,b |
| isoamyl decanoate | 0.12 ± 0.03 a,a | 0.11 ± 0.05 a,a | 0.09 ± 0.03 a,a | 0.09 ± 0.01 a,a |
| isoamyl dodecanoate | <LOD | <LOD | <LOD | <LOD |
| ∑ isoamyl esters | 0.22 ± 0.08 a,a | 0.16 ± 0.07 a,a | 0.18 ± 0.06 b,a | 0.11 ± 0.04 a,a |
| diethyl succinate | 4.58 ± 1.44 a,a | 4.86 ± 0.61 a,a | 2.42 ± 1.10 b,a | 2.33 ± 1.17 b,a |

[a]Different letters before the comma in the same row indicate a significant difference ($p \leq 0.05$) with respect to the distillation system (within the same yeast strain). Different letters after the comma in the same row indicate a significant difference ($p \leq 0.05$) with respect to the yeast strain (within the same distillation system). [b]LOD, limit of detection. [c]∑ Ethyl hexanoate, ethyl octanoate, ethyl decanoate, and ethyl dodecanoate.

After inoculation, Albariño pomace was allowed to ferment, and then it was stored until distillation. In order to evaluate the prevalence of the added yeast strain for fermentation and during the storage period, pomace samples from each container were taken before distillation. The presence of both bacteria and yeast was found in almost all samples, although only yeast isolates were characterized. The results showed that in all *S. cerevisiae* L1 fermentations except for L1-5, the inoculated strain was the dominant yeast even after the storage period. In L1-5, a different strain of *S. cerevisiae* (strain IV) was isolated. In addition, a non-*Saccharomyces* yeast species appeared with a frequency higher than *Saccharomyces*. The later was characterized as *Pichia membranifaciens*, a film-forming yeast that has oxidative activity,[36] suggesting that anaerobic conditions were not adequately kept in this container. This yeast is considered a common food spoilage species,[37] and its presence has been also reported at the end of fermentations of Prosecco marc.[14] On the basis of microbiological results, L1-5 was not considered for chemical analysis and ethanol yield, to avoid misleading conclusions.

The commercial yeast L2 did not show the same ability to ferment and survive in Albariño pomace as the native EVEGA strain. It only appeared as the leader strain in four out of the six fermentations performed; in one of them, L2-5, it was isolated as the dominant strain (frequency 93%), but in the remaining containers it fermented in codominance with indigenous strains from pomace, reaching frequencies close to 50%. These findings confirm the suitability of L1 for grape pomace fermentation, since this strains is able to control fermentation when added as starter and also in spontaneous processes.[38] The ability of inoculated yeast strains to prevail over the autochthonous microorganisms during grape marc fermentation and storage has also been reported for grappa production.[15] All L2 fermentations were considered for chemical analysis and ethanol yield determination.

**Distillation.** *Ethanol Yield.* Table 1 summarizes the yield of ethanol recovery and the alcoholic strength for alembic and column distillations. For packed-column distillation, the heart-fraction ethanol yield was higher than that for alembic distillation for both yeast strains. Moreover, packed-column distillates also showed higher alcoholic strength of heart fraction (between 13.9% and 24.4% v/v) than alembic distillates. In addition, with the yeast strain L1 a higher heart-fraction ethanol yield was obtained, mainly when the alembic was used.

**Table 4. Microconstituent Content of Distillates (Heart Fraction) Obtained from Albariño Grape Pomace Fermented with Different Yeast Strains[a]**

| | microconstituent (g/hL p.a.) | | | |
|---|---|---|---|---|
| | copper charentais alembic | | packed column | |
| compd | L1 ($n$ = 5) | L2 ($n$ = 6) | L1 ($n$ = 5) | L2 ($n$ = 6) |
| | | Minor Alcohols | | |
| *trans*-3-hexen-1-ol | 0.12 ± 0.01 a,a | 0.15 ± 0.02 a,a | 0.10 ± 0.02 a,a | 0.13 ± 0.02 a,a |
| *cis*-3-hexen-1-ol | 0.19 ± 0.03 a,a | 0.21 ± 0.04 a,a | 0.17 ± 0.02 a,a | 0.20 ± 0.02 a,a |
| *trans*-2-hexen-1-ol | 0.32 ± 0.14 a,a | 0.05 ± 0.03 a,b | 0.22 ± 0.09 a,a | 0.12 ± 0.10 a,b |
| ∑ *trans*/*cis* hexenols | 0.63 ± 0.06 a,a | 0.41 ± 0.01 a,b | 0.49 ± 0.05 a,a | 0.45 ± 0.05 a,a |
| 1-pentanol | 0.77 ± 0.05 a,a | 0.77 ± 0.04 a,a | 0.63 ± 0.05 a,a | 0.65 ± 0.04 a,a |
| 1-heptanol | 0.12 ± 0.04 a,a | 0.10 ± 0.03 a,a | 0.08 ± 0.01 b,a | 0.08 ± 0.01 a,a |
| 1-octanol | 0.15 ± 0.04 a,a | 0.13 ± 0.01 a,a | 0.08 ± 0.01 b,a | 0.07 ± 0.01 b,a |
| 1-nonanol | 0.08 ± 0.03 a,a | 0.10 ± 0.01 a,a | 0.08 ± 0.02 a,a | 0.08 ± 0.02 a,a |
| 1-decanol | <LOD[b] | <LOD | <LOD | <LOD |
| benzyl alcohol | 0.76 ± 0.35 a,a | 0.81 ± 0.15 a,a | 0.38 ± 0.21 b,a | 0.38 ± 0.16 b,a |
| 2-phenylethanol | 6.90 ± 3.28 a | 6.83 ± 0.99 a | 2.70 ± 1.34 b | 3.42 ± 1.85 b |
| ∑ linear alcohols[c] | 0.37 ± 0.09 a,a | 0.35 ± 0.04 a,a | 0.24 ± 0.05 b,a | 0.25 ± 0.03 b,a |
| | | Other Compounds | | |
| benzaldehyde | 0.65 ± 0.57 a,a | 0.13 ± 0.04 a,b | 0.54 ± 0.38 a,a | 0.14 ± 0.07 a,a |
| furfuraldehyde | <LOD | 0.16 ± 0.10 a,a | 0.07 ± 0.06 a,a | 0.33 ± 0.32 b,b |
| 3-ethoxy-1-propanol | 0.39 ± 0.10 a,a | 0.47 ± 0.09 a,a | 0.18 ± 0.10 b,a | 0.30 ± 0.16 b,b |
| 1-octen-3-ol | 0.12 ± 0.02 a,a | 0.10 ± 0.03 a,a | 0.09 ± 0.02 b,a | 0.09 ± 0.02 a,a |
| 3-hydroxy-2-butanone | <LOD | <LOD | 0.12 ± 0.06 a,a | 0.06 ± 0.04 a,a |
| | | Monoterpenols | | |
| *trans*-furan linalool oxide | 0.47 ± 0.06 a,a | 0.47 ± 0.02 a,a | 0.35 ± 0.07 b,a | 0.41 ± 0.13 a,a |
| *cis*-furan linalool oxide | 0.20 ± 0.08 a,a | 0.07 ± 0.05 a,b | 0.07 ± 0.05 b,a | 0.08 ± 0.06 a,a |
| linalol | 0.55 ± 0.03 a,a | 0.60 ± 0.06 a,a | 0.43 ± 0.04 b,a | 0.48 ± 0.03 b,a |
| α-terpineol | <LOD | <LOD | 0.05 ± 0.01 b,a | 0.05 ± 0.03 a,a |
| citronellol | 0.08 ± 0.01 a,a | 0.08 ± 0.01 a,a | 0.06 ± 0.01 a,a | 0.06 ± 0.02 a,a |
| nerol | 0.06 ± 0.01 a,a | 0.04 ± 0.01 a,b | 0.03 ± 0.01 b,a | 0.05 ± 0.01 a,b |
| hotrienol | 0.23 ± 0.03 a,a | 0.27 ± 0.03 a,a | 0.22 ± 0.03 a,a | 0.27 ± 0.09 a,a |
| ∑ monoterpenols | 1.67 ± 0.37 a,a | 1.60 ± 0.20 a,a | 1.21 ± 0.23 b,a | 1.39 ± 0.38 a,a |

[a]Different letters before the comma in the same row indicate a significant difference ($p \leq 0.05$) with respect to the distillation system (within the same yeast strain). Different letters after the comma in the same row indicate a significant difference ($p \leq 0.05$) with respect to the yeast strain (within the same distillation system). [b]LOD, limit of detection. [c]∑ 1-heptanol, 1-octanol, 1-nonanol, and 1-decanol.

*Major Volatile Compounds in Albariño Grape Pomace Distillates.* Table 2 summarizes the average concentrations of macroconstituents and the ANOVA test results for the Albariño heart distillates grouped according to yeast strain and distillation system. From this table, differences in some components of the different distillates are revealed. The methanol content of the distillates obtained from pomace inoculated with L2 yeast was 34−40% higher than those obtained from pomace fermented with L1 regardless of the distillation system employed. No differences in methanol content were found between distillation systems, and its concentration remained under the legal limits of 1000 g/hL p.a.[2] in all cases. Although methanol formation depends on plant enzymes,[39] it was reported that differences in yeast growth might affect the conditions for pectin methyl esterase activity[16] and to the evolution of the volatiles compounds of the marc during the process of storage.[40] Our results support these findings. The concentration of ethyl acetate was almost 2-fold higher in the L1 distillates (mean value of 221.00 g/hL p.a.) than in the L2 ones (mean value 126.43 g/hL p.a.) when alembic distillation was used, whereas no differences were found according to yeast strain when packed-column distillation was used (mean values around 105−110 g/hL p.a.). In all cases, the values of this compound were within the permitted maximum concentration (250 g/hL) by the Regulation of the Geographic Indication of the Spirits and Traditional Liqueurs from Galicia and Its Regulating Council.[3] Acetaldehyde and 1,1-diethoxyethane are the major aldehydes in grape marc distillates, accounting for more than 90% of total aldehydes.[41] The values of acetaldehyde obtained in this study were low (ranging between 21 and 32 g/hL) and within the orujo regulation limits (150 g/hL), indicating that the grape marc has been properly stored and distilled. No effect of yeast strain and/or distillation system on the concentration of acetaldehyde and 1,1-diethoxyethane was found. Similarly, no significant differences were found for the concentration of higher alcohols among the distillates, though their contents were slightly higher in alembic distillates (Table 2). The lower concentration is due to dilution by the higher recovery performance of ethanol in the heart fraction with packed-column distillation, since the recovery of higher alcohols is similar for both distillation systems (Table 1). From this group, the only compound that showed significant differences among yeasts was 1-propanol, being higher in L2 distillates (Table 2). The concentration of 2-butanol was below 2.0 g/hL p.a. in all cases, indicating a minimum presence of bacteria in the pomace; their activity did not affect the distillate quality. When the total sum of higher alcohols was compared with those reported for spontaneously

fermented grape pomace distillates,[9,34] higher values were obtained in this study. This confirmed the fact that the amount of fusel alcohols is higher in inoculated fermentations.[16] The concentration of 1-hexanol was mainly influenced by the distillation system, with alembic distillates having the highest values (around 7.5 g/hL p.a.), although none surpassed the level (10−15 g/hL p.a) at which it can contribute negatively to the flavor of wine distillates.[42] The content of ethyl lactate, a typical tail compound, was significantly higher in heart fractions of distillates from alembic than those from packed columns (Table 2). No effect of the yeast strain was observed. The values obtained in this study were lower than 150 g/hL p.a, indicating no spoilage by lactic acid bacteria during fermentation, and the distillates obtained could have favorable characteristics, since ethyl lactate is able to stabilize and soften the harsh flavours of distillates.[43,44]

*Minor Volatile Compounds in Albariño Grape Pomace Distillates.* Tables 3 and 4 summarize the average concentrations of microconstituents and ANOVA test results for the Albariño heart distillates grouped according to yeast strain and distillation system. Among the minor volatile compounds identified, the low molecular weight ethyl esters (C6−C12) were the most influenced by both distillation system and yeast strain (Table 3). Distillates fermented with L1 yeast and distilled with a packed column had the highest concentration values. Previous studies also reported similar results comparing distillations of fruits via batch column and alembic.[23,45,46] It is interesting to note that the concentration of C6−C12 ethyl esters obtained with L1 yeast, independent of the distillation system used, was higher than those obtained for L2 distillates, and the values were also higher than those reported for grape pomace distillates.[9,34] This yeast strain (L1) has already been reported to produce higher amounts of ethyl esters and fatty acids than other yeast strains in Albariño wines.[26] Similar behavior was observed in the sum of acetates of higher alcohols; higher values were obtained for the L1 and packed-column distillates in comparison with the L2 and alembic ones, although this difference was not significant when the distillation system is compared. These compounds are of fermentative origin and contribute fruity (banana and apple) notes to distillates.[47,48] In contrast, a clear effect was not found on the total amount of high molecular weight ethyl esters (C14−C18) with respect to distillation system and yeast strain. However, within this group, ethyl hexadecanoate was significantly higher in packed-column distillates independent of the yeast strain used (mean values of 3.63 and 4.38 g/hL p.a. for L1 and L2, respectively). The concentration of isoamyl esters was low (<0.13 g/hL p.a.) in all distillates; significant differences were found for isoamyl octanoate according to yeast strain. These compounds are produced by yeast during fermentation[49] and have been identified with fruity aroma in grappa from Moscato.[50] The levels of isoamyl esters referenced in other varieties of grape pomace were lower than the detection limits;[34] thus our results suggest that L1 yeast may increase these values in less aromatic varieties.

Regarding minor alcohols (Table 4), no differences were appreciated between strains, except for *trans*-2-hexen-1-ol, whose concentration was higher for L1 distillates. In contrast, differences were observed in the sum of linear alcohols (C7−C10) according to distillation system; benzyl alcohol, 2-phenylethylethanol, and 3-ethoxy-1-propanol concentrations were higher in alembic distillates. As shown in Table 4, the overall concentration of monoterpenols, typical varietal compounds that impart fruity notes to distillates, was similar in all distillates (ranged between 1.67 and 1.21 g/hL p.a.). Significant differences were found only for linalool according to distillation system, being higher when alembic was used.

On the other hand, diethyl succinate (Table 3), a compound linked to the intensity of the tail-fraction aroma, ranged from 2.33 to 4.86 g/hL p.a., showing higher levels in the distillates from the alembic than in those obtained with the column. This result is in accordance with those found for other typical tail-fraction compounds (ethyl lactate, 2-phenylethanol, and benzyl alcohol). Other minor compounds detected were less affected by yeast strain or distillation system; however, from Table 4 it is possible to observe that L1 yeast produced a higher concentration of benzaldehyde and a lower concentration of furfuraldehyde than L2, although the difference was significant only for one of the two distillation systems (alembic for benzaldehyde and packed column for furfuraldehyde).

**Principal Component Analysis.** Those compounds that showed significant differences among systems and/or yeasts were considered for principal component analysis (PCA), except for those influenced by cut supervision at the distillation process like 2-phenylethanol, diethyl succinate, ethyl lactate, and benzyl alcohol. To simplify the analysis, the concentration of ethyl esters C6−C12, acetates of higher alcohols, and linear alcohols were grouped as family sums. Two principal components were obtained (PC1 and PC2), which explained 73.75% of the variance (Table 5). These components are shown in Figure 1, in which the separation of samples according to yeast and distillation system used can be clearly seen. PC1 accounts for 38.70% of the total variance and clearly differentiates the spirits according to yeast strain. L1 distillates were located on the positive side of PC1, whereas those from L2 where plotted on the negative side of this component. L1 distillates were characterized by higher concentrations of ethyl esters C6−C12, isoamyl octanoate, *trans*-2-hexenol, and acetates of higher alcohols than L2 ones. On the contrary, L2 distillates were defined by a higher content of methanol and 1-propanol. PC2 accounts for 35.05% of the total variance and differentiates the spirits according to distillation system. Alembic distillates (top) were characterized by higher levels of linear alcohols, linalool, 1-hexanol, and 3-ethoxy-1-propanol,

**Table 5. Principal Component Analysis Results for Volatile Compounds Analyzed in Heart Fractions of Different Distillates**

| compd | loading | explained variance (%) | total variance (%) |
|---|---|---|---|
| | Principal Component 1 | | |
| ∑ ethyl esters C6−C12 | 0.922 | 38.70 | 38.7 |
| isoamyl octanoate | 0.915 | | |
| methanol | −0.912 | | |
| *trans*-2-hexen-1-ol | 0.809 | | |
| ∑ acetates of higher alcohols | 0.671 | | |
| propanol | −0.639 | | |
| | Principal Component 2 | | |
| ∑ linear alcohols | 0.934 | 35.05 | 73.75 |
| linalool | 0.930 | | |
| 1-hexanol | 0.878 | | |
| ethyl hexadecanoate | −0.796 | | |
| 3-ethoxy-1-propanol | 0.610 | | |

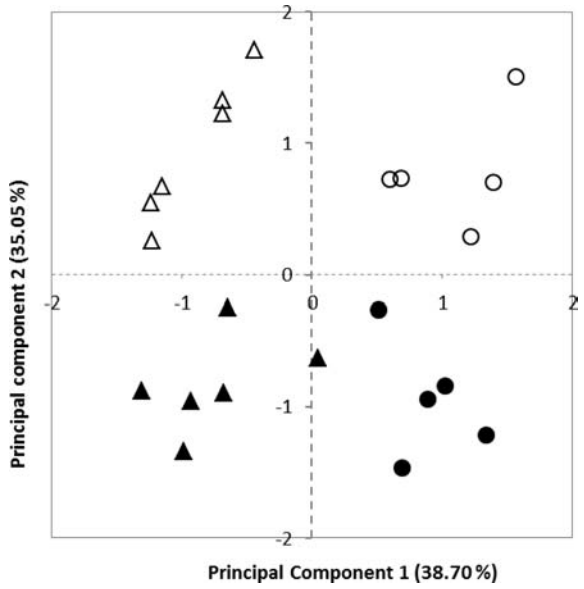


**Figure 1.** Principal component analysis of volatile composition of Albariño grape pomace distillates (heart fraction): L1 yeast (circles) and L2 yeast (triangles); alembic spirits (open symbols) and packed-column spirits (solid symbols).

whereas column distillates (bottom) were characterized by higher concentrations of ethyl hexadecanoate.

**Sensory Analysis.** The preference test did not show any significant taste and aroma difference (Friedman test $p < 0.05$) among the distillates according to the distillation system and yeast strain. In contrast, a noticeable difference according to the distillation system and/or yeast strain is observed for results obtained from the descriptive test (Figure 2). For aroma (Figure 2A), the distillates obtained from column and L1 yeast were scored with the highest PGI (positive general impression) and described by fruity character. This could be related to ethyl esters C6−C12 and acetates of higher alcohols, which were present in higher concentrations in these distillates (Table 3). The distillates obtained from alembic and L2 yeast received the lowest scores in some aromas (fruity, herbaceous, and spicy). However, the distillates obtained from L1 and distilled in alembic had the highest punctuation in oxidized and solvent attributes, which may be due to the fact that this distillate was the only one with concentrations of acetaldehyde (31.96 g/hL) and ethyl acetate (221 g/hL) close to the perception thresholds (30−50 and 180 g/hL, respectively).[51,52] It also can be noted in Figure 2 that distillates obtained with alembic had higher concentration of compounds associated with floral nuances (1-linalool and linear alcohol). However, the difference in these concentrations was not large enough (Table 1) for the panel to be able to differentiate the distillates according to this characteristic.

The panel of experts was able to differentiate the distillation system by taste (Figure 2B) but not the yeast. Distillates obtained from alembic (independent of the yeast strain) were characterized by the highest scores in astringency and the lowest scores in positive attributes (sweet, harmony, mellowness, and general quality in mouth). This result may be attributed to the interactions of the different compounds present in the studied distillates.

In summary, a packed column is an excellent option to produce orujo distillates, which are characterized by positive sensations in mouth and reduced intensity of negative aromas

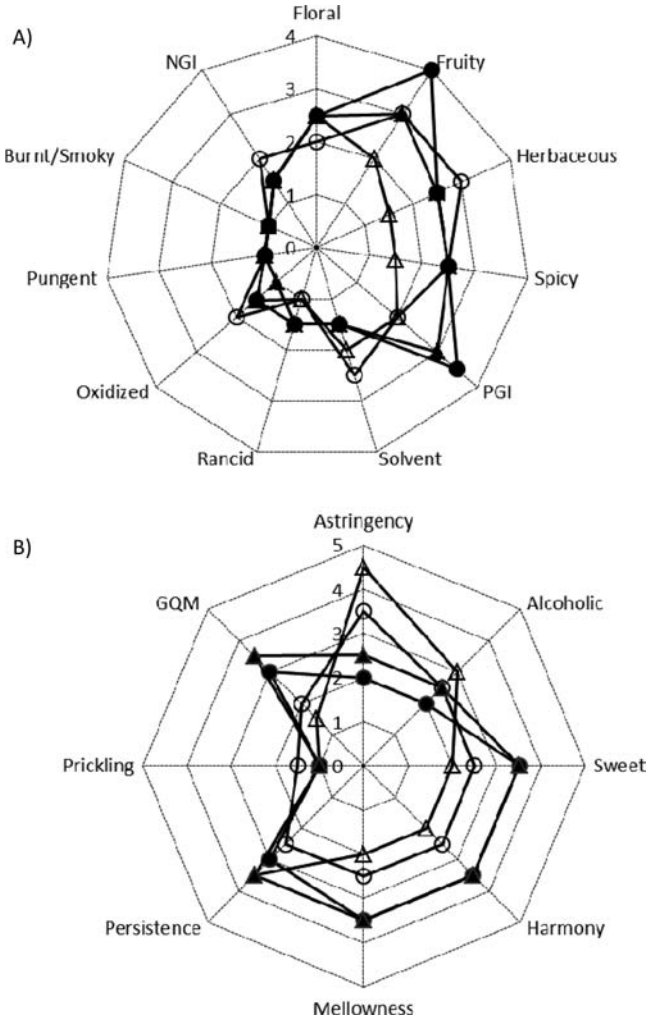


**Figure 2.** Spider diagram of descriptive sensory analysis for Albariño grape pomace distillates (heart fraction): (A) aroma profile and (B) taste profile. L1 yeast (circles) and L2 yeast (triangles) and alembic spirits (open symbols) and packed column (solid symbols) are shown. PGI, positive general impression; NGI, negative general impression; GQM, general quality in mouth.

(oxidized, solvent). Combined with an adequate yeast strain (L1 in this case), packed-column distillates present fruity notes attributable to their high concentrations of alcohols, acetates, and C6−C12 ethyl esters. Moreover, packed-column distillation combined with L1 fermentation resulted in higher ethanol yields and produced orujo distillates with low methanol concentration.

## AUTHOR INFORMATION

### Corresponding Author

*E-mail francisco.lopez@urv.cat.

### Funding

J.R.P. appreciates the support of AGAUR from the Generalitat de Catalunya through Grant 2007PIV-00017 and thanks Pontificia Universidad Católica de Chile for financial support for a sabbatical stay at Department D'Enginyeria Química at Universitat Rovira i Virgili. Part of this work was financially supported by Fondecyt Project 1100357-2010. J.J.R.-B. appreciates the fellowship from the program "Beatriu de Pinós" with the support of the Secretariat d'Universitats i Recerca del Departament d'Economia i Coneixement de la

Generalitat de Catalunya and the European Union. The reported research has been funded by Fondo Europeo de Desarrollo Regional (FEDER) and Instituto Nacional de Investigación y Tecnología Agraria y Alimentaria (RTA2009-00123-C02-01).

### Notes

The authors declare no competing financial interest.

## REFERENCES

(1) Orriols, I. As aguardientes de bagazo en Galicia. In *Serie Manuais Prácticos*; Conselleria de Agricultura, Gandería e Montes, Xunta de Galicia: Santiago de Compostela, Spain, 1989.

(2) European Commission.. EC Regulation 110/2008 of the European parliament and of the council on the definition, description, presentation, labelling and the protection of geographical indications of spirit drinks. *Off. J. Eur. Union, L: Legis. (Engl. Ed.)* **2008**, *L39*, 16−54 (13/2/2008).

(3) Reglamento de la denominación geográfica de los aguardientes y licores tradicionales de Galicia. *Diario Oficial de Galicia* **2012**, *10*, 2516−2545.

(4) Cortés, S.; Salgado, J. M.; Rodríguez, N.; Domínguez, J. M. The storage of grape marcs: Limiting factor in the quality of the distillate. *Food Control* **2010**, *21*, 1545−1549.

(5) Cortés-Diéguez, S.; Gil-de-la-Peña, M. L.; Fernández-Gómez, E. Concentration of volatiles in marc distillates from Galicia according to storage conditions of the grape pomace. *Chromatographia* **2011**, *53*, S406−S411.

(6) Orriols, I.; Bertrand, A. Los aguardientes tradicionales gallegos. Estudio de sus componentes volátiles y de la incidencia del estado de conservación del orujo sobre ellos. *Vitivinicultura* **1990**, *3*, 52−58.

(7) Diéguez, S. C.; de la Peña, M. L. G.; Gómez, E. F. Approaches to spirit aroma: Contribution of some aromatic compounds to the primary aroma in samples of orujo spirits. *J. Agric. Food Chem.* **2003**, *51*, 7385−7390.

(8) Diéguez, S. C.; de la Peña, M. L. G.; Gómez, E. F. Volatile Composition and Sensory Characters of Commercial Galician Orujo Spirits. *J. Agric. Food Chem.* **2005**, *53*, 6759−6765.

(9) López-Vázquez, C.; Bollaín, M. H.; Bertsch, K.; Orriols, I. Fast determination of principal volatile compounds in distilled spirits. *Food Control* **2010**, *21*, 1436−1441.

(10) Cortés, S.; Fernández, E. Differentiation of Spanish alcoholic drinks, orujo, obtained from red and white grape pomace distillation: Volatile composition. *Int. J. Food Sci. Technol.* **2011**, *14*, 1349−1357.

(11) Orriols, I.; Bollaín, M. H.; Bertch, K. Differentation varietale des eaux-de-vie de marc de la Galicia. In *First Symposium In Vino Analytica Scientia: Analytical Chemistry for Wine, Brandy and Spirits*; Ecole Européenne de Chimie Analytique: Bordeaux, France, 1997; pp 504−506.

(12) Iacumin, L.; Manzano, M.; Cecchini, F.; Orlic, S.; Zironi, R.; Comi, G. Influence of specific fermentation conditions on natural microflora of pomace in grappa production. *World J. Microbiol. Biotechnol.* **2012**, *28*, 1747−1759.

(13) Pina, C. G.; Hogg, T. Microbial and chemical changes during the spontaneous ensilage of grape pomace. *J. Appl. Microbiol.* **1999**, *86*, 777−784.

(14) Bovo, B.; Andriaghetto, C.; Carlot, M.; Corich, V.; Lombardi, A.; Giacomini, A. Yeast population dynamics during pilot-scale storage of grape marcs for the production of grappa, a traditional Italian alcoholic beverage. *Int. J. Food Microbiol.* **2009**, *129*, 221−228.

(15) Bovo, B.; Fontana, F.; Giacomini, A.; Corich, V. Effects of yeast inoculation on volatile compound production by grape marcs. *Ann. Microbiol.* **2011**, *61*, 117−124.

(16) Bovo, B.; Giacomini, A.; Corich, V. Effects of grape marcs acidification treatment on the evolution of indigenous yeast populations during the production of grappa. *J. Appl. Microbiol.* **2011**, *111*, 382−388.

(17) Bovo, B.; Nardi, T.; Fontana, F.; Carlot, M.; Giacomini, A.; Corich, V. Acidification of grape marc for alcoholic beverage production: Effects on indigenous microflora and aroma profile after distillation. *Int. J. Food Microbiol.* **2012**, *152*, 100−106.

(18) Orriols, I. Los aguardientes de orujo gallegos. Diferentes sistemas de elaboración, componentes volátiles característicos. *Vitivinicultura* **1991**, *7*, 58−63.

(19) Orriols, I.; Rodríguez, B.; Perez-Fernandez, J. F. L'eau-de-vie de marc ("aguardente") d'albarino: Influence de trois systèmes de distillation sur les teneurs en composés volatiles. In *Les eaux-de-vie traditionnelles d'origine viticole*; Bertrand, A., Ed.; Lavoisier: Paris, 1991; pp 43−49.

(20) Orriols, I.; Bollaín, M. H.; Bertch, K. Les marcs Orujo de Galicia. Difference entre les types d'élaboration. In *First Symposium In Vino Analytica Scientia: Analytical Chemistry for Wine, Brandy and Spirits*; Ecole Européenne de Chimie Analytique: Bordeaux, France, 1997; pp 507−511.

(21) Orriols, I.; Cortés, S. M.; Fornos, D. Caractérisation des différents systèmes de distillation utilisés dans l'élaboration Orujo de Galicia. In *Les eaux-de-vie traditionnelles d'origine viticole*; Bertrand, A., Ed.; Lavoisier Tec & Doc: Paris, 2008; pp 167−171.

(22) Orriols, I. ; Cortés, S. M., López, C., Fornos, D., Suárez, R. Application de la déméthylization dans l'élaboration d'eaux-de-vie de marc. In *Les eaux-de-vie traditionnelles d'origine viticole*; Bertrand, A., Ed.; Lavoisier Tec & Doc: Paris, 2008; pp 217−220.

(23) García-Llobodanin, L.; Roca, J.; López, J. R.; Pérez-Correa, J. R.; López, F. The lack of reproducibility of different distillation techniques and its impact on pear spirit composition. *Int. J. Food Sci. Technol.* **2011**, *46*, 1956−1963.

(24) Arrieta-Garay, Y.; García-Llobodanin, L.; Pérez-Correa, J. R.; López-Vázquez, C.; Orriols, I.; López, F. Aromatically enhanced pear distillates from blanquilla and conference varieties using a packed column. *J. Agric. Food Chem.* **2013**, *61*, 4936−4942.

(25) Arrieta-Garay, Y.; López-Vázquez, C.; Blanco, P.; Pérez-Correa, J. R.; Orriols, I.; López, F. Kiwi spirits with stronger floral and fruity characters were obtained with a packed column distillation system. *J. Inst. Brew.* **2014**, *120*, 111−118.

(26) Blanco, P.; Mirás-Avalos, J. M.; Pereira, E.; Orriols, I. Fermentative aroma compounds and sensory profiles of Godello and Albariño wines as influenced by *Saccharomyces cerevisiae* yeast strains. *J. Sci. Food Agric.* **2013**, *93*, 2489−2857.

(27) Blanco, P.; Mirás-Avalos, J. M.; Suárez, V.; Orriols, I. Inoculation of Treixadura musts with autochthonous *Saccharomyces cerevisiae* strains: fermentative performance and influence on the wine characteristics. *Food Sci. Technol. Int.* **2013**, *19*, 177−186.

(28) García-Llobodanin, L.; Achaerandio, I.; Ferrando, M.; Güell, C.; López, F. Pear distillates from pear juice concentrate: Effect of lees in the aromatic composition. *J. Agric. Food Chem.* **2007**, *55*, 3462−3468.

(29) Esteve-Zarzoso, E.; Belloch, C.; Uruburu, F.; Querol, A. Identification of yeasts by RFLP analysis of the 5.8S rRNA gene and the two ribosomal internal transcribed spacers. *Int. J. Syst. Bacteriol.* **1999**, *49*, 329−337.

(30) Kurtzman, C. P.; Robnett, C. J. Identification and phylogeny of ascomycetous yeasts from analysis of nuclear large subunit (26S) ribosomal DNA partial sequences. *Antonie van Leeuwenhoek* **1998**, *73*, 331−371.

(31) Altschul, S. F.; Gish, W.; Miller, W.; Myers, E. W.; Lipman, D. J. Basic local alignment search tool. *J. Mol. Biol.* **1990**, *215*, 403−410.

(32) Querol, A.; Barrio, E.; Ramón, D. A comparative study of different methods of yeast strain characterization. *Syst. Appl. Microbiol.* **1992**, *15*, 439−446.

(33) OIV, International Organization of Vine and Wine. Resolution OIV/OENO 379/2009. Update of the OIV international compendium of methods of analysis of spirit drinks of vitivinicultural origin, 2009.

(34) López-Vázquez, C.; Bollaín, M. H.; Moser, S.; Orriols, I. Characterization and differentiation of monovarietal grape pomace distillate from native varieties of Galicia. *J. Agric. Food Chem.* **2010**, *58*, 9657−9665.

(35) ISO 13299. Sensory analysis: Methodology. In *General guidance for establishing a sensory profile*; International Organization for Standardization: Geneva, Switzerland, 2003; http://www.iso.org.

(36) Fleet, G. H. Yeast interactions and wine flavor. *Int. J. Food Microbiol.* **2003**, *86*, 11−22.
(37) Loureiro, V.; Malfeito-Ferreira, M. Spoilage yeasts in the wine industry. *Int. J. Food Microbiol.* **2003**, *86*, 23−50.
(38) Blanco, P.; Tato, A.; Vázquez, M.; Cortés, S. Identificación de levaduras en orujo de la variedad Treixadura en función de las condiciones de ensilado. In *Nuevos Horizontes en la Viticultura y la Enología*; Falqué, E., Ed.; Servizo de publicacións da Universidade de Vigo: Vigo, Spain, 2009; pp 665−668.
(39) Zocca, F.; Lomolino, G.; Curioni, S. P.; Lante, A. Detection of pectinmethylesterase activity in presence of methanol during grape pomace storage. *Food Chem.* **2007**, *102*, 59−65.
(40) Usseglio-Tomasset, L. Le caratteristiche della grappa derivanti dall'evoluzione dei costituenti volatili delle vinacce durante il periodo di insilamento e dalle modificazioni apportate dal proceso di distillazione. *Vini Ital.* **1971**, *13*, 453−462.
(41) Silva, M. L.; Malcata, F. X.; de Revel, G. Volatile contents of grape marcs in Portugal. *J. Food Compost. Anal.* **1996**, *9*, 72−80.
(42) Cantagrel, R.; Lurton, L.; Vidal, J. P.; Galy, B. From vine to cognac. In *Fermented Beverage Production*, 1st ed.; Lea, A. G. H., Piggott, J. R., Eds.; Blackie Academic and Professional: London, 1997; pp 208−228.
(43) Apostolopoulou, A.; Flouros, A.; Demertzis, P.; Akrida-Demertzi, K. Differences in concentration of principal volatile constituents in traditional Greek distillates. *Food Control* **2005**, *16*, 157−164.
(44) Silva, M. L.; Malcata, F. X. Relationships between storage conditions of grape pomace and volatile composition of spirits obtained therefrom. *Am. J. Enol. Vitic.* **1998**, *49*, 56−64.
(45) Claus, M. J.; Berglund, K. A. Fruit brandy production by batch column distillation with reflux. *J. Food Process Eng.* **2005**, *28*, 53−67.
(46) García-Llobodanin, L.; Senn, T.; Ferrando, M.; Güell, C.; López, F. Influence of the fermentation pH on the final quality of Blanquilla pear spirits. *Int. J. Food Sci. Technol.* **2010**, *45*, 839−848.
(47) De Rosa, T.; Castagner, R. *Tecnologia delle grappe e dei distillati d'uva*; Edagricole: Bologna, Italy, 1994.
(48) Versini, G.; Franco, M. A.; Moser, S.; Barchetti, P.; Manca, G. Characterisation of apple distillates from native varieties of Sardinia island and comparison with other Italian products. *Food Chem.* **2009**, *113*, 1176−1183.
(49) Haefliger, O. P.; Jeckelmann, N. Stripping of aroma compounds during beer fermentation monitored in real-time using an automatic cryotrapping sampling system and fast gas chromatography/mass spectrometry. *Anal. Methods* **2013**, *5*, 4409−4418.
(50) Di Stefano, R. I Costituenti della Grappa di Moscato. *Vini Ital.* **1986**, *28*, 41−48.
(51) Odello, L.; Giomo, A.; Versini, G.; Zironi, R. *Grappa: Analisi Sensoriale e Tecnologia*; Centro Studi e Formacione Assaggiatori: Brescia, Italy, 1997
(52) Soufleros, E. H.; Mygdalia, A. S.; Natskoulis, P. Characterization and safety evaluation of the traditional Greek fruit distillate "Mouro" by flavor compounds and mineral analysis. *Food Chem.* **2004**, *86*, 625−636.

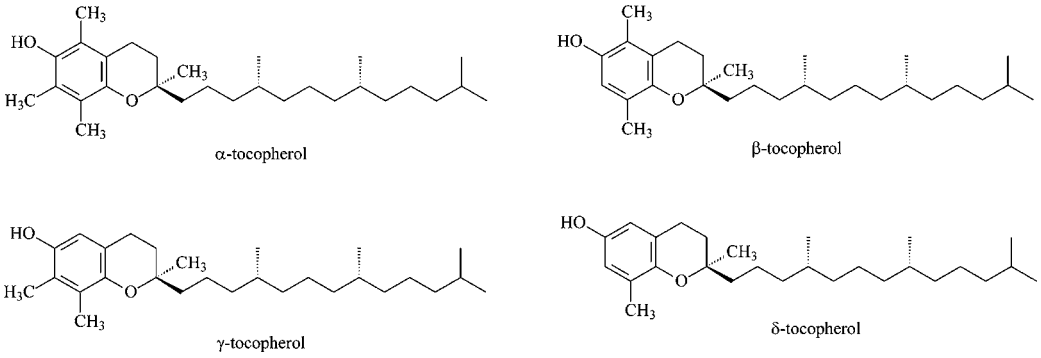


**Figure 1.** Structures of tocopherol homologues used in this study.

often explained by their differences in polarity.[12] Huang and coworkers[13] reported that the more polar $\gamma$-tocopherol was a more effective antioxidant than $\alpha$-tocopherol in corn O/W emulsions. Also, it was found that antioxidant activity of more polar $\delta$-tocopherol was better than $\alpha$-tocopherol in menhaden O/W emulsions, while in bulk menhaden oil, $\alpha$-tocopherol was a more effective antioxidant than $\delta$-tocopherol.[12] The physical location of antioxidants in O/W emulsions can be influenced by surfactant micelles, which can increase aqueous-phase antioxidant concentrations 2.3−7.5-fold.[14,15] In this study, we proposed to determine the effect of the Tween 20 concentration on the partioning behavior of $\alpha$-, $\gamma$-, and $\delta$-tocopherols and investigate how partitioning impacted the antioxidant activity of $\alpha$- and $\delta$-tocopherol in O/W emulsions. To accomplish this goal, the location of tocopherols in O/W emulsions was determined by high-performance liquid chromatography (HPLC), and antioxidant activity was determined by monitoring the formation of lipid peroxides and headspace hexanal.

## MATERIALS AND METHODS

**Chemicals and Materials.** Soybean oil was purchased from a local retail store in Hadley, MA. Iso-octane, 2-propanol, methanol, 1-butanol, *n*-hexane hydrochloric acid, and sodium phosphate dibasic were purchased from Fisher Scientific (Fair Lawn, NJ). Ethylenediaminetetraacetic acid (EDTA) was purchased from Chempure Ultra (Houston, TX). Silicic acid (100−200 mesh), activated charcoal (100−400 mesh), polyoxyethylene (20) sorbitan monolaurate (Tween 20), sodium phosphate monobasic, barium chloride dihydrate, ammonium thiocyanate, iron(II) sulfate heptahydrate, cumene hydroperoxide, hexanal, (±)-$\alpha$-tocopherol, (+)-$\gamma$-tocopherol, and (+)-$\delta$-tocopherol were purchased from Sigma-Aldrich (St. Louis, MO). The solvents were HPLC-grade, and all other chemicals were analytical-grade. Double-distilled and deionized water were used throughout the study. Glassware was incubated in 2 M HCl overnight to remove metals, followed by rinsing with double-distilled water before use.

**Preparation of Stripped Soybean Oil (SSO).** SSO was prepared according to the method by Boon et al.[16] and was used in all experiments. Briefly, silicic acid (100 g) was washed 3 times with a total of 3 L of distilled water and activated at 110 °C for 20 h. The activated silicic acid (22.5 g) and activated charcoal (5.63 g) were suspended in 100 and 70 mL of *n*-hexane, respectively. A chromatographic column (3.0 cm internal diameter × 35 cm height) was then packed sequentially with silicic acid, followed by activated charcoal, and then another layer of silicic acid. A total of 30 g of soybean oil was dissolved in 30 mL of *n*-hexane and passed through the column by eluting with 270 mL of *n*-hexane. To retard lipid oxidation during stripping, the collected soybean oil was held in an ice bath and covered with aluminum foil. After complete elution, *n*-hexane was removed with a vacuum rotary evaporator (model RE 111, Buchi, Flawil, Switzerland) at 37 °C, and traces of the remaining solvent were evaporated under a nitrogen stream. The SSO was flushed with nitrogen and stored at −80 °C until use. Removal of tocopherols in SSO was verified by HPLC.

**Emulsion Preparation.** O/W emulsions were prepared using 1.0 wt % SSO in a 10 mM phosphate buffer solution (pH 7.0). Tween 20 was used as an emulsifier at a 1:10 emulsifier/oil ratio. SSO, Tween 20, and phosphate buffer were added to a beaker, and a coarse emulsion was made by blending with a hand-held two-speed homogenizer (model M133/1281-0, Biospec Products, Inc., Bartlesville, OK) at the high speed setting for 2 min. The coarse emulsion was then homogenized with a microfluidizer (model M-110L, Microfluidics, Newton, MA) at a pressure of 9 kbar for three passes. During homogenization, ice was used to cover the homogenizer chamber and coil, to maintain the emulsion temperature at <25 °C.

After O/W emulsion was prepared, samples were mixed with 0, 0.1, 0.5, and 1.0 (w/w) Tween 20 and stirred by an electronic stirrer (model 2008, Thermo Fisher Scientific, Inc., Raleigh, NC) at 500 rpm for 1 h at room temperature. The emulsions (1 mL) were then transferred into 10 mL GC vials, capped with aluminum caps with polytetrafluoroethylene (PTFE)/silicone (tetrafluoroethylene) septa, and stored at 37 °C in the dark.

Particle size distributions of the final emulsions were measured using a dynamic light scattering instrument (Zetasizer Nano-ZS Malvern Instruments, Ltd., Worcestershire, U.K.). Samples for particle size distribution measurements were diluted into 10 mM phosphate buffer solution (pH 7.0) at an emulsion/buffer ratio of 1:50 to prevent the multiple scattering effects. Each measurement was determined in triplicate at room temperature. The average emulsion droplet size was 193.8 ± 14.4 nm, and there was no significant change in the droplet size of each emulsion over the course of studies (data not shown).

**Determination of Antioxidant Partitioning.** The physical location of $\alpha$-, $\gamma$-, and $\delta$-tocopherols in the emulsions were determined according to the procedure described by Panya et al.[15] Emulsions with various added Tween 20 concentrations (0, 0.1, 0.5, and 1.0, w/w) were prepared with 10 mM phosphate buffer, including 200 $\mu$M EDTA, to minimize oxidation of the antioxidants during analysis. $\alpha$-, $\gamma$-, and $\delta$-tocopherols in methanol were added to the emulsions at a final concentration of 100 $\mu$M. The emulsions were centrifuged at 162102*g* (46 000 rpm) for 1 h at 4 °C using a PTI F65L-6 × 13.5 rotor with a Sorvall WX Ultra 80 centrifuge (Thermo Fisher Scientific, Inc., Asheville, NC). After centrifugation, the aqueous phase was carefully collected with a needle and syringe. The aqueous phase (0.5 mL) was dried using a vacuum centrifuge drier and stored at −80 °C prior to further analyses. Aqueous-phase samples were dissolved in 200 $\mu$L of methanol, and tocopherol concentrations were determined by HPLC (Shimadzu, Kyoto, Japan) using a C18 reversed-phase column (150−4.6 mm, 5 $\mu$m, Beckman Coulter) equipped with a security guard column (C18, 4 × 3.0 mm, Phenomenex, Torrance, CA). An isocratic elution was carried out using methanol with a flow rate of 1 mL/min. Tocopherol homologues were detected with a fluorescence detector (scanning fluorescence detector, Waters 474, Milford, MA) at an excitation wavelength of 290 nm and emission wavelength of 330 nm. The concentration of tocopherols was calculated using a standard curve made from each tocopherol dissolved in methanol.

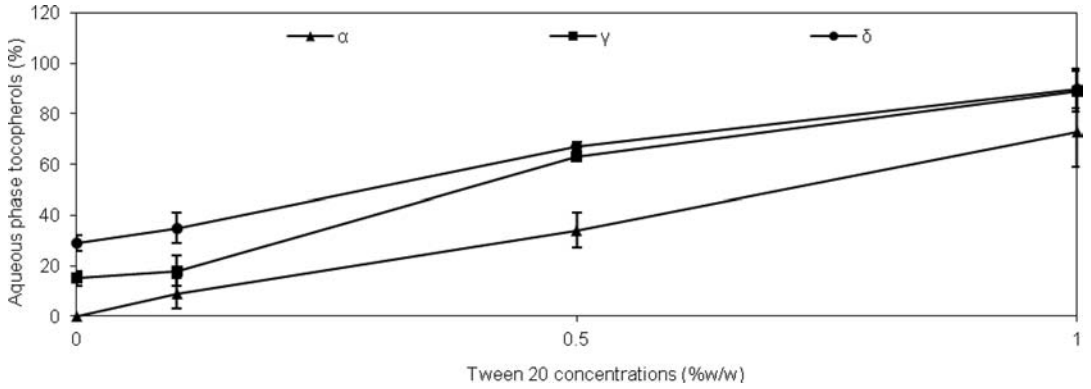


**Figure 2.** Effect of added Tween 20 (0, 0.1, 0.5, and 1%) on the partitioning of $\alpha$-, $\gamma$-, and $\delta$-tocopherols (100 $\mu$M) into the aqueous phase of 1% stripped soybean O/W emulsions. Data points and error bars represent means ($n$ = 3) ± standard deviations.

**Front-Face Fluorescence Measurements.** Front-face fluorescence of $\alpha$-tocopherol in O/W emulsions was determined by steady-state emission measurements recorded with a PTI spectrofluorometer (Photon Technology International, London, Ontario, Canada). Emulsions were prepared as described above with the addition of 30 $\mu$M $\alpha$-tocopherol. Final emulsions (1.5 mL) were transferred into triangular Suprasil cuvettes, and they were held in a sample holder at 25 °C. Emission was observed at 90° to the incident beam, that is, 22.5° with respect to the illuminated cell surface. The emission of $\alpha$-tocopherol was measured at 330 nm using an excitation wavelength of 299 nm. Spectral bandwidth for both excitation and emission slits was 2.0 nm; integration time was 1 s; and the wavelength increment was 2.5 nm. The intensity of the spectra of $\alpha$-tocopherol was determined as the emission signal intensity (counts per second) measured by means of a photomultiplier. The intensity ratio ($I_o/I$), where $I_o$ is the fluorescence intensity of $\alpha$-tocopherol, was plotted versus the concentrations of emulsifiers.

**Lipid Oxidation Studies.** For the lipid oxidation studies, $\alpha$- and $\delta$-tocopherols were added to the emulsions at a final concentration of 35 and 10 $\mu$M, respectively. Samples with methanol but without the addition of tocopherols were used as control samples. Lipid hydroperoxide formation was determined using the method adapted from Shanta and Decker.[17] Emulsion samples (0.3 mL) were mixed with 1.5 mL of isooctane/2-propanol solution (3:1, v/v) and vortexed (10 s, 3 times). The mixed solution was centrifuged at 3400$g$ for 10 min (Centrific centrifuge, Thermo Fisher Scientific, Inc., Fairlawn, NJ). The upper organic layer (0.2 mL or less according to the oxidation state) was mixed with 2.8 mL of methanol/butanol solution (2:1, v/v), followed by the addition of 15 $\mu$L of 3.94 M ammonium thiocyanate and 15 $\mu$L of $Fe^{2+}$ solution. The clear $Fe^{2+}$ solution was prepared freshly from the supernatant of a mixture of equal amounts of 0.132 M $BaCl_2$ (in 0.4 M HCl) and 0.144 M $FeSO_4$. The solution was vortexed, and after 20 min of incubation at room temperature, the absorbance of the samples were measured at 510 nm using an ultraviolet−visible (UV−vis) spectrophotometer (Genesys 20, Thermo Fisher Scientific, Inc., Waltham, MA). Hydroperoxide concentrations were determined using a standard curve prepared from cumene hydroperoxide.

Headspace hexanal was measured according to the method described by Panya et al.[18] using a gas chromatograph (GC, model GC-2014, Shimadzu Co., Tokyo, Japan) equipped with an autoinjector (model AOC-5000, Shimadzu Co., Tokyo, Japan). Emulsions (1 mL) in 10 mL glass vials capped with aluminum caps with PTFE/silicone septa were heated at 55 °C for 10 min in the autosampler heating block before measurements. A 50/30 $\mu$m divinylbenzene/carboxen/polydimethylsiloxane (DVB/carboxen/PDMS) stable flex solid-phase microextraction (SPME) fiber (Supelco Co., Bellefonte, PA) was then inserted into the vial headspace for 2 min to absorb volatiles. The fiber was transferred to the GC injector port (250 °C) for 3 min. The injection port was operated in split mode, and the split ratio was set at 1:7. Volatiles were separated on a fused-silica capillary Equity-1 Supelco column (30 m × 0.32 mm inner diameter × 1 $\mu$m) coated with 100% polydimethylsiloxane (PDMS) at 65 °C for 10 min. A flame ionization detector was used at a temperature of 250 °C. Hexanal concentrations were determined from peak areas using a standard curve made from authentic hexanal.

**Statistical Analysis.** All data shown represents the mean value ± standard deviation of triplicate measurements. The data obtained were analyzed by analysis of variance (ANOVA) using SPSS version 21 (SPSS, Inc., Chicago, IL). The differences between mean values were compared using Duncan's multiple-range test with a level of significance of $p < 0.05$.

## RESULTS AND DISCUSSION

**Impact of the Tween 20 Concentration on the Partitioning Behavior of Tocopherols in Stripped Soybean O/W Emulsions.** In this study, the effect of the surfactant concentration on the location of different tocopherol homologous in 1% stripped soybean O/W emulsions was determined by adding 0.1, 0.5, and 1.0% Tween 20 to the emulsions (Figure 2). The addition of all concentrations of Tween 20 increased the aqueous-phase concentration of all of the tocopherol homologues. Because the tocopherols are essentially insoluble in water,[19] the ability of Tween 20 to solubilize the tocopherols into the aqueous phase means that Tween 20 was forming comicelles with the tocopherols.

When the aqueous-phase concentration of the different forms of tocopherols were compared, they were in the order of $\delta$- > $\gamma$- > $\alpha$-tocopherols at all of the Tween 20 concentrations tested. At 1.0% Tween 20, the amount of $\alpha$-, $\gamma$-, and $\delta$-tocopherols in the aqueous phase was 73, 89, and 90%, respectively (Figure 2). $\delta$-Tocopherol is the most polar and most surface-active[20] of all of the tocopherols tested, which could explain why its solubilization into the aqueous phase by Tween 20 was greatest. Other researchers have reported that antioxidants in the emulsion droplet can migrate to the aqueous phase in the presence of surfactants. Richards et al.[14] found that Brij 700 was able to solubilize propyl gallate and butylated hydroxyltoluene out of emulsion droplets, with the more polar propyl gallate partitioning into the aqueous phase to a greater extent. Laguerre et al.[8] found that Brij 35 solubilized cholorogenic acid fatty acid esters out of emulsion droplets. Panya et al.[15] reported that Tween 20 solubilized rosmarinic acid esters out of the oil droplets, but in this case, the more nonpolar 20 carbon ester partitioned into the aqueous phase more than the 4 carbon ester.

It should be noted that the concentration of tocopherols in the presence of no added Tween 20 was in the order of $\delta$- > $\gamma$-

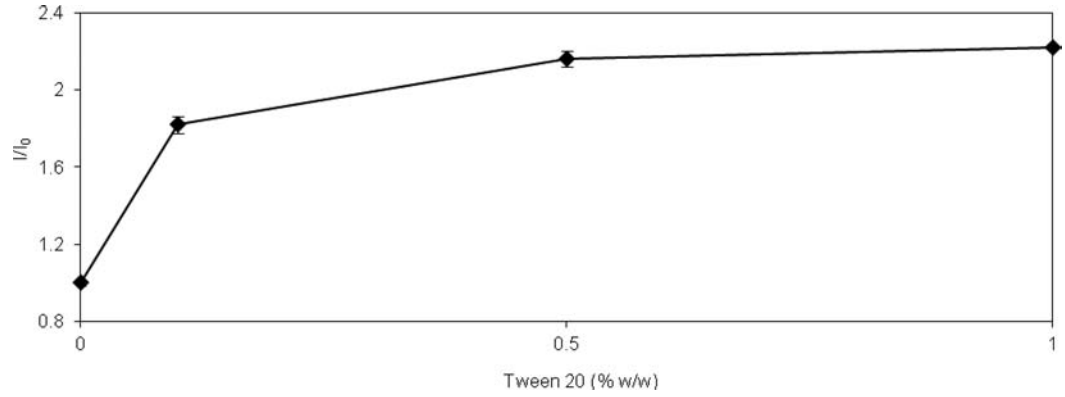


**Figure 3.** Front-face fluorescence measurements ($\lambda_{ex}$, 299; $\lambda_{em}$, 330) of 30 $\mu$M $\alpha$-tocopherol in 1% stripped soybean O/W emulsions with varying Tween 20 concentrations. Data points and error bars represent means ($n$ = 3) ± standard deviations.

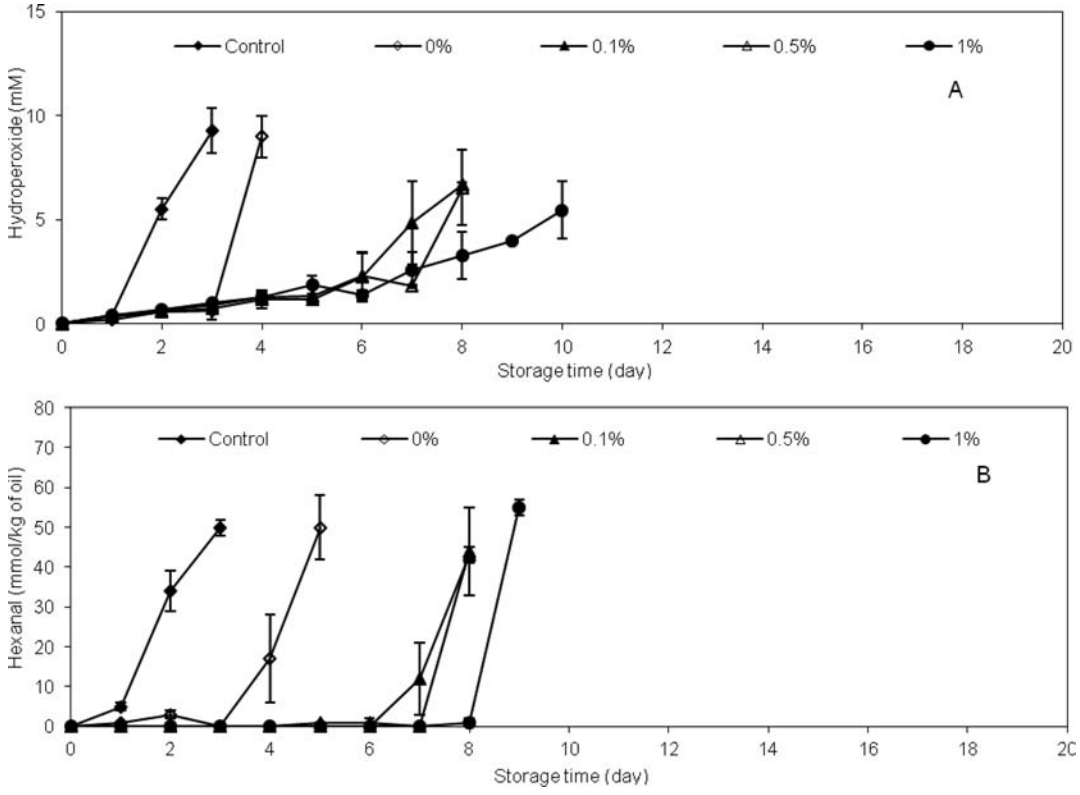


**Figure 4.** (A) Lipid hydroperoxide and (B) hexanal formation in 1% SSO−Tween 20 emulsions in the absence (control) or presence of $\alpha$-tocopherol (35 $\mu$M) as a function of added Tween 20 (0, 0.1, 0.5, and 1.0%, w/w) during storage at 37 °C. Data points and error bars represent means ($n$ = 3) ± standard deviations.

> $\alpha$-tocopherols at 0.1% Tween 20. All three tocopherol homologues are listed in the Merck Index as not being soluble in water.[21] During emulsion preparation, surfactants will concentrate at the droplet surface until the surface is saturated with the remaining surfactant partitioning into the aqueous phase.[14] Tween 20 has a low critical micelle concentration (cmc; <0.1 mM at 21 °C).[22] It is likely that Tween 20 present in the aqueous phase used in this study was at concentrations above the cmc, and these micelles were able to solubilize the tocopherols.

The process of measuring aqueous-phase antioxidant concentrations is time-consuming because of the need to separate the aqueous phase from the emulsion droplets by centrifugation. Therefore, we determined the possibility of measuring aqueous-phase tocopherol concentrations in the emulsions directly by fluorescence. In bulk oils, it is difficult to measure $\alpha$-tocopherol by fluoresce because of self-quenching.[5] However, if the tocopherols are present in the aqueous phase in surfactant micelles, this self-quenching could be decreased by physically separating the tocopherols into numerous micelles. The fluorescence intensity of $\alpha$-tocopherol with varying Tween 20 concentrations (0.1, 0.5, and 1.0%) as determined by front-faced fluoresce is shown in Figure 3. Increasing Tween 20 concentrations caused higher fluorescence intensity as $\alpha$-tocopherol was solubilized into the aqueous phase. Fluorescence intensity was 1.0-, 1.8-, 2.2-, and 2.2-fold higher in the presence of 0, 0.1, 0.5, and 1.0%, respectively. While the front-face fluorescence could detect the solubilization of $\alpha$-tocopherol into the aqueous phase, the increases in fluorescence did not strongly correspond to the aqueous-

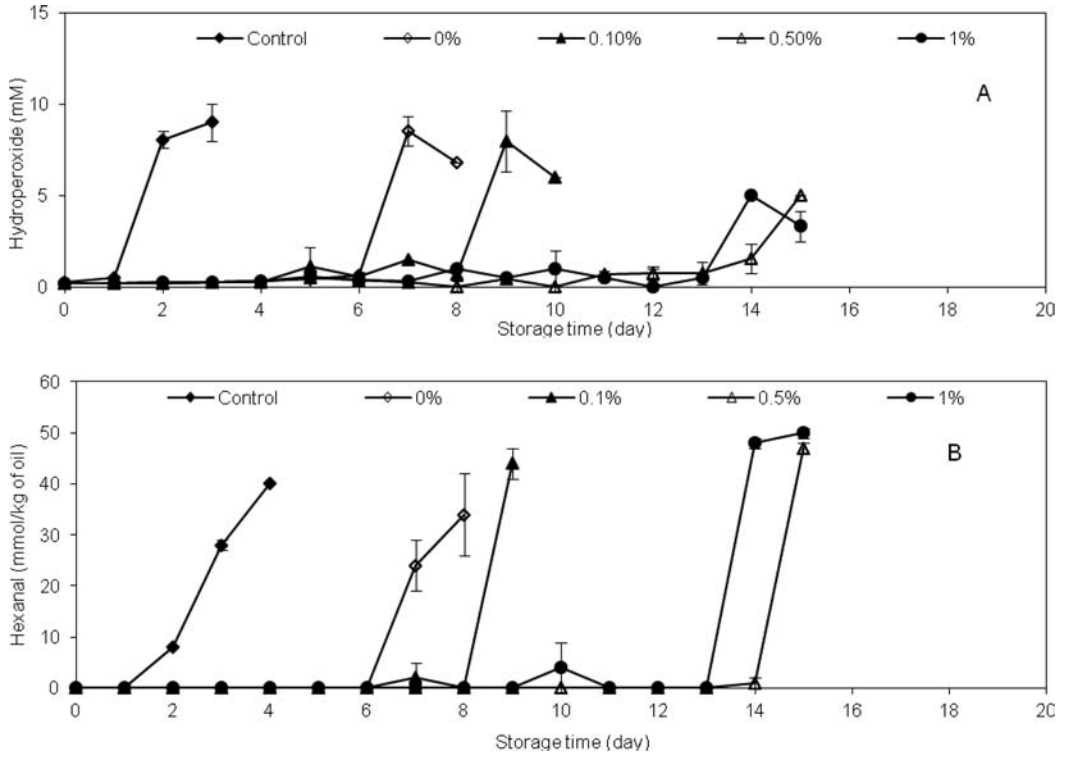


**Figure 5.** (A) Lipid hydroperoxide and (B) hexanal formation in 1% SSO−Tween 20 emulsions in the absence (control) or presence of $\delta$-tocopherol (10 $\mu$M) as a function of added Tween 20 concentrations (0, 0.1, 0.5, and 1.0%, w/w) during storage at 37 °C. Data points and error bars represent means ($n$ = 2) ± standard deviations.

phase concentrations determined by HPLC. For example, at 0.1% added Tween 20, fluorescence increased by over 80%, while actual aqueous-phase concentrations increased by less than 5%. Therefore, the front-faced fluorescence technique was not used for further studies.

**Impact of Partitioning on the Antioxidant Activity of Tocopherols.** The impact of the increasing concentrations of Tween 20 (0, 0.1, 0.5, and 1%) and, thus, the physical location of tocopherols on oxidative stability of 1% stripped soybean O/W emulsions were determined during incubation in the dark at 37 °C. Lipid oxidation rates of stripped soybean O/W emulsions with $\alpha$-tocopherol at a concentration of 35 $\mu$M were evaluated by lipid hydroperoxide and hexanal as indicators of primary and secondary oxidation products (panels A and B of Figure 4). The stripped soybean O/W emulsion without $\alpha$-tocopherol was used as a control. Lipid oxidation occurred rapidly in the absence of $\alpha$-tocopherol (control) with a lag phase of lipid hydroperoxide and hexanal formation of 1 day. The addition of 35 $\mu$M $\alpha$-tocopherol increased the lag phase for both lipid hydroperoxide and hexanal to 3 days. Increasing Tween 20 concentrations from 0.1 to 1.0% enhanced the antioxidant activity of $\alpha$-tocopherol in a concentration-dependent manner. The lag time of lipid hydroperoxide formation increased to 6−7 days, and hexanal formation improved oxidative stability to 6−9 days.

A similar trend was observed in O/W emulsions with $\delta$-tocopherol. In these experiments, $\delta$-tocopherol was added to the O/W emulsions at a concentration of 10 $\mu$M because preliminary studies showed that its activity was greater than $\alpha$-tocopherol. This was consistent with the study by Wagner et al., who reported that $\delta$-tocopherol was a better antioxidant in O/W emulsions than $\alpha$-tocopherol.[23] Huang et al. also reported that the more polar $\gamma$-tocopherol was more effective than $\alpha$-tocopherol in O/W emulsions.[13] As observed in the previous study, the lag phase of lipid hydroperoxide and hexanal formation in the control (without $\delta$-tocopherol) was 1 day (Figure 5). In the presence of 10 $\mu$M $\delta$-tocopherol, the lag phase for lipid hydroperoxide and hexanal increased to 6 days. Similar to $\alpha$-tocopherol, the activity of $\delta$-tocopherol was also enhanced by the presence of Tween 20 in the aqueous phase of the O/W emulsion. However, unlike $\alpha$-tocopherol, Tween 20 dramatically increased the ability of $\delta$-tocopherol to inhibit both lipid hydroperoxide and hexanal formation. The addition of 0.1% Tween 20 to the O/W emulsion increased the lag phase from 6 to 8 days. In the presence of 0.5 and 1.0% Tween 20, the activity of $\delta$-tocopherol was more than doubled, with lag phases of lipid hydroperoxide and hexanal formation of 14 and 13 days. Overall, the increased impact on $\delta$-tocopherol was not that unexpected; at both 0.5 and 1.0% Tween 20, the aqueous phase concentration of $\delta$-tocopherol was higher than $\alpha$-tocopherol (Figure 2).

This research and others[8,15] have found that increasing the concentration of hydrophobic antioxidants into the aqueous phase of O/W emulsions by surfactant micelles increases antioxidant activity. The reason for this phenomenon is currently unclear but has been proposed to be due to the ability of surfactant micelles to solubilize the antioxidant out of the emulsion droplet core, where they are ineffective antioxidants. However, this is contrary to the antioxidant polar paradox,[4] which states that the most effective antioxidants in lipid dispersions are those that remain in the emulsion droplet. The ability of surfactant micelles to increase the activity of hydrophobic antioxidants might be related to the hypothesis that antioxidants are most effective when they are at the interface of emulsion droplets.[7,15] Surfactant micelles can rapidly exchange lipid components between the micelles and

emulsion droplets.[24] Therefore, it is possible that the Tween 20−tocopherol comicelles could form a reservoir of tocopherols that could replace oxidized tocopherols in the emulsion droplets to maintain an optimum level of antioxidants. Alternately, it could be possible that reactive oxygen species could exist in the aqueous phase of the O/W emulsion, and the presence of the Tween 20−tocopherol comicelles could scavenge these radicals before they could oxidize the fatty acids in the oil droplets. This seems less likely because water-soluble antioxidants are often ineffective in O/W emulsions.[25]

This research highlights that tocopherols naturally occurring in refined oils are not reaching their maximum potential and could be made more effective in O/W emulsions if they can be solubilized into the aqueous phase by surfactant micelles. Unfortunately, this could be difficult in food emulsions because synthetic surfactant are not accepted by many consumers and many surfactants have unpleasant flavors. Therefore, more research is needed to gain a better understanding of how surfactant−antioxidant micelles impact the activity of antioxidants and how different surfactants effect antioxidant partitioning and activity, so that alternative strategies can be developed to increase the activity of tocopherols that are already present in the refined oils used in food emulsions.

## AUTHOR INFORMATION

### Corresponding Author

*Telephone: +90-312-203-3641. Fax: +90-0312-317-87-11. E-mail: sezertrhn@gmail.com.

### Notes

The authors declare no competing financial interest.

## REFERENCES

(1) Alamed, J.; Chaiyasit, W.; McClements, D. J.; Decker, E. A. Relationships between free radical scavenging and antioxidant activity in foods. *J. Agric. Food Chem.* **2009**, *57* (7), 2969−2976.

(2) Halliwell, B. Free radicals and antioxidants: Updating a personal view. *Nutr. Rev.* **2012**, *70* (5), 257−265.

(3) Decker, E. A.; Warner, K.; Richards, M. P.; Shahidi, F. Measuring antioxidant effectiveness in food. *J. Agric. Food Chem.* **2005**, *53* (10), 4303−4310.

(4) Porter, W. L.; Black, E. D.; Drolet, A. M. Use of polyamide oxidative fluorescence test on lipid emulsions: Contrast in relative effectiveness of antioxidants in bulk versus dispersed systems. *J. Agric. Food Chem.* **1989**, *37* (3), 615−624.

(5) Chen, B.; Han, A.; Laguerre, M.; McClements, D. J.; Decker, E. A. Role of reverse micelles on lipid oxidation in bulk oils: Impact of phospholipids on antioxidant activity of α-tocopherol and Trolox. *Food Funct.* **2011**, *2*, 302−309.

(6) Mosca, M.; Cuomo, F.; Lopez, F.; Ceglie, A. Role of emulsifier layer, antioxidants and radical initiators in the oxidation of olive oil-in-water emulsions. *Food Res. Int.* **2012**, *50* (1), 377−383.

(7) Frankel, E. N.; Huang, S. W.; Kanner, J.; German, J. B. Interfacial phenomena in the evaluation of antioxidants: Bulk oils vs emulsions. *J. Agric. Food Chem.* **1994**, *42* (5), 1054−1059.

(8) Laguerre, M.; Giraldo, L. J.; Lecomte, J.; Figueroa-Espinoza, M. C.; Barea, B.; Weiss, J.; Decker, E. A.; Villeneuve, P. Chain length affects antioxidant properties of chlorogenate esters in emulsion: The cutoff theory behind the polar paradox. *J. Agric. Food Chem.* **2009**, *57* (23), 11335−11342.

(9) Decker, E. A. Strategies for manipulating the prooxidative/antioxidative balance of foods to maximize oxidative stability. *Trends Food Sci. Technol.* **1998**, *9* (6), 241−248.

(10) Emerson, O. H. The structure of β- and γ-tocopherols. *J. Am. Chem. Soc.* **1938**, *60* (8), 1741−1742.

(11) Kim, H.; Kim, S.-G.; Choi, Y.; Jeong, H.-S.; Lee, J. Changes in tocopherols, tocotrienols, and fatty acid contents in grape seed oils during oxidation. *J. Am. Oil Chem. Soc.* **2008**, *85*, 487−489.

(12) Chaiyasit, W.; McClements, D. J.; Decker, E. A. The relationship between the physicochemical properties of antioxidants and their ability to inhibit lipid oxidation in bulk oil and oil-in-water emulsions. *J. Agric. Food Chem.* **2005**, *53* (12), 4982−4988.

(13) Huang, S. W.; Frankel, E. N.; German, J. B. Antioxidant activity of α- and γ-tocopherols in bulk oils and in oil-in-water emulsions. *J. Agric. Food Chem.* **1994**, *42* (10), 2108−2114.

(14) Richards, M. P.; Chaiyasit, W.; McClements, D. J.; Decker, E. A. Ability of surfactant micelles to alter the partitioning of phenolic antioxidants in oil-in-water emulsions. *J. Agric. Food Chem.* **2002**, *50* (5), 1254−1259.

(15) Panya, A.; Laguerre, M.; Bayrasy, C.; Lecomte, J.; Villeneuve, P.; McClements, D. J.; Decker, E. A. An ınvestigation of the versatile antioxidant mechanisms of action of rosmarinate alkyl esters in oil-in-water emulsions. *J. Agric. Food Chem.* **2012**, *60* (10), 2692−2700.

(16) Boon, C. S.; Xu, Z.; Yue, X.; McClements, D. J.; Weiss, J.; Decker, E. A. Factors affecting lycopene oxidation in oil-in-water emulsions. *J. Agric. Food Chem.* **2008**, *56* (4), 1408−1414.

(17) Shanta, N. C.; Decker, E. A. Rapid, sensitive, iron-based spectrophotometric methods for determination of peroxide values of food lipids. *J. AOAC Int.* **1994**, *77* (2), 421−424.

(18) Panya, A.; Laguerre, M.; Lecomte, J.; Villeneuve, P.; Weiss, J.; McClements, D. J.; Decker, E. A. Effects of chitosan and rosmarinate esters on the physical and oxidative stability of liposomes. *J. Agric. Food Chem.* **2010**, *58* (9), 5679−5684.

(19) Huang, S.-W.; Frankel, E. N.; Aeschbach, R.; German, J. B. Partition of selected antioxidants in corn oil-water model systems. *J. Agric. Food Chem.* **1997**, *45* (6), 1991−1994.

(20) Chaiyasit, W.; Elias, R. J.; McClements, D. J.; Decker, E. A. Role of physical structures in bulk oils on lipid oxidation. *Crit. Rev. Food Sci. Nutr.* **2007**, *47*, 299−317.

(21) Windholz, M.; Budavari, S.; Stroumtsos, L. Y.; Fertig, M. N. *The Merck Index: An Encyclopedia of Chemicals and Drugs*, 9th ed.; Merck & Co., Inc.: Rahway, NJ, 1976; pp 1221−1222.

(22) Kim, C.; Hsieh, Y.-L. Wetting and absorbency of nonionic surfactant solutions on cotton fabrics. *Colloids Surf., A* **2001**, *187−188*, 385−397.

(23) Wagner, K.; Isnardy, B.; Elmadfa, I. γ- and δ-tocopherols are more effective than α-tocopherol on the autoxidation of a 10% rapeseed oil triacylglycerol-in-water emulsion with and without a radical initiator. *Eur. J. Lipid Sci. Technol.* **2004**, *106*, 44−51.

(24) McClements, D. J.; Dungan, S. R.; German, J. B.; Kinsella, J. E. Oil exchange between oil-in-water emulsion droplets stabilized with a nonionic surfactant. *Food Hydrocolloids* **1992**, *6* (5), 415−422.

(25) Hu, M.; McClements, D. J.; Decker, E. A. Antioxidant activity of a proanthocyanidin-rich extract from grape seed in whey protein isolate stabilized algae oil-in-water emulsions. *J. Agric. Food Chem.* **2004**, *52* (16), 5272−5276.

inflammation mediators (e.g., IL-1$_\beta$, IFN-$\gamma$, TNF-$\alpha$, and IL-8) is considered a good approach to ascertain the status of the inflammation processes. Moreover, TNF-$\alpha$ released by monocytes/macrophages plays a key role in initiating the cascade of other pro-inflammatory cytokines, including IL-1$_\beta$, IL-6, and IFN-$\gamma$, which are important biomarkers in gastroenteric inflammation.[13] C-reactive protein[16] and fecal calprotectin[17,18] have been used widely as noninvasive markers of gut inflammation, including active IBD.

The aim of this study was to investigate the possible effects of moderate wine consumption on the gut immune status of healthy people through the study of a wide spectrum of fecal immune parameters, including several immunoglobulins, cytokines, chemokines, and growth factors. Possible relationships between contents of these immune parameters and of phenolic metabolites present in feces as a consequence of wine consumption were explored.

## MATERIALS AND METHODS

**Red Wines.** Initially, different enological parameters and practices, including grape variety and time of contact with seeds and skins, were optimized at the winery, with the aim of obtaining a red wine with especially high polyphenol content (data not shown). Finally, a young red wine (Pinot noir, vintage 2010) with a total phenolic content of 1758 mg of gallic acid equivalents/L and 12% ethanol was selected for the intervention study. Ethanol, pH, total acidity, and volatile acidity were determined in the wine according to the methods of the OIV (International Organization of Vine and Wine, 1990). The results were as follows: wine pH, 3.52; alcohol degree, 13.8% v/v; total acidity, 6.45 g/L tartaric acid; and volatile acidity, 0.56 g/L acetic acid. Wine phenolic composition determined by UPLC-ESI- MS/MS is shown in Table 1.

**Human Fecal Samples.** Fecal samples collected in a controlled and randomized human intervention study carried out at the CIAL-Institute of Food Science Research (CSIC-UAM) according to a computer-generated random-number table[19] involving 42 "healthy" volunteers (34 case and 8 control subjects; 23 women and 19 men; age range of 20−65 years) were selected for the present study. The participants were not suffering from any disease or intestinal disorder and were not receiving antibiotics or any other medical treatment for at least 6 months before the start of the study or during the study (including the washout period). All of the participants were fully informed about the study and gave written informed consent. The study was carried out according to the rules and approval of the Bioethics committee of Hospital "Ramón y Cajal" (Madrid, Spain).

The intervention study was divided into two consecutive periods: (a) an initial washout period of 2 weeks (baseline) during which the volunteers did not consume any wine or any other alcoholic beverage and followed a low-polyphenol diet and (b) a period of 4 weeks during which the case volunteers consumed a daily intake of red wine (250 mL) of red wine over 28 days (intervention period), divided into two doses. During this latter period, participants also maintained the restrictions for any other alcoholic beverages and followed a low-polyphenol diet. The control group ($n$ = 8) followed the same pattern as the case group ($n$ = 34), with the exception that no wine was ingested during this 4 week period.

Each participant provided samples of feces at two points: (a) after the washout period and (b) at the end of the study. Feces were immediately frozen and stored at −80 °C, no longer than 6 months, awaiting analysis. Only one freezing/thawing cycle was performed prior to the analysis and, after thawing, samples were kept on ice to prevent protease activity.

**Preparation of Fecal Solutions for Analysis of Immune Compounds.** Fecal samples (~0.1 g) were suspended in 1 mL of PBS. After homogenization, the samples were centrifuged (14000$g$, 15 min, 4 °C) and the supernatants (~200 $\mu$L) were collected.

**Detection and Quantification of Immune Compounds in the Fecal Samples.** Fecal concentration of immunoglobulins (Ig) Ig G1, Ig G2, Ig G3, Ig G4, Ig M, and Ig E, cytokines, chemokines, and growth factors, including interleukins (IL) 1$_\beta$, 2, 4, 5, 6, 7, 8, 10, 12(p70), 13, and 17, interferon-gamma (IFN-$\gamma$), tumor necrosis factor-alpha (TNF-$\alpha$), growth-regulated oncogene-alpha (Gro-$\alpha$), monocyte chemoattractant protein-1 (MCP-1), macrophage inflammatory protein-1$_\beta$ (MIP-1$_\beta$), granulocyte colony-stimulating factor (G-CSF), and granulocyte macrophage colony-stimulating factor (GM-CSF), were determined in fecal solutions by using the Bio-Plex Pro Human Isotyping assay and the Human Cytokine group I and II assay kits (Bio-Rad Laboratories, Hercules, CA, USA), following the manufacturer's protocol, in a Bioplex 200 system instrument (Bio-Rad Laboratories). Sample determinations were carried out in duplicate. Standard curves of each analyte were performed from triplicates of each assayed concentration on each plate, with the Bio-Plex Manager 6.0 software (Bio-Rad Laboratories). The variation coefficient for the standard curves between plates was <10%.

The concentration of Ig A in the fecal solution supernatants was determined using a specific enzyme-linked immunosorbent assay (ELISA) kit (Cusabio Biotech Co., Ltd., Wuhan, China), according to the manufacturer's instructions.

**Table 1. Phenolic Composition (Milligrams per Liter) of the Pinot noir Wine Used for the Intervention Study**

| | |
|---|---|
| benzoic acids | |
| gallic acid | 27.30 ± 0.20 |
| protocatechuic acid | 3.88 ± 0.01 |
| 3-*O*-methylgallic acid | 1.06 ± 0.06 |
| 4-hydroxybenzoic acid | 0.57 ± 0.01 |
| vanillic acid | 1.85 ± 0.03 |
| syringic acid | 2.30 ± 0.13 |
| benzoic acid | 1.14 ± 0.06 |
| salicylic acid | 0.22 ± 0.00 |
| phenols | |
| phloroglucinol | 0.33 ± 0.03 |
| tyrosol | 31.40 ± 1.40 |
| dihydroxyphenylpropan-2-ol | 0.30 ± 0.05 |
| cinnamic acids | |
| caffeic acid | 6.97 ± 0.26 |
| *p*-coumaric acid | 1.39 ± 0.02 |
| ferulic acid | 0.22 ± 0.02 |
| coutaric acid | 8.64 ± 0.01 |
| caftaric acid | 4.98 ± 0.33 |
| stilbenes | |
| resveratrol | 7.12 ± 0.29 |
| flavanols and others | |
| (+)-catechin | 51.60 ± 1.70 |
| (−)-epicatechin | 34.90 ± 2.90 |
| procyanidin B1 | 79.10 ± 0.90 |
| procyanidin B2 | 44.70 ± 0.60 |
| procyanidin B3 | 16.00 ± 1.00 |
| procyanidin B4 | 12.90 ± 0.30 |
| procyanidin B5 | 2.67 ± 0.01 |
| procyanidin B7 | 5.75 ± 0.15 |
| procyanidin C1 | 14.00 ± 0.40 |
| other trimers | 7.96 ± 1.05 |
| flavonols | |
| quercetin | 1.92 ± 0.01 |
| myricetin | 0.70 ± 0.03 |
| anthocyanins | |
| delphinidin-3-*O*-glucoside | 2.58 ± 0.11 |
| cyanidin-3-*O*-glucoside | 0.76 ± 0.04 |
| petunidin-3-*O*-glucoside | 4.06 ± 0.13 |
| peonidin-3-*O*-glucoside | 18.90 ± 2.00 |
| malvidin-3-*O*-glucoside | 36.70 ± 3.40 |

**Table 2. Median (IQR) Values of the Immune Parameters Analyzed in the Fecal Samples Provided by the 34 Case Volunteers before and after Wine Intake**

| case group ($n$ = 34) | | | | | |
|---|---|---|---|---|---|
| cytokines (ng/g feces) | | | immunoglobulins | | |
| | before | after | | before | after |
| IL-1$_\beta$ | 0.08 (0.02; 0.19) | 0.04 (0.01; 0.12) | Ig G1 ($\mu$g/g feces) | 1.09 (0.51; 9.16) | 2.55 (0.64; 5.60) |
| IL-2 | 0.00 (0.00; 1.87) | 0.07 (0.00; 0.57) | Ig G2 ($\mu$g/g feces) | 91.71 (27.96; 206.5) | 111.09 (31.13; 175.79) |
| IL-4 | 0.05 (0.03; 0.31) | 0.06 (0.03; 0.22) | Ig G3 ($\mu$g/g feces) | 0.98 (0.29; 3.39) | 1.65 (0.51; 2.99) |
| IL-5 | 0.06 (0.01; 1.50) | 0.02 (0.01; 0.71) | Ig G4 ($\mu$g/g feces) | 0.10 (0.00; 0.77) | 0.18 (0.06; 0.59) |
| IL-6 | 0.09 (0.07; 2.01) | 0.14 (0.05; 1.01) | Ig M (mg/g feces) | 0.05 (0.03; 0.14) | 0.06 (0.02; 0.13) |
| IL-7 | 0.02 (0.01; 0.05) | 0.01 (0.01; 0.02) | Ig A (mg/g feces) | 19.33 (13.79; 24.93) | 21.13 (12.52; 27.43) |
| IL-8 | 0.05 (0.00; 0.12) | 0.01 (0.00; 0.10) | | | |
| IL-10 | 0.08 (0.04; 0.81) | 0.09 (0.04; 0.69) | | | |
| IL-12(p70) | 0.46 (0.11; 25.61) | 0.36 (0.16; 10.06) | | | |
| IL-13 | 0.006 (0.006; 0.019) | 0.006[a] (0.006; 0.012) | | | |
| IL-17 | 0.84 (0.38; 14.11) | 0.98 (0.43; 4.85) | | | |
| IFN-$\gamma$ | 6.45 (2.67; 214.83) | 5.27 (0.18; 179.46) | | | |
| GRO-$\alpha$ | 1.21 (0.60; 1.55) | 0.99 (0.45; 1.31) | | | |
| MCP-1 | 0.50 (0.10; 4.38) | 0.32 (0.11; 2.07) | | | |
| MIP-1$_\beta$ | 0.15 (0.00; 0.42) | 0.12 (0.00; 0.32) | | | |
| TNF-$\alpha$ | 0.24 (0.10; 9.46) | 0.49 (0.13; 4.07) | | | |
| G-CSF | 1.51 (0.77; 10.01) | 1.16 (0.73; 7.40) | | | |
| GM-CSF | 8.57 (6.12; 15.85) | 9.70 (7.26; 14.67) | | | |

[a]Significant difference in the median values after intervention (nonparametric Wilcoxon test).

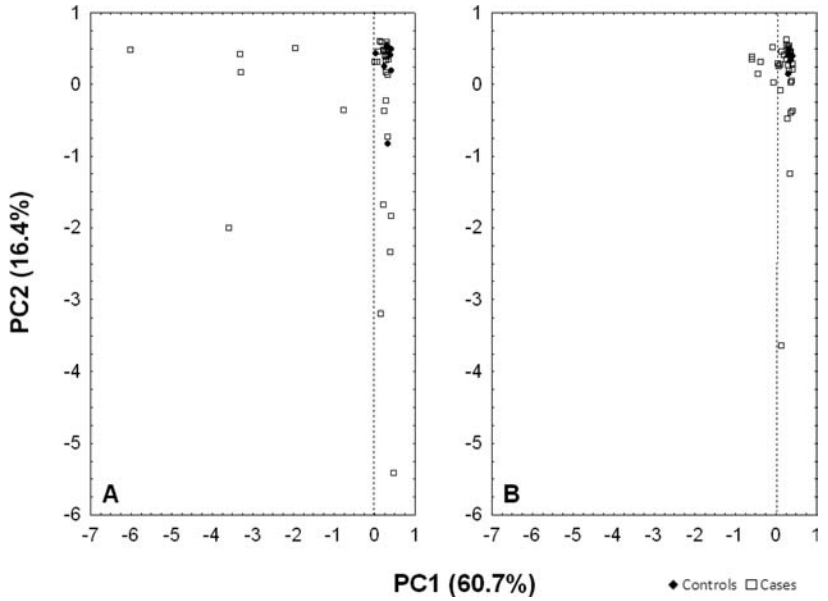


**Figure 1.** Representation of the volunteers (squares) and controls (rhombus), before (A) and after (B) intervention, in the plane defined by the two principal components.

**Quantification of Calprotectin.** Fecal calprotectin values were determined using a commercially available enzyme-linked immunosorbent assay (ELISA) Kit (Calpro, Lysaker, Norway). The standard curve of calprotectin was obtained from triplicates of each assayed concentration and fit to a four-parameter curve model according to the manufacturer's recommendations.

**Analysis of Phenolic Metabolites.** Phenolic metabolites were determined in the fecal samples as previously reported,[19] although in this paper data are arranged in a different manner according to the groups resulting from the analysis of immune compounds. Briefly, fecal samples were thawed at room temperature, homogenized, and weighed (1.0 g) in 15 mL sterile conical tubes. Ten milliliters of sterile saline solution (NaCl 0.9%, Fresenius Kabi, Spain) spiked with the internal standard (4-hydroxybenzoic-2,3,5,6-$d_4$ acid, Sigma-Aldrich, St. Louis, MO, USA) was added, vortexed, and centrifuged (10 min, 10000 rpm, 4 °C) twice. The supernatant (fecal solution) was filtered (0.22 $\mu$m) and diluted with acetonitrile (1:4, v/v, acetonitrile/fecal solution). Two microliters of sample was injected onto the chromatographic system. Fecal samples were analyzed by an UPLC-ESI-MS/MS method validated for the screening of >60 microbial-derived phenolic metabolites including phenols, valerolactones, and mandelic, benzoic, hippuric, phenylacetic, phenylpropionic, valeric, and cinnamic acids. The chromatographic conditions and MS/MS parameters (cone voltage, collision energy, and MRM transition) of the phenolic compounds targeted in our study were previously reported.[20] Fecal samples were analyzed in duplicate.

**Statistical Analysis.** The statistical analysis was performed using STATISTICA program for Windows, version 7.1 (Statsoft Inc., 2005,

Table 3. Median (IQR) Values (Nanograms per Gram Feces) of the Cytokines Analyzed in the Fecal Samples Provided by the 34 Case and 8 Control Volunteers before and after Wine Intake[a]

| | wine intake | | | | control group ($n$ = 8) | |
|---|---|---|---|---|---|---|
| | high-cytokine value subgroup($n$ = 6) | | low-cytokine value subgroup ($n$ = 28) | | | |
| | before | after | before | after | before | after |
| IL-1$_\beta$ | 0.13a (0.12; 0.22) | 0.17 (0.09; 0.36) | 0.05a (0.01; 0.17) | 0.03 (0.01; 0.10) | 0.01b (0.01; 0.04) | 0.01 (0.00; 0.01) |
| IL-2 | 60.95a (46.55; 75.54) | 1.38 (0.14; 2.72) | 0.00b (0.00; 0.09) | 0.05 (0.00; 0.50) | 0.04b (0.00; 0.25) | 0.00 (0.00; 0.10) |
| IL-4 | 10.51a (8.10; 10.95) | 0.31[b] (0.07; 0.54) | 0.04b (0.03; 0.07) | 0.06 (0.03; 0.14) | 0.04b (0.03; 0.08) | 0.03 (0.03; 0.06) |
| IL-5 | 9.80a (6.50; 13.73) | 0.43[b] (0.03;0.76) | 0.01b (0.01; 0.35) | 0.02 (0.01; 0.45) | 0.02b (0.01; 0.43) | 0.01 (0.01; 0.05) |
| IL-6 | 115.07a (78.38; 142.80) | 1.97[b] (0.25; 3.44) | 0.08b (0.06; 0.15) | 0.10 (0.04; 0.64) | 0.06b (0.02; 0.93) | 0.04 (0.03; 0.11) |
| IL-7 | 0.01a (0.01; 0.07) | 0.01 (0.01; 0.01) | 0.02a (0.01; 0.04) | 0.01 (0.01; 0.02) | 0.01a (0.01; 0.03) | 0.01 (0.01; 0.01) |
| IL-8 | 1.06a (0.62; 1.31) | 0.05[b] (0.00; 0.12) | 0.01b (0.00; 0.10) | 0.01 (0.00; 0.09) | 0.02b (0.00; 0.09) | 0.00 (0.00; 0.04) |
| IL-10 | 39.46a (27.63; 62.59) | 0.54[b] (0.17; 1.08) | 0.05b (0.03; 0.13) | 0.08 (0.04; 0.43) | 0.11b (0.06; 0.25) | 0.05 (0.01; 0.11) |
| IL-12(p70) | 556.47a (441.56; 682.70) | 9.86[b] (0.80; 17.71) | 0.27b (0.10; 0.94) | 0.29 (0.15; 4.12) | 0.09b (0.03; 5.57) | 0.13 (0.07; 0.83) |
| IL-13 | 0.20a (0.16; 0.34) | 0.02[b] (0.01; 0.03) | 0.01b (0.01; 0.01) | 0.01 (0.01; 0.01) | 0.01b (0.01; 0.01) | 0.01 (0.01; 0.01) |
| IL-17 | 319.25a (260.75; 417.16) | 11.97[b] (1.45; 25.23) | 0.71b (0.33; 1.80) | 0.71 (0.48; 4.28) | 0.96b (0.05; 4.15) | 0.66 (0.44; 0.96) |
| IFN-$\gamma$ | 3624.31a (2302.64; 3952.46) | 120.90[b] (15.99; 272.89) | 4.68b (1.91; 15.29) | 4.68 (0.01; 93.03) | 0.01b (0.01; 50.01) | 0.01 (0.01; 6.19) |
| GRO-$\alpha$ | 3.00a (2.60; 3.31) | 1.21[b] (0.88; 1.65) | 1.13b (0.56; 1.40) | 0.95 (0.18; 1.29) | 0.81b (0.01; 0.97) | 0.74 (0.33; 1.14) |
| MCP-1 | 27.23a (23.54; 34.02) | 1.29[b] (0.29; 1.94) | 0.26a (0.09; 2.42) | 0.27 (0.10; 2.52) | 0.26b (0.10; 0.66) | 0.10 (0.07; 0.52) |
| MIP-1$_\beta$ | 1.19a (0.76; 1.87) | 0.47[b] (0.12; 0.65) | 0.09b (0.00; 0.27) | 0.11 (0.00; 0.27) | 0.00b (0.00; 0.13) | 0.00 (0.00; 0.11) |
| TNF-$\alpha$ | 732.48a (561.02; 904.56) | 8.16[b] (0.81; 20.28) | 0.20b (0.09; 0.51) | 0.31 (0.12; 3.13) | 0.06b (0.02; 1.48) | 0.14 (0.03; 0.23) |
| G-CSF | 188.33a (123.79; 209.41) | 11.87[b] (2.16; 17.76) | 0.96b (0.64; 2.78) | 1.05 (0.72; 6.31) | 0.73b (0.48; 3.74) | 0.63 (0.46; 1.42) |
| GM-CSF | 180.79a (148.67; 259.47) | 17.18[b] (11.57; 21.68) | 7.53b (5.86; 10.34) | 9.31 (7.14; 11.23) | 7.06b (5.44; 7.55) | 7.24 (6.04; 7.72) |

[a]Median values, before intervention, with different letters are significantly different ($P < 0.05$) between groups (Mann−Whitney $U$ test). [b]Significant difference in the median values after intervention (nonparametric Wilcoxon test).

www.statsoft.com). As the data were not normally distributed, medians and interquartile ranges (IQR) were calculated for all of the groups. Principal component analysis (PCA) was used for exploration of the data and tentative classification of the case volunteers. For assessing significant differences between low- and high-cytokines-values subgroups before intervention, the nonparametric Mann−Whitney $U$ test was performed. For assessing significant differences before and after the intervention period for both the intervention group, either as a whole group ($n$ = 34) or divided into low-cytokines-values ($n$ = 28) and high-cytokines-values ($n$ = 6) subgroups, and the control group ($n$ = 8), the nonparametric Wilcoxon test was applied. In both cases, a value of $P$ = 0.05 was fixed for the level of significance of the tests. Finally, Pearson's correlation coefficients among the different immune parameters and between immune parameters and the total content of phenolic metabolites were calculated.

## RESULTS

**Changes in the Concentration of the Immune Parameters after Wine Consumption.** Without doubt, selection of the red wine for the intervention study is a key step in achieving maximum effects of wine active compounds in vivo. The wine used in this study was especially rich in flavan-3-ols, a class of compounds that represented 60% of the phenolic compounds identified (Table 1). Total flavan-3-ol content (270 mg/L) in this wine was relatively higher in comparison to that of other red wines.[21] After the wine intervention study, fecal samples from all of the subjects included in the intervention trial ($n$ = 42) were available for the immune parameters study. A high interindividual variability in the fecal concentration of the immune compounds analyzed in this study was observed either before or after the wine intervention (Table 2). Globally, no statistically significant differences in any fecal immune parameter were observed before or after wine consumption, except for IL-13 ($P$ = 0.044), when the whole intervention group ($n$ = 34) was considered (Table 2).

PCA was applied to all samples (before and after the intervention period), from both the intervention and control groups, to obtain a possible grouping of the volunteers according to their immune compound values. The first principal component (PC1) explained 60.7% of the total variance, whereas the second principal component (PC2) explained only 16.4% of the total variance (Figure 1). PC1 was highly correlated with the cytokine variables: G-CSF (−0.99326), IL-2 (−0.98931), IL-4 (−0.98626), TNF-$\alpha$ (−0.98531), IL-6 (−0.98453), IL-12(p70) (−0.98369), IFN-$\gamma$ (−0.98039), GM-CSF (−0.97632), IL-17 (−0.96915), IL-10 (−0.96162), IL-8 (−0.94341), MCP-1 (−0.93860), and IL-5 (−0.93454). Interestingly, the PCA representation allowed the detection of a volunteers' subgroup within the intervention group, which was characterized by significantly high concentrations for most of the cytokines before starting wine consumption (Figure 1A; Table 3), a fact that was in agreement with their low PC1 values. As a consequence, these six volunteers exhibiting high fecal cytokine values before intervention were considered as a subset (high-cytokines-values subgroup) clearly differentiated from the rest (low-cytokines-values subgroup, $n$ = 28) of the intervention group. The high-cytokines-values subgroup was formed by five men (age range 30−50 years) and one woman (age 50 years), all exhibiting BMI values within the normality (18.5−25). Then, the concentration of calprotectin in the samples of the six volunteers of the high-cytokines-values subgroup was determined to detect a potential intestinal inflammation. Results revealed that all of the volunteers from the high-cytokines-values subgroup exhibited normal fecal calprotectin values (2.07−37.73 mg/kg feces)[22,23] and inflammatory diseases were dismissed.

When the values obtained at the beginning and at the end of the study were compared, no significant differences in the concentrations of either immunoglobulins (data not shown) or cytokines, chemokines, and growth factors (Table 3) were found for the low-cytokines-values subgroup ($n$ = 28) or for the control group ($n$ = 8). However, significant differences were found for 16 of the 24 analyzed immune compounds (IL-2, IL-

4, IL-5, IL-6, IL-8, IL-10, IL-12(p70), IL-13, IL-17, IFN-$\gamma$, Gro-$\alpha$, MCP-1, MIP-1$_\beta$, TNF-$\alpha$, G-CSF, and GM-CSF) in the samples of the high-cytokines-values subgroup, after wine consumption (Figure 2; Table 3). Interestingly, among them, the medians of TNF-$\alpha$, IL-6, and IFN-$\gamma$ decreased 90-, 58-, and 30-fold, respectively, after the intervention period (Table 3).

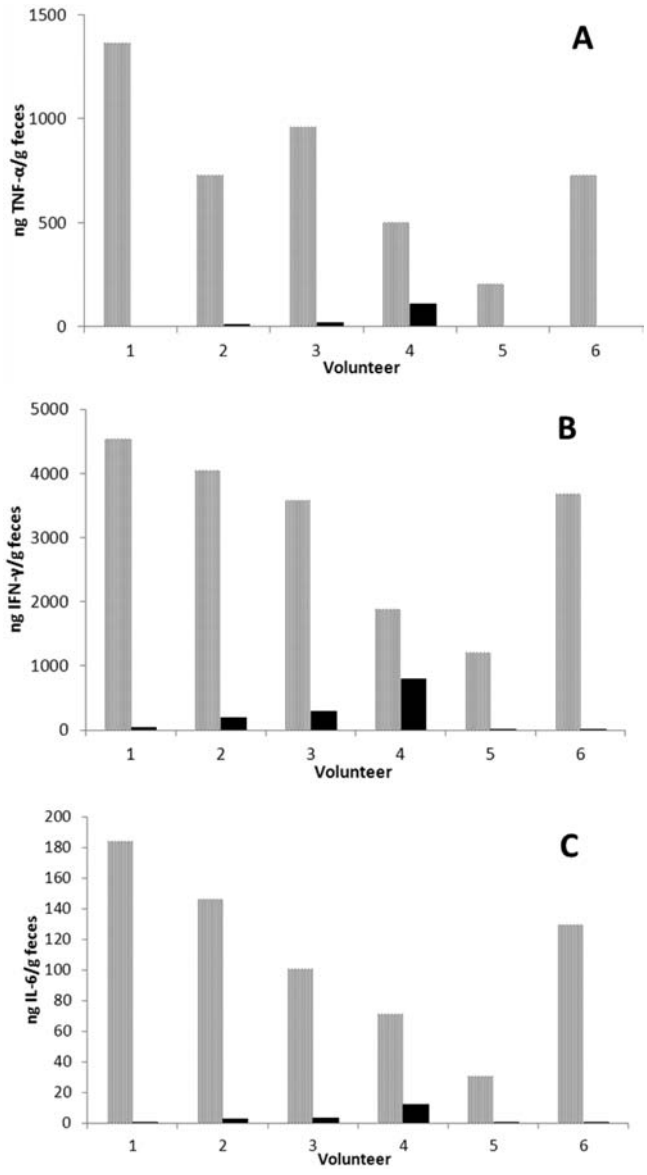


**Figure 2.** Line plots of variables TNF-$\alpha$ (A), IFN-$\gamma$ (B), and IL-6 (C) before (gray bars) and after (black bars) wine intervention in the high-cytokine-value subgroup.

**Relationships among Immune Compounds.** Pearson's correlation coefficients for cytokine values were determined for the samples of the two subgroups in which the case population was classified. Positive and significant correlations ($P < 0.01$) among the different cytokines were found for both the high- and low-cytokines-values subgroups before intervention (data not shown). In the high-cytokines-values subgroup, the highest correlations were established among the pro-inflammatory cytokines IL-2, IL-6, and IL-8 and also among IL-2, IL-4, and C-GSF. Correlations among cytokines in the low-cytokines-values subgroup were notably lower (data not shown). In both subgroups the cytokines with the lowest correlations were IL-1$_\beta$ and IL-7.

**Relationships between Immune Compounds and Fecal Phenolic Metabolites.** A total of 35 phenolic metabolites including mandelic acids, benzoic acids, phenols, hippuric acids, phenylacetic acids, phenylpropionic acids, valeric acids, valerolactones, and cinnamic acids were found in the fecal samples used in this study.[19] To better summarize changes after wine consumption and investigate a possible relationship with immune compounds, the sum of the concentration of all metabolites (total phenolic metabolite content) was calculated considering the subgroups exhibiting high and low cytokine content before wine intervention. For both groups, the range of variation (minimum−maximum interval) for the total fecal phenolic slightly moved forward after wine intake: from 122.2−501.1 to 169.2−864.6 $\mu$g/g (before and after wine intake, respectively) for the high-cytokines-value subgroup ($n = 6$) and from 46.2−1307.9 to 111.8−1364.5 $\mu$g/g (before and after wine intake, respectively) for the low-cytokines-values subgroup ($n = 27$, after excluding one volunteer not considered in our previous study[19]). Pearson's correlation coefficients between the content of immune parameters and the content of fecal phenolic were calculated separately for both the high- and low-cytokines-values subgroups, before and after wine consumption. For the high-cytokines-values subgroup and for data before the wine intervention, negative and significant correlations ($P < 0.05$) were found between the total content of phenolic metabolites and the immune markers IFN-$\gamma$ ($r = -0.892$), IL-8 ($r = -0.892$), and IL-6 ($r = -0.876$) (Figure 3). Interestingly, after wine intake, no significant correlations were found for any of these immune parameters, except for IL-8 ($r = 0.832$), but this fact was attributed to the high value obtained for the subject V25 in comparison to the rest of the group (Figure 3A). For the low-cytokines-values subgroup, no significant correlation between any cytokines and total phenolic metabolite content was found either before or after wine consumption (see Figure 3 for data corresponding to IFN-$\gamma$, IL-8, and IL-6).

## DISCUSSION

During recent years, the potential immunomodulatory and anti-inflammatory effects of wine have been investigated. These studies carried out so far have been performed in serum as biological fluid. Chiva-Blanch et al.[4] studied the seric concentrations of some inflammatory-related molecules after administration of red wine, dealcoholized red wine, or gin to high-cardiovascular-risk male volunteers and found that IL-6 concentration was significantly lower after the intake of wine or dealcoholized wine in comparison to that of gin. This finding suggested that wine compounds other than ethanol would be responsible for the IL-6 decrease. Another human intervention study with 35 healthy women who consumed white or red wine (~20 g ethanol/day) during two periods of 4 weeks also reported decreases in serum inflammatory biomarkers, such as C-reactive protein, and in IL-6 and MCP-1 after wine consumption.[24]

To our knowledge, this is the first paper to investigate the effects of wine in vivo on intestinal immunomodulation and inflammation in healthy volunteers. Our experimental design tried to assess changes in as many immune markers as possible to have the most complete overview of the immune status. The results of the study showed that moderate wine consumption for 4 weeks resulted in a significant decrease in the concentration of several cytokines among the volunteers of

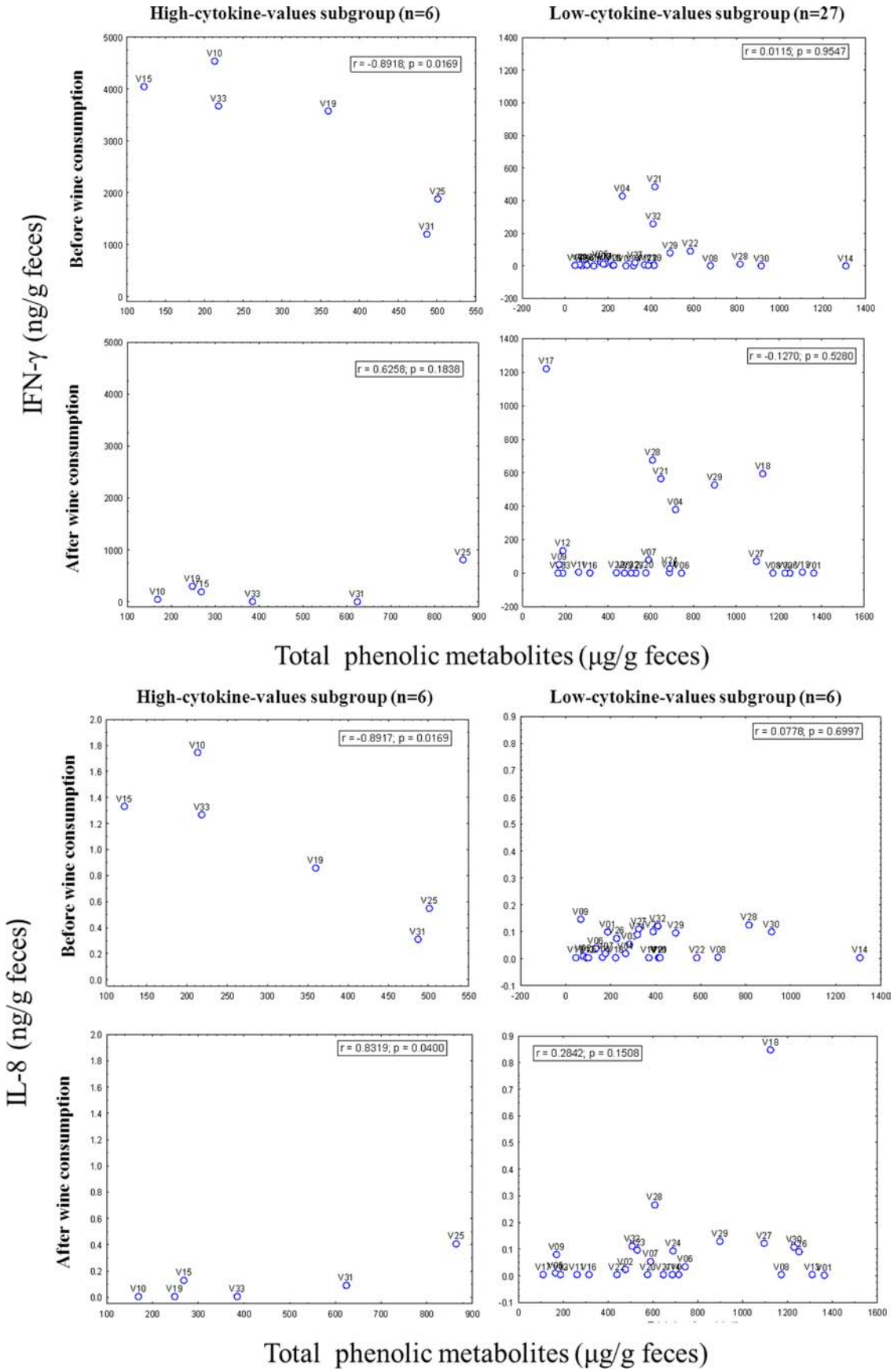


**Figure 3.** continued


dx.doi.org/10.1021/jf503310c | J. Agric. Food Chem. 2014, 62, 10567−10575

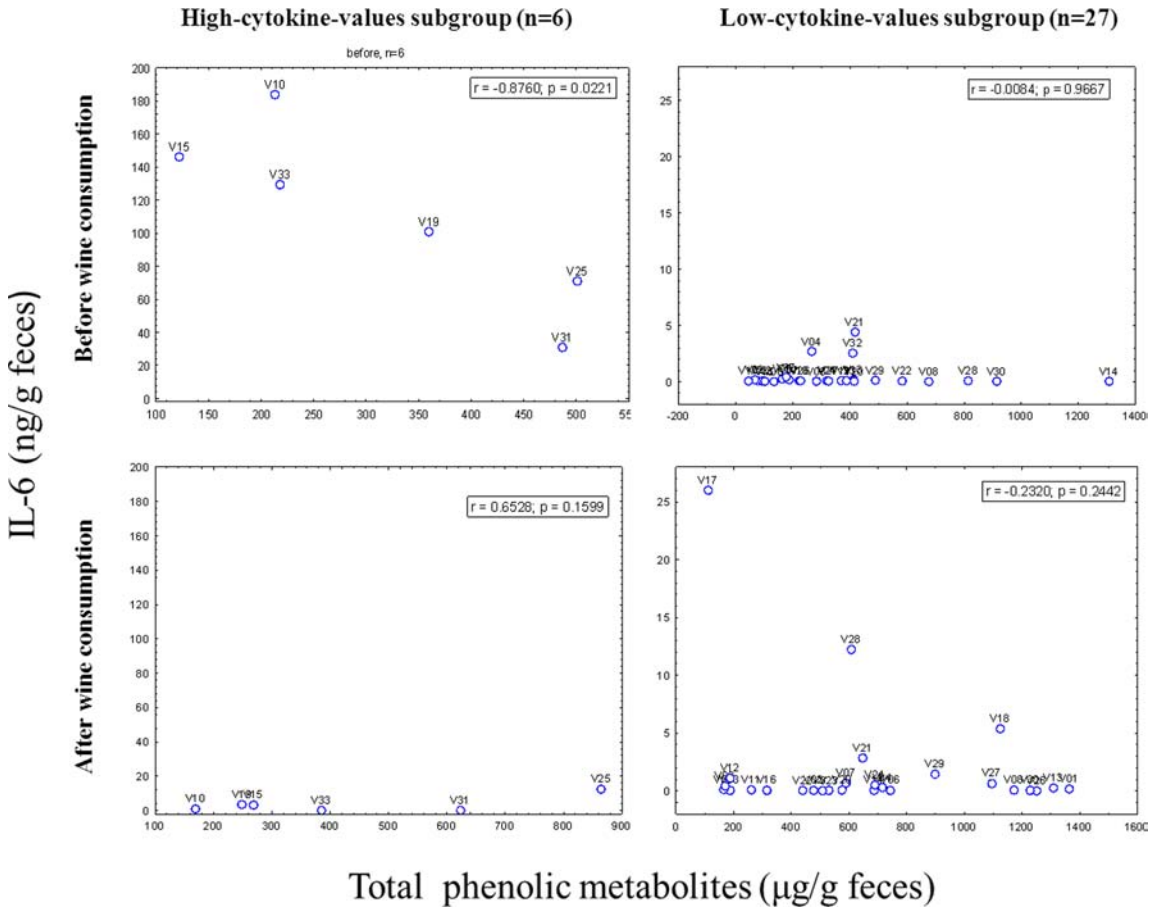


**Figure 3.** Correlation plots between contents of the immune compounds IFN-$\gamma$, IL-8, and IL-6 and of phenolic metabolites present in feces before and after wine intervention for both the high- and low- cytokine-value subgroups.

the subgroup that exhibited high cytokine values before the intervention (Table 3; Figure 2). No significant differences in the cytokine values were observed among the rest of the intervention volunteers after wine intake (Table 3; Figure 2). None of the control group's volunteers (no wine intake) exhibited high cytokine values in their initial samples, which could be due to its low number ($n$ = 8) in comparison to that of the intervention group ($n$ = 34).

Previous studies have shown anti-inflammatory effects of wine extracts in colonic cell models.[6,9,25] Nunes et al.[9] studied the effect of a red wine extract on a cytokine-stimulated HT-29 cell model and demonstrated that the extract significantly reduced the cytokine-induced overproduction of IL-8 in a dose-dependent manner. Angel-Morales et al.[26] used a red wine extract on an LPS-induced inflammation model of human colon CCD-18Co fibroblast cells and observed a decrease in the LPS-induced production of the pro-inflammatory cytokines IL-6 and TNF-$\alpha$. Another study assessed the effects of polyphenols on intestinal inflammation by using a Caco-2 Transwell model, and results confirmed that polyphenols from different sources, including red wine polyphenols, moderately modulate intestinal inflammation.[27] As red wine polyphenols comprise a great diversity of compounds, including phenolic acids, flavan-3-ols, and anthocyanins, studies with individual wine phenolic compounds have also been performed to specifically study the influence of the chemical structure on their anti-inflammatory properties. Bognar et al.[5] studied the anti-inflammatory effect of malvidin, a major red wine polyphenol, in an inflammation cell model and concluded that this compound was responsible, at least partially, for the positive effects of moderate red wine consumption on inflammation-mediated chronic maladies such as obesity, diabetes, hypertension, and cardiovascular disease. Other authors have studied the effect of polyphenols from different sources on experimentally induced gut inflammation in vitro and in vivo. Sergent et al.[11] tested different representative dietary phenolic compounds on an in vitro model of inflamed human intestinal epithelium and demonstrated that genistein and (−)-epigallocatechin-3-gallate provoked a decrease in IL-6 and IL-8 overproduction. Larrosa et al. and Sánchez-Fidalgo et al.[28,29] found significant reductions in the expression of IL-1$_\beta$, IL-8, IFN-$\gamma$, and TNF-$\alpha$ or IL-1$_\beta$ and TNF-$\alpha$, respectively, when administering hydrocaffeic acid or resveratrol, respectively, to the Dextran sulfate sodium (DSS)-treated rats used as a colitis model. Although most of these studies were conducted with the original phenolic forms present in wine or food, their derived metabolites may exhibit similar or enhanced anti-inflammatory properties.[28] In this context, a parallel study, focused on the phenolic metabolites present in the same set of fecal samples assayed in this paper, has revealed a great variability among subjects in the fecal content of phenolic metabolites (including benzoic, mandelic, hippuric, phenylacetic, phenylpropionic, cinnamic and valeric acids, phenols, valerolactones, and others).[19] Red wine phenolic content might be directly associated with the decrease observed in several cytokines after wine intake by the volunteers showing a high-

concentration cytokine profile before the intervention, because a significant increase of phenolic metabolites in the fecal profile was found after wine consumption. In this work, we demonstrated negative and significant correlations among the cytokines IFN-$\gamma$, IL-8, and IL-6 and the total content of phenolic metabolites for the high-cytokines-values subgroup before wine intake. This negative correlation between the content of certain cytokines and the content of phenolic metabolites at initial stages of gut inflammation (i.e., for the high-cytokine-value subgroup) suggested an anti-inflammatory action by phenolic metabolites at the epithelial level. In accordance with our findings, Chun et al.[30] found that intake of total flavonoid and also individual flavonol, anthocyanidin, and isoflavone intakes were inversely correlated with serum C-reactive protein in a large study ($n$ = 8335). Also, in another study with apparently healthy subjects ($n$ = 2115), Lanberg et al.[31] examined the association between the intake of total and six flavonoid subclasses as well as flavonoid-rich food sources in relation to plasma biomarkers of inflammation (including IL-6, IL-18, and C-reactive protein among others) and found negative correlations between several flavonoid classes and the pro-inflammatory cytokine IL-18. Cytokines play a key role in regulating the intestinal immune response and inflammation that is characterized by the loss of the physiological equilibrium between pro- and anti-inflammatory cytokines.[12] In our study, there was a significant decrease in the concentration of most of the tested cytokines after wine intake by the volunteers' subgroup characterized by high cytokines concentration in the initial sample. The decrease was especially noticeable in relation to those cytokines (TNF-$\alpha$, IL-6, and IFN-$\gamma$) that promote initial inflammation. Elevated values of fecal IFN-$\gamma$ and TNF-$\alpha$ have been observed in fecal samples from patients with bacterial diarrhea,[32] whereas increased concentrations of some pro-inflammatory cytokines, mainly TNF-$\alpha$, IL-1$_\beta$, and IL-6, have also been detected in feces of IBD patients.[33]

In summary, this study with healthy hosts showed, for the first time, that moderate consumption of a phenolic-rich red wine modulates the intestinal inflammatory response in vivo. This effect that could be attributed, at least partially, to the phenolic metabolites derived from wine polyphenols may be particularly beneficial for hosts with an initial (and still nonsymptomatic) stage of gut inflammation. These results will be the basis of further studies of wine consumption by patients affected by IBD.

## AUTHOR INFORMATION

### Corresponding Author

*(M.V.M.-A.) E-mail: victoria.moreno@csic.es. Phone: 34 91 0017900. Fax: 34 910017905.

### Funding

This work was funded by the MINECO (Spanish National Projects AGL2009-13361-C02-01, AGL2012-04172-C02-01, and CONSOLIDER INGENIO 2010 (FUN-C-FOOD, CSD2007-063), and the Comunidad de Madrid (ALIBIRD P2009/AGR-1469) Project. A.J.-G. and I.M.-G. thank the European Social Fund and JAE-Doc Program (CSIC) and the EPI Program for their research contracts, respectively.

### Notes

The authors declare no competing financial interest.

## ACKNOWLEDGMENTS

We thank winery Miguel Torres S.A. that kindly provided the wine used in the intervention study, as well as the volunteers for their kind participation.

## ABBREVIATIONS USED

G-CSF, granulocyte colony-stimulating factor; GM-CSF, granulocyte macrophage colony-stimulating factor; GRO, growth-regulated oncogene; IBD, inflammatory bowel disease; IFN, interferon; Ig, immunoglobulin; IL, interleukin; MCP, monocyte chemoattractant protein; MIP, macrophage inflammatory protein; PBS, phosphate buffer saline; PCA, principal component analysis; TNF, tumor necrosis factor

## REFERENCES

(1) Avellone, G.; Di Garbo, V.; Campisi, D.; De Simone, R.; Raneli, G.; Scaglione, R.; Licata, G. Effects of moderate Sicilian red wine consumption on inflammatory biomarkers of atherosclerosis. *Eur. J. Clin. Nutr.* **2006**, *60*, 41−47.

(2) Li, H.; Foerstermann, U. Red wine and cardiovascular health. *Circ. Res.* **2012**, *111*, 959−961.

(3) Chiva-Blanch, G.; Arranz, S.; Lamuela-Raventos, R. M.; Estruch, R. Effects of wine, alcohol and polyphenols on cardiovascular disease risk factors: evidences from human studies. *Alcohol Alcohol.* **2013**, *48*, 270−277.

(4) Chiva-Blanch, G.; Urpi-Sarda, M.; Llorach, R.; Rotches-Ribalta, M.; Guillen, M.; Casas, R.; Arranz, S.; Valderas-Martinez, P.; Portoles, O.; Corella, D. Differential effects of polyphenols and alcohol of red wine on the expression of adhesion molecules and inflammatory cytokines related to atherosclerosis: a randomized clinical trial. *Am. J. Clin. Nutr.* **2012**, *95*, 1506−1506.

(5) Bognar, E.; Sarszegi, Z.; Szabo, A.; Debreceni, B.; Kalman, N.; Tucsek, Z.; Sumegi, B.; Gallyas, F., Jr. Antioxidant and anti-inflammatory effects in RAW264.7 macrophages of malvidin, a major red wine polyphenol. *PLoS One* **2013**, *8*, No. e65355.

(6) Biasi, F.; Guina, T.; Maina, M.; Cabboi, B.; Deiana, M.; Tuberoso, C. I.; Calfapietra, S.; Chiarpotto, E.; Sottero, B.; Gamba, P.; Gargiulo, S.; Brunetto, V.; Testa, G.; Dessi, M. A.; Poli, G.; Leonarduzzi, G. Phenolic compounds present in Sardinian wine extracts protect against the production of inflammatory cytokines induced by oxysterols in CaCo-2 human enterocyte-like cells. *Biochem. Pharmacol.* **2013**, *86*, 138−145.

(7) Ramiro, E.; Franch, A.; Castellote, C.; Perez-Cano, F.; Permanyer, J.; Izquierdo-Pulido, M.; Castell, M. Flavonoids from theobroma cacao down-regulate inflammatory mediators. *J. Agric. Food Chem.* **2005**, *53*, 8506−8511.

(8) Garcia-Lafuente, A.; Guillamon, E.; Villares, A.; Rostagno, M. A.; Alfredo Martinez, J. Flavonoids as anti-inflammatory agents: implications in cancer and cardiovascular disease. *Inflammation Res.* **2009**, *58*, 537−552.

(9) Nunes, C.; Ferreira, E.; Freitas, V.; Almeida, L.; Barbosa, R. M.; Laranjinha, J. Intestinal anti-inflammatory activity of red wine extract: unveiling the mechanisms in colonic epithelial cells. *Food Funct.* **2013**, *4*, 373−383.

(10) Romier-Crouzet, B.; Van De Walle, J.; During, A.; Joly, A.; Rousseau, C.; Henry, O.; Larondelle, Y.; Schneider, Y. Inhibition of inflammatory mediators by polyphenolic plant extracts in human intestinal Caco-2 cells. *Food Chem. Toxicol.* **2009**, *47*, 1221−1230.

(11) Sergent, T.; Piront, N.; Meurice, J.; Toussaint, O.; Schneider, Y. Anti-inflammatory effects of dietary phenolic compounds in an in vitro model of inflamed human intestinal epithelium. *Chem.−Biol. Interact.* **2010**, *188*, 659−667.

(12) Cavaillon, J. Pro- versus anti-inflammatory cytokines: myth or reality. *Cell Mol. Biol.* **2001**, *47*, 695−702.

(13) Colombo, E.; Sangiovanni, E.; Dell'Agli, M. A review on the anti-inflammatory activity of pomegranate in the gastrointestinal tract. *Evidence-Based Complement. Altern. Med.* **2013**, No. 247145.

(14) Ardizzone, S.; Porro, G. Biologic therapy for inflammatory bowel disease. *Drugs* **2005**, *65*, 2253−2286.
(15) Wall, G.; Heyneman, C.; Pfanner, T. Medical options for treating Crohn's disease in adults: focus on antitumor necrosis factor-α chimeric monoclonal antibody. *Pharmacotherapy* **1999**, *19*, 1138−1152.
(16) Vermeire, S.; Van Assche, G.; Rutgeerts, P. C-reactive protein as a marker for inflammatory bowel disease. *Inflammtory Bowel Dis.* **2004**, *10*, 661−665.
(17) Lewis, J. D. The utility of biomarkers in the diagnosis and therapy of inflammatory bowel disease. *Gastroenterology* **2011**, *140*, 1817−U160.
(18) Ricanek, P.; Brackmann, S.; Perminow, G.; Lyckander, L. G.; Sponheim, J.; Holme, O.; Hoie, O.; Rydning, A.; Vatn, M. H.; IBSEN II Study Group. Evaluation of disease activity in IBD at the time of diagnosis by the use of clinical, biochemical, and fecal markers. *Scand. J. Gastroenterol.* **2011**, *46*, 1081−1091
(19) Munoz-Gonzalez, I.; Jiménez-Girón, A.; Martin-Alvarez, P. J.; Bartolome, B.; Victoria Moreno-Arribas, M. Profiling of microbial-derived phenolic metabolites in human feces after moderate red wine intake. *J. Agric. Food Chem.* **2013**, *61*, 9470−9479.
(20) Sánchez-Patán, F.; Monagas, M.; Moreno-Arribas, M. V.; Bartolomé, B. Determination of microbial phenolic acids in human feces by UPLC-ESI-TQ MS. *J. Agric. Food Chem.* **2011**, *59*, 2241−2247.
(21) García-Ruiz, A.; Bartolomé, B.; Martínez-Rodríguez, A. J.; Pueyo, E.; Martín-Álvarez, P. J.; Moreno-Arribas, M. V. Potential of phenolic compounds for controlling lactic acidbacteria growth in wine. *Food Control* **2008**, *19*, 835−841.
(22) Roseth, A.; Fagerhol, M.; Aadland, E.; Schjonsby, H. Assessment of the neutrophil dominating protein calprotectin in feces − a methodologic study. *Scand. J. Gastroenterol.* **1992**, *27*, 793−798.
(23) Johne, B.; Kronborg, O.; Ton, H.; Kristinsson, J.; Fuglerud, P. A new fecal calprotectin test for colorectal neoplasia − clinical results and comparison with previous method. *Scand. J. Gastroenterol.* **2001**, *36*, 291−296.
(24) Sacanella, E.; Vazquez-Agell, M.; Mena, M. P.; Antunez, E.; Fernandez-Sola, J.; Nicolas, J. M.; Lamuela-Raventos, R. M.; Ros, E.; Estruch, R. Down-regulation of adhesion molecules and other inflammatory biomarkers after moderate wine consumption in healthy women: a randomized trial. *Am. J. Clin. Nutr.* **2007**, *86*, 1463−1469.
(25) Tunon, M. J.; Garcia-Mediavilla, M. V.; Sanchez-Campos, S.; Gonzalez-Gallego, J. Potential of flavonoids as anti-inflammatory agents: modulation of pro- inflammatory gene expression and signal transduction pathways. *Curr. Drug Metab.* **2009**, *10*, 256−271.
(26) Angel-Morales, G.; Noratto, G.; Mertens-Talcott, S. Red wine polyphenolics reduce the expression of inflammation markers in human colon-derived CCD-18Co myofibroblast cells: potential role of microRNA-126. *Food Funct.* **2012**, *3*, 745−752.
(27) Nicod, N.; Chiva-Blanch, G.; Giordano, E.; Dávalos, A.; Parker, R. S.; Visioli, F. Green tea, cocoa, and red wine polyphenols moderately modulate intestinal inflammation and do not increase high-density lipoprotein (HDL) production. *J. Agric. Food Chem.* **2013**, *61*, 9470−9479.
(28) Larrosa, M.; Luceri, C.; Vivoli, E.; Pagliuca, C.; Lodovici, M.; Moneti, G.; Dolara, P. Polyphenol metabolites from colonic microbiota exert anti-inflammatory activity on different inflammation models. *Mol. Nutr. Food Res.* **2009**, *53*, 1044−1054.
(29) Sanchez-Fidalgo, S.; Cardeno, A.; Villegas, I.; Talero, E.; Alarcon de la Lastra, C. Dietary supplementation of resveratrol attenuates chronic colonic inflammation in mice. *Eur. J. Pharmacol.* **2010**, *633*, 78−84.
(30) Chun, O. K.; Chung, S. J.; Claycombe, K. J.; Song, W. O. Serum C-reactive protein concentrations are inversely associated with dietary flavonoid intake in U.S. adults. *J. Nutr.* **2008**, *138*, 753−760.
(31) Landberg, R.; Sun, Q.; Rimm, E. B.; Cassidy, A.; Scalbert, A.; Mantzoros, C. S.; Hu, F. B.; van Dam, R. M. Selected dietary flavonoids are associated with markers of inflammation and endothelial dysfunction in U.S. women. *J. Nutr.* **2011**, *141*, 618−625.
(32) Greenberg, D.; Jiang, Z.; Steffen, R.; Verenker, M.; DuPont, H. Markers of inflammation in bacterial diarrhea among travelers, with a focus on enteroaggregative *Escherichia coli* pathogenicity. *J. Infect. Dis.* **2002**, *185*, 944−949.
(33) Nikolaus, S.; Raedler, A.; Schreiber, S. Immunosenescence of the GI immune system: Increased secretion of proinflammatory cytokines by LPMNC. *Gastroenterology* **1998**, *114*, A897−A897.

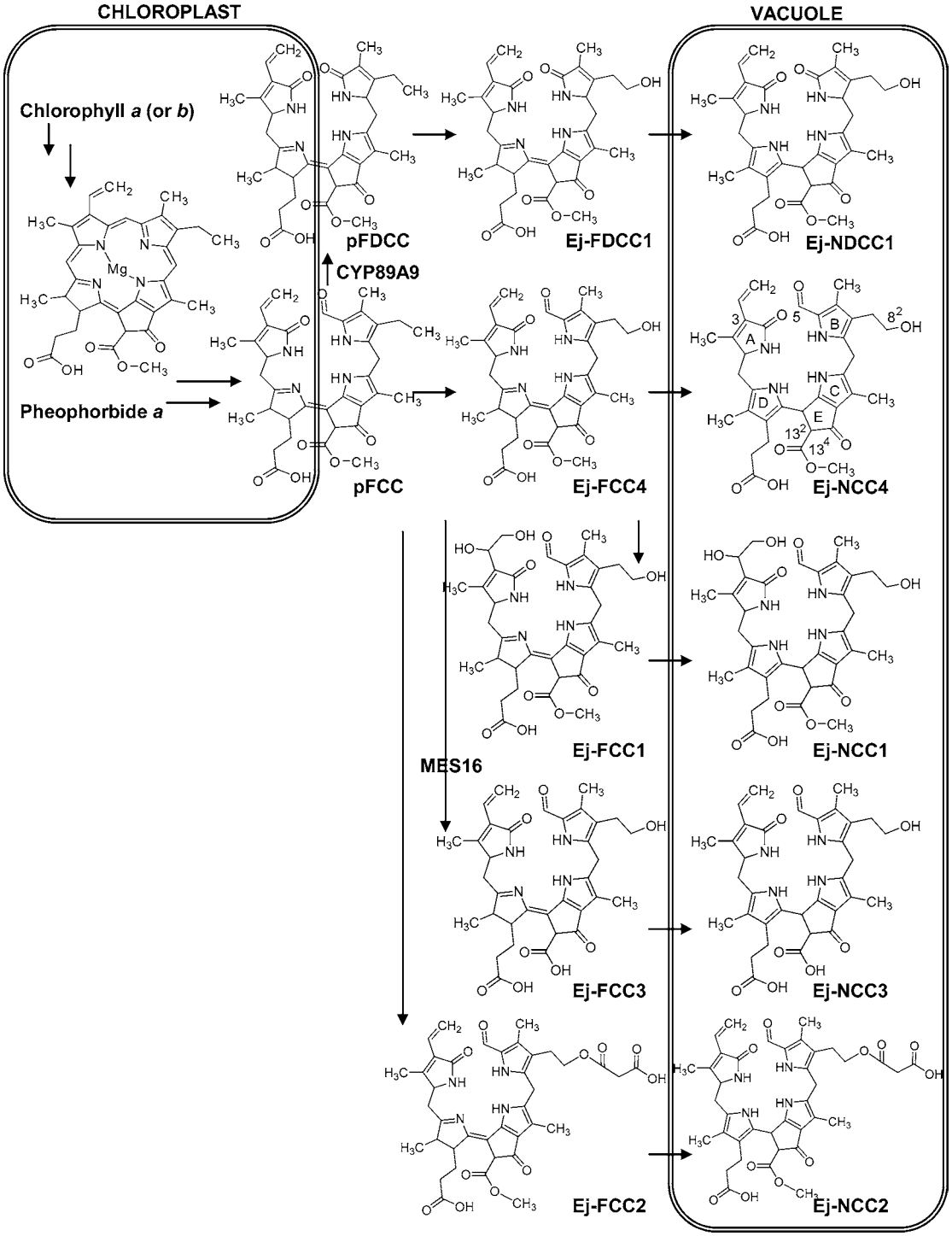


**Figure 1.** Proposed chlorophyll degradation pathway in senescent loquats fruits (*Eriobotrya japonica* Lindl.).

with electrospray ionization and mass spectrometry (HPLC–ESI–MS) with a couple of NCC/NDCC ratios equal to the catabolites identified in senescence leaves of maize (*Zea mays* L.) and barley (*Hordeum vulgare* L.), respectively, and a duo of two new structures.[13]

Autumn or early winter is time for loquats (*Eriobotrya japonica* Lindl.) to flower, and fruits are ripe in the market in late winter or early spring when few competitive fruits are available, so loquat fruits can be sold at higher prices.[14] The scientific literature describes the phenolics and antioxidative potential of loquat fruits,[15,16] but in relation to the chlorophyll fraction, only one publication[17] studied it considering its bioactive potential with medical purposes. Currently, numerous scientific studies point to tetrapyrroles as significant bioactive components related to cancer prevention, antioxidant and antimutagenic activity, mutagen trapping, modulation of xenobiotic metabolism, and induction of apoptosis.[18] Measurement of antioxidant capacity of NCCs brought new insights for the assignment of functionality to these molecules. It has been shown that NCCs display a similar antioxidant capacity to that of bilirubin, which points to a possible role of NCCs, to soften the stress induced by senescence.[11] This hypothesis is even


dx.doi.org/10.1021/jf503619s | J. Agric. Food Chem. 2014, 62, 10576–10584

more significant once it was shown that NCCs are resistant to digestion and absorbed by human intestinal epithelium.[19] The aim of this work was to determine NCCs/NDCCs profile in loquat fruits, a perennial species that may present an intricate process of chlorophyll catabolism, and produce a heterogeneous catabolites profile in comparison to the regular profile described in deciduous plant fruits described to date. To achieve this aim, a high-performance liquid chromatography coupled with electrospray ionization ion trap and quadropole time-of-flight mass spectrometry (HPLC/ESI-IT/qTOF-MS) method was applied to reach a high specificity for description of those already known NCCs and also to screen new structural rearrangements to expand knowledge of the chlorophyll breakdown route.

## MATERIALS AND METHODS

**Plant Material.** *Eriobotrya japonica* Lindl. trees (ca. 10 years old) were cultivated in an open field with a Mediterranean climate (Seville, Spain). Determination of the NCC profile was performed in naturally yellow fruits. Leaves of spinach (*Spinacea oleracea* L.) were bought at local market, and they were allowed to senescence by dark-incubation in distilled water in Petri dishes at 25 °C for 5−7 days.[20]

**Reagents.** Potassium phosphate was provided by Sigma-Aldrich Chemical Co. (Madrid, Spain). HPLC LC/MS grade solvents were supplied by Panreac (Barcelona, Spain). The deionized water used was obtained from a Milli-Q 50 system (Millipore Corp., Milford, MA, U.S.A.). Na (NaCOOH) (10 mM NaOH in 300 $\mu$L of formic acid) was used for calibration.

**NCCs Extraction.** Fresh material (ripened loquat fruits and senescent leaves of spinach) was homogenized in liquid nitrogen and extracted into four volumes of 20 mM potassium phosphate buffer (KPi), pH 7.0/methanol (1:3, v/v). The extract was centrifuged at 14 000 × *g* for 5 min, and the supernatant was concentrated[21] by a $C_{18}$ column (Bakerbond SPE, 500 mg/6 mL, J.T. Baker, Deventer, Holland). The SPE column was activated with two volumes of water and two volumes of methanol. Then, the extract, previously diluted to 80% with water, was applied to the column. The SPE with the sample was cleaned with four volumes of water for desalting, and the NCCs fraction was eluted with 1 mL of 20 mM KPi pH 7.0/methanol (1:9, v/v).[19]

**Liquid Chromatography/Electrospray Ionization Ion Trap/Time-of-Flight Mass Spectrometry.** The liquid chromatograph system was Dionex Ultimate3000RS U-HPLC (Thermo Fisher Scientific, Waltham, MA, U.S.A.). Chromatographic separation was performed as described earlier[22] but with modifications as follows. The eluent components were 0.1% (v/v) formic acid in water (A) and 0.1% (v/v) formic acid in methanol (B). The proportion of B was increased from 20% to 32% in 10 min, to 40% in 15 min, to 60% in 30 min, to 100% in 10 min, and held at 100% for 18 min. Initial conditions were reached in 2 min, and the equilibrium time was 10 min. The injection volume was 30 $\mu$L, and the flow rate was 1 mL/min. A stainless steel column (20 cm × 0.46 cm i.d.), packed with 3 $\mu$m $C_{18}$ Spherisorb ODS-2 (Teknokroma, Barcelona, Spain), was used. A split postcolumn of 0.4 mL/min was introduced directly on the mass spectrometer electrospray ion source. The HPLC/ESI-qTOF operated for mass analysis using a micrOTOF-QII High Resolution Time-of-Flight mass spectrometer (UHR-TOF) with qQ-TOF geometry (Bruker Daltonics, Bremen, Germany) equipped with an ESI interface. The HPLC/ESI-IT system operated for $MS^2$ analyses and selected an ion of a particular $m/z$ value to obtain exclusively its daughter ions. In this case, the instrument was operated in positive ion mode using a scan range from $m/z$ 50−1200. Mass spectra were acquired in MS fullscan mode, and data were used to perform multitarget-screening using TargetAnalysis 1.2 software (Bruker Daltonics, Bremen, Germany). $MS^2$ spectra were acquired in auto-$MS^2$ mode (data-dependent acquisition) and were used for structural confirmation of the compounds detected. Collision energy was estimated dynamically based on appropriate values for the mass and stepped across a ± 10% magnitude range to ensure good quality fragmentation spectra. The instrument control was performed using Bruker Daltonics HyStar 3.2.

**Data Analysis.** An in-house mass database created ex professo comprised monoisotopic masses, elemental composition, and, if known, retention time and characteristic product ions for 13 NCCs and the five NDCCs.[10,11,13,21−31] Additionally, elemental composition of new NCCs/NDCCs not described so far was included in the database. These new chlorophyll catabolites were generated holding two rules: (1) only those substituents already described in literature are allowed to enter in the basic NCC/NDCC structure and in the same carbon atom positions; and (2) dioxobilin-type chlorophyll catabolites are generated from all NCC structures (both known and new ones) by deformylation at C6 in ring B. Thus, some of the new NCC structures were the de-esterified form of *Nr*-NCC1 and the esterifed form of Bn-NCC1. Data evaluation was performed with Bruker Daltonics DataAnalysis 4.0. From the HPLC/TOF-MS acquisition data, an automated peak detection on the extracted ion currents (EICs) expected for the protonated molecule of each compound in the database was performed with Bruker Daltonics TargetAnalysis 1.2 software. The software performed the identification automatically according to mass accuracy and in combination with the isotopic pattern in the SigmaFit algorithm. This algorithm provides a numerical comparison of theoretical and measured isotopic patterns and can be utilized as an identification tool in addition to accurate mass determination. The calculation of mSigma values includes generation of the theoretical isotope pattern for the assumed protonated molecule and calculation of a match factor based on the deviations of the signal intensities. Only those hits with mass accuracy and mSigma values within the tolerance limits, which were set at 5 ppm and 50, respectively, are included in the final report list that was carried out using a Microsoft EXCEL-based script. This software has been successfully applied for screening of some other phytochemicals.[32,33] The interpretation of the $MS^2$ spectra was performed using the SmartFormula3D module included in the DataAnalysis software. This module includes an algorithm that estimates whether a formula for a product ion is a subset of a formula for the precursor ion. On the basis of expected chemistry, the elements carbon, hydrogen, oxygen, nitrogen, bromine, and iodine were allowed. Sodium and potassium were also included for the calculation of adduct masses. The number of nitrogen atoms was limited to an upper threshold of ten. The number of rings plus double bonds was checked to be chemically meaningful (between 0 and 50). For each NCC/NDCC detected in the sample, the module shows the original MS and $MS^2$ data as peak lists. From all possible formulas for the precursor ion, only one should fit with the elemental composition expected for the protonated molecule and satisfy thresholds for mass accuracy and mSigma values. Once the correct formula is selected, the module displays the formulas and neutral losses in the $MS^2$ spectrum fitting to the boundary conditions for the precursor ion, and they should be consistent with the $MS^2$ data peak list. The SmartFormula3D checks the consistency and highlights the monoisotopic peaks with formula suggestion and the related isotopic peaks. On the basis of this combined data evaluation, a fragmentation pattern for each NCC/NDCC can be generated to support its identification in the sample.

Mass Frontier 4.0 is a software package for the management, evaluation, and interpretation of mass spectra, including the automated generation of possible fragments and rearrangement mechanisms, starting from a user-supplied chemical structure. With this feature of the software, we can check the consistency between a chemical structure and its mass spectrum and recognize the structural differences between spectra of closely related compounds. The program generates a fragmentation scheme for the drawn molecular structure using fragmentation rules of mass spectrometry known in the literature as well as the selected ionization mode and the number of fragmentation steps. The program parameters used in this study were ESI ionization method, inductive cleavage, and five as the maximum number of reaction steps. The fragmentation reactions were selected to include hetero- and homolytic cleavage, neutral losses, and hydrogen rearrangements. Other parameters were left as their default values.

**Semipreparative HPLC Isolation of NCC Product(s).** To obtain enough quantity of *Ej*-NCC4, this catabolite was isolated from a NCC concentrated sample of loquat by semipreparative HPLC (injection volume, 500 $\mu$L; flow rate, 4.5 mL/min). Solvent A, 0.1% formic acid in water; solvent B, methanol; solvent composition (A/B) as a function of time (0−180 min), 0−5, 80:20; 5−120, 80:20 to 35:65; 120−180, 35:65 to 0:100. A stainless steel column (25 cm × 1 cm i.d.) packed with 3 $\mu$m C18 Spherisorb ODS-2 (Thermo Scientific Easy, Barcelona, Spain) was used. A split postcolumn of 0.30 mL/min was introduced directly on the mass spectrometer electrospray ion source using the same acquisition conditions described above. Three consecutive semipreparative HPLC runs were performed, and fractions containing *Ej*-NCC4 were collected at 59−61 min. For desalting, the aqueous solution was applied to a $C_{18}$ SPE column (Bakerbond SPE, 1 g/12 mL, J.T. Baker, Deventer, Holland) activated with two column volumes of methanol and preconditioned with two column volumes of water, washed with 20 mL of $H_2O$, and eluted with 4 mL of MeOH. The solvents were removed using a rotary evaporator.

**Chemical Derivatization of *Ej*-NCC4 Product.** Isolated compound was subjected to chemical derivatization for the identification of functional groups. Specific methylation of the hydroxyl function at the propionic acid group was performed with diazomethane.[34] An aliquot of the sample was dried with nitrogen and redissolved in methanol. Fresh diazomethane was generated from an ethereal solution of *N*-methyl-*N*-nitroso-*p*-toluene-sulfonamide in the presence of KOH and MeOH. A gentle stream of $N_2$ was bubbled from the reaction vessel, where diazomethane is generated, to the one containing the *Ej*-NCC4 solution to achieve the methylation reaction upon development of a light yellow color of the solution. For silylation, an aliquot of the isolated compound was dried with nitrogen and redissolved in 200 mL of bis(trimethylsilyl)trifluoroacetamide (BTSFA) in pyridine; the solution was heated at 90 °C for 20 min. Afterward, the final volume was evaporated with a nitrogen stream to 10 $\mu$L of MeOH for analysis by MS.[35]

## RESULTS AND DISCUSSION

**NCCs/NDCCs Profile in Senescent Fruits of Loquat.** Figure 2 depicts the HPLC 320 nm chromatogram obtained

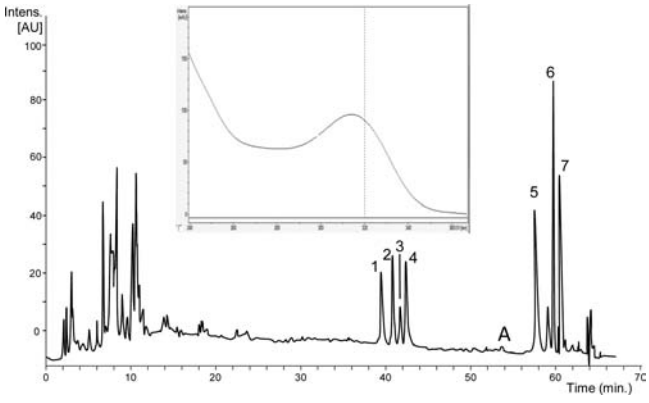


**Figure 2.** HPLC chromatogram of loquat senescent fruit extract acquired at 320 nm, showing the target compounds described in Table 1. Inserts correspond to UV spectrum of *Ej*-NCC4 (peak 9). A, artifact peak.

from the extract of ripened fruits of loquat and shows the NCCs/NDCCs identified through the application of the data-processing procedure from the acquired HPLC/ESI-TOF-MS data. Additionally, the UV−vis spectrum of the major NCC found (peak 9, *Ej*-NCC4) is included with the characteristic maximum absorbance peak at 320 nm as a consequence of the $\alpha$-formyl pyrrole moiety at ring B.[22] In ripened fruits of loquat, the nonfluorescent chlorophyll catabolite profile contains four different molecular formulas corresponding to NCCs and one to NDCC. Following the nomenclature convention (initials from latin species name followed by a number that indicates order in HPLC chromatogram),[36] these catabolites are designed as *Ej*-NCC1−*Ej*-NCC4 and *Ej*-NDCC1. Table 1 contains the mass spectroscopic characteristics of the NCC/NDCC detected in senescent fruits of loquat. Considering the elution order, *Ej*-NCC1 (peaks 1 and 3 in Figure 2) is the first NCC present in loquat fruits with a predicted elemental composition equal to $C_{35}H_{42}N_4O_{10}$, and with an experimental $m/z$ value equal to 679.2990 and 679.2974 for the protonated molecule (peaks 1 and 3, respectively). This compound should be equivalent to *So*-NCC2 described in senescent leaves of spinach,[22] and the results obtained for the standard *So*-NCC2 in our HPLC−MS system. The same elution time (39.4 min) with identical UV spectra and showing the same elemental composition and an experimental $m/z$ value equal to 679.2989 for the protonated molecule confirmed the hypothesis. Additionally, the characteristic product ions of *Ej*-NCC1 and *So*-NCC2 obtained by IT−$MS^2$ are the same. A signal at $m/z$ 647 corresponds to the product ion $[M+H-CH_3OH]^+$, $m/z$ 591, and $m/z$ 522 $[M+H\text{-ring A}]^+$. The high resolution ESI−TOF−$MS^2$ analysis of *So*-NCC2 from an extract of spinach senescent leaves and of its equivalent in loquat fruits confirms the consistency of the elemental composition and formulas of all product ions, which obtained positive records in all cases for both compounds. Consequently, *Ej*-NCC1 is the equivalent of *So*-NCC2 in loquat ripened fruits, which means a dihydroxylation in the vinyl group at C3, hydroxylation at $C8^2$, and keeps the esterification at $O13^4$ (Figure 1) .

*Ej*-NCC3 is the third NCC compound in elution order (57.7 min and 58.4 min, peaks 7 and 8, Figure 2) with an accurate mass for the protonated molecule of $m/z$ 631.2775 and 631.2762 and a predicted molecular formula of $C_{34}H_{38}N_4O_8$, identical to that of *So*-NCC3. The IT−$MS^2$ fragmentations of *Ej*-NCC3 are replicated in the corresponding analysis of the standard *So*-NCC3 in spinach extracts[22] and detailed in Table 1. Signals at $m/z$ 625 and 613 corresponding to the loss of $H_2O$ and that at $m/z$ 508 corresponding to the loss of ring A (both from the protonated molecule) were observed for *Ej*-NCC3 and *So*-NCC3. In addition, the elemental composition and formulas of all product ions were checked with the SmartFormula3D algorithm by high resolution ESI−TOF−$MS^2$ analysis of the *Ej*-NCC3 observed in loquat fruits and *So*-NCC3 in spinach, which obtained positive records for all fragments in both cases. The structure proposed for *Ej*-NCC3 maintained the vinyl group at C3, was hydoxylated at $C8^2$ and de-esterified at $O13^4$ (Figure 1).

The last chlorophyll NCC detected in loquat fruits was *Ej*-NCC4 (59.0 min and 60.4 min, peaks 8 and 9, Figure 2). The protonated molecule of this product was observed at $m/z$ 645.2910 in the high resolution ESI−qTOF−MS, with an elemental composition ($C_{35}H_{40}N_4O_8$) that fits with that of *So*-NCC4. The high resolution ESI−qTOF−MS data analysis of *So*-NCC4 showed the same predicted elemental composition as did *Ej*-NCC4 and an experimental $m/z$ value equal to 645.2918 for the protonated molecule (data not shown). The observed characteristic IT−$MS^2$ product ions for *Ej*-NCC4 and *So*-NCC4 were the same and are detailed in Table 1. The most prominent product ion was the one representing the loss of ring A, a characteristic fragmentation in the mass spectra of NCCs as well as the loss of methanol moiety from the protonated molecule that indicates the presence of a methyl

**Table 1. Nonfluorescent Chlorophyll Catabolites (NCCs and NDCC) Composition in Ripened Fruits of *Eriobotrya japonica* Lindl. Determined by HPLC/ESI-IT/TOF-MS**

| | | | time-of-flight | | | | ion trap |
|---|---|---|---|---|---|---|---|
| compound | peak number | $t_R$ (min) | error (ppm) | SigmaFit value | molecular formula | $[M + H]^+$ ($m/z$) | Product ions ($m/z$) |
| *Ej*-NCC1 | 1 | 39.4 | 2.7 | 23.3 | $C_{35}H_{42}N_4O_{10}$ | 679.2990 | 647 $[M+H-CH_3OH]^+$ |
| | | | | | | | 591 |
| | 3 | 41.9 | 0.9 | 19.2 | | 679.2974 | 522 $[M+H\text{-ring A}]^+$ |
| *Ej*-NCC2 | 2 | 40.1 | 0.2 | 39.7 | $C_{38}H_{42}N_4O_{11}$ | 731.2880 | 552 |
| | 4 | 42.2 | 1.9 | 42.4 | | 731.2878 | 522 $[M+H\text{-malonyl-ring A}]^+$ |
| *Ej*-NDCC1 | 5 | 50.4 | 5.9 | 45.9 | $C_{34}H_{40}N_4O_8$ | 633.2882 | 601 $[M+H-CH_3OH]^+$ |
| | 6 | 50.8 | 2.9 | 5.6 | | 633.2919 | 510 $[M+H\text{-ring A}]^+$ |
| *Ej*-NCC3 | 7 | 57.7 | 0.1 | 46.4 | $C_{34}H_{38}N_4O_8$ | 631.2775 | 625 |
| | | | | | | | 613 $[M+H-H_2O]^+$ |
| | 8 | 58.4 | 2.0 | 46.5 | | 631.2762 | 508 $[M+H\text{-ring A}]^+$ |
| *Ej*-NCC4 | 9 | 59.0 | 1.0 | 14.0 | $C_{35}H_{40}N_4O_8$ | 645.2910 | 613 $[M+H-CH_3OH]^+$ |
| | | | | | | | 522 $[M+H\text{-ring A}]^+$ |
| | 10 | 60.4 | 1.5 | 11.0 | | 645.2919 | 571 $[M+H-C_3H_6O_2]^+$ |

group at O13[4] as it has been previously described.[13,24,29] An additional product ion was observed corresponding to the loss of the propionic moiety at C17 ($m/z$ 571). This fragmentation has been described for chlorophyll derivatives[37] but not for NCCs so far. It is logical to assume that the fragmentation pattern of chlorophylls and their derivatives (NCCs) may display common product ions as in this case. To be sure that the signals obtained in the $MS^2$ analyses correspond to the predicted fragments, we checked the elemental composition and formulas of all product ions with the SmartFormula3D algorithm. Consistency of the monoisotopic peaks and the related isotopic peaks was determined by high resolution ESI−qTOF−$MS^2$ analyses, which obtained positive records for all fragments. The structure of *Ej*-NCC4 (and *So*-NCC4) is the simplest possible since it only implies the hydroxylation at C8[2], which maintains the vinyl group at C3 and the esterification at O13[4].

In addition, a chromatographic peak of the HPLC analysis (Rt: 55.8 min) of ripened fruits of loquat showed spectroscopic properties that match with those of a NCC (Supporting Information, S2). The MS spectrum of this "new" NCC indicated an elemental composition of $C_{36}H_{42}N_4O_9$, which means a molecular weight of 674.2951. The $MS^2$ spectrum, obtained by ESI−qTOF−MS to guarantee the interpretation with SmartFormula3D (Supporting Information, S3), shows two fragments corresponding to neutral losses of one or two molecules of methanol from the protonated molecule at $m/z$ 643.2762 $[M\text{-}CH_3OH+H]^+$ and at $m/z$ 611.2515 $[M\text{-}2 \times CH_3OH+H]^+$, respectively. In addition, the characteristic product ions corresponding to NCCs were also present, including the product ion at $m/z$ 552.2337 ($[M\text{-ring A}+H]^+$) and the product ion at $m/z$ 520.2105 $[M\text{-ring A-}CH_3OH+H]^+$ ion. With these data, the new NCC structure was tentatively assigned to the one presented in S3 of the Supporting Information. The compound derives from *Ej*-NCC4, to which a methoxy function was added at the C8[2] position. To confirm that the new NCC is an artifact produced during solvent extraction of the plant material from *Ej*-NCC4, ripened fruits of loquat were extracted with ethanol, and the HPLC gradient composition was changed by acetonitrile. A new compound was formed, with a protonated molecule at $m/z$ 689.3181, that is, the derivatization of *Ej*-NCC4 with ethanol; therefore, the new NCC is really an artifact produced during solvent extraction of the plant material. An FCC artifact formed during solvent isolation was reported recently[12] in banana fruits (*Musa acuminata* Colla) consisting of a trans-esterification by methanol at the propionic group. Special attention should be paid to the proper identification of noncolored chlorophyll catabolites since it seems they are prone to experiment modifications during solvent extraction.

**New NCC/NDCCs in Senescent Loquat Fruits.** Screening was not the sole strategy for NCC/NDCC determination; by exploiting the capabilities of this new methodology, we included in the target database elemental composition of new possible structures of NCCs/NDCCs not described so far. Of all of the plausible enzymes implicated in the modifications of FCCs (and consequently NCCs/NDCCs), only MES16, a methylesterase has been described, and taking into account that in loquat senescent fruits most NCCs (*Ej*-NCC1 and *Ej*-NCC4) are esterified, the ratio of esterified/de-esterified should be important in senescent fruits of loquat. Consequently, new theoretical structures were designed in base of de-esterifying or esterifying alternatives in already identified NCCs (not described to date). The methyl ester at the C13[2] form of *Bn*-NCC1 ($m/z$ 730.2850, $C_{38}H_{42}N_4O_{11}$) and the de-esterified forms of *Hv*-NDCC, *Zm*-NCC1, and *Nr*-NCC1 at C13[2], corresponding to the following masses and elemental compositions: $m/z$ 652.2744, $C_{33}H_{40}N_4O_{10}$; $m/z$ 826.3273, $C_{40}H_{50}N_4O_{15}$; and $m/z$ 878.3222, $C_{43}H_{50}N_4O_{16}$, respectively (Supporting Information, S1), were also included in the target database. Two positive matches (40.1 min and 42.2 min) with NCC UV absorption spectra were detected during the postprocessing procedure, both with an exact mass determined by high resolution ESI−TOF−MS of $m/z$ 731.2880 and 731.2878, corresponding to $C_{38}H_{42}N_4O_{11}$. Taking into account the structure of an NCC and the functional groups described, such an elemental composition could correspond to the ester form of *Bn*-NCC1, which means a vinyl group at C3, esterified at O13[4], and a malonyl group at C8[2] (Figure 1). Table 1 reports chromatographic characteristics of this NCC, designed as *Ej*-NCC2, following the nomenclature convention.[36] The $MS^2$ spectrum analyzed by IT−MS of *Ej*-NCC2 is shown in Figure 3, panel A. Besides the signal of the protonated molecule ion ($m/z$ 731), two signals of characteristic product ions of *Bn*-NCC1[20] are detected, one at $m/z$ 552 and the other at $m/z$ 522, corresponding to the $[M\text{-ring A-malonyl} +H]^+$ ion.

Within this strategy of including new possible structures in the target database of elemental composition for the screening

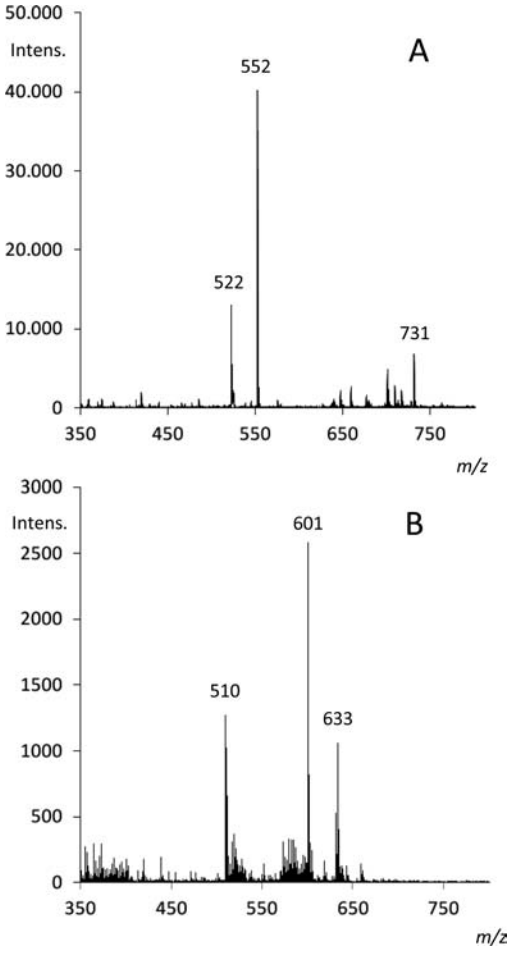


**Figure 3.** $MS^2$ spectra of (A) *Ej*-NCC2 and (B) *Ej*-NDCC1. The protonated molecule ion and the main product ions are shown.

procedure we also added the NDCCs theoretical alternatives that can be obtained from all the NCC structures described so far. NDCCs are generated from all NCC structures (both known and new ones) by deformylation at C6 in ring B. The screening showed the occurrence of *Ej*-NDCC1 (50.4 min and 50.8 min, peaks 5−6, Figure 2), both with the typical UV absorption spectrum of a NDCC[10,27] with broad bands near 237 nm and 274 nm. The only NDCCs detected in loquat fruits present in the high resolution ESI−TOF−MS a protonated molecule ion at *m/z* 633.2882 and 633.2919, both with a predicted elemental composition of $C_{34}H_{40}N_4O_8$. The $MS^2$ spectrum obtained by IT−MS (Figure 3B), besides the signal of the protonated molecule, showed two prominent signals of product ions, one at *m/z* 601 that corresponds to the neutral loss of methanol $[M\text{-}CH_3OH+H]^+$ and the other at *m/z* 510 in response to the ring A loss, $[M\text{-ring A}+H]^+$. Both losses are characteristics of NDDC MS fragmentation.[27] On the basis of previous configurations of NDCCs, the elemental composition of *Ej*-NDCC1 corresponds to the structure proposed in Figure 1, a vinyl group at C3, hydroxylated at $C8^2$, and keeping the esterification at $O13^4$. This means that *Ej*-NDCC1 is the NDCC that corresponds to *Ej*-NCC4. This compound has been identified previously in *Arabidopsis* MES16 mutant leaves,[31] a mutant that accumulates a different chlorophyll catabolite profile with novel and higher amounts of dioxobylins (FDCCs plus NDCCs, Figure 1). The results obtained show that at least *Ej*-NDCC1 is present as a consequence of a wild-type chlorophyll metabolism.

**Evidence for Tautomerism in NCCs Metabolism.** The description of the chlorophyll catabolites in extracts of fully developed loquat fruits shows a pair of isomers for each NCC/NDCC. For each catabolite, it detected a second product at a different retention time (see Table 1) with a feature UV-spectrum of NCC/NDCC, the same elemental composition, and an equivalent $MS^2$ fragmentation pattern. These compounds were assigned as isomers of *Ej*-NCC1, *Ej*-NCC2, *Ej*-NDCC1, *Ej*-NCC3, and *Ej*-NCC4. The possible effect of formic acid in the isomerization of NCCs was ruled out with a control experiment without formic acid in the HPLC gradient, which checked the presence of isomers in the control assay. This is not the first time that isomers of chlorophyll catabolites are described in senescent tissues. Four fractions of NDCCs produced by the activity of cytochrome P450 CYP89A9 have been described in *Arabidopsis* leaves,[30] and in senescent quince fruits, a pair of isomers for each NCC and two pairs for the NDCCs have been reported.[13] Although NCCs display three chiral centers at C1, $C13^2$, and C15, occurrence of different configurations is very constrained; thus, the possibility of epimerization at the chiral center C1 is excluded since this conformation is enzymatically originated and constant within the same vegetal species.[38] Structural configurations of the chiral centers $C13^2$ and C15 are *S* and *R*, respectively, for all NCCs described to date. This imposed spatial distribution is a sine qua non condition to carry out the spontaneous acid-catalyzed reaction of the FCC precursor to NCC in the weakly acidic vacuolar environment.[3] Consequently, few new structural rearrangements are available and hypothesized. One of those structural rearrangements to explain the NCC isomers is the keto−enol tautomerism at $C13^1$. This possible structural conformation is supported in the occurrence of enol forms of chlorophyll *a* and its derivatives at the isocyclic ring E. In fact, chlorophyll *a* keto−enol tautomerism was already evidenced by trapping the enol isomer as trimethylsilyl ether derivative.[39] By following the experimental approach that demonstrated keto−enol tautomerism in chlorophylls, the chemical derivatives of isolated *Ej*-NCC4 peaks (both isomers of the main NCC of loquat fruits) were obtained by semipreparative HPLC. To check the number of possible hydroxyl groups in the molecule(s) of *Ej*-NCC4 (two in the case of the keto tautomer, three for the enol configuration, Figure 4), a silylation reaction was performed with BSTFA, and the derivative compounds were analyzed by high resolution qTOF−MS. At 62.3 min, a derivative product was observed with a feature UV−vis spectrum of NCC, but regarding the original protonated molecule of *Ej*-NCC4, the atomic mass increased by 216 Da, which corresponds to the incorporation of three trimethylsilyl ether groups (TMSi) on the molecule (see Figure 4 for molecular rearrangement of *Ej*-NCC4 derivatives). At a different retention time the presence of di-TMSi derivative was also observed as shown in the table inserted in Figure 4 that contains retention time, elemental composition, and experimental atomic mass of the protonated molecules of the derivative products from *Ej*-NCC4 as well as the mass error and mSigma values from which the consistency of the isotopic pattern was ascertained. The incorporation of three TMSi groups to the *Ej*-NCC4 molecule is the hint for the presence of the enol isomer. The occurrence of the di-TMSi derivative should arise from the keto isomer. We also proceed to the specific methylation of the hydroxyl function from the

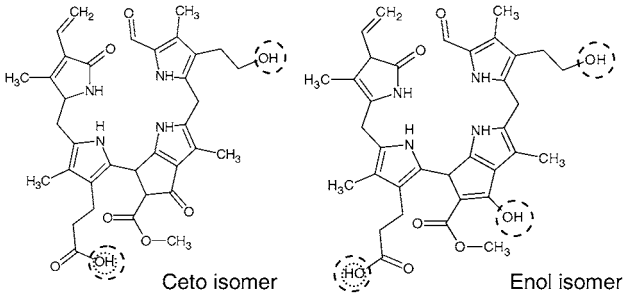


| | $t_R$ (min) | Error (ppm) | SigmaFit value | Molecular formula | $[M+H]^+$ cal. | $[M+H]^+$ meas. |
|---|---|---|---|---|---|---|
| Control | 59.3 | 0.9 | 9.9 | $C_{35}H_{40}N_4O_8$ | 645.2919 | 645.2925 |
| Methylation | 62.1 | 2.5 | 8.3 | $C_{36}H_{42}N_4O_8$ | 659.3075 | 659.3042 |
| Silylation | | | | | | |
| (1) | 63.7 | 1.1 | 30.3 | $C_{38}H_{48}N_4O_8Si$ | 717.3314 | 717.3322 |
| (2) | 61.7 | 0.2 | 17.9 | $C_{41}H_{56}N_4O_8Si_2$ | 789.3709 | 789.3711 |
| (3) | 62.3 | -3.8 | 15.4 | $C_{44}H_{64}N_4O_8Si_3$ | 861.4105 | 861.4072 |
| Methylation + silylation | 64.2 | 1.0 | 27.0 | $C_{42}H_{58}N_4O_8Si_2$ | 803.3866 | 803.3858 |

**Figure 4.** Scheme and results of *Ej*-NCC4 derivatization. Localizations for silylation (---) and methylation (·····) reactions are shown. Cal., calculated; meas., measured.

propionic group at C17 via diazomethane (see Figure 4), and then the silylation reaction was performed. In this case, we only observed the derivative products corresponding to the incorporation of one or two TMSi groups in the keto and enol isomer, respectively (see insert in Figure 4). Although specific analyses are required to definitively establish the structures of isomers found in senescent tissues, keto−enol tautomerism is a plausible possibility that should be elucidated in future research.

**Proposed NCC/NDCC Pathway in Loquat Senescent Fruits.** Figure 1 depicts a scheme for the structural rearrangements that originate the wide profile of FCCs in senescent loquat fruits by considering the pathway proposal outlined before.[22] It must be noted that the modification at C3, C8, and $C13^2$ takes place exclusively on the FCC/FDCC structure; however, FCC/FDCCs are very unstable, so we analyzed the NCC/NDCC structures.

The first structural modification of *p*FCC is the hydroxylation at the terminal carbon of the ethyl group at C8, which yields a secondary FCC (*s*FCC) that later is structurally modified by different catabolic enzymes,[6] which introduces new functions in the peripheral of the molecule and yields modified FCCs (*m*FCCs). In senescent loquat fruits, the major NCC is *Ej*-NCC4, which arises from a hydroxylation at $C8^2$ (resembles the rest of the structural features of FCC) and represents 80% of total NCCs. In parallel, three refunctionalization routes are available from *Ej*-NCC4.[22] First, the dihydroxylation at the vinyl group of ring A; second, the de-esterification process at ring E ($C13^2$). Certainly, esterified NCCs represent 95% of total NCCs in loquat senescent fruits. Remarkably, the only enzyme involved in the refunctionalization of NCCs that has been identified to date is MES16,[6] a member of the methylesterase protein family, which localizes to the cellular cytosol and specifically demethylates FCCs. It could be hypothesized that senescent fruits of loquat do not display a significant activity of MES16 as do some other vegetal species including *Zea mays* L., although no enzymatic determination has been developed. A third and new level of structural modification is the conjugation of the hydroxyl group at the $C8^2$ position with malonyl directly from *Ej*-NCC4, which means a complement to a previous proposal.[22] This new compound formed, *Ej*-NCC2, has a noncommon refunctionalization on $C8^2$ in plants, since the only vegetal species in that has been identified at the moment is *Brassica napus*.[20] In fact, *Brassica napus*, L., has three different NCCs, two of them with the same modifications in $C8^2$ as in loquat fruits. Nevertheless, no data are available in relation to the esterases enzymes implicated in the FCC modifications at $C8^2$. At this point, the identification of the enzymes responsible of such modifications will be very important for a better understanding of chlorophyll catabolism.

An alternative pathway (Figure 1) is the deformylation at C6 from *p*FCC by CYP89A9[6], which originates *p*FDCC. The hydroxylation at $C8^2$ is the reaction responsible for the formation of *Ej*-FDCC1. The esterase responsible for such hydroxylation should be very potent in loquat fruits since it is the dominating reaction in the refunctionalization of NCCs (*Ej*-NCC4, also hydroxylated in $C8^2$ is the major NCC). Later, *Ej*-FDCC1 is imported to the vacuole, where the low pH isomerizes to *Ej*-NDCC1. In loquats, CYP89A9 activity seems to be not very active, FDCC formation is very low and consequently so is *Ej*-NDCC1. The ratio among the sum of the UV-absorbance areas of NCCs (at 320 nm) and the sum of the UV-absorbance areas of NDCC (at 250 nm) in loquat fruits is about 1500. Clearly, there are two types of senescent tissues under the point of view of chlorophyll degradation, the NCCs species (most of the species analyzed so far) and the NDCCs species (Norway maple and *Arabidopsis thaliana* leaves). Recently, NDCCs were described for the first time in fruits,[13] and it was found that quince fruits have a dominated NDCC metabolism. The results obtained for loquats demonstrate that their major chlorophyll metabolism yields to NCC and consequently that the existing divergence between NCC or NDCC dominant metabolism in senescent leaves is also a reality in ripened fruits. This fact is another parallelism between chlorophyll catabolism in fruits and leaves.

## ■ ASSOCIATED CONTENT

### Ⓢ Supporting Information

Table with descriptions of the NCCs described up to now, MS chromatogram of *Ej*-NCC4 methanol derivative, and $MS^2$ chromatogram of *Ej*-NCC4 methanol derivative. This material is available free of charge via the Internet at http://pubs.acs.org.

## ■ AUTHOR INFORMATION

### Corresponding Author

*E-mail: aperez@cica.es. Phone: +00 34 954 691054. Fax: +00 34 954 691262.

### Funding

This work was supported by the Comisión Interministerial de Ciencia y Tecnología (CICYT-EU, Spanish and European Government, AGL 2012−39714) and by Junta de Andalucía (AGR 6271−2011).

### Notes

The authors declare no competing financial interest.

## ■ ABBREVIATIONS USED

FCC, fluorescent chlorophyll catabolite; NCCs, nonfluorescent chlorophyll catabolites; NDCC, urobilinogenoidic chlorophyll catabolite.

## ■ REFERENCES


(1) Hörtensteiner, S.; Kräutler, B. Chlorophyll breakdown in higher plants. *Biochim. Biophys. Acta* **2011**, *1807*, 977−988.

(2) Thomas, H.; Bortlik, K. H.; Rentsch, D.; Schellenberg, M.; Matile, P. Catabolism of chlorophyll in vivo: Significance of polar chlorophyll catabolites in a nonyellowing senescence mutant of *Festuca pratensis* Huds. *New Phytol.* **1989**, *111*, 3−8.

(3) Pružinská, A.; Anders, I.; Tanner, G.; Roca, M.; Hörtensteiner, S. Chlorophyll breakdown: Pheophorbide a oxygenase is a Rieske-type iron−sulfur protein, encoded by the accelerated cell death 1 gene. *Proc. Natl. Acad. Sci. U.S.A.* **2003**, *100*, 15259−15264.

(4) Roca, M.; James, C.; Pružinská, A.; Hörtensteiner, S.; Thomas, H.; Ougham, H. Analysis of the chlorophyll catabolism pathway in leaves of an introgression senescence mutant of *Lolium temulentum*. *Phytochemistry* **2004**, *65*, 1231−1238.

(5) Sato, Y.; Moria, R.; Katsuma, S.; Nishimura, M.; Tanaka, A.; Kusaba, M. Two short chain dehydrogenase/reductases, NON-YELLOW COLORING 1 and NYC1-LIKE, are required for chlorophyll *b* and light-harvesting complex II degradation during senescence in rice. *Plant J.* **2009**, *57*, 120−131.

(6) Christ, B.; Schelbert, S.; Aubry, S.; Süssenbacher, I.; Müller, T.; Kräutler, B.; Hörtensteiner, S. MES16, a member of the methylesterase protein family, specifically demethylates fluorescent chlorophyll catabolites during chlorophyll breakdown in *Arabidopsis*. *Plant Physiol.* **2012**, *158*, 628−641.

(7) Christ, B.; Hörtensteiner, S. Mechanism and significance of chlorophyll breakdown. *J. Plant Growth Regul.* **2014**, *33*, 4−20.

(8) Oberhuber, M.; Berghold, J.; Breuker, K.; Hörtensteiner, S.; Kräutler, B. Breakdown of chlorophyll: A nonenzymatic reaction accounts for the formation of the colorless "nonfluorescent" chlorophyll catabolites. *Proc. Natl. Acad. Sci. U.S.A.* **2003**, *100*, 6910−6915.

(9) Kräutler, B.; Jaun, B.; Bortlik, K. H.; Schellenberg, M.; Matile, P. On the enigma of chlorophyll degradation: The constitution of a secoporphinoid catabolite. *Angew. Chem., Int. Ed.* **1991**, *30*, 1315−1318.

(10) Losey, F. G.; Engel, N. Isolation and characterization of a urobilinogenoidic chlorophyll catabolite from *Hordeum vulgare* L. *J. Biol. Chem.* **2001**, *276*, 27233−27236.

(11) Müller, T.; Ulrich, M.; Ongania, K. H.; Kräutler, B. Colorless tetrapyrrolic chlorophyll catabolites found in ripening fruit are effective antioxidants. *Angew. Chem., Int. Ed.* **2007**, *46*, 8699−8702.

(12) Moser, S.; Müller, T.; Holzinger, A.; Lütz, C.; Kräutler, B. Structures of chlorophyll catabolites in bananas (*Musa acuminata*) reveal a split path of chlorophyll breakdown in a ripening fruit. *Chem.—Eur. J.* **2012**, *18*, 10873−10885.

(13) Ríos, J. J.; Pérez-Gálvez, A.; Roca, M. Non-fluorescent chlorophyll catabolites in quince fruits. *Food Res. Int.* **2014**, in press. DOI: 10.1016/j.foodres.2014.03.063.

(14) Caldeira, M. L.; Crane, H. Evaluation of loquats (*Eriobotrya japonica* (Thunb.) Lindl) at the Tropical Research and Education Center, Homestead. *Proc. Fla. State Hortic. Soc.* **1999**, *112*, 187−190.

(15) Ferreres, F.; Gomes, D.; Valentão, P.; Gonçalves, R.; Pio, R.; Chagasd, E. A.; Seabrab, R. M.; Paula, B. A. Improved loquat (*Eriobotrya japonica* Lindl.) cultivars: Variation of phenolics and antioxidative potential. *Food Chem.* **2009**, *114*, 1019−1027.

(16) Xu, H.; Chen, J. Commercial quality, major bioactive compound content, and antioxidant capacity of 12 cultivars of loquat (*Eriobotrya japonica* Lindl.) fruits. *J. Sci. Food Agric.* **2011**, *91*, 1057−1063.

(17) Zhou, C.; Li, X.; Sun, C.; Xu, C.; Chen, K. Effects of drying methods on the bioactive components in loquat (*Eriobotrya japonica* Lindl.) flowers. *J. Med. Plants Res.* **2011**, *5*, 3037−3041.

(18) Ferruzzi, M. G.; Blakeslee, J. Digestion, absorption, and cancer preventive activity of dietary chlorophyll derivatives. *Nutr. Res. (N.Y.)* **2007**, *27*, 1−12.

(19) Roca, M. In vitro digestive stability and uptake by Caco-2 human intestinal cells of nonfluorescent chlorophyll catabolites. *Food Chem.* **2012**, *130*, 134−138.

(20) Matile, P.; Ginsburg, S.; Schellenberg, M.; Thomas, H. Catabolites of chlorophyll in senescing barley leaves are localized in the vacuoles of mesophyll cells. *Proc. Natl. Acad. Sci. U.S.A.* **1988**, *85*, 9529−9532.

(21) Mühlecker, W.; Kräutler, B. Breakdown of chlorophyll: Constitution of nonfluorescing chlorophyll catabolites from senescent cotyledons of the dicot rape. *Plant Physiol. Biochem.* **1996**, *34*, 61−75.

(22) Berghold, J.; Breuker, K.; Oberhuber, M.; Hörtensteiner, S.; Kräutler, B. Chlorophyll breakdown in spinach: On the structure of five nonfluorescent chlorophyll catabolites. *Photosynth. Res.* **2002**, *74*, 109−119.

(23) Berghold, J.; Eichmüller, C.; Hörtensteiner, S.; Kräutler, B. Chlorophyll breakdown in tobacco: On the structure of two nonfluorescent chlorophyll catabolites. *Chem. Biodiversity* **2004**, *1*, 657−668.

(24) Berghold, J.; Müller, T.; Ulrich, M.; Hörtensteiner, S.; Kräutler, B. Chlorophyll breakdown in maize: On the structure of two nonfluorescent chlorophyll catabolites. *Monatsh. Chem.* **2006**, *137*, 751−763.

(25) Kräutler, B.; Jaun, B.; Amrein, W.; Bortlik, K.; Schellenberg, M.; Matile, P. Breakdown of chlorophyll: Constitution of a secoporphinoid chlorophyll catabolite isolated from senescent barley leaves. *Plant Physiol. Biochem.* **1992**, *30*, 333−346.

(26) Müller, T.; Oradu, S.; Ifa, D. R.; Cooks, G.; Kräutler, B. Direct plant tissue analysis and imprint imaging by desorption electrospray ionization mass spectrometry. *Anal. Chem.* **2011**, *83*, 5754−5761.

(27) Müller, T.; Rafelsberger, M.; Vergeiner, C.; Kräutler, B. A dioxobilane as product of a divergent path of chlorophyll breakdown in Norway maple. *Angew. Chem., Int. Ed.* **2011**, *50*, 1−5.

(28) Pružinská, A.; Tanner, G.; Aubry, S.; Anders, I.; Moser, S.; Müller, T.; Ongania, K. H.; Kräutler, B.; Youn, J. Y.; Liljegren, S. J.; Hörtensteiner, S. Chlorophyll breakdown in senescent *Arabidopsis* leaves: Characterization of chlorophyll catabolites and of chlorophyll catabolic enzymes involved in the degreening reaction. *Plant Physiol.* **2005**, *139*, 52−63.

(29) Scherl, M.; Müller, T.; Kraütler, B. Chlorophyll catabolites in senescent leaves of the Lime Tree (*Tilia cordata*). *Chem. Biodiversity* **2012**, *9*, 2605−2617.

(30) Christ, B.; Süssenbacher, I.; Moser, S.; Bichsel, N.; Egert, A.; Müller, T.; Kräutler, B.; Hörtensteiner, S. Cytochrome P450 CYP89A9 is involved in the formation of major chlorophyll catabolites during leaf senescence in *Arabidopsis*. *Plant Cell* **2013**, *25*, 1868−1880.

(31) Süssenbacher, I.; Christ, B.; Hörtensteiner, S.; Kräutler, B. Hydroxymethylated phyllobilins: A puzzling new feature of the dioxobilin branch of chlorophyll breakdown. *Chem.—Eur. J.* **2014**, *20*, 87−92.

(32) Iswaldi, I.; Arráez-Román, D.; Gómez-Caravaca, A. M.; Contreras, M. M.; Uberos, J.; Segura-Carretero, A.; Fernández-Gutierrez, A. Identification of polyphenols and their metabolites in human urine after cranberry-syrup consumption. *Food Chem. Toxicol.* **2013**, *55*, 484−492.

(33) Peters, R. J. B.; Rijk, J. C. W.; Bovee, T. F. H.; Nijrolder, A. W. J. M.; Lommen, A.; Nielen, M. W. F. Identification of anabolic steroids and derivatives using bioassay-guided fractionation, UHPLC/TOFMS analysis, and accurate mass database searching. *Anal. Chim. Acta* **2010**, *664*, 77−88.

(34) Darbre, A. Esterification. In *Handbook of Derivatives for Chromatography*; Balu, K., King, G., Eds.; Heyden: London, 1977; p 39.

(35) Poole, C. F. Recent advances in the sylilation of organic compounds for gas chromatography. In *Handbook of Derivatives for Chromatography*; Balu, K., King, G., Eds.; Heyden: London, 1977; p 153.

(36) Ginsburg, S.; Matile, P. Identification of catabolites of chlorophyll–porphyrin in senescent rape cotyledons. *Plant Physiol.* **1993**, *102*, 521–527.
(37) Van Breemen, R. B.; Canjura, F. L.; Schwartz, S. J. Identification of chlorophyll derivatives by mass spectrometry. *J. Agric. Food Chem.* **1991**, *39*, 1452–1456.
(38) Hörtensteiner, S.; Rodoni, S.; Schellenberg, M.; Vicentini, F.; Nandi, O. I.; Qui, Y. L.; Matile, Ph. Evolution of chlorophyll degradation: The significance of RCC reductase. *Plant Biol.* **2000**, *2*, 263–267.
(39) Hynninnen, P. H.; Wasielewski, M. R.; Katz, J. J.; Chlorophylls, V. I. Epimerization and enolization of chlorophyll *a* and its magnesium-free derivatives. *Acta Chem. Scand.* **1979**, *33*, 637–648.

protein in the presence or absence of lactose. These findings were then related to heat-induced viscosity measurements (with the addition of fat) in model IMF systems over a range of DM contents.

## MATERIALS AND METHODS

**Materials.** Whey protein isolate (WPI; Isolac; 90% protein) was obtained from Carbery (Cork, Ireland). Phosphocasein (PCN; 80% protein) was obtained from Sachsenmilch (Leppersdorf, Germany). Edible lactose (L) was obtained from Glanbia (Kilkenny, Ireland). Sunflower oil (SO; Solesta, Warwickshire, UK) was obtained from a local supermarket. Mineral salts (>98% purity) were obtained from Sigma-Aldrich (Wicklow, Ireland).

**Basis.** Heat-induced changes in dispersions of IMF constituents (protein, lactose, and fat) were studied for individual components and in combinations. Dispersions were prepared to correspond to an IMF intended for newborn infant feeding. The ratios of total protein to lactose and whey to casein were 1.4 to 7.2 and 6.0 to 4.0, respectively. For each combination of ingredients (WPI, PCN, and L) four concentration levels were prepared in simulated milk ultrafiltrate (SMUF), which approximated DM contents at various processing stages during IMF manufacture (i.e., 25.8−58.2% DM; Table 1). For example, at the lowest concentration studied, WPI solutions contained 2.4 g of whey protein per 100 g of SMUF, whereas WPI-PCN contained 2.4 g of whey protein and 1.6 g of casein per 100 g of SMUF. Table 2 shows the whey protein concentration of whey-containing solutions/dispersions as a function of overall weight of formulations (% w/w). For viscosity measurements, SO was also used in the systems at a protein to oil ratio of 1.4 to 3.6 (see Homogenization). All dispersions and emulsions were prepared and analyzed in triplicate.

**Table 1. IMF Constituents in Dispersion/Emulsions**

| concn level | whey (g) | casein (g) | fat[a] (g) | lactose (g) | SMUF (g) | DM (%) |
|---|---|---|---|---|---|---|
| 1 | 2.4 | 1.6 | 10.3 | 20.6 | 100.0 | 25.8 |
| 2 | 4.8 | 3.2 | 20.6 | 41.1 | 100.0 | 41.1 |
| 3 | 7.2 | 4.8 | 30.9 | 61.7 | 100.0 | 51.1 |
| 4 | 9.6 | 6.4 | 41.1 | 82.3 | 100.0 | 58.2 |

[a]Added to heat treatment experiments only.

**Table 2. Whey Protein as a Percentage of Total Matter in Whey-Containing Nonfat Systems**

| | % whey protein (w/w) | | | |
|---|---|---|---|---|
| concn level | WPI | WPI-L | WPI-PCN | WPI-PCN-L |
| 1 | 2.3 | 2.0 | 2.3 | 1.9 |
| 2 | 4.6 | 3.3 | 4.4 | 3.2 |
| 3 | 6.7 | 4.3 | 6.4 | 4.1 |
| 4 | 8.8 | 5.0 | 8.3 | 4.8 |

**Preparation of Dispersions.** SMUF was prepared using deionized water according to the method of Jenness and Koops.[17] Proteins, at levels stated in Table 1, were allowed to hydrate in SMUF overnight before use. The composition of SMUF was as follows: $KH_2PO_4$, 11.61 mM; $K_3$citrate·$H_2O$, 3.70 mM; $Na_3$citrate·$5H_2O$, 6.09 mM; $K_2SO_4$, 1.03 mM; $K_2CO_3$, 2.17 mM; KCl, 8.05 mM; $CaCl_2$·$2H_2O$, 8.98 mM; $MgCl_2$·$6H_2O$, 3.21 mM. Sodium azide (0.03% w/w) was added as a preservative. Dispersions and emulsions were standardized to pH 6.7 by the addition of 0.5 M NaOH. When necessary, lactose was added to dispersions at 25 °C and agitated for 2 h before use.

**Denaturation Temperature.** DSC was carried out using a Q2000 DSC (TA Instruments, New Castle, DE, USA). Samples (ca. 20 mg) were heated from 40 to 100 °C at a rate of 5 °C $min^{-1}$ in a nitrogen-purged environment. Heat flow to the sample was compared against an empty reference pan. The denaturation temperature ($T_d$) of $\beta$-lg was obtained using Universal Analysis 2000 software (TA Instruments), where $T_d$ was the temperature corresponding to the peak minimum of the denaturation endotherm.

**Fourier Transform Infrared Spectroscopy.** FTIR spectroscopy (Bruker Tensor 27, Bruker Optik GmbH, Germany) provided qualitative information on the physical state of proteins in dispersion. Attenuated total reflectance (ATR), mid-IR spectra were obtained using a thermally controlled BioATR cell II. Spectra used were an average of 300 scans at 4 $cm^{-1}$. Samples were measured, stepwise from 50 to 90 °C at 10 °C intervals, using fresh dispersions at each temperature. Background readings were taken against SMUF at each measurement temperature and subtracted automatically. Atmospheric corrections ($H_2O$ and $CO_2$ compensations), vector normalization, and Fourier self-deconvolution (Lorentzian shape with bandwidth and noise reduction factors of 20.31 and 0.36, respectively) of the amide I region (1700−1600 $cm^{-1}$) were carried out using OPUS 5.5 software.[18] FTIR measurements were carried out in triplicate at the highest whey protein concentration (9.6 g 100 $g^{-1}$ SMUF). In lactose-containing dispersions, the concentration of lactose (82.3 g 100 $g^{-1}$ SMUF) was present at levels greater than its theoretical solubility limit in water (42.4 g 100 $g^{-1}$ water at 49 °C[19]). Samples were centrifuged at 1000*g* for ca. 1 min to sediment crystalline lactose, and the supernatant was used for analyses.

**Viscosity.** Viscosity of dispersions/emulsions was monitored throughout heating using a starch pasting cell in a rheometer (AR 2000 rheometer, TA Instruments, New Castle, DE, USA). All samples (28 g) were heated from 40 to 95 °C at a rate of 22 °C $min^{-1}$ and then held at 95 °C for 5 min before cooling to 40 °C at a rate of 18 °C $min^{-1}$. During the measurement samples were sheared with the starch pasting cell impeller at a rate of 16.8 $s^{-1}$. For samples containing lactose, a solubilization step (60 °C for 30 min) was included prior to the heating ramp described above.

**Homogenization.** Emulsions were prepared (for viscosity experiments) by homogenizing mixtures of sunflower oil with dispersions (WPI, WPI-L, PCN, PCN-L, WPI-PCN, and WPI-PCN-L at each concentration level) prepared above. Homogenization was carried out at 65 °C using a two-stage, valve-type homogenizer, model NS2006H (Niro Soavi, Parma, Italy), employing a first-stage pressure of 15 MPa and a second-stage pressure of 5 MPa.

**Statistical Analysis.** Analysis of variance (ANOVA) was carried out using Minitab 15 (Minitab Ltd., Coventry, UK; 2007) statistical software. The significance of formulation type on heat-induced viscosity increase was estimated ($P < 0.05$).

Where the slope ($m$) of a regression line is reported, the 95% confidence limits associated with the slope are also specified ($m \pm t$ $SE_m$). The standard error of the estimated slope ($SE_m$) was calculated using Microsoft Excel's LINEST function. The confidence interval was then calculated as the product of $SE_m$ and $t$, the two-tailed $t$ value associated with $P = 0.05$ and $n - 2$ degrees of freedom.

## RESULTS AND DISCUSSION

**Denaturation Temperature.** Denaturation temperature ($T_d$) of $\beta$-lg was measured by DSC in the various dispersions, starting with WPI in deionized water, followed by the stepwise addition of the other constituents, mineral salts (SMUF), phosphocasein (PCN), and lactose (L). The effect of concentration was also studied; protein content of dispersions corresponded to concentrations found typically in IMF systems (Table 1). Figure 1 shows a representative trace of denaturation in a WPI solution. The shape of the thermograms is similar to those reported previously with the peak minimum corresponding to the $T_d$ of $\beta$-lg.[20,21] The $T_d$ of $\alpha$-lactalbumin was identified as a small shoulder occurring 10−15 °C lower than the $T_d$ $\beta$-lg on DSC thermograms but was detectable only at whey protein concentrations >8% w/w.

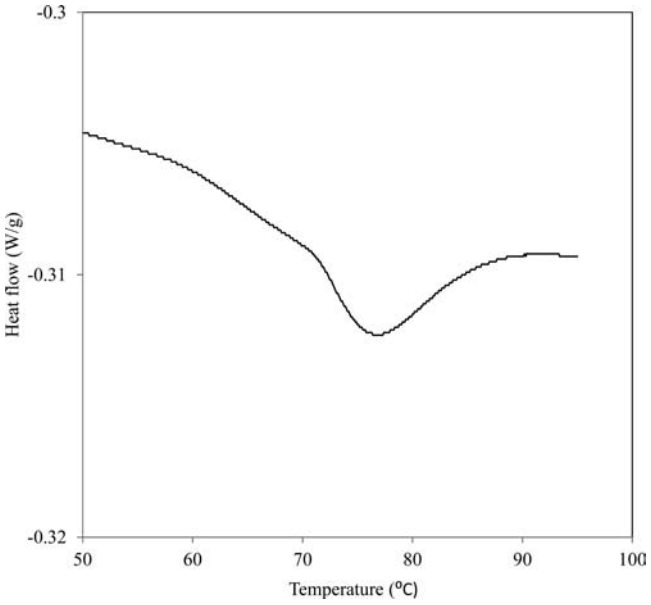


**Figure 1.** DSC thermogram of WPI solution (8.8% whey protein w/w in SMUF).

The $T_d$ of $\beta$-lg in WPI hydrated in deionized water and SMUF was within the range reported by previous studies, that is, 75−85 °C, depending on concentration, genetic variant of $\beta$-lg, scanning rate, etc.[22,23] In general, $T_d$ decreased with increasing protein concentration (Figure 2). Qi et al. reported

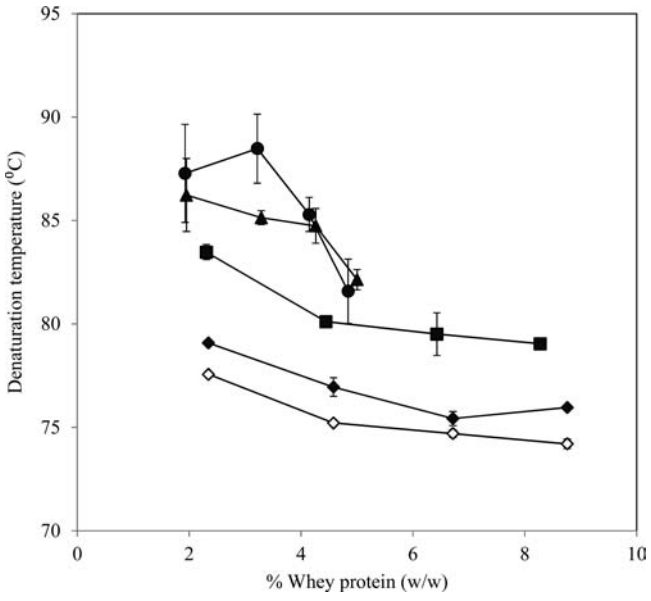


**Figure 2.** Denaturation temperature ($T_d$) in SMUF (solid symbols) and deionized water (open symbols), WPI (◇, ◆), WPI-PCN (■), WPI-L (▲), and WPI-PCN-L (●), at increasing protein concentrations. Error bars represent the standard deviation of three replicate trials.

that increasing the concentration of purified $\beta$-lg increased $T_d$.[23] $T_d$ values reported across a number of studies suggest that increasing protein concentration in nonpurified systems tends to decrease $\beta$-lg denaturation temperature.[20,22,24]

Hydrating WPI in SMUF, prior to DSC analysis, had the effect of increasing the $T_d$ of $\beta$-lg compared to that of WPI in deionized water (Figure 2) The effect of salts on denaturation temperature of proteins can be related to the Hoffmeister lyotropic series, according to which, ions are classified as chaotropic or kosmotropic, depending, respectively, on their destabilizing or stabilizing effects.[25] Chaotropes disrupt hydrophobic aggregation and promote unfolding of proteins and thereby reduce $T_d$. In contrast, kosmotropic agents promote hydrophobic interactions and lead to an increase in $T_d$.[26] The $T_d$ of $\beta$-lg in WPC has been shown to increase in the presence of NaCl and decrease in the presence of $MgCl_2$ or $CaCl_2$.[27,28] It appears from the present study that the net effect of the milk serum salts in SMUF is kosmotropic in nature; that is, the presence of mineral salts had the effect of increasing the $T_d$ of $\beta$-lg. These results show a clear effect of SMUF on $T_d$. Therefore, as SMUF plays an important role in stabilizing rehydrated PCN, all subsequent dispersions/solutions were hydrated in SMUF; this allowed comparisons to be made more easily between the various systems.

Addition of PCN to systems containing WPI increased the $T_d$ of $\beta$-lg (Figure 2). Casein micelles require a significant amount of water for hydration; extrapolating from previously reported data, casein micelles, at temperatures of 70−80 °C have a water content of approximately 2.2 g water $g^{-1}$ casein.[29] It could be argued that PCN increased the effective concentration of whey protein in the continuous phase due to the large voluminosity of casein micelles, rendering a significant proportion of solvation water unavailable to whey proteins. At the highest casein content of the present study (6.4 g 100 $g^{-1}$ SMUF) the propensity of casein micelles to hydrate and compete for water could decrease available water by ca. 14.1 g. On this basis, it might be expected that the addition of PCN should decrease $T_d$, given that increasing concentration of WPI dispersions resulted in a decrease in $T_d$. However, increased $T_d$ of $\beta$-lg in WPI-PCN dispersions suggests PCN had a stabilizing effect on whey protein denaturation. In previous studies, the effects of individual caseins ($\alpha$-, $\beta$-, $\kappa$-) on $T_d$ were inconsistent.[22,30,31] Imafidon et al.[22] found that $\kappa$-casein variants AB and BB decreased $T_d$, whereas variant AA increased $T_d$. Inconsistencies may be due to differences in buffer system source, genetic variants, and preprocessing of proteins used. Furthermore, these studies did not examine the effect of intact casein micelles on the $T_d$ of $\beta$-lg.

Addition of lactose to systems containing WPI resulted in an increase in $T_d$ of $\beta$-lg compared to lactose-free systems at equivalent protein concentrations (Figure 2). The stabilizing effect of sugars, including lactose, against whey protein denaturation has been well documented.[20,32−34] Interactions between sugars and the hydrophobic backbone of whey proteins are thermodynamically unfavorable.[35] As a result, sugars become preferentially excluded from the vicinity of the protein to minimize protein−carbohydrate contact.[36] Similarly, when heat is applied to whey protein, any potential interaction with a cosolvent sugar is unfavorable, which results in retention of the compact, native structure of the protein to higher temperatures. The stabilizing effect of lactose was least apparent at high protein levels, possibly due to low lactose solubility at high DM concentrations and particularly so in the presence of PCN.

**Fourier Transform Infrared Spectroscopy.** The amide I region (1700−1600 $cm^{-1}$) of FTIR spectra was examined in formulations equivalent to 58.2% DM (see Table 1). This region is associated with C═O and C—N stretching vibrations and is indicative of protein secondary structure.[18] Changes in

Table 3. Summary of Secondary Structural Changes with Respect to Temperature[a]

| | | 1684 $cm^{-1}$ | 1672 $cm^{-1}$ | 1654/1645 $cm^{-1}$ | 1630−1627 $cm^{-1}$ | 1616/1617 $cm^{-1}$ |
|---|---|---|---|---|---|---|
| | °C | intermolecular $\beta$-sheet[42,54] | turns[10] | $\alpha$-helix/random[10,54] | intramolecular $\beta$-sheet[10,37,38,54] | intermolecular $\beta$-sheet[10,37,38,54] |
| WPI | 50 | ○ | ○ | ○ | ○ | ○ |
| | 60 | - | - | - | ○ | + |
| | 70 | - | - | -- | -- | +++ |
| | 80 | - | - | - | - | + |
| | 90 | - | - | - | ○ | + |
| WPI-L | 50 | ○ | ○ | ○[b] | ○ | ○ |
| | 60 | - | - | -- | ○ | +++ |
| | 70 | + | + | - | ○ | ○ |
| | 80 | + | + | - | -- | + |
| | 90 | + | + | - | - | + |
| WPI-PCN | 50 | ○ | ○ | ○ | ○ | ○ |
| | 60 | + | + | + | + | + |
| | 70 | + | + | ○ | - | ○ |
| | 80 | ○ | ○ | -- | --- | + |
| | 90 | ○ | + | - | - | - |
| WPI-PCN-L | 50 | ○ | ○ | ○[b] | ○ | ○ |
| | 60 | ○ | + | - | ○ | +++ |
| | 70 | + | + | ○ | ○ | ○ |
| | 80 | + | ++ | ○ | -- | + |
| | 90 | ○ | + | ○ | -- | + |

[a](○) no change from previous temperature; (+/++/+++) small/intermediate/large increase; (-/--/---) small/intermediate/large decrease. [b]Increased absorbance compared to lactose-free dispersion. Analysis based on three replicate trials.

amide I spectra, with respect to temperature, are summarized in Table 3. As expected, little effect of temperature was observed for PCN dispersions, due to a relative lack of secondary structure in casein proteins. In the case of WPI, however, increasing temperature from 60 to 90 °C resulted in significant changes in secondary structure, particularly decreases in intramolecular $\beta$-sheet (1630−1627 $cm^{-1}$) and $\alpha$-helix (1654 $cm^{-1}$) conformations. A concomitant increase in the absorbance spectra in the region of 1617 $cm^{-1}$ indicated the formation of aggregates with intermolecular $\beta$-sheet structures.[37,38] The greatest changes in secondary structure and intermolecular aggregate formation occurred between 60 and 70 °C. Qi et al.[10] also reported a significant reduction in $\alpha$-helix conformation over these temperatures, which, it was suggested, plays an important role in the exposure of the free thiol group, Cys-121. Exposure of this group is of particular significance to IMF manufacture as it is associated with potentially large increases in viscosity, due to whey protein aggregation following intermolecular thiol−disulfide interchange reactions.

At 50 °C, the secondary structure of WPI-PCN dispersions was similar to that of WPI. The presence of PCN delayed temperature-induced losses of $\beta$-sheet structure. A major decrease in intramolecular $\beta$-sheet structure was not observed until >70 °C, compared to >60 °C for WPI in the absence of PCN. Delayed loss of secondary structure correlated well with DSC analysis, where PCN caused an increase in $T_d$. Surprisingly, between 80 and 90 °C, where intramolecular $\beta$-sheet structure decreased, intermolecular $\beta$-sheet structure also decreased. Increases in turns/random coil structure (~1672 $cm^{-1}$) were also observed as the temperature increased. Overall, it is evident that PCN altered the effects of temperature on secondary structural changes in whey proteins.

Addition of lactose to SMUF had negligible effect on absorbance of SMUF buffers in the amide I region. Lactose, however, did influence the spectra of WPI solutions in the amide I region (Figure 3A). A notable difference between the spectra of WPI and WPI-L is the relatively large absorbance peak in the region from 1670 to 1640 $cm^{-1}$ in lactose-containing samples. Peaks in this region (1654 and 1645 $cm^{-1}$) have been associated previously with $\alpha$-helical and random coil conformations.[10,38] However, it is also possible that the presence of lactose altered the local structure of water, resulting in preferential hydration of proteins.[39] Another notable difference occurred at ~1617 $cm^{-1}$, an area associated with intermolecular aggregates, where WPI-L systems had a lower absorbance in comparison to WPI (Figure 3A). It is also possible that spectral changes of WPI in the presence of lactose were due to the Maillard reaction. Czerwenka et al.[40] reported that lactosylation of $\beta$-lg (over 120 h at 60 °C) resulted in approximately 1.6 molecules of lactose bound to each $\beta$-lg molecule. It is suggested that the extent of the Maillard reaction was limited over the time frame of FTIR measurements reported here (approximately 6 min per analysis). Schiff base intermediates have been reported to absorb at 1647 $cm^{-1}$;[41] in the current study, the intensity at 1647 $cm^{-1}$ diminished with increasing temperature. On the basis of the above, it appears unlikely that possible spectral interferences due to lactosylation were a confounding factor.

Heating from 50 to 60 °C increased the aggregation band (1617 $cm^{-1}$) of WPI-L (Table 3). An accompanying reduction in the 1670−1640 $cm^{-1}$ region indicated that some of the additional secondary structure, due to the presence of lactose, was lost upon heating. Intramolecular $\beta$-sheet structure was preserved to a higher temperature in WPI-L solutions (Table 3), where no loss was observed until >70 °C, compared to

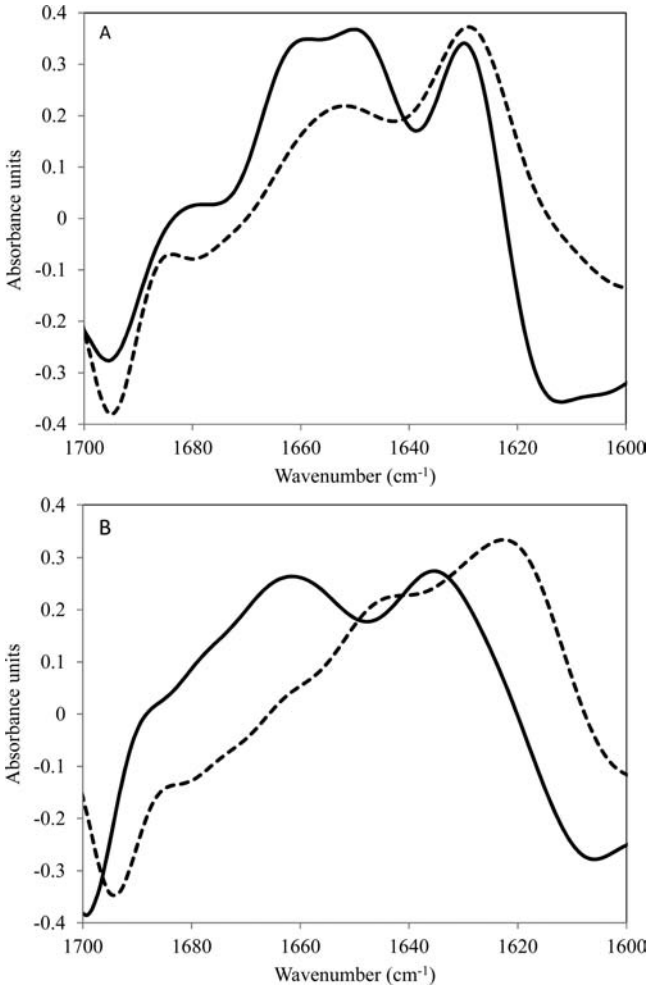


**Figure 3.** FTIR spectra of WPI (dashed line) and WPI-L (solid line) at 50 °C (A) and 80 °C (B).

>60 °C in the absence of lactose. Spectra of WPI-L solutions heated from 50 to 80 °C did not change in the same manner as WPI alone (compare panels A and B of Figure 3), in which the main peak shifted from intramolecular (1630 $cm^{-1}$) toward intermolecular $\beta$-sheet structure (1617 $cm^{-1}$). Delayed loss of structure and aggregation were most likely due to the stabilization effect of lactose, which has previously been shown to delay aggregation in $\beta$-lg solutions, albeit to a lesser extent than other sugars.[42] The findings are consistent with the DSC results reported above, which showed that $T_d$ of WPI in the presence of lactose was higher than in its absence. Increased absorbance at 1672 $cm^{-1}$ indicated an increase in turns/random coil structure upon heating, which was similar to the effect of PCN upon WPI.

Lactose in WPI-PCN dispersions had a similar effect as lactose in WPI solutions; that is, a relatively large peak, compared to lactose-free dispersions, in the range of 1640–1670 $cm^{-1}$ was observed. As with WPI-L dispersions, a decrease was observed in $\alpha$-helix/random conformation between 50 and 60 °C, and intramolecular $\beta$-sheet structure remained intact until the temperature exceeded 70 °C (Table 3).

**Heat Treatment Experiments.** The effect of heat treatment on viscosity of IMF formulations was determined by heat treatment at 95 °C for 5 min. Samples were heated from 40 to 95 °C at a rate of 22 °C $min^{-1}$. During this temperature ramp, viscosity first decreased, before a critical temperature was exceeded ($T_v$) and viscosity increased exponentially (Figure 4). Measurement of $T_v$ provides practical

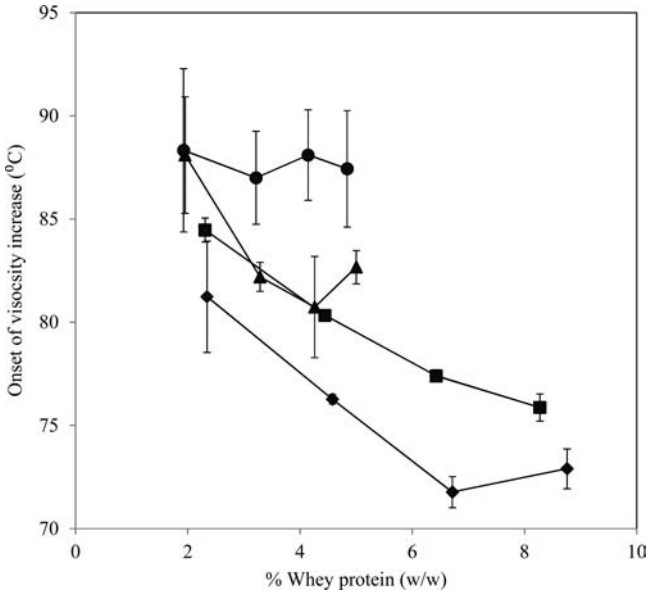


**Figure 4.** Onset of viscosity increase during heating, WPI (◆), WPI-PCN (■), WPI-L (▲), and WPI-PCN-L (●), at increasing protein concentrations. Error bars represent the standard deviation of three replicate trials.

information relevant to existing, industrial heat treatment scenarios, given that it was carried out under shear conditions and the rate of temperature increase was high (22 °C $min^{-1}$) compared to $T_d$ measurements. As observed by DSC and FTIR data reported above, $\beta$-lg in WPI is sensitive to heat denaturation and is highly reactive when unfolded due to the exposure of a free sulfhydryl (thiol) group.[11,12] During heat treatment, denatured and unfolded $\beta$-lg forms aggregates through self-association and association with other milk proteins.[43−46] Denatured whey proteins and aggregates have a greater hydrated volume than native proteins, which leads to significant increases in viscosity.[47,48] Therefore, it is not surprising that all WPI-containing systems increased in viscosity as the temperature approached $T_d$. The trends observed for $T_v$ were similar to those observed for $T_d$ (Figure 2); that is, addition of lactose and/or PCN increased $T_v$. In some cases it was observed that $T_v$ occurred prior to $T_d$, especially at higher whey protein concentrations. This could be explained by differences in heating and shearing rates between the rheometer and DSC methods. In the case of PCN and PCN-L dispersions viscosity did not increase due to the absence of whey protein.

The extent of viscosity change during heat treatment was calculated as the ratio of apparent viscosities (at 40 °C) after and before heating at 95 °C for 5 min (Figures 5 and 6). Heating for 5 min represents a more severe heat treatment than that generally applied during manufacture.[5,49] As a result, aggregates were observed in concentrated WPI-containing systems that would not be expected in an industrial process. The shearing action of the starch pasting cell ensured aggregates remained in suspension. Despite the severity of the treatment, it has the benefit of showing the potential for viscosity increase in a given system while providing indicative trends relevant to manufacture. Dispersions of PCN had lower viscosities following heat treatment (Figure 5). Viscosity in milk

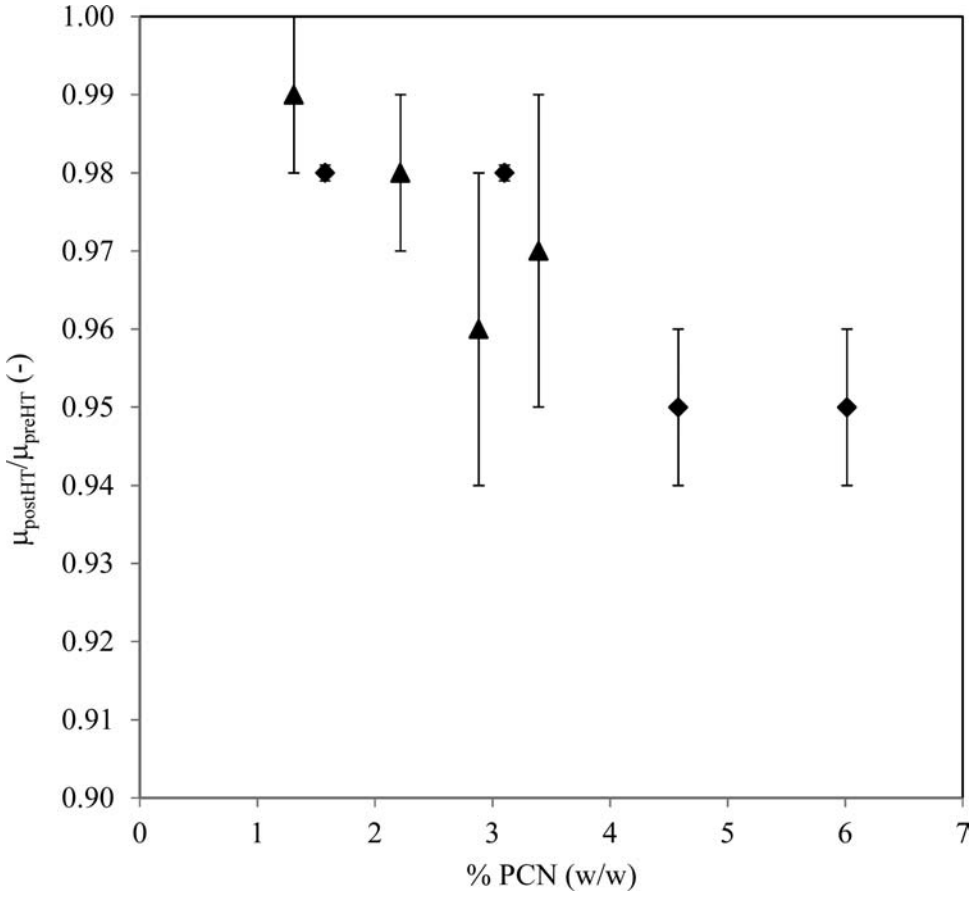


**Figure 5.** Ratio of apparent viscosity (40 °C; 16.8 $s^{-1}$) post ($\mu_{postHT}$) and pre ($\mu_{preHT}$) heat treatment (95 °C for 5 min) in PCN (◆) and PCN-L systems (▲). Error bars represent the standard deviation of three replicate trials.

protein dispersions is related to the hydrated volume of the micelle.[50] At higher temperatures the hydrophobic effect, responsible for much of the stability of the casein micelle, is greater, resulting in a "tightening" or deswelling of the micelle and a decrease in micellar hydration.[50] The lower viscosity of PCN dispersions after cooling is postulated to have been caused by high-temperature association of calcium phosphate with the micelles, which subsequently prevented reswelling of micelles upon cooling.[51]

Figure 6 shows the extent of viscosity increase in WPI containing dispersions/solutions as a result of heating. The large viscosity increases observed in systems containing WPI following heat treatment were related to the extensive water-holding capacity of denatured whey proteins and aggregates, an effect supported by the findings of O'Loughlin et al.[52] The extent of viscosity increase was a linear function of whey protein content (Figure 6). The 95% confidence intervals of both WPI and WPI-PCN dispersions overlap, suggesting there was no difference in extent of viscosity increase with whey protein concentration for these two systems. This was despite $T_d$ and $T_v$ occurring at higher temperatures in the presence on PCN; however, whey protein−casein interactions may also contribute to heat-induced increases in viscosity, depending on heating and solvent conditions and could explain the similar degree of viscosity increase.[13]

Lactose increased heat stability. The rate of change of viscosity increase per unit change in whey protein concentration (as indicated by the slope of regression lines in Figure 6) was lower for systems containing lactose; the 95% confidence intervals of the slopes did not overlap with those of lactose-free systems, suggesting lactose had a significant effect. Addition of lactose resulted in lower post heat treatment viscosity at higher DM content. For example, the most concentrated WPI solution had a DM content of 8.8% (w/w) compared to 47.9% (w/w) for the most concentrated WPI-L solution, yet the apparent viscosity of the former, post heat treatment, was twice that of the latter. Rich and Foegedding[16] found that the onset of WPI gelation was delayed in the presence of lactose and that subsequent gel strength was reduced.

As fat is a vital component in IMF, emulsions were also prepared and heat treated. In all cases addition of fat to formulations resulted in higher viscosities, post heat treatment, compared to corresponding oil-free systems. During homogenization, protein adsorbs to the oil−water interface and protects fat droplets from coalescence. Therefore, protein in emulsified systems can be divided into two classes: adsorbed and nonadsorbed. Despite this difference, the general trends observed upon heating of fat-free systems were reflected in emulsified systems. Major increases in viscosity were observed only in WPI-containing systems; PCN-stabilized emulsions were remarkably stable to heat treatment over the whole range of DM content studied. Lactose increased the heat stability of emulsions. Figure 7 shows the viscosity after heat treatment of the different formulations as a function of total DM content. In emulsified systems, a major increase in viscosity was observed between 25 and 35% DM (w/w) for lactose-free emulsions; similar viscosity increases were not observed before the DM

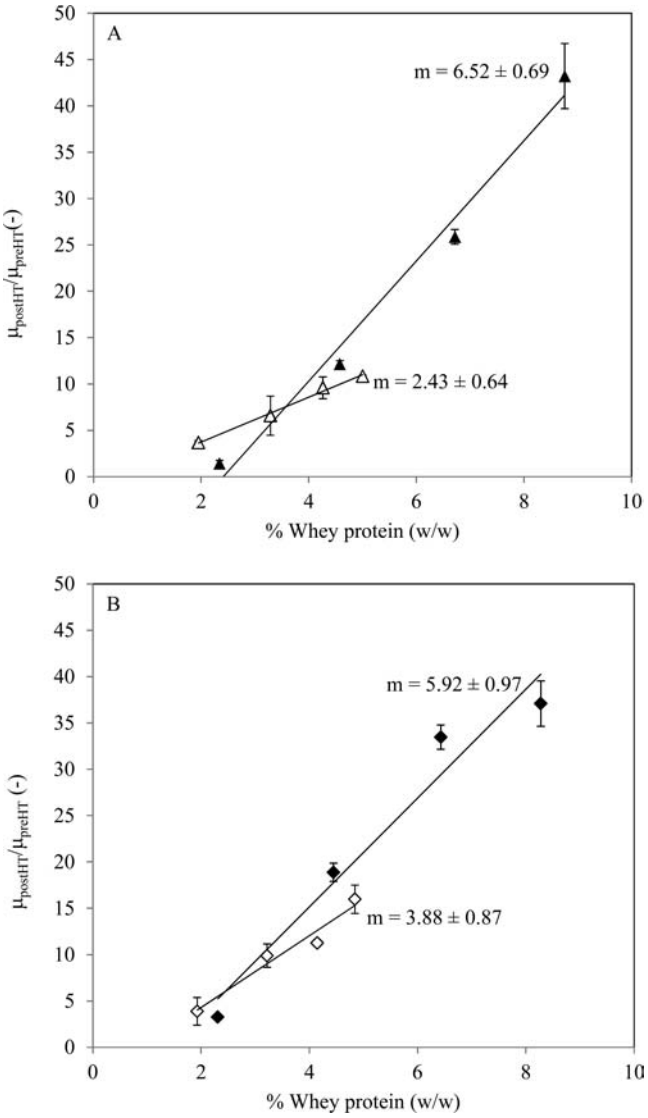


**Figure 6.** Ratio of apparent viscosity (40 °C; 16.8 $s^{-1}$) post ($\mu_{postHT}$) and pre ($\mu_{preHT}$) heat treatment (95 °C for 5 min) in WPI containing systems: (A) WPI (▲) and WPI-L (△); (B) WPI-PCN (◆) and WPI-PCN-L (◇). Error bars represent the standard devitation of three replicate trials. Slopes ($m$) are given ±95% confidence intervals.

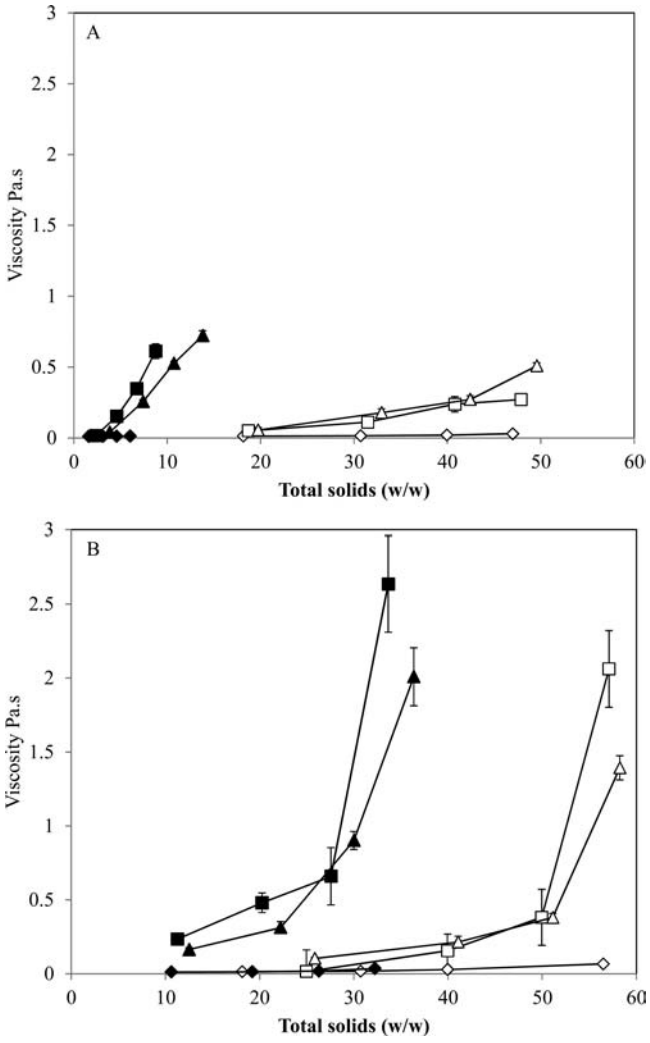


**Figure 7.** Apparent viscosities (40 °C; 16.8 $s^{-1}$) of oil-free (A) and homogenized oil-containing (B) IMF model systems after heat treatment (95 °C for 5 min). Solid symbols denote lactose-free dispersions/emulsions: PCN (◆), WPI (■), and WPI-PCN (▲). Open symbols denote lactose-containing dispersions/emulsions: PCN-L (◇), WPI-L (□), and WPI-PCN- L (△). Error bars represent the standard devitation of three replicate trials.

content reached 50% (w/w) in emulsions containing lactose. This is particularly relevant for ingredient/IMF manufacturers that produce lactose-depleted base powders with the intention of adding crystalline lactose at a later stage.[6] Maximizing DM content prior to heat treatment of lactose-depleted base mixtures could have a significant impact on the viscosity of concentrates, which in extreme cases causes problems such as inefficient atomization during spray-drying.[7] The extensive increases in viscosity following heat treatment of WPI-containing emulsions suggest that, during heat treatment, protein-stabilized oil droplets associated with nonabsorbed denatured whey proteins, and/or each other, to form a transient network of flocculated oil droplets, with an associated increase in volume fraction.[53] Such changes were sufficient to alter the viscoelastic properties of emulsions and confer a macro-structure with more "solid-like" properties.

The extent of whey protein structural changes and their influence on the viscosity of IMF dispersion/emulsions were significantly affected by their interactions with other macro-nutrient components. Lactose content, in particular, played an important protective role during the heat treatment of IMF, retarding and reducing viscosity increases in dispersions and emulsions alike. This is in keeping with the theory of preferential hydration of proteins in the presence of carbohydrates resulting in stabilization of the protein. Lactose content of wet-mixes should be a key consideration in the design of IMF manufacturing processes. PCN (micellar casein) also had a protective effect on $\beta$-lg denaturation. Despite increasing the denaturation temperature and delaying the onset of viscosity increase in WPI, in a manner similar (albeit diminished) to lactose, it seems that PCN interacted with WPI, during heating, in ways that led to similar levels of viscosity increase to that observed in WPI alone. Overall, this study provided insight into the relationships that exist between macronutrients as a function of concentration and temperature and should provide information of direct relevance to manufacturers of IMF.

## AUTHOR INFORMATION


### Corresponding Author

*(M.A.) E-mail: mark.fenelon@teagasc.ie. Phone: +353 (0) 2542355.


### Notes

The authors declare no competing financial interest.

## ABBREVIATIONS USED

IMF, infant milk formula; $T_d$, denaturation temperature; $T_v$, temperature of onset of viscosity increase; DM, dry matter; β-lg, β-lactoglobulin; DSC, differential scanning calorimetry; FTIR, Fourier transform infrared spectroscopy; WPI, whey protein isolate; PCN, phosphocasein; SO, sunflower oil; L, lactose; SMUF, simulated milk ultrafiltrate; ATR, attenuated total reflectance; ANOVA, analysis of variance

## REFERENCES


(1) Montagne, D. H.; Van Dael, P.; Skanderby, M.; Hugelshofer, W. Infant formulae − powders and liquids. In *Dairy Powders and Concentrated Products*; Tamime, A. Y., Ed.; Blackwell Publishing: Chichester, West Sussex, UK, 2009; pp 294−331.

(2) Nasripour, A.; Scher, J.; Desorby, S. Baby foods: formulations and interactions (a review). *Crit. Rev. Food Sci. Nutr.* **2006**, *46*, 665−681.

(3) U.S. FDA. Powdered Infant Formula: An Overview of Manufacturing Processes; http://www.fda.gov/OHRMS/DOCKETS/AC/03/briefing/3939b1_tab4b.htm.

(4) McCarthy, N. A.; Kelly, A. L.; O'Mahony, J. A.; Hickey, D. K.; Chaurin, V.; Fenelon, M. A. Effect of protein content on emulsion stability of a model infant formula. *Int. Dairy J.* **2012**, *25*, 80−86.

(5) McCarthy, N. A.; Gee, V. L.; Hickey, D. K.; Kelly, A. L.; O'Mahony, J. A.; Fenelon, M. A. Effect of protein content on the physical stability and microstructure of a model infant formula. *Int. Dairy J.* **2013**, *29*, 53−59.

(6) Mullane, N. R.; Whyte, P.; Wall, P. G.; Quinn, T.; Fanning, S. Application of pulsed-field gel electrophoresis to characterise and trace the prevalence of *Enterobacter sakazakii* in an infant formula processing facility. *Int. J. Food Microbiol.* **2007**, *116*, 73−81.

(7) Fox, M.; Akkerman, C.; Straatsma, H.; de Jong, P. Energy reduction by high dry matter concentration and drying. *New Food* **2010**, *2010*, 60−63.

(8) Thompkinson, D. K.; Kharb, S. Aspects of infant food formulation. *Compr. Rev. Food Sci. Food Saf.* **2007**, *6*, 79−102.

(9) Fox, P. F.; McSweeney, P. L. H. Heat induced changes of milk. In *Dairy Chemistry and Biochemistry*; Blackie Academic and Professional: London, UK, 1998; pp 347−378.

(10) Qi, X. L.; Holt, C.; McNulty, D.; Clarke, D. T.; Brownlow, S.; Jones, G. R. Effect of temperature on the secondary structure of β-lactoglobulin at pH 6.7, as determined by CD and IR spectroscopy: a test of the molten globule hypothesis. *Biochem. J.* **1997**, *324*, 341−346.

(11) Brownlow, S.; Cabral, J. H. M.; Cooper, R.; Flower, D. R.; Yewdall, S. J.; Polikarpov, I.; North, A. C. T.; Sawyer, L. Bovine β-lactoglobulin at 1.8 Å resolution − still an enigmatic lipocalin. *Structure* **1997**, 481−495.

(12) Papiz, M. Z.; Sawyer, L.; Eliopoulos, E. E.; et al. The structure of β-lactoglobulin and its similarity to plasma retinol-binding protein. *Nature* **1986**, *324*, 383−385.

(13) Anema, S. G.; Li, Y. Association of denatured whey proteins with casein micelles in heated reconstituted skim milk and its effect on casein micelle size. *J. Dairy Res.* **2003**, *70*, 73−83.

(14) Garrett, J. E.; Stairs, R. A.; Annett, R. G. Thermal denaturation and coagulation of whey proteins: effect of sugars. *J. Dairy Sci.* **1986**, *71*, 10−16.

(15) Kulmyrzaev, A.; Bryant, C.; McClements, D. J. Influence of sucrose on the thermal denaturation, gelation, and emulsion stabilization of whey proteins. *J. Agric. Food Chem.* **2000**, *48*, 1593−1597.

(16) Rich, L. M.; Foegeding, E. A. Effects of sugars on whey protein isolate gelation. *J. Agric. Food Chem.* **2000**, *48*, 5046−5052.

(17) Jenness, R.; Koops, J. Preparation and properties of a salt solution which simulates milk ultrafiltrate. *Neth. Milk Dairy J.* **1962**, *16*, 153−164.

(18) Hogan, S. A.; Chaurin, V.; O'Kennedy, B. T.; Kelly, P. M. Influence of dairy proteins on textural changes in high-protein bars. *Int. Dairy J.* **2012**, *26*, 58−65.

(19) Hunziker, O. F.; Nissen, B. H. Lactose solubility and lactose crystal formation: I. Lactose solubility. *J. Dairy Sci.* **1926**, *9*, 517−537.

(20) Boye, J. I.; Alli, I. Thermal denaturation of mixtures of α-lactalbumin and β-lactoglobulin: a differtial scanning calorimetric study. *Food Res. Int.* **2000**, *33*, 673−682.

(21) Fitzsimons, S. M.; Mulvihill, D. M.; Morris, E. R. Denaturation and aggregation processes in thermal gelation of whey proteins resolved by differential scanning calorimetry. *Food Hydrocolloids* **2007**, *21*, 638−644.

(22) Imafidon, G. I.; Ng-Kwai-Hang, K. F.; Harwalkar, V. R.; Ma, C. Y. Differential scanning calorimetric study of different genetic variants of β-lactoglobulin. *J. Dairy Sci.* **1991**, *74*, 2416−2422.

(23) Qi, X. L.; Brownlow, S.; Holt, C.; Sellers, P. Thermal denaturation of β-lactoglobulin: effect of protein concentration at pH 6.75 and 8.05. *Biochim. Biophys. Acta, Protein Struct. Mol. Enzymol.* **1995**, *1248*, 43−49.

(24) Haug, I. J.; Skar, H. M.; Vegarud, G. E.; Langsrud, T.; Draget, K. I. Electrostatic effects on β-lactoglobulin transitions during heat denaturation as studied by differential scanning calorimetry. *Food Hydrocolloids* **2009**, *23*, 2287−2293.

(25) Kendrick, B. S.; Li, T.; Chang, B. S. Physical stabilization of proteins in aqueous solution. In *Rational Design of Stable Protein Formulations − Theory and Practice*; Carpenter, J. F., Manning, M. C., Eds.; Kluwer Academic/Plenum Publishers: New York, 2002; pp 61−84.

(26) Tobias, D. J.; Hemminger, J. C. Getting specific about specific ion effects. *Science* **2008**, *319*, 1197−1198.

(27) Varunsatian, S.; Watanabe, K.; Hayakawa, S.; Nakamura, T. Effects of $Ca^{+2}$, $Mg^{+2}$ and $Na^{+}$ on heat aggregation of whey protein concentrates. *J. Food Sci.* **1983**, *48*, 42−70.

(28) Kunz, W.; Henle, J.; Ninham, B. W. 'Zur Lehre von der Wirkung der Salze' (about the science of the effect of salts): Franz Hofmeister's historical papers. *Curr. Opin. Colloid Interface Sci.* **2004**, *9*, 19−37.

(29) Sood, S. M.; Sidhu, K. S.; Dewan, R. K. Voluminosity of bovine and buffalo casein micelles at different temperatures. *Milchwissenschaft* **1976**, *31*, 470−474.

(30) Blanc, B. A.; Baer, A.; Ruegg, M. Etudes biochimiques et physico-chimiques de la denaturation thermique de la β-lactoglobuline dans le lait. *Schweiz. Milchwirtsch. Forsch.* **1977**, *6*, 21−32.

(31) Paulsson, M.; Dejmek, P. Thermal denaturation of whey proteins in mixtures with caseins studied by differential scanning calorimetry. *J. Dairy Sci.* **1990**, *73*, 590−600.

(32) Itoh, T.; Wada, Y.; Nakanshi, T. Differential thermal analysis of milk proteins. *Agric. Biol. Chem.* **1976**, *40*, 1083−1086.

(33) Bull, H. B.; Breese, K. Interaction of alcohols with proteins. *Biopolymers* **1978**, *17*, 2121−2132.

(34) De Wit, J. N.; Klarenbeek, G. A differential scanning calorimetric study of the thermal behaviour of bovine β-lactoglobulin at temperatures up to 100 °C. *J. Dairy Res.* **1981**, *48*, 293−302.

(35) Liu, Y.; Bolen, D. W. The peptide backbone plays a dominant role in protein stabilization by naturally occurring osmolytes. *Biochemistry* **1995**, *34*, 12884−12891.

(36) Timasheff, S. N. The control of protein stability and association by weak interactions with water: how do solvents affect these processes? *Annu. Rev. Biophys. Biomol. Struct.* **1993**, *22*, 67−97.

(37) Jackson, M.; Mantsch, H. H. Halogenated alcohols as solvents for proteins − FTIR spectroscopic studies. *Biochim. Biophys. Acta* **1992**, *1118*, 139−143.

(38) Kehoe, J. J.; Remondetto, G. E.; Subriade, M.; Morris, E. R.; Brodkorb, A. Tryptophan-mediated denaturation of β-lactoglobulin A by UV irradiation. *J. Agric. Food Chem.* **2008**, *56*, 4720−4725.

(39) Huang, P.; Dong, A.; Caughey, W. S. Effect of dimethyl sulfoxide, glycerol and ethylene glycol on secondary structures of cytochrome *c* and lysozyme as observed by inrared spectrosocpy. *J. Pharm. Sci.* **1995**, *4*, 387−392.
(40) Czerwenka, C.; Maier, I.; Pittner, F.; Linder, W. Investigation of the lactosylation of hhey proteins by liquid chromatography−mass spectrometry. *J. Agric. Food Chem.* **2006**, *54*, 8874−8882.
(41) Wnorowski, A.; Yaylayan, V. A. Monitoring carbonyl-amine reaction between pyruvic acid and $\alpha$-amino alcohols by FTIR spectroscopy: a possible route to Amadori products. *J. Agric. Food Chem.* **2003**, *51*, 6537−6543.
(42) Boye, J. I.; Ismail, A. A.; Alli, I. Effects of physicochemical factors on the secondary structure of $\beta$-lactoglobulin. *J. Dairy Res.* **1996**, *63*, 97−109.
(43) Manderson, G. A.; Herdman, M. J.; Creamer, L. K. Effect of heat treatment on the conformation and aggregation of $\beta$-lactoglobulin A, B, and C. *J. Agric. Food Chem.* **1998**, *46*, 5052−5061.
(44) Galani, D.; Apenten, R. K. O. Heat-induced denaturation and aggregation of $\beta$-lactoglobulin: kinetics of formation of hydrophobic and disulphide-linked aggregates. *Int. J. Dairy Technol.* **1999**, *34*, 467−476.
(45) Schokker, E. P.; Singh, H.; Creamer, L. K. Heat-induced aggregation of $\beta$-lactoglobulin A and B with $\alpha$-lactalbumin. *Int. Dairy J.* **2000**, *10*, 843−853.
(46) Fox, P. F.; Morrissey, P. A. Reviews of the progress of dairy science: the heat stability of milk. *J. Dairy Res.* **1977**, *44*, 627−646.
(47) Snoeren, T. H. M.; Damman, A. J.; Klok, H. J. The viscosity of skim-milk concentrates. *Neth. Milk Dairy J.* **1982**, *36*, 305−316.
(48) Ndoye, F. T.; Erabit, N.; Flick, D.; Alvarez, G. In-line characterization of a whey protein aggregation process: aggregates size and rheological measurements. *J. Food Eng.* **2013**, *115*, 73−82.
(49) Murphy, E. G.; Tobin, J. T.; Roos, Y. H.; Fenelon, M. A. A high-solids steam injection process for the manufacture of powdered infant milk formula. *Dairy Sci. Technol.* **2013**, *93*, 463−475.
(50) Horne, D. S. Casein interactions: casting light on the black boxes, the structure of dairy products. *Int. Dairy J.* **1998**, *8*, 171−177.
(51) Gaucheron, F. The minerals of milk. *Reprod. Nutr. Dev.* **2005**, *45*, 473−483.
(52) O'Loughlin, I. B.; Murray, B. A.; Kelly, P. M.; Fitzgerald, R. J.; Brodkorb, A. Enzymatic hydrolysis of heat-induced aggregates of whey protein isolate. *J. Agric. Food Chem.* **2012**, *60*, 4895−4904.
(53) Euston, S. R.; Finnigan, S. R.; Hirst, R. L. Aggregation kinetics of heated whey protein-stabilized emulsions. *Food Hydrocolloids* **2000**, *14*, 151−161.
(54) Barth, A.; Zscherp, C. What vibrations tell us about proteins. *Q. Rev. Biophys.* **2002**, *35*, 369−430.

**Table 1. Experimental Model and Levels of the Variables Used for Optimizing the Acidolysis of CCSO with Oleic Acid by RM IM**

| | *A* | *B* | *C* | *D* | |
|---|---|---|---|---|---|
| run | substrate mole ratio (oleic acid/CCSO) | enzyme concentration (%) | temperature (°C) | time (h) | oleic acid incorporation (%) |
| 1 | 2 (−1)[a] | 6 (−1) | 60 (0) | 24 (0) | 45.63 |
| 2 | 2 (−1) | 14 (+1) | 60 (0) | 24 (0) | 48.25 |
| 3 | 6 (+1) | 6 (−1) | 60 (0) | 24 (0) | 50.69 |
| 4 | 6 (+1) | 14 (+1) | 60 (0) | 24 (0) | 58.55 |
| 5 | 4 (0) | 10 (0) | 55 (−1) | 20 (−1) | 52.54 |
| 6 | 4 (0) | 10 (0) | 55 (−1) | 28 (+1) | 56.31 |
| 7 | 4 (0) | 10 (0) | 65 (+1) | 20 (−1) | 55.43 |
| 8 | 4 (0) | 10 (0) | 65 (+1) | 28 (+1) | 57.05 |
| 9 | 2 (−1) | 10 (0) | 60 (0) | 20 (−1) | 46.43 |
| 10 | 2 (−1) | 10 (0) | 60 (0) | 28 (+1) | 49.89 |
| 11 | 6 (+1) | 10 (0) | 60 (0) | 20 (−1) | 54.06 |
| 12 | 6 (+1) | 10 (0) | 60 (0) | 28 (+1) | 57.91 |
| 13 | 4 (0) | 6 (−1) | 55 (−1) | 24 (0) | 50.99 |
| 14 | 4 (0) | 6 (−1) | 65 (+1) | 24 (0) | 52.54 |
| 15 | 4 (0) | 14 (+1) | 55 (−1) | 24 (0) | 55.57 |
| 16 | 4 (0) | 14 (+1) | 65 (+1) | 24 (0) | 57.07 |
| 17 | 6 (+1) | 10 (0) | 55 (−1) | 24 (0) | 46.36 |
| 18 | 6 (+1) | 10 (0) | 65 (+1) | 24 (0) | 49.51 |
| 19 | 6 (+1) | 10 (0) | 55 (−1) | 24 (0) | 55.49 |
| 20 | 6 (+1) | 10 (0) | 65 (+1) | 24 (0) | 55.36 |
| 21 | 4 (0) | 6 (−1) | 60 (0) | 20 (−1) | 50.98 |
| 22 | 4 (0) | 6 (−1) | 60 (0) | 28 (+1) | 56.10 |
| 23 | 4 (0) | 14 (+1) | 60 (0) | 20 (−1) | 56.93 |
| 24 | 4 (0) | 14 (+1) | 60 (0) | 28 (+1) | 58.87 |
| 25 | 4 (0) | 10 (0) | 60 (0) | 24 (0) | 57.64 |
| 26 | 4 (0) | 10 (0) | 60 (0) | 24 (0) | 57.87 |
| 27 | 4 (0) | 10 (0) | 60 (0) | 24 (0) | 57.48 |
| 28 | 4 (0) | 10 (0) | 60 (0) | 24 (0) | 57.73 |
| 29 | 4 (0) | 10 (0) | 60 (0) | 24 (0) | 57.26 |

[a]The codes (−1, 0, 1) in parentheses represent different levels of independent variables for optimization.

group; then, a new ester bond is formed by the reaction between the newly created hydroxyl group and the incoming new free fatty acid.

Besides that, the fatty acids at different positions of the TAG affect the absorption efficiency; different lengths of fatty acids also have different absorption rates and different functions. Clinical experiments reveal that long-chain fatty acids (LCFAs, $C_{14}$−$C_{22}$) were more slowly absorbed than medium-chain fatty acids (MCFAs, $C_6$−$C_{12}$).[13] An increase in chain length of saturated fatty acids reduced their absorbability as well increased the loss of energy intake and calcium. MCFAs were absorbed more efficiently than LCFAs in the gastrointestinal tract via the portal system and rapidly provide energy for the body.[14] It has also been reported that MCFAs had greater antiviral and antibacterial activities than LCFAs.[15] Due to the predominance of LCFAs in infant formula and human milk fats, the incorporation of MCFAs into HMFS has been suggested to provide a concentrated source of energy by many clinical nutrition experts.[16] Recently, a commercial product named Neobee consisting of MCFAs (caprylic and capric acids) has been developed as a functional food for patients. To our knowledge, in the literature, few data can be found regarding the enrichment of human milk fat substitutes with MCFAs.[17]

Lipozyme RM IM, which is an immobilized lipase from *Rhizomucor miehei*, is widely used as a catalyst in pharmaceutical and drug production and lipid modifications. It has the characteristics of substrate specificity, stereospecificity, and regioselectivity.[18] In a recent study, different strategies of lipase immobilization were investigated to improve enzyme properties by positive alterations of structure, which may enhance enzyme activity, specificity, or selectivity and increase its mechanical strength, hydrophobic or hydrophilic character, and regeneration.[19]

*Cinnamomum camphora* (Lauraceae), known as an evergreen tree, is largely distributed south area of the Yangtze River in China. In a previous study, it has been reported that the oil from *C. camphora* (Lauraceae) seeds has a unique fatty acid profile that mainly contains MCFAs (capric acid, C10:0, 53.27%; lauric acid, C12:0, 39.93%).[20] Liu et al.[21] have also confirmed that *C. camphora* seed oil (CCSO) is nontoxic with no side effects, which could be used as a woody edible oil for its further development and utilization. Recently, our research group has managed to use CCSO for the production of medium-chain triacylglycerol (MCT) enriched plastic fats.[22−24]

The aim of this work was to synthesize HMFS enriched with MCFAs through enzymatic acidolysis of CCSO and oleic acid using immobilized Lipozyme RM IM lipase as a catalyst. The effects of reaction conditions (time, temperature, enzyme concentration, and substrate mole ratio) on oleic acid incorporation were optimized by response surface methodology (RSM). Subsequently, scale-up trials were conducted to determine the feasibility of enzymatic modification of CCSO for the production of HMFS and the reusability of Lipozyme RM IM.

## MATERIALS AND METHODS

**Materials and Chemicals.** Oleic acid (≥85%) was purchased from a local oil market (Nanchang, China). CCSO was extracted from *C. camphora* seeds by the $CO_2$ supercritical fluid method as described in Hu et al.[20] Lipozyme RM IM, a commercial immobilized 1,3-specific lipase from *R. miehei*, was purchased from Novozymes A/S (Bagsvaerd, Denmark). The specific activity of Lipozyme RM IM was 150 IU/g, having 0.35−0.45 g/mL bulk density and 0.3−0.6 mm particle diameter. Carbon dioxide (99.9%) was provided by Wanli Gas Corp (Nanchang, China). Four hundred and sixty-three standard fatty acid methyl esters (FAMEs) containing methyl esters $C_8$−$C_{20}$ saturated fatty acid, methyl myristate, methyl palmitoleate, methyl oleate, methyl linoleate, methyl linolenate, and four positional conjugated linoleic acid isomers were purchased from Nu-Chek Prep Inc. (Elysian, MN, USA). Tocopherol ($\alpha$, $\gamma$, and $\delta$) standards were acquired from Sigma Chemical Co. (St. Louis, MO, USA). All other chemicals used were of analytical or chromatographic grade.

**Acidolysis Reaction of Small-Scale Sample.** CCSO (1 g each) was blended with oleic acid at substrate mole ratios of 1:2, 1:4, and 1:6. Lipozyme RM IM of 6, 10, and 14% (w/w total reactants) was added to the blend in 50 mL screw-capped flask. The acidolysis was performed under 200 rpm orbital shaking water bath, and temperature was set at 55, 60, and 65 °C for 20, 24, and 28 h of incubation. After reaction, RM IM lipases were separated from the mixture through a 0.45 $\mu$m polytetrafluoroethylene (PTFE) syringe membrane filter. The filtrate was stored at −18 °C until analysis.

**Experimental Design for RSM Study.** Enzyme-catalyzed acidolysis was influenced by reaction conditions such as water content, substrate mole ratio, enzyme concentration, temperature, and reaction time.[12] Before models were set up by RSM, single-factor experiments were carried out to detect the effects of these five conditions on oleic acid incorporation. Then, four of the five factors were selected as independent variables, and the optimal reaction conditions for the acidolysis reaction were established via RSM. RSM, a useful mathematical tool, has been widely applied to the optimization of reaction conditions for the production of HMFS in several studies.[25,26] In our experiment, a four-factor and three-level full factorial design called Box−Behnken design (BBD) was employed to generate factor combinations by using Design Expert 7.1 software (Stat-Ease Inc., Minneapolis, MN, USA). The four selected factors were substrate mole ratio ($A$), enzyme concentration ($B$), temperature ($C$), and reaction time ($D$), and three levels were substrate mole ratios of 1:2, 1:4, and 1:6, Lipozyme RM IM of 6, 10, and 14% (w/w total reactants), temperature of 55, 60, and 65 °C, and reaction time of 20, 24, and 28 h. To avoid bias, 29 runs including 16 factorial points, 8 axial points, and 5 center points were performed in a random order. Oleic acid incorporation was acted as response value. The independent variables ($A$, $B$, $C$, $D$) and exact experimental model are presented in Table 1. Experiments were run randomly, and duplicate reactions were performed at all design points.

**Fatty Acid Profile.** The fatty acid compositions of substrates and products were determined. Thin-layer chromatography (TLC) analysis was carried out for the separation of newly synthesized product. About 50 $\mu$L of product was applied to TLC plates coated with silica gel G. The developing solvent was hexane/diethyl ether/acetic acid (50:50:1, v/v/v). Then, the bands were sprayed with 0.2% 2,7-dichlorofluorescein in methanol and visualized under UV light. Finally, the TAG band was scraped off into a screw-capped test tube and dissolved in 2 mL of hexane for fatty acid composition analysis. The TAG sample was converted to FAMEs following the procedure of Zhu et al.[27] and then analyzed by a gas−liquid chromatograph (GLC) (model 6890N, Agilent Technologies, Santa Clara, CA, USA) equipped with an autoinjector, a fused-silica capillary column (CP-Sil 88, 100 m × 0.25 mm × 0.2 $\mu$m i.d.), and a flame ionization detector (FID) and operated in splitless mode. The injector and detector temperatures were maintained at 250 and 260 °C, respectively. The column temperature was held at 45 °C for 3 min and then programmed to 175 °C for 27 min at the rate of 13 °C/min. The temperature was then further increased to 215 °C at the rate of 4 °C/min and held for 35 min. The carrier gas was nitrogen, and the total gas flow rate was 52 mL/min. The injecting sample volume was 0.3 $\mu$L.

**Sn-2 Positional Analysis.** Composition of sn-2 FAs was analyzed by the pancreatic hydrolysis method as previously described.[28] Likewise, TLC was used to separate 2-monoacylglycerol (2-MAG) from the hydrolysate. The 2-MAG band was scrapped off, methylated, and analyzed by GLC as also described above.

**Identification of TAG Species.** The different species of TAGs of CCSO and HMFS were separated by reversed-phase high-performance liquid chromatograph (HPLC) with a Nova-Pak C18 column (150 × 3.9 mm; Waters, Milford, MA, USA) and an evaporative light-scattering detector (Alltech 2000ES, USA) operating at 55 °C and a gas flow rate of 1.5 L/min. Samples were dissolved in methanol and filtered by 0.45 $\mu$m PTFE syringe membrane filter. Twenty microliters of filtered sample was injected and eluted by acetonitrile (solvent A) and 2-propanol/*n*-hexane (1:1, v/v) (solvent B) at a flow rate of 1.8 mL/min with the following profile: 0−20 min, 30% B; 21−36 min, 60% B; 37−40 min, 100% B, and then back to the initial flow rate. Last, the separated TAGs were identified by comparing the retention time and equivalent carbon number (ECN). ECN = CN − 2DB, used to predict the elution order, where CN is the total carbon number except three carbons of glycerol in the TAG and DB is the total number of double bonds on the fatty acids.

**Urea Inclusion for Separation and Purification of HMFS.** The mechanism of urea inclusion is traditionally explained as follows: separation of mixed fatty acids by urea inclusion occurs in terms of different saturation degrees and carbon chain lengths of the fatty acids.[29] Urea/HMFS mixed with 50 mL of 95% (v/v) ethanol was put into a round-bottom flask. Under the nitrogen gas flow, the mixture was refluxed at 60 °C in a water bath until the solution became clear. Then, the product was cooled at room temperature for 1 h and placed at −4 °C for 24 h. The mixture was separated by suction filtration using a Buchner funnel to obtain urea inclusion compounds and non-urea inclusion compounds. The non-urea inclusion compounds containing PUFA and acylglycerol were transferred to a round-bottom flask, and ethanol was evaporated as much as possible. Acylglycerol was separated and analyzed by HPLC.

**Tocopherol Analysis.** About 1 g of CCSO or HMFS sample was weighed into a flask and fully dissolved in 10 mL of hexane. After filtration with a 0.45 $\mu$m PTFE syringe filter, 3 $\mu$L samples were injected into the Agilent 1100 series HPLC. Then, the contents of tocopherol in prepared sample were determined by reversed-phase HPLC equipped with Hypersil ODS2 column (5 $\mu$m, 4.6 × 150 mm, Agilent Technologies) and a fluorescence detector (FLD). The mobile phase was methanol/water (98:2, v/v) with a flow rate of 0.8 mL/min. Standards of $\alpha$-, $\gamma$-, and $\delta$-tocopherol dissolved in hexane were used for identification and quantification.[30]

**Physicochemical Characteristics.** The determinations of CCSO and HMFS chemical properties, such as acid value, peroxide value, saponification value, and iodine value, were conducted following AOAC (1990) standard analytical methods.[31]

**Scale-up Trial.** Model verification was carried out from RSM design. To verify the feasibility of the scaled up acidolysis, a batch reaction (50 times scaleup) in a 500 mL flask was carried out at optimum conditions. The incorporation of oleic acid and productivity of TAG were determined to evaluate the feasibility of the scale-up trial.

**Statistical Analysis.** The effects of different substrate mole ratio, enzyme concentration, temperature, and reaction time studied in this work and their interactions were analyzed by using Design Expert 7.1 software. Mean values and standard deviations of a single-factor experiment, contents of tocopherol, and physicochemical characteristics were analyzed by using Statistical Analysis System software (SAS 2000, Cary, NC, USA).

## RESULTS AND DISCUSSION

**Effect of Water Content.** The water content in any quantity cannot be neglected because lipases are activated by a small amount of water,[32] and it is required for a first breaking of the triglyceride;[12] however, too much water can make the lipase

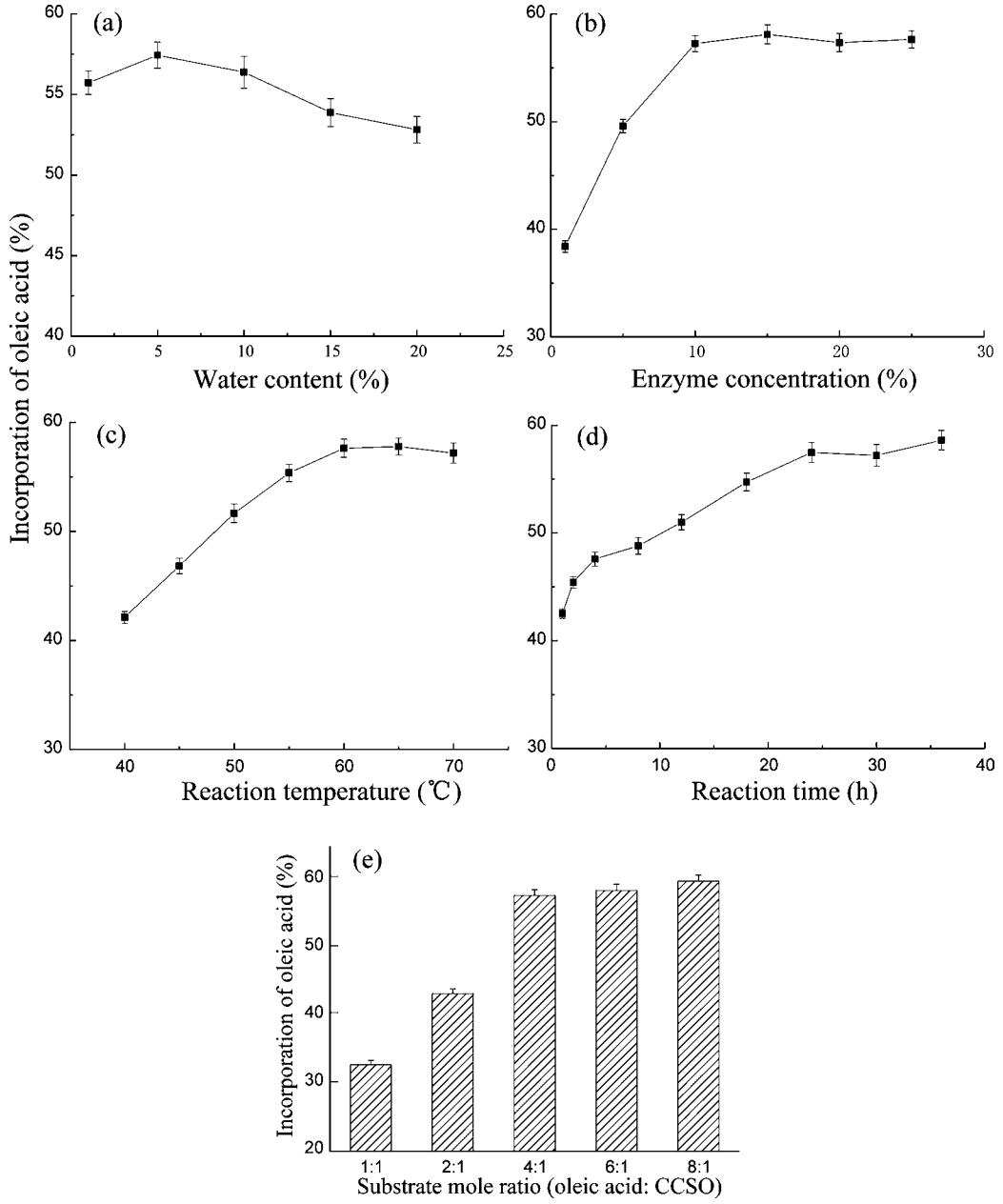


**Figure 1.** Effects of water content (a), enzyme concentration (b), reaction temperature (c), reaction time (d), and substrate mole ratio (oleic acid/CCSO) (e) on the incorporation of oleic acid.

unstable and have an adverse impact on activity, leading to a higher amount of byproducts.[33] Some authors reported that the optimum water contents were generally in the range of 0.2−3%;[34−36] however, a given enzymatic reaction depends on many factors (the selected enzyme, support, solvent, and quantities of substrates). Thus, it is necessary to optimize the water content in the reaction system. With enzyme of 10% (w/w total reactants), a 4:1 substrate mole ratio (oleic aid/CCSO), reaction temperature of 60 °C, and time of 24 h, the effects of water contents in the range of 1−20% (w/w total reactants) on the incorporation of oleic acid were studied (Figure 1a). The incorporation increased from 55.72 ± 0.31% to a maximum level of 57.44 ± 0.25% when the water content was increased from 1 to 5%. Then, a decrease to 52.81 ± 0.19% was observed when the water content was increased from 5 to 20%. Hence, we chose 5% water content for the ongoing study.

**Effect of Enzyme Concentration.** The effect of enzyme load, by varying from 1 to 25% (w/w total reactants) with constant substrate mole ratio of 4:1 and 60 °C reaction temperature after 24 h of incubation, on the oleic acid incorporation was also observed (Figure 1b). An increase in the catalyst percentage from 1 to 10% led to an incorporation increase from 38.41 ± 0.54 to 57.26 ± 0.75%. Further increase in the enzyme load from 10 to 25%, however, did not lead to further incorporation increase. This is possibly due to the saturation of the enzyme at the interface between CCSO and aqueous phase, in which an increase in enzyme concentration provided no significant changes on the incorporation.[37] Our results are similar to those reported by Rooney and Weatherley[37] and Raspe et al.[38] Considering the incorporation of oleic acid and the cost of Lipozyme RM IM, 10% (w/w total

Table 2. Estimated Regression Coefficients and Analysis of Variance (ANOVA) for the Acidolysis Reaction Catalyzed by *R. miehei* Lipase

| source of variance | sum of squares | degrees of freedom | means square | *F* value | *p* value | significant difference[a] |
|---|---|---|---|---|---|---|
| model | 455.95 | 14 | 32.57 | 129.72 | <0.0001 | significant |
| *A* | 176.26 | 1 | 176.26 | 702.05 | <0.0001 | * * |
| *B* | 66.79 | 1 | 66.79 | 266.02 | <0.0001 | * * |
| *C* | 7.84 | 1 | 7.84 | 31.23 | <0.0001 | * * |
| *D* | 32.54 | 1 | 32.54 | 129.60 | <0.0001 | * * |
| *AB* | 6.86 | 1 | 6.86 | 27.34 | 0.0001 | * * |
| *AC* | 2.69 | 1 | 2.69 | 10.71 | 0.0056 | * * |
| *AD* | 0.038 | 1 | 0.038 | 0.15 | 0.7030 | |
| *BC* | $6.250 \times 10^{-4}$ | 1 | $6.250 \times 10^{-4}$ | $2.489 \times 10^{-3}$ | 0.9609 | |
| *BD* | 2.53 | 1 | 2.53 | 10.07 | 0.0068 | * * |
| *CD* | 1.16 | 1 | 1.16 | 4.60 | 0.0499 | * |
| $A^2$ | 149.64 | 1 | 149.64 | 596.01 | <0.0001 | * * |
| $B^2$ | 20.97 | 1 | 20.97 | 83.52 | <0.0001 | * * |
| $C^2$ | 15.42 | 1 | 15.42 | 61.41 | <0.0001 | * * |
| $D^2$ | 1.67 | 1 | 1.67 | 6.63 | 0.0220 | * |
| residual | 3.51 | 14 | 0.25 | | | |
| lack of fit | 3.29 | 10 | 0.33 | 5.95 | 0.0502 | not significant |
| pure error | 0.22 | 4 | 0.055 | | | |
| total | 459.46 | 28 | | | | |
| | $R^2$ 0.9924 | | CV = 0.93 | | Adeq precision 35.275 | |

[a]*, *p* value <0.05 (* $p < 0.05$) is significant; **, *p* value <0.01 (** $p < 0.01$) is very significant.

reactants) enzyme concentration was chosen for the following optimization.

**Effect of Reaction Temperature.** Temperatures from 40 to 70 °C were evaluated in the present study. Substrate mole ratio (oleic acid/CCSO), water content, enzyme load, and reaction time were 4:1, 5%, 10%, and 24 h, respectively. Results are shown in Figure 1c. It can be noted that the increasing temperature in the range of 40−60 °C increased oleic acid incorporation from 42.11 ± 0.54 to 57.63 ± 0.83%. However, when the temperature further increased to 70 °C, the incorporation decreased to 57.19 ± 0.92%. This result is in good agreement with the results of Phuah et al.,[39] who investigated the effect of temperature on the hydrolysis of partial palm oil. It has been stated that enzyme activity and acyl migration are both increased by an increase in temperature until reaching the maximal rate.[40] Therefore, a higher temperature was not suggested. A temperature of 60 °C was suitable for further study.

**Effect of Reaction Time.** The reaction time was set from 1 to 36 h to investigate its influence on the incorporation. Substrate mole ratio (oleic acid/CCSO), water content, enzyme load, and reaction temperature were 4:1, 5%, 10%, and 60 °C, respectively. As shown in Figure 1d, the incorporation of oleic acid increased from 42.51 ± 0.43 to 57.48 ± 0.94% when the reaction time increased from 1 to 24 h. In 36 h, the oleic acid incorporation was 58.62 ± 0.90%. In a similar study the optimal reaction time was different depending on the use of enzyme and substrate.[41] Forty hours as the optimal reaction time was reported by Akoh et al. for the incorporation of EPA and capric acid into borage oil.[41]

**Effect of Substrate Mole Ratio (Oleic Acid/CCSO).** The effect of the molar ratio of oleic acid to CCSO on oleic acid incorporation was studied from 1:1 to 8:1 at a constant enzyme concentration (10%, w/w total reactants) and temperature of 60 °C for 24 h (Figure 1e). The incorporation increased from 32.75 ± 0.24 to 58.73 ± 0.13% as the substrate mole ratio changed from 1:1 to 4:1. Then, from 4:1 to 8:1, the incorporation increased until to 59.84 ± 0.26% was found. It was reported that the appropriate substrate molar ratio was in favor of the reaction equilibrium and increased the ratio of the collision between substrates and catalyst,[42] but higher substrate ratios were not desirable because a large amount of FFAs containing high levels of free or ionized carboxylic acid groups acidifies the enzyme layer, leading to absorption of water from the interface, which may decrease the activity of the enzyme.[43] Considering the stability of the enzyme and the cost of materials, a substrate mole ratio of 4:1 was chosen for further investigation.

**Experimental Design for RSM.** To find the optimal conditions of the greatest incorporation and also to see whether the reaction parameters have interactions on each other, RSM was used. According to the results of the single-fator experiment discussed above (Figure 1), the water content was set at constant 5% (w/w total reactants), and the substrate mole ratio (*A*, oleic acid/CCSO), enzyme load (*B*, w/w total reactants), temperature (*C*, °C), and reaction time (*D*, in hours) were chosen as the four optimizing factors. The experimental model is shown in Table 1.

**Model Fitting and Variance Analysis.** Quadratic models were well established by multiple regression and backward elimination using Design Expert 7.1 software. The model equation for the responses (% oleic acid incorporated) catalyzed by Lipozyme RM IM can therefore be written as

$$Y = 57.60 + 3.8A + 2.36B + 0.81C + 1.65D + 1.31AB - 0.82AC + 0.097AD - 0.012BC - 0.80BD - 0.54CD - 4.80A^2 - 1.80B^2 - 1.54C^2 - 0.51D^2$$

where *Y* is the oleic acid incorporation, *A* is substrate mole ratio, *B* is enzyme load, *C* is temperature, and *D* is reaction time.

The analysis of variance (ANOVA) of models for response variables is listed in Table 2. The very small *p* values (<0.0001) and nonsignificant lack of fit ($p = 0.0502$) from the ANOVA

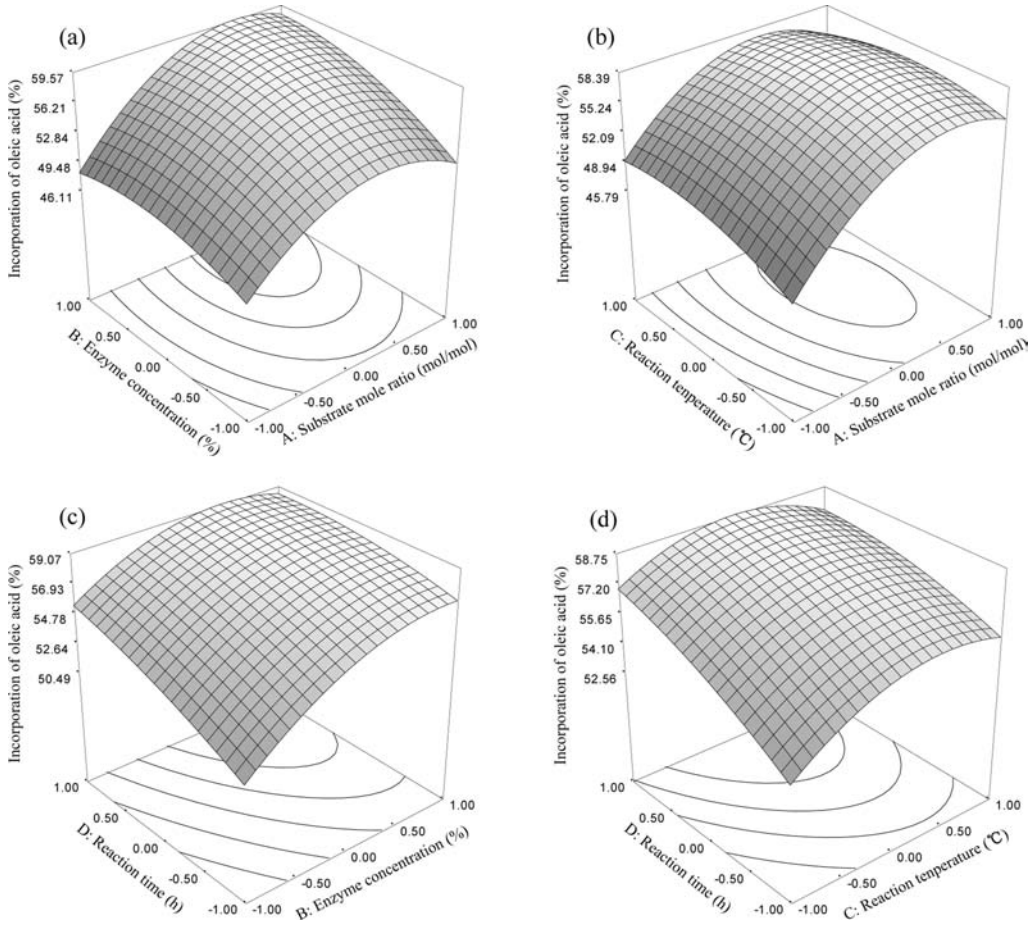


**Figure 2.** Response surface plots reflecting the pairwise interactive effects of the four selected factors on the acidolysis reaction catalyzed by RM IM.

indicated that the reduced cubic polynomial model was highly significant and sufficient to represent the actual relationship between responses (the incorporation of oleic acid) and the significant variables. The low pure error (0.055) demonstrated good reproducibility of the data. The high values of $R^2$ (0.9924) and adjusted $R^2$ (0.9847) showed a good agreement between the experimental results and predicted values, and the accuracy of the models was evaluated by coefficient of determination. The first-order parameters of substrate mole ratio ($A$, oleic acid/CCSO) had the greatest positive linear relation ($p < 0.01$) on the incorporation, followed by enzyme concentration ($B$), reaction time ($C$), and temperature ($D$), whereas the second-order parameters of $A^2$, $B^2$, and $C^2$ had significant quadratic relation. Interactions of $A$ and $B$, $A$ and $C$, $B$ and $D$, and $C$ and $D$ were found to be significant ($p < 0.05$) for the incorporation.

**Optimization.** The optimal conditions for the lipase-catalyzed synthesis of HMFS were predicted using the optimized function of the Design Expert Software. Figure 2a shows the predicted response surface of oleic acid incorporation as a function of enzyme concentration and substrate mole ratio, keeping the reaction temperature fixed at 60 °C and time at 24 h. An increase in oleic acid incorporation was observed by increasing the substrate mole ratio in an early stage of reaction. The trend was, however, reversed when the substrate mole ratio reached a certain value under the range of enzyme concentration in this work. At a fixed enzyme concentration of 10% and reaction time of 24 h, the effect of reaction temperature and substrate mole ratio on oleic acid incorporation is shown in Figure 2b. The elliptical contour plot showed that the interaction of substrate mole ratio and reaction temperature had a great influence on the incorporation. The oleic acid incorporation also increased as the increase of substrate mole ratio in an early stage of reaction and then decreased. The maximum increase of oleic acid incorporation was observed at a substrate mole ratio of 4:1 to 5:1 and a reaction temperature of 58−62 °C. Figure 2c shows the effect of varying enzyme concentration and reaction time on the oleic acid incorporation at a constant reaction temperature of 8 h with a substrate mole ratio of 4:1. The maximum increase of oleic acid was found at an enzyme concentration of 4:1−5:1 and time of 28 h. Figure 2d illustrates the effect of varying reaction temperature and time on the oleic acid incorporation at a constant enzyme concentration of 10% and substrate mole ratio of 4:1. The oleic acid incorporation increased from 55 to 62 °C and thereafter decreased with a dome shape observed. The effect of reaction time on the incorporation was more significant than reaction temperature. The maximum increase of oleic acid incorporation was found at a reaction temperature of 58−62 °C and time of 28 h.

**Model Verification.** By optimization, the optimum conditions yielding 60.19% of HMFS were as follows: a substrate molar ratio (oleic acid/CCSO) of 5:1, an enzyme concentration of 12.48% (w/w total reactants), a reaction temperature of 59.75 °C, and a reaction time of 28 h. To confirm the predicted results of this model, the experiment was done using optimized conditions with few modifications for the sake of experimental operating convenience. The modified conditions were as follows: a substrate molar ratio (oleic acid/

CCSO) of 5:1, an enzyme concentration of 12.5% (w/w total reactants), a reaction temperature of 60 °C, and a reaction time of 28 h. The incorporation of oleic acid from the experiments conducted according to the modified optimal conditions was 59.68%, which was in accordance with the predicted values and further verified the efficiency of the quadratic regression models.

**Fatty Acid Profile.** The fatty acid compositions of GC profiles of CCSO and HMFS are presented in Figure 3. The

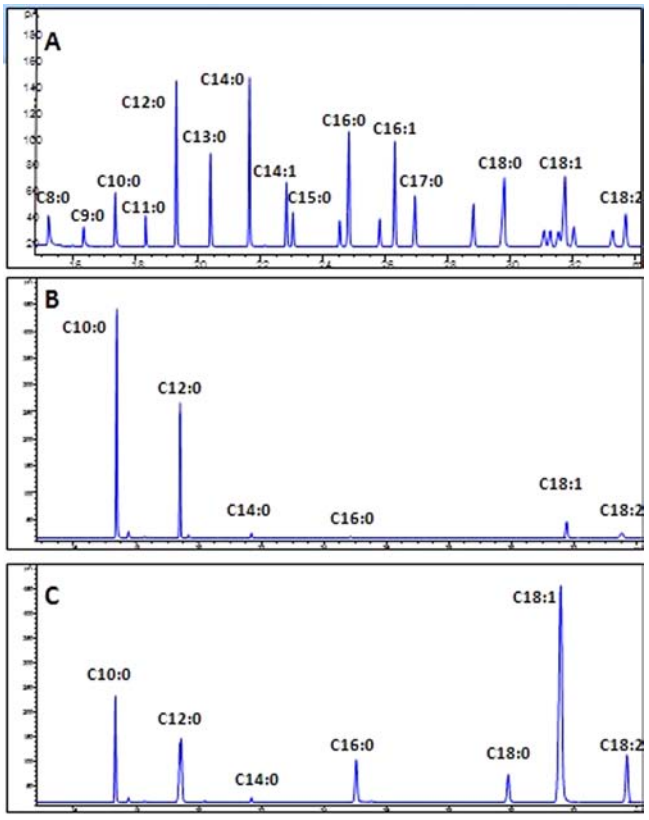


**Figure 3.** GC profile of fatty acid methyl esters of standards of glyceride (A), CCSO (B), and HMFS (C).

major fatty acids of CCSO were MCFAs including capric acid (C10:0, 54.76%, Table 3) and lauric acid (C12:0, 39.83%,

**Table 3. Fatty Acid Compositions (Area Percent) of CCSO and Interesterified Products**

| | CCSO | | | HMFS[a] | | |
|---|---|---|---|---|---|---|
| fatty acid | total | sn-2 | sn-1,3[b] | total | sn-2 | sn-1,3[b] |
| C8:0 | 0.38 | 0.11 | 0.57 | 0.09 | 0.03 | 0.12 |
| C10:0 | 54.76 | 64.28 | 50.00 | 13.91 | 41.62 | 0.06 |
| C12:0 | 39.83 | 32.04 | 43.73 | 11.35 | 28.96 | 2.55 |
| C14:0 | 1.14 | 0.81 | 1.31 | 0.60 | 0.44 | 0.68 |
| C16:0 | 0.56 | 0.86 | 0.41 | 5.50 | 1.95 | 7.28 |
| C18:0 | 0.25 | 0.03 | 0.36 | 3.04 | 1.09 | 4.02 |
| C18:1 | 2.04 | 1.23 | 2.43 | 59.68 | 21.67 | 78.69 |
| C18:2n-6 | 0.95 | 0.74 | 1.06 | 5.69 | 3.96 | 6.56 |
| C18:3n-3 | 0.09 | 0.25 | 0.01 | 0.14 | 0.28 | 0.07 |

[a]Human milk fat substitutes (HMFS) were synthesized with the Lipozyme RM IM of 12.5% (of the total substrate) and a molar ratio of 5:1 (oleic acid/CCSO) at 60 °C for the reaction of 28 h. [b]Sn-1,3 (percentage of the area) = (3*T* − sn-2)/2, where *T* is total fatty acids.

Table 3). The unsaturated fatty acid accounted for only 2−3%, mainly oleic acid and linoleic acid. The content of MCFAs at the sn-2 position of CCSO was up to 96%, and the ratio of C10:0 to C12:0 was 2:1, but only 1:1 at the sn-1,3 position. Compared with CCSO, MCFAs at the sn-2 position of the final product HMFS possessed >70%, whereas oleic acid was predominantly esterified at the sn-1,3 position, accounting for 78.69%. It can be concluded that the configuration of synthetic TAG rich in MCFAs can be expressed as sn-USU (U, unsaturated; S, saturated), which is similar to mother's milk and has the potential to be added to infant formula milk powder, especially to be used as a dietary treatment for premature infants who suffer from fat-absorption abnormalities and infant patients who need rapid fat absorption and energy supply.

**Triacylglycerol Analysis.** The TAG species of CCSO and HMFS product are shown in Figure 4, and respective

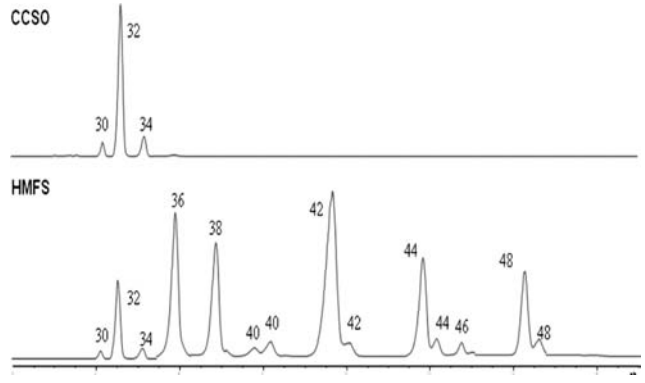


**Figure 4.** TAG of CCSO and HMFS (peak number represents ECN of the triacylglycerol group).

percentages are presented in Table 4. CCSO contained considerable amounts of LaCC/CLaC (82.21%), followed by MCC/LaLaC (11.82%) and CCC (5.97%). After acidolysis,

**Table 4. Triacylglycerol (TAG) Species (Area Percent) of CCSO and HMFS Product**

| ECN[a] | TAG[b] | CCSO | HMFS |
|---|---|---|---|
| 30 | CCC | 5.97 | 1.87 |
| 32 | LaCC/CLaC | 82.21 | 8.92 |
| 34 | MCC/LaLaC | 11.82 | 2.35 |
| 36 | CCO/LaCL | ND[c] | 14.94 |
| 38 | LaCO/LCL | ND | 13.58 |
| 40 | LaLaO/LaOLa | ND | 1.43 |
| 40 | SLaC/PCL | ND | 1.98 |
| 42 | COO/OCO | ND | 23.93 |
| 42 | PPC/PCP/PCO/SCL | ND | 1.82 |
| 44 | LaOO/OLaO | ND | 12.66 |
| 44 | PLaO/PLaP/SLaL | ND | 2.17 |
| 46 | LOO/OLO | ND | 1.64 |
| 46 | PLO/PLP/LLS | ND | 0.79 |
| 48 | OOO | ND | 11.13 |
| 48 | POO/OPO | ND | 2.14 |

[a]Equivalent carbon number (ECN) = CN − 2DB, where CN is carbon number of TAG and DB is total number of double bonds in TAG. [b]Abbreviations: C, capric acid; La, lauric acid; M, myristic acid; P, palmitic acid; S, stearic acid; O, oleic acid; L, linoleic acid. [c]Not detected under this analysis condition.

LaCC/CLaC was significantly reduced; however, COO/OCO, CCO/LaCL, LaCO/LCL, LaOO/OLaO, and OOO were observed as the major TAG species in HMFS accounting for 23.93, 14.94, 13.58, 12.66, and 11.13%, respectively. All five of these TAG species newly appeared in products compared to CCSO. This indicated that enzymatic acidolysis had taken place and HMFS rich in MCFAs were well synthesized. Considering that 70% of MCFAs are at the sn-2 position and 78.69% of oleic acid is at the sn-1,3 position in the final product of HMFS, we can speculate that OCO, CCO, LaCO, OLaO, OLaO, and OOO were the major TAG compositions in HMFS.

**Purification of HMFS Product.** Free fatty acid content in the raw product was higher, mainly of oleic acid and MCFAs, and the urea inclusion method was used to remove the saturated and unsaturated fatty acids. The determination of acid value and the content of TAG in non-urea inclusion compounds were used to evaluate the effect of different HMFS/urea ratios (1:1, 1:2, 1:3) on the purification. Relevant results are shown in Table 5. Acid values in the raw product were 51.47, 52.15, and 51.53 mg KOH/g respectively, higher than those in purified product (20.33, 2.46, and 2.94 mg KOH/g). When the HMFS/urea ratio was 1:2, the acid value lowered to the minimum (2.46 mg KOH/g), which showed that free fatty acids had been almost removed. By comparison of panels C and D of Figure 5, the purity of TAG improved, and the content of TAG improved to 77.28% when the HMFS/urea ratio was 1:2. Furthermore, the synthetic HMFS was a kind of light yellow liquid and its smell was the same as ordinary oil.

**Table 5. Acid Value and Triacylglycerol Content (Weight Percent) of Raw and Purified Products with Different Ratios of HMFS/Urea**

| | acid value (mg KOH/g) | | triacylglycerol (%) | |
|---|---|---|---|---|
| HMFS/urea | raw product | purified product | raw product | purified product |
| 1:1 | 51.47 | 20.33 | 38.49 | 52.96 |
| 1:2 | 52.15 | 2.46 | 38.12 | 77.28 |
| 1:3 | 51.53 | 2.94 | 39.04 | 61.42 |

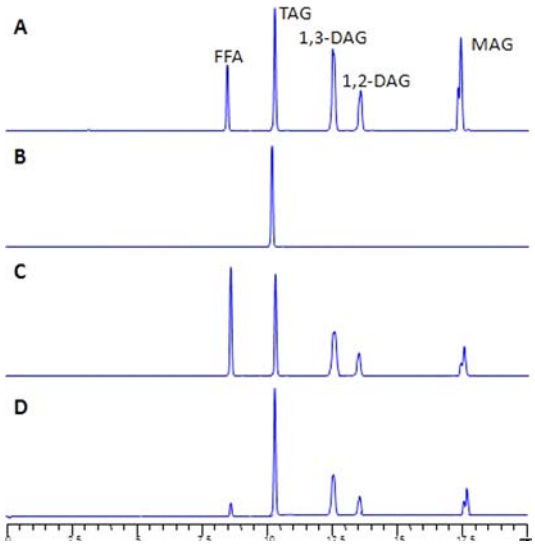


**Figure 5.** HPLC chromatograms of (A) glycerides standard, (B) CCSO, (C) raw product, and (D) purified product.

The urea inclusion product was of high purity and low damage; thus, the method was available for separation and purification of the product.

**Scale-up Trial and Physicochemical Properties.** To further verify the optimization model for mass production, a 50 times substrate (containg 50 g of CCSO) scale-up experiment was carried out under optimized condition, and the urea inclusion method was applied to purify the raw product. After purification, the incorporation of oleic acid was 58.36% as determined by GC analysis, and TAG were up to 76.95% by HPLC analysis. Table 6 shows the tocopherols content and physicochemical properties of the modified CCSO (HMFS) and CCSO. Tocopherols found naturally in vegetable oils function as antioxidants, having a physiological function of scavenging radicals in membrane and lipoprotein particles, thus preventing lipid peroxidation.[44] The contents of $\alpha$-tocopherol in CCSO and HMFS were 16.05 ± 0.62 and 5.86 ± 0.12 mg/100 g, respectively. Likewise, HMFS contained total tocopherols of 12.27 ± 0.19 mg/100 g, lower than that in CCSO (33.74 ± 1.15 mg/100 g). This indicated that the synthetic products contained a lower level of total tocopherols than the CCSO. This is a common phenomenon resulting from the acidolysis reaction and purification processes possibly due to the exposure to light and heat during these processes.[45] The acid value and peroxide value of HMFS were 1.46 ± 0.10 mg KOH/g oil and 1.87 ± 0.08 mmol/kg, respectively, higher than those of CCSO (0.21 ± 0.03 mg KOH/g oil, 0.25 ± 0.04 mmol/kg). This may be attributed to the lower level of total tocopherols in HMFS. The saponification value of HMFS (279.2 ± 2.40 mg KOH/g) was higher than that of CCSO (211.8 ± 1.70 mg KOH/g), illustrating the higher content of glyceride or fatty acid in HMFS per unit weight, which indicated that oleic acid was successfully incorporated into CCSO. The increased iodine value further proved the successful incorporation due to the inserted unsaturated oleic acid reducing the saturability of HMFS. This is in good agreement with Zhao's study.[24]

**Table 6. Contents of Tocopherol and Physicochemical Characteristics of CCSO and Human Milk Fat Substitutes (HMFS)[a]**

| | CCSO | HMFS[b] |
|---|---|---|
| tocopherol (mg/100 g) | | |
| $\alpha$-tocopherol | 16.05 ± 0.62 | 5.86 ± 0.12 |
| $\gamma$-tocopherol | 4.99 ± 0.24 | 1.73 ± 0.01 |
| $\delta$-tocopherol | 12.70 ± 0.29 | 4.68 ± 0.06 |
| total | 33.74 ± 1.15 | 12.27 ± 0.19 |
| physicochemical characteristics | | |
| acid value (mg KOH/g oil) | 0.21 ± 0.03 | 1.46 ± 0.10 |
| peroxide value (mmol/kg) | 0.25 ± 0.04 | 1.87 ± 0.08 |
| iodine value (g $I_2$/100 g oil) | 5.98 ± 0.23 | 54.52 ± 0.63 |
| saponification value (mg KOH/g) | 279.20 ± 2.40 | 211.8 ± 1.70 |

[a]Values presented as means of triplicates ± standard deviation. [b]Human milk fat substitutes (HMFS) was synthesized with the Lipozyme RM IM of 12.5% (of the total substrate) and molar ratio of 5:1 (oleic acid/CCSO) at 60 °C for the reaction of 28 h.

**Reusability of Lipozyme RM IM.** To investigate the reusability of Lipozyme RM IM, the modified optimal reaction conditions were used to detect the stability of the lipase. The activity was expressed as the incorporation of oleic acid in the produced HMFS. After each batch, the lipase was filtered and recovered. Ten batch cycles were conducted. The results

showed that the incorporation of oleic acid was maintained above 52% (87.13% of the first cycle oleic acid incorporation) at the 6th cycle, above 43% (72.05% of the 1st cycle oleic acid incorporation) at the 9th cycle, and about 38% (63.67% of the 1st cycle oleic acid incorporation) at the 10th cycle using Lipozyme RM IM (Figure 6). Therefore, Lipozyme RM IM could be reused 9 times without significant loss of activity.

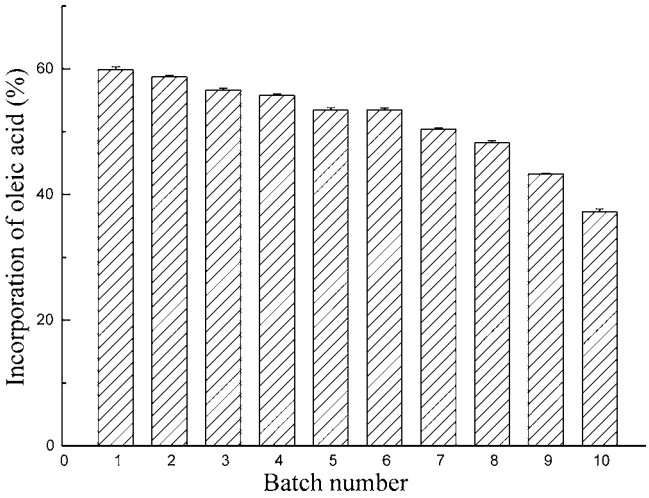


**Figure 6.** Stability of Lipozyme RM IM used for the acidolysis reaction after several usages.

**Conclusion.** This study has synthesized HMFS from CCSO with oleic acid by Lipozyme RM IM-catalyzed acidolysis in a solvent-free system, and the optimal reaction conditions were investigated by RSM and found to be a substrate molar ratio (oleic acid/CCSO) of 5:1, an enzyme concentration of 12.5% (w/w total reactants), a reaction temperature of 60 °C, and a reaction time of 28 h. Under these reaction conditions, the final product HMFS was achieved with >70% of MCFAs at the sn-2 position and 78.69% oleic acid at the sn-1,3 position. In a scale-up trial, the urea inclusion method can separate and purify the synthetic product to some extent, although it has limitations for production at the industrial scale. After purification, the contents of TAG and total tocopherols were 77.28% and 12.27 ± 0.19 mg/100 g, respectively. All of the physicochemical indices of product including acid value and peroxide value were within national standards. The present results showed that such HMFS enriched in MCFAs might have potential application in the infant formula industry, especially to be used as a dietary treatment for premature infants who suffer from fat-absorption abnormalities and infant patients who need rapid fat absorption and energy supply. All of these results may be further improved by the use of an immobilization-modified enzyme, which has enhanced stability and selectivity, and by the use of a better purification method such as molecule distillation for industrial production.

## AUTHOR INFORMATION

### Corresponding Authors

*(J.-N.H.) Phone: +86 88304449-8226. E-mail: hujiangning2005@hotmail.com.

*(Z.-Y.D.) Phone/fax: +86 791 88304402. E-mail: zeyuandeng@hotmail.com.

### Funding

We acknowledge Jiangxi Provincial Natural Science Foundation of China (20132BAB204001; 20122BAB214001) for supporting this project.

### Notes

The authors declare no competing financial interest.

## ACKNOWLEDGMENTS

We thank the Research Program of Sate Key Laboratory of Food Science and Technology in Nanchang University (Project SKLF-ZZB-201308) for providing the research platform.

## REFERENCES

(1) Wang, Y.-H.; Mai, Q.-Y.; Qin, X.-L.; Yang, B.; Wang, Z. L.; Chen, H. T. Establishment of an evaluation model for human milk fat substitutes. *J. Agric. Food Chem.* **2010**, *58*, 642−649.

(2) Xu, X. Production of specific-structured triacylglycerols by lipase-catalyzed reactions: a review. *Eur. J. Lipid Sci. Technol.* **2000**, *102*, 287−303.

(3) Sheila, M. I. Dietary triacylglycerol structure and its role in infant nutrition. *Adv. Nutr.* **2011**, *2*, 275−283.

(4) Koo, W. W. K.; Hockman, E. M.; Dow, M. Palm olein in the fat blend of infant formulas: effect on the intestinal absorption of calcium and fat, and bone mineralization. *J. Am. Coll. Nutr.* **2006**, *25*, 117−122.

(5) Lien, E. L. The role of fatty acid composition and positional distribution in fat absorption in infants. *J. Pediatr.* **1994**, *125*, 562−568.

(6) Srivastava, A.; Akoh, C. C.; Chang, S. W.; Lee, G. C.; Shaw, J. F. *Candida rugosa* lipase LIP1-catalyzed transesterification to produce human milk fat substitute. *J. Agric. Food Chem.* **2006**, *54*, 5175−5181.

(7) Nagachinta, S.; Akoh, C. C. Synthesis of structured lipid enriched with omega fatty acids and sn-2 palmitic acid by enzymatic esterification and its incorporation in powdered infant formula. *J. Agric. Food Chem.* **2013**, *61*, 4455−4463.

(8) Sahín, N.; Akoh, C. C.; Karaali, A. Lipase-catalyzed acidolysis of tripalmitin with hazelnut oil fatty acids and stearic acid to produce human milk fat substitutes. *J. Agric. Food Chem.* **2005**, *53*, 5779−5783.

(9) Nielsen, N. S.; Yang, T.; Xu, X.; Jacobsen, C. Production and oxidative stability of a human milk fat substitute produced from lard by enzyme technology in a pilot packed-bed reactor. *Food Chem.* **2006**, *94*, 53−60.

(10) Sahín, N.; Akoh, C. C.; Karaali, A. Enzymatic production of human milk fat substitutes containing γ-linolenic acid: optimization of reactions by response surface methodology. *J. Am. Oil Chem. Soc.* **2005**, *82*, 549−557.

(11) Sahín, N.; Akoh, C. C.; Karaali, A. Human milk fat substitutes containing omega-3 fatty acids. *J. Agric. Food Chem.* **2006**, *54*, 3717−3722.

(12) Rafael, C. R.; Roberto, F.-L. Lipase from Rhizomucor miehei as a biocatalyst in fats and oils modification. *J. Mol. Catal. B−Enzym.* **2010**, *66*, 15−32.

(13) Berit, M.; Maria, P.; Jürgen, S. Medium-chain triglycerides. *Int. Dairy J.* **2006**, *16*, 1374−1382.

(14) Lee, Y.-Y.; Tang, T.-K.; Lai, O.-M. Health benefits, enzymatic production, and application of medium- and long-chain triacylglycerol (MLCT) in food industries: a review. *J. Food Sci.* **2012**, *77*, 137−144.

(15) Isaacs, C. E.; Litov, R. E.; Thormar, H. Antimicrobial activity of lipids added to human milk, infant formula, and bovine milk. *J. Nutr. Biochem.* **1995**, *6*, 362−366.

(16) O'Shea, M.; Geritsen, J.; Moheda, I. Clinical benefit of a structured lipid (betapolTM) in infant formula. In *Handbook of Functional Lipids*; Akoh, C. C., Ed.; CRC Taylor & Francis Group: New York, 2005; pp 261−278.

(17) Huri, I.; Mine, G.-O.; Beraat, O. Production of human milk fat substitute with medium-chain fatty acids by lipase-catalyzed acidolysis: optimization by response surface methodology. *LWT−Food Sci. Technol.* **2011**, *44*, 999−1004.

(18) Rafael, C. R.; Roberto, F.-L. Lipase from *Rhizomucor miehei* as an industrial biocatalyst in chemical process. *J. Mol. Catal. B—Enzym.* **2010**, *64*, 1—22.
(19) Cristina, G.-G.; Angel, B.-M.; Roberto, F.-L.; Rafael, C. R. Potential of different enzyme immobilization strategies to improve enzyme performance. *Adv. Synth. Catal.* **2011**, *353*, 2885—2904.
(20) Hu, J. N.; Zhang, B.; Zhu, X. M.; Li, J.; Fan, Y. W.; Liu, R.; Tang, L.; Lee, K. T.; Deng, Z. Y. Characterization of medium-chain triacylglycerol (MCT)-enriched seed oil from *Cinnamomum camphora* (Lauraceae) and its oxidative stability. *J. Agric. Food Chem.* **2011**, *59*, 4771—4778.
(21) Liu, C. H.; Mishra, A. K.; Tan, R. X.; Yang, T. H.; Shen, Y. F. Repellent and insecticidal activities of essential oils from *Artemisia princeps* and *Cinnamomum camphora* and their effect on seed germination of wheat and broad bean. *Bioresour. Technol.* **2006**, *97*, 1969—1973.
(22) Tang, L.; Hu, J. N.; Zhu, X. M.; Luo, L. P.; Lei, L.; Deng, Z. Y.; Lee, K. T. Enzymatic interesterification of palm stearin with *Cinnamomum camphora* seed oil to produce zero-trans medium-chain triacylglycerols-enriched plastic fat. *J. Food Sci.* **2012**, *77*, 454—460.
(23) Zhao, M. L.; Tang, L.; Zhu, X. M.; Hu, J. N.; Li, H. Y.; Luo, L. P.; Lei, L.; Deng, Z. Y. Enzymatic production of zero-trans plastic fat rich in $\alpha$-linolenic acid and medium-chain fatty acids from highly hydrogenated soybean oil, *Cinnamomum camphora* seed oil, and perilla oil by lipozyme TL IM. *J. Agric. Food Chem.* **2013**, *61*, 1189—1195.
(24) Zhao, M. L.; Hu, J. N.; Zhu, X. M.; Li, H. Y.; Li, J.; Fan, Y. W.; Deng, Z. Y. Enzymatic synthesis of medium- and long-chain triacylglycerols-enriched structured lipid from *Cinnamomum camphora* seed oil and camellia oil by Lipozyme RM IM. *Int. J. Food Sci. Technol.* **2014**, *49*, 453—459.
(25) Rao, R.; Manohar, B.; Sambaiah, K.; Lokesh, B. R. Enzymatic acidolysis in hexane to produce n-3 or n-6 FA-enriched structured lipids from coconut oil: optimization of reactions by response surface methodology. *J. Am. Oil Chem. Soc.* **2002**, *79*, 885—890.
(26) Araújo, M. E. M. B.; Campos, P. R. B.; Noso, T. M.; Alberici, R. M.; Silva Cunha, I. B.; Simas, R. C.; Eberlin, M. N.; Carvalho, P. O. Response surface modelling of the production of structured lipids from soybean oil using *Rhizomucor miehei* lipase. *Food Chem.* **2011**, *127*, 28—33.
(27) Zhu, X. M.; Hu, J. N.; Xue, C. L.; Lee, J. H.; Shin, J. A.; Hong, S. T.; Sung, C. K.; Lee, K. T. Physiochemical and oxidative stability of interesterified structured lipid for soft margarine fat containing D 5-UPIFAs. *Food Chem.* **2011**, *10*, 101—106.
(28) Lee, K. T.; Foglia, T. A. Synthesis, purification, and characterization of structured lipids produced from chicken fat. *J. Am. Oil Chem. Soc.* **2000**, *77*, 1027—1034.
(29) Schlenk, H. Urea inclusion compounds of fatty acids. *Prog. Chem. Fats Other Lipids* **1954**, *2*, 243—267.
(30) Gimeno, E.; Castellote, A. I.; Lamuela-Raventos, R. M.; de la Torre, M. C.; Lopez-Sabater, M. C. Rapid determination of vitamin E in vegetable oils by reversed-phase high-performance liquid chromatography. *J. Chromatogr., A* **2000**, *881*, 251—254.
(31) AOAC. *Official Methods of Analysis*, 15th ed.; Association of Official Analytical Chemists: Washington, DC, USA, 1990.
(32) Vu, P. L.; Park, R. K.; Lee, Y. J.; Kim, Y. M.; Nam, H. Y.; Lee, J. H.; Akoh, C. C.; Lee, K. T. Two-step production of oil enriched in conjugated linoleic acids and diacylglycerol. *J. Am. Oil Chem. Soc.* **2007**, *84*, 123—128.
(33) Barahona, D.; Pfromm, P. H.; Rezac, M. E. Effect of water activity on the lipase catalyzed esterification of geraniol in ionic liquid [bmim] $PF_6$. *Biotechnol. Bioeng.* **2006**, *93*, 318—324.
(34) Rocha, J.; Gil, M.; Garcia, F. Optimisation of the enzymatic synthesis of noctyl oleate with immobilised lipase in the absence of solvents. *J. Chem. Technol. Biotechnol.* **1999**, *74*, 607—612.
(35) Yadav, G. D.; Piyush, S. L. Kinetics and mechanism of synthesis of butyl isobutyrate over immobilised lipases. *Biochem. Eng. J.* **2003**, *16*, 245—252.
(36) Iso, M.; Chen, B.; Eguchi, M.; Kudo, T.; Shrestha, S. Production of biodiesel fuel from triglycerides and alcohol using immobilized lipase. *J. Mol. Catal. B— Enzym.* **2001**, *16*, 53—58.
(37) Rooney, D.; Weatherley, L. R. The effect of reaction conditions upon lipase catalysed hydrolysis of high oleate sunflower oil in a stirred liquid-liquid reactor. *Process Biochem.* **2001**, *36*, 947—953.
(38) Raspe D. T.; Cardozo-Filho L.; Silva C. Effect of additives and process variables on enzymatic hydrolysis of macauba kernel oil (*Acrocomia aculeata*). *Int. J. Chem. Eng.* **2013**, ID 438270, 8 pp.
(39) Phuah, E.-T.; Lai, O.-M.; Choog, T. S.-H.; Tan, C.-P.; Lo, S.-K. Kinetic study on partial hydrolysis of palm oil catalyzed by *Rhizomucor miehei* lipase. *J. Mol. Catal. B—Enzym.* **2012**, *78*, 91—97.
(40) Mu, H.; Xu, X.; Høy, C. E. Production of specific-structured triacylglycerols by lipase-catalyzed interesterification in a laboratory-scale continuous reactor. *J. Am. Oil Chem. Soc.* **1998**, *75*, 1187—1193.
(41) Akoh, C. C.; Moussata, C. O. Lipase-catalyzed modification of borage oil: incorporation of capric acid and eicosapentaenoic acids to form structured lipids. *J. Am. Oil Chem. Soc.* **1998**, *75*, 697—701.
(42) Han, L.; Xu, Z. J.; Huang, J. H.; Meng, Z.; Liu, Y. H.; Wang, X. G. Enzymatically catalyzed synthesis of low-calorie structured lipid in a solvent-free system: optimization by response surface methodology. *J. Agric. Food Chem.* **2011**, *59*, 12635—12642.
(43) Yankah, V. V.; Akoh, C. C. Lipase-catalyzed acidolysis of tristearin with oleic or caprylic acids to produce structured lipids. *J. Am. Oil Chem. Soc.* **2000**, *77*, 495—500.
(44) Esterbauer, H.; Dieber-Rotheneder, M.; Striegl, G.; Waeg, G. Role of vitamin E in preventing the oxidation of low-density lipoprotein. *Am. J. Clin. Nutr.* **1991**, *53*, 314S—321S.
(45) Akoh, C. C.; Charment, O. M. Characterization and oxidative stability of enzymatically produced fish and canola oil-based structured lipids. *J. Am. Oil Chem. Soc.* **2001**, *78*, 25—30.

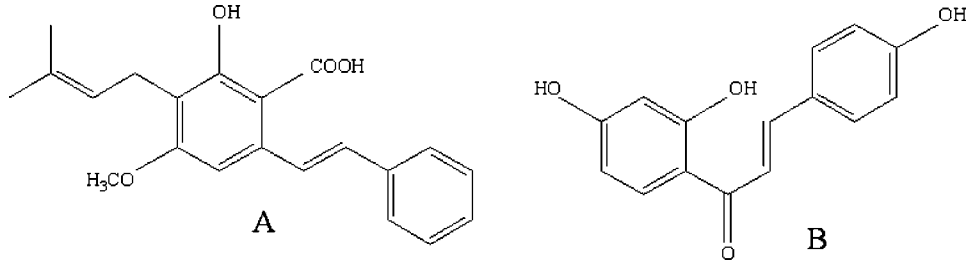


**Figure 1.** Chemical structures of (A) cajaninstilbene acid (CSA) and (B) isoliquiritigenin (ISL).

majority of drugs.[14,15] The activity alteration of these enzymes is the major cause of metabolic food−drug interactions.[16]

Hence, the aim of our study was to investigate the in vitro metabolism of CSA by human liver microsomes and recombinant human P450 enzymes to identify the CYP450 enzymes involved and evaluate potential CSA food−drug interactions.

## MATERIALS AND METHODS

**Chemicals and Reagents.** Cajaninstilbene acid (CSA, purity = 98%, HPLC grade) was isolated and purified in our laboratory. By comparing the IR, $^{1}H$ and $^{13}C$ nuclear magnetic resonance (NMR), and MS data with reported data,[17] we confirmed the structure of CSA. Isoliquiritigenin (ISL), paclitaxel, glucose 6-phosphate, glucose-6-phosphate dehydrogenase, NADPH- and CYP450-specific substrates, inhibitors, and inducers were purchased from Sigma-Aldrich (St. Louis, MO, USA). Human liver microsomes (pooled from 20 donors) and primary human hepatocytes (the human donor was a 47-year-old nonsmoking Chinese female with no known history of human immunodeficiency or virus exposure to hepatitis B or C) were purchased from iPhase Biosciences Co., Beijing, China. Recombinant human P450 enzymes (CYP1A2, CYP2A6, CYP2C9, CYP2C19, CYP2D6, CYP2E1, and CYP3A4) and human CYP-reductase coexpressed in *Escherichia coli*, supplemented with purified human cytochrome *b*5, were purchased from Cypex (Dundee, UK). All microsomal preparations were stored at −80 °C until used. The total P450 content, protein concentrations, and specific activity of each P450 isoform were supplied by the manufacturer. All other reagents and chemicals were of analytical grade. The chemical structures of CSA and ISL are shown in Figure 1.

**Incubations with Human Liver Microsomes for Metabolite Identification.** Incubation experiments were performed as described previously with slight modification.[18,19] Microsomal incubation mixture in phosphate buffer, pH 7.4 (0.1 mol/L), consisted of CSA (20 $\mu$M), 3 mM $MgCl_2$, 0.5 mg/mL microsomal protein, and the NADPH-regenerating system (0.5 mM $NADP^+$, 5 mM glucose 6-phosphate, and 0.5 unit of glucose-6-phosphate dehydrogenase/mL). Final volume was 500 $\mu$L. Samples were incubated at 37 °C for 5 min before the reaction was initiated by the addition of microsomal proteins. Thereafter, samples were carried out aerobically at 37 °C in a test tube placed on a temperature-controlled heating block for 60 min. To terminate the reaction, 500 $\mu$L of acetonitrile containing ISL (100 $\mu$L of 50 $\mu$M) was added. ISL was added as an internal standard to the incubation sample and vortexed for 3 min, and then the sample was extracted using 1 mL of ethyl acetate. The sample was centrifuged at 12000 rpm for 20 min at room temperature. The supernatant was then transferred to a separate tube and evaporated to dryness under nitrogen. The residues were dissolved in 0.1 mL of methanol and then vortex-mixed for 30 s and centrifuged at high speed for 5 min in an Eppendorf tube. All of the samples were injected into HPLC and LC-MS/MS for the analysis of CSA and its metabolites.

**Identification of P450s Involved in Metabolite Formation from CSA.** To determine the isozymes involved in metabolite formation in CSA, the chemical inhibitor and recombinant human P450 enzymes were used.

Formation rates of hydroxylation metabolites (M1, M2) from CSA were evaluated in the absence (control) and presence of known CYP450 isoform-specific inhibitors with pooled human liver microsomes. The inhibitors were 20 $\mu$M furafylline (CYP1A2 inhibitor), 50 $\mu$M pilocarpine (CYP2A6 inhibitor), 50 $\mu$M sulfaphenazole (CYP2C9 inhibitor), 5 $\mu$M ticlopidine (CYP2C19 inhibitor), 10 $\mu$M quinidine (CYP2D6 inhibitor), 50 $\mu$M diethylthiocarbamate (CYP2E1 inhibitor), and 5 $\mu$M ketoconazole (CYP3A4 inhibitor). The final concentration of acetonitrile in incubations was 0.1%. CSA (20 $\mu$M) was preheated for 5 min at 37 °C in an NADPH-generating system. Human liver microsomes (0.5 mg/mL) were added to initiate the reaction and incubated at 37 °C for 15 min. The inhibitors concentrations were chosen selectively for the respective CYP450 isoforms. Inhibition percent of metabolites' formation rate was calculated by comparing the inhibited activity with uninhibited controls (without inhibitors). Stock solutions of the chemical inhibitors were prepared in acetonitrile. Control solutions were prepared with the same amount of acetonitrile without inhibitors. The conditions for use of these inhibitors have been described in previous publications.[20−22]

The recombinant human P450 enzyme experiments were performed as described previously with slight modification,[23] The incubation system was the same as those applied to the liver microsomal incubations with the exception that microsomes were replaced by recombinant human P450 enzymes CYP1A2, 2A6, 2C9, 2C19, 2D6, 2E1, and 3A4. The enzyme concentration in the incubation system was 50 pmol/mL. The total volume of incubation was 500 $\mu$L. The incubation time was 60 min, and the sample treatment method was same as described under Incubations with Human Liver Microsomes for Metabolite Identification.

**Quantification and Chromatographic Analysis of Metabolites.** An LC-MS/MS analysis method was used to quantify CSA and its major metabolites M1 and M2. LC-MS/MS was carried out with an Agilent 1100 series LC system equipped with a UV detector (Agilent Technologies, Palo Alto, CA, USA). An HPLC system consisting of degasser G1379B, binary pump G1312B, a 7725i manual injector, and column thermostat G1316B was used. An HIQ Sil C 18 column (4.6 mm × 250 mm, KYA TEACH, made in Japan) was used. The mobile phase consisted of water and methanol (15:85, v/v) containing 0.1% formic acid. The flow rate was 1.0 mL/min, and the column eluate was monitored at a wavelength of 254 nm. The Agilent 1100 series LC system was series connected with an API5500Q trap triple-stage quadrupole mass spectrometer (Applied Biosystems, Concord, Canada) equipped with an electrospray ionization (ESI) source. The mass spectrometer was operated in negative ion mode with a capillary temperature of 300 °C and spray voltage of −4500 V. The nitrogen gas flow rate, collision energy, and declustering potential were adjusted to give maximum sensitivity for CSA (12 L/min, −25 V, −60 V, respectively).[9] The mass spectrometer was operated in multiple reaction monitoring (MRM) mode. For semiquantification of CSA and hydroxylation metabolites (M1, M2), ISL was added to each sample as internal standard and the following MRM transitions were selected on the basis of the fragmentation of $(M - H)^-$ ions (results observed in previous MS/MS analyses): 337.1/293.0 for CSA, 353.1/279.1 for M1, 353.4/253.9 for M2, and 255.1/119.3 for ISL.

An LC-MS/MS quantification method was used to quantify CYP450 enzyme activities in human liver microsomes and primary

Table 1. Experimental Conditions for Measuring Microsomal P450 Activity for Enzyme Inhibition Studies

| CYP isoform | substrate | substrate probe | parent ion | daughter ion | polarity | declustering potential (V) | collision energy (V) |
|---|---|---|---|---|---|---|---|
| 3A4 | testosterone | testosterone 6$\beta$-hydroxylation | 305.5 | 269 | ESI+ | 65 | 25 |
| 2D6 | dextromethorphan | dextromethorphan O-demethylation | 258.2 | 157 | ESI+ | 80 | 55 |
| 2C9 | tolbutamide | tolbutamide 4′-hydroxylation | 287.1 | 171.2 | ESI+ | 55 | 30 |
| 2A6 | coumarin | coumarin 7′-hydroxylation | 160.9 | 132.1 | ESI+ | 65 | 35 |
| 1A2 | phenacetin | phenacetin O-dealkylation | 151.9 | 110.1 | ESI+ | 60 | 25 |
| 2C19 | *S*-mephenytoin | *S*-mephenytoin 4 -hydroxylation | 233.4 | 190.2 | ESI− | −55 | −20 |
| 2E1 | chlorozoxazone | chlorozoxazone 6′-hydroxylation | 184 | 120.1 | ESI− | −40 | −15 |
| internal standard | | paclitaxel | 876 | 308.1 | ESI+ | −45 | −25 |

human hepatocytes. The ionization mode was electrospray, polarity positive. Electrospray jet stream conditions were as follows: capillary voltage, −4500 V; drying gas temperature, 300 °C; nebulizer pressure, 20 psi; sheath gas temperature, 350 °C. The mass spectrometer was operated in the MRM mode. MRM transitions, fragmentor voltage, and collision energy of the substrate probes are summarized in Table 1.

For structural identification, metabolites and major molecular ion peaks were determined using HPLC-MS, MS/MS, and MS/MS/MS spectra separately. Metabolites were identified on the basis of their accurate mass determination and fragmentation patterns in positive and negative modes.

**Enzyme Kinetic Analysis of CSA in Human Liver Microsomes and Recombinant Human P450 Enzymes.** The enzyme kinetics of CSA metabolism by pooled human liver microsomes and seven recombinant human P450 enzymes (CYP1A2, CYP2A6, CYP2C9, CYP2C19, CYP2D6, CYP2E1, or CYP3A4) was investigated. Kinetic constants were derived from incubations with the following CSA concentrations: 1, 2, 3.9, 7.8, 15.6, 31.3, 62.5, 125, 250, and 500 $\mu$M ($n$ = 3). Human liver microsomes and recombinant human P450 enzyme contents were 0.5 mg/mL and 50 pmol/mL, respectively. Incubation times were 30 and 15 min for human liver microsomes and recombinant human P450 enzymes, respectively. Reactions were stopped by adding 500 $\mu$L of protein precipitation/internal standard solution and were extracted as previously described. Incubation mixtures without NADPH incubated were used as controls.

**CSA Inhibition Study of CYP450 Enzymes.** The potential of CSA as an inhibitor of major drug-metabolizing CYP450 enzymes was evaluated with human liver microsomes using selective CYP450 probe substrates (Table1) in a reversible and time-dependent manner. Incubation in phosphate buffer, pH 7.4 (0.1 mol/L), was conducted at 37 °C, consisting of human liver microsomes, 0.5 mg/mL, and CYP450 probe substrate with the NADPH-regenerating system. In the assay of CSA inhibition in reversible manner, human liver microsomes were the last reagent added into the incubation system to initiate the reaction; after 10 min, the reaction was terminated by adding an equal volume of acetonitrile (v/v) containing paclitaxel as an internal standard. To examine CSA potential as a time-dependent inhibitor, CSA (20 $\mu$M) was preincubated at 37 °C with human liver microsomes and an NADPH-generating system for 30 min. After the preincubation period, the probe substrate was added, and the incubation was continued for 10 min to measure residual CYP450 activity. Reactions were terminated as described above. Samples were analyzed as described under Analytical Methods. The $IC_{50}$ value was determined by incubation of pooled human liver microsomes (0.5 mg/mL) with CYP450 probe substrates in the presence and absence of CSA (0.1−100 $\mu$M). The results were processed following a method described previously.[24]

**Analysis of CSA To Induce CYP450 Enzymes.** To investigate the potential of CSA to induce CYP450 enzymes, the enzyme activities of CYP1A2, CYP2A6, CYP2E1, CYP2C9, CYP2C19, and CYP3A4 in primary human hepatocytes were assessed. Primary human hepatocytes were treated with CSA (1, 10, and 30 $\mu$M) or one of three prototypical CYP450 inducers, omeprazole (100 $\mu$M), phenobarbital (750 $\mu$M), and rifampin (10 $\mu$M), as positive controls for 3 days. CSA and the positive controls were dissolved in DMSO, and hepatocytes treated with DMSO (final concentration = 0.1%, v/v) served as negative controls. Hepatocytes were harvested after 72 h of treatment, and microsomes were prepared from each culture, on the basis of the methods described previously.[25] The enzyme activity in microsomal samples was determined by incubating microsomal samples with probe substrates for 10 min at 37 °C. Microsomes were incubated with phenacetin (80 $\mu$M), tolbutamide (100 $\mu$M), coumarin (100 $\mu$M), chlorozoxazone (200 $\mu$M), *S*-mephenytoin (200 $\mu$M), and testosterone (250 $\mu$M) for various time periods (10−30 min). Then the activities of CYP1A2, CYP2A6, CYP2E1, CYP2C9, CYP2C19, and CYP3A4 were determined, respectively. Samples were analyzed as described under Quantification and Chromatographic Analysis of Metabolites. Hepatocytes' culture method and sample treatment method were described previously.[26]

**Data Analysis.** Nonlinear regression analysis, $V = V_{max}(S)/(K_m + (S))$, was used to describe the kinetics of biotransformation of CSA to M1 and M2 in human liver microsomes (GraphPad Prism 5.0).[27] $V$ is reaction rate, $(S)$ is substrate concentration, and $K_m$ is the Michaelis−Menten constant. The intrinsic clearance ($CL_{int}$) for formation of each CSA metabolite was calculated by $V_{max}/K_m$; it is a parameter commonly used for quantitative in vitro−in vivo allometric scaling.[28,29]

## RESULTS

**Identification of Metabolites Formed by Human Liver Microsomes.** When CSA was incubated with human liver microsomes in the presence of NADPH, two metabolites (M1 and M2) were detected by HPLC. The formation of the metabolites was dependent on the presence of NADPH, and the yield of metabolite appeared to be linear with respect to incubation time (up to 30 min). However, no metabolite could be clearly observed in the absence of NADPH. Typical chromatograms of CSA and its two main metabolites are shown in Figure 2. The HPLC retention times of metabolites, CSA, and the internal standard (ISL) were 6.8 (M1), 9.1 (M2), 15.7, and 3.9 min, respectively.

To characterize M1 and M2, LC-MS/MS and LC-MS/MS/MS methods were used. MS/MS and MS/MS/MS spectra of M1 and M2 are shown in Figure 3. First, precursor ion scanning identified two potential metabolites that exhibited 353.1 and 353.4 amu in the CSA microsomal incubates that consisted of human liver microsomes and NADPH system (but not in negative control experiments) in addition to the 337.3 amu of CSA. Second, to gain further structural information, MS/MS spectra of these potential metabolites were obtained by collision-induced dissociation of their molecular ions. The MS/MS spectra detected two major characteristic fragment ions for each potential metabolite: $m/z$ 309.1, 291.2, and 279.1 were obtained from $m/z$ 353.1; $m/z$ 309.3, 253.9, and 238.7 were obtained from $m/z$ 353.4. These transition ions were selected in the MRM modes for identification and quantification of the metabolites: The metabolite with 353.1 amu was measured with

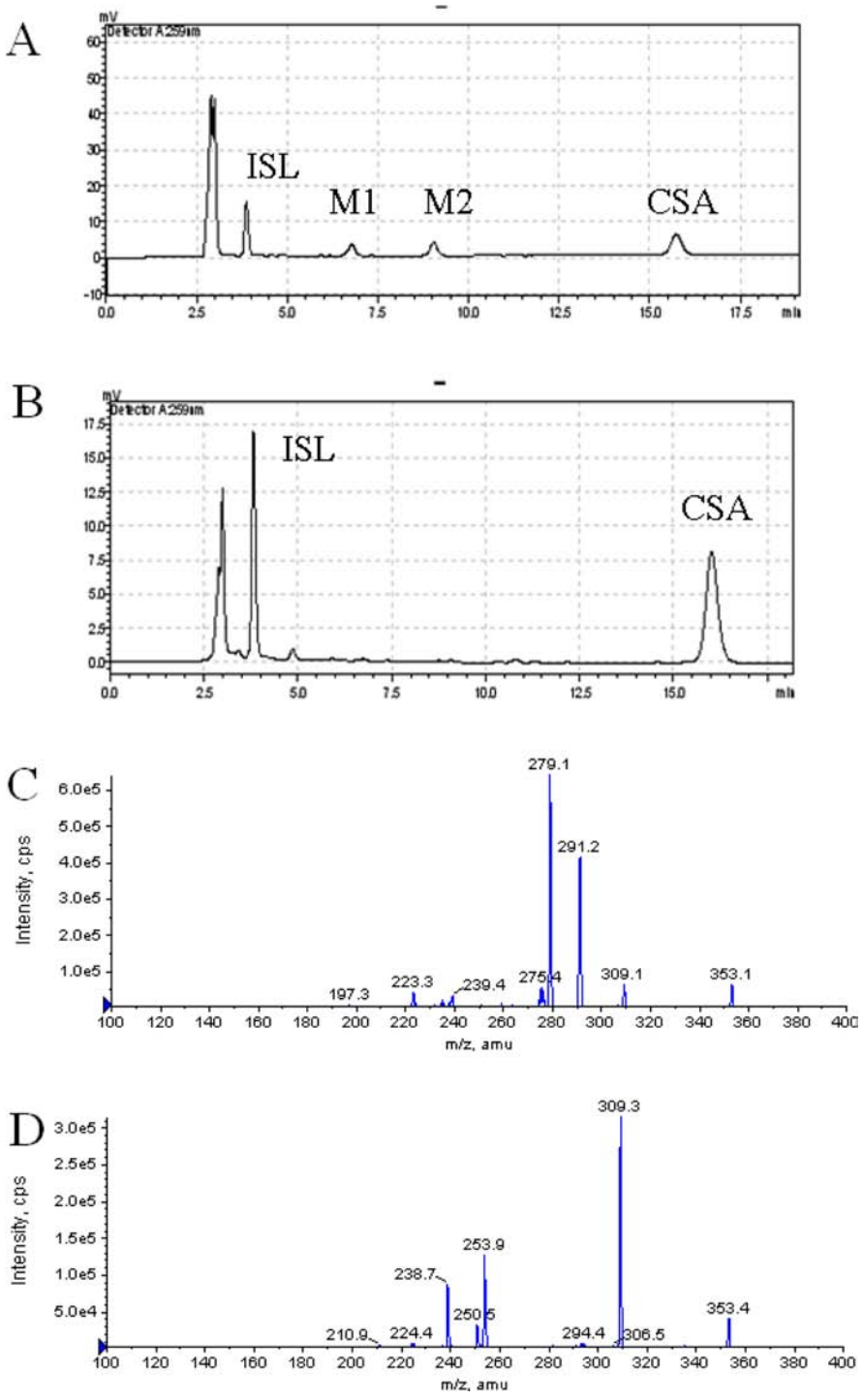


**Figure 2.** Representative chromatograms of CSA metabolites (M1 and M2) extracted from human liver microsomal incubates: (A) CSA incubated by human liver microsomes with NADPH-regenerating system; (B) CSA incubated by human liver microsomes without NADPH-regenerating system; MS/MS spectra of (C) M1 and (D) M2, the metabolite of CSA formed by human liver microsomes. ISL was used as an internal standard (IS). The retention times of M1, M2, CSA, and the internal standard (ISL) were 6.8, 9.1, 15.7, and 3.9 min, respectively.

the quantifier MRM $m/z$ 353.1/279.1 and confirmed with the qualifier MRM transition $m/z$ 353.1/291.2, and the metabolite with 353.4 amu was measured with the quantifier MRM $m/z$ 353.4/253.9 and confirmed with the qualifier MRM 353.4/238.7.

To determine the structures of M1and M2, the parent drug fragmentation pattern was used as a guide to identify CSA metabolites; metabolic pathways of CSA are shown in Figure 4. M1 and M2 showed the (M − H) ion at $m/z$ 353, which was 16 amu higher than that of the parent compound, suggesting that an oxygen atom was inserted into the molecule of CSA. To further confirm the structure of metabolites M1 and M2, MS/MS/MS experiments were performed. Fragment ions $m/z$ 309.1, 291.2, 279.1, and 239.4 from M1 and $m/z$ 309.3, 253.9, 250.5, and 238.7 from M2 were analyzed. The major fragment ions of $m/z$ 309.1, 291.2, 279.1, 239.4, 309.3, 253.9, 250.5, and 238.7 are shown in Figure 3. The fragment pathways of M1 and M2 are shown in Figure 5.

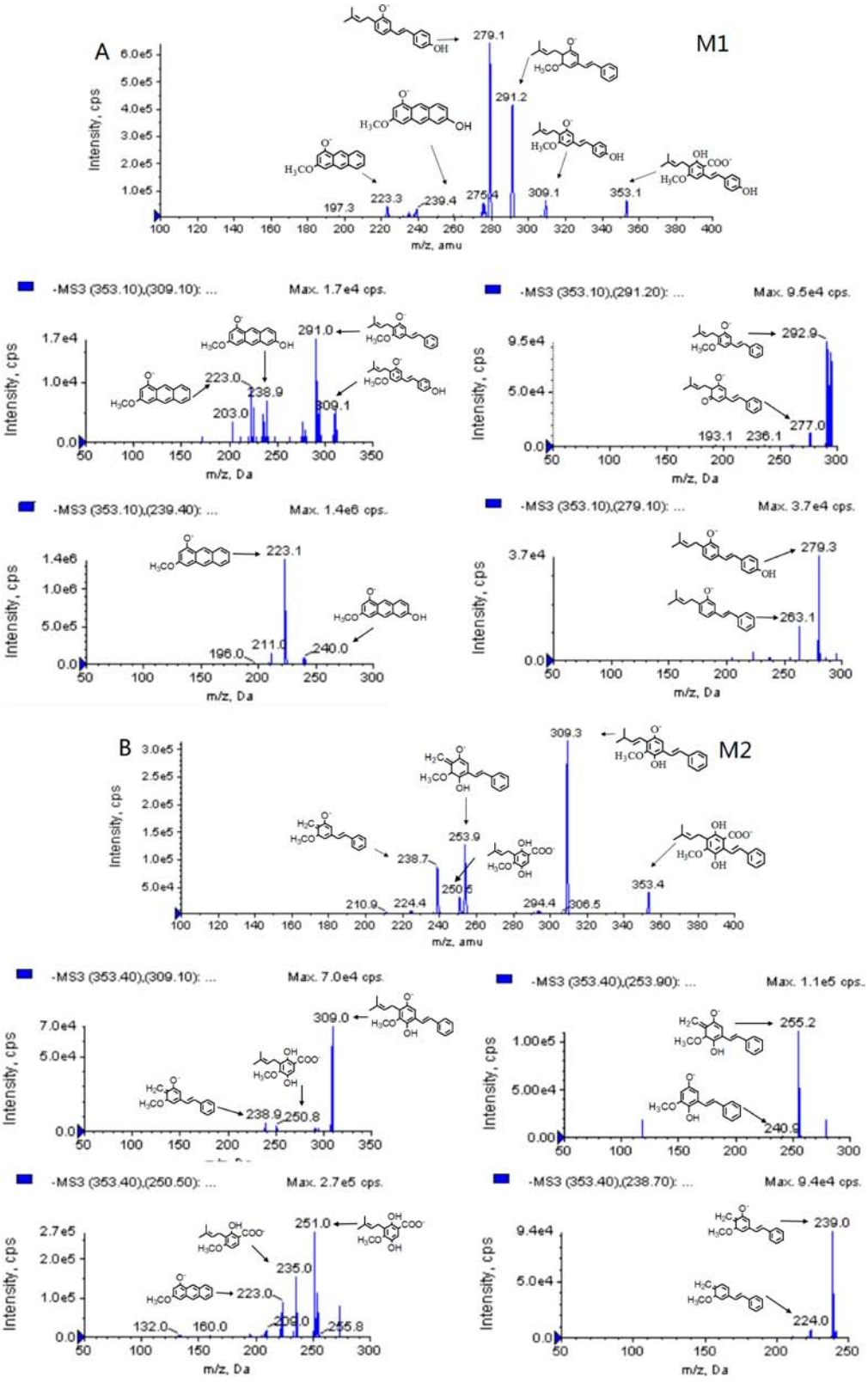


**Figure 3.** MS/MS and MS/MS/MS spectra of (A) M1 and (B) M2.

**Kinetic Analysis of CSA in Human Liver Microsomes.** Kinetic analysis for the formation of M1 and M2 was studied with pooled human liver microsomes. The formation rate of M1 and M2 revealed Michaelis−Menten saturation curves. A representative Michaelis−Menten plot for M1 and M2 formation in human liver microsomes is shown in Figure 6. The apparent $K_m$ values of M1 and M2 catalyzed by human liver microsomes are 28.8 and 23.6 $\mu$M, respectively (Table 2). $V_{max}$ (apparent) values were 141.6 and 122.7 pmol/mg/min, respectively. On average, the apparent intrinsic clearances ($Cl_{int}$) of M1 and M2 formation were 4.9 and 5.2 $\mu$L/mg protein/min, respectively.

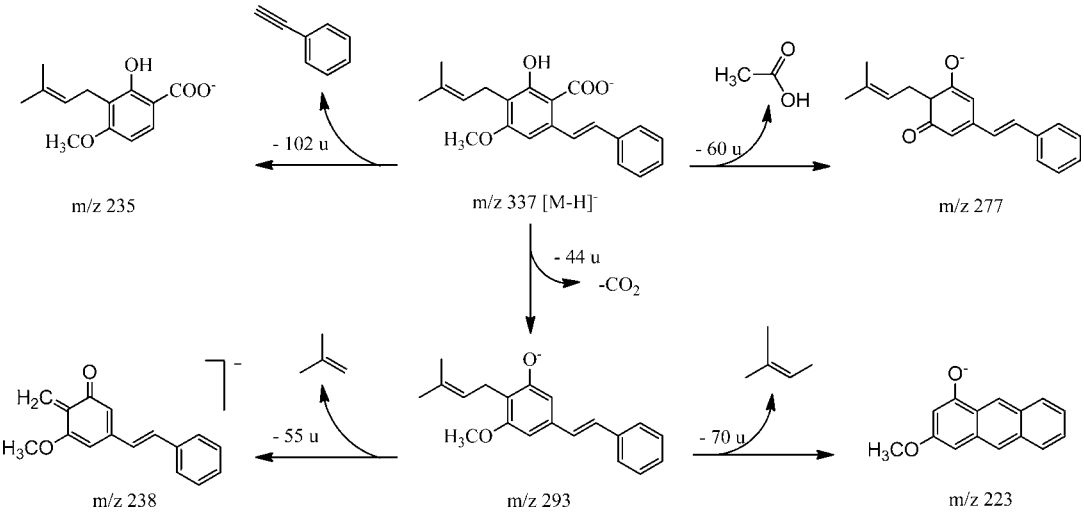


**Figure 4.** Formation and fragmentation pathways of CSA.

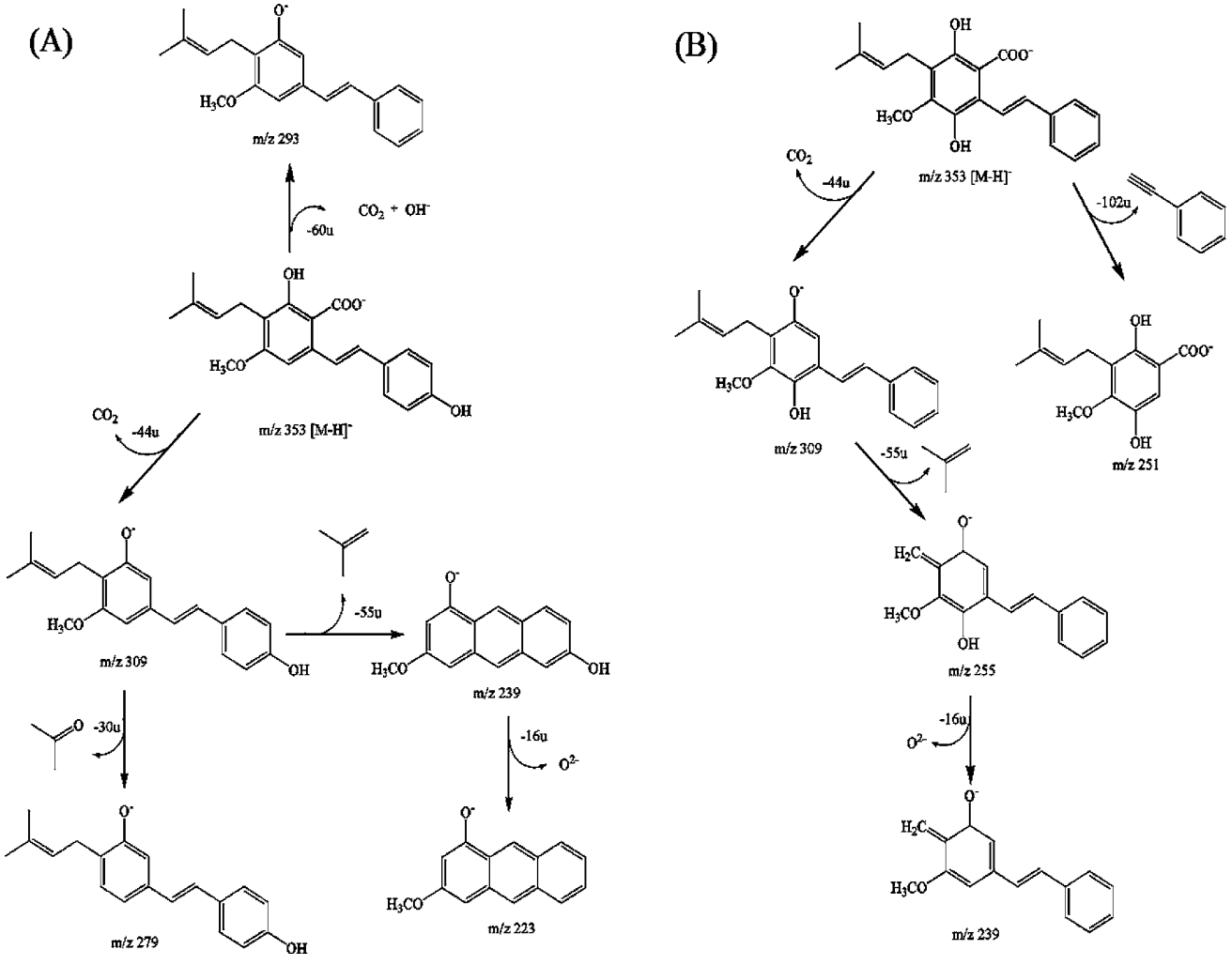


**Figure 5.** Formation and fragmentation pathways of (A) M1 and (B) M2.

**Metabolism of CSA by Recombinant Human P450 Enzymes.** Kinetic parameters of M1 and M2 from CSA are shown in Table 3. The formation rates of M1 and M2 revealed Michaelis–Menten saturation curves. The $K_m$ and $V_{max}$ of M1 formation from CSA were 5.9, 9.0, and 12.9 $\mu$M and 6.8, 15.0, and 28.9 pmol/mg/min for CYP1A2, CYP2C9, and CYP3A4, respectively. The $K_m$ and $V_{max}$ of M2 formation from CSA were 19.7 $\mu$M and 104.6 pmol/mg/min, respectively, for CYP2C9. To better assess the relative contribution of the individual P450 isoforms to the in vitro formation of CSA in human liver microsomes, the intrinsic clearances were calculated. The $CL_{int}$ values ($V_{max}/K_m$) for the formation of M1 by CYP1A2,


dx.doi.org/10.1021/jf501635a | J. Agric. Food Chem. 2014, 62, 10604–10614

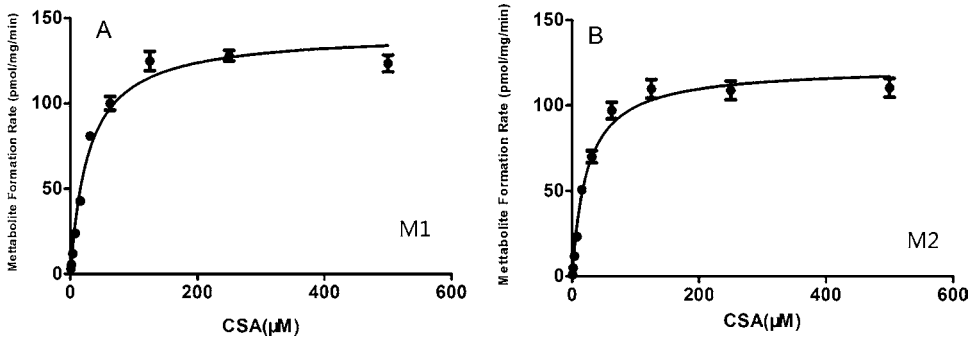


**Figure 6.** CSA concentration-dependent formation of (A) M1 and (B) M2 in the incubations with human liver microsomes. Data were fitted to a Michaelis–Menten substrate binding curve.

**Table 2. Kinetic Parameters for the Metabolism of CSA by Human Liver Microsomes**

| metabolite | pathway | $K_m$ ($\mu$M) | $V_{max}$ (pmol/mg/min) | $V_{max}/K_m$ ($\mu$L/mg protein/min) | kinetic model |
|---|---|---|---|---|---|
| M1 | phenyl hydroxylation | 28.8 | 141.6 | 4.9 | Michaelis–Menten |
| M2 | phenyl hydroxylation | 23.6 | 122.7 | 5.2 | Michaelis–Menten |

**Table 3. Kinetic Parameters for the Metabolism of CSA by Recombinant Human P450 Enzymes**

| metabolite | P450 | $K_m$ ($\mu$M) | $V_{max}$ (pmol/mg/min) | $V_{max}/K_m$ ($\mu$L/mg protein/min) | % of total $CL_{int}$ | kinetic model |
|---|---|---|---|---|---|---|
| M1 | CYP1A2 | 5.9 | 6.8 | 1.2 | 22.1 | Michaelis–Menten |
| | CYP2C9 | 9.0 | 15.0 | 1.7 | 31.7 | Michaelis–Menten |
| | CYP3A4 | 12.9 | 28.9 | 2.2 | 42.6 | Michaelis–Menten |
| M2 | CYP2C9 | 19.7 | 104.6 | 5.3 | 95.6 | |

CYP2C9, and CYP3A4 were 1.2, 1.7, and 2.2 $\mu$L/mg protein/min, respectively. The $CL_{int}$ value for the formation of M2 by CYP2C9 was 5.3 $\mu$L/mg protein/min.

**Chemical Inhibition Experiment.** Studies were conducted to evaluate the effect of CYP450 enzyme chemical inhibitors on the formation of M1 and M2 in pooled human liver microsomes (the concentration of CSA was 20 $\mu$M). According to the result above, M1 and M2 were identified as the metabolites derived from hydroxylation of CSA. Because of the very low yield of metabolites, they have not been separated or synthesized for technical reasons; metabolite formation was quantified by the loss of CSA relative to the internal standard (ISL) in each incubation sample on the basis of the MRM responses. Figure 7 presents the results of CSA biotransformation in the human liver microsome incubations after treatment with various inhibitors. Among seven kinds of inhibitors, ketoconazole (CYP3A4), sulfaphenazole (CYP2C9), and furafylline (CYP1A2) notably inhibited the formation of M1 from CSA. The percentages of inhibition of M1 formation by CYP1A2, CYP2C9, and CYP3A4 were 26.0, 35.5, and 38.5%, respectively. Sulfaphenazole showed significant inhibition to M2 formation, the percentage of inhibition reaching 97.8%. Percent inhibition of metabolite formation rate by isoform-specific inhibitors was calculated by comparing the inhibited activity with uninhibited controls (without inhibitors).

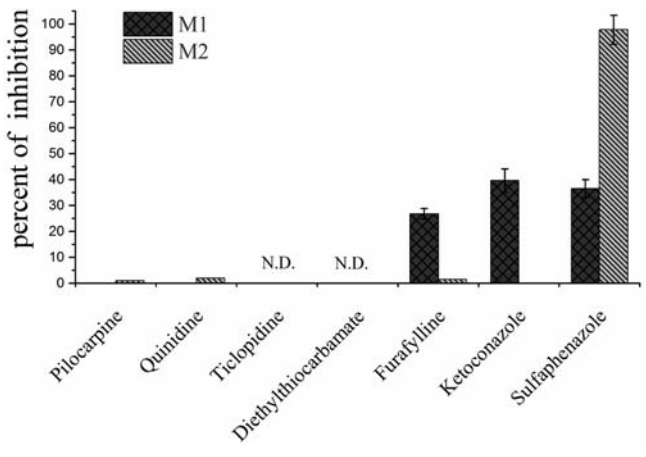


**Figure 7.** Inhibition percent of CSA with chemical inhibitor addition in the incubation system of human liver microsomes.

**CSA Inhibition Study of CYP450 Enzymes.** CSA (0.1–100 $\mu$M) was evaluated for its ability to inhibit CYP450 activity in pooled human liver microsomes using probe substrate. The results are presented in Table 4 and Figure 8. It is indicated that in a reversible manner CSA was an inhibitor of CYP3A4 and CYP2C9 ($IC_{50}$ values were 28.3 and 31.3 $\mu$M, respectively). CSA showed little or no inhibition to CYP1A2, 2A6, 2D6, 2C19, or 2E1 ($IC_{50} \geq 40$ $\mu$M).

**Table 4. CSA Inhibitory Activity against CYP1A2, CYP2A6, CYP2E1, CYP2C9, CYP2C19, CYP2D6, and CYP3A4 in Pooled Human Liver Microsomes**

| | $IC_{50}$ ($\mu$M) | |
|---|---|---|
| CYP isoform | 0 min of preincubation | 30 min of preincubation |
| 3A4 | 28.3 | 27.2 |
| 2D6 | >100 | >100 |
| 2C9 | 31.3 | 33.5 |
| 2A6 | >100 | >100 |
| 1A2 | >100 | >100 |
| 2C19 | >100 | >100 |
| 2E1 | 43.9 | 44.1 |

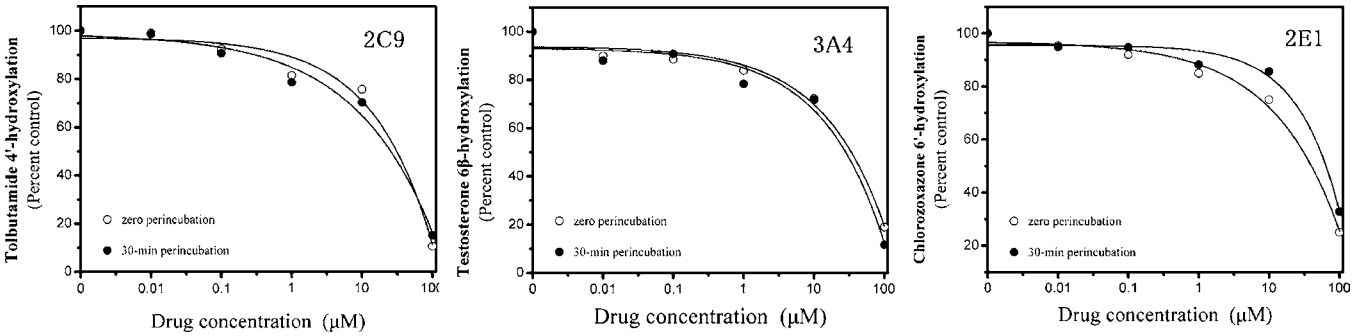


**Figure 8.** Effect of CSA on microsomal enzyme activity of CYP3A4, CYP2C9, and CYP2E1 with and without a 30 min preincubation with NADPH-fortified human liver microsomes.

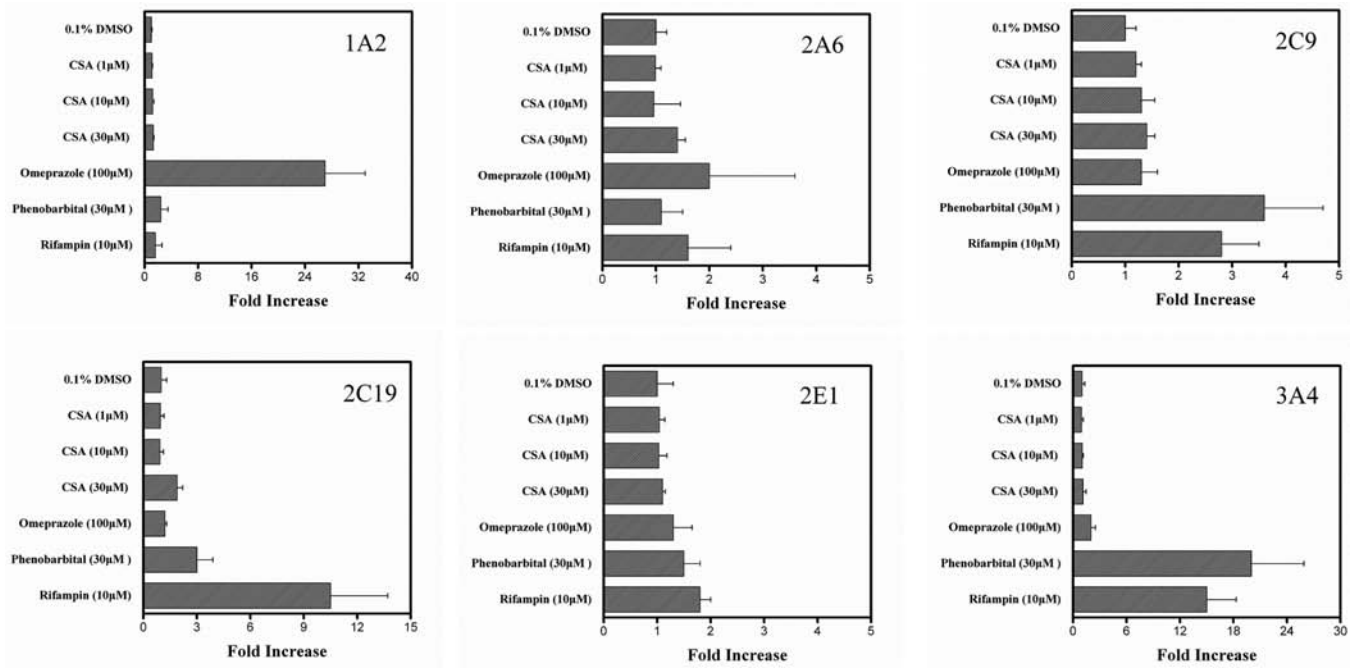


**Figure 9.** Effect of CSA or prototypical inducers on microsomal CYP450 activity in cultured human hepatocytes.

In the assay of time-dependent manner, the $IC_{50}$ values of CYP3A4 and CYP2C9 were 27.2 and 33.5 $\mu$M, respectively. $IC_{50}$ values of other enzymes were >40 $\mu$M.

**Analysis of CSA Potential To Induce CYP450 Enzymes.** To investigate the potential of CSA to induce the expression of CYP450 enzymes, freshly isolated and pretreated human hepatocytes were used. Three preparations of human hepatocytes were cultured and treated with CSA (1, 10, or 30 $\mu$M) or one of three prototypical enzyme inducers, omeprazole (100 $\mu$M), phenobarbital (750 $\mu$M), and rifampin (10 $\mu$M), once daily for 3 consecutive days. For the concentrations tested, CSA was not cytotoxic.

After treatment in all three preparations of human hepatocytes, prototypical CYP450 enzymes showed obviously sensitive to the inducers, as the result in Figure 9. Treatment with omeprazole produced a marked increase in CYP1A2 (27-fold), whereas it showed increases in CYP2C9 (3−4-fold), CYP2C19 (3−10-fold), and CYP3A4 (15−21-fold) after treatment with phenobarbital and rifampin. In the experiment of treatment with human hepatocytes for 3 consecutive days, with the concentration of CSA up to 30 $\mu$M, the activities of CYP1A2, CYP2A6, CYP2E1, CYP2C9, CYP2C19 , and CYP3A4 were almost not affected by CSA. The extent of enzyme activity induction did not reach significant levels, <2-fold increase (40% of the positive control).

## ■ DISSCUSSION

CSA has been shown to have effective antitumor, antioxidant, anti-inflammatory, and analgesic activities. However, up until now, the metabolism of CSA in vitro was unclear, and CSA metabolism in humans needs to be clarified. Therefore, metabolism of CSA with the CYP450 enzymes involved in vitro was identified in this study. Furthermore, experiments were conducted to explore the potential of CSA to cause food−drug interactions resulting from the inhibition or induction of the major human CYP450 enzymes.

LC-MS/MS, LC-MS/MS/MS, and parent drug fragmentation patterns were used as a guide to identify CSA metabolites. The fragmentation pathway of M1 was very similar to that of CSA. It was supposed that a hydroxyl group was conjugated on a simple benzene ring and dehydroxylation occurred easily. The most stable combination will occur at the para-position of the benzene ring, suggesting the structure of M1 was 12-hydroxycajaninstilbene acid. Fragment ions $m/z$ 250.5 and


dx.doi.org/10.1021/jf501635a | J. Agric. Food Chem. 2014, 62, 10604−10614

235.1 were found in fragment products of M2. It can be confirmed that $m/z$ 235.1 was obtained by styrene group removal on CSA according to the fragment pathway of CSA. $m/z$ 250.5 was 16 Da higher than $m/z$ 235.1, suggesting the hydroxyl occurred on $m/z$ 235.1 on the basis of MS/MS/MS results. Hence, it was supposed the hydroxyl was on the benzene ring that conjugated to isoprene, so the structure of M2 was 6-hydroxycajaninstilbene acid.

Hydroxylation to form metabolites M1 and M2 was the primary metabolic pathway of CSA in human liver microsomes. This indicates that CYP2C9 catalyzed the formation of all oxidative metabolites according to the results of incubations with recombinant human P450 enzymes and studies with human liver microsomes and selective P450 inhibitors, whereas CYP3A4 and CYP1A2 were only involved in the oxidization of CSA in the process of M1 formation.

The $CL_{int}$ values between human liver microsomes and recombinant human P450 enzymes indicated that CYP1A2, CYP2C9, and CYP3A4 were the predominant P450 enzymes forming M1. The $CL_{int}$ values for the formation of M1 by CYP3A4, CYP1A2, and CYP2C9 consistently were 1.2, 1.7, and 2.2 $\mu$L/mg protein/min, accounting for 22.1, 31.7, and 42.6% of the total $CL_{int}$. The inhibition effects of the chemical inhibitor toward M1 formation were consistent with the results of the contribution of each P450 involved in M1 formation. CYP1A2, CYP2C9, and CYP3A4 chemical inhibitors in human liver microsomes inhibited the formation of M1 by 26.0, 35.5, and 38.5%, respectively. This result was consistent with the $CL_{int}$ values of recombinant human P450 enzymes.

It is strongly suggested that M2 was primarily metabolized by CYP2C9 in human liver microsomes, on the basis of the present P450 reaction phenotype study. First, sulfaphenazole, a CYP2C9 specific inhibitor, significantly inhibited the formation of all major metabolites and the overall metabolism of M2; the inhibition rate was 97.8%. The chemical inhibitors selective to CYP1A2, CYP2A6, CYP2C9, CYP2C19, CYP2D6, and CYP2E1 showed little or no inhibitory effect on M2 formation. Second, recombinant CYP2C9 exhibited very high M2 oxidation activity, whereas other P450 isoforms had no or minimal M2 oxidation activity. The $CL_{int}$ values for the formation of M2 by CYP2C9 were 5.3 $\mu$L/mg protein/min, accounting for 95% of the total $CL_{int}$.

CYP2C9 was the only cytochrome P450 enzyme that converted CSA to M2, which raises the potential food−drug interactions. When two or more drugs competed for only one enzyme, and this enzyme catalyzing the metabolic reaction constitutes the major elimination pathway, a significant cytochrome P450 drug interaction may occur.[30,31] Compared with only one isozyme, three isozymes involved in the metabolism of CSA to M1 will reduce the potential food−drug interactions.

Inhibition studies were determined using the $(I)/K_i$ approach. $(I)$ is the maximum concentration of total drug at steady state $C_{max}$. $K_i$ wis the unbound inhibition constant determined in vitro. With a cutoff value of $(I)/K_i > 0.1$, drugs show an inhibition effect on enzymes. When $(I)/K_i < 0.1$, it is reasonable to assume that a drug had no clinically significant CYP450 inhibition. Although CSA metabolism studies in rats were reported recently,[9] there is no relative report of CSA metabolism in the human body until now. Herein, we assumed that $C_{max}$ is similar between rats and humans (with the addition of $IC_{50}$), and the potential of CSA in vitro food−drug interactions was evaluated using the $(I)/K_i$ approach. After 10 mg oral administration b.i.d. to rats, CSA resulted in a steady-state $C_{max}$ concentration of 2.03 $\mu$M (data not shown). The inhibitor concentration causing 50% inhibition ($IC_{50}$) was determined, and $K_i$ can be calculated as $IC_{50}/2$ by assuming competitive inhibition. Because $C_{max}/K_i$ was 0.14 for CYP3A4 and 0.13 for CYP2C9, it was possible for CSA to cause CYP3A4 and CYP2C9 inhibition. $C_{max}/K_i$ values were <0.1 for CYP1A2, CYP2A6, CYP2D6, CYP2C19, and CYP2E1, suggesting that CSA had a low tendency to inhibit these enzymes. CYP3A is the most abundant cytochrome P450 enzyme in humans, and it has been estimated that CYP3A4 is the major drug-metabolizing enzyme for nearly 50% of all currently marketed drugs.[32,33] A significant cytochrome P450 drug interaction may occur when two or more drugs compete for the same enzyme and when the metabolic reactions catalyzed by this enzyme constitute the major elimination pathway.[34] According to previous studies, resveratrol and naturally occurring stilbenes were suggested to be inhibitors of cytochrome P450 CYP3A4.[35−38] CSA belongs to the class of stilbene compounds, and our result showed its similar effect on CYP3A4, which was in accordance with results in the above references.

The preferred model for enzyme induction studies was primary human hepatocytes because primary human hepatocytes were mostly related to prediction of food−drug interactions.[39] The current study demonstrated that CSA was not an inducer of CYP1A2, CYP2A6, CYP2E1, CYP2C9, CYP2C19, or CYP3A4. CYP2D6 was not examined for its noninducible character recognized by the FDA (Draft Guidance for Industry: Drug Interaction Studies: Study Design, Data Analysis and Implications for Dosing and Labeling, 2006; http://www.fda.gov/downloads/Drugs/GuidanceComplianceRegulatoryInformation/Guidances/ucm072101). CSA did not cause more than a 2-fold induction in CYP1A2, CYP2A6, CYP2E1, CYP2C9, CYP2C19, or CYP3A4, and the relative response did not exceed 40% of the positive control.

In summary, major metabolism of CSA in human liver microsomes has been demonstrated. Of all the evaluated CYP450 isoforms, CYP3A4, CYP2C9, and CYP1A2 were the primary CYP450 enzymes responsible for the formation of these hydroxylation metabolites of CSA in human liver microsomes. These in vitro study results indicated that CYP3A4 and CYP2C9 were inhibited by CSA, which showed no inhibition for other CYP450 enzymes in a reversible manner. CSA did not show time-dependent inhibition potential on the CYP450 enzymes investigated here. In addition, the results of the present study suggested that CSA will not produce clinically significant induction of CYP450 enzymes.

## AUTHOR INFORMATION


### Corresponding Authors

*(Y.F.) Mail: Box 332, Hexing Road 26, Harbin 150040, PR China. Phone: +86 451 82190535. Fax: +86 451 82190535. E-mail: Yujie_fu2002@yahoo.com .

*(Y.Z.) Mail: Box 332, Hexing Road 26, Harbin 150040, PR China. Phone: +86 451 82191517. Fax: +86 451 82102082. E-mail: zygorl@vip.hl.cn

### Author Contributions

‖X.H. and X.P. contributed equally to this work.

## Funding

We gratefully acknowledge financial support from the Program for Importation of International Advanced Forestry Science and Technology, National Forestry Bureau (2012-4-06), Agricultural Science and Technology Achievements Transformation Fund Program (2012GB23600641), and Heilongjiang Province Science Foundation for Excellent Youths (JC200704).

## Notes

The authors declare no competing financial interest.

## REFERENCES

(1) Ingham, J. L. Induced isoflavonoids from fungus-infected stems of pigeonpea (*Cajanus cajan*). *Z. Naturforsch. C* **1976**, *31*, 504−508.

(2) Cooksey, C. J.; Dahiya, J. S.; Garratt, P. J.; Strange, R. N. Two novel stilbene-2-carboxylic acid phytoalexins from *Cajanus cajan*. *Phytochemistry* **1980**, *21*, 2935−2938.

(3) Inman, W. D.; Hoppe, D. C. *Compositions Containing Hyportriglyceridemically Active Stilbenenoids*; W. I. P. O. I. Bureau, 2002.

(4) Inman, W. D.; Hoppe, D. C. Compositions containing hypoglucemically active stilbenoids. U.S. Patent, Insemed Inc., Glen Allen, VA, USA, 2003.

(5) Zheng, Y. Y.; Yang, J.; Chen, D. H.; Sun, L. Effects of the stilbene extracts from *Cajanus cajan* L. on ovariectomy-induced bone loss in rats. *Acta Pharmacol. Sin.* **2007**, *42*, 562−565.

(6) Sun, S. M.; Song, Y. M.; Liu, J. Studies on the pharmacology of cajanin preparation. *Chin. Tradit. Herb Drugs* **1995**, *26*, 147−148.

(7) Wu, N.; Fu, K.; Fu, Y. J.; Zu, Y. G.; Chang, F. R.; Chen, Y. H.; Liu, X. L.; Kong, Y.; Liu, W.; Gu, C. B. Antioxidant activities of extracts and main components of pigeonpea (*Cajanus cajan* (L.) Millsp.) leaves. *Molecules* **2009**, *14*, 1032−1043.

(8) Fu, Y. J.; Zu, Y. G.; Liu, X.; Wu, N.; Kong, Y.; Luo, M.; Gu, C. B.; Peng, X. Apply of cajanin leaves supercritical carbon dioxide extraction and cajaninstilbene acid anti-tumor drug preparation. CN101569654B, 2011.

(9) Hua, X.; Fu, Y. J.; Zu, Y. G.; Wu, N.; Yu, K.; Li, j.; Peng, X.; Thomas, E. Plasma pharmacokinetics and tissue distribution study of cajaninstilbene acid in rats by liquid chromatography with tandem mass spectrometry. *J. Pharm. Biomed.* **2010**, *52*, 273−279.

(10) FDA. *Guidance for Industry: Drug Interaction Studies—Study Design, Data Analysis and Implications for Dosing and Labeling*, http://www.fda.gov/cber/guidelines.htm, 2006.

(11) Thompson, T. N. Early ADME in support of drug discovery, the role of metabolic stability studies. *Curr. Drug Metab.* **2000**, *1*, 215−241.

(12) Masimirembwa, C. M.; Thompson, R.; Andersson, T. B. *In vitro* high throughput screening of compounds for favorable metabolic properties in drug discovery. *Comb. Chem. High Throughput Screening* **2001**, *4*, 245−263.

(13) Bjornsson, T. D.; Callaghan, J. T.; Einolf, H. J.; Fischer, V.; Gan, L.; Grimm, S.; Kao, J.; King, S. P.; Miwa, G.; Ni, L. The conduct of *in vitro* and in vivo food-drug interaction studies, a Pharmaceutical Research and Manufacturers of America (PhRMA) perspective. *Drug Metab. Dispos.* **2003**, *31*, 815−832.

(14) Nebert, D. W.; Russell, D. W. Clinical importance of the cytochromes P450. *Lancet* **2002**, *360*, 1155−1162.

(15) Guengerich, F. P. Oxidative, reductive, and hydrolytic metabolism of drugs. In *Drug Metabolism in Drug Design and Development*; Zhang, D., Zhu, M., Humphreys, W. G., Eds.; Basic Concepts and Practice; Wiley: Hoboken, NJ, USA, 2007; pp 15−36.

(16) Hong, H.; Su, H.; Ma, L.; Yao, M.; Iyer, R. A.; Humphreys, W. G.; Christopher, L. J. *In vitro* characterization of the metabolic pathways and cytochrome P450 inhibition and induction potential of BMS-690514, an ErbB/vascular endothelial growth factor receptor inhibitor. *Drug Metab. Dispos.* **2011**, *39*, 1658−1667.

(17) Kong, Y.; Fu, Y. J.; Zu, Y. G.; Liu, W.; Wang, W.; Hua, X.; Yang, M. Ethanol modified supercritical fluid extraction and antioxidant activity of cajaninstilbene acid and pinostrobin from pigeonpea (*Cajanus cajan* (L.) Millsp.) leaves. *Food Chem.* **2009**, *117*, 152−159.

(18) Ward, B. A.; Gorski, J. C.; Jones, D. R.; Hall, S. D.; Flockhart, D. A.; Desta, Z. The cytochrome P450 2B6 (CYP2B6) is the main catalyst of efavirenz primary and secondary metabolism: implication for HIV/AIDS therapy and utility of efavirenz as a substrate marker of CYP2B6 catalytic activity. *J. Pharmacol. Exp. Ther.* **2003**, *306*, 287−300.

(19) Desta, Z.; Saussele, T.; Ward, B.; Blievernicht, J.; Li, L.; Klein, K.; Flockhart, D. A.; Zanger, U. M. Impact of CYP2B6 polymorphism on hepatic efavirenz metabolism in vitro. *Pharmacogenomics* **2007**, *8*, 547−558.

(20) Newton, D. J.; Wang, R. W.; Lu, A. Y. Cytochrome P450 inhibitors. Evaluation of specificities in the in vitro metabolism of therapeutic agents by human liver microsomes. *Drug Metab. Dispos.* **1995**, *23*, 154−158.

(21) Bourrié, M.; Meunier, V.; Berger, Y.; Fabre, G. Cytochrome P450 isoform inhibitors as a tool for the investigation of metabolic reactions catalyzed by human liver microsomes. *J. Pharmacol. Exp. Ther.* **1996**, *277*, 321−332.

(22) Rae, J. M.; Soukhova, N. V.; Flockhart, D. A.; Desta, Z. Triethylenethiophosphoramide is a specific inhibitor of cytochrome P450 2B6: implications for cyclophosphamide metabolism. *Drug Metab. Dispos.* **2002**, *30*, 525−530.

(23) Feidt, D. M.; Klein, K.; Hofmann, U.; Riedmaier, S.; Knobeloch, D.; Thasler, W. E.; Weiss, T. S.; Schwab, M.; Zanger, U. M. Profiling induction of cytochrome p450 enzyme activity by statins using a new liquid chromatography-tandem mass spectrometry cocktail assay in human hepatocytes. *Drug Metab. Dispos.* **2010**, *38*, 1589−1597.

(24) Wang, L.; Zhang, D.; Raghavan, N.; Yao, M.; Ma, L.; Frost, C. E.; Maxwell, B. D.; Chen, S. Y.; He, K.; Goosen, T. C.; Humphreys, W. G.; Grossman, S. J. In vitro assessment of metabolic drug-drug interaction potential of apixaban through cytochrome P450 phenotyping, inhibition, and induction studies. *Drug Metab. Dispos.* **2010**, *38*, 448−458.

(25) Wortelboer, H. M.; de Kruif, C. A.; van Iersel, A. A.; Falke, H. E.; Noordhoek, J.; Blaauboer, B. J. The isoenzymes pattern of cytochrome P450 in rat hepatocytes in primary culture, comparing different enzyme activities in microsomal incubations and intact monolayers. *Biochem. Pharmacol.* **1990**, *40*, 2525−2534.

(26) Robertson, P.; DeCory, H. H.; Madan, A.; Parkinson, A. In vitro inhibition and induction of human hepatic cytochrome P450 enzymes by modafinil. *Drug Metab. Dispos.* **2000**, *28*, 664−671.

(27) GraphPad Prism 5.0. GraphPad Software Inc., San Diego, CA, USA; www.graphpad.com.

(28) Ashforth, E. I.; Carlile, D. J.; Chenery, R.; Houston, J. B. Prediction of in vivo disposition from in vitro systems: clearance of phenytoin and tolbutamide using rat hepatic microsomal and hepatocyte data. *J. Pharmacol. Exp. Ther.* **1995**, *274*, 761−766.

(29) Houston, J. B.; Carlile, D. J. Prediction of hepatic clearance from microsomes, hepatocytes, and liver slices. *Drug Metab. Rev.* **1997**, *29*, 891−922.

(30) Rowland, M.; Matin, S. B. Kinetics of food-drug interactions. *J. Pharmacokinet. Biopharm.* **1973**, *1*, 553−567.

(31) Lin, J. H.; Lu, A. Y. Inhibition and induction of cytochrome P450 and the clinical implications. *Clin. Pharmacokinet.* **1998**, *35*, 361−390.

(32) Shimada, T.; Yamazaki, H.; Mimura, M.; Inui, Y.; Guengerich, F. P. Interindividual variations in human liver cytochrome P-450 enzymes involved in the oxidation of drugs, carcinogens and toxic chemicals, studies with liver microsomes of 30 Japanese and 30 Caucasians. *J. Pharmacol. Exp. Ther.* **1994**, *270*, 414−423.

(33) Yan, Z.; Caldwell, G. W. Metabolism profiling, and cytochrome P450 inhibition and induction in drug discovery. *Curr. Top. Med. Chem.* **2001**, *1*, 403−425.

(34) Lin, J. H.; Lu, A. Y. Inhibition and induction of cytochrome P450 and the clinical implications. *Clin. Pharmacokinet.* **1998**, *35*, 361−390.

(35) Gilly, R. S.; Oded, S.; Zohar, K. Influence of lipophilicity on the interaction s of hydroxy stilbenes with cytochrome P450 3A4. *Biochem. Biophys. Res. Commun.* **2004**, *323*, 668−673.

(36) Piver, B.; Berthou, F.; Dreano, Y.; Lucas, D. Inhibition of CYP3A, CYP1A and CYP2E1 activities by resveratrol and other non volatile red wine components. *Toxicol. Lett.* **2001**, *125*, 83−91.
(37) Chan, W. K.; Delucchi, A. B. Resveratrol, a red wine constituent, is a mechanism-based inactivator of cytochrome P450 3A4. *Life Sci.* **2000**, *67*, 3103−3112.
(38) Piver, B.; Berthou, F.; Dreano, Y.; Lucas, D. Differential inhibition of human cytochrome P450 enzymes by epsilon-viniferin, the dimer of resveratrol, comparison with resveratrol and polyphenols from alcoholizd beverages. *Life Sci.* **2003**, *73*, 1199−1213.
(39) LeCluyse, E. L. Pregnane X receptor, molecular basis for species differences in CYP3A induction by xenobiotics. *Chem.−Biol. Interact.* **2001**, *134*, 283−289.

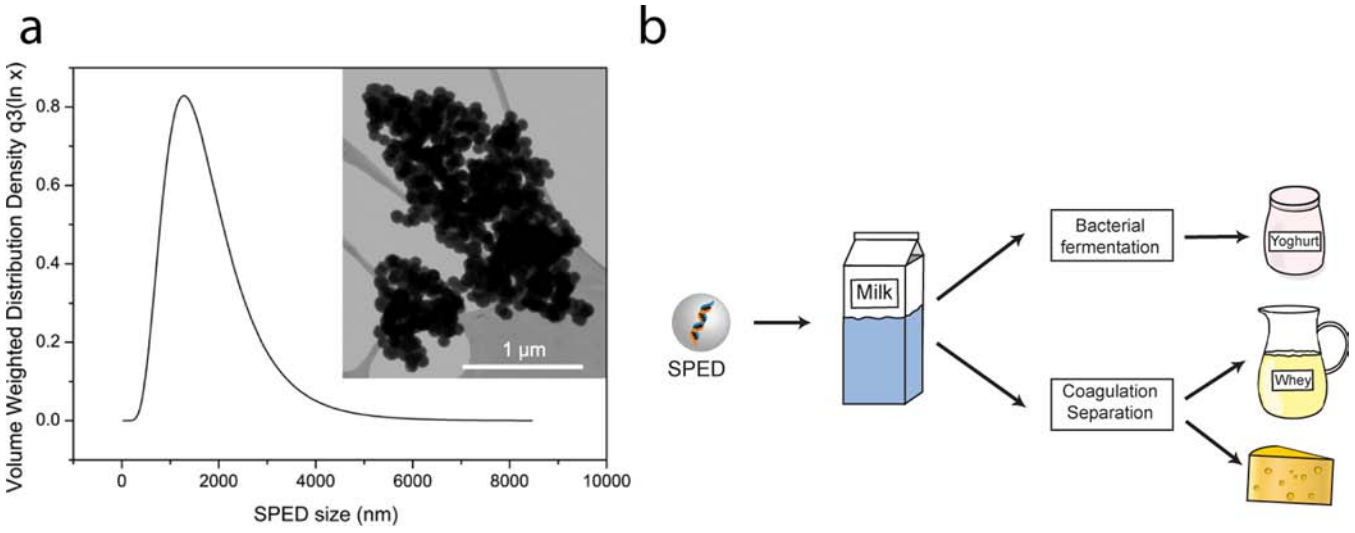


**Figure 1.** (a) Particle size distribution and a characteristic electron microscopy image of the applied Silica Particles with Encapsulated DNA (SPED). (b) Milk is complemented with SPED with a specific code and subsequently manufactured to yoghurt and cheese.

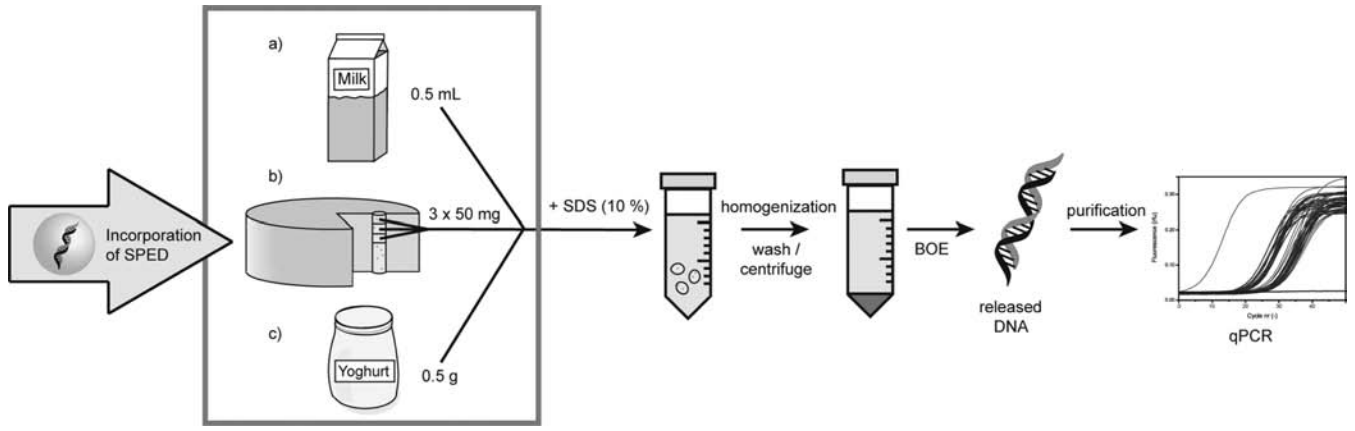


**Figure 2.** Flowchart for incorporation of SPED into milk, cheese, and yoghurt and subsequent extraction of the marker from the foodstuff by washing/centrifugation procedures for final analysis via qPCR.

solution (25 wt %), hydrogen peroxide ($H_2O_2$, 30 wt %), and ammonium hydrogen difluoride ($NH_4FHF$, pure) were purchased from Merck. Isopropanol (>99.8%), ammonium fluoride ($NH_4F$, puriss.), and ammonium hydroxide solution (25 wt %) were used as supplied from Sigma-Aldrich. Tetraethoxysilane (TEOS, ≥99.0%) was received from Aldrich, *N*-trimethoxysilylpropyl-*N*,*N*,*N*-trimethylammonium chloride (TMAPS, 50 wt % in methanol) from ABCR, L-ascorbic acid sodium salt (99%) from Acros Organics, and hexyltrimethoxysilane (>96%) from Tokyo Chemical Industry. Sodium dodecyl sulfate (SDS, >98%) was purchased from Sigma. Qubit dsDNA high-sensitivity (HS) assay was supplied by Invitrogen, QIAquick PCR purification kit from Quiagen, and EDTA disodium salt dihydrate (99%) from Biosolve. Ultrapure water (18.2 MΩ cm at 25 °C) was used. The double-stranded DNA solutions for the 116 base-pair (bp) amplicon MB1 and the 121 bp amplicon TOM1 (from tomato DNA sequence) as well as their corresponding primers were purchased from Microsynth. MB1 was used for the experiments with milk, yoghurt, cheese, and whey, while TOM1 was only used in one yoghurt experiment.

**Real-Time Quantitative PCR.** The qPCR was executed with a Roche Lightcycler 96. Based on the cycle of threshold (Ct), conclusions on the initial DNA concentration in the sample—and with that, the SPED concentration—can be drawn. The positive controls for the PCR were obtained by dissolving known SPED amounts directly in buffered oxide etch (BOE) solution. A PCR blank (no-template control) confirmed clean working conditions. Each sample well was filled with 5 µL of sample volume, 10 µL of master mix (Lightcycler 480 SYBR Green I Master, Roche), 3 µL of PCR-grade water, 1 µL of forward primer, and 1 µL of reverse primer (2 µM each). The qPCR consisted of a three-step amplification with 45 cycles. The samples were first heated to 95 °C for 15 s, then remained at 60 °C for 30 s, and last were held at 72 °C for 30 s. Each sample was analyzed in replicates (technical triplicates).

**Food Products.** Pasteurized milk (0.5 L, 3.9% fat, organic) and yoghurt (180 g, 4% fat, Naturaplan) were bought at Coop, ETH Hönggerberg. The rennet tablets were supplied by Swissmilk (Winkler AG, approximately 95% chymosin, 5% pepsin, salt as support material).

**DNA Codes.** Sequence *MB1* is a randomly generated DNA sequence, which was selected for good PCR amplification properties and checked for specificity using Basic Local Alignment Search Tool (BLAST):[26] (5′−3′) ATT GCA CCC TTA CCA CGA AGA CAG GTT TGT CCA ATC CCA TAT TGC GAC CTT GGC AGG GGG TTC GCA AGT CCC ACC CGA AAC GTT GCT GAA GGC TCA GGT TTC TGA GCG ACA AAA GC. Sequence *TOM1* is a short sequence taken from the tomato genome (species *Solanum lycopersicum*), Chromosome 1, NC_015438.1: (5′−3′) TGA AGG ACT GAA GCA ACA CGA AAC CTA TAC AAC TAA CTA GCA GAG CTC TCG ATT TTG CTA ATT CAT CAT AAC TCA TAC TAT GAG CAA AAA AGT AAA GGG AAA TTT TCG TGC ATG GTG TTG A.


dx.doi.org/10.1021/jf503413f | J. Agric. Food Chem. 2014, 62, 10615−10620

**Particle Synthesis.** To produce the SPED, the protocol of Paunescu et al.[22] was applied. Particles containing either the DNA sequence MB1 or the DNA sequence TOM1 were produced (for sequences, see above). Following their production, the SPED were tested on their radical treatment stability as previously described.[22] The particle structure was analyzed by scanning transmission electron microscopy (STEM, NovaNanoSEM 450, FEI) at 30 kV. The particle size was determined by volume-weighted sedimentation analysis (LUMiSizer, LUM GmbH).

**Labeling of Food.** *Milk.* SPED concentrations of 10, 1, and 0.1 ppb were prepared in milk. For every SPED concentration, ten 0.5 mL samples of pasteurized milk were labeled by adding a 5 $\mu$L of SPED dispersion at prediluted concentrations to give the final SPED concentration.

*Yoghurt.* The yoghurt was spiked with 100, 10, 1, and 0.1 ppb SPED containing the MB1 sequence. Additionally, yoghurt with 10 ppb SPED containing DNA code TOM1 was made. To produce 100 g of yoghurt, 87 g of pasteurized milk, 13 g of yoghurt, and 10 $\mu$L of prediluted SPED dispersion were used. After vortexing, the yoghurt was placed into an incubator at 42 °C for 5.5 h. Subsequently, the glasses were carefully transferred to a refrigerator ($T$ = 4−6 °C) and left there overnight. Experiments were performed in triplicates (three yoghurts for every concentration). From every yoghurt, two samples were analyzed. To ensure a representative sample, the yoghurt was stirred before sampling.

*Cheese.* For the cheese production, 5.8 g of yoghurt, 100 g of pasteurized milk, and a defined amount of SPED were mixed in a beaker. The mixture was added to 900 g of pasteurized milk. The detailed cheese recipe can be found in the Supporting Information.

**Label Extraction from Food.** *Milk.* For the extraction, the 0.5 mL sample was mixed with 1 mL of SDS solution (10 wt %) in a 2 mL Eppendorf tube (Figure 2). The sample was sonicated for 30 s using an ultrasonicator (Ultraschall-Prozessor UP50H, Huberlab) and then centrifuged for 3 min at 21500$g$. The supernatant was discarded, while 50 $\mu$L of ultrapure water was added to the pellet. The sample was vortexed for 1 min before 70 $\mu$L of the BOE solution was added. After the final purification with a QIAquick PCR Purification Kit, a qPCR was performed with a Roche Lightcycler 96. See Figure S5 in the Supporting Information for a flow diagram of the extraction method.

*Yoghurt.* To extract the SPED, 0.5 g of the yoghurt was mixed with 1 mL of SDS solution (10 wt %) in a 2 mL Eppendorf tube (Figure 2). After a quick vortex step, the sample was sonicated for 30 s. The tubes were centrifuged for 3 min at 21500$g$. The resulting supernatant was discarded, while 1 mL of SDS solution (10 wt %) was added to the pellet. One minute of vortexing was followed by another centrifugation step for 3 min at 21500$g$. The supernatant was discarded, while 50 $\mu$L of ultrapure water was given to the pellet. The sample was then vortexed for another minute. Finally, 70 $\mu$L of BOE solution was pipetted to the sample. As a last step, the QIAquick PCR Purification Kit was applied. The resulting liquid was directly used for qPCR analysis. See Figure S6 in the Supporting Information for a flow diagram of the extraction method.

*Cheese.* From the cheese, a cylindrical-shaped piece was cut out (Figure 2). From the cross section, three 50 mg samples from the cylinder's rind, core, and the space between the rind and the core were combined to a collective sample and placed into a 2 mL microtube. Next, 1.5 mL of SDS solution (10 wt %) and two speed mixing beads (chrome steel, $d$ = 6.35 mm) were added. The sample was then homogenized with a Mini-Beadbeater (Biospec Products) for 70 s at a speed of 4200 rpm. After the beads had been removed from the tubes, the latter were centrifuged for 7 min at 21500$g$. Following a repetition of the mechanical homogenization at the same conditions, the sample was washed twice with 1 mL of SDS solution (10 wt %) and once with ultrapure water, with intermediate centrifugation steps. After addition of 50 $\mu$L of ultrapure water, the sample was vortexed for 1 min, and 70 $\mu$L of the BOE solution was added. The sample was then shaken at 24 °C for 30 min before it was purified using the QIAquick PCR Purification Kit for qPCR analysis. See Figure S7 in the Supporting Information for a flow diagram of the extraction method.

**Statistical Analysis.** The validity of the SPED labeling method was proven. Please find the discussion on the necessary variables in the Supporting Information.

The experimental data were analyzed with Origin 8.6. The two-sample $t$ tests were based on a 5% significance level. One-way analysis of variance (ANOVA) was used to compare the sample means at different time points.

## RESULTS AND DISCUSSION

SPED are aggregated silica particles with a primary particle size of ∼140 nm and an agglomerate size of ∼1200 nm (see Figure 1a), much resembling the structure of commercial silica products (e.g., Aerosil, fumed silica, and precipitated silica). The particles are easily dispersed in water and can be directly mixed with aqueous liquids at various concentrations. The silica can be loaded with ∼0.1 wt % of DNA, and in this work both a random (MB1) and a naturally occurring (TOM1) DNA code were utilized. The DNA molecules are well encapsulated within the silica matrix, as proven by exposing the particles to aggressive radical oxygen species (stability >90%, see Table S2 in the Supporting Information).[23] Upon mixing with fluoride-containing solutions (e.g., buffered oxide etch (BOE), a pH-stabilized $NH_4F$ solution) the silica can be dissolved, releasing the DNA and allowing its analysis by qPCR without further treatment.[22] In the case of food products, the particles first have to be extracted from the complex matrix, as food components such as proteins and fats are known to interfere with PCR analysis. Therefore, for every food type, a processing procedure was elaborated (see Figure 2 and Figures S5−S7 in the Supporting Information). These processing procedures essentially include multiple SDS washing and particle centrifugation steps. In the case of the cheese, the semisolid matrix was first mechanically broken down utilizing a mini-bead-beater. Following the washing and centrifugation procedure, all cases resulted in (hardly visible) particle deposits in the tubes, without any visual residue of proteins or fat. The deposits were dissolved in BOE, and then the DNA was purified with commercial DNA purification kits and directly analyzed via qPCR using the corresponding primers. qPCR analysis was done in a traditional way, where the cycle was monitored (= Ct) at the point at which the fluorescence signal exceeded a given threshold (threshold computed automatically from signal-to-noise ratio by Lightcycler instrument). In this way the DNA, and by extension also the particles, could be detected down to 0.1 ppb for milk and yoghurt and down to 1 ppb for cheese (Figure 3 and Supporting Information). In comparison, the analysis of pesticide residues in fruit and vegetable samples with gas chromatography is possible to a limit of detection of 20 ppb.[27]

To investigate whether the DNA/particle detection method is quantitative, the foodstuffs under investigation were labeled with various SPED concentrations in the ppb range. Based on the exponential nature of the qPCR method, we did not expect to be able to measure small concentration differences, but rather concentrations on a logarithmic scale. Indeed, the Ct depended linearly ($R^2$ = 0.98 for yoghurt, $R^2$ = 0.99 for milk and cheese) on logarithmic particle concentration added to the individual foods (see Figure S1 and Table S1 in the Supporting Information). Additionally, in milk, yoghurt, and cheese, particle concentrations could be statistically discriminated on a log 10 scale, i.e., 0.1 ppb could be discriminated from 1 ppb, and 1/10 ppb samples were statistically different ($p$ < 0.05, Figure 3). Further control experiments (data not shown)

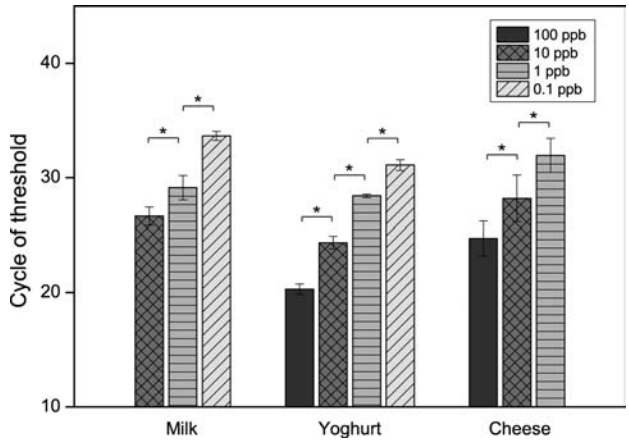


**Figure 3.** qPCR results (cycle of threshold, Ct) for the DNA within the particles detected at various particle loadings (ppb = $\mu$g particles per kg of food). *Denotes statistical significance at $p < 0.05$. The linearity of the Ct vs log particle concentration is shown in Figure S1 in the Supporting Information.

revealed that the particle concentration was independent of the sampling position in the cheese sample (yoghurt and milk samples were homogenized prior to particle extraction).

An additional aspect that is of importance with regard to quantitative analysis is the stability of the marker within the matrix over time. We have previously shown that, based on its encapsulation in silica, the DNA is protected from environmental decay over long storage times.[23] In order to display that this is true within the food products under investigation, additional tests were performed: SPED particles were added to cheese and yoghurt at 1 ppb and analyzed over time (2 weeks for yoghurt; 4 weeks for cheese). As visible in Figure 4, the

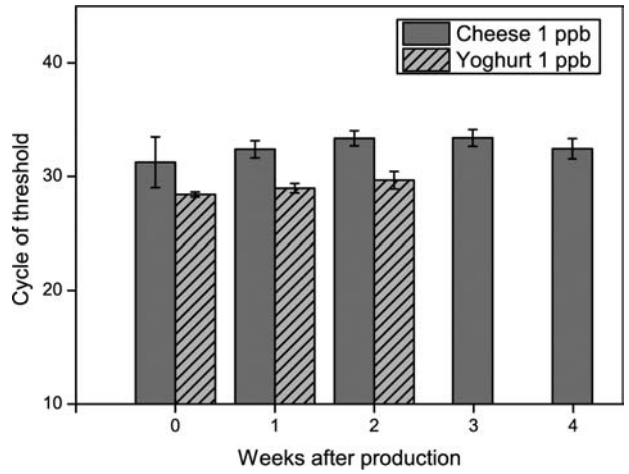


**Figure 4.** Cycle of threshold for cheese and yoghurt labeled with 1 ppb SPED. The samples remained stable over a course of 4 and 2 weeks for cheese and yoghurt, respectively.

qPCR readings (Ct values) did not increase over time, indicating that the DNA within the particles is unharmed during storage. This further shows that absolute quantification was feasible, even after several weeks of storage. Of course, for cheese, longer storage durations are of interest and are under current investigation.

The application of natural DNA as a unique sequence may be an advantage for consumer acceptance. For this reason we utilized a fragment (121 bp) of tomato DNA (species *Solanum lycopersicum*) as code. The sequence was selected from chromosome 1 of the tomato's DNA for optimal primers utilizing an online primer search algorithm (Primer3)[28] and tested for uniqueness using the Basic Local Alignment Search Tool (BLAST).[26] Yoghurt manufactured with 10 ppb of these particles could be identified by qPCR if the corresponding TOM1 primers were utilized (Ct = 28.77 ± 0.27). Utilizing the same procedure but analyzing with non-corresponding primers (MB1 primers) gave no significant PCR amplification (Ct = Ct(blank)), proving the selectivity of PCR analysis, which is well known and reported in medical diagnostics[29] and bacteria detection.[30]

The SPED labeling method is much more quantifiable compared to tagging approaches where a microbial cell with a DNA discriminable from the somatic cells of the milk was applied. Bacterial cells pass through a growth cycle with replication and decline. Their cell number and DNA amount is therefore not at all times the same. With our method, we could prove that the amount of DNA encapsulated in silica was stable over a course of several weeks. The SPED ensure, therefore, a more precise tagging than other methods do.

When silica particles loaded with the natural source DNA sequence (TOM1) are utilized to mark yoghurt at a particle loading of 1 ppb, a consumer eating 250 g of the yoghurt would consume 0.25 $\mu$g of silica and 0.25 ng of tomato DNA. This is equivalent to 0.0002% of the average daily dietary silica intake[31] and equivalent to the DNA present in 0.0001% of one fresh tomato.[32,33] Silica particles have a long history as food additives (E551) and are approved for several uses in European and U.S. markets. Based on the availability of billions of base-pair sequences from food sources, the use of naturally occurring DNA sequences as a coding tool can easily be envisioned. Combinations of mixtures of particles carrying several codes may further increase the variability of the code library.

In order to estimate the price of the DNA in silica food tagging technology presented here, we utilized currently available price data. The main cost driver of the technology is the synthetic DNA code, at a price of 9000 USD/g (as per commercial offer from Microsynth in March 2014; costs of additional raw materials are negligible). From 1 g of DNA, about 1 kg of particles can be produced (loading of ~1 $\mu$g/mg). If a SPED concentration of 10 ppb is applied to a food product, the labeling would cost 0.00009 USD per kg (i.e., 9¢ per ton) of food plus the labor costs, which will depend on the cost structure of the particle-producing company. This short calculation shows that in a potential application of the technology in tracing food, the cost of the DNA label is not critical.

From a purely technical and chemical point of view, above justification of material choice and cost estimation shows that the application of DNA in silica particles as a food-marking tool is of both low risk and low cost. Still, it will be evident to the reader that the ongoing public discussion on the risk of both DNA technology and nanotechnology (including discussions on the general use of amorphous silica as a food additive)[34] may slow down the application of these tracers in foodstuff. As with most new technologies, the potential risk of the additive must be balanced with the potential opportunity of uniquely tagging foodstuff. The answer to this question can only be the result of future discussions between many stakeholders, including consumers, producers, customs agencies, and local governments. In terms of food additive regulation, the use of an

additive as internal food label has not been addressed so far, so neither the Codex Alimentarius nor the European numbering system (EFSA) has a corresponding functional category.

This study shows that DNA-loaded silica particles can be utilized as tracers in milk, yoghurt, and cheese. The technology requires only marginal amounts of resources and has a broad range of label generation possibilities. While quantification has to be normalized for every food type (standard curve per food type), the result is quantitative on a logarithmic scale for tracer concentrations as low as 0.1 ppb (i.e., 0.1 $\mu$g of tracer per kg of foodstuff). The stability of the DNA tracer in the processing of milk to yoghurt and cheese shows the stability of the tracer over the production chain. The possibility of tracer read-out from food matrixes as complex as cheese and yoghurt displays the robustness of the method, and the applicability of the tracer to other food types is anticipated.

## ■ ASSOCIATED CONTENT

### Supporting Information

More information on the validity of the method, cheese manufacture, calculation of sedimentations times, and process flowcharts. This material is available free of charge via the Internet at http://pubs.acs.org.

## ■ AUTHOR INFORMATION

### Corresponding Author

*Tel: + 41 44 633 63 34. Fax: + 41 44 633 10 83. E-mail: robert.grass@chem.ethz.ch.

### Funding

The Institute for Chemical and Bioengineering (ICB) at ETH Zurich and the Swiss National Science Foundation (no. 200021-150179) provided financial support.

### Notes

The authors declare the following competing financial interest(s): R.N.G. and W.J.S. declare financial interest in the form of a patent application on DNA encapsulation licenced to TurboBeads Llc, of which R.N.G. and W.J.S. are shareholders and R.N.G. is a part-time employee. M.S.B., D.P., P.R.S., and C.A.M. have no competing financial interests..

## ■ REFERENCES

(1) European Union. Regulation (EU) No. 1151/2012 on Quality Schemes for Agricultural Products and Foodstuffs, 2012.

(2) Dalvit, C.; De Marchi, M.; Cassandro, M. Genetic Traceability of Livestock Products: A Review. *Meat Sci.* **2007**, *77*, 437−449.

(3) Chansud, W.; Wisanmongkol, J.; Ketprom, U. RFID for Poultry Traceability System at Animal Checkpoint. In *Electrical Engineering/Electronics, Computer, Telecommunications and Information Technology*; ECTI-CON 2008, 5th International Conference; IEEE: New York, 2008; Vol. 2, pp 753−756.

(4) Chao, C.-C.; Yang, J.-M.; Jen, W.-Y. Determining Technology Trends and Forecasts of RFID by a Historical Review and Bibliometric Analysis from 1991 to 2005. *Technovation* **2007**, *27*, 268−279.

(5) Regattieri, A.; Gamberi, M.; Manzini, R. Traceability of Food Products: General Framework and Experimental Evidence. *J. Food Eng.* **2007**, *81*, 347−356.

(6) Shanahan, C.; Kernan, B.; Ayalew, G.; McDonnell, K.; Butler, F.; Ward, S. A Framework for Beef Traceability from Farm to Slaughter Using Global Standards: An Irish Perspective. *Comput. Electron. Agric.* **2009**, *66*, 62−69.

(7) Cabana, G.; Rasmussen, J. B. Modelling Food Chain Structure and Contaminant Bioaccumulation Using Stable Nitrogen Isotopes. *Nature* **1994**, *372*, 255−257.

(8) Kelly, S.; Heaton, K.; Hoogewerff, J. Tracing the Geographical Origin of Food: The Application of Multi-Element and Multi-Isotope Analysis. *Trends. Food Sci. Technol.* **2005**, *16*, 555−567.

(9) Zhao, Y.; Zhang, B.; Chen, G.; Chen, A.; Yang, S.; Ye, Z. Tracing the Geographic Origin of Beef in China on the Basis of the Combination of Stable Isotopes and Multielement Analysis. *J. Agric. Food Chem.* **2013**, *61*, 7055−7060.

(10) Camin, F.; Wietzerbin, K.; Cortes, A. B.; Haberhauer, G.; Lees, M.; Versini, G. Application of Multielement Stable Isotope Ratio Analysis to the Characterization of French, Italian, and Spanish Cheeses. *J. Agric. Food Chem.* **2004**, *52*, 6592−6601.

(11) Scampicchio, M.; Mimmo, T.; Capici, C.; Huck, C.; Innocente, N.; Drusch, S.; Cesco, S. Identification of Milk Origin and Process-Induced Changes in Milk by Stable Isotope Ratio Mass Spectrometry. *J. Agric. Food Chem.* **2012**, *60*, 11268−11273.

(12) Versini, G.; Monetti, A.; Reniero, F. Monitoring Authenticity and Regional Origin of Wines by Natural Stable Isotope Ratios Analysis. *Wine: nutritional and therapeutic benefits*; ACS Symposium Series *661*; American Chemical Society: Washington, DC, 1997.

(13) Ehtesham, E.; Hayman, A. R.; McComb, K. A.; Van Hale, R.; Frew, R. D. Correlation of Geographical Location with Stable Isotope Values of Hydrogen and Carbon of Fatty Acids from New Zealand Milk and Bulk Milk Powder. *J. Agric. Food Chem.* **2013**, *61*, 8914−8923.

(14) Bugaud, C.; Buchin, S.; Coulon, J.-B.; Hauwuy, A.; Dupont, D. Influence of the Nature of Alpine Pastures on Plasmin Activity, Fatty Acid and Volatile Compound Composition of Milk. *Lait* **2001**, *81*, 401−414.

(15) Mauriello, G.; Moio, L.; Genovese, A.; Ercolini, D. Relationships Between Flavoring Capabilities, Bacterial Composition, and Geographical Origin of Natural Whey Cultures Used for Traditional Water-Buffalo Mozzarella Cheese Manufacture. *J. Dairy Sci.* **2003**, *86*, 486−497.

(16) Sampaio, O. M.; Reche, R. V.; Franco, D. W. Chemical Profile of Rums as a Function of Their Origin. The Use of Chemometric Techniques for Their Identification. *J. Agric. Food Chem.* **2008**, *56*, 1661−1668.

(17) Mafra, I.; Ferreira, I. M.; Oliveira, M. B. P. Food Authentication by PCR-Based Methods. *Eur. Food Res. Technol.* **2008**, *227*, 649−665.

(18) Conyers, C. M.; Allnutt, T. R.; Hird, H. J.; Kaye, J.; Chisholm, J. Development of a Microsatellite-Based Method for the Differentiation of European Wild Boar (Sus Scrofa Scrofa) from Domestic Pig Breeds (Sus Scrofa Domestica) in Food. *J. Agric. Food Chem.* **2012**, *60*, 3341−3347.

(19) Mininni, A. N.; Pellizzari, C.; Cardazzo, B.; Carraro, L.; Balzan, S.; Novelli, E. Evaluation of Real-Time PCR Assays for Detection and Quantification of Fraudulent Addition of Bovine Milk to Caprine and Ovine Milk for Cheese Manufacture. *Int. Dairy J.* **2009**, *19*, 617−623.

(20) Fang, W.; Meinhardt, L. W.; Mischke, S.; Bellato, C. M.; Motilal, L.; Zhang, D. Accurate Determination of Genetic Identity for a Single Cacao Bean, Using Molecular Markers with a Nanofluidic System, Ensures Cocoa Authentication. *J. Agric. Food Chem.* **2014**, *62*, 481−487.

(21) Casey, M. G.; Isolini, D.; Amrein, R.; Wechsler, D.; Berthoud, H. Naturally Occurring Genetic Markers in Lactobacilli and Their Use to Verify the Authenticity of Swiss Emmental PDO Cheese. *Dairy Sci. Technol.* **2008**, *88*, 457−466.

(22) Paunescu, D.; Puddu, M.; Soellner, J. O. B.; Stoessel, P. R.; Grass, R. N. Reversible DNA Encapsulation in Silica to Produce ROS-Resistant and Heat-Resistant Synthetic DNA "Fossils". *Nat. Protoc.* **2013**, *8*, 2440−2448.

(23) Paunescu, D.; Fuhrer, R.; Grass, R. N. Protection and Deprotection of DNA—High-Temperature Stability of Nucleic Acid Barcodes for Polymer Labeling. *Angew. Chem.* **2013**, *52*, 4269−4272.

(24) Mora, C. A.; Paunescu, D.; Grass, R. N.; Stark, W. J. Silica Particles with Encapsulated DNA as Trophic Tracers. *Mol. Ecol. Resour.* **2014**, DOI: 10.1111/1755-0998.12299.

(25) Puddu, M.; Paunescu, D.; Stark, W. J.; Grass, R. N. Magnetically Recoverable, Thermostable, Hydrophobic DNA/Silica Encapsulates

and Their Application as Invisible Oil Tags. *ACS Nano* **2014**, *8*, 2677−2685.
(26) Altschul, S. F.; Gish, W.; Miller, W.; Myers, E. W.; Lipman, D. J. Basic Local Alignment Search Tool. *J. Mol. Biol.* **1990**, *215*, 403−410.
(27) Fillion, J.; Sauvé, F.; Selwyn, J. Multiresidue Method for the Determination of Residues of 251 Pesticides in Fruits and Vegetables by Gas Chromatography/Mass Spectrometry and Liquid Chromatography with Fluorescence Detection. *J. AOAC Int.* **2000**, *83*, 698−713.
(28) Koressaar, T.; Remm, M. Enhancements and Modifications of Primer Design Program Primer3. *Bioinformatics* **2007**, *23*, 1289−1291.
(29) Rohr, U.-P.; Wulf, M.-A.; Stahn, S.; Steidl, U.; Haas, R.; Kronenwett, R. Fast and Reliable Titration of Recombinant Adeno-Associated Virus Type-2 Using Quantitative Real-Time PCR. *J. Virol. Methods* **2002**, *106*, 81−88.
(30) Hein, I.; Lehner, A.; Rieck, P.; Klein, K.; Brandl, E.; Wagner, M. Comparison of Different Approaches to quantifyStaphylococcus Aureus Cells by Real-Time Quantitative PCR and Application of This Technique for Examination of Cheese. *Appl. Environ. Microbiol.* **2001**, *67*, 3122−3126.
(31) Dekkers, S.; Krystek, P.; Peters, R. J.; Lankveld, D. P.; Bokkers, B. G.; van Hoeven-Arentzen, P. H.; Bouwmeester, H.; Oomen, A. G. Presence and Risks of Nanosilica in Food Products. *Nanotoxicology* **2011**, *5*, 393−405.
(32) Bertin, N.; Gautier, H.; Roche, C. Number of Cells in Tomato Fruit Depending on Fruit Position and Source-Sink Balance during Plant Development. *Plant Growth Regul.* **2002**, *36*, 105−112.
(33) Arumuganathan, K.; Earle, E. D. Nuclear DNA Content of Some Important Plant Species. *Plant Mol. Biol. Rep.* **1991**, *9*, 208−218.
(34) Dekkers, S.; Bouwmeester, H.; Bos, P. M.; Peters, R. J.; Rietveld, A. G.; Oomen, A. G. Knowledge Gaps in Risk Assessment of Nanosilica in Food: Evaluation of the Dissolution and Toxicity of Different Forms of Silica. *Nanotoxicology* **2013**, *7*, 367−377.

JOURNAL OF AGRICULTURAL AND FOOD CHEMISTRY

Addition/Correction

pubs.acs.org/JAFC

# Correction to Muscadine Grape (*Vitis rotundifolia*) and Wine Phytochemicals Prevented Obesity Associated Metabolic Complications in C57BL/6J Mice

Vishnupriya Gourineni, Neil F. Shay, Soonkyu Chung, Amandeep K. Sandhu, and Liwei Gu*

*J. Agric. Food Chem.* **2012**, *60* (31), 7674−7681. DOI: 10.1021/jf3013663

A recent review of the data related to this publication indicated several errors. Figure 3 and Table 5 in the original paper had typographical errors and should be replaced with the following.

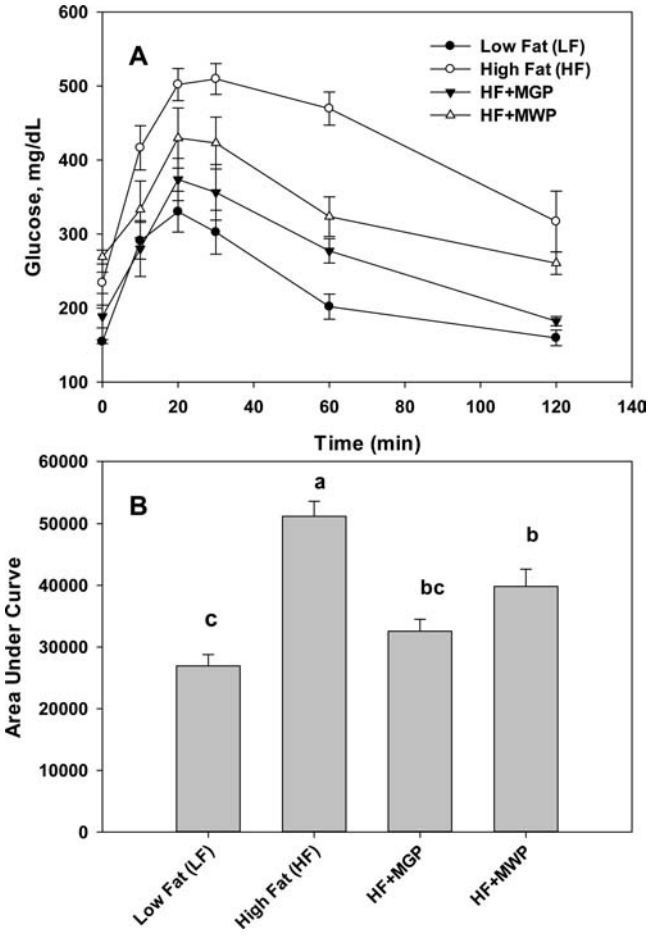


**Figure 3.** (A) Blood glucose levels in intraperitoneal glucose tolerance tests at week 12; (B) area under curve of blood glucose for 2 h after a glucose challenge ($n$ = 5).

Corrected Figure 3B shows that the AUC of glucose levels in the LF group was 47.4% lower ($p$ < 0.001) compared to HF controls. AUC levels in mice fed HF+MGP and HF+MWP were significantly lower than that of the HF group by 36.3 and 22.2%, respectively. AUC levels in mice fed HF+MGP were similar to those of mice receiving the low-fat diet. These data suggested that muscadine grape and wine phytochemicals improved glucose tolerance in mice fed a high-fat diet.

**Table 5. Effects of Muscadine Grape Phytochemicals (MGP) and Muscadine Wine Phytochemicals (MWP) on Plasma C-Reactive Protein (CRP) and Glutathione Peroxidase Activity**[a]

| group | plasma CRP (ng/mL) | plasma glutathione peroxidase activity (nmol/min/mL) |
|---|---|---|
| low fat (LF) | 23.2 ± 0.4 d | 1.1 ± 0.5 |
| high fat (HF) | 62.0 ± 0.2 a | 0.3 ± 0.07 |
| HF+MGP | 30.1 ± 0.6 c | 1.2 ± 0.3 |
| HF+MWP | 47.6 ± 0.8 b | 0.7 ± 0.2 |

[a]Values are the mean ± SEM $n$ = 9. Columns not sharing a common letter (a−d) are significantly different ($p \leq 0.05$).

Corrected values in Table 5 showed that muscadine grape or wine phytochemicals did not affect plasma glutathione peroxidase in mice; therefore, we cannot conclude that muscadine grape or wine phytochemicals alleviated oxidative stress.

Furthermore, there were, we believe, arithmetic errors in Table 4. Therefore, we withdraw the data in that table. As a result, we cannot conclude that muscadine grape or wine phytochemicals affect plasma insulin levels or insulin resistance in mice.

These corrections do not affect other conclusions in this paper.

**Published:** October 20, 2014

ACS Publications © 2014 American Chemical Society

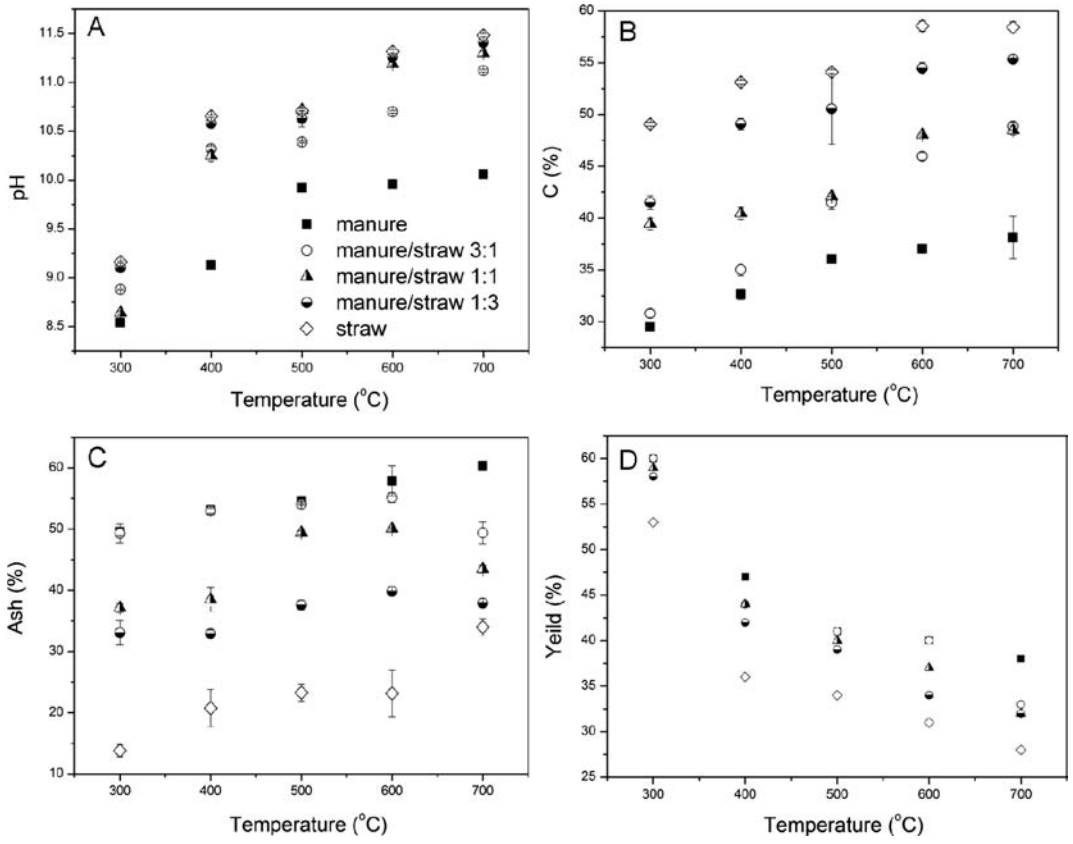


**Figure 1.** (A) pH, (B) total C (%), (C) ash content (%), and (D) yield (%) of the biochars at five pyrolysis temperatures.

disadvantages, and this new concept was quite different from previous studies.[16,17] Our aims were to (1) characterize the chemical and physical properties of biochars and investigate the mechanisms which led to these changes in properties; (2) investigate the heavy metal adsorption capacity of manure biochars, prepared with added straw feedstock using, as an example, Zn(II) adsorption; (3) assess the abilities of biochars prepared jointly from manures and plant materials as soil amendments, and suggest the appropriate proportions of straw addition and the pyrolysis temperature to suit different agronomic and environmental purposes.

## MATERIALS AND METHODS

**Preparation of Biochars.** The swine manure was obtained from a piggery in the suburbs of Hangzhou city, Zhejiang Province, China, where vegetables, corn, and wheat are provided as the diet of the pigs. The rice straw was collected from farmland near Zhejiang University, Zhejiang Province, China. The feedstocks were air-dried, crushed into pieces, and ground <0.154 mm. To change the properties of manure biochar, the straw was added to the manure feedstock at 3:1, 1:1, and 1:3 (w/w) manure/straw ratios respectively and then mixed thoroughly. The manure without straw addition and the straw without manure addition were regarded as the controls. The mixtures were placed in stainless steel bottles and pyrolyzed in a muffle furnace for 2 h without oxygen supply. The pyrolysis temperature was increased to the selected values of 300, 400, 500, 600, and 700 °C, respectively, at 26 °C/min. After cooling, all the biochars were ground, sieved <0.154 mm, and prepared for chemical and physical analysis. Throughout the paper, the biochars prepared from the feedstock mixtures at the ratio of 3:1, 1:1, and 1:3 (w/w) manure/straw are named "manure/straw 3:1 biochar", "manure/straw 1:1 biochar", and "manure/straw 1:3 biochar". The swine manure biochar and rice straw biochar are named "manure biochar" and "straw biochar" respectively.

**Chemical and Physical Analyses.** Yield (%) was calculated by the following equation: yield (%) = (weight of biochar)/(weight of feedstock) × 100. The ash content was determined as follows: 1.00 g of the ground biochar was heated at 700 °C for 2 h in a muffle furnace and the ash (%) calculated from ash (%) = (weight of ash)/(weight of biochar) × 100. The pH values of the biochars were determined in deionized water at the ratio of 1:10 w/w biochar/water with a pH meter. The total C, H, and N concentrations of the biochars were measured with a Flash EA 1112 elemental analyzer (Thermo Scientific, USA), and the total O concentration was determined by difference.[6] The exchangeable base cations (K, Na, Ca, and Mg) and heavy metal (Cu, Zn, and Fe) concentrations of the biochar samples were extracted by 1.0 mol/L ammonium acetate using a ratio of 1:25 w/v biochar/solution. The Ca, Mg, K, Na, Cu, Fe, and Zn concentrations were determined by a NovAA300 atomic absorption spectrometer (Analytikjena, Germany). The micropore area (MA), surface area (BET), total pore volume (TPV), average pore width (APW), and average particle size (APS) were measured using a Nova 2200e surface area analyzer (Quantachrome, USA) after degassing at 200 °C for 8 h.

**SEM-EDS, XRD, and FTIR Analyses.** A Sirion 100 thermal field emission scanning electron microscope (FEI, Netherlands) equipped with a Genesis 4000 X-ray energy dispersive spectroscope (EDAX, USA) (SEM-EDS) was used to determine the biochar morphology. X-ray diffraction (XRD) was used to observe the changes in mineral crystals in the biochars, using an X'Pert PRO computer-controlled diffractometer (PANalytical, The Netherlands). An Avatar370 Fourier transform infrared (FTIR) spectrometer with a Nicolet 380 spectrophotometer (ThermoNicolet, USA) was used to determine the functional groups on the biochar surface. The detail operations for the SEM-EDS, XRD, and FTIR analyses have been previously described.[5]

**Batch Zn(II) Adsorption Experiments.** Duplicate biochar samples of 0.1 g were added to 50 mL polypropylene tubes. The $Zn(NO_3)_2$ solutions were prepared with varying initial concentrations from 0 to 6.0 mM. The ionic strengths of the $Zn(NO_3)_2$ solutions

were adjusted to 10 mM $NaNO_3$. Then, 25 mL of Zn(II) solutions were added into each tube and mixed thoroughly. The mixtures were shaken at 160 rpm for 10 h at 25 °C, and the pH values of the suspensions in the tubes were adjusted to 5.0 before adsorption. After shaking, the suspensions were kept overnight and then centrifuged at 3500*g* for 10 min to separate the $Zn(NO_3)_2$ solutions from the biochar samples. The concentrations of Zn(II) were determined by atomic absorption spectroscopy, and the amount of Zn(II) absorbed by the biochars was calculated.

To investigate the Zn(II) adsorption capacity of the biochars, the Freundlich and Langmuir models were introduced to analyze the sorption isotherms data by the following equations:

$$\text{Freundlich: } q_e = K_F C_e^{\,n} \quad (1)$$

$$\text{Langmuir: } q_e = q_{max} C_e/(1/b + C_e) \quad (2)$$

where $q_e$ (mmol/kg) is the Zn(II) adsorbed by biochars at equilibrium; $C_e$ (mM) is the equilibrium Zn(II) concentration in the solution; $q_{max}$ (mmol/kg) is the maximum adsorption capacity; $n$ is the Freundlich constant without dimensions, which represents the degree of nonlinearity of the sorption isotherms; $K_F$ (mmol/kg)/(mmol/L)$^n$ and $b$ (mmol/L) are the adsorption constants of the Freundlich and Langmuir models, respectively.

**Statistical Analysis.** SPSS 18.0 software (SPSS Inc., Chicago, IL, USA) was used to perform statistical data analyses. Principal Components Analysis (PCA) was used to quantitate the relationships between biochar parameters and the differences in the biochar treatments.

## RESULTS AND DISCUSSION

**The Basic Properties of the Biochars.** The pH, total carbon, ash, and yield were all influenced by the pyrolysis temperature. Generally, as the pyrolysis temperature increased, the pH, ash, and C contents increased while the yield decreased (Figure 1), as previously reported.[5,18,19] The pH of the biochars is considered to be the most important parameter to correct soil acidity.[10,20] The formation of basic functional groups and carbonates or oxides of base cations (K, Na, Ca, and Mg) during the pyrolysis is the main mechanism for acidity correction, as these components can neutralize the $H^+$ in the soils. Thus, the temperature of 700 °C would be the best choice to increase the soil pH (Figure 1A). The total C in the biochars was divided into two pools: the aromatic portion and the aliphatic portion. The aliphatic portion, which can be readily mineralized, contributes to the biochar lability, whereas the aromatic portion, that is oxidized more slowly, can persist in the soils for thousands of years.[21,22] As the pyrolysis temperature increases from 300 to 700 °C, the aliphatic components will gradually be converted into aromatic components, as shown by the FTIR spectra (Figure 2), i.e., the peaks located in the region 2800−2950 $cm^{-1}$ associated with $CH_2$ and $CH_3$ disappeared. Thus, the biochar at 700 °C is an excellent material for soil C sequestration (Figure 1B). Similarly, the ash contents, which indirectly contribute to the soil nutrients, also reached the highest values when the temperature was 700 °C (Figure 1C). However, the yield rate markedly decreased as the pyrolysis temperature increased (Figure 1D), indicating that the more aliphatic fractions were evolved as methane, hydrogen, and carbon monoxide during pyrolysis. Thus, the yield rate should be also considered when selecting the most appropriate biochar with specific purposes for agronomic and environmental applications.

Compared with other straw amended biochars, manure biochar had the lowest pH and carbon content as well as the highest ash content and yield rate (Figure 1). The pH and C

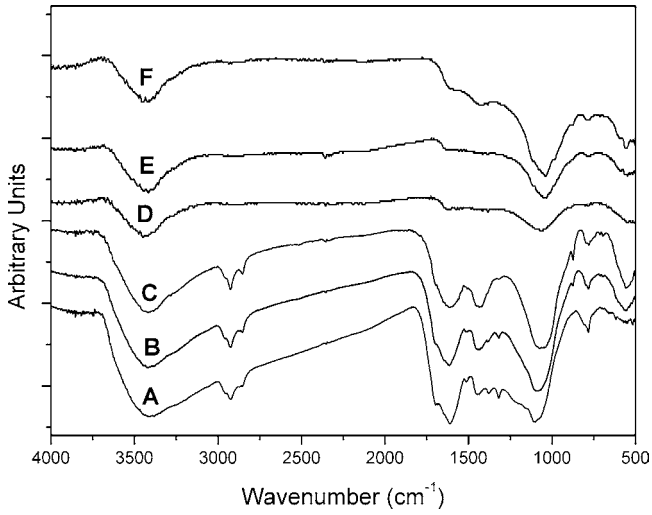


**Figure 2.** FTIR analyses of the biochars at pyrolysis temperature of 300 and 700 °C: (A) straw biochar-300 °C; (B) manure/straw 1:1 biochar-300 °C; (C) manure biochar-300 °C; (D) straw biochar-700 °C; (E) manure/straw 1:1 biochar-700 °C; (F) manure biochar-700 °C.

content increased consistently as the proportion of straw increased. For instance, the pH of manure biochar at 700 °C was 10.06, while the pH of the four other biochars (manure/straw 3:1, manure/straw 1:1, manure/straw 1:3, and straw biochars) were 11.12, 11.30, 11.41, and 11.48, respectively. This trend suggests that the added straw caused increases in pH and carbon content, giving the manure biochars the abilities to decrease soil acidity and soil C sequestration. However, with increased straw addition, the ash content and yield had the opposite trends (Figures 1C and 1D). This phenomenon indicated that the properties of manure biochar can be deliberately changed according to the different agronomic purposes required. To obtain higher yields from pyrolysis and to provide more nutrients for plant growth, the proportion of the straw added should be limited. However, to decrease soil acidity and to increase soil organic matter, increasing proportions of straw should be added. Normally, a soil which has a pH problem is always accompanied by other problems. Thus, the manure biochar blended with straw is probably the most comprehensive and effective soil amendment compared to the other biochars.

Measurements of physical parameters such as BET and micropore area of biochars are also essential to characterize their properties and to evaluate their agronomic and environmental potentials. From 300 to 500 °C, the BET and micropore area remained stable in all the biochars (except for straw biochar), at about 10 $m^2/g$ and 0 $m^2/g$, respectively (Figure 3). However, when the pyrolysis temperature increased to 600 and 700 °C, both the BET and micropore area increased rapidly, especially with the manure/straw 3:1, manure/straw 1:1, manure/straw 1:3, and straw biochars. For instance, the BET and micropore area in manure/straw 1:3 biochar at 700 °C were about 83 $m^2/g$ and 54 $m^2/g$, respectively, while the BET and micropore area in manure biochar at 700 °C were only 31 $m^2/g$ and 22 $m^2/g$, respectively (Figure 3). Normally, the biochars with high surface areas and more porous structures can provide large effective adsorption sites, for example as adsorbents for heavy metals and permanent organic pollutants.[23−25] This indicated that straw addition to the manure

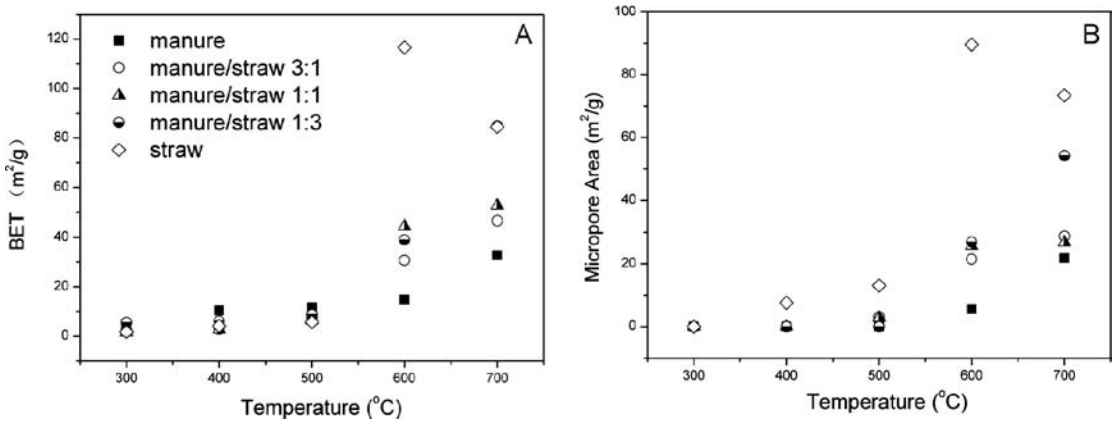


**Figure 3.** (A) BET and (B) micropore area of the biochars at five pyrolysis temperatures.

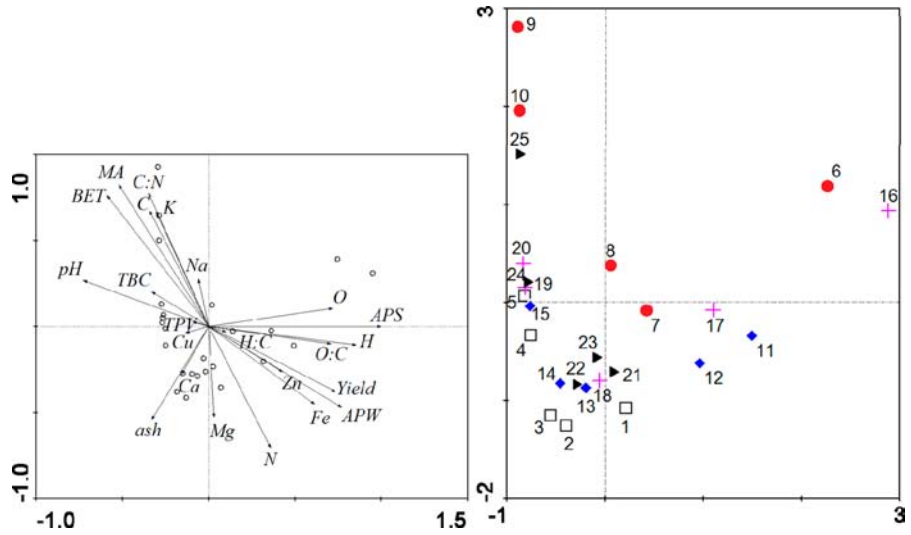


**Figure 4.** PCA analyses of the chemical and physical parameters in the biochars. 1, manure biochar-300 °C; 2, manure biochar-400 °C; 3, manure biochar-500 °C; 4, manure biochar-600 °C; 5, manure biochar-700 °C; 6, straw biochar-300 °C; 7, straw biochar-400 °C; 8, straw biochar-500 °C; 9, straw biochar-600 °C; 10, straw biochar-700 °C; 11, manure/straw 3:1 biochar-300 °C; 12, manure/straw 3:1 biochar-400 °C; 13, manure/straw 3:1 biochar-500 °C; 14, manure/straw 3:1 biochar-600 °C; 15, manure/straw 3:1 biochar-700 °C; 16, manure/straw 1:1 biochar-300 °C; 17, manure/straw 1:1 biochar-400 °C; 18, manure/straw 1:1 biochar-500 °C; 19, manure/straw 1:1 biochar-600 °C; 20, manure/straw 1:1 biochar-700 °C; 21, manure/straw 1:3 biochar-300 °C; 22, manure/straw 1:3 biochar-400 °C; 23, manure/straw 1:3 biochar-500 °C; 24, manure/straw 1:3 biochar-600 °C; 25, manure/straw 1:3 biochar-700 °C. MA, micropore area; BET, surface area; TPV, total pore volume; APW, average pore width; APS, average particle size.

during pyrolysis increased the manure biochar adsorption ability. Thus, the higher pyrolysis temperatures (600 and 700 °C) and the higher proportions of straw (1:1 and 1:3) would be the best choices to prepare the biochars for adsorption of pollutants, without consideration of production costs and yield rate. The porous structures are also supposed to be appropriate habitats for microbial growth and nutrient uptake.[26,27] However, the effects of pore numbers and sizes, and other factors (e.g., nutrient content, pH, labile organic carbon) of biochars, which may influence the microbial activity, remain unclear. Thus, the analyses of porous structure of the biochars provided valuable information for further studies of biochar effects on microbial growth and activity.

**The PCA of the Biochars.** To reach a conclusive interpretation of the effects of added straw to the manure, PCA was conducted to analyze the correlations between the biochar parameters, and determine the similarity and difference between the biochar samples. BET had a positive correlation with micropore area and total pore volume and a negative correlation with average pore width and average particle size (Figure 4), which is consistent with previous studies.[5,7] The H:C ratio was positively correlated with the O:C ratio and O concentrations, and negatively correlated with C concentrations. The results were attributed to the H and O loss (as $H_2$, $CH_4$, and CO) and the stable C formation during the pyrolysis process. In addition, the pH had a negative correlation with yield and had no correlation with ash content. Generally, some components of the ash (e.g., carbonates and bicarbonates) and functional groups ($-O^-$ and $-COO^-$) are both responsible for biochar pH. Thus, the ash content has no direct correlation with biochar pH because the functional groups also controlled the biochar pH and other components of ash are not alkaline. The first principal component was partially explained by the average particle size, total pore volume, O, and pH, whereas the second principal component was partially explained by K, Mg, Na, and ash.

The linear distances between two biochar samples demonstrated the degree of similarity between two biochars,


dx.doi.org/10.1021/jf504106v | J. Agric. Food Chem. 2014, 62, 10623−10631

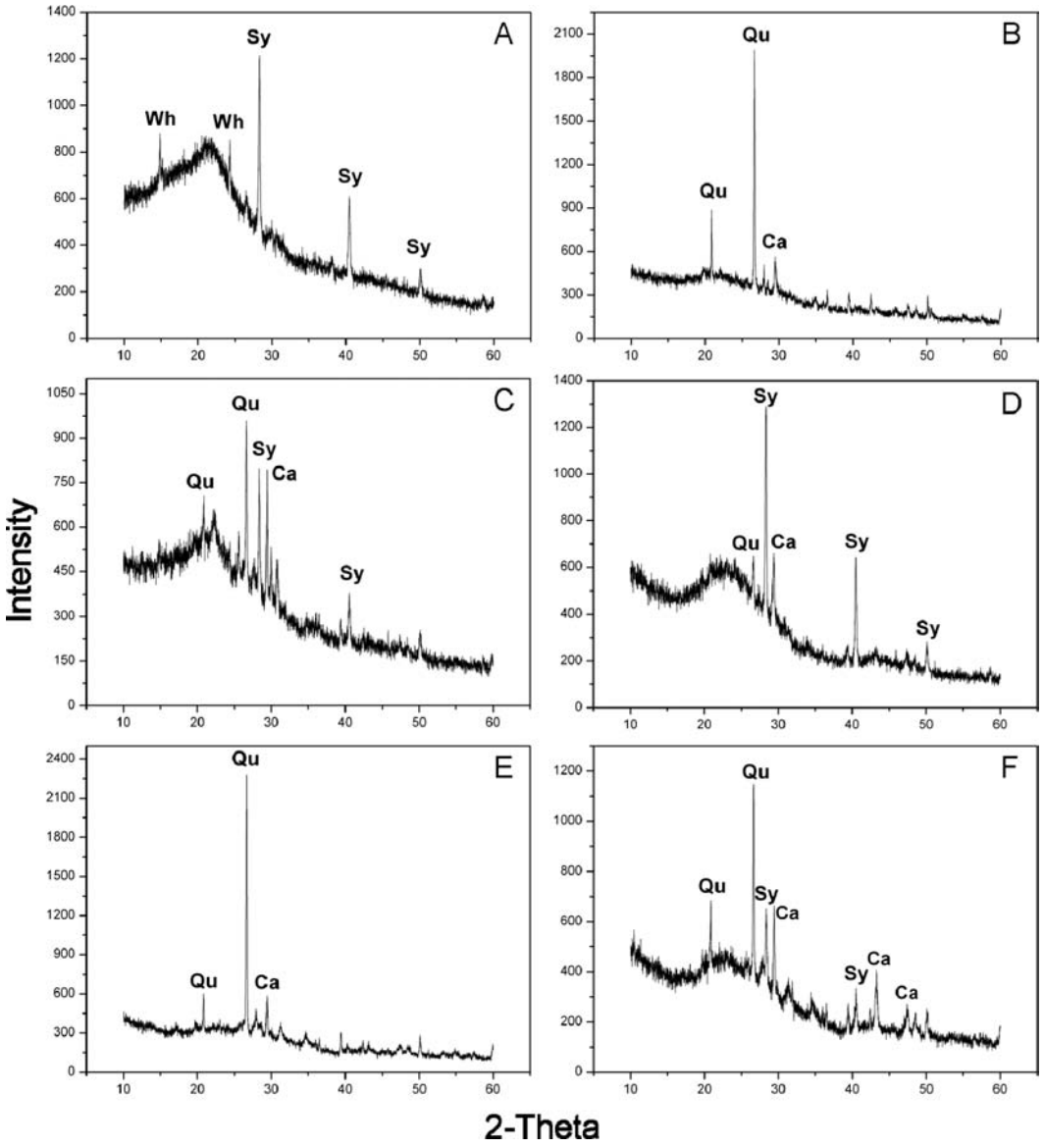


**Figure 5.** XRD analyses of the biochars at pyrolysis temperature of 300 and 700 °C: (A) straw biochar-300 °C; (B) manure biochar-300 °C; (C) manure/straw 1:1 biochar-300 °C; (D) straw biochar-700 °C; (E) manure biochar-700 °C; (F) manure/straw 1:1 biochar-700 °C. Sy, sylvite; Ka, kalicinite; Qu, quartz; Ca, calcite; Do, dolomite; Wh, Whewellite.

i.e., the larger the distance, the greater the difference (Figure 4). In most cases, the biochars at low pyrolysis temperatures (300 and 400 °C) had the most similar properties. When the temperature increased to 500 °C, the properties began to change slightly. At 600 and 700 °C, the properties were very different from those at the relatively lower temperatures (300, 400, and 500 °C), and the biochars at 600 and 700 °C only had small differences in the overall properties. In addition, at the same pyrolysis temperatures, the biochar properties gradually changed as the straw addition increased. For instance, the manure biochar had the largest differences with the manure/straw 1:3 and straw biochars. This statistical analysis indicates that the manure biochar can be adjusted to meet different agronomic and environmental purposes as a soil amendment, based on the pyrolysis temperatures and the proportion of straw added.

**XRD, FTIR, and SEM-EDS Spectra and Application Implications.** Based on results of the PCA analyses, the biochars from 300 to 500 °C and from 600 to 700 °C had similar properties, respectively (Figure 4). Thus, the typical biochars (manure, straw, and manure/straw 1:1 biochars) at 300 and 700 °C were selected for further analysis. The XRD spectra revealed the same mineral crystals in biochars at 300 and 700 °C, and the addition of straw had apparent influences on the mineral components in these biochars, i.e., the manure biochar at both 300 and 700 °C contained large quartz ($SiO_2$) and calcite ($CaCO_3$) concentrations, whereas the manure/straw 1:1 biochar at both 300 and 700 °C also contained some sylvite (KCl), which was from straw biochar (Figure 5). The mineral crystals, which can be detected by XRD, were the largest proportion of mineral components in the biochars and would play a great role in biochar applications, such as acidity correction and heavy metal adsorption. For instance, quartz and calcite can form silicate and calcite precipitates with some heavy metals in aqueous solutions,[15,28] and thus reduce their mobility and bioavailability. In addition, the calcite and sylvite, which are responsible for alkalinity, can also neutralize soil acidity and increase soil pH.

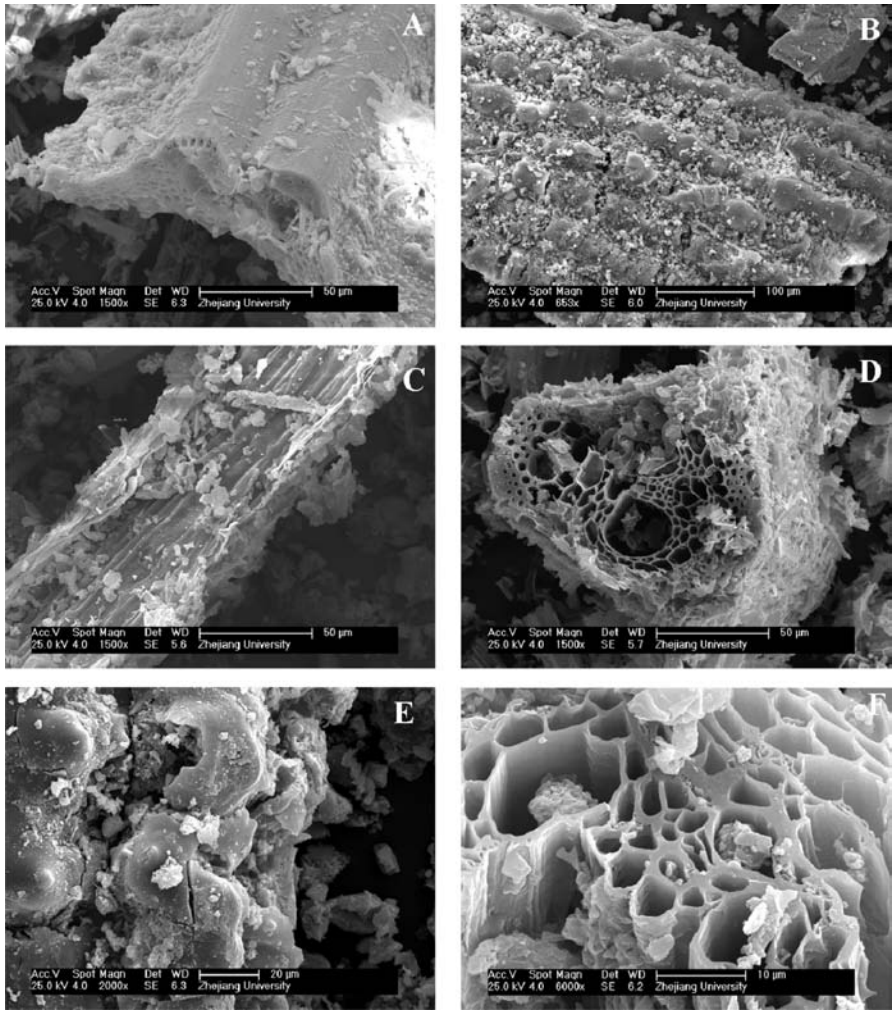


**Figure 6.** SEM analyses of the biochars at pyrolysis temperature of 300 and 700 °C: (A) straw biochar-300 °C; (B) manure biochar-300 °C; (C) manure/straw 1:1 biochar-300 °C; (D) straw biochar-700 °C; (E) manure biochar-700 °C; (F) manure/straw 1:1 biochar-700 °C.

The FTIR spectra of the biochars can indicate the changes in surface functional groups of the biochars (Figure 2). The biochars at 300 and 700 °C both had two big peaks, i.e., the peaks at 3418 $cm^{-1}$ and the peaks between 1000 and 1100 $cm^{-1}$. These two peaks were attributed to hydroxyl stretching and the aliphatic ether, alcohol C−O, or aromatic stretching, respectively.[29,30] Unlike the biochars at 700 °C, the peaks at 1614 and 1430 $cm^{-1}$ were detected in biochar at 300 °C, which were probably attributed to C═O stretching, respectively.[31] The oxygen functional groups, such as hydroxyl and carboxyl, can form complexes with heavy metals and thus increase the heavy metal adsorption ability of soil.[32] In addition, the carboxyl ($-COO^-$) and hydroxyl ($-O^-$) groups that can associate $H^+$ are the main contributions to the alkalinity of biochars[33] and play an important role in soil acidity correction.

The SEM images showed that both pyrolysis temperature and proportion of straw addition influenced the morphological structure of the biochars (Figure 6). At 300 °C, the manure biochar had few porous structures (Figure 6) and the lowest surface area (Figure 3). At 700 °C, the porous structure of manure biochar still had not been formed (Figure 6), which is consistent with the low values of BET and micropore area (Figure 3). However, the straw biochar and the manure/straw 1:1 biochar at 700 °C had large numbers of porous structures, in accordance with the larger surface area and porosity compared with the manure biochar. The reason was that the porous structures were more easily formed with the straw addition at the high pyrolysis temperature, due to the higher content of lignocellulose. However, at 300 °C, the straw biochar and the manure/straw 1:1 biochar also demonstrated low surface areas and porosities, suggesting that only high pyrolysis temperatures in combination with the straw addition can induce highly porous structures, not only providing large numbers of physical adsorption sites for heavy metals but also probably providing a suitable habitat for some specific microbes to colonize, reproduce, and grow. Therefore, the effects of the porous structure of biochar on microbial growth should be investigated further. The EDS images show the major elements in the biochars. The manure biochar contained more nutrients (K, P, Ca, and Mg) than the straw biochar, suggesting that a great number of minerals and nutrients adhered to the manure biochar surface. Overall, the biochars prepared from manure plus straw showed more comprehensive properties because of the increased ash from manure and the increased porous structure from straw. The proportion of the straw added should be carefully taken into account according to the results required for various agronomic and environmental applications.

**The Effect and Mechanism of Biochars on Zn(II) Adsoption.** The Zn(II) absorbed by all biochars at 300 °C decreased slightly as the proportion of straw addition increased

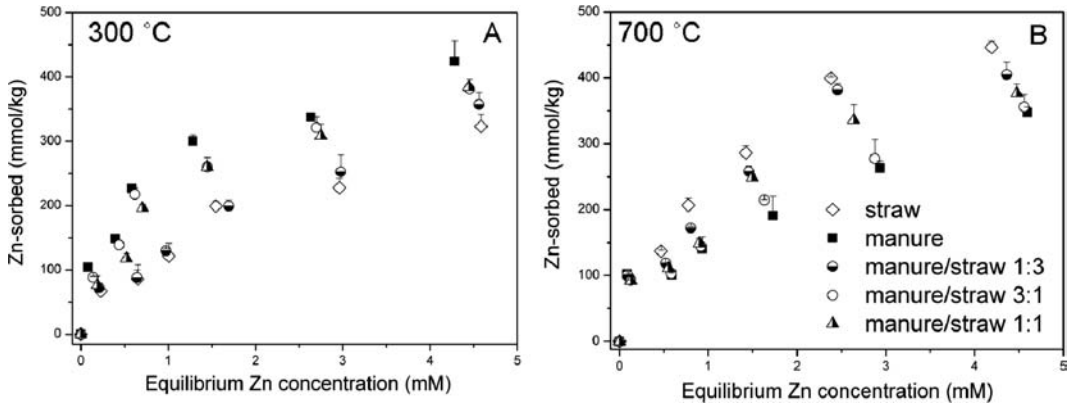


**Figure 7.** Adsorption isotherms of the biochars at pyrolysis temperature of (A) 300 and (B) 700 °C.

(Figure 7A). For instance, when the initial concentration of Zn(II) was 4 mM, the Zn(II) absorbed by biochars at 300 °C was 337, 321, 309, 253, and 228 mmol/kg with manure, manure/straw 3:1, manure/straw 1:1, manure/straw 1:3, and straw, respectively. However, the Zn(II) absorbed by biochars at 700 °C showed a trend opposite to that at 300 °C (Figure 7B). The Zn(II) absorbed by these biochars was 263, 277, 336, 382, and 400 mmol/kg for manure, manure/straw 3:1, manure/straw 1:1, manure/straw 1:3, and straw biochars, respectively, which suggests that the Zn(II) absorbed by biochars at 700 °C increased slightly as the proportion of straw addition increased.

The Freundlich and Langmuir models were introduced to fit the Zn(II) adsorption iostherms obtained from different biochars. The Freundlich model fitted the adsorption data better than the Langmuir model, with all correlation coefficients ($R^2$) being greater than 0.90, and mostly >0.94 (Table 1), and thus the Freundlich model could be used to explain the Zn(II) adsorption by biochars. At 300 °C, the Zn(II) adsorption capacity ($K_F$) decreased as the proportion of straw increased (except for straw biochar), i.e., 234, 210, 203, 136, and 146 (mmol/kg)/(mmol/L)$^n$ for manure, manure/straw 3:1, manure/straw 1:1, manure/straw 1:3, and straw biochars, respectively. However, At 700 °C, the Zn(II) adsorption capacity ($K_F$) increased as the proportion of straw increased, i.e., 139, 152, 174, 187, and 226 (mmol/kg)/(mmol/L)$^n$ for manure, manure/straw 3:1, manure/straw 1:1, manure/straw 1:3, and straw biochars, respectively. In addition, with the same proportion of straw added, the manure, manure/straw 3:1, and manure/straw 1:1 biochars at 300 °C had a larger Zn(II) adsorption capacity than that at 700 °C, whereas the manure/straw 1:3 and straw biochars had the opposite trend.

**Table 1. Constants and Correlation Coefficients of Freundlich and Langmuir Models for Zn(II) Adsorption by Feedstock Blending Biochars at 300 and 700 °C**

| | Freundlich | | | Langmuir | | |
|---|---|---|---|---|---|---|
| biochar | $K_F$ (mmol/kg) /(mmol/L)$^n$ | $n$ | $R^2$ | $q_{max}$ (mmol/kg) | $b$ | $R^2$ |
| straw-300 °C[a] | 146 | 0.52 | 0.97 | 324 | 1.08 | 0.95 |
| manure/straw 1:3[b]-300 °C | 136 | 0.62 | 0.95 | 595 | 0.29 | 0.88 |
| manure/straw 1:1-300 °C | 203 | 0.43 | 0.96 | 488 | 0.83 | 0.98 |
| manure/straw 3:1-300 °C | 210 | 0.44 | 0.96 | 377 | 2.07 | 0.94 |
| manure-300 °C | 234 | 0.38 | 0.99 | 410 | 1.75 | 0.96 |
| straw-700 °C | 226 | 0.63 | 0.99 | 683 | 0.58 | 0.94 |
| manure/straw 1:3-700 °C | 187 | 0.70 | 0.94 | 225 | 8.85 | 0.68 |
| manure/straw 1:1-700 °C | 174 | 0.58 | 0.90 | 580 | 0.46 | 0.90 |
| manure/straw 3:1-700 °C | 152 | 0.71 | 1.00 | 350 | 0.91 | 0.66 |
| manure-700 °C | 139 | 0.60 | 1.00 | 317 | 5.25 | 0.85 |

[a]The pyrolysis temperature at which biochars were prepared. [b]The ratio (w/w) of the swine manure and rice straw feedstocks.

Normally, the adsorption of heavy metals by biochars can be described by three main mechanisms: precipitation, cation exchange, and complexation.[34,35] In our study, the silicate and calcite from XRD in manure biochar, which can form the Zn-silicate and Zn-carbonate precipitates, were responsible for the higher Zn(II) adsorption in manure biochar at 300 °C. In addition, at 300 °C, as the proportion of straw increased, the EBC (sum of exchangeable K, Na, Ca, and Mg) decreased, resulting in less exchange with Zn(II). This is also the mechanism for the decrease in Zn(II) adsorption by the biochars with added straw compared to the manure biochar. At 700 °C, the adsorption capacity increased as the proportion of straw added increased, which was attributed to the large BET and micropore area (Figure 3). The large increases in BET and micropore area, especially with manure/straw 1:3 and straw biochars, provided more physical potential for adsorption sites, and the SEM images also showed the larger porous structures in manure/straw 1:3 and straw biochars. Overall, the biochars at 300 °C had greater Zn(II) adsorption capacities than 700 °C (except for the manure/straw 1:3 biochar and straw biochar), due to the high content of oxygen functional groups on biochar surfaces at low pyrolysis temperature (Figure 2). The −OH and −COOH, which can form complexes with Zn(II), were the main mechanism. Additionally, the extremely high number of adsorption sites in manure/straw 1:3 biochar and straw biochar at 700 °C caused higher Zn(II) adsorption capacities than at 300 °C.

**The Criteria To Select Biochars as Soil Amendments.** The criteria were to select biochars as soil amendments for varied purposes. It should be considered whether the soil can be improved by biochars for a specific purpose or not. For instance, biochars may have no positive effects on alkaline and calcareous soils,[36] which already have high pH values and organic matter. Second, the biochars should be classified into several groups based on the specific agronomic and environmental requirements. For instance, the properties of biochars used for heavy metal adsorption are quite different from those

required from biochars used for soil acidity correction. In our study, without considering the production costs, the manure/straw 3:1 biochar and manure biochar at 300 °C were suitable to absorb heavy metals such as Zn(II); the manure/straw 1:3 biochar and straw biochar at 700 °C can be used to correct soil acidity and increase soil carbon contents considerably; the manure/straw 3:1 biochar and manure biochar at 700 °C caused the largest increases in nutrients. In addition, the biochars prepared from two feedstocks may have more comprehensive and varied effects on soils rather than biochars prepared from a single feedstock. In conclusion, biochars prepared from manure plus straw had different physiochemical properties than the manure biochar. The addition of straw compensated for the disadvantages in the remedial effects of the manure biochar, while it decreased the advantages of the manure biochar. More detailed criteria should be established to prepare the most appropriate biochars as soil amendments for varied agronomic and environmental requirements, and the yield, production costs, and the long-term effects also should be taken into account.

## ■ ASSOCIATED CONTENT

### Supporting Information

The concentrations of exchangeable base cations and selected heavy metals of the biochar at 300 and 700 °C and the EDS analysis of the manure biochar at 700 °C and straw biochar at 700 °C. This material is available free of charge via the Internet at http://pubs.acs.org.

## ■ AUTHOR INFORMATION

### Corresponding Author

*Tel: +86-571-8898-2069. Fax: +86-571-8898-2069. E-mail: jmxu@zju.edu.cn.

### Funding

This work was financially supported by the National Basic Research Program of China (2011CB100502, 2014CB441002).

### Notes

The authors declare no competing financial interest.

## ■ REFERENCES

(1) Donham, K. J.; Yeggy, J.; Dague, R. R. Production rates of toxic gases from liquid swine manure: Health implications for workers and animals in swine confinement buildings. *Biol. Wastes* **1988**, *24*, 161−173.

(2) Zhang, H.; Dao, T. H.; Basta, N. T.; Dayton, E. A.; Daniel, T. C. Remediation techniques for manure nutrient loaded soils. In *Animal Agriculture and the Environment: National Center for Manure and Animal Waste Management White Papers*; Rice, J. M., Caldwell, D. F., Humenik, F. J., Eds.; ASABE: St. Joseph, MI, 2006; pp 482−504.

(3) Nicholson, F. A.; Chambers, B. J.; Williams, J. R.; Unwin, R. J. Heavy metal contents of livestock feeds and animal manures in England and Wales. *Bioresour. Technol.* **1999**, *70*, 23−31.

(4) Hsu, J. H.; Lo, S. L. Effect of composting on characterization and leaching of copper, manganese, and zinc from swine manure. *Environ. Pollut.* **2001**, *114*, 119−127.

(5) Dai, Z.; Meng, J.; Muhammad, N.; Liu, X.; Wang, H.; He, Y.; Brookes, P. C.; Xu, J. The potential feasibility for soil improvement, based on the properties of biochars pyrolyzed from different feedstocks. *J. Soils Sediments* **2013**, *13*, 989−1000.

(6) Enders, A.; Hanley, K.; Whitman, T.; Joseph, S.; Lehmann, J. Characterization of biochars to evaluate recalcitrance and agronomic performance. *Bioresour. Technol.* **2012**, *114*, 644−653.

(7) Tsai, W. T.; Liu, S. C.; Chen, H. R.; Chang, Y. M.; Tsai, Y. L. Textural and chemical properties of swine-manure-derived biochar pertinent to its potential use as a soil amendment. *Chemosphere* **2012**, *89*, 198−203.

(8) Singh, B.; Singh, B. P.; Cowie, A. L. Characterisation and evaluation of biochars for their application as a soil amendment. *Soil Res.* **2010**, *48*, 516−525.

(9) Qian, L.; Chen, B.; Hu, D. Effective alleviation of aluminum phytotoxicity by manure-derived biochar. *Environ. Sci. Technol.* **2013**, *47*, 2737−2745.

(10) Dai, Z.; Li, R.; Muhammad, N.; Brookes, P. C.; Wang, H.; Liu, X.; Xu, J. Principle component and hierarchical cluster analysis of soil properties following biochar incorporation. *Soil Sci. Soc. Am. J.* **2014**, *78*, 205−213.

(11) Uchimiya, M.; Wartelle, L. H.; Klasson, K. T.; Fortier, C. A.; Lima, I. M. Influence of pyrolysis temperature on biochar property and function as a heavy metal sorbent in soil. *J. Agric. Food Chem.* **2011**, *59*, 2501−2510.

(12) Beesley, L.; Moreno-Jimenez, E.; Gomez-Eyles, J. L.; Harris, E.; Robinson, B.; Sizmur, T. A review of biochars' potential role in the remediation, revegetation and restoration of contaminated soils. *Environ. Pollut.* **2011**, *159*, 3269−3282.

(13) Cao, X. D.; Ma, L. N.; Liang, Y.; Gao, B.; Harris, W. Simultaneous immobilization of lead and atrazine in contaminated soils using dairy-manure biochar. *Environ. Sci. Technol.* **2011**, *45*, 4884−4889.

(14) Uchimiya, M.; Bannon, D. I. Solubility of lead and copper in biochar-amended small arms range soils: influence of soil organic carbon and pH. *J. Agric. Food Chem.* **2013**, *61*, 7679−7688.

(15) Xu, X.; Cao, X.; Zhao, L.; Wang, H.; Yu, H.; Gao, B. Removal of Cu, Zn, and Cd from aqueous solutions by the dairy manure-derived biochar. *Environ. Sci. Pollut. Res.* **2013**, *20*, 358−368.

(16) Zhao, L.; Cao, X.; Wang, Q.; Yang, F.; Xu, S. Mineral constituents profile of biochar derived from diversified waste biomasses: Implications for agricultural applications. *J. Environ. Qual.* **2013**, *42*, 545−552.

(17) Novak, J. M.; Cantrell, K. B.; Watts, D. W.; Busscher, W. J.; Johnson, M. G. Designing relevant biochars as soil amendments using lignocellulosic-based and manure-based feedstocks. *J. Soils Sediments* **2014**, *14*, 330−343.

(18) Meng, J.; Wang, L.; Liu, X.; Wu, J.; Brookes, P. C.; Xu, J. Physicochemical properties of biochar produced from aerobically composted swine manure and its potential use as an environmental amendment. *Bioresour. Technol.* **2013**, *142*, 641−646.

(19) Cantrell, K. B.; Hunt, P. G.; Uchimiya, M.; Novak, J. M.; Ro, K. S. Impact of pyrolysis temperature and manure source on physicochemical characteristics of biochar. *Bioresour. Technol.* **2012**, *107*, 419−28.

(20) Yuan, J. H.; Xu, R. K.; Qian, W.; Wang, R. H. Comparison of the ameliorating effects on an acidic ultisol between four crop straws and their biochars. *J. Soils Sediments* **2011**, *11*, 741−750.

(21) Zimmerman, A. R. Abiotic and microbial oxidation of laboratory-produced black carbon (biochar). *Environ. Sci. Technol.* **2010**, *44*, 1295−1301.

(22) Lehmann, J.; Joseph, S. *Biochar for environmental management: science and technology*; Routledge: 2012.

(23) Chen, X.; Chen, G.; Chen, L.; Chen, Y.; Lehmann, J.; McBride, M. B.; Hay, A. G. Adsorption of copper and zinc by biochars produced from pyrolysis of hardwood and corn straw in aqueous solution. *Bioresour. Technol.* **2011**, *102*, 8877−8884.

(24) Chun, Y.; Sheng, G.; Chiou, C. T.; Xing, B. Compositions and sorptive properties of crop residue-derived chars. *Environ. Sci. Technol.* **2004**, *38*, 4649−4655.

(25) Luo, L.; Lou, L.; Cui, X.; Wu, B.; Hou, J.; Xun, B.; Xu, X.; Chen, Y. Sorption and desorption of pentachlorophenol to black carbon of three different origins. *J. Hazard. Mater.* **2011**, *185*, 639−646.

(26) Lehmann, J.; Rillig, M. C.; Thies, J.; Masiello, C. A.; Hockaday, W. C.; Crowley, D. Biochar effects on soil biota—A review. *Soil Biol. Biochem.* **2011**, *43*, 1812−1836.

(27) Luo, Y.; Durenkamp, M.; De Nobili, M.; Lin, Q.; Devonshire, B. J.; Brookes, P. C. Microbial biomass growth, following incorporation of

biochars produced at 350° C or 700° C, in a silty-clay loam soil of high and low pH. *Soil Biol. Biochem.* **2013**, *57*, 513−523.
(28) Meng, J.; Feng, X.; Dai, Z.; Liu, X.; Wu, J.; Xu, J. Adsorption characteristics of Cu (II) from aqueous solution onto biochar derived from swine manure. *Environ. Sci. Pollut. Res.* **2014**, *21*, 644−653.
(29) Keiluweit, M.; Nico, P. S.; Johnson, M. G.; Kleber, M. Dynamic molecular structure of plant biomass-derived black carbon (biochar). *Environ. Sci. Technol.* **2010**, *44*, 1247−1253.
(30) Mukome, F. N.; Zhang, X.; Silva, L. C.; Six, J.; Parikh, S. J. Use of chemical and physical characteristics to investigate trends in biochar feedstocks. *J. Agric. Food Chem.* **2013**, *61*, 2196−2204.
(31) Yaman, S. Pyrolysis of biomass to produce fuels and chemical feedstocks. *Energy Convers. Manage.* **2004**, *45*, 651−671.
(32) Tong, X.; Li, J.; Yuan, J.; Xu, R. Adsorption of Cu (II) by biochars generated from three crop straws. *Chem. Eng. J.* **2011**, *172*, 828−834.
(33) Yuan, J. H.; Xu, R. K.; Zhang, H. The forms of alkalis in the biochar produced from crop residues at different temperatures. *Bioresour. Technol.* **2011**, *102*, 3488−3497.
(34) Uchimiya, M.; Klasson, K. T.; Wartelle, L. H.; Lima, I. M. Influence of soil properties on heavy metal sequestration by biochar amendment: 1. Copper sorption isotherms and the release of cations. *Chemosphere* **2011**, *82*, 1431−1437.
(35) Jiang, T. Y.; Jiang, J.; Xu, R. K.; Li, Z. Adsorption of Pb (II) on variable charge soils amended with rice-straw derived biochar. *Chemosphere* **2012**, *89*, 249−256.
(36) Van Zwieten, L.; Kimber, S.; Morris, S.; Chan, K.; Downie, A.; Rust, J.; Joseph, S.; Cowie, A. Effects of biochar from slow pyrolysis of papermill waste on agronomic performance and soil fertility. *Plant Soil* **2010**, *327*, 235−246.

Table 1. Information of the Soil and Climate in the Test Locations Used for Residual Analysis at the Time of Harvest

| | | | | soil mechanical composition | | | | |
|---|---|---|---|---|---|---|---|---|
| location | type of soil | content of soil org matter (%) | pH of soil | sand (%) | silt (%) | clay (%) | av annu temp (°C) | av annu rainfall (mm) |
| Yongqing | clay | 1.50 | 5.8 | 27.7 | 38.0 | 34.3 | 12.0 | 540 |
| Jinan | cinnamon soil | 1.60 | 7.5 | 32.5 | 65.2 | 2.3 | 14.7 | 671 |
| Xiantao | alluvial soil | 1.61 | 6.2 | 11.5 | 87.3 | 1.2 | 16.0 | $1.21 \times 10^3$ |

sufficient to control white grubs during the later stages of the peanut-growing season. Fipronil and chlorpyrifos have different modes of action. Fipronil can be absorbed by roots and transported into plants whereas chlorpyrifos activity does not appear in plant tissues.[15] In this study, a microencapsulated mixture of fipronil and chlorpyrifos was applied through seed treatment to control white grubs in peanut fields, and the release kinetics and behaviors of the two active ingredients in the environment were investigated in comparison with those of the conventional formulation.

## MATERIALS AND METHODS

**Chemicals.** Technical-grade fipronil (95.0%) and chlorpyrifos (98.0%) were provided by the CAC Group Limited (Shanghai, China) and were used without further purification. Commercial-grade emulsifier 0203 (polyoxyethylene castor oil + calcium dodecylbenzenesulfonate, 1:1, w/w) and the NNO dispersant (2-naphthalenesulfonic acid) were purchased from Jiangsu GPRO Group Co. (Jiangsu, China). Xylene, melamine, acetonitrile, and a 37% formaldehyde solution were purchased from Sinopharm Chemical Reagent Beijing Co., Ltd. (Beijing, China). Hydroxyl poly(vinyl alcohol) (17-88) was purchased from Beijing Organic Chemical Plant (Beijing, China). PSA was purchased from Agela Technologies Inc. (Tianjin, China).

**Plant Material.** Peanut seeds (Jihua 4) were kindly supplied by the Cangzhou Seed Company (Cangzhou, China).

**Preparation of Microcapsules.** Microencapsulation was achieved using a modification of the in situ polymerization method.[16] Briefly, a mixture of 6.0 g of melamine and 11.6 g of 37% formaldehyde was adjusted to pH 8.5−9.0 with 10% $Na_2CO_3$ solution. The melamine−formalin precondensate was prepared by stirring the mixture at 70 °C until it became transparent. The temperature was then reduced to 40 °C. Simultaneously, an o/w emulsion was prepared by adding a mixture of 15.3 g of chlorpyrifos, 3.3 g of fipronil, 3.3 g of xylene, and 4.0 g of emulsifier 0203 to 26 g of water. The o/w emulsion was added to the melamine−formalin prepolymer. The reaction liquid was adjusted to pH 4.5 with 10% hydrochloric acid solution. The reaction system was then stirred at 70 °C for an hour.

The microcapsule slurry was centrifuged at $1.2 \times 10^4$ rev $min^{-1}$. The microencapsulated formulation for seed treatment was prepared by resuspending the sedimented material in an aqueous solution containing dispersant NNO (40 g $L^{-1}$) and poly(vinyl alcohol) (17-88) (10 g $L^{-1}$). The concentrations of chlorpyrifos and fipronil in this microencapsulated formulation for seed treatment were 150.0 g $L^{-1}$ and 30.0 g $L^{-1}$, respectively. The conventional formulation (flowable suspension for seed treatment) was prepared by milling 15.3 g of chlorpyrifos, 3.3 g of fipronil, 4.0 g of NNO, 1.0 g of 17-88, and 86.4 g of water using a Pulverisette 6 high-speed bead mill (Fritsch, Germany). The concentrations of chlorpyrifos and fipronil in the conventional formulation for seed treatment were the same as those in the microencapsulated formulation.

**Determination of Particle Sizes and Size Distribution.** The sizes of the microcapsule particle and their size distribution were determined using a BT-9300H laser particle-size analyzer (Dandong, China).

The encapsulation efficiency of the microcapsules was tested following a modification of the method of Asrar et al.[17] Briefly, 0.003 g of microcapsule formulation was mixed with 100 mL of 10% aqueous solution of methyl alcohol. The mixture was shaken for 1 min and was immediately filtered through a 0.45 μm PTFE filter, and then the amounts of fipronil and chlorpyrifos in the filtered solution were determined by HPLC using a VWD detector and a Hypersil ODS column (46 mm × 250 mm, 5 μm). The mobile phase was acetonitrile/water (90:10) flowing at a rate of 1.0 mL $min^{-1}$. The injected volume was 20 μL. Fipronil and chlorpyrifos were detected at wavelengths of 279 and 230 nm, respectively. The limits of quantification of fipronil and chlorpyrifos were 0.05 mg $L^{-1}$ and 0.04 mg $L^{-1}$, respectively. The filtered amount represented the REA, and the encapsulation efficiency was expressed as 100 − REA %.

**Field Experiments for Release Study.** Peanut seeds were coated with either the conventional formulation or the microencapsulated formulation. Each of the two formulations were applied to the seeds at rates of 1.8 g $kg^{-1}$ seed (fipronil:chlorpyrifos = 0.3 g:1.5 g) and 3.6 g $kg^{-1}$ seed (fipronil:chlorpyrifos = 0.6 g:3.0 g). All treatments were applied using the traditional method of stirring 100 g of seeds with a calculated dose of formulation after dilution with 1 mL of water. The untreated control seeds were stirred with 1 mL of tap water.

The treatments were arranged in a split-plot design and replicated three times in Cangzhou, China. Each subplot (45 $m^2$) consisted of 18, 5 m long rows spaced 0.5 m apart. The plants within the rows were spaced 0.3 m apart. There was 1.5 m spacing between the plots. Each planting hole was sowed with one coated peanut seed on May 13, 2012.

Five plants were randomly selected from each plot and dug out with approximately 200 g of soil adhering to the root zone at intervals of 15, 30, and 45 DAE. The sampled plants and adhering soil were stored at −20 °C for determining the dose dynamics of fipronil and chlorpyrifos. Thirty plants were randomly selected from each plot, and the plants and the adhering soil to a depth of 0.3 m were dug out at harvest to survey the white grub content.

**Field Experiments for Residual Analysis at the Time of Harvest.** The field experiments for the final residual analysis were conducted in Yongqing, Jinan, and Xiantao China in 2012. Table 1 lists the soil characteristics and climate information in three test locations. Peanut seeds were coated with the microencapsulated formulation at rates of 3.6 g $kg^{-1}$ seed and 5.4 g $kg^{-1}$ seed (fipronil:chlorpyrifos = 0.9 g:4.5 g). The untreated control seeds were treated with tap water. The insecticide-treatment and untreated-control plots were arranged randomly with three replications of each treatment. The area of each plot was 30 $m^2$.

Soil and plant samples were collected at harvest. The sampling method used was the same as that used for the release study in the field.

**Sample Preparation for Chemical Analysis.** The soil from each plot was pooled and sieved, and the extraneous matter, including stones and pieces of gravel, was removed. The sampled roots and pods were washed with water and were allowed to dry in the air. Afterward, 10 g of a sample (soil, roots, kernels, or pod hulls) was homogenized using a mortar. The homogenized sample was transferred to a centrifuge tube. Then, 20 mL of acetonitrile and 5 mL of 1% formic acid solution were added. The mixture was shaken for 1 h. Then, 3 g of NaCl was added, which was followed by vigorous shaking for 1 min. The mixture was centrifuged at $3.8 \times 10^3$ rev $min^{-1}$ for 5 min. A 6 mL aliquot of the supernatant was transferred to a 15 mL centrifuge tube containing 0.3 g of PSA. The sample was vigorously shaken for 1 min and then was centrifuged at $1.0 \times 10^4$ rev $min^{-1}$ for 3 min. A 1 mL aliquot of the supernatant was taken for fipronil analysis. Another 1 mL aliquot of the supernatant was transferred to a centrifuge tube containing 0.1 g of anhydrous $MgSO_4$ and then was vigorously shaken for 1 min. The sample was centrifuged at $1.0 \times 10^4$ rev $min^{-1}$ for 3 min. The supernatant was evaporated to dryness under a stream of

nitrogen. Finally, the residue was reconstituted using 1 mL of hexane prior to chlorpyrifos analysis.

**GC Analysis of the Chlorpyrifos Content.** The chlorpyrifos content was determined using an Agilent 7890A GC/FPD with an Agilent RTX-17 column (30 m × 0.25 mm × 0.25 $\mu$m) under the following conditions: column injector port temperature, 240 °C; injection volume, 1 $\mu$L with splitless mode; nitrogen as carrier gas at a flow rate of 1.0 mL min$^{-1}$; oven temperature program, 100 °C (1 min), increased at 20 °C min$^{-1}$ to 250 °C, and held for 3 min. The retention time of chlorpyrifos was 10.3 min. The limit of determination was 0.001 mg kg$^{-1}$. The recovery rates, relative standard deviations, and linearity of this method are provided in the Supporting Information (Table s1).

**LC−MS/MS Analysis of the Fipronil Content.** The fipronil content was determined using an Agilent 1200 HPLC system coupled online to an Agilent 6410 B LC-QQQ system. The LC separation was performed using an Agilent eclipse plus column (2.1 mm × 50 mm × 3.5 mm) at 30 °C. The mobile phase used was acetonitrile/water (containing 0.1% formic acid) (90:10) at a rate of 0.3 mL min$^{-1}$. The injected volume was 5 $\mu$L. For the mass spectrometric analysis, the ESI source was operated in the negative-ionization mode, and its parameters were as follows: gas temperature, 350 °C; gas flow, 8 L min$^{-1}$; nebulizer gas, 35 psi; and capillary voltage, 4000 V. Nitrogen gas served as the nebulizer, and argon gas was used as the collision gas. The MRM mode was selected to monitor the precursor-to-product ion transitions. The MRM parameters were the following: qualifying ion pair, 465/330 and 435/250; quantifying ion pair, 435/330; fragmentation voltage, 120 V; and collision energies, 8/25 eV. The retention time of fipronil was 0.64 min. The limit of determination was 0.001 mg kg$^{-1}$. The recovery rates, relative standard deviations and linearity of this method are provided in the Supporting Information (Table s1).

**Statistical Analysis.** Statistical analysis of the insecticide-efficacy values and the white-grub density values was conducted using SPSS 10.0 (SPSS Inc., Chicago, IL, USA) software at $\alpha = 0.05$. Fisher's least significant difference test was applied to compare the mean values, and $p < 0.05$ was accepted as significant. Before performing the statistical analysis, the values of white-grub density were transformed using $\log_{10} x$, and the efficacy of the insecticides was transformed using arcsine $\sqrt{x} \times 180/\pi$.

## RESULTS

**Characterization of the Microcapsules Containing the Mixture of Fipronil and Chlorpyrifos.** The size distribution of the microcapsules containing the mixture of fipronil and chlorpyrifos was found to be unimodal (Figure 1). The particle sizes ranged from 0.2 to 4.7 $\mu$m, with an average of 1.6 $\mu$m. The encapsulation efficiencies for fipronil and chlorpyrifos were 90.0% and 96.0%, respectively.

**Dynamic Changes in the Fipronil Concentration in the Soil and the Peanut Roots.** In the case of all of the treatments, fipronil was detectable in the soil and peanut roots during the experimental period. Microencapsulation effectively reduced the rate of fipronil degradation in the soil and peanut roots compared with that of the conventional formulation. As shown in Table 2, the fipronil concentration in the soil and the peanut roots of the microcapsule treatments at the same growth stage of the peanuts was higher than that of the conventional formulation treatments. The fipronil concentration in soil declined from 0.895 mg kg$^{-1}$ to 0.211 mg kg$^{-1}$ with the microencapsulated formulation, 2.5−4.9 times that of the conventional formulation when both were applied at a dose of 1.8 g kg$^{-1}$ seed and compared at the same peanut growth stage. When used at a dose of 3.6 g kg$^{-1}$ seed, this concentration decreased from 1.27 mg kg$^{-1}$ to 0.275 mg kg$^{-1}$ with the microcapsule formulation, 2.5−6.1 times that of the conventional formulation.

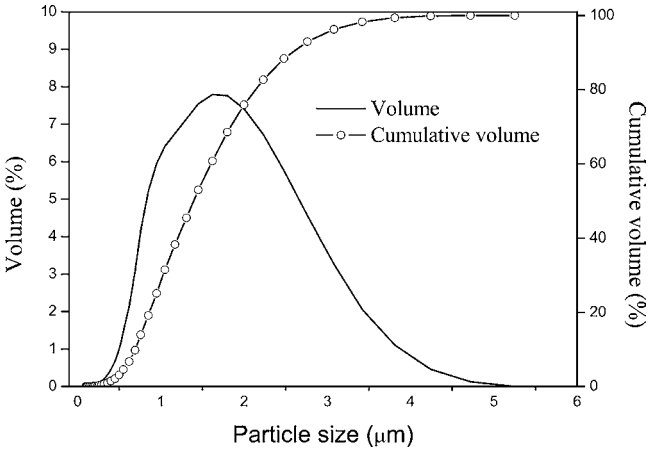


**Figure 1.** Size distribution of the microcapsules containing the mixture of fipronil and chlorpyrifos as determined using a BT-9300H laser particle-size analyzer.

The fipronil concentration in the peanut roots also declined gradually over the experimental period for both the microencapsulated and conventional formulations. These fipronil concentrations with the microencapsulated formulation were above 2.2 times that of the conventional formulation treatments when compared at the same peanut growth stage.

It was also observed that fipronil $C_r/C_s$ ratio for the conventional formulation declined gradually from 1.09 to 0.202 when applied at a dose of 1.8 g kg$^{-1}$ seed and from 1.36 to 0.273 when applied at a dose of 3.6 g kg$^{-1}$ seed. However, the fipronil $C_r/C_s$ ratio for the microencapsulated formulation peaked on 30 DAE.

**Dynamic Changes in the Chlorpyrifos Concentration in the Soil and Peanut Roots.** In contrast to fipronil, chlorpyrifos was detectable in both the soil and peanut roots on 15 DAE. After that point, it was detectable only in the soil (Table 3). Chlorpyrifos that was applied in microcapsules was effectively protected from degradation. On 15 DAE, its concentration for the microencapsulated formulation was 5.6 times that of the conventional formulation, and it increased to 10.3 times on 45 DAE when applied at a dose of 1.8 g kg$^{-1}$ seed. Similarly, the chlorpyrifos concentration for the microencapsulated formulation increased from 6.4 times that for the conventional formulation on 15 DAE to 28.1 times that for the conventional formulation on 45 DAE when applied at a dose of 3.6 g kg$^{-1}$ seed.

On 15 DAE, the $C_r/C_s$ ratio of chlorpyrifos for the conventional formulation was in the range of 2.55−2.80. For the microencapsulated formulation, that $C_r/C_s$ ratio was 2.48 when applied at a dose of 1.8 g kg$^{-1}$ seed, and 1.55 when applied at a dose of 3.6 g kg$^{-1}$ seed.

**Fipronil and Chlorpyrifos Residues in the Soil and Peanut Pods at Harvest.** As shown in Table 4, residues of fipronil were detectable in peanut kernels at harvest for all of the treatments, with the maximum residue level being 0.005 mg kg$^{-1}$, and the minimum residue level being 0.001 mg kg$^{-1}$. The amount of fipronil residue in the pod hulls and soil greatly varied depending on the location. The maximum residue level was found to be 0.040 mg kg$^{-1}$ in pod hulls and 0.059 mg kg$^{-1}$ in the soil when the formulations were applied at a dose of 5.4 g kg$^{-1}$ seed. Fipronil residues were also observed to be below the determination limit (0.001 mg kg$^{-1}$) in pod hulls and soil samples.

Table 2. Dynamic Changes in the Fipronil Concentration (mg kg$^{-1}$) in the Soil ($C_s$) and Roots ($C_r$) after a Single-Dose Application of Fipronil and Chlorpyrifos through Seed Treatment[a]

| | | soil | | | roots | | | $C_r/C_s$ | | |
|---|---|---|---|---|---|---|---|---|---|---|
| formulation | rate (g kg$^{-1}$ seed) | 15 DAE | 30 DAE | 45 DAE | 15 DAE | 30 DAE | 45 DAE | 15 DAE | 30 DAE | 45 DAE |
| conventional | 1.8 | 0.184 ± 0.070 | 0.141 ± 0.075 | 0.084 ± 0.013 | 0.200 ± 0.027 | 0.047 ± 0.074 | 0.017 ± 0.003 | 1.09 | 0.333 | 0.202 |
| | 3.6 | 0.275 ± 0.058 | 0.158 ± 0.028 | 0.110 ± 0.075 | 0.374 ± 0.036 | 0.056 ± 0.028 | 0.030 ± 0.001 | 1.36 | 0.354 | 0.273 |
| microencapsulated | 1.8 | 0.895 ± 0.172 | 0.606 ± 0.178 | 0.211 ± 0.027 | 0.434 ± 0.043 | 0.399 ± 0.107 | 0.056 ± 0.024 | 0.485 | 0.658 | 0.265 |
| | 3.6 | 1.27 ± 0.37 | 0.965 ± 0.061 | 0.275 ± 0.058 | 0.983 ± 0.086 | 0.870 ± 0.048 | 0.085 ± 0.002 | 0.772 | 0.902 | 0.204 |

[a]The results are presented as the mean values ± SD ($n$ = 3).

Table 3. Dynamic Changes in the Chlorpyrifos Concentration (mg kg$^{-1}$) in the Soil and Roots after a Single-Dose Application of Fipronil and Chlorpyrifos through Seed Treatment[a]

| | | soil | | | roots | | | $C_r/C_s$ |
|---|---|---|---|---|---|---|---|---|
| formulation | rate (g kg$^{-1}$ seed) | 15 DAE | 30 DAE | 45 DAE | 15 DAE | 30 DAE | 45 DAE | 15 DAE |
| conventional | 1.8 | 0.232 ± 0.038 | 0.111 ± 0.035 | 0.055 ± 0.007 | 0.591 ± 0.007 | ND[b] | ND | 2.55 |
| | 3.6 | 0.549 ± 0.166 | 0.140 ± 0.029 | 0.111 ± 0.035 | 1.54 ± 0.87 | ND | ND | 2.80 |
| microencapsulated | 1.8 | 1.29 ± 0.70 | 0.786 ± 0.398 | 0.567 ± 0.056 | 3.21 ± 0.14 | ND | ND | 2.48 |
| | 3.6 | 3.51 ± 0.51 | 3.34 ± 0.34 | 3.12 ± 0.07 | 5.43 ± 0.15 | ND | ND | 1.55 |

[a]The results are presented as the mean values ± SD ($n$ = 3). [b]ND, not detectable.

Table 4. Residues (mg kg$^{-1}$) of Fipronil and Chlorpyrifos in the Kernels, Pod Hulls, and Soil at Harvest after a Single-Dose Application of Microcapsule Formulation through Seed Treatment[a]

| | | fipronil | | | chlorpyrifos | | |
|---|---|---|---|---|---|---|---|
| | rate (g kg$^{-1}$ seed) | kernels | pod hulls | soil | kernels | pod hulls | soil |
| Yongqing | 3.6 | 0.005 ± 0.001 | 0.025 ± 0.002 | 0.036 ± 0.000 | ND[b] | ND | 0.015 ± 0.005 |
| | 5.4 | 0.005 ± 0.001 | 0.031 ± 0.001 | 0.059 ± 0.006 | ND | ND | 0.015 ± 0.001 |
| Jinan | 3.6 | 0.001 ± 0.000 | 0.007 ± 0.003 | 0.007 ± 0.001 | ND | ND | 0.002 ± 0.001 |
| | 5.4 | 0.004 ± 0.001 | 0.040 ± 0.000 | 0.014 ± 0.022 | 0.004 ± 0.001 | 0.015 ± 0.002 | 0.141 ± 0.004 |
| Xiantao | 3.6 | 0.001 ± 0.000 | ND | ND | ND | 0.003 ± 0.003 | 0.005 ± 0.000 |
| | 5.4 | 0.001 ± 0.000 | ND | ND | 0.002 ± 0.002 | 0.008 ± 0.007 | 0.010 ± 0.001 |

[a]The results are presented as the mean values ± SD ($n$ = 3). [b]ND, not detectable.

As shown in Table 4, the level of chlorpyrifos residues in the soil were always above the determination limit (0.001 mg kg$^{-1}$). The maximum residue level found in the soil was 0.141 mg kg$^{-1}$ when the formulations were applied at a dose of 5.4 g kg$^{-1}$ seed in Jinan. However, chlorpyrifos was detectable in less than half of the samples of pod hulls and kernels.

**The Efficacies of the Insecticides against White Grubs in Peanut Fields.** Microencapsulation greatly improved the efficacy of the mixture of fipronil and chlorpyrifos to control white grubs. As shown in Table 5, when the formulations were applied at a rate of 1.8 g kg$^{-1}$ seed, the populations of white grubs in the conventional formulation treated plots were not significantly lower than those in the control plots. When the formulations were applied at a rate of 3.6 g kg$^{-1}$ seed, the populations of white grub in the conventional formulation treated plots were significantly reduced, but the efficacy of this treatment was only 44.4%. In contrast, the microencapsulated mixture of fipronil and chlorpyrifos significantly reduced the populations of white grubs in the test fields and the efficacies of this formulation were greater than 71% when applied at both of the tested doses.

Table 5. Densities (Mean Values ± SD Numbers Per 30 Plants) of White Grubs and Efficacies (%) of the Insecticides at Harvest Time after a Single Dose Application of Fipronil and Chlorpyrifos through Seed Treatment[a]

| formulation | rate (g kg$^{-1}$ seed) | white grub density | efficacy |
|---|---|---|---|
| conventional formulation | 1.8 | 31.0 ± 1.0 a | 13.9 ± 2.8 c |
| | 3.6 | 20.0 ± 2.6 c | 44.4 ± 7.3 b |
| microcapsule formulation | 1.8 | 10.3 ± 1.5 b | 71.3 ± 4.2 a |
| | 3.6 | 9.0 ± 2.6 b | 75.9 ± 6.4 a |
| untreated control | | 36.0 ± 4.6 a | |

[a]The results are presented as the mean values ± SD ($n$ = 3). Values in the same column followed by different letters are significantly different at $\alpha$ = 0.05.

## DISCUSSION

Chlorpyrifos is often applied as a granular treatment along the peanut rows at pegging to control soil pests.[18,19] However, most growers choose to apply chlorpyrifos through seed treatment prior to planting because it is a more labor-efficient practice. Although the trials in this study were conducted by applying chlorpyrifos at planting, treatments at pegging or at both planting and pegging are more effective in controlling soil pests.[4,19] Our study indicated that applying a single dose of the conventional mixture of chlorpyrifos and fipronil through seed treatment did not meet the demands of peanut producers for the control of white grubs. The efficacy of this conventional formulation was in the range of only 13.9−44.4%. To better control this pest, a higher application rate or repeated

applications of the insecticides would be required, which is the commonly accepted practice for agricultural production.[20,21] A single dose of the microencapsulated mixture of chlorpyrifos and fipronil effectively controlled the white grubs throughout one growing season of peanuts, proving that microencapsulation can reduce the dosage and frequency of application of the insecticides (Table 5).

The degradation of chlorpyrifos in natural soil results from hydrolytic and microbial processes that often work in tandem.[10,22,23] However, hydrolysis constitutes the major route of chlorpyrifos degradation in soil, and a higher level of soil moisture increases the dissipation rate.[24,25] In this study, the concentration of chlorpyrifos in the soil for the microencapsulated formulation was 5.6−28.1 times that of the conventional formulation, which demonstrated the ability of microencapsulation to stabilize chlorpyrifos against degradation in the environment. However, chlorpyrifos is a compound without systemic activity. But it can strongly adhere to plants and soil.[10] When crop roots contact soil containing chlorpyrifos, no uptake of chlorpyrifos occurs. Chlorpyrifos adheres to the surface of roots and other underground tissues. In our study, chlorpyrifos was detectable in both the roots and soil on 15 DAE but was detectable only in the soil later in the growing season. This finding can be explained by gradual diffusion into the soil, as the peanut plants grew, of the chlorpyrifos coated on the surface of the peanut seeds, so that the level of chlorpyrifos in the roots decreased with the increasing experimental time. Additionally, although chlorpyrifos can adhere to the surface of roots, a great deal of the adsorbed chlorpyrifos might be washed away during the preparation of the root samples. The amounts of final chlorpyrifos residues in the soil, kernels, and pod hulls taken from the three tested locations were consistent with this hypothesis. At harvest, the levels of the final residues of chlorpyrifos were detectable in all of the soil samples but were detectable in less than half of the samples of pod hulls and kernels. Taken together, these results revealed that although microencapsulating chlorpyrifos retards its rate of degradation in the soil and improves its residual activity, there is a low risk that chlorpyrifos will contaminate the underground edible tissues following seed treatment because this compound is not taken up by plants.

In contrast, fipronil exhibits systemic activity against certain susceptible pests. Following application via seed treatment, fipronil can be absorbed by roots and transported upward in the xylem of plants.[15] In agreement with this chemical property, fipronil was detectable in all of the samples of the roots and soil within 45 DAE. At harvest, fipronil was detectable in all of the kernel and pod hull samples from Yongqing and Jinan, as well as in the kernel samples from Xiantao. Similarly, Aajoud et al. found that a great amount of fipronil was present in the tissues of sunflowers throughout the experiment course following seed coating application, as determined using $^{14}$C-fipronil. Therefore, they suggested that slow release strategies should be adopted when formulating a seed coating mixture using fipronil to maintain its efficiency to control soil-dwelling pests and to limit the uptake and transport of fipronil by plants.[15] In our study, the fipronil $C_r/C_s$ ratio for the conventional formulation exhibited a downward trend during the experiment period. This downward trend was due to the initially high dose of fipronil directly contacting the roots and the subsequent uptake of fipronil by the peanut roots occurring more slowly than the water uptake.[15] However, the fipronil $C_r/C_s$ ratio for the microencapsulated formulation peaked on 30 DAE, which revealed that the slow rate of fipronil release by the microcapsules limited its direct contact with the roots.

Fipronil is widely used in unencapsulated conventional formulation to control soil-dwelling pests, and the fipronil residues were often found to be below the detectable levels in the soil and plant tissues at the time of harvest.[9,11,26] At least a 2.2-fold higher concentration of fipronil in the soil and peanut root tissues was found with the microencapsulated treatment compared with the conventional treatment, which indicated that microencapsulation prolonged it activity. Besides this advantage of prolonged activity, the controlled release of pesticides can also reduce the adverse effects of pesticides on the biological systems. Many pesticides have been encapsulated within polymer beads for safer application, such as neem seed oil, chlorpyrifos, cypermethrin, and fenvalerate.[27−31] However, another risk should be taken into consideration. In this study, the greater persistence of the microencapsulated fipronil may result in a higher risk of exceeding the MRLs set by governments worldwide. The concentration of its final residue in kernels was in the range of 0.001−0.005 mg kg$^{-1}$. The official MRL for fipronil in peanuts set by the European Union is 0.005 mg kg$^{-1}$, and that of the Japanese government is 0.01 mg kg$^{-1}$. The level of fipronil residues in some kernel samples reached the MRL set by the European Union, which indicated that a higher application rate or repeated application of the microencapsulated fipronil at the tested dosages would not be acceptable.

In conclusion, white grubs are difficult to control because they can damage peanut plants throughout their growing season. A microencapsulated mixture of fipronil and chlorpyrifos effectively controlled this insect pest after a single dose applied via seed treatment. Microencapsulation protected both fipronil and chlorpyrifos against degradation in the environment. In this formulation, chlorpyrifos has a low risk of exceeding the MRLs at harvest in the underground edible tissues following seed treatment. However, the fipronil residues in some kernel samples at harvest reached the statutory MRL set by the European Union, which indicated that a higher rate of application or repeated application of the microencapsulated fipronil would not be acceptable.

## ■ ASSOCIATED CONTENT

### Ⓢ Supporting Information

The recovery rates, relative standard deviations, and linearity of methods determining the residual levels of fipronil and chlorpyrifos in soil, roots, kernels, and pod hulls (Table s1). This material is available free of charge via the Internet at http://pubs.acs.org.

## ■ AUTHOR INFORMATION

### Corresponding Author

*Tel/fax: +86-10-62815941. E-mail: hzhyuan@gmail.com.

### Funding

This study was supported by the National Key Technology R&D Program of China (Grant Number 2012BAD19B04) and the Public Welfare Project of the Ministry of Agriculture of the People's Republic of China (Grant Number 201003025).

### Notes

The authors declare no competing financial interest.

## ■ ACKNOWLEDGMENTS

The authors gratefully acknowledge Dr. Zhisheng Qin from the DuPont Pioneer Company for his helpful comments and suggestions for this manuscript.

## ■ ABBREVIATIONS USED

$C_r$, concentration in peanut roots; $C_s$, concentration in the soil; DAE, days after seedling emergence; MRL, maximum residue limit; MRM, multiple reaction monitoring; PSA, primary secondary amine; REA, readily extractable active ingredient; SD, standard deviation

## ■ REFERENCES

(1) Tsuji, K. Microencapsulation of pesticides and their improved handling safety. *J. Microencapsulation* **2001**, *18*, 137−147.
(2) Shirley, I. M.; Scher, H. B.; Perrin, R. M.; Wege, P. J.; Rodson, M.; Chen, J. L.; Rehmke, A. W. Delivery of biological performance via micro-encapsulation formulation chemistry. *Pest Manage. Sci.* **2001**, *57*, 129−132.
(3) Weeks, R.; Hagan, A.; Foshee, W.; Hartzog, D. L.; Everest, J. W. *Peanut pest management scout manual*; Alabama Cooperative Extension System Bulletin ANR-598; 2000.
(4) Abudulai, M.; Dzomeku, I. K.; Opare-Atakora, D.; Nutsugah, S. K.; Salifu, A. B.; Brandenburg, R. L.; Jordan, D. L. Survey of soil arthropod pests and assessment of yield loss in peanut in northern Ghana. *Peanut Sci.* **2012**, *39*, 113−120.
(5) Owusu-Akyaw, M.; Afun, J. V. K.; Mochiah, M. B.; Adu-Mensah, J.; Moses, E.; Bolfrey-Arku, G.; Osei, K.; Osei-Yeboah, S.; Dankyi, A. A.; Adama, I.; Brandenburg, R. L.; Jordan, D. L. Survey and management of soil arthropods in peanut (Arachis hypogaea L.) in southern Ghana, West Africa. *Peanut Sci.* **2005**, *32*, 136−143.
(6) Li, Y.; Han, J.; Yu, C.; Yu, W.; Mu, W. Toxicity and control effect of seven insecticides to *Holotrichia parallela*. *Acta Phytophylacica Sin.* **2012**, *39*, 147−152.
(7) Rajagopalan, N.; Bhaskar, C.; Bankar, V. S.; Pokharkar, V. B.; Shukla, P. G.; Regupathy, A.; Khilar, K. C. Starch urea formaldehyde matrix encapsulation of solid agrochemicals: III. Studies and bioefficacy trials on double encapsulation. *Pestic. Sci.* **1995**, *45*, 123−131.
(8) Ji, J.; Li, Y.; Gao, Z. S.; Liu, F. Influence of environmental factors on persistence of chlorpyrifos microcapsule suspension and emulsifiable concentrate in soils. *Chin. J. Pestic. Sci.* **2011**, *13*, 364−368.
(9) Mandal, K.; Singh, B. Dissipation of fipronil granule formulation in sugarcane field soil. *Ecotoxicol. Environ. Saf.* **2013**, *88*, 142−147.
(10) Gebremariam, S. Y.; Beutel, M. W.; Yonge, D. R.; Flury, M.; Harsh, J. B. Adsorption and desorption of chlorpyrifos to soils and sediments. *Rev. Environ. Contam. Toxicol.* **2012**, 123−175.
(11) Chopra, I.; Chauhan, R.; Kumari, B.; Dahiya, K. Fate of fipronil in cotton and soil under tropical climatic conditions. *Bull. Environ. Contam. Toxicol.* **2011**, *86*, 242−245.
(12) Pei, Z.; Yitong, L.; Baofeng, L.; Gan, J. J. Dynamics of fipronil residue in vegetable-field ecosystem. *Chemosphere* **2004**, *57*, 1691−1696.
(13) Mulrooney, J.; Wolfenbarger, D.; Howard, K. D.; Goli, D. Efficacy of ultra low volume and high volume applications of fipronil against the boll weevil. *J. Cotton Sci.* **1998**, *2*, 110−116.
(14) Racke, K. Environmental fate of chlorpyrifos. *Rev. Environ. Contam. Toxicol.* **1993**, *131*, 1−150.
(15) Aajoud, A.; Raveton, M.; Aouadi, H.; Tissut, M.; Ravanel, P. Uptake and xylem transport of fipronil in sunflower. *J. Agric. Food Chem.* **2006**, *54*, 5055−5060.
(16) Hong, K.; Park, S. Melamine resin microcapsules containing fragrant oil: synthesis and characterization. *Mater. Chem. Phys.* **1999**, *58*, 128−131.
(17) Asrar, J.; Ding, Y.; La Monica, R. E.; Ness, L. C. Controlled release of tebuconazole from a polymer matrix microparticle: release kinetics and length of efficacy. *J. Agric. Food Chem.* **2004**, *52*, 4814−4820.
(18) Chapin, J. W.; Thomas, J. S.; Joost, P. H. Tillage and chlorpyrifos treatment effects on peanut arthropods-an incidence of severe burrower bug injury. *Peanut Sci.* **2001**, *28*, 64−73.
(19) Jordan, D. L.; Brandenburg, R. L.; Johnson, P. D.; Royals, B. M.; Watson, B. Interactions of chlorpyrifos and herbicides applied to peanut (*Arachis hypogaea* L.). *Peanut Sci.* **2008**, *35*, 32−37.
(20) Racke, K. D.; Fontaine, D. D.; Yoder, R. N.; Miller, J. R. Chlorpyrifos degradation in soil at termiticidal application rates. *Pestic. Sci.* **1994**, *42*, 43−51.
(21) Murray, R. T.; von Stein, C.; Kennedy, I. R.; Sanchez-Bayo, F. Stability of chlorpyrifos for termiticidal control in six Australian soils. *J. Agric. Food Chem.* **2001**, *49*, 2844−2847.
(22) Chishti, Z.; Hussain, S.; Arshad, K. R.; Khalid, A.; Arshad, M. Microbial degradation of chlorpyrifos in liquid media and soil. *J. Environ. Manage.* **2013**, *114*, 372−380.
(23) Chai, L. K.; Wong, M. H.; Bruun Hansen, H. C. Degradation of chlorpyrifos in humid tropical soils. *J. Environ. Manage.* **2013**, *125*, 28−32.
(24) Racke, K. D.; Steele, K. P.; Yoder, R. N.; Dick, W. A.; Avidov, E. Factors affecting the hydrolytic degradation of chlorpyrifos in soil. *J. Agric. Food Chem.* **1996**, *44*, 1582−1592.
(25) Wang, L.; Jiao, W.; Jiang, X.; Liang, Y. Abiotic control on the dissipation of chlorpyrifos spiked in an Udic Ferrisol at a lower dosage. *Chem. Ecol.* **2013**, *29*, 724−732.
(26) Bhardwaj, U.; Kumar, R.; Kaur, S.; Kumar Sahoo, S.; Mandal, K.; Battu, R.; Singh, B. Persistence of fipronil and its risk assessment on cabbage *Brassica oleracea* var. capitata L. *Ecotoxicol. Environ. Saf.* **2012**, *79*, 301−308.
(27) Kulkarni, A. R.; Soppimath, K. S.; Aminabhavi, T. M.; Dave, A. M.; Mehta, M. H. Glutaraldehyde crosslinked sodium alginate beads containing liquid pesticide for soil application. *J. Controlled Release* **2000**, *63*, 97−105.
(28) Kumbar, S. G.; Kulkarni, A. R.; Dave, A. M.; Aminabhavi, T. M. Encapsulation efficiency and release kinetics of solid and liquid pesticides through urea formaldehyde crosslinked starch, guar gum, and starch + guar gum matrices. *J. Appl. Polym. Sci.* **2001**, *82*, 2863−2866.
(29) Kulkarni, A. R.; Soppimath, K. S.; Aminabhavi, T. M.; Dave, A. M. Polymeric sodium alginate interpenetrating network beads for the controlled release of chlorpyrifos. *J. Appl. Polym. Sci.* **2002**, *85*, 911−918.
(30) Kumbar, S. G.; Aminabhavi, T. M. Preparation and characterization of interpenetrating network beads of poly(vinyl alcohol)-grafted-poly(acrylamide) with sodium alginate and their controlled release characteristics for cypermethrin pesticide. *J. Appl. Polym. Sci.* **2002**, *84*, 552−560.
(31) Kumbar, S. G.; Dave, A. M.; Aminabhavi, T. M. Release kinetics and diffusion coefficients of solid and liquid pesticides through interpenetrating polymer network beads of polyacrylamide-*g*-guar gum with sodium alginate. *J. Appl. Polym. Sci.* **2003**, *90*, 451−457.

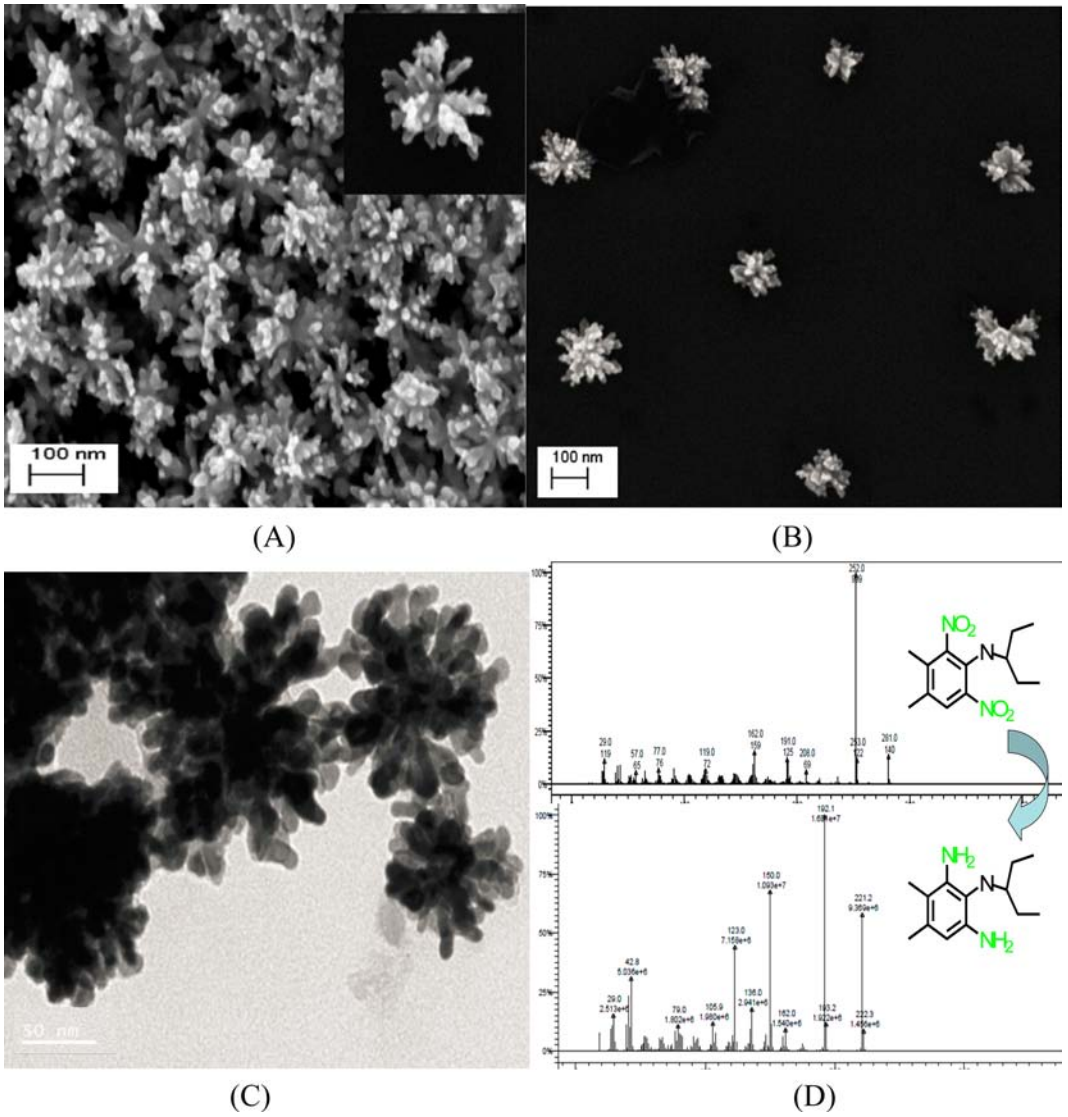


**Figure 1.** (A, B) SEM and (C) TEM images of gold nanoflower that were synthesized; Mass spectral data of (D) shows the process of degradation of pendimethalin (above) to *N*-(1-ethylpro-pyl)-2,6-diamino-3,4-xylidine (below).

the model contaminant due to its relatively long persistence in soil and its frequent use as a criterion for soil contamination by pesticide dealerships,[38] was effectively degraded by sodium borohydride. Pendimethalin is the common name for *N*-(1-ethylpro-pyl)-2,6-dinitro-3,4-xylidine, a representative member of the growing list of N-substituted 2,6-dinitroaniline herbicides used for selective control of most annual grasses and many annual broad-leaved weeds in several crops. Pendimethalin has approved uses in all countries of the European Union.[39] However, according to the label of pendimethalin, even in nanomolar concentration, it is toxic to aquatic organisms such as fish and may cause long-term adverse effects in the aquatic environment. What's more, pendimethalin has half-lives in soil usually ranging from a few days to several months.[40] Plieth and Boerner[41] reported approximately 10−15% remains of the 2.3 mg/kg pendimethalin 10 months after its application in the soil. Compared with previously reported ways of pendimethalin degradation, our method exhibited higher efficiency and faster reaction (within 5 min). In addition, degradation of pendimethalin in soil samples was performed to demonstrate enormous potential in the practical use of this platform. Furthermore, to verify the effectiveness of gold nanoflower as the catalyst in the degradation of nitroaromatic pesticides, additional experiments on trifluralin and *p*-nitrophenol, which are common nitroaromatic pesticides were carried out with satisfactory results.

## MATERIALS AND METHODS

**Chemicals and Apparatus.** Pendimethalin were purchased from Zouping Luda Pharmaceutical Co., Ltd. (Shandong, China). Trifluralin were purchased from Feng Shan Group Co., Ltd. (Jiangsu, China). *p*-Nitrophenol were purchased from Sinopharm Chemical Reagent Co.,Ltd. Two soil samples (A clay soil containing organic matter and sandy loam soil in absence of organic matter) came from Wuhan University. Other chemicals were of analytical grade and prepared with ultrapure water from a Millipore system (18.2 M resistivity).

The size distribution and structure of the Au nanoflower were probed by high-resolution transmission electron microscopy (HRTEM) using a JEM-2100 (HR) operated at an acceleration voltage of 200 kV and scanning electron microscope (SEM), respectively. Subsequently, gas chromatography−mass spectrometry (GC−MS) was used to ensure the product of degradation reaction. Finally, UV−vis absorption spectrometer (UV-2550, Hitachi Co. Ltd., Japan) was employed to record UV−vis absorption spectra.

**Synthesis of Au Nanoflower.** Modifications were made based on the literature[37,42] and Au nanoflower has been successfully synthesized with a simple, fast process without seeds and other surfactants. First, 50 $\mu$L of $HAuCl_4$ (wt 1%) aqueous solution was added to 2.5 mL of deionized water. Then, 10 $\mu$L of $NH_2OH$ (wt 50%) aqueous solution was injected into the solution with stirring, and after 1 min reaction, Au nanoflower dispersion was obtained. Finally, after half an hour standing, homogeneous Au nanoflower was obtained for use.

**UV−vis Spectra Measurements.** The color change was qualitatively measured by taking UV−vis spectra with 600 $\mu$L-optical-path-length quartz cuvettes at 1 min interval in the range of 200−700 nm. The rate constant of the degradation reaction of nitroaromatic pesticides was determined by the function of the measurement of the change of absorbance at the initially observed peak at 430 nm in relation to time. All experiments were reacted and measured at room temperature.

In order to investigate the feasibility of degrading pendimethalin by $NaBH_4$ in the presence of Au nanoflower (with stable particle size100 nm) as a degradation catalyst, three 2 mL test tubes (A,B,C) have been added into 500 $\mu$L of 2.34 mM pendimethalin aqueous solution. Then, pendimethalin aqueous solution in test A and test B was respectively mixed with 500 $\mu$L of 15 mM $NaBH_4$ aqueous solution and 500 $\mu$L ultrapure water was added into test C. 100 $\mu$L Au nanoflower was introduced into test A and 100 $\mu$L ultrapure water was added to test B and test C, respectively, to make each reaction solution 1100 $\mu$L. The final mixed solution was allowed to stand and react for 30 min at room temperature. The UV−vis absorption spectrum was measured at room temperature.

To save cost and time, kinetic analysis is necessary. A 500-$\mu$L portion of 2.34 mM pendimethalin aqueous solution was mixed with 500 $\mu$L of 15 mM $NaBH_4$ aqueous solution. After vibration, 100 $\mu$L Au nanoflower aqueous solution was added. The UV−vis absorption spectrum was measured at 1 min interval from zero to 10 min at room temperature. The rate constant of the degradation reaction of pendimethalin was determined by measuring the change in absorbance of the initially observed peak at 430 nm, for the pendimethalin, as a function of time.

The pH value is a very important factor to the reaction process. The pH value of pendimethalin aqueous solution was adjusted by 1 M HCl or 1 M NaOH aqueous solution and the final concentration was 2.34 mM. 500 $\mu$L of pendimethalin aqueous solution (2.34 mM) of different pH value (pH 1, 4, 7, 11, 14) were mixed with 500 $\mu$L 15 mM of $NaBH_4$ aqueous solution in 2.0 mL test tube respectively, and 100 $\mu$L Au nanoflower aqueous solution was added to make each solution 1.1 mL. Finally, these mixtures were detected by the UV−vis absorption spectrum at room temperature.

In order to optimize volume of Au nanoflower, 500 $\mu$L of 2.34 mM pendimethalin aqueous solution were mixed with 500 $\mu$L of 15 mM $NaBH_4$ aqueous solution. After vibration, different volumes (25−200 $\mu$L) of Au nanoflower solution were added in, respectively. Then appropriate aliquot of ultrapure water was introduced in to make each reaction solution 1.2 mL. Finally, the UV−vis absorption spectrum measurements were done at room temperature.

To verify the feasibility of this new platform for pendimethalin degradation in practical samples, two soil samples (clay soil containing organic matter and sandy loam soil in absence of organic matter) are applied to degrade pendimethalin. Two 10 g samples of air-dried soil were transferred to a 100 mL flask. Then 100 mL of water was added in and stirred for about 3 h; after the soil settled, the supernatant was filtered by 0.22 $\mu$m microporous membrane. Two 4.68 mM pendimethalin portions were diluted by two soil filtrates, and the final concentration was 2.34 mM. 500 $\mu$L 2.34 mM pendimethalin was mixed with 500 $\mu$L 15 mM $NaBH_4$ aqueous solution, then, 100 $\mu$L Au nanoflower aqueous solution was added into the mixtures. The UV−vis absorption spectrum measurements were done at room temperature.

To further explore the potential application of the platform in the practical samples, the development of new degradation platform was tested by other nitroaromatic pesticides, including trifluralin and *p*-nitrophenol. 500 $\mu$L of 1.43 mM trifluralin aqueous solution and 0.2 mM *p*-nitrophenol aqueous solution were mixed with 500 $\mu$L 15 mM NaBH4 aqueous solution respectively, then, 100 $\mu$L Au nanoflower aqueous solution was added into the mixtures. The UV−vis absorption spectrum measurements were done at room temperature.

## RESULTS AND DISCUSSION

**The Proposed Mechanism.** Gold-based catalysts have attracted intense interest in recent years following the discovery that small supported Au nanoparticles (NPs) can be effective catalysts for CO oxidation at low temperatures. They have been widely used and regarded as a new generation of catalysts to some reactions that are otherwise unfeasible. However, the properties of AuNPs depend strongly on their size and shape, which determine the surface structure of the particles.[29] In our experiment, Au nanoflower was synthesized through $NH_2OH$ reduction of $HAuCl_4$. To confirm the successful formation of Au nanoflower and its size and shape, the as-prepared Au nanoflower was characterized by SEM and HRTEM. As shown in Figure 1A−C, dendritic structures of Au nanoflower were synthesized, and the diameter of Au nanoflower was approximately 100 nm, exhibiting relatively narrow size distribution. Although reports of dendritic structure of gold nanoparticle are rarely seen,[37,42−44] dendritic nanostructures have often been reported in the synthesis of platinum nanocrystals.[45,46] According to diffusion-limited aggregation (DLA) model,[33,47] small Au nanoparticle has higher energy owing to a larger surface-to-volume ratio and of a higher collision frequency associated with their greater mobility, which leads to Au nanoparticle coalescence or attachment. The probability of finding a randomly diffusing AuNPs particle around the Au core is extremely low owing to the so-called screening effect. Due to the screening effect, the tips of most advanced branches of Au core can most effectively capture the incoming and randomly diffusing gold particles, forming particle coalescence, or attachment to the tips, thus homogeneous and stable gold nanoflower solution can be obtained in the end.

It can be observed that the yellow pendimethalin aqueous solution exhibited a large absorption peak at 430 nm without $NaBH_4$ and Au nanoflower. Upon the addition of aqueous solution of $NaBH_4$ (15 mM), the absorption peak at 430 nm of (B) and (C) remained unaltered and their solution color remained the same for a long duration, which indicated that the strong reducing agent $NaBH_4$ alone cannot degrade pendimethalin. Interestingly, the addition of an aliquot of Au nanoflower dispersion to the reaction system caused a fading and ultimate bleaching of the yellow color of pendimethalin in aqueous solution (A), suggesting the occurrence of the degradation reaction. The UV/vis spectra in Figure 2 unambiguously verifies this conclusion as well, as the absorption band of pendimethalin at 430 nm decreases and disappears in less than 5 min after the addition of Au nanoflower. To exclude the possibility that the degradation reaction could have been activated by the superfluous $NH_2OH$ instead of Au nanoflower, $NH_2OH$ alone was added into pendimethalin and $NaBH_4$ (15 mm) mixtures. No change in the color and position of the absorption band (at 430 nm) of pendimethalin was observed. Thus, the degradation of pendimethalin by $NaBH_4$ has been clearly demonstrated to be activated by the Au nanoflower. The samples of pendimethalin and degredation product were characterized using gas chromatography−mass spectrometry (GC−MS) for identification of compounds. The experimental results of mass spectrum (Figure 1 D) showed that the two

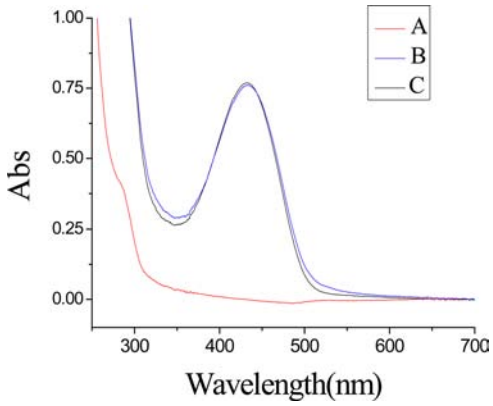


**Figure 2.** (A) UV−vis absorption spectra of degradation of pendimethalin catalyzed by Au nanoflower, (B) UV−vis absorption spectra during the reduction of pendimethalin by $NaBH_4$ without Au nanoflower, and (C) UV−vis absorption spectra of pendimethalin in aqueous solution.

nitro groups of pendimethalin were reduced to two amino groups of *N*-(1-ethylpro-pyl)-2,6-diamino-3,4-xylidine. On the basis of the above findings, a tentative reaction pathway for degradation of pendimethalin catalyzed by Au nanoflower processes is presented as follows (Scheme 1): in this process,

**Scheme 1. Reaction Pathway for Degradation of Pendimethalin Catalyzed by Au Nanoflower Processes**

the main oxidizing species is $H^-$ from $NaBH_4$. But $H^-$ is unstable in aqueous solution. Due to its large specific surface area and high specific activity, gold nanoflower could adsorb hydrogen anion ($H^-$) and provide places for the degradation of pendimethalin. Meanwhile, a large Fermi level shift caused the higher driving force of particle-mediated electron transfer from $BH_4^-$ ion to nitro compounds mediated by the Au nanoflower because that existing $H^-$ belong to highly electron-injecting species.[48] As seen from the principle above, pendimethalin are removed directly from the aqueous solution, leading to the formation of aromatic intermediates. Hence, this method is applicable to the degradation of all nitroaromatic pesticides rather than just a few particular nitrophenolic compounds.

**Kinetics for Pendimethalin Oxidation.** Hydrogen anion ($H^-$) from sodium borohydride ($NaBH_4$) is mainly used as a principal reducing agent in pendimethalin degradation. Hydrogen anion ($H^-$), as a nonspecific reductant, reacts with the target organic contaminants (pendimethalin) at rates close to diffusion rates in water. Thus, the kinetics for pendimethalin reducing by reduction of sodium borohydride catalyzed by Au nanoflower processes can be represented as follows:

$$dC(P)/dt = -k_P'C(P) \times C(NaBH_4) \quad (1)$$

A second-order rate equation can be applied to fit the data, where $C(P)$ is the concentration of pendimethalin, $C(NaBH_4)$ is the sodium borohydride concentration, and $k_P'$ is the second-order rate constant for the reaction. Since the concentration of $NaBH_4$ added in the system is much higher in comparison with that of pendimethalin, it is reasonable to assume that the concentration of $BH_4^-$ remains constant during the reaction. Equation 1 can be reduced to a pseudo-first-order rate equation:

$$dC(P)/dt = -k_PC(P) \quad (2)$$

where, $k_P$ is the pseudo-first-order rate constant. In case of Au nanoflower-catalyzed degradation processes, Au nanoflower remained almost constant during the experimental time and hence eq 2 was equated in evaluating the kinetics of pendimethalin during Au nanoflower-catalyzed degradation processes. When $t = 0$, $C(P)$ is equal to $C(P)_0$, and the solution of eq 2 becomes,

$$C(P) = C(P)_0 \exp(-k_Pt) \quad (3)$$

or

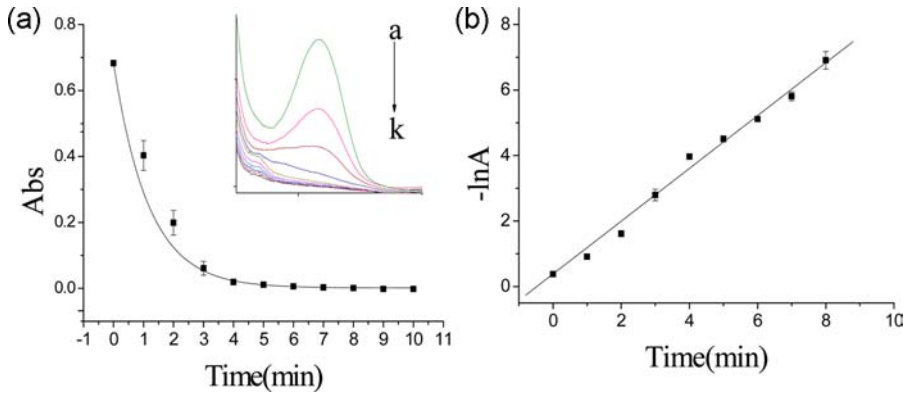


**Figure 3.** (a) Plot of absorbance (A) against time for the catalytic reduction of pendimethalin by Au nanoflower (the insets present the reaction kinetic graph for the degradation of pendimethalin catalyzed by Au nanoflower. (a–k): 0, 1, 2, 3, 4, 5, 6, 7, 8, 9, and 10 min) and (b) Plot of −ln(A) against time for the catalytic reduction of pendimethalin by Au nanoflower (conditions: 500 μL 2.34 mM pendimethalin + 500 μL 15 mM $NaBH_4$ + 100 μL Au nanoflower).


dx.doi.org/10.1021/jf5034015 | J. Agric. Food Chem. 2014, 62, 10638−10645

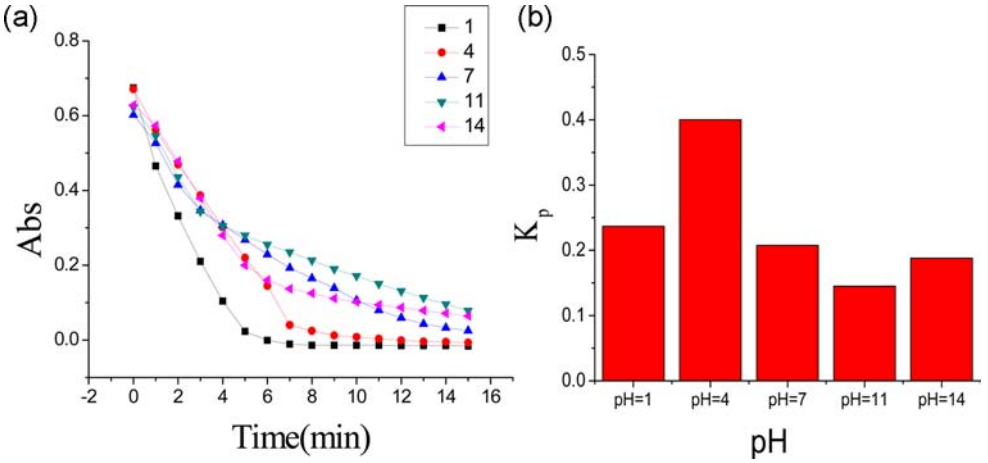


**Figure 4.** (A)Plot of the absorbance at $\lambda_{max}$ ($\lambda_{max}$ = 430 nm) of degradation pendimethalin versus time at different pH (B) Histogram of rate constant of degradation pendimethalin at different pH (pH 1, 4, 7, 11, and 14).

$$\ln[C(P)/C(P)_0] = -k_p t \quad (4)$$

On the basis of the above considerations, pseudo-first-order kinetics could be used to evaluate the kinetic reaction rate of the current catalytic reaction, together with the UV/vis absorption data in Figure 3. As expected, a good linear correlation of $\ln(A)$ versus time ($A$ is the absorption intensity of pendimethalin) was obtained (Figure 3), where $k$ is a kinetic reaction rate constant, $k$ = 0.8066 and $b$ = 0.3813. The linear fitting of the experimental data gives a linear correlation coefficient of 0.998 and standard deviation of 3.75. The equation is as follows:

$$-\ln A = kt + b$$

**Optimal pH Value.** We studied the effect of pH on the removal of pendimethalin because the degradation efficiency of the pendimethalin is pH dependent.[38] The changes of UV−vis absorption spectrum as a function of pH and time (Figure 4A) was taken into account. According to Figure 4A, when the pH value was increased from 1 to 11, the time of degradation was gradually prolonged, and the removal efficiency decreased. Despite the fact that velocity constant (Figure 4B) was improved slightly when the pH value was 14, it was accompanied by long degradation time and unsatisfactory removal efficiency. Under acidic conditions, protonation of nitrogen atoms of nitro of pendimethalin could easily be formed, giving them higher affinities with $H^-$ produced by $NaBH_4$. Nevertheless, $H^-$ is unstable in acidic solution because of the presence of $H^+$. Therefore, the degradation reaction was influenced by both the degree of protonation of nitrogen atom and the amount of $H^-$ existence. Under acidic conditions, nitrogen atoms of nitro of pendimethalin could achieve higher degree of protonation, while under alkaline conditions, $H^-$ is more stable. Due to redundant $NaBH_4$ in the designed system, the degradation reaction had little effect on $H^-$ under acidic condition. But under alkaline conditions, the reaction platform was largely influenced by the degree of protonation. Considering all these, pH under acidic condition, which is more conducive for pendimethalin degradation, was selected in the subsequent experiments, which is in accordance with the literature.[38] Since pendimethalin solution is naturally acidic (pH 4−5), no adjustments of pH were done in the experiments.

**Optimal Au nanoflower volume.** It is essential to carefully optimize the concentration of Au nanoflower due to its crucial role in the degradation of pendimethalin in aqueous solution and complex samples. A too low concentration of Au nanoflower could lead to low catalytic efficiency and longer time, while a too high concentration could have a slower effect on catalytic activity or cause a waste of the material. Both would result in bad rate of the degradation. Thus, the optimization of Au nanoflower concentration was performed (Figure 5). As shown in Figure 5, the degradation time decreased gradually with the increasing concentration of Au nanoflower, and a turning point of least degradation time was observed when the volume of Au nanoflower reached 150uL (Figure 5). Therefore, an optimized volume of 150 $\mu$L Au nanoflower was chosen in the experiments.

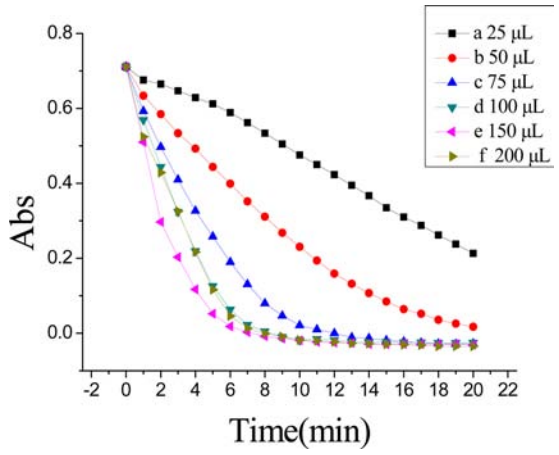


**Figure 5.** Plot of the absorbance at $\lambda_{max}$ of pendimethalin versus time at different volumes of Au nanoflower (a-f: 25, 50, 75, 100, 150, and 200 $\mu$L).

**Degradation of pendimethalin in soil.** To demonstrate the practical applicability of the designed strategy, we measured the UV−vis absorption spectra of soil diffusate containing pendimethalin at specific concentrations (Figure 6). It required about 7 min to complete the degradation of pendimethalin in the inorganic soil, and a little longer in organic soil yet within 10 min. Variations in pendimethalin removal efficiency between different soils were consistent with known effects from soil

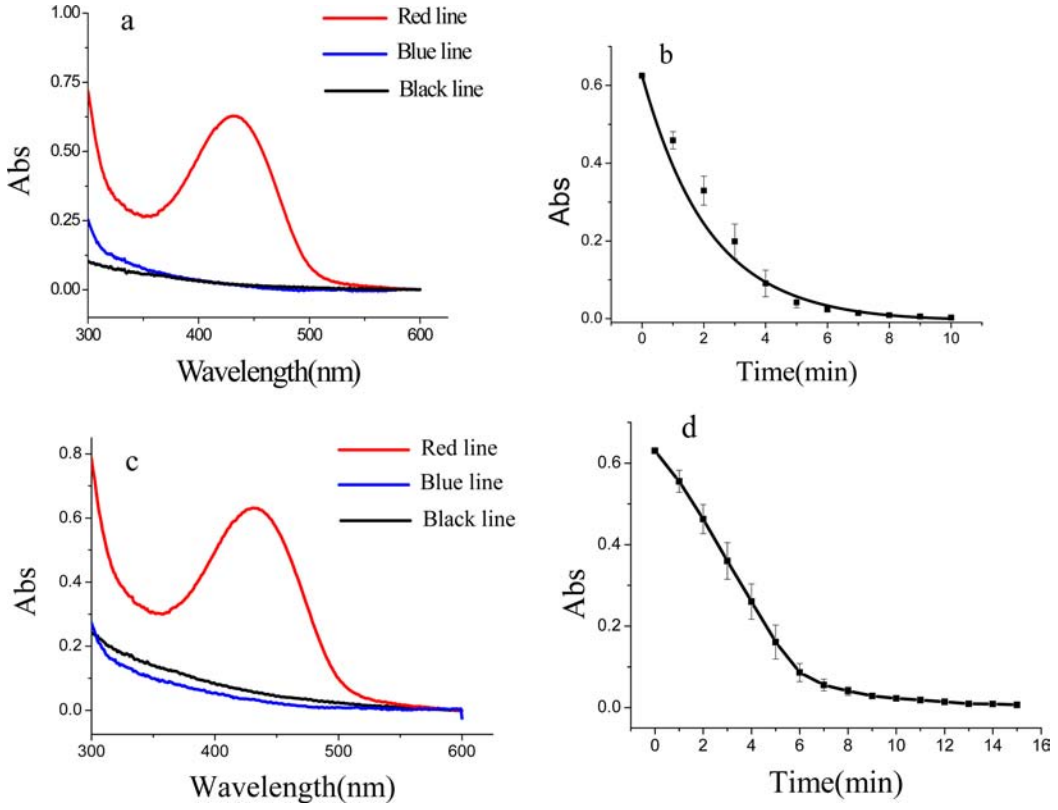


**Figure 6.** UV−vis spectrum of degradation pendimethalin in two soils (a) Red line is the UV−vis spectrum of sandy soil leachate containing pendimethalin. Blue line is UV−vis spectrum of sandy soil leachate. Black line is UV−vis spectrum of sandy soil leachate containing pendimethalin after reaction for about 10 min. (b) Plot of the absorbance at $\lambda$ max of pendimethalin degradation versus time in sandy soil. (c) Red line is UV−vis spectrum of organic soil leachate containing pendimethalin. Black line is UV−vis spectrum of organic soil leachate. Blue line is UV−vis spectrum of organic soil leachate containing pendimethalin after reaction about 10 min. (d) Plot of the absorbance at $\lambda$ max of pendimethalin degradation in organic soil versus time. Note: corresponding histograms with error bar (standard deviation from the mean, $n$ = 3).

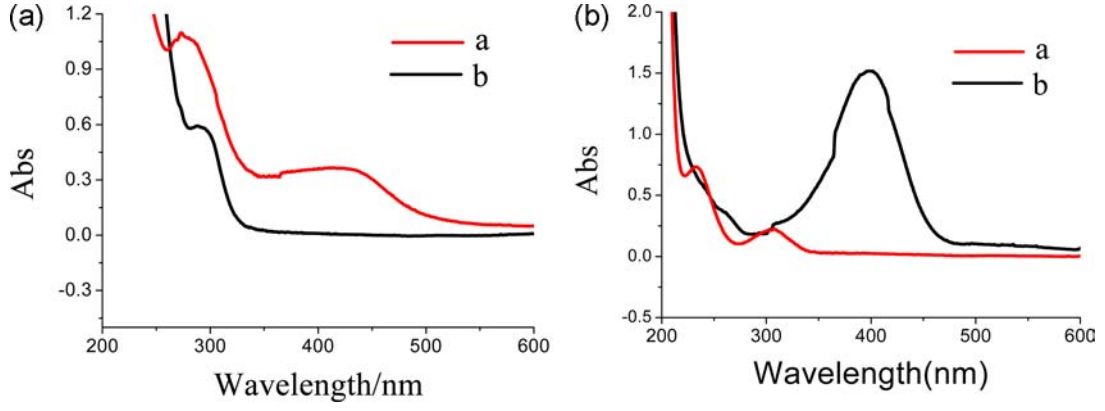


**Figure 7.** UV−visible spectra of (A) trifluralin and (B) *p*-nitrophenol during the reduction catalyzed by Au nanoflower, [$NaBH_4$] 2.34 mM and trifluralin 1.43 mM, *p*-nitrophenol 0.2 mM. Note: (a) is UV−vis spectrum before degradation reaction and (b) is UV−vis spectrum before degradation reaction. Corresponding histograms with error bar (standard deviation from the mean, $n$ = 3).

organic matter (i.e., removal efficiency decrease with organic content increase), which is in accordance with literature.[38] Delightfully, all pendimethalin could be degraded in a short time, hence achieving satisfactory contamination soil remediation. Therefore, this new degradation platform has a great potential in pendimethalin degradation in both organic and inorganic soil with interference.

**Degradation of Other Nitroaromatic Pesticides.** To exemplify the general applicability of our strategy to nitroaromatic pesticides, we applied the same principle and Au nanoflower to design a degradation platform targeting at trifluralin and *p*-nitrophenol. As expected, in the absence of Au nanoflower, this platform could not function and UV−vis absorption spectrum band (trifluralin at 425 nm and *p*-nitrophenol at 400 nm) did not change in a long duration (Figure 7); however, in the presence of Au nanoflower, the two solutions correspondingly changed from light yellow to transparency and a drop in UV−vis absorption spectrum band was observed (Figure 7). Amazingly, *p*-nitrophenol was degraded completely within 2 min and trifluralin within 10 min.


dx.doi.org/10.1021/jf5034015 | J. Agric. Food Chem. 2014, 62, 10638−10645

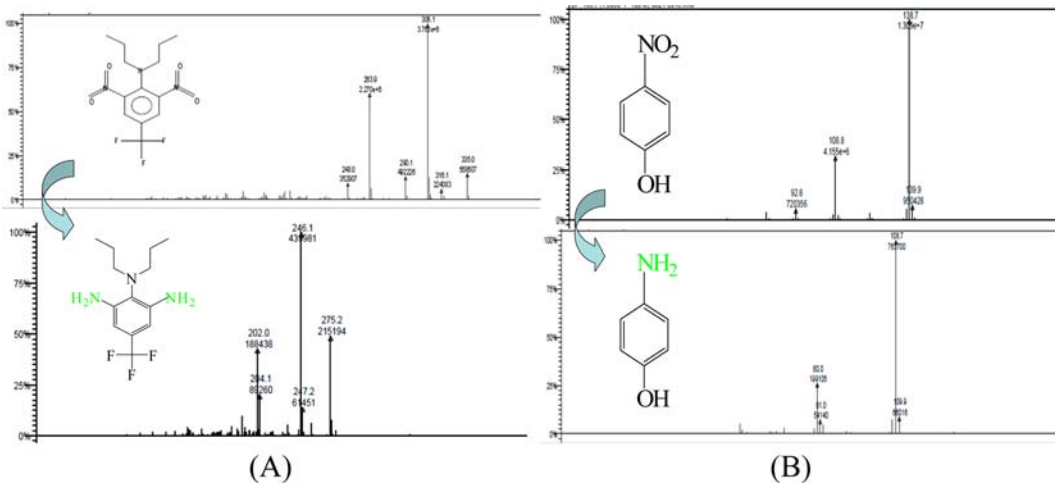


**Figure 8.** Mass spectral data of (A) shows the process of degradation of trifluralin (above) to 2,6-2-amino-*N*,*N*-2-4-propyl-3-fluorine methylanilines (below); Mass spectral data of (B) shows the process of degradation of *p*-nitrophenol (above) to *p*-aminophenol (below).

The degredation of the parent pesticide were confirmed by gas chromatography−mass spectrometry (GC−MS), Figure 8A,B shows that trifluralin and *p*-nitrophenol were reduced to 2,6-2-amino-*N*,*N*-2-4-propyl-3-fluorine methylanilines and *p*-aminophenol, respectively. Thus, when finished the degredation reaction, nitro groups of pesticides were reduced to amino groups of degredation product. The universality of the approach is achieved by virtue of catalyst of Au nanoflower without any change of the degradation platform structure.

In summary, we have developed a simple, rapid, facile, economically viable, and "green" growth approach without the use of seeds to synthesize branched gold nanocrystals which resemble the shape of a flower through $NH_2OH$ reduction of $HAuCl_4$. Under optimal conditions, the synthesized Au nanoflower can complete the degradation of pendimethalin in the presence of $NaBH_4$ within 4 min. In addition, the designed strategy is well applied not only to pendimethalin degradation in practical soil samples, but also to the degradation of common nitroaromatic pesticides including trifluralin and *p*-nitrophenol. We believe that this novel degradation platform can be very useful in the fields of environment protection, soil contamination remediation, and sewage treatment. It has also opened a window to the wide applications of synthesized Au nanoflower in pharmaceuticals, biomedicals, and biosensors in the future.

## AUTHOR INFORMATION

### Corresponding Author

*Fax: +86-027-68754067; e-mail: zhouxd@whu.edu.cn.

### Notes

The authors declare no competing financial interest.

## ACKNOWLEDGMENTS

We gratefully acknowledge the support from the Natural Science Foundation of China (NSFC) (No. 20927003, 90913013, 41273093, and 21175101), the National Major Scientific Instruments and Device Development Project (2012YQ16000701), and the Foundatio of China Geological Survey (Grant No. 12120113015200).

## REFERENCES

(1) Gatermann, R.; Hühnerfuss, H.; Rimkus, G.; Wolf, M.; Franke, S. The distribution of nitrobenzene and other nitroaromatic compounds in the North Sea. *Mar. Pollut. Bull.* **1995**, *30*, 221−227.

(2) Lange, J. H.; Thomulka, K. W. Use of the Vibrio harveyi Toxicity Test for Evaluating Mixture Interactions of Nitrobenzene and Dinitrobenzene. *Ecotoxicol. Environ. Saf.* **1997**, *38*, 2−12.

(3) Beltran, J.; López, F. J.; Hernández, F. Solid-phase microextraction in pesticide residue analysis. *J. Chromatogr. A* **2000**, *885*, 389−404.

(4) Kavitha, V.; Palanivelu, K. Degradation of nitrophenols by Fenton and photo-Fenton processes. *J. Photochem. Photobiol., A* **2005**, *170*, 83−95.

(5) Kelley, R.; Gauger, W. K.; Srivastava, V. J. *Application of Fenton's Reagent As a Pretreatment Step in Biological Degradation of Polyaromatic Hydrocarbons*; Institute of Gas Technology: Chicago, IL, 1990.

(6) Pal, S.; Moza, P. N.; Kettrup, A. Photochemistry of pendimethalin. *J. Agric. Food Chem.* **1991**, *39*, 797−800.

(7) Draper, W. M.; Crosby, D. G. Solar photooxidation of pesticides in dilute hydrogen peroxide. *J. Agric. Food Chem.* **1984**, *32*, 231−237.

(8) Anhalt, J. C.; Arthur, E. L.; Anderson, T. A.; Coats, J. R. Degradation of atrazine, metolachlor, and pendimethalin in pesticide-contaminated soils: Effects of aged residues on soil respiration and plant survival. *J. Environ. Sci. Health B* **2000**, *35*, 417−438.

(9) Ji, S.; Yang, Z.; Zhang, C.; Liu, Z.; Tjiu, W. W.; Phang, I. Y.; Zhang, Z.; Pan, J.; Liu, T. Exfoliated $MoS_2$ nanosheets as efficient catalysts for electrochemical hydrogen evolution. *Electrochim. Acta* **2013**, *109*, 269−275.

(10) Lukowski, M. A.; Daniel, A. S.; Meng, F.; Forticaux, A.; Li, L.; Jin, S. Enhanced Hydrogen Evolution Catalysis from Chemically Exfoliated Metallic $MoS_2$ Nanosheets. *J. Am. Chem. Soc.* **2013**, *135*, 10274−10277.

(11) Wang, T.; Zhu, H.; Zhuo, J.; Zhu, Z.; Papakonstantinou, P.; Lubarsky, G.; Lin, J.; Li, M. Biosensor Based on Ultrasmall $MoS_2$ Nanoparticles for Electrochemical Detection of $H_2O_2$ Released by Cells at the Nanomolar Level. *Anal. Chem.* **2013**, *85*, 10289−10295.

(12) Saha, K.; Agasti, S. S.; Kim, C.; Li, X.; Rotello, V. M. Gold nanoparticles in chemical and biological sensing. *Chem. Rev.* **2012**, *112*, 2739−2779.

(13) Turner, M.; Golovko, V. B.; Vaughan, O. P.; Abdulkin, P.; Berenguer-Murcia, A.; Tikhov, M. S.; Johnson, B. F.; Lambert, R. M. Selective oxidation with dioxygen by gold nanoparticle catalysts derived from 55-atom clusters. *Nature* **2008**, *454*, 981−983.

(14) Querlioz, D.; Dollfus, P. *The Wigner Monte-Carlo Method for Nanoelectronic Devices: A Particle Description of Quantum Transport and Decoherence*; John Wiley & Sons: New York, 2013.

(15) Jiang, Z. J.; Liu, C. Y.; Sun, L. W. Catalytic properties of silver nanoparticles supported on silica spheres. *J. Phys. Chem. B* **2005**, *109*, 1730−1735.

(16) Narayanan, K. B.; Sakthivel, N. Synthesis and characterization of nano-gold composite using Cylindrocladium floridanum and its

heterogeneous catalysis in the degradation of 4-nitrophenol. *J. Hazard. Mater.* **2011**, *189*, 519−525.
(17) Huang, X.; Liao, X.; Shi, B. Synthesis of highly active and reusable supported gold nanoparticles and their catalytic applications to 4-nitrophenol reduction. *Green Chem.* **2011**, *13*, 2801−2805.
(18) Remediakis, I. N.; Lopez, N.; Nørskov, J. K. CO Oxidation on Rutile-Supported Au Nanoparticles. *Angew. Chem.* **2005**, *44*, 1824−1826.
(19) Li, Y.; Shen, W. Morphology-dependent nanocatalysts: Rod-shaped oxides. *Chem. Soc. Rev.* **2014**, *43* (5), 1543−1574.
(20) Jana, N. R.; Gearheart, L.; Murphy, C. J. Seed-mediated growth approach for shape-controlled synthesis of spheroidal and rod-like gold nanoparticles using a surfactant template. *Adv. Mater.* **2001**, *13*, 1389.
(21) Sun, Y.; Yin, Y.; Mayers, B. T.; Herricks, T.; Xia, Y. Uniform silver nanowires synthesis by reducing $AgNO_3$ with ethylene glycol in the presence of seeds and poly (vinyl pyrrolidone). *Chem. Mater.* **2002**, *14*, 4736−4745.
(22) Pei, L.; Mori, K.; Adachi, M. Formation process of two-dimensional networked gold nanowires by citrate reduction of $AuCl_4^-$ and the shape stabilization. *Langmuir* **2004**, *20*, 7837−7843.
(23) Sadeghi, B.; Sadjadi, M.; Vahdati, R. Nanoplates controlled synthesis and catalytic activities of silver nanocrystals. *Superlattice Microst.* **2009**, *46*, 858−863.
(24) Lin, G.; Lu, W.; Cui, W.; Jiang, L. A Simple Synthesis Method for Gold Nano- and Microplate Fabrication Using a Tree-Type Multiple-Amine Head Surfactant. *Cryst. Growth Des.* **2010**, *10*, 1118−1123.
(25) Xie, J.; Lee, J. Y.; Wang, D. I. C. Synthesis of Single-Crystalline Gold Nanoplates in Aqueous Solutions through Biomineralization by Serum Albumin Protein. *J. Phys. Chem. C* **2007**, *111*, 10226−10232.
(26) Millstone, J. E.; Park, S.; Shuford, K. L.; Qin, L.; Schatz, G. C.; Mirkin, C. A. Observation of a quadrupole plasmon mode for a colloidal solution of gold nanoprisms. *J. Am. Chem. Soc.* **2005**, *127*, 5312−5313.
(27) Shankar, S. S.; Rai, A.; Ahmad, A.; Sastry, M. Controlling the optical properties of lemongrass extract synthesized gold nanotriangles and potential application in infrared-absorbing optical coatings. *Chem. Mater.* **2005**, *17*, 566−572.
(28) Millstone, J. E.; Hurst, S. J.; Métraux, G. S.; Cutler, J. I.; Mirkin, C. A. Colloidal Gold and Silver Triangular Nanoprisms. *Small* **2009**, *5*, 646−664.
(29) Liao, H. G.; Jiang, Y. X.; Zhou, Z. Y.; Chen, S. P.; Sun, S. G. Shape-Controlled Synthesis of Gold Nanoparticles in Deep Eutectic Solvents for Studies of Structure−Functionality Relationships in Electrocatalysis. *Angew. Chem.* **2008**, *120*, 9240−9243.
(30) Ahmadi, T.; Wang, Z.; Henglein, A.; El-Sayed, M. "Cubic" colloidal platinum nanoparticles. *Chem. Mater.* **1996**, *8*, 1161−1163.
(31) Tzitzios, V.; Niarchos, D.; Gjoka, M.; Boukos, N.; Petridis, D. Synthesis and characterization of 3D CoPt nanostructures. *J. Am. Chem. Soc.* **2005**, *127*, 13756−13757.
(32) Chen, H. M.; Liu, R. S. Architecture of Metallic Nanostructures: Synthesis Strategy and Specific Applications. *J. Phys. Chem. C* **2011**, *115*, 3513−3527.
(33) Lim, B.; Xia, Y. Metal nanocrystals with highly branched morphologies. *Angew. Chem.* **2011**, *50*, 76−85.
(34) Hutchings, G. J.; Haruta, M. A golden age of catalysis: A perspective. *Appl. Catal., A* **2005**, *291*, 2−5.
(35) Hashmi, A. S. K.; Hutchings, G. J. Gold catalysis. *Angew. Chem.* **2006**, *45*, 7896−7936.
(36) Lee, Y.; Park, T. G. Facile fabrication of branched gold nanoparticles by reductive hydroxyphenol derivatives. *Langmuir* **2011**, *27*, 2965−2971.
(37) Zou, X.; Ying, E.; Dong, S. Seed-mediated synthesis of branched gold nanoparticles with the assistance of citrate and their surface-enhanced Raman scattering properties. *Nanotechnology* **2006**, *17*, 4758.
(38) Miller, C. M.; Valentine, R. L.; Roehl, M. E.; Alvarez, P. J. J. Chemical and microbiological assessment of pendimethalin-contaminated soil after treatment with Fenton's reagent. *Water Res.* **1996**, *30*, 2579−2586.
(39) Tsiropoulos, N. G.; Miliadis, G. E. Field persistence studies on pendimethalin residues in onions and soil after herbicide post-emergence application in onion cultivation. *J. Agric. Food Chem.* **1998**, *46*, 291−295.
(40) Alister, C. A.; Gomez, P. A.; Rojas, S.; Kogan, M. Pendimethalin and oxyfluorfen degradation under two irrigation conditions over four years application. *J. Environ. Sci. Health B* **2009**, *44*, 337−343.
(41) Strandberg, M.; Scott-Fordsmand, J. J. Effects of pendimethalin at lower trophic levels—A review. *Ecotoxicol. Environ. Saf.* **2004**, *57*, 190−201.
(42) Yang, M.; Yang, X.; Huai, L. Synthesis and characterizations of hollow spheres and nanospheres of Au. *Appl. Phys. A: Mater. Sci. Process.* **2008**, *92*, 367−370.
(43) Xie, J.; Zhang, Q.; Lee, J. Y.; Wang, D. I. C. The Synthesis of SERS-Active Gold Nanoflower Tags for In Vivo Applications. *ACS Nano* **2008**, *2*, 2473−2480.
(44) Sau, T. K.; Rogach, A. L.; Döblinger, M.; Feldmann, J. One-Step High-Yield Aqueous Synthesis of Size-Tunable Multispiked Gold Nanoparticles. *Small* **2011**, *7*, 2188−2194.
(45) Song, Y.; Yang, Y.; Medforth, C. J.; Pereira, E.; Singh, A. K.; Xu, H.; Jiang, Y.; Brinker, C. J.; van Swol, F.; Shelnutt, J. A. Controlled synthesis of 2-D and 3-D dendritic platinum nanostructures. *J. Am. Chem. Soc.* **2004**, *126*, 635−645.
(46) Lim, B.; Jiang, M.; Camargo, P. H.; Cho, E. C.; Tao, J.; Lu, X.; Zhu, Y.; Xia, Y. Pd−Pt bimetallic nanodendrites with high activity for oxygen reduction. *Science* **2009**, *324*, 1302−1305.
(47) Witten, T., Jr; Sander, L. M. Diffusion-limited aggregation, a kinetic critical phenomenon. *Phys. Rev. Lett.* **1981**, *47*, 1400.
(48) Liu, J.; Qin, G.; Raveendran, P.; Ikushima, Y. Facile "Green" Synthesis, Characterization, and Catalytic Function of $\beta$-D-Glucose-Stabilized Au Nanocrystals. *Chem.—Eur. J.* **2006**, *12*, 2131−2138.

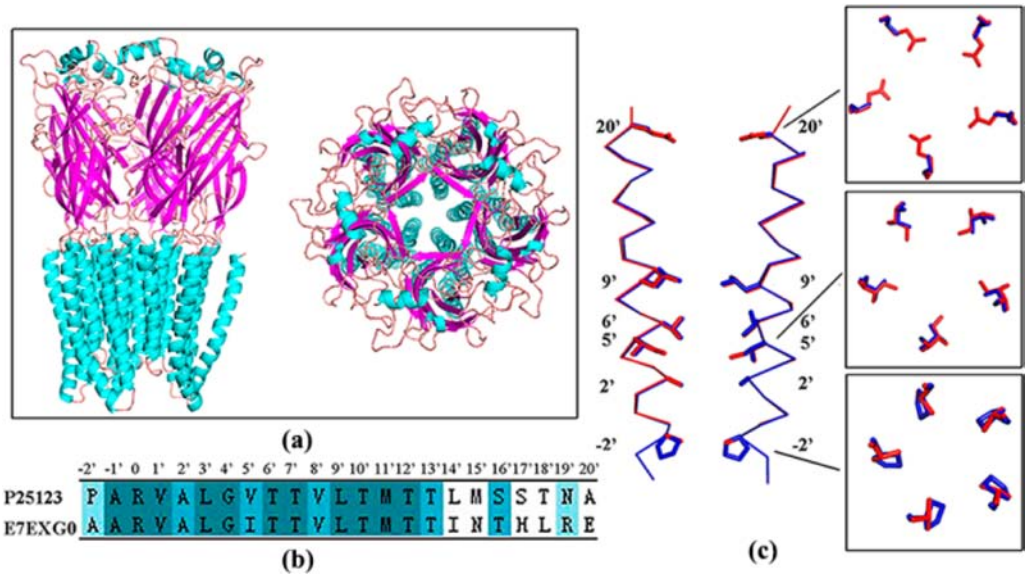


**Figure 1.** (a) Homology model of $GABA_AR$: side view (left), top view (right). (b) Index number (above) for the residues (bottom) of TM2 regions. (c) Reported key residues and different residues within the TM2 regions of fruitfly (blue) and zebrafish (red) $GABA_ARs$.

have exerted profound influences on the molecular design and interaction mechanism investigations of pesticides.[20−23] In the present study, the 3D structures of homopentamer of $GABA_ARs$ in representative insect (fruitfly Rdl) and fish (zebrafish $\beta3$) were established by the homology modeling method based on the open-state structure of an inhibitory glutamate-gated chloride channel[24] from *Caenorhabditis elegans*. The GluCl[24] showed high sequence similarity and was a good template for modeling the structures of the $GABA_ARs$, which was better than the nAChR and AChBP (acetylcholine binding protein) structures used in previous studies.[16−18] Finally, docking and molecular dynamics (MD) simulation studies were performed to explore the binding difference of fipronil with fruitfly Rdl and zebrafish $\beta3$ $GABA_ARs$.

## MATERIALS AND METHODS

**Homology Modeling.** The target sequences of fruitfly Rdl (UniProt ID P25123) and zebrafish $\beta3$ (UniProt ID E7EXG0) subunits were retrieved from UniProtKB (http://www.uniprot.org/). The sequences were subjected to template search using the BLAST program of the National Center for Biotechnology Information (NCBI) (http://www.ncbi.nlm.nih.gov/). Finally, the crystal structure of glutamate-gated chloride channel[24] (PDB ID 3RHW) was chosen as the template to build the 3D structures of both $GABA_ARs$.

As no intracellular portion of the Cys-loop receptor superfamily was resolved, the sequences of the long cytoplasmic loops of the intracellular domain were removed during homology modeling study. The ClustalW2 program[25−27] was used for sequence alignment. The identities of two $GABA_ARs$ of fruitfly and zebrafish with the same template were 40.6 and 37.6%, respectively. On the basis of the aligned sequences (Supporting InformationFigure S1), in which the blue squares stand for the conserved residues of extracellular loop A-F and the Cys-loop, the channel pore of $GABA_AR$ formed by the TM2 helices is magenta squares, and the rest of the TM helices are purple squares, the Build Homology Models Module encoded in the Discovery Studio 3.5 software package (Accelrys Inc., 2013) was applied to generate the $GABA_AR$ structures of fruitfly and zebrafish species. The quality of the established 3D structures was not only assessed by the PROCHECK[28] and the Profile-3D[29] approaches but also validated by the comparison between following docking investigations and the previous experimental mutation results within the TM2 domain.

**Ligand Docking.** Ligand docking was performed by the Glide approach integrated into Maestro 9.3 (Schrödinger, LLC, 2013), with default settings in standard precision mode. The binding site was set around the centroid of the −2′ and 2′ residues from five chains, with a size of 30 Å. In the docking run, 100 conformations were output and ranked by GlideScore. The superior pose with a reasonable binding orientation was selected as the initial binding conformation for further molecular dynamics (MD) simulation.

**Molecular Dynamics Simulation.** The obtained docking results of the fipronil−$GABA_AR$ complex were conducted for MD simulation using the GROMACS 4.5.5[30−32] package with the GROMOS53a6[33] force field for all atoms. The topology and other force field parameters for fipronil were obtained using the PRODRG beta server (http://davapc1.bioch.dundee.ac.uk/prodrg/).[34] The ESP partial atom charges were calculated at the B3LYP/6-31G(d,p) level using the Gaussian 09 package (Gaussian, Inc., Wallingford CT, USA; 2009) and determined using the Merz−Singh−Kollman scheme.[35,36] On the basis of the calculated electrostatic potential, the restrained electrostatic potential (RESP) charges were produced using the Antechamber module[37] of the Amber10 package. The fipronil−$GABA_AR$ complex structures were inserted into a pre-equilibrated 1-palmitoyl-2-oleylphosphatidylcholine (POPC) lipid bilayer using the "shrinking" method, where the shrinking cycles were performed with the InflateGRO script.[38] The bilayer structure used here was downloaded from Tieleman's Web site (http://moose.bio.ucalgary.ca/). The cubic periodic box comprising the simple point charge (SPC) water[39] model was built. The $Cl^-$ ions were inserted randomly into the solvent to preserve the electric neutrality in both systems.

The two systems were performed under the NPT ensemble, using the Nosé−Hoover thermostat[40,41] and Parrinello−Rahman barostat[42] to maintain the pressure at 1.02 bar, with the temperature maintained at 300 K. All bonds were constrained using the LINCS algorithm.[43] In the MD simulation, the cutoff distance was set to 1.2 nm for Lennard-Jones interactions. The long-range electrostatic interactions were handled using the particle-mesh Ewald (PME) method.[44,45] The time step of the simulation was set to 2 fs. Finally, the fruitfly and zebrafish $GABA_AR$ systems in the fipronil-bound state have 1695 and 1680 residues, 71635 and 71932 water molecules, 25 and 5 $Cl^-$ ions, and 502 POPC molecules, and the densities of the POPC lipid bilayers were 66.6 and 66.8 $Å^2$, respectively.

## RESULTS AND DISCUSSION

**Homology Models of $GABA_AR$s.** The modeled structure of $GABA_AR$ is depicted in Figure 1a, of which the $\beta$-sheets of extracellular region are shown in magenta and the $\alpha$-helices are in cyan. The channel pore of $GABA_AR$ was surrounded by five TM2 helices. The number for the residues of the TM2 region was indexed and is shown in Figure 1b for a convenient comparison between the two species. The interior residues in the TM2 channel of the $GABA_AR$ from fruitfly and zebrafish were −2′Pro (Ala), 2′Ala, 5′Val (Ile), 6′Thr, 9′Leu, and 20′Ala (Glu), which are shown as sticks in Figure 1c. Only three residues were different between the $GABA_AR$s of fruitfly and zebrafish, denoted −2′, 5′, and 20′, of which the 20′ residue was close to the extracellular region, the −2′ residue was near the intracellular domain, and 5′ was located in the lower part of the TM2 domain.

The quality of both modeled structures was evaluated by using the PROCHECK[28] and Profile-3D[29] approaches. In the fruitfly model, 99.3% residues were located in the allowed regions, and only 0.7% residues (Thr104 and Ser172 in the extracellular region) were located in the disallowed regions (Supporting Information Figure S2a). In the zebrafish model, 99.7% residues were observed in the allowed regions, whereas only 0.3% residues (Thr101 in the extracellular domain) were found in the disallowed regions (Supporting Information Figure S2b). The self-compatibility score by Profile-3D for the $GABA_AR$ structure of fruitfly was 543.87, which was close to the top score of 782.05. The corresponding score of the zebrafish $GABA_AR$ structure reached 546.56, which was also close to the top value of 775.07. Moreover, it could be seen that most residues were reasonable with positive score values; only a few residues far from the fipronil binding site, which located in the extracellular and TM3 regions, showed small negative profile-3D values (Supporting Information Figure S2c,d). The above results indicated that the homology models of fruitfly and zebrafish were reliable.

**Docking Results.** Docking studies were performed to explore the binding modes of fipronil with $GABA_AR$. The final docking pose was obtained by considering the GlideScore values and analyzing the binding mode, which is depicted in Figure 2. This showed that fipronil erected in both channels enclosed by the five TM2 helices, with the trifluoromethyl group of the benzene ring facing the intracellular domain, which was consistent with the previous modeling study by Cheng et al.[16] Also, the residues 2′Ala, 6′Thr, and 9′Leu were found to play important roles for the binding of fipronil (Supporting Information Figure S3), which was in accordance with the previously published investigations.[10−18,46−51] For example, Casida et al.[18] showed that the mutation of A2′C or A2′S and T6′C or T6′F, as well as L9′C or L9′S, in the human $\beta$3 homopentamer could abolish the binding sensitivity of NCAs.

The N−H···O H-bond between the amino group of fipronil and the side chain of 6′Thr was observed in both systems, which has been reported to be very important for binding by other researchers.[16−18] Moreover, it was found that the residues −2′Pro (Ala) and 5′Val (Ile) could also form interactions with fipronil (Supporting Information Figure S3). According to the docking results, both $GABA_AR$s showed favorable interactions with fipronil. All above docking analyses also confirmed that the modeled 3D structures of $GABA_AR$s were reasonable.

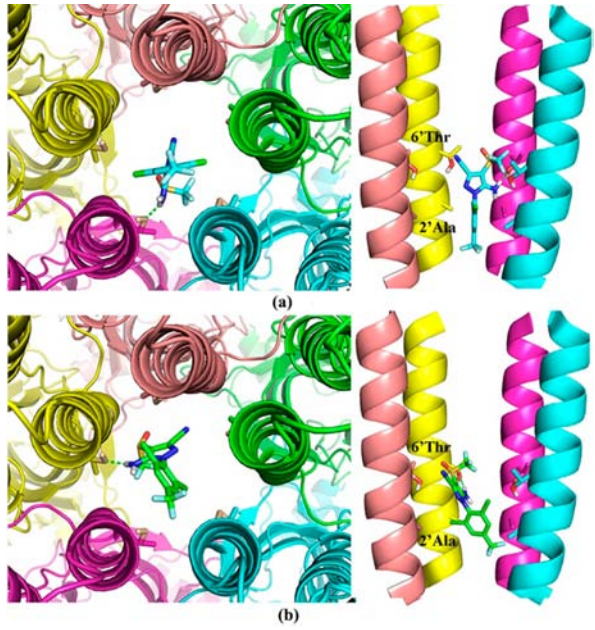


**Figure 2.** Docking poses of fipronil with fruitfly (a) and zebrafish (b) $GABA_AR$s. Dotted line, H-bond; stick, fipronil and the key residues.

**Molecular Dynamics Simulation.** *Root Mean Square Deviation (RMSD).* To evaluate the stability of the two systems during the MD simulation, the RMSD was plotted versus time. Figure 3 depicts the RMSD values for the backbone atoms of protein and ligand. The RMSD values for the backbone of fruitfly and zebrafish systems are colored in black and red, respectively; the two systems were stable after 16 ns simulations. However, during the last 14 ns of the simulations, the amplitude of the equilibrium deviation was slightly different in each trajectory. The RMSD values of the fruitfly system showed that the disruption of convergence was at about 0.46 nm, whereas the corresponding value was 0.43 nm for the zebrafish system. Meanwhile, the RMSD values of ligand atoms were also calculated and are depicted in Figure 3. The data indicated that the fipronil in both systems reached equilibrium states after a small fluctuation in the initial period of the simulation. The magnitude of fluctuations for ligand, together with the backbone of protein, led to the conclusion that the

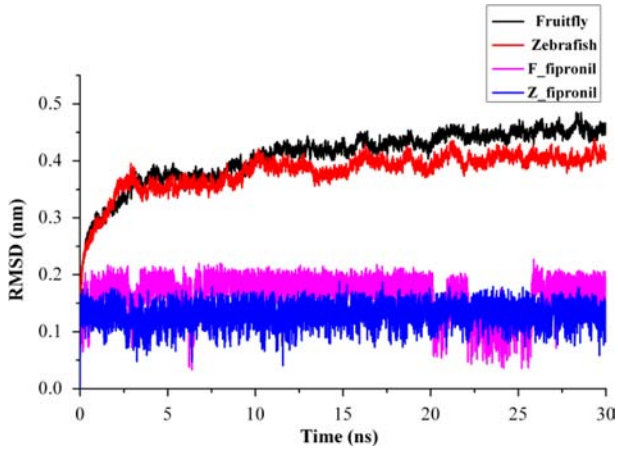


**Figure 3.** RMSD plots for the backbone of $GABA_AR$s and fipronil during MD simulation.


dx.doi.org/10.1021/jf503851z | J. Agric. Food Chem. 2014, 62, 10646−10653

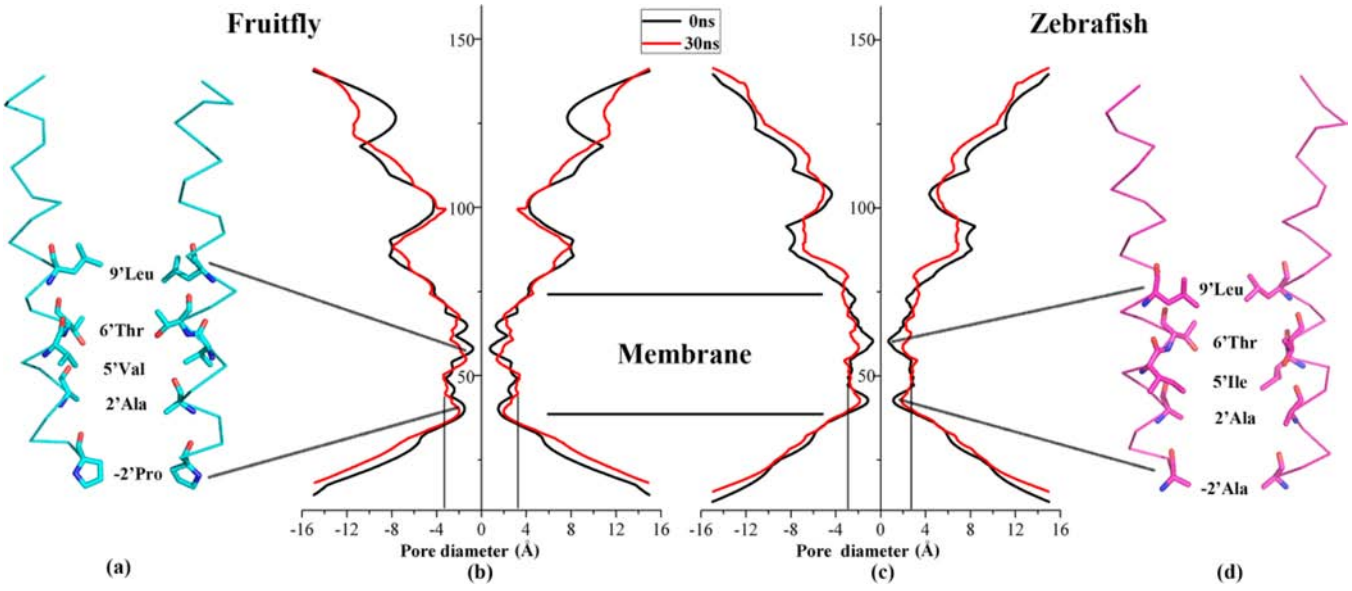


**Figure 4.** Pore diameter analysis at 0 and 30 ns snapshots of fruitfly (a, b) and zebrafish (c, d) systems: distance along the pore axis (Å) versus pore diameter. The key residues in the binding pocket from TM2 helices are shown as sticks.

simulation produced stable trajectories and provided a reliable basis for further analysis.

*Root Mean Square Fluctuation (RMSF).* With the aim of determining the mobility and flexibility of each residue in the MD simulation, the RMSF values were calculated. The RMSF values for the residues of TM domains were small, indicating that they were stable during the entire simulation (Supporting Information Figure S4a), whereas larger values were observed in the extracellular domain and the loops between TM3 and TM4, which implied that residues in these regions were flexible in the MD simulation. The fluctuating residues were observed far from the ligand binding site and might have weak influences on the interaction of fipronil with $GABA_AR$. For detailed analysis, the RMSF for the residues in ligand binding pocket within the TM2 domains is also depicted in Supporting Information Figure S4b. Clearly, the fruitfly system showed higher peaks around the fipronil binding pocket, compared with the zebrafish system, which indicated that such residues from the fruitfly system might undergo larger fluctuation than those from the zebrafish system. The smaller RMSF values in the zebrafish system also coincided with the above RMSD values.

*Pore Radius.* Ion channel radius is an important parameter to characterize the channel opening and closing, which has been widely used to measure the size of a channel pore. In the present study, the pore radius of the $GABA_AR$ was conducted using the HOLE program.[52−54] The pore radii at the 0, 5, 10, 20, and 30 ns snapshots, as well as on the average structure of the last 5 ns in the equilibrium state, have been calculated and analyzed (Supporting Information Figure S5). It could be observed that the pore radius variations were very similar at the 20 and 30 ns snapshots and on the average structure of the last 5 ns, especially in the region between the −2′Pro (Ala) and 9′Leu residues of the TM2 domain. The calculated pore diameters at 0 and 30 ns snapshots were analyzed and are depicted in Figure 4 to understand the changes of pore size after MD simulation.

The ion pores of both $GABA_ARs$ tilted radially from the extracellular domains down to the TM2 domain. The binding site of fipronil was located in the region between 9′Leu and −2′Pro (Ala) for both systems, where the side chain of 9′Leu defined the narrowest point in the middle of the two channels, whereas −2′Pro in the fruitfly system or −2′Ala in the zebrafish system determined the lowest narrow part of the channels. After a 30 ns simulation, the pore radius at 9′Leu that represented the top side of the binding pocket expanded for both systems, as well as the −2′Pro (Ala) that denoted the bottom of binding site. In the zebrafish system, no clear changes were found for the tunnel radius between 5′Ile and 2′Ala after simulation, whereas in the fruitfly system the corresponding radius between 5′Val and 2′Ala enlarged. It was also observed that the pore size between the 5′ and 2′ residues within the binding pocket of fruitfly system was wider than that in the zebrafish system, which might be a result of the smaller volume of 5′Val than of 5′Ile. Moreover, in the fruitfly system the pore radius defined by the 6′Thr narrowed, whereas in the zebrafish system the corresponding tunnel radius widened. The above differences in the binding pockets of the two systems might exert some influences on the binding modes of fipronil with the $GABA_ARs$ from the two species.

*Position and Orientation Changes of Fipronil during Simulation.* Figure 5a and b show the superposition for fipronil

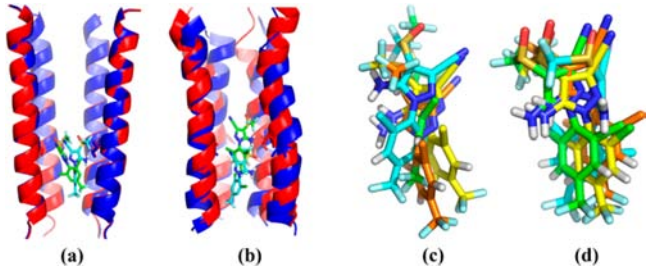


**Figure 5.** Alignment of the TM2 domain in the fruitfly (blue) and zebrafish (red) systems at 0 (a) and 30 ns (b). Cyan and green sticks represent the fipronil in fruitfly and zebrafish systems, respectively. Superimposition of the fipronil in fruitfly (c) and zebrafish (d) systems is shown as 0 ns (cyan), 10 ns (green), 20 ns (yellow), and 30 ns (orange) snapshots.


dx.doi.org/10.1021/jf503851z | J. Agric. Food Chem. 2014, 62, 10646−10653

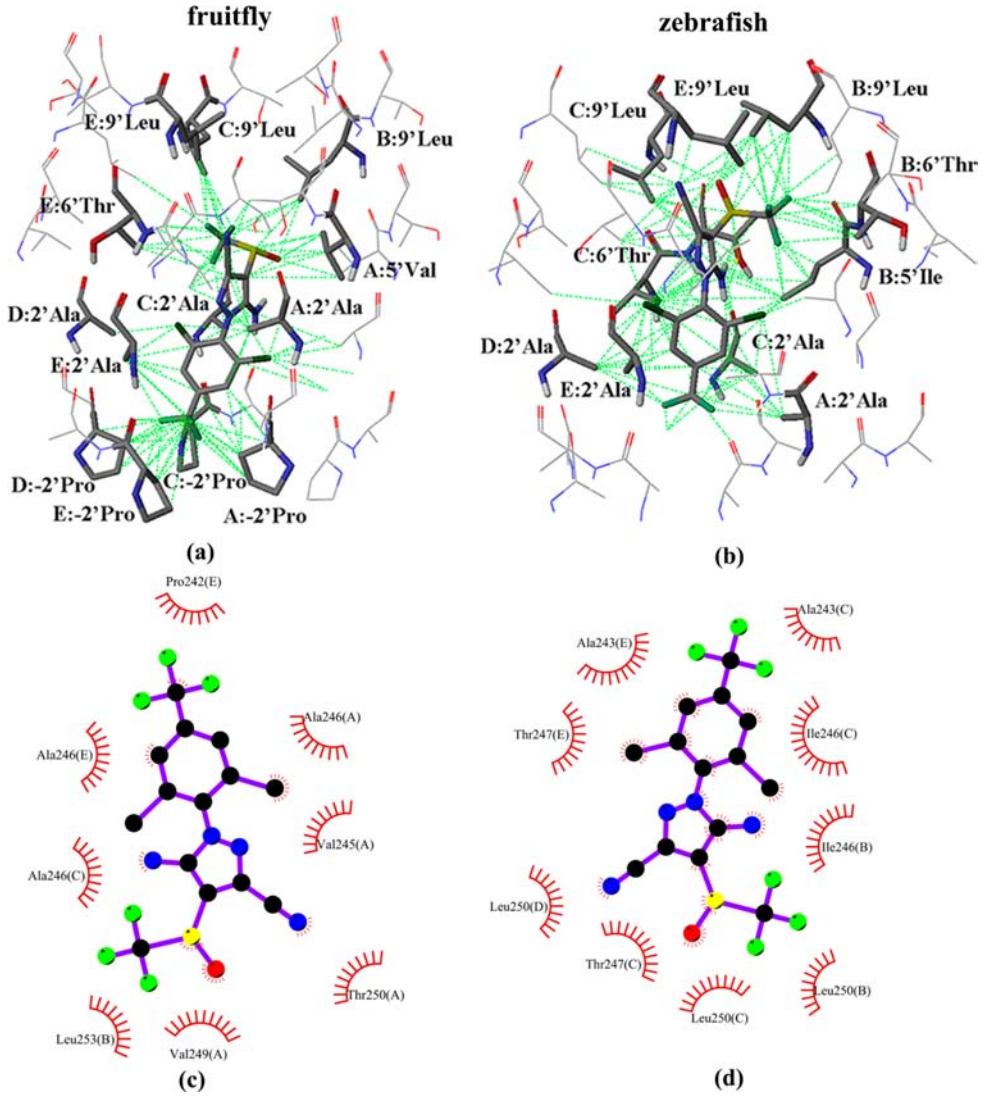


**Figure 6.** Interactions of fipronil with fruitfly (a) and zebrafish (b) $GABA_A$Rs at 30 ns snapshot after MD simulation: hydrophobic interactions between fipronil and the residues in fruitfly (c) and zebrafish (d) systems at the 30 ns snapshot.

and TM2 helices in the fruitfly and zebrafish systems at the snapshots of 0 and 30 ns of the simulation, respectively. Small position changes of fipronil were observed in the zebrafish system during the entire MD simulation, whereas the position of fipronil in the fruitfly system moved toward the lower part of the TM2 channel, as compared with its initial binding site. In other words, the binding site of fipronil in the fruitfly system was much closer to the intracellular domain than in the zebrafish system (Figure 5b).

Figure 5c and d display the superposition of fipronil in the snapshots at 0, 10, 20, and 30 ns in the MD trajectory from the fruitfly and zebrafish systems, respectively. It can be observed that fipronil went through large orientation changes in the fruitfly system relative to the zebrafish system. This might be a result of the different pore radius properties between the two systems. A wider tunnel dimension between 5′Thr and 2′Ala appeared in the binding pocket of the fruitfly system than in the zebrafish system, which might be an important reason for the observed larger position and orientation changes in the fruitfly system.

*Binding Difference of Fipronil with Fruitfly and Zebrafish $GABA_A$Rs.* To better understand the binding modes of fipronil with $GABA_A$Rs in fruitfly and zebrafish systems, the key residues for the binding of fipronil were fully analyzed on the structures at the equilibrium state. Panels a and b of Figure 6 depict the interaction between fipronil and the residues in the TM2 channel of $GABA_A$R at the 30 ns snapshots. The potential key residues displayed in sticks could also be observed in the 0, 5, 10, and 20 ns snapshots and in the average structure of the equilibrium state. It was found that residues 2′Ala, 6′Thr, and 9′Leu formed hydrophobic interactions with fipronil (Figure 6c,d), which were important for the binding of fipronil with both $GABA_A$Rs. The findings were in accordance with the previous modeling studies.[17,18] For example, Casida et al.[18] reported that 2′Ala, 6′Thr, and 9′Leu could form hydrophobic interactions with diverse antagonists, which had a critical influence on the recognition of NCAs. Moreover, in this study, the residue 5′Val (Ile) was observed forming hydrophobic interactions with fipronil in both.

Many researchers have reported that 6′Thr could form an H-bond with fipronil, which played key roles for the ligand−receptor recognition.[16−18] In the zebrafish system, an N−H···O H-bond was observed between the amino group of fipronil and the side chain of 6′Thr (Figure 7a). The distance between the


dx.doi.org/10.1021/jf503851z | J. Agric. Food Chem. 2014, 62, 10646−10653

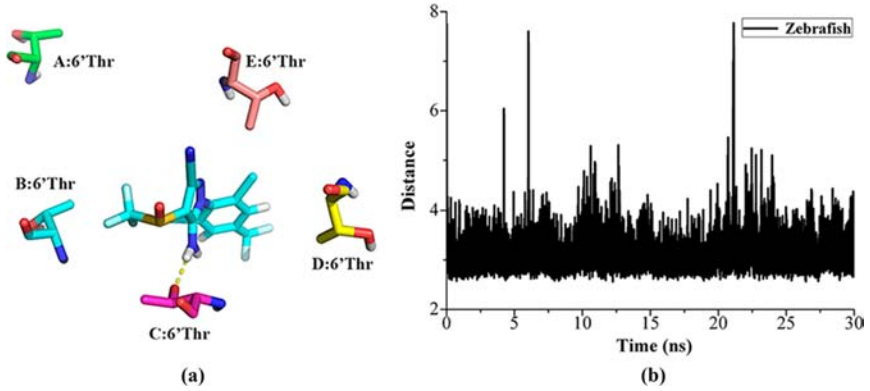


**Figure 7.** (a) N−H···O H-bond between fipronil and 6′Thr in zebrafish system; (b) N−H···O H-bond distance during the whole MD simulation.

N and O atoms versus the simulation time was monitored during the whole simulation (Figure 7b). It was found that the N−H···O H-bond was very stable, with an H-bond distance around 3.0 Å in the whole simulation. In the fruitfly system, the corresponding H-bond could be observed in the docking results and the initial snapshot of the simulation. However, it disappeared during the subsequent simulation. The detailed reasons for the disappearance of the N−H···O H-bond are still unclear. One of the reasons might be the above-mentioned large position and orientation changes of fipronil in the fruitfly system.

To gain detailed energy contributions of the key residues in the TM2 helices on the binding affinity of fipronil, a per-residue decomposition of the total energy was performed to evaluate the critical residues on the binding, using the Calculate Interaction Energy Protocol encoded in the Discovery Studio 3.5 software package (Accelrys Inc., 2013). The snapshots of two systems in the last 5 ns of MD simulation were extracted, respectively, for energy analysis. The residue-based energy decomposition results characterized the key residues in ligand binding and identified the contributions of different nonbonded interaction forces (van der Waals and electrostatic interactions). The energy contributions of each key residue are displayed in Table 1. They showed that 5′Val (Ile), 6′Thr, and 9′Leu were

**Table 1. Average Energy of Interaction between Individual Residues and Ligands for the Fruitfly and Zebrafish Systems**

| residue | fruitfly | zebrafish |
|---|---|---|
| 2′Ala | −1.05 | 1.01 |
| electrostatic term | −1.15 | 1.03 |
| 5′Val(Ile) | −1.19 | −1.54 |
| electrostatic term | −1.14 | −1.67 |
| 6′Thr | −0.82 | −1.94 |
| electrostatic term | −0.66 | −1.12 |
| 9′Leu | −0.67 | −1.23 |
| electrostatic term | −0.69 | −1.12 |

favorable for the binding of fipronil with both $GABA_A$Rs. Moreover, the average interaction energy between residue 2′Ala and fipronil, which was originated predominantly by the electrostatic interaction, was beneficial for complexation in the fruitfly system but unfavorable to binding in the zebrafish system. All of the data in Table 1 and Figures 6 and 7 indicated that residues 5′Val (Ile), 6′Thr, and 9′Leu played important roles for the binding of fipronil with both $GABA_A$Rs. Although the N−H···O H-bond between fipronil and 6′Thr could not be monitored during the MD simulation of the fruitfly system, the strong electrostatic interaction between 2′Ala and fipronil might compensate the binding force of fipronil with $GABA_A$R. Although 2′Ala and 6′Thr in the two systems, respectively, showed different roles in the recognition of fipronil, the favorable interactions enabled fipronil to erect steadily in both channels, which might contribute to the high toxicities to insects and fishes.

All of the data above indicated that residues 5′Val (Ile), 6′Thr, and 9′Leu played important roles in the binding of fipronil with both $GABA_A$Rs. Moreover, the H-bond between 6′Thr and fipronil in the zebrafish system was very stable during the whole MD simulations, which played a key role in the ligand−receptor recognition. However, such an H-bond was absent in the fruitfly system during simulation, although it could be observed in the docking results and the initial snapshot of the simulation. On the other hand, the electrostatic interaction between 2′Ala and fipronil was favorable to ligand recognition in the fruitfly system, but was detrimental to the binding in the zebrafish system. As a result, the observed strong electrostatic interaction between 2′Ala and fipronil compensated the absent contribution of the H-bond between 6′Thr and fipronil in the fruitfly system. The different roles of 2′Ala and 6′Thr marked the binding difference of fipronil with the $GABA_A$Rs of fruitfly and zebrafish, which might provide some clues for future design of new selective phenylpyrazole pesticides against insects over fishes.

## ■ ASSOCIATED CONTENT

### Ⓢ Supporting Information

Figures S1−S5. This material is available free of charge via the Internet at http://pubs.acs.org.

## ■ AUTHOR INFORMATION

### Corresponding Authors

*(J.C.) E-mail: jgcheng@ecust.edu.cn. Phone: +86-21-64251348. Fax: +86-21-64252603.
*(Z.L.) E-mail: lizhong@ecust.edu.cn.

### Funding

This work was financially supported by the National Key Technology R&D Program of China (2011BAE06B05), the National Natural Science Foundation of China (21172070), the National High Technology Research Development Program of China (2011AA10A207), and the Fundamental Research Funds for the Central Universities (222201314006)

### Notes

The authors declare no competing financial interest.

## ■ ABBREVIATIONS USED

$GABA_A$Rs, γ-aminobutyric acid type A receptors; LGIC, ligand gated ion channel; nAChRs, nicotinic acetylcholine receptors; GlyRs, glycine receptors; 5-$HT_3$R, serotonin type 3 receptors; GluCl, glutamate-gated chloride channels; CNS, central nervous system; NCAs, noncompetitive antagonists; TMD, transmembrane domain; Rdl, resistant to dieldrin; AChBP, acetylcholine binding protein; MD, molecular dynamics; NCBI, National Center for Biotechnology Information; RESP, restrained electrostatic potential; POPC, 1-palmitoyl-2-oleylphosphatidylcholine; SPC, simple point charge; PME, particle-mesh Ewald; RMSD, root-mean-square deviation; RMSF, root-mean-square fluctuation

## ■ REFERENCES


(1) Cole, L. M.; Nicholson, R. A.; Casida, J. E. Action of phenylpyrazole insecticides at the GABA gated chloride channel. *Pestic. Biochem. Physiol.* **1993**, *46*, 47−54.

(2) Tingle, C. C. D.; Rother, J. A.; Dewhurst, C. F.; Lauer, S.; King, W. J. Fipronil: environmental fate, ecotoxicology, and human health concerns. *Rev. Environ. Contam. Toxicol.* **2003**, *176*, 1−66.

(3) Novère, N. L.; Changeux, J. P. The Ligand Gated Ion Channel database: an example of a sequence database in neuroscience. *Philos. Trans. R. Soc. London B* **2001**, *356*, 1121−1130.

(4) Perret, P.; Sarda, X.; Wolff, M.; Wu, T. T.; Bushey, D.; Goeldner, M. Interaction of non-competitive blockers within the γ-aminobutyric acid type A chloride channel using chemically reactive probes as chemical sensors for cysteine mutants. *J. Biol. Chem.* **1999**, *274*, 25350−25354.

(5) Simon, J.; Wakimoto, H.; Fujita, N.; Lalande, M.; Barnard, E. A. Analysis of the set of $GABA_A$ receptor genes in the human genome. *J. Biol. Chem.* **2004**, *279*, 41422−41435.

(6) Ratra, G. S.; Kamita, S. G.; Casida, J. E. Role of human $GABA_A$ receptor β3 subunit in insecticide toxicity. *Toxicol. Appl. Pharmacol.* **2001**, *172*, 233−240.

(7) Olsen, R. W.; Tobin, A. J. Molecular biology of $GABA_A$ receptors. *FASEB J.* **1990**, *4*, 1469−1480.

(8) Xu, M.; Akabas, M. H. Identification of channel-lining residues in the M2 membrane-spanning segment of the $GABA_A$ receptor α1 subunit. *J. Gen. Physiol.* **1996**, *107*, 195−205.

(9) Horenstein, J.; Wagner, D. A.; Czajkowski, C.; Akabas, M. H. Protein mobility and GABA-induced conformational changes in $GABA_A$ receptor pore-lining M2 segment. *Nat. Neurosci.* **2001**, *4*, 477−485.

(10) Ffrench-Constant, R. H.; Mortlock, D. P.; Shaffer, C. D.; MacIntyre, R. J.; Roush, R. T. Molecular cloning and transformation of cyclodiene resistance in *Drosophila*: an invertebrate γ-aminobutyric acid subtype A receptor locus. *Proc. Natl. Acad. Sci. U.S.A.* **1991**, *88*, 7209−7213.

(11) Hosie, A. M.; Aronstein, K.; Sattelle, D. B.; Ffrench-Constant, R. H. Molecular biology of insect neuronal GABA receptors. *Trends Neurosci.* **1997**, *20*, 578−583.

(12) Gao, J. R.; Kozaki, T.; Leichter, C. A.; Rinkevich, F. D.; Shono, T.; Scott, J. G. The A302S mutation in Rdl that confers resistance to cyclodienes and limited crossresistance to fipronil is undetectable in field populations of house flies from the USA. *Pestic. Biochem. Physiol.* **2007**, *88*, 66−70.

(13) Ffrench-Constant, R. H.; Rocheleau, T. A.; Steichen, J. C.; Chalmers, A. E. A point mutation in a *Drosophila* GABA receptor confers insecticide resistance. *Nature* **1993**, *363*, 449−451.

(14) Ffrench-Constant, R. H.; Steichen, J. C.; Rocheleau, T. A.; Aronstein, K.; Roush, R. T. A single-amino acid substitution in a γ-aminobutyric acid subtype A receptor locus is associated with cyclodiene insecticide resistance in *Drosophila* populations. *Proc. Natl. Acad. Sci. U.S.A.* **1993**, *90*, 1957−1961.

(15) Ffrench-Constant, R. H.; Anthony, N.; Aronstein, K.; Rocheleau, T.; Stilwell, G. Cyclodiene insecticide resistance: from molecular to population genetics. *Annu. Rev. Entomol.* **2000**, *48*, 449−466.

(16) Cheng, J.; Ju, X. L.; Chen, X. Y.; Liu, G. Y. Homology modeling of human α1β2γ2 and house fly β3 GABA receptor channels and Surflex-docking of fipronil. *J. Mol. Model.* **2009**, *15*, 1145−1153.

(17) Ci, S. Q.; Ren, T. R.; Su, Z. G. Modeling the interaction of fipronil-related non-competitive antagonists with the GABA β3-receptor. *J. Mol. Model.* **2007**, *13*, 457−464.

(18) Chen, L.; Durkin, K. A.; Casida, J. E. Structural model for γ-aminobutyric acid receptor noncompetitive antagonist binding: widely diverse structures fit the same site. *Proc. Natl. Acad. Sci. U.S.A.* **2006**, *103*, 5185−5190.

(19) Wang, X. X.; Zhou, S. L.; Ding, X. F.; Zhu, G. N. Effect of triazophos, fipronil and their mixture on miRNA expression in adult zebrafish. *J. Environ. Sci. Health. Part B* **2010**, *45*, 648−657.

(20) Hao, G. F.; Wang, F.; Li, H.; Zhu, X. L.; Yang, W. C.; Huang, L. S.; Wu, J. W.; Berry, E. A.; Yang, G. F. Computational discovery of picomolar $Q_0$ site inhibitors of cytochrome $bc_1$ complex. *J. Am. Chem. Soc.* **2012**, *134*, 11168−11176.

(21) Zhao, P. L.; Wang, L.; Zhu, X. L.; Huang, X. Q.; Zhan, C. G.; Wu, J. W.; Yang, G. F. Subnanomolar inhibitor of cytochrome $bc_1$ complex designed by optimizing interaction with conformationally flexible residues. *J. Am. Chem. Soc.* **2010**, *132*, 185−194.

(22) Hao, G. F.; Yang, G. F. The role of Phe82 and Phe351 in auxin-induced substrate perception by TIR1 ubiquitin ligase: a novel insight from molecular dynamics simulations. *PLoS One* **2010**, *5*, No. e10742.

(23) Hao, G. F.; Yang, S. G.; Yang, G. F.; Zhan, C. G. Computational gibberellin-binding channel discovery unraveling the unexpected perception mechanism of hormone signal by gibberellin receptor. *J. Comput. Chem.* **2013**, *34*, 2055−2064.

(24) Hibbs, R. E.; Gouaux, E. Principles of activation and permeation in an anion-selective Cys-loop receptor. *Nature* **2011**, *474*, 54−60.

(25) Thompson, J. D.; Higgins, D. G.; Gibson, T. J. CLUSTAL W: improving the sensitivity of progressive multiple sequence alignment through sequence weighting, position-specific gap penalties and weight matrix choice. *Nucleic Acids Res.* **1994**, *22*, 4673−4680.

(26) Chenna, R.; Sugawara, H.; Koike, T.; Lopez, R.; Gibson, T. J.; Higgins, D. G.; Thompson, J. D. Multiple sequence alignment with the Clustal series of programs. *Nucleic Acids Res.* **2003**, *31*, 3497−3500.

(27) Larkin, M. A.; Blackshields, G.; Brown, N. P.; Chenna, R.; McGettigan, P. A.; McWilliam, H.; Valentin, F.; Wallace, I. M.; Wilm, A.; Lopez, R.; Thompson, J. D.; Gibson, T. J.; Higgins, D. G. Clustal W and Clustal X, version 2.0. *Bioinformatics* **2007**, *23*, 2947−2948.

(28) Laskowski, R. A.; MacArthur, M. W.; Moss, D. S.; Thornton, J. M. PROCHECK: a program to check the stereochemical quality of protein structures. *J. Appl. Crystallogr.* **1993**, *26*, 283−291.

(29) Lüthy, R.; Bowie, J. U.; Eisenberg, D. Assessment of protein models with three-dimensional profiles. *Nature* **1992**, *356*, 83−85.

(30) Berendsen, H. J. C.; Van Der Spoel, D.; Van Drunen, R. GROMACS: a message-passing parallel molecular dynamics implementation. *Comput. Phys. Commun.* **1995**, *91*, 43−56.

(31) Van Der Spoel, D.; Lindahl, E.; Hess, B.; Groenhof, G.; Mark, A. E.; Berendsen, H. J. C. GROMACS: fast, flexible, and free. *J. Comput. Chem.* **2005**, *26*, 1701−1718.

(32) Hess, B.; Kutzner, C.; van der Spoel, D.; Lindahl, E. GROMACS 4: algorithms for highly efficient, load-balanced, and scalable molecular simulation. *J. Chem. Theor. Comput.* **2008**, *4*, 435−447.

(33) Oostenbrink, C.; Villa, A.; Mark, A. E.; Van Gunsteren, W. F. A biomolecular force field based on the free enthalpy of hydration and solvation: the GROMOS force-field parameter sets 53A5 and 53A6. *J. Comput. Chem.* **2004**, *25*, 1656−1676.

(34) Schuttelkopf, A. W.; van Aalten, D. M. F. PRODRG: a tool for high-throughput crystallography of protein-ligand complexes. *Acta Crystallogr.* **2004**, *60*, 1355−1363.

(35) Singh, U. C.; Kollman, P. A. An approach to computing electrostatic charges for moleculars. *J. Comput. Chem.* **1984**, *5*, 129−145.
(36) Besler, B. H.; Merz, K. M.; Kollman, P. A. Atomic charges derived from semiempirical methods. *J. Comput. Chem.* **1990**, *11*, 431−439.
(37) Wang, J. M.; Wang, W.; Kollman, P. A.; Case, D. A. Antechamber: an accessory software package for molecular mechanical calculations. *J. Comput. Chem.* **2005**, *25*, 1157−1174.
(38) Kandt, C.; Ash, W. L.; Tieleman, D. P. Setting up and running molecular dynamics simulations of membrane proteins. *Methods* **2007**, *41*, 475−488.
(39) Berendsen, H. J. C.; Postma, J. P. M.; van Gunsteren, W. F.; Hermans, J. Interaction models for water in relation to protein hydration. *Intermolecular Forces*; Pullman, B., Ed.; Reidel: Dordrecht, The Netherlands, 1981; pp 331−342.
(40) Nosé, S. A molecular dynamics method for simulations in the canonical ensemble. *Mol. Phys.* **1984**, *52*, 255−268.
(41) Hoover, W. G. Canonical dynamics: equilibrium phase-space distributions. *Phys. Rev. A* **1985**, *31*, 1695−1697.
(42) Parrinello, M.; Rahman, A. Polymorphic transitions in single crystals: a new molecular dynamics method. *J. Appl. Phys.* **1981**, *52*, 7182−7190.
(43) Hess, B.; Bekker, H.; Berendsen, H. J. C.; Fraaije, J. G. E. M. LINCS: a linear constraint solver for molecular simulations. *J. Comput. Chem.* **1997**, *18*, 1463−1472.
(44) Darden, T.; York, D.; Pedersen, L. Particle mesh Ewald: an N. log(N) method for Ewald sums in large systems. *J. Chem. Phys.* **1993**, *98*, 10089−10092.
(45) Essmann, U.; Perera, L.; Berkowitz, M. L.; Darden, T.; Lee, H.; Pedersen, L. G. A smooth particle mesh Ewald method. *J. Chem. Phys.* **1995**, *103*, 8577−8593.
(46) Hosie, A. M.; Baylis, H. A.; Buckingham, S. D.; Sattelle, D. B. Actions of the insecticide fipronil, on dieldrin-sensitive and -resistant GABA receptors of *Drosophila melanogaster*. *Br. J. Pharmacol.* **1995**, *115*, 909−912.
(47) Charon, S.; Taly, A.; Rodrigo, J.; Perret, P.; Goeldner, M. Binding modes of noncompetitive GABA-channel blockers revisited using engineered affinity-labeling reactions combined with new docking studies. *J. Agric. Food Chem.* **2011**, *59*, 2803−2807.
(48) Goff, G. L.; Hamon, A.; Bergé, J. B.; Amichot, M. Resistance to fipronil in *Drosophila simulans*: influence of two point mutations in the RDL GABA receptor subunit. *J. Neurochem.* **2005**, *92*, 1295−1305.
(49) Nakao, T.; Naoi, A.; Kawahara, N.; Hirase, K. Mutation of the GABA receptor associated with fipronil resistance in the whitebacked planthopper *Sogatella furcifera*. *Pestic. Biochem. Physiol.* **2010**, *97*, 262−266.
(50) Casida, J. E.; Tomizawa, M. Insecticide interactions with γ-aminobutyric acid and nicotinic receptors: predictive aspects of structural models. *J. Pestic. Sci.* **2008**, *33*, 4−8.
(51) Hisano, K.; Ozoe, F.; Huang, J.; Kong, X.; Ozoe, Y. The channel-lining 6′ amino acid in the second membrane-spanning region of ionotropic GABA receptors has more profound effects on 4′-ethynyl-4-*n*-propylbicyclo-orthobenzoate binding than the 2′ amino acid. *Invert. Neurosci.* **2007**, *7*, 39−46.
(52) Smart, O. S.; Goodfellow, J. M.; Wallace, B. The pore dimensions of gramicidin A. *Biophys. J.* **1993**, *65*, 2455−2460.
(53) Smart, O. S.; Neduvelil, J. G.; Wang, X. N.; Wallace, B. A.; Sansom, M. S. P. HOLE: a program for the analysis of the pore dimensions of ion channel structural models. *J. Mol. Graphics* **1996**, *14*, 354−360.
(54) Wallace, B. A. Recent advances in the high resolution structures of bacterial channels: gramicidin A. *J. Struct. Biol.* **1998**, *121*, 123−141.

investigated the mechanism of citrate exudation by following the effect of DM on the transcription of the gene OSFRDL4 coding for an anion channel protein believed to mediate citrate efflux in plants[15] in the presence or absence of anthracene-9-carboxylase (a specific anion channel inhibitor).

## MATERIALS AND METHODS

**Culture Conditions and Herbicide Treatment.** The sterilized Japonica rice seeds (*Oryza sativa* L. *japonica* cv. Xiushui 63) were germinated on filter papers at 30 °C in the dark for 2 d. The germinated seeds were then transferred onto a net floating on a culture medium containing 0.5 mM $CaCl_2$ (initial pH ≈ 5.7) at 25 °C in the dark for 4 d. For the DM exposure experiments, the seedlings were uniformly placed in an environmentally controlled growth room under a 12 h/12 h light/dark cycle. The rice seedlings were exposed for 24, 48, and 72 h to DM concentrations of 0, 5, and 50 μg/L (or 0, 14.7, and 147 nM), which were added to the $CaCl_2$ culture medium. Note that DM may rapidly hydrolyze in diclofop acid (DH) on a time scale of hours to days.[4] Because DH has a $pK_a$ of 3.57,[16] the unprotonated or negatively charged species ($D^{-1}$) of DH is then expected to predominate over the protonated species at the pH of the culture medium. The rice seedlings were thus exposed to a mixture of DM, $D^{-1}$, and a low concentration of DH. The toxicity of DM on root growth and various biochemical targets in root explants of *O. sativa* L. was then investigated after 48 h of exposure. The transcription of genes related to citrate production and incorporation in fatty acids, as well as the activity of citrate synthase, were, however, measured after 24, 48, and 72 h of exposure to DM.

**Root Growth Measurement, Microscopic Observation of Leaf Protoplasts and Root Tissue Section.** The degree of inhibition in root elongation due to DM was measured using a vernier caliper. In parallel, we also isolated protoplasts from the leaves of rice seedlings using cellulase and pectinase incubation according to the protocol described in our previous study, and tissue sections were prepared from the roots of rice seedlings by paraffin block embedding.[17] The leaf protoplasts and root tissue sections were then observed with a light microscope at 1000×.

**Quantitative Real-Time PCR (qRT-PCR).** Root tissues were ground with a mortar and pestle in liquid nitrogen, and total RNA was extracted in 1 mL of RNAiso reagent according to the manufacturer's instructions (TaKaRa Company, Dalian, China). Total RNA was treated with DNase. RNA (500 ng) was then reverse transcripted in cDNA using a M-MLV reverse transcript kit (TaKaRa Company, Dalian, China). cDNA was diluted 10 times and used for real-time quantitative RT-PCR (qRT-PCR) which was carried out on an Eppendorf MasterCycler ep RealPlex[4] (Wesseling Berzdorf, Germany) according to the manufacturer's instructions using primers specific to the DNA sequence of several genes (Supporting Information (SI) Table SI.1). The housekeeping gene *25S* rDNA was used as an internal standard. qRT-PCR was performed in 10-μL aliquots, containing 1 μL of cDNA, 0.2 μL of each primer (10 μM), 5 μL of 2× mix buffer (Master mix, TOYOBO), and supplemented with sterile distilled water, with the following program: 95 °C 1 min; 40 cycles of 95 °C 15 s, and 60 °C 1 min. Gene expression normalized to 25S rDNA was analyzed by the $2^{-\Delta\Delta Ct}$ method, where $C_t$ is the cycle number at which the fluorescent signal rises statistically above the background.[18] qRT-PCR was repeated with three independent replicates.

**Enzyme Activity and Lipid Peroxidation Analyses.** To extract the enzymes, root tissues were ground and homogenized with a mortar and pestle in 1.5 mL of 20 mM phosphate buffer (pH 7.4) in an ice bath. The homogenate was centrifuged at 10 000*g* for 10 min at 4 °C and the supernatant was used for the enzyme, protein, and malondialdehyde assays. The activity of citrate synthase (CS) was measured according to the method of Srere.[19] The activity of superoxide dismutase (SOD) was determined with a SOD kit (SOD kit, Sangon Company, China). Peroxidase (POD) activity was measured according to Andrews et al.[20] Lipid peroxidation level was determined by following the root malondialdehyde (MDA) content according to Zhang and Kirkham.[21] The activity of each enzyme was normalized to protein concentration, which was determined using the bicinchoninic acid (BCA) method (BCA protein kit, Sangon Company, China).

**Intracellular and Extracellular Citrate Analyses by HPLC.** After the DM exposures, the root tissues of rice seedlings were rinsed with distilled water and homogenized with a mortar and pestle in 1.2 mL of ice-cold 0.6 M $HClO_4$. The homogenates were transferred into Eppendorf tubes, which were centrifuged at 14 000*g* at 4 °C for 5 min. Eighty microliters of 5 M $K_2CO_3$ was added to the homogenates to neutralize the $HClO_4$. The intracellular concentration of citrate was measured by HPLC using an ion-exclusion column (Shodex Rspak Kc811, 300 mm × 8 mm) and a spectrophotometry detector at the wavelength of 210 nm. The mobile phase was perchloric acid solution (pH 2.1) with a flow rate of 0.8 mL/min.

The dissolved concentration of citrate in the culture medium was also analyzed according to the following procedure. The culture medium was collected to purify the organic acids exuded in solution by *O. sativa* L. The medium was then passed through a cation-exchange column (16 mm × 20 cm) filled with 5 g of Amberlite IR-120B resin ($H^+$ form) and an anion-exchange column (16 mm × 20 cm) filled with 2 g of Dowex 1 × 8 (100−200 mesh, formate form). The organic acid anions retained on the anion-exchange resin were eluted with 2 M HCl. The eluate was then dried in a 40 °C water bath, redissolved in 1 mL of Milli-Q water, and filtered through a 0.45-μm filter membrane. Determination of dissolved citrate exuded in the culture medium was done by HPLC according to the same method as that used for the measurement of intracellular citrate.

**Measurements of Polysaccharides and Uronic Acid in Root Cell Wall.** Root tissues were disrupted with a mortar and pestle in liquid nitrogen, and put in 75% (v/v) ethanol for 20 min in a cool water bath. The sample was then centrifuged at 12 000*g* for 10 min. After the supernatant was removed, the pellet was washed with acetone, methanol/chloroform (1:1), and methanol, for 20 min each. The remaining pellet, composed of cell wall materials, was freeze-dried for further use. Two mg of cell wall was dissolved in 1 mL of water, and the pectin fraction was extracted with a 1-h heating treatment (100 °C). The samples were again centrifuged at 14 400*g* for 10 min, and the supernatants were collected into the tube. The above two steps were repeated three times. The pellet was further extracted with 1 mL of 24% (w/v) KOH and 0.1% (w/v) $KBH_4$ for 12 h and centrifuged at 12 000*g* for 10 min. The hemicellulose (HCl) fraction was recovered in the supernatant. Pectin extracts (200 μL) were then incubated with 1 mL of 98% (v/v) $H_2SO_4$ containing 0.0125 M $Na_2B_4O_7{\cdot}10H_2O$ at 100 °C for 5 min. After cooling, 20 μL of M-hydro-diphenyl (0.15%, w/v) was added to the solution and let to react with the samples for 20 min. The uronic acid concentration in the pectin fraction was then measured spectrophotometrically by following the absorbance at 520 nm. Extraction of total polysaccharides in the hemicellulose fraction of the cell wall was performed using the phenol sulfuric acid method in which 200 μL of hemicellulose was incubated in 1 mL of 98% $H_2SO_4$ and 10 μL of 80% (v/v) phenol for 15 min, followed by incubation in boiling water for 15 min. The total polysaccharide content in the HCl fraction was finally measured spectrophotometrically using an absorbance wavelength set to 490 nm.

**Statistical Analyses.** Significant differences among the means of different treatments were evaluated by using analyses of variance (ANOVA). The conditions of ANOVAs (the normality and homogeneity of variance) were evaluated with the Kolmogrov−Smirnov test and the Levene test, respectively. If the test conditions were not validated, the data were transformed prior to the ANOVAs. Statistical analyses were performed using the program StatView. Differences among means were considered to be significant when the probability ($p$) was less than 0.05. All means and standard errors were calculated from three independent replicates.

## RESULTS

**Effect of DM on Root Growth.** After a 48-h exposure to 5 and 50 μg/L DM, the mean root growth was only about 31.2%

($p < 0.01$) and 15.6% ($p < 0.01$) of the control value, respectively (Figure 1). DM also affected the shape and color of

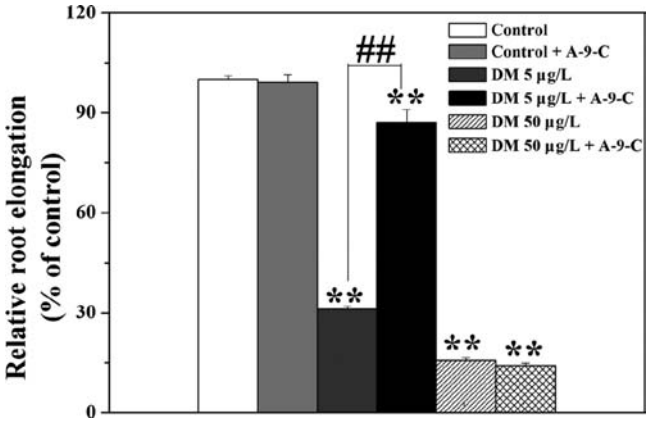


**Figure 1.** Relative root growth inhibition after a 48-h exposure to 5 and 50 $\mu$g/L DM in the presence or absence of the anion channel inhibitor anthracene-9-carboxylic acid (A-9-C). (*), (**) represent statistically significant differences relative to controls at $p < 0.05$ and at $p < 0.01$, respectively. (#), (##) show statistically significant differences due to the presence of A-9-C at $p < 0.05$ and at $p < 0.01$, respectively. Error bars represent the standard errors of three replicates.

cell walls and chloroplasts based on microscopic observations (SI Figure SI.1). Indeed, the root cell wall appeared darker and thicker after DM exposures (SI Figure SI.1). Moreover, at 50 $\mu$g/L DM, the chloroplasts could not be distinguished in the leaf protoplast and the green color of chlorophyll also weakened relative to that of the control (SI Figure SI.1).

**DM Effect on Cell Wall Composition.** Uronic acid and polysaccharides accounted for a relatively high proportion (>50%) of the pectin and hemicellulose fraction of the cell wall, respectively. The mean proportion of uronic acid significantly increased to a level 1.54-fold higher than that of the control after a 48-h exposure to 50 $\mu$g/L DM ($p < 0.01$) (SI Figure SI.2A). The proportion of polysaccharides in the cell wall also significantly increased by around 1.60-fold relative to that of the control after the 48 h exposure to 5 and 50 $\mu$g/L DM ($p < 0.01$) (SI Figure SI.2B). Furthermore, the transcription of five *pectin methylesterase* homologous genes was strongly induced by DM (SI Figure SI.2C). After the 48-h exposure to 50 $\mu$g/L DM, the transcripts of PME7, PME11, PME12, and PME22 significantly increased to levels 2.03-, 2.69-, 4.16-, and 3.10-fold higher than those of the control, respectively ($p < 0.01$ for PME11, PME12, PME22, but $p < 0.05$ for PME7) (SI Figure SI.2C). Gene transcription of PME29 was only significantly induced in response to the 5 $\mu$g/L DM treatment ($p < 0.05$), but did not change significantly at the highest DM concentration tested (50 $\mu$g/L) (SI Figure SI.2C). The microarray results also showed that the transcripts of many genes involved in the biosynthesis of cell wall can be induced in response to DM exposure (SI Table SI.2). The transcripts of phenylalanine ammonia-lyase (PAL) and peroxidases (PODs) were all induced by more than 2-fold in response to DM exposure.

**Effect of DM on Citrate Metabolism and Exudation.** Figure 2A shows that the transcript of ATP-cirate lyase (ACLY) already significantly decreased by 19.4% and 60.8% after 24 h of exposure to 5 and 50 $\mu$g/L DM, respectively ($p < 0.01$). Between 24 and 72 h, the transcript of ACLY continued to

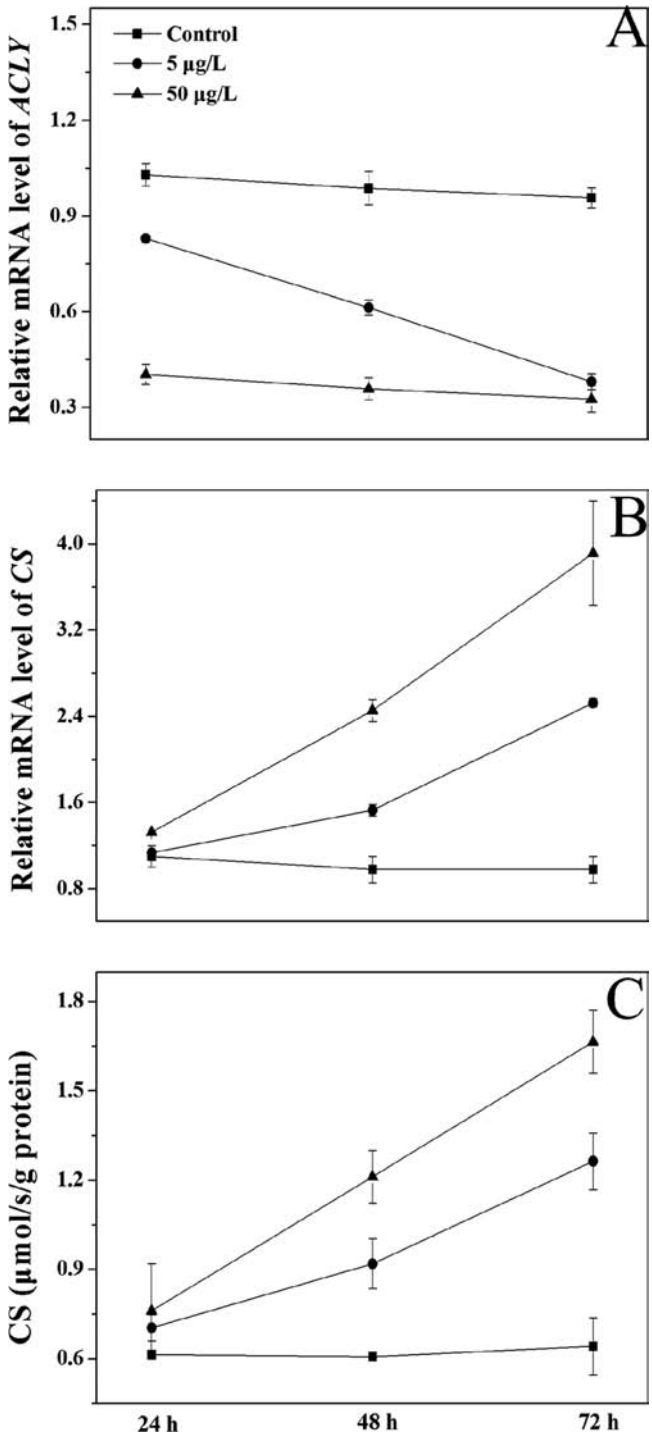


**Figure 2.** Effect of a 5 and 50 $\mu$g/L DM exposure for 24, 48, and 72 h on the transcription level of the citrate lyase (ACLY) gene (A) and the citrate synthase gene (B). Expression levels were normalized to that of the 25S rRNA gene. The effect of DM on CS activity (C). Error bars are the standard errors of three replicates.

decrease in the presence of 5 $\mu$g/L DM; at 72 h, the transcription of ACLY was inhibited by 63.0%. In contrast, at 50 $\mu$g/L DM, ACLY transcripts were inhibited by around 68% throughout the 72 h exposure ($p < 0.01$). The CS transcript level and CS enzyme activity both significantly increased in the presence of the two tested DM concentrations after 48 and 72 h exposure. After 72 h of exposure to 5 and 50 $\mu$g/L DM, CS


dx.doi.org/10.1021/jf503974t | J. Agric. Food Chem. 2014, 62, 10654−10660

enzyme activities reached levels 1.97- and 2.62-fold higher than those of the control, respectively (Figure 2B,C).

The citrate concentration in rice roots was not affected significantly after 24 h of exposure to 5 or 50 $\mu$g/L DM relative to control value, but significantly increased by approximately 15% after 48 h of exposure to 50 $\mu$g/L DM or 72 h of exposure to 5 or 50 $\mu$g/L DM. (Figure 3A). The amount of exuded

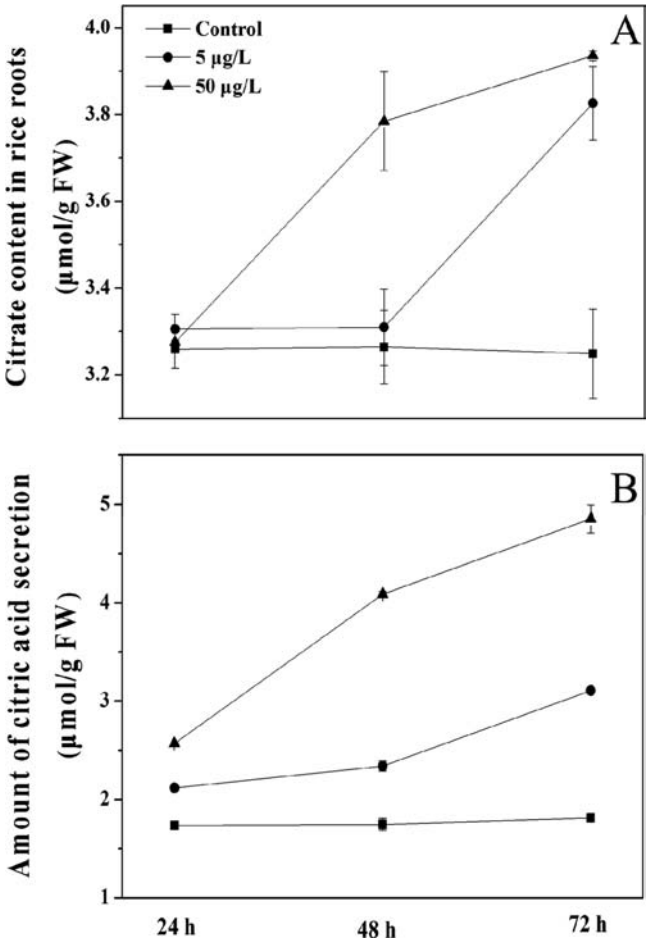


**Figure 3.** Citrate concentration in rice roots (A) and citrate concentration exuded in the medium normalized to root biomass (B) as a function of DM concentrations and time. Error bars are the standard errors of three replicates.

citrate in the culture medium normalized to root biomass showed a 1.79-fold increase after 72 h of exposure to 5 $\mu$g/L DM ($p < 0.01$) relative to that measured in control. The mean exudation of citrate increased by a factor of 1.48, 2.34, and 2.68 relative to control after 24, 48, and 72 h, respectively, of exposure to 50 $\mu$g/L DM (Figure 3B).

**Anion-Channel Inhibitor and Citrate Exudation.** Preliminary experiments demonstrated that 1 mg/L anthracene-9-carboxylic acid (A-9-C) did not affect the root growth of *O. sativa* L. over 48 h. In Figure 1A, we showed that addition of 1 mg/L A-9-C can even significantly decrease the toxicity of DM on root growth after 48 h of exposure to 5 $\mu$g/L DM, although 1 mg/L A-9-C did not affect significantly the toxicity of 50 $\mu$g/L DM. The results in Figure 4A shows that the transcription of *OsFRDL4* significantly increased in the presence of DM relative to control cultures without DM. Exposure of rice seedlings to 5 $\mu$g/L DM and 1 mg/L A-9-C

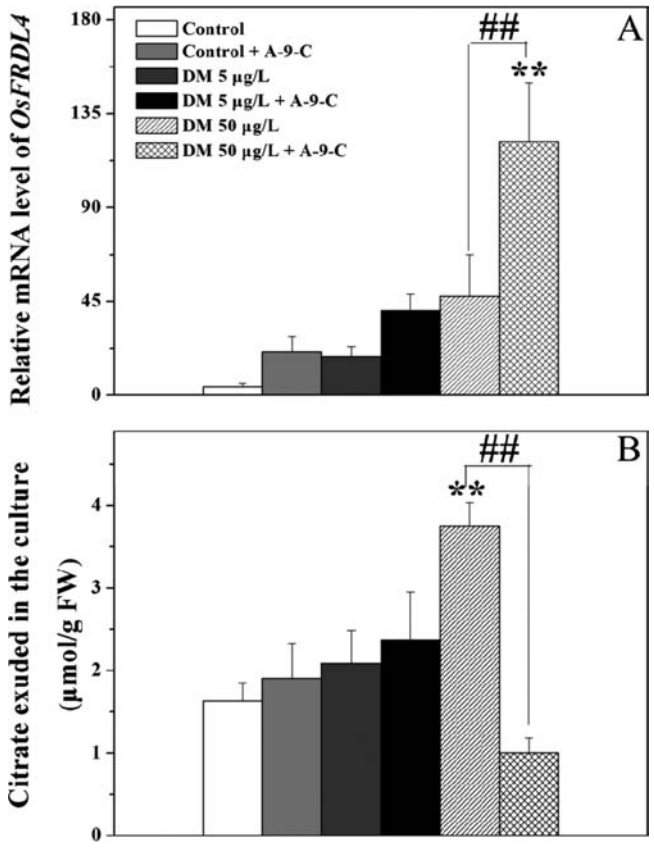


**Figure 4.** (A) Effect of a 5 and 50 $\mu$g/L DM exposure for 24, 48, and 72 h on the transcription level of the anion channel protein gene (OsFRDL4) normalized against 25S rRNA. The experiments in panel A were done in the presence or absence of the anion channel inhibitor Anthracene-9-carboxylic acid (A-9-C). B: Amount of citrate exuded in the culture medium normalized to root biomass. Error bars are the standard errors of three replicates. (*), (**) represent statistically significant differences relative to controls at $p < 0.05$ and at $p < 0.01$, respectively. (#), (##) show statistically significant differences due to the presence of A-9-C at $p < 0.05$ and at $p < 0.01$, respectively.

significantly increased the transcription of *OsFRDL4* relative to that measured after the exposure to 5 $\mu$g/L without A-9-C. In the presence of 50 $\mu$g/L DM and 1 mg/L A-9-C, the transcription of *OsFRDL4* was markedly induced by almost one order of magnitude with respect to its transcription at 50 $\mu$g/L DM without A-9-C (Figure 4A). A-9-C alone or combined with 5 $\mu$g/L DM did not affect significantly citrate exudation relative to control cultures, but addition of 1 mg/L A-9-C and 50 $\mu$g/L DM decreased citrate excretion by approximately 4-fold relative to that measured at 50 $\mu$g/L DM without A-9-C ($p < 0.01$)(Figure 4B).

**Antioxidant Enzymes and Oxidative Stress in Roots.** A 48-h exposure to 5 and 50 $\mu$g/L DM induced a significant increase in SOD activities relative to control values ($p < 0.05$ at 5 $\mu$g/L DM; $p < 0.01$ at 50 $\mu$g/L DM). In contrast, when 1 mg/L A-9-C was added in combination with DM, the SOD activity remained unaffected by the presence of DM (SI Figure SI.3A). The activity of total peroxidase (POD) also significantly increased in response to 5 or 50 $\mu$g/L DM ($p < 0.01$) and this stimulation of POD activity was less pronounced when A-9-C was added in combination with DM (SI Figure SI.3B). The malondialdehyde content in root tissues nearly doubled at 50 $\mu$g/L DM relative to control value, and the addition of A-9-C in


dx.doi.org/10.1021/jf503974t | J. Agric. Food Chem. 2014, 62, 10654−10660

combination with DM tended to decrease this effect, although this decrease was not statistically significant (SI Figure SI.3C).

## DISCUSSION

**DM Toxicity on Root Growth.** Residual low concentrations of the widely used herbicide diclofop-methyl have been shown to inhibit the growth of nontarget monocots and aquatic algae.[8,9,22] Qian et al.[9] have previously shown that exposures to 50 $\mu$g/L DM for 2 weeks significantly inhibited by around 50% the root growth of rice seedlings. Our results here show that DM toxicity on root growth of rice seedlings for a 48-h exposure period may be more important that that measured after a much longer exposure time of 2 weeks, indicating that DM toxicity may be particularly important in the first hours or days of exposure to DM (Figure 1A). This is consistent with a relatively rapid uptake of the hydrophobic DM species followed by a relatively rapid hydrolysis of DM in mostly deprotonated diclofop acid ($D^-$) (at pH of our culture medium).[4] Indeed, hydrophobic molecules such as DM (and perhaps DH) are typically taken up by living cells at a much higher rate compared to that of charged species (such as $D^-$).[12,23]

**Interaction between DM and Cell Wall Biosynthesis.** To exert its toxicity in plant cells, DM first needs to pass through the cell wall. Several studies have shown that both biotic stresses (e.g., bacteria, fungi, and virus) and abiotic stresses (metals, pesticide, UV−B, and temperature) may alter the composition of cell wall by inducing a thickening of cuticles or trichomes.[24,25] The present study confirms that the herbicide DM may strongly affect the cell wall of *O. sativa*. Our results show that a 48-h exposure to trace DM concentrations may increase the proportion of uronic acid and polysaccharides in cell wall fractions (SI Figure SI.2A, B) and induce the transcription of various genes involved in the biosynthesis of cell wall (*pectin methylesterase, pectinesterase, cellulose synthase, phenylalanine ammonia-lyase* genes) (SI Figure SI.2C; Table SI.1 and SI.2). Different hypotheses may explain this energy investment in cell wall biosynthesis: (1) The increased biosynthesis of cell wall components might be a toxic effect of DM with no cellular function per se. (2) If not accompanied by a net increase in the absolute amount of cell wall components, the DM-induced up-regulation of cell wall biosynthesis rate could be triggered to repair the cell wall damages caused by DM. (3) If accompanied by a net increase in the absolute amount of cell wall components, DM might trigger a cellular defense mechanism associated with the thickening of the cell wall, which could reduce DM or DH diffusive rate across the cell wall (depending on the cell wall porosity), as well as DM or DH uptake rate and its toxicity. Additionally, if the unprotonated diclofop acid species ($D^-$) could be internalized in cells of rice roots via a specific cell membrane transporter, then the increase in the activity of pectin methylesterase, which converts the methoxyl groups on the polygalacturonic acid chain of the cell wall into negatively charged carboxyl groups,[26] would decrease (to more negative values) the cell surface charge of plant cells, which could decrease the effective concentration of $D^-$ close to the cell surface and help decrease $D^-$ uptake rate. Further experiments are, however, needed to confirm or refute the above hypotheses stipulating that DM-induced cell wall thickening might decrease DM, DH, or $D^-$ uptake in rice roots.

**DM Toxicity on Fatty Acid Precursors.** The high toxicity of DM in monocots was previously shown to be due to the ability of DM to inhibit the activity of the enzyme acetyl-CoA carboxylase, which catalyzes the conversion of two acetyl-CoA molecules in one molecule of malonyl-CoA, the primary precursor for fatty acid biosynthesis in the chloroplast.[27] Another key enzyme upstream of the acetyl-CoA carboxylase that might also be affected by DM is the ATP-dependent citrate lyase (ACLY), which catalyzes the conversion of citrate and CoA in acetyl-CoA and oxaloacetate in the chloroplast.[28] This citrate comes from the mitochondrion matrix, where another important enzyme, citrate synthase (CS) produced citrate and initiates the tricarboxylic acid cycle. The present study shows that the activity and gene transcription of the enzyme CS increased in response to DM exposure, while DM decreased the gene transcription of the enzyme ACLY (Figure 2). This regulation pattern of CS and ACLY gene expression and enzyme activity will lead to an increase in citrate concentration in root cells as observed in Figure 3A.

**DM-Induced Citrate Exudation from Root Cells.** Our results show that the herbicide DM may increase citrate exudation from root cells since dissolved citrate concentrations increased over time in plant cultures exposed to DM (Figure 3B) as observed in the study of Ding et al.[10] who performed longer (2−3 weeks) DM exposure of rice seedlings.

Our data also show that the transcription level of *OsFRDL4* increased under DM exposure (Figure 4A) and that addition of the anion channel inhibitor A-9-C (at nontoxic concentration, Figure 1A) further increased the transcription of *OsFRDL4* (Figure 4A). Moreover, the amount of citrate exuded in the culture medium contaminated with 50 $\mu$g/L DM (but not with 5 $\mu$g/L DM) strongly decreased in response to the addition of the anion channel inhibitor A-9-C (Figure 4B). Together, the results strongly suggest that DM may up-regulate the synthesis of anion channel proteins in the plasma membrane of rice roots and may mediate the transport of excess intracellular citrate out of the cells (as shown in Figure 3B). However, this up-regulation of citrate channels and its associated increase in citrate exudation (only at 50 $\mu$g/L DM) caused by DM exposure did not decrease DM toxicity. Our results agree with those of previous reports showing that citrate exudation from plant roots probably involved a specific transport system in the plasma membrane.[14,29,30] The latter reports dealt with the effect of metals or phosphorus limitation, but, to our knowledge, the present study is the first showing that citrate exudation in the presence of an herbicide, DM, is mediated by an anion channel protein. Contrary to the protective effect of citrate exudation on Al toxicity,[14] our study shows that DM-induced citrate exudation did not protect rice roots against DM toxicity.

**DM Toxicity and Oxidative Stress.** Besides the toxicity of DM at the level of fatty acid biosynthesis, other studies of Shimabukuro et al.[31,32] have proposed that DM toxicity might be due to the DM-induced production of free radicals in plant cells. In the present study, we show that DM increased oxidative stress at the level of cell membranes (MDA production SI Figure SI.3C) in the roots of rice seedlings, and that the activity of two antioxidant enzymes may increase in response to this stress (SOD and POD) (SI Figure SI.3A,B). Furthermore, the addition of 1 mg/L A-9-C in cultures contaminated with 5 $\mu$g/L DM significantly decreased the level of oxidative stress in cell membrane (SI Figure SI.3C) as well as DM toxicity on root growth (Figure 1A). Then, our results are also consistent with a putative DM toxicity cellular mechanism based on the production of free radicals.

**Conclusions.** This study brings new insights into the key biochemical mechanisms leading to DM toxicity in rice. Here

we show that DM may increase the activity of CS and decrease the activity of ACLY, which increase the intracellular pool of citrate in rice roots. This cellular excess in citrate may be exuded by specific anion channels located in the cell membrane of root cells, but this DM-induced citrate exudation did not protect against DM toxicity on the root growth of rice seedlings. The exudation of citrate induced under DM stress is noteworthy since an increase in organic acid release in soils contaminated by residual herbicide concentrations may affect the chemistry of soil pore water (e.g., pH, organic carbon respiration) and the microbial community structure in the rhizosphere, which could in turn affect plant nutrition.

## ■ ASSOCIATED CONTENT

### Supporting Information

Table SI.1 Sequences of primer pairs used to measure the transcription of several genes by real-time PCR. Table SI.2 Changes in cell wall-related gene transcription relative to control after treatment with DM enantiomer (*S*-DM and *R*-DM), as analyzed by microarray. Figure SI.1 Microscopic observations of root tissue sections and leaf protoplasts of rice seedlings exposed to 0, 5, and 50 μg/L DM for 48 h. Figure SI.2 Effect of a 48-h exposure to 5 and 50 μg/L DM on the proportion of uronic acid in the pectin fraction of cell wall (A) and on the proportion of polysaccharides in the hemicellulose (HCl) fraction of cell wall (B). (C) Transcripts of five pectin methylesterase homologous genes normalized against 25s rRNA. Figure SI.3 Activity of superoxide dismutase (SOD) (A), and peroxidase (POD) (B) in rice roots after a 48-h exposure to 5 or 50 μg/L DM with and without the anion channel inhibitor, anthracene-9-carboxylic acid (A-9-C). Concentrations of malondialdehyde in rice roots (C) exposed for 48 h to 5 or 50 μg/L DM with or without A-9-C. This material is available free of charge via the Internet at http://pubs.acs.org.

## ■ AUTHOR INFORMATION

### Corresponding Author

*Tel.: +86 5718832 0742. Fax: +86 571 8832 0599. E-mail address: hfqian@zjut.edu.cn.

### Funding

This work was financially supported by the Natural Science Foundation of China (21277127), and Zhejiang Provincial Natural Science Foundation of China, China (LR14B070001).

### Notes

The authors declare no competing financial interest.

## ■ REFERENCES

(1) Burton, J. D.; Gronwald, J. W.; Somers, D. A.; Connelly, J. A.; Gengenbach, B. G.; Wyse, D. L. Inhibition of plant acetyl-coenzyme a carboxylase by herbicides sethoxydim and haloxyfop. *Biochem. Biophys. Res. Commun.* **1987**, *148*, 1039−1044.

(2) Alban, C.; Baldet, P.; Douce, R. Localization and characterization of two structurally different forms of acetyl-CoA carboxylase in young pea leaves, of which one is sensitive to aryloxyphenoxypropionate herbicides. *Biochem. J.* **1994**, *300*, 557−565.

(3) Alban, C.; Jullien, J.; Job, D.; Douce, R. Isolation and characterization of biotin carboxylase from pea chloroplasts. *Plant Physiol.* **1995**, *109*, 927−935.

(4) U.S. Environmental Protection Agency. *Pesticide Registration: Diclofop-Methyl*; EPA-738-F-00-007; Office of Prevention, Pesticides, and Toxic Substances: Washington, DC, 2000.

(5) Liu, W. P.; Jin, M. Q.; Cai, X. Y.; Ye, J. Progress in the mechanism of action and ecological effects of the herbicide diclofop methyl. *Chin. J. Pestic. Sci.* **2008**, *10*, 384−391 In Chinese.

(6) Gavrilescu, M. Fate of pesticides in the environment and its bioremediation. *Eng. Life Sci.* **2005**, *5*, 497−525.

(7) Dalton, R.; Boutin, C. Comparison of the effects of glyphosate and atrazine herbicides on non-target plants grown singly and in microcosms. *Environ. Toxicol. Chem.* **2010**, *29*, 2304−2315.

(8) Ye, J.; Zhang, Q.; Zhang, A. P.; Wen, Y. Z.; Liu, W. P. Enantioselective effects of chiral herbicide diclofop acid on rice Xiushui 63 seedlings. *Bull. Environ. Contam. Toxicol.* **2009**, *83*, 85−91.

(9) Qian, H. F.; Wang, R. Q.; Chen, J.; Ding, H. Y.; Wei, Y.; R, S. L.; Fu, Z. W. Analysis of enantioselective biochemical, physiological, and transcriptional effects of the chiral herbicide diclofop methyl on rice seedlings. *J. Agric. Food Chem.* **2012**, *60*, 5515−5523.

(10) Ding, H. Y.; Wen, D. N.; Fu, Z. W.; Qian, H. F. The secretion of organic acids is also regulated by factors other than aluminum. *Environ. Monit. Assess.* **2014**, *186*, 1123−1131.

(11) Jones, D. L. Organic acids in the rhizosphere - A critical review. *Plant Soil* **1998**, *205*, 25−44.

(12) Ryan, P. R.; Delhaize, E.; Jones, D. L. Function and mechanism of organic anion exudation from plant roots. *Annu. Rev. Plant Physiol. Plant Mol. Biol.* **2001**, *52*, 527−560.

(13) Haynes, R. J.; Mokolobate, M. S. Amelioration of Al toxicity and P deficiency in acid soils by additions of organic residues: A critical review of the phenomenon and the mechanisms involved. *Nutr. Cycl. Agroecosyst.* **2001**, *59*, 47−63.

(14) Yokosho, K.; Yamaji, N.; Ma, J. F. An Al-inducible MATE gene is involved in external detoxification of Al in rice. *Plant J.* **2011**, *68*, 1061−1069.

(15) Shen, H.; Yan, X. L.; Zhao, M.; Zheng, S. L.; Wang, X. R. Exudation of organic acids in common bean as related to mobilization of aluminum- and iron-bound phosphates. *Environ. Exp. Bot.* **2002**, *48*, 1−9.

(16) DiTomaso, J. M.; Brown, P. H.; Stowe, A. E.; Linscott, D. L.; Kochian, L. V. Effects of diclofop and diclofop-methyl on membrane potentials in roots of intact oat, maize, and pea seedlings. *Plant Physiol.* **1991**, *95*, 1063−1069.

(17) Qian, H. F.; Wang, R. Q.; Hu, H. J.; Lu, T.; Chen, X. L.; Ye, H. Q.; Liu, W. P.; Fu, Z. W. Enantioselective phytotoxicity of the herbicide imazethapyr and its effect on rice physiology and gene transcription. *Environ. Sci. Technol.* **2011**, *45*, 7036−7043.

(18) Livak, K. J.; Schmittgen, T. D. Analysis of relative gene expression data using real-time quantitative PCR and the $2^{-\Delta\Delta Ct}$ method. *Methods* **2001**, *25*, 402−408.

(19) Srere, P. A. Citrate synthase. *Methods Enzymol.* **1969**, *13*, 3−11.

(20) Andrews, J.; Malone, M.; Thompson, D. S.; Ho, L. C.; Burton, K. S. Peroxidase isozyme patterns in the skin of the maturing tomato fruit. *Plant Cell. Environ.* **2000**, *23*, 415−422.

(21) Zhang, J. X.; Kirkham, M. B. Drought-stress-induced changes in activities of superoxide-dismutase, catalase, and peroxidase in wheat species. *Plant Cell. Physiol.* **1994**, *35*, 785−791.

(22) Cai, X. Y.; Liu, W. P.; Sheng, G. Y. Enantioselective degradation and ecotoxicity of the chiral herbicide diclofop in three freshwater alga cultures. *J. Agric. Food Chem.* **2008**, *56*, 2139−2146.

(23) Boullemant, A.; Lavoie, M.; Fortin, C.; Campbell, P. G. C. Uptake of hydrophobic metal complexes by three freshwater algae: Unexpected influence of pH. *Environ. Sci. Technol.* **2009**, *43*, 3308−3314.

(24) O'Looney, N.; Fry, S. C. Oxaziclomefone, a new herbicide, inhibits wall expansion in maize cell-cultures without affecting polysaccharide biosynthesis, xyloglucan transglycosylation, peroxidase action or apoplastic ascorbate oxidation. *Ann. Bot.* **2005**, *96*, 1097−1107.

(25) Moura, J. C.; Bonine, C. A.; Viana, J. D.; Dornelas, M. C.; Mazzafera, P. Abiotic and biotic stresses and changes in the lignin content and composition in plants. *J. Integr. Plant Biol.* **2010**, *52*, 360−376.

(26) Bosch, M.; Hepler, P. K. Pectin methylesterases and pectin dynamics in pollen tubes. *Plant Cell* **2005**, *17*, 3219−3226.
(27) Hoppe, H. H. Differential effect of diclofop-methyl on fatty acid biosynthesis in leaves of sensitive and tolerant plant species. *Pestic. Biochem. Physiol.* **1985**, *23*, 297−308.
(28) Fatland, B. L.; Nikolau, B. J.; Wurtele, E. S. Reverse genetic characterization of cytosolic acetyl-CoA generation by ATP-citrate lyase in *Arabidopsis*. *Plant Cell* **2005**, *17*, 182−203.
(29) Neumann, G.; Römheld, V. Root excretion of carboxylic acids and protons in phosphorus-deficient plants. *Plant Soil* **1999**, *211*, 121−130.
(30) Liu, J. P.; Piñeros, M. A.; Kochian, L. V. The role of aluminum sensing and signaling in plant aluminum resistance. *J. Integr. Plant Biol.* **2014**, *56*, 221−230.
(31) Shimabukuro, R. H.; Hoffer, B. L. Enantiomers of diclofop-methyl and their role in herbicide mechanism of action. *Pestic. Biochem. Physiol.* **1995**, *51*, 68−82.
(32) Shimabukuro, R. H.; Davis, D. G.; Hoffer, B. L. The effect of diclofop-methyl and its antagonist, vitamin E, on membrane lipids in oat (*Avena sativa* L.) and leafy spurge (*Euphorbia esula* L.). *Pestic. Biochem. Physiol.* **2001**, *69*, 13−26.

fatty acids (FFAs), peroxide value (PV), two UV absorption parameters ($K_{232}$ and $K_{268}$), 1,2-diacylglycerol content (DAGs), and pyropheophytins (PPPs)), some or all of which are considered by various national and international standards as quality or grade indicators of olive oil,[21−23] have been linked to results provided by trained sensory panelists to, in the end, be able to provide a quality assessment of blind olive oil samples.

## MATERIALS AND METHODS

**Olive Oil Samples.** Two hundred and twenty samples of extra virgin olive oil were collected before their best-before date during 2010−2012, when this information was included on labels; some samples did not have labels indicating such information. Samples were stored in an air-conditioned laboratory (20−25 °C) away from light. Nitrogen gas was used to displace air in the space above the oil.

Sampled olive oils are a blend of different olive varieties and came from various olive oil producing countries, such as Spain, Italy, Greece, Tunisia, and the United States.

**Chemical and Sensory Analyses of the Olive Oil Samples.** Six different chemical parameters were obtained from the 220 olive oil samples studied. They are FFA, PV, two UV absorption parameters ($K_{232}$ and $K_{268}$), DAGs, and PPP. These were selected as they have been linked in the past to olive oil quality evaluation by multiple national and international sources. Specifically, FFA, PV, and both UV absorption parameters are associated with olive oil grades by numerous relevant organizations like the International Olive Council (IOC)[22] and United States Department of Agriculture (USDA),[23] while DAGs and PPP are related to olive oil quality, for instance, by Australian Standards[21] or Guillaume et al. (2014).[24]

In addition, sensory analyses were carried out by a trained taste panel (IOC-certified Australian Oils Research Laboratory (AORL))[25] to attain a reliable olive oil grading of the samples. The reasons for the parameter selection, protocols followed, and equipment employed are described in the following subsections.

*Free Fatty Acids.* The FFA is linked to olive oil quality as it manifests the carefulness taken during the production process as well as the intrinsic quality of the employed fruit.[23] FFAs are formed when triacylglycerols in olive oils suffer hydrolysis during extraction, processing, distribution, and storage. For this reason, high levels of FFA can be linked to poor-quality olive oils.

FFA values were determined by the method of the American Oil Chemists Society (AOCS), Ca 5a-40, and expressed as a percentage of oleic acid.[26]

*Peroxide Values.* The PV of an olive oil is a crude measurement of its primary oxidation due to oxygen exposure. This oxidation leads to secondary oxidation products which give undesirable flavors and odors. In general, high PVs imply an oxidized oil and, therefore, a lower quality product.[23]

PVs were determined according to International Standard ISO 3960:2007 and expressed as meq $O_2$/kg.[27]

*Ultraviolet Absorption Measurements.* The information gathered from these tests offers evidence concerning quality, state of preservation, and modifications originated by the processing method.[23] Conjugated double bonds are formed from natural nonconjugated molecules in olive oil due to oxidation. This means that an elevated UV absorbance (high $K_{232}$ and $K_{268}$) is related to oxidized and low-grade oils.

Ultraviolet absorbance was determined using IOC method COI/T.20/Doc. 19.[28]

*1,2-Diacylglycerol Content.* DAGs have shown to be reliable markers of olive oil freshness and quality in the past and are employed by Australian Standards as a quality assessing parameter.[21] They are excellent indicators of initial poor-quality or low-grade olive oils, and high temperatures affect their values. High-quality and fresh olive oils contain a high level of 1,2-diacylglycerols.[24,29]

1,2-Diacylglycerols were determined using the method ISO 29822:2009.[30,31] A miniaturized chromatography column of silica gel 60 at 5% moisture was used to separate the isomeric diacylglycerols. The diacylglycerol profiles were determined by gas chromatography using a SGE BP5 capillary column (30 m, 0.25 mm, 0.25 μm film) and a flame ionization detector (FID).

*Pyropheophytin Quantification.* Determination of PPPs can also be used as an indicator of general quality and freshness of olive oil samples.[24] Comparable to DAGs, PPPs are utilized by Australian Standards for quality evaluation processes,[21] but in contrast, these are not influenced by the initial quality of the olive oil. In fact, cultivar or growing conditions do not affect PPPs either. High temperatures and light exposure are responsible for PPP amount alteration.[24] Their values increase upon thermal degradation of olive oil, thus being related to lower quality products.

Pyropheophytin A was measured using method ISO 29841:2009.[32,33] A miniaturized chromatography column of silica gel 60 at 5% moisture was used to separate the pheophytins. Separated sample was dissolved in 200 μL of acetone and analyzed by HPLC with a mobile phase of water:methanol:acetone/4:36:60 using a Phenomonex Luna 5 μ silica column (250 × 4.60 mm). Separated components were measured at 410 nm using a photodiode array detector, and data was analyzed with Waters Empower Pro version 5.00.

*Sensory Analyses.* The sensory profiles of the oils collected in the study were evaluated following official IOC procedures by the Taste Panel of the Australian Oils Research Laboratory (AORL).[25]

The sensory attributes which were rated under official IOC procedures were defects (fusty/muddy sediment, musty/humid/earthy, winey/vinegary/acid/sour, rancid, and other) and desirable attributes (fruity (green and ripe), pungent, and bitter). Olive oils were graded to either "EVOO" or other grades by the sensory taste panel.

**Artificial Neural Networks.** The mathematical model designed to classify olive oil samples according to their quality is based on nonlinear ANNs. These intelligent algorithms have been used to link chemical information from 220 olive oil samples, which came from different geographical origins and olive types with the sensory results provided by trained panelists to achieve a potential tool for accurate quality control. Of the 220 olive oil samples, the panelists considered 94 of them to be EVOOs.

The specific type of ANN that has been selected to fulfill the objective is a supervised multilayer perceptron (MLP), which relies on target data to be adequately optimized.[34] These particular ANNs have offered successful results in terms of accurate estimations and classifications in multiple fields such as chemistry or food technology.[11,19,35,36] It is important to note that these tools are designed to carry out accurate interpolations; in other words, they originate large errors when tests are done with data points outside the operational window of the ANN.[19] For this reason, the final optimized model will perform adequately with samples that possess the nature of some of those included into the training data set. This confers a great additional value to the vast analytical work carried out during sampling and to the wide variety of olive oil types found in the database assembled in terms of olive variety, geographic origin, and quality grade.

MLPs possess a layer topology. The first one is the input layer, which is formed by nodes that are used to introduce all the desired independent variables into the nonlinear model.[37] In this case, the inputs correspond to six chemical parameters (FFAs, PV, $K_{232}$, $K_{268}$, DAGs, and PPPs) from the olive oil samples. The second layer of the MLP contains neurons, which are the calculation centers of the ANN, and it is known as the hidden layer. The hidden neuron number (HNN) should be optimized appropriately to get the most out of the MLP (vide infra).[38] Finally, the third and last layer is the output layer, which is also formed by neurons. These define the dependent variables of the mathematical tool, which in the end allow evaluation of the statistical performance of the ANN.[35] In the designed model, the single output resembles the quality of the olive oil samples.

Every node from the input layer is connected to all the neurons from the hidden layer, while these last ones are also connected to each neuron from the output layer. Each individual connection is controlled by a specific weighted coefficient or weight, which initially is a random value but is optimized during the training phase of the MLP. This optimization is crucial because the final performance of the model (in

this case, correct olive oil classification percentage) will strictly depend on it.[39] Additionally, so it can take place, a suitable training function should be selected according to the database variables and size (vide infra).

Prior to training the model, and so its optimization can be successfully carried out, the initial database (220 data points) was randomly divided into two. This led to the appearance of training and verification data sets, which approximately possessed 85% and 15% of the data points, respectively. The training data set is comprised of the data that the MLP employs to modify the values of the weights in order to attain lower estimation or, in this case, classification errors. On the other hand, the role of the verification data set is to ensure that the system is not only able to correctly classify data points from the training data set but also capable of correctly classifying data outside it, which allows assessing the generalization and applicability range of the designed, and now optimized, ANN. This second data set is vital in order to avoid obtaining overfit models that are not accurate for samples outside the data used to train it because the mentioned second data set is never involved in the weight modification process.[19]

There are additional parameters, different from the weights, which should be optimized to get the best possible results. For instance, the HNN has been optimized following a heuristic approach,[35] testing possibilities from 10 to 25 neurons due to the size of the database. The HNN selected is the one that provides the most accurate model. This step is very important because ANNs with a low HNN will offer a poor learning capability, while an excessive one may lead toward overfit systems.[38] Moreover, other parameters that should be optimized are the Marquardt adjustment parameter (Lc), the decrease factor for Lc (Lcd), and the increase factor for Lc (Lci).[40] The Lc parameter acts like the learning coefficient in usual back-propagation algorithms. Its value is modified by Lcd and Lci up until the Lc changes originate a less accurate MLP.[38] These three parameters have been optimized following a "Box-Wilson Central Composite Design $2^3$ + star points" experimental design,[38] and, once again, the combination selected has been the one that provided the best statistical performance. The range analyzed for Lc and Lcd was between 0.001 and 1, while for Lci it was between 2 and 100.[35]

All of the ANN-related calculations have been completed using Matlab version 7.0.1.24704 (R14),[40] while experimental design has been carried out with Statgraphics Centurion 16.1.18.

## RESULTS AND DISCUSSION

**Selection and Optimization of Multilayer Perceptron Parameters.** Design of an ANN requires a series of steps that must be followed to attain the most accurate nonlinear model possible. First of all, the architecture or topology of the MLP must be defined by selecting the independent and dependent variables as well as optimizing the HNN. Furthermore, a well-suited training function must be chosen depending on the database, and a set of ANN parameters (Lc, Lcd, and Lci) should be optimized.

*Topology of the Model.* The independent variables, or MLP inputs, selected have been the six chemical parameters obtained from different measurements of all the olive oil samples. They are FFA, PV, $K_{232}$, $K_{268}$, DAG, and PPP. On the other hand, the single dependent variable, or output, of the ANN is the quality evaluation of the olive oil provided by trained panelists. The output was transformed into a qualitative response based on the results from the panel. Ones (1s) were assigned to the samples that were identified as EVOOs by the panelists, while zeroes (0s) were given to all other lower quality samples (VOO and OVOO) found in the database.

After testing all HNN possibilities between 10 and 25, it was observed that the accuracy of the model was stable throughout the whole range. For example, when physicochemical property estimation is the goal of the MLP, every different HNN provides different prediction errors.[35,38] However, when single-output classifications are attempted, as is the case, and estimations are converted into 1s or 0s, the different HNNs provide very similar results. In fact, all HNN tests offered the same exact accuracy in terms of percentage classification of olive oil samples according to their quality. HNN 10 was finally chosen in order to lower the required calculations and obtain a more manageable model. It is worth mentioning that the optimal threshold found was 0.64, and therefore, estimations >0.64 were turned into 1s and ≤0.64 into 0s.

In Figure 1, a schematic representation of the architecture of the designed and optimized MLP can be seen.

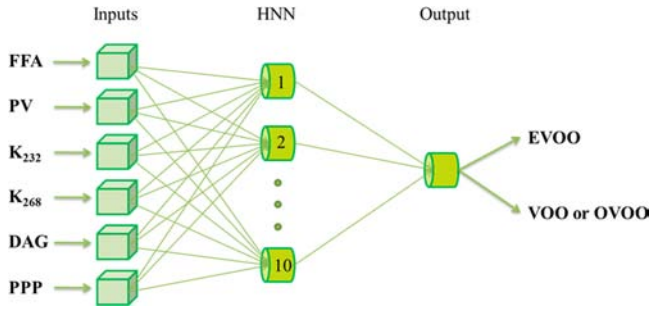


**Figure 1.** Schematic representation of the topology of the designed MLP. It is formed by six input nodes that correspond with chemical parameters measured from different olive oil samples, 10 hidden neurons, and a single output neuron, which classifies samples according to their quality.

*Training Function Selection.* Correct selection of a training function that is well suited for accomplishing the desired task is essential. Due to the database size and attempted goal, training function trainBR (Bayesian regularization function) has been designated. It is a modified version of the Levenberg–Marquardt training algorithm and employed to create MLPs that are able to generalize well, thus avoiding overfit systems. It reduces the difficulty of determining the optimum network topology and regularly updates the values of the weights turning trainBR into a compelling and an adaptable option.[41]

*Neural Network Parameter Optimization.* An experimental design based on a "Box-Wilson Central Composite Design $2^3$ + star points" was carried out in order to define the combination of Lc, Lcd, and Lci that offers the model with the highest accuracy (greatest correct classification rate). Nonetheless, similar to the HNN, the correct classification percentage did not practically vary with different values of these parameters due to the defined objective. Therefore, the following optimized values were selected: Lc = 0.005, Lcd = 0.1, and Lci = 10.

**Statistical Performance of the Model.** In order to evaluate the statistical performance of the designed and optimized MLP and to confirm that it is applicable for the entire database, a *K*-fold cross-validation ($K = 6$) was implemented so every data point is used to test the model (except for data points with the highest or the lowest values of any independent variable to limit the MLP to interpolations (vide supra); for this reason, only 203 out of 220 data points have been used to test the model).[35] The main and only difference between all six tests carried out is that the verification data set is completely different for each one of the ANNs (randomly divided into six). The role of these verification data sets is to permit the design of widely applicable models that can generalize well. They have been used to test each individual

system as well, due to the fact that they are not involved in the weight optimization process (vide supra), thus avoiding potential overfitting issues.[42] The results for all 6 tests can be found in Table 1.

**Table 1. Statistical Performance of the MLP Represented by the Results of the *K*-Fold Cross-Validation**

| | classification accuracy | |
|---|---|---|
| tests ($K$ = 6) | correctly classified | percentage of corrects (%) |
| 1 | 32/33 | 97.0 |
| 2 | 30/34 | 88.2 |
| 3 | 33/34 | 97.0 |
| 4 | 34/34 | 100 |
| 5 | 34/34 | 100 |
| 6 | 32/34 | 94.1 |
| total/average | 195/203 | 96.0 |

As shown, the MLP offers accurate results for every different data set employed to test the tool, proving its wide applicability range and generalization capability. It shows a correct classification rate of about 96% on average, verifying that the chemical information provided has a clear relationship with the results from the trained panelists.

Nevertheless, to further validate this statement, three blind tests were carried out. In this case, the database has been randomly divided into three data sets: training, verification, and simulation (or internal validation) data sets containing 80%, 10%, and 10% of the data points, respectively.[43] The MLP was optimized following the same procedure previously explained using the training and verification data sets. The only difference is that now the model was tested with the simulation data set, which has never been seen by the ANN for any purpose, instead of with the verification one. The results of these three internal validations are shown in Table 2.

**Table 2. Statistical Performance of the MLP for Three Independent Blind Tests**

| | classification accuracy | |
|---|---|---|
| blind tests | correctly classified | percentage of corrects (%) |
| 1 | 20/22 | 90.9 |
| 2 | 21/22 | 95.4 |
| 3 | 22/22 | 100 |
| total/average | 63/66 | 95.4 |

These results imply that the tool designed could be employed as an accurate quality control for diverse olive oil samples outside of the database employed in the present study. The tool could be set as a yes/no (EVOO/not EVOO) test for olive oil samples prior to being evaluated by trained panelists. This could allow lowering the amount of necessary tastings when the panelists are looking for only specific types of olive oil, classified by their quality, for sensory analysis.

The successful performance and accuracy of the MLP model corroborates that there is at least an indirect relation between the selected independent variables (six chemical parameters) and the results from the sensory analyses that can be adequately interpreted through nonlinear modeling. The manifestation of negatively affecting factors such as excessive amounts of fatty acids, peroxides, or PPPs, elevated absorption indices, and low quantities of 1,2-DAGs[21,23,24,29] can be related to low-quality grade olive oils which present one or more of the main sensory defects (vinegary, humid, fusty, and/or rancid). In other words, the appearance and emission of volatile organic compounds that characterize determined olive oil defects is nonlinearly correlated with the variables selected to train the MLP model presented.

It must be noted that ANNs are dynamic tools that can improve their performance and robustness with new data. In other words, tests carried out with new data points from more olive oil samples can be incorporated into the model leading to an enhanced version of the nonlinear model, with a greater applicability span. Ideally, in the end there will be enough data from such a wide variety of olive oils and panel results that the tool will be able to convert a subjective interpretation into an objective classification.

In summary, in the present article, a nonlinear model based on artificial neural networks has been designed and optimized to discriminate between extra virgin olive oil samples and other lower quality ones. The mathematical tool employs six chemical parameters (percentage of free acidity, peroxide value, two UV absorption parameters ($K_{232}$ and $K_{268}$), 1,2-diacylglycerol content, and pyropheophytins) as independent variables to accurately classify the olive oil samples. Two tests were carried out to determine the statistical performance of the model: (a) a *K*-fold cross-validation ($K$ = 6) that showed 96.0% of correct classifications and (b) three blind tests which provided 95.4% on average. These successful results prove the existence of a relationship between the six parameters utilized and the quality of the olive oil, leading to potential design of an objective evaluating method of the quality of diverse olive oil samples.

## AUTHOR INFORMATION


### Corresponding Author

*Tel.: +34 91 394 42 44; Fax: +34 91 394 42 43. E-mail: jstorre@ucm.es.



### Funding

The research leading to these results has received funding from the European Union Seventh Framework Programme (FP7/2007−2013) under grant agreement no. HEALTH-F4-2011-258868.

### Notes

The authors declare no competing financial interest.


## REFERENCES


(1) Willett, W. C.; Sacks, F.; Trichopoulou, A.; Drescher, G.; Ferroluzzi, A.; Helsing, E.; Trichopoulos, D. Mediterranean Diet Pyramid−A Cultural Model for Healthy Eating. *Am. J. Clin. Nutr.* **1995**, *61*, S1402−1406.

(2) Kris-Etherton, P. M.; Hecker, K. D.; Bonanome, A.; Coval, S. M.; Binkoski, A. E.; Hilpert, K. F.; Griel, A. E.; Etherton, T. D. Bioactive compounds in foods: Their role in the prevention of cardiovascular disease and cancer. *Am. J. Med.* **2002**, *113*, 71−88.

(3) Estruch, R.; Martínez-González, M. A.; Corella, D.; Salas-Salvado, J.; Ruiz-Gutiérrez, V.; Coyas, M. I.; Fiol, M.; Gómez-García, E.; López-Sabater, M. C.; Vinyoles, E.; Aros, F.; Conde, M.; Lahoz, C.; Lapetra, J.; Sáez, G.; Ros, E. Effects of a Mediterranean-style diet on cardiovascular risk factors - A randomized trial. *Ann. Int. Med.* **2006**, *145*, 1−11.

(4) Owen, R. W.; Giacosa, A.; Hull, W. E.; Haubner, R.; Spiegelhalder, B.; Bartsch, H. The antioxidant/anticancer potential of phenolic compounds isolated from olive oil. *Eur. J. Cancer* **2000**, *36*, 1235−47.

(5) Mateos, R.; Espartero, J. L.; Trujillo, M.; Ríos, J. J.; León-Camacho, M.; Alcudia, F.; Cert, A. Determination of phenols, flavones,

and lignans in virgin olive oils by solid-phase extraction and high-performance liquid chromatography with diode array ultraviolet detection. *J. Agric. Food Chem.* **2001**, *49*, 2185−2192.
(6) Morales, M. T.; Ríos, J. J.; Aparicio, R. Changes in the volatile composition of virgin olive oil during oxidation: Flavors and off-flavors. *J. Agric. Food Chem.* **1997**, *45*, 2666−2673.
(7) Zhu, H. J.; Li, X. Q.; Shoemaker, C. F.; Wang, S. C. Ultrahigh Performance Liquid Chromatography Analysis of Volatile Carbonyl Compounds in Virgin Olive Oils. *J. Agric. Food Chem.* **2013**, *61*, 12253−12259.
(8) Baeten, V.; Meurens, M.; Morales, M. T.; Aparicio, R. Detection of virgin olive oil adulteration by Fourier transform Raman spectroscopy. *J. Agric. Food Chem.* **1996**, *44*, 2225−2230.
(9) Torrecilla, J. S.; Cancilla, J. C.; Matute, G.; Díaz-Rodríguez, P.; Flores, A. I. Self-organizing maps based on chaotic parameters to detect adulterations of extra virgin olive oil with inferior edible oils. *J. Food Eng.* **2013**, *118*, 400−405.
(10) López-Feria, S.; Cardenas, S.; García-Mesa, J. A.; Valcárcel, M. Classification of extra virgin olive oils according to the protected designation of origin, olive variety and geographical origin. *Talanta* **2008**, *75*, 937−943.
(11) Torrecilla, J. S.; Cancilla, J. C.; Matute, G.; Díaz-Rodríguez, P. Neural network models to classify olive oils within the protected denomination of origin framework. *Int. J. Food Sci. Technol.* **2013**, *48*, 2528−2534.
(12) Escuderos, M. E.; Sánchez, S.; Jiménez, A. Quartz Crystal Microbalance (QCM) sensor arrays selection for olive oil sensory evaluation. *Food Chem.* **2011**, *124*, 857−862.
(13) García-González, D. L.; Aparicio, R. Classification of different quality virgin olive oils by metal-oxide sensors. *Eur. Food Res. Technol.* **2004**, *218*, 484−487.
(14) Poulli, K. I.; Mousdis, G. A.; Georgiou, C. A. Classification of edible and lampante virgin olive oil based on synchronous fluorescence and total luminescence spectroscopy. *Anal. Chim. Acta* **2005**, *542*, 151−156.
(15) Ruiz-Samblás, C.; Cuadros-Rodríguez, L.; González-Casado, A.; García, F. D. R.; de la Mata Espinosa, P.; Bosque-Sendra, J. M. Multivariate analysis of HT/GC-(IT)MS chromatographic profiles of triacylglycerol for classification of olive oil varieties. *Anal. Bioanal. Chem.* **2011**, *399*, 2093−2103.
(16) López-Feria, S.; Cardenas, S.; García-Mesa, J.; Valcárcel, M. Usefulness of the direct coupling headspace-mass spectrometry for sensory quality characterization of virgin olive oil samples. *Anal. Chim. Acta* **2007**, *583*, 411−417.
(17) Garrido Delgado, R.; Arce, L.; Valcárcel, M. Multi-capillary column-ion mobility spectrometry: a potential screening system to differentiate virgin olive oils. *Anal. Bioanal. Chem.* **2012**, *402*, 489−498.
(18) Baldwin, E. A.; Bai, J. H.; Plotto, A.; Dea, S. Electronic Noses and Tongues: Applications for the Food and Pharmaceutical Industries. *Sensors* **2011**, *11*, 4744−4766.
(19) Wang, B.; Cancilla, J. C.; Torrecilla, J. S.; Haick, H. Artificial Sensing Intelligence with Silicon Nanowires for Ultraselective Detection in the Gas Phase. *Nano Lett.* **2014**, *14*, 933−938.
(20) Cajka, T.; Hajslova, J.; Pudil, F.; Riddellova, K. Traceability of honey origin based on volatiles pattern processing by artificial neural networks. *J. Chromatogr. A* **2009**, *1216*, 1458−1462.
(21) Olive oils and olive-pomace oils. AS 5264-2011. Australian Standard. Australia, 2011.
(22) *Trade standard applying to olive oils and olive pomace oils*; International Olive Council (IOC): Madrid, Spain, 2013; T.15/NC No.3/Rev.7.
(23) *United States Standards for Grades of Olive Oil and Olive-Pomace Oil*; USDA: Washington D.C., 2010.
(24) Guillaume, C.; Gertz, C.; Ravetti, L. Pyropheophytin a and 1,2-Diacyl-glycerols Over Time Under Different Storage Conditions in Natural Olive Oils. *J. Am. Oil Chem. Soc.* **2014**, *91*, 697−709.
(25) Sensory analysis of olive oil. COI/T.20/Doc. 15, 2011. International Olive Oil Council, Spain.
(26) Method Ca 5a-40: Free Fatty Acids. *Official methods and recommended practices of the American Oil Chemists' Society*, 5th ed.; AOCS Press: Champaign, 1998.
(27) *ISO 3960:2007: Animal and vegetable fats and oils-Determination of peroxide value-Iodometric (visual endpoint determination)*; International Organization for Standardization (ISO): Geneva, 2007.
(28) Spectrophotometric investigation in the ultraviolet. *COI/T.20/Doc. 19*; International Olive Oil Council: Spain, 2008.
(29) Masao, S.; Naoto, K.; Yoshinobu, N.; Noboru, M.; Yoshihisa, K.; Ichiro, T.; Isabel, B.; Catalina, M.; Francisca, B. Acidity and DAG content of olive oils recently produced on the Island of Mallorca. *J. Am. Oil Chem. Soc.* **2008**, *85*, 1051−1056.
(30) Gertz, C.; Fiebig, H. J. Isomeric diacylglycerols-Determination of 1,2-and 1,3-diacylglycerols in virgin olive oil. *Eur. J. Lipid Sci. Technol.* **2006**, *108*, 1066−1069.
(31) *ISO 29822:2009 (E): Vegetable fats and oil-Isomeric diacylglycerols-Determination of relative amounts of 1,2- and 1,3-diacylglycerols*; International Organization for Standardization (ISO): Geneva, 2009.
(32) Gertz, C.; Fiebig, H. J. Pyropheophytin a-Determination of thermal degradation products of chlorophyll a in virgin olive oil. *Eur. J. Lipid Sci. Technol.* **2006**, *108*, 1062−1065.
(33) *ISO 29481:2009 (E): Vegetable fats and oils-Determination of the degradation products of chlorophylls a and a' (pheophytins a, a' and pyropheophytins)*; International Organization for Standardization (ISO), Geneva, 2009.
(34) Hush, D. R.; Horne, B. G. Progress in supervised neural networks. *IEEE Signal Process Mag.* **1993**, *10*, 8−39.
(35) Díaz-Rodríguez, P.; Cancilla, J. C.; Plechkova, N. V.; Matute, G.; Seddon, K. R.; Torrecilla, J. S. Estimation of the refractive indices of imidazolium-based ionic liquids using their polarisability values. *Phys. Chem. Chem. Phys.* **2014**, *16*, 128−134.
(36) Torrecilla, J. S.; Otero, L.; Sanz, P. D. A neural network approach for thermal/pressure food processing. *J. Food Eng.* **2004**, *62*, 89−95.
(37) Torrecilla, J. S.; Tortuero, C.; Cancilla, J. C.; Díaz-Rodríguez, P. Estimation with neural networks of the water content in imidazolium-based ionic liquids using their experimental density and viscosity values. *Talanta* **2013**, *113*, 93−98.
(38) Díaz-Rodríguez, P.; Cancilla, J. C.; Matute, G.; Torrecilla, J. S. Determination of Physicochemical Properties of Pyridinium-Based Ionic Liquid Binary Mixtures with a Common Component through Neural Networks. *Ind. Eng. Chem. Res.* **2014**, *53*, 1015−1019.
(39) Knoerzer, K.; Juliano, P.; Roupas, P.; Versteeg, C. *Innovative Food Processing Technologies: Advances in Multiphysics Simulation*. Wiley-Blackwell; Oxford (UK), 2011.
(40) Demuth, H.; Beale, M.; Hagan, M. *Neural Network Toolbox for Use with MATLAB User's Guide*, Version 4.0.6, Ninth printing Revised for Version 4.0.6 (Release 14SP3); The MathWorks, Inc.: Natick, MA, 2005.
(41) Torrecilla, J. S.; Aragón, J. M.; Palancar, M. Optimization of an Artificial Neural Network by Selecting the Training Function. Application to Olive Oil Mills Waste. *Ind. Eng. Chem. Res.* **2008**, *47*, 7072−7080.
(42) Cancilla, J. C.; Díaz-Rodríguez, P.; Izquierdo, J. G.; Bañares, L.; Torrecilla, J. S. Artificial neural networks applied to fluorescence studies for accurate determination of N-butylpyridinium chloride concentration in aqueous solution. *Sens. Actuators, B: Chem.* **2014**, *198*, 173−179.
(43) Torrecilla, J. S.; Tortuero, C.; Cancilla, J. C.; Díaz-Rodríguez, P. Neural networks to estimate the water content of imidazolium-based ionic liquids using their refractive indices. *Talanta* **2013**, *116*, 122−126.

showed an average BaP content level of 1.62 μg/kg of chocolate sweet.[13] Representative analyses on the occurrence of PAH4 in cocoa, derived products, and chocolate products on the German market were not available at the start of this study.

The pertinent literature contains a plethora of analysis methods for detecting the various relevant PAH individual substances. These methods are based on gas chromatography measurement procedures[21−26] and detection procedures using UV, fluorescence,[14−19] and MS.[20] GC-MS is the method most frequently used to detect PAH.[27] HPLC coupled with mass spectrometry (LC-MS) is only seldom used due to the nonionic and unpolar property of PAH.[20,28]

Currently, the European cocoa and chocolate industry is aware of the recent discussion at the European level about the possibility of a review into how to express PAH levels detected in cocoa beans and derived products. The ongoing discussion was triggered by the results of a recent proficiency test carried out by the European Reference Laboratory (EU-RL).[29] This showed that the results obtained in laboratories are less favorable if the analyses are conducted on a fat basis rather than on a product basis. It seems that converting the analytical results obtained on a product basis into results on a fat basis leads to variations in the final results obtained. For this reason it is considered that the best approach to addressing this issue is to use a standardized "fat extraction method" for cocoa beans and derived products. The current study consistently sidestepped this issue by using only cocoa butter obtained from products by way of cold extraction for PAH analysis. This did away with the need to use an additional fat determination method.

The objective of this research work was to develop a suitable internal standard (ISTD) method of routine analysis for quantitating the relevant PAH in cocoa and cocoa products and to give a situation assessment of the occurrence of these substances in the tested products. Due to the entry into force on April 1, 2013, of Regulation (EU) No. 835/2011, amending the EU Contaminants Regulation with regard to "cocoa beans and derived products" and stipulating a maximum level of 5.0 μg/kg fat for BaP and 35 μg/kg fat for PAH4 (30 μg/kg fat for PAH4 as of 01.04.2015), the focus of analytical methods was especially placed on BaP and PAH4 levels in cocoa, derived products, and chocolate products. In addition, a combined pool of 218 samples was analyzed, composed of samples of cocoa butter, cocoa masses, and raw cocoa plus monitoring samples of finished cocoa and chocolate products from the German market. Specific examination of cocoa butter samples from various growing and harvest years was also aimed at tracing the development and pattern of PAH4 content levels from 1999 to 2012.

## MATERIALS AND METHODS

**Samples.** In the period from 2010 to 2012, a total of 218 samples were analyzed for PAH4: of these, 12 were raw cocoa beans, 22 were cocoa masses, 67 were cocoa butter samples, and 117 were cocoa and chocolate products. The cocoa beans and semifinished cocoa products (cocoa masses and butter) came from the main growing regions in Africa, Asia, and America, in the harvest period from 1999 to 2012. The cocoa products and chocolate products were purchased quarterly in retail shops in the period from 2009 to 2012.

Definitions of the cocoa and chocolate products we analyzed in our research work are as follows: **Cocoa beans** (including raw cocoa) are the unshelled, fermented, and dried seeds of *Theobroma cacao* L. They have a thin shell (**cocoa shell**, botanical description: seed shell consisting of testa and rest of pulp). **Cocoa nibs** (botanical description: seed leaves [cotyledons] without seed shell) are the roasted, unshelled, mostly already broken up cocoa kernels. **Cocoa mass** is made up of finely ground cocoa nibs; **cocoa powder** is the finely ground cocoa press cake, which, in addition to **cocoa butter**, is what remains after pressing out the **cocoa mass**.[30] Cocoa nibs, cocoa masses, cocoa powder, and cocoa butter are collectively referred to as **semifinished cocoa products**. The term **cocoa products and chocolate products** covers products defined under Annex 1 of the German Cocoa Regulation, such as whole milk chocolate, dark chocolate, and chocolate coating.[31] The term cocoa and cocoa products used in this research work is a collective term and implies all products defined in this section.

**Chemicals.** The solvents used were petroleum benzene, *n*-hexane, and ethanol for analysis, as well as dichloromethane and acetonitrile, both of HPLC grade (>99.9%). Other reagents and materials used were potassium hydroxide and Strata EPH (200 μ, 70 Å) 5 g/20 mL (part 8B-SO31_LEG), Giga tube. All of the solvents, reagents, and materials mentioned are commercially available from Phenomenex (Aschaffenburg, Germany), Sigma-Aldrich (Steinheim, Germany), and Merck (Darmstadt, Germany).

The following PAH standards were used for the identification and quantitation of the PAH4 present in the samples: benzo[*a*]anthracene, chrysene, benzo[*b*]fluoranthene, benzo[*a*]pyrene, and benzo[*b*]-chrysene, which was used as an internal standard. All standards were obtained from Dr. Ehrenstorfer (Augsburg, Germany) and LCG (Wesel, Germany).

**Methodology.** To extract the cocoa butter, the samples are first defatted; depending on the respective matrix, this means weighing 10−15 g (raw cocoa, cocoa nibs, cocoa mass, and chocolate) or 50 g (cocoa powder) into a 250 mL centrifuge tube. Seventy milliliters of petroleum benzene and a magnetic stir bar are added to the samples. This mixture is then stirred for 1 h and centrifuged. The supernatant is transferred via pipet into a 500 mL round flask. This process is repeated three times, and the combined petroleum benzene residues are removed via rotary evaporator. The isolated fat, which is dried overnight in a desiccator cabinet (at 50 °C), can subsequently be used for further PAH analysis. Cocoa butter samples are melted at approximately 50 °C and can be immediately used for PAH analysis without additional preparation.

For saponification, 2 g of cocoa butter was weighed, spiked with 5 ng of benzo[*b*]chrysene as internal standard, and incubated for 30 min. After the addition of 8 mL of ethanol and 2 mL of potassium hydroxide solution (10%), the solution was heated at 60 °C for 30 min in an ultrasonic bath. After saponification, 5 mL of demineralized water was added and, after cooling, 10 mL of hexane. After centrifugation (20 °C, 2000 rpm), the upper hexane phase was put on a Strata EPH Giga Tube (conditioned with 30 mL of hexane). This extraction procedure was repeated twice with 8 and 7 mL of hexane. PAH were eluted with 20 mL of dichloromethane, and the solvent was removed using a rotary evaporator and further evaporated to just dryness under a nitrogen stream. The residue was redissolved in 2 mL of acetonitrile and finally transferred into an autosampler vial for HPLC-FD-analysis.

For the identification and quantitation of PAH4, extracts were analyzed using HPLC coupled to a fluorescence detector (FD). The HPLC system consists of a gradient pump, a column oven, an autosampler, and a fluorescence detector (Dionex Ultimate 3000, Idstein, Germany). A Multosphere PAH-III column (250 × 4.6 mm i.d., CS-Chromatographie Service, Langerwehe, Germany) was used along with a precolumn filled with the same material (20 × 4 mm). Separation was performed using the following gradient: acetonitrile/water (85:15, v/v) for 13.5 min, followed by a 2 min ramp to 100% acetonitrile, this solvent being further maintained for 15 min. The total flow rate was 1 mL/min. The analytical column was placed in an oven, and the following temperature program was performed: 25 °C for 4 min, followed by direct heating to 45 °C. Detection was performed at selected excitation and emission wavelengths, programmed as follows: 0−8.3 min, 290/470 nm; 8.3−11 min, 270/390 nm; 11−11.5 min, 290/470 nm.

**Table 1. Validation Parameters Obtained for the Four Individual PAH**

| parameter | BaA | Chr | BbF | BaP |
|---|---|---|---|---|
| calibration range (μg/kg) | 0.02−15.57 ($r^2$ > 0.999) | 0.02−9.45 ($r^2$ > 0.999) | 0.13−36.32 ($r^2$ > 0.999) | 0.17−67.33 ($r^2$ > 0.999) |
| recovery rate (%) | 81−101 | 66−91 | 94−103 | 90−100 |
| limit of detection (LOD, μg/kg) | 0.01 | 0.01 | 0.04 | 0.07 |
| limit of quantitation (LOQ, μg/kg) | 0.02 | 0.02 | 0.13 | 0.17 |
| intraday accuracy ($N$ = 12, %) | 10 | 13 | 7 | 6 |
| interday precision ($N$ = 12, %) | 11 | 13 | 9 | 7 |
| $HORRAT_r$ | 0.66 | 0.88 | 0.46 | 0.42 |

**Table 2. Overview of Raw Cocoa and Semifinished Cocoa Products (Cocoa Butter and Cocoa Masses) Examined within the Scope of This Study[a]**

| treatment | (μg/kg) | BaA | Chr | BbF | BaP | PAH4 |
|---|---|---|---|---|---|---|
| **Cocoa Butter** | | | | | | |
| all ($N$ = 67) | mean | 4.46 | 6.05 | 0.98 | 0.96 | 12.44 |
| | median | 3.40 | 4.18 | 0.70 | 0.66 | 9.94 |
| | range | 0.72−32.77 | 1.12−45.03 | ≤LOD[b]−6.86 | ≤LOD[b]−7.86 | 2.09−92.53 |
| deodorized ($N$ = 29) | mean | 3.07 | 3.81 | 0.84 | 0.86 | 8.55 |
| | median | 2.27 | 3.27 | 0.55 | 0.48 | 6.32 |
| | range | 0.76−13.42 | 1.32−11.23 | ≤LOD[b]−2.32 | 0.14−3.82 | 2.67−24.21 |
| not deodorized ($N$ = 8) | mean | 5.70 | 6.57 | 1.08 | 0.94 | 14.29 |
| | median | 5.93 | 5.65 | 0.64 | 0.63 | 13.56 |
| | range | 1.74−9.99 | 2.26−14.16 | 0.32−2.28 | 0.33−2.03 | 4.82−25.73 |
| unknown ($N$ = 30) | mean | 5.47 | 8.07 | 1.24 | 1.09 | 15.72 |
| | median | 4.16 | 5.51 | 1.12 | 0.92 | 12.20 |
| | range | 0.72−32.77 | 1.12−45.03 | ≤LOD[b]−6.86 | ≤LOD[b]−7.86 | 2.07−92.53 |
| **Cocoa Mass** | | | | | | |
| all ($N$ = 22) | mean | 1.32 | 2.59 | 0.33 | 0.32 | 4.57 |
| | median | 1.04 | 2.48 | 0.29 | 0.26 | 3.80 |
| | range | 0.71−3.37 | 1.18−5.56 | ≤LOD[b]−1.06 | ≤LOD[b]−0.76 | 2.59−9.29 |
| alkalized ($N$ = 3) | mean | 0.88 | 1.50 | 0.26 | 0.28 | 2.83 |
| | median | 0.80 | 1.51 | 0.26 | 0.34 | 2.61 |
| | range | 0.75−1.08 | 1.39−1.60 | ≤LOD[b]−0.29 | 0.12−0.38 | 2.56−3.32 |
| unknown ($N$ = 19) | mean | 1.39 | 2.76 | 0.36 | 0.35 | 4.84 |
| | median | 1.13 | 2.50 | 0.31 | 0.26 | 3.83 |
| | range | 0.71−3.37 | 1.18−5.56 | 0.17−1.06 | ≤LOD[b]−0.84 | 2.59−9.29 |
| **Raw Cocoa** | | | | | | |
| ($N$ = 12) | mean | 2.18 | 3.49 | 1.27 | 1.28 | 8.21 |
| | median | 0.86 | 2.03 | 0.41 | 0.24 | 2.91 |
| | range | 0.27−9.55 | 0.47−15.89 | ≤LOD[b]−8.86 | ≤LOD[b]−9.98 | 0.88−44.28 |

[a]All content levels are on a fat basis. [b]Calculation of mean and median was performed using 50% LOD (LOD: BaA = 0.01 μg/kg fat, chrysene = 0.01 μg/kg fat, BbF = 0.04 μg/kg fat, BaP = 0.07 μg/kg fat).

## RESULTS AND DISCUSSION

**Method Validation.** The presented method was validated on the basis of the guidelines provided by Kromidas.[32] For this purpose a cocoa butter sample without detectable PAH4 content was spiked with a PAH4 solution, prepared in keeping

**Table 3. PAH4 Content Levels in Cocoa Butter Samples from Various Sample Years[a]**

| sample year: | | 1999 | 2010 | 2011/2012 |
|---|---|---|---|---|
| $N$: | | 28 | 26 | 13 |
| PAH4 (μg/kg fat) | maximum | 92.53 | 24.42 | 21.94 |
| | mean | 17.12 | 8.81 | 9.63 |
| | minimum | 2.09 | 2.67 | 3.28 |
| BaP (μg/kg fat) | maximum | 7.86 | 1.61 | 3.82 |
| | mean | 1.00 | 0.78 | 1.27 |
| | minimum | ≤LOD[b] | 0.14 | 0.30 |

[a]All content levels are on a fat basis. [b]LOD: BaP = 0.07 μg/kg fat.

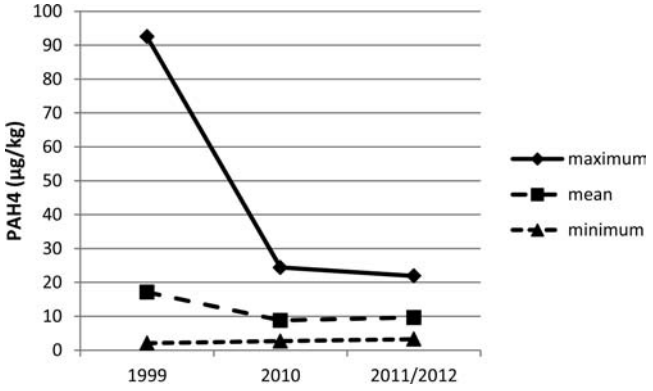


**Figure 1.** Time line of PAH4 content levels in cocoa butter samples for 1999−2012 (for data see Table 3).

Table 4. PAH4 Content Levels in Cocoa and Chocolate Products[a]

| | | milk chocolate/chocolate coatings | dark chocolate/chocolate coatings | cocoa powder | cocoa drink powder | total |
|---|---|---|---|---|---|---|
| | *N*: | 27 | 69 | 12 | 9 | 117 |
| PAH4 (μg/kg fat) | maximum | 17.08 | 17.42 | 21.56 | 19.98 | 21.56 |
| | mean | 10.11 | 5.88 | 8.86 | 9.48 | 6.66 |
| | median | 8.76 | 5.25 | 8.49 | 8.90 | 6.22 |
| | 90th percentile | 11.10 | 10.34 | 13.96 | 15.08 | 11.20 |
| BaP (μg/kg fat) | maximum | 1.96 | 1.56 | 2.44 | 2.92 | 2.92 |
| | mean | 0.70 | 0.57 | 1.07 | 1.00 | 0.69 |
| | median | 0.65 | 0.44 | 0.92 | 0.81 | 0.61 |
| | 90th percentile | 1.41 | 1.02 | 2.07 | 1.81 | 1.35 |

[a]All content levels are on a fat basis.

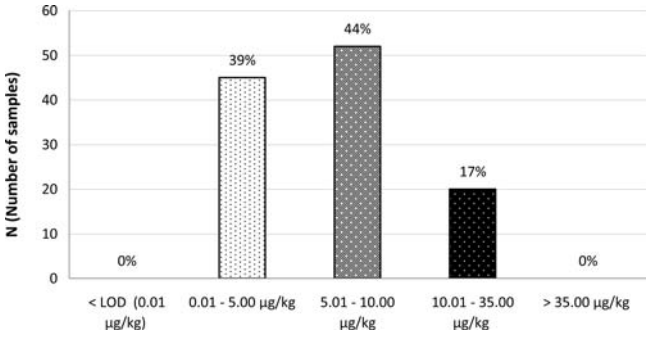


**Figure 2.** Distribution of PAH4 content levels in cocoa and chocolate products (*N* = 117). All content levels are on a fat basis (for data see Table 4).

with the method developed in this study, and analyzed. A series of validation data, such as calibration range, recovery rate, inter- and intraday precision, limit of detection (LOD), and limit of quantitation (LOQ), are compiled in Table 1. As a result, it is noted that the described method for analyzing the PAH4 shows linearity over a wide measuring range, has a good reproducibility, and is extremely sensitive (possessing an LOD of between 0.01 and 0.07 μg/kg). Regulation (EU) No. 836/2011 lays down the analytical performance criteria for the determination of PAH4 in food as recovery rates of 50−120%, LOD ≤ 0.30 μg/kg, LOQ ≤ 0.90 μg/kg, and $HORRAT_r$ < 2 for each of the four substances.[8] The method developed by the LCI optimally fulfills these requirements.

**PAH4 in Raw Cocoa and Semifinished Cocoa Products.** Using the successfully developed and validated analytical methods for determining PAH4, a selection of 101 samples of raw cocoa and semifinished cocoa products was examined. An overall view of the corresponding test results for PAH4 and the individual PAH benzo[*a*]anthracene (BaA), chrysene (Chr), benzo[*b*]fluoranthene (BbF), and benzo[*a*]-pyrene (BaP) is presented in Table 2. The analysis of PAH examinations of cocoa butter samples (*N* = 67) of various origins and treatments produced an overall mean for all cocoa butter samples of 12.44 μg PAH4/kg fat and 0.96 μg BaP/kg fat (median = 9.94 μg PAH4/kg fat and 0.66 μg BaP/kg fat) within a range of 2.09−92.53 μg PAH4/kg fat and <LOD−7.86 μg BaP/kg fat. This large range in PAH measurements is a result of the variation of the analyzed samples of different years from different origins.

The deodorized samples tended to show lower PAH4 content levels than the nondeodorized samples. The reason for this observation is the calcination of volatile compounds within the thermal treatment of the deodoration process.[10]

The maximum PAH4 content of 92.53 μg/kg fat was determined in a cocoa butter sample of unknown origin and treatment. The cocoa mass samples examined within the scope of this study (*N* = 22) contained a mean of 4.57 μg PAH4/kg fat and 0.32 μg BaP/kg fat (median = 3.80 μg/kg PAH4/kg fat and 0.26 μg BaP/kg fat) within a range of 2.59−9.29 μg PAH4/kg fat and <LOD−0.76 μg BaP/kg fat. The alkalized cocoa mass samples included in the examinations (*N* = 3) showed a low mean of 2.83 μg/PAH4/kg fat (median = 2.61 μg PAH4/kg fat). Our examinations for PAH4 of a comparatively small selection of raw cocoa samples (*N* = 12) produced an overall mean of 8.21 μg PAH4/kg fat and 1.28 μg BaP/kg fat (median =2.91 μg PAH4/kg fat and 0.24 μg BaP/kg fat) within a range of 0.88−44.28 μg PAH4/kg fat and <LOD−9.98 μg BaP/kg fat. One raw cocoa sample produced the maximum level measured in this category, showing a PAH4 content of 44.28 μg/kg fat.

All in all, however, among all of the examined product groups, we found a comparatively low contamination level in the 101 analyzed raw cocoa and semifinished cocoa products. Only two samples showed higher PAH content levels. This concerned one cocoa butter sample from the sample year 1999, showing a PAH4 content of 92.53 μg/kg fat, and a raw cocoa sample from the harvest year 2007 originating from Java, showing a PAH4 content of 44.28 μg/kg fat. All other samples were largely well below the legally stipulated maximum levels.

**Trend in PAH4 Content Levels Since 1999.** The cocoa butter samples analyzed for PAH4 during testing originated from various sample years. In particular, samples of cocoa butter stemming from the sample years 1999 and 2010 as well as 2011/2012 were examined. The results of these tests are compiled in Table 3 and Figure 1.

Given the trend in BaP and PAH4 content levels in the analyzed cocoa butter samples, a distinct decrease in these contaminants was observed throughout the sample years 1999−2012. This drop in contamination was particularly significant from 1999 to 2010, almost halving the PAH4 content levels determined in the samples we analyzed, falling from a mean of 17.12 μg/kg fat in 28 cocoa butter samples stemming from 1999 to a mean of 8.81 μg PAH4/kg fat in 26 cocoa butter samples originating from 2010.

The reason for the observed very significant decrease in PAH contents in cocoa butter samples over the years with respect to this project is of course a result of actions the cocoa producers applied, following the instructions of the "Code of Practice for the Reduction of Contamination of Food with PAH from Smoking and Direct Drying Processes" which was released by

Codex Alimentarius Commission in 2009.[33] This Code of Practice gives farmers in the cocoa-producing countries a very explicit toolset to avoid PAH contamination in cocoa beans within the postharvest process such as drying and fermenting.

**PAH4 in Cocoa and Chocolate Products.** In the final part of our research work, 117 samples taken from the food retail trade over the period 2009−2012 were analyzed for their PAH4 and BaP contents. Our test samples included milk chocolate and milk chocolate coatings, dark chocolate and dark chocolate coatings, cocoa-containing drink powders, and cocoa powder. The corresponding analysis results are compiled in Table 4 and Figure 2. It was observed that none of the analyzed samples exceeded the maximum levels set by Regulation (EU) No. 835/2011 of 5 μg/kg fat for BaP and 35 μg/kg fat for PAH4 (30 μg/kg as of April 1, 2015). Moreover, the data show that the samples of cocoa powder and cocoa-containing drink powders with a BaP mean of 1.07 and 1.00 μg/kg fat, respectively, had slightly higher content levels than the samples of milk chocolate and dark chocolate with BaP means of 0.70 and 0.57 μg/kg fat, respectively. However, contamination of the monitoring samples, showing an overall mean of 6.66 μg PAH4/kg fat and a median of 6.22 μg PAH4/kg fat, can be considered very low, particularly taking into account the maximum limits for cocoa beans and derived products set by Regulation (EU) No. 835/2011.

**Resume.** Within the scope of this research project it was shown that, for the period 1999−2012, raw cocoa and semifinished cocoa products (raw cocoa, cocoa masses, and cocoa butter) from various growing years and origins ($N$ = 218) underwent a steep downward trend in contamination with polycyclic aromatic hydrocarbons (PAH), especially in the years 1999−2010. Therefore, the assumption is suggested that the application of the "Code of Practice for the Reduction of Contamination of Food with PAH from Smoking and Direct Drying Processes" in the cocoa-producing countries since 2009 seems to be very successful.

No samples exceeding the maximum limits set by Regulation (EU) No. 835/2011 for cocoa beans and derived products have been found since the regulation came into effect.

## AUTHOR INFORMATION


### Corresponding Author

*(M.R.) Phone: ++49-221-623061. Fax: ++49-221-610477. E-mail: marion.raters@lci-koeln.de.



### Funding

We thank the German Cocoa and Chocolate Foundation (Stiftung der Deutschen Kakao- und Schokoladenwirtschaft) for its financial sponsorship of this project.


### Notes

The authors declare no competing financial interest.

## ACKNOWLEDGMENTS

We thank Saskia Krisch and Sven Rosendahl for their excellent technical support.

## REFERENCES


(1) World Health Organization (WHO). *Summary and Conclusions of the Sixty-Fourth Meeting of the Joint FAO/WHO Expert Committee on Food Additives*; World Health Organization: Rome, Italy, 2005.

(2) Purcaro, G.; Moret, S.; Lanfranco, S. C. Overview on polycyclic aromatic hydrocarbons: occurrence, legislation and innovative determination in foods. *Talanta* **2013**, *105*, 292−305.

(3) IARC (International Agency for Research on Cancer). Polynuclear aromatic compounds. Part 1. Chemical, environmental and experimental data. In *IARC Monographs on the Evaluation of the Carcinogenic Risk of Chemicals to Humans Vol. 32*; Lyon, France, 1983; 77 pp.

(4) IARC (International Agency for Research on Cancer). Overall evaluation of carcinogenicity: an updating of IARC monographs. In *IARC Monographs on the Evaluation of Carcinogenic Risks of Chemicals to Humans, Suppl. 7, Vol. 1−42*; Lyon, France, 1987; 440 pp.

(5) European Commission. Commission regulation (EC) no. 1881/2006 of 19 December 2006 setting maximum levels for certain contaminants in foodstuffs. *Off. J. Eur. Union* **2006**, *L364*, 5−24.

(6) European Commission. Commission regulation (EC) no. 835/2011 of 19 August 2011 amending regulation (EC) no. 1881/2006 as regards maximum levels for polycyclic aromatic hydrocarbons in foodstuffs. *Off. J. Eur. Union* **2011**, *L215*, 4−8.

(7) Wenzl, T.; Simon, R.; Anklam, E.; Kleiner, J. Analytical methods for polycyclic aromatichydrocarbons (PAHs) in food and the environment needed for new food legislation in the European Union. *TrAC, Trends Anal. Chem.* **2006**, *25*, 716−725.

(8) European Commission. Commission regulation (EC) no. 836/2011 of 19 August 2011 amending regulation (EC) no. 333/2007 laying down the methods of sampling and analysis for the official control of the levels of lead, cadmium, mercury, inorganic tin, 3-MCPD and benzo(a)pyrene in foodstuffs. *Off. J. Eur. Union* **2011**, *L215*, 9−16.

(9) Göbel, A. Sachstandsbericht: Polycyclische aromatische Kohlenwasserstoffe (PAH) − Ermitt-lung von Herstellungs- und Verarbeitungsverfahren mit dem Ziel der Reduzierung und Vermeidung von PAH in Lebensmitteln. *J. Verbr. Lebensm.* **2006**, *1*, 271−284.

(10) Lowor, S. T.; Jacquet, M.; Vrielink, T.; Aculey, P.; Cros, E.; Takrama, J. Post-harvest sources of polycyclic aromatic hydrocarbon contamination of cocoa beans: a simulation. *Int. J. AgriSci.* **2012**, *2*, 1043−1052.

(11) Stiftung Warentest. Dunkler Genuss. *Test* **2007**, *12*, 16−22.

(12) Ziegenhals, K.; Speer, K.; Jira, W. Polycyclic aromatic hydrocarbons (PAH) in chocolate on the German market. *J. Verbr. Lebensm.* **2009**, *4*, 128−135.

(13) Kumari, R.; Chaturvedi, P.; Ansari, N. G.; Murthy, R. C.; Patel, D. K. Optimization and Validation of an extraction method for the analysis of polycyclic aromatic hydrocarbons in chocolate candies. *J. Food Sci.* **2012**, *71*, T34−T40.

(14) Van Stijn, F. Determination of PAH in edible oil and fats by donor-acceptor complex chromatograpy and HPLC with fluorescence detection. *J. Chromatogr.* **1996**, *750*, 263−272.

(15) DGF-Einheitsmethode C-III 17 a. Bestimmung von polyzyklischen, aromatischen Kohlenwasserstoffen in Fetten und Ölen. Deutsche Einheitsmethoden zur Untersuchung von Fetten, Fettprodukten. *Tensiden und verwandten Stoffen*, Abteilung C; Wissenschaftliche Verlagsgesellschaft mbH: Stuttgart, Germany, 1997.

(16) Pagluica, G.; Gazotti, T.; Zironi, E.; Serrazanetti, G. P.; Mollica, D.; Rosmini, R. Determination of high molecular mass polycyclic aromatic hydrocarbons in a typical Italian smoked cheese by HPLC-FL. *J. Agric. Food Chem.* **2003**, *51*, 5111−5115.

(17) Maio, G.; Arnold, F.; Franz, H. Analysis of PAH in edible oils by DACC-HPLC coupling with fluorescence detection. *Poster Presented at the 25th International Symposium on Chromatography*, Paris, France, Oct 4−8, LPN 1663; Dionex Corp.: Sunnyvale, CA, USA, 2004.

(18) Martinez-Lopez, S.; Morales-Noe, A.; Pastor-Garcia, A.; Morables-Rubio, A.; de la Guradia, M. Sample preparation in polycyclic aromatic hydrocarbons in olive oils by gel permeation chromatography with fluorescence detection. *J. AOAC Int.* **2005**, *88*, 1247−1254.

(19) Matissek, R.; Steiner, G.; Fischer, M. *Lebensmittelanalytik*, 5th completely reworked ed.; Springer-Spektrum: Berlin, Germany, 2013.

(20) Doerge, D. R.; Clayton, J.; Fu, P. P.; Wolfe, D. A. Analysis of polycyclic aromatic-hyrocarbons using liquid-chromatography particle-beam mass spectrometry. *Biol. Mass Spectrom.* **1993**, *22*, 654−660.

(21) Grimmer, G.; Böhnke, H. Polycyclic aromatic hydrocarbon profile analysis on high protein foods, oils, and fats by gas-chromatography. *J. AOAC Int.* **1975**, *58*, 725−733.
(22) Wang, G. D.; Lee, A. S.; Lewis, M.; Kamath, B.; Archer, R. K. Accelerated solvent extraction and gas chromatography mass spectrometry for determination of polycyclic aromatic hydrocarbons in smoked food samples. *J. Agric. Food Chem.* **1999**, *47*, 1062−1066.
(23) Jira, W. A GC/MS method for the determination of carcinogenic polyphenol aromatic hydrocarbons (PAH) in smoked meat products and liquid smokes. *Eur. Food Res. Technol.* **2004**, *218*, 208−212.
(24) Guillen, M. D.; Sopelana, P.; Partearroyo, M. A. Determination of polycyclic aromatic hydrocarbons in commercial liquid smoke flavorings of different compositions by gas chromatography-mass spectrometry. *J. Agric. Food Chem.* **2000**, *48*, 126−131.
(25) Guillen, M. D.; Sopelana, P.; Palencia, G. Polycyclic aromatic hydrocarbons ald olive pomace oil. *J. Agric. Food Chem.* **2004**, *52*, 2123−2132.
(26) Klein, S.; Knepper, T.; Kron, J. Bestimmung acht polycyclischer aromatischer Kohlenwasserstoffe (PAK) in Lebensmitteln durch Extraktion nach modifizierter DIN EN 12393, schneller GPC- und Kiesegel-Aufreinigung mit nachfolgender GC-Bestimmung. *Lebensmittelchemie* **2011**, *65*, 49−80.
(27) Moret, S.; Lanfranco, S. C. Polycyclic aromatic hydrocarbons in edible fats and oils: occurrence and analytical methods. *J. Chromatogr.* **2000**, *882*, 245−253.
(28) Gonzales-Pinuela, C.; Alonso-Salces, R. M.; Andres, A.; Ortiz, I.; Viquri, J. I. Validated analytical strategy for the determination of polycyclic aromatic compounds in marine sediments by liquid chromatography coupled with diode-array detection and mass spectrometry. *J. Chromatogr.* **2006**, *1129*, 189−200.
(29) Lizak, R.; Zelinkova, Z.; Verlinde, P.; Wenzl, T. Report on the 10th inter-laboratory comparison organised by the European Union Reference Laboratory for Polycyclic Aromatic Hydrocarbons − four marker PAHs in chocolate and cocoa butter. European Union, 2013; ISBN 978-92-79-28532-5 (pdf).
(30) Fincke, A. *Handbuch der Kakaoerzeugnisse. 2. Auflage*; Springer-Verlag: Berlin, Germany, 1965.
(31) KakaoVO. Verordnung über Kakao- und Schokoladenerzeugnisse (Kakaoverordnung) vom15. Dezember 2003 (BGBl. I S. 2738) zuletzt geändert durch Artikel 2 der Verordnung vom 3,. September 2008 (BGBl. I S. 1911).
(32) Kromidas, S. *Handbuch Validierung in der Analytik*; Wiley-VCH: Weinheim, Germany, 2000; pp 1−40.
(33) Codex Alimentarius Commision. *Code of practice for the reduction of contamination of food with polycyclic aromatic hydrocarbons (PAH) from smoking and direct drying processes*; CAC/RCP 68-2009, 2009; pp 1−15.

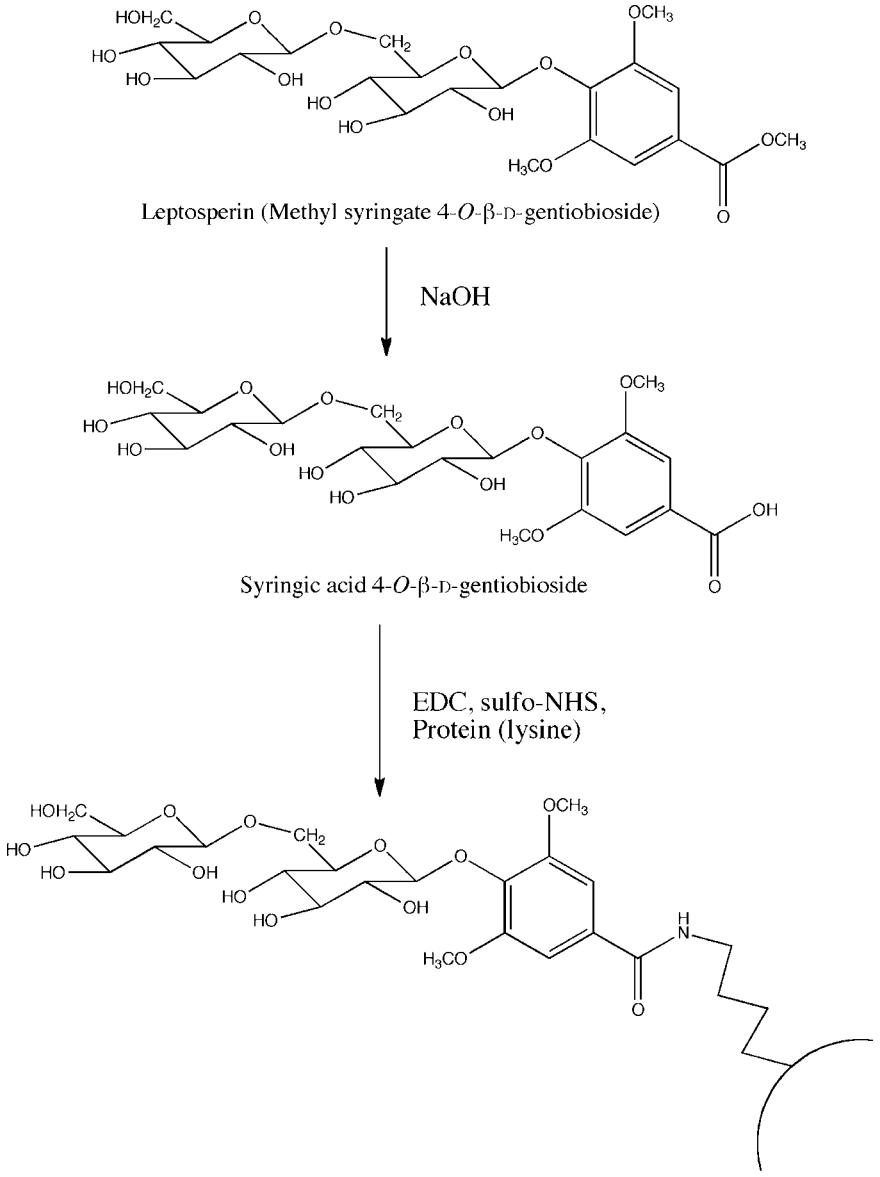


**Figure 1.** Scheme for the preparation of the immunogen to leptosperin. The methyl ester of leptosperin was hydrolyzed with a 1 M NaOH solution, and the successive syringic acid 4-*O*-*β*-D-gentiobioside was used as a hapten and conjugated with carrier protein, keyhole limpet hemocyanin (KLH), using carbodiimide through the carboxyl group of the hapten. Mice were immunized with the conjugated KLH, and monoclonal antibodies were then established.

HPLC or LC−MS/MS is much higher relative to that for an ELISA.

Recent studies have demonstrated the preparation and application of an antibody for the detection of phytochemicals or their derivatives.[6−10] Immunochemical approaches, in particular an ELISA, may allow the handling of multiple samples. The cost of an ELISA is much lower than that of HPLC or LC−MS/MS. For example, to quantify an antigen by an ELISA, only a microplate reader is needed.

In this paper, on the basis of the specific monoclonal antibody against leptosperin, we established an ELISA to quantify leptosperin levels in honey for the first time.

## EXPERIMENTAL PROCEDURES

**Materials and Methods.** Methyl syringate was purchased from Alfa Aesar, Johnson Matthey Co. (Ward Hill, MA). Maltose, sucrose, and glucose were obtained from Nacarai Tesque Inc. (Kyoto, Japan). 2-Methoxybenzoic acid and bovine serum albumin (BSA) were obtained from Sigma-Aldrich Japan (Tokyo, Japan). Syringic acid (4-hydroxy-3,5-dimethoxybenzoic acid), 5-hydroxymethyl-2-furaldehyde (HMF), and gentiobiose were purchased from TCI Co., Ltd. (Tokyo, Japan). 4-Hydroxyphenylacetic acid was purchased from Wako Pure Chemical Industries, Ltd. (Osaka, Japan). Sulfo-*N*-hydroxysuccinimide (sulfo-NHS), 1-ethyl-3-[3-(dimethylamino)propyl]carbodiimide (EDC), and keyhole limpet hemocyanin (KLH) were purchased from Pierce (Thermo Fisher Scientific K. K., Yokohama, Japan). Leptosperin was isolated from manuka honey as described previously.[2] Twenty certified honey samples were obtained from the Unique Manuka Factor Honey Association (UMFHA). Other kinds of honey samples were obtained from retail stores in Japan, China, Brazil, and New Zealand between 2011 and 2014.

**Preparation of the Immunogen.** Leptosperin was treated with a 1 M NaOH aqueous solution for 30 min at room temperature. After neutralization by the addition of Dowex 50W, the solution was centrifuged, and the modified leptosperin (syringic acid 4-*O*-*β*-D-gentiobioside, in the supernatant) was then purified by reversed-phase HPLC using a Combi-RP column (20 mm × 100 mm, Nomura Chemical Co. Ltd., Aichi, Japan) with a 0.1% acetic acid/$CH_3CN$

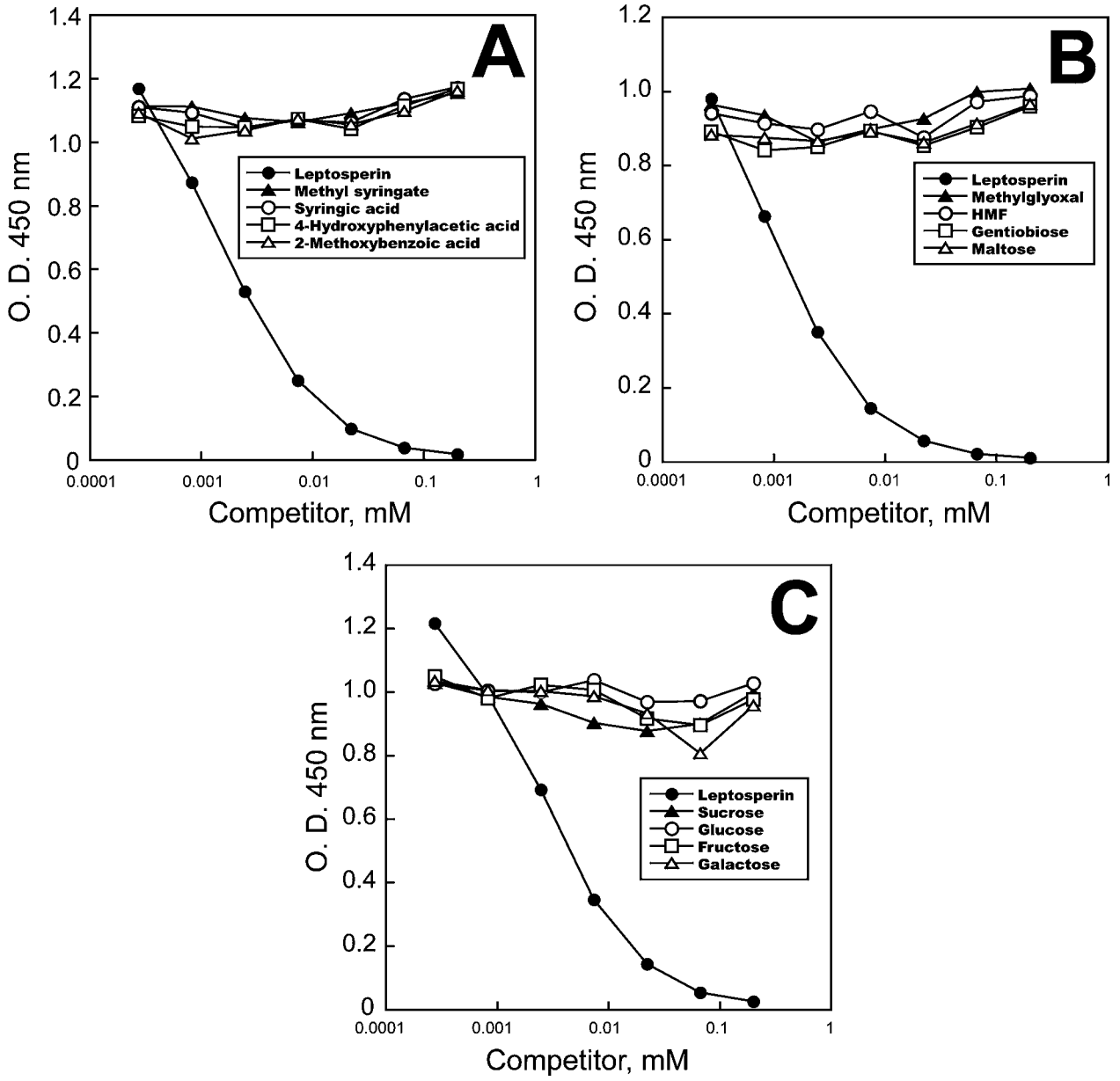


**Figure 2.** Characterization of monoclonal antibody 2H3 to leptosperin. The competitor and the antibody 2H3 were added to a well, which had been precoated with leptosperin-conjugated BSA. The antibody binding to the immobilized leptosperin-BSA was evaluated with a second antibody–peroxidase conjugate treatment. Each point represents the mean of duplicate determinations. (A) Cross-reactivity against phenolics: (●) leptosperin, (▲) methyl syringate, (○) syringic acid, (□) 4-hydroxyphenylacetic acid, and (△) 2-methoxybenzoic acid. (B) Cross-reactivity against aldehydes or disaccharides: (●) leptosperin, (▲) methylglyoxal, (○) HMF (5-hydroxymethyl-2-furaldehyde), (□) gentiobiose, and (△) maltose. (C) Cross-reactivity against saccharides: (●) leptosperin, (▲) sucrose, (○) glucose, (□) fructose, and (△) galactose.

mixture (85/15) at a flow rate of 5 mL/min. The modified leptosperin was then conjugated with KLH for an immunogen or BSA for a positive control antigen using EDC and sulfo-NHS. Briefly, 21 mg of modified leptosperin, 7.7 mg of EDC, and 8.7 mg of sulfo-NHS were dissolved in 700 μL of dimethylformamide, and then the mixture was incubated for 24 h at room temperature. Then, 350 μL of the reaction mixture reacted with KLH [8.5 mg/1.6 mL of 0.1 M phosphate buffer (pH 7.4)] for 4 h and then dialyzed against phosphate-buffered saline (PBS) for 3 days at 4 °C. The obtained leptosperin–KLH conjugate was stored at −80 °C until it was used. For the positive control antigen, BSA [13 mg/1.6 mL of 0.1 M phosphate buffer (pH 7.4)], instead of KLH, was mixed with 350 μL of reaction mixture and then dialyzed against PBS. The conjugation of leptosperin to BSA was confirmed by the loss of free amines by the reaction with 2,4,6-trinitrobenzenesulfonic acid (Thermo Scientific) according to the manufacturer's instructions and also an increase in absorbance at 262 nm, which was derived from absorption by the leptosperin moiety. The leptosperin–BSA antigen was used as the antigen for screening, cloning, and characterization by an ELISA.

**Preparation of the Monoclonal Antibody.** The monoclonal antibodies were prepared as described previously.[11] Three clones, 2H3, 2B5, and 1C10, which are all of the IgG1 class, were finally obtained. By simple characterization using culture media, the three antibodies showed strong reactivity against leptosperin and did not cross-react with gentiobiose, glucose, or methyl syringate. The 2H3 antibody from the clone was the most sensitive to leptosperin compared to the other two antibodies and then selected. The clone was cultivated, and the secreted antibody was purified from the cultured medium by a protein G column (HiTrap, Protein G HP, 1 mL, GE Healthcare) according to the manufacturer's instructions and then used for experiments.

**Characterization of the Antibody by an ELISA.** The leptosperin–BSA conjugate (5 μg/mL, 50 μL in PBS) was coated

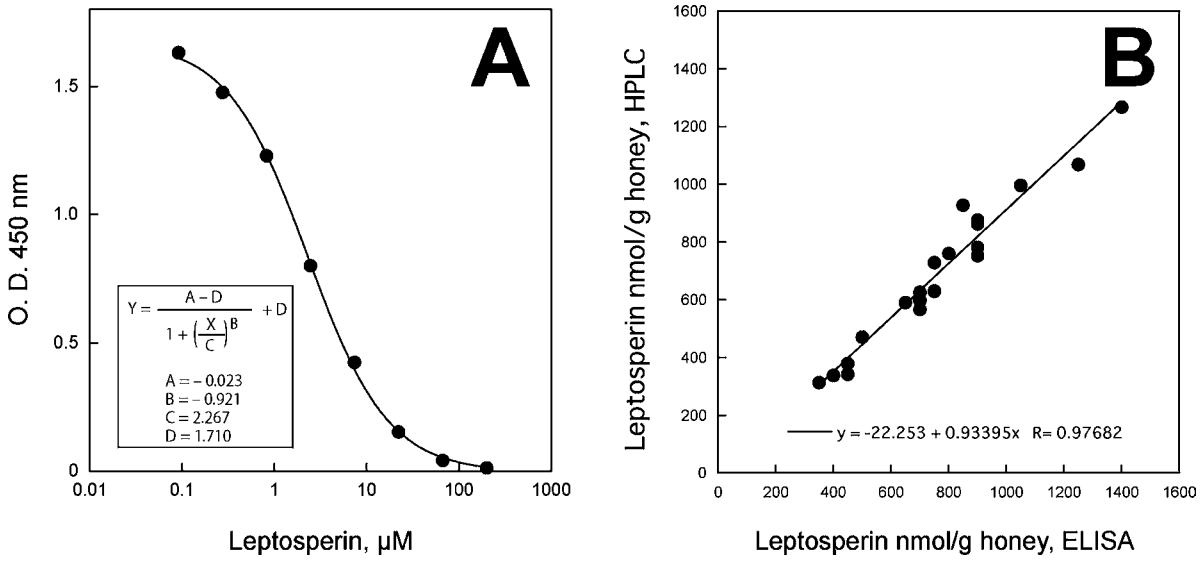


**Figure 3.** (A) Standard curve for an ELISA and (B) correlation between HPLC and ELISA. (A) A typical standard curve is shown with the equation (a four-parameter curve fitting). (B) The contents of leptosperin in the 20 certified manuka honey samples estimated by an ELISA significantly correlate with those determined by HPLC.[5] The ELISA for honey samples was performed four times, and the average was used.

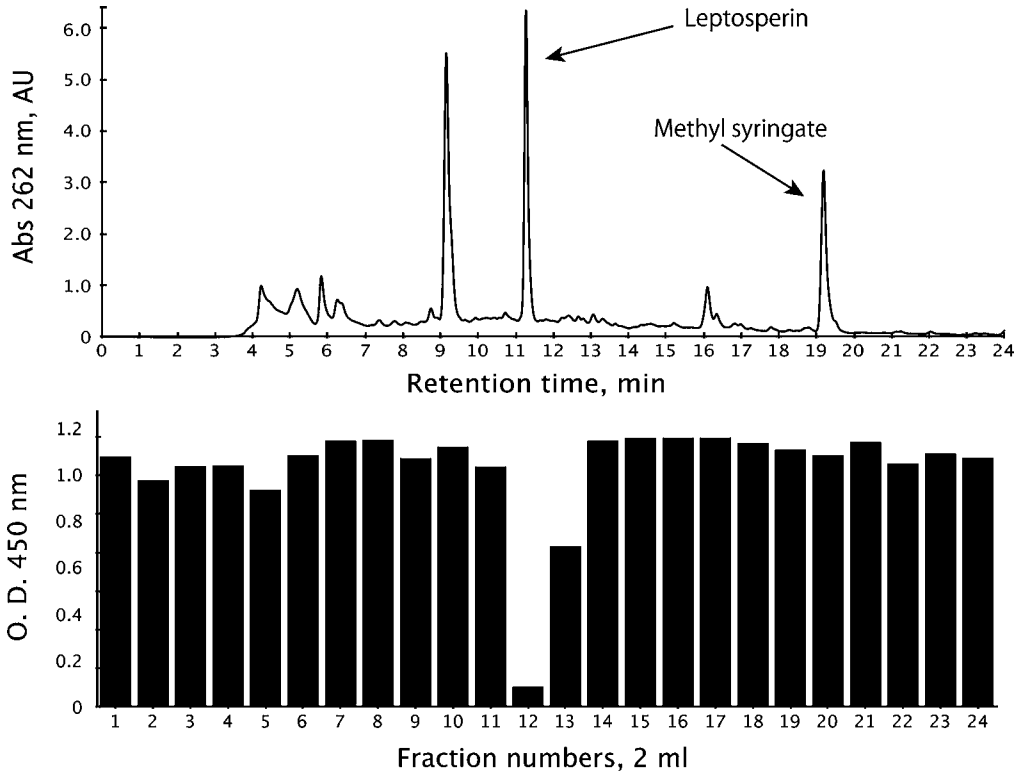


**Figure 4.** Fractionation and identification of antigen in manuka honey. An aqueous solution of manuka honey was injected into a semipreparative HPLC instrument, and the eluate was fractionated every minute (each 2 mL). The top panel shows the separation chromatogram with monitoring at an absorbance of 262 nm. The elution positions of leptosperin and methyl syringate are shown with arrows. The bottom panel indicates the immunoreactivity of fractionated samples estimated by a competitive ELISA.

on microtiter plate wells and kept overnight at 4 °C. The wells were washed with PBS containing 0.05% Tween 20 (PBST) and then blocked with 200 μL of 1% Block Ace (Dainihon Sumitomo Seiyaku, Osaka, Japan) for 1 h at 37 °C. Competitor (0−0.1 mM) or authentic leptosperin was mixed with the 2H3 antibody (0.02 μg/mL) in a well and further incubated for 2 h at 37 °C. The plate was washed and treated with 1/5000 diluted anti-mouse immunoglobulins labeled with peroxidase (DAKO) in PBST for 1 h at 37 °C. Color development was performed using 100 μL of 3,3′,5,5′-tetramethylbenzidine reagent (Popular, Nacalai Tesque) and terminated by the addition of 100 μL of 1 M aqueous phosphoric acid.

**Quantitation of Leptosperin in Honey Samples.** For an ELISA, manuka honey was dissolved in water at a concentration of 0.02 g/mL of water. Nonmanuka honey was dissolved at a concentration of 0.1 g/mL. The samples were centrifuged, and supernatants were then used. Authentic leptosperin (0−0.1 mM) and the honey samples (duplicate) were analyzed by an indirect competitive ELISA as described above. The concentration of

leptosperin was calculated by MPM-III software (version 6.0, Bio-Rad) with a four-parameter curve fitting. For analysis of 20 manuka honeys, an ELISA was performed four times and the averages were used. Commercial honeys were analyzed twice, and the averages were used. For chemical measurement of leptosperin, HPLC−PDA was used as described previously.[5]

**Fractionation of Honey by Semipreparative HPLC.** Manuka honey (UMF10+) was dissolved in water (1 g/mL of aqueous 10% $CH_3CN$) and then centrifuged. The supernatant (100 $\mu$L) of the sample was injected into a semipreparative HPLC instrument. The separation was achieved using a Develosil ODS-HG-5 column (8 mm × 250 mm, Nomura Chemical Co. Ltd.) and a 0.1% formic acid (A)/$CH_3CN$ (B) gradient system at a flow rate of 2 mL/min. The program was as follows: 90% A at 0 min, 70% A at 25 min, 90% A at 30 min, and 90% A at 55 min. The eluate was fractionated every minute (each 2 mL) in a test tube and dried with a centrifugal evaporator. The samples were dissolved in PBS, and 50 $\mu$L of the sample (duplicate) was then used for a competitive ELISA as described above.

**Statistics.** The relationship between two groups was calculated by IBM SPSS Statistics version 22 with Spearman's correlation.

## RESULTS

**Preparation of the Immunogen and Monoclonal Antibody.** The methyl ester (-$COOCH_3$) of leptosperin was hydrolyzed by alkali, and successive demethylated leptosperin was conjugated via carboxylic acid with a carrier protein, KLH, using a conventional carbodiimide method (Figure 1). To prepare a positive antigen, conjugation of demethylated leptosperin to BSA was simultaneously performed. The conjugation was confirmed by a 20% loss of the free amino moiety on the BSA, which was estimated by reactivity against trinitrobenzenesulfonic acid. The increase in absorption at 262 nm also indicated the adduction (data not shown). The immunogen was injected into mice, and hybridomas between spleen cells and myeloma cells were prepared by a typical polyethylene glycol method. Three clones (2H3, 2B5, and 1C10), which secreted the respective antibody to the immunogen, were obtained, and the 2H3 clone was then selected on the basis of simple characterization by an ELISA.

**Specificity of the Antibody to Leptosperin.** The detailed characterization of the 2H3 antibody was performed by a competitive ELISA. As shown in panels A and B of Figure 2, the antibody recognized leptosperin but not its component, methyl syringate or gentiobiose. Though manuka honey contains some characteristic compounds, HMF, 4-hydroxyphenylacetic acid, 2-methoxybenzoic acid, and methylglyoxal,[12−14] they did not cross-react with the 2H3 antibody. The antibody did not react with other saccharides such as glucose, fructose, sucrose, and galactose, which are the major components of honey (Figure 2C). These results suggest that the established antibody specifically reacts with leptosperin.

**Quantification of Leptosperin in 20 Certified Manuka Honey Samples.** Using the antibody, we established an ELISA method for the detection and quantitation of leptosperin. The range of quantitation was approximately 0.3−200 $\mu$M (Figure 3A). Twenty certified manuka honey samples were analyzed by an ELISA and then compared with previous data by HPLC.[5] As shown in Figure 3B, a significant correlation between the results of ELISA and HPLC was observed ($r = 0.97$; $p < 0.001$). An ELISA tended to produce a value higher than that produced by HPLC. The fitting equation (Figure 3B, inset; $y = -22 + 0.93x$) indicated that approximately 22 nmol of leptosperin per gram of honey should be calculated in manuka honey by an ELISA; even actual leptosperin was under the HPLC detection limit. This result suggested that some contaminants present in honey interfered with the assay. The amounts of leptosperin in the honey correlated with their nonperoxide-dependent antibacterial activities or the content of methylglyoxal.[2,5,12] The amount of leptosperin measured by an ELISA also correlated with this (data not shown). These results indicate that immunochemical quantification of leptosperin may be applicable for authentication of manuka honey.

**Identification of the Antigen as Leptosperin in Manuka Honey.** To confirm that the antigen in the honey was leptosperin, honey was fractionated by HPLC and the reactivities of the fractions with the antibody were then analyzed by a competitive ELISA. As shown in Figure 4, the antibody significantly reacted with fraction 12. Fraction 12 corresponded to a retention time of 11−12 min, which coincided with the elution time of leptosperin (11.5 min). This indicated that the antibody specifically reacts with leptosperin

**Table 1. Quantitation of Leptosperin in Certified Manuka Honeys by HPLC and ELISA**

| | | | | nmol/g of honey | |
|---|---|---|---|---|---|
| sample, information | certified | purchased | origin | HPLC[a] | ELISA |
| UMF[b] (Manuka Honey) | | | | | |
| 1 | UMF 15+ | China | New Zealand | 860 | 1023 |
| 2 | UMF 15+ | China | New Zealand | 530 | 494 |
| 3 | UMF 15+ | China | New Zealand | 758 | 752 |
| 4, similar label with samples 26 and 27 | UMF 15+ | Japan | New Zealand | 835 | 930 |
| 5 | UMF 15+ | Japan | New Zealand | 414 | 436 |
| 6 | UMF 15+ | Japan | New Zealand | 579 | 508 |
| 7 | UMF 12+ | Japan | New Zealand | 487 | 482 |
| 8, beech trees, blended, Southern Alps | UMF 5+ | New Zealand | New Zealand | 852 | 897 |
| Active + (Manuka Honey or Jelly Bush Honey) | | | | | |
| 9 | Active 15+ | China | New Zealand | 396 | 381 |
| 10, certified chloramphenicol-free | Active 15+ | China | New Zealand | 262 | 288 |
| 11, stick type | Active 13+ | Japan | New Zealand | 483 | 446 |
| 12 | Active 12+ | New Zealand | New Zealand | 294 | 326 |
| 13 | Active 10+ | New Zealand | New Zealand | 147 | 179 |
| 14, 100% raw unpasteurized | Active 5+ | New Zealand | New Zealand | 1044 | 1099 |
| 15, jelly bush honey | Active 5+ | Japan | Australia | 58 | 83 |
| MGO[c] (Manuka Honey) | | | | | |
| 16 | MGO 250+ | Japan | New Zealand | 690 | 673 |
| 17 | MGO 250+ | China | New Zealand | 386 | 434 |

[a]Data (samples 1−17) determined by HPLC were acquired previously.[5] [b]UMF means unique manuka factor, which is used as an index of antibacterial activity. [c]MGO is used for an index of the level of methylglyoxal in honey.

Table 2. Quantitation of Leptosperin in Noncertified and Other Honeys by HPLC and ELISA

| sample, information | certified | purchased | origin | nmol/g of honey HPLC[b,c] | nmol/g of honey ELISA[a] |
|---|---|---|---|---|---|
| Noncertified (or Self-Certified) Manuka Honey (or Jelly Bush Honey) | | | | | |
| 18 | – | Japan | New Zealand | 113 | 135 |
| 19, "self-rigid inspection passed" | – | Japan | New Zealand | 372 | 412 |
| 20, bottled in Japan, liquid type | – | Japan | New Zealand | 438 | 364 |
| 21 | – | Japan | New Zealand | 767 | 806 |
| 22, with kiwi fruit (2%) | – | Japan | New Zealand | 74 | 129 |
| 23, South Island | – | Japan | New Zealand | 592 | 666 |
| 24, "high grade manuka honey, 92.5%" | – | Japan | New Zealand | 720 | 665 |
| 25, with 0.25% propolis, 5+ certificated by a laboratory | – | Japan | New Zealand | 258 | 223 |
| 26, same jar and label as sample 27 | – | Japan | New Zealand | ND[d] | ND[d] (16) |
| 27, same jar and label as sample 26 | – | New Zealand | New Zealand | 164 | 157 |
| 28, squeeze type, jelly bush honey | – | Japan | Australia | 35 | ND[d] (31) |
| Other Honeys (Non-manuka Honey) | | | | | |
| 29, scottish heather honey | – | Japan | U.K. | ND[d] | ND[d] (41) |
| 30 | – | Brazil | Brazil | ND[d] | ND[d] (31) |
| 31, buckwheat | – | Japan | Japan | ND[d] | ND[d] (19) |
| 32, multifloral honey, Awaji Island | – | Japan | Japan | ND[d] | ND[d] (30) |
| 33, multifloral honey | – | Japan | Japan | ND[d] | ND[d] (11) |
| 34, kiawe tree | – | Japan | United States | ND[d] | ND[d] (27) |
| Other Honeys (Non-manuka Honey) | | | | | |
| 35, acacia | – | Japan | Hungary | ND[d] | ND[d] (20) |
| 36, asphodel | – | Japan | Italy | ND[d] | ND[d] (17) |
| 37, agrumi (citrus) | – | Japan | Italy | ND[d] | ND[d] (16) |
| 38, lavender (*Lavandula stoechas*) | – | Japan | Italy | ND[d] | ND[d] (15) |
| 39, millefiori (Tuscan honey) | – | Japan | Italy | ND[d] | ND[d] (19) |
| 40, eucalyptus | – | Japan | Italy | ND[d] | ND[d] (17) |
| 41, cardoon (*Galactites tomentosa*) | – | Japan | Italy | ND[d] | ND[d] (21) |
| 42, borragine (*Borago officinalis*) | – | Japan | Italy | ND[d] | ND[d] (28) |
| 43, orange | – | Japan | Italy | ND[d] | ND[d] (20) |
| 44, eucalyptus | – | Japan | Spain | ND[d] | ND[d] (18) |
| 45, lemon | – | Japan | Spain | ND[d] | ND[d] (19) |
| 46, lavender (*Lavandula stoechas*) | – | Japan | France | ND[d] | ND[d] (26) |
| 47, sunflower (*Helianthus annuus*) | – | Japan | France | ND[d] | ND[d] (27) |
| 48, oak (honeydew honey) | – | Japan | Spain | ND[d] | ND[d] (33) |
| 49, fir (Abies) (honeydew honey) | – | Japan | France | ND[d] | ND[d] (31) |
| 50, leather wood (*Eucryphia lucida*) | | Japan | Australia | ND[d] | ND[d] (20) |

[a]The calculated data are given in parentheses. [b]Data (for samples 18–34) determined by HPLC were acquired previously.[5] [c]Data (for samples 35–50) determined by HPLC were acquired previously.[2] [d]Not detected.

in manuka honey. In addition, syringic acid 4-*O*-β-D-gentiobioside (demethylated leptosperin) could not be detected.

**Application of the Determination of Leptosperin in Honey and Vodka by an ELISA.** Leptosperin has been found almost exclusively in manuka honey and jelly bush honey.[2,5,12,15] As shown in Table 1, leptosperin was detected in almost all manuka honey samples by an ELISA. The data for certified and noncertified manuka honey are fairly linear with respect to data determined previously by HPLC ($p < 0.001$).[2,5] There were no strong signals from non-manuka honey (Table 2), even if the honey was rich in methyl syringate (sample 36, from Sardinia, Italy).[16] After taking each datum into consideration, we decided that 70 nmol of leptosperin/g of honey was the detection limit for this ELISA. For reference, calculated data are given in parentheses in Table 2. In addition, leptosperin was also found (approximately 4 μmol/mL) in vodka to which manuka honey had been added. The concentration in vodka was almost identical to that measured by HPLC in our previous report.[5]

## DISCUSSION

The leptosperin levels in manuka honey correlated with the nonperoxide-dependent antibacterial activity of honey, which is used for authentication of manuka honey as UMF.[5] Because leptosperin is found exclusively in manuka honey,[2,12] the quantification of leptosperin could be an authentication marker for manuka honey. To detect the leptosperin, chemical methods are available, and these methods provide accurate measures of leptosperin levels.[5] Some products contain trace amounts of manuka honey, making it difficult to detect leptosperin using conventional HPLC–PDA (UV). However, mass spectrometry could resolve the problem. In contrast, immunochemical methods such as an ELISA can analyze many samples simultaneously; therefore, the cost of the required equipment, such as a conventional microplate reader, is lower than those required for chemical methods like HPLC–PDA (UV) or LC–MS/MS. Needless to say, a specific antibody is required for the construction of an ELISA.

There are several reports on antibodies to phytochemicals or their metabolites. Kawai et al. prepared antibodies to quercetin glucuronide and proved the localization of the metabolite in atherosclerotic plaques or the brain immunohistochemically.[7−9] Recently, a monoclonal antibody to liquiritin, a glucoside of liquiritigenin, has been developed to assist in the quality control of licorice products.[10] Antibodies developed specifically for a phytochemical may be useful for analyzing the metabolism of compounds and for the quality control of products. In this study, we aimed to obtain the antibody specific to leptosperin.

In preliminary experiments, we tried to prepare the antibody using an immunogen, which was prepared by conjugation of the carrier protein with leptosperin by a periodate oxidation method.[17] The obtained antibody recognized leptosperin; however, it also recognized its aglycone, methyl syringate (data not shown). In the study presented here, the methyl ester of methyl syringate in the leptosperin molecule was treated with a weak alkaline solution to expose the carboxyl moiety (-COOH); i.e., the methyl syringate moiety was transformed into a syringic acid moiety. Using the generated terminal COOH group, the leptosperin molecule was conjugated with a lysine residue of a carrier protein, KLH. The novel antibody that was obtained did not recognize gentiobiose, syringic acid, or methyl syringate (Figure 2). This result suggests that the antibody is highly specific for leptosperin.

We have found that the antigen in manuka honey completely coincides with the fraction containing leptosperin (Figure 4). Figure 3B and Tables 1 and 2 show good linearity between the data determined by HPLC and ELISA, indicating that the reliability of leptosperin analyses by an ELISA is sufficient for practical purposes.

The antibacterial activity is a key property of manuka honey, and this activity can be changed during storage, transport to a store, or its display at the store. A recent study showed that quantitation of leptosperin could identify falsified manuka honey or low-quality manuka honey[5] sold in the market. These findings suggest that the quantitation of leptosperin along with the measurement of antibacterial activity should be applicable for authentication of manuka honey. Immunochemical methods, such as an ELISA, using the antibody specific to leptosperin provide a simple method for novel immunochemical authentication of manuka honey.

## AUTHOR INFORMATION


### Corresponding Author

*Telephone: +81-79-292-9413. Fax: +81-79-293-5710. E-mail: yojikato@shse.u-hyogo.ac.jp.


### Notes

The authors declare no competing financial interest.

## ACKNOWLEDGMENTS

We sincerely thank John Rawcliff (Manager, UMFHA) for the supply of the 20 certified manuka honey samples and Hill Laboratories in New Zealand for providing the analytical data. We also thank Kazuo Sakai (Nikken Zeil Corp.) for his technical advice concerning the establishment of the ELISA protocol.

## ABBREVIATIONS USED

HPLC, high-performance liquid chromatography; PDA, photodiode array; UV, ultraviolet light; MS/MS, tandem mass spectrometry; HMF, 5-(hydroxymethyl)-2-furaldehyde; NHS, *N*-hydroxysuccinimide; EDC, 1-ethyl-3-[3-(dimethylamino)-propyl]carbodiimide; KLH, keyhole limpet hemocyanin; UMFHA, unique manuka factor honey association; BSA, bovine serum albumin; PBS, phosphate-buffered saline; PBST, PBS containing 0.05% Tween 20

## REFERENCES


(1) Adams, C. J.; Manley-Harris, M.; Molan, P. C. The origin of methylglyoxal in New Zealand manuka (*Leptospermum scoparium*) honey. *Carbohydr. Res.* **2009**, *344*, 1050−1053.

(2) Kato, Y.; Umeda, N.; Maeda, A.; Matsumoto, D.; Kitamoto, N.; Kikuzaki, H. Identification of a novel glycoside, leptosin, as a chemical marker of manuka honey. *J. Agric. Food Chem.* **2012**, *60*, 3418−3423.

(3) Takahashi, C.; Numata, A.; Ito, Y.; Matsumura, E.; Araki, H.; Iwaki, H.; Kushida, K. Leptosins, antitumour metabolites of a fungus isolated from a marine alga. *J. Chem. Soc., Perkin Trans. 1* **1994**, 1859−1864.

(4) Takahashi, C.; Numata, A.; Matsumura, E.; Minoura, K.; Eto, H.; Shingu, T.; Ito, T.; Hasegawa, T. Leptosins I and J, cytotoxic substances produced by a Leptosphaeria sp. Physico-chemical properties and structures. *J. Antibiot.* **1994**, *47*, 1242−1249.

(5) Kato, Y.; Fujinaka, R.; Ishisaka, A.; Nitta, Y.; Kitamoto, N.; Takimoto, Y. Plausible authentication of manuka honey and related products by measuring leptosperin with methyl syringate. *J. Agric. Food Chem.* **2014**, *62*, 6400−6407.

(6) Ban, Y.; Watanabe, T.; Miyazaki, A.; Nakano, Y.; Tobe, T.; Idei, T.; Iguchi, T.; Katagiri, T. Impact of increased plasma serotonin levels and carotid atherosclerosis on vascular dementia. *Atherosclerosis* **2007**, *195*, 153−159.

(7) Ishisaka, A.; Mukai, R.; Terao, J.; Shibata, N.; Kawai, Y. Specific localization of quercetin-3-*O*-glucuronide in human brain. *Arch. Biochem. Biophys.* **2014**, *557*, 11−17.

(8) Kawai, Y.; Ishisaka, A.; Saito, S.; Uchida, K.; Shibata, N.; Kobayashi, M.; Fukuchi, Y.; Naito, M.; Terao, J. Immunochemical detection of flavonoid glycosides: Development, specificity, and application of novel monoclonal antibodies. *Arch. Biochem. Biophys.* **2008**, *476*, 124−132.

(9) Kawai, Y.; Nishikawa, T.; Shiba, Y.; Saito, S.; Murota, K.; Shibata, N.; Kobayashi, M.; Kanayama, M.; Uchida, K.; Terao, J. Macrophage as a target of quercetin glucuronides in human atherosclerotic arteries: Implication in the anti-atherosclerotic mechanism of dietary flavonoids. *J. Biol. Chem.* **2008**, *283*, 9424−9434.

(10) Fujii, S.; Morinaga, O.; Uto, T.; Nomura, S.; Shoyama, Y. Development of a monoclonal antibody-based immunochemical assay for liquiritin and its application to the quality control of licorice products. *J. Agric. Food Chem.* **2014**, *62*, 3377−3383.

(11) Kato, Y.; Kawai, Y.; Morinaga, H.; Kondo, H.; Dozaki, N.; Kitamoto, N.; Osawa, T. Immunogenicity of a brominated protein and successive establishment of a monoclonal antibody to dihalogenated tyrosine. *Free Radical Biol. Med.* **2005**, *38*, 24−31.

(12) Oelschlaegel, S.; Gruner, M.; Wang, P. N.; Boettcher, A.; Koelling-Speer, I.; Speer, K. Classification and characterization of manuka honeys based on phenolic compounds and methylglyoxal. *J. Agric. Food Chem.* **2012**, *60*, 7229−7237.

(13) Stephens, J. M.; Schlothauer, R. C.; Morris, B. D.; Yang, D.; Fearnley, L.; Greenwood, D. R.; Loomes, K. M. Phenolic compounds and methylglyoxal in some New Zealand manuka and kanuka honeys. *Food Chem.* **2010**, *120*, 78−86.

(14) Mavric, E.; Wittmann, S.; Barth, G.; Henle, T. Identification and quantification of methylglyoxal as the dominant antibacterial constituent of Manuka (*Leptospermum scoparium*) honeys from New Zealand. *Mol. Nutr. Food Res.* **2008**, *52*, 483−489.

(15) Beitlich, N.; Koelling-Speer, I.; Oelschlaegel, S.; Speer, K. Differentiation of manuka honey from kanuka honey and from jelly bush honey using HS-SPME-GC/MS and UHPLC-PDA-MS/MS. *J. Agric. Food Chem.* **2014**, *62*, 6435−6444.

(16) Tuberoso, C. I.; Bifulco, E.; Jerkovic, I.; Caboni, P.; Cabras, P.; Floris, I. Methyl syringate: A chemical marker of asphodel (*Asphodelus microcarpus* Salzm. et Viv.) monofloral honey. *J. Agric. Food Chem.* **2009**, *57*, 3895−3900.

(17) Tanaka, H.; Shoyama, Y. Formation of a monoclonal antibody against glycyrrhizin and development of an ELISA. *Biol. Pharm. Bull.* **1998**, *21*, 1391−1393.

identify the ligands isolated. Moreover, using a fluorescence quenching method and molecular docking, the binding affinity and potential interaction mechanism between the ligands and lipase were investigated.

## MATERIALS AND METHODS

**Reagents and Chemicals.** Dried lotus leaves were obtained from Sichuan province, China. $FeCl_3 \cdot 6H_2O$, $FeCl_2 \cdot 4H_2O$, and *N*,*N*-dimethylformamide (DMF) were purchased from Chengdu Tianhua Chemical Technology Co., Ltd. (Chengdu, China). *N*-Hydroxysuccinimide (NHS), 2-(*N*-morpholino)ethanesulfonic acid (MES), 1-(3-(dimethylamino)propyl)-3-ethylcarbodiimide hydrochloride (EDC·HCl), orlistat, 4-methylumbelliferyl oleate (4-MUO), and porcine pancreatic lipase (type VI-S, from porcine pancreas) were purchased from Sigma Chemical Co. (St. Louis, MO, USA). Tetraethyl orthosilicate (TEOS), succinic anhydride, and 3-aminopropyltrimethoxysilane (APTMS) were purchased from TCI (Tokyo, Japan). The acetonitrile used for HPLC was of chromatographic grade (J. T. Baker, Phillipsburg, NJ, USA). HPLC grade water was produced by a Milli-Q (18.2 MΩ) system (Millipore, Bedford, MA, USA). The other chemicals and solvents were all of analytical reagent grade. Sephadex LH-20 was from Amresco (Solon, OH, USA). D101 macroporous resin, which was a cross-linked polystyrene copolymer, was purchased from the Chemical Plant of Nankai University (Tianjin, China).

**Apparatus and Instruments.** A TSP HPLC system consisting of quaternary pump and DAD detector (Thermo Separation Products Inc., Waltham, MA, USA) was used for HPLC analysis and ultraviolet (UV) measurement. A Thermo-Quest Finnigan $LCQ^{DECA}$ system equipped with an electrospray ionization source (Thermo-Quest LC/MS Division, USA) was used for HPLC-MS/MS measurements. Fluorescence spectra were recorded by an RF-5301 spectrofluorometer equipped with a 150 W xenon lamp (Shimadzu, Japan). Thermo Scientific Varioskan Flash equipped with a 96-well microplate (Thermo, USA) was used for lipase inhibition assay of active compounds. Ligand fishing was performed in a constant-temperature incubator shaker (Zhengzhou Zhicheng Device Works, Zhengzhou, China). The pH values were measured with a pHS-3 digital pH-meter (Shanghai LeiCi Device Works, Shanghai, China). Preparative separation of active compounds was performed using a Waters 2545 HPLC on a C-18 preparative column (5 μm, 250 × 10 mm i.d.).

**Preparation of Lipase-Functionalized MNPs (LMNPs).** Lipase-functionalized MNPs were prepared following a previously reported process with a little modification.[18] Briefly, $Fe_3O_4$ nanoparticles (MNPs) were prepared by coprecipitation of $FeCl_2$ and $FeCl_3$ with ammonia water. Using TEOS and APTMS, the MNPs were first coated with $SiO_2$, and then the $SiO_2$ was terminated with amino groups. These amine-terminated MNPs were then treated with 10% succinic anhydride in DMF to obtain carboxyl group-terminated MNPs. Lipase-MNPs coupling was achieved by activating the carboxyl groups with EDC/NHS followed by covalently cross-linking the primary amino groups of the lipase amino acids. LMNPs were suspended in $NH_4OAc$ buffer and stored before use at −4 °C. The immobilized yield of lipase on the MNPs was measured as 50 mg/g MNPs.

**Ligand Fishing from Lotus Leaf Extract.** Air-dried, powdered lotus leaves (5.0 g) were refluxed with 80% ethanol at 80 °C for 90 min, three times. The extractions were filtered, and all of the filtrates were combined and concentrated to dryness in vacuum at 45 °C to give the crude extract (456.0 mg). The crude extract was suspended in water and fractionated with petroleum ether and ethyl acetate successively. The ethyl acetate fraction was absorbed with a D101 macroporous resin-packed column, washed with water and 30, 50, and 75% alcohol successively. The 50% alcohol eluent was concentrated in vacuum to dryness (named $S_0$) and used for the following ligand fishing experiment.

Ligand fishing was performed according to the method we reported previously.[11] A 1.0 mg/mL $S_0$ solution was prepared in ammonium acetate buffer (10 mM, pH 7.4). Twenty milligrams of LMNPs was added to the Eppendorf tube containing 1 mL of $S_0$ solution. The tube was shaken vigorously for 30 min at 25 °C before being placed on a magnet for 1 min to carry out magnetic liquid−solid separation. The LMNPs were washed three times using 3 × 1 mL buffer to remove nonspecifically bound compounds. Finally, LMNPs were eluted with 1 mL of 50% acetonitrile to release the active compounds. The eluent was stored as solution $S_5$. $S_0$ and $S_5$ were then analyzed with HPLC-MS/MS.

**HPLC-DAD-MS/MS Analysis and Compounds Identification.** A Tianhe Kromasil C18 column (5 μm, 250 mm × 4.6 mm) kept at 35 °C with a guard column (C18, 5 μm, 4.0 mm × 3.0 mm) was used for chromatographic analysis. The injection volume was 20 μL. The mobile phase was composed of 0.1% HAc (A) and acetonitrile (B), and the column was eluted with a gradient of 10−90% B for 0−50 min at a flow rate of 0.8 mL/min. The peaks were detected by a UV detector set at 280 nm. A Thermo-Quest Finnigan $LCQ^{DECA}$ mass spectrometer equipped with an electrospray ionization source (Thermo-Quest LC/MS Division, USA) was used for HPLC-MS/MS analysis, which gave information on the molecular weights and fragmentation patterns. The mass spectrometry detector parameters were set as follows: nebulizer sheath gas $N_2$ was 80 units; nebulizer auxiliary gas $N_2$ was 20 units; capillary temperature was 300 °C; spray voltage was 4.5 kV; capillary voltage was −13 V; and lens voltage was 18 V. All of the data were processed using Finnigan Xcalibur core data system rev. 2.0 (Thermo, USA). Identification of compounds **1**−**6** was realized by comparison of the retention time as well as MS/MS data with those of the known compounds reported previously.[19]

**Purification and Identification of the Active Compounds.** Five hundred grams of the powdered lotus leaves was extracted and processed according to the method described above. The 50% alcohol eluent fraction was concentrated and redissolved in 50% methanol aqueous solution to submit to Sephadex LH-20 column chromatography eluated with 50% methanol. Elution of fraction A-2 was evaporated under vacuum and recrystallized in methanol to afford compound **1** (15 mg). Elution of fraction B-2 was concentrated and separated by a preparative HPLC system eluated with 40% methanol to give compound **4** (38 mg). Although identified as described above, chemical structures of compound **1** and **4** were further confirmed by comparing the $^1H$ and $^{13}C$ NMR data with the published ones. The two isolated compounds were used for subsequent lipase inhibition assay and fluorescence quenching experiment.

**Lipase Inhibition Assay.** The two bioactive compounds fished out from lotus leaves and the crude extract ($S_0$) used for ligand fishing process were subjected to lipase inhibition assay with the well-known lipase inhibitor orlistat as positive control.[20] Samples were dissolved in water, whereas both lipase and 4-MUO were dissolved in a buffer containing 13 mM Tris-HCl, 150 mM NaCl, and 1.3 mM $CaCl_2$ (pH 8.0). Briefly, 50 μL of a 0.1 mM 4-MUO solution was mixed with 25 μL of the sample solution into the well of a 96-well microtiter plate, to which 25 μL of the lipase solution (50 U/mL) was added to start the enzymatic reaction. After incubation for 30 min at 25 °C, the enzymatic reaction was stopped by adding 0.1 mL of 0.1 M sodium citrate (pH 4.2). The product of the enzymatic reaction, 4-methylumbelliferone, was quantified with a fluorometric microplate reader (Thermo Scientific Varioskan Flash system) at 355 nm (excitation wavelength) and 460 nm (emission wavelength). All of the assays were performed in triplicate to calculate the mean ± standard deviation values.

**Fluorescence Quenching Measurements of Active Compounds with PPL.** In the fluorescence quenching experiment, 1.0 μM lipase solution was used. Series concentrations of compounds **1** and **4** (0.013−0.26 mM) were prepared in a buffer of DMSO/$H_2O$ (9:1). Each 0.25 mL of sample solution was added to a 3 mL lipase solution to give a sample concentration in the range of 0.001−0.02 mM. Each mixture was then incubated at 300 K for 0.5 h. The intensity of the fluorescence emission of each mixture at 340 nm was measured at the excitation wavelength of 280 nm, which was repeated three times. Neither compound **1** nor **4** gave out fluorescence emission around 340 nm (in the range of 300−450 nm) at the excitation wavelength. The fluorescence intensities were measured with a Shimadzu RF5301 spectrophotometer with 5.0 nm of excitation and emission slit widths.

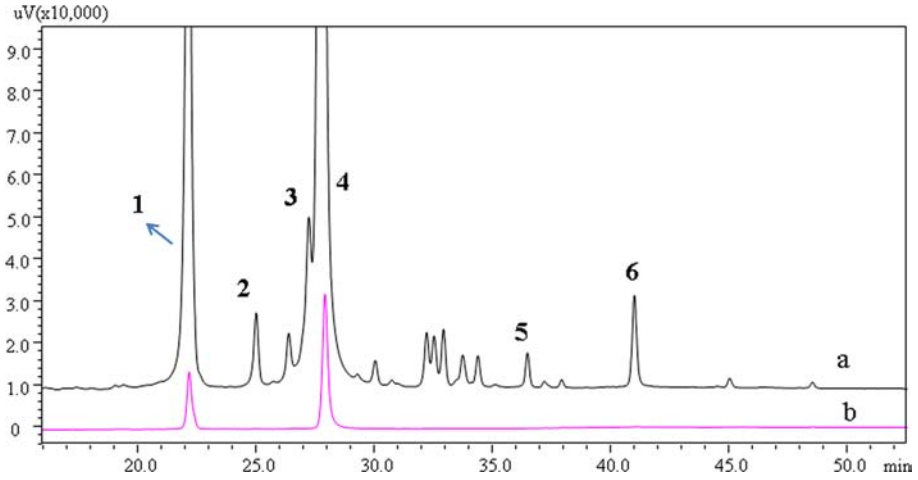


**Figure 1.** HPLC chromatograms obtained from (a) the extract of lotus leaf ($S_0$) and (b) the eluent from LMNPs after extraction ($S_5$). Peaks: 1, quercetin-3-*O*-*β*-D-arabinopyranosyl-(1→2)-*β*-D-galactopyranoside; 2, quercetin-3-*O*-rhamnopyranosyl-(1 → 6)-glucopyranoside; 3, quercetin-3-*O*-glucoside; 4, quercetin-3-*O*-glucuronide; 5, isorhamnetin 3-*O*-*β*-D-xylopyranosyl-(1→2)-*β*-D-glucopyranoside; 6, isorhamnetin 3-*O*-glucoside (**6**).

**Table 1. UV−Vis Absorption Maxima ($\lambda_{max}$) in HPLC and Main ESI-MS$^n$ Ions of Ingredients in Extracts of Lotus Leaves**[a]

| compd | identification | $t_R$ (min) | $\lambda_{max}$ (nm) | NI$^-$ | MS/MS |
|---|---|---|---|---|---|
| **1** | quercetin-3-*O*-*β*-D-arabinopyranosyl-(1→2)-*β*-D-galactopyranoside | 22.1 | 227, 254, 354 | 595 | 300 |
| **2** | quercetin-3-*O*-rhamnopyranosyl-(1→6)-glucopyranoside | 25.0 | 227, 254, 354 | 609 | 301, 150 |
| **3** | quercetin-3-*O*-glucoside | 27.2 | 227, 254, 354 | 463 | 300 |
| **4** | quercetin-3-*O*-glucuronide | 27.9 | 229, 254, 354 | 477 | 301 |
| **5** | isorhamnetin 3-*O*-*β*-D-xylopyranosyl-(1→2)-*β*-D-glucopyranoside | 36.4 | 234, 265, 354 | 609 | 299, 314 |
| **6** | isorhamnetin 3-*O*-glucoside | 41.0 | 236, 254, 354 | 477 | 314, 299 |

[a]Compound numbering is in accordance with peak numbering in Figure 1.

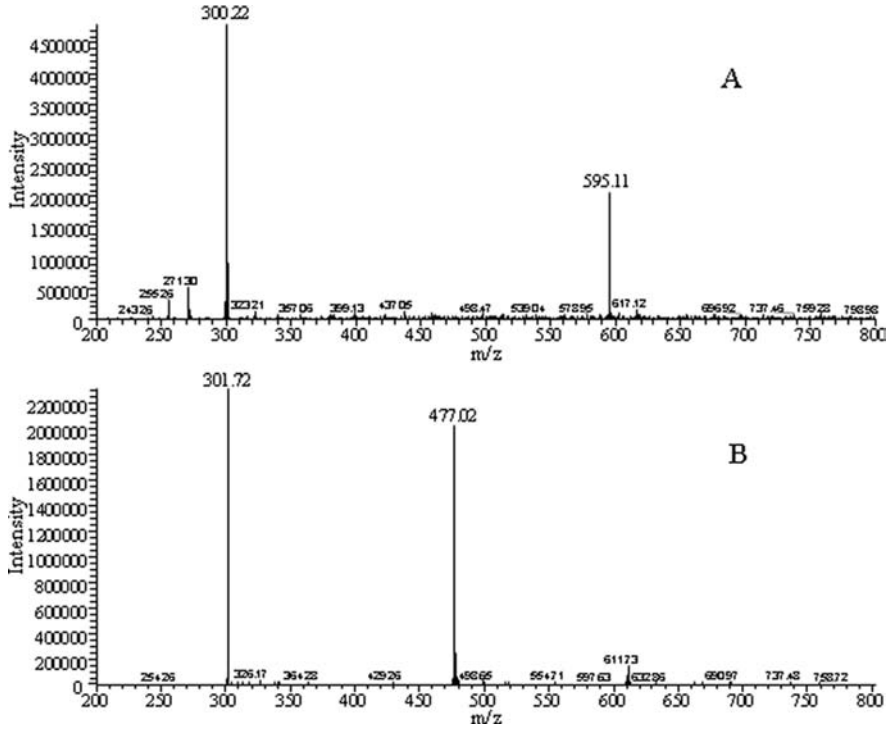


**Figure 2.** Negative ion CID mass spectra of the two compounds: (A) MS/MS of Qc-3-*O*-AraGal ($m/z$ 595); (B) MS/MS of Qc-3-*O*-Glu ($m/z$ 477).

In addition, synchronous fluorescence spectra of lipase ($T$ = 300 K, pH 7.4) were measured, and the range of synchronous scanning was $\Delta\lambda$ = 60 nm.

The quenching emission data were plotted as a Stern−Volmer plot of $F_0/F$ against [Q], and the quenching constant was calculated by linear regression. Binding constants ($K_a$) and binding sites ($n$) were calculated in static quenching by the following equation:

$$\lg[(F_0 - F)/F] = \lg K_a + n \lg[Q] \quad (1)$$


dx.doi.org/10.1021/jf503687e | J. Agric. Food Chem. 2014, 62, 10679−10686

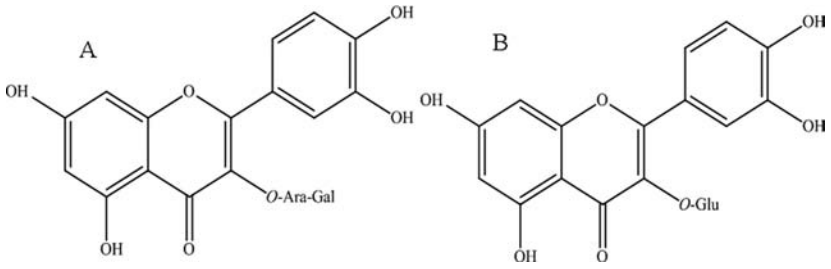


**Figure 3.** Chemical structures of the ligands isolated from the extract of *Nelumbo nucifera* leaves.

Thermodynamic evaluation of the active compounds with lipase was assessed according to a previously reported method.[20]

**Molecular Docking Studies.** To investigate the interactions between compounds **1** and **4** with porcine pancreas lipase (PPL), we tried to dock them onto the enzyme. Autodock Vina program was used for in silico molecular docking of the compounds in the active site of lipase.[17] Both compounds were drawn in mol2 format with all hydrogen atoms added, and then the energy was minimized using Hamiltonian-Force-Field-MMFF94x by Molecular Operating Environment (MOE) software. The partial charges were calculated, which were finally saved in pdbqt format. The X-ray crystallographic structure of PPL (Protein Data Bank, PDB entry code 1ETH, 2.80 Å resolution[21]) was downloaded from the Protein Data Bank and opened with Deep View software to check whether the amino acids of the protein were complete or not. Subsequently, all hydrogen atoms and the charges were added for the PPL and also saved as a pdbqt file.

The structure was complexed respectively with the two inhibitors by AutoDock Vina. The catalytic serine residue of the lipase was replaced by glycine residue, and docking runs were subsequently performed to enable the ligand to adopt a suitable position corresponding to the prebound intermediate before the nucleophilic attack in the lipase active site. To fit the active site cleft and allow nonconstructive binding, the appropriate box size for PPL was selected. Using the center of the bound compound, the center of the grid enclosing the box could be defined. The dimensions of the enclosing box were deduced according to the compound size Grid utility program within the Dock 4.0.1 to generate docking grid, which was calculated using box dimensions of 52.65, 45.404, and 123.331. Binding free energies of Qc-3-*O*-AraGal and Qc-3-*O*-Glu were also calculated.

## RESULTS AND DISCUSSION

**Ligand Fishing from Lotus Leaves Extract with Lipase-Functionalized MNPs.** The HPLC chromatograms of lotus leaf extracts before ($S_0$) and after ($S_5$) incubation with

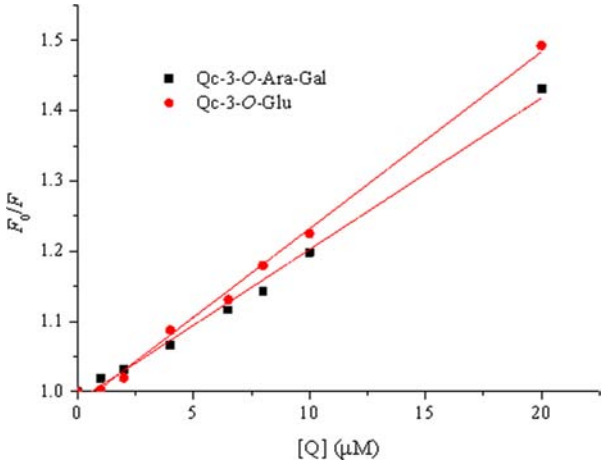


**Figure 4.** Stern–Volmer plots for the quenching of Qc-3-*O*-AraGal and Qc-3-*O*-Glu on the PPL at 300 K.

**Table 2. Stern–Volmer Quenching Constants for the Interaction of Qc-3-*O*-AraGal and Qc-3-*O*-Glu with PPL at 300 K**

| compd | temp (K) | $K_{SV}/10^4$ (L mol$^{-1}$) | $k_q/10^{12}$ (L mol$^{-1}$ s$^{-1}$) | $R^2$ |
|---|---|---|---|---|
| Qc-3-*O*-AraGal | 300 | 2.157 | 2.157 | 0.992 |
| Qc-3-*O*-Glu | 300 | 2.521 | 2.521 | 0.995 |

**Table 3. Relative Thermodynamic Parameters of the Interaction of Active Compounds with PPL**

| compd | temp (K) | $\Delta G$ (kJ mol$^{-1}$) | $\Delta H$ (kJ mol$^{-1}$) | $\Delta S$ (J mol$^{-1}$ K$^{-1}$) |
|---|---|---|---|---|
| Qc-3-*O*-AraGal | 300 | −24.890 | 3.091 | 93.270 |
| Qc-3-*O*-Glu | 300 | −25.278 | 9.782 | 116.867 |

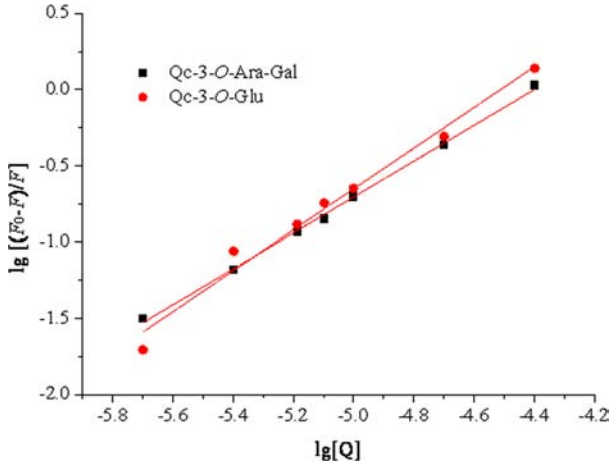


**Figure 5.** Plots of lg[$(F_0 - F)/F$] versus lg[Q] for Qc-3-*O*-AraGal and Qc-3-*O*-Glu at 300 K.

**Table 4. Binding Constant $K_a$ and the Number of Binding Sites ($n$) at Different Temperatures**

| compd | temp (K) | $K_a/10^5$ (L mol$^{-1}$) | $n$ | $R^2$ |
|---|---|---|---|---|
| Qc-3-*O*-AraGal | 300 | 1.491 | 1.176 | 0.998 |
| Qc-3-*O*-Glu | 300 | 10.926 | 1.338 | 0.979 |

LMNPs are shown in Figure 1. As in Figure 1a, the crude extracts ($S_0$) from lotus leaves possessed a complicated composition containing a variety of flavonoid compounds. The chromatographic and MS data of the main flavonoids from $S_0$ are listed in Table 1. By comparison of HPLC retention time, molecular weight, and MS/MS data with those reported in the literature previously,[19] six flavonoids were identified as quercetin-3-*O*-*β*-D-arabinopyranosyl-(1→2)-*β*-D-galactopyranoside (**1**), quercetin-3-*O*-rhamnopyranosyl-(1→6)-glucopyrano-

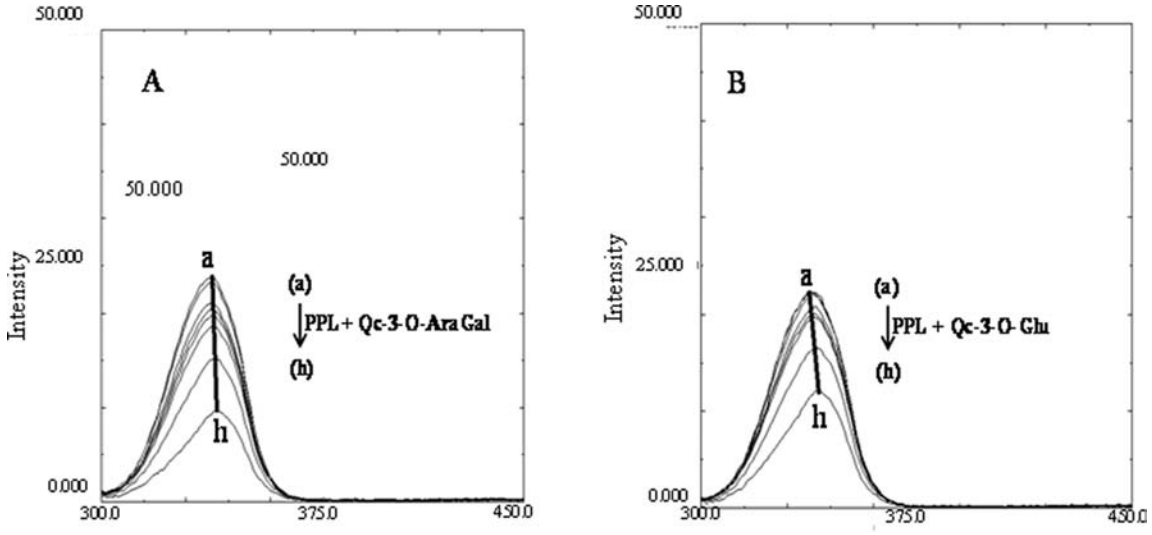


**Figure 6.** Synchronous fluorescence spectra of PPL at various concentrations of Qc-3-*O*-AraGal (A) and Qc-3-*O*-Glu (B) at 60 nm wavelength interval, $T$ = 310 K, $c$(PPL) = $1.0 \times 10^{-6}$ mol $L^{-1}$; $c$(Qc-3-*O*-AraGal), and $c$(Qc-3-*O*-Glu)/($10^{-6}$ mol $L^{-1}$) a–h: 0, 1, 2, 4, 6.5, 8, 10, 20, respectively.

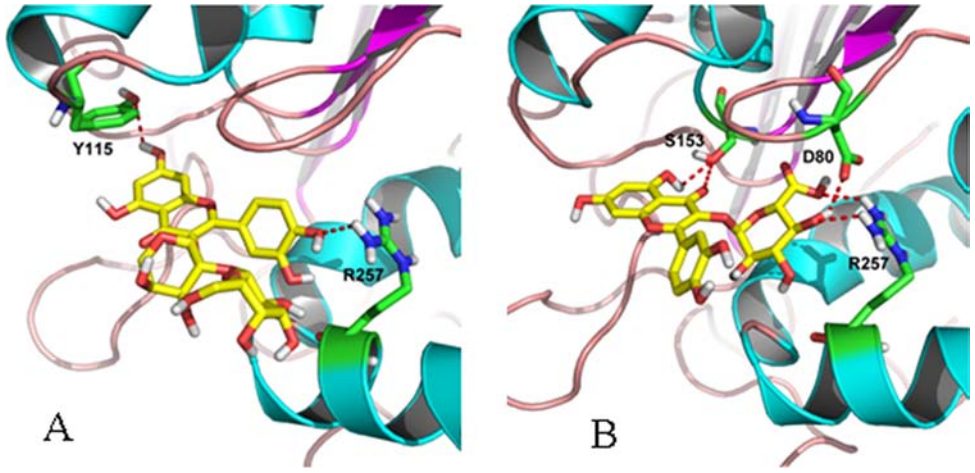


**Figure 7.** Superimposition of the top-scoring docking positions of (A) Qc-3-*O*-AraGal and (B) Qc-3-*O*-Glu in PPL active sites. Each inhibitor is represented in atom color-code sticks (oxygen, red). Structures were drawn with PyMOL Molecular Graphics System (version 1.3, Schrodinger, LLC), using the following PDB file: 1ETH for PPL.

side (**2**), quercetin-3-*O*-glucoside (**3**), quercetin-3-*O*-glucuronide (**4**), isorhamnetin 3-*O*-*β*-D-xylopyranosyl-(1→2)- *β*-D-glucopyranoside (**5**), and isorhamnetin 3-*O*-glucoside (**6**). Two compounds (**1** and **4**) were found in $S_5$ as shown in Figure 1b, indicating that there were only two lipase ligands in the lotus leaf crude extracts which can bind to LMNPs. They were isolated from the extracts for subsequent lipase inhibition assay and fluorescence quenching experiment, and their chemical structures were confirmed as following.

The UV absorption maximum ($\lambda_{max}$, nm) of both **1** and **4** were at ∼254 nm (Figure 2), which were consistent with those of quercetin type flavonoids.[22] Compound **1** has a molecular weight of 596 ($m/z$ 595, $[M - H]^-$). The radical aglycone ion at $m/z$ 300 $[A - 2H]^-$ in $MS^2$ (Figure 2A) indicated that the interglycosidic linkage between the two monosaccharides was C1→C2.[22] Therefore, this compound was identified as quercetin-3-*O*-*β*-D-arabinopyranosyl-(1→2)-*β*-D-galactopyranoside (Qc-3-*O*-AraGal). Compound **2** was found to have a molecular weight of 478 ($m/z$ 477, $[M - H]^-$). A significantly strong aglycone ion peak was observed at $m/z$ 301 $[A - H]^-$ in $MS^2$ (Figure 2B), indicating that it was a glucuronic acid glycoside. Therefore, compound **2** was identified as quercetin 3-*O*-D-glucuronide (Qc-3-*O*-Glu), which was the dominant flavonoid in lotus leaves.[19] Their chemical structures are shown in Figure 3.

It is worth noting that only two flavonoids (compounds **1** and **4**) were fished out from the mixture of many flavonoids present in the extract, and only these two exhibited potent binding ability to PPL. As all six identified flavonoids have the same aglycones, that is, quercetin or isorhamnetin, we speculated that it was the complicated conformation of the different sugar chains that caused such difference in lipase binding. This result corresponds largely to a previous study in which lipase immobilized on hollow fiber was used to select lipase inhibitors from lotus leaf.[23] The only difference is that, apart from compounds **1** and **4**, another kaempferol type flavonoid was extracted in the study. However, it showed significantly lower bioactivity and binding capacity compared with compounds **1** and **4**.

**Lipase Inhibition Assay.** The beneficial effects of lotus leaves have been mainly attributed to their high flavonoid contents. To our knowledge, this is the first screening of lipase

inhibitors from lotus leaves by LMNP-based ligand fishing. The PPL inhibitory activities of the two PPL-bound flavonoids, Qc-3-*O*-AraGal (**1**) and Qc-3-*O*-Glu (**2**), together with the crude extract of lotus leaves ($S_0$) were evaluated by a traditional PL inhibitor assay[20] with orlistat as the positive control. The lipase inhibitory activities of the samples were determined using 4-MUO as the substrate of the lipase-catalyzing reaction. They were determined by measuring the fluorescence intensity increment arising from the fluorescent product 4-methylumbelliferone (4-MU) at an excitation wavelength of 360 nm and an emission wavelength of 450 nm using a 96-well microplate reader. Compared to the $IC_{50}$ value of orlistat (1.53 ± 0.02 μM), those for compounds **1**, **4**, and $S_0$ were 52.9 ± 3.2 μg/mL (88.8 ± 5.4 μM), 17.1 ± 1.5 μg/mL (35.8 ± 3.1 μM), and 95.0 ± 5.1 μg/mL, respectively. The two active compounds (**1** and **4**) showed significantly stronger inhibitory effects than the crude extracts ($S_0$). These results indicate that both compounds fished out by this method are effective inhibitors of lipase. This finding is in agreement with a previous report.[24] Therefore, this method is expected to be useful for activity-guided separation of active compounds from natural products.

**Fluorescence Quenching Measurements of Active Compounds with PPL.** *Fluorescence Quenching Mechanism.* The intrinsic fluorescence is usually used to investigate the structure and dynamics of proteins; therefore, it is a good tool in the study of association reactions between proteins and bioactive compounds.[24] When the excitation wavelength was set at 280 nm, the fluorescence emission peaks of PPL (at 340 nm) mixed with a series concentrations of the quencher provided information on tryptophan residues, which are the main contributors to intrinsic fluorescence of proteins.[25] Fluorescence quenching can thus be used to measure binding affinity. Fluorescence quenching is described by the Stern−Volmer equation as follows:

$$\frac{F_0}{F} = 1 + k_q\tau_0[Q] = 1 + K_{SV}[Q] \quad (2)$$

$F_0$ and $F$ are the fluorescence intensity before and after quencher was added to PPL; $k_q$ is the quenching rate constant, $K_{SV}$ is the Stern−Volmer dynamic quenching constant, $\tau_0$ is the average lifetime of bimolecular fluorescence without quencher ($\tau_0 = 10^{-8}$ s), and [Q] is the concentration of the quencher. $K_{SV}$ was determined by linear regression of a plot of $F_0/F$ against [Q], and it is the slop of linear regression of eq 2. In this work, Stern−Volmer plots for PPL fluorescence quenching by Qc-3-*O*-AraGal and Qc-3-*O*-Glu are shown in Figure 4, and $K_{SV}$ and $k_q$ at pH 7.4 are summarized in Table 2. A linear Stern−Volmer plot usually indicates a single way of quenching, in which the fluorophores are all equally accessible to the quencher. On the other hand, when the fluorophores are quenched by both collision and complex formation with the quencher, the Stern−Volmer plot will exhibit an upward curvature, corresponding to the occurrence of both dynamic and static quenching. In this work, the plots of the two flavonoids were in good agreement with the linear Stern−Volmer plot, whereas no obvious deviation toward the *y*-axis was observed, indicating that either dynamic quenching or static quenching was predominant.[26]

The $k_q$ value reflects the efficiency of quenching or the accessibility of the fluorophores to the quencher and, thus, is used to judge whether the formation of a complex can lead to the quenching.[27]The $k_q$ value near $1 \times 10^{10}$ $M^{-1}$ $s^{-1}$ is typical for dynamic quenching mechanism. In this work, the $k_q$ values of Qc-3-*O*-AraGal and Qc-3-*O*-Glu were 200-fold ($2.157 \times 10^{12}$ L $mol^{-1}$ $s^{-1}$) and 250-fold ($2.521 \times 10^{12}$ L $mol^{-1}$ $s^{-1}$) higher than $1 \times 10^{10}$ $M^{-1}$ $s^{-1}$, respectively. This result suggested that both compounds formed a complex with PPL and both belonged to static quenching mechanism. Moreover, Qc-3-*O*-Glu showed higher fluorescence quenching effects on PPL than Qc-3-*O*-AraGal.

*Thermodynamic Parameters and the Characteristic of the Binding Forces.* The binding of ligands to proteins is mainly affected by noncovalent interactions including hydrogen bonds, van der Waals forces, electrostatic interactions, and hydrophobic interactions. These acting forces can be confirmed by thermodynamic parameters of the binding reaction. Therefore, the interaction of the two flavonoids with PPL identified by thermodynamic parameters dependent on temperature are calculated from van't Hoff equations:

$$\ln(K_2/K_1) = \left(\frac{1}{T_1} - \frac{1}{T_2}\right)\Delta H/R \quad (3)$$

$$\Delta G = \Delta H - T\Delta S = -RT\ln K \quad (4)$$

where $T$ is the experimental temperature, $\Delta H$ is the enthalpy change, $R$ is the gas constant, $\Delta S$ is the entropy change, $K_2$ and $K_1$ are the binding constants ($K_a$) at the corresponding $T$, and $\Delta G$ is the free energy change.

The values of $\Delta H$, $\Delta S$, and $\Delta G$ obtained are shown in Table 3. The negative value for $\Delta G$ indicated a spontaneous interaction process. For both Qc-3-*O*-AraGal (+93.270 J $mol^{-1}$ $K^{-1}$) and Qc-3-*O*-Glu (+116.867 J $mol^{-1}$ $K^{-1}$), from the point of water structure, the positive $\Delta S$ values reflected a hydrophobic interaction.[28] In particular, the specific positive $\Delta H$ and $\Delta S$ values indicated that hydrophobic interaction was the major acting force and the reaction was mainly driven by entropy. These interactions could proceed through aromatic rings and other hydrophobic groups of the two active compounds. In addition to hydrophobic forces, hydrogen bonding between OH groups and the side chain of amino acids was also involved in the interaction of the two active compounds with PPL at the molecular level.

*Numbers of Binding Sites (n) and Binding Constants ($K_a$).* For static quenching, the binding sites and constants were calculated according to the following double-logarithm equation:[29]

$$\lg\frac{F_0 - F}{F} = \lg K_a + n\lg[Q] \quad (1)$$

$F_0$ and $F$ are the fluorescence intensities of PPL in the absence and presence of both compounds; $K_a$ is the binding constant; $n$ is the number of binding sites; and [Q] is the concentration of the quencher. The dependence of $\lg[(F_0 - F)/F]$ on $\lg[Q]$ value was linear, the slope of which equals $n$, and intercept to $\lg[K_a]$. Plots of $\lg[(F_0 - F)/F]$ versus $\lg[Q]$ for Qc-3-*O*-AraGal and Qc-3-*O*-Glu to PPL are shown in Figure 5. The double-logarithm curves for both active compounds were obviously linear. The corresponding calculated $K_a$ ($n$) values between Qc-3-*O*-AraGal or Qc-3-*O*-Glu and PPL were $1.491 \times 10^5$ (1.176) and $10.926 \times 10^5$ (1.338) at 300 K, respectively. The active compound Qc-3-*O*-Glu showed an obviously stronger binding capacity than Qc-3-*O*-AraGal (Table 4).

*Characteristics of Synchronous Fluorescence Spectra.* To investigate the effect of active compounds on the structural change of PPL, synchronous fluorescence spectra of PPL with different concentrations of active compounds were measured by simultaneously scanning the excitation and emission mono-

chromators. Qc-3-O-AraGal and Qc-3-O-Glu were measured individually under the same condition to exclude the possible interruption. Because none of them showed signals, no background control was needed in the following experiment. The synchronous fluorescence spectra have advantages of reducing bandwidth and avoiding various perturbations. It shows only the characteristics of tyrosine and tryptophan residues of PPL under wavelength interval ($\Delta\lambda$) between 15 and 60 nm, respectively. The maximum excitation and emission wavelengths of the residues correlate to the polarity of the microenvironment and, thus, can be used to judge the conformational change of proteins.

The effect of the two active compounds on PPL synchronous fluorescence spectroscopy is shown in Figure 6. The emission maximum of tryptophan residues exhibited a significant red shift (from 338 to 342 nm) for both Qc-3-O-AraGal and Qc-3-Glu, indicating an increase of polarity around the tryptophan residues and a decrease of the hydrophobicity. The results showed the conformational change of PPL tryptophan microregion by addition of active compounds during the binding process.

*Molecular Docking.* In silico molecular docking provided additional explanation for the experimental inhibition activity of Qc-3-*O*-AraGal and Qc-3-*O*-Glu. The porcine pancreatic lipase possesses two domains. Its N-terminal domain is an $\alpha/\beta$ hydrolase fold, which contains the catalytic sites of Ser153, Asp177, and His264. The crystal structure of the ternary porcine lipase-colipase-tetraethylene glycol monooctyl ether showed that the overall position of the three catalytic sites is conservative in different species.[21] The crystal structure of PPL (1ETH) was determined at a resolution of 2.80 Å, and the lipase active site was fully accessible so that docking experiments with the two inhibitors could be carried out. The in silico docking experiment showed that Qc-3-*O*-AraGal mostly interacted with PPL through hydrogen bonding of Tyr115 with the 7-hydroxyl group on ring A and Arg257 with the 3′-hyroxyl group on ring B (Figure 7A). Docking of Qc-3-*O*-Glu to PPL also showed an apparent hydrogen-bonding network resulting from the interaction of the 5-hyrdoxyl group on ring A and carbonyl group on ring C with the PPL catalytic residue Ser153. Additionally, the carboxyl and hydroxyl moieties on the sugar residue together had strong hydrogen-bonding interactions with the side chain of the PPL catalytic residue Arg257; the hydroxyl group on the sugar residue also showed hydrogen-bonding interaction with PPL residue Asp80 (Figure 7B). The estimated binding energies were −9.2 kcal $mol^{-1}$ for Qc-3-*O*-Glu and −7.9 kcal $mol^{-1}$ for Qc-3-*O*-AraGal, respectively. The docking results suggested that the two compounds from the screen might be potential inhibitors of PPL. In addition, the different binding free energies of Qc-3-*O*-Glu and Qc-3-*O*-AraGal suggested that Qc-3-*O*-Glu had a higher affinity than Qc-3-*O*-AraGal for PPL, which was consistent with the results of the lipase inhibition assay in vitro and fluorescence quenching analysis.

In conclusion, an effective method based on ligand fishing was developed to screen lipase inhibitors from complex chemical mixtures. Pancreatic porcine lipase immobilized onto magnetic nanoparticles was used to bind the ligands from the complex mixtures, and then the bound ligands could be easily separated magnetically for HPLC-MS/MS analysis. This method was first employed in lotus leaf extract to identify two flavonoids that showed significant inhibitory effect toward lipase, and the mechanism of PPL inhibition of the two ligands was investigated by fluorescence quenching together with molecular docking. The result of this study adds to the understanding of the mechanism of health effects of lotus leaves, and the method proposed shows great potential in screening enzyme inhibitors from edible and medicinal plants.

## AUTHOR INFORMATION


### Corresponding Author

*(X.L.) Phone/fax: +86 28 82890402. E-mail: liaoxun@cib.ac.cn.



### Funding

We appreciate the financial support from the National Natural Science Foundation of China (81173536 and 21072184 to X.L.) and the U.S. National Institutes of Health (GM 089557 to Y.-M.L.).


### Notes

The authors declare no competing financial interest.

## ABBREVIATIONS USED

MNPs, magnetic nanoparticles; Qc-3-*O*-AraGal, quercetin-3-*O*-$\beta$-D-arabinopyranosyl-(1→2)-$\beta$-D-galactopyranoside; Qc-3-*O*-Glu, quercetin-3-*O*-$\beta$-D-glucuronide; $IC_{50}$, 50% inhibitory concentration; 4-MUO, 4-methylumbelliferyl oleate; 4-MU, 4-methylumbelliferone; PPL, porcine pancreas lipase; LMNPs, lipase-functionalized MNPs; $NI^-$, negative ion mode

## REFERENCES


(1) Tang, W.; Eisenbrand, G. *Nelumbo nucifera* Gaertn. In *Chinese Drugs of Plant Origin*; Springer: Berlin, Germany, 1992; pp 697−701.

(2) Guo, H. Cultivation of lotus (*Nelumbo nucifera* Gaertn. ssp. *nucifera*) and its utilization in China. *Genet. Resour. Crop Evol.* **2009**, *56*, 323−330.

(3) Liu, S.; Li, D.; Huang, B.; Chen, Y.; Lu, X.; Wang, Y. Inhibition of pancreatic lipase, $\alpha$-glucosidase, $\alpha$-amylase, and hypolipidemic effects of the total flavonoids from *Nelumbo nucifera* leaves. *J. Ethnopharmacol.* **2013**, *149*, 263−269.

(4) Tho Chau Minh Vinh, D.; Tuan Duc, N.; Hung, T.; Stuppner, H.; Ganzera, M. Analysis of alkaloids in lotus (*Nelumbo nucifera* Gaertn.) leaves by non-aqueous capillary electrophoresis using ultraviolet and mass spectrometric detection. *J. Chromatogr., A* **2013**, *1302*, 174−180.

(5) Mukherjee, P. K.; Mukherjee, D.; Maji, A. K.; Rai, S.; Heinrich, M. The sacred lotus (*Nelumbo nucifera*) − phytochemical and therapeutic profile. *J. Pharm. Pharmacol.* **2009**, *61*, 407−422.

(6) Li, M.; Xu, Z. Quercetin in a lotus leaves extract may be responsible for antibacterial activity. *Arch. Pharmacal Res.* **2008**, *31*, 640−644.

(7) Ono, Y.; Hattori, E.; Fukaya, Y.; Imai, S.; Ohizumi, Y. Anti-obesity effect of *Nelumbo nucifera* leaves extract in mice and rats. *J. Ethnopharmacol.* **2006**, *106*, 238−244.

(8) Birari, R. B.; Bhutani, K. K. Pancreatic lipase inhibitors from natural sources: unexplored potential. *Drug Discovery Today* **2007**, *12*, 879−889.

(9) Moaddel, R.; Marszall, M.; Bighi, F.; Yang, Q.; Duan, X.; Wainer, I. Automated ligand fishing using human serum albumin-coated magnetic beads. *Anal. Chem.* **2007**, *79*, 5414−5417.

(10) Yasuda, M.; Wilson, D.; Fugmann, S.; Moaddel, R. Synthesis and characterization of SIRT6 protein coated magnetic beads: Identification of a novel inhibitor of SIRT6 deacetylase from medicinal plant extracts. *Anal. Chem.* **2011**, *83*, 7400−7407.

(11) Qing, L.-S.; Xue, Y.; Zheng, Y.; Xiong, J.; Liao, X.; Ding, L.-S.; Li, B.-G.; Liu, Y.-M. Ligand fishing from *Dioscorea nipponica* extract using human serum albumin functionalized magnetic nanoparticles. *J. Chromatogr., A* **2010**, *1217*, 4663−4668.

(12) Qing, L. S.; Tang, N.; Xue, Y.; Liang, J.; Liu, Y. M.; Liao, X. Identification of enzyme inhibitors using therapeutic target protein−magnetic nanoparticle conjugates. *Anal. Methods* **2012**, *4*, 1612−1615.
(13) Yanagisawa, M.; Sugiya, M.; Iijima, H.; Nakagome, I.; Hirono, S.; Tsuda, T. Genistein and daidzein, typical soy isoflavones, inhibit TNF-$\alpha$-mediated downregulation of adiponectin expression via different mechanisms in 3T3-L1 adipocytes. *Mol. Nutr. Food. Res.* **2012**, *56*, 1783−1793.
(14) Wang, Y. Q.; Zhang, H. M.; Zhang, G. C.; Tao, W.-H.; Tang, S.-H. Binding of brucine to human serum albumin. *J. Mol. Struct.* **2007**, *830*, 40−45.
(15) Li, Y. Q.; Zhou, F. C.; Gao, F.; Bian, J. S.; Shan, F. Comparative evaluation of quercetin, isoquercetin and rutin as inhibitors of $\alpha$-glucosidase. *J. Agric. Food Chem.* **2009**, *57*, 11463−11468.
(16) Park, H.; Hwang, K. Y.; Oh, K. H.; Kim, Y. H.; Lee, J. Y.; Kim, K. Discovery of novel $\alpha$-glucosidase inhibitors based on the virtual screening with the homology-modeled protein structure. *Bioorg. Med. Chem.* **2008**, *16*, 284−292.
(17) Point, V.; Kumar, K. V. P. P.; Marc, S.; Delorme, V.; Parsiegla, G.; Amara, S.; Carriere, F.; Buono, G.; Fotiadu, F.; Canaan, S.; Leclaire, J.; Cavalier, J.-F. Analysis of the discriminative inhibition of mammalian digestive lipases by 3-phenyl substituted 1,3,4-oxadiazol-2(3*H*)-ones. *Eur. J. Med. Chem.* **2012**, *58*, 452−463.
(18) Qing, L. S.; Xiong, J.; Xue, Y.; Liu, Y. M.; Guang, B.; Ding, L. S.; Liao, X. Using baicalin-functionalized magnetic nanoparticles for selectively extracting flavonoids from *Rosa chinensis*. *J. Sep. Sci.* **2011**, *34*, 3240−3245.
(19) Chen, S.; Wu, B. H.; Fang, J. B.; Liu, Y. L.; Zhang, H. H.; Fang, L. C.; Guan, L.; Li, S. H. Analysis of flavonoids from lotus (*Nelumbo nucifera*) leaves using high performance liquid chromatography/photodiode array detector tandem electrospray ionization mass spectrometry and an extraction method optimized by orthogonal design. *J. Chromatogr., A* **2012**, *1227*, 145−153.
(20) Nakai, M.; Fukui, Y.; Asami, S.; Toyoda-Ono, Y.; Iwashita, T.; Shibata, H.; Mitsunaga, T.; Hashimoto, F.; Kiso, Y. Inhibitory effects of oolong tea polyphenols on pancreatic lipase in vitro. *J. Agric. Food Chem.* **2005**, *53*, 4593−4598.
(21) Hermoso, J.; Pignol, D.; Kerfelec, B.; Crenon, I.; Chapus, C.; FontecillaCamps, J. C. Lipase activation by nonionic detergents − the crystal structure of the porcine lipase-colipase-tetraethylene glycol monooctyl ether complex. *J. Biol. Chem.* **1996**, *271*, 18007−18016.
(22) Qing, L. S.; Xue, Y.; Zhang, J. G.; Zhang, Z. F.; Liang, J.; Jiang, Y.; Liu, Y.-M.; Liao, X. Identification of flavonoid glycosides in *Rosa chinensis* flowers by liquid chromatography−tandem mass spectrometry in combination with $^{13}C$ nuclear magnetic resonance. *J. Chromatogr., A* **2012**, *1249*, 130−137.
(23) Tao, Y.; Zhang, Y.; Wang, Y.; Cheng, Y. Hollow fiber based affinity selection combined with high performance liquid chromatography-mass spectroscopy for rapid screening lipase inhibitors from lotus leaf. *Anal. Chim. Acta* **2013**, *785*, 75−81.
(24) Wang, Y.-Q.; Zhang, H.-M.; Zhang, G.-C.; Tao, W.-H.; Tang, S.-H. Interaction of the flavonoid hesperidin with bovine serum albumin: a fluorescence quenching study. *J. Lumin.* **2007**, *126*, 211−218.
(25) Ladokhin, A. S. Fluorescence spectroscopy in peptide and protein analysis. In *Encyclopedia of Analytical Chemistry*; Wiley: New York, 2000; pp 5762−5769.
(26) Soares, S.; Mateus, N.; De Freitas, V. Interaction of different polyphenols with bovine serum albumin (BSA) and human salivary $\alpha$-amylase (HSA) by fluorescence quenching. *J. Agric. Food Chem.* **2007**, *55*, 6726−6735.
(27) Eftink, M. R. Fluorescence quenching reactions. In *Biophysical and Biochemical Aspects of Fluorescence Spectroscopy*; Springer: Berlin, Germany, 1991; pp 1−41.
(28) Daneshgar, P.; Moosavi-Movahedi, A. A.; Norouzi, P.; Ganjali, M. R.; Madadkar-Sobhani, A.; Saboury, A. A. Molecular interaction of human serum albumin with paracetamol: spectroscopic and molecular modeling studies. *Int. J. Biol. Macromol.* **2009**, *45*, 129−134.
(29) Wang, Y. P.; Wei, Y. L.; Dong, C. Study on the interaction of 3,3-bis(4-hydroxy-1-naphthyl)-phthalide with bovine serum albumin by fluorescence spectroscopy. *J. Photochem. Photobiol. A* **2006**, *177*, 6−11.

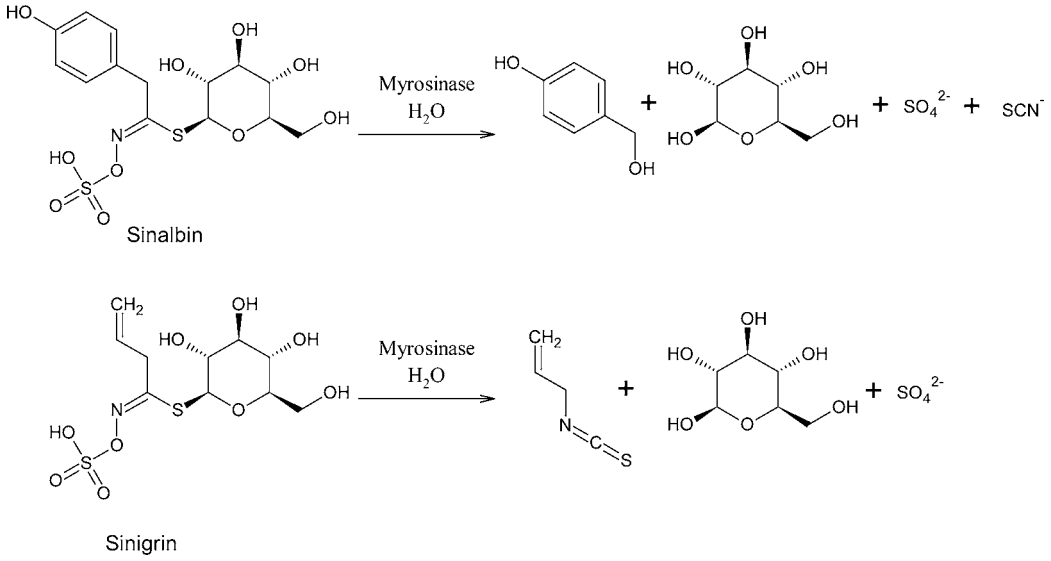


**Figure 1.** Myrosinase-catalyzed hydrolysis of mustard glucosinolates sinalbin and sinigrin.

quantification provides a measure of glucosinolate hydrolysis based on reaction stoichiometry. Thus, for *B. juncea*, sinigrin and $SO_4^{2-}$ can be quantified prior to seed meal application to predict biopesticidal potential.

Intact glucosinolates are ionic compounds that can be quantified by ion chromatography (IC) along with $SCN^-$ and $SO_4^{2-}$; however, there is no reported method for simultaneous analysis of mustard glucosinolates and their anionic hydrolysis products. Our objective was to develop and evaluate an IC method for the simultaneous quantification of sinigrin, sinalbin, $SO_4^{2-}$, and $SCN^-$ in mustard seed. The advantages of using IC for analysis include simplicity, selectivity, and relatively low cost. Ion chromatography is a commonly used technique in agricultural and environmental laboratories and, as such, a method that can be easily implemented in routine quality control analyses. The availability of a simple and inexpensive method of analysis is critical in encouraging the development of plant-derived biopesticides to improve agricultural sustainability.

## MATERIALS AND METHODS

**Materials.** Mustard seeds (*S. alba* and *B. juncea*) were obtained locally (Latah County, ID, USA). Two varieties of *B. juncea* (Pacific Gold and Kodiak) and one variety of *S. alba* (IdaGold) were used (Table 1). Oil contents of seeds and meals were analyzed gravimetrically after extraction with hexane. A sinigrin standard and sulfatase (EC 3.1.6) were purchased from Sigma-Aldrich (St. Louis, MO, USA). Glucolimnanthin (3-methoxybenzyl glucosinolate) and sinalbin were isolated from meadowfoam (*Limnanthes alba*) and *S. alba*, respectively, in our laboratory. Acetonitrile, water, methanol, and other solvents were of HPLC or LC/MS grade. Solvents and all other chemicals (at least of analytical grade) were purchased from Sigma-Aldrich or ThermoFisher (Pittsburgh, PA, USA).

**Table 1. Mustard Seeds and Seed Meals Used in IC Analysis**

| sample | species | variety | form | oil content[a] (%) |
|---|---|---|---|---|
| Sa_1 | *S. alba* | IdaGold | seed | 32 |
| Sa_2 | *S. alba* | IdaGold | seed | 41 |
| Sa_3 | *S. alba* | IdaGold | meal | 22 |
| Sa_4 | *S. alba* | IdaGold | meal | 29 |
| Sa_5 | *S. alba* | IdaGold | meal | 18 |
| Bj_1 | *B. juncea* | Pacific Gold | meal | 33 |
| Bj_2 | *B. juncea* | Kodiak | meal | 26 |
| Bj_3 | *B. juncea* | Pacific Gold | meal | 29 |
| Bj_4 | *B. juncea* | Pacific Gold | seed | 46 |
| Bj_5 | *B. juncea* | Kodiak | seed | 40 |

[a]Oil content was calculated on a weight basis.

**Extraction of Intact Glucosinolates.** Mustard seed and meal samples were ground and analyzed as schematically depicted in Figure 2. Prior to analysis, mustard samples were homogenized and milled

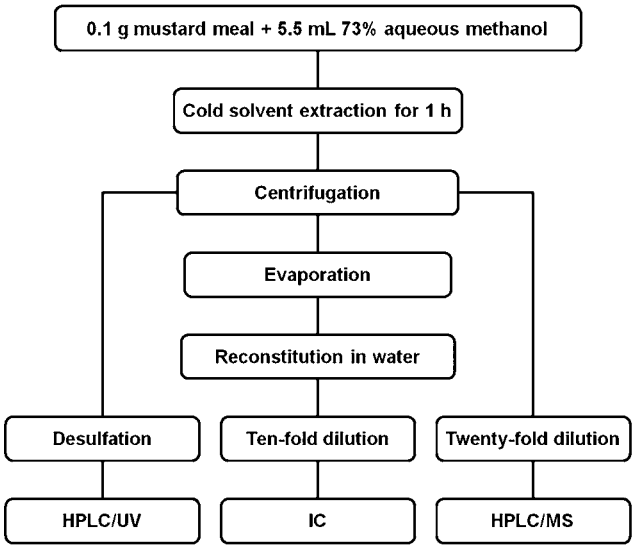


**Figure 2.** Scheme for optimization of the IC method for analysis of sinalbin and sinigrin in mustard seed meals.

with a coffee grinder to a fine powder. Seed meal (0.1 g) was extracted with 5.5 mL of 73% (v/v) methanol using an end-to-end shaker at room temperature for 1 h. To account for extraction recoveries, 1 mL of glucolimnanthin was added as an internal standard. Seed debris was separated by centrifugation at 2400 rpm for 20 min. An aliquot (1000 $\mu$L) of supernatant was (1) evaporated to dryness under a gentle stream of $N_2$ in a heating block at 60 °C, reconstituted in water, diluted 10 times with deionized water, and analyzed by IC; (2) diluted 20 times with deionized water and analyzed directly by HPLC/TOF MS; or (3) desulfated and analyzed by HPLC/UV.

**Desulfation of Glucosinolates for HPLC/UV Analysis.** Desulfation of intact glucosinolates was carried out according to the ISO 9167-1 procedure.[17] A 1-mL aliquot of the filtered methanol extract was transferred onto a column containing 500 mg of DEAE-Sephadex A-25 anion exchanger and allowed to drain freely. The column was washed twice with 1 mL of deionized water and finally with 1 mL of 0.1 M ammonium acetate buffer (pH 4.0). One hundred microliters of a 1 mg/L sulfatase enzyme (Sigma-Aldrich) solution was added to the column, the column was covered to prevent evaporation, and hydrolysis was allowed to continue for 12 h. Desulfated glucosinolates were eluted directly into 2-mL HPLC autosampler vials with two consecutive 1-mL volumes of deionized water.

**HPLC/DAD/TOF MS Analysis.** HPLC analysis was performed using an Agilent 1200 series HPLC with a diode array detection (DAD) system coupled to an Agilent G1969A TOF-MS equipped with an ESI source (Agilent, Santa Clara, CA, USA). Chromatographic separation of desulfated glucosinolates was conducted using a Phenomenex 4u Hydro-RP, 250 mm × 2 mm, 4 μm, column (Phenomenex, Torrance, CA, USA) maintained at 30 °C. The injection volume was 5 μL. The mobile phase consisted of water (solvent A) and acetonitrile (solvent B). The gradient elution program started with 2% B and followed a linear gradient to 30% B during a 30-min period, after which solvent B was increased to 70% in 1 min and held for 2 min; solvent B was then reduced to 2% at 32 min and held for 13 min. The flow rate was 0.25 mL/min. The UV signal was recorded at 229 nm with the reference set to 360 nm.

The chromatographic separation of intact glucosinolates was performed using a Zorbax XDB-C18, 50 mm × 4.6 mm, 1.8 μm, column (Agilent) maintained at 30 °C. The injection volume was 5 μL. The mobile phase consisted of 0.1% formic acid in water (solvent A) and 0.1% formic acid in methanol (solvent B). The gradient program started with isocratic elution using 5% B for 3 min, followed by a linear gradient to 70% B from 3 to 5 min, and then held at 70% B for 5 min; solvent B was then reduced to 5% at 10 min and held for 5 min. For the first 1.5 min of the analysis, the flow was diverted from the MS to prevent MS contamination and ion suppression with salts and other polar species. The flow rate was 0.4 mL/min, and spectra were recorded from 190 to 400 nm. Electrospray ionization was operated in the negative mode, and electrospray ionization potential was set at −3500 V. The collision-induced dissociation potential was set at 200 V. Gas temperature was 350 °C, drying gas ($N_2$) flow rate was 12 L/min, and nebulizer pressure was $2.4 \times 10^5$ Pa. Analyses were conducted in a profile mode with an $m/z$ range from 90 to 1000 amu. Quantification was performed using deprotonated molecules ($[M - H]^-$) with $m/z$ of 424.0378, 358.0272, and 438.0534 to quantify sinalbin, sinigrin, and glucolimnanthin, respectively.

**Ion Chromatographic Analysis of Intact Glucosinolates.** Ion chromatography was performed using Dionex Ion Analyzer (Dionex, Sunnyvale, CA, USA) equipped with a GP40 gradient pump, an ED40 electrochemical detector, and an AS40 autosampler. Three Dionex, 4 × 210 mm anion-exchange columns were tested: Ion-Pac AS11, Ion-Pac AS16, and Ion-Pac AS18. Sodium hydroxide (100 mM) was used as the mobile phase. Flow rate was varied from 0.5 to 0.9 mL/min. The detector stabilizer temperature was set at 30 °C with temperature compensation of 1.7% per °C. Anion suppressor current was set to 300 mA. The injection volume was 20 μL. The solution used for optimization included 1 mM sinigrin, 1.5 mM sinalbin, 1 mM glucolimnanthin, 0.1 mM $SO_4^{2-}$, and 0.25 mM $SCN^-$ in deionized water.

**Calibration Curves, Accuracy, and Precision.** Eight calibration standards (0.015625, 0.03125, 0.0625, 0.125, 0.25, 0.5, 1.0, and 2.0 mM) containing equimolar concentrations of sinigrin, sinalbin, $SO_4^{2-}$, and $SCN^-$ were included in calibration curves for glucosinolates and their hydrolysis products. Limits of detection (LOD) and limits of quantification (LOQ) for glucosinolates were determined under the optimized conditions for IC analysis based on a least-squares regression analysis as $3.3s_y/b$ and $10s_y/b$, respectively, where $b$ is the slope of the calibration curve and $s_y$ is the residual standard deviation of the regression line. The precision of the developed IC method was evaluated on the basis of intra- and interday reproducibility of analyses. The accuracy of the IC method for glucosinolate analysis was evaluated on the basis of statistical differences in IC concentrations compared to concentrations detected by the ISO 9167-1 HPLC/UV and HPLC/TOF MS methods.

**Matrix Effects, Analyte Recoveries, and Sample Stabilities.** The chemical compositions of the two mustard species are similar with the exception of the major glucosinolates. *B. juncea* contains sinigrin, but not sinalbin, and *S. alba* contains sinalbin, but not sinigrin. For evaluation of matrix effects, recovery, and sample stability, methanol extracts of *S. alba* (Sa_4) and *B. juncea* (Bj_5) were spiked with sinigrin and sinalbin, respectively, to yield a final glucosinolate concentration of 5 mM. Thus, for the evaluation of matrix effects on sinigrin, methanolic extracts of *S. alba* were used to prepare calibration standards. Similarly, methanolic extracts of *B. juncea* were used to evaluate matrix effects on sinalbin. Recoveries of analytes evaluated at three representative concentrations were expressed as percent of spiked concentrations in the extracts relative to concentrations of the same analytes prepared in water. Stabilities of the analytes were evaluated in *B. juncea* and *S. alba* extracts spiked with known amounts of sulfate, thiocyanate, and sinalbin or sinigrin, respectively. Analyte concentrations were quantified at 3, 6, 12, and 24 h after sample storage at room temperature.

Oil contents of mustard meals and seeds analyzed in the present study ranged from 18 to 46% (Table 1), thus potentially introducing additional matrix effects. To test for oil-introduced matrix effects, sinigrin in whole and defatted (DF) seed of Bj_5 and sinalbin in whole and DF seed of Sa_4 were quantified and respective samples of the same species compared.

A final concern was that the evaporation/reconstitution step included in the proposed IC method may cause glucosinolate loss (Figure 2). Sinigrin concentrations in three *B. juncea* samples (Bj_2, Bj_4, and Bj_5) were analyzed by HPLC/TOF MS to address this possibility. One set of extracts was evaporated and reconstituted in water as described previously under Extraction of Intact Glucosinolates (Figure 2), and another set of extracts were not evaporated, but diluted 20 times. Both sets of samples were analyzed using HPLC/TOF MS, and sinigrin concentrations in each respective sample were compared.

**Glucosinolate Hydrolysis in Solutions of Varied Methanol Concentrations.** For evaluation of sinalbin and sinigrin hydrolysis in methanol solutions, 0.1 g of seed (Sa_2 and Bj_4) was hydrolyzed for 1 h in 5.5 mL of solution containing 10, 40, or 70% methanol (v/v). Extracts were prepared and analyzed by IC as described under Ion Chromatographic Analysis of Intact Glucosinolates.

**Statistical Analysis.** All experiments were performed at least in triplicate and are presented as means ± one standard deviation. Calibrations were conducted both before and after the analysis of each sequence of samples. The accuracy of the proposed method was evaluated on the basis of statistical differences determined using one-way analysis of variance (ANOVA) with a $p < 0.05$ level of significance. Precision was evaluated using the relative standard deviations of standards at three representative concentrations as well as biological replicates. For evaluation of sample extract stability, mean values of peak areas for each analyte in freshly prepared samples were compared to corresponding peak areas at 3, 6, 12, and 24 h. Differences were assessed on the basis of Student's $t$-test. All analyses were performed using JMP software (version 10, SAS Institute Inc., Cary, NC, USA).

## RESULTS AND DISSCUSION

**Optimization of the IC Method.** IC conditions including anion-exchange column, mobile phase compositions, and the elution program were optimized to obtain baseline separation of mustard glucosinolates (sinigrin and sinalbin), their hydrolysis products ($SO_4^{2-}$ and $SCN^-$), and the internal standard (glucolimnanthin). All three Dionex anion-exchange columns evaluated for analyte separation were hydroxide-selective, cross-linked alkanol, quaternary ammonium-based columns. The Ion-Pac AS11 (45 μequiv) column has a low capacity, whereas Ion-Pac AS16 (170 μequiv) and Ion-Pac

AS18 (185 μequiv) columns have higher capacities. On the basis of preliminary results, conditions were initiated with 100 mM NaOH at a 0.5 mL/min flow rate.

The Ion-Pac AS11 column provided a good separation for inorganic anions; however, glucosinolates were not baseline separated under initial isocratic conditions (Table 2). When gradient elution (10−100 mM NaOH in 15 min) was used, the critical $SO_4^{2-}$/sinigrin pair could be valley separated, but not the glucolimnanthin/sinalbin pair. Glucolimnanthin and sinalbin have similar structures with comparable polarizabilities of 35.86 ± 0.5 × $10^{-24}$ and 37.83 ± 0.5 × $10^{-24}$ $cm^3$, respectively (calculated using ACDLabs 12, Advanced Chemistry Development Inc., Canada). Decreasing the gradient steepness from 6 to 4 mM NaOH/min resulted in unacceptable $SCN^-$ peak broadening and long run times. The use of Ion-Pac AS16 and Ion-Pac AS18 columns provided baseline separation of the five analytes under isocratic conditions (Table 2). Late-eluting sinalbin and $SCN^-$ peaks exhibited significant broadening on the Ion-Pac AS18 column (peak widths were 2.0 and 3.1 min, respectively), and their retention factors exceeded 20. The Ion-Pac AS16 column provided a reasonable run time as all five analytes were baseline separated in 13 min with retention factors ranging from 4.1 to 12.0 and resolutions ranging from 3.1 to 5.7. The Ion-Pac AS16 column was used for all subsequent analyses.

**Table 2. Performance Characteristics of Three Tested Anion-Exchange Columns for the Separation of Glucosinolates (Sinigrin, Sinalbin, and Glucolimnanthin) and Anionic Hydrolysis Products ($SO_4^{2-}$ and $SCN^-$)[a]**

| analyte | $t_r$ (min) | $T_f$ | $k$ | $N$ | $R_s$ |
|---|---|---|---|---|---|
| | | | **IonPac AS11** | | |
| sulfate | 2.6 | 1.0 | 1.6 | 1146 | na[b] |
| sinigrin | 2.9 | 1.2 | 1.9 | 1284 | 0.8 |
| glucolimnanthin | 3.6 | 0.8 | 2.6 | 7056 | 2.9 |
| sinalbin | 3.7 | 1.5 | 2.7 | 5040 | 0.8 |
| thiocyanate | 4.5 | 1.1 | 3.5 | 2374 | 2.7 |
| | | | **IonPac AS16** | | |
| sulfate | 5.1 | 1.6 | 4.1 | 4879 | na |
| sinigrin | 6.9 | 1.1 | 5.9 | 6540 | 5.7 |
| glucolimnanthin | 9.0 | 1.5 | 8.0 | 8100 | 5.7 |
| sinalbin | 11.2 | 1.4 | 10.2 | 5535 | 4.3 |
| thiocyanate | 13.0 | 1.2 | 12.0 | 7792 | 3.1 |
| | | | **IonPac AS18** | | |
| sulfate | 5.1 | 1.2 | 4.1 | 149 | na |
| sinigrin | 9.4 | 1.4 | 8.4 | 704 | 2.8 |
| glucolimnanthin | 19.8 | 2.0 | 18.8 | 2518 | 7.0 |
| sinalbin | 22.0 | 2.0 | 21.0 | 1912 | 1.2 |
| thiocyanate | 35.0 | 1.6 | 34.0 | 2040 | 5.1 |

[a]Separation was carried out in an isocratic mode with 100 mM NaOH at room temperature. $T_f$, tailing factor; $k$, retention factor; $N$, number of plates; $R_s$, resolution; $t_r$, retention time. [b]na, not applicable.

To increase throughput of the analysis, a series of runs with flow rates ranging from 0.5 to 0.9 mL/min were evaluated. An increase in flow rate of 0.1 mL/min resulted in a 10−12% decrease in retention time and a 6−14% decrease in peak width. Using a 0.9 mL/min flow rate, elution of the five analytes was achieved in 7.5 min with resolution and retention factors ranging from 2.4 to 5.4 and from 1.8 to 6.2, respectively. Thus, optimum conditions of the IC method were as follows: isocratic elution with 100 mM NaOH at a flow rate of 0.9 mL/min on a Dionex Ion-Pac AS16 column (Figure 3).

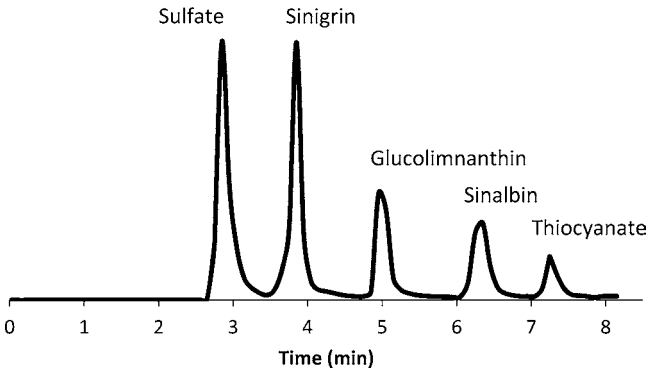


**Figure 3.** IC chromatogram for glucosinolates, $SCN^-$, and $SO_4^{2-}$ obtained using a 0.9 mL/min flow rate.

**Linearity and Detection and Quantification Limits of the IC Method.** Calibration curves for all analytes were linear for the entire calibration range (Table 3). Regression analysis of triplicates for each concentration level yielded correlation coefficients ($r$) of 0.9998 and 0.9986 for sinigrin and sinalbin, respectively. The LOD for sinigrin and sinalbin were 0.03 mM (Table 3). These LOD are comparable with those of the HPLC/UV method (0.06 mM) and up to 5 times higher than those of the HPLC/TOF MS method (0.01 mM).[20] The LODs for $SO_4^{2-}$ and $SCN^-$ were 0.02 and 0.04 mM, respectively. The LOQ for sinigrin, sinalbin, sulfate and thiocyanate were 0.09, 0.10, 0.07, and 0.09 mM, respectively.

When concentrations of sinigrin and sinalbin in the final solution are at the LOQ (0.09−0.10 mM), the corresponding concentrations in mustard meal would be 5.37 and 5.70 μmol/g meal (Table 3). The typical concentrations of glucosinolates in mustard meal are significantly higher and range from 60 to 220 μmol/g meal. Similarly, the concentrations of $SO_4^{2-}$ and $SCN^-$ in mustard hydrolysates are >200 times higher than the corresponding LOQ. Thus, the proposed IC method is sufficiently sensitive for the quantification of sinigrin and sinalbin concentrations in mustard meal. When concentrations of glucosinolates in mustard are expected to be low, 10-fold dilution of methanol extracts (Figure 2) can be omitted and more concentrated extracts can be analyzed.

**Precision.** Precision was evaluated by intraday and interday reproducibility of analysis. When standards were analyzed by the proposed method, intraday and interday relative standard deviations were 1.0−2.6 and 1.3−2.6%, respectively (Table 4 and Figure 4). The ranges of detected concentrations were 64−189 and 126−201 μmol/g in DF meal for sinigrin and sinalbin, respectively. The relative standard deviations for sinigrin were 2−9% and 2−6% for sinalbin. The precision of the IC method for both glucosinolates was comparable with those of the reference HPLC/UV method (1−7%) and the HPLC/TOF MS method developed in our laboratory (2−6%)[20] (Figure 4).

**Accuracy.** The accuracy of the proposed method was compared to that of the ISO HPLC/UV and HPLC/TOF MS methods for concentrations of sinigrin and sinalbin in the same respective samples (Figure 4). No differences in the concentrations of sinigrin and sinalbin detected by IC, HPLC/UV, and HPLC/TOF MS methods were observed.

**Matrix Effects and Analyte Recoveries.** When mustard meal is extracted, other compounds may be coextracted along

**Table 3. Calibration Curve Parameters, Limits of Detection (LOD), and Limits of Quantification (LOQ) for Two Intact Glucosinolates (Sinigrin and Sinalbin) and Anionic Hydrolysis Products ($SO_4^{2-}$ and $SCN^-$) As Determined by the Proposed IC Method**

| analyte | sinigrin | sinalbin | sulfate | thiocyanate |
|---|---|---|---|---|
| concentration range (mM) | 0.016−2.0 | 0.016−2.0 | 0.016−2.0 | 0.016−2.0 |
| slope | 1.12 | 1.21 | 4.13 | 1.61 |
| intercept | 0.00 | −0.01 | 0.01 | −0.02 |
| correlation coefficient | 0.9998 | 0.9991 | 0.9995 | 0.9997 |
| linearity (mM) | 0.03−2.0 | 0.01−2.0 | 0.03−2.0 | 0.01−2.0 |
| range (mM) | 0.08−2.0 | 0.09−2.0 | 0.08−2.0 | 0.08−2.0 |
| LOD (mM) | 0.03 | 0.03 | 0.02 | 0.04 |
| LOQ (mM) | 0.09 | 0.10 | 0.07 | 0.09 |
| LOD ($\mu$mol/g meal) | 1.6 | 1.9 | 1.2 | 1.6 |
| LOQ ($\mu$mol/g meal) | 5.0 | 5.8 | 3.7 | 5.0 |

**Table 4. Reproducibility and Recovery of Two Intact Glucosinolates (Sinigrin and Sinalbin) and Anionic Hydrolysis Products ($SO_4^{2-}$ and $SCN^-$) As Determined by the Proposed IC Method**

| concentration (mM) | sinigrin | sinalbin | sulfate | thiocyanate |
|---|---|---|---|---|
| | Intraday Reproducibility (Relative Standard Deviation) | | | |
| 0.1 | 1.1 | 1.3 | 2.1 | 2.1 |
| 0.5 | 1.5 | 1.2 | 2.2 | 2.6 |
| 1.0 | 1.2 | 1.0 | 1.9 | 2.2 |
| | Interday Reproducibility (Relative Standard Deviation) | | | |
| 0.1 | 1.3 | 1.5 | 2.6 | 2.4 |
| 0.5 | 2.1 | 1.9 | 2.3 | 2.5 |
| 1.0 | 2.4 | 1.4 | 2.2 | 2.0 |
| | Recovery (%) | | | |
| 0.1 | 85 ± 1 | 98 ± 8 | 101 ± 3 | 87 ± 9 |
| 0.5 | 100 ± 1 | 95 ± 1 | 98 ± 3 | 83 ± 1 |
| 1.0 | 102 ± 4 | 95 ± 4 | 101 ± 2 | 95 ± 1 |

with glucosinolates including proteins, phenolics, and carbohydrates.[21,22] Whereas only anions are detected by IC, positively charged and neutral compounds may affect detected concentrations of target analytes. For example, if glucosinolates are strongly associated with other matrix components, they may not be quantified by IC.[23]

First, the effect of coextracted matrix components was evaluated (Table 4). Recoveries for all four analytes at three representative concentrations ranged from 83 to 102% as determined by comparing conductivity peak areas for each calibration standard spiked with mustard extracts containing the corresponding standard prepared in deionized water (Table 4).

The effect of oil content in mustard seed on method performance was then evaluated. Concentrations of sinigrin in whole mustard seed (sample Bj_5) with 40% oil content did not differ significantly from sinigrin concentrations in the same DF seed meal (155 ± 4 vs 152 ± 2 $\mu$mol/g DF meal, respectively). Concentrations of sinalbin in whole mustard seed (sample Sa_4) with 29% oil content did not differ significantly from sinigrin concentrations in the same DF seed meal (165 ± 3 vs 165 ± 2 $\mu$mol/g DF meal, respectively) (data not shown). These results demonstrate that the proposed method can be used for the analysis of mustard meals with a wide range of oil contents. The possibility of analysis with no required oil removal shortens overall analysis time.

Finally, the effect of methanol evaporation on glucosinolate concentrations was evaluated. The two most commonly used

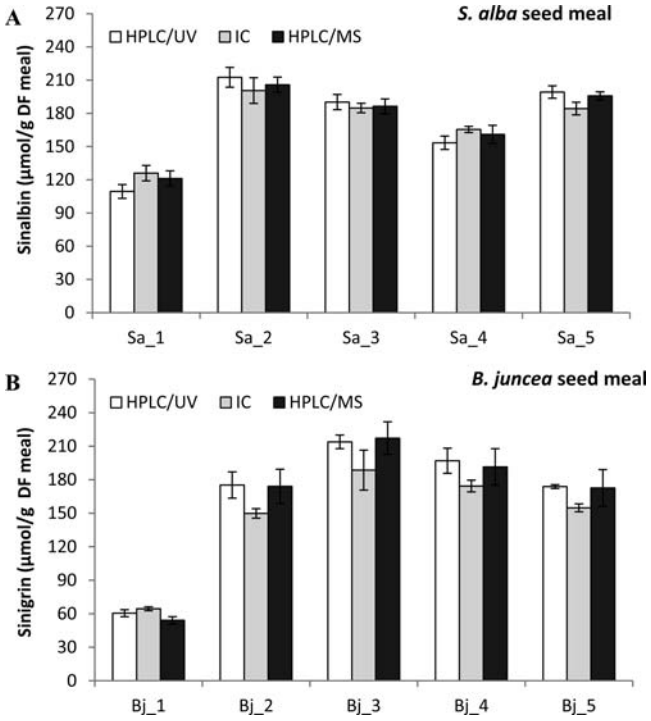


**Figure 4.** Concentrations of sinalbin in *S. alba* Sa_1−Sa_5 samples (A) and sinigrin in *B. juncea* Bj_1− Bj_5 samples (B) in mustard meal determined by the developed IC method as compared with ISO 9167-1 HPLC/UV and HPLC/TOF MS methods. Concentration is expressed as a mean value of three replicates with a verticle line representing the associated standard deviation for that mean.

procedures for the extraction of intact glucosinolates from mustard meals are extraction with boiling water and extraction with 73% aqueous methanol. High temperature and methanol prevent enzymatic hydrolysis of intact glucosinolates by myrosinase naturally present in mustard. When glucosinolates are extracted by boiling water, the filtered supernatant can be analyzed by IC with no additional sample preparation. However, during boiling extraction mustard meal can swell up to 400% by weight and a colloidal suspension may be formed. Also, a significant amount of protein (constituting up to 45% of mustard meal by weight) coextracted by boiling water may interfere with analysis and typically requires precipitation with lead acetate or barium acetate.[24] The use of methanol reduces the formation of colloids and minimizes coextraction of proteins. However, when aqueous methanol is used, methanol should be removed, and extracts require

reconstitution in water prior to IC injection. On the basis of the HPLC/TOF MS analysis of methanolic *B. juncea* extracts and corresponding evaporated and reconstituted in water extracts, no significant differences were found and, consequently, no loss of glucosinolates by evaporation was observed (Figure 5). The relative standard deviation for both sets of extracts did not exceed 8%.

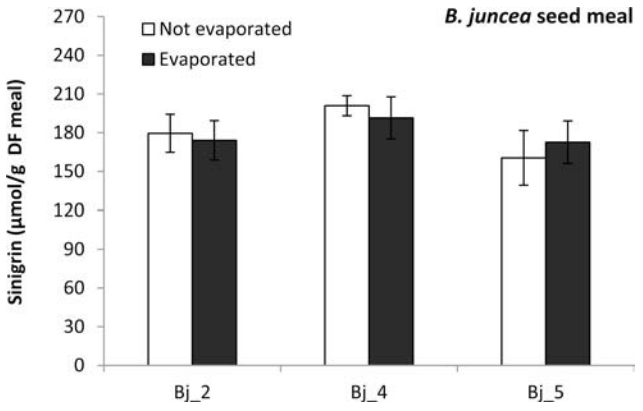


**Figure 5.** Effect of evaporation on sinigrin concentrations in *B. juncea* seed meal (Bj_2, Bj_4, and Bj_6 meal samples) as determined by the HPLC/TOF MS method. Concentration is expressed as a mean value of three replicates with a verticle line representing the associated standard deviation for that mean.

**Stability of Sample Extracts.** The stability of the extracts was evaluated during a 24 h time period, which is a reasonable time interval for sample preparation and analysis that includes a sample preparation time of <90 min and an analysis run time of 10 min (Figure 6). Samples of three representative concentrations (0.1, 0.5, and 1.0 mM) covering the expected concentration range of detected glucosinolates in mustard meal extracts were analyzed immediately after preparation and again at 3, 6, 12, and 24 h. On the basis of the results of Student's *t*-test, peak areas of all four analytes at the three representative concentrations were not significantly different from the corresponding peak areas of freshly prepared samples (Figure 6).

**Glucosinolate Hydrolysis in Solutions of Varied Methanol Concentrations.** One application for the proposed method is monitoring glucosinolate hydrolysis during extraction of biopesticidal compounds from mustard meal. To prepare extracts with the highest concentration of biologically active compounds, glucosinolate hydrolysis and recoveries of hydrolysis products are monitored. Intact glucosinolates are typically extracted with 70% methanol, whereas lower methanol concentrations result in partial glucosinolate hydrolysis and the associated production of multiple hydrolysis products. Thus, to demonstrate the applicability of the proposed IC method, we assessed the extent of glucosinolate extraction and hydrolysis in aqueous solutions containing 10, 40, and 70% methanol by quantifying sinigrin, sinalbin, $SCN^-$, and $SO_4^{2-}$ by the proposed IC method (Figure 7). On the basis of stoichiometric conversion of glucosinolates to $SO_4^{2-}$ (Figure 1), the mass balance was within 90% of that expected for both mustards (Figure 7). For *S. alba* seed, the use of $SCN^-$ or $SO_4^{2-}$ resulted in similar total moles of products. These results demonstrate the use of ion chromatography for simultaneous analysis of intact mustard glucosinolates and their anionic hydrolysis products, providing a technique with high utility for studies involving the hydrolysis of glucosinolates contained in mustard seed and seed meals.

The proposed method can be used for the fast analysis of intact glucosinolates in mustard seeds and meals for screening and quality control. The method may also be useful for

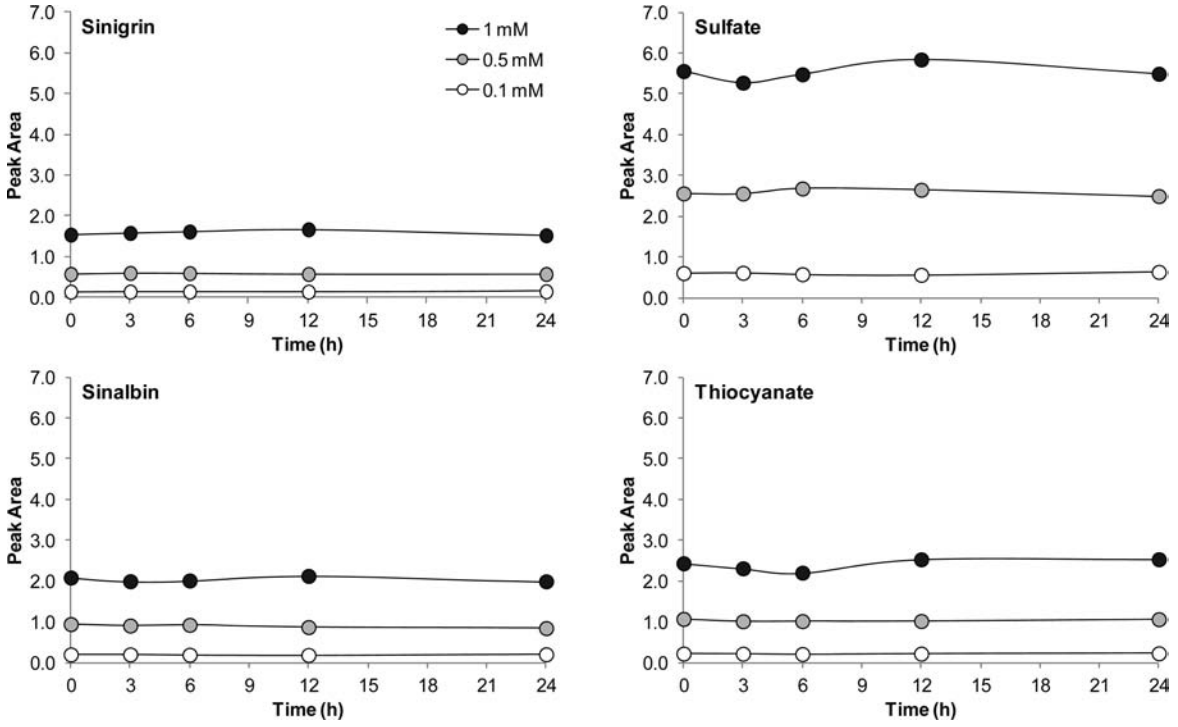


**Figure 6.** Stability of mustard glucosinolates $SO_4^{2-}$ and $SCN^-$ in sample extracts within 24 h of sample preparation. Peak areas are expressed as a mean value of three replicates. Standard deviations are smaller than the symbol for each respective mean and are therefore not shown.

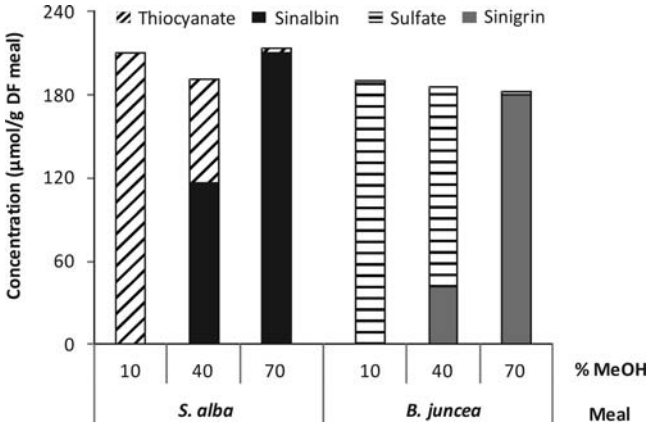


**Figure 7.** Concentrations (μmol/g DF meal) of intact glucosinolates and anionic hydrolysis products in *S. alba* and *B. juncea* hydrolysates with different methanol contents.

studying enzyme kinetics using glucosinolate−myrosinase systems. To the best of our knowledge, the proposed IC procedure is the only reported method that allows for simultaneously monitoring intact glucosinolates and their anionic hydrolysis products in the same sample extract in one chromatographic run.

## AUTHOR INFORMATION

### Corresponding Author

*(I.E.P.) Phone: (208) 885-4953. Fax: (208) 885-7760. E-mail: ipopova@uidaho.edu.

### Funding

This project was supported by Agriculture and Food Research Initiative competitive grant 2011-67009-20094 from the USDA National Institute of Food and Agriculture.

### Notes

The authors declare no competing financial interest.

## REFERENCES

(1) Heap, The International Survey of Herbicide Resistant Weeds; http://www.weedscience.org (accessed June 2, 2014).

(2) Ferguson, G. M.; Hamill, A. S.; Tardif, F. J. ALS inhibitor resistance in populations of Powell amaranth and redroot pigweed. *Weed Sci.* **2001**, *49*, 448−453.

(3) Hoy, M. A. Myths, models and mitigation of resistance to pesticides. *Philos. Trans. R. Soc. London B* **1998**, *353*, 1787−1795.

(4) Datta, A.; Knezevic, S. Z. Chapter 6. Flaming as an alternative weed control method for conventional and organic agronomic crop production systems: a review. In *Advances in Agronomy*; Donald, L. S., Ed.; Academic Press: San Diego, CA, USA, 2013; Vol. 118, pp 399−428.

(5) Boydston, R. A.; Morra, M. J.; Borek, V.; Clayton, L.; Vaughn, S. F. Onion and weed response to mustard (*Sinapis alba*) seed meal. *Weed Sci.* **2011**, *59*, 546−552.

(6) Yu, J.; Morishita, D. W. Response of seven weed species to corn gluten meal and white mustard (*Sinapis alba*) seed meal rates. *Weed Technol.* **2014**, *28*, 259−265.

(7) Avato, P.; D'Addabbo, T.; Leonetti, P.; Argentieri, M. P. Nematicidal potential of Brassicaceae. *Phytochem. Rev.* **2013**, *12*, 791−802.

(8) Beckie, H. J.; Johnson, E. N.; Blackshaw, R. E.; Gan, Y. Weed suppression by canola and mustard cultivars. *Weed Technol.* **2008**, *22*, 182−185.

(9) Brown, J.; McCaffrey, J. P.; Harmon, B. L.; Davis, J. B.; Brown, A. P.; Erickson, D. A. Effect of late season insect infestation on yield, yield components and oil quality of *Brassica napus*, *B. rapa*, *B. juncea* and *Sinapis alba* in the Pacific Northwest region of the United States. *J. Agric. Sci.* **1999**, *132*, 281−288.

(10) Rosa, E.; Heaney, R.; Fenwick, G.; Portas, C. Glucosinolates in crop plants. *Hortic. Rev.* **1997**, *19*, 99−215.

(11) Borek, V.; Morra, M. J. Ionic thiocyanate ($SCN^-$) production from 4-hydroxybenzyl glucosinolate contained in *Sinapis alba* seed meal. *J. Agric. Food Chem.* **2005**, *53*, 8650−8654.

(12) Hansson, D.; Morra, M. J.; Borek, V.; Snyder, A. J.; Johnson-Maynard, J. L.; Thill, D. C. Ionic thiocyanate ($SCN^-$) production, fate, and phytotoxicity in soil amended with Brassicaceae seed meals. *J. Agric. Food Chem.* **2008**, *56*, 3912−3917.

(13) Dai, R.; Lim, L.-T. Release of allyl isothiocyanate from mustard seed meal powder. *J. Food Sci.* **2014**, *79*, E47−E53.

(14) Dosz, E. B.; Ku, K. M.; Juvik, J. A.; Jeffery, E. H. Total myrosinase activity estimates in Brassica vegetable produce. *J. Agric. Food Chem.* **2014**, *62*, 8094−8100.

(15) Hennig, K.; Verkerk, R.; Dekker, M.; Bonnema, G. Quantitative trait loci analysis of non-enzymatic glucosinolate degradation rates in *Brassica oleracea* during food processing. *Theor. Appl. Genet.* **2013**, *126*, 2323−2334.

(16) Bones, A. M.; Rossiter, J. T. The myrosinase-glucosinolate system, its organisation and biochemistry. *Physiol. Plant.* **1996**, *97*, 194−208.

(17) ISO 9167-1: Rapeseed − Determination of glucosinolate content − Part 1: Method using high-performance liquid chromatography, 1992.

(18) Campbell, L. D.; Slominski, B. A. Extent of thermal-decomposition of indole glucosinolates during the processing of canola seed. *J. Am. Oil Chem. Soc.* **1990**, *67*, 73−75.

(19) Bell, J. M.; Keith, M. O. A survey of variation in the chemical-composition of commercial canola-meal produced in western canadian crushing plants. *Can. J. Anim. Sci.* **1991**, *71*, 469−480.

(20) Popova, I. E.; Morra, M. J. High performance liquid chromatography/time-of-flight mass spectrometry for fast quantification of sinigrin and sinalbin in mustard seed. *J. Food Compos. Anal.* **2014**, *35*, 120−126.

(21) Dubie, J.; Stancik, A.; Morra, M.; Nindo, C. Antioxidant extraction from mustard (*Brassica juncea*) seed meal using high-intensity ultrasound. *J. Food Sci.* **2013**, *78*, E542−E548.

(22) Katepa-Mupondwa, F.; Raney, J. P.; Rakow, G. Recurrent selection for increased protein content in yellow mustard (*Sinapis alba* L.). *Plant Breed.* **2005**, *124*, 382−387.

(23) Bjergegaard, C.; Buskov, S.; Sørensen, H.; Soerensen, M.; Soerensen, S. Reactions between glucosinolate products and thiol groups in food components. *Czech. J. Food Sci.* **2000**, *18*, 193−195.

(24) Marnoch, R.; Diosady, L. L. Production of mustard protein isolates from oriental mustard seed (*Brassica juncea* L.). *J. Am. Oil Chem. Soc.* **2006**, *83*, 65−69.

and pancreatin were purchased from Wako Pure Chemical Industries Ltd. (Osaka, Japan). Phosphatidylcholine and lysozyme (Ly) were obtained from Kewpie Corp. (Tokyo, Japan).

**Animals, Diets, and Permanent Thoracic Lymph Duct Cannulation.** Seven-week-old male Sprague−Dawley rats (Kud:SD) were obtained from Kyudo (Kumamoto, Japan). The rats were housed individually in metal cages in a temperature-controlled room (21−23 °C) under a 12 h light/dark cycle. Experimental diets were prepared according to the recommendations of the AIN-93G[17] and contained the following ingredients (in weight, %): casein or EWP (20), $\alpha$-cornstarch (13.2), sucrose (10), cellulose (5), mineral mixture (3.5), vitamin mixture (1), choline bitartrate (0.25), soybean oil (7), cholesterol (0.5), cholic acid (0.125), *tert*-butylhydroquinone (0.0014), and $\beta$-cornstarch (39.4236). The rats were trained to consume the casein diet as a basal diet twice a day from 10:00 to 11:00 a.m. and from 4:00 to 5:00 p.m., respectively, for 5 days. On day 6, the rats were anesthetized using nembutal before permanent cannulation of the thoracic duct lymph, as described previously.[14,15] In brief, a cannula [SH silicon tube, 0.5 mm inner diameter (i.d.) and 1.0 mm outer diameter (o.d.), Kaneka Medics, Osaka, Japan] filled with heparinized saline was inserted into the thoracic duct and secured within the abdominal cavity. After surgery, the rats were returned to their cages and provided free access to isotonic glucose solution (139 mM glucose and 85 mM NaCl in distilled water). On days 7 and 8, the rats were provided with the casein diet twice a day, as described. On day 9, the rats were attached to a long polyethylene cannula (0.58 mm i.d. and 0.97 mm o.d.; Becton, Dickinson, and Co., Franklin Lakes, NJ, USA). The end of the cannula was 5−10 cm below the bottom of the cage to allow the lymph to drain. After a 20 min collection period, the rats were provided free access to the casein diet or the EWP diet for 30 min. Then, the lymph was collected every hour for 7 h. The rats had free access to deionized water throughout the feeding periods and during lymph collection. The collected lymph was maintained at 4 °C overnight before the fibrin was removed, and the samples were stored at −30 °C until lipid analysis. Following lymph collection, the rats were anesthetized with nembutal and sacrificed by exsanguination. This experiment was conducted according to the Guidelines for Animal Experiments of Kyushu University (Fukuoka, Japan) and the law (no. 105) and notification (no. 6) of the government of Japan. The authorization number was A19-195-0.

**Lymphatic Lipid Transport Measurement.** Total cholesterol, triacylglycerol (TAG), and phospholipid levels in the lymph were measured using commercial enzyme assay kits (T-CHO Kainos from Kainos Laboratories, Inc., Tokyo, Japan; Triglyceride E-Test and Phospholipid C-Test from Wako Pure Chemicals, Tokyo, Japan). If the lymphatic lipid levels exceeded the range of a standard curve, the lymph was diluted with physiological saline and retested.

**Preparation of Micellar Solutions.** Micellar solutions containing 6.6 mM sodium taurocholate, 0.6 mM phosphatidylcholine, 50 $\mu$M cholesterol, 1.0 mM oleic acid, 0.5 mM monoolein, and 132 mM NaCl in 15 mM sodium phosphate buffer (pH 6.8) were prepared by sonication. The micelles were passed through a 0.2 $\mu$m syringe filter (DISMIC-25CS, Toyo Roshi Kaisha Ltd., Tokyo, Japan) and maintained at 37 °C for 24 h for stabilization of the micelles.

**Preparation of Casein, EWP, and EWP Constituent Protein Hydrolysates.** Ten grams of casein, EWP, OA, OT, OM, and Ly was hydrolyzed by 400 mL of experimental gastric juice [0.1% (w/v) pepsin in 100 mM KCl] at pH 2.0 with HCl and 37 °C for 24 h.[18] The reaction mixtures were adjusted to pH 7.0 with 1 M KOH, freeze-dried, and powdered to obtain casein pepsin hydrolysate (C-ph), EWP pepsin hydrolysate (EWP-ph), OA pepsin hydrolysate (OA-ph), OT pepsin hydrolysate (OT-ph), OM pepsin hydrolysate (OM-ph), and Ly pepsin hydrolysate (Ly-ph). The degree of hydrolysis of casein and EWP was determined by SDS-PAGE. The protein content of casein, C-ph, EWP, and EWP-ph was determined according to the method discussed by Lowry et al.[19] The samples in the SDS-PAGE sample buffer were incubated at 95 °C for 5 min using a thermal cycler, and 5 $\mu$g of protein from each sample was then electrophoresed on a 5−20% gradient polyacrylamide gel. The gel was stained using a silver staining kit (Wako Pure Chemical Industries Ltd.).

**Micellar Solubility of Cholesterol in Vitro.** The micellar solubility of cholesterol was measured according to the method of Ikeda et al.[20] A solution containing C-ph, EWP-ph, ovalbumin, ovotransferrin, ovomucoid, or lysozyme was added to the micelles. In the experiments shown in Figure 3A,C, the samples were added at a final concentration of 10 mg/mL to the micelles. In the experiment shown in Figure 4A, the samples were added at a final concentration of 5 mg/mL to the micelles. In the experiment shown in Figure 4B, EWP-ph was added at a final concentration of 10 mg/mL to the micelles, whereas the reconstituted EWP-ph was added at a final concentration of 8 mg/mL to the micelles. In accordance with a previous study,[21] the reconstituted EWP-ph included 54% OA-ph, 13% OT-ph, 11% OM-ph, and 3.5% Ly-ph. The samples were incubated at 37 °C for 1 h and passed through the 0.2 $\mu$m syringe filter. In the experiment shown in Figure 3A, pancreatin was added at a final concentration of 0.15 mg/mL during the incubation time. After lipid extraction from the filtrate, cholesterol levels were measured by gas chromatography (GC).[20]

**Transfer of Cholesterol from the Bile Acid Micelle to Triolein.** The transfer rate of triolein to cholesterol was measured according to the method of Hamada et al.[22,23] One and a half milliliters of the micellar solution, 0.5 mL of triolein, and C-ph or EWP-ph (final concentration, 10 mg/mL) were placed in a plastic tube, which was flushed with $N_2$ and sealed. The tubes were incubated at 37 °C for 1 h with shaking. After incubation, the contents of each tube were transferred to a sealed tube, and the oil and aqueous phases were separated by centrifugation at 100000*g* for 1 h at 37 °C. The oil and micellar phases were collected, and the cholesterol levels in each phase were analyzed by GC using 5$\alpha$-cholestane as an internal standard.

**Water-Holding Capacities (WHCs) of Casein, EWP, and Its Pepsin Hydrolysate.** The WHCs of casein, EWP, C-ph, and EWP-ph were measured as described previously.[24] Samples (0.1 g) were placed on two filter papers fitted in a stainless steel container (hole diameter, 2.5 cm; diameter, 5 cm; height, 1.5 cm) with a polypropylene net. This weight was measured as dry weight. After being placed in a case with distilled water for 24 h at room temperature, the container was removed and weighed. The WHCs of casein, EWP, C-ph, and EWP-ph were evaluated by measuring the difference between the wet and dry weights. Each measurement was repeated three times.

**Settling Volumes (SVs) in Water of Casein, EWP, and Its Pepsin Hydrolysate.** The SVs of casein, EWP, C-ph, and EWP-ph were measured as described previously.[24] Samples (7 mg) were blended with 7 mL of distilled water in 10 mL graduated cylinders. The cylinders were left to stand for 24 h at room temperature. The SVs of casein, EWP, C-ph, and EWP-ph were evaluated on the basis of precipitation volume. Each measurement was repeated three times.

**Viscosities of Casein, EWP, and Its Pepsin Hydrolysate.** The viscosities of casein, EWP, C-ph, and EWP-ph were measured using an Ostwald viscometer (Sansyo Co., Ltd., Tokyo, Japan) with a 0.75 mm capillary diameter, as described previously.[24] Samples (1 g) were blended with distilled water. After being stored for 24 h at room temperature, 1% (v/v) suspending solutions were prepared in 100 mL volumetric flasks. The solutions were preheated at 37 °C for 15 min and the flow times determined. Each measurement was repeated three times. The viscosities of casein, EWP, C-ph, and EWP-ph were calculated relative to the viscosity of distilled water.

**Statistical Analysis.** All values are expressed as the mean ± standard error of mean (SEM). Comparisons between two groups were performed by Student's *t* test, whereas those among more than three groups were performed by using one-way ANOVA followed by the Tukey−Kramer multiple-comparison post hoc test. Differences were considered to be significant at $P < 0.05$. Statistical analysis was performed using StatView version 4.5 (Abacus Concept Inc., Berkeley, CA, USA).

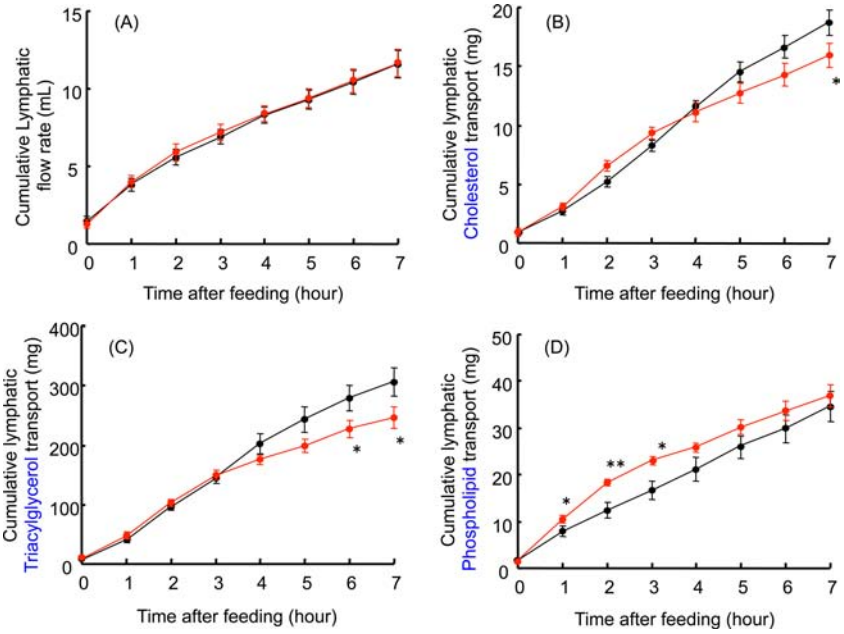


**Figure 1.** Cumulative lymph flow (A), lymphatic transport of cholesterol (B), triacylglycerol (C), and phospholipids (D) in rats fed diets containing casein (black circles) or EWP (red circles). Values are expressed as the mean ± SEM for six rats. (∗) $P < 0.05$ and (∗∗) $P < 0.01$ versus casein group by Student's $t$ test.

## RESULTS

**Effects of Dietary EWP on Lymphatic Lipid Transport.** The two groups of rats did not differ in final body weight (casein, 232.3 ± 3.7; EWP, 228.4 ± 6.5 g). The rats consumed the casein and EWP diets for 30 min (4.6 ± 0.3 and 4.4 ± 0.4 g, respectively). Figure 1 shows the cumulative lymph flow and lipid transport. There was no significant difference in lymph flow (Figure 1A). The lymphatic transport of total cholesterol at 7 h (Figure 1B) and TAG at 6 and 7 h (Figure 1C) after feeding was significantly decreased in the EWP group compared with that in the casein group. In addition, the lymphatic transport of phospholipids at 1, 2, and 3 h after feeding was significantly increased in the EWP group compared with that in the casein group (Figure 1D).

**Degree of Hydrolysis of Casein and EWP by Pepsin.** Figure 2 shows the degree of hydrolysis of casein and EWP by pepsin. Two bands were recognized in the gel. These bands were identified as ovalbumin (45 kDa) and lysozyme (14.3 kDa) in EWP-ph.[25] The casein was almost digested with pepsin.

**Effects of EWP Pepsin Hydrolysate and EWP Constituent Protein Pepsin Hydrolysates on the Micellar Solubility of Cholesterol.** EWP-ph significantly inhibited the micellar solubility of cholesterol to a greater extent than C-ph did (Figure 3A). There was no effect of pancreatin on micellar solubility (Figure 3A). The inhibitory effect of EWP-ph on micellar solubility was dose-dependent and reached a plateau at a final concentration of 10 mg/mL (Figure 3B). There was no effect of the presence of phosphatidylcholine in bile acid micelles on micellar solubility (Figure 3C). Compared with C-ph, EWP-ph, OA-ph, and OT-ph significantly inhibited micellar solubility (Figure 4A). Furthermore, there was no significant difference in micellar solubility between EWP-ph and reconstructed EWP-ph (Figure 4B).

**Effects of EWP on Transfer of Cholesterol from Micelles to Triolein.** EWP-ph significantly inhibited the transfer of cholesterol from micelles to triolein (Figure 5). That is, EWP-ph inhibited cholesterol monomer release from micelles.

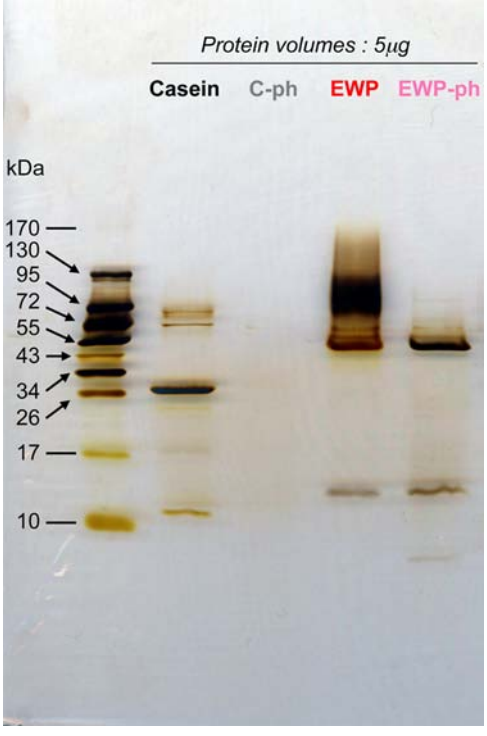


**Figure 2.** Results of electrophoresis of casein, EWP, and its pepsin hydrolysate.

**Effects of EWP and Its Pepsin Hydrolysate on Water-Holding Capacity, Settling Volume in Water, and Relative Viscosity.** Table 1 summarizes the effects of EWP and its pepsin hydrolysate on WHC, SV, and relative viscosity. There was no significant difference in WHC between casein and EWP. However, the WHC of EWP-ph was approximately

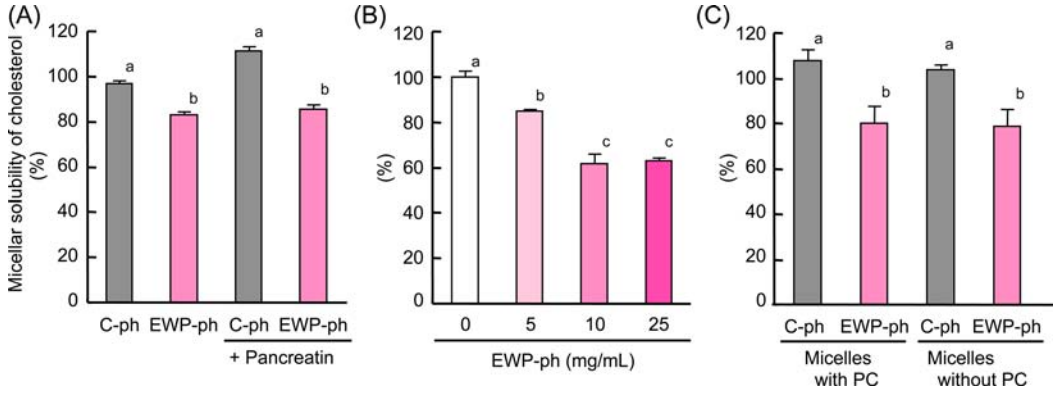


**Figure 3.** Effects of EWP hydrolysate on the micellar solubility of cholesterol in vitro: (A) effects of EWP pepsin hydrolysate or EWP pepsin + pancreatin hydrolysate; (B) dose-dependent effects of EWP pepsin hydrolysate; (C) effects of phosphatidylcholine containing the micelles. C-ph, casein pepsin hydrolysate; EWP-ph, egg white protein pepsin hydrolysate; PC, phosphatidylcholine. Data were calculated using the following formula: micellar cholesterol contents incubated with protein/micellar cholesterol contents incubated without protein × 100. Values are expressed as the mean ± SEM for three samples. Different letters (a–c) show a significant difference by the Tukey–Kramer test ($P < 0.05$).

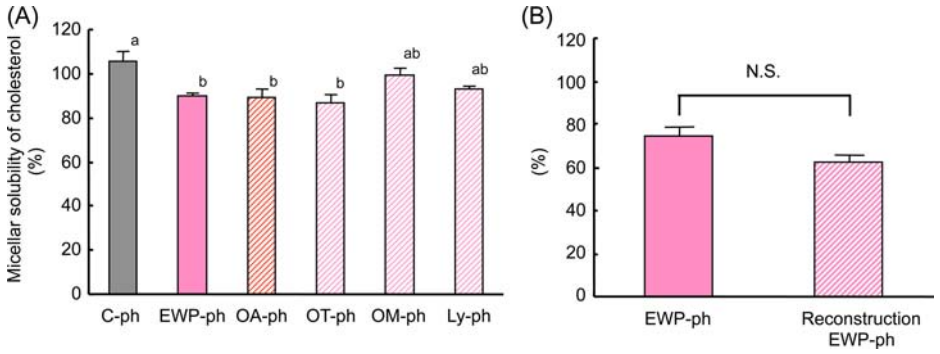


**Figure 4.** Effects of EWP constituent protein pepsin hydrolysates and reconstructed EWP-ph on the micellar solubility of cholesterol in vitro: (A) effects of EWP-ph and EWP constituent protein pepsin hydrolysates (each protein was added at a final concentration of 5 mg/mL); (B) effects of EWP-ph and reconstruction EWP-ph (reconstructed EWP-ph included 54% OA-ph, 13% OT-ph, 11% OM-ph, and 3.5% Ly-ph; EWP-ph was added at a final concentration of 10 mg/mL; reconstruction EWP-ph was added at a final concentration of 8 mg/mL). C-ph, casein pepsin hydrolysate; EWP-ph, egg white protein pepsin hydrolysate; OA-ph, ovalbumin pepsin hydrolysate; OT-ph, ovotransferrin pepsin hydrolysate; OM-ph, ovomucoid pepsin hydrolysate; Ly, lysozyme pepsin hydrolysate. Data were calculated using the following formula: micellar cholesterol contents incubated with protein/micellar cholesterol contents incubated without protein × 100. Values are expressed as the mean ± SE for three samples. Different letters(a–c) show a significant difference by the Tukey–Kramer test ($P < 0.05$).

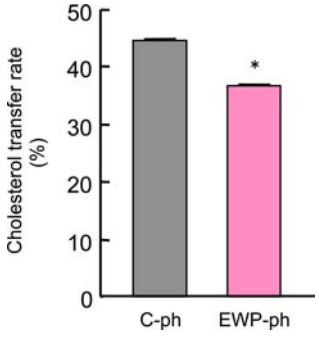


**Figure 5.** Effects of EWP-ph on the transfer of micellar cholesterol to triolein in vitro. Data were calculated using the following formula: cholesterol contents in the triolein phase/original micellar cholesterol contents × 100. Values are expressed as the mean ± SEM for three samples. (*) $P < 0.05$ versus casein group by Student's $t$ test.

7.6 times higher than that of C-ph. In addition, the SV of casein was higher than that of EWP, whereas the SV of EWP-ph was approximately 4.5 times higher than that of C-ph. In accordance with the behavior of SV, the relative viscosity of casein was higher than that of EWP, whereas that of EWP-ph was significantly higher than that of C-ph.

## DISCUSSION

We confirmed that dietary EWP inhibited intestinal cholesterol absorption in thoracic lymph duct-cannulated rats (Figure 1B). These data supported the serum and hepatic cholesterol-lowering action of EWP in our previous paper.[11] In that previous paper, evidence for the inhibition of cholesterol absorption was the fecal excretion of neutral steroids in rats fed the 20% EWP diet compared with that in rats fed the 20% casein diet. Most of the dietary lipids are absorbed in the proximal small intestine and then transported by the lymphatic system. We hypothesized that EWP hydrolysate by pepsin in the stomach may play a major contributing role to the inhibition of cholesterol absorption by EWP. To test the hypothesis, we prepared EWP-ph and then conducted the in vitro experiments. The results showed that EWP-ph inhibited the micellar solubility of cholesterol (Figures 3A–C and 4A) and cholesterol monomer release from micelles (Figure 5). In addition, there was no effect of pancreatin on the micellar solubility of cholesterol (Figure 3A).

Table 1. Water-Holding Capacities, Settling Volumes in Water, and Relative Viscosities of Casein, EWP, and Its Pepsin Hydrolysate[a]

| | casein | EWP | C-ph | EWP-ph |
|---|---|---|---|---|
| water-holding capacity [wet (g)/dry (g)] | 2.87 ± 0.03a | 2.87 ± 0.13a | 0.32 ± 0.09b | 2.11 ± 0.09c |
| settling volume (mL/g) | 4.14 ± 0.22a | 0.95 ± 0.13b | 1.80 ± 0.17b | 8.09 ± 0.34c |
| relative viscosity ($\eta$) | 1.115 ± 0.000a | 1.096 ± 0.001b | 1.054 ± 0.001c | 1.059 ± 0.001d |

[a]Different letters (a–d) show a significant difference by the Tukey–Kramer test. Mean ± SE of three samples.

The hypocholesterolemic manners of EWP resemble those of plant sterols, which have hypocholesterolemic activity.[12,23] The efficiency of lymphatic cholesterol transport inhibition by $\beta$-sitosterol, a major plant sterol, was 57% in thoracic lymph duct-cannulated rats administered lipid emulsions in the stomach.[12] The efficiency of a hypocholesterolemic effect of $\beta$-sitosterol in rats fed a 0.5% cholesterol-containing diet for 2 weeks was 21%.[26] According to a comparison of these calculated data, it was estimated that dietary $\beta$-sitosterol inhibited intestinal cholesterol absorption more strongly than dietary EWP did. However, the hypocholesterolemic effect of dietary plant sterol was similar to that of dietary EWP. To assess intestinal lipid absorption, the administration of two types of diets containing lipids and infusion lipid emulsions into the stomach or duodenum was used. The method that used lipid emulsions failed to consider the interaction of the lipid emulsion with other dietary components, particularly proteins and carbohydrates.[27] Therefore, differences in the methods of administration may contribute to the fact that the hypocholesterolemic effects of dietary plant sterols and EWP were similar. Otherwise, EWP may have other functions for the hypocholesterolemic effect. It has been reported that a commercially available EWP hydrolysate produced by microbial proteases, with an average molecular weight of approximately 1100, as well as EWP, have hypocholesterolemic effects in rats and mice.[28] In this study, the hypocholesterolemic effect of EWP through its physicochemical properties depended on its protein structure, which resisted protease digestion in the gut and inhibited intestinal cholesterol absorption. The commercial EWP hydrolysate primarily comprises peptides and amino acids. The hypocholesterolemic effect of the hydrolysate may be exerted on the intestinal mucosa after absorption as smaller size peptides except for the physiological properties of the hydrolysate described above.

Many studies have reported that other dietary proteins such as soy protein isolate[29] and whey protein[30] can provide several peptides that can exert a hypocholesterolemic effect. Therefore, some peptides derived from EWP may have a hypocholesterolemic effect inside animal bodies. In this study, the efficiency of the inhibition of lymphatic cholesterol transport was approximately 14%. In the previous study, the decrease in serum cholesterol levels in rats fed the EWP diet was approximately 17%.[11] The serum cholesterol-lowering activities of several dietary proteins compared with those of casein were found to depend on their amino acid compositions.[31] Serum cholesterol levels were found to be similar in rats fed a casein diet supplemented with cystine as an amino acid rich in EWP and those fed a casein diet, as described in the previous paper.[11] To exert the serum cholesterol-lowering action of EWP, protein structures, including the primary structure, may be important; however, the amino acid composition does not obviously. Further studies are needed to investigate whether a reconstructed amino acid mixture of the EWP amino acid composition has a hypocholesterolemic effect. Therefore, we concluded that the primary mechanism underlying the hypocholesterolemic effect of dietary EWP was the inhibition of dietary cholesterol absorption.[11] In addition, in this study, lymphatic cholesterol transport was decreased by dietary EWP (Figure 1B).

As shown in Figure 2, there were proteins that were resistant to pepsin in EWP. On the other hand, there was no band in the C-ph lane. Two major bands were recognized in the EWP lane after pepsin digestion (EWP-ph lane). These bands were individually identified as ovalbumin (MW 45 kDa) and lysozyme (MW 14.3 kDa). EWP contains 54% ovalbumin and 3.5% lysozyme.[21] Ovalbumin is the most abundant protein in EWP. Ovalbumin almost remained in EWP digestion by pepsin. We attempted to do a reverse experiment. A reconstructed EWP-ph was used; four pepsin hydrolysates of the EWP protein components were mixed with the EWP-ph while considering an intact ratio for the EWP composition, as described in Figure 4. The cholesterol micellar solubility was found to be similar for reconstructed EWP-ph and EWP-ph (Figure 4B). There was no ingredient in EWP that altered the solubility. According to the results of inhibition of cholesterol-micellar solubility, ovalbumin is responsible for the cholesterol-lowering activity. The solubility of EWP-ph was as low as that of OA-ph (Figure 4A). Ovalbumin may pass through the intestine, as evidenced by difficulty in its digestion according to the results of the in vitro protease digestion experiment (Figure 2). When EWP was the only dietary protein source in the rats fed the EWP diet, approximately half the dietary protein could not be absorbed. However, in the previous study, body weight gain in rats fed the EWP diet was not different from that in rats fed the casein diet.[11]

From the perspective of nutrition, the EWP diet supplemented with biotin did not cause growth inhibition in animal models, similar to that observed with egg white injury. It was reported that nitrogen excretion in the feces of rats fed EWP was not high.[32] Furthermore, EWP exhibits greater net protein utilization compared with other protein sources.[32] It has also been reported that EWP includes protease inhibitors.[33] Protease inhibition by EWP components or ovalbumin may be selective for proteases during gastric digestion. In this study, ovalbumin was resistant to stomach pepsin, but it may not be resistant to the other proteases in the intestine.

We newly observed that EWP inhibited lymphatic triacylglycerol (TAG) transport (Figure 1C). This observation reflected on serum and hepatic TAG levels from the previous study, where the efficiency of inhibition in rats fed the EWP diet for 3 weeks was 26 and 37%, respectively.[11] However, there were no significant differences in serum and hepatic TAG levels between the casein and EWP diets. These TAG-lowering effects were not observed in rats fed the EWP diet for 1 week; however, the hypocholesterolemic effect of EWP was evident. Ovalbumin has a pancreatic lipase inhibitory activity.[34] It is not digested by pepsin in the stomach because of its protease inhibitory activity as described above; it reaches the intestine to

act as a lipase inhibitor. Therefore, the intestinal absorption and lymphatic transport of TAG decreased and serum and hepatic TAG levels decreased. The difference in sensitivities for the inhibition of intestinal absorption of dietary cholesterol and TAG may rely on the feeding periods. The inhibition of cholesterol absorption may be more sensitive to its accumulation in the animal body compared with the inhibition of TAG.

As shown in Figure 1D, the mechanisms underlying temporal promotion of lymphatic phospholipid transport are not clear for the EWP diet without phospholipids. The rats may have temporarily experienced a condition of less intestinal phospholipid from 1 to 4 h after consuming the EWP diet. As shown in Figure 3C, there was no effect of the presence of PC in the bile acid micelles on the micellar solubility of cholesterol. Also, EWP-ph has better physicochemical properties of WHC, SV, and relative viscosity compared with casein and C-ph. These characteristics of EWP-ph are similar to those of water-soluble fibers such as guar gum.[24] Under alkaline conditions, fatty acids, water, and EWP combine in the intestine after ingestion, and EWP turns into a gel because of its physicochemical properties.[35−39] According to these results and information, the gel form of EWP may hold the micelles. Moreover, the gel mixture that contained EWP, fatty acids, and water may lead to inhibited fatty acid absorption. The time-dependent effect of dietary EWP on lymphatic transport of lipids was totally exerted after 3 h of feeding. In research on the effects of dietary protein on gastric emptying, compared to casein, gluten, and fish protein, whey protein delays gastric emptying time to suppress plasma FFA levels because of their controlling gastric hormone secretion and/or their physicochemical properties such as solubility of acidic solution.[40] Physicochemical properties and stimulation of gastric hormone secretion of dietary protein influence gastric emptying time, and then the influences reach intestinal absorption of nutrients. In fact, the protein form of EWP partly remained after the digestion (Figure 2). In the early phase of lipid transfer, EWP may stay in the stomach and the TAG and cholesterol may reach the duodenum more rapidly than EWP-ph. In the late phase, EWP-ph may exert effects of inhibition of intestinal lipid absorption. In this study, the lymphatic phospholipids may be derived from bile, intestinal mucosa exfoliation, bacterial flora, etc., but not from the diets and stomach. The lymphatic phospholipid transport may primarily suffer from the influence of phase shifting of gastric emptying. Taken together, the differences of the time course of lymphatic lipid transport may depend on the differences of gastric emptying time of protein. These mechanisms remain a hypothesis. Therefore, we have to organize acceptable plans for each dietary lipid in future studies.

The efficiency of intestinal cholesterol absorption is approximately 50%.[17,41] It assumes a one-to-one relationship between a passive diffusion process and a process through the Niemann−Pick C1-like 1 (NPC1L1) protein, a cholesterol transporter.[17,41] Possible findings about the effect of dietary EWP on NPC1L1 would be of great interest for future study, although none of the studies have shown that dietary components inhibit NPC1L1 protein. Further studies are also needed to investigate whether dietary EWP affects the assembly and secretion of chylomicrons.

In summary, dietary EWP inhibited dietary cholesterol absorption via decreased cholesterol passage in and out of the micelles and increased WHC, SV, and relative viscosity. Ovalbumin, a major protein in EWP, resisted protease digestion and may possess properties capable of exerting a hypocholesterolemic effect.

## AUTHOR INFORMATION


### Corresponding Author

*(M.S.) Phone/fax: +81-92-642-3004. E-mail: masaos@agr.kyushu-u.ac.jp.

### Author Contributions

‖R.M. and B.S. contributed equally to the study.


### Author Contributions

R.M. and B.S. wrote the manuscript and contributed equally to the study. R.M., B.S., S.K., S.B., S.S., and K.N. participated in the experimental work and collected and analyzed data. K.I. and M.S. supervised the study design and commented on the manuscript. All authors read and approved the final manuscript.

### Notes

The authors declare no competing financial interest.

## ACKNOWLEDGMENTS

We thank Enago (www.enago.jp) for the English language review.

## REFERENCES


(1) Hegsted, D. M.; McGandy, R. B.; Myers, M. L.; Stare, F. J. Quantitative effects of dietary fat on serum cholesterol in man. *Am. J. Clin. Nutr.* **1965**, *17*, 281−295.

(2) Schnohr, P.; Thomsen, O. O.; Riis Hansen, P.; Boberg-Ans, G.; Lawaetz, H.; Weeke, T. Egg consumption and high-density-lipoprotein cholesterol. *J. Int. Med.* **1994**, *235*, 249−251.

(3) Homma, Y.; Kobayashi, T.; Yamaguchi, H.; Ozawa, H.; Homma, K.; Ishiwata, K. Apolipoprotein-E phenotype and basal activity of low-density lipoprotein receptor are independent of changes in plasma lipoprotein subfractions after cholesterol ingestion in Japanese subjects. *Nutrition* **2001**, *17*, 310−314.

(4) Knopp, R. H.; Retzlaff, B.; Fish, B.; Walden, C.; Wallick, S.; Anderson, M.; Aikawa, K.; Kahn, S. E. Effects of insulin resistance and obesity on lipoproteins and sensitivity to egg feeding. *Arterioscler. Thromb. Vasc. Biol.* **2003**, *23*, 1437−1443.

(5) Katz, D. L.; Evans, M. A.; Nawaz, H.; Njike, V. Y.; Chan, W.; Comerford, B. P.; Hoxley, M. L. Egg consumption and endothelial function: a randomized controlled crossover trial. *Int. J. Cardiol.* **2005**, *99*, 65−70.

(6) Murata, M.; Imaizumi, K.; Sugano, M. Effect of dietary phospholipids and their constituent bases on serum lipids and apolipoproteins in rats. *J. Nutr.* **1982**, *112*, 1805−1808.

(7) Buang, Y.; Wang, Y. M.; Cha, J. Y.; Nagao, K.; Yanagita, T. Dietary phosphatidylcholine alleviates fatty liver induced by orotic acid. *Nutrition* **2005**, *21*, 867−873.

(8) Hamada, T.; Ikeda, I.; Takashima, K.; Kobayashi, M.; Kodama, Y.; Inoue, T.; Matsuoka, R.; Imaizumi, K. Hydrolysis of micellar phosphatidylcholine accelerates cholesterol absorption in rats and Caco-2 cells. *Biosci., Biotechnol., Biochem.* **2005**, *69*, 1726−1732.

(9) Imaizumi, K.; Mawatari, K.; Murata, M.; Ikeda, I.; Sugano, M. The contrasting effect of dietary phosphatidylethanolamine and phosphatidylcholine on serum lipoproteins and liver lipids in rats. *J. Nutr.* **1983**, *113*, 2403−2411.

(10) Asato, L.; Wang, M. F.; Chan, Y. C.; Yeh, S. H.; Chung, H. M.; Chung, S. Y.; Chida, S.; Uezato, T.; Suzuki, I.; Yamagata, N.; Kokubu, T.; Yamamoto, S. Effect of egg white on serum cholesterol concentration in young women. *J. Nutr. Sci. Vitaminol.* **1996**, *42*, 87−96.

(11) Matsuoka, R.; Kimura, M.; Muto, A.; Masuda, Y.; Sato, M.; Imaizumi, K. Mechanism for the cholesterol-lowering action of egg white protein in rats. *Biosci., Biotechnol., Biochem.* **2008**, *72*, 1506−1512.

(12) Ikeda, I.; Tanaka, K.; Sugano, M.; Vahouny, G. V.; Gallo, L. L. Inhibition of cholesterol absorption in rats by plant sterols. *J. Lipid Res.* **1988**, *29*, 1573−1582.
(13) Ikeda, I.; Imasato, Y.; Sasaki, E.; Nakayama, M.; Nagao, H.; Takeo, T.; Yayabe, F.; Sugano, M. Tea catechins decrease micellar solubility and intestinal absorption of cholesterol in rats. *Biochim. Biophys. Acta* **1992**, *29* (1127), 141−146.
(14) Stitcher, J. E.; Jolliff, C. R.; Hill, R. M. Comparison of Dumas and Kjeldahl methods for determination of nitrogen in feces. *Clin. Chem.* **1969**, *15*, 248−254.
(15) Reeves, P. G.; Nielsen, F. H.; Fahey, G. C., Jr. AIN-93 purified diets for laboratory rodents: final report of the American Institute of Nutrition ad hoc writing committee on the reformulation of the AIN-76A rodent diet. *J. Nutr.* **1993**, *123*, 1939−1951.
(16) Sato, M.; Ueda, T.; Nagata, K.; Shiratake, S.; Tomoyori, H.; Kawakami, M.; Ozaki, Y.; Okubo, H.; Shirouchi, B.; Imaizumi, K. Dietary kakrol (*Momordica dioica* Roxb.) flesh inhibits triacylglycerol absorption and lowers the risk for development of fatty liver in rats. *Exp. Biol. Med. (Maywood)* **2011**, *236*, 1139−1146.
(17) Shirouchi, B.; Nakamura, Y.; Furukawa, Y.; Shiraishi, A.; Tomoyori, H.; Imaizumi, K.; Sato, M. Ezetimibe inhibits lymphatic transport of esterified cholesterol but not free cholesterol in thoracic lymph duct-cannulated rats. *Cardiovasc. Drugs Ther.* **2012**, *26*, 427−431.
(18) Hashimoto, T.; Kurose, M.; Oku, K.; Nishimoto, T.; Chaen, H.; Fukuda, S.; Tsujisaka, Y. Digestibility and suppressive effect on rats' body fat accumulation of cyclic tetrasaccharide. *J. Appl. Glycosci.* **2006**, *53*, 233−239.
(19) Lowry, O. H.; Rosebrough, N. J.; Farr, A. L.; Randall, R. J. Protein measurement with the Folin phenol reagent. *J. Biol. Chem.* **1951**, *193*, 265−275.
(20) Ikeda, I.; Tsuda, K.; Suzuki, Y.; Kobayashi, M.; Unno, T.; Tomoyori, H.; Goto, H.; Kawata, Y.; Imaizumi, K.; Nozawa, A.; Kakuda, T. Tea catechins with a galloyl moiety suppress postprandial hypertriacylglycerolemia by delaying lymphatic transport of dietary fat in rats. *J. Nutr.* **2005**, *135*, 155−159.
(21) Nakamura, R.; Takeyama, M.; Nakamura, K.; Umemura, O. Constituent proteins of globulin fraction obtained from egg white. *Agric. Biol. Chem.* **1980**, *44*, 2357−2362.
(22) Hamada, T.; Ikeda, I.; Takashima, K.; Kobayashi, M.; Kodama, Y.; Inoue, T.; Matsuoka, R.; Imaizumi, K. Hydrolysis of micellar phosphatidylcholine accelerates cholesterol absorption in rats and Caco-2 cells. *Biosci., Biotechnol., Biochem.* **2005**, *69*, 1726−1732.
(23) Hamada, T.; Goto, H.; Yamahira, T.; Sugawara, T.; Imaizumi, K.; Ikeda, I. Solubility in and affinity for the bile salt micelle of plant sterols are important determinants of their intestinal absorption in rats. *Lipids* **2006**, *41*, 551−556.
(24) Shirouchi, B.; Kawamura, S.; Matsuoka, R.; Baba, S.; Nagata, K.; Shiratake, S.; Tomoyori, H.; Imaizumi, K.; Sato, M. Dietary guar gum reduces lymph flow and diminishes lipid transport in thoracic duct-cannulated rats. *Lipids* **2011**, *46*, 789−793.
(25) Sakai, K.; Ushiyama, Y.; Manabe, S. Peptic and pancreatic digestibility of raw and heat-treated hen's egg white protein (in Japanese). *Jpn. J. Pediatr. Allergy Clin. Immunol.* **1999**, *13*, 36−42.
(26) Sugano, M.; Morioka, H.; Ikeda, I. A comparison of hypocholesterolemic activity of beta-sitosterol and beta-sitostanol in rats. *J. Nutr.* **1977**, *107*, 2011−2019.
(27) Carey, M. C.; Hernell, O. Digestion and absorption of fat. *Semin. Gastrointest. Dis.* **1992**, *3*, 189−208.
(28) Yamamoto, S.; Kina, T.; Yamagata, N.; Kokubu, T.; Shinjo, S.; Asato, L. Favorable effects of egg white protein on lipid metabolism in rats and mice. *Nutr. Res. (N.Y.)* **1993**, *13*, 1453−1457.
(29) Sugano, M.; Goto, S. Steroid-binding peptides from dietary proteins. *J. Nutr. Sci. Vitaminol.* **1990**, *Suppl. 2*, S147−S150.
(30) Nagaoka, S.; Futamura, Y.; Miwa, K.; Awano, T.; Yamauchi, K.; Kanamaru, Y.; Tadashi, K.; Kuwata, T. Identification of novel hypocholesterolemic peptides derived from bovine milk $\beta$-lactoglobulin. *Biochem. Biophys. Res. Commun.* **2001**, *281*, 11−17.
(31) Morita, T.; Oh-hashi, A.; Takei, K.; Ikai, M.; Kasaoka, S.; Kiriyama, S. Cholesterol-lowering effects of soybean, potato and rice proteins depend on their low methionine contents in rats fed a cholesterol-free purified diet. *J. Nutr.* **1997**, *127*, 470−477.
(32) Eckferdt, G. A.; Sheffner, A. L.; Spector, H. The pepsin-digest-residue (PDR) amino acid index of net protein utilization. *J. Nutr.* **1956**, *60*, 105−120.
(33) Snook, J. T. Factors in whole-egg protein influencing dietary induction of increases in enzyme and RNA levels in rat pancreas. *J. Nutr.* **1969**, *97*, 286−294.
(34) Gargouri, Y.; Julien, R.; Sugihara, A.; Verger, R.; Sarda, L. Inhibition of pancreatic and microbial lipases by proteins. *Biochim. Biophys. Acta* **1984**, *795*, 326−331.
(35) Yuno-Ohta, N.; Toryu, H.; Higasa, T.; Maeda, H.; Okada, M.; Ohta, H. Gelation properties of ovalbumin as affected by fatty acid salts. *J. Food Sci.* **1996**, *61*, 906−910.
(36) King, A. J.; Ball, H. R., Jr.; Catignani, G. L.; Swaisgood, H. E. Physicochemical properties of ovalbumin and lysozyme treate with oleic acid. *J. Food Sci.* **1989**, *54*, 1639−1641.
(37) King, A. J.; Ball, H. R., Jr.; Catignani, G. L.; Swaisgood, H. E. Modification of egg white proteins with oleic acid. *J. Food Sci.* **1984**, *49*, 1240−1243.
(38) Yuno-Ohta, N. Mechanism for formation of ovalbumin-fatty acid salt mixed gels. *Food Hydrocolloids* **2006**, *20*, 375−360.
(39) Yuno-Ohta, N.; Higasa, T.; Tatsumi, E.; Sakurai, H.; Asano, R.; Hirose, M. Formation of fatty acid salt induced gel of ovalbumin and the mechanism for gelation. *J. Agric. Food Chem.* **1998**, *46*, 4518−4523.
(40) Stanstrup, J.; Schou, S. S.; Holmer-Jensen, J.; Hermansen, K.; Dragsted, L. O. Whey protein delays gastric emptying and suppresses plasma fatty acids and their metabolites compared to casein, gluten, and fish protein. *J. Proteome Res.* **2014**, *13*, 2396−2408.
(41) Sudhop, T.; Lütjohann, D.; Kodal, A.; Igel, M.; Tribble, D. L.; Shah, S.; Perevozskaya, I.; von Bergmann, K. Inhibition of intestinal cholesterol absorption by ezetimibe in humans. *Circulation* **2002**, *106*, 1943−1948.

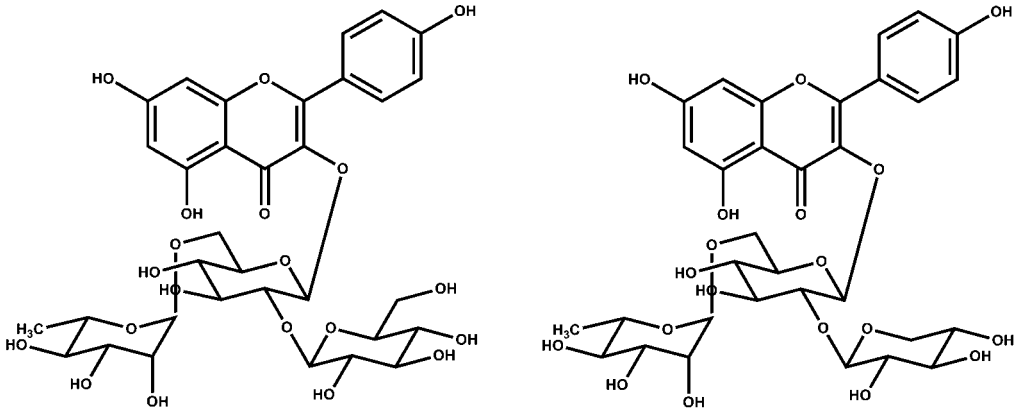

kaempferol 3-O-(2''-glucopyranosyl)-rutinoside kaempferol 3-O-(2''-xylopyranosyl)-rutinoside

**Figure 1.** Structures of two phytochemicals in fraction 3 from the methanol extracts of tea seed pomace from *Camellia tenuifolia*: kaempferol 3-*O*-(2″-glucopyranosyl)-rutinoside and kaempferol 3-*O*-(2″-xylopyranosyl)-rutinoside.

Given that it is an inexpensive and residual resource, we explored the potential beneficial health effects from the main biowaste, tea seed pomace, produced when tea seed from *C. tenuifolia* is processed. DPPH radical scavenging and total phenolic content assays were performed to evaluate the in vitro activities of the extracts. *C. elegans* was used as an in vivo model to evaluate the beneficial health effects, including antioxidant activity, delayed aging, and reduced amyloid-$\beta$ toxicity.

## MATERIALS AND METHODS

**Plant Materials.** All chemicals unless otherwise stated were purchased from Sigma-Aldrich (Poole, Dorset, UK). Tea seed pomace of *C. tenuifolia* was collected in October 2011 from the *Camellia* tree farm located in Taichung county, Taiwan. The species were identified by the Taiwan Forestry Research Institute.

**Tea Seed Pomace Extract Preparation and Identification of Compounds.** The dried samples (in triplicate 100 g batches) were incubated with water, hot water (100 °C), ethyl acetate (EtOAc), ethanol (EtOH), *n*-hexane (Hex), and methanol (MeOH) at room temperature for 1 h (sample/solvent = 1:5). The extracts were decanted, filtered under vacuum, concentrated in a rotary evaporator, and then lyophilized. The MeOH-soluble fraction was further divided into six fractions (1−6) by chromatography with a Diaion HP-20 column eluted with water/MeOH (gradient elution was performed by changing from 100/0 to 0/100).

The phytochemicals from fraction 3 were separated and purified by semipreparative high-performance liquid chromatography (HPLC) on an Agilent model 1100 pump equipped with a UV detector (Agilent 1100) and a 250 mm × 10.0 mm i.d., 5 $\mu$m, Luna RP-18 column (Phenomenex, Torrance, CA, USA). The mobile phase used was solvent A (ultrapure water) and solvent B (MeOH). Elution conditions were 0−5 min, 55% B (isocratic gradient); 5−20 min, 55−65% B (linear gradient); 20−30 min, 65−100% B (linear gradient). ESI-MS data were collected using a Finnigan LCQ mass spectrometer, and NMR spectra were recorded by a Bruker AVIII 500 MHz FT-NMR spectrometer. The structures of chemical compounds (as shown in Figure 1) were identified by ESI-MS and NMR, and the data were consistent with those reported in the studies.[16,17]

**1,1-Diphenyl-2-picrylhydrazyl (DPPH) Free Radical Scavenging Assay.** The DPPH free radical scavenging activities of MeOH extracts and their derived fractions were measured. Extracts with a series of concentrations were dissolved in EtOH (50 $\mu$L) and mixed with 1000 $\mu$L of 0.1 mM DPPH−EtOH solution and 450 $\mu$L of 50 mM Tris-HCl buffer (pH 7.4). EtOH (50 $\mu$L) was used as the control for this experiment. After 30 min of incubation at room temperature, the reduction of the DPPH free radical was determined by reading the absorbance at 517 nm. Ascorbic acid, a well-known antioxidant, was used as the positive control, and the inhibition ratio (%) was calculated as follows:

$$\%\ \text{inhibition} = [(\text{absorbance of control} - \text{absorbance of test sample})/\text{absorbance of control}] \times 100$$

Each test was repeated three times, and the results were averaged.

**Determination of Total Phenolic Contents.** Total phenolic contents were analyzed according to the Folin−Ciocalteu method, using gallic acid as a standard. The samples were dissolved in 10 mL of EtOH/water (50:50, v/v). Subsequently, the sample solution (0.5 mL) was mixed with 0.5 mL of 1 N Folin−Ciocalteu reagent and then incubated at room temperature for 5 min followed by the addition of 1 mL of 20% $Na_2CO_3$. After 10 min, the mixture was centrifuged for 8 min (12000*g*), and the absorbance of the supernatant was measured at 730 nm. The total phenolic contents were presented as gallic acid equivalents (GAE) in milligrams per gram of test sample. Each test was repeated three times, and the results were averaged.

***C. elegans* Strains and Culture Conditions.** *C. elegans* strains used in this study were Bristol N2 (wild-type) and CL4176 (smg-1ts [myo-3/A$\beta$1−42 long 3′-UTR]). *C. elegans* was maintained and assayed (unless otherwise stated) at 20 °C on nematode growth medium (NGM) agar plates carrying a lawn of *Escherichia coli* OP50. All chemicals in NGM plates and liquid are expressed as the final concentrations.

***C. elegans* Oxidative Stress Resistance Assays.** Oxidative stress assays were performed as previously described.[18−20] Briefly, synchronized wild-type L1 larvae were incubated in liquid S-basal containing *E. coli* OP50 bacteria at $10^9$ cells/mL in the presence or absence of tea seed pomace extracts (1 and 10 $\mu$g/mL) for 72 h at 20 °C followed by 250 $\mu$M juglone (5-hydroxy-1,4-naphthoquinone) (Sigma, St. Louis, MO, USA) exposure for 3 h and then scored for viability. The survival of worms was determined by touch-provoked movement as described.[21] Nematodes were scored as dead when they failed to respond to repeated touching with a platinum wire pick. The test was performed on at least three independent biological replicates.

***C. elegans* Intracellular Reactive Oxygen Species (ROS) Measurement.** *C. elegans* was pretreated with tea seed pomace extracts (1 and 10 $\mu$g/mL) as the oxidative stress assays. After 72 h at 20 °C, nematodes were washed with K-medium three times and then transferred to 500 $\mu$L of K-medium containing 100 $\mu$M CM-$H_2$DCFDA (Molecular Probes, Eugene, OR, USA) for 2.5 h at 20 °C. At least 20 randomly selected worms from each set of experiments were mounted onto microscope slides coated with 3% agarose, anesthetized with 2% sodium azide, and capped with coverslips. Epifluorescence images were captured with an epifluorescence

microscope (Leica, Wetzlar, Germany) using a suited filter set (excitation, 480 ± 20 nm; emission, 510 ± 20 nm) with a cooled charge-coupled device (CCD) camera. Total fluorescence for each whole worm was quantified by Image-Pro Plus software (Media Cybernetics, Bethesda, MD, USA).

***C. elegans* Lifespan Assays.** Lifespan analyses were performed in the same manner for all treatments at 20 °C. Synchronized eggs were placed on fresh NGM plates containing UV-inactivated *E. coli* OP50 in the absence or presence of tea seed pomace extracts (1 and 10 μg/mL), and nematodes were allowed to develop to adulthood. UV inactivation was used to avoid the effects of live *E. coli* on the conditions of tea seed pomace extracts examined in this study.[22] Surviving and dead worms were scored daily (starting on the first day of adulthood) until all nematodes had died. Nematodes that did not move when gently prodded (with a platinum wire) were judged to be dead. Nematodes suffering from internal hatch (a defect in egg laying) and those that crawled off the NGM plate were not included in the lifespan scores. During the reproductive period, adult nematodes were transferred to fresh NGM plates every day and then every other day thereafter. The test was performed on at least three independent biological replicates.

***C. elegans* Paralysis Assays.** Strain CL4176[23] maintained at 16 °C was egg-synchronized onto the NGM plates containing *E. coli* OP50 in the absence or presence of tea seed pomace extracts. At 50 h after egg laying, A$\beta$ transgene expression was induced by increasing the temperature from 16 to 23 °C and continued to the end of the paralysis assays.[23] Paralysis was scored at 2 h intervals until the last worm became paralyzed.[24] The definition of paralysis of worms in this study was that worms exhibited pharyngeal pumping, but failed to complete one sinusoidal turn within 5 s of being touched on the head and tail with a platinum wire.[24] The test was performed on at least three independent biological replicates.

**Statistical Analysis.** Statistical analysis was performed using SPSS Statistics 17.0 software (SPSS, Inc., Chicago, IL, USA; 2008). The results are presented as the mean ± standard errors of mean (SEM). Comparisons and $p$ value calculations were made between treated and untreated animals of the same strain using one-way ANOVA and the LSD post hoc test. Differences were considered significant at $p < 0.05$ (see figures). For the lifespan and paralysis assays, animal survival was plotted using Kaplan–Meier survival curves and analyzed by log-rank test using GraphPad Prism (GraphPad Software, Inc., La Jolla, CA, USA).

## RESULTS AND DISCUSSION

**Solvent Selection.** Direct extraction using various types of solvents is the most common technique employed to obtain extracts with high antioxidant activity from plants. To examine the extraction process of compounds with antioxidant properties from tea seed pomace of *C. tenuifolia*, tea seed pomace was initially extracted by various types of solvents, including $H_2O$ (room temperature), hot $H_2O$ (100 °C), EtOAc, EtOH, Hex, and MeOH.

*C. elegans* was used to investigate whether extracts from different solvents exert oxidative stress resistance. Wild-type N2 *C. elegans* was pretreated with different solvent extracts followed by exposure to juglone-induced oxidative stress. Figure 2 shows that pretreatments with extracts from $H_2O$, hot $H_2O$ (100 °C), EtOH, and MeOH significantly increased the survival of *C. elegans* exposed to juglone-induced oxidative stress (Figure 2). It is noted that the extracts from hot $H_2O$ (100 °C) showed a protective effect at lower dose (1 μg/mL), whereas the higher dose (10 μg/mL) did not. It is possible that the higher concentration of extracts from hot $H_2O$ might be toxic, alleviating the antioxidant effects on wild-type *C. elegans*. Therefore, it is likely that a linear dose–response curve was not observed. Moreover, MeOH extract exhibited the highest *C. elegans* survival against juglone-induced oxidative stress (Figure 2). Herein, we selected the extract from MeOH-extracted tea seed pomace for further investigation.

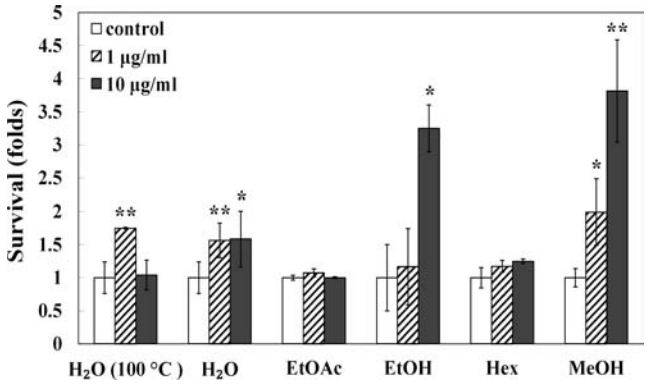


**Figure 2.** Protective effects of tea seed pomace extracts with different solvents extraction on wild-type *C. elegans* N2 under oxidative stress. Synchronized wild-type L1 larvae were pretreated with 1 and 10 μg/mL of different solvent extracts or with 0.1% DMSO as the solvent control for 72 h at 20 °C. Nematodes were then subjected to oxidative stress assays. Tea seed pomace extract-treated (1 and 10 μg/mL) and untreated control nematodes were exposed to 250 μM juglone for 3 h and then scored for viability. Solvents used for the extractions were water ($H_2O$, room temperature), hot water ($H_2O$, 100 °C), ethyl acetate (EtOAc), ethanol (EtOH), *n*-hexane (Hex), and methanol (MeOH). At least three independent biological replicates were performed, and approximately 60–80 worms were scored in each experiment. Data are normalized to the untreated control. Results are presented as the mean ± standard error of mean (SEM). Differences compared to the untreated control were considered significant at $p < 0.05$ (*) and $p < 0.01$ (**) by one-way ANOVA and LSD post hoc test.

**Fraction Selection from the Methanol Extract.** The MeOH extract was further fractionated by column chromatography with a Diaion HP-20 column, and six fractions (1–6) were obtained. For the in vitro assay, the DPPH radical scavenging activity of MeOH-soluble extract and the derived fractions of tea seed pomace were performed. DPPH contains a proton free radical, which significantly reduces on exposure to proton radical scavengers.[25] Therefore, the DPPH assay has been commonly used to examine in vitro antioxidant activity.[26] Figure 3A shows that the lowest $IC_{50}$ value (the concentration required to inhibit radical formation by 50%) was observed in fraction 3 ($IC_{50}$ = 49.5 μg/mL), whereas fraction 4 ($IC_{50}$ = 93.0 μg/mL) and the MeOH-soluble extract ($IC_{50}$ = 133.4 μg/mL) also exhibited good inhibitory effects.

The total phenolic contents were also examined as most plant phenolics are highly effective free radical scavengers and antioxidants. The total phenolics in the MeOH extract and their derived fractions were determined according to the Folin–Ciocalteu method and expressed as GAE. As shown in Figure 3B, fraction 3 showed the highest total phenolic contents (101.2 mg of GAE/g), followed by fraction 4 (99.9 mg of GAE/g) and the MeOH extract (50.1 mg of GAE/g). These results indicated that the free radical scavenging activity of the MeOH extract of tea seed pomace could be effectively enriched in fractions 3 and 4.

For the in vivo assay, the antioxidant activity of the MeOH-soluble extract and their derived fractions was examined in *C. elegans*. Wild-type N2 *C. elegans* was pretreated with 1 and 10 μg/mL of MeOH-soluble extract and their derived fractions. Figure 3C showed that pretreatment with fractions 1 and 3 significantly enhanced the survival of worms. Although fraction

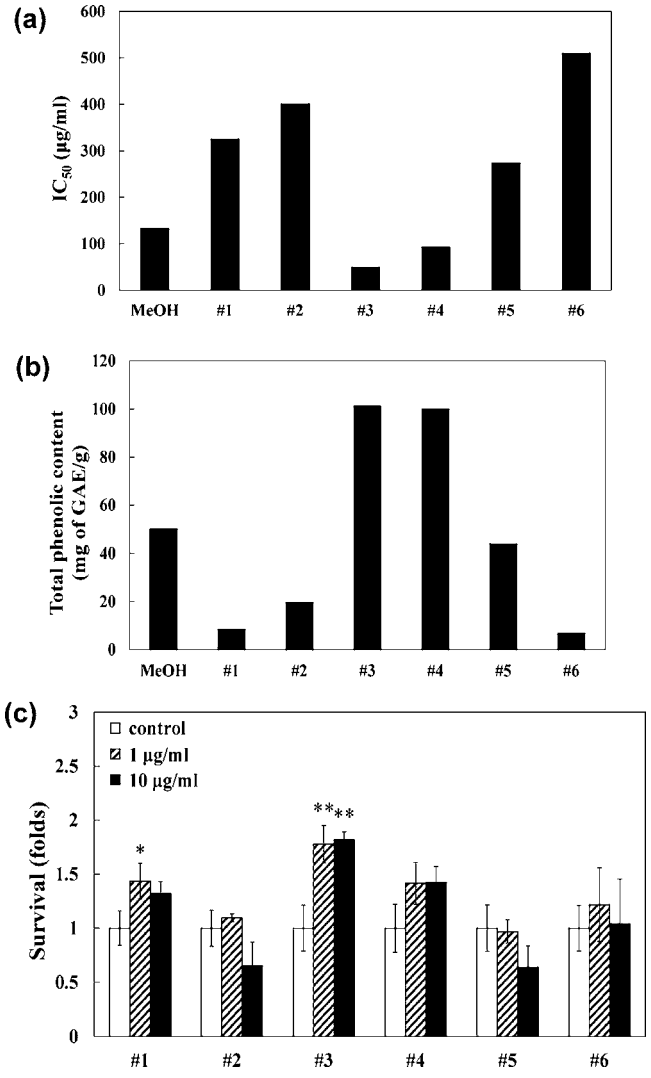


**Figure 3.** In vitro and in vivo antioxidant activity of different fractions from the methanol extracts of tea seed pomace. The MeOH-soluble extraction was divided into six fractions (1−6) by chromatography with a Diaion HP-20 column eluted with water/MeOH. (A) The DPPH scavenging activity of each test sample is presented as $IC_{50}$ values (μg/mL). Each test was repeated three times, and the results were averaged. (B) Total phenolic contents in each sample are expressed as gallic acid equivalent (mg of GAE/g of test sample). Each test was repeated three times, and the results were averaged. (C) Oxidative stress was performed as described above. At least three independent biological replicates were performed, and approximately 60−80 worms were scored in each experiment. Data are normalized to the untreated control. Results are presented as the mean ± standard error of mean (SEM). Differences compared to the untreated control were considered significant at $p < 0.05$ (*) and $p < 0.01$ (**) by one-way ANOVA and LSD post hoc test.

4 pretreatment did not show statistically increased survival of nematodes ($p = 0.0716$ for 1 μg/mL; $p = 0.053$ for 10 μg/mL), the observed protective effect to *C. elegans* against juglone-induced oxidative stress was obvious (Figure 3C). In contrast, fractions 2, 5, and 6 did not produce a significant increase in the survival of worms exposed to juglone-induced oxidative stress. Furthermore, it was observed that fraction 3 (both 1 and 10 μg/mL) exhibited the best performance in oxidative stress resistance in *C. elegans*.

Taken together, the aforesaid results suggested that the free radical scavenging effect of each fraction and their phenolic contents correlates closely with their oxidative stress resistance in *C. elegans*. Moreover, fraction 3 of the MeOH extract from tea seed pomace not only had the highest phenolic contents but also had the best antioxidant activity in both in vitro and in vivo tests (Figure 3). Accordingly, fraction 3 was selected for further investigation in the *C. elegans* model.

**Fraction 3 from the Methanol Extract of Tea Seed Pomace Reduces Intracellular ROS Production in *C. elegans*.** To gain insight into which fraction 3 from the MeOH extract suppresses the juglone-induced oxidative stress in *C. elegans*, intracellular ROS production in *C. elegans* after fraction 3 pretreatment was measured. Figure 4 shows that both 1 and

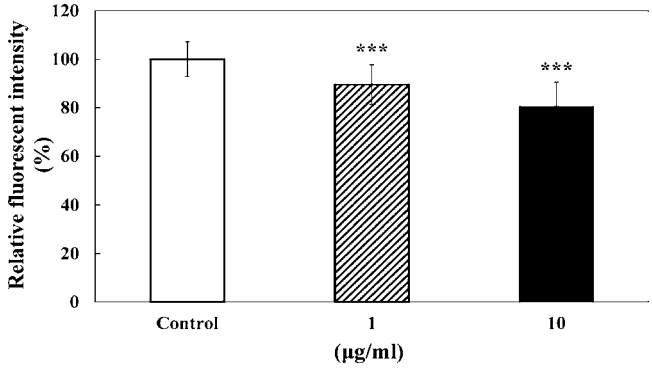


**Figure 4.** Effects of fraction 3 from the methanol extracts of tea seed pomace on intracellular ROS production in wild-type *C. elegans* N2. Synchronized wild-type L1 larvae were pretreated with fraction 3 from the methanol extracts (1 and 10 μg/mL) of tea seed pomace for 72 h at 20 °C. Subsequently, worms were treated with 100 μM CM−$H_2$DCFDA for 2.5 h at 20 °C, and intracellular ROS for adult animals was measured. Twenty randomly selected worms from each set of experiments were directly measured for the total GFP fluorescence for each whole worm and quantified by Image-Pro Plus software (Media Cybernetics, Bethesda, MD, USA). At least three independent biological replicates were performed. Data are normalized to the untreated control. Results are presented as the mean ± standard error of mean (SEM). Differences compared to the untreated control were considered significant at $p < 0.001$ (***) by one-way ANOVA and LSD post hoc test.

10 μg/mL of fraction 3 significantly inhibited the production of ROS compared to that in the untreated control ($p < 0.001$) (Figure 4). This suggests that pretreatment of fraction 3 from the MeOH extract may reduce juglone-induced toxicity as observed in Figure 3, by decreasing the levels of intracellular ROS in *C. elegans*.

**Fraction 3 from the Methanol Extracts of Tea Seed Pomace Significantly Prolongs *C. elegans* Lifespan.** Aging has been correlated to oxidative stress in *C. elegans*.[27] An increased lifespan was shown to be closely associated with increased survival under oxidative stress.[21,28] Therefore, we evaluated whether fraction 3 from the MeOH extract of tea seed pomace has an effect on the lifespan of *C. elegans* or not.

The lifespans of untreated (control) and fraction 3-treated wild-type nematodes were compared. Adult wild-type nematodes grown on control NGM plates and fed UV-killed bacteria at 20 °C have a median lifespan of 16 days with a maximum lifespan of 24 days (the age at death of the oldest animals). When nematodes grown on medium containing fraction 3 (1 and 10 μg/mL) were fed UV-killed bacteria at 20 °C, the

fraction 3-treated worms showed a statistically significantly increased lifespan compared to the untreated ones (log-rank, $p$ = 0.0372 for 1 $\mu$g/mL; $p$ = 0.0044 for 10 $\mu$g/mL, treated vs untreated control) (Figure 5). The median lifespans for both 1

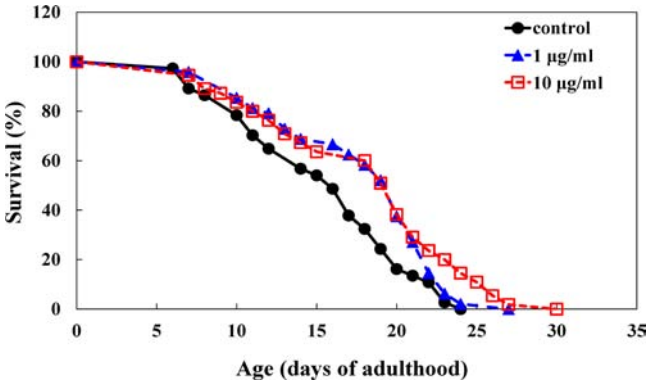


**Figure 5.** Effects of fraction 3 from the methanol extracts of tea seed pomace on the lifespan of wild-type *C. elegans* N2. Synchronized wild-type L1 larvae were incubated on NGM plates in the absence (control) or presence of fraction 3 (1 and 10 $\mu$g/mL), and worms were allowed to develop to adulthood. Surviving and dead animals were counted daily until all nematodes had died. Survival curves are of untreated control compared to fraction 3-treated worms. Day 1 refers to the first day of adulthood. At least three independent biological replicates were performed. Approximately 60 worms were scored in each experiment. Statistical significance of the difference between the curves (treated vs untreated control) was demonstrated by log-rank test using the Kaplan–Meier survival analysis. Differences at the $p < 0.05$ level were considered significantly different.

and 10 $\mu$g/mL fraction 3-treated worms are 20 days, respectively, with maximum lifespans of 27 days (1 $\mu$g/mL) and 30 days (10 $\mu$g/mL) (Figure 5). Taken together, the results suggest that fraction 3 from the MeOH extract of tea seed pomace has a beneficial effect on *C. elegans* in longevity.

**Fraction 3 from the Methanol Extracts of Tea Seed Pomace Delays Amyloid-$\beta$-Induced Paralysis in Transgenic *C. elegans* Expressing Human A$\beta$.** Production of oxidative stress by amyloid-$\beta$ (A$\beta$) is a possible cause for neurodegenerative diseases such as Alzheimer's disease (AD).[29,30] It has previously been shown that certain small molecules inhibit A$\beta$ oligomers, thereby reducing its toxicity.[31,32] However, most of these studies were conducted in vitro. In addition, it is time- and cost-consuming using a transgenic mice model of AD for pharmacological evaluation and mechanistic studies. Therefore, *C. elegans* has been increasingly used as a model of neurodegenerative diseases as it offers experimental advantages to address many basic cellular processes/functions that are conserved among animals.[33] *Ginkgo biloba* extract EGb 761 and aqueous coffee extracts were previously shown to associate A$\beta$ toxicity with A$\beta$-induced pathological behaviors in *C. elegans*.[24,34]

To examine whether fraction 3 has protective effects on AD, we investigated the effects of fraction 3 in a *C. elegans* model of A$\beta$ toxicity.[23] In the transgenic *C. elegans* strain CL4176 model, a temperature increase from 16 to 23 °C induced human A$\beta_{42}$ expression in body wall muscle of *C. elegans*, resulting in an A$\beta$-dependent paralysis phenotype.[23] In the present study, synchronized eggs from transgenic CL4176 worms were placed on *E. coli* OP50 food in the presence or absence of fraction 3 (1 and 10 $\mu$g/mL) for 50 h at 16 °C, and then the temperature was increased to 23 °C to induce A$\beta$ transgene expression. Figure 6 shows that A$\beta$-induced muscle paralysis was

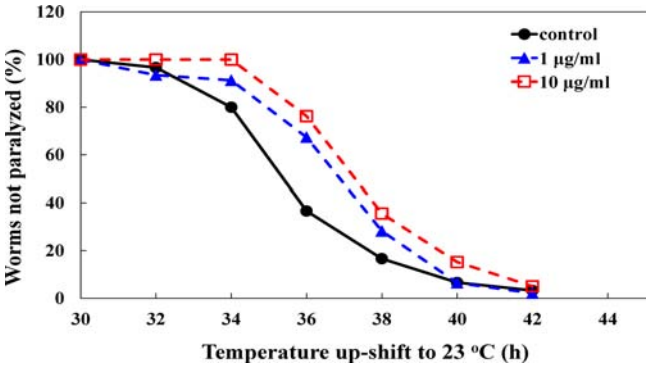


**Figure 6.** Effects of fraction 3 from the methanol extracts of tea seed pomace on A$\beta$-induced paralysis in transgenic *C. elegans* CL4176 strain. Strain CL4176 (muscle A$\beta$ strain) maintained at 16 °C was egg-synchronized onto the NGM plates with *E. coli* OP50 in the absence or presence of fraction 3 (1 and 10 $\mu$g/mL). At 50 h after egg laying, the temperature was shifted to 23 °C to induce A$\beta$ transgene expression. The paralysis phenotype was scored at 2 h intervals. Data are expressed as percentage of nonparalyzed worms from at least three independent assays of 100 worms in each set of experiments. Statistical significance of the difference between the curves (treated vs untreated control) was demonstrated by log-rank test using the Kaplan–Meier survival analysis. Differences at the $p < 0.05$ level were considered significantly different.

significantly delayed in nematodes fed fraction 3 (1 and 10 $\mu$g/mL) compared with the untreated controls (log-rank, $p$ = 0.008 for 1 $\mu$g/mL; $p < 0.001$ for 10 $\mu$g/mL, treated vs untreated control) (Figure 6). This suggests that fraction 3 from the MeOH extract has protective effects on *C. elegans* against A$\beta$ toxicity.

**Constituents of Fraction 3 from the Methanol Extracts of Tea Seed Pomace from *C. tenuifolia*.** Constituents of fraction 3 were further determined by the bioactivity-guided fractionation procedure. Semipreparative HPLC was employed to isolate phytochemicals in fraction 3 from the MeOH extracts of *C. tenuifolia* tea seed pomace. ESI-MS and NMR were applied to determine two constituents, namely, kaempferol 3-*O*-(2″-glucopyranosyl)-rutinoside (23 ± 0.11% of crude extracts) and kaempferol 3-*O*-(2″-xylopyranosyl)-rutinoside (20.65 ± 0.25% of crude extracts).

In Figure 3C, as low as 1 $\mu$g/mL fraction 3 from the MeOH extract showed good oxidative stress resistance in *C. elegans*. Thus, we further examined the antioxidant activity of kaempferol 3-*O*-(2″-glucopyranosyl)-rutinoside and kaempferol 3-*O*-(2″-xylopyranosyl)-rutinoside with 0.24 and 0.21 $\mu$g/mL, respectively, for the juglone-induced oxidative stress assays. The results showed that both phytochemicals exhibited higher *C. elegans* survival than the control (Figure 7).

In the present study, kaempferol derivatives were identified from *C. tenuifolia* tea seed pomace. Kaempferol triglycosides have been identified from a variety of plants.[35] The flavonoid kaempferol is commonly found in many edible plants and used in traditional medicine. Many studies have reported that kaempferol and some glycosides of kaempferol have a wide range of biological activities, including antioxidant, anti-inflammatory, antimicrobial, and anticancer activities.[35,36] In the *C. elegans* model, previous studies have shown that kaempferol decreases the intracellular ROS level, prolongs

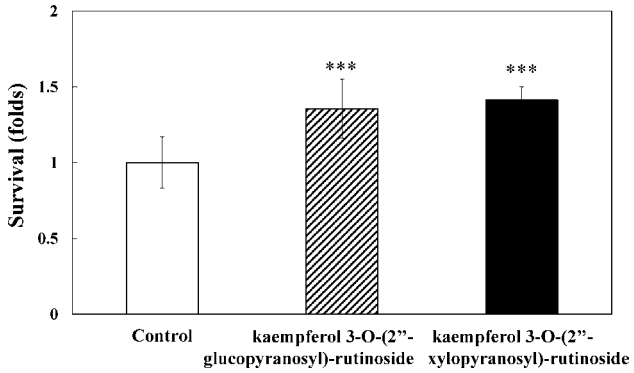


**Figure 7.** Antioxidant activity of kaempferol 3-*O*-(2″-glucopyranosyl)-rutinoside and kaempferol 3-*O*-(2″-xylopyranosyl)-rutinoside on wild-type *C. elegans* N2. Oxidative stress was performed as described above except that L1 nematodes were pretreated with kaempferol 3-*O*-(2″-glucopyranosyl)-rutinoside (0.24 μg/mL) and kaempferol 3-*O*-(2″-xylopyranosyl)-rutinoside (0.21 μg/mL). At least three independent biological replicates were performed, and approximately 60−80 worms were scored in each experiment. Data are normalized to the untreated control. Results are presented as the mean ± standard error of mean (SEM). Differences compared to the untreated control were considered significant at $p < 0.01$ (**) and $p < 0.001$ (***) by one-way ANOVA and LSD post hoc test.

lifespan, and attenuates amyloid-β-induced toxicity.[37−39] The aforesaid studies were in good agreement with our present findings (Figures 3−6). Therefore, the extracts from *C. tenuifolia* tea seed pomace are important and valuable and should be explored for further development of potential applications.

In conclusion, to the best of our knowledge, this is the first report demonstrating that the extracts from *C. tenuifolia* tea seed pomace exert multiple beneficial health effects in an intact organism. The MeOH extract of tea seed pomace from *C. tenuifolia* significantly decreases intracellular ROS level, prolongs *C. elegans* lifespan, and delays amyloid-β-induced paralysis in transgenic *C. elegans* expressing human $A\beta_{42}$. Aging is considered as one of the major risk factors in AD, and oxidative stress has been correlated to aging and amyloid-β toxicity. Therefore, the observed delay in aging and reduced amyloid-β toxicity by MeOH extract of tea seed pomace might be due to its antioxidant properties. Moreover, two phytochemicals, namely, kaempferol 3-*O*-(2″-glucopyranosyl)-rutinoside and kaempferol 3-*O*-(2″-xylopyranosyl)-rutinoside, were identified from the extract and exhibited excellent in vivo antioxidant activity. Our results showed that extracts of tea seed pomace from *C. tenuifolia* have multiple beneficial health effects, suggesting that biowaste might be valuable and should be explored for further development as nutraceutical products. Furthermore, the reuse of agricultural byproduct tea seed pomace also fulfills the environmental perspective.

## AUTHOR INFORMATION

### Corresponding Authors

*(V.H.-C.L.) Phone: +886-2-33665239. Fax: +886-2-33663462. E-mail: vivianliao@ntu.edu.tw.

*(F.-L.H.) Phone: +886-2-23039978, ext. 2173. Fax: +886-2-23077306. E-mail: flhsu@tfri.gov.tw.

### Author Contributions

‖C.-C.W. and C.-W.Y. contributed equally to this work.

### Notes

The authors declare no competing financial interest.

## ACKNOWLEDGMENTS

All nematode strains used in this work were provided by the *Caenorhabditis* Genetics Center, which is funded by the NIH National Center for Research Resources.

## REFERENCES

(1) Kroyer, G. T. Impact of food processing on the environment − an overview. *Lebensm. Wiss. Technol.* **1995**, *28*, 547−552.

(2) Dorta, E.; Lobo, M. G.; Gonzalez, M. Reutilization of mango byproducts: study of the effect of extraction solvent and temperature on their antioxidant properties. *J. Food Sci.* **2012**, *77*, C80−C88.

(3) Plaza, M.; Abrahamsson, V.; Turner, C. Extraction and neoformation of antioxidant compounds by pressurized hot water extraction from apple byproducts. *J. Agric. Food Chem.* **2013**, *61*, 5500−5510.

(4) Lee, C. P.; Yen, G. C. Antioxidant activity and bioactive compounds of tea seed (*Camellia oleifera* Abel.) oil. *J. Agric. Food Chem.* **2006**, *54*, 779−784.

(5) Lee, C. P.; Shih, P. H.; Hsu, C. L.; Yen, G. C. Hepatoprotection of tea seed oil (*Camellia oleifera* Abel.) against $CCl_4$-induced oxidative damage in rats. *Food Chem. Toxicol.* **2007**, *45*, 888−895.

(6) Chen, Y. F.; Yang, C. H.; Chang, M. S.; Ciou, Y. P.; Huang, Y. C. Foam properties and detergent abilities of the saponins from *Camellia oleifera*. *Int. J. Mol. Sci.* **2010**, *11*, 4417−4425.

(7) Zhang, X. F.; Han, Y. Y.; Bao, G. H.; Ling, T. J.; Zhang, L.; Gao, L. P.; Xia, T. A new saponin from tea seed pomace (*Camellia oleifera* Abel) and its protective effect on PC12 cells. *Molecules* **2012**, *17*, 11721−11728.

(8) Dai, D. F.; Chiao, Y. A.; Marcinek, D. J.; Szeto, H. H.; Rabinovitch, P. S. Mitochondrial oxidative stress in aging and healthspan. *Longev. Healthspan* **2014**, *3*, 6.

(9) Mao, P.; Reddy, P. H. Aging and amyloid β-induced oxidative DNA damage and mitochondrial dysfunction in Alzheimer's disease: implications for early intervention and therapeutics. *Biochim. Biophys. Acta* **2011**, *1812*, 1359−1370.

(10) Ansari, N.; Khodagholi, F. Natural products as promising drug candidates for the treatment of Alzheimer's disease: molecular mechanism aspect. *Curr. Neuropharmacol.* **2014**, *11*, 414−429.

(11) Sadowska-Bartosz, I.; Bartosz, G. Effect of antioxidants supplementation on aging and longevity. *Biomed Res. Int.* **2014**, *2014*, No. 404680.

(12) Guarente, L.; Kenyon, C. Genetic pathways that regulate ageing in model organisms. *Nature* **2000**, *408*, 255−262.

(13) McColl, G.; Roberts, B. R.; Pukala, T. L.; Kenche, V. B.; Roberts, C. M.; Link, C. D.; Ryan, T. M.; Masters, C. L.; Barnham, K. J.; Bush, A. I.; Cherny, R. A. Utility of an improved model of amyloid-β (Aβ(1−42)) toxicity in *Caenorhabditis elegans* for drug screening for Alzheimer's disease. *Mol. Neurodegener.* **2012**, *7*, 57.

(14) Kaletta, T.; Hengartner, M. O. Finding function in novel targets: *C. elegans* as a model organism. *Nat. Rev. Drug Discov.* **2006**, *5*, 387−398.

(15) Shaye, D. D.; Greenwald, I. OrthoList: a compendium of *C. elegans* genes with human orthologs. *PLoS One* **2011**, *6*, No. e20085.

(16) Budzianowski, J. Kaempferol glycosides from *Hosta ventricosa*. *Phytochemistry* **1990**, *29*, 3643−3647.

(17) Park, J. S.; Rho, H. S.; Kim, D. H.; Chang, I. S. Enzymatic preparation of kaempferol from green tea seed and its antioxidant activity. *J. Agric. Food Chem.* **2006**, *54*, 2951−2956.

(18) Hsu, F. L.; Li, W. H.; Yu, C. W.; Hsieh, Y. C.; Yang, Y. F.; Liu, J. T.; Shih, J.; Chu, Y. J.; Yen, P. L.; Chang, S. T.; Liao, V. H. *In vivo* antioxidant activities of essential oils and their constituents from leaves of the Taiwanese *Cinnamomum osmophloeum*. *J. Agric. Food Chem.* **2012**, *60*, 3092−3097.

(19) Shi, Y. C.; Liao, V. H.; Pan, T. M. Monascin from red mold dioscorea as a novel antidiabetic and antioxidative stress agent in rats and *Caenorhabditis elegans*. *Free Radical Biol. Med.* **2012**, *52*, 109−117.
(20) Yu, C. W.; Wei, C. C.; Liao, V. H. Curcumin-mediated oxidative stress resistance in *Caenorhabditis elegans* is modulated by *age-1*, *akt-1*, *pdk-1*, *osr-1*, *unc-43*, *sek-1*, *skn-1*, *sir-2.1*, and *mev-1*. *Free Radical Res.* **2014**, *48*, 371−379.
(21) Lithgow, G. J.; White, T. M.; Melov, S.; Johnson, T. E. Thermotolerance and extended life-span conferred by single-gene mutations and induced by thermal stress. *Proc. Natl. Acad. Sci. U.S.A.* **1995**, *92*, 7540−7544.
(22) Honda, Y.; Tanaka, M.; Honda, S. Modulation of longevity and diapause by redox regulation mechanisms under the insulin-like signaling control in *Caenorhabditis elegans*. *Exp. Gerontol.* **2008**, *43*, 520−529.
(23) Link, C. D.; Taft, A.; Kapulkin, V.; Duke, K.; Kim, S.; Fei, Q.; Wood, D. E.; Sahagan, B. G. Gene expression analysis in a transgenic *Caenorhabditis elegans* Alzheimer's disease model. *Neurobiol. Aging* **2003**, *24*, 397−413.
(24) Wu, Y.; Wu, Z.; Butko, P.; Christen, Y.; Lambert, M. P.; Klein, W. L.; Link, C. D.; Luo, Y. Amyloid-$\beta$-induced pathological behaviors are suppressed by *Ginkgo biloba* extract EGb 761 and ginkgolides in transgenic *Caenorhabditis elegans*. *J. Neurosci.* **2006**, *26*, 13102−13113.
(25) Yamaguchi, T.; Takamura, H.; Matoba, T.; Terao, J. HPLC method for evaluation of the free radical-scavenging activity of foods by using 1,1-diphenyl-2-picrylhydrazyl. *Biosci., Biotechnol., Biochem.* **1998**, *62*, 1201−1204.
(26) Sanchez-Moreno, C. Review: Methods used to evaluate the free radical scavenging activity in foods and biological systems. *Food Sci. Technol. Int.* **2002**, *8*, 121−137.
(27) Vanfleteren, J. R. Oxidative stress and ageing in *Caenorhabditis elegans*. *J. Biochem.* **1993**, *292*, 605−608.
(28) Munoz, M. J.; Riddle, D. L. Positive selection of *Caenorhabditis elegans* mutants with increased stress resistance and longevity. *Genetics* **2003**, *163*, 171−180.
(29) Butterfield, D. A. Amyloid $\beta$-peptide [1−42]-associated free radical-induced oxidative stress and neurodegeneration in Alzheimer's disease brain: mechanisms and consequences. *Curr. Med. Chem.* **2003**, *10*, 2651−2659.
(30) Caldeira, G. L.; Ferreira, I. L.; Rego, A. C. Impaired transcription in Alzheimer's disease: key role in mitochondrial dysfunction and oxidative stress. *J. Alzheimer's Dis.* **2013**, *34*, 115−131.
(31) Walsh, D. M.; Townsend, M.; Podlisny, M. B.; Shankar, G. M.; Fadeeva, J. V.; El Agnaf, O.; Hartley, D. M.; Selkoe, D. J. Certain inhibitors of synthetic amyloid $\beta$-peptide (A$\beta$) fibrillogenesis block oligomerization of natural A$\beta$ and thereby rescue long-term potentiation. *J. Neurosci.* **2005**, *25*, 2455−2462.
(32) Yang, F.; Lim, G. P.; Begum, A. N.; Ubeda, O. J.; Simmons, M. R.; Ambegaokar, S. S.; Chen, P. P.; Kayed, R.; Glabe, C. G.; Frautschy, S. A.; Cole, G. M. Curcumin inhibits formation of amyloid $\beta$ oligomers and fibrils, binds plaques, and reduces amyloid *in vivo*. *J. Biol. Chem.* **2005**, *280*, 5892−5901.
(33) Link, C. D. Invertebrate models of Alzheimer's disease. *Genes Brain Behav.* **2005**, *4*, 147−156.
(34) Dostal, V.; Roberts, C. M.; Link, C. D. Genetic mechanisms of coffee extract protection in a *Caenorhabditis elegans* model of beta-amyloid peptide toxicity. *Genetics* **2010**, *186*, 857−866.
(35) Calderon-Montano, J. M.; Burgos-Moron, E.; Perez-Guerrero, C.; Lopez-Lazaro, M. A review on the dietary flavonoid kaempferol. *Mini Rev. Med. Chem.* **2011**, *11*, 298−344.
(36) Chen, A. Y.; Chen, Y. C. A review of the dietary flavonoid, kaempferol on human health and cancer chemoprevention. *Food Chem.* **2013**, *138*, 2099−2107.
(37) Grunz, G.; Haas, K.; Soukup, S.; Klingenspor, M.; Kulling, S. E.; Daniel, H.; Spanier, B. Structural features and bioavailability of four flavonoids and their implications for lifespan-extending and antioxidant actions in *C. elegans*. *Mech. Ageing Dev.* **2012**, *133*, 1−10.
(38) Kampkotter, A.; Gombitang Nkwonkam, C.; Zurawski, R. F.; Timpel, C.; Chovolou, Y.; Watjen, W.; Kahl, R. Effects of the flavonoids kaempferol and fisetin on thermotolerance, oxidative stress and FoxO transcription factor DAF-16 in the model organism *Caenorhabditis elegans*. *Arch. Toxicol.* **2007**, *81*, 849−858.
(39) Smith, J. V.; Luo, Y. Elevation of oxidative free radicals in Alzheimer's disease models can be attenuated by *Ginkgo biloba* extract EGb 761. *J. Alzheimer's Dis.* **2003**, *5*, 287−300.

HR62 allows more comprehensive understanding of the mechanisms involved in this biocontrol system. The objectives of this work were as follows: (1) to assess the capability of a new bioorganic fertilizer containing *B. amyloliquefaciens* HR62 to control bacterial wilt of tomato under greenhouse conditions and (2) to purify and to identify the antibacterial compounds produced by *B. amyloliquefaciens* HR62 that are responsible for the in vitro antagonism of *R. solanacearum*.

## MATERIALS AND METHODS

**Bacterial Strains and Culture Conditions.** HR62 was isolated from the rhizosphere soil of healthy tomato plants from a heavily wilt diseased field using dilution plate techniques. The strain was identified as *B. amyloliquefaciens* based on its biochemical characteristics and partial 16s rRNA.[23]

*B. amyloliquefaciens* HR62 was cultured on Luria−Bertani medium (LB) plates and stored at −70 °C in a mixture of LB liquid broth and 30% glycerol for further use. *R. solanacearum* QL-Rs1115 was provided by the Soil-Microbe-Interaction Laboratory at Nanjing Agricultural University in Nanjing, China.[11] The strain was maintained on KB plates supplemented with 0.005% triphenyltetrazolium chloride (m/v) for 2 days at 30 °C. A single colony was transferred into sterilized water for storage at room temperature.

For the production of antibiotics, *B. amyloliquefaciens* HR62 was grown in an optimized culture.[24]

**Preparation of Bioorganic Fertilizers.** The preparation of the bioorganic fertilizer (BIO62) followed the procedure described by Zhang et al.[36] The organic fertilizers (OF) consisted of a compost of pig manure and rice straw containing 33.7% OM (organic material), 2.51% N, 2.4% $P_2O_5$, 1.13% $K_2O$, and 22.3% $H_2O$ (Jiangsu Tianniang Agri-technology Ltd., Jiangsu, China) and an amino acid organic fertilizer containing a biologically hydrolyzed rapeseed cake with 44.2% OM, 8.0% amino acids, 4.4% N, 3.5% $P_2O_5$, 0.67% $K_2O$, and 28.5% $H_2O$[36] provided by Jiangsu Xintiandi Ltd. (Jiangsu, China). The two organic fertilizers were evenly mixed (1:1, w/w). *B. amyloliquefaciens* HR62 was incubated in 1 L of optimized culture in a 5 L fermentation tank on a shaker at 170 rpm at 30 °C for 36 h. The bacterial culture was centrifuged (at 10 000*g* for 10 min at 4 °C), and the collected cell pellets were resuspended in sterile water. The suspension of HR62 ($5.0 \times 10^9$ cfu $mL^{-1}$) was mixed with the OF mixture at a 1:5 (v/w) ratio. The final concentration of HR62 in the fortified organic fertilizer was approximately $10^9$ cfu $g^{-1}$ dry soil (ds).

**Design of the Pot Experiment under Greenhouse Conditions.** Tomato seedlings were grown in nursery cups (8.5 × 11 cm) containing 300 g of healthy nursery soil (i.e., soil that had been previously planted with tomato). One seedling was maintained in each cup. The seedlings were grown in a greenhouse, with temperatures ranging from 26 to 35 °C, until the seedlings had four true leaves. The seedlings were then transplanted to pots with 5 kg of *R. solanacearum*-infested soil. The following three treatments were included in the pot experiment: (1) CK treatment, where OF was applied to the soil; (2) HR62 treatment, where OF and a cell-free fermentation of HR62 was applied to the soil; and (3) BIO62 treatment, where BIO62 was added in the pot soil. The rate of the OF and BIO applications was 0.5% (dry weight basis). The OF and BIO applications were mixed separately into the soil prior to the transplantation of the tomato seedlings. Seedlings with four leaves were transplanted into the ceramic pots (5 kg soil per pot). One week after the transplantation, a 1 mL suspension of the *R. solanacearum* strain QL-Rs1115 ($5 \times 10^7$ cfu $mL^{-1}$) was poured into the soil to give a final bacterial concentration of $10^4$ cfu $g^{-1}$ ds. A total of 45 pots (15 pots with 30 plants for each treatment) were placed on a glasshouse bench in a completely randomized design and watered regularly. The experiment was repeated twice.

Disease development, expressed as disease incidence (DI), was based on a disease index (di) scale of 0−4,[25] where 0 = no wilting, 1 = 1−25% wilting, 2 = 26−50% wilting, 3 = 51−75% wilting, and 4 = 76−100% wilting or dead. The di was recorded daily for 28 days after pathogen challenge. The DI was calculated according to the following equation:[26]

$$DI = [\sum(\text{number of diseased plants in the index} \times \text{di})/(\text{total number of plants investigated} \times \text{highest di})] \times 100\%$$

To evaluate the *R. solanacearum* populations in the rhizosphere soils and crown sections, three tomato plants were uprooted from each treatment at 1, 7, 14, 21, and 28 days after pathogen challenge. Ten grams of rhizosphere soils or tomato crown sections was added to 90 mL of sterile water (crown sections were ground beforehand). The suspensions were shaken for 30 min on a rotary shaker at 200 rpm. Several 10-fold dilutions were made, and 0.1 mL aliquots were spread on the surface of M-SMSA medium.[27] After 2 days of incubation at 30 °C, colonies typical of *R. solanacearum* were counted. Colony forming units (cfu) were calculated per gram (dry weight) of soil and the values were log-transformed before statistical analysis was performed.

**Amplification of HR62 Antagonistic Genes.** The primers used to amplify the genes encoding bioactive compounds in HR62 were either used as previously described by Arguelles-Arias et al.[19] and Joshi and Gardener[28] or designed using Primer 5 software from Premier Biosoft based on consensus sequences of known *Bacillus subtilis* lipopeptide antibiotic genes that were deposited in GenBank (Table S1, Supporting Information).[29,30] PCR reactions were carried out in a 25 μL reaction volume containing 1 μL of genomic DNA, 2.5 μL of 10× PCR buffer, 20 mM $MgCl_2$, 0.2 mM of each dNTP, 0.5 μM of each primer, and 1.25 U of Taq DNA polymerase (Takara, Dalian). Amplification was performed using a PCR System DNA thermal cycler (Bio-Rad) programmed for one cycle of 94 °C for 5 min, followed by 30 cycles of 94 °C for 30 s, annealing for 30 s at 51 °C, extension for 1 min and 30 s, and a final extension at 72 °C for 10 min. A negative control without DNA was included in each PCR run. Each PCR reaction had three replicates. The amplified products were visualized by gel electrophoresis in 1% agarose gels; gels were stained with ethidium bromide. Expected PCR fragments were extracted using a gel extraction kit (Axygen, China). The obtained fragments were sequenced by Majorbio Co. (Shanghai, China). Nucleotide sequences were compared with those from GenBank using the BlastN software provided online by the National Center for Biotechnology Information.

**Isolation and Purification of Antibacterial Compounds from *B. amyloliquefaciens* HR62.** To select the best extractant, HR62 was incubated in an optimized culture (100 mL) for 36 h and extracted twice (for 1 h each) in an equal volume for five the following extractants: toluene, hexane, chloroform, ethyl acetate, and *n*-butyl alcohol. Among these, *n*-butyl alcohol was found to be the best extractant and was therefore used in subsequent experiments. Then, 5 mL of an overnight optimized culture of HR62 was used to inoculate 500 mL of fresh liquid optimized culture. The culture was then placed in an incubator shaker (at 170 rpm and 30 °C) for 36 h. The liquid culture was centrifuged at 10 000*g* for 10 min, and the supernatants were pooled together. Active compounds were extracted twice (for 1 h each) with an equal volume of *n*-butyl alcohol. The extract was concentrated using a rotary evaporator, and the residues were dissolved in 100 mL of distilled water. The sample was adjusted to pH 2.0 with 6 mol $L^{-1}$ HCl and stored overnight at 4 °C. The precipitate was recovered by centrifugation at 8000 g for 20 min. The pellet was washed twice with acidic deionized waster (pH 2.0) and extracted twice with methanol.[31] The solution was dried in a rotary vacuum evaporator, and the residue was dissolved in 10 mL of 0.01 mol $L^{-1}$ phosphate buffer solution (PBS) at pH 7.4.

A chloroform and methanol gradient (e.g., 100 mL of chloroform, 90 mL of chloroform + 10 mL of methanol, 80 mL of chloroform + 20 mL of methanol, and so on, up to 100 mL of methanol) was used to elute active compounds from a silica gel column (2 × 24 cm). Twenty-eight fractions (10 50-mL fractions and 18 30-mL fractions) were collected. The fractions were dried using a rotary evaporator and dissolved separately in 2 mL of PBS buffer. Active fractions were identified by an agar diffusion assay against *R. solanacearum* on KB plates; these fractions were then pooled and eluted further using a water and methanol gradient (e.g., 100 mL of water, 90 mL of water + 10 mL of methanol, 80 mL of water + 20 mL of methanol, and so on, up to 100 mL of methanol) in a Sephadex LH-20 column (2 × 24 cm). Active fractions were found using a bioassay and were then pooled. The pooled fractions were purified further using an HPLC device (1200 series, Agilent, Santa Clara, CA).

A 20 μL of sample was injected into an HPLC column (Eclipse XDB-C18, 4.6 × 250 mm, 5 μm, Agilent, Santa Clara, CA). Two conditions were applied. In condition 1, the temperature of the column was maintained at 30 °C throughout the experiment. The purification was performed using a solvent containing 40% A ($CH_3CN$) and 60% B [0.1% (v/v) $CH_3COOH$], with a flow rate of 0.6 mL $min^{-1}$ for 30 min. In condition 2, the temperature of the column was maintained at 35 °C throughout the experiment. The sample was eluted in 60−93% A ($CH_3CN$) and 40−7% B [0.1% (v/v) $CH_3COOH$] over 9 min. The ratio was then kept stable until the end of the experiment, with a flow rate of 0.84 mL $min^{-1}$ for 25 min. A standard sample of surfactin was also tested using condition 2. An ultraviolet (UV) detector was used to detect peaks at 210 nm. A fraction collector (Analyt FC, G1364C, Agilent, Santa Clara, CA) was used to collect the pure compounds; the fractions were collected using the time and peaks mode. The injections were performed repeatedly to allow for the collection of a sufficient quantity of antibiotics. The fractions were lyophilized, and the residues were dissolved in 500 μL of methanol. After an agar diffusion assay against *R. solanacearum* on KB plates, the active peaks were located.

**Mass Spectrometry Analysis.** The antibacterial material was subjected to a liquid chromatography/electrospray ionization-mass spectrometry (LC/ESI-MS) system (1200 series, Agilent, Santa Clara, CA, and ESI-MS, 6410 Triple Quad LC/MS, Agilent, Santa Clara, CA) with a C18 column (4.6 × 250 mm, 5 μm). Two conditions were used; these conditions were the same as those described for the purification in the HPLC section. For the MS analysis, the electrospray needle was operated at a spray voltage of 4.5 kV. The capillary temperature was 300 °C. The fractions eluted in condition 1 were measured in the both positive and negative ion modes to determine the accurate molecular weights of the antibiotics. The fractions eluted in condition 2 were measured in positive ion mode. The mass spectra were acquired in an *m*/*z* range of 100−2000 at a scan rate of 500 atomic mass units (amu)/s.

**Sensitivity of the Antibacterial Compounds to Temperature, pH, Enzymes, and Organic Solvents.** For the thermal stability test, the antibacterial compounds were exposed to temperatures of 30, 40, 50, 60, 70, 80, 90, and 100 °C for 1 h; 115 °C for 30 min; or 121 °C for 20 min. For the pH stability test, the antibacterial compounds were solubilized in a buffer containing 100 mM citrate and 200 mM phosphate buffer (pH 1−8), a buffer containing 100 mM phosphate and 100 mM HCl (pH 9−11), or a buffer containing 200 mM KCl and 200 mM NaOH (pH 12−14), followed by an incubation at 30 °C for 12 h. The residual antibacterial activity was assessed after neutralizing the samples to pH 7.0 with an appropriate weak base or weak acid. The sensitivity of the antibacterial compounds to various enzymes was tested. The enzymes used were as follows: pepsin (800−2500 U $mg^{-1}$; P8160, Solarbio), recombinant proteinase K (600−100 U $mg^{-1}$; 03115828001, Roche Applied Science), albumin fraction V (≥95% protein; A8020, Solarbio), and trypsin from bovine pancreas (≥2500 U $mg^{-1}$; 64008834, SCRS). All of the enzyme solutions were prepared in 25 mM phosphate buffer (pH 7.0). Each solution contained 1 mg $mL^{-1}$ of its respective enzyme. Solutions containing the antibacterial compounds were prepared by centrifuging the HR62 fermentation. The stock solutions of the antibacterial compounds and the enzymes were mixed at a 1:1 ratio (v/v) and incubated at 37 °C for 1 h before the residual antibacterial activity was measured using an agar diffusion assay against *R. solanacearum*. The sensitivity of the antibacterial compounds to the following organic solvents was tested: acetone, methanol, isopropyl alcohol, and ethanol. A 100 mL aliquot of cultured HR62 was centrifuged at 10 000*g* for 10 min, and the supernatants were added to the organic solvents in equal volumes. The mixture was then placed at room temperature for 4 h. The mixtures were dried using a rotary evaporator, and the residues were dissolved in 100 mL of PBS buffer. The resistance activity of the PBS solutions to *R. solanacearum* was determined using KB plates.

**Statistical Analysis.** The arcsin conversion was performed before the data were analyzed for percentages. Differences were assessed by one-way ANOVA. Duncan's multiple-range test was applied when one-way ANOVA revealed significant differences ($P < 0.05$). All statistical analyses were performed with SPSS 16.0 (SPSS Inc.) and SigmaPlot 11.0 (Systat Software Inc.).

## RESULTS

**Biological Control Assays against Bacterial Wilt of Tomato.** Treating plants with BIO62 resulted in reduced disease incidence (Figure 1). Disease symptoms were apparent 7 days after the pathogen challenge in all treatments. The BIO62-treated plants had significantly lower disease incidence compared with the control at 14, 21, and 28 days after the pathogen challenge. At the end of the experiment, the disease incidence in HR62- and BIO62-treated plants was reduced by 53% and 65%, respectively. The disease incidence in the control was 85%.

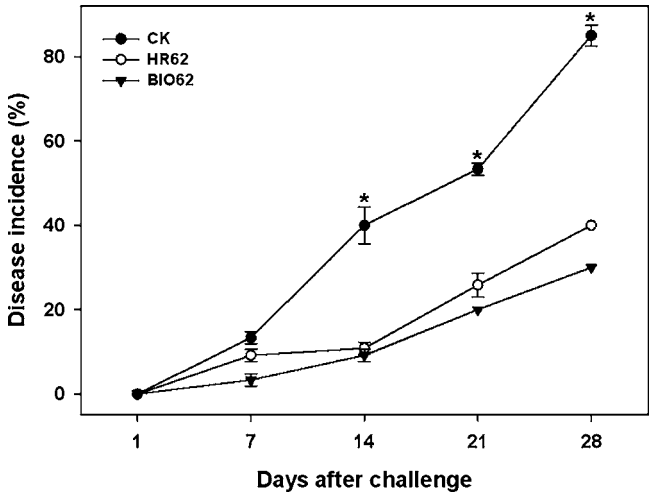


**Figure 1.** Effect of different treatments on bacterial wilt disease incidences at 1, 7, 14, 21, and 28 days after challenge. All values are means of three blocks with ten replicates per block. Bars show standard errors of the mean. An asterisk on the top of the bar represents significance at $P < 0.05$ (Duncan's multiple range test).

**Population Dynamics of *R. solanacearum* in the Rhizosphere Soil and Crown Sections of Tomato.** Populations of *R. solanacearum* in the rhizosphere soil of CK-treated tomatoes were significantly higher than those observed in HR62 and BIO62 treatments (Figure 2A) throughout the challenge period. The rhizosphere soil of BIO62-treated plants had the lowest population density at 8.04 log cfu $g^{-1}$ ds. For the CK treatment, the observed population density was 9.30 log cfu $g^{-1}$ ds at the end of experiment.

The same trend was observed in the dynamics of *R. solanacearum* among three treatments in the crown sections of tomatoes (Figure 2B). BIO62-treated plants had the lowest population density at 5.63 log cfu $g^{-1}$ fresh plant section (fps). For the CK treatment, the observed population density was 8.08 log cfu $g^{-1}$ fps at the end of experiment.

**Identification of Antibiotic Biosynthesis Genes from *B. amyloliquefaciens* HR62.** PCR was used to detect the genes involved in the biosynthesis of the six antibiotics reported to be produced by *B. amyloliquefaciens*. A total of 10 gene fragments of expected sizes correlated with biological control activities were efficiently amplified from HR62 (Figure S2, Supporting Information). The DNA sequences obtained from these amplifications confirmed the identity of these genes (Table 1). FenBF/FenBR and FNDF/FNDR primers amplified fragments with 99% and 96% homology, respectively, to the gene that encodes fengycin (synonymous with plipastatin) synthetase. The analysis of sequences amplified by the primers ituAF/ituAR, bamB1F/bamB1R, ituCF/ituCR, and ituD2F/ituD2R showed

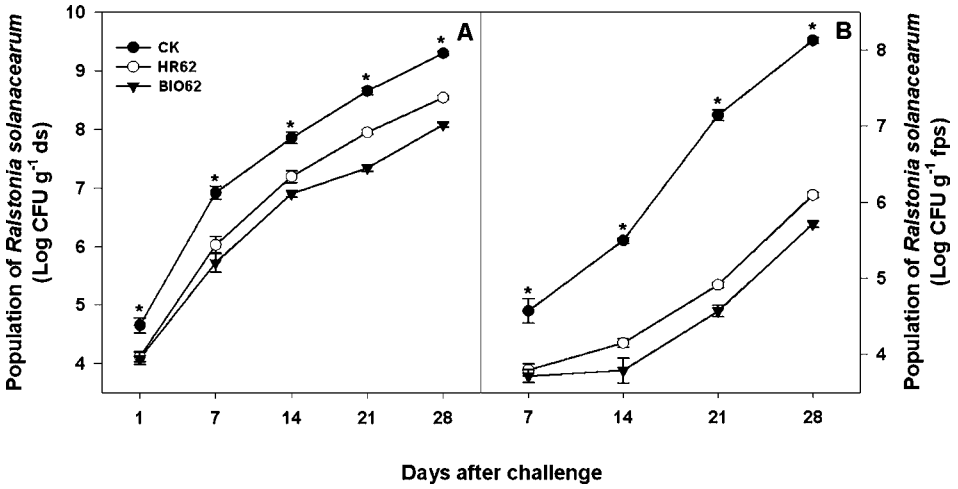


**Figure 2.** Populations of *R. solanacearum* in the rhizosphere soil (A) and crown section (B) of tomato plants were determined using the plate count method at 1, 7, 14, 21, and 28 days after challenge with *R. solanacearum* QL-Rs1115. Bars show standard errors of the mean. An asterisk on the top of the bar represents significance (Duncan's multiple range test, $P < 0.05$).

**Table 1. Genes Showing the Highest Similarity to the Sequenced Products Obtained from PCR Amplification of Biosynthetic Genes**

| primer names | isolate | match with proper genes by BlastN | GenBank accession numbers of matching genes | e value of BlastN | % identity of corresponding gene by BlastN |
|---|---|---|---|---|---|
| BacF/BacR | *B. subtilis* 916 | bacillorin synthetase A | FJ194462.1 | 0.0 | 98 |
| ituAF/ituAR | *B. subtilis* MH25 | iturin A operon | EU263005.1 | 0.0 | 99 |
| bamB1F/bamB1R | *B. subtilis* SQR9 | iturin A synthetase B (ituB) gene | JN093026.1 | 0.0 | 97 |
| ituCF/ituCR | *B. subtilis* | iturin A synthetase C | AB050629.1 | 0.0 | 99 |
| ituD2F/ituD2R | *B. subtilis* SQR9 | malonyl-CoA transacylase (ituD) | JN093033.1 | 0.0 | 97 |
| FNDF/FNDR | *B. amyloliquefaciens* Q-426 | fengycin synthetase D | JQ271536.1 | 4e-108 | 96 |
| fenBF/fenBR | *B. amyloliquefaciens* Lx-11 | fengycin synthetase B | JN086144.1 | 0.0 | 99 |
| BACDF1/BACDR1 | *B. subtilis* ME488 | BacD gene product | EU334357.1 | 0.0 | 99 |
| 110F/110R | *B. subtilis* B006 | srfAB gene | GU062711.1 | 8e-115 | 95 |
| mln1F/mln1R | *B. amyloliquefaciens* FZB42 | macrolactin synthesis | CP000560.1 | 0.0 | 98 |

97−99% identity with regions of genes encoding iturin synthetase or enzymes synthesizing closely related compounds in the iturin family. A sequence with 95% (e value = 8e-115) homology to the surfactin synthetase gene was detected in HR62 by the primer pair 110F/110R. BacF/BacR primers amplified a fragment similar to the Bacillorin operon with 98% homology. The Macrolactin gene cluster was amplified by mLn1F/mLn1R primers with 98% homology. Moreover, the analysis of sequences amplified by BACDF1/BACDR1 primers revealed 99% identity with the bacilysin synthetase gene cluster.

**Characterization of the Antibacterial Compounds from *B. amyloliquefaciens* HR62.** After the final purification with RP-HPLC, the fractions eluted at 4.740 and 5.808 min (Figure 3A) in condition 1 showed pathogen antagonism; these fractions were recorded as HR62-1 and HR62-2, respectively. To determine the molecular weight and molecular formula of the HPLC-purified antibiotics, the samples were subjected to HPLC analysis coupled with ESI-Q-trap MS. The data from the HPLC/ESI-MS analyses are shown in Figure 4. The spectra of HR62-1 revealed molecular masses of 401.3 $[M - H]^-$ in negative ion mode (Figure 4B) and 425.2 $[M + Na]^+$, 441.2 $[M + K]^+$, 385.2 $[M + H - H_2O]^+$, 367.2 $[M + 2K - 2H_2O]^{2+}$, and 349.1 $[M + 2K - 3H_2O]^{3+}$ in positive ion mode (Figure 4A). Therefore, HR62-1 contained macrolactin A, with a molecular weight of 402 Da.[16] The spectra of HR62-2 exhibited molecular masses of 435.5 $[M - OH - H_2O]^-$ in negative ion mode (Figure 4D) and 511.2 $[M + Na]^+$ and 367.2 $[M -$ malonic acid $- 2H_2O + H]^+$ in positive ion mode (Figure 4C). This fraction was identified as containing 7-*O*-malonyl macrolactin A, with a molecular weight of 488 Da.[16]

In addition, five fractions collected from sample HR62 showed antagonism to *R. solanacearum* QL-Rs1115. These fractions were collected at almost the same retention time as the standard surfactin sample (Figure 3B,C). The collection times were 14.385, 15.563, 17.476, 18.303, and 20.248 min (Figure 3B); the fractions were named HR62-1′, HR62-2′, HR62-3′, HR62-4′, and HR62-5′, respectively. The mass spectra of HR62-1′, HR62-2′, HR62-3′, HR62-4′, and HR62-5′ exhibited $m/z$ ratios of 516.8, 523.7, 530.9, 530.9, and 537.8, respectively. According to the already available information about surfactin, the molecular weight of surfactin is approximately 1000 Da. We deduced that the sample took two charges after ionization and analyzed the $m/z$ results as 516.8 $[M + K + H]^{2+}$, 523.7 $[M + K + H]^{2+}$, 530.9 $[M + K + H]^{2+}$, 530.9 $[M + K + H]^{2+}$, and 537.8 $[M + K + H]^{2+}$ in positive ion mode; these fractions were identified as surfactin with molecular weights of 994 ($C_{13}$), 1008 ($C_{14}$), 1022 ($C_{15}$), 1022 ($C_{15}$), and 1036 ($C_{16}$), respectively. The prominent masses from the HPLC/ESI-MS spectra and the molecular weights are listed in Table 2.

**The Effect of Temperature, pH, Organic Solvents and Enzymes on Antibacterial Activity.** The antibacterial

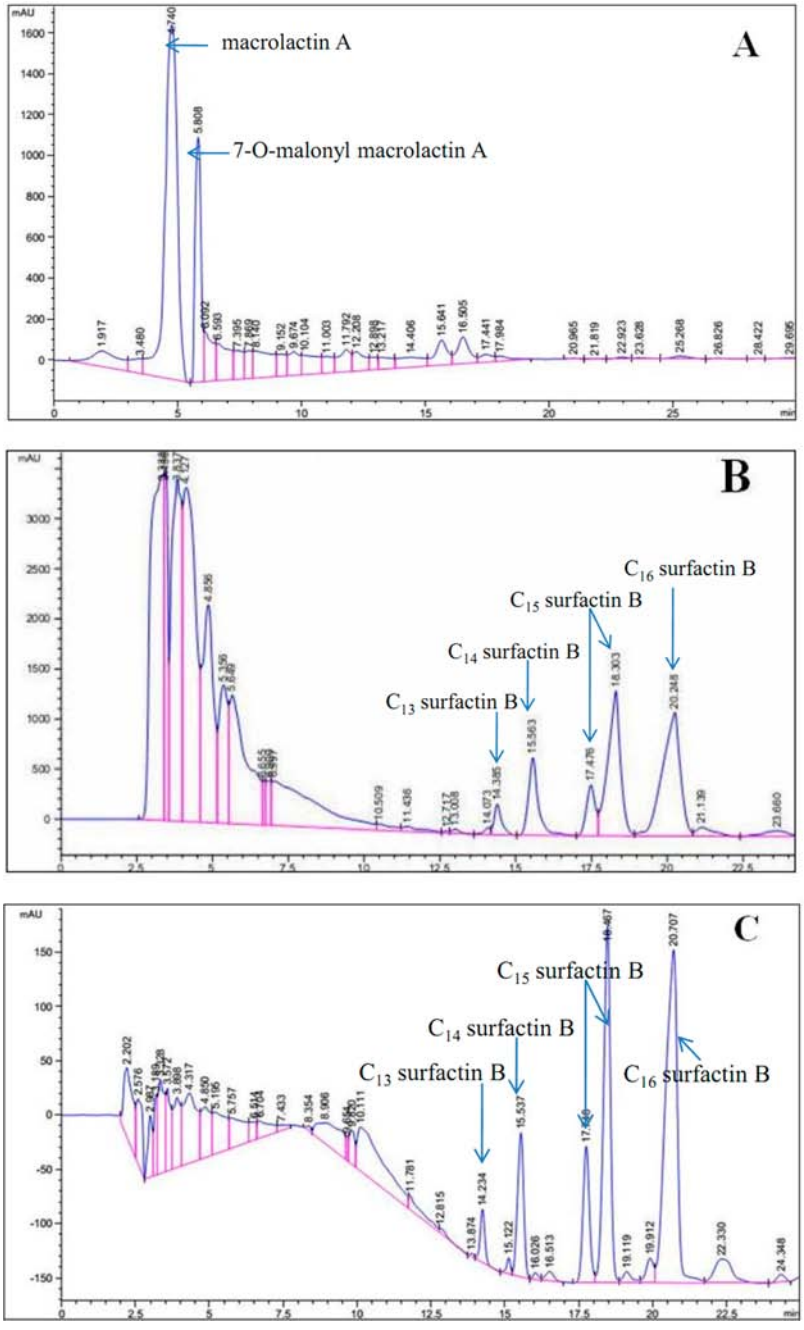


**Figure 3.** Reversed-phase HPLC chromatograms of antibiotics produced by *B. amyloliquefaciens* HR62 by condition 1 (A) and condition 2 [B and C (standard sample)]. Antibacterial activities were found in peaks located at 4.740 and 5.808 min (A) and at 14.385, 15.563, 17.476, 18.303, and 20.248 min (B).

compounds were stable at different temperatures (40, 50, and 60 °C) (Figure 5A) and at a pH range of 5−7 (Figure 5B). Antibacterial activities were decreased at 100, 115, and 121 °C. In addition, the antibacterial compounds were stable in methanol, ethanol, acetone, and isopropyl alcohol (Figure 5C). The enzymes pepsin (800−2500 U $mg^{-1}$; P8160, Solarbio), recombinant proteinase K (600−100 U $mg^{-1}$; 03115828001, Roche Applied Science), albumin fraction V (≥95% protein; A8020, Solarbio), and trypsin from bovine pancreas (≥2500 U $mg^{-1}$; 64008834, SCRS) were unable to degrade the antibacterial compounds (Figure 5D).

## DISCUSSION

Bacterial wilt of tomato was significantly suppressed by both of the treatments tested in the present study. The application of organic fertilizer and antagonists separately (treatment HR62) reduced the incidence of bacterial wilt disease by 53% (Figure 1), in agreement with the established effect of organic amendments and biocontrol agents such as *Bacillus* on soilborne diseases.[32−34] The application of BIO62 conferred a biocontrol efficacy of 65% (Figure 1). The combination of antagonists with a suitable organic fertilizer may provide sufficient nutrients to the antagonists to ensure high inoculum to the plants at the time of treatment, promote the root-colonization capacity of the antagonist, and prevent the invasion of the pathogen.[35,36]


dx.doi.org/10.1021/jf503136a | J. Agric. Food Chem. 2014, 62, 10708−10716

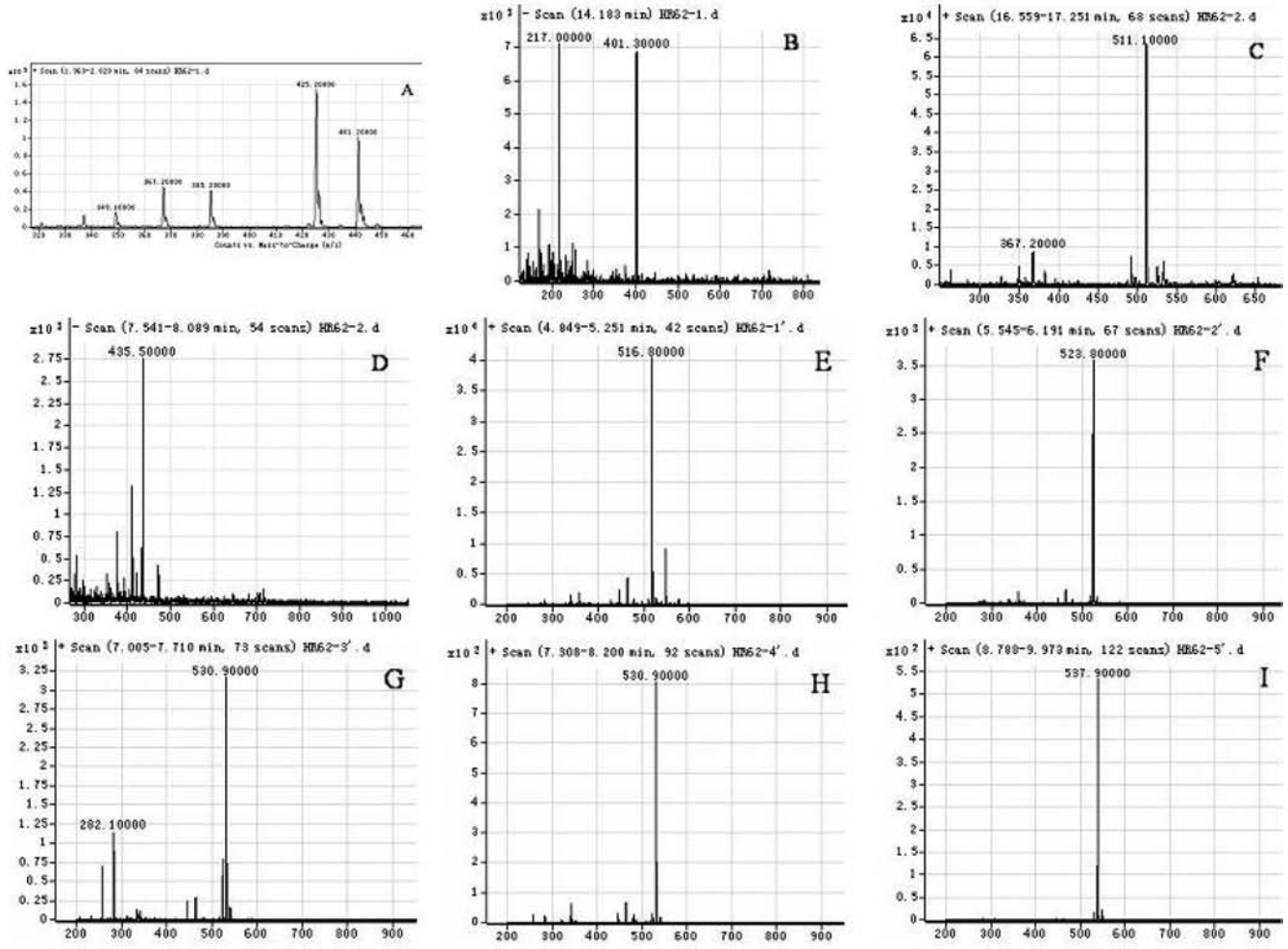


**Figure 4.** Mass spectroscopic analysis of antibacterial compounds observed in peaks eluted at 4.740 min (A and B), 5.808 min (C and D), 14.385 min (E), 15.563 min (F), 17.476 min (G), 18.303 min (H), and 20.248 min (I) by reversed-phase HPLC.

**Table 2. Active Compound Production by *B. amyloliquefaciens* HR62 Detected by HPLC/ESI-MS in Positive and (or) Negative Modes**

| | | *m/z* | | product ions | | | |
|---|---|---|---|---|---|---|---|
| name of sample | retention time (min) | negative | positive | negative | positive | mol wt | compd |
| HR62-1 | 4.740 | 401.3 | 425.2 | $[M - H]^-$ | $[M + Na]^+$ | 402 | macrolactin A |
| | | | 441.2 | | $[M + K]^+$ | | |
| | | | 385.2 | | $[M + H - H_2O]^+$ | | |
| | | | 367.2 | | $[M + 2K - 2H_2O]^{2+}$ | | |
| | | | 349.1 | | $[M + 2K - 3H_2O]^{3+}$ | | |
| HR62-2 | 5.808 | 435.5 | 511.2 | $[M - OH - H_2O]^-$ | $[M + Na]^+$ | 488 | 7-*O*-malonyl macrolactin A |
| | | | 367.2 | | $[M -$ malonic acid $- 2H_2O + H]^+$ | | |
| HR62-1′ | 14.385 | ND | 516.8 | ND | $[M + K + H]^{2+}$ | 994 | $C_{13}$ surfactin B |
| HR62-2′ | 15.563 | ND | 523.7 | ND | $[M + K + H]^{2+}$ | 1008 | $C_{14}$ surfactin B |
| HR62-3′ | 17.476 | ND | 530.9 | ND | $[M + K + H]^{2+}$ | 1022 | $C_{15}$ surfactin B |
| HR62-4′ | 18.303 | ND | 530.9 | ND | $[M + K + H]^{2+}$ | 1022 | $C_{15}$ surfactin B |
| HR62-5′ | 20.248 | ND | 537.8 | ND | $[M + K + H]^{2+}$ | 1036 | $C_{16}$ surfactin B |

Biomass yields of plants treated with HR62 and BIO62 were significantly higher than that of the control (Figure S1, Supporting Information). This result demonstrates that BIO62 not only reduced bacterial wilt of tomato but also promoted plant growth. This was most likely due to the beneficial contribution of the enriched microorganism community in the compost.[37] These results were in agreement with the report published by Wei et al.,[11] which indicated that the application of bioorganic fertilizers significantly reduced the incidence of bacterial wilt disease both in the greenhouse and in field conditions.

Several *B. amyloliquefaciens* strains have been used as biological control agents of plant diseases.[21,38,39] The most convincing antagonism properties are the broad-spectrum antibiotic and antimicrobial compounds synthesized by these microorgan-


dx.doi.org/10.1021/jf503136a | J. Agric. Food Chem. 2014, 62, 10708−10716

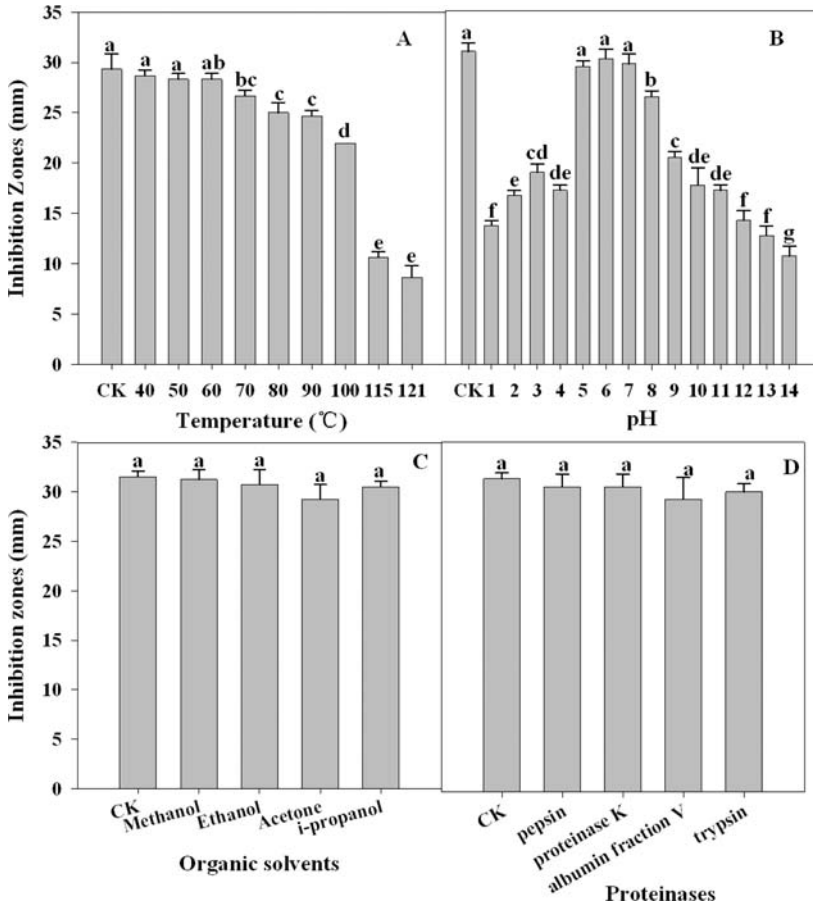


**Figure 5.** Sensitivities of antibacterial compounds produced by *B. amyloliquefaciens* HR62 to temperature (A), pH (B), organic solvents (C), and proteinases (D).

isms.[20] Antibiotics from *Bacillus* protect plants either by hampering the pathogens directly or by inducing systemic resistance in the host.[40,41] In the present study, *B. amyloliquefaciens* HR62 showed antagonism against seven soil-borne fungi pathogens (Table S2, Supporting Information). This result suggests that a large range of antibiotics may be secreted by HR62. Furthermore, PCR analysis of the HR62 genome revealed the existence of lipopeptide-synthetic genes encoding for surfactin, fengycin, iturin, and bacillicon; polyketide-synthetic genes coding for macrolactin; and dipeptide-synthetic genes encoding for bacilysin synthetase (Table 1). Therefore, *B. amyloliquefaciens* HR62 is an effective biocontrol agent. We focused on its antagonism to *R. solanacearum*, a causative agent of bacterial wilt of tomato, both in vitro and in vivo. In this study, we tried to isolate the antibiotics produced by HR62 to explain another biocontrol mechanism. After purification and characterization using extraction, precipitation, and purification using silica gel columns (Sephadex LH-20, RP-HPLC and LC−MS), two types of polyketides were identified, macrolactin A and 7-*O*-malonyl macrolactin A. One type of lipopeptide, surfactin B ($C_{13}$, $C_{14}$, $C_{15}$, $C_{15}$, and $C_{16}$), was observed and identified according to previous studies.[16,19,42]

Macrolactin, which consists of a 24-membered lactone ring, was first isolated from a deep-sea bacterium. Macrolactin was used in clinical antibiosis because of its selective antibacterial activities, its cytotoxicity against murine melanoma cancer cells, and its antiviral activities against Herpes simplex virus (HSV) and human immunodeficiency virus (HIV).[43,45] 7-*O*-Malonyl macrolactin A (MMA) has the same configuration as its parent molecule macrolactin A. MMA is a bacteriostatic antibiotic that inhibits a number of multidrug-resistant Gram-positive pathogens, such as *B. subtilis*, *Staphylococcus aureus*, and *Burkholderia cepacia*.[44,45] Dunlap et al.[46] identified and confirmed the presence of the PKS cluster that encodes the synthesis of macrolactin from antagonist *B. amyloliquefaciens* AS 43.3, which showed antagonism to *Fusarium* head blight. In this present study, we observed the inhibition activities of these compounds to the phytopathogen *R. solanacearum*; this activity was supported by the results published by Yuan et al.[16]

In the present study, the antibiotic surfactin was also shown to act as an antagonist to *R. solanacearum* QL-Rs1115. This compound is applied in an extremely wide variety of industrial processes involving emulsification, foaming, detergency, wetting, dispersing, and solubilization. Kim et al.[42] reported that surfactin isolated from *Bacillus polyfermenticus* KJS-2 showed antimicrobial activity to several Gram-positive and Gram-negative bacteria. Zhu et al.[47] tested the antagonism of lipopeptides produced by *B. amyloliquefaciens* XZ-173 to *R. solanacearum* QL-Rs1115; one of these lipopeptides was surfactin. Bacon et al.[48] reported that *Bacillus mojavensis* produce a considerable amount of surfactin A to inhibit of the maize mycotoxic fungus *Fusarium verticillioides*. Surfactin resists soil-borne pathogens by stimulating plant growth, increasing the adhesion of biocontrol agents to plant surfaces, inhibiting the formation of biofilms by pathogenic organisms, and activating systemic resistance in a wide range of plants.[24,49,50]

In this work, the combination of organic fertilizers with *B. amyloliquefaciens* HR62 significantly reduced the disease

incidence of bacterial wilt of tomato. Macrolactin and surfactin analogs were detected in an HR62 culture filtrate. Although these two compounds have been previously reported in the literature, here they were found in one strain that could inhibit *R. solanacearum* for the first time. Polyketide and lipopeptide production were pursued as another possible mechanism underlying the biocontrol of bacterial wilt disease by HR62. These data provide a theoretical basis for the development of commercial bioorganic fertilizers with different functional biocontrol agents.

## ■ ASSOCIATED CONTENT

### Supporting Information

Figures S1 and S2 and Tables S1 and S2, as noted in the text. This material is available free of charge via the Internet at http://pubs.acs.org.

## ■ AUTHOR INFORMATION


### Corresponding Author

*Tel.: +86 25 84396824. Fax: +86 25 84396824. E-mail: ycxu@njau.edu.cn.



### Funding

This research was financially supported by the National Natural Science Foundation of China (41301262), the Jiangsu Province Science Foundation for Youths (BK20130677), the Innovative Research Team Development Plan of the Ministry of Education of China (IRT1256), the Priority Academic Program Development (PAPD) of Jiangsu Higher Education Institutions, and the 111 project (B12009).


### Notes

The authors declare no competing financial interest.

## ■ REFERENCES


(1) Xue, Q. Y.; Chen, Y.; Li, S. M.; Chen, L. F.; Ding, G. C.; Guo, D. W.; Guo, J. H. Evaluation of the strains of *Acinetobacter* and *Enterobacter* as potential biocontrol agents against Ralstonia wilt of tomato. *Biol. Control* **2009**, *48*, 252−258.

(2) Quimby, P. C.; King, L. R.; Grey, W. E. Biological control as a means of enhancing the sustainability of crop/land management systems. *Agric. Ecosyst. Environ.* **2002**, *88*, 147−152.

(3) Ji, X. L.; Lu, G. B.; Gai, Y. P.; Zheng, C. C.; Mu, Z. M. Biological control against bacterial wilt and colonization of mulberry by an endophytic *Bacillus subtilis* strain. *FEMS Microbiol. Ecol.* **2008**, *65*, 565−573.

(4) Vanitha, S. C.; Niranjana, S. R.; Mortensen, C. N.; Umesha, S. Bacterial wilt of tomato in Karnataka and its management by *Pseudomonas fluorescens*. *BioControl* **2009**, *54*, 11.

(5) Frey, P.; Prior, P.; Marie, C.; Kotoujansky, A.; Demery, D. T.; Trigalet, A. Hrp$^-$ Mutants of *Pseudomonas solanacearum* as potential biocontrol agents of tomato bacterial wilt. *Appl. Environ. Microbiol.* **1994**, *60*, 3175−3181.

(6) El-Hassan, S. A.; Gowen, S. R. Formulation and delivery of the bacterial antagonist *Bacillus subtilis* for management of lentil vascular wilt caused by *Fusarium oxysporum* f. sp. lentis. *J. Phytopathol.* **2006**, *154*, 148−155.

(7) Kokalis-Burelle, N.; Vavrina, C. S.; Rosskopf, E. N.; Shelby, R. A. Field evaluation of plant growth-promoting rhizobacteria amended transplant mixes and soil solarization for tomato and pepper production in Florida. *Plant Soil* **2002**, *238*, 257−266.

(8) Cotxarrera, L.; Trillas-Gay, M. I.; Steinberg, C.; Alabouvette, C. Use of sewage sludge compost and *Trichoderma asperellum* isolates to suppress Fusarium wilt of tomato. *Soil Biol. Biochem.* **2002**, *34*, 467−476.

(9) Trillas, M. I.; Casanova, E.; Cotxarrera, L.; Ordovás, J.; Borrero, C.; Avilés, M. Composts from agricultural waste and the *Trichoderma asperellum* strain T-34 suppress *Rhizoctonia solani* in cucumber seedlings. *Biol. Control* **2006**, *39*, 32−38.

(10) Luo, J.; Ran, W.; Hu, J.; Yang, X.; Xu, Y.; Shen, Q. Application of bio-organic fertilizer significantly affected fungal diversity of soils. *Soil Sci. Soc. Am. J.* **2010**, *74*, 2039−2048.

(11) Wei, Z.; Yang, X. M.; Yin, S. X.; Shen, Q. R.; Ran, W.; Xu, Y. C. Efficacy of bacillus-fortified organic fertiliser in controlling bacterial wilt of tomato in the field. *Appl. Soil Ecol.* **2011**, *48*, 152−159.

(12) Yuan, S. F.; Wang, L. L.; Wu, K.; Shi, J. X.; Wang, M. S.; Yang, X. M.; Shen, Q. R.; Shen, B. Evaluation of bacillus-fortified organic fertilizer for controlling tobacco bacterial wilt in greenhouse and field experiments. *Appl. Soil Ecol.* **2014**, *75*, 86−94.

(13) Lee, S. C.; Kim, S. H.; Park, I. H.; Chung, S. Y.; Chandra, M. S.; Choi, Y. L. Isolation, purification and characterization of novel fengycin S from *Bacillus amyloliquefaciens* LSC04 degrading-crude oil. *Biotechnol. Bioproc. E* **2010**, *15*, 246−253.

(14) Scholz, R.; Molohon, K. J.; Nachtigall, J.; Vater, J.; Markley, A. L.; Süssmuth, R. D.; Mitchell, D. A.; Borriss, R. Plantazolicin, a novel microcin B17/streptolysin S-like natural product from *Bacillus amyloliquefaciens* FZB42. *J. Bacteriol.* **2011**, *193*, 215−224.

(15) Wang, X. X.; Huang, L. L.; Kang, Z. S.; Buchenauer, H.; Gao, X. N. Optimization of the fermentation process of *Actinomycete* strain Hhs.015$^T$. *J. Biomed. Biotechnol.* **2010**, *2010*, 141876.

(16) Yuan, J.; Li, B.; Zhang, N.; Waseem, R.; Shen, Q. R.; Huang, Q. W. Production of bacillomycin- and macrolactin-type antibiotics by *Bacillus amyloliquefaciens* NJN-6 for suppressing soilborne plant pathogens. *J. Agric. Food Chem.* **2012**, *60*, 2976−2981.

(17) Lee, S. C.; Kim, S. H.; Park, I. H.; Chung, S. Y.; Choi, Y. L. Isolation and structural analysis of bamylocin A, novel lipopeptide from *Bacillus amyloliquefaciens* LP03 having antagonistic and crude oil-emulsifying activity. *Arch. Microbiol.* **2007**, *188*, 307−312.

(18) Yu, G. Y.; Sinclair, J. B.; Hartman, G. L.; Bertagnolli, B. L. Production of iturin A by *Bacillus amyloliquefaciens* suppressing *Rhizoctonia solani*. *Soil Biol. Biochem.* **2002**, *34*, 955−963.

(19) Arguelles-Arias, A.; Ongena, M.; Halimi, B.; Lara, Y.; Brans, A.; Joris, B.; Fickers, P. *Bacillus amyloliquefaciens* GA1 as a source of potent antibiotics and other secondary metabolites for biocontrol of plant pathogens. *Microb. Cell Fact.* **2009**, *8*, 63.

(20) Chen, X. H.; Koumoutsi, A.; Scholz, R.; Schneider, K.; Vater, J.; Süssmuth, R.; Piel, J.; Borriss, R. Genome analysis of *Bacillus amyloliquefaciens* FZB42 reveals its potential for biocontrol of plant pathogens. *J. Biotechnol.* **2009**, *140*, 27−37.

(21) Kim, P. I.; Chung, K.-C. Production of an antifungal protein for control of *Colletotrichum lagenarium* by *Bacillus amyloliquefaciens* MET0908. *FEMS Microbiol Lett.* **2004**, *234*, 177−83.

(22) Rapp, C.; Jung, G.; Katzer, W.; Loeffler, W. Chlorotetain from *Bacillus subtilis*, an antifungal dipeptide with an unusual chlorine-containing amino acid. *Angew. Chem. Int. Ed.* **1988**, *27*, 1733−1734.

(23) Huang, J. F.; Wei, Z.; Tan, S. Y.; Mei, X. L.; Yin, S. X.; Shen, Q. R.; Xu, Y. C. The rhizosphere soil of diseased tomato plants as a source for novel microorganisms to control bacterial wilt. *Appl. Soil Ecol.* **2013**, *72*, 79−84.

(24) Jourdan, E.; Henry, G.; Duby, F.; Dommes, J.; Barthélemy, J. P.; Thonart, P.; Ongena, M. Insights into the defense-related events occurring in plant cells following perception of surfactin-type lipopeptide from *Bacillus subtilis*. *Mol. Plant−Microbe Interact.* **2009**, *22*, 456−468.

(25) Tans-Kersten, J.; Brown, D.; Allen, C. Swimming motility, a virulence trait of *Ralstonia solanacearum*, is regulated by FlhDC and the plant host environment. *Mol. Plant−Microbe Interact.* **2004**, *17*, 686.

(26) Guo, J. H.; Qi, H. Y.; Guo, Y. H.; Ge, H. L.; Gong, L. Y.; Zhang, L. X.; Sun, P. H. Biocontrol of tomato wilt by plant growth-promoting rhizobacteria. *Biol. Control* **2004**, *29*, 66−72.

(27) French, E. B.; Elphinstone, J. Culture media for *Ralstonia solanacearum* isolation, identification and maintenance. *Fitopatologia* **1995**, *30*, 126−130.

(28) Joshi, R.; Gardener, B. B. M. Identification and characterization of novel genetic markers associated with biological control activities in *Bacillus subtilis*. *Phytopathology* **2006**, *96*, 145−54.

(29) Chung, S.; Kong, H.; Buyer, J. S.; Lakshman, D. K.; Lydon, J.; Kim, S. D.; Roberts, D. P. 2008. Isolation and partial characterization of *Bacillus subtilis* ME488 for suppression of soilborne pathogens of cucumber and pepper. *Appl. Microbiol. Biotechnol.* **2008**, *80*, 115−123.
(30) Tapi, A.; Chollet-Imbert, M.; Scherens, B.; Jacques, P. New approach for the detection of non-ribosomal peptide synthetase genes in *Bacillus* strains by polymerase chain reaction. *Appl. Microbiol. Biotechnol.* **2010**, *85*, 1521−1531.
(31) Roongsawang, N.; Thaniyavarn, J.; Thaniyavarn, S.; Kameyama, T.; Haruki, M.; Imanaka, T.; Morikawa, M.; Kanaya, S. Isolation and characterization of a halotolerant *Bacillus subtilis* BBK-1 which produces three kinds of lipopeptides: Bacillomycin L, plipastatin, and surfactin. *Extremophiles* **2002**, *6*, 499−506.
(32) Zanón, M. J.; M. I, F.; Jordá, C. Use of tomato crop residues into soil for control of bacterial wilt caused by *Ralstonia solanacearum*. *Crop Prot.* **2011**, *30*, 1138−1143.
(33) Yogev, A.; Raviv, M.; Kritzman, G.; Hadar, Y.; Cohen, R.; Kirshner, B.; Katan, J. Suppression of bacterial canker of tomato by composts. *Crop Prot.* **2009**, *28*, 97−103.
(34) Cao, Y.; Zhang, Z. H.; Ling, N.; Yuan, Y. J.; Zheng, X. Y.; Shen, B.; Shen, Q. R. *Bacillus subtilis* SQR 9 can control *Fusarium* wilt in cucumber by colonizing plant roots. *Biol. Fert Soils* **2011**, *47*, 495−506.
(35) Ling, N.; Xue, C.; Huang, Q. W.; Yang, X. M.; Xu, Y. C.; Shen, Q. R. Development of a mode of application of bioorganic fertilizer for improving the biocontrol efficacy to Fusarium wilt. *BioControl* **2010**, *55*, 673−683.
(36) Zhang, N.; Wu, K.; He, X.; Li, S. Q.; Zhang, Z. H.; Shen, B.; Yang, X. M.; Zhang, R. F.; Huang, Q. W.; Shen, Q. R. A new bioorganic fertilizer can effectively control banana wilt by strong colonization with *Bacillus subtilis* N11. *Plant Soil* **2011**, *344*, 87−97.
(37) Swain, M. R.; Ray, R. C. Biocontrol and other beneficial activities of *Bacillus subtilis* isolated from cowdung microflora. *Microb. Res.* **2009**, *164*, 121−130.
(38) Correa, O. S.; Montecchia, M. S.; Berti, M. F.; Ferrari, M. C. F.; Pucheu, N. L.; Kerber, N. L.; García, A. F. *Bacillus amyloliquefaciens* BNM122, a potential microbial biocontrol agent applied on soybean seeds, causes a minor impact on rhizosphere and soil microbial communities. *Appl. Soil Ecol.* **2009**, *41*, 185−194.
(39) Wang, Y.; Lu, Z. X.; Bie, X. M.; Lv, F. X. Separation and extraction of antimicrobial lipopeptides produced by *Bacillus amyloliquefaciens* ES-2 with macroporous resin. *Eur. Food Res. Technol.* **2010**, *231*, 189−196.
(40) Asaka, O.; Shoda, M. Biocontrol of *Rhizoctonia solani* damping off of tomato with *Bacillus subtilis* RB14. *Appl. Environ. Microb.* **1996**, *62*, 4081−4085.
(41) Berg, G.; Roskot, N.; Steidle, A.; Eberl, L.; Zock, A.; Smalla, K. Plant-dependent genotypic and phenotypic diversity of antagonistic rhizobacteria isolated from different *Verticillium* host plants. *Appl. Environ. Microbiol.* **2002**, *68*, 3328−3338.
(42) Kim, K. M.; Lee, J. Y.; Kim, C. K.; Kang, J. S. Isolation and characterization of surfactin produced by *Bacillus polyfermenticus* KJS-2. *Arch Pharm. Res.* **2009**, *32*, 711−715.
(43) Gustafson, K.; Roman, M.; Fenical, W. The macrolactins, a novel class of antiviral and cytotoxic macrolides from a deep-sea marine bacterium. *J. Am. Chem. Soc.* **1989**, *111*, 7519−7524.
(44) Jaruchoktaweechai, C.; Suwanborirux, K.; Tanasupawatt, S.; Kittakoop, P.; Menasveta, P. New macrolactins from a marine *Bacillus* sp. Sc026. *J. Nat. Prod.* **2000**, *63*, 984−986.
(45) Romero-Tabarez, M.; Jansen, R.; Sylla, M.; Lünsdorf, H.; Häußler, S.; Santosa, D. A.; Timmis, K. N.; Molinari, G. 7-*O*-Malonyl macrolactin A, a new macrolactin antibiotic from *Bacillus subtilis* active against methicillin-resistant *Staphylococcus aureus*, vancomycin-resistant enterococci, and a small-colony variant of *Burkholderia cepacia*. *Antimicrob. Agents Chem.* **2006**, *50*, 1701−1709.
(46) Dunlap, C. A.; Bowman, M. J.; Schisler, D. A. Genomic analysis and secondary metabolite production in *Bacillus amyloliquefaciens* AS 43.3: A biocontrol antagonist of Fusarium head blight. *Biol. Control* **2013**, *64*, 166−175.
(47) Zhu, Z.; Zhang, F. G.; Luo, Y.; Ran, W.; Shen, Q. R. Production of lipopeptides by *Bacillus amyloliquefaciens* XZ-173 in solid state fermentation using soybean flour and rice straw as the substrate. *Bioresour. Technol.* **2012**, *112*, 254−60.
(48) Bacon, C. W.; Hinton, D. M.; Mitchell, T. R.; Snook, M. E.; Olubajo, B. Characterization of endophytic strains of *Bacillus mojavensis* and their production of surfactin isomers. *Biol. Control.* **2012**, *62*, 1−9.
(49) Chen, Y.; Yan, F.; Chai, Y. R.; Liu, H. X.; Kolter, R.; Losick, R.; Guo, J. H. Biocontrol of tomato wilt disease by *Bacillus subtilis* isolates from natural environments depends on conserved genes mediating biofilm formation. *Environ. Microbiol.* **2013**, *15*, 848−864.
(50) Haggag, W. M.; Timmusk, S. Colonization of peanut roots by biofilm-forming *Paenibacillus polymyxa* initiates biocontrol against crown rot disease. *J. Appl. Microbiol.* **2008**, *104*, 961−969.

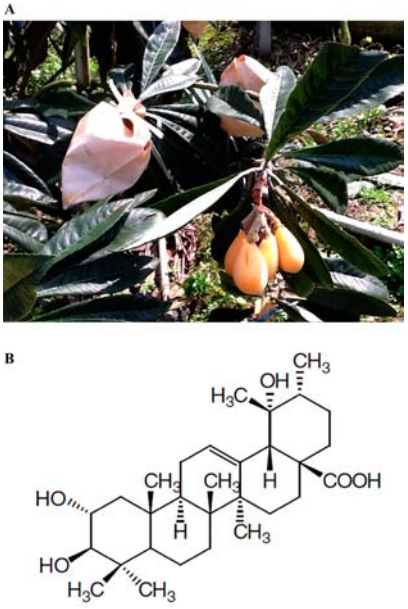


**Figure 1.** (A) The plant *Eriobotrya japonica* Lindl. (B) Structure of tormentic acid (PTA).

of loquat is reported to produce large amounts of triterpenes.[16] We have recently shown that loquat leaf extract as well as its cell suspension culture (which contains five main bioactive constituents including tormentic acid (PTA), see chemical structure in Figure 1B) could improve insulin sensitivity and hyperlipidemia;[17,18] we think it is possible that the five constituents act synergistically (a synergistic effect is one in which the combined effect of two chemicals is greater than the sum of the effect of each agent given alone) on diabetes and lipid. Nevertheless, the effect of single and pure PTA of antidiabetes and antidyslipidemia is still not fully understood. The aerial part of *Poterium ancistroides* Desf. contained tormentic acid and exhibited antidiabetic activity.[19] Tormentic acid has been shown to lower blood glucose in normoglycemic and glucose-induced hyperglycemic rats[19] and initiates insulin secretion by isolated rat islets of Langerhans.[20]

The mouse C57BL/6 model fed a high-fat (HF) diet could induce insulin resistance, obesity, hyperlipidemia, hyperinsulinemia, hyperleptinemia, and excess circulating free fatty acid.[21,22] Therefore, we conducted our animal study using HF diet-induced diabetic and hyperlipidemic states. AMPK activity is dependent on the phosphorylation of Thr 172 of $\alpha$ subunits.[23] This study also examined the effect of PTA on the expression or protein of genes involved in antidiabetes and lipogenesis, including GLUT4, Akt, AMPK, phosphoenol pyruvate carboxykinase (PEPCK), glucose-6-phosphatase (G6 Pase), sterol regulatory element binding protein-1c (SREBP-1c), peroxisome proliferator-activated receptor $\alpha$ (PPAR$\alpha$), and apolipoprotein C-III (apo-CIII).

## MATERIALS AND METHODS

**Chemicals.** GLUT4 was purchased from Santa Cruz Biotechnology (Santa Cruz, CA, USA); phospho-AMPK was purchased from Abcam Inc. (Cambridge, MA, USA); phospho-Akt, total AMPK, and total Akt were obtained from Cell Signaling Technology, Inc. (Danvers, MA, USA); the BCA protein assay kit was from Thermo Scientific (Rockford, IL, USA); and the ECL reagent kit was from GE Healthcare BioSciences (Buckinghamshire, UK). Secondary antibody anti-rabbit was from Jackson ImmunoResearch Laboratories, Inc. (West Grove, PA, USA). Structural proteins GAPDH and $\beta$-actin were from Santa Cruz Biotechnology.

**Isolation of Tormentic Acid.** PTA was obtained from Jen Li Biotech Co. Callus induction, suspension cultures, and extraction and isolation of tormentic acid from suspension cells of *E. japonica* were performed as previously described.[16,24] Briefly, sterilized seeds after callus induction were cultured in a bioreactor, and the cell suspension (ca. 844.5 g) was dried and extracted with ethanol and then concentrated to afford the white powder fraction (ca. 6.1 g).[24] The white powder (0.5 g) was chromatographed on a reverse silica gel column (LiChroprep RP-18, E. Merck, 40−63 $\mu$m) and then further purified by preparative high-performance liquid chromatography (PHPLC) to yield tormentic acid.[24] Tormentic acid (230.5 mg): $^1$H NMR (pyridine-$d_5$) $\delta$ 1.00 (H-25), 1.07 (H-24), 1.10 (H-26), 1.11 (H-30), 1.26 (H-23), 1.42 (H-29), 1.71 (H-27), 3.04 (H-18), 3.36 (H-3$\alpha$), 4.09 (H-3$\beta$), 5.58 (H-12). $^1$H NMR (400 MHz) spectra were measured by using a Bruker AMX-400 spectrometer as previously described.[24]

**Animals and Experimental Design.** Part 1, an oral glucose tolerance (OGTT), test was performed on 12 h fasted ICR mice ($n$ = 5) that were allowed access to 0.2, 0.4, and 0.8 g/kg PTA or an equivalent amount of vehicle (water), which were given orally 30 min before an oral glucose load (1 g/kg body wt). The control group was given glucose, whereas the normal group was not. Blood samples were collected from the retro-orbital sinus of fasted mice at the time of the glucose administration (0) and every 30 min until 120 min after glucose administration. The blood glucose level was monitored. For part 2, C57BL/6J mice (4 weeks old) were obtained from the National Laboratory Animal Breeding and Research Center. The mice were divided randomly into two groups after 7 days acclimation. The control (CON) group ($n$ = 9) was fed a low-fat diet (diet 12450B, Research Diets, Inc., New Brunswick, NJ, USA), whereas the experimental group was fed a 45% high-fat diet (diet 12451, Research Diets, Inc.) for 12 weeks.[18,25] The compositions of the experimental diets are given in previous studies.[18,25] After 8 weeks, the high-fat treated mice were randomly subdivided into four groups ($n$ = 9) including PTA (0.06, 0.12 g/kg/day) or rosiglitazone (Rosi; 1% methylcellulose, 10 mg/kg body weight) (GlaxoSmithKline) or vehicle and treated by oral gavage one time per day from the 9th to 12th weeks, while the mice were still on the high-fat diet, whereas the CON and high-fat control (HF) mice were treated with vehicle only. At the end, food was withheld from the animals (from 10 p.m. to 10 a.m.). The next day, the mice were sacrificed for blood and tissue collection and analysis. Livers, skeletal muscles, and white adipose tissues (WATs) (including epididymal, mesenteric, and retroperitoneal WAT) were weighed and excised, followed by immediate freezing, and kept at −80 °C for target gene analysis. Heparin (30 units/mL) (Sigma) was added to blood samples. Plasma samples were collected within 30 min by centrifugation at 1600$g$ for 15 min at 4 °C. Plasma was obtained for insulin and leptin assay.[18,25]

**Measurement of Body Weight, Body Weight Gain, and Food Intake.** Body weight was measured daily at the same time throughout the study. Body weight gain is defined as the difference between one day and the next day. The pellet food was weighed and placed in a food container. After 24 h, the remaining food was weighed, and the difference represented the daily food intake.

**Analysis of Blood Parameters.** Blood samples (0.8 mL) were collected from the retro-orbital sinus of fasted mice, and the glucose level was analyzed by the glucose oxidase method (model 1500; Sidekick Glucose Analyzer; YSI Inc., Yellow Springs, OH, USA).[18,25] Plasma triglycerides (TG), total cholesterol (TC), and free fatty acids (FFA) were measured using commercial assay kits according to the manufacturer's directions (Triglycerides-E test, Cholesterol-E test, and FFA-C test, Wako Pure Chemical, Osaka, Japan).[17,18] The levels of insulin and leptin in blood were analyzed by ELISA using a commercial assay kit according to the manufacturer's directions (mouse insulin ELISA kit, Sibayagi, Gunma, Japan; and mouse leptin ELISA kit, Morinaga, Yokohama, Japan).[18,25]

**Analysis of Histopathology.** Small pieces of epididymal WAT and liver tissue were fixed with formalin (200 g/kg) neutral buffered

**Table 1. Primers Used in This Study**

| gene | accession no. | forward and reverse primers | PCR product (bp) | annealing temp (°C) |
|---|---|---|---|---|
| | | **Liver** | | |
| PEPCK | NM_011044.2 | F: CTACAACTTCGGCAAATACC<br>R: TCCAGATACCTGTCGATCTC | 330 | 52 |
| G6 Pase | NM_008061.3 | F: GAACAACTAAAGCCTCTGAAAC<br>R: TTGCTCGATACATAAAACACTC | 350 | 50 |
| 11$\beta$-HSD1 | NM_008288.2 | F: AAGCAGAGCAATGGCAGCAT<br>R: GAGCAATCATAGGCTGGGTCA | 300 | 50 |
| DGAT2 | NM_026384.3 | F: AGTGGCAATGCTATCATCATCGT<br>R: AAGGAATAAGTGGGAACCAGATCA | 149 | 50 |
| PPAR$\alpha$ | NM_011144 | F: ACCTCTGTTCATGTCAGACC<br>R: ATAACCACAGACCAACCAAG | 352 | 55 |
| SREBP1c | NM_011480 | F: GGCTGTTGTCTACCATAAGC<br>R: AGGAAGAAACGTGTCAAGAA | 219 | 50 |
| FAS | NM_007988 | F: TGGAAAGATAACTGGGTGAC<br>R: TGCTGTCGTCTGTAGTCTTG | 240 | 50 |
| apo C-III | NM_023114.3 | F: CAGTTTTATCCCTAGAAGCA<br>R: TCTCACGACTCAATAGCTG | 349 | 47 |
| GAPDH | NM_031144 | F: TGTGTCCGTCGTGGATCTGA<br>R: CCTGCTTCACCACCTTCTTGA | 99 | 55 |

solution and embedded in paraffin. Sections (8 $\mu$m) were cut and stained with hematoxylin and eosin. For microscopic examination, a microscope (Leica, DM2500) was used, and the images were taken using a Leica Digital camera (DFC-425-C).[18]

**Analysis of Hepatic Lipids.** Hepatic lipids were extracted using a previously described protocol.[17] For the hepatic lipid extraction, 0.375 g liver samples were homogenized with 1 mL of distilled water for 5 min. Finally, the dried pellet was resuspended in 0.5 mL of ethanol and analyzed using a triglycerides kit as used for serum lipids.[18]

**Isolation of RNA and Relative Quantization of mRNA Indicating Gene Expression.** Total RNA from the liver tissue was isolated with a Trizol reagent (Molecular Research Center, Inc., Cincinnati, OH, USA) according to the manufacturer's directions. The integrity of the extracted total RNA was examined by 2% agarose gel electrophoresis, and the RNA concentration was determined by ultraviolet (UV) light absorbency at 260 and 280 nm (spectrophotometer U-2800A, Hitachi). Total RNA (1 $\mu$g) was reverse transcribed to cDNA with 5 $\mu$L of Moloney murine leukemia virus reverse transcriptase (Epicenter, Madison, WI, USA) as a previously described protocol.[17,25] The polymerase chain reaction (PCR) was performed in a final 25 $\mu$L containing 1 U of Blend Taq-Plus (TOYOBO, Japan), 1 $\mu$L of the RT first-strand cDNA product, 10 $\mu$M of each forward (F) and reverse (R) primer, 75 mM Tris-HCl (pH 8.3) containing 1 mg/L Tween 20, 2.5 mM dNTP, and 2 mM $MgCl_2$.[17,18,25] The primers are shown in Table 1. The products were run on 2% agarose gels and stained with ethidium bromide. The relative density of the band was evaluated using AlphaDigiDoc 1201 software (Alpha Innotech Co., San Leandro, CA, USA). All of the measured PCR products were normalized to the amount of cDNA of GAPDH in each sample.[17,18,25]

**Western Immunoblotting Analysis.** This follows a previous paper;[18,26,27] protein extractions and immunoblots for the determination of GLUT4, phospho-AMPK (Thr172), and phospho-Akt (Ser 473) proteins were carried out on frozen skeletal muscle and liver tissue from mice. Briefly, samples of liver tissue (0.1 g) were homogenized with lysis buffer (pH 6.4) and protease inhibitors. Forty micrograms of each homogenate was used for SDS-PAGE and immunoblotting as in a previously described protocol.[18,26,27] Additionally, GLUT4 was carried out on frozen skeletal muscle from mice, as briefly described: Skeletal muscle (1 g) was powdered under liquid nitrogen and homogenized for 20 s in buffer (pH 7.4). The total membrane fractions were collected with buffer and centrifuged as a previously described.[28,29] The protein contents of GLUT4, phospho-AMPK, phospho-Akt, total AMPK, and total Akt were detected by immunoblotting using a rabbit polyclonal antibody. The protein concentration in supernatant was determined with a BCA protein assay kit. The membranes were blocked with 5% skim milk in Tris-buffered saline (TBS) (Amersham BioSciences, Uppsala, Sweden) containing 0.05% Tween-20 (Bio-Rad, Hercules, CA, USA) and incubated overnight at 4 °C with anti-GLUT4, antiphospho-AMPK, and antiphospho-Akt at 1:200 dilution and anti-total-AMPK and anti-total-Akt at 1:1000 dilution. Subsequently, the membranes were washed three times with TBS containing 0.05% Tween-20 and incubated with secondary antibody anti-rabbit (1:1000) for 1 h. Immunoreactive bands were detected with ECL reagent kit. The density blotting was analyzed using Alpha Easy FC software (Alpha Innotech Corp., Randburg, South Africa). Structural proteins GAPDH and $\beta$-actin were obtained by stripping the nitrocellulose membrane proteins of liver and skeletal muscle, respectively.[18,26,27]

**Statistical Analysis.** All results are presented as the mean and standard error. Statistical significance is calculated by Dunnett's multiple-range tests, using SPSS software (SPSS Inc., Chicago, IL, USA).

## RESULTS

**OGTT Assay.** Administration of 0.2, 0.4, and 0.8 g/kg tormentic acid decreased the levels of blood glucose from 30 to 120 min following a glucose loading.

**Body Weight and Food Parameters.** Body weights of mice were measured at the end of the study. Feeding with a high-fat diet increased body weight and body weight gain, whereas the 4 week average food intake of the HF group was

Table 2. Absolute Tissue Weight, Food Intake, Liver Lipids, and Blood Profiles[a]

| parameter | CON | HF | HF+PTA1 0.06[b] | HF+PTA2 0.12[b] | HF+Rosi 0.01[b] |
|---|---|---|---|---|---|
| absolute tissue weight (g) | | | | | |
| EWAT | 0.598 ± 0.021 | 1.629 ± 0.169### | 1.042 ± 0.089* | 0.945 ± 0.079** | 1.074 ± 0.154* |
| RWAT | 0.168 ± 0.011 | 0.715 ± 0.063### | 0.490 ± 0.022** | 0.418 ± 0.046*** | 0.472 ± 0.059** |
| MWAT | 0.288 ± 0.016 | 0.518 ± 0.070### | 0.414 ± 0.032 | 0.345 ± 0.038* | 0.233 ± 0.034** |
| visceral fat wt (g) | 0.766 ± 0.028 | 2.344 ± 0.199### | 1.532 ± 0.108* | 1.363 ± 0.122** | 1.546 ± 0.160* |
| BAT | 0.146 ± 0.020 | 0.187 ± 0.023 | 0.145 ± 0.020 | 0.125 ± 0.009* | 0.156 ± 0.034 |
| liver (g) | 0.984 ± 0.057 | 1.177 ± 0.107 | 0.927 ± 0.038 | 0.913 ± 0.035 | 0.954 ± 0.037 |
| spleen | 0.062 ± 0.004 | 0.077 ± 0.004 | 0.078 ± 0.004 | 0.072 ± 0.003 | 0.077 ± 0.053 |
| final body wt (g) | 24.04 ± 0.33 | 31.91 ± 1.95### | 29.43 ± 1.05 | 29.17 ± 0.80 | 31.85 ± 1.75 |
| body wt gain (g) | 0.21 ± 0.32 | 2.56 ± 0.39### | 0.88 ± 0.29** | 0.84 ± 0.38** | 2.58 ± 0.31 |
| food intake (g/day/mouse) | 2.21 ± 0.03 | 1.84 ± 0.06### | 1.71 ± 0.04 | 1.69 ± 0.03 | 1.83 ± 0.04 |
| liver lipids | | | | | |
| total lipid (mg/g) | 55.2 ± 5.1 | 98.7 ± 6.4### | 80.1 ± 4.6* | 68.2 ± 5.9** | 74.7 ± 5.7** |
| triacylglycerol (μmol/g) | 31.5 ± 4.2 | 68.5 ± 7.1### | 51.7 ± 5.1* | 35.2 ± 4.9*** | 43.8 ± 4.7*** |
| blood profiles | | | | | |
| FFA (mequiv/L) | 1.63 ± 0.14 | 2.75 ± 0.42# | 2.15 ± 0.35* | 1.88 ± 0.29* | 1.85 ± 0.28* |
| TC (mg/dL) | 87.7 ± 5.7 | 188.5 ± 10.2### | 167.0 ± 6.1 | 153.7 ± 6.9* | 140.7 ± 14.1* |
| leptin (μg/mL) | 1.523 ± 0.072 | 3.124 ± 0.065### | 2.345 ± 0.092*** | 1.780 ± 0.094*** | 2.151 ± 0.099*** |
| insulin (μU/mL) | 31.3 ± 5.9 | 162.6 ± 16.5### | 101.7 ± 15.2* | 73.9 ± 11.8** | 56.4 ± 13.8** |

[a]All values are means ± SE ($n$ = 9). #, $p < 0.05$; ##, $p < 0.01$; and ###, $p < 0.001$ compared with the control (CON) group. *, $p < 0.05$; **, $p < 0.01$; and ***, $p < 0.001$ compared with the high-fat + vehicle (distilled water) (HF) group. Tormentic acid (PTA) (PTA1:0.06 and PTA2:0.12 g/kg body wt); Rosi, rosiglitazone (0.01 g/kg body wt); BAT, brown adipose tissue; RWAT, retroperioneal white adipose tissue; MWAT, mesenteric white adipose tissue; visceral fat, sum of epididymal and retroperioneal WAT; FFA, plasma free fatty acid; TC, total cholesterol; TG, triglyceride. [b]Dose (g/kg/day).

decreased. Final body weight and food intake were unchanged between the PTA-treated groups and the HF group. The PTA1- and PTA2-treated groups decreased the body weight gain over 4 weeks of treatment (Table 2).

**White Adipose Tissue Fat Accumulation.** The final weights of epididymal, mesenteric and retroperitoneal WATs, and visceral fat of the HF group were increased. Administration of PTA1, PTA2, and Rosi reduced epididymal WAT, mesenteric and retroperitoneal WATs, and visceral fat weights (Table 2).

**Blood Parameter, Leptin, Insulin, and Liver Lipid.** HF-diet increased blood glucose, and administration of PTA1, PTA2, and Rosi lowered blood glucose levels (Figure 2B). High-fat diets caused increases in circulating TG, FFA, leptin, and insulin levels. The PTA1-, PTA2-, and Rosi-treated mice displayed decreased TG, FFA, leptin, and insulin. The PTA2- and Rosi-treated mice showed decreased TC levels. The HF diet increased the total lipids of liver and concentrations of triacylglycerol, whereas mice administrated PTA1, PTA2, and Rosi showed significant decreases in these phenomena.

**Pathological Diagnosis.** HF induced adipocyte hypertrophy (the average areas of adipocytes in the HF group and CON group were 6515.9 ± 495.1 and 2584.6 ± 205.8 $\mu m^2$, respectively), whereas mice administered PTA1 (2380.9 ± 108.6 $\mu m^2$) and PTA2 (2243.2 ± 100.9 $\mu m^2$) showed significantly lower hypertrophy. The average area of the Rosi-treated mice was 4574.4 ± 162.7 $\mu m^2$ (Figure 3A). According to a previous study,[30] designation of histological hepatocellular ballooning findings included grade 0, none; grade 1, a few cells; grade 2, many cells. The ballooning phenomenon in liver is visible on the HF diet (mean score = 1.7 ± 0.2). The ballooning phenomenon is lower in the PTA1-treated (1.0 ± 0.2), PTA2-treated (0.7 ± 0.2), and Rosi-treated (0.9 ± 0.2) mice (Figure 3B).

**Hepatic Target Gene Expressions.** The mRNA levels of PEPCK, G6 Pase, 11$\beta$-hydroxysteroid dehydrogenase 1 (11$\beta$-HDS1), diacyl glycerol acyltransferase 2 (DGAT2), PPAR$\alpha$, SREBP1c, fatty acid synthase (FAS), and apo C-III were increased in the HF group. Following treatment, the PTA1-, PTA2-, and Rosi-treated groups decreased the mRNA level of PEPCK, G6 Pase, DGAT2, 11$\beta$-HSD1, SREBP1c, FAS, and apo C-III. The PTA1- and PTA2-treated groups showed increased mRNA levels of PPAR$\alpha$ (Figure 4).

**Protein Contents of Phospho-AMPK (Thr172), GLUT4, and Phospho-Akt (Ser 473)/Total Akt in Different Tissues.** The protein contents of phospho-AMPK protein were decreased in the HF group, whereas the PTA1-, PTA2-, and Rosi- treated groups increased the protein contents of both hepatic and skeletal muscular phospho-AMPK. HF-induced the protein contents of GLUT4 and phospho-Akt decreased, whereas PTA1-, PTA2-, and Rosi-treated mice increased the protein contents of GLUT4 and phospho-Akt in skeletal muscle (Figure 5).

## DISCUSSION

The present results demonstrated that PTA is effective in lowering blood glucose and circulating triglyceride levels in HF-fed mice. We have previously shown that loquat leaf extract as well as its cell suspension culture (total contents of five triterpenes were 85.35% including tormentic acid, 44.30%; corosolic acid, 19.50%; maslinic acid, 14.65%; oleanolic acid, 1.60%; and ursolic acid, 5.30%),[18] could improve insulin sensitivity and hyperlipidemia.[17,18] Because the cell suspension culture contained 44.3% tormetic acid, it is possible that the five constituents act synergistically and exert a more potent effect on diabetes and lipid. Nevertheless, the effect of single and pure tormentic acid (PTA) on diabetes and dyslipidemia is still not fully understood; therefore, we hypothesized that the present

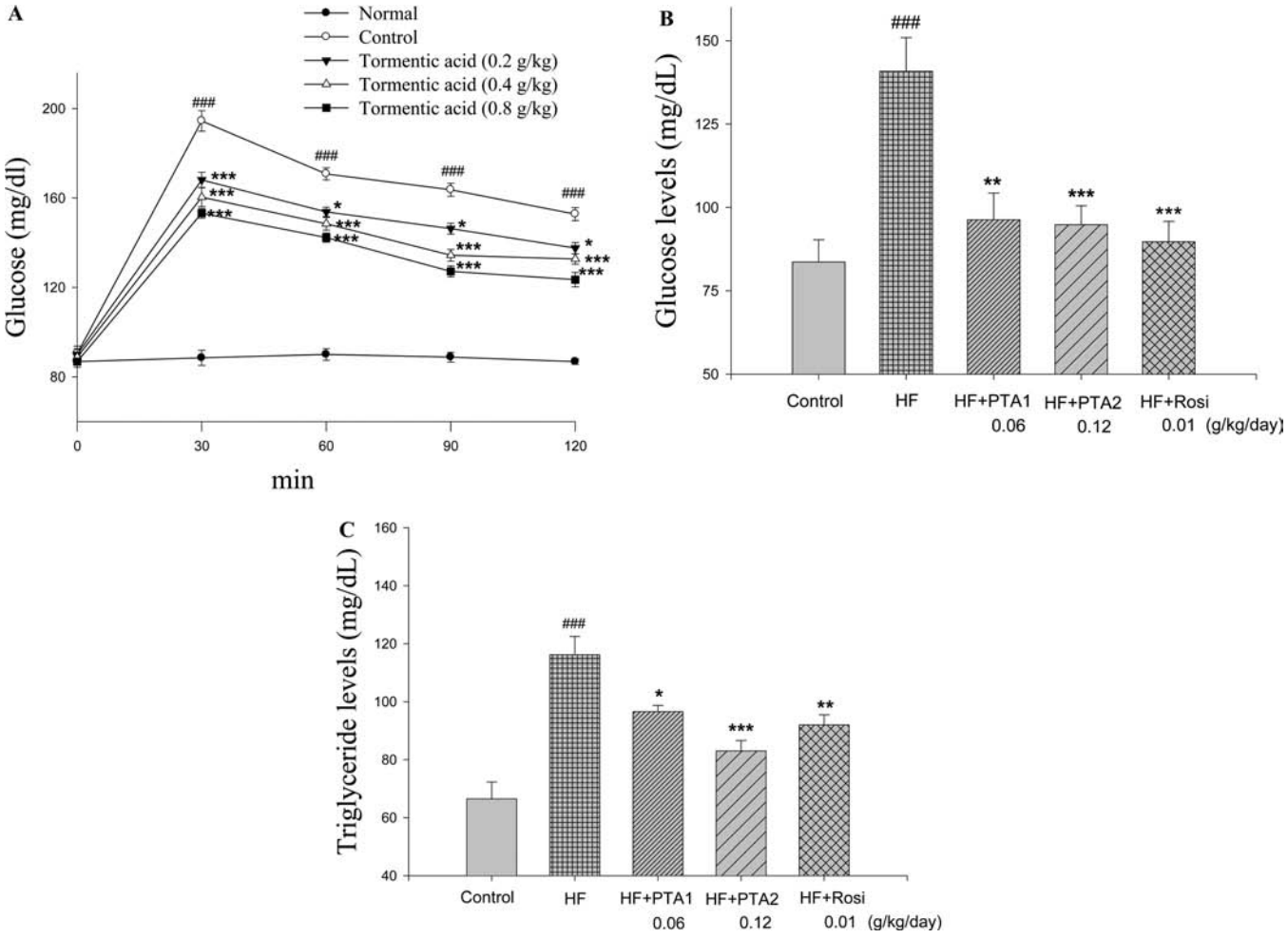


**Figure 2.** (A) Effects of tormentic acid on oral glucose tolerance test (OGTT) in normal mice. Animals in all groups received oral glucose 30 min after tormentic acid administration. Blood samples were collected and centrifuged at 3000 rpm for 10 min. Each point is the mean ± SE of five separate mice. (###) $p < 0.001$ compared with the control (CON) group; (∗) $p < 0.05$ and (∗∗∗) $p < 0.001$ were significantly different compared with the control group in the same time by ANOVA. (B, C) Effects of tormentic acid (PTA) on (B) blood glucose levels and (C) circulating triglyceride levels at week 12. Mice were fed a 45% high-fat diet (HF) or low-fat diet (CON) for 12 weeks. After 8 weeks, the HF mice were treated with vehicle or tormentic acid (PTA) or rosiglitazone (Rosi) accompanied by HF diet for 4 weeks. All values are means ± SE ($n = 9$). (#) $p < 0.05$, (##) $p < 0.01$, and (###) $p < 0.001$ compared with the control (CON) group; (∗) $p < 0.05$, (∗∗) $p < 0.01$, and (∗∗∗) $p < 0.001$ compared with the high-fat plus vehicle (distilled water) (HF) group by ANOVA. Tormentic acid (PTA1:0.06 and PTA2:0.12 g/kg body wt); Rosi, rosiglitazone (0.01 g/kg body wt); WAT, white adipose tissue; epididymal WAT+retroperitoneal WAT, visceral fat.

study of pure PTA could exhibit an effect in glucose control and lipid metabolism. Indeed, treatment with PTA displayed hypoglycemic and hypolipidemic effects.

C57BL/6J mice fed a high-fat diet is a mouse model to induce type 2 diabetes.[31] The HF-induced model had also elevated levels of triglycerides.[31] Therefore, this model was used in the present study for investigating PTA's effects on diabetes and dyslipidemia. In the present study, feeding C57BL/6J mice a HF diet induced hyperglycemia, obesity, hyperinsulinemia, hypertriglyceridemia, hyperleptinemia, and excess circulating free fatty acid, consistent with earlier observations.[31] Following treatment with PTA, blood glucose levels, circulating triglycerides, and visceral fat mass were lowered along with a reduction in free fatty acid and improved insulin resistance.

One of the difficulties in pursuing the mechanism of action of this compound is its limited availability, although at present PTA could be produced in great quantity. Therefore, PTA was first administered at concentrations of 0.2, 0.4, and 0.8 g/kg in OGTT by ICR mice. It was found PTA could lower blood glucose levels. Then, PTA was administered at concentrations of 0.06 and 0.12 g/kg in chronic HF-fed mice. On the basis of the few amounts of PTA and the duration of the 4 week chronic treatment experimental design, tormentic acid at a dosage of 30 mg/kg exerted an antihyperglycemic effect but did not act in rats with severe diabetes induced by an injection of streptozotocin,[19,20] so the concentration of PTA was lowered to 0.06 and 0.12 g/kg (duplicated or four times) in HF-fed mice; the daily dosage is expected to have a cumulative effect and a long-lasting effectiveness.

The primary aim is to investigate the antidiabetic mechanism of PTA, and we evaluate the GLUT4 protein content in the skeletal muscle. The present study showed that PTA2 caused marked increases of GLUT4 protein, and PTA1 displayed GLUT4 levels similar to those of Rosi, which is an antidiabetic agent and directly targets insulin resistance and increases peripheral glucose uptake (GLUT4), leading to improved glycemic control.[32] These findings are the first to reveal that PTA caused increased GLUT4 proteins as well as a direct relationship exhibiting antidiabetic activity. Thus, PTA

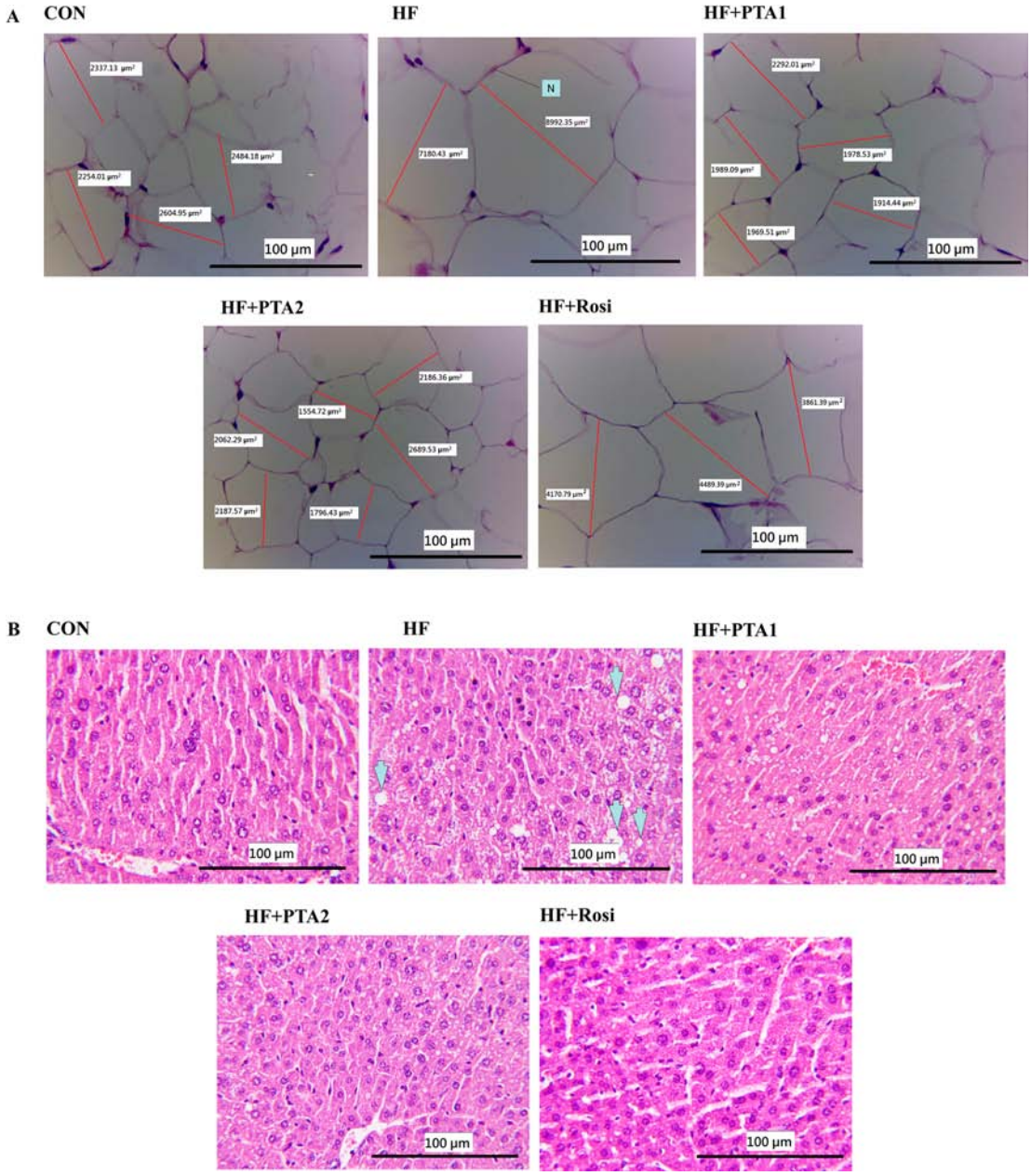


**Figure 3.** Effects of tormentic acid (PTA) on (A) epididymal WAT and (B) liver tissue morphology in the low-fat (CON), high-fat (HF), HF + PTA1, HF + PTA2, or HF + Rosi groups. Pictures of hematoxylin and eosin-stained sections of (A) mean area of adipocytes ($\mu m^2$) for epididymal WAT (magnification: 10 (ocular) × 20 (object lens)) from mice fed with PTA. The high-fat diet induced the hepatic ballooning degeneration in the HF group as compared with the CON group. The ballooning degeneration is a form of liver parenchymal cell death, and the nucleolus was squeezed into the other side named balloon (as the arrow indicates). This may be due to the heap of glycogen in the nucleus. The high-fat diet induced obesity and insulin resistance. Insulin levels affected the storage of hepatic glycogen. Treatment with PTA1 and PTA2 significantly decreased the degree of ballooning degeneration. Each presented is typical and representative of nine mice. Tormentic acid (PTA1:0.06 and PTA2:0.12 g/kg body wt); Rosi, rosiglitazone (0.01 g/kg body wt).

displayed a very marked enhancement of GLUT4 accompanied by ameliorated insulin resistance.

There are two pathways in regulated GLUT4 translocation including insulin signaling (those involving phosphatidylinositol 3′ kinase (PI3K)/Akt) and the AMPK pathway.[33] To monitor the mechanism of enhanced GLUT4 by PTA, we evaluated its effects on the phosphorylation of Akt in the skeletal muscle. The results demonstrated that PTA had a significantly increased effect on skeletal muscular phosphorylation of Akt, suggesting that PTA increased muscular GLUT4 contents are likely to be partly mediated by Akt phosphorylation; moreover, PTA enhanced Akt phosphorylation and increased insulin sensitivity.

Furthermore, it was evaluated that PTA acts on the phosphorylation of AMPK to the same effect as in people who exercise or take antidiabetic agents such as AICAR and metformin,[34,35] and rosiglitazone could activate AMPK. TZDs act as an AMPK activator, but differently from metformin, reduce liver fat accumulation, and ameliorate insulin resistance due to their effect on plasma adipocytokine (including adiponectin and leptin) and more AMPK activation.[36,37] Indeed, PTA increases skeletal muscular phosphorylation of

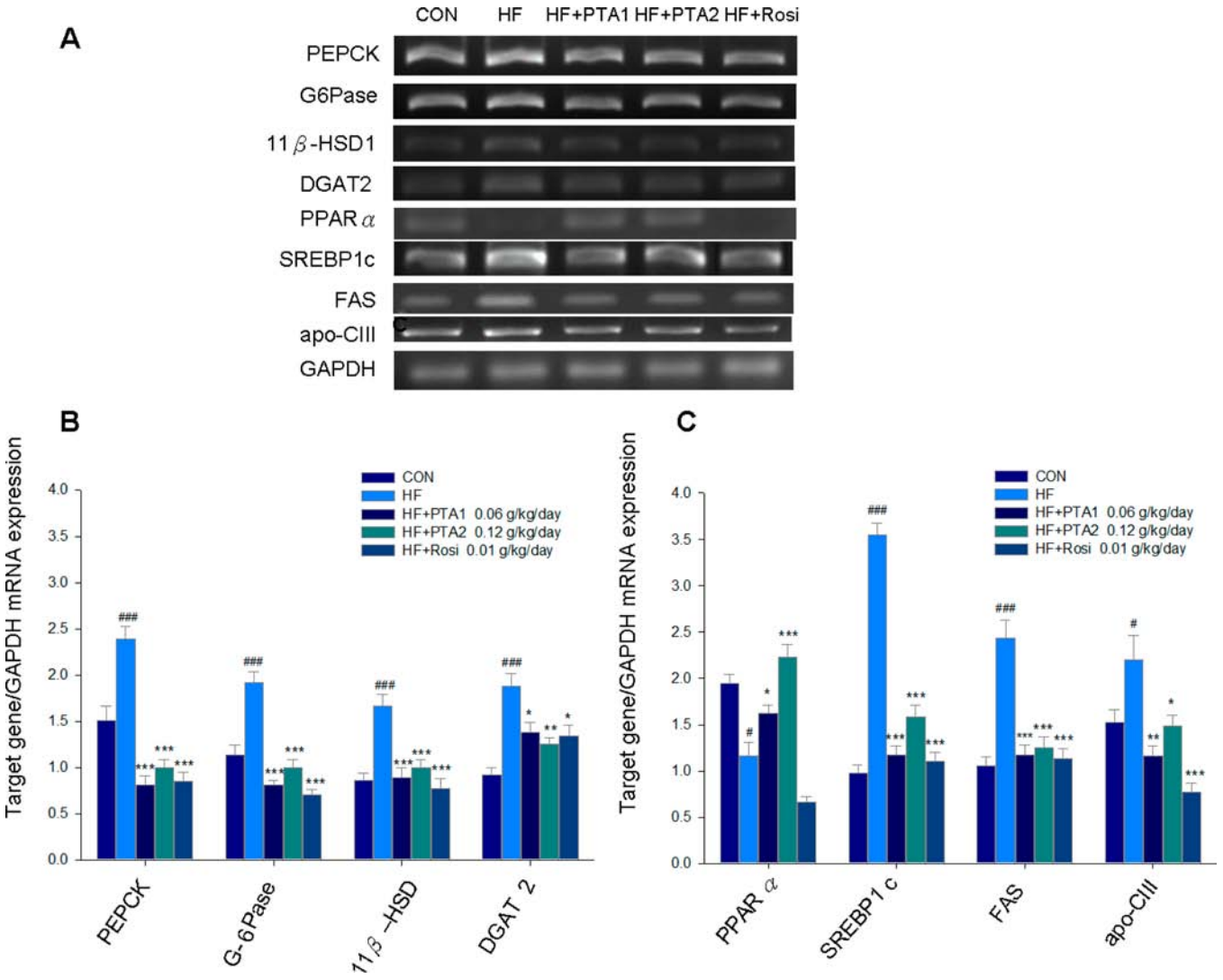


**Figure 4.** Semiquantative RT-PCR analysis on PEPCK, G6 Pase, 11$\beta$-HSD1, DGAT2, PPAR$\alpha$, SREBP1c, FAS, and apo C-III mRNA expression in liver tissue of the mice receiving oral gavage extracts of tormentic acid (PTA) for 4 weeks. All values are means ± SE ($n$ = 9). (#) $p < 0.05$ and (###) $p < 0.001$ compared with the control (CON) group; (∗) $p < 0.05$, (∗∗) $p < 0.01$, and (∗∗∗) $p < 0.001$ compared with the high-fat + vehicle (distilled water) (HF) group. Tormentic acid (PTA) (PTA1:0.06 and PTA2:0.12 g/kg body wt); Rosi, rosiglitazone (0.01 g/kg body wt). Total RNA (1 $\mu$g) isolated from tissue was reverse transcripted by MMLV-RT, and 10 $\mu$L of RT products was used as template for PCR. Signals were quantitated by image analysis; each value was normalized by GAPDH.

AMPK, suggesting that it is possibly partly responsible for increased GLUT4 translocation. Further study on the phosphorylation of AS160 is needed.

The liver is the organ responsible for the majority of hepatic gluconeogenesis.[38] A number of hormones regulate a set of genes (including PEPCK and G6 Pase) in the liver that modulates the rate of glucose synthesis. PEPCK is a rate-controlling step of gluconeogenesis in animals, and G6 Pase plays a vital role in glucose homeostasis.[39] Overexpression of the PEPCK enzyme in mice results in symptoms of type 2 diabetes. The hepatic G6 Pase activities of diabetic animals were increased.[40] PTA treatment reduced the expressions of PEPCK and G6 Pase. Therefore, the antidiabetic effect of PTA is due to down-regulation of PEPCK and G6 Pase. Furthermore, PEPCK is controlled by hormonal mechanisms including 11$\beta$-HSD1. 11$\beta$-HSD1 knockout mice fed a HF diet are protected from developing insulin resistance.[18,41] Therefore, compounds that down-regulate 11$\beta$-HSD1 might contribute to antidiabetic activities.[18] Besides PEPCK and G6 Pase, PTA-decreased hepatic 11$\beta$-HSD1 expressions also lead to enhanced insulin sensitivity.

AMPK activation is beneficial in the management of type 2 diabetes.[42] Metformin is a medication for the treatment of type 2 diabetes causing increased skeletal muscular glucose uptake and reduced gluconeogenesis in the liver.[20] HF-induced reduced phospho-AMPK in the liver, with increased in PTA- and Rosi-treated groups, indicates improved hyperglycemia by AMPK activation. Besides increasing muscular glucose uptake (GLUT4), PTA is likely to reduce hepatic glucose production by down-regulations of PEPCK and G6 Pase via AMPK.

To monitor the mechanism of PTA on antihyperlipidemia, we found that PTA increased PPAR$\alpha$ expressions. PPAR$\alpha$ ligands (such as fibrates) have been shown to reduce the expression of the apo C-III gene,[43] thus resulting in lowering fat values in the blood and liver and exhibiting a hypotriglyceridemic effect. We also measured DGAT2 expressions. DGAT2 catalyzes the final step in the synthesis of triglycerides.[18,44] It was found that PTA decreased circulating TG levels, and this

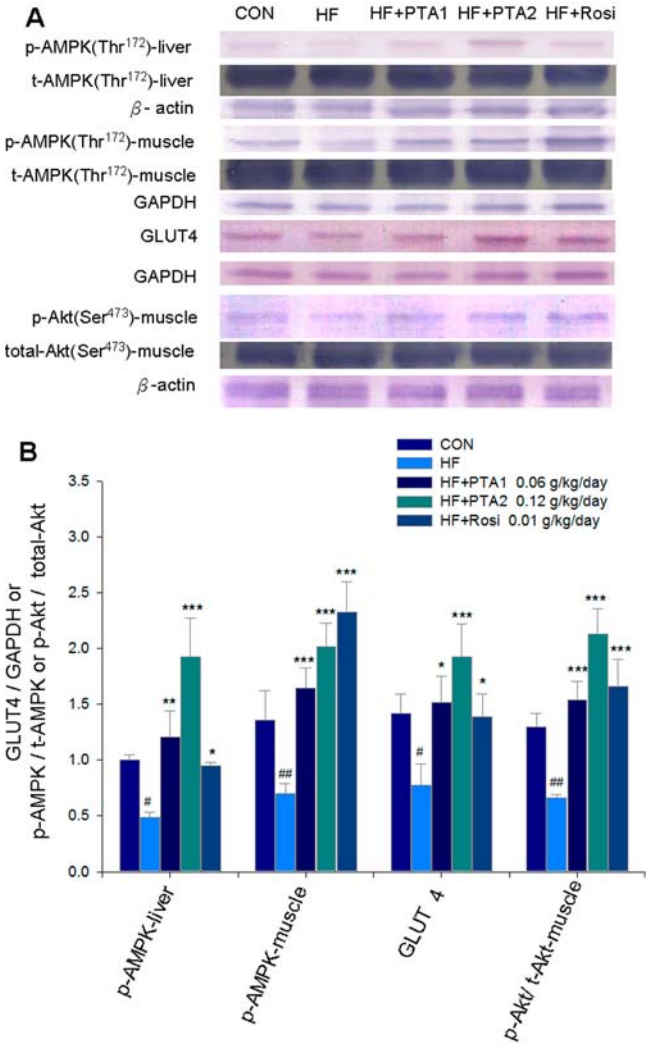


**Figure 5.** Protein contents of GLUT4 in skeletal muscle, the ratio of phospho-AMPK (Thr172) to total AMPK in liver tissue and skeletal muscle, and quantified results for the phosphorylation status of Akt (p-Akt normalized to total Akt (pAkt/Akt)) in skeletal muscle of the mice receiving tormentic acid (PTA) by oral gavage for 4 weeks. Protein was separated by 12% SDS-PAGE detected by Western blot. All values are means ± SE ($n$ = 9). (#) $p < 0.05$ and (##) $p < 0.01$ compared with the control (CON) group; (*) $p < 0.05$, (**) $p < 0.01$, and (***) $p < 0.001$ compared with the high-fat plus vehicle (HF) group. Tormentic acid (PTA) (PTA1:0.06 and PTA2:0.12 g/kg body wt); Rosi, rosiglitazone (0.01 g/kg body wt).

may be associated with decreased DGAT2 expressions. Previous study showed that leptin activated AMPK.[45] It is possible that PTA directly caused AMPK phosphorylation or altered leptin secretion by PTA, inducing AMPK activation. The blood leptin level is markedly reduced in PTA-treated mice, which is consistent with the reduced fat mass.[46] PTA significantly reduced SREBP1c, a key transcription factor controlling de novo lipogenesis.[47] Moreover, PTA suppressed the expression of FAS, which is a key enzyme in fatty acid synthesis. The glucose-induced SREBP1c and FAS mRNA levels were also down-regulated by AMPK.[48] The AMPK activator metformin has been shown to down-regulate FAS expression via AMPK activation.[7] Therefore, it is possible that PTA down-regulated these genes through AMPK activation.

The evidence for morphological analysis comes from the finding that treatment with PTA1 and PTA2 decreased the hypertrophy of adipocytes. The liver is a major organ metabolizing fat. The level of circulating TG fluctuates;[49] it is possible that PTA caused fat to move from adipose to liver tissue by increasing hepatic lipid catabolism, thus resulting in decreased size of adipocytes and almost the complete absence of liver lipid droplets.

In conclusion, this study demonstrated that PTA effectively lowers hyperglycemia and hypertriglycemia in HF-fed mice. PTA improves glycemic control primarily via increased skeletal muscular GLUT4 proteins to elevate glucose uptake but suppresses hepatic glucose production (down-regulations of PEPCK and G6 Pase). PTA enhanced AMPK phosphorylation both in skeletal muscle and in the liver. PTA enhanced skeletal muscular Akt phosphorylation and increased insulin sensitivity. PTA increased hepatic fatty acid oxidation (PPAR$\alpha$), but suppressed lipogenic enzyme expression (including SREBP1c and FAS), thus contributing to lowering triglyceride levels. Therefore, tormentic acid is effective on type 2 diabetes and hyperlipidemia in HF-fed mice.

## AUTHOR INFORMATION


### Corresponding Author

*(C.-C.S.) Phone:+886-4-22391647, ext. 3978. Fax: +886-4-22394256. E-mail: ccshih@ctust.edu.tw


### Notes

The authors declare no competing financial interest.

## ABBREVIATIONS USED

AMPK, AMP-activated protein kinase; apo C-III, apolipoprotein C-III; BAT, brown adipose tissue; 11$\beta$-HSD1, 11$\beta$-hydroxysteroid dehydroxygenase; CON, control; DGAT, acyl-coenzyme A:diacylglycerol acyltransferase; FAS, fatty acid synthase; FFA, free fatty acid; GAPDH, glyceraldehyde-3-phosphate dehydrogenase; G6 Pase, glucose-6-phosphatase; GLUT4, glucose transporter 4; HF, high-fat control; OGTT, oral glucose tolerance test; PEPCK, phosphenolpyruvate carboxykinase; PPAR$\alpha$, peroxisome proliferator-activated receptor $\alpha$; PTA, tormentic acid; Rosi, rosiglitazone; RT-PCR, reverse transcription-polymerase chain reaction; SREBP-1c, sterol regulatory element binding protein 1c; TC, total cholesterol; TG, triglyceride; WAT, white adipose tissue

## REFERENCES


(1) Stumvoll, M.; Goldstein, B. J.; Van Haeften, T. W. Type 2 diabetes: principles of pathogenesis and therapy. *Lancet* **2005**, *365*, 1333−1346.

(2) Basu, A.; Caumo, A.; Bettini, F.; et al. Impaired basal glucose effectiveness in NIDDM; contribution of defects in glucose disappearance and production, measured using an optimized minimal model independent protocol. *Diabetes* **1997**, *46*, 421−432.

(3) Minokoshi, Y.; Kahn, C. R.; Kahn, B. B. Tissue-specific ablation of the GLUT4 glucose transporter or the insulin receptor challenges assumptions about insulin action and glucose homeostasis. *J. Biol. Chem.* **2003**, *278* (36), 33609−33612.

(4) Joost, H. G.; Bell, G. I.; Best, J. D.; Birnbaum, M. J.; Charron, M. J.; Chen, Y. T.; Dieg, H.; James, D. E.; Lodish, H. J.; Moley, K. H.; Moly, J. F.; Mueckler, M.; Rogers, S.; Schurmann, A.; Seino, S.; Thotens, B. Nomenclature of the GLUT4/SLC2A family of sugar/phylol transport facilitators. *Am. J. Physiol. Endocrinol. Metab.* **2002**, *282*, 974−976.

(5) Watson, R. T.; Pessin, J. E. Intracellular organization of insulin signaling and GLUT4 translocation. *Recent Prog. Horm. Res.* **2001**, *56*, 175−193.
(6) Sujatha, S.; Anand, S.; Scangeetha, K. N.; Shilpa, K.; Lakshmi, J.; Balakrishnan, A.; Lakshmi, B. S. Biological evaluation of (3$\beta$)-stigmast-5-en-3-ol as potent anti-diabetic agent in regulating glucose transport using in vitro model. *Int. J. Diabetes Mellitus* **2010**, *2*, 101−109.
(7) Zhou, G.; Myers, R.; Li, Y.; Chen, T.; Shen, X.; Fenyk-Melody, J.; Wu, M.; Ventre, J.; Doebber, T.; Fujii, N.; Musi, N.; Hirshman, M. E.; Goodyear, L. J.; Möller, D. E. Role of AMP-activated protein kinase in mechanism of metformin action. *J. Clin. Invest.* **2001**, *108* (8), 1167−1174.
(8) Foretz, M.; Taleux, N.; Guigas, B.; Horman, S.; Beauloye, C.; Andreelli, F.; et al. Regulation of energy metabolism by AMPK: a novel therapeutic approach for the treatment of metabolic and cardiovascular diseases. *Med. Sci. (Paris)* **2006**, *22*, 381−383.
(9) Viollet, B.; Lantier, L.; Devin-Leclerc, J.; Hebrard, S.; Amouyal, C.; Mounier, R.; Foretz, M.; Andreelli, F. Targeting the AMPK pathway for the treatment of type 2 diabetes. *Front. Biosci. (Landmark Ed.)* **2009**, *14*, 3380−3400.
(10) Musi, N. AMP-activated protein kinase and type 2 diabetes. *Curr. Med. Chem.* **2006**, *13* (5), 583−589.
(11) Noreen, W.; Wadood, A.; Hidayat, H. K.; Wahid, S. A. Effect of *Eriobotrya japonica* on blood glucose levels of normal and alloxan-diabetic rabbits. *Planta Med.* **1988**, *54*, 196−199.
(12) Tommasi, N. D.; Shimone, F. D.; Pizza, C. Constituents of *Eriobotrya japonica*: a study of their antiviral properties. *J. Nat. Prod.* **1992**, *55*, 1067−1073.
(13) Liu, J. Oleanolic acid and ursolic acid: research perspectives. *J. Ethnopharmacol.* **2005**, *100*, 92−94.
(14) Ivorra, M. D.; Paya, M.; Villar, A. Hypoglycemic and insulin release effects of tormentic acid: a new hypoglycemic natural product. *Planta Med.* **1988**, *54*, 282−285.
(15) Wen, X.; Sun, H.; Liu, J.; Wu, G.; Zhang, L.; Wu, X.; Ni, P. Pentacyclic triterpenes. Part 1: The first examples of naturally occurring pentacyclic triterpenes as a new class of inhibitors of glycogen phosphorylases. *Bioorg. Med. Chem. Lett.* **2005**, *15*, 4944−4948.
(16) Taniguchi, S.; Imayoshi, Y.; Kobayashi, E.; Takamatsu, Y.; Ito, H.; Hatano, T.; Sakagami, H.; Tokuda, H.; Nishino, H.; Sugita, D.; Shimura, S.; Yoshida, T. Production of bioactive triterpenes by *Eriobotrya japonica* calli. *Phytochemistry* **2002**, *59*, 315−323.
(17) Shih, C. C.; Lin, C. H.; Wu, J. B. *Eriobotrya japonica* improves hyperlipidaemia and reverses insulin resistance in high-fat-fed mice. *Phytother. Res.* **2010**, *24* (12), 1769−1780.
(18) Shih, C. C.; Ciou, J. L.; Lin, C. H.; Wu, J. B.; Ho, H. Y. Cell suspension culture of *Eriobotrya japonica* regulates the diabetic and hyperlipidemic signs of high-fat-fed mice. *Molecules* **2013**, *18* (3), 2726−2753.
(19) Villar, A.; Payá, M.; Hortiguela, M. D.; Cortes, D. Tormentic acid, a new hypoglycemic agent from *Poterium ancistroides*. *Planta Med.* **1986**, *52*, 43−45.
(20) Ivorra, M. D.; Payá, M.; Villar, A. Effect of tormentic acid on insulin secretion in isolated rat islets of Langerhans. *Phytother. Res.* **1989**, *3* (4), 145−147.
(21) Harte, R. A.; Kirk, E. A.; Rosenfeld, M. E.; LeBoeuf, R. C. Initiation of hyperinsulinemia and hyperleptinemia is diet dependent in C57BL/6 mice. *Horm. Metab. Res.* **1999**, *31*, 570−575.
(22) Arner, P. Insulin resistance in type 2 diabetes: role of fatty acid. *Diabetes Metab. Res. Rev.* **2002**, *18*, S5−S9.
(23) Shen, Q. W.; Jones, C. S.; Kalchayanand, N.; Zhu, M. J.; Du, M. J. Effect of dietary alpha-lipoic acid on growth, body composition, muscle pH, and AMP-activated protein kinase phosphorylation in mice. *J. Anim. Sci.* **2005**, *83*, 2611−2617.
(24) Chang, C. T.; Huang, S. S.; Lin, S. S.; Amagaya, S.; Ho, H. Y.; Hou, W. C.; Shie, P. H.; Wu, J. B.; Huang, G. J. Anti-inflammatory activities of tormentic acid from suspension cells of *Eriobotrya japonica* ex vivo and in vivo. *Food Chem.* **2011**, *127*, 1131−1137.
(25) Shih, C. C.; Lin, C. H.; Lin, W. L. Effects of *Momordica charantia* on insulin resistance and visceral obesity in mice on high-fat diet. *Diabetes Res. Clin. Pract.* **2008**, *81* (2), 134−143.
(26) Shih, C. C.; Lin, C. H.; Lin, Y. J.; Wu, J. B. Validation of the antidiabetic and hypolipidemic effects of hawthorn by assessment of gluconeogenesis and lipogenesis related genes and AMP-activated protein kinase phosphorylation. *Evidence-Based Complement. Altern. Med.* **2013**, *2013*, No. 597067.
(27) Shih, C. C.; Shlau, M. T.; Lin, C. H.; Wu, J. B. *Momordica charantia* ameliorates insulin resistance and dyslipidemia with altered hepatic glucose production and fatty acid synthesis and AMPK phosphorylation in high-fat-fed mice. *Phytother. Res.* **2014**, *28* (3), 363−371.
(28) Klip, A.; Ramlal, T.; Young, D. A.; Holloszy, J. O. Insulin-induced translocation of glucose transporters in rat hindlimb muscles. *FEBS Lett.* **1987**, *224* (1), 224−230.
(29) Shih, C. C.; Lin, C. H.; Lin, W. L.; Wu, J. B. *Momordica charantia* extract on insulin resistance and the skeletal muscle GLUT4 protein in fructose-fed rats. *J. Ethnopharmacol.* **2009**, *123* (1), 82−90.
(30) Kleiner, D. E.; Brunt, E. M.; Van Natta, M.; Sanyal, A. J. Design and validation of a histological scoring system for nonalcoholic fatty liver disease. *Hepatology* **2005**, *41*, 1313−1321.
(31) Petro, A. E.; Cotter, J.; Cooper, D. A.; Peters, J. C.; Surwit, S. J.; Surwit, R. S. Fat, carbohydrate and calories in the development of diabetes and obesity in the C57BL/6J mouse. *Metabolism* **2004**, *53*, 454−457.
(32) Martinez, L.; Berenguer, M.; Bruce, M. C.; Le Marchand-Brustel, Y.; Govers, R. Rosiglitazone increases cell surface GLUT4 levels in 3T3-L1 adipocytes through an enhancement of endosomal recycling. *Biochem. Pharmacol.* **2010**, *79* (9), 1300−1309.
(33) Huang, S.; Czech, M. P. The GLUT4 glucose transporter. *Cell Metab.* **2007**, *5*, 237−252.
(34) Iglesias, M. A.; Ye, J. M.; Frangioudakis, G.; Saha, A. K.; Tomas, E.; Ruderman, N. B.; Cooney, G. J.; Kraegen, E. W. AICAR administration causes an apparent enhancement of muscle and liver action in insulin-resistant high-fat-fed rats. *Diabetes* **2002**, *51*, 2886−2894.
(35) Ye, J. M.; Ruderman, N. B.; Kraegen, E. W. AMP-activated protein kinase and malonyl-CoA: targets for treating insulin resistance? *Drug Discovery Today: Ther. Strategies* **2005**, *2* (2), 157−163.
(36) Fryer, L. G.; Parbu-Patel, A.; Patel, A. The anti-diabetic drugs rosiglitazone and metformin stimulate AMP-activated protein kinase through distinct signaling pathways. *J. Biol. Chem.* **2002**, *277*, 25226−25232.
(37) Ahmed, M. H.; Byrne, C. D. Modulation of sterol regulatiry element binding proteins (SREBPs) as potential treatments for non-alcoholic fatty liver disease (NAFLD). *Drug Discovery Today* **2007**, *12* (17−18), 740−747.
(38) Kurukulasuriya, R.; Link, J. T.; Madar, D. J.; et al. Prospects for pharmacologic inhibition of hepatic glucose production. *Curr. Med. Chem.* **2003**, *10* (2), 99−121.
(39) Guignot, L.; Mithieux, G. Mechanisms by which insulin, associated or not with glucose, may inhibit hepatic glucose production in the rat. *Am. J. Physiol.* **1999**, *227* (6, Part 1), E984−E989.
(40) Berg, J. M.; Tymoczko, J. L.; Stryer, L. Glycolysis and glyconeogenesis. In *Stryer Biochemistry*; Berg, J. M., Tymoczko, J. L., Eds.; Freeman: New York, 2001; pp 425−464.
(41) Kotelevtsev, Y.; Holmes, M. C.; Burchell, A.; Houston, P. M.; Schmoll, D.; Jamieson, P.; Best, R.; Brown, R.; Edwards, C. R.W.; Seckl, J. R.; Mullins, J. J. 11$\beta$-hydroxysteroid dehydrogenase type 1 knockout mice show attenuated glucocorticoid-inducible responses and resist hyperglycemia on obesity or stress. *Proc. Natl. Acad. Sci. U.S.A.* **1997**, *94*, 14924−14929.
(42) Mackenzie, R. W.; Elliot, B. T. Akt/PKB activation and insulin signaling: a novel insulin signaling pathway in the treatment of type 2 diabetes. *Diabetes Metab. Syndr. Obes.* **2014**, *7*, 55−64.
(43) Staels, B.; Dallongeville, J.; Auwerx, K.; Schoonjans, K.; Leitersdorf, E.; Fruchart, J.-C. Mechanism of action of fibrates on lipid and lipoprotein metabolism. *Circulation* **1998**, *98*, 2088−2093.

(44) Cases, S.; Stone, S. J.; Zhou, P.; Yen, E.; Tow, B.; Lardizabal, K. D.; Voelker, T.; Farese, R. V., Jr. Cloning of DGAT2, a second mammalian diacylglycerol acyltransferase, and related family members. *J. Biol. Chem.* **2001**, *276*, 38870−38876.
(45) Minokoshi, Y.; Kim, Y.-B.; Peroni, O. D.; Fryer, L. G. D.; Muller, C.; Carling, D.; Kahn, B. B. Leptin stimulates fattyacid oxidation by activating AMP-activated protein kinase. *Nature (London)* **2002**, *415*, 339−343.
(46) Myers, M. G.; Cowley, M. A.; Műnzberg, H. Mechanism of leptin action and leptin resistance. *Annu. Rev. Physiol.* **2008**, *70*, 537−556.
(47) Moon, Y. A.; Hammer, R. E.; Horton, J. D. Deletion of ELOVL5 leads to fatty liver through activation of SREBP-1c in mice. *J. Lipid Res.* **2008**, *50*, 412−423.
(48) Foretz, M.; Carling, D.; Guichard, C.; Ferre, P.; Foufelle, F. AMP-activated protein kinase inhibits the glucose-activated expression of fatty acid synthase gene in rat hepatocytes. *J. Biol. Chem.* **1998**, *273*, 14767−14771.
(49) Bourgeois, F.; Alexiu, A.; Lemonnier, D. Dietary-induced obesity: effect of dietary fats on adipose tissue cellularity in mice. *Br. J. Nutr.* **1983**, *49*, 17−26.

in vivo of verbascose was evaluated by using animal models through the measurement of immune organ index, lysozyme activity, hemolysin level, and swelling rate of earlap in delayed-type hypersensitivity (DTH) reaction.

## MATERIALS AND METHODS

**Materials and Chemicals.** Mung beans were obtained from a local market (Nanjing, China). The RAW264.7 murine macrophage cell line was purchased from Nanjing University of Chinese Medicine (Nanjing, China). The Kunming mice (8 weeks old), grade of specific pathogen free (SPF) with body weights (BWs) of 20 ± 2 g, were purchased from the Experiment Animal Center of Academy of Military Medical Sciences (Beijing, China). Mulbecco's modified Eagle medium (DMEM), newborn calf serum, 4-(2-hydroxyethyl)-1-piperazine-ethane-sulfonic acid (HEPES), and trypan blue dye were purchased from Gibco/Invitrogen (Carlsbad, CA, USA). Sheep blood and guinea pig serum were purchased from Chuanxiang Biotechnology Co. (Shanghai, China). Lipopolysaccharide (LPS), neutral red, penicillin–streptomycin stock solution, and 3-(4,5-dimethylthiazol-2-yl)-2,5-diphenyltetrazolium bromide (MTT) were obtained from Sigma-Aldrich Chemical Co., Ltd. (St. Louis, MO, USA). Cyclophosphamide (CPA) was purchased from Jiangsu Hengrui Medcine Co. (Nanjing, China). Dinitrofluorobenzene (DNFB) was purchased from Xiya Reagent Co., Ltd. (Chengdu, China). Levamisole hydrochloride was purchased from Jinan Aodekai Pharmaceutical Co., Ltd. (Jinan, China). Lysozyme kit and NO kit, as well as IL-6, IL-1$\beta$, INF-$\alpha$, and INF-$\gamma$ ELISA kits were purchased from Nanjing Jiancheng Bioengineering Institute (Nanjing, China). Chromogenic TAL/TAL end point assay kit for determination of endotoxin was purchased from Chinese Horseshoe Crab Reagent Manufactory Co., Ltd. (Xiamen, China). All other reagents used were of analytical grade.

**Preparation of Verbascose from Mung Beans.** The preparation of verbascose from mung beans was carried out according to the reported method.[21] Full grains of pest-free mung beans were selected and crushed with a grinder, and the powder was extracted two times with 80% aqueous ethanol in a ratio of 10:1 (ethanol solution to material, mL/g) at 70 °C for 60 min. The extract was centrifuged at 2800*g* for 10 min. The supernatants of two extractions were combined and concentrated by using a rotary vacuum evaporator (Heidolph, Germany). The resulting residue was loaded onto a column (2.0 × 30.0 cm) of charcoal/Celite (1:1, w/w), and the column was successively eluted with a linear gradient of 0–50% aqueous ethanol. The fractions were collected (40 mL/tube) and screened by reaction with naphthoresorcinol, and those with sugars were further analyzed by using an Agilent 1100 series HPLC system (Agilent, USA) with a refraction index detector (RID). The separation of sugars was completed on a Sugar-D column (4.6 × 250 mm, Nacalai Tesque Inc., Kyoto, Japan) by using acetonitrile/water (75:25, v/v) as the mobile phase at a flow rate of 1.0 mL/min. Sugars were identified by comparing the retention times with those of standard sugars. The fractions containing verbascose only were combined, concentrated in vacuo, and further purified by gel filtration chromatography of Biogel P-2 (1.5 × 100.0 cm). The fractions (2.5 mL/tube) containing verbascose checked by HPLC were combined, concentrated/ and freeze-dried, affording high-purity verbascose. The structure of verbascose prepared was characterized by HPLC, mass spectrometry (Mariner system 5304 mass spectrometer, Applied Biosystems, Foster City, CA, USA), and nuclear magnetic resonance (NMR) spectroscopy. $^{1}$H and $^{13}$C NMR spectra of the sample, dissolved in deuterated water, were recorded on a Burker Avance DRX-500 spectrometer (Bruker, Karlsruhe, Germany) at a temperature of 298 K. Data for verbascose: $^{1}$H NMR (500 MHz, $D_2O$) $\delta$ 5.42 (d, 1H, $J$ = 3.7 Hz), 4.98 (t, 2H); $^{13}$C NMR (500 MHz, $D_2O$) $\delta$ 106.44, 100.98, 100.57, 100.41, 94.74, 83.98, 79.00, 76.64, 75.39, 73.90, 73.59, 72.14, 72.03, 71.88, 71.48, 71.30, 71.08, 70.91, 69.10, 68.95, 68.49, 65.12, 64.08, 63.80; MS $m/z$ 851.27 for $[M + Na]^+$ (calcd for $C_{30}H_{52}O_{26}$ $[M + Na]^+$, 851.2639).

**Determination of Endotoxin Contamination.** The concentration of endotoxin in the verbascose sample was measured by using a chromogenic TAL/TAL end point assay kit according to the manufacturer's instruction.

**Cell Culture.** The RAW264.7 cells cryopreserved in liquid nitrogen were rapidly thawed in a water bath at 37 °C, transferred to sterile tissue culture dishes, suspended in DMEM supplemented with 10% newborn calf serum, 100 IU/mL penicillin, and 100 IU/mL streptomycin, and incubated in a humidified 5% $CO_2$ incubator at 37 °C. When the cells spread to >80% of the bottom of the culture dishes, the adherent cells were kept for cell passage and used for further culture.

**Assay of RAW264.7 Cell Viability.** Measurement of RAW264.7 cell viability was done according to the MTT-based colorimetric method.[39] Briefly, the RAW264.7 cells, suspended at a density of 1 × $10^5$ cells/mL in DMEM supplemented with 10% newborn calf serum, 100 IU/mL penicillin, and 100 IU/mL streptomycin, were seeded into a 96-well flat-bottom plate (100 $\mu$L/well) and inoculated in a humidified 5% $CO_2$ incubator at 37 °C for 12 h. The nonadherent cells in the wells were removed by washing three times with DMEM. After that, a series of concentrations of verbascose solution (final concentrations of 25.0, 50.0, 100.0, 200.0, and 400.0 $\mu$g/mL) were added (100 $\mu$L/well). LPS (final concentration of 10.0 $\mu$g/mL) and complete DMEM alone were used as positive control and blank control, respectively. The cells were incubated as mentioned above for 12, 24, 36, and 48 h, respectively. After each incubation, 200 $\mu$L of MTT solution (0.5 mg/mL) was added to each well, and the plate was further incubated at 37 °C for 4 h. Finally, the reaction was stopped by adding 150 $\mu$L of DMSO to each well for the dissolution of formazan crystals. The absorbance (Abs) at 570 nm was determined by a Synergy 2 Multimode Microplate Reader (BioTeK Instruments, Inc., Winooski, VT, USA), and the cell viability rate was calculated according to the formula below:

$$\text{cell viability rate (\%)} = \text{Abs}_{\text{sample}}/\text{Abs}_{\text{control}} \times 100$$

**Assay of Phagocytosis of RAW264.7 Cells.** Phagocytosis of RAW264.7 cells was measured according to the reported method with modification.[40] The prior stage culture of RAW264.7 cells was done as previously described. The verbascose solutions with different concentration (25.0, 50.0, 100.0, 200.0, and 400.0 $\mu$g/mL) as well as a blank control (complete DMEM) and positive control (LPS, 10.0 $\mu$g/mL) were added to a 96-well plate (100 $\mu$L/well), and the plate was incubated at 37 °C in a 5% $CO_2$ incubator for 24 h. Subsequently, the neutral red solution at a concentration of 0.075% was added to each well (100 $\mu$L/well). After further incubation for 1 h, the cells were washed with phosphate-buffered saline (PBS) two times to remove excess neutral red. After that, a mixture of glacial acetic acid (0.1 M) and ethanol (1:1, v/v) was added to each well (100 $\mu$L/well), and the plate was incubated again overnight at 37 °C. Finally, Abs at 540 nm of each well was measured by using an ELISA plate reader. The phagocytosis index of devouring neutral red of peritoneal macrophages was calculated by using the following equation:

$$\text{phagocytosis rate (\%)} = \text{Abs}_{\text{sample}}/\text{Abs}_{\text{control}} \times 100$$

**Assay of NO and Cytokines.** The NO amount released by peritoneal macrophages was determined by measuring the nitrite level in the cell supernatant with Greiss reaction.[41] Briefly, the collected cell supernatant from the assay of phagocytosis of peritoneal macrophages was mixed in 96-well cell plates with Griess reagent (1% sulfanilamide and 0.1% *N*-1-naphthylethylenediamine dihydrochloride in 5% phosphoric acid) in equal volume and incubated at room temperature for 10 min. Abs at 492 nm was then measured by an ELISA plate reader by using sodium nitrite ($NaNO_2$) as a standard. The levels of cytokines (IL-6, IL-1$\beta$, IFN-$\alpha$, and IFN-$\gamma$) were measured by using an ELISA kit according to the manufacturer's protocol.

**Animal Grouping and Experimental Design.** All animals were treated according to the previously reported method,[42] and the procedures involving animals were conducted in strict accordance with the Chinese legislation on the use and care of latoratory animals. Briefly, female Kunming mice were housed in an air-conditioned animal room with constant temperature (21 ± 1 °C), 50–60% relative

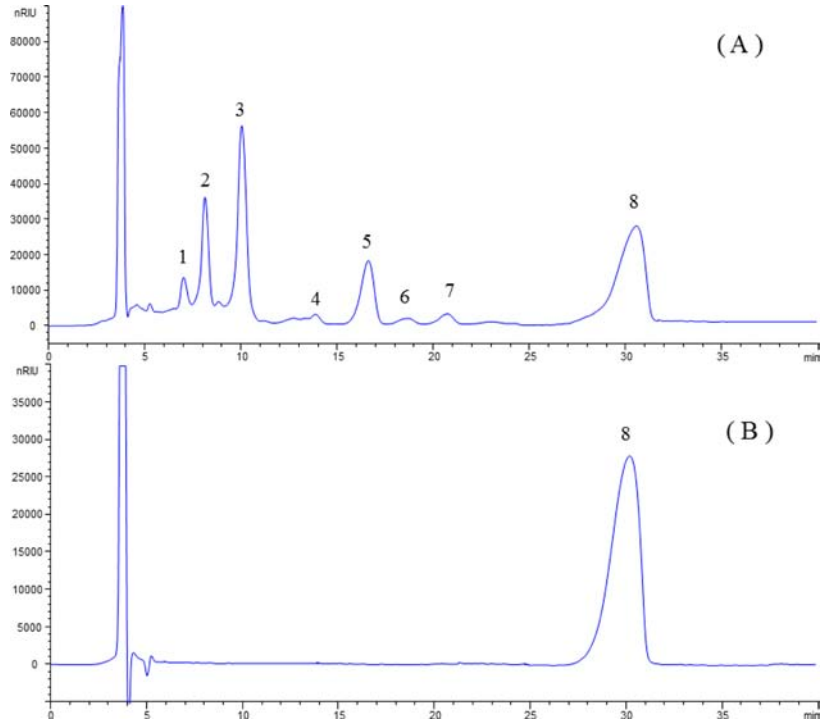


**Figure 1.** HPLC chromatograms of soluble sugars (A) and purified verbascose (B) from mung beans. HPLC conditions: column, Sugar-D (4.6 × 250 mm); mobile phase, acetonitrile/water (75:25, v/v); flow rate, 1.0 mL/min; detector, RID. Peaks: 1, fructose; 2, glucose; 3, sucrose; 4, melibiose; 5, raffinose; 6, unknown compound; 7, stachyose; 8, verbascose.

humidity, and a 12 h light/dark cycle with free acess to laboratory chow and water. After acclimatization for 7 days, the mice were randomly assigned to six groups (eight for each group). The mice in group I (normal control) were given a hypodermic injection of 0.9% NaCl once daily for 8 days. The mice in group II (model control group) were given a hypodermic injection of 0.9% NaCl once daily as well as a hypodermic injection of CPA (100 mg/kg BW) on days 2, 3, and 4. Group III was positive control, in which 0.9% NaCl was replaced with levamisole hydrochloride on the basis of group II. Groups IV–VI were verbascose treatment groups at doses of 30, 90, and 270 mg/kg BW, respectively. Different doses of verbascose were given for 8 consecutive days, and a hypodermic injection of CPA (100 mg/kg BW) was performed on days 2, 3, and 4. At 12 h after the last administration, all of the mice were sacrificed by using a cervical dislocation method and the spleen index, thymus index, swelling rate of earlap, lysozyme activity, and serum 50% hemolytic value ($HC_{50}$) were measured.

**Lymphoid Organ and Body Weights.** The BWs of mice in each group were measured during the experimental period. Furthermore, the weights of vital organs (spleen and thymus) were recorded after cervical dislocation of the mice. The viscera index was calculated as

$$\text{viscera index (mg/g)} = W_1/W_0$$

where $W_1$ is the weight of the spleen or thymus and $W_0$ is the BW of mouse.

**DTH Response.** DNFB solution was prepared with acetone and vegetable oil in a ratio of 1:1 (v/v) in advance. On the third day of inspection, abdomenal hair on the mice was cut off (3.0 × 3.0 cm), and 30 μL of 1% DNFB was smeared slowly on the shaved abdomen. After 7 days of treatment, both sides of the right ears of the mice were embrocated with 20 μL of 1% DNFB, whereas the left ears were not treated (as control). After cervical dislocation of the mice, a 6 mm diameter round ear piece was taken from each earlap by using a puncher. The swelling rate of the earlap was calculated as follows:

$$\text{swelling rate of earlap (\%)} = (W_{\text{right ear}} - W_{\text{left ear}})/W_{\text{left ear}} \times 100$$

**Assay for Serum Hemolysis to Sheep Red Blood Cell (SRBC).** On the fourth day of treatment, the mice were sensitized by intraperitoneal injection of 0.2 mL of 2% SRBC suspension. At 24 h after the last inspection, the serum was collected through the eye orbit of the mouse and diluted with normal saline. The diluted serum (200 μL) was taken into a centrifuge tube, and 200 μL of SRBC (2%) and 200 μL of guinea pig serum were added in sequence. The diluted serum was substituted with normal saline as a blank control. The mixtures were incubated at 37 °C for 30 min and then centrifuged at 10000*g* for 5 min. The Abs of the supernatant was measured at 540 nm ($Abs_{sample}$). In addition, the Abs at which SRBC reached the half hemolytic situation was measured ($Abs_{SRBC}$). Briefly, 2% SRBC (1.0 mL) was centrifuged and the sediment was diluted with distilled water to a volume of 950 μL. After 10 min, 17% NaCl solution (50 μL) was added to afford a 0.2% hemoglobin solution. To the resulting hemoglobin solution (50 μL), 50 μL of SRBC suspension and 400 μL of normal saline were added. Finally, the Abs at 540 nm of the supernatant from centrifugation was measured as $Abs_{SRBC}$. The content of serum hemolysin antibody was expressed by $HC_{50}$ as follows:

$$HC_{50} = Abs_{sample}/Abs_{SRBC}$$

**Determination of Lysozyme Activity in Spleen and Serum.** The spleen and serum were obtained as previously described. The lysozyme activity was measured by an ELISA kit according to the manufacturer's protocol.

**Statistical Analysis.** Data are expressed as means ± SD and subjected to one-way analysis of variance (ANOVA). Duncan's new multiple-range test was performed to determine the significant difference using SPSS 18.0 software (SPSS Inc., Chicago, IL, USA).

## RESULTS AND DISCUSSION

**Preparation of Verbascose.** As shown in Figure 1A, the soluble sugars extracted from mung bean were effectively separated by HPLC. According to the retention times of standard sugars, fructose, glucose, sucrose, melibiose, raffinose,

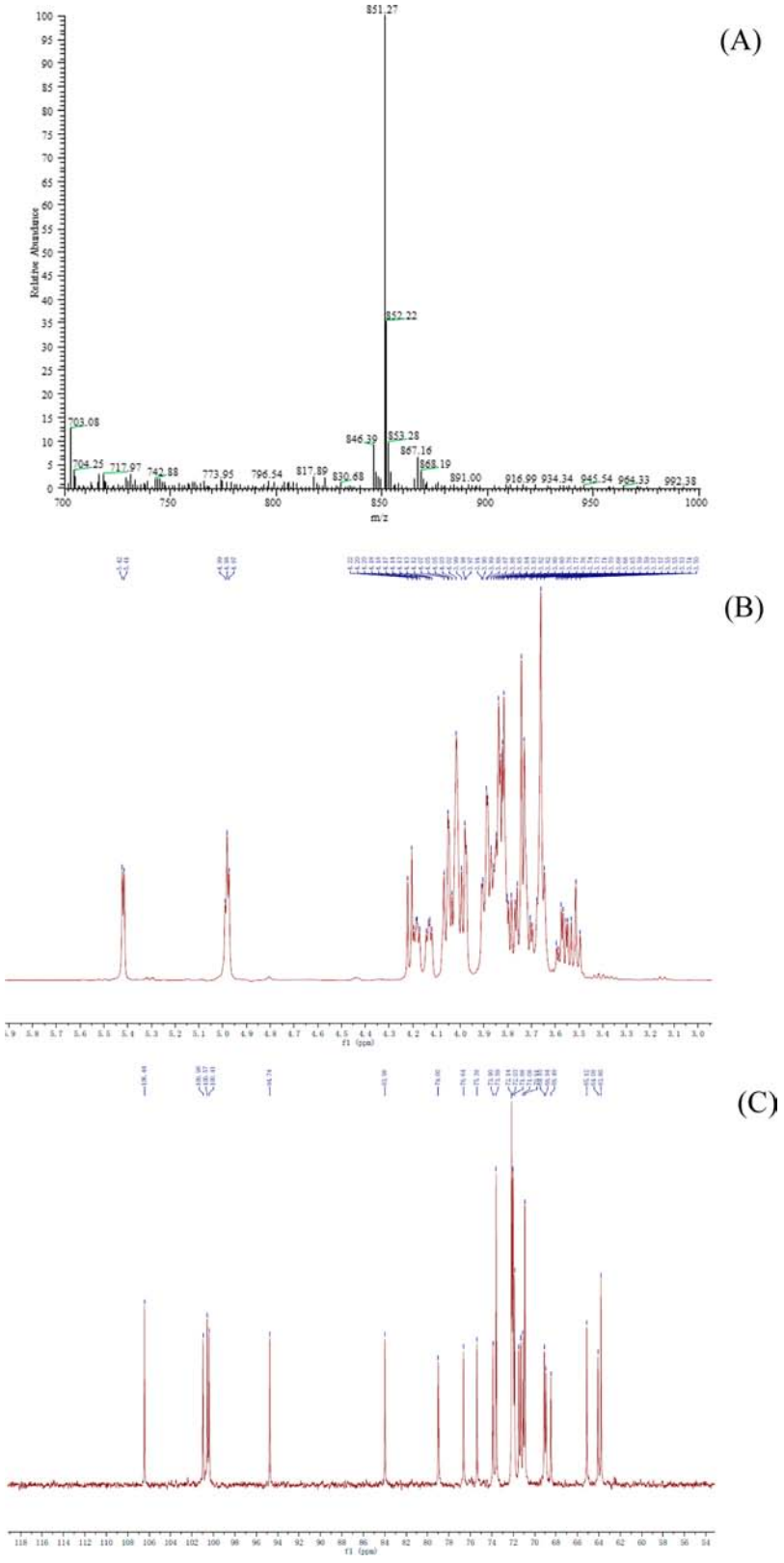


**Figure 2.** Mass spectrum (A) and $^{1}H$ (B) and $^{13}C$ NMR (C) spectra of verbascose prepared from mung bean.

stachyose, and verbascose were identified in mung beans. Notably, the three most abundant sugars were verbascose, sucrose, and raffinose, accounting for 41.8, 26.7, and 12.5% of the total soluble sugars in mung beans, respectively. The contents of monosaccharides and disaccharides including fructose, glucose, sucrose, and melibiose accounted for only 42.4% of the total soluble sugars, only slightly greater than the content of verbascose. Despite the low level of stachyose, $\alpha$-GOS still accounted for >50% of total soluble sugars. The results clearly demonstrate that nodigestible $\alpha$-GOS are the

Table 1. Effects of Verbascose on RAW264.7 Cell Viability[a]

| | cell viability | | | | | | |
|---|---|---|---|---|---|---|---|
| | | | verbascose | | | | |
| incubation time (h) | control | LPS | 25 μg/mL | 50 μg/mL | 100 μg/mL | 200 μg/mL | 400 μg/mL |
| 12 | 1 ± 0.08a | 1.29 ± 0.14c | 1.04 ± 0.02a | 1.13 ± 0.02ab | 1.23 ± 0.07bc | 1.34 ± 0.12c | 1.34 ± 0.16c |
| 24 | 1 ± 0.09a | 1.76 ± 0.19cd | 1.21 ± 0.10b | 1.25 ± 0.30b | 1.56 ± 0.21c | 1.82 ± 0.25d | 1.78 ± 0.11cd |
| 36 | 1 ± 0.12a | 1.67 ± 0.17c | 1.29 ± 0.17b | 1.34 ± 0.29b | 1.43 ± 0.20b | 1.60 ± 0.15c | 1.62 ± 0.24c |
| 48 | 1 ± 0.05a | 1.50 ± 0.14d | 1.23 ± 0.28b | 1.26 ± 0.13b | 1.31 ± 0.22bc | 1.44 ± 0.11cd | 1.41 ± 0.12cd |

[a]Different lower case letters represent a significant difference ($p < 0.05$) between different samples of the same time.

major oligosaccharides present in mung bean. Therefore, mung bean is one of the most suitable materials for verbascose preparation, which is consistent with the previous study.[20]

To prepare verbascose, the soluble sugars extracted from mung bean were separated by charcoal/Celite column chromatography combined with Biogel P-2 gel filtration chromatography. Charcoal/Celite column chromatography can isolate different carbohydrates mainly through their hydrophobic properties. However, stachyose and verbascose showed similar hydrophobicities, and both were eluted out by 15% aqueous ethanol in the present study. The mixture of stachyose and verbascose was further separated by Biogel P-2 gel filtration chromatography, due to the distinct difference in their molecular sizes. The data of MS and NMR (Figure 2) for the resulting fractions of verbascose clearly demonstrated that it was verbascose,[36] and the purity of verbascose obtained was 98.5% (Figure 1B).

**Endotoxin Contents.** Endotoxin, as a contaminant in biological preparations, has a capacity of immune stimulation. In the present work, we measured the endotoxin content in verbascose sample by TAL chromogenic method for the sake of endotoxin influence. As a result, the endotoxin contamination of verbascose sample was quite low (0.0056%), suggesting that the interference from endotoxin to the immunity could be ignored.

**Effects of Verbascose on RAW264.7 Cell Viability.** The viability of RAW264.7 cells is an indicator for further experiments of immune activation. The assay is dependent on the ability of viable cells to metabolize a water-soluble tetrazolium salt into a water-insoluble formazan product. Therefore, we investigated the effects of verbascose on the viability of RAW264.7 cells. As shown in Table 1, the viabilities of treatments by verbascose (100.0, 200.0, and 400.0 μg/mL) were significantly increased ($p < 0.05$) as compared with that of blank control after 12 h of incubation. However, after incubation for 24, 36, and 48 h, all of the doses of verbascose showed significant differences ($p < 0.05$) compared with the blank control, indicating that they all had positive influences on the viability of RAW264.7 cells. The cell viability increased with the increase of sample concentration and reached the maximum value at a concentration of 200.0 μg/mL. Furthermore, both treatments at concentrations of 200.0 and 400.0 μg/mL showed striking differences compared with the other treatments, but there was no significant difference between the two concentrations. The results suggested that the influence of verbascose on RAW264.7 cell viability was in a dose-dependent manner at lower concentrations. The treatments at 100.0, 200.0, and 400.0 μg/mL of verbascose with incubation time of 24 h exhibited the best effects on cell viability. Therefore, 24 h was selected for the cell culture time in the following experiments.

**Effects of Verbascose on Phagocytic Activity of RAW264.7 Cells.** Activated macrophage not only participates in both specific and nonspecific immune reactions but also is the "bridge cell" of these two kinds of immune reactions.[43] The increase in phagocytic activity is one of the most distinguished features of macrophage activation. Therefore, the neutral red phagocytosis assay was applied to evaluate the effects of verbascose on phagocytic activity of RAW264.7 cells, and the results are presented in Figure 3. The phagocytosis indices of

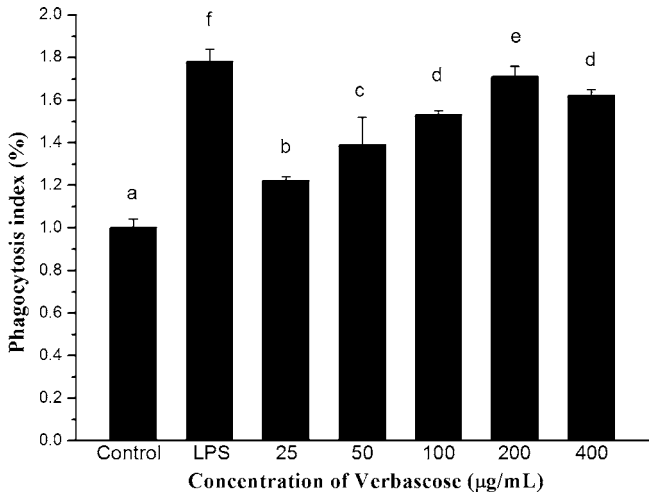


Figure 3. Effects of verbascose on phagocytosis of RAW264.7 cells. Letters a–f represent a significant difference ($p < 0.05$) between different concentrations of samples.

different doses of verbascose on devouring neutral red of peritoneal macrophages all exceeded 1.0, and all of the stimulating indices at different concentrations were comparable to that stimulated by LPS (positive control). The results demonstrated that verbascose had notable activity of promoting peritoneal macrophages to devour neutral red at a low dose. Furthermore, the promoting effects increased with the increases of sample concentration ranging from 25 to 200 μg/mL. Nevertheless, the phagocytosis index for treatment at 400 μg/mL was significantly lower ($p < 0.05$) than that of treatment at 200 μg/mL, which confirmed that verbascose exhibited its maximum activity of cell phagocytosis at a concentration of 200 μg/mL.

**Effects of Verbascose on NO and Cytokine Production.** Once activated, macrophages release a large number of cell factors, such as NO, INF, and $PGE_2$, to exert joint efficacy against microbial infections and cancer.[44] NO is a modulator of neurotransmission that can act as a vasorelaxant and defend against pathogens. It has been reported that the antitumor and antiviral activities, inflammatory reaction, and immune response

have a strong relationship with the release of NO.[45] Thus, we considered NO as an index to evaluate the immunomodulatory effects of verbascose. As shown in Figure 4, a minimum amount

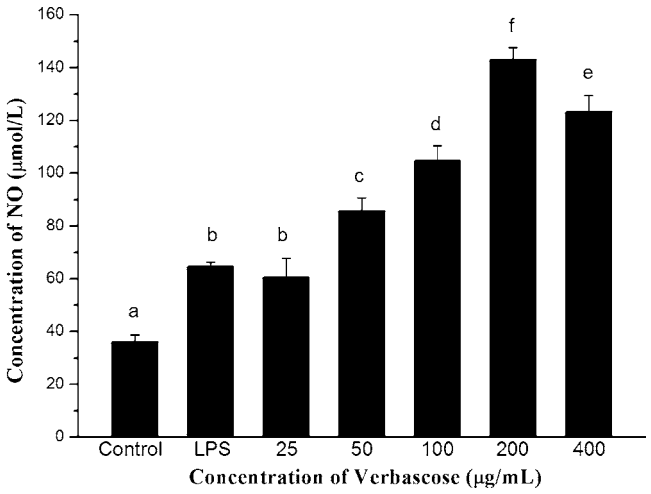


**Figure 4.** Effects of verbascose on nitric oxide level of RAW264.7 cells. Letters a–f represent a significant difference ($p < 0.05$) between different concentrations of samples.

of NO was produced in the blank control group, which might be due to the low expression of inducible NO synthase (iNOS) in static status RAW264.7 cells, whereas treatments with verbascose induced significant increases of NO production ($p < 0.05$), indicating that verbascose had the ability to activate macrophages to release NO. At concentrations of verbascose from 25.0 to 200.0 μg/mL, the levels of NO production showed a dose-dependent effect. In addition, between every two concentrations there was a significant difference ($p < 0.05$). It might be related to the expression of iNOS induced by verbascose.

Cytokines are small molecule proteins produced by immune cells with immunomodulatory and anti-inflammatory abilities. It is well-known that mature T cells, following antigen recognition, are induced to differentiate into three distinct functional subsets of Th1, Th2, and Th0 cells, which can be discriminated on the basis of the array of cytokines produced. Th1 cells secrete IL-2, IFN-$\gamma$, and TNF-$\beta$, and Th2 cells secrete IL-4, IL-5, and IL-6, whereas Th0 cells, having the capacity to produce both Th1 and Th2 cytokines, are believed to represent a stage of differentiation before commitment to the Th1 or Th2 lineage. Thus, the section of IFN-$\gamma$ and IL-6 may represent the function of mature T cells.[46,47] IL-1 (IL-1$\alpha$ and IL-1$\beta$) is the prototypic "multifunctional" cytokine, which affects nearly every cell type and often in concert with other cytokines or small mediator molecules. IFN-$\alpha$, produced by leukocytes, is mainly involved in innate immune response against viral infection.[34] Accordingly, the effects of verbascose on cytokine production (IL-1$\beta$, IL-6, IFN-$\alpha$, and IFN-$\gamma$) were investigated in the present study. Compared with those of the normal control group (Table 2), the concentrations of cytokines (IL-1$\beta$, IL-6, IFN-$\alpha$, and IFN-$\gamma$) secreted by RAW264.7 cells in all treatments of verbascose were significantly higher ($p < 0.05$). In the range of 25–200 μg/mL verbascose, the production of cytokines was enhanced in a dose-dependent manner, whereas there was no significant difference in the secretion of IL-6, IFN-$\alpha$, and IFN-$\gamma$ between the treatments of verbascose at concentrations of 400 and 200 μg/mL. The results indicated that verbascose could stimulate immune responses through the release of immune cell factors (IL-1$\beta$, IL-6, IFN-$\alpha$, and IFN-$\gamma$) as well as inflammatory mediators (NO).

**Effects of Verbascose on the Immune Organ Index.** Thymus decline is an important marker of immune system aging because the immune system degeneration is expressed as an aging process from center to periphery piloted by thymus involution. Thus, the immunomodulatory effect is closely related to the change of immune organ index.[48] CPA, a DNA alkylating agent with striking immunomodulatory properties being used as a chemotherapeutic and immunosuppression drug, may cause the decline of lymphocyte percent, peripheral blood leucocyte, macrophage phagocytosis, spleen index, thymus index, DTH earlap swelling, carbon clearance, and serum hemolysin. Therefore, it is often used to establish the immunosuppressed model.[49] In this study, the effects of verbascose on the thymus and spleen indices were investigated. Compared with the normal control group (Figure 5), significant decreases in indices of spleen and thymus were observed after treatment by CPA in model control group ($p < 0.05$). However, treatment of verbascose could improve the spleen index as compared with the model control group. Furthermore, the medium-dose treatment (90 mg/kg BW) exhibited the best effect (significant difference with the other treatments at $p < 0.05$), even though no significant difference was observed for medium-dose treatment and the normal group. For the thymus index, there were no significant difference between the treatment and model control group ($p > 0.05$), but the medium-dose treatment showed some improvements on the thymus index. The results suggested that verbascose was able to act against immunosuppression induced by CPA in vivo to some extent.

**Effects of Verbascose on DTH.** DTH is a protective localized cell-mediated immune response mediated by $CD4^+$ and $CD8^+$ T-cells, primarily against intracellular pathogens. In

**Table 2. Effects of Verbascose on Cytokine (IL-6, IL-1$\beta$, IFN-$\alpha$, and IFN-$\gamma$) Levels of RAW264.7 Cells[a]**

| treatment | concn of IL-6 (pg/mL) | concn of IL-1$\beta$ (pg/mL) | concn of INF-$\alpha$ (pg/mL) | concn of INF-$\gamma$ (pg/mL) |
|---|---|---|---|---|
| control | 113.33 ± 2.32a | 53.51 ± 1.83a | 63.77 ± 4.54a | 142.22 ± 11.98a |
| LPS | 231.26 ± 12.31d | 137.02 ± 3.69cd | 118.98 ± 7.73b | 350.24 ± 13.20d |
| verbascose | | | | |
| 25 μg/mL | 158.17 ± 8.16b | 108.15 ± 0.26b | 118.30 ± 3.38b | 237.78 ± 0.45b |
| 50 μg/mL | 158.33 ± 2.85b | 118.19 ± 1.14bc | 128.53 ± 8.31bc | 251.22 ± 5.35bc |
| 100 μg/mL | 162.67 ± 6.69b | 142.55 ± 1.83d | 136.12 ± 10.88c | 255.56 ± 9.43bc |
| 200 μg/mL | 198.33 ± 4.00c | 143.76 ± 9.41d | 134.82 ± 3.46c | 280.67 ± 8.17c |
| 400 μg/mL | 195.00 ± 1.21c | 150.31 ± 7.33d | 132.31 ± 6.57c | 274.00 ± 6.25bc |

[a]Different lower case letters represent a significant difference ($p < 0.05$) between different concentrations of samples.

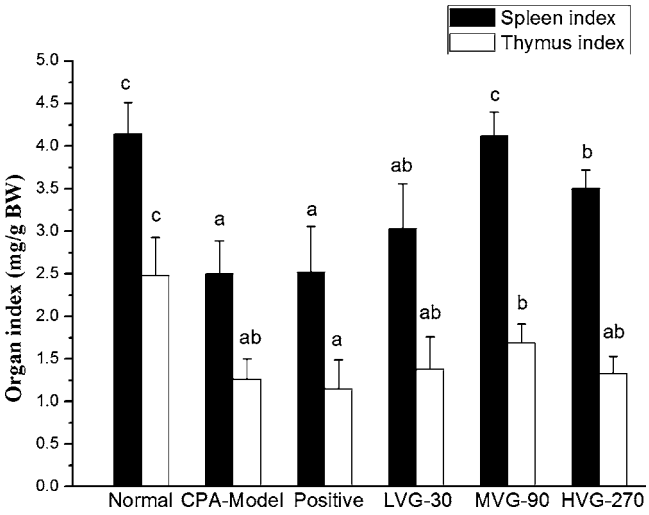


**Figure 5.** Effects of verbascose on the spleen and thymus indices. Letters a−c represent a significant difference ($p < 0.05$) between different concentrations of samples. Normal, normal control group, given a hypodermic injection of 0.9% NaCl once daily for 8 days; CPA-Model, model control group, given 0.9% NaCl once daily as well as a hypodermic injection of cyclophosphamide (CPA, 100 mg/kg body weight (BW)) on days 2, 3, and 4; Positive, positive control group, which replaced NaCl with levamisole hydrochloride on the basis of model control group; LVG-30, low dose of verbascose (30 mg/kg BW); MVG-90, medium dose of verbascose (90 mg/kg BW); HVG-30, high dose of verbascose (270 mg/kg BW).

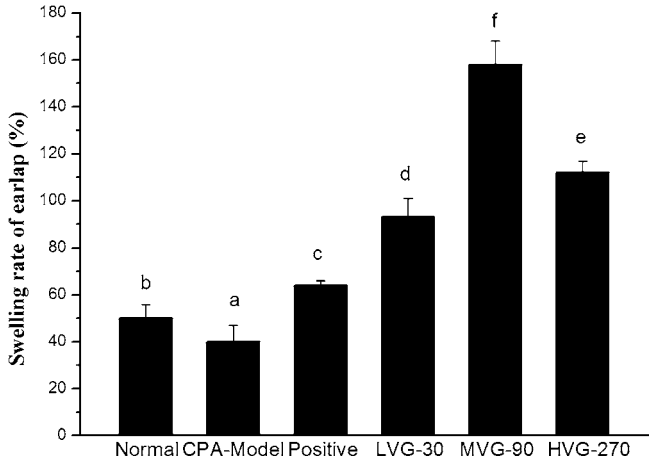


**Figure 6.** Effects of verbascose on the swelling rate of earlap in delayed type of hypersensitivity reaction. Letters a−f represent a significant difference ($p < 0.05$) between different concentrations of samples. Normal, normal control group, given a hypodermic injection of 0.9% NaCl once daily for 8 days; CPA-Model, model control group, given 0.9% NaCl once daily as well as a hypodermic injection of cyclophosphamide (CPA, 100 mg/kg body weight (BW)) on days 2, 3, and 4; Positive, positive control group, which replaced NaCl with levamisole hydrochloride on the basis of model control group; LVG-30, low dose of verbascose (30 mg/kg BW); MVG-90, medium dose of verbascose (90 mg/kg BW); HVG-30, high dose of verbascose (270 mg/kg BW).

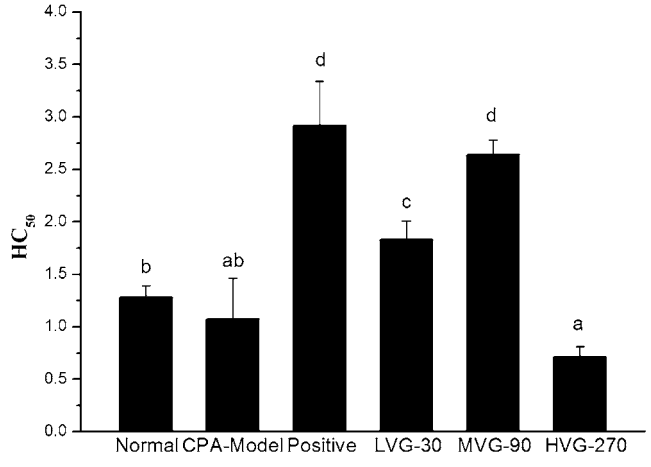


**Figure 7.** Effects of verbascose on hemolysin in serum ($HC_{50}$). Letters a−c represent a significant difference ($p < 0.05$) between different concentrations of samples. Normal, normal control group, given a hypodermic injection of 0.9% NaCl once daily for 8 days; CPA-Model, model control group, given 0.9% NaCl once daily as well as a hypodermic injection of cyclophosphamide (CPA, 100 mg/kg body weight (BW)) on days 2, 3, and 4; Positive, positive control group, which replaced NaCl with levamisole hydrochloride on the basis of model control group; LVG-30, low dose of verbascose (30 mg/kg BW); MVG-90, medium dose of verbascose (90 mg/kg BW); HVG-30, high dose of verbascose (270 mg/kg BW).

the case of allergenic effect, T-lymphocyte may become sensitized lymphocyte and will generate a regional abnormal reactive inflammation when it encounters the allergen again. This allergic inflammation is delayed (starting after 12 h and peaking at 24−72 h) and characterized by cell degeneration and necrosis.[50] It has been reported that DNFB (a hapten) may become a complete antigen when binding with skin protein. It will then stimulate T-lymphocyte to form sensitized lymphocyte. After it is painted on the earlap of mice, regional earlap swelling would be observed 4−7 days later and the swelling rate of earlap is associated with the degree of DTH reaction. As shown in Figure 6, a significant decrease of earlap swelling rate was observed between the model control group compared and the normal control group ($p < 0.05$), which indicated the feasibilty of the present immunosuppressed model. When mice received positive drug or verbascose, they showed a significant DTH response in vivo ($p < 0.05$) compared with the normal control group. Compared with the positive control group, all of the treatments of different verbascose doses exhibited significant DTH responses. However, a notably significant immunological effect was observed for the treatment with the middle dose (90 mg/kg) of verbascose compared to the other two dose treatments ($p < 0.05$). The results suggested that verbascose might strengthen immune function by increasing DTH earlap swelling.

**Effects of Verbascose on Serum Hemolysin ($HC_{50}$).** Serum hemolysin antibody, secreted by B-lymphocytes when stimulated by a variety of antigens, is a reliable indicator reflected by the level of humoral immunity.[51] Therefore, we evaluated the levels of serum hemolysin antibody in response to SRBC in mice. As shown in Figure 7, the daily treatments of mice with 30 or 90 mg/kg doses of verbascose resulted in a significant enhancement of serum hemolysin level as compared with the model control group ($p < 0.05$). Particularly, there was no significant difference between the treatments of the middle dose of verbascose and positive control, and both treatments exhibited the best effects. However, the high-dose treatment (270 mg/kg BW) showed a sharp decrease in hemolysin level, indicating that the high-dose verbascose treatment might suppress the production of serum hemolysin to SRBC. From the above results, it was concluded that low-dose verbascose

treatment possessed the potential of immune-enhancing activity.

**Effects of Verbascose on Lysozyme in Serum and Spleen.** Lysozyme, also called muramidase or peptidoglycan *N*-acetylmuramoyl-hydrolase, existing extensively in animals, plants, and microorganisms, is considered to be a potent innate immunity molecule.[52] In vivo, lysozyme catalyzes the hydrolysis of the $\beta$-(1→4) glycosidic linkage between *N*-acetylmuramic acid and *N*-acetylglucosamine, alternates the sugar residues in the bacterial peptidoglycan, and causes bacterial cell lysis.[53] As a consequence, lysozyme occupies an important position in normal and nonspecific immunity. In the present study, the effects of verbascose on lysozyme activity in serum and spleen were evaluated, and the results are presented in Table 3.

**Table 3. Effects of Verbascose on Activity of Lysozyme in Mouse Spleen and Serum**[a]

| sample | lysozyme in serum (U/mL) | lysozyme in spleen (U/mg) |
|---|---|---|
| normal | 347.2 ± 19.14bcd | 142.96 ± 29.80d |
| CPA-model | 182.66 ± 25.91a | 77.23 ± 7.93a |
| levamisole | 486.15 ± 39.82d | 273.31 ± 15.08f |
| low dose of verbascose (30 mg/kg BW) | 272.69 ± 43.12abc | 90.68 ± 3.26b |
| medium dose of verbascose (90 mg/kg BW) | 427.63 ± 26.76cd | 146.91 ± 12.56e |
| high dose of verbascose (270 mg/kg BW) | 236.89 ± 20.35ab | 105.14 ± 15.19c |

[a]Different lower case letters represent a significant difference ($p < 0.05$) between different concentrations of samples.

Compared with the normal control group, the activities of lysozyme in the three doses of verbascose and positive drug were significantly enhanced ($p < 0.05$). In addition, it was found that treatment with a medium dose of verbascose (90 mg/kg BW) could significantly improve the activity of lysozyme compared with the other two treatment doses ($p < 0.05$) and restored the activity of lysozyme to normal level. The results suggested that verbascose could reinforce the immune function by raising the activity of lysozyme.

In conclusion, we demonstrated that verbascose could promote the proliferation in vitro of RAW264.7 cells, strengthen peritoneal macrophages to devour neutral red, and enhance the production of NO and cytokines (IL-1$\beta$, IL-6, IFN-$\alpha$, and IFN-$\gamma$). In in vitro experiments, treatment with 200 $\mu$g/mL verbascose exhibited the most significant immunomodulatory activity. As for in vivo experiments, the results demonstrated that verbascose could raise the spleen index, elevate the activity of lysozyme in serum, and increase the level of serum hemolysin and the swelling rate of earlap in DTH reaction. The results suggested that verbascose had potent immunostimulatory activity, and further works on its potential mechanisms are in progress.

## AUTHOR INFORMATION


### Corresponding Author

*(X.Z.) Phone/fax: +86 25 84396791. E-mail: zengxx@njau.edu.cn.



### Funding

This work was partly supported by Grants-in-Aid for Scientific Fesearch from the National Natural Science Foundation of China (31171750) and a project funded by the Priority Academic Program Development of Jiangsu Higher Education Institutions (PAPD).

### Notes

The authors declare no competing financial interest.


## REFERENCES


(1) Roberfroid, M. Prebiotics: the concept revisited. *J. Nutr.* **2007**, *137*, 830S−837S.

(2) Steed, H.; Macfarlane, G. T.; Macfarlane, S. Prebiotics, synbiotics and inflammatory bowel disease. *Mol. Nutr. Food Res.* **2008**, *52*, 898−905.

(3) Macfarlane, G. T.; Steed, H.; Macfarlane, S. Bacterial metabolism and health-related effects of galacto-oligosaccharides and other prebiotics. *J. Appl. Microbiol.* **2008**, *104*, 305−344.

(4) Rastall, R. A. Gluco and galacto-oligosaccharides in food: update on health effects and relevance in healthy nutrition. *Curr. Opin. Clin. Nutr. Metab. Care* **2013**, *16*, 675−678.

(5) Ye, E. Q.; Chacko, S. A.; Chou, E. L.; Kugizaki, M.; Liu, S. M. Greater whole-grain intake is associated with lower risk of type 2 diabetes, cardiovascular disease, and weight gain. *J. Nutr.* **2012**, *142*, 1304−1313.

(6) Maslowski, K. M.; Vieira, A. T.; Ng, A.; Kranich, J.; Sierro, F.; Yu, D.; Schilter, H. C.; Rolph, M. S.; Mackay, F.; Artis, D.; Xavier, R. J.; Teixeira, M. M.; Mackay, C. R. Regulation of inflammatory responses by gut microbiota and chemoattractant receptor GPR43. *Nature* **2009**, *461*, 1282−1286.

(7) Torres, D. P. M.; Goncalves, M. P.; Teixeira, J. A.; Rodrigues, L. R. Galacto-oligosaccharides: production, properties, applications, and significance as prebiotics. *Compr. Rev. Food Sci. Food Saf.* **2010**, *9*, 438−454.

(8) Park, A. R.; Oh, D. K. Galacto-oligosaccharide production using microbial $\beta$-galactosidase: current state and perspectives. *Appl. Microbiol. Biotechnol.* **2010**, *85*, 1279−1286.

(9) Shadid, R.; Haarman, M.; Knol, J.; Theis, W.; Beermann, C.; Rjosk-Dendorfer, D.; Schendel, D. J.; Koletzko, B. V.; Krauss-Etschmann, S. Effects of galactooligosaccharide and long-chain fructooligosaccharide supplementation during pregnancy on maternal and neonatal microbiota and immunity − a randomized, double-blind, placebo-controlled study. *Am. J. Clin. Nutr.* **2007**, *86*, 1426−1437.

(10) Gosling, A.; Stevens, G. W.; Barber, A. R.; Kentish, S. E.; Gras, S. L. Recent advances refining galactooligosaccharide production from lactose. *Food Chem.* **2010**, *121*, 307−318.

(11) Ariefdjohan, M. W.; Martin, B. R.; Lachcik, P. J.; Weaver, C. M. Acute and chronic effects of honey and its carbohydrate constituents on calcium absorption in rats. *J. Agric. Food Chem.* **2008**, *56*, 2649−2654.

(12) Rastall, R. A.; Gibson, G. R.; Gill, H. S.; Guarner, F.; Klaenhammer, T. R.; Pot, B.; Reid, G.; Rowland, I. R.; Sanders, M. E. Modulation of the microbial ecology of the human colon by probiotics, prebiotics and synbiotics to enhance human health: an overview of enabling science and potential applications. *FEMS Microbiol. Ecol.* **2005**, *52*, 145−152.

(13) Li, W.; Xiang, X. L.; Tang, S. F.; Hu, B.; Tian, L.; Sun, Y.; Ye, H.; Zeng, X. Effective enzymatic synthesis of lactosucrose and its analogues by $\beta$-D-galactosidase from *Bacillus circulans*. *J. Agric. Food Chem.* **2009**, *57*, 3927−3933.

(14) Peacock, K. S.; Ruhaak, L. R.; Tsui, M. K.; Mills, D. A.; Lebrilla, C. B. Isomer-specific consumption of galactooligosaccharides by bifidobacterial species. *J. Agric. Food Chem.* **2013**, *61*, 12612−12619.

(15) Weaver, C. M.; Martin, B. R.; Nakatsu, C. H.; Armstrong, A. P.; Clavijo, A.; McCabe, L. D.; McCabe, G. P.; Duignan, S.; Schoterman, M. H. C.; van den Heuvel, E. G. H. M. Galactooligosaccharides improve mineral absorption and bone properties in growing rats through gut fermentation. *J. Agric. Food Chem.* **2011**, *59*, 6501−6510.

(16) Taniguchi, Y.; Mizote, A.; Kohno, K.; Iwaki, K.; Oku, K.; Chaen, H.; Fukuda, S. Effects of dietary lactosucrose ($4^G$-$\beta$-D-galactosylsucrose) on the IgE response in mice. *Biosci., Biotechnol., Biochem.* **2007**, *71*, 2766−2773.

(17) Teramoto, F.; Rokutan, K.; Sugano, Y.; Oku, K.; Kishino, E.; Fujita, K.; Hara, K.; Kishi, K.; Fukunaga, M.; Morita, T. Long-term administration of $4^{G}$-$\beta$-D-galactosylsucrose (lactosucrose) enhances intestinal calcium absorption in young women: a randomized, placebo-controlled 96-wk study. *J. Nutr. Sci. Vitaminol.* **2006**, *52*, 337−346.
(18) Martinez-Villaluenga, C.; Frias, J.; Vidal-Valverde, C. $\alpha$-Galactosides: antinutritional factors or functional ingredients? *Crit. Rev. Food Sci. Nutr.* **2008**, *48*, 301−316.
(19) Kadlec, P.; Dostalova, J.; Houska, M.; Strohalm, J.; Bubnik, Z. Evaluation of $\alpha$-galactosides decrease during storage of germinated pea seeds treated by high pressure. *J. Food Eng.* **2006**, *77*, 364−367.
(20) Kuo, T. M.; Vanmiddlesworth, J. F.; Wolf, W. J. Content of raffinose oligosaccharides and sucrose in various plant seeds. *J. Agric. Food Chem.* **1988**, *36*, 32−36.
(21) Xiang, X. L.; Yang, L. Y.; Hua, S.; Li, W.; Sun, Y.; Ma, H.; Zhang, J. S.; Zeng, X. Determination of oligosaccharide contents in 19 cultivars of chickpea (*Cicer arietinum* L) seeds by high performance liquid chromatography. *Food Chem.* **2008**, *111*, 215−219.
(22) Yang, X. B.; Zhao, Y.; He, N. W.; Croft, K. D. Isolation, characterization, and immunological effects of $\alpha$-galacto-oligosaccharides from a new source, the herb *Lycopus lucidus* Turcz. *J. Agric. Food Chem.* **2010**, *58*, 8253−8258.
(23) Teixeira, J. S.; McNeill, V.; Ganzle, M. G. Levansucrase and sucrose phoshorylase contribute to raffinose, stachyose, and verbascose metabolism by lactobacilli. *Food Microbiol.* **2012**, *31*, 278−284.
(24) Montilla, A.; Corzo, N.; Olano, A.; Jimeno, M. L. Identification of oligosaccharides formed during stachyose hydrolysis by Pectinex Ultra SP-L. *J. Agric. Food Chem.* **2009**, *57*, 5007−5013.
(25) Abou Hachem, M.; Fredslund, F.; Andersen, J. M.; Larsen, R. J.; Majumder, A.; Ejby, M.; Van Zanten, G.; Lahtinen, S. J.; Barrangou, R.; Klaenhammer, T. Raffinose family oligosaccharide utilisation by probiotic bacteria: insight into substrate recognition, molecular architecture and diversity of GH36 $\alpha$-galactosidases. *Biocatal. Biotransform.* **2012**, *30*, 316−325.
(26) Ishizuka, S.; Iwama, A.; Dinoto, A.; Suksomcheep, A.; Maeta, K.; Kasai, T.; Hara, H.; Yokota, A. Synbiotic promotion of epithelial proliferation by orally ingested encapsulated *Bifidobacterium breve* and raffinose in the small intestine of rats. *Mol. Nutr. Food Res.* **2009**, *53*, S62−S67.
(27) Gulewicz, P.; Szymaniec, S.; Bubak, B.; Frias, J.; Vidal-Valverde, C.; Trajanowska, K.; Gulewicz, K. Biological activity of $\alpha$-galactoside preparations from *Lupinus angustifolius* L. and *Pisum sativum* L. seeds. *J. Agric. Food Chem.* **2002**, *50*, 384−389.
(28) Hayakawa, K.; Mizutani, J.; Wada, K.; Masai, T.; Yoshiara, I.; Mitsuoka, T. Effects of soybean oligosaccharides on human fecal microflora. *Microb. Ecol. Health Dis.* **1990**, *3*, 293−303.
(29) Kelly-Quagliana, K. A.; Nelson, P. D.; Buddington, R. K. Dietary oligofructose and inulin modulate immune functions in mice. *Nutr. Res. (N.Y.)* **2003**, *23*, 257−267.
(30) Schley, P. D.; Field, C. J. The immune-enhancing effects of dietary fibres and prebiotics. *Br. J. Nutr.* **2002**, *87*, S221−S230.
(31) Jeurink, P. V.; van Esch, B. C. A. M.; Rijnierse, A.; Garssen, J.; Knippels, L. M. J. Mechanisms underlying immune effects of dietary oligosaccharides. *Am. J. Clin. Nutr.* **2013**, *98*, 572S−577S.
(32) Lorsbach, R. B.; Murphy, W. J.; Lowenstein, C. J.; Snyder, S. H.; Russell, S. W. Expression of the nitric-oxide synthase gene in mouse macrophages activated for tumor cell killing: molecular basis for the synergy between interferon-$\gamma$ and lipopolysaccharide. *J. Biol. Chem.* **1993**, *268*, 1908−1913.
(33) Schmidt, H. H. H. W.; Walter, U. NO at work. *Cell* **1994**, *78*, 919−925.
(34) Akira, S.; Uematsu, S.; Takeuchi, O. Pathogen recognition and innate immunity. *Cell* **2006**, *124*, 783−801.
(35) Laskin, D. L.; Pendino, K. J. Macrophages and inflammatory mediators in tissue injury. *Annu. Rev. Pharmacol. Toxicol.* **1995**, *35*, 655−677.
(36) Zhao, Y. T.; Niu, S.; Huang, L. B.; Wang, J. M.; Yin, Z. J.; Li, Q.; Li, Z. J. Synthesis of raffinose family oligosaccharides by regioselective de-O-benzylation with $Co_2(CO)_8/Et_3SiH/CO$ system. *Tetrahedron* **2013**, *69*, 5022−5028.
(37) Peterbauer, T.; Mucha, J.; Mach, L.; Richter, A. Chain elongation of raffinose in pea seeds: Isolation, charcterization, and molecular cloning of a multifunctional enzyme catalyzing the synthesis of stachyose and verbascose. *J. Biol. Chem.* **2002**, *277*, 194−200.
(38) Peterbauer, T.; Richter, A. Galactosylononitol and stachyose synthesis in seeds of adzuki bean: purification and characterization of stachyose synthase. *Plant Physiol.* **1998**, *117*, 165−172.
(39) Luo, J. G.; Liu, J.; Ke, C. L.; Qiao, D. L.; Ye, H.; Sun, Y.; Zeng, X. Optimization of medium composition for the production of exopolysaccharides from *Phellinus baumii* Pilat in submerged culture and the immuno-stimulating activity of exopolysaccharides. *Carbohydr. Polym.* **2009**, *78*, 409−415.
(40) Zhang, W. Y.; Yang, J. Y.; Chen, J. P.; Hou, Y. Y.; Han, X. D. Immunomodulatory and antitumour effects of an exopolysaccharide fraction from cultivated *Cordyceps sinensis* (Chinese caterpillar fungus) on tumour-bearing mice. *Biotechnol. Appl. Biochem.* **2005**, *42*, 9−15.
(41) Green, L. C.; Wagner, D. A.; Glogowski, J.; Skipper, P. L.; Wishnok, J. S.; Tannenbaum, S. R. Analysis of nitrate, nitrite, and [$^{15}$N]nitrate in biological fluids. *Anal. Biochem.* **1982**, *126*, 131−138.
(42) Liu, C. H.; Xi, T.; Lin, Q. X.; Xing, Y. Y.; Ye, L.; Luo, X. G.; Wang, F. S. Immunomodulatory activity of polysaccharides isolated from *Strongylocentrotus nudus* eggs. *Int. Immunopharmacol.* **2008**, *8*, 1835−1841.
(43) Chen, X. M.; Lu, J. X.; Zhang, Y. D.; He, J. T.; Guo, X. Z.; Tian, G. Y.; Jin, L. Q. Studies of macrophage immuno-modulating activity of polysaccharides isolated from *Paecilomyces tenuipes*. *Int. J. Biol. Macromol.* **2008**, *43*, 252−256.
(44) Karnjanapratum, S.; You, S. Molecular characteristics of sulfated polysaccharides from *Monostroma nitidum* and their *in vitro* anticancer and immunomodulatory activities. *Int. J. Biol. Macromol.* **2011**, *48*, 311−318.
(45) Mayer, B.; Hemmens, B. Biosynthesis and action of nitric oxide in mammalian cells. *Trends Biochem. Sci.* **1997**, *22*, 477−481.
(46) Han, S. B.; Kim, Y. H.; Lee, C. W.; Park, S. M.; Lee, H. Y.; Ahn, K. S.; Kim, I. H.; Kim, H. M. Characteristic immunostimulation by angelan isolated from *Angelica gigas* Nakai. *Immunopharmacology* **1998**, *40*, 39−48.
(47) Chen, J. R.; Yang, Z. Q.; Hu, T. J.; Yan, Z. T.; Niu, T. X.; Wang, L.; Cui, D. A.; Wang, M. Immunomodulatory activity in vitro and in vivo of polysaccharide from *Potentilla anserina*. *Fitoterapia* **2010**, *81*, 1117−1124.
(48) Schiavoni, G.; Mattei, F.; Di Pucchio, T.; Santini, S. M.; Bracci, L.; Belardelli, F.; Proietti, E. Cyclophosphamide induces type I interferon and augments the number of CD44$^{hi}$ T lymphocytes in mice: implications for strategies of chemoimmunotherapy of cancer. *Blood* **2000**, *95*, 2024−2030.
(49) Pelaez, B.; Campillo, J. A.; Lopez-Asenjo, J. A.; Subiza, J. L. Cyclophosphamide induces the development of early myeloid cells suppressing tumor cell growth by a nitric oxide-dependent mechanism. *J. Immunol.* **2001**, *166*, 6608−6615.
(50) Heriazon, A.; Yager, J. A.; Sears, W.; Mallard, B. A. Induction of delayed-type hypersensitivity and interferon-gamma to *Candida albicans* and anti-hen-egg white lysozyme antibody as phenotypic markers of enhanced bovine immune response. *Vet. Immunol. Immunopathol.* **2009**, *129*, 93−100.
(51) Tsai, J. P.; Chen, H. W.; Cheng, M. L.; Liu, H. K.; Lee, Y. P.; Hsieh, C. L.; Luh, K. T.; Wu, C. W.; Hsu, L. H.; Chao, T. Y.; Wang, W. H.; Chang, C. M.; Ting, C. C. Analysis of host versus tumor interaction in cancer patients: opposing role of transforming growth factor-$\beta$1 and interleukin-6 in the development of in situ tumor immunity. *Immunobiology* **2005**, *210*, 661−671.
(52) Shuai, X. H.; Hu, T. J.; Liu, H. L.; Su, Z. J.; Zeng, Y.; Li, Y. H. Immunomodulatory effect of a *Sophora subprosrate* polysaccharide in mice. *Int. J. Biol. Macromol.* **2010**, *46*, 79−84.
(53) Rodriguez, M. C.; Rivas, G. A. Label-free electrochemical aptasensor for the detection of lysozyme. *Talanta* **2009**, *78*, 212−216.

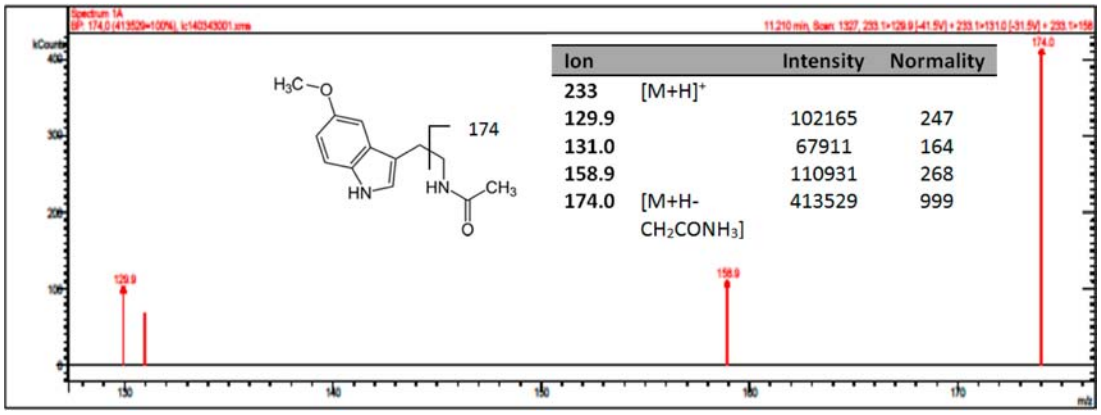


**Figure 1.** Melatonin spectrum and mass accuracy.

## MATERIALS AND METHODS

**Plant Materials.** Two varieties of common legumes: lentil (*Lens culinaris* L., var. *Salmantina*) and kidney bean (*Phaseolus vulgaris* L., var. *Pinta*) were provided by Institute of Food Science, Technology and Nutrition (CSIC, Madrid). They were stored in dark and dry conditions under refrigeration.

**Processing Conditions.** Three batches of seeds (20 g of lentils and 50 g of beans) were sterilized in 1% NaClO solution for 30 min to reduce bacterial and fungal growth. Seeds were washed three times with distilled water and then soaked in distilled water for 5 h for seed hydration (ratio 1 g:20 mL, seed:water). They were germinated in an incubator (Construcciones Frigoríficas, Confri, S.L.) at 20 °C and 80% RH, illumination conditions of photoperiodic cycle (12 h light/12 h dark) and darkness (24 h dark) for 3, 6, and 8 days. Lentil and kidney bean sprouts were withdrawn, frozen in $N_2$, freeze-dried, and milled. Flours were passed through a 50-$\mu$m sieve and stored at 4−6 °C for further analysis.

**Melatonin Extraction and Quantification by HPLC-MS/MS.** Extraction was conducted according to Manchester et al.[22] and Ansari et al.[23] with some modifications. Briefly, lentil and kidney bean flours (2 g) were extracted with 10 mL of methanol (MeOH). Extracts were stored for 16 h at 4 °C in darkness. After a brief centrifugation at 2000*g* for 15 min at room temperature; the supernatants were filtered under vacuum by a filter (11 $\mu$m, Whatman) and they were evaporated to dryness under $N_2$ (g). The residues were resuspended in 2 mL of water, after a mild ultrasonic treatment for 2 min at room temperature; the reconstituted extracts were filtered using the solid phase extraction (SPE, cartridge C-18, Waters). The extracts obtained were evaporated to dryness by use of evaporator centrifuge (Speed Vac SC 200, Savant, USA). The residues were dissolved in MeOH/$H_2O$ (80:20; v/v) + 0.1% formic acid. Melatonin was determined by HPLC-ESI-MS/MS triple quadrupole (Varian 1200L with API-ES between 10 and 1500 Da range mass). Melatonin was recorded using multiple reaction monitoring (MRM) mode by selecting ion 233 ($M + H^+$) at the first quadrupole (Q1), fragmented in Q2 using Ar and analyzing resulting ion $m/z$ 130, 131, 159, and 174 at Q3, measuring at 174 (Figure 1). The system consisted of two pumps, Varian Prostar 210, and an Intensity Trio C18 (150 mm × 2.0 mm ID, S-3 $\mu$m, 12 nm BRYTC18032150) (Bruker) column, at a flow rate of 0.2 mL/min. Acetonitrile containing 0.1% formic acid (solvent A) and 0.1% formic acid in $H_2O$ (solvent B) as mobile phase were pumped with the following gradient: 5% solvent A (0−4 min), 5−100% solvent A (4−15 min), 100% solvent A (15−18 min), and 100−5% solvent A (18−25 min) to recover initial conditions. The injection volume was 50 $\mu$L. Quantification was performed using external standard method, using pure melatonin (Sigma-Aldrich Química, Spain) dissolved in MeOH/$H_2O$ (80:20; v/v) containing 0.1% formic acid, showing good regression coefficient ($R^2$ = 0.9989). Samples and standard solutions were analyzed in triplicate. Melatonin content was expressed as ng/g dry weight (DW).

**Phenolic Compounds Extraction and Determination.** Extraction of phenolic compounds was carried out following the Gou et al.[24] method with some modifications. Germinated flours (2 g) were blended using 30 mL of 80% chilled acetone (1:2, w/v) for 5 min and vortex for 10 min. The homogenates were then centrifuged at 2054*g* for 5 min. Supernatants were collected, and the extraction was repeated three times. All the supernatants were pooled and evaporated until 10% of the supernatants remained. The soluble phytochemical extracts were brought to 10 mL in water and were kept at −40 °C until analysis. For the extractions of bound phytochemicals, the residues from above soluble free extraction were flushed with $N_2$ and hydrolyzed directly with 20 mL of 4 M NaOH at room temperature for 1 h with shaking. The mixture was acidified to pH 2 with concentrated HCl, centrifuged at 2958*g* for 5 min, and extracted three times with ethyl acetate. The ethyl acetate fractions were evaporated to dryness, and were reconstituted into 1.5 mL of methanol and stored at −40 °C until analysis.

The phenolic compounds were determined by Folin−Ciocalteu colorimetric method according to Singleton et al.[25] using gallic acid (GAE) as standard. Phenolic compounds were expressed as mg GAE/100 g DW.

**Oxygen Radical Absorbing Capacity (ORAC) Assay.** The above methanol extracts were used for determining the radical absorbance activity by ORAC method using fluorescein as a fluorescence probe.[26] Briefly, the reaction was carried out at 37 °C in 75 mM phosphate buffer (pH 7.4) and the final assay mixture (200 $\mu$L) contained fluorescein (70 nM), 2,2-azobis (2-methyl-propionamidine)-dihydrochloride (12 mM), and antioxidant standard (Trolox [10−80 $\mu$M] or sample extracts). A Polarstar Galaxy plate reader (BMG Labtechnologies GmbH, Offenburg, Germany) was used to read fluorescence at wavelengths of 485 nm excitation and 520 nm emission. The equipment was controlled by the Fluostar Galaxy software version (4.31-0) for fluorescence measurement. Black 96-well untreated microplates (PS Balck, Porvair, Leatherhead, UK) were used. The plate was automatically shaken before preincubation, and the fluorescence was recorded every minute for 80 min. All reaction mixtures were prepared in duplicate and at least 3 independent runs were performed for each sample. Fluorescence measurements were normalized to the oxidation control (phosphate buffer) and stability control (no antioxidant). From the normalized curves, the area under the fluorescence decay curve (AUC) was calculated as

$$\mathrm{AUC} = 1 + \sum_{i=1}^{i=80} f_i/f_0$$

where $f_0$ is the initial fluorescence reading at 0 min and $f_i$ is the fluorescence reading at time $i$. The net AUC corresponding to a sample was calculated as follows:

$$\text{net AUC} = \text{AUC antioxidant} - \text{AUC blank}$$

The net AUC was plotted against the antioxidant concentration, and the regression equation of the curve was calculated. The ORAC

value was obtained by dividing the slope of the latter curve between the slopes of the Trolox curve obtained in the same assay. Final ORAC values were expressed as μmol of Trolox equivalents/g of dry sample (μmol TE/g DW).

**Statistical Analysis.** Each sample was analyzed in triplicate. Data were expressed as mean ± standard deviation (SD). The data were analyzed by one-way analysis of variance (ANOVA) and posthoc Duncan test. Differences were considered to be significant at $p < 0.05$. The statistical analysis was performed by SPSS 17.0.

## RESULTS AND DISCUSSION

**Germination Process.** The changes in biomass and percents of germination under different germination conditions are shown in Table 1. Legume biomass increased from 111% to 162% and lentil sprouts showed higher levels than bean sprouts at the same germination conditions. The highest rise was reached in lentil under eighth day 12 h light/12 h dark. The success of this processing exhibited good viability for both legumes, reaching 100% in case of bean sprouts at 12 h light/12 h dark on the eighth germination day. However, lentil exhibited lower germination percentage on the eighth day due to fungal growth. The parameter of development of radicle was different not only dependent on the kind of leguminous seeds, but also on process conditions (i.e., the presence of light and germination time). The length of bean radicle was higher than of lentils, irrespective of light conditions and germination time. These differences could be attributed to changes in bioactive compounds (melatonin) that promote vegetative plant growth.[12]

**Table 1. Changes in Seed/Seedlings Biomass and Percent of Germination at Different Illumination Conditions of Germination**[a]

| illumination conditions of germination | germination time (day) | % increase in fresh weight of seeds/ seedlings | % germination | development of radicle (cm) |
|---|---|---|---|---|
| | | Lentil | | |
| 12 h light/ 12 h dark | 3 | 137 ± 8 a | 92 ± 8 b | 1.4 ± 0.1 a |
| | 6 | 141 ± 9 a | 58 ± 5 a | 2.6 ± 0.1 b |
| | 8 | 162 ± 5 b | 59 ± 5 a | 4.5 ± 0.2 c |
| 24 h dark | 3 | 138 ± 5 a | 83 ± 7 b | 1.4 ± 0.1 a |
| | 6 | 150 ± 6 b | 83 ± 7 b | 4.1 ± 0.2 c |
| | 8 | 156 ± 10 b | 65 ± 6 a | 7.3 ± 0.2 d |
| | | Bean | | |
| 12 h light/ 12 h dark | 3 | 104 ± 6 a | 47 ± 3 a | 1.0 ± 0.1 a |
| | 6 | 126 ± 9 b | 84 ± 5 b | 3.7 ± 0.2 b |
| | 8 | 133 ± 9 c | 100 ± 4 c | 6.1 ± 0.4 d |
| 24 h dark | 3 | 90 ± 7 a | 46 ± 4 a | 1.9 ± 0.1 a |
| | 6 | 104 ± 8 a | 89 ± 5 b | 5.6 ± 0.2 c |
| | 8 | 111 ± 9 a | 96 ± 5 b | 10.6 ± 0.6 e |

[a]Results are reported as mean ± SD ($n = 3$). Mean values of each row of different illumination conditions followed by different superscript letter significantly differ when subjected to Duncan's multiple range test ($p < 0.05$).

**Melatonin.** Different methods have been developed for melatonin identification in plant extracts. Melatonin was detected in raw lentil and kidney beans varieties studied, and chromatograms are shown in Figure 2. From the results, kidney beans exhibited higher melatonin content than lentils (1.0 and 0.4 ng/g DW, respectively). These data explain the different elongation showed by legume sprouts that could be due to melatonin levels. This molecule exhibits auxinic activity in a way similar to indole-3-acetic acid (IAA).[12] In comparison to other plant foods, the results obtained were higher than those reported in other seeds such as sweet corn and rice,[27] indicating a good dietary melatonin source. The available scientific data of melatonin in foods are scarce because only a few food items have been analyzed. Melatonin levels are greatly variable among plant species, apart from seeds, fruits (12−36 pg/g WW), roots protected from light such as carrots and onions, or processed foods such as fermented drinks (0.1−35 ng/mL) and olive oil (108 pg/mL) are also natural sources of melatonin.[19]

Germination brought about a noticeable increase in melatonin ($p < 0.05$) and this effect was time-dependent in all seeds studied (Figure 3). Reports indicated higher melatonin levels at complete darkness[28] and relative increases in cucumber and red cabbage germinated seeds.[29,30] To our knowledge, the present work is the first report on the melatonin content of lentil and bean sprouts to improve the content of this bioactive compound. In this sense, melatonin content increased significantly in lentil sprouts during both germination processes, showing similar values under 12 h light/12 h dark and 24 h dark conditions (Figure 3a). In both illumination conditions, the highest contents were shown on the sixth germination day (2.3 and 2.5 ng/g DW under 12 h light/12 h dark and 24 h dark, respectively). After the sixth germination day, the levels of melatonin decreased in lentil sprouts, being more pronounced under 24 h dark (72% of decrease with respect to the sixth germination day). Similar behavior was found in bean sprouts (Figure 3b). On the sixth processing day, germination significantly influenced melatonin accumulation in both germination conditions, up to 2.4-fold at 12 h light/12 h dark and more accentuated, up to 9.4-fold at 24 h dark conditions. Finally, it is worth emphasizing that a sharp melatonin decrease (94%) from the sixth to eighth germination day was observed at 24 h darkness (0.6 ng/g DW) and less accentuated (38% of decrease) at 12 h light/12 h dark (1.5 ng/g DW). Thus, germination in darkness for 8 days did not cause melatonin increase either in lentils or beans. Our data were in agreement with those of Zielinski et al.,[31] who found contents of melatonin in lentil, vetch, and soybean seeds, as well as increases in melatonin during 7 days of germination. Hence, melatonin content in lentil showed maximum levels at sixth germination day either at 12 or 24 h dark, while melatonin content in bean reached the highest content at 24 h dark. From our results, melatonin was mainly influenced by photoperiods; darkness regimes led to more of this bioactive compound in kidney bean and these results were in agreement with those of Murch et al.[27]

The melatonin originated from these sprouts may play a role as a health promoting substance with clear antioxidant and anti-inflammatory properties; its genomic effects, and its capacity to modulate mitochondrial homeostasis, are linked to the redox status of cells and tissues.[16] From our results, the sprout intake, especially germinated beans, could be considered as a food source of dietary melatonin.

**Phenolic Compounds.** The free, bound (cell wall-associated), and total phenolic compounds (TPC) of lentil and bean sprouts are shown in Figure 4. TPC in raw lentil and bean seeds were 488 and 379 mg GAE/100 g DW, respectively. These legume seeds seem to be a good source of phenolic compounds and our results are within the range of previously reported data.[32−34] The predominant phenolic compounds in lentils and beans are catechins and procyanidins;[35,36] however, the phenolic composition of legume seeds may vary among

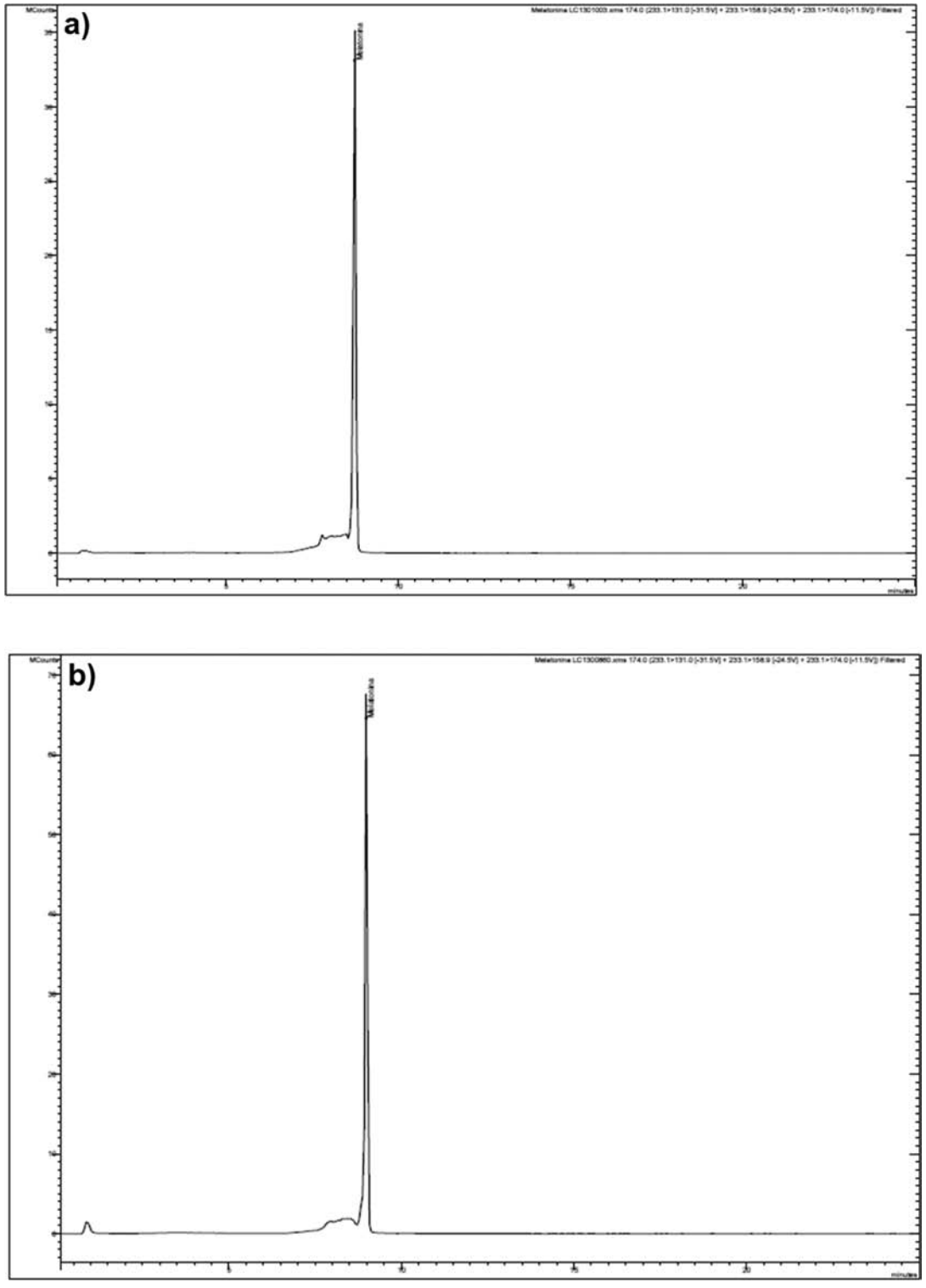


**Figure 2.** HPLC-MS/MS chromatograms of raw lentil (a) and raw kidney bean (b).

cultivars and genotypes. Differences among them may be attributed to differences in the color of the seed coat as has been reported in the literature,[32] lentil was darker than kidney bean. Lentil seeds showed 88% of free phenolic contents with respect to TPC (Figure 4a), while kidney bean seeds exhibited a higher percentage of free phenols (92%) and consequently, a lower percentage of bound phenols (8%) (Figure 4b). These results are in agreement with those found in other legume seeds.[24,37]

Our results exhibited that TPC decreased dramatically in lentil sprouts at both darkness germination conditions (12 and 24 h dark), while kidney bean sprouts exhibited relevant decreases at 12 h light/12 h dark but no relevant changes at 24 h dark germination conditions. These results are in agreement with the findings of Khandelwal et al.[32] and Troszyńska et al.[38]

With respect to lentil, decreases of phenolic compounds (total, free, and bound forms) were initiated at the third germination day and maintained during germination conditions

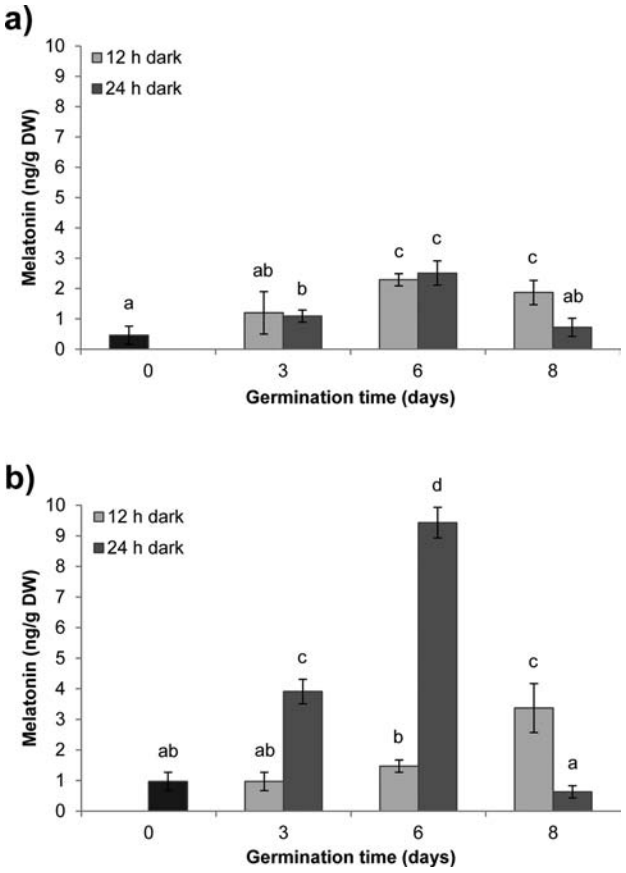


**Figure 3.** Melatonin content in raw and germinated lentils (a) and kidney beans (b).

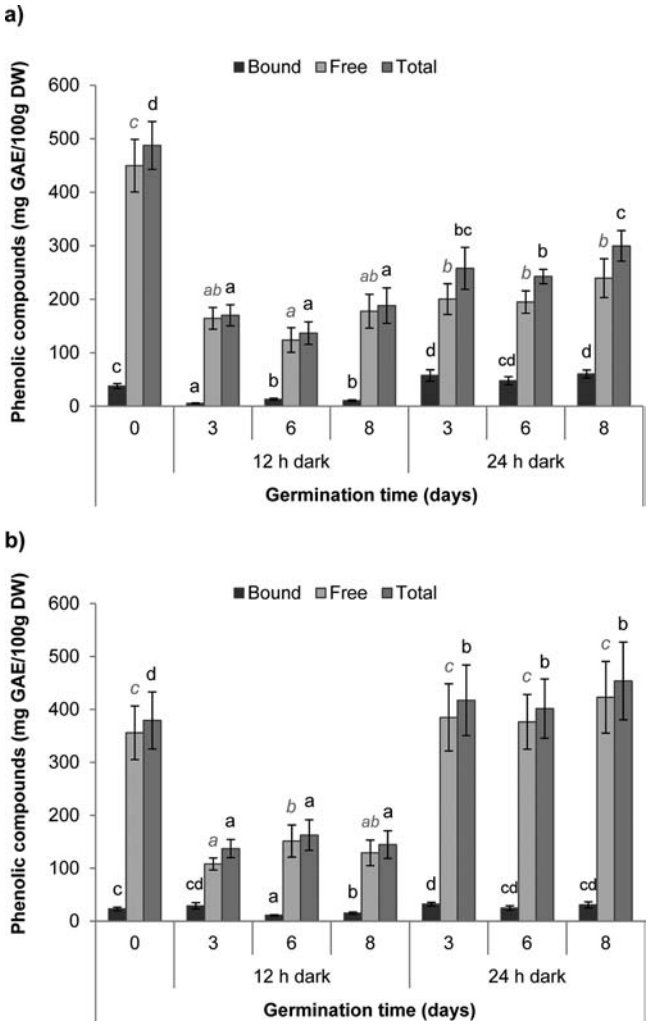


**Figure 4.** Bound, free, and total phenolic compounds in raw and germinated lentils (a) and kidney beans (b).

(12 and 24 h dark) (Figure 4a). The germination process of 12 h light/12 h dark reduces significantly up to 72% with respect to raw lentil on the sixth germination day, but any further process did not exhibit any significant changes ($p < 0.05$). In this sense, the concentration of free phenolic acids showed the maximum decrease on the sixth germination day (from 450 to 124 mg GAE/100 g DW). Decreasing tendency was also observed in bound phenols, being more accentuated on the third germination day (from 38 to 5 mg GAE/100 g DW). Regarding 24 h dark lentil germination, a similar trend was observed but lower reduction in TPC was detected (50% of decrease at the sixth germination respect to control). This may be due to the relative amounts of free phenolic compounds present in these sprouts and, also, the significant increases of bound phenolics (up to 1.6-fold respect to raw lentil seed) exhibited under 24 h darkness (Figure 4a). Although this fraction is hardly noticeable in both legumes, bound phenols are more likely glycoside flavonols, subjected to the action of colonic microflora, releasing aglycones that might be absorbed in a lesser extent and, probably, degraded to simpler phenolic derivatives and thus, they may play a special role on health.[39]

Concerning kidney beans, 12 h light/12 h dark led to a TPC reduction in a time-dependent manner (Figure 4b). The contents of free phenolic under 12 h light/12 h dark exhibited decreases (70% reduction at the third germination day as compared to raw bean) and contributed up to 93% of TPC of bean sprouts. Bean sprouts at 24 h dark exhibited an increase of TPC due to the increases either of free or bound phenol forms but these were not significant ($p < 0.05$) in a time-dependent manner. A similar trend was also observed in germinated black beans (*Phaseolus vulgaris* L.) with no significant difference of phenolic contents among them.[34] However, decreases in phenolic contents of legumes following germination have been reported by several authors.[32,40] These decreases may be attributed to the increases in the activity of enzymes responsible for the oxidation of endogenous phenolic compounds and other catabolic enzymes in raw and processed legumes. During germination, enzymes are activated, resulting in the hydrolysis of various components, including carbohydrate, protein, fiber, and lipid, as well as phenolic compounds.[32] Thus, the phytochemical quality of sprouts depends on many factors such as legume cultivar and germination conditions. This means that optimum germination conditions need to be defined for legume seeds to improve the functional quality of the sprout.

**Antioxidant Activity.** The antioxidant capacities of lentil and bean seeds (Figure 5) were similar (20.2 and 24.0 $\mu$mol TE/g DW, respectively). The results obtained were lower than those reported by Xu et al.[41] and Aguilera et al.,[35] but similar to those of Xu and Chang[37] and Guajardo-Flores et al.[34] in common beans. In general, germination brought about an enhancement of the antioxidant potential of legumes, in agreement with other studies.[7,10,34,42] Germination time directly affected the antioxidant activity of lentil and bean

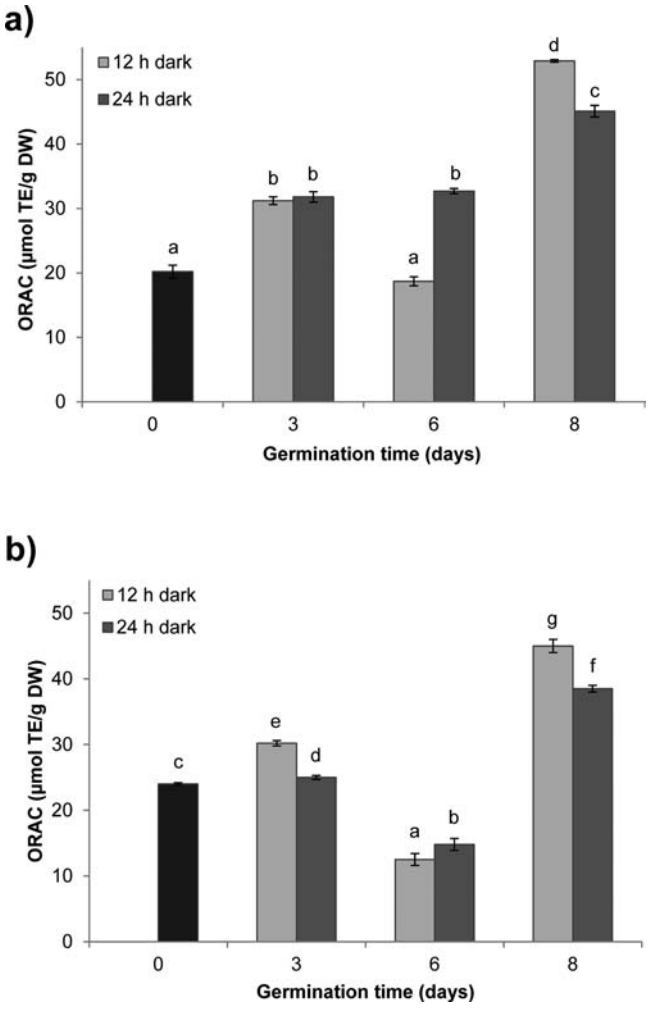


**Figure 5.** Antioxidant activity in raw and germinated lentils (a) and kidney beans (b).

sprouts. The antioxidant activity of both sprouts increased with longer germination time ($p < 0.05$), except at day 6. Among legume seeds, antioxidant activity also varied following different germination conditions. ORAC values were up to 2.4- and 2.2-fold higher after sprouting on the eighth germination day at 12 and 24 h dark for lentil sprouts, respectively. In general, lower increases were detected in bean sprouts (1.6- and 1.9-fold on the sixth germination day at 12 and 24 h dark, respectively). In addition, it should be pointed out that different light conditions during germination significantly influenced the antioxidant capacity of sprouts.[43] Among all of the sprouted legumes tested, it was noted that both samples germinated on the sixth germination day under 12 and 24 h dark showed the lowest antioxidant activities, with values ranged from 14.8 to 18.9 μmol TE/g DW. Interestingly, these samples corresponded to those exhibiting the lowest phenolic compound levels but the maximum contents of melatonin. In general, the antioxidant properties of melatonin and its ability to scavenge several radical species as part of its bioactivity have been described in the literature.[44,45] Melatonin has been found to neutralize the most toxic oxidizing agents generated within cells, such as hydroxyl radical (·OH) and peroxynitrite anion (ONOO−). In addition, melatonin reportedly scavenges singlet oxygen ($^1O_2$), superoxide anion radical ($O_2^{\bullet-}$), hydrogen peroxide ($H_2O_2$), nitric oxide (NO·), and hypochlorous acid (HClO).[46]

Finally, after the eighth germination day, a significant increase of antioxidant activity was also detected for both legume sprouts as mentioned before. Thus, this effect could be attributed to higher accumulation of compounds as melatonin degradation with radical scavenging activity. Longer application of germination resulted in further increment of antioxidant capacity, showing major ability of sprouts to prevent oxidative stress on the eighth germination day. The pronounced values of antioxidant capacity on day eight have an inverse correlation with values of melatonin in sprouts ($r = 0.61-0.75$, $p < 0.01$). This behavior may result from the indirect antioxidant properties of melatonin, as the activation of several antioxidant enzymatic cascades, including glutathione peroxidase, superoxide dismutase, and glutathione reductase, and the accumulation of degradation products, highly effective scavengers (AFMK, AMK, and cyclic 3-hydroxymelatonin),[46,47] bringing about the increased antioxidant capacity levels of bean sprouts on the eighth germination day.[48] Thus, the legume sprouts obtained in this study are valuable sources of natural antioxidants that most likely could positively influence the overall antioxidant status in humans.

Germination led to decreases in phenolic compounds and relative improvements in melatonin levels, bringing about significant increases of antioxidant activity in lentil and bean sprouts. Optimal germination conditions for melatonin levels seemed to be under 24 h dark at the sixth germination day for both sprouts, even though antioxidant activity increased on the eighth day. These germinated legume seeds with improved levels of melatonin might play a role because of the potential enhancement of the nutraceutical value of these seeds. Thus, considering the potent antioxidant activity of melatonin, these sprouts can be consumed as direct foods or adopted in the future consumer's food practices and be offered as preventive food strategies in combating chronic diseases through the diet.

## AUTHOR INFORMATION

### Corresponding Author

*E-mail: maria.martin@uam.es. Tel.: 0034 91 497 8678. Fax: 0034 91 497 3826.

### Funding

This research was financially supported by Second Call for Interuniversity Cooperation Projects University Autónoma de Madrid and Santander Bank with United States (2013−2014).

### Notes

The authors declare no competing financial interest.

## ABBREVIATIONS USED

AFMK, N(1)-acetyl-N(2)-formyl-5-methoxykynuramine; AMK, N(1)-acetyl-5-methoxykynuramine; DW, Dry weight; GAE, Gallic acid equivalents; HPLC-MS/MS, High-performance liquid chromatography tandem mass spectrometry; MRM, Multiple reaction monitoring; TE, Trolox equivalents; TPC, Total phenolic compounds; WW, Wet weight

## REFERENCES

(1) Adebowale, Y. A.; Adeyemi, A.; Oshodi, A. A. Variability in the physicochemical, nutritional and antinutritional attributes of six *Mucuna* species. *Food Chem.* **2005**, *89*, 37−48.

(2) Martín-Cabrejas, M. A.; Díaz, M. F.; Aguilera, Y.; Benítez, V.; Mollá, E.; Esteban, R. M. Influence of germination on the soluble carbohydrates and dietary fibre fractions in non-conventional legumes. *Food Chem.* **2008**, *107*, 1045−1052.

(3) Vadivel, V.; Stuetz, W.; Scherbaum, V.; Biesalski, H. K. Total free phenolic content and health relevant functionality of Indian wild legume grains: Effect of indigenous processing methods. *J. Food Compos. Anal.* **2011**, *24*, 935−943.
(4) Aguilera, Y.; Díaz, M. F.; Jiménez, T.; Benítez, V.; Herrera, T.; Cuadrado, C.; Martín-Pedrosa, M.; Martín-Cabrejas, M. A. Changes in nonnutritional factors and antioxidant activity during germination of nonconventional legumes. *J. Agric. Food Chem.* **2013**, *61*, 8120−8125.
(5) Benítez, V.; Cantera, S.; Aguilera, Y.; Mollá, E.; Esteban, R. M.; Díaz, M. F.; Martín-Cabrejas, M. A. Impact of germination on starch, dietary fiber and physicochemical properties in non-conventional legumes. *Food Res. Int.* **2013**, *50*, 64−69.
(6) Arts, I. C.; Hollman, P. C. Polyphenols and disease risk in epidemiologic studies. *Am. J. Clin. Nutr.* **2005**, *81*, 317S−325S.
(7) Dueñas, M.; Hernández, T.; Estrella, I.; Fernández, D. Germination as a process to increase the polyphenol content and antioxidant activity of lupin seeds (*Lupinus angustifolius* L.). *Food Chem.* **2009**, *117*, 599−607.
(8) Mohd Esa, N.; Abdul Kadir, K. K.; Amom, Z.; Azlan, A. Antioxidant activity of white rice, brown rice and germinated brown rice (*in vivo* and *in vitro*) and the effects on lipid peroxidation and liver enzymes in hyperlipidaemic rabbits. *Food Chem.* **2013**, *141*, 1306−1312.
(9) Paucar-Menacho, L. M.; Berhow, M. A.; Mandarino, J. M. G.; de Mejia, E. G.; Chang, Y. K. Optimisation of germination time and temperature on the concentration of bioactive compounds in Brazilian soybean cultivar BRS 133 using response surface methodology. *Food Chem.* **2010**, *119*, 636−642.
(10) Cáceres, P. J.; Martínez-Villaluenga, C.; Amigo, L.; Frías, J. Maximising the phytochemical content and antioxidant activity of Ecuadorian brown rice sprouts through optimal germination conditions. *Food Chem.* **2014**, *152*, 407−414.
(11) García, J. J.; López-Pingarrón, L.; Almeida-Souza, P.; Tres, A.; Escudero, P.; García-Gil, F. A.; Tan, D. X.; Reiter, R. J.; Ramírez, J. M.; Bernal-Pérez, M. Protective effects of melatonin in reducing oxidative stress and in preserving the fluidity of biological membranes: A review. *J. Pineal Res.* **2014**, *56*, 225−237.
(12) Park, W. J. Melatonin as an endogenous plant regulatory signal: Debates and perspectives. *J. Plant Biol.* **2011**, *54*, 143−149.
(13) Hernández-Ruiz, J.; Arnao, M. B. Distribution of melatonin in different zones of lupin and barley plants at different ages in the presence and absence of light. *J. Agric. Food Chem.* **2008**, *56*, 10567−10573.
(14) Tan, D. X.; Reiter, R. J.; Manchester, L. C.; Yan, M. T.; El-Sawi, M.; Sainz, R. M.; Mayo, J. C.; Kohen, R.; Allegra, M.; Hardeland, R. Chemical and physical properties and potential mechanisms: Melatonin as a broad spectrum antioxidant and free radical scavenger. *Curr. Top. Med. Chem.* **2002**, *2*, 181−197.
(15) Tan, D. X.; Hardeland, R.; Manchester, L. C.; Korkmaz, A.; Ma, S.; Rosales-Corral, S.; Reiter, R. J. Functional roles of melatonin in plants, and perspectives in nutritional and agricultural science. *J. Exp. Bot.* **2012**, *63*, 577−597.
(16) Acuña-Castroviejo, D.; Escames, G.; Venegas, C.; Díaz-Casado, M. E.; Lima-Cabello, E.; López, L. C.; Rosales-Corral, S.; Tan, D. X.; Reiter, R. J. Extrapineal melatonin: Sources, regulation, and potential functions. *Cell. Mol. Life Sci.* **2014**, 1−29.
(17) Dubbels, R.; Reiter, R. J.; Klenke, E.; Goebel, A.; Schnakenberg, E.; Ehlers, C.; Schiwara, H. W.; Schloot, W. Melatonin in edible plants identified by radioimmunoassay and by high performance liquid chromatography-mass spectrometry. *J. Pineal Res.* **1995**, *18*, 28−31.
(18) Iriti, M.; Varoni, E. M.; Vitalini, S. Melatonin in traditional Mediterranean diets. *J. Pineal Res.* **2010**, *49*, 101−105.
(19) Garcia-Parrilla, M. C.; Cantos, E.; Troncoso, A. M. Analysis of melatonin in foods. *J. Food Comp. Anal.* **2009**, *22*, 177−183.
(20) Claustrat, B.; Brun, J.; Chazot, G. The basic physiology and pathophysiology of melatonin. *Sleep Med. Rev.* **2005**, *9*, 11−24.
(21) Liu, F.; Ng, T. B. Effect of pineal indoles on activities of the antioxidant defense enzymes superoxide dismutase, catalase, and glutathione reductase, and levels of reduced and oxidized glutathione in rat tissues. *Biochem. Cell Biol.* **2000**, *78*, 447−453.
(22) Manchester, L. C.; Tan, D.; Reiter, R. J.; Park, W.; Monis, K.; Qi, W. High levels of melatonin in the seeds of edible plants: Possible function in germ tissue protection. *Life Sci.* **2000**, *67*, 3023−3029.
(23) Ansari, M.; Kh, R.; Yasa, N.; Vardasbi, S.; Naimi, S. M.; Nowrouzi, A. Measurement of melatonin in alcoholic and hot water extracts of *Tanacetum parthenium, Tripleurospermum disciforme* and *Viola odorata*. *DARU, J. Pharm. Sci.* **2010**, *18*, 173−178.
(24) Guo, X.; Li, T.; Tang, K.; Liu, R. H. Effect of germination on phytochemical profiles and antioxidant activity of mung bean sprouts (*Vigna radiata*). *J. Agric. Food Chem.* **2012**, *60*, 11050−11055.
(25) Singleton, V. L.; Orthofer, R.; Lamuela-Raventós, R. M. Analysis of total phenols and other oxidation substrates and antioxidants by means of Folin-Ciocalteu reagent. *Methods Enzymol.* **1998**, *299*, 152−178.
(26) Dávalos, A.; Gómez-Cordovés, C.; Bartolomé, B. Extending applicability of the Oxygen Radical Absorbance Capacity (ORAC-Fluorescein) Assay. *J. Agric. Food Chem.* **2004**, *52*, 48−54.
(27) Hattori, A.; Migitaka, H.; Iigo, M.; Itoh, M.; Yamamoto, K.; Ohtani-Kaneko, R.; Hara, M.; Suzuki, T.; Reiter, R. J. Identification of melatonin in plants and its effects on plasma melatonin levels and binding to melatonin receptors in vertebrates. *Biochem. Mol. Biol. Int.* **1995**, *35*, 627−634.
(28) Murch, S. J.; Campbell, S. S. B.; Saxena, P. K. The role of serotonin and melatonin in plant morphogenesis: Regulation of auxin-induced root organogenesis in *in vitro*-cultured explants of St. John's wort (*Hypericum perforatum* L.). *In Vitro Cell. Dev. Biol. Plant* **2001**, *37*, 786−793.
(29) Posmyk, M. M.; Kuran, H.; Marciniak, K.; Janas, K. M. Presowing seed treatment with melatonin protects red cabbage seedlings against toxic copper ion concentrations. *J. Pineal Res.* **2008**, *45*, 24−31.
(30) Posmyk, M. M.; Janas, K. M. Melatonin in plants. *Acta Physiol. Plant.* **2009**, *31*, 1−11.
(31) Zielinski, H.; Lewczuk, B.; Przybylska-Gornowicz, B.; Kozłowska, H. Melatonin in germinated legume seeds as a potentially significant agent for health. In *Biologically-Active Phytochemicals in Food: Analysis, Metabolism, Bioavailability and Function*; Pfannhauser, W., Fenwick, G. R., Khokhar, S., Eds.; Royal Society of Chemistry: Cambridge, Great Britain, 2001; pp 110−117.
(32) Khandelwal, S.; Udipi, S. A.; Ghugre, P. Polyphenols and tannins in Indian pulses: Effect of soaking, germination and pressure cooking. *Food Res. Int.* **2010**, *43*, 526−530.
(33) Xu, B.; Chang, S. K. C. Phenolic substance characterization and chemical and cell-based antioxidant activities of 11 lentils grown in the Northern United States. *J. Agric. Food Chem.* **2010**, *58*, 1509−1517.
(34) Guajardo-Flores, D.; Serna-Saldívar, S. O.; Gutiérrez-Uribe, J. A. Evaluation of the antioxidant and antiproliferative activities of extracted saponins and flavonols from germinated black beans (*Phaseolus vulgaris* L.). *Food Chem.* **2013**, *141*, 1497−1503.
(35) Aguilera, Y.; Dueñas, M.; Estrella, I.; Hernández, T.; Benitez, V.; Esteban, R. M.; Martín-Cabrejas, M. A. Evaluation of phenolic profile and antioxidant properties of *Pardina* lentil as affected by industrial dehydration. *J. Agric. Food Chem.* **2010**, *58*, 10101−10108.
(36) Aguilera, Y.; Estrella, I.; Benitez, V.; Esteban, R. M.; Martín-Cabrejas, M. A. Bioactive phenolic compounds and functional properties of dehydrated bean flours. *Food Res. Int.* **2011**, *44*, 774−780.
(37) Xu, B. J.; Chang, S. K. C. A comparative study on phenolic profiles and antioxidant activities of legumes as affected by extraction solvents. *J. Food Sci.* **2007**, *72*, S159−S166.
(38) Troszyńska, A.; Estrella, I.; Lamparski, G.; Hernández, T.; Amarowicz, R.; Pegg, R. B. Relationship between the sensory quality of lentil (*Lens culinaris*) sprouts and their phenolic constituents. *Food Res. Int.* **2011**, *44*, 3195−3201.
(39) Kroon, P. A.; Clifford, M. N.; Crozier, A.; Day, A. J.; Donovan, J. L.; Manach, C.; Williamson, G. How should we assess the effects of exposure to dietary polyphenols in vitro? *Am. J. Clin. Nutr.* **2004**, *80*, 15−21.

(40) Gupta, N. K.; Agarwal, S.; Agarwal, V. P.; Nathawat, N. S.; Gupta, S.; Singh, G. Effect of short-term heat stress on growth, physiology and antioxidative defence system in wheat seedlings. *Acta Physiol. Plant.* **2013**, *35*, 1837−1842.
(41) Xu, B. J.; Yuan, S. H.; Chang, S. K. C. Comparative analyses of phenolic composition, antioxidant capacity, and color of cool season legumes and other selected food legumes. *J. Food Sci.* **2007**, *72*, S167−S177.
(42) López-Amorós, M. L.; Hernández, T.; Estrella, I. Effect of germination on legume phenolic compounds and their antioxidant activity. *J. Food Comp. Anal.* **2006**, *19*, 277−283.
(43) Swieca, M.; Gawlik-Dziki, U.; Kowalczyk, D.; Zlotek, U. Impact of germination time and type of illumination on the antioxidant compounds and antioxidant capacity of *Lens culinaris* sprouts. *Sci. Hortic.* **2012**, *140*, 87−95.
(44) Allegra, M.; Reiter, R. J.; Tan, D. X.; Gentile, C.; Tesoriere, L.; Livrea, M. A. The chemistry of melatonin's interaction with reactive species. *J. Pineal Res.* **2003**, *34*, 1−10.
(45) Reiter, R. J.; Tan, D. X.; Mayo, J. C.; Sainz, R. M.; Leon, J.; Czarnocki, Z. Melatonin as an antioxidant: biochemical mechanisms and pathophysiological implications in humans. *Acta Biochim. Polym.* **2003**, *50*, 1129−1146.
(46) Reiter, R. J.; Tan, D. X.; Lorena, F.-B. Melatonin: A multitasking molecule. *Prog. Brain Res.* **2010**, *181*, 127−151.
(47) Korkmaz, A.; Reiter, R. J.; Tan, D.; Manchester, L. C. Melatonin; From pineal gland to healthy foods. *Spatula DD* **2011**, *1*, 33−36.
(48) Mekhloufi, J.; Bonnefont-Rousselot, D.; Yous, S.; Lesieur, D.; Couturier, M.; Thérond, P.; Legrand, A.; Jore, D.; Gardès-Albert, M. Antioxidant activity of melatonin and a pinoline derivative on linoleate model system. *J. Pineal Res.* **2005**, *39*, 27−33.

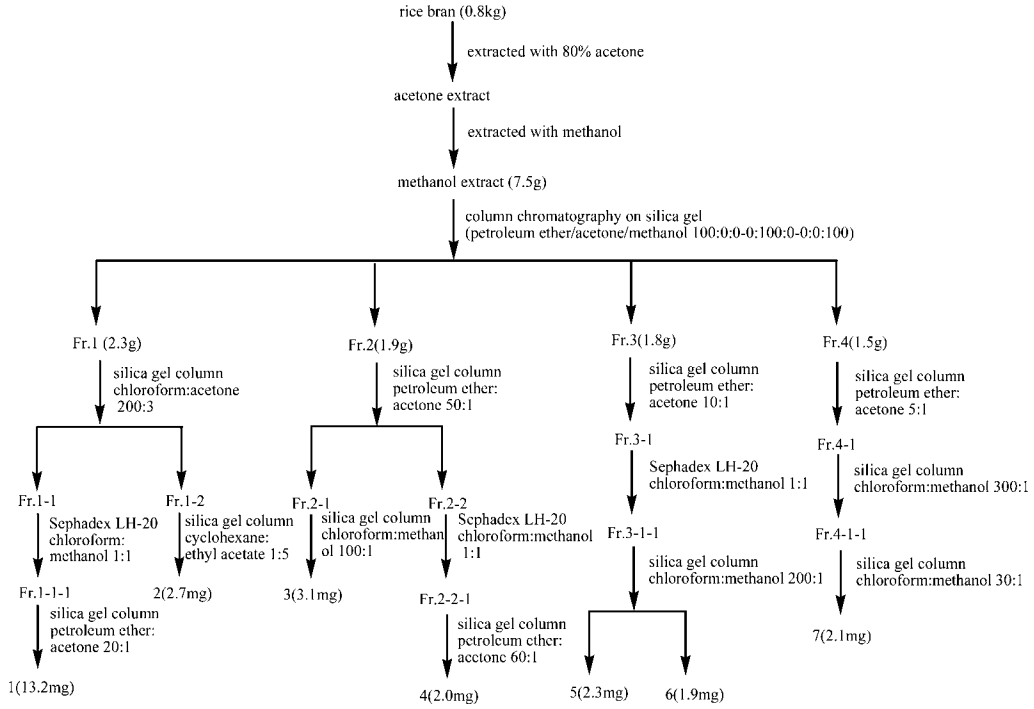


**Figure 1.** Extraction and separation process for the methanol extract of rice bran.

**Extraction and Isolation.** Rice bran (0.8 kg) was homogenized using a Polytron homogenizer before being extracted three times with 8 L of 80% acetone at ambient temperature for 24 h. The resulting mixture was then filtered after each extraction, and the filtrate was collected and concentrated under vacuum at 38 °C until approximately 90% of the solvent had been evaporated. The final solution was then extracted three times with equal volumes of methanol, and the combined extracts were concentrated under vacuum at 40 °C to give the crude methanol extract (7.5 g).

The crude methanol extract (7.5 g) was separated into four fractions (Fr. 1-4; Figure 1) by normal-phase silica gel CC (20 g of silica gel, 300−400 mesh) using a stepwise gradient elution of petroleum ether:acetone:MeOH (100:0:0 to 0:100:0 to 0:0:100, v/v/v).

Fraction 1 (2.3 g) was separated into two subfractions (Fr. 1-1 and Fr. 1-2) on a silica gel CC with a $CHCl_3$: acetone eluent (200:3, v/v). Fr. 1-1 was passed through a Sephadex LH-20 column with a $CHCl_3$:MeOH eluent (1:1, v/v) to give Fr. 1-1-1, which was purified over a silica gel CC using a petroleum ether:acetone eluent (20:1, v/v) to give **1** (13.2 mg). Fr. 1-2 was purified by CC over silica gel with a cyclohexane:ethyl acetate eluent (1:5, v/v) to give **2** (2.7 mg).

Fraction 2 (1.9 g) was purified over a silica gel CC with a petroleum ether:acetone eluent (50:1, v/v) to yield Fr. 2-1 and Fr. 2-2. Fr. 2-1 was then purified over a silica gel CC with a $CHCl_3$:MeOH eluent (100:1, v/v) to give **3** (3.1 mg). Fr. 2-2 was separated through a Sephadex LH-20 column with a $CHCl_3$:MeOH eluent (1:1, v/v) to yield Fr. 2-2-1, which was further purified on a silica gel CC using a petroleum ether:acetone eluent (60:1, v/v) to yield **4** (2.0 mg).

Fraction 3 (1.8 g) was also purified on a normal-phase silica gel CC using a petroleum ether:acetone eluent (10:1, v/v) to yield Fr. 3-1. Fr. 3-1 was purified over a Sephadex LH-20 column with a $CHCl_3$:MeOH eluent (1:1, v/v) to give Fr. 3-1-1, which was further purified on a silica gel CC using a $CHCl_3$:MeOH eluent (200:1, v/v) to give **5** (2.3 mg) and **6** (1.9 mg).

Fraction 4 (1.5 g) was subjected to CC over silica gel using a petroleum ether:acetone eluent (5:1, v/v) to yield Fr. 4-1. Fr. 4-1 was subsequently purified on a silica gel CC using a $CHCl_3$:MeOH eluent (300:1, v/v) to give Fr. 4-1-1, which was purified by CC over silica gel, eluting with $CHCl_3$:MeOH (30:1, v/v) to yield 7 (2.1 mg).

**Assay of $ABTS^+$ and DPPH Radical Scavenging.** Radical-scavenging activity against $ABTS^+$ was performed as described in the literature.[14] DPPH radical-scavenging assay was performed according to a previously reported protocol.[15] Vitamin C was employed as a positive control. The antioxidant activities of the test compounds were expressed as $IC_{50}$, with the $IC_{50}$ being defined as the concentration of the test compounds required to inhibit the formation of radicals by 50%.[16] All of the samples were analyzed in triplicate.

**Antimicrobial Bioassay.** The antimicrobial assay was carried out on the pure compounds using the disc diffusion method described in the literature.[17] The commercial antimicrobial agent, gentamicin (National Institute for the Control of Pharmaceutical and Biological products, Beijing, China), was employed as a positive control. Several test microorganisms were used, including *Escherichia coli* (*E. coli*; ATCC 25922), *Staphylococcus aureus* (S. aureus; ATCC 25923), *Bacillus subtilis* (B. subtilis; ATCC 6633), *Mycobacterium smegmatis* (*My. smegmatis*; CMCC 93321), *Clostridium perfringens* (*C. perfringens*; ATCC 13124), *Micrococcus tetragenus* (*Mi. tetragenus*; ATCC 35098), *Candida albicans* (*C. albicans*; CMCC 98001), and *Mycobacterium phlei* (*My. phlei*; AS 4.1180). The tested strains were incubated in Luria−Bertani (LB) agar plates for bacteria and in YPD agar plates for *C. albicans* at 37 °C. The minimal inhibitory concentrations (MICs) were determined. After an incubation period of 24 h, the zones of inhibition (millimeters in diameter) were recorded, and the MICs values were determined.

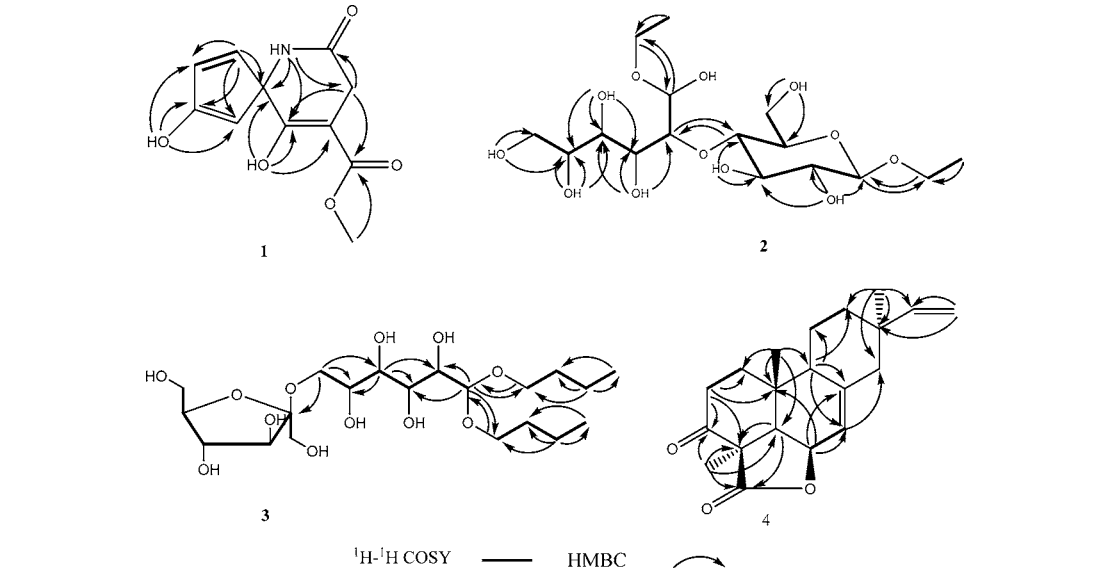


**Figure 2.** Key $^1$H−$^1$H COSY and HMBC correlations for compounds **1**, **2**, **3**, and **4**.

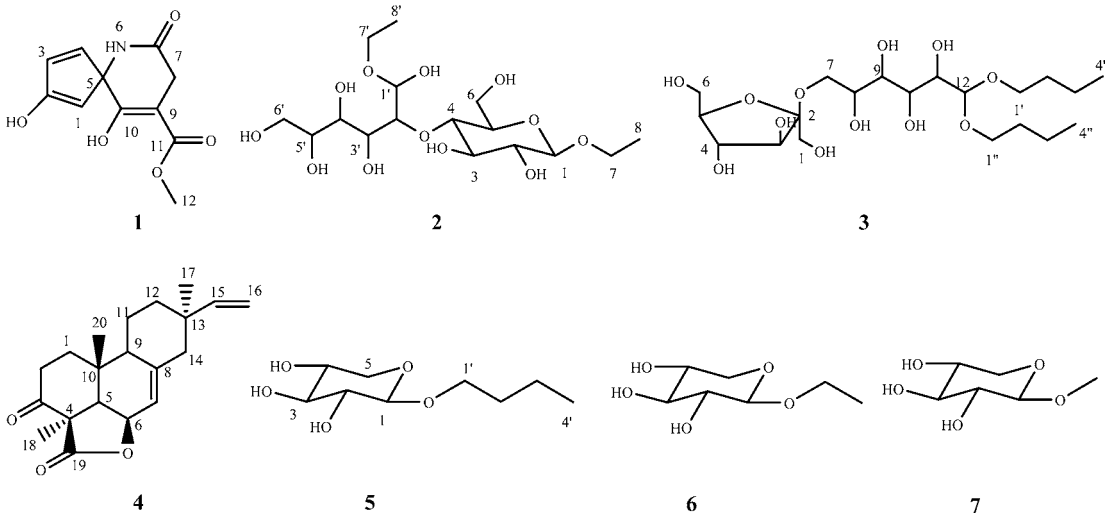


**Figure 3.** Structures of the compounds isolated from the methanol extract of rice bran.

**Statistical Analysis.** All of the data were analyzed according to Duncan's multiple comparison test ($p < 0.05$), using version 8.1 of the SAS software package. The resulting data were presented as mean ± SD.

## RESULTS AND DISCUSSION

**Structural Elucidation of the Isolated Compounds.** Compound **1** was isolated as a yellow amorphous powder. Its molecular formula was determined to be $C_{11}H_{11}NO_5$ based on HRESIMS analysis of the pseudomolecular ion peak at $m/z$ 260.0542 $[M + Na]^+$ (calcd 260.0535), indicating seven degrees of unsaturation. The UV spectrum of compound **1** revealed three strong absorption bands at 210, 265, and 320 nm. The IR spectrum displayed strong absorption bands at 3274, 1721, 1478, and 1204 cm$^{-1}$, which were attributed to hydroxyl, amide, ester carboxyl, and olefinic functionalities. The $^1$H NMR spectrum showed three exchangeable protons in the downfield at $\delta$ 10.01 (s, 1H), 9.01 (s, 1H), and 6.07 (s, 1H) corresponding to two hydroxyl group linked to C-10 and C-2, and an amide group at the position of 6-NH, respectively, these three functionalities were further confirmed by the key HMBC correlations (Figure 2) from 2-OH to C-1, C-2, and C-3, from 10-OH to C-5, C-9, and C-10, and from 6-NH to C-5, C-8, and C-10. The double bond at C-3 and C-4 was supported by COSY correlations between H-3 and H-4, as well as confirmed by the key correlation from H-4 to C-1, C-2, C-3, and C-5. The proton signal at $\delta$ 2.91 was assigned to C-8 on the basis of the results provided by the HSQC and HMBC spectra, respectively. A key correlation from H-12 to C-11was observed in the HMBC experiment, indicating that a methoxy at C-12 was connected to the carbonyl at C-11. Consequently, the structure of **1** was determined to be methyl 2,10-dihydroxy-7-oxo-6-azaspiro[4.5]deca-1,3,9-triene-9-carboxylate and named Oryzalactam (Figure 3).

Compound **2** was isolated as a white amorphous powder, and its molecular formula was determined to be $C_{16}H_{32}O_{12}$ based on HRESIMS analysis of the pseudomolecular ion peak at $m/z$ 415.1826 $[M - H]^-$ (calcd 415.1816). The UV spectrum of compound **2** revealed only one strong absorption band at 205 nm. The IR spectrum displayed strong absorption bands at 3416 and 1029 cm$^{-1}$ which are characteristic of glycosidic-type structures. The $^1$H NMR spectrum of **2** showed the presence of


dx.doi.org/10.1021/jf5037273 | J. Agric. Food Chem. 2014, 62, 10744−10751

two anomeric protons at $\delta$ 4.12 (d, $J$ = 7.77 Hz, 1H) and 4.63 (d, $J$ = 3.72 Hz, 1H), which was further supported by the chemical shift at $\delta$ 103.0 and 98.7 in the $^{13}$C NMR spectrum. Analysis of the $^{1}$H−$^{1}$H COSY, HSQC, and HMBC spectra (Figure 2) of compound **2** allowed for the complete assignment of the $^{1}$H and $^{13}$C NMR spectral data. The sequence from an anomeric proton H-1 to oxymethylene proton H-6 through oxymethine protons H-2, H-3, H-4, and H-5, as well as H-7 to H-8, was confirmed by $^{1}$H−$^{1}$H COSY. Similarly, the fragments from H-1′ to H-6′ and from H-7′ to H-8′ were also established. Three sets of mutual key long-range couplings from H-1 to C-7 and from H-7 to C-1, and from H-1′ to C-7′ and from H-7′ to C-1′, as well as from H-2′ to C-4 and from H-4 to C-2′, were observed in the HMBC experiments, indicating that two ethyl groups and another sugar unit in a ring-opening form were connected directly to the C-1, C-1′, and C-4 by ether linkages. The pyranosyl sugar units were identified as a $\beta$-glucopyranosyl group on the basis of its $^{3}J_{\text{H-1,H-2}}$ coupling constant of 7.77 Hz. On the basis of this evidence, the structure of **2** was characterized as shown Figure 3 and trivially named oryzasaccharide A.

Compound **3** was obtained as a white amorphous powder. Its molecular formula was established as $C_{20}H_{40}O_{12}$ by negative HRESIMS $[M - H]^-$ at $m/z$ 471.2451 (calcd 471.2444). The UV spectrum of compound **3** revealed only one strong absorption band at 205 nm. The IR spectrum displayed strong absorption bands at 3420 and 1033 cm$^{-1}$ which are typical of glycosidic-type structures. The 1D NMR data (Table 3) revealed the presence of a fructofuranose, a ring-opening pyranose moiety and two butyl group fragments. The $^{13}$C NMR of **3** revealed the presence of 20 carbon signals, with six of these signals being assigned to the fructofuranose, six to the ring-opening pyranose moiety, and the remaining eight to two butyl ether fragments. The chemical shifts of all of the protons and carbons belonging to these three parts were assigned using a combination of $^{1}$H−$^{1}$H COSY, HSQC, and HMBC analysis (Figure 2). Several key correlations in the HMBC spectra, including correlations from H-7 to C-2, and two mutual long-range couples from H-12 to C-1′ and H-1′ to C-12, and from H-12 to C-1″ and H-1″ to C-12, were observed, indicating that two butyl groups and the ring-opening pyranose moiety were connected directly to the C-1′, C-1″, and C-2 by three ether linkages, respectively. Taken together, these data were indicative of a typical sugar ether structure with unique ring-opening moiety and two butyl groups. Consequently, the structure of **3** was elucidated, as shown in Figure 3 and named oryzasaccharide B (Figure 3).

Compound **4** was isolated as a colorless needle. The molecular formula of the material was determined to be $C_{20}H_{26}O_3$ on the basis of its $^{1}$H and $^{13}$C NMR and ESI-MS data. ESI-MS analysis of the material revealed a peak at $m/z$ 337.2, corresponding to $[M + Na]^+$, indicating that the molecular weight of **4** was 314. The $^{1}$H NMR and $^{13}$C NMR spectra revealed the presence of three tertiary methyls at $\delta$ 0.94 (s, 3H), 1.58 (s, 3H), and 1.04 (s, 3H), three vinylic protons at $\delta$ 5.90 (dd, $J$ = 10.76, 17.48 Hz, 1H), 5.01 (d, $J$ = 17.48 Hz, 1H), and 4.98 (d, $J$ = 10.76 Hz, 1H), one oxygenated methane at $\delta$ 4.89 (t, $J$ = 5.12 Hz, 1H), and one trisubstituted olefinic protons at $\delta$ 5.76 (d, $J$ = 5.00 Hz, 1H), as well as one $\gamma$-lactone carbon at $\delta$ 174.5 and one carbonyl carbon at $\delta$ 205.3 in the molecule. The structure of **4** was further confirmed by the COSY and HMBC correlations (Figure 2) and by comparing the NMR data with those of momilactone A in the literature.[18] Compound **4** was consequently identified as momilactone A (Figure 3).

Compound **5** was isolated as a white amorphous powder. The molecular formula was determined to be $C_9H_{18}O_5$ on the basis of its $^{1}$H NMR, $^{13}$C NMR, and ESI-MS spectra. ESI-MS analysis gave $m/z$ values of 205.1 and 229.1, corresponding to $[M - H]^-$ and $[M + Na]^+$. The $^{1}$H and $^{13}$C NMR spectra of **5** were typical of a sugar ether compound. The $^{13}$C NMR spectrum revealed the presence of nine carbons corresponding to one xylopyranose unit and one butyl group, respectively. Analysis of the $^{1}$H−$^{1}$H COSY, HSQC, and HMBC spectra of compound **5** allowed for the complete assignment of the $^{1}$H and $^{13}$C NMR spectral data. From the $^{1}$H−$^{1}$H COSY spectrum, the molecular fragments from C-1 to C-5 and from C-1′ to C-4′ could be established. Key mutual correlations from H-1 to C-1′ and from H-1′ to C-1 were observed in the HMBC experiments, indicating that the xylopyranose unit and the butyl group were connected by ether linkages. The xylopyranose unit was identified as a $\beta$-xylopyranose group on the basis of its $^{3}J_{\text{H-1,H-2}}$ coupling constant of 6.90 Hz. Based on a comparison of these data with data published in the literature,[19] compound **5** was identified as butyl $\beta$-D-xylopyranose (Figure 3).

Compound **6** was isolated as a white amorphous powder, and its molecular formula was determined to be $C_7H_{14}O_5$ on the basis of its $^{1}$H and $^{13}$C NMR and ESI-MS spectra. ESI-MS analysis of the material gave $m/z$ values of 177.1 and 201.1, corresponding to $[M - H]^-$ and $[M + Na]^+$, respectively. A careful comparison of the $^{1}$H and $^{13}$C NMR spectra of **6** with those of **5** revealed the existence of a close structural relationship between the two compounds. Compared to the spectra of **5**, five ethyoxyl proton signals at $\delta$ 3.51 (m, 2H, H-1′), 1.25 (t, $J$ = 6.87 Hz, 3H, H-2′) in **6** instead of nine butyoxyl proton signals at $\delta$ 3.54 (m, 2H, H-1′), 1.61 (m, 2H, H-2′), 1.38 (m, 2H, H-3′), and 0.93 (t, $J$ = 7.35 Hz, 3H, H-4′) in **5** were observed in the $^{1}$H NMR spectrum. As expected, two methene carbon signals at $\delta$ 31.6 (C-2′) and 19.1 (C-3′) in **5** were missed in the $^{13}$C NMR spectrum of **6**. By a comparison with data available in the literature,[19] compound **6** was determined to be ethyl $\beta$-D-xylopyranose (Figure 3).

Compound **7** was isolated as a white amorphous powder. The molecular formula was determined to be $C_6H_{12}O_5$ on the basis of its $^{1}$H NMR, $^{13}$C NMR, and ESI-MS spectra. ESI-MS analysis gave $m/z$ values of 163.0 and 187.1, corresponding to $[M - H]^-$ and $[M + Na]^+$, respectively. The $^{1}$H and $^{13}$C NMR spectra for **7** and **6** are very similar, with the exception that an ethyoxyl group in **6** was replaced by a methoxy group in **7**. Based on a comparison of these data with information reported in the literature,[19] compound **7** was identified as methyl $\beta$-D-xylopyranose (Figure 3).

**Antioxidant Activities of the Pure Compounds Isolated from Rice Bran.** The antioxidant activities of the seven pure compounds were tested according to their ABTS$^+$ and DPPH radical-scavenging assay. The results of these experiments have been shown in Figure 4 and Figure 5. Only compound **1** showed 98.57% and 77.33% of ABTS$^+$ and DPPH radical-scavenging ability at the concentration of 100 $\mu$M, respectively (Figure 4A,B) and were comparable to that of positive control vitamin C; other compounds were inactive. Based on the data obtained, compound **1** was selected to further determine whether their ABTS$^+$ and DPPH radical-scavenging capacity was in a dose-dependent manner , and the results are shown in Figure 5. The ABTS$^+$ radical-scavenging activities for compound **1** and vitamin C were comparable and

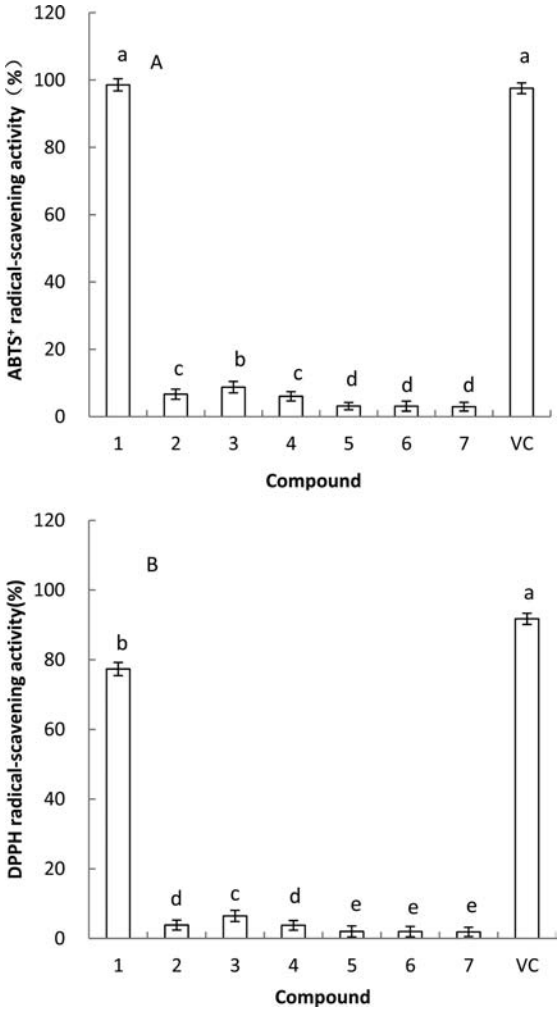


**Figure 4.** ABTS$^+$ radical-scavenging activity (A), DPPH radical-scavenging activity (B) of the isolated compounds. oryzalactam (**1**), oryzasaccharide A (**2**), oryzasaccharide B (**3**), momilactone A (**4**), butyl $\beta$-D-xylopyranose (**5**), ethyl $\beta$-D-xylopyranose (**6**), and methyl $\beta$-D-xylopyranose (**7**). Each value has been presented as the mean ± SD of three experiments. Note: a−e, results with a different letter differ significantly ($p < 0.05$).

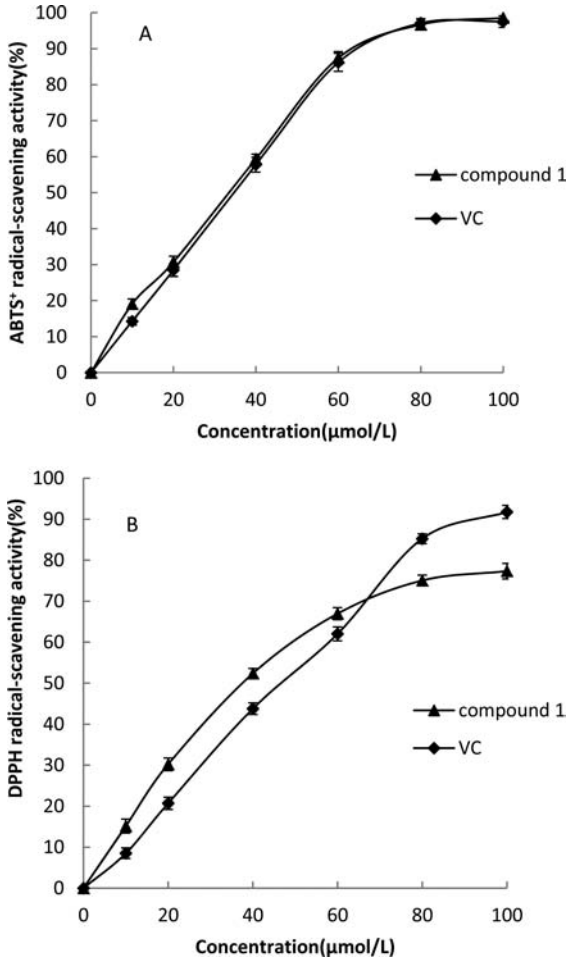


**Figure 5.** ABTS$^+$ radical-scavenging activity (A) and DPPH radical-scavenging activity (B) of compound **1** under different concentrations.

increased sharply with increasing concentration in a dose-dependent manner at the range of 0−80 $\mu$M, increased to maximal values of 96.70% and 97.10% ABTS$^+$ inhibitory effect at the concentration of 80 $\mu$M, and then were kept constant, and their $IC_{50}$ values were 33.38 ± 1.58 and 34.70 ± 1.19 $\mu$M, respectively. The results suggested that the ABTS$^+$ radical-scavenging activity of compound **1** was almost identical to that of vitamin C. Similarly, as shown in Figure 4B and Figure 5B, compound **1** and vitamin C showed antioxidant activity profiles that resembled one another and a dose-dependent manner in DPPH scavenging-radical assay, and their $IC_{50}$ values were 40.2 ± 1.34 and 47.59 ± 1.41 $\mu$M, respectively, indicating that the DPPH scavenging-radical activity of compound **1** was slightly weaker than that of Vitamin C.

**Antimicrobial Bioassay.** Seven pure compounds were tested for their antimicrobial activities against eight pathogenic strains. Only compound **4** exhibited a significant inhibition zone against *E. coli* with a MIC value of 5 $\mu$M, indicating that compound **4** possessed high levels of selectivity toward *E. coli*. All of the other compounds isolated were found to be inactive.

**NMR and ESI-MS Spectroscopic Data.** Oryzalactam (**1**). Yellow amorphous powder. $^1$H NMR and $^{13}$C NMR data, see Table 1. ESI-MS $m/z$ 260.0542 $[M + Na]^+$.

Oryzasaccharide A (**2**). White amorphous powder. $^1$H NMR and $^{13}$C NMR data, see Table 2. ESI-MS $m/z$ 415.1826 $[M - H]^-$.

Oryzasaccharide B (**3**). White amorphous powder. $^1$H NMR and $^{13}$C NMR data, see Table 3. ESI-MS $m/z$ 471.2451 $[M - H]^-$.

Momilactone A (**4**). Colorless needles. $^1$H NMR (400 MHz, $CDCl_3$, TMS): $\delta$ 5.90 (dd, $J$ = 10.76, 17.48 Hz, 1H, H-15), 5.76 (d, $J$ = 5.00 Hz, 1H, H-7), 5.01 (d, $J$ = 17.48 Hz, 1H, H-16b), 4.98 (d, $J$ = 10.76 Hz, 1H, H-16a), 4.89 (t, $J$ = 5.12 Hz, 1H, H-6), 2.67 (m, 2H, H-2), 2.37 (d, $J$ = 5.08 Hz, 1H, H-5), 2.26 (d, $J$ = 12.04 Hz, 1H, H-14b), 2.11 (d, $J$ = 12.04 Hz, 1H, H-14a), 1.84 (m, 1H, H-9), 1.78 (m, 2H, H-11), 1.66 (m, 2H, H-1),1.60 (m, 2H, H-12), 1.58 (s, 3H, H-18), 1.04 (s, 3H, H-20), 0.94 (s, 3H, H-17); $^{13}$C NMR: $\delta$ 31.4 (C-1), 35.0 (C-2), 205.3 (C-3), 53.7 (C-4), 46.5 (C-5), 73.1 (C-6), 114.1 (C-7), 148.9 (C-8), 50.3 (C-9), 32.6 (C-10), 24.1 (C-11), 37.4 (C-12), 40.3 (C-13), 47.7 (C-14), 149.1 (C-15), 110.3 (C-16), 22.1 (C-17), 21.4 (C-18), 174.5 (C-19), 21.9 (C-20). ESI-MS $m/z$ 337.2 $[M + Na]^+$.

Butyl $\beta$-D-xylopyranose (**5**). Colorless amorphous powder. $^1$H NMR (500 MHz, $CDCl_3$, TMS): $\delta$ 4.28 (d, $J$ = 6.90 Hz, 1H, H-1), 3.98 (m, 1H, H-5a), 3.85 (m, 1H, H-4), 3.54 (m, 2H, H-1′), 3.53 (m, 1H, H-3), 3.41 (m, 1H, H-2), 3.28 (m, 1H, H-5b),


dx.doi.org/10.1021/jf5037273 | J. Agric. Food Chem. 2014, 62, 10744−10751

Table 1. NMR Spectral Data for Compound 1 in DMSO-$d_6$ at 400 ($^1$H) and 100 MHz ($^{13}$C)

| position | $H$ ($J$, Hz) | HSQC | HMBC (H→C) | $^1$H–$^1$H COSY |
|---|---|---|---|---|
| 1 | 6.59 (d, $J$ = 1.44 Hz, 1H) | 115.5 | C-3, C-4, C-5 | |
| 2 | | 152.8 | | |
| 2-OH | 9.01 (s, 1H) | | C-2, C-3, C-4 | |
| 3 | 6.77 (t, $J$ = 1.44 Hz, 1H) | 112.5 | C-1, C-2, C-4, C-5 | H-4 |
| 4 | 6.59 (d, $J$ = 1.44 Hz, 1H) | 110.3 | C-1, C-2, C-3, C-5 | |
| 5 | | 73.5 | | |
| 6 | 6.07 (s, 1H) | | C-1, C-8, C-10 | |
| 7 | | 178.1 | | |
| 8 | 2.91 (d, $J$ = 4.32 Hz, 2H) | 41.9 | C-7, C-10, C-11 | |
| 9 | | 134.5 | | |
| 10 | | 132.3 | | |
| 10-OH | 10.01 (s, 1H) | | C-1, C-10, C-9 | |
| 11 | | 169.5 | | |
| 12 | 3.42 (s, 3H) | 51.6 | C-11 | |

Table 2. NMR Spectral Data for Compound 2 in DMSO-$d_6$ at 400 ($^1$H) and 100 MHz ($^{13}$C)

| position | $H$ ($J$, Hz) | HSQC | HMBC (H→C) | $^1$H–$^1$H COSY |
|---|---|---|---|---|
| 1 | 4.12 (d, $J$ = 7.77 Hz, 1H) | 103.0 | C-3, C-7 | H-2 |
| 2 | 2.92 (m, 1H) | 73.8 | C-1, C-3 | |
| 2-OH | 4.91 (d, $J$ = 4.83 Hz, 1H) | | C-1, C-2, C-3 | H-2 |
| 3 | 3.04 (m, 1H) | 77.2 | | H-2 |
| 3-OH | 4.80 (d, $J$ = 5.40 Hz, 1H) | | C-3, C-4 | H-3 |
| 4 | 3.06 (m, 1H) | 70.5 | | H-3 |
| 5 | 3.39 (m, 1H) | 73.8 | | H-4 |
| 6 | 3.62 (m, 1H), 3.43 (m, 1H) | 61.5 | C-4, C-5 | H-5 |
| 6-OH | 4.40 (m, 1H) | | C-6 | H-6 |
| 7 | 3.81 (m, 1H), 3.52 (m, 1H) | 64.2 | C-1 | H-8 |
| 8 | 1.14 (m, 3H) | 15.5 | C-7 | |
| 1′ | 4.63 (d, $J$ = 3.72 Hz, 1H) | 98.7 | C-2′, C-7′ | H-2′ |
| 1′-OH | 4.56 (d, $J$ = 6.36 Hz, 1H) | | C-1′, C-2′ | H-1′ |
| 2′ | 3.17 (m, 1H) | 72.4 | C-2′, C-3′ | |
| 3′ | 3.40 (m, 1H) | 73.1 | C-2′, C-3′, C-4′ | H-2′, H-4′ |
| 3′-OH | 4.66 (d, $J$ = 4.68 Hz, 1H) | | C-3′, C-4′ | H-3′ |
| 4′ | 3.04 (m, 1H) | 70.9 | | |
| 4′-OH | 4.63 (m, 1H) | | C-3′, C-4′, C-5′ | H-4′ |
| 5′ | 3.12 (m, 1H) | 77.2 | | H-4′ |
| 5′-OH | 4.86 (d, $J$ = 5.04, 7.59 Hz, 1H) | | C-4′, C-5′ | H-5′ |
| 6′ | 3.43 (m, 1H), 3.62 (m, 1H) | 61.5 | | H-5′ |
| 6′-OH | 4.40 (m, 1H) | | C-6′ | H-6′ |
| 7′ | 3.40 (m, 1H), 3.64 (m, 1H) | 62.7 | C-1′ | H-8′ |
| 8′ | 1.14 (m, 3H) | 15.6 | C-7′ | |

1.61 (m, 2H, H-2′), 1.38 (m, 2H, H-3′), 0.93 (t, $J$ = 7.35 Hz, 3H, H-4′). $^{13}$C NMR: $\delta$ 102.9 (C-1), 72.9 (C-2), 76.0 (C-3), 69.6 (C-4), 64.9 (C-5), 69.7 (C-1′), 31.6 (C-2′), 19.1 (C-3′), 13.8(C-4′). ESI-MS $m/z$ 205.1 $[M - H]^-$, 229.1 $[M + Na]^+$.

Ethyl $\beta$-D-xylopyranose (**6**). Colorless amorphous powder. $^1$H NMR (300 MHz, $CDCl_3$, TMS): $\delta$ 4.28 (d, $J$ = 6.84 Hz, 1H, H-1), 4.19 (m, 1H, H-5a), 3.94 (m, 1H, H-4), 3.51 (m, 2H, H-1′), 3.50 (m, 1H, H-3), 3.38 (m, 1H, H-2), 3.26 (m, 1H, H-5b), 1.25 (t, $J$ = 6.87 Hz, 3H, H-2′). $^{13}$C NMR: $\delta$ 102.9 (C-1), 72.9 (C-2), 76.0 (C-3), 69.6 (C-4), 65.4 (C-5), 65.3 (C-1′), 15.1 (C-2′). ESI-MS $m/z$ 177.1 $[M - H]^-$, 201.1 $[M + Na]^+$.

Methyl $\beta$-D-xylopyranose (**7**). Colorless amorphous powder. $^1$H NMR (300 MHz, DMSO-$d_6$, TMS): $\delta$ 3.99(d, $J$ = 7.5 Hz, 1H, H-1), 3.70 (m, 1H, H-5a), 3.41 (m, 1H, H-4), 3.34 (s, 3H, 1-$OCH_3$), 3.30 (m, 1H, H-3), 3.01 (m, 1H, H-2), 2.94 (m, 1H, H-5b). $^{13}$C NMR: $\delta$ 105.2 (C-1), 73.7 (C-2), 77.0 (C-3), 70.1 (C-4), 66.1 (C-5), 56.4 (C-1′). ESI-MS $m/z$ 163.0 $[M - H]^-$, 187.1 $[M + Na]^+$.

An investigation of the methanol extract of rice bran allowed for the isolation of a new screw lactam and two new oligosaccharide derivatives, oryzalactam (**1**), oryzasaccharide A (**2**), and oryzasaccharide B (**3**), as well as four known compounds, including momilactone A (**4**), butyl $\beta$-D-xylopyranose (**5**), ethyl $\beta$-D-xylopyranose (**6**), and methyl $\beta$-D-xylopyranose (**7**), and the structures of all seven of these compounds were elucidated using a combination of spectroscopic methods. To the best of our knowledge, this is the first report concerning the isolation of compounds **1**, **2**, **3**, **5**, **6**, and **7** from rice bran.

Oryzalactam is a new screw lactam and extremely rare. To date, there are no compounds with this particular skeleton have been isolated from natural sources. This compound exhibited strong antioxidant activity against $ABTS^+$ and DPPH radical and might represent a new potential natural antioxidant agent.


dx.doi.org/10.1021/jf5037273 | J. Agric. Food Chem. 2014, 62, 10744−10751

Table 3. NMR Spectral Data for Compound 3 in Methanol-$d_4$ at 400 ($^1$H) and 100 MHz ($^{13}$C)

| position | $H$ ($J$, Hz) | HSQC | HMBC (H→C) | $^1$H–$^1$H COSY |
|---|---|---|---|---|
| 1 | 3.50 (m, 1H), 3.67 (m, 1H) | 60.8 | C-2, C-3 | |
| 2 | | 103.7 | | |
| 3 | 4.13 (d, $J$ = 8.08 Hz, 1H) | 77.0 | | H-4 |
| 4 | 3.94 (t, $J$ = 7.72 Hz, 1H) | 75.9 | C-3, C-5, C-6 | H-5 |
| 5 | 3.75 (m, 1H) | 81.9 | C-4, C-6 | |
| 6 | 3.60 (m,1H) | 63.6 | C-4, C-5 | H-5 |
| | 3.75 (m, 1H) | | | |
| 7 | 3.70 (t, $J$ = 2.80 Hz, 1H) | 61.3 | C-2, C-8, C-9 | H-8 |
| | 3.80 (d, $J$ = 2.36 Hz, 1H) | | | |
| 8 | 3.60 (m, 1H) | 72.2 | | H-9 |
| 9 | 3.30 (d, $J$ = 9.64 Hz, 1H) | 70.4 | C-7, C-8, C-10, C-11 | |
| 10 | 3.66 (dd, $J$ = 3.20, 5.76 Hz, 1H) | 73.7 | C-8, C-12 | H-11 |
| 11 | 3.40 (dd, $J$ = 3.76, 9.68 Hz, 1H) | 72.2 | | |
| 12 | 4.79 (d, $J$ = 3.72 Hz, 1H) | 98.6 | C-10, C-11, C-1′, C-1″ | H-11 |
| 1′ | 3.77 (m, 2H) | 67.4 | C-2′, C-3′, C-12 | H-2′ |
| 2′ | 1.65 (m, 2H) | 31.3 | C-1′ | H-3′ |
| 3′ | 1.45 (m, 2H) | 19.0 | C-1′, C-2′, C-4′ | H-4′ |
| 4′ | 0.97 (m, 3H) | 12.8 | C-2′ | |
| 1″ | 3.46 (m, 2H) | 67.4 | C-2″, C-3″, C-12 | H-2″ |
| 2″ | 1.65 (m, 2H) | 32.0 | C-1″ | H-3″ |
| 3″ | 1.45 (m, 2H) | 18.9 | C-1″, C-2″, C-4″ | H-4″ |
| 4″ | 0.97 (m, 3H) | 12.9 | C-2″ | |

It is worth mentioning, however, the bioactivities of this compound *in vitro* are not necessarily equal to its actual beneficial effects on human health. It is determined by the bioaccessibility and bioavailability of the compound *in vivo* where it is commonly mixed with different macromolecules such as carbohydrates, lipids, and proteins to form the food matrix.[20] Several factors interfere with the real effects of a compound, such as food source and chemical interactions with other phytochemicals and biomolecules present in the food matrix. Therefore, research concerning the bioaccessibility and bioavailability of a compound from rice bran are important, since a compound is only released from the food matrix by the action of digestive enzymes in the small intestine or bacterial microflora in the large intestine and then can be absorbed to exert their beneficial effects.[2] Oryzasaccharides A and B and the three other known compounds are carbohydrate derivatives with a diverse side chain. It has been reported that rice bran contains about 6.5% free sugars on a dry-weight basis, more than 50% of the sugar being simple saccharides (mainly glucose and sucrose); therefore, the current research indicated that the free sugar in the rice bran might exist in more complex forms. Momilactone A obtained in this study is one of the diterpenoid phytoalexins and originally isolated from the seed husk of rice. So far, three momilactones members (momilactone A–C) have been found from rice in all.[21,22] It has been reported that momilactones are accumulated in rice during vegetative growth and are released into the soil, causing growth inhibition of neighboring plants, and responding to UV irradiation and pathogenesis such as fungal invasion, suggesting that momilactones in rice also play a role in plant defense.[23,24]

In summary, the current study has effectively demonstrated that various compounds with antioxidant and antimicrobial activities are present in rice bran. Oryzalactam, in particular, has been identified as a new screw lactam and showed strong antioxidant activities. The results of the current study represent a useful addition to understanding the potential application and health benefits of rice bran and confirming the interesting potential of rice bran as natural antioxidant to the food industry, as well as enhancing our better understanding of the relationships between the individual component and human health in rice bran. Further studies should be carried out to assess the bioactivities to validate the real effects of the compounds on the prevention and therapy of some chronic human diseases in future, especially on antioxidant activities of the compounds isolated, e.g., bioaccessibility, bioavailability, and enrichment for developing a food by using these compounds, as well as possibilities of interactions with other biomolecules.

## AUTHOR INFORMATION


### Corresponding Author

*Tel./Fax: +86 25 8439 5618. E-mail: xzhfood@njau.edu.cn.



### Funding

This work was financially supported by the Fundamental Research Funds for the Central Universities (Grant KYZ201118), the Project of National Key Technology Research and Development Program for the 12th Five-year Plan (Grant 2012BAD33B10), the special funds of agro-product quality safety risk assessment of Ministry of Agriculture of the People's Republic of China (Grant 2014FP11), and a project funded by the Priority Academic Program Development of Jiangsu Higher Education Institution.


### Notes

The authors declare no competing financial interest.

## REFERENCES


(1) Li, P.; Feng, X.; Qiu, G. Methylmercury exposure and health effects from rice and fish consumption: A review. *Int. J. Environ. Res. Public Health* **2010**, *7*, 2666–2691.

(2) Ti, H.; Li, Q.; Zhang, R.; Zhang, M.; Deng, Y.; Wei, Z.; Chi, J.; Zhang, Y. Free and bound phenolic profiles and antioxidant activity of milled fractions of different indica rice varieties cultivated in southern China. *Food Chem.* **2014**, *159*, 166–174.

(3) Saxena, M.; Mir, A. H.; Sharma, M.; Malla, M. Y.; Qureshi, S.; Mir, M. I.; Chaturvedi, Y. Phytochemical screening and in-vitro antioxidant activity isolated bioactive compounds from Tridax procumbens Linn. *Pak. J. Biol. Sci.* **2013**, *16*, 1971−1977.
(4) Xu, Z.; Hua, N.; Godber, J. S. Antioxidant activity of tocopherols, tocotrienols, and γ-oryzanol components from rice bran against cholesterol oxidation accelerated by 2, 2′-azobis (2-methylpropionamidine) dihydrochloride. *J. Agric. Food Chem.* **2001**, *49*, 2077−2081.
(5) Rogers, E.; Rice, S.; Nicolosi, R.; Carpenter, D.; McClelland, C.; Romanczyk, L., Jr. Identification and quantitation of γ-oryzanol components and simultaneous assessment of tocols in rice bran oil. *J. Am. Oil Chem. Soc.* **1993**, *70*, 301−307.
(6) Zullaikah, S.; Lai, C.-C.; Vali, S. R.; Ju, Y.-H. A two-step acid-catalyzed process for the production of biodiesel from rice bran oil. *Bioresour. Technol.* **2005**, *96*, 1889−1896.
(7) Dunford, N.; King, J. Phytosterol enrichment of rice bran oil by a supercritical carbon dioxide fractionation technique. *J. Food Sci.* **2000**, *65*, 1395−1399.
(8) Butsat, S.; Siriamornpun, S. Antioxidant capacities and phenolic compounds of the husk, bran and endosperm of Thai rice. *Food Chem.* **2010**, *119*, 606−613.
(9) Qureshi, A. A.; Sami, S. A.; Khan, F. A. Effects of stabilized rice bran, its soluble and fiber fractions on blood glucose levels and serum lipid parameters in humans with diabetes mellitus Types I and II. *J. Nutr. Biochem.* **2002**, *13*, 175−187.
(10) Henderson, A. J.; Ollila, C. A.; Kumar, A.; Borresen, E. C.; Raina, K.; Agarwal, R.; Ryan, E. P. Chemopreventive properties of dietary rice bran: Current status and future prospects. *Adv. Nutr.* **2012**, *3*, 643−653.
(11) Liu, R. H. Whole grain phytochemicals and health. *J. Cereal Sci.* **2007**, *46*, 207−219.
(12) Ferguson, L.; Harris, P. Protection against cancer by wheat bran: Role of dietary fibre and phytochemicals. *Eur. J. Cancer Prev.* **1999**, *8*, 17−26.
(13) Tham, D. M.; Gardner, C. D.; Haskell, W. L. Potential Health Benefits of Dietary Phytoestrogens: A Review of the Clinical, Epidemiological, and Mechanistic Evidence. *J. Clin. Endocrinol. Metab.* **1998**, *83*, 2223−2235.
(14) Miller, N. J.; Rice-Evans, C. A. Factors influencing the antioxidant activity determined by the $ABTS^{+}$ radical cation assay. *Free Radical Res.* **1997**, *26*, 195−199.
(15) Mensor, L. L.; Menezes, F. S.; Leitão, G. G.; Reis, A. S.; Santos, T. C. d.; Coube, C. S.; Leitão, S. G. Screening of Brazilian plant extracts for antioxidant activity by the use of DPPH free radical method. *Phytother. Res.* **2001**, *15*, 127−130.
(16) Mahakunakorn, P.; Tohda, M.; Murakami, Y.; Matsumoto, K.; Watanabe, H. Antioxidant and free radical-scavenging activity of Choto-san and its related constituents. *Biol. Pharm. Bull.* **2004**, *27*, 38−46.
(17) Wang, X.; Wang, H.; Liu, T.; Xin, Z. A PKS I gene-based screening approach for the discovery of a new polyketide from Penicillium citrinum Salicorn 46. *Appl. Microbiol. Biotechnol.* **2014**, *98*, 4875−4885.
(18) Nozaki, H.; Hayashi, K.-i.; Nishimura, N.; Kawaide, H.; Matsuo, A.; Takaoka, D. Momilactone A and B as allelochemicals from moss Hypnum plumaeforme: first occurrence in bryophytes. *Biosci., Biotechnol., Biochem.* **2007**, *71*, 3127−3130.
(19) Jiang, Z.; Zhu, Y.; Li, L.; Yu, X.; Kusakabe, I.; Kitaoka, M.; Hayashi, K. Transglycosylation reaction of xylanase B from the hyperthermophilic Thermotoga maritima with the ability of synthesis of tertiary alkyl beta-D-xylobiosides and xylosides. *J. Biotechnol.* **2004**, *114*, 125−134.
(20) Palafox-Carlos, H.; Ayala-Zavala, J. F.; Gonzalez-Aguilar, G. A. The role of dietary fiber in the bioaccessibility and bioavailability of fruit and vegetable antioxidants. *J. Food Sci.* **2011**, *76*, R6−R15.
(21) Kato-Noguchi, H.; Ino, T. Concentration and release level of momilactone B in the seedlings of eight rice cultivars. *J. Plant Physiol.* **2005**, *162*, 965−969.
(22) Liu, N.; Wang, S.; Lou, H. A new pimarane-type diterpenoid from moss Pseudoleskeella papillosa (Lindb.) Kindb. *Acta Pharm. Sin. B* **2012**, *2*, 256−259.
(23) Kato-Noguchi, H.; Ino, T. Possible involvement of momilactone B in rice allelopathy. *J. Plant Physiol.* **2005**, *162*, 718−721.
(24) Kodama, O.; Suzuki, T.; Miyakawa, J.; Akatsuka, T. Ultraviolet-induced accumulation of phytoalexins in rice leaves. *Agric. Biol. Chem.* **1988**, *52*, 2469−2473.

## MATERIALS AND METHODS

**Cells and Chemicals.** Human prostate cancer LNCaP, VCaP, and CWR22Rv1cells were obtained from the ATCC (Rockville, MD, U.S.A.). α-T, γ-T and δ-T were from Sigma Co. (St. Louis, MO, U.S.A.). A mixture of tocopherol γ-TmT was purchased from the Cogns Corp. (Cincinnati, OH, U.S.A.). The extracellular matrix Matrigel was obtained from Corning Co. (Tewksbury, MA, U.S.A.). The various human prostate cancer cells were maintained in RPMI-1640 culture medium as described in our earlier study.[17]

**Cell Viability.** Cell viability was determined by the trypan blue exclusion assay. At the end of the experiments, the cells were trypsinized. Trypan blue solution (0.4%) was mixed with cell suspension in a ratio of 1:4, and the mixtures were kept at room temperature for 2 min for the cells to be stained with the dye. The number of viable cells was counted under a microscope (Nikon Optiphot, Tokyo, Japan). Cells absorbed the dye were counted as dead cells. The cells that did not absorb the dye were counted as live cells.[18]

**Determination of Apoptosis.** Apoptotic cells were identified in propidium iodide (PI) stained cells by morphology.[19] At the end of the experiment, cells were spined to slides using a Shandon cytospin centrifuge (Thermo Scientific, Waltham, MA, U.S.A.) and fixed in a solution containing 50% acetone and 50% methanol. The cells were then stained with PI at a concentration of 1 μg/mL. A microscope (Nikon Optiphot, Tokyo, Japan) was used to identified apoptotic cells according to the morphological changes characteristic of apoptosis as described earlier.[19]

**Western Blotting.** After treatment, the cell lysates were prepared as described earlier.[20] Proteins were subjected to sodium dodecyl sulfate polyacrylamide gel electrophoresis (SDS-PAGE) and transferred to nitrocellulose membrane. After blocking nonspecific binding sites with blocking buffer, the membrane was incubated overnight at 4 °C with PSA primary antibody (CBL-252, Millipore Co, Billerica, MA, U.S.A.). The β-actin was used as a loading control. Following removal of the primary antibody, the membrane was washed three times with TBS (PBS containing 0.05% tween 20) buffer at room temperature and then incubated with fluorochrome-conjugated secondary antibody (Santa Cruz Biotechnology Inc., CA, U.S.A.). The membrane was then washed with TBS three times. Final detection was done with an Odyseey infrared imaging system (Li-Cor Biotechnology, Lincoln, NE, U.S.A.).

**AR Luciferase Reporter Assay.** The CWR-22Rv1/AR cell line that stably expresses the AR-luciferase reporter gene was used in the present study.[21] CWR-22Rv1/AR cells were treated with dihydrotestosterne (DHT), α-T and δ-T for 24 h. After treatment, the cells were harvested in a reporter lysis buffer and the luciferase activities were measured using luciferase assay kits from Promega (Madison, WI, U.S.A.), as described in our recent study.[21]

**Subcutaneous LNCaP Tumors in SCID Mice.** SCID mice originally obtained from Taconic Farms (Germantown, NY, U.S.A.) were bred in the animal facility in the Susan Lehman Cullman Laboratory for Cancer Research. Eight-week old SCID mice were housed in microisolator cages. Human prostate cancer LNCaP cells ($2.0 \times 10^6$ cells/mouse) were suspended in culture medium and Matrigel (1:1) and injected subcutaneously into the back of the animals.[22] The mice were randomly assigned to 3 experimental groups in the same day of the tumor cell injection. Group 1 was the control and the mice in this group were fed AIN 93 M diet. Mice in group 2 received AIN 93 M diet containing 0.3% α-T. Mice in group 3 were fed 0.3% δ-T in AIN 93 M diet. There were 10 animals in each experimental group. The experimental duration was 48 days. The mice were examined every day for the formation of subcutaneous tumors. When the subcutaneous tumor formed, tumor length and tumor width were measured once every third day and calculated as tumor size (length × width, $cm^2$). The animal experiment was carried out under the Rutgers University Institutional Animal Care and Use Committee (IACUC)-approved protocol (RU02-001).

**Tumor Cell Proliferation and Apoptosis.** Proliferation of LNCaP tumor cell was measured by determining the number of mitotic cells, and apoptosis of the tumor cells was assessed by immunohistochemical staining for activated caspase-3. At the end of the experiment, tumors were excised from each mouse and weighted. Tumor tissues were fixed in buffered formalin for 24 h and then with ethanol for 48 h. Paraffin blocks of tumor tissues were prepared and paraffin sections of tumor tissues were processed for H&E staining. A microscope (Nikon Optiphot, Tokyo, Japan) was used to examine the tumor sections for mitotic cells. Activated caspase-3 was determined immunohistochemically using an anti activated caspase-3 antibody (#AF835, R&D Systems Ltd., Minneapolis, MN). Immunohistochemical staining was performed as described earlier.[23] The number of cells with positive staining of activated caspase-3 was counted and expressed as % caspase-$3^+$ cells.

**Statistical Analyses.** We used ANOVA (analysis of variance) and multiple comparison (Tukey-Kramer test) to perform statistical analyses in the present study. Differences in cell viability, apoptosis and AR activity in cells from different treatment groups were analyzed. Differences in tumor size and body weight between different treatment group in the in vivo study were also analyzed.

## RESULTS

**Effects of Different Tocopherols on Growth and Apoptosis of Human Prostate Cancer Cells.** In initial studies, the effects of α-T, γ-T, δ-T, and γ-TmT on growth and apoptosis in human prostate cancer LNCaP cells were determined. As shown in Figure 1A, the different tocopherols dose-dependently inhibited the growth of cultured LNCaP cells. δ-T had a stronger inhibitory effect on the growth of LNCaP cells than the other tocopherols (Figure 1A). Additional experiments showed that treatment of LNCaP

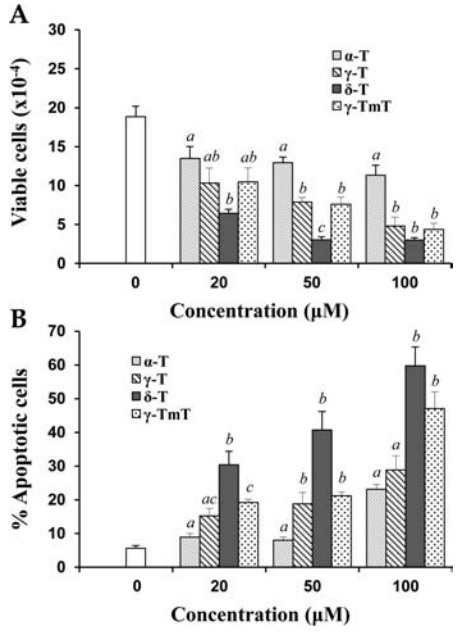


**Figure 1.** Inhibition of growth and induction of apoptosis in LNCaP cells by α-T, γ-T, δ-T, and γ-TmT. Human prostate cancer LNCaP cells ($0.5 \times 10^5$ cells/mL) were seeded in RPMI medium with 10% FBS and incubated 24 h to allow the cells attach to the dish. Then the cells were cultured in medium containing 1% FBS and treated with various concentrations of α-T, γ-T, δ-T, or γ-TmT. The treatment time was 96 h. The trypan blue exclusion assay was used to determine cell viability. Number of viable cells after treatment is shown in (A). Morphological assessment of PI-stained cells was used to determine apoptosis and the number of apoptotic cells is shown in (B). Different superscripts (*a*, *b*, and *c*) indicate statistical differences in the number of viable cells or percent apoptotic cells among different tocopherol isoforms ($p < 0.05$).

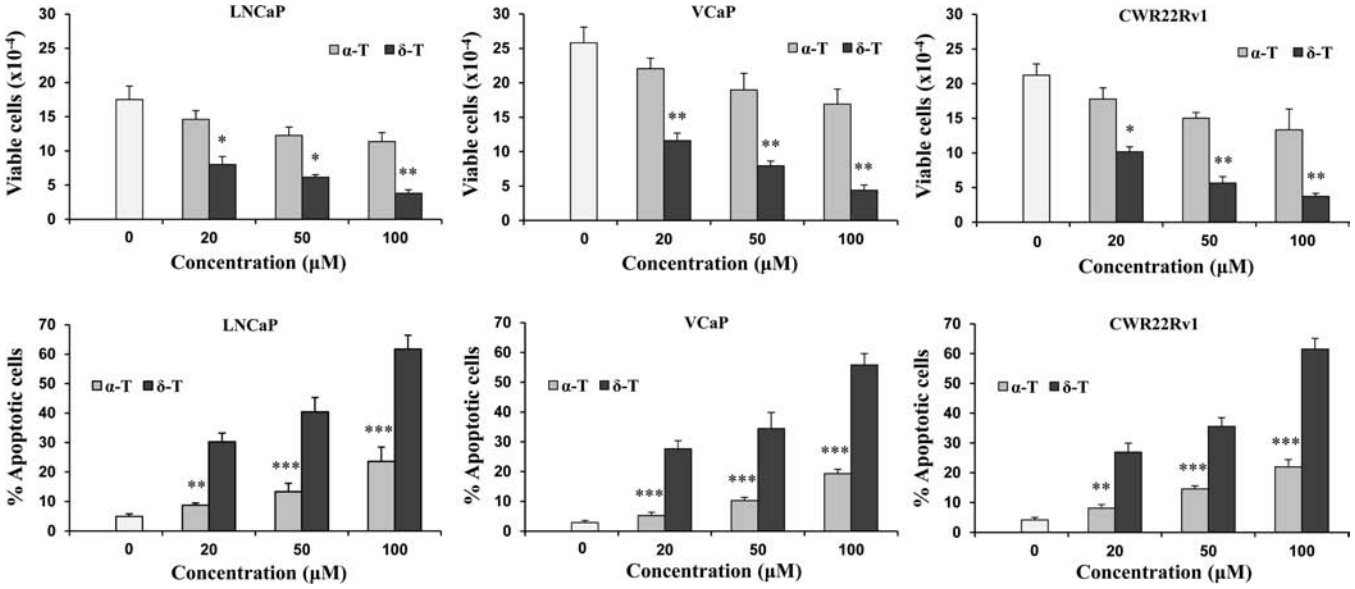


**Figure 2.** Effects of $\alpha$-T and $\delta$-T on growth (upper panel) and apoptosis (lower panel) of cultured human prostate cancer cells. LNCaP, VCaP, and CWR22Rv1 cells (all at $0.5 \times 10^5$ cells/mL) were seeded in RPMI medium containing 10% FBS. After 24 h incubation, the cells were cultured in medium containing 1% FBS and treated with $\alpha$-T or $\delta$-T. The treatment time was 96 h. Graphs in the upper panel show the number of viable cells as determined by the trypan blue exclusion assay. Graphs in the lower panel show the number of apoptotic cells determined by morphological assessment. Differences for the number of viable or apoptotic cells between the $\alpha$-T-treated group and the $\delta$-T-treated group at different concentrations were statistically analyzed. $^*p < 0.05$, $^{**}p < 0.01$, and $^{***}p < 0.001$.

cells with different tocopherols resulted in a concentration-dependent increase in apoptosis. As shown in Figure 1B, $\delta$-T had a more potent effect on inducing apoptosis in LNCaP cells than other tocopherols.

Since $\delta$-T had stronger effects on growth inhibition and apoptosis induction than other tocopherols tested, we subsequently determined the effects of $\delta$-T on different prostate cancer cells and compared its effects with $\alpha$-T, the most common form of vitamin E. As shown in the upper panel of Figure 2, treatment with $\delta$-T and $\alpha$-T inhibited the growth of cultured LNCaP, VCaP, and CWR22Rv1 prostate cancer cells in a dose-dependent manner. $\delta$-T had a stronger inhibitory effect on the growth of all three prostate cancer cell lines than $\alpha$-T (upper panel of Figure 2). Treatment of different prostate cancer cells with $\alpha$-T and $\delta$-T also induced apoptosis in a dose-dependent manner. As shown in the lower panel of Figure 2, $\delta$-T had a more potent effect on induction of apoptosis in different prostate cancer cells than $\alpha$-T.

**Effects of $\delta$-T and $\alpha$-T on AR Activity in CWR-22Rv1/AR Cells.** The effects of $\delta$-T and $\alpha$-T on AR activation was determined using the AR-luciferase reporter gene expression assay. AR activity in CWR-22Rv1/AR cells was stimulated by treatment with DHT and the inhibitory effect of $\delta$-T and $\alpha$-T on DHT-induced AR activation was determined. As shown in Figure 3, treatment with $\alpha$-T and $\delta$-T dose-dependently inhibited DHT-induced AR activation in CWR-22Rv1/AR cells. A stronger inhibitory effect of $\delta$-T on AR activation than $\alpha$-T was observed (Figure 3).

**Effects of $\delta$-T and $\alpha$-T on the Level of PSA in CWR-22Rv1 and LNCaP Cells.** To investigate whether decrease in AR activity by tocopherols leads to inhibition of AR signaling, we determined the level of PSA which is a down stream target of the AR signaling pathway. Treatment of CWR-22Rv1 and LNCaP cells with DHT caused an increase in the level of PSA (Figure 4). Treatment of the cells with $\delta$-T strongly inhibited the DHT-induced increase in PSA while $\alpha$-T only had small to

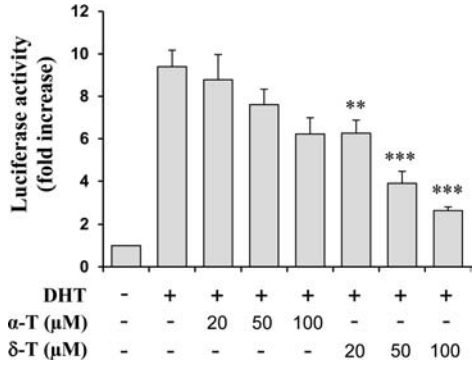


**Figure 3.** Effect of $\alpha$-T and $\delta$-T on AR reporter activity in CWR-22Rv1/AR cells. CWR-22Rv1/AR cells were seeded at a density of $0.5 \times 10^5$ cells/mL of medium for 24 h. The medium was then changed to RPMI supplemented with 1% FBS, and the cells were treated with vehicle (control), with DHT (10 nM) alone or in combination with $\alpha$-T or $\delta$-T (20, 50, or 100 $\mu$M) for 24 h. The luciferase activity and protein concentration of the CWR-22Rv1/AR cells were measured. Each value represents the mean ± SE from three separate experiments. Differences for the relative luciferase activities between the $\alpha$-T-treated group and the $\delta$-T-treated group were analyzed by ANOVA with the Tukey-Kramer Multiple Comparison Test $^{**}p < 0.01$, $^{***}p < 0.001$.

moderate effects (Figure 4). The Western blots were analyzed by optical density measurement and normalized for actin. In the Western blot with LNCaP cells, the level of PSA relative to control (1.00) was 1.97 ± 0.12 in cells treated with DHT, 1.46 ± 0.09 in cells treated with DHT + $\alpha$-T and 0.91 ± 0.08 in cells treated with DHT + $\delta$-T. In the Western blot with CWR22Rv1 cells, the relative level of PSA was 1.00 in control, 2.01 ± 0.15 in cells treated with DHT, 1.02 ± 0.05 in cells treated with DHT + $\alpha$-T and 0.48 ± 0.06 in cells treated with DHT + $\delta$-T. Statistical analysis showed that the differences for density measurement between DHT + $\alpha$-T and DHT + $\delta$-T groups are statistically significant ($p < 0.01$) in both LNCaP and

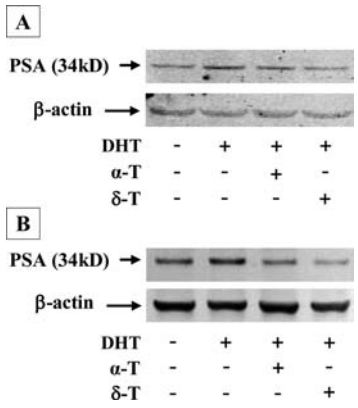


**Figure 4.** Effect of $\alpha$-T and $\delta$-T on the level of PSA in prostate cancer cells. CWR-22Rv1 and LNCaP cells were seeded at a density of $1 \times 10^5$ cells/mL of medium in 100 mm culture dishes (10 mL/dish) and incubated for 24 h. The medium was changed to RPMI supplemented with 1% FBS, and the cells were then treated with vehicle, with 10 nM DHT alone or together with $\alpha$-T (50 $\mu$M) or $\delta$-T (50 $\mu$M) for 48 h. PSA was determined by the Western blot analysis with anti-PSA antibody. The extent of protein loading was determined by blotting for $\beta$-actin. Representative blots for LNCaP (A) and CWR22Rv1 (B) cells are shown.

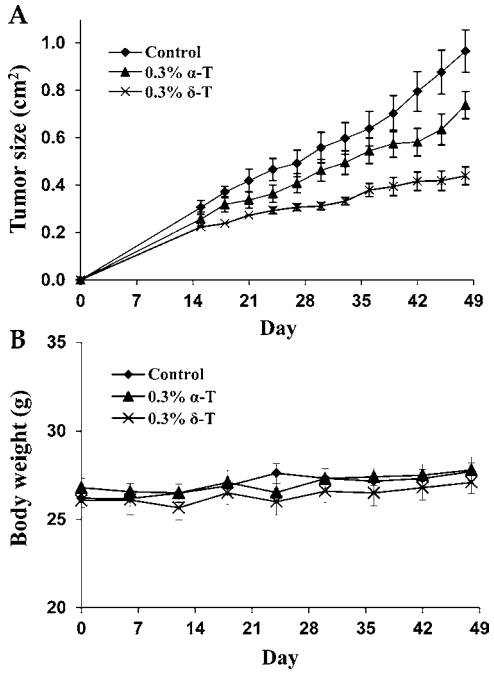


**Figure 5.** In vivo effects of $\alpha$-T and $\delta$-T. Human prostate cancer LNCaP cells were injected subcutaneously into male SCID mice. The mice received AIN93 M diet (10 mice), AIN93 M diet containing 0.3% $\alpha$-T (10 mice), or AIN93 M diet containing 0.3% $\delta$-T (10 mice) for 48 days. (A) Tumor growth curve (measured as tumor size; $cm^2$) in the control, 0.3% $\alpha$-T-treated, and 0.3% $\delta$-T-treated groups. (B) Body weight (g) of the mice in each group. Each value represents the mean ± SE.

CWR22Rv1 cells. The result indicates that $\delta$-T more potently inhibits activation of AR and its downstream target PSA as compared to $\alpha$-T.

**In Vivo Effects of $\delta$-T and $\alpha$-T.** SCID mice were injected subcutaneously with LNCaP cells and received 0.3% $\alpha$-T or 0.3% $\delta$-T in diet. The tumor take rate was 100% in the control group, 70% in the $\alpha$-T-treated group, and 50% in the $\delta$-T-treated group. This result indicates that $\delta$-T has a more potent inhibitory effect on the development of transplant prostate tumors than $\alpha$-T. Treatment with $\delta$-T also more potently inhibited the growth of LNCaP tumors than $\alpha$-T (Figure 5). As shown in Table 1, the average tumor size at the end of the experiment (day 48) in the $\delta$-T-treated group was significantly smaller than the $\alpha$-T-treated group ($p < 0.05$). The tumor weight (g) was also measured at the end of the experiment (day 48). A statistically significant difference ($p < 0.05$) in the tumor weight between the $\delta$-T-treated group and the $\alpha$-T-treated group was found (Table 1). As shown in Figure 5B, mice in different treatment group had similar body weight during the experiment period. No statistically significant difference in body weight between any two groups was found at the end of the experiment ($p > 0.05$).

**Decreased Proliferation and Increased Apoptosis in LNCaP Tumors by $\alpha$-T and $\delta$-T.** Tumor cell proliferation was measured by determining the number of mitotic cells in the xenograft tumors. We found that treatment of the mice with $\delta$-T in diet resulted in a strong inhibition of tumor cell mitosis (Table 2). The differences in % mitotic cells between the $\delta$-T-treated group and the control group, and between the $\delta$-T-treated group and the $\alpha$-T-treated group were statistically significant ($p < 0.001$). We found no statistically significant difference ($p > 0.05$) in % mitotic cells between the control group and the $\alpha$-T-treated group (Table 2). As shown in Table 2 and Figure 6, treatment with $\delta$-T also resulted in a strong increase in the number of caspase-$3^+$ cells. The differences in the percentage of caspase-$3^+$ between the $\delta$-T-treated group and the control group, and between the $\delta$-T-treated group and the $\alpha$-T-treated group were statistically significant ($p < 0.001$). Treatment with $\alpha$-T did not significantly increase the percentage of caspase-$3^+$ cells ($p > 0.05$).

**Table 1. Effects of $\delta$-T and $\alpha$-T on Tumor Growth and Body Weight of SCID Mice[a]**

| treatment group | tumor size ($cm^2$) | tumor weight (g) | body weight (g) |
|---|---|---|---|
| control | 0.97 ± 0.08 | 0.62 ± 0.05 | 27.7 ± 0.50 |
| 0.3% $\alpha$-T | 0.74 ± 0.05 | 0.54 ± 0.09 | 28.1 ± 0.74 |
| 0.3% $\delta$-T | 0.44 ± 0.04[b,d] | 0.28 ± 0.06[c,d] | 27.5 ± 0.64 |

[a]Human prostate cancer LNCaP cells were injected subcutaneously into SCID mice as indicated in the Materials and Methods. The mice were fed diet with 0.3% $\alpha$-T or 0.3% $\delta$-T. Tumor size ($cm^2$) and tumor weight (g) were measured at the end of the experiment. Each value is the mean ± SE. [b]Indicates $p < 0.001$ compared to the control. [c]Indicates $p < 0.01$ compared to the control. [d]Indicates $p < 0.05$ compared to the 0.3% $\alpha$-T-treated group.

**Table 2. Effects of $\delta$-T and $\alpha$-T on Tumor Cell Proliferation and Apoptosis[a]**

| treatment group | number of tumors | % mitotic cells | % caspase-$3^+$ cells |
|---|---|---|---|
| control | 10 | 0.88 ± 0.03 | 0.57 ± 0.03 |
| 0.3% $\alpha$-T | 7 | 0.78 ± 0.03 | 0.68 ± 0.05 |
| 0.3% $\delta$-T | 5 | 0.50 ± 0.02[b] | 1.01 ± 0.05[b] |

[a]The tumors from mice at the end of the experiment were analyzed for proliferation and apoptosis. Tumor cell proliferation was measured by determining mitotic cells. Apoptosis was measured by immunohistochemical staining with activated caspase-3. Each value is the mean ± SE. [b]Indicates $p < 0.001$ compared to the control or to the 0.3% $\alpha$-T-treated group.


dx.doi.org/10.1021/jf504058f | J. Agric. Food Chem. 2014, 62, 10752−10758

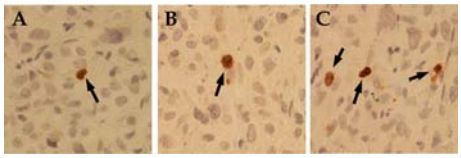


**Figure 6.** Effects of $\alpha$-T and $\delta$-T on expression of activated caspase-3 in prostate LNCaP xenograft tumors. Immunohistochemistry with an activated caspase-3 antibody was performed in paraffin sections of LNCaP tumors collected from the experiment described in Figure 5. Representative micrographs of caspase-3 immunostaining in LNCaP tumors from the control (A), $\alpha$-T-treated (B), and $\delta$-T-treated (C) mice are shown. Arrows indicate caspase-3 positive cells.

## DISCUSSION

In the present study, we demonstrated for the first time that $\delta$-T had a potent inhibitory effect on the growth of prostate cancer cells cultured in vitro and grown as subcutaneous xenograft tumors in SCID mice. In initial studies, we determined the effects of $\alpha$-T, $\gamma$-T, $\delta$-T, and a mixture of tocopherols on cultured prostate cancer cells and found that $\delta$-T had stronger effects on growth inhibition and apoptosis stimulation than $\alpha$-T, $\gamma$-T, and the tocopherol mixture. In subsequent studies, we found that $\delta$-T more potently inhibited the growth of LNCaP tumors in SCID mice than $\alpha$-T. Most of the previous studies on vitamin E have focused on $\alpha$-T. Studies on the effects of $\alpha$-T on prostate cancer reveal inconsistent results.[24−29] It has recently been shown by a number of laboratories that $\gamma$-T or a mixture of different tocopherols, $\gamma$-TmT, are more active than $\alpha$-T for inhibiting prostate cancer.[14,17,30−32] Accumulating evidence from experimental studies suggests that the $\alpha$-T used in clinical trials may not be the correct form of vitamin E for cancer prevention. The strong inhibitory effect of $\delta$-T on prostate cancer shown in our present studies indicates that $\delta$-T may be a good candidate for future clinical trial of prostate cancer prevention.

The mechanisms by which different tocopherols inhibit the growth and induce apoptosis in prostate cancer cells are still largely unknown. Although many studies investigated the mechanisms of action for $\alpha$-T and $\gamma$-T in cancer cells, there are very few studies for the mechanisms of anticancer activities of $\delta$-T. A previous study showed that combination of $\gamma$-T with $\delta$-T induced apoptosis in LNCaP cells by induction of cytochrome *c* release, activation of caspase-9 and caspase-3, and cleavage of poly-ADP-ribose polymerase.[30] Recent studies by our collaboration team demonstrated that suppression of lung tumorigenesis by $\delta$-T was associated with its ability to inhibit the formation of 8-OHdG, $\gamma$-H2AX, and nitrotyrosine, as well as to induce cell apoptosis.[33] In another study, $\delta$-T was found to induce PPAR-$\gamma$ and PTEN, and reduce pAkt levels in breast cancer cells.[34] The mechanisms for the effects of $\delta$-T on prostate cancer are not clear. It is known that the AR signaling pathway is important for growth and survival of prostate cancer cells. Earlier studies have shown that analogues of $\alpha$-T induced transcriptional repression of AR, inhibited AR activity and decreased the level of PSA.[35,36] However, the effect of $\delta$-T on AR signaling was not reported. In the present study, we demonstrated that $\delta$-T had a more potent inhibitory effect than $\alpha$-T on AR activation in prostate cancer cells as determined by the luciferase reporter gene expression assay. In addition, $\delta$-T more potently decreased the level of PSA than $\alpha$-T. Suppression of the AR signaling may be one of the mechanisms by which $\delta$-T inhibits the growth and induces apoptosis in androgen sensitive prostate cancer cells. Preliminary results from our recent studies showed inhibitory effect of $\delta$-T on the growth of PC-3 and Du145 cells (data not shown). This result indicates that $\delta$-T also inhibited androgen-independent prostate cancer cells and that mechanisms other than AR signaling may be involved. Further studies are needed to explore the mechanisms of action for $\delta$-T in androgen-independent prostate cancer cells.

Since $\delta$-T showed strong effects on growth inhibition and apoptosis in cultured prostate cancer cells, we used the xenograft prostate tumor model to determine the in vivo effect of this tocopherol. We found in our earlier studies that 0.3% of different tocopherols in diet were effective.[13−15] Therefore, 0.3% of $\alpha$-T and $\delta$-T in diet were used in our present in vivo study. Our study showed that treatment with 0.3% $\alpha$-T in diet decreased the number of mice that formed LNCaP tumors. However, $\alpha$-T administration did not significantly inhibit the growth of the tumors. Administration of 0.3% $\delta$-T in the diet strongly inhibited the formation and growth of subcutaneous LNCaP tumors. In a recent pilot study, we found low plasma levels of $\delta$-T (0.16−0.47 $\mu$M) in prostate cancer patients received 2 capsules of mix-tocopherol (containing 128 mg $\alpha$-T, 200 mg $\gamma$-T, and 71 mg $\delta$-T per capsule) for 7 or 14 days (data presented in the 2011 AACR annual meeting). The concentrations of $\alpha$-T and $\delta$-T to inhibit cultured prostate cancer cells are higher than the plasma levels of these compounds. It is possible that the in vivo effects of $\delta$-T were cumulative. In addition, $\delta$-T may interact with endogenous factors such as cytokines within tumor tissues leading to stronger anticancer effects. Mechanistic studies showed that treatment of mice with $\delta$-T inhibited proliferation as reflected by decreased mitosis, and stimulated apoptosis as reflected by increased caspase-3 in LNCaP tumors. This result indicates that the strong inhibitory effect of $\delta$-T on the growth of LNCaP tumors in SCID mice may be mediated by inhibition of proliferation and stimulation of apoptosis in the tumors. To our knowledge, this is the first report for an inhibitory effect of $\delta$-T on the formation and growth of human prostate tumors in a xenograft model.

In summary, the present study showed that $\delta$-T had more potent effects on inhibiting proliferation and inducing apoptosis in prostate cancer cells than $\alpha$-T. The strong activities of $\delta$-T were associated with suppression of AR activity and decreased level of PSA. Results from the in vivo study demonstrated a strong inhibitory effect of $\delta$-T on the formation and growth of LNCaP tumors in SCID mice without apparent toxicity. Clinical studies for determining the potential preventive efficacy of $\delta$-T on prostate cancer patients are warranted.

## AUTHOR INFORMATION

### Corresponding Author

*Phone: 848-445-8069; fax: 732-445-0687; e-mail: xizheng@pharmacy.rutgers.edu.

### Author Contributions

⊥These two authors contributed equally to this work.

### Funding

The present study was supported by the Guangdong Province Leadership Grant, China National Science Foundation Grants (Grant No. 81272452, 21102020, and 21272043), and the Rutgers Cancer Institute of New Jersey (CCSG P30-CA072720 RSD).

### Notes

The authors declare no competing financial interest.
[#]Deceased.

## ■ ACKNOWLEDGMENTS

The authors dedicate this paper to Dr. Allan H. Conney, an outstanding and widely recognized cancer researcher who passed away on September 10, 2013. We thank Dr. Philip Fumanski for his valuable suggestions for the manuscript.

## ■ ABBREVIATIONS USED

$\alpha$-T,($\alpha$-tocopherol); $\beta$-T,($\beta$-tocopherol); $\gamma$-T,($\gamma$-tocopherol); $\delta$-T,($\delta$-tocopherol); AR,(androgen receptor); PSA,(prostate specific antigen); SCID,(severe combined immunodeficient); ANOVA,(analysis of variance)

## ■ REFERENCES

(1) Constantinou, C.; Papas, A.; Constantinou, A. I. Vitamin E and cancer: An insight into the anticancer activities of vitamin E isomers and analogs. *Int. J. Cancer* **2008**, **15**, *123* (4), 739−752.
(2) Herrera, E.; Barbas, C. Vitamin E: action, metabolism and perspectives. *J. Physiol. Biochem.* **2001**, *57* (1), 43−56.
(3) Ju, J.; Picinich, S. C.; Yang, Z.; Zhao, Y.; Suh, N.; Kong, A. N.; Yang, C. S. Cancer preventive activities of tocopherols and tocotrienols. *Carcinogenesis* **2010**, *31* (4), 533−542.
(4) Jiang, Q. Natural forms of vitamin E: metabolism, antioxidant, and anti-inflammatory activities and their role in disease prevention and therapy. *Free Rad. Biol. Med.* **2014**, *72*, 76−90.
(5) Gilbert, R.; Metcalfe, C.; Fraser, W. D.; Donovan, J.; Hamdy, F.; Neal, D. E.; Lane, J. A.; Martin, R. M. Associations of circulating retinol, vitamin E, and 1,25-dihydroxyvitamin D with prostate cancer diagnosis, stage, and grade. *Cancer Causes Control.* **2012**, *23* (11), 1865−1873.
(6) Yang, C. S.; Suh, N.; Kong, A. N. Does vitamin E prevent or promote cancer? *Cancer Prev. Res. (Phila)* **2012**, *5* (5), 701−705.
(7) Banim, P. J.; Luben, R.; McTaggart, A.; Welch, A.; Wareham, N.; Khaw, K. T.; Hart, A. R. Dietary antioxidants and the aetiology of pancreatic cancer: A cohort study using data from food diaries and biomarkers. *Gut.* **2013**, *62* (10), 1489−1496.
(8) Epplein, M.; Shvetsov, Y. B.; Wilkens, L. R.; Franke, A. A.; Cooney, R. V.; Le Marchand, L.; Henderson, B. E.; Kolonel, L. N.; Goodman, M. T. Plasma carotenoids, retinol, and tocopherols and postmenopausal breast cancer risk in the Multiethnic Cohort Study: A nested case-control study. *Breast Cancer Res.* **2009**, *11* (4), R49.
(9) The Alpha-tocopherol, Beta-carotene Cancer Prevention Group. The effect of vitamin E and beta carotene on the incidence of lung cancer and other cancers in male smokers. The Alpha-Tocopherol, Beta Carotene Cancer Prevention Study Group. *N. Engl. J. Med.* **1994**, *330*(15), 1029−1035.
(10) Albanes, D.; Till, C.; Klein, E. A.; Goodman, P. J.; Mondul, A. M.; Weinstein, S. J.; Taylor, P. R.; Parnes, H. L.; Gaziano, J. M.; Song, X.; Fleshner, N. E.; Brown, P. H.; Meyskens, F. L., Jr.; Thompson, I. M. Plasma Tocopherols and Risk of Prostate Cancer in the Selenium and Vitamin E Cancer Prevention Trial (SELECT). *Cancer Prev. Res. (Phila)* **2014**, *7* (9), 886−95.
(11) Lee, I. M.; Cook, N. R.; Gaziano, J. M.; Gordon, D.; Ridker, P. M.; Manson, J. E.; Hennekens, C. H.; Buring, J. E. Vitamin E in the primary prevention of cardiovascular disease and cancer: The Women's Health Study: A randomized controlled trial. *JAMA* **2005**, *294* (1), 56−65.
(12) Gaziano, J. M.; Glynn, R. J.; Christen, W. G.; Kurth, T.; Belanger, C.; MacFadyen, J.; Bubes, V.; Manson, J. E.; Sesso, H. D.; Buring, J. E. Vitamins E and C in the prevention of prostate and total cancer in men: The Physicians' Health Study II randomized controlled trial. *JAMA* **2009**, *301* (1), 52−62.
(13) Smolarek, A. K.; So, J. Y.; Thomas, P. E.; Lee, H. J.; Paul, S.; Dombrowski, A.; Wang, C. X.; Saw, C. L.; Khor, T. O.; Kong, A. N.; Reuhl, K.; Lee, M. J.; Yang, C. S.; Suh, N. Dietary tocopherols inhibit cell proliferation, regulate expression of ER$\alpha$, PPAR$\gamma$, and Nrf2, and decrease serum inflammatory markers during the development of mammary hyperplasia. *Mol. Carcinog.* **2013**, *52* (7), 514−525.
(14) Huang, Y.; Khor, T. O.; Shu, L.; Saw, C. L.; Wu, T. Y.; Suh, N.; Yang, C. S.; Kong, A. N. A $\gamma$-tocopherol-rich mixture of tocopherols maintains Nrf2 expression in prostate tumors of TRAMP mice via epigenetic inhibition of CpG methylation. *J. Nutr.* **2012**, *142* (5), 818−823.
(15) Lu, G.; Xiao, H.; Li, G. X.; Picinich, S. C.; Chen, Y. K.; Liu, A.; Lee, M. J.; Loy, S.; Yang, C. S. A gamma-tocopherol-rich mixture of tocopherols inhibits chemically induced lung tumorigenesis in A/J mice and xenograft tumor growth. *Carcinogenesis* **2010**, *31* (4), 687−694.
(16) Yang, C. S.; Suh, N. Cancer prevention by different forms of tocopherols. *Top. Curr. Chem.* **2013**, *329*, 21−33.
(17) Zheng, X.; Cui, X. X.; Khor, T. O.; Huang, Y.; Dipaola, R. S.; Goodin, S.; Lee, M. J.; Yang, C. S.; Kong, A. N.; Conney, A. Inhibitory Effect of a $\gamma$-Tocopherol-Rich Mixture of Tocopherols on the Formation and Growth of LNCaP Prostate Tumors in Immunodeficient Mice. *Cancers (Basel)* **2011**, *3* (4), 3762−3772.
(18) Altiok, N.; Ersoz, M.; Koyuturk, M. Estradiol induces JNK-dependent apoptosis in glioblastoma cells. *Oncol Lett.* **2011**, *2* (6), 1281−1285.
(19) Motyl, T.; Grzelkowska, K.; Zimowska, W.; Skierski, J.; Wareski, P.; Płoszaj, T.; Trzeciak, L. Expression of bcl-2 and bax in TGF-beta 1-induced apoptosis of L1210 leukemic cells. *Eur. J. Cell Biol.* **1998**, *75* (4), 367−374.
(20) Ma, L.; Li, W. Emodin inhibits LOVO colorectal cancer cell proliferation via the regulation of the Bcl-2/Bax ratio and cytochrome *c*. *Exp. Ther. Med.* **2014**, *8* (4), 1225−1228.
(21) Zhou, D. Y.; Ding, N.; Du, Z.; Cui, X.; Wang, H.; Wei, X.; Conney, A.; Zhang, K.; Zheng, X. Curcumin analogues with high activity for inhibiting human prostate cancer cell growth and androgen receptor activation. *Mol. Med. Rep.* **2014**, *10*, 1315−1322.
(22) Hu, G.; Li, F.; Ouyang, K.; Xie, F.; Tang, X.; Wang, K.; Han, S.; Jiang, Z.; Zhu, M.; Wen, D.; Qin, X.; Zhang, L. Intrinsic gemcitabine resistance in a novel pancreatic cancer cell line is associated with cancer stem cell-like phenotype. *Int. J. Oncol.* **2012**, *40* (3), 798−806.
(23) Qu, J.; Lu, W.; Li, B.; Lu, C.; Wan, X. WWOX induces apoptosis and inhibits proliferation in cervical cancer and cell lines. *Int. J. Mol. Med.* **2013**, *31* (5), 1139−1147.
(24) Venkateswaran, V.; Fleshner, N. E.; Klotz, L. H. Synergistic effect of vitamin E and selenium in human prostate cancer cell lines. *Prostate Cancer Prostatic Dis.* **2004**, *7* (1), 54−56.
(25) Nakamura, A.; Shirai, T.; Takahashi, S.; Ogawa, K.; Hirose, M.; Ito, N. Lack of modification by naturally occurring antioxidants of 3,2′-dimethyl-4-aminobiphenyl-initiated rat prostate carcinogenesis. *Cancer Lett.* **1991**, *58* (3), 241−246.
(26) McCormick, D. L.; Rao, K. V. Chemoprevention of hormone-dependent prostate cancer in the Wistar-Unilever rat. *Eur. Urol.* **1999**, *35* (5−6), 464−467.
(27) Limpens, J.; Schröder, F. H.; de Ridder, C. M.; Bolder, C. A.; Wildhagen, M. F.; Obermüller-Jevic, U. C.; Krämer, K.; van Weerden, W. M. Combined lycopene and vitamin E treatment suppresses the growth of PC-346C human prostate cancer cells in nude mice. *J. Nutr.* **2006**, *136* (5), 1287−1293.
(28) Fleshner, N.; Fair, W. R.; Huryk, R.; Heston, W. D. Vitamin E inhibits the high-fat diet promoted growth of established human prostate LNCaP tumors in nude mice. *J. Urol.* **1999**, *161* (5), 1651−1654.
(29) Basu, A.; Grossie, B.; Bennett, M.; Mills, N.; Imrhan, V. Alpha-tocopheryl succinate (alpha-TOS) modulates human prostate LNCaP xenograft growth and gene expression in BALB/c nude mice fed two levels of dietary soybean oil. *Eur. J. Nutr.* **2007**, *46* (1), 34−43.
(30) Jiang, Q.; Wong, J.; Ames, B. N. Gamma-tocopherol induces apoptosis in androgen-responsive LNCaP prostate cancer cells via caspase-dependent and independent mechanisms. *Ann. N.Y. Acad. Sci.* **2004**, *1031*, 399−400.

(31) Singh, C. K.; Ndiaye, M. A.; Siddiqui, I. A.; Nihal, M.; Havighurst, T.; Kim, K.; Zhong, W.; Mukhtar, H.; Ahmad, N. Methaneseleninic acid and γ-Tocopherol combination inhibits prostate tumor growth in vivo in a xenograft mouse model. *Oncotarget* **2014**, *5* (11), 3651−3661.
(32) Torricelli, P.; Caraglia, M.; Abbruzzese, A.; Beninati, S. γ-Tocopherol inhibits human prostate cancer cell proliferation by up-regulation of transglutaminase 2 and down-regulation of cyclins. *Amino Acids* **2013**, *44* (1), 45−51.
(33) Li, G. X.; Lee, M. J.; Liu, A. B.; Yang, Z.; Lin, Y.; Shih, W. J.; Yang, C. S. δ-Tocopherol is more active than α - or γ -tocopherol in inhibiting lung tumorigenesis in vivo. *Cancer Prev. Res. (Phila)* **2011**, *4* (3), 404−413.
(34) Smolarek, A. K.; So, J. Y.; Burgess, B.; Kong, A. N.; Reuhl, K.; Lin, Y.; Shih, W. J.; Li, G.; Lee, M. J.; Chen, Y. K.; Yang, C. S.; Suh, N. Dietary administration of δ- and γ-tocopherol inhibits tumorigenesis in the animal model of estrogen receptor-positive, but not HER-2 breast cancer. *Cancer Prev. Res. (Phila)* **2012**, *5* (11), 1310−1320.
(35) Zhang, H.; Wu, Y.; Malewicz, B.; Lu, J.; Li, S.; Marshall, J.; Ip, C.; Dong, Y. Augmented suppression of androgen receptor signaling by a combination of alpha-tocopheryl succinate and methylseleninic acid. *Cancer* **2006**, *107* (12), 2942−2948.
(36) Huang, P. H.; Wang, D.; Chuang, H. C.; Wei, S.; Kulp, S. K.; Chen, C. S. alpha-Tocopheryl succinate and derivatives mediate the transcriptional repression of androgen receptor in prostate cancer cells by targeting the PP2A-JNK-Sp1-signaling axis. *Carcinogenesis* **2009**, *30* (7), 1125−1131.

lignin could replace 55% of phenol in phenol−formaldehyde resins. Gromov and Pormale[10] performed hydrogenation of lignin directly during hydrotropic treatment with a nickel catalyst to obtain phenols. Kreicberg and Grabovskij[7] carried out nitrobenzene oxidation of aspen hydrotropic lignin in alkaline media and obtained aromatic aldehydes with a yield of 8.8% based on Klason lignin of the hydrotropic lignin. Another paper[11] describes oxidative degradation of aspen hydrotropic lignin with oxygen in an alkaline media in the presence of copper oxide. The yield of low molecular weight products was 39.3% based on Klason lignin of the hydrotropic lignin. The products were further fractionated into aldehyde, acidic, phenolic, and neutral fractions.[11]

All of these studies have shown that hydrotropic lignin is a valuable biobased polymer that can be used to produce chemicals and as a substituent of phenol in phenol−formaldehyde resins. Despite all of the research, there is no detailed information about the composition and chemical structure of this, rather novel, type of technical lignin. However, characterization of lignin has a great importance for the evaluation of its potential for various applications. In this study, hydrotropic lignin was isolated from industrial birch wood chips by conventional (reference) and modified hydrotropic treatments.[5] The difference between these two processes is that in the latter the hydrotropic solution was modified by the addition of formic acid and hydrogen peroxide. Such modification led to a better delignification, and the obtained pulp had higher cellulose content than the reference one; however, the modified process was more severe, which resulted in a lower yield of pulp with a lower viscosity.[5] Therefore, it was interesting to investigate how the modification of hydrotropic solution with hydrogen peroxide and formic acid would affect the chemical composition of lignin. The lignins were characterized with Fourier transform infrared spectroscopy (FTIR), pyrolysis−gas chromatography−mass spectrometry (pyrolysis-GC-MS), semi-quantitative $^{1}H-^{13}C$ HSQC NMR, $^{31}P$ NMR spectroscopy techniques, and size exclusion chromatography (SEC) to elucidate their structures and functional groups. The chemical and elemental compositions of the lignins were studied as well. We believe that the characterization of hydrotropic lignins presented will facilitate their utilization and promote the hydrotropic process in the pulp and biorefinery industry.

## MATERIALS AND METHODS

**Materials.** Birch wood chips collected from a Finnish pulp and paper mill were screened in the laboratory, and a 4−6 mm fraction was used for the hydrotropic treatments. Technical grade sodium xylenesulfonate having purity >90% (Sigma-Aldrich) was used as a hydrotropic agent. Other chemicals were obtained from commercial sources and were used without further purification.

**Isolation of Hydrotropic Lignins.** Hydrotropic lignins were extracted in a 10 L rocking digester using a 36% aqueous hydrotropic solution. Two treatments were performed, namely, a conventional reference method and one with the addition of formic acid and hydrogen peroxide. Lignins obtained with these treatments were designated R and M lignins, respectively. A dosage of hydrogen peroxide for the modified treatment was 2.5% based on wood, and the amount of formic acid was added to lower the pH to 3.5. The conditions of the extractions were the following: liquor-to-wood ratio, 4 (w/w); heating rate, 1.5 °C/min; dwell temperature, 170 °C; and dwell time, 120 min. The pH values of the prepared hydrotropic solutions were 9.2 and 3.5 for the reference and modified solutions, respectively. Prior to the extractions, the chips were vacuum-impregnated with the hydrotropic solutions at room temperature for 30 min using a water pump. The solid residues (or pulps) after the treatments were disintegrated and washed as described elsewhere[5] and screened in a Valmet TAP03 rotary screen using a 0.1 mm slit basket. The accepted fraction was used for the determination of residual lignin content.

Hydrotropic lignins from the collected spent solutions were precipitated by dilution with 10-fold (v/v) of hot distilled water. After addition of the hot water, the temperature of the diluted solution was around 75 °C. The precipitated lignin was separated by filtration through a glass filter funnel no. 2. At the beginning of the filtration, some amount of the filtrate was recirculated back onto the filter until the filtrate became free of lignin particles. The precipitate was further washed with around 8-fold (v/v, based on the volume of spent solution taken for precipitation) of hot distilled water. The temperature of the suspension during the washing was maintained at 75−80 °C. The washed lignins were freeze-dried and stored in a cold room at a temperature of 10 °C.

The amounts of dissolved, precipitated, and nonprecipitated lignins were calculated according to eqs 1−4.

dissolved lignin (or degree of delignification) based on lignin in wood, %

$$L_{dis} = (L_{wood} - L_{pulp} \times m_{pulp}/m_{wood})/L_{wood} \times 100 \quad (1)$$

precipitated lignin (lignin yield) based on wood, %

$$L_{precip/wood} = L_{precip\ ss} \times m_{ss}/m_{wood} \times 100 \quad (2)$$

precipitated lignin (lignin yield) based on the original lignin in wood, %

$$L_{precip/lignin} = L_{precip\ ss} \times m_{ss}/m_{lignin\ wood} \times 100 \quad (3)$$

nonprecipitated lignin based on the original lignin in wood, %

$$L_{nonprecip} = L_{dis} - L_{precip/lignin} \quad (4)$$

$L_{wood}$ and $L_{pulp}$ are lignin contents in birch wood and in pulp, %; $m_{pulp}$ and $m_{wood}$ are the amounts of pulp and wood, g; $L_{precip\ ss}$ is the amount of lignin precipitated from spent solution, g/g; $m_{ss}$ is the amount of spent solution calculated as a sum of hydrotropic solution, water in wood, and dissolved wood, g; $m_{lignin\ wood}$ is the amount of lignin in birch wood, g.

**Chemical Composition of Lignins.** Residual carbohydrates in the lignin samples were determined using acid methanolysis and gas chromatography (GC) as described elsewhere.[5] The analysis was carried out using an AutosystemXL (PerklinElmer, Norwalk, CT, USA) gas chromatograph. The columns used were 25 m × 0.200 mm i.d., 0.11 μm, HP-1 (Agilent Technologies, Santa, Clara, CA, USA) and 25 m × 0.199 mm i.d., 0.11 μm, HP-5 (Agilent Technologies). The operating parameters of the GC were the following: injection amount, 1 μL; split ratio, 1:25; injector temperature, 250 °C; temperature program of the oven, 100 °C, held for 1 min, increased at 4 °C/min to 170 °C and then at 12 °C/min to 300 °C, and, finally, held for 7 min. The temperature of the detector (flame ionization detector, FID) was 310 °C. Hydrogen was used as a carrier gas.

Extractives in lignins were analyzed by GC after silylation. The amount of samples weighed for the analysis was about 8 mg with the accuracy of 0.1 mg. Two milliliters of the internal standard containing 0.02 mg/mL cholesterol, heneicosanoic acid, 1,3-dipalmitoyl-2-oleoylglycerol, and cholesteryl heptadecanoate in methyl *tert*-butyl ether was added to the samples. The samples were mixed well with the internal standard and evaporated under a nitrogen flow at 50 °C. To ensure complete removal of the solvent, the samples were kept in a vacuum oven for 20 min at 40 °C. The dried samples were dissolved in 40 μL of pyridine and silylated with 80 μL of *N*,*O*-bis(trimethylsilyl)-trifluoroacetamide and 40 μL of trimethylchlorosilane at 70 °C for 45 min. After cooling at room temperature, the samples were transferred

into GC vials and analyzed by Clarius 500 (PerkinElmer) and AutosystemXL (PerkinElmer) gas chromatographs equipped with 6−7 m × 0.530 mm i.d., 0.15 μm, HP-1 (Agilent Technologies) and 25 m × 0.200 mm i.d., 0.11 μm, HP-1 (Agilent Technologies) columns, respectively. The injection parameters and temperature programs are described elsewhere.[12] The short column was used to analyze groups of components, whereas the long column was used for the analysis of individual substances (except for steryl esters and triglycerides). The identification and assignment of the peaks were done with the help of GC-MS.[13]

**Elemental Analysis.** Carbon, hydrogen, nitrogen, and sulfur contents of the lignins were measured with a Thermo Scientific Flash 2000 series elemental analyzer. The description of the analysis can be found elsewhere.[14] Oxygen content was calculated by subtracting the sum of C, H, N, and S from 100%. The elemental compositions of lignins obtained by the reference and modified treatments were as follows: carbon, 65.51 and 64.50%; hydrogen, 5.87 and 5.54%; nitrogen, 0.23 and 0.22%; sulfur, 0.16 and 0.39%; oxygen, 28.23 and 29.35%, respectively.

**Pyrolysis-GC-MS.** The mass ratios of the *p*-hydroxyphenyl (H), guaiacyl (G), and syringyl units (S) in the hydrotropic lignins as well as in the lignin in the wood were determined using pyrolysis-GC-MS. Before the analysis, the wood was ground using a cutting mill with a sieve cassette with 1 mm openings. After that, the wood meal was sieved to obtain a fraction <250 μm and freeze-dried.

The pyrolysis-GC-MS was done on a foil pulse Pyrola 2000 pyrolyzer (Pyrol AB, Lund, Sweden) connected to the GC-MS instrument.[13] The analyses were performed as described previously.[13] The tentative identification was mainly based on the mass spectra library created at the Laboratory of Wood and Paper Chemistry at Åbo Akademi University and partly on the Wiley 10/NIST 2012 mass spectral libraries. A sample amount of about 100 μg and one drop of acetone was applied onto the Pt filament, the sample was allowed to dry, and the analysis was started 2 min after the filament was added into the probe.

**FTIR.** The FTIR spectra were recorded in transmission mode using a Thermo Scientific Nicolet iS50 instrument. The concentration of lignin in a KBr pellet was about 1%. The number of scans was 32, and the resolution was 4 $cm^{-1}$.

**$^{1}H-^{13}C$ HSQC NMR.** Around 50 mg was dissolved in 1 mL of DMSO-$d_6$. NMR spectra were recorded at 25 °C on a Bruker AVANCE III 400 MHz instrument equipped with a 5 mm BBI probe (5 G/cmA). Heteronuclear single-quantum coherence (HSQC) experiments used Bruker's "hsqcetgpsi2" pulse program with spectral widths of 5000 Hz (from 10 to 0 ppm) and 20843 Hz (from 165 to 0 ppm) for the $^{1}H$ and $^{13}C$ dimensions. The number of collected complex points was 1024 for the $^{1}H$ dimension with a recycle delay of 1.5 s. The number of transients was 32, and 256 time increments were always recorded in the $^{13}C$ dimension. The $^{1}J_{CH}$ used was 145 Hz. Processing used squared cosine-bell apodization in both dimensions. Prior to Fourier transformation, the data matrices were zero-filled to 1024 points in the $^{13}C$ dimension. The central solvent peak was used as an internal reference ($\delta_C$ 39.5; $\delta_H$ 2.49). HSQC correlation peaks were assigned by comparison with the literature.[15−18] A semi-quantitative analysis[15] of the volume integrals (uncorrected) of the HSQC correlation peaks was performed using Mnova 7 processing software. In the aliphatic oxygenated region, the relative abundances of side chains involved in the various interunit linkages were estimated from the $C_\alpha-H_\alpha$ correlations to avoid possible interference from homonuclear $^{1}H-^{1}H$ couplings. In the aromatic/unsaturated region, $C_2-H_2$ and/or $C_6-H_6$ correlations from H, G, and S lignin units were used to estimate their relative abundances.

**$^{31}P$ NMR.** Hydroxyl and carboxyl functional groups were quantified by $^{31}P$ NMR after derivatization with 2-chloro-4,4,5,5-tetramethyl-1,3,2-dioxaphospholane. The detailed description of the analysis can be found elsewhere.[19]

**SEC.** Number-average ($M_n$) and weight-average ($M_w$) molar mass distributions and polydispersity were determined with alkaline SEC analysis according to the method of Gosselink et al.[19]

**Other Analysis.** Contents of lignin in the birch wood and in the wood residues (pulps) after the treatments were determined as described elsewhere.[5]

## RESULTS AND DISCUSSION

**Isolation of Hydrotropic Lignins.** As expected, the addition of hydrogen peroxide and formic acid to a hydrotropic solution resulted in a more efficient lignin removal from the wood in comparison with the reference process. The contents of residual lignins in the pulps were 4.5 and 1.7% for the reference and modified treatments, which corresponded to degrees of delignification of 91 and 97%, respectively. The yield of the residue after the modified treatment was also lower, 43 against 48% in the case of the reference treatment. Such a low yield of pulp from the modified process, besides the higher degree of delignification, can be attributed to a higher rate of carbohydrate degradation, mainly hemicelluloses, as has been shown previously.[5]

The yield of lignin from both treatments was 16.1% calculated on the dry wood basis or 160 kg of lignin from 1 t of wood. This amount corresponded to around 67.0% of the original lignin contained in the birch wood. Some amount of lignin did not precipitate upon dilution with water and, therefore, was not recovered. This fraction constituted 23.9 and 30.0% of the original lignin in birch for the reference and modified treatments, respectively. These numbers also include losses of lignin during the washing step. Similar behavior of lignin during precipitation was also described by Gromov and Odincov.[20,21] In their studies of hydrotropic treatment of aspen wood, the amount of nonprecipitated lignin fractions varied in the range from 10 to 50% based on the original lignin in the wood.[20] The authors assumed that this fraction was composed of low molecular weight lignin. In another study,[21] they partially isolated this fraction by acidification and heating the diluted spent solution. According to Gromov and Odincov,[20,21] the quantity of nonprecipitated lignin depended on the treatment conditions. Some low molecular weight phenolic compounds (syringaldehyde, syringic acid, vanillin, vanillic acid, stilbenes, and syringaresinol) were also detected in the hydrotropic lignins by GC during analysis of the extractives, although their total quantity was <1%.

Interestingly, water-soluble lignin degradation products were also found in spent liquors from other autocatalyzed and moderately acidic treatments, such as in hydrolysates after hot water treatment of eucalyptus[22] and sugar maple,[23] and in a spent solution after ethanol−water treatment (Alcell process) of a mixture of hardwoods.[24] In the last studies, the amount of nonprecipitated lignin varied from 20 to 40% of the original lignin in wood.

**Chemical and Elemental Composition of Lignins.** The purity of lignins was analyzed indirectly and expressed through the contents of non-lignin substances. Such substances could originate, for example, from the raw material and the hydrotropic reagent. The former includes wood constituents such as extractives, carbohydrates, and proteins. The latter consists of the hydrotropic salt itself and contaminants present in the salt.

The contents of extractives in the lignins were determined to be 0.50 and 0.44% for R and M lignins, respectively. The detected extractives were in a free form, meaning that they were not strongly bound to lignin. Therefore, they could be analyzed by silylation and GC, that is, a procedure which does not include any destructive steps, such as hydrolysis. The free

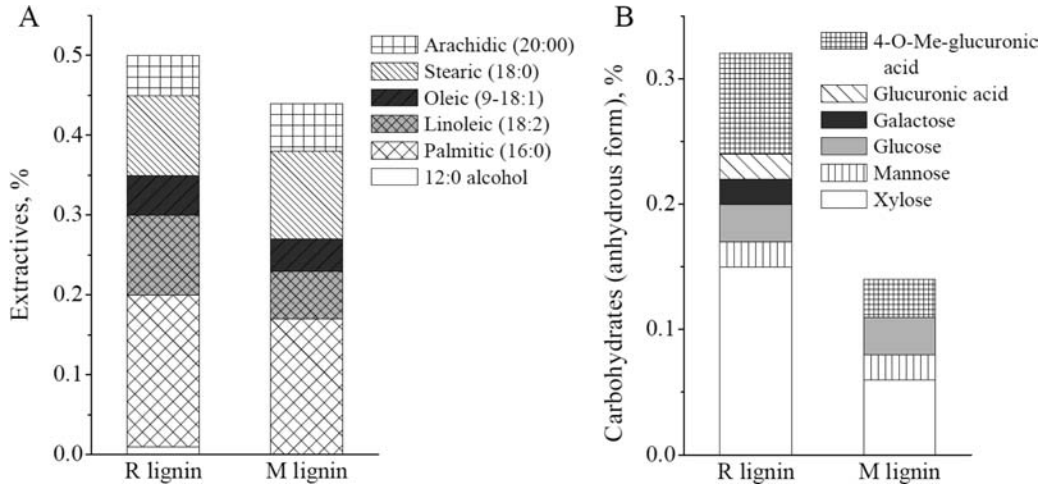


**Figure 2.** (A) Extractives and (B) carbohydrates (as anhydrous units) in the hydrotropic lignins.

extractable matter of the lignins consisted exclusively of fatty acid with palmitic acid being the most abundant (Figure 2A). The only exception was a very small amount of 12-carbon alcohol found in the reference lignin.

The lignins had a very small amount of residual carbohydrates (Figure 2B) owing to extensive hydrolytic reactions, which took place during the treatment. The reactions were catalyzed by the organic acids liberated from wood, mainly acetic and formic.[2] In the case of the modified treatment, destruction of hemicelluloses was additionally intensified by formic acid added to the hydrotropic solution. Therefore, M lignin contained less residual carbohydrates than the reference sample, 0.14 versus 0.32%, respectively. In contrast to the extractives, the residual carbohydrates are covalently bound to lignin and form so-called lignin−carbohydrate complexes. This was also a reason why the carbohydrates were not removed completely during the hydrotropic treatment and lignin recovery. As expected, xylose was the main contaminating sugar, because it was present in the birch wood in a large quantity, around 20%.[5] In the lignins, residual xylose is present in its polymeric form, xylan.

Both lignins exhibited elemental composition typical of technical lignins, for example, kraft and EtOH/$H_2O$ lignins from the literature.[25] Technical lignins usually have a higher content of carbon and lower contents of oxygen and hydrogen than the original lignin in wood (milled wood lignins in the literature[25]). Nitrogen in both samples presumably originated from a small amount of proteins from the wood. Assuming a conversion factor of 6.25,[26] this content of nitrogen corresponded to approximately 1.4% of proteins in the samples. The proteins are most likely strongly bound to the lignins as has been shown by other studies.[26,27]

Both lignins contained sulfur, which indicates that the samples were possibly contaminated with the hydrotropic salt. In that case the salt must be strongly associated with the lignins, because it could not be removed during the washing step. Alternatively, the sulfur might originate from impurities present in the hydrotropic reagent. One such compound, 2,2′,5,5′-tetramethyldiphenylsulfone, or its isomers, was found during the analysis of extractives by GC. The same substance was also detected in the salt and lignins by pyrolysis-GC-MS. Tetramethyldiphenylsulfone is probably a byproduct of manufacturing sodium xylenesulfonate, and it is most likely insoluble in water. The water solubility for different tetramethyldiphenylsulfone isomers varies from 0.026 to 0.037 mmol/L (predicted using Advanced Chemistry Development (ACD/Laboratories) software V11.02). Therefore, it survived the washing step and remained in the lignins. This compound may contribute 0.09 and 0.08%-units to the total sulfur content in R and M lignins, correspondingly. Interestingly, lignin from the modified treatment had a higher content of sulfur. However, the sulfur level in both lignins was substantially lower than in commercially produced kraft lignins (1.0−3.0%) and lignosulfonates (3.5−8.0%).[28]

**H/G/S Ratio by Pyrolysis-GC-MS.** The mass ratios of the *p*-hydroxyphenyl, guaiacyl, and syringyl units were found to be 1:25:74 for R and 2:26:71 for M lignins. The corresponding ratio for the original birch wood lignin was 3:26:71. Hence, the results show that the relative content of the units in the lignins was almost the same as in birch wood lignin; therefore, it can be concluded that the ratio did not change over the course of the hydrotropic treatments. Also, both hydrotropic lignins were comparable with each other, which means that the addition of hydrogen peroxide and formic acid did not affect the unit ratio of lignins. Both lignins can be regarded as SG lignins according to Faix's classification[29] with a high content of S units. It should be noted that small amounts of low molecular weight phenols detected in the lignins by GC (analysis of extractives) were predominantly derived from the S units (syringaresinol, syringaldehyde, and syringic acid).

Another observation made from the results of pyrolysis-GC-MS was related to the formation of catechol units during hydrotropic treatments. Several types of catechols were detected in the pyrograms of the hydrotropic lignins, namely, catechol, 3-methylcatechol, 4-methylcatechol, and 3-methoxycatechol. The pyrogram of birch wood meal did not have such units. Most likely, these structures were formed by demethylation of methoxyl groups of G and S units. The ratios of the sum of H, G, and S units and catechol units were 94:6 and 93:7 for the R and M lignins, respectively.

**FTIR.** Lignin is a complex material and has many bonds and functional groups in its structure. This is reflected in its IR spectrum, which shows many bands, most of which overlap with each other, especially in the fingerprint area. However, IR studies can provide some basic information about lignin purity and its structure and can be further complemented with more sophisticated methods of analysis. FTIR spectra of hydrotropic

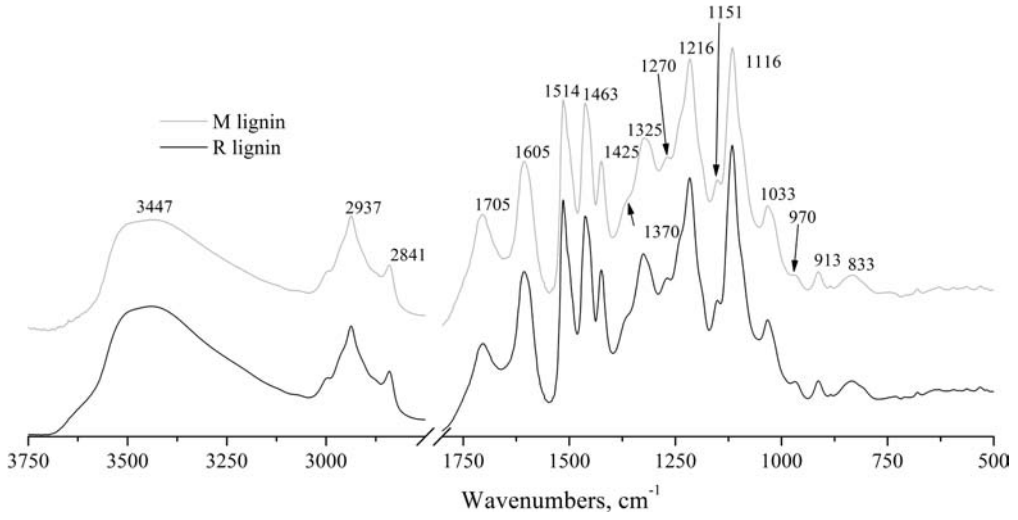


**Figure 3.** FTIR spectra of the hydrotropic lignins.

lignins are shown in Figure 3. The bands were assigned according to the data found in the literature (Table 1).[29,30]

**Table 1. Band Assignment in FTIR**

| wavenumber, $cm^{-1}$ | band assignment |
|---|---|
| 3447 | O—H stretch in aliphatic and phenolic −OH |
| 2937, 2841 | C—H stretch in methyl and methylene groups |
| 1705 | C═O stretching in unconjugated ketones and carboxyl groups; aryl and *α,β* unsaturated esters |
| 1605 | aromatic skeletal vibration (S > G) + C═O stretch |
| 1514 | aromatic skeletal vibrations (G > S) |
| 1463 | C—H asymmetric deformations in methyl and methylene groups |
| 1425 | aromatic skeletal vibrations |
| 1370 | aliphatic C—H symmetric deformation in methyl (not methoxyl) + O—H deformation in phenols |
| 1325 | S ring breathing + G ring substituted in position 5 |
| 1270 | G ring breathing and C—O stretching |
| 1216 | C—O stretching in phenols and ethers |
| 1116 | aromatic C—H in-plane deformations (S units) |
| 1033 | aromatic C—H in-plane deformations in G units + C—O deformations in primary alcohols |
| 970 | C—H out-of-plane deformation of trans-double bond (conjugated with an aromatic ring, *α,β*-double bond) |
| 913 | aromatic C—H out-of-plane deformation (only in GS lignin type) |
| 833 | aromatic C—H out-of-plane deformation (only in GS and H lignin types) |

The spectra showed bands typical of hardwood lignin. A relatively high peak at 1325 $cm^{-1}$ and a strong band at 1116 $cm^{-1}$ are characteristic for an IR spectrum of hardwood lignins.[29,30] In the case of softwood lignin, the former is usually very small, and the latter appears at 1140 $cm^{-1}$. Such shifts have been explained by Faix,[29] who found that the band at 1140 $cm^{-1}$ is shifted toward lower wavenumbers as the content of S units in lignin increases. Bands at 833 and 913 $cm^{-1}$ are also specific to hardwood lignins, and they are absent in spectra of softwood lignins.[29,30] The spectra of both hydrotropic lignins were almost identical, implying that the lignins have similar structures. Compared to other lignins,[31] the spectra look very similar to the spectrum of Alcell lignin. This could suggest that the structures of the hydrotropic and Alcell lignins are close to each other.

A weak band at 970 $cm^{-1}$ is attributed to the *α,β*-double bond. A small amount of low molecular weight stilbenes was found in the lignins in the GC (analysis of extractives). Such compounds are not present in birch wood in either extractives or lignin. In addition, FTIR spectra of milled wood lignins (MWL) do not show absorbance at this wavenumber.[29] Therefore, it can be concluded that such structures were formed during the treatments. A possible route of formation of stilbenes in moderately acidic conditions is described elsewhere.[32] The sequence involves homolysis of a *β-O*-4′ linkage and formation of a *β*-1′ structure, which in acidic media is converted to stilbenes.

**Characterization of Lignins with $^{1}H-^{13}C$ HSQC NMR.** 2D NMR spectrometry was used to estimate the main linkages in the lignins. The spectra are shown in Figure 4, and the main lignin linkages and structures are depicted in Figure 5. The results of the 2D NMR studies are shown in Table 2. Both lignins still contained *β-O*-4′ linkages (structure A), and this type of linkage was the predominant type of bond; *β*-5′ (structure B) and *β-β*′ (structure C) linkages were present in hydrotropic lignins in lower quantities (Table 2). Generally, *β-O*-4′ is the main type of bond in native lignins, and the contents of *β*-5′ and *β-β*′ linkages are much lower. In native birch wood lignin *β-O*-4′ accounts for about 40 per 100 units, and the amounts of *β*-5′ and *β-β*′ are 2−5 and 7−10 per 100 units, respectively.[33−35] Hence, it is clearly seen for *β-O*-4′ and *β-β*′ linkages that their contents decreased during the hydrotropic process. On the other hand, it seems that the amount of *β*-5′ bonds was not affected significantly by the hydrotropic treatments.

Such changes in the structure of the lignins are consequences of the chemical reactions that took place during the hydrotropic treatments. The pH of the process was around 3.5 (pH values of spent solutions from the modified and reference treatments were 3.3 and 3.5, respectively) and, therefore, the type of reactions that happened with the lignin during the treatment are probably those that take place during pulping under moderately acidic conditions and autocatalyzed processes, such as hydrothermal or ethanol−water treatment. It is suggested that the main reaction in such conditions is homolytic cleavage of a *β-O*-4′ bond through quinone methide intermediate


dx.doi.org/10.1021/jf5037728 | J. Agric. Food Chem. 2014, 62, 10759−10767

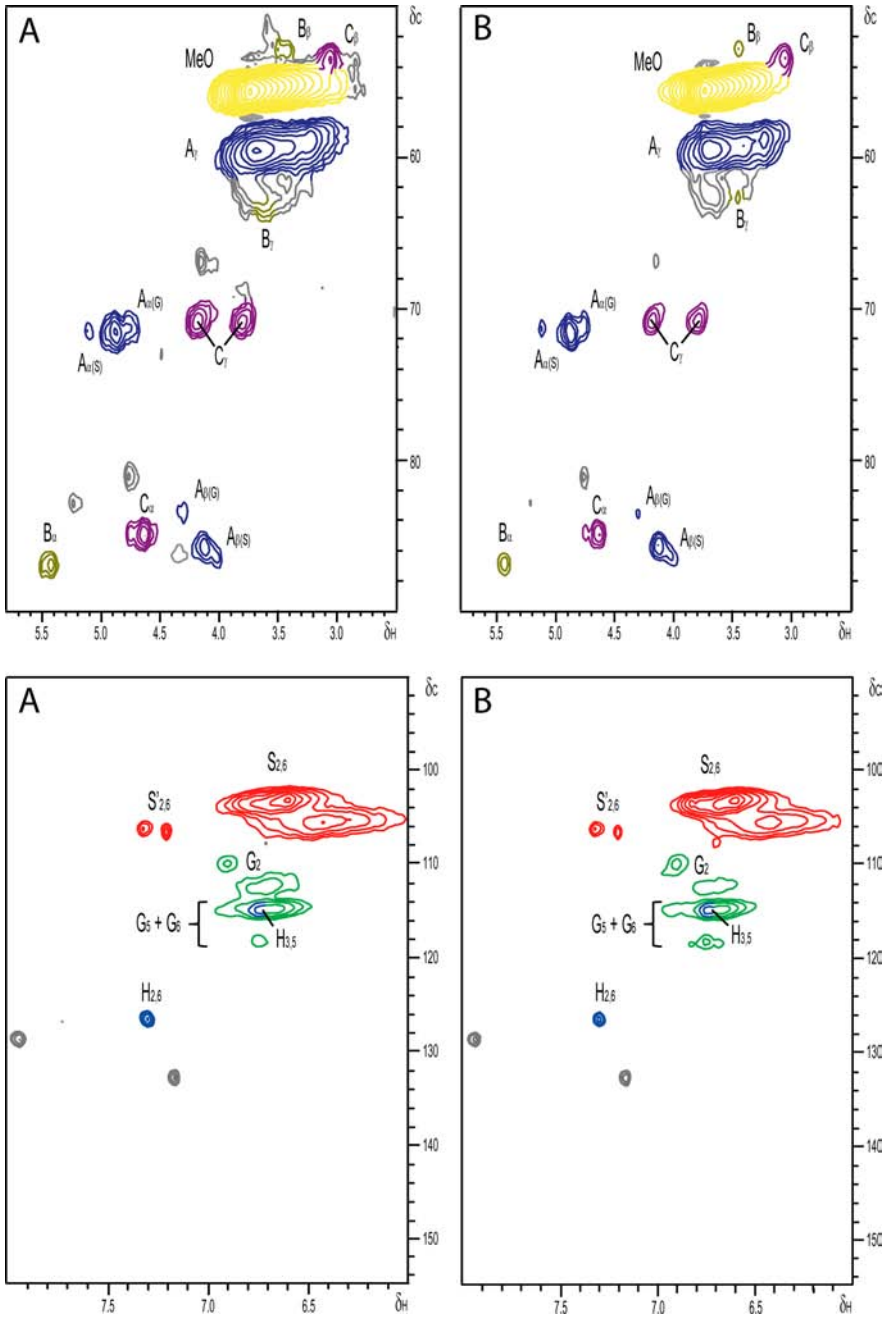


**Figure 4.** HSQC spectra of hydrotropic lignins: (A) R and (B) M. The assigned lignin structures are shown in Figure 5.

followed by radical coupling and radical exchange reactions.[22,32,36] The former path leads to the formation of *β*-1′, *β*-*β*′, and *β*-5′ structures.[32] *β*-1′ and *β*-5′ can be converted to stilbenes (as was discussed under FTIR) with the loss of a C*γ*–OH group as formaldehyde.[32,37] Besides these reactions, lignin also undergoes counterproductive condensation reactions. In the case of the modified process, additional various reactions could take place due to added hydrogen peroxide.[5]

The ratio of the units (H/G/S) calculated from the NMR data differs from the values obtained by pyrolysis-GC-MS, especially the results for the reference lignin (Table 2). However, the results of NMR can be considered more accurate than those of pyrolysis-GC-MS. According to the NMR, both lignins showed difference in the ratio of the units.

Both lignins were quite similar in the amount of bonds. The only difference was the amount of *β*-*O*-4′ linkage. With respect to this, the M lignin seems to be more degraded than the reference one. The reason for this is more severe conditions during the modified treatment due to a higher acidity and the presence of an oxidant. This fact can be also supported by the lower yield of cellulosic pulp obtained with the modified process and lower content of residual lignin in the pulp. In addition, it has been shown previously[5] that the pulp from the modified process has lower viscosity and a smaller amount of residual hemicelluloses in comparison with the reference one, which also indicates the severity of the modified treatment.

**$^{31}$P NMR.** The data from other analyses were extended by quantitative $^{31}$P NMR spectrometry. Before $^{31}$P NMR measurements, the sample is derivatized with 2-chloro-4,4,5,5-


dx.doi.org/10.1021/jf5037728 | J. Agric. Food Chem. 2014, 62, 10759−10767

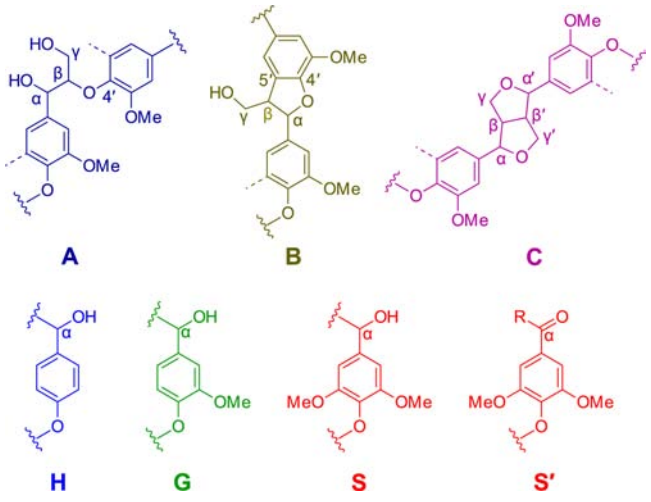


**Figure 5.** Lignin structures detected by 2D NMR: (A) *β-O*-4′; (B) *β*-5′ (phenylcoumaran structure); (C) *β*-*β*′ (resinol structure); (H) *p*-hydroxyphenylpropane unit; (G) guaiacylpropane unit; (S) syringyl-propane unit; (S′) syringylpropane unit with a carbonyl group at $C_\alpha$.

**Table 2. Content of the Main Linkages in the Hydrotropic Lignins, Lignin Units, and Their Ratio Determined by $^1H-^{13}C$ HSQC NMR**

| | linkages, per 100 units | | | units, % | | | | |
|---|---|---|---|---|---|---|---|---|
| lignin | *β-O*-4′ (A) | *β*-5′ (B) | *β*-*β*′ (C) | H, % | G, % | S, % | S′, % | S/G |
| R | 15.0 | 3.3 | 3.2 | 1 | 19 | 78 | 2 | 4.2 |
| M | 11.8 | 3.2 | 3.0 | 2 | 22 | 73 | 3 | 3.4 |

tetramethyl-1,3,2-dioxaphospholane, which reacts with OH moieties of functional groups. Therefore, this technique is used for estimation of aromatic and aliphatic hydroxyl and carboxyl groups in lignin samples.

The amount of functional groups calculated from the $^{31}P$ NMR is summarized in Table 3. Both lignins had a relatively high content of phenolic hydroxyls attached to 5-substituted units. The signal of these units consisted of two poorly resolved signals of S phenolic units and G phenolic units substituted at the fifth position (condensed structures).[38] Therefore, it is quite likely that such a high amount of 5-substituted phenolic hydroxyls was affected by a high content of S units in the lignins.

**Table 3. Some Characteristics of the Hydrotropic and Two Hardwood Technical Lignins**

| | lignins | | | |
|---|---|---|---|---|
| | hydrotropic | | | |
| | R | M | Alcell[a] | HW soda[a] |
| carbohydrates, % | 0.32 | 0.14 | 0.30 | 8.04 |
| sulfur, % | 0.16 | 0.39 | | |
| aliphatic OH, mmol/g | 1.38 | 1.13 | 1.08 | 1.34 |
| 5-substituted (condensed + S) phenolic OH, mmol/g | 2.43 | 2.39 | 1.81 | 1.62 |
| G−OH, mmol/g | 0.64 | 0.60 | 0.70 | 0.51 |
| H−OH, mmol/g | 0.15 | 0.17 | 0.20 | 0.34 |
| total phenolic, mmol/g | 3.22 | 3.16 | 2.71 | 2.47 |
| COOH, mmol/g | 0.30 | 0.32 | 0.30 | 1.06 |
| $M_w$, g/mol | 5306 | 5910 | 3470 | 4570 |
| $M_n$, g/mol | 1035 | 1143 | 850 | 1105 |
| polydispersity | 5.1 | 5.2 | 4.1 | 4.0 |

[a]Data for Alcell and HW soda are from the literature.[19]

The contents of phenolic and aliphatic hydroxyl groups in birch (*Betula pendula*) MWL determined by $^{31}P$ NMR are 1.2 and 5.4 mmol/g, respectively.[39] By comparison of these numbers with the contents of aliphatic and phenolic hydroxyl groups of the hydrotropic lignins, it is clearly seen that the content of phenolic hydroxyl groups in the lignins increased after the treatment, whereas the amount of aliphatic hydroxyls decreased (Table 3). Both the increase of phenolic hydroxyl groups and the decrease of aliphatic OH are consequences of the reactions discussed above. Aliphatic hydroxyls could also be converted into carboxyl groups as a result of oxidation reactions.[36] The amounts of carboxyl groups were 0.30 and 0.32 mmol/g for R and M lignins (Table 3). The contributions of the extractives to the total content of carboxyl groups were not significant and were 6.0 and 4.9% in the case of R and M lignins, respectively.

Generally, the lignins did not differ from each other in the amount of functional groups, except the contents of aliphatic hydroxyl groups. Again, as was discussed previously, the reason for this was the different composition of the hydrotropic solutions employed in the treatments.

**SEC.** The molecular weights of lignins determined by alkaline SEC are shown in Table 3. The values do not differ considerably; however, the M lignin has higher $M_w$ than the reference one. Because the M lignin underwent greater changes due to the severity of the process, the difference between the molecular weights can be explained by the higher degree of condensation in the case of lignin obtained according to a modified process.

**Comparison with Other Technical Lignins.** Table 3 displays some characteristics of two commercial hardwood technical lignins and the hydrotropic lignins. The data are presented only for hardwoods, because lignins from nonwood and softwood raw materials are different by nature. The lignin obtained from the alkaline process has a higher content of carboxyl groups in comparison to the lignins isolated in acidic conditions. This can be explained by the higher oxidation rate of phenolic units by air in alkaline media in comparison to an acidic one.[40] A similar trend as with the carboxylic groups can be observed for carbohydrates. Lower contents of carbohydrates of Alcell and hydrotropic lignins can be attributed to the extensive hydrolytic processes taking place in the acidic media, as was discussed earlier in this paper.

Among the listed lignins, hydrotropic lignins are expected to be closer to Alcell lignin due to the similarity of the nature of the processes. Indeed, the contents of carbohydrates and carboxyl groups are quite similar (Table 3). In addition, the FTIR spectra of thhate hydrotropic lignins were similar to the spectrum of the Alcell lignin. However, due to the difference in the wood species and treatment agents as well as the process conditions (temperature, duration, liquor to solid ratio, etc.), the lignins also showed differences. For example, the Alcell lignin has a lower molecular weight and a lower content of phenolic hydroxyl groups than the hydrotropic lignins (Table 3) Also, the Alcell lignin is sulfur-free, and the hydrotropic lignins contain small amounts of sulfur, which, however, might be due to contamination in the hydrotropic agent.

In conclusion, the present study showed that 67% of the original birch wood lignin could be recovered by conventional

and modified hydrotropic treatments. The structure of lignins was altered during the hydrotropic treatments; the content of phenolic hydroxyl groups increased and that of aliphatic hydroxyls decreased. The lignin from the modified treatment underwent more considerable changes than the reference one, although generally both lignins were quite similar to each other. Also, the lignins showed some similarities with technical organosolv Alcell lignin. Both hydrotropic lignins have very little non-lignin contaminants and potentially present valuable raw materials for further chemical and thermal conversion or for making shaped biobased materials.

## ■ ASSOCIATED CONTENT

### Supporting Information

Material balance of lignin for the reference (Figure S1A) and modified (Figure S1B) hydrotropic treatments and $^{31}$P NMR spectra of the reference lignin (Figure S2A) and lignin from the modified hydrotropic process (Figure S2B). This material is available free of charge via the Internet at http://pubs.acs.org.

## ■ AUTHOR INFORMATION

### Corresponding Author

*(P.F.) Phone: +358 504096424. E-mail: pfardim@abo.fi.

### Funding

The Graduate School for Biomass Refining (BIOREGS) is acknowledged for its financial support.

### Notes

The authors declare no competing financial interest.

## ■ ACKNOWLEDGMENTS

Jacinta van der Putten and Guus Frissen are kindly acknowledged for the SEC analysis and NMR analysis, respectively.

## ■ REFERENCES

(1) Lapierre, C. Determining lignin structure by chemical degradations. In *Lignin and Lignans − Advances in Chemistry*; Heitner, C., Dimmel, D., Schmidt, J. A., Eds.; CRC Press: Boca Raton, FL, USA, 2010; pp 11−48.

(2) Procter, A. R. A review of hydrotropic pulping. *Pulp Pap. Mag. Can.* **1971**, *72*, 67−74.

(3) Balasubramanian, D.; Friberg, S. E. Hydrotropes − recent developments. In *Surface and Colloid Science*; Matijevic, E., Ed.; Plenum Press: New York, 1993; Vol. 15, pp 197−220.

(4) Korpinen, R.; Fardim, P. Lignin extraction from wood biomass by a hydrotropic solution. *Papel* **2009**, *70*, 69−82.

(5) Gabov, K.; Fardim, P.; da Silva Junior, F. G. Hydrotropic fractionation of birch wood into cellulose and lignin: a new step towards green biorefinery. *BioResources* **2013**, *8*, 3518−3531.

(6) McKee, R. H. Use of hydrotropic solutions in industry. *Ind. Eng. Chem.* **1946**, *38*, 382−384.

(7) Kreicberg, Z. N.; Grabovskij, J. K. Oxidation of hydrotropic lignin from aspen. *Tr. Inst. Lesokhoz. Probl. Khim. Drev., Akad. Nauk Latv. SSR* **1960**, *21*, 69−75.

(8) Zoldners, J. A.; Surna, J. A. Comparison of the reactivities of hydrotropic, alkali, and dioxane lignins from aspen. *Khim. Drev.* **1969**, *3*, 123−127.

(9) Kalninsh, A. I.; Surna, J. A.; Zoldners, J. A. The utilization of hydrotropic lignin for the preparation of molding powders. *Tr. Inst. Lesokhoz. Probl. Khim. Drev., Akad. Nauk Latv. SSR* **1962**, *24*, 65−70.

(10) Gromov, V.; Pormale, M. Hydrotropic and alkaline pulping of deciduous woods with simultaneous hydrogenation of lignin. II. Fractionation of the products of hydrogenation of lignin and separation of phenols. *Latv. PSR Zinat. Akad. Vestis* **1961**, *4*, 85−92.

(11) Telysheva, G. M.; Sergeeva, V. N.; Mozheiko, L. N. Alkaline oxidative decomposition of hydrotropic and sulfuric acid lignins. *Latv. PSR Zinat. Akad. Vestis, Kim. Ser.* **1966**, *6*, 720−728.

(12) Strand, A.; Sundberg, A.; Vähäsalo, L.; Holmbom, B. Influence of pitch composition and wood substances on the phase distribution of resin and fatty acids at different pH levels. *J. Dispersion Sci. Technol.* **2011**, *32*, 702−709.

(13) Smeds, A. I.; Eklund, P. C.; Monogioudi, E.; Willför, S. M. Chemical characterization of polymerized products formed in the reactions between matairesinol and pinoresinol with the stable radical 2,2-diphenyl-1-picrylhydrazyl. *Holzforschung* **2012**, *66*, 283−294.

(14) Vega, B.; Wondraczek, H.; Zarth, C. S. P.; Heikkilä, E.; Fardim, P.; Heinze, T. Charge-directed fiber surface modification by molecular assemblies of functional polysaccharides. *Langmuir* **2013**, *29*, 13388−13395.

(15) Ralph, J.; Marita, J. M.; Ralph, S. A.; Hatfield, R. D.; Lu, F.; Ede, R. M.; Peng, J.; Quideau, S.; Helm, R. F.; Grabber, J. H.; Kim, H.; Jimenez-Monteon, G.; Zhang, Y.; Jung, H.-J. G.; Landucci, L. L.; MacKay, J. J.; Sederoff, R. R.; Chapple, C.; Boudet, A. M. Solution-state NMR of lignins. In *Advances in Lignocellulosics Characterization*; Argyropoulos, D. S., Ed.; TAPPI Press: Atlanta, GA, USA, 1999; pp 55−108.

(16) Ralph, S. A.; Ralph, J.; Landucci, L. NMR database of lignin and cell wall model compounds. U.S. Forest Products Laboratory, Madison, WI, USA, http://ars.usda.gov/Services/docs.htm?docid=10491, 2004 (accessed January 2009).

(17) Martínez, A. T.; Rencoret, J.; Marques, G.; Gutiérrez, A.; Ibarra, D.; Jiménez-Barbero, J.; del Río, J. C. Monolignol acylation and lignin structure in some nonwoody plants: a 2D NMR study. *Phytochemistry* **2008**, *69*, 2831−2843.

(18) Ralph, J.; Landucci, L. L. NMR of lignins. In *Lignin and Lignans: Advances in Chemistry*; Heitner, C., Dimmel, D. R., Schmidt, J. A., Eds.; CRC Press (Taylor & Francis Group): Boca Raton, FL, USA, 2010; pp 137−234.

(19) Gosselink, R. J. A.; van Dam, J. E. G.; De Jong, E.; Scott, E. L.; Sanders, J. P. M.; Li, J.; Gellerstedt, G. Fractionation, analysis, and PCA modeling of properties of four technical lignins for prediction of their application potential in binders. *Holzforschung* **2010**, *64*, 193−200.

(20) Gromov, V. S.; Odincov, P. N. The hydrotropic pulping of aspen wood and the influence of various factors on it. *Tr. Inst. Lesokhoz. Probl. Akad. Nauk Latv. SSR, Vopr. Lesokhim. Khim. Drev.* **1957**, *12*, 79−90.

(21) Gromov, V. S.; Odincov, P. N. Composition and properties of the lignin hydrotropically isolated from hardwood. *Tr. Inst. Lesokhoz. Probl. Akad. Nauk Latv. SSR, Vopr. Lesokhim. Khim. Drev.* **1957**, *12*, 91−100.

(22) Leschinsky, M.; Zuckerstätter, G.; Weber, H. K.; Patt, R.; Sixta, H. Effect of autohydrolysis of *Eucalyptus globulus* wood on lignin structure. Part 1: comparison of different lignin fractions formed during water prehydrolysis. *Holzforschung* **2008**, *62*, 645−652.

(23) Goundalkar, M. J.; Bujanovic, B.; Amidon, T. E. Analysis of non-carbohydrate based low-molecular weight organic compounds dissolved during hot-water extraction of sugar maple. *Cellul. Chem. Technol.* **2010**, *44*, 27−33.

(24) Hergert, H. L.; Goyal, G. C.; Lora, J. H. Limiting molecular weight of lignin from autocatalysed organosolv pulping of hardwood. In *Lignin: Historical, Biological, and Materials Perspectives*; Glasser, W. G., Northey, R. A., Schultz, T. P., Eds.; ACS Symposium Series 742; American Chemical Society: Washington, DC, USA, 2000; pp 265−277.

(25) Fengel, D.; Wegener, G. *Wood: Chemistry, Ultrastructure, Reactions*; de Gruyter: Berlin, Germany, 1984; p 613.

(26) Gosselink, R. J. A.; Abächerli, A.; Semke, H.; Malherbe, R.; Käuper, P.; Nadif, A.; van Dam, J. E. G. Analytical protocols for characterization of sulfur-free lignin. *Ind. Crops Prod.* **2004**, *19*, 271−281.

(27) Pan, X.-J.; Sano, Y. Comparison of acetic acid lignin with milled wood and alkaline lignins from wheat straw. *Holzforschung* **2000**, *54*, 61−65.
(28) Vishtal, A.; Kraslawski, A. Challenges in industrial applications of technical lignins. *BioResources* **2011**, *6*, 3547−3568.
(29) Faix, O. Classification of lignins from different botanical origins by FT-IR spectroscopy. *Holzforschung* **1991**, *45*, S21−S27.
(30) Hergert, H. L. Infrared spectra. In *Lignins: Occurrence, Formation, Structures and Reactions*; Sarkanen, K. V., Ludwig, C. H., Eds.; Wiley Interscience: New York, 1971; pp 267−297.
(31) Boeriu, C. G.; Bravo, D.; Gosselink, R. J. A.; van Dam, J. E. G. Characterization of structure-dependent functional properties of lignin with infrared spectroscopy. *Ind. Crops Prod.* **2004**, *20*, 205−218.
(32) Li, S.; Lundquist, K.; Westermark, U. Cleavage of arylglycerol *β*-aryl ethers under neutral and acid conditions. *Nord. Pulp Pap. Res. J.* **2000**, *15*, 292−299.
(33) Lundquist, K. $^{1}$H NMR spectral studies of lignins. Quantitative estimates of some types of structural elements. *Nord. Pulp Pap. Res. J.* **1991**, *6*, 140−146.
(34) Lundquist, K. $^{1}$H NMR spectral studies of lignins. Results regarding the occurrence of *β*-5 structures, *β*-*β* structures, non-cyclic benzyl aryl ethers, carbonyl groups and phenolic groups. *Nord. Pulp Pap. Res. J.* **1992**, *1*, 4−8, 16.
(35) Balakshin, M.; Capanema, E.; Gracz, H.; Chang, H. M.; Jameel, H. Quantification of lignin-carbohydrate linkages with high-resolution NMR spectroscopy. *Planta* **2011**, *233*, 1097−1110.
(36) Hallac, B. B.; Pu, Y.; Ragauskas, A. J. Chemical transformations of *Buddleja davidii* lignin during ethanol organosolv pretreatment. *Energy Fuels* **2010**, *24*, 2723−2732.
(37) Li, S.; Lundquist, K. Acid reactions of lignin models of *β*-5 type. *Holzforschung* **1999**, *53*, 39−42.
(38) Berlin, A.; Balakshin, M. Industrial lignins: analysis, properties, and applications. In *Bioenergy Research: Advances and Applications*; Gupta, V. K., Tuohy, M. G., Kubicek, C. P., Saddler, J., Xu, F., Eds.; Elsevier: Amsterdam, The Netherlands, 2014; pp 315−336.
(39) Rauhala, T.; King, A. W. T.; Zuckerstätter, G.; Suuronen, S.; Sixta, H. Effect of autohydrolysis on the lignin structure and the kinetics of delignification of birch wood. *Nord. Pulp Pap. Res. J.* **2011**, *26*, 386−391.
(40) Liu, Y.; Carriero, S.; Pye, K.; Argyropoulos, D. S. A comparison of the structural changes occurring in lignin during Alcell and kraft pulping of hardwoods and softwoods. In *Lignin: Historical, Biological, and Materials Perspectives*; Glasser, W. G., Northey, R. A., Schultz, T. P., Eds.; ACS Symposium Series 742; American Chemical Society: Washington, DC, USA, 2000; pp 447−464.

related to whether *A. confusa* is suited to produce sugars for bioenergy application is limited, and this hinders the effective utilization of this species. Therefore, the objective of this study was to evaluate the potential of the extractive-free *A. confusa* heartwood for producing fermentable sugars based on two acid-based pretreatments: dilute acid (DA) and sulfite pretreatment (SP). The changes of the chemical characteristics in the cell wall of this species during these pretreatments were evaluated. Original *A. confusa* heartwood with high extractive content was also investigated for comparison.

## MATERIALS AND METHODS

**Wood Materials.** Shavings of a 40-year-old *A. confusa* heartwood were soaked in ethanol at ambient temperature for 3 weeks to remove valuable extracts. The yield of this ethanolic extract was 8.2%.[4] After air-dried at ambient temperature, these shavings were ground to 40−60 mesh wood meals. The wood meals were further extracted with toluene/ethanol (2:1, v/v) and ethanol in a Soxhlet apparatus for 48 h. The extractive yield of this further extraction was 1.1%. A total of 9.3% extractives were obtained from all of the extraction processes. The extractive-free wood meals were further dried over $P_2O_5$ under vacuum for later experiments.

**Pretreatments.** All pretreatments were performed in a cylindrical stainless reactor (25 mL) with a dry-heating system. The solid/liquid ratio (w/v) for all pretreatments was 1:10. For dilute acid pretreatments, 1 g of wood meals was reacted with 0.1% (w/w) $H_2SO_4$ at 150 or 170 °C for 10 or 20 min (150C10M, 150C20M, 170C10M, and 170C20M; Table 1). For sulfite pretreatments, 1 g of wood meals was reacted with 4 or 8% (w/w) $NaHSO_3$ and 1 or 2% (w/w) $H_2SO_4$ at 180 °C for 30 min (4B1A, 4B2A, 8B1A, and 8B2A; Table 1). The initial pH values of the SP liquors were between pH 2.1 and 2.6. After individual pretreatment, the sample was filtered by a sintered glass filter to separate the solid residues [pretreatment residues (PRs)] and pretreatment hydrolysates (PHs). An additional double-distilled water ($ddH_2O$) rinse (50 mL) of the PRs to remove residual pretreatment chemicals and inhibitors was also filtered, collected, and combined into PHs. An aliquot of the pretreatment hydrolysates was used for determination of the neutral sugar contents and other components.

**Table 1. Lists of Different Pretreatment Conditions Used**

| | | condition | |
|---|---|---|---|
| pretreatment | sample | temperature (°C) | time (min) |
| dilute acid[a] | 150C10M | 150 | 10 |
| | 150C20M | 150 | 20 |
| | 170C10M | 170 | 10 |
| | 170C20M | 170 | 20 |
| | | $NaHSO_3$ charge (wt % of wood) | $H_2SO_4$ charge (wt % of wood) |
| sulfite[b] | 4B1A | 4 | 1 |
| | 4B2A | 4 | 2 |
| | 8B1A | 8 | 1 |
| | 8B2A | 8 | 2 |

[a] $H_2SO_4$ (0.1%, w/w). [b] At 180 °C and 30 min.

**Enzymatic Saccharification.** The PRs were further vibration-milled (Wig-L-Bug) for 2.5 min, and the milled solid residues (0.5 g) were subjected to enzymatic saccharification. Enzymatic saccharification was carried out at 1% (w/v) consistency with the enzyme loading of 10.4 filter paper units (FPU)/g of substrate at pH 4.5 (sodium acetate buffer) and 45 °C for 72 h. The enzyme (FiberZyme LBL CONC, Dyadic International, Inc.) was a preparation of carbohydrate hydrolases with cellulase and xylanase activities. After the enzymatic saccharification, the mixtures were centrifuged to collect the supernatant. An aliquot of the supernatant [enzymatic hydrolysates (EHs)] was used for determination of the neutral sugar contents.

The overall performance of individual pretreatment was evaluated by the sugar recovery (%).

$$\text{sugar recovery (\%)} = (\text{sugar from PHs} + \text{sugar from EHs}) \times 100/\text{sugar in the original wood}$$

**Analytical Methods.** All analyses were conducted with three replicates, and all calculations were based on the oven-dried weight basis. The lignin content was determined according to the Klason lignin method,[19] combining both the Klason lignin and acid-soluble lignin to be the total lignin content. The extinction coefficient for acid-soluble lignin was 110 L $g^{-1}$ $cm^{-1}$ at 205 nm.[19]

Neutral sugar contents of samples were determined from the acid-soluble fraction of lignin determinations by the alditol−acetate method[20] and quantified by gas chromatography with a flame ionization detector (GC−FID, Agilent 7890A) and a DB-225 GC column. For the sugar contents released from the pretreatment processes (PHs) or enzymatic saccharification (EHs), aliquots of the corresponding hydrolysates were used for determining the sugar contents by the same alditol−acetate method.

Furfural contents in PHs were also determined by GC−FID (Agilent 7890A) with a Supelcowax 10 GC column. An aliquot of the PHs was diluted in acetone and used for determination of the furfural contents according to a GC method.[21]

Lignin monomeric composition was determined by the nitrobenzene oxidation (NBO) using original wood or pretreated residues according to a previous protocol,[22] and 5-iodovanillin was used as the internal standard.[23] The amounts of each lignin degradation product were quantified by GC−FID (Agilent 7890A) equipped with a DB-5 GC

**Table 2. Chemical Composition of *A. confusa* Cell Walls before and after Different Pretreatments[a]**

| | | composition (%)[b] | | | |
|---|---|---|---|---|---|
| sample[c] | pretreatment yield (%)[d] | total lignin | glucan | xylan | all polysaccharides |
| wood[e] | | 24.7 ± 0.4 D | 36.5 ± 0.8 C | 16.1 ± 0.3 A | 57.1 ± 1.5 A,B |
| 150C10M | 79.1 ± 1.7 A | 25.3 ± 0.3 D | 33.0 ± 1.1 C | 16.8 ± 0.2 A | 53.0 ± 1.4 B,C |
| 150C20M | 77.9 ± 2.2 A | 28.2 ± 1.3 B,C | 37.6 ± 0.6 C | 10.7 ± 0.8 B | 51.6 ± 1.2 B,C |
| 170C10M | 71.7 ± 0.6 B | 26.4 ± 0.4 C,D | 36.9 ± 0.4 C | 4.1 ± 0.3 C,D | 41.1 ± 0.1 D |
| 170C20M | 70.1 ± 0.4 B | 29.0 ± 0.0 A,B | 45.2 ± 0.2 B | 5.4 ± 0.3 C | 51.8 ± 0.9 C |
| 4B1A | 64.1 ± 0.2 C | 31.3 ± 0.3 A | 55.1 ± 1.2 A | 2.4 ± 0.6 D | 58.9 ± 0.7 A |
| 4B2A | 64.1 ± 0.2 C | 29.7 ± 0.1 A,B | 53.7 ± 1.7 A | 2.6 ± 0.1 D | 59.3 ± 0.8 A |
| 8B1A | 63.7 ± 1.1 C | 24.4 ± 0.2 D | 56.9 ± 0.2 A | 2.7 ± 1.1 D | 59.8 ± 0.6 A |
| 8B2A | 62.5 ± 0.3 C | 28.5 ± 0.6 B,C | 46.0 ± 0.7 B | 1.7 ± 0.0 D | 48.0 ± 0.7 C |

[a] Values in the same column with different letters are statistically different under Tukey's HSD test ($\alpha = 0.05$) [mean ± standard error (SE); $n = 3$; numbers are rounded up to the first decimal place]. [b] Percentage based on original or pretreated samples subjected for chemical analyses. [c] Please refer to Table 1 for the sample name. [d] Percentage of starting materials recovered as insoluble residues. [e] Extractive-free.


dx.doi.org/10.1021/jf504461c | J. Agric. Food Chem. 2014, 62, 10768−10775

column. H-type lignin was calculated from *p*-hydroxybenzaldehyde; G-type lignin was calculated from the sum of vanillin and vanillic acid; and S-type lignin was from the sum of syringaldehyde and syringic acid. No *p*-hydroxybenzoic acid was found in the nitrobenzene oxidation products.

The cellulose crystallinity indexes (CrIs) of different samples were calculated from the X-ray diffractogram (XRD) of the wood meal with the mesh size ranging from 40 to 60 with or without pretreatments. The XRDs were recorded on a Bruker D2 PHASER diffractometer. All scans were collected at 30 kV and 10 mA in the range of $5° < 2\theta < 40°$ using Cu K$\alpha$ radiation ($\lambda$ = 0.1544 nm). A peak fitting software (PeakFit, Systat Software, Inc.) was used to deconvolute the individual peaks, assuming Gaussian function for each peak and a broad peak at around 20.04° assigned to the amorphous component. Peak fittings were continued until the maximum *F* values were achieved. In all cases, the *F* values were greater than 2700, which corresponding to an $r^2 > 0.98$. The CrI was calculated by dividing the diffractogram area because of the crystalline components (sum of peak areas from 002, 021, 101, 10$\bar{1}$, and 040 peaks) by the total area of the original diffractogram.[24]

Properties of different treatment groups were compared all together by multiple mean comparisons [Tukey's honest significant difference (HSD) test; $\alpha = 0.05$] to test the significant differences among groups (SAS 9.3, SAS Institute, Inc., Cary, NC). Correlation analysis of the specific property pair was also performed with the same software using the multivariate function.

## RESULTS AND DISCUSSION

**Cell Wall Chemical Composition before and after Pretreatments.** Table 2 shows changes in the chemical composition before and after pretreatments. A typical *A. confusa* wood contains about 24.7% lignin and 57.1% polysaccharides. The pretreatment yields of the DA pretreatments were between 70.1 and 79.1%. As the reaction temperatures increased, the yields were reduced. The total lignin contents of the DA-pretreated residues slightly increased as the reaction times became longer. The glucan contents of the DA-pretreated residues did not change, except for the 170C20M sample. However, if the glucan contents of the DA-pretreated residues were calculated back to the glucan contents of the original wood, about 13−28% original glucan was actually lost during the DA pretreatment processes. The xylan contents reduced dramatically as the reaction temperatures increased from 150 to 170 °C. The increased glucan and lignin and reduced xylan contents in pretreated residues were also reported from the dilute-acid-pretreated *Populus trichocarpa*[18,25] and mixed hardwood species.[17,26]

The pretreatment yields of the sulfite pretreatments (62.5−64.1%) were lower than those in the DA pretreatments, as displayed in Table 2. The pretreatment yields from different sulfite pretreatments were similar to each other. The lignin contents of the SP-pretreated residues were increased when compared to that of the original wood, except for the 8B1A sample. The glucan contents of the SP-pretreated residues (46.0−56.9%) were much higher when compared to that of the original wood, and these contents were also higher than those of the DA-pretreated residues. If the glucan contents of the SP-pretreated residues were calculated back to the glucan contents of the original wood, about 1−6% original glucan was lost during the sulfite pretreatment processes except for the 8B2A sample. These glucan losses were lower than those in the DA-pretreated processes. The xylan contents of the SP-pretreated residues (1.7−2.7%) were lower than those of the DA-pretreated residues (4.1−16.8%). These results are consistent with the observation from other researchers, who applied SPORL on various hardwood species.[15,17]

Nitrobenzene oxidation was used to profile the lignin composition of *A. confusa* wood before and after pretreatments, as illustrated in Figure 1. The major monomeric components of

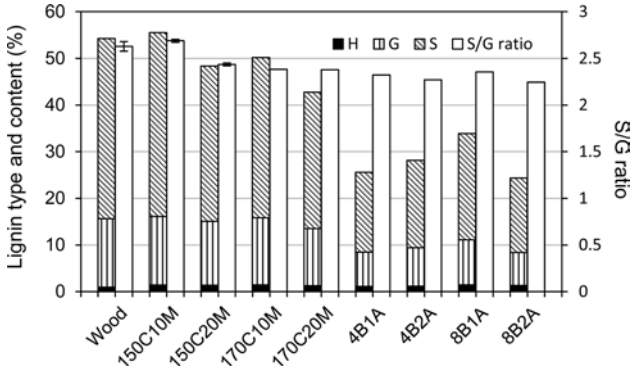


**Figure 1.** Lignin composition of samples before and after different pretreatments. Percentage based on moles of lignin from each sample assuming the molecular weight of one lignin C9 unit to be 210 g/mol. H, *p*-hydroxybenzaldehyde; G, sum of vanillin and vanillic acid; and S, sum of syringaldehyde and syringic acid. Mean ± SE; $n$ = 3. Please refer to Table 1 for the sample name.

*A. confusa* lignin were S- and G-type lignin, and they were about 38.6 and 14.7% based on moles of lignin, respectively. H-type lignin was the minor component and was only about 0.9% (Figure 1). The S/G ratio of *A. confusa* lignin was about 2.6, and the total yield of the nitrobenzene oxidation products was about 54.2%. The total yields of the nitrobenzene oxidation products decreased as the reaction temperatures or times increased during the DA pretreatments, indicating that the noncondensed lignin structures, such as 4-O-alkylated, $\alpha$-O-4, and $\beta$-O-4 lignin structures,[22] were reduced. This suggests that the lignin structures retained in the DA-pretreated residues were more condensed-type than that of the original wood. Recent evidence also revealed that the condensed lignin structures were increased after dilute acid pretreatments in spruce.[16] The DA pretreatments removed more S-type lignin than G-type lignin from the original wood lignin structures as the reaction temperatures or times increased (Figure 1). This caused the S/G ratios of lignin to decrease gradually from 2.7 (150C10M) to 2.4 (170C20M) as the reaction conditions became severe. The H-type lignin was rather stable (~1%) when compared to S- or G-type lignin under these pretreatments. Current results are consistent with the previous reports that $\beta$-O-4 linkages and S/G ratios were reduced during the DA pretreatment on hardwood species and the relative content of H-type lignin was rather unchanged during this process.[18,26]

During the sulfite pretreatments, *A. confusa* lignin was partially sulfonated, and the sulfonated lignin structures were removed by dissolving in the pretreatment liquors. The removals of noncondensed S- and G-type lignin structures in the sulfite pretreatments were more significant when compared to those in the DA pretreatments (Figure 1). The removal of the S-type lignin in the sulfite pretreatments seemed higher than that of the G-type lignin, causing the S/G ratios to reduce to 2.2−2.4 compared to that of the original wood (2.6; Figure 1). The total yields of the nitrobenzene oxidation products from the SP-pretreated samples were reduced in the range from 24% (8B2A) to 34% (8B1A), indicating that the residual lignin in acid bisulfite-pretreated samples was a more condensed type of lignin than that in DA-pretreated samples or modified lignin structures,

which could not be analyzed by the nitrobenzene oxidation. The occurrence of the lignin condensation reaction was reported in acidic sulfite pulping[27] and the SPORL-pretreated spruce,[16] suggesting that a similar condensation reaction might occur in the SP-pretreated *A. confusa* and, hence, increase the condensed lignin structures.

The CrI of original wood without any pretreatment was estimated to be 59.1% (Figure 2). DA pretreatments increased

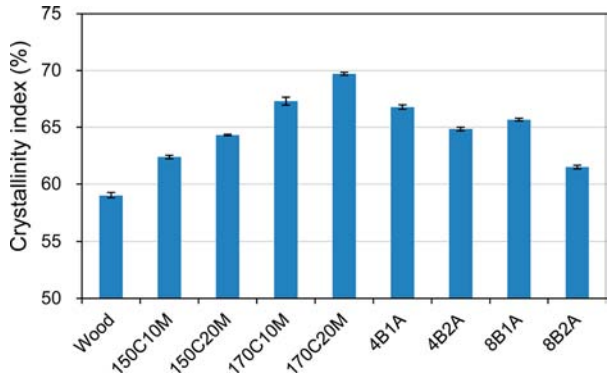


**Figure 2.** CrIs of samples before and after different pretreatments. Mean ± SE; $n$ = 3. Please refer to Table 1 for the sample name.

the CrIs of the pretreated residues when compared to that of the original wood. The increases of these CrIs were positively correlated to the reaction temperatures and times, and the highest CrI was 69.7% (170C20M). The sulfite pretreatments also increased the CrIs of the pretreated residues (61.5−66.8%) compared to that of the original wood. The increasing values of CrIs in pretreated residues were consistent with previous reports that dilute acid or acid bisulfite pretreatments usually elevated the crystallinity of lignocellulosics.[28,29] The increase of the biomass CrI was usually attributed to that of the amorphous hemicelluloses and partial lignin, and amorphous regions of native cellulose were removed and disrupted during the pretreatment process; hence, these would relatively increase the crystalline portion of the pretreated residue. However, current results cannot rule out the possibility that the aggregation of cellulose fibrils might occur because of thermally induced crystallization and aggregate growth under hydrothermal conditions.[28] The increments in CrIs of the SP-pretreated residues were reduced as the charges of bisulfite or acid increased. The reduced increments in CrIs of the SP-pretreated residues were likely attributed to the relatively increased amorphous components resulting from the condensed lignin aggregation.

**Composition of Hydrolysates Released from Pretreatments.** The monosugar components of the pretreatment hydrolysates were further analyzed and expressed as polysaccharide forms, as shown in Figure 3. Both DA and sulfite pretreatments hydrolyzed lots of xylan into the hydrolysates (Figure 3). In the DA pretreatments, 3.4% xylan was recovered from the 150C10M PHs and about 9−10% xylan was recovered from other PHs (Figure 3A). In the sulfite pretreatments, about 12−13% xylan was recovered from the 4% bisulfite-charged PHs and only about 6% xylan was recovered from the 8% bisulfite-charged PHs. The furfural contents in the SP hydrolysates were about 3.9−5.4% (Figure 3B), which were higher than those in the DA hydrolysates (∼2.0%; Figure 3A). Studies have shown that xylan, in comparison to other polysaccharides, can easily be hydrolyzed under acidic conditions and release xylose into the pretreatment hydrolysates,[8] and these xyloses might continue to be broken down into furfural and other degradation products.[30] Hence, by considering the mass balance of xylan, the lower xylan contents of 8% SP hydrolysates compared to those of 4% SP hydrolysates indicated that further degradation might occur during the pretreatment processes.

The DA pretreatments broke down about 1.7−3.3% lignin into the pretreatment hydrolysates (Figure 3A). The same extinction coefficient for acid-soluble lignin was assumed and used to calculate the sulfonated acid-soluble lignin in the SP hydrolysates. The acid-soluble lignin contents in the SP hydrolysates were about 4.6−6.9% (Figure 3B), which were higher than those in the DA hydrolysates. This indicated that more lignins were actually removed from the original wood during the sulfite pretreatments when compared to those during the dilute acid pretreatments. The disrupted and sulfonated

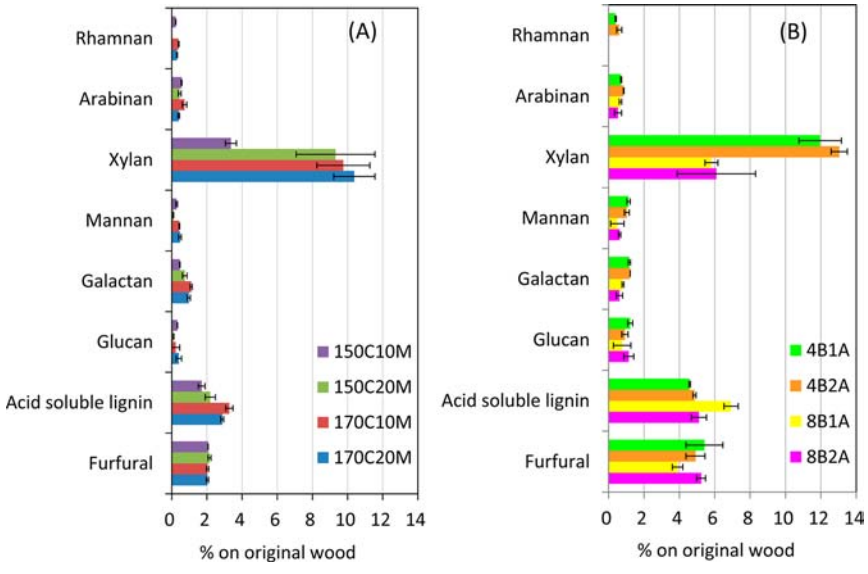


**Figure 3.** Chemical components in different pretreatment hydrolysates: (A) dilute acid pretreatments and (B) sulfite pretreatments. Mean ± SE; $n$ = 3. Please refer to Table 1 for the sample name.


dx.doi.org/10.1021/jf504461c | J. Agric. Food Chem. 2014, 62, 10768−10775

lignin could facilitate cellulose susceptibility to the following enzymatic hydrolysis.[16]

The glucan contents recovered from the pretreatment hydrolysates were not high. It was 0.1−0.4% from the DA hydrolysates (Figure 3A) and 0.8−1.2% from the SP hydrolysates (Figure 3B). Thus, about 12−28% original glucan was degraded to other products during the pretreatments, especially in the DA pretreatments (cf. Table 2 and Figure 3). These degradation products were not measured in the current study. However, previous studies have suggested that fermentation inhibitor compounds, such as 5-hydroxymethylfurfural, 5-methylfurfual, levulinic acid, and formic acid, might come from glucose degradation.[16,30] In spruce, DA pretreatments produced more than twice these inhibitor compounds when compared to those from SPORL pretreatments.[16] These could attribute to the low mass balances of glucan in the DA-pretreated samples (cf. Table 2 and Figure 3).

**Enzymatic Saccharification and Cell Wall Properties.** Without any pretreatment, *A. confusa* wood released about 15% xylose or glucose based on the xylose or glucose contents of the original wood during the enzymatic saccharification (Figure 4).

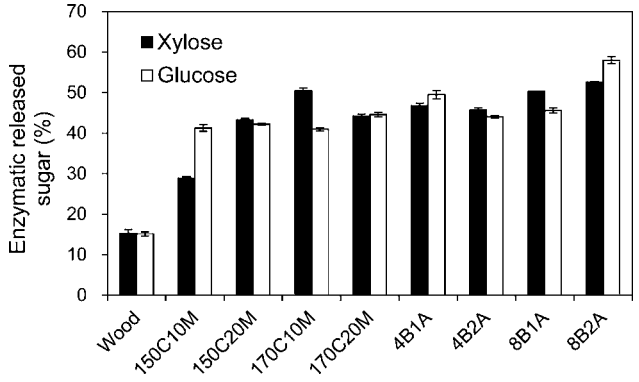


**Figure 4.** Enzymatic released sugar of different samples after 72 h of enzymatic saccharification. Percentage based on xylose or glucose contents in the substrates subjected to enzymatic hydrolysis. Mean ± SE; $n = 3$. Please refer to Table 1 for the sample name.

Both DA and sulfite pretreatments increased the enzymatic saccharification of pretreated residues when compared to that of the original wood without any pretreatment. Because the xylan contents in many of the pretreated residues were rather low (Table 2), the enzymatic saccharification of glucan was more significant than that of xylan in the pretreated residues. A generally higher glucose yield (44.0−58.0%) was obtained from the SP-pretreated residues when compared to that from the DA-pretreated residues (40.9−44.6%; Figure 4). These enzymatic saccharification yields are rather comparable to those obtained in the previous studies, in which various pretreatments, including dilute acid, SPORL, green liquor, autohydrolysis, and ozone pretreatments, were applied on various poplar woods.[17,25]

To further understand the cell wall properties that might have influences on the enzymatic saccharification of glucan, correlation analysis was further performed to profile the relationships (Figure 5). Among the cell wall properties measured in this study, only the xylan content, total yield of nitrobenzene oxidation, and S/G ratio were found to have significant correlations ($p < 0.05$) to the enzymatic saccharification of glucan. Other properties, such as total lignin, glucan content, and CrIs, were tested without significant correlations ($p > 0.13$). Our results indicated that lower xylan contents in the

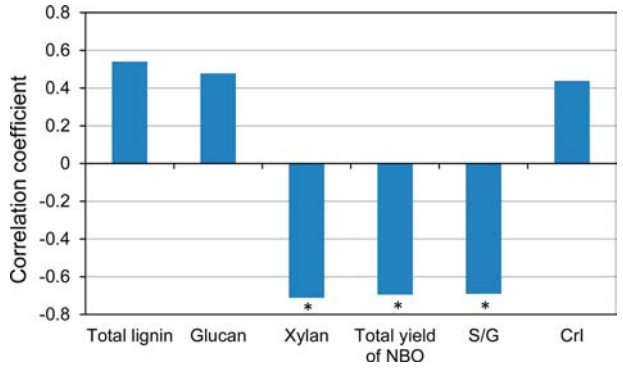


**Figure 5.** Correlation coefficient between enzymatic saccharification of glucan and the cell wall properties. NBO, nitrobenzene oxidation; S/G, S/G ratio; and CrI, crystallinity index. (*) $p < 0.05$.

pretreated residues would increase the enzymatic saccharification of glucan ($r = -0.7122$; Figure 5). Similar results were reported that decreasing the xylan content in the DA-pretreated corn stover[31] and SPORL-pretreated Douglas fir[32] would improve the extent of cellulose digestibility. Xylan is the major hemicellulose of *A. confusa*, and hemicelluloses are spatially associated with cellulose. Removal of hemicelluloses is important to enhance the cellulose digestibility.

The total yield of nitrobenzene oxidation reflects the portion of the noncondensed lignin in the overall lignin structures.[22] The correlation analysis indicated that, if the pretreated residues had less noncondensed lignin (more condensed lignin), the pretreated residues were more enzymatically hydrolyzable ($r = -0.6952$; Figure 5). Similarly, if the lignin S/G ratios of these pretreated residues were lower, the pretreated residues were more enzymatically hydrolyzable ($r = -0.6908$; Figure 5). The influence of lignin composition on cell wall digestibility still remains uncertain, and the results can be very different using various biomass and pretreatment techniques.[33−37] In the current study, the results can be explained by considering the cellulose accessible surface after the pretreatments. Our results indicated that both DA and sulfite pretreatments could break down the lignin barriers to loosen the ultrastructures of the cell walls and the sulfite pretreatments removed more lignin than the DA processes (Figure 3). The removal of lignin was more on the noncondensed lignin (high S/G ratio moieties), and this action left more condensed lignin (low S/G ratio moieties) retained in the SP-pretreated residues (Figure 1). The S/G ratios of the SP-pretreated residues were lower than those of the DA-pretreated residues (Figure 1), indicating that more severe lignin removal and loosened cell walls might exist in the SP-pretreated residues compared to those in the DA-pretreated residues. A previous study in comparing the cell wall structure changes after DA and SPORL pretreatments has demonstrated that the cellulose accessible surfaces from the SPORL-pretreated pine cell wall were about 3 times more than those from the DA-pretreated samples.[38] The cellulose accessible surface was actually created because of the lignin removal and loosened structures during the pretreatments. More cellulose accessible surfaces in the SP-pretreated residues might be created in comparison to those in the DA-pretreated residues, and hence, the enzymatic saccharification of the SP-pretreated residues (low S/G ratio and more condensed lignin) was increased in comparison to those in the DA-pretreated residues. The sulfonated lignin structures of the SP-pretreated residues might also play a significant role in the enzymatic efficiency and enhance the glucose yields.[12]

**Total Sugar Recovery.** To further evaluate the overall performance of different pretreatments, sugar recovery, combining the sugar contents from both PHs and EHs, was calculated. Without any pretreatment, *A. confusa* wood yielded only about 15% sugar recovery based on xylose, glucose, or total sugar of the original wood (Figure 6). All pretreatments could enhance the sugar recovery (>30%) based on xylose, glucose, or total sugar of the original wood. The recoveries of xylose exceeded 65% for many of the pretreatments in either the DA or sulfite pretreatment. These high xylose recoveries (Figure 6) mainly resulted from the xylose contents in the PHs (cf. Table 2 and Figure 3).

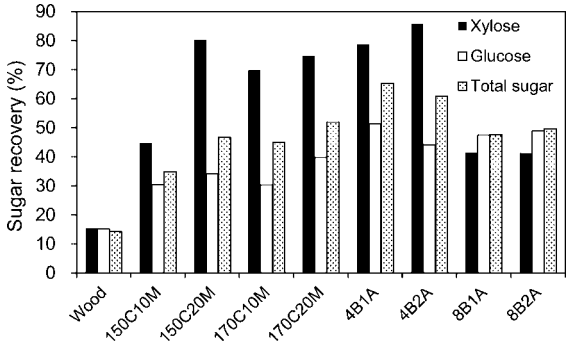


**Figure 6.** Sugar recovery (%) based on xylose, glucose, and total sugar of the original wood after individual pretreatment and enzymatic saccharification. Please refer to Table 1 for the sample name.

All glucose recoveries from different pretreatments were more than 30%, and the highest glucose recovery was from the 4% $NaHSO_3$ and 1% $H_2SO_4$ pretreatment (51.2%; Figure 6). Current glucose recoveries seem lower than the high glucose recovery suggested by the previous report, which showed a near-complete cellulose conversion to glucose in aspen using SPORL pretreatment.[15] About 60−80% original lignin was still remained in the pretreated residues (Table 2), and this residual condensed-type lignin and also the ultrastructures of the pretreated cell walls were still barriers limiting the full accessibility of enzymes during enzymatic saccharification. This indicates that further efforts either chemically or mechanically to increase the accessibility of the hydrolytic enzymes will help to enhance the glucose recoveries of current results. Studies even suggested that post-treatments after the pretreatment process, such as oxygen delignification[39] and mechanical refining,[12,40] would open up the surface areas and pore volumes, which would ultimately improve the enzymatic hydrolysis and finally increase the sugar recovery.

In the DA pretreatments, total sugar recoveries increased when the reaction temperatures and times increased. In the sulfite pretreatments, 4% bisulfite-pretreated samples yielded better total sugar recoveries than 8% bisulfite-pretreated samples. Overall, these total sugar recoveries were comparable to the results of the DA and SPORL pretreatments on various poplar species.[17] In the current study, the best total sugar recoveries from the DA and sulfite pretreatments are 52.0% (170C20M) and 65.3% (4B1A).

**Comparison of Samples with and without Extractives.** A high extractive content (9.3%) was obtained from the *A. confusa* heartwood. The best two pretreatments in the current study, 170C20M and 4B1A, were further chosen to evaluate the influences of extractives on the pretreatment and enzymatic saccharification. Figure 7 shows the sugar recoveries of wood, with and without extractives, after each pretreatment and enzymatic saccharification. Without any pretreatment, the original wood samples performed similarly either with or without extractives, and the total sugar recoveries were 13.0% for wood with extractives and 14.2% for wood without extractives, respectively (Figure 7). For the 170C20M-pretreated sample, the existence of extractives reduced the sugar recovery majorly from the PHs, especially in the recovery of xylose (Figure 7). For the 4B1A-pretreated sample, the existence of extractives reduced the sugar recoveries from both the pretreatment hydrolysates and enzymatic hydrolysates (Figure 7). The combined reductions of total sugar recoveries were 11.7% in the 170C20M-pretreated sample and 17.7% in the 4B1A-pretreated sample, indicating that the existence of extractives would reduce the sugar recoveries from both the DA and sulfite pretreatments.

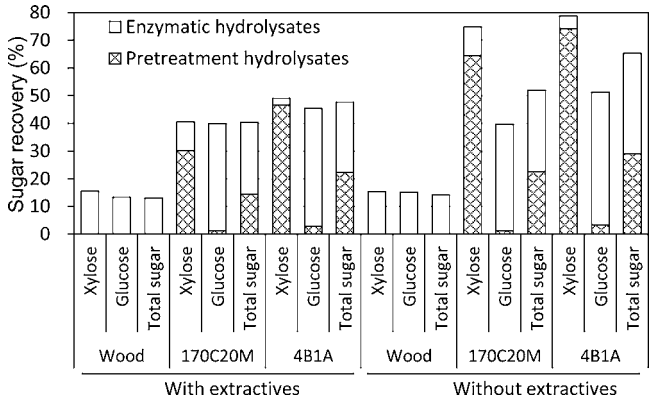


**Figure 7.** Sugar recovery (%) based on xylose, glucose, and total sugars of the original wood with and without extractives after specific pretreatments and enzymatic saccharification. Please refer to Table 1 for the sample name.

The major constituents in the extractives of *A. confusa* heartwood are phenolic compounds, flavonoids, and condensed tannins.[4,41] These compounds are chemically reactive species able to react with other molecules or through condensation reactions under acid treatments or acidic sulfite conditions.[27,42] These side reactions rerouted the pretreatment reactions, which were originally arranged to decrease the recalcitrance of cell walls to facilitate followed enzymatic saccharification. The non-productive adsorption of enzymes onto the condensation adducts from extractives can also be disadvantageous to enzymatic saccharification and, hence, reduce overall sugar recovery efficiency. Therefore, it is worth performing an extraction process in advance to remove the valuable extractives from *A. confusa* heartwood for biomedical purposes, and the resulting extractive-free wood residues will then go for deconstructing the cell walls for bioethanol utilization to maximize the benefits.

In summary, extractive-free *A. confusa* heartwood was subjected to different dilute acid and sulfite pretreatments. Reduced 4-O-alkylated lignin structures, lower S/G ratios, decreased xylan contents, and increased cellulose CrIs were found in all pretreated residues. All pretreated samples showed better sugar recoveries than the untreated wood. Cell wall properties, such as 4-O-alkylated lignin structures, S/G ratios, and xylan contents, of the pretreated residues showed significant correlations with the enzymatic saccharification of glucan. Increased cellulose accessible surfaces in the SP-pretreated samples compared to those in the DA-pretreated samples might enhance the enzymatic saccharification of the SP-pretreated samples. As a result, 4% bisulfite-pretreated samples yielded

higher sugar recovery than the DA-pretreated samples. The best sugar recovery was from the 4% $NaHSO_3$ and 1% $H_2SO_4$ pretreated sample. Current results also revealed that the existence of extractives in *A. confusa* reduced the sugars released from both the pretreatments and enzymatic saccharification.

## AUTHOR INFORMATION


### Corresponding Author

*Telephone: +886-2-33664655. Fax: +886-2-23654520. E-mail: stfyeh@ntu.edu.tw.



### Funding

This study was sponsored part by a grant (Grant 100AS-8.4.1-FB-e1(5)) from the Forestry Bureau, Council of Agriculture, Taiwan.


### Notes

The authors declare no competing financial interest.

## ACKNOWLEDGMENTS


The authors sincerely thank Dyadic International, Inc. (Jupiter, FL) for providing the enzymes. The authors gratefully acknowledge Prof. Shang-Tzen Chang for instrument access and suggestions to the manuscript. The authors also thank Prof. Jinn P. Chu for access to the X-ray diffractometer.


## REFERENCES


(1) Wang, Y. C. Carbon sequestration and foliar dust retention by woody plants in the greenbelts along two major Taiwan highways. *Ann. Appl. Biol.* **2011**, *159*, 244−251.

(2) Chen, Y. H.; Ho, C. K.; Hsiu, Y. R. Lowland forestation of *Acacia confusa*. *For. Res. Newsl.* **2014**, *21*, 1−5.

(3) Tung, Y. T.; Wu, J. H.; Huang, C. C.; Peng, H. C.; Chen, Y. L.; Yang, S. C.; Chang, S. T. Protective effect of *Acacia confusa* bark extract and its active compound gallic acid against carbon tetrachloride-induced chronic liver injury in rats. *Food Chem. Toxicol.* **2009**, *47*, 1385−1392.

(4) Wu, J. H.; Tung, Y. T.; Wang, S. Y.; Shyur, L. F.; Kuo, Y. H.; Chang, S. T. Phenolic antioxidants from the heartwood of *Acacia confusa*. *J. Agric. Food Chem.* **2005**, *53*, 5917−5921.

(5) Lin, H. Y.; Chang, S. T. Antioxidant potency of phenolic phytochemicals from the root extract of *Acacia confusa*. *Ind. Crops Prod.* **2013**, *49*, 871−878.

(6) Tung, Y. T.; Hsu, C. A.; Chen, C. S.; Yang, S. C.; Huang, C. C.; Chang, S. T. Phytochemicals from *Acacia confusa* heartwood extracts reduce serum uric acid levels in oxonate-induced mice: Their potential use as xanthine oxidase inhibitors. *J. Agric. Food Chem.* **2010**, *58*, 9936−9941.

(7) Wu, J. H.; Tung, Y. T.; Chien, S. C.; Wang, S. Y.; Kuo, Y. H.; Shyur, L. F.; Chang, S. T. Effect of phytocompounds from the heartwood of *Acacia confusa* on inflammatory mediator production. *J. Agric. Food Chem.* **2008**, *56*, 1567−1573.

(8) Hendriks, A. T. W. M.; Zeeman, G. Pretreatments to enhance the digestibility of lignocellulosic biomass. *Bioresour. Technol.* **2009**, *100*, 10−18.

(9) Himmel, M. E.; Ding, S. Y.; Johnson, D. K.; Adney, W. S.; Nimlos, M. R.; Brady, J. W.; Foust, T. D. Biomass recalcitrance: Engineering plants and enzymes for biofuels production. *Science* **2007**, *315*, 804−807.

(10) Johnson, D. K.; Elander, R. T. Pretreatment for enhanced digestability of feedstocks. In *Biomass Recalcitrance*; Himmel, M. E., Ed.; Blackwell Publishing: Oxford, UK, 2008; pp 436−453.

(11) Lloyd, T. A.; Wyman, C. E. Combined sugar yields for dilute sulfuric acid pretreatment of corn stover followed by enzymatic hydrolysis of the remaining solids. *Bioresour. Technol.* **2005**, *96*, 1967−1977.

(12) Zhu, J. Y.; Pan, X. J.; Wang, G. S.; Gleisner, R. Sulfite pretreatment (SPORL) for robust enzymatic saccharification of spruce and red pine. *Bioresour. Technol.* **2009**, *100*, 2411−2418.

(13) Jin, Y.; Jameel, H.; Chang, H. M.; Phillips, R. Green liquor pretreatment of mixed hardwood for ethanol production in a repurposed kraft pulp mill. *J. Wood Chem. Technol.* **2010**, *30*, 86−104.

(14) Teymouri, F.; Laureano-Perez, L.; Alizadeh, H.; Dale, B. E. Optimization of the ammonia fiber explosion (AFEX) treatment parameters for enzymatic hydrolysis of corn stover. *Bioresour. Technol.* **2005**, *96*, 2014−2018.

(15) Wang, G. S.; Pan, X. J.; Zhu, J. Y.; Gleisner, R.; Rockwood, D. Sulfite pretreatment to overcome recalcitrance of lignocellulose (SPORL) for robust enzymatic saccharification of hardwoods. *Biotechnol. Prog.* **2009**, *25*, 1086−1093.

(16) Shuai, L.; Yang, Q.; Zhu, J. Y.; Lu, F. C.; Weimer, P. J.; Ralph, J.; Pan, X. J. Comparative study of SPORL and dilute-acid pretreatments of spruce for cellulosic ethanol production. *Bioresour. Technol.* **2010**, *101*, 3106−3114.

(17) Wang, Z. J.; Zhu, J. Y.; Zalesny, R. S., Jr.; Chen, K. F. Ethanol production from poplar wood through enzymatic saccharification and fermentation by dilute acid and SPORL pretreatments. *Fuel* **2012**, *95*, 606−614.

(18) Cao, S.; Pu, Y.; Studer, M.; Wyman, C.; Ragauskas, A. J. Chemical transformations of *Populus trichocarpa* during dilute acid pretreatment. *RSC Adv.* **2012**, *2*, 10925−10936.

(19) Dence, C. W. The determination of lignin. In *Methods in Lignin Chemistry*; Lin, S. Y., Dence, C. W., Eds.; Springer-Verlag: New York, 1992; pp 34−40.

(20) Blakeney, A. B.; Harris, P. J.; Henry, R. J.; Stone, B. A. A simple and rapid preparation of alditol acetates for monosaccharide analysis. *Carbohydr. Res.* **1983**, *113*, 291−299.

(21) Cantarella, M.; Cantarella, L.; Gallifuoco, A.; Spera, A.; Alfani, F. Effect of inhibitors released during steam-explosion treatment of poplar wood on subsequent enzymatic hydrolysis and SSF. *Biotechnol. Prog.* **2004**, *20*, 200−206.

(22) Chen, C. L. Nitrobenzene and cupric oxide oxidation. In *Methods in Lignin Chemistry*; Lin, S. Y., Dence, C. W., Eds.; Springer-Verlag: New York, 1992; pp 301−321.

(23) Katahira, R.; Nakatsubo, F. Determination of nitrobenzene oxidation products by GC and $^1$H-NMR spectroscopy using 5-iodovanillin as a new internal standard. *J. Wood Sci.* **2001**, *47*, 378−382.

(24) Park, S.; Baker, J. O.; Himmel, M. E.; Parilla, P. A.; Johnson, D. K. Cellulose crystallinity index: Measurement techniques and their impact on interpreting cellulase performance. *Biotechnol. Biofuels* **2010**, *3*, 10.

(25) Min, D.; Li, Q.; Jameel, H.; Chiang, V.; Chang, H. M. Comparison of pretreatment protocols for cellulase-mediated saccharification of wood derived from transgenic low-xylan lines of cottonwood (*P. trichocarpa*). *Biomass Bioenergy* **2011**, *35*, 3514−3521.

(26) Lim, W. S.; Kim, J. Y.; Kim, H. Y.; Choi, J. W.; Choi, I. G.; Lee, J. W. Structural properties of pretreated biomass from different acid pretreatments and their effects on simultaneous saccharification and ethanol fermentation. *Bioresour. Technol.* **2013**, *139*, 214−219.

(27) Gellerstedt, G. Chemistry of chemical pulping. In *Pulp and Paper Chemistry and Technology. Volume 2, Pulping Chemistry and Technology*; Ek, M., Gellerstedt, G., Henriksson, G., Eds.; Walter de Gruyter GmbH & Co.: Berlin, Germany, 2009; Vol. 2, pp 91−120.

(28) Foston, M.; Ragauskas, A. J. Changes in lignocellulosic supramolecular and ultrastructure during dilute acid pretreatment of *Populus* and switchgrass. *Biomass Bioenergy* **2010**, *34*, 1885−1895.

(29) Kumar, R.; Mago, G.; Balan, V.; Wyman, C. E. Physical and chemical characterizations of corn stover and poplar solids resulting from leading pretreatment technologies. *Bioresour. Technol.* **2009**, *100*, 3948−3962.

(30) Zheng, R.; Zhang, H.; Zhao, J.; Lei, M.; Huang, H. Direct and simultaneous determination of representative byproducts in a lignocellulosic hydrolysate of corn stover via gas chromatography−mass spectrometry with a Deans switch. *J. Chromatogr. A* **2011**, *1218*, 5319−5327.

(31) Jeoh, T.; Ishizawa, C. I.; Davis, M. F.; Himmel, M. E.; Adney, W. S.; Johnson, D. K. Cellulase digestibility of pretreated biomass is limited by cellulose accessibility. *Biotechnol. Bioeng.* **2007**, *98*, 112−122.

(32) Leu, S. Y.; Zhu, J. Y.; Gleisner, R.; Sessions, J.; Marrs, G. Robust enzymatic saccharification of a Douglas-fir forest harvest residue by SPORL. *Biomass Bioenergy* **2013**, *59*, 393−401.
(33) Chen, F.; Dixon, R. A. Lignin modification improves fermentable sugar yields for biofuel production. *Nat. Biotechnol.* **2007**, *25*, 759−761.
(34) Grabber, J. H.; Ralph, J.; Hatfield, R. D.; Quideau, S. *p*-Hydroxyphenyl, guaiacyl, and syringyl lignins have similar inhibitory effects on wall degradability. *J. Agric. Food Chem.* **1997**, *45*, 2530−2532.
(35) Mechin, V.; Argillier, O.; Menanteau, V.; Barriere, Y.; Mila, I.; Pollet, B.; Lapierre, C. Relationship of cell wall composition to *in vitro* cell wall digestibility of maize inbred line stems. *J. Sci. Food Agric.* **2000**, *80*, 574−580.
(36) Santos, R. B.; Lee, J. M.; Jameel, H.; Chang, H. M.; Lucia, L. A. Effects of hardwood structural and chemical characteristics on enzymatic hydrolysis for biofuel production. *Bioresour. Technol.* **2012**, *110*, 232−238.
(37) Zhang, Y.; Culhaoglu, T.; Pollet, B.; Melin, C.; Denoue, D.; Barriere, Y.; Baumberger, S.; Mechin, V. Impact of lignin structure and cell wall reticulation on maize cell wall degradability. *J. Agric. Food Chem.* **2011**, *59*, 10129−10135.
(38) Li, X. P.; Luo, X. L.; Li, K. C.; Zhu, J. Y.; Fougere, J. D.; Clarke, K. Effects of SPORL and dilute acid pretreatment on substrate morphology, cell physical and chemical wall structures, and subsequent enzymatic hydrolysis of lodgepole pine. *Appl. Biochem. Biotechnol.* **2012**, *168*, 1556−1567.
(39) Koo, B. W.; Treasure, T. H.; Jameel, H.; Phillips, R. B.; Chang, H. M.; Park, S. Reduction of enzyme dosage by oxygen delignification and mechanical refining for enzymatic hydrolysis of green liquor-pretreated hardwood. *Appl. Biochem. Biotechnol.* **2011**, *165*, 832−844.
(40) Ertas, M.; Han, Q.; Jameel, H.; Chang, H. M. Enzymatic hydrolysis of autohydrolyzed wheat straw followed by refining to produce fermentable sugars. *Bioresour. Technol.* **2014**, *152*, 259−266.
(41) Wei, S. D.; Zhou, H. C.; Lin, Y. M.; Liao, M. M.; Chai, W. M. MALDI-TOF MS analysis of condensed tannins with potent antioxidant activity from the leaf, stem bark and root bark of *Acacia confusa*. *Molecules* **2010**, *15*, 4369−4381.
(42) Ping, L.; Brosse, N.; Sannigrahi, P.; Ragauskas, A. Evaluation of grape stalks as a bioresource. *Ind. Crops Prod.* **2011**, *33*, 200−204.

**Table 1. Percent Fatty Acid Composition of Purified Oils and of Monoacylglycerols (MAG) Obtained from Soybean Purified Oil**

| | purified oil | | | | | |
|---|---|---|---|---|---|---|
| fatty acid | peanut | palm | olive | sunflower | soybean | purified MAG |
| $C_{14:0}$ | 0.21 ± 0.03 | 0.72 ± 0.14 | 0.03 ± 0.01 | 0.12 ± 0.02 | 0.57 ± 0.15 | 0.29 ± 0.04 |
| $C_{16:0}$ | 11.39 ± 0.75 | 36.45 ± 1.65 | 9.59 ± 0.65 | 6.42 ± 0.46 | 12.67 ± 0.33 | 14.29 ± 0.27 |
| $C_{16:1}$ | 0.23 ± 0.09 | 0.52 ± 0.06 | 0.36 ± 0.06 | 0.06 ± 0.01 | 0.39 ± 0.13 | 0.35 ± 0.08 |
| $C_{17:0}$ | 0.23 ± 0.08 | 0.44 ± 0.09 | 0.27 ± 0.03 | 0.05 ± 0.01 | 0.32 ± 0.14 | 0.33 ± 0.09 |
| $C_{17:1}$ | 0.09 ± 0.02 | 0.40 ± 0.05 | 0.26 ± 0.03 | 0.05 ± 0.01 | 0.22 ± 0.09 | 0.26 ± 0.14 |
| $C_{18:0}$ | 1.57 ± 0.15 | 5.05 ± 0.24 | 2.53 ± 0.11 | 3.56 ± 0.22 | 3.68 ± 0.29 | 3.02 ± 0.43 |
| $C_{18:1}$ | 53.42 ± 1.01 | 45.90 ± 0.39 | 75.91 ± 1.22 | 29.29 ± 0.31 | 31.16 ± 1.01 | 29.47 ± 0.69 |
| $C_{18:2}$ | 30.98 ± 0.78 | 8.87 ± 0.08 | 9.55 ± 0.55 | 58.93 ± 0.97 | 44.01 ± 1.14 | 47.03 ± 1.02 |
| $C_{18:3}$ | 0.22 ± 0.05 | 0.46 ± 0.04 | 0.63 ± 0.12 | 0.38 ± 0.09 | 4.71 ± 0.24 | 4.18 ± 0.23 |
| $C_{20:0}$ | 0.88 ± 0.09 | 0.64 ± 0.11 | 0.59 ± 0.04 | 0.21 ± 0.03 | 1.13 ± 0.13 | 0.37 ± 0.06 |
| $C_{20:1}$ | 0.76 ± 0.05 | 0.55 ± 0.10 | 0.30 ± 0.09 | 0.94 ± 0.17 | 1.15 ± 0.16 | 0.40 ± 0.07 |
| iodine value[a] | 101.55 | 61.88 | 85.99 | 115.30 | 114.03 | |

[a]Calculated as reported by Kyriakidis and Katsiloulis.[26]

solution in methanol and vortexed for 3 min. Then, 200 mL of distilled water and 200 mL of diethyl ether were added. After mixing, the aqueous phase was removed while the etheric phase was repeatedly washed with distilled water (80 mL each time), until neutrality of the discarded water. Then, after filtration on sodium sulfate anhydrous, the ether was removed in a rotary evaporator. The adopted saponification method led to the formation of 98% of MAG, as confirmed by the HPSEC analysis. Obtained MAG were added to each PO (olive, peanut, sunflower, soybean, and palm) to obtain the following MAG/PO proportions: 0.5% (MAG0.5); 1% (MAG1); 2% (MAG2); 3% (MAG3). For each type of oil, as control (C) was used the PO with no added MAG.

**Oven Test.** Five grams of each PO was weighed in 50 mL glass vials and kept for 18 days at 60 °C, which represents the temperature commonly employed in a forced air oven. Fifty vials were prepared for each PO. At 4, 6, 10, 14, and 18 days 10 vials for each PO (two for control and for each MAG/PO proportion) were taken and submitted to analyses.

**Chemical Analyses.** The determinations of the free fatty acids (FFA), peroxide value (PV), and spectrophotometric constants were carried out according to the *Official Journal of the European Communities*.[24]

Fatty acids composition was carried out by gas chromatographic analysis of fatty acid methyl esters, according to the official methods.[24,25] In particular, the oil was treated with 2 N potassium hydroxide solution in methanol and vortexed for 5 min, and then 1 mL of hexane was added. Then, 1 μL of the hexane fraction was injected. The gas chromatographic system was composed of an Agilent model 7890A gas chromatograph (Cernusco, MI, Italy), equipped with a flame ionization detector (FID) and a WCOT fused-silica capillary column, FFAP-CB coating, 0.32 mm i.d. × 25 m length and 0.30 μm film thickness (Chrompack, Middleburg, The Netherlands). The temperature of the split injector was 210 °C, with a splitting ratio of 1:17; the detector temperature was 220 °C. The oven temperature was isothermally at 180 °C. Helium at flow rate of 1 mL $min^{-1}$ was utilized as carrier gas. The identification of each fatty acid was carried out by comparing the retention time with that of the corresponding standard methyl ester purchased from Sigma-Aldrich (St. Louis, MO, USA). RSD was about 5%.

The iodine value (IV) was determined as proposed by Kyriakidis and Katsiloulis,[26] which uses the percentage of fatty acid methyl esters determined from analysis of the fatty acid composition and an equation with coefficients specific for every type of vegetable oil.

The equation proposed is

$$IV = xC_1 + yC_2 + zC_3$$

where $C_1$, $C_2$, and $C_3$ correspond to the sum of the relative percentage concentrations of the unsaturated fatty acids with one, two, and three double bonds respectively, whereas $x$, $y$, and $z$ are the relative coefficients.

TAGP and ox-TAG were determined by means of high-performance size exclusion chromatography (HPSEC) of polar compounds (PCs), previously separated from the oil samples by silica gel column chromatography according to AOAC method 982.27.[27] After elution of the nonpolar components with 150 mL of petroleum ether/diethyl ether (87:13, v/v), the PCs were recovered with 150 mL of diethyl ether. After removal of the diethyl ether, the PCs were recovered in THF and the efficacy of separation was checked by thin layer chromatography as recommended by the same method. The chromatographic system consisted of a PerkinElmer pump, series 200, a 50 μL injector loop, a PL-gel guard column (PerkinElmer, Beaconsfield, UK) of 5 cm length × 7.5 mm i.d., and a series of two PL-gel columns (PerkinElmer) of 7.5 mm i.d. × 30 cm in length each. The columns were packed with highly cross-linked styrene divinylbenzene copolymers with a particle diameter of 5 μm and pore diameters of 500 Å. The detector was a differential refractometer (series 200A, PerkinElmer). The elution solvent used was THF for HPLC at a flow rate of 1.0 mL $min^{-1}$. The identification and quantification of individual peaks was carried out as described in previous papers.[28,29] The precision of the HPSEC method, expressed as RSD% ($n$ = 10), was 1.9% for PCs, 3.2% for TAGP, and 2.3% for ox-TAG.

Three replicates were analyzed per sample for each determination.

**Statistical Analysis.** Analysis of variance (two-way ANOVA) was carried out on the experimental data by using XLStat software (Addinsoft SARL, New York, NY, USA). Two-way ANOVA was performed considering the amount of MAG added to PO (MAG) and the different vegetable oils considered (oil), as well as their first -order interaction, as independent variables; Tukey's HSD test was applied for multiple comparisons.

The surface response regression analysis was carried out by Minitab 16 software (Minitab Inc., State College, PA, USA).

## RESULTS AND DISCUSSION

**Characterization of Raw Materials.** Table 1 reports the fatty acid composition of PO of olive, peanut, sunflower, soybean, and palm oils and of the MAG obtained from the purified soybean oil. The observed values agreed with those of the botanic species they derived from; higher saturated fatty acid levels were detected in palm oil, whereas higher monounsaturated levels were observed in olive, followed by peanut, palm, soybean, and sunflower oils. Linoleic acid was markedly more represented in sunflower, soybean, and peanut oils than in olive and palm oils; soybean oil, finally, showed the highest contents of linolenic acid. The differences in the

**Table 2. Chemical Characteristics of Purified Oils**

| | oil | | | | |
|---|---|---|---|---|---|
| parameter[a] | peanut | palm | olive | sunflower | soybean |
| FFA (g 100 $g^{-1}$) | 0.00 ± 0.00 | 0.00 ± 0.00 | 0.00 ± 0.00 | 0.00 ± 0.00 | 0.00 ± 0.00 |
| PV (mequiv $O_2$ $kg^{-1}$) | 0.00 ± 0.00 | 0.00 ± 0.00 | 0.00 ± 0.00 | 0.00 ± 0.00 | 0.00 ± 0.00 |
| $K_{232}$ | 0.46 ± 0.05 | 0.53 ± 0.05 | 0.59 ± 0.04 | 0.96 ± 0.06 | 1.29 ± 0.07 |
| $K_{270}$ | 0.09 ± 0.01 | 0.02 ± 0.00 | 0.04 ± 0.01 | 0.08 ± 0.01 | 0.09 ± 0.01 |
| TAGP (g 100 $g^{-1}$) | 0.02 ± 0.00 | 0.00 ± 0.00 | 0.00 ± 0.00 | 0.03 ± 0.00 | 0.00 ± 0.00 |
| ox-TAG (g 100 $g^{-1}$) | 0.00 ± 0.00 | 0.02 ± 0.00 | 0.00 ± 0.00 | 0.02 ± 0.00 | 0.08 ± 0.01 |
| DAG (g 100 $g^{-1}$) | 0.08 ± 0.01 | 0.07 ± 0.01 | 0.03 ± 0.00 | 0.06 ± 0.01 | 0.03 ± 0.00 |
| PCs (g 100 $g^{-1}$) | 0.09 ± 0.01 | 0.10 ± 0.01 | 0.04 ± 0.01 | 0.11 ± 0.01 | 0.11 ± 0.01 |

[a]FFA, free fatty acids; PV, peroxide value; $K_{232}$, specific absorption at 232 nm; $K_{270}$, specific absorption at 270 nm; TAGP, triacylglycerol oligopolymers; ox-TAG, oxidized triacylglycerols; DAG, diacylglycerols; PCs, polar compounds.

**Table 3. Mean Values of the Analyses Carried out on Purified Oils (POs) and on the Same with Added 0.5, 1, 2, and 3% of Monoacylglycerols (MAG0.5, MAG1, MAG2, MAG3) after 10 Days at 60 °C, as well as Results of Statistical Analysis (Two-Way ANOVA followed by Tukey's HSD Test for Multiple Comparisons)**

| | | | oil | | | | |
|---|---|---|---|---|---|---|---|
| determination[a] | | MAG % | peanut | palm | olive | sunflower | soybean |
| PV | PO | 0 A[b] | 180.0 ± 3.9e[b] | 79.5 ± 1.7j | 139.9 ± 3.0h | 389.1 ± 8.4a | 155.9 ± 1.2fg |
| | MAG0.5 | 0.5 B | 146.0 ± 3.1fgh | 64.2 ± 1.4k | 47.5 ± 1.0l | 355.6 ± 7.7b | 158.8 ± 0.2f |
| | MAG1 | 1 C | 111.3 ± 2.4i | 46.3 ± 1.0l | 13.5 ± 0.3m | 332.6 ± 7.2c | 159.5 ± 0.6f |
| | MAG2 | 2 D | 91.6 ± 2.0j | 17.7 ± 0.4m | 8.7 ± 0.2m | 329.0 ± 7.1c | 148.0 ± 1.4fgh |
| | MAG3 | 3 E | 85.7 ± 1.8j | 13.8 ± 0.3m | 6.3 ± 0.1m | 289.6 ± 6.2d | 143.7 ± 1.6gh |
| TAGP | PO | 0 A | 2.53 ± 0.02fg | 0.87 ± 0.02l | 1.01 ± 0.01l | 4.22 ± 0.03a | 2.44 ± 0.01g |
| | MAG0.5 | 0.5 B | 2.05 ± 0.02h | 0.63 ± 0.01m | 0.19 ± 0.01no | 3.90 ± 0.02b | 2.56 ± 0.01efg |
| | MAG1 | 1 C | 1.83 ± 0.08i | 0.59 ± 0.01m | 0.06 ± 0.01op | 3.40 ± 0.10c | 2.72 ± 0.01e |
| | MAG2 | 2 D | 1.66 ± 0.01j | 0.51 ± 0.01m | 0.04 ± 0.00op | 3.27 ± 0.13c | 2.66 ± 0.02ef |
| | MAG3 | 3 E | 1.38 ± 0.03k | 0.31 ± 0.01n | 0.02 ± 0.00p | 2.92 ± 0.02d | 2.43 ± 0.03g |
| ox-TAG | PO | 0 B | 8.85 ± 0.02e | 4.26 ± 0.04m | 7.13 ± 0.03jk | 12.98 ± 0.09a | 7.62 ± 0.01hi |
| | MAG0.5 | 0.5 B | 8.07 ± 0.06f | 2.95 ± 0.09n | 2.42 ± 0.08o | 12.22 ± 0.02b | 7.73 ± 0.01gh |
| | MAG1 | 1 A | 7.39 ± 0.29ij | 2.04 ± 0.02p | 0.66 ± 0.01qr | 11.54 ± 0.07c | 7.99 ± 0.01fg |
| | MAG2 | 2 A | 7.06 ± 0.02k | 0.85 ± 0.01q | 0.48 ± 0.01rs | 11.31 ± 0.12cd | 7.85 ± 0.02fgh |
| | MAG3 | 3 B | 6.01 ± 0.12l | 0.51 ± 0.01rs | 0.32 ± 0.01s | 11.20 ± 0.04d | 7.70 ± 0.04ghi |

[a]PV, peroxide value (mequiv $O_2$ $kg^{-1}$); TAGP, triacylglycerol oligopolymers (g 100 $g^{-1}$); ox-TAG, oxidized triacylglycerols (g 100 $g^{-1}$). [b]Upper case letters are used to compare the samples considering the amount of monoacylglycerols added to purified oil; lower case letters are used to compare the samples considering the combined effect of MAG (%), oilm and MAG × oil interaction: different letters mean significant differences at $p \leq 0.05$.

unsaturation degree were paralleled by the IV, which was higher in sunflower and soybean oils than in the others.

Table 1 shows also that the fatty acid composition of MAG was similar to that of the corresponding soybean purified oil used for their preparation.

POs were constituted by unaltered triacylglycerols (>99.9%) and showed FFA and PV values equal to zero and low values for the spectrophotometric constants (Table 2), similar to those detected in a previous study.[14]

**Oven Test: Oxidation after 10 Days at 60 °C.** Table 3 reports the results of the analyses carried out on each PO and on the same PO with added 0.5, 1, 2, and 3% MAG (MAG0.5, MAG1, MAG2, and MAG3, respectively) after 10 days at 60 °C, as well as the results of statistical analysis (two-way ANOVA followed by Tukey's HSD test for multiple comparisons). The data of oxidation after 10 days were reported as representative of the overall trend during time, to exclude, in the first instance, "time" as a third source of variability, besides MAG amount and type of oil.

The addition of increasing amounts of MAG significantly influenced the oxidative process. In particular, less marked oxidative phenomena were observed when MAG were added to PO derived from olive, palm, peanut, and sunflower, confirming previous results obtained by adding MAG prepared from olive oil to the same olive oil.[21] A different and particular trend, instead, was observed when MAG were added to soybean PO. In this case, all of the analytical indices considered, apart from PV, significantly increased when MAG amounts up to 1% were added, confirming other research,[19,20,22] and decreased at higher MAG doses.

**Oven Test: Surface Response Regression.** In a recent review, Chen and collaborators[30] pointed out the presence of discordant data about MAG behavior toward oxidation. Moreover, the effect of compositional characteristics of MAG (chain length, unsaturation level) have been investigated, but the role of fatty acid composition of the oil to which MAG are added has been scarcely studied, as well as the relationships between the two compositions. We adopted surface response regression analysis to point out the effect of MAG on oxidation in oils having different fatty acid compositions.

Table 4 reports the coefficients of the regressions and the corresponding $p$ values. The use of coded units enables

**Table 4. Results of the Surface Response Regression: Regression Coefficients and Respective *p* Values**

| | peroxide value[a] | | ox-TAG[a] | | TAGP[a] | |
|---|---|---|---|---|---|---|
| term | coefficient | *p* value | coefficient | *p* value | coefficient | *p* value |
| **Soybean Oil** | | | | | | |
| constant | 176.511 | **<0.001** | 8.376 | **<0.001** | 2.874 | **<0.001** |
| time | 119.497 | **<0.001** | 3.818 | **<0.001** | 1.986 | **<0.001** |
| MAG | −2.023 | 0.323 | −0.114 | 0.060 | −0.120 | **0.001** |
| time × time | 110.945 | **0.004** | −1.237 | **<0.001** | 0.287 | **<0.001** |
| MAG × MAG | −9.711 | **0.010** | −0.370 | **0.001** | −0.319 | **<0.001** |
| MAG × time | 6.544 | **0.022** | −0.050 | 0.539 | −0.043 | 0.351 |
| **Sunflower Oil** | | | | | | |
| constant | 345.23 | **<0.001** | 12.216 | **<0.001** | 3.788 | **<0.001** |
| time | 286.83 | **<0.001** | 7.240 | **<0.001** | 4.481 | **<0.001** |
| MAG | −28.58 | **<0.001** | −0.831 | **<0.001** | −0.698 | **<0.001** |
| time × time | −9.54 | 0.292 | −1.886 | **<0.001** | 1.385 | **<0.001** |
| MAG × MAG | 5.38 | 0.556 | 0.131 | 0.522 | 0.112 | 0.199 |
| MAG × time | −3.22 | 0.643 | 0.045 | 0.770 | −0.589 | **<0.001** |
| **Peanut Oil** | | | | | | |
| constant | 138.85 | **<0.001** | 7.521 | **<0.001** | 1.912 | **<0.001** |
| time | 162.99 | **<0.001** | 5.316 | **<0.001** | 1.898 | **<0.001** |
| MAG | −25.25 | **<0.001** | −0.740 | **<0.001** | −0.415 | **<0.001** |
| time × time | 34.68 | **<0.001** | −1.601 | **<0.001** | 0.214 | **0.001** |
| MAG × MAG | 15.50 | **0.001** | 0.121 | 0.541 | 0.056 | 0.381 |
| MAG × time | −11.87 | **0.001** | −0.148 | 0.327 | −0.273 | **<0.001** |
| **Palm Oil** | | | | | | |
| constant | 38.64 | **<0.001** | 1.708 | **<0.001** | 0.482 | **<0.001** |
| time | 56.44 | **<0.001** | 2.177 | **<0.001** | 0.326 | **<0.001** |
| MAG | −42.94 | **<0.001** | −1.574 | **<0.001** | −0.309 | **0.009** |
| time × time | 13.23 | **0.006** | 0.231 | 0.100 | 0.102 | **0.008** |
| MAG × MAG | 20.88 | **<0.001** | 0.853 | **<0.001** | 0.124 | **0.002** |
| MAG × time | −42.79 | **<0.001** | −1.431 | **<0.001** | −0.199 | **<0.001** |
| **Olive Oil** | | | | | | |
| constant | 5.640 | 0.358 | 0.474 | 0.077 | −0.059 | 0.371 |
| days | 47.130 | **<0.001** | 1868 | **<0.001** | 0.331 | **<0.001** |
| MAG | −68.435 | **<0.001** | −2.943 | **<0.001** | −0.478 | **<0.001** |
| time × time | 20.049 | **0.006** | 0.499 | 0.103 | 0.141 | 0.066 |
| MAG × MAG | 65.648 | **<0.001** | 2.747 | **<0.001** | 0.514 | **<0.001** |
| MAG × time | −54.630 | **<0.001** | −2.094 | **<0.001** | −0.505 | **<0.001** |

[a]Peroxide value (mequiv $O_2$ $kg^{-1}$); TAGP, triacylglycerol oligopolymers (g 100 $g^{-1}$); ox-TAG, oxidized triacylglycerols (g 100 $g^{-1}$). *p* values <0.05 are in bold.

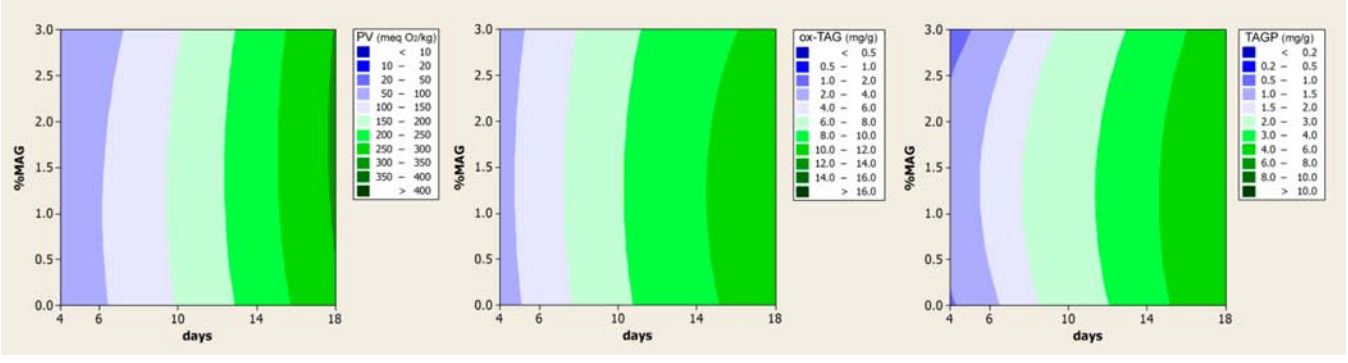


**Figure 1.** Response surface regressions for PV, ox-TAG, and TAGP in soybean oil as a function of time (oven test at 60 °C) and amount of added MAG.

comparisons among different variables. The results will be discussed separately for each type of oil, followed by the comparison among different oils.

Figure 1 shows the response surface regressions for PV, ox-TAG, and TAGP in soybean oil as a function of time and amount of added MAG. The addition of MAG to soybean PO determined a limited effect on PV, with a slight pro-oxidant activity at MAG doses up to 2% and antioxidant activity at higher doses (significant second-degree coefficient, denoted by the curved profile of isometric lines). This trend was more


dx.doi.org/10.1021/jf5025888 | J. Agric. Food Chem. 2014, 62, 10776−10782

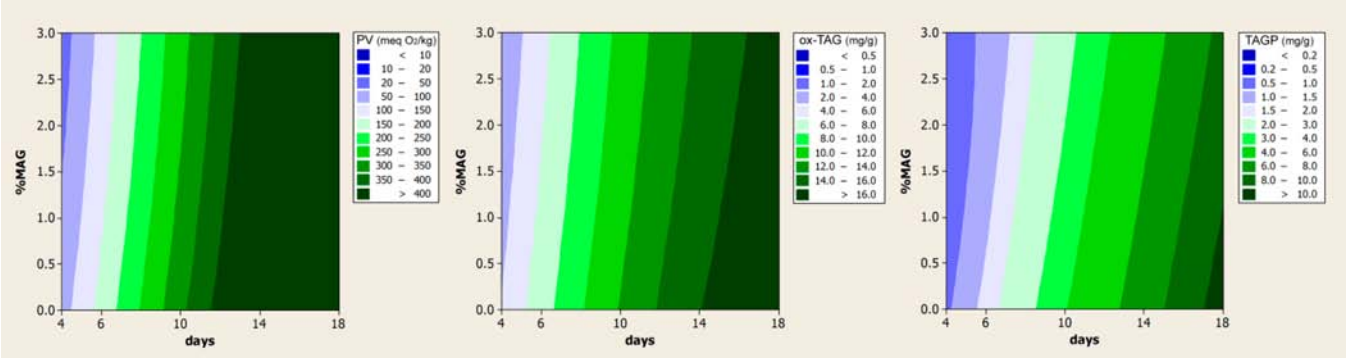


**Figure 2.** Response surface regressions for PV, ox-TAG, and TAGP in sunflower oil as a function of time (oven test at 60 °C) and amount of added MAG.

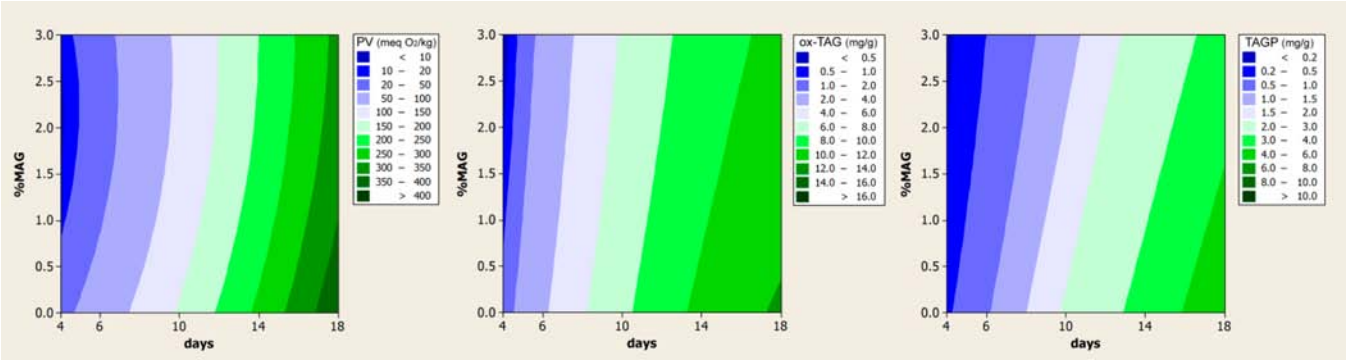


**Figure 3.** Response surface regressions for PV, ox-TAG, and TAGP in peanut oil as a function of time (oven test at 60 °C) and amount of added MAG.

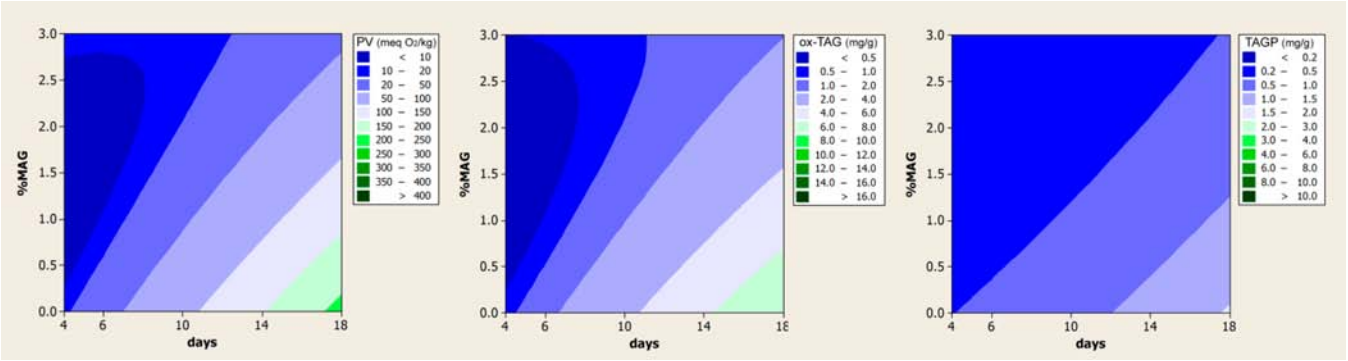


**Figure 4.** Response surface regressions for PV, ox-TAG, and TAGP in palm oil as a function of time (oven test at 60 °C) and amount of added MAG.

evident considering ox-TAG and TAGP, which showed, during the oven test, lower values in MAG3 than in control (PO).

Sunflower PO showed faster oxidation rates than the other oils tested, as evidenced by coefficients of the "time" variable. This result was probably due to higher content of linoleic acid than the other oils. The addition of MAG to sunflower PO induced exclusively antioxidant effect (Figure 2). PV and ox-TAG showed a linear negative correlation with MAG content. TAGP were significantly influenced by the interaction "MAG × time": the antioxidant activity of MAG on TAGP was more evident at longer times.

The addition of MAG to peanut oil had antioxidant effects (Figure 3), as observed in sunflower oil. The influence of MAG on PV increased progressively during time ($p$ value <0.001 for the interaction "MAG × time") and decreased with the increase of MAG amount. The effect observed on ox-TAG, although antioxidant as well, was linear. With regard to TAGP, the MAG amount effect was more evident in the advanced oxidation phases (only the interaction "MAG × time" was significant), confirming the intrinsic nature of these substances that are known to be related to the final steps of oxidative.

Palm oil, characterized by high contents of saturated fatty acids, enabled the observation of a marked antioxidant activity of MAG (Figure 4). The regression coefficients evidenced that the "MAG" variable had a greater contribution than "time". The antioxidant effect did not show a perfectly linear trend and was progressively more evident during time, as evidenced by the significant coefficient of the interaction "MAG × time".

In the case of olive oil (Figure 5) the addition of "MAG" had an impact comparable to that of the "time" variable on the


dx.doi.org/10.1021/jf5025888 | J. Agric. Food Chem. 2014, 62, 10776−10782

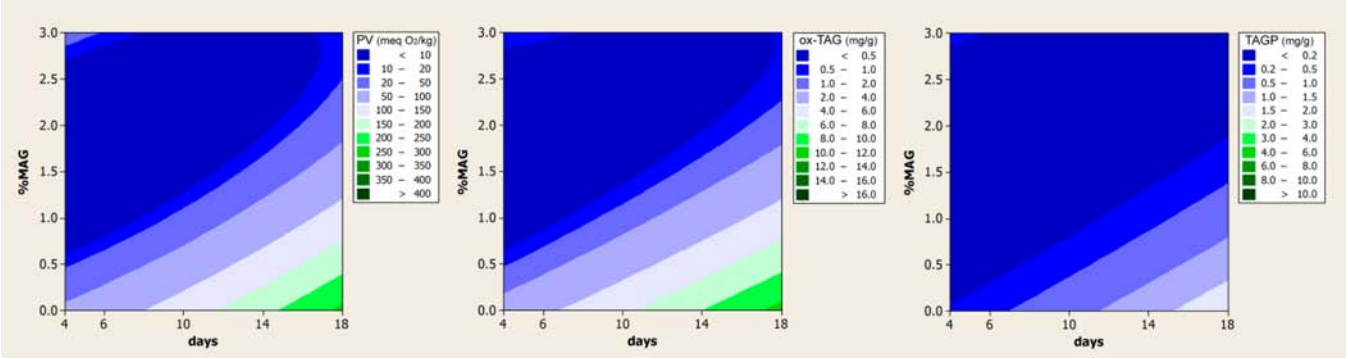


**Figure 5.** Response surface regressions for PV, ox-TAG, and TAGP in olive oil as a function of time (oven test at 60 °C) and amount of added MAG.

variations of the oxidative indices. The intensification of antioxidant activity during time compensated a not perfect linearity observed at the beginning of the forced oxidation in oven.

**Relationships between MAG Activity and Fatty Acid Composition of Oil.** As above-discussed, evident differences were observed in the effects induced by the addition of increasing MAG doses to different types of PO. The antioxidant effect of MAG was significantly higher in oil at low unsaturation level, such as palm and olive oils, with the most positive effects for the latter. Among the most unsaturated oils, peanut and sunflower encountered a linear slowdown of oxidation, slightly less pronounced in sunflower oil, which was the most susceptible to oxidation due to its high content of linoleic acid. A peculiar trend was highlighted for soybean oil, where the antioxidant effect of high amounts of MAG was opposed to a pro-oxidant effect observed up to 1%, coupled to a more limited overall oxidation than in other oils. Mistry and Min[20] observed a pro-oxidant activity of MAG in soybean oil up to 1% and attributed this result to the ability of MAG to situate at the interface oil/air (due to their high polarity) so as to facilitate oxygen solubilization into oil. It is possible that, at higher doses, interface MAG constituted a preferential substrate of oxidation. These phenomena could be more pronounced when differences in fatty acid composition between MAG and triacylglycerols further limit the interactions between oil mass and interface MAG. Hence, the observed results should be interpreted in relation to the fatty acid composition of the MAG used, and it has to be taken into account that we adopted soybean oil as starting oil to prepare MAG; then we obtained highly unsaturated MAG with high content of linolenic (about 5%) and linoleic acid. It remains unclear why olive oil, less unsaturated than palm oil, amplifies the antioxidant behavior of MAG.

## AUTHOR INFORMATION

### Corresponding Author

*(F.C.) Mail: Università degli Studi di Bari Aldo Moro, DiSSPA, Sezione di Scienze e Tecnologie Alimentari, Via Amendola 165/a, I-70126 Bari, Italy. Fax: +39 080 5443467. E-mail: francesco.caponio@uniba.it.

### Notes

The authors declare no competing financial interest.

## ABBREVIATIONS USED

ANOVA, analysis of variance; FFA, free fatty acids; HPSEC, high-performance size exclusion chromatography; IV, iodine value; MAG, monoacylglycerols; MUFA, monounsatured fatty acids; ox-TAG, oxidized triacylglycerols; PCs, polar compounds; PO, purified oil; PUFA, polyunsaturated fatty acids; PV, peroxide value; TAGP, triacylglycerol oligopolymers

## REFERENCES

(1) Billek, G. Health aspects of thermoxidized oils and fats. *Eur. J. Lipid Sci. Technol.* **2000**, *102*, 587−593.

(2) Udilova, N.; Jurek, D.; Marian, B.; Gille, L.; Schulte-Hermann, R.; Nohl, J. Induction of lipid peroxidation in biomembranes by dietary oil components. *Food Chem. Toxicol.* **2003**, *41*, 1481−1489.

(3) Chung, H. J.; Colakoglu, A. S.; Min, D. B. Relationships among headspace, oxygen, peroxide value, and conjugated diene content of soybean oil oxidation. *J. Food Sci.* **2004**, *69*, 83−88.

(4) Antolovich, M.; Prenzler, P. D.; Patsalides, E.; Mcdonald, S.; Robard, K. Methods for testing antioxidant activity. *Analyst* **2002**, *127*, 183−198.

(5) Chayasit, W.; Elias, R. J.; McClements, D. J.; Decker, E. A. Role of physical structures in bulk oil on lipid oxidation. *Crit. Rev. Food Sci.* **2007**, *47*, 299−317.

(6) Min, D. B.; Boff, J. M. Chemistry and reaction of singlet oxygen in foods. *Compr. Rev. Food Sci. Food Saf.* **2002**, *1*, 57−72.

(7) Gutteridge, J. M. C. Biological origin of free radicals, and mechanisms of antioxidant protection. *Chem.−Biol. Interact.* **1994**, *91*, 133−144.

(8) Benjelloun, B.; Talou, T.; Delmas, M.; Gaset, A. Oxidation of rapeseed oil: effect of metal traces. *J. Am. Oil Chem. Soc.* **1991**, *68*, 210−211.

(9) Frankel, E. N. *Lipid Oxidation*; Oily Press: Dundee, Scotland, 1998.

(10) Jadhav, S. J.; Nimbalkar, S. S.; Kulkami, A. D.; Madhavi, D. L. Lipid oxidation in biological and food systems. In *Food Antioxidants*; Madhavi, D. L., Deshpande, S. S., Salunke, D. K., Eds.; Dekker: New York, 1996; pp 5−64.

(11) Mistry, B. S.; Min, D. B. Effects of fatty acids on the oxidative stability of soybean oil. *J. Food Sci.* **1987**, *52*, 380−381.

(12) Miyashita, K.; Takagi, T. Study on the oxidative rate and pro-oxidant activity of free fatty acids. *J. Am. Oil Chem. Soc.* **1986**, *63*, 1380−1384.

(13) Paradiso, V. M.; Gomes, T.; Nasti, R.; Caponio, F.; Summo, C. Effects of free fatty acids on the oxidative processes in purified olive oil. *Food Res. Int.* **2010**, *43*, 1389−1394.

(14) Gomes, T.; Delcuratolo, D.; Paradiso, V. M. Pro-oxidant action of polar triglyceride oligopolymers in edible vegetable oils. *Eur. Food Res. Technol.* **2008**, *226*, 1409−1414.

(15) Gomes, T.; Delcuratolo, D.; Paradiso, V. M.; Summo, C.; Caponio, F. Pro-oxidant activity of oxidized triacylglycerols in olive oil

and comparison with pro-oxidant action of polar triacylglycerol oligopolymers. *LWT—Food Sci. Technol.* **2011**, *44*, 1236−1239.
(16) Yoon, S. H.; Jung, M. Y.; Min, D. B. Effect of thermally oxidized triglycerides on the oxidative stability of soybean oil. *J. Am. Oil Chem. Soc.* **1988**, *65*, 1652−1656.
(17) Mistry, B. S.; Min, D. B. Prooxidant effects of monoglycerides and diglycerides in soybean oil. *J. Food Sci.* **1988**, *53*, 1896−1897.
(18) Aubourg, S. P. Effect of partially hydrolysed lipids on inhibition of oxidation of marine lipids. *Eur. Food Res. Technol.* **2001**, *212*, 540−545.
(19) Colakoglu, A. S. Oxidation kinetics of soybean oil in the presence of monoolein, stearic acid and iron. *Food Chem.* **2006**, *101*, 724−728.
(20) Mistry, B. S.; Min, D. B. Isolation of sn-$\alpha$-monolinolein from soybean oil and its effect on oil oxidative stability. *J. Food Sci.* **1987**, *52*, 786−790.
(21) Gomes, T.; Caponio, F.; Bruno, G.; Summo, C.; Paradiso, V. M. Effect of monoacylglycerols on the oxidative stability of olive oil. *J. Sci. Food Agric.* **2010**, *90*, 2228−2232.
(22) Caponio, F.; Paradiso, V. M.; Bruno, G.; Summo, C.; Pasqualone, A.; Gomes, T. Do monoacylglycerols act as pro-oxidants in purified soybean oil? Evidence of a dose-dependent effect. *Ital. J. Food Sci.* **2011**, *23*, 239−244.
(23) Lee, S. H.; Min, D. B. Effects, quenching mechanism and kinetics of carotenoids in chlorophyll-sensitized photooxidation of soybean oil. *J. Agric. Food Chem.* **1990**, *38*, 1630−1634.
(24) EC Regulation 2568/91. *Off. J. Eur. Communities* **1991**, *L 248*.
(25) AOCS. *Official Methods and Recommended Practices of the American Oil Chemists' Society*; AOCS Press: Champaign, IL, USA, 1993; method Ch 12b-92.
(26) Kyriakidis, N. B.; Katsoulis, T. Calculation of iodine value from measurement of fatty acid methyl esters of some oils: comparison with the relevant American Chemists' Society method. *J. Am. Oil Chem. Soc.* **2000**, *77*, 1235−1238.
(27) AOAC. *Official Methods of Analysis of Association of Official Analytical Chemists International*, 17th ed.; Horwitz, W., Ed.; AOAC Press: Arlington, VA, USA, 2003; method 982.27.
(28) Gomes, T.; Caponio, F. Effort to improve the quantitative determination of oxidation and hydrolysis compound classes in edible vegetable oils. *J. Chromatogr., A* **1999**, *844*, 77−86.
(29) Caponio, F.; Gomes, T.; Summo, C. Assessment of the oxidative and hydrolytic degradation of oils used as liquid medium of in-oil preserved vegetable. *J. Food Sci.* **2003**, *68*, 147−151.
(30) Chen, B.; McClements, D. J.; Decker, E. A. Minor components in food oils: a critical review of their roles on lipid oxidation chemistry in bulk oils and emulsions. *Crit. Rev. Food Sci.* **2011**, *51*, 901−916.

protein isolate was compared for its water-binding, emulsification, and gelation properties with egg white and soy protein isolates[11] and was found to have similar or better properties compared to egg white protein,[33] for example, in higher foam stability.[11] With regard to gelation, RuBisCO from alfalfa, tobacco, and spinach were reported to yield strong gels.[6] Libouga et al.[34] determined the critical gelation concentration of RuBisCO (from alfalfa) by heating sealed tubes. Unfortunately, this method yields no information on gelation kinetics. Lamsal et al.[31] performed stress relaxation tests on heat-set soluble leaf protein gels (alfalfa) that were found softer and faster to relax compared to whey protein.

Up to now, the gelation properties of RuBisCO were studied only for limited conditions (concentrations, pH) and experimental setup. No information is available on large deformation, texture properties, or microstructure of heat-induced gels of RuBisCO. For application purposes in food products, information on these properties and comparison with existing (e.g., whey protein, egg white protein) and other plant proteins (e.g., soy, pea, lupine) is essential. Hence, the objective of this study is to obtain insight into the gelation behavior of RuBisCO and the subsequent gel properties with regard to fracture behavior and microstructure. In addition, the heat-induced gelation of RuBisCO is compared to whey protein and egg white protein, which have been studied extensively for their gelation behavior, and to plant proteins such as soy, pea, and lupine. This study aims to show the potential of RuBisCO as a functional ingredient, giving opportunities for the design of new textures at low protein concentration.

## MATERIAL AND METHODS

**Materials.** WPI (BiPRO) was obtained from Davisco (Eden Prairie, MN, USA). Egg white protein was kindly supplied by Bouwhuis Enthoven (Raalte, The Netherlands). Water was purified using a Milli-Q system (Millipore Systems, Molsheim, France). Polyvinylpolypyrrolidone (PVPP), sodium metabisulfite, and Tris-base were obtained from Sigma-Aldrich (St. Louis, MO, USA). Q-Sepharose, Sephadex G75, and Superdex 200 were obtained from GE Healthcare (The Netherlands).

**Extraction RuBisCO.** Fresh spinach was pressed using an Angel juicer (Slowjuice, Naarden, The Netherlands); the juice was collected into a container and mixed with wet PVPP and 0.1% sodium metabisulfite. During collection the juice was stirred and cooled in ice water and stored at 4 °C until further use. To remove the chlorophyll, the collected juice was heated at 50 °C for 30 min while stirring and flushing the headspace with nitrogen. After heating, the juice was cooled to 4−6 °C while stirring in a cold room and centrifuged (15000*g*, 35 min, 6−8 °C). The clear juice was set to pH 8 with solid Tris-base (4 g/L) and 4 M NaOH. The juice was filtered over a 0.45 μm filter before being loaded on a Q-Sepharose fast flow (FF). The clear juice containing the RuBisCO was diluted with Milli-Q water and eluens until conductivity was below 6.5 mS/cm. The resulting solution was loaded on a Q-sepharose FF column (1.4 L, diameter = 10 cm, height = 23 cm) previously equilibrated with 20 mM Tris/HCl, pH 8.0. Immediately after the Q-Sepharose, soluble fractions containing RuBisCO were desalted into 20 mM Tris/HCl, pH 8, using a Sephadex G75 column. The desalted fractions were colorless, treated with a 0.22 μm sterile filter, and stored as a protein concentrate (12.4 mg/mL, 20 mM Tris/HCl, pH 8) at 4 °C until further use. For gelation experiments, this solution was diafiltrated against demineralized water and concentrated to the desired concentration using an Amicon 8200 stirred cell (Merck Millipore, Darmstadt Germany) with a 3K membrane filter. pH was set at pH 7. Yield of RuBisCO from spinach was 10 g/10 kg of spinach.

**Extraction of Plant Proteins.** Pea was extracted from a commercial brand of dry peas (HAK, Almkerk, The Netherlands). The protein content of this source is 22% of proteins. The dried peas were ground to get a flour. Then, the flour was sieved, and only the fraction with size smaller than 180 μm was used for extraction. Lupine was extracted from a lupine flour (*Lupinus angustifolius*, unknown cultivar) product called FRALU CON, from L. I. Frank (Twello, The Netherlands). Soy was extracted from defatted soybean flour (Cargill, Amsterdam, The Netherlands) having a protein content of ∼50 wt %.

For all plant proteins the following steps were performed. Flour was dissolved in Milli-Q water, ratio 1:10. The pH was adjusted to 8, and the mixture was incubated for 1 h at room temperature while stirring. Centrifugation of the suspension was done at 6000*g* for 30 min at 7 °C, and the supernatant was taken for isoelectric precipitation at pH 4.5 (lupine and soy) or pH 4.8 (pea). Incubation was performed for at least 2 h (overnight in the case of soy) at 4 °C. After centrifugation (6000*g* for 30 min at 7 °C), the pellet was washed with cold Milli-Q water and dispersed using an Ultra Rurrax at low speed. For soy, three wash steps (1:3 volume ratio with Milli-Q water) were carried out, whereas for pea and lupine only one wash step (1:10 volume ratio) was done. Centrifugation and collection of the pellet were repeated followed by dispersion of the pellet in 3 volumes of Milli-Q water and adjustment of the pH to 7. Protein solutions were stirred overnight for complete dissolution. A final centrifugation step (10000*g*, 30 min at 10 °C) was performed to get rid of the insoluble material. Sodium azide (0.02%) was added as preservative, and the samples were kept at 4 °C until further use. All protein solutions were set at pH 7.

**Differential Scanning Calorimetry (DSC).** Thermal analysis was performed with a TA Instruments type Q200 modulated differential scanning calorimeter. About 30 mg samples (containing 10% protein) were weighed in MD cups, which were hermetically sealed. The temperature scan in linear mode was performed from 20 to 140 °C with increasing temperature with a rate of 2 °C/min. During this scan the heat flow was measured. Measurements were performed in duplicate, and results are presented as mean values.

**Gelation.** Gelation kinetics were studied as a function of time using a stress-controlled AR2000 rheometer (TA Instruments, Etten-Leur, The Netherlands). A concentric cylinder system with a bob diameter of 14 mm was used. A temperature range was applied in which the temperature increased from 25 to 95 °C with a heating rate of 5 °C $min^{-1}$. It was kept at this temperature for 1 h (strain $10^{-3}$, 6.27 rad $s^{-1}$, frequency 1 Hz) before cooling back to 25 °C. The applied strain was within linear region. $G'$, $G''$, and tan $\delta$ were measured during both steps as a function of time. At the end of the measurement a strain sweep was performed from 0.001 to 1 (25 °C). Samples were covered with a thin layer of paraffin oil to prevent evaporation. Measurements were performed in duplicate, and results are presented as mean values ± standard deviation (SD).

**Texture Analysis.** Samples for large deformation were prepared by heating 10−15% protein solutions (in a skin similar to that of a sausage) in a water bath (95 °C) for 45 min. Heated protein gels were prepared 1 day prior to texture analysis and stored overnight in the refrigerator. Gels were cut into cylindrical pieces (2 cm × 2 cm) using a steel wire. Samples were compressed in a single compression test to 90% of their initial height at a compression speed of 1 mm/s using a Texture Analyzer (TA Instruments) with a flat plate probe (diameter = 75 mm). The compressive stress and strain were determined and recalculated to true Hencky's stress and strain. Young's modulus was calculated from the linear part of the stress over strain curve. Each measurement was performed in triplicate, and results are presented as mean values ± standard deviation (SD).

**Microscopy.** Microstructure was visualized using confocal laser scanning microscopy (CLSM). Protein gels were cut using a wet knife, and protein was colored with a Rhodamine B solution (0.2%). Measurements were performed on a TCS SP2 AOBS Leica Confocal (Leica-microsystems, Mannheim, Germany) mounted on a DM IRE2. Two objectives were used, a 20× objective (HC PL apo CS 20×/0.70 D) and a 63× objective (HCX Pl apo 63×/1.40). An excitation wavelength of 561 nm and an emission wavelength of 571−660 nm were employed. Four pictures were averaged, and a scanning speed of 400 Hz was used.

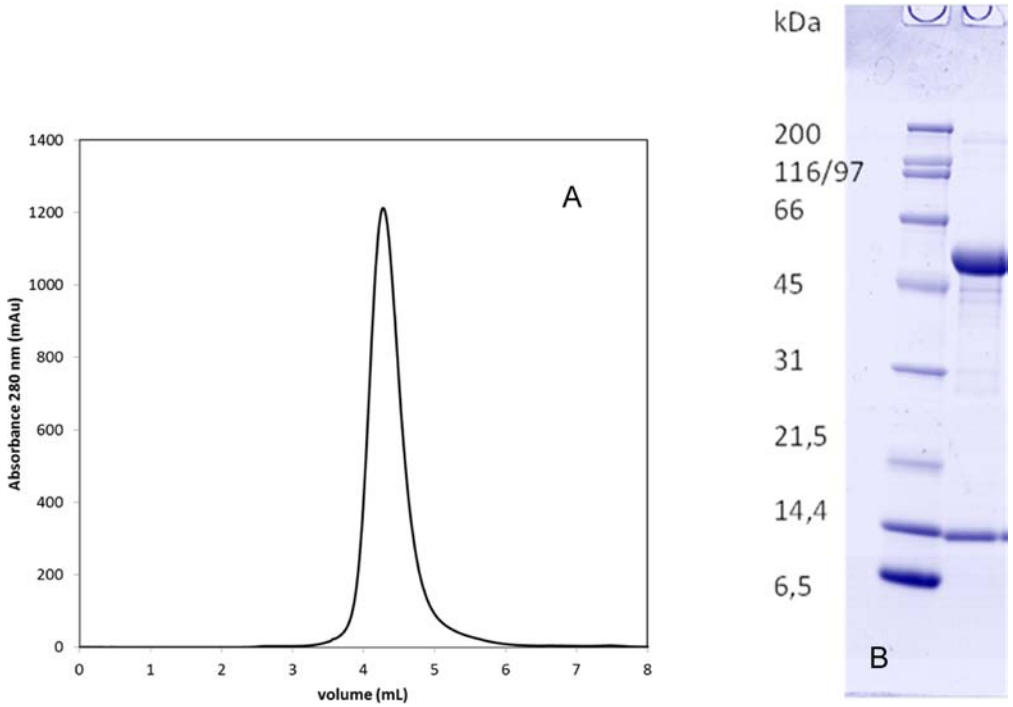


**Figure 1.** Characterization of RuBisCO using (A) size exclusion chromatography and (B) SDS-PAGE, with the left lane being molecular weight markers and the right lane being RuBisCO.

**Protein Interactions.** Solutions of 10% RuBisCO, 10% WPI with 0.2 M NaCl, and 10% egg white protein were heated for 30 min 90 °C in a microwell plate. After heating, the gels were removed from the microwell plate and rolled (roller mixer) in a 15 mL greiner tuber for 24 h with the following solutions: (1) Milli-Q water, (2) Milli-Q + 2% $\beta$-mercaptoethanol, (3) 2 M NaCl, (4) 2 M NaCl + 2% $\beta$-mercaptoethanol, (5) 8 M urea, (6) 8 M urea +2% $\beta$-mercaptoethanol, (7) 2% SDS, or (8) 2% SDS + 2% $\beta$-mercaptoethanol, as previously described by Liu et al.[35] Gels were visually inspected whether they were solubilized or remained intact.

## RESULTS AND DISCUSSION

**Characterization RuBisCO Isolate.** Following the isolation procedure, the purity of the obtained protein isolate was measured with size exclusion chromatography on a Superdex 200 column and gel electrophoresis (see Figure 1). Size exclusion results showed one peak with a narrow distribution indicating a 95% purity of RuBisCO. In addition, the electrophoresis shows two bands at 12.5 and 55 kDa indicating the presence of the small and large subunits of RuBisCO, respectively. Both analyses show that a pure RuBisCO isolate was obtained using the current extraction procedure. UV−vis analysis of the final RuBisCO solution showed no clear sign of any polyphenol absorbance at 340 nm (data not shown). In fact, the ratio between the absorbance at 280 nm and that at 340 nm was >40, indicative of the almost complete absence of polyphenols.

To verify the nativity of the isolated RuBisCO as well as the other plant proteins that were isolated, DSC was performed. Figure 2 shows the thermograms for RuBisCO, isolated plant proteins from soy (SPI), pea (PPI), and lupine (LPI), and, in addition, egg white protein (EWP) and whey protein isolate (WPI). For all proteins clear enthalpic peaks were found indicating the presence of native protein. For RuBisCO the denaturation temperature ($T_d$) was found to be 64.9 °C, which is slightly lower than values found by Libouga et al.[34] and

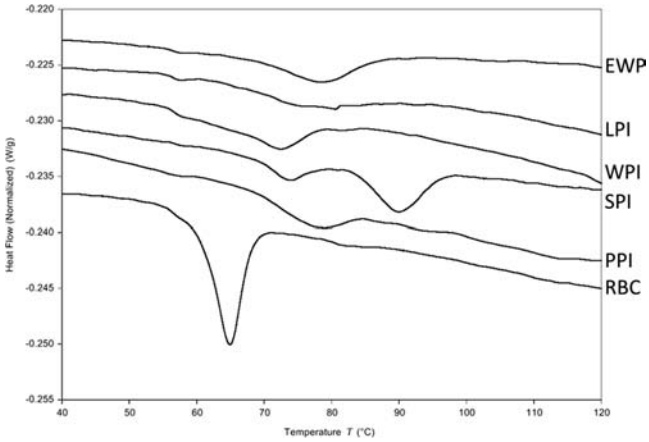


**Figure 2.** DSC thermograms for isolated proteins from (top to bottom) EWP, LPI, WPI, SPI, PPI, and RuBisCO (measured at 10% protein concentration).

Beghin et al.[36] Libouga et al.[34] and Beghin et al.[35] report $T_d$ values of 66.5 and 67.5 °C, respectively, for RuBisCO isolated from alfalfa. The difference is caused by the known higher thermostability of RuBisCO from alfalfa. Compared to WPI, EWP, and especially plant proteins such as SPI, RuBisCO has a relatively low $T_d$. For WPI and EWP, $T_d$ was found to be 72 and 78 °C, similar to the literature.[37,38] For SPI two major peaks were found at ∼73 and ∼90 °C assigned to the main fractions $\beta$-conglycinin and glycinin, respectively, similar to values found by Renkema et al.[39] For pea protein the individual proteins of legumins and vicilins overlap and one endothermic peak was observed with a $T_d$ of 82 °C, which is slightly lower compared to values reported by Shand et al.[40] but similar to those reported by Munialo et al.[41] and Mession et al.[42] For lupine protein also different protein fractions are expected, that is, vicilin ($\beta$-conglutin) and legumin ($\alpha$-conglutin), but the

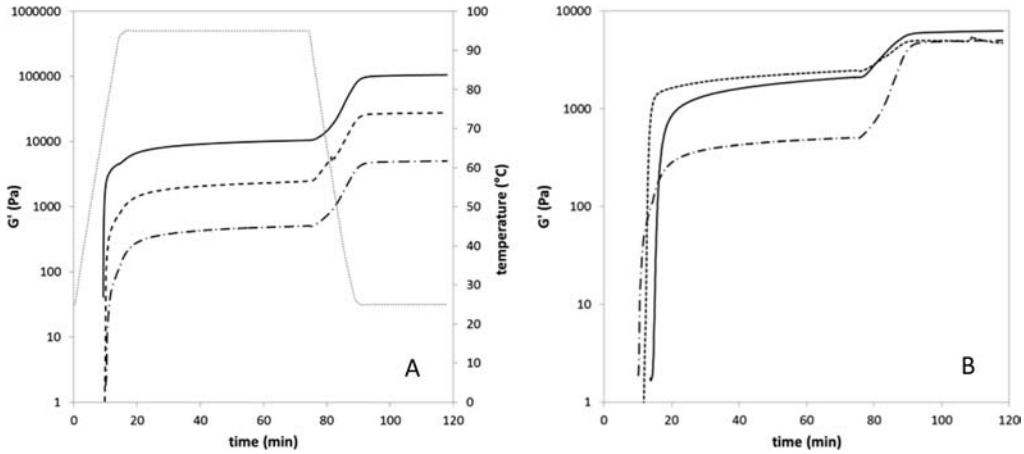


**Figure 3.** Storage modulus $G'$ (Pa) as a function of time during a heating−cooling profile (··· temperature) for (A) (—)10% RuBisCO, (− −) 5% RuBisCO, and (−·−) 2.5% RuBisCO, and (B) (−·−) 2.5% RuBisCO, (—) 10% EWP, and (- - -) 12.5% WPI.

thermogram could not distinguish between these fractions with separate peaks and shows one broad endothermic peak between 66 and 85 °C. Sirtori et al.,[43] however, found two peaks, at 71.5 and 91 °C for the vicilin and legumin, respectively.

**Gelation Properties.** The gelation of RuBisCO was followed by measuring the storage modulus ($G'$) as a function of time during a given heating profile. For 2.5, 5, and 10% protein concentrations, the increase in $G'$ with time is given in Figure 3A. Having a low denaturation temperature, RuBisCO readily gels as shown by the steep increase in $G'$ at short time scale, after which a plateau value is quickly reached. When cooled to room temperature, a further increase in $G'$ is observed, which generally can be appointed to hydrophobic and electrostatic interactions and hydrogen bonds. Already at very low protein concentration (2.5%) RuBisCO was found to form gels with a $G'$ of 5 kPa. With increasing protein concentration $G'$ increases to 104 kPa for 10% RuBisCO, which is extremely high compared to whey protein and egg white protein. Moreover, Figure 3B shows that $G'$ values were obtained in the same order of magnitude for 2.5% RuBisCO, 10% EWP, and 12.5% WPI. The onset in gelation is directly related to the denaturation temperature of the protein as the point at which $G'$ starts to increase (onset gelation time) from RuBisCO to WPI to EWP agrees with $T_d$ of 65, 72, and 78 °C, respectively. The increase in $G'$ during heating, however, is much larger for WPI and EWP than for RuBisCO, whereas during cooling the opposite occurred, in the end leading to similar values for $G'$. Typically, during heating covalent bonds are formed, strengthening the network, whereas during cooling hydrogen bonds and hydrophobic interactions play a role. It can be postulated that for RuBisCO the latter type of interactions are more dominant in determining the final gel strength.

The gelation behavior of RuBisCO was fitted using first-order kinetics

$$G'(t) = G'_{\infty}(1 - e^{-k(t-t_g)}) \quad (1)$$

in which $G'_{\infty}$ is the estimated $G'$ value at infinite time after the heating cycle (at 95 °C), $k$ is a constant, and $t_g$ is the onset gelation time. Table 1 summarizes the findings for $G'_{\infty}$ and $t_g$ for the three different protein concentrations. With increasing protein concentration, $G'_{\infty}$ and $t_g$ increase and decrease, respectively. Similarly, the gelation behaviors of WPI, EWP, SPI, PPI, and LPI were fitted, and the results for $t_g$ and $G'_{\infty}$ are given in Table 2. At a protein concentration of 10%, RuBisCO has the lowest $t_g$ and the highest $G'_{\infty}$ followed by EWP and SPI.

**Table 1. Onset Gelation Time $t_g$, Estimated Infinite $G'_{\infty}$ at 95 °C, and Critical Strain $\gamma_c$ for Different Concentrations of RuBisCO**

| RBC concn (%) | $t_g$ (s) | $G'_{\infty}$ (kPa) | $\gamma_c$ (-) |
|---|---|---|---|
| 2.5 | 630 | 0.5 ± 0.1 | 0.0436 ± 0.004 |
| 5 | 594 | 2.4 ± 0.3 | 0.0397 ± 0.003 |
| 10 | 546 | 10.4 ± 0.2 | 0.0374 ± 0.002 |

**Table 2. Effect of 0.2 M NaCl on Onset Gelation Time $t_g$ and Estimated $G'_{\infty}$ at 95 °C of RuBisCO in Comparison to Other Proteins**

| | 0 M NaCl | | +0.2 M NaCl | |
|---|---|---|---|---|
| protein concn (%) | $t_g$ (s) | $G'_{\infty}$ (kPa) | $t_g$ (s) | $G'_{\infty}$ (kPa) |
| 10% RBC | 546 | 10.4 ± 0.2 | 590 | 6.6 ± 0.4 |
| 10% WPI | no gel | | 726 | 7.7 ± 0.1 |
| 10% EWP | 740 | 4.1 ± 0.2 | 720 | 4.4 ± 0.2 |
| 10% SPI | 790 | 0.40 ± 0.01 | 798 | 0.81 ± 0.04 |
| 15% PPI | no gel | | 438 | 2.8 ± 0.1 |
| 21.5% LPI | 1038 | 0.34 ± 0.03 | 768 | 1.8 ± 0.1 |

Note that WPI does not form a gel at 10% protein concentration, and neither does PPI give a significant value for $G'_{\infty}$ at 95 °C at a concentration of 15%. For the latter, gel formation did occur during cooling. Upon the addition of 0.2 M NaCl, $t_g$ decreased and $G'_{\infty}$ increased for all proteins except for RuBisCO, and now WPI and PPI form a gel as well. The addition of small amounts of salt to globular proteins promotes aggregation due to reduced steric repulsion. Hence, network formation is enhanced and stronger networks are formed. Apparently, the effect of salt on the gelation behavior of RuBisCO is opposite, as $t_g$ increased and $G'$ at infinite time decreased upon addition of 0.2 M NaCl.

During cooling from 95 to 25 °C, $G'$ further increased for all proteins. However, differences in the increase in $G'$ during cooling were observed, and values for $G'$ at 95 and 25 °C are given in Table 3. Two important features can be observed here, that is, a much higher increase in $G'$ during cooling for RuBisCO compared to the other proteins and the higher tan $\delta$ of the same gel when cooled. As postulated before, RuBisCO

**Table 3. Estimated $G'_\infty$ at 95 °C (End of Heating) and 25 °C (End of Cooling) and tan $\delta$ for Proteins Gels Made of RuBisCO (RBC), Whey Protein Isolate (WPI), Egg White Protein (EWP), Soy Protein Isolate (SPI), Pea Protein Isolate (PPI), and Lupine Protein Isolate (LPI)**

| protein concn (%) | $G'_\infty$ (kPa) at 95 °C | $G'_\infty$ (kPa) at 25 °C | increase in $G'_\infty$ at 25/95 °C | tan $\delta$ at 25 °C |
|---|---|---|---|---|
| 2.5% RBC | 0.5 ± 0.1 | 5.0 ± 0.9 | ~10 | 0.21 |
| 5% RBC | 2.4 ± 0.3 | 26.8 ± 7.9 | ~10 | 0.22 |
| 10% RBC | 10.4 ± 0.2 | 104.2 ± 10.8 | ~10 | 0.20 |
| 12.5% WPI | 1.9 ± 0.2 | 6.3 ± 0.2 | ~3 | 0.09 |
| 15% WPI | 5.0 ± 0.1 | 11.5 ± 0.4 | ~2 | 0.07 |
| 10% EWP | 4.1 ± 0.2 | 8.2 ± 0.9 | ~2 | 0.09 |
| 12.5% EWP | 10.2 ± 0.4 | 20.4 ± 0.3 | ~2 | 0.10 |
| 10% SPI | 0.40 ± 0.01 | 1.5 ± 0.1 | ~4 | 0.11 |
| 17.5% PPI | 1.0 ± 0.2 | 3.1 ± 0.2 | ~3 | 0.08 |
| 21.5% LPI | 0.34 ± 0.03 | 9.7 ± 0.2 | ~30 | 0.15 |

forms a network in which different types of interactions play a role, giving it its specific behavior.

After cooling to 25 °C, $G'$ reached a steady state value for all proteins. Plotting this $G'$ value as a function of protein concentration for RuBisCO in comparison to other proteins, it is obvious that the gelation potential of RuBisCO exceeds that of WPI and EWP and by far that of plant proteins such as SPI, LPI, and PPI (see Figure 4). For each protein an increase in $G'$ was found with increasing protein concentration, and the critical gelation concentration for each protein could be estimated from the graph. For RuBisCO the critical gelation concentration ($c_{gel}$) is <2.5%. For RuBisCO from alfalfa, Libouga et al.[34] reported values for $c_{gel}$ of 0.5% at pH 7.5 and 1% at pH 8, well below 2.5% protein. Differences in $c_{gel}$ can be explained by the difference in p$I$ between alfalfa and spinach. For the latter p$I$ values of 5.5, 4.9, or 5.0 were found, whereas for alfalfa p$I$ ~6.[3] At neutral pH, RuBisCO from spinach has a higher net charge compared to alfalfa, leading to enhanced steric repulsion and hence a higher $c_{gel}$. Nevertheless, $c_{gel}$ for RuBisCO is much lower compared to the other proteins given in Figure 4, where the minimum concentration needed to form a gel at pH 7 starts from ~5% (SPI) and the order in which it increases follows SPI < EWP < WPI < PPI < LPI. For SPI the highest concentration that could be measured was 10% as above that concentration the (native) protein solution became too viscous to handle. Critical gelation concentrations for SPI, EWP, and WPI agree with literature values.[44,45]

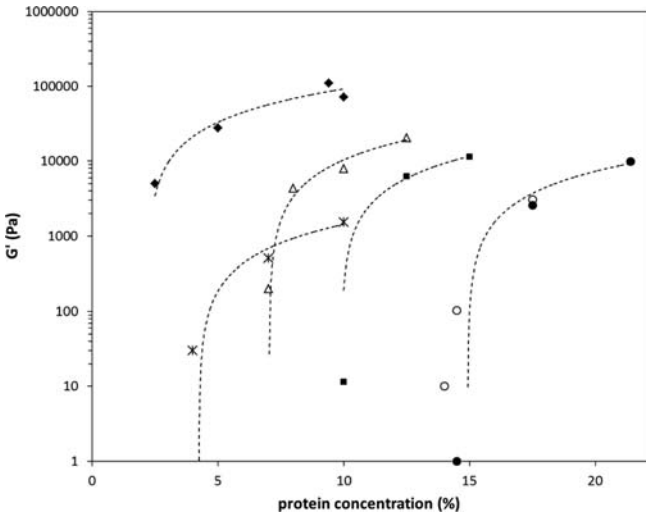


**Figure 4.** Storage modulus $G'$ as a function of protein concentration for (◆) RuBisCO, (■) WPI, (△) EWP, (×) SPI, (●) LPI, and (○) PPI. Dotted lines are to guide the eye.

After a heating and cooling profile had been applied, a strain sweep was performed to study the linear region and breakdown behavior of RuBisCO gels. Figure 5A shows the decrease in $G'$ when the strain increased from 0.001 to 1 for three concentrations of RuBisCO (2.5, 5, and 10%). For all concentrations, it appeared that the linear region for RuBisCO is quite small and, as a result, the critical strain ($\gamma_c$) is low as well. Values for $\gamma_c$ are given in Table 1 and show that with increasing RuBisCO concentration, $\gamma_c$ decreases. In comparison to gels made from WPI and EWP, RuBisCO exhibits a brittle character prone to early breakdown. Figure 5B clearly shows the early breakdown of RuBisCO compared to protein gels made from WPI and EWP and indicates once more that the type of interactions in a RuBisCO gel are of a different, weaker kind. In fact, covalent bonds between protein molecules and aggregates (as commonly found in WPI and EWP gels) tend to be stronger than hydrophobic interactions and hydrogen bonds.

In summary, RuBisCO typically has a very low critical gelling concentration and a low $t_g$, resulting in gels that have a very high $G'$ but also a high tan $\delta$. In addition, early breakdown of RuBisCO gels during the strain sweep was observed. It is postulated that the type of interactions that are formed during aggregation and network formation play a role in RuBisCO's specific behavior. To further investigate this, fracture properties and microstructure were determined. As WPI, EWP, and SPI form self-supporting gels at much lower concentrations than PPI and LPI, the latter two are not further taken into account for comparison with RuBisCO.

**Fracture Properties.** Fracture properties were determined to establish information on (true) fracture stress and (true) fracture strain during compression, as is relevant for textural and sensory properties. Fracture properties of RuBisCO were compared with those of WPI, EWP, and SPI, and true fracture stress ($\sigma_f$) was plotted against true fracture strain ($\varepsilon_f$) for protein gels without and with 0.2 M NaCl (see Figure 6). RuBisCO (10%) has a higher $\sigma_f$ (125 kPa) compared to 10% WPI (no gel), 10% EWP (90 kPa), and 10% SPI (31 kPa) but a similar $\varepsilon_f$ to SPI. The relatively low $\varepsilon_f$ indicates that RuBisCO forms a brittle gel as is commonly observed for SPI.[44] As for 10% WPI no self-supporting gel is formed, a 15% concentration was used for comparison. The higher $\sigma_f$ of 15% WPI compared to that of 10% RuBisCO gels is most probably caused by the higher protein concentration. In addition, WPI (and also EWP) forms more elastic gels. For EWP, WPI, and SPI, the addition of 0.2 M NaCl led to similar or slightly increased values for $\sigma_f$ and lower $\varepsilon_f$. For RuBisCO, however, both $\sigma_f$ and $\varepsilon_f$ decreased drastically when salt was added, similar to the reduction in gel strength observed with small deformation measurements ($G'$ values). In addition, the brittleness of RuBisCO in large deformation is in line with the early breakdown observed for RuBisCO with small deformation experiments.

**Microstructure.** To understand the differences in small and large deformation properties between RuBisCO and other proteins, the microstructure of RuBisCO is probed with CLSM as a function of NaCl concentration for 5 and 10% RuBisCO (see Figure 7) and compared to 10% WPI. Whereas WPI and also EWP and SPI form transparent and hence fine-stranded

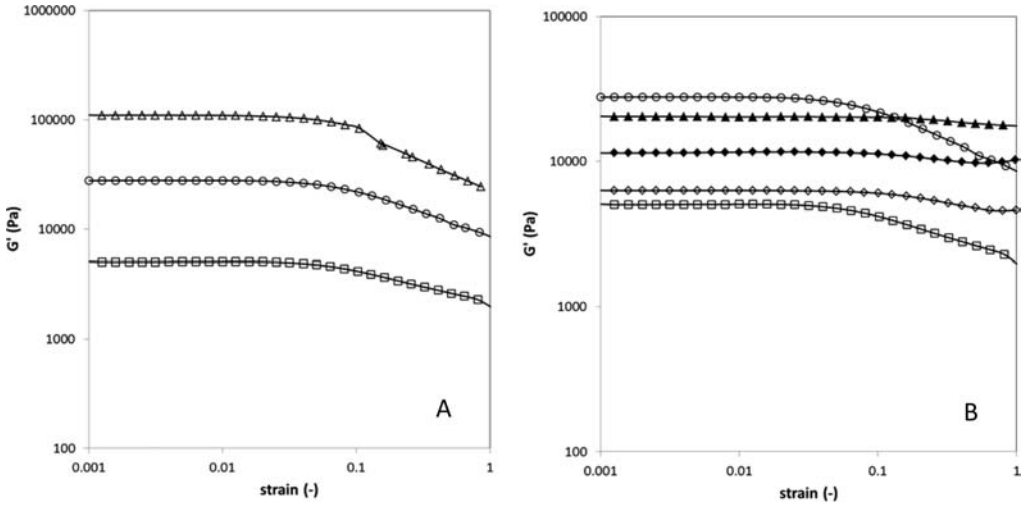


**Figure 5.** (A) Strain sweep for (△) 10% RuBisCO, (○) 5% RuBisCO, (□) 2.5% RuBisCO. (B) Comparison between RuBisCO and (▲) 12.5% EWP, (◇) 12.5% WPI, and (◆) 15% WPI.

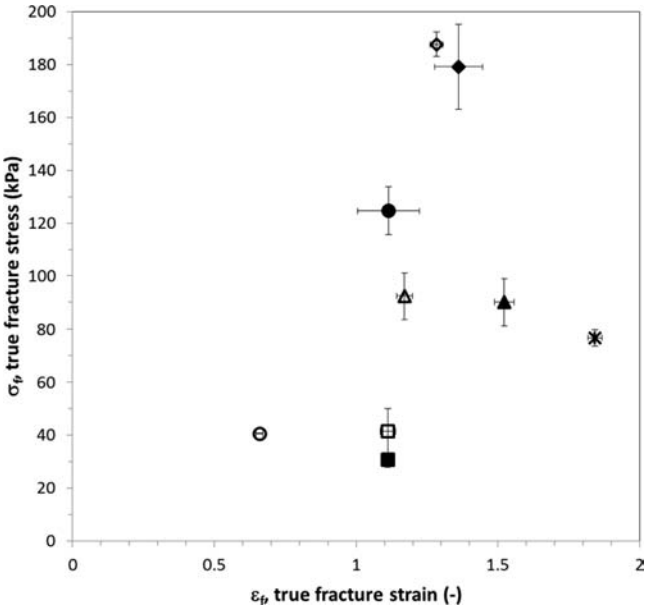


**Figure 6.** Fracture properties in terms of fracture stress (kPa) and fracture strain of various protein gels without salt (solid symbols) and with 0.2 M NaCl (open symbols) for (●) 10% RuBisCO, (◆) 15% WPI, (×) 10% WPI + 0.2 M NaCl, (▲) 10% EWP, and (■) 10% SPI.

gels at neutral pH, RuBisCO formed a white turbid gel. Upon addition of NaCl to WPI and EWP, the transparency of the gels disappeared as a transition occurred from fine-stranded to coarse-stranded gel. This indicates that the aggregation mechanism and how aggregates together build the microstructure of protein network are clearly different for RuBisCO relative to WPI or EWP. Note that the molecular weight for RuBisCO (~550 kDa) is >10 times higher than that for WPI (with $\beta$-lactoglobulin of 18 kDa in monomeric form as most prevalent protein) and EWP (containing predominantly ovalbumin of 44 kDa) and that reported values for hydrodynamic radius, $R_g$, for RuBisCO range from 5 to 7 nm,[7] where ovalbumin and $\beta$-lactoglobulin, the major proteins of EWP and WPI, have values of ~3 and ~2 nm, respectively.[45,46]

With regard to the microstructure as observed with CLSM, the density of the RuBisCO network increased with increasing protein concentration. For 10% protein the addition of 0.2 (B2) and 0.5 M NaCl (B3) does not seem to have a large influence on the network density, although a small increase in coarseness from 0 to 0.2 M NaCl could be observed. For 5% RuBisCO (A1) however, it seems that the network becomes coarser with higher salt concentration (A2 and A3). Addition of 0.2 M NaCl clearly resulted in a coarser network, but upon further increasing NaCl concentration, the coarseness decreased again. By comparing RuBisCO to WPI the following was observed. At 10% WPI (C1) no gel was formed, but from the literature it is known that at 15% WPI a fine-stranded network is formed when no salt is present.[46] The features of such a network cannot be probed with CLSM. With increasing salt concentration (C2), the network becomes more coarse-stranded as charges are screened. When the NaCl concentration is further increased (C3), the coarseness is strongly enhanced. The effect of salt on the microstructure is far more pronounced for WPI than for RuBisCO.

The increase in coarseness with addition of NaCl can be related to the decrease in fracture strain. Fine-stranded gels (without addition of NaCl) tend to be more elastic than coarse-stranded gels (formed when NaCl is added). However, a clear relationship between the microstructure and rheological properties could not be found for RuBisCO. Changes in the type of interactions between RuBisCO molecules as a result of salt addition affect the rheological properties to a greater extent than the microstructure itself. As native RuBisCO is held together by numerous ionic bridges and most of these salt bridges are ruptured during denaturation, dissociation of the subunits occurs and hence a more open structure is created.[34] When salt is added, electrostatic repulsions between the charged groups of the subunits are screened and will drive aggregation. The type of interactions that are formed in the presence of salt may be weaker than when no salt is added.

**Protein−Protein Interactions.** To gain an understanding of the type of interactions that occur between RuBisCO molecules and the relationship with the brittleness of RuBisCO gels, protein−protein interactions were investigated. During aggregation and gelation of globular proteins, different types of interactions play a role. During the heating phase, covalent bonds (e.g., disulfide bridges) can be formed, whereas during the cooling phase, noncovalent interactions such as hydro-

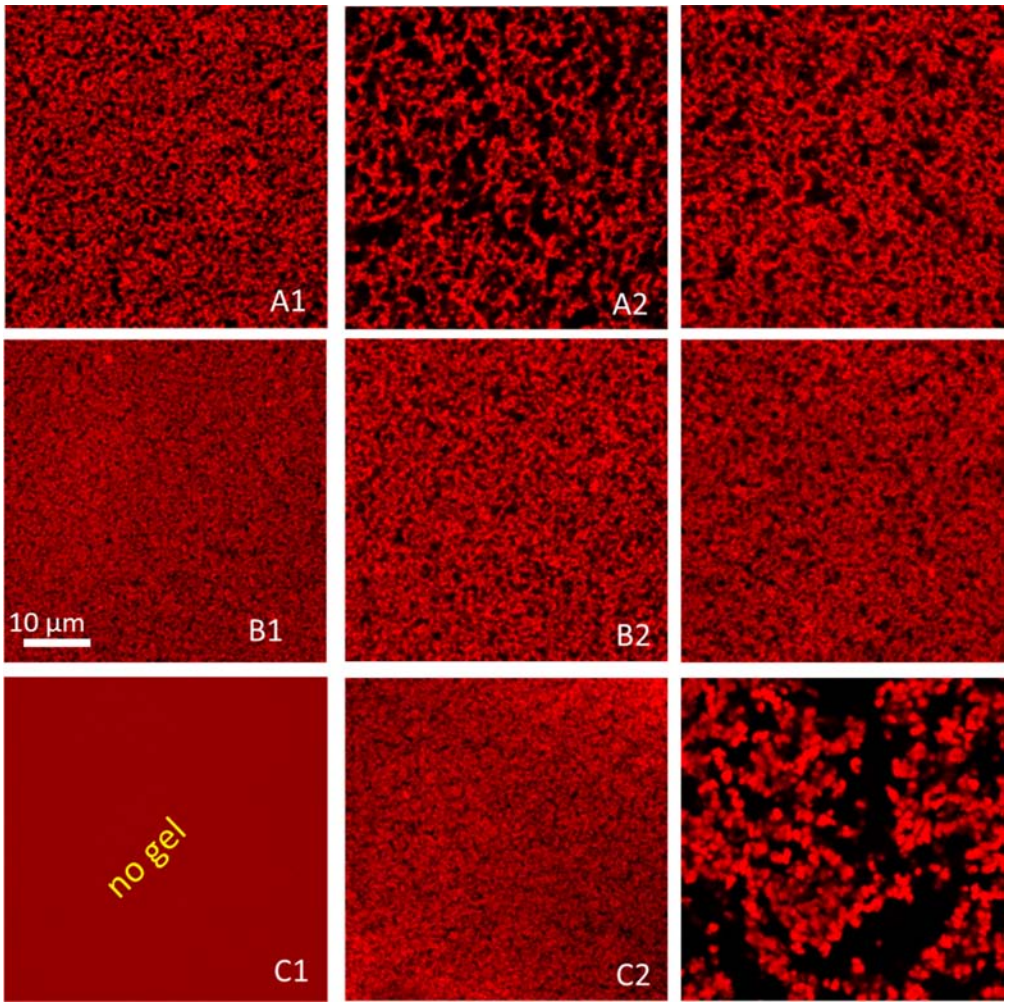


**Figure 7.** Microstructure of RuBisCO gels (A, 5% protein concentration; B, 10% protein concentration) and WPI (C, 10%) as a function of NaCl concentration (1, no salt; 2, 0.2 M; 3, 0.5 M) as measured by CLSM. The scale bar presented in image B1 applies to all images.

phobic interactions and hydrogen bonds come into play. In small deformation rheology a distinction can be made between the increase in $G'$ during the heating phase and the second increase in $G'$ during the cooling phase. From Table 3 it is clear that for RuBisCO the increase in $G'$ during cooling is much higher than for the other proteins, suggesting that noncovalent interactions play a much larger role in strengthening the protein network. To further investigate this, RuBisCO gels were subjected to a series of solvents that each break specific interactions in proteins gels (see Table 4). $\beta$-Mercaptoethanol (ME), NaCl, urea, SDS, and combinations of these solvents were used to distinguish between disulfide bridges, hydrogen bonds, hydrophobic, and electrostatic interactions. Both WPI and EWP gels stayed intact when dissolved in water, ME, 2 M NaCl, or 2 M NaCl+ME. RuBisCO gels, however, changed in size. Upon addition of NaCl, both in the absence and in the presence of ME, the gels shrank, indicating contraction of the protein network due to enhanced hydrophobic interactions. Addition of ME alone resulted in swelling of the RuBisCO gel. As disulfide bridges are present within the large subunits, ME may disrupt these when accessible, leading to a looser and open structure. Urea and SDS are known to disrupt hydrogen bonds and/or hydrophobic interactions. When added to RuBisCO, these gels are partially dissolved, suggesting that hydrogen bonds and hydrophobic interactions play a role in holding the protein network together. The falling apart by urea or SDS is confirmed by Douillard et al.,[7] who reported on dissociation of small subunits from the large ones for spinach RuBisCO already at 3 M urea. As only the small subunits are dissociated, this may explain the partial dissolvement of the gel as opposed to complete dissolvement. Addition of urea or SDS to WPI or EWP led to swelling of the gel. Here, internal hydrogen bonds and hydrophobic interactions are broken, but the presence of disulfide bridges holds the protein network together, acting as a frame with more open pores. For both WPI and EWP the

**Table 4. Solvents to Break up Protein−Protein Interactions**

| | type of interaction | | | |
|---|---|---|---|---|
| solvent | S−S | H-bonds | hydrophobic | electrostatic |
| (1) water | | | | |
| (2) ME[a] | × | | | |
| (3) 2 M NaCl | | | × | × |
| (4) 2 M NaCl + ME | × | | × | × |
| (5) 8 M urea | | × | | |
| (6) 8 M urea + ME | × | × | | |
| (7) 2% SDS[b] | | × | × | |
| (8) 2% SDS + ME | × | × | × | |

[a]ME, $\beta$-mercaptoethanol. [b]SDS, sodium dodecyl sulfate.


dx.doi.org/10.1021/jf502905g | J. Agric. Food Chem. 2014, 62, 10783−10791

importance of disulfide bridges in aggregation was frequently studied,[47,48] and hence this confirms the results obtained here. A combination of urea and ME or SDS and ME, targeting all interactions, dissolved all three protein gels. Hence, no differences were observed between RuBisCO, EWP, and WPI.

Using solvents to study the type of interactions resulted in a validation of the hypothesis that hydrophobic interactions and H-bonds play a larger role in RuBisCO gels than in WPI or EWP gels. This explains the higher increase in $G'$ upon cooling (Table 3) and the higher brittleness as these bonds are weaker than the covalent bonds that occur with WPI and EWP.

In conclusion, heat-induced aggregation and network formation of RuBisCO resulted in gels with unique characteristics compared to well-known proteins such as WPI and EWP and plant proteins such as SPI, PPI, and LPI. Having a very low critical gelling concentration and low denaturation temperature, RuBisCO could be applied in a wide range of products that need mild processing conditions. Product categories of interest include meat replacers, either as a bulk ingredient or as a binder, but it could also be applied as a meat improvement agent. The gelation functionality could also be applied in potato starch based products, surimi, or fish cakes. In these applications RuBisCO would be a more sustainable alternative to soy or egg white protein. In general, RuBisCO would be very suitable to partially replace proteins with poorer functional properties to enhance, for example, the gelation behavior. Moreover, the unique set of properties of RuBisCO allows for expansion of the application area, as it forms a strong network at low concentrations (high $G'$, high fracture stress) but upon deformation (oral processing) it has a brittle character (low critical strain, low fracture strain). In relation to fracture properties of food gels made from different types of hydrocolloids or mixtures thereof, the fracture strain of RuBisCO is in the same region as different tofu model systems[44] and of mixtures of whey protein and κ-carrageenan, where κ-carrageenan forms the continuous phase.[49] Selectively mixing RuBisCO with other types of biopolymers would give the opportunity to deliver new textures at low concentrations, similarly to mixtures of soy protein and gelatin.[50] The typical breakdown behavior of RuBisCO can be explained by the dominant role of hydrophobic and electrostatic interactions and H-bonds and by the coarse microstructure, as opposed to disulfide bridges and (more) fine-stranded networks for WPI and EWP. These findings enhance the knowledge currently available on RuBisCO functionality, especially in the area of understanding the mechanical and microstructural properties of RuBisCO gels.

## AUTHOR INFORMATION

### Corresponding Author

*(A.H.M.) E-mail: anneke.martin@tno.nl. Phone: +31 (0)88 866 1815.

### Notes

The authors declare no competing financial interest.

## ACKNOWLEDGMENTS

Helene Mocking and Ron van den Dool are acknowledged for their help in extraction of RuBisCO, soy protein, pea protein, and lupine protein.

## REFERENCES

(1) Wanadundra, J. P. Proteins of Brassicaceae oilseeds and their potential as a plant protein source. *Crit. Rev. Food Sci. Nutr.* **2011**, *51*, 635−677.

(2) Day, L. Proteins from land plants − potential resources for human nutrition and food security. *Trends Food Sci. Technol.* **2013**, *32*, 25−42.

(3) Dijkstra, D. S.; Linneman, A. R.; van Boekel, T. A. J. S. Towards sustainable production of protein-rich foods: appraisal of eight crops for Western Europe. Part II: Analysis of the technological aspects of the production chain. *Crit. Rev. Food Sci. Nutr.* **2003**, *43*, 481−506.

(4) Boland, M. J.; Rae, A. N.; Vereijken, J. M.; Meuwissen, M. P. M.; Fischer, A. R. H.; van Boekel, M. A. J. S.; Rutherfurd, S. M.; Gruppen, H.; Moughan, P. J.; Hendriks, W. H. The future supply of animal-derived protein for human consumption. *Trends Food Sci. Technol.* **2013**, *29*, 62−73.

(5) Ellis, R. J. The most abundant protein in the world. *Trends Biochem. Sci.* **1979**, *4*, 241−244.

(6) Barbeau, W. E.; Kinsella, J. E. Ribulose biphosphate carboxylase/oxygenase (rubisco) from green leaves − potential as food protein. *Food Rev. Int.* **1988**, *4*, 93−127.

(7) Douillard, R.; de Mathan, O. Leaf protein for food use: potential of Rubisco. In *New and Developing Sources of Proteins*; Hudson, B. J. F., Ed.; Springer: New York, 1994; pp 307−342.

(8) Hartman, F. C.; Harpel, M. R. Structure, function, regulation, and assembly of D-ribulose-1,5-bisphosphatecarboxylase oxygenase. *Annu. Rev. Biochem.* **1994**, *63*, 197−234.

(9) Hilditch, C. M.; Jones, P. B.; Balding, P.; Smith, A. J.; Rogers, L. J. Ribulose biphosphate carboxylases from macroalgae − proteolysis during extraction and properties of the enzyme from *Porphyra umbilicalis*. *Phytochemicals* **1991**, *30*, 745−750.

(10) Patel, M.; Berry, J. O. Rubisco gene expression in C4 plants. *J. Exp. Bot.* **2008**, *59*, 1625−1634.

(11) Sheen, S. J.; Sheen, V. L. Functional properties of fraction-1 protein from tobacco leaf. *J. Agric. Food Chem.* **1985**, *33*, 79−83.

(12) Hassiotou, E.; Tsaftaris, A. Comparison of three procedures for rubisco purification from green tobacco leaves. *Chim. Chronica* **1995**, *24*, 147−158.

(13) Fantozzi, P.; Sensidoni, A. Protein extraction from tobacco-leaves − technological, nutritional and agronomical aspects. *Qual. Plant. − Plant Foods Hum. Nutr.* **1983**, *32*, 351−368.

(14) Fu, H.; Machado, P. A.; Hahm, T. S.; Kratochvil, R. J.; Wei, C. I.; Lo, Y. M. Recovery of nicotine-free proteins from tobacco leaves using phosphate buffer system under controlled conditions. *Bioresour. Technol.* **2010**, *101*, 2034−2042.

(15) Carmo-Silva, A. E.; Barta, C.; Salvucci, M. E. Isolation of ribulose-1,5-bisphosphate carboxylase/oxygenase from leaves. *Methods Mol. Biol.* **2011**, *684*, 339−347.

(16) Salvucci, M. E.; Portis, A. R.; Ogren, W. L. Purification of ribulose-1,5-bisphosphate carboxylase oxygenase with high specific activity by fast protein liquid-chromatography. *Anal. Biochem.* **1986**, *153*, 97−101.

(17) Paulsen, J. M.; Lane, M. D. Spinach ribulose diphosphate carboxylase. I. Purification and properties of enzyme. *Biochemistry* **1966**, *5*, 2350−2357.

(18) Betschar, A.; Kinsella, J. E. Extractability and solubility of leaf protein. *J. Agric. Food Chem.* **1973**, *21*, 60−65.

(19) Knuckles, B. E.; Kohler, G. O. Functional properties of edible protein concentrates from alfalfa. *J. Agric. Food Chem.* **1982**, *30*, 748−752.

(20) Lu, P. S.; Kinsella, J. E. Extractability and properties of protein from alfalfa leaf meal. *J. Food Sci.* **1972**, *37*, 94−99.

(21) Edwards, R. H.; Miller, R. E.; Fremery, D. D.; Knuckles, B. E.; Bickoff, E. M.; Kohler, G. O. Pilot-plant production of an edible white fraction leaf protein concentrate from alfalfa. *J. Agric. Food Chem.* **1975**, *23*, 620−626.

(22) D'Alvise, N.; Lesueur-Lambert, C.; Fertin, B.; Dhulster, P.; Guillochon, D. Removal of polyphenols and recovery of proteins from

alfalfa white protein concentrate by ultrafiltration and adsorbent resin separations. *Sep. Sci. Technol.* **2000**, *35*, 2453−2472.
(23) Jwanny, E. W.; Montanari, L.; Fantozzi, P. Protein-production for human use from sugar-beet byproducts. *Bioresour. Technol.* **1993**, *43*, 67−70.
(24) Merodio, C.; Sabater, B. Preparation of a white protein fraction in high yield from sugar beet (*Beta vulgaris* L) leaves. *J. Sci. Food Agric.* **1988**, *44*, 237−243.
(25) Schwenzfeier, A.; Wierenga, P. A.; Gruppen, H. Isolation and characterization of soluble protein from the green microalgae *Tetraselmis* sp. *Bioresour. Technol.* **2011**, *102*, 9121−9127.
(26) Satoh, H.; Okada, M.; Nakayama, K.; Miyaji, K. Purification and further characterization of pyrenoid proteins and ribulose-1,5-bisphosphate carboxylase-oxygenase from the green-alga *Bryopsis maxima*. *Plant Cell Physiol.* **1984**, *25*, 1205−1214.
(27) Sheen, S. J. Whole-plant utilization − the potential of soybean. *Biomass* **1986**, *10*, 195−206.
(28) Barbeau, W. E.; Kinsella, J. E. Factors affecting the binding of chlorogenic acid to fraction 1 leaf protein. *J. Agric. Food Chem.* **1983**, *31*, 993−998.
(29) Wang, D.; Naidu, S. L.; Portis, A. R., Jr.; Moose, S. P.; Long, S. P. Can the cold tolerance of C4 photosynthesis in *Miscanthus giganteus* relative to *Zea mays* be explained by differences in activities and thermal properties of Rubisco? *J. Exp. Bot.* **2008**, *59*, 1779−1787.
(30) Whitney, S. M.; Kane, H. J.; Houtz, R. L.; Sharwood, R. E. Rubisco oligomers composed of linked small and large subunits assemble in tobacco plastids and have higher affinities for CO2 and O2. *Plant Physiol.* **2009**, *149*, 1887−1895.
(31) Lamsal, B. P.; Koegel, R. G.; Gunasekaran, S. Some physicochemical and functional properties of alfalfa soluble leaf proteins. *LWT−Food Sci. Technol.* **2007**, *40*, 1520−1526.
(32) Zhong, C.; Wang, R.; Zhou, Z.; Jia, S.-R.; Tan, Z.-L.; Han, P.-P. Functional properties of protein isolates from *Caragana korshinskii* Kom. extracted by three different methods. *J. Agric. Food Chem.* **2012**, *60*, 10337−10342.
(33) Barbeau, W. E. Functional properties of leaf proteins: criteria required in food applications. *Ital. J. Food Sci.* **1990**, *4*, 213−225.
(34) Libouga, D. G.; AguieBeghin, V.; Douillard, R. Thermal denaturation and gelation of Rubisco: effects of pH and ions. *Int. J. Biol. Macromol.* **1996**, *19*, 271−277.
(35) Liu, K.; Hsieh, F.-H. Protein−protein interactions during high-moisture extrusion for fibrous meat analogues and comparison of protein solubility methods using different solvent systems. *J. Agric. Food Chem.* **2008**, *56*, 2681−2687.
(36) Beghin, V.; Bizot, H.; Audebrand, M.; Lefebvre, J.; Libouga, D. G.; Douillard, R. Differential scanning calorimetric studies of the effects of ions and pH on ribulose 1,5-bisphosphate carboxylase/oxygenase. *Int. J. Biol. Macromol.* **1993**, *15*, 195−200.
(37) Verheul, M.; Roefs, S. P. F. M.; de Kruif, C. G. Kinetics of heat-induced aggregation of β-lactoglobulin. *J. Agric. Food Chem.* **1998**, *46*, 896−903.
(38) de Groot, J.; de Jongh, H. H. J. The presence of heat-stable conformers of ovalbumin affects properties of thermally formed aggregates. *Protein Eng.* **2003**, *16*, 1035−1040.
(39) Renkema, J. M. S.; Lakemond, C.; de Jongh, H. H. J.; Gruppen, H.; van Vliet, T. The effect of pH on heat denaturation and gel forming properties of soy proteins. *J. Biotechnol.* **2000**, *79*, 223−230.
(40) Shand, P. J.; Ya, H.; Pietrasik, Z.; Wanasundara, P. K. J. P. D. Physicochemical and textural properties of heat-induced pea protein isolate gels. *Food Chem.* **2007**, *102*, 1119−1130.
(41) Munialo, C. D.; van der Linden, E.; de Jongh, H. H. J. The ability to store energy in pea protein gels is set by network dimensions smaller than fifty nanometers. *Food Res. Int.* **2014**, *64*, 482−491.
(42) Mession, J.-L.; Sok, N.; Assifaoui, A.; Saurel, R. Thermal denaturation of pea globulins (*Pisum sativum* L.) − molecular interactions leading to heat-induced protein aggregation. *J. Agric. Food Chem.* **2013**, *61*, 1196−1204.
(43) Sirtori, E.; Resta, D.; Brambilla, F.; Zacherl, C.; Arnoldi, A. The effects of various processing conditions on a protein isolate from *Lupinus angustifolius*. *Food Chem.* **2010**, *120*, 496−504.
(44) Urbonaite, V.; de Jongh, H. H. J.; van der Linden, E.; Pouvreau, L. Origin of water loss from soy protein gels. *J. Agric. Food Chem.* **2014**, *62*, 7550−7558.
(45) Weijers, M.; Nicolai, T.; Visschers, R. W. Influence of the ionic strength on the structure of heat-set globular protein gels at pH 7. Ovalbumin. *Macromolecules* **2004**, *37*, 8709−8714.
(46) Verheul, M.; Roefs, S. P. F. M. Structure of particulate whey protein gels: effect of NaCl concentration, pH, heating temperature and protein composition. *J. Agric. Food Chem.* **1998**, *46*, 4909−4916.
(47) Hoffmann, M. A. M.; van Mil, P. J. J. M. Heat-induced aggregation of β-lactoglobulin: role of the free thiol group and disulphide bonds. *J. Agric. Food Chem.* **1997**, *45*, 2942−2948.
(48) Arntfield, S. D.; Murray, E. D.; Ismond, M. A. H. Role of disulfide bonds in determining the rheological and microstructural properties of heat-induced protein networks from ovalbumin and vicilin. *J. Agric. Food Chem.* **1991**, *39*, 1378−1385.
(49) Çakir, E.; Foegeding, E. A. Combining protein micro-phase separation and protein-polysaccharide segregative phase separation to produce gel structures. *Food Hydrocolloids* **2011**, *25*, 1538−1546.
(50) Ersch, E.; ter Laak, I.; van der Linden, E.; Venema, P.; Martin, A. H. Modulating fracture properties of mixed protein systems. *Food Hydrocolloids* **2015**, *44*, 59−65.

screening of free and/or bound water-soluble manganese fractions from samples with minimal sample preparation.

## MATERIALS AND METHODS

**Reagents and Samples.** A manganese(II) standard solution at a concentration of 1000 $\mu$g mL$^{-1}$ was purchased from Inorganic Ventures (Lakewood, NJ, USA). Suprapure $HNO_3$ (65%, v/v), HCl (30%, v/v), and all other reagents and chemicals used in the fractionation studies were of liquid chromatography (LiChrosolv) or analytical reagent grade and were obtained from Merck (Darmstadt, Germany). The digestive enzymes, pepsin (P7000, from porcine gastric mucosa), pancreatin (P1750, from porcine pancreas), and bile extract (B8631), were obtained from the local suppliers of Sigma-Aldrich (St. Louis, MO, USA) and used for the simulation of in vitro gastric and intestinal digestions. Sodium hydrogen carbonate was a Carlo Erba RPE reagent (Rodano, Milan, Italy) and was used for the preparation of the digestion solutions. Activated carbon (AOX Batch, PPTRE0049, Euroglas, Okehampton, UK) in powder form was used to evaluate the adsorption capabilities of manganese. All of the standards and samples were filtered through Double Rings 103 (12.5 cm filter paper) blue ribbon filter paper, followed by filtration through 0.45 $\mu$m hydrophilic polyvinylidene fluoride (PVDF) syringe filters (Millex-HV, Millipore) prior to analysis. Certified reference materials, NIST 1567a wheat flour (Gaithersburg, MD, USA) and Conostan (S-21-10 $\mu$g g$^{-1}$) oil-based multielement calibration standard (LGC Standards, London, UK), were used for validation purposes. A FAME (fatty acid methyl ester) Mix C4−C24 (Supelco 18919-1AMP, Sigma-Aldrich) standard mixture was used for fatty acid analysis. The water used was of ultrapure grade (18.3 MΩ·cm, Zeener Power I, Human Corp., Seoul, Korea). Highly pure (99.999%) argon and nitrogen gases were purchased from Orsez (Bursa, Turkey). Helium gas (99.999%) was supplied by Linde Gas A.Ş. (Bursa, Turkey).

Among the many varieties of hazelnuts that are cultivated in Turkey, Tombul hazelnuts are known as Giresun or premium quality and are mainly grown in Giresun, Turkey.[9] Thus, Fiskobirlik Efit A.Ş. (hazelnut processing company in Giresun) brand or Giresun quality unshelled and processed (Tombul) hazelnut samples were purchased from markets in Giresun and Bursa.

**Apparatus and Instrumentation.** Total manganese (Mn) analyses were performed after sample digestion using a microwave digestion system (Microwave Labstation MLS 1200 mega, Milestone, Italy). An Elma LC-30H model ultrasonic bath (Singen, Germany) operated at an ultrasonic frequency of 35 kHz and a power of 240 W was used for the sample preparation. A pH meter (Minilab IQ125 Isfet pH tester, IQ Scientific Instruments Inc., Carlsbad, CA, USA) was obtained from PerkinElmer (PerkinElmer SCIEX, Shelton, CT, USA). An unstirred thermostatic water bath (Clifton NE1-22, Nickel Electro Ltd., UK) and an MSE Mistral 2000 centrifuge (MSE Scientific Instruments, UK) were used for the bioaccessibility studies.

A PerkinElmer 200 series high-performance liquid chromatography (HPLC) system consisting of a series 200 quaternary pump, a series 225 autosampler, a series 200 column oven, and a vacuum degasser was used for the chromatographic analyses. The separation and identification of manganese fractions was achieved using a Brownlee DB Aq. C-18 (150 mm × 4.6 mm i.d. and 5 $\mu$m film thickness) analytical column (PerkinElmer SCIEX) equipped with a guard column (40 mm) with the same stationary phase material. The column was maintained at 26 °C, and the elution was performed with filtered and degassed ultrapure water. A methanol/water mixture as a gradient mobile phase was also used to evaluate the separation. The gradient program began with 100:0 (A%/B%, v/v) for 0−1 min, then the following steps were applied: 95:5 (A%/B%, v/v) for 1 min, 97:3 (A%/B%, v/v) for 2 min, and 98:3 (A%/B%, v/v) for 2 min. The elution was performed using a 1.5 mL min$^{-1}$ flow rate, and the injection volume was 30 $\mu$L.

The determination of the total manganese in the samples/fractions and the monitoring of manganese fractions in the extracts were performed by an Elan 9000 ICP-MS (PerkinElmer SCIEX) composed of a PerkinElmer Ryton cross-flow nebulizer, a Scott-type double-pass spray chamber, and a standard glass torch. The sampler and skimmer cones were made of nickel. The operating conditions of the ICP-MS were as follows: RF power, 1000 W; plasma argon flow rate, 17.0 L min$^{-1}$; nebulizer flow rate, 0.85 L min$^{-1}$; sample uptake rate, 1.5 mL min$^{-1}$. The other plasma conditions and acquisition parameters were the same as those reported in our earlier studies.[12] Additionally, total manganese analyses were performed by a Varian (Australia) AA240FS fast sequential atomic absorption spectrometer (AAS) for validation purposes. The optimum parameters for manganese determination were as follows: wavelength, 279.5 nm; HCL current, 10 mA; acetylene flow rate, 2.0 L min$^{-1}$; slit width, 0.2 mm; and flame height, 7 mm. The fatty acid profiles in the hazelnut samples were identified by gas chromatography with flame ionization detection (GC-FID, Shimadzu, Kyoto, Japan) consisting of a DB-WAX analytical column (30 m × 0.25 mm × 0.25 $\mu$m). The injector and detector temperatures were 250 °C. The GC oven was maintained at 210 °C (isothermal). The injection volume was 1 $\mu$L, and the injection mode was split (1:20 ratio). Helium was used as the carrier gas with a flow rate of 1 mL min$^{-1}$.

HPLC was coupled online with ICP-MS through a Rheodyne switching valve apparatus (PerkinElmer SCIEX), which accomplished sample introduction from the outlet of the column to the nebulizer of the ICP-MS instrument via high-purity fluoropolymer tubing (PFA, Poly Fluorinated Alkoxy, 0.019 in. i.d., $^1/_{16}$ in. o.d., and 580 mm length, PerkinElmer SCIEX). The software Chromera version 1.2.254.0 (PerkinElmer SCIEX) was used to assess the online HPLC-ICP-MS chromatograms and data. The $^{55}$Mn isotope was measured on the basis of peak height using three replicates.

**Sample Preparation.** Three packages (90−250 g) of unshelled and processed (peeled, roasted, and ready-to-eat) Giresun-quality hazelnut samples obtained from the same manufacturer were mixed, and a portion of the homogenized sample was ground to a fine powder in a porcelain mortar and then transferred to polyethylene bottles. This preparation procedure described in detail above was separately applied to three different samples of the same quality purchased at different times and markets. Then, the obtained hazelnut samples were coded as samples 1, 2, and 3. The following sample preparation procedures were applied to preweighed samples.

**Major Constituents Analysis.** The moisture contents were determined according to ISO 771:1997.[20] The oil contents of the samples were determined according to TS 765:1969[21] after diethyl ether extraction. Additionally, chloroform/methanol (2:1 v/v) extraction[22] was applied to the samples to compare their lipid contents. The dietary fiber, crude fiber, crude ash, and sugar contents were determined according to AOAC 985.29 1986, ISO 5498:1981, and ISO 5984:2002 standard methods and the Luff Scroll method,[23−26] respectively. Methyl esters of the fatty acids were prepared and analyzed according to methods TS 4504 EN ISO 5509[27] and TS 4664 EN ISO 5508,[28] respectively, with some modifications. Briefly, transesterification was performed with 0.1 g of oil residue remaining from the samples after the application of method TS 765:1969.[21] Isooctane (4 mL) and methanolic KOH (0.8 mL) solutions were used for the transesterification. After vortexing for 30 s at room temperature, the upper isooctane layers of the samples were injected into the GC-FID column.

**Total Manganese Validation Analysis.** To minimize contamination, all of the glassware, polyethylene bottles, polypropylene centrifuge tubes, and pipet tips were soaked in 10% (v/v) nitric acid for at least 48 h and then rinsed several times with ultrapure water before drying in an oven at 40 °C. The hazelnut samples were digested prior to AAS and ICP-MS analyses. The detailed sample preparation procedure based on the DS/EN 14084 method,[29] together with the microwave digestion operating conditions, was reported in our earlier studies.[12] Briefly, 0.5 g of homogenized samples was digested with 6 mL of $HNO_3$ and 1 mL of $H_2O_2$. The microwave digestion operating conditions were as follows: 250 W (2 min), 0 W (2 min), 250 W (6 min), 400 W (5 min), and finally 600 W (5 min). An open-wet digestion method with the same proportion of nitric acid and hydrogen peroxide used in the microwave digestion was also applied. After cooling to room temperature, the samples were transferred to

polypropylene centrifuge tubes and diluted to 25 mL. Three independent replicates were prepared for each of the samples, spiked samples, and reagent blanks. Working solutions of manganese were prepared on a daily basis by appropriate dilution of a single stock solution and used for external calibration. The calibration curve was constructed from eight data points for standard solution concentrations ranging from 0.5 to 80 $\mu$g $L^{-1}$ for ICP-MS analysis and from six data points ranging from 0.1 to 2.0 mg $L^{-1}$ for AAS analysis. Because no hazelnut type certified reference material was available, each of the three hazelnut samples was spiked with aqueous manganese standard solutions at one level (0.1 mg $L^{-1}$) prior to microwave digestion for recovery studies. The calibration methods using aqueous standards and standard addition were compared on the basis of their slopes. Additionally, wheat flour certified reference material (for the defatted hazelnut samples) and the Conostan S-21 oil analysis standard (for the oil fraction of the hazelnut samples) were used to determine the accuracy of the manganese determinations by ICP-MS after the microwave and/or open-wet digestion methods. All microwave-digested samples were analyzed by AAS, followed by ICP-MS. The open-wet digested samples were analyzed only by ICP-MS.

**Fractionation Studies.** Manganese was extracted from 0.1 g of hazelnut sample using 15 mL of various solvents, including water, diethyl ether, *n*-hexane, and methanol. The extractions were performed in closed clear glass vials for 1.5 h at room temperature in an ultrasonic bath. Reagent blanks were also prepared in the same manner. The organic solvents in each fraction were filtered through blue ribbon filter paper and evaporated to dryness under nitrogen gas, and the residue was analyzed by ICP-MS after dissolving in 10 mL of 1% (v/v) $HNO_3$. All of the fractionation studies were performed in triplicate. The final extracts were then analyzed for manganese content by ICP-MS. The fractionation scheme is summarized in Figure 1. Additionally,

**Figure 1.** Fractionation scheme of manganese in hazelnut samples.

the lipids were extracted using a chloroform/methanol (2:1 v/v) extraction. Two grams of the samples was subjected to extraction in an ultrasonic bath for 30 min using 15 mL of the solvent mixture. The samples were filtered through blue ribbon filter paper, and 15 mL of fresh solvent mixture was added to the filtered sample. The entire procedure was applied in triplicate for one sample (hazelnut 1), and the number of independent applications for this sample was five. After this sequential extraction, the samples were dried and the fat content per 100 g was determined on the basis of mass loss. The fractionation approach based on activated carbon adsorption was performed using the method introduced by Kowalewska et al. with some modifications.[30] Briefly, a mixture of 30 mL of ultrapure water, 2.5 mL of methyl isobutyl ketone, and 0.03 g of activated carbon was added to each 0.1 g of sample. After extraction in an ultrasonic bath for 1 h at room temperature, the samples were filtered through blue ribbon filter paper and dried. The manganese contents in the samples were leached with 10 mL of 10% (v/v) nitric acid and determined by ICP-MS after appropriate dilution.

**HPLC-ICP-MS Analysis.** The water-soluble fractions were subjected to online analysis by HPLC-ICP-MS. After fractionation with water, all of the solutions were filtered through 0.45 $\mu$m PVDF filters and stored in clear polypropylene centrifuge tubes at 4 °C until analysis. The calibration standards ranged in concentration from 136 to 595 $\mu$g $L^{-1}$. The retention times of the standards and the samples, together with the peak heights, were compared to screen the manganese levels and the fractions.

**Bioaccessibility Assessments.** The bioaccessible manganese levels were determined after an in vitro enzymatic digestion procedure with appropriate solutions of pepsin and pancreatin. The simulated gastric digestion was initiated by adding 2 mL of freshly prepared pepsin−HCl solution (0.2 g of pepsin in 5 mL of 0.1 M HCl) to 0.03 g of sample. A 15 mL volume of ultrapure water was then added to the samples. The pH values of the solutions were adjusted to 1.9 with 0.1 M HCl. The solutions were incubated in a water bath at 37 °C for 1 h. The enzyme residues were removed by centrifugation at 2135*g* for 5 min, and the manganese contents of the samples determined by ICP-MS were designated the pepsin-digestible amounts. For the simulated intestinal digestion, 2.5 mL of freshly prepared enzyme solution (pancreatin/bile: 0.45 g of bile extract and 0.075 g of pancreatin in 37.5 mL of 0.1 M $NaHCO_3$) was added to 15 mL of the solutions containing 0.03 g of the samples. The pH values of the solutions were adjusted to 6.9 with 0.1 M $NaHCO_3$ or 0.1 M HCl. The solutions were incubated in a water bath at 37 °C for 2 h, and the manganese contents of the samples were determined by ICP-MS after the removal of the enzyme residues. The manganese levels in these solutions were designated the pancreatin-digestible amounts. The simulated gastrointestinal digestion was designated as the pepsin+pancreatin-digestible amount and was prepared by adding 4.5 mL of water to 3 mL of gastric extract. After pH adjustment, 3 mL of the pancreatin/bile solution was added to the samples. The pH values of the solutions were adjusted to 6.9, and the solutions were incubated in a water bath at 37 °C for 2 h.[12,17,31] The gastrointestinal digests were centrifuged at 2135*g* for 5 min. The supernatants were filtered immediately to remove any enzyme residue through PVDF syringe filters prior to being stored at 4 °C and analyzed by ICP-MS. The contents of the digests were analyzed to ensure the inactivity of any remaining enzyme residue. The manganese contents of the enzymatic digestions, together with the total element digestions, were used to calculate the percent bioaccessibility according to the equation

$$\text{bioaccessibility (\%)} = ([Mn^{2+}]_2/[Mn^{2+}]_1) \times 100$$

where $[Mn^{2+}]_2$ and $[Mn^{2+}]_1$ are the total manganese contents determined by ICP-MS after in vitro digestion and microwave-assisted acid digestion, respectively.[17] Additionally, 0.1 g samples were extracted with 15 mL of *n*-octanol to compare with the results obtained from intestinal pancreatic digestion. The extraction was performed in an ultrasonic bath for 1.5 h. Subsequently, a liquid−liquid extraction was performed using 5 mL of 1% (v/v) $HNO_3$ (in

**Table 1. Major Matrix Components of the Three Different Hazelnut Samples[a]**

| sample | moisture (%) | dietary fiber (%) | crude fiber (%) | crude protein (%) | oil (%) | sugar (%) | crude ash (%) |
|---|---|---|---|---|---|---|---|
| 1 | 2.03 ± 0.01 | 11.90 ± 0.41 | 5.45 ± 0.24 | 18.2 ± 0.8 | 64.6 ± 0.7 | 2.22 ± 0.24 | 2.20 ± 0.18 |
| 2 | 1.65 ± 0.02 | 10.48 ± 0.45 | 5.97 ± 0.42 | 18.3 ± 0.2 | 61.2 ± 0.7 | | 2.13 ± 0.17 |
| 3 | 1.89 ± 0.03 | 10.29 ± 1.05 | 5.95 ± 0.40 | 17.0 ± 0.2 | 64.7 ± 0.6 | | 2.33 ± 0.07 |

[a]Results represent the mean ± standard deviation ($N$ = 3).

triplicate), and the nitric acid fractions were analyzed by ICP-MS. To evaluate its compatibility, *n*-octanol extraction was applied to the spiked samples (at two levels) for recovery studies.[17]

## RESULTS AND DISCUSSION

**Fractionation Studies.** Manganese fractionation studies are important for establishing the relationship between metal mobility in organisms and nutrition. Additionally, understanding the role of major components of hazelnut is important for predicting manganese-binding food structures, which will provide valuable insights for further bioaccessibility studies. The major food components of hazelnut samples are outlined in Table 1. According to this table, most of the manganese could be present in oil-, protein-, or fiber-bound structures, with the hazelnuts consisting primarily of oil (60%) and protein (18%). The organic solvents selected for fractionation studies should represent these components, and these fractions are important for bioaccessibility assessments. The oil contents were 64.6, 61.2, and 64.7% for samples 1, 2, and 3, respectively. We focused only on the oily matrix for fractionation purposes; the protein contents were discussed within an online method by HPLC-ICP-MS. For fractionation purposes, diethyl ether, *n*-hexane, and methanol extractions were applied to remove the neutral, free, and bound polar lipids,[17,22] respectively. The manganese contents in these fractions ranged from 0.67 to 0.79 mg $kg^{-1}$ in the diethyl ether fractions, from 0.36 to 0.67 mg $kg^{-1}$ in the *n*-hexane fractions, and from 0.15 to 0.42 mg $kg^{-1}$ in the methanol fractions (Table 2). As discussed in the literature, diethyl ether extraction is important for neutral lipids, whereas methanol extraction is important for cell-membrane lipids (phospholipids, glycoproteins, and cholesterol).[22] We can conclude that the manganese content in any lipid fraction will be small compared to the total manganese content, and no substantial differences were observed among them. Thus, manganese should be naturally and mostly bound to other parts of the matrix constituents, the structures of which will help to assess manganese bioaccessibility. The oil contents of the samples achieved by chloroform/methanol extraction were compared with those obtained by standard methods using Soxhlet extraction.[21] The results were comparable, with 64.6 ± 0.7% for the standard method and 61.8 ± 5.6% for the proposed extraction method. The only difference between the two methods was the wide standard deviation in the latter method. This result also shows the similar levels of neutral and total lipids in the hazelnut matrix. Additionally, as reported in the literature, Mn(II) is most likely bound strongly to the carboxylate ends of the fatty acids.[32] To evaluate the fatty acid binding site, fatty acid characterization studies were performed by GC-FID. The results were evaluated according to the chromatographic retention times and peak areas of the corresponding methyl ester standard in the FAME mixture. The fatty acid contents of the three hazelnut samples per 100 g are outlined in Table 3. As observed in this table, the most abundant fatty acids per 100 g in the hazelnut samples, in decreasing order, were oleic, linoleic, palmitic, and stearic acids. The bound manganese levels (methanol fractions) might be associated with the most abundant fatty acid (oleic acid) for the following reasons. First, it is indicated in the literature that the foliar application of $MnCl_2$ to sunflower plants (seed produces oil up to 50% by weight) positively affects the palmitic and oleic acid levels and increases their amounts, whereas it negatively affects the stearic, linoleic, and linolenic acid levels.[33] Palmitic and oleic acids are the saturated and unsaturated fatty acids, respectively. Mn potentially influences the fatty acid profile via promoting acetyl-CoA carboxylase activity, which is important in fatty acid synthesis.[34] From these results, together with the similar oil contents of the seeds and our matrix, oleic and palmitic acids are the most probable manganese complexes among the fatty acids in hazelnuts. Second, it has been reported that $C_{18}$ fatty acids have a tendency to be expelled from water to reduce the total energy and therefore arrange themselves into oligomers or clusters. Fatty acids with straight alkyl chains are known to pack closer together; therefore, it is difficult to strip away the acidic proton in solution. Additionally, trans double bonds are known to pack closer than cis double bonds, subsequently leading to higher $pK_a$ values for trans double bonds.[35] Given this information, the observed $pK_a$ of palmitic acid ($C_{16}$ fatty acid) is expected to be higher than that of oleic acid ($C_{18}$ fatty acid with a cis double bond); therefore, oleic acid may be a preferable manganese binding fatty acid structure. This acid is also the most abundant fatty acid in hazelnuts, as shown in Table 3.

**Table 2. Manganese Levels Released from the Samples Using Fractionation Methods[a]**

| sample | water | diethyl ether | *n*-hexane | methanol |
|---|---|---|---|---|
| 1 | 10.89 ± 2.62 | 0.78 ± 0.15 | 0.36 ± 0.03 | 0.15 ± 0.05 |
| 2 | 13.38 ± 0.02 | 0.79 ± 0.24 | 0.67 ± 0.02 | 0.23 ± 0.01 |
| 3 | 7.33 ± 0.32 | 0.67 ± 0.05 | 0.40 ± 0.02 | 0.42 ± 0.04 |

[a](Mean ± SD, mg $kg^{-1}$, $N$ = 3).

**Table 3. Fatty Acids in the Three Hazelnut Samples Based on the Methyl Ester Compositions[a]**

| fatty acid | sample 1 (%) | sample 2 (%) | sample 3 (%) |
|---|---|---|---|
| myristic (C14:0) | <0.1 | <0.1 | <0.1 |
| palmitic (C16:0) | 5.02 ± 0.04 | 5.03 ± 0.02 | 5.04 ± 0.01 |
| palmitoleic (C16:1) | 0.13 ± 0.01 | 0.13 ± 0.01 | 0.14 ± 0.01 |
| stearic (C18:0) | 2.52 ± 0.01 | 2.45 ± 0.01 | 2.20 ± 0.01 |
| oleic (C18:1) | 84.2 ± 0.10 | 83.9 ± 0.10 | 84.1 ± 0.10 |
| linoleic (C18:2) | 7.95 ± 0.05 | 8.29 ± 0.03 | 8.34 ± 0.01 |
| linolenic (C18:3) | <0.1 | <0.1 | 0.11 ± 0.01 |
| arachidic (C20) | 0.11 ± 0.01 | 0.11 ± 0.01 | 0.10 ± 0.01 |
| eicosenoic (C20:1) | <0.1 | <0.1 | <0.1 |
| behenic (C22:0) | <0.1 | <0.1 | <0.1 |
| erucic (C22:1) | <0.1 | <0.1 | <0.1 |
| total | 100.00 | 100.00 | 100.00 |

[a]Injection count = 4.

**Validation Analysis.** Although the total Mn validation could be conducted using only reference material after microwave acid extraction and ICP-MS analysis, there is no hazelnut-type reference material. Consequently, additional validation was performed by AAS via total manganese determination in our study. The method detection and quantification limits for AAS analysis were 0.64 and 2.13 mg $kg^{-1}$, respectively. Under the optimum conditions, the accuracy was evaluated using recovery studies. Manganese recoveries of 100.0, 94.7, and 102.4% and manganese contents of 74.6 ± 1.0, 85.8 ± 2.8, and 65.5 ± 10.9 mg $kg^{-1}$ were determined by AAS for hazelnut samples 1, 2, and 3, respectively. The total manganese levels in samples 1, 2, and 3 were determined to be 79.9 ± 1.3, 95.5 ± 1.9, and 76.7 ± 9.3 mg $kg^{-1}$, respectively, based on the wet weight basis by ICP-MS, and the moisture

Table 4. Manganese Levels Released from the Samples after Treatment with Digestive Enzymes (Pepsin, Pancreatin, Bile Salts Mixture), Water, *n*-Octanol, and Activated Carbon Shown with the Bioavailability of Manganese from the Three Samples[a]

| | pepsin | | pancreatin | | pepsin + pancreatin[b] | | activated carbon adsorbability[c] | |
|---|---|---|---|---|---|---|---|---|
| sample | mg kg$^{-1}$ | % | mg kg$^{-1}$ | % | mg kg$^{-1}$ | % | mg kg$^{-1}$ | % |
| 1 | 47.57 ± 0.42 | 59.5 | 30.80 ± 4.50 | 38.5 | 46.03 ± 2.25 | 57.6 | 27.33 ± 0.50 | 34.2 |
| 2 | 44.79 ± 3.15 | 46.9 | 25.86 ± 3.01 | 27.1 | 30.55 ± 3.00 | 32.0 | 21.73 ± 2.30 | 22.8 |
| 3 | 65.68 ± 4.06 | 85.6 | 26.13 ± 2.12 | 34.1 | 47.60 ± 4.81 | 62.1 | 21.65 ± 3.05 | 28.2 |

| | water extractability | | bioavailability[d] | *n*-octanol extractability[e] | | corrected *n*-octanol extractability[f] |
|---|---|---|---|---|---|---|
| sample | mg kg$^{-1}$ | % | % | mg kg$^{-1}$ | % | mg kg$^{-1}$ |
| 1 | 10.89 ± 2.62 | 13.6 | 57.6 | 1.11 ± 0.43 | 1.4 | 2.26 ± 0.28 |
| 2 | 13.38 ± 0.02 | 14.0 | 32.0 | 1.54 ± 0.86 | 1.6 | 4.51 ± 1.23 |
| 3 | 7.33 ± 0.32 | 9.6 | 62.1 | 1.25 ± 0.21 | 1.6 | 3.16 ± 0.20 |

[a]Mean ± SD, $N = 3$. [b]Gastrointestinal fraction. [c]Activated carbon-absorbable amount/total amount of manganese . [d]Simulated in vitro pepsin +pancreatin-digestible amount/total amount of manganese . [e]*n*-Octanol-extractable amount/total amount of manganese . [f]$c \times$ correction factor.

levels for the samples were 2.03, 1.65, and 1.89%, respectively, as shown in Table 1. The instrumental detection and quantification limits for ICP-MS (also for further HPLC-ICP-MS) analysis were calculated as 3 and 10 times the standard deviations of the concentrations derived from the lowest detectable and quantified levels, respectively, near the reagent blanks with reasonable certainty ($k = 3$, a confidence level of 99.86%).[17,36] The sample mass and dilution factors were considered to calculate the method detection and quantification limits. The limits of detection and quantification for manganese by ICP-MS were 0.031 and 0.103 mg kg$^{-1}$, respectively. The calibration equation was $y = 38593x$, with a correlation coefficient ($r^2$) of 0.999960. The intraday precision was 3.3%, whereas the interday precision was 4.5%. The intraday mean value was calculated from the relative standard deviation (%) of six separately prepared samples at the smallest concentration of manganese (0.5 $\mu$g L$^{-1}$) that were analyzed on the same day. Additionally, the interday mean value was calculated from the same smallest concentration of manganese analyzed over a period of a week.[12] Because of the lack of a standard reference material with the same matrix, the accuracy of the ICP-MS method was also evaluated by recovery studies. The recoveries were 100.3, 96.5, and 95.3% for samples 1, 2, and 3, respectively, by ICP-MS. Additionally, two different types of certified reference materials representing the defatted and fatty portions of the hazelnut samples were evaluated. The measured manganese concentration of 12.2 ± 3.4 mg kg$^{-1}$ obtained by ICP-MS after open-wet digestion was in good agreement with the certified value of 9.4 ± 0.9 mg kg$^{-1}$ at the 95% confidence level for wheat flour. In addition, the measured manganese concentration of 11.5 ± 1.7 mg kg$^{-1}$ was in good agreement with the standard value of 10 mg kg$^{-1}$ from the Conostan calibration and verification standard. Because microwave digestion systems are available in many laboratories, the open-wet digestion method was applied as an alternative to the microwave digestion system, and manganese contents of 84.2 ± 11.6, 88.0 ± 1.2, and 74.6 ± 6.1 mg kg$^{-1}$ were determined in the samples by ICP-MS. This method has proven the minimal effect of fat-bound manganese to total manganese levels and might serve as an alternative to microwave digestion. The paired $t$ test was applied to the AAS and ICP-MS results, from which no significant difference between the results at the 95% confidence level was observed.

Open-wet digestion was also applied to the defatted samples remaining after Soxhlet extraction to investigate whether the manganese originated primarily from the protein structures (the most abundant component after oil). The manganese concentrations in the defatted samples were found to be 49.0 ± 4.8, 43.0 ± 8.9, and 65.2 ± 10.2 mg kg$^{-1}$. According to these results, 54−87% of manganese may be associated with the protein components, with a maximum of 67% of the manganese observed to be associated with protein in sample 1, as discussed under HPLC-ICP-MS Analysis.

**In Vitro Bioaccessibility Studies.** The total concentration of metals in foods may not represent the bioavailable amounts for humans. A better approach to assess metal content is to determine the amount of metal released during gastrointestinal digestion.[12] For this purpose, pepsin, pancreatin, or *n*-octanol extraction processes were performed to determine the absorption levels of manganese through the stomach and intestinal pathway. The compatibilities for intestinal absorption of pancreatin and *n*-octanol were thus compared. As stated in our previous studies, *n*-octanol fractions cannot be used to assess the daily intake as an alternative to pancreatic digestion unless an appropriate correction factor is applied.[12,17] To determine this factor, spiked studies were performed, together with *n*-octanol fractionation by Mn(II) standard solutions, at two concentration levels (5 and 10 $\mu$g L$^{-1}$), and recoveries for the three hazelnut samples were 49.07, 34.1, and 39.5%. These values reflect the complexation possibilities of Mn(II) in the *n*-octanol fraction.[17] The recoveries of the samples were used as a correction factor for the *n*-octanol extraction results before comparison with pancreatic digestion. Nevertheless, higher digestible amounts were achieved using pancreatin. Kowalevska et al. determined the metal adsorption on activated carbon from a vegetable oil matrix. As a general approach, activated carbon adsorption represents any bound compounds that can be adsorbed onto the surface.[12,30] Activated carbon adsorption studies were thus performed to assess the presence of bound manganese species that are water- or organic solvent-soluble. Activated carbon can adsorb complexes and aromatic manganese-bound structures,[12] and one of these species may originate from the oily matrix (primarily from fatty acids) of hazelnut. Hazelnut contains a significant amount of fiber, containing approximately 5 and 10% crude and dietary fiber, respectively (Table 1). Previous studies have suggested that the dietary fiber present in many plants is important for metal absorption. Additionally, dietary fiber can facilitate Mn excretion and reduce its accumulation in many tissues.[37] These evaluations suggest that nondigestible or unavailable manganese levels might originate from the dietary fiber or crude fiber contents of nut matrices. The digestible or

absorbable fractions of manganese are shown in Table 4. The manganese levels in the water fractions were found to be 7.3−13.4 mg $kg^{-1}$, varying in the range from 9.6 to 14%. This fraction may represent the free Mn(II) or ionic Mn(II) originating from soluble manganese complexes, hydrolyzable lipids, or sugar compounds.[12] Soluble proteins might also be considered in this context. Because hazelnut predominantly contains oil and proteins, manganese complexes will associate with these structures. None of the organic solvents used in the fractionation analysis were sensitive enough, and validation studies will not be meaningful unless these groups can be precisely identified.[17]

The bioavailability was calculated by dividing the total contents of manganese after in vitro digestion by the contents of manganese in the microwave-assisted acid digests of the samples. The bioavailability of the manganese was found to be 57.6, 32.0, and 62.1% for samples 1, 2, and 3, respectively. The bioavailability of manganese from three hazelnut samples is presented in Table 4. The difference between the total and the gastrointestinal-digested amounts can be attributed to the unavailable manganese originating primarily from the dietary fiber-bound content, as mentioned above, and also to the manganese in particulate form. Importantly, a portion of unavailable manganese could become bioavailable if it can be directly absorbed in the stomach from calcium channels, such as in the form of calcium ions.[38] The pancreatin-digestible and activated carbon-adsorbable values as well as the pepsin- and gastrointestinal-digestible values showed similar tendencies. Because of these similar results, the approaches are interchangeable in assessing bioavailability. Additionally, the similarity of the pepsin and gastrointestinal (pepsin+pancreatin consecutive digestion) bioavailabilities shows that protein structures are the most important food components for manganese bioaccessibility, and the oil-bound structures have a minimal effect. Consequently, it can be concluded that most of the free and/or soluble Mn(II) originated from the water-extractable fractions, which together with the protein-bound manganese are important for hazelnut bioaccessibility. Thus, these fractions were undertaken for a hyphenated technique analysis. As expected, HPLC-ICP-MS provided valuable information regarding the free Mn(II) content and the soluble protein complexes. Only two peaks were extracted as water-soluble manganese fractions, corresponding to well-defined free manganese and most likely charged and complexed Mn(II), which coeluted on the column. As previously mentioned, nuts contain relatively high levels of protein compared to other plant materials,[39] as confirmed by our fractionation studies detailed above. For this reason, it is likely that this fraction is associated with soluble, protein-bound manganese. An elution solvent with an acceptable amount of methanol for ICP-MS analysis was also applied under different gradient elution conditions, and the two peaks were not well separated. This can be attributed to the two charged manganese species. The first peak contained 32.8% of the water-soluble manganese, and the second peak contained 18.2%. There were no significant variations among the samples after qualitative analysis, and for this reason, quantitative online analysis was applied for only one sample (sample 1). The other samples displayed similar chromatograms. The baselines between the extractions were monitored with Chromera software, and the two peaks were well differentiated from the baseline. Because manganese possesses only a single isotope ($^{55}Mn$), possible matrix interferences originating from $^{40}Ar^{14}N^{1}H^{+}$, $^{37}Cl^{18}O^{+}$, $^{40}Ar^{15}N^{+}$, $^{38}Ar^{17}O^{+}$, $^{36}Ar^{18}O^{1}H^{+}$, $^{38}Ar^{16}O^{1}H^{+}$, and $^{37}Cl^{17}O^{1}H^{+}$[40,41] can be reduced by dilution in the online system and by using correction equations from the software. In addition, to eliminate the possibility of interference in the manganese determinations, the peak heights were selected for monitoring instead of the peak areas.

After analysis of the oil contents according to TS 765:1969,[21] the HPLC-ICP-MS chromatograms of the residues (defatted samples) were compared with those of the original samples after the water extraction procedure. As expected from the results of the fractionation studies and as confirmed by the chromatograms obtained by this technique, the defatted hazelnut samples exhibited chromatograms similar to those of the original samples, which were considered sufficient for quantitative analytical purposes. Additionally, there were no significant variations among the samples after fractionation analysis, and for this reason quantitative online analysis was used for only one sample. There is no certified reference material for hazelnut, as mentioned above, and recovery studies with spiked samples are not valuable for speciation studies by HPLC−ICP-MS. For this reason, an external calibration method was applied for free manganese as a Mn(II) standard solution, and peak confirmation was achieved by the standard addition method. Identification was based on the retention times of the samples and the standards. Chromatographic identification was achieved within 5 min with isocratic elution using water. The retention times were 2.5 min for the Mn(II) standard and the first peak of the hazelnut sample. In addition, the second peaks in the chromatograms of the hazelnut samples were detected at $t_R$ = 3.0 min. For HPLC-ICP-MS analysis, the detection limit was 3.6 $\mu g\ L^{-1}$ and the quantification limit was 12 $\mu g\ L^{-1}$. The calibration equation was $y = 1181x - 13609$ with an $r^2$ of 0.975. Additionally, the repeatability calculated from the relative standard deviation (%RSD) was 6.1%. Water-soluble fractions are also important in terms of bioaccessibility, and the amount of manganese in the first and second peaks observed in the HPLC-ICP-MS chromatogram was 51% of the total water-soluble manganese. The bioaccessibility and the water-soluble manganese levels were compatible with one another, and the water-soluble manganese can be attributed to the bioavailable fraction from the hazelnuts. The difference between the total bioavailable fraction and this fraction (11.1%) originates from the bioaccessibility of the lipid and/or the manganese bound to other microconstituents.

In conclusion, a method for the screening and measurement of manganese fractions in hazelnut samples was presented herein. Fractionation, speciation, and matrix characterization can be regarded as three pillars of bioaccessibility assessment. From this perspective, matrix characterization by major constituent analysis and fractionation studies was evaluated in the context of bioaccessibility to increase the accuracy of in vitro methods. This analytical approach can be considered a new method for the evaluation of manganese binding sites in plant-based food matrices together with the fractionation of manganese. Our preliminary results provided good experimental foreknowledge, and future studies are in progress to apply and evaluate this online technique for the speciation of essential elements in hazelnut samples.

## AUTHOR INFORMATION

### Corresponding Author

*(U.S.E.) Phone: +90 224 294 1739. Fax: +90 224 294 1899. E-mail: useven@uludag.edu.tr.

### Funding

This work was supported by the Commission of Scientific Research Projects of Uludag University (Project F-2008/25).

### Notes

Part of this study was presented at the 1st International Conference on Food Properties (ICFP2014) in Kuala Lumpur, Malaysia.

The authors declare no competing financial interest.

## ■ ACKNOWLEDGMENTS

This work is part of the Ph.D. thesis of the first author, which was accepted on July 10, 2013, by the Graduate School of Natural and Applied Sciences of Uludag University.

## ■ REFERENCES

(1) Pelvan, E.; Alasalvar, C.; Uzman, S. Effects of roasting on the antioxidant status and phenolic profiles of commercial Turkish hazelnut varieties (*Corylus avellana* L.). *J. Agric. Food Chem.* **2012**, *60*, 1218−1223.

(2) Açkurt, F.; Özdemir, M.; Biringen, G.; Löker, M. Effects of geographical origin and variety on vitamin and mineral composition of hazelnut (*Corylus avellana* L.) varieties cultivated in Turkey. *Food Chem.* **1999**, *65*, 309−313.

(3) Altun, M.; Çelik, S. E.; Güçlü, K.; Özyürek, M.; Erçağ, E.; Apak, R. Total antioxidant capacity and phenolic contents of Turkish hazelnut (*Corylus avellana* L.) kernels and oils. *J. Food Biochem.* **2013**, *37*, 53−61.

(4) Simsek, A.; Aykut, O. Evaluation of the microelement profile of Turkish hazelnut (*Corylus avellana* L.) varieties for human nutrition and health. *Int. J. Food Sci. Nutr.* **2007**, *58*, 677−688.

(5) Alasalvar, C.; Shahidi, F.; Cadwallader, K. R. Comparison of natural and roasted Turkish Tombul hazelnut (*Corylus avellana* L.) volatiles and flavor by DHA/GC/MS and descriptive sensory analysis. *J. Agric. Food Chem.* **2003**, *51*, 5067−5072.

(6) Amaral, J. S.; Casal, S.; Citova, I.; Santos, A.; Seabra, R. M.; Oliveira, B. P. P. Characterization of several hazelnut (*Corylus avellana* L.) cultivars based in chemical, fatty acid and sterol composition. *Eur. Food Res. Technol.* **2006**, *222*, 274−280.

(7) Köksal, A.İ.; Artik, N.; Şimşek, A.; Güneş, N. Nutrient composition of hazelnut (*Corylus avellana* L.) varieties cultivated in Turkey. *Food Chem.* **2006**, *99*, 509−515.

(8) Şimşek, A.; Korkmaz, D.; Velioğlu, Y. S.; Ataman, O. Y. Determination of boron in hazelnut (*Corylus avellana* L.) varieties by inductively coupled plasma optical emission spectrometry and spectrophotometry. *Food Chem.* **2003**, *83*, 293−296.

(9) Alasalvar, C.; Shahidi, F.; Liyanapathirana, C. M.; Ohshima, T. Turkish Tombul hazelnut (*Corylus avellana* L.). 1. Compositional characteristics. *J. Agric. Food Chem.* **2003**, *51*, 3790−3796.

(10) Alasalvar, C.; Amaral, J. S.; Satır, G.; Shahidi, F. Lipid characteristics and essential minerals of native Turkish hazelnut varieties (*Corylus avellana* L.). *Food Chem.* **2009**, *113*, 919−925.

(11) Gomez-Ariza, J. L.; Arias-Borrego, A.; Garcia-Barrera, T. Multielemental fractionation in pine nuts (*Pinus pinea*) from different geographic origins by size-exclusion chromatography with UV and inductively coupled plasma mass spectrometry detection. *J. Chromatogr., A* **2006**, *1121*, 191−199.

(12) Erdemir, U. S.; Gucer, S. Fractionation analysis and bioaccessibility of manganese in spinach (*Spinacia oleracea* L.) leaves. *Chem. Speciation Bioavailability* **2013**, *25*, 265−272.

(13) Dugo, G.; Pera, L. L.; Turco, V. L.; Palmieri, R. M.; Saitta, M. Effect of boiling and peeling on manganese content of some vegetables determined by derivative anodic stripping chronopotentiometry (dASCP). *Food Chem.* **2005**, *93*, 703−711.

(14) Pearson, G. F.; Greenway, G. M. Recent developments in manganese speciation. *TrAC, Trends Anal. Chem.* **2005**, *24*, 803−809.

(15) Kim, M. H.; Choi, M. K. Seven dietary minerals (Ca, P, Mg, Fe, Zn, Cu, and Mn) and their relationship with blood pressure and blood lipids in healthy adults with self-selected diet. *Biol. Trace Elem. Res.* **2013**, *153*, 69−75.

(16) Santos, E. E.; Lauria, D. C.; Porto da Silveira, C. L. Assessment of daily intake of trace elements due to consumption of foodstuffs by adult inhabitants of Rio de Janeiro city. *Sci. Total Environ.* **2004**, *327*, 69−79.

(17) Erdemir, U. S.; Gucer, S. Assessment of copper bioaccessibility in spinach (*Spinacia oleracea* L) leaves by chemical fractionation. *Food Anal. Methods* **2014**, *7*, 994−1001.

(18) Sun, S. S. M.; Leung, F. W.; Tomic, J. C. Brazil nut (*Bertholletia excelsa* H. B. K.) proteins: fractionation, composition, and identification of a sulfur-rich protein. *J. Agric. Food Chem.* **1987**, *35*, 232−235.

(19) Goncalves, A. M.; Fernandes, K. G.; Ramos, L. A.; Cavalheiro, E. T. G.; Nobrega, J. A. Determination and fractionation of barium in Brazil nuts. *J. Braz. Chem. Soc.* **2009**, *20*, 760−769.

(20) ISO 771:1977, Oilseed residues − determination of moisture and volatile matter content; ISO, Geneva, Switzerland, 1977.

(21) TS 765:1969, Oilseed residues − determination of diethyl ether extract; BSI Group, London, UK, 1969.

(22) Ferraz, T. P. L.; Fiuza, M. C.; dos Santos, M. L. A.; Pontes de Carvalhoa, L.; Soares, J. N. M. Comparison of six methods for the extraction of lipids from serum in terms of effectiveness and protein preservation. *J. Biochem. Biophys. Methods* **2004**, *58*, 187−193.

(23) AOAC 985.29:1986, Total dietary fiber in foods, enzymatic-gravimetric method; AOAC International, Gaithersburg, MD, USA, 1986.

(24) ISO 5498:1981, Agricultural food products − determination of crude fibre content; ISO, Geneva, Switzerland, 1981.

(25) ISO 5984:2002, Animal feeding stuffs − determination of crude ash; ISO, Geneva, Switzerland, 2002.

(26) Egan, H.; Kirk, R.; Sawyer, R. In *Pearson's Chemical Analysis of Foods*; Longman Scientific and Technical: Harlow, UK, 1981; 591 pp.

(27) TS 4504 EN ISO 5509, Animal and vegetable fats and oils − preparation of methyl esters of fatty acids; BSI Group, London, UK.

(28) TS 4664 EN ISO 5508, Animal and vegetable fats and oils − analysis by gas chromatography of methyl esters of fatty acids; BSI Group, London, UK.

(29) DS/EN 14084:2003, Foodstuffs − determination of trace elements: determination of lead, cadmium, zinc, copper and iron by atomic absorption spectrometry (AAS) after microwave digestion; BSI Group, London, UK, 2003.

(30) Kowalewska, Z.; Izgi, B.; Saracoglu, S.; Gucer, S. Application of liquid-liquid extraction and adsorption on activated carbon to the determination of different forms of metals present in edible oils. *Chem. Anal. (Warsaw)* **2005**, *50*, 1007−1019.

(31) Liu, C. S.; Glahn, R. P.; Liu, R. H. Assessment of carotenoid bioaccessibility of whole foods using a Caco-2 cell culture model coupled with an in vitro digestion. *J. Agric. Food Chem.* **2004**, *52*, 4330−4337.

(32) Yoo, H. J.; Hakansson, K. Determination of double bond location in fatty acids by manganese adduction and electron induced dissociation. *Anal. Chem. (Washington, DC, U.S.)* **2010**, *82*, 6940−6946.

(33) Jabeen, N.; Ahmad, R.; Sultana, R.; Saleem, R.; Ambrat, E. Investigations on foliar spray of boron and manganese on oil content and concentrations of fatty acids in seeds of sunflower plant raised through saline water irrigation. *J. Plant Nutr.* **2013**, *36*, 1001−1011.

(34) Scorpio, R. M.; Masoro, E. J. Differences between manganese and magnesium ions with regard to fatty acid biosynthesis, acetyl-coenzyme A carboxylase activity and malonyl-coenzyme A decarboxylation. *Biochem. J.* **1970**, *118* (3), 391−399.

(35) Kanicky, J. R.; Shah, D. O. Effect of degree, type, and position of unsaturation on the p$K_a$ of long-chain fatty acids. *J. Colloid Interface Sci.* **2002**, *256*, 201−207.

(36) Corley, J. Best practices in establishing detection and quantification limits for pesticide residues in foods. In *The Handbook of Residue Analytical Methods for Agrochemicals*; Lee, P. W., Aizawa, H.,

Barefoot, A. C., Murphy, J. J., Eds.; Wiley: Chichester, UK, 2003, Vol. 1, pp 59−75.
(37) Shi, X.-Q.; Yan, W.; Wang, K.-Y.; Fan, Q.-Y.; Zou, Y. Protective effects of dietary fibre against manganese-induced neurobehavioral aberrations in rats. *Arh. Hig. Rada Toksikol.* **2012**, *63*, 263−270.
(38) Petkova-Kirova, P. S.; Lubomirov, L. T.; Gagov, H. S.; Kolev, V. B.; Duridanova, D. B. Thyrotropin-releasing hormone activates K-Ca channels in gastric smooth muscle cells via intracellular $Ca^{2+}$ release. *Gen. Physiol. Biophys.* **2001**, *20*, 46−60.
(39) Kannamkumarath, S. S.; Wrobel, K.; Wrobel, K.; Vonderheide, A.; Caruso, J. A. HPLC−ICP−MS determination of selenium distribution and speciation in different types of nut. *Anal. Bioanal. Chem.* **2002**, *373*, 454−460.
(40) Quintana, M.; Klouda, A. D.; Ochsenkuhn-Petropoulou, M.; Michalke, B. Size characterization of manganese species from liver extracts using size exclusion chromatography inductively coupled plasma mass spectrometry. *Anal. Chim. Acta* **2005**, *554*, 130−135.
(41) D'Ilio, S.; Violante, N.; Caimi, S.; Di Gregorio, M.; Petrucci, F.; Senofonte, O. Determination of trace elements in serum by dynamic reaction cell inductively coupled plasma mass spectrometry. Developing of a method with a desolvating system nebulizer. *Anal. Chim. Acta* **2006**, *573−574*, 432−438.

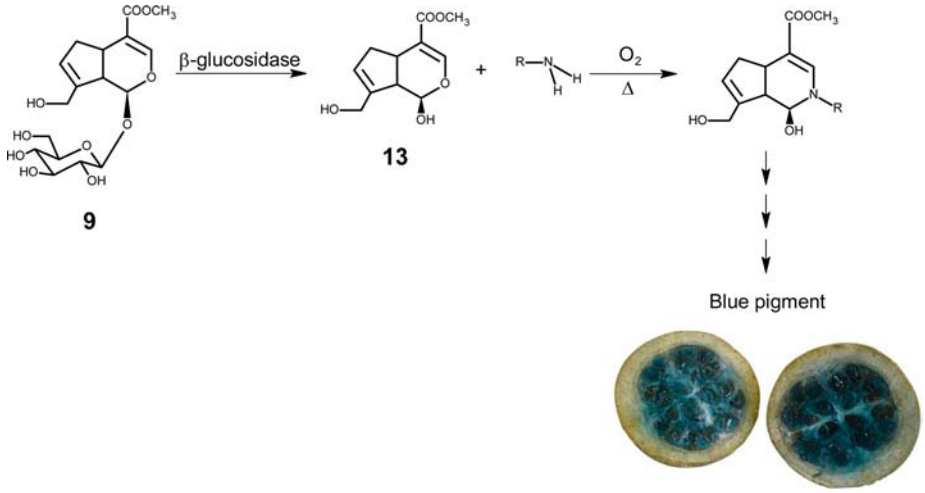


**Figure 2.** Formation reaction for the blue pigment and its appearance in genipap fruit (compounds numbered according to retention time given in Table 2).

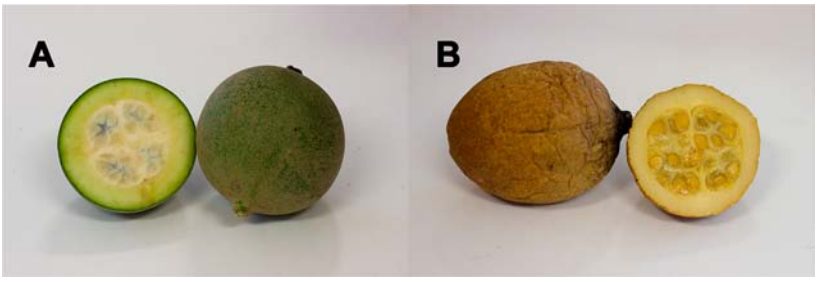


**Figure 3.** Photographs of genipap fruit at two ripening stages: unripe (left) and ripe (right).

from a Milli-Q system (Billerica, MA, USA), and the Folin−Ciocalteu reagent was acquired from Dinâmica (São Paulo, Brazil). The samples and standards were filtered through 0.22 $\mu$m Millipore membranes.

**Materials.** The genipap fruits (Figure 3) were harvested from a tree situated inside the University of Campinas (UNICAMP) campus, located in the city of Campinas (São Paulo State, Brazil), corresponding to the following coordinates: latitude 22°49′88″, longitude 47°04′21″, and altitude of 606 m. The plant material was authenticated by Professor Jorge Yoshio Tamashiro; Department of Plant Biology at the Institute of Biology, UNICAMP, and a voucher specimen was deposited in the UNICAMP Herbarium (UEC 11713).

Three batches of fruits were harvested, with an interval of 10 days between each harvest. All harvests occurred in the months of January and February 2013. The genipap fruits were manually washed and peeled. The portions of mesocarp and endocarp were separated and frozen immediately in liquid nitrogen. Each sample was then freeze-dried (Liobrás, São Paulo, Brazil) and ground in a domestic food processor. The three batches of each sample were mixed together to form a composite sample and vacuum packed in polyethylene bags. The samples were stored in a freezer at −36 °C until analysis.

The moisture of the genipap fruit samples was determined in triplicate according to an AOAC method.[21] The samples exhibited the following moisture contents: unripe endocarp, 85.7 ± 0.1 g/100 g; unripe mesocarp, 80.9 ± 0.1 g/100 g; ripe endocarp, 70.2 ± 0.1 g/100 g; ripe mesocarp, 75.3 ± 0.1 g/100 g.

**Differentiation between Unripe and Ripe Fruits.** The ripeness of the fruits was determined by firmness and peel color analysis. These techniques were chosen for being minimally invasive, because tissue damage can both release the enzyme and expose the interior of the unripe fruits to oxygen, which leads to the formation of the blue pigment. All of the fruits used in this study were submitted to firmness and color analysis.

The firmness was evaluated by determining the maximum force of penetration (MFP) using a TA-XT Plus texturometer (Stable Micro Systems Ltd., Surrey, UK) equipped with a P/2N needle probe. The MFP was determined on two opposite faces in the equatorial region of each fruit. The analysis was performed under the following conditions: pretest speed, 5 mm/s; test speed, 2 mm/s; post-test speed, 10 mm/s; and penetration depth, 10 mm. The results were expressed in newtons (N). Fruits with MFP values >10 N were considered unripe, and fruits with MFP values <2 N were considered ripe. Fruits with intermediate MFP values were discarded. Thus, the samples were composed of 45 ripe and 45 unripe fruits, after preliminary ripeness classification.

The fruit color was determined at four equidistant points around the equatorial region using a Hunter ColorQuest XE (Reston, VA, USA) spectrocolorimeter calibrated in the reflectance mode, with specular excluded, using the illuminant D65 and an observation angle of 10°. The parameters $L^*$, $a^*$, and $b^*$ of the CIELAB color system were determined.

**Determination of the Iridoid and Phenolic Compound Compositions.** The iridoids and phenolic compounds were extracted from the freeze-dried sample (0.4 g) with 20 mL of a methanol/water [8:2 (v/v)] solution in a Teflon tube by vortexing for 5 min at room temperature (22 ± 3 °C), followed by centrifugation (Beckman Coulter, Allegra 64R, Palo Alto, CA, USA) at 22000*g* for 10 min at 4 °C. The supernatant was collected, another aliquot of solvent was added to the tube, and the extraction procedure was repeated until extraction of the sample was complete. The absence of iridoids and phenolic compounds in the residue was confirmed using the Folin−Ciocalteu reagent. In general, five extractions were enough to achieve complete extraction; the supernatants were then combined to form a single extract, which was made up to a final volume of 100 mL using the same extraction solvent.

The extract was analyzed by high-performance liquid chromatography (HPLC) using a Shimadzu chromatograph (Kyoto, Japan) equipped with a quaternary pump (LC-20AD), a degasser (DGU-20A5), and a Rheodyne injection valve with a 20 $\mu$L loop, connected in series to a diode array detector (DAD) (SPD-M20A) and a Amazon

speed ETD mass spectrometer (MS) (Bruker Daltonics, Bremen, Germany), with an electrospray ionization source (ESI) and an ion trap analyzer.

The column used was a 250 × 4.6 mm i.d., 4 μm, $C_{18}$ Synergi Hydro RP80A (Phenomenex, Torrance, CA, USA) at a flow rate of 0.9 mL/min and column temperature set at 29 °C, using as mobile phase water (A) and acetonitrile (B), both containing 0.1% formic acid (v/v), in a linear gradient (v/v) from A/B 99:1 to 50:50 in 50 min, then to 1:99 in 5 min, maintaining this proportion for 5 min, returning to 99:1 in 5 min, and finally maintaining this proportion for 10 min to re-equilibrate the column.[22] The UV−vis spectra were obtained between 200 and 600 nm and the chromatograms were processed at 250 and 320 nm. For the MS analysis, the flow from the DAD was split, allowing the entrance of only 0.15 mL/min onto the ESI source. The MS was configured with the following parameters: negative ionization mode; voltage on the capillary, 2 kV; capillary exit voltage, −110 V; skimmer 1, 10 V; skimmer 2, 5 V; end plate offset, −500 V; drying gas ($N_2$) temperature, 310 °C; flow rate, 5 L/min; and nebulizer, 30 psi.[22] The fragmentation energy to obtain the MS/MS was 1.4 and 1.8 V for the $MS^3$ fragmentation energy. The mass spectra were acquired with a scan range from $m/z$ 100 to 1000.

The iridoids and phenolic compounds were identified through the combined information from the following parameters: elution order and retention time on the $C_{18}$ column, characteristics of the UV−vis and mass spectra as compared to standards analyzed under the same conditions, and information available in the literature.[23−29]

The iridoids were quantitated by HPLC-DAD, using an external analytical curve of genipin (0.5−100 μg/mL), with a detection limit of 0.75 μg/mL and quantification limit of 2.25 μg/mL. The phenolic compounds were quantitated with an external analytical curve of 5-caffeoylquinic acid (0.5−55 μg/mL), with a detection limit of 0.85 μg/mL and quantitation limit of 2.34 μg/mL. The two curves were linear ($r^2$ = 0.99). The limits of detection (LOD) and quantitation (LOQ) were calculated using the parameters of the analytical curves (standard deviation and slope).[30]

**Statistical Analysis of the Results.** The mean and standard deviation results were calculated using the software Origin version 8. The mean values were compared by analysis of variance (ANOVA), complemented by the Tukey test when significant differences were detected, using the software Statistica version 12. A confidence interval of 95% was used.

## RESULTS AND DISCUSSION

**Differences between the Unripe and Ripe Fruits.** Table 1 shows the mean results obtained for the firmness and skin color analyses. After the fruits had been classified, their weights (g) and dimensions (mm) were determined in both ripening stages. The unripe fruits (Figure 3A) were significantly lighter and shorter than ripe fruits (Figure 3B), although the values for the transversal diameter were very similar, independent of the ripening stage. All color parameter values were statistically different between fruit skins from both ripening stages (Table 1). According to these values, the skins of the unripe fruits tended to green color, indicated by negative $a^*$ values, whereas the skins of ripe fruits were yellow-reddish, with positive $a^*$ and high $b^*$ values.

**Table 1. Physical Characteristics, Maximum Force, and CIELAB Parameters for the Unripe and Ripe Genipap Fruits[a]**

| parameter | unripe fruit ($n$ = 45) | ripe fruit ($n$ = 45) |
|---|---|---|
| weight (g) | 96.4 ± 14.9a | 141.4 ± 19.8b |
| longitudinal diameter (mm) | 59.1 ± 3.3a | 78.1 ± 4.7b |
| transversal diameter (mm) | 57.9 ± 3.0a | 59.0 ± 2.9a |
| maximal force of penetration (N) | 13.8 ± 1.7a | 0.6 ± 0.2b |
| $L^*$ | 51.7 ± 0.9a | 47.3 ± 4.9b |
| $a^*$ | −2.8 ± 0.8a | 9.2 ± 1.7b |
| $b^*$ | 20.7 ± 1.3a | 23.4 ± 3.4b |

[a]Results are expressed as the mean ± standard deviation. Means with the lower case letter in the same row show no significant difference between them ($P$ > 0.05). $L^*$, $a^*$, and $b^*$ are CIELAB color system parameters.

**Identification of Iridoids and Phenolic Compounds.** Eighteen compounds (14 iridoids, 3 phenolic compounds, and 1 unidentified compound) were separated by HPLC from the genipap extracts, 14 being from unripe and 13 from ripe fruits (Figure 4). Among the separated compounds, the identities of 2 were confirmed with commercial standards, and 15 were tentatively identified considering their chromatographic and spectroscopic characteristics (Table 2), and 1 was not identified. The proposed structures are presented in Figure 5, and of the 17 identified compounds, 10 had never previously been found in genipap fruits.

Because no access to commercial standards of iridoid glycosides was possible, and the structures of the same iridoids were already determined by nuclear magnetic resonance as containing glucose as their hexose component,[14,15,31−35] in the present study all of the hexoses were identified as glucose.

Peaks 1 and 3 presented the same mass to charge ratio ($m/z$) value for the deprotonated molecule ($[M - H]^-$), and similar maximum absorption wavelengths ($\lambda_{max}$) in the UV spectrum. However, in the MS/MS spectrum of peak 1, the major fragment was an ion at $m/z$ 193, whereas for peak 3 it was at $m/z$ 211. The difference in mass between these fragments (18 Da) was relative to the elimination of one water molecule. When there is an OH at C-8 or the carbon directly bonded to C-8, a hydrogen bond is formed with the oxygen of the glycosidic bond, making it difficult to lose this oxygen during fragmentation, resulting in a neutral loss of 162 Da, as can be seen in the spectrum of peak 3. In the absence of this hydroxyl group, the most common loss is 180 Da, as observed in the MS/MS spectrum of peak 1.[23] The fragment at $m/z$ 149, resulting from the loss of $CO_2$ (44 Da), indicated the presence of a carboxyl group in both molecules. Thus, peaks 1 and 3 were tentatively identified as gardoside and geniposidic acid, respectively, on the basis of the similarities with the same compounds previously found in *Gardenia jasminoides*.[23] This was the first time that gardoside, **1**, was detected in *Genipa americana* L.

Peak 2 presented $[M - H]^-$ at $m/z$ 391 and neutral losses corresponding to a hexose unit (162 Da), $H_2O$ (18 Da), and $CO_2$ (44 Da). Considering the hexose as glucose, this compound was tentatively identified as shanzhiside. The same characteristics were reported by Ren et al.[24] for the standard of this compound.

Peaks 4, 5, and 6 presented in common a formate-adducted ion $[M + HCOO]^-$ at $m/z$ 449 and a deprotonated molecule $[M - H]^-$ at $m/z$ 403 in the MS/MS spectrum. These three peaks showed the same $\lambda_{max}$ in the UV and similar MS/MS fragmentation profiles. However, only peaks 4 and 6 presented the $MS^3$ fragment at $m/z$ 139, formed by the loss of a molecule of methyl 3-oxopropanoate (102 Da). This loss resulted from the cleavage of the basic skeleton of iridoid glycosides of the type 7,8-cyclopentane.[25] Thus, compound **5** was tentatively identified as gardenoside, and compounds **4** and **6** were tentatively identified as deacetylasperulosidic methyl ester (DAME) and scandoside methyl ester (SME). However, DAME and SME are epimers, and the detection methods

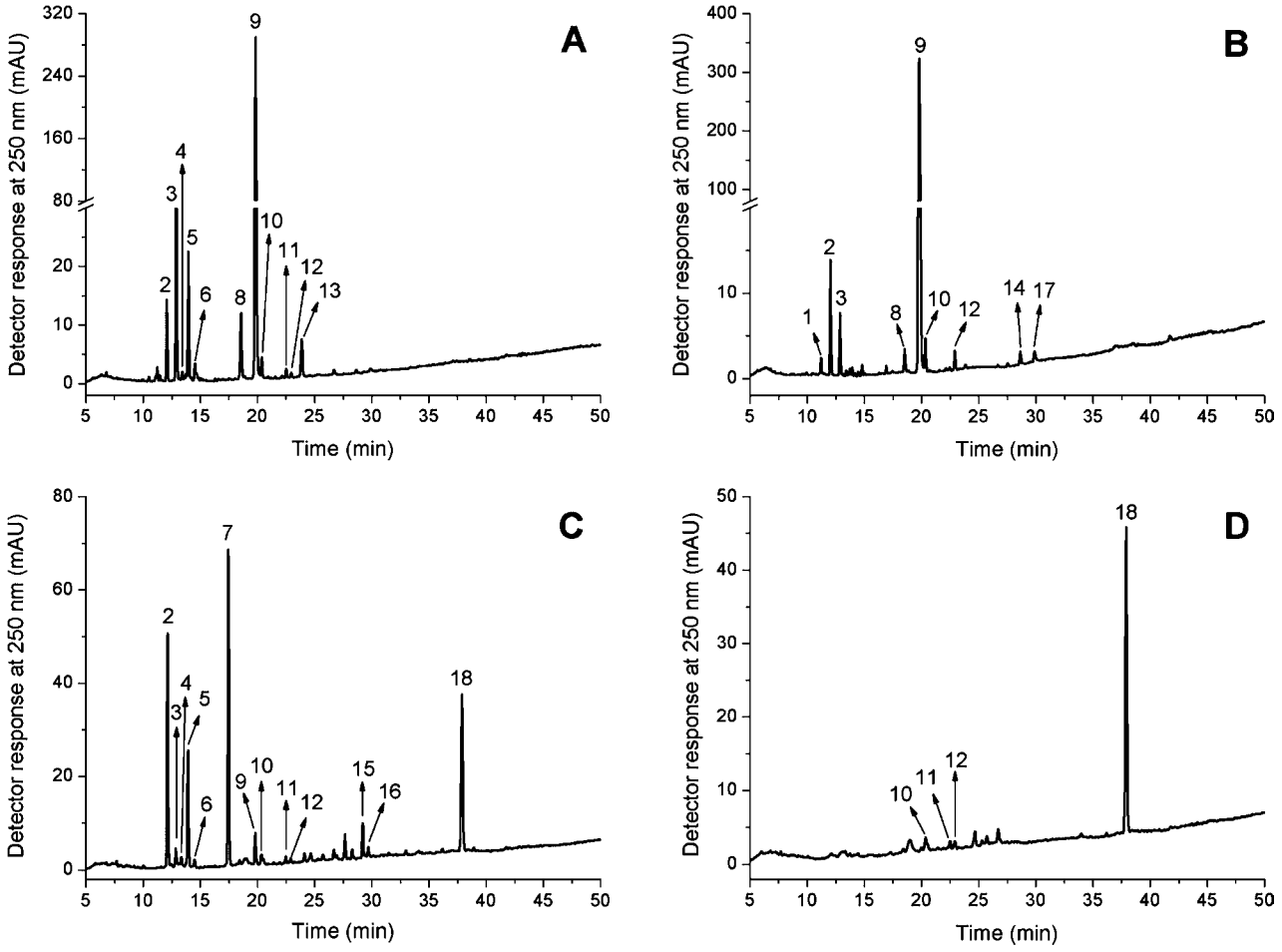


**Figure 4.** HPLC-DAD chromatograms of the iridoids and phenolic compounds of genipap fruits in two ripening stages: (A) unripe endocarp; (B) unripe mesocarp; (C) ripe endocarp; (D) ripe mesocarp. Peak identification is presented in Table 2.

used in this study did not allow the two compounds to be differentiated. Therefore, it was not possible to determine which of the two peaks corresponded to each isomer.

Peaks 7 and 9 also formed adducts with the formate ion ($[M - H + HCOO]^-$). Using MS/MS, the $[M - H]^-$ fragments at $m/z$ 549 and 387 were observed for peaks 7 and 9, respectively. On the $MS^3$ of the deprotonated molecules of both compounds, the major fragment at $m/z$ 225 corresponded to the aglycone genipin after the loss of one (peak 9) or two (peak 7) hexose units. From the fragmentation pattern, peaks 7 and 9 were tentatively identified as genipin-1-$\beta$-D-gentiobioside and geniposide, respectively, on the basis of the similarity of their characteristics with the same compounds found in *Gardenia jasminoides* Ellis.[23] These compounds are the major iridoids in gardenia fruits.[26]

Peak 8 was identified as 5-caffeoylquinic acid on the basis of the same retention time and UV and mass spectra characteristics as an authentic standard of 5-caffeoylquinic acid. The $[M - H]^-$ was detected at $m/z$ 353, and the MS/MS fragments showed 191 and 179 Da due to, respectively, the loss of caffeoyl and quinoyl groups. This is the first study to report the presence of chlorogenic acids in *Genipa americana* L.

Peaks 10 and 11 presented $[M - H]^-$ at $m/z$ 535 and at $m/z$ 519, respectively. Using MS/MS, both compounds presented a common loss of 212 Da. This loss could correspond either to the aglycone of gardoside, **1**, or geniposidic acid, **3**. Considering the same principle used to differentiate compounds **1** and **3**, the loss of the whole aglycone (212 Da) is characteristic of the presence of an OH group linked to C-8, indicating that the aglycone under question was geniposidic acid, **3**.[23] For peak 10, the $MS^3$ from the $m/z$ at 323 resulted in fragments with 179 and 161 Da, which correspond to ionized and dehydrated caffeic acid, respectively. For peak 11, the $MS^3$ from the ion with 307 Da resulted in fragments at $m/z$ 217 and 145, which correspond to the sugar moiety and ionized *p*-coumaric acid, respectively. Thus, compounds **10** and **11** were tentatively identified as caffeoyl geniposidic acid and *p*-coumaroyl geniposidic acid, respectively. Up to now, the presence of iridoid glycosides esterified with acids in genipap fruits has never been reported in the literature.

Peak 12 presented the $[M - H]^-$ at $m/z$ 549 and MS/MS fragments at $m/z$ 355 $[M - H - 194]^-$ and at $m/z$ 337 $[M - H - 194 - 18]^-$, relative to the loss of one dehydrated and one nondehydrated aglycone, respectively. Considering the above discussion, this fragmentation indicates the absence of an OH group on C-8 or on the carbon directly bound to it.[23] Thus, the aglycone present in compound **12** was tentatively identified as that from gardoside, **1**. The $MS^3$ of the ion at $m/z$ 355 produced, in addition to the ion at $m/z$ 337 (loss of $H_2O$), an ion at $m/z$ 193, which corresponded to ionized ferulic acid. Thus, compound **12** was tentatively identified as feruloyl gardoside, which was also found in gardenia fruits.[31]

Peak 13 was identified as genipin, because it showed the same retention time and UV and mass spectra characteristics as

**Table 2. Chromatographic and Spectroscopic Characteristics of the Iridoids and Phenolic Compounds Obtained from Genipap**

| peak[a] | compound | $t_R$ (min)[b] | $\lambda_{max}$ (nm)[c] | $[M - H]^-$ ($m/z$) | $[M - H + HCOO]^-$ ($m/z$) | MS/MS ($m/z$)[d] | $MS^3$ ($m/z$)[d] |
|---|---|---|---|---|---|---|---|
| 1 | gardoside | 11.2 | 235 | 373 | nd[e] | 211 $[M - H - 162]^-$, **193** $[\mathbf{M - H - 162 - 18}]^-$, 149 $[M - H - 162 - 44 - 18]^-$, 123 $[M - H - 162 - 44 - 44]^-$ | 211→**193**, 149, 123 |
| 2 | shanzhiside | 12.0 | 235 | 391 | nd | 229 $[M - H - 162]^-$, **185** $[\mathbf{M - H - 162 - 44}]^-$, 167 $[M - H - 162 - 44 - 18]^-$, 149 $[M - H - 162 - 44 - 18 - 18]^-$ | 229→**185**, 167, 149 |
| 3 | geniposidic acid | 12.9 | 236 | 373 | nd | **211** $[\mathbf{M - H - 162}]^-$, 167 $[M - H - 162 - 44]^-$, 149 $[M - H - 162 - 44 - 18]^-$, 123 $[M - H - 162 - 44 - 44]^-$ | 211→167, 149, **123** |
| 4 | DAME or SME[f] | 13.4 | 241 | nd | 449 | 403 $[M - H]^-$, **241** $[\mathbf{M - H - 162}]^-$, 223 $[M - H - 162 - 18]^-$, 139 $[M - H - 162 - 102]^-$ | 403→**241**, 223, 139 |
| 5 | gardenoside | 13.9 | 241 | nd | 449 | 403 $[M - H]^-$, **241** $[\mathbf{M - H - 162}]^-$, 223 $[M - H - 162 - 18]^-$ | 403→**241**, 223 |
| 6 | DAME or SME | 14.5 | 241 | nd | 449 | 403 $[M - H]^-$, **241** $[\mathbf{M - H - 162}]^-$, 223 $[M - H - 162 - 18]^-$, 139 $[M - H - 162 - 102]^-$ | 403→**241**, 139 |
| 7 | genipin-1-$\beta$-D-gentiobioside | 17.4 | 241 | nd | 595 | **549** $[\mathbf{M - H}]^-$, 225 $[M - H - 162 - 162]^-$ | 549→**225** |
| 8 | 5-caffeoylquinic acid | 18.5 | 300 (sh), 328 | 353 | nd | **191** $[\mathbf{M - H - 162}]^-$, 179 $[M - H - 174]^-$, 173 $[M - H - 162 - 18]^-$ | 191→**173**, 127, 109 |
| 9 | geniposide | 19.8 | 241 | nd | 433 | 387 $[M - H]^-$, **225** $[\mathbf{M - H - 162}]^-$, 123 $[M - H - 162 - 102]^-$ | 387→**225**, 123 |
| 10 | caffeoylgeniposidic acid | 20.4 | 298 (sh), 328 | 535 | nd | 491 $[M - H - 44]^-$, **323** $[\mathbf{M - H - 212}]^-$, 161 $[M - H - 212 - 162]^-$ | 323→179 $[M - H - 212 - 144]^-$, **161** |
| 11 | *p*-coumaroylgeniposidic acid | 22.5 | 294 (sh), 313 | 519 | nd | **307** $[\mathbf{M - H - 212}]^-$, 187, 163 $[M - H - 212 - 144]^-$, 145 $[M - H - 212 - 162]^-$ | 307→**217**, 145 |
| 12 | feruloyl gardoside | 22.9 | 298 (sh), 328 | 549 | nd | 355 $[M - H - 194]^-$, 337 $[M - H - 194 - 18]^-$, **217**, 193 $[M - H - 212 - 144]^-$, 175 $[M - H - 212 - 162]^-$ | 355→337, **217**, 193 |
| 13 | genipin | 23.9 | 238 | 225 | nd | 207 $[M - H - 18]^-$, **123** $[\mathbf{M - H - 102}]^-$, 101 | - |
| 14 | 3,5-dicaffeoylquinic acid | 28.7 | 302 (sh), 328 | 515 | nd | **353** $[\mathbf{M - H - 162}]^-$, 191 $[M - H - 162 - 162]^-$ | 353→**191**, 179 $[M - H - 162 - 174]^-$, 173 $[M - H - 162 - 162 - 18]^-$ |
| 15 | *p*-coumaroylgenipin gentiobioside | 29.2 | 296(sh), 313 | 695 | nd | 663, **469** $[\mathbf{M - H - 226}]^-$, 367 $[M - H - 226 - 102]^-$, 307 $[M - H - 226 - 102 - 60]^-$, 265, 235, 205 | 469→**367**, 307, 265, 235, 163 $[M - H - 226 - 162 - 144]^-$, 145 $[M - H - 226 - 180]^-$ |
| 16 | feruloylgenipin gentiobioside | 29.7 | 296(sh), 328 | 725 | nd | 693, **499** $[\mathbf{M - H - 226}]^-$, 397 $[M - H - 226 - 102]^-$, 337 $[M - H - 226 - 102 - 60]^-$, 295, 265, 235 | 499→**397**, 295, 265, 235, 193 $[M - H - 226 - 162 - 144]^-$, 175 $[M - H - 226 - 180]^-$ |
| 17 | 4,5-dicaffeoylquinic acid | 29.9 | 302 (sh), 328 | 515 | nd | **353** $[\mathbf{M - H - 162}]^-$, 335 $[M - H - 162 - 18]^-$, 173 $[M - H - 162 - 162 - 18]^-$ | 353→191, 179, **173**, 135 $[M - H - 162 - 174 - 44]^-$ |
| 18 | not identified | 37.9 | 276 | nd | nd | | |

[a]Numbered according to the chromatograms in Figure 4. [b]Retention time on the $C_{18}$ column. [c]Solvent: linear gradient of water and acetonitrile, both containing 0.1% formic acid. [d]Ions in bold type represent the major fragment. [e]nd, not detected; [f]DAME, deacetylasperulosidic methyl ester; SME, scandoside methyl ester



dx.doi.org/10.1021/jf503378k | J. Agric. Food Chem. 2014, 62, 10800−10808

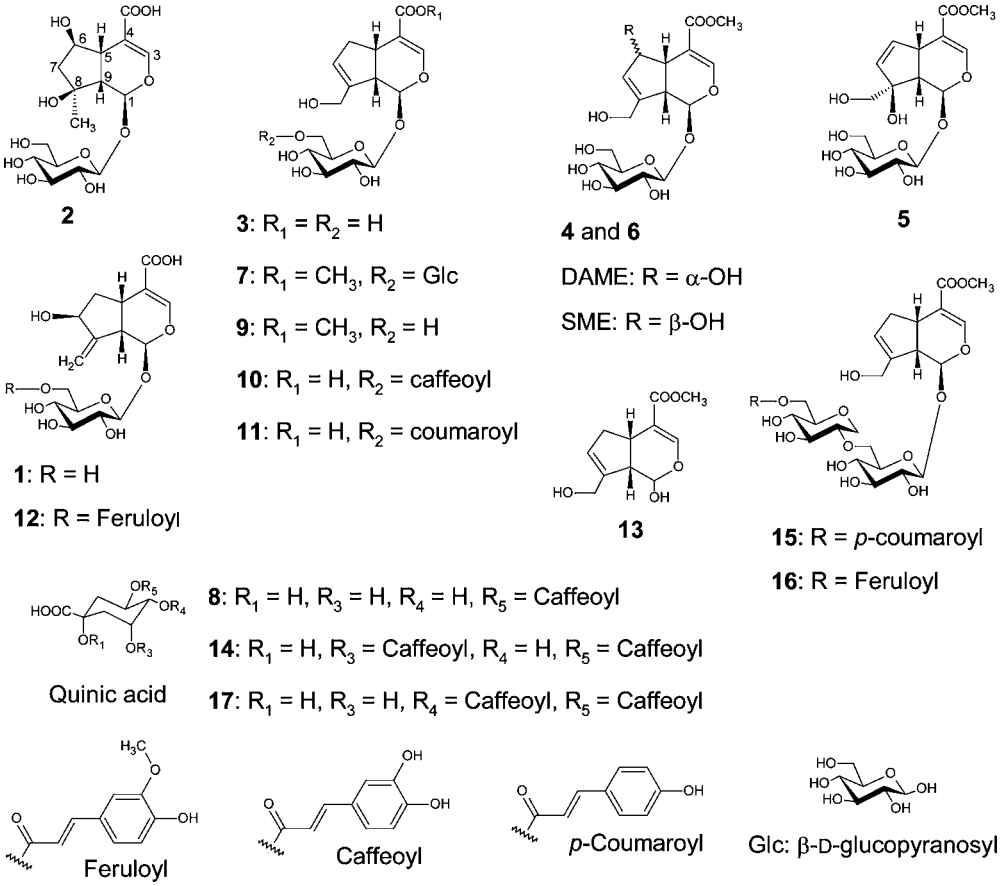


**Figure 5.** Proposed chemical structures for the compounds found in genipap fruits. The compounds are numbered according to their elution order from the $C_{18}$ column (Table 2).

**Table 3. Iridoid and Phenolic Compound Contents in the Endocarp and Mesocarp of Ripe and Unripe Genipap Fruits**[a]

| | | unripe fruit | | ripe fruit | |
|---|---|---|---|---|---|
| peak | compound | endocarp | mesocarp | endocarp | mesocarp |
| 1 | gardoside[b] | nd[c] | 0.76 ± 0.03 | nd | nd |
| 2 | shanzhiside[b] | 4.34 ± 0.03 | 4.23 ± 0.04 | 1.64 ± 0.06 | nd |
| 3 | geniposidic acid[b] | 19.86 ± 0.09 | 2.54 ± 0.05 | 0.19 ± 0.01 | nd |
| 4 | DAME or SME[b] | 0.80 ± 0.02 | nd | 0.11 ± 0.00 | nd |
| 5 | gardenoside[b] | 7.05 ± 0.13 | nd | 0.90 ± 0.03 | nd |
| 6 | DAME or SME[b] | 1.37 ± 0.05 | nd | 0.09 ± 0.00 | nd |
| 7 | genipin-1-β-D-gentiobioside[b] | nd | nd | 2.45 ± 0.13 | nd |
| 8 | 5-caffeoylquinic acid[d] | 5.59 ± 0.06 | 1.72 ± 0.03 | nd | nd |
| 9 | geniposide[b] | 107.11 ± 0.74 | 117.99 ± 0.93 | 0.29 ± 0.01 | nd |
| 10 | caffeoylgeniposidic acid[d] | 1.34 ± 0.02 | 1.44 ± 0.02 | 0.07 ± 0.00 | 0.06 ± 0.00 |
| 11 | *p*-coumaroylgeniposidic acid[d] | 1.43 ± 0.02 | nd | 0.12 ± 0.00 | 0.12 ± 0.00 |
| 12 | feruloyl gardoside[d] | 0.75 ± 0.01 | 1.12 ± 0.04 | 0.07 ± 0.00 | 0.08 ± 0.00 |
| 13 | genipin[b] | 3.40 ± 0.11 | nd | nd | nd |
| 14 | 3,5-dicaffeoylquinic acid[d] | nd | 1.23 ± 0.03 | nd | nd |
| 15 | *p*-coumaroylgenipin gentiobioside[d] | nd | nd | 0.38 ± 0.00 | nd |
| 16 | feruloylgenipin gentiobioside[d] | nd | nd | 0.10 ± 0.01 | nd |
| 17 | 4,5-dicaffeoylquinic acid[d] | nd | 1.22 ± 0.04 | n.d | nd |
| 18 | not identified[b] | nd | nd | 1.76 ± 0.05 | 1.07 ± 0.00 |
| | total iridoids | 147.45 ± 0.88 | 128.07 ± 1.09 | 6.43 ± 0.22 | 0.25 ± 0.00 |
| | total phenolic compounds | 5.59 ± 0.06 | 4.17 ± 0.07 | 0.00 ± 0.00 | 0.00 ± 0.00 |

[a]Values of mean ± standard deviation are expressed in mg/g of freeze-dried sample; analyses were carried out in triplicate from the sample pool composed of three batches. [b]Quantitated as genipin equivalents. [c]nd, not identified. [d]Quantitated as 5-caffeoylquinic acid equivalents.


dx.doi.org/10.1021/jf503378k | J. Agric. Food Chem. 2014, 62, 10800−10808

the authentic genipin standard. This compound presented the $[M - H]^-$ at $m/z$ 225 and the following MS/MS fragments: $m/z$ 207 relative to the loss of a water molecule; $m/z$ 123 generated by the loss of a methyl 3-oxopropanoate group (102 Da); and $m/z$ 101, corresponding to the ionized methyl 3-oxopropanoate group.

Peaks 14 and 17 both presented the same $[M - H]^-$ at $m/z$ 515 and a major MS/MS fragment at $m/z$ 353, which is characteristic of dicaffeoylquinic acids. The $MS^3$ fragmentations of the ion at $m/z$ 353 of both compounds were very similar, differing only with respect to the intensity of the major peak. Compound **14** presented a major fragment at $m/z$ 191, resulting from the loss of a caffeoyl group (162 Da), whereas for compound **17** the major fragment was observed at $m/z$ 173, representing a dehydrated quinic acid. The fragmentation pattern of isomers of chlorogenic acids depends on the position of attachment of the caffeoyl group to quinic acid.[28] Thus, peaks 14 and 17 were tentatively identified as 3,5-dicaffeoylquinic acid and 4,5-dicaffeoylquinic acid, respectively. The chlorogenic acids were also found in gardenia fruits.[27]

Peak 15 showed the $[M - H]^-$ at $m/z$ 695 and a major MS/MS fragment at $m/z$ 469, due to the loss of a genipin molecule (226 Da). The $MS^3$ of this ion showed fragments with 367, 307, 265, and 235 Da, characteristic of the fragmentation of two hexose molecules, and also fragments at $m/z$ 163 and 145, which correspond to ionized and dehydrated *p*-coumaric acid, respectively. Taking into account all of the information provided, peak 15 was tentatively identified as *p*-coumaroyl genipin gentiobioside, which was also found in gardenia fruits and in a formulation of a Chinese medicine based on gardenia fruits and fermented soybean.[29,36]

Peak 16 was tentatively identified as feruloyl genipin gentiobioside, considering the same MS fragmentation mechanism and a difference of 30 Da as compared to *p*-coumaroylgenipin gentiobioside, **15**. However, in this case ions at $m/z$ 193 and 175 were obtained on the $MS^3$, representing ionized and dehydrated ferulic acid, respectively. Feruloyl genipin gentiobioside, **16**, has been previously also detected in gardenia fruits.[31,37]

Peak 18 was not identified, because this compound was detected only on the UV spectrum, but was not ionized under the conditions used in this study, neither in the positive nor in the negative mode. Its late elution on the reversed-phase column indicated low polarity in relation to the other compounds. This was the major compound found in the mesocarp of ripe fruits.

**Contents of Iridoids and Phenolic Compounds.** Because genipap (*Genipa americana* L.) and *Gardenia jasminoides* fruits belong to the same family, it is not a surprise that their qualitative compositions of iridoids and chlorogenic acids are very similar.

As in gardenia, geniposide, **9**, was the major iridoid in the unripe genipap fruits (Table 3), corresponding to 72 and 92% of the total iridoids in the endocarp and mesocarp, respectively. Furthermore, the geniposide, **9**, contents in the endocarp and mesocarp of unripe genipap fruits (107.11 and 117.99 mg/g freeze-dried sample, respectively) were higher than those reported for gardenia fruits from different varieties and origins (43.19−95.51 mg/g dry sample).[16,38] In addition, the unripe genipap also presented higher geniposidic acid, **3** (endocarp and mesocarp), and gardenoside, **5** (endocarp), contents than those found in gardenia fruits (0.80 and 1.08 mg/g dry sample, respectively).[26] Genipin-1-$\beta$-D-gentiobioside, **7**, was the major iridoid in the ripe endocarp and was not detected in unripe genipap fruits. This indicates that ripening favors the addition of a second hexoside group to the geniposide, **9**.

According to the biosynthetic pathway of iridoids, geniposidic acid, **3**, is the precursor of geniposide, **9**, that further gives rise to gardenoside, **5**.[7] These three compounds are the major ones found in the unripe genipap endocarp and are among the main compounds of the unripe mesocarp, but their contents indicate that in the unripe genipap fruits, the formation of geniposide, **9**, is the favored route.

Another difference observed between both ripeness stages was the absence of chlorogenic acids in the ripe genipap fruits. In addition, the ripe genipap fruits presented a 90% reduction in the iridoid contents, especially geniposide, **9**, in relation to the green fruits. This behavior was also observed in *Gardenia jasminoides* fruits, in which the geniposide, **9**, contents decreased throughout the fruit-ripening process.[39,40] This fact can be explained by the highest expression levels of the enzyme responsible for iridoid glycosylation in the earlier stages of *Gardenia jasminoides* ripening.[41] This phenomenon was attributed to the fact that the iridoids as well as the phenolic acids act as defense compounds against herbivores, and their synthesis demands precursors of low molecular mass and low enzymatic activity, making their synthesis energetically favorable in the initial developmental stages.[42−44]

**Blue Color and Genipap Ripeness Stage.** Although the endocarp of the unripe fruits showed a low concentration of genipin, **13** (3.40 mg/g of the freeze-dried sample), small lines of blue color were visually observed, most probably due to formation of the blue pigment as the result of a reaction, shown in Figure 2, between amino acids and free genipin, **13**, present in endocarp.

In addition, we verified that extracts from unripe genipap fruit kept at room temperature for a few hours resulted in increased intensity of the genipin, **13**, peak in the endocarp extract or its appearance in the mesocarp extract (data not shown). In addition, reduction of the geniposide, **9**, concentration and formation of a new peak ($t_R$ = 21.1 min, $[M - H]^-$ at $m/z$ 387 and MS/MS fragments at $m/z$ 285 $[M - H - 102]^-$, 207 $[M - H - 162 - 18]^-$, 179 $[M - H - 162 - 18 - 28]^-$, and 179 $[M - H - 162 - 18 - 28 - 18]^-$) were also observed. This new peak may be an intermediate in the reaction shown in Figure 2. These facts indicate the presence of $\beta$-glucosidase in the fruit, which was possibly released by tissue rupture. As shown in Figure 2, the enzyme hydrolyzes the glycosidic bond of geniposide, **9**, furnishing genipin, **13**, that reacts with primary amine sources present in the matrix. The drastic reduction of geniposide, **9**, contents and the absence of genipin, **13**, in the ripe fruit may explain the nonoccurrence and/or formation of the blue pigment in the ripe fruits.

The present study was the first to relate the iridoid and phenolic compound compositions to both ripening stage and part of the fruit (mesocarp and endocarp). Our results show that the stage of ripeness influences both the iridoid and phenolic compound profiles. The unripe genipap fruits were shown to be a very good source of geniposide, **9**, which can be used to produce genipin, **13**, and subsequently the blue pigment for use by the natural dye industry. In addition, the fact that geniposide, **9**, was almost nonexistent in the ripe genipap fruits could explain the nonformation of the blue pigment in this ripeness stage.

## AUTHOR INFORMATION


### Corresponding Author

*(A.Z.M.) Phone: +55-19-35212163. Fax: +55-19-35212153. E-mail: azmercadante@gmail.com or azm@fea.unicamp.br.



### Funding

We thank the Brazilian funding agencies Coordination of Improvement of Higher Education Personnel (CAPES) and São Paulo Research Foundation (FAPESP, proc. 2013/07914-8) for their financial support.


### Notes

The authors declare no competing financial interest.

## REFERENCES


(1) Dinda, B.; Debnath, S.; Harigaya, Y. Naturally occurring iridoids. A review, part 1. *Chem. Pharm. Bull.* **2007**, *55*, 159−222.

(2) Bianco, A. Recent developments in iridoids chemistry. *Pure Appl. Chem.* **1994**, *66*, 2335−2338.

(3) Villasenor, I. M. Bioactivities of iridoids. *Anti-Inflamm. Anti-Allergy Agents Med. Chem.* **2007**, *6*, 307−314.

(4) Al-Hazimi, H. M. G.; Alkhathlan, H. Z. Naturally occurring iridoids during the period 1990−1993. *J. Chem. Soc. Pak.* **1996**, *18*, 336−357.

(5) Yu, Y.; Xie, Z.-l.; Gao, H.; Ma, W.-w.; Dai, Y.; Wang, Y.; Zhong, Y.; Yao, X.-s. Bioactive iridoid glucosides from the fruit of *Gardenia jasminoides*. *J. Nat. Prod.* **2009**, *72*, 1459−1464.

(6) Lee, J.-H.; Lee, D.-U.; Jeong, C.-S. *Gardenia jasminoides* Ellis ethanol extract and its constituents reduce the risks of gastritis and reverse gastric lesions in rats. *Food Chem. Toxicol.* **2009**, *47*, 1127−1131.

(7) Sampaio-Santos, M. I.; Kaplan, M. A. C. Biosynthesis significance of iridoids in chemosystematics. *J. Braz. Chem. Soc.* **2001**, *12*, 144−153.

(8) Francis, F. J. Food colorings. In *Colour in Food: Improving Quality*; MacDougall, D. B., Ed.; CRC Press: Boca Raton, FL, USA, 2002; pp 297−330.

(9) Fujikawa, S.; Fukui, Y.; Koga, K.; Kumada, J. Brilliant skyblue pigment formation from gardenia fruits. *J. Ferment. Technol.* **1987**, *65*, 419−424.

(10) Cho, Y. J.; Kim, S. Y.; Kim, J.; Choe, E. K.; Kim, S. I.; Shin, H. J. One-step enzymatic synthesis of blue pigments from geniposide for fabric dyeing. *Biotechnol. Bioprocess Eng.* **2006**, *11*, 230−234.

(11) Paik, Y. S.; Lee, C. M.; Cho, M. H.; Hahn, T. R. Physical stability of the blue pigments formed from geniposide of gardenia fruits: effects of pH, temperature, and light. *J. Agric. Food Chem.* **2001**, *49*, 430−432.

(12) Park, J. E.; Lee, J. Y.; Kim, H. G.; Hahn, T. R.; Paik, Y. S. Isolation and characterization of water-soluble intermediates of blue pigments transformed from geniposide of *Gardenia jasminoides*. *J. Agric. Food Chem.* **2002**, *50*, 6511−6514.

(13) Touyama, R.; Takeda, Y.; Inoue, K.; Kawamura, I.; Yatsuzuka, M.; Ikumoto, T.; Shingu, T.; Yokoi, T.; Inouye, H. Studies on the blue pigments produced from genipin and methylamine. I. Structures of the brownish-red pigments, intermediates leading to the blue pigments. *Chem. Pharm. Bull.* **1994**, *42*, 668−673.

(14) Ono, M.; Ueno, M.; Masuoka, C.; Ikeda, T.; Nohara, T. Iridoid glucosides from the fruit of *Genipa americana*. *Chem. Pharm. Bull.* **2005**, *53*, 1342−1344.

(15) Ono, M.; Ishimatsu, N.; Masuoka, C.; Yoshimitsu, H.; Tsuchihashi, R.; Okawa, M.; Kinjo, J.; Ikeda, T.; Nohara, T. Three new monoterpenoids from the fruit of *Genipa americana*. *Chem. Pharm. Bull.* **2007**, *55*, 632−634.

(16) Yang, Q. J.; Fan, M. S.; Wu, B.; Sun, Z. L.; Cui, X. L.; Du, X. W.; Huang, C. G. Quality assessment for fructus Gardeniae by multi-component quantification, chromatographic fingerprint and related chemometric analysis. *J. Med. Plant Res.* **2011**, *5*, 4126−4137.

(17) UNCTAD, Market brief in the European Union for selected natural ingredients derived from native species: *Genipa americana*. United Nations Conference on Trade and Development/BioTrade Facilitation Programme, 2005.

(18) Cavalcante, P. B. *Frutas Comestíveis da Amazônia*, 5th ed.; CEJUP/Museu Paraense Emílio Goeldi: Belém, Brazil, 1991; p 279.

(19) Djerassi, C.; Gray, J. D.; Kincl, F. A. Naturally occurring oxygen heterocyclics. IX. Isolation and characterization of genipin. *J. Org. Chem.* **1960**, *25*, 2174−2177.

(20) Silva, D. B.; Silva, J. A.; Junqueira, N. T. V.; Andrade, L. R. M. *Frutas do Cerrado*; Embrapa Informação Tecnológica: Brasília, Brazil, 2001.

(21) AOAC. *Official Mehods of Analysis*, 18th ed.; AOAC International: Gaithersburg, MD, USA, 2005.

(22) Chisté, R. C.; Mercadante, A. Z. Identification and quantification, by HPLC-DAD-MS/MS, of carotenoids and phenolic compounds from the Amazonian fruit *Caryocar villosum*. *J. Agric. Food Chem.* **2012**, *60*, 5884−5892.

(23) Zhou, T. T.; Liu, H.; Wen, J.; Fan, G. R.; Chai, Y. F.; Wu, Y. T. Fragmentation study of iridoid glycosides including epimers by liquid chromatography-diode array detection/electrospray ionization mass spectrometry and its application in metabolic fingerprint analysis of *Gardenia jasminoides* Ellis. *Rapid Commun. Mass Spectrom.* **2010**, *24*, 2520−2528.

(24) Ren, L.; Xue, X. Y.; Zhang, F. F.; Wang, Y. C.; Liu, Y. F.; Li, C. M.; Liang, X. M. Studies of iridoid glycosides using liquid chromatography/electrospray ionization tandem mass spectrometry. *Rapid Commun. Mass Spectrom.* **2007**, *21*, 3039−3050.

(25) Li, C. M.; Zhang, X. L.; Xue, X. Y.; Zhang, F. F.; Xu, Q.; Liang, X. M. Structural characterization of iridoid glucosides by ultra-performance liquid chromatography/electrospray ionization quadrupole time-of-flight tandem mass spectrometry. *Rapid Commun. Mass Spectrom.* **2008**, *22*, 1941−1954.

(26) Sheu, S. J.; Hsin, W. C. HPLC separation of the major constituents of Gardeniae fructus. *J. High Resolut. Chromatogr.* **1998**, *21*, 523−526.

(27) Clifford, M. N.; Wu, W. G.; Kirkpatrick, J.; Jaiswal, R.; Kuhnert, N. Profiling and characterisation by liquid chromatography/multi-stage mass spectrometry of the chlorogenic acids in Gardeniae Fructus. *Rapid Commun. Mass Spectrom.* **2010**, *24*, 3109−3120.

(28) Clifford, M. N.; Johnston, K. L.; Knight, S.; Kuhnert, N. Hierarchical scheme for LC-MSn identification of chlorogenic acids. *J. Agric. Food Chem.* **2003**, *51*, 2900−2911.

(29) Zhao, X.; Long, Z.; Dai, J.; Bi, K.; Chen, X. Identification of multiple constituents in the traditional Chinese medicine formula Zhi-zi-chi decoction and rat plasma after oral administration by liquid chromatography coupled to quadrupole time-of-flight tandem mass spectrometry. *Rapid Commun. Mass Spectrom.* **2012**, *26*, 2443−2453.

(30) ICH. *ICH Harmonised Tripartite Guideline − Guidance for Industry, Q2B Validation of Analytical Procedures: Methodology*; International Conference on Harmonization of Technical Requirements for the Registration of Pharmaceuticals for Human Use, 2005; p 13.

(31) Qin, F. M.; Meng, L. J.; Zou, H. L.; Zhou, G. X. Three new iridoid glycosides from the fruit of *Gardenia jasminoides* var. radicans. *Chem. Pharm. Bull.* **2013**, *61*, 1071−1074.

(32) Nishizawa, M.; Izuhara, R.; Kaneko, K.; Koshihara, Y.; Fujimoto, Y. 5-Lipoxygenase inhibitors isolated from Gardeniae fructus. *Chem. Pharm. Bull.* **1988**, *36*, 87−95.

(33) Shaker, K. H.; Elgamal, M. H. A.; Seifert, K. Iridoids from *Avicennia marina*. *Z. Naturforsch., C, J. Biosci.* **2001**, *56*, 965−968.

(34) Fu, X. M.; Chou, G. X.; Wang, Z. T. Iridoid glycosides from *Gardenia jasminoides* Ellis. *Helv. Chim. Acta* **2008**, *91*, 646−653.

(35) Yang, L. G.; Peng, K. F.; Zhao, S. Z.; Chen, L. X.; Qiu, F. Monoterpenoids from the fruit of *Gardenia jasminoides* Ellis (Rubiaceae). *Biochem. Syst. Ecol.* **2013**, *50*, 435−437.

(36) Fu, Z.; Xue, R.; Li, Z.; Chen, M.; Sun, Z.; Hu, Y.; Huang, C. Fragmentation patterns study of iridoid glycosides in fructus Gardeniae by HPLC-Q/TOF-MS/MS. *Biomed. Chromatogr.* **2014**, DOI: 10.1002/bmc.3223.

(37) Li, H. B.; Yu, Y.; Wang, Z. Z.; Dai, Y.; Gao, H.; Xiao, W.; Yao, X. S. Iridoid and bis-iridoid glucosides from the fruit of *Gardenia jasminoides*. *Fitoterapia* **2013**, *88*, 7−11.
(38) Tsai, T. R.; Tseng, T. Y.; Chen, C. F.; Tsai, T. H. Identification and determination of geniposide contained in *Gardenia jasminoides* and in two preparations of mixed traditional Chinese medicines. *J. Chromatogr., A* **2002**, *961*, 83−88.
(39) Chen, Y.; Zhang, H.; Li, Y. X.; Cai, L.; Huang, J.; Zhao, C.; Jia, L.; Buchanan, R.; Yang, T.; Jiang, L. J. Crocin and geniposide profiles and radical scavenging activity of gardenia fruits (*Gardenia jasminoides* Ellis) from different cultivars and at the various stages of maturation. *Fitoterapia* **2010**, *81*, 269−273.
(40) Gao, L.; Zhu, B. Y. The accumulation of crocin and geniposide and transcripts of phytoene synthase during maturation of *Gardenia jasminoides* fruit. *Evidence-Based Complement. Altern. Med.* **2013**, *2013*, 6.
(41) Nagatoshi, M.; Terasaka, K.; Nagatsu, A.; Mizukami, H. Iridoid-specific glucosyltransferase from *Gardenia jasminoides*. *J. Biol. Chem.* **2011**, *286*, 32866−32874.
(42) Baby, S.; Raj, G.; Thaha, A. R. M.; Dan, M. Volatile chemistry of a plant: mono-sesquiterpenoid pattern in the growth cycle of *Curcuma haritha*. *Flavour Fragrance J.* **2010**, *25*, 35−40.
(43) Hosni, K.; Jemli, M.; Dziri, S.; M'rabet, Y.; Ennigrou, A.; Sghaier, A.; Casabianca, H.; Vulliet, E.; Ben Brahim, N.; Sebei, H. Changes in phytochemical, antimicrobial and free radical scavenging activities of the Peruvian pepper tree (*Schinus molle* L.) as influenced by fruit maturation. *Ind. Crops Prod.* **2011**, *34*, 1622−1628.
(44) Crozier, A.; Jaganath, I. B.; Clifford, M. N. Phenols, polyphenols and tannins: an overview. In *Plant Secondary Metabolites: Occurrence, Structure and Role in the Human Diet*; Crozier, A., Clifford, M. N., Ashihara, H., Eds.; Blackwell Publishing: Oxford, UK, 2006; pp 1−24.

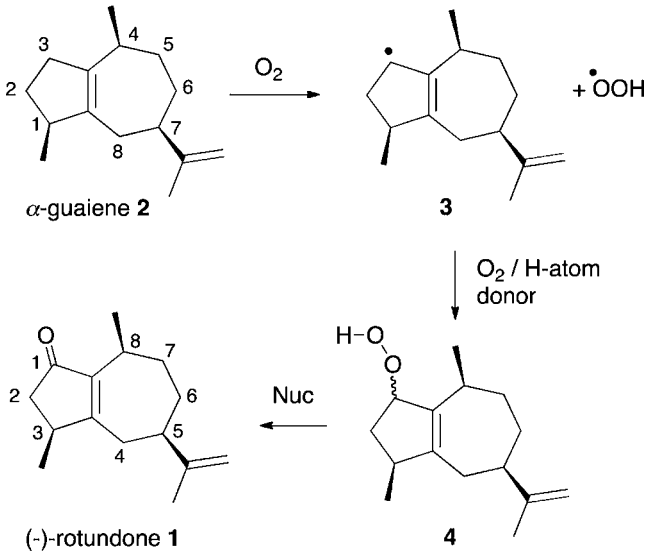


**Figure 1.** Hypothetical aerial oxidation of $\alpha$-guaiene, **2**, to form rotundone, **1**. IUPAC chemical names: (−)-(3*S*,5*R*,8*S*)-3,8-dimethyl-5-(prop-1-en-2-yl)-3,4,5,6,7,8-hexahydroazulene-1(2*H*)-one **1** and (−)-(1*S*,4*S*,7*R*)-1,4-dimethyl-7-(prop-1-en-2-yl)-1,2,3,4,5,6,7,8-octahydroazulene, **2**.

some precursor substrate. Mechanistically, any proposed aerial oxidation of $\alpha$-guaiene, **2**, is likely to begin with a traditional free radical initiation step, namely, hydrogen atom abstraction from $C_3$ to produce the resonance stabilized allylic radical, **3** (Figure 1). This initiation could be caused by dioxygen ($O_2$) itself or by other initiators such as reactive oxygen species (ROS) or the breakdown of $H_2O_2$ produced due to plant−pathogen interactions. Indeed, $H_2O_2$ has recently been identified in distinct cellular compartments of the skins of grapes during grape berry ripening, and as mentioned above, both rotundone and $\alpha$-guaiene have clearly been identified on the skins of grapes.[24] The allylic radical, **3**, could then enter a propagation sequence by first reacting with dioxygen to form an allylic hydroperoxy radical, which in turn abstracts another hydrogen atom from either another guaiene molecule or some other abstractable hydrogen atom source to produce the guaiene hydroperoxide, **4**. Exposure of this hydroperoxide to trace metals (e.g., copper sprays in vineyards) or nucleophiles (e.g., basic amines of plant proteins or pathogens) would allow for decomposition to the ketone rotundone, **1**, via well established chemical mechanisms (Figure 1).[25]

Given this background, the current study has been carried out to evaluate whether $\alpha$-guaiene could be a natural precursor to rotundone via the process of simple aerial oxidation. Autoxidation was carried out both in organic solvents and also on filter paper derived from cellulose to mimic more closely biological matrices of some plant products.

## MATERIALS AND METHODS

**General Experimental Procedures.** Acetic anhydride (≥98% ACS reagent grade), pyridinium dichlorochromate, *tert*-butyl hydroperoxide (5−6 M in decane), and *m*-chloroperbenzoic acid (max 77%) were purchased from Sigma-Aldrich (Saint Louis, MO, USA). $d_6$-Benzene was purchased from Cambridge Isotope Laboratories, Inc. (Tewksbury, MA, USA). All reagents were used directly unless otherwise stated. Solvents for synthesis were dried according to known procedures where necessary.[26] Solvents for general chromatography were AR grade except that those used for GC−MS and HRMS analysis were HPLC grade. NMR data were recorded with a Varian-Inova 600 MHz spectrometer (Agilent Technologies, USA). All compounds for NMR analysis were dissolved in $C_6D_6$. All $^1H$ and $^{13}C$ NMR spectra were calibrated with residual deuterated solvent signals set at 7.16 and 128.06 ppm. HRMS (ESI-TOF) analysis was performed with a triple TOF 5600 mass spectrometer from AB Sciex Instruments. Whatman grade 1 cellulose filter paper was used to mimic the oxidation of $\alpha$-guaiene on plant cell wall cellulose.[27] Silica column chromatography was performed using either LC60A 40−63 $\mu$m silica (Grace Davison) or silica gel 60 (0.015−0.040 mm) from Merck. TLC was conducted with TLC silica gel 60 $F_{254}$ plates (Merck KGaA) using standard vanillin stain for visualization. Guaiac wood essential oil (steam-distilled from *Bulnesia sarmientoi,* Paraguay) was purchased from the Australian Botanical Products Company as viscous oil. This oil contains ca. 40% (−)-guaiol as determined by GC−MS analysis.

**Preparation of Standards.** $\alpha$-Guaiene, **2**, was prepared as follows. Recrystallization of guaiac wood essential oil from warm acetonitrile several times afforded (−)-guaiol as white needles in an overall yield of approximately 14% by weight in a similar fashion to that described previously.[1] Treatment with acetic anhydride under reflux conditions afforded the guaiyl acetate in a good yield of 71.9% after workup. Elimination of acetic acid from the guaiyl acetate through pyrolysis was achieved under nitrogen at 210 °C in a similar fashion to that reported previously.[28] Workup and purification by flash chromatography afforded $\alpha$-guaiene, **2**, in a very good yield of 84%. Analysis by GC−MS indicated that the purity of the $\alpha$-guaiene, **2**, was >98% with traces of $\beta$-guaiene and $\delta$-guaiene also present. Rotundone, **1**, was synthesized as follows. Pyridinium dichlorochromate (37.6 g, 0.1 mol) was added to $CH_2Cl_2$ (400 mL) and the resulting mixture cooled in an ice-bath before introduction dropwise of a solution of *tert*-butyl hydroperoxide (5−6 M in decane, 20 mL) in $CH_2Cl_2$ (80 mL) with stirring for 20 min. To this mixture was added dropwise a solution of $\alpha$-guaiene, **2** (20.4 g, 0.1 mol), in $CH_2Cl_2$ (80 mL), and the resulting mixture was stirred at 0 °C under $N_2$ for 4.5 h. The reaction was terminated by filtering through a plug of silica (ca. 80 g). The residue in the flask was further extracted with $CH_2Cl_2$ (2 × 100 mL), which was filtered through the same silica plug. The combined $CH_2Cl_2$ extracts were concentrated under vacuum at 40 °C and the concentrate purified by silica column chromatography (*n*-hexane:$Et_2O$, gradient elution from 100:0 to 85:15) to yield rotundone, **1** (1.39 g, 27% based on 25% conversion), as a pale yellow oil with the recovery of unreacted $\alpha$-guaiene, **2** (15.28 g, 75% recovery). Spectroscopic data of **1** including NMR and MS were in agreement with those reported.[1]

**Aerial Oxidation of $\alpha$-Guaiene, 2, and GC−MS Analysis.** $\alpha$-Guaiene, **2** (1.0 g, 4.9 mmol), was dissolved in $CH_2Cl_2$ (200 mL) at ambient temperature. The mixture was stirred while being purged slowly with a stream of oxygen (ca. 1 mL/min) through a glass frit. Small aliquots (0.2 mL) were removed daily, diluted with $CH_2Cl_2$, and analyzed by GC−MS using an Agilent 6890 gas chromatograph coupled with a 5973N mass spectrometer detector (MSD) and a Gerstel multipurposed autosampler (Gerstel, Germany) and equipped with a HP-wax bonded polyethylene glycol capillary column (DB-Wax 30 m × 250 $\mu$m i.d. × 0.25 $\mu$m film thickness, Agilent Technologies). Samples were prepared in dry dichloromethane and analyzed in split mode with a split ratio of 50.1:1. The inlet and transfer line temperatures were set at 250 °C. Injection volume was 1 $\mu$L. The column flow was set at 1.9 mL/min with a pressure of 15.96 psi. Helium was used as carrier gas. The oven temperature was initially set at 50 °C and held for 0.5 min and ramped up to 240 °C at 10 °C/min and held for a further 6 min. The MSD was operated in full scan mode scanning $m/z$ ions from 50 to 550 amu with EI energy set at 70 eV. MS source and quadrupole temperatures were set at 230 and 150 °C, respectively. The total and selected ion response ratios of $\alpha$-guaiene and its oxidation products were used as indicators for the extent of autoxidation of $\alpha$-guaiene under the different conditions. At the same concentrations and under the same GC−MS conditions, the total ion (TI) response ratio of $\alpha$-guaiene (**2**):epoxy guaienes (**5a**/**b**):rotundone (**1**) was ca. 36:33:31 and the response ratio of $\alpha$-guaiene (204) and rotundone (218) was found to be 1.0:1.11 (Figure 3).

**Preparation of Epoxides 5a/b.** To a stirred solution of $\alpha$-guaiene, **2** (103 mg, 0.50 mmol), in $CH_2Cl_2$ (3 mL) at −78 °C was

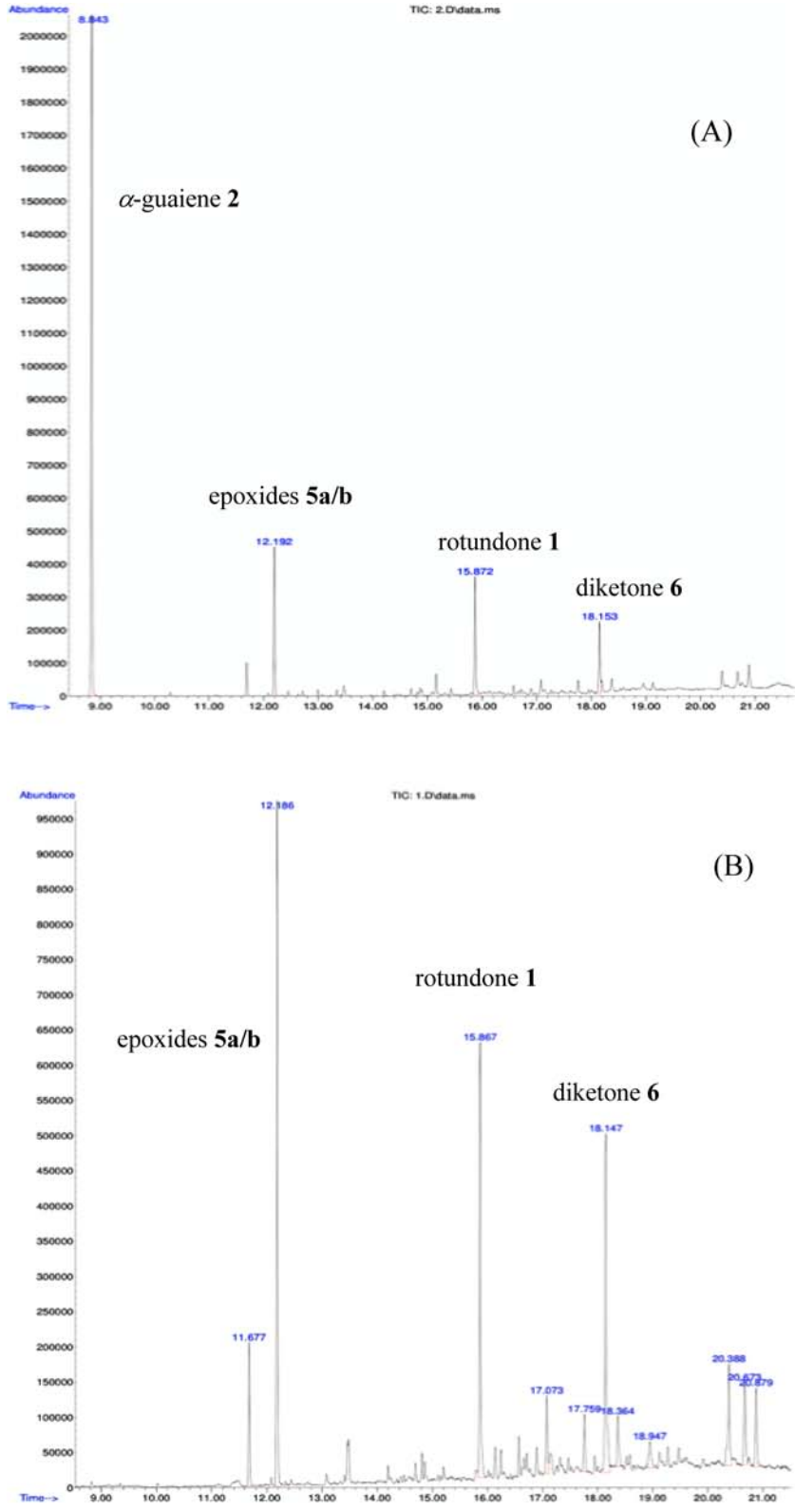


**Figure 2.** GC−MS traces of the aerial oxidation of α-guaiene, **2**, after (A) 4 days and (B) 29 days.

added dropwise a solution of *m*-CPBA (128 mg, 0.57 mmol) in $CH_2Cl_2$ (3 mL). After stirring at −78 °C for 30 min, the reaction was quenched with KI (10 mg), saturated aqueous $Na_2S_2O_3$ (1 mL) and aqueous $NaHCO_3$ (3 mL). The resulting mixture was extracted with $Et_2O$ (3 × 10 mL). The combined ether layers were washed with brine (10 mL), dried over anhydrous $MgSO_4$, and filtered. The filtrate was concentrated in vacuo and purified on neutral alumina to furnish the pair of epoxy diastereomers, **5a**:**5b** (ca. 1:2, 103 mg, 93%), as a colorless oil. **5a**: $^1$H NMR (600 MHz, $C_6D_6$) $\delta$ 4.77 (m, 1H, $H_{12a}$), 4.71 (dq, $J$ = 1.8, 1.5 Hz, 1H, $H_{12b}$), 2.15 (ddd, $J$ = 12.0, 10.8, 6.0 Hz, 1H, $H_7$), 1.94 (br d, $J$ = 14.4 Hz, 1H, $H_{6a}$), 1.88 (dd, $J$ = 13.8, 8.4 Hz, 1H, $H_{3a}$), 1.84−1.78 (m, 2H, $H_{6b\ and\ 10}$), 1.72 (ddq $J$ = 9.6, 7.2, 7.2 Hz, 1H, $H_4$), 1.65 (m, 1H, $H_{9a}$), 1.58 (br s, 3H, $H_{13}$), 1.55 (m, 1H, $H_{8a}$), 1.47 (ddd, $J$ = 14.4, 10.8, 4.8 Hz, 1H, $H_{8b}$), 1.42 (dd, $J$ = 12.6, 8.4 Hz,


dx.doi.org/10.1021/jf504693e | J. Agric. Food Chem. 2014, 62, 10809−10815

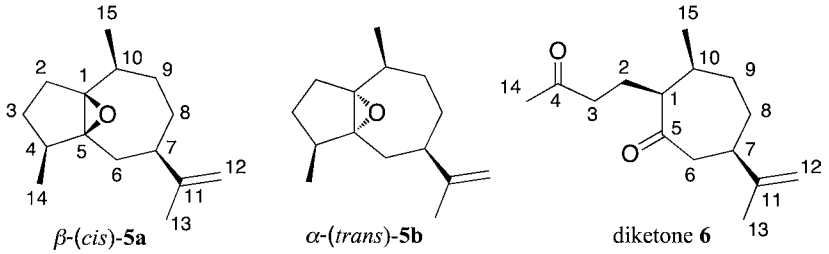


**Figure 3.** Structures of epoxides **5a** and **5b** and diketone **6**.

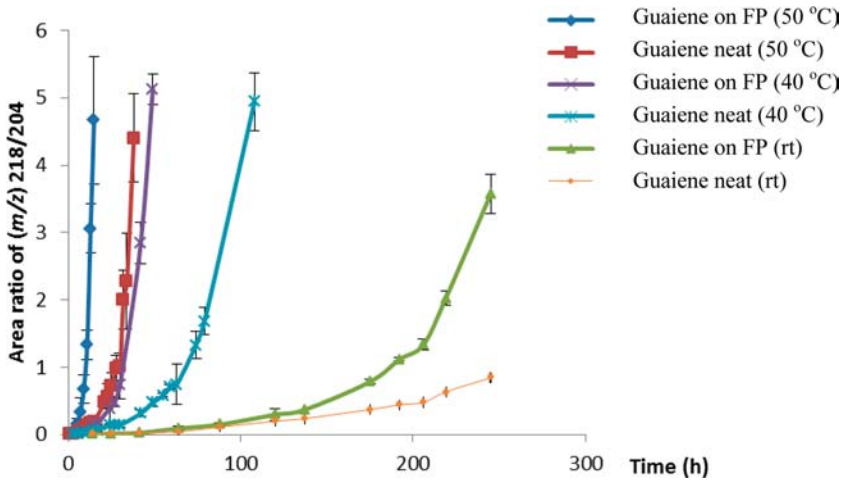


**Figure 4.** Autoxidation of α-guaiene, **2**, and formation of rotundone, **1**, on cellulose filter paper vs none at various temperatures.

1H, $H_{2a}$), 1.28 (ddd, $J$ = 13.8, 10.8, 8.4 Hz, 1H, $H_{3b}$), 1.16 (m, 1H, $H_{9b}$), 1.09 (ddd, $J$ = 12.6, 10.8, 8.4 Hz, 1H, $H_{2b}$), 1.06 (d, $J$ = 7.2 Hz, 3H, $H_{15}$), 1.02 (d, $J$ = 7.2 Hz, 3H, $H_{14}$); $^{13}$C NMR (150 MHz, $C_6D_6$) $\delta$ 150.6 ($C_{11}$), 109.1($C_{12}$), 72.6 ($C_5$), 72.5($C_1$), 43.5 ($C_7$), 38.5 ($C_4$), 34.5 ($C_{10}$), 32.2 ($C_8$), 31.8 ($C_6$), 31.4 ($C_3$), 28.6 ($C_9$), 28.4 ($C_2$), 20.0 ($C_{13}$), 18.5 ($C_{15}$), 13.9 ($C_{14}$); EI-MS $m/z$ (rel intensity) 220 (8), 205 (32), 162 (87), 147 (46), 107 (95), 81 (89), 67 (100). **5b**: $^1$H NMR (600 MHz, $C_6D_6$) $\delta$ 4.78 (m, 1H, $H_{12a}$), 4.73 (dq, $J$ = 1.8, 1.5 Hz, 1H, $H_{12b}$), 2.47 (dddd, $J$ = 12.6, 12.0, 2.4, 1.8 Hz, 1H, $H_7$), 2.24 (m, 1H, $H_{10}$), 2.05 (dd, $J$ = 14.4, 2.4 Hz, 1H, $H_{6a}$), 2.02 (br q, $J$ = 7.2 Hz, 1H, $H_4$), 1.98 (dddd, $J$ = 13.8, 12.6, 3.0, 1.8 Hz, 1H, $H_{8a}$), 1.86 (dd, $J$ = 14.4, 12.0 Hz, 1H, $H_{6b}$), 1.83−1.76 (m, 2H, $H_{2a,\ 3a}$), 1.64 (s, 3H, $H_{13}$), 1.58 (m, 1H, $H_{9a}$), 1.52−1.48 (m, 1H, $H_{9b}$), 1.34 (dddd, $J$ = 13.8, 6.6, 4.2, 1.8 Hz, 1H, $H_{8b}$), 1.24 (dddd, $J$ = 14.4, 13.2, 12.6, 1.8 Hz, 1H, $H_{3b}$), 0.94 (m, 1H, $H_{2b}$), 0.89 (d, $J$ = 7.2 Hz, 3H, $H_{15}$), 0.70 (d, $J$ = 7.2 Hz, 3H, $H_{14}$); $^{13}$C NMR (150 MHz, $C_6D_6$) $\delta$ 151.8 ($C_{11}$), 108.9 ($C_{12}$), 73.0 ($C_5$), 71.9 ($C_1$), 43.8 ($C_7$), 40.6 ($C_4$), 34.2 ($C_6$), 32.7 ($C_{10}$), 31.3 ($C_8$), 29.77 ($C_3$), 29.74 ($C_9$), 27.7 ($C_2$), 21.0 ($C_{13}$), 17.0 ($C_{14}$), 16.0 ($C_{15}$); EI-MS $m/z$ (rel intensity) 220 (7), 205 (22), 162 (63), 145 (52), 107 (94), 81 (85), 67 (100). These NMR data were consistent with low field data reported previously.[29]

**Identification of (2*S*,3*S*,6*R*)-3-Methyl-2-(3-oxobutyl)-6-(prop-1-en-2-yl)cycloheptanone; 7-*epi*-Chabrolidione A, 6.** A portion of the autoxidation mixture was subjected to silica (40−60 μm, ca. 100 g) column chromatography using a gradient elution of $Et_2O$:hexanes (200 mL, 2:98, 8:92, 12:88, 15:85, 17:83, 20:80, 23:77, 26:74, 50:50). Fractions from gradient 20:80 $Et_2O$:hexanes (ca. 100 mg) containing diketone **6** were further purified using ultrafine silica (15−40 μm, 10 g, $Et_2O$:hexanes, 15:85, 200 mL) column chromatography repeatedly to furnish **6** (2 mg) as a colorless oil: $R_f$ = 0.1 (30% $Et_2O$:hexanes); $^1$H NMR (600 MHz, $C_6D_6$) $\delta$ 4.66 (br s, 1H, $H_{12a}$), 4.63 (appr quint, $J$ = 1.5 Hz, 1H, $H_{12b}$), 2.65 (ddd, $J$ = 9.6, 4.2, 2.4 Hz, 1H, $H_1$), 2.37 (td, $J$ = 10.2, 1.2 Hz, 1H, $H_{6a}$), 2.35 (d, $J$ = 10.2 Hz, 1H, $H_{6b}$), 2.30 (m, 1H, $H_7$), 2.23 (dddd, $J$ = 13.8, 9.6, 8.4, 6.0 Hz, 1H, $H_{2a}$), 2.13 (ddd, $J$ = 16.8, 8.4, 6.0 Hz, 1H, $H_{3a}$), 1.88 (ddd, $J$ = 16.8, 8.4, 6.6 Hz, 1H, $H_{3b}$), 1.65 (s, 3H, $H_{14}$), 1.67−1.62 (m, 1H, $H_{10}$), 1.53−1.46 (m, 2H, $H_{9a,b}$), 1.48 (s, 3H, $H_{13}$), 1.45−1.38 (m, 2H, $H_{2b\ and\ 8a}$), 1.29−1.25 (m, 1H, $H_{8b}$), 0.67 (d, $J$ = 7.2 Hz, 3H, $H_{15}$); $^{13}$C NMR (150 MHz, $C_6D_6$) $\delta$ 210.7 ($C_5$), 206.5 ($C_4$), 149.8 ($C_3$), 109.6 ($C_{12}$), 54.2 ($C_1$), 50.2 ($C_6$), 43.4 ($C_7$), 41.7 ($C_3$), 37.1 ($C_9$), 35.0 ($C_{10}$), 29.9 ($C_8$), 29.3 ($C_{14}$), 24.8 ($C_2$), 19.9 ($C_{13}$), 14.1 ($C_{15}$); EI-MS $m/z$ (rel intensity): 236 (9), 221 (15), 203 (6), 179 (27), 161 (21), 150 (19), 135 (25), 123 (53), 109 (70), 95 (100), 67 (87); HRMS (ESI-TOF) $m/z$ $[M + H]^+$ calcd for $C_{15}H_{25}O_3$ 237.1855, found 237.1847.

**Aerial Oxidation of α-Guaiene, 2, on Filter Paper.** Autoxidation of α-guaiene, **2**, on filter paper was carried out on 50 mg quantities in duplicate at ambient temperature, 40 °C, and 50 °C. Filter paper (10 $cm^2$) was finely cut into approximately 2 $mm^2$ shreds, and these were placed into 20 mL, 75 mm × 25 mm glass vials. Six vials (3 treatments in duplicate) contained approximately 50 filter paper shreds while another six vials contained no filter paper shreds and were used as controls. α-Guaiene, **2** (neat, 50 mg), was added to each of the vials followed by the addition of $CH_2Cl_2$ (0.5 mL), and the mixtures were gently shaken for several minutes. The solvent was then removed under a gentle stream of $N_2$ at 10 °C, which ensured an even coating of guaiene onto the filter paper. The control experiments were identical except for the fact that they did not contain filter paper and were also conducted at ambient temperature, 40 °C, and 50 °C at the same time. The process of autoxidation was monitored by GC−MS by sampling a small fraction of the substrate from each control experiment and by removing one piece of filter paper shred from each filter paper treatment at various time points. A portion of the substrate from the control experiments or the filter paper sheds were placed in dry $CH_2Cl_2$ (1.5 mL) for GC−MS analysis. The selected ion response ratio of rotundone to α-guaiene at their corresponding retention times in the GC chromatogram was used as an indicator for the extent of the aerial oxidation of α-guaiene. The ratio of the areas of rotundone ($m/z$ 218) to those of α-guaiene ($m/z$ 204) under the different autoxidation conditions were plotted against time (Figure 4). Note that the total ion (TI) or other selected ion response ratios of rotundone and α-guaiene can also be used as indicators for the reaction rates of autoxidation of α-guaiene under the different

conditions without altering the trend of the curves shown in Figure 4. At the same concentrations and under the same GC−MS conditions, the total ion (TI) response ratio of α-guaiene (**2**):epoxy guaienes (**5a**/**b**):rotundone (**1**) is ca. 36:33:31 and the response ratio of α-guaiene ($m/z$ 204) and rotundone ($m/z$ 218) was found to be 1.0:1.11. GC−MS analysis was performed on the same instrument (6890 GC-5973N MSD) and with the same capillary column (DB-Wax 30 m × 0.25 mm i.d. × 0.25 μm film thickness, Agilent Technologies). Acquisition parameters were as follows: initial oven temperature set at 100 °C, ramped up to 200 °C at 8 °C/min and then to 240 °C at 20 °C/min and held at 240 °C for 3 min. Injection was in a splitless mode with a purge flow of 6 mL/min in 0.05 min. The inlet temperature was set at 240 °C with a pressure of 12.92 psi. Injection volume was 2 μL and gas flow rate set at 1.2 mL/min. Helium was the carrier gas. MSD was in full scan mode (50−550 Da). Gain factor was 1.0 and EI 70 eV. Transfer line temperature was set at 240 °C, MS source at 230 °C, and MS quadrupole at 150 °C.

## RESULTS AND DISCUSSION

With pure α-guaiene, **2**, in hand we placed 1 g in dichloromethane and bubbled oxygen through the solution over a number of weeks and followed the autoxidation by GC−MS on a daily basis. Figure 2A shows the oxidation at day 4 while Figure 2B displays the progress of oxidation of α-guaiene after 29 days. We indeed found that the aerial oxidation of α-guaiene, **2** ($t_R$ 8.84 min), after 4 days resulted in the formation of rotundone, **1** ($t_R$ 15.87 min), as one of the major products (Figure 2A). Identification was confirmed by comparison with an authentic sample via MS, by symmetrical peak enhancement on coinjection with synthetic rotundone utilizing several column types, and through isolation by column chromatography and comparison by $^1$H NMR.

In addition, two reaction products at retention times of 11.69 and 12.19 min displayed molecular masses of $m/z$ 220 ($C_{15}H_{24}O$) indicating that they had incorporated one oxygen atom when compared to α-guaiene ($m/z$ 204, $C_{15}H_{24}$) itself. These two compounds were identified as the monoepoxides (β-(*cis*)-**5a**, $t_R$ 11.69, and α-(*trans*)-**5b**, $t_R$ 12.19) by comparison with synthetic samples. One other major product at retention time 18.15 min was clearly observable after 4 days of oxidation (Figure 2A). It displayed a molecular mass of $m/z$ 236 indicating that it was likely to be an oxidized product ($C_{15}H_{24}O_2$) with two oxygen atoms incorporated. After careful column chromatography of the autoxidation mixture, this product was isolated and identified as the diketone, **6**, by $^1$H, $^{13}$C, and 2D NMR analysis. This oxidation product presumably results from the oxidative cleavage of the $C_1-C_{8a}$ carbon bond within α-guaiene itself. Indeed, such a cleavage has been proposed for the formation of several related epimers of this diketone isolated from various soft coral extracts in nature.[30]

We followed the aerial oxidation for 29 days, at which point complete consumption of α-guaiene, **2**, was observed (Figure 2B). Again, formation of rotundone, **1**, the two epoxides (**5a** and **5b**), and the diketone, **6**, were clearly visible. In addition, numerous other minor oxidation products were now present, many of which displayed molecular masses of 220 or 236 indicating the incorporation of one or two oxygen atoms when compared to α-guaiene ($m/z$ 204). Conducting the aerial oxidation in a range of other organic solvents (e.g., ether, chloroform or acetonitrile) also resulted in the same four major compounds being formed in very similar time frames.

Table 1 displays the relative GC peak area of the four major products formed at various stages of the autoxidation process (days 0, 4, 7, 9, 17, and 29) as a percentage of the peak area of α-guaiene plus total products observed by GC-MS.

**Table 1. Percentages Determined by GC−MS of Major Products Formed and α-Guaiene Remaining on Aerial Oxidation over Time**

| time (days) | α-guaiene (**2**) | β-*cis*-**5a** | α-*trans*-**5b** | rotundone (**1**) | diketone **6** | total (%) |
|---|---|---|---|---|---|---|
| 0 | 100.0 | 0.0 | 0.0 | 0.0 | 0.0 | 100.0 |
| 4 | 49.9 | 2.5 | 11.3 | 9.5 | 6.0 | 79.2 |
| 7 | 25.0 | 3.9 | 18.6 | 13.6 | 10.0 | 71.2 |
| 9 | 15.8 | 4.5 | 20.2 | 15.1 | 12.2 | 67.8 |
| 17 | 2.4 | 5.2 | 24.6 | 17.3 | 14.9 | 64.3 |
| 29 | 0.2 | 5.0 | 23.6 | 16.7 | 15.1 | 60.6 |

As can be seen from Table 1, the concentration of α-guaiene, **2**, steadily decreased over time, However, the relative proportions of the oxidation products, rotundone, **1**, monoepoxides **5a** and **5b**, and the diketone, **6**, remain approximately constant over the time period, suggesting that they are all being produced from a common intermediate such as the hydroperoxide **4**, as shown in Figure 1, formed first along the reaction coordinate. Removal of the proton α to the peroxide linkage by trace amounts of external nucleophiles would result in the formation of rotundone, **1**, and the loss of $H_2O$.[25] Furthermore, the formation of the monoepoxides (**5a** and **5b**) is highly consistent with the initial formation of hydroperoxide **4**. Once **4** is formed in solution it would be expected to act as an epoxidizing agent, reacting with the more electron rich internally bridged C=C of α-guaiene, **2**, to produce either the *cis* or *trans* epoxides (**5a** and **5b**) in a similar fashion to the action of *m*-CPBA on α-guaiene, **2**, reported herein. The hydroperoxide **4** could act as an epoxidizing agent toward any substrate containing C=C bonds, a situation which may well lead to some of the minor oxidized products seen in the later stages of this autoxidation sequence.

A matrix or scaffold that may well mimic the cellulose biolayers of some processed plant materials is filter paper. Indeed, filter paper disks which are made from compacted cellulose fibers have been used to monitor the disruption of hydrogen bonding between plant cell wall polymers by proteins that induce wall extension and in assays for the measurement of lipid biosynthesis.[27,31] With this scenario in mind, we coated α-guaiene onto cellulose filter paper shreds and allowed it to undergo autoxidation at various temperatures. The selected ion response ratio of rotundone to α-guaiene at their corresponding retention times in the GC chromatogram was used as an indicator for the extent of guaiene degradation (Figure 4). Again the same major products were formed over time, and it was observed that the extent of aerial oxidation of α-guaiene in general rose significantly with increasing temperature. Oxidation of α-guaiene on filter paper was more advanced than that without filter paper at the same temperature. These observations are consistent with the fact that coating α-guaiene onto the surface of filter paper would greatly enlarge the overall contact area between molecular oxygen and the substrate α-guaiene, thus leading to a substantial increase in oxidation rate.

Sesquiterpenes such as α-guaiene are mainly biosynthesized via the mevalonate acid (MVA) pathway in the cytosol of plant cells[32] though the newly discovered plastidial 2-*C*-methyl-D-erythritol-4-phosphate (MEP) pathway also generate sesquiterpenes and takes place in plastids.[33,34] A recent labeling study has suggested that the precursors supplied for the biosynthesis

of sesquiterpenes in the grape berry exocarp are mainly transported from plastids to the cytosol in cells of grape berry skin.[35] Dried grape skins consist of ca. 15% of cell wall materials which are made up of ca. 30−35% of neutral polysaccharides and ca. 20% of acidic pectic substances with 62% moderately methyl-esterified.[36] The only barrier between the cytosol and the plant cell wall is the cell membrane which is permeable to small hydrophobic molecules such as sesquiterpenes according to the well-established solubility−diffusion model (Overton's rule).[37−40] While enzymic oxidation of terpenes by plant or fungal oxidases is well-known,[41] it is possible that hydrophobic sesquiterpenes formed in the cytosol of plant cell matrices such as grapes could also be secreted onto their cell wall matrices and accumulate thereafter, and in the case for $\alpha$-guaiene might be further oxidized into sesquiterpenoids such as rotundone by ROS or atmospheric oxygen.

Overall our studies have shown that simple aerial oxidation of $\alpha$-guaiene, **2**, results in significant formation of the peppery aroma compound rotundone, **1**. Therefore, the mode of formation of rotundone in processed plant products, including dried herbs and spices, may simply be a result of air contact rather than rotundone being a product of enzymatically controlled processes. Furthermore, this autoxidation sequence is enhanced at higher temperatures as indicated by our findings when exploiting cellulose filter paper to mimic nature's biological scaffolds and may have significance when considering the amount of rotundone that may be formed during the cooking, heating, or drying of foodstuffs.

## AUTHOR INFORMATION


### Corresponding Author

*Phone: +61-8-8313-7239. Fax: +61-8-8313-4711. E-mail: dennis.taylor@adelaide.edu.au.



### Funding

This project was supported by the School of Agriculture, Food and Wine, the University of Adelaide, as well as by Australia's grape growers and winemakers through their investment body, the Grape and Wine Research and Development Corporation, with matching funds from the Australian Government. A.-C.H is indebted to the University of Adelaide and the China Scholarship Council for a joint Ph.D. scholarship. S.B. thanks the Faculty of Science for a Ph.D. scholarship.


### Notes

The authors declare no competing financial interest.

## REFERENCES


(1) Wood, C.; Siebert, T. E.; Parker, M.; Capone, D. L.; Elsey, G. M.; Pollnitz, A. P.; Eggers, M.; Meier, M.; Vössing, T.; Widder, S.; Krammer, G.; Sefton, M. A.; Herderich, M. J. From wine to pepper: rotundone, an obscure sesquiterpene, is a potent spicy aroma compound. *J. Agric. Food Chem.* **2008**, *56*, 3738−3744.

(2) Menon, A. N. The aromatic compounds of pepper. *J. Med. Aromat. Plant Sci.* **2000**, *22*, 185−190.

(3) Jagella, T.; Grosch, W. Flavour and off-flavour compounds of black and white pepper (Piper nigrum L.) I. Evaluation of potent odorants of black pepper by dilution and concentration techniques. *Eur. Food Res. Technol.* **1999**, *209*, 16−21.

(4) Jagella, T.; Grosch, W. Flavour and off-flavour compounds of black and white pepper (*Piper nigrum* L.) II. Odour activity values of desirable and undesirable odorants of black pepper. *Eur. Food Res. Technol.* **1999**, *209*, 22−26.

(5) Mattivi, F.; Caputi, L.; Carlin, S.; Lanza, T.; Minozzi, M.; Nanni, D.; Valenti, L.; Vrhovsek, U. Effective analysis of rotundone at below-threshold levels in red and white wines using solid-phase micro-extraction gas chromatography/tandem mass spectrometry. *Rapid Commun. Mass Spectrom.* **2011**, *25*, 483−488.

(6) Caputi, L.; Carlin, S.; Ghiglieno, I.; Stefanini, M.; Valenti, L.; Vrhovsek, U.; Mattivi, F. Relationship of changes in rotundone content during grape ripening and winemaking to manipulation of the 'peppery' character of wine. *J. Agric. Food Chem.* **2011**, *59*, 5565−5571.

(7) Capone, D. L.; Jeffery, D. W.; Sefton, M. A. Vineyard and fermentation studies to elucidate the origin of 1,8-cineole in Australian red wine. *J. Agric. Food Chem.* **2011**, *60*, 2281−2287.

(8) Scarlett, N. J.; Bramley, R. G. V.; Siebert, T. E. Within-vineyard variation in the 'pepper' compound rotundone is spatially structured and related to variation in the land underlying the vineyard. *Aust. J. Grape Wine Res.* **2014**, *20*, 214−222.

(9) Mayr, C. M.; Geue, J. P.; Holt, H. E.; Pearson, W. P.; Jeffery, D. W.; Francis, I. L. Characterization of the key aroma compounds in Shiraz wine by quantitation, aroma reconstitution, and omission studies. *J. Agric. Food Chem.* **2014**, *62*, 4528−4536.

(10) Vierling, E.; Kimpel, J. A. Plant responces to environmental stress. *Curr. Opin. Biotechnol.* **1992**, *3*, 164−170.

(11) Dicke, M.; Baldwin, I. T. The evolutionary context for herbivore-induced plant volatiles: beyond the 'cry for help'. *Trends Plant Sci.* **2010**, *15*, 167−175.

(12) Kapadia, V. H.; Naik, V. G.; Wadia, M. S.; Dev, S. Sesquiterpenes from the essential oil of *Cyperus rotundas*. *Tetrahedron. Lett.* **1967**, *47*, 4661−4667.

(13) Tajuddin, S. N.; Yusoff, M. M. Chemical composition of volatile oil of *Aquilaria malaccensis* (Thymelaeaceae) from Malaysia. *Nat. Prod. Commun.* **2010**, *5*, 1965−1968.

(14) Pripdeevech, P.; Khummueng, W.; Park, S.-K. Identification of odor-active components of agarwood essential oils from Thailand by solid phase microextraction-GC/MS and GC-O. *J. Essent. Oil Res.* **2011**, *23*, 46−53.

(15) Naef, R. The volatile and semi-volatile constituents of agarwood, the infected heartwood of Aquilaria species: A review. *Flavour Fragrance J.* **2011**, *26*, 73−89.

(16) Chanko, S.; Jayalekshmy, A.; Gopalakrishnan, M.; Narayanan, C. S. Roasting studies on Black Pepper (*Piper nigrum* L.). *Flavour Fragrance J.* **1996**, *11*, 305−310.

(17) Wei, A.; Shibamoto, T. Antioxidant activities and volatile constituents of various essential oils. *J. Agric. Food Chem.* **2007**, *55*, 1737−1742.

(18) Sundaresan, V.; Singh, S. P.; Mishra, A. N.; Shasany, A. K.; Darokar, M. P.; Kaira, A.; Naqvi, A. A. Composition and comparison of essential oils of *Pogostemon cablin* (Blanco) Benth. (Patchouli) and *Pogostemon travancoricus* Bedd. var. *travancoricus*. *J. Essent. Oil Res.* **2009**, *21*, 220−222.

(19) Vaze, K. Lesser known essential oils of India, their composition and uses. *FAFAI* **2003**, *5* (314), 47−58.

(20) Pandey, A. K.; Chowdhury, A. R. Essential oil of *Cyperus scariosus* R. Br. tubers from central India. *Indian Perfum.* **2002**, *46*, 325−328.

(21) Schreier, P.; Drawert, F.; Junker, A. Identification of volatile constituents from grapes. *J. Agric. Food Chem.* **1976**, *24*, 331−336.

(22) Coelho, E.; Rocha, S. M.; Delgadillo, I.; Coimbra, M. A. Headspace- SPME applied to varietal volatile components evolution during *Vitis vinifera* L. cv. 'Baga' ripening. *Anal. Chim. Acta* **2006**, *563*, 204−214.

(23) Ishihara, M.; Tsuneya, T.; Uneyama, K. Guaiene sesquiterpenes from agarwood. *Phytochemistry* **1991**, *30*, 3343−3347.

(24) Pilati, S.; Brazzale, D.; Guella, G.; Milli, A.; Ruberti, C.; Biasioli, F.; Zottini, M.; Moser, C. The onset of grapevine berry ripening is characterized by ROS accumulation and lipoxygenase-mediated membrane peroxidation in the skin. *BMC Plant Biol.* **2014**, *14*, 1−15.

(25) Yin, H.; Xu, L.; Porter, N. Free radical lipid peroxidation: Mechanisms and analysis. *Chem. Rev.* **2011**, *111*, 5944−5972.

(26) Armarego, W. L. F.; Chai, C. L. L. *Purification of Laboratory Chemicals*, 5th ed.; Elsevier Inc.: 2003.

(27) McQueen-Mason, S.; Cosgrove, D. J. Disruption of hydrogen bonding between plant cell wall polymers by proteins that induce wall extension. *Proc. Natl. Acad. Sci. U.S.A.* **1994**, *91*, 6574−6578.
(28) Marshall, J. A.; Ruden, R. A. Selective degradation of guaiol. The synthesis of 7-epiguaiol. *J. Org. Chem.* **1971**, *36*, 2569−2571.
(29) Pesnelle, P. The epoxides of guaiol. *Recherches (Paris)* **1966**, *15*, 33−40.
(30) Su, J.-H.; Chiang, M. Y.; Wen, Z.-H.; Dai, C.-F.; Hsu, C.-H.; Sheu, J.-H. Sespuiterpenoids from the Formosan Soft Coral Sinularia leptoclados. *Chem. Pharm. Bull.* **2010**, *58*, 250−253.
(31) Gutensohn, M.; Nagegowda, D.; Dudareva, N., Involvement of Compartmentalization in Monoterpene and Sesquiterpene Biosynthesis in Plants. In *Isoprenoid Synthesis in Plants and Microorganisms*, Bach, T. J., Rohmer, M., Eds.; Springer: New York, 2013; pp 155−169.
(32) Rohmer, M.; Knani, M.; Simonin, P.; Sutter, B.; Sahm, H. Isoprenoid biosynthesis in bacteria: A novel pathway for the early steps leading to isopentenyl diphosphate. *Biochem. J.* **1993**, *295*, 517−24.
(33) Rohmer, M. The discovery of a mevalonate-independent pathway for isoprenoid biosynthesis in bacteria, algae and higher plants. *Nat. Prod. Rep.* **1999**, *16*, 565−574.
(34) May, B.; Lange, B. M.; Wüst, M. Biosynthesis of sesquiterpenes in grape berry exocarp of *Vitis vinifera* L.: Evidence for a transport of farnesyl diphosphate precursors from plastids to the cytosol. *Phytochemistry.* **2013**, *95*, 135−144.
(35) Lecas, M.; Brillouet, J. M. Cell wall composition of grape berry skins. *Phytochemistry* **1994**, *35*, 1241−1243.
(36) Overton, E. *Studien über die Narkose*; Gustav Fischer Verlag: Jena, 1901.
(37) Meyer, H. Zur Theorie der Alkoholnarkose. *Arch. Exp. Pathol. Pharmakol.* **1899**, *42*, 109−118.
(38) Missner, A.; Pohl, P. 110 Years of the Meyer−Overton rule: Predicting membrane permeability of gases and other small compounds. *ChemPhysChem* **2009**, *10*, 1405−1414.
(39) Lodish, H.; Berk, A.; Zipursky, S. L.; Matsudaira, P.; Baltimore, D.; Darnell, J. The Dynamic Plant Cell Wall. In *Molecular Cell Biology*, 4th ed.; W. H. Freeman: New York, 2000.
(40) Goldfine, H. Use of a filter paper disk assay in the measurement of lipid biosynthesis. *J. Lipid Res.* **1966**, *7*, 146−149.
(41) Cankar, K.; Houwelingen, A. v.; Bosch, D.; Sonke, T.; Bouwmeester, H.; Beekwilder, J. A chicory cytochrome P450 monooxygenase CYP71AV8 for the oxidation of (+)-valencene. *FEBS Lett.* **2011**, *585*, 178−182.

isoelectric point of around pH 5.0 and a single thermal denaturation temperature (around 70 °C).[31,32] However, to our knowledge, the interaction between thermally modified LF and EGCG was not characterized. LF has two lobes, and each one consists of two domains and a single, high affinity metal binding site, which binds, very tightly but reversibly, one ferric ion together with one carbonate as the synergistic anion.[33] When LF is heated, one of the lobes unfolds at around 60 °C, and the other unfolds at around 85 °C,[34−37] leading to a conformational change irreversibly in the LF molecules.[30]

There are some reports available on the heat-induced structural and conformational changes of LF.[6,30,33] None of the papers, however, focused on the interaction between LF and EGCG. Until now, the information for the interaction and structure−affinity relationship of thermally modified LF and polyphenol was not available at different pH values.

In this study, we examined whether protein−EGCG nanoparticles or submicrometer particles could be formed using native and thermally modified LF at different pH values. The effects of LF and EGCG interactions at different pH values on the structure of LF are tested. The binding constant and the number of binding sites of EGCG with native and thermally modified LF were also compared by fluorescence spectroscopy. LF has a much high isoelectric point, and LF−EGCG nanoparticles or submicrometer particles may be positively charged over a wider pH range. These LF−EGCG complexes may be useful functional ingredients in food, cosmetic, and pharmaceutical applications, e.g., to modify the optical or rheological properties of products.

## MATERIALS AND METHODS

**Materials.** Lactoferrin from bovine whey was purchased from New Image International Limited (New Zealand). Its composition was protein (dry basis) 99.41%, of which LF was 92.0% of total proteins, ash 0.31%, and moisture 15.0%. The iron saturation of the LF powder was reported to be 15%. EGCG (purity ≥98%) from green tea was purchased from BSZH Science Company (Beijing, China). All other chemicals used were of analytical grade, unless otherwise stated.

**Solution Preparation.** LF and EGCG aqueous solutions were prepared freshly by dissolving the proper amount of each powder in citrate buffer (pH 3.5, 10 mM), acetate buffer (pH 5.0, 10 mM), and phosphate buffer (pH 6.5, 10 mM) at room temperature and stirring for 2 h. If necessary, pH was adjusted with HCl (10 mM) or NaOH (10 mM). LF was dispersed in buffers to get a final concentration of 200 $\mu$M. The protein solutions were filled in plastic tubes (1 cm diameter). The thermally denatured experiments were conducted in a thermostatic water bath at 70 or 90 °C for 20 min. The two temperatures correspond approximately to the first and second unfolding transition of LF, respectively.[30,34,35,38] After the thermal treatment, the tubes were immediately cooled in ice water to prevent further denaturation. All measurements were performed within 3 min after the heat treatment. The mixtures of Lf and EGCG were prepared by blending the appropriate volume of native LF or thermally modified LF and EGCG solutions in order to achieve the desired final concentrations. All spectroscopic studies were carried out on the heated−cooled protein, implying that only irreversible/permanent structural changes were detected.

The abbreviations $LF_x$ ($x$ = 3.5, 5.0, or 6.5) were used to represent the LF in the buffer solutions at pH 3.5, 5.0, and 6.5, respectively. The abbreviations $LF_{x\text{-}25°C}$ were used to represent the native LF in the corresponding buffer solutions. The abbreviations $LF_{x\text{-}70°C}$ and $LF_{x\text{-}90°C}$ were used to represent the LF heated at 70 and 90 °C for 20 min in the corresponding buffer solutions, respectively.

**ζ-Potential Measurements.** The ζ-potential of the complexes was determined by a particle electrophoresis instrument using a Zetasizer Nano-ZS90 (Malvern Instruments, U.K.). Samples were loaded in the cell and temperature was set at 25 °C without further dilution. The ζ-potential measurements were reported as the average of measurements for three fresh samples, with three readings recorded for each sample.

**Haze and Particle Size Measurements.** LF and EGCG solutions with different concentrations were mixed to obtain final EGCG levels of 0.5, 1.0, 1.5, 2.0, 2.5, 3.0, 3.5, and 4.0 mM with a constant LF concentration of 0.1 mM. Haze formation was monitored by DLS and nephelometry when the mixture was kept at 25 °C for 2 h.[39]

Nephelometry experiments were performed in a HACH 2100N laboratory turbidimeter (Loveland, USA), and the aggregation behavior of LF and EGCG in aqueous solution was evaluated. The optical apparatus was equipped with a tungsten-filament lamp with three detectors: a 90° scattered-light detector, a forward-scatter light detector, and a transmitted light detector. The calibration was performed using a Gelex Secondary Turbidity Standard Kit (HACH, Loveland, USA), which consists of stable suspensions of a metal oxide in a gel.[39] All experiments were performed in triplicate.

Particle size and size distribution of LF−EGCG complexes were determined by dynamic light scattering (DLS) using a Zetasizer Nano-ZS90 (Malvern Instruments, Worcestershire, U.K.). The intensity of light scattered was monitored at a 90° angle. Results were described as cumulants mean diameter (size, nm) for particle size and polydispersity index (PDI) for size distribution. All experiments were performed in triplicate.

**Fourier Transform Infrared (FTIR) Spectroscopy.** The infrared spectra of samples were measured with the potassium bromide (KBr) pellet method using a Spectrum 100 Fourier transform spectrophotometer (PerkinElmer, U.K.) in the 500−4000 $cm^{-1}$ range, with a resolution of 4 $cm^{-1}$. Potassium bromide was used as a reference. For each measurement, 11 scans were taken. The samples analyzed were free LF, free EGCG, and freeze-dried LF−EGCG complexes.

**Circular Dichroism Measurements.** The CD spectra were recorded using a CD spectropolarimeter (Pistar $\pi$-180, Applied Photophysics Ltd., U.K.) at both far-UV (190−250) and near-UV (250−320) regions under a constant nitrogen flush. Path lengths were 0.1 cm for the far-UV region and 1 cm for the near-UV region. Ellipticity was recorded at a speed of 100 nm/min, 0.2 nm resolution, 20 accumulations, and 2.0 nm bandwidth. The collected data were analyzed using Dichroweb: the online Circular Dichroism Web site http://dichroweb.cryst.bbk.ac.uk.[40,41] Each spectrum presented was the average of three consecutive measurements.

**Fluorescence Spectroscopy.** Fluorescence measurements were carried out using a fluorescence spectrophotometer (F-7000, Hitachi, Japan). LF and EGCG solutions with various concentrations were mixed to prepare final EGCG levels of 10, 20, 30, 40, 50, 60, and 70 $\mu$M with a constant LF concentration of 0.1 mM. Spectra were collected when the mixture was kept at 25 °C for 2 h. The interaction between LF and EGCG was investigated using tryptophan fluorescence quenching. Fluorescence emission spectra of LF were recorded with the excitation wavelength at 292 nm. Both excitation and emission slit widths were set at 5 nm.

The fluorescence quenching data were analyzed by fitting to the Stern−Volmer equation (eq 1):

$$\frac{F_0}{F} = 1 + k_q\tau_0[Q] = 1 + K_{sv}[Q] \quad (1)$$

where $F_0$ and $F$ are the fluorescence intensities in the absence and presence of quencher, $k_q$ is the biomolecular quenching constant, $\tau_0$ is the lifetime of fluorescence in the absence of a quencher, [Q] is the concentration of the quencher, and $K_{sv}$ is the Stern−Volmer quenching constant.[33,42]

The binding constant $K_a$ and the number of binding sites $n$ can be calculated according to a double-logarithmic equation (eq 2):

$$\log\frac{F_0 - F}{F} = \log K_a + n\log[Q] \quad (2)$$

The intercept of the double logarithmic Stern−Volmer plot provides the binding constant ($K_a$), and the slope yields the number of binding sites ($n$).

**Statistical Analysis.** The experiments were conducted in duplicate, and all the analyses were done in triplicate. The results were presented as the means ± standard deviation. Data were analyzed by one-way analysis of variance using the SPSS 16.0 package (SPSS Inc., Chicago, IL, USA), and the means were analyzed by Duncan's multiple-range test. The correlations analysis was carried out using the Pearson mode. The concordance between experimental data and calculated values was established by the root mean squared deviation (RMSD).

## RESULTS AND DISCUSSION

**The Turbidity Measurements.** The turbidity of the LF−EGCG solutions was measured to obtain some information about LF−EGCG complexes' aggregation (Figure 1). The order of turbidity of single protein solutions was as follows: pH 6.5 > pH 3.5 > pH 5.0. At pH 6.5, native LF might undergo a pH-induced self-assembly that led to the formation of increasingly larger particles with time extension than those at pH 3.5 and 5.0.[43] This result could be attributed to the fact that the protein particles had a low net charge around pH 6.5 (see Figure 2), therefore, there might be a weak electrostatic repulsion between the particles. Thermally modified LF at pH 3.5 and 5.0 did not display thermal aggregation behavior whereas LF associated into large insoluble aggregates at pH 6.5. Abe et al. and Sreedhara et al. reported that LF was more thermoresistant at acidic pH whereas turbidity and sometimes gelation were observed upon heating at neutral and alkaline pH.[44,45] The thermal aggregation of LF at pH 6.5 probably exposed sites normally buried inside the molecule that increased protein association by noncovalent interactions, with intermolecular thiol/disulfide reactions.[46] There is a simple relationship between turbidity and ζ-potential at different thermal denaturation temperatures and pH values, that is, at pH 3.5, 5.0, and 6.5, the turbidity of free LF solution becomes higher with the increase of ζ-potential as the two lobes of LF unfold successively (see Figure 2).

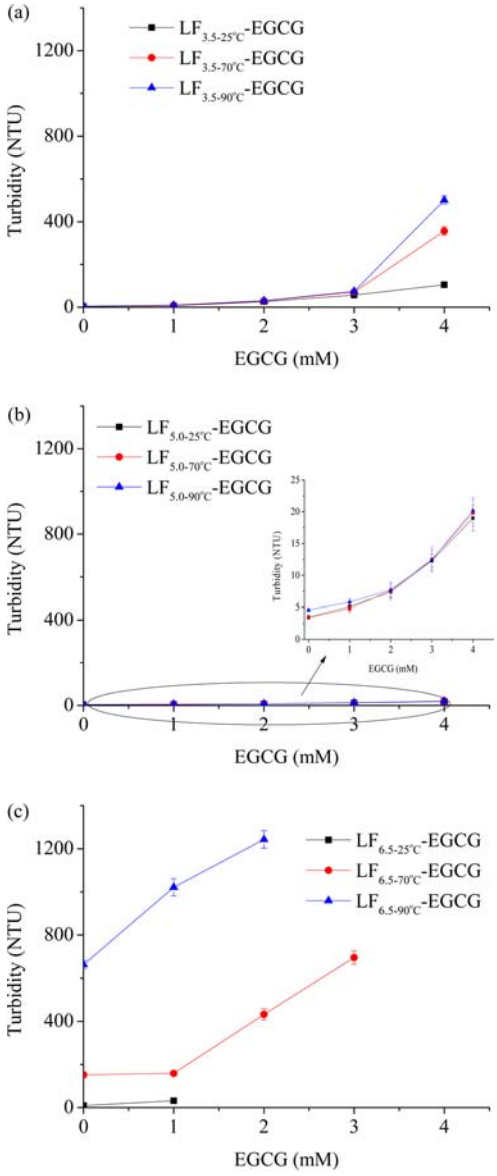


**Figure 1.** Influence of pH and EGCG concentration on the turbidity of LF and LF−EGCG complexes.

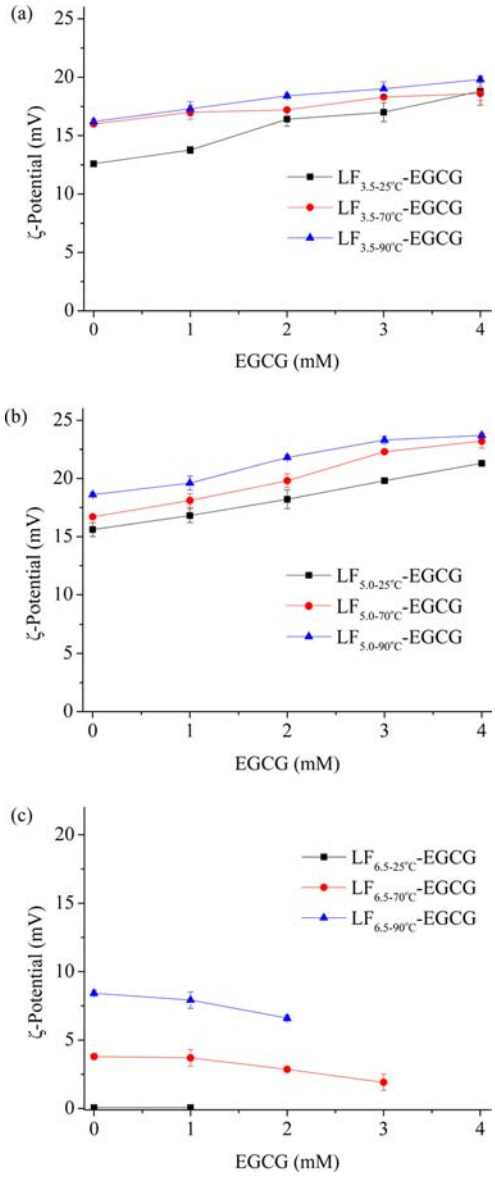


**Figure 2.** Influence of pH and EGCG concentration on the ζ-potential of LF and LF−EGCG complexes.


dx.doi.org/10.1021/jf5038147 | J. Agric. Food Chem. 2014, 62, 10816−10827

In the presence of EGCG, LF−EGCG complexes were formed as indicated by the appearance of increasing turbidity at pH 3.5, 5.0, and 6.5. The precipitations of LF−EGCG complexes resulting from polyphenol−protein interactions were pH sensitive. At pH 3.5 and 5.0, no precipitation was observed for LF−EGCG complexes. This might be ascribed to two reasons: one was the high net surface charge (>13.0 mV) of protein−polyphenol complexes (see Figure 2), which prevented them from coming into close contact and forming large aggregates;[47,48] the other was the small size of complexes formed (see Figure 3). The minimum level of turbidity

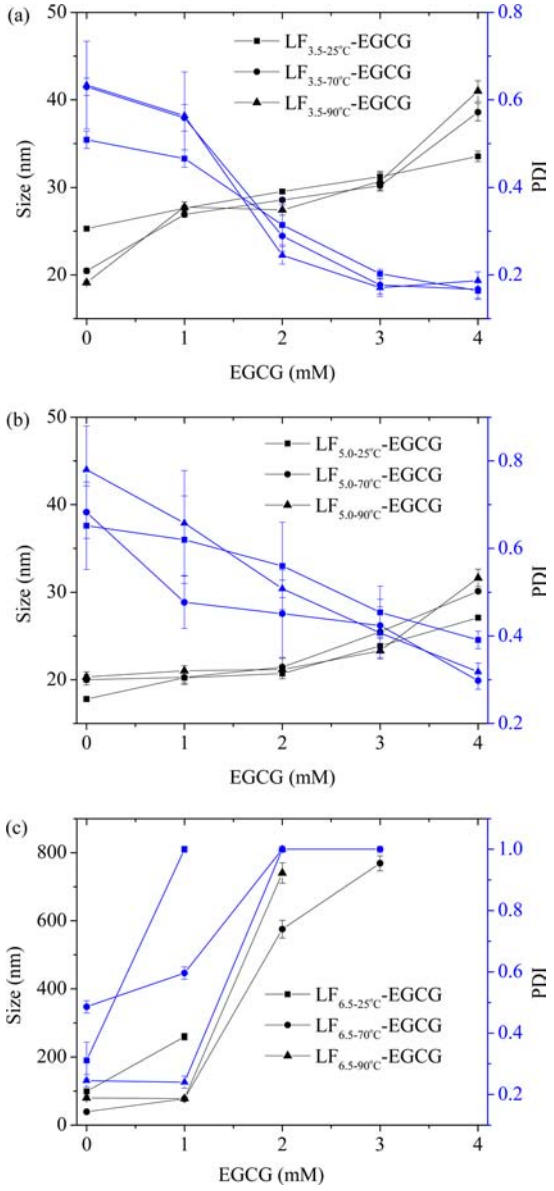


**Figure 3.** Influence of pH and EGCG concentration on the particle size of LF and LF−EGCG complexes.

occurred at pH 5.0 for LF−EGCG complexes; this might be attributed to the higher ζ-potential and smaller size of $LF_{5.0}$−EGCG complex than $LF_{3.5}$−EGCG complex and $LF_{6.5}$−EGCG complex (see Figures 2 and 3), and/or the secondary structure profiles of LF, which presented lower unordered content but higher α-helix content at pH 5.0, while higher unordered content but lower α-helix content at pH 3.5 and 6.5 (see Figure 5 (b)).

It should be noted that the addition of 1.0 mM EGCG resulted in significant sedimentation of $LF_{6.5\text{-}25°C}$−EGCG aggregates. The extensive precipitation could be related to the fact that the ζ-potential of $LF_{6.5\text{-}25°C}$ was very close to neutrality (0.613 ± 0.1 mV for $LF_{6.5\text{-}25°C}$) (see Figure 2) allowing the formation of large aggregates that precipitate.[49] Naczk et al. studied the effect of pH on the formation of crude tannin canola extract and protein (BSA, fetuin, gelatin, and lysozyme) complexes. It was suggested that the lowest solubility of polyphenol−protein complexes occurred at 0.3−3.1 pH units below the isoelectric point of the proteins.[50] Indeed, increased precipitation of protein/polyphenol complex close to the isoelectric point might be attributed to the minimum solubility of the protein at this pH. $LF_{6.5\text{-}70°C}$−EGCG complex and $LF_{6.5\text{-}90°C}$−EGCG complex, having a uniform cloudy appearance, remained relatively stable against particle aggregation until the concentrations of EGCG were more than 2.0 and 3.0 mM, respectively. The low ζ-potential (see Figure 2) explained the low stability of these LF−EGCG complexes at this pH, where particles tended to flocculate and precipitate.

In general, polyphenols normally have a strong binding affinity with proteins, which often leads to precipitation,[51] but some factors, such as pH, temperature, protein type, structure and concentration, and the type and structure of phenolic compounds, basically affect protein−phenolic interactions. The results from aforementioned experiments indicated that the turbidity of LF−EGCG complexes could be manipulated by controlling the pH of solutions, the structure of LF, and the concentration of EGCG.

**ζ-Potential Measurements.** The charge of single LF and LF−EGCG complexes at different pH values is presented in Figure 2. It is interesting to note that the ζ-potential of the $LF_{6.5\text{-}25°C}$ was around 0 mV, despite this pH being below the reported isoelectric point of lactoferrin. The most likely explanation for this result was that the cationic groups on the adsorbed LF bound some anionic phosphate ions present in the buffer.[52]

There were appreciable differences in the influence of pH and thermal treatment on the ζ-potential of LF. As shown in Figure 2, the ζ-potential of LF was increased with the rise of thermal denaturation temperature in different buffer systems. We speculated that the two lobes of the protein are so close that they mask potential interactive sites buried within the interdomains of both lobes of the protein.[46] As the two lobes of LF unfold successively when the protein was heated at 70 and 90 °C, more cationic groups originally located in the hydrophobic interior of LF exposed successively to buffer solutions and/or the thermally modified LF weaken the adsorbed ability of anion present in the buffers, leading to the increased ζ-potential of the thermally modified LF in different buffer solutions.

Some researchers reported that the addition of green tea polyphenols hardly affected the ζ-potential of protein.[47] However, in our study, we interestingly found that the ζ-potential of LF−EGCG complexes was affected by the presence of EGCG. At pH 3.5 and 5.0, the LF had a higher ζ-potential which was further increased by the addition of EGCG. The high net charge of LF−EGCG complexes played an important role in preventing precipitation, which was consistent with the turbidity result that showed a low turbidity at pH 3.5 and 5.0. It should be noted that EGCG bears negative ζ-potential at pH

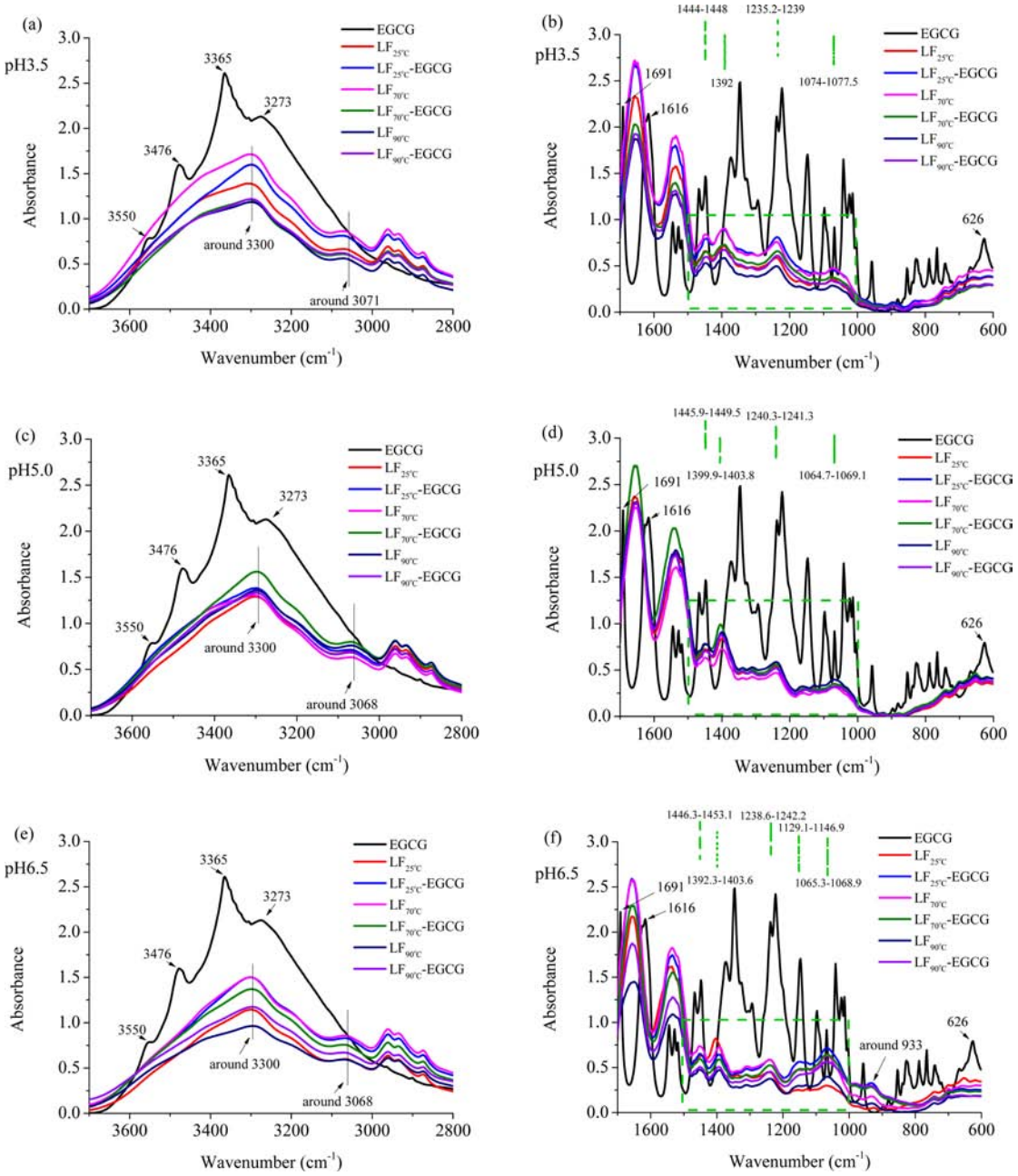


**Figure 4.** FTIR spectra of EGCG, LF, and LF−EGCG complexes (containing 1.0 mM EGCG) at pH 3.5, 5.0, and 6.5.

3.5 and 5.0, opposite to LF. This result revealed that other factors except for the net charge affected the ζ-potential of LF−EGCG complexes, for example, the molecule of EGCG is much smaller than LF, therefore, EGCG might insert into the LF molecule and surround the LF molecule surface, resulting in reorganization of protein secondary and tertiary structures, thereby changing the protein surface charge distribution. At pH 6.5, close to the p$K_a$, the protonated phenolic groups of EGCG could be deprotonated and the generated oxygen center imparts a high negative charge density,[47] which further decreased the ζ-potential value of the complexes, leading to particle aggregation at higher concentration of EGCG.

**The Particle Size Measurements.** Figure 3 shows the particle size and the polydispersity of the LF−EGCG complexes present in buffer solutions. The particle size of thermally modified LF underwent only slight changes compared with native LF at pH 3.5, 5.0, and 6.5. EGCG induced an increase of size of the LF−EGCG complexes at desired pH values, forming larger aggregates that enhanced the scattered light, which was in agreement with the observed increase of nephelometric measurements.

Single LF showed a particle size of 19−25 nm at pH 3.5, and 17.8−20.31 nm at pH 5.0. In the presence of EGCG, this value was increased significantly ($P < 0.05$), but it was always smaller than 41 nm at pH 3.5, and 32 nm at pH 5.0. These nanosized particles were soluble at pH 3.5 and 5.0, in other words, the large-scale aggregation was suppressed in the mixture of LF and EGCG at these two pH values. It is interesting to find that, as the EGCG concentration was increased, the aggregation of LF−EGCG complexes at pH 3.5 and 5.0 was hardly changed, but a narrow range of the particle size distribution was observed (a decreased PDI value, from 0.6 to 0.16 at pH 3.5, and 0.78 to


dx.doi.org/10.1021/jf5038147 | J. Agric. Food Chem. 2014, 62, 10816−10827

0.298 at pH 5.0), indicating a very homogeneous population of these aggregates.

At pH 6.5, the particle size of native LF was larger than 99.35 ± 6.0 nm at the original state because the ζ-potential of LF at pH 6.5 was very close to neutrality (0.613 ± 0.1 mV), and the association was promoted.[53] In the presence of EGCG, this value was increased significantly ($P < 0.05$) and submicrometer particles (0.6−0.8 μm) could be formed. The PDI values, which were different from those at pH 3.5 and 5.0, were enhanced as the size of LF−EGCG complexes increased at pH 6.5, indicating a very heterogeneous population of the aggregates formed. Larger particles remained unstable in solution (see Figure 1) at pH 6.5, which was attributed to the low net charge, with only weak electrostatic repulsion between the particles.

It can be concluded that pH and the structure of LF significantly affected the interaction between LF and EGCG. This interpreted the possibility of monitoring LF−EGCG particle size (nanometer or submicrometer) and morphology with pH and heat treatment as factors. Overall, the sensitivity of the particle size to pH and the structure of LF facilitated the control of the physical properties of LF−EGCG complexes.

**Fourier Transform Infrared (FTIR) Spectroscopy.** EGCG is known to form complexes with proteins leading to changes in the structural, functional, and nutritional properties of both compounds. Figure 4 shows the infrared spectra of LF and LF−EGCG complexes (1.0 mM EGCG). FTIR profiles revealed some pronounced differences between native LF at different pH values, and distinguished LF−EGCG complexes from the native LF.

EGCG has four typical peaks around 3550, 3476, 3365, and 3273 $cm^{-1}$, probably due to the vibration of the O−H linkage of phenolic and hydroxyl groups,[54−56] and two large peaks around 1691 and 1616 $cm^{-1}$, probably due to the carbonyl stretching of the gallic acid,[57] while those peaks were not found in the complexes at all. At the same time, the disappearance of other typical characteristic bands of EGCG, such as peaks in the regions of 1000−1500 and 700−900 $cm^{-1}$, also confirmed the formation of the LF−EGCG complex by noncovalent interaction.

In this study, all complexes showed a broad feature around 3300 $cm^{-1}$, due to intermolecular H-bonded and O−H stretching modes. Slight change of the peak around 3300 $cm^{-1}$ in all LF−EGCG complexes compared to the native LF was an indication of the interaction between LF and EGCG induced by hydrogen bonds.[55] This result was in agreement with previous findings suggesting that polyphenols were bound to the protein partially via H-bonds.[15,58] The absorption bands of LF located at 2936 and 2875 $cm^{-1}$ were attributed to antisymmetric and symmetric $CH_2$ stretching vibrations of proteins.[59] The spectral changes of these vibrations were monitored in order to locate the presence of hydrophobic contact in the LF−EGCG complex. Upon the interaction with EGCG, no shifts of absorption peaks were observed in the LF−EGCG complex compared to native LF (Figure 4), which suggested that the hydrophobic interaction was not the main force when the LF−EGCG complex formed.

Peaks around 1653 and 1535 $cm^{-1}$ in the FTIR spectra of native LF were attributed to C═O stretching vibrations of amide I band[60,61] and N−H bending vibrations and C−N stretching vibrations of amide II band,[62−65] respectively. Both the C═O bonds and the C−N bonds were involved in the hydrogen bonds which took place between the different elements of secondary structure of proteins.[66] LF showed slight or no obvious difference in the amide I band (at 1600−1700 $cm^{-1}$) before and after the addition of EGCG (1.0 mM), but there was some major spectral shifting for LF amide II band at 1535 $cm^{-1}$ upon EGCG interaction. The peak position of amide II blue-shifted from 1535 to 1537 $cm^{-1}$ for $LF_{3.5}$ and $LF_{5.0}$ and red-shifted from 1537.3, 1535.4, and 1533.7 $cm^{-1}$ to 1535.6, 1534.9, and 1533.3 $cm^{-1}$ for $LF_{6.5\text{-}25°C}$, $LF_{6.5\text{-}70°C}$, and $LF_{6.5\text{-}90°C}$, respectively. Peaks around 1448 $cm^{-1}$ for $LF_{3.5}$, 1449 $cm^{-1}$ for $LF_{5.0}$, 1446.3 $cm^{-1}$ for $LF_{6.5\text{-}25°C}$, and 1453 $cm^{-1}$ for $LF_{6.5\text{-}90°C}$ also had obvious red shift (about 1−4 $cm^{-1}$) (Tables 1−3). These results implied that EGCG interacted with the C═O and C−N groups in the protein structural subunits (hydrophilic interaction).

**Table 1. FTIR Spectral Peak Position of LF and LF−EGCG Complexes (1.0 mM EGCG) at pH 3.5**

| | peak wavenumber ($cm^{-1}$) | | | | | |
|---|---|---|---|---|---|---|
| | $LF_{3.5\text{-}25°C}$ | | $LF_{3.5\text{-}70°C}$ | | $LF_{3.5\text{-}90°C}$ | |
| region | 0 mM[a] | 1.0 mM | 0 mM | 1.0 mM | 0 mM | 1.0 mM |
| amide A | 3304.0 | 3298.0 | 3301.0 | 3299.9 | 3299.3 | 3299.6 |
| amide B | 3071.0 | 3075.0 | 3072.0 | 3072.7 | 3071.7 | 3077.0 |
| amide I | 1656.6 | 1657.8 | 1657.0 | 1656.3 | 1656.3 | 1656.1 |
| amide II | 1535.5 | 1536.6 | 1535.0 | 1537.5 | 1535.8 | 1536.6 |
| | 1448.0 | 1446.0 | 1448.0 | 1444.5 | 1447.7 | 1445.2 |
| amide III | 1239.0 | 1236.0 | 1238.6 | 1236.8 | 1238.5 | 1236.0 |
| | 1075.0 | 1077.0 | 1074.0 | 1077.0 | 1074.9 | 1077.3 |

[a]EGCG concentration.

**Table 2. FTIR Spectral Peak Position of LF and LF−EGCG Complexes (1.0 mM EGCG) at pH 5.0**

| | peak wavenumber ($cm^{-1}$) | | | | | |
|---|---|---|---|---|---|---|
| | $LF_{5.0\text{-}25°C}$ | | $LF_{5.0\text{-}70°C}$ | | $LF_{5.0\text{-}90°C}$ | |
| region | 0 mM[a] | 1.0 mM | 0 mM | 1.0 mM | 0 mM | 1.0 mM |
| amide A | 3301.0 | 3299.7 | 3307.9 | 3299.2 | 3298.5 | 3299.4 |
| amide B | 3066.4 | 3071.4 | 3069.0 | 3067.6 | 3067.5 | 3070.1 |
| amide I | 1657.9 | 1658.0 | 1656.3 | 1657.0 | 1656.0 | 1656.0 |
| amide II | 1535.5 | 1543.7 | 1535.1 | 1537.1 | 1536.2 | 1537.0 |
| | 1449.3 | 1447.0 | 1449.5 | 1447.0 | 1448.9 | 1448.3 |
| amide III | 1160.8 | 1151.4 | 1160.3 | 1151.1 | 1159.9 | 1151.4 |
| | 1069.4 | 1067.6 | 1069.1 | 1067.4 | 1067.8 | 1064.7 |

[a]EGCG concentration.

It is interesting to find that FTIR profiles also revealed some pronounced differences in the region of 1500−1000 $cm^{-1}$ at pH 3.5, 5.0, and 6.5. In this region, there existed four peaks at

**Table 3. FTIR Spectral Peak Position of LF and LF−EGCG Complexes (1.0 mM EGCG) at pH 6.5**

| | peak wavenumber ($cm^{-1}$) | | | | | |
|---|---|---|---|---|---|---|
| | $LF_{6.5\text{-}25°C}$ | | $LF_{6.5\text{-}70°C}$ | | $LF_{6.5\text{-}90°C}$ | |
| region | 0 mM[a] | 1.0 mM | 0 mM | 1.0 mM | 0 mM | 1.0 mM |
| amide A | 3299.9 | 3300.9 | 3302.7 | 3296.8 | 3296.3 | 3297.2 |
| amide B | 3066.6 | 3069.2 | 3066.7 | 3070.0 | 3070.2 | 3071.2 |
| amide I | 1656.7 | 1657.1 | 1656.9 | 1657.1 | 1656.0 | 1656.0 |
| amide II | 1537.3 | 1535.6 | 1535.4 | 1534.9 | 1533.7 | 1533.3 |
| | 1446.3 | 1451.9 | 1452.9 | 1453.1 | 1452.8 | 1451.5 |
| amide III | 1242.2 | 1240.4 | 1240.7 | 1238.6 | 1239.0 | 1238.8 |

[a]EGCG concentration.

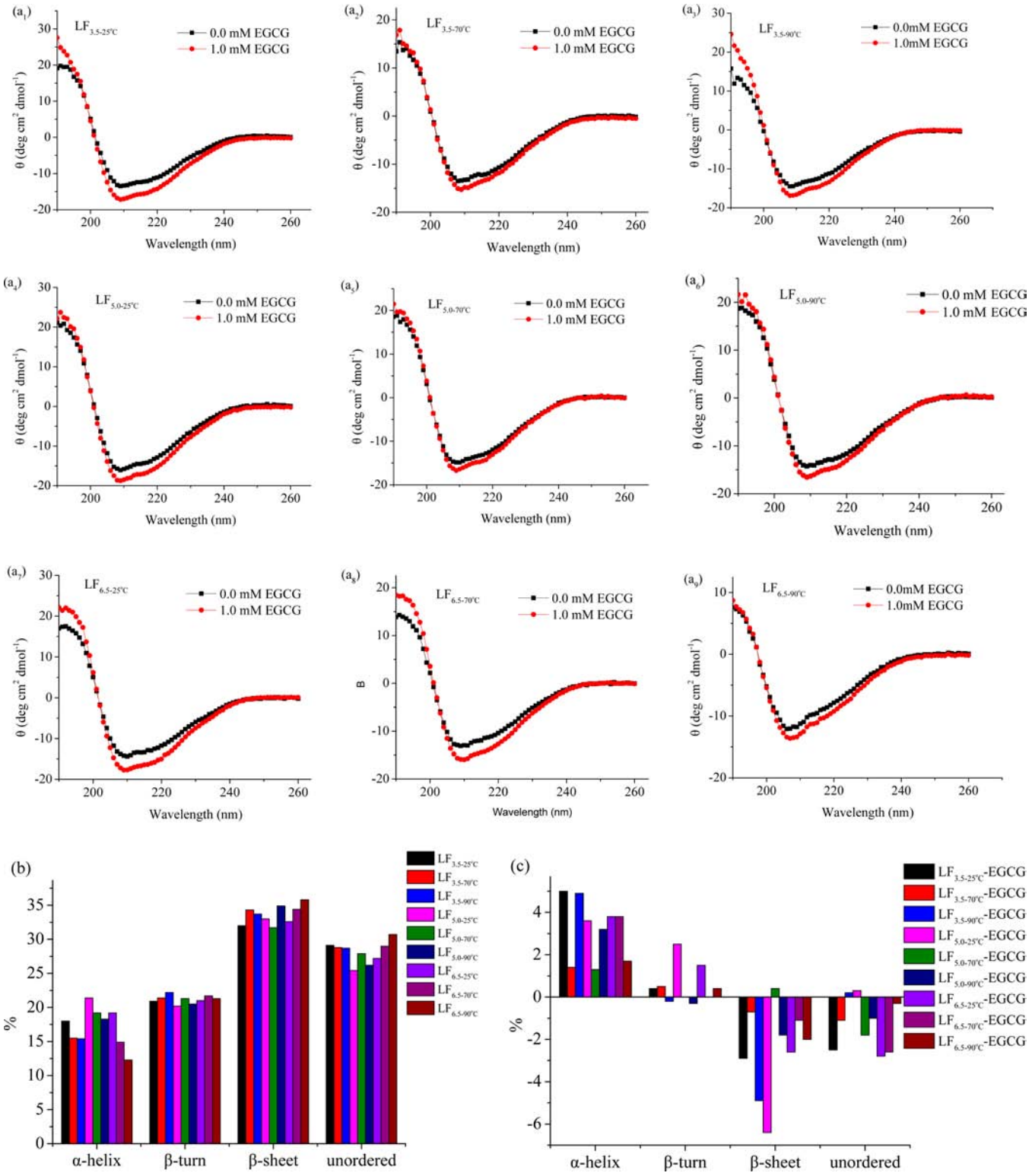


**Figure 5.** (a, $a_1$−$a_9$) Far-UV CD spectra of native and thermally modified LF in the absence and presence of 1.0 mM EGCG at pH 3.5, 5.0, and 6.5. (b) Secondary structure of native and thermally modified LF at pH 3.5, 5.0, and 6.5. (c) Changes in secondary structure of native and thermally modified LF−EGCG complexes (containing 1.0 mM EGCG) at pH 3.5, 5.0, and 6.5.

pH 3.5 and 5.0, and five peaks at pH 6.5 (Figure 4). The shape and intensity of those peaks were varied due to the pH of solutions. The two bands around 1392 and 1446 $cm^{-1}$ associated with the C−O stretching bond of carboxyl groups and the C−H deformation (asymmetrical) vibration in R−$CH_3$,[67,68] respectively; the occurrence of the band at 1238 or 1242 $cm^{-1}$ was assigned to N−H in plane bending of the amide III band;[61] the band observed at 1062 $cm^{-1}$ was attributed to the asymmetrical C−O vibration.[67,69] The characteristic bands of LF in the region of 1500−1000 $cm^{-1}$ were shifted to higher wavelength or lower wavelength, revealing the presence of


dx.doi.org/10.1021/jf5038147 | J. Agric. Food Chem. 2014, 62, 10816−10827

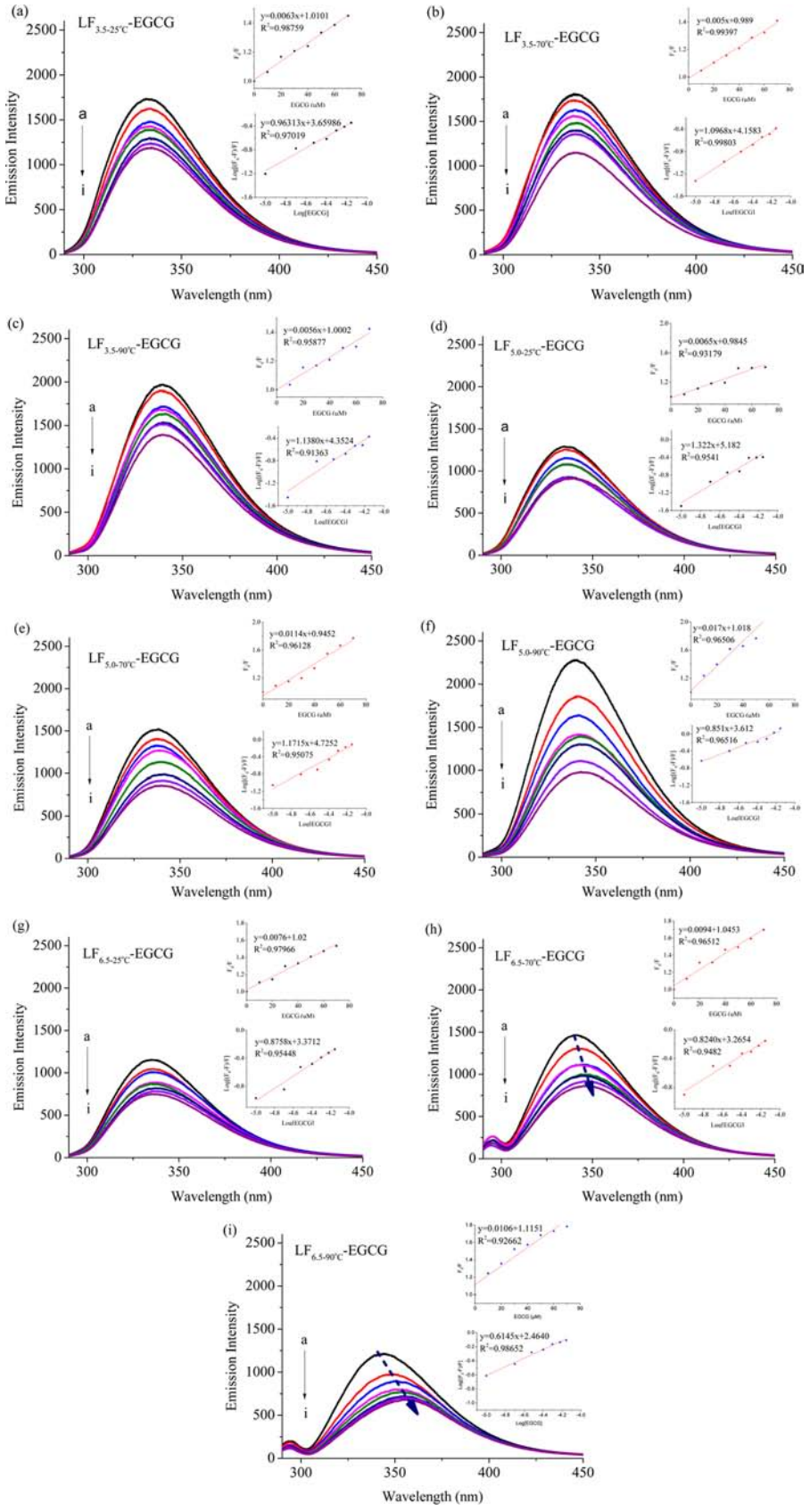


**Figure 6.** Fluorescence emission spectra of LF−EGCG complexes at different EGCG to LF molar ratios at pH 3.5, 5.0, and 6.5. Insets: Plot of $F_0/F$ versus [EGCG] as per eq 1 (top); $\log[(F_0 - F)/F]$ vs log [EGCG] as per eq 2 (bottom).

specific interactions between LF and EGCG at specific pH values.

It should be noted that the occurrence of a new band at 933 $cm^{-1}$ in thermally modified LF and LF−EGCG complexes at


dx.doi.org/10.1021/jf5038147 | J. Agric. Food Chem. 2014, 62, 10816−10827

pH 6.5 (except $LF_{6.5\text{-}25°C}$) might be associated with the denaturation of LF from thermal treatment or from the interaction with EGCG.[70]

**Analysis of the Secondary Structures of LF and LF−EGCG Complex Using Circular Dichroism (CD).** Far-UV CD was used to obtain information about the changes occurring at the secondary folding level of protein. In this section, the influence of pH on the secondary structure of LF formed by thermal treatment and EGCG-induced conformational transitions of LF (the concentration of EGCG was 1.0 mM) are monitored by far-UV CD spectroscopy (Figure 5).

As shown in Figure 5a, $a_1$−$a_9$, in the 190−260 nm region, the spectra of $LF_{3.5\text{-}25°C}$ were composed of a broad negative band centered at 208−210 nm and a shoulder at 218−220 nm. In the presence of 1.0 mM EGCG, the peak showed a significant decrease in negative ellipticities for all wavelengths of the far-UV CD spectrum, which was a characteristic of $LF_{3.5\text{-}25°C}$ secondary structure conformation change. Similar spectra were obtained for other native and thermally modified LF. The secondary structure content was estimated using the DICHROWEB procedure, which was an online server for protein secondary structure analyses from circular dichroism spectroscopic data.[41] The fractions of $\alpha$-helix, $\beta$-sheet, turn, and unordered coil were estimated by SELCON3 and are shown in Figure 5b.

It should be noted that Sreedhara et al. recently studied the pH-induced change in the structure of bovine lactoferrin, which was similar to our results in this work, finding a structure change for native LF with a relatively low content of $\alpha$-helix structure (18%, 21.4%, and 19.2% for $LF_{3.5\text{-}25°C}$, $LF_{5.0\text{-}25°C}$, and $LF_{6.5\text{-}25°C}$, respectively), but still rich in $\beta$-structure (32%, 33%, and 32.6% for $LF_{3.5\text{-}25°C}$, $LF_{5.0\text{-}25°C}$, and $LF_{6.5\text{-}25°C}$, respectively) (Figure 5b).[45] On the other hand, some researchers reported that LF released iron at pH 3.0−4.0, resulting in a less compact structure.[3,36] Therefore, the structure of LF at pH 3.5 might be less compact than those at pH 5.0 and 6.5. The results in our study were consistent with the reports for LF at pH 3.5 with a relatively higher content (29.1%) of unordered structure than those at pH 5.0 (25.4%) and 6.5 (27.2%).

The protein conformational analysis based on CD data indicated that the thermal process led to changes in the secondary structure of LF. In the presence of 1.0 mM EGCG, the $\alpha$-helical content was increased with a concomitant reduction of $\beta$-sheet and unordered coil contents; whereas the content of $\beta$-turn did not exhibit obvious change (Figure 5c). Therefore, it could be concluded that EGCG induced a progressive increase in the proportion of $\alpha$-helix structure at the cost of $\beta$-sheet and unordered coil structure of LF (both native and thermally modified LF) at pH 3.5, 5.0, and 6.5. In other words, it indicated that EGCG contributed largely to the stability of LF helical conformation and LF became a slightly looser conformation due to the increase of unordered coil fraction.

**Comparison of Binding Constant and Site of EGCG with Native LF and Thermally Modified LF.** In general, heating induces conformational (secondary/tertiary structure) changes of proteins, and exposes previously buried hydrophobic sites, which may influence LF affinity with EGCG. Aromatic residues (Phe, Trp, and Tyr) contribute to hydrophobic interactions that stabilize the core of protein interiors because they have relatively large apolar surface areas.[71] The tryptophan (Trp) residues are often found fully or partially buried in the hydrophobic core of protein interiors, at the interface between two protein domains or subdomains, or at the subunit interface in oligomeric protein systems.[72] There exist 13 Trp residues in the LF structure.[33] By monitoring the emission peak change, some information might be obtained concerning the structural changes and the microenvironment surrounding the fluorophore in the proteins.[73] As shown in Figure 6, the thermal treatment at 70 or 90 °C induced an increase in the fluorescence intensity. The fluorescence intensities of LF solutions exhibited the increases of 6.1% and 16.3% at pH 3.5, 18.7% and 77.4% at pH 5.0, and 26% and 2.4% at pH 6.5 when heated at 70 and 90 °C for 20 min, respectively. This might be attributed to the irreversibly changed conformation of LF as the two lobes successively unfolded and the side chains of LF became more exposed to buffer solutions, leading to the Trp residues gradually exposed to water and the decrease of intramolecular quenching.[33]

The emission of tryptophan may be blue-shifted if the group is buried within a native protein, and its emission may be red-shifted when the protein is unfolded.[74] The fluorescence spectra of LF after the addition of EGCG are shown in Figure 6. It was obvious that the fluorescence intensity of LF was regularly decreased with the rise of EGCG concentration, and this implied that there existed binding behavior between LF and EGCG at pH 3.5, 5.0, and 6.5. There were no obvious shifts of the maximum $\lambda_{em}$ (338 nm) of LF fluorescence at pH 3.5 and 5.0, while the maximum $\lambda_{em}$ of $LF_{6.5\text{-}70°C}$ and $LF_{6.5\text{-}90°C}$ was obviously red-shifted (from 341 to 346 nm for $LF_{6.5\text{-}70°C}$ and from 344 to 355 nm for $LF_{6.5\text{-}90°C}$) in the presence of EGCG (Figure 6h,i). These results revealed that there was a larger change in the immediate environment of the tryptophan residues of thermally modified LF at pH 6.5 than pH 3.5 and 5.0, and then EGCG was situated in close proximity to the tryptophan residues for quenching to occur.

Table 4 summarizes the results correspondingly estimated according to eqs 1 and 2. Figure 6 shows the Stern−Volmer plots for LF fluorescence quenching by EGCG. In the linear range of the Stern−Volmer regression curve, the average quenching constants ($K_{sv}$) of LF were estimated as 6.3, 5.8, and 5.6 × $10^4$ $M^{-1}$ for $LF_{3.5\text{-}25°C}$, $LF_{3.5\text{-}70°C}$, and $LF_{3.5\text{-}90°C}$, respectively; 6.5, 11.4, and 17.6 × $10^4$ $M^{-1}$ for $LF_{5.0\text{-}25°C}$, $LF_{5.0\text{-}25°C}$, and $LF_{5.0\text{-}25°C}$, respectively; 7.6, 9.4, and 10.6 × $10^4$ $M^{-1}$ for $LF_{6.5\text{-}25°C}$, $LF_{6.5\text{-}70°C}$, and $LF_{6.5\text{-}90°C}$, respectively. It is well-known that Trp $\tau_0$ depends on pH and buffer composition. In buffer solutions at pH < 7.0, Trp $\tau_0$ is in the range of 2.33 ± 0.15 ns (at pH 2.55) to 3.16 ± 0.10 ns (at pH 6.8).[75] The lowest $K_{sv}$ value estimated in our study was 5.6 × $10^4$ $M^{-1}$ (for

**Table 4. Stern−Volmer Quenching Constant ($K_{sv}$), the Binding Constant ($K_a$), and the Number of Binding Sites ($n$) for the Interaction of EGCG with Native and Thermally Modified LF at pH 3.5, 5.0, and 6.5**

| pH | | $K_{sv}$ [$10^4$ $M^{-1}$] | $R^2$ | $K_a$ [$10^4$ $M^{-1}$] | $n$ | $R^2$ |
|---|---|---|---|---|---|---|
| 3.5 | $LF_{25°C}$ | 6.30 | 0.988 | 0.46 | 0.96 | 0.970 |
| | $LF_{70°C}$ | 5.77 | 0.994 | 1.44 | 1.09 | 0.998 |
| | $LF_{90°C}$ | 5.60 | 0.959 | 2.55 | 1.14 | 0.914 |
| 5.0 | $LF_{25°C}$ | 6.50 | 0.932 | 15.23 | 1.32 | 0.954 |
| | $LF_{70°C}$ | 11.40 | 0.961 | 5.31 | 1.17 | 0.951 |
| | $LF_{90°C}$ | 17.60 | 0.965 | 0.41 | 0.85 | 0.965 |
| 6.5 | $LF_{25°C}$ | 7.61 | 0.980 | 0.24 | 0.86 | 0.954 |
| | $LF_{70°C}$ | 9.43 | 0.965 | 0.18 | 0.82 | 0.948 |
| | $LF_{90°C}$ | 10.60 | 0.927 | 0.03 | 0.61 | 0.987 |

$LF_{3.5\text{-}25°C}$), yielding $k_q$ above $2.4 \times 10^{13}$ $M^{-1}$ $s^{-1}$, at least 3 orders of magnitude higher than $2.0 \times 10^{10}$ $M^{-1}$ $s^{-1}$, the maximum collisional (dynamic) quenching constant for various quenchers interacting with biopolymers.[76,77] These results thus implied that the quenching process was static quenching involving the formation of LF−EGCG complexes.

For the static mechanism of quenching, the double logarithmic Stern−Volmer equation (eq 2) could be used to analyze the quenching data and calculation of the apparent binding constants ($K_a$) of the LF−EGCG complexes formed.

As illustrated in Table 4, the binding constants ($K_a$) and the number of binding sites per LF molecule ($n$) for EGCG with LF were increased with the rise of denaturation temperature at pH 3.5, while they were decreased at pH 5.0 and 6.5. Most of the $K_a$ values were in the range of $10^3$−$10^5$ $M^{-1}$, except $LF_{6.5\text{-}90°C}$, which displayed great thermal aggregation behavior at pH 6.5. The association constants obtained were in agreement with previously published data for other proteins (such as bovine serum albumin, whey protein isolate, sodium caseinate) and EGCG by applying the same methodology ($10^4$−$10^5$ $M^{-1}$).[12,13,31] The $K_a$ values were estimated as $LF_{5.0\text{-}25°C}$ > $LF_{5.0\text{-}70°C}$ > $LF_{3.5\text{-}90°C}$ > $LF_{3.5\text{-}70°C}$ > $LF_{3.5\text{-}25°C}$ > $LF_{5.0\text{-}90°C}$ > $LF_{6.5\text{-}25°C}$ > $LF_{6.5\text{-}70°C}$ > $LF_{6.5\text{-}90°C}$. Based on the aforementioned result, we concluded that if we do not take $LF_{5.0\text{-}90°C}$ into account, the affinity of EGCG toward LF was pH dependent and had the following order: pH 5.0 > pH 3.5 > pH 6.5. Lower pH led to stronger binding because the dissociation of protein had more binding sites at lower pH.[78] Therefore, we hypothesized that when pH changes away from the p$I$ of LF, the electrostatic repulsion between LF molecules increases, which inhibits the self-association of the protein and facilitates the binding of EGCG to LF. The interactions between chlorogenic acid and several proteins such as BSA, lysozyme, and $\alpha$-lactalbumin at pH ≤ 7 resulted from noncovalent bonds and the amount of chlorogenic acid bound by BSA (per molecule) was somewhat higher at lower pH.[79] Some researchers reported that the EGCG-binding capacity of thermally modified $\beta$-lactoglobulin could be enhanced compared to the native protein at pH 7.0,[31] while, with the rise of thermal denaturation temperature, the binding constant decreased at pH 5.0 and 6.5, which implied that EGCG had strong affinity for native LF but weak affinity for thermally modified LF. It seemed that the probably more unfolded structure of $LF_{5.0\text{-}70°C}$ and $LF_{5.0\text{-}90°C}$ decreased the exposure of noncovalent sites normally located on the surface of both lobes of the protein, reducing the binding constant when LF−EGCG complexes formed. Moreover, the thermal aggregation of LF at pH 6.5 probably exposed nonpolar groups normally buried in the LF nonpolar interior, which increased the self-association of the protein through hydrophobic attraction and decreased the binding of EGCG to LF. In contrast, EGCG had weak affinity for native LF but strong affinity for thermally modified LF at pH 3.5. This might be ascribed to the difference of pH in the solution and the secondary structure of the protein at pH 3.5.

In this study, the native and thermally modified LF had potential to form coassembled vehicles for the delivery of EGCG. The changes of pH in the solution and the structure of protein were the crucial factors influencing the noncovalent interaction between LF and EGCG. LF−EGCG nanoparticles have good transparency at pH 3.5 and 5.0, which could be applied in clear beverages and liquid foods. At the same time, LF−EGCG submicrometer particles remained relatively stable to particle aggregation and were formed at pH 6.5, which could be applied in cloudy beverages and liquid foods. Overall, LF−EGCG nano- and submicrometer particles as protective vehicles for EGCG could be obtained by choosing the appropriate reaction parameters, which was beneficial for the development of controlled release of other bioactive materials.

## AUTHOR INFORMATION


### Corresponding Author

*Tel: +86-10-62737034. Fax: +86-10-62737986. E-mail: gyxcau@126.com.



### Funding

The research work was funded by the National Natural Science Foundation of China under Grant No. 31371835.


### Notes

The authors declare no competing financial interest.

## REFERENCES


(1) Wakabayashi, H.; Yamauchi, K.; Takase, M. Lactoferrin research, technology and applications. *Int. Dairy J.* **2006**, *16*, 1241−1251.

(2) Levay, P. F.; Viljoen, M. Lactoferrin: a general review. *Acta Haematol.* **1995**, *80*, 252−267.

(3) Steijns, J. M.; Van Hooijdonk, A. C. M. Occurrence, structure, biochemical properties and technological characteristics of lactoferrin. *Br. J. Nutr.* **2000**, *84*, 11−17.

(4) Satué-Gracia, M. T.; Frankel, E. N.; Rangavajhyala, N.; German, J. B. Lactoferrin in infant formulas: effect on oxidation. *J. Agric. Food Chem.* **2000**, *48*, 4984−4990.

(5) Soejima, T.; Yamauchi, K.; Yamamoto, T.; Ohara, Y.; Nagao, E.; Kanbara, K.; Fujisawa, M.; Okuda, Y.; Namba, S. Determination of bovine lactoferrin in lactoferrin-supplemented dairy products and raw milk by an automated latex assay. *J. Dairy Res.* **2007**, *74*, 100−105.

(6) Sui, Q.; Roginski, H.; Williams, R. P. W.; Versteeg, C.; Wan, J. Effect of pulsed electric field and thermal treatment on the physicochemical properties of lactoferrin with different iron saturation levels. *Int. Dairy J.* **2010**, *20*, 707−714.

(7) Kao, Y. H.; Chang, H. H.; Lee, M. J.; Chen, C. L. Tea, obesity, and diabetes. *Mol. Nutr. Food Res.* **2006**, *50*, 188−210.

(8) Levites, Y.; Weinreb, O.; Maor, G.; Youdim, M. B. H.; Mandel, S. Green tea polyphenol (−)-epigallocatechin-3-gallate prevents N-methyl-4-phenyl-1,2,3,6-tetrahydropyridine-induced dopaminergic neurodegeneration. *J. Neurochem.* **2001**, *78*, 1073−1082.

(9) Chyu, K. Y.; Babbidge, S. M.; Zhao, X. N.; Dandillaya, R.; Rietveld, A. G.; Yano, J.; Dimayuga, P.; Cercek, B.; Shah, P. K. Differential effects of green tea-derived catechin on developing versus established atherosclerosis in apolipoprotein E-null mice. *Circulation* **2004**, *109*, 2448−2453.

(10) Cabrera, C.; Artacho, R.; Gimenez, R. Beneficial effects of green tea-a review. *J. Am. Coll. Nutr.* **2006**, *25*, 79−99.

(11) Nagle, D. G.; Ferreira, D.; Zhou, Y. D. Epigallocatechin-3-gallate (EGCG): chemical and biomedical perspectives. *Phytochemistry* **2006**, *67*, 1849−1855.

(12) Kanakis, C. D.; Hasni, I.; Bourassa, P.; Tarantilis, P. A.; Polissioiu, M. G.; Tajmir-Riahi, H.- A. Milk $\beta$-lactoglobulin complexes with tea polyphenols. *Food Chem.* **2011**, *127*, 1046−1055.

(13) Hasni, I.; Bourassa, P.; Hamdani, S.; Samson, G.; Carpentier, R.; Tajmir-Riahi, H.-A. Interaction of milk $\alpha$-and $\beta$-caseins with tea polyphenols. *Food Chem.* **2011**, *126*, 630−639.

(14) Ishii, T.; Ichikawa, T.; Minoda, K.; Kusaka, K.; Ito, S.; Suzuki, Y.; Nakayama, T. Human serum albumin as an antioxidant in the oxidation of (−)-epigallocatechin gallate: participation of reversible covalent binding for interaction and stabilization. *Biosci., Biotechnol., Biochem.* **2011**, *75*, 100−106.

(15) Wang, X.; Ho, C.-T.; Huang, Q. Investigation of Adsorption Behavior of (−)-Epigallocatechin Gallate on Bovine Serum Albumin Surface Using Quartz Crystal Microbalance with Dissipation Monitoring. *J. Agric. Food Chem.* **2007**, *55*, 4987−4992.

(16) Bohin, M. C.; Vincken, J. P.; van der Hijden, H. T.; Gruppen, H. Efficacy of food proteins as carriers for flavonoids. *J. Agric. Food Chem.* **2012**, *60*, 4136−4143.
(17) Rodríguez-Franco, D. A.; Vázquez-Moreno, L.; Ramos-Clamont, M. G. Actividad antimicrobiana de la lactoferrina: Mecanismos y aplicaciones clínicas potenciales. *Rev. Latinoam. Microbiol.* **2005**, *47*, 101−11.
(18) Takakura, N.; Wakabayashi, H.; Ishibashi, H.; Teraguchi, S.; Tamura, Y.; Yamaguchi, H.; Abe, S. Oral lactoferrin treatment of experimental oral candidiasis in mice. *Antimicrob. Agents Chemother.* **2003**, *47*, 2619−2623.
(19) Ward, P. P.; Uribe-Luna, S.; Conneely, O. M. Lactoferrin and host defense. *Biochem. Cell Biol.* **2002**, *80*, 95−102.
(20) Yamauchi, K.; Tomita, M.; Giehl, T. J.; Ellison, R. 3. Antibacterial activity of lactoferrin and a pepsin-derived lactoferrin peptide fragment. *Infect. Immun.* **1993**, *61*, 719−728.
(21) Medina, I.; Tombo, I.; Satué-Gracia, M. T.; German, J. B.; Frankel, E. N. Effects of natural phenolic compounds on the antioxidant activity of lactoferrin in liposomes and oil-in-water emulsions. *J. Agric. Food Chem.* **2002**, *50*, 2392−2399.
(22) Mohan, K. V. P.; Gunasekaran, P.; Varalakshmi, E.; Hara, Y.; Nagini, S. In vitro evaluation of the anticancer effect of lactoferrin and tea polyphenol combination on oral carcinoma cells. *Cell. Biol. Int.* **2007**, *31*, 599−608.
(23) Chandra Mohan, K. V. P.; Letchoumy, P. V.; Hara, Y.; Nagini, S. Combination chemoprevention of hamster buccal pouch carcinogenesis by bovine milk lactoferrin and black tea polyphenols. *Cancer. Invest.* **2008**, *26*, 193−201.
(24) Letchoumy, P. V.; Mohan, K. C.; Stegeman, J. J.; Gelboin, H. V.; Hara, Y. In vitro antioxidative potential of lactoferrin and black tea polyphenols and protective effects in vivo on carcinogen activation, DNA damage, proliferation, invasion and angiogenesis during experimental oral carcinogenesis. *Oncol. Res.* **2008**, *17*, 193.
(25) Bromley, E. H. C.; Krebs, M. R. H.; Donald, A. M. Mechanisms of structure formation in particulate gels of $\beta$-lactoglobulin formed near the isoelectric point. *Eur. Phys. J. E: Soft Matter Biol. Phys.* **2006**, *21*, 145−152.
(26) Donato, L.; Schmitt, C.; Bovetto, L.; Rouvet, M. Mechanism of formation of stable heat-induced $\beta$-lactoglobulin microgels. *Int. Dairy J.* **2009**, *19*, 295−306.
(27) Hoffmann, M. A. M.; Roefs, S. P. F. M.; Verheul, M.; Mil, P. J. J. M. v.; Kruif, K. G. d. Aggregation of $\beta$-lactoglobulin studied by in situ light scattering. *J. Dairy Res.* **1996**, *63*, 423−440.
(28) Jones, O. G.; Decker, E. A.; McClements, D. J. Comparison of protein−polysaccharide nanoparticle fabrication methods: Impact of biopolymer complexation before or after particle formation. *J. Colloid Interface Sci.* **2010**, *344*, 21−29.
(29) Santipanichwong, R.; Suphantharika, M.; Weiss, J.; McClements, D. J. Core-Shell Biopolymer Nanoparticles Produced by Electrostatic Deposition of Beet Pectin onto Heat-Denatured $\beta$-Lactoglobulin Aggregates. *J. Food Sci.* **2008**, *73*, N23−N30.
(30) Bengoechea, C.; Peinado, I.; McClements, D. J. Formation of protein nanoparticles by controlled heat treatment of lactoferrin: Factors affecting particle characteristics. *Food Hydrocolloids* **2011**, *25*, 1354−1360.
(31) Shpigelman, A.; Israeli, G.; Livney, Y. D. Thermally-induced protein−polyphenol co-assemblies: beta lactoglobulin-based nanocomplexes as protective nanovehicles for EGCG. *Food Hydrocolloids* **2010**, *24*, 735−743.
(32) Chanasattru, W.; Jones, O. G.; Decker, E. A.; McClements, D. J. Impact of cosolvents on formation and properties of biopolymer nanoparticles formed by heat treatment of $\beta$-lactoglobulin-Pectin complexes. *Food Hydrocolloids* **2009**, *23*, 2450−2457.
(33) Stănciuc, N.; Aprodu, I.; Râpeanu, G.; van der Plancken, I.; Bahrim, G.; Hendrickx, M. Analysis of the thermally induced structural changes of bovine lactoferrin. *J. Agric. Food Chem.* **2013**, *61*, 2234−2243.
(34) Kussendrager, K. D. Effects of heat treatment on structure and iron-binding capacity of bovine lactoferrin. *IDF Bull.* **1994**, No. Indigenous antimicrobial agents of milk: recent developments, 133−146.
(35) Paulsson, M. A.; Svensson, U.; Kishore, A. R.; Satyanarayan Naidu, A. Thermal behavior of bovine lactoferrin in water and its relation to bacterial interaction and antibacterial activity. *J. Dairy Sci.* **1993**, *76*, 3711−3720.
(36) Baker, E. N.; Baker, H. M. Molecular structure, binding properties and dynamics of lactoferrin. *Cell. Mol. Life Sci.* **2005**, *62*, 2531−2539.
(37) Baker, E. N.; Baker, H. M. A structural framework for understanding the multifunctional character of lactoferrin. *Biochimie* **2009**, *91*, 3−10.
(38) Bokkhim, H.; Bansal, N.; Grøndahl, L.; Bhandari, B. Physico-chemical properties of different forms of bovine lactoferrin. *Food Chem.* **2013**, *141*, 3007−3013.
(39) de Freitas, V.; Carvalho, E.; Mateus, N. Study of carbohydrate influence on protein-tannin aggregation by nephelometry. *Food Chem.* **2003**, *81*, 503−509.
(40) Lobley, A.; Whitmore, L.; Wallace, B. A. DICHROWEB: an interactive website for the analysis of protein secondary structure from circular dichroism spectra. *Bioinformatics* **2002**, *18*, 211−212.
(41) Whitmore, L.; Wallace, B. A. DICHROWEB, an online server for protein secondary structure analyses from circular dichroism spectroscopic data. *Nucleic Acids Res.* **2004**, *32* (Suppl. 2), W668−W673.
(42) Zhang, Y.; Zhong, Q. Probing the binding between norbixin and dairy proteins by spectroscopy methods. *Food Chem.* **2013**, *139*, 611−616.
(43) Persson, B. A.; Lund, M.; Forsman, J.; Chatterton, D. E. W.; Åkesson, T. Molecular evidence of stereo-specific lactoferrin dimers in solution. *Biophys. Chem.* **2010**, *151*, 187−189.
(44) Abe, H.; Saito, H.; Miyakawa, H.; Tamura, Y.; Shimamura, S.; Nagao, E.; Tomita, M. Heat stability of bovine lactoferrin at acidic pH. *J. Dairy Sci.* **1991**, *74*, 65−71.
(45) Sreedhara, A.; Flengsrud, R.; Prakash, V.; Krowarsch, D.; Langsrud, T.; Kaul, P.; Devold, T. G.; Vegarud, G. E. A comparison of effects of pH on the thermal stability and conformation of caprine and bovine lactoferrin. *Int. Dairy J.* **2010**, *20*, 487−494.
(46) Brisson, G.; Britten, M.; Pouliot, Y. Heat-induced aggregation of bovine lactoferrin at neutral pH: Effect of iron saturation. *Int. Dairy J.* **2007**, *17*, 617−624.
(47) Von Staszewski, M.; Jara, F. L.; Ruiz, A. L. T. G.; Jagus, R. J.; Carvalho, J. E.; Pilosof, A. M. R. Nanocomplex formation between $\beta$-lactoglobulin or caseinomacropeptide and green tea polyphenols: Impact on protein gelation and polyphenols antiproliferative activity. *J. Funct. Foods* **2012**, *4*, 800−809.
(48) Wang, S. H.; Liu, F. F.; Dong, X. Y.; Sun, Y. Thermodynamic analysis of the molecular interactions between amyloid $\beta$-peptide 42 and (−)-epigallocatechin-3-gallate. *J. Phys. Chem. B* **2010**, *114*, 11576−11583.
(49) Charlton, A. J.; Baxter, N. J.; Khan, M. L.; Moir, A. J.; Haslam, E.; Davies, A. P.; Williamson, M. P. Polyphenol/peptide binding and precipitation. *J. Agric. Food Chem.* **2002**, *50*, 1593−601.
(50) Naczk, M.; Oickle, D.; Pink, D.; Shahidi, F. Protein precipitating capacity of crude canola tannins: effect of pH, tannin, and protein concentrations. *J. Agric. Food Chem.* **1996**, *44*, 2144−2148.
(51) Xia, S. Q.; Li, Y.; Xia, Q. Y.; Zhang, X. M.; Huang, Q. R. Glycosylation of bovine serum albumin via maillard reaction prevents epigallocatechin-3-gallate-induced protein aggregation. *Food Hydrocolloids* **2014**, DOI: 10.1016/j.foodhyd.2014.05.022.
(52) Tokle, T.; Lesmes, U.; McClements, D. J. Impact of electrostatic deposition of anionic polysaccharides on the stability of oil droplets coated by lactoferrin. *J. Agric. Food Chem.* **2010**, *58*, 9825−9832.
(53) Von Staszewski, M.; Jagus, R. J.; Pilosof, A. M. R. Influence of green tea polyphenols on the colloidal stability and gelation of WPC. *Food Hydrocolloids* **2011**, *25*, 1077−1084.
(54) Robb, C. S.; Geldart, S. E.; Seelenbinder, J. A.; Brown, P. R. Analysis of green tea constituents by HPLC-FTIR. *J. Liq. Chromatogr. Relat. Technol.* **2002**, *25* (5), 787−801.

(55) Chen, Y. C.; Yu, S. H.; Tsai, G. J.; Tang, D. W.; Mi, F. L.; Peng, Y. P. Novel technology for the preparation of self-assembled catechin/gelatin nanoparticles and their characterization. *J. Agric. Food Chem.* **2010**, *58*, 6728−6734.
(56) Zhu, B.; Li, J.; He, Y.; et al. Hydrogen-Bonding Interaction and Crystalline Morphology in the Binary Blends of Poly (ε-caprolactone) and Polyphenol Catechin. *Macromol. Biosci.* **2003**, *3*, 684−693.
(57) Peña, C.; Larranaga, M.; Gabilondo, N.; Tejado, A.; Echeverria, J. M.; Mondragon, I. Synthesis and characterization of phenolic novolacs modified by chestnut and mimosa tannin extracts. *J. Appl. Polym. Sci.* **2006**, *100*, 4412−4419.
(58) Frazier, R. A.; Deaville, E. R.; Green, R. J.; Stringano, E.; Willoughby, I.; Plant, J.; Mueller-Harvey, I. Interactions of tea tannins and condensed tannins with proteins. *J. Pharmaceut. Biomed.* **2010**, *51*, 490−495.
(59) Ye, J.; Fan, F.; Xu, X.; Liang, Y. Interactions of black and green tea polyphenols with whole milk. *Food Res. Int.* **2013**, *53*, 449−455.
(60) Renugopalakrishnan, V.; Chandrakasan, G.; Moore, S.; Hutson, T. B.; Berney, C. V.; Bhatnagar, R. S. Bound water in collagen: evidence from Fourier transform infrared and Fourier transform infrared photoacoustic spectroscopic study. *Macromolecules* **1989**, *22*, 4121−4124.
(61) Sessa, D. J.; Mohamed, A.; Byars, J. A. Chemistry and physical properties of melt-processed and solution-cross-linked corn zein. *J. Agric. Food Chem.* **2008**, *56*, 7067−7075.
(62) Beauchemin, R.; N'Soukpoe-Kossi, C. N.; Thomas, T. J.; Thomas, T.; Carpentier, R.; Tajmir-Riahi, H. A. Polyamine analogues bind human serum albumin. *Biomacromolecules* **2007**, *8*, 3177−3183.
(63) Bandekar, J. Amide modes and protein conformation. *Biochim. Biophys. Acta* **1992**, *1120*, 123−143.
(64) Krimm, S.; Bandekar, J. Vibrational spectroscopy and conformation of peptides, polypeptides, and proteins. *Adv. Protein Chem.* **1986**, *38*, 181−364.
(65) Eissa, A. S.; Puhl, C.; Kadla, J. F.; Khan, S. A. Enzymatic cross-linking of β-lactoglobulin: conformational properties using FTIR spectroscopy. *Biomacromolecules* **2006**, *7*, 1707−1713.
(66) Kong, J.; Yu, S. Fourier transform infrared spectroscopic analysis of protein secondary structures. *Acta Biochim. Biophys. Sin.* **2007**, *39*, 549−559.
(67) Constantinescu, C.; Palla-Papavlu, A.; Rotaru, A.; Florian, P.; Chelu, F.; Icriverzi, M.; Nedelcea, A.; Dinca, V.; Roseanu, A.; Dinescu, M. Multifunctional thin films of lactoferrin for biochemical use deposited by MAPLE technique. *Appl. Surf. Sci.* **2009**, *255*, 5491−5495.
(68) Sadeghi, S.; Madadlou, A.; Yarmand, M. Microemulsification−cold gelation of whey proteins for nanoencapsulation of date palm pit extract. *Food Hydrocolloids* **2014**, *35*, 590−596.
(69) Bagheri, L.; Madadlou, A.; Yarmand, M.; Mousavi, M. E. Nanoencapsulation of date palm pit extract in whey protein particles generated via desolvation method. *Food Res. Int.* **2013**, *51*, 866−871.
(70) Yang, W.; Liu, F.; Xu, C.; Fang, Y.; Gao, Y. Molecular interaction between (−)-epigallocatechin-3-gallate and bovine lactoferrin using multi-spectroscopic method and isothermal titration calorimetry. *Food Res. Int.* **2014**, *64*, 141−149.
(71) Kuznetsova, I. M.; Turoverov, K. K.; Uversky, V. N. Use of the phase diagram method to analyze the protein unfolding-refolding reactions: fishing out the "invisible" intermediates. *J. Proteome Res.* **2004**, *3*, 485−494.
(72) Royer, C. A. Probing protein folding and conformational transitions with fluorescence. *Chem. Rev.* **2006**, *106*, 1769−1784.
(73) Xiao, J.; Shi, J.; Cao, H.; Wu, S.; Ren, F.; Xu, M. Analysis of binding interaction between puerarin and bovine serum albumin by multi-spectroscopic method. *J. Pharm. Biomed. Anal.* **2007**, *45*, 609−615.
(74) Lakowicz, J. R.; Masters, B. R. Principles of fluorescence spectroscopy. *J. Biomed. Opt.* **2008**, *13*, 9901.
(75) Gudgin, E.; Lopez-Delgado, R.; Ware, W. R. The tryptophan fluorescence lifetime puzzle: A study of decay times in aqueous solution as a function of pH and buffer composition. *Can. J. Chem.* **1981**, *59*, 1037−1044.
(76) Lange, D. C.; Kothari, R.; Patel, R. C.; Patel, S. C. Retinol and retinoic acid bind to a surface cleft in bovine β-lactoglobulin: a method of binding site determination using fluorescence resonance energy transfer. *Biophys. Chem.* **1998**, *74*, 45−51.
(77) Gonçalves, R.; Mateus, N.; De Freitas, V. Study of the interaction of pancreatic lipase with procyanidins by optical and enzymatic methods. *J. Agric. Food Chem.* **2010**, *58*, 11901−11906.
(78) Sastry, M. C. S.; Rao, M S N. Binding of chlorogenic acid by the isolated polyphenol-free 11 S protein of sunflower (Helianthus annuus) seed. *J. Agric. Food Chem.* **1990**, *38*, 2103−2110.
(79) Prigent, S. V. E.; Gruppen, H.; Visser, A. J. W. G.; Van Koningsveld, G. A.; De Jong, G. A.; Voragen, A. G. Effects of non-covalent interactions with 5-O-caffeoylquinic acid (chlorogenic acid) on the heat denaturation and solubility of globular proteins. *J. Agric. Food Chem.* **2003**, *51*, 5088−5095.

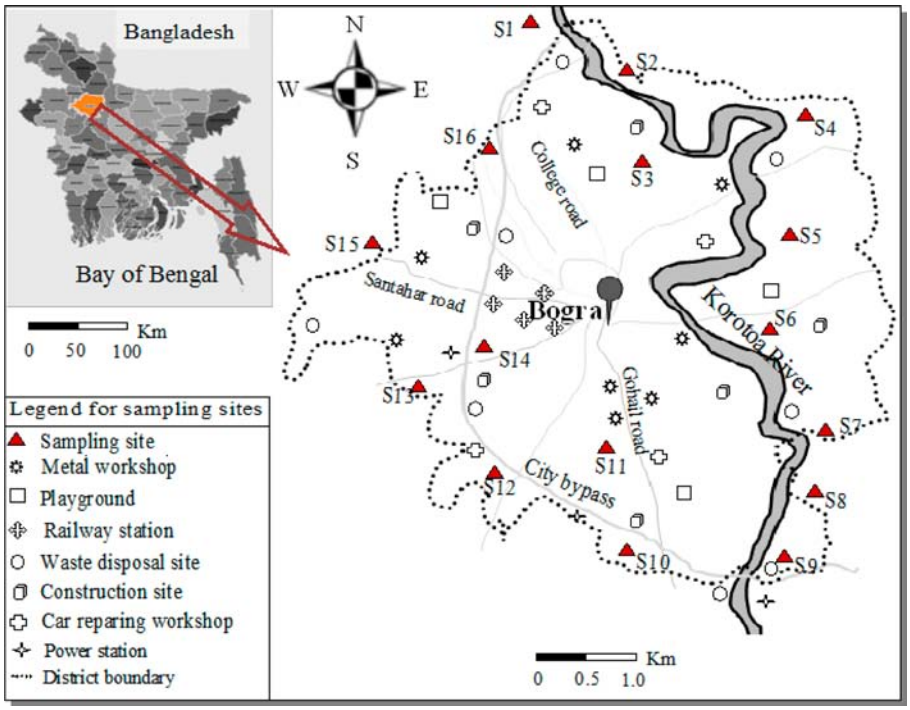


**Figure 1.** Map of the study area of agricultural fields in Bogra district situated at the northern part of Bangladesh.

the middle- and low-income group of the population in Bangladesh, to establish baseline information on the levels of heavy metals (Cr, Ni, Cu, Zn, As, Cd, and Pb) and to estimate their risk to human through dietary intake.

## MATERIALS AND METHODS

**Sample Collection and Preparation.** The per capita per day intake of major food items and intakes of individual food items were used to characterize the food consumption pattern for adults in Bangladesh.[18] The five most consumed types of grains and pulses, i.e., rice (*Oryza sativa*), wheat (*Triticum aestivum*), maize (*Zea mays*), lentil (*Lens culinaris*), and black gram (*Vigna mungo*), were collected from an urban area situated at the northern part in Bangladesh (Figure 1). Wheat, maize, and pulses were collected during February−March 2012, and rice samples were collected during August−September, 2013. In the process of sample transport and storage, we ensured that the samples did not make contact with metal instruments in order to avoid cross-contamination. From each sampling site a composite sample for each food item was prepared and homogenized using a food processor. After collection from the field, about 200 g of fresh food samples were put in the rotary type food processor. The pretreated samples were first mixed and homogenized and then oven-dried at 105 °C for 24 h to remove the moisture content. The dried samples were then stored at −20 °C in the laboratory of the Institute of Nutrition and Food Science (INFS), University of Dhaka, Bangladesh. About 48 composite soil samples were also collected from the same fields of collected food samples. At each sampling station, soil sample (up to 10 cm depth) was collected in the form of subsamples, which were thoroughly mixed to form a composite sample. Soil samples were air-dried at room temperature for 2 weeks, then ground, and homogenized. The dried soil samples were crumbled and pulverized with a porcelain mortar and pestle, sieved through a 2 mm nylon sieve, and stored in an airtight clean zipper bag in freezer conditions until chemical analysis was carried out.

**Measurement of Soil Properties.** The physicochemical parameters of soil such as pH, EC, % C, and texture were measured. The pH of sediments was measured in 1:2.5 soil to water ratio. The soil/deionized water mixture was stirred with a clean glass rod, and the slurry was allowed to equilibrate for 30 min.[19] The pH values were recorded using a Horiba U-23 instrument with the calibration of pH 4.0, pH 7.0, and pH 9.0 standards. For electrical conductivity (EC) determination, 5.0 g of sediment was taken in 50 mL polypropylene tubes. Then, 30 mL of distilled water was added to the tube. The lid was closed properly and was shaken for 5 min. After that, EC was measured using an EC meter (Horiba D-52).[20] Percent organic carbon of soil was measured using an elemental analyzer (model type: Vario EL III, Elenemtar, Germany). The catalytic combustion was carried out at a permanent temperature of up to 1200 °C. The element concentration from the detector signal and the sample weight based on stored calibration curves were measured. Particle size distribution was determined using the hydrometer method.[21] The soils were classified using the United States Department of Agriculture (USDA) classification system (gravel [>2 mm], sand [2−0.05 mm], silt [0.05−0.002 mm], and clay [<0.002 mm]).

**Chemicals and Analytical Methods.** A microwave digestion system (Berghof, Germany) was used in preparation of samples to analyze various metals. The microwave digestion system has been designed to perform chemical digestion procedures under extreme pressure and temperature conditions in chemical laboratories. Digestion reagents that were used included 5 mL of 69% $HNO_3$ acid (Kanto Chemical Co. Japan) and 2 mL of 30% $H_2O_2$ (Wako Chemical Co. Japan). The weighed samples of 0.3 g were then placed into the digestion reagent in a Teflon vessel (DAP-60K type). After digestion, samples were then transferred into a Teflon beaker and total volume was made up to 25 mL with Milli-Q water (Elix UV5 and Milli-Q, Millipore, USA). The digest solution was then filtered (DISMIC 25HP PTFE syringe filter (pore size = 0.45 mm, Toyo Roshi Kaisha, Ltd., Japan) and stored in a screw cap plastic tube (Nalgene, New York).

**Quality Control.** All test batches were evaluated using an internal quality approach and validated if they satisfied the defined internal quality controls (IQCs). For each experiment, a run included blank, certified reference materials (CRM) as internal standard in samples, and samples analyzed in triplicate to eliminate any batch-specific error. Standard stock solutions containing 10 μg/L of each element (Cd, As, Pb, Cr, Ni, Zn, Se, Cu, Mo, Mn, Sb, Ba, V, and Ag) and internal standard solutions containing 1.0 mg/L of indium (In), yttrium (Y), beryllium (Be), telium (Te), cobalt (Co), and titanium (Ti) were purchased from Spex CertiPrep USA. Multielement standard solution

was used to prepare a standard curve. Before starting the sequence, relative standard deviation (RSD < 5%) was checked by using tuning solution purchased from Agilent Company. Metals in samples were analyzed using an inductively coupled plasma mass spectrometer (ICP-MS).

**Transfer Factor of Metals.** The transfer factor (TF) of metals from soil to the edible parts of food was defined as the ratio of the metal concentration in the plant's tissues to the metal concentration in soil. The transfer factor was calculated for each food at each site separately. Transfer factor can be used to evaluate the potential capability of plants to transfer metals from soil to edible tissues. TF was calculated as follows:

$$\mathrm{TF} = \frac{C_{\mathrm{food}}}{C_{\mathrm{soil}}} \quad (1)$$

where $C_{\mathrm{food}}$ and $C_{\mathrm{soil}}$ represent the total metal concentration in the edible part of foods (mg/kg) and total metal concentration in soil (mg/kg) on a dry weight basis.[22]

**Estimated Daily Intakes.** Estimated daily intakes (EDIs) for heavy metals were calculated using the respective average concentration in food samples by the weight of food item consumed by an individual (body weight 60 kg for adult[23] in Bangladesh), which was obtained from the household income and expenditure survey,[18] and calculated by using the following formula:

$$\mathrm{EDI} = \frac{\mathrm{FIR} \times C}{\mathrm{BW}} \quad (2)$$

where FIR is the food ingestion rate (g/person/day), $C$ is the metal concentration in food samples (mg/kg), and BW is the body weight.

**Noncarcinogenic Risk.** The equation used for estimating the target hazard quotient is as follows:[17]

$$\mathrm{THQ} = \frac{\mathrm{EFr} \times \mathrm{ED} \times \mathrm{FIR} \times C}{\mathrm{RfD} \times \mathrm{BW} \times \mathrm{AT}} \times 10^{-3} \quad (3)$$

$$\mathrm{TTHQ\,(individual\,food)} = \mathrm{THQ}_{\mathrm{toxicant1}} + \mathrm{THQ}_{\mathrm{toxicant2}} + \ldots + \mathrm{THQ}_{\mathrm{toxicant}n} \quad (4)$$

In order to assess the overall potential for noncarcinogenic effects from more than one heavy metal, a hazard index (HI) has been formulated based on the Guidelines for Health Risk assessment of Chemical Mixtures of USEPA[12] as follows:

$$\mathrm{HI} = \sum \mathrm{TTHQ} = \mathrm{TTHQ}_{\mathrm{food1}} + \mathrm{TTHQ}_{\mathrm{food2}} + \ldots + \mathrm{TTHQ}_{\mathrm{food}n} \quad (5)$$

where THQ is the target hazard quotient (dimensionless), EFr is the exposure frequency (365 days/year), ED is the exposure duration (70 years), FIR is the food ingestion rate (g/person/day), $C$ is the metal concentration in foods (mg/kg), RfD is the oral reference dose (mg/kg/day), and AT is the averaging time for noncarcinogens (365 days/year × number of exposure years). The oral reference doses were based on 1.5, 0.02, 0.04, 0.3, 0.0003, 0.003, and 0.0035 mg/kg/day for Cr, Ni, Cu, Zn, As, Cd, and Pb.[24] If the THQ is less than 1, the exposed population is unlikely to experience obvious adverse effects. If the THQ is equal to or higher than 1, there is a potential health risk[25] and related interventions and protective measurements should be taken.

**Carcinogenic Risk.** The equation used for estimating the target carcinogenic risk factor (lifetime cancer risk)[12] is as follows:

$$\mathrm{TR} = \frac{\mathrm{EFr} \times \mathrm{ED} \times \mathrm{FIR} \times C \times \mathrm{CSFo}}{\mathrm{BW} \times \mathrm{AT}} \times 10^{-3} \quad (6)$$

where TR represents the target cancer risk or the risk of cancer over a lifetime, AT is the averaging time for carcinogens (365 days/year × ED), and CSFo is the oral carcinogenic slope factor from the Integrated Risk Information System USEPA[24] database, which was 1.5 and 8.5 × $10^{-3}$ (mg/kg/day)$^{-1}$ for As and Pb.

**Statistical Analysis.** Data were statistically analyzed using the statistical package SPSS 16.0 (SPSS, USA). The mean and standard deviation of heavy metals in food samples were calculated. Post hoc Tukey tests were employed to examine the statistical significance ($P$ < 0.05) among mean concentrations of heavy metals among different food groups.

## RESULTS AND DISCUSSION

**Physicochemical Properties and Metals in Soil.** The physicochemical properties of soil are presented in Table 1.

**Table 1. Physicochemical Properties of Soil at Different Sites of Bogra District Urban Area, Bangladesh**

| | | | | (% in <2 mm) | | | |
|---|---|---|---|---|---|---|---|
| land types | pH (1:5 $H_2O$) | EC ($\mu$S/cm) | organic carbon (%) | sand | silt | clay | soil type |
| S1 | 5.6 | 39 | 1.4 | 52 | 25 | 23 | sandy clayey loam |
| S2 | 7.2 | 79 | 2.8 | 51 | 31 | 18 | loam |
| S3 | 6.7 | 120 | 2.4 | 53 | 25 | 22 | sandy clayey loam |
| S4 | 8.2 | 36 | 1.1 | 57 | 24 | 19 | sandy clayey loam |
| S5 | 7.2 | 16 | 0.88 | 67 | 24 | 9 | sandy loam |
| S6 | 6.5 | 22 | 0.36 | 91 | 5.0 | 4.0 | sand |
| S7 | 6.3 | 39 | 0.51 | 92 | 6.0 | 2.0 | sand |
| S8 | 7.1 | 17 | 1.1 | 69 | 18 | 13 | sandy loam |
| S9 | 5.7 | 17 | 0.58 | 89 | 6.0 | 5.0 | sand |
| S10 | 6.4 | 34 | 0.61 | 68 | 20 | 12 | sandy loam |
| S11 | 6.3 | 41 | 1.3 | 75 | 15 | 10 | sandy loam |
| S12 | 6.1 | 12 | 0.84 | 58 | 18 | 24 | sandy clayey loam |
| S13 | 5.8 | 35 | 0.43 | 81 | 15 | 4.0 | loamy sand |
| S14 | 7.6 | 44 | 1.3 | 67 | 21 | 12 | sandy loam |
| S15 | 6.0 | 26 | 3.1 | 18 | 27 | 55 | clay loam |
| S16 | 5.7 | 38 | 2.9 | 16 | 24 | 60 | clay loam |

[a]According to the United States Department of Agriculture soil classification system.

The studied soils were slightly acidic to neutral except the S4 site, which was alkaline (Table 1) due to the decomposition of organic matter and subsequent formation of carbonic acid.[26] The range of organic carbon (% C) was 0.36 to 3.1, and the highest value was observed in soil collected from the S15 site. According to the United States soil texture classification, the textural analysis revealed that the soil belonged to the sand, sandy loam, sandy clayey loam, loam, loamy sand, and clay loam class (Table 1). The concentrations of heavy metals were measured to estimate the transfer factor in cereals and pulses. Mean concentrations of Cr, Ni, Cu, Zn, As, Cd, and Pb in soil were 41, 45, 42, 75, 10, 4.2, and 44 mg/kg, respectively (Table 2). Metals in soils were compared with the other studies in Bangladesh and other countries. Chromium concentrations of the present study were higher than those of the study conducted in China, Spain, and Turkey and one study in Bangladesh (Table 2), indicating that soils were contaminated

Table 2. Comparison of Metal Concentration in Soil of Present Study with Other Studies and Guideline Values[a]

| district (country) | Cr | Ni | Cu | Zn | As | Cd | Pb | refs |
|---|---|---|---|---|---|---|---|---|
| Bogra (Bangladesh) | 41 (6.6–87)[b] | 45 (15–95) | 42 (6.4–107) | 75 (24–205) | 10 (2.0–36) | 4.2 (0.7–10) | 44 (13–96) | present study |
| Noakhali (Bangladesh) | 29 (18–46) | 64 (37–93) | 22 (13–63) | 75 (50–116) | 3.3 (1.5–9.2) | 0.07 (0.03–0.2) | 13 (8–22) | 40 |
| Dhaka (Bangladesh) | 54 (34–68) | 58 (36–74) | 39 (31–45) | 115 (103–123) | NA | 11 (6–16) | 50 (44–52) | 8 |
| Guandong (China) | 12.3 (9.66–19) | 8.83 (7.04–10.3) | 324 (210–450) | 122 (92–142) | NA | 0.9 (0.26–1.17) | 96 (73–134) | 37 |
| Maharashtra (India) | 164 (66–279) | 171 (69–465) | 155 (52–373) | 689 (63–7120) | 2.8 (NA–11.2) | 30 (22–39) | 42 (36–49) | 41 |
| Murcia (Spain) | 18 (10–60) | 14 (5.1–31) | 11 (3.8–65) | 18 (4.5–93) | NA | 0.22 (0.06–1.1) | 49 (11–674) | 42 |
| Kayseri (Turkey) | 29 (17–81) | 45 (16–217) | 37 (12–144) | 112 (33–733) | NA | 2.5 (0.98–15) | 75 (28–312) | 43 |
| Dutch soil quality standard (Target Value) | 100 | 35 | 36 | 140 | 29 | 0.8 | 85 | 30 |
| Dutch soil quality standard (Intervention Value) | 380 | 210 | 190 | 720 | 55 | 12 | 530 | 30 |
| Canadian Environmental Quality Guidelines | 64 | 50 | 63 | 200 | 12 | 1.4 | 70 | 44 |
| Department of Environmental Protection, Australia | 50 | 60 | 60 | 200 | 20 | 3 | 300 | 45 |

[a]All values are expressed as mg/kg. [b]Data in parentheses indicates range.

by Cr. In Bangladesh, the main sources of Cr in agricultural soils where the farmers grow cereals and pulses are the repeated uses of untreated or poorly treated wastewater from industrial establishments (e.g., textile and tannery sludge) and the application of chemical fertilizers and pesticides.[2,27] Like Cr, other metals were slightly higher than found in the other studies conducted in Bangladesh and other countries. This can be ascribed to the fact that metal processing, battery manufacturing, and smelting industries responsible for severe metal pollution have been reported from many countries.[28] During our sampling campaign, we observed leachates from defused Ni–Cd batteries, Cd plated items, casting lead, and lead product manufacturing at the sampling sites. Used metal fittings, rubber, plastics, tires, paints, etc. are materials emitting Cd to the environment.[29] The mean concentrations of Ni, Cu, and Cd in the present study were above the Dutch soil quality standard[30] (Table 2). The functional properties of these soils such as nutrients and contaminants storage, transformation and biomass production, etc. were seriously hampered or threatened, which could potentially cause an adverse effect on humans, plants, and animals.[30] Therefore, the contaminations of these agricultural fields' soils are a major concern because foods are still being grown on these soils. The Dutch soil quality standard is regarded as the most comprehensive guideline considering all possible exposure pathways for protecting humans, plants, and animals. If any metal concentration in soil is below its respective Dutch Target Value, the soil is considered clean. If the concentration level lies between the target values and intervention values, the soil is regarded to be slightly to moderately contaminated. In contrast, if the value is above the Dutch Intervention Value, the soil is considered detrimental to humans, plants, and animals. According to Table 2, Cd was in the worst situation among the studied metals as the mean concentration of Cd was more than 5 times higher than the Dutch Target value.

**Metals in Cereals and Pulses.** In the present study, concentrations of Cr, Ni, Cu, Zn, As, Cd, and Pb (mg/kg) were determined in the composite samples of most commonly consumed cereals (rice, wheat, and maize) and pulses (lentil and black gram) by the Bangladeshi population and are listed in Table 3. Average concentration of heavy metals among the food groups showed the descending order of maize > black gram > lentil > wheat > rice. The observed variation in metal concentrations for analyzed foodstuffs might be due to variable capabilities of absorption and accumulation of metals by the cereal crops.[31]

An elevated level of Cr was found in black gram (2.4 mg/kg) followed by lentil, maize, rice, and wheat (Table 3). The mean Cr concentration in rice was 1.8 mg/kg (range, 0.26–4.2 mg/kg, $n$ = 32). A previous study by Fu et al.[16] reported mean Cr concentration in Chinese rice of 0.20 mg/kg (range, 0.062–0.42 mg/kg, $n$ = 4), which is lower than in the present study. In the present study, the highest mean concentration of Ni was found in black gram, 1.4 mg/kg (range, 0.047–4.0 mg/kg). In rice, Ni concentration was observed (mean, 1.0; range, 0.03–2.6 mg/kg). However, Ni concentration in all rice samples of the present study was considerably lower than those of Chinese rice (mean, 0.48 mg/kg; range, 0.20–0.82 mg/kg, $n$ = 4)[16] and Indian state of West Bengal (mean, 0.87 mg/kg; range, 0.0002–1.8 mg/kg).[32] Among the studied metals, significant difference of Zn concentration was observed in the studied foods (Table 3), therefore, Zn measured in the current study is more likely to be having a micronutrient effect rather than

**Table 3. Heavy Metals (mg/kg) in Cereals and Pulses Collected from Agricultural Fields of Bogra District, Bangladesh**

| name | | | | | | | | |
|---|---|---|---|---|---|---|---|---|
| common | scientific | Cr | Ni | Cu | Zn | As | Cd | Pb |
| rice ($n$ = 32)[a] | *Oryza sativa* | | | | | | | |
| | range | 0.26−4.2 | 0.028−2.6 | 0.50−3.3 | 0.55−3.5 | 0.06−1.6 | 0.001−0.073 | 0.07−1.3 |
| | mean ± SD[b] | 1.8 ± 1.4 a[c] | 1.0 ± 0.73 a | 1.7 ± 0.68 a | 2.1 ± 0.64 b | 0.47 ± 0.39 a | 0.045 ± 0.017 a | 0.71 ± 0.29 a |
| wheat ($n$ = 32) | *Triticum aestivum* | | | | | | | |
| | range | 0.24−3.4 | 0.095−3.6 | 0.52−4.3 | 1.1−6.0 | 0.08−1.5 | 0.0010−0.66 | 0.028−1.1 |
| | mean ± SD | 1.3 ± 0.92 a | 1.3 ± 1.1 a | 1.9 ± 0.91 a | 2.9 ± 1.2 a | 0.57 ± 0.39 a | 0.16 ± 0.19 b | 0.26 ± 0.30 b |
| maize ($n$ = 32) | *Zea mays* | | | | | | | |
| | range | 0.39−4.0 | 0.24−2.8 | 0.87−4.5 | 1.5−7.3 | 0.08−1.7 | 0.018−0.53 | 0.044−1.3 |
| | mean ± SD | 1.9 ± 0.99 a | 1.4 ± 0.66 a | 2.3 ± 0.94 a | 3.6 ± 1.6 c | 0.64 ± 0.44 a | 0.10 ± 0.11 ab | 0.31 ± 0.31 bc |
| lentil ($n$ = 24) | *Lens culinaris* | | | | | | | |
| | range | 0.39−6.5 | 0.036−4.0 | 0.61−4.5 | 1.5−3.9 | 0.10−1.8 | 0.018−0.13 | 0.14−1.6 |
| | mean ± SD | 2.3 ± 1.8 a | 1.1 ± 1.0 a | 2.3 ± 1.1 a | 2.3 ± 0.71 ab | 0.66 ± 0.45 a | 0.044 ± 0.037 a | 0.60 ± 0.38 a |
| black gram ($n$ = 24) | *Vigna mungo* | | | | | | | |
| | range | 0.29−6.5 | 0.047−4.0 | 0.43−4.1 | 0.61−3.9 | 0.06−1.6 | 0.0012−0.13 | 0.08−1.6 |
| | mean ± SD | 2.4 ± 2.0 a | 1.4 ± 1.0 a | 2.1 ± 1.2 a | 2.5 ± 0.81 ab | 0.62 ± 0.44 a | 0.046 ± 0.041 a | 0.55 ± 0.37 ac |

[a] $n$ = number of samples analyzed for this study. [b] SD = standard deviation. [c] Different letter (a, b, c) indicates statistical significance ($p < 0.05$).

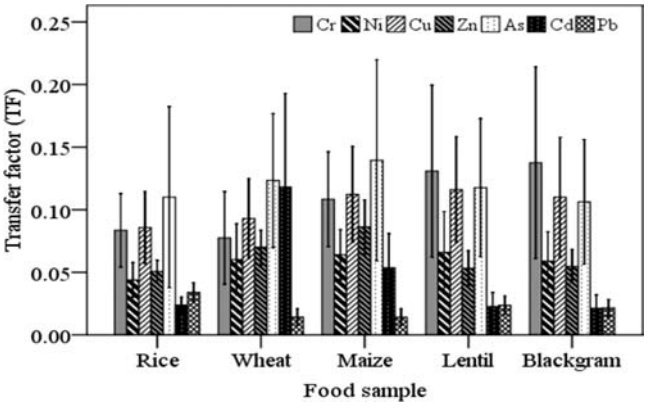


**Figure 2.** Transfer factor of metals from soil to cereals and pulses collected from agricultural fields of Bogra district, Bangladesh (bars represent standard error at 95% CI).

posing a significant risk of toxicity. However, the highest Zn concentration was found in maize (mean, 3.6 mg/kg; range, 1.5−7.3 mg/kg, $n$ = 32) (Table 3). The mean concentration of As in rice was 0.47 mg/kg, which was higher than in the previous study conducted by Williams et al.,[33] where As concentration in Bangladeshi rice was 0.13 mg/kg. The elevated As concentration in rice was attributed to the higher accumulation of As from soil to grain in the anaerobic paddy soil systems for rice production and uncontrolled application of As enriched fertilizers and pesticides.[34] Cadmium is a metallic element that occurs naturally at low levels in the environment. Food, rather than air or water, represents the major source of cadmium exposure.[35] The highest Cd concentration was observed in wheat (mean, 0.16; range, 0.001−0.66 mg/kg).

**Transfer Factor of Metals.** The accumulation of metals in the edible parts of cereals and pulses could have a direct impact on human health through the food chain. Metals with high TF are more easily transferred from soil to the edible parts of

**Table 4. Food Intake and Intake of Heavy Metals (mg/day) through the Diet of Cereals and Pulses of the Present Study (Mean ± SD)**

| | | estimated daily intake (EDI) (mg/day) | | | | | | |
|---|---|---|---|---|---|---|---|---|
| foods | consumption rate (g/day/person)[18] | Cr | Ni | Cu | Zn | As | Cd | Pb |
| rice | 445[38] | 0.79 ± 0.62 | 0.46 ± 0.32 | 0.78 ± 0.30 | 0.95 ± 0.28 | 0.21 ± 0.17 | 0.020 ± 0.01 | 0.32 ± 0.13 |
| wheat | 26.09 | 0.035 ± 0.024 | 0.033 ± 0.028 | 0.050 ± 0.024 | 0.077 ± 0.030 | 0.015 ± 0.010 | 0.004 ± 0.005 | 0.007 ± 0.008 |
| maize | 26.09 | 0.050 ± 0.026 | 0.036 ± 0.017 | 0.061 ± 0.025 | 0.095 ± 0.042 | 0.017 ± 0.012 | 0.003 ± 0.003 | 0.008 ± 0.008 |
| lentil | 14.3 | 0.033 ± 0.026 | 0.016 ± 0.014 | 0.033 ± 0.016 | 0.033 ± 0.010 | 0.009 ± 0.006 | 0.001 ± 0.001 | 0.009 ± 0.005 |
| black gram | 14.3 | 0.034 ± 0.028 | 0.020 ± 0.015 | 0.030 ± 0.016 | 0.035 ± 0.012 | 0.009 ± 0.006 | 0.001 ± 0.001 | 0.008 ± 0.005 |
| total intake from foods | 0.95 | 0.57 | 0.95 | 1.2 | 0.26 | 0.028 | 0.35 | |
| maximum tolerable daily intake (MTDI) | 0.2[46] | 0.3[47] | 30[48] | 60[47] | 0.13[23] | 0.021[49] | 0.21[50] | |

Table 5. Target Hazard Quotients (Noncarcinogenic) and Carcinogenic Risk (CR) of Heavy Metals (Mean ± SD) Due to Food Consumption in Bogra District Urban Area, Bangladesh

| foods | target hazard quotients (THQs) | | | | | | | TTHQ[a] | carcinogenic risk (CR) | |
|---|---|---|---|---|---|---|---|---|---|---|
| | Cr | Ni | Cu | Zn | As | Cd | Pb | | As[b] | Pb |
| rice | 0.009 ± 0.007 | 0.39 ± 0.27 | 0.32 ± 0.13 | 0.05 ± 0.02 | 12 ± 10 | 0.11 ± 0.04 | 1.5 ± 0.61 | 14 | $4.7 \times 10^{-3}$ | $4.5 \times 10^{-5}$ |
| wheat | 0.0004 ± 0.0003 | 0.027 ± 0.023 | 0.021 ± 0.010 | 0.004 ± 0.002 | 0.83 ± 0.56 | 0.023 ± 0.028 | 0.033 ± 0.037 | 0.94 | $3.4 \times 10^{-4}$ | $1.1 \times 10^{-6}$ |
| maize | 0.0006 ± 0.0003 | 0.030 ± 0.014 | 0.025 ± 0.010 | 0.005 ± 0.002 | 0.93 ± 0.64 | 0.014 ± 0.016 | 0.038 ± 0.038 | 1.0 | $3.8 \times 10^{-4}$ | $1.1 \times 10^{-6}$ |
| lentil | 0.0004 ± 0.0003 | 0.013 ± 0.012 | 0.014 ± 0.007 | 0.002 ± 0.001 | 0.52 ± 0.36 | 0.003 ± 0.003 | 0.041 ± 0.026 | 0.59 | $2.1 \times 10^{-4}$ | $1.2 \times 10^{-6}$ |
| black gram | 0.0004 ± 0.0003 | 0.017 ± 0.012 | 0.013 ± 0.007 | 0.002 ± 0.001 | 0.49 ± 0.35 | 0.004 ± 0.003 | 0.037 ± 0.026 | 0.56 | $2.0 \times 10^{-4}$ | $1.1 \times 10^{-6}$ |
| total | 0.011 | 0.47 | 0.40 | 0.066 | 14 | 0.16 | 1.7 | 17 (HI)[c] | $5.8 \times 10^{-3}$ | $4.9 \times 10^{-5}$ |

[a]The total metals THQs (TTHQ, sum of individual metal THQs). [b]Carcinogenic risk for As was calculated based on 90% inorganic As in cereals and pulses. [c]HI: the sum of THQ values of heavy metals due to consuming the diet.

plants than the ones with low TF. As seen from Figure 2, large variations in TFs were observed among different samples and metals. The average TF of metals in all crops was in the following order: As > Cr > Cu > Zn > Ni > Cd > Pb. In rice, average values of TF were 0.084, 0.044, 0.086, 0.051, 0.11, 0.024, and 0.034, in wheat, average values of TF were 0.078, 0.060, 0.093, 0.070, 0.12, 0.12, and 0.014, and in maize, average values of TF were 0.11, 0.064, 0.11, 0.086, 0.14, 0.054, and 0.014 for Cr, Ni, Cu, Zn, As, Cd, and Pb, respectively. The TF of Cd in wheat was higher than those of any other metals examined. It was noticeable that Cd was considered as a very dangerous substance for human health by the long-term effects.[36] Therefore, the risks of Cd for health should be highlighted by its high toxicity and mobility from soil to wheat grain. In lentil, average values of TF were 0.13, 0.066, 0.12, 0.053, 0.12, 0.023, and 0.024, and in black gram, average values of TF were 0.14, 0.059, 0.11, 0.055, 0.11, 0.021, and 0.022 for Cr, Ni, Cu, Zn, As, Cd, and Pb, respectively. The major pathway for Pb to enter the above-ground tissues of plants is through atmospheric deposition.[37] Therefore, the factual TF of Pb should be lower than the calculated value. In this study, the soil-to-plant TF for various metals and for most common cereals and pulses consumed by local residents were calculated (Figure 2), and our data showed that TF values slightly varied among metals within the same crop. The difference in TFs between metals and species might be related to soil properties, nutrient management, crop genetic features, and physicochemical properties of pollutants.[22] For instance, soils from S2, S3, S15, and S16 were generally higher in organic matter and clay content might be responsible for higher metal transfer from soil to plants.

**Estimated Daily Intakes (EDIs).** The EDIs of seven metals (Cr, Ni, Cu, Zn, As, Cd, and Pb) were evaluated according to the average concentration of each metal in each food crop from each site and the respective consumption rates. The EDI and maximum tolerable daily intake (MTDI) of studied metals from consumption of grain crops are shown in Table 4. Total daily intake of Cr, Ni, Cu, Zn, As, Cd, and Pb were 0.95, 0.57, 0.95, 1.2, 0.26, 0.28, and 0.35 mg/day, respectively (Table 4). The maximum contribution of daily intake of studied metals came from rice; this is due to the highest consumption rate of rice (445 g/person/day).[38] The total EDIs of Cr, Ni, As, Cd, and Pb from all examined food items were higher than the MTDI values recommended by the international regulatory bodies (Table 4), indicating that these foods might pose health risks to consumers.

**Noncarcinogenic Risk.** Risk assessment is the process that evaluates the potential health effects from doses to humans of one contaminant received through one or more exposure pathways. The health risks from consumption of cereals and pulses by adult populations were assessed based on the target hazard quotients (THQs). The THQ is a ratio of determined dose of a pollutant to a reference dose level. If the ratio is greater than 1, the exposed population is likely to experience obvious adverse effects.[25] The methodology for estimation of THQs does not provide a quantitative estimate on the probability of an exposed population experiencing a reverse health effect, but it offers an indication of the risk level due to contaminant exposure. The estimated THQs of studied metals are shown in Table 5, indicating that THQ values of As and Pb were above 1 through consumption of rice, suggesting that people would experience significant health risks if they only ingest these two metals from rice. The consumption of rice per

capita in Bangladesh is 445 g/day.[38] Therefore, consuming rice containing high As and Pb might put pregnant women at a higher risk. Among all the metals studied, the TTHQ through consuming rice was 14, suggesting that Bangladeshi people might have significant noncarcinogenic health risk through only consuming rice. However, the total target hazard quotient (TTHQ) values through consuming other cereals and pulses were equal to or less than 1, indicating that there were no potential significant health risks in terms of these food items. The hazard index (HI) value expresses the combined noncarcinogenic effects of multiple elements. In Table 5, the HI value through selected food consumption was 17, indicating that consumers of the studied foodstuffs may experience adverse health effects.

**Carcinogenic Risk of As and Pb.** Concerning the carcinogenic risk, the CR values of As were $4.7 \times 10^{-3}$, $3.4 \times 10^{-4}$, $3.8 \times 10^{-4}$, $2.1 \times 10^{-4}$, and $2.0 \times 10^{-4}$ (assuming 90% of inorganic As[39]) and of Pb were $4.5 \times 10^{-5}$, $1.1 \times 10^{-6}$, $1.1 \times 10^{-6}$, $1.2 \times 10^{-6}$, and $1.1 \times 10^{-6}$ for rice, wheat, maize, lentil, and black gram, respectively, which were clearly higher than the USEPA threshold level ($10^{-6}$) or residual level ($10^{-4}$) for causing cancer,[24] indicating carcinogenic risks for all adults of the study area.

The concentrations of heavy metals widely varied among the samples. Among cereals and pulses, rice contributes the highest intake of the studied metals. Considering the transfer factor of metals from soil to cereals and pulses, As showed higher TF values than the other metals. Total intake of Cr, Ni, As, Cd, and Pb for the exposed people was slightly higher than that recommended as the MTDI (for a person weighing 60 kg), indicating that people would experience significant risks. From the human health point of view, the THQ values for As and Pb were higher than 1, suggesting that people would experience significant health risks if they ingest these two vital metals through consuming the studied foodstuffs. However, consumption of all foodstuffs could lead to a potential health risk to the consumers since HI value was higher than 1. Concerning the carcinogenic risk, the total CR values of As and Pb were clearly higher than the USEPA threshold level ($1 \times 10^{-6}$). However, health risks associated with food consumption are not negligible and the sources of metal pollution should be controlled to achieve safe foodstuffs. The present study is of great interest in terms of toxicology and food safety for the Bogra district urban population, given the absence of previous studies to determine dietary intake of heavy metals, not only for the district urban population but also at the national level.

## AUTHOR INFORMATION


### Corresponding Author

*Department of Soil Science, Patuakhali Science and Technology University, Dumki, Patuakhali, 8602, Bangladesh. Phone: +88-01717372057. Fax: +88-04427-56009. E-mail: msaifulpstu@yahoo.com.


### Notes

The authors declare no competing financial interest.

## ACKNOWLEDGMENTS

The authors thank the authority of Patuakhali Science and Technology University, Bangladesh, and Yokohama National University, Japan, for providing laboratory facilities. The authors are also delighted to express their gratefulness and sincerest thanks to Professor Dr. Md. Shams-Ud-Din (Vice Chancellor, PSTU), for his valuable suggestions and cooperation to carry out this research.

## REFERENCES


(1) Khan, S.; Cao, Q.; Zheng, Y. M.; Huang, Y. Z.; Zhu, Y. G. Health risks of heavy metals in contaminated soils and food crops irrigated with wastewater in Beijing, China. *Environ. Pollut.* **2008**, *152*, 686−692.

(2) Rahman, S. H.; Khanam, D.; Adyel, T. M.; Islam, M. S.; Ahsan, M. A.; Akbor, M. A. Assessment of heavy metal contamination of agricultural soil around Dhaka Export Processing Zone (DEPZ), Bangladesh, implication of seasonal variation and indices. *Appl. Sci.* **2012**, *2*, 584−601.

(3) Cameron, R. E. *Guide to site and soil description for hazardous waste site characterization. Vol. 1: Metals*; Environmental Protection Agency EPA/600/4-91/029; US EPA: Washington, DC. http://nepis.epa.gov/Adobe/PDF/200097F6.PDF. 1992.

(4) Lei, M.; Zhang, Y.; Khan, S.; Qin, Pu.; Liao, Bo. Pollution, fractionation and mobility of Pb, Cd, Cu, and Zn in garden and paddy soils from a Pb/Zn mining area. *Environ. Monit. Assess.* **2010**, *168*, 215−222.

(5) Fabietti, G.; Biasioli, M.; Barberis, R.; Ajmone-Marsan, F. Soil contamination by organic and inorganic pollutants at the regional scale: the case of Piedmont, Italy. *J. Soils Sediments* **2010**, *10*, 290−300.

(6) Micó, C.; Recatalá, L.; Peris, M.; Sánchez, J. Assessing heavy metal sources in agricultural soils of an European Mediterranean area by multivariate analysis. *Chemosphere* **2006**, *65*, 863−872.

(7) Kabata-Pendias, A.; Mukherjee, A. B. *Trace elements from soil to human*; Springer-Verlag: Berlin, 2007.

(8) Ahmad, J. U.; Goni, M. A. Heavy Metal Contamination in Water, Soil, and Vegetables of the Industrial Areas in Dhaka, Bangladesh. *Environ. Monit. Assess.* **2010**, *166*, 347−357.

(9) Ji, K.; Kim, J.; Lee, M.; Park, S.; Kwon, H.; Cheong, H.; Jang, J.; Kim, D.; Yu, S.; Kim, Y.; Lee, K.; Yang, S.; Jhung, I. k.; Yang, W.; Paek, D.; Hong, Y.; Choi, K. Assessment of exposure to heavy metals and health risks among residents near abandoned metal mines in Goseong, Korea. *Environ. Pollut.* **2013**, *178*, 322−328.

(10) Kachenko, A. G.; Singh, B. Heavy metals contamination in vegetables grown in urban and metal smelter contaminated sites in Australia. *Water Air Soil Pollut.* **2006**, *169*, 101−123.

(11) Sharma, R. K.; Agrawal, M.; Marshall, F. Heavy metal contamination of soil and vegetables in suburban areas of Varanasi, India. *Ecotoxicol. Environ. Saf.* **2007**, *66*, 258−266.

(12) USEPA (US Environmental Protection Agency). *Risk Assessment Guidance for Superfund, Human Health Evaluation Manual (Part A). Interim Final, Vol. I*; United States Environmental Protection Agency: Washington, DC; 1989; EPA/540/1-89/002.

(13) Schaaf, F. *The brightest stars: Discovering the universe through the sky's most brilliant stars*. John Wiley: Hoboken, NJ, 2008; p 211.

(14) WHO (World Health Organization). *Evaluation of certain food additives and contaminants fifty-seventh report of the Joint FAO/WHO Expert Committee on Food Additives*; WHO technical report series 909; WHO: Geneva, 2002.

(15) Seyfferth, A. L.; McCurdy, S.; Schaefer, M. V.; Fendorf, S. Arsenic Concentrations in Paddy Soil and Rice and Health Implications for Major Rice-Growing Regions of Cambodia. *Environ. Sci. Technol.* **2014**, *48*, 4699−4706.

(16) Fu, J.; Zhou, Q.; Liu, J.; Liu, W.; Wang, T.; Zhang, Q.; Jiang, G. High levels of heavy metals in rice (Oryza sativa L.) from a typical E-waste recycling area in southeast China and its potential risk to human health. *Chemosphere* **2008**, *71*, 1269−1275.

(17) FAO/WHO. Food standards programme codex committee on contaminants in foods. Fifth session. The Netherlands: The Hague, 2011.

(18) HIES. *Preliminary report on household income and expenditure survey-2010. Bangladesh Bureau of Statistics, Statistics division, Ministry of planning*: Dhaka, Bangladesh, 2011.

(19) Ahmed, F.; Bibi, M. H.; Asaeda, T.; Mitchell, C. P. J.; Ishiga, H.; Fukushima, T. Elemental composition of sediments in Lake Jinzai,

Japan: Assessment of sources and pollution. *Environ. Monit. Assess.* **2012**, *184*, 4383−4396.
(20) Niwa, Y.; Sugai, T.; Saegusa, Y.; Ogami, T.; Sasao, E. Use of electrical conductivity to analyze depositional environments: Example of a Holocene delta sequence on the Nobi Plain, central Japan. *Q. Int.* **2011**, *230*, 78−86.
(21) Zhao, L.; Xu, Y.; Hou, H.; Shangguan, Y.; Li, F. 2014. Source identification and health risk assessment of metals in urban soils around the Tanggu chemical industrial district, Tianjin, China *Sci. Total Environ.* **2014**, 468−469, 654−662.
(22) Li, Q. S.; Chen, Y.; Fu, H.; Cui, Z.; Shi, L.; Wang, L.; Liu, Z. Health risk of heavy metals in food crops grown on reclaimed tidal flat soil in the Pearl River Estuary, China *J. Hazard. Mater.* **2012** 227−228, 148−154.
(23) FAO (Food and Agriculture Organization). *Arsenic contamination of irrigation water, soil and crops in Bangladesh: Risk implications for sustainable agriculture and food safety in Asia*; Food and agriculture organization of the United Nations regional office for Asia and the Pacific: Bangkok, Thailand, 2006.
(24) USEPA (US Environmental Protection Agency). *Risk-based Concentration Table*. Available from http://www.epa.gov/reg3hwmd/risk/human/index.htm, 2010.
(25) Wang, X.; Sato, T.; Xing, B.; Tao, S. Health risks of heavy metals to the general public in Tianjin, China via consumption of vegetables and fish. *Sci. Total Environ.* **2005**, *350*, 28−37.
(26) Ahmad, S.; Siddiqui, E. N.; Khalid, S. Studies on certain physico chemical properties of soil of two fresh water ponds of Darbhanga. *Environ. Pollut.* **1996**, *31*, 31−39.
(27) Islam, M. M.; Halim, M. A.; Safiullah, S.; Hoque, S. A. M. W.; Islam, M. S. Heavy metal (Pb, Cd, Zn, Cu, Cr, Fe and Mn) content in textile sludge in Gazipur, Bangladesh. *Res. J. Environ. Sci.* **2009**, *3*, 311−315.
(28) Martley, E.; Gulson, B. L.; Pfeifer, H. R. Metal Concentrations in Soils Around the Copper Smelter and Surrounding Industrial Complex of Port Kembla, NSW, Australia. *Sci. Total Environ.* **2004**, *325*, 113−127.
(29) Hossain, M. Z.; Ullah, S. M.; Ahad, S. A.; Ullah, M. B. Transfer of Cadmium from Soil to Vegetable Crops. *Bangladesh J. Sci. Ind. Res.* **2007**, *42*, 327−334.
(30) VROM (Volkshuisvesting, Ruimtelijke Ordening enMilieubeheer). Spatial Planning and Environment. Circular on target values and intervention values for soil remediation. Spatial Planning and Environment, Ministry of Housing, Netherlands, 2000.
(31) Pandey, J.; Pandey, U. Accumulation of heavy metals in dietary vegetables and cultivated soil horizon in organic farming system in relation to atmospheric deposition in a seasonally dry tropical region of India. *Environ. Monit. Asses.* **2009**, *148*, 61−74.
(32) Roychowdhury, T.; Tokunaga, H.; Ando, M. Survey of arsenic and other heavy metals in food composites and drinking water and estimation of dietary intake by the villagers from an arsenic-affected area of West Bengal, India. *Sci. Total Environ.* **2003**, *308*, 15−35.
(33) Williams, P. N.; Price, A. H.; Raab, A.; Hossain, A. A.; Feldmann, J.; Meharg, A. A. Variation in arsenic speciation and concentration in paddy rice related to dietary exposure. *Environ. Sci. Technol.* **2005**, *39*, 5531−5540.
(34) Neumann, R. B.; Ashfaque, K.; Badruzzaman, A. B. M.; Ali, M. A.; Shoemaker, J.; Harvey, C. Anthropogenic influences on groundwater arsenic concentrations in Bangladesh. *Nat. Geosci.* **2010**, *3*, 46−52.
(35) Rahman, M. A.; Rahman, M. M.; Reichman, S. M.; Lim, R. P.; Naidu, R. Heavy metals in Australian grown and imported rice and vegetables on sale in Australia: Health hazard. *Ecotoxicol. Environ. Saf.* **2014**, *100*, 53−60.
(36) Lavado, R. S. Concentration of potentially toxic elements in field crops grown near and far from cities of the Pampas (Argentina). *J. Environ. Manage.* **2006**, *80*, 116−119.
(37) Luo, C.; Liu, C.; Wang, Y.; Liu, X.; Li, F.; Zhang, G.; Li, X. Heavy metal contamination in soils and vegetables near an e-waste processing site, south China. *J. Hazard. Mater.* **2011**, *186*, 481−490.
(38) Meharg, A. A.; Williams, P. N.; Adomako, E.; Lawgali, Y. Y.; Deacon, C.; Villada, A.; Cambel, R. C. J.; Sun, G.; Zhu, Y. G.; Feldmann, J.; Raab, A.; Zhao, F. J.; Islam, R.; Hossain, S.; Yanai, J. Geographical variation in total and inorganic arsenic content of polished (white) rice. *Environ. Sci. Technol.* **2009**, *43*, 1612−1617.
(39) Smith, N. M.; Lee, R.; Heitkemper, D. T.; Cafferky, K. D.; Haque, A.; Henderson, A. K. Inorganic arsenic in cooked rice and vegetables from Bangladeshi households. *Sci. Total Environ.* **2006**, *370*, 294−301.
(40) Rahman, M. M.; Asaduzzaman, M.; Naidu, R. Consumption of arsenic and other elements from vegetables and drinking water from an arsenic-contaminated area of Bangladesh. *J. Hazard. Mater.* **2013**, *262*, 1056−1063.
(41) Bhagure, G. R.; Mirgane, S. R. Heavy Metal Concentrations in Groundwaters and Soils of Thane Region of Maharashtra, India. *Environ. Monit. Assess.* **2011**, *173*, 643−652.
(42) Acosta, J. A.; Faz, A.; Martínez-Martínez, S.; Arocena, J. M. Enrichment of Metals in Soils Subjected to Different Land Uses in a Typical Mediterranean Environment (Murcia City, Southeast Spain). *Appl. Geochem.* **2011**, *26*, 405−414.
(43) Tokalıoğlu, Ş.; Kartal, S. Multivariate analysis of the data and speciation of heavy metals in street dust samples from the organized industrial district in Kayseri (Turkey). *Atmos. Environ.* **2006**, *40*, 2797−2805.
(44) CCME (Canadian Council of Ministers of the Environment). *Canadian Environmental Quality Guidelines*, 2003.
(45) DEP (Department of Environmental Protection). Assessment Levels for Soil, Sediment and Water Contaminated Sites Management Series. Perth's, Australia, 2003.
(46) RDA (Recommended Dietary Allowance). *Recommended Dietary Allowance*, 10th ed.; National Academic Press: Washington, DC, 1989.
(47) WHO. *Guidelines for Drinking-Water Quality*, 2nd ed.; World Health Organization: Geneva, Switzerland, 1996; Vol. *2*.
(48) JECFA. *Summary and conclusions of the 61st meeting of the Joint FAO/WHO Expert Committee on Food Additives (JECFA)*; JECFA/61/SC; Rome, Italy, 2003.
(49) EFSA (European Food Safety Authority). Scientific opinion of the Panel on Contaminants in the Food Chain on a request from the European Commission on cadmium in food. *EFSA J.* **2009**, *980*, 1−139.
(50) JECFA (Joint FAO/WHO expert Committee on Food Additives). *Evaluation of Certain Food Additives and Contaminants*; 41st Report of JECFA; Technical Reports Series No. 837; World Health Organization: Geneva, 1993.

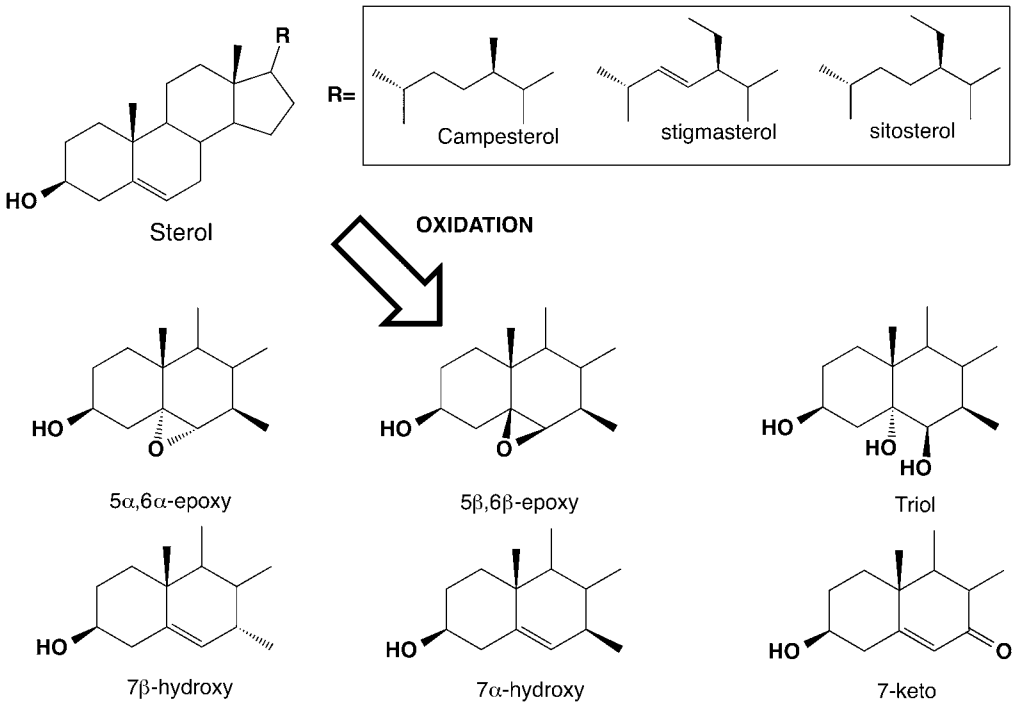


**Figure 1.** Structures of campesterol, stigmasterol, sitosterol, and their main oxidation products (POPs).

storage; in fact, the presence of OTA in green coffee was reported for the first time in 1974,[22] and thereafter, many authors have determined the OTA content in green and roasted coffee or in coffee beverages.[5,21,23−25] Contradictory results about the effect of roasting on the reduction of OTA in coffee beans have been reported. However, it seems that roasting can diminish OTA content, as reported by Napolitano et al.[5] and Romani et al.,[23] who observed an OTA reduction >90% in green coffee after roasting. Although the latter could be an effective process for reducing OTA content in coffee, it should be pointed out that roasting conditions (time/temperature) could differently impact OTA destruction. On the other hand, several studies mention physical removal of OTA by elimination of coffee silverskin before and during the roasting process;[5] in fact, since CS covers and protects the coffee bean, it is possible that a high amount of OTA is concentrated in CS. Nevertheless, only a few papers reported the presence (<4 μg/kg) of OTA in CS.[4,15]

Also, the lipid fraction of CS could be potentially a source of bioactive molecules, such as phytosterols (PS) (Figure 1), which are known to reduce the low-density lipoproteins (LDL) cholesterol concentration and are thus often incorporated into functional foods.[26] However, PS are prone to oxidation, like cholesterol,[27] leading to a wide range of oxidation products[26] (POPs; Figure 1). While the toxicological aspects of cholesterol oxidation products are well-documented,[28] the information about the biological impact of POPs is limited.[26] Recently, O'Callaghan et al.[29] reported the role of POPs in many different biological mechanisms (cholesterol uptake and metabolism, atherosclerosis, inflammation, cytotoxicity, oxidative stress, etc.), while Adcox et al.[30] demonstrated that β-sitosterol and campesterol oxides display a similar toxicity to that of COPs in a culture-derived macrophage cell line (C57BL6). To the best of our knowledge, no data about the content of PS and/or POPs in CS have been reported in the literature. However, in order to propose some reuse of CS, it is of outmost importance to define the potential safety risks.

The aim of this paper was to evaluate the CS suitability as possible source of bioactive compounds, as well as the presence of potentially hazardous compounds, in usual storage conditions employed for this waste product. A full characterization study focused on both lipophilic and hydrophilic components of CS was carried out. OTA and POPs were determined, together with the fiber content, the total phenolic compounds, the carbohydrate composition, and the caffeine amount. Different methods for extracting the lipid fraction were tested, and its total fatty acid composition and total PS content were investigated.

## 2. MATERIALS AND METHODS

**2.1. Samples.** CS was obtained from a mix of Arabica and Robusta coffee, supplied by a local coffee-roasting enterprise (Bologna, Italy). CS was removed during roasting through a cyclone and then stored in closed containers kept in a separate locale at uncontrolled room temperature and relative humidity. Two-kilogram CS samples were weekly collected in triplicate for a total of 5 weeks ($n$ = 15). For OTA determination, the CS sampling was extended to 10 weeks ($n$ = 30).

**2.2. Reagents and Solvents.** All chemicals and solvents were of analytical grade. HPLC-grade methanol (≥99.9%) and water (≥99.8%) were purchased from Merck (Darmstadt, Germany), while bidistilled water (100%) was supplied by Panreac (Castellar del Vallès, Spain).

Caffeine (assay ≥99%) and magnesium oxide (MgO) were purchased from Caelo (Hilden, Germany) and Riedel-de-Haen (Seelze, Germany), respectively. A fiber kit was provided by Megazyme International Ireland Ltd. (Wicklow, Ireland). The standard mixture of fatty acid methyl esters (GLC 463) was purchased from Nu-Chek (Elysian, MN). 19-Hydroxycholesterol (19-HC) were supplied by Steraloids (Newport, RI). Triolein (≥99.0%), tripalmitin (≥99.0%), tristearin (≥99.0%), 1,3-diolein (≥99.0%), 1,2(3)-dipalmitin (≥99.0%), cholesteryl palmitate (≥97%), 1-oleoyl-*rac*-glycerol (≥99.0%), tridecanoic acid (≥99.0%), methyl tridecanoate (≥99.5%), gallic acid (≥98%, GA), D-dulcitol (≥99%), D-mannitol (≥98%), D-

sucrose (≥99.5%), D-glucose (≥99.5%), D-inositol (≥99.5%), (±)-α-tocopherol (≥96%), rac-β-tocopherol (≥96%), (+)-δ-tocopherol (≥96%), (+)-γ-tocopherol (≥96%), Folin−Ciocalteu phenol reagent, 5α-cholestan-3β-ol (dihydrocholesterol, ≥95%), stigmasterol (≥95%), β-sitosterol (≥95%), betulinol (≥98%), and tetramethylbenzidine (TMB) were purchased from Sigma (St. Louis, MO). The purity of sterols was controlled by GC−FID. No. 1 filters (70 mm diameter) were used (Whatmann, Maidstone, England). Aminopropyl solid-phase extraction (SPE-$NH_2$) cartridges (Strata $NH_2$-55 mm, 500 mg/3 mL) from Phenomenex (Torrence, CA), were utilized for sterol oxide purification. The silylation mixture was prepared with dried pyridine, hexamethyldisilazane, and trimethylchlorosilane at a ratio of 5:2:1 by volume. Silylating agents and large silica TLC plates (20 cm × 20 cm × 0.25 mm film thickness) were supplied by Merck (Darmstadt, Germany).

**2.3. Extraction and Determination of Caffeine from CS.** CS was pulverized and subjected to caffeine extraction as reported by the ISO 20481:2008 method.[31] Briefly, 1 g of CS was placed in a flask and extracted with 250 mL of bidistilled water in the presence of 5 g of magnesium oxide for 20 min, under continuous stirring in a water bath at 90 °C. The supernatant was filtered through a nylon filter (0.45 μm) and diluted at 50% with methanol, and 10 μL of the extract was injected into a high-performance liquid chromatography (HPLC) system (HP1050 series; Hewlett-Packard, Palo Alto, CA). The latter was equipped with a quaternary pump, an autosampler Series 1100 (Agilent, Santa Clara, CA), an UV−vis photodiode, and a Poroshell 120 EC-C18 (Phenomenex, Torrance, CA) analytical column (50 × 3.0 mm, 2.7 μm particle size). An isocratic elution with HPLC-water:methanol (76:24, v/v) at a flow rate of 0.4 mL/min was carried out at room temperature. Data were acquired with Chemstation for LC3D software (Agilent Technologies, Palo Alto, CA). The caffeine determination and quantification was performed at the wavelength of maximum absorbance ($\lambda$ = 272 nm).

Caffeine was quantified by using an external standard calibration curve with a concentration range of 8.08−40.40 μg/mL. The linear regression equation and correlation coefficient were calculated for caffeine ($y = 71.933x + 11.127$; $R^2 = 0.999$). Limit of detection and limit of quantitation were calculated as 3- and 10-fold the signal-to-noise ratio. Caffeine content of CS samples is expressed as grams per 100 g of CS (g/100 g CS), and each determination was performed in triplicate.

**2.4. Determination of Moisture.** The moisture content of CS was determined as reported by AOAC.[32] Samples were kept under vacuum (2 mbar) at 70 °C for 16 h. The moisture and dry weight were gravimetrically determined in triplicate.

**2.5. Determination of Insoluble, Soluble, and Total Dietary Fiber.** The insoluble (IDF), soluble (SDF), and total (TDF) dietary fiber contents were determined by using the total dietary fiber assay kit, according to the enzymatic−gravimetric method suggested by Borrelli et al.[15]

One gram of CS was suspended in 40 mL of Tris-Mes buffer (0.05 mM) and added with 50 μL of α-amylase. The mixture was heated at 95 °C for 35 min. Then the solution was cooled down at 60 °C, 10 μL of the protease was added, and the mixture incubated at 60 °C for 30 min. In order to stop the reaction, 5 mL of HCl (0.56 M) was added and pH was adjusted to a value between 4.1 and 4.8, by using NaOH (0.5 M) and HCl (0.5 M). Finally, 200 μL of amyloglucosidase was added and the solution was incubated at 60 °C for 30 min (A).

For the IDF determination, the enzymatically digested solution (A) was filtered on the crucible and the insoluble material (which contains the IDF) was washed with 10 mL of warm bidistilled water (60 °C). Two identical aliquots of insoluble matter were prepared. Both aliquots were placed at 103 °C overnight and then weighed. Afterward, one of them was placed in a muffle furnace at 525 °C for 5 h and then weighed to quantify the ashes; the other one was used to quantify the protein amount ($p$) by the Kjeldahl method.[33] The digestion was performed with $H_2SO_4$ (96%) at 420 °C for 2 h.

The protein amount was subtracted from IDF by applying the following formula:

$$\text{IDF}\ (\%) = [[R - (p + (\text{As}/100))R] - B]/100m$$

where $R$ is the total solids from $m$, $m$ is the sample weight (g), $p$ is the protein weight (g), As is the ashes weight (g) from $R$, and $B$ is the weight of blank (g) (enzymes + solvents without sample). $B$ was calculated as follows:

$$B = \text{total solid weight} - (\text{protein weight} + \text{ashes of solid weight})$$

For SDF determination, 300 mL of ethanol (95%) at 60 °C was added to filtered fractions collected from IDF separation, in order to precipitate the fiber fraction; after 1 h, SDF was recovered by filtration on the crucible. The insoluble matter was washed with 10 mL of ethanol (78%), followed by 10 mL of ethanol (90%). The following steps were performed as above-described for the IDF determination. The percentage of SDF was calculated using the same formula for IDF evaluation.

For TDF determination, 300 mL of ethanol (95%) at 60 °C was added to the enzymatically digested solution (A), and after 1 h, this solution was filtered. The TDF was obtained by filtering the ethanol solution through a crucible with a Celite filter (1 g). Subsequently, insoluble material was repeatedly washed with 15 mL of ethanol (78%), followed by 10 mL of ethanol (90%) and 10 mL of acetone. The following steps were performed as aforementioned for IDF determination. The percentage of TDF was calculated from the same formula used for IDF evaluation.

The results are expressed as a percentage (%).

**2.6. Extraction and Determination of Soluble Carbohydrates.** The soluble carbohydrates were extracted from 10 g of CS using 250 mL of bidistilled water at 50 °C and ultrasound (Branson 2510, Thermo Fischer Scientific, Waltham, MA) for 30 min. After cooling, the supernatant was filtered through a nylon filter (0.45 μm) and injected into HPLC system by autosampler. The soluble carbohydrate amount and composition were determined using an HPLC equipped with a LC-10 A (JASCO, Tokyo, Japan) quaternary pump, a Rezex RPM-Monosaccharides $Pb^{2+}$ column (300 mm × 7.8 mm × 8.0 μm) at 75 °C, and a refractive index (RI) detector. HPLC-grade water was used as mobile phase at flow rate of 0.7 mL/min. The identification of soluble carbohydrates was carried out by injecting a standard mixture containing D-dulcitol, D-inositol, D-mannitol, D-sucrose, D-glucose, and D-fructose. Soluble carbohydrates were quantified by using an external standard calibration curve of glucose. Soluble carbohydrate content of CS samples are expressed as a percentage of glucose equivalent. The determination was performed in triplicate.

**2.7. Determination of Total Phenolic Compounds.** Phenolic compounds were extracted from CS by solid−liquid extraction, according to a modified version of the method suggested by Pirisi et al.[34] Ten milliliters of $CH_3OH$:$H_2O$ solution (60:40, v/v) were added to 1 g of CS, and total phenols were extracted at 45 °C for 15 min. The sample was then centrifuged for 20 min at 1000$g$ and the supernatant was collected; other two extractions were performed using the same conditions. The supernatant fraction was collected, and after solvent evaporation by rotary evaporator, the phenolic fraction was dissolved in 8 mL of $CH_3OH$:$H_2O$ solution (50:50, v/v).

Folin−Ciocalteu reactive solution (0.5 mL) was added to 100 μL of the extracted phenolic fraction and incubated in the presence of $Na_2CO_3$ (15%, p/v) for 2 h at room temperature. The absorbance was measured at 750 nm, using a double-beam UV−visible spectrophotometer (JASCO model V-550, JASCO International, Tokyo, Japan). For the quantification of total phenolic compounds, a calibration curve of gallic acid (GA) was used with a concentration range of 2.01−10.1 μg/mL ($y = 128.65x + 0.0492$; $R^2 = 0.996$). The results are expressed as milligrams of GA equivalents per 100 g of CS (mg GA equiv/100 g CA).

**2.8. Determination of Lipid Content.** Different extraction methods were tested and compared: a modified version of the method proposed by Folch et al.[35] (A), the Soxhlet method[36] performed with $n$-hexane (B) and petroleum ether (40−60 °C) (C), and a direct solid−liquid extraction with $n$-hexane:CS (1:100, v/w) (D). In the latter case, 1 g of CS was added to the solvent,

homogenized by Ultra-Turrax for 3 min, and then subjected to ultrasound for 20 min. The organic layer (containing the lipid matter) was separated by centrifugation (1620*g* for 20 min); this procedure was carried out in triplicate. The lipid fraction was collected and dried with a rotary evaporator; the fat amount was determined gravimetrically.

Each method for lipid extraction was performed in triplicate ($n = 3$).

**2.9. Chromatographic Lipid Profile.** Twenty milligrams of the lipid extract was dissolved in 1 mL of *n*-hexane, and 1 μL was injected in the GC−FID. A fused silica capillary column (Restek RTX-5, 10 m × 0.25 mm i.d. × 0.1 μm film thickness; Bellefonte, PA), coated with 95% dimethyl- and 5% diphenylpolysiloxane, was used. The temperature was programmed from 100 to 350 °C at 6 °C/min. The injector and FID temperatures were set at 350 °C. The injection was performed in the split mode (1:50), and helium at a flow of 1 mL/min was used as the carrier gas. The different lipid classes (free fatty acids, free and esterified sterols, monoacylglycerols, diacylglycerols, triacylglycerols) were identified using diverse commercial standards. The data are expressed as area percentage.

**2.10. Determination of Total Fatty Acids Methyl Esters.** About 20 mg of lipid extract were methylated with 200 μL of diazomethane;[37] 1.01 mg of tridecanoic acid methyl ester was added (as internal standard), and the mixture was transmethylated with 40 μL of 2 N KOH in methanol.[38] The composition of total fatty acid methyl esters was determined by injecting 1 μL of the supernatant of transmethylated solution into a GC−FID, as reported by Cardenia et al.[39] The data are expressed as a percentage of CS and total fatty acids.

**2.11. Determination of Sterols in CS.** A 150 mg subfraction of the lipid extract was added with known amounts of the internal standard solution (1.6 mg of dihydrocholesterol and 0.125 mg of 19-HC for the determination of total sterols and POPs, respectively). Subsequently, the sample was dried under nitrogen stream and treated with 10 mL of 1 N KOH solution in methanol to perform a cold saponification at room temperature for 18 h, as reported by Sander et al.[40]

One-tenth of the unsaponifiable matter was used for the determination of total sterols, whereas the remaining part was utilized for POP analysis.

Two milligrams of unsaponifiable matter was dissolved in chloroform and loaded on a 20 × 20 cm silica TLC plate, which had been previously immersed in a 0.2 N KOH solution in ethanol. The mobile phase was a mixture of *n*-hexane:diethyl ether (65:35, v/v). The TLC bands of the unsaponifiable components were visualized by spraying with a 0.2% ethanolic solution of 2′,7′-dichlorofluorescein sodium salt, under UV light (254 nm). The bands were separately scraped off, transferred in tubes, and extracted three times with 3 mL of chloroform each time. The fractions were collected, dried under nitrogen flow at room temperature, silylated,[41] and analyzed by Fast GC/MS.

Fast GC/MS analysis was performed using a GC Shimadzu QP 2010 Plus (Kyoto, Japan) equipped with a split−splitless injector and coupled to an electron impact (EI) mass spectrometric detector. A Restek RTX-5 fused silica capillary column (10 m × 0.1 mm i.d. × 0.1 μm film thickness; Bellefonte, PA), coated with 95% dimethyl- and 5% diphenylpolysiloxane, was used. A nonsilanized standard split liner (95 mm × 5 mm o.d. × 3.4 mm i.d.) was utilized. The temperature was programmed from 220 to 325 °C at 5 °C/min. The injector and the ion source temperatures were set at 325 and 200 °C, respectively. The injection was performed in the split mode (1:50), and helium at a linear velocity of 47.7 cm/s was used as the carrier gas. The electron energy was 70 eV. A mass range from 50 to 650 *m*/*z* was scanned at a rate of 2500 amu/s, which corresponded to 0.3 event time. The acquisition and integration modes were full scan (TIC) and single ion monitoring (SIM), respectively. PS were recognized and quantified by their corresponding characteristic ions, as reported by Inchingolo et al.:[42] 215 *m*/*z*, dihydrocholesterol (internal standard); 382 *m*/*z*, campesterol; 83 *m*/*z*, stigmasterol; 396 *m*/*z*, β-sitosterol; 488 *m*/*z*, sitostanol; and 459 *m*/*z*, campestanol. The data are expressed as percentage of CS and lipid matter.

**2.12. Determination of Phytosterol Oxidation Products (POPs).** The $^{9}/_{10}$ of the unsaponifiable matter was purified by silica solid-phase extraction (SPE-SI), as reported by Guardiola et al.[43] TMSE derivatives of POPs were analyzed by Fast GC−MS, as suggested by Cardenia et al.[45] with minor modifications. A Shimadzu GC-MS QP 2010 Plus (Kyoto, Japan) was fitted with an RTX-5 Restek capillary column (10 m × 0.1 mm i.d. × 0.1 μm film thickness; Supelco, Bellefonte, PA), and helium was used as carrier gas (0.5 mL/min). The oven temperature was programmed from 220 to 325 °C at the rate of 5 °C/min. The injector and transfer line temperatures were set at 325 and 320 °C, respectively. Manual injection of 1 μL of the solution containing POPs and the solutions obtained from samples was performed in the split mode at a 1:50 ratio. The filament emission current was 70 eV. A mass range from 40 to 650 *m*/*z* was scanned at a rate of 1500 amu/s. The acquisition and integration modes were full scan (TIC) and single ion monitoring (SIM), respectively.

Identification of POPs was performed by comparing their retention times and mass spectra with an internal laboratory library, as well as with those reported in the literature. POPs were recognized and quantified by their corresponding characteristic ions, which show a high abundance in SIM mode: 353 *m*/*z*, 19-hydroxycholesterol (19-HC, internal standard); 470 *m*/*z*, 7α/β-hydroxycampesterol (7α/β-HCA); 482 *m*/*z*, 7α/β-hydroxystigmasterol (7α/β-HST); 484 *m*/*z*, 7α/β-hydroxysitosterol (7α/β-HSI); 488 *m*/*z* α/β-epoxycampesterols (α/β-ECA); 500 *m*/*z*, α/β-epoxystigmasterols (α/β-EST); 412 *m*/*z*, α/β-epoxysitosterols (α/β-ESI); 417 *m*/*z*, campestanetriol (CATr); 429 *m*/*z*, stigmastentriol (STTr); 431 *m*/*z*, sitostanetriol (SITr); 486 *m*/*z*, 7-ketocampesterol (7-KCA); 498 *m*/*z*, 7-ketostigmasterol (7-KST); 500 *m*/*z*, 7-ketositosterol (7-KSI). The full MS fragmentation of POPs is reported in Figures S.1−S.18 and Table S.1 in the Supporting Information. Considering that POP standards are not commercially available and that POP fragmentation is similar to that of cholesterol oxidation products (COPs), POPs quantification was performed by using the calibration curves obtained for cholesterol oxides in SIM mode.[44] The data are expressed as milligrams per 100 g of CS (mg/100 g CS).

**2.13. Determination of Ochratoxin A (OTA).** A Helica Ochratoxin A Assay Kit (Helica Biosystem Inc., Santa Ana, CA), which is a solid-phase direct enzyme immunoassay, was used for the determination of OTA in CS. OTA was extracted from 25 g of CS with 125 mL of methanol (70%) and the extracted fluid was filtered by Whatman filter (No. 1; Whatman International Ltd., Maidstone, England). The latter (100 μL) was allowed to react with 200 μL of horseradish peroxidase (HRP), put in polystyrene microwells coated by antibody with high affinity for OTA, and incubated for 5 min. Thereafter, the wells were washed with water and TMB, and substrate was added, which develops a blue color in the presence of the enzyme that is inversely proportional to the content of OTA. The reaction was stopped by adding 100 μL of diluted $H_2SO_4$, and the blue color of the solution became yellow. The absorbance was determined at 450 nm, by using an ELISA reader. OTA was quantified by using a calibration curve of OTA with a concentration range of 0.4−8.0 ng/mL, which corresponded to 20.0−40.0 μg/kg OTA. The results are expressed as micrograms per kilogram of CS (μg/mg CS).

**2.14. Statistical Analysis.** For all analytical determinations, the data are reported as median values and the standard deviation of 15 independent replicates ($n = 15$), except for OTA, where 30 independent replicates ($n = 30$) were analyzed. Statistical analysis of the data was performed by R 3.0.2 (R Foundation for Statistical Computing, 2013).

## 3. RESULTS AND DISCUSSION

**3.1. Caffeine Content.** A noticeable amount of caffeine in CS samples was found. In general, the average caffeine content (0.8−1.0%) was in agreement with those reported by Napolitano et al.[5] (0.83−1.37%). However, other authors found higher caffeine levels (1.7−4.1 and 8.9−11.1%).[1,16,45] Such differences could be attributed to the diverse methods used for caffeine extraction from CS.

Table 1. Chemical Composition of CS [moisture (g/100 g CS), dietary fiber (g/100 g CS), caffeine (g/100 g CS), carbohydrates (g/100 g CS), and polyphenols (g GA/100 g CS)] and Its Comparison with Literature Data[a]

| | Present work | Ref 15 | Ref 17 | Ref 3 | Ref 16 | Ref 1 |
|---|---|---|---|---|---|---|
| Moisture | 2.59−10.34 (4.26; 2.79) | 7.30 ± 0.4 | 7.1 ± 0.21 | NR | NR | NR |
| TDF | 67.7−80.0 (74.15; 4.49) | 62.4 ± 0.6 | 62.4 ± 0.5 | 80.0 ± 0.6 | NR | NR |
| IDF | 54.4−79.5 (66.50; 7.58) | 53.7 ± 0.2 | 53.7 ± 0.4 | 64.0 ± 0.8 | NR | NR |
| SDF | 8.2−14.2 (10.90; 1.79) | 8.8 ± 0.4 | 8.8 ± 0.6 | 16.0 ± 0.5 | NR | NR |
| Caffeine | 0.77−1.03 (0.91; 0.09) | NR | NR | NR | 0.41−0.44 | 0.89−1.1 |
| Soluble Carbohydrates | 0.8−1.6 (1.07; 0.26) | 0.21 ± 0.01 | NR | NR | 1.5−4.0 | NR |
| Sucrose | 0.1−0.3 (0.13; 0.08) | NR | NR | NR | NR | NR |
| Glucose | nd−0.3 (0.15; 0.07) | NR | NR | NR | NR | NR |
| fructose | 0.3−0.7 (0.43; 0.12) | NR | NR | NR | NR | NR |
| Inositol | 0.1−0.2 (0.15; 0.05) | NR | NR | NR | NR | NR |
| Mannitol | 0.1−0.3 (0.17; 0.06) | NR | NR | NR | NR | NR |
| Others | nd−0.1 (0.06; 0.01) | NR | NR | NR | NR | NR |
| Polyphenols | 0.39−0.73 (0.56; 0.13) | NR | NR | 1.5 ± 0.9 | 0.5−3.6 | 1.5−1.7 |

[a]The results are expressed as min−max (median; standard deviation, $n$ = 45). Literature data are expressed either as min−max or as mean ± standard deviation. Abbreviations: nd = not detected, NR, not reported.

Table 2. Total Lipid Content (g/100 g CS) and Lipid Composition (% of total lipid matter) of CS As Related to the Extraction Methods Used (A, B, C, and D)[a]

| | Method A | Method B | Method C | Method D | Stat Signif[b] |
|---|---|---|---|---|---|
| Lipid | 5.2 ± 0.0 a | 3.4 ± 0.2 b | 3.61 ± 0.7 b | 1.9 ± 0.1 c | ** |
| FFA | 58.4 ± 2.3 a | 20.7 ± 3.8 b | 24.1 ± 3.4 b | 30.9 ± 7.0 b | ** |
| S | 16.7 ± 0.3 b | 12.9 ± 0.4 b | 13.7 ± 0.9 b | 32.9 ± 5.6 a | ** |
| DG | 11.9 ± 1.0 a | 4.2 ± 1.1 b | 6.8 ± 1.3 bc | 8.1 ± 1.9 bc | * |
| ES | 3.7 ± 0.5 b | 14.6 ± 2.7 a | 6.4 ± 1.4 b | 9.1 ± 1.8 ab | * |
| TG | 9.2 ± 0.1 c | 47.6 ± 0.9 a | 48.9 ± 1.0 a | 18.9 ± 2.6 b | *** |

[a]The results are expressed as mean ± standard deviation ($n$ = 15). Different letters in each row denote statistically different means (Tukey's test; $P \leq 0.05$). Abbreviations: method A, Folch et al.'s method;[35] method B, Soxhlet[36] performed with $n$-hexane; method C, Soxhlet[36] performed with petroleum ether (40−60 °C); method D, direct solid−liquid extraction with $n$-hexane:CS (1:100, v/w); stat signif, statistical significance. [b]The asterisks denote the level of significance: *significant at $P \leq 0.05$; **significant at $P \leq 0.01$; ***significant at $P \leq 0.001$.

**3.2. Moisture Content.** Since microbial growth is greatly affected by humidity,[46] the moisture content of CS was determined during storage. After CS removal during the roasting process, it was collected and pressed in the presence of water; however, a noncontrolled hydration system was used, and this could have affected the moisture content of the CS samples (Table 1). In fact, high data dispersion was observed (average values 2.6−8.2%), with the highest and lowest moisture levels found in the first and the fourth weeks, respectively. Nevertheless, the present data are in agreement with those reported in the literature.[4,15]

**3.3. Content of Dietary Fibers.** TDF, IDF, and SDF were determined (Table 1). Average TDF (70−79%) was composed of about 85% IDF and 15% SDF, which are in agreement with the results reported by Murthy et al.;[47] however, the present data were higher than those found by Borrelli et al.,[15] which might be due to the different extraction conditions used. The high content of fibers confirms that CS could be utilized in the food industry, to develop functional food and beverages for the control of human body weight, for prevention of pathologies related to carbohydrates metabolism (such as obesity, diabetes, etc.),[8] or as an alternative source of dietary fiber for bread making.[17]

**3.4. Soluble Carbohydrate Content.** As shown in Table 1, the average total amount of soluble carbohydrates ranged from 0.87 to 1.39% and were mainly composed of fructose (0.34−0.58% CS), sucrose (0.09−0.25% CS), mannitol (0.11−0.23% CS), glucose (0.08−0.21% CS), and inositol (0.08−0.19% CS). It must be pointed out that CS is mainly constituted by two polysaccharides, cellulose and hemicellulose, which contain glucose, xylose, galactose, mannose, and arabinose; however, Mussatto et al.[7] found that glucose was the main carbohydrate in CS, which is in contrast with data found here. Furthermore, other authors found a wide range of total sugar content (1.6−12%) in CS.[16] These differences might be related to the extraction procedures used, as they might have led to a diverse hydrolysis degree of the native polysaccharides, thus being reflected in a different final content of the single mono- and disaccharides.

**3.5. Content of Phenolic Compounds.** Phenolic compounds are well-known for their antioxidant activity and their defense role, so many authors have studied their presence in CS.[1,3,15,16,48] The total phenolic compounds were determined by the Folin−Ciocalteau method, and their average content ranged from 0.46 to 0.71 g/100 g CS; these levels agree with those found by Murthy and Naidu[3] and Bresciani et al.,[1] but they were lower than those reported by Narita and Inouye,[16] who used subcritical water. It might be possible that, during coffee roasting, phenols were degraded due the high processing temperature and that melanoidins were formed, thus affecting the Folin−Ciocalteau method, probably due to a chemical redox-based principle as described by Bresciani et al.,[1] who reported that the phenolic matter of CS was mostly

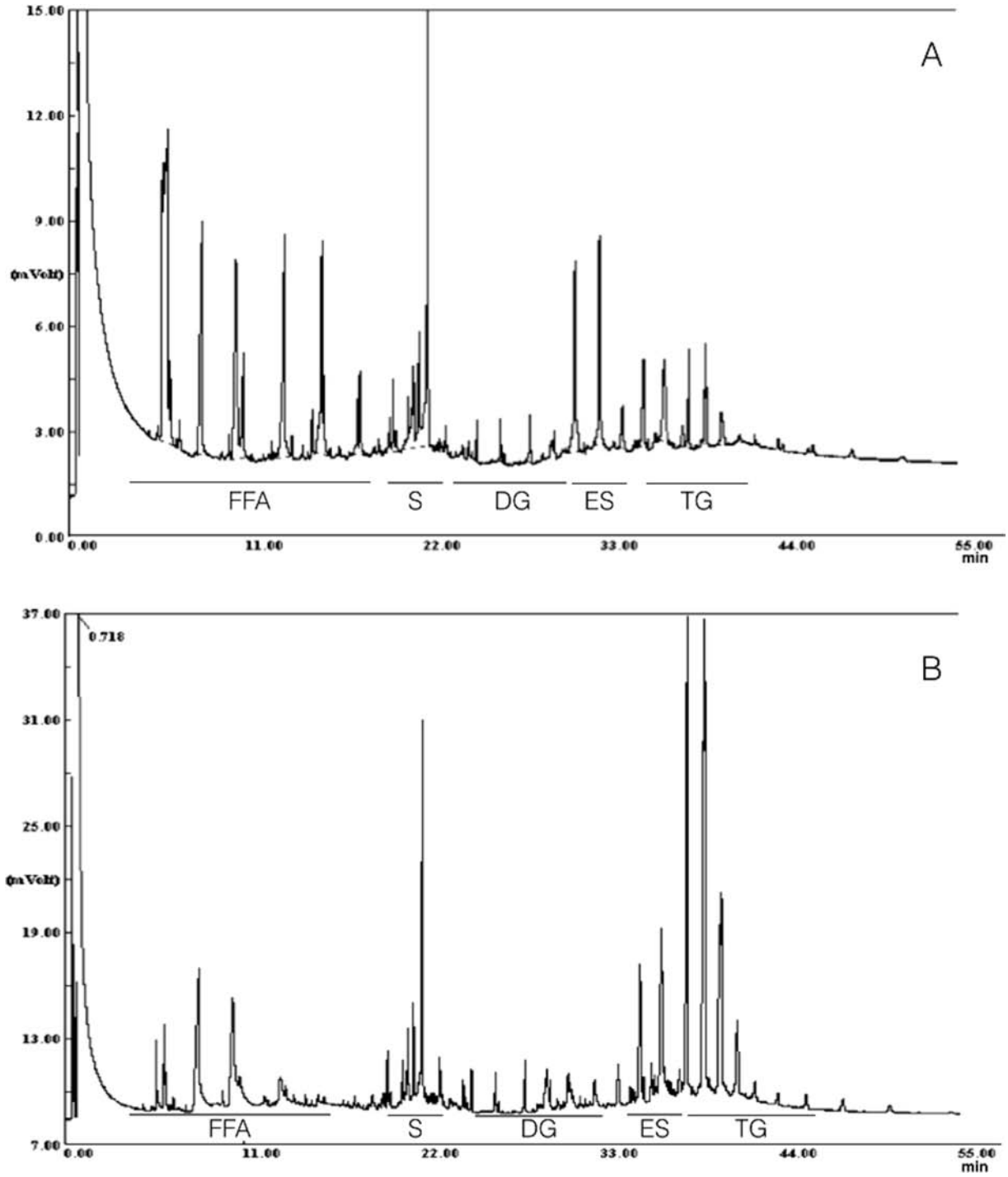


**Figure 2.** Chromatographic lipid profile of CS, obtained after extraction with two different methods (A and B). Abbreviations: FFA, free fatty acids; S, free sterols; DG, diacylglycerols; ES, esterified sterols; TG, triacylglycerols.

constituted by chlorogenic acids (coumaroylquinic, feruloylquinic, and caffeoylquinic acids).

**3.6. Lipid and Fatty Acid Composition.** Many authors have suggested the potential reuse of CS, mainly due to its content of antioxidant compounds, fiber, and caffeine. However, there are few data available about the lipid composition; in fact, only three studies report the lipid content of CS, which varies from 2.0 to 7.0%.[6,15,17]

In the present paper, different extraction methods were tested to obtain the lipid fraction; in particular, the method suggested by Folch et al.[35] (A) was compared with the Soxhlet one[36] using *n*-hexane (B) and petroleum ether (40−60 °C) (C), and a liquid extraction with *n*-hexane (D). The method A led to the highest amount of extracted lipids (5.2%), but no significant differences were found with respect to methods B and C (3.4% and 3.61%, respectively); method D, instead, resulted in the significantly ($P \leq 0.05$) lowest amount of extracted lipids (about 1.9%) (Table 2). The different extraction procedures greatly impacted the lipid composition, as shown in Figure 2. When method A was used, the lipid fraction was mainly composed of free fatty acids (FFA; 58%), free sterols (S; 17%), diacylglycerols (DG; 12%), triacylglycer-

Table 3. Total Fatty Acid Composition of CS, Expressed in Matrix (g/100 g CS) and Lipid Basis (% of total fatty acids)[a]

| Fatty Acids | CS | | Lipid | |
|---|---|---|---|---|
| C14:0 | 0.010−0.013 | (0.01; 0.00) | 0.55−0.93 | (0.76; 0.13) |
| C15:0 | 0.002−0.003 | (0.00; 0.00) | 0.12−1.98 | (0.19; 0.57) |
| C16:0 | 0.323−0.633 | (0.39; 0.11) | 26.61−30.55 | (27.52; 1.37) |
| C16:1 *n*-7 | 0.001−0.002 | (0.00; 0.00) | 0.07−0.12 | (0.09; 0.02) |
| C17:0 | 0.002−0.003 | (0.00; 0.00) | 0.13−0.20 | (0.16; 0.02) |
| C18:0 | 0.077−0.151 | (0.10; 0.02) | 6.34−7.21 | (6.71; 0.29) |
| C18:1 *n*-9 | 0.068−0.152 | (0.10; 0.03) | 5.65−7.51 | (6.93; 0.65) |
| C18:1 *c*11 | 0.007−0.010 | (0.01; 0.00) | 0.50−0.59 | (0.55; 0.04) |
| C18:2 *n*-6 | 0.339−0.708 | (0.42; 0.13) | 28.22−33.90 | (29.22; 2.14) |
| C20:0 | 0.137−0.169 | (0.16; 0.01) | 7.77−11.22 | (10.83; 1.54) |
| C18:3 *n*-3 | 0.012−0.026 | (0.02; 0.00) | 1.01−1.34 | (1.27; 0.13) |
| CLA | 0.004−0.006 | (0.01; 0.00) | 0.24−0.39 | (0.35; 0.05) |
| C22:0 | 0.133−0.182 | (0.17; 0.02) | 7.73−13.16 | (11.48; 1.86) |
| C20:4 | 0.005−0.007 | (0.01; 0.00) | 0.31−0.45 | (0.43; 0.05) |
| C24:0 | 0.036−0.044 | (0.04; 0.00) | 1.73−3.00 | (2.82; 0.47) |
| ∑SFA | 0.758−1.172 | (0.92; 0.14) | 55.96−63.42 | (60.63; 2.50) |
| ∑UFA | 0.442−0.919 | (0.62; 0.16) | 36.58−39.72 | (39.37; 2.50) |
| ∑UFA/∑SFA | 1.271−1.714 | (1.48; 0.15) | 1.27−1.73 | (1.54; 0.15) |

[a]The results are expressed as min−max (median; standard deviation, $n$ = 45). Abbreviations: CLA, conjugated linoleic acid *cis*-9,*trans*-11-isomer; ∑SFA total saturated fatty acids; ∑UFA, total unsaturated fatty acids.

ols (TG; 9%), and esterified sterols (ES; 3.7%), whereas the lipid matter obtained with method B was essentially constituted by TG (48%), followed by FFA (21%), S (13%), ES (15%), and DG (4%) (Table 2). A slightly polar solvent (method A) increased the extraction of FFA in spite of TG, whereas when apolar solvent was used (e.g., method B), TG became the most abundant lipid class and the polar fraction (e.g., FFA) decreased. No significant differences ($P \geq 0.05$) were found on lipids extracted by method C with respect to method B (except for ES content), while method D led to a higher amount of FFA and a lower content of TG than B and D methods (Table 2). Comparing the different methods for the quantitavely extraction of lipids, method B was the most sustainable choice, and thus, all lipid analytical determinations (FAMEs, unsaponifiable composition, and POPs content) were carried out on the lipid extract obtained with method B.

Table 3 reports the total FA composition of CS. In general, the mean FA composition of the lipid fraction was principally constituted by saturated fatty acids (SFA) (0.9% CS, which corresponded to 60.6% lipid matter); in particular, palmitic acid (PA; C16:0) (0.39% CS; 27.5% lipid) was the main SFA, followed by behenic acid (BA; C22:0) (0.17% CS; 11.5% lipid), arachidic acid (AA; C20:0) (0.16% CS; 10.8% lipid), and stearic acid (SA; C18:0) (0.10% CS; 6.7% lipid). The unsaturated fraction (UFA) (0.6% CS; 39.4% lipid matter) was mainly composed of the essential fatty acids (EFAs) linoleic acid (LA; C18:2 *n*-6) (0.42% CS; 29.2% lipid) and oleic acid (OA; C18:1 *n*-9) (0.10% CS; 6.9% lipid), whereas only traces of the EFA α-linolenic acid (ALA; C18:3 *n*-3) (0.02% CS; 1.3% lipid) and conjugated linoleic acid *cis*-9,*trans*-11-isomer (CLA) (0.01% CS; 0.35% lipid) were found. No data about the FA composition of CS are available in literature, but it seems to be similar to that of crude coffee beans[49] and roasted coffee.[50] The average UFA/SFA ratio was about 1.5, which could be used as a potential tool to understand the oxidative stability of CS as related to storage. In fact, a higher presence of SFA, together with a considerable content of phenolic compounds, could limit CS degradation due to lipid oxidation. It should be noted that a negative relationship between the LA intake and LDL-cholesterol concentrations has been found, while a positive effect on HDL cholesterol concentrations and a consequent reduction of cardiovascular events have been reported.[51] Nevertheless, to the best of our knowledge, this is the first report of the fatty acid composition of CS, and according to the data here obtained, CS could also represent a possible source of EFAs.

**3.7. Sterol Composition.** Before investigating the sterol composition of CS, a qualitative analysis of the unsaponifiable matter was carried out by TLC. As shown in Figure 3, five

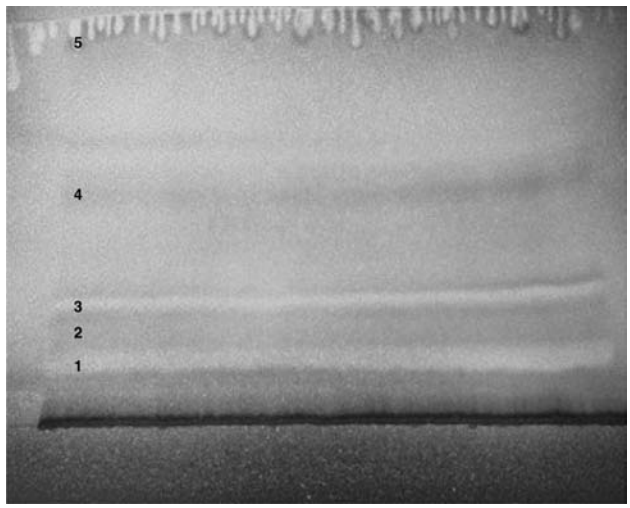


**Figure 3.** TLC fractionation of the unsaponifiable matter of CS. Identification of the TLC bands: (1) sterols, (2) 4-methylsterols, (3) 4,4′-dimethylsterols, (4) tocopherols, and (5) hydrocarbons.

different bands were well-separated, which corresponded (from the bottom to the top of the TLC elution direction) to sterols, 4-methylsterols, 4,4′-dimethylsterols, triterpenes, tocopherols, and hydrocarbons, respectively. Qualitative determination of the extracted TLC bands by GC/MS confirmed the presence of citrostadienol, α-amirine, β-amirine, cycloartenol, 24-methyl-

enecycloartenol, α-tocopherol, β-tocopherol, campesterol, stigmasterol, β-sitosterol, and 5-avenasterol.

The average total amount of sterols ranged from 7.0 to 12.1% of lipid, which corresponded to 0.21−0.36% of CS and was mainly composed of β-sitosterol (71.1%), campesterol (14.0%), stigmasterol (10.5%), and 5-avenasterol (4.4%). Comparing the data found here with those described for green coffee,[49,52] it is possible to observe that CS contains a lower amount of sterols; however, it should be considered that, during roasting, sterols could have been involved in a different degradation process (dehydration, oxidation, etc.), which could have led to their reduction[53]

**3.8. Composition of Phytosterol Oxidation Products (POPs).** Table 4 reports the amount of POPs in CS. The average total POPs was about 114.11 mg/100 g CS, the most abundant being those arising from β-sitosterol (93.26 mg/100 g CS, which corresponded to 2.98% lipid matter); in fact, 7α-hydroxysitosterol (1.70% lipids) was the main oxyphytosterol, followed by 7-ketositosterol (0.62% lipids), 7β-hydroxysitosterol (0.42% lipids), β-epoxysitosterol (0.09% lipids), α-epoxysitosterol (0.07% lipids), and triolsitosterol (0.07% lipids). Lower average amounts of POPs deriving from oxidation of campesterol (11.24 mg/100 g CS) and stigmasterol (9.60 mg/100 g CS) were found, 7α-hydroxyl and 7-keto derivatives being the main ones (Table 4). Epoxy isomers of these minor phytosterols and 5-avenasterol oxidation products were not found, probably due to the low amount of such sterols present in CS. The average phytosterol oxidation rate was determined (% POPs/PS; OR) and varied from 27.6 to 48.1%, which indicated that a high amount of PS was oxidized, probably due to the extensive heating during coffee roasting. It should be pointed out that while the toxicological aspects of cholesterol oxidation products are well-documented, the information about the biological impact of POPs is still limited. Some authors[26,29] have reported the role of POPs in many different biological mechanisms (cholesterol uptake and metabolism, atherosclerosis, inflammation, cytotoxicity, oxidative stress, etc.); Adcox et al.[30] have demonstrated that β-sitosterol and campesterol oxides have a similar toxicity in culture-derived macrophage cell (line C57BL6) as compared to COPs. In addition, according the threshold of toxicological concern (TTC) for unclassified compounds (0.15 μg per person/day[54]), the level of POPs found in CS could represent a risk for human health. Therefore, before suggesting the reuse of CS in foodstuffs, a deeper investigation on the presence of POPs and the prevention of their formation is indispensable.

**Table 4. Total Phytosterol Oxidation Products (POPs, expressed as mg/100 g CS) and Phytosterol Oxidation Ratio (OR, %) in CS[a]**

| | Derivative | POPs | OR |
|---|---|---|---|
| Campesterol | 7α-H | 6.88 ± 2.01 | 2.28 ± 0.67 |
| | 7β-H | 1.62 ± 0.37 | 0.54 ± 0.12 |
| | β-E | nd | nd |
| | α-E | nd | nd |
| | triol | 0.27 ± 0.22 | 0.09 ± 0.07 |
| | 7-K | 2.47 ± 1.10 | 0.82 ± 0.36 |
| Stigmasterol | 7α-H | 6.58 ± 1.49 | 2.18 ± 0.49 |
| | 7β-H | 1.62 ± 0.51 | 0.54 ± 0.17 |
| | β-E | nd | nd |
| | α-E | nd | nd |
| | triol | 0.16 ± 0.05 | 0.05 ± 0.02 |
| | 7-K | 1.24 ± 0.53 | 0.41 ± 0.18 |
| Sitosterol | 7α-H | 53.28 ± 19.89 | 17.66 ± 6.59 |
| | 7β-H | 13.26 ± 4.89 | 4.40 ± 1.64 |
| | β-E | 2.90 ± 1.48 | 0.96 ± 0.49 |
| | α-E | 2.25 ± 0.05 | 0.74 ± 0.02 |
| | triol | 2.10 ± 1.05 | 0.70 ± 0.35 |
| | 7-K | 19.48 ± 10.05 | 6.46 ± 3.33 |
| ∑POPs | | 114.11 ± 43.74 | 37.83 ± 14.50 |

[a]The results are expressed as mean ± standard deviation ($n$ = 15). Abbreviations: 7α-H, 7α-hydroxy derivatives; 7β-H, 7β-hydroxy derivatives; β-E, 5,6β-epoxy derivatives; α-E, 5,6α-epoxy derivatives; triol, triol derivatives; 7-K, 7-keto derivatives; nd, not detected.

**3.9. Ochratoxin A (OTA) Content.** In addition to the presence of a high level of POPs in CS, the occurrence of OTA could represent a further safety problem. The level of OTA in CS was controlled for 10 weeks. The content of OTA ranged from 17.8 to 36.1 μg/kg CS, being 5−9 times higher than those reported by Borrelli et al.[15] Since CS is considered a waste, there is no specific OTA regulation limit and there are very little OTA data in the literature. Considering the OTA limit fixed for coffee, the European Commission regulation[55] states that the maximum level of OTA in roasted coffee and soluble coffee should be 5 and 10 μg/kg, respectively, which is more than 3 times lower than the data found in the present study. Moreover, some authors[21,23] reported that the temperature used during roasting leads to an OTA reduction in coffee; however, it is important to consider that CS was removed during roasting and stored, so it is reasonable that the isolated CS showed a higher level of such mycotoxin. It is well-known that the presence of OTA is correlated to human nephropathy and urothelial urinary tract tumors, while in mice it increases the incidence of hepatocellular tumors, renal-cell adenomas, and carcinomas.[20] Therefore, a possible solution for the removal or dilution of OTA from CS should be studied, if CS is intended for human or livestock consumption.

In conclusion, data obtained in the present work suggest that CS could be used as a source of cellulose for paper production, as well as a source of bioactive compounds (such as fiber and polyphenols) to be employed as ingredients in pharmaceutical/cosmetic industries or for development of functional foods. However, the noticeable amounts of POPs and OTA found in CS might represent a risk for human safety if intended for human or livestock use; therefore, it is very important to set up a rigorous quality control and to develop a suitable procedure for the reduction of the aforementioned contaminants.

## ■ ASSOCIATED CONTENT

### Supporting Information

Table S.1, summarizing characteristic ions of phytosterol oxidation products, and Figures S.1−S.18, showing the mass spectra of compounds of interest. This material is available free of charge via the Internet at http://pubs.acs.org.

## ■ AUTHOR INFORMATION

### Corresponding Author

*Tel: +39-051-2096015. Fax: +39-051-2096017. E-mail: vladimiro.cardenia3@unibo.it.

### Funding

Co. Ind. S.c. (Bologna, Italy) provided financial support.

### Notes

The authors declare no competing financial interest.

## ■ ACKNOWLEDGMENTS

The authors thank Co. Ind. S.c. (Bologna, Italy) for providing the samples and RVF Ambiente S.R.L. (Ferrara, Italy) for the collaboration.

## ■ REFERENCES

(1) Bresciani, L.; Calani, L.; Bruni, R.; Brighenti, F.; Del Rio, D. *Food Res. Int.* **2014**, *61*, 196−201.
(2) Andrade, K. S.; Gonçalvez, R. T.; Maraschin, M.; Ribeiro-do-Valle, R. M.; Martínez, J.; Ferreira, S. R. S. *Talanta* **2012**, *88*, 544−552.
(3) Murthy, P. S.; Naidu, M. M. *Food Bioprocess. Technol.* **2010**, *5*, 897−903.
(4) Narita, Y.; Inouye, K. *Food Res. Int.* **2014**, 1−7.
(5) Napolitano, A.; Fogliano, V.; Tafuri, A.; Ritieni, A. *J. Agric. Food Chem.* **2007**, *55*, 10499−10504.
(6) Esquivel, P.; Jiménez, V. M. *Food Res. Int.* **2012**, *46*, 488−495.
(7) Mussatto, S. I.; Machado, E. M. S.; Martins, S.; Teixeira, J. A. *Food Bioprocess. Technol.* **2011**, *4*, 661−672.
(8) Martinez-Saez, N.; Ullate, M.; Martin-Cabrejas, M. A.; Martorell, P.; Genovés, S.; Ramon, D.; del Castillo, M. D. *Food Chem.* **2014**, *150*, 227−234.
(9) Mussatto, S. I.; Ballesteros, L. F.; Martins, S.; Teixeira, J. A. *Sep. Purif. Technol.* **2011**, *83*, 173−179.
(10) Marchei, E.; De Orsi, D.; Guarino, C.; Dorato, S.; Pacifici, R.; Pichini, S. *Anal. Methods* **2013**, *5*, 376.
(11) Glade, M. J. *Nutrition (Burbank, CA, U. S.)* **2010**, *26*, 932−938.
(12) O'Keefe, J. H.; Bhatti, S. K.; Patil, H. R.; DiNicolantonio, J. J.; Lucan, S. C.; Lavie, C. J. *J. Am. Coll. Cardiol.* **2013**, *62*, 1043−1051.
(13) Lupi, O.; Semenovitch, I. J.; Treu, C.; Bottino, D.; Bouskela, E. *J. Cosmet. Dermatol.* **2007**, *6*, 102−107.
(14) Herman, A.; Herman, A. P. *Skin Pharmacol. Physiol.* **2013**, *26*, 8−14.
(15) Borrelli, R. C.; Esposito, F.; Napolitano, A.; Ritieni, A.; Fogliano, V. *J. Agric. Food Chem.* **2004**, *52*, 1338−1343.
(16) Narita, Y.; Inouye, K. *Food Chem.* **2012**, *135*, 943−949.
(17) Pourfarzad, A.; Mahdavian-Mehr, H.; Sedaghat, N. *LWT—Food Sci. Technol.* **2013**, *50*, 599−606.
(18) Furusawa, M.; Narita, Y.; Iwai, K.; Fukunaga, T.; Nakagiri, O. *Biosci. Biotechnol. Biochem.* **2011**, *75*, 1205−1207.
(19) Jaquet, M.; Rochat, I.; Moulin, J.; Cavin, C.; Bibiloni, R. *Int. J. Food Microbiol.* **2009**, *130*, 117−121.
(20) IARC. *IARC Monographs on the Evaluation of Carcinogenic Risks to Humans*; International Agency of Research on Cancer: Lyon, France, 1993; Vol. *56*, p 489.
(21) Ferraz, M. B. M.; Farah, A.; Iamanaka, B. T.; Perrone, D.; Copetti, M. V.; Marques, V. X.; Vitali, A. A.; Taniwaki, M. H. *Food Control* **2010**, *21*, 872−877.
(22) Studer-Rohr, I.; Dietrich, D. R.; Schlatter, J.; Schlatter, C. *Food Chem. Toxicol.* **1995**, *5*, 341−355.
(23) Romani, S.; Pinnavaia, G. G.; Dalla Rosa, M. *Food Chem.* **2003**, *51*, 5168−5171.
(24) Vanesa, D.; Ana, P. *Food Control* **2013**, *30*, 675−678.
(25) Castellanos-Onorio, O.; Gonzalez-Rios, O.; Guyot, B.; Fontana, T. A.; Guiraud, J. P.; Schorr-Galindo, S.; Durand, N.; Suárez-Quiroz, M. *Food Control* **2011**, *22*, 1184−1188.
(26) García-Llatas, G.; Rodríguez-Estrada, M. T. *Chem. Phys. Lipids* **2011**, *164*, 607−624.
(27) Boselli, E.; Cardenia, V.; Rodriguez-Estrada, M. T. *Eur. J. Lipid Sci. Technol.* **2012**, *114*, 644−655.
(28) Otaegui-Arrazola, A.; Menendez-Carreno, M.; Ansorena, D.; Astiasarán, I. *Food Chem. Toxicol.* **2010**, *48*, 3289−3303.
(29) O'Callaghan, Y.; McCarthy, F. O.; O'Brien, N. M. *Biochem. Biophys. Res. Commun.* **2014**, 1−6.
(30) Adcox, C.; Boyd, L.; Oehrl, L.; Allen, J.; Fenner, G. *J. Agric. Food Chem.* **2001**, *49*, 2090−2095.
(31) ISO. *ISO 20481:2008*; International Organization for Standardization: Geneva, 2008.
(32) AOAC. In *Association of Official Analytical Chemists*, 13th ed.; Horwitz, W., Latimer, G., Eds.; AOAC: Washington, DC, 1980; pp 376−384.
(33) Kjeldahl, J. Z. *Anal. Chem.* **1883**, *22*, 366−382.
(34) Pirisi, F. M.; Cabras, P.; Falqui Cao, C.; Migliorini, M.; Muggelli, M. *J. Agric. Food Chem.* **2000**, *48*, 1191−1196.
(35) Folch, J.; Lees, M.; Stanley, G. H. S. *J. Biol. Chem.* **1957**, *226*, 497−509.
(36) Soxhlet, F. *Dinglers Polytech. J.* **1879**, *232*, 461−465.
(37) Fieser, L. F.; Fieser, M. In *Reagents for Organic Chemistry*; Wiley: New York, 1967; pp 101−192.
(38) European Commision. *Off. J. Eur. Communities* **2002**, L128/14, Allegate B.
(39) Cardenia, V.; Rodriguez-Estrada, M. T.; Baldacci, E.; Lercker, G. *Food Chem. Toxicol.* **2013**, *57*, 32−38.
(40) Sander, B. D.; Addis, P. B.; Park, S. W.; Smith, D. E. *J. Food Prot.* **1989**, *52*, 109−114.
(41) Sweeley, C. C.; Bentley, R.; Makita, M.; Wells, W. W. *J. Am. Chem. Soc.* **1963**, *85*, 2497−2507.
(42) Inchingolo, R.; Cardenia, V.; Rodriguez-Estrada, M. T. *J. Sep. Sci.* **2014**, *37*, 2911−2919.
(43) Guardiola, F.; Codony, R.; Rafecas, M.; Boatella, J. *J. Chromatogr. A* **1995**, *705*, 289−304.
(44) Cardenia, V.; Rodriguez-Estrada, M. T.; Baldacci, E.; Savioli, S.; Lercker, G. *J. Sep. Sci.* **2012**, *35*, 424−430.
(45) Ribeiro, V. S.; Leitão, A. E.; Ramalho, J. C.; Lidon, F. C. *Food Res. Int.* **2014**, *61*, 39−47.
(46) Machado, E. M. S.; Rodriguez-Jasso, R. M.; Teixeira, J. A.; Mussatto, S. I. *Biochem. Eng. J.* **2012**, *60*, 87−90.
(47) Murthy, P. S.; Madhava Naidu, M. *Resour. Conserv. Recycl.* **2012**, *66*, 45−58.
(48) Ballesteros, L. F.; Teixeira, J. A.; Mussatto, S. I. *Food Bioprocess Technol.* **2014**, *7*, 1322−1332.
(49) Nikolova-Damyanova, B.; Velikova, R.; Jham, G. N. *Food Res. Int.* **1999**, *31*, 479−486.
(50) Toci, A. T.; Neto, V. J. M. F.; Torres, A. G.; Farah, A. *LWT—Food Sci. Technol.* **2013**, *50*, 581−590.
(51) EFSA Panel on Dietetic Products Nutrition and Allergies. *EFSA J.* **2010**, *8*, 1−107.
(52) Speer, K.; Kölling-speer, I. *Braz J. Plant Physiol.* **2006**, *18*, 201−216.
(53) Lercker, G.; Frega, N.; Bocci, E.; Rodriguez-Estrada, M. T. *Chromatographia* **1995**, *41*, 29−33.
(54) Kroes, R.; Renwick, A. G.; Cheeseman, M.; Kleiner, J.; Mangelsdorf, I.; Piersma, A.; Schilter, B.; Schlatter, J.; Van Schothorst, F.; Vos, J. G.; Wurtzen, G. *Food Chem. Toxicol.* **2004**, *42*, 65−83.
(55) Commission Regulation (EC). *Off. J. Eur. Communities* **2006**, L 364/5, 5−24.

JOURNAL OF AGRICULTURAL AND FOOD CHEMISTRY

Addition/Correction

pubs.acs.org/JAFC

# Correction to Utilization of Phosphate Rock from Lisina for Direct Application: Release of Plant Nutrients in the Exchange-Fertilizer Mixtures

Marija Mihajlović, Nebojša Perišić,* Lato Pezo, Mirjana Stojanović, Jelena Milojković, Zorica Lopičić, and Marija Petrović

*J. Agric. Food Chem.* **2014**, *62* (41), 9965−9973. DOI: 10.1021/jf502704j

Table 1 erroneously gave the composition of Ca-Cp when it should have been K-Cp. The corrected table is given below.

**Table 1. Chemical Composition of the Clinoptilolite (Cp) Used in the Study**

| oxide | $SiO_2$ | $Al_2O3$ | $Fe_2O_3$ | CaO | MgO | $TiO_2$ | $Na_2O$ | $K_2O$ | loi |
|---|---|---|---|---|---|---|---|---|---|
| % (w/w) | 65.89 | 12.86 | 2.06 | 4.90 | 0.95 | 0.17 | 0.97 | 1.14 | 11.26 |

**Published:** October 27, 2014

ACS Publications © 2014 American Chemical Society

model server and processed using SwissPDB viewer.[18] Conversion of receptor and ligand from.pdb to.pdbqt format, also grid map and other docking parameters were set using AutoDock 4.2 software.[19] Virtual screening was carried out using AutoDock Vina software and the Lamarckian genetic algorithm as a searching procedure.[20] Binding energy obtained for each complex was represented in heat map format using MeV software packages (http://www.tm4.org/mev/). The gradient ruler is an indicator of interaction strength. Represented molecules showing strong binding against all the selected targets, represented by lower free energy, were selected for further in vitro and simulation study.

**Methodology of Chemical Derivatization of Caffeic Acid.** Four derivatives (1a−d) were procured from Sigma Chemical Co., and other derivatives (1e−j) were synthesized in laboratory. A detailed methodology is given in the Supporting Information (SI).

**Inhibition Kinetics Study.** Concentration-dependent reduction in trypsin activity by CA was also estimated through a BA*p*NA assay using chromogenic substrate Benzoyl-L-arginyl *p*-nitroanilide (BA*p*NA; Purity: >99%; Sigma Chemical Co., St. Louis, MO, U.S.A.). BA*p*NA assays were performed as previously described.[21] A minimum three replicates of each experiment were performed. Michaelis−Menten constant (Km) for trypsin was calculated by using various concentrations of BA*p*NA substrate (1 to 5 mM), and then plotting the double reciprocal curve with 1/(v) and 1/[S]. The kinetic properties of CA were analyzed over a range of concentration of inhibitors (1 $\mu$M to 1 mM). $IC_{50}$ values for each inhibitor were calculated from the sigmoid curve, indicating the best fit for the percentage inhibition data obtained. The values of $K_i$ values for each inhibitor were calculated directly from $IC_{50}$ values using Cheng-Prusoff's classical equation.[21]

$$K_i = \frac{IC_{50}}{\left(1 + \frac{[S]}{Km}\right)}$$

**Feeding Assay and Nutritional Indexing.** Bioassays were conducted by feeding *H. armigera* larvae on artificial diet containing 5 to 200 ppm/g of CA. Three independent sets ($n$ = 30 insects larvae of first instar) were used for feeding on control and CA containing AD. Detailed method is as previously described.[22] The insect growth, development, and survival of insect fed on control and CA containing diet were analyzed on each alternate day for 10 days.

**Semiquantitative Gene Expression Analysis.** Total RNA was extracted from whole larval body using Trizol reagent (Invitrogen, CA, U.S.A.), followed by RQ1 DNase treatment (Promega, U.S.A.). cDNA was synthesized from 2 $\mu$g of the DNA-free RNA samples by reverse transcription using oligo dT primers and reverse transcriptase (Promega, U.S.A.) following the manufacturer's recommendations. Primers pairs were designed for Acetylcholinesterase, Amylase, Chymotrypsin, CYP450, GSTs and Trypsin genes of *H. armigera*. cDNA was diluted (1:10) before use in a PCR. Semiquantitative RT-PCR performed under the following conditions: initial denaturation at 95 °C for 2 min; 30 cycles at 95 °C for 30 s; 60 °C for 30 s; 72 °C for 30 s and a final extension at 72 °C for 5 min.[23]

**Fluorescence Quenching Assay.** Fluorometric experiments were carried out on a fluorescence spectrometer from Thermo Scientific (Waltham, MA, U.S.A.). Stock solutions of CA (1 mM) in ethanol and Bovine Trypsin (1 mM) in 100 mM TrisHCl (pH 7.8) was prepared at room temperature. The final concentration of CA was from 0.2 to 30.0 $\mu$M with a constant bovine trypsin content of 1 $\mu$M. The fluorescence spectra were recorded at $\lambda_{exc}$ = 280 nm and $\lambda_{em}$ from 300 to 500 nm.[24−27]

**MALDI-TOF Analysis.** Different molar concentration of CA and trypsin were mixed and incubated for 20 min at 37 °C. The mass spectral analysis of the reaction mix was done on Q-TOF-MALDI-TOF-MS with a standard instrumental protocol (High Definition Mass spectrometer, ABSCIX, MA, U.S.A.). Sample preparation, spectral acquisition, and processing were done as described earlier.[28]

**Isothermal Titration Calorimetry.** ITC was performed using Microcal Auto-iTC instrument (GE Healthcare, Buckinghamshire, U.K.). Nineteen injections of 2 $\mu$L bovine trypsin (Stock = 2.0 mM) was titrated against 0.1 mM solution of CA. Experiments were carried out at 37 °C in a Tris buffer, pH 7.8. Reference titration was carried out by injecting the same concentration of trypsin into buffer. Reference titration was subtracted from experimental titration. Origin 6.0 software was used to derive affinity constants ($K_d$), the molar reaction enthalpy (CH), and the stoichiometry of binding (N), by fitting the integrated titration peaks.[29]

**Circular Dichroism Spectroscopy.** A Jasco J-810 spectropolarimeter (Jasco, Easton, MD, U.S.A.) running the software Jasco J815CD was used to collect spectra at wavelengths 190−240 nm (far-UV) and 240−300 nm (near-UV). Quartz cuvettes of path lengths 5 mm was used for spectral scan. The scanning speed was 20 nm/min, the response was 4 s, and the bandwidth was 1 nm. Trypsin (10 $\mu$M) was incubated with CA in 1:2, 1:1, and 2:1 ratio for 4 h at room temperature, a similar process was done for chymotrypsin. Baseline corrections were performed by subtracting the spectra of the buffer and phenolic compounds from the sample spectra. The data are reported as mean residue ellipticity ([Θ]) in $deg^3cm^2$ $3dmol^{-1}$. Each spectrum is the result of three accumulations. The CD spectra were analyzed using the DicroWeb server and applying the CONTIN/LL program with a reference database, SP175, containing 70 proteins with complex structures including trypsin.[28]

**Molecular Dynamic Simulation.** The structures with 27 CA molecules (aggregation study) and bovine trypsin-CA complex were relaxed using all-atom MD simulation in explicit water with GROMACS software package using the AMBER99SB force field[21] and the simple point charge (SPC) water model.[30] The time step used in the simulation was 0.002 ps while list of neighbors was updated every 0.01 ps with the grid method and a cut off radius of 14 Å. The coordinates of all atoms in the simulation were saved every 2 ps. The initial velocities were chosen randomly. NPT ensemble was used with the user-defined box dimension. The temperature and pressure were kept at the desired value using the Berendsen method and an isotropic coupling for the pressure ($T$ = 300 K, $\zeta T$ = 0.1 ps, $P_0$ = 1 bar, coupling time = $\zeta T$ = 1 ps). The electrostatic term was calculated using the Particle Mesh Ewald (PME) algorithm with the radius of 16 Å with Fast Fourier Transform (FTT) optimization (with an order of 4 for the cubic interpolation). The cut off algorithm was applied for the noncoulomb potential with a radius of 9 Å. Initial minimization was done for a total of 50 000 steps, followed by volume and pressure equilibration each for 1 ns. The production MD run for the complexes were then carried out.

Both of these systems were then simulated using the simulation parameters mentioned in the previous section. The parameters for CA were retrieved from the SWISSPARAM server (http://www.swissparam.ch/).[30,31] Both of these simulations were performed and analyzed using the supercomputing facility provided by BRAF cluster using GROMACS.[32]

**Enzymatic Assays.** Five hundred milligrams of whole insect tissue of *H. armigera* were ground to a fine powder and extracted in 500 mL of 200 mM Glycine-NaOH buffer (pH 10) for 2 h at 4 °C. The extract was then centrifuged at 12 000*g* (4 °C; 10 min) and the clear supernatant was used as a source of enzyme for all solution assays. Control and CA fed insects protein lysate (50 $\mu$g) was used to carry out the following functional assays: (a) total proteaseactivity;[21] (b) Trypsin-like activity;[22] (c) Chymotrypsin like activity;[22] (d) Amylase activity;[23] (e) Lipase activity;[32] (f) Acetylcholinesterase activity;[33] (g) GSTs activity;[34] and (h) CYP450 activity.[34] The detailed methodology is described in corresponding references.

**Statistical Analysis.** All the experiments were performed three times independently. Student's $t$ test was used for statistical analysis. Data were expressed as mean ± SD. A $p$-value< 0.05 was considered as statistically significant.

## RESULTS AND DISCUSSION

**Protease Inhibition Potential of Hydroxycinnamic Acid Derivatives.** Comparison of binding energies of various HCA derivatives against bovine and *H. armigera* proteases displayed variability in binding affinity (Figure 1A). Caffeic,

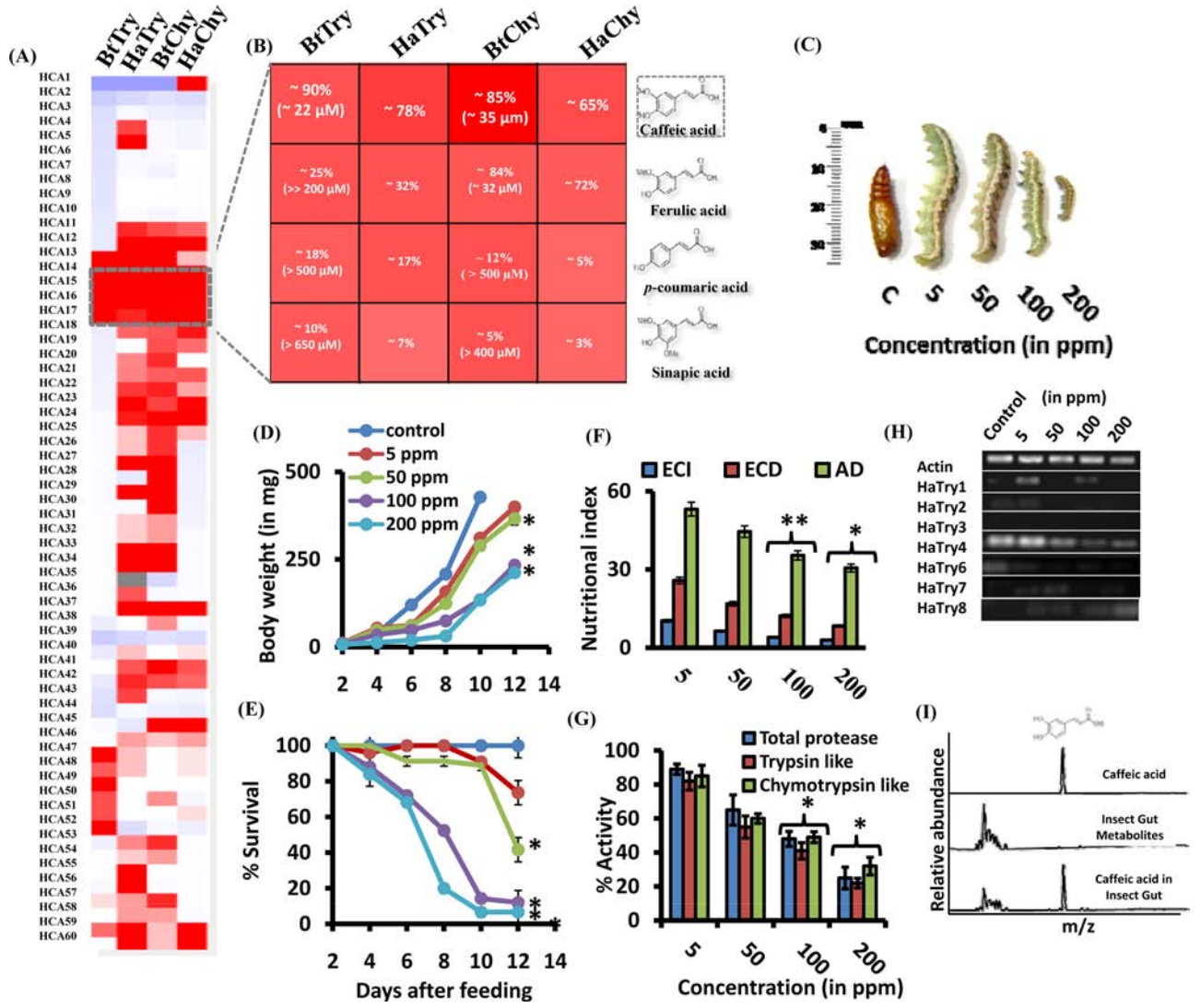


**Figure 1.** (A) Interaction energy of binding of various hydroxycinnamic acid derivatives with bovine and *H. armigera* proteases is compared by using Heatmap analysis. Relative free binding energy (obtained from docking study) normalized by mean values of cumulative free energy was obtained from *Bos taurus* (Bovine) trypsins, bovine chymotrypsin, *H. armigera* trypsin, and chymotrypsin binding with different derivatives. The gradient ruler is an indicator of interaction strength, where the blue color indicates weak binding and red indicates strong binding. Values in parentheses indicate $K_i$. (B) Derivatives with strong binding affinities are marked with dash board. *H. armigera* larvae were raised on artificial diets containing 5 to 200 ppm/g of CA. (C) Average size of larvae recorded on day 10. (D) Insect growth and (E) survival rate normalized with control (F) nutritional parameters ECI, ECD, and Ad and (G) In vivo proteolytic activity of insect fed on control and CA containing dietwere assessed. Bars represent means (±) SE from three independent experiments at *$p$_0.05 (H) Protease gene expression analysis at the transcript level by performing semiquantitative RT-PCR using total RNA isolated from control and CA fed larvae. All samples were analyzed on 2% agarose gels containing gel red. This analysis showed differential expression of protease gene in CA fed larvae. (I) HRMS analysis of insect gut metabolites indicated the fate of CA in insect gut environment. Results are representative of three independent experiments.

ferulic, sinapic, and *p*-coumaric acid emerged as strong inhibitors of candidate proteases (Figure 1B). It was observed that caffeic acid (CA) showed strong competitive inhibition of bovine (*Bos tarus*) trypsin ($K_i \approx 22\ \mu M$) and bovine chymotrypsin ($K_i \approx 32\ \mu M$), while ferulic acid (FA) showed exclusive inhibition of bovine chymotrypsin with $K_i \approx 32\ \mu M$. CA and FA showed significant inhibition of *H. armigera* trypsin and chymotrypsin activity (Figure 1B). Molecular docking analysis and binding energy comparison indicated that natural phenols have affinity toward insect proteases. Moreover, the interaction between phenols and the proteases from different insects is conserved. (Polyphagous: *H. armigera and Ptullae xylostella*; Monophagous: *Menduca sexta*) (SI Figure S1). Analysis of 130 docked complexes revealed that CA had strong interaction (low binding energy) with various insect serine proteases, especially with trypsin like proteases. This observation might support the fact that elevated concentration of CA and other similar natural phenols in plant tissues upon insect infestation might have direct role in inhibition of digestive function of the insects.[12−16]

**Molecular Response of *H. armigera* to CA Ingestion.** Delayed pupation indicates the retardation of development in larvae fed on CA (Figure 1C). CA appeared to have significant and concentration-dependent negative impact on growth and survival of *H. armigera*. Larvae fed on diet containing 50 to 200 ppm of CA showed ∼20 to 50% less body mass (in g) as compared to control (Figure 1D). Furthermore, CA fed leave had ∼50 to 80% reductions in survival rate (Figure 1E).


dx.doi.org/10.1021/jf503437r | J. Agric. Food Chem. 2014, 62, 10847−10854

Evaluation of nutritional parameters like Efficiency of Conversion of Ingested Food (ECI), Efficiency of Conversion of Digested Food (ECD) and Approximate Digestibility (AD) revealed that the ingestion of CA had deleterious effect on growth and rudimentary metabolism of the insect (Figure 1F). Insects fed on CA exhibited a substantial reduction in trypsin-like (~20 to 60%) and thus total protease (~15 to 50%) activity (Figure 1G). Inhibition of digestive proteases by CA probably causes starvation in insects. It might lead to nutritional scarcity, less pool of free amino acids, and also energy required for metabolism, thus causing the growth retardation followed by insect death.[12,15]

Candidate protease gene expression analysis indicated that ingestion of CA also led to a differential response. Several of the *H. armigera* trypsin's and chymotrypsin's (HaTry1 to 8; HaChy1 to 4) were down-regulated, except HaTry4 (Figure 1H). Overexpression of HaTry4 and HaChy4 in CA fed insects might have been resulted in response to compensate for reduced the protease activity. HaTry4 and HaChy4 might be inhibitor resistant/insensitive proteases, and thus overexpression of these proteases might be help in rescuing the insect from growth retardation, which could further predominate and hijack the insect digestive system to fulfill the insect's growth requirement.[35−37]

**The Fate of CA in the Insect Gut Environment.** Stability of CA in insect gut environment and probability of formation of subsequent metabolites were investigated by LC-ESI (−)-HRMS analysis (Figure 1I). Chromatograms of gut metabolite extract of CA fed larvae in 1:1 acetonitrile and methanol showed the presence of intact CA molecule and no additional peaks in comparison to control. Thus, it excluded the possibility of the formation of degraded products of CA in digestive tract of insect. Stability of CA in insect gut leads to maximum availability and hence causes it to be constitutively active as protease inhibitor. In vivo stability of CA made it a lucrative molecule to be used as an insecticidal agent.[38]

**Structure−Activity Relationship of CA as Protease Inhibitor.** Functional group-activity relationships provide a detailed insight into the essentiality of individual functional groups to maintain the inhibitory potency (Table 1). Semisynthesized derivatives were structurally characterized by mass spectrometric and NMR data (SI) which were well in agreement with the previous reports.[39−44] Masking of 3-hydroxyl group as methoxy on the phenolic ring (FA, **1b**) resulted in the considerable reduction in gut protease inhibition (40 to 60%). Even the addition of another methoxy group at 5-position (**1c**, sinapic acid) on the phenolic ring led to further reduction in inhibitory potencies (20 to 30%). Removal of the 3-hydroxyl group (**1d**, cinnamic acid) from the CA structure resulted in drastic reduction in the inhibitory activity (15 to 25%). Masking of the terminal carboxylic acid as a methyl (**1e**) ester also caused a significant lowering in inhibitory activities (35 to 50%). Further increment in the chain length as an ethyl ester (**1f**) showed far more reduction in inhibitory potency (25 to 30%). Hydrogenation (reduction) of the double bond in the side chain of CA (**1g**) reduced the activity extensively (12 to 20%). A similar effect was observed when methyl ester of CA was subjected to hydrogenation (**1h**) (inhibition 25 to 50%). Protection of both the hydroxyl groups on the phenolic ring by acetylation (**1i** and **1j**) drastically attenuated its inhibitory potential (10 to 20%). In brief, modification in any of the functional groups (phenolic hydroxyl, carboxylic acid, and double bond) on CA structure led to reduction in the inhibitory activity against proteases with variable extent and all of them were found to be essentially responsible for the activity. Therefore, the parent natural product (**1a**) found to be most potent among all the derivatives screened.

**Table 1. IC50 ($\mu$M) Values of Bovine Trypsin and Chymotrypsin and % Inhibition of HGP for Derivatives of CA**

| | Compound | Inhibition | | |
|---|---|---|---|---|
| | | Trypsin (~ $IC_{50}$ in μM) | Chymotrypsin (~ $IC_{50}$ in μM) | % Inhibition (~) of HGP activity |
| 1a | 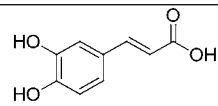 | 22 | 35 | 70-80 |
| 1b | 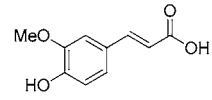 | 120 | 32 | 40-60 |
| 1c | 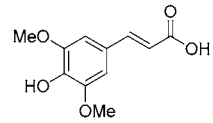 | 650 | 460 | 20-30 |
| 1d | 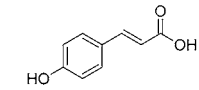 | 780 | 525 | 15-25 |
| 1e | 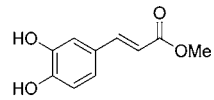 | 80 | 125 | 35-50 |
| 1f | 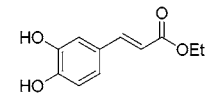 | 165 | 205 | 25-30 |
| 1g | 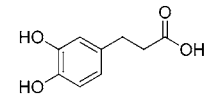 | 225 | 320 | 12-20 |
| 1h | 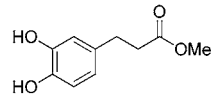 | 109 | 165 | 25-50 |
| 1i | 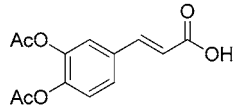 | 380 | 520 | 10-20 |
| 1j | 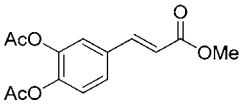 | 350 | 451 | 10-20 |

**Binding of CA Causes Structural and Conformational Change in Target Protein.** Bovine trypsin showed reduction in tryptophan fluorescence in response to titration with CA, suggesting the change of the molecular environment of tryptophan (Figure 2A). A red shift is observed in this case, indicating the conformational change in protease on ligand binding. Furthermore, it was found that multiple CA molecules were interacting noncovalently with proteases. It was validated

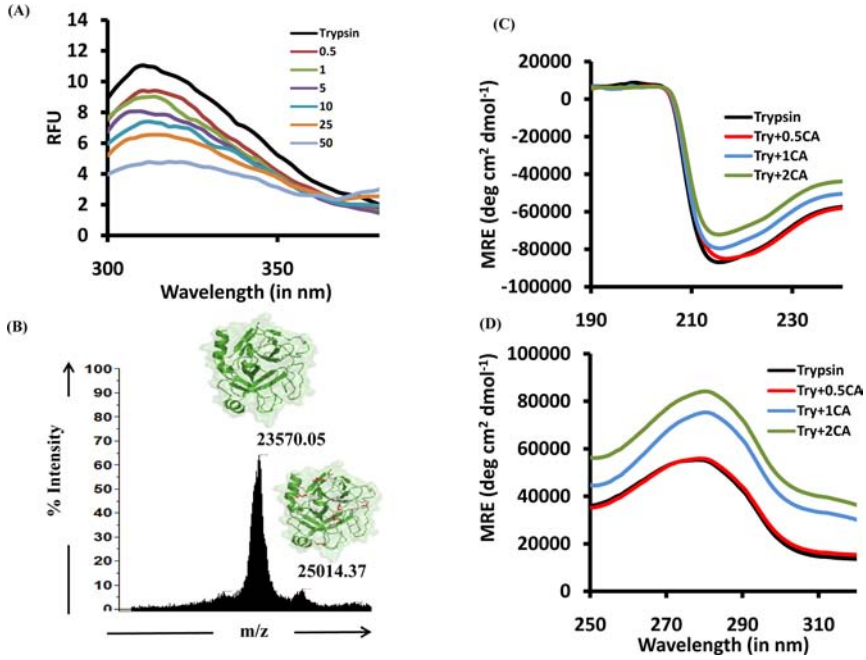


**Figure 2.** Biophysical characterization of CA and protease interaction: (A) Fluorescence emission of bovine trypsin in the presence of various concentration of CA and (B) binding of multiple CA to protease molecule was analyzed by MALDI TOF analysis. Structural change in protease on CA binding was examined at secondary level by (C) near UV CD spectra and at tertiary level by (D) far UV CD spectra.

by mass spectrometric analysis, where shift in mass ($m/z$) was observed in comparison to native enzymes due to binding of multiple CA molecules to the proteases (Figure 2B). Circular dichroism (CD) spectroscopy of proteins in near and far UV regions suggested the secondary and tertiary structure alteration in the protease respectively, on CA binding (Figure 2C,D). Fluorescence quenching and CD spectroscopy analysis together indicated that binding of CA caused environmental alteration around the tryptophan residue, resulting in structural and conformational changes in the protease, which might further be attributed to the reduced enzyme activity.[23−26]

**CA Showed Sequential Binding to Protease and Exhibit Heterogonous Mode of Inhibition.** In the set of simulation systems to study the impact of CA binding on the structure of protease, the system containing *H. armigera* trypsin 4 (HaTry4, predominant trypsin from *H. armigera* gut) with multiple CA in the vicinity was simulated for1 $\mu$S, and the trajectory was analyzed. The CA molecules in this simulation were initially restrained at discrete positions on the protease molecule, and the restrain was released, until 10 ns of the simulation. Out of these 5 CA molecules, one was found to remain in the active site for the rest of the simulation, interacting with Ser200 of HaTry4 (Figure 3A). Hydroxyl groups of CA can form multiple transient interactions with the protease active site, however, the H-bond between the OH group of CA and Tyr45 and Ser200 was found to be stable throughout the simulation time (Figure 3B). Further, after around 208 and 300 ns of the simulation, two more CA molecules were found to be located near the mouth of the active site (Figure 3C). These three CA clubbed near active site to form stacked triad via $\pi-\pi$ interactions and maintains its position through another set of $\pi-\pi$ interaction with lining residues of active site mouth, i.e., Tyr45, Trp144, and Tyr154 (Figure 3D). In this way, CA binding to *H. armigera* trypsin might cause heterogeneous type of inhibition by (i) competitively binding to the active site residue i.e. Ser200 (ii) blocking the mouth of the active site, leads to inaccessibility to the substrate. This suggests that CA might be having some crucial interactions with the active site residues and longer time-scale simulation might be required to explore major structural changes in the protein.

Thermodynamic studies of trypsin-CA interaction was carried out using isothermal titration calorimetry (ITC) as it is one of the most widely used quantitative technique for direct measurement of the enthalpy change when two species interact, allowing the determination of heat of association, stoichiometry, and binding affinity from a single experiment. The raw data and corresponding thermogram of the binding experiment is depicted in Figure 3E. Binding was strongly exothermic and showed 1:3 stoichiometry for trypsin and CA. The spontaneity of the process was evidenced by a negative change in the enthalpy, CH, and a positive change in the entropy, CS. Binding of first CA molecule showed lower $\Delta G$ as compared to the second and third molecule binding. This thermodynamic pattern of binding indicates that binding of first CA molecule was strong as compared to the second and third CA molecule.

To investigate the aggregation propensity of CA in solution and its effect on protein binding, 27 CA molecules (aggregation study) were relaxed using all-atom MD simulation in explicit water with GROMACS software package using the AMBER99SB force field and the simple point charge (SPC) water model.[29] The 50 ns trajectory of this system was analyzed to see how individual CA molecules display the phenomenon of aggregation. At around 1 to 2 ns of simulation, formation of aggregates were initiated (Figure 2F). These aggregates were observed in different clusters with varying number of CA molecules in individual clusters. Initially after 2 ns of the simulation, two major clusters were observed having 12 CA molecules each and remaining 3 CA in none of them. Likewise, a big cluster of 21 CA molecules was observed after 6.5 ns and just after 30 ns of the simulation, a cluster of 27 CA molecules was also observed. Some of these aggregated CA molecules also


dx.doi.org/10.1021/jf503437r | J. Agric. Food Chem. 2014, 62, 10847−10854

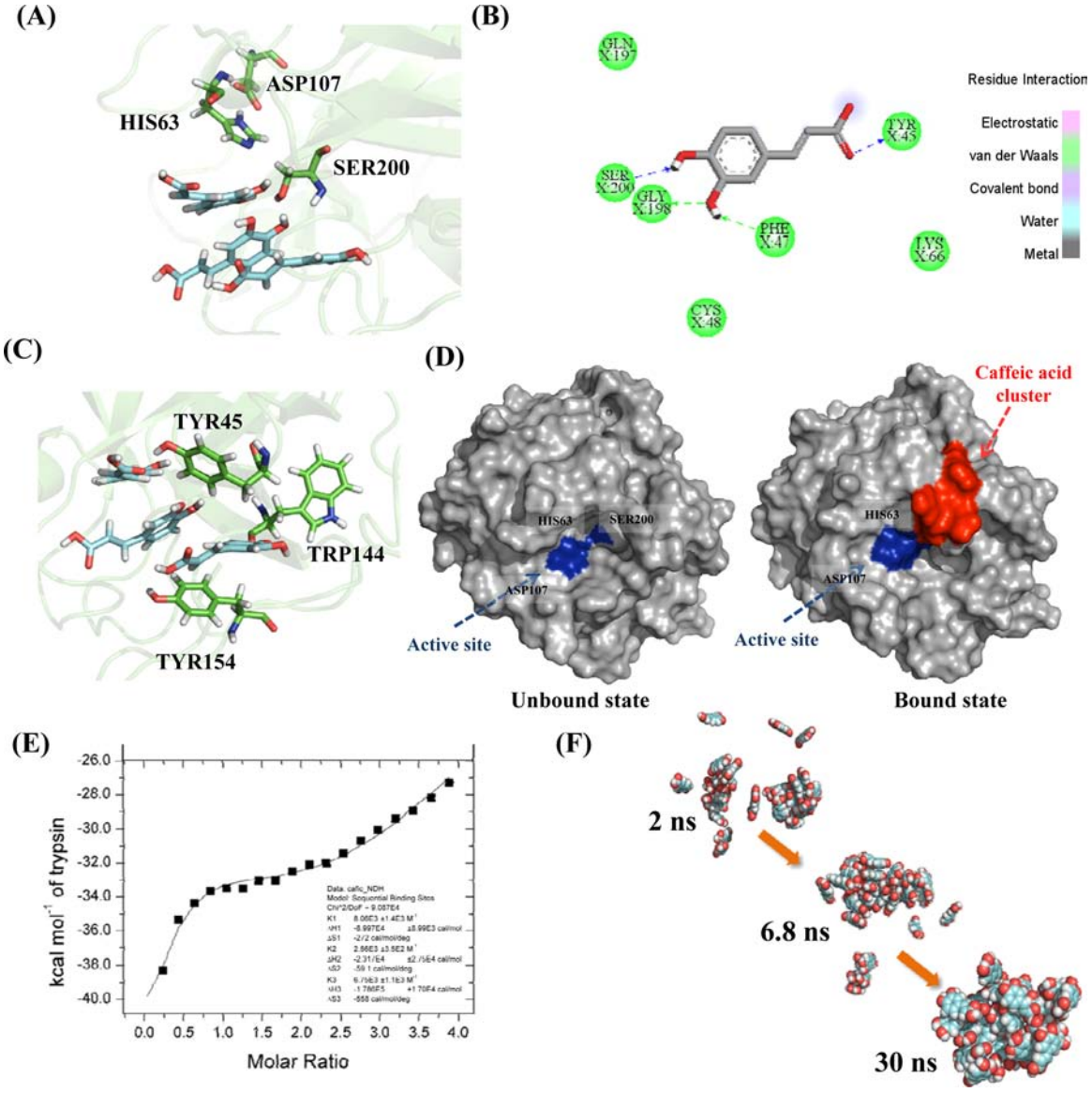


**Figure 3.** Simulation of bovine trypsin and CA in one system illustrates (A) binding of single CA molecule at the active site residue SER200. (B) 2D interaction map showed establishment of multiple interactions of CA with trypsin binding pocket. Strong binding of CA at active site leads to (C) formation of nucleation center for aggregation of other two CA molecules in the active site. (D) Aggregate formation in binding pocket further blocks complete access to the active site, which is shown in the surface model. (E) Simulation of only CA in the solvation box showed that CA has intrinsic propensity to form aggregate and this might enhance its chances to interact with the proteases.

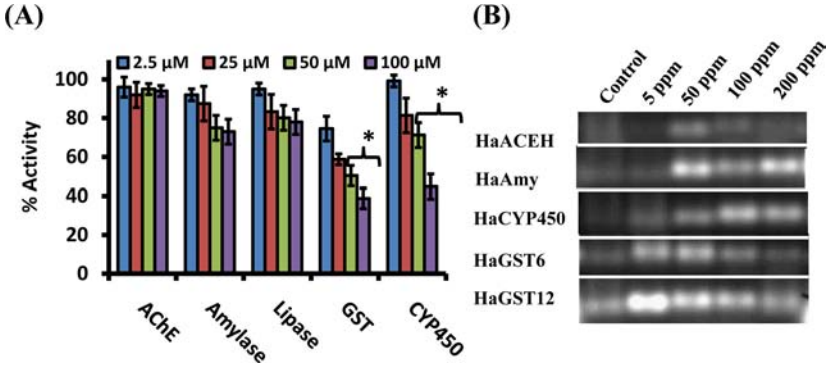


**Figure 4.** Enzymatic activities of (A)AChE, Amylase, lipase, GST, and CYP450 were analyzed for control and CA treated insects using protocols described in corresponding references. In CAfed insects, significant and concentration dependent reduction in GST and CYP450 activity was observed. Bars represent means (±) SE from three independent experiments at *$p$_0.05 (B) Gene expression analysis of AChE, Amylase, lipase, GST, and CYP450 genes at the transcript level by performing semiquantitative RT-PCR using total RNA isolated from control and CA fed larvae.


dx.doi.org/10.1021/jf503437r | J. Agric. Food Chem. 2014, 62, 10847−10854

formed stacked orientation with one another during the simulation. This suggested that the CA had an intrinsic property of displaying stacking interactions as well as self-aggregation. Formation of aggregates might enhance the probability of CA to interact with proteases. Kinetic, simulation, and ITC data demonstrated the binding of single molecule of CA to the active site of trypsin initiates the sequential binding of CA molecules at the active site.

**CA Inhibits the Insect Detoxification Machinery.** Estimation of different enzyme activities and semiquantitative gene expression analysis indicated that other than protease inhibition activity, CA also had adverse effects on various enzymes primarily involved in detoxification mechanism. It was observed that activity of Glutathion S-tranferase (GST) and Cytochrome P450 (CYP450) reduced drastically in insects fed with CA containing diet (Figure 4A), and insect attempted to compensate this activity reduction by overexpression of these genes at transcript level (Figure 4B). Reduction in these enzyme activities was concentration dependent and almost 60% GST and CYP450 enzyme activity was reduced at 200 ppm concentration. Other than these enzymes, various other digestive enzymes activities like amylase, lipase was found to be maintained in the presence of CA even at concentration of 200 ppm. Amylase, proteases, and lipases are three major enzymes contributing to the insect digestive system. Proteases are more crucial for insect development, growth, metamorphosis, and immunity, and thus their inhibition is found to be significantly detrimental as compared to amylase and lipase inhibition. Inhibition of detoxification enzymes by natural phenols might intensify the detrimental effect on insect growth and development.

In conclusion, CA has been found and validated as a potential insecticidal molecule. All the functional groups contributed to its protease inhibitor property, and it also remains stable in the insect gut environment. Ingestion of CA causes differential molecular responses at transcriptional and translational level. Structural investigation showed that CA showed sequential binding at the active site of major insect protease, thus inhibiting its activity. Although overexpression of proteases was observed in CA fed larvae, the strong inhibition potential of CA overcomes the effect of the enhanced expression of insect proteases. All these finding suggests that exploration of natural phenols could be an effective approach to develop a "Dietary pesticide" against *H. armigera* infestation.

## ■ ASSOCIATED CONTENT

### Supporting Information

SI 1: Methodology of chemical derivatization of caffeic acid. SI II: HRMS data of caffeic acid derivatives. SI III: NMR spectra of caffeic acid derivatives. Interaction energy of binding of various hydroxycinnamic acid derivatives with (A) *M. sexta* and (B) *P. xylostella* proteases is compared by using Heatmap analysis (Figure S1) and additional figures. This material is available free of charge via the Internet at http://pubs.acs.org.

## ■ AUTHOR INFORMATION


### Corresponding Author

*Phone: 0091-(0)20-25902710; fax: 0091-(0)20-25902648; e-mail: ap.giri@ncl.res.in.

### Present Address

∥(R.S.J.) Institute of Bioinformatics and Biotechnology, University of Pune, Pune 411007, Pune, India.


### Notes

The authors declare no competing financial interest.

## ■ ACKNOWLEDGMENTS

The authors acknowledge Saikat Haldar, Aarohi Summanwar, and Nidhi Saikhedkar for their technical help in planning experiments. The authors acknowledge Dr. A. Das, CSIR-NCL, Pune, India for providing access to ITC instrument.

## ■ REFERENCES


(1) Gavrilescu, M. Fate of pesticides in the environment and its bioremediation. *Eng. Life Sci.* **2005**, *5*, 497−526.

(2) Abdollahi, M.; Ranjbar, A.; Shadnia, S.; Nikfar, S.; Rezaiee, A. Pesticides and oxidative stress: a review. *Med. Sci. Monitor* **2004**, *10*, 141−147.

(3) Lattanzio, V.; Kroon, P. A.; Quideau, S.; Treutter, D. Plant phenolics—Secondary metabolites with diverse functions. *Recent Adv. Poly. Res.* **2008**, *1*, 1−35.

(4) Boerjan, W.; Ralph, J.; Baucher, M. Lignin biosynthesis. *Annu. Rev. Plant. Biol.* **2003**, *54*, 519−546.

(5) Asakawa, Y.; Ludwiczuk, A.; Nagashima, F. Phytochemical and biological studies of bryophytes. *Phytochemistry* **2013**, *91*, 52−80.

(6) Bi, J.; Felton, G. Foliar oxidative stress and insect herbivory: primary compounds, secondary metabolites, and reactive oxygen species as components of induced resistance. *J. Chem. Ecol.* **1995**, *21*, 1511−1530.

(7) Horváth, E.; Szalai, G.; Janda, T. Induction of abiotic stress tolerance by salicylic acid signaling. *J. Plant Growth Regul.* **2007**, *26*, 290−300.

(8) Ingersoll, C. M.; Niesenbaum, R. A.; Weigle, C. E.; Lehman, J. H. Total phenolics and individual phenolic acids vary with light environment in *Lindera benzoin*. *Botany* **2010**, *88*, 1007−1010.

(9) Mahmood, K.; Khan, M. B.; Song, Y. Y.; Ijaz, M.; Luo, S. M.; Zeng, R. S. UV-irradiation enhances rice allelopathic potential in rhizosphere soil. *J. Plant Growth Regul.* **2013**, *71*, 21−29.

(10) Green, P. W.; Stevenson, P. C.; Simmonds, M. S.; Sharma, H. C. Phenolic compounds on the pod-surface of pigeonpea, *Cajanus cajan*, mediate feeding behavior of *Helicoverpa armigera* larvae. *J. Chem. Ecol.* **2003**, *29*, 811−821.

(11) Magalhães, S. T.; Fernandes, F. L.; Demuner, A. J.; Picanço, M. C.; Guedes, R. N. C. Leaf alkaloids, phenolics, and coffee resistance to the leaf miner *Leucoptera coffeella* (Lepidoptera: Lyonetiidae). *J. Econ. Entomol.* **2010**, *103*, 1438−1443.

(12) Rani, P. U.; Devanand, P. Bioactivities of caffeic acid methyl ester (methyl-(*E*)-3-(3, 4-dihydroxyphenyl) prop-2-enoate): a hydroxycinnamic acid derivative from *Solanum melongena* L. fruits. *J. Pest Sci.* **2013**, *86*, 579−589.

(13) Usha Rani, P.; Pratyusha, S. Defensive role of *Gossypium hirsutum* L. anti-oxidative enzymes and phenolic acids in response to *Spodoptera litura* F. feeding. *J. Asia Pac. Entomol.* **2013**, *16*, 131−136.

(14) War, A. R.; Paulraj, M. G.; Ahmad, T.; Buhroo, A. A.; Hussain, B.; Ignacimuthu, S.; Sharma, H. C. Mechanisms of plant defense against insect herbivores. *Plant Signal Behav.* **2012**, *7*, 1306−1320.

(15) War, A. R.; Paulraj, M. G.; Hussain, B.; Buhroo, A. A.; Ignacimuthu, S.; Sharma, H. C. Effect of plant secondary metabolites on legume pod borer *Helicoverpa armigera*. *J. Pest Sci.* **2013**, *86*, 399−408.

(16) Kimmins, F. M.; Padgham, D. E.; Stevenson, P. C. Growth inhibition of the cotton bollworm *Helicoverpa armigera* larvae by caffeoylquinic acids from the wild groundnut, *Arachis paraguariensis*. *Insect Sci. Appl.* **1997**, *16*, 363−368.

(17) Dawkar, V. V.; Chikate, Y. R.; Lomate, P. R.; Dholakia, B. B.; Gupta, V. S.; Giri, A. P. Molecular insights into resistance mechanisms of lepidopteran insect pests against toxicants. *J. Proteome Res.* **2013**, *12*, 4727−4737.

(18) Kaplan, W.; Littlejohn, T. G. Swiss-PDB viewer (deep view). *Brief Bioinform.* **2001**, *2*, 195−197.

(19) Morris, G.; Goodsell, D.; Pique, M.; Lindstrom, W.; Huey, R.; Forli, S.; Hart, W.; Halliday, S.; Belew, R.; Olson, A. AutoDock 4.2 with AutoDock Tools, 2009.
(20) Trott, O.; Olson, A. J. AutoDock Vina: improving the speed and accuracy of docking with a new scoring function, efficient optimization, and multithreading. *J. Comput. Chem.* **2010**, *31*, 455−461.
(21) Joshi, R. S.; Mishra, M.; Tamhane, V. A.; Ghosh, A.; Sonavane, U.; Suresh, C. G.; Joshi, R.; Gupta, V. S.; Giri, A. P. The remarkable efficiency of a Pin-II proteinase inhibitor sans two conserved disulfide bonds is due to enhanced flexibility and hydrogen bond density in the reactive site loop. *J. Biomol. Struct. Dyn.* **2014**, *32*, 13−26.
(22) Joshi, R. S.; Gupta, V. S.; Giri, A. P. Differential antibiosis against *Helicoverpa armigera* exerted by distinct inhibitory repeat domains of *Capsicum annuum* proteinase inhibitors. *Phytochemistry* **2014**, *101*, 16−22.
(23) Kotkar, H. M.; Bhide, A. J.; Gupta, V. S.; Giri, A. P. Amylase gene expression patterns in *Helicoverpa armigera* upon feeding on a range of host plants. *Gene* **2012**, *501*, 1−7.
(24) Jin, X. L.; Wei, X.; Qi, F. M.; Yu, S. S.; Zhou, B.; Bai, S. Characterization of hydroxycinnamic acid derivatives binding to bovine serum albumin. *Org. Biomol. Chem.* **2012**, *10*, 3424−3431.
(25) Bian, H.; Zhang, H.; Yu, Q.; Chen, Z.; Liang, H. Studies on the interaction of cinnamic acid with bovine serum albumin. *Chem. Pharma. Bull.* **2007**, *55*, 871−875.
(26) Jiang, M.; Xie, M. X.; Zheng, D.; Liu, Z.; Li, X. Y.; Chen, X. Spectroscopic studies on the interaction of cinnamic acid and its hydroxyl derivatives with human serum albumin. *J. Mol. Struct.* **2004**, *692*, 71−80.
(27) Kang, J.; Liu, Y.; Xie, M. X.; Li, S.; Jiang, M.; Wang, Y. D. Interactions of human serum albumin with chlorogenic acid and ferulic acid. *Biochim. Biophys. Acta* **2004**, *1674*, 205−214.
(28) Mishra, M.; Joshi, R. S.; Gaikwad, S.; Gupta, V. S.; Giri, A. P. Structural-functional insights of single and multi-domain *Capsicum annuum* protease inhibitors. *Biochem. Biophys. Res. Commun.* **2013**, *430*, 1060−1065.
(29) Weber, P. C.; Salemme, F. R. Applications of calorimetric methods to drug discovery and the study of protein interactions. *Curr. Opin. Struct. Biol.* **2003**, *13*, 115−121.
(30) Ghosh, A.; Sonavane, U.; Andhirka, S.; Aradhyam, G.; Joshi, R. Structural insights into human GPCR protein OA1, a computational perspective. *J. Mol. Model.* **2012**, *18*, 2117−2133.
(31) Zoete, V.; Cuendet, M. A.; Grosdidier, A.; Michielin, O. SwissParam: A fast force field generation tool for small organic molecules. *J. Comput. Chem.* **2011**, *32*, 2359−2368.
(32) Sarate, P. J.; Tamhane, V. A.; Kotkar, H. M.; Ratnakaran, N.; Susan, N.; Gupta, V. S.; Giri, A. P. Developmental and digestive flexibilities in the midgut of a polyphagous pest, the cotton bollworm *Helicoverpa armigera*. *J. Insect Sci.* **2012**, *12*, 42.
(33) Ellman, G. L.; Courtney, D.; Andres, V.; Featherston, R. M. A new and rapid colorimetric determination of acetylcholinesterase activity. *Biochem. Pharmacol.* **1961**, *7*, 88−95.
(34) Dawkar, V. V.; Chikate, Y. R.; Gupta, V. S.; Slade, S. E.; Giri, A. P. Assimilatory potential of *Helicoverpa armigera* reared on host (Chickpea) and nonhost (*Cassia tora*) diets. *J. Proteome Res.* **2011**, *10*, 5128−5138.
(35) Bown, D. P.; Wilkinson, H. S.; Gatehouse, J. A. Differentially regulated inhibitor-sensitive and insensitive protease genes from the phytophagous insect pest, *Helicoverpa armigera*, are members of complex multigene families. *Insect Biochem. Mol. Biol.* **1997**, *27*, 625−638.
(36) Broadway, R. M. Dietary regulation of serine proteinases those are resistant to serine proteinase inhibitors. *J. Insect Physiol.* **1997**, *43*, 855−874.
(37) Chikate, Y. R.; Tamhane, V. A.; Joshi, R. S.; Gupta, V. S.; Giri, A. P. Differential protease activity augments polyphagy in *Helicoverpa armigera*. *Insect Mol. Biol.* **2013**, *22*, 258−272.
(38) Yang, W.; Fang, D. M.; He, H. P.; Hao, X. J.; Wu, Z. J.; Zhang, G. L. Analysis of mexicanolide-and phragmalin-type limonoids from *Heynea trijuga* using high-performance liquid chromatography/electrospray tandem mass spectrometry. *Rapid Commun. Mass Spectrom.* **2013**, *27*, 1203−1212.
(39) Barontini, M.; Bernini, R.; Carastro, I.; Gentili, P.; Romani, A. Synthesis and DPPH radical scavenging activity of novel compounds obtained from tyrosol and cinnamic acid derivatives. *New J. Chem.* **2014**, *38*, 809−816.
(40) Percec, V.; Peterca, M.; Sienkowska, M. J.; Ilies, M. A.; Aqad, E.; Smidrkal, J.; Heiney, P. A. Synthesis and retrostructural analysis of libraries of AB3 and constitutional isomeric AB2 phenylpropyl ether-based supramolecular dendrimers. *J. Am. Chem. Soc.* **2006**, *128*, 3324−3334.
(41) Roche, M.; Dufour, C.; Mora, N.; Dangles, O. Antioxidant activity of olive phenols: mechanistic investigation and characterization of oxidation products by mass spectrometry. *Org. Biomol. Chem.* **2005**, *3*, 423−430.
(42) Takahashi, T.; Miyazawa, M. Tyrosinase inhibitory activities of cinnamic acid analogues. *Pharmazie* **2010**, *65*, 913−918.
(43) Uwai, K.; Osanai, Y.; Imaizumi, T.; Kanno, S. I.; Takeshita, M.; Ishikawa, M. Inhibitory effect of the alkyl side chain of caffeic acid analogues on lipopolysaccharide-induced nitric oxide production in RAW264.7 macrophages. *Bioorgan. Med. Chem.* **2008**, *16*, 7795−7803.
(44) Zhu, Y.; Zhang, L. X.; Zhao, Y.; Huang, G. D. Unusual sesquiterpene lactones with a new carbon skeleton and new acetylenes from *Ajania przewalskii*. *Food Chem.* **2010**, *118*, 228−238.

soil and the surface chemistry of fresh and aged biochar was characterized. Knowledge gained on the mechanisms of mineral incorporation with biochar would be useful to reveal the interactions and aggregation of biochar and soil materials and how this affects the fate and behavior of herbicides.

## MATERIALS AND METHODS

**Chemicals.** Pure analytical (>99%) standards and radiochemicals of indaziflam (*N*-[(1*R*,2*S*)-2,3-dihydro-2,6-dimethyl-1*H*-inden-1-yl]-6-[(1*R*)-1-fluoroethyl]-1,3,5-triazine-2,4-diamine) (3.96 MBq $mg^{-1}$, 97.9% radiochemical purity) and fluoroethyldiaminotriazine (6-[(1*R*)-1-fluoroethyl]-1,3,5-triazine-2,4-diamine) (3.79 MBq $mg^{-1}$, 90% radiochemical purity) were graciously supplied by Bayer Crop Science (Wuppertal, Germany). Nicosulfuron (2-[[[[(4,6-dimethoxy-2-pyrimidinyl)amino]carbonyl]amino]sulfonyl]-*N*,*N*-dimethyl-3-pyridinecarboxamide) (2.33 MBq $mg^{-1}$, >98% radiochemical purity) was provided by DuPont Crop Protection. Unlabeled MCPA (4-chloro-2-methylphenoxyacetic acid) (purity = 98.9%) and terbuthylazine (6-chloro-*N*-ethyl-*N*′-(2-methyl-2-propanyl)-1,3,5-triazine-2,4-diamine) (purity = 99.6%) were purchased by Dr. Ehrenstorfer Lab. Chemical structures of the pesticides are shown in Figure 1 and physicochemical characteristics in Table 1 (data from www.eu-footprint.org[17] and www.chemaxon.com[18]).

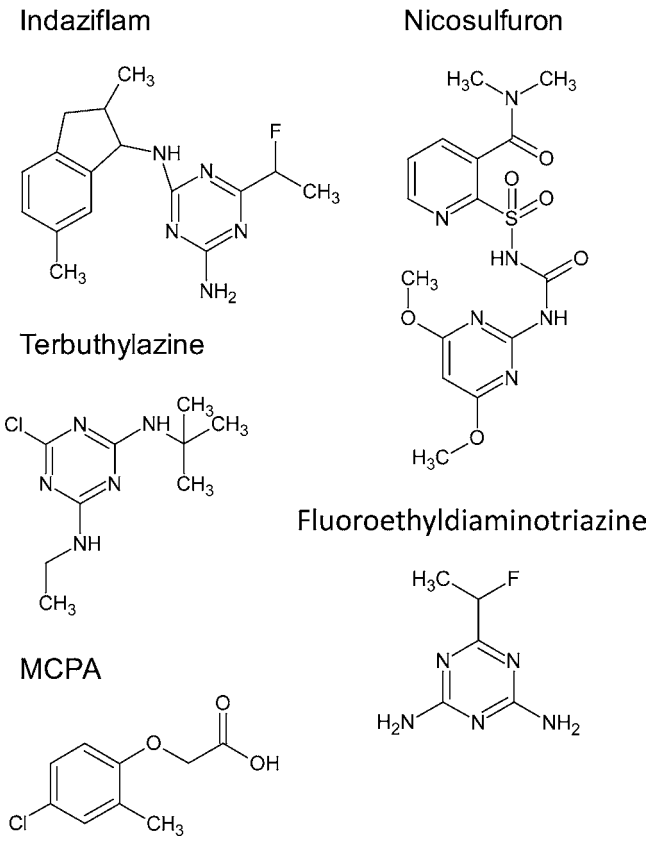


**Figure 1.** Chemical structures of indaziflam, nicosulfuron, terbuthylazine, fluoroethyldiaminotriazine, and MCPA.

**Biochar.** Three macadamia nut shell biochars, ranging in soil equilibration time (zero, one, and two years), were used as pesticide sorbents (Table 2). The biochar was aged in a Waukegan silt loam containing approximately 22% sand, 55% silt, and 23% clay with a pH (1:1 $H_2O$) of 6.3−6.6, and 2.6% organic carbon (OC). Average annual temperature is 6.85 °C with 887 mm of annual precipitation (102 cm snowfall).[19]

The specific surface area of the biochars was measured by nitrogen surface sorption, using a Micromeritics ASAP 2420 and the Brunauer, Emmett, and Teller (BET) method on a previously degassed 0.2 g sample at 8 °C during a 24 h period. The pH was determined in a 1:5 biochar:deionized water slurry. Dissolved organic carbon (DOC) was extracted from biochar by shaking 5 g of the sorbent with 20 mL of 0.01 M $CaCl_2$ for 15 min. The suspension was centrifuged at 8000 rpm for 15 min and filtered through a 0.45 $\mu$m pore nylon filter. The solution was diluted (1:5) in 0.01 M $CaCl_2$ and analyzed using a total carbon analyzer (Shimadzu TOC-V). The absorbance of the extracted DOC was measured with a VWR UV-3100 PC at 254 nm. The estimated aromaticity, $SUVA_{254}$ (L $mg^{-1}$ $m^{-1}$), was calculated using the equation

$$SUVA_{254} = a_{254}/DOC$$

where $a_{254}$ is the absorbance coefficient measured at 254 nm ($m^{-1}$) and was defined as $a_\lambda = 2.303A_\lambda/l_L$; $A_\lambda$ is the absorbance, and $l_L$ is the path length of the optical cell in meters (here $l_L$ = 0.01 m). DOC is the dissolved organic carbon expressed in (mg $L^{-1}$). $SUVA_{254}$ has previously been found to be a useful parameter for estimating the dissolved aromatic carbon content.[20]

The surface morphology of the sample was studied using a JEOL 6500 scanning electron microscope. The functional groups of the biochars were determined using a Nicolet Series II Magna-IR System 750 FTIR spectrometer, recording the spectral region from 4000 to 400 $cm^{-1}$ with a resolution of 2 $cm^{-1}$ (University of Minnesota CharFac facility).

**Sorption Experiments.** Sorption experiments were conducted using the batch equilibrium technique according to OECD guideline 106.[21] Duplicate 0.1 g biochar samples were equilibrated with 8 mL of 0.01 M $CaCl_2$ solution containing initial concentrations of 1 mg $L^{-1}$ terbuthylazine and MCPA, 0.3 mg $L^{-1}$ fluoroethyldiaminotriazine and indaziflam, and 0.2 mg $L^{-1}$ nicosulfuron. Radiolabeled chemicals were added to nonradioactive solutions to give a final solution concentration of ∼174 Bq $mL^{-1}$ for fluoroethyldiaminotriazine, indaziflam, and nicosulfuron. The 0.01 M $CaCl_2$ solution was used as the background electrolyte to maintain constant ionic strength of sorption and desorption equilibration solutions and to facilitate flocculation of the soil. Suspensions were shaken mechanically at 21 ± 2 °C for 24 h and centrifuged at 370*g* for 30 min, and the supernatant was removed for analysis of the equilibrium concentration.

For fluoroethyldiaminotriazine, indaziflam, and nicosulfuron, 1 mL aliquots of the clear supernatant were mixed with 5 mL of scintillation cocktail (Ecolite, ICN Biomedicals, Costa Mesa, CA) and the amount of radioactivity was determined by liquid scintillation counting for 1 min in a liquid scintillation analyzer (1500 TRI-CARB, Packard Instruments, Downers Grove, IL). The amount of the chemicals in solution was calculated by considering the specific activity of each chemical. The equilibrium concentrations ($C_e$) of terbuthylazine and

**Table 1. Physicochemical Characteristics of the Pesticides Used**

| pesticide | mol wt (g $mol^{-1}$) | solubility in water (pH 7, 20 °C) (mg $L^{-1}$) | $K_{ow}$ (log *P*) (pH 7, 20 °C) | $pK_a$ |
|---|---|---|---|---|
| terbuthylazine | 229.71 | 6.6 | 3.4 | 1.9 |
| indaziflam | 301.36 | 2.8 | 2.8 | 3.5 |
| MCPA | 200.62 | 29390 | −0.81 | 3.7 |
| fluoroethyldiaminotriazine | 157.00 | | | 4.10 |
| nicosulfuron | 410.41 | 7500 | 0.61 | 4.78 |

**Table 2. Physicochemical Properties of the Biochars**

| biochar | pH | SSA ($m^2$ $g^{-1}$) | DOC (mg $L^{-1}$) | abs[a] (254 $nm^{-1}$) | $SUVA_{254}$ (L $mg^{-1}$ $m^{-1}$) |
|---|---|---|---|---|---|
| BC-fr | 6.5 | 0.09 | 80.4 | 1.29 | 3.70 |
| BC-1yr | 6.6 | 69.77 | 31.6 | 0.84 | 6.12 |
| BC-2yr | 6.7 | 5.79 | | | |

[a]Absorbance.

MCPA were determined by HPLC with a Waters 600E chromatograph coupled to a Waters 996 diode array detector, under the following conditions: Nova-Pak C18 column (150 mm length × 3.9 mm i.d.); flow rate, 1 mL $min^{-1}$, 25 $\mu$L injection; eluent system for terbuthylazine 50:50 (v/v) water/acetonitrile mixture and UV detection at 220 nm; eluent system for MCPA 60:40 (v/v) methanol/diluted $H_3PO_4$ (pH 2) mixture and UV detection at 230 nm. Differences between the initial ($C_i$) and equilibrium ($C_e$) solution concentration were assumed to be sorbed ($C_s$). The sorption coefficient ($K_d$) was calculated as $C_s/C_e$.

## RESULTS AND DISCUSSION

**Biochar.** Fourier transform infrared spectra (FTIR) of the fresh biochar (BC-fr) and biochars aged 1 (BC-1yr) or 2 (BC-2yr) years are displayed in Figure 2. The appearance of new peaks in the infrared spectra of the aged biochars compared to those present in the spectra of the fresh biochar provides evidence for chemical alteration of the surface moieties due to the interactions between the soil and biochar. Additional bands at 3695 and 1003 $cm^{-1}$ for BC-1yr and BC-2yr, corresponding to the O−H stretching and Si−O vibrations of clay minerals, could be due to soil mineral incorporation onto the surface of the biochars (see Figure 3c−e). The band at ∼2660 $cm^{-1}$ can be assigned to O−H stretching vibration of carboxylic groups from fatty acids that coat the surface of the fresh biochar. The band close to 1700 $cm^{-1}$ corresponds to C═O stretching vibration mode, and the group of bands between 1030 and 1090 $cm^{-1}$ can be assigned to C−O stretching vibrations corresponding to the carboxylic acid group. The decrease of the intensity of the band at about 1700 $cm^{-1}$ and the increase of the band at 1400 $cm^{-1}$ correspond to the C−H bending and the carboxylate anion stretching[22] for the aged biochars and, in comparison with the BC-fr, reveal a partial elimination of the unsaturated fatty acid with the aging process and a partial interaction of the carboxylate anion.

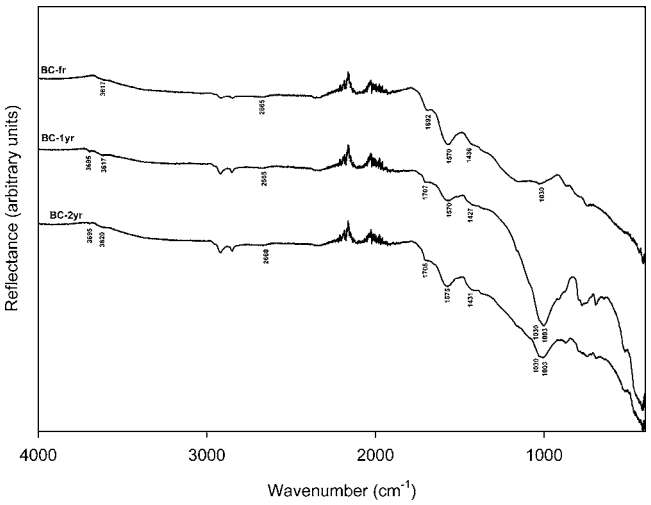


**Figure 2.** Attenuated total reflectance (ATR) infrared spectra of fresh biochar (BC-fr) and biochars aged 1 (BC-1yr) and 2 years (BC-2yr).

Figure 3 shows the SEM images of the fresh biochar (BC-fr) (Figure 3a,b), the biochar aged 1 year and a biochar aged 4 years in soil (Figure 3c−f). SEMs of fresh biochar show a macropore (Figure 3a) with an organic layer coating the micropores and remaining surface structures (Figure 3b). In contrast, the surface of the BC-1yr shows a highly porous surface, with only some of the pores having a range of organic and mineral matter (Figure 3c,d). The SEM image of the biochar aged 2 years show that most of the pores were filled after longer exposure in the soil (Figure 3e,f). Lin et al.[23] observed that clay and mineral particles were adhered to the biochar surface, the mineral attachment occurred preferentially around the biochar external surface, and most of the pores inside the biochar were free of mineral phases. This agrees with our observations.

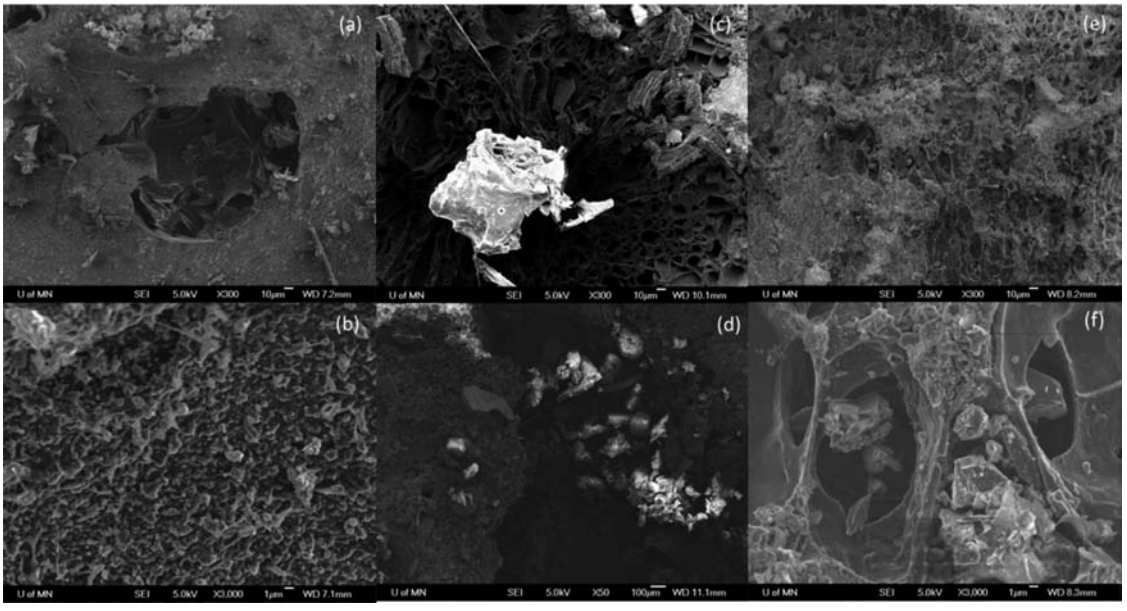


**Figure 3.** (a) SEM image showing a macropore on the fresh biochar (×300 magnification). (b) Fatty lipid surface (organic layer) on the fresh biochar (×3000). (c) Soil particles on the porous surface of BC-1yr (×300). (d) Soil particles on the porous surface of BC-1yr (×50). (e) Surface and pores covered with soil particles for biochar aged 4 years (×300). (f) Surface and pores covered with soil particles on the porous surface of BC-4yr (×3000). Note the significant difference in the appearance of the BC surface in panels b and f, which are at the same magnification (×3000).

Table 3. Sorption Coefficients ($K_d$) for the Pesticides in the Biochars

| | $K_d$ (L kg$^{-1}$) | | | | |
|---|---|---|---|---|---|
| biochar | terbuthylazine | indaziflam | MCPA | fluoroethyldiaminotriazine | nicosulfuron |
| BC-fr | 595 ± 9 | 162 ± 20 | 7.49 ± 2.00 | 0.26 ± 0.15 | 0.00 ± 0.00 |
| BC-1yr | 312 ± 27 | 156 ± 18 | 2.23 ± 0.00 | 1.18 ± 0.75 | 0.00 ± 0.00 |
| BC-2yr | 221 ± 4 | 237 ± 25 | 2.48 ± 0.00 | 2.95 ± 0.92 | 0.03 ± 0.02 |

The specific surface area (SSA) of the biochars (Table 1) increased with time after soil application, from 0.095 m$^2$ g$^{-1}$ for the fresh biochar (BC-fr) to 69.774 m$^2$ g$^{-1}$ for biochar aged 1 year. The increase in SSA is assumed to be due to the elimination of the organic film from the BC-fr surface exposing the underlying micropores. The SSA was still higher than the initial biochar after 2 years (5.786 m$^2$ g$^{-1}$), even though some pores were filled with organic and mineral matter (Figure 3e,f).

Complex reactions take place on biochar surfaces, especially for those biochars that have high mineral content. Due to the high-temperature pyrolysis (850 °C) of the biochar, a high mineral-ash biochar with characteristics of a highly aromatic composition and recalcitrant microbial decomposition are expected.[3] Several mechanisms for interactions between biochar and minerals or biochar and organic matter have been hypothesized:

(i) The interactions at mineral surfaces could be cation−$\pi$ interactions between mineral surface cations and with the negative electrostatic surface of the aromatic ring,[24] hydrogen−$\pi$ interactions between the face of electron-rich $\pi$-system of the aromatic ring of the biochar and the H silanol groups of the minerals, or n−$\pi$ electron donor−acceptor interactions (n = nonbonding electrons at siloxane surface) between a nitroaromatic compound ($\pi$-acceptor) and a basal siloxane surface.

(ii) $\pi$−$\pi$ interactions could happen between the $\pi$-donor or $\pi$-acceptor system of the biochar with the natural organic matter (NOM) or polar−$\pi$ interactions between aromatic systems with positively polarized or charged organic moieties. It has been shown that NOM can suppress sorption of organic contaminants on environmental black carbon by blocking micropores.[25]

The decline in DOC of BC-1yr (31.6 mg L$^{-1}$) in comparison to BC-fr (80.4 mg L$^{-1}$) (Table 2) could be a result of the natural elimination in soil of the organic covering on the fresh biochars and also for the degradation of the more labile fraction of DOC, which would enhance the proportion of recalcitrant aromatics,[26] increasing the aromaticity ($SUVA_{254}$) (6.12 L mg$^{-1}$ m$^{-1}$ for BC-1yr and 3.70 L mg$^{-1}$ m$^{-1}$ for BC-fr). Cox et al.[27] found that the humification index (HIX) of DOC from a solid organic amended with a high amount of aromatic molecules after two months of soil incubation shows just a small increase with residence time. This can be attributed to the sorption of organic matter that must be more humified and have higher adsorption capacities. Lin et al.[23] noticed that the hydrophobic DOC fraction decreased in a biochar mineral complex indicating that hydrophobic DOC could be immobilized in the complex because of a strong affinity toward clays.[28]

**Sorption Experiments.** The greatest sorption for the fresh and two aged biochars was for indaziflam and terbuthylazine, both weak bases (Table 3). At the pH of the solutions (6.5−6.7) while >99% of both chemicals would be molecular species, cationic species may significantly contribute to the net sorption through (1) an interaction of a positively charged ion with the negative electrostatic potential surface of the aromatic ring of the biochars,[23] (2) carboxylic groups of the organic surface covering of the fresh biochar, and (3) partially being sorbed in the pores of the aged biochar. As the cation is sorbed, a portion of the molecular species is protonated to reestablish the solution equilibrium. The greatest sorption of terbuthylazine is due to a high number of cationic species at the same pH as compare to indaziflam. In addition, dispersive and hydrophobic forces are thought to act in support of this type of association.[29] For pesticides with low water solubility, organic matter provides important sorbent surfaces in soil because phase partitioning is driven by hydrophobic interactions.[30] Cox et al.[31] found a high sorption of simazine in a soil amended with humified organic matter. Sorption values ($K_d$) of indaziflam and terbuthylazine found in different soil were 27.44−4.86 (Alonso et al., 2011)[32] and 3.7−0.4 (Alister et al., 2011),[33]respectively. These values are around 10 and 300 times higher than the adsorption observed for biochars for indaziflam and terbuthylazine.

The $K_d$ values for the aged biochars (BC-1yr and BC-2yr) decreased for terbuthylazine ∼52% for BC-1yr and ∼63% for BC-2yr with respect to BC-fr because of a decrease of the number of the cationic molecules with the increase of the pH and due to a decrease of the carboxylic groups of the surface of the aged biochars for a natural elimination or a sorption of the unsaturated acid in soil. Conversely, for indaziflam the BC-2yr $K_d$ value increased ∼43% in comparison with BC-fr and BC-1yr. Indaziflam sorption could be more affected for the hydrophobic interactions than terbuthylazine due to its lower solubility, so the increase of the number of available pores from removal of the organic layer aids sorption. As we mentioned above, aging may have altered the qualitative DOC character affecting its chemical affinity.

Nicosulfuron and MCPA are weak acids and at the pH of the solutions (6.7−6.5) >98% of the molecules are anionic. This negatively charged species could create a repulsion to negative groups on the biochar surface, and only the molecular species are sorbed. Cabrera et al.[34] evaluated several biochars made from different feedstocks under different pyrolysis conditions and observed a correlation between MCPA sorption and the biochar surface area, where BC2 biochar with the same characteristic of BC-fr had the smaller SSA value (3.3 m$^2$/g) and showed the lower $K_d$ value. No sorption of nicosulfuron was observed on the biochars, which may be due to higher repulsion of anionic molecules (>99%). Unlike other sulfonylureas for which adsorption is usually controlled by organic C content, different results show that clay mineralogy plays an important role in nicosulfuron adsorption.[35−37] For MCPA, an increase of anionic molecules is expected at more alkaline conditions, which decreases the sorption of the molecular species and enhances the charge repulsion interaction for BC-1yr and BC-2yr. Oliveira et al. (2001)[38] found $K_d$ values for nicosulfuron of 0.14−1.38 in six Brazilian soils, and Reginato and Koskinen (2008)[39] determined in three American soils and two Brazilian soils values in the range of 0.14−1.81. Lopez Piñeiro (2013)[40] established $K_d$ values of

MCPA in different soils of 0.29−0.43. The increase on MCPA sorption in biochar was 18 times even for this herbicide where biochar surface repulsion happened and only the molecular species are sorbed. Nicosulfuron $K_d$ values are higher in soils than in biochars.

According to the $K_d$ values of biochar in the four herbicides mentioned above, it appears that the sorption depends on the p$K_a$ and hydrophobicity of the chemical. This indicates that the metabolite of indaziflam (fluoroethyldiaminotriazine) would be more polar than the parent compound, which explains the lower values of $K_d$ (0.26−2.95) than the parent and its dependency on the biochar pH explaining the sorption increase in BC-1yr and BC-2yr. Using a theoretical p$K_a$ value for fluoroethyldiaminotriazine of 4.10 (www.chemaxon.com),[18] a higher percentage of cationic molecules and sorption than indaziflam is predicted, so the difference in the observed sorption could be due to the differences in the hydrophobic biochar interactions.

These results indicate that, for a biochar made under high pyrolysis conditions, the sorption of pesticides depends highly on the hydrophobicity of the chemicals. The aging process of the biochars modified the pH of the solution and correspondingly affected the sorption behavior of the herbicides. Even so, the aged biochars are highly effective in adsorbing terbuthylazine and indaziflam, due to its high initial adsorptivity.

Our results indicate that biochar and soil components interaction happened in the surface of the aged biochars and the specific surface area (SSA) increased with this process. For this biochar the major facet of the aging process was loss of the sorbed organic films present on the fresh biochar particle. The adsorption of pesticides is highly dependent not only on biochar characteristics but also on the physicochemical characteristics of the pesticides. For the biochar examined here, aged biochars in soils still remain highly effective at adsorbing pesticides, due to the high initial adsorptivity. Due to the variable nature of biochars, individual characterization of the biochar used as soil amendment is recommended prior to field applications. However, these results do indicate the potential for increased sorption behavior to exist 2 years after the initial biochar application, despite the observed clogging of biochar pore space with soil particles. In addition, it is important to match the target chemical characteristics with the correct biochar properties to optimize the sorption potential of biochar in a particular application.

## AUTHOR INFORMATION

### Corresponding Author

*E-mail: kurt.spokas@ars.usda.gov.

### Funding

We acknowledge the postdoctoral fellowship MINECO/FECYT for C.T. and the funding project AGL2013-48446-C3-1-R.

### Notes

The authors declare no competing financial interest.

## ACKNOWLEDGMENTS

Parts of this work were carried out in the Characterization Facility, University of Minnesota, which receives partial support from NSF through the MRSEC program.

## REFERENCES

(1) Joseph, S. D.; Camps-Arbestain, M.; Lin, Y.; Munroe, P.; Chia, C. H.; Hook, J.; Van Zwieten, L.; Kimber, S.; Cowie, A.; Singh, B. P.; Lehmann, J.; Foidl, N.; Smernik, R. J.; Amonette, J. E. An investigation into the reactions of biochar in soil. *Aust. J. Soil Res.* **2010**, *48*, 501−515.

(2) Schmidt, M. W. I.; Noack, A. G. Black carbon in soils and sediments: Analysis, distribution, impplications and current challenges. *Global Biogeochem. Cycles* **2000**, *14* (3), 777−793.

(3) Singh, B. P.; Cowie, A. L. A novel approach, using $^{13}C$ natural abundance, for measuring decomposition of biochars in soil. In *Carbon and Nutrient Management in Agriculture, Fertilizer and Lime Research Centre Workshop proceedings*; Currie, L. D., Yates, L. J., Eds.; Massey University: Palmerston North, New Zealand, 2008; 549 pp.

(4) Kuzyakov, Y.; Subbotina, I.; Chen, H.; Bogomolova, I.; Xu, X. L. Black carbon decomposition and incorporation into soil microbial biomass estimated by $^{14}C$ labeling. *Soil Biol. Biochem.* **2009**, *41* (2), 210−219.

(5) Kleber, M.; Sollins, P.; Sutton, R. A conceptual model or organo-mineral interactions in soils: self-assembly or organic molecular fragments into zonal structures on mineral surfaces. *Biogeochemistry* **2007**, *85*, 9−24.

(6) Nguyen, B. T.; Lehmann, J.; Kinyangi, J.; Smernik, R.; Riha, S. J.; Engelhard, M. H. Long-term black carbon dynamics in cultivated soil. *Biogeochemistry* **2008**, *89*, 295−308.

(7) Spokas, K.; Koskinen, W. C.; Baker, J. M.; Reicosky, D. C. Impacts of wood biochar additions on greenhouse gas production and sorption/degradation of two herbicides in a Minnesota soil. *Chemosphere* **2009**, *77*, 574−581.

(8) Wang, H.; Lin, K.; Hou, Z.; Richardson, B.; Gan, J. Sortion of the herbicide terbuthylazine in two New Zealand forest soils amended with biosolids and biochars. *J. Soils Sediments* **2010**, *10*, 283−289.

(9) Yu, X.; Pan, L.; Ying, G.; Kookana, R. S. Enhanced and irreversible sorption of pesticide Pyrimethanil by soil amended with biochars. *J. Environ. Sci.* **2010**, *22*, 615−620.

(10) Kookana, R. S. The role of biochar in modifying the environmental fate, bioavailability, and efficacy of pesticides in soils: a review. *Aust. J. Soil Res.* **2010**, *48*, 627−637.

(11) Yang, Y.; Sheng, G. Pesticide Adsorptivity of Aged Particulate Matter Arising from Crop Residue Burns. *J. Agric. Food Chem.* **2003**, *51*, 5047−5051.

(12) Brown, H. R. Mode of action, crop selectivity, and soil relations of the sulfonylurea herbicides. *Pestic. Sci.* **1990**, *29*, 261−281.

(13) Felding, G. Leaching of phenoxyalkanoic acid herbicides from farmland. *Sci. Total Environ.* **1995**, *168*, 11−18.

(14) REGLAMENTO DE EJECUCIÓN (UE) N° 820/2011 DE LA COMISION de 16 de agosto de 2011 (17.8.2011).

(15) Trigo, C.; Koskinen, W. C.; Kookana, R. Sorption-desorption of indaziflam and its three metabolites in sandy soils. *J. Environ. Sci. Health, Part B* **2014**, *49*, 836−843.

(16) Tang, J.; Zhu, W.; Kookana, R.; Watayama, A. Characteristics of biochar and its application in remediation of contaminated soil. *J. Biosci. Bioeng.* **2013**, *116* (6), 653−659.

(17) http://www.eu-footprint.org/ppdb.html (accessed April 2014).

(18) Chemaxon-cheminformatics platforms and desktop applications. Available at https://www.chemaxon.com/products/calculatorplugins/property-predictors/ (accessed Apr 2014).

(19) US Climate Data, 2014. Web Resource, http://www.usclimatedata.com/climate/rosemount/minnesota/united-states/usmn0642/2014/1 (accessed on July 7, 2014).

(20) Weishaar, J. L.; Aiken, G. R.; Bergamaschi, B. A.; Fram, M. S.; Fuji, R.; Mopper, K. Evaluation of specific ultraviolet absorbance as an indicator of the chemical composition and reactivity of dissolved organic carbon. *Environ. Sci. Technol.* **2003**, *37*, 4702−4708.

(21) OECD. Test No. 106: adsorption-desorption using a batch equilibrium method. *OECD guidelines for the testing of chemicals, section 1*; OECD Publishing: 2000.

(22) Bellamy, L. J. *The Infrared Spectra of Complex Molecules*, 3rd ed.; Chapman and Hall: London, U.K., 1975; Vol. *I*.

(23) Lin, Y.; Munroe, P.; Joseph, S.; Kimber, S.; Van Zwieten, L. Nanoscale organo-mineral reactions of biochars in ferrosol: an investigation using microscopy. *Plant Soil* **2012**, *357*, 369−380.
(24) Mecozzi, S.; West, A. P.; Dougherty, D. A. Cation-pi interactions in aromatics of biological and medical interest: Electrostatic potential surfaces as a useful qualiative guide. *Proc. Natl. Acad. Sci. U.S.A.* **1996**, *93* (20), 10566−10571.
(25) Pignatello, J. J.; Kwon, S.; Lu, Y. Effect of natural organic substances on the surface and adsorptive properties of environmental black carbon (char): attenuation of surface activity by humic and fulvic acids. *Environ. Sci. Technol.* **2006**, *40* (24), 7757−7763.
(26) Jamieson, T.; Sager, E.; Guéguen, C. Characterization of biochar-derived disolved organic matter using UV-visible absorption and excitation-emission fluorescence. *Chemosphere* **2014**, *103*, 197−204.
(27) Cox, L.; Fernandes, M. C.; Zsolnay, A.; Hermosín, M. C.; Cornejo, J. Changes in Dissolved Organic Carbon in Soil Amendments with Aging: Effect on Pesticide Adsorption Behavior. *J. Agric. Food Chem.* **2004**, *52*, 5635−5642.
(28) Specht, C.; Kumke, M.; Frimmel, F. Characterization of NOM adsorption to clay minerals by size exclusion chromatography. *Water Res.* **2000**, *34*, 4063−4069.
(29) Keiluweit, M.; Kleber, M. Molecular-Level Interactions in Soils and Sediments: The Role of Aromatic π-Systems. *Environ. Sci. Technol.* **2009**, *43*, 3421−3429.
(30) Hamaker, J. W., Thompson, J. M. Adsorption. In *Organic Chemicals in the Soil Environment*. Goring, C. A. I., Hamaker, J. W., Eds.; Marcel Dekker: New York, 1972; Vol. *1*, pp 49−143.
(31) Cox, L.; Celis, R.; Hermosín, M. C.; Cornejo, J.; Zsolnay, A.; Zeller, K. Effect of Organic Amendments on Herbicide Sorption as Related to the Nature of the Dissolved Organic Matter. *Environ. Sci. Technol.* **2000**, *34*, 4600−4605.
(32) Alonso, D.; Koskinen, W.; Oliveira, R.; Constantin, J.; Mislankar, S. Sorption-Desorption of Indaziflam in Selected Agricultural Soils. *J. Agric. Food Chem.* **2011**, *59*, 13096−13101.
(33) Alister, C.; Araya, M.; Kogan, M. Effects of physicochemical soil properties of five agricultural soils on herbicide soil adsorption and leaching. *Cienc. Invest. Agrar.* **2011**, *38*, 243−251.
(34) Cabrera, A.; Cox, L.; Spokas, K.; Celis, R.; Hermosín, M. C.; Cornejo, J.; Koskinen, W. Comparative sorption and leaching study of the herbicides fluometuron and 4-chloro-2-methylphenoxyacetic acid (MCPA) in a soil amended with biochars and other sorbents. *J. Agric. Food Chem.* **2011**, *59*, 12550−12560.
(35) Ukrainczyk, L.; Rashid, N. Irreversible sorption of nicosulfuron on clay minerals. *J. Agric. Food Chem.* **1995**, *43*, 855−857.
(36) Gonzalez, J.; Ukrainczyk, L. Adsorption and Desorption of Nicosulfuron in Soils. *J. Environ. Qual.* **1996**, *25*, 1186−1192.
(37) Carrizosa, M. J.; Hermosín, M. C.; Koskinen, W. C.; Cornejo, J. Interactions of two sulfonilurea herbicides with organoclays. *Clays Clay Miner.* **2004**, *52* (5), 643−649.
(38) Oliveira, R., Jr.; Koskinen, W. C.; Ferreira, F. A. Sorption and leaching potential of herbicides on Brazilian soils. *Weed Res.* **2001**, *41*, 97−110.
(39) Reginato, J. B.; Koskinen, W. C. Characterization of nicosulfuron availability in aged soils. *J. Agric. Food Chem.* **2008**, *56*, 5801−5805.
(40) López-Piñeiro, A.; Peña, D.; Albarrán, A.; Sánchez-Llerena, J.; Becerra, D. Behavior of MCPA in four intensive cropping soils amended with fresh, composted, and aged olive mill waste. *J. Contam. Hydrol.* **2013**, *152*, 137−146.

varietal dependents, so such composition can be associated with the so-called "terroir character" of their vineyards and their wines.

There are a number of solid−liquid extraction (SLE) techniques used for the extraction of phenolic compounds from different vegetable waste materials, most of them using organic solvents (mainly ethanol), high temperatures (up to 240 °C), and long extraction times (up to 1 h) to exhaust the materials.[20−22] However, such long extraction times can cause the generation of artifact compounds, and the use of organic solvents limits the search for new applications, due to their negative environmental impact and other human health issues. SLE procedures may be assisted by other parameters such as as ultrasound (UAE),[23] pressure (PSE),[13,24] or the use of supercritical fluids[25] among others.

Nowadays there is a trend that encourages the use of free environmental techniques to enhance sustainability; it is the so-called "green chemistry". Such techniques are developed to reduce and/or eliminate the use of organic solvents, and the use of water as extractant should be preferred. As well, the resulting aqueous extracts will have the advantage of being exempt from certification based on their vegetal origin,[26] although the compounds' concentration in such extracts may be lower than when other techniques are used as the exhaustion of the vegetable material does not take place. Other SLE techniques that may be in agreement with this new green postulated may be based on the Naviglio principle[27,28] or on microwave extraction (ME).[29,30] Whereas the Naviglio solid−liquid extraction technique is carried out at room temperature and compression/decompression times are modified, ME uses higher temperatures but shorter extraction times.

Extraction techniques to get aromatic plant extracts are very limited, except for essential oil production.[31] Delgado de la Torre et al.[15] have only refereed vine-shoot aroma description where ethanolic water mixtures at 220 °C for 60 min were the selected extraction conditions. Volatile phenols and furanic derivates were described in the previous work as the main components in vine-shoots, the same compounds found in oak aqueous extracts with biostimulant properties.[18]

Consequently, the aim of this work was to compare Airén vine-shoot waste aqueous extracts produced by four solid−liquid extraction techniques (conventional solid−liquid extraction (CSLE), solid−liquid dynamic extraction (SLDE-Naviglio), solvent free microwave extraction (ME), and pressurized solvent extraction (PSE) and to study their chemical composition in terms of phenolic, volatile, and mineral valuable compounds as they may have agricultural applications such as plant biostimulants or foliar fertilizers.

## MATERIALS AND METHODS

**Vine-Shoot Samples.** One hundred kilograms of Airén white *V. vinifera* vine-shoot wastes was sampled in D.O. Mancha, located in the Castilla-La Mancha Spanish region, 4 months after the harvest of 2013, by randomized selection. Samples were dried for 72 h at room temperature until a final humidity of 6.5% ($g_{water}$/100 g $_{of\ sample}$). Dry vine-shoot wastes were ground by using a hammer miller (LARUS Impianti, Skid Sinte 1000, Zamora, Spain) to get a homogeneous 40 mesh sieve sampling. Samples were kept under vacuum until their use at room temperature (25−27 °C).

**Vine-Shoot Extraction Procedures.** All vine-shoot waste aqueous extracts were submitted twice for each extraction technique and condition tested.

*CSLE.* Fifty grams of ground Airén vine-shoot waste samples was extracted with 250 mL of boiling water, and then the solution was kept at 100 °C. The extraction time was set at 15, 30, and 60 min (CSLE-15, CSLE-30, and CSLE-60, respectively).

*SLDE-Naviglio.* A dynamic solid−liquid extraction was carried out using a Naviglio Extractor (FT 110, Armfield, UK) following the Naviglio methodology.[27] The Naviglio extraction is based on a suction effect generated by a compression of water, used as extracting solvent, on solids at room temperature (25−27 °C) and a pressure of 8 bar, followed by immediate decompression at atmospheric pressure. Two hundred grams of ground vine-shoot wastes was placed inside the extraction chamber, and 1.1 L of water was added as a solvent. The conditions tested for compound extraction were as follows: 20 extractive cycles of 6.5 min (5 min in the static phase and 1.5 min in the dynamic phase; SLDE-Naviglio-6.5), 8 min (5 min in the static phase and 3 min in the dynamic phase; SLDE-Naviglio-8), and 12 min (9 min in the static phase and 3 min in the dynamic phase; SLDE-Naviglio-12) each.

*ME.* Microwave extraction was carried out with a NEOS apparatus (Milestone, Italy). Fifty grams of ground vine-shoot waste samples was placed into the reactor with 250 mL of water at 100 °C. The extraction program was set at 600 W (held for 5, 10, and 15 min; ME-5, ME-10, ME-15, respectively). A rotating microwave diffuser ensured homogeneous microwave distribution throughout the plasma-coated PTFE cavity. The temperature was monitored by an external IR sensor.

*PSE.* Twenty grams of ground vine-shoot wastes was placed into each cell (four cells) with 100 mL of water and extracted using a pressurized extractor (Speed Extractor BUCHI E-914, Barcelona, Spain). The extractor parameters were set at temperature of 30 °C ($T_1$) and 100 °C ($T_2$), pressure of 50 bar ($P_1$) and 100 bar ($P_2$), three cycles (heat up, 1 min; hold (10, 15, 30 min), and discharge (9 min) named PSE-time, pressure, temperature (PSE-10$P_1T_1$, PSE-10$P_1T_2$, PSE-10$P_2T_1$, PSE-10$P_2T_2$, PSE-15$P_1T_1$, PSE-15$P_1T_2$, PSE-15$P_2T_1$, PSE-15$P_2T_2$, PSE-30$P_1T_1$, PSE-30$P_1T_2$, PSE-30$P_2T_1$, PSE-30$P_2T_2$). After the discharge of the last cycle, the extraction cells were flushed with water for 3 min and with $N_2$ gas for 5 min.

All extracts were filtered through a PVDF Durapore filter of 0.45 μm (Millipore, Bedford, MA, USA).

**Extract Analysis.** Extracts general parameters such as °Brix, pH, and total phenol index (TPI, measured at 280 nm by means of an UV−vis spectrophotometer Lambda 25 (PerkinElmer, Norwalk, CT, USA) were determined.

*Determination of Phenolic Compounds by HPLC-DAD-MS.* This method was based on Pardo-García et al.'s[19] work, but the gradient condition was slightly modified to improve the resolution of new standards. The HPLC grade solvents used were water/formic acid/acetonitrile (97.5:1.5:1 v/v/v) as solvent A and acetonitrile/formic acid/solvent A (78.5:1.5:20 v/v/v) as solvent B. The elution gradient was set up for solvent B as 0 min, 5%; 2 min, 10%; 4 min, 14%; 9 min, 14%; 37 min, 18.5%; 35 min, 20%; 50 min, 25%; 55 min, 50%; 60 min, 5%; and 65 min, 5%. The loop volume was 20 μL.

Phenolic acid, stilbene, and flavanol detections were carried out with the DAD by comparison with the corresponding UV−vis spectra and retention time of their pure standards in the chromatogram. Acids *trans*-caftaric and *trans*-*p*-coutaric were not available, so they were identified with the molecular ion and the spectral parameters, which were very close to their analogous *trans*-caffeic and *trans*-*p*-coumaric acids. Compounds were quantified and identified at different wavelengths: (+)-catechin, (−)-epicatechin, gallic acid, protocatechuic acid, pyrogallol, and syringic acid at 280 nm; ellagic, ferulic, and vanillic acids at 256 nm; *trans*-caffeic acid, *trans*-caftaric acid, and sinapaldehyde at 324 nm; *trans*-resveratrol, piceid (*t*-resveratrol-3-glucoside), *trans*-*p*-coumaric acid, and *trans*-*p*-coutaric acid at 308 nm.

Quantification was based on calibration curves of the respective standards (Sigma-Aldrich, Steinheim, Germany) at five different concentrations (0.70−175 mg/L) ($R^2$ > 0.97). All analyses were made in duplicate.

*Determination of Volatile Compounds by HS-SBSE-GC-MS.* Volatiles were extracted by means of headspace stir bar sorptive extraction (HS-SBSE) according to Pardo-Garcia et al.'s[32] method. The volatile analysis was performed using an automated thermal

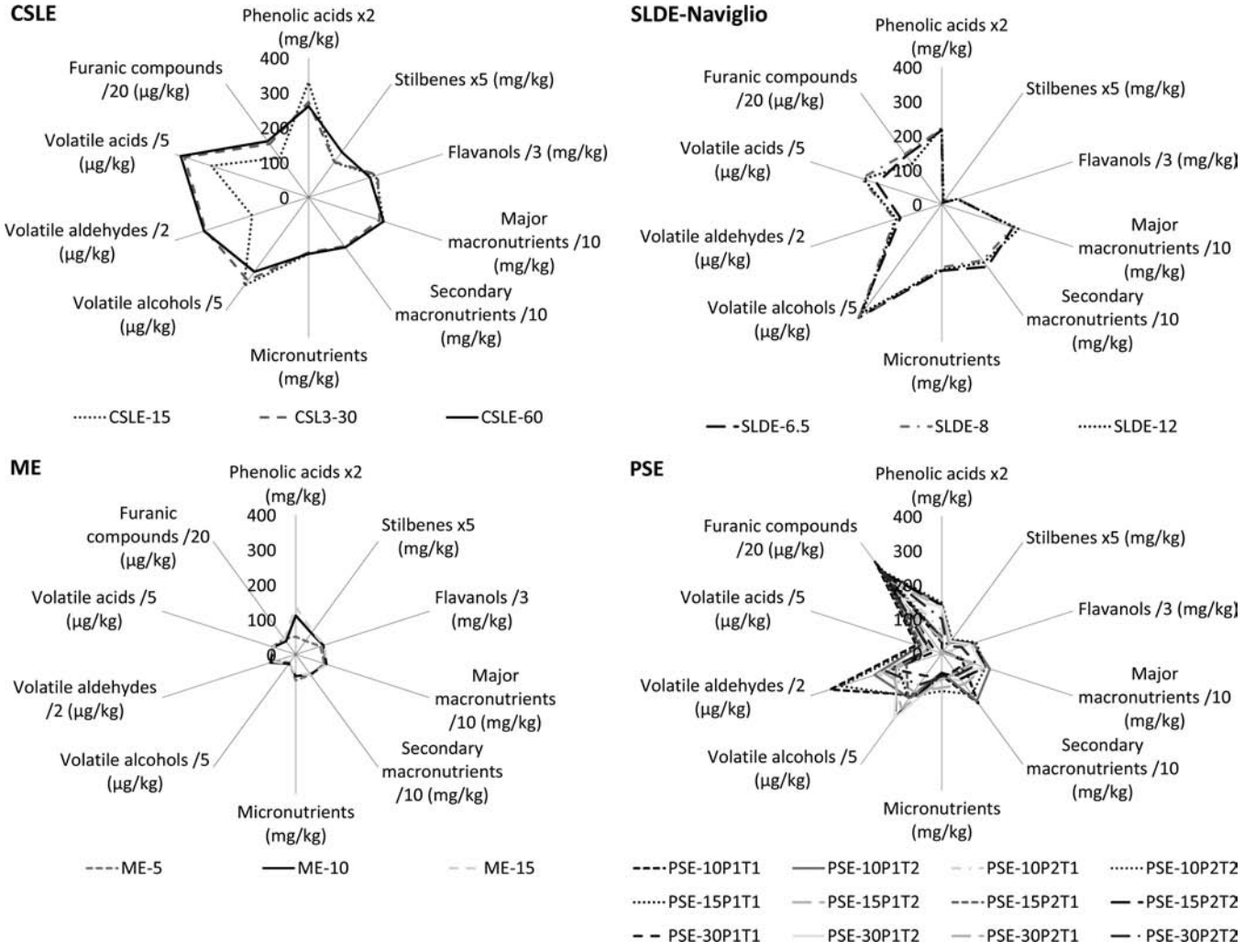


**Figure 1.** Total composition, in terms of the main chemical families, for the aqueous vine-shoot waste extracts obtained under different extraction systems and conditions. ME, solvent-free microwave extraction (ME-5, 5 min; ME-10, 10 min; ME-15, 15 min); CSLE, conventional solid−liquid extraction (CSLE-15, 15 min; CSLE-30, 30 min; CSLE-60, 60 min); SLDE-Naviglio, solid−liquid dynamic extraction (SLDE-Naviglio-6.5, 5 min in the static phase and 1.5 min in the dynamic phase; SLDE-Naviglio-8, 5 min in the static phase and 3 min in the dynamic phase; SLDE-Naviglio-12, 9 min in the static phase and 3 min in the dynamic phase); PSE, pressurized solvent extraction (extraction temperature, 30 °C ($T_1$) and 100 °C ($T_2$); pressure, 50 ($P_1$) and 100 bar ($P_2$); cycles, 3 (heat up, 1 min, hold (10, 15, 30 min), and discharge (9 min) named PSE-time, pressure, temperature (PSE-10$P_1T_1$, PSE-10$P_1T_2$, PSE-10$P_2T_1$, PSE-10$P_2T_2$, PSE-15$P_1T_1$, PSE-15$P_1T_2$, PSE-15$P_2T_1$, PSE-15$P_2T_2$, PSE-30$P_1T_1$, PSE-30$P_1T_2$, PSE-30$P_2T_1$, PSE-30$P_2T_2$).

desorption unit (TDU, Gerstel, Mülheim and der Ruhr, Germany) mounted on an Agilent 7890A gas chromatograph system (GC) coupled to a quadrupole Agilent 5975C electron ionization mass spectrometric detector (Agilent Technologies, Palo Alto, CA, USA) equipped with a fused silica capillary column (BP21 stationary phase, 30-m length, 0.25 mm i.d., and 0.25 μm film thickness) (SGE, Ringwood, Australia). The carrier gas was helium with a constant column pressure of 20.75 psi.

The stir bars were thermally desorbed in a stream of helium carrier gas at a flow rate of 75 mL/min with the TDU programmed from 40 to 295 °C (held 5 min) at a rate of 60 °C/min. The analytes were focused in a programmed temperature vaporizing injector (PTV) (CIS-4, Gerstel), containing a packed liner (20 mg tenax TA), held at 25 °C with Peltier cooling prior to injection. After desorption and focusing, the CIS-4 was programmed from 25 to 260 °C (held for 5 min) at 12 °C/s to transfer the trapped volatiles onto the analytical column. The TDU was operated in the splitless desorption mode, whereas the CIS-4 was operated in the PTV solvent vent mode (purge flow to split vent of 80 mL/min, vent 75 mL/min, and pressure 20.85 psi). The GC oven temperature was programmed to 40 °C (held for 2 min), raised to 80 °C (5 °C/min, held for 2 min), raised to 130 °C (10 °C/min, held for 5 min), raised to 150 °C (5 °C/min, held for 5 min), and then raised to 230 °C (10 °C/min, held for 5 min). The MS was operated in scan acquisition (27−300 u) with an ionization energy of 70 eV. The temperature of the MS transfer line was maintained at 230 °C. The identification of the compounds was performed using the NIST library and confirmed by comparison with the mass spectra and retention time of chromatographic standards. To avoid matrix interferences, the MS quantification was performed in the single ion-monitoring mode using characteristic $m/z$ values. The standards employed to identify and quantify volatiles (GC-MS) were purchased from Sigma-Aldrich (Steinheim, Germany) (the numbers in parentheses indicate the $m/z$ used for quantification): D-limonene ($m/z$ 69), 1-hexanol ($m/z$ 56), 3-hexen-1-ol (*Z*) ($m/z$ 67), nonanal ($m/z$ 57), 1-octen-3-ol ($m/z$ 57), furfural ($m/z$ 96), benzaldehyde ($m/z$ 106), linalool ($m/z$ 71), linalyl acetate ($m/z$ 93), 5-methylfurfural ($m/z$ 110), 1-nonanol ($m/z$ 56), α-terpineol ($m/z$ 59), hexanoic acid ($m/z$ 60), geranyl acetone ($m/z$ 43), guaiacol ($m/z$ 109), benzyl alcohol ($m/z$ 108), *trans*/*cis*-whiskey lactones ($m/z$ 99), 2-phenylethanol ($m/z$ 91), β-ionone ($m/z$ 177), octanoic acid ($m/z$ 60), decanoic acid ($m/z$ 60), and vanillin ($m/z$ 151), together with the internal standards 3-methyl-1-pentanol and γ-hexalactone. Quantifica-


dx.doi.org/10.1021/jf503929v | J. Agric. Food Chem. 2014, 62, 10861−10872

a)

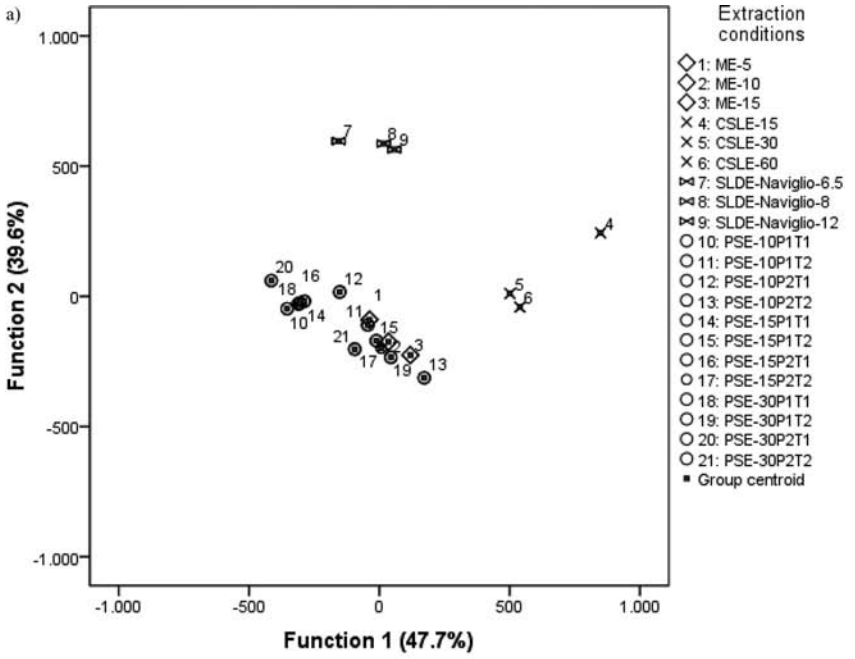


b)

| Compounds* | Function 1 | Function 2 |
|---|---|---|
| Gallic acid | 24,527 | -0,671 |
| Pyrogallol | 2,659 | -1,471 |
| Protocatechuic acid | -3,176 | -10,757 |
| *trans*-Caftaric acid | 15,160 | -1,007 |
| (+)-Catechin | -4,054 | -0,020 |
| *trans-p*-Coutaric | -1,903 | 12,457 |
| *trans*-Caffeic acid | -6,657 | -1,561 |
| Vanillic acid | 15,110 | 8,286 |
| (-) -Epicatechin | -17,127 | -1,674 |
| Syringic acid | -6,935 | -0,304 |
| *trans-p*-Coumaric acid | 7,055 | -2,807 |
| Piceid | 1,184 | -1,465 |
| Ellagic acid | 20,920 | 3,952 |
| Ferulic acid | -11,690 | 5,965 |
| *trans*-Resveratrol | -6,103 | -0,244 |
| Boron | 1,193 | -10,058 |
| Calcium | -11,177 | 18,417 |
| Iron | 5,890 | -4,422 |

*Coefficients with values lower than |1.00| are not shown.

**Figure 2.** (a) Canonical discriminant analysis of the 21 vine-shoot waste aqueous extracts obtained by four extraction systems. (b) Standarized canonical coefficients of the main discriminant variables in functions 1 and 2 obtained for phenolic compounds, volatile compounds, and mineral composition data. ME, solvent-free microwave extraction (ME-5, 5 min; ME-10, 10 min; ME-15, 15 min); CSLE, conventional solid–liquid extraction (CSLE-15, 15 min; CSLE-30, 30 min; CSLE-60, 60 min); SLDE-Naviglio, solid–liquid dynamic extraction (SLDE-Naviglio-6.5, 5 min in the static phase and 1.5 min in the dynamic phase; SLDE-Naviglio-8, 5 min in the static phase and 3 min in the dynamic phase; SLDE-Naviglio-12, 9 min in the static phase and 3 min in the dynamic phase); PSE, pressurized solvent extraction (extraction temperature, 30 °C ($T_1$) and 100 °C ($T_2$); pressure, 50 ($P_1$) and 100 bar ($P_2$); cycles, 3 (heat up, 1 min, hold (10, 15, 30 min), and discharge (9 min) named PSE-time, pressure, temperature (PSE-10$P_1T_1$, PSE-10$P_1T_2$, PSE-10$P_2T_1$, PSE-10$P_2T_2$, PSE-15$P_1T_1$, PSE-15$P_1T_2$, PSE-15$P_2T_1$, PSE-15$P_2T_2$, PSE-30$P_1T_1$, PSE-30$P_1T_2$, PSE-30$P_2T_1$, PSE-30$P_2T_2$).

tion was based on calibration curves of the respective standards at five different concentrations (2 μg/L–15 mg/L) ($R^2$ > 0.97). All analyses were made in triplicate.

*Mineral Composition.* Al, As, B, Be, Bi, Ca, Cd, Co, Cr, Cu, Fe, K, Li, Mg, Mn, Mo, Na, Ni, P, Pb, S, Sb, Se, Sr, Ti, Tl, V, and Zn were quantified in vine-shoot waste aqueous extracts by inductively coupled plasma–optical emission spectrometry (ICP-OES) using an ICP spectrometer (Thermo Scientific ICAP 6500 Duo, Madrid, Spain). Anion quantifications such as P, S, Cl, F, N (as $NO_3^-$ and $NO_2^-$) were determined by ion chromatography (850 Professional IC Anion, Suppressor Module MSM, Metrohm, Herisau, Switzerland) coupled with a conductivity detector (model 819, Metrohm). Aliquots of 20 μL were injected after filtering through a 0.45 μm PTFE filter in a Metrosep A Supp 7 analytical column (4.0 mm i.d. × 250 mm, 5 μm particle size, Metrohm) at 50 °C. An isocratic elution was performed with 3.6 mM $Na_2CO_3$ at a flow of 0.8 mL/min.

Quantification was based on calibration curves of the respective standards (Sigma-Aldrich, Steinheim, Germany) at five different concentrations (0.01–25.00 mg/L) ($R^2$ > 0.99). All analyses were made in duplicate.

**Statistical Analysis.** The statistical elaboration of the data was performed using SPSS version 19.0 statistical package for Windows (SPSS, Chicago, IL, USA). Phenolic, volatile, and mineral compound data were processed using the variance analysis (ANOVA). Differences between means were compared using the least significant difference (LSD) test at a 99.95% probability level.

## ■ RESULTS AND DISCUSSION

The first approach of this paper was to produce aqueous extracts from vine-shoot wastes of Airén white *V. vinifera*. Four extraction systems (CSLE, SLDE-Naviglio, ME, and PSE) were assayed with the same vine-shoot sample/water ratio, combining, according to the system selected, parameters such as time, temperature, and pressure, resulting in 21 different aqueous vine-shoot waste extracts for their study. Different extraction yields were obtained, so all data have been homogenized and expressed as milligrams per kilogram or micrograms per kilogram of dry vine-shoot matter. Extracts were characterized in terms of phenolic, volatile, and mineral compounds. All extracts had a pH value ranging from 5.93 (ME) to 6.62 (PSE).

Due to the large quantity of compositional data, some chemical associations were carried out to have a general look at each extraction system and their respective conditions (Figure 1). The most concentrated family of compounds, independent of the extraction technique used, were macronutrients (major and secondary), followed by flavanols and phenolic acids, all of

**Table 1. Non-Flavonoid and Flavonoid Composition (Milligrams per Kilogram Dry Weight) of Different Vine-Shoot Waste Aqueous Extracts[a]**

| | CSLE | | | SLDE-Naviglio | | |
|---|---|---|---|---|---|---|
| compound | CSLE-15 | CSLE-30 | CSLE-60 | SLDE-Naviglio-6.5 | SLDE-Naviglio-8 | SLDE-Naviglio-12 |
| **flavanols** | | | | | | |
| (+)-catechin | 390.88 ± 5.11 c | 402.21 ± 8.95 c | 353.47 ± 0.29 b | 80.35 ± 1.69 a | 83.64 ± 0.65 a | 76.41 ± 1.67 a |
| (−)-epicatechin | 214.46 ± 30.38 b | 217.79 ± 17.33 b | 197.34 ± 3.17 b | 66.30 ± 1.87 a | 67.21 ± 0.00 a | 62.99 ± 0.94 a |
| **total** | **605.33 ± 25.27 bc** | **619.99 ± 26.28 c** | **550.81 ± 3.46 b** | **146.65 ± 3.55 a** | **150.84 ± 0.64 a** | **139.39 ± 2.61 a** |
| **phenolic acids** | | | | | | |
| *trans*-caffeic acid | 1.92 ± 0.15 a | 2.17 ± 029 ab | 2.14 ± 0.03 ab | 2.83 ± 0.57 abc | 3.06 ± 0.04 bc | 3.43 ± 0.21 c |
| *trans-p*-coumaric acid | 8.49 ± 0.43 d | 7.31 ± 0.11 bcd | 7.68 ± 0.51 cd | 5.63 ± 0.22 a | 6.22 ± 0.34 ab | 6.76 ± 0.20 abc |
| ferulic acid | 2.20 ± 0.24 b | 2.05 ± 0.05 b | 2.36 ± 0.02 b | 1.12 ± 0.11 a | 0.93 ± 0.05 a | 0.92 ± 0.02 a |
| *trans*-caftaric acid | 77.60 ± 2.74 b | 60.59 ± 2.95 a | 55.21 ± 0.59 a | 59.83 ± 5.44 a | 60.34 ± 2.41 a | 59.96 ± 0.14 a |
| *trans-p*-coutaric acid | 19.39 ± 0.83c | 16.58 ± 0.85 abc | 14.70 ± 0.04 a | 17.85 ± 0.16 b | 16.18 ± 0.82 ab | 16.08 ± 0.20 ab |
| ellagic acid | 14.10 ± 2.88 c | 13.38 ± 1.40 c | 10.28 ± 0.74 bc | 3.89 ± 0.43 a | 4.98 ± 0.69 ab | 5.57 ± 0.70 ab |
| gallic acid | 19.40 ± 0.13 b | 18.53 ± 0.75 b | 20.53 ± 0.36 b | 8.37 ± 2.20 a | 7.21 ± 0.72 a | 7.80 ± 0.12 a |
| protocatechuic acid | 6.94 ± 0.86 b | 6.67 ± 0.12 b | 6.94 ± 0.23 b | 3.62 ± 0.75 a | 3.34 ± 0.25 a | 3.25 ± 0.08 a |
| syringic acid | 6.37 ± 0.09 b | 6.50 ± 0.41 b | 6.05 ± 0.25 b | 4.59 ± 0.15 a | 4.91 ± 0.21 a | 4.62 ± 0.11 a |
| vanillic acid | 8.38 ± 1.15 c | 3.45 ± 0.14 ab | 4.72 ± 0.04 b | nd[b] | 2.56 ± 0.23 a | 2.70 ± 0.11 a |
| **total** | **164.79 ± 2.35 c** | **137.22 ± 3.38 b** | **130.61 ± 0.34 b** | **107.74 ± 0.60 a** | **109.72 ± 2.94 a** | **111.10 ± 1.05 a** |
| **stilbenes** | | | | | | |
| piceid | 3.73 ± 0.48 b | 3.80 ± 0.19 b | 3.50 ± 0.03 b | 0.50 ± 0.04 a | 0.50 ± 0.12 a | 0.58 ± 0.01 a |
| *trans*-resveratrol | 21.03 ± 4.96 b | 21.22 ± 5.30 b | 28.56 ± 3.90 b | 0.66 ± 0.05 a | 0.79 ± 0.20 a | 1.32 ± 0.09 a |
| **total** | **24.76 ± 5.44 b** | **25.02 ± 5.49 b** | **32.06 ± 3.93 b** | **1.16 ± 0.09 a** | **1.29 ± 0.32 a** | **1.90 ± 0.10 a** |
| **others** | | | | | | |
| pyrogallol | 21.46 ± 0.19 a | 20.49 ± 0.64 a | 19.91 ± 0.32 a | 36.43 ± 0.38 b | 34.09 ± 2.44 b | 33.57 ± 0.09 b |
| sinapaldehyde | 2.32 ± 0.26 a | 2.32 ± 0.11 a | 2.19 ± 0.00 a | nd | nd | nd |
| **total** | **23.78 ± 0.45 a** | **22.81 ± 0.74 a** | **22.11 ± 0.32 a** | **34.43 ± 0.38 b** | **34.09 ± 2.44 b** | **33.57 ± 0.09 b** |

[a]CSLE, conventional solid−liquid extraction (CSLE-15, 15 min; CSLE-30, 30 min; CSLE-60, 60 min); SLDE-Naviglio, solid−liquid dynamic extraction (SLDE-Naviglio-6.5, 5 min in the static phase and 1.5 min in the dynamic phase; SLDE-Naviglio-8, 5 min in the static phase and 3 min in the dynamic phase; SLDE-Naviglio-12, 9 min in the static phase and 3 min in the dynamic phase). Different letters in the same row indicate significant differences among extraction conditions according to the LSD test ($\alpha < 0.05$). The mean values ($n = 4$) are shown with their standard deviation. [b]nd, not detected.

them expressed in milligrams per kilogram. The volatile content was the lowest, expressed in micrograms per kilogram, the most abundant being furanic compounds. CSLE and SLDE-Naviglio techniques produced the most concentrated extracts in relation to the groups of compounds previously discussed. Both extraction techniques are very different from one another, equating a conventional solid−liquid extraction technique with a novel technique based on a suction effect generated by a compression/decompression cycle (SLDE-Naviglio). The other two innovative extraction systems tested, ME and PSE, showed lower compositional data in comparison with CSLE and SLDE-Naviglio, and, more importantly, they did not show significant differences between any of the conditions test.

It has to be pointed out that all SLE systems extracted the same number of compounds, except for vanillic acid and ferulic acid (not found in PSE system) and sinapaldehyde, D-limonene, and linalyl acetate (not found in SLDE-Naviglio).

To differentiate extracts according to the different extraction conditions, a discriminant analysis was performed (Figure 2a). Three main groups can be distinguished, which were clearly separated by two canonic discriminating functions, explaining 47.7% of the total variance with the first function and 87.3% together with the second function. One of the groups encompasses the ME and PSE systems, whereas the other two groups account for CSLE and SLDE-Naviglio systems. The compounds that contributed most to the differentiation (Figure 2b) are phenolic compounds, especially gallic acid, ellagic acid, (−)-epicatechin, and *trans*-caftaric acid. In terms of minerals, calcium, iron, and boron showed the highest weight on the canonic coefficients. However, no volatile compound contributed to this differentiation. It is surprising that general parameters such as total phenolic index (TPI) or °Brix values were not selected for these differentiations. TPI and °Brix higher values were found in ME (61.60 and 3.55, respectively) and CSLE (45.8 and 2.88, respectively) techniques, followed by SLDE-Naviglio (13.90 and 2.0, respectively) and PSE (11.13 and 0.9, respectively).

The objective of the present research is to get aqueous extracts for agricultural purposes to be applied as a mix. For this reason, the composition discussion will focus on the CSLE and SLDE-Naviglio extraction systems as they are the ones with the highest concentration of valuable compounds (phenolic and volatile compounds, minerals), although they may be in detriment of a specific compound extracted by the other tested techniques.

Furthermore, it is interesting to point out that both systems are not of remarkable energy requirements with respect to other extractive processes. For example, CSLE is the process traditionally more used in industries.

**Phenolic Composition by HPLC-DAD-MS.** Table 1 lists the concentration of the phenolic compounds identified within the Airén vine-shoot waste aqueous extracts obtained by CSLE and SLDE-Naviglio. Significant differences were found among both extraction systems, as CSLE extracts were more concentrated that SLDE-Naviglio ones, independent of the extraction conditions tested, except for the group named "others".

(+)-Catechin and (−)-epicatechin were the only flavanol compounds detected in all extracts. By CSLE it was possible to extract 4 times more flavanols than with SLDE-Naviglio (Table 1), suggesting that higher temperature (100 °C) favored their release in comparison with room temperature conditions (25−27 °C). (+)-Catechin represented 60% of the CSLE total flavanol fraction, whereas in SLDE-Naviglio it was approximately 80% of the total content. When Airén vine-shoots were extracted by ethanol superheated liquid extraction (SHLE), (+)-catechin, pyrogallol, and syringic acid were the most abundant compounds.[13]

Among phenolic acids, *trans*-caffeic acid was the only compound for which the concentration was higher when the SLDE-Naviglio extraction system was used. *trans*-Caffeic acid concentration (Table 1) was higher in the present extracts than the one found (19 μg/kg) in other vine canes of which extracts were obtained by CSLE with an ethanol aqueous solution.[14] This compound was not detected when SHLE was used as extraction system.[13] *trans*-*p*-Coumaric and ferulic acids were highly extracted in terms of temperature, due to the high concentrations found in CSLE extracts. The presence of the hydroxycinnamoyltartaric acids (*trans*-*p*-coutaric and *trans*-caftaric) has not been previously reported in the literature in any type of wood. Such compounds are identified as oxidation substrates and browning precursors in white wines.[33] *trans*-Caftaric acid was the third compound in abundance within the phenolic pool (Table 1), especially when CSLE-15 was used. The content of *trans*-*p*-coutaric acid was significantly higher for CSLE-15 and CSLE-30 than for the other conditions tested.

The presence of low molecular weight compounds such as gallic and ellagic acids indicated that vine-shoots contain as well hydrolyzable tannins, although other authors[13] did not found ellagic acid in Airén vine-shoots. The concentration of gallic acid was higher than that of ellagic acid, favored by the CSLE system that produced a 50% more concentrated extract than SLDE-Naviglio, independent of the conditions tested on each system (Table 1). Protocatechuic acid, related to gallic acid by dealcoholization, was extracted by CSLE rather than by SLDE-Naviglio. An opposite behavior was found by pyrogallol, included in the "others" chemical group (Table 1) and which is related to gallic acid by decarboxylation. This latest compound, together with *trans*-caffeic acid, was highly extracted at room temperature (25−27 °C) (SLDE-Naviglio) rather than at 100 °C (CSLE), but no significant differences were observed when the different compression/decompression times were tested (Table 1).

Syringic acid was highly extracted by the CSLE system, showing the same behavior as most phenolic compounds. Vanillic acid behavior was different between the assayed extracts, as the higher concentration was quantified in CSLE-15, which indicated that higher extraction temperature but shorter times favored its extraction. This observation may be also justified by the fact that 3 mg/kg of this compound was quantified when SHLE was used.[13]

An important group of phenolic compounds is the stilbenes, which are best represented by *trans*-resveratrol, and it is identified in a wide variety of plant spices, especially in grapevines.[34−36] *trans*-Resveratrol has attracted research interest because of its demonstrated therapeutic effects, anti-inflammatory or even anticancer ones.[34] The glycosylated form of resveratrol, piceid, may also be found in the same or lower proportion depending on grape variety. The higher concentration of *trans*-resveratrol has been reported by some authors, between 1100 and 5000 mg/kg, in different vine-shoot cultivars, especially high in Pinot noir,[12] whereas in Turkish cultivars the concentration was around 2.5 μg/kg.[14] Although Delgado de la Torre et al.[13] did not find *trans*-resveratrol in Airén vine-shoots, it was found in the present aqueous extracts. Especially interesting is the CSLE concentration, which was approximately 20 times more concentrated than by SLDE-Naviglio (Table 1). The differences found between both systems indicate that the extraction temperature is an important parameter to enhance the extraction of this compound, but no significant differences were found in terms of time when the CSLE conditions were tested. Several factors could produce the differences found with other authors' references, not only by the grape variety, but the health of the grape vine and grape canes, together with the differences on the extraction system used.[11,35] The other identified stilbene, piceid, was not detected by any other authors, and it had the same behavior as its nonglycosylated derivate when CSLE was compared with the SLDE-Naviglio. The concentration of the piceid was 7 times lower than that of *trans*-resveratrol. Other stilbenes (*trans*-piceatannol, *trans*-ε-viniferin, or vitisinol among others) have been also characterized in other vine-shoot cultivars,[11,12] but those compounds could not be detected in the present aqueous extracts.

It is surprising that sinapaldehyde was not found in SLDE-Naviglio extracts in comparison with CSLE extracts, but it was quantified in those extracts previously reported.[13] Compounds such as acetovanillone, pyrocatechol, 4-hydroxybenzoic acid, and coniferaldehyde referred to in the Delgado de la Torre et al.[13] study were looked for but not found in our extracts.

**Volatile Composition by HS-SBSE-GC-MS.** Table 2 summarizes the results of volatile compounds identified, classified into different families according to their chemical structure, within the Airén vine-shoot waste aqueous extracts obtained by CSLE and SLDE-Naviglio. It is the first time that vine-shoot waste aqueous extract volatile composition is quantified, as only a qualitative profile was carried out by Delgado de la Torre et al.[15] Because the vine-shoots are subjected to a degradation process while extracting, cellulose and lignin may release such important aroma compounds. In all extracts, the furanic compounds were the most abundant followed by alcohols and acids. For both extraction systems, furanics showed around 48% of the total content; however, alcohols and acids presented some differences. If in SLDE-Naviglio alcohols reached around 30% of the total content, in the CSLE extraction system they were about 20%. With regard to acids, the higher proportion within the total content was observed by CSLE, 24 versus the 16% reached by the SLDE-Naviglio system.

Significant differences were found among the extraction systems used, depending on the extraction conditions tested; both extraction systems did not extract the same number of compounds. For example, D-limonene and linalyl acetate were not found in SLDE-Naviglio extraction system.

Table 2. Volatile Composition (Micrograms per Kilogram Dry Weight) of Different Vine-Shoot Waste Aqueous Extracts[a]

| | CSLE | | | SLDE-Naviglio | | |
|---|---|---|---|---|---|---|
| compound | CSLE-15 | CSLE-30 | CSLE-60 | SLDE-Naviglio-6.5 | SLDE-Naviglio-8 | SLDE-Naviglio-12 |
| **acids** | | | | | | |
| hexanoic acid | 1126.93 ± 133.19 a | 1671.27 ± 100.04 b | 1760.76 ± 36.37 b | 743.18 ± 92.32 a | 893.62 ± 158.87 a | 875.45 ± 71.32 a |
| octanoic acid | 252.67 ± 41.05 bc | 138.84 ± 1.47 ab | 110.27 ± 2.70 a | 175.30 ± 11.14 abc | 267.35 ± 36.73 c | 244.53 ± 45.64 bc |
| decanoic acid | 78.49 ± 0.21 c | 49.45 ± 5.65 ab | 41.95 ± 6.92 a | 68.53 ± 2.65 c | 62.81 ± 4.22 bc | 66.54 ± 0.90 c |
| **total** | **1458.09 ± 174.46 ab** | **1859.56 ± 104.21 b** | **1912.98 ± 26.75 b** | **987.00 ± 83.83 a** | **1223.78 ± 199.83 a** | **1186.51 ± 24.77 a** |
| **alcohols** | | | | | | |
| 1-hexanol | 1135.84 ± 56.94 c | 889.09 ± 43.66 b | 554.49 ± 38.03 a | 1476.35 ± 4.84 e | 1350.74 ± 64.54 de | 1242.91 ± 22.57 cd |
| 3-hexen-1-ol, (*Z*) | 76.45 ± 7.03 ab | 69.38 ± 9.31 a | 66.03 ± 3.41 a | 84.11 ± 1.08 ab | 85.59 ± 1.57 ab | 94.65 ± 4.14 c |
| 1-octen-3-ol | 14.87 ± 2.42 bc | 10.92 ± 1.70 ab | 8.94 ± 1.50 a | 13.84 ± 0.51 abc | 17.19 ± 0.09 c | 12.09 ± 1.22 abc |
| 1-nonanol | 7.58 ± 0.06 ab | 7.03 ± 1.48 a | 5.44 ± 0.82 a | 12.05 ± 0.71 c | 14.18 ± 0.92 c | 10.94 ± 0.37 bc |
| linalool | 0.94 ± 0.00 ab | 0.93 ± 0.01 ab | 0.99 ± 0.01 b | nd[b] | nd | 1.83 ± 0.60 b |
| *α*-terpineol | 26.83 ± 2.25 ab | 15.51 ± 2.08 a | 40.19 ± 8.22 b | 14.14 ± 1.26 a | 42.31 ± 2.70 b | 32.95 ± 3.54 b |
| guaiacol | 53.98 ± 8.71 a | 49.54 ± 8.23 a | 92.07 ± 1.82 b | 82.51 ± 7.30 b | 46.71 ± 4.08 a | 45.94 ± 3.48 a |
| benzyl alcohol | 269.60 ± 15.84 c | 428.92 ± 16.57 d | 582.43 ± 19.33 e | 177.45 ± 0.88 a | 264.21 ± 4.08 bc | 216.34 ± 9.53 ab |
| 2-phenylethanol | 29.58 ± 2.46 a | 32.91 ± 2.87 a | 20.85 ± 0.21 a | 221.93 ± 4.81 b | 289.39 ± 6.42 c | 354.09 ± 5.71 d |
| **total** | **1615.67 ± 78.16 a** | **1504.23 ± 82.92 a** | **1371.43 ± 73.33 a** | **2082.38 ± 6.36 b** | **2110.31 ± 76.24 b** | **2011.73 ± 51.16 b** |
| **aldehydes** | | | | | | |
| benzaldehyde | 12.16 ± 0.68 a | 90.16 ± 2.89 c | 93.84 ± 1.73 c | 12.10 ± 0.88 a | 11.86 ± 0.83 a | 60.73 ± 6.40 b |
| nonanal | 3.90 ± 0.93 ab | 2.96 ± 0.08 a | 2.93 ± 0.95 a | 6.46 ± 1.26 b | 5.28 ± 0.57 ab | 6.69 ± 0.80 b |
| vanillin | 322.72 ± 21.44 b | 523.49 ± 30.62 c | 528.12 ± 37.82 c | 233.94 ± 26.46 ab | 268.81 ± 27.56 ab | 208.71 ± 12.39 a |
| **total** | **338.78 ± 19.83 a** | **616.61 ± 33.59 b** | **624.89 ± 37.04 b** | **252.50 ± 28.60 a** | **285.95 ± 28.96 a** | **276.13 ± 5.20 a** |
| **furanic compounds** | | | | | | |
| furfural | 1460.00 ± 84.85 a | 1920.00 ± 169.71 ab | 2200.00 ± 141.42 b | 1762.50 ± 159.10 ab | 1812.50 ± 17.68 ab | 1475.00 ± 212.13 a |
| 5-hydroxymethylfurfural[c] | 1192.04 ± 43.42 a | 1630.10 ± 78.49 a | 1560.07 ± 128.93 a | 1523.27 ± 209.61 a | 1522.83 ± 172.36 a | 1286.38 ± 249.10 a |
| 5-methylfurfural | 54.27 ± 5.02 a | 85.41 ± 8.27 a | 88.28 ± 10.63 a | 96.63 ± 27.26 a | 113.88 ± 23.97 a | 61.65 ± 6.99 a |
| 2-furanmethanol[c] | 54.38 ± 1.70 a | 82.27 ± 6.11 c | 67.83 ± 4.11 bc | 51.94 ± 6.56 a | 87.72 ± 11.56 c | 70.77 ± 1.92 bc |
| methyl furoate[c] | 40.05 ± 1.15 a | 62.54 ± 9.66 a | 55.58 ± 8.23 a | 61.28 ± 21.34 a | 73.52 ± 27.97 a | 47.48 ± 6.06 a |
| **total** | **2800.74 ± 136.14 a** | **3680.32 ± 86.49 a** | **3971.05 ± 272.05 a** | **3495.61 ± 423.87 a** | **3610.45 ± 149.65 a** | **2923.29 ± 476.21 a** |
| **lactones** | | | | | | |
| *trans*-whiskey lactone | 44.65 ± 5.47 a | 34.96 ± 3.31 a | 42.88 ± 5.63 a | 69.54 ± 6.35 b | 31.54 ± 4.58 a | 34.06 ± 3.77 a |
| *cis*-whiskey lactone | 27.59 ± 1.09 a | 26.40 ± 8.12 a | 49.58 ± 5.66 bc | 89.49 ± 5.04 d | 43.94 ± 2.10 ab | 64.00 ± 3.85 c |
| **total** | **72.24 ± 4.38 ab** | **61.36 ± 11.42 a** | **92.46 ± 11.29 ab** | **159.03 ± 11.38 c** | **75.48 ± 2.47 ab** | **98.06 ± 0.09 b** |
| **others** | | | | | | |
| D-limonene | 0.08 ± 0.03 bc | 0.09 ± 0.01 c | 0.03 ± 0.01 ab | nd | nd | nd |
| geranyl acetone | 4.20 ± 0.49 ab | 5.84 ± 0.44 bc | 3.35 ± 0.56 a | 4.55 ± 0.50 ab | 6.38 ± 0.02 c | 2.94 ± 0.34 a |
| linalyl acetate | 0.17 ± 0.01 b | 0.13 ± 0.04 ab | 0.08 ± 0.02 a | nd | nd | nd |
| *β*-ionone | 2.65 ± 0.81 a | 3.13 ± 0.33 a | 2.64 ± 0.45 a | 2.34 ± 0.02 a | 1.64 ± 0.58 a | 2.28 ± 0.07 a |



dx.doi.org/10.1021/jf503929v | J. Agric. Food Chem. 2014, 62, 10861−10872

Table 2. continued

| | CSLE | | | SLDE-Naviglio | | |
|---|---|---|---|---|---|---|
| compound | CSLE-15 | CSLE-30 | CSLE-60 | SLDE-Naviglio-6.5 | SLDE-Naviglio-8 | SLDE-Naviglio-12 |
| stilbene 1[d] | 2.24 ± 0.37 a | 2.60 ± 0.14 a | 3.70 ± 4.02 a | 3.49 ± 1.08 a | 2.61 ± 0.55 a | 2.80 ± 0.14 a |
| stilbene 2[d] | 4.47 ± 0.27 a | 6.59 ± 0.44 a | 8.04 ± 1.24 a | 8.28 ± 3.01 a | 8.52 ± 0.43 a | 7.75 ± 1.06 a |
| **total** | **13.81 ± 1.94 a** | **18.38 ± 0.39 a** | **17.84 ± 2.84 a** | **18.65 ± 4.57 a** | **19.15 ± 1.58 a** | **15.76 ± 0.50 a** |

[a]SLE, conventional solid−liquid extraction (CSLE-15, 15 min; CSLE-30, 30 min; CSLE-60, 60 min); SLDE-Naviglio, solid−liquid dynamic extraction (SLDE-Naviglio-6.5, 5 min in the static phase and 1.5 min in the dynamic phase; SLDE-Naviglio-8, 5 min in the static phase and 3 min in the dynamic phase; SLDE-Naviglio-12, 9 min in the static phase and 3 min in the dynamic phase). Different letters in the same row indicate significant differences among extraction conditions according to the LSD test ($\alpha < 0.05$). The mean values ($n = 6$) are shown with their standard deviation. [b]nd, not detected. [c]Identification only tentative and expresed as μg/kg of furfural. [d]Expresed as μg/kg of 3-methyl-1-pentanol.

The obtained extracts were rich in acids, especially in hexanoic. No significant differences in total acids were observed among the extraction systems used, except for CSLE-30 and CSLE-60, with the highest concentrations due to the hexanoic acid; thus, longer times favor its extraction. In other woods, such as seasoned oak wood chips of American origin, these acid compounds were also found.[37,38]

Total alcohols showed significant differences regarding the extraction system, as SLDE-Naviglio produced the highest content, independent of the extraction conditions tested. A clear behavior for each compound was not observed under SLDE-Naviglio conditions, such as the case of the 1-hexanol, the most abundant alcohol. The presence of 1-hexanol was expected, because it is derived from the unsaturated fatty acids, which are present in all plants.[39] On the other hand, 3-hexen-1-ol (*Z*) content was affected significantly by SLDE-Naviglio-12 conditions; guaiacol content was significantly higher in SLDE-Naviglio-6.5, being quantified as 4% of the total alcohols fraction, whereas in SLDE-Naviglio-8 and SLDE-Naviglio-12 conditions it was only about 2%. α-Terpineol concentration was significantly lower under SLDE-Naviglio-6.5 conditions. The compounds more influenced by SLDE-Naviglio were linalool and 2-phenylethyl alcohol, the first quantified only in SLDE-Naviglio-12 and the second increasing when the compression/decompression times were longer.

About the influence of CSLE conditions, 1-hexanol content decreased significantly with extraction time, going from 71% of the total alcohols fraction by CSLE-15 to 40% with CSLE-60. With regard to linalool, although no statistical differences were observed, it is worth mentioning that it is an important odorant terpene present in grapes, especially in Muscat varieties, which gives them their characteristic aroma.[40] Benzyl alcohol and guaiacol contents were highest in CSLE-60 conditions, reaching 42.5 and 6.7%, respectively, of the total alcohols. Guaiacol is a volatile phenol common in other types of woods, such as oak, chestnut, ash, acacia, or cherry, because their source is lignin,[41,42] and it is one of the most abundant compounds in commercial aqueous oak extracts (0.21 mg/L).[19] These oak extracts, when applied to vineyard by a foliar treatment, increased the concentration of glycosidically bound aroma precursors of guaiacol in grapes and the concentration of this compound in their respective wines.[18] In the same way, recent works have also shown that the application of an aqueous solution of guaiacol stimulated the varietal aroma composition of grapes, showing an important influence in the aroma of wines.[19]

Total aldehydes showed significant differences with regard to the extraction system, as CSLE-30 and CSLE-60 had the highest content with around twice those of the CSLE-15 and SLDE-Naviglio systems. Vanillin was the major aldehyde, having a big influence in the total aldehydes content, its concentration ranging from 76% for SLDE-Naviglio-12 to 95% for CSLE-15. Vanillin is one of the most important odorant compounds present in commercial aqueous oak extracts used within grapevines,[19] providing them a vanilla aroma. In wines from such grapevines, a significant increase in vanillin content and woody aroma was observed.[18] The reported levels of these compounds were similar to those found in some varieties of oak chips.[41,42] Besides, Delgado de la Torre et al.[15] suggested the possibility of using vine-shoots in wines as flavoring agents, after observing similar chromatographic peak areas of a comparative study with oak chips. As vanillin, the highest benzaldehyde content was at CSLE-30 and CSLE-60, around

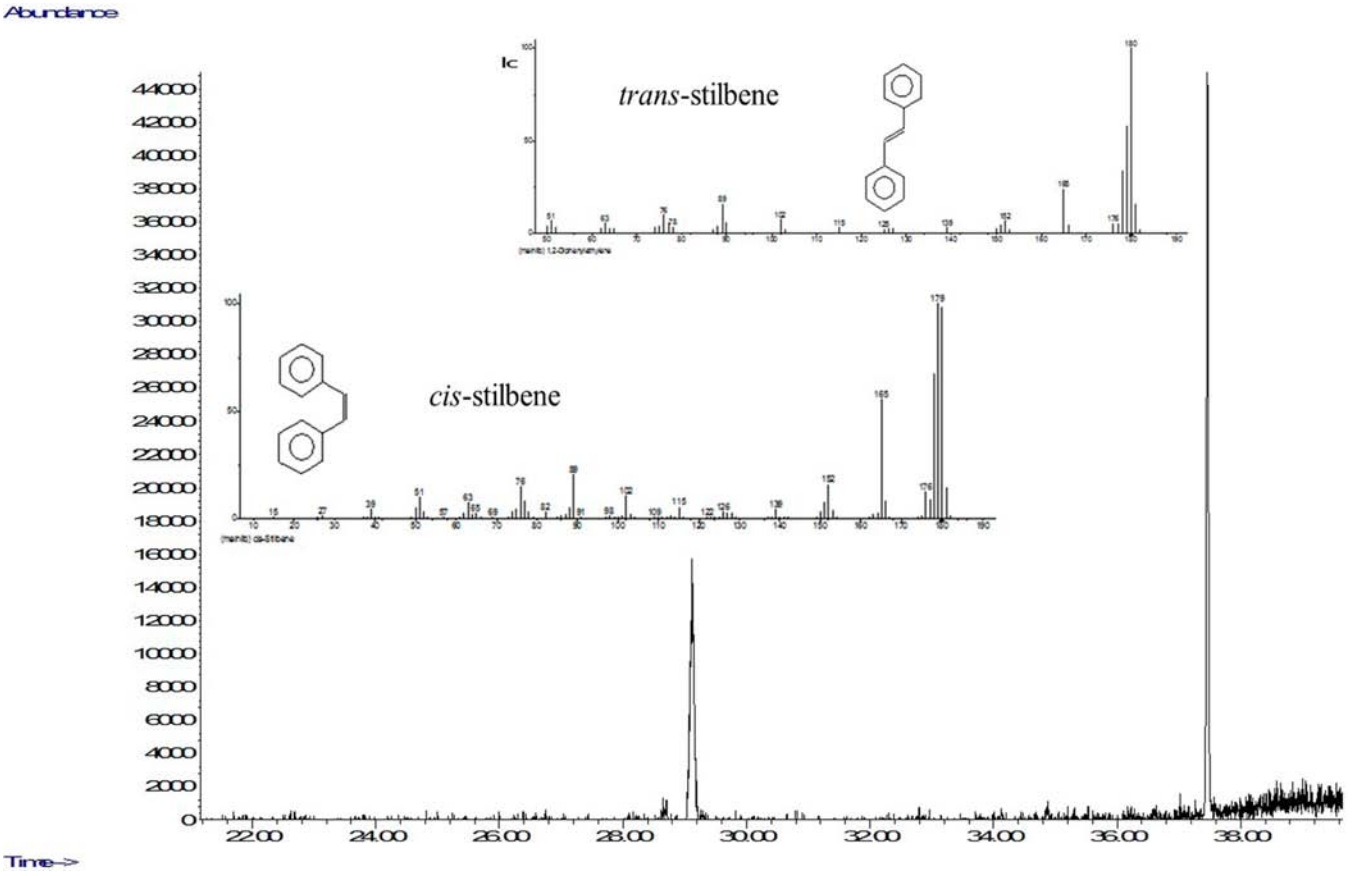


**Figure 3.** Chromatographic peaks corresponding to volatile *cis*- and *trans*-stilbenes at SIM mode, with characteristic $m/z$ at 179 and 180, respectively, identified for the first time in vine-shoots.

**Table 3. Mineral Composition (Milligrams per Kilogram Dry Weight) of Different Vine-Shoot Waste Aqueous Extracts[a]**

| | CSLE | | | SLDE-Naviglio | | |
|---|---|---|---|---|---|---|
| | CSLE-15 | CSLE-30 | CSLE-60 | SLDE-Naviglio-6.5 | SLDE-Naviglio-8 | SLDE-Naviglio-12 |
| **major macronutrients** | | | | | | |
| nitrogen (as nitrate) | 6.36 ± 0.22 d | 3.49 ± 0.12 b | 6.15 ± 0.21 d | 2.05 ± 0.07 a | 4.36 ± 0.15 c | 4.36 ± 0.15 c |
| nitrogen (as nitrite) | 1.23 ± 0.04 a | 1.44 ± 0.05 a | 1.44 ± 0.05 a | 6.50 ± 0.22 b | 7.37 ± 0.25 c | 7.79 ± 0.27 c |
| phosphorus | 249.90 ± 8.62 a | 229.19 ± 7.91 a | 258.30 ± 8.91 a | 301.61 ± 10.40 b | 306.99 ± 10.59 b | 323.90 ± 11.17 b |
| potassium | 1534.63 ± 52.93 a | 1467.80 ± 50.63 a | 1413.07 ± 48.74 a | 1435.00 ± 49.50 a | 1421.42 ± 49.03 a | 1541.34 ± 53.17 a |
| **total** | **1792.11 ± 61.82 a** | **1701.91 ± 58.70 a** | **1678.65 ± 57.91 a** | **1745.15 ± 60.20 a** | **1740.13 ± 60.02 a** | **1877.39 ± 64.76 a** |
| **secondary macronutrients** | | | | | | |
| calcium | 236.16 ± 8.15 a | 266.91 ± 9.21 a | 260.56 ± 8.99 a | 388.73 ± 13.41 b | 367.21 ± 12.67 b | 394.11 ± 13.59 b |
| magnesium | 254.61 ± 8.78 a | 267.94 ± 9.24 ab | 261.58 ± 9.02 ab | 316.73 ± 10.92 c | 297.76 ± 10.27 bc | 275.73 ± 9.51 ab |
| sulfur | 1278.38 ± 44.10 ab | 1197.41 ± 41.30 a | 1374.32 ± 47.40 abc | 1546.98 ± 53.36 c | 1357.61 ± 46.83 ab | 1425.78 ± 49.18 bc |
| **total** | **1769.15 ± 61.02 ab** | **1732.25 ± 59.75 a** | **1896.46 ± 65.41 abc** | **2252.44 ± 77.69 d** | **2022.58 ± 69.76 bcd** | **2095.61 ± 72.28 cd** |
| **micronutrients** | | | | | | |
| boron | 0.66 ± 0.02 b | 0.80 ± 0.03 c | 0.92 ± 0.03 d | 0.40 ± 0.01 a | 0.39 ± 0.01 a | 0.42 ± 0.01 a |
| iron | 0.83 ± 0.03 b | 1.36 ± 0.05 d | 1.13 ± 0.04 c | 0.35 ± 0.01 a | 0.30 ± 0.01 a | 0.30 ± 0.01 a |
| copper | 0.17 ± 0.01 a | 0.24 ± 0.01 a | 0.20 ± 0.01 a | 0.97 ± 0.03 bc | 0.96 ± 0.03 b | 1.06 ± 0.04 c |
| zinc | 1.49 ± 0.05 a | 1.56 ± 0.05 a | 1.59 ± 0.05 a | 1.63 ± 0.06 a | 1.61 ± 0.06 a | 2.20 ± 0.08 b |
| manganese | 2.05 ± 0.07 a | 2.38 ± 0.08 ab | 2.34 ± 0.08 ab | 2.42 ± 0.08 b | 2.34 ± 0.08 ab | 2.58 ± 0.09 b |
| chlorine | 156.83 ± 5.41 ab | 151.29 ± 5.22 a | 159.08 ± 5.49 ab | 187.83 ± 6.48 c | 178.35 ± 6.15 bc | 184.76 ± 6.37 c |
| **total** | **162.04 ± 5.59 ab** | **157.61 ± 5.44 a** | **165.25 ± 5.70 ab** | **193.60 ± 6.68 c** | **183.95 ± 6.35 bc** | **191.32 ± 6.60 c** |

[a]CSLE, conventional solid−liquid extraction (CSLE-15, 15 min; CSLE-30, 30 min; CSLE-60, 60 min); SLDE-Naviglio, solid−liquid dynamic extraction (SLDE-Naviglio-6.5, 5 min in the static phase and 1.5 min in the dynamic phase; SLDE-Naviglio-8, 5 min in the static phase and 3 min in the dynamic phase; SLDE-Naviglio-12, 9 min in the static phase and 3 min in the dynamic phase). Different letters in the same row indicate significant differences among extraction conditions according to the LSD test ($\alpha < 0.05$). The mean values ($n = 4$) are shown with their standard deviation.


dx.doi.org/10.1021/jf503929v | J. Agric. Food Chem. 2014, 62, 10861−10872

15% of total aldehydes, followed by SLDE-Naviglio-12, where its percentage was the highest, 22% of total aldehydes.

As expected, furanic compounds were the most abundant volatile compounds found in the vine-shoot aqueous extracts, because they are carbohydrate derivatives appearing in other woods such as oak, chestnut, cherry, or ash.[42] Their total content was not dependent on the extraction system used, as no significant differences were observed between them. Furfural and 5-hydroxymethylfurfural were the most abundant furanic compounds (53 and 43%, respectively), as it was observed in the aqueous oak extracts used as plant biostimulants.[19] Compounds such as 5-methylfurfural and methyl furoate were not influenced by the extraction system and conditions used. Most furanic compounds were also found in previous vine-shoot aroma research.[15]

It is important to emphasize the presence of whiskey lactone compounds, which are characteristic mainly in oak woods, but they were not previously detected in other vine-shoot wastes;[15] however, these lactones come from the degradation of lipids, and they are abundant in oak green wood.[43] They were influenced by the extraction system, especially *cis*-whiskey lactone, which reached the highest concentration when SLD-Naviglio-6.5 was used. Both whiskey lactones are compounds present in aqueous oak extract,[19] and recently it has been observed that when a solution of whiskey lactones was used in grapevines, wines from such grapes had enhanced varietal aroma after the malolactic fermentation.[44] Because it has been shown that some of these compounds presented in both vine-shoots and oak aqueous extracts, then the same applications carried out with the latest could be performed.

With regard to the compounds grouped as "others", no significant differences were found between the extraction systems used, except for D-limonene and linalyl acetate, which were not present in SLDE-Naviglio extracts. The latest behavior suggests that the extraction of such compounds was temperature dependent (CSLE vs SLDE-Naviglio). Geranyl acetone, which appears in all extracts, did not show a clear behavior.

*β*-Ionone is a norisoprenoid compound known as an important varietal aroma in grapes and wines, but it was not affected by the extraction system and conditions used.

Although the stilbenes fraction has been widely studied in different vine canes,[11,12] until now no reference about the two volatile stilbenes found in the present extracts has been mentioned in other woods. However, such compounds were detected during the lignin pyrolysis produced in pulping of corn.[45] Figure 3 illustrates the chromatographic profiles of such compounds, with $m/z$ 179 and 180. Neither stilbene showed significant differences among SLDE-Naviglio and CSLE extraction systems and their respective conditions, but according to previous authors,[45] stilbene structures are stable even at pyrolysis temperature.

**Mineral Composition by ICP-OES.** The mineral composition of the different vine-shoot extracts is listed in Table 3, excluding the ones with a concentration <0.03 mg/kg. All minerals shown are essential nutrients for plant growth, so they are used in fertilization. Regardless of the extraction system used, the higher concentration (>1 g/kg) corresponded to potassium and sulfur nutrients, followed by calcium, magnesium, and phosphorus with concentrations around 0.3 g/kg. Among the other nutrients, the most abundant was chlorine (approximately 0.2 g/kg), followed by nitrogen as nitrate or nitrite depending on the extraction system used. As cation micronutrients, the most abundant was manganese and the lowest was iron.

The mineral contents quantified in Airén vine-shoot aqueous extracts were lower than the ones referred for other cultivars,[10,14] although it was dependent on the grape variety and the soil composition. Anyway, the mineral content found in Airén aqueous vine-shoot extracts could be sufficient to support the plant nutrition whether they are directly applied on the leaves or suitably diluted, as other byproducts.[46]

From a long time ago, foliar fertilization based on micronutrients has been used, because it reduces the need for soil-applied fertilizer and the leaching of nutrients, decreasing the impact on the environment of fertilizers' salts. It does not totally replace soil-applied fertilizer, but it does increase the uptake and hence the efficiency of the nutrients applied to the soil.[46] In such a way, the presence of small quantities of major nutrients such as N, P, and K, in the vine-shoot aqueous extracts, may leave the opportunity to be applied at any time depending on the needs of the crop. In the case of grapevines it is known that N is the major nutrient affecting vigor and must quality; for this reason it is used in great quantities, but it results as well in poorer wine quality.[47] In the case of K, it is widely used in viticulture as it can increase grape yield, as a result of increased cluster number and weight.[48] Phosphorus is also an essential nutrient for vines as it favors root development,[49] although their quantity requirements are lower than those for N and K.

The extraction technique used did not modify the potassium content in all extracts, but it increased significantly the content of nitrogen as nitrite and phosphorus when SLDE-Naviglio was used, whereas nitrogen, in the form of nitrate, which is the preferable form to be taken up by plants, was significantly higher when CSLE-15 or CSLE-60 was used. Such nutrients (N, P, K) are the main nutritive sources for plants, so foliar fertilization can be one of their possible uses, because they are already dissolved in water, which is the main requisite to be assimilated by the plants. In should be pointed out that when nutrients are applied to the soil in forms available to the plants, important losses are produced because they can react with soil components, giving insoluble forms.

Secondary macronutrient and micronutrient contents were higher in extracts from the SLDE-Naviglio system than in the CSLE one, independent of the extraction conditions tested. It is worth mentioning that the highest boron content is by CSLE-60 and that of iron by CSLE-30. The SLDE-Naviglio extraction technique did not show a clear behavior related to micronutrients.

In conclusion, it has been observed that vine-shoot waste aqueous extracts from *V. vinifera* Airén variety obtained by CSLE and SLDE-Naviglio were the highest concentrated extracts in phenolic, volatile, and mineral valuable compounds. Such compositions suggest that these wastes may have a new potential uses as bioestimulants or foliar fertilizers in the vineyard. It could be implemented in the "Sustainable Viticulture" concept, where the cycle of the vine could be closed, as such vine-shoot extracts may modulate the grape quality, returning to the grapevines what they took from the soil, and even enhancing the terroir effect. Moreover, these extracts may be produced in the owner wineries, using the facilities available once the winemaking process ends.

## AUTHOR INFORMATION


### Corresponding Author

*(M.R.S.) Phone: +34 967 599210. Fax: +34 967 599238. E-mail: Rosario.Salinas@uclm.es.



### Funding

Many thanks for the financial support given by the Ministerio de Economía y Competitividad of the Spanish government to Project AGL2012-33132.


### Notes

The authors declare no competing financial interest.

## REFERENCES


(1) European Parliament. Directive 2008/98/EC of the European Parliament and of the Council on waste and repealing certain directives. *Off. J. Eur. Union* **2008**, 3−4.

(2) SEVI. *Rev. Semana Vitivinicola* **2014**, *3421*, 467−470.

(3) Cheng, V. J.; Bekhit, A. E. A.; Sedcole, R.; Hamid, N. The impact of grape skin bioactive functionality information on the acceptability of tea infusions made from wine by-products. *J. Food Sci.* **2010**, *75*, 167−172.

(4) Pedroza, M. A.; Carmona, M.; Salinas, M. R.; Zalacain, A. Use of dehydrated waste grape skins as a natural additive for producing rosé wines: study of extraction conditions and evolution. *J. Agric. Food Chem.* **2011**, *59*, 10976−10986.

(5) Jiménez Gómez, S.; Cartagena Causapé, M. C.; Arce Martínez, A. Distribution of nutrients in anaerobic digestion of vine shoots. *Bioresour. Technol.* **1993**, *45*, 93−97.

(6) Pardo, J.; Gea, F. J.; Pardo, A.; Navarro, M. J. Characterization of some materials derived from the grapevine industry and their use in traditional composting in Castilla-La Mancha (Spain). *Mushroom Sci.* **1995**, *14*, 213−221.

(7) Corcho-Corral, B.; Olivares-Marín, M.; Fernández-González, C.; Gómez-Serrano, V.; Macías-García, A. Preparation and textural characterisation of activated carbon from vine shoots (*Vitis vinifera*) by $H_3PO_4$-chemical activation. *Appl. Surf. Sci.* **2006**, *252*, 5961−5966.

(8) Portilla, O. M.; Rivas, B.; Torrado, A.; Moldes, A. B.; Domínguez, J. M. Revalorisation of vine trimming wastes using *Lactobacillus acidophilus* and *Debaryomyces hansenii*. *J. Sci. Food Agric.* **2008**, *88*, 2298−2308.

(9) Jiménez, L.; Angulo, V.; Ramos, E.; De la Torre, J. L.; Ferrer, A. Comparison of various pulping processes for producing pulp from vine shoots. *Ind. Crops Prod.* **2006**, *23*, 122−130.

(10) Mendívil, M. A.; Muñoz, P.; Morales, M. P.; Juárez, M. C.; García-Escudero, E. Chemical characterization of pruned vine shoots from la Rioja (Spain) for obtaining solid bio-fuels. *J. Renewable Sustainable Energy* **2013**, *5*, No. 033113.

(11) Gorena, T.; Saez, V.; Mardones, C.; Vergara, C.; Winterhalter, P.; Von Baer, D. Influence of post-pruning storage on stilbenoid levels in *Vitis vinifera* L. canes. *Food Chem.* **2014**, *155*, 256−263.

(12) Vergara, C.; Von Baer, D.; Mardones, C.; Wilkens, A.; Wernekinck, K.; Damm, A.; Winterhalter, P. Stilbene levels in grape cane of different cultivars in southern Chile: determination by HPLC-DAD-MS/MS method. *J. Agric. Food Chem.* **2012**, *60*, 929−933.

(13) Delgado de la Torre, M. P.; Ferreiro-Vera, C.; Priego-Capote, F.; Pérez-Juan, P. M.; Luque De Castro, M. D. Comparison of accelerated methods for the extraction of phenolic compounds from different vine-shoot cultivars. *J. Agric. Food Chem.* **2012**, *60*, 3051−3060.

(14) Çetin, E. S.; Altiñöz, D.; Tarçan, E.; Göktürk Baydar, N. Chemical composition of grape canes. *Ind. Crops Prod.* **2011**, *34*, 994−998.

(15) Delgado de la Torre, M. P.; Priego-Capote, F.; Luque de Castro, M. D. Comparative profiling analysis of woody flavouring from vine-shoots and oak chips. *J. Sci. Food Agric.* **2014**, *94*, 504−514.

(16) Martínez-Gil, A. M.; Angenieux, M.; Pardo-García, A. I.; Alonso, G. L.; Ojeda, H.; Salinas, M. R. Glycosidic aroma precursors of Syrah and Chardonnay grapes after an oak extract application to the grapevines. *Food Chem.* **2013**, *138*, 956−965.

(17) Martínez-Gil, A. M.; Garde-Cerdán, T.; Zalacain, A.; Pardo-García, A. I.; Salinas, M. R. Applications of an oak extract on Petit Verdot grapevines. Influence on grape and wine volatile compounds. *Food Chem.* **2012**, *132*, 1836−1845.

(18) Martínez-Gil, A. M.; Garde-Cerdán, T.; Martínez, L.; Alonso, G. L.; Salinas, M. R. Effect of oak extract application to Verdejo grapevines on grape and wine aroma. *J. Agric. Food Chem.* **2011**, *59*, 3253−3263.

(19) Pardo-García, A. I.; Martínez-Gil, A. M.; Cadahía, E.; Pardo, F.; Alonso, G. L.; Salinas, M. R. Oak extract application to grapevines as a plant biostimulant to increase wine polyphenols. *Food Res. Int.* **2014**, *55*, 150−160.

(20) Luque-Rodríguez, J. M.; Luque de Castro, M. D.; Pérez-Juan, P. Dynamic superheated liquid extraction of anthocyanins and other phenolics from red grape skins of winemaking residues. *Bioresour. Technol.* **2007**, *98*, 2705−2713.

(21) Luque-Rodríguez, J. M.; Pérez-Juan, P.; Luque De Castro, M. D. Extraction of polyphenols from vine shoots of *Vitis vinifera* by superheated ethanol-water mixtures. *J. Agric. Food Chem.* **2006**, *54*, 8775−8781.

(22) Spigno, G.; Tramelli, L.; De Faveri, D. M. Effects of extraction time, temperature and solvent on concentration and antioxidant activity of grape marc phenolics. *J. Food Eng.* **2007**, *81*, 200−208.

(23) Vilkhu, K.; Mawson, R.; Simons, L.; Bates, D. Applications and opportunities for ultrasound assisted extraction in the food industry. A review. *Innovative Food Sci. Emerging Technol.* **2008**, *9*, 161−169.

(24) Mustafa, A.; Turner, C. Pressurized liquid extraction as a green approach in food and herbal plants extraction. A review. *Anal. Chim. Acta* **2011**, *703*, 8−18.

(25) Pourmortazavi, S. M.; Rahimi-Nasrabadi, M.; Hajimirsadeghi, S. S. Supercritical fluid technology in analytical chemistry. A review. *Curr. Anal. Chem.* **2014**, *10*, 3−28.

(26) Wissgott, U.; Bortlik, K. Prospects for new natural food colorants. *Trends Food Sci. Technol.* **1996**, *7*, 298−302.

(27) Naviglio, D. Naviglio's principle and presentation of an innovative solid-liquid extraction technology: Extractor Naviglio®. *Anal. Lett.* **2003**, *36*, 1647−1659.

(28) Naviglio, D.; Pizzolongo, F.; Ferrara, L.; Aragòn, A.; Santini, A. Extraction of pure lycopene from industrial tomato by-products in water using a new high-pressure process. *J. Sci. Food Agric.* **2008**, *88*, 2414−2420.

(29) Chan, C. H.; Yusoff, R.; Ngoh, G. C.; Kung, F. W. L. Microwave-assisted extractions of active ingredients from plants. *J. Chromatogr., A* **2011**, *1218*, 6213−6225.

(30) Teo, C. C.; Chong, W. P. K.; Ho, Y. S. Development and application of microwave-assisted extraction technique in biological sample preparation for small molecule analysis. *Metabolism* **2013**, *9*, 1109−1128.

(31) Rubiolo, P.; Sgorbini, B.; Liberto, E.; Cordero, C.; Bicchi, C. Essential oils and volatiles: Sample preparation and analysis. A review. *Flavour Fragrance J.* **2010**, *25*, 282−290.

(32) Pardo-García, A. I.; Martínez-Gil, A. M.; López-Córcoles, H.; Zalacain, A.; Salinas, M. R. Effect of eugenol and guaiacol application on tomato aroma composition determined by headspace stir bar sorptive extraction. *J. Sci. Food Agric.* **2013**, *93*, 1147−1155.

(33) Ferrandino, A.; Carra, A.; Rolle, L.; Schneider, A.; Schubert, A. Profiling of hydroxycinnamoyl tartrates and acylated anthocyanins in the skin of 34 *Vitis vinifera* genotypes. *J. Agric. Food Chem.* **2012**, *60*, 4931−4945.

(34) Shakibaei, M.; Harikumar, K. B.; Aggarwal, B. B. Review: Resveratrol addiction: to die or not to die. *Mol. Nutr. Food Res.* **2009**, *53*, 115−128.

(35) Karacabey, E.; Mazza, G. Optimization of solid-liquid extraction of resveratrol and other phenolic compounds from milled grape canes (*Vitis vinifera*). *J. Agric. Food Chem.* **2008**, *56*, 6318−6325.

(36) Teissedre, P. L. Wine and health. *Biochem. Grape Berry* **2012**, 269−285.

(37) Alañón, M. E.; Ramos, L.; Díaz-Maroto, M. C.; Pérez-Coello, M. S.; Sanz, J. Extraction of volatile and semi-volatile components from oak wood used for aging wine by miniaturised pressurised liquid technique. *Int. J. Food Sci. Technol.* **2009**, *44*, 1825−1835.
(38) Fernández de Simón, B.; Sanz, M.; Cadahía, E.; Poveda, P.; Broto, M. Chemical characterization of oak heartwood from Spanish forests of *Quercus pyrenaica* (Wild.). Ellagitannins, low molecular weight phenolic, and volatile compounds. *J. Agric. Food Chem.* **2006**, *54*, 8314−8321.
(39) Schwab, W.; Davidovich-Rikanati, R.; Lewinsohn, E. Biosynthesis of plant-derived flavor compounds. *Plant J.* **2008**, *54*, 712−732.
(40) Agosin, E.; Belancic, A.; Ibacache, A.; Baumes, R.; Bordeu, E.; Crawford, A.; Bayonove, C. Aromatic potential of certain Muscat grape varieties important for Pisco production in Chile. *Am. J. Enol. Vitic.* **2000**, *51*, 404−408.
(41) Culleré, L.; Fernández de Simón, B.; Cadahía, E.; Ferreira, V.; Hernández-Orte, P.; Cacho, J. Characterization by gas chromatography-olfactometry of the most odor-active compounds in extracts prepared from acacia, chestnut, cherry, ash and oak woods. *LWT−Food Sci. Technol.* **2013**, *53*, 240−248.
(42) De Simón, B. F.; Esteruelas, E.; Muñoz, A. M.; Cadahía, E.; Sanz, M. Volatile compounds in acacia, chestnut, cherry, ash, and oak woods, with a view to their use in cooperage. *J. Agric. Food Chem.* **2009**, *57*, 3217−3227.
(43) Doussot, F.; De Jéso, B.; Quideau, S.; Pardon, P. Extractives content in cooperage oak wood during natural seasoning and toasting; influence of tree species, geographic location, and single-tree effects. *J. Agric. Food Chem.* **2002**, *50*, 5955−5961.
(44) Pardo-García, A. I.; De La Hoz, K. S.; Zalacain, A.; Alonso, G. L.; Salinas, M. R. Effect of vine foliar treatments on the varietal aroma of Monastrell wines. *Food Chem.* **2014**, *163*, 258−266.
(45) Bai, X.; Kim, K. H.; Brown, R. C.; Dalluge, E.; Hutchinson, C.; Lee, Y. J.; Dalluge, D. Formation of phenolic oligomers during fast pyrolysis of lignin. *Fuel* **2014**, *128*, 170−179.
(46) Tejada, M.; Gonzalez, J. L. Effects of foliar application of a byproduct of the two-step olive oil mill process on rice yield. *Eur. J. Agron.* **2004**, *21*, 31−40.
(47) Pérez-Álvarez, E. P.; Martínez-Vidaurre, J. M.; Martín, I.; García-Escudero, E.; Peregrina, F. Relationships among soil nitrate nitrogen and nitrogen nutritional dtatus, yield components, and must quality in semi-arid vineyards from Rioja AOC, Spain. *Commun. Soil Sci. Plant Anal.* **2013**, *44*, 232−242.
(48) Amiri, M. E.; Fallahi, E. Influence of mineral nutrients on growth, yield, berry quality, and petiole mineral nutrient concentrations of table grape. *J. Plant Nutr.* **2007**, *30*, 463−470.
(49) Mengel, K.; Kirkby, E. A. *Principles of Plant Nutrition*, 4th ed.; International Potash Institute: Worblaufen-Bern, Switzerland, 1987.

of the volatile fraction, DDG was milled to particles less than 500 μm using an Ultra Centrifugal Mill ZM200 from Retsch (Haan, Germany) by 5000−6000 rpm.

**Chemicals.** Chemicals were obtained from the following sources: diethyl ether (≥99.5%) and anhydrous sodium sulfate (≥99.0%) from Sigma−Aldrich (Taufkirchen, Germany), sodium carbonate (≥99.5%) from Merck (Darmstadt, Germany), sodium chloride from Avantor Performance Materials (Deventer, Netherlands), and hydrochloric acid (37%) from Roth (Karlsruhe, Germany). Reference standards of aroma compounds were purchased from commercial sources: Alfa Aesar, Karlsruhe, Germany; Merck, Darmstadt, Germany; Sigma−Aldrich, Taufkirchen, Germany; others were kindly provided from flavor companies (Firmenich, Switzerland; Symrise, Holzminden, Germany).

**Sample Preparation for HS-SPME.** A 3.0 g amount of DDG was weighed in a 20 mL headspace vial and sealed with flanged caps. The septum was pierced with the SPME needle, and subsequently, the fiber was manually exposed to the sample for a normal adsorption time of 1 h and a prolonged adsorption time of 6 h for a better enrichment of medium and low volatile compounds. The adsorption process was performed in a tempered water bath at 30 and 70 °C. SPME fiber material was 50/30 μm divinylbenzol/carboxen/PDMS (Supelco Inc., Bellefonte, PA, USA). Fibers were conditioned in a GC injector at 270 °C for 1 h. After adsorption, the fiber was directly transferred to the injection port of the gas chromatograph. Volatiles then were desorbed at 250 °C for 30 s. Before the next analysis, the fiber was reconditioned at 250 °C for 15 min in the GC injector to avoid carry-over of compounds from previous samples.

**Sample Preparation for SDE.** SDE was performed in a Likens−Nickerson apparatus, as modified by Schultz et al.[8] using 100 g of DDG suspended in 500 mL of water. The sample−water mixture and 100 mL of diethyl ether were boiled for 2 h. After cooling down to room temperature, diethyl ether was dried over sodium sulfate and concentrated to 1 mL using a Vigreux column (30 cm × 1 cm i.d.).

**Sample Preparation for SAFE.** A 150 g amount of DDG was mixed with diethyl ether (2 × 100 mL) and extracted for 2 h. For quantitation, 500 μL of methyl decanoate ($c$ = 0.81 mg/L) as the internal standard was added to the DDG−diethyl ether mixture. After filtration, the volatile fraction of the diethyl ether extract was isolated by means of the SAFE technique,[9] dried over sodium sulfate, and subsequently, concentrated to 1 mL using a Vigreux column.

**Separation into Neutral-Basic and Acidic Fraction.** The distillate obtained by SAFE was fractionated into a neutral-basic fraction (NBF) and an acidic fraction (AF) by treatment with 0.5 M sodium carbonate solution (2 × 50 mL, pH 10.0). After drying over anhydrous sodium sulfate, the NBF was concentrated to 1 mL using a Vigreux column. The AF was treated with a solution of 100 mL of saturated sodium chloride, and the pH was adjusted to pH 1.0 with hydrochloric acid. After treatment with diethyl ether, the organic phase was dried over anhydrous sodium sulfate and concentrated to 1 mL as described above.

**GC-Olfactometry and GC/MS.** Identification of aroma compounds was carried out on a SiChromat II gas chromatograph (Siemens, München, Germany) directly coupled to a Finnigan MAT 8222 magnetic sector mass spectrometer. At the end of the capillary column, the effluent was split into two equal parts using a Life-T effluent splitter to the mass spectrometer and a sniffing port.[10] The sniffing port was heated to 250 °C and rinsed with humidified air, to avoid dehydration of nasal membranes of assessors. Samples were separated using a silica capillary column SPB5 (Supelco) (30 m × 0.53 mm i.d., 1.5 μm film thickness). The column carrier gas was helium at a constant flow of 3 mL/min. A 2 μL amount of samples was applied with a split ratio of 1:10. The injector temperature was 250 °C, and the transfer line temperature was 200 °C. The oven program started with an initial temperature of 100 °C and subsequently was raised to finally 250 °C at a rate of 5 °C/min. MS detection was performed with an electron impact (EI) energy of 70 eV. The analyzed mass range was 35−350 amu in EI mode. For quantitation, an internal standard was added (500 μL of methyl decanoate with $c$ = 0.81 mg/L) at the beginning of the sample preparation step. Calculated concentrations are semiquantitative, since no response factors were determined.

**Aroma Compound Identification.** Identification of aroma compounds was based on the following criteria: odor description, linear retention indices (RIs), comparison with reference substances, and mass spectrometric data from the literature and the NIST library. In the case that MS data were too weak for unequivocal identification, aroma compounds were tentatively identified based on the remaining criteria. Linear RIs were determined after van Den Dool et al.[11] using a mixture of linear alkanes $C_6$−$C_{20}$ under the same chromatographic conditions described above.

**Sensory Analysis.** The sensory analysis of DDG was performed twice by a group of at least 10 panelists from the Institute of Brewing and Beverage Technology on different days. The analysis took place in a room for sensory analysis at room temperature. Panelists were trained weekly after DIN 10961 in general odor and taste perception and especially on cereal-based food products. In a preliminary session, panelists were asked to define attributes, which describe the odor of DDG. Subsequently, in the following sessions, panelists evaluated the intensity of the prior defined attributes on a scale of 0 (not present) to 5 (very intensive).

## RESULTS AND DISCUSSION

**Sensory Analysis of DDG from Wheat.** The incorporation of DDG in food products was a topic for many studies during the late 1980s, but unfortunately, the investigated products did not have a sufficient odor for being a popular food product.[1] Since no research has been done on the systematic study of flavor volatiles of DDG, a sensory analysis of the aroma profile was performed first.

For the development of an aroma profile, panelists were asked to list and evaluate perceptible odor impressions and the overall odor impression. In the following sessions, panelists rated these impressions in their intensity on a scale from 0 (not present) to 5 (very intensive). The three impressions caramellike, roasty, and brothlike were rated as most frequently mentioned impressions. The evaluation of the intensity during the following sessions emphasizes these results as it is shown in Figure 1 with seasoninglike and roasty, breadlike as the most

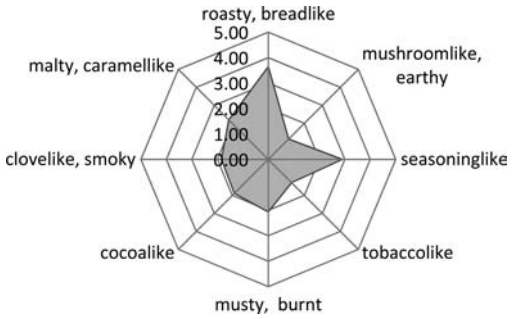


**Figure 1.** Flavor profile of DDG from wheat after sensory analysis; intensities of descriptors on a scale from 0 (not present) to 5 (very intensive), $n \geq 20$, results where averaged.

intensive odor impressions in DDG from wheat. High intensities could be determined for malty, caramellike and musty, burnt as well. During the production of DDG, fermentation, distillation and drying steps play an important role. In the distillation process, highly volatile compounds can be distilled together with ethanol, and new components can be formed during the drying process. Thus, odor-active compounds from Maillard reaction, byproducts of yeast fermentation, or thermal reaction compounds of the drying process are expected to contribute to the odor of DDG. The results of

**Table 1. Odor-Active Compounds in DDG from Wheat**

| odor-active volatiles identified with SPME, SDE, and SAFE | | | | | |
|---|---|---|---|---|---|
| odor-active compound | odor quality[a] | RI (DB-5)[b] | SPME | SDE | SAFE |
| butanoic acid[d] | cheesy | 743 | x | x | x |
| 3-methylbutanoic acid[d] | cheesy | 810 | x | x | x |
| 2-methylbutanoic acid[d] | cheesy, fruity | 830 | x | x | x |
| 1-octen-3-one[c] | mushroomlike | 978 | x | x | x |
| 1,5-octadien-3-one[c] | metallic | 986 | x | x | x |
| dimethyl trisulfide[d] | cooked, cabbagelike | 995 | x | x | x |
| 2-phenylacetaldehyde[d] | flowery | 1055 | x | x | x |
| 2-ethyl-3,6-dimethylpyrazine[d] | breadlike | 1089 | x | x | x |
| 2-ethyl-3,5-dimethylpyrazine[d] | roasty | 1095 | x | x | x |
| 2-methoxyphenol[d] | smoky | 1102 | x | x | x |
| 3-hydroxy-4,5-dimethyl-2(5H)-furanone[c] | seasoninglike | 1106 | x | x | x |
| 2-phenylethanol[d] | flowery | 1124 | x | x | x |
| (*Z*)-2-nonenal[c] | cucumberlike, fatty | 1149 | x | x | x |
| (*E*,*Z*)-2,6-nonadienal[c] | cucumberlike | 1159 | x | x | x |
| 3-hydroxy-4-methyl-5-ethyl-2(5*H*)-furanone[c] | fatty, brothlike | 1191 | x | x | x |
| 4-vinylphenol[c] | clovelike, phenolic | 1222 | x | x | x |
| 2-methoxy-4-vinylphenol[d] | clovelike | 1329 | x | x | x |
| *β*-damascenone[d] | fruity, cooked applelike | 1402 | x | x | x |
| 4-hydroxy-3-methoxybenzaldehyd[d] | vanillalike | 1419 | x | x | x |
| odor-active volatiles identified with specific technique (marked with an "x") | | | | | |
| odor-active compound | odor quality[a] | RI (DB-5)[b] | SPME | SDE | SAFE |
| acetic acid[d] | acetic | 589 | x | | |
| 2,3-butanedione[d] | buttery | 600 | x | | |
| 3-methylbutanal[d] | breadlike | 675 | x | | |
| 2,3-pentanedione[d] | mushroomlike, cheesy | 707 | x | | |
| 2-methylpropionic acid[d] | sweet | 716 | | x | |
| hexanal[d] | green | 798 | | x | |
| n.i.[e] | caramellike | 883 | x | x | |
| n.i.[e] | mushroomlike, seasoninglike | 898 | | x | x |
| 3-methylthiopropanal[d] | cooked potato | 913 | x | x | |
| 2,5-dimethylpyrazine[d] | breadlike, roasty | 915 | | x | |
| n.i.[e] | musty, burnt | 920 | | x | |
| n.i.[e] | musty, earthy | 926 | x | | |
| 2-ethyl-5-methylpyrazine[d] | roasty | 1011 | | x | |
| 4-hydroxy-5-methyl-3(2*H*)-furanone[c] | caramellike, sweet | 1039 | x | | x |
| 4-hydroxy-2,5-dimethyl-3(2*H*)-furanone[c] | caramellike | 1054 | x | | x |
| n.i.[e] | caramellike, sweet | 1083 | x | | |
| (*E*)-2-nonenal[d] | dusty, rancid | 1164 | x | | |
| 2-phenylacetic acid[dd] | honeylike | 1248 | x | | x |
| 2-phenylethyl acetate[d] | flowery | 1264 | | x | x |
| n.i.[e] | roasty, nutty | 1283 | x | x | |
| (*E*,*Z*)-2,4-decadienal[d] | fatty | 1298 | | x | |
| (*E*,*E*)-2,4-decadienal[d] | fatty, rancid | 1324 | | x | |
| 3-methylindole[c] | fecal | 1409 | x | x | |

[a]Odor quality perceived at the sniffing port. [b]RIs on a DB-5 column. [c]Tentatively identified by RIs, odor quality, and comparison with reference substances. [d]Identified by RIs, odor quality, and mass spectra obtained in EI. [e]n.i. = not identified.

sensory analysis indicate the presence of volatiles from thermal processing such as pyrazines (roasty and breadlike, burnt) or sugar degradation products (caramellike, seasoninglike). The analysis of odor-active volatiles was carried out in the next step to substantiate the results of the sensory evaluation.

**Analysis of Odor-Active Volatiles in DDG.** Sample preparation and isolation procedures applied before the analysis can determine the composition of aroma extracts. Since there is no knowledge concerning odor-active compounds in DDG, the sample preparation step is performed with multiple techniques to avoid misinterpretations and to work out a representative classification of odor-active volatiles. For this purpose, one headspace technique (HS-SPME) and two solvent-extraction techniques (SDE, SAFE) were carried out.

With the three applied methods, 42 odor-active compounds could be found in total in DDG from wheat. Nineteen of the 42 compounds were identified in accordance with the application of every specific method (upper part, Table 1). Twenty-three compounds (lower part, Table 1) could only be identified with one respectively two specific techniques and confirms the dependence of traceability and the sample preparation step. Classification of identified aroma compounds reveals four

**Table 2. Peak Areas of Characteristic Mass Fragments of Selected Compounds after HS-SPME at Different Enrichment Conditions (1 and 6 h; 30 and 70 °C)**

| odor-active compound | RI (DB-5)[a] | *m/z* | 30 °C, 1 h[b] | 30 °C, 6 h[b] | 70 °C, 1 h[b] | 70 °C, 6 h[b] |
|---|---|---|---|---|---|---|
| acetic acid | 589 | 60 | 1540.0 | 1890.0 | 1800.0 | 1470.0 |
| 2,3-butanedione | 600 | 86 | 9.5 | 6.6 | 21.5 | 13.7 |
| 3-methylbutanal | 675 | 58 | 47.8 | 28.0 | 19.0 | 30.0 |
| 2,3-pentanedione | 707 | 100 | 5.7 | 2.7 | 10.0 | 3.9 |
| butanoic acid | 746 | 60 | 15.2 | 13.9 | 16.9 | 5.2 |
| hexanal | 798 | 82 | 7.1 | 2.6 | 5.0 | 3.5 |
| 3-methylbutanoic acid | 810 | 60 | 53.2 | 35.7 | 19.0 | 10.8 |
| 2-methylbutanoic acid | 830 | 74 | 31.3 | 30.4 | 14.7 | 7.9 |
| dimethyl trisulfide | 995 | 126 | 21.0 | 10.7 | 14.8 | 10.0 |
| 2-phenylacetaldehyde | 1055 | 120 | 3.3 | 9.1 | 25.9 | 19.9 |
| 2-ethyl-3,5-dimethylpyrazine | 1095 | 135 | 12.0 | 30.7 | 20.5 | 6.5 |
| 2-phenylethanol | 1124 | 120 | 1050.0 | 1720.0 | 1760.0 | 1390.0 |
| 2-phenylacetic acid | 1248 | 136 | 0.0 | 0.0 | 4.0 | 5.6 |
| 2-phenylethyl acetate | 1287 | 104 | 18.2 | 96.9 | 113.0 | 55.4 |
| 2-methoxy-4-vinylphenol | 1329 | 150 | 0.9 | 7.0 | 72.5 | 204.0 |
| 4-hydroxy-3-methoxybenzaldehyde | 1419 | 151 | 0.0 | 24.9 | 90.2 | 307.0 |

[a]RIs on a DB-5 column. [b]Values show peak areas × $10^8$.

furanones (3(2*H*)- and 2(5*H*)-furanones), four pyrazines (2,5-dimethylpyrazine, 2-ethyl-5-methylpyrazine, 2-ethyl-3,6-dimethyl-, and 2-ethyl-3,5-dimethylpyrazine), and six acids (acetic and butanoic acids, 2-methylpropanoic acid, 3- and 2-methylbutanoic acids, and 2-phenylacetic acid). Moreover, four phenolic compounds (2-methoxyphenol, 2-methoxy-4-vinylphenol, 4-vinylphenol, and 4-hydroxy-3-methoxybenzaldehyd), two sulfur-containing compounds (dimethyl trisulfide and 3-methylthiopropanal), and a number of aldehydes and ketones (2,3-butanedione, 3-methylbutanal, 2,3-pentanedione, hexanal, 1-octen-3-one, 1,5-octadien-3-one, 2-phenylacetaldehyde, (*E*)- and (*Z*)-2-nonenal, (*E*,*Z*)-(2,6)-nonadienal, (*E*,*E*)- and (*E*,*Z*)-2,4-decadienal, and $\beta$-damascenone) were determined. Besides 2-phenylethanol and 2-phenylethyl acetate, no alcohols and esters were determined. 3-Methylindole was determined as single N-heterocyclic compound.

Unequivocal MS data could not be obtained for 10 compounds ((*Z*)-2-nonenal, (*E*,*Z*)-2,6-nonadienal, 5-ethyl-3-hydroxy-4-methyl-2(5*H*)-furanone, 4-vinylphenol, 3-hydroxy-4,5-dimethyl-2(5*H*)-furanone, 1-octen-3-one, 1,5-octadien-3-one, 3-methylindole, 4-hydroxy-5-methyl-3(2*H*)-furanone, and 4-hydroxy-2,5-dimethyl-3(2*H*)-furanone), so the identification was based on the remaining criteria. Further, six odor-active regions in the GC chromatogram could not be identified by any of the applied methods, because of low concentrations and insufficient MS data.

**Identification of Odor-Active Compounds in DDG from Wheat via SPME.** To get a first impression of volatile compounds in a matrix, HS-SPME is a reasonable technique for a qualitative overview. Moreover, HS-SPME is a proven method for the analysis of volatiles in food and wheat products such as partially baked bread.[12,13] The application of SPME on DDG from wheat revealed 33 odor active regions in the gas chromatogram, of which 29 could be identified. The four compounds acetic acid, 2,3-butanedione, 3-methylbutanal, and 2,3-pentanedione could only be determined by HS-SPME, due to the coelution and overlay with diethyl ether used as the solvent in the distillation methods. Odor-active compounds eluting before or simultaneously with the solvent cannot be determined. Therefore, a headspace method complements information caused by solvent delay.

Furthermore, the isolation of flavor compounds by SPME reveals strong dependence of adsorption behavior on the SPME fiber from adsorption time and temperature as it is shown in Table 2. Low-temperature adsorption (30 °C) and prolonging of adsorption time from 1 to 6 h results in lower peak areas for highly volatile compounds (e.g., dimethyl trisulfide) and increased peak areas for medium and low volatile compounds (e.g., 4-hydroxy-3-methoxybenzaldehyde). The prolonging of adsorption time shifts the spectrum of volatiles to medium and low volatile compounds. High-temperature adsorption (70 °C) and prolonging of adsorption time leads to a reduction of peak areas of high volatile compounds (e.g., 2-phenylethyl acetate, 2-phenylethanol, and acetic acid). The odor perception of 4-hydroxy-5-methyl-3-(2*H*)-furanone, 3-methylindole, and an unknown compound with green, metallic odor at the sniffing port ($RI_{DB5}$ = 1197) is enabled only at a longer adsorption time and a higher temperature (6 h and 70 °C). Moreover, prolonging of adsorption time to 6 h made the odor perception of 1,5-octadien-3-one, 2-phenylacetaldehyde, (*Z*)-2-nonenal, 2-phenylacetic acid, and two unknown compounds ($RI_{DB5}$ = 1083, sweet, caramellike; $RI_{DB5}$ = 1283, roasty, nutty) possible. Basically, an enhanced intensity of odor perception could be obtained by higher temperature and prolonging of adsorption time (70 °C and 6 h); nevertheless, artifact formation at these conditions cannot be excluded.

**Identification of Odor-Active Compounds in DDG from Wheat via SDE.** SDE, as developed by Likens and Nickersson[14] and modified by Schultz et al.,[8] is a method for continuous and concurrent vapor distillation and solvent extraction. For the isolation of volatiles from a food matrix, SDE still represents a standard procedure.[15−17] In the case of DDG from wheat, 32 odor-active areas could be located in total in the GC chromatogram obtained by an aroma extract derived by means of SDE, of which 29 could be identified. The isolation of volatile compounds with SDE revealed an extract with intensive roasty and breadlike aroma. Besides 2-ethyl-3,6-dimethyl- and 2-ethyl-3,5-dimethylpyrazine, two additional pyrazines (2-ethyl-5-methylpyrazine and 2,5-dimethylpyrazine) were determined. Since it is well known that pyrazines contribute to the roasty odor of processed food, the increased

number of pyrazines in the SDE extract might contribute to the intensified roasty odor.

Further, the aldehydes hexanal (green), (*E*,*Z*)- and (*E*,*E*)-2,4-decadienal (fatty, rancid) were detected in the SDE extract. Since these aldehydes were not detectable or perceptible with SPME or SAFE, the artifact formation during the distillation process cannot be excluded. Moreover, lipid oxidation products are enriched due to the temperature treatment during extraction. After isolation with SDE and in accordance to SPME, 3-(methylthio)-propanal, 3-methylindole, and two additional unidentified compounds ($RI_{DB5}$ = 883, caramellike; $RI_{DB5}$ = 1283, roasty) could be determined. In accordance to SAFE, SDE was able to determine (*Z*)-4-heptenal and 2-phenylethylacetat. In addition, an unidentified compound ($RI_{DB5}$ = 920) was determined. Because of the musty and burnt odor quality, it might be an artifact. SDE was not able to isolate 2-phenylacetic acid, as well as the two furanones 4-hydroxy-5-methyl-3(2*H*)-furanone and 4-hydroxy-2,5-dimethyl-3(2*H*)-furanone. The good solubility in water leads to poor extractability and retention in the water matrix, which was already reported by Siegmund et al.[18] Since highly hydrophilic compounds are prevented from extraction out of the water suspension and thus remain in the extraction residue during SDE, an important part for a responsible aroma profile is missing. For this reason, SAFE was applied as an additional extraction procedure on DDG from wheat.

**Identification of Odor-Active Compounds in DDG from Wheat via SAFE.** SAFE as developed in 1999 by Engel et al.[9] was chosen as the second solvent-extraction method, since SAFE is known as a gentle isolation process preserving the native profile of odor-active compounds in a food product. An extract derived with SAFE generally neither contains or enriches oxidation products and thermal reaction compounds nor supports the formation of artifacts. The isolation of volatile compounds of DDG from wheat with SAFE revealed an extract with strong seasoninglike, breadlike, and spicy odor impression. By contrast to SDE, the aroma of the extract was less roasty and breadlike but showed a strong seasoninglike odor impression. Twenty-four odor-active areas were located in the gas chromatogram after injection of an extract derived via SAFE. Present results confirm that SAFE represents a gentle isolation process of volatile compounds, because Strecker aldehydes (e.g., 3-methylthiopropanal) and possible artifacts isolated via SPME and SDE could not be confirmed with SAFE under moderate conditions. Because of the native odor profile, the SAFE extract was chosen for further analysis.

In the last step of aroma analysis, the extract derived via SAFE was fractionated into an AF and NBF, to determine coelutions and improve the separation behavior on the capillary column. The fractionation revealed five additional odor-active areas in the GC chromatogram. One could be identified as 3-hydroxy-2-methylpyran-4-one ($RI_{DB5}$ = 1123, caramellike), already identified as an odor-active volatile in the crust of wheat and rye bread.[19] Because of the coelution with 2-phenylethanol ($RI_{DB5}$ = 1124) and the similar odor impression, 3-hydroxy-2-methylpyran-4-one could not be determined without fractionation. Four of the five additional compounds could not be identified due to unequivocal MS data.

**Key Aroma Compounds in DDG from Wheat.** To investigate key odorants in DDG from wheat, the distillate obtained by SAFE was analyzed by means of AEDA. Therefore, the gas chromatogram was compared to the flavor dilution (FD) chromatogram (Figure 2), and eight compounds with a

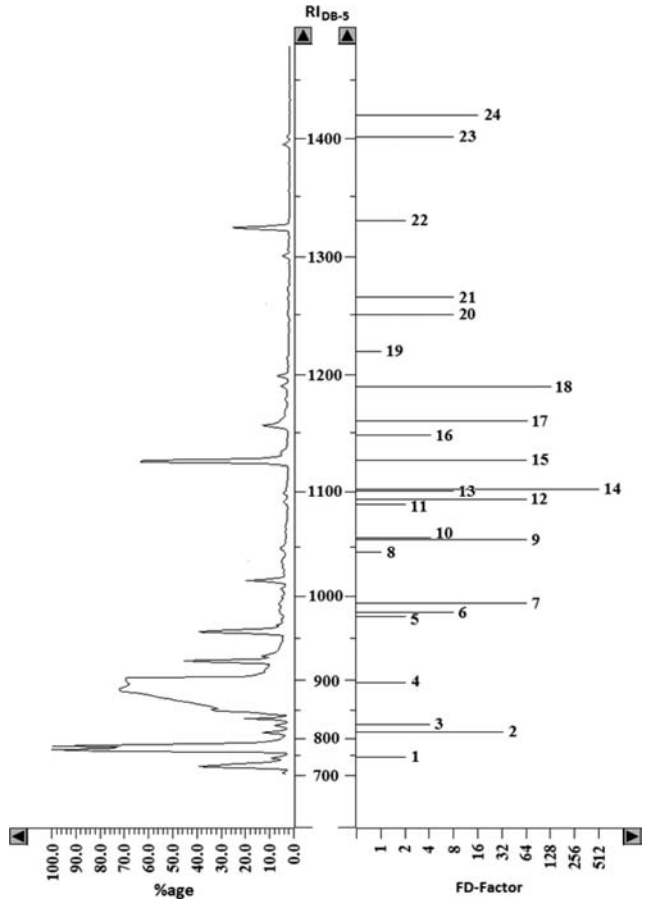


**Figure 2.** FD chromatogram compared to the gas chromatogram of a SAFE distillate from DDG from wheat; numbers indicate flavor-active compounds as identified in Table 3.

FD factor ≥ 32 could be determined. The highest FD factor of 512 was determined for 3-hydroxy-4,5-dimethyl-2(5*H*)-furanone (sotolon) with seasoninglike odor and a slightly lower FD factor of 128 for the ethyl-homologue 5-ethyl-3-hydroxy-4-methyl-2(5*H*)-furanone (brothlike, spicy). These furanones were revealed as the most influential odor-active volatiles in DDG from wheat, which is in accordance with the results of the sensory evaluation shown in Figure 1. 3-Hydroxy-4,5-dimethyl-2(5*H*)-furanone is the character impact compound of fenugreek and has also been identified in white and whole wheat flour and Bavarian wheat beer as an important odor-active volatile with high FD factors of 256 for the formers and 512 for the latter.[20−22] Blank et al.[20] proposed that, in the case of fenugreek, 3-hydroxy-4,5-dimethyl-2(5*H*)-furanone originates from thermally induced oxidative deamination of 4-hydroxyisoleucine and its lactone 3-amino-4,5-dimethyl-3,4-dihydro-2(5*H*)-furanone as shown in Figure 4. Moreover, it was revealed that the yield is improved by boiling several hours at acidic conditions. Regarding the thermal conditions of the drying process and the acidic pH of 3.8 of DDG, it can be concluded that the formation of 3-hydroxy-4,5-dimethyl-2(5*H*)-furanone can be enhanced.

Further, a high FD factor of 64 could be determined for 4-hydroxy-2,5-dimethyl-3(2*H*)-furanone (Furaneol) with caramellike odor. 3(2*H*)-Furanones are an important group of hydroxyl furanones, usually responsible for the sweet and caramellike odor impression of processed food. 4-Hydroxy-2,5-dimethyl-3(2*H*)-furanone could already be identified in wheat

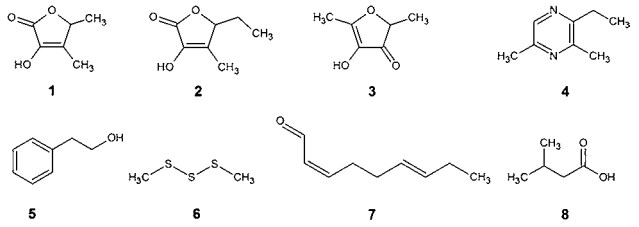

**Figure 3.** Chemical structures of key aroma compounds in DDG obtained by AEDA with FD factor ≥ 32: 3-hydroxy-4,5-dimethyl-2(5*H*)-furanone (**1**), 3-hydroxy-4-methyl-5-ethyl-2(5*H*)-furanone (**2**), 4-hydroxy-2,5-dimethyl-3(2*H*)-furanone (**3**), 2-ethyl-3,5-dimethylpyrazine (**4**), 2-phenylethanol (**5**), dimethyl trisulfide (**6**), (*E*,*Z*)-2,6-nonadienal (**7**), and 3-methylbutanoic acid (**8**).

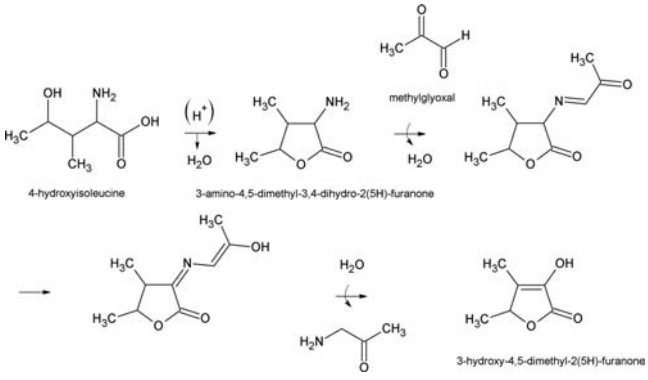

**Figure 4.** Formation pathway leading to 3-hydroxy-4,5-dimethyl-2(5*H*)-furanone from 4-hydroxyisoleucine, modified according to Blank et al.[20]

beer and wheat bread crumb.[19,22] The formation pathway of 4-hydroxy-2,5-dimethyl-3(2*H*)-furanone in wheat bread crust is known to descend from yeast as the most important source, with fructose-1,6-diphosphate as the predominant precursor.[23] The roasty and breadlike odor impression revealed during sensory analysis can be attributed to 2-ethyl-3,5-dimethylpyrazine with a FD factor of 64. Besides the seasoning and caramellike odor impression, the roasty character represents a central odor impression of DDG. It is well known that a number of volatile pyrazines contribute to the flavor of thermal processed foods originating from nonenzymatic browning of food products. Schieberle and Grosch identified 2-ethyl-3,5-dimethylpyrazine as an odor-active compound in wheat bread crust[19] and rye bread crust,[24] with FD factors of 16 and 64, respectively. Moreover, 2-ethyl-3,6-dimethylpyrazine with a FD factor of 4 and the identification of 2,5-dimethylpyrazine and 2-ethyl-5-methylpyrazine substantiate the contribution of pyrazines to the roasty odor impression of DDG from wheat. With a FD factor of 32, dimethyl trisulfide, the cabbagelike odor typically arising in plants of the genera *Brassica* and *Allium,* plays an important role in DDG odor as well. In processed wheat products, dimethyl trisulfide has not been found as a relevant key odorant by now. Nevertheless, Lee at al. showed that the analysis of volatiles from a wheat gluten hydrolysate thermally processed with glucose or fructose revealed dimethyl trisulfide as a product from Maillard reaction.[25] Because of the high FD factor and very low odor threshold of 0.01 μg/L in $H_2O$, dimethyl trisulfide could be a possible source for the off flavor in DG from wheat described previously.[26] The differences in DDG flavor to the flavor of wheat products might occur especially due to the presence of dimethyl trisulfide, which is not known as a key odorant of processed

**Table 3. Odor-Active Volatiles and Corresponding FD Factors Obtained by AEDA in DDG from Wheat**

| no.[a] | odor-active compound | odor quality[b] | RI (DB-5)[c] | FD factor[d] |
|---|---|---|---|---|
| 1 | butanoic acid[f] | rancid | 743 | 2 |
| 2 | 3-methylbutanoic acid[f] | cheesy | 810 | 32 |
| 3 | 2-methylbutanoic acid | cheesy | 830 | 4 |
| 4 | n.i. | spicy, brothlike | 900 | 2 |
| 5 | 1-octen-3-one[e] | mushroomlike | 978 | 2 |
| 6 | 1,5-octadien-3-one[e] | metallic | 986 | 8 |
| 7 | dimethyl trisulfide[f] | sulphurous | 995 | 32 |
| 8 | 4-hydroxy-5-methyl-3(2*H*)-furanone | caramellike | 1045 | 1 |
| 9 | 4-hydroxy-2,5-dimethyl-3(2*H*)-furanone[e] | caramellike | 1054 | 64 |
| 10 | phenylacetaldehyde[f] | flowery | 1055 | 4 |
| 11 | 2-ethyl-3,6-dimethylpyrazine[f] | breadlike | 1089 | 4 |
| 12 | 2-ethyl-3,5-dimethylpyrazine[f] | roasty | 1095 | 64 |
| 13 | 2-methoxyphenol[f] | smoky | 1102 | 8 |
| 14 | 3-hydroxy-4,5-dimethyl-2(5*H*)-furanone[e] | seasoninglike | 1100 | 512 |
| 15 | 2-phenylethanol[f] | flowery | 1126 | 64 |
| 16 | (*Z*)-2-nonenal[e] | cucumberlike | 1160 | 2 |
| 17 | (*E*,*Z*)-2,6-nonadienal[f] | fatty | 1189 | 64 |
| 18 | 5-ethyl-3-hydroxy-4-methyl-2(5*H*)-furanone[e] | brothlike | 1196 | 128 |
| 19 | 4-vinylphenol[f] | phenolic, sweet | 1222 | 1 |
| 20 | 2-phenylacetic acid[f] | honeylike | 1250 | 8 |
| 21 | 2-phenylethyl acetat[f] | flowery | 1263 | 8 |
| 22 | 2-methoxy-4-vinylphenol[f] | clovelike | 1329 | 2 |
| 23 | β-damascenone[f] | applelike | 1404 | 8 |
| 24 | 4-hydroxy-3-methoxybenzaldehyd[f] | vanillalike | 1422 | 4 |

[a]Numbering refers to Figure 2. [b]Odor quality perceived at the sniffing port. [c]RIs on a DB-5 column. [d]Flavor dilution factor. [e]Tentatively identified by RIs, odor quality, and comparison with reference substances. [f]Identified by RIs, odor quality, and mass spectra obtained in EI; n.i. = not identified.

wheat products by now. 2-Phenylethanol with a FD factor of 64 is also one of the eight most important odor-active volatiles in DDG and consequently contributing to its sweet and floral odor. It is formed as byproduct in the fermentation of yeasts by enzymatic reactions via Ehrlich pathway.[27,28] The presence of 2-phenylethanol in processed wheat products is already known, since it was revealed as an important odor-active volatile in wheat bread crumb.[29] Likewise, 3-methylbutanoic acid with a FD factor of 32 was enlightened as an important odor-active volatile in DDG from wheat. Together with 2-methylbutanoic acid, the two methyl-substituted butanoic acids are responsible for the rancid off flavor in wheat bread.[30] (*E*,*Z*)-2,6-Nonadienal, a degradation product of linolenic acid, is another of the most important odorants of DDG from wheat with a FD factor of 64. It is already identified in wheat bread crust and white wheat flour.[19,21] A number of other unsaturated aldehydes such as (*E*)-/(*Z*)-2-nonenal and (*E*,*Z*)-/(*E*,*E*)-2,4-decadienal were also identified in DDG from wheat. These unsaturated aldehydes are well known to contribute to the fatty and rancid odor impression.

In summary, 42 odor-active compounds could be identified in total in DDG from wheat. Ranges of concentrations and odor activity values of selected important odor-active volatiles can be seen in Tables 4 and 5. Eight compounds were determined as key aroma compounds with a FD factor ≥ 32 as shown in Figure 3. These eight key odorants of DDG from wheat point out that the overall aroma of DDG is based on reaction compounds and precursors from thermal food processing, in particular Maillard reaction and Strecker degradation. This is also supported by a view on the production process of DDG. Regarding the further processing of the yeast fermented grain matrix, the mash is distilled for separation of ethanol at 78 °C. After a temporary storage (75−80 °C, 2−8 h), the thickening process of the thin stillage to syrup (55−65 °C, 2−4 h) follows. Subsequently, the main drying process takes place, where the stillage is dried at 100−105 °C for 1−3 h. These conditions markedly favor the formation of oxidation products and the continuation of Maillard and Strecker reactions. Aroma volatiles and key aroma compounds in DDG from wheat show high compliance to wheat processed products such as white wheat bread. DDG represents a thermal processed wheat product, which is supported by its composition of flavor volatiles.

**Table 4. Odor-Activity Values Greater Than 1 of Selected Compounds in DG from Wheat**

| odor-active compound | odor quality[a] | RI (DB-5)[b] | OAV[c] |
|---|---|---|---|
| butanoic acid | cheesy | 743 | 3.0 |
| 3-methylbutanoic acid | cheesy, | 810 | 15.5 |
| 2-methylbutanoic acid | cheesy, fruity | 830 | 4.55 |
| dimethyl trisulfide | cooked, cabbagelike | 995 | 965.0 |
| 2-phenylacetaldehyde | flowery | 1055 | 22.0 |
| 2-ethyl-3,5-dimethylpyrazine | roasty | 1095 | 90.5 |
| 2-methoxyphenol | smoky | 1102 | 1.8 |
| 2-phenylethanol | flowery | 1124 | 8.7 |
| 2-phenylethyl acetate | flowery | 1264 | 2.7 |
| 2-methoxy-4-vinylphenol | clovelike | 1329 | 2.3 |
| *β*-damascenone | fruity, cooked applelike | 1402 | 50.0 |

[a]Odor quality perceived at sniffing port. [b]RIs on a DB-5 column. [c]Odor-activity value based on odor thresholds known from literature and concentrations calculated with methyl decanoate as the internal standard.

**Table 5. Concentrations of Selected Compounds in DDG from Wheat**

| odor-active compound | odor quality[a] | RI (DB-5)[b] | conc[c] (*μ*g/kg) |
|---|---|---|---|
| 2-methylpropionic acid | sweet | 716 | >100 |
| butanoic acid | rancid | 746 | >100 |
| hexanal | green | 798 | >100 |
| 3-methylbutanoic acid | cheesy | 810 | >100 |
| 2-methylbutanoic acid | cheesy, fruity | 819 | >100 |
| 2,5-dimethylpyrazine | breadlike, roasty | 915 | >100 |
| dimethyl trisulfide | cooked, cabbagelike | 995 | 10−100 |
| 2-phenylacetaldehyde | flowery | 1055 | 10−100 |
| 2-ethyl-3,6-dimethylpyrazine | breadlike | 1089 | 1−10 |
| 2-ethyl-3,5-dimethylpyrazine | roasty | 1095 | 10−100 |
| 2-methoxyphenol | smoky | 1102 | 1−10 |
| 2-phenylethanol | flowery | 1124 | >10 000 |
| 2-phenylacetic acid | honeylike | 1248 | 10−100 |
| 2-phenylethyl acetate | flowery | 1264 | 10−100 |
| 2-methoxy-4-vinylphenol | clovelike | 1329 | 10−100 |
| *β*-damascenone | fruity, cooked applelike | 1402 | 1−10 |
| 4-hydroxy-3-methoxybenzaldehyde | vanillalike | 1419 | 10−100 |

[a]Odor quality perceived at sniffing port. [b]RIs on a DB-5 column. [c]Concentration in *μ*g/kg.

## AUTHOR INFORMATION

### Corresponding Author

*E-mail: mjekle@tum.de.

### Notes

The authors declare no competing financial interest.

## ABBREVIATIONS USED

DG, distiller's grains; DDG, dried distiller's grains; HS-SPME, headspace solid-phase microextraction; SAFE, solvent-assisted flavor evaporation; SDE, simultaneous distillation extraction; AEDA, aroma extract dilution analysis; GC-O/MS, gas chromatography-olfactometry/mass spectrometry; AACC, American Association of Cereal Chemists; PDMS, polydimethylsiloxane; NBF, neutral-basic fraction; AF, acidic fraction; RI, retention index; DIN, Deutsches Institut für Normung; FD, flavor dilution

## REFERENCES

(1) Rosentrater, K. A.; Krishnan, P. G. Incorporating distillers grains in food products. *Cereal Foods World* **2006**, *51*, 52−60.

(2) Liu, K. Chemical composition of distillers grains, a review. *J. Agric. Food Chem.* **2011**, *59*, 1508−1526.

(3) Bookwalter, G. N.; Warner, K.; Wall, J. S.; Wu, Y. V. Corn distillers grains and other byproducts of alcohol production in blended foods. II. Sensory, stability and processing studies. *Cereal Chem.* **1984**, *61*, 509−513.

(4) Bookwalter, G. N.; Warner, K.; Wu, Y. V. Processing corn distillers' grains to improve flavor: Storage stability in corn-soy-milk blends. *J. Food Sci.* **1988**, *53*, 523−526.

(5) Abbott, J.; O'Palka, J.; McGuire, C. Dried distillers' grains with solubles: Particle size effects on volume and acceptability of baked products. *J. Food Sci.* **1991**, *56*, 1323−1326.

(6) Rasco, B. A.; Hashisaka, A. E.; Dong, F. M.; Einstein, M. A. Sensory evaluation of baked foods incorporating different levels of distillers' dried grains with solubles from soft white winter wheat. *J. Food Sci.* **1989**, *54*, 337−342.
(7) Biswas, S.; Staff, C. Analysis of headspace compounds of distillers grains using SPME in conjunction with GC/MS and TGA. *J. Cereal Sci.* **2001**, *33*, 223−229.
(8) Schultz, T. H.; Flath, R. A.; Mon, T. R.; Eggling, S. B.; Teranishi, R. Isolation of volatile components from a model system. *J. Agric. Food Chem.* **1977**, *25*, 446−449.
(9) Engel, W.; Bahr, W.; Schieberle, P. Solvent assisted flavour evaporation − A new and versatile technique for the careful and direct isolation of aroma compounds from complex food matrices. *Eur. Food Res. Technol.* **1999**, *209*, 237−241.
(10) Nitz, S.; Drawert, F.; Gellert, U. A variable effluent splitter for simultaneous sniffing-MS-monitoring. *Chromatographia* **1986**, *22*, 51−54.
(11) van Den Dool, H.; Kratz, P. D. A generalization of the retention index system including linear temperature programmed gas-liquid partition chromatography. *J. Chromatogr.* **1963**, *11*, 463−471.
(12) Poinot, P.; Grua-Priol, J.; Arvisenet, G.; Rannou, C.; Semenou, M.; Bail, A. Le; Prost, C. Optimisation of HS-SPME to study representativeness of partially baked bread odorant extracts. *Food Res. Int.* **2007**, *40*, 1170−1184.
(13) Kollmannsberger, H.; Rodríguez-Burruezo, A.; Nitz, S.; Nuez, F. Volatile and capsaicinoid composition of ají (*Capsicum baccatum*) and rocoto (*Capsicum pubescens*), two Andean species of chile peppers. *J. Sci. Food Agric.* **2011**, *91*, 1598−1611.
(14) Likens, S.; Nickerson, G. Detection of certain hop oil constituents in brewing products. *Am. Soc. Brew. Chem. Proc.* **1964**, 5−13.
(15) Díaz-Maroto, M. C.; Díaz-Maroto Hidalgo, I. J.; Sánchez-Palomo, E.; Pérez-Coello, M. S. Volatile components and key odorants of fennel (*Foeniculum vulgare* Mill.) and thyme (*Thymus vulgaris* L.) oil extracts obtained by simultaneous distillation-extraction and supercritical fluid extraction. *J. Agric. Food Chem.* **2005**, *53*, 5385−5389.
(16) Strohalm, H.; Dregus, M.; Wahl, A.; Engel, K.-H. Enantioselective analysis of secondary alcohols and their esters in purple and yellow passion fruits. *J. Agric. Food Chem.* **2007**, *55*, 10339−10344.
(17) Du, L.; Li, J.; Li, W.; Li, Y.; Li, T.; Xiao, D. Characterization of volatile compounds of pu-erh tea using solid-phase microextraction and simultaneous distillation−extraction coupled with gas chromatography−mass spectrometry. *Food Res. Int.* **2014**, *57*, 61−70.
(18) Siegmund, B.; Leitner, E.; Mayer, I.; Farkas, P. Untersuchungen zur problematik der extraktion von aromastoffen mit der SDE nach likens-nickersson. *Dtsch. Lebensm.-Rundsch.* **1996**, *92*, 286−290.
(19) Schieberle, P.; Grosch, W. Identification of the volatile flavour compounds of wheat bread crust - Comparison with rye bread crust. *Z. Lebensm.-Unters. Forsch.* **1985**, 474−478.
(20) Blank, I.; Lin, J.; Devaud, S.; Fumeaux, R.; Laurent, B. The principal flavor components of fenugreek (*Trigonella foenum-graecum* L.). In *Spices: Flavor Chemistry and Antioxidant Properties*; Risch, S. J., Ho, C.-T., Eds.; American Chemical Society: Washington, DC, 1997; pp 12−28.
(21) Czerny, M.; Schieberle, P. Important aroma compounds in freshly ground wholemeal and white wheat flour − Identification and quantitative changes during sourdough fermentation. *J. Agric. Food Chem.* **2002**, 6835−6840.
(22) Langos, D.; Granvogl, M.; Schieberle, P. Characterization of the key aroma compounds in two bavarian wheat beers by means of the sensomics approach. *J. Agric. Food Chem.* **2013**, *61*, 11303−11311.
(23) Schieberle, P. Formation of furaneol in heat processed foods. In *Flavor Precursors. Thermal and Enzymatic Conversions*; Teranishi, R., Takeoka, G. R., Güntert, M., Eds.; American Chemical Society: Washington, DC, 1992; pp 164−174.
(24) Schieberle, P.; Grosch, W. Potent odorants of rye bread crust − Differences from the crumb and from wheat bread crust. *Z. Lebensm.-Unters. Forsch.* **1994**, 292−296.
(25) Lee, S. E.; Chung, H.; Kim, Y.-S. Effects of enzymatic modification of wheat protein on the formation of pyrazines and other volatile components in the Maillard reaction. *Food Chem.* **2012**, *131*, 1248−1254.
(26) Buttery, R. G.; Teranishi, R.; Flath, R. a.; Ling, L. C. Identification of additional tomato paste volatiles. *J. Agric. Food Chem.* **1990**, *38*, 792−795.
(27) Fabre, C. E.; Blanc, P. J.; Goma, G. Screening of yeasts producing 2-phenylethylalcohol. *Biotechnol. Technol.* **1997**, *11*, 523−525.
(28) Hazelwood, L. A.; Daran, J.-M.; van Maris, A. J. A; Pronk, J. T.; Dickinson, J. R. The Ehrlich pathway for fusel alcohol production: A century of research on Saccharomyces cerevisiae metabolism. *Appl. Environ. Microbiol.* **2008**, *74*, 2259−2266.
(29) Schieberle, P.; Grosch, W. Potent odorants of the wheat bread crumb: Differences to the crust and effect of a longer dough fermentation. *Z. Lebensm.-Unters. Forsch.* **1991**, *192*, 130−135.
(30) Grosch, W.; Schieberle, P. Flavor of cereal products- A review. *Cereal Chem.* **1997**, *74*, 91−97.

in 1988.[8] However, appreciable amounts of coumarin have been found in various foods, such as bakery products, breakfast cereals, confectionary, and so on.[9,10] Vanilla extracts adulterated with coumarin as a fragrance enhancer[11] are other potential paths for baby's coumarin exposure.

Recently, China's authorities and the media have reported the illegal use of flavorings in some infant formulas. Meanwhile, considering the low limits of the usage and the complex matrix of formula samples, a reliable analytical method must be established for their simultaneous identification and quantification. Several methods have been developed for analyzing the four above-mentioned flavorings in various samples. High-performance liquid chromatography (HPLC),[12] liquid chromatography−tandem mass spectrometry (LC-MS/MS),[13] and gas chromatography−mass spectrometry (GC-MS)[14] have been used for the simultaneous analysis of vanillin, ethylvanillin, and coumarin in vanilla extracts. Meanwhile, more attention has been focused on the simultaneous analysis of vanillin and ethylvanillin both in vanilla extracts and in foods, and various methods were investigated including gas chromatography (GC),[15] HPLC,[16,17] capillary electrophoresis (CE),[18,19] chemiluminometry,[20] atmospheric pressure solids analysis probe,[21] and so on. However, there have only HPLC methods been reported for the analysis of methylvanillin in industrial waste waters[22] and food.[23] To the best of the authors' knowledge, there is no paper focused on the simultaneous determination of these four flavorings in any samples.

Recently, we proposed a sufficient LC-MS/MS method for the simultaneous determination of vanillin, ethylvanillin, and coumarin in infant formula samples,[24] but methylvanillin was unnoticed. Except for LC-MS/MS, gas chromatography−tandem mass spectrometry (GC-MS/MS) has become one of the most widely used methods for the identification and quantification of residues in food because of its higher selectivity, sensitivity, and necessity for confirmation.[25−27] Therefore, in this study we developed a GC-MS/MS method for the simultaneous determination of vanillin, methylvanillin, ethylvanillin, and coumarin in infant formula samples, and this is the first trial performed for this objective.

## MATERIALS AND METHODS

**Chemicals.** Certified standards of vanillin (CAS Registry No. 121-33-5, 99.9% purity) and ethylvanillin (CAS Registry No. 121-32-4, 97.3% purity) were purchased from Chroma Dex (Irvine, CA, USA). Coumarin (CAS Registry No. 91-64-5, 98% purity) was purchased from Dr. Ehrenstorfer GmbH (Augsburg, Germany). Methylvanillin (CAS Registry No. 120-14-9, 98.0% purity), methylvanillin-$^{13}C$ (CAS Registry No. 1173022-44-0, 98.0% purity), vanillin-$^{13}C_6$ (CAS Registry No. 201595-58-6, 98%), and coumarin-$D_4$ (CAS Registry No. 185056-83-1, 98%) were purchased from Toronto Research Chemicals Inc. (North York, Canada). The structures of these standards are shown in Figure 1. The water used was purified with a Milli-Q water purification system from Millipore (Bedford, MA, USA). HPLC grade methanol was obtained from Merck (Darmstadt, Germany).

**Preparation of Standard Solutions.** Individual standard stock solutions were prepared at a concentration of 500 mg $L^{-1}$ in methanol and stored at 4 °C in the dark. A multistandard mixture working solution, containing 5 mg $L^{-1}$ of each standard compound, was prepared by diluting each above stock solution with methanol and was then used for spiking blank infant formula samples and for preparation of matrix-matched calibration solutions. Matrix-matched calibration standards with six final concentration levels of 0.001, 0.002, 0.005, 0.01, 0.02, and 0.05 mg $L^{-1}$ were prepared by adding to infant formula blank extracts appropriate volumes of the standard working solutions.

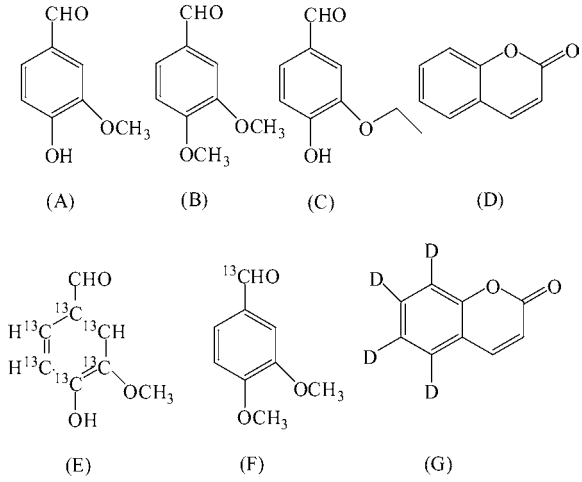


**Figure 1.** Chemical structures of vanillin (A), methylvanillin (B), ethylvanillin (C), coumarin (D), vanillin-$^{13}C_6$ (E), methylvanillin-$^{13}C$ (F), and coumarin-$D_4$ (G).

Vanillin-$^{13}C_6$, methylvanillin-$^{13}C$, and coumarin-$D_4$ were used as internal standards, and the final concentration was 0.01 mg $L^{-1}$.

**Sample Preparation.** Twenty infant formula samples for 0−12-, 6−12-, and 6−18-month-old babies were randomly purchased from local supermarkets, and the brands covered both Chinese domestic brands and foreign brands. Sample preparation was based on a previously reported process developed by our group[24] with few adaptations. A 1.00 g infant formula sample was weighed into a 50 mL polypropylene centrifuge tube. Before the addition of 25 mL of methanol/water (v/v, 1:1) for extraction, 500 μL of vanillin-$^{13}C_6$, methylvanillin-$^{13}C$, and coumarin-$D_4$ mixed internal standards solution (0.4 mg $L^{-1}$) was first added. The sample was vortexed for 1 min, and then an ultrasonic extraction was performed for 30 min at 30 °C. After extraction, the suspension was centrifuged at 8875*g* for 15 min, and then the supernatant layer was transferred into a 50 mL volumetric flask and diluted with water. This extract was then forwarded to the next cleanup procedure.

**Solid-Phase Extraction.** The cleanup procedure based on a solid-phase extraction was also referenced to our previous paper.[24] An Oasis HLB solid phase extraction (SPE) cartridge (60 mg, 3 mL, Waters, Milford, MA, USA) was used and conditioned with 5 mL of methanol and then 5 mL of water before use. Five milliliters of sample extracting solution was then introduced to the conditioned cartridge and allowed to elute by gravity. The cartridge was washed with 5 mL of pure water, followed by 5 mL of a methanol/water (v/v, 1:9) mixture, and then dried under vacuum for 1 min. Finally, the cartridge was eluted with 6 mL of methanol into a glass culture tube, and the eluate was evaporated to dryness under vacuum at 45 °C. The dried extract was reconstituted in 2.0 mL of methanol, vortex mixed for 60 s, and then filtered through a 0.22 μm nylon membrane into a glass GC vial ready for analysis.

Blank infant formula samples were prepared in the same way as mentioned above without the addition of the internal standard solution. The matrix-matched standard solutions were prepared from the blank extracts as mentioned earlier.

**GC-MS/MS Analysis.** A Thermo Fisher Trace 1300 GC coupled with a Thermo Fisher TSQ 8000 triple-quadrupole mass spectrometer and a Triplus RSH autosampler (Thermo Fisher Scientific, Waltham, MA, USA) was used in the GC-MS/MS system. The separation of analytes was performed on a Thermo Scientific TG-SQC 15 m × 0.25 mm × 0.25 μm capillary column. Splitless injection mode was used, and the injection volume was 1.0 μL. The GC oven temperature program was as follows: initial at 80 °C, held for 1 min, increased to 200 °C at a rate of 30 °C $min^{-1}$, then increased to 280 °C at a rate of 15 °C $min^{-1}$, and held for 5 min. The injector temperature was set at 250 °C. Helium (99.9999% purity) was used as carrier gas at a constant flow rate of 1.0 mL $min^{-1}$ and Argon (99.999% purity) was

Table 1. Analytical Conditions for MS/MS (Thermo Fisher TSQ 8000 Triple-Quadrupole Mass Spectrometer, Waltham, MA, USA)

| compound | retention time (min) | parent ion ($m/z$) | product ion ($m/z$) | collision energy (eV) | ratio of abundance (qualitative/quantitative) |
|---|---|---|---|---|---|
| vanillin | 6.10 | 152.0 | 123.0[a] | 20 | 24 |
| | | | 109.0 | 18 | |
| ethylvanillin | 6.23 | 166.0 | 137.0[a] | 15 | 21 |
| | | | 109.0 | 25 | |
| vanillin-$^{13}C_6$ | 6.10 | 158.0 | 129.0[a] | 20 | 23 |
| | | | 115.0 | 20 | |
| methylvanillin | 6.53 | 166.0 | 95.0[a] | 15 | 138 |
| | | | 137.0 | 18 | |
| methylvanillin-$^{13}C$ | 6.53 | 167.0 | 95.0[a] | 15 | 104 |
| | | | 137.0 | 18 | |
| coumarin | 6.55 | 146.0 | 118.0[a] | 10 | 17 |
| | | | 90.0 | 23 | |
| coumarin-$D_4$ | 6.54 | 150.0 | 122.0[a] | 10 | 20 |
| | | | 94.0 | 25 | |

[a]The MS/MS transition was used for quantitation.

used as collision gas in the ion trap chamber of the MS/MS system. The mass spectrometer was operated in electron ionization (EI) mode. The ion source and transfer line temperatures were set at 250 and 280 °C, respectively. Retention times of the four flavorings were detected in full scan mode by recording the mass range between $m/z$ 50 and 300. For the determination of target analytes, MS/MS mode was selected and performed in selected reaction monitoring (SRM) mode.

## RESULTS AND DISCUSSION

**Optimization of MS/MS Conditions.** For the unambiguous identification and accurate quantification of vanillin, methylvanillin, ethylvanillin, and coumarin in real infant formula samples at trace levels, MS/MS conditions were optimized. First, individual flavoring and isotope-labeled standards were performed in full scan mode separately in the $m/z$ 50−300 scan range to identify the optimal precursor ions. Molecular ions present in all seven target substances appeared and were selected as the parent ions beyond doubt. High masses were preferred as the precursor ions because it could avoid interferences from isobaric masses resulting from common molecule fragments.[28] Once the precursor ions were chosen, the MS/MS conditions were further optimized to obtain maximum resolution and sensitivity. The collision energies with different values between 10 and 30 eV were applied to find the two most abundant fragments for further qualitative and quantitative intentions. The dwell time was 200 ms for each compound, and the optimal collision energies for each transition are listed in Table 1. Moreover, one precursor ion and two daughter ions were applied, which well fitted the European Union (EU) criteria.[29] Although the precursor ions of methylvanillin and ethylvanillin were the same due to their completely same molecular formula, their daughter ions were different due to their different chemical structures. This permitted their separate recognition even if insufficient GC separation was encountered.

A complete SRM chromatogram of a real blank infant formula sample spiked with 10 $\mu g\ kg^{-1}$ of four flavorings and three isotopic labels is shown in Figure 2. It was observed that vanillin, methylvanillin, and ethylvanillin were well separated, whereas methylvanillin and coumarin had almost the same retention time from 6.5 to 6.6 min. However, in SRM mode, they could be unambiguously identified without any question. In the MS/MS analysis mode, the target was initially identified by the retention time and typical SRM transitions and then further confirmed by the relative ion abundance ratio between the qualitative ion and the quantitative ion (shown in Table 1). Meanwhile, a clean background was obtained in spiked sample analysis as shown in Figure 2, which indicated that no chromatographic interference occurred from the sample matrix.

The GC-MS/MS product scan spectra of the investigated compounds were obtained and are shown in Figure 3. Moreover, on the basis of the fragment information given by Figure 3, plausible interpretation of the MS/MS fragmentation was proposed and is presented in Figure 4. Note that we have interpreted the MS/MS fragmentation of vanillin, vanillin-$^{13}C_6$, ethylvanillin, coumarin, and coumarin-$D_4$ obtained in HPLC-MS/MS using a positive electrospray ionization (ESI) mode in our earlier study.[24] The obviously different cracking behavior was noted for all compounds, and this might be attributed to the different ionization mode. At this point, there is no related reported work as reference.

**Method Validation.** To investigate the applicability of the developed method for routine real analysis, general analytical merits including linearity, limits of quantification (LOQ), specificity, precision, and accuracy (recovery) were detected.

Matrix effects, expressed as suppression or enhancement of instrument signals, have been generally recognized as an important and serious error source in the quantitative analysis of trace-level compounds in food samples by using either the GC-MS/MS or LC-MS/MS method.[30−32] In our previous trial on analysis flavorings in infant formula by LC-MS/MS,[24] the matrix effects were discussed and verified by contrastive experiments. To correct matrix effects, a combination of isotope-labeled internal standards and matrix-matched calibration solutions was performed, and satisfactory results were obtained.

Quantification was performed on the basis of calibration plots using the peak area of the most intense MS/MS transition of the analyte, which was defined as the quantitative ion shown in Table 1. The calibration curves with $1/x$ weighting were plotted for each individual target compound, and the response data were adjusted according to the relative ratios of responses to the stable isotope internal standards in the standards. Good linearity was achieved, and the correlation coefficients were in the range from 0.9991 to 0.9995. The LOQ was calculated as 10 times the standard deviation, and it was 10.0 $\mu g\ kg^{-1}$ for vanillin, methylvanillin, ethylvanillin, and coumarin. For vanillin

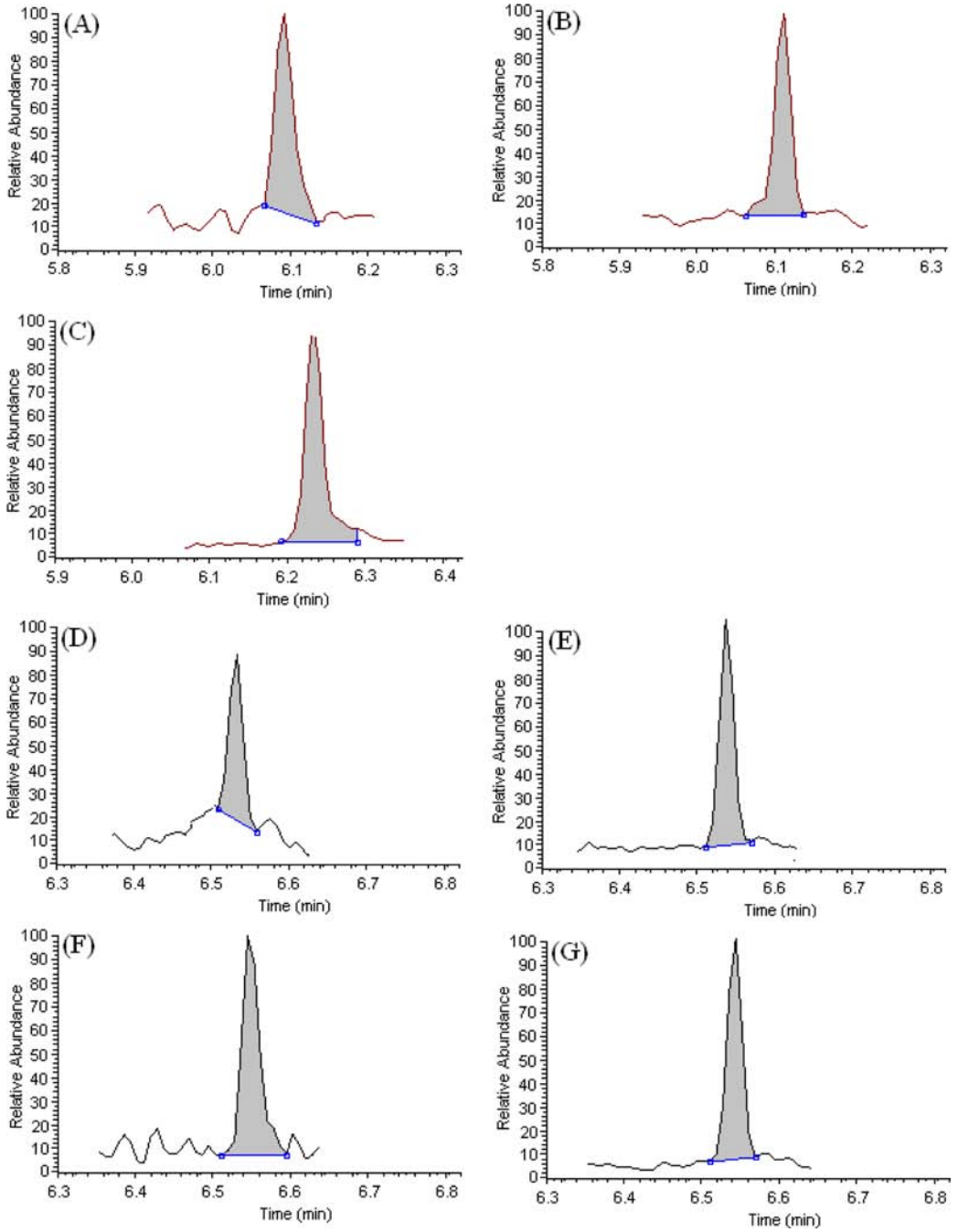


**Figure 2.** GC-MS/MS SRM chromatograms of a blank infant formula sample spiked at 10 $\mu$g kg$^{-1}$ with four flavorings: vanillin (A); vanillin-$^{13}C_6$ (B); ethylvanillin (C); methylvanillin (D); methylvanillin-$^{13}C$ (E); coumarin (F); coumarin-$D_4$ (G).

and ethylvanillin, which are permitted to be added to follow-up formula (for >6-month-old infants and children) in China with maximum usage amount of 5 mg/100 mL, the LOQ is available without any doubt. According to the general average use instructions of infant formula, there are approximatly 13−17 g of milk powder contained in 100 mL of ready-to-use liquid nutrition for babies; thus, a vanillin or ethylvanillin content of 294−385 mg kg$^{-1}$ in powder samples (average 333 mg kg$^{-1}$) complies with the regulations of China's usage limit. For coumarin, the LOQ of 10.0 $\mu$g kg$^{-1}$ is also far below the limit of 2 mg kg$^{-1}$ set by Codex Alimentarius and the EU. This indicated that this method is suitable for analysis of these flavoring agents in infant formula samples.

To evaluate the specificity of the developed method, 10 different blank infant formula samples were investigated. No interfering peaks from endogenous compounds of sample extracts were observed at or near the retention times of all target analytes, indicative of the specificity of the method.

To evaluate the precision of this method, both intraday and interday repeatabilities were examined by determination of a fortified sample at three different concentrations (low, medium, and high) at 10, 50, and 100 $\mu$g kg$^{-1}$. Good stability and satisfactory repeatability were achieved, and the relative standard deviation (RSDs) values were <3.62%.

The method accuracy was evaluated by analyzing series of fortified spiking samples using the developed method. The

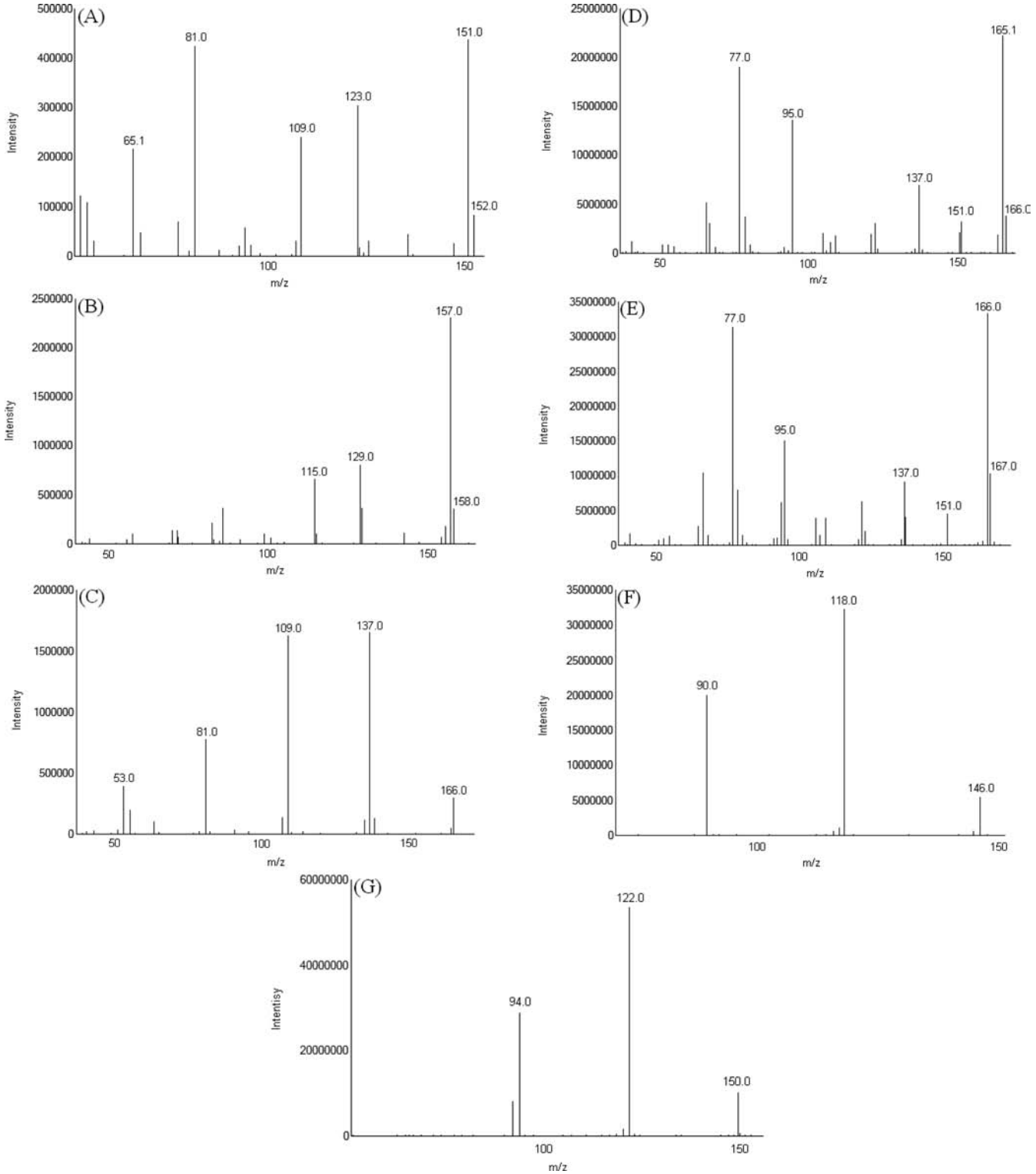


**Figure 3.** GC-MS/MS product scan spectrum of vanillin (A), vanillin-$^{13}C_6$ (B), ethylvanillin (C), methylvanillin (D), methylvanillin-$^{13}C$ (E), coumarin (F), and coumarin-$D_4$ (G). Collision energy (eV): A, 20; B, 20; C, 15; D, 15; E, 15; F, 10; G, 10.

appropriate amounts of the standard target compounds were spiked into the "blank" infant formula samples and given at three final concentration levels of 10, 50, and 100 $\mu g\ kg^{-1}$. The spiked samples were treated following the same procedure as mentioned and determination by GC-MS/MS. Average recoveries ranging within 82.8−107.5% (Table 2) were achieved, and RSDs were <8.9%, indicative of the good recovery and precision of the method.

**Application to Real Samples.** Twenty infant formula samples were purchased from local supermarkets and analyzed following the proposed method, and the blanks were periodically run during the sample analysis sequence to confirm the absence of contamination. Neither ethylvanillin nor


dx.doi.org/10.1021/jf5013083 | J. Agric. Food Chem. 2014, 62, 10881−10888

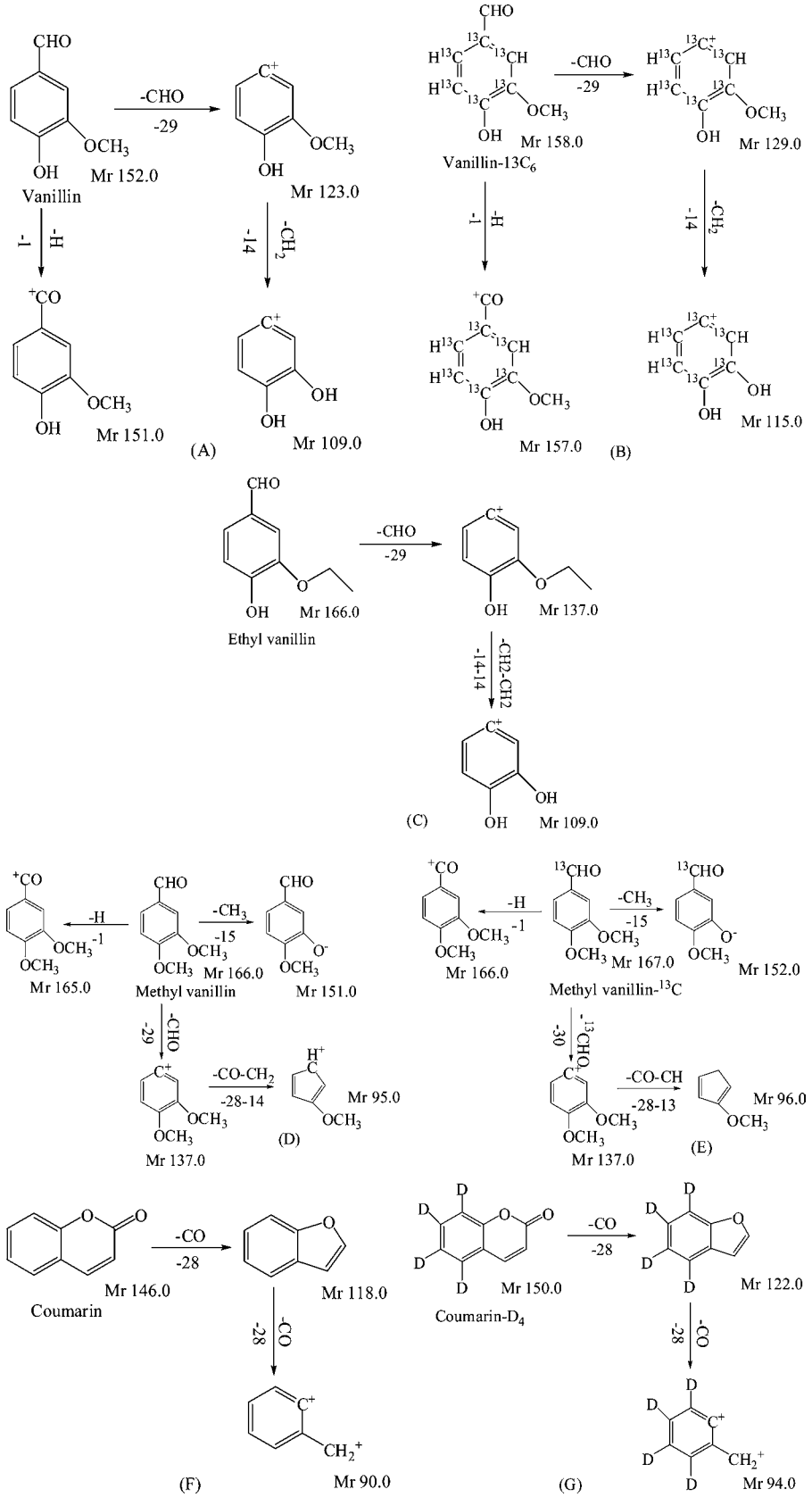


**Figure 4.** Proposed fragmentation pattern with tentative structures for the product ions of vanillin (A), vanillin-$^{13}C_6$ (B), ethylvanillin (C), methylvanillin (D), methylvanillin-$^{13}C$ (E), coumarin (F), and coumarin-$D_4$ (G).

coumarin was detected in any sample, whereas vanillin was detected at concentration levels ranging from 2.4 to 706.8 mg $kg^{-1}$ in four samples; these results were highly consistent with our previous study using the LC-MS/MS method.[24] At the


dx.doi.org/10.1021/jf5013083 | J. Agric. Food Chem. 2014, 62, 10881−10888

**Table 2. Mean Recoveries and Repeatability of the Developed Method at Three Concentration Levels with LOQs ($n$ = 6)**

| compound | spiking level ($\mu$g kg$^{-1}$) | recovery (%) | RSD (%) | LOQ ($\mu$g kg$^{-1}$) |
|---|---|---|---|---|
| vanillin | 10 | 82.8 | 5.8 | 10 |
| | 50 | 88.5 | 4.2 | |
| | 100 | 94.3 | 3.6 | |
| methylvanillin | 10 | 87.3 | 4.9 | 10 |
| | 50 | 92.6 | 4.1 | |
| | 100 | 107.5 | 3.5 | |
| ethylvanillin | 10 | 85.1 | 5.6 | 10 |
| | 50 | 90.6 | 3.8 | |
| | 100 | 93.4 | 3.3 | |
| coumarin | 10 | 88.6 | 8.9 | 10 |
| | 50 | 93.8 | 6.4 | |
| | 100 | 105.2 | 3.7 | |

same time, methylvanillin was detected at concentration levels ranging from 0.78 to 0.94 mg kg$^{-1}$ in three samples. The detailed results are summarized in Table 3, and the SRM chromatograms of a real positive sample are shown in Figure 5. Vanillin was considered as being added intentionally to the four vanillin-positive samples because the concentration is high. Especially the sample containing 706.8 mg kg$^{-1}$ vanillin, according to previous analysis on Chinese vanillin usage limit, is certainly against China's national standard. These samples should be a matter of concern when applied to infants and even children. Meanwhile, the occurrence of methylvanillin was considered as being contaminated during the production process and not added intentionally, because its concentrations were so small that it could not effectively act as a flavoring ingredient.

**Table 3. Content of Vanillin and Methylvanillin in Infant Formula Samples ($n$ = 3)**

| | vanillin | | methylvanillin | |
|---|---|---|---|---|
| sample | content[a] | RSDs (%) | content[a] | RSDs (%) |
| 1 | 2.4 | 2.5 | 0.85 | 2.8 |
| 2 | 32.6 | 2.1 | 0.78 | 3.1 |
| 3 | 80.3 | 2.3 | 0.94 | 2.4 |
| 4 | 706.8 | 1.8 | *b* | |

[a]Content in mg kg$^{-1}$. Ethylvanillin and coumarin were below LOQ. [b]Contents were below LOQ.

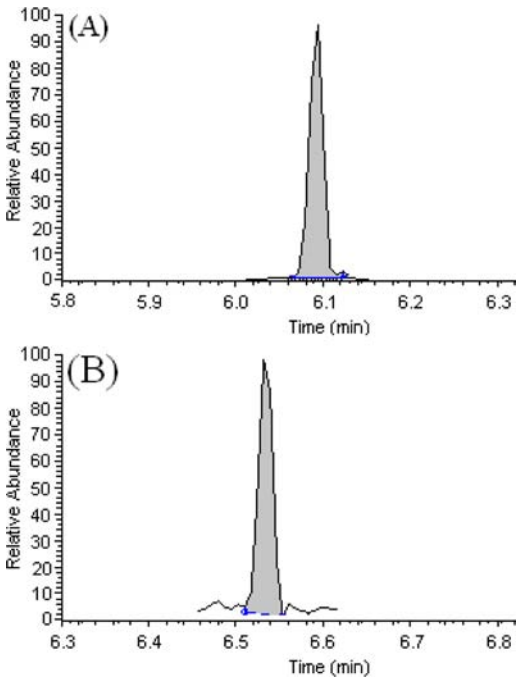


**Figure 5.** SRM chromatograms of a real positive sample: vanillin (A); methylvanillin (B).

The developed method allows the simple, rapid, and sensitive determination of four flavorings in infant formula samples. The method showed good recoveries (82.8−107.5%) and precision (RSDs < 8.9%) and could be applied for the unequivocal simultaneous identification and quantification of target analytes in complex formula samples.

## AUTHOR INFORMATION


### Corresponding Authors

*(Y.S.) Phone: 86-577-88373937. Fax: 86-577-88373937. E-mail: shenyan@wzu.edu.cn.

*(C.H.) E-mail: chaohan96@hotmail.com.



### Funding

Financial support from the Science Technology Department of Zhejiang Province (2013C37065), NSFC (21207102), AQSIQ (2009IK172), and Wenzhou Municipal Science and Technology Bureau project (2013G0007) is gratefully acknowledged.


### Notes

The authors declare no competing financial interest.

## REFERENCES


(1) The Japan Food Chemical Research Foundation. *Japan's Specifications and Standards for Food Additives*, 7th ed.; The Ministry of Health and Welfare: Tokyo, Japan, 2000; http://www.ffcr.or.jp/zaidan/FFCRHOME.nsf/pages/list-desin.add-x (updated to June 18, 2014).

(2) Center for Food Safety and Applied Nutrition. *Everything Added to Food in the United States (EAFUS): A Food Additive Database*; U.S. Food and Drug Administration; http://www.usc.es/caa/EdulcWeb/EAFUS.pdf.

(3) GB 2760-2011, National food safety standard, standard of using food additives; Ministry of Health: People's Republic of China, 2011.

(4) Nia, Y. N.; Zhang, G. W.; Kokot, S. Simultaneous spectrophotometric determination of maltol, ethyl maltol, vanillin and ethyl vanillin in foods by multivariate calibration and artificial neural networks. *Food Chem.* **2005**, *89*, 465−473.

(5) Hazleton, L. W.; Tusing, T. W.; Zeitlin, B. R.; Thiessen, R.; Murer, H. K. Toxicity of coumarin. *J. Pharmacol. Exp. Ther.* **1956**, *118*, 348−358.

(6) *Code of Federal Regulations*, Title 21 Part 189.130; Government Printing Office: Washington, DC, USA, 2006

(7) Codex alimentarius. General requirements for natural flavourings (CAC/GL 29.1987), 1985; www.codexalimentarius.net (accessed Nov 28, 2007).

(8) European Council. Council Directive (EEC) No. 88/388 on the approximation of the laws of the Member States relating to flavourings for use in foodstuffs and to source materials for their production. *Off. J. Eur. Communities* **1998**, *L184*, 61−66.

(9) Sproll, C.; Ruge, W.; Andlauer, C.; Godelmann, R.; Lachenmeier, D. W. HPLC analysis and safety assessment of coumarin in foods. *Food Chem.* **2008**, *109*, 462−469.

(10) Raters, M.; Matissek, R. Analysis of coumarin in various foods using liquid chromatography with tandem mass spectrometric detection. *Eur. Food Res. Technol.* **2008**, *227*, 637−642.
(11) Thompson, R. D.; Hoffmann, T. J. Determination of coumarin as an adulterant in vanilla flavoring products by high-performance liquid chromatography. *J. Chromatogr. A* **1988**, *438*, 369−382.
(12) Lavine, B. K.; Corona, D. T.; Perera, U. D. N. T. Analysis of vanilla extract by reversed phase liquid chromatography using water rich mobile phases. *Microchem. J.* **2012**, *103*, 49−61.
(13) De Jager, L. S.; Perfetti, G. A.; Diachenko, G. W. Determination of coumarin, vanillin, and ethyl vanillin in vanilla extract products: liquid chromatography mass spectrometry method development and validation studies. *J. Chromatogr. A* **2007**, *1145*, 83−88.
(14) De Jager, L. S.; Perfetti, G. A.; Diachenko, G. W. Comparison of headspace-SPME-GC−MS and LC−MS for the detection and quantification of coumarin, vanillin, and ethyl vanillin in vanilla extract products. *Food Chem.* **2008**, *107*, 1701−1709.
(15) Sostaric, T.; Boyce, M. C.; Spickett, E. E. Analysis of the volatile components in vanilla extracts and flavorings by solid-phase microextraction and gas chromatography. *J. Agric. Food Chem.* **2000**, *48*, 5802−5807.
(16) Lamprecht, G.; Pichlmayer, F.; Schmid, E. R. Determination of the authenticity of vanilla extracts by stable isotope ratio analysis and component analysis by HPLC. *J. Agric. Food Chem.* **1994**, *42*, 1722−1727.
(17) Kahoun, D.; Řezková, S.; Veškrnová, K.; Královský, J.; Holčapek, M. Determination of phenolic compounds and hydroxymethylfurfural in meads using high performance liquid chromatography with coulometric-array and UV detection. *J. Chromatogr. A* **2008**, *1202*, 19−33.
(18) Ohashi, M.; Omae, H.; Hashida, M.; Sowa, Y.; Imai, S. Determination of vanillin and related flavor compounds in cocoa drink by capillary electrophoresis. *J. Chromatogr. A* **2007**, *1138*, 262−267.
(19) Avila, M.; Gonzalez, M. C.; Zougagh, M.; Escarpa, A.; Ríos, A. Rapid sample screening method for authenticity controlling vanilla flavors using a CE microchip approach with electrochemical detection. *Electrophoresis* **2007**, *28*, 4233−4239.
(20) Timotheou-Potamia, M.; Calokerinos, A. C. Chemiluminometric determination of vanillin in commercial vanillin products. *Talanta* **2007**, *71*, 208−212.
(21) Lee, P. J.; Ruel, A. M.; Balogh, M. P. Analysis of vanilla flavoured food products using atmospheric-pressure solids analysis probe. *Agro. Food Ind. Hi-Technol.* **2010**, *21*, 25−28.
(22) Cserháti, T.; Forgfiás, E. Simultaneous determination of 3,4-dimethoxybenzaldehyde and 3,4-dimethoxyphenylacetone in industrial waste waters by high performance liquid chromatography-diode array detection. *J. Chromatogr. A* **1996**, *750*, 257−261.
(23) Kumar, A.; Singh, B.; Malik, A. K. Determination of some aldehydes by using solid-phase microextraction and high-performance liquid chromatography with UV detection. *J. AOAC Int.* **2007**, *90*, 1689−1694.
(24) Shen, Y.; Han, C.; Liu, B.; Lin, Z. F.; Zhou, X. J.; Wang, C. J.; Zhu, Z. O. Determination of vanillin, ethyl vanillin and coumarin in infant formula by liquid chromatography-quadrupole linear ion trap mass spectrometry. *J. Dairy Sci.* **2014**, *97*, 679−686.
(25) Chen, X. S.; Bian, Z. Y.; Hou, H. W.; Yang, F.; Liu, S. S.; Tang, G. L.; Hu, Q. Y. Development and validation of a method for the determination of 159 pesticide residues in tobacco by gas chromatography-tandem mass spectrometry. *J. Agric. Food Chem.* **2013**, *61*, 5746−5757.
(26) Lu, J.; Wu, J.; Stoffella, P. J.; Wilson, P. C. Analysis of bisphenol A, nonylphenol, and natural estrogens in vegetables and fruits using gas chromatography-tandem mass spectrometry. *J. Agric. Food Chem.* **2013**, *61*, 84−89.
(27) Martins, J.; Esteves, C.; Simoes, T.; Correia, M.; Delerue-Matos, C. Determination of 24 pesticide residues in fortified wines by solid-phase microextraction and gas chromatography-tandem mass spectrometry. *J. Agric. Food Chem.* **2011**, *59*, 6847−6855.
(28) Rodríguez-Carrasco, Y.; Berrada, H.; Font, G.; Mañes, J. Multimycotoxin analysis in wheat semolina using an acetonitrile-based extraction procedure and gas chromatography-tandem mass spectrometry. *J. Chromatogr. A* **2012**, *1270*, 28−40.
(29) Commission Decision 2002/657/EC of 12 August 2002, Implementing Council Directive 96/23/EC: concerning the Performance of Analytical Methods and the Interpretation of Results. European Union: Brussels, Belgium, 2002.
(30) Yu, S.; Xu, X. M. Study of matrix-induced effects in multi-residue determination of pesticides by online gel permeation chromatography-gas chromatography/mass spectrometry. *Rapid Commun. Mass Spectrom.* **2012**, *26*, 963−977.
(31) Lehotay, S. J.; Son, K. A.; Kwon, H.; Koesukwiwat, U.; Fu, W.; Mastovska, K.; Hoh, E.; Leepipatpiboon, N. Comparison of QuEChERS sample preparation methods for the analysis of pesticide residues in fruits and vegetables. *J. Chromatogr. A* **2010**, *1217*, 2548−2560.
(32) Niessen, W. M. A.; Manini, P.; Andreoli, R. Matrix effects in quantitative pesticide analysis using liquid chromatography-mass spectrometry. *Mass Spectrom. Rev.* **2006**, *25*, 881−899.

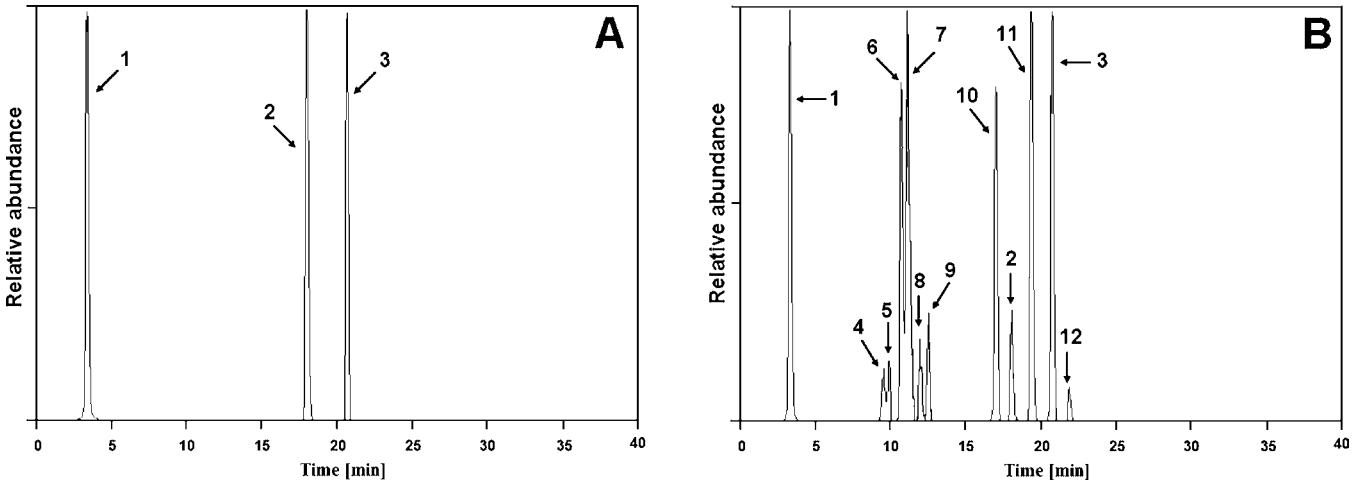


**Figure 1.** Chromatogram of supernatant from blueberry pulp obtained before (A) and after 5 h of thermal processing (B).

**Table 1. Names, Abbreviations, and Peak or Structure Numbers of Estimated 5-*O*-Caffeoylquinic Transformation Products**

| compd name | abbrev | peak no.[a] | structure no.[b] |
|---|---|---|---|
| quinic acid | QA | 1 | 1 |
| 5-*O*-caffeoylquinic acid | 5-CQA | 2 | 2 |
| caffeic acid | CA | 3 | 3 |
| (1*S*,3*R*,4*R*,5*R*)-3-[3-(3,4-dihydroxyphenyl)-3*R*-hydroxypropanoyl]-1,4,5-trihydroxycyclohexanecarboxylic acid | 3-CQA-3*R*-OH | 4 or 5 | 4 |
| (1*S*,3*R*,4*R*,5*R*)-3-[3-(3,4-dihydroxyphenyl)-3*S* -hydroxypropanoyl]-1,4,5-trihydroxycyclohexanecarboxylic acid | 3-CQA-3*S*-OH | 4 or 5 | 5 |
| (1*S*,3*R*,4*R*,5*R*)-5-[3-(3,4-dihydroxyphenyl)-3*R*-hydroxypropanoyl]-1,3,4-trihydroxycyclohexanecarboxylic acid | 5-CQA-3*R*-OH | 6 or 7 | 6 |
| (1*S*,3*R*,4*R*,5*R*)-5-[3-(3,4-dihydroxyphenyl)-3*S*-hydroxypropanoyl]-1,3,4-trihydroxycyclohexanecarboxylic acid | 5-CQA-3*S*-OH | 6 or 7 | 7 |
| (1*S*,3*R*,4*R*,5*R*)-4-[3-(3,4-dihydroxyphenyl)-3*R*-hydroxypropanoyl]-1,3,5,-trihydroxycyclohexanecarboxylic acid | 4-CQA-3*R*-OH | 8 or 9 | 8 |
| (1*S*,3*R*,4*R*,5*R*)-4-[3-(3,4-dihydroxyphenyl)-3*S*-hydroxypropanoyl]-1,3,5,-trihydroxycyclohexanecarboxylic acid | 4-CQA-3*S*-OH | 8 or 9 | 9 |
| 3-*O*-caffeoylquinic acid | 3-CQA | 10 | 10 |
| 4-*O*-caffeoylquinic acid | 4-CQA | 11 | 11 |
| *cis*-5-*O*-caffeoylquinic acid | *cis*-5-CQA | 12 | 12 |

[a]See Figure 1. [b]See Figure 2.

experiments. The same equipment as above was used for this purpose. The solvents were heated for 5 h.

*HPLC Measurements.* Chromatographic measurements were performed using LC/ESI/IT/MS from Finnigan (LCQ Adventage Max) equipped with the ion-trap mass spectrometric system (Thermo-Electron Corp., San Jose, CA, USA) and a diode array detector from Finningan (Surveyer PDA Plus Detector). The column used was a 100 mm × 4.6 mm i.d., 3 $\mu$m, Gemini C18 (Phenomenex, Torrance, CA, USA). Chromatographic separation was performed using gradient elution. Mobile phase A was 25 mM formic acid in water; mobile phase B was 25 mM formic acid in acetonitrile. The gradient program started at 5% B, increasing to 35% for 30 min, next from 35 to 100% B for 5 min, followed by isocratic elution (100% B) for 5 min. The total run time was 40 min at the mobile phase flow rate of 0.4 mL/min.

In each run, PDA spectra in the range of 200−600 nm and MS spectra in the range of $m/z$ 100−1000 were collected continuously. SIM function was used to better visualize the chromatographic separation and to remove the signal connected with the interfering components of the blueberry pulp. The time periods and monitored ions were as follows: 0−9 min, $m/z$ 191; 9−15 min, $m/z$ 371; 15−20 min, $m/z$ 353; 20−21.5 min, $m/z$ 179; 21.5−40 min, $m/z$ 353.

The column effluent was ionized by electrospray (ESI). The ESI needle potential was 4.5 kV in the negative ionization mode. To identify the chlorogenic acid isomers and the chlorogenic acid transformation products, the functions of secondary ($MS^n$) ion fragmentation were applied. The collision energy was chosen individually for each group of the examined compounds.

To identify 5-*O*-caffeoylquinic acid derivatives in the examined samples, LC/ESI/TOF/MS analysis was additionally performed. LC/ESI/TOF/MS analysis was carried out on the Agilent (Agilent Technologies, Palo Alto, CA, USA) liquid chromatography system. MS analysis was performed on the orthogonal TOF/MS equipped with an electrospray interface (Agilent Technologies, Santa Clara, CA, USA). Negative mode using full scan mode in TOF/MS analysis was applied, and the mass range was set at 100−600 Da. Chromatographic separation was performed using the same chromatographic column and the same gradient elution as described for LC/ESI/IT/MS analysis.

Due to the lack of standards of CQA isomers and their hydroxyl derivatives, the amounts of these compounds were calculated by relating their chromatographic responses to the calibration curve for 5-CQA. Quantitative evaluations of all examined compounds were performed on the basis of the signal from the MS detector.

## RESULTS AND DISCUSSION

Figure 1 presents the chromatogram of supernatant from blueberry pulp obtained before (Figure 1A) and after 5 h of thermal processing (Figure 1B). As seen in Figure 1A, the supernatant from unprocessed blueberries contains three main components: 5-CQA and quinic and caffeic acid. They are all known as the main components of blueberries,[11] but they additionally were confirmed on the basis of retention coefficients of their standards and MS and PDA spectra. As shown in Figure 1B, the supernatant from the processed blueberries contains, besides the parent substances, nine additional components formed as a result of 5-CQA transformation and degradation: hydroxyl derivatives of 3-CQA, peaks 4 and 5; hydroxyl derivatives of 5-CQA, peaks 6 and 7; hydroxyl derivatives of 4-CQA, peaks 8 and 9; 3-CQA, peak 10; 4-CQA,

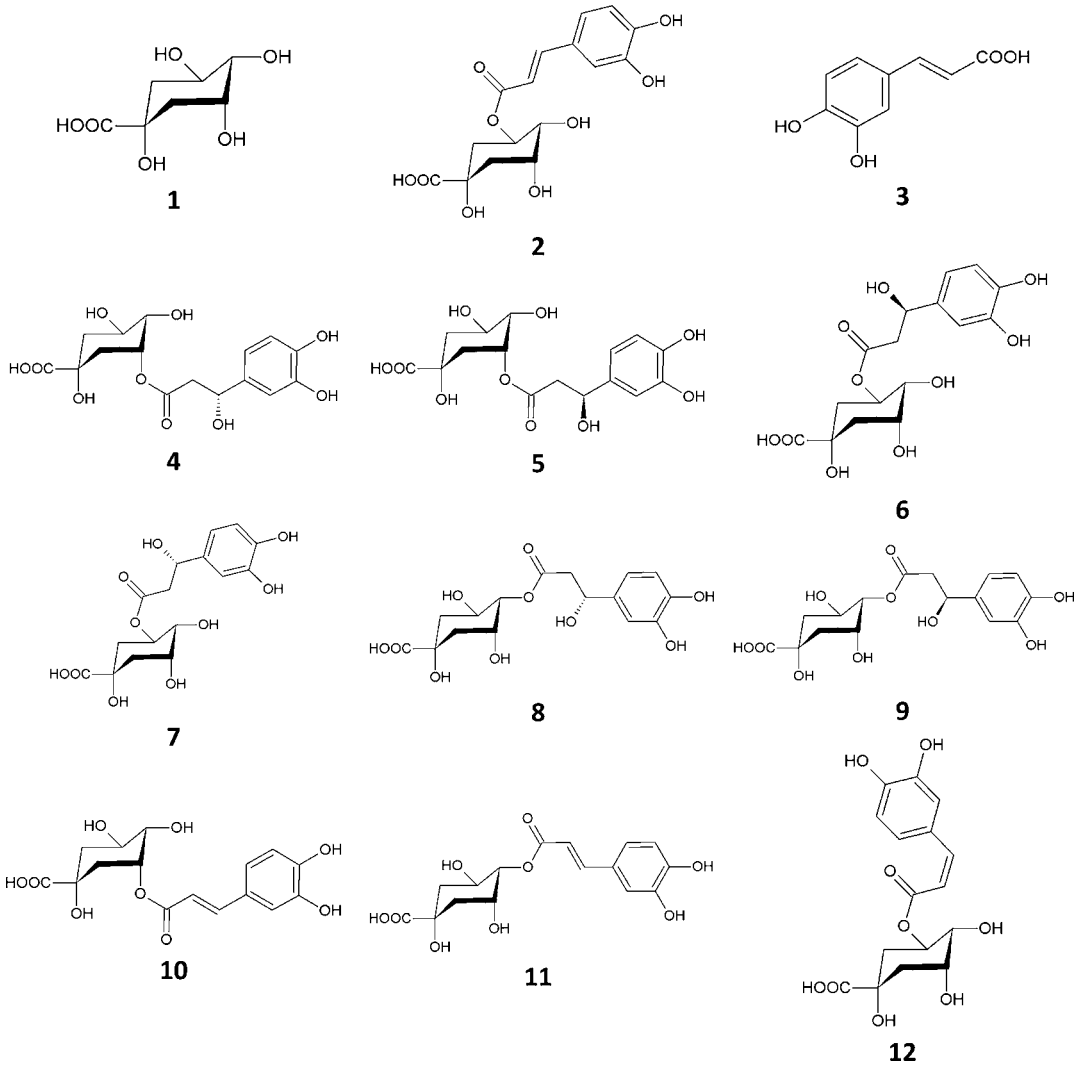


**Figure 2.** Molecular structures of 5-CQA and its transformation products identified in blueberry pulp before and after thermal processing.

peak 11; and *cis*-5-CQA, peak 12. Their presence was identified and confirmed by the PDA, $MS^n$,[10,12,13] and HRMS data. All of these components were reported earlier as transformation and degradation products of 5-CQA in buffered 5-CQA solution,[10] so it turns out that the 5-CQA transformation and degradation in thermally processed blueberry pulp is almost the same as its transformation in the model system. The matrix components have no impact on the process.

For clarity, the names of all the identified compounds, their peak and structure numbers, abbreviations, and chemical structures are collected in Table 1 and graphically presented in Figure 2. The $MS^n$ and HRMS data for the compounds are collected in Tables 2 and 3. To eliminate the concentration differences resulting from the presence of sucrose in the examined samples, the amounts of 5-CQA and its transformation products were recalculated and related to the mass of pure fresh blueberry pulp.

The influence of heating time of the blueberry pulp on the amount of individual formed components is presented in Figures 3−5. Each figure contains three curves. The dash-dotted line corresponds to the processed pulp without sucrose addition, whereas the dotted line and dashed line are the relationships for blueberry pulps with added sucrose at two concentration levels (10 and 30%, respectively). The presented relationships

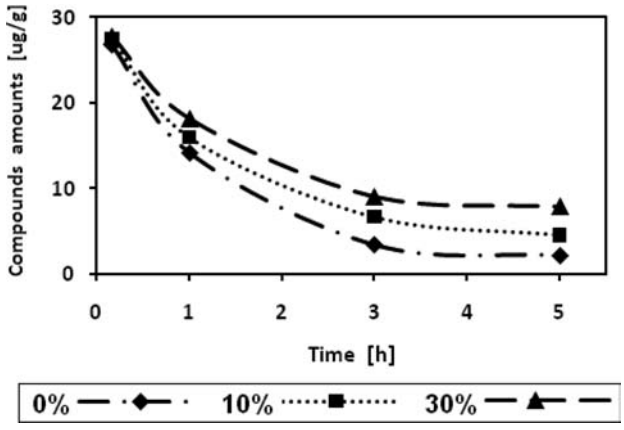


**Figure 3.** Influence of time and sucrose concentration on the amount of 5-CQA in blueberry pulp during its thermal processing.

show the following: (i) The concentration of 5-CQA decreases in the pulp (see Figure 3). This behavior is obvious as 5-CQA is a precursor to other already described products. Significantly, the 5-CQA transformation process was the quickest in the blueberry pulp containing no sucrose. (ii) The concentrations of CQA isomers (3- and 4-CQA), their hydroxyl derivatives


dx.doi.org/10.1021/jf503993q | J. Agric. Food Chem. 2014, 62, 10889−10895

**Table 2. Negative Ion MS$^n$ Data for 5-*O*-Caffeoylquinic Acid and Product of Its Transformation**

| | MS$^1$ | MS$^2$ | | | MS$^3$ | | | | MS$^4$ | | | | |
|---|---|---|---|---|---|---|---|---|---|---|---|---|---|
| | parent ion | base peak | secondary peak | | parent ion | base peak | secondary peak | | parent ion | base peak | secondary peak | | |
| peak no. | $m/z$ | $m/z$ | $m/z$ | intensity (%) | $m/z$ | $m/z$ | $m/z$ | intensity (%) | $m/z$ | $m/z$ | $m/z$ | intensity (%) | compd |
| 1 | 191.2 | 127.1 | 85.1 | 9.1 | | | | | | | | | QA |
| | | | 93.1 | 44.3 | | | | | | | | | |
| | | | 173.2 | 33.3 | | | | | | | | | |
| 2 | 352.9 | 191.1 | 179.2 | 6.6 | 191.1 | 127.2 | 85.1 | 9.5 | | | | | 5-CQA |
| | | | | | | | 93.2 | 47.7 | | | | | |
| | | | | | | | 173.3 | 26.6 | | | | | |
| 3 | 179.2 | 135.2 | | | | | | | | | | | CA |
| 4 | 371.1 | 352.9 | 179.1 | 5.2 | 352.8 | 191.1 | 135.1 | 18.1 | 191.1 | 127.1 | 85.1 | 8.2 | 3-CQA-3*R*-OH or 3-CQA-3*S*-OH |
| | | | | | | | 173.2 | 4.0 | | | 93.1 | 49.4 | |
| | | | 191.2 | 5.7 | | | 179.2 | 78.8 | | | 173.3 | 31.5 | |
| 5 | 371.2 | 352.8 | 179.1 | 5.1 | 352.9 | 191.1 | 135.2 | 25.5 | 191.1 | 127.1 | 85.2 | 8.9 | 3-CQA-3*R*-OH or 3-CQA-3*S*-OH |
| | | | 191.1 | 6.2 | | | 173.2 | 3.3 | | | 93.1 | 53.7 | |
| | | | | | | | 179.2 | 86.4 | | | 173.2 | 28.5 | |
| 6 | 371.2 | 352.9 | 191.1 | 5.2 | 352.9 | 191.1 | 179.2 | 8.4 | 191.1 | 127.1 | 85.1 | 7.5 | 5-CQA-3*R*-OH or 5-CQA-3*S*-OH |
| | | | | | | | | | | | 93.1 | 43.9 | |
| | | | | | | | | | | | 173.2 | 38.5 | |
| 7 | 371.1 | 352.8 | 191.2 | 5.7 | 352.8 | 191.2 | 179.1 | 7.4 | 191.1 | 127.1 | 85.2 | 8.8 | 5-CQA-3*R*-OH or 5-CQA-3*S*-OH |
| | | | | | | | | | | | 93.2 | 43.1 | |
| | | | | | | | | | | | 173.1 | 36.3 | |
| 8 | 371.1 | 352.9 | 173.2 | 5.5 | 352.9 | 179.1 | 135.2 | 8.4 | 179.1 | 135.1 | | | 4-CQA-3*R*-OH or 4-CQA-3*S*-OH |
| | | | | | | | 173.2 | 84.2 | | | | | |
| | | | 179.2 | 6.3 | | | 191.1 | 16.7 | | | | | |
| 9 | 371.1 | 352.9 | 173.2 | 5.7 | 352.9 | 179.2 | 135.3 | 7.9 | 179.1 | 135.2 | | | 4-CQA-3*R*-OH or 4-CQA-3*S*-OH |
| | | | | | | | 173.2 | 82.4 | | | | | |
| | | | 179.2 | 5.2 | | | 191.2 | 16.7 | | | | | |
| 10 | 352.8 | 191.2 | 135.2 | 20.5 | 191.2 | 127.1 | 85.2 | 8.1 | | | | | 3-CQA |
| | | | 173.3 | 3.6 | | | 93.2 | 44.4 | | | | | |
| | | | 179.2 | 86.9 | | | 173.1 | 32.3 | | | | | |
| 11 | 352.9 | 179.1 | 135.3 | 10.2 | 179.2 | 135.2 | | | | | | | 4-CQA |
| | | | 173.1 | 85.5 | | | | | | | | | |
| | | | 191.1 | 23.6 | | | | | | | | | |
| 12 | 352.8 | 191.1 | 179.1 | 9.1 | 191.1 | 127.1 | 85.2 | 13.2 | 127.1 | 85.1 | | | *cis*-5-CQA |
| | | | | | | | 93.1 | 58.4 | | | | | |
| | | | | | | | 173.2 | 48.8 | | | | | |

(3- and 4-CQA-OH), and CQA hydrolysis products (QA and CA) increase (see Figure 4). The amounts of QA and CA formed are similar, which agrees with the reaction stoichiometry of 5-CQA hydrolysis. The concentration increase of 3- and 4-CQA-3R/S-OH is consistent with the concentration increase of their precursors, 3- and 4-CQA. In contrast to 5-CQA, the increase of sucrose concentration slows the speed of the formation of these compounds. (iii) The initial increase of the amount of *cis*-5-CQA and hydroxylated 5-CQA derivates (5-CQA-3*R*-OH and 5-CQA-3*S*-OH) is followed by the decrease of their amount (see Figure 5). This shape of the relationships, most evident for *cis*-5-CQA, can be explained by the simultaneous occurrence of two competitive reactions: the formation and degradation of the transformation products. For this group of components, as for the components mentioned previously, the sucrose concentration increase slows the speed of their formation.

The comparative analysis of the presented results and those obtained for 5-CQA transformation in artificial systems[10] leads to the conclusion that the transformation of this acid in the processed blueberry pulp is very similar to that occurring in acidic


dx.doi.org/10.1021/jf503993q | *J. Agric. Food Chem.* 2014, 62, 10889−10895

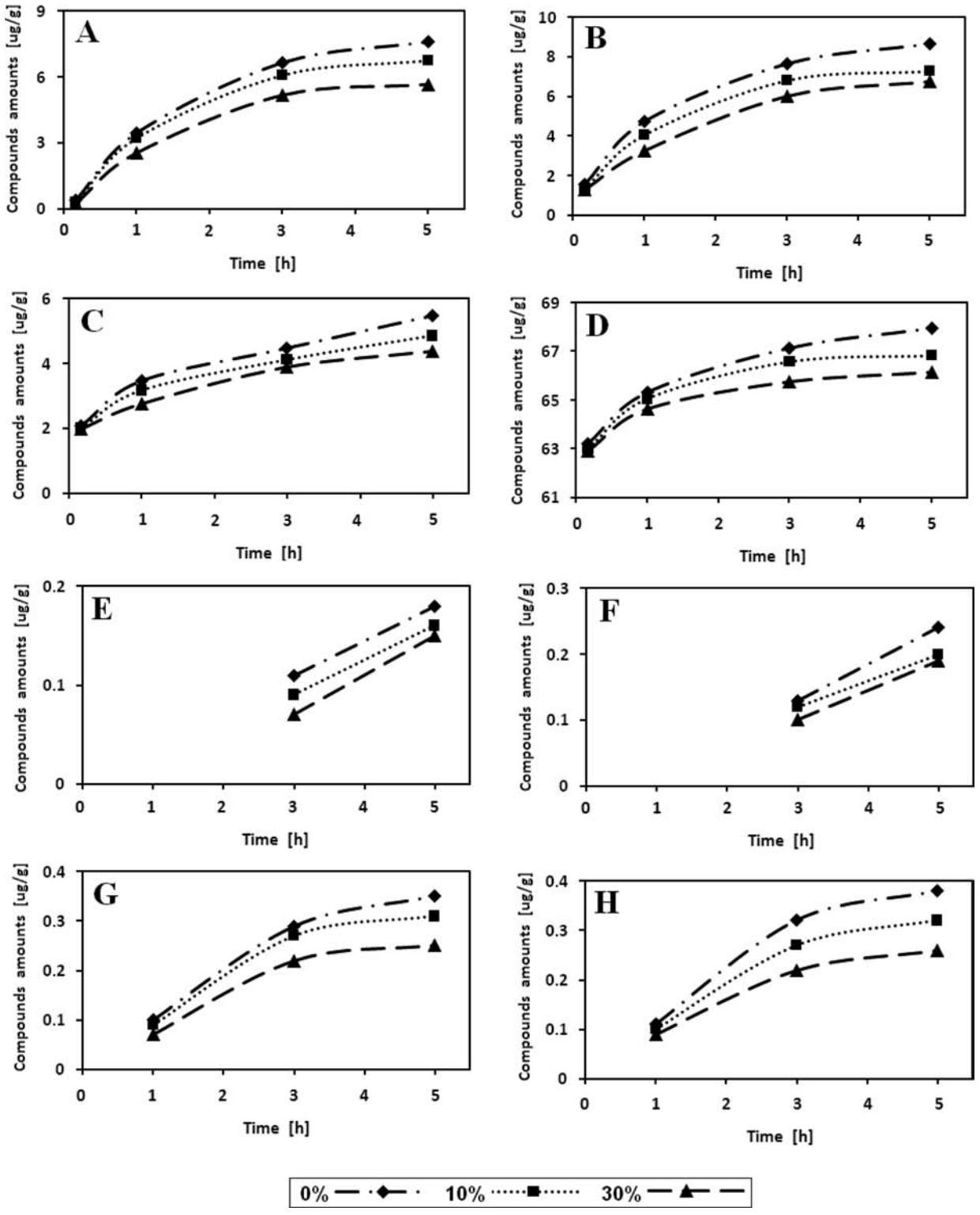


**Figure 4.** Influence of time and sucrose concentration on the amount of 3-CQA (A), 4-CQA (B), CA (C), QA (D), 3-CQA-3*R*-OH (E, F), 3-CQA-3*S*-OH (E, F), 4-CQA-3*R*-OH (G, H), and 4-CQA-3*S*-OH (G, H) forming in blueberry pulp during its thermal processing.

water solution.[10] The experiments concerning 5-CQA transformation in water solution have revealed a larger number of 5-CQA transformation and degradation products[10] than those in the processed blueberries, but the absence of some 5-CQA transformation products in blueberry pulp probably results from the significantly lower concentration level of 5-CQA in the processed fruits than in the previously reported experiments.[10]

Slow transformation and degradation of 5-CQA in the presence of sucrose is the most striking result. To confirm this finding, the transformation of 5-CQA in water solution with and without the addition of sucrose was examined. The experiments were performed using a 5-CQA water solution containing a similar amount of the acid in 1 mL of solvent to 1 g of blueberry pulp. The results of these experiments are collected in Table 4.


dx.doi.org/10.1021/jf503993q | *J. Agric. Food Chem.* 2014, 62, 10889−10895

**Table 3. HRMS Data for 5-*O*-Caffeoylquinic Acid and Product of Its Transformation**

| | | $[M-H]^-$ (Da) | | error | | |
|---|---|---|---|---|---|---|
| peak no. | elemental composition $[M-H]^-$ | exptl | calcd | ppm | mDa | compd |
| 1 | $C_9H_{11}O_6$ | 191.0561 | 191.0556 | 2.6 | 0.5 | QA |
| 2 | $C_{16}H_{17}O_9$ | 353.0879 | 353.0873 | 1.7 | 0.6 | 5-CQA |
| 3 | $C_9H_7O_4$ | 179.0338 | 179.0344 | 3.4 | −0.6 | CA |
| 4 | $C_{16}H_{19}O_{10}$ | 371.0979 | 371.0978 | 0.3 | 0.1 | 3-CQA-3*R*-OH or 3-CQA-3*S*-OH |
| 5 | $C_{16}H_{19}O_{10}$ | 371.0982 | 371.0978 | 1.1 | 0.4 | 3-CQA-3*R*-OH or 3-CQA-3*S*-OH |
| 6 | $C_{16}H_{19}O_{10}$ | 371.0979 | 371.0978 | 0.3 | 0.1 | 5-CQA-3*R*-OH or 5-CQA-3*S*-OH |
| 7 | $C_{16}H_{19}O_{10}$ | 371.0971 | 371.0978 | 1.9 | −0.7 | 5-CQA-3*R*-OH or 5-CQA-3*S*-OH |
| 8 | $C_{16}H_{19}O_{10}$ | 371.0982 | 371.0978 | 1.1 | 0.4 | 4-CQA-3*R*-OH or 4-CQA-3*S*-OH |
| 9 | $C_{16}H_{19}O_{10}$ | 371.0976 | 371.0978 | 0.5 | −0.2 | 4-CQA-3*R*-OH or 4-CQA-3*S*-OH |
| 10 | $C_{16}H_{17}O_9$ | 353.0871 | 353.0873 | 0.6 | −0.2 | 3-CQA |
| 11 | $C_{16}H_{17}O_9$ | 353.0879 | 353.0873 | 1.7 | 0.6 | 4-CQA |
| 12 | $C_{16}H_{17}O_9$ | 353.0876 | 353.0873 | 0.8 | 0.3 | *cis*-5-CQA |

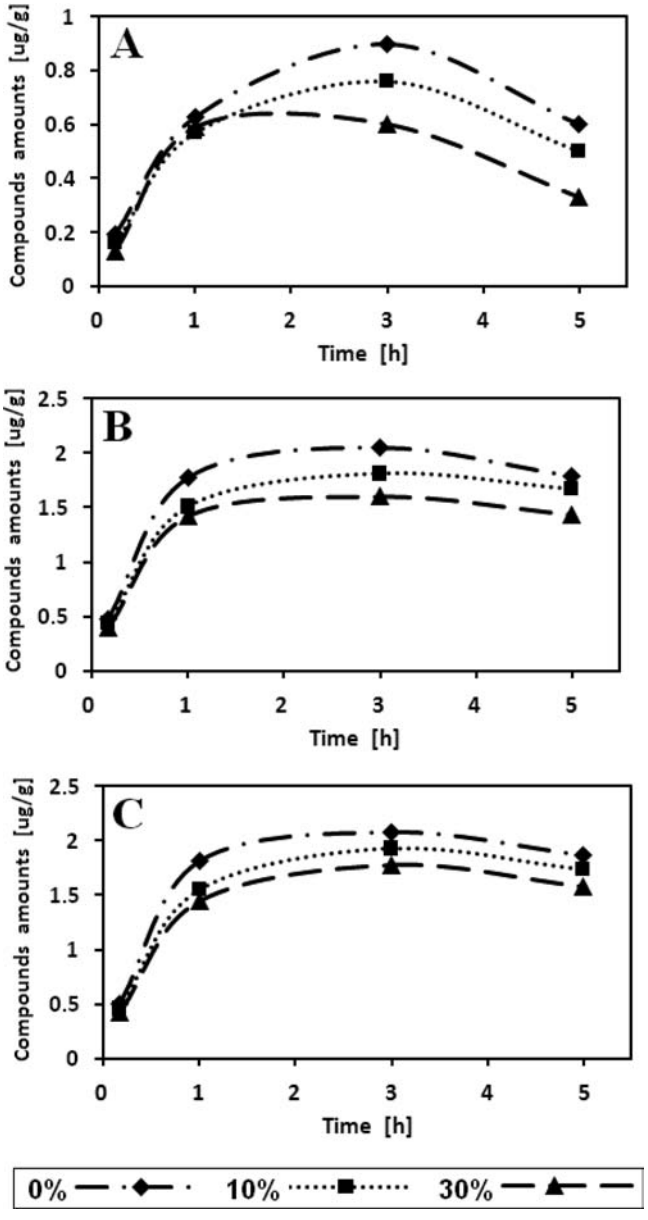


**Figure 5.** Influence of time and sucrose concentration on the amount of *cis*-5-CQA (A), 5-CQA-3*R*-OH (B, C), and 5-CQA-3*S*-OH (B, C) forming in blueberry pulp during its thermal processing.

**Table 4. Influence of Sucrose Concentration for the CQA and Its Transformation Products**

| | | compd amounts ($\mu$g/g) | |
|---|---|---|---|
| peak no. | compd | sucrose concn (0%) | sucrose concn (30%) |
| 1 | QA | 4.28 | 3.13 |
| 2 | 5-CQA | 6.01 | 9.82 |
| 3 | CA | 3.89 | 2.93 |
| 4 | 3-CQA-3*R*-OH or 3-CQA-3*S*-OH | 0.23 | 0.11 |
| 5 | 3-CQA-3*R*-OH or 3-CQA-3*S*-OH | 0.25 | 0.14 |
| 6 | 5-CQA-3*R*-OH or 5-CQA-3*S*-OH | 1.13 | 1.03 |
| 7 | 5-CQA-3*R*-OH or 5-CQA-3*S*-OH | 1.23 | 1.06 |
| 8 | 4-CQA-3*R*-OH or 4-CQA-3*S*-OH | 0.28 | 0.18 |
| 9 | 4-CQA-3*R*-OH or 4-CQA-3*S*-OH | 0.31 | 0.19 |
| 10 | 3-CQA | 5.92 | 5.12 |
| 11 | 4-CQA | 7.12 | 6.13 |
| 12 | *cis*-5-CQA | 0.41 | 0.29 |

As appears from the table, the presence of sucrose clearly slows the transformation speed also in the artificial system. The observed phenomenon can be attributed to the increase of the pulp's viscosity resulting from the presence of the sugar or can be connected with the competition of sucrose and 5-CQA molecules for water molecules.

The presented results prove that high-temperature processing of blueberries causes 5-*O*-caffeoylquinic acid isomerization and transformation. It has been found that as many as 11 components (5-CQA derivatives and its reaction product with water) can be formed from 5-CQA during the processing of blueberries. As results from the experiments, the transformation of this acid in the processed blueberry pulp is very similar to that occurring in acidic water solution.[10] Moreover, the speed of these transformations depends on the sucrose concentration in the processing system, which is another paper novelty. It can be anticipated that 5-CQA, during the high-temperature processing of other fruits and plants containing this acid, is transformed in a similar way.

These results are important not only for food technologists but also for researchers examining plant materials, who may mistakenly treat the 5-CQA transformation products as new components not previously found in examined plants and, thus, erroneously estimate their composition.


dx.doi.org/10.1021/jf503993q | *J. Agric. Food Chem.* 2014, 62, 10889−10895

## AUTHOR INFORMATION

### Corresponding Author

*(A.L.D.) Phone: +48 81 537 55 45. Fax: +48 81 533 33 48. E-mail: dawid@poczta.umcs.lublin.pl.

### Notes

The authors declare no competing financial interest.

## REFERENCES

(1) Jassim, S. A. A.; Naji, M. A. Novel antiviral agents: a medicinal plant perspective. *J. Appl. Microbiol.* **2003**, *95*, 412−427.

(2) Rodriguez de Sotillo, D.; Hadley, M.; Wolf-Hall, C. Potato peel extract a nonmutagenic antioxidant with potential antimicrobial activity. *J. Food Sci.* **1998**, *63*, 907−911.

(3) Bowles, B. L.; Miller, A. J. Caffeic acid activity against *Clostridium botulinum* spores. *J. Food Sci.* **1994**, *59*, 905−908.

(4) Marinova, E. M.; Toneva, A.; Yanishlieva, N. Comparison of the antioxidative properties of caffeic and chlorogenic acids. *Food Chem.* **2009**, *114*, 1498−1502.

(5) Paynter, N. P.; Yeh, H. C.; Voutilainen, S.; Schmidt, M. I.; Heiss, G.; Folsom, A. R.; Brancati, F. L.; Kao, W. H. Coffee and sweetened beverage consumption and the risk of type 2 diabetes mellitus. *Am. J. Epidemiol.* **2006**, *164*, 1075−1084.

(6) Prabhakar, P. K.; Doble, M. Synergistic effect of phytochemicals in combination with hypoglycemic drugs on glucose uptake in myotubes. *Phytomedicine* **2009**, *16*, 1119−1126.

(7) Johnston, K. L.; Clifford, M. N.; Morgan, L. M. Coffee acutely modifies gastrointestinal hormone secretion and glucose tolerance in humans: glycemic effects of chlorogenic acid and caffeine. *Am. J. Clin. Nutr.* **2003**, *78*, 728−733.

(8) Ludwig, I. A.; Clifford, M. N.; Lean, M. E. J.; Ashihara, H.; Crozier, A. Coffee: biochemistry and potential impact on health. *Food Funct.* **2014**, *5*, 1695−1717.

(9) Dawidowicz, A. L.; Typek, R. Thermal stability of 5-*O*-caffeoylquinic acid in aqueous solutions at different heating conditions. *J. Agric. Food Chem.* **2010**, *58*, 12578−12584.

(10) Dawidowicz, A. L.; Typek, R. The influence of pH on the thermal stability of 5-*O*-caffeoylquinic acids in aqueous solutions. *Eur. Food Res. Technol.* **2011**, *233*, 223−232.

(11) Kalt, W.; McDonald, J. E. Chemical composition of blueberry cultivars. *J. Am. Soci. Hortc. Sci.* **1996**, *121*, 142−146.

(12) Clifford, M. N.; Johnston, K. L.; Knight, S.; Kuhnert, N. A hierarchical scheme for LC-MS$^n$ identification of chlorogenic acids. *J. Agric. Food Chem.* **2003**, *51*, 2900−2911.

(13) Clifford, M. N.; Kirkpatrick, J.; Kuhnert, N.; Roozendaal, H.; Salgado, P. R. LC-MS$^n$ analysis of the cis isomers of chlorogenic acids. *Food Chem.* **2008**, *106*, 379−385.

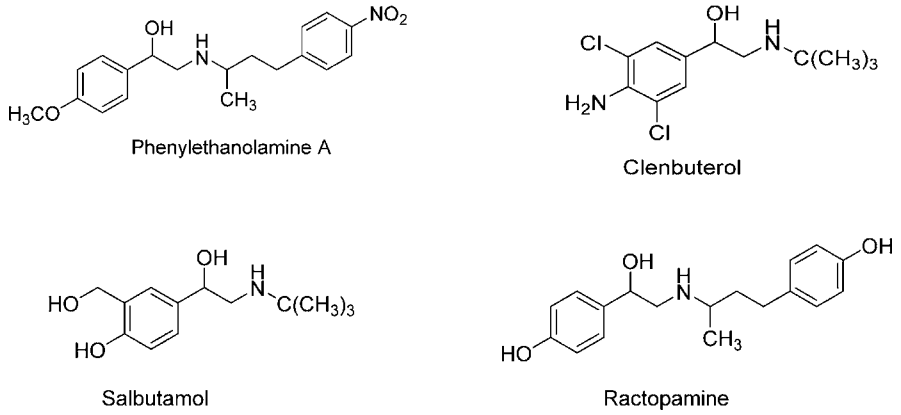


**Figure 1.** Molecular structures of phenylethanolamine A, clenbuterol, ractopamine, and salbutamol.

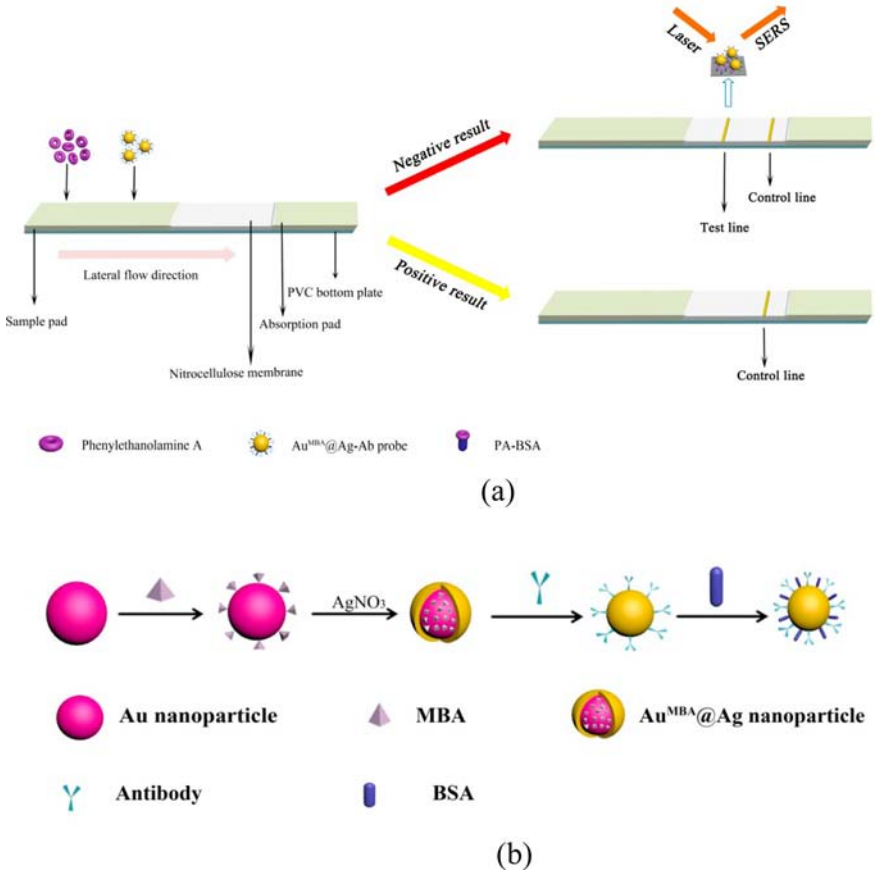


**Figure 2.** (a) Schematic diagrams of the assembly of the ICA strip and the principle of SERS-based ICA for PA detection; (b) preparation of $Au^{MBA}$@Ag-Ab probe.

primary drawback is its time-consuming and laborious incubation washing and rinsing procedures. The electrochemical method is disturbed by many interferents.

Immunochromatography assay (ICA) represents a popular and widely used test principle for point-of-care applications. The main features of the normal Au colloidal particle-based ICA are the user-friendly operation, quickly obtained results, less interference due to chromatographic separation, relatively low cost, and fairly good shelf life.[16] At present, ICA has been widely used for the rapid detection of toxic or harmful substances in many fields such as food safety monitoring[17−20] and point-of-care diagnostics.[21−24] However, although the conventional qualitative analysis can meet the needs of detection of some analytes (e.g., pregnancy testing), it is not suitable in some cases when the quantitative level of an analyte is important.[25] In past years, some attempts of ICA using fluorescence or quantum dots for quantitative analysis were made.[26,27] Nevertheless, a significant limitation of these modified ICA methods is that the results may suffer from optical interference (e.g., photobleaching). Fluorescence ICAs are often complicated by the requirement of an elaborate excitation and detection scheme and by broad emission bands.

Surface-enhanced Raman scattering (SERS) is one of the most sensitive analytical techniques available for the scientist today.[28] Colloidal Au and Ag in solution can render SERS-active by adsorbate-induced particle aggregation.[29,30] Au


dx.doi.org/10.1021/jf503599x | J. Agric. Food Chem. 2014, 62, 10896−10902

colloids have advantages of easy preparation, homogeneity, and biocompatibility with biomolecules such as proteins, antibodies, and DNA, in contrast to Ag NPs, which are not biocompatible and less stable under biological conditions.[31] However, the extinction coefficient of the surface plasmon band of Ag NP is approximately 4 times as large as that for an Au NP of the same size.[32] Currently, the SERS activity of the Ag@Au or Au@Ag core−shell bimetallic nanoparticles were investigated and compared.[33−35] The Au@Ag core−shell nanoparticles were found to have a higher SERS activity mainly due to electronic ligand effect and localized electric field enhancement in core−shell naoparticles.[35] Au@Ag core−shell nanoparticles have been explored for biological applications such as oligonucleotide conjugation and SERS-based immunoassay.[36]

Herein, we describe a novel ICA based on SERS for the detection of PA in urine samples for the first time. The principle and procedures of this approach (Figure 2a) were similar to those based on normal Au colloidal particles. To develop this ICA, a new probe (e.g., $Au^{MBA}$@Ag-Ab) was synthesized (Figure 2b) by immobilizing a polyclonal antibody against PA on the surface of Au/Ag core−shell nanoparticles that have been sandwiched with a Raman reporter (MBA, which is the most common Raman reporter with specific Raman peaks at 1074 and 1583 $cm^{-1}$ applied to the development of a SERS-based immunoassay). After ICA procedures, the specific Raman scattering intensity of MBA on the test line was measured for the quantitative detection of PA. The proposed ICA displayed the properties of high sensitivity, specificity, accuracy, and precision for PA detection.

## MATERIALS AND METHODS

**Materials and Apparatus.** Bovine serum albumin (BSA) and Tween-20 were purchased from Sigma (St. Louis, MO, USA). 4-Mercaptobenzoic acid (MBA) was purchased from Aladdin China Ltd. (Shanghai, China). Chloroauric acid ($HAuCl_4$), silver nitrate ($AgNO_3$, 99%), ascorbic acid (99%), and trisodium citrate were obtained from Sinopharm Chemical Reagent Co., Ltd. (Shanghai, China). Phenylethanolamine A (PA) was bought from Toronto Research Chemicals Inc. (Toronto, ON, Canada). Clenbuterol, ractopamine, and salbutamol were obtained from Zhongmu Pharmaceutical Co., Ltd. (Hubei, China). All other chemicals were of analytical grade. The polyclonal Ab against PA and coating antigen (PA−BSA conjugate) were prepared by our group.[14] Nitrocellulose (NC) membranes were purchased from Whatman (Shanghai, China). PVC sheets, adhesive tape, and filter paper were purchased from Jieyi Biotechnology Co. Ltd. (Shanghai, China). A deionized-RO water machine (Dura 12FV) was purchased from THE LAB Co. (USA). The digital photographs of the samples were taken with a Cannon IXUS 125 HS digital camera (Cannon Inc., Japan). Transmission electron microscopy (TEM) photographs were taken on a Tecnai G220 from USA FEI Co. The portable Raman Analyzer RamTracer-200-HS was obtained from OptoTrace Technologies, Inc. (Suzhou, China).

**Preparation of $Au^{MBA}$@Ag-Ab Probe.** The preparation of the $Au^{MBA}$@Ag-Ab probe is illustrated in Figure 2b. The colloidal gold particles were first prepared according to ref37. Briefly, 1.5 mL of 1% trisodium citrate solution was added rapidly to the boiling aqueous solution of 100 mL of 0.01% $HAuCl_4$ with vigorous stirring. The mixture was kept boiling for 15 min until the color did not change. After the solution cooled down, 10 $\mu$L of 1 mmol $L^{-1}$ MBA solution was added to 10 mL of colloidal gold solution and stirred for 3 h. The MBA modified Au colloids (e.g., $Au^{MBA}$) were purified by centrifugation and resuspension with the same volume of ultrapure water.

After pH adjustment with 0.01 mol $L^{-1}$ HCl, 10 mL of the above $Au^{MBA}$ colloid was mixed with 2 mL of 0.1 mol $L^{-1}$ ascorbic acid in a beaker under stirring. Then 1 mmol $L^{-1}$ $AgNO_3$ was dropwise added into the above mixture. With the continuous addition of $AgNO_3$ solution in amounts of 0.08, 0.12, 0.16, 0.20, 0.25, 0.30, and 0.40 $\mu$mol to 1 mL of $Au^{MBA}$ solution, silver nitrate was reduced by ascorbic acid and the resultant Ag shells continuously grew on the surface of Au seeds. When the purple-red of solution changed to orange-yellow, the solution was further stirred for 30 min and centrifuged at 9000 rpm for 10 min. After removal of the supernatant, the $Au^{MBA}$@Ag NPs were obtained.

The pH value of $Au^{MBA}$@Ag solution was adjusted to 9.0 with 0.1 mol $L^{-1}$ $K_2CO_3$, and then 1 mL of the solution was mixed with Ab against PA for 3.5 h. Finally, 100 $\mu$L of 5% BSA was added to the mixtures and incubated overnight to block the immune complex probes. The final $Au^{MBA}$@Ag-Ab probes were separated from solutions by centrifugation at 8500 rpm for 10 min. Sediment was diluted with an equal volume of phosphate (PB) buffer and stored at 4 °C until use.

**Preparation of ICA Strip.** The ICA strip consisting of an absorbent pad, a nitrocellulose membrane with a test line and a control line, a sample pad, and a PVC bottom plate in a length of 6 cm was assembled (Figure 2a). The test and control lines were formed by spreading 10 $\mu$L of PA−BSA (5.0 mg $mL^{-1}$) and 10 $\mu$L of goat anti-rabbit IgG (1:100 dilution), respectively, and then dried for 20 min at room temperature. The NC membrane was pasted on the center of the PVC bottom plate. The absorbent pad and the sample pad were pasted to both ends of the NC membrane, overlapping it about 1.5 mm. The assembled plate was cut to 4 mm in width. Strips were sealed into glass bottles in the presence of desiccant gel and nitrogen gas and stored at 4 °C until use.

**Procedure of SERS-ICA and SERS Signal Acquisition.** Six microliters of $Au^{MBA}$@Ag-Ab was added onto the sample pad 1.0 cm near the NC membrane, and then 150 $\mu$L of PA standard/sample solution was pipetted onto the sample pad at 0.5 cm from the end of the strip. The standard/sample solutions together with the $Au^{MBA}$@Ag-Ab probes were flowing toward the absorbent pad by capillary action. The color was developed on the test and control zones visually. All ICA procedures were completed within 15 min. The immune complex probes captured by the coating antigen on the test line could be measured with the portable laser Raman Analyzer coupled with a microscope (Eplan, 40 × 0.6). Excitation source was tuned at 785 nm with a laser power of 20 mW at the test line area. The typical integration time used in this assay was 10 s, average with 2 and boxcar with 1. The peak intensity at 1074 $cm^{-1}$ arose from MBA measured from an average of spectra collected at 10 different spots along the middle part of the test line used for quantification.

## RESULTS AND DISCUSSION

**Principle of the SERS-Based ICA.** As illustrated in Figure 2a, the principle of SERS-based ICA is similar to that based on conventional gold colloidal particles. When 150 $\mu$L of PA standard/sample solution was pipetted onto the sample pad at 0.5 cm from the end of the strip, the standard/sample solutions would move toward the absorbent pad and $Au^{MBA}$@Ag-Ab would migrate together with liquid solution. If there was no PA in the standard/sample solution (e.g., negative result), the $Au^{MBA}$@Ag-Ab would be captured by PA−BSA coated on the membrane (test line). Excess $Au^{MBA}$@Ag-Ab would be moved continuously to get the control line and be captured by goat anti-rabbit IgG. Two orange-yellow bands on the test line and control line would appear due to the accumulation of orange-yellow $Au^{MBA}$@Ag-Ab. In contrast, for standard/sample solution containing a large amount of PA (e.g., positive result), the specific antibody binding sites on the probe would be occupied first by PA, leaving no binding sites for PA−BSA. Consequently, no $Au^{MBA}$@Ag-Ab would remain at the PA−BSA location on the NC membrane, but $Au^{MBA}$@Ag-Ab would move continuously to get to the control line and be captured by goat anti-rabbit IgG. In this case, only the orange-yellow band on the control line appeared. Thus, the degree of intensity of

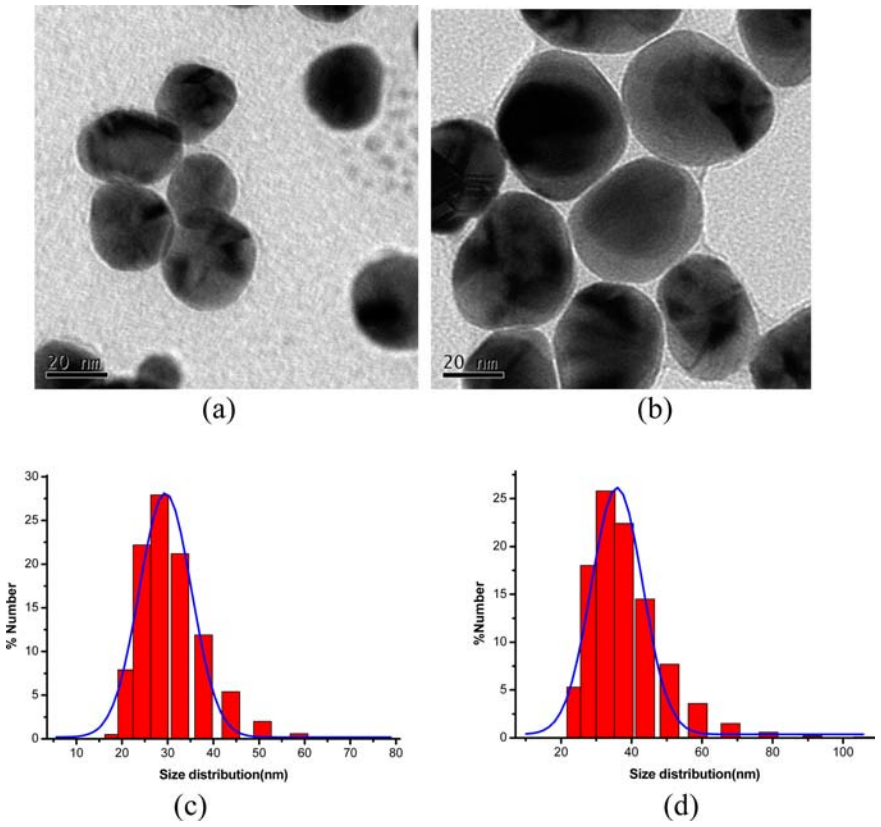


**Figure 3.** (a, c) TEM images and DLS of Au NPs; (b, d) TEM images and DLS of $Au^{MBA}$@Ag NPs with Ag shell thickness of 2.5 nm.

$Au^{MBA}$@Ag-Ab color on the test line was the reverse of the concentration of PA. With the portable Raman analyzer, the SERS scattering intensity arising from the MBA captured on the test line was measured for the quantitative analysis of PA.

**Preparation and Characterization of $Au^{MBA}$@Ag NPs.** The colloidal gold NPs were first prepared and characterized. The TEM images and dynamic light scattering (DLS) of 100 individual Au NPs are shown in Figure 3a,c. The TEM images revealed that the colloidal gold NPs were homogeneous with a diameter size about 30 nm, whereas the DLS results showed that the Au NPs size distribution was in the range of 30 ± 5 nm.

To increase the sensitivity of the SERS-based ICA for PA, it will be desirable to have more MBA sandwiched in the probe. MBA could be easily attached to Au NPs via the thiol group in the MBA molecule. When 10.0 mL of the Au colloids was mixed with different amounts of MBA, more MBA addition to Au colloid solution would make the Au NPs aggregate and even precipitate. We found that 10.0 $\mu$L of MBA solution at the concentration of $1 \times 10^{-3}$ mol $L^{-1}$ was considered the appropriate amount of MBA required to mix with 10.0 mL of the Au colloids to form the $Au^{MBA}$ NPs.

The effect of the amount of $AgNO_3$ in the preparation of $Au^{MBA}$@Ag NPs on the SERS enhancement of MBA was investigated. With the amount of $AgNO_3$ increasing in the range of 0.08, 0.12, 0.16, 0.20, 0.25, 0.30, and 0.40 $\mu$mol to 1 mL of $Au^{MBA}$ solution, silver nitrate was reduced by ascorbic acid and the Ag shells continuously grew on the surface of $Au^{MBA}$ seeds. Accordingly, the color of the resultant $Au^{MBA}$@Ag NPs was gradually changed from purple-red to orange-yellow to yellow (Supporting Information, Figure S1a). The Raman intensity of the $Au^{MBA}$@Ag solutions was tested by the portable Raman Analyzer. As illustrated in Figure S1b, there is a strong dependence of the Raman intensity on the amount of $AgNO_3$ for NPs preparation, for example, on the Ag shell thickness. The maximal Raman intensity was obtained for the $Au^{MBA}$@Ag solution by employing 0.25 $\mu$mol of $AgNO_3$ for NPs preparation. Apparently, the Ag shell of $Au^{MBA}$@Ag NPs plays an important role in enhancing the MBA signals in the SERS detection.

The TEM image and DLS of 100 individual $Au^{MBA}$@Ag NPs using 0.25 $\mu$mol of $AgNO_3$ for NPs preparation are presented in Figure 3, panels b and d, respectively. The TEM image indicated the size of $Au^{MBA}$@Ag NPs was about 35 nm. The DLS results showed that the $Au^{MBA}$@Ag NPs size distribution was in the range of 35 ± 5 nm. Compared with the size of gold NPs, the thickness of the Ag shell in $Au^{MBA}$@Ag NP was estimated to be 2.5 nm.

**Test of Nonspecific Adsorption.** Before PA detection, whether there was nonspecific adsorption was tested. The ICA procedures at zero concentration of analyte in three situations were performed: (a) $Au^{MBA}$@Ag-Ab as a probe, PA−BSA coated on the test line; (b) $Au^{MBA}$@Ag-BSA as a probe, PA−BSA coated on the test line; (c) $Au^{MBA}$@Ag-Ab as a probe, $Na_2CO_3$−$NaHCO_3$ solution spread on the test line. The Raman spectra in the above three situations are illustrated in Figure S2. From Raman spectrum a, it was seen that both specific Raman scattering peaks of the MBA at 1074 and 1583 $cm^{-1}$ with the signal values of 9200 (AU) and 8100 (AU) appeared, which clearly demonstrated that the probe of $Au^{MBA}$@Ag-Ab was specifically bound with PA−BSA at the test line on the membrane. From Raman spectra b and c, there were almost no SERS signals appearing either at 1074 $cm^{-1}$ or

at 1583 $cm^{-1}$, indicating that there was no nonspecific adsorption.

**Optimization of Assay Conditions.** The sensitivity of the SERS-based ICA was improved by optimizing a series of conditions such as the amount of the antibody used for preparing $Au^{MBA}$@Ag-Ab probes, the coating antigen, and the probe utilized on the strip. Here we used the inhibition ratio ($B_0/B_{0.1}$) to evaluate the optimization. $B_0$ and $B_{0.1}$ are the SERS intensities at 1074 $cm^{-1}$ when PA concentrations were at 0 and 0.1 ng $mL^{-1}$, respectively. The bigger the inhibition ratio value, the higher the sensitivity of the assay.

In the preparation of $Au^{MBA}$@Ag-Ab probe, different amounts of antibody were consecutively coupled to 1.0 mL of $Au^{MBA}$@Ag NPs. The effects of the amount of Ab on the inhibition ratio were investigated (Figure S3a). It was found that when different volumes of antibody (at concentration of 2.0 mg $mL^{-1}$) from 0.5 to 3.0 $\mu$L were applied, the highest value of $B_0/B_{0.1}$ was achieved at 2.0 $\mu$L. Thus, the optimal amount of Ab for $Au^{MBA}$@Ag probe preparation was 2.0 $\mu$L.

The amount of coating antigen (PA−BSA) immobilized on the test line and the $Au^{MBA}$@Ag-Ab probe applied in the ICA strip significantly influence the assay sensitivity. As shown in Figure S3b,c, when 10 $\mu$L of PA−BSA at concentrations from 3.0 to 7.0 mg $mL^{-1}$ was applied to the ICA procedure, the highest value of $B_0/B_{0.1}$ was achieved at 5.0 mg $mL^{-1}$, whereas when volumes of $Au^{MBA}$@Ag-Ab from 2.0 to 10 $\mu$L were tested, the highest value of $B_0/B_{0.1}$ was obtained at 6.0 $\mu$L. Therefore, the optimal conditions applied to one ICA strip were 10 $\mu$L of PA-BSA at a concentration of 5.0 mg $mL^{-1}$ and 6.0 $\mu$L of $Au^{MBA}$@Ag-Ab.

**Sensitivity of the Assay.** Under optimal assay conditions, the SERS-based ICA for PA detection was developed. The PA standard solutions were in a range of 0−100 ng $mL^{-1}$. After the addition of 150 $\mu$L of PA standard solution to the sample pad, 15 min later, the color arising from $Au^{MBA}$@Ag-Ab on the test line was visualized by the naked eye (Figure 4a). With PA concentration increasing, the intensity of the color on test lines was gradually decreased. The SERS intensity at 1074 $cm^{-1}$ generated from MBA on the test lines was measured by SERS analyzer. As illustrated in Figure 4b, with PA concentration increasing, the SERS intensity at 1074 $cm^{-1}$ gradually decreased. The standard curve of the SERS-based ICA for PA was constructed in the form of $B/B_0 \times 100\%$ versus log $C$ (Figure 4c), where $B$ and $B_0$ were the SERS intensities when PA solutions were at the standard points and zero concentration. It was seen from Figure 4c that values of $IC_{50}$ and LOD at 3 × SD were 0.064 ng $mL^{-1}$ and 0.32 pg $mL^{-1}$, respectively. The comparison of the $IC_{50}$ and LOD values achieved in this study with those obtained in other immunoassays for PA detection is given in Table S1. It can be seen from Table S1 that $IC_{50}$ and LOD values in this work are 1−3 orders of magnitude lower than those obtained by other immunoassays, indicating the ultrasensitivity of the SERS-based ICA.

**Reproducibility of the SERS Signals.** To investigate the reproducibility of the SERS signals, three strips set up with PA standard solutions at 0, 0.1, and 1.0 ng $mL^{-1}$ after ICA procedures were tested. The SERS intensities at 1074 $cm^{-1}$ from 10 different spots along the middle parts of the test line in the strips were measured and are illustrated in Figure S4a. It was seen that among the three strips, the higher the PA concentration, the lower the SERS intensities; in each strip, the RSD value of the SERS intensities at 10 measurements were

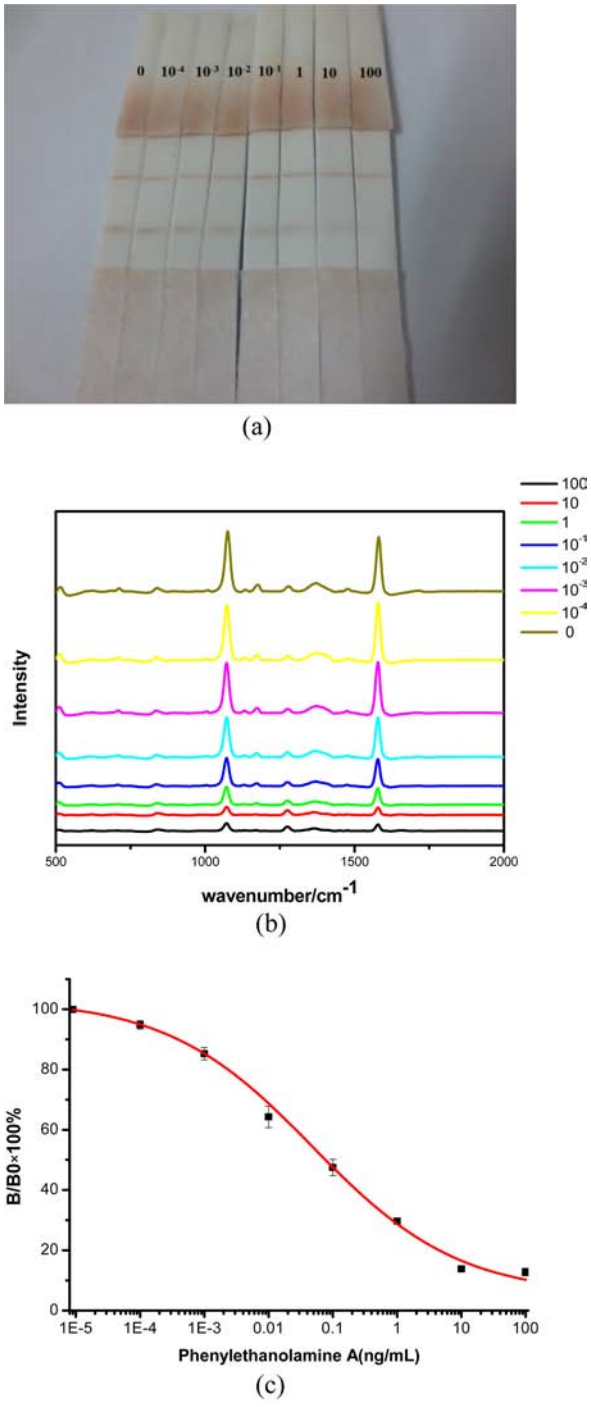


**Figure 4.** (a) Digital photograph of the strips after ICA procedure. The numbers on the test lines are the standard concentration of analyte (ng $mL^{-1}$). (b) Raman spectra arising from MBA on test lines. (c) Standard curve of the SERS-based ICA for PA. The bars represent the standard deviation of the 10 measurements of the intensities of MBA at 1074 $cm^{-1}$ on test lines.

5.17, 7.93, and 5.64%, respectively, indicating high precision of the SERS signal.

**Specificity of the Assay.** The specificity of a competitive immunoassay is often expressed by cross-reactivity (CR) value. Here we chose another three $\beta$-adrenergic agonists (ractopamine, salbutamol, and clenbuterol hydrochloride) to test the specificity of this assay. All compounds including PA were prepared at concentrations of 0, 0.01, 0.1, and 1 ng $mL^{-1}$ and


dx.doi.org/10.1021/jf503599x | J. Agric. Food Chem. 2014, 62, 10896−10902

applied to ICA procedures. The CR values were calculated according to CR (%) = [$IC_{50}$ of PA)]/[$IC_{50}$ of tested compound] × 100%. As shown in Figure S4b, for all three $\beta$-agonists, with the concentration increasing, the SERS intensities were almost constant, suggesting that there was almost no cross-reactivity of this SERS-based ICA with these three $\beta$-agonists, which demonstrated the high specificity of the proposed assay.

**Test of Recovery.** We chose pig urine samples for the spiking experiment. After dilution of the urine to 1:50 with PVP−PBST (polyvinylpyrrolidone−phosphate buffer saline with 0.1% Tween-20, v/v = 1:1, 1%), the urine sample was spiked with PA to concentrations of 0.01, 0.1, and 1.0 ng $mL^{-1}$, then 150 $\mu$L of the diluted urine sample was applied to ICA procedures. The contents of PA in spiked samples were quantified according to the standard curve run in the same day. As shown in Table 1, the recoveries of the PA from spiked samples were 99.9−101.2% with RSD values in range of 3.6−5.8% ($n$ = 3), indicating that this new approach was an applicable method to effectively detect the target analyte in urine samples.

**Table 1. Recoveries of PA from Spiked Urine Samples Measured by SERS-Based ICA**

| concn spiked (ng $mL^{-1}$) | recovery measured (100%) | | | average | RSD (100%) |
|---|---|---|---|---|---|
| 0.01 | 101.9 | 94.7 | 106.3 | 100.9 | 5.8 |
| 0.1 | 97.5 | 101 | 105 | 101.2 | 3.7 |
| 1 | 96.36 | 103.6 | 99.7 | 99.9 | 3.6 |

In conclusion, a novel ICA based on SERS using $Au^{MBA}$@Ag-Ab as a probe for the sensitive and quantitative detection of PA was developed in this study. Under optimal conditions, the $IC_{50}$ and LOD values of this new approach for PA were 0.06 ng $mL^{-1}$ and 0.32 pg $mL^{-1}$, respectively, indicating the ultrasensitivity of the assay. This ICA also displayed high specificity and reproducibility. Furthermore, by sandwich format, the proposed SERS-based ICA might be applied for the detection of macromolecular compounds; and by immobilizing more than two different kinds of coating antigens on the NC membrane as test lines and utilizing corresponding $Au^{MBA}$@Ag-Ab probes, it might be used for multiplex assays. The proposed SERS-based ICA was proven to be a rapid, simple, and ultrasensitive analytical method for PA and might be also applied for the determination of various target analytes in clinical, biological, food, and environmental analyses.

## ■ ASSOCIATED CONTENT

### Supporting Information

Figures S1−S4 and Table S1. This material is available free of charge via the Internet at http://pubs.acs.org.

## ■ AUTHOR INFORMATION


### Corresponding Authors

*(A.P.) Phone: +86 512 65882362. Fax: +86 512 65882362. E-mail: denganping@suda.edu.cn.

*(J.L.) Phone: +86 512 65882362. Fax: +86 512 65882362. E-mail: lijgsd@suda.edu.cn.



### Funding

We thank the National Natural Science Foundation of China (NSFC, Contracts 20835003, 21075087, and 21175097) and a Project Funded by the Priority Academic Program Development of Jiangsu Higher Education Institutions for financial support of this study.


### Notes

The authors declare no competing financial interest.

## ■ REFERENCES


(1) Vestergaard, M.; Sejrsen, K.; Klastrup, S. G. Composition and eating quality of longissimus dorsi from young bulls fed the $\beta$-agonist cimaterol at consecutive developmental stages. *Meat Sci.* **1994**, *38*, 55−66.

(2) Prezelj, A.; Obreza, A.; Pecar, S. Abuse of clenbuterol and its detection. *Curr. Med. Chem.* **2003**, *10*, 281−290.

(3) Mitchell, G. A.; Dunnavan, G. Illegal use of adrenergic agonists in the United States. *J. Anim. Sci.* **1998**, *76*, 208−211.

(4) Chan, T. Y. K. Food-borne clenbuterol may have potential for cardiovascular effects with chronic exposure (commentary). *J. Toxicol. Clin. Toxicol.* **2001**, *39*, 345−348.

(5) Bulletin of the Ministry of Agriculture of the People's Republic of China, No. 1519, 2010.

(6) Zhang, Y. T.; Zhang, Z. J.; Sun, Y. H.; Wei, Y. Development of an analytical method for the determination of $\beta_2$-agonist residues in animal tissues by high-performance liquid chromatography with on-line electrogenerated $[Cu(HIO_6)_2]^{5-}$-luminol chemiluminescence detection. *J. Agric. Food Chem.* **2007**, *55*, 4949−4956.

(7) Courant, F.; Pinel, G.; Bichon, E.; Monteau, F.; Antignac, J. P.; LeBizec, B. Development of a metabolomic approach based on liquid chromatography-high resolution mass spectrometry to screen for clenbuterol abuse in calves. *Analyst* **2009**, *134*, 1637−1646.

(8) Mazzarino, M.; Fiacco, I.; delaTorre, X.; Botrèa, F. Screening and confirmation analysis of stimulants, narcotics and beta-adrenergic agents in human urine by hydrophilic interaction liquid chromatography coupled to mass spectrometry. *J. Chromatogr., A* **2011**, *1218*, 8156−8167.

(9) Blanca, J.; Muñz, P.; Morgado, M.; Méndez, N.; Aranda, A.; Reuvers, T.; Hooghuis, H. Determination of clenbuterol, ractopamine and zilpaterol in liver and urine by liquid chromatography tandem mass spectrometry. *Anal. Chim. Acta* **2005**, *529*, 199−205.

(10) Caban, M.; Stepnowski, P.; Kwiatkowski, M.; Migowska, N.; Kumirska, J. Determination of $\beta$-blockers and $\beta$-agonists using gas chromatography and gas chromatography−mass spectrometry − a comparative study of the derivatization step. *J. Chromatogr., A* **2011**, *1218*, 8110−8122.

(11) Bulletin of the Ministry of Agriculture of the People's Republic of China, No. 1486-1-2010, Beijing, 2010.

(12) Zhang, M. X.; Li, C.; Wu, Y. L. Determination of phenylethanolamine a in animal hair, tissues and feeds by reversed phase liquid chromatography tandem mass spectrometry with QuEChERS. *J. Chromatogr., B* **2012**, *900*, 94−99.

(13) Bai, Y. H.; Liu, Z. H.; Bi, Y. F.; Wang, X.; Jin, Y. Z.; Sun, L.; Wang, H. J.; Zhang, C. M.; Xu, S. X. Preparation of polyclonal antibodies and development of a direct competitive enzyme-linked immunosorbent assay to detect residues of phenylethanolamine a in urine samples. *J. Agric. Food Chem.* **2012**, *60*, 11618−11624.

(14) Cao, B. Y.; He, G. Z.; Yang, H.; Chang, H. F.; Li, S. Q.; Deng, A. P. Development of a highly sensitive and specific enzyme-linked immunosorbent assay (ELISA) for the detection of phenylethanolamine a in tissue and feed samples and confirmed by liquid chromatography tandem mass spectrometry (LC−MS/MS). *Talanta* **2013**, *115*, 624−630.

(15) Lai, Y. J.; Bai, J.; Zhu, W.; Xian, Y. Z.; Jin, L. T. Electrochemical determination of phenylethanolamine a based on Nafion/MWCNTs/AuNPs modified carbon electrode. *Chin. J. Chem.* **2013**, *31*, 221−229.

(16) Posthuma-Trumpie, G. A.; Korf, J.; Amerongen, A. Lateral flow(immuno)assay: its strengths, weaknesses, opportunities, and threats − a literature survey. *Anal. Bioanal. Chem.* **2009**, *393*, 569−582.

(17) Liu, B. H.; Tsao, Z. J.; Wang, J. J.; Yu, F. Y. Development of a monoclonal antibody against ochratoxin A and its application in

enzyme-linked immunosorbent assay and gold nanoparticle immunochromatographic strip. *Anal. Chem.* **2008**, *80*, 7029−7035.
(18) Molinelli, A.; Grossalber, K.; Fuhrer, M.; Baumgartner, S.; Sulyok, M.; Krska, R. Development of qualitative and semiquantitative immunoassay-based rapid strip tests for the detection of T-2 toxin in wheat and oat. *J. Agric. Food Chem.* **2008**, *56*, 2589−2594.
(19) Sheibani, A.; Tabrizchi, M.; Ghaziaskar, H. S. Determination of aflatoxins B1 and B2 using ion mobility spectrometry. *Talanta* **2008**, *75*, 233−238.
(20) Xu, Y.; Huang, Z. B.; He, Q. H.; Deng, S. Z.; Li, L. S.; Li, Y. P. Development of an immunochromatographic strip test for the rapid detection of deoxynivalenol in wheat and maize. *Food Chem.* **2010**, *119*, 834−839.
(21) Krajaejun, T.; Imkhieo, S.; Intaramat, A.; Ratanabanangkoon, K. Development of an immunochromatographic test for rapid serodiagnosis of human pythiosis. *Clin. Vaccine Immunol.* **2009**, *16*, 506−509.
(22) Sithigorngul, P.; Rukpratanporn, S.; Pecharaburanin, N.; Suksawat, P.; Longyant, S.; Chaivisuthangkura, P.; Sithigorngul, W. A simple and rapid immunochromatographic test strip for detection of pathogenic isolates of *Vibrio harveyi*. *J. Microbiol. Methods* **2007**, *71*, 256−264.
(23) Sithigorngul, W.; Rukpratanporn, S.; Sittidilokratna, N.; Pecharaburanin, N.; Longyant, S.; Chaivisuthangkura, P.; Sithigorngul, P. A convenient immunochromatographic test strip for rapid diagnosis of yellow head virus infection in shrimp. *J. Virol. Methods* **2007**, *140*, 193−199.
(24) Sundar, S.; Maurya, R.; Singh, R. K.; Bharti, K.; Chakravarty, J.; Parekh, A.; Rai, M.; Kumar, K.; Murray, H. W. Rapid, noninvasive diagnosis of visceral *Leishmaniasis* in India: comparison of two immunochromatographic strip tests for detection of anti-K39 antibody. *J. Clin. Microbiol.* **2006**, *44*, 251−253.
(25) Liu, G.; Lin, Y. Y.; Wang, J.; Wu, H.; Wai, C. M.; Lin, Y. Disposable electrochemical immunosensor diagnosis device based on nanoparticle probe and immunochromatographic strip. *Anal. Chem.* **2007**, *79*, 7644−7653.
(26) Zou, Z. X.; Du, D.; Wang, J.; Smith, J. N.; Timchalk, C.; Li, Y. Q.; Lin, Y. H. Quantum dot-based immunochromatographic fluorescent biosensor for biomonitoring trichloropyridinol, a biomarker of exposure to chlorpyrifos. *Anal. Chem.* **2010**, *82*, 5125−5133.
(27) Kim, Y. M.; Oh, S. W.; Jeong, S. Y.; Pyo, D. J.; Choi, E. Y. Development of an ultrarapid one-step fluorescence immunochromatographic assay system for the quantification of microcystins. *Envrion. Sci. Technol.* **2003**, *37*, 1899−1904.
(28) Petry, R.; Schmitt, M. J. Raman spectroscopy − a prospective tool in the life sciences. *ChemPhysChem* **2003**, *4*, 14−30.
(29) Senapati, D.; Dasary, S. S. R.; Singh, A. K.; Senapati, T.; Yu, H. T.; Ray, P. C. A label-free gold-nanoparticle-based SERS assay for direct cyanide detection at the parts-per-trillion level. *Chem.−Eur. J.* **2011**, *17*, 8445−8451.
(30) Lee, P. C.; Meisel, D. Adsorption and surface-enhanced Raman of dyes on silver and gold sols. *J. Phys. Chem.* **1982**, *86*, 3391−3395.
(31) Chandran, S. P.; Ghatak, J.; Satyam, P. V.; Sastry, M. Interfacial deposition of Ag on Au seeds leading to Au core Ag shell in organic media. *J. Colloid Interface Sci.* **2007**, *312*, 498−505.
(32) Cao, Y. W.; Jin, R.; Mirkin, C. A. DNA-modified core-shell Ag/Au nanoparticles. *J. Am. Chem. Soc.* **2001**, *123*, 7961−7962.
(33) Rivas, L.; Sanchez-Cortes, S.; Garca-Ramos, J. V.; Morcillo, G. Mixed silver/gold colloids: a study of their formation, morphology, and surface-enhanced Raman activity. *Langmuir* **2000**, *16*, 9722−9728.
(34) Yang, Y.; Shi, J.; Kawamura, G.; Nogami, M. Preparation of Au−Ag, Ag−Au core−shell bimetallic nanoparticles for surface enhanced Raman scattering. *Scr. Mater.* **2008**, *58*, 862−865.
(35) Huang, Y.; Yang, Y.; Chen, Z.; Li, X.; Nogami, M. Fabricating Au−Ag core-shell composite films for surface-enhanced Raman scattering. *J. Mater. Sci.* **2008**, *43*, 5390−5393.
(36) Cui, Y.; Ren, B.; Yao, J. L.; Gu, R. A.; Tian, Z. Q. Synthesis of $Ag_{core}Au_{shell}$ bimetallic nanoparticles for immunoassay based on surface-enhanced Raman spectroscopy. *J. Phys. Chem. B* **2006**, *110*, 4002−4006.
(37) Frens, G. Controlled nucleation for the regulation of the particle size in monodisperse gold suspensions. *Nat. Phys. Sci.* **1973**, *241*, 20−22.

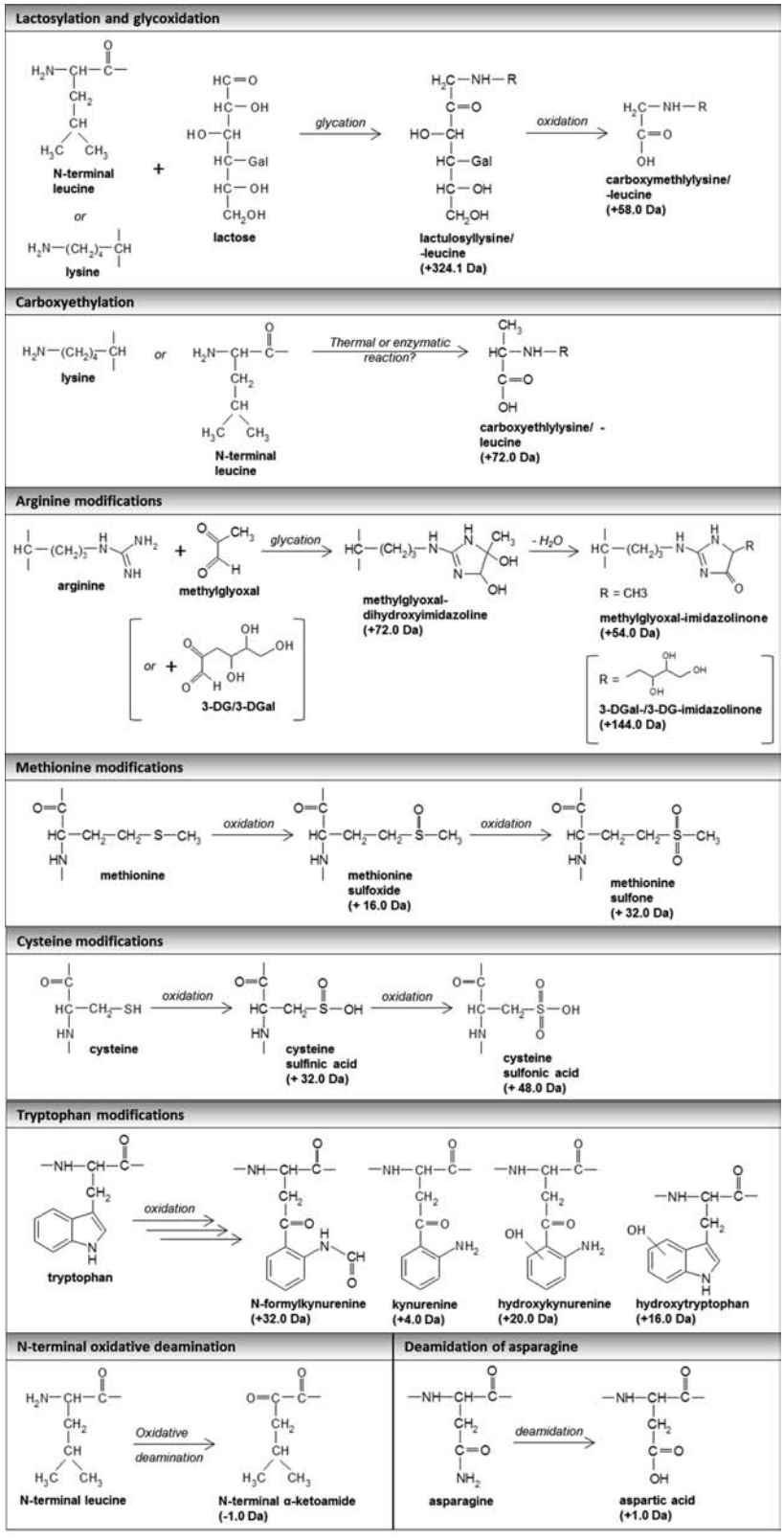


**Figure 1.** Reactions leading to the analyzed protein modifications in heated milk.

quantification of the modified peptides in diverse commercial milk products was performed to confirm their relevance for industrial processes. Furthermore, the data were applied to evaluate the potential of novel marker compounds to reflect milk processing conditions.

## MATERIALS AND METHODS

**Materials.** Formic acid (eluent additive for LC-MS), acetonitrile (LC-MS Chromasolv), disodium phosphate purum p.a., and monosodium phosphate purum p. a. were obtained from Sigma-Aldrich (Taufkirchen, Germany). 1,4-Dithiothreitol (DTT) was purchased from Roth (Karlsruhe, Germany). Endoproteinase GluC was supplied

by Roche (Mannheim, Germany). All water used was ultrapure water (18.2 MΩ cm resistivity).

**Milk Samples.** Raw milk samples ($n$ = 5) were provided by local farmers. Each sample was taken from pooled milk of at least 20 cows. Pasteurized milk ($n$ = 5; 1.5−3.5% fat), extended shelf life (ESL) milk ($n$ = 5; 3.5−3.8% fat), ultrahigh-temperature (UHT) milk ($n$ = 5; 3.5−3.8% fat), evaporated milk ($n$ = 6; 3.0−7.5% fat), and coffee cream ($n$ = 2; 10−12% fat) were purchased at local supermarkets. The day of purchase was generally about 3.5 months (UHT milk), 16 days (ESL milk), and 3−6 days (pasteurized milk) before the respective expiration date, indicating only a moderate storage time between production and purchase. Sterilized milk ($n$ = 1; 1.5% fat) was obtained from a German producer via an Internet shop. All samples were analyzed directly after purchase or kept at −21 °C until analysis.

**Defatting of Raw Milk and Milk Samples.** Fat from raw milk and milk samples was removed by centrifugation in a Hettich (Tuttlingen, Germany) Universal 16/32 R centrifuge for 60 min at 1650$g$ and 4 °C. The upper fat layer was carefully removed with a spatula. Visual evaluation indicated that the major part of the fat had been separated from the aqueous layer. Minor lipid contaminations in the samples did not interfere noticeably with chromatography, enzymatic hydrolysis, or mass analysis. Defatted milk samples were either stored at −80 °C prior to analysis or worked up directly after defatting. Samples were permanently kept on ice during sample preparation to minimize enzymatic activity.

**Heating of Raw Milk.** Aliquots of 25 μL of defatted raw milk were transferred to Eppendorf (Hamburg, Germany) tubes and heated in an Eppendorf thermo mixer at 99 °C for 0, 5, 10, 15, and 23 min. After heating, samples were immediately cooled in ice. All heating experiments were performed in triplicate.

Because industrial heating of milk is more efficient than heating in the laboratory scale, the heating conditions had to be adapted to obtain similar modification pattern as observed in commercial products. As shown later, the applied heating conditions modeled the extent of modifications in industrial products well.

**Specific Enzymatic Hydrolysis.** Milk samples (25 μL each) were transferred to Eppendorf tubes and specifically hydrolyzed by the addition of 75 μL of endoproteinase GluC (0.08 μg/μL) in 25 mM phosphate buffer, pH 7.8. The tubes were shaken in an Eppendorf thermo mixer for 16 h at 37 °C. Hydrolyzed proteins were reduced by adding 10 μL of 1 M DTT. Following 30 min of incubation at room temperature, 890 μL of water was added and samples were filtered (PVDF, 0.22 μm; Roth, Karlsruhe, Germany). Under these conditions, 95−100% of the cleavage sites in β-lactoglobulins were specifically hydrolyzed, which was monitored by targeted analysis of peptides with missed cleavages in full scan chromatograms.

**LC-MS/MS Analysis.** LC-MS/MS experiments were carried out on a Dionex (Germering, Germany) Ultimate 3000 RS UHPLC system from Thermo Scientific, coupled to a QTrap 4000, equipped with an electrospray ionization (ESI) source (AB Sciex, Foster City, CA, USA). Aliquots of 10 μL of the protein hydrolysates were separated on a C18 column (Waters (Eschborn, Germany) Acquity UPLC BEH 300, 2.1 × 100 mm, 1.7 μm) at a flow rate of 0.3 mL/min, with a gradient program as follows: 0 min, 5% B; 5 min, 5% B; 55 min, 50% B; 55.5 min, 95% B; and 60 min, 95% B, using 0.1% formic acid as eluent A and acetontrile as eluent B. Equilibration of the column was performed with initial conditions for 6 min prior to each injection. The column was operated at 30 °C. After 1 min, the LC flow was directed into the mass spectrometer for 54 min. Experiments were carried out in the positive mode with the resolution of the quadrupoles set to unit.

**Scheduled Multiple Reaction Monitoring (sMRM).** A sMRM method was developed as described previously.[6] Briefly, sMRM data were acquired using a list that defined transitions for each single modification (one quantifier and two qualifiers per modified peptide as shown in the Supporting Information), indicating the expected retention times and determining a detection window of 40 s. Target scan time was set to 1.2 s. Collision energies and declustering potentials were optimized for each single transition as detailed in the Supporting Information.

**Calculation of Modification Indices.** Modification indices for each modification were calculated from the extracted ion chromatograms of the sMRM runs as follows:

$$\text{index} = \frac{\text{area extracted ion chromatogram (modified peptide)}}{\text{area extracted ion chromatogram (internal standard)}} \times 100$$

Areas of extracted ion chromatograms were obtained by signal integration, which was performed in Analyst 1.5.1 (AB Sciex). The multiplier of 100 was arbitrarily chosen to obtain easily manageable numbers for the indices. The peptide AA 159−162 (QCHI) from β-lactoglobulin was selected as internal standard because its unreactive amino acids were expected not to be modified during thermal treatment (see below).

**Statistical Data Evaluation.** Statistical data evaluation was performed in Microsoft Office Excel 2007. Variance homogeneity was tested with an $F$ test. Levels of significance were then calculated using an unpaired two-tailed Student $t$ test for homoscedastic or heteroscedastic distribution, respectively. A $p$ value <0.05 was considered as significant.

## RESULTS AND DISCUSSION

The goal of the present study was to investigate if the β-lactoglobulin modifications, which had previously been identified in milk, were indeed formed by thermal processes or if they originated from other mechanisms. Therefore, kinetics of the site-specific formation of protein modifications in β-lactoglobulin during thermal treatment of raw milk was systematically investigated by UHPLC-ESI-MS/MS in sMRM mode after specific enzymatic hydrolysis. β-Lactoglobulin was chosen because the structures and binding sites of nePTMs formed during milk processing are well characterized, which is a prerequisite of the present quantitative studies.[6] The method, however, can easily be adapted to other milk proteins, such as the caseins. To confirm that the results are of relevance for industrial processes, the modifications were also semiquantified in commercially available dairy samples. With the aim to cover a broad range of different industrial heating procedures, the following product types were chosen for analysis: raw milk as unheated control, pasteurized milk, ESL milk, UHT milk, sterilized milk, evaporated milk, and coffee cream. Altogether, 52 modifications were analyzed, with 19 different structures at 26 binding sites. Among these modifications were N-terminal and lysine- or arginine-bound glycation or glycoxidation products, oxidation products of methionine, tryptophan, cysteine, and the N-terminus, and, finally, the hydrolysis product of asparagine. Table 1 gives a detailed overview of analyzed modifications and their position in the amino acid sequence. Figure 1 displays the reactions leading to the corresponding protein modifications in thermally processed milk.

**Semiquantification by Means of an Internal Peptide as Standard for Normalization.** Because absolute site-specific quantification of protein modifications is not practicable in default of available standards, we performed semiquantification by normalizing the peak area of a specific modified peptide to an internal standard peptide released during specific enzymatic hydrolysis from β-lactoglobulin, as applied in previous studies.[20] The peptide AA 159−162 (QCHI) from β-lactoglobulin was selected as internal standard because its unreactive amino acids were expected not to be modified during thermal treatment. When raw milk was heated over 23 min, no significant decrease of signal areas could be observed for the peptide AA 159−162 (Figure 2), confirming that the selected peptide was obviously not significantly modified indeed. Furthermore, the enzymatic digestibility of β-lactoglobulin by GluC was not detectably impaired by thermally induced modification. Thus, it could be

**Table 1. Overview of Modifications of $\beta$-Lactoglobulin Detected in Heated Milk and in Commercially Available Milk Products**

| AA[a] | sequence | modification | localization | heated milk | raw milk | past[b] milk | ESL[c] milk | UHT[d] milk | steril[e] milk | evap[f] milk | coffee cream |
|---|---|---|---|---|---|---|---|---|---|---|---|
| 1−11 | LIVTQTMKGLD | lactulosylleucine | N-terminus[g] | x | x | x | x | x | x | x | x |
| | | $N^{\alpha}$-carboxymethylleucine | N-terminus | – | – | – | – | t[h] | x | t | t |
| | | $N^{\varepsilon}$-carboxymethyllysine | K8 | t | – | – | – | t | t | t | t |
| | | $N^{\alpha}$-carboxyethylleucine | N-terminus | – | – | – | – | – | – | – | – |
| | | methionine sulfoxide | M7[g] | x | x | x | x | x | x | x | x |
| | | methionine sulfone | M7 | – | – | – | – | – | – | – | – |
| | | N-terminal $\alpha$-ketoamide | N-terminus[g] | x | x | x | x | x | x | x | x |
| 12−28 | IQKVAGTWYSLAMAASD | lactulosyllysine | K14[g] | x | – | – | – | x | x | x | x |
| | | $N^{\varepsilon}$-carboxymethyllysine | K14 | t | – | – | – | – | t | t | t |
| | | methionine sulfoxide | M24[g] | x | x | x | x | x | x | x | x |
| | | methionine sulfone | M24 | – | – | – | – | – | – | – | – |
| | | hydroxytryptophan | W19 | t | – | – | – | – | t | – | – |
| | | *N*-formylkynurenine | W19 | – | – | – | – | – | – | – | – |
| | | kynurenine | W19[g] | x | x | x | x | x | x | x | x |
| 34−45 | AQSAPLRVYVEE | methylglyoxal-dihydroxyimidazoline | R40 | – | – | – | – | – | – | – | – |
| | | methylglyoxal-imidazolinone | R40 | – | – | – | – | – | x | t | t |
| | | 3-DGal-/3-DG-imidazolinone | R40 | – | – | – | – | – | – | – | – |
| 46−51 | LKPTPE | lactulosyllysine | K47[g] | x | x | x | x | x | x | x | x |
| 46−55 | LKPTPEGDLE | $N^{\varepsilon}$-carboxymethyllysine | K47[g] | x | – | – | – | t | x | x | t |
| 56−62 | ILLQKWE | lactulosyllysine | K60[g] | x | x | x | x | x | x | x | x |
| | | $N^{\varepsilon}$-carboxymethyllysine | K60[g] | x | t | t | x | x | x | x | x |
| | | $N^{\varepsilon}$-carboxyethyllysine | K60[g] | x | x | x | x | x | x | x | x |
| | | *N*-formylkynurenine | W61[g] | x | x | x | x | x | x | x | x |
| | | kynurenine | W61[g] | x | x | x | x | x | x | x | x |
| | | hydroxykynurenine | W61 | – | – | – | – | – | – | – | – |
| | | hydroxytryptophan | W61[g] | x | x | x | x | x | x | x | x |
| 56−65 | ILLQKWENGE | deamidation | N63[g] | x | x | x | x | x | x | x | x |
| 66−74 | CAQKKIIAE | $N^{\varepsilon}$-carboxymethyllysine | K69 | t | – | – | – | t | x | x | x |
| | | $N^{\varepsilon}$-carboxymethyllysine | K70 | t | – | – | – | t | x | x | x |
| | | $N^{\varepsilon}$-carboxyethyllysine | K69/K70 | t | t | t | t | t | x | x | t |
| | | sulfonic acid | C66[g] | x | x | x | x | x | x | x | x |
| 75−89 | KTKIPAVFKIDALNE | lactulosyllysine | K75/K77/K83[g,i] | x | x | | x | x | x | x | x |
| | | $N^{\varepsilon}$-carboxymethyllysine | K75/K77[i] | t | – | – | – | t | x | x | x |
| | | $N^{\varepsilon}$-carboxymethyllysine | K83 | – | – | – | – | t | t | t | t |



dx.doi.org/10.1021/jf503664y | J. Agric. Food Chem. 2014, 62, 10903−10915

**Table 1. continued**

| AA[a] | sequence | modification | localization | heated milk | raw milk | past[b] milk | ESL[c] milk | UHT[d] milk | steril[e] milk | evap[f] milk | coffee cream |
|---|---|---|---|---|---|---|---|---|---|---|---|
| 90–96 | NKVLVLD | lactulosyllysine | K91[g] | x | x | x | x | x | x | x | x |
| | | $N^{\epsilon}$-carboxymethyllysine | K91[g] | x | x | x | x | x | x | x | x |
| | | $N^{\epsilon}$-carboxyethyllysine | K91 | t | – | t | – | x | x | x | t |
| 97–108 | TDYKKYLLFCME | $N^{\epsilon}$-carboxymethyllysine | K100 | – | – | – | – | – | t | t | t |
| | | $N^{\epsilon}$-carboxymethyllysine | K101 | t | – | – | – | – | t | t | t |
| | | $N^{\epsilon}$-carboxyethyllysine | K100 | – | – | – | – | – | – | – | – |
| | | $N^{\epsilon}$-carboxyethyllysine | K101 | – | – | – | – | – | – | – | – |
| | | methionine sulfoxide | M107[g] | x | x | x | x | x | x | x | x |
| | | methionine sulfone | M107[g] | x | x | x | x | x | x | x | x |
| 115–127 | QSLACQCLVRTPE | sulfinic acid | C119 | t | t | t | t | x | x | x | t |
| | | sulfinic acid | C121 | – | – | – | – | – | – | – | – |
| | | sulfonic acid | C119 | – | – | t[k] | – | – | – | – | – |
| | | sulfonic acid | C121 | – | – | t[k] | – | – | – | – | – |
| | | methylglyoxaldihydroxyimidazoline | R124 | – | – | – | – | – | t | t | – |
| | | methylglyoxalimidazolinone | R124 | – | – | – | – | t | x | t | t |
| 135–137 | KFD | lactulosyllysine | K135[g] | | x | x | x | x | x | x | x |
| | | $N^{\epsilon}$-carboxymethyllysine | K135[g] | x | – | – | – | x | x | x | x |
| 135–158 | KFDKALKALPMHIRLSFNPTQLEE | methionine sulfoxide | M145[g] | x | x | x | x | x | x | x | x |

[a]Amino acid. [b]Pasteurized. [c]Extended shelf life. [d]Ultrahigh temperature. [e]Sterilized. [f]Evaporated. [g]Quantitative data shown in Figure 3. [h]Detected in traces. [i]Localization not possible. [k]Detected in only one sample.



dx.doi.org/10.1021/jf503664y | J. Agric. Food Chem. 2014, 62, 10903−10915

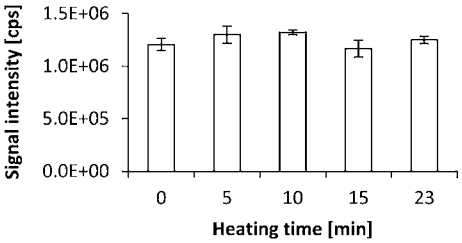


**Figure 2.** Absolute signal intensities of the peptide AA 159−162 (QCHI). $\beta$-Lactoglobulin from raw and heated milk was digested with GluC and analyzed by UHPLC-MS/MS. Intensities were not significantly altered by the heating process. The mean of a triplicate ± standard deviation is displayed.

expected that the normalization of signal areas of the analytes to the signal area of the internal standard peptide compensated for differences in the mass spectrometric performance during different runs. In commercially available dairy products, the concentration of $\beta$-lactoglobulin depends, for example, on the cattle breed or feeding conditions. Industrial processing such as evaporation further influences the protein concentration. Thus, normalizing the signal areas of modified peptides by the signal area of the internal standard peptide also compensates for differences in protein concentrations between different products.

It was expected that protein modifications in milk are present in very small quantities. Therefore, a sensitive sMRM method was developed that considered only the most intense charge state for quantification.[6] Although this approach did not allow for the direct comparison of the modification degree of different modification sites, it provided information on the relative amount of one specific modification site in different samples. Figure 3 summarizes the results obtained for the detected modifications in raw milk heated on a laboratory scale and those found in commercially available milk products.

**Kinetics of N-Terminal Lysine- and Arginine-Bound Glycation Products.** Heating of raw milk at 99 °C resulted in detectable lactosylation of the lysine residues K14, K47, K60, K75/77/83, K91, and K135 (Table 1; Figure 3B−G). Furthermore, glycation of the N-terminal amino group was observed (Figure 3A). Modification indices ranged between 0.99 (K14) and 56.3 (N-terminus). Similar profiles for the formation of the Amadori products were obtained for all affected lysine residues with very low modification rates in raw milk and increasing modification with extended heating. The modification indices of some lysine residues (e.g., K91, see Figure 3F) reached a plateau after prolonged heating. These findings are in very good agreement with previous studies on the kinetics of lactulosyllysine formation in milk proteins, showing a linear function of time in the early phase of milk heating and ending up in a plateau after prolonged heating.[2] It should be noted that the indices do not necessarily correlate with the concentration of modifications, because lower peptide ionization leads to lower modification indices. Nevertheless, it is interesting that only the N-terminus was already remarkably glycated in raw milk (index 16.1), whereas all other Amadori products were of very low intensity in raw milk (indices <1). The presence of the Amadori product in raw milk has been detected before.[7,21] Those initial levels of lactosylated lysine may be formed in vivo or during storage by nonenzymatic, but possibly also by enzymatic reactions. Furthermore, artificial formation during sample workup cannot be fully excluded. However, the background levels in raw milk have been observed not only in the present study but also through the use of other analytical methods including different methods of sample preparation.[7,21] At all lysine residues, a (highly) significant increase of lactulosyllysine was observed after only 5 min of heating, confirming that this modification is a good marker for milk products that underwent a low degree of processing.

In dairy products, clear differences in the modification indices were observed in relation to industrial treatment. In most cases, the glycation degree determined in pasteurized samples was not significantly different from raw milk, whereas ESL treatment led to a significantly higher lactosylation rate at three sites (K60, K75/77/83, K135; Figure 3AA−GG). Depending on the lactosylation site in the amino acid sequence, either sterilized milk and evaporated milk, or coffee cream, or UHT milk showed the highest modification indices. Obviously, the particular sites in protein structures are prone to glycation to variable extent and undergo different subsequent reactions, when the processing conditions vary.[22] It could be concluded from the comparison of evaporated milk with sterilized milk and coffee cream, for example, that the evaporation step led to a particularly severe modification of K47 and K60, whereas K14 and K91 were less affected. The evaporation process leads to a higher concentration of the reactants lactose and lysine residues, which should promote lactosylation in general. However, this effect was not observed for all lysine residues. Most likely, evaporation influenced the conformation of $\beta$-lactoglobulin differently from sole heating. The different process-induced changes of protein conformation may then lead to different molecular environments of the particular lysine residues. The lactosylation of the sites K60, K75/77/83, and K135 reflected moderate heating during the production of ESL milk more sensitively, so that it can be assumed that site-specific analysis of lactulosyllysine may be a more sensitive marker of low-impact heat treatment than the recording of overall lactulosylation as determined, for example, by the furosine method.[21] A previous study already achieved site-specific semiquantification of the Amadori product in $\beta$-lactoglobulin in dairy products by mass spectrometry, applying matrix-assisted laser desorption ionization time-of-flight mass spectrometry (MALDI-TOF-MS) after in-gel digest.[8] However, the former study detected modifications at only three sites (K47, K138/141), probably because the method was less sensitive. The present results of the lactosylation index at K47 in different milk products match former data very well, whereas the present method did not cover K138/141.

CML, the best characterized degradation product of the Amadori product, could be detected in traces in heated raw milk at K8, K14, K69, K70, K75/77, and K101 (Table 1). Higher modification indices of CML, which allowed semiquantifiction, were observed at K47, K60, K91, and K135 (Figure 3H−K). After a lag phase, CML indices increased linearly as a function of heating time and reached final values between 0.03 (K47) and 1.6 (K60). In commercially available milk products, CML was also detected in traces at K83 and K100 as well as at the N-terminus, in addition to the aforementioned sites (Table 1). However, these signals were close to the detection level so that further analyses are required to determine if this observation is indeed related to industrial processing. CML could not be detected at all or only in very low amounts in raw, pasteurized, and ESL milk. All other analyzed milk products showed a clear connection of CML formation to heat treatment (Figure 3HH−KK), with the highest modification indices in sterilized and evaporated milk and coffee cream, which is consistent with previous studies.[4] Thus, it can be

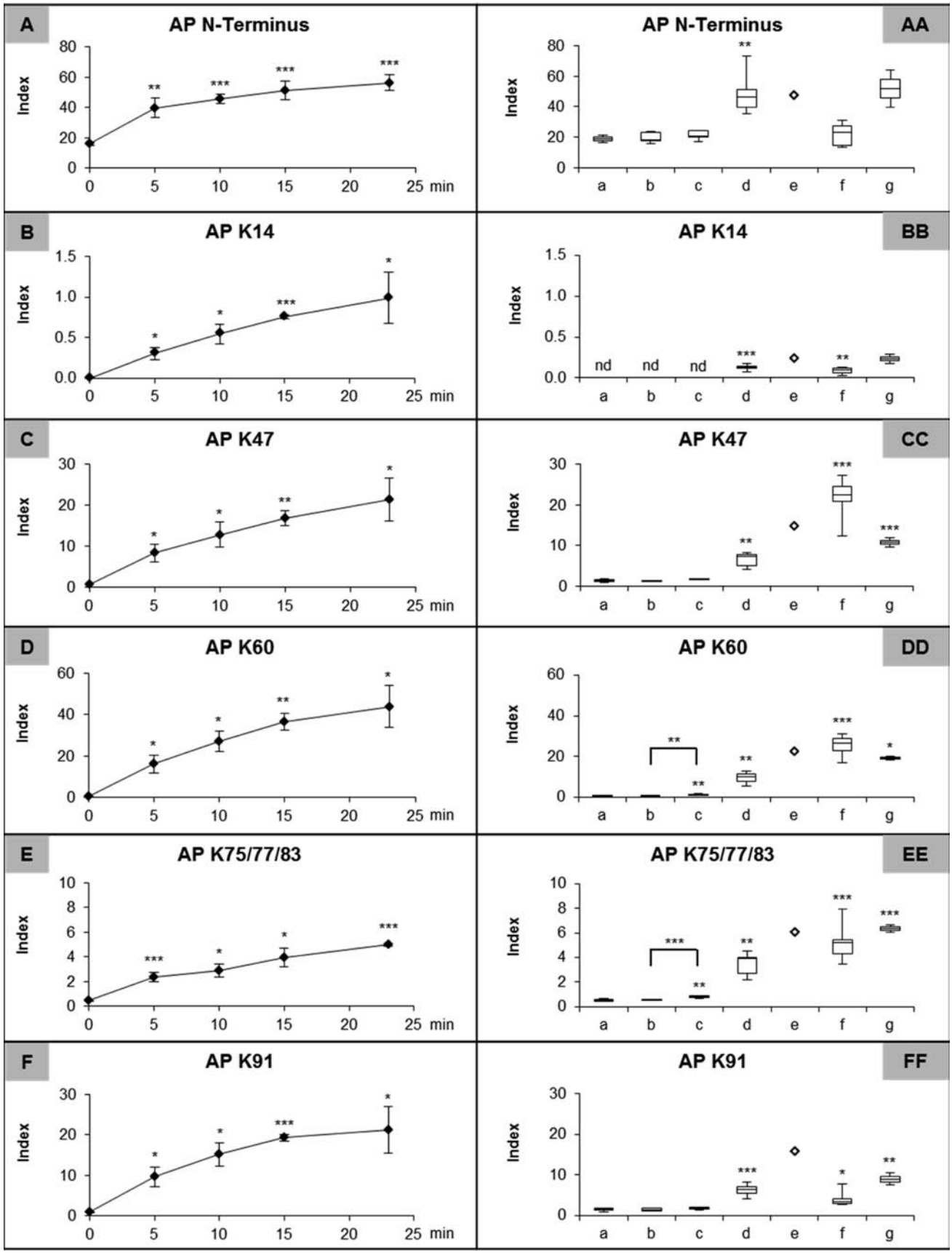


**Figure 3.** continued


dx.doi.org/10.1021/jf503664y | J. Agric. Food Chem. 2014, 62, 10903−10915

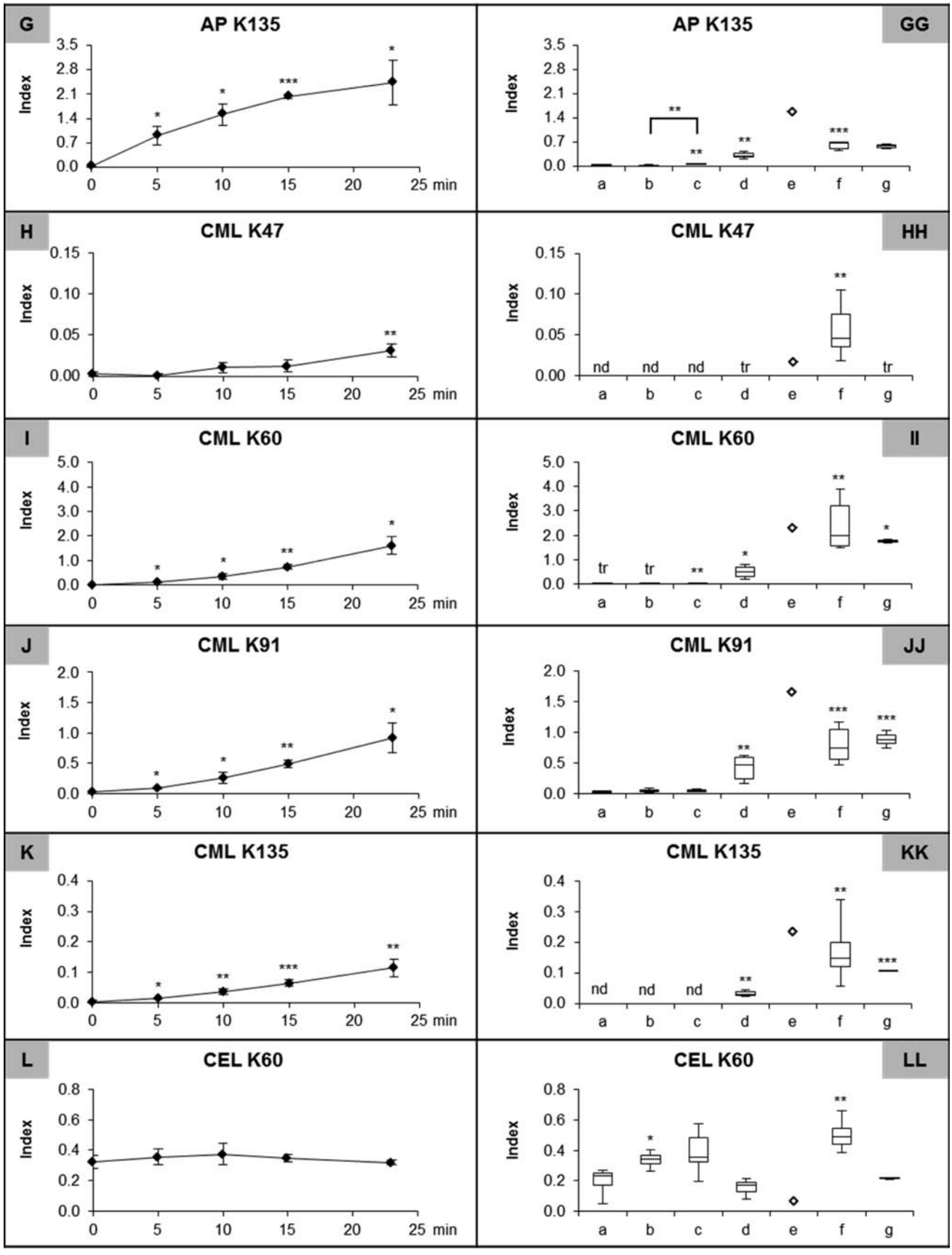


**Figure 3.** continued


dx.doi.org/10.1021/jf503664y | *J. Agric. Food Chem.* 2014, 62, 10903−10915

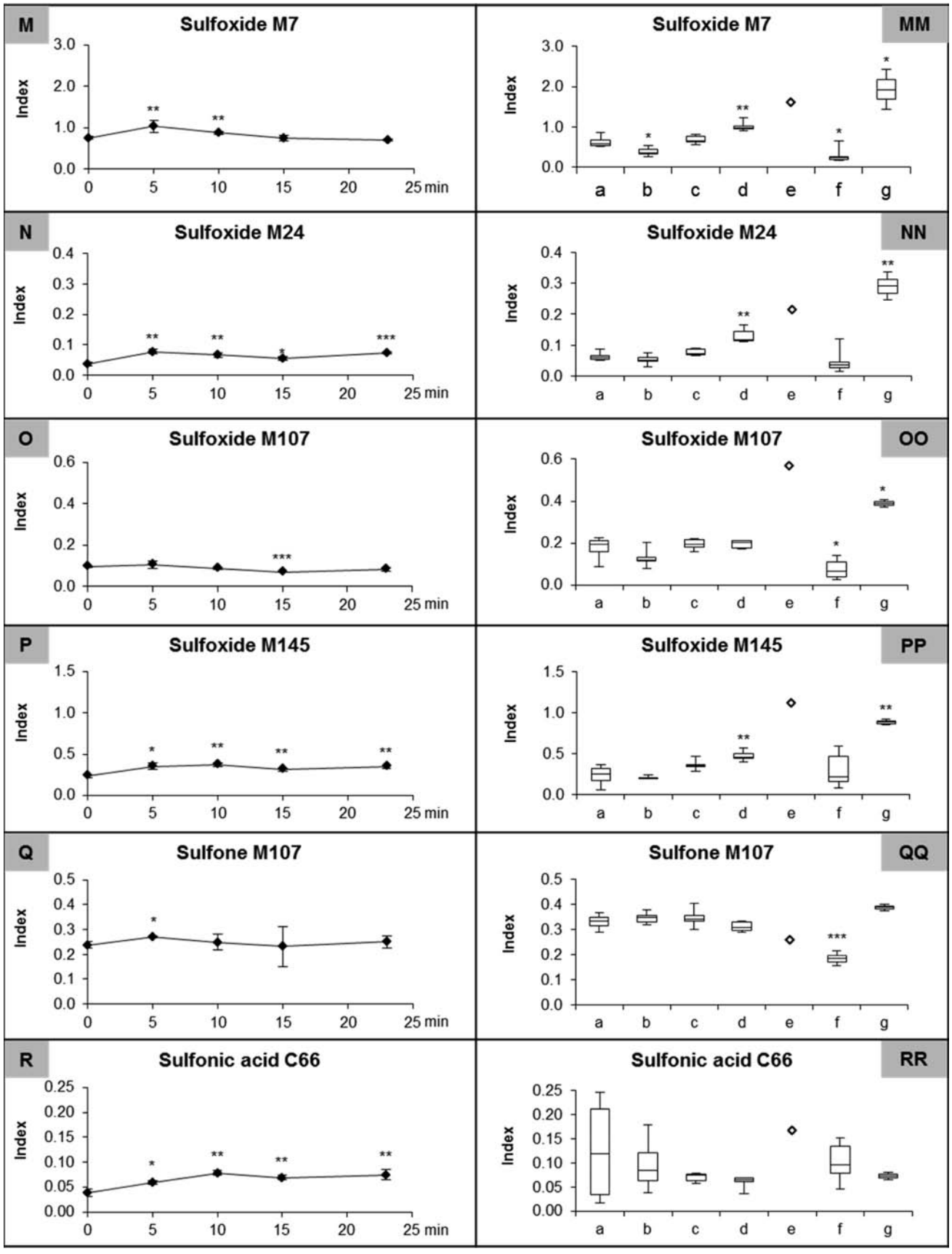


**Figure 3.** continued


dx.doi.org/10.1021/jf503664y | J. Agric. Food Chem. 2014, 62, 10903−10915

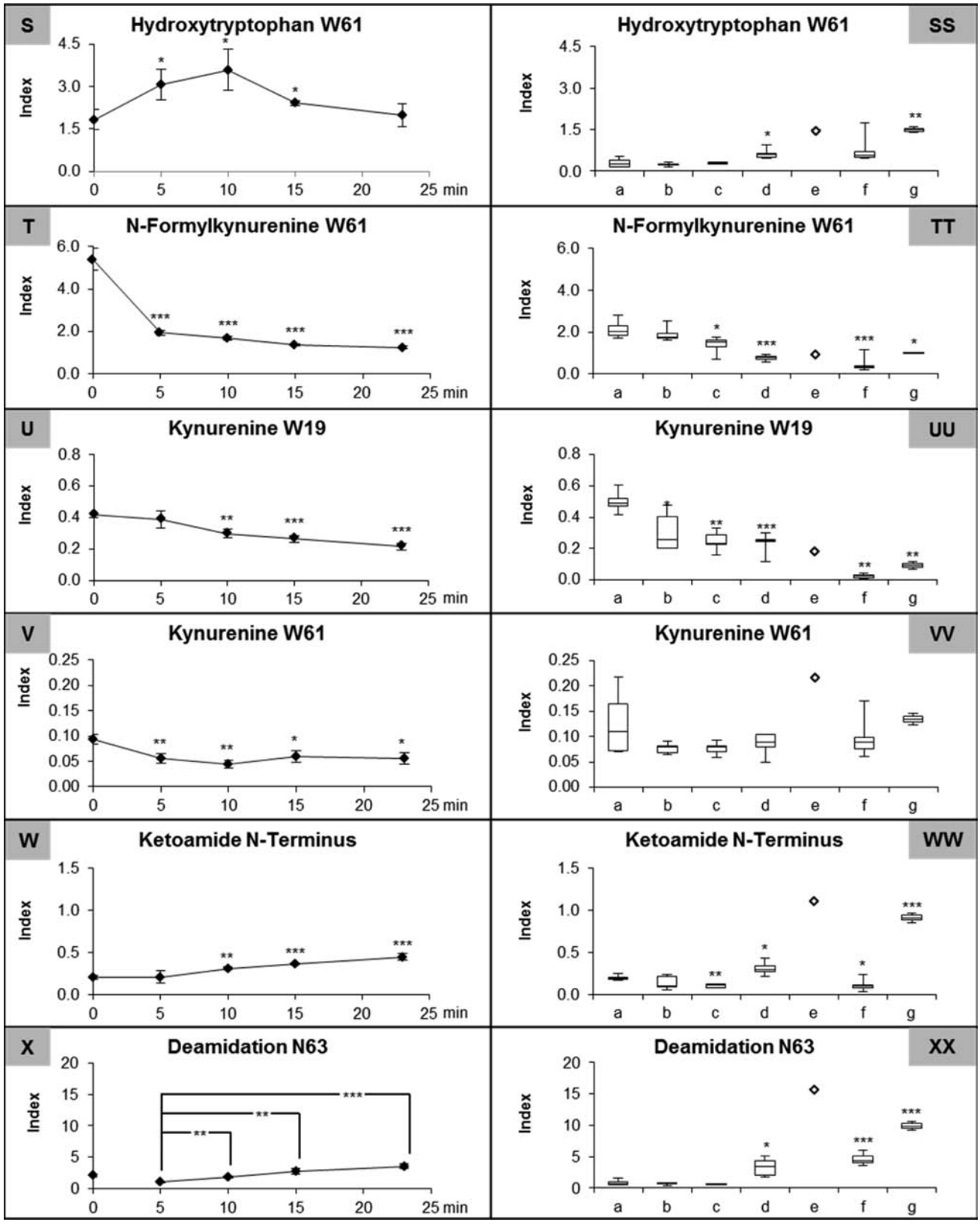


**Figure 3.** Modification indices of modifications detected in milk and dairy products. (A–X) Raw milk was heated at 99 °C for up to 23 min. The mean of a triplicate ± standard deviation is displayed. (AA–XX) Commercially available products: (a) raw milk ($n = 5$); (b) pasteurized milk ($n = 5$); (c) ESL milk ($n = 5$); (d) UHT milk ($n = 5$); (e) sterilized milk ($n = 1$); (f) evaporated milk ($n = 6$); (g) coffee cream ($n = 2$). The median, the first and the third quartiles, the minimum, and the maximum are displayed. AP, Amadori product; CML, $N^{\varepsilon}$-carboxymethyllysine. (∗) $p < 0.05$; (∗∗) $p < 0.01$; (∗∗∗) $p < 0.001$ (reference, if not marked differently, raw milk).


dx.doi.org/10.1021/jf503664y | J. Agric. Food Chem. 2014, 62, 10903–10915

concluded that the presence of CML in milk products is strictly related to thermal treatment during processing. In contrast to lactulosyllysine, different processing conditions did not site-specifically affect the CML formation. As a marker, it may reflect rather intensive heating conditions as applied during UHT treatment and beyond.

CEL was semiquantified in heated milk at K60 (Figure 3L) and detected in traces at K69/70 and K91 (Table 1). The modification index at K60 did not increase significantly during heating at 99 °C, nor could we establish a clear correlation of the modification indices for K60 in commercially available milk products to the heating process (Figure 3LL). On the other hand, CEL at K69/70 and K91 could be clearly detected only in sterilized, evaporated, and UHT milk, but not in coffee cream (Table 1), which may indicate some influence from the processing conditions. It has been shown before that dehydrogenases from *Lactococcus (Streptococcus) lactis* are able to form CEL by reductive alkylation of lysine with pyruvate.[4] Thus, the microbial activity may be a more important source of CEL in some samples than thermal processes. Ahmed et al. measured protein-bound CEL in three samples of raw, pasteurized, and sterilized milk and found significantly higher concentrations in pasteurized and sterilized milk compared to raw milk, but not in sterilized milk compared to pasteurized milk.[23] Altogether, the findings indicate that nonthermal processes may also be an important source of CEL in milk products, so that this modification cannot be used as convincing marker for heat treatment in this product group.

No arginine glycation products could be detected in $\beta$-lactoglobulin from heated raw milk (Table 1), although the presence of methylglyoxal-dihydroxyimidazoline, methylglyoxal-imidazolinone, and 3-deoxygalactosone-/3-deoxyglucosone-imidazolinone has been reported for $\beta$-lactoglobulin after heating with lactose.[6] Due to their relatively low stability, they may react further with other milk ingredients. However, traces of methylglyoxal-dihydroxyimidazoline were detected at R124 in sterilized and evaporated milk (Table 1) and, furthermore, small amounts of methylglyoxal-imidazolinone were shown to be present at R40 and R124 in more severely heated products (Table 1). As with CEL, Ahmed et al. detected protein-bound methylglyoxal-imidazolinone in significantly higher concentrations in pasteurized and sterilized milk samples compared to raw milk, but not in sterilized compared to pasteurized milk.[23] Thus, the present results suggest that methlyglyoxal-derived arginine modifications are formed to some extent upon thermal milk processing, but their relevance is low compared to other protein modifications.

**Kinetics of Oxidation Products.** When defatted milk was heated at 99 °C, we could observe oxidation of methionine to the sulfoxide, of cysteine to the sulfonic acid, and of tryptophan to hydroxytryptophan (Table 1; Figure 3M−P,R,S).

Methionine is very easily oxidized, in a first step yielding methionine sulfoxide, which has already been reported to be present in heated milk and, particularly, in whey protein and caseinate preparation.[8,9] Methionine sulfoxide could be detected in raw milk at all four methionine residues (M7, M24, M107, M145), which may be partially caused by oxidation processes during sample preparation or by enzymatic processes, for example, through lactoperoxidase (Table 1).[24] When raw milk was heated for a short time, relatively low, but significant, increases in the indices of methionine sulfoxide were found at M7, M24, and M145 (Figure 3M−P). However, prolonged heating did not lead to a further increase of methionine oxidation. In the case of M107, in contrast, no formation of methionine sulfoxide was observed as a consequence of thermal treatment. On the other hand, a clear tendency toward higher indices of methionine sulfoxide was observed with increasing severity of the thermal treatment in pasteurized, ESL, UHT, and sterilized milk, and, at all methionine residues, even higher indices were measured in sterilized milk and coffee cream (Figure 3MM−PP). Evaporated milk, in contrast, had surprisingly low indices, indicating further reactions of methionine residues during the concentration step (Figure 3MM−PP). In coffee cream, which has the highest fat content of all samples, the generation of reactive oxygen species during lipid oxidation very likely promoted oxidation of methionine to the sulfoxide.[20] This hypothesis is supported by the results for evaporated milk: the product with the highest fat content (7.5%) had very high indices for methionine sulfoxide at M7 and M24 (0.65 and 0.12, respectively), whereas the other five products were much less affected (0.17−0.28 and 0.02−0.05, respectively) (Figure 3MM,NN). Because lipid oxidation may be an important contributor to the formation of methionine sulfoxide, it can be assumed that heating of whole milk has a greater effect than heat treatment of defatted milk as performed in the present study. Thus, it may be concluded that methionine sulfoxide is a rather poor indicator of thermal impact but may reflect the lipid oxidation rate during processing very well.

Although methionine sulfone could be detected at M107, its index was stable during the heating of raw milk, and the indices measured in commercially available milk samples did not suggest that formation of the sulfone was dependent on the process parameters (Figure 3Q). In evaporated milk, the intensities of sulfone were very low, indicating once more that methionine underwent further reactions during the evaporation processes (Figure 3QQ). Thus, it is likely that methionine sulfone in milk results from enzymatic post-translational modification rather than from chemical modification during thermal treatment.

Oxidation of cysteine to the sulfinic acid during heating of raw milk was detected only in traces at C119 (Table 1). In the peptide used as internal standard (AA 159−162, QCHI), oxidation of cysteine could not be detected.[6] A trend toward higher concentration of sulfinic acid at C119 was observed in commercially available products (Table 1), suggesting heat-dependent oxidation. At C66, significantly higher indices for cysteine sulfonic acid were also found as a result from the heating of raw milk (Figure 3R). However, the analysis of commercial milk products did not confirm these findings, because the products showed high variations of the cysteine sulfonic acid concentration at C66, C119, and C121 without clear correlation with the heat treatment (Table 1; Figure 3RR). Obviously, the nonenzymatic oxidation of cysteine to the sulfonic acid is of minor importance in heated milk products. Cysteine sulfenic acid is not covered by the method because it is reduced by the addition of DTT prior to mass analysis.

When $\beta$-lactoglobulin was heated in a milk-resembling system, hydroxytryptophan, *N*-formylkynurenine, kynurenine, and hydroxykynurenine were reported as oxidation products of tryptophan.[6] Only traces of hydroxytryptophan were detected at W19, when raw milk was heated at 99 °C (Table 1). Semiquantification at W61 revealed that the indices for hydroxytryptophan first significantly increased during heating but that the amino acid approached its initial concentration during prolonged reaction (Figure 3S). Thus, formation of hydroxytryptophan is probably promoted by thermal processing, although the product is not stable, but further degraded. UHT, sterilized, and evaporated milk as well as coffee cream contained

higher levels of hydroxytryptophan than less severely heated milk, confirming heat-dependent oxidation of tryptophan (Figure 3SS). It is interesting to note that the striking variance in the indices of evaporated milk is due to a single sample which contained more fat (7.5%; index 1.75), whereas the five other products with fat contents between 3 and 4% showed indices between 0.45 and 0.75. Probably, lipid-dependent generation of reactive oxygen species led to the higher oxidation degree of tryptophan at W61 observed in the outlier. However, it cannot be excluded that differences in the heating process also contributed to the observed variance.

*N*-Formylkynurenine at W61 was naturally present in raw milk and significantly decreased from an index of 5.4 to 1.2 when the raw milk was heated (Figure 3T). It seems likely that it was further degraded. However, kynurenine, a possible degradation product of *N*-formylkynurenine, also decreased significantly at W19 and W61 during heating (Figure 3U,V) indicating that further/other degradation reactions must be responsible for the decrease of *N*-formylkynurenine and kynurenine. The observation that tryptophan was hydroxylated (see above) and that hydroxykynurenine has been detected in a model system, when $\beta$-lactoglobulin was heated in a milk-resembling system with lactose,[6] gives rise to the assumption that the aromatic rings of *N*-formylkynurenine and kynurenine were oxidized. The oxidized products could, however, not be detected in heated milk (see Table 1) and were apparently below the detection limit of the applied method. The analyzed milk products showed the same trend as heated raw milk, with high contents of *N*-formylkynurenine and kynurenine at W19 and W61, respectively, in mildly treated milk and lower contents in more severely heated products (Figure 3TT−VV).

Altogether, these results lead to the assumption that enzymatic processes probably contribute largely to the presence of tryptophan modifications in raw milk. Additionally, further degradation reactions of primary tryptophan modifications, which have not been elucidated yet, must take place during thermal treatment.

Recently, N-terminal $\alpha$-ketoamide was detected in $\beta$-lactoglobulin in sterilized milk, resulting from the oxidation of the N-terminal amine functional group.[6] The present study revealed that detectable amounts of the $\alpha$-ketoamide were already present in raw milk, with a modification index of 0.2 (Figure 3W). The index increased during heating of raw milk and reached a final value of 0.45. Possibly, reactive intermediate products from the Maillard reaction such as dicarbonylic structures favored the oxidation, as proposed by Akagawa et al.[25] In commercial milk products, significantly higher indices were observed in UHT milk, sterilized milk, and coffee cream, reflecting the heat-dependent formation (Figure 3WW). In evaporated milk, in contrast, the concentrations of the N-terminal $\alpha$-ketoamide were very low. The examined structure has a highly reactive $\alpha$-dicarbonyl group and, probably, underwent further reactions during the industrial concentration of the product.

**Kinetics of the Hydrolysis of Asparagine.** Heating of raw milk resulted in the hydrolysis of asparagine N63 to aspartic acid. The hydrolysis occurred linearly (Figure 3X). Interestingly, the modification index in raw milk was higher (index 2.1) than in milk heated for 5 min at 99 °C (index 1.0). This leads to the assumption that the deamidation in raw milk was partially catalyzed by milk asparaginase during sample preparation. Thermal treatment probably deactivated the asparaginase, preventing any additional deamidation during sample workup of the heated samples. The results obtained for the analyzed milk samples also reflected the heat-dependent hydrolysis of N63, with sterilized milk having the highest modification index (Figure 3XX). Deamidation of N63 has already been observed during the storage of UHT milk[26] and, thus, the presented modification indices might have been partially influenced by different storage periods of the products. Still, the heat-dependent formation is clearly visible and in good accordance with a previous study,[27] providing evidence for the heat-induced deamidation of milk protein.

Previously, it has been shown that a great variety of protein modifications are present in processed milk affecting, for example, lysine, arginine, methionine, cysteine, tryptophan, asparagine, and the N-terminus.[6] The present study performed semiquantitative analyses of these modifications to reveal the origin of the compounds. As expected, lactosylation of lysine and the N-terminus as well as CML formation was observed as consequences of thermal treatment. Additionally, hydroxytrypophan and the ketoamide of the N-terminus as well as deamidation of asparagine were detected as thermal reaction products. The formation of CEL, cysteine sulfonic acid, methionine sulfone, *N*-formylkynurenine, and kynurenine, in contrast, rather seems to depend on enzymatic processes in the raw milk. Further degradation of *N*-formylkynurenine and kynurenine, however, was detected again as thermal reaction. Finally, the formation of methionine sulfoxide reflected heat treatment only to some extent, but was obviously more strongly related to lipid oxidation processes. Thus, product-specific semiquantification of a variety of post-translational modifications helped to shed light on different enzymatic and nonenzymatic processes that occur during the heating and storage of milk. The newly acquired information may be helpful to develop custom-tailored markers for different industrial processes and storage conditions. Additionally, site-specific semiquantification revealed that the site-specific analysis of a modification may lead to highly sensitive markers. For example, lactosylation of K60, K75/77/83, and K135 indicated a difference between pasteurized milk and ESL milk, whereas lactosylation of other lysine residues and the N-terminus did not reflect the minor differences in the thermal impact of these two production processes.

In the future, highly sensitive and truly untargeted methods will be required to comprehensively elucidate all post-translational protein modifications that have escaped identification so far. Furthermore, controlled storage experiments are required to differentiate between storage and heating effects in commercial samples.

## ■ ASSOCIATED CONTENT

### Supporting Information

Overview of modified peptides of $\beta$-lactoglobulin which were selected for the MRM-method. This material is available free of charge via the Internet at http://pubs.acs.org.

## ■ AUTHOR INFORMATION

### Corresponding Author

*(M.P.) Mail: Henriette Schmidt-Burkhardt Chair of Food Chemistry, Food Chemistry Unit, Department of Chemistry and Pharmacy, Emil Fischer Center, Friedrich-Alexander Universität Erlangen-Nürnberg (FAU), Schuhstr. 19, 91052 Erlangen, Germany. Phone: +49-9131-8524102. Fax: +49-9131-8522587. E-mail: monika.pischetsrieder@fau.de.

### Author Contributions

[‖]J.M. and J.W. equally contributed to this work.

### Notes

The authors declare no competing financial interest.

## ■ ABBREVIATIONS USED

CML, $N^{\varepsilon}$-carboxymethyllysine; CEL, $N^{\varepsilon}$-carboxyethyllysine; UHPLC-MS/MS, ultrahigh-performance liquid chromatography−tandem mass spectrometry; DTT, 1,4-dithiothreitol; ESL, extended shelf life; UHT, ultrahigh temperature; ESI, electrospray ionization; sMRM, scheduled multiple reaction monitoring; MALDI-TOF-MS, matrix-assisted laser desorption ionization−time-of-flight−mass spectrometry

## ■ REFERENCES


(1) van Boekel, M. A. J. S. Effect of heating on Maillard reactions in milk. *Food Chem.* **1998**, *62*, 403−414.

(2) Claeys, W. L.; Ludikhuyze, L. R.; Hendrickx, M. E. Formation kinetics of hydroxymethylfurfural, lactulose and furosine in milk heated under isothermal and non-isothermal conditions. *J. Dairy Res.* **2001**, *68*, 287−301.

(3) Lan, X. Y.; Wang, J. Q.; Bu, D. P.; Shen, J. S.; Zheng, N.; Sun, P. Effects of heating temperatures and addition of reconstituted milk on the heat indicators in milk. *J. Food Sci.* **2010**, *75*, C653−C658.

(4) Delatour, T.; Hegele, J.; Parisod, V.; Richoz, J.; Maurer, S.; Steven, M.; Buetler, T. Analysis of advanced glycation endproducts in dairy products by isotope dilution liquid chromatography-electrospray tandem mass spectrometry. The particular case of carboxymethyllysine. *J. Chromatogr., A* **2009**, *1216*, 2371−2381.

(5) Assar, S. H.; Moloney, C.; Lima, M.; Magee, R.; Ames, J. M. Determination of $N^{\varepsilon}$-(carboxymethyl)lysine in food systems by ultra performance liquid chromatography-mass spectrometry. *Amino Acids* **2009**, *36*, 317−326.

(6) Meltretter, J.; Wuest, J.; Pischetsrieder, M. Comprehensive analysis of non-enzymatic post-translational $\beta$-lactoglobulin modifications in processed milk by ultrahigh-performance liquid chromatography−tandem mass spectrometry. *J. Agric. Food Chem.* **2013**, *61*, 6971−6981.

(7) Hegele, J.; Buetler, T.; Delatour, T. Comparative LC-MS/MS profiling of free and protein-bound early and advanced glycation-induced lysine modifications in dairy products. *Anal. Chim. Acta* **2008**, *617*, 85−96.

(8) Meltretter, J.; Becker, C. M.; Pischetsrieder, M. Identification and site-specific relative quantification of $\beta$-lactoglobulin modifications in heated milk and dairy products. *J. Agric. Food Chem.* **2008**, *56*, 5165−5171.

(9) Baxter, J. H.; Lai, C. S.; Phillips, R. R.; Dowlati, L.; Chio, J. J.; Luebbers, S. T.; Dimler, S. R.; Johns, P. W. Direct determination of methionine sulfoxide in milk proteins by enzyme hydrolysis/high-performance liquid chromatography. *J. Chromatogr., A* **2007**, *1157*, 10−16.

(10) Calabrese, M. G.; Mamone, G.; Caira, S.; Ferranti, P.; Addeo, F. Quantitation of lysinoalanine in dairy products by liquid chromatography-mass spectrometry with selective ion monitoring. *Food Chem.* **2009**, *116*, 799−805.

(11) Kislinger, T.; Humeny, A.; Peich, C. C.; Zhang, X.; Niwa, T.; Pischetsrieder, M.; Becker, C. M. Relative quantification of $N(\varepsilon)$-(carboxymethyl)lysine, imidazolone A, and the Amadori product in glycated lysozyme by MALDI-TOF mass spectrometry. *J. Agric. Food Chem.* **2003**, *51*, 51−57.

(12) Meyer, B.; Baum, F.; Vollmer, G.; Pischetsrieder, M. Distribution of protein oxidation products in the proteome of thermally processed milk. *J. Agric. Food Chem.* **2012**, *60*, 7306−7311.

(13) Meyer, B.; Al-Diab, D.; Vollmer, G.; Pischetsrieder, M. Mapping the glycoxidation product $N(\varepsilon)$-carboxymethyllysine in the milk proteome. *Proteomics* **2011**, *11*, 420−428.

(14) Meltretter, J.; Seeber, S.; Humeny, A.; Becker, C. M.; Pischetsrieder, M. Site-specific formation of Maillard, oxidation, and condensation products from whey proteins during reaction with lactose. *J. Agric. Food Chem.* **2007**, *55*, 6096−6103.

(15) Arena, S.; Renzone, G.; Novi, G.; Paffetti, A.; Bernardini, G.; Santucci, A.; Scaloni, A. Modern proteomic methodologies for the characterization of lactosylation protein targets in milk. *Proteomics* **2010**, *10*, 3414−3434.

(16) Le, T. T.; Deeth, H. C.; Bhandari, B.; Alewood, P. F.; Holland, J. W. Quantification of lactosylation of whey proteins in stored milk powder using multiple reaction monitoring. *Food Chem.* **2013**, *141*, 1203−1210.

(17) Fogliano, V.; Monti, S. M.; Visconti, A.; Randazzo, G.; Facchiano, A. M.; Colonna, G.; Ritieni, A. Identification of a $\beta$-lactoglobulin lactosylation site. *Biochim. Biophys. Acta* **1998**, *1388*, 295−304.

(18) Distler, L.; Georgieva, A.; Kenkel, I.; Huppert, J.; Pischetsrieder, M. Structure- and concentration-specific assessment of the physiological reactivity of $\alpha$-dicarbonyl glucose degradation products in peritoneal dialysis fluids. *Chem. Res. Toxicol.* **2014**, *27*, 1421−1430.

(19) Ahmed, N.; Dobler, D.; Dean, M.; Thornalley, P. J. Peptide mapping identifies hotspot site of modification in human serum albumin by methylglyoxal involved in ligand binding and esterase activity. *J. Biol. Chem.* **2005**, *280*, 5724−5732.

(20) Brock, J. W.; Cotham, W. E.; Thorpe, S. R.; Baynes, J. W.; Ames, J. M. Detection and identification of arginine modifications on methylglyoxal-modified ribonuclease by mass spectrometric analysis. *J. Mass Spectrom.* **2007**, *42*, 89−100.

(21) Elliott, A. J.; Datta, N.; Amenu, B.; Deeth, H. C. Heat-induced and other chemical changes in commercial UHT milks. *J. Dairy Res.* **2005**, *72*, 442−446.

(22) Gadgil, H. S.; Bondarenko, P. V.; Pipes, G.; Rehder, D.; McAuley, A.; Perico, N.; Dillon, T.; Ricci, M.; Treuheit, M. The LC/MS analysis of glycation of IgG molecules in sucrose containing formulations. *J. Pharm. Sci.* **2007**, *96*, 2607−2621.

(23) Ahmed, N.; Mirshekar-Syahkal, B.; Kennish, L.; Karachalias, N.; Babaei-Jadidi, R.; Thornalley, P. J. Assay of advanced glycation endproducts in selected beverages and food by liquid chromatography with tandem mass spectrometric detection. *Mol. Nutr. Food Res.* **2005**, *49*, 691−699.

(24) Ostdal, H.; Bjerrum, M. J.; Pedersen, J. A.; Andersen, H. J. Lactoperoxidase-induced protein oxidation in milk. *J. Agric. Food Chem.* **2000**, *48*, 3939−3944.

(25) Akagawa, M.; Sasaki, T.; Suyama, K. Oxidative deamination of lysine residue in plasma protein of diabetic rats. Novel mechanism via the Maillard reaction. *Eur. J. Biochem.* **2002**, *269*, 5451−5458.

(26) Holland, J. W.; Gupta, R.; Deeth, H. C.; Alewood, P. F. Proteomic analysis of temperature-dependent changes in stored UHT milk. *J. Agric. Food Chem.* **2011**, *59*, 1837−1846.

(27) Metwalli, A. A. M.; van Boekel, M. A. J. S. On the kinetics of heat-induced deamidation and breakdown of caseinate. *Food Chem.* **1998**, *61*, 53−61.

deoxyanthocyanidins, which otherwise have only been found in the flowers of sinningia (*Sinningia cardinalis*), the silk tissues of maize (*Zea mays*), and the stalks of sugar cane (*Saccharum* sp.).[17−19]

In sorghum grains, polyphenol compounds can be found in the pericarp (outer seed coat) and the testa (inner layer of tissue between the pericarp and the endosperm). A number of classical loci identified by their effects on grain color and testa presence control the presence or absence of polyphenol compounds in sorghum.[20] Genotypes with dominant alleles at the B1 and B2 loci have proanthocyanidins in the testa. Genotypes with a dominant allele at the spreader (S) locus, as well as dominant alleles at the B1 and B2 loci, have proanthocyanidins in both the pericarp and the testa, often, but not always, resulting in a brown appearance to the grain. The base pericarp color is red, yellow, or white, and these colors are controlled by the R and Y loci. The S locus and additional loci, such as intensifier (I) and mesocarp thickness (Z), modify the base pericarp color, resulting in a range of colors from brilliant white to black with various shades of red, yellow, pink, orange, and brown among sorghum genotypes (see Figure 1). Using mutants for seed color traits, the

**Figure 1.** Natural variation in sorghum grain color. Three accessions (with three seeds of each accession) of grain with the appearance of (A) brown (PI597965, PI533927, PI35038), (B) white (PI533755, PI533845, PI534028), (C) yellow (PI659691, PI656011, PI533776), and (D) red (PI576418, PI534047, PI564165) pericarps. The outer coat has been scraped off of some samples, revealing the presence or absence of a pigmented testa.

biochemical and regulatory pathways underlying flavonoids and flavonoid products have been almost completely elucidated in *Arabidopsis* and maize, and extensively studied in other species (Table S1 in the Supporting Information).[21] Therefore, homology can be used as a guide to discover genes involved in the sorghum flavonoid pathway. The gene underlying the B2 locus was recently cloned and designated *Tannin1*, along with two nonfunctional alleles of *Tannin1*, *tan1-a* and *tan1-b*.[22] *Tannin1* encodes a WD40 protein homologous to the *Arabidopsis* proanthocyanidin regulator *transparent testa glabra1* (*TTG1*). The gene underlying the Y locus has also been cloned and designated *Yellow seed1*. *Yellow seed1* encodes a MYB protein, orthologous to the maize 3-deoxyanthocyanidin regulator *P1*, that is needed for accumulation of 3-deoxyanthocyanidins in the sorghum pericarp.[23] The R locus has been mapped to chromosome 3 between 57 and 59 Mb, and the Z locus has been mapped to chromosome 2 between 56 and 57 Mb,[24] but the underlying genes have not been identified.

While the genetic controls of polyphenol presence/absence have been well-studied using mutant lines and nonfunctional polymorphisms, there has been little study of quantitative natural variation in polyphenols.[25] Polyphenol nonfunctional mutations were strongly selected during cereal domestication, when bitter tasting and/or dark compounds were partly or completely lost in most cereals, including wheat, rice, and maize.[26] However, sorghum provides a valuable resource for polyphenol diversity, as adaptation to different environments has led to extensive phenotypic and genetic diversity in the crop.[13,27] This diversity can be useful for biofortification and crop improvement (e.g., desirable traits can be bred into existing elite varieties), but quantitative phenotyping is needed to identify alleles responsible for quantitative trait variation in grain polyphenols (reviewed by Flint-Garcia[28]). The goals of this study were to quantify the natural variation of two of the major sorghum grain polyphenols (proanthocyanidins and 3-deoxyanthocyanidins) and to identify single-nucleotide polymorphisms (SNPs) that are associated with low or high polyphenol concentrations using genome-wide association studies (GWAS). GWAS are used to map the genomic regions underlying phenotypic variation (known as quantitative trait loci) by scanning the genome for statistical associations between genetic variation and phenotypic variation.[29] In contrast to the biparental linkage mapping approach, GWAS takes advantage of historical recombinations in a diverse panel and linkage disequilibrium between causal variants and nearby SNP markers. Although it has been used extensively to identify putative genetic controls of human disease,[30] it is a relatively new but promising tool in plant genomics.[27,31,32] Here we present a survey of the quantitative natural variation of polyphenols in a diverse worldwide panel of sorghum and a catalog of flavonoid-associated loci across the sorghum genome.

## MATERIALS AND METHODS

**Plant Materials.** We investigated a total of 381 sorghum accessions, comprising 308 accessions from the Sorghum Association Panel (SAP)[33] and an additional 73 accessions selected based on presence of a pigmented testa using the U.S. National Plant Germplasm System's Germplasm Resources Information Network (GRIN).[34] The SAP includes accessions from all major cultivated races and geographic centers of diversity in sub-Saharan Africa and Asia, as well as important breeding lines from the United States. The 73 additional accessions were included to increase the proportion of accessions with high proanthocyanidins.

Seeds were obtained through GRIN and planted in late April 2012 at Clemson University Pee Dee Research and Education Center in Florence, SC. A 2-fold replicated complete randomized block design was used. Panicles from each plot were collected at physiological maturity (signified by a black layer at the base of the seed that normally forms about 35 days after anthesis). Due to differences in maturity among these accessions, harvest occurred between September and October. Once harvested, panicles were air-dried in a greenhouse and then mechanically threshed, and any remaining glumes were removed with a wheat head thresher (Precision Machine Company, Lincoln, NE).

**Phenotyping.** Twenty grams of cleaned whole grain from one replicate was scanned with a FOSS XDS spectrometer (FOSS North America, Eden Prairie, MN, USA) at a wavelength range of 400−2500 nm. To determine reproducibility, duplicates on a subset of 218 accessions available from replicate plots were also scanned. The NIR reflectance spectra were recorded using the ISIscan software (Version 3.10.05933) and converted to estimates of total phenol, proanthocyanidin, and 3-deoxyanthocyanidin concentrations. The spectrometer, software, and calibration curves used in this study were recently described.[35] Samples with unusual reflectance were visually inspected, and near-infrared spectroscopy (NIRS) was repeated. Seventeen samples were removed from further analysis either because they

contained mixed grain (mixed size, shape, or color) or because their readings were outside the range of the available NIRS calibration curve. Total phenol, proanthocyanidin, and 3-deoxyanthocyanidin data are expressed as mg gallic acid equivalents (GAE)/g, mg catechin equivalents (CE)/g, and absorbance (abs)/mL/g, respectively. These were the units used in creating the calibration curves, which measured total phenols with the Folin−Ciocalteu method, 3-deoxyanthocyanidins with the colorimetric method of Fuleki and Francis, and proanthocyanidins with the modified vanillin/HCl assay.[35] For the purposes of this study, we use a cutoff of greater than 10.00 mg CE/g to define proanthocyanidin-containing varieties and greater than 50.00 abs/mL/g to define 3-deoxyanthocyanidin-containing varieties.

Visual appearance of grain was classified independently by two people by visually scoring three seeds per accession as white, yellow, red, or brown. Testa presence was identified with three seeds per accession by cutting a thin layer off the pericarp and examining under a dissecting microscope. The total grain weight of 100 seeds per accession was recorded.

**Genomic Analysis.** Genotypes were available for the 324 accessions that were part of the SAP.[27] Genotyping-by-sequencing (GBS) was performed for the 73 additional accessions by the Institute for Genomic Diversity using the methods by Elshire et al.[36] Briefly, we provided seeds of the 73 additional accessions (the same seeds obtained from GRIN that we used to grow our panel) to the Institute for Genomic Diversity, where the following work was performed: Seedlings were grown to obtain tissue, DNA was isolated using the Qiagen DNeasy Plant kit, genomic DNA was digested individually using ApeKI, 96X multiplexed GBS libraries were constructed, and DNA sequencing was performed on the Illumina Genome Analyzer *IIx*. To extract SNP genotypes from sequence data, the GBS pipeline 3.0 in the TASSEL software package[57] was used, with mapping to the BTx623 sorghum reference genome.[37] Missing genotype calls were imputed using the FastImputationBitFixedWindow plugin in TASSEL 4.0.[38]

GWAS was carried out on 404,628 SNP markers, using the statistical genetics package Genome Association and Prediction Integrated Tool (GAPIT)[39] with both a general linear model (GLM) and a mixed linear model (MLM) with kinship. In a previous study we found that an MLM[40] with kinship (K), which controls for relatedness among the accessions in the panel, performs well to identify causative loci for sorghum polyphenols.[41] Bonferroni correction (family wise *P*-value of 0.01, $P < 10^{-6}$) was used to identify significant associations. Pseudoheritability (proportion of phenotypic variation explained by genotype) was estimated from the kinship (K) model in GAPIT[42] as the *R*-squared of a model with no SNP affects. A previously developed a priori candidate gene list was used, and 35 additional candidate genes were added (see Supporting Information).[41]

## RESULTS

**Quantitative Variation in Grain Polyphenols.** We first sought to determine the reliability of the NIRS estimates across the diverse material in the panel. Phenotypic variation for grain polyphenol concentrations was determined using a diverse association panel with 381 accessions (Figure 2). The standard deviation between the duplicates was similar across all concentrations of polyphenols ($r^2$ = 0.06, $P$ = 0.0001) and proanthocyanidins ($r^2$ = 0.01, $P$ = 0.12), with an average difference of 47% and 4%, respectively. However, the standard deviation between the 3-deoxyanthocyanidin duplicates becomes much larger for samples with higher 3-deoxyanthocyanidin concentrations ($r^2$ = 0.32, $P = 10^{-17}$), with an average difference of 72% (Figure 2C). To determine if the NIRS measurements of proanthocyanidin concentration were concordant with the known distribution of testa and *tan1-a* nonfunctional allele,[22] we plotted proanthocyanidin concentration of accessions with or without a pigmented testa (Figure

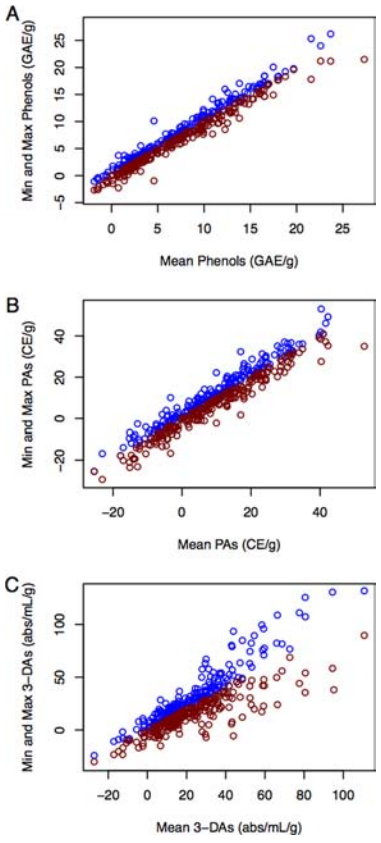


**Figure 2.** Phenotypic variation of grain polyphenol concentrations in 381 sorghum varieties. Samples are ordered on the *x*-axis according to their mean value for the accession. The observed value for each replicate is given on the *y*-axis, with the higher value of the duplicates in red and the lower value of the duplicates in blue. (A) Total polyphenols, (B) proanthocyanidins (PAs), and (C) 3-deoxyanthocyanidins (3-DAs).

S1A in the Supporting Information), and accessions with the wild-type *Tannin1* allele or the *tan1-a* allele (Figure S1B in the Supporting Information). As expected, the absence of a testa and presence of *tan1-a* were primarily found in accessions containing less than 10 mg CE/g of proanthocyanidins. The mean proanthocyanidin concentrations in accessions with a pigmented testa were significantly higher than in accessions without a pigmented testa (18.17 versus 1.45 mg CE/g; $P = 10^{-17}$), and the mean proanthocyanidin concentrations in accessions with the wild-type *Tannin1* were significantly higher than in accessions with *tan1-a* (12.28 versus 0.86 mg CE/g; $P = 10^{-11}$).

Next we investigated the range of total phenol, proanthocyanidin, and 3-deoxyanthocyanidin concentrations and their covariation with each other and grain weight (Figure 3). Overall, proanthocyanidins were detected in 55% of the samples, while only 13% contained 3-deoxyanthocyanidins, and only 6% contained both polyphenols. The mean total polyphenol concentration was 7.00 mg (GAE)/g, the mean proanthocyanidin concentration was 7.73 mg CE/g, and the mean 3-deoxyanthocyanidin concentration was 27.40 abs/mL/g (Table 1 and Figure 3). Pearson's correlations were calculated between total phenols, proanthocyanidins, and 3-deoxyanthocyanidins. There was no significant correlation between proanthocyanidins and 3-deoxyanthocyanidins (0.02, $P$ = 0.7), consistent with independent genetic control. In contrast,

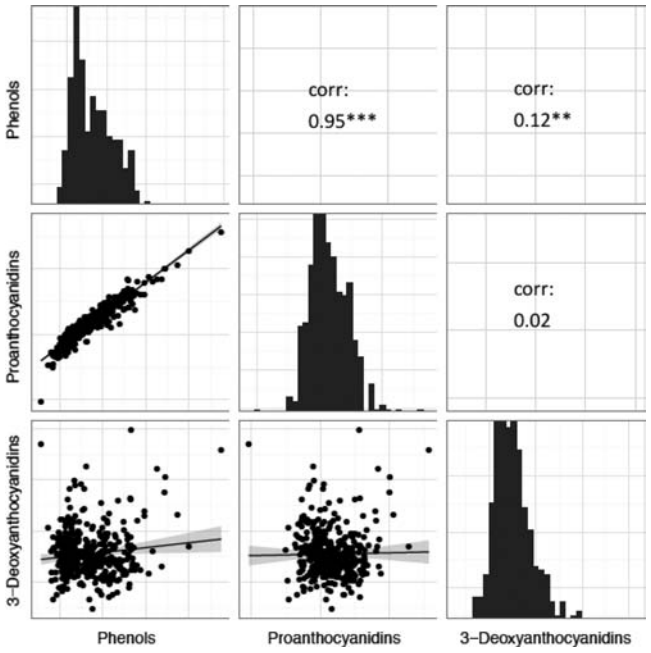


**Figure 3.** Relationship within and between grain polyphenol traits in a global sorghum germplasm collection. The center diagonal presents histograms of the mean concentrations of each trait ($n$ = 381). The lower corner contains scatter plots with regression lines showing the relationships between the traits. The upper corner shows Pearson's correlations between the traits. Units are mg GAE/g for total phenols, mg CE/g for proanthocyanidins, and abs/mL/g for 3-deoxyanthocyanidins.

**Table 1. Polyphenol Concentrations in 373 Sorghum Varieties**

| constituent | mean | range | SD |
|---|---|---|---|
| total phenols (mg GAE/g) | 7.00 | ND−37.46 | 5.92 |
| proanthocyanidins (mg CE/g) | 7.73 | ND−78.51 | 15.45 |
| 3-deoxyanthocyanidins (abs/mL/g) | 27.40 | ND−149.21 | 24.05 |

there were a strong positive correlation between total phenols and proanthocyanidins (0.95, $P < 10^{-15}$) and a weak positive correlation between total phenols and 3-deoxyanthocyanidins (0.12, $P$ = 0.02). Variance in proanthocyanidins accounted for 90% of all the variance in total phenols (Figure 3). Since the seed coat (pericarp and testa) contains most of the polyphenols in the grain, and the ratio of seed coat (surface area) to endosperm is generally greater in smaller grains, we wondered if differences in grain size might be underlying variation in polyphenol concentrations. In other words, are high grain polyphenol concentrations limited to small-grain varieties, which have a high proportion of seed coat to endosperm? No significant correlation was found between grain weight and either proanthocyanidins (−0.02, $P$ = 0.7) or 3-deoxyanthocyanidins (−0.02, $P$ = 0.7), and a small negative correlation was found between grain weight and total polyphenols (−0.10, $P$ = 0.04). Pseudoheritability was 81.7% for proanthocyanidins and 66.5% for 3-deoxyanthocyanidins.

**Population Structuring of Polyphenol Concentrations.** To determine the distribution of polyphenol traits with respect to global genetic diversity, we conducted a principal component analysis and highlighted the variation in polyphenol concentration (Figures S2A and S2B in the Supporting Information), as well as morphological races (Figure S2C in the Supporting Information). At least some high proanthocyanidin accessions were found in most subpopulations, whereas high 3-deoxyanthocyanidin accessions were more restricted (Table 2). Bicolor (21.18 mg CE/g) and guinea-caudatum (17.89 mg CE/g) had the highest mean concentration of proanthocyanidins. Caudatum had moderate concentrations (13.20 mg CE/g), and the other botanical races and intermediate groups showed an average less than 10.00 mg CE/g. The highest mean concentrations of 3-deoxyanthocyanidins were found in bicolor-durra (36.95 abs/mL/g) and guinea (35.63 abs/mL/g) accessions (Table 2). We also determined the mean concentrations by country to better understand the geographic patterns for sorghum polyphenols (Table 3). Accessions from Uganda (19.03 mg CE/g) had the highest mean proanthocyanidin concentrations, accessions from South Africa (12.23 mg CE/g) and Sudan (10.33 mg CE/g) had moderate concentrations, while accessions from the other countries showed an average less than 10.00 mg CE/g. The highest mean concentrations of 3-deoxyanthocyanidins were found in accessions from Nigeria (36.39 abs/mL/g) and Ethiopia (32.87 abs/mL/g).

**Genome-Wide Association Studies.** To investigate the genetic basis of natural variation in sorghum grain polyphenols, we conducted GWAS using 404,628 SNP markers. We were able to obtain genotype data for 373 out of the 381 phenotyped accessions. As a data quality check, we first collapsed the quantitative proanthocyanidin data to qualitative (presence or absence) data, and were able to repeat findings from previous GWAS and linkage studies (Figures S3 and S4 and Tables S2 and S3 in the Supporting Information). Next, to identify novel alleles associated with quantitative variation of proanthocyani-

**Table 2. Polyphenol Concentrations by Race**

| | | total phenols (mg GAE/g) | | PA (mg CE/g) | | 3-DA (abs/mL/g) | |
|---|---|---|---|---|---|---|---|
| race[a] | $n$ | mean | range | mean | range | mean | range |
| bicolor | 15 | 13.68 ± 6.69 | 0.74−24.49 | 21.18 ± 17.68 | ND−50.16 | 26.91 ± 33.65 | ND−102.96 |
| bicolor-durra | 19 | 6.59 ± 4.28 | ND−13.38 | 3.89 ± 12.06 | ND−23.35 | 36.95 ± 28.24 | 1.30−113.42 |
| caudatum | 86 | 9.08 ± 5.86 | ND−27.32 | 13.20 ± 14.15 | ND−52.83 | 28.22 ± 21.06 | ND−110.73 |
| caudatum-kafir | 20 | 6.27 ± 5.41 | ND−15.68 | 7.00 ± 15.13 | ND−31.98 | 26.65 ± 16.87 | 6.70−58.25 |
| durra | 15 | 2.17 ± 3.61 | ND−11.68 | ND | ND−17.64 | 22.17 ± 21.33 | ND−71.10 |
| guinea | 11 | 1.95 ± 5.25 | ND−15.44 | ND | ND−33.45 | 35.63 ± 36.88 | 0.93−135.34 |
| guinea-caudatum | 15 | 10.01 ± 3.13 | 2.54−15.87 | 17.89 ± 9.76 | ND−34.92 | 19.72 ± 15.69 | 0.40−60.10 |
| kafir | 29 | 6.02 ± 4.05 | 1.32−14.71 | 6.50 ± 10.20 | ND−28.72 | 17.59 ± 20.65 | ND−94.49 |

[a]If a race contained a small sample size (less than 10 accessions), it was not included in this analysis. PA, proanthocyanidins; 3-DA, 3-deoxyanthocyanidins; ND, not detected (absorbance was less than 0.001).

**Table 3. Polyphenol Concentrations by Geographic Origin**

| | | total phenols (mg GAE/g) | | PA (mg CE/g) | | 3-DA (abs/mL/g) | |
|---|---|---|---|---|---|---|---|
| country[a] | *n* | mean | range | mean | range | mean | range |
| Uganda | 44 | 10.99 ± 5.17 | 1.17−27.32 | 19.03 ± 12.02 | ND−52.83 | 27.37 ± 20.8 | 1.30−110.73 |
| South Africa | 31 | 9.11 ± 5.21 | 1.11−20.63 | 12.23 ± 12.37 | ND−43.75 | 13.52 ± 14.1 | ND−38.82 |
| Sudan | 31 | 7.50 ± 3.34 | ND−14.67 | 10.33 ± 8.93 | ND−25.26 | 27.15 ± 15.1 | 4.13−60.10 |
| Nigeria | 21 | 5.0 ± 6.46 | ND−24.49 | 1.21 ± 21.36 | ND−50.16 | 36.39 ± 35.8 | ND−135.34 |
| Ethiopia | 29 | 5.71 ± 5.43 | ND−15.94 | 1.53 ± 13.13 | ND−23.53 | 32.87 ± 21.1 | ND−77.59 |
| India | 21 | 3.90 ± 5.09 | ND−16.98 | ND | ND−32.13 | 28.74 ± 28.7 | ND−113.42 |
| USA | 71 | 5.09 ± 5.25 | ND−29.93 | 3.6 ± 12.55 | ND−63.80 | 27.50 ± 24.2 | ND−95.20 |

[a]If a country contained a small sample size (less than 10 accessions), it was not included in this analysis. PA, proanthocyanidins; 3-DA, 3-deoxyanthocyanidins; ND, not detected (absorbance was less than 0.001).

dins, we conducted a GWAS on the 373 accessions (Figure 4; Table S4 in the Supporting Information). A GLM identified 3,272 significant SNPs (Figure 4A), while the MLM identified 24 significant SNPs after accounting for population structure (Figure 4B). The genomic locations of the association peaks were generally similar between methods. A peak on chromosome 4 at ∼61 Mb colocalized with *Tannin1* (Sb04g031730), as well as three a priori candidate genes in the region: a putative *Zm1* homologue (Sb04g031110), a putative *TTG1* homologue (Sb04g030840), and a putative *TT16* homologue (Sb04g031750) (Figure 4C). The GLM identified a peak at 58.6 Mb on chromosome 7 (S7_58603858; $P < 10^{-15}$), which was not present in the MLM.

In order to reduce the effects of known *Tannin1* nonfunctional alleles and identify additional quantitative loci, samples with the *tan1-a* and *tan1-b* alleles were removed and a GWAS was conducted on the remaining samples (Figure 5 and Table S5 in the Supporting Information). The GLM identified 2,641 significant SNPs (Figure 5A). The association peak on chromosome 7 was again identified in the GLM and not in the MLM (Figure 5B). Additionally, there was a peak on chromosome 2 around 8 Mb (S2_8258226; $P < 10^{-11}$) identified in the GLM, near a putative *TT8* homologue (Sb02g006390). Both the GLM and the MLM identified a peak on chromosome 4, again around 61 Mb, and another peak on chromosome 4 between 53 Mb and 55 Mb, close to an F3′H *Pr1* coorthologue.

To further map loci controlling quantitative proanthocyanidin variation, we ran a GWAS only on samples that contained proanthocyanidins (greater than 10.00 mg CE/g) and/or had a visible pigmented testa (Figure 6 and Table S6 in the Supporting Information). With this subset, there were 676 significant SNPs identified in the GLM, but association peaks were more diffuse (Figure 6A). The most significant SNP was on chromosome 6 (S6_56992521, $P < 3 \times 10^{-10}$) near a *TT16* a priori candidate (Sb06g028420). The MLM identified two significant SNPs, with a peak on chromosome 4, again around 61 Mb, and another peak on chromosome 4 between 53 Mb and 55 Mb (Figure 6B). Both the GLM and the MLM identified significant SNPs around 61.1 Mb on chromosome 1, which is near *yellow seed1*.

Next, a GWAS was conducted to identify genetic controls of 3-deoxyanthocyanidin variation among the 373 accessions (Figure 7 and Table S7 in the Supporting Information). The GLM identified 233 significant SNPs, with distinct association peaks on chromosomes 3 and 4 (Figure 7A). The peak on chromosome 3 was between 71 and 72 Mb and colocalized with a gene (Sb03g045170) homologous to both *TT18* (ANS) and *TT6* (F3H). The peak on chromosome 4 was between 53 Mb and 55 Mb, close to *TT1* and *TT2* homologues, and an F3′H *Pr1* coorthologue. While there was not a distinct peak on chromosome 1, the strongest association signal in the GWAS was found in a diffuse peak on chromosome 1 around 55 Mb ($P < 10^{-9}$). The closest a priori candidates were putative *TTG2* (Sb01g032120) and *TT2* (Sb01g032770) homologues. There were no distinct peaks or significant associations identified in the MLM (Figure 7B).

**Grain Color.** Since grain color is commonly used as a visual marker for sorghum polyphenol content, we used our data set to better understand both the correlation between visually scored grain color and polyphenol concentration, and the potential shared genetic basis for these traits. Based on visual assessment of grain appearance, we designated 142 white, 35 yellow, 48 red, and 152 brown grain accessions. An analysis of variance (ANOVA) showed significant variation among the grain color groups, so we conducted a post hoc Tukey test. Grain classified as red contained significantly more 3-deoxyanthocyanidins than brown ($P < 10^{-5}$) or white grain ($P < 10^{-5}$) accessions, but no significant difference was found between red and yellow accessions (Figure 8A and Table 4). Brown grain accessions contained significantly more proanthocyanidins than accessions with red ($P = 0.0001$), white ($P = 0.001$), or yellow ($P = 0.001$) grain (Figure 8B and Table 4). This was expected as most of the sorghums with testa layers were classified as brown (57%). We also compared proanthocyanidin concentrations between grain color in proanthocyanidin-containing (greater than 10.00 mg CE/g or presence of pigmented testa) accessions. Brown grain color classes contained significantly more proanthocyanidins than nonbrown (brown $n = 120$, nonbrown $n = 85$, $P < 10^{-13}$). However, when brown grain color classes were compared to each color class individually, they only contained significantly more proanthocyanidins than white color classes ($P < 10^{-4}$). Red and lemon-yellow grain color classes also contained significantly more proanthocyanidins than white in the proanthocyanidin-containing accessions ($P = 0.001$ and $P = 0.02$).

To identify genes associated with brown grain, we conducted a presence/absence (brown versus nonbrown) GWAS on all 373 of the accessions (Figures S5A and S5B and Table S8 in the Supporting Information) and another presence/absence (brown versus nonbrown) GWAS on the 203 proanthocyanidin-containing accessions (Figures S5C and S5D and Table S9 in the Supporting Information). A distinct association peak on chromosome 8 at 52.9 Mb was observed in both GWAS. The nearest a priori candidate was a putative *TT12* homologue within 400 Kb (Sb08g021640). The GWAS conducted on all 373 accessions identified a peak on chromosome 3 at 63.6 Mb,

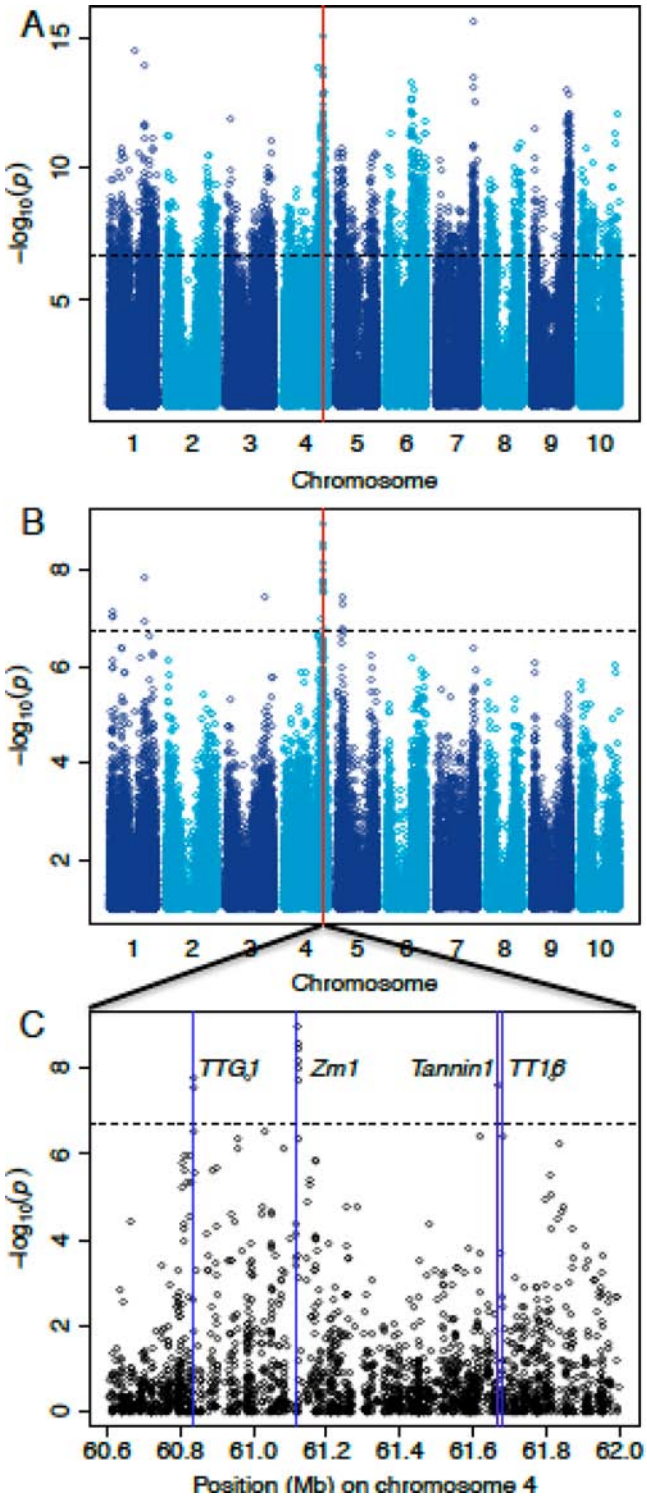


**Figure 4.** GWAS for proanthocyanidin concentration in sorghum grain. Manhattan plot of association results from (A) a GLM analysis, (B) an MLM analysis, and (C) a closeup of the peak on chromosome 4 showing *Tannin1* and other candidate genes in the region, using 404,628 SNP markers and 373 accessions. Axes: the $-\log_{10}$ *p*-values (*y* axis) plotted against the position on each chromosome (*x* axis). Each circle represents a SNP. The dashed horizontal line represents the genome-wide significance threshold as determined by Bonferroni correction. Regions with $-\log_{10}$ *p*-values above the threshold are candidates. The vertical lines indicate the location of *Tannin1* and a priori candidate genes in the *Tannin1* region (~61 Mb).

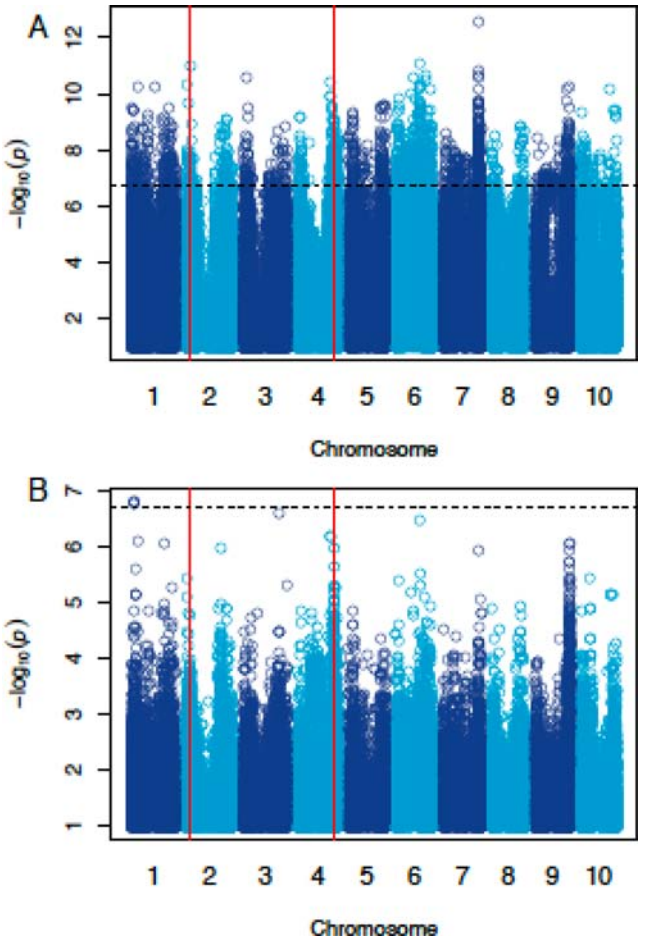


**Figure 5.** GWAS for proanthocyanidin concentration in sorghum grain with accessions containing *tan1-a* and *tan1-b* nonfunctional alleles removed. Manhattan plot of association results from (A) a GLM analysis and (B) an MLM analysis, using 404,628 SNP markers and 312 accessions. Axes: the $-\log_{10}$ *p*-values (*y* axis) plotted against the position on each chromosome (*x* axis). Each circle represents a SNP. The dashed horizontal line represents the genome-wide significance threshold as determined by Bonferroni correction. Regions with $-\log_{10}$ *p*-values above the threshold are candidates. The red vertical lines highlight the location of candidate genes. (TT8 on chrm. 2 and *TTG1*, *Zm1*, and *TT16* on chrm. 4)

within 100 Kb of another putative *TT12* homologue (Sb03g035610), and also a peak on chromosome 6 (S6_56992521, $P < 3 \times 10^{-10}$) near a *TT16* a priori candidate (Sb06g028420) (Figures S4A and S4B in the Supporting Information). The GWAS conducted on the proanthocyanidin-containing accessions identified a peak on chromosome 2 around 69.6 Mb, very near another *TT12* homologue (Sb02g034720) (Figures S5C and S5D in the Supporting Information). This peak was also identified in the GWAS conducted on all 373 accessions, but was more diffuse. There were no peaks on chromosome 4 around *Tannin1* or on chromosome 2 around the Z locus.

To identify genes associated with red grain, we conducted a presence/absence (red versus nonred) GWAS on all of the samples (Figure S6 and Table S10 in the Supporting Information). Two association peaks on chromosome 4 were identified by both the GLM and MLM, in the same region as the peak in the 3-deoxyanthocyanidin GWAS. The first peak, at 54.5 Mb, colocalized with a priori candidate Sb04g024710, the


dx.doi.org/10.1021/jf503651t | J. Agric. Food Chem. 2014, 62, 10916−10927

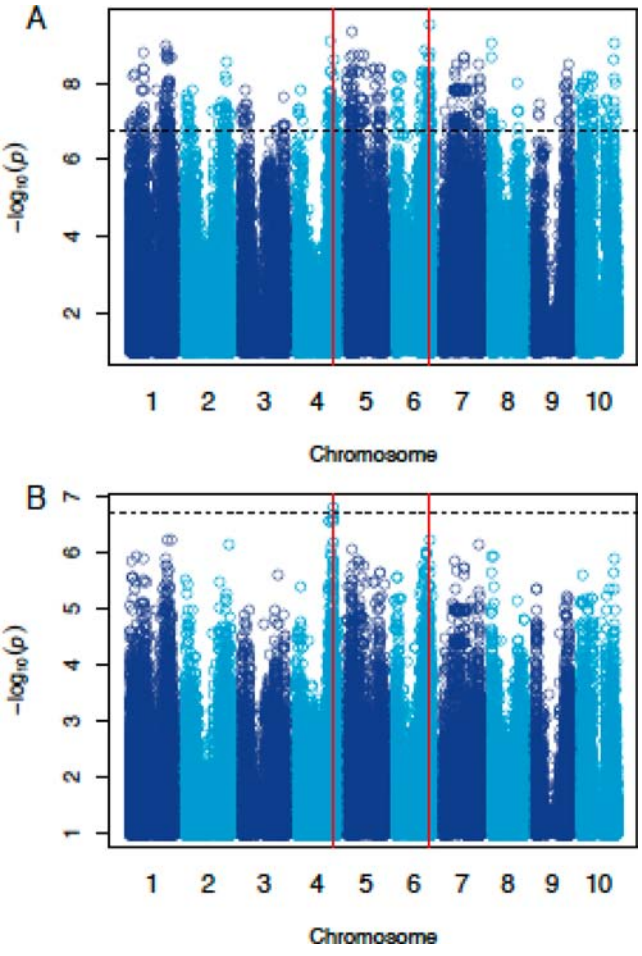


**Figure 6.** GWAS for proanthocyanidin concentration in proanthocyanidin-containing sorghum grain (greater than 10.00 mg CE/g or pigmented testa). Manhattan plot of association results from (A) a GLM analysis and (B) an MLM analysis, using 404,628 SNP markers and 208 accessions. Axes: the $-\log_{10}$ *p*-values (*y* axis) plotted against the position on each chromosome (*x* axis). Each circle represents a SNP. The dashed horizontal line represents the genome-wide significance threshold as determined by Bonferroni correction. Regions with $-\log_{10}$ *p*-values above the threshold are candidates. The red vertical lines highlight the location of candidate genes (*TT16*, *Tannin1* region, *Pr1*/*TT7*).

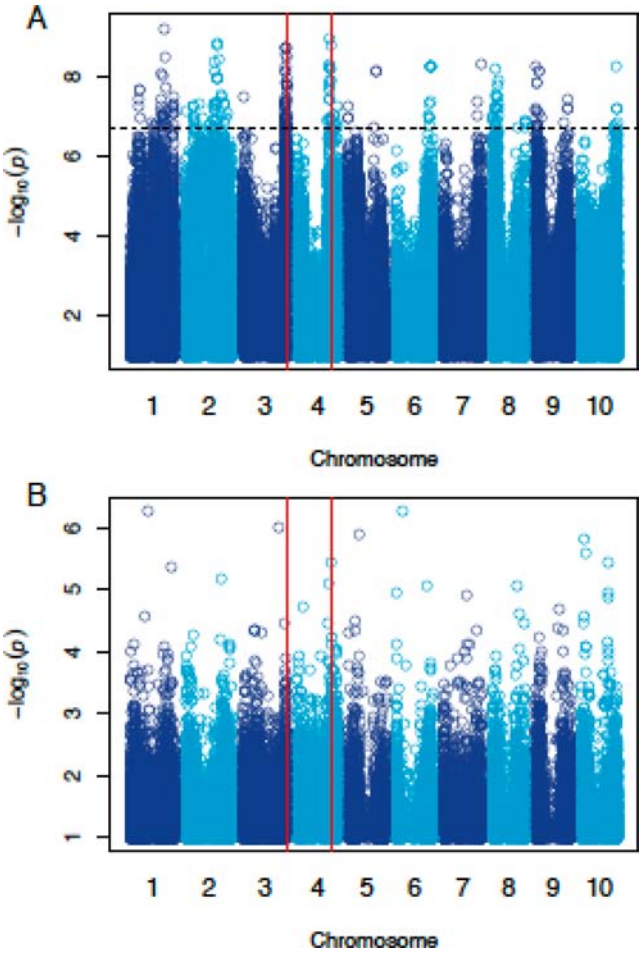


**Figure 7.** GWAS for 3-deoxyanthocyanidin concentration in sorghum grain. Manhattan plot of association results from (A) a GLM analysis and (B) an MLM analysis, using 404,628 SNP markers and 373 accessions. Axes: the $-\log_{10}$ *p*-values (*y* axis) plotted against the position on each chromosome (*x* axis). Each circle represents a SNP. The dashed horizontal line represents the genome-wide significance threshold as determined by Bonferroni correction. Regions with $-\log_{10}$ *p*-values above the threshold are candidates. The red vertical lines highlight the location of candidate genes (*TT18*/*ANS*, *TT6*/*F3H*, *Pr1*/*TT7*).

F3′H *Pr1* coorthologue that was also in one of the 3-deoxyanthocyanidin GWAS peaks. The second peak, at 55.9 Mb, was very close to a priori candidate Sb04g026480, a putative MYB homologue. There was also a peak around 72 Mb on chromosome 3, in the same region as the peak in the 3-deoxyanthocyanidin GWAS, near a priori candidate Sb03g044980, a putative *TT19* homologue. A peak was identified on chromosome 6 between 7 and 8 Mb, which was not near any a priori genes, but was near a putative vacuolar sorting protein gene (Sb06g003780). There were no peaks on chromosome 3 around the R locus.

## DISCUSSION

**Genetic Controls of Sorghum Polyphenols.** The genetic controls of the flavonoid pathway (Figure 9) have been well studied in many economically important food plants, including grape (*Vitis vinifera*), barley (*Hordeum vulgare*), maize (*Zea mays*), rice (*Oryza sativa*), and wheat (*Triticum* spp.).[43] Much of our understanding of flavonoid genetics, including biosynthetic enzymes, transporters, and regulatory proteins, come from analysis of Transparent Testa (TT) mutants in *Arabidopsis*.[44] Transcriptional regulation occurs through a ternary complex made up of *TT2*, *TT8*, and *TTG1*, which encode for MYB, bHLH, and WD40 proteins (MBW complex), respectively.[44] This ternary complex is highly conserved among plant species.[45] In the sorghum proanthocyanidin pathway, the WD40 (*Tannin1*) component of the MBW complex has been identified, as well as a likely candidate for the bHLH; several studies have found a significant linkage and association on sorghum chromosome 2 around 8 Mb, near a putative bHLH transcription factor orthologous to *Arabidopsis TT8*.[22,24,41,46,47] The MYB transcription factor that would complete the ternary complex has not been found in sorghum. The *Zm1* homologue on chromosome 4 at 61.1 Mb (Sb04g031110, 66.8% similarity), which was mapped in all of our proanthocyanidin GWAS, is a possible candidate for the missing MYB. The maize *Zm1* gene is a MYB transcription factor, homologous to classical maize grain pigmentation gene *C1* that can induce transcription of DFR, an essential structural enzyme in the flavonoid pathway.[48]

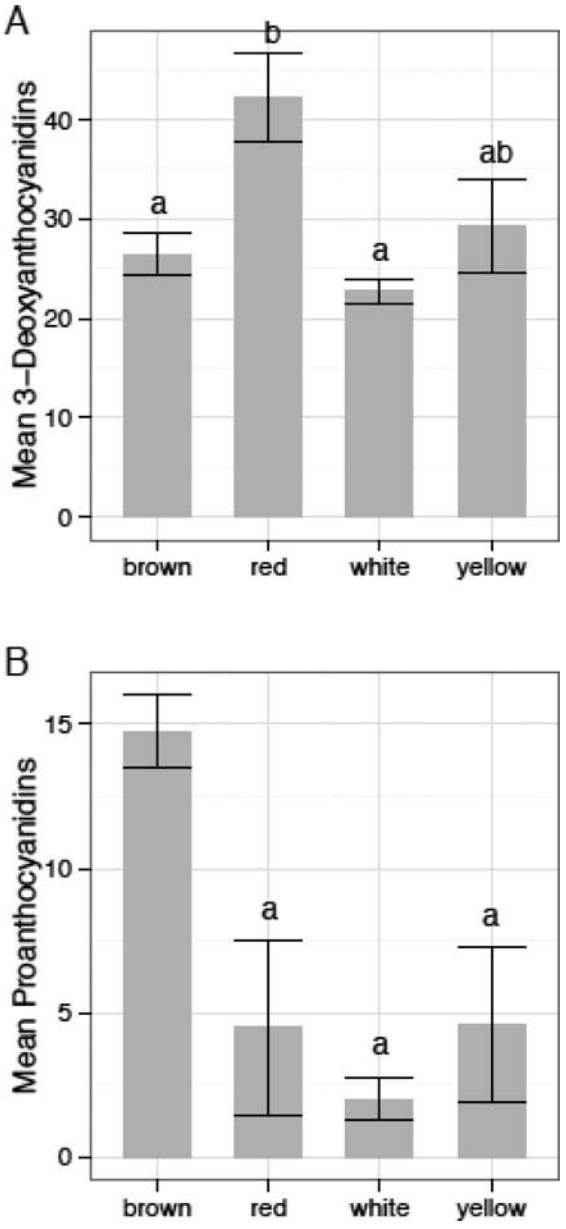


**Figure 8.** Polyphenol differences between grain colors. Mean concentrations of (A) proanthocyanidins and (B) 3-deoxyanthocyanidins in accessions of each grain color. Color categories share the same letter if they are not significantly different from each other, based on a post hoc Tukey HSD test (brown, $n$ = 152; red, $n$ = 48; white, $n$ = 142; yellow, $n$ = 35).

Another possible explanation for the significant SNPs at this location is an indirect association with an undescribed allele at *Tannin-1*.

About two-thirds of the SAP accessions we studied were "converted" tropical accessions, meaning that alleles for reduced height and early flowering have been introgressed so they can be grown in temperate regions.[49] Surprisingly, the proanthocyanidin GWAS association peak on chromosome 7 (~58.6 Kb) precisely colocalizes with *dw3* (Sb07g023730), a dwarfing loci used in the conversion, in conjunction with *dw1*, *dw2*, and *dw4*.[27] Smaller peaks on chromosomes 6 (~39 Kb) and 9 (~57 Kb) were near the *dw2* and *dw1* loci. The association peaks on chromosomes 6, 7, and 9 may be artifacts arising from a lower mean proanthocyanidin concentration in the converted lines (4.4 mg CE/g) which all shared the same *dw* alleles, compared to the unconverted lines (11.0 mg CE/g). Accordingly, when we conducted a proanthocyanidin GWAS using only converted accessions to control for this spurious phenotypic covariation between proanthocyanidin and height, the peaks near *dw1*, *dw2*, and *dw3* disappeared, while the *Tannin1* peak remained (Figure S7 in the Supporting Information).

As a phytoalexin,[15,16] the effect of the environment may make it more difficult to map the genetic basis of 3-deoxyanthocyanidins than the genetic basis of proanthocyanidins. Although the GLM was able to identify significant SNP associations for 3-deoxyanthocyanidins, there were few peaks, and the MLM did not identify any significant associations. Detection of alleles contributing to variance of 3-deoxyanthocyanidins may require a larger sample size, additional replication, a biparental mapping population, or controlled fungal inoculations to induce biosynthesis of polyphenol compounds.[23] However, our results did provide a promising candidate for followup. A *Pr1* orthologue (Sb04g024750) lies within a distinct peak on chromosome 4, about 400 Kb from the top SNP identified in the 3-deoxyanthocyanidin GWAS (S4_54975391; $P < 10^{-8}$), and 100 Kb from the top SNP in the red grain GWAS (S4_54555458, $P < 10^{-13}$). *Pr1* is a maize F3′H enzyme, homologous to *TT7* in *Arabidopsis*. The F3′H enzyme is essential for production of 3-deoxyanthocyanidins, as well as the red phlobaphene pigments visible in maize,[18] and has been implicated in production of these compounds in sorghum (Figure 9).[50] Overall, we observe a 1.6-fold difference in 3-deoxyanthocyanidin concentrations between accessions carrying the high concentration alleles and low concentration alleles for the top red grain-associated SNP ($P$ = 0.001). F3′H is necessary for proanthocyanidin production as well, and, indeed, significant associations with SNPs in the ~54 Mb region on chromosome 4 were also identified in the GWAS with *tan1-a* and *tan1-b* samples removed, as well as the GWAS with only proanthocyanidin-containing samples.

Our study identified many peaks and SNPs significantly associated with proanthocyanidins and 3-deoxyanthocyanidins, hence there appear to be many small effect genes controlling natural variation of these traits. Consequently, a larger association panel, or a targeted biparental mapping population,

**Table 4. Polyphenol Concentrations by Color**

| | | total phenols (mg GAE/g) | | PA (mg CE/g) | | 3-DA (abs/mL/g) | |
|---|---|---|---|---|---|---|---|
| color | $n$ | mean | range | mean | range | mean | range |
| white | 142 | 4.0 ± 3.10 | ND−14.67 | 2.00 ± 8.84 | ND−25.26 | 22.74 ± 14.03 | ND−58.41 |
| yellow | 35 | 6.0 3 ± 6.18 | ND−23.69 | 4.60 ± 15.98 | ND−42.30 | 29.30 ± 27.89 | ND−98.90 |
| red | 48 | 6.97 ± 7.30 | ND−27.32 | 4.48 ± 21.10 | ND−52.83 | 42.21 ± 30.43 | ND−135.34 |
| brown | 152 | 10.01 ± 6.01 | ND−37.46 | 14.74 ± 15.63 | ND−78.51 | 26.46 ± 26.64 | ND−149.21 |

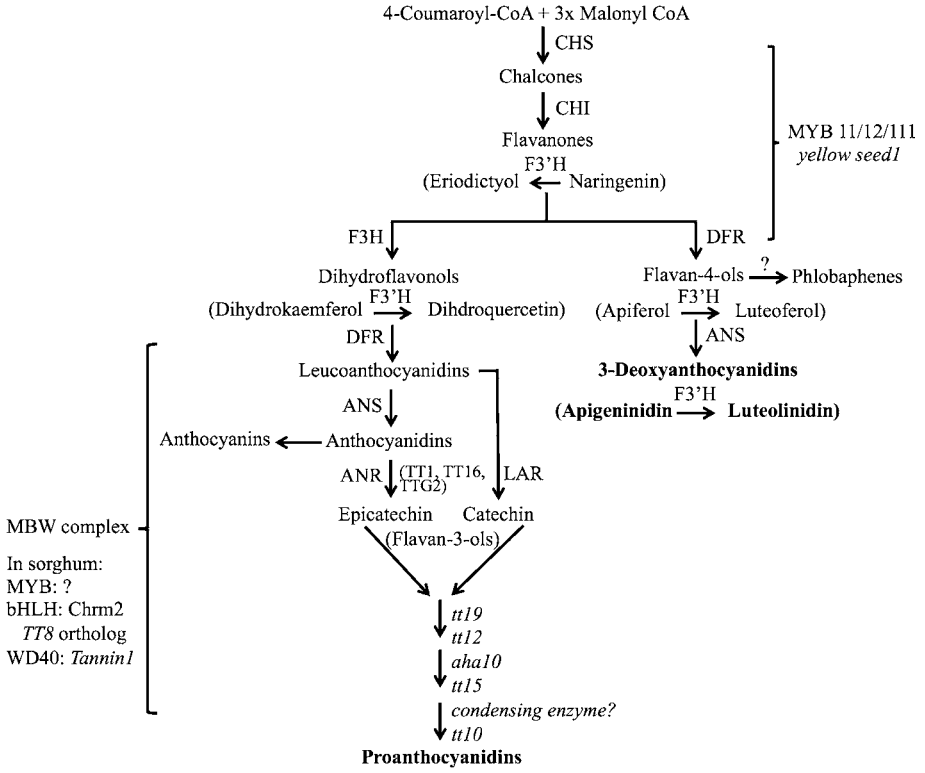


**Figure 9.** Simplified scheme of flavonoid biosynthetic pathway in sorghum grain with candidate genes noted. Enzyme abbreviations are in uppercase letters, while gene abbreviations are in italics. Question marks depict unknown steps. Chalcone synthase (CHS), chalcone-flavanone isomerase (CHI), flavanone 3-hydroxylase (F3H), flavanone 3′-hydroxylase (F3′H), dihydroflavonol-4-reductase (DFR), anthocyanidin synthase (ANS), anthocyanidin reductase (ANR), leucoanthocyanidin reductase (LAR); MYB-bHLH-WD40 (MBW).

may be more effective in precisely identifying causal alleles. Moving forward, sequence analysis and expression analysis of the candidate genes are needed to identify causal polymorphisms and lay the groundwork for the use of polyphenol genetic variation in crop improvement.

**Crop Improvement for Sorghum Polyphenols.** Efforts to characterize polyphenols, with the goal of producing high polyphenol specialty varieties, have been undertaken in several grain crops, including purple wheat,[51] black rice,[52] multicolored maize,[53] multicolored barley,[54] and black sorghum.[55] Our diverse association panel contained a wide range of proanthocyanidin and 3-deoxyanthocyanidin concentrations, and this genetic variation may be useful in breeding programs to produce high polyphenol specialty varieties. Bicolor sorghums had the highest mean proanthocyanidin concentrations, but their grain weight is significantly less (20% less) than that of non-bicolor sorghums ($P < 10^{-9}$). Combined with low yield potential, the small grain size makes it difficult to use bicolor race sorghums in a grain sorghum breeding program, but may still be of interest to breeders wanting to produce specialty varieties. In addition to bicolor sorghums, caudatum and guinea-caudatum sorghums also had high mean proanthocyanidin concentrations, and are promising sources for increasing proanthocyanidin concentrations in sorghum. In particular, among the caudatum and guinea-caudatum sorghums, caudatum sorghums from tropical climates such as Uganda had the highest mean proanthocyanidin concentrations, so they may be good material for breeding high polyphenol sorghums. While bicolor-durra and guinea sorghums had the highest mean 3-deoxyanthocyanidin concentrations, the difference among all the races was not significant, so it may be more important to simply identify unique genotypes across the sorghum collection. Chemical analysis is underway on the samples that were outside of the NIRS calibration curves, and true biological outliers may open up new avenues for future work on sorghum varieties with extreme polyphenol concentrations.

Increasing 3-deoxyanthocyanidin production may be challenging, since, as phytoalexins, they are not constitutively expressed, but rather synthesized by plants under pathogen attack.[15,16] We note in our comparison of 3-deoxyanthocyanidin concentrations from duplicate samples that the difference between duplicates becomes larger for accessions with higher 3-deoxyanthocyanidin concentrations. One possibility is that there is greater technical variation in the 3-deoxyanthocyanidin NIRS estimates, but Dykes et al.[35] demonstrated the same correlation coefficient between the NIRS-predicted values and the values in the validation set for proanthocyanidins ($r = 0.81$) and 3-deoxyanthocyanidins ($r = 0.82$). Therefore, we would not expect to see differences in accuracy of the NIRS predictions for proanthocyanidins and 3-deoxyanthocyanidins in our study. As this was a field study, another possibility is that uncontrolled environmental variation may have contributed to the difference between the duplicate samples. Accessions with the genetic capability to produce grain 3-deoxyanthocyanidins may be producing low or high 3-deoxyanthocyanidin concentrations depending on the exposure to inducing agents on a given panicle. Controlled inoculation studies are needed to further explore this possibility.[23]

The spreader gene is a promising target for increasing grain proanthocyanidin concentrations, and a previous report using a small number of varieties has shown higher proanthocyanidin

concentrations in varieties with a functional spreader.[56] Given that three peak SNP associations in the brown grain GWAS were near putative MATE transporter *TT12* homologues, we propose that the spreader gene may be a *MATE* transporter. A biparental mapping population segregating the spreader gene would be needed to confirm this hypothesis. To get a sense of the effect these loci may have on proanthocyanidin concentrations, we compared concentrations of each allele in proanthocyanidin-containing accessions. There was a 1.8-fold (S3_63633634, $P$ = 0.04), a 1.5-fold (S2_69656067, $P$ = 0.0003), and a 1.7-fold (S8_52906014, $P$ = 0.0002) difference between accessions carrying the high concentration alleles and low concentration alleles. When the three polymorphisms are considered together, accessions with all three high-alleles (S2_69656067 = "A", S3_63633634 = "A", S8_52906014 = "G") have 1.7- to 2.7-fold higher proanthocyanidin concentrations ($P = 10^{-8}$), consistent with an additive effect more than doubling the concentration of proanthocyanidins in sorghum grain.

Appearance of grain color is predominantly due to polyphenols, but can also be influenced by endosperm color and grain weathering. Taken in total, the color classes used for our analysis represent general groups and are not definitive descriptors of any specific trait. For example, it is possible to have a sorghum classified as brown that does not have a testa layer, as well to have a sorghum classified as white that has a testa layer (see Figure 1). However, our results support the use of visual categorization of grain color as a simple assessment of polyphenol concentrations in crop improvement programs; brown grain has significantly higher proanthocyanidin concentrations than nonbrown, red grain has significantly higher 3-deoxyanthocyanidin concentrations than nonred, and white grain has significantly lower concentrations of these polyphenols than nonwhite. Additionally, the genetic architecture of grain color reflects, to an extent, that of the polyphenols with which they are associated. For instance, the red grain GWAS and the 3-deoxyanthocyanidin GWAS produced similar association peaks on chromosome 4 (~54 Mb), which may map to the sorghum *Pr1* orthologue, and chromosome 3 (~72 Mb), which colocalizes with putative homologues of *ANS*, *F3H*, and *TT19*. The brown grain GWAS and the proanthocyanidin-containing GWAS produced similar association peaks on chromosome 6 (~57 Mb) near a priori candidate *TT16*, a key regulatory protein in the proanthocyanidin branch of the flavonoid pathway. Overall, to increase sorghum proanthocyanidin and 3-deoxyanthocyanidin concentrations quantitatively, there are many associated alleles available, but none of them have large effect. This survey of grain polyphenol variation in sorghum germplasm and catalog of flavonoid pathway-associated loci contributes toward the goal of producing sorghum crops that will contribute to marker-assisted breeding of sorghum crops that will benefit human health.

## ■ ASSOCIATED CONTENT

### Supporting Information

Proanthocyanidin concentration in accessions with *Tannin1* and *tan1-a* (Figure S1), population structure of polyphenols (Figure S2), GWAS for proanthocyanidin presence/absence (Figures S3, S4), GWAS for grain color (Figures S5, S6), GWAS for converted lines (Figure S7), flavonoid pathway-related genes (Table S1), significant SNPs identified in each GWAS (Tables S2–S10), and flavonoid pathway a priori candidate gene list. This material is available free of charge via the Internet at http://pubs.acs.org.

## ■ AUTHOR INFORMATION

### Corresponding Author

*Tel: 773-603-2897. Fax: 785-532-6094. E-mail: rhodesdh@email.sc.edu.

### Present Address

[‖]Institute for Genomic Diversity, Cornell University, Ithaca, NY, 14853, USA.

### Notes

The authors declare no competing financial interest.

## ■ ACKNOWLEDGMENTS

We thank Zach Brenton for considerable help with sample preparation, and Scott Bean, Prini Gadgil, Tom Herald, Amy Murphy, and the reviewers for their thoughtful comments.

## ■ ABBREVIATIONS USED

abs, absorbance; ANOVA, analysis of variance; CE, catechin equivalents; GAE, gallic acid equivalent; GBS, genotyping-by-sequencing; GAPIT, Genome Association and Prediction Integrated Tool; GLM, general linear model; GRIN, Germplasm Resources Information Network; GWAS, genome-wide association study; K, kinship; MLM, mixed linear model; NIRS, near-infrared spectroscopy; SAP, Sorghum Association Panel; SNP, single-nucleotide polymorphism

## ■ REFERENCES

(1) Tsao, R. Chemistry and biochemistry of dietary polyphenols. *Nutrients* **2010**, *2*, 1231–1246.

(2) Hichri, I.; Barrieu, F.; Bogs, J.; Kappel, C.; Delrot, S.; Lauvergeat, V. Recent advances in the transcriptional regulation of the flavonoid biosynthetic pathway. *J. Exp. Bot.* **2011**, *62*, 2465–2483.

(3) Buer, C. S.; Imin, N.; Djordjevic, M. A. Flavonoids: new roles for old molecules. *J. Integr. Plant Biol.* **2010**, *52*, 98–111.

(4) Del Rio, D.; Rodriguez-Mateos, A.; Spencer, J. P. E.; Tognolini, M.; Borges, G.; Crozier, A. Dietary (poly)phenolics in human health: structures, bioavailability, and evidence of protective effects against chronic diseases. *Antioxid. Redox Signaling* **2013**, *18*, 1818–1892.

(5) Hellstrom, J. K.; Törrönen, A. R.; Mattila, P. H. Proanthocyanidins in common food products of plant origin. *J. Agric. Food Chem.* **2009**, *57*, 7899–7906.

(6) Santos-Buelga, C.; Scalbert, A. Proanthocyanidins and tannin-like compounds—nature, occurrence, dietary intake and effects on nutrition and health. *J. Sci. Food Agric.* **2000**, *80*, 1094–1117.

(7) Dixon, R. A.; Xie, D.-Y.; Sharma, S. B. Proanthocyanidins—a final frontier in flavonoid research? *New Phytol.* **2005**, *165*, 9–28.

(8) FAO. Sorghum and millets in human nutrition. http://www.fao.org/docrep/T0818E/T0818E04.htm (accessed Feb 18, 2014).

(9) Janzen, E. L.; Wilson, W. W. *Cooperative marketing in specialty grains and identity preserved grain markets*; Agribusiness & Applied Economics Report No. 500; North Dakota State University, Department of Agribusiness and Applied Economics: Fargo, ND, September 2002.

(10) Taylor, J. R. N.; Schober, T. J.; Bean, S. R. Novel food and non-food uses for sorghum and millets. *J. Cereal Sci.* **2006**, *44*, 252–271.

(11) Elbehri, A. *The changing face of the U.S. grain system: differentiation and identity preservation trends*; Economic Research Report 7185; United States Department of Agriculture, Economic Research Service: 2007.

(12) Cureton, P.; Fasano, A. The increasing incidence of celiac disease and the range of gluten-free products in the marketplace. In *Gluten-Free Food Science and Technology*; Gallagher, E., Ed.; Wiley-Blackwell: Oxford, U.K., 2009; pp 1–15.

(13) Harlan, J. R.; de Wet, J. M. J. A simplified classification of cultivated sorghum. *Crop Sci.* **1972**, *12*, 172−176.
(14) Awika, J. M.; Rooney, L. W. Sorghum phytochemicals and their potential impact on human health. *Phytochemistry* **2004**, *65*, 1199−1221.
(15) Nicholson, R. L.; Kollipara, S. S.; Vincent, J. R.; Lyons, P. C.; Cadena-Gomez, G. Phytoalexin synthesis by the sorghum mesocotyl in response to infection by pathogenic and nonpathogenic fungi. *Proc. Natl. Acad. Sci. U.S.A.* **1987**, *84*, 5520−5524.
(16) Dixon, R. A. Natural products and plant disease resistance. *Nature* **2001**, *411*, 843−847.
(17) Winefield, C. S.; Lewis, D. H.; Swinny, E. E.; Zhang, H.; Arathoon, H. S.; Fischer, T. C.; Halbwirth, H.; Stich, K.; Gosch, C.; Forkmann, G.; Davies, K. M. Investigation of the biosynthesis of 3-deoxyanthocyanins in *Sinningia cardinalis*. *Physiol. Plant.* **2005**, *124*, 419−430.
(18) Sharma, M.; Chai, C.; Morohashi, K.; Grotewold, E.; Snook, M. E.; Chopra, S. Expression of flavonoid 3′-hydroxylase is controlled by *p1*, the regulator of 3-deoxyflavonoid biosynthesis in maize. *BMC Plant Biol.* **2012**, *12*, 196.
(19) Malathi, P.; Viswanathan, R.; Padmanaban, P.; Mohanraj, D.; Kumar, V. G.; Salin, K. P. Differential accumulation of 3-deoxy anthocyanidin phytoalexins in sugarcane varieties varying in red rot resistance in response to colletotrichum falcatum infection. *Sugar Tech* **2008**, *10*, 154−157.
(20) Rooney, W. L. Genetics and cytogenetics. In *Sorghum: Origin, History, Technology, and Production*, 1st ed.; Smith, C. W., Frederiksen, R. A., Eds.; John Wiley & Sons: New York, NY, 2000; pp 261−307.
(21) Morohashi, K.; Casas, M. I.; Ferreyra, L. F.; Mejía-Guerra, M. K.; Pourcel, L.; Yilmaz, A.; Feller, A.; Carvalho, B.; Emiliani, J.; Rodriguez, E.; Pellegrinet, S.; McMullen, M.; Casati, P.; Grotewold, E. A genome-wide regulatory framework identifies maize *pericarp color1* controlled genes. *Plant Cell* **2012**, *24* (7), 2745−2764.
(22) Wu, Y.; Li, X.; Xiang, W.; Zhu, C.; Lin, Z.; Wu, Y.; Li, J.; Pandravada, S.; Ridder, D. D.; Bai, G.; Wang, M. L.; Trick, H. N.; Bean, S. R.; Tuinstra, M. R.; Tesso, T. T.; Yu, J. Presence of tannins in sorghum grains is conditioned by different natural alleles of *Tannin1*. *Proc. Natl. Acad. Sci. U.S.A.* **2012**, *109* (26), 10281−10286.
(23) Ibraheem, F.; Gaffoor, I.; Chopra, S. Flavonoid phytoalexin-dependent resistance to anthracnose leaf blight requires a functional *yellow seed1* in *Sorghum bicolor*. *Genetics* **2010**, *184*, 915−926.
(24) Mace, E. S.; Jordan, D. R. Location of major effect genes in sorghum (*Sorghum bicolor* (L.) Moench). *Theor. Appl. Genet.* **2010**, *121*, 1339−1356.
(25) Routaboul, J.-M.; Dubos, C.; Beck, G.; Marquis, C.; Bidzinski, P.; Loudet, O.; Lepiniec, L. Metabolite profiling and quantitative genetics of natural variation for flavonoids in arabidopsis. *J. Exp. Bot.* **2012**, *63* (10), 3749−3764.
(26) Olsen, K. M.; Wendel, J. F. Crop plants as models for understanding plant adaptation and diversification. *Front. Plant Sci.* **2013**, *4*.
(27) Morris, G. P.; Ramu, P.; Deshpande, S. P.; Hash, C. T.; Shah, T.; Upadhyaya, H. D.; Riera-Lizarazu, O.; Brown, P. J.; Acharya, C. B.; Mitchell, S. E.; Harriman, J.; Glaubitz, J. C.; Buckler, E. S.; Kresovich, S. Population genomic and genome-wide association studies of agroclimatic traits in sorghum. *Proc. Natl. Acad. Sci. U.S.A.* **2013**, *110*, 453−458.
(28) Flint-Garcia, S. A. Genetics and consequences of crop domestication. *J. Agric. Food Chem.* **2013**, *61*, 8267−8276.
(29) Myles, S.; Peiffer, J.; Brown, P. J.; Ersoz, E. S.; Zhang, Z.; Costich, D. E.; Buckler, E. S. Association mapping: critical considerations shift from genotyping to experimental design. *Plant Cell* **2009**, *21*, 2194−2202.
(30) Hirschhorn, J. N.; Daly, M. J. Genome-wide association studies for common diseases and complex traits. *Nat. Rev. Genet.* **2005**, *6*, 95−108.
(31) Huang, X.; Wei, X.; Sang, T.; Zhao, Q.; Feng, Q.; Zhao, Y.; Li, C.; Zhu, C.; Lu, T.; Zhang, Z.; Li, M.; Fan, D.; Guo, Y.; Wang, A.; Wang, L.; Deng, L.; Li, W.; Lu, Y.; Weng, Q.; Liu, K.; Huang, T.; Zhou, T.; Jing, Y.; Li, W.; Lin, Z.; Buckler, E. S.; Qian, Q.; Zhang, Q.-F.; Li, J.; Han, B. Genome-wide association studies of 14 agronomic traits in rice landraces. *Nat. Genet.* **2010**, *42*, 961−967.
(32) Shu, X.; Backes, G.; Rasmussen, S. K. Genome-wide association study of resistant starch (RS) phenotypes in a barley variety collection. *J. Agric. Food Chem.* **2012**, *60*, 10302−10311.
(33) Casa, A. M.; Pressoir, G.; Brown, P. J.; Mitchell, S. E.; Rooney, W. L.; Tuinstra, M. R.; Franks, C. D.; Kresovich, S. Community resources and strategies for association mapping in sorghum. *Crop Sci.* **2008**, *48*, 30.
(34) USDA. GRIN National Genetic Resources Program. http://www.ars-Grin.gov (2014-07-25).
(35) Dykes, L.; Hoffmann, L., Jr.; Portillo-Rodriguez, O.; Rooney, W. L.; Rooney, L. W. Prediction of total phenols, condensed tannins, and 3-deoxyanthocyanidins in sorghum grain using near-infrared (NIR) spectroscopy. *J. Cereal Sci.* **2014**, *60* (1), 138−142.
(36) Elshire, R. J.; Glaubitz, J. C.; Sun, Q.; Poland, J. A.; Kawamoto, K.; Buckler, E. S.; Mitchell, S. E. A robust, simple genotyping-by-sequencing (GBS) approach for high diversity species. *PLoS One* **2011**, *6*, e19379.
(37) Paterson, A. H.; Bowers, J. E.; Bruggmann, R.; Dubchak, I.; Grimwood, J.; Gundlach, H.; Haberer, G.; Hellsten, U.; Mitros, T.; Poliakov, A.; Schmutz, J.; Spannagl, M.; Tang, H.; Wang, X.; Wicker, T.; Bharti, A. K.; Chapman, J.; Feltus, F. A.; Gowik, U.; Grigoriev, I. V.; Lyons, E.; Maher, C. A.; Martis, M.; Narechania, A.; Otillar, R. P.; Penning, B. W.; Salamov, A. A.; Wang, Y.; Zhang, L.; Carpita, N. C.; Freeling, M.; Gingle, A. R.; Hash, C. T.; Keller, B.; Klein, P.; Kresovich, S.; McCann, M. C.; Ming, R.; Peterson, D. G.; Mehboob-ur-Rahman; Ware, D.; Westhoff, P.; Mayer, K. F. X.; Messing, J.; Rokhsar, D. S. The sorghum bicolor genome and the diversification of grasses. *Nature* **2009**, *457*, 551−556.
(38) Buckler Lab for Maize Genetics and Diversity. TASSEL. http://sourceforge.net/projects/tassel (7/25/14).
(39) Lipka, A. E.; Tian, F.; Wang, Q.; Peiffer, J.; Li, M.; Bradbury, P. J.; Gore, M. A.; Buckler, E. S.; Zhang, Z. GAPIT: genome association and prediction integrated tool. *Bioinformatics* **2012**, *28*, 2397−2399.
(40) Yu, J.; Pressoir, G.; Briggs, W. H.; Bi, I. V.; Yamasaki, M.; Doebley, J. F.; McMullen, M. D.; Gaut, B. S.; Nielsen, D. M.; Holland, J. B.; Kresovich, S.; Buckler, E. S. A unified mixed-model method for association mapping that accounts for multiple levels of relatedness. *Nat. Genet.* **2006**, *38*, 203−208.
(41) Morris, G. P.; Rhodes, D. H.; Brenton, Z.; Ramu, P.; Thayil, V. M.; Deshpande, S.; Hash, C. T.; Acharya, C.; Mitchell, S. E.; Buckler, E. S.; Yu, J.; Kresovich, S. Dissecting genome-wide association signals for loss-of-function phenotypes in sorghum flavonoid pigmentation traits. *G3: Genes, Genomes, Genet.* **2013**, *3*, 2085−2094.
(42) Zhang, Z.; Ersoz, E.; Lai, C.-Q.; Todhunter, R. J.; Tiwari, H. K.; Gore, M. A.; Bradbury, P. J.; Yu, J.; Arnett, D. K.; Ordovas, J. M.; Buckler, E. S. Mixed linear model approach adapted for genome-wide association studies. *Nat. Genet.* **2010**, *42*, 355−360.
(43) Liu, Z.; Liu, Y.; Pu, Z.; Wang, J.; Zheng, Y.; Li, Y.; Wei, Y. Regulation, evolution, and functionality of flavonoids in cereal crops. *Biotechnol. Lett.* **2013**, *35*, 1765−1780.
(44) Lepiniec, L.; Debeaujon, I.; Routaboul, J.-M.; Baudry, A.; Pourcel, L.; Nesi, N.; Caboche, M. Genetics and biochemistry of seed flavonoids. *Annu. Rev. Plant Biol.* **2006**, *57*, 405−430.
(45) Petroni, K.; Tonelli, C. Recent advances on the regulation of anthocyanin synthesis in reproductive organs. *Plant Science* **2011**, *181*, 219−229.
(46) Nesi, N.; Debeaujon, I.; Jond, C.; Pelletier, G.; Caboche, M.; Lepiniec, L. The *tt8* gene encodes a basic helix-loop-helix domain protein required for expression of *DFR* and *BAN* genes in arabidopsis siliques. *Plant Cell* **2000**, *12*, 1863−1878.
(47) Furukawa, T.; Maekawa, M.; Oki, T.; Suda, I.; Iida, S.; Shimada, H.; Takamure, I.; Kadowaki, K. The *Rc* and *Rd* genes are involved in proanthocyanidin synthesis in rice pericarp. *Plant J.* **2007**, *49*, 91−102.
(48) Franken, P.; Schrell, S.; Peterson, P. A.; Saedler, H.; Wienand, U. Molecular analysis of protein domain function encoded by the *myb*-

homologous maize genes *C1*, *Zm 1* and *Zm 38*. *Plant Journal* **1994**, *6*, 21−30.
(49) Smith, C. W.; Finlayson, S. A. physiology and genetics of maturity and height. In *Sorghum: Origin, History, Technology, and Production*, 1st ed.; Smith, C. W., Frederiksen, R. A., Eds.; John Wiley & Sons: New York, NY, 2000; pp 261−307.
(50) Boddu, J.; Svabek, C.; Sekhon, R.; Gevens, A.; Nicholson, R. L.; Jones, A. D.; Pedersen, J. F.; Gustine, D. L.; Chopra, S. Expression of a putative flavonoid 3′-hydroxylase in sorghum mesocotyls synthesizing 3-deoxyanthocyanidin phytoalexins. *Physiol. Mol. Plant Pathol.* **2004**, *65*, 101−113.
(51) Chen, W.; Müller, D.; Richling, E.; Wink, M. Anthocyanin-rich purple wheat prolongs the life span of *Caenorhabditis elegans* probably by activating the DAF-16/FOXO transcription factor. *J. Agric. Food Chem.* **2013**, *61*, 3047−3053.
(52) Sriseadka, T.; Wongpornchai, S.; Rayanakorn, M. Quantification of flavonoids in black rice by liquid chromatography-negative electrospray ionization tandem mass spectrometry. *J. Agric. Food Chem.* **2012**, *60*, 11723−11732.
(53) Zilic, S.; Serpen, A.; Akıllıoğlu, G.; Gökmen, V.; Vančetović, J. Phenolic compounds, carotenoids, anthocyanins, and antioxidant capacity of colored maize (*Zea mays* l.) Kernels. *J. Agric. Food Chem.* **2012**, *60*, 1224−1231.
(54) Kim, M.-J.; Hyun, J.-N.; Kim, J.-A.; Park, J.-C.; Kim, M.-Y.; Kim, J.-G.; Lee, S.-J.; Chun, S.-C.; Chung, I.-M. Relationship between phenolic compounds, anthocyanins content and antioxidant activity in colored barley germplasm. *J. Agric. Food Chem.* **2007**, *55*, 4802−4809.
(55) Dykes, L.; Rooney, W. L.; Rooney, L. W. Evaluation of phenolics and antioxidant activity of black sorghum hybrids. *J. Cereal Sci.* **2013**, *58*, 278−283.
(56) Dykes, L.; Rooney, L. W.; Waniska, R. D.; Rooney, W. L. Phenolic compounds and antioxidant activity of sorghum grains of varying genotypes. *J. Agric. Food Chem.* **2005**, *53*, 6813−6818.
(57) Glaubitz, J. C.; Casstevens, T. M.; Lu, F.; Harriman, J.; Elshire, R. J.; Sun, Q.; Buckler, E. S. TASSEL-GBS: A High Capacity Genotyping by Sequencing Analysis Pipeline. *PLoS ONE* **2014**, *9*, e90346.

York) at 37 °C in a 5% $CO_2$ incubator with 10 μL of the RES storage solutions for 48 h. A 10 μL portion of DMSO was added to each control group to exclude its effect on cells. In addition, caspase inhibitor (z-VAD-FMK, Beyotime Institute of Biotechnology, Haimen, China) and JNK inhibitor (SP600125, Beyotime Institute of Biotechnology, Haimen, China) were used here to assess the relevant RES signaling pathway.

**Cell Viability and Cytotoxicity Assay.** After 48 h RES treatment, Jurkat cells and NK cells in each group were centrifuged at 1000 × *g* for 5 min, washed with PBS, and resuspended in 600 μL of RPMI-1640 media (IL-2 free). A 20 μL portion of CCK-8 (Cell Counting Kit-8, Dojindo, Japan) was added to a 200 μL cell suspension per well in a 96-well plate in triplicate for each group. The cells were then incubated for 2 h at 37 °C in a 5% $CO_2$ incubator. The optical density (OD) values per well were recorded at 450 nm in microplate reader (BioTek Synergy-4).

The procedure of NK cell cytotoxicity assay was described by Li et al.[12] Briefly, NK cells ($8 \times 10^5$) were separated from each RES treated group, washed three times with PBS, and resuspended in 400 μL of RPMI-1640 (IL-2 free). A 100 μL portion of NK cells ($2 \times 10^5$) was plated into each well of a 96-well plate with 100 μL of K562 cells ($4 \times 10^4$) in triplicate to make the effector-to-target ratio (E:T) at 5:1. The effector control wells contained 100 μL of NK cells ($2 \times 10^5$ cells) and 100 μL of medium. The target control wells contained 100 μL of K562 cells ($4 \times 10^4$ cells) and 100 μL of medium. Plates were incubated at 37 °C in a 5% $CO_2$ incubator. After 4 h coculture, 20 μL of CCK-8 was added to each well, and the plate was then incubated for another 2 h with OD values recorded at 450 nm. Cytotoxicity was determined by evaluating the rate at which NK cells killed K562 cells; the killing rate was calculated as following equation:[13]

$$\text{killing rate (\%)} = [1 - (OD_{e+t} - OD_e)/OD_t] \times 100\%$$

The notation is defined as follows: $OD_e$, average $OD_{450}$ of triplicate wells for NK cell control; $OD_t$, average $OD_{450}$ of triplicate wells for K562 cells control; $OD_{e+t}$, average $OD_{450}$ of triplicate wells for NK cells plus K562 cells.

**mRNA Expression Analysis.** Total RNA was isolated from RES treated NK cells ($1 \times 10^7$) by using TRIzol reagent (Invitrogen, Carlsbad, CA). The mRNA levels of three cytokines, IFN-γ, perforin, granzyme-B, and four receptors related to the cytotoxicity of NK cell, NKG2A, NKG2D, NKp30, and NKp44, were evaluated by relative quantification PCR (RT-qPCR) with SYBR Green random mixing method. Glyceraldehyde-3-phosphate dehydrogenase (GAPDH) was used as the internal control. The $2^{-\Delta\Delta Ct}$ method was used to calculate relative changes in gene expression.[14] All primers used here are shown in Table 1. RT-qPCR was performed as the instructions of the TransStart Top Green qPCR SuperMix kit (TransGen Biotech, Beijing, China). The reaction mixtures were incubated for 30 min at 48 °C, followed by 40 cycles of PCR at 94 °C for 5 s, 55 °C for 15 s, and 72 °C for 10 s. At the end of 40 cycles, a melting curve analysis was performed to confirm the presence of only a single amplified product of the expected size.

**ELISA Assay of IFN-γ, Perforin, and Granzyme-B.** The secretions of IFN-γ, perforin, and granzyme-B were assessed by corresponding ELISA Kits (BD Bioscience, CA). After RES treatment, NK cells ($8 \times 10^5$) were centrifuged and washed with PBS, resuspended in 400 μL RPMI-1640 (IL-2 free), mixed with $1.6 \times 10^5$ K562 cells in 100 μL RPMI-1640 (IL-2 free), and then incubated for 4 h at 37 °C in 5% $CO_2$ incubator (K562 cells were used to activate the cytokine secretion of NK cells according the literature).[15] In the ELISA assay, each condition was performed twice, and OD values were recorded at 450 nm. Curve Expert 13.0 was employed to create the standard curve according to the OD values of standards. The quantities of these cytokine secreted by NK were calculated from these standard curves.

**Apoptosis and Receptor Expression Assay.** AnnexinV-FITC Apoptosis Detection Kit (Beyotime Institute of Biotechnology, Haimen, China) was used to assess the apoptosis of Jurkat cells and NK cells. After treatment with RES in presence or absence of the z-VAD-FMK (caspase inhibitor, 50 μg/mL, Beyotime Institute of Biotechnology, Haimen, China), cells were centrifuged and washed 3 times with PBS, and then labeled with AnnexinV-FITC and PI following the instructions. NK cells treated by RES were centrifuged and washed with PBS, and then divided into 4 groups ($1 \times 10^5$ cells each) and labeled with PE-conjugated mouse antihuman NKG2A (R&D Systems, Minnesota), NKG2D, NKp30, and NKp44 (BD Bioscience, California). All the cells were analyzed using flow cytometry.

**Data Analysis.** Statistical analysis was performed using SPSS 16.0 statistical software (IBM, New York). The data were presented as the mean ± SD. The results were analyzed using the analysis of variance (ANOVA). Multiple comparisons used LSD test to evaluate the significance of differences between groups. Statistical significance was defined as $p < 0.05$.

**Table 1. Primer Pairs Used for RT-qPCR Analysis**

| primer | sequence (5′-3′) | amplicon size (bp) |
|---|---|---|
| IFN-γ | F: TGCAGGTCATTCAGATGTAGC | 248 |
| | R: GGACATTCAAGTCAGTTACCG | |
| perforin | F: GGGACAATAACAACCCCATCT | 174 |
| | R:GGAATTTTAGGTGGCCATGAT | |
| granzyme-B | F:AGATCGAAAGTGCGAATCTGA | 138 |
| | R: TTCGTCCATAGGAGACAATGC | |
| NKG2A | F: TCATTGTGGCCATTGTCCTGAGG | 291 |
| | R: AGCACTGCACAGTTAAGTTCAGC | |
| NKG2D | F: ATCGCTGTAGCCATGGGAATCCG | 213 |
| | R: AGACATACAAGAGACCTGGCTCTC | |
| NKp30 | F: TGAGATTCGTACCCTGGAAGG | 235 |
| | R: CACTCTGCACACGTAGATGCT | |
| NKp44 | F: TCCAAGGCTCAGGTACTTCAA | 163 |
| | R: GATTGTGAATCGAGAGGTCCA | |
| GAPDH | F: TCCTGCACCACCAACTGCTTAGC | 254 |
| | R: ACACGGAAGGCCATGCCAGTGAGC | |

## RESULTS

**NK Cell Purity.** After 3 weeks of *ex vivo* expansion, primary human NK cells were harvested, stained with CD56-PE and CD3-FITC mAbs, and analyzed by flow cytometry. The percentage of NK cells ($CD56^+CD3^-$) was determined. The mean percentage of NK cells from 12 donors was 91.21 ± 1.78% ($n = 12$).

**Cell Viability.** RES (12.5−50 μM) shows concentration-dependent effects on the viability of both Jurkat cells and NK cells. In the concentration of 50 μM, RES can inhibit the viability of both cells. Figure 1 shows the OD values were significantly reduced, which were 1.94 ± 0.33, 1.8 ± 0.34, 1.79 ± 0.37 1.74 ± 0.23, 1.85 ± 0.26, 1.47 ± 0.21, 1.41 ± 0.36, and 1.18 ± 0.29 in Jurkat cells, and 0.77 ± 0.05, 0.76 ± 0.03, 0.77 ± 0.04, 0.76 ± 0.03, 0.76 ± 0.04, 0.74 ± 0.02, 0.62 ± 0.03, and 0.48 ± 0.03, respectively, in NK cells with the concentration of RES increased from 0 to 50 μM (Figure 1A). It was noticed that when the concentration of RES reduced to 12.5 μM, there was no obvious inhibited effect on NK cells, but the Jurkat cells still could be affected until it reduced to 6.25 μM. This suggested that Jurkat cells are more sensitive than NK cells in response to RES causing cell death. On the other hand, inhibitors were employed here to assess the relevant signaling pathway RES may act with (Figure 1B). After pretreatment by inhibitors (z-VAD-FMK and SP600125), RES (50 μM) no longer showed the inhibited effect on Jurkat cells and NK cells in z-VAD-FMK group. The OD values in z-VAD-FMK group

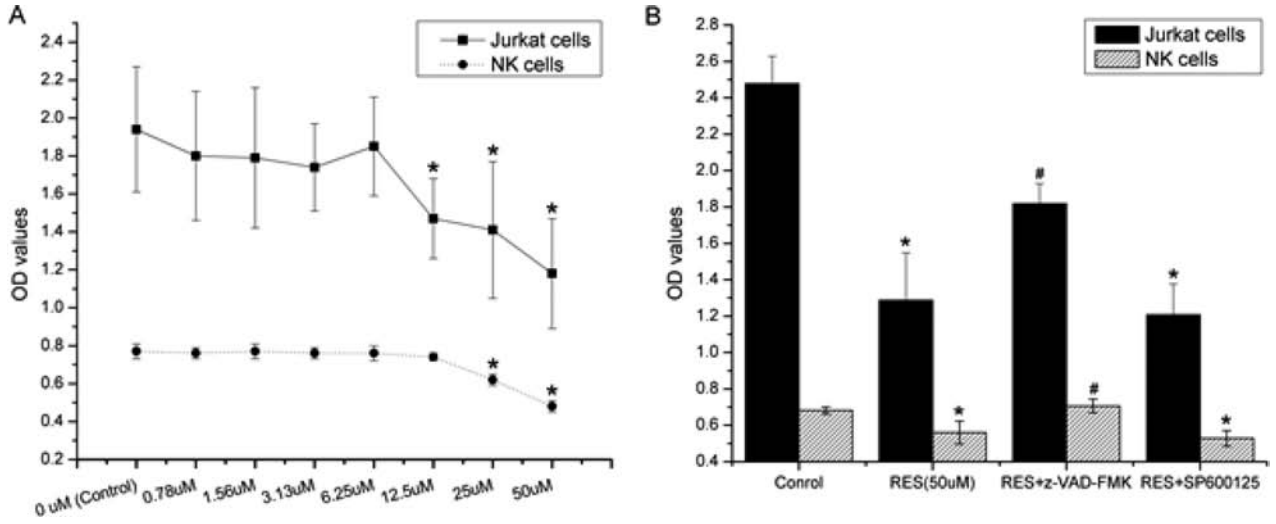


**Figure 1.** OD values of cells treated with RES and inhibitors ($n = 4$). (A) Cells treated with RES in concentration gradient (0−50 $\mu$M) for 48 h. (B) Cells treated with RES (50 $\mu$M) in present or absent of z-VAD-FMK and SP600125 (50 $\mu$M each) for 48 h. Data represent the mean ± SD of four independent experiments. One-way ANOVA and LSD tests were performed: * $p < 0.05$ compared with the control; # $p < 0.05$ compared with the RES treated group.

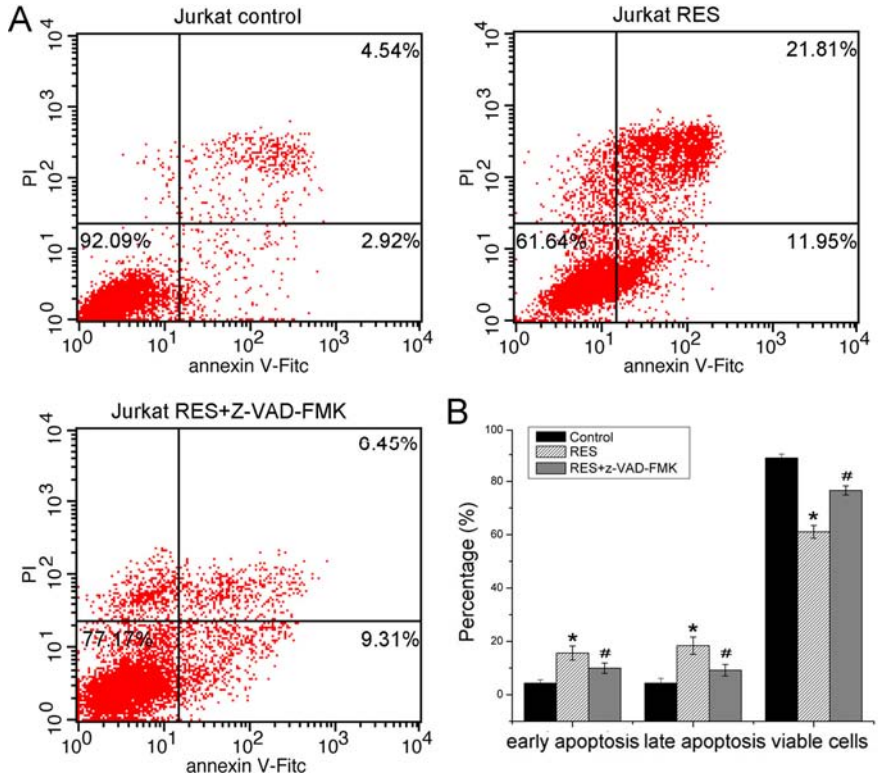


**Figure 2.** Apoptosis and necrosis of Jurkat cells after RES treatment ($n = 4$). (A) A representative flow cytometry plot of Jurkat cells from one donor. The percentages of viable (Annexin $V^-/PI^-$), early apoptotic (Annexin $V^+/PI^-$), and late apoptotic/necrotic (Annexin $V^+/PI^+$) cells are shown. (B) The percentage of apoptosis in these cells is summarized in the bar graph; each column represents the mean ± SD from four independent experiments. Multivariate ANOVA and LSD tests were performed: * $p < 0.05$ compared with the control; # $p < 0.05$ compared with the RES treated group.

were 1.82 ± 0.11 and 0.71 ± 0.04, respectively, compared with the 1.29 ± 0.26 (Jurkat cells) and 0.56 ± 0.06 (NK cells) in RES groups. However, the OD values in SP600125 groups of the two cells showed no significant changes compared with the RES groups. It is suggested that RES may inhibit the viability of cells by causing them apoptosis/death via caspase signal pathway.

**Cell Apoptosis.** Cells stained by AnnexinV and PI after 48 h RES (50 $\mu$M) treatment in presence or absence of z-VAD-FMK were shown in Figures 2 and 3. Apoptosis of both Jurkat cells and NK cells increased comparing with the controls, and the apoptosis of Jurkat cells was more damaged than the latter. Early apoptosis (Annexin$V^+/PI^-$) occurred in 15.9 ± 1.99% in NK cells and 15.59 ± 2.67% in Jurkat cells after RES treated


dx.doi.org/10.1021/jf502950u | J. Agric. Food Chem. 2014, 62, 10928−10935

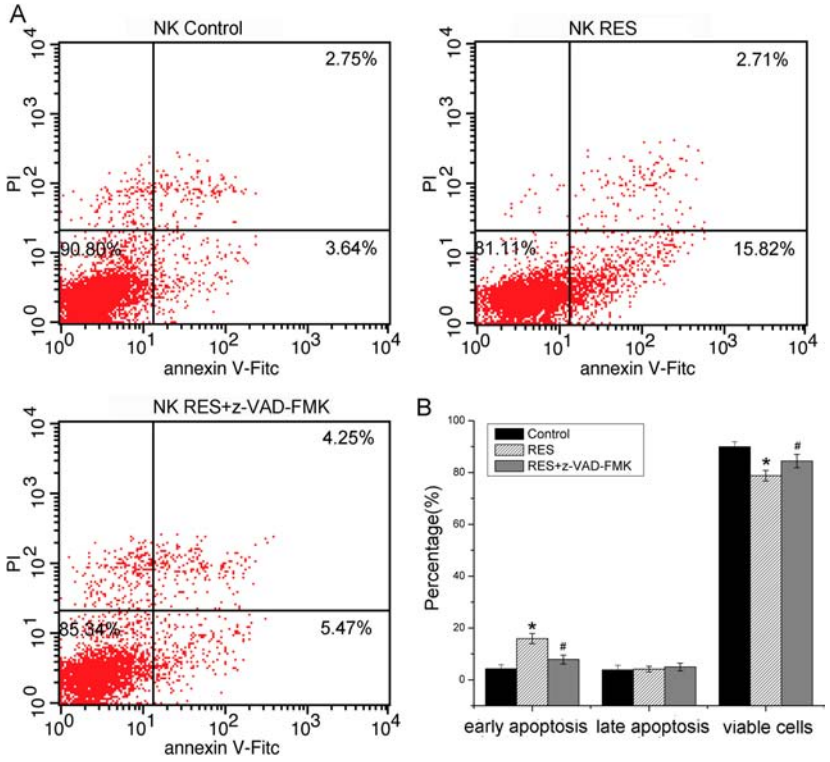


**Figure 3.** Apoptosis and necrosis of NK cells after RES treatment ($n = 4$). (A) A representative flow cytometry plot of NK cells from one donor. The percentages of viable (Annexin $V^-/PI^-$), early apoptotic (Annexin $V^+/PI^-$), and late apoptotic/necrotic (Annexin $V^+/PI^+$) NK cells are shown. (B) The percentage of apoptosis in these cells is summarized in the bar graph; each column represents the mean ± SD from four independent experiments. Multivariate ANOVA and LSD tests were performed: * $p < 0.05$ compared with the control; # $p < 0.05$ compared with the RES treated group.

compared with 4.24 ± 1.57% and 4.29 ± 1.25%, respectively, of the control ($p < 0.05$). Meanwhile, the late apoptosis/necrosis NK cells were 4.12 ± 1.08%, with no significant difference compared with 3.8 ± 1.79% of the control. However, the late apoptosis/necrosis Jurkat cells were 18.35 ± 3.24%, increased significantly compared with the 4.3 ± 1.82% in the control. Correspondingly, the percentages of viable cells were 78.78 ± 2.06% (NK cells) and 61.06 ± 2.4% (Jurkat cells) in RES treated groups compared with 89.98 ± 1.93% (NK cells) and 88.79 ± 1.5% (Jurkat cells) in control, respectively ($p < 0.05$). Furthermore, the RES-induced apoptosis and necrosis of cells were blocked by caspase inhibitor (z-VAD-FMK). After pretreatment by z-VAD-FMK, the apoptosis rates of Jurkat cells and NK cell were reduced partially. These results suggested that RES could induce Jurkat cell and NK cell apoptosis in 50 μM, which may be relevant with caspase signaling pathways. NK cells showed more resistance than Jurkat cells on RES induced apoptosis at dose tested.

**NK Cells Cytotoxicity.** In this assay, NK cells were treated with RES in concentration gradient for 48 h. The cytotoxicity of the NK cells was tested. As shown in Figure 4, the cytotoxicity of NK cells was significantly decreased when the concentration of RES was above 25 μM, 61.42 ± 3.93% and 71.28 ± 3.55% in 50 and 25 μM treated groups compared with the 90.22 ± 1.43% in the control ($p < 0.05$). Unexpectedly, RES in low concentration (3.13 and 1.56 μM) increased the cytotoxicity of NK cells, 95.86 ± 1.56% and 94.73 ± 1.62% compared with control ($p < 0.05$). Therefore, in the following experiments, the mechanism underlying the increased NK cells cytotoxicity was studied under 3.13 μM treatment of RES.

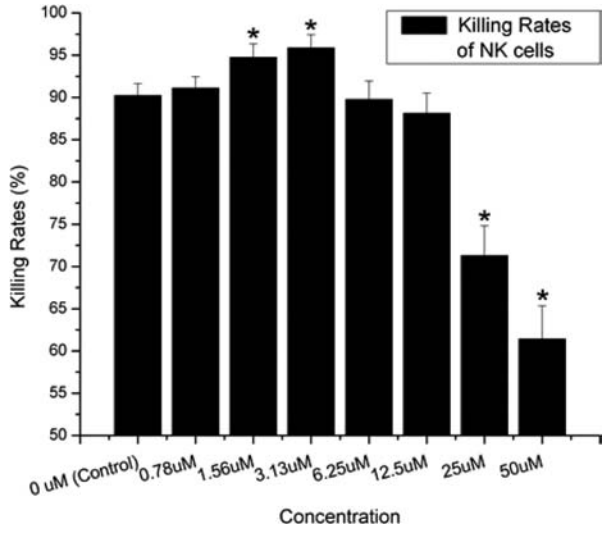


**Figure 4.** Effect of RES on NK cell cytotoxicity ($n = 4$). Each column represents the mean ± SD from four independent experiments. One-way ANOVA and LSD tests were performed: * $p < 0.05$ compared with the control.

**RT-qPCR.** Table 2 depicted the expression profiles of genes involved in NK cell functions after low concentration RES (3.13 μM) treatment. The mRNA level of IFN-γ increased significantly in the RES-treated group to 4.5-fold compared with the control ($p < 0.05$). Meanwhile, the mRNA levels of triggering receptors NKG2D were also up-regulated signifi-


dx.doi.org/10.1021/jf502950u | J. Agric. Food Chem. 2014, 62, 10928−10935

Table 2. RES in Low Concentration Regulated NK Cell Functional Proteins at the mRNA Level ($n$ = 6)[a]

| gene | IFN-$\gamma$ | perforin | granzyme-B | NKG2A | NKG2D | NKp30 | NKp44 |
|---|---|---|---|---|---|---|---|
| compared with control | 4.5(fold)[b] | 2.14(fold) | 1.77(fold) | 0.53(fold) | 6.36(fold)[b] | 1.39(fold) | 1.71(fold) |

[a]SYBR green-based RTq-PCR was used to examine the mRNA levels of genes that are important for NK cell functions. The data represent the mean ± SD of six independent experiments. One-way ANOVA and LSD test. [b]$p < 0.05$ compared with 1.

cantly in the RES treated group, which increased 6.36-fold compared with control ($p < 0.05$).

**ELISA.** The levels of cytokine and cytolytic proteins in the NK cell supernatants are illustrated in Figure 5. It is noticed that the IFN-$\gamma$ level was increased under 3.13 $\mu$M RES treatment, which was increased to 730 ± 41 pg/mL compared with the 400 ± 35 pg/mL in the control ($p < 0.05$). The concentration of perforin was not changed significantly. They were about 800 ng/mL in RES treated and control groups. However, the granzyme-B was hardly detected in the supernatants of two groups.

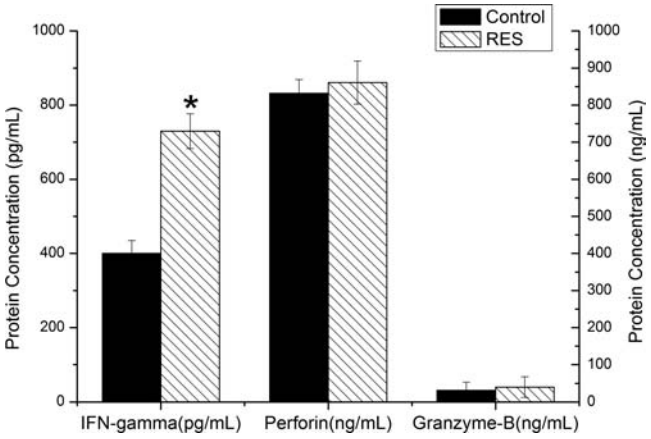


**Figure 5.** IFN-$\gamma$, perforin, and granzyme-B secretion of NK cells after RES treatment. RES (3.125 $\mu$M) treated NK cells were stimulated with K562 cells, supernatants were collected, and then the concentrations of IFN-$\gamma$, perforin, and granzyme-B were detected. Each column represents mean ± SD of four independent experiments. One-way ANOVA and LSD tests were performed: * $p < 0.05$ compared with control.

**Receptor Expression.** Flow cytometry assays indicate that NK cells display a significant up-regulation of NKG2D (Figure 6). The positive percentage of NKG2D increased from 83.52 ± 5.64% in the control group to 94.2 ± 4.67% in RES treated group ($p < 0.05$). The positive percentages of NKG2A, NKp30, and NKp44 were not changed obviously.

## DISCUSSION

As a small polyphenol, RES was found in various plant sources,[16] and has been demonstrated to have many beneficial effects and received a lot of attention in recent years. RES was well-known for use in various areas including anti-inflammatory, antioxidant, antidiabetic, and antiaging.[17−19] Also, it showed the positive effects of triggering cell death in a great variety of human tumor cells, such as colon, prostate, breast, lymphoma, and leukemia.[20−24] For these reasons, RES has been recognized as a potential adjuvant in cancer chemotherapy.[25,26]

NK cells play a pivotal role in innate and adaptive immunity, especially in tumor surveillance. The effect of RES on human NK cells should be assessed carefully if it has been used as antitumor drug. In this study, primary human NK cells were treated by RES with concentration gradient. The viability, apoptosis, and cytotoxicity of NK cells were detected. Jurkat cells were used to assess if there was a sensitivity difference for RES between primary cells and tumor cells.

When RES was employed as a drug or adjuvant to inhibit viability or induce apoptosis on tumor cells *in vitro*, the common working concentrations were 25−200 $\mu$M.[27−30] In the present study we noticed that when the concentration of RES above 12.5 $\mu$M, the significant inhibiting effect was observed on Jurkat cells, but the threshold in NK cells was 25 $\mu$M. It indicated that tumor cell lines such as Jurkat are more sensitive than NK cells to the toxicity effect of RES. Jazirehi et al. reported that, in 10 $\mu$M concentration, RES did not show any toxicity on human PBMCs, but it caused cell death in Roma cell lines.[31] Another study reported that RES reduced the viability and DNA synthesis capability of the promyelocytic leukemia (HL-60) cell;[32] it also inhibited growth of human colon tumorigenic cells mediated by cell cycle arrest.[33] Tumor cells grow more actively than primary cells, the DNA synthesis reduction and cell cycle arrest caused by RES affect the tumor cell proliferation more serious than primary cells, which may explain the sensitivity difference of RES between the two kinds of cells.

Many studies have indicated the biphasic effects of RES on cells. It was reported that RES can promote GH3 cells proliferation at low concentrations (1 $\mu$M) and inhibit it at high concentrations (>10 $\mu$M), and the RES-induced GH3 cell apoptosis was caspase-dependent.[25] Suzuki et al. observed cleavage of caspase-3 and poly(ADP-ribose) polymerase in RES-treated cells, which indicated that RES induces caspase-dependent apoptosis in MT-2 and HUT-102 cells.[34] Our results showed, at the high concentration (50 $\mu$M), RES reduces OD values of both Jurkat cells and NK cells, while caspase inhibitor z-VAD-FMK can prevent RES caused cell death. The flow cytometry assay confirmed these results; after pretreatment by z-VAD-FMK, the early and late apoptosis/necrosis cells caused by RES were reduced significantly, which suggests that RES promotes cell apoptosis via caspase signaling pathway. Kashif et al. reported that RES (4−8 $\mu$M) treatment inhibited the caspase activation, and $H_2O_2$ induced apoptosis in HL60 cells.[35] Another study showed that RES in 2 and 5 $\mu$M increased the percentage of CD19+ cell in human PBMCs. However, 10 $\mu$M RES inhibited the proliferation of B lymphocyte.[36] In our results, RES (in 1.56−6.25 $\mu$M) did not show the promote proliferation or antiapoptosis effects (data not shown) on either Jurkat cells or NK cells, but it actually promoted the cytotoxicity of NK cells in 1.56−3.13 $\mu$M.

The cytotoxicity of NK cells plays a key role in tumor identification and surveillance. NK cells kill malignant cells by secretion of IFN-$\gamma$, perforin, and granzyme-B. NKG2D is the most important triggering receptor on NK cells which trigger cytotoxicity and mediate the secretion of IFN-$\gamma$.[37] RT-qPCR and flow cytometry assays indicated that RES in 3.13 $\mu$M can increase the expression of NKG2D both in mRNA and protein level. Results from Lu et al. show that RES pretreatment increases NK cell cytotoxicity in a dose-dependent (1.56−12.5

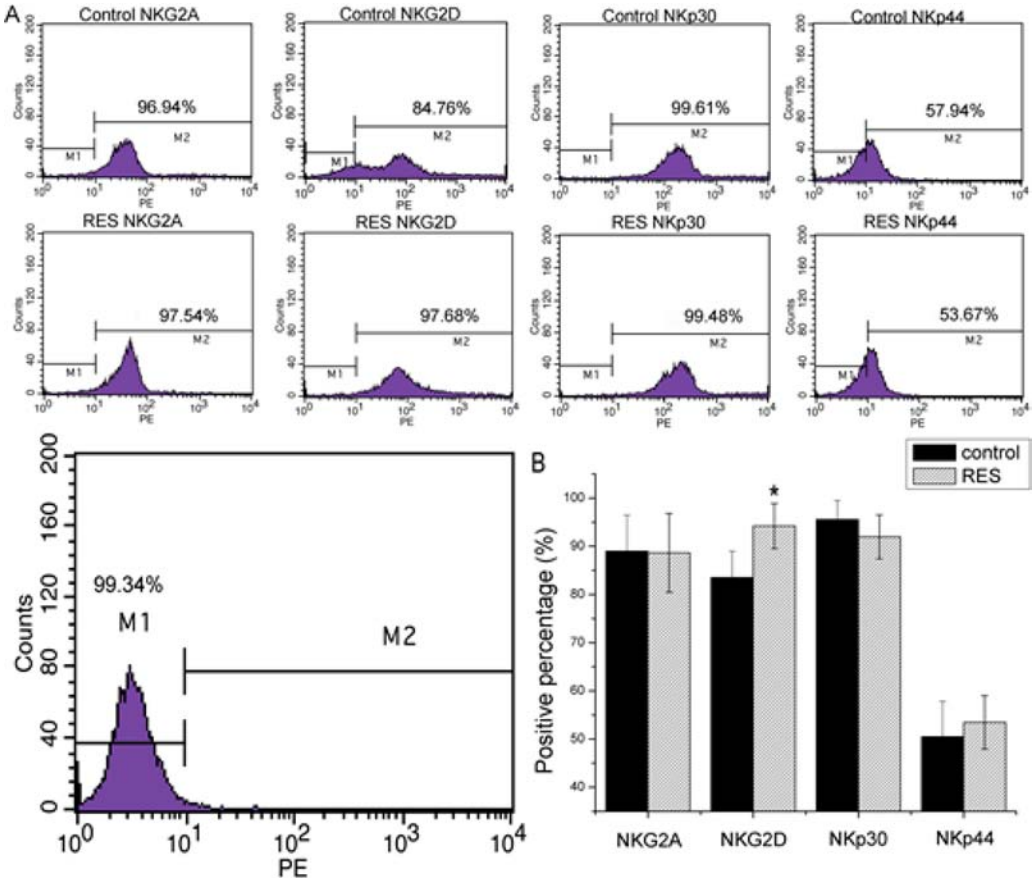


**Figure 6.** Protein expression profiles for the NK cell receptors NKG2A, NKG2D, NKp30, and NKp44 after low concentration RES treatment. (A) NK cells were stained with PE-conjugated mAbs and analyzed by flow cytometry (for example). (B) The bar graph represents the mean ± SD from three independent experiments. One-way ANOVA and LSD test: * $p < 0.05$ compared with control.

$\mu$M) manner by up-regulation of the expression of NKG2D and perforin expression.[38] In our results, the change of perforin expression was not obvious, but the IFN-$\gamma$ expression was up-regulated significantly. Increased expression of NKG2D and IFN-$\gamma$ may be the reason for enhanced cytotoxicity of NK cells. Hu et al. reported that RES treatment also increases the cell-surface expression of NKG2D ligands on human promyelo-blastic leukemia KG-1a cells.[39] It indicated that RES can enhance the CIK (cytokine-induced killer) via up-regulation of the expression of both NKG2D and NKG2D ligands on effector and target cells, respectively.

Thought that the effects of RES on NK cytotoxic activity may be due to partial agonistic activity of RES on aryl hydrocarbon receptor (AhR).[40] They speculated that RES is a partial agonist of human AhR and exerts its effect on NK cells by the mechanism involving activation of JNK (c-Jun N-terminal kinase) and ERK (extracellular-regulated kinase).[38,40] Unlike caspase inhibitor, JNK inhibitor SP600125 did not show the abolished effects on high concentration RES induced NK cell apoptosis in our study. However, JNK may relate to the positive effect of RES on NK cells.

The present study indicated that RES has biphasic effects on human NK cells. Other biphasic effects of RES on tumor cells or several parasitic diseases were also reported (reviewed by Calabrese et al.[41]). In line with these findings, it indicated that RES acts via multiple target pathways (AhR, JNK, and ERK).[42] Due to rapid metabolism in human body, RES may hardly reach the body tissues in sufficient dosage to exert the beneficial health effects by oral consumption.[43] Using RES as one kind of injection may be part of the solution. Therefore, it was very important to confirm and calculate the effective concentration of RES accurately when it was used as a potential antitumor or health product.

## AUTHOR INFORMATION

### Corresponding Author

*Phone:+86-029-88460332. Fax: +86-029-88460332. E-mail: huangqingsheng1963@aliyun.com.

### Funding

We gratefully acknowledge financial support from the Natural Science Foundation of Shaanxi Province (Grant 2014JM4171) and the Fundamental Research Funds for the Central Universities (Grant 3102014JKY15008).

### Notes

The authors declare no competing financial interest.

## ABBREVIATIONS USED

CCK-8, cell counting kit-8; E:T, effector versus target; FBS, fetal bovine serum; GAPDH, glyceraldehyde-3-phosphate dehydrogenase; IFN, interferon; IL, interleukin; LSD, least significant difference; mAbs, monoclonal antibodies; NK, natural killer; OD, optical density; PBMC, peripheral blood mononuclear cell; PBS, phosphate-buffered saline; RES, resveratrol

## REFERENCES


(1) Dudka, J.; Gieroba, R.; Korga, A.; Burdan, F.; Matysiak, W.; Jodlowska-Jedrych, B.; Mandziuk, S.; Korobowicz, E.; Murias, M. Different effects of resveratrol on dose-related Doxorubicin-induced heart and liver toxicity. *Evidence-Based Complementary Altern. Med.: eCAM* **2012**, *2012*, 606183.

(2) Sadruddin, S.; Arora, R. Resveratrol: Biologic and therapeutic implications. *J. CardioMetab. Syndr.* **2009**, *4*, 102−6.

(3) Tome-Carneiro, J.; Larrosa, M.; Gonzalez-Sarrias, A.; Tomas-Barberan, F. A.; Garcia-Conesa, M. T.; Espin, J. C. Resveratrol and clinical trials: The crossroad from in vitro studies to human evidence. *Curr. Pharm. Des.* **2013**, *19*, 6064−93.

(4) Pangeni, R.; Sahni, J. K.; Ali, J.; Sharma, S.; Baboota, S. Resveratrol: Review on therapeutic potential and recent advances in drug delivery. *Expert Opin. Drug Deliv.* **2014**, *11*, 1285−98.

(5) Liu, Y. Z.; Wu, K.; Huang, J.; Liu, Y.; Wang, X.; Meng, Z. J.; Yuan, S. X.; Wang, D. X.; Luo, J. Y.; Zuo, G. W.; Yin, L. J.; Chen, L.; Deng, Z. L.; Yang, J. Q.; Sun, W. J.; He, B. C. The PTEN/PI3K/Akt and Wnt/beta-catenin signaling pathways are involved in the inhibitory effect of resveratrol on human colon cancer cell proliferation. *Int. J. Oncol.* **2014**, *45*, 104−12.

(6) Ferruelo, A.; Romero, I.; Cabrera, P. M.; Arance, I.; Andres, G.; Angulo, J. C. Effects of resveratrol and other wine polyphenols on the proliferation, apoptosis and androgen receptor expression in LNCaP cells. *Actas Urol. Esp.* **2014**, *38*, 397−404.

(7) Frazzi, R.; Tigano, M. The multiple mechanisms of cell death triggered by resveratrol in lymphoma and leukemia. *Int. J. Mol. Sci.* **2014**, *15*, 4977−93.

(8) Cooper, M. A.; Fehniger, T. A.; Caligiuri, M. A. The biology of human natural killer-cell subsets. *Trends Immunol.* **2001**, *22*, 633−40.

(9) Trinchieri, G. Biology of natural killer cells. *Adv. Immunol.* **1989**, *47*, 187−376.

(10) Huang, Q. S.; Li, Q.; Huang, Y.; Shang, P.; Zhang, M. J. Expansion of human natural killer cells ex vivo. *Xibao yu Fenzi Mianyixue Zazhi* **2008**, *24*, 1167−9.

(11) Imai, C.; Iwamoto, S.; Campana, D. Genetic modification of primary natural killer cells overcomes inhibitory signals and induces specific killing of leukemic cells. *Blood* **2005**, *106*, 376−83.

(12) Li, Q.; Mei, Q.; Huyan, T.; Xie, L.; Che, S.; Yang, H.; Zhang, M.; Huang, Q. Effects of simulated microgravity on primary human NK cells. *Astrobiology* **2013**, *13*, 703−14.

(13) Chen, Y.; Wang, Y.; Zhuang, Y.; Zhou, F.; Huang, L. Mifepristone increases the cytotoxicity of uterine natural killer cells by acting as a glucocorticoid antagonist via ERK activation. *PloS One* **2012**, *7*, e36413.

(14) Livak, K. J.; Schmittgen, T. D. Analysis of relative gene expression data using real-time quantitative PCR and the 2(-Delta Delta C(T)) Method. *Methods* **2001**, *25*, 402−8.

(15) Denman, C. J.; Senyukov, V. V.; Somanchi, S. S.; Phatarpekar, P. V.; Kopp, L. M.; Johnson, J. L.; Singh, H.; Hurton, L.; Maiti, S. N.; Huls, M. H.; Champlin, R. E.; Cooper, L. J.; Lee, D. A. Membrane-bound IL-21 promotes sustained ex vivo proliferation of human natural killer cells. *PloS One* **2012**, *7*, e30264.

(16) Baur, J. A.; Sinclair, D. A. Therapeutic potential of resveratrol: the in vivo evidence. *Nat. Rev. Drug Discov.* **2006**, *5*, 493−506.

(17) Pezzuto, J. M. The phenomenon of resveratrol: Redefining the virtues of promiscuity. *Ann. N.Y. Acad. Sci.* **2011**, *1215*, 123−30.

(18) Howitz, K. T.; Bitterman, K. J.; Cohen, H. Y.; Lamming, D. W.; Lavu, S.; Wood, J. G.; Zipkin, R. E.; Chung, P.; Kisielewski, A.; Zhang, L. L.; Scherer, B.; Sinclair, D. A. Small molecule activators of sirtuins extend Saccharomyces cerevisiae lifespan. *Nature* **2003**, *425*, 191−6.

(19) Lee, C. W.; Yen, F. L.; Huang, H. W.; Wu, T. H.; Ko, H. H.; Tzeng, W. S.; Lin, C. C. Resveratrol nanoparticle system improves dissolution properties and enhances the hepatoprotective effect of resveratrol through antioxidant and anti-inflammatory pathways. *J. Agric. Food Chem.* **2012**, *60*, 4662−71.

(20) Lee, Y. J.; Im, J. H.; Won, S. Y.; Kim, Y. B.; Cho, M. K.; Nam, H. S.; Choi, Y. J.; Lee, S. H. Synergistic anti-cancer effects of resveratrol and chemotherapeutic agent clofarabine against human malignant mesothelioma MSTO-211H cells. *Food Chem. Toxicol.* **2013**, *52*, 61−8.

(21) Castillo-Pichardo, L.; Dharmawardhane, S. F. Grape polyphenols inhibit Akt/mammalian target of rapamycin signaling and potentiate the effects of gefitinib in breast cancer. *Nutr. Cancer* **2012**, *64*, 1058−69.

(22) Can, G.; Cakir, Z.; Kartal, M.; Gunduz, U.; Baran, Y. Apoptotic effects of resveratrol, a grape polyphenol, on imatinib-sensitive and resistant K562 chronic myeloid leukemia cells. *Anticancer Res.* **2012**, *32*, 2673−8.

(23) Iguchi, K.; Toyama, T.; Ito, T.; Shakui, T.; Usui, S.; Oyama, M.; Iinuma, M.; Hirano, K. Antiandrogenic activity of resveratrol analogs in prostate cancer LNCaP cells. *J. Androl.* **2012**, *33*, 1208−15.

(24) Juan, M. E.; Alfaras, I.; Planas, J. M. Colorectal cancer chemoprevention by trans-resveratrol. *Pharmacol. Res.* **2012**, *65*, 584−91.

(25) Chao, W.; Xuexin, Z.; Jun, S.; Ming, C.; Hua, J.; Li, G.; Tan, C.; Xu, W. Effects of resveratrol on cell growth and prolactin synthesis in GH3 cells. *Exp. Ther. Med.* **2014**, *7*, 923−928.

(26) Yang, X.; Li, X.; Ren, J. From French Paradox to cancer treatment: anti-cancer activities and mechanisms of resveratrol. *Anti-Cancer Agents Med. Chem.* **2014**, *14*, 806−25.

(27) Park, D. G. Antichemosensitizing effect of resveratrol in cotreatment with oxaliplatin in HCT116 colon cancer cell. *Ann. Surg. Treat. Res.* **2014**, *86*, 68−75.

(28) Yan, H. W.; Hu, W. X.; Zhang, J. Y.; Wang, Y.; Xia, K.; Peng, M. Y.; Liu, J. Resveratrol induces human K562 cell apoptosis, erythroid differentiation, and autophagy. *Tumor Biol.* **2014**, *35*, 5381−8.

(29) Ge, J.; Liu, Y.; Li, Q.; Guo, X.; Gu, L.; Ma, Z. G.; Zhu, Y. P. Resveratrol induces apoptosis and autophagy in T-cell acute lymphoblastic leukemia cells by inhibiting Akt/mTOR and activating p38-MAPK. *Biomed. Environ. Sci.* **2013**, *26*, 902−11.

(30) Zou, T.; Yang, Y.; Xia, F.; Huang, A.; Gao, X.; Fang, D.; Xiong, S.; Zhang, J. Resveratrol inhibits CD4+ T cell activation by enhancing the expression and activity of Sirt1. *PloS One* **2013**, *8*, e75139.

(31) Jazirehi, A. R.; Bonavida, B. Resveratrol modifies the expression of apoptotic regulatory proteins and sensitizes non-Hodgkin's lymphoma and multiple myeloma cell lines to paclitaxel-induced apoptosis. *Mol. Cancer Ther.* **2004**, *3*, 71−84.

(32) Surh, Y. J.; Hurh, Y. J.; Kang, J. Y.; Lee, E.; Kong, G.; Lee, S. J. Resveratrol, an antioxidant present in red wine, induces apoptosis in human promyelocytic leukemia (HL-60) cells. *Cancer Lett.* **1999**, *140*, 1−10.

(33) Gonzalez-Sarrias, A.; Gromek, S.; Niesen, D.; Seeram, N. P.; Henry, G. E. Resveratrol oligomers isolated from Carex species inhibit growth of human colon tumorigenic cells mediated by cell cycle arrest. *J. Agric. Food Chem.* **2011**, *59*, 8632−8.

(34) Suzuki, Y.; Ito, S.; Sasaki, R.; Asahi, M.; Ishida, Y. Resveratrol suppresses cell proliferation via inhibition of STAT3 phosphorylation and Mcl-1 and cIAP-2 expression in HTLV-1-infected T cells. *Leuk. Res.* **2013**, *37*, 1674−9.

(35) Ahmad, K. A.; Clement, M. V.; Hanif, I. M.; Pervaiz, S. Resveratrol inhibits drug-induced apoptosis in human leukemia cells by creating an intracellular milieu nonpermissive for death execution. *Cancer Res.* **2004**, *64*, 1452−9.

(36) Zunino, S. J.; Storms, D. H. Resveratrol alters proliferative responses and apoptosis in human activated B lymphocytes in vitro. *J. Nutr.* **2009**, *139*, 1603−8.

(37) Krzewski, K.; Strominger, J. L. The killer's kiss: The many functions of NK cell immunological synapses. *Curr. Opin. Cell Biol.* **2008**, *20*, 597−605.

(38) Lu, C. C.; Chen, J. K. Resveratrol enhances perforin expression and NK cell cytotoxicity through NKG2D-dependent pathways. *J. Cell. Physiol.* **2010**, *223*, 343−51.

(39) Hu, L.; Cao, D.; Li, Y.; He, Y.; Guo, K. Resveratrol sensitized leukemia stem cell-like KG-1a cells to cytokine-induced killer cells-mediated cytolysis through NKG2D ligands and TRAIL receptors. *Cancer Biol. Ther.* **2012**, *13*, 516−26.

(40) Bachleda, P.; Vrzal, R.; Dvorak, Z. Resveratrol enhances NK cell cytotoxicity: Possible role for aryl hydrocarbon receptor. *J. Cell. Physiol.* **2010**, *225*, 289−90.
(41) Calabrese, E. J.; Mattson, M. P.; Calabrese, V. Resveratrol commonly displays hormesis: Occurrence and biomedical significance. *Hum. Exp. Toxicol.* **2010**, *29*, 980−1015.
(42) Timmers, S.; Auwerx, J.; Schrauwen, P. The journey of resveratrol from yeast to human. *Aging* **2012**, *4*, 146−58.
(43) Goldberg, D. M.; Yan, J.; Soleas, G. J. Absorption of three wine-related polyphenols in three different matrices by healthy subjects. *Clin. Biochem.* **2003**, *36*, 79−87.

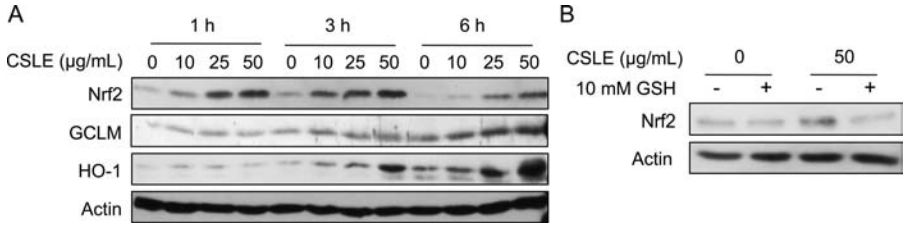


**Figure 1.** CSLE-mediated activation of Nrf2 in HepG2 cells and modification of purified Keap1. (A) Cells were exposed to CSLE (10, 25, or 50 $\mu$M) for 1, 3, or 6 h, and then total cell proteins were subjected to Western blot analysis with the indicated antibodies. (B) CSLE was incubated with GSH (10 mM) for 30 min at room temperature. The cells were treated with GSH-incubated CSLE (50 $\mu$g/mL) for 1 h, and total cell proteins were subjected to Western blot analysis with the indicated antibodies.

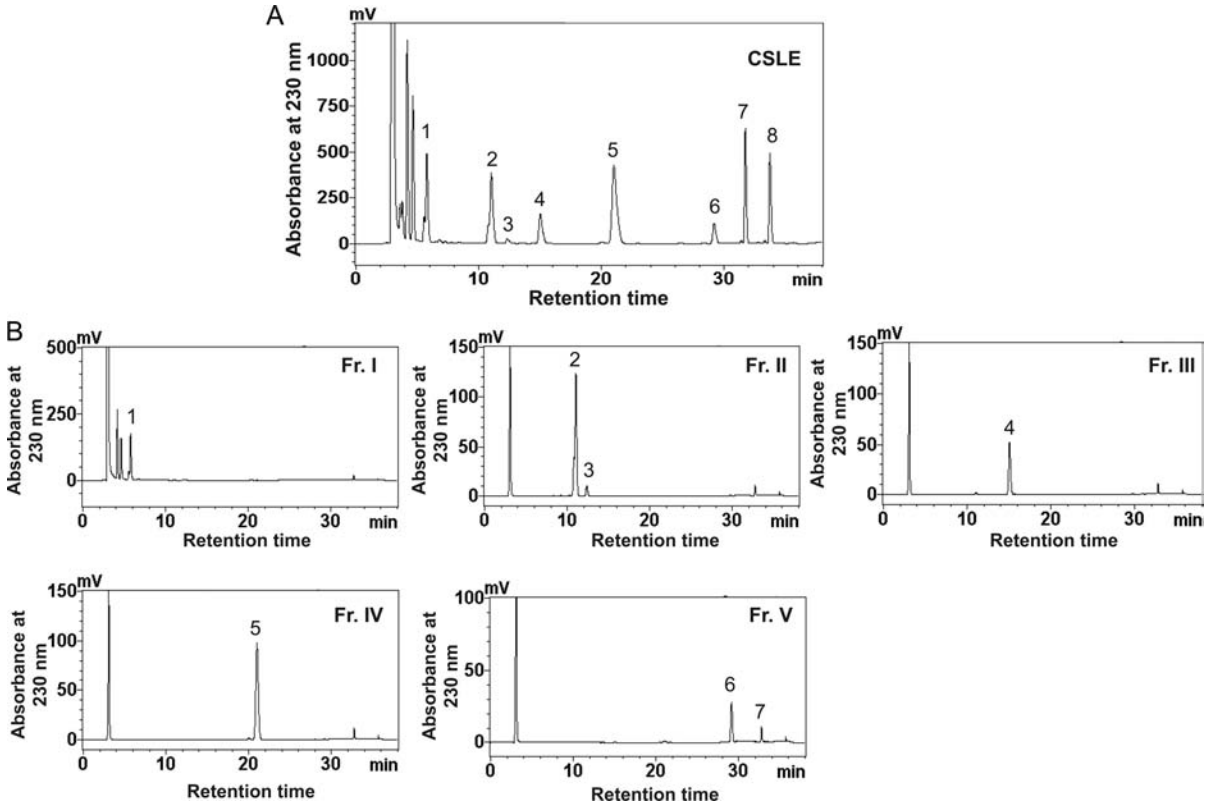


**Figure 2.** HPLC analysis of CSLE (A) and fractions separated by Ultra Pack ODS-S-50B column chromatography (B). Detection at 230 nm.

(Beverly, MA, USA), and Invitrogen (Carlsbad, CA, USA), respectively. All other reagents were of the highest grade available.

**Cell Culture.** HepG2 cells were obtained from RIKEN Cell Bank (Tsukuba, Japan). The cells were cultured in minimal essential medium (MEM; Wako) containing 10% fetal bovine serum, antibiotics (100 U/mL penicillin and 100 $\mu$g/mL streptomycin), and 2 mM L-alanyl-L-glutamine (Invitrogen) in an incubator supplemented with 5% $CO_2$ at 37 °C. In extracting total protein, $8 \times 10^5$ cells were seeded in 35 mm dishes. The cells were preincubated in serum-free medium for 12 h before treatment with compounds.

**CSLE Extraction.** *C. sativum* leaves (78 g) were frozen in liquid nitrogen and transferred to a 1 L flask containing 80 mL of distilled deionized water and 160 mL of *n*-hexane. The flask was refluxed in an oil bath at 80 °C for 2 h, and the *n*-hexane layer was collected using a separating funnel. The *n*-hexane layer was passed over anhydrous sodium sulfate to remove any trace of water and then treated with argon gas. The *n*-hexane layer was evaporated in vacuo to remove *n*-hexane, and the residues were redissolved in acetonitrile or dimethyl sulfoxide (DMSO). Samples were stored at −80 °C prior to use.

**Separation of CSLE.** The CSLE (70 mg) in DMSO was separated into five fractions by preparative column chromatography using an Ultra Pack ODS-S-50B column (300 × 26 mm i.d., 50 $\mu$m; Yamazen Science Inc., Osaka, Japan); elution was with 25% acetonitrile in water at a flow rate of 5 mL/min. Phytochemicals with retention times of 2−60 min (fraction I, 10 mg), 60−100 min (fraction II, 10 mg), 100−150 min (fraction III, 10 mg), 150−220 min (fraction IV, 20 mg), and 220−300 min (fraction V, 10 mg) were collected, evaporated in vacuo, and freeze-dried. Phytochemicals in each fraction were monitored using analytical high-performance liquid chromatography (HPLC) [YMC-Pack, ODS-AM, 250 × 4.6 mm, i.d., 5 $\mu$m (YMC CO Ltd., Kyoto, Japan); mobile phase, acetonitrile/water, 25:75 (v/v); flow rate, 1 mL/min; detection, 230 nm].

**Detection of the Covalent Modification of Keap1 by Electrophiles.** The covalent modification of Keap1 by electrophiles was detected using a BPM-labeling assay as previously described.[22] Recombinant murine Keap1 was expressed as a C-terminal His-tagged fusion protein from BL21-CodonPlus (DE3)-RIPL cells (Stratagene, La Jolla, CA, USA) and purified using Ni-NTA agarose (Qiagen, Valencia, CA, USA).[23] Samples, including Keap1−decenal and −dodecenal adducts, were incubated with 25 $\mu$M BPM for 30 min at 37 °C and then subjected to Western blot analysis with an HRP-linked antibiotin antibody (Cell Signaling Technology).

**Detection of 2-Alkenals Using DAIH Labeling Analysis.** Each sample (17 $\mu$L) was incubated with 85 $\mu$L of a derivatization reagent


dx.doi.org/10.1021/jf5030592 | J. Agric. Food Chem. 2014, 62, 10936−10944

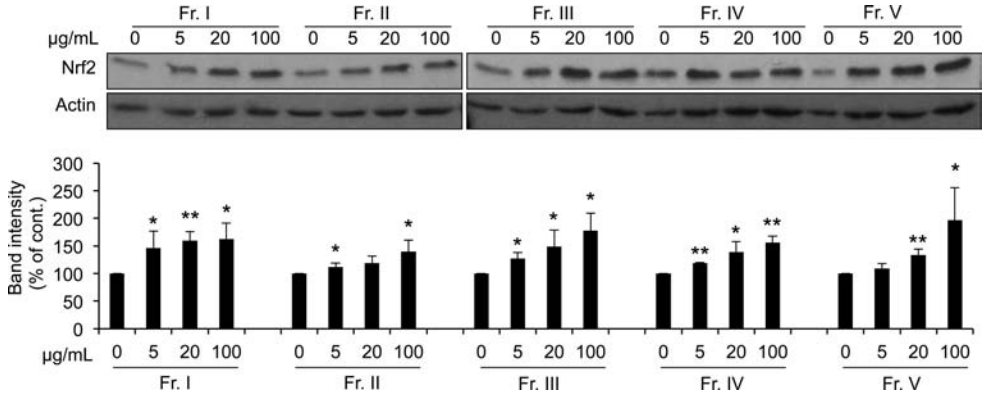


**Figure 3.** Nrf2 activation during exposure of HepG2 cells to the CSLE fractions. The cells were exposed to each fraction (5, 20, or 100 $\mu$M) for 1 h, and then the cell lysates were subjected to Western blot analysis with the indicated antibodies. The bands were quantified using ImageJ software, and the density of each band was normalized to that of actin. Each value is the mean ± SE of three determinations. (*) $p < 0.05$ and (**) $p < 0.01$ versus control.

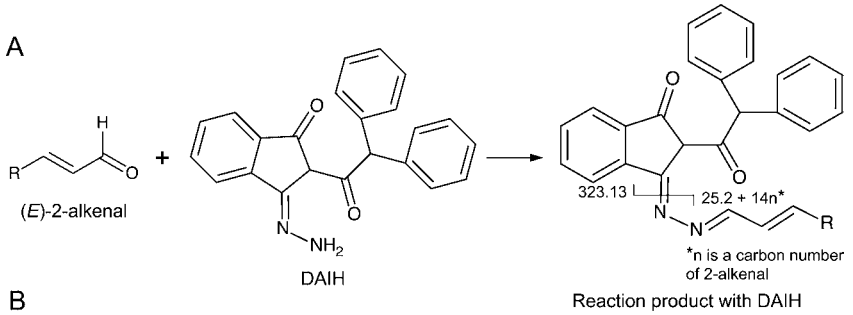


B

| Compound | R | MW | MS of reaction products with DAIH | Fragment MS of the reaction products |
|---|---|---|---|---|
| (*E*)-2-hexenal | $CH_3(CH_2)_2$ | 98.15 | 433.2 | 109.1 |
| (*E*)-2-decenal | $CH_3(CH_2)_6$ | 154.25 | 489.3 | 165.2 |
| (*E*)-2-undecenal | $CH_3(CH_2)_7$ | 168.28 | 503.3 | 179.2 |
| (*E*)-2-dodecenal | $CH_3(CH_2)_8$ | 182.31 | 517.3 | 193.2 |
| (*E*)-2-tridecenal | $CH_3(CH_2)_9$ | 196.33 | 531.4 | 207.2 |
| (*E*)-2-tetradecenal | $CH_3(CH_2)_{10}$ | 210.36 | 545.4 | 221.2 |
| (*E*)-2-pentadecenal | $CH_3(CH_2)_{11}$ | 224.38 | 559.4 | 235.2 |
| (*E*)-2-hexadecenal | $CH_3(CH_2)_{12}$ | 238.41 | 573.4 | 249.3 |
| (*E*)-2-heptadecenal | $CH_3(CH_2)_{13}$ | 252.43 | 583.4 | 263.3 |

**Figure 4.** Identification of (*E*)-2-alkenals in CSLE and fractions by UPLC-MS/MS following reaction with DAIH: (A) reaction of (*E*)-2-alkenal with DAIH leading to the dehydrated reaction product [predicted MS numbers of the fragments are $m/z$ 323.13 derived from DAIH and $m/z$ 25.2 + 14$n$ derived from the (*E*)-2-alkenal residue of the (*E*)-2-alkenal-DAIH adduct]; (B) observed MS number of the reaction products with DAIH and fragments derived from the 2-alkenal−DAIH adduct by UPLC-MS/MS analysis.

consisting of 0.06% DAIH, 140 $\mu$M HCl, and 93% acetonitrile for 15 min on ice. A 10 $\mu$L sample of the reaction mixture was analyzed by ultraperformance liquid chromatography (UPLC) and liquid chromatography−tandem mass spectrometry (LC-MS/MS). Briefly, the reaction products were characterized using an Acquity UPLC system (Waters Co., Milford, MA, USA) equipped with an Acquity BEH $C_{18}$ column (2.1 mm × 50 mm i.d., 1.7 $\mu$m) held at 35 °C in the direct injection mode. Mobile phases A [water containing 0.1% (v/v) formic acid] and B [acetonitrile containing 0.1% (v/v) formic acid] were linearly mixed using a gradient program, and the instrument was calibrated immediately prior to each series of experiments. The flow rate was 0.3 $\mu$L/min, and the mobile phase composition was as follows: 15% B for 10 min; linear increase over 20 min to 95% B; maintained at 95% B for 2 min before a linear return to 15% B over 3 min. The total running time, including conditioning the column to the initial conditions, was 35 min. The eluted chemical compounds were then transferred to the electrospray source of the Synapt High Definition MS system (Waters Co.). The system control and analysis of the mass spectra were performed using Waters MassLynx software ver. 4.1. Electrospray ionization was used with a capillary voltage of 2.8 kV and a sampling cone voltage of 35 V. Low (6 eV) or elevated (stepped from 15−60 eV) collision energy was used to generate either intact precursor ions (low energy) or product ions (elevated energy). The source temperature was 80 °C, and the detector was operated in the negative ion mode. Data were collected from $m/z$ 50−1000. All analyses were acquired with an independent reference; leucine enkephalin $[M - H]^-$ ion as lock mass ($m/z$ 554.2615) was infused via the LockSpray ion source to ensure accuracy and reproducibility. Data were analyzed with MassLynx version 4.1 software and MassFragment version 1.1 software.

**Luciferase Assay.** Transient transfection of cDNAs was performed using Lipofectamin 2000 (Invitrogen) according to the manufacturer's instructions. Briefly, HepG2 cells were seeded at 0.5 × $10^5$ cells/cm$^2$ in 12-well plates. After the cells were incubated overnight, 1.6 $\mu$g of ARE-Luciferase cDNA and 0.16 $\mu$g of pRL-TL cDNA or Lipofectamin 2000 reagent were mixed with OPTI-MEM (Invitrogen) in separate tubes and incubated for 20 min at room temperature to allow the


dx.doi.org/10.1021/jf5030592 | J. Agric. Food Chem. 2014, 62, 10936−10944

formation of complexes. These solutions were then added to the cells and incubated for 12 h, followed by a further 12 h of incubation in serum-free medium. The cDNA-transfected cells were then exposed to the samples, washed with phosphate-buffered saline (PBS), and lysed with Passive Lysis Buffer (Promega, Madison, WI, USA). Luciferase activity was measured using a Dual-Luciferase Reporter Assay System (Promega) according to the manufacturer's instructions.

**Western Blot Analysis.** HepG2 cells were exposed to CSLE, butanal (99.85% purity, Sigma-Aldrich, St. Louis, MO, USA), (*E*)-2-butenal (99% purity, Nacalai), (*E*)-2-decenal, or (*E*)-2-dodecenal, washed with ice-cold PBS, and then collected by scraping into a 2% sodium dodecyl sulfate (SDS) solution. After the cells were lysed at 95 °C for 20 min, protein concentrations were determined using the BCA Protein Assay (Piece, Rockford, IL, USA). Each sample was mixed with a half-volume of SDS−polyacrylamide gel electrophoresis (PAGE) loading buffer (62.5 mM Tris-HCl, pH 6.8; 6% SDS; 24% glycerol; 50 mM TCEP; and 0.015% bromophenol blue) and incubated at 95 °C for 5 min. The cellular proteins were then separated using SDS-PAGE and transferred to polyvinylidene difluoride membranes (Bio-Rad Laboratories, Hercules, CA, USA). The membranes were blocked with 5% skim milk in TTBS (20 mM Tris-HCl, pH 7.5; 150 mM NaCl; and 0.1% Tween 20) and then incubated with primary antibody in TTBS. To detect immunoreactive proteins, HRP-conjugated anti-rabbit IgG and an enhanced system (Chemi-Lumi One L; Nacalai, Kyoto, Japan) were used. Representative blots were from three independent experiments.

**Determination of Electrophilicity Index.** The lowest unoccupied molecular orbital energy ($E_{LUMO}$) and highest occupied molecular orbital energy ($E_{HOMO}$) were determined using Gaussian 09 (ver. 8.0) software (Conflex, San Diego, CA, USA). The ground state equilibrium geometries of each structure were calculated with density-functional RB3LYP 6-31G(d). The global hardness ($\eta$) was calculated as $\eta \approx (E_{LUMO} - E_{HOMO})/2$, softness ($\sigma$) was calculated as $\sigma = 1/\eta$, and the electronic chemical potential ($\mu$) was calculated as $\mu \approx (E_{HOMO} + E_{LUMO})/2$. The electrophilicity index ($\omega$) was calculated as $\omega = \mu^2/2\eta$.[24,25]

**Statistical Analysis.** Statistical significance was assessed using Student's *t* test or Dunnett's post hoc test after a one-way analysis of variance with Microsoft Excel for Mac 2011 version 14.4.3; $p < 0.05$ was considered significant.

## RESULTS

**Activation of Nrf2 by CSLE.** Exposure of HepG2 cells to CSLE resulted in activation of Nrf2 and up-regulation of downstream proteins, such as GCLM and HO-1 (Figure 1A); however, CSLE at a concentration of 100 $\mu$g/mL repressed the Nrf2 activation and thus GCLM and HO-1 gene expression. Pretreatment with GSH markedly diminished CSLE-mediated activation of Nrf2 in the cells (Figure 1B), suggesting electrophiles contributed to the activation. Consistent with this, the thiol groups of Keap1, the negative regulator for Nrf2, were modified by CSLE in a concentration-dependent manner as determined by a BPM assay (Supporting Information Figure S1).

**Separation of Nrf2 Activators in CSLE.** As shown in Figure 2A, the CSLE contained eight major compounds detected at 230 nm; compounds **2** and **5** were identical to authentic (*E*)-2-decenal and (*E*)-2-dodecenal, respectively (Figure 2 and Figure S2 in the Supporting Information). The CSLE components were separated into five fractions by Ultra Pack ODS-S-50B column chromatography (Figure 2B), and then the Nrf2 activation potential of each fraction was evaluated in HepG2 cells. Unexpectedly, fractions I−V all activated Nrf2 to a similar extent (Figure 3), suggesting that the observed Nrf2 activation might be due to electrophiles with (*E*)-2-alkenal substituents, as various (*E*)-2-alkenals have been observed previously in a CSLE.[3,9]

**Analysis of (*E*)-2-Alkenals in CSLE.** To investigate whether or not the components in each fraction contained (*E*)-2-alkenal moieties, we performed UPLC-MS/MS analysis in the negative ion mode of the CSLE components after derivatization with DAIH (see Figure 4A).[26]

Authentic (*E*)-2-decenal and (*E*)-2-dodecenal were converted into DAIH derivatives with retention times of 16.61 min ($m/z$ 489.3) and 20.95 min ($m/z$ 517.3), respectively (Figure 4 and Figure S3 in the Supporting Information), whereas no such peaks and corresponding molecular masses were seen without DAIH (Figure S3A). Using the DAIH derivative method, we identified (*E*)-2-alkenal-related chemicals, including (*E*)-2-decenal (compound **2** in fraction II), (*E*)-2-undecenal (compound **4** in fraction III), and (*E*)-2-dodecenal (compound **5** in fraction IV) (Figures 4 and 5). Compound **3** was not an (*E*)-2-alkenal because

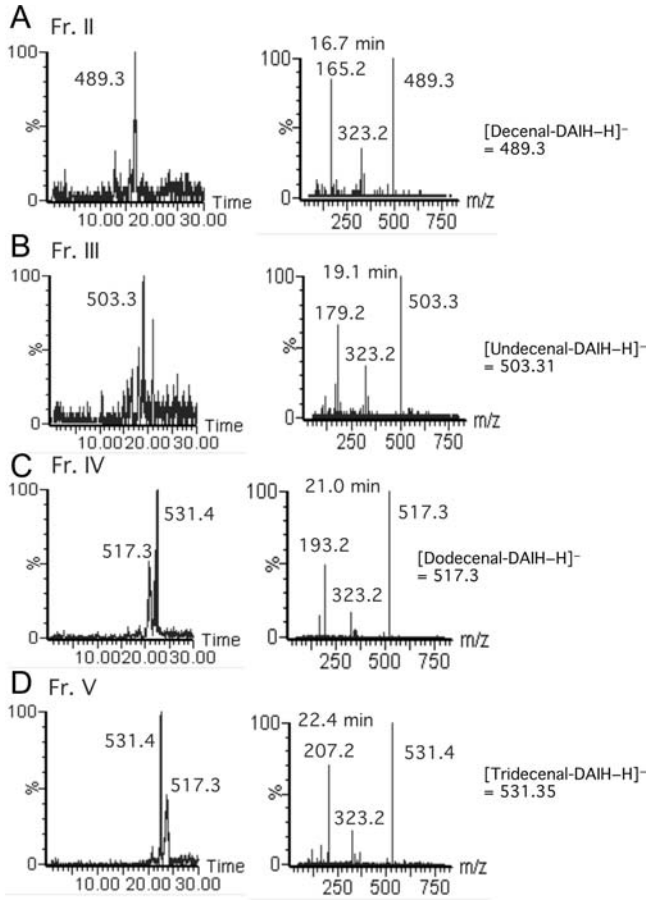


**Figure 5.** UPLC and LC-MS/MS spectra of reaction products after reaction of each fraction with DAIH: (A−D) UPLC/MS chromatograms of derivatives of 2-alkenal with DAIH (left) monitored at $m/z$ 323.1, respectively. The mass spectra were obtained from derivatives with retention times of 16.7 min (A), 19.1 min (B), 21.0 min (C), 22.6 min (C) and 22.4 min (D), corresponding to the DAIH adducts.

this molecule could not be converted to a DAIH derivative (data not shown). Fraction V contained (*E*)-2-tridecenal, although we did not examine whether (*E*)-2-tridecenal is compound **6**, **7**, or **8** (Figures 4 and 5). (*E*)-2-Hexenal, (*E*)-2-tetradecenal, (*E*)-2-pentadecenal, (*E*)-2-hexadecenal, and (*E*)-2-heptadecenal were also detected in the CSLE by DAIH derivatization (Figure 4 and Figure S4 in the Supporting Information). These results suggest that there are a variety of aliphatic electrophiles with an (*E*)-2-alkenal group in the CSLE, which is in agreement with previous studies.[3,9,16]

**Activation of Nrf2 Is Coupled to Covalent Modification of Keap1 by (*E*)-2-Decenal and (*E*)-2-Dodecenal.** Exposure of HepG2 cells to (*E*)-2-decenal and (*E*)-2-dodecenal under

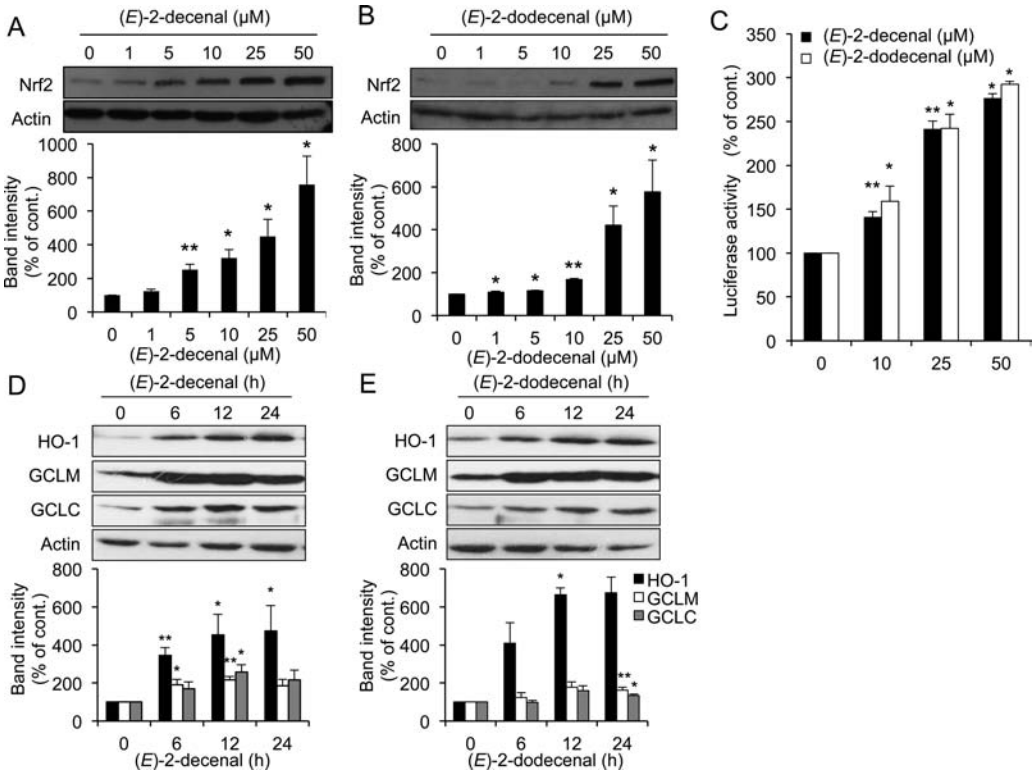


**Figure 6.** (*E*)-2-Decenal- or (*E*)-2-dodecenal-mediated activation of Nrf2 and up-regulation of downstream gene products. (A, B) The cells were exposed to (*E*)-2-decenal (A) or (*E*)-2-dodecenal (B) for 3 h, and total cell proteins were subjected to Western blot analysis with the indicated antibodies. (C) ARE-luciferase and pRL-TK cDNAs were transfected into HepG2 cells. After exposure of the cells to (*E*)-2-decenal or (*E*)-2-dodecenal for 6 h, luciferase activity was measured. (D, E) The cells were exposed to 25 $\mu$M (*E*)-2-decenal (D) or (*E*)-2-dodecenal (E) for 6, 12, or 24 h, and total cell proteins were subjected to Western blot analysis with the indicated antibodies. The bands were quantified using ImageJ software, and the density of each band was normalized to that of actin. Each value is the mean ± SE of three determinations. (*) $p < 0.05$ and (**) $p < 0.01$ versus control.

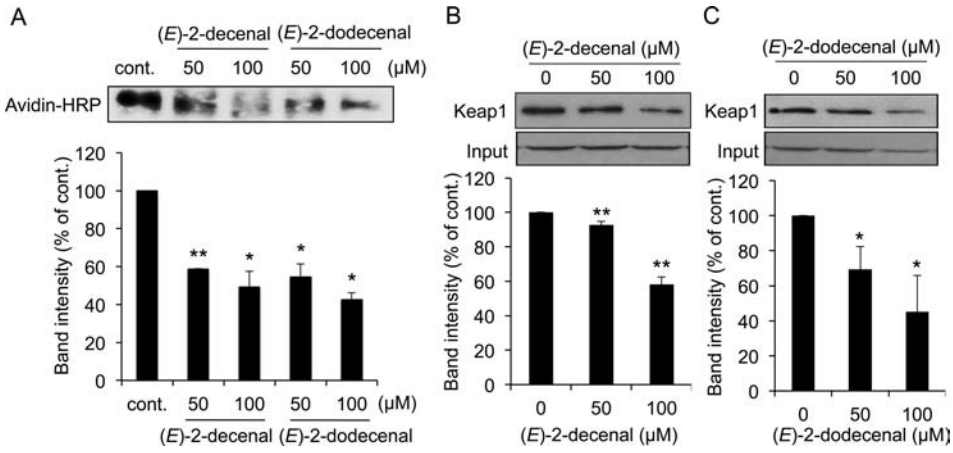


**Figure 7.** Modification of cellular Keap1 and purified Keap1 by (*E*)-2-decenal and (*E*)-2-dodecenal. (A) Recombinant murine Keap1 was incubated with (*E*)-2-decenal and (*E*)-2-dodecenal in 20 mM Tris-HCl (pH 8.5) at 37 °C for 20 min and allowed to react with 25 $\mu$M BPM (30 min at 37 °C). The reaction mixture was subjected to Western blot analysis with avidin−horseradish peroxidase conjugate. The bands were quantified using ImageJ software, and the band densities were normalized to that of Keap1. Each value is the mean ± SE of three determinations. (*) $p < 0.05$ and (**) $p < 0.01$ versus control. (B, C) HepG2 cells were incubated with (*E*)-2-decenal (B) and (*E*)-2-dodecenal (C) for 30 min and then lysed with RIPA buffer. Cell lysates were incubated with BPM (50 $\mu$M) for 30 min and then immunoprecipitated with avidin−agarose. The precipitated proteins were subjected to Western blot analysis with an anti-Keap1 antibody. The bands were quantified using ImageJ software. Each value is the mean ± SE of three determinations. (*) $p < 0.05$ and (**) $p < 0.01$ versus control.

nontoxic conditions (<50 $\mu$M) resulted in Nrf2 activation in a concentration-dependent manner (Figure 6A,B). These (*E*)-2-alkenal-related aliphatic electrophiles were able to transactivate Nrf2, as evaluated by ARE-dependent luciferase activity (Figure 6C), and to up-regulate the downstream gene products GCLC, GCLM, and HO-1 (Figure 6D,E). As shown in Figure 7A, recombinant Keap1 underwent covalent modification by (*E*)-2-decenal and (*E*)-2-dodecenal, as evaluated in the BPM assay. Cellular Keap1 was also modified in HepG2 cells exposed to (*E*)-2-decenal and (*E*)-2-dodecenal (Figure 7B,C).


dx.doi.org/10.1021/jf5030592 | J. Agric. Food Chem. 2014, 62, 10936−10944

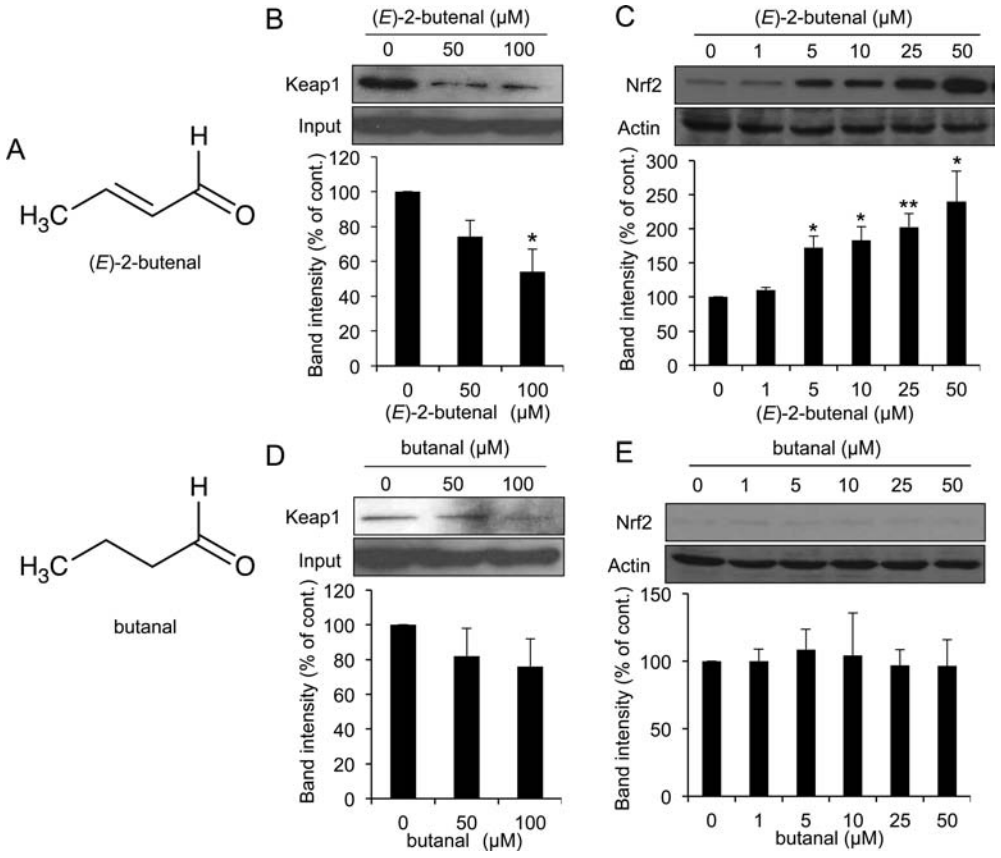


**Figure 8.** S-Alkylation of the cellular Keap1 and activation of Nrf2 during exposure of HepG2 cells to (*E*)-2-butenal or butanal. Panel A shows structures of (*E*)-2-butenal and butanal. (B, D) Cells were incubated with (*E*)-2-butenal (B) or butanal (D) for 30 min and then lysed with RIPA buffer. The cell lysates were incubated with BPM (50 $\mu$M) for 30 min and then immunoprecipitated with avidin−agarose. The precipitated proteins were subjected to Western blot analysis with an anti-Keap1 antibody. (C, E) The cells were exposed to (*E*)-2-butenal (C) or butanal (E) for 3 h, and total cell proteins were subjected to Western blot analysis with the indicated antibodies. The bands were quantified by using ImageJ software. Each value is the mean ± SE of three determinations. (*) $p < 0.05$ and (**) $p < 0.01$ versus control.

**(*E*)-2-Alkenal Structure Is Essential for Nrf2 Activation.** On the basis of the results described above, we postulated that the (*E*)-2-alkenal moiety is required for the covalent modification of Keap1 that leads to Nrf2 activation during exposure of cells to isolated CSLE phytochemicals because of its electrophilic properties. To confirm this hypothesis, we calculated the electrophilicity of (*E*)-2-butenal and butanal as model compounds (Figure 8A). The electrophilicity index of (*E*)-2-butenal, calculated using Gaussian09 (ver. 8.0) software, was 3.23 eV, and the electrophilicity indices of related chemicals were similar (Table 1). These results suggest that the electrophilic potentials of (*E*)-2-alkenals are unaffected by differences in the carbon number of these chemicals. In contrast, butanal was weaker in electrophilicity and harder than (*E*)-2-butenal ($\eta$ = 2.64 eV, $\sigma$ = 0.38, Table 1). Consistent with this, butanal only minimally reacted with the thiol groups of GSH (Supporting Information Figure S5). In HepG2 cells, (*E*)-2-butenal modified intracellular Keap1, as detected by the BPM assay (Figure 8B), and activated Nrf2 in a concentration-dependent manner (Figure 8C), whereas exposure to butanal did not result in Keap1 modification and Nrf2 activation (Figure 8D,E).

**Table 1. Electrophilicity Index ($\omega$), Global Hardness ($\eta$), and Softness ($\sigma$) of Butanal and Various (*E*)-2-Alkenals[a]**

| compound | $\omega$ (eV) | $\eta$ (eV) | $\sigma$ (eV) |
|---|---|---|---|
| butanal | 2.29 | 3.07 | 0.33 |
| (*E*)-2-butenal | 3.23 | 2.64 | 0.38 |
| (*E*)-2-decenal | 3.21 | 2.61 | 0.38 |
| (*E*)-2-undecenal | 3.17 | 2.63 | 0.38 |
| (*E*)-2-dodecenal | 3.17 | 2.63 | 0.38 |
| (*E*)-2-tridecenal | 3.17 | 2.63 | 0.38 |

[a]Calculated as described under Materials and Methods.

## DISCUSSION

The present study indicates that phytochemicals involved in the Nrf2 activation are (*E*)-2-alkenal-related aliphatic electrophiles. Preparative ODS column chromatography and a DAIH labeling assay, followed by UPLC-MS/MS isolated nine phytochemicals from a CSLE that were identified as (*E*)-2-hexenal, (*E*)-2-decenal, (*E*)-2-undecenal, (*E*)-2-dodecenal, (*E*)-2-tetradecenal, (*E*)-2-pentadecenal, (*E*)-2-hexadecenal, and (*E*)-2-heptadecenal (Figure 4B and Figure S4 in the Supporting Information). Supporting our results, (*E*)-2-alkenals have been detected in an extract of *C. sativum* leaves by GC-MS.[3,5] Potter has shown that a pentane extract of the leaves of *C. sativum* contained a series of (*E*)-2-alkenals that accounted for approximately 69% of the *C. sativum* leaf oil, consisting mainly of (*E*)-2-decenal (46.1%) and (*E*)-2-dodecenal (10%).[3] Whereas 4-hydroxy-2-(*E*)-nonenal and acrolein are found to be aliphatic electrohiles, which are able to activate Nrf2,[27−29] to our knowledge there is no report that these compounds are components in *C. sativum* leaf oil. These


dx.doi.org/10.1021/jf5030592 | J. Agric. Food Chem. 2014, 62, 10936−10944

suggest, therefore, that (*E*)-2-alkenals would predominantly participate in CSLE-dependent Nrf2 activation. Matsutani et al.[30] have reported that (*E*)-2-hexenal enhances ARE-dependent luciferase activity in K562 cells, supporting our notion.

It is well-known that oxidative stress-mediated phosphorylation of Nrf2, oxidative modification and covalent modification of Keap1, and proteasome inhibition are associated with substantial Nrf2 activation.[20,31−33] In a preliminary study, we found that (*E*)-2-decenal and (*E*)-2-dodecenal could neither cause proteasome inhibition nor induce oxidative stress under the concentrations examined in the present study (data not shown). As shown in Figure 7 and Figure S1 in the Supporting Information, the BPM-labeling assay revealed that CSLE, (*E*)-2-decenal, and (*E*)-2-dodecenal are able to modify Keap1 through thiol groups, suggesting that these (*E*)-2-alkenals are able to incorporate into the cells presumably by passive diffusion and then modify the cellular proteins. Thus, it seems likely that *S*-alkylation of Keap1 participates in the Nrf2 activation (Figure 9).

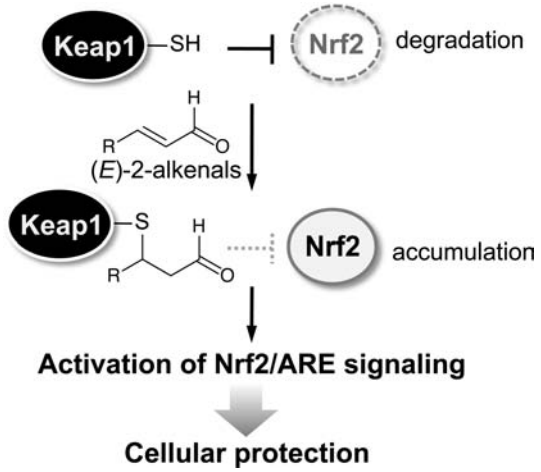


**Figure 9.** (*E*)-2-Alkenals in *C. sativum* leaves activate Nrf2/ARE signaling through covalent modification of Keap1.

(*E*)-2-Alkenals isolated from CSLE activated Nrf2 to a similar degree despite the different carbon numbers of these phytochemicals (Figures 3 and 5). This suggests that the (*E*)-2-alkenal groups are a common substituent required for the activation of Nrf2. Such a hypothesis was well supported by an estimation of the electrophilicity indices for (*E*)-2-alkenals with different carbon numbers (Table 1). Furthermore, experiments with (*E*)-2-butenal as a model of (*E*)-2-alkenals with an $\alpha,\beta$-unsaturated aldehyde group indicated that even (*E*)-2-butenal can modify cellular Keap1, thereby activating Nrf2 in HepG2 cells, whereas butanal had no effect on Keap1 modification and Nrf2 activation (Figure 8). Collectively, our study strongly indicates that CSLE contains several electrophiles, which can easily bind to soft nucleophiles,[34,35] and thus can activate Nrf2 through covalent modification of Keap1 through the (*E*)-2-alkenal group of these chemicals (Figure 9). Acrolein with an $\alpha,\beta$-unsaturated aldehyde is reported to up-regulate downstream protein of Nrf2 such as HO-1 through activation of phosphatidylinositol 3-kinase pathway.[36] Further study is required to clarify whether or not CSLE, (*E*)-2-decenal, and (*E*)-2-dodecenal could activate Nrf2 through activation of other signaling pathways in addition to covalent modification of Keap1 (Figure 7 and Figure S1 in the Supporting Information).

A variety of phytochemicals with different structures are known to have an effect on health through activation of Nrf2.[37,38] For example, sulforaphane in *Brassica oleracea* var. *italica*,[39] curcumin in *Curcuma longa* L., caffeic acid phenyl ester in honey,[37,38] perillaldehyde in *Perilla frutescens* (L.) Britt. and *Artemisia princeps* Pamp.,[30] diallyl trisulfide in *Allium sativum* L.,[40] and now (*E*)-2-alkenal derivatives in *C. sativum* leaves are able to activate Keap1/Nrf2 signaling. This Nrf2 activation results in up-regulation of downstream proteins associated with cellular protection such as phase II xenobiotic detoxification enzymes (GCLM and GCLC), phase III transporters (multidrug resistance-associated proteins), and antioxidant proteins (HO-1 and peroxiredoxin).[16−20] GCLM, GCLC, and HO-1 were induced during exposure of HepG2 cells to (*E*)-2-decenal or (*E*)-2-dodecenal (Figure 6). We have previously reported that sulforaphane can suppress arsenic-induced cytotoxicity through Nrf2 activation and induction of downstream proteins.[16] CSLE and (*E*)-2-alkenals also have a cytoprotective effect on arsenite-induced cytotoxicity (data not shown). (*E*)-2-Alkenals are contained not only in *C. sativum* leaves but also in other plants, including *Eryngium fetidum* L. belonging to the Umbelliferae family.[5,41] (*E*)-2-Hexenal, which is synthesized in green leaves from $\alpha$-linolenic and linolenic acids, is a component of the green odor for various classes of plants.[4] Therefore, we postulate that aliphatic electrophiles, such as (*E*)-2-alkenals in plants, possess a potential cytoprotective effect against environmental pollutants and oxidative stress through activation of electrophilic signaling mediated by the (*E*)-2-alkenal group.

## ■ ASSOCIATED CONTENT

### Supporting Information

Additional experimental details and Figures S1−S5. This material is available free of charge via the Internet at http://pubs.acs.org.

## ■ AUTHOR INFORMATION

### Corresponding Author

*(Y.K.) Phone: +81-29-853-3297. Fax: +81-29-853-3259. E-mail: yk-em-tu@md.tsukuba.ac.jp.

### Funding

This work was supported by a grant-in-aid (25220103 to Y.K.) for scientific research from the Ministry of Education, Culture, Sports, Science and Technology of Japan.

### Notes

The authors declare no competing financial interest.

## ■ ABBREVIATIONS USED

BPM, biotin−PEAC$_5$-maleimide; CSLE, *C. sativum* leaf extract; DAIH, 2-diphenylacetyl-1,3-inandione-1-hydrazone; GCLM, glutamate−cysteine ligase, modifier subunit; GCLC, glutamate−cysteine ligase, catalytic subunit; GSH, glutathione; HO-1, heme oxygenase-1; Keap1, Kelch-like erythroid cell-derived protein with Cap'n'collar homology-associated protein 1; Nrf2, NF-E2 related factor 2

## ■ REFERENCES

(1) Rajeshwari, A.; Somayaji, G.; Deviprasad, S. A rare cause of dysphagia: a case report. *Indian J. Otolaryngol. Head Neck Surg.* **2011**, *63*, 83−84.

(2) Tapsell, L. C.; Hemphill, I.; Cobiac, L.; Patch, C. S.; Sullivan, D. R.; Fenech, M.; Roodenrys, S.; Keogh, J. B.; Clifton, P. M.; Williams, P. G.; Fazio, V. A.; Inge, K. E. Health benefits of herbs and spices: the past, the present, the future. *Med. J. Aust.* **2006**, *185*, S4−S24.

(3) Potter, T. L. Essential oil composition of cilantro. *J. Agric. Food Chem.* **1996**, *44*, 1824−1826.
(4) Reyes, M. R.; Reyes-Esparza, J.; Angeles, O. T.; Rodriguez-Fragoso, L. Mutagenicity and safety evaluation of water extract of *Coriander sativum* leaves. *J. Food Sci.* **2010**, *75*, T6−T12.
(5) Eyres, G.; Dufour, J. P.; Hallifax, G.; Sotheeswaran, S.; Marriott, P. J. Identification of character-impact odorants in coriander and wild coriander leaves using gas chromatography-olfactometry (GCO) and comprehensive two-dimensional gas chromatography-time-of-flight mass spectrometry (GC×GC-TOFMS). *J. Sep. Sci.* **2005**, *28*, 1061−1074.
(6) Wu, T. T.; Tsai, C. W.; Yao, H. T.; Lii, C. K.; Chen, H. W.; Wu, Y. L.; Chen, P. Y.; Liu, K. L. Suppressive effects of extracts from the aerial part of *Coriandrum sativum* L. on LPS-induced inflammatory responses in murine RAW 264.7 macrophages. *J. Sci. Food Agric.* **2010**, *90*, 1846−1854.
(7) Wangensteen, H.; Samuelsen, A. B.; Malterud, K. E. Antioxidant activity in extracts from coriander. *Food Chem.* **2004**, *88*, 293−297.
(8) Park, G.; Kim, H. G.; Kim, Y. O.; Park, S. H.; Kim, S. Y.; Oh, M. S. *Coriandrum sativum* L. protects human keratinocytes from oxidative stress by regulating oxidative defense systems. *Skin Pharmacol. Physiol.* **2012**, *25*, 93−99.
(9) Potter, T. L.; Fagerson, I. S. Composition of coriander leaf volatiles. *J. Agric. Food Chem.* **1990**, *38*, 2054−2056.
(10) Bolton, J. L.; Trush, M. A.; Penning, T. M.; Dryhurst, G.; Monks, T. J. Role of quinones in toxicology. *Chem. Res. Toxicol.* **2000**, *13*, 135−160.
(11) Liebler, D. C. Protein damage by reactive electrophiles: targets and consequences. *Chem. Res. Toxicol.* **2008**, *21*, 117−128.
(12) Iwamoto, N.; Sumi, D.; Ishii, T.; Uchida, K.; Cho, A. K.; Froines, J. R.; Kumagai, Y. Chemical knockdown of protein-tyrosine phosphatase 1B by 1,2-naphthoquinone through covalent modification causes persistent transactivation of epidermal growth factor receptor. *J. Biol. Chem.* **2007**, *282*, 33396−33404.
(13) Sumi, D.; Akimori, M.; Inoue, K.; Takano, H.; Kumagai, Y. 1,2-Naphthoquinone suppresses lipopolysaccharide-dependent activation of IKK$\beta$/NF-$\kappa$B/NO signaling: an alternative mechanism for the disturbance of inducible NO synthase-catalyzed NO formation. *J. Toxicol. Sci.* **2010**, *35*, 891−898.
(14) Kwak, M. K.; Kensler, T. W.; Casero, R. A., Jr. Induction of phase 2 enzymes by serum oxidized polyamines through activation of Nrf2: effect of the polyamine metabolite acrolein. *Biochem. Biophys. Res. Commun.* **2003**, *305*, 662−670.
(15) Lee, S. E.; Jeong, S. I.; Kim, G. D.; Yang, H.; Park, C. S.; Jin, Y. H.; Park, Y. S. Upregulation of heme oxygenase-1 as an adaptive mechanism for protection against crotonaldehyde in human umbilical vein endothelial cells. *Toxicol. Lett.* **2011**, *201*, 240−248.
(16) Shinkai, Y.; Sumi, D.; Fukami, I.; Ishii, T.; Kumagai, Y. Sulforaphane, an activator of Nrf2, suppresses cellular accumulation of arsenic and its cytotoxicity in primary mouse hepatocytes. *FEBS Lett.* **2006**, *580*, 1771−1774.
(17) Shinkai, Y.; Sumi, D.; Toyama, T.; Kaji, T.; Kumagai, Y. Role of aquaporin 9 in cellular accumulation of arsenic and its cytotoxicity in primary mouse hepatocytes. *Toxicol. Appl. Pharmacol.* **2009**, *237*, 232−236.
(18) Toyama, T.; Sumi, D.; Shinkai, Y.; Yasutake, A.; Taguchi, K.; Tong, K. I.; Yamamoto, M.; Kumagai, Y. Cytoprotective role of Nrf2/Keap1 system in methylmercury toxicity. *Biochem. Biophys. Res. Commun.* **2007**, *363*, 645−650.
(19) Abiko, Y.; Miura, T.; Phuc, B. H.; Shinkai, Y.; Kumagai, Y. Participation of covalent modification of Keap1 in the activation of Nrf2 by *tert*-butylbenzoquinone, an electrophilic metabolite of butylated hydroxyanisole. *Toxicol. Appl. Pharmacol.* **2011**, *255*, 32−39.
(20) Itoh, K.; Wakabayashi, N.; Katoh, Y.; Ishii, T.; O'Connor, T.; Yamamoto, M. Keap1 regulates both cytoplasmic-nuclear shuttling and degradation of Nrf2 in response to electrophiles. *Genes Cells* **2003**, *8*, 379−391.
(21) Nioi, P.; McMahon, M.; Itoh, K.; Yamamoto, M.; Hayes, J. D. Identification of a novel Nrf2-regulated antioxidant response element (ARE) in the mouse NAD(P)H:quinone oxidoreductase 1 gene: reassessment of the ARE consensus sequence. *Biochem. J.* **2003**, *374*, 337−348.
(22) Toyama, T.; Shinkai, Y.; Kaji, T.; Kumagai, Y. Convenient method to assess chemical modification of protein thiols by electrophilic metals. *J. Toxicol. Sci.* **2013**, *38*, 477−484.
(23) Dinkova-Kostova, A. T.; Holtzclaw, W. D.; Cole, R. N.; Itoh, K.; Wakabayashi, N.; Katoh, Y.; Yamamoto, M.; Talalay, P. Direct evidence that sulfhydryl groups of Keap1 are the sensors regulating induction of phase 2 enzymes that protect against carcinogens and oxidants. *Proc. Natl. Acad. Sci. U.S.A.* **2002**, *99*, 11908−11913.
(24) Pearson, R. G. Chemical hardness and density functional theory. *J. Chem. Sci.* **2005**, *117*, 369−377.
(25) Parr, R. G.; Szentpaky, L.; Liu, S. Electrophilicity index. *J. Am. Chem. Soc.* **1999**, *121*, 1922−1924.
(26) Luth, A.; Neuber, C.; Kleuser, B. Novel methods for the quantification of (2*E*)-hexadecenal by liquid chromatography with detection by either ESI QTOF tandem mass spectrometry or fluorescence measurement. *Anal. Chim. Acta* **2012**, *722*, 70−79.
(27) Tirumalai, R.; Rajesh Kumar, T.; Mai, K. H.; Biswal, S. Acrolein causes transcriptional induction of phase II genes by activation of Nrf2 in human lung type II epithelial (A549) cells. *Toxicol. Lett.* **2002**, *132*, 27−36.
(28) Zhang, H.; Forman, H. J. Signaling pathways involved in phase II gene induction by $\alpha,\beta$-unsaturated aldehydes. *Toxicol. Ind. Health* **2009**, *25*, 269−278.
(29) Malone, P. E.; Hernandez, M. R. 4-Hydroxynonenal, a product of oxidative stress, leads to an antioxidant response in optic nerve head astrocytes. *Exp. Eye Res.* **2007**, *84*, 444−454.
(30) Masutani, H.; Otsuki, R.; Yamaguchi, Y.; Takenaka, M.; Kanoh, N.; Takatera, K.; Kunimoto, Y.; Yodoi, J. Fragrant unsaturated aldehydes elicit activation of the Keap1/Nrf2 system leading to the upregulation of thioredoxin expression and protection against oxidative stress. *Antioxid. Redox Signal.* **2009**, *11*, 949−962.
(31) Aono, J.; Yanagawa, T.; Itoh, K.; Li, B.; Yoshida, H.; Kumagai, Y.; Yamamoto, M.; Ishii, T. Activation of Nrf2 and accumulation of ubiquitinated A170 by arsenic in osteoblasts. *Biochem. Biophys. Res. Commun.* **2003**, *305*, 271−277.
(32) Bloom, D. A.; Jaiswal, A. K. Phosphorylation of Nrf2 at Ser40 by protein kinase C in response to antioxidants leads to the release of Nrf2 from INrf2, but is not required for Nrf2 stabilization/accumulation in the nucleus and transcriptional activation of antioxidant response element-mediated NAD(P)H:quinone oxidoreductase-1 gene expression. *J. Biol. Chem.* **2003**, *278*, 44675−44682.
(33) Motohashi, H.; Yamamoto, M. Nrf2-Keap1 defines a physiologically important stress response mechanism. *Trends Mol. Med.* **2004**, *10*, 549−557.
(34) Zhang, L.; Gavin, T.; Barber, D. S.; LoPachin, R. M. Role of the Nrf2-ARE pathway in acrylamide neurotoxicity. *Toxicol. Lett.* **2011**, *205*, 1−7.
(35) LoPachin, R. M.; Gavin, T.; Geohagen, B. C.; Das, S. Neurotoxic mechanisms of electrophilic type-2 alkenes: soft soft interactions described by quantum mechanical parameters. *Toxicol. Sci.* **2007**, *98*, 561−570.
(36) Zhang, H.; Forman, H. J. Acrolein induces heme oxygenase-1 through PKC-$\delta$ and PI3K in human bronchial epithelial cells. *Am. J. Respir. Cell Mol. Biol.* **2008**, *38*, 483−490.
(37) Surh, Y. J.; Kundu, J. K.; Na, H. K. Nrf2 as a master redox switch in turning on the cellular signaling involved in the induction of cytoprotective genes by some chemopreventive phytochemicals. *Planta Med.* **2008**, *74*, 1526−1539.
(38) Surh, Y. J. Cancer chemoprevention with dietary phytochemicals. *Nat. Rev. Cancer* **2003**, *3*, 768−780.
(39) Zhang, Y.; Talalay, P.; Cho, C. G.; Posner, G. H. A major inducer of anticarcinogenic protective enzymes from broccoli: isolation and elucidation of structure. *Proc. Natl. Acad. Sci. U.S.A.* **1992**, *89*, 2399−2403.
(40) Chen, C.; Pung, D.; Leong, V.; Hebbar, V.; Shen, G.; Nair, S.; Li, W.; Kong, A. N. Induction of detoxifying enzymes by garlic organosulfur

compounds through transcription factor Nrf2: effect of chemical structure and stress signals. *Free Radical Biol. Med.* **2004**, *37*, 1578−1590.
(41) Hatanaka, A. The biogeneration of green odour by green leaves. *Phytochemistry* **1993**, *34*, 1201−1218.

Table 1. $^{13}C$ NMR Data ($\delta_C$) of Compounds 1−9 (100 MHz)[a]

| position | | 1 | 2 | 3 | 4 | 5 | 6 | 7 | 8 | 9 |
|---|---|---|---|---|---|---|---|---|---|---|
| 1 | | 79.2 | 75.4 | 73.3 | 76.7 | 79.0 | 76.4 | 76.3 | 73.7 | 74.6 |
| 2 | | 23.3 | 22.1 | 22.2 | 73.4 | 23.5 | 69.4 | 69.3 | 21.3 | 22.2 |
| 3 | | 26.5 | 26.8 | 26.7 | 31.5 | 26.8 | 31.1 | 31.1 | 26.8 | 26.8 |
| 4 | | 33.5 | 39.8 | 39.7 | 33.4 | 39.8 | 39.3 | 39.2 | 33.8 | 39.8 |
| 5 | | 91.0 | 86.9 | 86.4 | 90.5 | 88.3 | 88.1 | 87.9 | 90.6 | 86.9 |
| 6 | | 74.7 | 36.7 | 36.8 | 75.3 | 36.6 | 35.5 | 36.1 | 75.5 | 36.4 |
| 7 | | 53.3 | 49.5 | 48.2 | 52.8 | 47.3 | 47.3 | 49.1 | 55.5 | 48.1 |
| 8 | | 71.4 | 72.6 | 71.5 | 73.5 | 78.2 | 76.3 | 75.8 | 74.7 | 72.0 |
| 9 | | 73.3 | 70.8 | 68.3 | 74.8 | 76.3 | 78.1 | 80.5 | 80.6 | 68.6 |
| 10 | | 51.1 | 52.8 | 51.5 | 48.3 | 51.1 | 52.6 | 50.5 | 49.5 | 52.9 |
| 11 | | 81.1 | 82.2 | 82.3 | 81.4 | 81.7 | 81.5 | 82.0 | 81.6 | 82.0 |
| 12 | | 14.9 | 16.8 | 17.2 | 18.7 | 17.0 | 18.8 | 18.4 | 17.3 | 17.0 |
| 13 | | 60.8 | 62.5 | 64.8 | 12.2 | 62.7 | 60.4 | 61.9 | 19.1 | 62.2 |
| 14 | | 24.2 | 25.1 | 25.0 | 24.0 | 24.7 | 24.6 | 24.8 | 25.7 | 25.1 |
| 15 | | 30.1 | 31.4 | 31.0 | 30.9 | 30.9 | 30.6 | 31.0 | 31.0 | 31.2 |
| 1-OR | 1 | 169.8 | 169.2 | 169.6 | | 130.4 | 169.7 | 169.8 | 170.0 | 169.3 |
| | 2/6 | 20.8 | 20.8 | 20.7 | | 129.7 | 21.3 | 21.4 | 21.4 | 20.8 |
| | 3/5 | | | | | 128.5 | | | | |
| | 4 | | | | | 133.1 | | | | |
| | 7 | | | | | 166.4 | | | | |
| 2-OR | 1 | | | | 130.0 | | 169.8 | 169.7 | | |
| | 2/6 | | | | 129.8 | | 20.6 | 20.4 | | |
| | 3/5 | | | | 128.6 | | | | | |
| | 4 | | | | 133.2 | | | | | |
| | 7 | | | | 167.4 | | | | | |
| 6-OR | 1 | 169.8 | | | 169.9 | | | | 170.0 | |
| | 2 | 20.5 | | | 21.3 | | | | 20.8 | |
| 8-OR | 1 | 130.6 | | 169.9 | 130.0 | 130.0 | 170.5 | | | 169.9 |
| | 2/6 | 130.1 | | 20.8 | 129.7 | 129.6 | 21.0 | | | 20.9 |
| | 3/5 | 128.8 | | | 128.5 | 128.4 | | | | |
| | 4 | 133.5 | | | 133.2 | 133.1 | | | | |
| | 7 | 166.2 | | | 166.3 | 166.1 | | | | |
| 9-OR | 1 | 130.0 | 129.4 | 129.3 | | | 129.8 | 129.7 | 129.0 | 129.7 |
| | 2/6 | 129.8 | 130.3 | 130.2 | | | 129.4 | 129.7 | 130.1 | 130.2 |
| | 3/5 | 128.7 | 128.3 | 128.3 | | | 128.8 | 128.7 | 128.4 | 128.3 |
| | 4 | 133.5 | 133.4 | 133.3 | | | 133.3 | 133.4 | 133.5 | 133.1 |
| | 7 | 165.2 | 167.7 | 165.9 | | | 165.4 | 167.4 | 165.7 | 166.0 |
| 13-OR | 1 | 170.5 | | 125.6 | | 125.9 | | 170.2 | | |
| | 2 | 21.2 | | 137.5 | | 137.2 | | 21.5 | | |
| | 3 | | | 123.6 | | 123.6 | | | | |
| | 4 | | | 153.8 | | 153.7 | | | | |
| | 5 | | | 151.2 | | 151.1 | | | | |
| | 6 | | | 165.3 | | 165.4 | | | | |

[a]Compound **1** was recorded in pyridine-$d_5$, and the others were in $CDCl_3$.

**Extraction and Isolation.** The air-dried fruits of *C. orbiculatus* (9.0 kg) were powdered and extracted with methanol three times (3 × 54 L) under reflux. The organic solvent was evaporated to afford a crude extract (1.2 kg). The extract was suspended in $H_2O$ (1.2 L) and then partitioned with petroleum ether (5 × 1.2 L) and ethyl acetate (5 × 1.2 L) successively. The ethyl acetate soluble part (190 g) was fractionated by silica gel column chromatography (silica gel, 1.2 kg; column, 9 × 70 cm), using a gradient solvent system of petroleum ether/acetone (100:0, 100:2, 100:4, 100:7, 100:10, 100:15, 100:20, and 100:28, 21 L for each gradient elution), to afford seven fractions ($F_1$−$F_7$) according to the TLC analyses. Fraction $F_3$ (eluted by petroleum ether/acetone, 100:4 and 100:7) was subjected to medium-pressure liquid chromatography (MPLC) over octadecylsilyl (ODS) eluting with a step gradient from 68 to 87% MeOH in $H_2O$ to give seven subfractions ($F_{3\text{-}1}$−$F_{3\text{-}7}$). Subfraction $F_{3\text{-}4}$ was further purified by preparative HPLC (YMC-pack ODS-AM, 250 × 20 mm i.d., 85% MeOH in $H_2O$) to afford compound **1** ($t_R$ = 29 min, 14.7 mg). Fraction $F_5$ (eluted by petroleum ether/acetone, 100:10 and 100:15), using the above MPLC (67−87% MeOH in $H_2O$), provided 12 subfractions $F_{5\text{-}1}$−$F_{5\text{-}12}$, and the following purification of $F_{5\text{-}1}$ by the

Table 2. $^1$H NMR Data ($\delta_H$) of Compounds 1−4 (400 MHz)[a]

| position | | 1 | 2 | 3 | 4 |
|---|---|---|---|---|---|
| 1 | | 5.87 dd (11.7, 4.7) | 5.60 dd (12.0, 4.0) | 5.60 dd (12.2, 4.1) | 4.31 d (3.6) |
| 2$\alpha$ | | 1.80 m | 1.63 m | 1.69 m | 5.52 dd (6.5, 3.6) |
| 2$\beta$ | | 1.90 m | 1.88 m | 1.77 m | |
| 3$\alpha$ | | 2.27 m | 2.25 m | 2.30 m | 2.36 m |
| 3$\beta$ | | 1.41 m | 1.56 m | 1.47 m | 2.00 m |
| 4 | | 2.25 m | 1.86 m | 1.94 m | 2.32 m |
| 6$\alpha$ | | | 2.18 overlapped | 2.22 overlapped | |
| $\beta$ | | 7.07 s | 2.23 d (13.2) | 2.26 overlapped | 6.14 s |
| 7 | | 2.66 d (3.7) | 2.26 overlapped | 2.28 overlapped | 2.60 d (4.7) |
| 8 | | 6.13 dd (5.6, 3.7) | 4.43 dd (6.2, 3.0) | 5.67 dd (6.4, 2.9) | 5.68 t (4.7) |
| 9 | | 6.20 d (5.6) | 6.03 d (6.2) | 5.94 d (6.4) | 4.37 d (4.7) |
| 12 | | 1.06 d (7.0) | 1.04 d (7.6) | 1.16 d (7.8) | 1.31 d (7.6) |
| 13 | | 5.24 d (13.2) | 4.30 d (12.0) | 4.86 d (12.4) | 1.59 s |
| | | 5.06 d (13.2) | 3.79 d (12.0) | 4.80 d (12.4) | |
| 14 | | 1.57 s | 1.56 s | 1.57 s | 1.48 s |
| 15 | | 1.48 s | 1.22 s | 1.24 s | 1.44 s |
| 1-OR | 2/6 | 2.17 s | 1.64 s | 1.56 s | |
| 2-OR | 2/6 | | | | 8.15 d (7.9) |
| | 3/5 | | | | 7.48 t (7.9) |
| | 4 | | | | 7.58 t (7.9) |
| 6-OR | 2 | 1.59 s | | | 2.09 s |
| 8-OR | 2/6 | 8.34 d (7.9) | | 1.92 s | 8.02 d (7.9) |
| | 3/5 | 7.47 t (7.9) | | | 7.45 t (7.9) |
| | 4 | 7.56 t (7.9) | | | 7.58 t (7.9) |
| 9-OR | 2/6 | 8.27 d (7.9) | 8.11 d (8.0) | 8.11 d (7.2) | |
| | 3/5 | 7.35 t (7.9) | 7.44 t (8.0) | 7.46 t (7.6) | |
| | 4 | 7.48 t (7.9) | 7.56 t (8.0) | 7.59 t (7.4) | |
| 13-OR | 2 | 2.18 s | | 8.56 dt (8.0,1.7) | |
| | 3 | | | 7.48 dd (8.0,4.6) | |
| | 4 | | | 8.83 d (4.0) | |
| | 5 | | | 9.44 s | |

[a]Compound **1** was recorded in pyridine-$d_5$, and the others were in $CDCl_3$.

same HPLC system (72% MeOH in $H_2O$) yielded compounds **2** ($t_R$ = 28 min, 13.5 mg) and **7** ($t_R$ = 31 min, 12.7 mg). By the same HPLC system, compound **3** ($t_R$ = 29 min, 40.6 mg) was obtained from subfraction $F_{5\text{-}5}$ (82% MeOH in $H_2O$). The further purification of subfractions $F_{5\text{-}2}$ (78% MeOH in $H_2O$) and $F_{5\text{-}10}$ (88% MeOH in $H_2O$) yielded compounds **4** ($t_R$ = 12 min, 8.7 mg) and **6** ($t_R$ = 48 min, 5.0 mg), respectively. Compounds **5** ($t_R$ = 23 min, 6.0 mg) and **10** ($t_R$ = 25 min, 6.9 mg) were acquired from the subfraction $F_{5\text{-}12}$ (91% MeOH in $H_2O$) with the same HPLC system. Compounds **8** ($t_R$ = 47 min, 4.9 mg) and **9** ($t_R$ = 45 min, 6.6 mg) were isolated from subfraction $F_{4\text{-}2}$ (72% MeOH in $H_2O$), which was obtained from $F_4$ (eluted by petroleum ether/acetone, 100:7 and 100:10) by the above MPLC (67−87% MeOH in $H_2O$).

**Celaspene A (1):** white powder; $[\alpha]_D^{21}$ −21.4 (*c* 0.19, $CH_2Cl_2$); CD ($CH_3CN$) 198 ($\Delta\varepsilon$ −19.3), 222 ($\Delta\varepsilon$ +9.4), 239 ($\Delta\varepsilon$ −13.9) nm; IR (KBr) $\nu_{max}$ 2955, 2917, 2849, 1736, 1602, 1369, 1279, 1229, 1114, 1069, and 1026 cm$^{-1}$; $^{13}$C NMR (100 MHz, pyridine-$d_5$) and $^1$H NMR (400 MHz, pyridine-$d_5$) data, Tables 1 and 2, respectively; ESIMS *m*/*z* 659 $[M + Na]^+$; HR-ESIMS *m*/*z* 659.2466 $[M + Na]^+$, calcd for $C_{35}H_{40}NaO_{11}$, 659.2468.

**Celaspene B (2):** colorless oil; $[\alpha]_D^{21}$ +8.2 (*c* 0.15, $CH_2Cl_2$); IR (KBr) $\nu_{max}$ 3432, 2917, 2849, 1734, 1654, 1374, 1277, 1236, and 1024 cm$^{-1}$; $^{13}$C NMR (100 MHz, $CDCl_3$) and $^1$H NMR (400 MHz, $CDCl_3$) data, Tables 1 and 2, respectively; ESIMS *m*/*z* 455 $[M + Na]^+$; HR-ESIMS *m*/*z* 455.2042 $[M + Na]^+$, calcd for $C_{24}H_{32}NaO_7$, 455.2046.

**Celaspene C (3):** colorless oil; $[\alpha]_D^{22}$ +23.0 (*c* 0.20, $CH_2Cl_2$); IR (KBr) $\nu_{max}$ 2918, 2850, 1729, 1540, 1452, 1367, 1273, 1228, 1150, and 1025 cm$^{-1}$; $^{13}$C NMR (100 MHz, $CDCl_3$) and $^1$H NMR (400 MHz, $CDCl_3$) data, Tables 1 and 2, respectively; ESIMS *m*/*z* 602 $[M + Na]^+$; HR-ESIMS *m*/*z* 602.2366 $[M + Na]^+$, calcd for $C_{32}H_{37}NNaO_9$, 602.2366.

**Celaspene D (4):** colorless oil; $[\alpha]_D^{21}$ +2.7 (*c* 0.15, $CH_2Cl_2$); IR (KBr) $\nu_{max}$ 3446, 2917, 2849, 1714, 1452, 1273, 1229, 1095, and 1032 cm$^{-1}$; $^{13}$C NMR (100 MHz, $CDCl_3$) and $^1$H NMR (400 MHz, $CDCl_3$) data, Tables 1 and 2, respectively; ESIMS *m*/*z* 575 $[M + Na]^+$; HR-ESIMS *m*/*z* 575.2246 $[M + Na]^+$, calcd for $C_{31}H_{36}NaO_9$, 575.2257.

**Celaspene E (5):** Colorless oil; $[\alpha]_D^{22}$ +1.9 (*c* 0.21, $CH_2Cl_2$); IR (KBr) $\nu_{max}$ 3431, 2917, 2849, 1705, 1463, 1276, 1082, and 1039 cm$^{-1}$; $^{13}$C NMR (100 MHz, $CDCl_3$) and $^1$H NMR (400 MHz, $CDCl_3$) data, Tables 1 and 3, respectively); ESIMS *m*/*z* 622 $[M + Na]^+$; HR-ESIMS *m*/*z* 622.2417 $[M + Na]^+$, calcd for $C_{35}H_{37}NNaO_8$, 622.2417.

**Celaspene F (6):** colorless oil; $[\alpha]_D^{22}$ +1.6 (*c* 0.25, $CH_2Cl_2$); IR (KBr) $\nu_{max}$ 3448, 2917, 2849, 1741, 1709, 1463, 1367, 1264, 1108, and 1071 cm$^{-1}$; $^{13}$C NMR (100 MHz, $CDCl_3$) and $^1$H NMR (400 MHz,


dx.doi.org/10.1021/jf503735t | J. Agric. Food Chem. 2014, 62, 10945−10953

Table 3. $^1$H NMR Data ($\delta_H$) of Compounds 5−9 ($CDCl_3$, 400 MHz)

| position | | 5 | 6 | 7 | 8 | 9 |
|---|---|---|---|---|---|---|
| 1 | | 5.80 dd (10.8, 5.9) | 5.46 d (3.2) | 5.51 d (3.3) | 5.43 dd (11.8, 4.1) | 5.55 dd (12.3, 4.0) |
| 2$\alpha$ | | 1.63 m | 5.38 dd (6.3, 3.2) | 5.37 dd (6.3, 3.3) | 1.66 m | 1.64 m |
| 2$\beta$ | | 1.87 m | | | 1.89 m | 1.88 m |
| 3$\alpha$ | | 1.60 m | 2.35 m | 2.39 m | 2.26 m | 2.27 m |
| 3$\beta$ | | 1.55 m | 1.70 m | 1.72 m | 1.48 m | 1.65 m |
| 4 | | 1.91 m | 1.91 m | 1.91 m | 2.27 m | 1.87 m |
| 6$\alpha$ | | 2.14 dd (12.7, 4.8) | 2.12 dd (12.7, 4.9) | 2.09 dd (12.6, 4.2) | | 2.15 dd (12.8, 4.2) |
| $\beta$ | | 2.68 d (12.7) | 3.04 d (12.7) | 2.64 d (12.6) | 5.91 s | 2.52 d (12.8) |
| 7 | | 2.47 t (4.8) | 2.40 t (4.9) | 2.38 t (4.2) | 2.41 d(3.2) | 2.26 t (4.2) |
| 8 | | 5.70 dd (9.5, 4.8) | 5.58 dd (9.5, 4.9) | 4.32 dd (9.2, 4.2) | 4.31 s | 5.52 dd (6.4, 4.2) |
| 9 | | 4.70 dd (9.5) | 5.97 d (9.5) | 5.80 d (9.2) | 4.89 s | 5.94 d (6.4) |
| 12 | | 1.21 d (7.7) | 1.36 d (8.0) | 1.28 d (8.0) | 1.03 d (7.3) | 1.09 d (7.8) |
| 13 | | 5.15 d (12.6) | 4.45 d (13.0) | 4.87 d (13.0) | 1.48 s | 4.25 d (11.7) |
| | | 5.07 d (12.6) | 4.20 d (13.0) | 4.80 d (13.0) | | 3.92 d (11.7) |
| 14 | | 1.64 s | 1.54 s | 1.63 s | 1.35 s | 1.53 s |
| 15 | | 1.22 s | 1.20 s | 1.23 s | 1.42 s | 1.21 s |
| 1-OR | 2/6 | 8.03 d (7.0) | 2.01 s | 2.08 s | 1.58 s | 1.65 s |
| | 3/5 | 7.41 t (7.0) | | | | |
| | 4 | 7.54 t (7.0) | | | | |
| 2-OR | 2 | | 1.56 s | 1.43 s | | |
| 6-OR | 2 | | | | 2.12 s | 1.89 s |
| 8-OR | 2/6 | 8.01 d (7.1) | 1.89 s | | | |
| | 3/5 | 7.40 t (7.1) | | | | |
| | 4 | 7.52 t (7.1) | | | | |
| 9-OR | 2/6 | | 7.95 d (7.2) | 7.99 d (7.5) | 8.05 d (7.2) | 8.11 d (7.3) |
| | 3/5 | | 7.48 t (7.2) | 7.46 t (7.5) | 7.45 t (7.2) | 7.46 t (7.3) |
| | 4 | | 7.59 t (7.2) | 7.57 t (7.5) | 7.57 t (7.2) | 7.57 t (7.3) |
| 13-OR | 2 | 8.50 dt (7.9, 1.8) | | 2.21 s | | |
| | 3 | 7.50 dd (7.9, 4.0) | | | | |
| | 4 | 8.84 d (4.0) | | | | |
| | 5 | 9.41 s | | | | |

$CDCl_3$) data, Tables 1 and 3, respectively; ESIMS $m/z$ 555 $[M + Na]^+$; HR-ESIMS $m/z$ 555.2207 $[M + Na]^+$, calcd for $C_{28}H_{36}NaO_{10}$, 555.2206.

**Celaspene G (7):** colorless oil; $[\alpha]_D^{21}$ −13.2 ($c$ 0.17, $CH_2Cl_2$); IR (KBr) $\nu_{max}$ 3450, 2917, 2849, 1743, 1721, 1464, 1367, 1279, and 1026 $cm^{-1}$; $^{13}C$ NMR (100 MHz, $CDCl_3$) and $^1H$ NMR (400 MHz, $CDCl_3$) data, Tables 1 and 3, respectively; ESIMS $m/z$ 555 $[M + Na]^+$; HR-ESIMS $m/z$ 555.2205 $[M + Na]^+$, calcd for $C_{28}H_{36}NaO_{10}$, 555.2206.

**Celaspene H (8):** colorless oil; $[\alpha]_D^{22}$ +3.2 ($c$ 0.25, $CH_2Cl_2$); IR (KBr) $\nu_{max}$ 3444, 2917, 2849, 1714, 1464, 1367, 1275, 1234, and 1096 $cm^{-1}$; $^{13}C$ NMR (100 MHz, $CDCl_3$) and $^1H$ NMR (400 MHz, $CDCl_3$) data, Tables 1 and 3, respectively; ESIMS $m/z$ 497 $[M + Na]^+$; HR-ESIMS $m/z$ 497.2144 $[M + Na]^+$, calcd for $C_{26}H_{34}NaO_8$, 497.2151.

**Celaspene I (9):** colorless oil; $[\alpha]_D^{22}$ −11.6 ($c$ 0.21, $CH_2Cl_2$); IR (KBr) $\nu_{max}$ 3499, 2918, 2850, 1737, 1711, 1462, 1367, 1283, 1265, and 1025 $cm^{-1}$; $^{13}C$ NMR (100 MHz, $CDCl_3$) and $^1H$ NMR (400 MHz, $CDCl_3$) data, Tables 1 and 3, respectively; ESIMS $m/z$ 497 $[M + Na]^+$; HR-ESIMS $m/z$ 497.2153 $[M + Na]^+$, calcd for $C_{26}H_{34}NaO_8$, 497.2151.

**Computational Methods.** Details have been previously reported.[11,12]

**Antifungal Activity Assay.** The antifungal activities of the isolated compounds were tested against six pathogenic fungi (*Gibberella zeae*, *Physalospora piricola*, *Alternaria solani*, *Cercospora arachidicola*, *Cladosporium cucumerinum*, and *Phytophthora capsici*) using a mycelium growth inhibition method.[13−17] The test solution (1 mL, 50 $\mu$g/mL) was poured into sterile culture plates (9 cm diameter), and agar culture medium (9 mL) was added. Sterile water (1 mL) and agar culture medium (9 mL) were used as controls. The inocula, 4 mm in diameter, were removed from the margins of actively growing colonies of mycelium, placed in the centers of the above plates, and incubated at 24 °C. After an incubation of 72 h, the diameter of the mycelium was measured. Each treatment was performed in two replicates. The inhibitory rate was used to describe the antifungal activities of compounds:

$$\text{inhibition rate (\%)} = (\text{av hyphal diam in control} - \text{av hyphal diam in treatment})/\text{av hyphal diam in control}$$

## RESULTS AND DISCUSSION

The ethyl acetate-soluble part of the methanol extract of the fruits of *C. orbiculatus* was subjected to silica gel column chromatography and further purified by HPLC to acquire nine new (**1**−**9**) and one known (**10**) compound (Figure 1). The known compound was identified by comparison of spectroscopic data with those reported in the literature as 6$\alpha$-acetoxy-1$\beta$,2$\beta$,9$\beta$-tribenzoyloxy-8$\beta$-nicotinoyloxy-$\beta$-dihydroagarofuran, **10**.[18]

Compound **1** was isolated as a white powder. Its molecular formula was determined as $C_{35}H_{40}O_{11}$ on the basis of HR-ESI-MS spectroscopic data, which were consistent with the NMR data. The $^1H$ NMR spectrum of **1** exhibited six methyl groups [$\delta_H$ 2.18 (3H, s, COC$H_3$-13), 2.17 (3H, s, COC$H_3$-1), 1.59 (3H, s, COC$H_3$-6), 1.57 (3H, s, $H_3$-14), 1.48 (3H, s, $H_3$-15), and 1.06 (3H, d, $J$ = 7.0 Hz, $H_3$-12)], four oxygenated methine protons [$\delta_H$ 5.87 (1H, dd, $J$ = 11.7, 4.7 Hz, H-1), 7.07 (1H, s, H-6), 6.13 (1H, dd, $J$ = 5.6, 3.7 Hz, H-8), and 6.20 (1H, d, $J$ =


dx.doi.org/10.1021/jf503735t | J. Agric. Food Chem. 2014, 62, 10945−10953

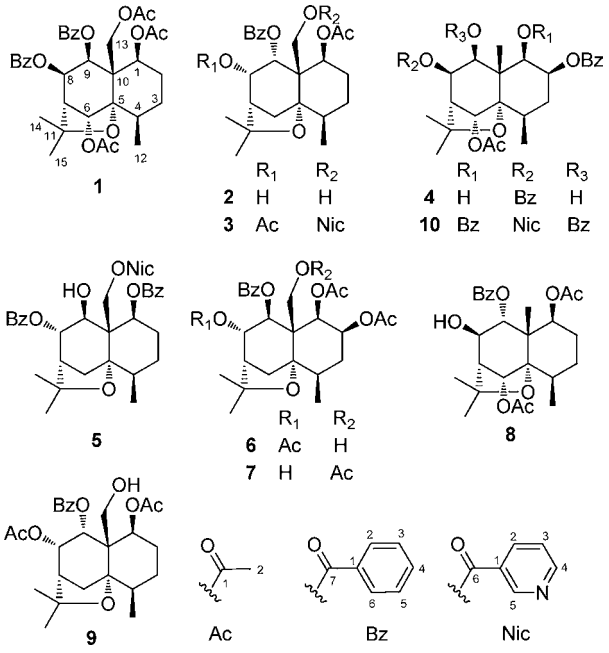


**Figure 1.** Structures of compounds **1**–**10** from *C. orbiculatus*.

5.6 Hz, H-9)], and a pair of methylene protons [$\delta_H$ 5.24 and 5.06 (each 1H, d, $J$ = 13.2 Hz, $H_2$-13)]. Additionally, 10 aromatic protons were also revealed by the $^1$H NMR spectrum. The $^{13}$C NMR spectrum of **1** showed 35 carbon resonances (Table 1). From the $^1$H and $^{13}$C NMR spectra, three acetyl groups and two benzoyl groups were deduced and defined from the above proton signals and the observation of the corresponding carbon signals (Tables 1 and 2).[5] In addition to the above 20 signals for the acyl groups, there are additional 15 resonances displayed for the parent skeleton in the $^{13}$C NMR spectrum. These skeletal carbon signals comprised three methyls [$\delta_C$ 14.9 (C-12), 24.2 (C-14), and 30.1 (C-15)], two methylenes [$\delta_C$ 23.3 (C-2), and 26.5 (C-3)], six methines [$\delta_C$ 79.2 (C-1), 33.5 (C-4), 74.7 (C-6), 53.3 (C-7), 71.4 (C-8), and 73.3 (C-9)], and four quaternary carbons [$\delta_C$ 91.0 (C-5), 51.1 (C-10), and 81.1 (C-11)] on the basis of the HMQC and DEPT spectra. The above spectroscopic features and the 15 skeletal carbons displayed in the $^{13}$C NMR spectrum suggested that compound **1** is a sesquiterpene having five acyloxy groups (three acetoxy and two benzoyloxy groups).[7−10] When the chemical shifts of skeletal carbons of **1** were compared with those of sesquiterpenes reported in the literature,[5,19] the presence of $\beta$-dihydroagarofuran skeleton for **1** was obvious. To corroborate the above deductions and confirm the $\beta$-dihydroagarofuran sesquiterpene skeleton, the HMBC and $^1$H−$^1$H COSY experiments were performed. By interpretation of the HMQC, HMBC, and $^1$H−$^1$H COSY spectra, the $\beta$-dihydroagarofuran sesquiterpene skeleton for **1** was elucidated, where the oxygenated methine and methylene carbon signals at $\delta_C$ 79.2, 74.7, 71.4, 73.3, and 60.8 were assigned to C-1, C-6, C-8, C-9, and C-13, respectively. The locations of the five acyloxy groups were determined via HMBC correlations. The long-range correlation of the proton H-1 ($\delta_H$ 5.87) with the carbonyl signal at $\delta_C$ 169.8 (CO of the acetoxy moiety) revealed the presence of the acetoxy group at C-1. Similarly, the long-range couplings of the protons H-6 ($\delta_H$ 7.07) and $H_2$-13 ($\delta_H$ 5.24 and 5.06), with the carbonyl carbon signals at $\delta_C$ 169.8 and 170.5 evidenced that the remaining two acetoxy groups were attached at C-6 and C-13, respectively. The two benzoyloxy groups located at C-8 and C-9 were verified by the HMBC correlations of H-8 and H-9 to the corresponding carbonyl carbons of two benzoyloxy groups. Further analyses of the 2D NMR spectra (Figure 2) led to the assignments of all the proton and carbon signals, and the planar structure for **1** was thus established.

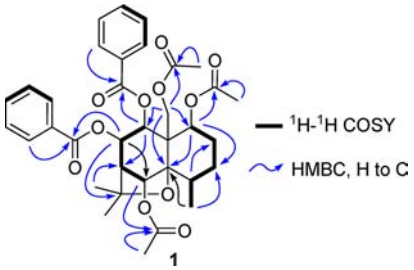


**Figure 2.** Selected HMBC and $^1$H−$^1$H COSY correlations of compound **1**.

The relative configuration of compound **1** was established on the basis of the NOESY spectrum and Chem3D modeling (Figure 3). NOESY correlations observed for $H_3$-12/$H_2$-13, $H_3$-12/H-2$\beta$, $H_2$-13/H-2$\beta$, $H_2$-13/H-6, $H_3$-12/H-6, H-1/H-9, H-9/$H_3$-14, H-8/$H_3$-14, and H-1/H-3$\alpha$ (Figure 3), but not for $H_2$-13/H-1, $H_2$-13/H-9, and $H_3$-12/H-1, and the Chem3D modeling indicated a conformation for compound **1** as shown in Figure 3, where the two six-membered rings B and A were *trans*-fused and existed in a twist-chair and chair conformation, and the furan ring C, almost perpendicular to the six-membered ring B, was located below ring B. The arrangement of the three rings and the NOESY correlations required that the C-12 methyl group and the C-13 methylene group were both $\beta$-axially oriented, the C-1 acetoxy group and the C-9 benzoyloxy group were both $\beta$-equatorially oriented, the C-6 acetoxy group was in an $\alpha$-equatorial position, and the C-8 benzoyloxy group was in a $\beta$-axial position.[5,19] Thus, the relative configuration of **1** was designated as shown in Figure 3. The absolute configuration of **1** was tentatively established by the TDDFT CD calculations[20,21] and substantiated by the CD exciton chirality method.[22] Through the systematic conformational search and optimization and TDDFT CD calculations, the calculated ECD spectra were obtained. The calculated ECD spectrum of **1a** (Figure 4) is agreement with the experimental result, which suggested an absolute configuration of 1*S*,4*R*,5*S*,6*R*,7*R*,8*R*,9*S*,10*S* for compound **1**, whereas the experimental CD spectrum of **1** showed a characteristic Davidoff-type split curve with a first negative Cotton effect at 239 nm ($\Delta\varepsilon$ −13.9) and a second positive effect at 222 nm ($\Delta\varepsilon$ +9.4), due to the couplings of the two benzoyloxy chromophores at C-8$\beta$ and C-9$\beta$, which confirmed the absolute configuration of 1*S*,4*R*,5*S*,6*R*,7*R*,8*R*,9*S*,10*S* unequivocally. On the basis of the above evidence, the structure of **1** was established as (1*S*,4*R*,5*S*,6*R*,7*R*,8*R*,9*S*,10*S*)-1$\beta$,6$\alpha$,13-triacetoxy-8$\beta$,9$\beta$-dibenzoyloxy-$\beta$-dihydroagarofuran, which has been named celaspene A.

Compound **2**, a colorless oil, had a molecular formula of $C_{24}H_{32}O_7$ as deduced from the HR-ESIMS. From the $^1$H NMR spectrum of **2**, four methyl groups, five aromatic protons, three oxygenated methine protons, and a pair of methylene protons were displayed (Table 2). The $^{13}$C NMR spectrum of **2** exhibited 24 carbon resonances. From the $^1$H and $^{13}$C NMR spectra, one acetyl group was apparent from the methyl singlet


dx.doi.org/10.1021/jf503735t | J. Agric. Food Chem. 2014, 62, 10945−10953

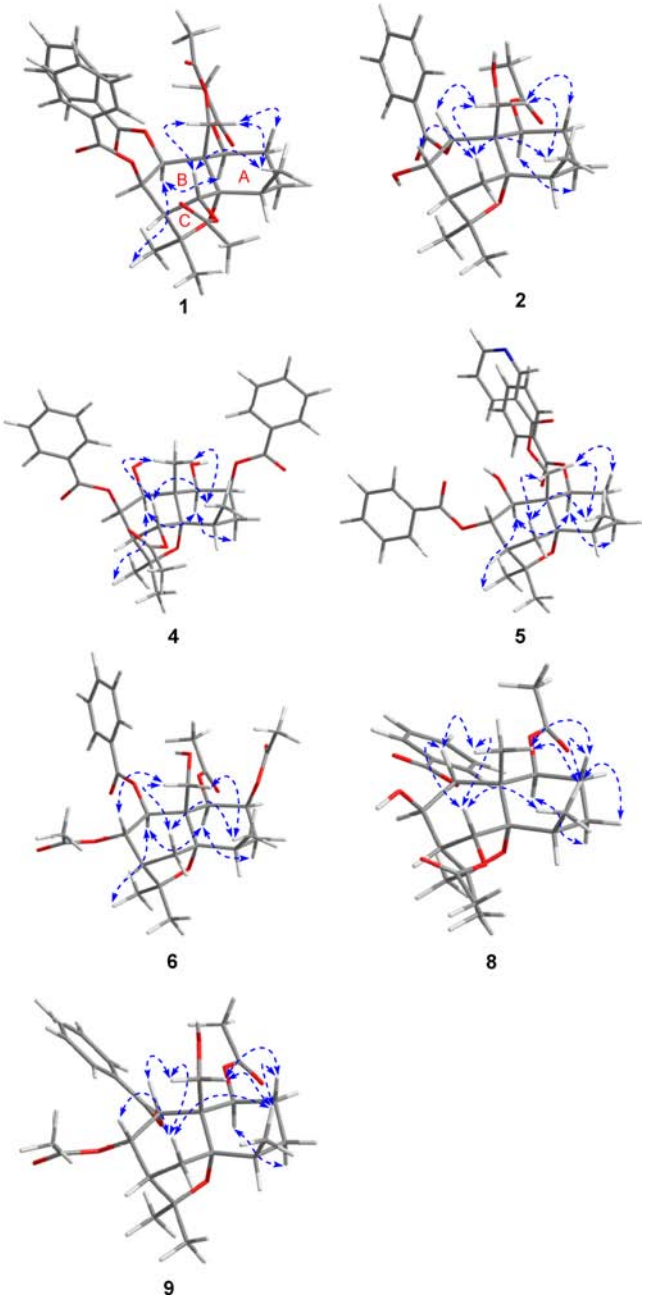


**Figure 3.** Key NOESY correlations of compounds **1**, **2**, **4**−**6**, **8**, and **9**.

and the corresponding carbon signals (Tables 1 and 2). In addition, one benzoyloxy group was also deduced and defined from the observation of the aromatic proton signals (Table 2) and the typical aromatic carbon signals (Table 1).[5−10] Apart from the above nine resonances for the substituent groups, the remaining 15 skeletal carbon resonances indicated in the $^{13}C$ NMR spectrum form a characteristic $\beta$-dihydroagrofuran skeleton.[5] To elucidate the skeleton and assign the substituent groups, the following HMQC, HMBC, and $^{1}H-^{1}H$ COSY experiments were performed. By interpretation of the 2D NMR spectra, the characteristic 1,8,9,13-tetrasubstituted-$\beta$-dihydroagrofuran sesquiterpene skeleton was confirmed, where the oxygenated methylene and methine carbons at $\delta_C$ 75.4, 72.6, 70.8, and 62.5 were ascribed to C-1, C-8, C-9, and C-13, respectively. The HMBC correlations of the protons H-1 ($\delta_H$ 5.60) and H-9 ($\delta_H$ 6.03) with the carbonyl carbons at $\delta_C$ 169.2

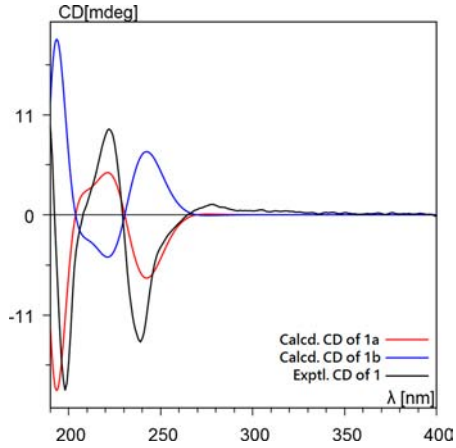


**Figure 4.** Calculated ECD spectra of **1a** (1*S*,4*R*,5*S*,6*R*,7*R*,8*R*,9*S*,10*S*)- and **1b** (1*R*,4*S*,5*R*,6*S*,7*S*,8*S*,9*R*,10*R*)-isomers and the experimental ECD spectrum of **1** in acetonitrile.

and 167.7 demonstrated that the acetoxy group was attached at C-1 and the benzoyloxy group was at C-9, respectively. There were no additional acyloxy groups in compound **2**, so the substituent groups at C-8 and C-13 could only be hydroxy groups, which was confirmed by the HR-ESIMS data. Further analyses of the HMQC, HMBC, and $^{1}H-^{1}H$ COSY spectroscopic data resulted in the assignments of all the proton and carbon signals. The planar structure with a $\beta$-dihydroagrofuran sesquiterpene skeleton for **2** was therefore disclosed. The relative configuration was elucidated on the basis of the NOESY spectrum and the coupling constants. NOESY correlations observed for $H_3$-12/$H_2$-13, $H_3$-12/H-2$\beta$, $H_2$-13/H-2$\beta$, $H_2$-13/H-6$\beta$, $H_3$-12/H-6$\beta$, $H_2$-13/H-9, H-8/H-6$\beta$, and H-1/H-3$\alpha$ (Figure 3), but not for H-1/H-9, $H_2$-13/H-1, $H_3$-14/H-8, H-9/$H_3$-14, and $H_3$-12/H-1, and the Chem3D modeling revealed a conformation for compound **2** as shown in Figure 3, where the C-1 acetoxy group was in a $\beta$-equatorial position and the C-9 benzoyloxy group was in an $\alpha$-axial position. The C-8 hydroxy group was determined as $\alpha$-equatorially oriented, which was supported by the coupling constant between H-9 and H-8 ($J_{8,9}$ = 6.2 Hz).[7,19] Thus, the relative configuration of **2** was characterized as in Figure 3. Considering the biosynthetic origin, the conformations of three skeletal rings, and the same relative configurations for C-4, C-5, and C-10 in compounds **2** and **1**, the absolute configurations of C-4, C-5, and C-10 were established to be 4*R*, 5*S*, and 10*S* and the absolute configurations of C-1, C-8, and C-9, consequently, were determined as 1*S*, 8*S*, and 9*R*.[5] Thus, compound **2** was characterized as (1*S*,4*R*,5*S*,7*S*,8*S*,9*R*,10*S*)-1$\beta$-acetoxy-9$\alpha$-benzoyloxy-8$\alpha$,13-dihydroxy-$\beta$-dihydroagarofuran, which was named celaspene B.

Compound **3** possessed the molecular formula of $C_{32}H_{37}NO_9$ on the basis of the HR-ESIMS. The $^{1}H$ and $^{13}C$ NMR spectra implied that **3** had the same 1,8,9,13-tetrasubstituted-$\beta$-dihydroagrofuran sesquiterpene skeleton as compound **2** and possessed four acyl groups.[5−10,19] Besides one benzoyl and two acetyl groups, an additional nicotinoyl group was deduced and defined on the basis of the proton signals and the typical carbon resonances (Tables 1 and 2).[19,23] The following 2D NMR experiments validated the above deductions. The locations of the acyl groups were elucidated by interpretation of the HMBC data as in the case of **2**. HMBC correlations of the protons at H-1 ($\delta_H$ 5.60), H-8 ($\delta_H$ 5.67), H-


dx.doi.org/10.1021/jf503735t | J. Agric. Food Chem. 2014, 62, 10945−10953

9 ($\delta_H$ 5.94), and $H_2$-13 ($\delta_H$ 4.86 and 4.80) with the corresponding carbonyl carbons at $\delta_C$ 169.6, 169.9, 165.9, and 165.3 indicated that two acetoxy, one benzoyloxy, and one nicotinoyloxy group were attached at C-1, C-8, C-9, and C-13, respectively. By further analyzing the 2D NMR spectra, the planar structure of **3** was established. The relative configuration of compound **3** was elucidated on the basis of the NOESY spectrum and Chem3D modeling as that of compound **2**. The NOESY correlations observed for $H_3$-12/$H_2$-13, $H_3$-12/H-2$\beta$, $H_2$-13/H-2$\beta$, $H_2$-13/H-6$\beta$, $H_3$-12/H-6$\beta$, $H_2$-13/H-9, H-8/H-6$\beta$, and H-1/H-3$\alpha$ (Figure 3), but not for $H_2$-13/H-1, H-1/H-9, H-9/$H_3$-14, and $H_3$-12/H-1, and the Chem3D modeling disclosed a molecular conformation for compound **3** as depicted in Figure 3, where all of the chiral carbons had the same relative configurations as those of compound **2**. On the basis of the above spectroscopic evidence and the biosynthetic standpoint, compound **3** was assigned as (1*S*,4*R*,5*S*,7*S*,8*S*,9*R*,10*S*)-1$\beta$,8$\alpha$-diacetoxy-9$\alpha$-benzoyloxy-13-nicotinoyloxy-$\beta$-dihydroagarofuran and named celaspene C, which is the C-8 isomer of the known compound 1$\beta$,8$\alpha$-diacetoxy-9$\beta$-benzoyloxy-13-nicotinoyloxy-$\beta$-dihydroagarofuran.[24,25]

Analyses of the $^{13}C$ and $^{1}H$ NMR data (Tables 1 and 2) of compound **4** revealed that **4** had the characteristic 1,2,6,8,9-pentasubstituted-$\beta$-dihydroagarofuran sesquiterpene skeketon.[5−10] The same acyl groups as those appearing in compounds **1**−**3** were apparent, which were deduced and determined as one acetyl and two benzoyl groups according to its $^{13}C$ and $^{1}H$ NMR spectra.[19,23] The residual substituent groups could only be hydroxy groups, which were validated by the HR-ESIMS data. Through the same 2D NMR experiments, especially HMBC and $^{1}H-^{1}H$ COSY experiments, as for compounds **1**−**3**, the positions of the substituent groups (one acetoxy and two benzoyloxy groups) of **4** were determined, which suggested that the two benzoyloxy groups were attached at C-2 and C-8, the two hydroxy groups were ascribed to C-1 and C-9, and the acetoxy group was at C-6, respectively. The NOESY spectrum and the coupling constants allowed the relative configuration of **4** to be assigned. The NOESY correlations observed for $H_3$-12/$H_3$-13, $H_3$-13/H-6, $H_3$-12/H-6, H-1/H-9, H-9/$H_3$-14, H-8/$H_3$-14, and H-1/H-3$\alpha$ (Figure 3), but not for $H_3$-13/H-1, $H_3$-13/H-9, $H_3$-12/H-1, and $H_3$-12(13)/H-2, and Chem 3D revealed that the two hydroxy groups attributed to C-1 and C-9 were both $\beta$-equatorially oriented, the two benzoyloxy groups ascribed to C-2 and C-8 were both $\beta$-axially oriented, and the acetoxy attached at C-6 was $\alpha$-equatorially oriented.[5,19] The coupling constants between H-9 and H-8 ($J_{8,9}$ = 4.7 Hz) and H-1 and H-2 ($J_{1,2}$ = 3.6 Hz) also confirmed that the protons H-1 and H-9 were in $\alpha$-axial positions and H-2 and H-8 were in $\alpha$-equatorial positions, respectively. According to the above spectroscopic evidence and the biosynthetic standpoint, the structure of compound **4** was therefore assigned as (1*R*,2*S*,4*R*,5*S*,6*R*,7*R*,8*R*,9*S*,10*S*)-6$\alpha$-acetoxy-2$\beta$,8$\beta$-dibenzoyloxy-1$\beta$,9$\beta$-dihydroxy-$\beta$-dihydroagarofuran,[5] which has been named celaspene D.

The HR-ESIMS provided a molecular formula of $C_{35}H_{37}NO_8$ for compound **5**. The $^{13}C$ and $^{1}H$ NMR spectra (Tables 1 and 3) suggested a 1,8,9,13-tetrasubstituted-$\beta$-dihydroagarofuran sesquiterpene skeketon for **5**.[5−10] The four substituent groups were deduced as two benzoyloxy groups, one nicotinoyloxy group,[19,23] and one hydroxy group according to its $^{13}C$ and $^{1}H$ NMR spectra, which was supported by the 2D NMR and HR-ESIMS data. As in the case of **1**−**4**, the acyloxy groups were positioned by interpretation of the HMBC spectrum. The HMBC correlations of the protons H-1, H-8, and $H_2$-13 with the carbonyl carbons at $\delta_C$ 166.4, 166.1, and 165.4 demonstrated that the two benzoyloxy groups were located at C-1 and C-8, and the nicotinoyloxy group was at C-13, respectively. Consequently, the substituent group at C-9 could only be hydroxy group. The coupling constants and the NOESY spectrum allowed the relative configuration of **5** to be assigned. The coupling constant ($J_{8,9}$ = 9.5 Hz) between H-9 and H-8 suggested that both H-8 and H-9 had an axial orientation, with a nearly 180° dihedral angle between H-8 and H-9.[7,19] The NOESY spectrum displayed the correlations of $H_3$-12/$H_2$-13, $H_3$-12/H-6$\beta$, $H_2$-13/H-6$\beta$, H-6$\beta$/H-8, $H_3$-12/H-2$\beta$, $H_2$-13/H-2$\beta$, $H_2$-13/H-8, H-1/H-9, H-9/$H_3$-14, and H-1/H-3$\alpha$ (Figure 3), but not for $H_2$-13/H-1, $H_2$-13/H-9, and $H_3$-12/H-1. According to the above evidence, the C-1 benzoyloxy group, the C-9 hydroxy group, and the C-8 benzoyloxy group were characterized as $\beta$-equatorial, $\beta$-equatorial, and $\alpha$-equatorial, respectively. The relative stereochemistry of **5** was therefore elucidated, where the orientation of the C-8 substituent group was different from those in compounds **1** and **4**. Also on the basis of the conformations of three skeletal rings and the biosynthetic origin, the absolute configuration of **5** was established as 1*S*,4*R*,5*S*,7*S*,8*S*,9*S*,10*R*.[5] Thus, compound **5** was elucidated as (1*S*,4*R*,5*S*,7*S*,8*S*,9*S*,10*R*)-1$\beta$,8$\alpha$-dibenzoyloxy-9$\beta$-hydroxy-13-nicotinoyloxy-$\beta$-dihydroagarofuran and named celaspene F.

Compounds **6** and **7** had the same molecular formula, $C_{28}H_{36}O_{10}$, on the basis of their HR-ESIMS data. Analyses of the $^{13}C$ and $^{1}H$ NMR spectra (Tables 1 and 3) of the two compounds revealed that compounds **6** and **7** had the same 1,2,8,9,13-pentasubstituted-$\beta$-dihydroagarofuran skeleton and the same substituent groups (one hydroxy, one benzoyloxy, and three acetoxy groups).[5,19] The difference was that the substituent groups in the two compounds were in different positions. Through the same 2D NMR experiments as those for compounds **1**−**5**, the positions of the hydrxoy and acyloxy groups in compounds **6** and **7** were determined. For compound **6**, the three acetoxy groups and the benzoyloxy group were attributed to C-1, C-2, and C-8, and C-9 by the HMBC correlations of H-1, H-2, H-8, and H-9 to the corresponding carbonyl carbons, and the remaining one hydroxy group could only be located at C-13. The following NOESY experiment and the coupling constants led to the elucidation of the relative configuration of **6**. The NOESY correlations observed for $H_3$-12/$H_2$-13, $H_3$-12/H-6$\beta$, $H_2$-13/H-6$\beta$, H-6$\beta$/H-8, $H_2$-13/H-8, H-1/H-9, H-9/$H_3$-14, and H-1/H-3$\alpha$ (Figure 3), but not for $H_2$-13/H-1(2), $H_2$-13/H-9, and $H_3$-12/H-1(2), the coupling constant of H-9 and H-8 ($J_{9,8}$ = 9.5 Hz), and the Chem3D modeling suggested a conformation for **6** as shown in Figure 3, where the C-1 acetoxy group and the C-9 benzoyloxy group were both in $\beta$-positions with an equatorial orientation, the C-2 acetoxy group was in a $\beta$-position with an axial orientation, and the C-8 acetoxy group was in an $\alpha$-position with an equatorial orientation. Compound **7** had the same substituent groups as compound **6**, and their relative locations were assigned by the HMBC spectrum, which demonstrated the three acetoxy groups and the benzoyloxy group were attached at C-1, C-2, C-13, and C-9, respectively. The only hydroxy group supported by the HR-ESIMS data was verified at C-8 by interpretation of the $^{1}H-^{1}H$ COSY spectrum. The same relative configuration for compounds **7** and **6** was inferred on the basis of the analyses

and the careful comparison of the NOESY spectra of **7** and **6**. On the basis of the same conformations of three skeletal rings in compounds **1**−**7** and the biosynthetic origin, compounds **6** and **7** were characterized as (1*R*,2*S*,4*R*,5*S*,7*S*,8*S*,9*S*,10*S*)-1*β*,2*β*,8*α*-triacetoxy-9*β*-benzoyloxy-13-hydroxy-*β*-dihydroagarofuran and (1*R*,2*S*,4*R*,5*S*,7*S*,8*S*,9*S*,10*R*)-1*β*,2*β*,13-triacetoxy-9*β*-benzoyloxy-8*α*-hydroxy-*β*-dihydroagarofuran, which have been named celaspenes G and H, respectively.

Compound **8** possessed the molecular formula of $C_{26}H_{34}O_8$ as determined by the HR-ESIMS. Its $^{13}C$ and $^{1}H$ NMR spectra (Tables 1 and 3) revealed that compound **8** was a 1,6,8,9-tetrasubstituted-*β*-dihydroagarofuran sesquiterpene with two acetyl, one benzoyl, and one hydroxy group, which was supported and confirmed by 2D NMR spectra. The further interpretation of 2D NMR spectra led to the determination of the relative positions of these substituent groups, which verified that the two acetoxy groups were located at C-1 and C-6, the benzoyloxy group was at C-9, and the hydroxy group was at C-8, respectively. By further analyzing the HMQC, HMBC, and $^{1}H-^{1}H$ COSY spectra, all of the proton and carbon signals were assigned unambiguously. On the basis of these assignments, the proton signals for H-8 and H-9 presented in the form of singlet, which implied the different configurations for C-8 and C-9 in **8**. The NOESY correlations of $H_3$-12/$H_3$-13, $H_3$-12/H-6, $H_3$-13/H-6, $H_3$-13/H-9, $H_3$-13/H-2*β*, $H_3$-12/H-2*β*, and H-1/H-3*α* (Figure 3), but not for H-6/H-8, H-1/H-9, H-9/$H_3$-14, $H_3$-13/H-1, and $H_3$-12/H-1, the coupling constant of H-9 and H-8 ($J_{9,8}$ = 0 Hz), and Chem3D modeling suggested that H-8 was *α*-equatorially oriented, H-9 was *β*-equatorially oriented, and H-1 was *α*-axially oriented.[5,19] Thus, the relative configuration of **8** was elucidated. According to the same conformations of three skeletal rings of compounds **1**−**7**, the absolute configuration of **8** was assigned as 1*S*,4*R*,5*S*,6*R*,7*R*,8*R*,9*R*,10*S*.[5,19] Compound **8** was therefore characterized as (1*S*,4*R*,5*S*,6*R*,7*R*,8*R*,9*R*,10*S*)-1*β*,6*α*-diacetoxy-9*α*-benzoyloxy-8*β*-hydroxy-*β*-dihydroagarofuran and named celaspene H, which is the C-9 isomer of the known compound 1*β*,6*α*-diacetoxy-9*β*-benzoyloxy-8*β*-hydroxy-*β*-dihydroagarofuran.[26−29]

Compound **9** possessed a molecular formula of $C_{26}H_{34}O_8$ from its HR-ESIMS. The molecular formula and its $^{13}C$ and $^{1}H$ NMR spectra (Tables 1 and 3) suggested that compound **9** was a 1,8,9,13-tetrasubstituted-*β*-dihydroagarofuran sesquiterpene with two acetoxy, one benzoyloxy, and one hydroxy group. To achieve the assignments of all the proton and carbon signals, the 2D NMR spectra were recorded. By interpretation and analyses of 2D NMR spectra, the planar structure of a 1,8,9,13-tetrasubstituted-*β*-dihydroagarofuran sesquiterpene was established, where the two acetoxy groups and one benzoyloxy group were ascribed to C-1, C-8, and C-9, and the residual hydroxy group was securely assigned to C-13. The coupling constant of H-9 and H-8 ($J_{9,8}$ = 6.4 Hz), Chem3D modeling, and the NOESY correlations of $H_3$-12/$H_2$-13, $H_3$-12/H-6*β*, $H_2$-13/H-6*β*, $H_2$-13/H-9, $H_2$-13/H-8, H-6*β*/H-8, $H_2$-13/H-2*β*, $H_3$-12/H-2*β*, and H-1/H-3*α* (Figure 3), but not for H-1/H-9, H-9/$H_3$-14, $H_2$-13/H-1, and $H_3$-12/H-1, revealed a molecular conformation for **9** as shown in Figure 3.[5] The proton H-1 was in an *α*-position with an axial orientation, H-8 was in a *β*-position with an axial orientation, and H-9 was in a *β*-position with an equatorial orientation. Similarly, from a biosynthetic standpoint, the absolute configuration was also assigned on the basis of the same conformations of the three skeletal rings.[5] Thus, compound **9** was elucidated as (1*S*,4*R*,5*S*,7*S*,8*S*,9*R*,10*S*)-1*β*,8*α*-diacetoxy-9*α*-benzoyloxy-13-hydroxy-*β*-dihydroagarofuran and named celaspene I.

To explore the potential biological effects of these new sesquiterpenes to serve agriculture, these isolated compounds from *C. orbiculatus* were preliminarily investigated for their antifungal activities against six pathogenic fungi (*G. zeae*, *P. piricola*, *A. solani*, *C. arachidicola*, *C. cucumerinum*, and *P. capsici*), which commonly infect crops, leading to severe crop yield reduction and dramatic economic losses in agriculture.[30] Chlorothalonil and carbendazol were used as the corresponding positive controls. At a concentration of 50 *μ*g/mL, all of the evaluated compounds exhibited antifungal activities. Their preliminary antifungal activities are shown in Figure 5

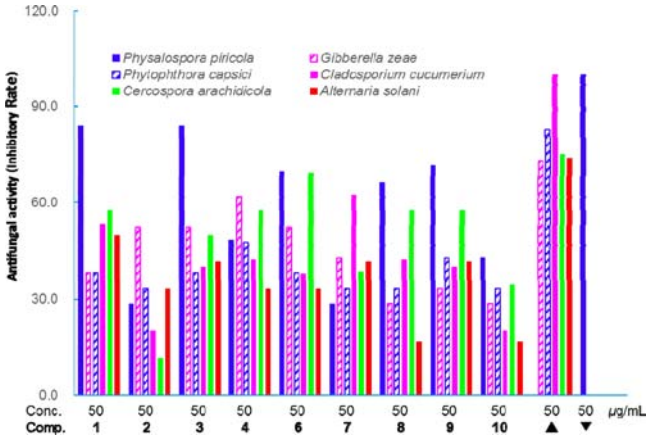


**Figure 5.** Antifungal effects of compounds **1**−**4** and **6**−**10** against six pathogenic fungi. Six common pathogenic fungi (*G. zeae*, *P. piricola*, *A. solani*, *C. arachidicola*, *C. cucumerinum*, and *P. capsici*) were selected to evaluate the antifungal activities of compounds **1**−**4** and **6**−**10**. The biological data presented are the mean scores for each treatment across replicates. The symbols ▲ and ▼ indicate the positive controls chlorothalonil and carbendazol, respectively.

(compound **5** was not assayed for the antifungal effects because of inadequate residual amount). For the pathogenic fungi *A. solani* and *P. capsici*, all of the compounds showed weak or moderate antifungal effects. For the fungus *G. zeae*, compound **4** showed a strong activity with an inhibitory rate of 62%. For the fungus *C. cucumerinum*, compound **7** showed a strong activity with an inhibitory rate of 62%. For the fungus *C. arachidicola*, compound **6** had a stronger activity with an inhibitory rate of 69% than other compounds. Compounds **1**, **3**, **6**, **8**, and **9** showed promising antifungal activities against the fungus *P. piricola* with inhibitory rates of 84, 84, 70, 66, and 71%, respectively. From the above antifungal data, there seem to be no obvious correlations among these activities against the six pathogenic fungi and the selectivity or sensitivity of each pathogenic fungus toward the same compound is different, which implies that the antifungal activity against different pathogenic fungus may have different mechanisms.

In conclusion, nine new and one known sesquiterpene were obtained from the fruits of the plant *C. orbiculatus*. Their structures, especially the stereochemical features, were elucidated by NMR data analyses, TDDFT CD calculations, and the CD exciton chirality method. The subsequent biological screenings exhibited that these isolated compounds showed antifungal activities against six phytopathogenic fungi. The results of our phytochemical investigation further revealed the chemical components of *C. orbiculatus* as an insecticidal and

medicinal plant, and the biological screenings implied that *C. orbiculatus* may be potentially useful to protect crops against phytopathogenic fungi and that the bioactive compounds may probably be considered as candidate agents of antifungal agrochemicals for crop protection products.

## ■ ASSOCIATED CONTENT

### Supporting Information

1D and 2D NMR and HR-MS spectra of compounds **1**−**9**. This material is available free of charge via the Internet at http://pubs.acs.org.

## ■ AUTHOR INFORMATION


### Corresponding Author

*(J.X.) Phone/fax: +86-22-23502595. E-mail: xujing611@nankai.edu.cn.



### Funding

This work was supported in part by the National Natural Science Foundation of China (No. 21372125).


### Notes

The authors declare no competing financial interest.

## ■ REFERENCES


(1) Nanjing University of Chinese Medicine. *Dictionary of Chinese Herb Medicines*, 2nd ed.; Shanghai Scientific and Technologic Press: Shanghai, China, 2006; pp 2205−2206.

(2) Wang, M. A.; Chen, F. H. Insect antifeedant sesquiterpenoids from *Celastrus orbiculatus*. *Gaodeng Xuexiao Huaxue Xuebao* **1995**, *16*, 1248−1250.

(3) Wang, L. Y.; Wu, J.; Yang, Z.; Wang, X. J.; Fu, Y.; Liu, S. Z.; Wang, H. M.; Zhu, W. L.; Zhang, H. Y.; Zhao, W. M. (*M*)- and (*P*)-bicelaphanol A, dimeric trinorditerpenes with promising neuroprotective activity from *Celastrus orbiculatus*. *J. Nat. Prod.* **2013**, *76*, 745−749.

(4) Wu, J.; Zhou, Y.; Wang, L.; Zuo, J.; Zhao, W. Terpenoids from root bark of *Celastrus orbiculatus*. *Phytochemistry* **2012**, *75*, 159−168.

(5) Zhu, Y.; Miao, Z.; Ding, J.; Zhao, W. Cytotoxic dihydroagarofuranoid sesquiterpenes from the seeds of *Celastrus orbiculatus*. *J. Nat. Prod.* **2008**, *71*, 1005−1010.

(6) Xu, J.; Jin, D. Q.; Zhao, P.; Song, X.; Sun, Z.; Guo, Y.; Zhang, L. Sesquiterpenes inhibiting NO production from *Celastrus orbiculatus*. *Fitoterapia* **2012**, *83*, 1302−1305.

(7) Jin, H. Z.; Hwang, B. Y.; Kim, H. S.; Lee, J. H.; Kim, Y. H.; Lee, J. J. Antiinflammatory constituents of *Celastrus orbiculatus* inhibit the NF-κB activation and NO production. *J. Nat. Prod.* **2002**, *65*, 89−91.

(8) Guo, Y. Q.; Li, X.; Xu, J.; Li, N.; Meng, D. L.; Wang, J. H. Sesquiterpene esters from the fruits of *Celastrus orbiculatus*. *Chem. Pharm. Bull.* **2004**, *52*, 1134−1136.

(9) Kim, S. E.; Kim, H. S.; Hong, Y. S.; Kim, Y. C.; Lee, J. J. Sesquiterpene esters from *Celastrus orbiculatus* and their structure-activity relationship on the modulation of multidrug resistance. *J. Nat. Prod.* **1999**, *62*, 697−700.

(10) Kim, S. E.; Kim, Y. H.; Lee, J. J.; Kim, Y. C. A new sesquiterpene ester from *Celastrus orbiculatus* reversing multidrug resistance in cancer cells. *J. Nat. Prod.* **1998**, *61*, 108−111.

(11) Wang, M.; Zhang, Q.; Wang, H.; Ren, Q.; Sun, Y.; Xie, C.; Xu, J.; Jin, D. Q.; Ohizumi, Y.; Guo, Y. Characterization and NO inhibitory activities of chemical constituents from an edible plant *Petasites tatewakianus*. *J. Agric. Food Chem.* **2014**, *62*, 9362−9367.

(12) Xu, J.; Zhang, Q.; Wang, M.; Ren, Q.; Sun, Y.; Jin, D. Q.; Xie, C.; Chen, H.; Ohizumi, Y.; Guo, Y. Bioactive clerodane diterpenoids from the twigs of *Casearia balansae*. *J. Nat. Prod.* **2014**, *77*, 2182−2189.

(13) Clough, J. M.; Godfrey, C. R. A. The strobilurin fungicides. In *Fungicidal Activity, Chemical and Biological Approaches to Plant Protection*; Hutson, D. H., Miyamoto, J., Eds.; Wiley Series in Agrochemicals and Plant Protection; Wiley: Surrey, UK, 1998; pp 109−148.

(14) Zhao, H.; Liu, Y.; Cui, Z.; Beattie, D.; Gu, Y.; Wang, Q. Design, synthesis, and biological activities of arylmethylamine substituted chlorotriazine and methylthiotriazine compounds. *J. Agric. Food Chem.* **2011**, *59*, 11711−11717.

(15) Li, X. J.; Zhang, Q.; Zhang, A. L.; Gao, J. M. Metabolites from *Aspergillus fumigatus*, an endophytic fungus associated with *Melia azedarach*, and their antifungal, antifeedant, and toxic activities. *J. Agric. Food Chem.* **2012**, *60*, 3424−3431.

(16) Zhang, Y.; Wang, J. S.; Wang, X. B.; Gu, Y. C.; Wei, D. D.; Guo, C.; Yang, M. H.; Kong, L. Y. Limonoids from the fruits of *Aphanamixis polystachya* (Meliaceae) and their biological activities. *J. Agric. Food Chem.* **2013**, *61*, 2171−2182.

(17) Wang, D. M.; Zhang, C. C.; Zhang, Q.; Shafiq, N.; Pescitelli, G.; Li, D. W.; Gao, J. M. Wightianines A−E, dihydro-β-agarofuran sesquiterpenes from *Parnassia wightiana*, and their antifungal and insecticidal activities. *J. Agric. Food Chem.* **2014**, *62*, 6669−6676.

(18) Takaishi, Y.; Tokura, K.; Noguchi, H.; Nakano, K.; Murakami, K.; Tomimatsu, T. Sesquiterpene esters from *Tripterygium wilfordii*. *Phytochemistry* **1991**, *30*, 1561−1566.

(19) Kennedy, M. L.; Cortés-Selva, F.; Pérez-Victoria, J. M.; Jiménez, I. A.; González, A. G.; Muñoz, O. M.; Gamarro, F.; Castanys, S.; Ravelo, A. G. Chemosensitization of a multidrug-resistant *Leishmania tropica* line by new sesquiterpenes from *Maytenus magellanica* and *Maytenus chubutensis*. *J. Med. Chem.* **2001**, *44*, 4668−4476.

(20) Conflex software, version 6.7; Conflex Corp., Tokyo, Japan, 2010.

(21) Gaussian 09, revision B.01; Gaussian Inc.: Pittsburgh, PA, USA, 2010.

(22) Harada, N.; Nakanishi, K. *Circular Dichroic Spectroscopy: Exciton Coupling in Organic Stereochemistry*; University Science Books: Mill Valley, CA, USA, 1983.

(23) Xu, J.; Jin, D. Q.; Guo, Y.; Xie, C.; Ma, Y.; Yamakuni, T.; Ohizumi, Y. New myrsinol diterpenes from *Euphorbia prolifera* and their inhibitory activities on LPS-induced NO production. *Bioorg. Med. Chem. Lett.* **2012**, *22*, 3612−3618.

(24) Wang, Y.; Yang, L.; Tu, Y.; Zhang, K.; Chen, Y.; Fan, J. Two new sesquiterpenoids from the seeds of *Celastrus angulatus*. *J. Nat. Prod.* **1998**, *61*, 942−944.

(25) Yang, L.; Wang, Y.; Tu, Y.; Chen, Y. Two sesquiterpenoids from *Celastrus angulatus*. *Zhongshan Daxue Xuebao, Ziran Kexueban* **1997**, *36*, 123−124.

(26) Guo, Y. Q.; Li, X.; Ma, Z. J.; Cui, W. S.; Wang, J. H.; Ju, Z. X. A new sesquiterpene ester from the fruits of *Celastrus orbiculatus*. *J. Asian Nat. Prod. Res.* **2005**, *7*, 157−160.

(27) Tu, Y.; Wang, Y. Complete proton and carbon-13 chemical shift assignments and the relationship between carbon-13 chemical shifts and stereochemistry for β-dihydroagarofuran sesquiterpene. *Bopuxue Zazhi* **1992**, *9*, 329−335.

(28) Tu, Y.; Wu, D.; Zhang, X.; Hao, X. Bioactive sesquiterpenoids from *Celastrus paniculatus*. *Gaodeng Xuexiao Huaxue Xuebao* **1992**, *13*, 1548−1550.

(29) Tu, Y. Q.; Chen, Y. Z.; Wu, D. G.; Zhang, X. M.; Hao, X. J. Sesquiterpenoids from *Celastrus paniculatus*. *J. Nat. Prod.* **1993**, *56*, 122−125.

(30) Savary, S.; Teng, P. S.; Willocquet, L.; Nutter, F. W., Jr. Quantification and modeling of crop losses: a review of purposes. *Annu. Rev. Phytopathol.* **2006**, *44*, 89−112.

carried out in the veterinary area due to the promising overall efficacy of aromatic herbs for the benefit of animals and the quality of animal-derived products. Some authors have even proposed these naturally occurring substances as substitutes for antibiotic growth promoters.[14] In a preliminary study conducted by our group, the bioaccessibility and phase II metabolism of thyme phenols were assessed by an in vitro digestion model combined with Caco-2 and HepG-2 cell models.[15] The results of this study showed different metabolic profiles depending on the phenolic compound. Whereas eriodictyol appeared in both its sulfated and glucuronidated forms after cell incubation, naringenin was only conjugated into its glucuronide form. To complement these studies, it becomes essential to study the microbial conversion of thyme phenolic compounds and the elucidation of their colonic pathways. In this sense, the main aim of the present study was to provide more complete, comprehensive, and convincing results about the gut metabolism of thyme phenolic compounds by using a combination of in vitro and in vivo experiments. For the in vitro fermentation study, the most representative compounds from different subclasses of thyme phenols were selected: (i) the monoterpene thymol and its isomer carvacrol; (ii) the flavonoid eriodictyol; and (iii) rosmarinic acid, a phenolic acid occurring in many common aromatic herbs from the Lamiaceae group. After studying the in vitro gut metabolism pathways of the aforementioned thyme phenols, we investigated their colonic metabolites in human fecal samples obtained before and after a 3 week intervention with a daily administered dose of 25 mL (23 g) of a thyme phenol-enriched olive oil (TPEOO).

## MATERIALS AND METHODS

**In Vitro Colonic Fermentation.** Fecal samples were collected from three healthy volunteers who followed normal dietary habits and declared that they had not taken antibiotics for at least 3 months prior to the sample collection. The fermentation medium was carbonate−phosphate buffer. This was prepared according to a previously described method[16] by mixing (all in g/L) 9.240 $NaHCO_3$, 3.542 $Na_2HPO_4{\cdot}2H_2O$, 0.470 NaCl, 0.450 KCl, 0.227 $Na_2SO_4{\cdot}10H_2O$, 0.055 $CaCl_2$ (anhydrous), 0.100 $MgCl_2{\cdot}6H_2O$, and 0.400 urea with 10 mL/L of added trace element solution (in mg/L) 3680 $FeSO_4{\cdot}7H_2O$, 1159 $MnSO_4{\cdot}H_2O$, 440 $ZnSO_4{\cdot}7H_2O$, 120 $CoCl_2{\cdot}6H_2O$, 98 $CuSO_4{\cdot}5H_2O$, and 17.4 $Mo_7(NH_4)_6O_24{\cdot}4H_2O$). Before its use, the culture medium was maintained in an anaerobic chamber for 48 h, using gas generator bags ($CO_2$) (Becton Dickinson, Sparks, MD, USA) to remove the oxygen. The anaerobic conditions were continuously monitored by using anaerobic indicator strips (Becton Dickinson). Standards of thymol, rosmarinic acid, and eriodictyol were purchased from Extrasynthese (Genay, France), whereas carvacrol was purchased from Sigma-Aldrich (St. Louis, MO, USA). For the selection of the phenolic compounds to carry out the in vitro experiments, we took into consideration the availability of commercial standards and the occurrence of these substances in the TPEOO.

The in vitro fermentation procedure used in this study was adapted from the method proposed by Serra and co-workers.[17] For each volunteer, 15 g of fresh feces was homogenized for 60 s in a stomacher with 300 mL of prereduced culture medium to obtain a 5% fecal slurry. Following the homogenization, the fecal slurry was filtered and left to stand for 30 min. Once done, 10 mL was taken and added to 15 mL disposable tubes. After the addition of the standard (phenol standard final concentration 500 $\mu$M for thymol, carvacrol, and eriodictyiol, and 200 $\mu$M for rosmarinic acid), the disposable tubes were incubated in anaerobic chambers at 37 °C in an orbital shaker (60 strokes/min) to mimic colon conditions (anaerobic conditions were controlled by anaerobic indicator strips). The high initial concentrations (500 and 200 $\mu$M) of the parent compounds were chosen to determine more clearly the microbial metabolites generated, even at relatively low concentrations. Aliquots of the fermented fecal samples (500 $\mu$L) were collected at 0, 2, 6, 12, 24, and 48 h of incubation and stored immediately at −80 °C until the chromatographic analysis. All of the fermentation samples were incubated in triplicate. In parallel, a control sample (fecal slurry without addition of phenolic standard) was prepared for each fermentation time. Also, the phenolic standards without feces (blank 1) were incubated at each time (0, 2, 6, 12, 24, and 48 h) to take into account the possible chemical degradation of phenolic compounds.

**Human Intervention Study.** Fecal samples from 10 volunteers were used to determine thyme phenolic metabolites identified in the in vitro fermentation model. The feces were obtained before and after the consumption (25 mL/day) of a thyme phenol-enriched olive oil (TPEOO) over a period of 3 weeks. The TPEOO was prepared by adding a thyme phenolic extract to an olive oil according to the methodology described by Rubió and co-workers.[18] The main phenolic compounds that were transferred from thyme to the olive oil were flavonoids, such as eriodictyol, thymusin, naringenin, and xanthomicrol, phenolic acids, such as rosmarinic acid, and the monoterpenes thymol and carvacrol (Table 1).

**Table 1. Phenolic Composition of Thyme Phenol-Enriched Olive Oil (TPEOO)[a]**

| compound | mg phenol/kg oil |
|---|---|
| rosmarinic acid | 16.3 ±1.2 |
| flavonoids | |
| eriodictyol | 6.9 ±0.5 |
| luteolin | 8.5 ±0.8 |
| apigenin | 3.8 ±0.2 |
| naringenin | 7.9 ±0.8 |
| thymusin | 48.6 ±3.6 |
| xanthomicrol | 21.3 ±2.2 |
| 7-methylsudachitin | 21.1 ±3.4 |
| monoterpenes | |
| thymol | 25.4 ±2.1 |
| carvacrol | 9.1 ±0.8 |

[a]Values are means ± SD ($n$ = 5) expressed as mg phenol/kg oil.

Prior to the TPEOO intervention, there was a 2 week wash-out period, in which common olive oil (a blend of refined olive oil and a small percentage of virgin olive oil) was the main fat consumed. To avoid an excessive intake of phenolic compounds during the intervention period, the participants were advised to limit the intake of phenol-rich foods. Fecal samples from each volunteer were collected after the wash-out period (pre TPEOO intake) and at the end of the 3 week intervention (post TPEOO intake). The subjects gave their written informed consent before participation (Ethics Committee for Human Research of the IMIM-Hospital del Mar, Barcelona, Spain; CEIC-PSMAR 2009/3347/I). Freshly voided fecal samples were collected by the volunteers into a sterile pot and brought to the laboratory under anaerobic conditions within 2 h of defecation, immediately mixed in a phosphate buffer (PBS; final concentration 10% of fecal sample), and centrifuged for 5 min at 13000 rpm. The supernatant was divided into aliquots of 500 $\mu$L and stored at −20 °C until chromatographic analysis of phenol metabolites.

**Treatment of Fecal Samples and Chromatographic Analysis of Thyme Metabolites.** The in vitro fermentation samples and the supernatants obtained from the human intervention study were slowly thawed in ice, transferred into a disposable tube (15 mL), and acidified with 60 $\mu$L of HCl to inactivate the microbiota. A liquid−liquid extraction was carried out by adding 5 mL of ethyl acetate, and after shaking for 10 min in a vortex, samples were centrifuged (10 min, 8784$g$, at room temperature). The supernatants resulting from two ethyl acetate extractions were combined and evaporated under nitrogen flow at 30 °C. The dry residue was reconstituted with 500 $\mu$L of water/acetonitrile/methanol (86:12:2, v/v/v), filtered with a

0.22 μm nylon syringe filter, and transferred into chromatographic vials for analysis.

The chromatographic analysis of rosmarinic acid, eriodictyol, and their metabolites and thymol and carvacrol metabolites was performed with a Waters Acquity Ultra-Performance liquid chromatography (UPLC-ESI-MS/MS) system (Waters, Milford MA, USA), according to the previously described method.[19] The tandem mass spectrometry (MS/MS) analyses were carried out on a triple-quadrupole detector (TQD) mass spectrometer (Waters) equipped with a Z-spray electrospray interface. The analyses were done in the negative ion mode, and the data were acquired with the selected reaction monitoring mode (SRM). The MS/MS parameters were as follows: capillary voltage, 3 kV; source temperature, 150 °C; cone gas flow rate, 80 L/h; desolvation gas flow rate, 800 L/h; desolvation temperature, 400 °C. Nitrogen (>99% purity) and argon (99% purity) were used as the nebulizing and collision gases, respectively. The cone voltages and collision energies were optimized for each analyte by injection of each standard compound in a mixture of acetonitrile/water (50:50, v/v) at a concentration of 10 mg/L. Two transitions were studied for each compound. The most abundant transition was used for quantification, whereas the second most abundant was used for confirmation purposes. The dwell time established for each transition was 30 ms. Data acquisition was carried out with MassLynx v 4.1 software. Catechol, phenylacetic acid, 4-hydroxybenzoic acid, 3-phenylpropionic acid, 2-(4′-hydroxyphenyl)acetic acid, 2-(3′-hydroxyphenyl)acetic acid, 4-coumaric acid, protocatechuic acid, 2-(3′,4′-dihydroxyphenyl)acetic acid, 3-(4′-hydroxyphenyl)propionic acid, 3-(3′,4′-dihydroxyphenyl)-propionic, caffeic acid, rosmarinic acid, and eriodictyol were quantified using the calibration curves of their respective standards.

Additionally, all samples were subjected to gas chromatography (GC) analyses to identify and quantify the volatile monoterpene thymol and carvacrol in their native forms. These compounds were first extracted from the in vitro fermentation samples and from the human fecal supernatants to the TPEOO intervention by hexane. For this purpose, 500 μL of sample was mixed with 1 mL of hexane and shaken during 1 h and then centrifuged for 10 min at 9000 rpm at room temperature. The volatile material collected from the supernatant was analyzed by gas chromatography (GC) (Agilent 7890A series) coupled to a flame ionization detector (FID) using a capillary column TRB-5SM (Teknocroma, Barcelona, Spain). The column temperature was programmed at 90 °C for 1 min, increased by 15 °C/min to 270 °C, and then maintained at 270 °C for 10 min (total run time of 25 min). Helium was the carrier gas (1 mL/min). Injector temperature was 250 °C, the detector temperature was 280 °C, and 1 μL of the solution was injected into the GC-FID system. Thymol and carvacrol were identified by comparing the retention times to those for the authentic standards and quantified by using the calibration curve of the respective standard.

**Statistical Analysis.** Each sample from the in vitro experiment was analyzed in triplicate (three replicates from three volunteers; $n = 9$), and the data are presented as the mean values of all samples at each time ($n = 9$ per each time) minus the concentration of the compound in the control (fecal culture medium without phenolic compound). In the in vivo study, to compare the baseline with the post-treatment concentration values of the metabolites in human fecal samples, the ANOVA analysis was employed using STAT-GRAPHICS Plus 5.1 software (Manugistics Inc., Rockville, MD, USA). The level of significance was 0.05.

## RESULTS AND DISCUSSION

**Kinetics of Thyme Phenol Colonic Metabolism in in Vitro Fermentation.** Changes in the precursor compounds (thymol, carvacrol, rosmarinic acid, and eriodictyiol) during the in vitro fermentation were monitored from 0 to 48 h. Results are reported as the average of three independent fermentations for each human fecal sample, obtaining nine replicates for each fermentation time (individual values are shown in Tables S1–S4 of the Supporting Information). The amounts of the phenolic compounds and their metabolites were corrected for the endogenous levels detected in the control fermentations (fecal culture medium without phenolic compound) (Human Intervention Study underMaterials and Methods).

**Monoterpenes: Thymol and Carvacrol.** On the basis of the volatile nature of thymol and carvacrol, these compounds were analyzed by GC, whereas colonic metabolites formed during in vitro fermentation were analyzed by liquid chromatography (UPLC-MS/MS). The kinetics of the generated metabolites after thymol and carvacrol fermentation is shown in Figure 1, panels A and 1B, respectively. In general,

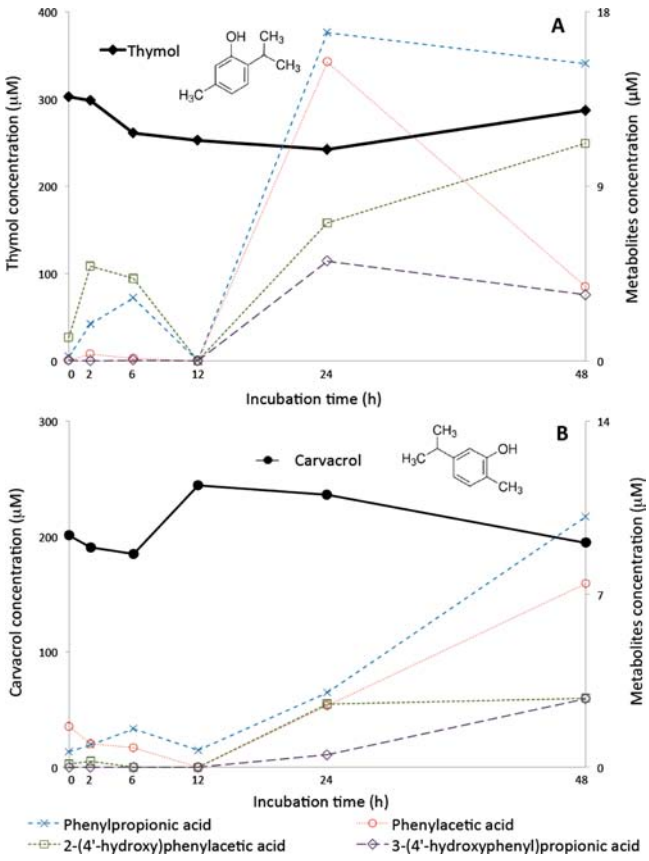


**Figure 1.** (A) Thymol concentration (solid line) and metabolite generation (dotted line) during in vitro fermentation. (B) Carvacrol concentration (solid line) and metabolite generation (dotted line) during in vitro fermentation.

carvacrol and thymol showed a similar behavior during the 48 h incubation, possibly due to the closely related chemical structure. Both compounds were poorly degraded and remained relatively stable until the end-time of the fermentation, indicating the nonexistent or low activity of gut microbiota in terms of monoterpene utilization. However, some metabolites were formed during the in vitro fermentation of thymol (Figure 1A): (i) phenylacetic acid, which reached its maximum concentration (16.91 μM) at 24 h of incubation; (ii) 2-(4′-hydroxyphenyl)acetic acid with a maximum recovery (15.39 μM) also at 24 h of incubation. Furthermore, (iii) phenylpropionic acid and (iv) 3-(4′-hydroxyphenyl)propionic acid reached the maximum concentration at 48 h (11.20 μM) and at 24 h (5.14 μM) of incubation, respectively. Interestingly, low concentrations of carvacrol were found at different times during the thymol fermentation (Supporting Information,

Table S1) but were also detected in thymol standard samples incubated without fecal slurry (blank 1), which may indicate that carvacrol is generated by the medium conditions as a consequence of the isomerization of thymol.

Similar results were observed when carvacrol was fermented. During the fermentation the main metabolites that appeared were (i) phenylpropionic acid (10.13 $\mu$M) and (ii) phenylacetic acid (7.43 $\mu$M), both by the end of fermentation. After the fermentation of carvacrol, (iii) 2-(4′-hydroxyphenyl)acetic acid and (iv) 3-(4′-hydroxyphenyl)propionic acid wer also detected. Both phenolic acids reached their maximum concentrations (2.78 and 2.77 $\mu$M, respectively) at 48 h of fermentation.

In vitro fermentation of monoterpenes using animal intestinal content as inocula also showed low microbial activity.[20,21] Michiels and co-workers have reported that thymol and carvacrol were degraded by 29% after the fermentation of both compounds using piglet cecal as inocula, but no degradation products were specified.[20] Varel and co-workers also observed high stability of thymol and carvacrol after anoxic swine waste fermentation, recovering close to 95% of both monoterpenes at 62 days.[21] Therefore, our results confirm that phenol terpenes remain stable during the fermentation, probably due to the complex carbon skeleton that may hamper their microbial degradation. To the best of our knowledge, there are no data available in the literature about thymol and carvacrol metabolism in human bowel. However, cholesterol and bile acids, which also have a terpenoid lipid structure, are daily exposed to gut microbiota, and their bacterial transformations have been extensively documented in humans. The reduction of the C7 double bond of the cholesterol molecule,[22] the 7$\alpha$-dehydroxylation, and the side chain degradation of functional groups in the case of bile acids are typically caused by bacteria activity, but in any case cholesterol, bile acids, and their metabolites suffer further degradation.[23] Similarly, our results suggest that thymol and carvacrol (phenolic terpenes) may be recalcitrant molecules to biodegradation in the human large intestine, probably as a consequence of the low number of functional groups and/or the lack of intestinal bacteria specialized in their metabolism. Therefore, the appearance of phenolic acids, especially within 24 h of incubation (Figure 1), may be explained by the loss of bacteria cell integrity due to the modification of membrane permeability, which could induce the release of endogenous metabolites into the culture medium. Linked to this, Thapa and co-workers[1] studied the effects of different essential oils and their pure compounds, including thymol, on pathogenic and commensal intestinal bacteria. The results showed that phenolic monoterpenes were the most active class of antibacterial agents and caused a dose-dependent loss of cell integrity in Gram-positive bacteria, probably by modifying the permeability of cellular membranes, thus promoting the loss of ATP and intracellular metabolites or enzymes. Therefore, in our study the release of endogenous microbial material could explain the presence of different phenylacetic and phenylpropionic acids in the thyme and carvacrol fermentation media.

**Rosmarinic Acid and Eriodictyol.** Analyses of the fermentation samples of rosmarinic acid and eriodictyol revealed a full degradation of the parent compounds and a high generation of microbial products over the incubation time (0−48 h). The kinetics of the rosmarinic acid fermentation showed that this compound was insignificant at 12 h of incubation (Figure 2A). The first intermediate microbial metabolite derived from the hydrolysis of rosmarinic acid was

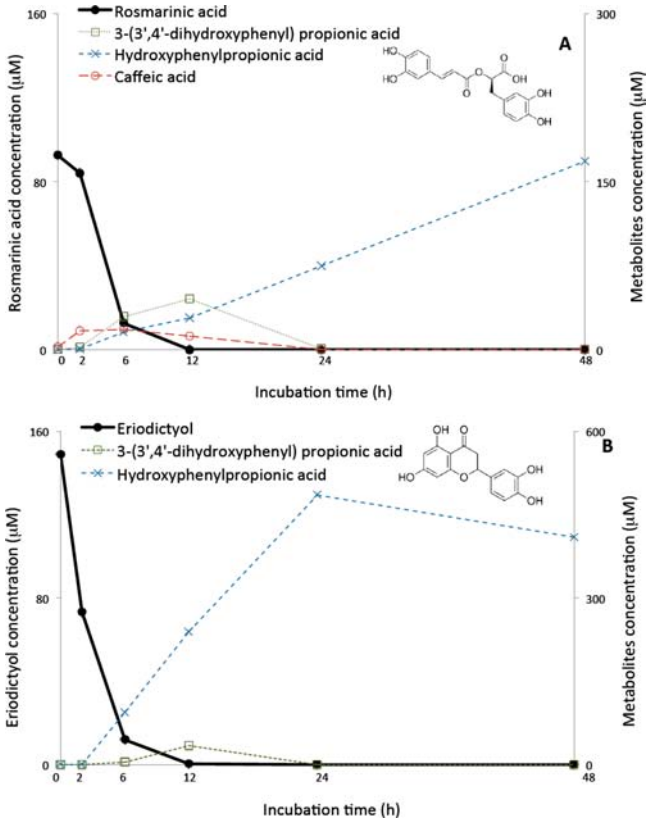


**Figure 2.** (A) Conversion of rosmarinic acid (solid line) during in vitro fermentation into its phenolic catabolites (dotted line). (B) Conversion of eriodictyol (solid line) during in vitro fermentation into its phenolic catabolites (dotted line).

caffeic acid, which reached its maximum concentration at 6 h (17.9 $\mu$M) (Figure 2A) before declining to trace levels at 48 h of fermentation. The gut metabolic pathway of rosmarinic acid is proposed in Figure 3. A previous study has also revealed a rapid transformation of rosmarinic acid when it was fermented in pure cultures of *Lactobacillus johnsonii*,[24] a type of lactic acid bacteria (LAB) commonly found in the human gut.[25] Degradation of rosmarinic acid seems to be mediated by microbial chlorogenate esterases.[24]

The second intermediate metabolite detected in the fecal culture medium was 3-(3′,4′-dihydroxyphenyl)propionic acid, probably formed as a result of the microbial transformation of caffeic acid (Figure 3) by the reduction of the aliphatic double bond of the second ring of the molecule. 3-(3′,4′-dihydroxyphenyl)propionic acid reached its highest peak of concentration at 12 h (24.2 M) coinciding with the decrease in the concentration of caffeic acid in the fermentation medium (Figure 2A). An isomer of 3-(4′-hydroxypehyl)propionic acid was identified as the main metabolite formed by the fermentation of rosmarinic acid, and this reached the highest concentration in the medium (168.2 $\mu$M) at 48 h of fermentation, parallel to the decrease in the concentration of its precursor, 3-(3′,4′-dihydroxyphenyl)propionic acid. The generation of hydroxyphenylpropionic acid probably came from the 4-dehydroxylation of 3-(3′,4′-dihydroxyphenyl)propionic acid, but we were not able to confirm this information. Caffeic acid is a hydroxycinammic acid widely present in foods, in both free and conjugated forms (normally with quinic acid to form chlorogenic acid). Microbial fermentation of free or conjugated caffeic acid has been studied, and our findings seem to be in line

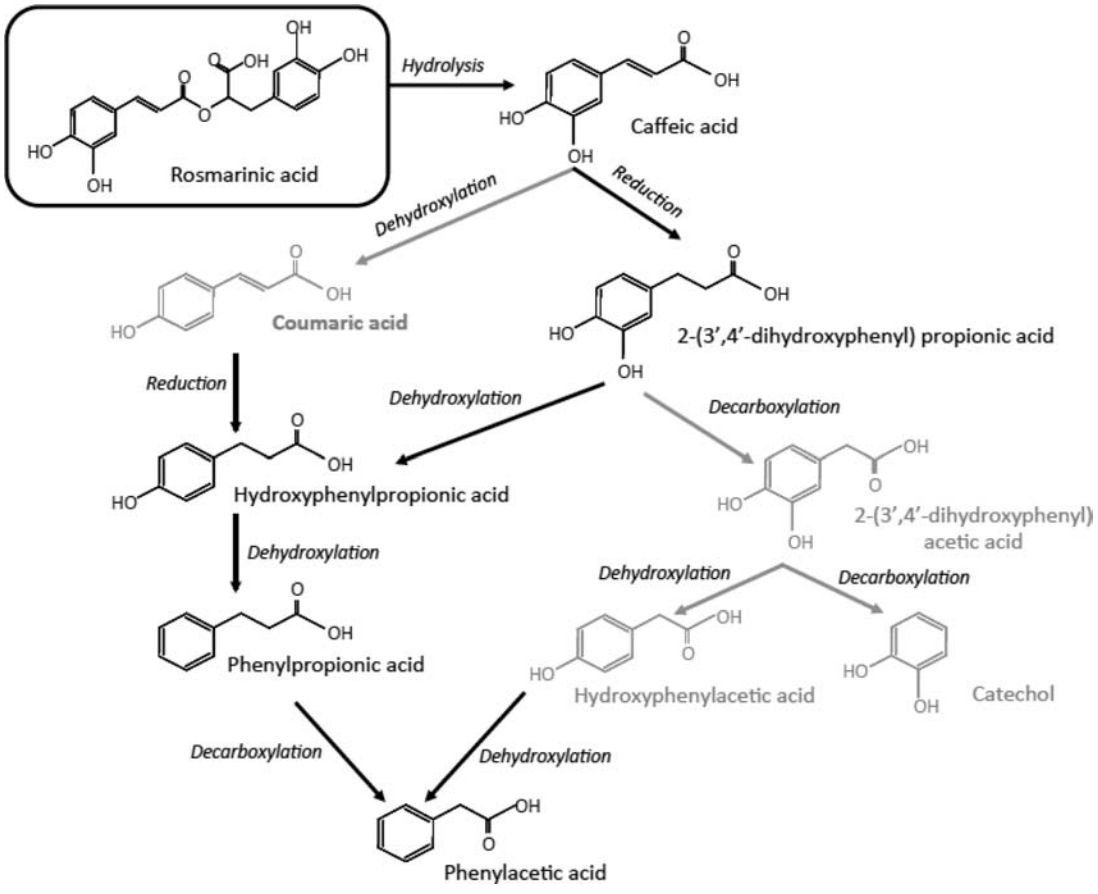


**Figure 3.** Proposed colonic pathway of rosmarinic acid. Compounds in bold were detected in the fermentation medium between 0 and 48 h. Compounds in gray were detected as minor metabolites in the fermentation medium.

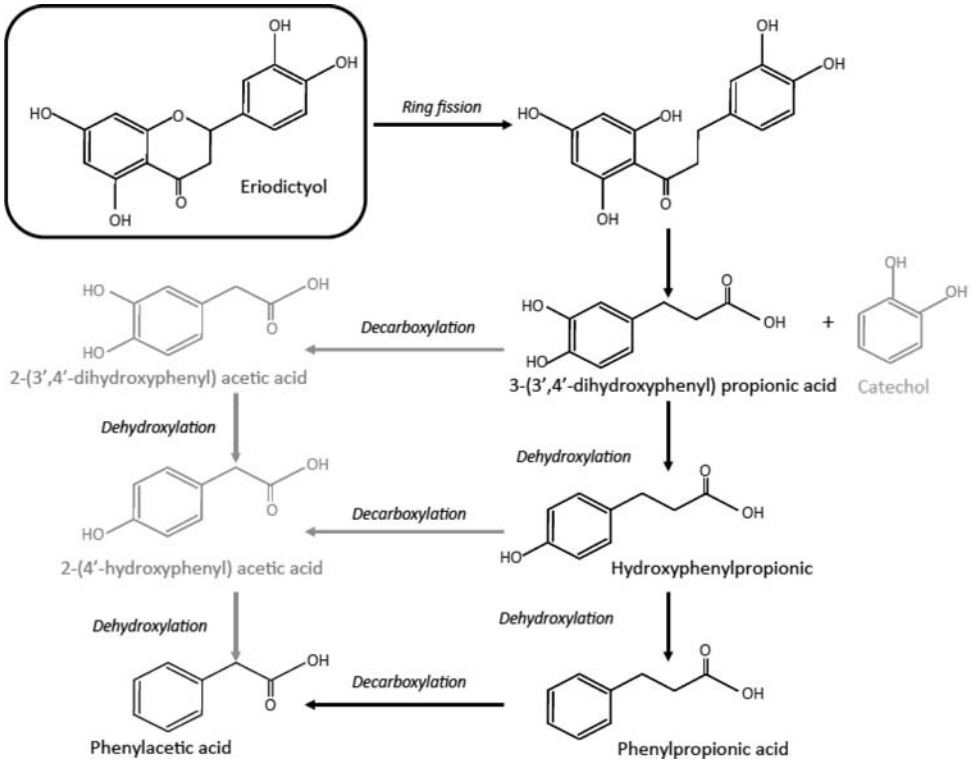


**Figure 4.** Proposed colonic pathway of eriodictyol. Compounds in bold were detected in the fermentation medium between 0 and 48 h. Compounds in gray were detected as minor metabolites in the fermentation medium.


dx.doi.org/10.1021/jf503748y | J. Agric. Food Chem. 2014, 62, 10954−10961

with previous works in which 3-(3′-hydroxyphenyl)propionic acid was recovered as the main bacteria metabolite.[13]

Chemically, rosmarinic acid is an ester of caffeic acid and 3-(3′,4′-dihydroxyphenyl)lactic acid. As a consequence of its hydrolysis, two molecules are released into the medium, but both yield hydroxyphenylpropionic acid as the final metabolite, which could explain the high molar ratio between the parent compound and its formed metabolite. In the proposed rosmarinic acid colonic pathway (Figure 3), other metabolites such as the nonhydroxylated form of phenylpropionic acid, coumaric acid, benzoic acid, and catechol have been described as other possible final metabolites. However, the low and variable amounts of these metabolites detected during the fermentation suggest that they could be attributed to other food precursors, as was reported after an in vitro fermentation of coffee polyphenols.[13]

With regard to the colonic metabolism of eriodictyol, the kinetic response of the generated microbial metabolites is shown in Figure 2B. Complete degradation of eriodictyiol before 48 h of fermentation has been seen in all of the samples analyzed, indicating high microbial activity. Total degradation of eriodictyol has also been reported in previous works using *Eubacterium ramulus*[26] and *Clostridium orbiscindens*[27] as inocula. On the basis of the different metabolic compounds detected at different collection times, we proposed a hypothetical colon degradation pathway for eriodictyol (Figure 4). Heterocyclic C-ring cleavage of eriodictyol was the first evidence of microbial action, yielding 3-(3′,4′-dihydroxyphenyl)propionic acid as an intermediate metabolite probably derived from the B-ring fragment. 3-(3′,4′-dihydroxyphenyl)propionic acid reached its maximum concentration (12.9 $\mu$M) at 12 h and declined thereafter (Figure 2C). Dehydroxylation of 3-(3′,4′-dihydroxyphenyl)propionic acid produced an isomer of hydroxyphenylpropionic acid, which represents the main phenolic end product. There was a progressive increase in the concentration of hydroxyphenylpropionic acid over the time course of fermentation with the maximum peak of concentration at 24 h (344.4 $\mu$M). These results are in line with those reported by other authors, who also detected 3-(3′,4′-dihydroxyphenyl)propionic acid as a fermentation product of eriodictyol.[26,27] However, no hydroxyphenylpropionic acid was described, probably because the experiments were carried out with two types of bacteria, *E. ramulus* and *Cl. orbiscinders*, that may not have dehydroxylation activity.

**Human Intervention Study.** The impact of human intestinal microbiota on the transformation of thyme phenols was investigated in 10 volunteers after the daily consumption of 25 mL of TPEOO over 3 weeks. The feces of the volunteers were analyzed at baseline and after the intervention period to elucidate eventual changes in the profile of the microbial metabolites. Although we observed that thymol and carvacrol were stable over 48 h during the in vitro incubation, only carvacrol was quantified in feces from one of the volunteers after the intake of TPEOO (data not shown). Nevertheless, an increment in the instrumental signal corresponding to the chromatographic peak of carvacrol (Treatment of Fecal Samples and Chromatographic Analysis of Thyme Metabolites under Material and Methods) was observed in 7 of the 10 fecal samples analyzed, although the carvacrol concentration was below to the limit of quantification (data not shown). This is in line with Anderson and co-workers, who failed to detect the aforementioned monoterpenes in pig feces after the intake of a thyme-rich diet.[28] In a similar study, only <10% of limonele was detected in the feces of animals (dog and guinea pig) after a high dose, whereas a high recovery was observed in urine.[29] In a preliminary human intervention study conducted by our research group in which hyperlipidemic adults consumed thyme-enriched olive oil, a high recovery of thymol metabolites (main glucuronide conjugates) in 24 h urine was observed.[30] The findings of the present survey, together with the previous reported data regarding the urinary excretion of monoterpenes,[18] support the hypothesis that phenol monoterpenes are effectively absorbed in the upper part of the gastrointestinal tract, and consequently the trace levels of carvacrol found in fecal samples actually represent only nonabsorbed remnants.

With regard to rosmarinic acid and eriodictyol, these compounds were not detected in the human fecal samples as their native structure after the sustained intake of TPEOO, which is in line with the complete degradation of these compounds observed in the in vitro study. In accordance with the in vitro fermentation, increased in the phenolic acids concentrations of 3-(3′,4′-dihydroxyphenyl)propionic acid, hydroxyphenylpropionic acid (the same isomer of acid reported in the in vitro experiments), 3-phenylpropionic acid, and 2-(4′-hydroxyphenyl)acetic acid were detected in human fecal samples after the intake of TPEOO. 3-(3′,4′-dihydroxyphenyl)-propionic acid and hydroxyphenylpropionic acid were identified in the in vitro colon fermentation study as the intermediate and main metabolites of rosmarinic acid (Figure 3) and eriodictyol (Figure 4). However, the increase in the concentrations of these catabolites was not statistically significant ($p > 0.05$) (Figure 5). Similarly, other in vivo studies also noted an increment in the concentration of hydroxyphenylpropionic acid in feces after the intake of grape seed extract and cranberries.[31,32]

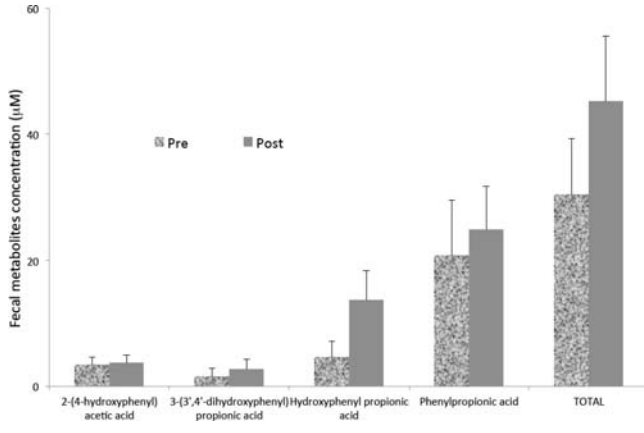


**Figure 5.** Phenolic metabolites detected in human fecal samples before (pre-) and after (post-) intake of thyme phenol-enriched olive oil (TPEOO).

Microbial metabolites produced in the large intestine could carry out their bioactive activity at a local level (intestinal lumen) or, if absorbed, they could be distributed by blood circulation to organs and tissues where they might accumulate or be detoxified by metabolizing enzymes (primarily in the liver) before being excreted in the urine.[8,12] Bioactivity investigations using human or animal cell lines have made extensive use of phenolic microbial catabolites to elucidate their possible mechanisms of action, and experiments have been widely reviewed by Del Rio and co-workers[33] and Rodriguez-Mateos and co-workers,[34] From this recent literature it is

apparent that polyphenols and itheir microbial catabolites do not act simply as antioxidants in vivo and that their diverse effects are, in most instances, based on more complex and specific modes of action, mainly related to cancer and cardiovascular diseases. In this sense, microbial catabolites derived from phenylacetic and phenylpropionic acids, which were also detected in large amounts in fecal samples following TPEOO intake, were proposed as anti-inflammatory agents.[35] Additional experiments were carried out with the advance glycation end products (AGEs) model and pointed to the glucose-mediated pathway as a likely site of action of several microbial catabolites derived from hydroxyphenylacetic acid.[36]

These minor changes in phenol metabolite concentrations observed in feces after the sustained intake of thyme phenols through TPEOO (Figure 5) could indicate a high rate of absorption of thyme phenolic compounds in the upper part of the gastrointestinal tract. There is in vitro evidence that suggests that minor constituents of herb and spice extracts could enhance the rate of absorption of hydrophilic compounds present in the lumen of the small intestine, thus increasing paracellular transport by the transient opening of tight junctions.[37,38]

Recent in vitro studies have proposed that aromatic herbs could inhibit the growth of colon cancer cells,[39] which suggests that these compounds might have antitumoral effects in contact with colon mucosa. Also, a promising use of aromatic herbs as natural antimicrobials of gut pathogens was proposed.[1] However, in our study the thyme phenolic compounds (thymol, carvacrol, rosmarinic acid, or eriodictyol) in their native structures were not detected in human feces.

In conclusion, the results of the present study provide very useful information regarding the gut metabolism of thyme phenols. Although the monoterpenes carvacrol and thymol were poorly metabolized by gut microbiota in the in vitro model fermentation, neither of these compounds, except for one volunteer, was quantified in human feces after the sustained intake (3 weeks) of a daily dose of 25 mL of TPEOO. These results support the idea suggested by other authors that thymol and carvacrol are well absorbed during small intestine passage. In contrast, rosmarinic acid and the flavonoid eriodictyol were extensively metabolized during in vitro colonic fermentation, yielding hydroxyphenylpropionic acid as the main metabolite. In accordance with these results, after the sustained intake of TPEOO, neither rosmarinic acid nor eriodictyol was detected in human feces, observing at the same time an increase in the concentration of hydroxyphenylpropionic and phenylpropionic acids, confirming the effective microbial degradation for these compounds. The most likely effective absorption in the upper part of the gastrointestinal tract, together with the intense colonic metabolism of other representative compounds of thyme phenolic fraction (rosmarinic acid and eriodictyol), opens the possibility of the application of technologic resources, such as microencapsulation, to facilitate the arrival of this type of compound to the colon. Further research is needed to understand the physiological effects of thyme phenols in the gut and their implications when thyme is used as such (dry leaf) or as an essential oil for food flavoring.

## ■ ASSOCIATED CONTENT

### Supporting Information

Tables S1−S4. This material is available free of charge via the Internet at http://pubs.acs.org.

## ■ AUTHOR INFORMATION


### Corresponding Author

*(M.-J.M.) Phone: +34 973 702817. Fax: + 34 973 702596. E-mail: motilva@tecal.udl.es.



### Funding

This work was supported by the Spanish Ministry of Economy and Competitiveness (MINECO) (AGL2009-13517-C03, AGL2012-40144-C03-03, AGL2012-40144-C03-02, and AGL2012-40144-C03-01 projects); Spanish Ministry of Health (FIS-FEDER; PI021307), CIBERDEM, and CIBEROBN (CB06/03); Health Institute of Carlos III (Sara Borrell CD10/00224); Generalitat de Catalunya through the J. Mosele grant, and the FPI contract (BES-2010-040766) through the M. Farràs grant in the context of Autonomous University of Barcelona (UAB) Ph.D. Program in Biochemistry, Molecular Biology and Biomedicine.

### Notes

The authors declare no competing financial interest.


## ■ REFERENCES


(1) Thapa, D.; Losa, R.; Zweifel, B.; Wallace, R. J. Sensitivity of pathogenic and commensal bacteria from the human colon to essential oils. *Microbiology* **2012**, *158*, 2870−2877.

(2) Wang, C. Y.; Wang, S. Y.; Yin, J.-J.; Parry, J.; Yu, L. L. Enhancing antioxidant, antiproliferation, and free radical scavenging activities in strawberries with essential oils. *J. Agric. Food Chem.* **2007**, *55*, 6527−6532.

(3) Rubió, L.; Motilva, M. J.; Romero, M. P. Recent advances in biologically active compounds in herbs and spices: a review of the most effective antioxidant and anti-inflammatory active principles. *Crit. Rev. Food Sci. Nutr.* **2013**, *53*, 943−953.

(4) Mihailovic-Stanojevic, N.; Belščak-Cvitanović, A.; Grujić-Milanović, J.; Ivanov, M.; Jovović, D.; Bugarski, D.; Miloradović, Z. Antioxidant and antihypertensive activity of extract from *Thymus serpyllum* L. in experimental hypertension. *Plant Foods Hum. Nutr.* **2013**, *68*, 235−240.

(5) Bhalla, Y.; Gupta, V. K.; Jaitak, V. Anticancer activity of essential oils: a review. *J. Sci. Food Agric.* **2013**, *93*, 3643−3653.

(6) Jabri-Karoui, I.; Bettaieb, I.; Msaada, K.; Hammami, M.; Marzouk, B. Research on the phenolic compounds and antioxidant activities of tunisian *Thymus capitatus*. *J. Funct. Foods* **2012**, *4*, 661−669.

(7) Mertens-Talcott, S. U.; Jilma-Stohlawetz, P.; Rios, J.; Hingorani, L.; Derendorf, H. Absorption, metabolism, and antioxidant effects of pomegranate (*Punica granatum* L.) polyphenols after ingestion of a standardized extract in healthy human volunteers. *J. Agric. Food Chem.* **2006**, *54*, 8956−8961.

(8) Serra, A.; Rubió, L.; Borràs, X.; Macià, A.; Romero, M. P.; Motilva, M. J. Distribution of olive oil phenolic compounds in rat tissues after administration of a phenolic extract from olive cake. *Mol. Nutr. Food Res.* **2012**, *56*, 486−496.

(9) Cardona, F.; Andrés-Lacueva, C.; Tulipani, S.; Tinahones, F. J.; Queipo-Ortuño, M. I. Benefits of polyphenols on gut microbiota and implications in human health. *J. Nutr. Biochem.* **2013**, *24*, 1415−1422.

(10) Dolara, P.; Luceri, C.; De Filippo, C.; Femia, A. P.; Giovannelli, L.; Caderni, G.; Cecchini, C.; Silvi, S.; Orpianesi, C.; Cresci, A. Red wine polyphenols influence carcinogenesis, intestinal microflora, oxidative damage and gene expression profiles of colonic mucosa in F344 rats. *Mutat. Res.−Fundam. Mol. Mech. Mutagen.* **2005**, *591*, 237−246.

(11) Crozier, A.; Jaganath, I. B.; Clifford, M. N. Dietary phenolics: chemistry, bioavailability and effects on health. *Nat. Prod. Rep.* **2009**, *26*, 1001−1043.

(12) Hanske, L.; Loh, G.; Sczesny, S.; Blaut, M.; Braune, A. The bioavailability of apigenin-7-glucoside is influenced by human intestinal microbiota in rats. *J. Nutr.* **2009**, *139*, 1095−1102.

(13) Gonthier, M. P.; Remesy, C.; Scalbert, A.; Cheynier, V.; Souquet, J. M.; Poutanen, K.; Aura, A.-M. Microbial metabolism of caffeic acid and its esters chlorogenic and caftaric acids by human faecal microbiota in vitro. *Biomed. Pharmacother.* **2006**, *60*, 536−540.
(14) Li, P.; Piao, X.; Ru, Y.; Han, X.; Xue, L.; Zhang, H. Effects of adding essential oil to the diet of weaned pigs on performance, nutrient utilization, immune response and intestinal health. *Asian−Aust. J. Anim. Sci.* **2012**, *25*, 1617−1626.
(15) Rubió, L.; Serra, A.; Chen, C. Y. O.; Macià, A.; Romero, M. P.; Covas, M. I.; Solà, R.; Motilva, M. J. Effect of the co-occurring olive oil and thyme extracts on the phenolic bioaccessibility and bioavailability assessed by in vitro digestion and cell models. *Food Chem.* **2014**, *149*, 277−284.
(16) Durand, M.; Dumay, C.; Beaumatin, P.; Morel, M. T. Use of rumen simulation technique (RUSITEC) to compare microbial digestion of various by-products. *Anim. Feed Sci. Technol.* **1988**, *21*, 197−204.
(17) Serra, A.; Maciá, A.; Romero, M.-P.; Anglés, N.; Morelló, J. R.; Motilva, M. J. Metabolic pathways of the colonic metabolism of procyanidins (monomers and dimmers) and alkaloids. *Food Chem.* **2011**, *126*, 1127−1137.
(18) Rubió, L.; Motilva, M. J.; Macià, A.; Ramo, T.; Romero, M. P. Development of a phenol-enriched olive oil with both its own phenolic compounds and complementary phenols from thyme. *J. Agric. Food Chem.* **2012**, *60*, 3105−3112.
(19) Rubió, L.; Serra, A.; Macià, A.; Borràs, X.; Romero, M. P.; Motilva, M. J. Validation of determination of plasma metabolites derived from thyme bioactive compounds by improved liquid chromatography coupled to tandem mass spectrometry. *J. Chromataogr., B: Anal. Technol. Biomed. Life Sci.* **2012**, *905*, 75−84.
(20) Michiels, J.; Missotten, J.; Dierick, N.; Fremaut, D.; Maene, P.; De Smet, S. In vitro degradation and in vivo passage kinetics of carvacrol, thymol, eugenol and *trans*-cinnamaldehyde along the gastrointestinal tract of piglets. *J. Sci. Food Agric.* **2008**, *88*, 2371−2381.
(21) Varel, V. H. Carvacrol and thymol reduce swine waste odor and pathogens: stability of oils. *Curr. Microbiol.* **2002**, *44*, 38−43.
(22) García, J. L.; Uhía, I.; Galán, B. Catabolism and biotechnological applications of cholesterol degrading bacteria. *Microb. Biotechnol.* **2012**, *5*, 679−699.
(23) Ridlon, J. M.; Kang, D.; Hylemon, P. B. Bile salt biotransformations by human intestinal bacteria. *J. Lipid Res.* **2006**, *47*, 241−259.
(24) Bel-Rhlid, R.; Crespy, V.; Pagé-Zoerkler, N.; Nagy, K.; Raab, T.; Hansen, C.-E. Hydrolysis of rosmarinic acid from rosemary extract with esterases and *Lactobacillus johnsonii* in vitro and in a gastrointestinal model. *J. Agric. Food Chem.* **2009**, *57*, 7700−7705.
(25) Buhnik-Rosenblau, K.; Matsko-Efimov, V.; Jung, M.; Shin, H.; Danin-Poleg, Y.; Kashi, Y. Indication for co-evolution of *Lactobacillus johnsonii* with its hosts. *BMC Microbiol.* **2012**, *12*, 10.1186/1471-2180-12-149.
(26) Schneider, H.; Blaut, M. Anaerobic degradation of flavonoids by *Eubacterium ramulus*. *Arch. Microbiol.* **2000**, *173*, 71−75.
(27) Schoefer, L.; Mohan, R.; Schwiertz, A.; Braune, A.; Blaut, M. Anaerobic degradation of flavonoids by *Clostridium orbiscindens*. *Appl. Environ. Microbiol.* **2003**, *69*, 5849−5854.
(28) Anderson, R. C.; Krueger, N. A.; Genovese, K. J.; Stanton, T. B.; Mackinnon, K. M.; Harvey, R. B.; Nisbet, A. J. Effect of thymol or diphenyliodonium chloride on performance, gut fermentation characteristics, and campylobacter colonization in growing swine. *J. Food Prot.* **2012**, *75*, 758−761.
(29) Kodama, R.; Yano, T.; Noda, K.; Ide, H. Studies on the metabolism of *d*-limonene (*p*-mentha-1,8-diene). *Xenobiotica* **1976**, *6*, 377−389.
(30) Rubió, L.; Farràs, M.; de La Torre, R.; Macià, A.; Romero, M.-P.; Valls, R. M.; Solà, R.; Farré, M.; Fitó, M.; Motilva, M. J. Metabolite profiling of olive oil and thyme phenols after a sustained intake of two phenol-enriched olive oils by humans: identification of compliance biomarkers. *Food Res. Int.* **2014**, DOI: 10.1016/j.foodres.2014.05.009.
(31) Ward, N. C.; Croft, K. D.; Puddey, I. B.; Hodgson, J. M. Supplementation with grape seed polyphenols results in increased urinary excretion of 3-hydroxyphenylpropionic acid, an important metabolite of proanthocyanidins in humans. *J. Agric. Food Chem.* **2004**, *52*, 5545−5549.
(32) Prior, R. L.; Rogers, T. R.; Khanal, R. C.; Wilkes, S. E.; Wu, X.; Howard, L. R. Urinary excretion of phenolic acids in rats fed cranberry. *J. Agric. Food Chem.* **2010**, *58*, 3940−3949.
(33) Del Rio, D.; Rodriguez-Mateos, A.; Spencer, J. P. E.; Tognolini, M.; Borges, G.; Crozier, A. Dietary (poly)phenolics in human health: structures, bioavailability, and evidence of protective effects against chronic diseases. *Antiox. Redox Signal.* **2013**, *18*, 1818−1892.
(34) Rodriguez-Mateos, A.; Vauzour, D.; Krueger, C. G.; Shanmuganayagam, D.; Jess Reed, J.; Calani, L.; Mena, P.; Del Rio, D.; Crozier, A. Bioavailability, bioactivity and impact on health of dietary flavonoids and related compounds: an update. *Arch. Toxicol.* **2014**, *88*, 1803−1853.
(35) Russell, W. R.; Labat, A.; Scobbie, L.; Duncan, S. H. Availability of blueberry phenolics for microbial metabolism in the colon and the potential inflammatory implications. *Mol. Nutr. Food Res.* **2007**, *51*, 726−731.
(36) Verzelloni, E.; Pellacani, C.; Tagliazucchi, D.; Tagliaferri, S.; Calani, L.; Costa, L. G.; Brighenti, F.; Borges, G.; Crozier, A.; Conte, A.; Del Rio, D. Antiglycative and neuroprotective activity of colon-derived polyphenol catabolites. *Mol. Nutr. Food Res.* **2011**, *55*, S35−S43.
(37) Konishi, Y. Modulations of food-derived substances on intestinal permeability in Caco-2 cell monolayers. *Biosci., Biotechnol., Biochem.* **2003**, *67*, 2297−2299.
(38) Laitinen, L. A.; Tammela, P. S. M.; Galkin, A.; Vuorela, H. J.; Marvola, M. L. A.; Vuorela, P. M. Effects of extracts of commonly consumed food supplements and food fractions on the permeability of drugs across Caco-2 cell monolayers. *Pharm. Res.* **2004**, *21*, 1904−1916.
(39) Kaliora, A. C.; Kogiannou, D. A. A.; Kefalas, P.; Papassideri, I. S.; Kalogeropoulos, N. Phenolic profiles and antioxidant and anticarcinogenic activities of Greek herbal infusions; balancing delight and chemoprevention? *Food Chem.* **2014**, *142*, 233−241.

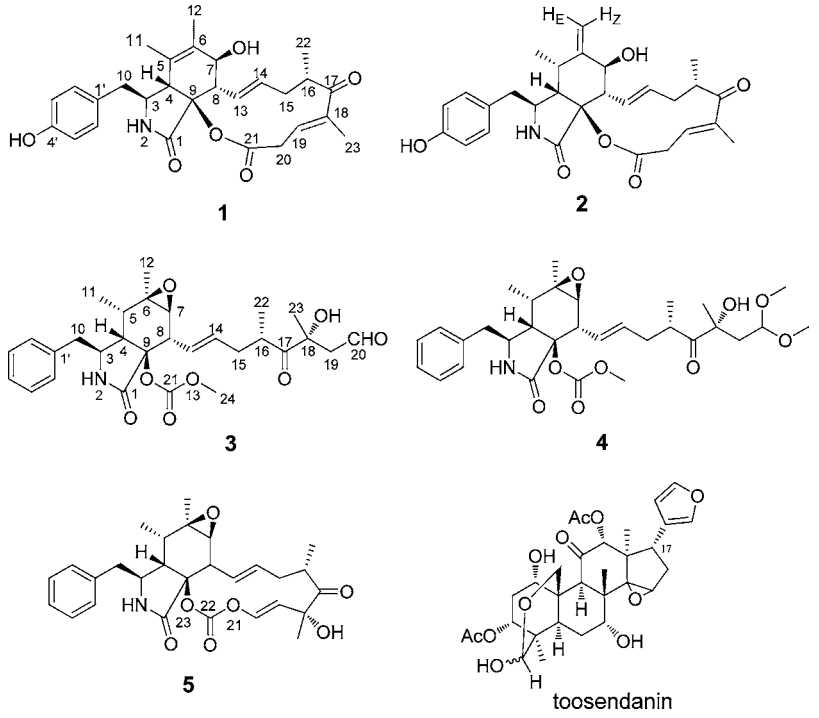


**Figure 1.** Structures of cytochalasins **1**–**5** isolated from *Xylaria* sp. XC16 and toosendanin.

(Mitsubishi Chemical Corp., Tokyo, Japan), Sephadex LH-20 (40–70 μm) (Amersham Pharmacia Biotech AB, Uppsala, Sweden), and Lichroprep RP-18 gel (40–63 μm) (Merck, Darmstadt, Germany). $GF_{254}$ plates (Qingdao Marine Chemical Inc., Qingdao, China) were used for thin-layer chromatography (TLC). High-performance liquid chromatography (HPLC) analysis was performed on an Agilent TC-C18 column (250 mm × 4.6 mm, 5 μm, Agilent Technologies Ltd., CA, USA) on a Waters 1525 instrument (Waters Corp., MA, USA). Brine shrimp eggs (*Artemia* cysts) (Advanced Hatchery Technology Inc., Xiamen, China) were used for bioguided assay.

**Fungal Material.** Plant material was collected in Yangling, Shaanxi province, China, in April 2011. Isolation, maintenance, and preservation of endophytic fungi were performed according to the reported protocols.[21] All isolated fungal strains (28 in total, XC1–XC28) were prescreened for their toxicity toward brine shrimp.[19] The most toxic strain XC16 belonged to the genus *Xylaria*, identified by internal transcribed spacer (ITS) rDNA region sequence comparison, and was designated as *Xylaria* sp.

**Fermentation, Extraction, and Isolation.** All 28 isolated fungal strains (XC1–XC28) were fermented on solid rice medium. Toxicity of the fermented culture (20 μg/mL) against brine shrimp were assayed according to our previously reported protocol.[19] The most toxic strain XC16 was selected to be cultivated on rice medium (40 g rice and 100 mL distilled water, sterilized under 121 °C for 30 min) in 200 Erlenmeyer flasks (500 mL each). The flask cultures were incubated under 28 °C for 3 weeks.

The fungal cultures of *Xylaria* sp. XC16 grown on rice medium were extracted with petroleum ether and EtOAc three times, respectively, and tested by brine shrimp lethality assay. The toxic EtOAc crude extract was fractionated by silica gel CC using $CHCl_3$–MeOH gradient elution to provide five fractions (Fr.1–Fr.5). Fr.2 (4.93 g) indicated the highest activity and was further chromatographed on Sephadex LH-20 eluted with MeOH as an eluent to give two fractions A and B. These two fractions were analyzed by a Thermo BDS Hypersil column (250 × 10 mm, 5 μm, Thermo Fisher Scientific Inc., MA, U.S.), eluted with gradient 60–90% MeOH/$H_2O$ at a flow rate of 2.0 mL/min over 30 min. Then fractions A and B were chromatographed on the same HPLC column, respectively. Fraction A was separated with 70% MeOH/$H_2O$ as eluent to yield compounds **3** (8.7 mg), **4** (5.8 mg), and **5** (3.9 mg). Fraction B was purified with 82% MeOH/$H_2O$ to afford compounds **1** (12.3 mg) and **2** (8.2 mg).

*Cytochalasin Z27,* ***1:*** White solid; $[\alpha]_D^{22}$ + 77.8 (*c* 0.16, $CH_3OH$); UV (MeOH) $\lambda_{max}$ (log $\varepsilon$) 206 (4.30), 252 (3.96); CD (MeOH) $\lambda_{max}$ ($\Delta\varepsilon$) 198 (+48.4), 238 (−12.8), 265 (+4.9), 315 (+4.2); IR (KBr) $\nu_{max}$ 3395, 2922, 1707, 1668, 1516, 1451, 1265, 1225, 1135, 980 $cm^{-1}$; $^1H$ and $^{13}C$ NMR data, see Table 1; ESI MS (positive) *m*/*z* 502.30 $[M + Na]^+$; HR-ESI-MS *m*/*z* 502.2212 ($[M + Na]^+$, calcd. $C_{28}H_{33}NO_6Na^+$, 502.2206).

*Cytochalasin Z28,* ***2:*** White solid; $[\alpha]_D^{22}$ + 68.9 (*c* 0.14, $CH_3OH$); UV (MeOH) $\lambda_{max}$ (log $\varepsilon$) 206 (4.21), 251 (3.82); CD (MeOH) $\lambda_{max}$ ($\Delta\varepsilon$) 194 (+25.6), 229 (−5.4), 262 (+3.3), 317 (+2.1); IR (KBr) $\nu_{max}$ 3425, 3258, 2866, 2931, 1701, 1559, 1516, 1440, 1269, 1228, 1019 $cm^{-1}$; $^1H$ and $^{13}C$ NMR data, see Table 1; ESI MS (positive) *m*/*z* 502.29 $[M + Na]^+$; HR-ESI-MS *m*/*z* 502.2205 ($[M + Na]^+$, calcd. $C_{28}H_{33}NO_6Na^+$, 502.2206).

*seco-Cytochalasin E,* ***3:*** Colorless oily solid; $[\alpha]_D^{25}$ +114.8 (*c* 0.08, MeOH); UV (MeOH) $\lambda_{max}$ (log $\varepsilon$) 222 (2.61), 258 (0.69); IR (KBr) $\nu_{max}$ 3368, 2969, 1694, 1454, 1015, 697 $cm^{-1}$; $^1H$ and $^{13}C$ NMR data see Table 1; ESI MS *m*/*z* 550 $[M + Na]^+$.

**Computational Section.** MMFF and DFT calculations were run with Spartan 10 (Wave function Inc., Irvine, CA) with standard parameters and convergence criteria. TDDFT calculations were run with Gaussian 09,[22] with default grids and convergence criteria. Conformational searches were run with the Monte Carlo algorithm implemented in Spartan 10 using Merck molecular force field (MMFF). All structures thus obtained were optimized with DFT method using B3LYP functional, using first the 6-31G(d) basis set and then 6-311+G(d,p) basis set. TDDFT calculations were run using B3LYP and CAM-B3LYP functionals and TZVP basis set, including 64 and 42 excited states, respectively. UV and CD spectra were generated using the program SpecDis[23] by applying a Gaussian band shape with 0.3–0.4 eV exponential half-width, from dipole-length rotational strengths.

**Toxicity Bioassay.** All the isolated metabolites were tested for their toxicity activity against brine shrimp (*Artemia* cysts) as previously reported method.[19]

**Phytotoxicity Bioassay.** The seeds of two herbaceous plants, lettuce (*Lactuca sativa*) and radish (*Raphanus sativus*) were used for the bioassay. The procedure was conducted according to the


dx.doi.org/10.1021/jf503846z | J. Agric. Food Chem. 2014, 62, 10962–10969

Table 1. $^{1}H$ and $^{13}C$ NMR Data of Compounds 1−3

| | 1[b] | | 2[b] | | 3[c] | |
|---|---|---|---|---|---|---|
| | $\delta_H$, multi ($J$ in Hz) | $\delta_C$ | $\delta_H$, multi ($J$ in Hz) | $\delta_C$ | $\delta_H$, multi ($J$ in Hz) | $\delta_C$ |
| 1 | | 172.4 | | 171.3 | | 170.1 |
| 2 | 9.56, s | | 9.21, s | | 8.52, br.s | |
| 3 | 3.86, t (7.1) | 59.9 | 3.64,[a] m | 53.9 | 3.66,[a] m | 52.8 |
| 4 | 4.02, br. s | 49.6 | 3.02,[a] m | 48.6 | 2.44, dd (5.2, 2.1) | 47.0 |
| 5 | | 125.4 | 3.44,[a] m | 32.4 | 1.84, m | 35.6 |
| 6 | | 134.8 | | 151.9 | | 57.1 |
| 7 | 4.56, d (9.8) | 70.1 | 4.45, d (11.3) | 69.8 | 2.67, d (5.2) | 60.0 |
| 8 | 3.81, t (9.8) | 50.9 | 3.68, t (10.4) | 50.3 | 2.76, m | 45.6 |
| 9 | | 85.3 | | 84.6 | | 85.2 |
| 10 | 3.21, dd (13.9, 7.1) | 43.3 | 3.00,[a] m | 43.1 | 2.88, dd (13.0, 5.2) | 43.2 |
| | 3.10, dd (13.9, 7.1) | | | | 2.63, m | |
| 11 | 1.52, s | 17.5 | 1.06, d (6.6) | 14.2 | 0.59,d (7.8) | 12.4 |
| 12 | 1.88, s | 14.8 | 5.62, br. s (H-12*Z*) | 112.7 | 1.13, s | 19.2 |
| | | | 5.21, br. s (H-12*E*) | | | |
| 13 | 6.67, dd (15.1, 10.1) | 128.6 | 6.27, ddd (15.0, 9.5, 1.3) | 128.7 | 6.01, dd (15.8, 8.8) | 127.9 |
| 14 | 5.66, ddd (15.1, 10.1, 3.8) | 134.5 | 5.74, ddd (15.0, 11.1, 3.8) | 134.2 | 5.35, m | 130.6 |
| 15 | 2.18,[a] m | 40.5 | 2.23, br. d (11.0) | 40.6 | 2.27, ddd (13.5, 6.7, 2.1) | 35.5 |
| | 2.01, ddd (25.2, 11.4, 0.63) | | 2.13, br. d (12.0) | | 1.97, ddd (14.0, 7.3, 2.6) | |
| 16 | 3.38, m | 40.0 | 3.44,[a] m | 39.4 | 3.31,[a] m | 38.7 |
| 17 | | 205.4 | | 202.0 | | 217.0 |
| 18 | | 142.6 | | 142.3 | | 77.0 |
| 19 | 6.53, dd (10.6, 6.1) | 133.0 | 6.71, t (8.0) | 133.7 | 2.70, m | 52.5 |
| | | | | | 2.54, dd (16.1, 3.1) | |
| 20 | 3.74, t (10.9) | 37.8 | 3.51, dd (12.6, 9.8) | 36.7 | 9.55, t (2.1) | 201.1 |
| | 3.18, dd (11.4, 6.3) | | 3.29, dd (12.6, 6.9) | | | |
| 21 | | 169.4 | | 169.3 | | 153.1 |
| 22 | 1.131 d (6.6) | 17.3 | 1.13, d (6.6) | 17.7 | 0.97, d (7.3) | 16.4 |
| 23 | 2.15, s | 13.0 | 2.17, s | 12.6 | 1.26, s | 25.3 |
| 24 | | | | | 3.68, s | 54.6 |
| 1′ | | 128.6 | | 128.4 | | 137.0 |
| 2′ | 7.30, d (8.2) | 131.0 | 7.22, d (8.5) | 131.2 | 7.16, t (7.3) | 129.6 |
| 3′ | 7.17, d (8.2) | 116.2 | 7.12, d (8.5) | 116.0 | 7.30, t (7.3) | 128.3 |
| 4′ | | 157.6 | | 157.5 | 7.22, t (7.3) | 126.5 |
| 5′ | 7.17, d (8.2) | 116.2 | 7.12, d (8.5) | 116.0 | 7.30, t (7.3) | 128.3 |
| 6′ | 7.30, d (8.2) | 131.0 | 7.22, d (8.5) | 131.2 | 7.16, t (7.3) | 129.6 |

[a]Overlapped signal. [b]pyridine-$d_5$; [c]DMSO-$d_6$.

previously reported protocol.[20,24−26] Glyphosate was selected as the positive control. Triplicate experiments were conducted on 6-well plates, and the phytotoxic effects [response index (RI)] were calculated according to the equation:

$$\text{If } T > C, \text{ then RI} = 1 - C/T; \text{ if } T < C, \text{ then RI} = T/C - 1$$

where $T$ is the length of the treatment, $C$ is the length of the blank control, and RI is the response index. RIs are expressed as averages ± standard deviation (SD) for three replicates.

**Antifungal Bioassay.** All the isolated metabolites were tested in vitro for the antifungal activity against agriculturally important four phytopathogenic fungi: *Fusarium solani*, *Gibberella saubinetti*, *Botrytis cinerea*, and *Alternaria solani*, according to our reported bioassay.[19] All these pathogenic organisms tested were deposited at the College of Science, Northwest A&F University. Antifungal activity was assessed by the microbroth dilution method in 96-well flat-microtiter plates using a potato dextrose (PD) medium. Initial concentrations of compounds tested were made up to 4 mM in DMSO. Two commercial fungicides, carbendazim and hymexazol (Aladdin Chemistry Co. Ltd., Shanghai, China) were used as positive control. A DMSO solution of equal concentration was used as a negative control. The fungi were incubated in the PD medium for 18−36 h at 28 ± 0.5 °C at 150 rpm, and spores of different microorganism concentrations were diluted to approximately $1 \times 10^6$ colony-forming units/mL (CFU/mL) with PD medium. In flat-microtiter plates, tested compounds, fungal suspension, and sterile water were added to made up final concentrations of the compounds in the range of 1.57−200 μM. Cultures were then grown in the dark at 28 ± 0.5 °C for 48 h. Minimum inhibitory concentrations (MICs) were inspected as the lowest concentrations in which no fungal growth could be observed.

## RESULTS AND DISCUSSION

**Identification of the Bioactive Fungal Endophytic Strain XC16.** Brine shrimp test has been proved to be a simple and reliable benchtop bioassay for screening toxicity for natural extracts and synthetic products.[27−29] Twenty-eight strains (XC1−XC28) of endophytic fungi were isolated from the healthy leaves of *Toona sinensis*. All isolates were screened for their toxicity against brine shrimp at 20 μg/mL level. Among the isolates, the secondary metabolites of the two strains XC16 and XC20 exhibited remarkable toxicity to the organism. The culture filtrate from strain XC16 killed all brine shrimp larvae, showing the greatest activity, and was therefore selected for the isolation and characterization of bioactive metabolites. To identify this active strain XC16, a GenBank search with the nuclear ribosomal ITS1 sequence and 18S rDNA of XC16 was

carried out. The results revealed a species of *Xylaria* as the closest match, with sequence identities 99%. The most similar sequence was that of *Xylaria* sp. JW38−4 (accession number GQ906959). On the basis of its ITS and 18S rDNA sequences, the fungus XC16 clearly belongs to the member of the genus *Xylaria*, identified as *Xylaria* sp. XC16, a mycelial fungus under scanning electron microscope.

**Isolation, Purification, and Structure Elucidation.** The active EtOAc extracts of the cultures of this strain *Xylaria* sp. XC-16 were submitted to column chromatography on silica gel to provide five fractions (Fr. 1-Fr. 5). Among these fractions, Fr.2 showed strong toxicity to brine shrimp at 20 $\mu$g/mL level. As a result, Fr. 2 was fractionated through silica gel column chromatography, gel filtration over Sephadex LH-20, ODS column chromatography, and semipreparative HPLC to afford two new cytochalasins **1** and **2**, together with three known cytochalasin derivatives, **3**−**5** (Figure 1). Their structures were elucidated by a combination of spectroscopic analyses (UV, CD, IR, MS, 1D, and 2D NMR) and by comparison to literature data.

Cytochalasin $Z_{27}$, **1**, was obtained as white powder. Its molecular formula was assigned as $C_{28}H_{33}NO_6$ based on the pseudomolecular ion in HR-ESI-MS, requiring 13 degrees of unsaturation. The IR absorptions at 1707, 1667, 1614, and 1516 $cm^{-1}$ indicated the presence of carbonyl and benzene ring groups in the structure. The $^1H$ and $^{13}C$ NMR data of **1** (Table 1) suggested four methyls, three methenes, 12 methines (including seven unsaturated ones), and nine quaternary carbons (including eight unsaturated ones). The unsaturated carbon signals in $^{13}C$ NMR suggested six carbon−carbon double bonds and three C═O groups ($\delta_C$ 205.4, 172.4, and 169.4). In particular, the AA′XX′ spin system [$\delta_H$ 7.30 (*d*, *J* = 8.2 Hz), 7.17 (*d*, *J* = 8.2 Hz)] indicated a 1,4-disubstituted benzene ring in **1**. Apart from the ten degrees of unsaturation due to the unsaturated bonds and the benzene ring, the remaining ones indicated that **1** possesses a tricyclic framework, which was elucidated by means of extensive analysis of the 2D NMR spectra (HSQC, $^1H-^1H$ COSY, and HMBC). All protons directly bonded to the carbon atoms were first assigned on the basis of the HSQC data. Five fragments were deduced from the COSY spectrum (Figure 2). Further detailed HMBC correlations (Figure 2) revealed the whole planar structure of **1**, a 4′-hydroxyl derivative of cytochalasin $Z_{17}$, which was obtained from *Aspergillus flavipes*, an endophytic fungus of the mangrove plant *Acanthus ilicifolius*.[30]

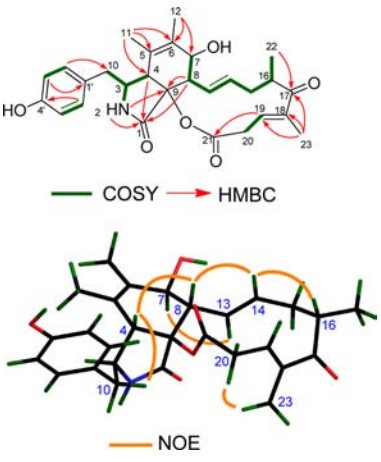


**Figure 2.** Selected HMBC, $^1H-^1H$ COSY, and NOESY correlations of **1**.

The relative configuration of **1** was assigned by $^{13}C$ NMR data in comparison with reported ones, and by NOESY results with the help of molecular modeling. As shown in Figure 2, the observed correlations of H-10a/H-4 and H-4/H-8 indicated that C-10, H-4, and H-8 are on the same side of the molecule and were arbitrarily assigned as $\beta$-oriented. The NOE correlation of H-7/H-13 indicated H-7 to be $\alpha$-oriented. Further confirmation of the stereochemistry at C-7 and C-8 was provided by the NOE correlation of H-8/H-14. Moreover, the NOE correlation H-14/H-16, when checked against molecular modeling results (Figure 2), offered the proof of the $\alpha$-orientation of Me-22. Finally, the 18*E* configuration of the C-18/C-19 double bond was proved by H-20/Me-23 NOE correlation and the absence of H-19/Me-23 correlation. Previous studies suggested that the stereochemistry of the essential elements of cytochalasins skeleton is well retained along the series. These include (1) the stereochemistry of the macrocyclic ring, with a trans C-8/C-9 junction and a cis C-4/C-9 junction;[31,32] (2) the $\beta$ orientation of the oxygen at C-7;[11,33,34] (3) the $\alpha$-orientation of Me-22;[31,32] and (4) the *E* configuration of the C-18/C-19 double bond.[30,34,35] The $^{13}C$ NMR spectrum of **1** (Table 1) showed similar chemical shifts to that of cytochalasin $Z_{17}$,[30] especially of the macrocyclic ring moiety. In particular, the similarities between the chemical shifts of C-7, C-9, and C-16 indicated that the relative configurations of these centers in **1** are consistent with those in cytochalasin $Z_{17}$, as shown in Figure 2. Furthermore, compound **1** showed a CD spectrum (Figure 3A) consistent with that of cytochalasin $Z_{17}$.[35] This is not surprising because of the structural analogy between the two compounds; still, an independent proof of the absolute configuration of **1** was obtained by quantum mechanical calculations of its CD spectrum. It was concluded that **1** has the same configuration of cytochalasin $Z_{17}$, and its structure is determined as (+)-(3*S*,4*S*,7*S*,8*S*,9*S*,13*E*,16*S*,18*E*)-7-hydroxy-5,6,16,18- tetramethyl-10-(4′-hydroxyphenyl)-22-oxa-[12]-cytochalasa-6,13,18-trien-1,17,21-trione.

Molecular modeling of compound **1** was run through a well-established protocol.[36] The most stable energy minima thus obtained had a very similar conformation of the macrocycle (Figure 2), which was in keeping with the NOE correlations discussed above, and differed only for the orientation of the 4′-hydroxyphenylmethyl and the hydroxyl groups. CD calculations were run of DFT geometries with TDDFT method,[37] using B3LYP and CAM-B3LYP functionals and TZVP basis set, and averaged at 300 K using Boltzmann populations. The weighted-average CD spectra (Figure 3B) are in good agreement with the experimental one. In particular, the B3LYP functional performed better in the long-wavelength region, where TDDFT method is intrinsically more accurate.[38] Conversely, the CAM-B3LYP functional reproduced better the short-wavelength region. In conclusion, the absolute configuration of cytochalasin $Z_{27}$ was definitely established as (+)-(3*S*,4*S*,7*S*,8*S*,9*S*,16*S*)-**1**.

Cytochalasin $Z_{28}$, **2**, was obtained as white solid. Its molecular formula $C_{28}H_{33}NO_6$ is the same as **1**, as deduced from the pseudomolecular ion in HR-ESI-MS, suggesting that **2** was an isomer of **1**. Comparison of its $^1H$ and $^{13}C$ NMR data with those of **1** (Table 1) revealed that compound **2** also had a quite similar skeleton to that of **1**. A significant difference was that the two carbon signals at $\delta_C$ 125.4 (C-5, s) and 134.8 (C-6,

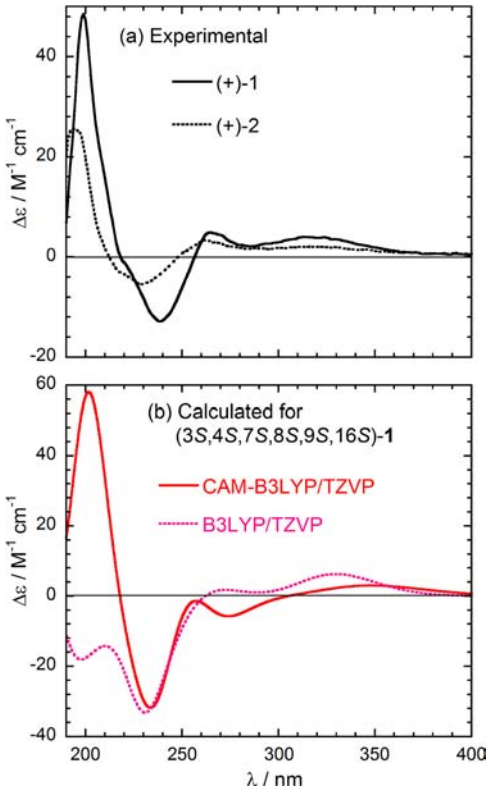


**Figure 3.** (A) Experimental CD spectra of (+)-**1** and (+)-**2** in methanol (0.5 mM, 0.5 mm cell). (B) CD spectra calculated for (3*S*,4*S*,7*S*,8*S*,9*S*,16*S*)-**1** at B3LYP/TZVP//B3LYP/6-311+G(d,p) and CAM-B3LYP/TZVP//B3LYP/6-311+G(d,p) levels as Boltzmanns average on 8 structures. Gaussian band-shape with 0.3 (B3LYP) and 0.4 eV (CAM-B3LYP) exponential width; CAM-B3LYP spectrum red-shifted by 30 nm.

s), attributable to the tetrasubstituted endocyclic double bond in **1**, were replaced by the two exocyclic double-bond carbon signals at $\delta_C$ 151.9 (C-6, s) and 112.7 (C-12, t) in **2**. This portion of the spectrum was also similar to that observed in the $^{13}$C spectrum of 10-phenyl[12]cytochalasin $Z_{16}$.[35] Furthermore, in the $^1$H NMR spectrum of **2**, the C-11 methyl proton signal ($\delta_H$ 1.06, d, $J$ = 6.6 Hz), appearing as a doublet instead of the singlet ($\delta_H$ 1.52, s) as in **1**, was also consistent with a methyl-substituted six-membered ring as seen in cytochalasin $Z_{16}$.[35] This difference between **1** and **2** was further confirmed by $^1$H−$^1$H COSY and HMBC correlations as shown in Figure 4. The similar $^{13}$C NMR data of the macrocyclic rings in **1** and **2** (Table 1) and the consistency of NOESY results (Figures 2 and 4) suggested that the cyclic moieties in both **1** and **2** possess the same relative configurations. Additionally, the relative configuration of the chirality center at C-5 in **2** was assigned through the NOE correlations H-3/$H_3$-11, proving that Me-11 is $\alpha$-oriented.

The absolute configuration of compound (+)-**2** was established by spectroscopic comparison. Compound (+)-**2** has in fact a CD spectrum very similar to that of (+)-**1** (Figure 3A), and also consistent with that reported for cytochalasin $Z_{16}$.[35] It can therefore be assumed that cytochalasins **1** and **2** have the same absolute configuration of the corresponding chirality centers, as established above for (+)-**1**. Thus, the structure of **2** was determined as (+)-(3*S*,4*S*,5*S*,7*S*,8*S*,9*S*,13*E*,16*S*,18*E*)-7-hydroxy-5,16,18-trimethyl-10-(4′-hydroxy)phenyl-22-oxa-[12]-cytochalasa-6-(12),13,18-trien-1,17,21-trione.

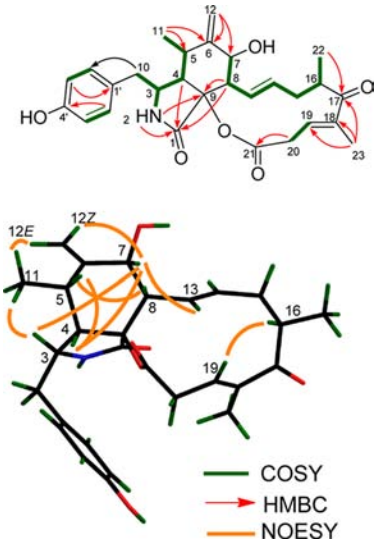


**Figure 4.** Selected HMBC, $^1$H−$^1$H COSY, and NOESY correlations of **2**.

*seco*-Cytochalasin E, **3**, was isolated as colorless oily solid. Its molecular formula was tentatively established as $C_{29}H_{37}NO_8$ based on ESI-MS peak at $m/z$ 550.11 ([M + Na]$^+$) associated with $^{13}$C NMR data. The $^1$H NMR signals (Table 1) at $\delta_H$ 7.15 (2H, d, $J$ = 7.3 Hz), 7.22 (1H, d, $J$ = 7.3 Hz), and 7.30 (2H, *d*, $J$ = 7.3 Hz) indicated a phenyl group in the structure. The large coupling constant ($J$ = 15.6 Hz) at $\delta_H$ 7.15 indicated a trans double bond in the structure. The similar $^{13}$C NMR data of compound **3** and cytochalasin $Z_{18}$ (**4**)[30] revealed a typical octahydro-1*H*-isoindol-1-one moiety of cytochalasin skeleton. Further detailed analysis of HSQC and $^1$H−$^1$H COSY suggested fragments as shown in Figure 5. Connections

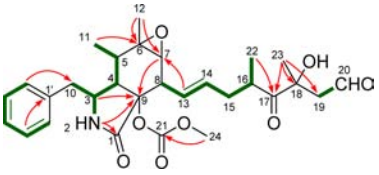

**Figure 5.** Selected HMBC and COSY correlations of **3**.

among the fragments showing COSY cross-peaks, quaternary carbons and methyl groups were further confirmed by HMBC correlations (Figure 5). The whole planar structure was elucidated as *seco*-cytochalasin E, a ring-opened derivative of cytochalasin E, which had been previously obtained as a semisynthetic derivative of **5**,[39] but without detailed spectroscopic data reported in the literature. Herein, all the $^1$H NMR and $^{13}$C NMR data were assigned unambiguously according to the 2D NMR experiments (Table 1). This is the first report of *seco*-cytochalasin E as a natural product.

Compounds **4** and **5** were identified as cytochalasin $Z_{18}$[30] and cytochalasin E,[30,33] respectively, on the basis of their spectroscopic features (NMR, MS) and by comparison with the published data in the literature.

**Biological Activity.** All the compounds **1**−**5** were examined for toxicity against brine shrimp, for phytotoxicity and antiphytopathogens in vitro.


dx.doi.org/10.1021/jf503846z | *J. Agric. Food Chem.* 2014, 62, 10962−10969

**Toxicity to Brine Shrimp.** In the screening assay on brine shrimp, cytochalasin E, **5**, at 50 $\mu$M displayed 100% lethality. In contrast, the other compounds **1**−**4** displayed very weak toxicity toward brine shrimp larvae with lethality below 10%. Compound **5** produced strong toxic effects on brine shrimp in a concentration-dependent manner (0.625−20.0 $\mu$M (Figure 6),

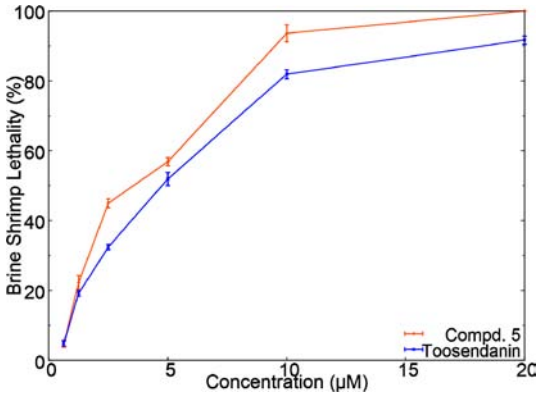


**Figure 6.** Brine shrimp lethality of **5** and the positive control drug toosendanin in concentrations 0.625−20.0 $\mu$M.

with a $LC_{50}$ value of 2.79 $\mu$M, which was comparable to that of the commercial insecticidal agent toosendanin, showing a $LC_{50}$ value of 4.03 $\mu$M. By comparison of the isolated structures of **1**−**5**, the toxicity against brine shrimp of **5** may be rationalized as due to the 13-membered macrocycle with a vinyl carbonate ester group.

**Phytotoxic Activity.** Among the five compounds tested, only cytochalasin E, **5**, bearing a vinyl carbonate ester and an epoxy group, demonstrated the highest seedling growth inhibition on *Lactuca sativa* and *Raphanus sativus* at concentrations in the range of 10−80 $\mu$M (Figure 7). The phytotoxicity of **5** was higher than that of the positive control, glyphosate, a broad-spectrum systemic herbicide in agriculture. In contrast, the remaining compounds **1**−**4** showed no effect on both seedlings even at a concentration of 100 $\mu$M. These

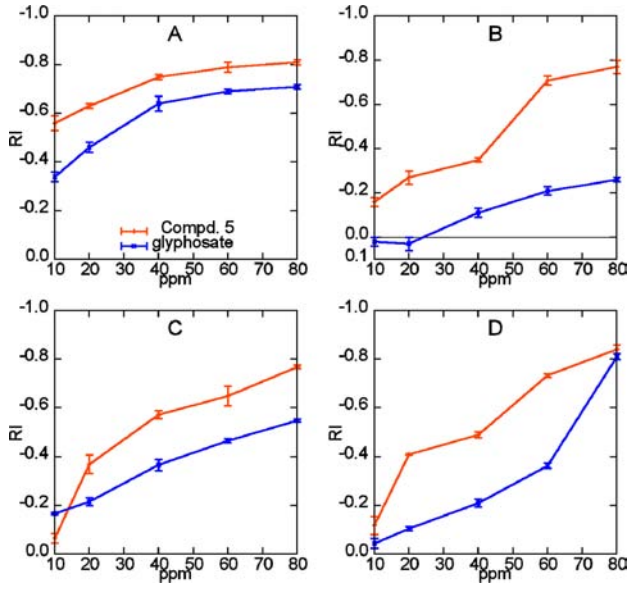


**Figure 7.** Phytotoxic activities of **5** and glyphosate on (A) *Lactuca sativa* root, (B) shoot, (C) *Raphanus sativus* L. Root, and (D) shoot.

findings demonstrated again that the 13-membered macrocyclic vinyl carbonate ester moiety in cytochalasins could be a determinant feature for activity. In fact, the macrocyclic ring opening of **5** to yield *seco*-cytochalasin E, **3**, leads to a loss of activity; 22-oxa[12]cytochalasins (e.g., cytochalasins $Z_{27}$, **1**, and $Z_{28}$, **2**), possessing the secondary hydroxyl group on C-7, were inactive; and open-chain cytochalasins (e.g., *seco*-cytochalasin E, **3**, and cytochalasin $Z_{18}$, **4**) without a perihydroisoindolyl scaffold were also inactive. Interestingly, the bioassay results of cytochalasin E, **5**, show an agreement between phytotoxic and insecticidal activity.

Cytochalasins have been considered as potential mycotoxins, and some of them have been found to be phytotoxic to different plants. Cytochalasin H, a toxic [11]cytochalasan of *Phomopsis* sp. isolated from weevil-damaged pecans, was markedly inhibitory to the growth of the floral development of tobacco plants.[40] Two [11]cytochalasans, pyrichalasin H, produced by the fungus *Pyricularia grisea*, and zygosporin D, isolated from the culture of the insect pathogenic fungus *Metarrhizium anisopliae*, were found to strongly inhibit the growth of rice seedlings.[41,42] Cytochalasin $Z_6$, an 24-oxa[14]-cytochalasan isolated from the culture of *Phoma exigua* var. *heteromorpha*, caused inhibition of rootlet elongation of tomato seedlings.[43] In addition, three 24-oxa[14]cytochalasans, namely cytochalasins $Z_3$, B, F, and an [13]cytochalasan, deoxaphomin, from the culture of *Pyrenophora semeniperda*, a promising mycoherbicide for the biological control of grass weeds, showed a remarkable ability to inhibit root elongation of wheat and tomato seedlings.[44] Of the test cytochalasins B, F, $Z_2$, and $Z_3$, and deoxaphomin, produced by *Phoma exigua* var. *exigua*, a potential mycoherbicide against the perennial weeds *Sonchus arvensis* and *Cirsium arvense*, deoxaphomin demonstrated the highest level of toxicity on leaves of *S. arvensis*, whereas other cytochalasins showed lower activity.[11] These observations promoted structure−activity relationship (SAR) studies leading to the conclusions that a [11] or a [13]carbocyclic or a [14]lactonic macrocyclic ring fused to an intact perihydroisoindolyl-1-one motif is an important feature for toxicity, and that the role played by the hydroxyl group on C-7 also appears crucial in imparting toxicity.[44−48] However, these results are not in accordance with our results, which indicated instead that the presence of 7-OH group in 22-oxa[12]cytochalasin motif has no major role in conferring activity. This discrepancy may depend on different crop species, varying sensitivity, and cytochalasin type. This is the first report of phytotoxicity of the tested cytochalasins, especially, a small type of 21,23-dioxa[13]-cytochalasin containing the unique vinyl carbonate moiety (e.g., **5**), to *Lactuca sativa* and *Raphanus sativus* seedlings.

**Antifungal Activity.** The antiphytopathogenic activity of the isolated cytochalsins was also evaluated on four different pathogens, namely, *Fusarium solani*, *Gibberella saubinetti*, *Botrytis cinerea*, and *Alternaria solani*, and the results are shown in Table 2. The antifungal activity of cytochalsin derivatives strongly depends on the fungal species. Among the compounds tested, only compound **2** showed strong fungicidal effect (MIC of 12.5 $\mu$M) against *G. saubinetti*, compared with that of the positive control hymexazol (MIC of 25 $\mu$M). In contrast, other compounds displayed quite weak properties with MIC values of greater than 50 $\mu$M against the pathogens tested.

In conclusion, five cytochalasins **1**−**5** have been characterized in the endophytic *Xylaria* sp., including two new compounds cytochalasin $Z_{27}$, **1**, and cytochalasin $Z_{28}$, **2**, and one new

**Table 2. Inhibitory Effects of Compounds 1−5 on Phytopathogenic Fungi**

| | phytopathogenic fungi (MIC, μM) | | | |
|---|---|---|---|---|
| compound | *Alternaria solani* | *Botrytis cinerea* | *Fusarium solani* | *Gibberella saubinetti* |
| **1** | 50 | 100 | 100 | 50 |
| **2** | 50 | 100 | 50 | 12.5 |
| **3** | 100 | 100 | >100 | 100 |
| **4** | 50 | >100 | 100 | >100 |
| **5** | 50 | 100 | >100 | 100 |
| carbendazim | 3.13 | 6.25 | 6.25 | 3.13 |
| hymexazol | 12.5 | 50 | 50 | 25 |

natural product *seco*-cytochalasin E. To the best of our knowledge, this is the first report of these three types of cytochalasan alkaloids in the genus *Xylaria*.[49] Cytochalasin E was identified as the most active component in brine shrimp toxicity and phytotoxicity potency in the fungal endophyte. The preliminary SAR analysis suggested that cytochalasin E with a characteristic 13-membered macrocyclic vinyl carbonate group could most likely result in strong activity. Fungal endophytes are well-known for their ability to produce a wide range of antimicrobial substances and enhance plant resistance to pathogens and pests. Therefore, a chemical interaction between the endophyte *Xylaria* sp. and the plant *T. sinensis* produces the mycotoxins as chemical defense compounds that could protect the host.

## ■ ASSOCIATED CONTENT

### Supporting Information

Photographs of isolated strains, SEM photographs and rDNA ITS sequence of XC16, bioassay-guided results of the fungal exteacts of *Xylaria* sp., NMR spectra of compounds **1**−**3**. This material is available free of charge via the Internet at http://pubs.acs.org.

## ■ AUTHOR INFORMATION


### Corresponding Author

* Tel: +86-29-87092515. Fax: +86-29-87092226. E-mail: jinminggao@nwsuaf.edu.cn.



### Funding

This work was financially supported by the Natural Science Foundation of Shaanxi Province (2015YFJZ0115), as well as by the National Natural Science Foundation of China (31371886 and 21102114) and the Chinese Universities Scientific Fund (QN2011118).


### Notes

The authors declare no competing financial interest.

## ■ REFERENCES


(1) Qin, J. C.; Zhang, Y. M.; Gao, J. M.; Bai, M. S.; Yang, S. X.; Laatsch, H.; Zhang, A. L. Bioactive metabolites produced by *Chaetomium globosum*, an endophytic fungus isolated from *Ginkgo biloba*. *Bioorg. Med. Chem. Lett.* **2009**, *19*, 1572−1574.

(2) Whalley, A. J. S.; Edwards, R. L. Secondary metabolites and systematic arrangement within the Xylariaceae. *Can. J. Bot.* **1995**, *73*, 802−810.

(3) Stadler, M.; Hellwig, V. Chemotaxonomy of the Xylariaceae and remarkable bioactive compounds from *Xylariales* and their associated asexual stages. *Recent Res. Dev. Phytochem.* **2005**, *9*, 41−93.

(4) Vicente, F.; Basilio, A.; Platas, G.; Collado, J.; Bills, G. F.; González Del Val, A.; Martín, J.; Tormo, J. R.; Harris, G. H.; Zink, D. L.; Justice, M.; Kahn, J. N.; Peláez, F. Distribution of the antifungal agents sordarins across filamentous fungi. *Mycol. Res.* **2009**, *113*, 754−770.

(5) Boonphong, S.; Kittakoop, P.; Isaka, M.; Pittayakhajonwut, D.; Tanticharoen, M.; Thebtaranonth, Y. Multiplolides A and B, New antifungal 10-membered lactones from *Xylaria multiplex*. *J. Nat. Prod.* **2001**, *64*, 965−967.

(6) Rothweiler, W.; Tamm, C. Isolation and structure of phomin. *Experientia* **1966**, *22*, 750−752.

(7) Aldridge, D. C.; Armstrong, J. J.; Speake, R. N.; Turner, W. B. Cytochalasins, A new class of biologically active mold metabolites. *Chem. Commun.* **1967**, 26−27.

(8) Zhang, Q.; Li, H. Q.; Zong, S. C.; Gao, J. M.; Zhang, A. L. Chemical and bioactive diversities of the genus *Chaetomium* secondary metabolites. *Mini-Rev. Med. Chem.* **2012**, *12*, 127−148.

(9) Dagne, E.; Gunatilaka, A. A. L.; Asmellash, S.; Abate, D.; Kingston, D. G. I.; Hofmann, G. A.; Johnson, R. K. Two new cytotoxic cytochalasins from *Xylaria obovata*. *Tetrahedron* **1994**, *50*, 5615−5620.

(10) Wagenaar, M. M.; Corwin, J.; Strobel, G.; Clardy, J. Three new cytochalasins produced by an endophytic fungus in the genus *Rhinocladiella*. *J. Nat. Prod.* **2000**, *63*, 1692−1695.

(11) Cimmino, A.; Andolfi, A.; Berestetskiy, A.; Evidente, A. Production of phytotoxins by *Phoma exigua* var. *exigua*, A potential mycoherbicide against perennial thistles. *J. Agric. Food Chem.* **2008**, *56*, 6304−6309.

(12) Li, H.; Xiao, J.; Gao, Y.-Q.; Tang, J.-J.; Zhang, A.-L.; Gao, J.-M. Chaetoglobosins from *Chaetomium globosum*, An endophytic fungus in *Ginkgo biloba*, and their phytotoxic and cytotoxic activities. *J. Agric. Food Chem.* **2014**, *62*, 3734−3741.

(13) Li, J.-X.; Eidman, K.; Gan, X.-W.; Haefliger, O. P.; Carroll, P. J.; Pika, J. Identification of (*S*,*S*)-γ-glutamyl-(*cis*-*S*-1-propenyl)thioglycine, a naturally occurring norcysteine derivative, from the Chinese vegetable *Toona sinensis*. *J. Agric. Food Chem.* **2013**, *61*, 7470−7476.

(14) Hseu, Y.-C.; Chen, S.-C.; Lin, W.-H.; Hung, D.-Z.; Lin, M.-K.; Kuo, Y.-H.; Wang, M.-T.; Cho, H.-J.; Wang, L.; Yang, H.-L. *Toona sinensis* (leaf extracts) inhibit vascular endothelial growth factor (VEGF)-induced angiogenesis in vascular endothelial cells. *J. Ethnopharmacol.* **2011**, *134*, 111−121.

(15) Gao, J.-M.; Yang, S.-X.; Qin, J.-C. Azaphilones: Chemistry and biology. *Chem. Rev.* **2013**, *113*, 4755−4811.

(16) Xue, M.; Zhang, Q.; Gao, J.-M.; Li, H.; Tian, J.-M.; Pescitelli, G. Chaetoglobosin $V_b$ from endophytic *Chaetomium globosum*: Absolute configuration of chaetoglobosins. *Chirality* **2012**, *24*, 668−674.

(17) Yang, S.-X.; Gao, J.-M.; Laatsch, H.; Tian, J.-M.; Pescitelli, G. Absolute configuration of fusarone, A new azaphilone from the endophytic fungus *Fusarium* sp isolated from *Melia azedarach*, and of related azaphilones. *Chirality* **2012**, *24*, 621−627.

(18) Li, X.-J.; Gao, J.-M.; Chen, H.; Zhang, A.-L.; Tang, M. Toxins from a symbiotic fungus, *Leptographium qinlingensis* associated with *Dendroctonus armandi* and their in vitro toxicities to *Pinus armandi* seedlings. *Eur. J. Plant Pathol.* **2012**, *134*, 239−247.

(19) Li, X.-J.; Zhang, Q.; Zhang, A.-L.; Gao, J.-M. Metabolites from *Aspergillus fumigatus*, an endophytic fungus associated with *Melia azedarach*, and their antifungal, antifeedant, and toxic activities. *J. Agric. Food Chem.* **2012**, *60*, 3424−3431.

(20) Zhang, Q.; Wang, S.-Q.; Tang, H.-Y.; Li, X.-J.; Zhang, L.; Xiao, J.; Gao, Y.-Q.; Zhang, A.-L.; Gao, J.-M. Potential allelopathic indole diketopiperazines produced by the plant endophytic *Aspergillus fumigatus* using the one strain−many compounds method. *J. Agric. Food Chem.* **2013**, *61*, 11447−11452.

(21) Schulz, B.; Wanke, U.; Draeger, S.; Aust, H. J. Endophytes from herbaceous plants and shrubs: Effectiveness of surface sterilization methods. *Mycol. Res.* **1993**, *97*, 1447−1450.

(22) Frisch, M. J.; Trucks, G. W.; Schlegel, H. B.; Scuseria, G. E.; Robb, M. A.; Cheeseman, J. R.; Scalmani, G.; Barone, V.; Mennucci, B.; Petersson, G. A.; Nakatsuji, H.; Caricato, M.; Li, X.; Hratchian, H. P.; Izmaylov, A. F.; Bloino, J.; Zheng, G.; Sonnenberg, J. L.; Hada, M.; Ehara, M.; Toyota, K.; Fukuda, R.; Hasegawa, J.; Ishida, M.; Nakajima, T.; Honda, Y.; Kitao, O.; Nakai, H.; Vreven, T.; Montgomery, J. A., Jr.; Peralta, J. E.; Ogliaro, F.; Bearpark, M.; Heyd, J. J.; Brothers, E.; Kudin,

K. N.; Staroverov, V. N.; Kobayashi, R.; Normand, J.; Raghavachari, K.; Rendell, A.; Burant, J. C.; Iyengar, S. S.; Tomasi, J.; Cossi, M.; Rega, N.; Millam, J. M.; Klene, M.; Knox, J. E.; Cross, J. B.; Bakken, V.; Adamo, C.; Jaramillo, J.; Gomperts, R.; Stratmann, R. E.; Yazyev, O.; Austin, A. J.; Cammi, R.; Pomelli, C.; Ochterski, J. W.; Martin, R. L.; Morokuma, K.; Zakrzewski, V. G.; Voth, G. A.; Salvador, P.; Dannenberg, J. J.; Dapprich, S.; Daniels, A. D.; Farkas, O.; Foresman, J. B.; Ortiz, J. V.; Cioslowski, J.; Fox, D. J. *Gaussian 09*, revision D.01; Gaussian, Inc.: Wallingford, CT, 2013.

(23) Bruhn, T.; Schaumloeffel, A.; Hemberger, Y.; Bringmann, G. SpecDis: Quantifying the comparison of calculated and experimental electronic circular dichroism spectra. *Chirality* **2013**, *25*, 243−249.

(24) Zhang, H.; Gao, J.-M.; Liu, W.-T.; Tang, J.-C.; Zhang, X.-C.; Jin, Z.-G.; Xu, Y.-P.; Shao, M.-A. Allelopathic substances from walnut (*Juglans regia* L.) leaves. *Allelopathy J.* **2008**, *21*, 426−432.

(25) Tang, H.-Y.; Zhang, Q.; Li, H.; Gao, J.-M. Antimicrobial and allelopathic metabolites produced by *Penicillium brasilianum*. *Nat. Prod. Res.* **2014**, DOI: 10.1080/14786419.2014.940347.

(26) Williamson, G. B.; Richardson, D. Bioassays for allelopathy: Measuring treatment responses with independent controls. *J. Chem. Ecol.* **1988**, *14*, 181−187.

(27) Himri, I.; Guaadaoui, A.; Souna, F.; Bouakka, M.; Melhaoui, A.; Hakkou, A.; Saalaoui, E. Toxicity testing of tartrazine using the nematode *Caenorhabditis elegans*, brine shrimp larvae (*Artemia salina*) and KGN granulosa cell line. *J. Appl. Pharm. Sci.* **2013**, *3*, 051−058.

(28) Solis, P. N.; Wright, C. W.; Anderson, M. M.; Gupta, M. P.; Phillipson, J. D. A microwell cytotoxicity assay using *Artemia salina* (brine shrimp). *Planta Med.* **1993**, *59*, 250−252.

(29) Fan, N. J.; Tang, J. J.; Li, H.; Li, X. J.; Luo, B.; Gao, J. M. Synthesis and cytotoxic activity of some novel steroidal C-17 pyrazolinyl derivatives. *Eur. J. Med. Chem.* **2013**, *69*, 182−190.

(30) Lin, Z.-J.; Zhang, G.-J.; Zhu, T.-J.; Liu, R.; Wei, H.-J.; Gu, Q.-Q. Bioactive cytochalasins from *Aspergillus flavipes*, An endophytic fungus associated with the mangrove plant *Acanthus ilicifolius*. *Helv. Chim. Acta* **2009**, *92*, 1538−1544.

(31) Scherlach, K.; Boettger, D.; Remme, N.; Hertweck, C. The chemistry and biology of cytochalasans. *Nat. Prod. Rep.* **2010**, *27*, 869−886.

(32) Feng, Y.; Blunt, J. W.; Cole, A. L. J.; Munro, M. H. G. Three novel cytochalasins X, Y, and Z from *Pseudeurotium zonatum*. *J. Nat. Prod.* **2002**, *65*, 1274−1277.

(33) Liu, R.; Gu, Q.; Zhu, W.; Cui, C.; Fan, G.; Fang, Y.; Zhu, T.; Liu, H. 10-Phenyl-[12]-cytochalasins $Z_7$, $Z_8$, and $Z_9$ from the marine-derived fungus *Spicaria elegans*. *J. Nat. Prod.* **2006**, *69*, 871−875.

(34) Liu, J.-T.; Hu, B.; Gao, Y.; Zhang, J.-P.; Jiao, B.-H.; Lu, X.-L.; Liu, X.-Y. Bioactive tyrosine-derived cytochalasins from fungus *Eutypella* sp D-1. *Chem. Biodiversity* **2014**, *11*, 800−806.

(35) Zhang, H.-W.; Zhang, J.; Hu, S.; Zhang, Z.-J.; Zhu, C.-J.; Ng, S. W.; Tan, R.-X. Ardeemins and cytochalasins from *Aspergillus terreus* residing in *Artemisia annua*. *Planta Med.* **2010**, *76*, 1616−1621.

(36) Pescitelli, G.; Di Bari, L.; Berova, N. Conformational aspects in the studies of organic compounds by electronic circular dichroism. *Chem. Soc. Rev.* **2011**, *40*, 4603−4625.

(37) Autschbach, J. Computing chiroptical properties with first-principles theoretical methods: background and illustrative examples. *Chirality* **2009**, *21*, E116−E152.

(38) Casida, M. E.; Jamorski, C.; Casida, K. C.; Salahub, D. R. Molecular excitation energies to high-lying bound states from time-dependent density-functional response theory: Characterization and correction of the time-dependent local density approximation ionization threshold. *J. Chem. Phys.* **1998**, *108*, 4439−4449.

(39) Steyn, P. S.; van Heerden, F. R.; Rabie, C. J. Cytochalasins E and K, Toxic metabolites from *Aspergillus clavatus*. *J. Chem. Soc., Perkin Trans. 1* **1982**, 541−544.

(40) Wells, J. M.; Cutler, H. G.; Cole, R. J. Toxicity and plant growth regulator effects of cytochalasin H isolated from *Phomopsis* sp. *Can. J. Microbiol.* **1976**, *22*, 1137−1143.

(41) Nukina, M. Pyrichalasin H, A new phytotoxic metabolite belonging to the cytochalasans from *Pyricularia grisea* (Cooke) Saccardo. *Agric. Biol. Chem.* **1987**, *51*, 2625−2628.

(42) Fujii, Y.; Tani, H.; Ichinoe, M.; Nakajima, H. Zygosporin D and two new cytochalasins produced by the fungus *Metarrhizium anisopliae*. *J. Nat. Prod.* **2000**, *63*, 132−135.

(43) Evidente, A.; Andolfi, A.; Vurro, M.; Zonno, M. C.; Motta, A. Cytochalasins Z4, Z5, and Z6, Three new 24-oxa[14]cytochalasans produced by *Phoma exigua* var. *heteromorpha*. *J. Nat. Prod.* **2003**, *66*, 1540−1544.

(44) Evidente, A.; Andolfi, A.; Vurro, M.; Zonno, M. C.; Motta, A. Cytochalasins $Z_1$, $Z_2$ and $Z_3$, Three 24-oxal[14]cytochalasans produced by *Pyrenophora semeniperda*. *Phytochemistry* **2002**, *60*, 45−53.

(45) Capasso, R.; Evidente, A.; Vurro, M. Cytochalasins from *Phoma exigua* var. *heteromorpha*. *Phytochemistry* **1991**, *30*, 3945−3950.

(46) Vurro, M.; Bottalico, A.; Capasso, R.; Evidente, A. Cytochalasins from phytopatogenic *Ascochyta* and *Phoma* species. In *Toxins in Plant Disease Development and Evolving Biotechnology*; Upadhyay, R. K.;, Mukerji, K. G., Eds.; Oxford & IBH Publishing Co.: New Delhi, India, 1997; pp 127−147.

(47) Bottalico, A.; Capasso, R.; Evidente, A.; Randazzo, G.; Vurro, M. Cytochalasins: Structure−activity relationships. *Phytochemistry* **1990**, *29*, 93−96.

(48) Berestetskiy, A.; Dmitriev, A.; Mitina, G.; Lisker, I.; Andolfi, A.; Evidente, A. Nonenolides and cytochalasins with phytotoxic activity against *Cirsium arvense* and *Sonchus arvensis*: A structure−activity relationships study. *Phytochemistry* **2008**, *69*, 953−960.

(49) Song, F.; Wu, S. H.; Zhai, Y. Z.; Xuan, Q. C.; Wang, T. Secondary metabolites from the genus *Xylaria* and their bioactivities. *Chem. Biodiversity* **2014**, *11*, 673−694.

**Bacterial Strains and Growth Media.** *Bifidobacterium dentium* KCTC 3361, *Clostridium leptum* KCTC 5155, *Enterococcus saccharolyticus* KCTC 3643, *Mitsuokella multacida* KCTC 5453, *Pediococcus acidilactici* KCTC 15064, *Clostridium nexile* KCTC 5578, *Clostridium scindens* KCTC 5591, *Ruminococcus gnavus* KCTC 5920, and *Weissella paramesenteroides* KCTC 3531 were purchased from the Korean Collection for Type Cultures. *Megamonas funiformis* JCM 14723 was purchased from the Japan Collection of Microorganisms. *Marvinbryantia formatexigens* DSM 14469 and *Ruminococcus obeum* DSM 25238 were purchased from the Leibniz Institute DSMZ (German Collection of Microorganisms and Cell Cultures). *Lactobacillus acidophilus* ATCC 4356, *Lactobacillus delbrueckii* subsp. *bulgaricus* ATCC 11842, *Lactobacillus fermentum* ATCC 14931, and *Lactobacillus plantarum* subsp. *plantarum* ATCC 14917 were kindly provided by Professor Heping Zhang (Inner Mongolia Agricultural University, China). *Bifidobacterium adolescentis* CICC 6070 was purchased from the China Center of Industrial Culture Collection. *Clostridium perfringens* ATCC 13124 was purchased from the American Type Culture Collection. *Lactobacillus reuteri* CCFM 8217 and *Leuconostoc mesenteroides* CCFM 8220 were obtained from the Culture Collection of Food Microorganisms, Jiangnan University.

The medium used to isolate the bacteria was modified from gut microbiota medium (GMM),[19] which was modified from the supplemented tryptone−yeast−glucose medium by Gordon and co-workers[19] to culture fecal microbiota. The modified GMM contained 4 g of lactulose, 2 g of peptone, 1 g of yeast extract, 2 g of $KH_2PO_4$, 0.002 g of $MgSO_4{\cdot}7H_2O$, 0.08 g of NaCl, 8 mg of $CaCl_2$, 0.73 mg of $FeSO_4{\cdot}7H_2O$, 1.2 mg of hematin, 10 mL of ATCC vitamin mix, 10 mL of ATCC trace mineral mix, 0.5 mL of Tween 80, and 0.5 g of L-cysteine per liter. The pH was adjusted to 7.0 ± 0.1 by use of NaOH, and the medium was sterilized at 115 °C for 20 min. Lactulose was filter-sterilized through a 0.22-$\mu$m filter and added to the autoclaved medium as the sole carbon source. Solid medium was obtained by adding 18 g of agar/L of liquid medium. A total of 15 mL of 0.5% bromocresol purple was added to the GMM agar medium as the indicator of pH change.

**Database Preparation.** Site-specialized protein multifasta (PEP) files for reference genomes can be downloaded from the HMP Data Analysis and Coordination Center. These files record all HMP isolates that have completed sequencing and annotation. The gastrointestinal-tract PEP file (382 rows) was downloaded from http://hmpdacc.org/HMRGD/. A customized script was used to eliminate redundance.

The output of HMP's mothur community profiling of metagenomic 16S rRNA sequence data generated by a low-stringency approach (http://hmpdacc.org/HMMCP/) was also used for reference. One hundred seven of the genera depicted in the mothur community profiling output were not found in the list of reference genomes. Therefore, the 98 available genome coding sequences for these 107 genera were downloaded from the National Center for Biotechnology Information and merged into the gastrointestinal-tract PEP file, followed by BLAST database formatting.

**Genes Responsible for Uptake and Hydrolysis of Galactooligosaccharides.** By use of literature mining, 41 genes were identified as responsible for the transport or catabolism of GOS (Table 1). However, no genes have been reported to be responsible for the metabolism of lactulose. Like lactulose, GOS is formed by a $\beta$-1,4-glycosidic bond. Therefore, the genes related to GOS metabolism were used in this study to predict potential lactulose-metabolizing bacteria.

**Alignment of Transporters and Glycosidases against the Local Protein Database.** BLASTP searches were run against the local protein database with transporters and glycoside hydrolases used as queries. When the alignment length was found to exceed 70% of the transporter/glycoside hydrolase sequence and the identity was greater than 40%, the strain was inferred to have homologous proteins for corresponding functions.

**Isolation and Identification of Lactulose-Metabolizing Bacteria.** Fresh fecal samples were collected from five healthy donors aged 25−29 years. The fecal samples were placed in prereduced 0.1 M phosphate-buffered saline (PBS; 80 g of NaCl, 2 g of KCl, 14.4 g of $Na_2PO_4$, 2.4 g of $KH_2PO_4$, and 0.5 g of L-cysteine per liter; pH 7.0), with 15 mL/g of feces per sample.[19] The samples were dispersed and suspended by vortexing with sterilized glass beads for 5 min. Serial dilution was performed with 0.1 M PBS, and the diluted ($10^{-3}$) samples (0.1 mL) were plated. Six plates were used for each fecal sample, as recommended by Gordon and co-workers,[19] and the medium without lactulose was used for negative controls. The plates were incubated in an anaerobic workstation (Whitley DG250, Don Whitley Scientific Limited, West Yorkshire, U.K.) at 37 °C for 24 h under an atmosphere of 80% $N_2$, 10% $CO_2$, and 10% $H_2$. Colonies

**Table 1. Genes Responsible for Transport and Catabolism of Galactooligosaccharides**

| gene | annotation |
|---|---|
| *Bifidobacterium lactis* Bl-04[20] | |
| *lacS*-balac_0475 | MFS permease |
| balac_0485 | permease |
| balac_0486 | permease |
| *lacZ*-balac_0476 | $\beta$-galactosidase |
| balac_0484 | $\beta$-galactosidase |
| *Bifidobacterium longum* LMG13197[21] | |
| bl1523 | permease |
| bl0260 | permease |
| bl0261 | permease |
| bl0259 | $\beta$-galactosidase |
| bl0976 | galactoside transporter |
| bl0978 | $\beta$-galactosidase |
| *Bifidobacterium longum* subsp. *infantis* ATCC15697[22] | |
| blon_0267 | permease |
| blon_0268 | $\beta$-galactosidase |
| blon_2331 | permease |
| blon_2332 | permease |
| blon_2334 | $\beta$-galactosidase |
| blon_2016 | $\beta$-galactosidase |
| blon_2123 | $\beta$-galactosidase |
| blon_2416 | $\beta$-galactosidase |
| blon_2414[a] | solute binding protein |
| blon_2453[a] | $\beta$-galactosidase |
| *Bifidobacterium breve* UCC2003[24] | |
| bbr_0417 *galC* | solute binding protein |
| bbr_0418 *galD* | permease |
| bbr_0419 *galE* | permease |
| bbr_0420 *galG* | $\beta$-galactosidase |
| bbr_1551 *lacS* | galactoside symporter |
| bbr_1552 *lacZ* | $\beta$-galactosidase |
| bbr_0530 *gosC* | solute binding protein |
| bbr_0527 *gosD* | permease |
| bbr_0528 *gosE* | permease |
| bbr_0529 *gosG* | $\beta$-galactosidase |
| *Geobacillus stearothermophilus* T-6[25] | |
| *ganA* | extracellular endo-$\beta$-1,4-galactanase precursor |
| *ganE* | solute binding protein |
| *ganF* | permease |
| *ganG* | permease |
| *ganB* | $\beta$-galactosidase |
| *Lactobacillus acidophilus*[26] | |
| lacS-lba1463 | permease |
| *Lactobacillus acidophilus* NCFM[27] | |
| *lacZ*-lba1462 | $\beta$-galactosidases |
| *lacL*-lba1467 | $\beta$-galactosidases |
| *lacM*-lba1468 | $\beta$-galactosidases |
| *Bifidobacterium bifidum* NCIMB41171[28] | |
| bbgII | $\beta$-galactosidase |

[a]This entry from ref 23.

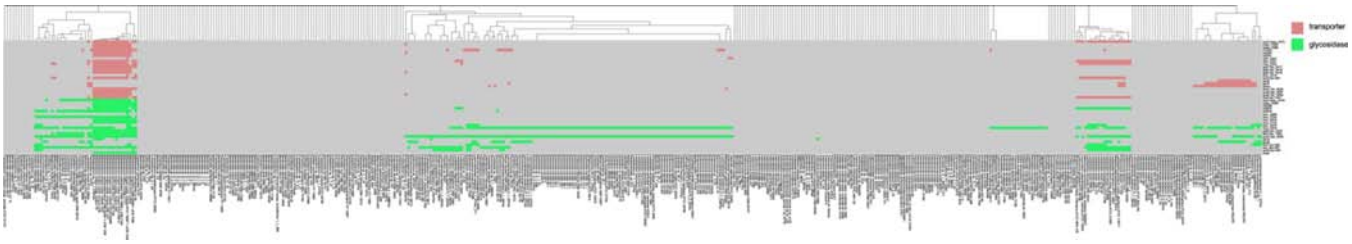

**Figure 1.** Distribution of homologue proteins of transporters and glycosidases for lactulose (vertical axis) among GIT bacteria (horizontal axis). Positive results for transporters and glycosidases are indicated in red and green, relatively.

with yellow surroundings on the GMM plates were picked up, reinoculated into liquid medium, and cultured anaerobically. The bacteria were isolated and purified by the standard streak-plate technique. The isolated bacteria were Gram-stained and identified by amplification and sequencing of 16S rRNA. The polymerase chain reaction (PCR) procedure was as follows: 95 °C for 5 min; 95 °C for 30 s, 50 °C for 30 s, and 72 °C for 1 min 30 s, 30 cycles; 72 °C for 10 min; 12 °C for 10 min. The resulting PCR product was sequenced by Sangon Biotech (Shanghai) Co., Ltd.

**Characterization of Bacterial Growth on Lactulose.** Bacteria were cultured anaerobically in GMM at 37 °C for 24 h, with lactulose as the sole carbon source. Absorbance at 600 nm ($OD_{600}$) and pH were recorded every 2 h to characterize the growth. The amount of lactulose in the culture supernatant was determined by the method developed by Zhang et al.[29]

**Fermentation of Galactooligosaccharides by Lactulose-Metabolizing Bacteria.** Bacteria capable of metabolizing lactulose were inoculated on GMM plates with GOS as the sole carbon source and bromocresol purple as the indicator. GMM plates without GOS were set as negative controls. The bacteria on the GMM−GOS plates that were capable of growing and coloring their surroundings yellow were considered to have the ability to metabolize GOS.

## RESULTS

**Homologous Proteins for Lactulose Transporters and Glycosidases in 453 Gastrointestinal-Tract Bacteria Strains.** The results of aligning the transporters and glycosidases with the local protein database are shown in Figure 1. Surprisingly, homologue proteins for the glycosidases appeared in 222 of the 453 strains, which accounted for 56 of the 114 genera. In contrast, homologue proteins for the transporters were found in only 90 strains, accounting for 29 of the 114 genera. These 90 strains also possessed homologue proteins for the glycosidases. In general, lactulose metabolism requires transporters and galactosidases. In addition to *Bifidobacterium* and *Lactobacillus*, 27 genera with homologue proteins for both transporters and glycosidases were found (Figure 1), indicating that lactulose may not be exclusively a stimulant of probiotics.[30] However, it remains unclear whether the predicted bacteria are able to utilize lactulose; further investigation is required.

**Utilization of Lactulose by *Cronobacter sakazakii*, *Enterococcus casseliflavus*, *Enterococcus faecalis*, and *Klebsiella pneumoniae*.** Compared with GOS, lactulose has an accurate chemical structure and metabolic process, and its purity can reach 99.3%. In the current study, fecal samples collected from five healthy adults were plated on GMM with lactulose as the sole carbon source. Ninety-six strains belonging to 18 species of nine genera were identified (Table 2). To our knowledge, *Cronobacter*, *Enterococcus*, *Klebsiella*, and *Pseudomonas* are first reported in our study to be capable of utilizing lactulose. One strain from each species was selected and its growth on lactulose was characterized (Figure 2). $OD_{600}$ increased during the 24-h culture period, along with a decrease in pH and a reduction in the lactulose amount, which provided direct proof of lactulose utilization.

**Table 2. Identified Lactulose-Metabolizing Bacteria in Healthy Adult Feces[a]**

| genus and species | strains |
|---|---|
| *Cronobacter sakazakii* | CCFM 8305, 8306, 8307, 8308, 8309, 8310, 8311, 8312 |
| *Enterobacter aerogenes* | CCFM 8313 |
| Enterobacteriaceae bacterium | CCFM 8314, 8315 |
| *Enterococcus casseliflavus* | CCFM 8316, 8317, 8318, 8319 |
| *Enterococcus faecalis* | CCFM 8320 |
| *Enterococcus faecium* | CCFM 8321, 8322, 8323, 8324 |
| *Enterococcus gallinarum* | CCFM 8325 |
| *Escherichia coli* | CCFM 8326, 8327, 8328, 8329, 8330, 8331, 8332, 8333, 8334, 8335, 8336, 8337, 8338, 8339, 8340, 8341, 8342 |
| *Escherichia fergusonii* | CCFM 8343, 8344, 8345, 8346 |
| *Klebsiella pneumoniae* | CCFM 8347, 8348, 8349, 8350, 8351, 8352, 8353, 8354, 8355, 8356, 8357, 8358, 8359, 8360, 8361, 8362, 8363, 8364, 8365, 8366, 8367, 8368, 8369, 8370 |
| *Klebsiella* sp. | CCFM 8371, 8372, 8373, 8374, 8375, 8376, 8377, 8378, 8379, 8380, 8381, 8382, 8383, 8384, 8385, 8386 |
| *Klebsiella variicola* | CCFM 8387 |
| *Pseudomonas putida* | CCFM 8388 |
| *Streptococcus anginosus* | CCFM 8389 |
| *Streptococcus equinus* | CCFM 8390, 8391 |
| *Streptococcus sanguinis* | CCFM 8392, 8393, 8394 |
| *Bifidobacterium pseudocatenulatum* | CCFM 8395, 8396, 8397, 8398 |
| *Bifidobacterium* sp. | CCFM 8399, 8400 |

[a]16S rRNA nucleotide acid sequences of the identified strains are shown in Table S1 in Supporting Information.

In addition, the ability of 21 strains to metabolize lactulose was assessed, and 17 strains were proven to be able to grow on lactulose (Table 3 and Figure 3). Thirteen of the 15 strains with homologue proteins for both transporters and glycosidases were capable of utilizing lactulose, indicating that searching for transporter and glycosidase homology may be an effective method of predicting lactulose-metabolizing bacteria.

**Galactooligosaccharide Utilization by Lactulose-Metabolizing Bacteria.** Due to the structural similarity of lactulose and GOS, the 18 strains isolated (Figure 2) and the 17 strains found to be capable of metabolizing lactulose (Table 3) were tested for their ability to ferment GOS. The results showed that 32 strains were capable of GOS utilization (Table

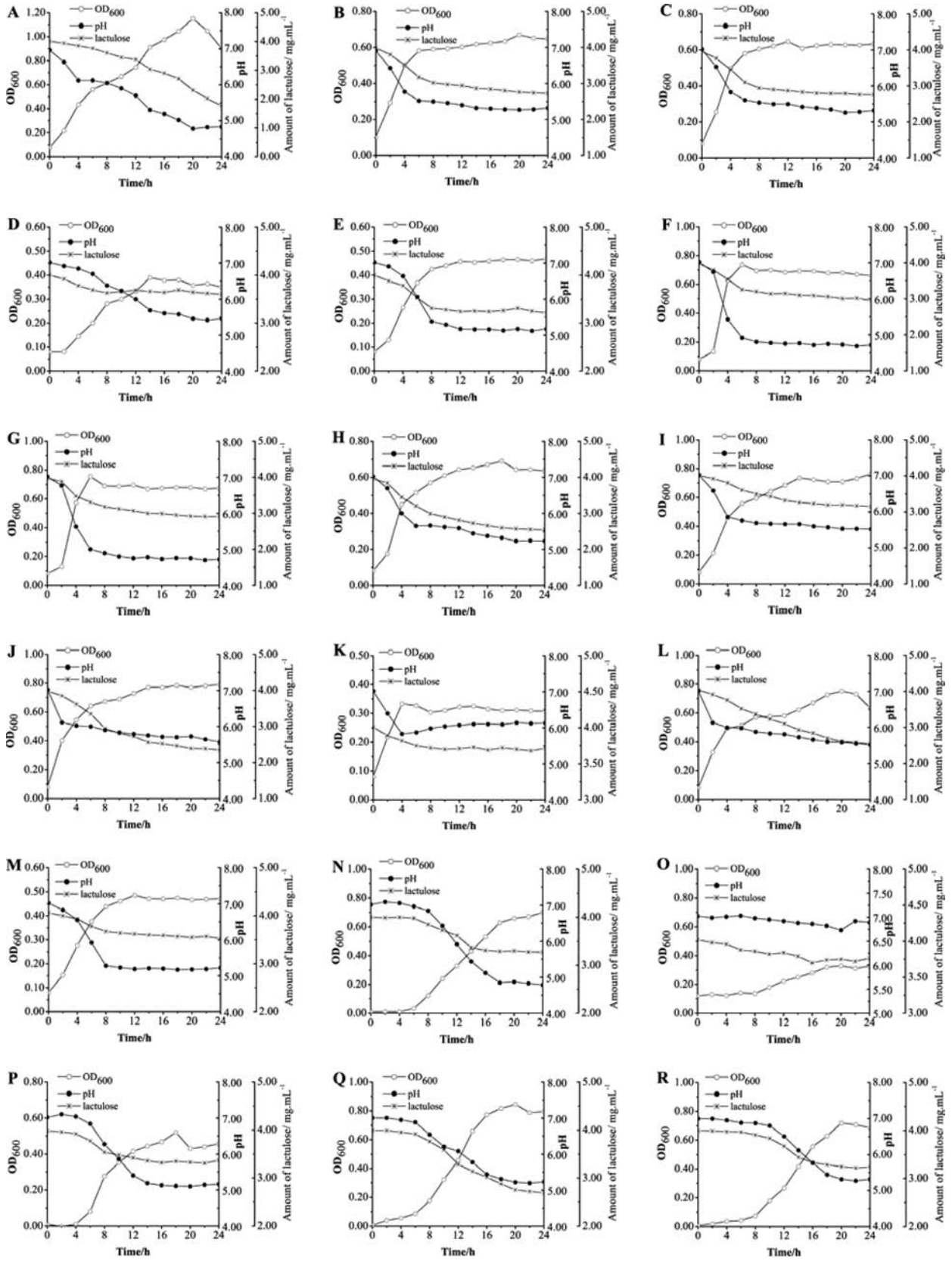


**Figure 2.** Growth of isolated strains on GMM medium with lactulose as the sole carbon source. $OD_{600}$ (○), pH (●), and the amount of lactulose (×) were recorded every 2 h, and the strains are presented as follows: (A) *C. sakazakii* CCFM 8306, (B) *E. aerogenes* CCFM 8313, (C) Enterobacteriaceae bacterium CCFM 8315, (D) *E. casseliflavus* CCFM 8316, (E) *E. faecalis* CCFM 8320, (F) *E. faecium* CCFM 8321, (G) *E. gallinarum* CCFM 8325, (H) *E. coli* CCFM 8331, (I) *E. fergusonii* CCFM 8343, (J) *K. pneumoniae* CCFM 8358, (K) *Klebsiella* sp. CCFM 8371, (L) *K. variicola* CCFM 8387, (M) *P. putida* CCFM 8388, (N) *S. anginosus* CCFM 8389, (O) *S. equinus* CCFM 8390, (P) *S. sanguinis* CCFM 8392, (Q) *B. pseudocatenulatum* CCFM 8395, and (R) *Bifidobacterium* sp. CCFM 8399.


dx.doi.org/10.1021/jf503484d | J. Agric. Food Chem. 2014, 62, 10970−10977

**Table 3. Bacteria Obtained on the Basis of Alignment Analysis[a]**

| strain | source | transporters | glycosidases | lactulose |
|---|---|---|---|---|
| *Bifidobacterium adolescentis* CICC 6070 | CICC | Y | Y | + |
| *Bifidobacterium dentium* KCTC 3361 | KCTC | Y | Y | + |
| *Clostridium leptum* KCTC 5155 | KCTC | N | Y | + |
| *Clostridium perfringens* ATCC 13124 | ATCC | N | Y | + |
| *Enterococcus saccharolyticus* KCTC 3643 | KCTC | N | Y | + |
| *Eubacterium rectale* ATCC 33656 | KCTC | Y | Y | + |
| *Lactobacillus acidophilus* ATCC 4356 | Zhang | Y | Y | + |
| *Lactobacillus delbrueckii* subsp. *bulgaricus* ATCC 11842 | Zhang | N | Y | + |
| *Lactobacillus fermentum* ATCC 14931 | Zhang | Y | Y | + |
| *Lactobacillus plantarum* subsp. *plantarum* ATCC 14917 | Zhang | Y | Y | + |
| *Lactobacillus reuteri* CCFM8217 | CCFM | Y | Y | + |
| *Leuconostoc mesenteroides* CCFM8220 | CCFM | Y | Y | + |
| *Marvinbryantia formatexigens* DSM 14469 | DSM | Y | Y | + |
| *Megamonas funiformis* JCM 14723 | JCM | Y | Y | + |
| *Mitsuokella multacida* KCTC 5453 | KCTC | Y | Y | + |
| *Pediococcus acidilactici* KCTC 15064 | KCTC | Y | Y | + |
| *Weissella paramesenteroides* KCTC 3531 | KCTC | Y | Y | + |
| *Clostridium nexile* KCTC 5578 | KCTC | N | Y | − |
| *Clostridium scindens* KCTC 5591 | KCTC | N | Y | − |
| *Ruminococcus gnavus* KCTC 5920 | KCTC | Y | Y | − |
| *Ruminococcus obeum* DSM 25238 | DSM | Y | Y | − |

[a]Symbols: Y, positive for alignment search; N, negative for alignment search; +, positive growth on lactulose; −, negative growth on lactulose.

4). Although lactulose is a disaccharide composed of fructose and galactose, while GOS is a complex with different degrees of galactose polymerization, they may share the same transporters or glycosidases. Moreover, the 17 lactulose-metabolizing strains obtained from the alignment search contained homologue proteins for transporters and glycosidases that have been reported to be responsible for metabolizing GOS. Thus, there seems to be a significant correlation between lactulose and GOS.

## DISCUSSION

Lactulose has generally been regarded as a special substrate used by probiotic bifidobacteria and lactobacilli. However, *Faecalibacterium prausnitzii*, *Bacteroides oralis*, *E. coli*, and *C. perfringens* have also been reported to utilize lactulose in vitro.[10,31] It remains unclear which species are able to utilize lactulose in the gut. The gut is a complex ecosystem, with about $10^{14}$ bacteria categorized into more than 1000 species,[32] and the aim of the current study was to identify lactulose-metabolizing bacteria within this ecosystem.

Transporters and glycosidases are of great importance to the utilization of oligosaccharides. Thus far, however, no encoding genes for lactulose metabolism have been identified. Therefore, the genes for GOS metabolism acquired through literature mining were used instead. Moreover, the unculturability of most gut microbes has limited our understanding of the metabolic characteristics of individual strains. To date, HMP has failed to reach its goal of isolating 3000 reference genomes from human body sites. In the current study, the site-specialized reference genome data provided by HMP were combined with the output of mothur community profiling to build a local protein database. As shown in Figure 1, the genes for lactulose metabolism appeared in 222 GIT bacteria strains, of which 90 strains possessed homologue proteins for both transporters and glycosidases. It is reasonable to infer from the existence of transporters in a given strain that the strain contains corresponding glycosidases. If no corresponding glycosidases were available, the strain would be unlikely to contain transporters.

To identify lactulose-metabolizing bacteria in the gut, 18 species were isolated from fecal samples (Table 2), and 17 strains were proven to have the ability to utilize lactulose (Table 3). This indicates that bioinformatic analysis is an effective tool for predicting lactulose-metabolizing bacteria, thereby narrowing the scope of experimental research. Unlike the results of previous studies,[10,31,33] the findings of the current study indicated for the first time that the genera *Cronobacter*, *Enterococcus*, *Klebsiella*, and *Pseudomonas* are able to utilize lactulose. To the best of our knowledge, *C. sakazakii*, *E. aerogenes*, Enterobacteriaceae bacterium, *E. casseliflavus*, *E. faecalis*, *E. faecium*, *E. gallinarum*, *E. fergusonii*, *K. pneumoniae*, *Klebsiella* sp., *K. variicola*, *P. putida*, *S. anginosus*, *S. equinus*, and *B. pseudocatenulatum* have never been reported to be capable of utilizing lactulose.

Therefore, lactulose was shown to have the potential to stimulate the growth of many commensal bacteria in addition to bifidobacteria and lactobacilli. More gut bacteria capable of utilizing lactulose may exist than previously supposed. Additionally, lactulose exhibited similar metabolic characteristics to GOS (Table 4), which may be derived from lactulose.[34] Therefore, lactulose may be considered a type of GOS with a lower degree of polymerization, and lactulose and GOS may possess similar genes for transporters or galactosidases. In the human gut, competition for limited food takes place among the bacteria, and those capable of utilizing prebiotic substrates might have advantages during the competition with other bacteria.[35]

In conclusion, the combination of a homology search and the traditional isolation method assisted in the identification of lactulose-metabolizing bacteria. Thirty-five species were found, most of which were reported for the first time to be capable of utilizing lactulose. The commensal gut bacteria *Cronobacter*, *Enterococcus*, *Escherichia*, *Klebsiella*, *Pseudomonas*, and *Streptococcus* were found to be able to ferment lactulose. In addition, significant correlations were observed between lactulose and GOS metabolism. This work offers greater insight into the utilization of oligosaccharides by gut bacteria. To further explore the relationship between functional oligosaccharides

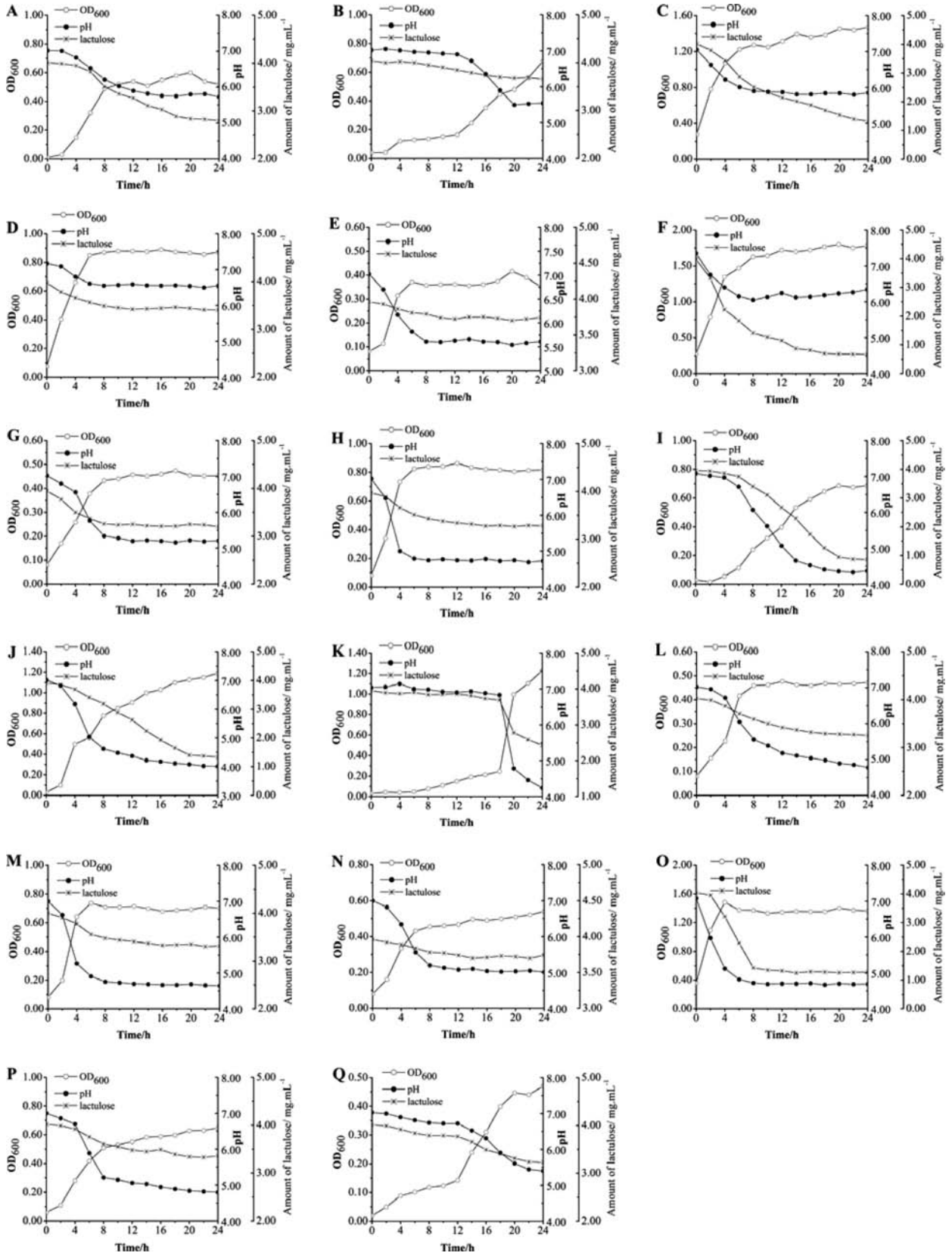


**Figure 3.** Growth of obtained strains on GMM medium with lactulose as the sole carbon source. $OD_{600}$ (○), pH (●), and the amount of lactulose (×) were recorded every 2 h, and the strains are presented as follows: (A) *B. adolescentis* CICC 6070, (B) *B. dentium* KCTC 3361, (C) *C. leptum* KCTC 5155, (D) *C. perfringens* ATCC 13124, (E) *E. saccharolyticus* KCTC 3643, (F) *E. rectale* ATCC 33656, (G) *L. acidophilus* ATCC 4356, (H) *L. delbrueckii* subsp. *bulgaricus* ATCC 11842, (I) *L. fermentum* ATCC 14931, (J) *L. plantarum* subsp. *plantarum* ATCC 14917, (K) *L. reuteri* CCFM 8217, (L) *L. mesenteroides* CCFM 8220, (M) *M. formatexigens* DSM 14469, (N) *M. funiformis* JCM 14723, (O) *M. multacida* KCTC 5453, (P) *P. acidilactici* KCTC 15064, and (Q) *W. paramesenteroides* KCTC 3531.


dx.doi.org/10.1021/jf503484d | *J. Agric. Food Chem.* 2014, 62, 10970−10977

**Table 4. Growth of Lactulose-Metabolizing Strains on Galactooligosaccharides[a]**

| strain | GOS | strain | GOS |
|---|---|---|---|
| *C. sakazakii* CCFM8306 | + | *B. adolescentis* CICC 6070 | + |
| *E. aerogenes* CCFM8313 | + | *B. dentium* KCTC 3361 | + |
| Enterobacteriaceae bacterium CCFM8315 | + | *C. leptum* KCTC 5155 | − |
| *E. casseliflavus* CCFM8316 | + | *C. perfringens* ATCC 13124 | + |
| *E. faecalis* CCFM8320 | + | *E. saccharolyticus* KCTC 3643 | + |
| *E. faecium* CCFM8321 | − | *E. rectale* ATCC 33656 | + |
| *E. gallinarum* CCFM8325 | + | *L. acidophilus* ATCC 4356 | + |
| *E. coli* CCFM8331 | + | *L. delbrueckii* subsp. *bulgaricus* ATCC 11842 | + |
| *E. fergusonii* CCFM8343 | + | *L. fermentum* ATCC 14931 | + |
| *K. pneumoniae* CCFM8358 | + | *L. plantarum* subsp. *plantarum* ATCC 14917 | + |
| *Klebsiella* sp. CCFM8371 | + | *L. reuteri* CCFM8217 | + |
| *K. variicola* CCFM8387 | + | *L. mesenteroides* CCFM8220 | + |
| *P. putida* CCFM8388 | + | *M. formatexigens* DSM 14469 | + |
| *S. anginosus* CCFM8389 | + | *M. funiformis* JCM 14723 | + |
| *S. equinus* CCFM8390 | + | *M. multacida* KCTC 5453 | + |
| *S. sanguinis* CCFM8392 | − | *P. acidilactici* KCTC 15064 | + |
| *B. pseudocatenulatum* CCFM8395 | + | *W. paramesenteroides* KCTC 3531 | + |
| *Bifidobacterium* sp. CCFM8399 | + | | |

[a]+, positive growth on GOS; −, negative growth on GOS.

and gut bacteria, more attention should be paid to bacteria other than bifidobacteria and lactobacilli.

## ■ ASSOCIATED CONTENT

### Ⓢ Supporting Information

One table listing 16S rRNA nucleotide acid sequences of the identified strains. This material is available free of charge via the Internet at http://pubs.acs.org.

## ■ AUTHOR INFORMATION


### Corresponding Authors

*Telephone/fax 86-510-85912155; e-mail zhanghao@jiangnan.edu.cn.

*Telephone/fax 86-510-85912155; e-mail chenwei66@jiangnan.edu.cn.

### Author Contributions

[§]B.M. and D.L. contributed equally to this work.



### Funding

This work was supported by the National Science Fund for Distinguished Young Scholars (31125021), Key Projects in the National Science and Technology Pillar Program during the 12th five-year plan period (2013BAD18B01, 2013BAD18B02, 2012BAD28B07, 2012BAD28B08), the 111 Project B07019, and the Program for Changjiang Scholars and Innovative Research Team in University (IRT1249).


### Notes

The authors declare no competing financial interest.

## ■ ACKNOWLEDGMENTS


We thank all adults who provided fecal samples. We also thank Professor H. Zhang for providing *Lactobacillus acidophilus* ATCC 4356, *Lactobacillus delbrueckii* subsp. *bulgaricus* ATCC 11842, *Lactobacillus fermentum* ATCC 14931, and *Lactobacillus plantarum* subsp. *plantarum* ATCC 14917.


## ■ ABBREVIATIONS

GOS, galactooligosaccharides; HMP, Human Microbiome Project; GMM, gut microbiota medium; GIT, gastrointestinal tract

## ■ REFERENCES


(1) Gibson, G. R.; Probert, H. M.; Loo, J. V.; Rastall, R. A.; Roberfroid, M. B. Dietary modulation of the human colonic microbiota: Updating the concept of prebiotics. *Nutr. Res. Rev.* **2004**, *17*, 259−275.

(2) Roberfroid, M. Prebiotics: The concept revisited. *J. Nutr.* **2007**, *130*, 830S−837S.

(3) Panesar, P. S.; Kumari, S. Lactulose: Production, purification and potential applications. *Biotechnol. Adv.* **2011**, *29*, 940−948.

(4) Buddington, R. K.; Williams, C. H.; Chen, S. C.; Witherly, S. A. Dietary supplement of neosugar alters the fecal flora and decreases activities of some reductive enzymes in human subjects. *Am. J. Clin. Nutr.* **1996**, *63*, 709−716.

(5) Rycroft, C. E.; Jones, M. R.; Gibson, G. R.; Rastall, R. A. A comparative in vitro evaluation of the fermentation properties of prebiotic oligosaccharides. *J. Appl. Microbiol.* **2001**, *91*, 878−887.

(6) Cardelle-Cobas, A.; Olano, A.; Corzo, N.; Villamiel, M.; Collins, M.; Kolida, S.; Rastall, R. A. In vitro fermentation of lactulose-derived oligosaccharides by mixed fecal microbiota. *J. Agric. Food Chem.* **2012**, *60*, 2024−2032.

(7) Boler, B. M. V.; Serao, M. C. R.; Faber, T. A.; Bauer, L. L.; Chow, J.; Murphy, M. R.; Fahey, G. C., Jr. In vitro fermentation characteristics of select nondigestible oligosaccharides by infant fecal inocula. *J. Agric. Food Chem.* **2013**, *61*, 2109−2119.

(8) Sahota, S. S.; Bramley, P. M.; Menzies, I. S. The fermentation of lactulose by colonic bacteria. *J. Gen. Microbiol.* **1982**, *128*, 319−325.

(9) Porcheron, G.; Kut, E.; Canepa, S.; Maurel, M. C.; Schouler, C. Regulation of fructo-oligosaccharide metabolism in an extra-intestinal pathogenic *Escherichia coli* strain. *Mol. Microbiol.* **2011**, *81*, 717−733.

(10) Buddington, K. K.; Donahoo, J. B.; Buddington, R. K. Dietary oligofructose and inulin protect mice from enteric and systemic pathogens and tumor inducers. *J. Nutr.* **2002**, *132*, 472−477.

(11) Wollowski, I.; Rechkemmer, G.; Pool-Zobel, B. L. Protective role of probiotics and prebiotics in colon cancer. *Am. J. Clin. Nutr.* **2001**, *73*, 451S−455S.

(12) Marcobal, A.; Barboza, M.; Froehlich, J. W.; Block, D. E.; German, J. B.; Lebrilla, C. B.; Mills, D. A. Consumption of human milk oligosaccharides by gut-related microbes. *J. Agric. Food Chem.* **2010**, *58*, 5334−5340.

(13) Hernandez-Hernandez, O.; Côté, G. L.; Kolida, S.; Rastall, R. A.; Sanz, M. L. In vitro fermentation of alternansucrase raffinose-derived oligosaccharides by human gut bacteria. *J. Agric. Food Chem.* **2011**, *59*, 10901−10906.

(14) Schluter, J.; Foster, K. R. The evolution of mutualism in gut microbiota via host epithelial selection. *PLoS Biol.* **2012**, *10*, 1−9.

(15) Diard, M.; Garry, L.; Selva, M.; Mosser, T.; Denamur, E.; Matic, I. Pathogenicity-associated islands in extraintestinal pathogenic *Escherichia coli* are fitness elements involved in intestinal colonization. *J. Bacteriol.* **2010**, *192*, 4885−4893.

(16) Ganzle, M. G.; Follador, R. Metabolism of oligosaccharides and starch in lactobacilli: A review. *Front. Microbiol.* **2012**, *3*, 340.

(17) Petuely, F. *Lactobacillus bifidus* flora produced in artificially-fed infants by bifidogenic substances (bifidus factor). *Z. Kinderheilkd.* **1957**, *79*, 174−179.

(18) Panesar, P. S.; Kumari, S. Lactulose: Production, purification and potential applications. *Biotechnol. Adv.* **2011**, *29*, 940−948.

(19) Goodman, A. L.; Kallstrom, G.; Faith, J. J.; Reyes, A.; Moore, A.; Dantas, C.; Gordon, J. I. Extensive personal human gut microbiota culture collections characterized and manipulated in gnotobiotic mice. *Proc. Natl. Acad. Sci. U.S.A.* **2011**, *108*, 6252−6257.

(20) Andersen, J. M.; Barrangou, R.; Hachem, M. A.; Lahtinen, S. J.; Goh, Y. J.; Svensson, B.; Klaenhammeret, T. R. Transcriptional

analysis of oligosaccharide utilization by *Bifidobacterium lactis* Bl-04. *BMC Genomics* **2013**, *14*, 312.
(21) González, R.; Klaassens, E. S.; Malinen, E.; de Vos, W. M.; Vaughan, E. E. Differential transcriptional response of *Bifidobacterium longum* to human milk, formula milk, and galactooligosaccharide. *Appl. Environ. Microb.* **2008**, *74*, 4686−4694.
(22) Garrido, D.; Ruiz-Moyano, S.; Jimenez-Espinoza, R.; Eom, H. J.; Block, D. E.; Mills, D. A. Utilization of galactooligosaccharides by *Bifidobacterium longum* subsp. *infantis* isolates. *Food Microbiol.* **2013**, *33*, 262−270.
(23) Kim, J. H.; An, H. J.; Garrido, D.; German, J. B.; Lebrilla, C. B.; Millset, D. A. Proteomic analysis of *Bifidobacterium longum* subsp. *infantis* reveals the metabolic insight on consumption of prebiotics and host glycans. *PLoS One* **2013**, *8*, 1−13.
(24) O'Connell, M. M.; Kinsella, M.; Fitzgerald, G. F.; van Sinderen, D. Transcriptional and functional characterization of genetic elements involved in galacto-oligosaccharide utilization by *Bifidobacterium breve* UCC2003. *Microb. Biotechnol.* **2013**, *6*, 67−79.
(25) Tabachnikov, O.; Shoham, Y. Functional characterization of the galactan utilization system of *Geobacillus stearothermophilus*. *FEBS J.* **2013**, *28*, 950−964.
(26) Andersen, J. M.; Barrangou, R.; Hachem, M. A.; Lahtinen, S.; Goh, Y. J.; Svensson, B.; Klaenhammer, T. R. Transcriptional and functional analysis of galactooligosaccharide uptake by lacS in *Lactobacillus acidophilus*. *Proc. Natl. Acad. Sci. U.S.A.* **2011**, *108*, 17785−17790.
(27) Andersen, J. M.; Barrangou, R.; Hachem, M. A.; Lahtinen, S. J.; Goh, Y. J.; Svensson, B.; Klaenhammer, T. R. Transcriptional analysis of prebiotic uptake and catabolism by *Lactobacillus acidophilus* NCFM. *PLoS One* **2012**, *7*, 1−12.
(28) Goulas, T.; Goulas, A.; Tzortzis, G.; Gibson, G. R. Expression of four beta-galactosidases from *Bifidobacterium bifidum* NCIMB41171 and their contribution on the hydrolysis and synthesis of galactooligosaccharides. *Appl. Microbiol. Biotechnol.* **2009**, *84*, 899−907.
(29) Zhang, Z.; Wang, H.; Yang, R. J.; Jiang, X. A novel spectrophotometric method for quantitative determination of lactulose in food industries. *Int. J. Food Sci. Technol.* **2010**, *45*, 258−264.
(30) Roberfroid, M. B. Prebiotics: Preferential substrates for specific germs? *Am. J. Clin. Nutr.* **2001**, *73*, 406S−409S.
(31) Cecchini, D. A.; Laville, E.; Laguerre, S.; Robe, P.; Leclerc, M.; Doré, J.; Henrissat, B.; Remaud-Siméon, M.; Monsan, P.; Potocki-Véronèse, G. Functional metagenomics reveals novel pathways of prebiotic breakdown by human gut bacteria. *PLoS One* **2013**, *8*, No. e72766.
(32) Whitman, W. B.; Coleman, D. C.; Wiebe, W. J. Prokaryotes: The unseen majority. *Proc. Natl. Acad. Sci. U.S.A.* **1998**, *95*, 6578−6583.
(33) Moynihan, P. J.; Ferrier, S.; Blomley, S.; Wright, W. G.; Russell, R. R. Acid production from lactulose by dental plaque bacteria. *Lett. Appl. Microbiol.* **1998**, *27*, 173−177.
(34) Marín-Manzano, M. C.; Abecia, L.; Hernandez-Hernandez, O.; Sanz, M. L.; Montilla, A.; Olano, A.; Rubio, L. A.; Moreno, F. J.; Clemente, A. Galacto-oligosaccharides derived from lactulose exert a selective stimulation on the growth of *Bifidobacterium animalis* in the large intestine of growing rats. *J. Agric. Food Chem.* **2013**, *61*, 7560−7567.
(35) Ignatova, T.; Iliev, I.; Kirilov, N.; Vassileva, T.; Dalgalarrondo, M.; Haertlé, T.; Chobert, J. M.; Ivanova, I. Effect of oligosaccharides on the growth of *Lactobacillus delbrueckii* subsp. *bulgaricus* strains isolated from dairy products. *J. Agric. Food Chem.* **2009**, *57*, 9496−9502.

Table 1. Range of Average Leaf and Stem Particle Sizes, Stem Diameters, and Country of Origin (According to Manufacturer Information) of the Four Analyzed *C. incanus* Herbal Teas (Samples 1−4)

| | sample 1 | | sample 2 | | sample 3 | | sample 4 | |
|---|---|---|---|---|---|---|---|---|
| compound | leaves | stems | leaves | stems | leaves | stems | leaves | stems |
| particle size (mm) | 1.0−7.0 | 2.0−15.0 | 1.0−7.0 | 4.0−15.0 | 1.0−5.0 | 3.0−10.0 | 1.0−4.0 | 3.0−7.0 |
| diameter (mm) | | 0.5−4.0 | | 0.5−3.0 | | 0.5−3.0 | | 0.5−1.0 |
| country of origin | Greece | | Greece | | unknown | | Turkey | |

stem parts in their *C. incanus* herbal teas. As a result, the particle size also varies widely in such products.

So far, some studies have investigated the phenolic compounds in different *Cistus* species, but in these studies only the leaves[19,20] or aerial parts of *Cistus* plants have been analyzed, which presumably consisted of an undefined mixture of leaves and a few stems as well as some blossoms.[2,12,21−23] Especially in some regions in northern Greece, hot water extracts from aerial parts consisting of dominantly woody and less leafy parts of *C. incanus* have been traditionally used as remedies.[3] However, until today no reliable scientific data seem to be available for the distribution of bioactive phenolic compounds in the leaves or the woody stem parts of *C. incanus*.

With regard to the brewing references recommended (by the manufacturers), hot water extractability represents a very critical factor in yielding herbal tea infusions with high concentrations of phenolic compounds. In a previous work, the influence of brewing process factors such as the type of water, temperature, and brewing duration on the phenolic compounds in *C. incanus* infusions was demonstrated.[10] To augment these results, a potential influence of herbal particle size on the extractability of bioactive phenolic compounds in *C. incanus* infusions should be taken into consideration in the current study.

For investigating the presence of bioactive phenolic compounds in *C. incanus* herbal tea, four commercially available products were manually divided into leaves and woody stems. However, there are only a few manufacturers that sell products with a high amount of woody stems, but especially these products are highly advertised for their health-preventive properties. The resulting infusions were analyzed for the presence and concentration of phenolic compounds. Additionally, the separated plant parts were reconstituted into three defined mixtures. As chemical analytical marker, the amount of woody parts of these model samples was determined by cellulose concentrations and sugar profiles.

Furthermore, one *C. incanus* herbal tea was exemplarily separated by the use of a laboratory sieving machine into six fractions of different particle sizes with recognizable leafy and woody parts to investigate the extractability and the influence of particle size on the phenolic substances in the corresponding infusions. By use of LC-DAD-ESI-MS/MS the phenolic compounds were identified, and 22 substances were quantitated by LC-DAD. The chemical reactivity of these quantitated phenolic compounds was estimated using LC-onlineTEAC data published previously for the Trolox equivalent antioxidant capacity (TEAC) of the single compounds in *C. incanus* infusions.[10]

The aim of this study was to investigate the influence of the herbal leaf content and particle size on the concentration of quantitated bioactive phenolic compounds in *C. incanus* infusions. Besides the importance for the consumers with regard to potential health beneficial effects, these data might be of certain importance for a re-evaluation of the persisting *Novel Food* status of *C. incanus* products in the European Community.

## MATERIALS AND METHODS

**Chemicals.** Gallocatechin (≥98%), myricitrin (≥99%), quercitrin hydrate (≥78%), procyanidin B1 (≥90%), *trans*-ferulic acid (99%), copper(II) sulfate pentahydrate (Ph. Eur.), and sodium carbonate (99.5%) were purchased from Sigma-Aldrich Chemie GmbH (Schnelldorf, Germany). Catechin (∼CHR), formic acid (≥98%), D-(+)-xylose (>99%), and D-(+)-glucose (≥99.5%) were purchased from Carl Roth GmbH & Co. KG (Karlsruhe, Germany). Tiliroside (96%) was purchased from PhytoLab GmbH & Co. KG (Vestenbergsgreuth, Germany). Gallic acid (98%) was purchased from Acros Organics BVBA (Geel, Belgium). Ellagic acid (≥98%) and myricetin-3-*O*-galactoside (≥99%) were purchased from Extrasynthese SAS (Genay, France). Ammonia solution (25% p.a.) and petroleum ether (40−60 °C) were purchased from Th. Geyer GmbH & Co. KG. (Renningen, Germany). Acetone, ethanol, sulfuric acid (>95%), boric acid, and bicinchoninic acid were purchased from Fisher Scientific GmbH (Schwerte, Germany). Glacial acetic acid, methanol, and acetonitrile were purchased from VWR International GmbH (Darmstadt, Germany). Potassium tetraborate (99.5%) was purchased from ChemPur GmbH (Karlsruhe, Germany). MCI Gel CA08F was purchased from Mitsubishi Chemical Corp. (Tokyo, Japan). L-Aspartic acid (Ph. Eur.) and amylase was purchased from Merck KGaA (Darmstadt, Germany). Amyloglucosidase was purchased from Roche Diagnostics GmbH (Mannheim, Germany). Polyamide 6 (particle size = 0.05−0.16 mm) was purchased from Macherey-Nagel GmbH & Co. KG (Düren, Germany). All solvents were of LC grade, and water was of Milli-Q-quality.

**Plant Material.** Four commercially available products of *C. incanus* herbal teas were used as a basis for this study. Leaf particles and woody stem parts as well as some blossoms were recognizable in all samples. The average sizes of leaves and stems, the stem diameters, and the country of origin of the four herbal teas are presented in Table 1. For the determination of a possible influence of the leaf and wood contents on the presence of phenolic compounds in the infusions, the four herbal samples were manually sorted into woody stems and leaves. Furthermore, three mixtures of sample 1 were reconstituted exemplarily from the stems (st1; "st" stands for *sorted*) and leaves (st5), resulting in preparations with (st2) 25% (w/w), (st3) 50% (w/w), and (st4) 75% (w/w) leaf content and corresponding woody stem contents of 75% (w/w), 50% (w/w), and 25% (w/w). In Figure 1A samples st1, st3, and st5 are shown for the manually sorted herbal teas. In a second series of experiments, investigating the extractability of the phenolic compounds with regard to particle size, *C. incanus* herbal tea sample 1 was exemplarily separated by use of a laboratory sieving machine Typ 3D from Retsch GmbH (Haan, Germany) into six fractions with the sizes (sample sv1; "sv" stands for *sieved*) 2.5−3.1 mm, (sv2) 2.0−2.5 mm, (sv3) 1.4−2.0 mm, (sv4) 1.0−1.4 mm, (sv5) 0.5−1.0 mm, and (sv6) <0.5 mm. All fractions contained recognizable parts of leaves and stem parts (Figure 1B).

**Sample Preparation.** *C. incanus* herbal tea (1.25 g) was brewed in 45 mL of water at a temperature of 95 °C for 5 min. The brewing time and temperature were used according to manufacturer recommendations for the preparation of the infusions. After centrifugation (centrifuge 5810 R, Eppendorf GmbH, Hamburg, Germany) for 10 min at 3220*g*, an aliquot of 35 mL was taken of the supernatant. Lyophilization of the aliquot using a lyophilizer (Alpha 1-4 LSC,

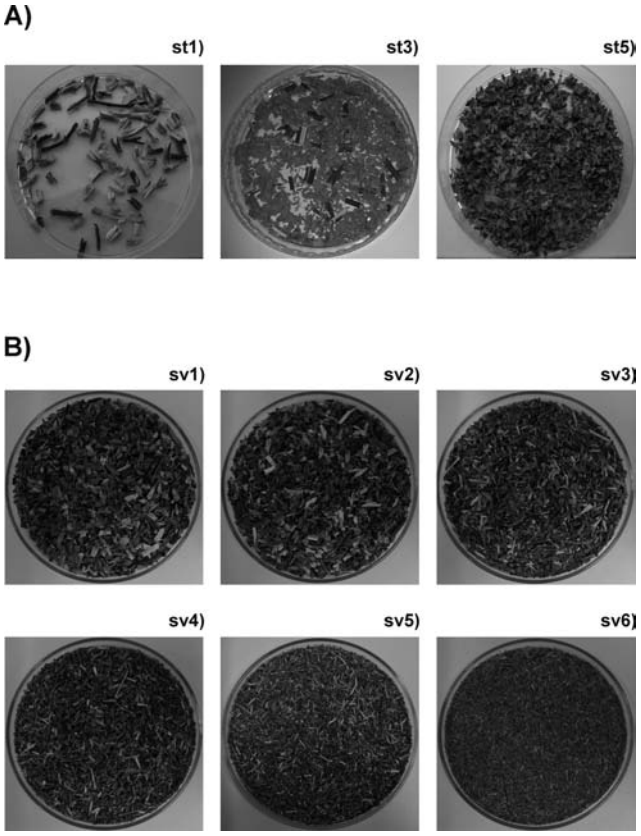


**Figure 1.** (A) Three manually sorted *C. incanus* herbal teas (of sample 1). Plant part composition of samples: (st1) 0% (w/w) leaves and 100% (w/w) woody stems; (st3) 50% (w/w) leaves and 50% (w/w) woody stems; (st5) 100% (w/w) leaves and 0% (w/w) woody stems. (B) Sieved *C. incanus* herbal teas (of sample 1) containing leaves and woody stem parts. Average particle sizes of herb material: (sv1) 2.8 mm; (sv2) 2.3 mm; (sv3) 1.7 mm; (sv4) 1.2 mm; (sv5) 0.8 mm; (sv6) 0.3 mm.

Martin Christ GmbH, Osterode, Germany) and dissolving the dry residues in 4 mL of water followed. The next step in sample preparation included a solid phase extraction (SPE) according to a method of Breitfellner et al.[24] using polyamide 6 as stationary phase and two elutions, one with methanol and one with ammonia containing methanol, for purification and fractionation. After drying under a stream of nitrogen overnight, redissolving in 4 mL of methanol 70%, and syringe filtration (0.45 $\mu$m nylon membrane), the extracts were ready for analyses.[10] The extracted herb was air-dried at room temperature for about 72 h. An accelerated solvent extraction (ASE) with four solvents of different polarities followed for a ful extraction of all soluble substances of herb material. The insoluble cellulose was determined of the fully extracted *C. incanus* herb resulting from the brewing process and ASE. The used methods for ASE and determination of wood sugar and cellulose concentrations are described below.

**Analysis of the Wood Content.** For analyzing the wood content in the sorted leaf and woody stem samples (st1−st5), the cellulose concentrations and sugar profiles of the stems were measured as analytical markers. Following the determination of the dry weight, 0.5 g of each manually sorted sample was extracted in duplicate by use of an accelerated solvent extraction system ASE 200 (Dionex GmbH, Idstein, Germany). Two extraction cycles with 10 mL of solvent were performed for 10 min at 70 °C and 10 MPa for each solvent. The following solvents were used gradually: petroleum ether, acetone/water (9:1), ethanol/water (8:2), and water. After air-drying at room temperature for about 24 h ("climatization") and milling with a laboratory disk mill Typ T 1000 from Siebtechnik GmbH (Mühlheim, Germany), the ASE residues were subjected to a two-stage hydrolysis. For the prehydrolysis 200 mg of the milled material was mixed with 2 mL of 72% sulfuric acid in a reaction tube and hydrolyzed under repeated stirring at 30 °C for 1 h on a thermostat. The reaction was stopped by adding 6 mL of water. Afterward, the prehydrolyzed sample was transferred with 50 mL of water in a 100 mL volumetric flask. For posthydrolysis the pretreated sample was hydrolyzed at 120 °C and 0.12 MPa for 30 min in an autoclave. After cooling, filling to the calibration mark with water and subsequent agitation, filtration over a G4 sintered glass crucible, and washing the hydrolysis residue acid-free with water followed. After drying at 105 °C, the residue was determined gravimetrically. With regard to wood chemistry, this residue represents the acid-insoluble lignin (Klason lignin). The hydrolysates were analyzed with regard to their glucose and xylose contents by borate anion exchange chromatography.[25] Additionally, a test on starch was carried out for the 100% (w/w) woody stem (st1) and the 100% (w/w) leaf sample (st5) to evaluate if the glucose results from cellulose or from starch hydrolysis. For this purpose, the two samples described were finely milled by use of a disk mill, 200 mg was weighed in a 25 mL volumetric flask, and 20 mL of methanol/water (3:1) was added. After shaking thoroughly by hand, the solution was incubated for about 15 h and filtered over a G4 sintered glass filter. The filtration residues were washed with 20 mL of methanol/water (3:1) and climatized for 5 days. Afterward, 25 mg of the residues was incubated with 0.75 mL of enzyme solution (0.05% amylase and 0.05% amyloglucosidase in 0.1 M ammonium acetate buffer, pH 4.7) at 45 °C for 24 h. After filtration of the solutions, the glucose concentration was determined by borate anion exchange chromatography[25] and corrected for an enzyme blank. All monosaccharide and starch concentrations were based on the original raw material under consideration of the various extraction losses. The cellulose content of samples was calculated from the glucose concentration by subtracting the glucose from starch and considering the weight gain due to water addition during hydrolysis (−10%).

**Identification and Quantification of the Phenolic Compounds.** Identification of the phenolic compounds was previously described by Riehle et al.[10] Following SPE cleanup of the *C. incanus* infusions, the phenolic substances in both eluates, one methanolic and one ammonia−methanol eluate, were identified by LC-DAD-ESI-MS/MS.

For the quantitation of the phenolic compounds, stock solutions of standard substances were prepared at a concentration level of 1 mg/mL. For the calibration curves, seven equidistant concentrations of each standard were prepared, and the purity of standard substances was considered in the calculations. A coefficient of determination with $R^2 = 0.99$ resulted for all calibrations curves. As there are no standards commercially available for all compounds, some were quantitated by the use of structural relatives. Thus, methyl gallate was quantitated as gallic acid and gallocatechin−catechin as procyanidin B1, myricetin-*O*-xyloside as myricitrin, myricetin-3-*O*-glucoside as myricetin-3-*O*-galactoside, glycosides of quercetin as quercitrin, hexahydroxydiphenoyl-glucose and ellagic acid-7-*O*-xyloside as ellagic acid, and hydroxyferulic acid-*O*-rhamnosides and hydroxyferuloyl-rhamnose as *trans*-ferulic acid. The corresponding correction factors for the difference in molecular weight were included in the calculation of substance concentrations. For the quantitation of gallocatechin−catechin as procyanidin B1, it has to be considered that the absorption of the gallocatechin subunit was lower compared to the absorption of the catechin subunit in procyanidin B1. Consequently, the absolute results for gallocatechin−catechin concentrations are slightly higher. For the measurements, the LC-DAD method according to Riehle et al.[10] was used. Hydroxybenzoic acids, ellagitannins, and flavanols were detected at a wavelength of 280 nm, hydroxycinnamic acids at 325 nm, and the flavonols at 350 nm.

**Statistical Analysis.** Two *C. incanus* infusions of each sample were brewed and analyzed twice. The standard deviation was calculated, and the averaged values along with the standard deviations are documented in the corresponding figures. The calibration curves for quantitation were also analyzed twice.

**Table 2. Quantitated Phenolic Compounds in *C. incanus* Infusions: Compound no., MS Data, Retention Times, and Corresponding SPE Eluates**

| no. | compound | $[M-H]^-$ ($m/z$) | MS/MS fragments (relative intensity %) ($m/z$) | | | | | | | | | | $t_R$[a] (min) | SPE eluate[b] |
|---|---|---|---|---|---|---|---|---|---|---|---|---|---|---|
| **1** | gallic acid | 169 | 125 | (100) | | | | | | | | | 2.9 | MeOH |
| **2** | gallocatechin | 305 | 287 | (4) | 261 | (35) | 221 | (82) | 219 | (90) | 179 | (100) | 5.6 | MeOH |
| **3** | gallocatechin-(4$\alpha$-8)-catechin or catechin-(4$\alpha$-8)-gallocatechin | 593 | 575 | (3) | 467 | (10) | 425 | (100) | 407 | (28) | 289 | (14) | 6.6 | MeOH |
| **4** | catechin | 289 | 271 | (3) | 245 | (100) | 205 | (38) | 179 | (14) | | | 11.6 | MeOH |
| **5** | myricetin-3-*O*-galactoside | 479 | 461 | (1) | 317 | (87) | 316 | (94) | 271 | (2) | 179 | (4) | 19.5 | MeOH |
| **6** | myricetin-3-*O*-glucoside | 479 | 461 | (3) | 317 | (94) | 316 | (98) | 271 | (1) | 179 | (4) | 19.8 | MeOH |
| **7** | myricetin-*O*-xyloside | 449 | 431 | (4) | 317 | (51) | 316 | (100) | 271 | (1) | 179 | (4) | 21.9 | MeOH |
| **8** | myricitrin | 463 | 445 | (1) | 317 | (83) | 316 | (100) | 179 | (4) | | | 23.0 | MeOH |
| **9** | quercetin-3-*O*-galactoside | 463 | 445 | (1) | 301 | (100) | 179 | (3) | | | | | 23.7 | MeOH |
| **10** | quercetin-3-*O*-glucoside | 463 | 445 | (1) | 301 | (100) | 179 | (2) | | | | | 23.2 | MeOH |
| **11** | quercetin-*O*-xyloside | 433 | 301 | (100) | 179 | (2) | | | | | | | 26.6 | MeOH |
| **12** | quercitrin | 447 | 429 | (1) | 301 | (100) | 179 | (1) | | | | | 28.3 | MeOH |
| **13** | *trans*-tiliroside | 593 | 447 | (13) | 307 | (7) | 285 | (100) | 257 | (2) | | | 41.1 | MeOH |
| **14** | *cis*-tiliroside | 593 | 447 | (13) | 307 | (7) | 285 | (100) | 257 | (2) | | | 42.5 | MeOH |
| **15** | methyl gallate | 183 | 139 | (100) | | | | | | | | | 2.6 | MeOH/$NH_3$ |
| **16** | hydroxyferulic acid-5-*O*-rhamnoside | 355 | 337 | (20) | 209 | (24) | 191 | (100) | 173 | (3) | 147 | (4) | 15.3 | MeOH/$NH_3$ |
| **17** | hydroxyferulic acid-4-*O*-rhamnoside | 355 | 337 | (14) | 209 | (24) | 191 | (100) | 173 | (3) | 147 | (2) | 17.7 | MeOH/$NH_3$ |
| **18** | hydroxyferuloylrhamnose | 355 | 337 | (17) | 209 | (22) | 191 | (100) | 173 | (3) | 147 | (3) | 22.3 | MeOH/$NH_3$ |
| **19** | HHDP-glucose[c] isomer | 482 | 464 | (3) | 450 | (33) | 406 | (3) | 300 | (100) | 271 | (5) | 27.1 | MeOH/$NH_3$ |
| **20** | HHDP-glucose isomer | 481 | 463 | (20) | 449 | (100) | 405 | (16) | 299 | (54) | 270 | (7) | 28.7 | MeOH/$NH_3$ |
| **21** | ellagic acid-7-*O*-xyloside | 433 | 301 | (100) | | | | | | | | | 35.8 | MeOH/$NH_3$ |
| **22** | ellagic acid | 301 | 257 | (11) | 229 | (7) | 185 | (1) | | | | | 33.8 | MeOH/$NH_3$ |

[a] $t_R$, retention time during LC-DAD analysis. [b] MeOH, methanolic SPE eluate; MeOH/$NH_3$, ammonia containing methanolic SPE eluate. [c] HHDP-glucose, hexahydroxydiphenoylglucose.

**Table 3. Total ASE Extract Content, Hydrolysis Residues, Contents of Glucose, Xylose, and Sum of Glucose and Xylose as well as Cellulose Contents of Sample 1 Sorted *C. incanus* Herbal Teas (st1−st5)[a]**

| sample | leaf parts (% w/w) | stem parts (% w/w) | total ASE extract content (%) | hydrolysis residue (%) | glucose (%) | xylose (%) | glucose + xylose (%) | cellulose (%) | glucose (from starch) (%) |
|---|---|---|---|---|---|---|---|---|---|
| st1 | 0 | 100 | 2 | 26 | 34 | 21 | 55 | 30 | 1 |
| st2 | 25 | 75 | 7 | 26 | 29 | 17 | 46 | 26 | |
| st3 | 50 | 50 | 12 | 28 | 24 | 13 | 37 | 21 | |
| st4 | 75 | 25 | 18 | 31 | 19 | 9 | 28 | 17 | |
| st5 | 100 | 0 | 22 | 35 | 14 | 5 | 19 | 12 | 1 |

[a] Glucose values of the starch test are shown for samples st1 and st5.

## RESULTS AND DISCUSSION

**Identification of the Phenolic Compounds.** *C. incanus* infusions include a wide range of phenolic compounds of different substance classes. According to Riehle et al.,[10] 32 phenolic compounds, belonging to the subclasses of phenolic acids, flavonoids, and ellagitannins, were detected. In addition to the previously identified phenolic compounds, a 4-*O*-rhamnoside and a 5-*O*-rhamnoside of hydroxyferulic acid as well as a hydroxyferuloyl-rhamnose have been tentatively identified by LC-DAD-ESI-MS/MS in this study. Such *O*-glycosylated phenolic acids were also previously identified by Barrajón-Catalán et al.[2] for *Cistus albidus*, another species of the plant family Cistaceae. From the substances identified, the 22 dominant phenolic compounds in the *C. incanus* infusions have been quantitated with LC-DAD. Table 2 gives an overview of these compounds, their retention times, and MS and MS/MS data as well as their distribution in the two SPE eluates.

**Leaf and Wood Contents of the Manually Sorted Samples.** For the investigation of the influence of herbal leaf and wood content on the composition of phenolic compounds in *C. incanus* infusions, four herbal tea samples were manually sorted into woody stems and leaves. Besides sample st1 with 100% (w/w) and st5 with 0% (w/w) woody stem parts, *C. incanus* herbal tea sample 1 was exemplarily reconstituted into three defined mixtures of stems and leaves on the basis of their dry weight: (st2) 75% (w/w), (st3) 50% (w/w), and (st4) 25%


dx.doi.org/10.1021/jf504119s | J. Agric. Food Chem. 2014, 62, 10978−10988

Table 4. Concentration (Milligrams per 100 mL) of Phenolic Compounds in Four Samples of *C. incanus* Infusions Brewed from Manually Sorted Herbal Teas Including 100% (w/w) Leaves and 100% (w/w) Stems

| | | sample 1 | | sample 2 | | sample 3 | | sample 4 | |
|---|---|---|---|---|---|---|---|---|---|
| no. | compound | leaves | stems | leaves | stems | leaves | stems | leaves | stems |
| 1 | gallic acid | 1.1 ± 0.03 | 0.1 ± 0.00 | 1.1 ± 0.02 | 0.2 ± 0.01 | 1.1 ± 0.01 | 0.3 ± 0.01 | 1.2 ± 0.01 | 0.4 ± 0.03 |
| 2 | gallocatechin | 1.7 ± 0.17 | nd[a] | 1.6 ± 0.06 | 0.2 ± 0.02 | 1.0 ± 0.10 | 0.2 ± 0.02 | 0.7 ± 0.04 | nd |
| 3 | gallocatechin-(4$\alpha$-8)-catechin or catechin-(4$\alpha$-8)-gallocatechin | 0.8 ± 0.06 | nd | 0.9 ± 0.10 | 0.2 ± 0.01 | 0.7 ± 0.02 | 0.2 ± 0.02 | 0.8 ± 0.08 | 0.3 ± 0.02 |
| 4 | catechin | 0.8 ± 0.04 | 0.5 ± 0.05 | 1.2 ± 0.06 | 1.1 ± 0.07 | 0.6 ± 0.06 | 0.9 ± 0.04 | 0.4 ± 0.02 | 0.3 ± 0.02 |
| 5 | myricetin-3-*O*-galactoside | 3.2 ± 0.16 | nd | 1.4 ± 0.06 | 0.1 ± 0.00 | 2.1 ± 0.03 | 0.1 ± 0.01 | 1.4 ± 0.03 | 0.1 ± 0.01 |
| 6 | myricetin-3-*O*-glucoside | 0.4 ± 0.03 | nd | 0.2 ± 0.01 | nd | 0.2 ± 0.01 | nd | 0.2 ± 0.01 | nd |
| 7 | myricetin-*O*-xyloside | 1.1 ± 0.11 | nd | 0.4 ± 0.01 | nd | 0.7 ± 0.03 | nq[b] | 0.4 ± 0.02 | nq |
| 8 | myricitrin | 8.4 ± 0.22 | nd | 5.8 ± 0.12 | 0.1 ± 0.02 | 4.7 ± 0.09 | 0.2 ± 0.01 | 8.4 ± 0.19 | 0.5 ± 0.01 |
| 9 | quercetin-3-*O*-galactoside | 0.8 ± 0.03 | nd | 0.6 ± 0.03 | 0.1 ± 0.01 | 1.3 ± 0.06 | 0.1 ± 0.01 | 0.5 ± 0.02 | 0.1 ± 0.01 |
| 10 | quercetin-3-*O*-glucoside | 0.1 ± 0.01 | nd | 0.1 ± 0.01 | nq | 0.2 ± 0.02 | nq | 0.1 ± 0.01 | nq |
| 11 | quercetin-*O*-xyloside | 0.4 ± 0.03 | nd | 0.4 ± 0.17 | nq | 0.4 ± 0.18 | 0.1 ± 0.01 | 0.3 ± 0.02 | nq |
| 12 | quercitrin | 1.6 ± 0.04 | nd | 1.0 ± 0.05 | 0.1 ± 0.01 | 0.8 ± 0.01 | 0.2 ± 0.01 | 1.8 ± 0.04 | 0.1 ± 0.01 |
| 13 | *trans*-tiliroside | 0.9 ± 0.04 | nd | 0.9 ± 0.05 | 0.1 ± 0.01 | 0.8 ± 0.02 | 0.2 ± 0.01 | 0.6 ± 0.03 | 0.1 ± 0.01 |
| 14 | *cis*-tiliroside | 0.3 ± 0.01 | nd | 0.3 ± 0.00 | nq | 0.3 ± 0.01 | nq | 0.2 ± 0.01 | nq |
| 15 | methyl gallate | 0.2 ± 0.01 | 0.1 ± 0.01 | 0.3 ± 0.02 | 0.1 ± 0.00 | 0.5 ± 0.02 | 0.2 ± 0.00 | 0.3 ± 0.03 | 0.2 ± 0.00 |
| 16 | hydroxyferulic acid-5-*O*-rhamnoside | 1.0 ± 0.06 | nd | 2.6 ± 0.25 | 0.1 ± 0.04 | 1.7 ± 0.06 | 0.4 ± 0.04 | 1.9 ± 0.11 | 0.2 ± 0.06 |
| 17 | hydroxyferulic acid-4-*O*-rhamnoside | 2.2 ± 0.18 | nd | 2.6 ± 0.15 | 0.4 ± 0.02 | 2.6 ± 0.10 | 0.9 ± 0.09 | 1.9 ± 0.11 | 0.5 ± 0.06 |
| 18 | hydroxyferuloyl-rhamnose | 0.6 ± 0.04 | nd | 1.0 ± 0.13 | nq | 1.3 ± 0.08 | 0.2 ± 0.03 | 1.1 ± 0.11 | nq |
| 19 | HHDP-glucose[c] isomer | 0.5 ± 0.03 | nd | 0.7 ± 0.15 | nd | 0.5 ± 0.01 | nd | 0.2 ± 0.02 | nd |
| 20 | HHDP-glucose isomer | 0.9 ± 0.07 | nd | 2.0 ± 0.10 | 0.1 ± 0.02 | 2.1 ± 0.05 | 0.3 ± 0.02 | 0.5 ± 0.05 | nd |
| 21 | ellagic acid-7-*O*-xyloside | 0.1 ± 0.03 | nd | 0.1 ± 0.03 | nd | 0.1 ± 0.01 | nd | 0.1 ± 0.02 | nd |
| 22 | ellagic acid | 0.7 ± 0.05 | nd | 0.4 ± 0.01 | 0.1 ± 0.01 | 0.4 ± 0.02 | 0.1 ± 0.01 | 0.2 ± 0.02 | 0.1 ± 0.01 |

[a]nd, not detectable. [b]nq, not quantitatable. [c]HHDP-glucose, hexahydroxydiphenoylglucose.

(w/w) woody stem parts. To monitor the biochemical "real" wood contents of these exemplarily sorted *C. incanus* herbal teas, the results from acid hydrolysis and carbohydrate analysis were considered (Table 3). With regard to wood chemistry, the residue from a sulfuric acid hydrolysis represents the acid-insoluble lignin content of the sample (Klason lignin). However, for the various *C. incanus* samples, the hydrolysis residue was always in a similar order of magnitude and did not correlate with the ratio of stem and leaf material. This indicates that other components, for example, protein from the leaves, are as well incorporated into the residue. Accordingly, this value is not suitable to monitor the proportion of leaf and stem material. Alternatively, the polysaccharide components of the material have been considered. The sum of glucose and xylose combines the main components, representing the cellulose and hemicelluloses content of the samples. In addition, the cellulose content was calculated. In Table 3, the corresponding values of the five samples (st1−st5) prepared from the leaves and stems of sample 1, manually separated and then mixed according to fixed ratios, as well as the concentrations of glucose resulting of starch of the 100% (w/w) woody stem (st1), and 100% (w/w) leaf sample (st5) are presented. Strongly linear positive correlating concentrations of glucose and xylose with an increasing amount of woody plant parts ($R^2$ = 0.99) were revealed. The low glucose values of 1% in the starch test indicated that the glucose, which was used for the calculation of cellulose, did not significantly result from starch hydrolysis. On the basis of the starch test results, a correction factor of 1% was included in the calculation of the absolute cellulose concentration. Altogether, the cellulose contents of manually sorted *C. incanus* herbal teas can be used as a valid analytical marker for wood contents.

**Presence of Phenolic Compounds Depending on the Plant Parts of the Herbal Tea Mixture.** The presence of the 22 quantitated phenolic compounds in the resulting infusions brewed from the four herbal tea samples sorted into woody stems and leaves is shown in Table 4. In all four samples higher concentrations of quantitated phenolic compounds were present in the infusions brewed from the sorted leaves compared to the stems. Furthermore, several of the 22 quantitated compounds were not even detectable in the infusions brewed from stems. Especially in sample 1, which included the longest stems with the largest diameters of the four *C. incanus* herbal tea samples analyzed, only gallic acid, catechin, and methyl gallate were detected in infusions brewed from stems. A remarkable exception was the catechin concentration. In the four infusions brewed from *C. incanus* stems, comparatively high concentrations of this phenolic compound from 0.3 to 1.1 mg/100 mL infusion were quantitated. In sample 3, the concentration in the infusion brewed from stems (0.9 mg/100 mL) was even higher compared to the infusion brewed from *C. incanus* leaves (0.6 mg/100 mL). Altogether there were differences in the concentrations of the quantitated phenolic compounds between the infusions brewed from four *C. incanus* herbal teas. These differences were maybe a result from different plant origins, ecophysiological factors, cultivation conditions, or harvest time. For example, the plant materials of samples 1 and 2 were harvested in Greece, sample 4 was from Turkey, and the origin of sample 3 was not available. In the discussion of the varying presence of phenolic compounds in *C. incanus* plant parts, the plant physiological properties and harvest time of these Mediterranean shrubs should be considered, too. These plants have been classified as malakophyllous xerophytes[4,26]

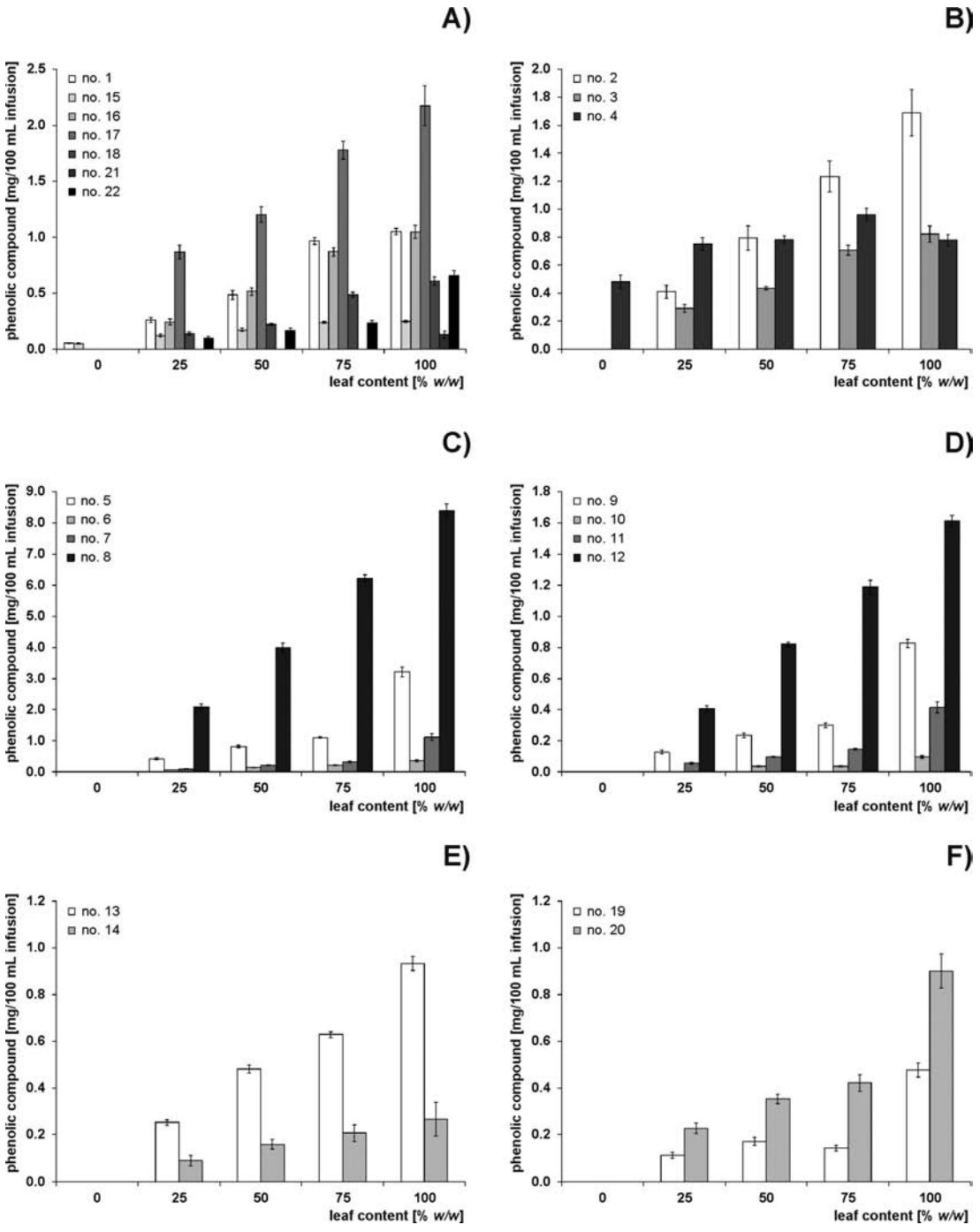


**Figure 2.** Contents of 22 phenolic compounds in five *C. incanus* infusions brewed from herbal mixtures (of sample 1) with leaf contents of 0% (w/w), 25% (w/w), 50% (w/w), 75% (w/w), and 100% (w/w) and corresponding woody stem contents of 100% (w/w), 75% (w/w), 50% (w/w), and 0% (w/w): (A) phenolic acids; (B) flavan-3-ols and dimers; (C) myricetin glycosides; (D) quercetin glycosides; (E) tiliroside isomers; (F) ellagitannins. For compound no. refer to Table 2.

and are drought resistant with seasonal dimorphism of the leaves.[27] The plants of this genus develop small leaves with numerous trichomes during dry summer periods for minimization of transpiration and leaves with only few trichomes in winter.[27] According to Christodoulakis et al.,[28] the prominent feature of *C. incanus* summer leaves is an intense accumulation of phenolic secondary metabolites, whereas in less climatically stressed winter leaves, a lower accumulation can be observed. Similar effects have been already shown for environmental stress factors such as drought, which significantly increased concentrations of bioactive phenolic compounds in *Cistus clusii* leaves, for example.[29] Therefore, investigating the influence of seasonal leaf polymorphism on the presence of phenolic compounds in *C. incanus* can be a scientific basis for further research. Altogether, a tentative indication of the ecophysiological variation in the concentrations of phenolic compounds in different *C. incanus* herbal products and plant parts is represented by the results of the four traditional herbal tea samples of this work.

Subsequently, the concentrations of the 22 quantitated phenolic compounds in the infusions brewed from the mixtures (st1−st5) of *C. incanus* sample 1 are shown along six chosen phenolic substance classes. In Figure 2, the influence of the leaf content on the concentration of phenolic acids (A), flavan-3-ols and their dimers (B), myricetin glycosides (C), quercetin glycosides (D), tiliroside isomers (E), and ellagitannins (F) is shown for *C. incanus* woody stems (st1) and leaves (st5) as well as for the three reconstituted mixtures (samples st2−st4). The strongest correlations in the class of phenolic acids between leaf content and presence of substance resulted for gallic acid ($R^2$ = 0.96) and methyl gallate ($R^2$ = 0.95). Furthermore, these two compounds were present in infusions brewed from the 100% (w/w) woody stem sample (st1), too. Concentrations for both gallic acid derivatives ranged from 0.1 mg/100 mL infusion (st1) to 1.1 mg/100 mL infusion (st5) and for methyl gallate from 0.1 mg/100 mL infusion (st1) to 0.3 mg/100 mL infusion (st5). This result illustrates that up to 11-fold higher concentrations of gallic acid can be yielded when *C. incanus* infusions are brewed from a herbal preparation consisting of 100% (w/w) pure leaves. As shown in a previous work, gallic acid is one of the most reactive phenolic compounds in *C. incanus* infusions, as it is responsible for about 11% of the total TEAC.[10] For the other phenolic acids a similar occurrence in woody stem and leaf parts was observed, too.

With regard to the class of flavan-3-ols (catechins) and their oligomers, the strongest correlation between leaf content of *C. incanus* herbal tea sample 1 and the presence of phenolic substance was found for gallocatechin ($R^2$ = 0.99). The gallocatechin concentrations ranged from 0.0 mg/100 mL infusion (st1) to 1.7 mg/100 mL infusion (st5). For the antioxidant capacity and bioactivity of *C. incanus* infusions, the presence of gallocatechin is an important aspect. This substance contributes 14% of total TEAC.[10]

In contrast to the gallocatechin concentrations, remarkably high catechin concentrations of 0.5 mg/100 mL infusion were quantitated in the sample consisting of 100% (w/w) stems (st1). These comparatively high concentrations of catechin in woody parts of *C. incanus* may also be an argument for the traditional application of the aerial parts, including woody stems, for herbal infusions.[3,30] The presence of catechin and further flavan-3-ol derivatives in stems or bark is known for many other plants of different plant families and orders.[31−33] Besides the occurrence of catechin in woody plant parts, higher concentrations were reported for leaves.[34,35] The presence of catechin in leaves and woody stems of *C. incanus* also explains the quite low correlation of $R^2$ = 0.55 for the influence between the concentrations of this substance and leaf content of reconstituted samples. However, the presence of notable amounts of catechin in infusions brewed from woody stem parts of *C. incanus* is also important for antioxidant capacity. Catechin was responsible for 11% of total TEAC.[10]

Furthermore, for sensory properties of the infusion, the content of phenolic compounds can be important, too. According to Peleg et al.,[36] catechin monomers are responsible as they have a strong bitter taste and elicit a slight astringency. However, Scharbert et al.[37] described the catechin threshold concentration for astringency being approximately 11.9 mg/100 mL aqueous solution. Bitterness and astringency in *C. incanus* infusions therefore should be expected only at levels of 10-fold higher catechin concentrations. Furthermore, black and green teas provide astringency, and the content of catechin is almost similar in *C. incanus* infusions as given in polyphenol databases[14−16] and shown herein. Therefore, the combination and synergisms of different phenolic compounds have been taken into account. Again, Scharbert et al.[37] showed for some flavonol glycosides really low sensory threshold levels.

For the flavor of herbal infusions it should be also considered that an infusion brewed from 100% (w/w) *C. incanus* leaves exhibits a persistent "green odor". This odor arises from volatile compounds based on $C_6$-aldehydes and $C_6$-alcohols.[38,39]

With regard to the presence of flavonols in the five reconstituted herbal tea mixtures, the highest concentrations as well as the strongest correlations between leaf contents and amounts of phenolic compounds in *C. incanus* infusions were observed for myricitrin and quercitrin. Additionally, both can be detected only in samples that contained pure leaves. For myricitrin, the concentrations reached from 0.0 mg/100 mL infusion (st1) to 1.1 mg/100 mL infusion (st5) and for quercitrin from 0.0 mg/100 mL infusion (st1) to 1.6 mg/100 mL infusion (st5). The coefficient of determination for the leaf content of sample and concentrations of myricitrin as well as for quercitrin was $R^2$ = 0.99. Moreover, high concentrations of myricitrin in *C. incanus* infusions seem to be an important marker of bioactivity, as it is highly responsible for the infusion's total antioxidant capacity. This substance contributes to 17% of total TEAC.[10]

A similar distribution in herbal plant material was observed for the isomers of tiliroside. Both isomers were present in samples that contained only leaves (st5), but not in pure woody stems (st1). For the dominant isomer *trans*-tiliroside, concentrations ranged between 0.0 mg/100 mL infusion (st1) and 0.9 mg/100 mL infusion (st5). The correlation coefficient of $R^2$ = 0.99 again suggests a very good linearity between the amount of substance and leaf content in a sample.

With the exception of catechin an exclusive occurrence of all quantitated flavonoids in *C. incanus* infusions brewed from leafy parts was observed in this work for sample 1. In woody stem parts this substance class was not present.

For the presence of the class of ellagitannins, a similar trend but slightly weaker linear correlation was observed in samples st1−st5. For the hexahydroxydiphenoyl-glucose isomers, concentrations of 0.0 mg/100 mL infusion (st1) to 0.5 mg/100 mL infusion (st5) together with a correlation of $R^2$ = 0.76 were detected for the first isomer at a retention time of 27.1 min. Concentrations from 0.0 mg/100 mL infusion (st1) to 0.9 mg/100 mL infusion (st5) together with $R^2$ = 0.90 were analyzed for the second isomer at a retention time of 28.7 min. Both isomers are also important antioxidants. The first isomer is responsible for 6% and the second isomer for 14% of total TEAC in *C. incanus* infusions.[10]

From the results of this study, it can be concluded that most of the phenolic compounds in *C. incanus* are present in the leafy parts. The dominant presence in leaves was generally observed for most of the flavonoids, phenolic acids, and ellagitannins. Nevertheless, for consumer's acceptance, a balanced flavor is of equal importance, besides the amount of bioactive phenolic compounds. Infusions brewed from 100% (w/w) leaf material may be rejected because of an overpowering "green odor". However, there might be some unidentified or under the actual brewing conditions nonextractable compounds in woody stem parts of *C. incanus*. Varying extraction conditions, for example, multiple maceration or use of other solvents, can lead to different results. In this context, it also has to be considered that short-term boiled hot water extracts of the aerial parts have been traditionally used for the therapy of inflammatory skin

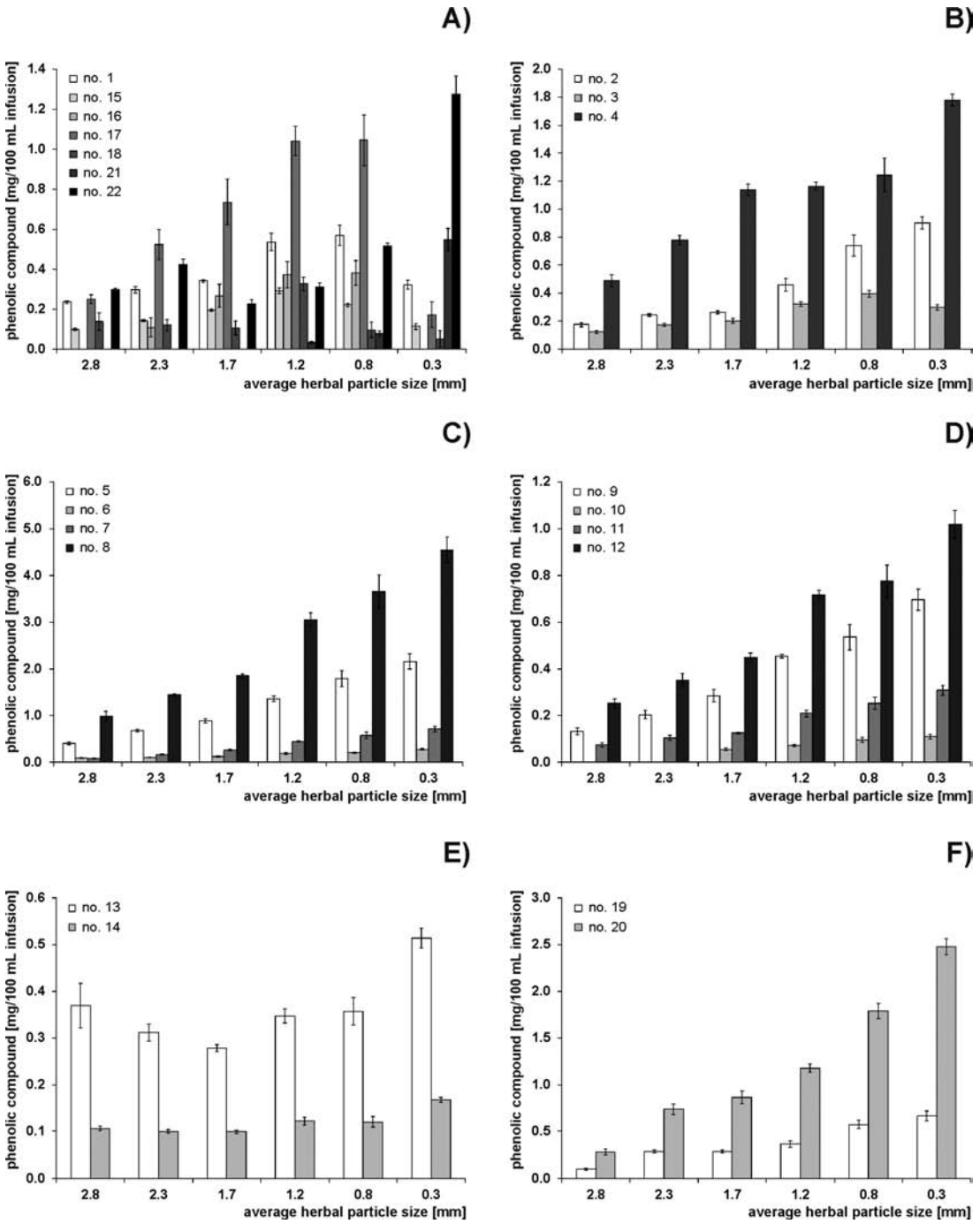


**Figure 3.** Contents of 22 phenolic compounds in six *C. incanus* infusions brewed from herbal material (of sample 1) with average particle sizes of 2.8, 2.3, 1.7, 1.2, 0.8, and 0.3 mm, all including recognizable leaf and stem parts (Figure 1 B): (A) phenolic acids; (B) flavan-3-ols and dimers; (C) myricetin glycosides; (D) quercetin glycosides; (E) tiliroside isomers; (F) ellagitannins. For compound no. refer to Table 2.

diseases, as well as for improved wound healing, whereas hot water extracts boiled for a longer time have been used as antidiarrhetics.[3] For this reason product optimization regarding stem and leaf contents of herbal tea mixtures and preparation guidelines are very important for infusions containing high concentrations of bioactive phenolic compounds with reference to the corresponding physiological property aimed at.

**Influence of Herbal Particle Size on the Extractability of Phenolic Compounds.** Besides the question of the presence of phenolic compounds in leaves or woody stem material of *C. incanus*, the different particle sizes of the herbal material may be also important for the extractability of bioactive compounds during the brewing process. To investigate a correlation between extractability of phenolic compounds and herbal particle size, exemplarily *C. incanus* herbal tea sample 1 was separated by use of a laboratory sieving machine into six fractions with different particle sizes (samples sv1−sv6). As obvious from Figure 1B, all sieved fractions contained recognizable parts of both leaves and woody stem parts. Figure 3 shows the influence of the herbal particle size on the concentration of 22 phenolic compounds in the resulting *C. incanus* infusions. This influence is demonstrated for the

phenolic substance classes of phenolic acids (A), flavan-3-ols and their dimers (B), myricetin glycosides (C), quercetin glycosides (D), tiliroside isomers (E), and ellagitannins (F).

For most of the phenolic acids quantitated in the six measured *C. incanus* infusions brewed from plant material with different average particle sizes from 0.3 to 2.8 mm, concentrations increased with decreasing particle size. For example, the concentration of hydroxyferulic acid-4-*O*-rhamnoside increased gradually from 0.3 mg/100 mL infusion (sv1) up to 1.1 mg/100 mL infusion (sv5). However, the lowest content of 0.2 mg/100 mL infusion for this compound was detected for infusions brewed from 0.3 mm herbal material (sv6). A similar negative correlation between particle size and concentration of phenolic compound was observed for gallic acid, methyl gallate, and hydroxyferulic acid-5-*O*-rhamnoside. For ellagic acid and ellagic acid-7-*O*-xyloside, the highest extraction yields were reached by use of herb material with an average particle size of 0.3 mm (sv6). Additionally, ellagic acid-7-*O*-xyloside only was present in quantitatable amounts in infusions brewed from herbal tea with particle size <1.7 mm (sv3). Furthermore, hydroxyferuloyl-rhamnose reached the highest concentration in the infusion resulting of *C. incanus* herbal tea with an average particle size of 1.2 mm (sv4). Altogether, the coefficients of correlation between particle size and concentration of phenolic compound were very low for phenolic acids in *C. incanus* infusions. However, all results for the extractability were based on actual preparation recommendations of the manufacturer. Longer extraction times or other extraction temperatures can lead to varying concentrations of antioxidant phenolic substances in *C. incanus* infusions, as shown in a recent study.[10]

With regard to the group of flavan-3-ols and dimers, the highest extractability for gallocatechin and catechin was achieved when using herbal tea consisting of an average particle size of 0.3 mm (sv6). Altogether, gallocatechin concentrations ranged from 0.2 mg/100 mL infusion (sv1) to 0.9 mg/100 mL infusion (sv6) and for catechin from 0.5 mg/100 mL infusion (sv1) to 1.8 mg/100 mL infusion (sv6). The correlation coefficients for the influence of the particle size on the concentration of phenolic compound in the infusion were $R^2$ = 0.89 for gallocatechin and $R^2$ = 0.93 for catechin. These results for the extractability of some phenolic compounds were also supported by a study of Lang and Wai,[40] who described the sample particle size being a generally critical factor for a satisfactory extraction in herbal and natural products. In the present work, catechin, which was detected not only in leaves but also in remarkably high contents in woody stem parts, the extraction yield was almost 4-fold higher when extracting out of herbal material with an average particle size of 0.3 mm (sv6) compared to a particle size of 2.8 mm (sv1). However, controversial results were reported for black tea infusions. Astill et al.[41] measured higher catechin concentrations in infusions brewed from whole tea leaves compared to infusions resulting from tea dust. In the case of black tea, a higher degradation of catechin in tea dust due to an enzymatic degradation (e.g., phenoloxidases) is the main explanation.[41] In *C. incanus* herbal teas with small particle sizes, such an endogenous degradation of phenolic compounds seems to be negligible or may be overlaid by higher extraction yields.

A similar extractability was observed for the myricetin and quercetin glycosides. The concentrations of myricitrin reached from 1.0 mg/100 mL infusion (sv1) to 4.6 mg/100 mL infusion (sv6) and for quercitrin from 0.3 mg/100 mL infusion (sv1) to 1.0 mg/100 mL infusion (sv6) with decreasing particle size. This means 5-fold higher concentrations for myricitrin and 3-fold higher concentrations of quercitrin in *C. incanus* infusions brewed from herb material with a comparatively small particle size. The coefficients of correlation between particle size and concentration of phenolic compound were $R^2$ = 0.97 for myricitrin and $R^2$ = 0.96 for quercitrin.

For the tiliroside isomers extractability seems to be different. For both isomers only an approximately 1.5-fold higher amount was extracted from herbal tea with 0.3 mm average particle size (sv6) compared to the infusion brewed from plant material with 2.8 mm herbal particle size (sv1). From all of these results it can be concluded that these acylated flavonol glucosides were extracted very efficiently from plant material even at a rather large particle size.

With regard to the extractability of the ellagitannins, a strong influence of particle size on the concentration in the corresponding infusions was observed for both hexahydroxydiphenoyl-glucose isomers. For the first isomer at a retention time of 27.1 min a 7-fold higher concentration and for the second isomer at a retention time of 28.7 min an 8-fold higher concentration was yielded when the infusion was brewed from herbal tea with a particle size of 0.3 mm (sv6) instead of using material with 2.8 mm average particle size (sv1). The absolute concentrations for the second isomer reached from 0.3 mg/100 mL infusion (sv1) to 2.5 mg/100 mL infusion (sv6). Overall, for ellagitannin-rich *C. incanus* infusions, a small herbal particle size is decisive under the actual brewing recommendations.

Altogether, the herbal particle size should be considered as an important factor for the extractability of phenolic compounds in *C. incanus* infusions. For most of the bioactive phenolic compounds quantitated in this work, infusions brewed from herbal tea with a comparatively small particle size between 0.3 mm (sv6) and 0.8 mm (sv5) contained the highest concentrations.

## AUTHOR INFORMATION

### Corresponding Author

*(S.R.) E-mail: rohn@chemie.uni-hamburg.de. Phone: +49 40/42838-7979. Fax: +49 40/42838-4342.

### Notes

The authors declare no competing financial interest.

## ACKNOWLEDGMENTS

We thank Anna Knöpfle (Chemical Wood Technology, University of Hamburg, Germany) for excellent technical assistance.

## REFERENCES

(1) Attaguile, G.; Russo, A.; Campisi, A.; Savoca, F.; Acquaviva, R.; Ragusa, N.; Vanella, A. Antioxidant activity and protective effect on DNA cleavage of extracts from *Cistus incanus* L. and *Cistus monspeliensis* L. *Cell Biol. Toxicol.* **2000**, *16*, 83−90.

(2) Barrajón-Catalán, E.; Fernández-Arroyo, S.; Roldán, C.; Guillén, E.; Saura, D.; Segura-Carretero, A.; Micol, V. A systematic study of the polyphenolic composition of aqueous extracts deriving from several *Cistus* genus species: evolutionary relationship. *Phytochem. Anal.* **2011**, *22*, 303−312.

(3) Petereit, F. *Polyphenolische Inhaltsstoffe und Untersuchungen zur entzündungs-hemmenden Aktivität der traditionellen Arzneipflanze Cistus incanus L. (Cistaceae)*. Ph.D. thesis, University of Münster, Germany, 1992.

(4) Pott, R. Naturwirkstoffe aus Pflanzen. Biodiversitätsforschung. *Chem. Unserer Zeit* **2010**, *44*, 260−274.

(5) Droebner, K.; Ehrhardt, C.; Poetter, A.; Ludwig, S.; Planz, O. CYSTUS052, a polyphenol-rich plant extract, exerts anti-influenza virus activity in mice. *Antiviral Res.* **2007**, *76*, 1−10.
(6) Ehrhardt, C.; Hrincius, E. R.; Korte, V.; Mazur, I.; Droebner, K.; Poetter, A.; Dreschers, S.; Schmolke, M.; Planz, O.; Ludwig, S. A polyphenol rich plant extract, CYSTUS052, exerts anti influenza virus activity in cell culture without toxic side effects or the tendency to induce viral resistance. *Antiviral Res.* **2007**, *76*, 38−47.
(7) Droebner, K.; Haasbach, E.; Mueller, C.; Ludwig, S.; Planz, P. The polyphenol rich plant extract CYSTUS052 is highly effective against H5N1 and pandemic H1N1v influenza A viruses. *Influenza Other Respir. Viruses* **2011**, *5*, 230−251.
(8) Kalus, U.; Grigorov, A.; Kadecki, O.; Jansen, J.-P.; Kiesewetter, H.; Radtke, H. *Cistus incanus* (CYSTUS052) for treating patients with infection of the upper respiratory tract. A prospective, randomised, placebo-controlled clinical study. *Antiviral Res.* **2009**, *84*, 267−271.
(9) Hannig, C.; Spitzmüller, B.; Al-Ahmad, A.; Hannig, M. Effects of *Cistus*-tea on bacterial colonization and enzyme activities of the *in situ* pellicle. *J. Dent.* **2008**, *36*, 540−545.
(10) Riehle, P.; Vollmer, M.; Rohn, S. Phenolic compounds in *Cistus incanus* herbal infusions − antioxidant capacity and thermal stability during the brewing process. *Food Res. Int.* **2013**, *53*, 891−899.
(11) Scalbert, A.; Manach, C.; Morand, C.; Rémésy, C.; Jiménez, L. Dietary polyphenols and the prevention of diseases. *Crit. Rev. Food Sci. Nutr.* **2005**, *45*, 287−306.
(12) Pomponio, R.; Gotti, R.; Santagati, N.; Cavrini, V. Analysis of catechins in extracts of *Cistus* species by microemulsion electrokinetic chromatography. *J. Chromatogr., A* **2003**, *990*, 215−223.
(13) Arts, I. C. W.; Hollmann, P. C. H.; Feskens, E. J. M.; De Mesquita, H. B. B.; Kromhout, D. Catechin intake might explain the inverse relation between tea consumption and ischemic heart disease: the Zutphen Elderly Study. *Am. J. Clin. Nutr.* **2001**, *74*, 227−232.
(14) Neveu, V.; Perez-Jiménez, J.; Vos, F.; Crespy, V.; Du Chaffaut, L.; Mennen, L.; Knox, C.; Eisner, R.; Cruz, J.; Wishart, D.; Scalbert, A. Phenol-Explorer: an online comprehensive database on polyphenol contents in foods. *Database* **2010**, DOI: 10.1093/database/bap024.
(15) Rothwell, J. A.; Urpi-Sarda, M.; Boto-Ordoñez, M.; Knox, C.; Llorach, R.; Eisner, R.; Cruz, J.; Neveu, V.; Wishart, D.; Manach, C.; Andres-Lacueva, C.; Scalbert, A. Phenol-Explorer 2.0: a major update of the Phenol-Explorer database integrating data on polyphenol metabolism and pharmacokinetics in humans and experimental animals. *Database* **2012**, DOI: 10.1093/database/bas031.
(16) Rothwell, J. A.; Pérez-Jiménez, J.; Neveu, V.; Medina-Ramon, A.; M'Hiri, N.; Garcia Lobato, P.; Manach, C.; Knox, K.; Eisner, R.; Wishart, D.; Scalbert, A. Phenol-Explorer 3.0: a major update of the Phenol-Explorer database to incorporate data on the effects of food processing on polyphenol content. *Database* **2013**, DOI: 10.1093/database/bat070.
(17) Goto, T.; Teraminami, A.; Lee, J.-Y.; Ohyama, K.; Funakoshi, K.; Kim, Y.-I.; Hirai, S.; Uemura, T.; Yu, R.; Takahashi, N.; Kawada, T. Tiliroside, a glycosidic flavonoid, ameliorates obesity-induced metabolic disorders via activation of adiponectin signaling followed by enhancement of fatty acid oxidation in liver and skeletal muscle in obese-diabetic mice. *J. Nutr. Biochem.* **2012**, *23*, 768−776.
(18) Silva, G. C.; Pereira, A. C.; Rezende, B. A.; Da Silva, J. F. P.; Cruz, J. S.; De Souza, M. de F. V.; Gomes, R. A.; Teles, Y. C. F.; Cortes, S. F.; Lemos, V. S. Mechanism of antihypertensive and vasorelaxant effects of the flavonoid tiliroside in resistance ateries. *Planta Med.* **2013**, *79*, 1003−1008.
(19) Chaves, N.; Rios, J. J.; Gutierrez, C.; Escudero, J. C.; Olias, J. M. Analysis of secreted flavonoids of *Cistus ladanifer* L. by high-performance liquid chromatography particle beam mass spectrometry. *J. Chromatogr., A* **1998**, *799*, 111−115.
(20) Saracini, E.; Tattini, M.; Traversi, M. L.; Vincieri, F. F.; Pinelli, P. Simultaneous LC-DAD and LC-MS determination of ellagitannins, flavonoid glycosides, and acyl-glycosyl flavonoids in *Cistus salvifolius* L. leaves. *Chromatographia* **2005**, *62*, 245−249.
(21) Santagati, N. A.; Salerno, L.; Attaguile, G.; Savoca, F.; Ronsisvalle, G. Simultaneous determination of catechins, rutin, and gallic acid in *Cistus* species extracts by HPLC with diode array detection. *J. Chromatogr. Sci.* **2008**, *46*, 150−156.
(22) Fernández-Arroyo, S.; Barrajón-Catalán, E.; Micol, V.; Segura-Carretero, A.; Fernández-Gutiérrez, A. High-performance liquid chromatography with diode array detection coupled to electrospray time-of-flight and ion-trap tandem mass spectrometry to identify phenolic compounds from a *Cistus ladanifer* aqueous extract. *Phytochem. Anal.* **2009**, *21*, 307−313.
(23) Qa'Dan, F.; Petereit, F.; Mansoor, K.; Nahrstedt, A. Antioxidant oligomeric proanthocyanidins from *Cistus salvifolius*. *Nat. Prod. Res.* **2006**, *20*, 1216−1224.
(24) Breitfellner, F.; Solar, S.; Sontag, G. Effect of gamma-irradiation on phenolic acids in strawberries. *J. Food Sci.* **2002**, *67*, 517−521.
(25) Willför, S.; Pranovich, A.; Tamminen, T.; Puls, J.; Laine, C.; Suurnäkki, A.; Saake, B.; Uotila, K.; Simolin, H.; Hemming, J.; Holmbom, B. Carbohydrate analysis of plant materials with uronic acid-containing polysaccharides − a comparison between different hydrolysis and subsequent chromatographic analytical techniques. *Ind. Crops Prod.* **2009**, *29*, 571−580.
(26) Pott, R.; Hüppe, J. 9 Anpassungen der Pflanzen. In *Spezielle Geobotanik: Pflanze − Klima − Boden*; Springer-Verlag: Berlin, Germany, 2007; pp 232−282.
(27) Aronne, G.; De Micco, V. Seasonal dimorphism in the Mediterranean *Cistus incanus* L. subsp. *incanus*. *Ann. Bot.* **2001**, *87*, 789−794.
(28) Christodoulakis, N. S.; Georgoudi, M.; Fasseas, C. Leaf structure of *Cistus creticus* L. (rock rose), a medicinal plant widely used in folk remedies since ancient times. *J. Herbs, Spices Med. Plants* **2014**, *20*, 103−114.
(29) Hernández, I.; Alegre, L.; Munné-Bosch, S. Drought-induced changes in flavonoids and other low molecular weight antioxidants in *Cistus clusii* grown under Mediterranean field conditions. *Tree Physiol.* **2004**, *4*, 1303−1311.
(30) Meyer-Buchtela, E. *Tee-Rezepturen: Ein Handbuch für Apotheker und Ärzte*, mit 2, Ergänzungslieferung; Deutscher Apotheker Verlag: Stuttgart, Germany, 2001.
(31) Souquet, J.-M.; Labarbe, B.; Le Guernevé, C.; Cheynier, V.; Moutounet, M. Phenolic composition of grape stems. *J. Agric. Food Chem.* **2000**, *48*, 1076−1080.
(32) Lavola, A.; Karjalainen, R.; Julkunen-Tiitto, R. Bioactive polyphenols in leaves, stems, and berries of Saskatoon (*Amelanchier alnifolia* Nutt.) cultivars. *J. Agric. Food Chem.* **2012**, *60*, 1020−1027.
(33) Jürgenliemk, G.; Petereit, F.; Nahrstedt, A. Flavan-3-ols and procyanidins from the bark of *Salix purpurea* L. *Pharmazie* **2007**, *62*, 231−234.
(34) Harris, C. U.; Burt, A. J.; Saleem, A.; Maile, P.; Martineau, L. C.; Haddad, P. S.; Bennett, S. A. L.; Aanason, J. T. A single HPLC-PAD-APCI/MS method for the quantitative comparison of phenolic compounds found in leaf, stem, root and fruit extracts of *Vaccinium angustifolium*. *Phytochem. Anal.* **2007**, *18*, 161−169.
(35) Tian, C.; Wang, M.; Liu, X.; Wang, H.; Zhao, C. HPLC quantification of nine chemical constituents from the five parts of *Abutilon theophrasti* Medic. *J. Chromatogr. Sci.* **2014**, *52*, 258−263.
(36) Peleg, H.; Gacon, K.; Schlich, P.; Noble, A. C. Bitterness and astringency of flavan-3-ol monomers, dimers and trimers. *J. Agric. Food Chem.* **1999**, *79*, 1123−1128.
(37) Scharbert, S.; Hofmann, T. Molecular definition of black tea taste by means of quantitative studies, taste reconstitution, and omission experiments. *J. Agric. Food Chem.* **2005**, *53*, 5377−5384.
(38) Hatanaka, A. The biogeneration of green odor by green leaves. *Phytochemistry* **1993**, *34*, 1201−1218.
(39) Hongsoongnern, P.; Chambers, E., IV. A lexicon for green odor or flavor and characteristics of chemicals associated with green. *J. Sens. Stud.* **2008**, *23*, 205−221.
(40) Lang, Q.; Wai, C. M. Supercritical fluid extraction in herbal and natural product studies − a practical review. *Talanta* **2001**, *53*, 771−782.

(41) Astill, C.; Birch, M. R.; Dacombe, C.; Humphrey, P. G.; Martin, P. T. Factors affecting the caffeine and polyphenol contents of black and green tea infusions. *J. Agric. Food Chem.* **2001**, *49*, 5340−5347.

addition of phytase into the precipitated SPI would make the SPI processing have an additional step (the addition of water for phytase treatment). Therefore, the addition of phytase into the water extract of soybean flour should be the best strategy. In addition, the phytase used in this study is recommended to hydrolyze phytate at 55 °C and pH 5.0, which is well used in the phytase treatment. To examine whether this condition could produce SPI with high quality, the hydrolysis conditions (25−55 °C, pH 5.0−6.5) for phytase were examined, and the optimal condition was selected to prepare SPI samples with different phytate contents by prolonging the hydrolysis time. The effects of phytate content on the yield, components, and physicochemical (solubility, ζ-potential, denaturation temperature, and secondary structure) and functional properties (emulsifying activity, foaming activity, gelation, and in vitro digestibility) of SPI were systematically examined. This study will provide some valuable information for the application of phytase on SPI processing.

## MATERIALS AND METHODS

**Materials.** Defatted low-heat soybean meal (protein content, 52.9%, dry basis; moisture, 7.9%) was purchased from Shandong Wonderful Industrial Group Co., Ltd. (Dongying, China). Phytase from *Aspergillus niger* with an activity of 45000 U/g was purchased from Sukahan Bio-Technology Co., Ltd. (Weifang, China), and hydrolysis condition of pH 5.0 and 55 °C was recommended by the manufacturer. Its activity was about 200000 PU/g after simple purification.

**Purification of Phytase and Determination of Phytase Activity.** The phytase purchased from Sukahan was dissolved in 50 mM sodium acetate buffer (pH 5.5), stirred for 30 min at 4 °C, and then centrifuged (9690*g*, 20 min, 4 °C) to obtain supernatant and precipitate. The supernatant was subjected to ammonium sulfate precipitation (80% saturation) with constant stirring. The precipitate was collected by centrifugation (9690*g*, 20 min, 4 °C) and dissolved in a minimum volume of 50 mM sodium acetate buffer (pH 5.5). The enzyme solution was dialyzed overnight at 4 °C against deionized (DI) water and freeze-dried to obtain purified phytase. Phytase activity was analyzed according to the method described by Quan et al.[19] and Harland et al.[20] with minor modifications, and one phytase unit (PU) was the amount of enzyme that released 1 μmol of inorganic phosphorus from 5 mM sodium phytate in 1 min at pH 5.5 and 37 °C.

**Phytase Treatment.** Defatted soybean meal was ground three times at a 30 s interval and sieved through an 80 mesh sieve to obtain soybean flour. The procedure for extracting soybean protein isolate (SPI) is shown in Figure 1. SPI samples with different contents of phytate were obtained at room temperature (about 25 °C) and pH 5.0 by prolonging hydrolysis time (5, 10, 20, 40, and 60 min). There were two control samples in this study: SPI0 was prepared under the same condition without phytase according to the traditional method; SPI2 was prepared under the same condition with phytase at the optimal condition (pH 5.0, 55 °C) of phytase recommended by the manufacturer. SPI samples were sealed in polythene bags and stored at 4 °C until further analysis.

**Determination of Phytate Content.** Phytate content was determined as described by Gao et al.[21] with minor modifications. Approximately 0.5 g of SPI was extracted with 10 mL of 2.4% HCl, magnetically stirred at 220 rpm for 2 h at room temperature, and centrifuged at 1000*g* at 10 °C for 20 min. Crude extract was transferred into a 25 mL beaker containing 1 g of NaCl, which was magnetically stirred at 350 rpm for 20 min to dissolve the salt and then allowed to settle at 4 °C for 60 min. The mixture was centrifuged at 1000*g* at 10 °C for 20 min, and supernatant was transferred into a 200 mL volumetric flask followed by the addition of DI water to the final volume. The diluted solution (5 mL) was thoroughly mixed with 4 mL of Wade reagent (0.03% $FeCl_3 \cdot 6H_2O$ + 0.3% sulfosalicylic acid) and centrifuged (1000*g*, 10 min, 10 °C). Absorbance of color reaction products for both samples and standards was read at 500 nm. Sodium phytate solutions (0.1−0.5 mg/mL; Sigma-Aldrich, Shanghai, China) were used to make the standard curve ($R^2 > 0.99$).

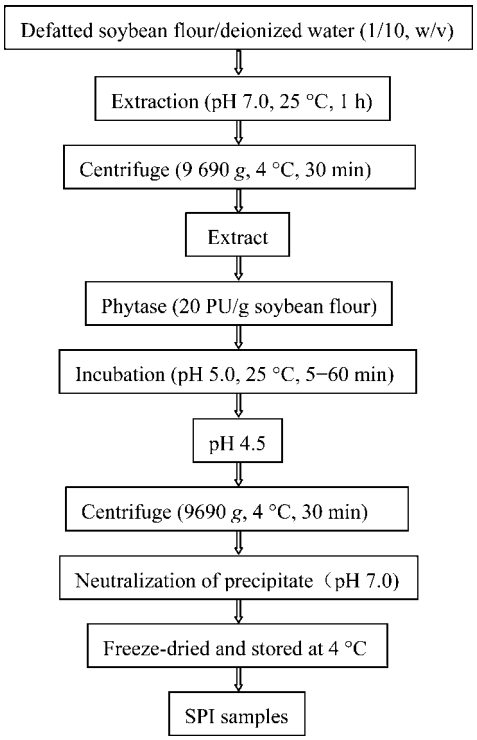


**Figure 1.** Procedure for preparation of soybean protein isolate from defatted low-heat soybean flour.

**ζ-Potential.** The ζ-potentials of SPI suspensions (0.05%, w/v) were measured by using a Zetasizer Nano ZS (Mastersizer X, Malvern Instruments Ltd., Malvern, UK).

**Protein Solubility.** Protein solubility of SPI was determined according to the method of Li et al.[18] with minor modifications. Aliquots (200 mg) of SPI samples were dispersed and stirred in 20 mL of DI water (pH 6.8) at 200 rpm for 30 min at room temperature. Then, the suspensions were centrifuged at 4000*g* for 30 min. Nitrogen contents of the supernatants were measured by using the micro-Kjeldahl method (N × 6.25), and the measurements were performed in duplicate. Percent nitrogen solubility (NS) was calculated as follows (eq 1):

$$\text{NS}\,(\%) = (\text{N in supernatant/total N in 200 mg sample}) \times 100\% \quad (1)$$

**Differential Scanning Calorimetry (DSC).** The thermal characteristics of SPI were examined by using a TA Q100-DSC thermal analyzer (TA Instruments, New Castle, DE, USA), according to the procedure of Wang et al.[22] with some modifications. SPI (10.0 mg) was dispersed into 40 μL of 0.01 M phosphate buffer (pH 7.0), and 10 μL was hermetically sealed into a coated aluminum pan and heated from 20 to 110 °C at a rate of 5 °C/min. A sealed empty pan was used as control. Peak or denaturation temperature ($T_d$) and total enthalpy of denaturation ($\Delta H$, J/g dry matter) were computed from the thermograms by Universal Analysis 2000 software, version 4.7A (TA Instruments-Waters LLC). All experiments were conducted in duplicate. In all cases, the sealed pans were equilibrated at 25 °C for >6 h.

**Measurement of Circular Dichroism (CD).** CD spectra were obtained using an MOS-450 spectropolarimeter (BioLogic Science Instrument, France). The CD spectroscopic measurement was done according to the method of Tang et al.,[23] which was performed in a quartz cuvette of 2 mm with a protein concentration of 0.1 mg/mL in DI water at pH 6.8. The sample was scanned from 190 to 250 nm, and the spectra were an average of eight scans. The following parameters were used: step resolution, 1 nm; acquisition duration, 1 s; bandwidth,

0.5 nm; sensitivity, 100 mdeg. The cell was thermostated with a Peltier element at 25 °C, unless specified otherwise. Recorded spectra were corrected by subtraction of the spectrum of DI water. The secondary structure composition was estimated from the CD spectra using the CONTIN/LL program in CDPro software.

**Emulsifying Activity.** The emulsifying activity index (EAI) and emulsion stability index (ESI) of SPI were determined according to the method of Wang et al.[22] An SPI suspension (9 mL; 0.2% (w/v)) and 3 mL of soybean oil were homogenized using one high-speed homogenizer (FA25, Fluko Co., Germany) for 1 min at 10000 rpm to form an emulsion. An aliquot (50 $\mu$L) of the emulsion was collected from the bottom of the emulsion, immediately (0 min) or 10 min after homogenization, and diluted (1:100, v/v) in 0.1% (w/v) sodium dodecyl sulfate (SDS) solution. After thorough mixing, the absorbance of the diluted emulsion was read at 500 nm.

EAI and ESI values were calculated by using eqs 2 and 3

$$\text{EAI}\ (\text{m}^2/\text{g}) = 2 \times 2.303 \times A_0 \times \text{DF}/[c \times \varphi \times (1 - \theta)] \quad (2)$$

$$\text{ESI}\ (\text{min}) = A_0/(A_0 - A_{10}) \times 10 \quad (3)$$

where DF is the dilution factor (100), $c$ is the initial concentration of SPI (0.2 g/100 mL), $\varphi$ is the optical path (0.01 m), $\theta$ is the fraction of oil used to form the emulsion (0.25), and $A_0$ and $A_{10}$ are the absorbance of the diluted emulsions at 0 and 10 min, respectively. Measurements were performed in triplicate.

**Foaming Activity.** The foam capacity and stability were determined according to the method of Venktesh et al.[24] with slight modifications. Two grams of SPI was dispersed in 100 mL of DI water (pH 6.8). Then, it was whipped in the high-speed homogenizer (FA25, Fluko Co.) at 10000 rpm for 1 min and poured into a 250 mL graduated cylinder. The volume of the foam after 30 s was recorded, and the volume increase was expressed as percent foam capacity. The foam stability was determined by measuring the decrease in foam volume as a function of time up to 30 min.

$$\text{foam capacity}\ (\%) = [\text{vol after whipping}\ (\text{mL}) - \text{vol before whipping}\ (\text{mL})] \times 100/\text{vol before whipping}\ (\text{mL}) \quad (4)$$

Measurements were performed in triplicate.

**Textural Measurements of SPI Gels.** The methods of preparing SPI gels and determining the texture of SPI gels were according to the method of Li et al.[18] Briefly, gels were prepared by heating 15% (w/v) SPI suspension in cylindrical glass molds with an inner diameter of 20 mm and a height of 40 mm. The molds were filled three-fourths full, and the air bubbles in suspension were removed using a vacuum pump. The sample was heated in a 95 °C water bath for 30 min and immediately cooled in an ice water bath. Then the sample was kept at 4 °C for 24 h for further analysis. Then, the gels were taken out of the molds and transferred to a Texture Analyzer (TMS-PRO, Food Technology Corp., USA). A cylinder probe with a diameter of 10 mm was chosen. The probe test speed, starting trigger force, depth, back-off distance, and holding time between two cycles were set as follows: 120 mm/min, 0.05 N, 10 mm, 40 mm, and 0 s, respectively. The tests were performed in triplicate at 25 °C. The hardness was analyzed by Rheology Advantage Data Analysis software.

**In Vitro Digestibility of Protein and Bioavailability of Minerals.** The in vitro digestibility of protein and bioavailability of minerals were respectively evaluated according to the methods of Dinnella et al.[25] and Lestinenne et al.[26] with minor modifications. About 1 g of SPI was precisely weighed in an enzymolysis reactor and dispersed into 20 mL of DI water. After 10 min of conditioning in a shaking water bath at 37 °C, the pH was adjusted to 2.0 with 1 M HCl solution under magnetic stirring. Next, 2% (w/w) of pepsin (Sigma-Aldrich, Shanghai, China) was added, and the mixture was incubated for 2 h. The pH was then increased to about 5.3 with 1 M $NaHCO_3$, 6% (w/w) of bile salts (Sigma-Aldrich) was added, and the pH was adjusted to 7.5 with 1 M NaOH. Then 4% (w/w) of pancreatin (Sigma-Aldrich) was added and incubated for 2 h under low magnetic stirring. Then, the obtained emulsion was divided into two aliquots.

One aliquot (10 g) was mixed with 10 mL of 20% (w/v) trichloroacetic acid (TCA). The mixture was kept for 10 min at room temperature and then centrifuged (4000g, 30 min) to obtain the precipitate. After a washing with 10 mL of TCA (20%, w/v), the final precipitate was obtained by centrifugation at the same parameters above. The nitrogen (N) content was determined by using the Kjeldahl method. The percent N release after the digestion was calculated as

$$\%\ \text{N release} = (N_0 - N_t) \times 100/N_{\text{total}} \quad (5)$$

$N_t$ (mg) is the TCA-insoluble N after digestion, $N_0$ (mg) is the TCA-insoluble N in SPI sample, and $N_{\text{total}}$ (mg) is the total N of SPI sample. Measurements were performed in duplicate.

The other aliquot (10 g) was dialyzed using a cellulose dialysis tube (cutoff 12 kDa) containing 25 mL of NaCl solution (9 mg/mL). The solution was dialyzed under stirring at 37 °C for 2 h. The dialyzed solution in the tube was then removed and stored at 4 °C in an amber bottle under a nitrogen blanket. The amounts of dialyzable calcium (Ca) and zinc (Zn) corresponded to those obtained outside the dialysis membrane (analyzed by atomic absorption spectrophotometer), expressed as percentages of total calcium and zinc present in the test sample, were used as an indicator of mineral bioavailability. Measurements were performed in duplicate.

**Determination of Ca and Zn.** Ca and Zn contents in SPI were measured by atomic absorption spectrophotometer (SperctrAA220/22Z, Varian, USA) according to the method of Kamchan et al.[27] SPI (0.5 g) was weighed into a preweighed porcelain crucible (predried in an oven at 105 °C overnight) and put into a muffle furnace (550 °C, 8 h). The resulting white ash was weighed, dissolved into 3 mL of concentrated nitric acid, and diluted with distilled water in a 25 mL volumetric flask. The solution was used to determine Ca and Zn contents.

**Trypsin Inhibitor Activity (TIA) Assay.** TIA of SPI was measured according to the method of Xu et al.,[28] with slight modifications. For the TIA standard curve, 0−1.0 mL of trypsin inhibitor standard solution (0.01%, w/v) was pipetted into a set of test tubes, and the volume was made up to 2 mL with DI water. The test tubes were placed and warmed in a 37 °C water bath. Then 5 mL of 0.04% (w/v) $N^{\alpha}$-benzoyl-L-arginine 4-nitroanilide hydrochloride (BAPA) in pH 8.2 Tris-HCl buffer (1% dimethyl sulfoxide, v/v; 0.02 M $CaCl_2$), which should be prepared freshly and prewarmed in 37 °C water bath, was pipetted into test tubes followed by 2 mL of 0.01% (w/v) trypsin in 0.04 mM HCl solution. Exactly 10 min later, the reaction was terminated by adding 1 mL of 30% acetic acid (v/v) into each tube. After mixing, the content of each tube was centrifuged at 3000 rpm for 10 min, and the absorbance of the filtrate was measured at 410 nm by using a UV-2100 spectrophotometer (UNICO, WFZ UV-2100) against a reagent blank. The reagent blank was prepared by adding 1 mL of 30% acetic acid (v/v) to a test tube containing trypsin and water before 5 mL of BAPA solution was added. The linearity of the calibration curve was $r = 1$. TIA of SPI should be diluted to the point where 1 mL produces trypsin inhibition of 40−60%. Then 1 mL of diluted sample was added to tubes, and it was done just as above. One TIA unit is arbitrarily defined as an increase of 0.01 absorbance unit at 410 nm per 10 mL of the reaction mixture under the conditions used.

**Statistical Analysis.** Data reported are mean values ± standard deviations. Data were analyzed using SPSS for Windows (version 13.0, SPSS Inc. Chicago, IL, USA) following an analysis of variance (ANOVA) one-way linear model. Mean comparisons were performed using the Duncan test, and the significance level was established for $P < 0.05$.

## RESULTS AND DISCUSSION

**Hydrolysis Condition.** The condition (pH 5.0 and 55 °C) was recommended by the manufacturer for the hydrolysis of phytate by phytase. In the beginning of this study, this condition was used to produce SPI samples, but it was found

that the obtained samples had bad solubility. By increasing the hydrolysis pH (pH 5.0, 5.5, 6.0, and 6.5; 25 °C), the degree of phytate degradation was decreased (Supporting Information Table S1); by decreasing the hydrolysis temperature (55, 45, 35, and 25 °C (room temperature); pH 5.0), it was found that the solubility of SPI sample was increased (Supporting Information Table S2). As a result, two hydrolysis conditions (pH 5.0, 25 °C, 60 min, 20 PU/g soybean flour; pH 5.0, 55 °C, 60 min, 10 PU/g soybean flour) were selected for the following research, and the obtained SPI samples were named SPI1 and SPI2, respectively. In addition, SPI was also produced by the traditional method without phytase (SPI0).

Table 1 shows that SPI0 has a phytate content of 19.86 mg/g, which is in agreement with the results of Saito et al. (20.5 mg/g)[29] and Kumar et al. (1−2%).[1] Phytate contents of SPI1 (0.11 mg/g) and SPI2 (0.11 mg/g) are very low, revealing that phytate also can be efficiently hydrolyzed at 25 °C by increasing the addition of phytase. Table 1 also shows that SPI0 has the highest solubility, EAI, and FC, whereas SPI1 has the highest ESI, FS, and gel hardness; SPI2 shows the worst properties. The results revealed that phytase treatment at 55 °C had bad effects on the properties of low-phytate SPI. Therefore, room temperature (25 °C) was selected for the low-phytate SPI production.

**Table 1. Physicochemical and Functional Properties of SPI with or without Phytase According to the Procedure Described in Figure 1**[a]

| | SPI0[b] | SPI1[c] | SPI2[d] |
|---|---|---|---|
| phytate content (mg/g) | 19.86 ± 0.56a | 0.11 ± 0.06b | 0.11 ± 0.04b |
| protein solubility (%) | 98.89 ± 1.16a | 95.57 ± 0.87b | 72.36 ± 1.07c |
| EAI ($m^2$/g) | 24.99 ± 0.33a | 15.26 ± 0.46b | 4.12 ± 0.45c |
| ESI (min) | 40.01 ± 0.71b | 55.93 ± 1.15a | 15.05 ± 1.02c |
| FC (%) | 75.1 ± 1.5a | 60.2 ± 1.1b | 39.2 ± 1.6c |
| FS (%) | 53.0 ± 2.3b | 70.0 ± 1.3a | 35.0 ± 2.0c |
| hardness of gel (N) | 0.51 ± 0.05b | 0.68 ± 0.06a | 0.25 ± 0.05c |

[a]The data are shown as means ± SD. Means with different letters in the same row are significantly different at the 5% level. [b]SPI0, traditional method. [c]SPI1, pH 5.0, 20 PU/g soy flour, 25 °C, 60 min. [d]SPI2, pH 5.0, 10 PU/g soy flour, 55 °C, 60 min.

**Effects of Phytase-Assisted Processing Method on the Components of SPI.** To systematically examine the effects of phytase-induced phytate degradation on SPI, the water extract of soy flour was respectively hydrolyzed by phytase (pH 5.0, 25 °C, 20 PU/g soybean flour) for 5, 10, 20, 40, and 60 min and acid-precipitated to obtain SPI1 samples. SPI0 was used as control. Table 2 shows that phytate contents of SPI samples are 19.86 (SPI0), 14.58 (5 min), 8.64 (10 min), 4.42 (20 min), 1.89 (40 min), and 0.11 (60 min) mg/g, respectively; interestingly, protein recovery ($R^2$ = 0.781; 52.26−54.83%) and content ($R^2$ = 0.876; 90.57−92.85%) in SPI are linearly and slightly increased, whereas ash content is linearly ($R^2$ = 0.940) and significantly decreased from 5.15 to 3.62% with decreasing phytate content. Two important minerals (Zn and Ca) in SPI are also significantly decreased with prolonged hydrolysis time, which is in good agreement with the behavior of ash content. Ca content in SPI0 (818.6 μg/g) was in agreement with the results of Honig and Wolf[30] (1.05−1.66 mg/g) and Kroll et al.[31] (0.076%, w/w), and the Zn content in SPI0 (21 μg/g) was also consistent with the results of Honig and Wolf[30] (29−36 μg/g).

Generally, the interaction between phytate and protein was electrostatic, and both phytate and soybean proteins were negatively charged at neutral pH.[32] As a result, phytate did not bind to soybean proteins at neutral pH,[31] but the binding of phytate did happen in the presence of $Ca^{2+}$ (or $Zn^{2+}$ and some other divalent ions), which was considered that phytate−mineral ($Ca^{2+}$, $Zn^{2+}$, and some other divalent ions)−protein complexes were formed.[33,34] By phytase treatment, phytate was hydrolyzed to phosphorus and inositol, and mineral−protein complexes remained. By deceasing the pH from neutral pH to acidic pH (acid-precipitation for SPI), the number of bound $Ca^{2+}$ on soybean proteins was decreased,[31] which might be the reason that ash content in SPI1 was decreased with prolonged hydrolysis time. For SPI0, some phytate−mineral complexes (insoluble) might be released from proteins by decreasing the pH, but they would be mixed with soybean proteins in the precipitate, which should be the reason that ash content in SPI0 was still larger than that in SPI0.[35]

Phytate is one kind of salt rich in negative charge, so it was considered that phytate−mineral−protein complexes would be more acidic than mineral−protein complexes, revealing that the former should be more hydrophilic than the latter, which might be one reason for the higher protein recovery induced by phytase.

**ζ-Potential and Protein Solubility.** Figure 2a shows that the ζ-potential value of the SPI suspension is linearly ($R^2$ = 0.793) and significantly increased from −26.1 to −35.4 mV with increasing phytate content, which is consistent with the hypothesis stated above. Figure 2b shows that the protein solubility of SPI is linearly ($R^2$ = 0.983) and slightly increased from 94.81 to 98.89% with increasing phytate content, which is

**Table 2. Components of SPI Treated by Phytase for Different Times (5, 10, 20, 40, 60 min; pH 5.0, 25 °C, 20 PU/g Soybean Flour)**[a]

| | | SPI1 | | | | |
|---|---|---|---|---|---|---|
| time (min) | SPI0 | 5 | 10 | 20 | 40 | 60 |
| phytate content (mg/g) | 19.86 ± 0.61a | 14.58 ± 0.20b | 8.64 ± 0.42c | 4.42 ± 0.51d | 1.89 ± 0.24e | 0.11 ± 0.10f |
| degree of phytate degradation (%) | 0f | 26.59 ± 0.94e | 56.50 ± 1.32d | 77.74 ± 1.07c | 90.50 ± 0.98b | 99.56 ± 1.12a |
| protein content (%) | 90.57 ± 0.62c | 91.26 ± 0.51b | 92.52 ± 0.40a | 92.15 ± 0.61a | 92.45 ± 0.54a | 92.85 ± 0.42a |
| moisture (%) | 1.49 ± 0.21a | 1.48 ± 0.14a | 1.24 ± 0.16a | 1.29 ± 0.17a | 1.32 ± 0.20a | 1.31 ± 0.12a |
| ash content (%) | 5.15 ± 0.11a | 4.38 ± 0.12b | 4.26 ± 0.09b | 3.73 ± 0.14c | 3.63 ± 0.13c | 3.62 ± 0.20c |
| Ca (μg/g SPI) | 818.6 ± 18.2a | 739.9 ± 20.4b | 694.8 ± 28.7c | 657.2 ± 19.5d | 619.9 ± 14.4e | 562.2 ± 22.3f |
| Zn (μg/g SPI) | 20.94 ± 0.65a | 19.73 ± 0.48a | 18.67 ± 0.51b | 15.17 ± 0.76 c | 14.08 ± 0.32c | 12.71 ± 0.28d |
| protein recovery (%) | 52.26 ± 1.11c | 53.84 ± 1.14b | 54.67 ± 1.02b | 54.37 ± 0.81a | 54.54 ± 0.65a | 54.83 ± 0.90a |

[a]The data are shown as means ± SD. Means with different letters in the same row are significantly different at the 5% level.

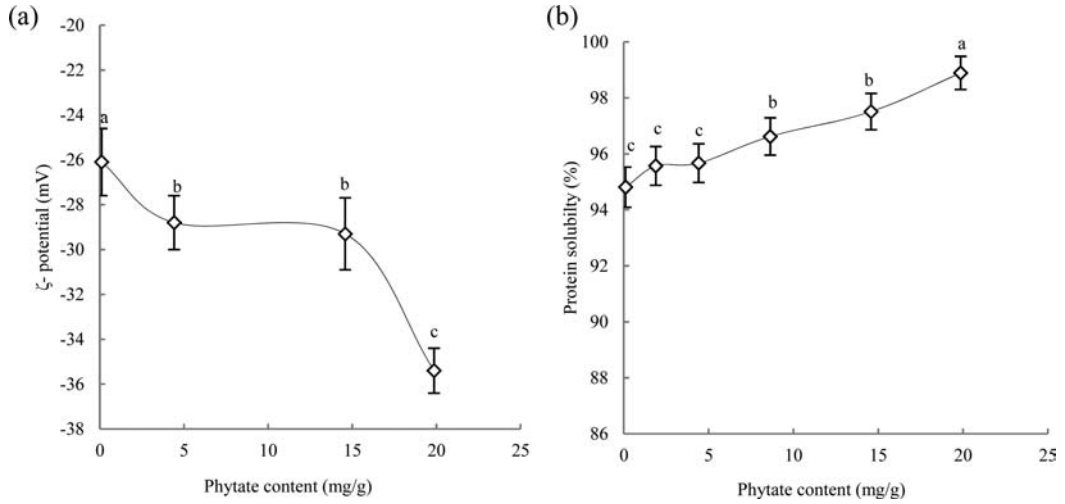


**Figure 2.** Effects of phytate content on ζ-potential (a) and protein solubility (b) of SPI. Means with different letters on the same line are significantly different at the 5% level.

in agreement with the results in Figure 2a. This is because the ζ-potential value reflects the degree of repulsion between the adjoining charged colloids: colloids with higher ζ-potential values are more electrically stable and vice versa. Ishiguro et al.[36] reported that the solubility of soy milk protein was positively correlated with soy milk phytate content and that a greater amount of coagulant was needed to coagulate high-phytate soy milk to form tofu compared to low-phytate soy milk. In addition, Liu and Chang[37] reported similar results as above.

**Thermal Behaviors.** All SPI samples showed typical DSC thermograms of soybean isolates in which two endothermic transitions corresponded to the denaturation of β-conglycinin and glycinin, respectively. $T_{d1}$ (denaturation temperature of β-conglycinin), $T_{d2}$ (denaturation temperature of glycinin), and $\Delta H$ (total enthalpy change of SPI) were obtained from DSC thermograms and are shown in Table 3. β-Conglycinin and glycinin of SPI0 exhibited two endothermic peaks at about 79.4 ($T_{d1}$) and 96.2 °C ($T_{d2}$), and $\Delta H$ was 10.2 J/g. With decreasing phytate content, $T_{d1}$ ($R^2$ = 0.941), $T_{d2}$ ($R^2$ = 0.977), and $\Delta H$ ($R^2$ = 0.963) were all linearly decreased. When SPI had a phytate content of 0.11 mg/g, $T_{d1}$, $T_{d2}$, and $\Delta H$ were 71.2 °C, 92.1 °C, and 9.3 J/g, respectively. These results showed that SPI with higher phytate content had higher denaturation temperatures than that with lower phytate content.

**Table 3. DSC Characteristics of SPI with Different Phytate Contents**[a]

| phytate content in SPI (mg/g) | $T_{d1}$[b] (°C) | $T_{d2}$[c] (°C) | $\Delta H$[d] (J/g) |
|---|---|---|---|
| 19.86 ± 0.61a | 79.4 ± 0.5a | 96.2 ± 0.7a | 10.2 ± 0.5a |
| 14.58 ± 0.20b | 78.5 ± 0.3b | 94.5 ± 0.5b | 9.8 ± 0.6b |
| 4.42 ± 0.51c | 74.8 ± 0.4c | 92.8 ± 0.4c | 9.5 ± 0.4c |
| 0.11 ± 0.10d | 71.2 ± 0.1d | 92.1 ± 0.4d | 9.3 ± 0.1d |

[a]The data are shown as means ± SD. Means with different letters in the same column are significantly different at the 5% level. [b]$T_{d1}$, denaturation temperature of β-conglycicin. [c]$T_{d2}$, denaturation temperature of glycicin. [d]$\Delta H$, total enthalpy change of β-conglycicin and glycicin.

In food processing and biological processes, many kinds of molecules (i.e., proteins, lipids, anions, metal ions, ions, odorant molecules, and others, collectively known as ligands) would bind to proteins, and it was widely accepted that the liganded proteins were more thermally stable than the nonliganded ones. As the hypothesis stated above, the phytate in phytate−mineral−protein complexes was gradually hydrolyzed with prolonged hydrolysis time, and mineral−protein complexes remained. The ash content, including Ca and Zn, in SPI was also decreased with prolonged hydrolysis time (Table 2). These showed that SPI obtained from long hydrolysis time contained lower bound phytate and minerals than that from short hydrolysis time. Scilingo and Anon[38] reported that the Ca content increase could cause an increase in thermal stability of SPI, and Martins et al.[39] reported that the binding of phytate derivatives could also enhance the thermal stability of proteins. Therefore, it was reasonable that SPI with low phytate and ash contents was less thermally stable that that with high phytate and ash contents.

**Secondary Structure of Proteins in SPI.** SPI0 and SPI1 (phytate content, 0.11 mg/g) were selected to be examined by CD spectrometry between 190 and 250 nm. The ratios of α-helix, β-sheet, β-turn, and random coil were calculated from their CD spectra and are shown in Table 4. It was found that the ratios of β-sheet and β-turn were increased, whereas that of random coil was decreased for SPI1 compared to SPI0; the ratio of α-helix was slightly decreased. Phytate could inhibit the activities of many kinds of digestive enzymes, revealing that it might change the conformations of those enzymes.[1] Therefore, it was reasonable that phytate could affect the secondary structure of proteins in SPI.

**Table 4. Ratio of Secondary Structure of Proteins in SPI0 and SPI1 with Phytate Contents of 19.86 and 0.11 mg/g, Respectively**

| | α-helix | β-sheet | β-turn | random coil | total |
|---|---|---|---|---|---|
| SPI0 | 0.324 | 0.167 | 0.199 | 0.308 | 0.998 |
| SPI1 | 0.321 | 0.185 | 0.211 | 0.280 | 0.997 |

Similar to the digestive enzymes, it was considered that soybean proteins should be slightly denatured by the binding of phytate, and Wang et al.[22] reported that the slight denaturation of soybean proteins by high hydrostatic pressure could increase

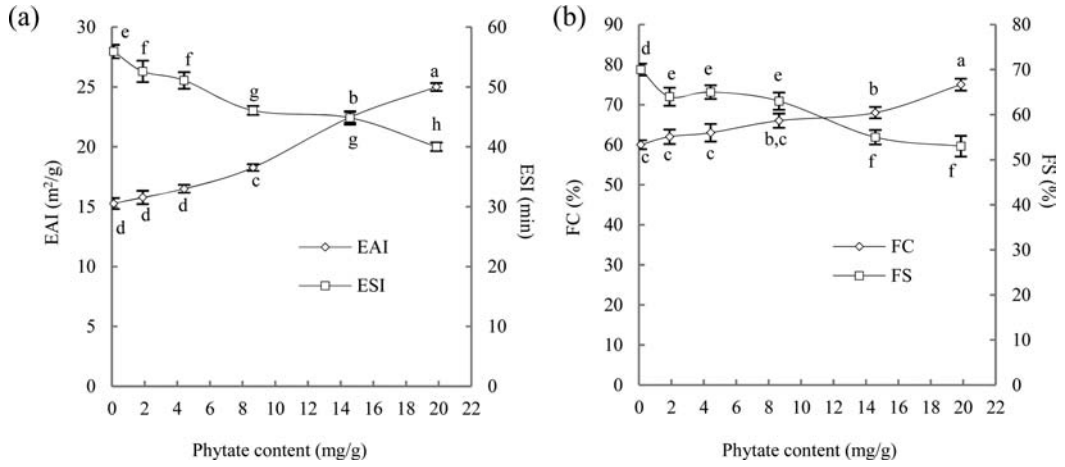


**Figure 3.** Effects of phytate content on EAI and ESI (a) and FC and FS (b) of SPI. Means with different letters on the same line are significantly different at the 5% level.

the denaturation temperatures and solubility, which was consistent with the results in Figure 2b and Table 3. Unfortunately, they did not give the data concerning the secondary structure.

**Emulsifying and Foaming Properties.** Figure 3a shows that the EAI of SPI is linearly ($R^2$ = 0.983) and significantly increased from 15.26 to 25.00 $m^2/g$, whereas the ESI of SPI is linearly ($R^2$ = 0.953) and significantly decreased from 55.93 to 40.01 min, with increasing phytate content. Li et al.[18] reported that high hydrostatic pressure could significantly increase solubility and EAI but significantly decrease ESI of SPI in the ranges of 0−300 MPa and 5−15 min, which was in agreement with the results above. Wang et al.[22] used high hydrostatic pressure to treat SPI and obtained results similar to those of Li et al.[18] It is known that protein solubility is a key factor for its emulsifying activity. Generally, high solubility corresponds to high emulsifying activity and vice versa. Table 3 shows that the denaturation temperature of SPI is increased with increasing phytate content, revealing that the molecular flexibility of SPI is decreased.[40] It is known that molecular flexibility is positively correlated with its emulsion stability. In addition, phytate−mineral−protein complexes (high-phytate SPI) were more hydrophilic than mineral−protein complexes (low-phytate SPI), meaning that the former had larger surface hydrophilicity/hydrophobicity ratios (similar to the hydrophilic−lipophilic balance of a surfactant) than the latter, which could be well evidenced by the results in Figure 2b. Therefore, the balance between protein solubility and flexibility could be used to explain the different behaviors of EAI and ESI of SPI.

Figure 3b shows that the FC of SPI is linearly ($R^2$ = 0.955) and significantly increased from 60 to 75%, whereas the FS of SPI is linearly ($R^2$ = 0.919) and significantly decreased from 70 to 53%, with increasing phytate content. Li et al.[18] reported that high hydrostatic pressure also could significantly increase FC but significantly decrease FS of SPI in the ranges of 200−300 MPa and 5−15 min. Foaming activity, similar to emulsifying activity, belongs to the functional properties related to the protein surface. Therefore, the different behaviors of FC and FS of SPI could be explained by the same theory as above.

**Hardness of SPI Gels.** SPI samples with different phytate contents were used to prepare gels, and the hardness, a typical parameter of gel, was determined and is shown in Figure 4. It was found that hardness was linearly ($R^2$ = 0.893) and significantly decreased from 0.69 to 0.50 N with increasing

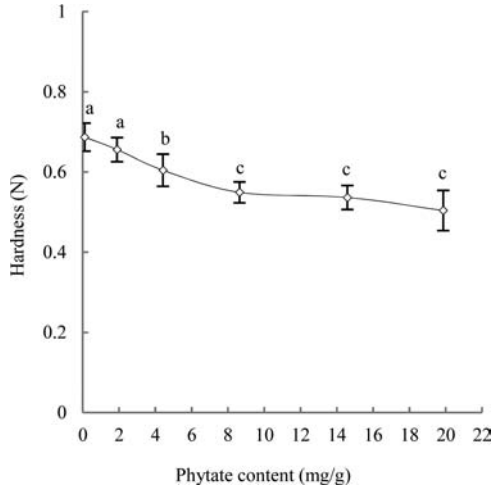


**Figure 4.** Effects of phytate content on hardness of SPI gel. Means with different letters are significantly different at the 5% level.

phytate content. Toda et al.[41] prepared soy milks with different phytate contents by using different soybean varieties, and breaking stress (hardness) of filled tofu (coagulant: low concentration (0.25%) of $MgCl_2$) was highly and negatively ($P$ < 0.001, $r$ = −0.73) correlated with soy milk phytate content. Ishiguro et al.[37] prepared soy milks with different phytate contents by the addition of different levels of phytate, and filled tofu with higher phytate content had lower breaking stress. Hou and Chang[42] prepared soy milks with different phytate contents by using phytase, and it was found that the yield of momen tofu was increased; breaking stress was decreased with decreasing phytate content, showing a different trend from the two research studies above. However, it was considered that the different trend should be induced by the different preparation methods of tofu. For momen tofu, the step of pressing was used to remove the whey fraction, and a lower yield of menon tofu was obtained from high-phytate soy milk compared to low-phytate soy milk, indicating that low-phytate momen tofu had a higher moisture content than high-phytate momen tofu. It was considered that the high-moisture content glossed over the real effects of phytate on the hardness of tofu. Additionally, it is widely accepted that the gel network formation is the result of a combination of hydrophobic and

electrostatic interactions.[43] As stated above, SPI with a high phytate content was more acidic than that with a low phytate content (Figure 2a), revealing that proteins in the former SPI had stronger electrostatic repulsion, and phytate−mineral−protein complexes (high-phytate SPI) had lower surface hydrophobicity/hydrophilicity ratios than mineral−protein complexes. These could be used to well explain the results in Figure 4.

**In Vitro Digestibility of Protein and Bioavailability of Minerals.** Figure 5 shows the in vitro protein digestibility and TIA of SPI with different phytate contents. It was found that the in vitro digestibility was linearly ($R^2$ = 0.96) and significantly decreased from 72 to 59%, whereas the TIA was linearly ($R^2$ = 0.821) and significantly increased from 71934 to 78500 U/g with increasing phytate content. It was calculated that the TIA in SPI with a phytate content of 0.11 mg/g was about 92% of that with a phytate content of 19.86 mg/g, revealing that phytate had some effects on inhibiting the activity of trypsin. Ritter et al.[44] reported that low-phytate SPI obtained from sequential ion exchange process was more digestible than high-phytate SPI, and Knuckles et al.[45] found that the inhibitory effect of the phytate on in vitro digestibility of casein and bovine serum albumin was positively correlated with phytate content. Borowsk et al.[46] found that protein isolates from fava bean and soybean with low phytate contents also had low TIA, and Singh et al.[47] reported that the activity of trypsin could be substantially inhibited by low levels of phytate.

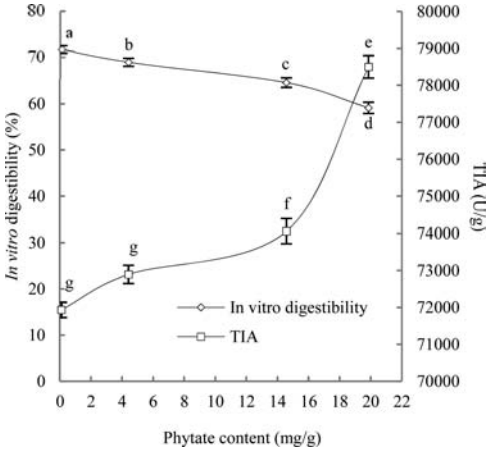


**Figure 5.** Effects of phytate content on in vitro digestibility and TIA of SPI. Means with different letters on the same line are significantly different at the 5% level.

Table 5 shows the dialyzable Ca and Zn in SPI with different phytate contents by simulated gastrointestinal digestion. With increasing phytate content, Zn and Ca contents in SPI are significantly increased from 12.71 to 20.94 μg/g and from 562.2 to 818.6 μg/g, respectively; percentages of dialyzable Zn and Ca are significantly decreased from 15.4 to 2.5% and from 27.64 to 20.13%, respectively; interestingly, the amount of dialyzable Zn is significantly decreased from 1.96 to 0.53 μg/g, whereas that of dialyzable Ca is significantly increased from 155.39 to 164.78 μg/g. These results showed that phytase should be able to increase the amount of bioavailable Zn, although it decreased the Zn content in SPI, and that phytase increased the percentage of bioavailable Ca, but decreased the amount of bioavailable Ca, which should result from the phytase-induced Ca content decrease in SPI. The results were in agreement with many research studies which revealed that the removal of phytate could enhance the bioavailability of minerals.[1] Wise et al.[48] reported that Ca-bound phytate increased chelation with trace minerals, especially Zn, to form coprecipitates that make the Zn unavailable, which might be used to explain the amount decrease of bioavailable Zn with increasing phytate content. This was because Ca content was decreased with decreasing phytate content. In addition, the low percentages of dialyzable Zn (2.5−15.4%) and Ca (20.13−27.64%) may result from the binding of Zn and Ca to protein hydrolysates.[49,50]

In this study, it was found that hydrolysis condition at low temperature (25 °C) and pH 5.0 was better than that (55 °C, pH 5.0) recommended by the manufacturer for retaining the properties of SPI, so the former condition was used to prepare SPI sample with decreasing phytate content by prolonged hydrolysis time. The results showed that protein content, protein recovery, solubility, ζ-potential value, denaturation temperatures, EAI, FC, and TIA were highly and positively correlated, whereas ash content (including Ca and Zn), ESI, FS, gel hardness, and in vitro protein digestibility were highly and negatively correlated with phytate content of SPI. Simulated gastrointestinal digestion and subsequent dialysis showed that the percentages of dialyzable Zn and Ca were increased with decreasing phytate content in SPI but that the amounts of dialyzable Zn and Ca revealed different behaviors: the former was increased and the latter was decreased. CD spectra revealed that the phytase treatment could change the secondary structure of SPI. In all, these results showed that the phytase-assisted processing method could produce low-phytate SPI with better gelling and nutritional properties than the traditional method by slightly losing solubility and partially losing emulsifying activity and foaming activity. It was considered that this kind of SPI would be a good ingredient in the production of sausage and similar products.

**Table 5. Dialyzable Ca and Zn in SPI with Different Phytate Contents by Simulated Gastrointestinal Digestion[a]**

| phytate content (mg/g SPI) | Zn content (μg/g SPI) | dialyzable Zn (μg/g SPI) | dialyzable Zn (%) | Ca content (μg/g SPI) | dialyzable Ca (μg/g SPI) | dialyzable Ca (%) |
|---|---|---|---|---|---|---|
| 19.86 ± 0.61a | 20.94 ± 0.31a | 0.53 ± 0.04e | 2.5 ± 0.4f | 818.6 ± 5.6a | 164.8 ± 1.2a | 20.13 ± 1.21e |
| 14.58 ± 0.20b | 19.73 ± 0.16b | 0.81 ± 0.12d | 4.1 ± 0.2e | 739.9 ± 4.2b | 158.7 ± 2.2b | 21.46 ± 0.62d |
| 8.64 ± 0.42c | 18.67 ± 0.24b | 1.08 ± 0.16c | 5.8 ± 0.1d | 694.8 ± 5.0c | 158.1 ± 2.4b | 22.75 ± 1.02d |
| 4.42 ± 0.51d | 15.17 ± 0.33c | 1.18 ± 0.11c | 7.8 ± 0.4c | 657.2 ± 3.7d | 159.5 ± 1.5b | 24.27 ± 0.48c |
| 1.89 ± 0.24e | 14.08 ± 0.42c | 1.35 ± 0.07b | 9.6 ± 0.3b | 619.9 ± 4.3e | 157.3 ± 1.8b | 25.38 ± 0.46b |
| 0.11 ± 0.10f | 12.71 ± 0.35d | 1.96 ± 0.15a | 15.4 ± 0.5a | 562.2 ± 2.8f | 155.4 ± 1.0b | 27.64 ± 0.63a |

[a]A cellulose dialysis tube (cutoff 12 kDa) was used. Means with different letters in the same column are significantly different at the 5% level.

## ■ ASSOCIATED CONTENT

### Supporting Information

Tables S1 and S2. This material is available free of charge via the Internet at http://pubs.acs.org.

## ■ AUTHOR INFORMATION


### Corresponding Author

*(Y.H.) Phone: 0510-85917812. Fax: 0510-85329091. E-mail: yfhua@jiangnan.edu.cn.



### Funding

The work received financial support from the National Natural Science Foundation of China (No. 21276107), the National Great Project of Scientific and Technical Supporting Programs funded by the Ministry of Science and Technology of China during the 12th five-year plan (No. 2012BAD34B04-1), and the 863 Program (Hi-tech research and development program of China, No. 2013AA102204-3).


### Notes

The authors declare no competing financial interest.

## ■ REFERENCES


(1) Kumar, V.; Sinha, K.; Makkar, H.; Becker, K. Dietary roles of phytate and phytase in human nutrition: a review. *Food Chem.* **2010**, *120*, 945−959.

(2) Sandstrom, B.; Kivistö, B.; Cederblad, A. Absorption of zinc from soy protein meals in humans. *J. Nutr.* **1987**, *117*, 321−327.

(3) Lo, G. S.; Settle, S. L.; Steinke, F. H.; Hopkins, D. T. Effect of phytate: zinc molar ratio and isolated soybean protein on zinc bioavailability. *J. Nutr.* **1981**, *111*, 2223−2235.

(4) Lopez, H.; Leenhardt, F.; Coundray, C.; Renesy, C. Minerals and phytic acid interactions: is it a real problem for human nutrition? *Int. J. Food Sci. Technol.* **2002**, *37*, 727−739.

(5) Wise, A. Phytate and zinc bioavailability. *Int. J. Food Sci. Nutr.* **1995**, *46*, 53−63.

(6) Hurrel, R. F.; Juillerat, M. A.; Reddy, M. B.; Lynch, S. R.; Dassenko, S. A.; Cook, J. D. Soy protein, phytate, and iron absorption in humans. *Am. J. Clin. Nutr.* **1992**, *56*, 573−578.

(7) Greiner, R.; Konietzny, U. Phytase for food application. *Food Technol. Biotechnol.* **2006**, *44*, 125−140.

(8) Sandberg, A. S. Bioavailability of minerals in legumes. *Br. J. Nutr.* **2002**, *88*, 281−285.

(9) Fredrikson, M.; Biot, P.; Alminger, M. L.; Carlsson, N. G.; Sandberg, A. S. Production process for high-quality pea-protein isolate with low content of oligosaccharides and phytate. *J. Agric. Food Chem.* **2001**, *49*, 1208−1212.

(10) Brooks, J. R.; Morr, C. V. phytate removal from soybean protein isolates using ion exchange processing treatment. *J. Food Sci.* **1982**, *47*, 1280−1282.

(11) Sandberg, A. S.; Hulthen, L. R.; Turk, M. Dietary *Aspergillus niger* phytase increases iron absorption in humans. *J. Nutr.* **1996**, *126*, 476−480.

(12) Hurrel, R. F.; Reddy, M. B.; Juillerat, M. A.; Cook, J. D. Degradation of phytic acid in cereal porridges improves iron absorption by human subjects. *Am. J. Clin. Nutr.* **2003**, *77*, 1213−1219.

(13) Segueilha, L.; Moulin, G.; Galzy, P. Reduction of phytate content in wheat bran and glandless cotton flour by *Schwanniomyces castellii*. *J. Agric. Food Chem.* **1993**, *41*, 2451−2454.

(14) Haros, M.; Rosell, C. M.; Benedito, C. Fungal phytase as a potential bread-making additive. *Eur. Food Res. Technol.* **2001**, *213*, 317−322.

(15) Caransa, A.; Simell, M.; Vaara, M.; Vaara, T. A novel enzyme application in corn wet milling. *Starch/Staerke* **1988**, *40*, 409−411.

(16) Wang, M.; Hettiarachchy, N. S.; Qi, M.; Burks, W.; Siebenmorgen, T. Preparation and functional properties of rice bran protein isolate. *J. Agric. Food Chem.* **1999**, *47*, 411−416.

(17) Han, Y. W.; Wilfred, A. G. Phytate hydrolysis in soybean and cottonseed meals by *Aspergillus ficuum* phytase. *J. Agric. Food Chem.* **1988**, *36*, 262−269.

(18) Li, H. J.; Zhu, K. X.; Zhou, H. M.; Wei, P. Effects of high hydrostatic pressure on some functional and nutritional properties of soy protein isolate for infant formula. *J. Agric. Food Chem.* **2011**, *59*, 12028−12036.

(19) Quan, C. S.; Tian, W. J.; Fan, S. D.; Kikuchi, J. I. Purification and properties of a low-molecular-weight phytase from *Cladosporium* sp. FP-1. *J. Biosci. Bioeng.* **2004**, *97*, 260−266.

(20) Harland, B. F.; Harland, J. Fermentative reduction of phytate in rye, white and whole wheat breads. *Cereal Chem.* **1980**, *57*, 226−229.

(21) Gao, Y.; Shang, C.; Saghai, M. A.; Biyashev, R. M.; Grabau, E. A.; Kwanyuen, P.; Burton, J. W.; Buss, G. R. A modified colorimetric method for phytic acid analysis in soybean. *Crop Sci.* **2007**, *47*, 1797−1803.

(22) Wang, X. S.; Tang, C. H.; Lia, B. S.; Yang, X. Q.; Li, L.; Ma, C. Y. Effects of high-pressure treatment on some physicochemical and functional properties of soy protein isolates. *Food Hydrocolloids* **2008**, *22*, 560−567.

(23) Tang, C. H.; Sun, X. A comparative study of physicochemical and conformational properties in three vicilins from *Phaseolus legumes*: implications for the structure-function relationship. *Food Hydrocolloids* **2011**, *25*, 315−324.

(24) Venktesh, A.; Prakash, V. Functional properties of total sunflower (*Helianthus annuus* L.) seed-effect of physical and chemical. *J. Agric. Food Chem.* **1993**, *41*, 18−23.

(25) Dinnella, C.; Minichino, P.; Andrea, A. M.; Monteleone, E. Bioaccessibility and antioxidant activity stability of phenolic compounds from extra-virgin olive oils during in vitro digestion. *J. Agric. Food Chem.* **2007**, *55*, 8423−8429.

(26) Lestienne, I.; Besancon, P.; Caporiccio, B.; Pellerin, V. L.; Treche, S. Iron and zinc in vitro availability in pearl millet flours (*Pennisetum glaucum*) with varying phytate, tannin, and fiber contents. *J. Agric. Food Chem.* **2005**, *53*, 3240−3247.

(27) Kamchan, A.; Puwastien, P.; Sirichakwal, P. P.; Kongkachuichai, R. In vitro calcium bioavailability of vegetables, legumes and seeds. *J. Food Compos. Anal.* **2004**, *17*, 311−320.

(28) Xu, Z. C.; Chen, Y. M.; Zhang, C. M.; Kong, X. Z.; Hua, Y. F. The heat-induced protein aggregate correlated with trypsin inhibitor inactivation in soymilk processing. *J. Agric. Food Chem.* **2012**, *60*, 8012−8019.

(29) Saito, T.; Kohno, M.; Tsumura, K.; Kugimiya, W.; Kito, M. Novel methods using phytase for separating soybean $\beta$-conglycinin and glycinin. *Biosci., Biotechnol., Biochem.* **2001**, *65*, 884−887.

(30) Honig, D. H.; Wolf, W. J. Mineral and phytate content and solubility of soybean protein isolates. *J. Agric. Food Chem.* **1987**, *35*, 583−588.

(31) Kroll, R. D. Effect of pH on the binding of calcium ions by soybean proteins. *Cereal Chem.* **1984**, *61*, 490−495.

(32) Jordan, W. B.; Nathan, P. C.; Aaron, J. C.; Peter, H. S.; Robert, J. F. Dual effects of sodium phytate on the structural stability and solubility of proteins. *J. Agric. Food Chem.* **2013**, *61*, 290−295.

(33) Saio, K.; Koyama, E.; Watanabe, T. Protein-calcium-phytic acid relationships in soybean. Part II. effects of phytic acid on combination of calcium with soybean meal protein. *Agric. Biol. Chem.* **1968**, *32*, 448−452.

(34) Nosworthy, N.; Caldwell, R. A. The interaction of zinc(II) and phytic acid with soya bean glycinin. *J. Sci. Food Agric.* **1988**, *44*, 143−150.

(35) Delezie, E.; Maertens, L.; Huyghebaert, G. Consequences of phosphorus interactions with calcium, phytase, and cholecalciferol on zootechnical performance and mineral retention in broiler chickens. *Poult. Sci.* **2013**, *91*, 2523−2531.

(36) Ishiguro, T.; Ono, T.; Wada, T.; Tsukamoto, C.; Kono, Y. Changes in soybean phytate content as a result of field growing conditions and influence on tofu texture. *Biosci., Biotechnol., Biochem.* **2006**, *70*, 874−880.

(37) Liu, Z. S.; Chang, S. K. C. Effect of soy milk characteristics and cooking conditions on coagulant requirements for making filled tofu. *J. Agric. Food Chem.* **2004**, *52*, 3405−3411.
(38) Scilingo, A. A.; Anon, M. C. Calorimetric study of soybean protein isolates: effect of calcium and thermal treatments. *J. Agric. Food Chem.* **1996**, *44*, 3751−3756.
(39) Martins, L. O.; Carreto, L. S.; Da Costa, M. S.; Santos, H. New compatible solutes related to di-myo-inositol-phosphate in members of the order *Thermotogales*. *J. Bacteriol.* **1996**, *178*, 5644−5651.
(40) Fields, P. A. Review: Protein function at thermal extremes: balancing stability and flexibility. *Comp. Biochem. Physiol. A* **2001**, *129*, 417−431.
(41) Toda, K.; Takahashi, K.; Ono, T.; Kitamura, K.; Nakamura, Y. Variation in the phytic acid content of soybeans and its effect on consistency of tofu made from soybean varieties with high protein content. *J. Sci. Food Agric.* **2006**, *86*, 212−219.
(42) Hou, H. J.; Chang, K. C. Yield and textural properties of tofu as affected by the changes of phytate content during soybean storage. *J. Food Sci.* **2003**, *68*, 1185−1191.
(43) Uruakpa, F. O. Gelling behavior of plant proteins and polysaccharides in food systems. *J. Food Sci. Eng.* **2012**, *2*, 247−256.
(44) Ritter, M. A.; Morr, C. V.; Thoma, R. L. In vitro digestibility of phytate-reduced and phenolics-reduced soy protein isolates. *J. Food Sci.* **1987**, *52*, 325−327.
(45) Knuckles, B. E.; Kuzmicky, D. D.; Betschart, A. A. Effect of phytate and partially hydrolyzed phytate on invitro protein digestibility. *J. Food Sci.* **1985**, *50*, 1980−1982.
(46) Borowska, J.; Kozlows, H. Isolates from faba bean and soybean with lowered content of phytic acid and activity of the trypsin inhibitors. *Nahrung* **1986**, *30*, 11−18.
(47) Singh, M.; Krikorian, A. D. Inhibition of trypsin activity in vitro by phytate. *J. Agric. Food Chem.* **1982**, *30*, 799−800.
(48) Wise, A. Dietary factors determining the biological activities of phytate. *Nutr. Abstr. Rev.* **1980**, *53*, 791−806.
(49) Bao, X. L.; Lv, Y.; Yang, B. C.; Ren, C. G.; Guo, S. T. A study of the soluble complexes formed during calcium binding by soybean protein hydrolysates. *J. Food Sci.* **2008**, *73*, 117−121.
(50) Hegde, U.; Lakshmi, A. J.; Radha, C.; Kumar, P. R.; Prakash, J. Effect of soya protein on the dialysability of exogenous iron and zinc. *Food Chem.* **2009**, *117*, 577−581.

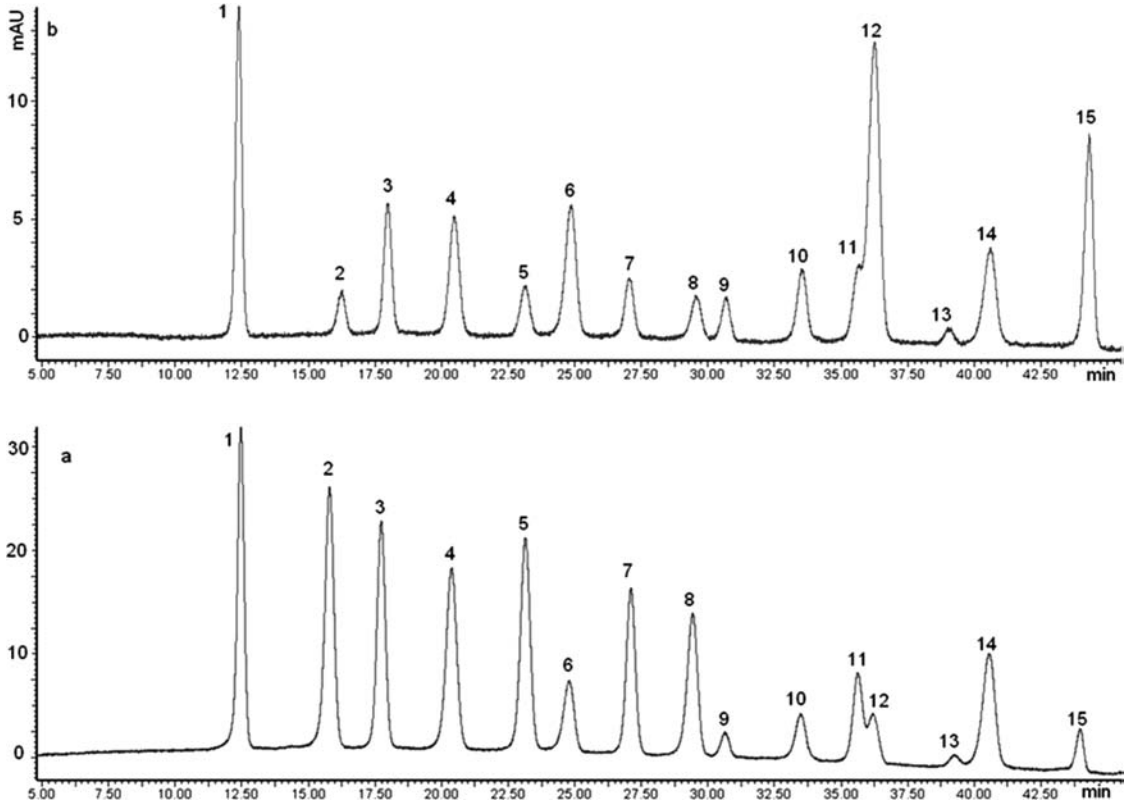


**Figure 1.** Chromatograms integrated at 520 nm of bilberry fruits at higher (a) and lower (b) content in glucosylated anthocyanidins. Peaks: 1, D-gal ($[M]^+$, *m/z* 465; MS/MS, *m/z* 303); 2, D-glc ($[M]^+$, *m/z* 465; MS/MS, *m/z* 303); 3, Cy-gal ($[M]^+$, *m/z* 449; MS/MS, *m/z* 287); 4; D-ara ($[M]^+$, *m/z* 435; MS/MS, *m/z* 303); 5, Cy-glc ($[M]^+$, *m/z* 449; MS/MS, *m/z* 287); 6, Pt-gal ($[M]^+$, *m/z* 479; MS/MS, *m/z* 317); 7, Cy-ara ($[M]^+$, *m/z* 419; MS/MS, *m/z* 287); 8, Pt-glc ($[M]^+$, *m/z* 479; MS/MS, *m/z* 317); 9, Pe-gal ($[M]^+$, *m/z* 463; MS/MS, *m/z* 301); 10, Pt-ara ($[M]^+$, *m/z* 449; MS/MS, *m/z* 317); 11, Pe-glc ($[M]^+$, *m/z* 463; MS/MS, *m/z* 301); 12, Mv-gal ($[M]^+$, *m/z* 493; MS/MS, *m/z* 331); 13, Pe-ara ($[M]^+$, *m/z* 433; MS/MS, *m/z* 301); 14 Mv-glc ($[M]^+$, *m/z* 493; MS/MS, *m/z* 331); 15, Mv-ara ($[M]^+$, *m/z* 463; MS/MS, *m/z* 331).

anthocyanins including glucoside, galactoside, and arabinoside of delphinidin, cyanidin, peonidin, petunidin, and malvidin.[11] The aim of this study was to establish a routine methodology to assess the possible adulteration of commercial extracts and dietary supplements containing *V. myrtillus*. Thus, the anthocyanin profiles and their relative percentages in the berries of *V. myrtillus* from different countries were analyzed by LC. The resultant information was used as a baseline to evaluate the quality of 14 extracts, 6 dietary supplements, and 6 juices containing bilberry found in marketplaces and herbalist's shops.

## MATERIALS AND METHODS

**Chemicals and Materials.** Standards of cyanidin (Cy)-, delphinidin (D)-, petunidin (Pt)-, peonidin (Pe)-, malvidin (Mv)-, and their 3-*O*-glucoside (glc), Cy-, Pt-, Pe-, Mv-3-*O*-galactoside (gal), Cy-arabinoside (Cy-ara), and Cy-rutinoside (Cy-rut) were purchased from Polyphenols Laboratory (Sandnes, Norway). Potassium chloride, hydrochloric acid, methanol, acetonitrile, and phosphoric and trifluoroacetic acid (TFA) were from Merck (Darmstadt, Germany). Amaranth and ammonium acetate were purchased from Sigma-Aldrich (St. Louis, MO, USA), and water was obtained from a Milli-Q apparatus (Millipore, Milford, MA, USA). Frozen bilberries (*V. myrtillus*) originating from Italy ($n$ = 5), Finland ($n$ = 3), Sweden ($n$ = 1), Germany ($n$ = 3), Croatia ($n$ = 2), Argentina ($n$ = 2), and Slovenia ($n$ = 3) were purchased in local supermarkets and stored immediately at −20 °C. Bilberry extracts (E1−E14) were from different manufacturers, whereas food supplements (S1−S6) and juices (J1−J6) were acquired in herbal shops and local markets. The extracts of berries such as chokeberry (*Aronia melanocarpa*), elderberry, blackberry, black currant, red raspberry, sweet cherry, black beans, and black soybean and the fruits of mulberry (*Morus nigra*) were a gift from Specchiasol (Bussolengo, VR, Italy).

**Sample Preparation.** *Bilberry Fruit.* Approximately 10 g of frozen berries was mixed with 30 mL of a solution of methanol/TFA 2% in water (10:90, v/v) and homogenized by an Ultra-Turrax (IKA-Werke, Staufen, Germany) for 1 min. The homogenate was extracted for 30 min under agitation in the dark at room temperature. The suspension was centrifuged at 1000*g* for 10 min at 4 °C and the supernatant recovered. The residue was extracted again until disappearance of the red color (4 × 20 mL) with a solution of methanol/TFA 2% in water (10:90, v/v) and treated as described above. The supernatants were combined, and the volume was adjusted to 200 mL by solution of 2% TFA in water. All extracts were stored at −20 °C and centrifuged at 3000*g* for 1 min before the LC analysis.

*Bilberry Extracts.* Approximately 100 mg of powder was dissolved in approximately 20 mL of a solution of methanol/water (10:90, v/v), the suspension was sonicated for 5 min and centrifuged at 1000*g* for 5 min, and the supernatant was recovered. The residue, if present, was extracted four times with 15 mL of a methanol/water (10:90, v/v) solution and treated as described above. The supernatants were combined, and then the final volume was adjusted to 100 mL with water.

*Food Supplements and Juices Containing Bilberry Extract.* The contents of 10 capsules were mixed, and approximately 300 mg was dissolved in approximately 5 mL of methanol. This suspension was sonicated for 5 min and centrifuged at 1000*g* for 5 min, and the supernatant was recovered. The residue was extracted three times with 5 mL of water and treated as previously described. The supernatants were combined, and then the final volume was adjusted to 25 mL with water. The juice (2 mL) was diluted in 7 mL of a methanol/water

**Table 1. Anthocyanin Composition of Authentic Bilberry, Mulberry, Chokeberry, and Blackberry Samples**

| | name: | D-gal | D-glc | Cy-gal | D-ara | Cy-glc | Pt-gal | Cy-ara | Pt-glc | Pe-gal | Pt-ara | Pe-glc | Mv-gal | Pe-ara | Mv-glc | Mv-ara | ACNs |
|---|---|---|---|---|---|---|---|---|---|---|---|---|---|---|---|---|---|
| country | peak: | 1 | 2 | 3 | 4 | 5 | 6 | 7 | 8 | 9 | 10 | 11 | 12 | 13 | 14 | 15 | %[a] |
| Italy | RP[b] | 15.0 | –[c] | 2.0 | 8.5 | – | 0.9 | 10.8 | – | 1.5 | 5.5 | – | 36.2 | – | 0.8 | 19.0 | 0.16 |
| Italy | RP | 16.2 | 1.8 | 5.7 | 9.3 | 1.6 | 2.1 | 8.5 | – | 3.5 | 5.3 | 2.1 | 23.3 | 3.3 | 3.6 | 13.7 | 0.31 |
| Finland | RP | 20.5 | – | 2.7 | 15.0 | – | 1.7 | 11.3 | 0.5 | 3.9 | 7.4 | – | 19.0 | – | – | 18.0 | 0.25 |
| Germany | RP | 16.2 | – | 3.4 | 9.4 | 0.5 | 1.9 | 11.9 | – | 3.3 | 7.1 | – | 23.1 | 4.1 | – | 19.1 | 0.33 |
| Finland | RP | 14.0 | 16.7 | 7.7 | 10.2 | 8.6 | 7.0 | 8.5 | 7.6 | 1.2 | 3.6 | 3.4 | 1.7 | 0.2 | 7.2 | 2.4 | 0.22 |
| Finland | RP | 13.2 | 15.2 | 9.6 | 11.6 | 9.8 | 7.0 | 4.4 | 7.7 | 1.2 | 3.1 | 4.1 | 2.4 | 0.3 | 7.6 | 2.8 | 0.59 |
| Sweden | RP | 13.8 | 14.3 | 10.5 | 12.3 | 10.6 | 3.5 | 8.1 | 7.9 | 0.9 | 2.2 | 4.0 | 2.3 | 0.4 | 7.7 | 1.5 | 1.10 |
| Croatia | RP | 12.2 | 12.9 | 9.4 | 11.3 | 11.6 | 8.2 | 4.3 | 7.4 | 1.2 | 2.3 | 4.7 | 4.2 | 0.3 | 7.8 | 2.2 | 0.45 |
| Croatia | RP | 12.3 | 13.0 | 9.7 | 10.7 | 11.9 | 7.5 | 3.5 | 8.4 | 1.0 | 2.9 | 5.0 | 3.7 | 0.2 | 8.1 | 2.1 | 0.54 |
| Argentina | RP | 14.1 | 13.3 | 9.6 | 10.5 | 9.8 | 6.9 | 5.5 | 7.7 | 0.6 | 2.1 | 5.2 | 3.8 | 0.5 | 8.9 | 1.5 | 0.15 |
| Argentina | RP | 13.8 | 12.2 | 9.4 | 11.5 | 10.0 | 7.5 | 5.3 | 8.2 | 0.4 | 2.3 | 4.1 | 4.4 | 0.6 | 8.2 | 2.1 | 0.19 |
| Slovenia | RP | 12.8 | 13.7 | 10.2 | 12.6 | 10.9 | 5.2 | 9.2 | 8.4 | 1.1 | 2.0 | 4.7 | 2.2 | 0.4 | 5.6 | 1.1 | 1.20 |
| Slovenia | RP | 13.0 | 12.9 | 10.5 | 11.7 | 12.0 | 4.7 | 10.1 | 8.4 | 1.0 | 2.4 | 5.0 | 2.3 | 0.3 | 5.1 | 0.7 | 1.00 |
| Slovenia | RP | 13.3 | 13.1 | 9.8 | 13.0 | 9.7 | 5.9 | 7.4 | 9.3 | 1.1 | 2.2 | 4.3 | 2.4 | 0.3 | 6.8 | 1.4 | 1.31 |
| Germany | RP | 13.5 | 17.0 | 6.9 | 9.9 | 7.4 | 7.4 | 9.1 | 7.9 | 1.5 | 3.9 | 4.1 | 2.1 | 0.3 | 6.8 | 2.2 | 0.41 |
| Germany | RP | 13.0 | 14.2 | 9.4 | 10.4 | 7.1 | 7.4 | 10.3 | 7.8 | 1.8 | 3.4 | 3.6 | 2.7 | 0.3 | 6.5 | 2.1 | 0.92 |
| Italy | RP | 16.2 | 14.3 | 8.6 | 10.8 | 8.3 | 5.3 | 4.4 | 8.4 | 0.8 | 2.5 | 7.2 | 3.7 | 0.2 | 8.1 | 1.4 | 0.57 |
| Italy | RP | 16.0 | 14.1 | 10.0 | 13.8 | 9.5 | 6.9 | 4.0 | 7.7 | 0.7 | 2.7 | 3.4 | 3.0 | 0.2 | 6.6 | 1.6 | 0.40 |
| Italy | RP | 13.6 | 13.9 | 10.8 | 11.2 | 10.6 | 7.4 | 4.2 | 8.3 | 1.2 | 2.5 | 3.5 | 3.4 | 0.4 | 7.2 | 1.8 | 0.35 |
| mulberry[d] | RP | – | – | – | 0.5 | 77.2 | – | – | 2.2 | – | – | 0.3 | 0.2 | 1.4 | – | – | 0.23 |
| chokeberry[e] | RP | – | – | 51.3 | – | 33.8 | – | 11 | – | – | – | 2.3 | – | – | – | – | 0.36 |
| blackberry[f] | RP | – | – | – | – | 91.5 | – | – | – | – | – | 4.5 | – | – | – | – | 0.12 |

[a]Mean value (g/100 g FW, RSD% <12). [b]RP, relative percentage (individual compounds reported as percentage of total ACN monitored at 520 nm). [c]–, not found. [d]Contains also cyanidin-rutinoside (RP = 18.3). [e]Contains also cyanidin-xyloside (RP = 1.6). [f]Contains also cyanidin-rutinoside (RP = 4.0).

(10:90, v/v) solution, the suspension was sonicated for 5 min and centrifuged at 1000*g* for 5 min, and the supernatant was recovered. The residue was extracted with 7 mL of water and treated as previously described. The supernatants were combined, and then the final volume was adjusted to 20 mL with water. The sample was stored at 4 °C before the qualitative and quantitative analyses.

**Determination of Total Anthocyanins.** The total content of ACNs was determined spectrophotometrically (PerkinElmer Lambda 20, Waltham, MA, USA) by two methods.

Method A was described by Giusti et al.[22] Extracts were diluted in 0.1% HCl, the absorbance was measured at 520 nm, and the total percentage of ACNs was calculated as

$$\text{total ACNs (\%)} = \frac{A \times \text{MW} \times V \times D}{\varepsilon_{\text{mol}} \times W} \times 100$$

where $A$ = absorbance (AU), $\varepsilon_{\text{mol}}$ = Cy-glc molar extinction coefficient (26900), MW = Cy-glc molecular weight (449 Da), $W$ = sample weight (mg), $V$ = volume (mL), and $D$ = dilution factor.

Method B was described by Lee et al.[13] The absorbance was measured twice for each sample and buffer at the following wavelengths: 520 and 700 nm. The absorbance $A$ was calculated as follows:

$$A = (A_{520\text{nm}} - A_{700\text{nm}})_{\text{pH1}} - (A_{520\text{nm}} - A_{700\text{nm}})_{\text{pH4.5}}$$

The total ACN content (mg ACNs/100 mg) was calculated as described above.

**Anthocyanin Determination by Liquid Chromatography–Diode Array–Mass Spectrometry.** The UPLC system was a model Acquity (Waters, Milford, MA, USA) equipped with a model E-Lambda photodiode array detector (Waters) and a tandem mass spectrometer model Quattromicro (Waters). The separation was carried out by a BEH Shield $C_{18}$ column (150 × 2.1 mm, 1.7 μm, Waters) maintained at 45 °C. The flow rate was 0.5 mL/min, and the eluents were (A) 0.3% TFA and (B) $CH_3CN/CH_3OH$/TFA 0.5% (22:22:56, v/v/v). The elution gradient was linear as follows: 0–20 min, 20% B; 20–30 min, from 20 to 26% B; 30–40 min, from 26 to 30% B; 40–45 min, from 30 to 40% B; 45–47 min, from 40 to 60% B; 47–50 min, from 60 to 90% B; 90% for 3 min. Chromatographic data were acquired from 200 to 700 nm and integrated at 520 nm. Anthocyanin stock solutions (1 mg/mL) were prepared in methanol/TFA 2% (10:90, v/v) and stored at −20 °C. Working solutions ($n$ = 5) were prepared in the range of 2–50 μg/mL, and each analysis was carried out in duplicate. Fifty microliters was injected into the chromatographic system. The concentration of the ACNs not commercially available (D-gal, D-ara, Mv-ara, and Pt-ara) was estimated using the calibration curve equation of the same anthocyanidin linked to glucose. The ACNs were also determined by the Cy-glc curve, and the resulting data were corrected by molecular weight ratio.

Mass analyses were performed in positive scan mode in the range of 100–1000 Da, and the fragmentations were performed using cone voltage, collision energy, and argon gas at 20 V, 30 eV, and $2.0 \times 10^{-3}$ mbar, respectively.

**Amaranth Determination by UPLC-MS/MS.** The UPLC system was a model Acquity (Waters) coupled to a tandem mass spectrometer model Quattromicro (Waters). Separations were performed using a 1.7 μm BEH $C_{18}$ column (100 × 2.1 mm, Waters). The eluent was 1 mM ammonium acetate, pH 4.5/acetonitrile (80:20, v/v). The flow rate was 0.5 mL/min, the column temperature was 35 °C, and the injection volume was 2 μL. The capillary voltage was set to 3.0 kV, the cone voltage was 30 V, the source temperature was 130 °C, the desolvating temperature was 350 °C, the collision energy (CE) was specific for each transition, and argon was used at $2.0 \times 10^{-3}$ mbar to improve fragmentation in the collision cell. Amaranth was determined in multiple reaction monitoring (MRM) mode, and the data were acquired by MassLynx 4.0 software (Waters). The mass spectrometer was operated in the electrospray ionization (ESI) negative mode, and the fragmentation transitions were $(m/z)^-$ 537 → 317 (CE 30), 457 (CE 40), with a dwell time of 0.2 s. Calibration curves were obtained from amaranth stock solutions prepared by dissolving 10 mg of standard powder in 10 mL of methanol, and their quantitative determination was performed in the range of 50–500 ng/mL.

**Table 2. Total Anthocyanin Content (Percent, Mean ± SD) in Bilberry Extracts (E1−E14) and Commercial Products (Capsules, S1−S6; Juices, J1−J6) Determined by Different Analytical Methods**

| sample | declared | method A | method B | method C |
|---|---|---|---|---|
| E1 | 36[a] | 33.9 ± 0.7 | 29.5 ± 0.5 | 29.9 ± 0.4 |
| E2 | 25[b] | 24.8 ± 0.6 | 20.4 ± 0.5 | 15.9 ± 0.3 |
| E3 | 25[a] | 23.4 ± 0.8 | 19.6 ± 0.5 | 17.8 ± 0.3 |
| E4 | 30[b] | 29.0 ± 0.5 | 24.3 ± 0.5 | 22.4 ± 0.4 |
| E5 | 25[b] | 30.0 ± 0.7 | 26.2 ± 0.6 | 24.9 ± 0.4 |
| E6 | 1.4[b] | 1.4 ± 0.0 | 1.0 ± 0.0 | 0.3 ± 0.0 |
| E7 | 25[c] | 9.8 ± 0.4 | 7.0 ± 0.2 | 2.4 ± 0.1 |
| E8 | 25[a] | 25.7 ± 0.3 | 23.6 ± 0.3 | 22.3 ± 0.1 |
| E9 | 25[a] | 1.3 ± 0.1 | 1.0 ± 0.0 | 0.7 ± 0.0 |
| E10 | 1[c] | 0.2 ± 0.0 | 0.1 ± 0.0 | 0.05 ± 0.0 |
| E11 | 2.5[b] | 2.6 ± 0.1 | 2.2 ± 0.1 | 2.4 ± 0.1 |
| E12 | 1[b] | 1.5 ± 0.1 | 1.2 ± 0.0 | 1.2 ± 0.0 |
| E13 | 25[a] | 21.3 ± 0.7 | 17.0 ± 0.3 | 18.8 ± 0.4 |
| E14 | 25[a] | 19.6 ± 0.4 | 16.2 ± 0.5 | 17 ± 0.3 |
| S1 | nr[d] | 0.1 ± 0.0 | 0.0 ± 0.0 | 0.0 ± 0.0 |
| S2 | 1.7 | 1.5 ± 0.1 | 1.2 ± 0.0 | 1.2 ± 0.0 |
| S3 | 3.5 | 3.0 ± 0.1 | 1.9 ± 0.1 | 1.8 ± 0.0 |
| S4 | 8.6 | 13.3 ± 0.4 | 11.7 ± 0.3 | 8.9 ± 0.0 |
| S5 | 0.7 | 1.3 ± 0.0 | 0.8 ± 0.0 | 0.8 ± 0.0 |
| S6 | 0.8 | 0.7 ± 0.0 | 0.7 ± 0.0 | 0.5 ± 0.0 |
| J1 | nr | 0.11 ± 0.01 | 0.07 ± 0.01 | 0.06 ± 0.00 |
| J2 | nr | 0.01 ± 0.00 | 0.01 ± 0.00 | 0.00 ± 0.00 |
| J3 | nr | 0.10 ± 0.01 | 0.08 ± 0.01 | 0.07 ± 0.00 |
| J4 | nr | 0.03 ± 0.00 | 0.02 ± 0.00 | 0.01 ± 0.00 |
| J5 | 0.2 | 0.10 ± 0.00 | 0.02 ± 0.00 | 0.00 ± 0.00 |
| J6 | nr | 0.05 ± 0.00 | 0.04 ± 0.00 | 0.03 ± 0.00 |

[a]ACN content by HPLC. [b]ACN content by spectrophotometer. [c]Method not reported in the analytical certificate. Method A, spectrophotometric at 520 nm; method B, spectrophotometric (520 nm) at two different pH values; method C, LC-DAD. [d]nr, not reported in the packaging.

**Statistical Analysis.** The statistical analysis was performed by means of Excel software. To demonstrate the similarity or differentiation between the chemical profiling chromatograms between reference (fruits) and target products (extracts, commercial preparations), the total deviation percentage (TD%) was introduced and calculated by using the equation

$$\mathrm{TD\%} = \sum_{i}^{n} \frac{|A_s' - A_t'|}{A_s' n}$$

where TD% = total deviation percentage, $A_s$ = relative percentage of the peak in the reference chromatogram (bilberry fruits), $A_t$ = relative percentage of the peak in the target chromatogram, and $n$ = the number of peaks.

## RESULTS AND DISCUSSION

Anthocyanins in bilberry fruit and their commercial preparations were identified by cochromatography, online UV−vis spectra, molecular weight, and MS/MS fragmentation. The chromatograms relating to fruits, obtained at 520 nm, showed the presence of 15 anthocyanins, whereas the respective aglycones were absent in all of the samples (Figure 1a) and several fruits ($n$ = 3) displayed a lower amount of anthocyanidin glucosides (Figure 1b). Therefore, there were two types of bilberry, which differed in the relative percentages of glucosylated anthocyanidins. Lower percentages of glucosylated ACN have already been found in several cultivars of bilberry[1] and highbush blueberry,[16] but the factors responsible for these differences are not yet clear. They could include differences in the genotype, environment, such as light, temperature, and altitude, or both factors. Table 1 reports the individual and total anthocyanin content in bilberries from different countries. The monomeric anthocyanin pigment content of the analyzed berry samples ranged from 151 to 1310 mg/100 g FW with a mean of 551 mg/100 g (Table 1), and D-, Cy-, Pt-, Mv-, and Pe-glycosides comprised about 39, 24, 18, 14, and 5% of the total ACNs, respectively. The average contents of these ACNs were comparable to those reported by Latti et al.,[1] but lower than those reported by other authors.[17] Quantification of the ACNs was based on authentic standards and by the Cy-glc equivalents, which are the methods generally used in quality control laboratories. The latter type of quantification underestimated the content of D-glycosides by approximately 30%, as shown by Kähkönen et al.[18]

**ACNs in Bilberry Extracts.** Amaranth, a dye used to adulterate the extracts of bilberry, was not detected in any sample analyzed. The quantitative analysis of the standardized bilberry extracts showed marked differences among them (Table 2). The spectrophotometric determinations have provided quantitative data up to 75% higher than those obtained by chromatography, and the differences may be due to the presence of other pigments, polymerized anthocyanins, or both. Despite this, the pH differential method could be used to quickly determine the presence of dyes that do not change color in varying pH conditions, such as amaranth.

The chromatographic analyses showed that 35% of the tested extracts (E2, E4, E7, E9, and E10) did not qualitatively and quantitatively conform to the analytical report provided by the supplier. Extracts E1, E3, E6, E13, and E14 did qualitatively conform, but their content in anthocyanins was lower than declared by the supplier. In particular, the ACN amount found in E6 was lower than about 80%. The remaining extracts (E5 and E11) were qualitatively and quantitatively in accordance with those stated by the manufacturer.

Figure 2 shows the chromatograms, integrated at 520 nm, corresponding to samples E2, E7, and E9. The chromatographic profile of the E2 extract, similar to E4, showed the presence of two main ACNs that seemed to match, separation factor ($\alpha$) = 1, Cy-glc and Pt-glc. The mass spectra showed that peaks 5 and 8 (Figure 2I) had molecular weights of 449 and 595, respectively, and at lower collision energy values these ions gave an ion product with $(m/z)^+$ 287, likely corresponding to the aglycone moiety. Thus, the mass spectrometry data, combined with the UV−vis and chromatographic behavior, suggest that peaks 5 and 8 were Cy-glc and Cy-rut, respectively. The latter compound, Cy-rut, is not normally present in bilberry fruit extracts, but has been found in berries such as *Morus nigra* (black mulberry). Thus, the reference extract of bilberry fruit was spiked with a commercial extract of mulberry, and chromatographic analysis revealed that the E2 and E4 samples contained approximately 50 and 30% mulberry, respectively.

The chromatographic profiles of the E7 and E8 extracts differed significantly from that of the bilberry; they contained three main ACNs corresponding to Cy-gal, Cy-glc, and Cy-ara and two minor compounds identified as Pe-glc and Cy-xyloside (Figure 2II). These ACNs were present in a reference extract of *Aronia melanocarpa* (chokeberry), and they have also been

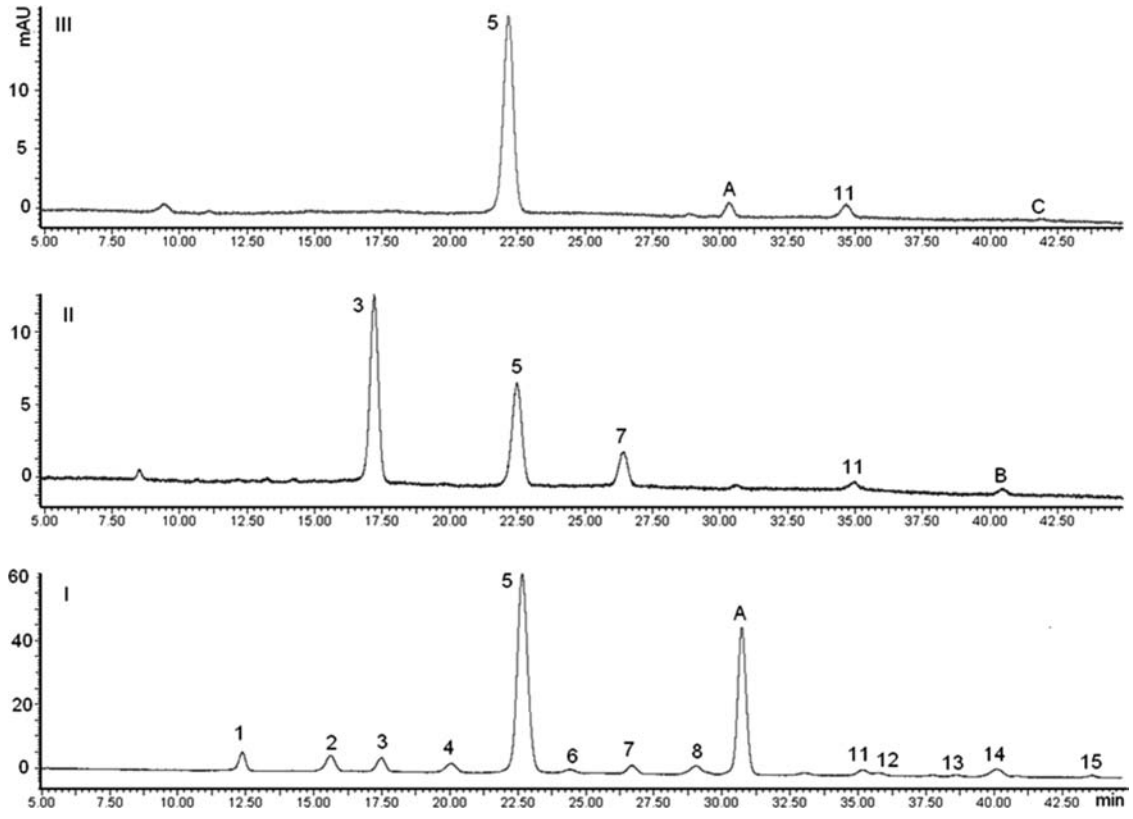


**Figure 2.** Chromatograms integrated at 520 nm of extracts E2 (I), E7 (II), and E9 (III). Peaks: A, Cy-rutinoside ($[M]^+$, $m/z$ 595; MS/MS, $m/z$ 287); B, Cy-xyloside ($[M]^+$, $m/z$ 419; MS/MS, $m/z$ 287); C, Cy-derivative (($[M]^+$, $m/z$ 569; MS/MS, $m/z$ 287). The chromatographic profiles of samples E2, E7, and E9 were comparable to those of mulberry, chokeberry, and blackberry extract, respectively. See Figure 1 for peak attribution.

found in chokeberries by different authors,[19,15] although in different proportions from those present in our chokeberry extracts. Thus, it seems that samples E7 and E8 were extracts of chokeberries and not bilberries. In addition, sample E9 did not contain the 15 typical bilberry ACNs. Indeed, it contained mainly Cy-glc and lower amounts of Cy-rut, Pe-glc, pelargonidin-hexoside, and an unknown anthocyanin (Figure 2III, peak C). The mass spectra showed that peak C had a molecular weight of 569 Da, and at lower collision energy values it gave an ion product with $(m/z)^+$ 287, likely corresponding to the aglycone moiety, thus suggesting that it was a cyanidin derivative. We found these ACNs in an extract of blackberry (*Rubus nigra*). Furthermore, Jacobeck et al.[15] reports a chromatographic profile of the blackberry very similar to that of extract E9. Thus, the sample E9 is not bilberry, but may be a blackberry extract. Finally, extract E10 did not contain ACNs, and the spectrophotometric data revealed significantly less than the declared percentage.

**ACNs in Food Supplements Containing Bilberry.** The ACN spectrophotometric determinations (Table 2) in 12 food supplements have provided quantitative data up to 80% higher than those obtained by chromatography, as already obtained from analyzing the extracts. The LC-DAD-MS analyses showed that the food supplements formulated in capsules (S1−S6) did not qualitatively and/or quantitatively conform (Table 2). In particular, the chromatographic profiles of products S2, S4, and S5 were comparable to those of extracts E2 and E4, identified as black mulberry extracts. The quantitative data suggest that S4, S5, and S2 contain approximately 50, 70, and 70% of mulberry extract, respectively, suggesting that these dietary supplements have been manufactured using an extract of the E2-type. Products S3 and S6 contained bilberry extract, but the ACN content determined by LC-DAD was less than that declared on the label (Table 2). Moreover, sample S6 contained aglycones comprising approximately 20% of the total ACNs, which suggests the use of an extract of lower quality, inadequate/incorrect processing, or both. Product S1 did not contain ACNs, and the package did not report the ACN percentage.

With regard to juices, their chromatographic profiles were comparable to those of the reference extracts except for sample J5. In this product, ACNs were not detected and the chromatographic profile showed a "hump" at about 45 min, which could suggest the presence of polymerized ACNs. The ACN content was only reported on the label of product J5, which was much lower than that determined spectrophotometrically (Table 2). The quantitative data show that the ACN daily intake is in the ranges of 5−33 and 0.5−9.3 mg for products S1−S6 and J1−J6, respectively, which corresponds to <20 g of fresh bilberry fruits containing 0.2% in ACNs. Moreover, it should be pointed out that these quantities are much lower than those demonstrated to be effective in the treatment of some pathologies, such as peripheral vascular disease and venous sensitivity (100−200 mg ACNs)[20] or in reducing the levels of oxidized DNA bases and increasing the resistance to oxidatively induced DNA damage (375 mg ACNs).[21]

Overall, the picture is discouraging and, therefore, it would be appropriate for producers to standardize their extracts and food supplements with chromatographic techniques, as reported in pharmacopoeia, to effectively declare the amounts of anthocyanins.

**Total Deviation Percentage.** The extracts and food supplements showed chromatographic profiles of ACNs similar

Table 3. Chemical Profiling Data of the ACNs in Bilberry Fruits and Commercial Products (Peak Area in Percentage)[a]

| peak:[b] | 1 | 2 | 3 | 4 | 5 | 6 | 7 | 8 | 9 | 10 | 11 | 12 | 13 | 14 | 15 | |
|---|---|---|---|---|---|---|---|---|---|---|---|---|---|---|---|---|
| mean:[c] | 13.6 | 14.1 | 9.2 | 11.4 | 9.6 | 6.5 | 7.3 | 8.1 | 1.0 | 2.8 | 4.3 | 2.9 | 0.3 | 7.1 | 1.9 | |
| SD: | 1.1 | 1.4 | 1.6 | 1.1 | 2.0 | 1.4 | 3.5 | 0.6 | 0.5 | 0.8 | 1.2 | 0.9 | 0.2 | 1.3 | 0.9 | TD% |
| E1 | 12.5 | 13.3 | 10.3 | 11.0 | 11.4 | 7.6 | 3.7 | 8.0 | 1.0 | 2.6 | 4.5 | 3.8 | 0.3 | 8.3 | 1,9 | 12 |
| E2 | 6.3 | 5.6 | 4.1 | 4.6 | 60.1 | 3.2 | 1.9 | 3.1 | 0.4 | 1.3 | 2.0 | 2.2 | 0.1 | 4.3 | 0.9 | 86 |
| E3 | 14.3 | 11.6 | 11.8 | 10.8 | 10.8 | 7.4 | 4.0 | 6.7 | 0.8 | 2.6 | 4.4 | 4.8 | 0.1 | 7.7 | 1.9 | 21 |
| E4 | 8.8 | 8.7 | 7.7 | 7.3 | 37.4 | 5.2 | 2.6 | 6.9 | 0.6 | 1.8 | 3.3 | 2.7 | 0.2 | 5.5 | 1.2 | 47 |
| E5 | 13.3 | 12.8 | 10.9 | 11.1 | 11.1 | 7.5 | 3.9 | 7.6 | 0.9 | 2.6 | 4.6 | 4.0 | 0.3 | 8.0 | 1.8 | 13 |
| E6 | 12.9 | 11.9 | 11.1 | 10.5 | 13.6 | 8.3 | 3.7 | 6.8 | 1.0 | 2.3 | 4.0 | 4.0 | 0.3 | 7.8 | 1.6 | 18 |
| E7 | –[d] | – | 46.3 | – | 32.9 | – | 18.0 | – | – | – | 1.9 | 1.1 | – | – | – | 129 |
| E8 | – | – | 40.0 | – | 40.0 | – | 20.0 | – | – | – | – | – | – | – | – | 135 |
| E9 | – | – | 0.0 | – | 87.6 | – | – | 3.9 | – | – | 4.5 | – | – | 4.1 | – | 138 |
| E10 | – | – | 0.0 | – | 0.0 | – | – | – | – | – | 0.0 | – | – | – | – | |
| E11 | 12.7 | 12.1 | 11.1 | 11.1 | 10.9 | 8.4 | 3.9 | 8.0 | 1.3 | 2.7 | 4.3 | 3.9 | 0.6 | 7.2 | 1.8 | 21 |
| E12 | 13.6 | 12.8 | 10.3 | 11.4 | 10.5 | 7.7 | 3.9 | 8.3 | 1.1 | 2.7 | 4.2 | 3.8 | 0.3 | 7.7 | 1.8 | 11 |
| E13 | 13.8 | 12.0 | 11.0 | 11.5 | 10.4 | 7.6 | 3.9 | 7.2 | 1.1 | 2.8 | 4.3 | 4.2 | 0.5 | 7.7 | 2.1 | 17 |
| E14 | 13.3 | 14.0 | 10.1 | 10.8 | 11.4 | 7.0 | 3.6 | 8.1 | 0.9 | 2.5 | 4.5 | 3.6 | 0.4 | 7.9 | 1.8 | 13 |
| S1 | – | – | – | – | – | – | – | – | – | – | – | – | – | – | – | |
| S2 | 0.9 | 0.7 | 0.5 | 0.7 | 88.1 | 0.3 | 0.2 | 6.4 | 0.6 | 0.1 | 0.2 | 0.2 | – | 0.7 | 0.1 | 135 |
| S3 | 11.8 | 13.2 | 11.0 | 8.9 | 12.4 | 7.5 | 3.7 | 8.4 | 1.0 | 2.5 | 5.6 | 4.0 | – | 8.6 | 1.5 | 26 |
| S4 | 4.0 | 5.8 | 6.4 | 5.3 | 51.7 | 2.9 | 1.6 | 6.5 | 0.6 | 1.3 | 2.0 | 4.6 | 2.2 | 3.5 | 1.2 | 116 |
| S5 | 10.2 | 5.9 | 7.3 | 5.8 | 47.0 | 4.0 | 3.3 | 1.3 | 1.0 | 1.2 | 1.9 | 5.4 | 0.9 | 3.3 | 1.1 | 82 |
| S6 | 14.1 | 11.3 | 10.8 | 10.5 | 11.7 | 7.5 | 4.1 | 6.6 | 0.5 | 2.9 | 4.5 | 5.1 | 0.1 | 7.9 | 2.0 | 24 |
| J1 | 12.8 | 14.0 | 10.1 | 8.1 | 11.6 | 5.5 | 4.3 | 8.4 | 0.8 | 2.2 | 4.8 | 5.4 | 0.3 | 9.7 | 2.1 | 21 |
| J2 | 8.7 | 13.9 | 8.4 | 5.9 | 16.1 | 5.9 | 3.3 | 9.7 | 0.6 | 2.0 | 6.2 | 6.7 | 0.0 | 10.3 | 2.4 | 44 |
| J3 | 14.0 | 12.0 | 11.8 | 11.1 | 11.0 | 7.2 | 4.1 | 6.5 | 0.7 | 2.6 | 4.4 | 4.6 | 0.1 | 7.7 | 2.1 | 21 |
| J4 | 12.5 | 12.8 | 10.2 | 12.2 | 11.2 | 6.0 | 3.4 | 8.2 | 0.7 | 2.1 | 4.2 | 5.2 | 0.1 | 8.6 | 2.3 | 24 |
| J5 | – | – | – | – | – | – | – | – | – | – | – | – | – | – | – | |
| J6 | 11.8 | 12.9 | 11.9 | 7.3 | 13.4 | 6.3 | 3.9 | 9.3 | 1.1 | 2.3 | 5.1 | 4.1 | 0.0 | 9.1 | 1.6 | 28 |

[a]E1–E14, bilberry extracts; S1–S6 and J1–J6, food supplements in capsules (S) and juice (J). [b]Peaks: 1, D-gal; 2, D-glc; 3, Cy-gal, 4; D-ara, 5, Cy-glc; 6, Pt-gal; 7, Cy-ara; 8, Pt-glc; 9, Pe-gal; 10, Pt-ara; 11, Pe-glc; 12, Mv-gal; 13, Pe-ara; 14, Mv-glc; 15, Mv-ara. [c]Average determined by analyzing frozen bilberries samples ($n$ = 19) from different countries ($n$ = 7). [d]–, not found.

to those of fruits with higher glucosylated anthocyanidin contents. Therefore, fruits with a fingerprinting shown in Figure 1a were used as a reference for the determination of the relative percentages of ACNS. Fourteen extracts and 12 finished products were analyzed on the basis of the established chromatographic profiling (Figure 1a), and the normalized peak areas of the typical 15 ACNs are provided in Table 3. The total deviation percentage (TD%) was chosen as the parameter to compare the chromatograms of the reference and target products. The last column of Table 3 shows the TD% values of 26 commercial products versus the reference bilberry. The TD% data for the bilberry extracts suggested that products E1, E3, E5, E6, and E11–14 were similar to the given reference, but the others (about 57%) differed significantly from it. The food supplements in capsules or juice showed higher values of TD% in about 60 and 33% of the products, respectively. The TD% does not provide quantitative data, but it can be a valuable tool to verify the conformity of a product. The limiting value of TD% beyond which the product is not to be considered bilberry remains to be determined.

## AUTHOR INFORMATION


### Corresponding Author

*(C.G.) Phone: +39-02-50316722. Fax: +39-02-50316721. E-mail: claudio.gardana@unimi.it.


### Notes

The authors declare no competing financial interest.

## ABBREVIATIONS USED

$\alpha$, separation factor; ACN(s), anthocyanin(s); Dp-gal, delphinidin-galactoside; Dp-glc, delphinidin-glucoside; Dp-ara, delphinidin-arabinoside; CE, collision energy; Cy-gal, cyanidin-galactoside; Cy-glc, cyanidin-glucoside; Cy-ara, cyanidin-arabinoside; Cy-rut, cyanidin-rutinoside; E1–E14, bilberry extracts; J1–J6, juices containing bilberry; Pt-gal, petunidin-galactoside; Pt-glc, petunidin-glucoside; Pt-ara, petunidin-arabinoside; Pe-gal, peonidin-galctoside; Pe-glc, peonidin-glucoside; Pe-ara, eonidin-arabinoside; S1–S6, food supplements; Mv-gal, malvidin-galctoside; Mv-glc, malvidin-glucoside; Mv-ara, malvidin-arabinoside; TFA, trifluoroacetic acid

## REFERENCES


(1) Latti, A. K.; Riihinen, K. R.; Kainulainen, P. S. Analysis of anthocyanin variation in wild populations of bilberry (*Vaccinium myrtillus* L.) in Finland. *J. Agric. Food Chem.* **2008**, *56*, 190–196.

(2) Seeram, N. P.; Adams, L. S.; Zhang, Y.; Lee, R.; Sand, D.; Sheuller, H. S.; Heber, D. Blackberry, black raspberry, blueberry, cranberry, red raspberry, and strawberry extracts inhibit growth and stimulate apoptosis of human cancer cells in vitro. *J. Agric. Food Chem.* **2006**, *54*, 9329–9339.

(3) Steigerwalt, R. D., Jr.; Gianni, B.; Paolo, M.; Bombardelli, E.; Burki, C.; Schönlau, F. Effect of Mirtogenol® on ocular blood flow and intraocular hypertension in asymptomatic subjects. *Mol. Vis.* **2008**, *14*, 1288–1292.

(4) Takikawa, M.; Inoue, S.; Horio, F.; Tsuda, T. Dietary anthocyanin-rich bilberry extract ameliorates hyperglycemia and insulin sensitivity via activation of amp-activated protein kinase in diabetic mice. *J. Nutr.* **2010**, *140*, 527−533.
(5) Mauray, A.; Felgines, C.; Morand, C.; Mazur, A.; Scalbert, A.; Milenkovic, D. Bilberry anthocyanin-rich extract alters expression of genes related to atherosclerosis development in aorta of apo E-deficient mice. *Nutr. Metab. Cardiovasc. Dis.* **2012**, *22*, 72−80.
(6) Bridle, P.; Timberlake, C. F. Anthocyanins as natural food colours-selected aspects. *Food Chem.* **1997**, *58*, 103−109.
(7) Takeoka, G. R.; Dao, L. T.; Full, G. H.; Wong, R. Y.; Harden, L. A.; Edwards, R. H.; Berrios, J. Characterization of black bean (*Phaseolus vulgaris* L.) anthocyanins. *J. Agric. Food Chem.* **1997**, *45*, 3395−3400.
(8) Lee, J. H.; Kang, N. S.; Shin, S. O.; Shin, S. H.; Lim, S.; Suh, D. Y.; Baek, I. Y.; Park, K. Y.; Ha, T. J. Characterization of anthocyanins in the black soybean (*Glycine max* L.) by HPLC-DAD-ESI/MS analysis. *Food Chem.* **2009**, *112*, 226−231.
(9) Pennman, K. G.; Halstead, C. W.; Stuhe, U.; Bone, K. M.; Lehmann, R. P. Bilberry adulteration using the food dye amaranth. *J. Agric. Food Chem.* **2006**, *54*, 7378−7382.
(10) Artaria, C.; Pace, R.; Maramaldi, G.; Appendino, G. Different brands of bilberry extract. A comparison of selected components. *Nutrafood* **2007**, *6*, 13−18.
(11) Cassinese, C.; de Combarieu, E.; Falzoni, M.; Fuzzati, N.; Pace, R.; Sardone, N. New liquid chromatography method with ultraviolet detection for analysis of anthocyanins and anthocyanidins in *Vaccinium myrtillus* fruit dry extracts and commercial preparations. *J. AOAC Int.* **2007**, *90*, 911−919.
(12) Wrolstad, R. E.; Durst, R. W.; Lee, J. Tracking color and pigment changes in anthocyanin products. *Trends Food Sci. Technol.* **2005**, *16*, 423−428.
(13) Lee, J.; Durst, R. W.; Wrolstad, R. E. Determination of total monomeric anthocyanin pigment content of fruit juices, beverages, natural colorants, and wines by the pH differential method: collaborative study. *J. AOAC Int.* **2005**, *88*, 1269−1278.
(14) Díaz-García, M. C.; Obón, J. M.; Castellar, M. R.; Collado, J.; Alacid, M. Quantification by UHPLC of total individual polyphenols in fruit juices. *Food Chem.* **2013**, *138*, 938−949.
(15) Jakobek, L.; Seruga, M.; Medvidovic-Kosanovic, M.; Novak, I. Anthocyanin content and antioxidant activity of various red fruit juices. *Dtsch. Lebensm.-Rundsch.* **2007**, *103*, 58−64.
(16) Wang, J.; Kalt, W.; Sporns, P. Comparison between HPLC and MALDI-TOF MS analysis of anthocyanins in highbush blueberries. *J. Agric. Food Chem.* **2000**, *48*, 3330−3335.
(17) Määttä-Riihinen, K. R.; González-Paramás, A. M.; Törrönen, A. R.; Kamal-Eldin, A.; Mattila, P. H. Distribution and contents of phenolic compounds in eighteen Scandinavian berry species. *J. Agric. Food Chem.* **2004**, *52*, 4477−4486.
(18) Kähkönen, M. P.; Heinämäki, J.; Ollilainen, V.; Heinonen, M. Berry anthocyanins: isolation, identification and antioxidant activities. *J. Sci. Food Agric.* **2003**, *83*, 1403−1411.
(19) Myrtilli fructus. *European Scientific Cooperative on Phytotherapy (ESCOP) Monographs*, 2nd ed.; Thieme Publishers: New York, 2003; pp 345−350.
(20) Bräunlich, M.; Slimestad, R.; Wangensteen, H.; Brede, C.; Malterud, K. E.; Barsett, H. Extracts, anthocyanins and procyanidins from *Aronia melanocarpa* as radical scavengers and enzyme inhibitors. *Nutrients* **2013**, *5*, 663−678.
(21) Riso, P.; Klimis-Zacas, D.; Del Bó, C.; Martini, D.; Campolo, J.; Vendrame, S.; Møller, P.; Loft, S.; De Maria, R.; Porrini, M. Effect of a wild blueberry (*Vaccinium angustifolium*) drink intervention on markers of oxidative stress, inflammation and endothelial function in humans with cardiovascular risk factors. *Eur. J. Nutr.* **2013**, *52*, 949−961.
(22) Giusti, M. M.; Rodríguez-Saona, L. E.; Wrolstad, R. E. Molar absorptivity and color characteristics of acylated and non-acylated pelargonidin-based anthocyanins. *J. Agric. Food Chem.* **1999**, *47*, 4631−4637.

**Table 1. Parameters[a] from LC-Neg-ESI-MS/MS Data for Curcuminoids Curcumin, DMC, Bis-DMC, Known Metabolites DHC, THC, and FA, and a New Compound Detected in the Fermentation Culture**

| | | MRM parameters | | | | |
|---|---|---|---|---|---|---|
| compound | Rt (min) | MRM transitions ($m/z$) | fragmentor voltage | collision energy (CE) | LOD ($\mu$M) | LOQ ($\mu$M) |
| curcumin | 5.99 | 367−134[b] | 100 | 20 | 0.01 | 0.025 |
| | | 367−149 | 100 | 20 | | |
| | | 367−173 | 100 | 10 | | |
| DMC | 5.97 | 337−217[b] | 110 | 10 | 0.01 | 0.025 |
| | | 337−173 | 110 | 10 | | |
| Bis-DMC | 5.94 | 307−143[b] | 110 | 10 | 0.01 | 0.025 |
| | | 307−119 | 110 | 10 | | |
| DHC[c] | 5.10 | 369−219[b] | 110 | 10 | | |
| | | 369−134 | 110 | 10 | | |
| | | 369−149 | 110 | 25 | | |
| THC | 5.60−6.05 | 371−235[b] | 120 | 10 | 0.025 | 0.05 |
| | | 371−99 | 120 | 30 | | |
| | | 371−135 | 120 | 30 | | |
| ferulic acid (FA) | 1.35 | 193−134[b] | 100 | 10 | 0.01 | 0.025 |
| | | 193−178 | 100 | 10 | | |
| curcumin adduct (curcumin−L-cysteine)[d] | 5.46 | 470−167[b] | 120 | 10 | | |
| | | 470−392 | 120 | 10 | | |
| | | 470−152 | 120 | 10 | | |
| $\beta$-estradiol-17-acetate | 6.34 | 313−185 | 230 | 35 | | |

[a]Rt, retention time; LOD, limit of detection; LOQ, limit of quantification. [b]Peak area from this transition was used for quantification. [c]Identification and confirmation based on molecular weight and MS/MS fragmentation patterns. [d]Compound confirmation based on accurate mass from FT-ICR-MS and structural identification based on MS/MS fragmentation patterns. Response for DHC and curcumin adduct (curcumin−L-cysteine) was assumed to be the same as that for curcumin.

then THC in the presence of nicotinamide adenine dinucleotide phosphate (NADPH).[19] The mechanism of *CurA* is presumed to occur through the reduction of C═C bonds only and not C═O bonds on the heptadienone linkage of curcumin.[19] To gain more information on the metabolism of curcuminoids by gut bacteria, we studied the in vitro interaction of curcuminoids with a pure culture of *Escherichia fergusonii* (ATCC 35469 (E469)) and two strains of *E. coli* (ATCC 8739 (E739) and DH10B (E10B)). These bacteria were chosen as they all contain the YncB gene that encodes for *CurA*. A basic local alignment search tool (BLAST) program revealed that the predicted amino acid sequence of *Escherichia fergusonii* ATCC 35469 (E469) and *E. coli* ATCC 8739 (E739) exhibited 90% and 97% similarity, respectively, to the deduced amino acid sequence of *CurA* from *E. coli* DH10B (E10B). The amount of curcuminoids degraded by the three *Escherichia* bacteria was quantified using liquid chromatography−mass spectrometry (LC-MS) and multiple reaction monitoring (MRM). The breakdown products produced were identified and characterized using tandem mass spectrometry (MS/MS) and high-resolution Fourier Transform-ion cyclotron resonance MS (FT-ICR-MS) and then quantified using MRM.

## MATERIALS AND METHODS

**Materials.** Commercially available curcumin, which consists of a mixture of three naturally occurring curcuminoids, curcumin (80.1%), DMC (15.6%), and Bis-DMC (2.6%), pure standards of two possible breakdown products, THC and FA, and the internal standard (IS) used, $\beta$-estradiol-17-acetate, were purchased from Sigma-Aldrich (Castle Hill, NSW, Australia). Acetonitrile was purchased from Burdick & Jackson (Gillman, SA, Australia), methanol and ethyl acetate were supplied by Merck Pty Ltd. (Kilsyth, Vic, Australia), and all solvents were of HPLC grade. Formic acid and ammonium acetate (analytical grade) were from Ajax FineChem (Waltham, MA, USA). Redistilled deionized water with a resistivity of 18.2 m$\Omega$ was used in all experiments.

Pig cecal fluid (PCF) was sourced from an abattoir (Laverton, VIC, Australia). The PCF was centrifuged at 16000*g* for 40 min (Sorvall RC-6, Thermo Scientific) to remove solid particles, and the supernatant was stored at −20 °C until further use.

**Bacterial Strains.** *Escherichia fergusonii* ATCC 35469 (E469) and *E. coli* ATCC 8739 (E739) from human fecal isolates were obtained from American Type Culture Collection (Manassas, VA, USA). *E. coli* DH10B (E10B) was from Invitrogen (VIC, Australia). All strains were stored at −80 °C in de Man−Rogosa−Sharpe medium (MRS medium; Oxoid; SA, Australia) supplemented with 30% (v/v) glycerol as a cryoprotectant.

**Medium and Growth Conditions for Fermentation Experiments.** Modified medium for colon bacteria (mMCB), which supports the growth of colonic bacteria,[20] was selected for fermentation experiments. The medium consisted of 0.65% (all w/v) bacteriological peptone (Oxoid), 0.5% soy peptone (Oxoid), 0.3% yeast extract (Oxoid), 0.25% tryptone (Oxoid), 0.45% NaCl, 0.2% KCl, 0.05% $MgSO_4 \cdot 7H_2O$, 0.045% $CaCl_2 \cdot 2H_2O$, 0.02% $NaHCO_3$, 0.02% $MnSO_4 \cdot H_2O$, 0.0005% $FeSO_4 \cdot 7H_2O$, 0.0005% $ZnSO_4 \cdot 7H_2O$, 0.04% L-cysteine $HCl \cdot H_2O$ as a reducing agent, and 1.0 mL of resazurin solution (made from 0.01% w/v) as an anaerobic indicator. This growth medium was supplemented with 5% (v/v) PCF for selected experiments. This

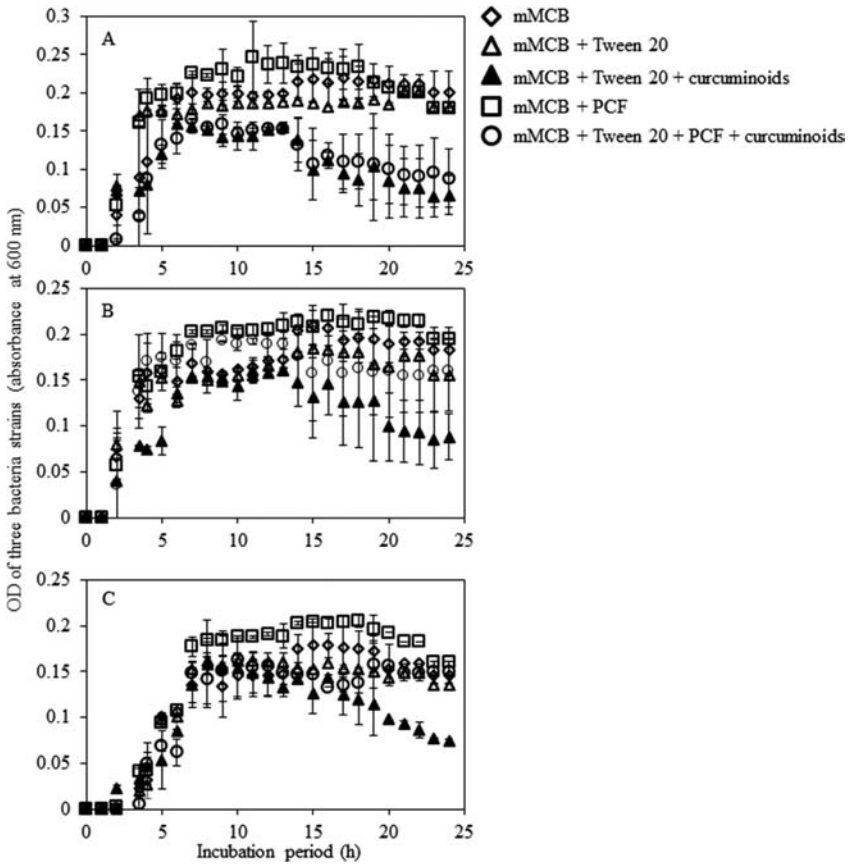


**Figure 1.** Growth of *Escherichia fergusonii* (E469) (A), *E. coli* 739 (E739) (B), and *E. coli* DH10B (E10B) (C) in mMCB with or without Tween 20 and PCF and supplemented with curcuminoids. Each data point is the average of three biological replicates ± SD.

medium was prepared anaerobically and transferred (10 mL) to glass tubes in an anaerobic culturing hood.

For subculture preparations, *Escherichia fergusonii* and *E. coli* were cultured individually on lysogeny agar plates containing 1% (all w/v) tryptone, 0.5% yeast extract, 1% NaCl, and 2% agar (Oxoid). Under these conditions colonies were visible after 24 h of incubation at 37 °C. One colony of each culture was then grown in separate glass tubes containing 10 mL of mMCB, as above, under anaerobic conditions at 37 °C for 2 h.

For fermentation assays, 100 $\mu$L of the subculture was inoculated into separate glass tubes containing 10 mL of mMCB and supplemented with curcuminoids at a concentration of 0.3 mM (solubilized in 3% (v/v) of Tween 20). Blank control samples containing only mMCB or mMCB + PCF but without curcuminoids were also inoculated. The initial pH of the fermentation medium was pH 6.27 ± 0.02. A set of abiotic samples with or without curcuminoids in mMCB or mMCB + PCF were maintained to account for the stability of curcuminoids at the start and end of fermentation. Fermentation temperature was kept constant at 37 °C and maintained for 36 h. Samples were acquired at 12 different time points for further analysis. The fermentation was performed on three separate occasions.

**Bacterial Growth.** The growth curves of bacterial strains were obtained by measuring the optical density (OD) at 600 nm using a Nanodrop 2000C spectrophotometer with a UV−vis detector (Thermo-Fisher Scientific). Triplicate measurements were obtained, and data are presented as the mean ± SD.

**Quenching and Cell Lysis.** Following incubation, bacterial metabolism was quenched by adding 2 mL of cold methanol/water (60%, v/v) solution to 1 mL of cell culture. To lyse the cell, samples were frozen in liquid nitrogen, thawed on dry ice, and then sonicated in a microfuge tube within a sonicator bath for ∼3 min. This lysis procedure was repeated 10 times. The samples were then vortexed and centrifuged at 805*g* for 5 min at 0 °C (Eppendorf centrifuge 5810R) to remove cell debris. The supernatant was kept at −20 °C prior to extraction.

**Curcuminoids and Metabolite Extraction.** The procedure for extraction of curcuminoids and transformed metabolites was adapted and optimized from that of Saradhi et al.[21] Briefly, 0.5 mL of supernatant and 1 mL of ethyl acetate with 100 $\mu$g/mL IS ($\beta$-estradiol-17-acetate) were mixed. The sample was then vortexed and centrifuged at 11000*g* for 5 min (Eppendorf Centrifuge 5424). The upper organic layer (∼1 mL) was transferred to a clean microfuge tube. The same extraction procedure was repeated using the lower aqueous layer. Both upper organic layers were then combined and dried (SpeedVac, Christ RVC 2-33, John Morris Scientific) for about 2 h at 20 °C or until completely dry. The dried extracts were then resuspended in 100 $\mu$L of LC-MS running buffer containing 10 mM ammonium acetate in an acetonitrile/water (50%, v/v) solution, vortexed, and further diluted by combining 10 $\mu$L of resuspended extract and 90 $\mu$L of LC-MS running buffer. This solution was then vortexed and centrifuged at 11000*g* for 5 min, and 80 $\mu$L was transferred to vials, which were capped and ready for LC-MS analysis.

**Identification and Quantification of Extracted Curcuminoids and Metabolites.** Chromatographic separation of curcuminoids and metabolites was performed with an LC 1200 series system (Agilent Technologies, Santa Clara, CA, USA), which consisted of a Binary Pump SL and Hi-P-Autosampler (with injection volume of 2 $\mu$L). Elution was achieved with an Agilent Poroshell 120 EC-C8 column (2.1 × 50 mm, with a particle size of 2.7 $\mu$m). The mobile phases consisted of 10 mM ammonium acetate and 0.1% (v/v) formic acid in water (A) or in acetonitrile (B). A linear gradient was applied as follows with a flow rate of 0.3 mL min$^{-1}$: 0−5 min, 20% B; 5−8.1 min, 80% B; 8.1−10.0 min, 20% B; with a total run time of 10 min. Analysis was performed using a 6460 triple-quadrupole mass spectrometer (Agilent Technologies) equipped with an electrospray ionization (ESI) source operating in negative mode. For the identification and quantification of compounds,

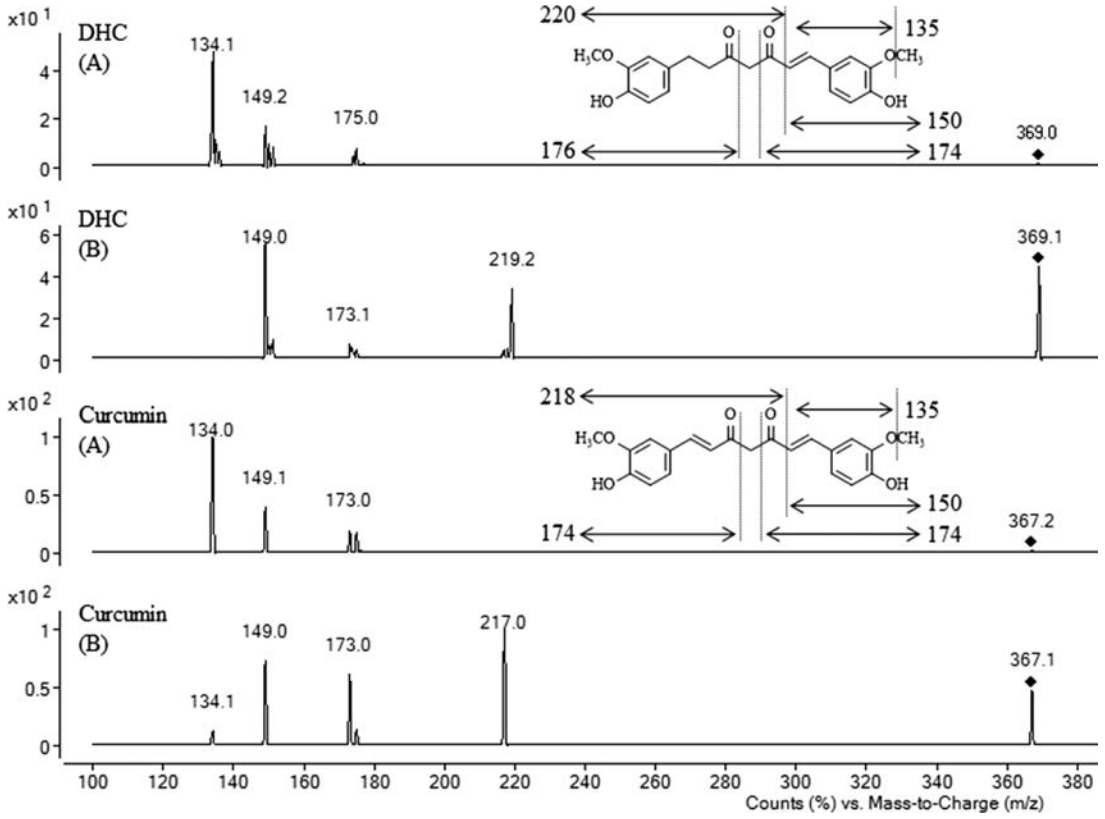


**Figure 2.** MS/MS spectra of DHC and curcumin from triple-quadrupole mass spectrometer operating in negative mode with a fragmentor voltage of 110 V and collision energy of 25 V (A) and 10 V (B) and their neutral chemical structures and fragmentation sites, DHC (top) and curcumin (bottom). The product ions shown on the spectra are the $[M - H]^-$ ions formed by loss of a proton from either of the phenol moieties.

a MRM analysis was employed, tracking the transition indicative of parent and product ion specific for each compound. Previous direct infusion experiments were performed to optimize the fragmentor voltage and collision energy (CE). After infusion had been performed, the following parameters were fixed: drying $N_2$ temperature, 300 °C; gas flow, 7 L $min^{-1}$; nebulizer pressure, 15 psi; sheath gas temperature, 400 °C; sheath gas flow, 10 L $min^{-1}$; capillary voltage, 2000 V; nozzle voltage, 1000 V; cell accelerator voltage, 7 V; dwell time, 20 ms. Detailed transitions of parent molecules and product ions, MS parameters (fragmentor voltage and CE), limits of detection (LODs), and limits of quantification (LOQs) are listed in Table 1.

The concentrations of curcuminoids curcumin, DMC, and Bis-DMC were quantified on the basis of a calibration curve for curcumin. It was assumed that the response factors for DMC and Bis-DMC were the same as that for curcumin. The metabolites THC and FA were also quantified using standards. For the quantification of the metabolite with $m/z$ $[M - H]^-$ 369 and the compound with $m/z$ $[M - H]^-$ 470, it was assumed that these also had the same response factor as curcumin. The area under the curve from the LC-MS spectra of each compound was normalized using the IS and then converted to concentration using the standard calibration curves.

Separate spiking experiments with known quantities of the curcuminoids, and the metabolites THC and FA in mMCB medium were carried out. Recoveries for all five compounds were ∼80%. All values given in the tables and figures were corrected for recovery (assuming 80% for all compounds).

**Identification of Compounds with $m/z$ $[M - H]^-$ 369 and $m/z$ $[M - H]^-$ 470.** LC-MS/MS using a triple-quadrupole mass spectrometer and accurate mass using FT-ICR-MS were used to confirm the identity of compounds with $m/z$ $[M - H]^-$ 369 and $m/z$ $[M - H]^-$ 470.

*LC-MS/MS.* Chromatographic separation conditions were as described above. Analysis was performed using a 6460 triple-quadrupole mass spectrometer (Agilent Technologies) equipped with an ESI ion source operating in negative mode. A product ion scan was employed for confirmation of the metabolite. The acquisition parameters were as follows: CE, 10, 20, and 35 V; fragmentor voltage, 110 V; MS scan range from 50 $m/z$ (min) to 500 $m/z$ (max); drying $N_2$ temperature, 300 °C; gas flow, 7 L $min^{-1}$; nebulizer pressure, 15 psi; sheath gas temperature, 400 °C; sheath gas flow, 10 L $min^{-1}$; capillary voltage, 2000 V; noozle voltage, 1000 V.

*FT-ICR-MS.* A Bruker Daltonics (Bremen, Germany) SolariX 7 T Hybrid MALDI/ESI-FT-ICR-MS was used for isolation and high mass resolution analysis. The instrument was operated in ESI negative ionization mode with TD acquisition = 1M, MS detection (resolution 260000 at $m/z$ 400) using an external calibration of sodium trifluoroacetate solution, and MS/MS detection (resolution 45000 at $m/z$ 400). The sample was infused at a rate of 2 $\mu$L $min^{-1}$ using the syringe pump, and a total of 20 scans were collected and averaged. The following general instrument conditions were set: capillary voltage, 4200 V; drying gas flow, 4.0 L $min^{-1}$; drying gas temperature, 180 °C; nebulizer gas flow rate, 0.8 bar; source accumulation, 0.001 s; ion accumulation, 0.5 s; ion cooling time, 0.01 s; flight time, 0.001 s. Various collision voltages were used with a collision gas flow rate of 40%. Data were analyzed using Bruker Compass Data Analysis 4.2 (Build 383.1) software.

**Statistical Analysis.** Statistical analysis was performed using the statistical package Minitab for Windows (version 17). Differences in the data were analyzed using one-way analysis of variance (ANOVA). The effect of two different treatments, (i) without PCF and (ii) with PCF, on the ability of the three bacterial strains to degrade curcuminoids at 36 h of fermentation was also tested. Tukey pairwise comparisons were used to identify the differences and statistical significance defined as $p < 0.05$.

## RESULTS AND DISCUSSION

**Growth of *Escherichia fergusonii* and Two *E. coli* Strains.** The three *Escherichia* bacterial strains demonstrated a

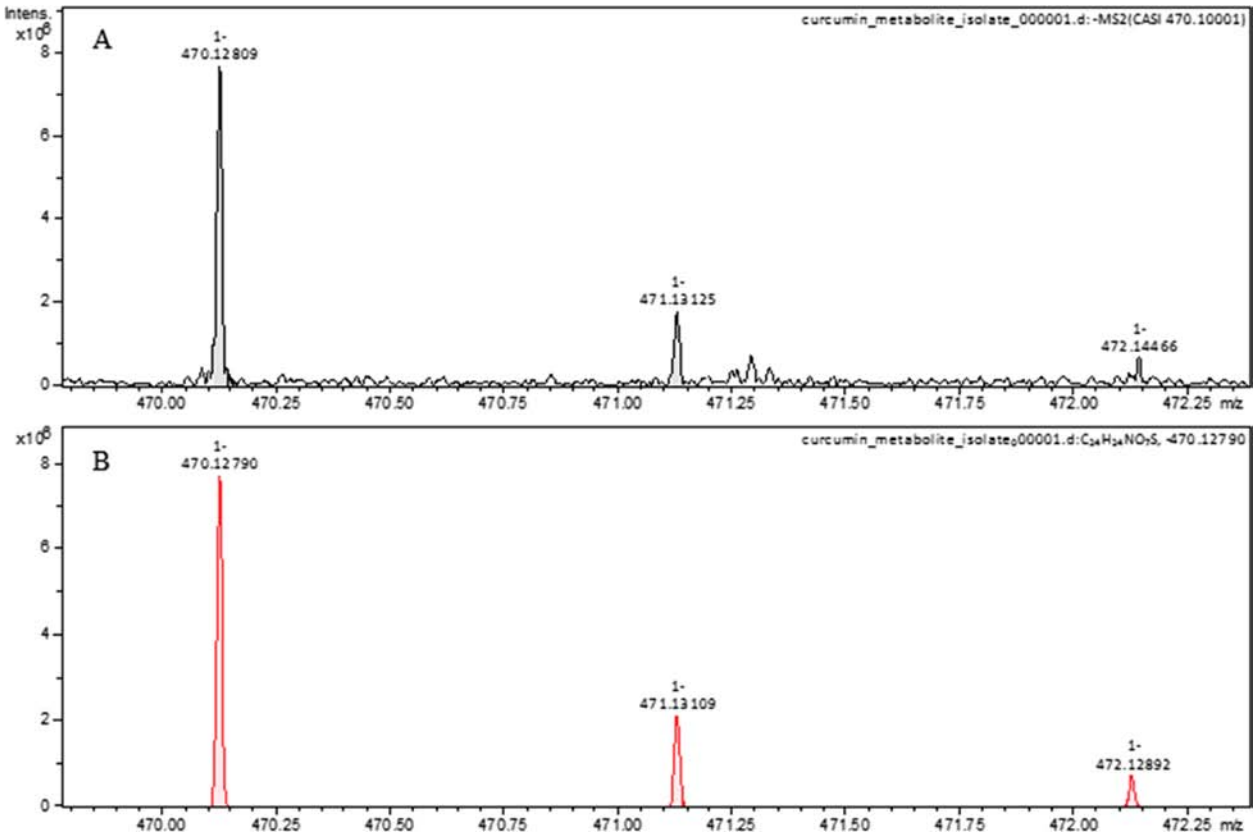


**Figure 3.** Full scan MS mass spectra of isolated curcumin adduct displaying isotopic profile (A) and the calculated isotopic profile of the predicted $C_{24}H_{25}NO_7S$ compound (B).

growth curve typical of batch culture in mMCB media, with a lag phase of around 2−3 h followed by exponential growth and a stationary phase beyond 8 h (Figure 1). The growth of all strains was not markedly affected by the addition of Tween 20 to solubilize the curcumin (3%, v/v) (Figure 1). Others have observed that Tween 20 (0.5%, w/w) in 0.1 M phosphate buffer disintegrated the cell wall and cytoplasmic membrane of *Listeria monocytogenes* and *Salmonella typhimurium*.[22] It is likely that differences in the responses of bacteria to curcumin may vary with growth medium and microbial species. Indeed, the addition of medium was observed to counter the nonreversible damage caused to cells grown in buffer.[23]

The addition of PCF (5%, v/v) slightly increased bacterial growth and the $OD_{600\ nm}$ increased by ∼0.02−0.05 units (Figure 1). PCF is known to assist the growth of facultative anaerobic bacteria. Similar findings were observed previously when media containing either ruminal fluid or pig cecal extract supported the growth of a larger number of gut bacteria compared to a medium rich in nutrients.[24]

The growth of E469, E739, and E10B in the first 8 h of fermentation was not affected by the supplementation of 0.3 mM curcuminoids, as shown by the profiles (Figure 1). However, a decline in $OD_{600\ nm}$ was observed for E469 and E10B during the stationary phase, indicating a change in metabolism. A similar decline was observed for E469 in the presence of PCF and Tween 20.

The pH values at the start and end of the fermentation were 6.27 ± 0.02 and 6.00 ± 0.05, respectively. Curcumin is stable at these pH values, but at alkaline pH >7.5, it degraded chemically within 30 min to ferulic acid, feruloylmethane, and vanillin.[25,26] Therefore, changes in curcumin are likely to be due to bacterial metabolism.

**Identity of Compounds Formed in Fermentation Cultures with Curcumin.** The upper organic and lower aqueous fractions for all extracted samples were examined by LC-MS using a full MS scan operating in both negative and positive modes from $m/z$ 50 to 800 (method S1, Supporting Information).

Four compounds, in addition to the curcuminoids added, were identified from the full scan LC-MS spectra of the upper organic fraction of inoculated samples supplemented with curcuminoids. The full scan LC-MS spectra showing the total ion chromatogram of sample with 0.3 mM curcuminoids inoculated with E469 in mMCB and the extracted full mass spectra of one of the compounds are shown in Figure S1 (Supporting Information). Two of these additional compounds, THC and FA, were identified by comparison to standards. The other two compounds with $m/z$ (all in $[M - H]^-$) 369 and 470 were identified using LC-MS/MS and FT-ICR-MS, respectively. Compounds with $m/z$ $[M - H]^-$ 369 and 470 were confirmed to be dihydrocurcumin (DHC) and a curcumin adduct (curcumin−L-cysteine), respectively, as discussed below. No metabolites could be identified in the lower aqueous fractions.

*Confirmation of Compounds with m/z [M − H]⁻ 369.* Full scan LC-MS of samples grown in the presence of curcuminoids gave rise to product ion with $m/z$ $[M - H]^-$ 369 (data not shown), consistent with the $[M - H]^-$ ion of DHC (370 MW). To ensure that this compound putatively identified as DHC was not an isotope of curcumin, LC-MS/MS of DHC and curcumin in negative mode were performed and their spectra together with neutral chemical structures are shown in Figure 2. A fragmentor


dx.doi.org/10.1021/jf5031168 | J. Agric. Food Chem. 2014, 62, 11005−11015

**Table 2. Calculation of Molecular Formulas from High-Resolution FT-ICR-MS Analysis of the Compound ($m/z$ $[M - H]^-$ 470) and Most Abundant Fragment Ions Observed from the Analysis of Collision-Induced Decay (CID) MS/MS Data**

| metabolite | formula | calcd formula | neutral mass | calcd $m/z$, $[M - H]^-$ | obsd $m/z$, $[M - H]^-$ | error (ppm) |
|---|---|---|---|---|---|---|
| curcumin | $C_{21}H_{20}O_6$ | | 368.12544 | 367.11871 | 367.11876 | −0.25 |
| L-cysteine | $C_3H_7NO_2S$ | | | | | |
| curcumin + cysteine | | $C_{24}H_{27}NO_8S$ | 489.14574 | | | |
| curcumin−L-cysteine | | $C_{24}H_{25}NO_7S$ | 471.13462 | 470.12789 | 470.12809 | −0.41 |
| 392 fragment | | $C_{23}H_{22}NO_5^-$ | 393.15762 | 392.15035 | 392.15045 | −0.27 |
| 167 fragment | | $C_8H_7O_2S^-$ | 168.0245 | 167.01722 | 167.01725 | −0.14 |

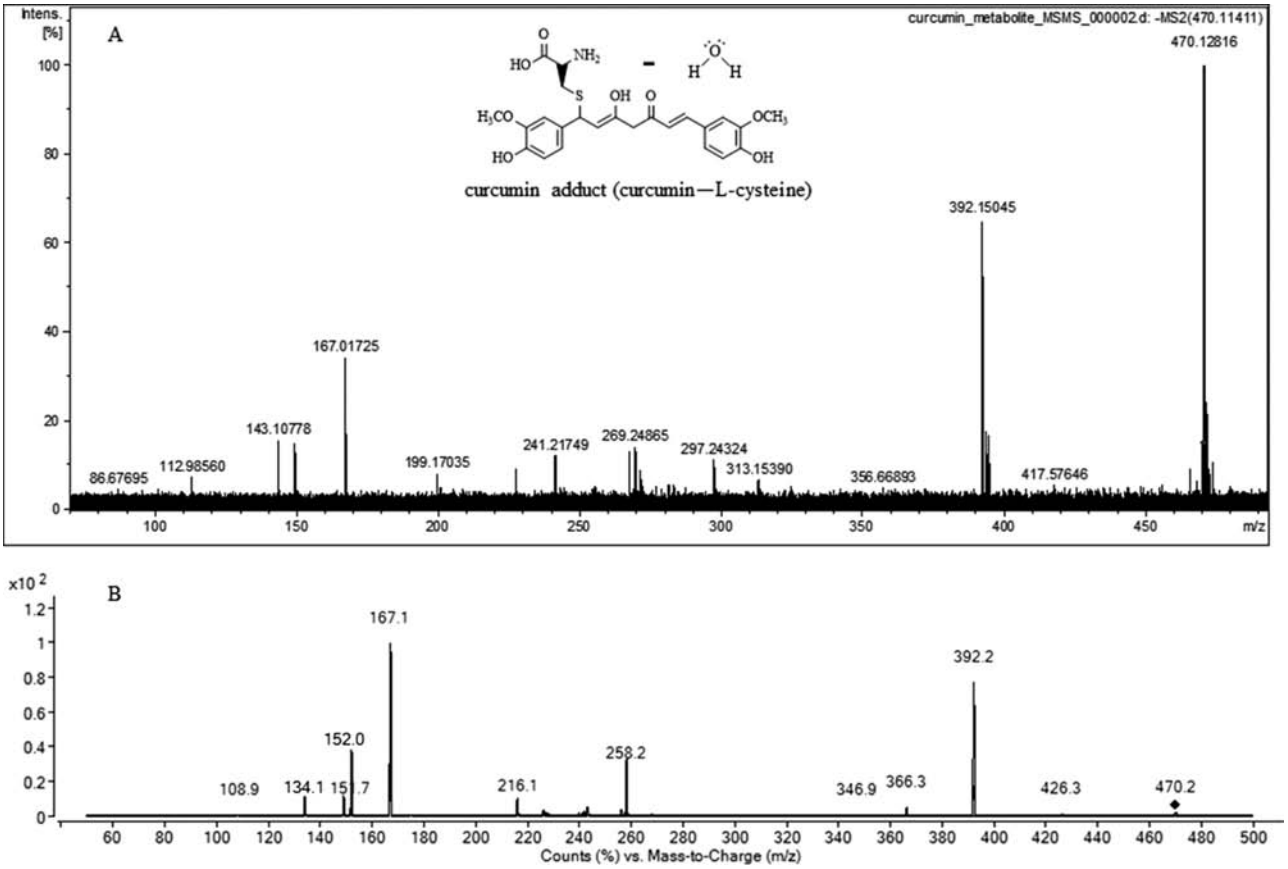


**Figure 4.** MS/MS analysis of curcumin adduct (curcumin−L-cysteine) from FT-ICR-MS (A) and triple-quadrupole mass spectrometer (B) and the proposed chemical structure of the adduct. MS/MS fragmentation patterns of curcumin adduct (curcumin−L-cysteine) from both instruments showed two intense fragment ions at nominal masses of 392 and 167.

voltage of 110 V and CE of 25 and 10 V were applied to both compounds, producing product ions of $m/z$ 134, 149, 173, 175, and 219 for DHC and $m/z$ 134, 149, 173, and 217 for curcumin (Figure 2).

Differences between the product ions of DHC and curcumin were attributed to their chemical structures. Curcumin possesses two alkenyl C═C bonds within the heptadienone backbone,[1] whereas DHC is the reduced form of curcumin in which one of the alkenes has been reduced.[19] DHC has been previously reported as the intermediate breakdown product of curcumin by the enzyme *CurA*, through the reduction of an alkene present on the heptadienone chain.[19] The common product ions of both curcumin and DHC can be rationalized through the presence of at least one C═C bond, where the observed $[M - H]^-$ product ions $m/z$ 134 and 149 correspond to fragmentation across the enone functionality (149) with a further loss of a single methyl group (134) (Figure 2). The other product ions for curcumin, 173 and 217, correspond to fragmentation at the ketone functionality. For DHC, which possesses a reduced alkene with two hydrogen atoms, the corresponding mass shifted product ions 175 and 219 were observed (Figure 2). The product ion 173 was also observed for DHC, where the presence of a single alkene functionality and corresponding fragmentation at the ketone produce an identical product ion to that of curcumin.

*Confirmation of Compound with m/z [M − H]⁻ 470.* To putatively identify the compound with $m/z$ $[M - H]^-$ 470, high mass accuracy FT-ICR-MS mass spectra of the compound were collected. Direct infusion of the crude culture media provided a complex signal; further isolation of a narrow mass range (10 $m/z$) centered around $m/z$ of 470 found a single peak at $m/z$ $[M - H]^-$ 470.12809 as shown in Figure 3. Calculation of the molecular formula from the accurate mass gave only a single possible formula, $C_{24}H_{25}NO_7S$ (calculated $m/z$ $[M - H]^-$ 470.12789), with a very low mass error of −0.41 ppm, as shown in Table 2. The isotopic pattern of the compound with $m/$


dx.doi.org/10.1021/jf5031168 | J. Agric. Food Chem. 2014, 62, 11005−11015

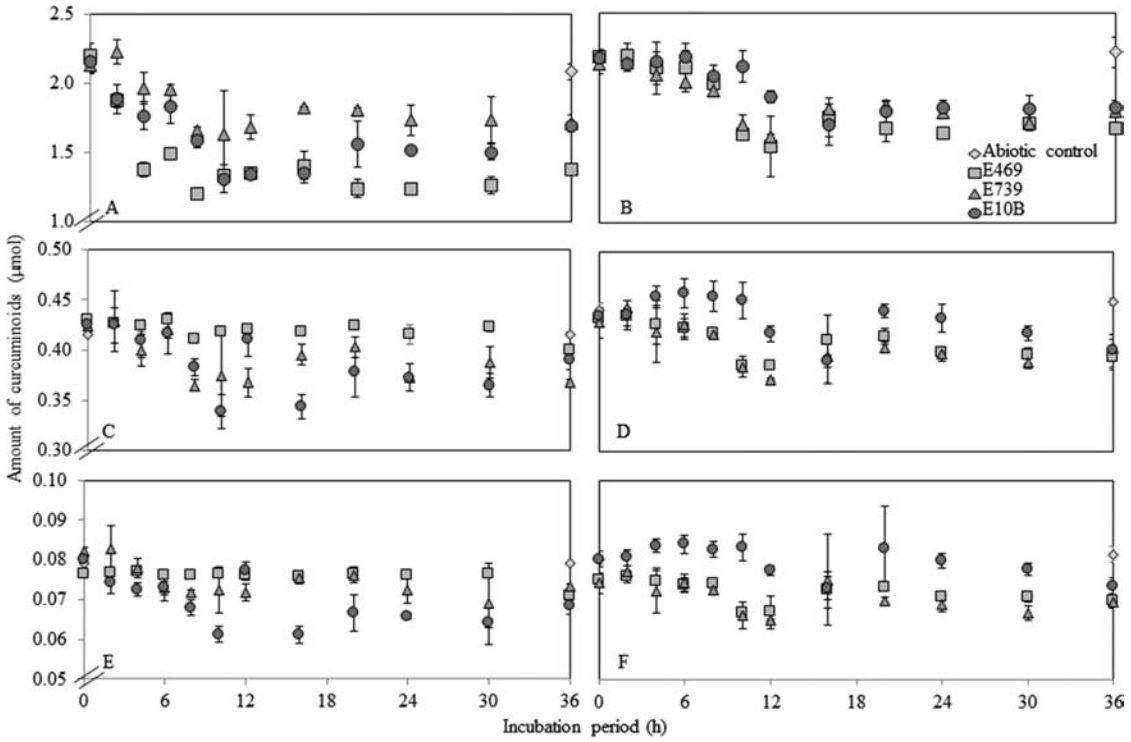


**Figure 5.** Amount of curcuminoids: curcumin (A, B), DMC (C, D), and Bis-DMC (E, F) measured during fermentation with *Escherichia fergusonii* (E469), *E. coli* 739 (E739), and *E. coli* DH10B (E10B) in mMCB without PCF (A, C, E) or with PCF (5%, v/v) (B, D, F). The amount of curcuminoids in the upper organic extracts was quantified using LC-MS/MS and expressed as total micromoles in the original experimental broth of 10.1 mL. The amounts of curcuminoids in the control (abiotic) samples were measured at 0 and 36 h. Each data point is the average of three biological replicates ± SD.

$z$ $[M - H]^-$ 470 from FT-ICR-MS is similar to the calculated isotopic peak spacing of the compound, as shown in Figure 3.

L-Cysteine was present in the growth medium (mMCB) to reduce the oxido/reduction potential. The amount added far exceeds that required for the formation of the curcumin−L-cysteine adduct. The predicted formula of the metabolite matches an addition product of curcumin ($C_{21}H_{20}O_6$) and L-cysteine ($C_3H_7NO_2S$) with a loss of water. We propose an initial 1,4-addition product, curcumin adduct (curcumin−L-cysteine), with a possible chemical structure as shown in Figure 4, which undergoes dehydration either in vitro or within the MS source. In support of our putative assignment, curcumin possesses two $\alpha,\beta$-unsaturated ketone moieties that can act as Michael acceptors to nucleophilic attack through a Michael-type addition reaction mechanism.[27] Furthermore, curcumin has previously been found to bind covalently to nucleophilic sulfhydryls and the selenol moiety of selenocysteine.[28,29] Thioredoxin reductase, a selenocysteine-containing enzyme, was irreversibly inhibited by curcumin through a Michael-type addition reaction only in the presence of NADPH, with inhibition persisting after the removal of curcumin.[28]

To explore the mechanism of formation of the putatively identified curcumin adduct, we performed a separate experiment by incubating mMCB with and without 0.3 mM curcuminoids at 37 °C for 24 h and removed the bacterial cells to produce spent media. Both spent media samples were further supplemented with 0.3 mM curcuminoids and incubated for another 24 h. The curcumin adduct was observed only in spent media where curcuminoids were co-incubated with mMCB (data not shown). This suggests that the curcumin adduct is formed only in the presence of bacteria. We propose that this curcumin adduct may be formed through a Michael-type addition, possibly in the presence of NADPH. It is probable that NADPH was produced in the fermentation cultures in this study through bacterial synthesis or another biological reductant may be employed.

Additional MS/MS analysis by FT-ICR-MS and triple-quadrupole MS showed two intense fragment ions at nominal masses of 392 and 167, as demonstrated in Figure 4. Accurate mass analysis gave masses of 392.15045 and 167.01725 with calculation of the molecular formula indicating empirical formulas of $C_{23}H_{22}NO_5^-$ (calculated, 392.15035; mass error, −0.26 ppm) and $C_8H_7O_2S^-$ (calculated mass, 167.01722; mass error, −0.14 ppm) as probable fragmentation products of a curcumin−L-cysteine adduct, as shown in Table 2. Although isolation and elucidation of the exact chemical structure is beyond the scope of the current study, data presented here can be used to assist in future determination of the exact chemical structure of the compound with $m/z$ $[M - H]^-$ 470.

**Quantification of Compounds Formed in Fermentation Cultures with Curcumin.** *Change in Curcuminoid Concentrations during Fermentation.* The extent to which the three curcuminoids (curcumin, DMC, and Bis-DMC) were degraded by the bacteria E469, E739, and E10B during batch fermentation for 36 h was determined using LC-MS. The effect of supplementing the media with PCF (5%, v/v) on the ability of all three strains to degrade curcuminoids was examined. Blank control samples containing only mMCB or mMCB with PCF without curcuminoids showed no or negligible signal interference in the LC-MS spectra of curcuminoids and metabolites.

The amounts of curcuminoids (curcumin, DMC, and Bis-DMC) present in abiotic control samples in mMCB (Figure 5A,C,E) and in mMCB with PCF (Figure 5B,D,F) did not change at the start and end of fermentation. This may be expected as curcumin is stable at the pH of the fermentation


dx.doi.org/10.1021/jf5031168 | J. Agric. Food Chem. 2014, 62, 11005−11015

**Table 3. Measured Curcuminoids Curcumin, DMC, Bis-DMC, Metabolite FA, and Curcumin Adduct Curcumin−L-Cysteine Detected in the Fermentation Culture[a]**

| | fermentation medium: mMCB | | | fermentation medium: mMCB with 5% (v/v) PCF | | |
|---|---|---|---|---|---|---|
| compound | *E. fergusonii* E469 | *E. coli* E739 | *E. coli* E10B | *E. fergusonii* E469 | *E. coli* E739 | *E. coli* E10B |
| curcumin | | | | | | |
| initial $t$ = 0 h ($\mu$mol) | 2.20 ± 0.09 | 2.13 ± 0.06 | 2.16 ± 0.02 | 2.19 ± 0.04 | 2.13 ± 0.07 | 2.17 ± 0.01 |
| final $t$ = 36 h ($\mu$mol) | 1.38 ± 0.03 | 1.71 ± 0.06 | 1.69 ± 0.01 | 1.68 ± 0.03 | 1.80 ± 0.04 | 1.82 ± 0.05 |
| % converted | 37.3 ± 3.79a | 19.9 ± 1.65bc | 20.8 ± 0.42bc | 23.2 ± 1.24b | 15.8 ± 1.45c | 16.1 ± 2.09c |
| DMC | | | | | | |
| initial $t$ = 0 h ($\mu$mol) | 0.43 ± 0.004 | 0.42 ± 0.005 | 0.42 ± 0.002 | 0.43 ± 0.007 | 0.43 ± 0.015 | 0.43 ± 0.006 |
| final $t$ = 36 h ($\mu$mol) | 0.40 ± 0.003 | 0.37 ± 0.002 | 0.39 ± 0.010 | 0.39 ± 0.011 | 0.40 ± 0.008 | 0.40 ± 0.016 |
| % change | 7.09 ± 1.42ab | 16.3 ± 5.57a | 8.10 ± 2.11ab | 9.12 ± 2.21ab | 5.69 ± 1.69b | 7.78 ± 4.91ab |
| Bis-DMC | | | | | | |
| initial $t$ = 0 h ($\mu$mol) | 0.08 ± 0.001 | 0.08 ± 0.001 | 0.08 ± 0.001 | 0.08 ± 0.001 | 0.07 ± 0.002 | 0.08 ± 0.002 |
| final $t$ = 36 h ($\mu$mol) | 0.07 ± 0.001 | 0.07 ± 0.001 | 0.07 ± 0.001 | 0.07 ± 0.002 | 0.07 ± 0.001 | 0.07 ± 0.002 |
| % change | 7.22 ± 0.76b | 10.8 ± 1.33ab | 14.8 ± 2.40a | 7.21 ± 2.04b | 6.58 ± 1.65b | 9.60 ± 2.79b |
| ferulic acid (FA) | | | | | | |
| final $t$ = 36 h ($\mu$mol) | 0.13 ± 0.005 | 0.06 ± 0.002 | 0.05 ± 0.005 | 0.14 ± 0.003 | 0.04 ± 0.003 | 0.03 ± 0.003 |
| curcuminoid equiv[b] ($\mu$mol) | 0.07 ± 0.003b | 0.03 ± 0.001c | 0.03 ± 0.003c | 0.08 ± 0.002a | 0.02 ± 0.002d | 0.02 ± 0.002d |
| curcumin−L-cysteine | | | | | | |
| final $t$ = 36 h ($\mu$mol) | 0.43 ± 0.02 | 0.23 ± 0.01 | 0.21 ± 0.01 | 0.28 ± 0.02 | 0.17 ± 0.01 | 0.22 ± 0.01 |
| curcuminoid equiv[c] ($\mu$mol) | 0.43 ± 0.02a | 0.23 ± 0.01c | 0.21 ± 0.01cd | 0.28 ± 0.02b | 0.17 ± 0.01d | 0.22 ± 0.01c |
| % curcuminoids accounted[d] | 86.8 ± 2.96b | 90.8 ± 2.57ab | 90.4 ± 0.91ab | 92.6 ± 1.32a | 93.5 ± 1.06a | 94.4 ± 2.22a |

[a]The values for the amounts have been corrected for the recoveries of compounds and represent the amount present in 10.1 mL of fermentation medium. This was 80% for curcumin, DMC, Bis-DMC, and FA, as determined from separate spiking experiments. As curcumin−L-cysteine was not commercially available, spiking experiments could not be carried out, and the values are those as determined without correction for recovery. Means with the same letters within the same row are not significantly different. [b]Curcuminoid equivalents (equiv) were calculated assuming the following: (i) 1 mol of curcumin gives 2 mol of FA and 1 mol of DMC gives 1 mol of FA. (ii) The initial curcuminoid mixture contained 80.1:15.6 (curcumin/DMC); therefore, FA obtained from this mixture on a molar basis would be 1.837. [c]Curcuminoid equivalents (equiv) were calculated assuming 1 mol of curcumin gives 1 mol of curcumin−L-cysteine. [d]Percent curcuminoids accounted for {[$\mu$mol of remaining curcuminoids + $\mu$mol FA/1.837) + $\mu$mol curcumin−L-cysteine)]/(initial $\mu$mol curcumin + initial $\mu$mol DMC + initial $\mu$mol Bis-DMC)} × 100.

media (pH 6.00−6.27 over the fermentation course of 36 h). It is only at pH >7.5 that curcumin is unstable.[25,26] The absence of an observable change in abiotic samples shows that there is no chemical degradation of curcuminoids over this time and confirms that any change in curcuminoids in the presence of the cultures is the result of bacterial metabolism.

The degradation profiles of curcuminoids (curcumin, DMC, and Bis-DMC) in the presence of bacteria over the 36 h fermentation period are also shown in Figure 5. In the absence of PCF, a decrease in curcumin was observed until about 8−10 h, coincident with the onset of the stationary phase (Figure 1); the level of curcumin then stayed relatively constant until 36 h (Figure 5A), whereas with PCF, the level of curcumin decreased until around 12 h and then stayed relatively constant until 36 h (Figure 5B). A slight decrease was also observed in the amounts of DMC and Bis-DMC following 36 h of fermentation, as demonstrated in Figure 5C,D and E,F, respectively.

The initial measured amounts of curcuminoids in fermentation cultures at 0 and 36 h are given in Table 3. The significant differences between the ability of the three bacterial strains to degrade curcuminoids in mMCB with or without PCF at 36 h were compared. The ability of all three strains to convert curcumin, in mMCB media with or without PCF, was in the order E469 > E10B ∼ E739. Whereas E469 degraded 37.3% of curcumin, which is significantly higher ($p < 0.05$) than that with E739 (19.9%) and E10B (20.8%), there were no significant differences ($p > 0.05$) between degradation by E739 and E10B in the absence of PCF. Similar results were obtained in the presence of PCF, where curcumin conversion was significantly higher ($p < 0.05$) with E469 (23.2%) compared to E739 (15.8%) and E10B (16.1%). The effects of PCF addition on curcumin degradation were strain dependent. In the presence of PCF, the degradation of curcumin by E469 was significantly reduced ($p < 0.05$). However, the addition of PCF had no significant effect ($p > 0.05$) on the ability of E739 and E10B to degrade curcumin.

The amounts of DMC altered in the fermented cultures for all strains in mMCB were not significantly different ($p > 0.05$). This was also the case for all strains in mMCB with added PCF (Table 3). The change in the amount of DMC in the presence of E739 was significantly higher ($p < 0.05$) in mMCB (16.3%) than in mMCB with added PCF (5.7%), but changes in DMC amounts were not significantly affected by the addition of PCF ($p > 0.05$) when E469 or E10B was used.

The amount of Bis-DMC in mMCB changed by E10B (14.8%) was significantly higher ($p < 0.05$) than that changed by E469 (7.2%), but there were no significant differences ($p > 0.05$) between E739 and E469. The ability of all three strains to convert curcumin in mMCB was in the order E10B > E739 ∼ E469. The changes in the amounts of Bis-DMC in the presence of all three strains were not significantly different ($p > 0.05$) in mMCB with

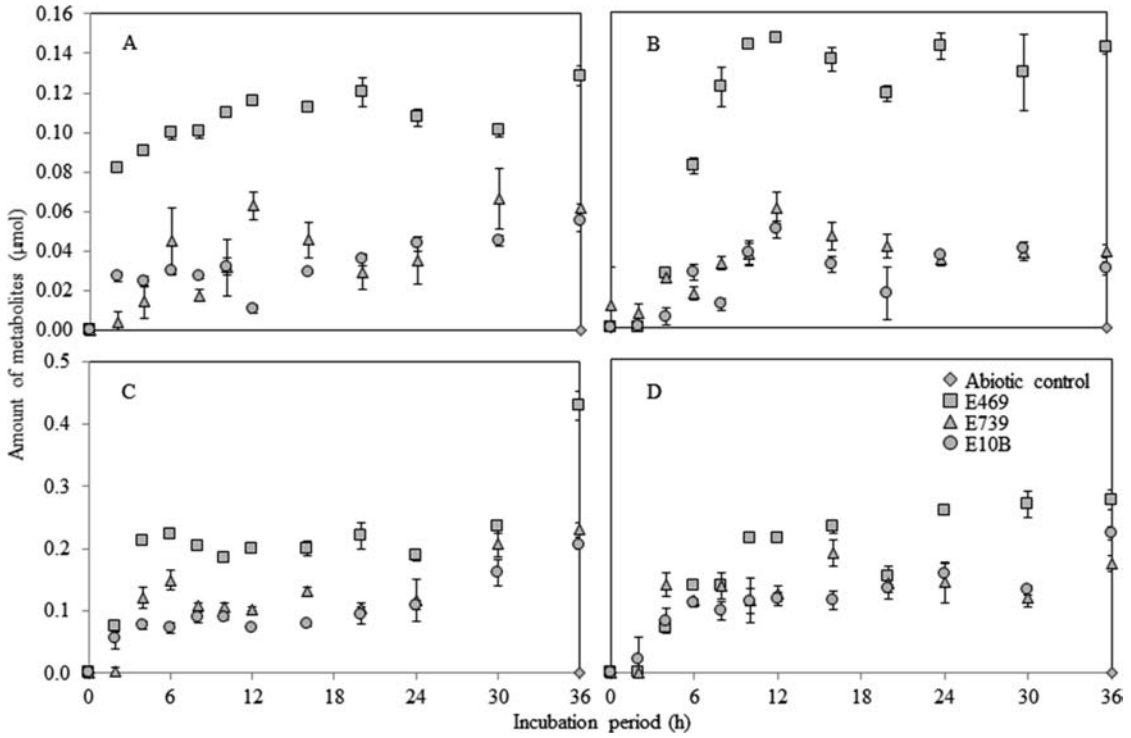


**Figure 6.** Measured amounts of FA (A, B) and curcumin adduct (curcumin−L-cysteine) (C, D) during fermentation with *Escherichia fergusonii* (E469), *E. coli* 739 (E739), and *E. coli* DH10B (E10B) in mMCB without PCF (A, C) or with PCF (5%, v/v) (B, D). The amount of FA and curcumin adduct (curcumin−L-cysteine) in the upper organic extracts were quantified using LC-MS/MS and expressed as total micromoles in experimental broth of 10.1 mL. Each data point is the average of three biological replicates ± SD.

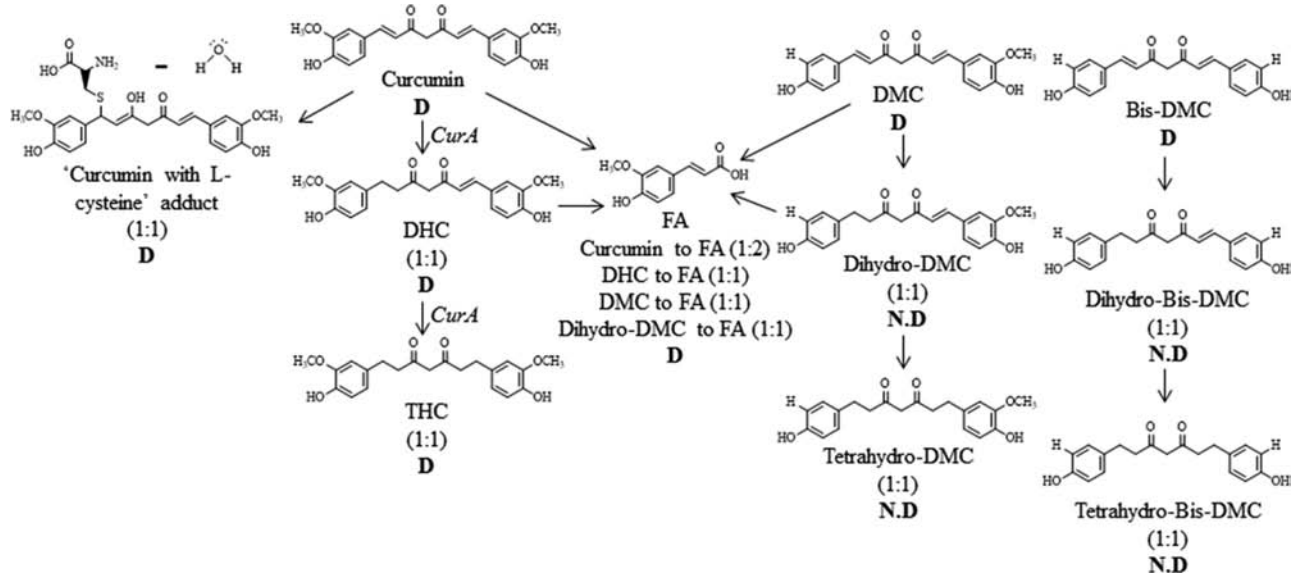


**Figure 7.** Proposed degradation of the three curcuminoids (curcumin, DMC, and Bis-DMC) and breakdown products formed by *Escherichia fergusonii* (E 469), *E. coli* 739 (E739), and *E. coli* DH10B (E10B). Numbers in parentheses represent the theoretical conversion of curcuminoids to metabolites. D, detected; N.D, not detected in this study.

added PCF. The ability of E469 and E739 to convert Bis-DMC was not significantly affected by the addition of PCF ($p > 0.05$). However, a significant increase ($p < 0.05$) was observed for changes in Bis-DMC when PCF was not added to mMCB in the presence of E10B (14.8% compared from 9.6%).

*Quantification of Compounds Formed in Fermentation Cultures with Curcumin.* DHC and THC were minor metabolites of curcumin degradation, and they constitute <1% of the total metabolites recovered. The formation of FA and curcumin−L-cysteine during fermentation is shown in Figure 6, and the amounts quantified after 36 h are given in Table 3. In mMCB without PCF, the formation of FA by E469 (0.07 μmol) was significantly higher ($p < 0.05$) than the amounts formed by E739 and E10B (0.03 μmol), but there were no significant differences ($p > 0.05$) between E739 and E10B. In mMCB with PCF, the formation of FA by E469 (0.08 μmol) was also significantly higher ($p < 0.05$) than that by E739 and E10B (0.02 μmol), but there were no significant differences ($p > 0.05$)


dx.doi.org/10.1021/jf5031168 | J. Agric. Food Chem. 2014, 62, 11005−11015

between E739 and E10B. The formation of FA by E469 in the presence of PCF (0.08 μmol) was significantly higher ($p < 0.05$) than in mMCB alone (0.07 μmol). The formation of FA by E739 and E10B in the presence of PCF (0.02 μmol) was significantly lower ($p < 0.05$) than in mMCB alone (0.03 μmol).

In mMCB without PCF, the formation of curcumin−L-cysteine by E469 (0.43 μmol) was significantly higher ($p < 0.05$) than those by E739 (0.23 μmol) and E10B (0.21 μmol), but there were no significant differences ($p > 0.05$) between E739 and E10B. In mMCB with PCF, the formation of curcumin−L-cysteine by E469 (0.28 μmol) was significantly higher ($p < 0.05$) than those by E10B (0.22 μmol) and E739 (0.17 μmol). In the same medium, the formation of curcumin−L-cysteine by E10B was also significantly higher ($p < 0.05$) than that by E739. The formation of curcumin−L-cysteine by E469 and E739 in the absence of PCF (0.43 and 0.23 μmol, respectively) was significantly higher ($p < 0.05$) than in the presence of PCF (0.28 and 0.17 μmol, respectively). The formation of curcumin−L-cysteine by E10B was not significantly different ($p > 0.05$) in the absence (0.21 μmol) or presence of PCF (0.22 μmol).

*Accountability for Curcuminoids.* The amount of curcumin accounted for was also calculated and found to be 87−94%. The amount of curcumin accounted for was not significantly different ($p > 0.05$) between the three *Escherichia* bacteria in mMCB or mMCB with PCF (Table 3). However, the amount of curcumin accounted for E469 in the presence of PCF (92.6%) was significantly higher ($p < 0.05$) than in the absence of PCF (86.8%), but there were no significant differences ($p > 0.05$) for E739 and E10B in the presence or absence of PCF. The level of accountability, which represents remaining curcuminoids (curcumin, DMC, and Bis-BMC) and curcuminoid equivalents for conversion into ferulic acid and curcumin−L-cysteine, is high. In a different system, when curcuminoids were incubated with rat liver slices, there was ∼50% of curcumin and DMC and ∼75% for Bis-DMC accounted for.[11] These authors attributed the lack of accountability for the total amount of curcuminoids to possible spontaneous chemical degradation in aqueous solution and conversion to other breakdown products that were not detected by the methods used.[11]

**Proposed Pathways of Degradation of Curcuminoids by Bacterial Strains Examined.** The proposed pathways of degradation of the three curcuminoids are demonstrated in Figure 7. Curcumin is converted to DHC and then THC by the enzyme *CurA*, through the reduction of C═C bonds on the heptadienone chain.[19] In studies involving ingestion of curcumin in humans and animals it was found that this pathway was rapid and that curcumin and metabolites were subsequently glucuronidated or sulfated by enzymes present in the liver.[10,11]

Both curcumin and DHC can also be converted to FA, as shown in Figure 7. FA was found to be one of the major metabolites in the serum, urine, and feces of humans after consumption of encapsulated curcumin in bread, and the authors suggested that the presence of FA was probably as a result of gut bacteria metabolism.[12] Our data are consistent with this hypothesis.

In our in vitro system, the presence of a curcumin adduct, curcumin−L-cysteine, was also found. This adduct was observed only in fermented samples in the presence of curcuminoids and bacteria and not present in abiotic samples. The adduct was also observed only in spent media where curcuminoids were co-incubated with mMCB, confirming that the presence of bacteria was necessary for the formation of the curcumin adduct. However, from these studies alone it is not possible to assign this to bacterial transformation. It is possible that under the conditions used in this study, the formation of the adduct was due to a chemical reaction induced by the presence of the changed composition of the media due to the formation of bacterial metabolites.

DMC and Bis-DMC follow the same pathway as curcumin, with similar reductive products.[11] Therefore, DMC is predicted to be converted to dihydro-DMC and then tetrahydro-DMC (Figure 7). DMC and dihydro-DMC can also be converted to FA as shown in Figure 7. Furthermore, Bis-DMC is converted to dihydro-Bis-DMC and then tetrahydro-Bis-DMC (Figure 7). Metabolites from DMC and Bis-DMC degradation were not detected in this study, probably due to the lower concentration of these compounds in the starting material.

Pure culture experiments provide insights into possible products formed by bacteria in the presence of curcuminoid. Our studies have demonstrated that the metabolism of curcuminoids (curcumin, DMC, and Bis-DMC) by three different *Escherichia* bacteria in vitro in batch culture resulted in the metabolism of curcumin to DHC, THC, and FA. In addition, the formation of a curcumin adduct (curcumin−L-cysteine) was also observed. Although the result obtained is fundamental, it is limited to the capability of *Escherichia* bacteria to metabolize curcuminoids. Further in vitro studies should be expanded to include the incubation of curcuminoids with a complex microbial population such as fecal samples to determine any differences in metabolism and metabolite production. It is also necessary to carry out in vivo trials to ascertain whether similar microbial metabolites and a curcumin adduct are formed under conditions in the body where there is consortia of microbes in the lower gut environment. Our data contribute to a possible map of curcumin breakdown products and show the relative abundance of different curcumin metabolites. The methods presented here will facilitate further studies of these pathways, including the flux of metabolite production under biologically relevant conditions.

## ■ ASSOCIATED CONTENT

### Supporting Information

Method S1, profiling of breakdown products using full scan LC-MS; Figure S1. This material is available free of charge via the Internet at http://pubs.acs.org.

## ■ AUTHOR INFORMATION

### Corresponding Author

*(M.A.A.) E-mail: maryann.augustin@csiro.au.

### Funding

S.T. is supported by a CSIRO OCE Postgraduate Scholarship and a University of Melbourne MIFRS Scholarship.

### Notes

The authors declare no competing financial interest.

## ■ ACKNOWLEDGMENTS

We thank A/Prof Stuart Dashper of University of Melbourne for the use of the anaerobic culturing facilities. We also thank Patrick Daniel of Department of Primary Industries for supplying the pig cecal fluid.

## ■ ABBREVIATIONS USED

DMC, demethoxycurcumin; Bis-DMC, bis-demethoxycurcumin; DHC, dihydrocurcumin; THC, tetrahydrocurcumin; FA, ferulic acid; *E. coli*, *Escherichia coli*; NADPH, nicotinamide

adenine dinucleotide phosphate; LC-MS, liquid chromatography−mass spectrometry; IS, internal standard; PCF, pig cecal fluid; E469, *Escherichia fergusonii* ATCC 35469; E739, *Escherichia coli* ATCC 8739; E10B, *Escherichia coli* DH10B; mMCB, modified medium for colon bacteria; OD, optical density; ESI, electrospray ionization; MRM, multiple reaction monitoring; CE, collision energy; Rt, retention time; LOD, limit of detection; LOQ, limit of quantification; AUC, area under the curve; FT-ICR-MS, Fourier transform-ion cyclotron resonance-mass spectrometer

## REFERENCES


(1) Sharma, R. A.; Gescher, A. J.; Steward, W. P. Curcumin: the story so far. *Eur. J. Cancer* **2005**, *41*, 1955−1968.

(2) Strimpakos, A. S.; Sharma, R. A. Curcumin: preventive and therapeutic properties in laboratory studies and clinical trials. *Antioxid. Redox Signal.* **2008**, *10*, 511−545.

(3) Begum, A. N.; Jones, M. R.; Lim, G. P.; Morihara, T.; Kim, P.; Heath, D. D.; Rock, C. L.; Pruitt, M. A.; Yang, F. S.; Hudspeth, B.; Hu, S. X.; Faull, K. F.; Teter, B.; Cole, G. M.; Frautschy, S. A. Curcumin structure-function, bioavailability, and efficacy in models of neuroinflammation and Alzheimer's disease. *J. Pharmacol. Exp. Ther.* **2008**, *326*, 196−208.

(4) Aggarwal, B. B.; Sundaram, C.; Malani, N.; Ichikawa, H. Curcumin: the Indian solid gold. In *Molecular Targets and Therapeutic Uses of Curcumin in Health and Disease*; Springer: New York, 2007; Vol. 595, pp 1−75.

(5) Joe, B.; Vijaykumar, M.; Lokesh, B. R. Biological properties of curcumin-cellular and molecular mechanisms of action. *Crit. Rev. Food Sci. Nutr.* **2004**, *44*, 97−111.

(6) Ireson, C.; Orr, S.; Jones, D. J. L.; Verschoyle, R.; Lim, C. K.; Luo, J. L.; Howells, L.; Plummer, S.; Jukes, R.; Williams, M.; Steward, W. P.; Gescher, A. Characterization of metabolites of the chemopreventive agent curcumin in human and rat hepatocytes and in the rat in vivo, and evaluation of their ability to inhibit phorbol ester-induced prostaglandin E-2 production. *Cancer Res.* **2001**, *61*, 1058−1064.

(7) Ireson, C. R.; Jones, D. J. L.; Orr, S.; Coughtrie, M. W. H.; Boocock, D. J.; Williams, M. L.; Farmer, P. B.; Steward, W. P.; Gescher, A. J. Metabolism of the cancer chemopreventive agent curcumin in human and rat intestine. *Cancer Epidemiol. Biomarkers Prev.* **2002**, *11*, 105−111.

(8) Williamson, G.; Clifford, M. N. Colonic metabolites of berry polyphenols: the missing link to biological activity? *Br. J. Nutr.* **2010**, *104*, S48−S66.

(9) Holder, G. M.; Plummer, J. L.; Ryan, A. J. Metabolism and excretion of curcumin (1,7-bis-(4-hydroxy-3-methoxyphenyl)-1,6-heptadiene-3,5-dione) in the rat. *Xenobiotica* **1978**, *8*, 761−768.

(10) Pan, M. H.; Huang, T. M.; Lin, J. K. Biotransformation of curcumin through reduction and glucuronidation in mice. *Drug Metab. Dispos.* **1999**, *27*, 486−494.

(11) Hoehle, S. I.; Pfeiffer, E.; Solyom, A. M.; Metzler, M. Metabolism of curcuminoids in tissue slices and subcellular fractions from rat liver. *J. Agric. Food Chem.* **2006**, *54*, 756−764.

(12) Vitaglione, P.; Lumaga, R. B.; Ferracane, R.; Radetsky, I.; Mennella, I.; Schettino, R.; Koder, S.; Shimoni, E.; Fogliano, V. Curcumin bioavailability from enriched bread: the effect of micro-encapsulated ingredients. *J. Agric. Food Chem.* **2012**, *60*, 3357−3366.

(13) Ravindranath, V.; Chandrasekhara, N. In vitro studies on the intestinal absorption of curcumin in rats. *Toxicology* **1981**, *20*, 251−257.

(14) Wahlstrom, B.; Blennow, G. A study on the fate of curcumin in the rat. *J. Acta Pharmacol. Toxicol.* **1978**, *43*, 86−92.

(15) Fava, F.; Danese, S. Intestinal microbiota in inflammatory bowel disease: friend of foe? *World J. Gastroenterol.* **2011**, *17*, 557−566.

(16) Tuohy, K. M.; Conterno, L.; Gasperotti, M.; Viola, R. Up-regulating the human intestinal microbiome using whole plant foods, polyphenols, and/or fiber. *J. Agric. Food Chem.* **2012**, *60*, 8776−8782.

(17) Aura, A. M. Microbial metabolism of dietary phenolic compounds in the colon. *Phytochem. Rev.* **2008**, *7*, 407−429.

(18) Jazayeri, S. D.; Mustafa, S.; Manap, M. Y.; Ali, A. M.; Ismail, A.; Faujan, N. H.; Shaari, M. Y. Survival of Bifidobacteria and other selected intestinal bacteria in TPY medium supplemented with curcumin as assessed in vitro. *Int. J. Probiotics Prebiotics* **2009**, *4*, 15−22.

(19) Hassaninasab, A.; Hashimoto, Y.; Tomita-Yokotani, K.; Kobayashi, M. Discovery of the curcumin metabolic pathway involving a unique enzyme in an intestinal microorganism. *Proc. Natl. Acad. Sci. U.S.A., Early Ed.* **2011**, 1−6.

(20) Van der Meulen, R.; Makras, L.; Verbrugghe, K.; Adriany, T.; De Vuyst, L. In vitro kinetic analysis of oligofructose consumption by Bacteroides and Bifidobacterium spp. indicates different degradation mechanisms. *Appl. Environ. Microbiol.* **2006**, *72*, 1006−1012.

(21) Saradhi, U.; Ling, Y. H.; Wang, J. A.; Chiu, M.; Schwartz, E. B.; Fuchs, J. R.; Chan, K. K.; Liu, Z. F. A liquid chromatography-tandem mass spectrometric method for quantification of curcuminoids in cell medium and mouse plasma. *J. Chromatogr., B* **2010**, *878*, 3045−3051.

(22) Cherepova, N.; Veljanov, D. Effect of sorbitan monolaurate polyoxyalkylene (Tween 20) on the ultrastructure of some bacteria. *Cytobios* **1994**, *80*, 179−185.

(23) Ingram, L. O. Ethanol tolerance in bacteria. *Crit. Rev. Biotechnol.* **1990**, *9*, 305−319.

(24) Salanitro, J. P.; Muirhead, P. A. Quantitative method for gas-chromatographic analysis of short chain monocarboxylic and dicarboxylic-acids in fermentation media. *Appl. Microbiol.* **1975**, *29*, 374−381.

(25) Tonnesen, H. H.; Karlsen, J. Studies on curcumin and curcuminoids. 5. Alkaline-degradation of curcumin. *Z. Lebensm.-Unters. -Forsch.* **1985**, *180*, 132−134.

(26) Tonnesen, H. H.; Karlsen, J. Studies on curcumin and curcuminoids. 6. Kinetics of curcumin degradation in aqueous-solution. *Z. Lebensm.-Unters. -Forsch.* **1985**, *180*, 402−404.

(27) Gupta, S. C.; Prasad, S.; Kim, J. H.; Patchva, S.; Webb, L. J.; Priyadarsini, I. K.; Aggarwal, B. B. Multitargeting by curcumin as revealed by molecular interaction studies. *Nat. Prod. Rep.* **2011**, *28*, 1937−1955.

(28) Fang, J. G.; Lu, J.; Holmgren, A. Thioredoxin reductase is irreversibly modified by curcumin − a novel molecular mechanism for its anticancer activity. *J. Biol. Chem.* **2005**, *280*, 25284−25290.

(29) Jung, Y. J.; Xu, W. P.; Kim, H.; Ha, N.; Neckers, L. Curcumin-induced degradation of ErbB2: a role for the E3 ubiquitin ligase CHIP and the Michael reaction acceptor activity of curcumin. *Biochim. Biophys. Acta−Mol. Cell Res.* **2007**, *1773*, 383−390.

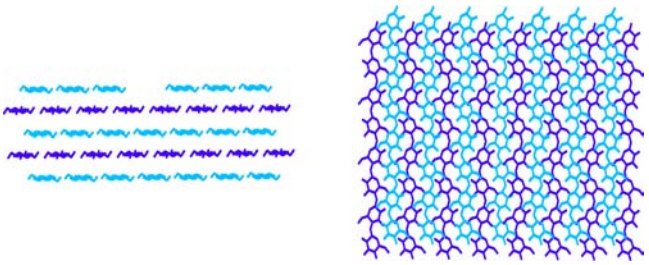

**Figure 1.** End-on (left) and "bottom" (right) views of the initial structure of the cellulose microcrystallite simulated in this study. As one can see from the end view, the center chain on the upper 100 surface has been removed. The analysis of the water structuring over the 100 surface reported here thus was confined to the uninterrupted "bottom" surface.

## EXPERIMENTAL PROCEDURES

The MD simulations reported here were conducted in the *NPT* ensemble using the CHARMM molecular mechanics program.[11,12] The sugar atoms were modeled using parameters specifically developed for carbohydrates, denoted as CSFF.[13,14] Water molecules were represented using the modified TIP3P force field.[15,16]

The initial cellulose structure for the simulations was taken from the reported native cellulose I$\beta$ crystal structure.[6] It thus differs significantly from that apparently used by Biermann et al. in that all exocyclic C6 primary alcohol groups were initially set in the TG conformation.[1] The cellulose model consisted of 36 chains, each with a degree of polymerization of eight, arranged into a small microcrystallite as shown in Figure 1. This microcrystallite consisted of five layers of parallel chains, with three even layers and two odd layers. The two odd layers contained eight chains each, and two of the even layers had seven chains each; the third consisted of only six chains, with the central chain removed, to model the effects on solvent structuring from the removal of a single chain, which might occur in the hydrolysis conducted by a processive exocellulase. In this model, the "top" and "bottom" of the microcrystallite consisted of approximately planar 100 surfaces, which permitted an analysis of how water interacts with this hydrophobic surface. Deletion of the middle chain of the "top" 100 even layer created a trough ~8 Å wide and ~4 Å deep that ran the length of the crystal. Chain numbers were assigned as chains 1−36 from the left on the first layer of the cellulose crystal. The constructed microcrystallite was placed in an equilibrated cubic box of TIP3P water molecules with a box length of 73.8 Å. All those water molecules that overlapped with the carbohydrate heavy atoms were deleted. The simulation contained 11821 water molecules and 41619 atoms in total. For the purpose of comparison, a simulation of $\beta$-D-glucopyranose in aqueous solution using the same carbohydrate force field and water model was also conducted to analyze how water molecules orient over an individual glucose monomer.

Chemical bonds to hydrogen atoms were kept fixed using the general constraint algorithm SHAKE.[17,18] van der Waals interactions were smoothly truncated on an atom-by-atom basis using switching functions from 12.0 to 14.0 Å.[11] Electrostatic interactions were treated using the particle-mesh Ewald method[19] with a real space cutoff of 15 Å and a $\kappa$ value of 0.3 Å$^{-1}$. The simulation was run at a constant temperature of 300 K and a constant pressure of 1 atm, maintained using a Hoover constant pressure/temperature algorithm, with a Hoover piston mass of 2000 amu.[20−22] Initial velocities were assigned from a Boltzmann distribution at 300 K, and the trajectories were run for 11 ns with a step size of 1 fs using full periodic boundary conditions. The last 10 ns of the simulation time was used for analysis. This simulation time is more than adequate to allow complete convergence of the water structuring[23] but is not long enough to allow the crystallite to undergo the structural transition that is known to occur with all of the highly developed carbohydrate force fields.[24]

Molecular graphics were generated with Visual Molecular Dynamics (VMD1.9),[25] and atomic density analyses of the trajectories were calculated using this program.[25] For each saved frame of the trajectory, a coordinate transformation was conducted so that the positions of the water molecules could be specified relative to the crystal surfaces in a coordinate frame fixed on its center of mass. The solvent density was then averaged relative to bulk solvent density. Average orientational and distributional properties were analyzed for those water molecules located in cylinders above the 100 crystal face with positions defined and located as shown in Figure 2, to evaluate the structuring influences

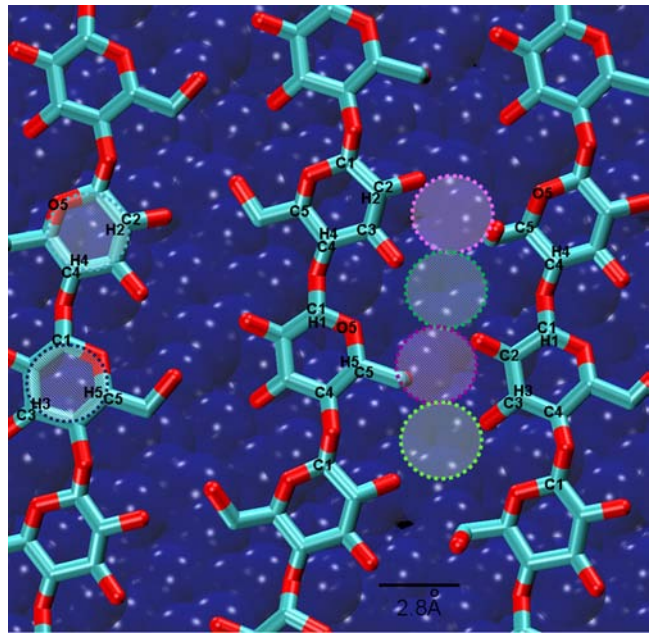


**Figure 2.** Illustration of the central portion of the "bottom" surface of the simulated microcrystal, illustrating the atom labeling employed as well as the footprints of the six cylindrical volumes for which orientational structuring was computed. Only carbon and oxygen atoms are shown for the sake of clarity, but the locations of the nonpolar H1, H2, H3, H4, and H6 hydrogen atoms are indicated by labels located on the appropriate carbon atoms. Also indicated is the coloring scheme used to distinguish these regions in subsequent figures: black, above the glucose H1−H3−H5 plane; turquoise, above the glucose H2−H4 atoms; dark purple, between two residues (O5−C5−C2−C3); pink, between two residues (C2−C3−O5−C5); dark green, among four residues (C4−C1−C4−C1); light green, among four residues (C4−C1−C4−C1).

of different features on the surface, including directly over both types of faces in the chains and over several positions in the more polar grooves between the chains. The same color schemes used in Figure 2 for these different regions are employed in Figures 5 and 7 to distinguish the behaviors of water molecules over the various parts of the surface.

## RESULTS AND DISCUSSION

Because the chains that make up the microcrystallite were completely unconstrained in these simulations, the entire crystal quickly developed a twist as the individual chains distorted away from the flat 2-fold screw geometry of the crystal structure (Figure 3). Such twisting has been observed in previous simulations of this crystal structure with all three of the most commonly used molecular mechanics force fields (CHARMM, GLYCAM, and GROMACS).[8,24,26] To minimize edge effects on the calculated local density profiles, only the volume above the middle three chains of the 100 face was used, and only for the middle four residues of these chains, as shown in Figure 2. Over this approximately square area, the solvent

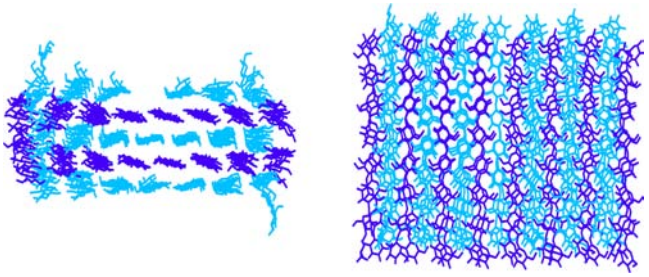

**Figure 3.** End-on (left) and "bottom" (right) views of the instantaneous final structure of the cellulose microcrystallite simulated in this study, illustrating the twist that developed in the crystal.

density and orientation were characterized in various cylindrical subvolumes centered over specific locations on the surface, as indicated in Figure 2. These volumes were selected to sample the effects of both types of faces of the monomer rings, as well as different portions of the hydrophilic, hydrogen-bonded groove between the chains. Because the twist in the substrate surface is minimal over the center of the surface, its effects on the calculated densities are also minimal and would primarily arise at long distances, where the overlap with the edges of similar adjacent cylinders would be greatest, but are of less interest because of the distance from the surface.

As one would expect for this topologically complex surface, the average density of neighboring water molecules varied with position over the surface as well as with distance from the surface. Figure 4 illustrates examples of the variation in solvent density as a function of distance from the surface in cylinders located at various places in the crystal face, including over the H2−H4 face (Figure 4a), over the H1−H3−H5 face (Figure 4b) of a glucose ring, and over two different spots between different chains (Figure 4c,d). Even within most of these cylindrical volumes, the density varies across the diameter of the cylinder, reflecting the changes in the underlying molecular geometry. For example, for the cylinder over the H2−H4 face (Figure 4a), it can be seen in the figure that the water molecules approach the ring more closely over the O5 atom on the right side of the cylinder, to which they can weakly hydrogen bond, than they do over the nonpolar H2 and H4 atoms that point directly up and prevent the closer approach of solvent.

The density over the H1−H3−H5 face is more uniform (Figure 4b) and clearly indicates two pronounced nearby layers, as does the density over the H2−H4 face, with a clear minimum between layers. The decreased density between the second and third layers is harder to detect in these figures. The density between the O2−O6 interchain hydrogen bond penetrates most closely between the hydroxyl groups (Figure 4c), as would be expected. The density between the chains, but not centered over any hydroxyl groups (Figure 4d), is more complex. Note that the fact that the edges at longer distances do not exhibit higher densities in any of these cylinders indicates that the twist of the surface is not significantly affecting the calculated densities.

Figure 5 displays the averaged solvent density in the various cylinders whose bases are illustrated in Figure 2 as a function of distance above the average plane defined by the sugar rings. As one can see, these distributions fall into three groups: those centered over the glucose rings, with first peaks located around 3.7 Å, those centered between the O2 and O6 groups of different chains, and those centered between the O2 and O3 groups of different chains, where the water molecules can

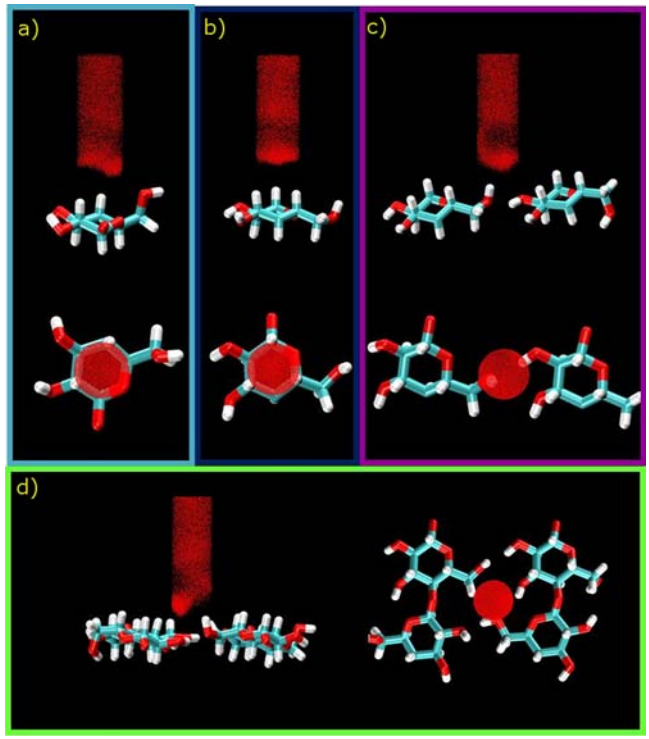


**Figure 4.** Examples of the variation in density in selected cylinders located over different positions in the surface, as seen from top and sides: (a) centered over the H2−H4 face of a glucose monomer, (b) centered over the H1−H3−H5 surface of a glucose ring, (c) centered over the HO2−O6 hydrogen bond between chains, and (d) centered over a region between the interchain hydrogen bonds. The red dots represent water oxygen positions at regular intervals over the entire simulation.

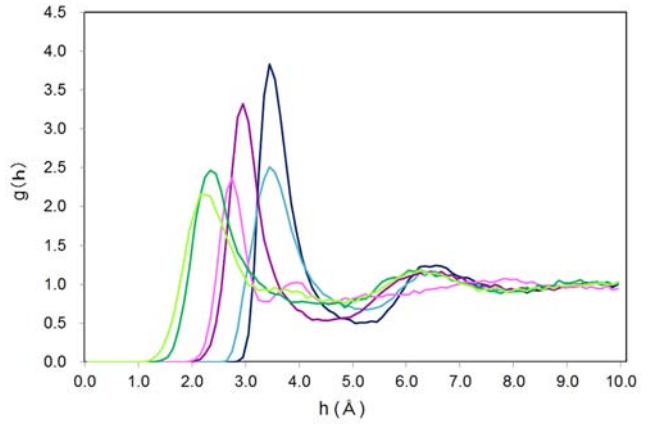


**Figure 5.** Solvent density profiles in the cylinders centered over various positions in the average crystal face: black, above the glucose H1−H3−H5 plane; turquoise, above the glucose H2−H4 atoms; dark purple, between two residues (O5−C5−C2−C3); pink, between two residues (C2−C3−O5−C5); dark green, among four residues (C4−C1−C4−C1); light green, among four residues (C4−C1−C4−C1).

approach much more closely, with first peaks centered around 2.0−2.2 Å. Note that all of these distributions exhibit distinct second peaks but with significantly lower amplitudes, and no longer-range structure. Uniquely among these distributions, that for the cylinder centered between the O2 hydroxyl of the center chain and the O6 hydroxyl of the outer chain, colored pink, exhibits a significant additional peak around 4.0 Å that


dx.doi.org/10.1021/jf501763r | J. Agric. Food Chem. 2014, 62, 11017−11023

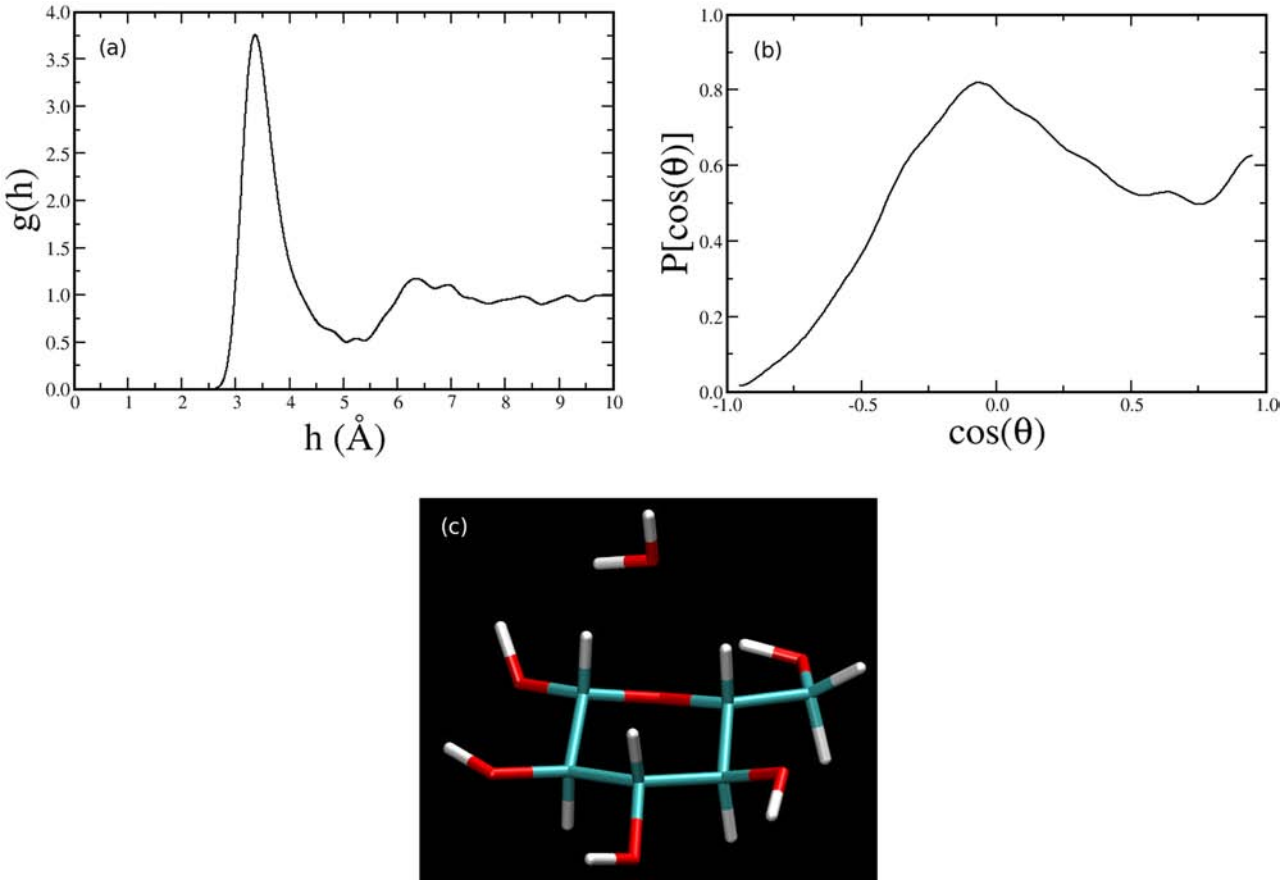


**Figure 6.** (a) Density distribution as a function of distance above the average H1−H3−H5 plane and (b) angular orientational distribution function for water molecules in a cylinder centered over the H1−H3−H5 face of $\beta$-D-glucopyranose in aqueous solution. (c) Typical example of a water molecule over this face with one of its protons pointing directly away from the face.

apparently represents first peak water molecules from the adjacent cylinder centered between the O3 and O2 hydroxyl groups of the same chains. The cylinder centered in this groove between the O2 hydroxyl of the center chain and the O3 group of the outer chain, colored light green, also exhibits a similar but less distinct shoulder at the same distance. In general, sharp narrow peaks in radial distribution functions are a signature of hydrogen bonding, while lower-magnitude, broader peaks generally are taken to indicate nonspecific packing (it should be remembered, however, that the density profiles shown in Figure 5 are not radial distribution functions). None of the density distributions seen in Figure 5 display the conventional structure of either hydrophilic or hydrophobic radial distribution functions.

Recent theories of the hydration of nonpolar species have found that extended planar surfaces should hydrate in a manner different from that of smaller hydrophobic molecules.[27−31] For hydrophobic solutes with a small spatial extent and a high convex curvature, such as methane or methylene, water molecules in the first "hydration shell" can straddle the solute to make hydrogen bonds to other water molecules off to the sides, with neither their protons nor lone pairs directly pointing at the solute, which would involve the loss of a hydrogen bond.[32] The cost of this structuring is entropic, because the translational and rotational freedom of the water molecules is restricted. As a result, such species are driven to aggregate in aqueous solutions,[33] which liberates water molecules to regain their motional freedom. The calorimetric signature of this type of hydrophobic aggregation at room temperature is that it is entropy-driven, with a heat capacity change that is negative, because the initial solvation of such hydrophobic species is accompanied by an increase in the level of solvent structuring and thus heat capacity.

However, as the spatial dimensions of hydrophobic species increase, it becomes impossible for water molecules to straddle the hydrophobic surface and still make hydrogen bonds to other water molecules off to its sides.[9,34−37] Under these conditions, the water molecules point one hydrogen atom or lone pair directly at the hydrophobic surface,[9] because the resulting loss of one hydrogen bond is nevertheless energetically better than the loss of the two or three hydrogen bonds that would result if they adopted the orientation of waters adjacent to a methane molecule.[9,29,34,37,38] The aggregation of such extended surfaces in aqueous solution would then be enthalpically dominated, because the pairing of two such surfaces would allow the liberated water molecules to regain their lost hydrogen bonds as well as their motional freedom. Orientational structuring of this type has been observed in simulation studies of extended featureless surfaces as well as of benzene and silica.[9,31,33,35,39] It has been demonstrated that there is a gradual transition from entropic to enthalpic domination of the solvation free energy as a function of size for the case of a spherical cavity, with a characteristic length scale for the transition of ∼1 nm.[28,29] This type of hydration also results in a depletion of water molecule density close to the hydrophobic surface, unlike the case for the small spherical

solutes such as methane, where there is a peak in water density at approximately the contact distance,[38] so that the hydration of these surfaces is characterized by a dewetting, with a more extended zone from which water is excluded.[29,31]

The nonpolar H1−H3−H5 triad face of a single glucose molecule in the $^4C_1$ conformation presents a rather limited hydrophobic surface to adjacent water molecules, with the average length of the sides of this triangle being only ∼2.5 Å. Thus, water molecules directly over this face can straddle this hydrophobic surface much as they would a smaller convexly curved nonpolar species like methane, making hydrogen bonds to other water molecules off to the side of the sugar ring, including those that might also be hydrogen bonding to the sugar's hydroxyl groups, and thus approach the surface more closely. This similarity to the hydration of methane can be seen in the density distribution function for water oxygen atoms above the H1−H3−H5 plane (Figure 6a), which strongly resembles the radial density distribution function for water molecules above the approximately spherical methane.

As is also the case for water molecules around a hydrated methane,[38] the first neighbor water molecules in the simulation of a single β-D-glucopyranose molecule in solution tend to point one of their protons directly away from the surface as shown in Figure 6c for a typical instantaneous "snapshot" example. This tendency can be characterized quantitatively using an orientational probability distribution function for the O−H bonds of the water molecules, calculated as the probability of observing an angle $\theta$ between the bond vector and the normal to the surface from the oxygen atom. Figure 6b displays this orientational distribution function $P[\cos(\theta)]$ [plotted as a function of $\cos(\theta)$ to eliminate cosine law effects], which exhibits a peak at +1 (i.e., $\theta = 0$), indicating a proton pointing directly away from the surface, with the other proton then oriented at a tetrahedral angle, producing the broad central peak in the distribution centered between −0.33 (the tetrahedral angle) and 0. The weakness of the peak at +1, and both the broadness and shift toward 0 of the maximum of the position of the central peak of the distribution, as compared to a more classical nonpolar distribution for solutes like argon or methane,[38] are a reflection of the larger extent of the flat hydrophobic surface here, compared to that of methane, requiring the water molecules to shift off-center and tilt to accommodate the hydrogen bonds to other water molecules. Nonetheless, this orientational behavior for a single glucose molecule qualitatively strongly resembles that for solvated methane and hydrocarbon chains.

Embedding such a glucose monomer in a cellulose chain, however, and then packing that chain into a 100 face of a cellulose crystal, presents the nearest neighbor water molecules with a significantly different topological landscape. The effects of this different surface have been characterized previously in terms of the anisotropic density distribution of water molecules over the surface,[8] but not in terms of their orientations. In the troughs between the chains, made up of the hydrogen-bonding hydroxyl groups, water molecules can approach more closely as they also attempt to hydrogen bond to these groups, as reflected in the density distributions illustrated in Figure 5. Angular orientational distribution functions for water molecules in the cylinders centered over different regions of the cellulose surface were calculated for those first-layer water molecules closer to the surface than the first minimum in each individual distance distribution, as shown in Figure 5, and are plotted in Figure 7. As one can see in this figure, the water molecules

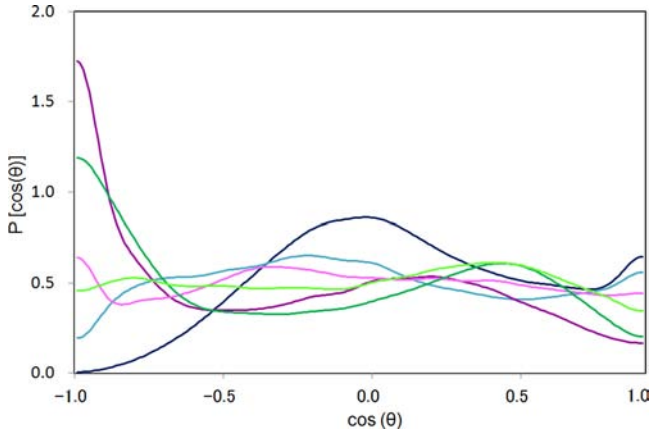


**Figure 7.** Orientational distribution function $P[\cos(\theta)]$ as a function of $\cos(\theta)$ for water molecules in selected regions above the 100 surface of the crystallite: black, above the glucose H1−H3−H5 plane; turquoise, above the glucose H2−H4 atoms; dark purple, between two residues (O5−C5−C2−C3); pink, between two residues (C2−C3−O5−C5); dark green, among four residues (C4−C1−C4−C1); light green, among four residues (C4−C1−C4−C1).

centered over the H1−H3−H5 face of the cellulose monomers exhibit the same sort of hydrophobic orientational structuring as for the free glucose molecule (Figure 6), which again qualitatively resembles that for methane, indicating that these ribbons of hydrophobicity are not acting like more extended hydrophobic surfaces (where a proton would be pointing directly at the surface), but more like the hydrocarbon chains of a fatty acid. Qualitatively similar behavior is seen for the H2−H4 face, but with a lower peak maximum at +1; in this case, the orientational structuring is even weaker.

For water molecules located in some of the cylinders centered between the chains, over the hydrophilic troughs occupied by the hydroxyl groups, strong orientational structuring is seen, particularly for the cylinders indicated in Figure 7 by purple and green, while for the other two there is very little structuring. This is somewhat surprising because these volumes are essentially equivalent positions. In these distributions, a hydrogen atom is directed down toward the surface to make a hydrogen bond to one of the glucose hydroxyl groups, as indicated by the peaks in the angular distribution function at $\cos(\theta) = -1$, the opposite of that seen in Figure 6. This orientational effect is much stronger than the nonpolar structuring, because of the strength and geometric requirements of the hydrogen bonds to the cellulose.

Recently, we demonstrated that the special water solvent structuring above extended flat surfaces is a dominant factor in the aggregation of the planar purine molecule caffeine in aqueous solution.[36] Although caffeine is <1 nm in size, in a narrow volume over the center of the molecular plane, water molecules indeed are unable to straddle the plane and make hydrogen bonds to water molecules around the periphery of the ring. Solvent molecules in this small volume point one hydrogen atom or lone pair directly at the center of the caffeine solute, even though this entails the loss of a hydrogen bond. The liberation of this structured water molecule when the face of caffeine binds to another molecule drives the association of caffeine with hydrophobic solutes, including other caffeine molecules, and from calorimetry, it is known that such aggregation is enthalpically dominated.[40,41]

Another study has found that in MD simulations of β-D-glucopyranose, the monomer repeat unit of cellulose, interacting in aqueous solution with indole, the side chain of the amino acid tryptophan, and the triad of H1−H3−H5 hydrophobic protons in glucose exhibited a pronounced tendency to bind to the flat hydrophobic face of the indole, with an association energy of approximately 1.2 kcal/mol.[42] Similar binding of glucose to caffeine has also been observed, with a very similar binding energy,[43] and glucose has been shown to bind to tryptophan side chains in cellulases and other proteins.[42,44−46] Thus, the hydration of planar surfaces like those in tryptophan, phenylalanine, and tyrosine may play an important part in molecular recognition involving protein−carbohydrate interactions. However, from these results, it appears that this is a property of these larger planar surfaces alone but is not a characteristic of the H1−H3−H5 hydrophobic triad of the $^4C_1$ conformation of the β-D-glucopyranose monomer that constitutes the largest part of the hydrophobicity of the cellulose 100 surface. As evidence of this observation, it should be noted that at normal biological concentrations glucose molecules do not exhibit any significant tendency to self-associate, and to the extent that they do interact at high concentrations (1.5 mol $kg^{-1}$), it tends to be by hydrogen-bonding interactions rather than by pairing of these triad faces.[47]

A significant factor contributing to the insolubility of cellulose is the fact that the chains exhibit considerable hydrophobicity, with nonpolar "tops" and "bottoms" in the extended 2-fold screw conformation of the reported crystal structure. These hydrophobic faces constitute the bulk of the exposed area of the 100 crystal surface. However, while the total surface of a crystalline cellulose fibril can be extensive, with diameters in the tens of nanometers, these surfaces are structurally very complex, and predominantly hydrophilic, with the hydrophobic 100 faces constituting only a portion of the fibril surface. Even this 100 surface is not completely hydrophobic, because the grooves between the chains are lined with the hydrogen-bonding hydroxyl groups of the monomers. Thus, the 100 surface exhibits a complex character with alternating hydrophobic and hydrophilic bands, rather than a single extended hydrophobic plane, and with the hydrophobic bands raised slightly higher than the average surface plane and the hydrophilic bands recessed slightly lower. Although the fibrils are quite large, the hydrophobic nature of their interactions with water more resembles that of the hydration of lipids than that of larger hydrophobic surfaces, as characterized by the orientational effects of these hydrophobic regions on the adjacent water molecules, and apparently does not involve the form of structuring seen in planar hydrophobic species like indole and the purines, in spite of its larger size. These results also might seem to suggest that the aggregation of cellulose chains and microfibrils by hydrophobic association would be dominated by entropy, as is the case of methane and lipids, rather than enthalpy, as is the case for caffeine aggregation. However, in the case of the aggregation of cellulose chains into layers such as those seen in the reported crystal structure, the water molecules hydrogen bonded to the hydroxyl-lined grooves between the chain would also be excluded by the aggregation, with the enthalpic cost due to the loss of these hydrogen bonds disfavoring aggregation. Because cellulose is not soluble, this factor is evidently smaller than the hydrophobic contribution, but this contribution to the energetic balance sheet for cellulose chain aggregation was not examined in our previous calculation of the factors contributing to cellulose insolubility.[2]

Finally, it should be remembered that the system simulated here is highly idealized; it is quite small and does not have the quasi-cylindrical cross section that might be expected for a real microfibril. In addition, any rotations of the primary alcohol groups to the GG orientation, perpendicular to the ribbon plane, particularly if they are randomly distributed, would significantly complicate the surface hydration patterns, as described by Biermann et al.[1] Additionally, real *in vivo* microfibrils might interact not only with other cellulose microfibrils but also with hemicellulose and lignin in ways that would further complicate hydration patterns. The hydration patterns seen here may help rationalize how such interactions arise.

## AUTHOR INFORMATION

### Corresponding Author

*E-mail: jwb7@cornell.edu. Phone: (607) 255-2897.

### Funding

This work was supported under the SciDAC Program by the U.S. Department of Energy Office of Biological and Environmental Research and the Office of Advanced Scientific Computing Research.

### Notes

The authors declare no competing financial interest.

## REFERENCES

(1) Biermann, O.; Hädicke, E.; Koltzenburg, S.; Müller-Plathe, F. Hydrophilicity and lipophilicity of cellulose crystal surfaces. *Angew. Chem., Int. Ed.* **2001**, *40*, 3822−3825.

(2) Bergenstråhle, M.; Wohlert, J.; Himmel, M. E.; Brady, J. W. Simulation Studies of the Insolubility of Cellulose. *Carbohydr. Res.* **2010**, *345*, 2060−2066.

(3) Wohlert, J.; Schnupf, U.; Brady, J. W. Free Energy Surfaces for the Interaction of Glucose with Planar Aromatic Groups in Aqueous Solution. *J. Chem. Phys.* **2010**, *133*, 155103.

(4) Medronho, B.; Romano, A.; Miguel, M. G.; Stigsson, L.; Lindman, B. Rationalizing cellulose (in)solubility: Reviewing basic physicochemical aspects and role of hydrophobic interactions. *Cellulose* **2012**, *19*, 581−587.

(5) Glasser, W. G.; Atalla, R. H.; Blackwell, J.; Brown, R. M.; Burchard, W.; French, A. D.; Klemm, D. O.; Nishiyama, Y. About the structure of cellulose: Debating the Lindman hypothesis. *Cellulose* **2012**, *19*, 589−598.

(6) Langan, P.; Sukumar, N.; Nishiyama, Y.; Chanzy, H. Synchrotron X-ray Structures of Cellulose Iβ and Regerated Cellulose II at Ambient Temperature and 100 K. *Cellulose* **2005**, *12*, 551−562.

(7) Nishiyama, Y.; Langan, P.; Chanzy, H. Crystal Structure and Hydrogen-Bonding System in Cellulose Iβ from Synchrotron X-ray and Neutron Fiber Diffraction. *J. Am. Chem. Soc.* **2002**, *124*, 9074−9082.

(8) Matthews, J. F.; Skopec, C. E.; Mason, P. E.; Zuccato, P.; Torget, R. W.; Sugiyama, J.; Himmel, M. E.; Brady, J. W. Computer Simulation Studies of Microcrystalline Cellulose Iβ. *Carbohydr. Res.* **2006**, *341*, 138−152.

(9) Lee, C. Y.; McCammon, J. A.; Rossky, P. J. The Structure of Liquid Water at an Extended Hydrophobic Surface. *J. Chem. Phys.* **1984**, *80*, 4448−4455.

(10) Lum, K.; Chandler, D.; Weeks, J. D. Hydrophobicity at small and large length scales. *J. Phys. Chem. B* **1999**, *103*, 4570−4577.

(11) Brooks, B. R.; Bruccoleri, R. E.; Olafson, B. D.; Swaminathan, S.; Karplus, M. CHARMM: A Program for Macromolecular Energy, Minimization, and Dynamics Calculations. *J. Comput. Chem.* **1983**, *4*, 187−217.

(12) Brooks, B. R.; Brooks, C. L.; MacKerell, A. D., Jr.; Nilsson, L.; Petrella, R. J.; Roux, B.; Won, Y.; Archontis, G.; Bartels, C.; Boresch, S.; Caflisch, A.; Caves, L.; Cui, Q.; Dinner, A. R.; Feig, M.; Fischer, S.; Gao, J.; Hodoscek, M.; Im, W.; Kuczera, K.; Lazaridis, T.; Ma, J.; Ovchinnikov, V.; Paci, E.; Pastor, R. W.; Post, C. B.; Pu, J. Z.; Schaefer, M.; Tidor, B.; Venable, R. M.; Woodcock, H. L.; Wu, X.; Yang, W.; York, D. M.; Karplus, M. CHARMM: The Biomolecular Simulation Program. *J. Comput. Chem.* **2009**, *30*, 1545−1614.

(13) Palma, R.; Himmel, M. E.; Brady, J. W. Calculation of the Potential of Mean Force for the Binding of Glucose to Benzene in Aqueous Solution. *J. Phys. Chem. B* **2000**, *104*, 7228−7234.

(14) Kuttel, M.; Brady, J. W.; Naidoo, K. J. Carbohydrate Solution Simulations: Producing a Force Field with Experimentally Consistent Primary Alcohol Rotational Frequencies and Populations. *J. Comput. Chem.* **2002**, *23*, 1236−1243.

(15) Jorgensen, W. L.; Chandrasekhar, J.; Madura, J. D.; Impey, R. W.; Klein, M. L. Comparison of Simple Potential Functions for Simulating Liquid Water. *J. Chem. Phys.* **1983**, *79*, 926−935.

(16) Durell, S. R.; Brooks, B. R.; Ben-Naim, A. Solvent-Induced Forces Between Two Hydrophilic Groups. *J. Phys. Chem.* **1994**, *98*, 2198−2202.

(17) Miyamoto, S.; Kollman, P. A. SETTLE: An Analytical Version of the SHAKE and RATTLE Algorithms for Rigid Water Models. *J. Comput. Chem.* **1992**, *13*, 952−962.

(18) van Gunsteren, W. F.; Berendsen, H. J. C. Algorithms for Macromolecular Dynamics and Constraint Dynamics. *Mol. Phys.* **1977**, *34*, 1311−1327.

(19) Darden, T.; York, D.; Pedersen, L. Particle Mesh Ewald: An N log(N) Method for Ewald Sums in Large Systems. *J. Chem. Phys.* **1993**, *98*, 10089−10092.

(20) Hoover, W. G. Canonical Dynamics: Equilibrium Phase-Space Distributions. *Phys. Rev. A* **1985**, *31*, 1695−1697.

(21) Martyna, G. J.; Tobias, D. J.; Klein, M. L. Constant Pressure Molecular Dynamics Algorithms. *J. Chem. Phys.* **1994**, *101*, 4177−4189.

(22) Feller, S. E.; Zhang, Y.; Pastor, R. W.; Brooks, B. R. Constant Pressure Molecular Dynamics Simulation: The Langevin Piston Method. *J. Chem. Phys.* **1995**, *103*, 4613−4621.

(23) Mark, P.; Nilsson, L. Structure and Dynamics of the TIP3P, SPC, and SPC/E Water Models at 298 K. *J. Phys. Chem. A* **2001**, *105*, 9954−9960.

(24) Matthews, J. F.; Beckham, G. T.; Bergenstråhle-Wohlert, M.; Brady, J. W.; Himmel, M. E.; Crowley, M. Comparison of Cellulose I$\beta$ Simulations with Three Carbohydrate Force Fields. *J. Chem. Theory Comput.* **2012**, *8*, 735−748.

(25) Humphrey, W.; Dalke, A.; Schulten, K. VMD: Visual Molecular Dynamics. *J. Mol. Graphics* **1996**, *14*, 33−38.

(26) Matthews, J. F.; Bergenstråhle, M.; Beckham, G. T.; Himmel, M. E.; Nimlos, M. R.; Brady, J. W.; Crowley, M. F. The High Temperature Behavior of Cellulose I. *J. Phys. Chem. B* **2011**, *115*, 2155−2166.

(27) Ashbaugh, H. S.; Paulaitis, M. E. Effect of Solute Size and Solute-Water Attractive Interactions on Hydration Water Structure around Hydrophobic Solutes. *J. Am. Chem. Soc.* **2001**, *123*, 10721−10728.

(28) Huang, D. M.; Chandler, D. The Hydrophobic Effect and the Influence of Solute-Solvent Attractions. *J. Phys. Chem. B* **2002**, *106*, 2047−2053.

(29) Chandler, D. Interfaces and the driving force of hydrophobic assembly. *Nature* **2005**, *437*, 640−647.

(30) Choudhury, N.; Pettitt, B. M. The Dewetting Transition and The Hydrophobic Effect. *J. Am. Chem. Soc.* **2007**, *129*, 4847−4852.

(31) Zangi, R.; Berne, B. J. Temperature Dependence of Dimerization and Dewetting of Large-Scale Hydrophobes: A Molecular Dynamics Study. *J. Phys. Chem. B* **2008**, *112*, 8634−8644.

(32) Stillinger, F. H. Water Revisited. *Science* **1980**, *209*, 451−457.

(33) Raschke, T. M.; Tsai, J.; Levitt, M. Quantification of the Hydrophobic Interaction by Simulations of the Aggregation of Small Hydrophobic Solutes in Water. *Proc. Natl. Acad. Sci. U.S.A.* **2001**, *98*, 5965−5969.

(34) Lee, S. H.; Rossky, P. J. A Comparison of the Structure and Dynamics of Liquid Water at Hydrophobic and Hydrophilic Surfaces: A Molecular Dynamics Simulation Study. *J. Chem. Phys.* **1994**, *100*, 3334−3345.

(35) Stirnemann, G.; Rossky, P. J.; Hynes, J. T.; Laage, D. Water reorientation, hydrogen-bond dynamics and 2-D-IR spectroscopy next to an extended hydrophobic surface. *Faraday Discuss.* **2010**, *146*, 263−281.

(36) Tavagnacco, L.; Schnupf, U.; Mason, P. E.; Saboungi, M.-L.; Cesàro, A.; Brady, J. W. Molecular Dynamics Simulation Studies of Caffeine Aggregation in Aqueous Solution. *J. Phys. Chem. B* **2011**, *115*, 10957−10966.

(37) Brady, J. W.; Tavagnacco, L.; Ehrlich, L.; Chen, M.; Schnupf, U.; Himmel, M. E.; Saboungi, M.-L.; Cesàro, A. Weakly-hydrated surfaces and the binding interactions of small biological solutes. *Eur. Biophys. J.* **2012**, *41*, 369−377.

(38) Tsunekawa, N.; Miyagawa, H.; Kitamura, K.; Hiwatari, Y. A study of water-water interactions in hydrophobic association by a molecular dynamics simulation with an optimized umbrella sampling method. *J. Chem. Phys.* **2002**, *116*, 6725−6730.

(39) Schravendijk, P.; van der Vegt, N. F. A. From Hydrophobic to Hydrophilic Solvation: An Application to Hydration of Benzene. *J. Chem. Theory Comput.* **2005**, *1*, 643−652.

(40) Cesàro, A.; Russo, E.; Crescenzi, V. Thermodynamics of Caffeine Aqueous Solutions. *J. Phys. Chem.* **1976**, *80*, 335−339.

(41) Stoesser, P. R.; Gill, S. J. Calorimetric Study of Self-Association of 6-Methylpurine in Water. *J. Phys. Chem.* **1967**, *71*, 564−567.

(42) Mason, P. E.; Lerbret, A.; Saboungi, M.-L.; Neilson, G. W.; Dempsey, C. E.; Brady, J. W. The Interactions of Glucose with a Model Peptide. *Proteins: Struct., Funct., Bioinf.* **2011**, *79*, 2224−2232.

(43) Tavagnacco, L.; Engström, O.; Schnupf, U.; Saboungi, M.-L.; Himmel, M.; Widmalm, G.; Cesàro, A.; Brady, J. W. Caffeine and Sugars Interact in Aqueous Solutions: A Simulation and NMR Study. *J. Phys. Chem. B* **2012**, *116*, 11701−11711.

(44) Linder, M.; Mattinen, M.-L.; Kontteli, M.; Lindeberg, G.; Ståhlberg, J.; Drakenberg, T.; Reinikainen, T.; Pettersson, G.; Annila, A. Identification of Functionally Important Amino Acids in the Cellulose-Binding Domain of *Trichoderma reesei* Cellobiohydrolase I. *Protein Sci.* **1995**, *4*, 1056−1064.

(45) Beckham, G. T.; Matthews, J. F.; Bomble, Y. J.; Bu, L.; Adney, W. S.; Himmel, M. E.; Nimlos, M. R.; Crowley, M. F. Identification of Amino Acids Responsible for Processivity in a Family I Carbohydrate-Binding Module from a Fungal Cellulase. *J. Phys. Chem. B* **2010**, *114*, 1447−1453.

(46) Tavagnacco, L.; Mason, P. E.; Schnupf, U.; Pitici, F.; Zhong, L.; Himmel, M. E.; Crowley, M.; Cesàro, A.; Brady, J. W. Sugar Binding Sites on the Surface of the Carbohydrate Binding Module of CBH I from *Trichoderma reesei*. *Carbohydr. Res.* **2011**, *346*, 839−846.

(47) Mason, P. E.; Neilson, G. W.; Enderby, J. E.; Saboungi, M.-L.; Brady, J. W. The Structure of Aqueous Glucose Solutions as Determined by Neutron Diffraction with Isotopic Substitution Experiments and Molecular Dynamics Calculations. *J. Phys. Chem. B* **2005**, *109*, 13104−13111.

the farm and its surroundings was conducted daily. All experiments with ostriches were performed according to protocols approved by the Huazhong Agricultural University Animal Care and Utilization Committee.

**Experimental Diets and Nutrient Levels.** The ostriches were fed with a blend of custom-made premix diet and pak choi based on their physiological needs, developmental stage, and breeding experience.[15] Moreover, to aid in digestion, some sand must be added in sufficient but not excessive quantities.[16] The nutrient composition of the diets and of each ingredient is reported in Table 1.

**Table 1. Ingredients and Composition of the Basal Diets[a]**

| ingredients | content (g/kg) | chemical composition | content (g/kg) |
|---|---|---|---|
| custom-made premix | 670 | crude protein | 193 |
| pak choi | 330 | lysine | 10.0 |
| | | cystine | 3.90 |
| | | crude fiber | 76.5 |
| | | crude fat | 29.1 |
| | | methionine | 3.41 |
| | | ash | 87.8 |
| | | metabolic energy | $2.94 \times 10^3$ kcal |
| | | boron in premix | 1.78 mg |
| | | boron in pakchoi | 2.45 mg |

[a]Supplied per kilogram of diet: 6.30 g of phosphorus, 14.7 g of calcium, 80.0 mg of manganese, 500 mg of magnesium, 11.0 mg of copper, 87.0 mg of zinc, 0.27 mg of selenium, 3.00 mg of iodine, 150 mg of ferrum, 12 000 IU of vitamin A, 3000 IU of vitamin $D_3$, 3.50 mg of vitamin K, 100 IU of vitamin E, 3.50 mg of vitamin $B_1$, 8.10 mg of vitamin $B_2$, 4.00 mg of vitamin $B_6$, 50.4 mg of niacin, 20.9 mg of pantothenic acid, 2.00 mg of folic acid, 0.20 mg of biotin, 1500 mg of choline, and 0.01 mg of vitamin $B_{12}$.

**Sample Collection and Processing.** At 90 days of age, the birds were weighed after a fasting period of 24 h, and cumulative weight gain and feed intake were determined. Using these values, cumulative feed to gain ratios were calculated. Following these measurements, the birds were electrically stunned and terminated in an ostrich abattoir. The iliofibularis muscles were removed from the left and right legs of each carcass, after removal of the external fat and the epimysium. The muscle samples of every ostrich were divided in two; one was kept at 4 °C until the completion of the physical analysis, and the other was frozen at −20 °C for further chemical analysis. Each sample was ground, homogenized, and vacuum-packed in plastic bags.

**Meat Physical Analyses.** At 24 h post-mortem, meat pH was measured on the iliofibularis muscles with a Testo 205 pH meter (Testo AG, Germany), equipped with an insertion glass electrode (calibrated at pH 4.01 and 7.00 at the abattoir temperature). Three readings were made on each sample, and the mean was recorded.

Meat color was measured on 4 cm thick muscle slices (cut 24 h post-mortem), according to the CIE $L^*a^*b^*$ color system (where $L^*$ measures relative lightness, $a^*$ measures relative redness, and $b^*$ measures relative yellowness) using a Colorgard System 2000 colorimeter (Pacific Scientific, Silver Spring, MD). Three measurements were taken per sample at random positions to determine $L^*$, $a^*$, and $b^*$ values; the average of the three readings was used in the statistical analysis.

Drip loss (%) was determined according to the method described by Zhang et al.[17] Briefly, the muscles were cut into 2 × 2 × 2 cm thick slices, weighed, and suspended in individual plastic bags. After storage for 24 h at 4 °C, the samples were removed from their individual bags, dried with absorbent paper, and weighed again. Drip loss was calculated as weight loss expressed as a percentage of the initial weight of the sample.

Cooking loss (%) was determined by placing weighed samples of approximately 100 g into sealed plastic bags and immersing in water at 75 °C (for the sufficient heat penetration without causing excessive denaturation of the collagen present in the meat). Samples were then removed from the water; the bagged samples were allowed to cool in running water to ±25 °C, and then the samples were blotted dry with tissue paper and reweighed. Cooking losses were then calculated by measuring the weight difference before and after cooking, and values were expressed as a percentage of the fresh (uncooked) sample weight.

Warner−Bratzler shear force (WBS) was determined on the same samples used for the cooking loss determination. Cooked muscle was cooled to room temperature, and three cylindrical cores were randomly removed from each cooked sample using a 1.27 cm diameter bore to determine Warner−Bratzler shear force values.[18] The samples were cut parallel to the direction of the muscle fiber to measure the influence of the myofibrillar proteins. Maximum shear force values were recorded for each cylindrical core of cooked muscle (repeated three times), and the mean values attained from the three samples were used in the statistical analysis. A larger value (kg) indicated a greater shear force and therefore tougher meat.

**Meat Chemical Analyses.** Chemical analyses were carried out on meat samples stored at −20 °C. Moisture, fat, protein, and ash contents were assessed according to AOAC standard techniques[19] on minced meat samples after 24 h of thawing at 4 °C.

For fatty acid composition, lipid was extracted according to the method used by Folch et al.[20] on *M. iliofibularis* (5 g of ground meat), after which the lipids were analyzed for fatty acids. Fatty acids were quantified as methyl esters, prepared according to the method described by Butte.[21] Methyl esters were separated on an Agilent model GC-6400 gas chromatograph equipped with a DB-23 capillary column (length 60 m, internal diameter 0.25 mm, film thickness 0.25 μm). The GC program was set to the following conditions: a helium flow rate of 1 mL/min, FID detector at 250 °C, split−splitless injector at 220 °C, and an injection volume of 0.5 mL. The fatty acid methyl esters (FAME) were identified by comparison of the retention times to those of the FAME standards. Fatty acids were expressed as a percentage of total methylated fatty acids.

The determination of cholesterol was performed using the method of Duckett and Wagner.[22] This method involved direct saponification of the samples and extraction of the unsaponifiable compounds with cyclohexane. Samples were separated using a Drug Three Mega bore column (10 m, 0.53 mm) maintained at a constant temperature of 285 °C, with the injector temperature set at 300 °C and detector temperature at 320 °C. Helium was the carrier gas (flow rate: 12 mL/min). The content of cholesterol was quantified using regression equations obtained from cholesterol standards and then corrected using stigmasterol (50 μg/mL) as an internal standard; cholesterol content was expressed as mg/100 g of meat.

**Table 2. Effect of Boron on Growth Performance of African Chicks[a]**

| items | group 1 | group 2 | group 3 | group 4 | group 5 | group 6 |
|---|---|---|---|---|---|---|
| final BW/kg | 32.0 ± 0.04 b | 32.7 ± 0.02 ab | 32.9 ± 0.70 ab | 33.4 ± 0.30 a | 31.9 ± 1.04 c | 30.8 ± 1.05 c |
| ADFI/g | 364 ± 1.21 b | 364 ± 0.94 b | 371 ± 2.25 ab | 376 ± 1.83 a | 364 ± 0.04 b | 360 ± 2.13 b |
| ADG/g | 214 ± 2.31 c | 215 ± 1.02 bc | 219 ± 0.96 b | 224 ± 1.01 a | 210 ± 0.63 d | 208 ± 0.74 d |
| feed conversion | 1.71 ± 0.31 | 1.70 ± 0.88 | 1.69 ± 0.74 | 1.68 ± 0.05 | 1.71 ± 0.92 | 1.71 ± 1.49 |

[a]In the same row, values with different letters indicate significant differences ($p < 0.05$), while the same or no letters indicate no significant difference ($p > 0.05$). The same applies for all tables.

Table 3. Mean Values (Mean ± Standard Deviation) for the Physical Meat Quality Parameters Measured in *M. iliofibularis* (Groups 1−6)

| parameter | group 1 | group 2 | group 3 | group 4 | group 5 | group 6 |
|---|---|---|---|---|---|---|
| pH | 6.01 ± 1.32 b | 6.03 ± 0.55 b | 6.07 ± 0.12 ab | 6.13 ± 0.28 a | 6.15 ± 1.17 a | 6.18 ± 0.03 a |
| CIE $L^*$ | 37.7 ± 1.04 | 37.3 ± 0.25 | 37.1 ± 1.44 | 37.0 ± 0.83 | 36.6 ± 0.52 | 36.3 ± 1.51 |
| CIE $a^*$ | 15.9 ± 0.33 | 15.7 ± 0.16 | 15.9 ± 0.64 | 16.0 ± 0.03 | 16.0 ± 0.06 | 16.3 ± 0.17 |
| CIE $b^*$ | 9.73 ± 0.03 | 9.82 ± 0.31 | 9.80 ± 0.52 | 9.61 ± 1.31 | 9.91 ± 0.42 | 9.84 ± 0.34 |
| drip loss (%) | 2.36 ± 0.06 a | 2.34 ± 0.43 a | 2.29 ± 1.06 ab | 2.20 ± 0.59 b | 2.14 ± 1.04 b | 2.10 ± 0.76 c |
| cooking loss (%) | 36.7 ± 0.02 a | 36.2 ± 0.23 a | 36.1 ± 0.91 ab | 35.3 ± 1.14 b | 35.2 ± 0.06 bc | 35.0 ± 0.41 c |
| WBS (kg) | 3.61 ± 0.27 | 3.60 ± 0.81 | 3.60 ± 0.93 | 3.59 ± 0.19 | 3.58 ± 0.40 | 3.59 ± 1.73 |

**Statistical Analysis.** All of the samples were measured in triplicate; the average of the three values was used in the statistical analysis. Data were analyzed using the SPSS 17.0 software (SPSS Inc., Chicago, IL). A one-way analysis of variance (ANOVA) was used to evaluate the effects of different concentrations of boron on the performance and meat quality of the African ostrich chicks. Duncan's multiple range tests were performed to denote differences between the groups when differences were significant (a probability level of 5% was considered significant ($p < 0.05$) for all tests). All values were expressed as the means ± standard deviations.

## RESULTS AND DISCUSSION

**Growth Performance.** The results of the growth performance of the birds are presented in Table 2. The final BW of the birds fed 160 mg/L boron was significantly higher than that of the control group (0 mg/L) ($P < 0.05$), and the addition of 320 and 640 mg/L boron significantly decreased the final BW of the ostrich chicks when compared to the other groups ($P < 0.05$). The ADFI of the birds was significantly increased by 160 mg/L supplemental boron in drinking water ($P < 0.05$); however, the other boron levels had no significant effect on ADFI. Adding 80 and 160 mg/L boron significantly increased the ADG of the birds, and 320 and 640 mg/L boron significantly decreased the ADG of the birds ($P < 0.05$). Boron had no effect on feed conversion.

In the present study, final BW, ADFI, and ADG of the birds significantly increased ($P < 0.05$) with supplementation of boron at 160 mg/L level (Table 2). Similar results were obtained in broilers fed 60−120 mg/kg boron[8] and hens fed 100 and 200 mg/kg boron.[23] Final BW and ADG were depressed by the higher levels of boron (320 and 640 mg/L) (Table 2), agreeing with results obtained in broilers fed 300 mg/kg boron,[8] layers fed 400 mg/kg boron,[9,23] hens fed 400 mg/kg boron,[24] and Japanese quails fed 10, 60, 120, and 240 mg/kg boron.[25] However, there were no differences in feed conversion between the groups (Table 2). In previous studies, feed conversion was not affected by 80 mg/kg boron in broilers,[26] by 5, 10, 50, 100, 200, and 400 mg/kg boron in the hens,[24] or by 5 and 15 mg/kg boron in pigs.[27] The results (Table 2) of this study indicated that 160 mg/L boron supplementation improved growth performance in ostrich chicks, but 320 and 640 mg/L boron supplementation inhibited growth performance.

**Physical Meat Quality Parameters.** The effects of different concentrations of boron on the physical meat quality parameters of the ostrich chicks are reported in Table 3. The drip loss and cooking loss of meat were significantly decreased by supplemental boron at 160, 320, and 640 mg/L. Further, the addition of 160, 320, and 640 mg/L boron to drinking water significantly increased the pH value of the meat ($p < 0.05$). The color and WBS values of meats did not differ among the birds administered different boron levels ($P > 0.05$).

To the best of our knowledge, there are no reports of the effect of boron on physical meat quality parameters. The data clearly showed that the pH value of the meat was significantly increased by supplemental boron at 160, 320, and 640 mg/L ($P < 0.05$) (Table 3). The pH value of meat depends on the content of lactic acid in the muscles, and after the slaughter, muscle glycogen glycolysis is the main source of lactic acid.[28] It is widely accepted that there is a close correlation between muscle pH values and glycogen.[29] The high ultimate pH of the meat is a consequence of depleted muscular glycogen reserves prior to slaughter and greatly affects meat quality.[30] Boron has a major role in controlling certain metabolic pathway processes using hydrolases or oxidoreductases.[4,31] These enzymes need pyridine or flavin nucleotides (NAD+, NADP, or FAD) to promote the enzyme activity. Boron reversibly inhibits their activity by forming transition state analogs or competing for NAD or FAD.[4,31] Boron can also inhibit NAD directly to affect enzyme activity.[32−34] NAD is an important reaction substrate of glycolysis; boron inhibits the glycolytic pathway by acting on NAD, thus reducing the lactic acid content of muscle and increasing pH value. Geyikoğglu and Türkez[35] reported that high boric acid doses (3.375 and 4.5 mmol B/kg b.wt.) caused decreased metabolite concentrations (glucose, glycogen, lactate, and ATP) in breast muscle of broiler chickens, thus increasing the muscle pH value. In the present study, the pH value of the meat was significantly increased by 160, 320, and 640 mg/L boron in the drinking water, which could be due to the additional boron reducing lactic acid and glycogen content in the muscles.

The drip loss and cooking loss were significantly decreased by supplemental boron at 160, 320, and 640 mg/L ($P < 0.05$) (Table 3). Meat that has a higher pH has a stronger water holding capacity (WHC) and lower moisture loss.[36] Lower drip loss and cooking loss were, therefore, expected for the samples of groups 4, 5, and 6. The results confirmed that the drip loss and cooking loss of these groups were significantly decreased as compared to those of the control group ($P < 0.05$). The significant increase in the ultimate pH of groups 4, 5, and 6 could account for this finding.

There were no significant differences between treatments with regard to meat color or shear force values ($P > 0.05$) (Table 3). At a higher meat pH, protein can bind more strongly with water, allowing less free water; therefore, meat will be darker in color because there is less free water to reflect light.[37] Although not significant, groups 4, 5, and 6 had lower $L^*$ values. Lanza et al.[38] reported that there was a negative correlation ($r = -0.41$; $P < 0.05$) between shear force values and ultimate pH, but in this study, no significant changes were detected for the shear force values with increasing pH value, suggesting that the inclusion of boron in the drinking water of

Table 4. Mean Values (Mean ± Standard Deviation) for the Chemical Meat Quality Parameters Measured in *M. iliofibularis* (Groups 1−6)

| parameter | group 1 | group 2 | group 3 | group 4 | group 5 | group 6 |
|---|---|---|---|---|---|---|
| moisture (%) | 77.8 ± 1.44 | 77.9 ± 1.46 | 77.0 ± 0.83 | 76.9 ± 1.23 | 76.8 ± 0.31 | 76.8 ± 1.20 |
| fat (%) | 0.49 ± 0.40 | 0.50 ± 0.07 | 0.50 ± 0.42 | 0.51 ± 0.33 | 0.51 ± 0.26 | 0.52 ± 0.03 |
| protein (%) | 21.0 ± 0.41 a | 20.9 ± 1.36 a | 20.7 ± 1.05 ab | 20.7 ± 0.66 ab | 20.5 ± 1.21 b | 20.4 ± 1.74 c |
| ash (%) | 1.00 ± 0.03 b | 1.01 ± 0.13 b | 1.03 ± 0.24 ab | 1.13 ± 0.08 ab | 1.20 ± 0.04 ab | 1.35 ± 0.01 a |
| FA (%) SFA | | | | | | |
| C12:0 | 0.04 ± 0.02 | 0.04 ± 0.03 | 0.04 ± 0.13 | 0.05 ± 0.42 | 0.04 ± 0.07 | 0.05 ± 0.53 |
| C14:0 | 1.06 ± 0.04 | 1.03 ± 0.01 | 1.01 ± 0.01 | 1.12 ± 0.42 | 1.10 ± 0.72 | 1.07 ± 0.18 |
| C15:0 | 0.23 ± 0.01 | 0.23 ± 0.02 | 0.23 ± 0.23 | 0.24 ± 0.33 | 0.23 ± 0.11 | 0.23 ± 0.21 |
| C16:0 | 21.7 ± 0.72 | 21.6 ± 0.34 | 21.9 ± 0.21 | 22.0 ± 0.10 | 21.1 ± 0.02 | 21.2 ± 0.81 |
| C18:0 | 14.9 ± 0.01 | 14.9 ± 0.03 | 14.9 ± 0.21 | 14.8 ± 0.03 | 14.9 ± 0.01 | 15.0 ± 0.03 |
| FA (%) MUFA | | | | | | |
| C16:1 | 6.13 ± 0.32 | 6.13 ± 0.02 | 6.14 ± 0.07 | 6.13 ± 0.11 | 6.14 ± 0.43 | 6.13 ± 0.01 |
| C18:1 | 29.8 ± 0.33 a | 29.0 ± 0.04 a | 28.8 ± 0.30 a | 28.7 ± 0.14 a | 28.4 ± 0.17 ab | 28.2 ± 0.65 b |
| C20:1 | 0.31 ± 0.05 | 0.31 ± 0.04 | 0.30 ± 0.13 | 0.30 ± 0.12 | 0.29 ± 0.02 | 0.27 ± 0.31 |
| C22:1 | 5.77 ± 0.01 | 5.74 ± 0.02 | 5.74 ± 0.05 | 5.71 ± 0.13 | 5.79 ± 0.04 | 5.73 ± 0.02 |
| FA (%) PUFA | | | | | | |
| C18:2$\omega$6 | 18.0 ± 0.03 | 18.9 ± 0.01 | 19.1 ± 0.37 | 19.0 ± 0.03 | 18.0 ± 0.32 | 19.2 ± 0.96 |
| C18:3$\omega$3 | 2.81 ± 0.04 a | 2.80 ± 0.13 a | 2.80 ± 0.32 a | 2.77 ± 0.01 ab | 2.71 ± 0.03 ab | 2.60 ± 0.51 b |
| C20:2$\omega$6 | 0.29 ± 0.01 | 0.29 ± 0.01 | 0.28 ± 0.04 | 0.30 ± 0.45 | 0.27 ± 0.03 | 0.30 ± 0.19 |
| C20:5$\omega$3 | 0.52 ± 0.32 | 0.51 ± 0.03 | 0.49 ± 0.04 | 0.50 ± 0.90 | 0.48 ± 0.38 | 0.53 ± 1.42 |
| C22:6$\omega$3 | 0.31 ± 0.53 | 0.31 ± 0.01 | 0.28 ± 0.06 | 0.30 ± 0.42 | 0.29 ± 0.03 | 0.32 ± 0.73 |
| cholesterol (mg/100 g) | 60.4 ± 0.87 | 60.0 ± 0.42 | 59.9 ± 0.12 | 59.7 ± 1.33 | 59.7 ± 0.92 | 59.5 ± 1.42 |

ostrich chicks does not have any effect on the tenderness of meat.

**Chemical Meat Quality Parameters.** The effects of different levels of boron on chemical meat quality parameters of ostrich chicks are reported in Table 4. The parameters that differed in the current study were protein, ash, C18:1, and C18:3$\omega$3; significantly lower protein was found in the treatments of 320 and 640 mg/L boron; lower C18:1 and C18:3$\omega$3 were found with the dose of 640 mg/L boron, and higher ash was found with the 640 mg/L boron ($p < 0.05$) dose. No significant effects of the boron treatment for moisture, fat, SFA, or cholesterol of meat were found for any birds in the trial.

The moisture of muscle was decreased with increasing dosages of the boron supplement in the drinking water, but no significant difference ($P > 0.05$) was observed between the treatment groups. Eren et al.[25] reported that boron had no effect on the moisture of Japanese quail meat, which was consistent with our results.

Eren et al.[25] also reported that fat in the meat of male Japanese quails was increased with boron supplements of 10, 60, 120, 240 mg/kg, and in females, 120 and 240 mg/kg boron increased fat percentages in the meat ($P < 0.05$). In the present study, the fat of the muscle increased with increasing doses of boron, but it was not significant ($P < 0.05$). This trend for fat was similar to previous research.

The ash content of muscle is representative of mineral and trace element content.[39] Boron has a regulatory role in the metabolism of several minerals such as magnesium, phosphorus, molybdenum, and calcium.[23] Shang et al.[40] showed that the addition of boron in drinking water could improve the contents of iron and zinc in chicken meat. Similarly, Eren et al.[25] reported that 240 mg/kg boron increased ash percentages in the meat of Japanese quails ($P < 0.05$). Our results also showed that ash of muscle was increased with increasing dosage of boron, and ash content was significantly ($P < 0.05$) higher at the high dose (640 mg/L) than at the low doses (0, 40, 80, 160, 320 mg/L). The ash content increased gradually due to the boron raising the mineral content of the muscle, but more research is needed to further quantify this.

As mentioned above, boron can inhibit the activity of NAD,[32−34] and, because serine proteases require pyridine or flavin nucleotides ($NAD^+$, NADP, or FAD), boron can inhibit the activity of serine proteases. Serine proteases are one of the most abundant groups of proteolytic enzymes; they are involved in many physiological processes through the proteolytic activation of precursor proteins.[41] The addition of boron inhibited the activity of serine proteases, so that macromolecule proteins cannot be broken down into smaller proteins, resulting in the relatively low protein content of the ostrich meat. This may be the cause of the decrease in muscle protein with increasing doses of boron supplementation.

Hall et al.[42] reported that when boron was orally administered (8 mg/kg/day) to rats, daily for 14 days, TG levels and LDL cholesterol decreased. Basoglu et al.[43] suggested that boron had positive effects on hepatic steatosis and visceral fat by affecting the lipid profile and reducing oxidative stress. The administration of sodium borate decreased concentrations of total cholesterol, triglyceride, high-density lipoprotein, low-density lipoprotein, and nonesterified fatty acids in the blood.[3] Several studies have indicated that boron could improve lipid metabolic profiles. Until now, the research has only been conducted in serum; there is no literature reporting changes of lipid substances in the muscle when boron is administered. Our experiment showed that boron had no influence on the percentages of SFA and cholesterol in meat, but the proportion of C18:1 and C18:3$\omega$3 significantly ($P < 0.05$) decreased at the highest dosage (640 mg/L).

In conclusion, we investigated the effect of boron on the growth performance and meat quality of African ostrich chicks, and our results showed that additional boron improved these parameters, but a high dose of boron had a negative effect.

According to our results, 160 mg/L boron was the optimal dosage for growth performance and meat quality of African ostrich chicks.

## AUTHOR INFORMATION


### Corresponding Author

*Tel.: 86-27-87286970. Fax: 86-27-87280408. E-mail: pengkm@mail.hzau.edu.cn.



### Funding

This study was supported by the National Natural Science Foundation of China no. 31272517.


### Notes

The authors declare no competing financial interest.

## ACKNOWLEDGMENTS

We thank Lingqiao Ma for her skillful assistance in conducting this experiment.

## ABBREVIATIONS USED

BW, body weight; AOAC, Association of Official Analytical Chemists; ADFI, average daily feed intake; ADG, average daily gain; NAD, nicotinamide adenine dinucleotide; NADP, nicotinamide-adenine dinucleotide phosphate; FAD, flavin adenine dinucleotide; ATP, adenosine triphosphate; TG, triglyceride; LDL, low density lipoprotein; SFA, saturated fatty acid; MUFA, monounsaturated fatty acid; PUFA, polyunsaturated fatty acid

## REFERENCES


(1) Criste, R. D.; Grossu, D. V.; Scorei, R.; Duca, R. C.; Mitrut, M.; Ciurascu, C. New investigations on the effect of the dietary boron on broilers and layers: boron and food quality. *Arch. Zootec.* **2005**, *8*, 65−78.

(2) Mondy, N. I.; Munshi, C. B. Effect of boron on enzymic discoloration and phenolic and ascorbic acid contents of potatoes. *J. Agric. Food Chem.* **1993**, *41*, 554−556.

(3) Kabu, M.; Civelek, T. Effects of propylene glycol, methionine and sodium borate on metabolic profile in dairy cattle during periparturient period. *Rev. Med. Vet. (Toulouse, Fr.)* **2012**, *163*, 419−430.

(4) Hunt, C. D. Dietary boron: progress in establishing essential roles in human physiology. *J. Trace Elem. Med. Biol.* **2012**, *26*, 157−160.

(5) Kabu, M.; Akosman, M. S. Biological effects of boron. *Reviews of Environmental Contamination and Toxicology*; Springer: New York, 2013; pp 57−75.

(6) Nielsen, F. H. Is boron nutritionally relevant? *Nutr. Rev.* **2008**, *66*, 183−191.

(7) Hunt, C. D.; Herbel, J. L.; Idso, J. P. Dietary boron modifies the effects of vitamin D3 nutrition on indices of energy substrate utilization and mineral metabolism in the chick. *J. Bone Miner. Res.* **1994**, *9*, 171−182.

(8) Rossi, A.; Miles, R.; Damron, B.; Flunker, L. Effects of dietary boron supplementation on broilers. *Poult. Sci.* **1993**, *72*, 2124−2130.

(9) Wilson, J.; Ruszler, P. Long term effects of boron on layer bone strength and production parameters. *Br. Poult. Sci.* **1998**, *39*, 11−15.

(10) Tavil Sabuncuoglu, B.; Aribal Kocaturk, P.; Yaman, O.; Ozelci Kavas, G.; Tekelioglu, M. Effects of subacute boric acid administration on rat kidney tissue. *Clin. Toxicol.* **2006**, *44*, 249−253.

(11) Cheng, J.; Peng, K.; Jin, E.; Zhang, Y.; Liu, Y.; Zhang, N.; Song, H.; Liu, H.; Tang, Z. Effect of additional boron on tibias of African ostrich chicks. *Biol. Trace Elem. Res.* **2011**, *144*, 538−549.

(12) Sales, J.; Hayes, J. Proximate, amino acid and mineral composition of ostrich meat. *Food Chem.* **1996**, *56*, 167−170.

(13) Özsaraç, N.; Kolsarici, N.; Demirok, E. A study on nutritional characteristics of ostrich meat. *Electronic J. Food Technol.* **2013**, *8*, 63−68.

(14) Majewska, D.; Jakubowska, M.; Ligocki, M.; Tarasewicz, Z.; Szczerbińska, D.; Karamucki, T.; Sales, J. Physicochemical characteristics, proximate analysis and mineral composition of ostrich meat as influenced by muscle. *Food Chem.* **2009**, *117*, 207−211.

(15) Cilliers, S.; Hayes, J.; Chwalibog, A.; Sales, J.; Du Preez, J. Determination of energy, protein and amino acid requirements for maintenance and growth in ostriches. *Anim. Feed Sci. Technol.* **1998**, *72*, 283−293.

(16) Liang, C. Z.; Yang, Y. J. *Ostrich-Raising Management and Disease Control*; Beijing Agricultural University Press: Beijing, 1996; pp 42−56.

(17) Zhang, W.; Xiao, S.; Lee, E. J.; Ahn, D. U. Consumption of oxidized oil increases oxidative stress in broilers and affects the quality of breast meat. *J. Agric. Food Chem.* **2010**, *59*, 969−974.

(18) Jiang, Z.; Lin, Y.; Zhou, G.; Luo, L.; Jiang, S.; Chen, F. Effects of dietary selenomethionine supplementation on growth performance, meat quality and antioxidant property in yellow broilers. *J. Agric. Food Chem.* **2009**, *57*, 9769−9772.

(19) AOAC. *Official Methods of Analysis*; Association of Official Analytical Chemists: Washington, DC, 2000.

(20) Folch, J.; Lees, M.; Sloane-Stanley, G. A simple method for the isolation and purification of total lipids from animal tissues. *J. Biol. Chem.* **1957**, *226*, 497−509.

(21) Butte, W. Rapid method for the determination of fatty acid profiles from fats and oils using trimethylsulphonium hydroxide for transesterification. *J. Chromatogr., A* **1983**, *261*, 142−145.

(22) Duckett, S. K.; Wagner, D. G. Effect of laidlomycin propionate on bovine longissimus muscle fatty acid and cholesterol content. *J. Agric. Food Chem.* **1997**, *45*, 1725−1728.

(23) Wilson, J.; Ruszler, P. Effects of dietary boron supplementation on laying hens. *Br. Poult. Sci.* **1996**, *37*, 723−729.

(24) Eren, M.; Uyanik, F.; Küçükersan, S. The influence of dietary boron supplementation on egg quality and serum calcium, inorganic phosphorus, magnesium levels and alkaline phosphatase activity in laying hens. *Res. Vet. Sci.* **2004**, *76*, 203−210.

(25) Eren, M.; Kocaoglu-Güclü, B.; Uyanik, F.; Karabulut, N. The effects of dietary boron supplementation on performance, carcass composition and serum lipids in Japanese quails. *J. Anim. Vet. Adv.* **2006**, *5*, 1105−8.

(26) Elliot, M. A.; Edwards, H. M. Studies to determine whether an interaction exists among boron, calcium, and cholecalciferol on the skeletal development of broiler chickens. *Poult. Sci.* **1992**, *71*, 677−690.

(27) Armstrong, T.; Spears, J. Effect of dietary boron on growth performance, calcium and phosphorus metabolism, and bone mechanical properties in growing barrows. *J. Anim. Sci.* **2001**, *79*, 3120−3127.

(28) Zhong, Q. Z.; Wang, D.; Lou, Y. J. Research development in effects of heat stress on meat quality of poultry. *China Anim. Husb. Vet. Med.* **2011**, *38*, 231−234.

(29) Warriss, P. D. *Meat Science: An Introductory Text*; CABI Publishing: Wallingford, UK, 2010.

(30) Silva, J.; Patarata, L.; Martins, C. Influence of ultimate pH on bovine meat tenderness during ageing. *Meat Sci.* **1999**, *52*, 453−459.

(31) Hunt, C. D. Regulation of enzymatic activity. *Biol. Trace Elem. Res.* **1998**, *66*, 205−225.

(32) Strittmatter, P. Reversible direct hydrogen transfer from reduced pyridine nucleotides to cytochrome b5 reductase. *J. Biol. Chem.* **1964**, *239*, 3043−3050.

(33) Deitrich, R. A. Diphosphopyridine nucleotide-linked aldehyde dehydrogenase: III. Sulfhydryl characteristics of the enzyme. *Arch. Biochem. Biophys.* **1967**, *119*, 253−263.

(34) Deal, W. C., Jr. Metabolic control and structure of glycolytic enzymes. IV. Nicotinamide adenine dinucleotide-dependent in vitro reversal of dissociation and possible in vivo control of yeast glyceraldehyde-3-phosphate dehydrogenase synthesis. *Biochemistry* **1969**, *8*, 2795−2805.

(35) Geyikoğglu, F.; Türkez, H. Acute toxicity of boric acid on energy metabolism of the breast muscle in broiler chickens. *Biologia* **2007**, *62*, 112−117.
(36) Page, J.; Wulf, D.; Schwotzer, T. A survey of beef muscle color and pH. *J. Anim. Sci.* **2001**, *79*, 678−687.
(37) Johnston, D.; Knight, M.; Ledward, D. A. *The Chemistry of Muscle-Based Foods*; The Royal Society of Chemistry: Thomas Graham House, Science Park, Cambridge, U.K., 1992; pp 128−139.
(38) Lanza, M.; Fasone, V.; Galofaro, V.; Barbagallo, D.; Bella, M.; Pennisi, P. Citrus pulp as an ingredient in ostrich diet: effects on meat quality. *Meat Sci.* **2004**, *68*, 269−275.
(39) Liu, X. *Integrated Study on the Characters of Fish Meat*; Xiamen University: Xiamen, 2007; pp 3−4.
(40) Shang, Z. F.; Gu, Y. F.; Chen, H. L.; Yang, J. F.; Pu, X. M.; Zha, L.; Wu, Q. T.; Wang, Y. Influence of boron on content of copper, zinc, iron and manganese in chicken meat. *Stud. Trace Elem. Health* **2004**, *11*, 31−33.
(41) Neurath, H. Evolution of proteolytic enzymes. *Science* **1984**, *224*, 350−357.
(42) Hall, I.; Spielvogel, B.; Griffin, T.; Docks, E.; Brotherton, R. The effects of boron hypolipidemic agents on LDL and HDL receptor binding and related enzyme activities of rat hepatocytes, aorta cells and human fibroblasts. *Res. Commun. Chem. Pathol. Pharmacol.* **1989**, *65*, 297−317.
(43) Basoglu, A.; Baspinar, N.; Ozturk, A. S.; Akalin, P. P. Effects of boron administration on hepatic steatosis, hematological and biochemical profiles in obese rabbits. *Trace Elem. Electrolytes* **2010**, *27*.

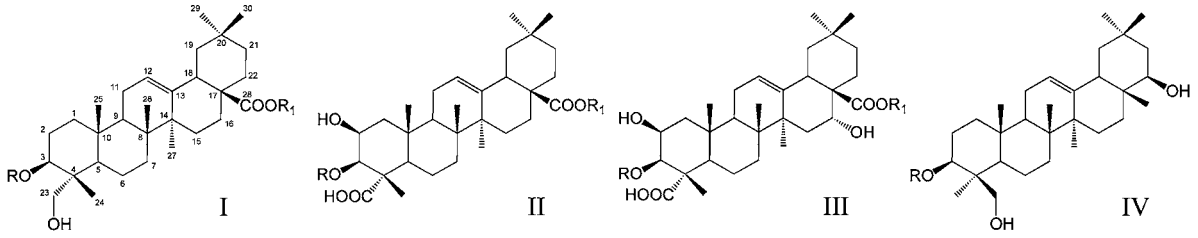


| Compound | Aglycone | R | $R_1$ |
|---|---|---|---|
| **1** | I | α-L-Ara-(1→2)-β-D-Glc | β-D-Glc |
| **2** | I | α-L-Ara-(1→2)-β-D-Glc-(1→2)-α-L-Ara | H |
| **3** | I | α-L-Ara-(1→2)-β-D-Glc-(1→2)-α-L-Ara | β-D-Glc |
| **4** | II | β-D-Glc | H |
| **5** | II | β-D-Glc | β-D-Glc |
| **6** | II | β-D-Glc | β-D-Xyl-(1→4)-α-L-Rha-(1→2)-α-L-Ara |
| **7** | II | β-D-GlcA | β-D-Xyl-(1→4)-α-L-Rha-(1→2)-α-L-Ara |
| **8** | II | β-D-Glc-(1→2)-β-D-Glc | β-D-Glc |
| **9** | II | β-D-Glc-(1→2)-β-D-Glc | β-D-Xyl-(1→4)-α-L-Rha-(1→2)-α-L-Ara |
| **10** | III | β-D-Glc-(1→2)-β-D-Glc-(1→2)-β-D-Glc | β-D-Xyl-(1→4)-α-L-Rha-(1→2)-α-L-Ara |
| **11** | III | β-D-Glc-(1→2)-β-D-Glc-(1→2)-β-D-Glc | β-D-Xyl-(1→4)-α-L-Rha-(1→2)-α-L-Ara β-D-Api-(1→3)┘ |
| **12** | IV | α-L-Rha-(1→2)-β-D-Gal-(1→2)-β-D-GlcA | H |
| **13** | I | H | H |
| **14** | II | H | H |
| **15** | III | H | H |

**Figure 1.** Chemical structure of purified saponins (**1**−**12**) and sapogenins (**13**−**15**) used in this investigation (I, hederagenin; II medicagenic acid; III, zanhic acid; and IV, soyasapogenol B).

has been extensively investigated.[17,20−22] In some cases, their structure−activity relationship has been assessed.[16,23] In addition, the main genes involved in their biosynthesis have been identified.[24−27]

In the present study, data on the antifungal properties of saponin extracts from alfalfa (*Medicago sativa* L.) against the causal agent of rice blast *P. oryzae* were obtained. The *P. oryzae* strains used in these investigations were isolated from five different rice varieties cultivated in Lombardy, in the Po valley, a typical Italian area of rice production. Saponins from *M. sativa* tops and roots, the corresponding mixture of prosapogenins, and pure saponins and sapogenins were tested against *P. oryzae* isolates in *in vitro* experiments. A prosapogenin mixture from alfalfa leaves was used to evaluate their antifungal activity by means of the *in planta* tests. These assays were performed in controlled conditions, using three different rice cultivars known to possess high, medium, and low pathogen resistance, infected with a mixture of the isolated strains of *P. oryzae*. Results of the antifungal properties of saponins from *M. sativa* are also discussed on the basis of their structure−activity relationship. To our knowledge, no previous investigations have been reported on the antifungal activity of saponins from *M. sativa* against the rice pathogen *P. oryzae* in both *in vitro* and *in planta* tests.

## MATERIALS AND METHODS

**Chemicals and Reagents.** Ethanol (EtOH) and penicillin G were purchased from Sigma-Aldrich s.r.l. (Milan, Italy). Water was deionized by a filter through a Direct-Q system (Millipore, Bedford, MA). Potato dextrose agar (PDA) was purchased from BioLife (Milan, Italy).

**Extraction and Purification of *M. sativa* Saponins and Preparation of Prosapogenins and Sapogenins.** Alfalfa (*M. sativa* cv. Equipe) plants were grown in an open field at CRA-FLC (Lodi, Italy). Leaf samples (collected at anthesis) and roots (collected in autumn) were oven-dried at 50 °C for 2 days, ground, and used for saponin extraction. Saponins used in this study were newly extracted and purified, following general procedures previously reported.[16,21,22,28,29] Pure saponins, compounds **1**−**12** (Figure 1), were obtained by a combination of chromatographic separation steps [silica gel open-column chromatograpy and semi-preparative reversed-phase high-performance liquid chromatography (RP-HPLC)] from the crude saponin mixtures from leaves and roots as described.[21,22,28] The saponin mixture from leaves was used to prepare prosapogenins and


dx.doi.org/10.1021/jf5049063 | J. Agric. Food Chem. 2014, 62, 11030−11036

sapogenins. Prosapogenins were obtained after basic hydrolysis,[19,30] and acid hydrolysis afforded the related sapogenins, compounds **13**−**15** (Figure 1), that were obtained in a pure form after silica gel open-column chromatography.[16,31]

**Analysis of Saponin Extracts.** Purified mixtures of saponins were obtained as whitish powder in a purity of 90−95% and analyzed by silica gel 60H ready-to-use thin-layer chromatography (TLC) plates (Merck, Darmstadt, Germany) as previously described[20] and by high-performance liquid chromatography (HPLC) as reported.[21,22,28] Purified saponin and prosapogenin mixtures were characterized for their quantitative aglycone composition by gas chromatography−flame ionization detection (GC−FID) and gas chromatography−mass spectrometry (GC−MS) analyses of derivatized sapogenins.[20,32] Detailed structural elucidation of pure saponins, compounds **1**−**12**, and sapogenins, compounds **13**−**15**, was obtained by nuclear magnetic resonance (NMR) and electrospray ionization−tandem mass spectrometry (ESI−MS/MS) analysis.[17,21,22,27−29] Evaluation of the saponin composition in the plant extracts was also performed by liquid chromatography−tandem mass spectrometry (LC−MS/MS) experiments.

**Saponin Preparation for *in Vitro* and *in Planta* Bioassays.** For the *in vitro* tests, crude saponin mixtures from alfalfa leaves and roots, prosapogenins, and pure saponins, compounds **1**−**12**, were dissolved in EtOH/$H_2O$ solutions (from 30 to 70% EtOH according to their solubility), while pure sapogenins, compounds **13**−**15**, were dissolved in 100% EtOH. All samples were prepared in a final concentration of 0.5 mg/mL. Serial dilutions (2-fold) were prepared from the starting standardized stock solutions to obtain a concentration range from 500 to 15.625 μg/mL for each sample. Sonication of each sample was generally adopted to facilitate solubilization of the metabolites. A series of EtOH/$H_2O$ control solutions at different concentrations were also tested against *P. oryzae*. For the *in planta* bioassays, under controlled conditions, prosapogenins were dissolved at 1% (w/v) in water with added 0.5% (w/v) gelatin, which is used in the rice infection standard protocol, with mild heating to facilitate solubilization. Prosapogenins were also tested in the same water/gelatin mixture at the same concentration in the *in vitro* experiments.

**Microorganism Growth Conditions.** Antifungal activity was tested against different isolates of *P. oryzae* [formerly called *Pyricularia grisea* (Cooke) Saccardo],[33] obtained from leaf lesions of the following rice Italian varieties: Augusto, Nembo, Italico, Karnak, and Vialone Nano, with isolate number PatVeg 202 a, b, c, d, and e, respectively, included in a large collection of *P. oryzae* partially used for the study of the genetic structure of the Italian pathogen population. The isolates were maintained in the Laboratory of Mycology of the University of Pavia and grown on potato dextrose agar or rice seed flour medium, adding 500 000 units of penicillin G. Petri dishes with the cultures were maintained at 25 °C in a growth chamber with a 12 h photoperiod for 7−9 days before the antifungal assays.[34] Each of the five *P. oryzae* isolates from the above-cited rice varieties were individually used for the *in vitro* tests and further used as a mixture (50 000 conidia/mL each) for the *in planta* experiments.

***In Vitro* Antifungal Assay.** The *in vitro* antifungal activities of all of the tested saponins were determined as the minimum inhibitory concentration (MIC) and the minimum fungicidal concentration (MFC) against the *P. oryzae* isolates described above, following reported procedures,[35−37] with some modifications. MIC was defined as the lowest drug concentration that completely inhibited the growth of the test fungal pathogens after 7 days of incubation at 25 °C. To determine the lowest concentration required to kill completely the test fungus (MFC), the initial inoculum was sub-cultured from 7-day-old microwell plates containing the extract where no fungal growth was observed (100% of inhibition) in a fresh cultural medium free of the extract and examined at 24 h intervals for 10 days. The MFC was defined as the lowest drug dilution, allowing for a total reduction (99.9%) of the initial inoculum on the culture medium.[38] MIC and MFC values were determined by a 2-fold serial broth microdilution method in multi-well plates. All of the tested samples were diluted in a Sabouraud culture medium to the following final concentrations (1 mL final volume): 0.500, 0.250, 0.125, 0.060, 0.030, 0.015, and 0.0075 mg/mL. Flutriafol Pestanal, containing the antifungal compound (*R*,*S*)-2,4-difluoro(1*H*-1,2,4-triazol-1-ylmethyl)benzhydryl alcohol, was used at the following concentrations: 0.250, 0.125, 0.060, 0.030, 0.015, and 0.0075 mg/mL. The MIC and MFC of the EtOH/$H_2O$ solutions were also recorded at the concentrations described above to exclude any antifungal effect because of the solvent. All bioassays were performed in triplicate.

***In Planta* Antifungal Assays.** Two *in planta* bioassays were performed. The first experiment aimed to compare the *in vitro* results and was performed using the Italian rice (*O. sativa* L. ssp. *japonica*) cultivar Maratelli, highly susceptible to rice blast. The protection against the disease exerted by prosapogenins was compared versus that of commercial fungicide Flutriafol Pestanal. In a second assay, the prosapogenin effect on rice genotypes was evaluated using the rice cultivars Baldo and Selenio, characterized by medium and low susceptibility to blast disease, respectively. The resistance/susceptibility to *P. oryzae* of the three rice cultivars has been reported[39] and was confirmed by previous pathogenicity assays (data not shown).

In both assays, rice plants were grown from seeds in trays filled with compost kept in a greenhouse under a daytime temperature of 27 °C and a nighttime temperature of 22 °C, with a 12 h photoperiod and 60% humidity. Nitrogen fertilization with 8.6 g of nitrogen equivalent (corresponding to standard levels used during rice crop cultivation) was applied 2 days before inoculation with the fungus. The fungal conidia suspension used to infect the rice plants was obtained by mixing the same amounts of the five isolates of *P. oryzae* (50 000 conidia/mL each) with 0.5% (w/v) gelatin to ensure conidial adhesion on rice leaves. Inoculation was performed as described,[40] by spraying 30 mL of conidia suspension on a block of 150 rice seedlings 4 weeks after sowing. Prosapogenin treatments were performed by spraying a solution [50 mL of 10 g/L in 0.5% (w/v) gelatin]. The Flutriafol Pestanal formulation was applied at field dosage (125−150 g/ha). All treatments (prosapogenin and fungicide) were applied at two different times, viz., 24 h before and 3 days after inoculation of rice plantlets with *P. oryzae*. Positive control plants were sprayed with conidial suspensions (30 mL as above) without further treatment. All bioassays were performed in three replicates. After 7 days, the macroscopic disease symptoms on the second rice leaf were scored on all plants to assess the effect of the treatments. The disease severity (DS) was estimated on the basis of a visual 5-level scale from 1 (no disease) to 5 (serious disease), as described in Figure 2. Efficacy classes were then created by merging DS score levels as follows: DS1 and DS2 were associated with high efficacy of the treatment, and the corresponding efficacy class was "protection" (P), with no reduction of the grain yield; DS3 was considered of moderate efficacy, and the class was "medium protection" (MP), with reduction of the grain yield; and DS4 and DS5 were associated with low efficacy of the treatment, and the efficacy class was "no protection" (NP), with considerable grain loss. Efficacy classes were subsequently used in the statistical analysis.

**Statistical Analysis.** For each cultivar, treatment, and replicate, the frequency of the three efficacy classes was computed as a percentage of evaluated plants. The angular transformation was applied to the percentage values, and the transformed data were subjected to analysis of variance (ANOVA).[41] A first ANOVA compared the frequency of the three efficacy classes in each treatment of each individual cultivar (Table 2). In a second ANOVA, the effect of treatments on plant protection was assessed by comparing, within each cultivar, the frequency of plants from different treatments within each efficacy class (Figure 3). In both ANOVAs, mean values were compared by Duncan's multiple range test (at $p < 0.05$) when the $F$ test from the analysis was significant at $p < 0.05$.

## RESULTS AND DISCUSSION

The saponin composition from alfalfa extracts was evaluated by TLC and HPLC analyses as previously reported.[21,22,28] LC−MS/MS analyses of the total extracts were also performed, and several mass peaks corresponding to the different saponins were identified (data not shown). GC−FID and GC−MS analyses of the aglycone moieties, obtained by acid hydrolyses from the

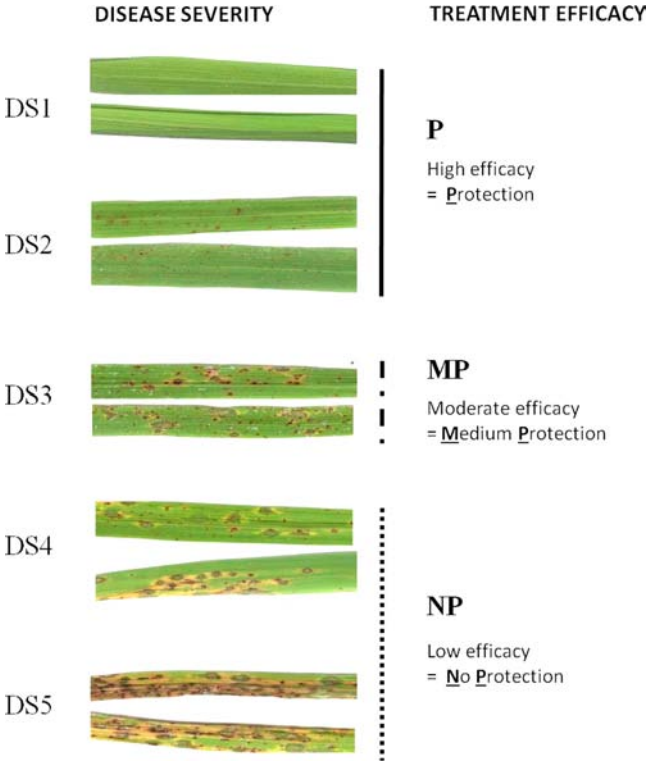


**Figure 2.** DS scale of rice leaves based on a visual 5-level scale: DS1, highly resistant (no symptoms); DS2, resistant (necrotic spots); DS3, partially resistant (mixture of necrotic spots and small gray lesions); DS4, susceptible (typical diamond-shaped blast lesions, lengthened, gray inside and brown outside, and yellow edges); and DS5, highly susceptible (blast lesions with wide yellow edges on the whole leaf surface). The treatment efficacy classes were then created by merging DS score levels: (P) DS1 and DS2, (MP) DS3, and (NP) DS4 and DS5.

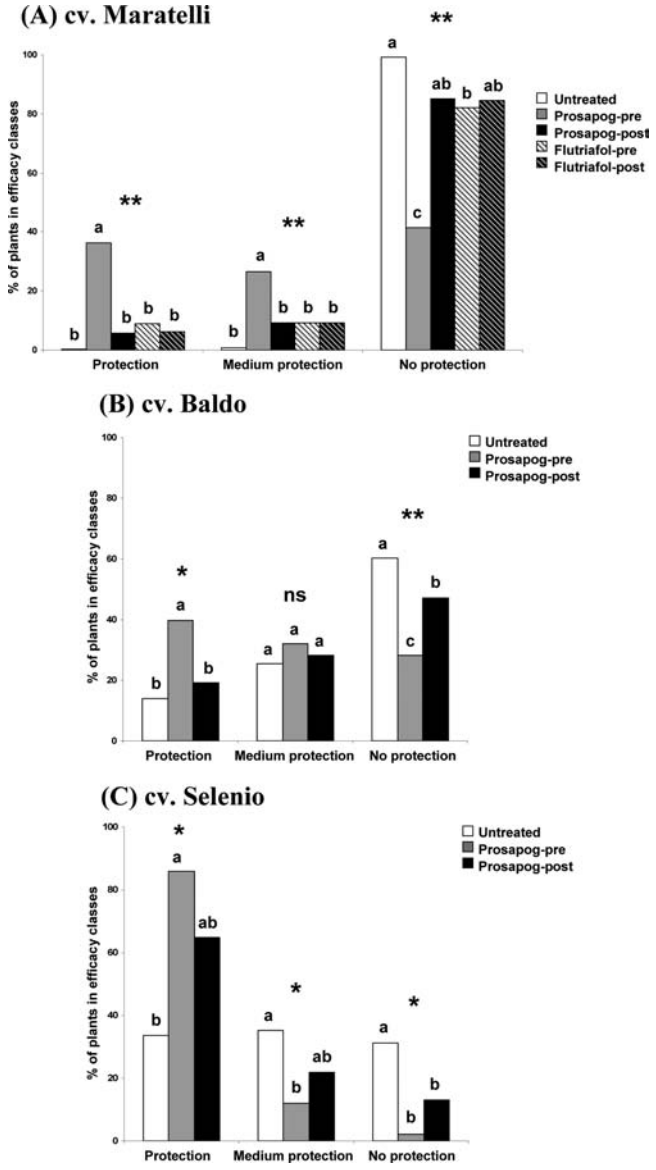


**Figure 3.** Frequency of plants (percentage of evaluated plants) classified in three efficacy classes (protection, medium protection, and no protection) after treatments against *P. oryzae* infection (untreated control and application of prosapogenins or Flutriafol Pestanal fungicide before and after plant inoculation with the pathogen) in three rice cultivars. For a symptom description of efficacy classes, see Figure 2. ns, ∗, and ∗∗, variation among treatments within each cultivar and efficacy classes not significant and significant at $p < 0.05$ and $p < 0.01$, respectively. In each cultivar and efficacy class, treatment mean values followed by different letters are different at $p < 0.05$ according to Duncan's multiple range test.

corresponding saponin mixtures, showed that saponins from alfalfa leaves are characterized by a high concentration of medicagenic acid (51% of the total sapogenins), followed by zanhic acid (25%), soyasapogenol B (16%), bayogenin (3%), hederagenin (1%), and soyasapogenol A (1%), while saponins from alfalfa roots are characterized by the presence of medicagenic acid (68%), hederagenin (18%), soyasapogenol B (6%), bayogenin (3%), and zanhic acid (2%) (Figure 1). Composition of purified saponin mixtures used in these assays was consistent with previously obtained results.[19,20,29] From the TLC and HPLC analyses, a different saponin composition was confirmed for the two plant organs, e.g., the presence of compound **4**, the 3-*O*-$\beta$-D-glucopyranosyl derivative of medicagenic acid (Figure 1), only in roots.[17] In addition, monodesmosidic saponins, compounds **2**, **4**, and **12**, were found to be more abundant in alfalfa root extracts, representing about 45% of the total saponins, while saponins from tops were predominantly composed of bidesmosidic compounds **1**, **3**, and **5**−**11**, accounting for about 80% of the total saponins (data not shown). Prosapogenins that were obtained from the leaf saponin mixture after basic hydrolyses showed the same chemical aglycone composition of the saponins from which they were prepared, but they were entirely composed of monodesmosidic compounds. Individual pure saponins, compounds **1**−**12**, and sapogenins, compounds **13**−**15**, were obtained by means of chromatographic purification steps, and their chemical structure (Figure 1) was determined by LC−MS/MS and NMR experiments.

The *in vitro* biological effects of saponin extracts from alfalfa leaves and roots, single purified saponins, prosapogenins, and sapogenins were investigated for activity against five strains of the rice fungal pathogen *P. oryzae* isolated from five different Italian rice varieties. All of these isolates showed a similar response (in terms of MIC/MFC) to the different tested compounds. Results from these bioassays are reported as MIC and MFC values in Table 1. All of the tested compounds showed a broad spectrum of antifungal activity. The lowest

**Table 1. Antifungal Activity (MIC and MFC) of Alfalfa Saponins, Prosapogenins, and Sapogenins Tested *in Vitro* against the Fungus *P. oryzae* Isolated from *O. sativa*[a]**

| samples | | MIC (mg/mL) | MFC (mg/mL) |
|---|---|---|---|
| total saponins | *M. sativa* tops | 2.0 | nd |
| | *M. sativa* roots | 0.25 | 0.5 |
| prosapogenins | *M. sativa* tops | 0.03 | 0.25 |
| pure saponins | **1** | >0.5 | >0.5 |
| | **2** | 0.25 | nd |
| | **3** | >0.5 | >0.5 |
| | **4** | 0.03 | 0.125 |
| | **5** | 0.125 | 0.25 |
| | **6** | 0.125 | nd |
| | **7** | 0.25 | 0.5 |
| | **8** | 0.5 | >0.5 |
| | **9** | 0.125 | >0.5 |
| | **10** | 0.25 | 0.5 |
| | **11** | >0.5 | >0.5 |
| | **12** | >0.5 | >0.5 |
| pure sapogenins | **13**, hederagenin | >0.5 | >0.5 |
| | **14**, medicagenic acid | 0.01 | 0.03 |
| | **15**, zanhic acid | 0.25 | 0.25 |
| Flutriafol Pestanal | | 0.01 | 0.01 |

[a]Flutriafol Pestanal was tested as a positive control. For chemical structures, see Figure 1.

activity (MIC = 2.0 mg/mL) was observed for the saponin mixture from alfalfa leaves, while the corresponding prosapogenins showed the highest inhibition activity, with MIC and MFC values of 0.03 and 0.25 mg/mL, respectively. Intermediate values (MIC = 0.25 mg/mL, and MFC = 0.5 mg/mL) were instead recorded for pure saponins, compounds **1**−**12** (Table 1). Among pure saponins, the bidesmosidic hederagenin derivatives, compounds **1** and **3** (Figure 1), did not show any antifungal activity (MIC and MFC values of >0.5 mg/mL) against *P. oryzae*, while a moderate inhibition (MIC and MFC values from 0.125 to 0.5 and from 0.125 to >0.5 mg/mL, respectively) was in general observed for the bidesmosidic saponins of medicagenic and zanhic acid (compounds **5**−**10**). The only exception was saponin **11**, a bidesmoside of zanhic acid, which revealed no activity (MIC and MFC values of >0.5 mg/mL). A moderate inhibition (MIC = 0.25 mg/mL) was observed for saponin **2**, a trisaccharide monodesmoside of hederagenin, while a strong inhibition was observed for compound **4**, the 3-*O*-*β*-D-glucopyranosyl derivative of medicagenic acid, for which a MIC of 0.03 mg/mL and a MFC of 0.125 mg/mL were recorded. As expected, no growth inhibition was instead observed for compound **12**, a saponin of soyasapogenol B, that is known for its very low or null antifungal activity.[17] A similar trend (Table 1) could also be observed for the three pure sapogenins **13**−**15**: no activity was recorded for hederagenin **13** (MIC and MFC values of >0.5 mg/mL); a moderate activity was observed for zanhic acid **15** (MIC and MFC values of 0.25 mg/mL); and a high antifungal activity was observed for medicagenic acid **14** with a MIC = 0.01 mg/mL and MFC = 0.03 mg/mL. Among all of the tested compounds, this last sapogenin and its 3-*O*-*β*-D-glucopyranosyl derivative, compound **4**, showed the highest antifungal activity similar to that of the Flutriafol Pestanal, which is a systemic fungicide currently applied in rice fields to control the blast disease and, hence, assayed as a standard for *P. oryzae* positive control.

Previous investigations on the structure−activity relationship of saponins have led to contrasting results:[16,42,43] some authors suggested that sugar moieties are important for their antifungal effects, while according to others, sapogenins are more active. The data reported here clearly demonstrate that medicagenic acid, the main aglycone among *M. sativa* saponins, and its derivatives are responsible for the highest antifungal inhibition against *P. oryzae* (in comparison to hederagenin and zanhic acid saponins). In addition, as previously stated,[16,17,42,43] the monodesmosidic compounds (prosapogenins from *M. sativa* tops and compound **4**) are, in general, more active against rice blast pathogen than the corresponding bidesmosides.

Concerning the mechanism of action of these antifungal compounds, some considerations on their biocidal activities can be deduced. It is known that Flutriafol Pestanal is a triazole derivative, and it is able to inhibit the ergosterol biosynthesis, causing the rupture of fungi cell membranes.[44] In addition, there is evidence that saponins are able to alter membrane permeability, to complex cholesterol or other membrane components, leading to the rupture of the cell.[15,45] The results obtained in our experiments show that monodesmosides of medicagenic acid and compound **4** are as bioactive as Flutriafol and support a mechanism of action affecting the cell membrane integrity.

On the basis of the highest antifungal activity shown in the *in vitro* tests by the monodesmosidic prosapogenins, these compounds were employed for the *in planta* assays on three Italian rice varieties, Maratelli, Baldo, and Selenio, chosen for their different levels of susceptibility to the pathogen. The *in planta* assays confirmed the different degrees of susceptibility to the disease shown by the three cultivars evaluated. The frequency of highly symptomatic plants (represented by the efficacy class "no protection") was indeed generally very high in cv. Maratelli, regardless of the applied treatment, moderate or low in cv. Selenio, and somewhat intermediate between the previous two in cv. Baldo (Table 2). In the tolerant cv. Selenio, the frequency of the three efficacy classes (protection, medium protection, and no protection) did not differ in the inoculated untreated condition, whereas with either application of prosapogenins, the frequency of "protection" was significantly greater ($p < 0.05$) than those of the two other classes (Table 2). Interestingly, in both the susceptible cv. Maratelli and the moderately susceptible cv. Baldo, the three efficacy classes did not differ under the pre-inoculation prosapogenin application, as a consequence of an increase of frequency of protected plants and a decrease of frequency of non-protected plants, in comparison to the other treatments in each cultivar (Table 2).

The latter finding is shown better in Figure 3, where the results of the second ANOVA are graphically reported. In particular, in Figure 3A, it is evident that, for cv. Maratelli, the pre-inoculation application of prosapogenins enhanced remarkably the frequency of plants with "protection" and "medium protection" and reduced the frequency of those with "no protection" compared to the control and all other treatments. Similarly, the application of saponins before the inoculation also increased the frequency of protected plants and decreased that of non-protected plants in cv. Baldo compared to the control and post-inoculation application (Figure 3B). Only in the tolerant cv. Selenio was the post-inoculation application of prosapogenins able to exert some protective efficacy against the

**Table 2. Comparison among Efficacy Classes within Individual Treatments against *P. oryzae* Infection (Untreated Control and Application of Prosapogenins or Flutriafol Pestanal before and after Plant Inoculation with the Pathogen) in Three Rice Cultivars[a]**

| | | treatment efficacy class[b] | | |
|---|---|---|---|---|
| treatment | *F* test probability[c] | protection | medium protection | no protection |
| | | cv. Maratelli | | |
| untreated | 0.0001 | 0.2 b | 0.7 b | 99.1 a |
| prosapogenins pre-inoculation | ns | 36.3 a | 26.5 a | 41.5 a |
| prosapogenins post-inoculation | 0.05 | 5.8 b | 9.2 b | 85.0 a |
| Flutriafol pre-inoculation | 0.01 | 8.9 b | 9.1 b | 82.0 a |
| Flutriafol post-inoculation | 0.01 | 6.3 b | 9.2 b | 84.5 a |
| | | cv. Baldo | | |
| untreated | 0.05 | 14.1 b | 25.6 b | 60.3 a |
| prosapogenins pre-inoculation | ns | 39.8 a | 32.0 a | 28.2 a |
| prosapogenins post-inoculation | 0.05 | 19.2 c | 33.7 c | 47.1 a |
| | | cv. Selenio | | |
| untreated | ns | 33.5 a | 35.2 a | 31.2 a |
| prosapogenins pre-inoculation | 0.05 | 85.9 a | 11.9 a | 2.2 b |
| prosapogenins post-inoculation | 0.05 | 64.8 a | 22.0 a | 13.2 b |

[a]Values are percentages of plants recorded in each class for each treatment and cultivar. For a symptom description of efficacy classes, see Figure 2. [b]In each cultivar and treatment, class values followed by different letters are different at $p < 0.05$ according to Duncan's multiple range test. Analysis was carried out after angular transformation of original percentage values reported in the table for the sake of clarity. [c]Among efficacy classes within each treatment; ns, not significant.

fungus, while the pre-inoculation treatment had the same positive effect exhibited for the two other cultivars (Figure 3C).

The results reported herein indicate that prosapogenins are active compounds against *P. oryzae*, especially in prevention of the fungal attack, and they were active against all five *P. oryzae* isolates used in both the *in vitro* and *in planta* experiments. The toxicity of the commercial formulation Flutriafol Pestanal has been poorly described.[46,47] Nevertheless, this compound is extremely persistent in soil, possesses high mobility potential, and is considered a groundwater contaminant.[48] Therefore, saponins from *M. sativa* could represent, if properly formulated, a promising and environmentally friendly treatment for control of rice blast.

In conclusion, data presented here make a point about the potential use of saponins, related prosapogenins, or aglycones from *M. sativa* for new fungicidal formulations. The highest antifungal activity shown by prosapogenins makes these saponin-derived compounds good candidates for practical use in agriculture. The large biomass produced by alfalfa, together with the selection of new varieties with high content of selected saponins with a defined chemical structure,[49] should make the industrial extraction of saponins economically viable.

## AUTHOR INFORMATION


### Corresponding Author

*Telephone: +39-0371-40471. Fax: +39-0371-31853. E-mail: aldo.tava@entecra.it.



### Funding

This work was supported by the Regione Lombardia within the framework of the project Biogesteca (Decreto 4779 14052009).

### Notes

The authors declare no competing financial interest.

## ACKNOWLEDGMENTS

The authors are grateful to Prof. M. Mella (Università di Pavia) and and Mr. G. Dipinto (Università degli Studi di Bari Aldo Moro) for their valuable help in the chemical analysis of saponins.


## REFERENCES


(1) Couch, B. C.; Kohn, L. M. A multilocus gene genealogy concordant with host preference indicates segregation of a new species, *Magnaporthe oryzae*, from *M. grisea*. *Mycologia* **2002**, *94*, 683−693.

(2) Zeigler, R. S.; Leong, S. A.; Teeng, P. S. *Rice Blast Disease*; CAB International: Wallingford, U.K., 1994.

(3) Khush, G. S.; Jena, K. K. Current status and future prospects for research on blast resistance in rice (*Oryza sativa* L.). In *Advances in Genetics, Genomics and Control of Rice Blast Disease*; Wang, G. L., Valent, B., Eds.; Springer Science + Business Media: New York, 2009; pp 1−10, ISBN: 9781402094996.

(4) Roumen, E. C. Partial resistance to neck blast influenced by stage of panicle development and rice genotype. *Euphytica* **1992**, *64*, 173−182.

(5) Manibhushan Rao, K. *Rice Blast Disease*; Daya Publishing House: New Delhi, India, 1994; ISBN: 8170351308.

(6) Scheuermann, K. K.; Vieira Raimondi, J.; Marschalek, R.; de Andrade, A.; Wickert, E. *Magnaporthe oryzae* genetic diversity and its outcomes on the search for durable resistance. In *The Molecular Basis of Plant Genetic Diversity*; Caliskan, M., Ed.; InTech Europe: Rijeka, Croatia, 2012; Chapter 15, ISBN: 978-953-51-0157-4.

(7) Joe, M. M.; Islam, Md. R.; Karthikeyan, B.; Bradeepa, K.; Sivakumaar, P. K.; Sa, T. Resistance responses of rice to rice blast fungus after seed treatment with the endophytic *Achromobacter xylosoxidans* AUM54 strains. *Crop Prot.* **2012**, *42*, 141−148.

(8) Shan, H.; Zhao, M.; Chen, D.; Cheng, J.; Li, J.; Feng, Z.; Ma, Z.; An, D. Biocontrol of rice blast by the phenaminomethylacetic acid producer of *Bacillus methylotrophicus* strain BC79. *Crop Prot.* **2013**, *44*, 29−37.

(9) Su, Z. Z.; Mao, L. J.; Li, N.; Feng, X. X.; Yuan, Z. L.; Wang, L. W.; Lin, F. C.; Zhang, C. L. Evidence for biotrophic lifestyle and biocontrol potential of dark septate endophyte *Harpophora oryzae* to rice blast disease. *PLoS One* **2013**, *8*, No. e61332.

(10) Hu, K.; Dong, A.; Sun, Q.; Yao, X. Bioactivity of 247 traditional chinese medicines against *Pyricularia oryzae*. *Pharm. Biol.* **2001**, *39*, 47−53.

(11) Du, Z.; Zhu, N.; Ze-Ren-Wang-Mu, N.; Shen, Y. Two new antifungal saponins from the Tibetan herbal medicine *Clematis tangutica*. *Planta Med.* **2003**, *69*, 547−551.

(12) Yoon, M. Y.; Kim, Y. S.; Ryu, S. Y.; Choi, G. J.; Choi, Y. H.; Yang, K. S.; Cha, B.; Han, S. S.; Kim, J. C. In vitro and in vivo antifungal activities of decursin and decursinol angelate isolated from *Angelica gigas* against *Magnaporthe oryzae*, the causal agent of rice blast. *Pestic. Biochem. Physiol.* **2011**, *101*, 118−124.

(13) Brusotti, G.; Tosi, S.; Tava, A.; Picco, A. M.; Grisoli, P.; Cesari, I.; Caccialanza, G. Antimicrobial and phytochemical properties of stem bark extracts from *Piptadeniastrum africanum* (Hook f.) Brenan. *Ind. Crops Prod.* **2013**, *43*, 612−616.

(14) Inagaki, Y. S.; Yoshiteru, N.; Keiko, F.; Atsuko, I.; Sakae, A.; Kazuhiro, T.; Tomonori, S.; Yuki, I. Infection-inhibition activity of avenacin saponins against the fungal pathogens *Blumeria graminis* f. sp. *hordei*, *Bopolaris oryzae* and *Magnaporthe oryzae*. *J. Gen. Plant Pathol.* **2013**, *79*, 69−73.
(15) Hostettmann, K.; Marston, A. In *Saponins (Chemistry and Pharmacology of Natural Products)*; Phillipson, J. D., Baxter, H, Eds.; Cambridge University Press: Cambridge, U.K., 1995.
(16) Avato, P.; Bucci, R.; Tava, A.; Vitali, C.; Rosato, A.; Bialy, Z.; Jurzjsta, M. Antimicrobial activity of saponins from *Medicago* sp.: Structure−activity relationship. *Phytother. Res.* **2006**, *20*, 454−457.
(17) Tava, A.; Avato, P. Chemical and biological activity of triterpene saponins from *Medicago* species. *Nat. Prod. Commun.* **2006**, *1*, 1159−1180.
(18) D'Addabbo, T.; Carbonara, T.; Leonetti, P.; Radicci, V.; Tava, A.; Avato, P. Control of plant parasitic nematodes with active saponins and biomass from *Medicago sativa*. *Phytochem. Rev.* **2011**, *10*, 503−519.
(19) Argentieri, M. P.; D'Addabbo, T.; Tava, A.; Agostinelli, A.; Jurzysta, M.; Avato, P. Evaluation of nematicidal properties of saponins from *Medicago* spp. *Eur. J. Plant Pathol.* **2008**, *120*, 189−197.
(20) Pecetti, L.; Tava, A.; Romani, M.; De Benedetto, M. G.; Corsi, P. Variety and environment effects on the dynamics of saponins in lucerne (*Medicago sativa* L.). *Eur. J. Agron.* **2006**, *25*, 187−192.
(21) Tava, A.; Mella, M.; Avato, P.; Biazzi, E.; Pecetti, L.; Bialy, Z.; Jurzysta, M. New triterpenic saponins from the aerial parts of *Medicago arabica* (L.) Huds. *J. Agric. Food Chem.* **2009**, *57*, 2826−2835.
(22) Tava, A.; Pecetti, L.; Romani, M.; Mella, M.; Avato, P. Triterpenoid glycosides from the leaves of two cultivars of *Medicago polymorpha* L. *J. Agric. Food Chem.* **2011**, *59*, 6142−6149.
(23) Tava, A.; Pecetti, L. Chemical investigation of saponins from twelve *Medicago* species and their bioassay with the brine shrimp *Artemia salina*. *Nat. Prod. Commun.* **2012**, *7*, 837−840.
(24) Tava, A.; Scotti, C.; Avato, P. Biosynthesis of saponins in the genus *Medicago*. *Phytochem. Rev.* **2011**, *10*, 459−469.
(25) Carelli, M.; Biazzi, E.; Panara, F.; Tava, A.; Scaramelli, L.; Porceddu, A.; Graham, N.; Odoardi, M.; Piano, E.; Arcioni, S.; May, S.; Scotti, C.; Calderini, O. *Medicago truncatula* CYP716A12 is a multifunctional oxidase involved in the biosynthesis of hemolytic saponins. *Plant Cell* **2011**, *23*, 3070−3081.
(26) Fukushima, E. O.; Seki, H.; Ohyama, K.; Ono, E.; Umemoto, N.; Mizutani, M.; Saito, K.; Muranaka, T. CYP716A subfamily members are multifunctional oxidases in triterpenoid biosynthesis. *Plant Cell Physiol.* **2011**, *52*, 2050−2061.
(27) Pollier, J.; Moses, T.; Gonzallez-Guzman, M.; De Geyter, N.; Lippens, S.; Vanden Bossche, R.; Marhavy, P.; Kremer, A.; Morreel, K.; Guerin, C. J.; Tava, A.; Oleszek, W.; Thevelein, J. M.; Campos, N.; Goormachtig, S.; Goossens, A. The protein quality control system manages plant defense compound synthesis. *Nature* **2013**, *504*, 148−152.
(28) Tava, A.; Mella, M.; Avato, P.; Argentieri, M. P.; Bialy, Z.; Yurzysta, M. Triterpene saponins from leaves of *Medicago arborea* L. *J. Agric. Food Chem.* **2005**, *53*, 9954−9965.
(29) Bialy, Z.; Jurzysta, M.; Oleszek, W.; Piacente, S.; Pizza, C. Saponins in alfalfa (*Medicago sativa* L.) root and their structural elucidation. *J. Agric. Food Chem.* **1999**, *47*, 3185−3192.
(30) Oleszek, W.; Jurzysta, M.; Ploszynski, M.; Coloquhoun, I. J.; Price, K. R.; Fenwick, G. R. Zahnic acid tridesmoside and other dominant saponins from alfalfa (*Medicago sativa* L.) aerial parts. *J. Agric. Food Chem.* **1992**, *40*, 191−196.
(31) Jurzysta, M. A method for isolation of medicagenic acid from plant material. Polish Patent 114,171, 1982.
(32) Tava, A.; Oleszek, W.; Jurzysta, M.; Berardo, N.; Odoardi, M. Alfalfa saponins and sapogenins: Isolation and quantification in two different cultivars. *Phytochem. Anal.* **1993**, *4*, 269−274.
(33) Hebert, T. T. The perfect stage of *Pyricularia grisea*. *Phytopathology* **1971**, *61*, 83−87.
(34) Piotti, E.; Rigano, M. M.; Rodino, D.; Rodolfi, M.; Castiglione, S.; Picco, A. M.; Sala, F. Genetic structure of *Pyricularia grisea* (Cooke) Sacc. isolates from Italian paddy fields. *J. Phytopathol.* **2005**, *153*, 80−86.
(35) Gadd, G. M. Toxicity screening using fungi and yeasts. In *Microbial Toxicity Testing*; Dutka, B., Bitton, G., Eds.; CRC Press: Boca Raton, FL, 1986; Vol. 2, pp 43−77.
(36) Clinical and Laboratory Standards Institutes (CLSI). *Reference Methods for Broth Dilution Antifungal Susceptibility Testing of Yeasts; Approved Standard*, 3rd ed.; CLSI: Wayne, PA, 2008; M27-A3.
(37) Clinical and Laboratory Standards Institutes (CLSI). *Reference Methods for Broth Dilution Antifungal Susceptibility Testing of Filamentous Fungi; Approved Standard*, 2nd ed.; CLSI: Wayne, PA, 2008; M38-A2.
(38) National Committee for Clinical Laboratory Standards (NCCLS). *Reference Method for Broth Dilution Antifungal Susceptibility Testing of Yeasts; Approved Standard*, 2nd ed.; NCCLS: Wayne, PA, 2002; M27-A2.
(39) Faivre-Rampant, O.; Bruschi, G.; Abbruscato, P.; Cavigliolo, S.; Borgo, L.; Lupotto, E.; Piffanelli, P. Assessment of genetic diversity in Italian rice germplasm related to agronomic traits and blast resistance (*Magnaporthe oryzae*). *Mol. Breed.* **2011**, *27*, 233−246.
(40) Faivre-Rampant, O.; Thomas, J.; Allègre, M.; Morel, J. B.; Tharreau, D.; Nottéghem, J. L.; Lebrun, M. H.; Schaffrath, U.; Piffanelli, P. Characterization of the model system rice−*Magnaporthe* for the study of nonhost resistance in cereals. *New Phytol.* **2008**, *180*, 899−910.
(41) Steel, R. G.; Torrie, J. H. *Principles and Procedures of Statistics: A Biometrical Approach*, 2nd ed.; McGraw-Hill: New York, 1980.
(42) Oleszek, W. Alfalfa saponins: Structure, biological activity, and chemotaxonomy. In *Saponins Used in Food and Agriculture*; Waller, G. R., Yamasaki, K, Eds.; Plenum Press: New York, 1996; pp 155−170.
(43) Oleszek, W. Saponins. In *Natural Food Antimicrobial Systems*; Naidu, A. S., Ed.; CRC Press: Boca Raton, FL, 2000; pp 1−30.
(44) Griffiths, K. M.; Bacic, A.; Howlett, B. J. Sterol composition of mycelia of the plant pathogenic ascomycete *Leptosphaeria maculans*. *Phytochemistry* **2003**, *62*, 147−153.
(45) Oakenful, D.; Sidhu, G. S. Toxicant of plant origin. In *Glycosides*; Cheeke, P. R., Ed.; CRC Press: Boca Raton, FL, 1989; Vol. 2, Chapter 4, pp 97−141.
(46) Middleton, M. C.; Milne, C. M.; Moreland, S.; Hasmall, R. L. Ovulation in rats is delayed by a substituted triazole. *Toxicol. Appl. Pharmacol.* **1986**, *83*, 230−239.
(47) Milne, C. M.; Hasmall, R. L.; Russel, A.; Watson, S. C.; Vaughan, Z.; Middelton, M. C. Reduced estradiol production by a substituted triazole results in delayed ovulation in rats. *Toxicol. Appl. Pharmacol.* **1987**, *90*, 427−435.
(48) United States Environmental Protection Agency (U.S. EPA). *U.S. EPA Pesticide Monitoring, Phase II Fact Sheet Series 7 (of 14)*; U.S. EPA: Washington, D.C., 1991.
(49) Carelli, M.; Biazzi, E.; Gaudenzi, P.; Tava, A.; Scotti, C. *M. sativa* × *M. arborea* cross (SAC) derivatives for saponin production in *Medicago* spp. *Proceedings of TERPNET 2013*; Kolymvari, Crete, Greece, June 1−5, 2013; p 235.

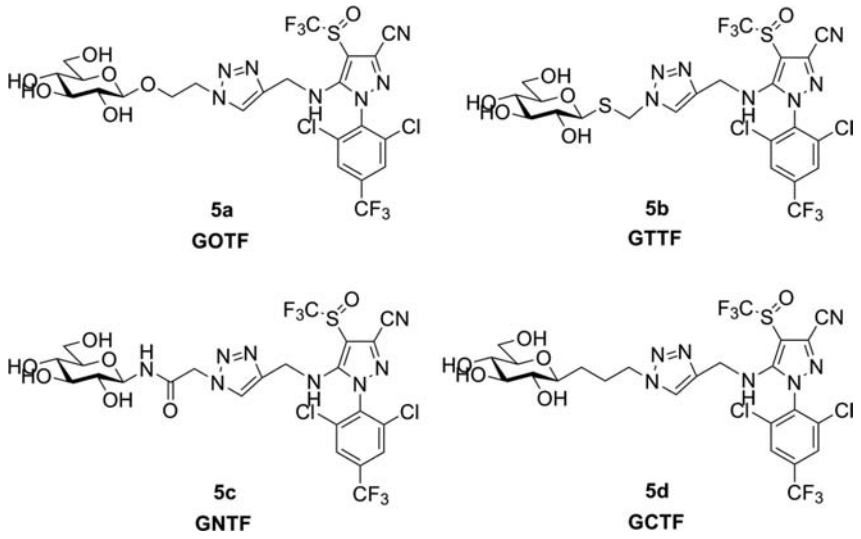


**Figure 1.** Chemical structures of O-, S-, N-, and C-glycosidic bonds in glucose−fipronil conjugates.

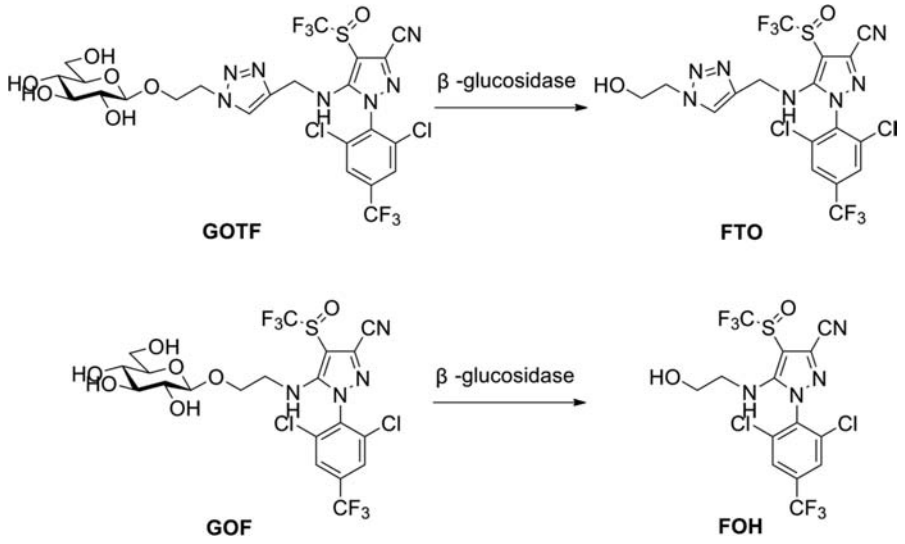


**Figure 2.** Metabolism of O-glycosidic bond in glucose−fipronil conjugates as catalyzed by $\beta$-glucosidase.

be recognized and hydrolyzed by endogenous $\beta$-glucosidases to bioactivate aglycons and control pests, which are also performed by plant defense systems. Secondary plant metabolites are glycosylated within plants to O (OH− and COOH−), N, S, and C atoms by glycosyltransferases.[16−18] In this study, we synthesize O-, S-, N-, and C-glycosidic bonds of glucose−fipronil conjugates (Figure 1) to investigate their metabolisms in vitro and in vivo. To verify metabolism and insecticidal activity, we introduce another synthesized O-glycosidic bond conjugate *N*-{3-cyano-1-[2,6-dichloro-4-(trifluoromethyl)phenyl]-4-[(trifluoromethyl)-sulfinyl]-1*H*-pyrazol-5-yl}-2-aminoethyl-$\beta$-D-glucopyranoside (GOF; Figure 2), which possesses moderate phloem mobility.[6] This study aimed to determine metabolic differences between four glycosidic bond conjugates and the activity of endogenous $\beta$-glucosidase, which is involved in the hydrolysis of exogenous glucose−pesticide conjugates in the plant. The results can help establish methods of circumventing the mutual exclusivity of phloem mobility and biological activity through the hydrolysis of endogenous $\beta$-glucosidases.

## MATERIALS AND METHODS

**General Information on Synthesis.** All reagents and solvents were purchased from a commercial company. $^1$H NMR and $^{13}$C NMR spectra were obtained with a Bruker AV-600 instrument. Chemical shifts were expressed in parts per million with TMS as internal standard. High-resolution electrospray ionization mass spectra (HR-ESI-MS) were recorded on a Bruker maXis impact ESI-Q-TOF instrument. Analytical thin-layer chromatography (TLC) was carried out on precoated plates (silica gel $GF_{254}$), and spots were visualized with a ZF-20D ultraviolet (UV) analyzer. Silica gel (200−300 mesh) was used for column chromatography.

*Synthesis of 2,3,4,6-Tetra-O-acetyl-(2-azidoethyl)-$\beta$-D-glucopyranoside (**3a**; Scheme 1).* $\beta$-D-Glucose pentaacetate (5 g, 12.81 mmol) and 2-bromoethanol (3.2 g, 25.62 mmol, 2 equiv) were dissolved in 25 mL of anhydrous $CH_2Cl_2$. The solution was stirred under nitrogen and cooled to 0 °C, and then $BF_3{\cdot}Et_2O$ (2.1 mL, 16.65 mmol, 1.3 equiv) was added dropwise over a period of 30 min. The reaction was stirred for 1 h at 0 °C and overnight at room temperature. After dilution with $CH_2Cl_2$ and washing with cold water and saturated aqueous $NaHCO_3$, the organic phase was dried over anhydrous $Na_2SO_4$ and evaporated under reduced pressure to yield **2a** (4.55 g, 78%) as colorless oil. The product was subjected to the next step without further purification.

**Scheme 1**[a]

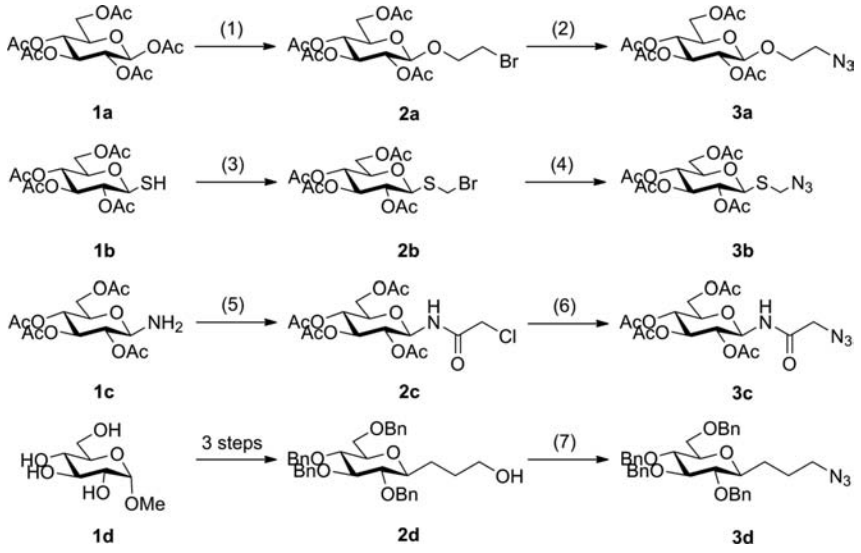


[a]Reagents and conditions: (1) 2-bromoethanol, $BF_3{\cdot}Et_2O$, and $CH_2Cl_2$ overnight; (2) $NaN_3$, 2:1 acetone/$H_2O$, and reflux for 20 h; (3) $CH_2Br_2$, $K_2CO_3$, 6 h; (4) $NaN_3$ and DMF at 90 °C for 12 h; (5) $(ClCH_2CO)_2O$, TEA, $CH_2Cl_2$, 0 °C and room temperature for 2 h and overnight, respectively; (6) $NaN_3$ and DMF at 90 °C for 12 h; (7) DPPA, DBU, and DMF at 100 °C for 4 h; $NaN_3$ at 100 °C for 12 h.

$NaN_3$ (3.25 g, 50 mmol, 5 equiv) was added to a solution of **2a** (4.55 g, 10.0 mmol) in acetone (20 mL) and water (10 mL). The reaction mixture was heated under reflux for 20 h, diluted with $CH_2Cl_2$, and sequentially washed with saturated aqueous $NaHCO_3$, water, and brine. The organic layer was dried over anhydrous $Na_2SO_4$ and evaporated to a residue, which was purified by column chromatography (hexane/EtOAc 3:2) to afford 2-azidoethyl glycoside (**3a**) (3.75 g, 85%) as a clear glass: $^1$H NMR ($CDCl_3$) $\delta$ 5.18 (t, $J$ = 9.5 Hz, 1H), 5.06 (t, $J$ = 9.7 Hz, 1H), 4.99 (t, $J$ = 8.8 Hz, 1H), 4.57 (d, $J$ = 8.0 Hz, 1H), 4.22 (dd, $J$ = 12.3, 4.7 Hz, 1H), 4.13 (dd, $J$ = 12.3, 2.0 Hz, 1H), 4.00 (dt, $J$ = 10.5, 4.1 Hz, 1H), 3.72−3.63 (m, 2H), 3.46 (ddd, $J$ = 11.7, 7.6, 3.3 Hz, 1H), 3.26 (dt, $J$ = 13.4, 4.0 Hz, 1H), 2.06 (s, 3H), 2.02 (s, 3H), 1.99 (s, 3H), 1.97 (s, 3H); $^{13}$C NMR ($CDCl_3$) $\delta$ 170.65, 170.26, 169.41(2C), 100.69, 72.81, 71.96, 71.10, 68.58, 68.36, 61.87, 50.55, 20.75, 20.69, 20.61 (2C). HRMS (ESI) calcd for $C_{16}H_{23}N_3NaO_{10}$ $(M + Na)^+$ 440.1281, found 440.1276.

*Synthesis of Bromomethyl 2,3,4,6-Tetra-O-acetyl-1-thio-β-D-glucopyranoside (**2b**; Scheme 1).* 2,3,4,6-Tetra-*O*-acetyl-β-D-1-thio-glucopyranosyl[19] (**1b**) was synthesized as previously described.

$K_2CO_3$ (3.03 g, 21.9 mmol, 2 equiv) was added to a stirred solution of **1b** (4 g, 10.95 mmol) in $CH_2Br_2$ (20 mL), and the mixture was stirred at room temperature. TLC was used to determine the disappearance of the starting material (about 6 h), and then the solid was removed by filtration and the filtrate was concentrated. The residue was purified by column chromatography (hexane/EtOAc 3:2) to afford product **2b** (3.51 g, 70%) as a clear glass: $^1$H NMR ($CDCl_3$) $\delta$ 5.28 (t, $J$ = 9.4 Hz, 1H), 5.13−5.06 (m, 2H), 4.81 (d, $J$ = 10.2 Hz, 1H), 4.76 (d, $J$ = 11.0 Hz, 1H), 4.55 (d, $J$ = 11.0 Hz, 1H), 4.25 (dd, $J$ = 12.5, 5.0 Hz, 1H), 4.17 (dd, $J$ = 12.4, 2.3 Hz, 1H), 3.78 (ddd, $J$ = 10.1, 5.0, 2.3 Hz, 1H), 2.08 (s, 3H), 2.05 (s, 3H), 2.03 (s, 3H), 2.00 (s, 3H); $^{13}$C NMR ($CDCl_3$) $\delta$ 170.71, 170.22, 169.54, 169.50, 82.05, 76.39, 73.86, 69.91, 68.34, 62.01, 32.11, 20.86, 20.75, 20.71, 20.70. HRMS (ESI) calcd for $C_{15}H_{21}BrNaO_9S$ $(M + Na)^+$ 478.9988, found 478.9982.

*Synthesis of Azidomethyl 2,3,4,6-Tetra-O-acetyl-1-thio-β-D-glucopyranoside (**3b**; Scheme 1).* $NaN_3$ (2.13 g, 32.8 mmol, 5 equiv) was added to a solution of **2b** (3.0 g, 6.56 mmol) in 30 mL of DMF. The reaction mixture was stirred at 90 °C for 12 h, diluted with $CH_2Cl_2$, and washed with saturated aqueous $NaHCO_3$, water, and brine. The organic layer was dried over anhydrous $Na_2SO_4$ and evaporated under reduced pressure. The residues was purified by column chromatography (hexane/EtOAc 2:1) to afford product **3b** (2.48 g, 90%) as a white amorphous solid: $^1$H NMR ($CDCl_3$) $\delta$ 5.23 (t, $J$ = 9.4 Hz, 1H), 5.10 (t, $J$ = 9.8 Hz, 1H), 5.06 (t, $J$ = 9.7 Hz, 1H), 4.70 (d, $J$ = 10.1 Hz, 1H), 4.41 (d, $J$ = 13.5 Hz, 1H), 4.32 (d, $J$ = 13.5 Hz, 1H), 4.23 (dd, $J$ = 12.4, 4.9 Hz, 1H), 4.14 (dd, $J$ = 12.4, 2.2 Hz, 1H), 3.74 (ddd, $J$ = 10.1, 4.9, 2.3 Hz, 1H), 2.06 (s, 3H), 2.05 (s, 3H), 2.01 (s, 3H), 2.00 (s, 3H); $^{13}$C NMR ($CDCl_3$) $\delta$ 170.71, 170.21, 169.53, 169.45, 81.81, 76.31, 73.79, 70.12, 68.18, 62.05, 51.12, 20.81, 20.74, 20.69, 20.68. HRMS (ESI) calcd for $C_{15}H_{21}N_3NaO_9S$ $(M + Na)^+$ 442.0896, found 442.0891.

*Synthesis of 2,3,4,6-Tetra-O-acetyl-N-chloroacetyl-β-D-glucopyranosylamine (**2c**; Scheme 1).* 2,3,4,6-Tetra-*O*-acetyl-β-D-glucopyranosylamine[20] (**1c**) was synthesized as previously described.

The solution of **1c** (1.74 g, 5.0 mmol) in anhydrous $CH_2Cl_2$ (30 mL) was cooled to 0 °C, anhydrous TEA (1.4 mL, 10.0 mmol, 2 equiv) was added dropwise, and then chloroacetic anhydride (1.28 g, 7.5 mmol, 1.5 equiv) was added to the solution in portions. The reaction mixture was stirred for 2 h at 0 °C, followed by stirring at room temperature overnight. After dilution with $CH_2Cl_2$ and washing with cold water and saturated aqueous $NaHCO_3$, the organic phase was dried over anhydrous $Na_2SO_4$ and evaporated in vacuo. The residues were purified by column chromatography (hexane/EtOAc 1:1) to afford the product **2c** (1.17 g, 55%) as a white solid: $^1$H NMR ($CDCl_3$) $\delta$ 7.31 (d, $J$ = 8.9 Hz, 1H), 5.32 (t, $J$ = 9.5 Hz, 1H), 5.20 (t, $J$ = 9.2 Hz, 1H), 5.07 (t, $J$ = 9.7 Hz, 1H), 5.00 (t, $J$ = 9.6 Hz, 1H), 4.29 (dd, $J$ = 12.5, 4.4 Hz, 1H), 4.13−3.95 (m, 3H), 3.83 (ddd, $J$ = 10.1, 4.3, 2.1 Hz, 1H), 2.08 (s, 3H), 2.05 (s, 3H), 2.03 (s, 3H), 2.02 (s, 3H); $^{13}$C NMR ($CDCl_3$) $\delta$ 170.88, 170.69, 169.97, 169.60, 166.95, 78.63, 73.92, 72.68, 70.38, 68.21, 61.69, 42.36, 20.83−20.68 (4C). HRMS (ESI) calcd for $C_{16}H_{22}ClNNaO_{10}$ $(M + Na)^+$ 446.0830, found 446.0824.

*Synthesis of 2,3,4,6-Tetra-O-acetyl-N-azidoacetyl-β-D-glucopyranosylamine (**3c**; Scheme 1).* $NaN_3$ (650.0 mg, 10.0 mmol, 5 equiv) was added to a solution of **2c** (847.6 mg, 2 mmol) in 20 mL of DMF. The reaction mixture was stirred at 90 °C for 12 h, diluted with $CH_2Cl_2$, and washed with saturated aqueous $NaHCO_3$, water, and brine. The organic layer was dried over anhydrous $Na_2SO_4$ and evaporated under reduced pressure. The residue was purified by column chromatography (hexane/EtOAc 2:1) to afford product **3c** (780 mg, 91%) as a white amorphous solid: $^1$H NMR ($CDCl_3$) $\delta$ 7.11 (d, $J$ = 9.1 Hz, 1H), 5.31 (t, $J$ = 9.5 Hz, 1H), 5.22 (t, $J$ = 9.3 Hz, 1H), 5.07 (t, $J$ = 9.8 Hz, 1H), 4.97 (t, $J$ = 9.6 Hz, 1H), 4.29 (dd, $J$ = 12.5, 4.4 Hz, 1H), 4.09 (dd, $J$ = 12.5, 2.1 Hz, 1H), 4.03−3.90 (m, 2H), 3.83 (ddd, $J$ = 10.1, 4.3, 2.1 Hz, 1H), 2.08 (s, 3H), 2.05 (s, 3H), 2.03 (s, 3H), 2.02 (s, 3H); $^{13}$C NMR ($CDCl_3$) $\delta$ 170.96, 170.68, 169.96, 169.62, 167.57, 78.25, 73.90, 72.71, 70.58, 68.22, 61.71, 52.69, 20.81,


dx.doi.org/10.1021/jf5034575 | J. Agric. Food Chem. 2014, 62, 11037−11046

**Scheme 2**[a]

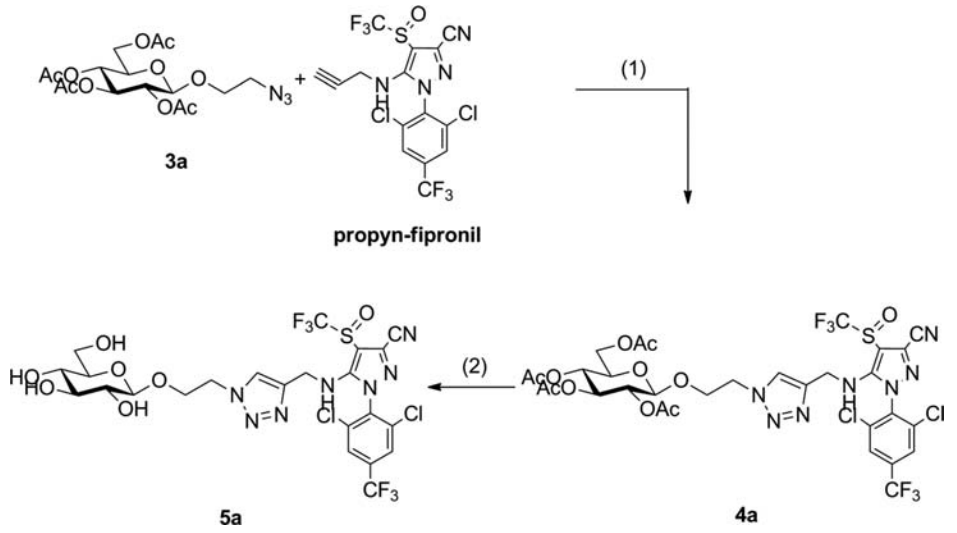


[a]Reagents and conditions: (1) $CuSO_4 \cdot 5H_2O$, sodium ascorbate, and 1:1 t-BuOH/$H_2O$ at 60 °C for 3 h; (2) 1 M NaOMe/MeOH at room temperature for 30 min.

**Scheme 3**[a]

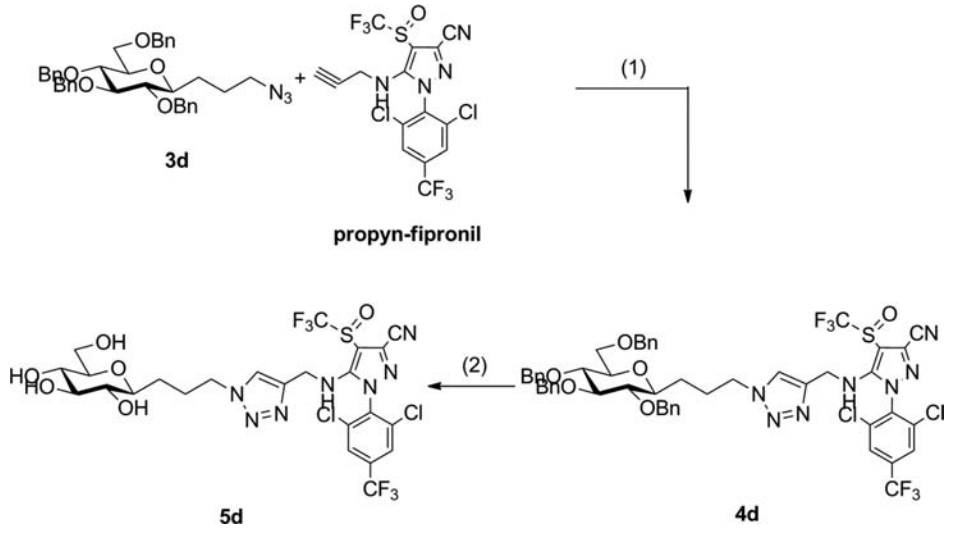


[a]Reagents and conditions: (1) $CuSO_4 \cdot 5H_2O$, sodium ascorbate, and 1:1 t-BuOH/$H_2O$ at 60 °C for 3 h; (2) anhydrous $FeCl_3$ and $CH_2Cl_2$ at room temperature.

20.70, 20.66 (2C). HRMS (ESI) calcd for $C_{16}H_{22}N_4NaO_{10}$ $(M + Na)^+$ 453.1234, found 453.1228.

*3-(2,3,4,6-Tetra-O-benzyl-β-D-glucopyranosyl)-1-propanol*[21] ***(2d; Scheme 1).*** **2d** was synthesized as previously described to afford the compound as a white amorphous solid: $^1$H NMR ($CDCl_3$) $\delta$ 7.35−7.26 (m, 18H), 7.15−7.10 (m, 2H), 4.93 (d, $J$ = 10.9 Hz, 1H), 4.80 (dd, $J$ = 14.1, 10.9 Hz, 2H), 4.70 (d, $J$ = 11.7 Hz, 1H), 4.61 (dd, $J$ = 11.8, 10.1 Hz, 2H), 4.48 (dd, $J$ = 18.7, 11.5 Hz, 2H), 4.07−4.00 (m, 1H), 3.80−3.53 (m, 9H), 1.82−1.77 (m, 2H), 1.72−1.58 (m, 2H); $^{13}$C NMR ($CDCl_3$) $\delta$ 138.86, 138.42, 138.30, 138.07, 128.58−127.74 (20C), 82.54, 80.36, 78.39, 75.60, 75.17, 74.52, 73.66, 73.30, 71.32, 69.33, 62.54, 29.39, 21.10. HRMS (ESI) calcd for $C_{37}H_{42}NaO_6$ $(M + Na)^+$ 605.2879, found 605.2874.

*Synthesis of 3-(2,3,4,6-Tetra-O-benzyl-β-D-glucopyranosyl)-1-azidopropyl* ***(3d; Scheme 1).*** Compound **2d** (582.73 mg, 1 mmol) was dissolved in anhydrous DMF (15 mL), DPPA (650 μL, 3 mmol, 3 equiv), and DBU (150 μL, 1 mmol, 1 equiv) added dropwise. The solution was stirred at 100 °C for 4 h and then cooled to room temperature. Sodium azide (195 mg, 3 mmol, 3 equiv) was added to the solution in one portion, and the reaction mixture was stirred at 100 °C for an additional 12 h. After cooling to room temperature, the solution was diluted with diethyl ether (100 mL). The organic phase was then washed with $H_2O$ (100 mL) and saturated aqueous NaCl (100 mL), dried over anhydrous $Na_2SO_4$, and then evaporated in vacuo. The residue was purified by column chromatography (hexane/EtOAc 8:1) to afford **3d** (2.48 g, 90%) as a colorless oil: $^1$H NMR ($CDCl_3$) $\delta$ 7.43−7.27 (m, 18H), 7.16−7.07 (m, 2H), 4.92 (d, $J$ = 10.9 Hz, 1H), 4.80 (dd, $J$ = 10.8, 4.7 Hz, 2H), 4.71 (d, $J$ = 11.7 Hz, 1H), 4.66−4.55 (m, 2H), 4.47 (dd, $J$ = 11.4, 7.1 Hz, 2H), 4.05−3.91 (m, 1H), 3.82−3.21 (m, 9H), 1.85−1.67 (m, 3H); $^{13}$C NMR ($CDCl_3$) $\delta$ 138.88, 138.38, 138.32, 138.16, 128.61−127.75 (20C), 82.59, 80.25, 78.29, 75.63, 75.21, 73.91, 73.68, 73.43, 71.35, 69.22, 51.31, 25.16, 22.01. HRMS (ESI): calcd for $C_{37}H_{41}N_3NaO_5$ $(M + Na)^+$ 630.2944, found 630.2938.

**General Procedure for the Synthesis of Title Compounds (4a−4d; Schemes 2 and 3).** The propyn-fipronil donor[5] was synthesized as previously described. Compounds **3a−3d** (1 mmol) were added to a solution of propyn-fipronil donor (1 mmol) in 3 mL

**Scheme 4**[a]

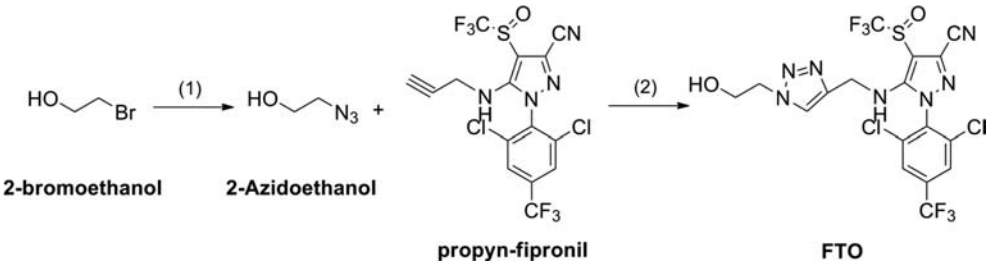


[a]Reagents and conditions: (1) $NaN_3$ and water at 85 °C for 16 h; (2) $CuSO_4{\cdot}5H_2O$, sodium ascorbate, and 1:1 t-BuOH/$H_2O$ at 60 °C for 3 h.

of *tert*-butyl alcohol. Then, a solution of $CuSO_4{\cdot}5H_2O$ (100 mg, 0.4 mmol) and sodium ascorbate (173 mg, 0.8 mmol) in distilled water (3 mL) was further added. The yellow solution was vigorously stirred at 60 °C for 3 h and quenched by adding water (10 mL). The aqueous layer was extracted with $CH_2Cl_2$ (10 mL × 3). The combined organic extracts were washed with aqueous sodium hydrogen carbonate and brine, dried with anhydrous $Na_2SO_4$, filtered, and evaporated in vacuo. The residues were purified by column chromatography (hexane/EtOAc 1:1) to afford the desired products as solids.

*N-{3-Cyano-1-[2,6-dichloro-4-(trifluoromethyl)-phenyl]-4-[(trifluoromethyl)sulfinyl]-1H-pyrazol-5-yl}-1-[2,3,4,6-tetra-O-acetyl-(2-triazolethyl)-β-D-glucopyranoside]-1H-1,2,3-triazole-4-methanamine (**4a**):* white solid; yield 85%; $^1$H NMR ($CDCl_3$) $\delta$ 7.75 (d, $J$ = 10.2 Hz, 2H), 7.53 (s, 1H), 6.24 (t, $J$ = 5.6 Hz, 1H), 5.16 (t, $J$ = 9.5 Hz, 1H), 5.03 (t, $J$ = 9.7 Hz, 1H), 4.86 (dd, $J$ = 9.5, 7.9 Hz, 1H), 4.50 (t, $J$ = 4.9 Hz, 2H), 4.46 (d, $J$ = 7.8 Hz, 1H), 4.37 (ddd, $J$ = 30.0, 14.7, 5.6 Hz, 2H), 4.21 (dd, $J$ = 12.4, 5.0 Hz, 1H), 4.17−4.10 (m, 1H), 4.08 (dd, $J$ = 12.4, 2.3 Hz, 1H), 3.91 (dt, $J$ = 10.8, 5.4 Hz, 1H), 3.68 (ddd, $J$ = 9.9, 4.9, 2.3 Hz, 1H), 2.03 (s, 3H), 2.01 (s, 3H), 2.00 (s, 3H), 1.89 (s, 3H); $^{13}$C NMR ($CDCl_3$) $\delta$ 170.64, 170.11, 169.60, 169.47, 151.24, 142.78, 136.66, 136.53, 135.48, 135.06 (q, $J$ = 34.4 Hz), 127.32, 126.49, 126.32, 125.46 (q, $J$ = 336.3 Hz), 123.77, 121.93 (q, $J$ = 274.1 Hz), 110.53, 100.70, 96.18, 72.32, 72.14, 71.10, 68.26, 67.84, 61.79, 50.37, 41.21, 20.71, 20.62 (2C), 20.59. HRMS (ESI): calcd for $C_{31}H_{30}Cl_2F_6N_7O_{11}S$ $(M+H)^+$ 892.1005, found 892.1000.

*N-{3-Cyano-1-[2,6-dichloro-4-(trifluoromethyl)-phenyl]-4-[(trifluoromethyl)sulfinyl]-1H-pyrazol-5-yl}-1-(2,3,4,6-Tetra-O-acetyl-β-D-glucopyranosylthiomethyl)-1H-1,2,3-triazole-4-methanamine (**4b**).* White solid; yield 85%. $^1$H NMR ($CDCl_3$) $\delta$ 7.77 (s, 2H), 7.70 (d, $J$ = 2.7 Hz, 1H), 6.19 (d, $J$ = 6.3 Hz, 1H), 5.61 (dd, $J$ = 14.7, 10.2 Hz, 1H), 5.31 (dd, $J$ = 14.7, 10.5 Hz, 1H), 5.19 (td, $J$ = 9.4, 3.4 Hz, 1H), 5.09−4.99 (m, 2H), 4.59 (dd, $J$ = 10.1, 5.6 Hz, 1H), 4.45 (dd, $J$ = 15.0, 6.0 Hz, 1H), 4.32 (dd, $J$ = 14.8, 5.0 Hz, 1H), 4.09−4.00 (m, 2H), 3.67−3.63 (m, 1H), 2.02 (s, 3H), 2.01 (s, 3H), 2.00 (s, 3H), 1.99 (s, 3H); $^{13}$C NMR ($CDCl_3$) $\delta$ 170.78, 170.09, 169.53, 169.43, 151.24, 143.94, 136.62 (2C), 135.37, 135.26 (q, $J$ = 34.7 Hz), 127.44, 126.65, 126.44, 125.49 (q, $J$ = 336.1 Hz), 122.60, 121.96 (q, $J$ = 274.0 Hz), 110.46, 96.06, 82.30, 76.52, 73.49, 69.55, 68.02, 61.44, 49.04, 40.84, 20.86, 20.66 (3C). HRMS (ESI): calcd for $C_{30}H_{28}Cl_2F_6N_7O_{10}S_2$ $(M + H)^+$ 894.0620, found 894.0615.

*N-{3-Cyano-1-[2,6-dichloro-4-(trifluoromethyl)-phenyl]-4-[(trifluoromethyl)sulfinyl]-1H-pyrazol-5-yl}-1-(2,3,4,6-tetra-O-acetyl-N-triazolylacetyl-β-D-glucopyranosylamine)-1H-1,2,3-triazole-4-methanamine (**4c**):* white solid; yield 85%; $^1$H NMR ($CDCl_3$) $\delta$ 7.75 (s, 2H), 7.67 (d, $J$ = 9.7 Hz, 1H), 7.00 (dd, $J$ = 26.1, 8.9 Hz, 1H), 6.29 (dd, $J$ = 10.4, 6.1 Hz, 1H), 5.28 (t, $J$ = 9.5 Hz, 1H), 5.19 (t, $J$ = 9.2 Hz, 1H), 5.09−4.94 (m, 3H), 4.84 (dt, $J$ = 11.9, 9.6 Hz, 1H), 4.52 (dd, $J$ = 15.0, 6.7 Hz, 1H), 4.37−4.18 (m, 2H), 4.07 (d, $J$ = 11.2 Hz, 1H), 3.84−3.78 (m, 1H), 2.04 (s, 3H), 2.02 (s, 3H), 2.00 (s, 6H); $^{13}$C NMR ($CDCl_3$) $\delta$ 171.18, 170.73, 169.94, 169.68, 165.58, 151.19, 143.78, 136.55 (2C), 135.29, 135.12 (q, $J$ = 34.5 Hz), 127.36, 126.46 (2C), 125.45 (q, $J$ = 336.7 Hz), 124.08, 121.91 (q, $J$ = 274.1 Hz), 110.51, 96.29, 78.37, 73.89, 72.59, 70.62, 68.13, 61.74, 52.58, 40.83, 20.77, 20.70, 20.65, 20.60. HRMS (ESI): calcd for $C_{31}H_{28}Cl_2F_6N_8NaO_{11}S$ $(M + Na)^+$ 927.0777, found 927.0772.

*N-{3-Cyano-1-[2,6-dichloro-4-(trifluoromethyl)phenyl]-4-[(trifluoromethyl)sulfinyl]-1H-pyrazol-5-yl}-1-(2,3,4,6-tetra-O-benzyl-β-D-glucopyranosyl)propyl-1H-1,2,3-triazole-4-methanamine (**4d**):* white solid; yield 85%; $^1$H NMR ($CDCl_3$) $\delta$ 7.73 (d, $J$ = 5.7 Hz, 2H), 7.41 (s, 1H), 7.35−7.23 (m, 18H), 7.17−7.10 (m, 2H), 6.20 (d, $J$ = 16.0 Hz, 1H), 4.89 (d, $J$ = 10.9 Hz, 1H), 4.79 (t, $J$ = 11.1 Hz, 2H), 4.70 (d, $J$ = 11.7 Hz, 1H), 4.57 (dd, $J$ = 11.6, 9.3 Hz, 2H), 4.52−4.21 (m, 6H), 3.98 (d, $J$ = 9.8 Hz, 1H), 3.71 (d, $J$ = 2.4 Hz, 2H), 3.64 (s, 2H), 3.57−3.48 (m, 2H), 2.04−1.85 (m, 2H), 1.79−1.63 (m, 2H); $^{13}$C NMR ($CDCl_3$) $\delta$ 151.43, 143.08, 138.65, 138.18, 138.08, 137.99, 136.52 (2C), 135.50, 135.24 (q, $J$ = 34.7 Hz), 128.65−127.76 (20C), 127.34, 126.54, 126.38, 125.50 (q, $J$ = 336.5 Hz), 121.89 (q, $J$ = 274.1 Hz), 121.73, 110.38, 95.61, 82.26, 79.86, 78.03, 75.54, 75.19, 73.68, 73.66, 73.47, 71.55, 69.22, 50.25, 40.95, 26.71, 21.89. HRMS (ESI): calcd for $C_{52}H_{48}Cl_2F_6N_7O_6S$ $(M + H)^+$ 1082.2668, found 1082.2663.

**General Procedure for the Synthesis of Title Compounds (5a−5c; Scheme 2).** The peracetylated compounds **4a**−**4c** (1 mmol) were dissolved in 10 mL of dry MeOH. To this solution was added freshly prepared NaOMe (1 M, 0.5 mL) with stirring at room temperature for 30 min. The reaction mixture was neutralized with Amberlite IR 120 ($H^+$) resin and filtered, and then the filtrate was evaporated. The residues were purified by column chromatography (chloroform/methanol 15:1) to afford the desired products as solids.

*N-{3-Cyano-1-[2,6-dichloro-4-(trifluoromethyl)phenyl]-4-[(trifluoromethyl)sulfinyl]-1H-pyrazol-5-yl}-1-(2-triazolethyl-β-D-glucopyranoside)-1H-1,2,3-triazole-4-methanamine (**5a**):* white solid; yield 60%; $^1$H NMR (MeOD) $\delta$ 8.08 (d, $J$ = 3.9 Hz, 2H), 8.00 (s, 1H), 4.66−4.57 (m, 3H), 4.45 (d, $J$ = 16.1 Hz, 1H), 4.31 (dd, $J$ = 7.8, 5.5 Hz, 1H), 4.20 (ddd, $J$ = 10.1, 6.9, 4.0 Hz, 1H), 3.99 (dq, $J$ = 6.6, 3.7 Hz, 1H), 3.86 (d, $J$ = 11.9 Hz, 1H), 3.66−3.60 (m, 1H), 3.39−3.32 (m, 1H), 3.29−3.22 (m, 2H), 3.17 (ddd, $J$ = 9.1, 7.9, 4.9 Hz, 1H); $^{13}$C NMR (MeOD) $\delta$ 151.87, 144.90, 137.90 (2C), 136.13, 136.12 (q, $J$ = 34.3 Hz), 127.95, 127.86, 126.95 (q, $J$ = 335.8 Hz), 125.13 (2C), 123.63 (q, $J$ = 273.2 Hz), 112.18, 104.75, 97.59, 78.13, 78.03, 74.96, 71.62, 69.28, 62.78, 51.72, 41.20. HRMS (ESI): calcd for $C_{23}H_{22}Cl_2F_6N_7O_7S$ $(M + H)^+$ 724.0582, found 724.0577.

*N-{3-Cyano-1-[2,6-dichloro-4-(trifluoromethyl)phenyl]-4-[(trifluoromethyl)sulfinyl]-1H-pyrazol-5-yl}-1-(β-D-glucopyranosylthiomethyl)-1H-1,2,3-triazole-4-methanamine (**5b**):* white solid; yield 60%; $^1$H NMR (MeOD) $\delta$ 8.08 (d, $J$ = 3.1 Hz, 1H), 8.06 (s, 2H), 5.82 (dd, $J$ = 14.6, 2.7 Hz, 1H), 5.53 (dd, $J$ = 14.6, 2.4 Hz, 1H), 4.61 (dd, $J$ = 16.1, 3.3 Hz, 1H), 4.50−4.40 (m, 2H), 3.92−3.82 (m, 1H), 3.62 (dd, $J$ = 11.9, 5.7 Hz, 1H), 3.35−3.17 (m,4H); $^{13}$C NMR (DMSO) $\delta$ 150.18, 143.54, 136.02 (2C), 134.50, 133.61 (q, $J$ = 33.7 Hz), 126.87 (2C), 125.73, 125.46 (q, $J$ = 337.7 Hz), 123.51, 122.23 (q, $J$ = 274.2 Hz), 111.53, 95.59, 83.32, 81.29, 79.16, 78.07, 73.30, 70.16, 61.40, 47.44. HRMS (ESI): calcd for $C_{22}H_{20}Cl_2F_6N_7O_6S_2$ $(M + H)^+$ 726.0197, found 726.0192.

*N-{3-Cyano-1-[2,6-dichloro-4-(trifluoromethyl)phenyl]-4-[(trifluoromethyl)sulfinyl]-1H-pyrazol-5-yl}-1-(N-triazolylacetyl-β-D-glucopyranosylamine)-1H-1,2,3-triazole-4-methanamine (**5c**):* white solid; yield 60%; $^1$H NMR (MeOD) $\delta$ 8.00 (d, $J$ = 2.3 Hz, 2H), 7.81 (s, 1H), 5.20−5.08 (m, 2H), 4.92 (d, $J$ = 9.1 Hz, 1H), 4.43 (s, 2H), 3.82 (dd, $J$ = 11.9, 2.1 Hz, 1H), 3.65 (dd, $J$ = 11.9, 5.2 Hz, 1H), 3.41 (t, $J$ = 8.8 Hz, 1H), 3.36−3.33 (m, 1H), 3.32−3.26 (m, 2H); $^{13}$C NMR (MeOD) $\delta$ 175.20, 161.33, 152.19, 145.12 (2C), 144.21,

143.30 (q, $J$ = 34.2 Hz), 137.76, 136.39 (2C), 133.91, 131.86 (q, $J$ = 274.2 Hz), 129.39 (q, $J$ = 325.2 Hz), 119.61, 100.91, 89.14, 88.65, 88.19, 86.82, 82.12, 79.38, 70.35, 49.67. HRMS (ESI): calcd for $C_{23}H_{21}Cl_2F_6N_8O_7S$ $(M + H)^+$ 737.0535, found 737.0530.

**General Procedure for the Synthesis of Title Compound 5d (Scheme 3).** Anhydrous $FeCl_3$ (12 mmol) was added to a stirred solution of compound **4d** (1 mmol) in dry $CH_2Cl_2$ (10 mL) at room temperature under nitrogen. The reaction was left undisturbed until the color of the reaction mixture became brown. The solution was then evaporated under reduced pressure, and the residue was purified by column chromatography (chloroform/methanol 15:1) to afford the desired product **5d** as a white solid.

*N-{3-Cyano-1-[2,6-dichloro-4-(trifluoromethyl)phenyl]-4-[(trifluoromethyl)sulfinyl]-1H-pyrazol-5-yl}-1-(β-D-glucopyranosyl)-propyl-1H-1,2,3-triazole-4-methanamine (**5d**):* white solid; yield 55%; $^1$H NMR (MeOD) $\delta$ 8.08 (s, 2H), 7.87 (d, $J$ = 2.3 Hz, 1H), 4.61 (dd, $J$ = 16.1, 3.8 Hz, 1H), 4.50−4.36 (m, 3H), 3.93−3.87 (m, 1H), 3.78 (dd, $J$ = 11.8, 2.1 Hz, 1H), 3.59 (ddd, $J$ = 15.3, 10.6, 6.0 Hz, 2H), 3.47 (t, $J$ = 9.0 Hz, 1H), 3.36−3.32 (m, 1H), 3.24−3.17 (m, 1H), 2.13−2.02 (m, 1H), 1.96−1.85 (m, 1H), 1.74−1.58 (m, 2H); $^{13}$C NMR (MeOD) $\delta$ 151.87, 145.11, 137.88 (2C), 136.14, 136.13 (q, $J$ = 34.6 Hz), 127.97, 127.85, 126.94 (q, $J$ = 335.8 Hz), 123.98 (2C), 123.62 (q, $J$ = 272.9 Hz), 112.17, 97.60, 76.66, 75.18, 74.67, 72.94, 72.35, 63.24, 51.23, 41.18, 27.78, 22.65. HRMS (ESI): calcd for $C_{24}H_{24}Cl_2F_6N_7O_6S$ $(M + H)^+$ 722.0790, found 722.0785.

*Synthesis of N-{3-Cyano-1-[2,6-dichloro-4-(trifluoromethyl)-phenyl]-4-[(trifluoromethyl)sulfinyl]-1H-pyrazol-5-yl}-1-ethanol-1H-1,2,3-triazole-4-methanamine (FTO; Scheme 4).* 2-Bromoethanol (3.2 g, 25.62 mmol) was dissolved in water (12 mL), and sodium azide (2.5 g, 38.5 mmol, 1.5 equiv) was added to the solution. The reaction mixture was stirred at 85 °C for 16 h and quenched by adding cold water (10 mL). Diethyl ether (50 mL) was added, and the organic layer was washed with saturated aqueous $NaHCO_3$, water, and brine. The organic layer was dried over anhydrous $Na_2SO_4$ and evaporated under reduced pressure to yield 2-azidoethanol (1.56 g, 70%) as a colorless oil. The product was subjected to the next step without further purification.

2-Azidoethanol (0.5 g, 5.74 mmol) was added to a solution of propyn-fipronil (2.72 g, 5.74 mmol) in 15 mL of *tert*-butyl alcohol. Then, a solution of $CuSO_4{\cdot}5H_2O$ (575 mg, 2.3 mmol, 0.4 equiv) and sodium ascorbate (911.3 mg, 4.6 mmol, 0.8 equiv) in distilled water (15 mL) was added. The yellow solution was vigorously stirred at 60 °C for 3 h and then quenched by adding water (10 mL). The aqueous layer was extracted with $CH_2Cl_2$ (15 mL × 3). The combined organic extracts were washed with aqueous sodium hydrogen carbonate and brine, dried with anhydrous $Na_2SO_4$, filtered, and evaporated in vacuo. The residues were purified by column chromatography (hexane/EtOAc 2:3) to afford FTO (2.64 g, 82%) as a white solid: $^1$H NMR ($CDCl_3$) $\delta$ 7.76 (d, $J$ = 2.6 Hz, 1H), 7.60 (s, 1H), 6.04 (t, $J$ = 5.6 Hz, 1H), 4.47−4.44 (m, 1H), 4.40 (dd, $J$ = 15.1, 6.2 Hz, 1H), 4.28 (dd, $J$ = 15.1, 5.8 Hz, 1H), 4.08−4.01 (m, 1H), 2.23 (s, 1H); $^{13}$C NMR ($CDCl_3$) $\delta$ 153.75, 146.32, 137.81 (2C), 136.59, 136.03 (q, $J$ = 34.6 Hz), 129.81, 127.53, 126.78 (q, $J$ = 334.6 Hz), 125.79 (2C), 122.13 (q, $J$ = 272.8 Hz), 110.90, 96.81, 60.58, 48.74, 43.17. HRMS (ESI): calcd for $C_{17}H_{12}Cl_2F_6N_7O_2S$ $(M + H)^+$ 562.0055, found 562.0049.

**β-Glucosidase Enzymes.** β-Glucosidase from almonds was purchased from Sigma-Aldrich. A 10 U/mL solution was prepared.

**Growth of Plants.** This procedure is reported in detail elsewhere.[22,23] Six-day-old castor bean seedlings were selected for cotyledon absorption experiments. Adult plants of castor bean were grown in half-strength Hoagland's solution for 3−4 weeks until they possessed four true leaves. The cotyledons and primary leaves were cut, and the plants were tested 2−3 days later.

**Glucoside Metabolism Assays in Vitro.** A modification of the phosphate-based method of Masayuki[24] was used for glucoside metabolism assays. Glucosides were hydrolyzed in 0.1 M citrate−0.2 M phosphate buffer (pH 5.5) containing 1 unit of β-glucosidase, and the volume was brought up to 1 mL. Then, 5 μL of 20 mM concentrated standard solution was added to these centrifugal tubes. After incubation at 37 °C for 1 h, the reaction was stopped by boiling for 3 min.

The reaction mixture was analyzed with an Agilent 1100 HPLC system on a $C_{18}$ reversed-phase column (5 μm; 250 × 4.6 mm i.d.; Agilent Co.) with a flow rate of 1.0 mL min$^{-1}$ at 30 °C, and the eluent was made of water and acetonitrile (50:50, v/v). Glucoside and aglycon were detected by UV absorption at 210 nm.

For the identification of reaction products, UHPLC-HRMS analyses were performed. The UHPLC system consisting of an autosampler, a binary pump, and a diode array detector (Agilent Technologies 1290 infinity) was interfaced to a time-of-flight (TOF) mass spectrometer (Bruker Maxis, Germany). SB-$C_{18}$ RRHD (1.8 μm, 50 × 2.1 mm, Agilent Technologies) was used for the separation. Column temperature was set at 30 °C, and injection volume was 5 μL. The binary mobile phase consisted of (A) 100% water and (B) 100% acetonitrile, and the 8 min gradient was described as follows: 0−1 min, 10% B isocratic; 1−4 min, 90% B; 4−8 min, 10% B, at a flow rate of 0.2 mL min$^{-1}$. The detection wavelength was 210 nm. Electrospray ionization in positive mode was performed under the following conditions: nebulizer, 0.3 bar; drying gas, 4.0 L min$^{-1}$; drying temperature, 180 °C; and capillary, 3500 V. The full scan mass spectra of the compounds were recorded within $m/z$ 50−1000.

**Glucoside Metabolism Assays in Vivo.** These assays were performed following a previous method.[25] In a typical procedure, an aqueous solution (10 mM, equal volumes of 10 μL in each petiole) was injected into the petioles of the two mature leaves using a 10 μL microsyringe. After the application of glucosides, the plants were grown for 4 h, and then the blades of the mature leaves were separated from the plants.

The compounds were extracted from the leaves (2.0 g) by grinding in 10 mL of methanol with a glass mortar and pestle. After ultrasonic treatment for 20 min, a portion (2.0 mL) of the extract was centrifuged at 15000 rpm for 5 min and the supernatant passed through a 0.22 μm filter. Then, the treated solutions were analyzed by HPLC. Recoveries of parent compound were >85% conducted by adding known amounts of glucosides with three replicates.

**Insects.** Larvae of *S. litura* F. were obtained from the Guangzhou Biological Control Station and raised with artificial feed under cage conditions for three generations. Healthy larvae of *P. xylostella* L. were collected from the experimental farm of Dongguan Agricultural Science Research Center, Guangdong, China, and reared on Chinese cabbage (*Brassica rapa*) under cage conditions for three generations. The feeding conditions were as follows: temperature, 26 ± 2 °C; relative humidity, 70%; and photoperiod, 16:8 h (light/dark).

**Insecticidal Activity.** To investigate the insecticidal activities of FTO (Scheme 4) and FOH,[6] we synthesized the aglycons beforehand. The insecticidal activities of the compounds GOTF, FTO, GOF, FOH, and fipronil against *P. xylostella* L. and *S. litura* F. were evaluated by leaf disk dipping assay.[26] The leaf disks (1.8 cm diameter) were cut from fresh cabbage grown in a greenhouse. The compounds were dissolved in acetone and suspended in distilled water containing Tween 80 (0.1%). Leaf disks were dipped in each test solution for 30 s and allowed to dry for 2 h. After air-drying, the treated leaf disks were placed in Petri dishes (9 cm diameter) lined with filter paper, and then the second-instar larvae of *P. xylostella* L. and *S. litura* F. were transferred to a Petri dish. Three replicates (10 larvae per replicate) were carried out. Fipronil was used as a standard. Petri dishes were kept in an incubator at 26 °C and 85% relative humidity under a photoperiod of 16:8 h (light/dark). Mortalities were determined 24 h after treatment.

## RESULTS AND DISCUSSION

**Synthesis and Characterization.** Click chemistry[27] was performed to create four glucose−fipronil conjugates, **4a−4d** (Figure S1). $CuSO_4{\cdot}5H_2O$/sodium ascorbate and CuI/DIPEA are commonly used as catalysts for this method. The $CuSO_4{\cdot}5H_2O$/sodium ascorbate system[28] was selected to optimize the reaction yield (>85%) and ensure the stability of conjugates. Compounds **4a−4c** were deprotected using 1 M NaOMe in

MeOH to yield products **5a**–**5c** with 60% yields. The structures of **4a**–**4c** and **5a**–**5c** were confirmed by $^{1}$H NMR, $^{13}$C NMR, and mass spectrometry. The acetyl groups of **4a** exhibited characteristic signals at 1.89, 2.00, 2.01, and 2.03 ppm in the $^{1}$H NMR spectra, as well as 20.59, 20.62, and 20.71 ppm in the $^{13}$C NMR spectra. However, the characteristic $^{1}$H NMR and $^{13}$C NMR spectrum signals of **5a** were not observed. The acetyl groups of **4a** disappeared after deprotection.

Generally, palladium-catalyzed hydrogenolysis was used to deprotect benzyl ether. However, **4d** exhibited a sulfur atom in sulfinyl that could cause permanent catalytic poisoning. Accordingly, $FeCl_3$ was introduced to synthesize **5d** with 55% yield because of its high efficacy.[29] The structures of **4d** and **5d** were confirmed by $^{1}$H NMR, $^{13}$C NMR, and mass spectrometry. Debenzylation was proved by $^{1}$H and $^{13}$C NMR spectra. The characteristic peaks between 7.35 and 7.1 ppm in the $^{1}$H NMR spectra, as well as the peaks at 128.65–127.76, 137.99, 138.08, 138.18, and 138.65 ppm in the $^{13}$C NMR spectra, were not observed after deprotection.

**Hydrolysis of Glucosides.** To examine the ability of *β*-glucosidase to hydrolyze glucose–pesticide conjugates in vitro, 1 mL of buffer solutions containing 1 unit of almond *β*-glucosidase was individually incubated with four glucose–fipronil conjugates for 1 h. Each solution was analyzed by HPLC upon termination of the reaction to detect potential hydrolysis products. Figure 3A shows that GOTF solution displayed a novel peak, and the original peak at the GOTF position cannot be clearly detected. This result indicated that 1 unit of *β*-glucosidase could hydrolyze nearly all GOTF within 1 h. However, no peak was observed from the other conjugate solutions, indicating that these analogues could not be hydrolyzed by *β*-glucosidases under experimental conditions (Figure 3B–D). In the absence of enzymes, hydrolysis was not observed in the control reaction, demonstrating the stability of glucosides. Considering the metabolite accumulation caused by the *β*-glucosidase-mediated degradation of GOTF, the single metabolite observed in the in vitro assay was analyzed by UHPLC-HRMS to determine its structure and define the enzymatic reactions (Figure 4A,B). The GOTF metabolite in the positive-ion mode resulted in pseudomolecular $[M + Na]^+$ at $m/z$ 583.9904, which was consistent for its reduced mass (mass loss = 162) indicating the removal of a single glucose molecule. This result determined the chemical structure (FTO) of the metabolite (Figure 2). The identity of the GOTF metabolite was verified by $^{1}$H NMR (Figure S2). These data indicated that the almond *β*-glucosidase hydrolyzed GOTF to FTO and exhibited high specificity for the O-glycosidic bond.

The in vitro activity of *β*-glucosidases implied that it could hydrolyze glucose–fipronil conjugates in vivo. To confirm this result, tests were conducted in adult *Ricinus communis* L. A peak was detected by HPLC in the leaf extracts when 20 *μ*L of a 10 mM GOTF solution was injected into the petioles after 4 h (Figure 3A). The retention time of the metabolic product suggested that for GOTF the observed products of castor bean in vivo were similar to those generated from the in vitro assays using *β*-glucosidase solutions (UHPLC-HRMS, Figure 4C–E). GOTF was also identified in the leaf extract (Figure 4C,D). By contrast, peaks were undetected in the extracted solution by HPLC when analogues were treated under the same experimental condition (Figure 3B–D). Thus, the analogues were stable within 4 h of injection, but we cannot rule out the possibility of other metabolism mechanisms occurring within the plant with prolonged time. Given the results of in vivo and

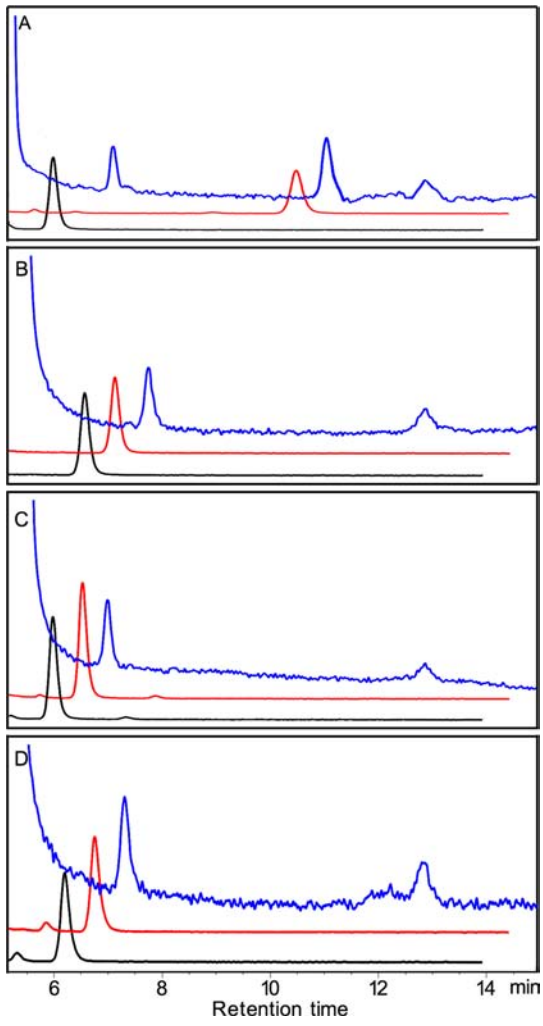


**Figure 3.** HPLC chromatograms of four glucosides measured at 210 nm for (A) GOTF, (B) GTTF, (C) GNTF, and (D) GCTF. Lane 1 (black line) describes the standard solutions of the corresponding glucosides. Lane 2 (red line) represents the glucosides incubated in buffer solutions containing of 1 unit of *β*-glucosidase for 1 h. Lane 3 (blue line) corresponds to the leaf extraction of castor bean at 4 h after injection.

in vitro assays, *β*-glucosidase was associated with the metabolism of glucose–fipronil conjugates in the body of adult castor beans and was specific for the hydrolysis of O-glycosidic bonds.

*β*-Glucosidase mediated the hydrolysis of glucose–pesticide conjugates, in which glucose was tethered to pesticides by O-glycosidic bonds. To verify this result, another glucose–fipronil conjugate, GOF, was selected for additional tests under the same experimental condition; this conjugate has been synthesized, and its phloem mobility in the castor bean system has been examined.[6] After 1 h of incubation with *β*-glucosidase, a peak in the HPLC chromatogram was observed and analyzed by UHPLC-HRMS (Figure 5A). Results showed that GOF (molecular mass = 642.0177) had $[M + Na]^+$ at $m/z$ 665.0077 (calculated for $C_{20}H_{18}Cl_2F_6N_4NaO_7S$; Figure 5B). The hydrolysis products (FOH) indicated a reduction in glucose molecule, and the majority of these displayed $[M + H]^+$ at $m/z$ 480.9733 (calculated for $C_{14}H_9Cl_2F_6N_4O_2S$; Figure 5C). The glucose–pesticide conjugate was metabolized within the body of an adult castor bean 4 h after injection. The reaction


dx.doi.org/10.1021/jf5034575 | J. Agric. Food Chem. 2014, 62, 11037–11046

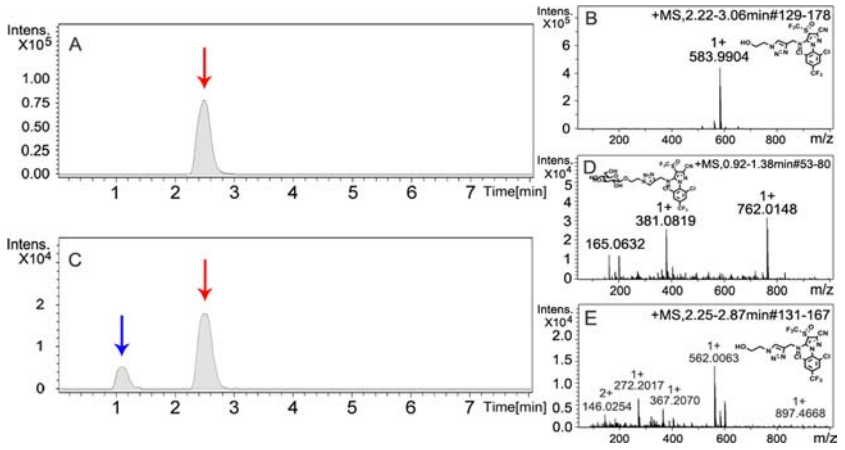


**Figure 4.** UHPLC-HRMS analysis of the metabolites present in the buffer solution of $\beta$-glucosidases and adult castor bean after GOTF application: (A) UV chromatogram of the reaction products in vitro; (B) positive-ion ESI mass spectrum of the peak in panel A (red arrow) showing $[M + Na]^+$ at $m/z$ 583.9904; (C) UV chromatogram of the leaf extracts; (D) positive-ion ESI mass spectrum of the peak in panel C (blue arrow) showing $[M + K]^+$ at $m/z$ 762.0148, which corresponds to the mass of GOTF; (E) positive-ion ESI mass spectrum of the peak in panel C (red arrow) indicating $[M + H]^+$ at $m/z$ 562.0063, which corresponds to the metabolite in vitro.

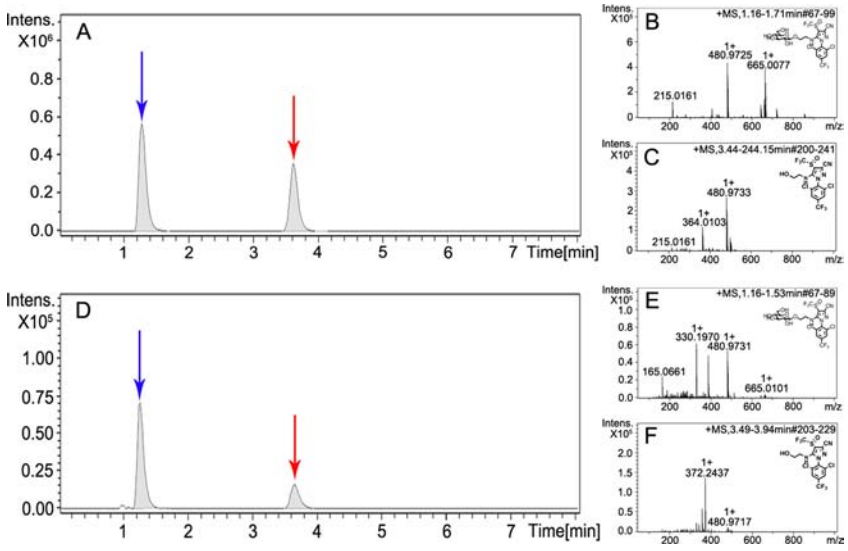


**Figure 5.** UHPLC-HRMS analysis of metabolites present in the buffer solution of $\beta$-glucosidases and leaf extract after treatment with GOF: (A) GOF solution incubated with $\beta$-glucosidases in vitro; (B) positive-ion ESI mass spectrum of the peak in panel A (blue arrow) showing $[M + Na]^+$ at $m/z$ 665.0077, which corresponds to the mass of GOF; (C) positive-ion ESI mass spectrum of the peak in panel A (red arrow) showing the reduced mass of the hydrolysis products to remove the glucose molecule; $[M + H]^+$ is located at $m/z$ 480.9733; (D) UV chromatogram of the leaf extracts; (E) positive-ion ESI mass spectrum of the peak in panel D (blue arrow) indicating $[M + Na]^+$ at $m/z$ 665.0101; (F) positive-ion ESI mass spectrum of the peak in panel D (red arrow) showing $[M + H]^+$ at $m/z$ 480.9717, which corresponds to the metabolite in vitro.

products identified by UHPLC-HRMS (Figure 5D–F) were similar to those of $\beta$-glucosidase hydrolysis in vitro. These data demonstrated that $\beta$-glucosidase was associated with the hydrolysis of GOF within the plant and the O-glycosidic bond.

To determine whether the O-glycosidic bond conjugates GOTF and GOF would be hydrolyzed in epidermal or mesophyll cells before reaching the phloem, a cotyledon absorption experiment was performed using castor bean seedlings (Supporting Information, Materials and Methods). After 15 min of incubation, both GOTF and GOF were hydrolyzed. GOTF was almost entirely hydrolyzed to be FTO within the cotyledons, whereas about 75% of GOF was hydrolyzed (Figure S3). Combined with in vitro and in vivo hydrolysis, GOF can be speculated to be not as readily hydrolyzed as GOTF. Given that the phloem mobility of GOF has been confirmed,[6] the slow hydrolysis and moderate phloem mobility of GOF is considered to be preferred over GOTF to be loaded in the phloem and achieve the slow release of insecticidal activities. The difference in hydrolyzing degree between GOF and GOTF may be due to the distinction of $\beta$-glucosidase affinity. Thus, the effects of different glucose–pesticide conjugates' chemical construction on hydrolyzing degree is worthy of further investigation.

A pro-drug was designed to solve the incompatibility between phloem mobility and activity. This material could be cleaved inside the plant or pest organism by spontaneous chemical conversion or enzyme-catalyzed metabolism. The enzyme unique to the plant crucially determines the proper approach to the preparation of pro-drugs.[2,30] Related works have achieved this enzyme through engineering mechanisms to release the active molecule within the plants. For instance, a sulfonylurea pro-herbicide can be activated in transgenic


dx.doi.org/10.1021/jf5034575 | J. Agric. Food Chem. 2014, 62, 11037–11046

tobacco using the TA29 promoter to express a bacterial P450 gene in a tissue-specific manner.[31] Tobacco could hydrolyze oxamyl glucuronide into its active compound by expressing the gene of *E. coli* β-glucuronidase in the root meristem and central cylinder.[2] However, the environmental effects of genetically modified crops could limit the use of this approach.[32] Plants contain endogenous β-glucosidases that catalyze the hydrolysis of glucosidic bonds to bioactivate plant glucosides (e.g., pro-hormones and phytoanticipins) and design parts as special active sites.[33] Although the importance of β-glucosidase in catalyzing glucoside hydrolysis is well documented, few studies have focused on the utilization of endogenous β-glucosidase to hydrolyze exogenous glucosides. This study revealed the involvement of endogenous β-glucosidase in the hydrolysis of glucose−pesticide conjugates. Furthermore, tethering of the mobility-conferring glucose to the pesticide through O-glycosidic bonds can circumvent the conflicting functions of mobility and activity.

**Insecticidal Activity.** The insecticidal activities of GOTF, FTO, GOF, and FOH were evaluated and compared with those of fipronil over a wide range of concentrations (Tables 1 and 2). GOTF and GOF exhibited negligible insecticidal activities against the second-instar larvae of *P. xylostella* L. and *S. litura* F. (mortality rate at 500 mg $L^{-1}$, <20%; Table 1). The low insecticidal activity of glucose−fipronil conjugates verified the theory of Hsu et al.,[2] in which the incompatibility between mobility and activity was observed. However, FOH (aglycon of GOF) exhibited excellent activity comparable to that of commercialized fipronil (Tables 1 and 2). $LC_{50}$ value (95% confidence limits, CL) after 24 h was found to be 31.49 mg $L^{-1}$ (18.19−54.49 mg $L^{-1}$) against the larvae of *P. xylostella* L., which was analogous to that of fipronil (25.50 mg $L^{-1}$ (16.10−40.40 mg $L^{-1}$)). Meanwhile, the $LC_{50}$ (95% CL) of FOH was 36.34 mg $L^{-1}$ (26.15−50.52 mg $L^{-1}$) against the second-instar larvae of *S. litura* F; the $LC_{50}$ for fipronil was 33.87 mg $L^{-1}$ (25.81−44.45 mg $L^{-1}$). FTO (the aglycon of GOTF) exhibited unsatisfactory insecticidal activity at 500 mg $L^{-1}$, with mortality rates of only 30% against *P. xylostella* L. and 9.7% against *S. litura* F. after 24 h (Table 1). Thus, we inferred that triazolyl could significantly reduce the insecticidal activity of fipronil. However, the results of this study should be further analyzed.

Overall, four glucose−fipronil conjugates were designed and synthesized by click chemistry. Metabolic assays of conjugates in vitro and in vivo were performed. Results demonstrated that the O-glycosidic bond could be recognized and hydrolyzed only by β-glucosidases. Another O-glycosidic bond conjugate GOF was metabolized in *R. communis* L., which released the aglycon FOH with highly analogous efficacy to the commercialized fipronil against *P. xylostella* L. and *S. litura* F. However, further analyses of the location and rate of GOF hydrolysis are required. These results conformed to our initial hypothesis that endogenous β-glucosidases were involved in the hydrolysis of exogenous phloem-mobile conjugates and the release of active aglycons, which can reasonably and feasibly achieve phloem mobility and biological activity of pesticides.

**Table 1. Insecticidal Activities of GOTF, FTO, GOF, FOH, and Fipronil against *P. xylostella* L. and *S. litura* F.**

| | toxicities against *P. xylostella* L. | | toxicities against *S. litura* F. | |
|---|---|---|---|---|
| compd | concn (mg $L^{-1}$) | larvicidal activity (%) | concn (mg $L^{-1}$) | larvicidal activity (%) |
| GOTF | 500 | 16.6 | 500 | 4.0 |
| | 250 | 0 | 250 | 3.3 |
| | 125 | | 125 | 0 |
| FTO | 500 | 30.0 | 500 | 9.7 |
| | 250 | 10.0 | 250 | 0 |
| | 125 | 0 | 125 | |
| GOF | 500 | 20.0 | 500 | 17.2 |
| | 250 | 16.6 | 250 | 10.0 |
| | 125 | 6.70 | 125 | 3.3 |
| FOH | 50 | 63.3 | 100 | 86.7 |
| | 25 | 50.0 | 50 | 43.3 |
| | 12.5 | 20.0 | 25 | 30.0 |
| fipronil | 50 | 73.3 | 100 | 90.0 |
| | 25 | 36.7 | 50 | 50.0 |
| | 12.5 | 33.3 | 25 | 33.3 |

## ■ ASSOCIATED CONTENT

### Ⓢ Supporting Information

Additional spectra. This material is available free of charge via the Internet at http://pubs.acs.org.

## ■ AUTHOR INFORMATION


### Corresponding Author

*(H.-H.X.) Phone: +86-20-85285127. E-mail: hhxu@scau.edu.cn.

### Author Contributions

‖Q.X. and Y.-J.W. contributed equally to this work.



### Funding

Financial support was from the National Natural Science Foundation of China (Grant 31171886) and the Specialized Research Fund for the Doctoral Program of Education of China (Grant 20134404130003).


### Notes

The authors declare no competing financial interest.

## ■ ABBREVIATIONS USED

GTF, *N*-{3-cyano-1-[2,6-dichloro-4-(trifluoromethyl)phenyl]-4-[(trifluoromethyl)sulfinyl]-1*H*-pyrazol-5-yl}-1-(β-D-glucopyranosyl)-1*H*-1,2,3-triazole-4-methanamine; ABA, abscisic acid; ABA-GE, ABA glucose ester; DMF, *N*,*N*-dimethylformamide; TEA, triethylamine; DPPA, diphenylphosphoryl azide; DBU,

**Table 2. $LC_{50}$ Values of FOH and Fipronil against *P. xylostella* L. and *S. litura* F**

| | *P. xylostella* L. | | | *S. litura* F. | | |
|---|---|---|---|---|---|---|
| compd | regression eq | *r* | $LC_{50}$ (mg $L^{-1}$) (95% CL) | regression eq | *r* | $LC_{50}$ (mg $L^{-1}$) (95% CL) |
| FOH | $y = 3.0739 + 1.2857x$ | 0.9489 | 31.49 (18.19−54.49) | $y = 2.3350 + 1.7079x$ | 0.9280 | 36.34 (26.15−50.52) |
| fipronil | $y = 3.0394 + 1.3939x$ | 0.9550 | 25.50 (16.10−40.40) | $y = 1.8019 + 2.0906x$ | 0.9675 | 33.87 (25.81−44.45) |

1,8-diazabicyclo[5.4.0]undec-7-ene; DIPEA, *N*,*N*-diisopropylethylamine; $LC_{50}$, median lethal concentration

## REFERENCES


(1) Lichtner, F. Phloem mobility of crop protection products. *Aust. J. Plant Physiol.* **2000**, *27*, 609−614.

(2) Hsu, F. C.; Sun, K.; Kleier, D. A.; Fielding, M. J. Phloem mobility of xenobiotics VI. A phloem-mobile pro-nematicide based on oxamyl exhibiting root-specific activation in transgenic tobacco. *Pestic. Sci.* **1995**, *44*, 9−19.

(3) Kleier, D. A. Phloem mobility of xenobiotics V. Structural requirements for phloem-systemic pesticides. *Pestic. Sci.* **1994**, *42*, 1−11.

(4) Kleier, D. A. Phloem mobility of xenobiotics I. Mathematical model unifying the weak Acid and intermediate permeability theories. *Plant Physiol.* **1988**, *86*, 803−810.

(5) Yang, W.; Wu, H. X.; Xu, H. H.; Hu, A. L.; Lu, M. L. Synthesis of glucose−fipronil conjugate and its phloem mobility. *J. Agric. Food Chem.* **2011**, *59*, 12534−12542.

(6) Yuan, J. G.; Wu, H. X.; Lu, M. L.; Song, G. P.; Xu, H. H. Synthesis of a series of monosaccharide-fipronil conjugates and their phloem mobility. *J. Agric. Food Chem.* **2013**, *61*, 4236−4241.

(7) Hsu, F. C.; Kleier, D. A. Phloem mobility of xenobiotics VIII. A short review. *J. Exp. Bot.* **1996**, *47*, 1265−1271.

(8) Chollet, J. F.; Rocher, F.; Jousse, C.; Deletage-Grandon, C.; Bashiardes, G.; Bonnemain, J. L. Acidic derivatives of the fungicide fenpiclonil: effect of adding a methyl group to the N-substituted chain on systemicity and fungicidal activity. *Pest Manage. Sci.* **2005**, *61*, 377−382.

(9) Poulton, J. E. Cyanogenesis in plants. *Plant physiol.* **1990**, *94*, 401−405.

(10) Letham, D. S.; Palni, L. M. S. The biosynthesis and metabolism of cytokinins. *Annu. Rev. Plant Physiol.* **1983**, *34*, 163−197.

(11) Morant, A. V.; Jørgensen, K.; Jørgensen, C.; Paquette, S. M.; Sánchez-Pérez, R.; Møller, B. L.; Bak, S. $\beta$-Glucosidases as detonators of plant chemical defense. *Phytochemistry* **2008**, *69*, 1795−1813.

(12) Kleczkowski, K.; Schell, J. Phytohormone conjugates: nature and function. *Crit. Rev. Plant Sci.* **1995**, *14*, 283−298.

(13) Brzobohaty, B.; Moore, I.; Kristoffersen, P.; Bako, L.; Campos, N.; Schell, J.; Palme, K. Release of active cytokinin by a $\beta$-glucosidase localized to the maize root meristem. *Science* **1993**, *262*, 1051−1054.

(14) Lee, K. H.; Piao, H. L.; Kim, H. Y.; Choi, S. M.; Jiang, F.; Hartung, W.; Hwang, I.; Kwak, J. M.; Lee, I. J.; Hwang, I. Activation of glucosidase via stress-induced polymerization rapidly increases active pools of abscisic acid. *Cell* **2006**, *126*, 1109−1120.

(15) Morant, A. V.; Bjarnholt, N.; Kragh, M. E.; Kjaergaard, C. H.; Jorgensen, K.; Paquette, S. M.; Piotrowski, M.; Imberty, A.; Olsen, C. E.; Møller, B. L.; Bak, S. The $\beta$-glucosidases responsible for bioactivation of hydroxynitrile glucosides in *Lotus japonicus*. *Plant Physiol.* **2008**, *147*, 1072−1091.

(16) Coleman, J.; Blake-Kalff, M.; Davies, E. Detoxification of xenobiotics by plants: chemical modification and vacuolar compartmentation. *Trends Plant Sci.* **1997**, *2*, 144−151.

(17) Jones, P.; Vogt, T. Glycosyltransferases in secondary plant metabolism: tranquilizers and stimulant controllers. *Planta* **2001**, *213*, 164−174.

(18) Frear, D. S. Pesticide conjugates-glycosides. In *Bound and Conjugated Pesticide Residues*; Kaufman, D. D., Still, G. G., Paulson, G. D., Bandal, S. K., Eds.; American Chemical Society: Washington, DC, USA, 1976; Vol. 29, Chapter 3, pp 35−54.

(19) Fulton, D. A.; Stoddart, J. F. Synthesis of cyclodextrin-based carbohydrate clusters by photoaddition reactions. *J. Org. Chem.* **2001**, *66*, 8309−8319.

(20) Badía, C.; Souard, F.; Vicent, C. Sugar−oligoamides: synthesis of DNA minor groove binders. *J. Org. Chem.* **2012**, *77*, 10870−10881.

(21) Miller, G. J.; Gardiner, J. M. Adaptable synthesis of C-glycosidic multivalent carbohydrates and succinamide-linked derivatization. *Org. Lett.* **2010**, *12*, 5262−5265.

(22) Bromilow, R. H.; Rigitano, R. L. O.; Briggs, G. G.; Chamberlain, K. Phloem translocation of non-ionised chemicals in *Ricinus communis*. *Pestic. Sci.* **1987**, *19*, 85−99.

(23) Chollet, J. F.; Rocher, F.; Jousse, C.; Delétage Grandon, C.; Bashiardes, G.; Bonnemain, J. L. Synthesis and phloem mobility of acidic derivatives of the fungicide fenpiclonil. *Pest Manage. Sci.* **2004**, *60*, 1063−1072.

(24) Sue, M.; Ishihara, A.; Iwamura, H. Purification and characterization of a hydroxamic acid glucoside beta-glucosidase from wheat (*Triticum aestivum* L.) seedlings. *Planta* **2000**, *210*, 432−438.

(25) Bromilow, R. H.; Chamberlain, K.; Patil, S. G. A rapid method using *Ricinus communis* for the estimation of phloem translocation of xenobiotics. *Pestic. Sci.* **1990**, *30*, 1−12.

(26) Jiang, D. X.; Lu, X. L.; Hu, S.; Zhang, X. B.; Xu, H. H. A new derivative of fipronil: effect of adding a glycinyl group to the 5-amine of pyrazole on phloem mobility and insecticidal activity. *Pestic. Biochem. Physiol.* **2009**, *95*, 126−130.

(27) Tornoe, C. W.; Christensen, C.; Meldal, M. Peptidotriazoles on solid phase: [1,2,3]-triazoles by regiospecific copper(I)-catalyzed 1,3-dipolar cycloadditions of terminal alkynes to azides. *J. Org. Chem.* **2002**, *67*, 3057−3064.

(28) Wilkinson, B. L.; Bornaghi, L. F.; Poulsen, S. A.; Houston, T. A. Synthetic utility of glycosyl triazoles in carbohydrate chemistry. *Tetrahedron* **2006**, *62*, 8115−8125.

(29) Padrón, J. I.; Vázquez, J. T. Ferric chloride: an excellent reagent for the removal of benzyl ethers in the presence of *p*-bromobenzoate esters. *Tetrahedron: Asymmetry* **1995**, *6*, 857−858.

(30) Flury, T.; Hall, R. G.; Karrer, F.; Kienast, H.; Leuenberger, K.; Pascual, A.; Rindlisbacher, A.; Trah, S.; Widmer, H. J. Substituted $\alpha$-(phenylhydrazono) phenylacetonitrile derivatives. Part 2: synthesis and biological activity of pro-pesticides. *Pest Manage. Sci.* **2006**, *62*, 236−241.

(31) O'Keefe, D. P.; Tepperman, J. M.; Dean, C.; Leto, K. J.; Erbes, D. L.; Odell, J. T. Plant expression of a bacterial cytochrome P450 that catalyzes activation of a sulfonylurea pro-herbicide. *Plant Physiol.* **1994**, *105*, 473−482.

(32) Dale, P. J.; Clarke, B.; Fontes, E. M. G. Potential for the environmental impact of transgenic crops. *Nat. Biotechnol.* **2002**, *20*, 567−574.

(33) Minic, Z. Physiological roles of plant glycoside hydrolases. *Planta* **2008**, *227*, 723−740.

controlled, and more comprehensive research should be conducted.

In this Article, field experiments of penconazole were conducted, and then cucumber, tomato, head cabbage, and pakchoi samples were collected for analysis. A simple pretreatment method was adopted on the basis of buffered QuEChERS (quick, easy, cheap, effective, rugged, and safe) for the extraction, cleanup, and preconcentration of penconazole.[27,28] The chiral analysis method of penconazole was established by liquid chromatography−tandem mass spectrometry (LC−MS/MS) equipped with a Lux Cellulose-2 chiral column. Finally, the result suggested that penconazole showed enantioselective dissipation in head cabbage and pakchoi, but not in the cucumber and tomato samples. The results in this Article might also provide some sufficient information on penconazole during the food and environment risk assessment.

## MATERIALS AND METHODS

**Chemicals and Materials.** The analytical standard of (±)-penconazole (purity 99.0%) was purchased form Dr. Ehrenstorfer (Augsburg, Germany). The commercial product of penconazole-EC (10% of (±)-penconazole) was obtained from the Hangzhou Udragon Chemical Co. Ltd. (Zhejiang, China). Purified water was prepared by using a Milli-Q water purification system (Millipore Corp., Billerica, U.S.). LC grade methanol ($CH_3OH$) and acetonitrile ($CH_3CN$) were obtained from Merck (Darmstadt, Germany). Formic acid and ammonium acetate were obtained from TEDIA (Fairfield, U.S.). Acetic acid was obtained from Sigma-Aldrich (St. Louis, U.S.). Silica-based sorbents including $C_{18}$ (40 μm particle size) and primary secondary amine (PSA) (40 μm particle size) were obtained from Agilent (Wilmington, U.S.). All other chemicals and solvents were of analytical grade and were purchased from commercial sources.

**Field Experiments.** The vegetable (cucumber, tomato, head cabbage, and pakchoi) seeds purchased from Longda Seeds (Hangzhou, China) were sown in greenhouse conditions on 7 February 2012. The field experiments were conducted from March to May 2012 in Zhejiang Academy of Agricultural Sciences (Hangzhou, China). Every experiment treatment for a vegetable contained three replicate plots and a control plot without penconazole. The area of each plot was 30 (10 × 3) $m^2$, and the buffer zone was set up between plots. These plots had never been treated with penconazole for more than 3 years. (±)-Penconazole 10% EC was applied as foliar spray at the dose of 47.6 g a.i. $ha^{-1}$ (gram of active ingredient per hectare), dissolving in 2 L of water. Approximately 2 kg of vegetable samples was collected from nine randomly selected sampling points within each plot, at 0 (1 h after spraying), 1, 2, 3, 5, 7, 10, 14, and 21 days after spray. All vegetable samples were homogenized by a blender (Philips, China), and then stored at −20 °C until further analysis.

**Enantioselective LC−MS/MS Analysis.** LC−MS/MS analyses were performed on a Surveyor liquid chromatograph equipped with a TSQ Discovery triple quadrupole mass spectrometer (Thermo Fisher Scientific, U.S.). Thermo Fisher Xcalibur software (version 2.0.7) was used for data quantitation and documentation.

A satisfactory enantioseparation of penconazole was performed on a Lux Cellulose-2 chiral column (150 mm × 2.0 mm i.d., 3 μm, Phenomenex, U.S.) packed with cellulose tris (3-chloro-4-methylphenylcarbamate). The analysis was isocratic at 0.2 mL $L^{-1}$ flow rate using mobile phase A (LC grade methanol) and mobile phase B (0.1% formic acid and 2 mM ammonium acetate in water) in a 70:30 v/v ratio. The column temperature was kept at 25 °C, and the autosampler temperature was set at 4 °C. The sample injection volume was 10 μL, and the total run time was 25 min.

The ESI−MS/MS (electrospray ionization coupled with tandem mass spectrometry) was performed in positive ion mode, and the monitoring conditions were optimized for penconazole. The typical ESI source conditions were as follows: ion spray voltage, 4200 V; ion capillary temperature, 350 °C; sheath gas flow ($N_2$), 35 (arbitrary) units; aux gas flow ($N_2$), 8 U; collision gas pressure (Ar), 1.5 mTorr. Multiple reactions monitoring (MRM) mode was applied to determine the fragmentation of the protonated pseudomolecular ions of penconazole. The transitions $m/z$ 284 > 159 and $m/z$ 284 > 70 were used for quantification and confirmation, respectively. The corresponding collision energies were 15 and 20 eV.

**Elution Order Determination of Penconazole Enantiomers.** The optical rotation dispersion (ORD) signal of (+) or (−) was used to distinguish the elution order of the enantiomers by an Agilent 1200 HPLC system equipped with a G1315B diode array detector (Wilmington, U.S.) and online CHIRALYSER-MP optical rotation detector (IBZ Messtechnik, Germany). The signal was received and processed by Agilent 1200 chemstation and N2000 SP1 chromatographic chemstation (Zhida, China) software. The chiral separation was performed under the same LC conditions as LC−MS/MS, but the injection volume was 20 μL and the flow rate was set at 1.0 mL/min with the UV detection at 230 nm.

**Sample Preparation.** Samples were thawed previously at room temperature. A 15 g triturated vegetable sample was weighed into a 50 mL polypropylene centrifuge tube, and 15 mL of acetonitrile containing 1% of acetic acid was added. The mixture was shaken by a vortex mixer for 1 min and then sonicated for 15 min. Subsequently, 6 g of anhydrous magnesium sulfate and 1.5 g of anhydrous sodium acetate were added, and the tube was shaken vigorously by hand for 5 min and centrifuged at 6000 rpm for 5 min. A 1 mL aliquot of upper acetonitrile supernatant was transferred into a 2 mL centrifuge tube containing 50 mg of PSA sorbent, 50 mg of C18 sorbent, and 150 mg of anhydrous magnesium sulfate for cleanup. The tube was shaken by vortex mixer for 1 min and centrifuged at 6000 rpm for 5 min. A 0.5 mL portion of the upper extracts was transferred into a 2 mL centrifuge tube containing 0.5 mL of water. The resulting solution was filtered through a 0.22 μm Teflon syringe filter for LC−MS/MS analysis.

**Method Validation.** A series of working standard solutions and matrix-matched calibration standard of (±)-penconazole for linearity of the method were prepared at 0.5, 1, 2.5, 5, 25, 100, and 500 μg $L^{-1}$ for each enantiomer. The calibration curves were generated by plotting the peak area of quantification ion transition versus the concentration of each enantiomer. Linear regression analysis was performed using Microsoft Excel 2007, and the correlation coefficient was used to evaluate linearity of the method.

The accuracy and precision of the method were investigated to evaluate its reliability. The blank vegetable samples obtained from the field experiment were fortified with standard solutions of each enantiomer at three levels (2.5, 50, and 500 μg $kg^{-1}$). Recovery experiments were carried out with five replicates for each level, and fortified samples were equilibrated for 1 h at room temperature prior to extraction as described above. The precision of the method was investigated by the repeatability (intraday assays) and reproducibility (interday assays), expressed by relative standard deviation (RSD). The repeatability assays were measured in five replicates at three concentration levels on the same day, with the same instrument and by the same operator. The reproducibility assays were evaluated in five replicates at the earlier stated concentration levels on three different days, with the same instrument but by different operators.

The limits of detection (LODs) for each enantiomer were calculated as 3 times the signal-to-noise (peak to peak) ratio of the quantitative ion transition by the lowest spiked analytes concentration assayed with five replicates. The limits of quantification (LOQs) were defined as the lowest concentration with acceptable accuracy for 70−120% and precision for 15% variability.

## RESULTS AND DISCUSSION

**Enantioseparation and Identification Elution Order of Penconazole.** Under the LC−MS/MS condition, the enantiomers of penconazole were separated completely on a Lux Cellulose-2 column (as shown in Figure 4). In this work, an online ORD was used to distinguish the elution order information on penconazole enantiomers based on the difference of the refractive index between left (−) and right

Table 1. Comparison of Matrix-Matched Calibration and Solvent Calibration (0.5−500 $\mu$g $L^{-1}$)

| compound | matrix | standard linear equation | $R^2$ | slope of matrix/slope of solvent |
|---|---|---|---|---|
| (+)-penconazole | solvent | $Y = 130131X + 50683$ | 0.9983 | |
| | cucumber | $Y = 128910X + 23523$ | 0.9998 | 0.991 |
| | tomato | $Y = 129063X + 37715$ | 0.9992 | 0.992 |
| | head cabbage | $Y = 121242X + 47990$ | 0.9986 | 0.937 |
| | pakchoi | $Y = 128443X + 46901$ | 0.9988 | 0.987 |
| (−)-penconazole | solvent | $Y = 128074X + 51929$ | 0.9982 | |
| | cucumber | $Y = 125365X + 39602$ | 0.9991 | 0.979 |
| | tomato | $Y = 127859X + 39504$ | 0.9989 | 0.998 |
| | head cabbage | $Y = 118915X + 45003$ | 0.9987 | 0.928 |
| | pakchoi | $Y = 125778X + 37255$ | 0.9987 | 0.982 |

Table 2. Recovery and Precision of the Method in Vegetable Samples

| | | mean recoveries ($n$ = 15; %) (RSD[a] %, RSD[b] %) | | |
|---|---|---|---|---|
| | | fortified level ($\mu$g $kg^{-1}$) | | |
| compound | matrix[c] | 2.5 | 50 | 500 |
| (+)-penconazole | C | 89.5 (4.8, 7.5) | 98.7 (8.2, 7.3) | 101 (7.6, 8.3) |
| | T | 85.9 (5.4, 6.6) | 79.4 (5.7, 8.2) | 100 (4.7, 5.3) |
| | H | 98.9 (5.9, 8.5) | 86.5 (4.2, 8.9) | 87.0 (3.6, 8.5) |
| | P | 78.5 (5.4, 10.4) | 82.2 (2.8, 9.2) | 86.0 (5.1, 8.3) |
| (−)-penconazole | C | 90.3 (5.2, 7.6) | 98.0 (9.2, 7.7) | 101 (8.0, 8.5) |
| | T | 88.3 (4.1, 6.2) | 80.4 (4.1, 7.8) | 97.4 (7.2, 8.4) |
| | H | 102 (5.3, 7.4) | 86.8 (7.8, 11.5) | 89.3 (3.9, 9.8) |
| | P | 79.6 (6.5, 9.6) | 84.6 (4.9, 6.3) | 87.9 (5.8, 6.0) |

[a]RSD represents the relative standard deviation of intraday ($n$ = 5). [b]RSD represents the relative standard deviation of interday ($n$ = 15). [c]C represents cucumber. T represents tomato. H represents head cabbage. P represents pakchoi.

(+) linearly polarized lights. The results showed that the first eluted enantiomer was confirmed as (+)-penconazole, while the second eluted enantiomer was (−)-penconazole under the LC condition described above.

**Method Development and Validation.** The sample extraction and cleanup procedure for penconazole enantiomers in vegetables followed the buffered QuEChERS method. Validation of the proposed method included linearity, recovery, and precision. Good linear calibration curves for both enantiomers were obtained over the range of 0.5−500 $\mu$g $L^{-1}$. The linear equations for each enantiomer in standard solutions and matrix-matched solutions are listed in Table 1. The matrix effect was calculated by comparing the slope of matrix-matched standard curve with the slope of solvent standard calibration curve.[29] The slope ratios of matrix-matched to solvent-based calibration listed in Table 1 were in the range of 0.928−0.998, which implied no significant matrix effect for enantiomers of penconazole in the four vegetable matrixes.

The recoveries of penconazole enantiomers in vegetable matrixes at three spiked levels ranged from 78.5% to 102%, and the RSDs of repeatability and reproducibility ranged from 2.8% to 11.5% (see Table 2). The results of recoveries and precisions obtained in the method validation portion proved that the method was efficient and reliable to determine the enantiomers of penconazole in the four vegetables with LC−MS/MS. The LODs for both enantiomers in the tested vegetables were estimated to be 0.5 $\mu$g $kg^{-1}$, while the LOQs of enantiomers in vegetables were 2.5 $\mu$g $kg^{-1}$ based on the lowest fortified level in the tested vegetables.

**Residues Dissipation of Penconazole in Cucumber and Tomato.** Penconazole residue dissipation in cucumber and tomato was investigated under field conditions. In Figure 2, the data were plotted from cucumber and tomato as normalized concentrations ($100C/C_0$) versus treatment time. Figure 2 shows that the residues of penconazole decreased quickly with time in cucumber and tomato when the (±)-penconazole was sprayed, and the dissipation processes followed first-order kinetics. The depletion rate constant were obtained by fitting the enantiomer of penconazole residue data from each experiment to the first-order kinetic equation $\ln(C/C_0) = -kt$, where $C_0$ is the initial concentration of the enantiomer ($\mu$g $kg^{-1}$), $C$ is its concentration ($\mu$g $kg^{-1}$) at time $t$ (days), $k$ is the depletion rate constant, and the corresponding half-lives ($t_{1/2}$) were calculated as $t_{1/2} = \ln 2/k = 0.693/k$.[30] The depletion rate constant, half-life, and correlation coefficient ($R^2$) of the two enantiomers are shown in Table 3, and the data show that the depletion rates of the two enantiomers in cucumber and tomato were similar to $t_{1/2}$ ranging from 1.52 to 1.98 days.

In this study, the enantiomeric ratio (ER) was used as a measure of the enantioselectivity of the residues dissipation of penconazole in vegetables. The ER value was defined as the concentration of the first eluting (+)-enantiomer divided by the concentration of the later eluting (−)-enantiomer.[31] It was shown in Figure 3 that the ER values of (±)-penconazole were constant with time in cucumber and tomato. Student's $t$-tests were made to compare the mean ER values of (±)-penconazole in the two vegetables with ER = 1 at a 95% confidence interval. The statistical test results indicated that the dissipation of penconazole enantiomers was not enantioselective either in cucumber ($p$ = 0.17) or in tomato ($p$ = 0.30).

**Residue Dissipation of Penconazole in Head Cabbage and Pakchoi.** The residue dissipation of penconazole enantiomers in head cabbage and pakchoi was investigated under field conditions with (±)-penconazole foliage sprayed. Generally, the residues of both enantiomers of penconazole decreased quickly with time elapsed in the head cabbage and

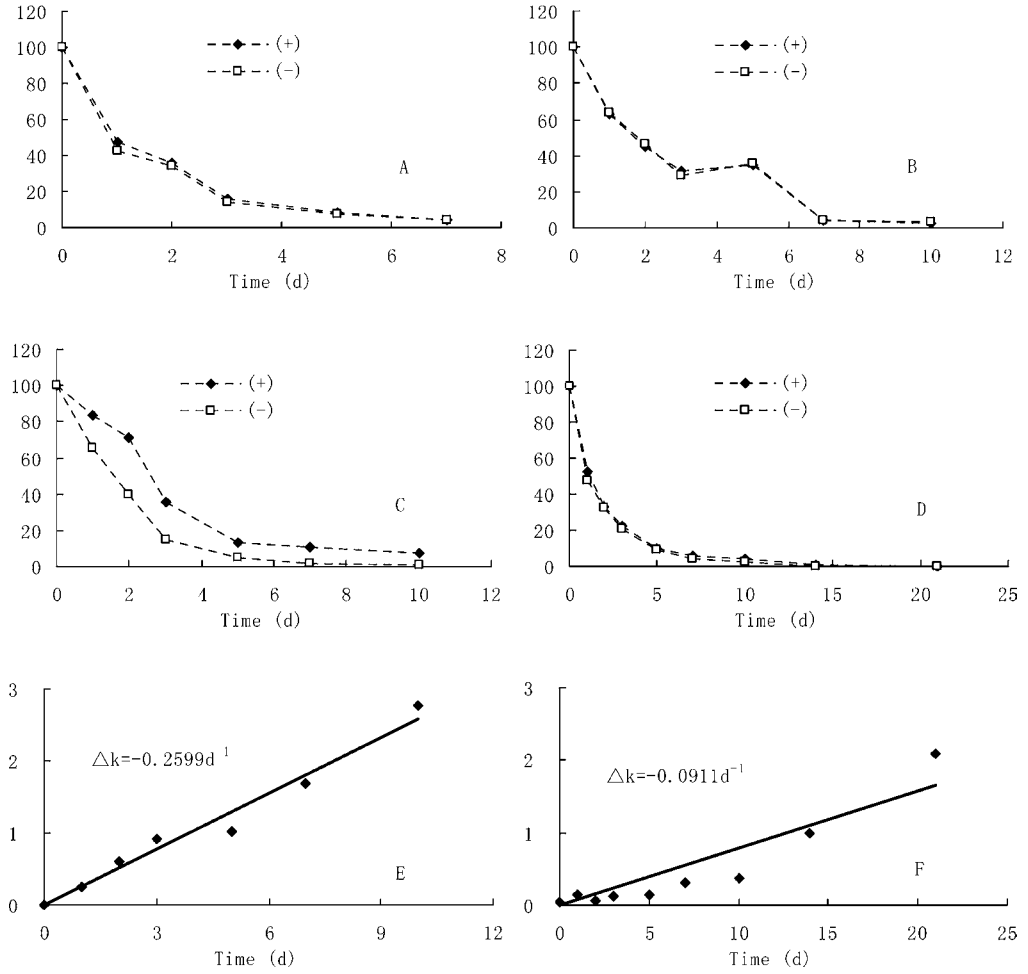


**Figure 2.** Degradation of penconazole enantiomers in (A) cucumber, (B) tomato, (C) head cabbage, and (D) pakchoi. Normalized concentrations ($100C/C_0$) are plotted versus treatment time (d). Note the faster degradation of the (−)-enantiomer. Plot of ln(ER) from (E) head cabbage and (F) pakchoi after treatment with (±)-penconazole versus treatment time showing a linear relationship.

**Table 3. First-Order Depletion Rate Constant ($k$), Initial Concentration ($C_0$), Half-Life ($t_{1/2}$), and Correlation Coefficient ($R^2$) for the Enantioselective Dissipation of Penconazole**

| experiment | compound | $k$ (day$^{-1}$) | $C_0$ ($\mu$g kg$^{-1}$)[a] | $t_{1/2}$ (day)[a] | $R^2$ |
|---|---|---|---|---|---|
| cucumber | (+)-penconazole | 0.4536 | 39.3 ± 3.6 | 1.53 ± 0.07 | 0.9756 |
| | (−)-penconazole | 0.4547 | 43.1 ± 1.9 | 1.52 ± 0.09 | 0.9667 |
| tomato | (+)-penconazole | 0.3636 | 49.6 ± 4.0 | 1.90 ± 0.12 | 0.9117 |
| | (−)-penconazole | 0.3491 | 50.9 ± 1.9 | 1.98 ± 0.06 | 0.9025 |
| head cabbage | (+)-penconazole | 0.2899 | 119.6 ± 7.7 | 2.39[b] ± 0.05 | 0.9165 |
| | (−)-penconazole | 0.5497 | 118.4 ± 5.1 | 1.26[b] ± 0.11 | 0.9895 |
| pakchoi | (+)-penconazole | 0.2720 | 449.3 ± 8.7 | 2.55[b] ± 0.03 | 0.9553 |
| | (−)-penconazole | 0.3632 | 435.0 ± 6.7 | 1.91[b] ± 0.07 | 0.9861 |

[a]Values represent the means ± SDs ($n$ = 3). [b]Significantly different from each other, $p < 0.05$ (paired $t$ test).

pakchoi (see Figure 2), and the typical LC−MS/MS chromatograms are shown in Figure 4. In Figure 2C and D, the data were plotted from head cabbage and pakchoi as normalized concentration ($100C/C_0$) versus time, and it was obvious that the second-eluted (−)-enantiomer dissipated more rapid than the other enantiomer, leading to residues enriched in (+)-form. By calculation, the depletion rate constant followed first-order kinetics and the half-life of each enantiomers is listed in Table 3, and these data also demonstrated that (−)-enantiomer ($t_{1/2}$ = 1.26 and 1.91 days, respectively) degraded faster than (+)-enantiomer ($t_{1/2}$ = 2.39 and 2.55 days, respectively) in the two tested vegetables. The statistical analysis was also performed, and the result suggested that the difference of the two enantiomers was significant ($p < 0.05$, student's paired $t$ test).

In Figure 3C and D, the variation curve of ER value was plotted versus time from head cabbage and pakchoi, and it could be found that the ER values of penconazole consistently increased with time in both vegetables. Student's $t$ tests were made to compare the mean ER values of (±)-penconazole in the two vegetables with ER = 1 at a 95% confidence interval. The statistical test results indicated there was substantial enantioselectivity on the dissipation of (±)-penconazole in

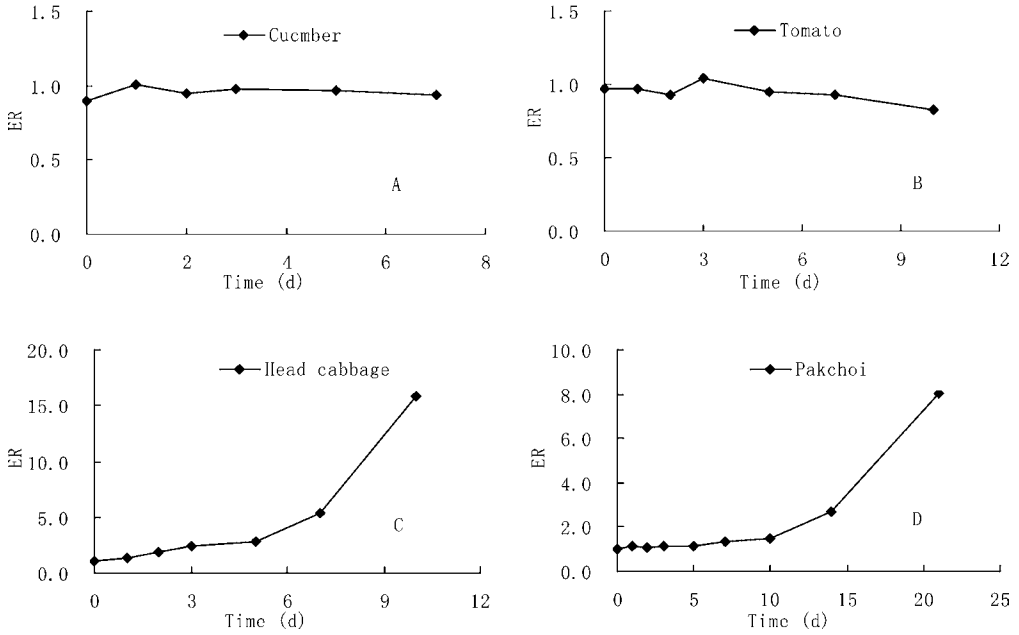


**Figure 3.** Enantiomeric ratio (ER) of penconazole residues in (A) cucumber, (B) tomato, (C) head cabbage, and (D) pakchoi.

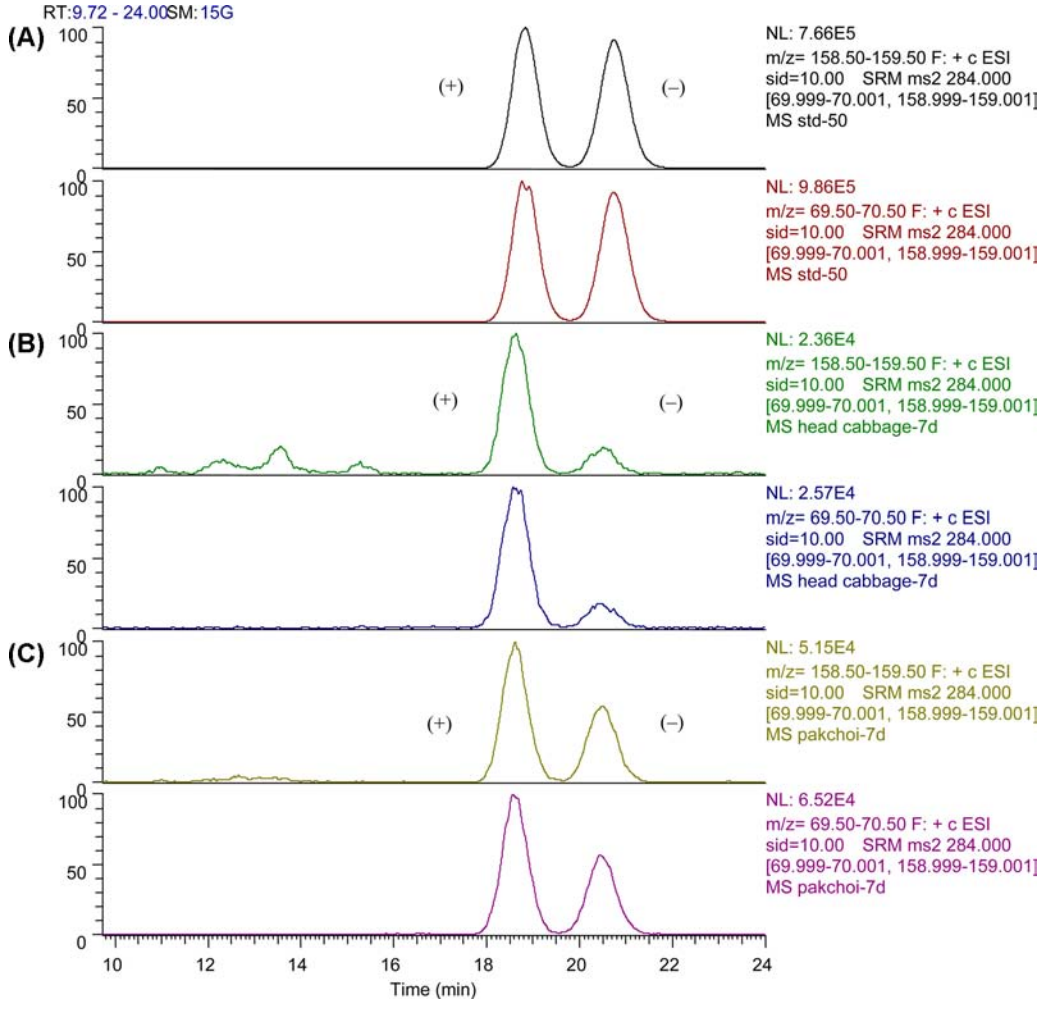


**Figure 4.** Representative chromatograms of (A) (±)-penconazole standard (50 $\mu$g L$^{-1}$), (B) extract from head cabbage at 7 d after treatment with (±)-penconazole, and (C) extract from pakchoi at 7 d after treatment with (±)-penconazole.


dx.doi.org/10.1021/jf5034653 | J. Agric. Food Chem. 2014, 62, 11047−11053

head cabbage ($p$ = 0.005) and pakchoi ($p$ = 0.016) under the field experiments.

The dissipation processes of penconazole enantiomers in the test vegetables followed first-order kinetics with a depletion rate constant of $k_{(+)}$ for the (+)-enantiomer, and a depletion rate constant of $k_{(-)}$ for the (−)-form; ER may be expressed as an equation of time ($t$) in the following relationship:[32,33]

$$ER_t = [+]/[-] = ER_0 \times e^{\{k_{(-)} - k_{(+)}\}} = ER_0 \times e^{\Delta k} \quad (1)$$

where $ER_0$ is the initial ER value at 1 h after spraying with (±)-penconazole in head cabbage and pakchoi, [+] and [−] are the concentrations of (+)-enantiomer and (−)-enantiomer at time $t$, respectively, and $\Delta k$ is the difference from $ER_0$ over time. The above relationship can be further expressed in a linear form after logarithmic transformation of ER:

$$\ln(ER_t) = \ln(ER_0) + \Delta k \quad (2)$$

Equation 2 indicated a linear relationship between $\ln(ER_t)$ and time ($t$), and we showed the data plotted in Figure 2E and F, which could be used to determine the rate difference $\Delta k$ and thus enantioselectivity. The $\Delta k$ calculated from these plots for head cabbage and pakchoi is 0.2599 and 0.0911 $d^{-1}$, respectively. The results also suggested that greater enantioselectivity of penconazole occurred in head cabbage than that in pakchoi.

In the present study, the dissipation of the two enantiomers of penconazole was investigated in the four test vegetables. The results showed that the (−)-penconazole degraded faster than the (+)-isomer in head cabbage and pakchoi, which meant enantioselectivity happened. However, no obvious enantioselectivity of dissipation behavior existed in cucumber and tomato. Some studies[16,17,20,23,24] verified that other triazole fungicides, such as hexaconazole, tebuconazole, and myclobutanil, exhibited stereoselectivity of degradation in cucumber or tomato. Many researchers[34−38] indicated that whether enantioselective behavior occurred or not may be related to the metabolic enzyme system in plant during the process of chiral pesticide biotransformation. Further research should be done to identify the metabolic enzyme systems related to penconazole biotransformation in vegetables. Meanwhile, research concerning the bioactivities and toxicities of individual enantiomer of penconazole also should be conducted to provide adequate information for further food safety risk evaluation of penconazole enantiomers.

## AUTHOR INFORMATION


### Corresponding Author

*Phone: 86-571-86404355. Fax: 86-571-86401834. E-mail: wangqiang2003@sina.com.



### Funding

This study was supported by the National High Technology Research and Development Program of China (The 863 Program, Grant No. 2011AA100806), and the Special Fund for Agro-scientific Research in the Public Interest (Grant No. 201303088).


### Notes

The authors declare no competing financial interest.

## REFERENCES


(1) Buchenauer, H. Mechanism of action of triazolyl fungicides and related compounds. In *Modern Selective Fungicides: Properties, Applications, Mechanisms of Action*; Lyr, H., Ed.; Longman Scientific and Technical: Harlow, 1987; pp 205−231.

(2) Crofton, K. A structure-activity relationship for the neurotoxicity of triazole fungicides. *Toxicol. Lett.* **1996**, *84*, 155−159.

(3) Filipov, N. M.; Lawrence, D. A. Developmental toxicity of a triazole fungicide: consideration of interorgan communication. *Toxicol. Sci.* **2001**, *62*, 185−186.

(4) Liu, W.; Gan, J.; Schlenk, D.; Jury, W. A. Enantioselectivity in environmental safety of current chiral insecticides. *Proc. Natl. Acad. Sci. U.S.A.* **2005**, *102*, 701−706.

(5) Zhang, Q.; Wang, C.; Zhang, X.; Jin, D.; Huang, C.; Zhao, M. Enantioselective aquatic toxicity of current chiral pesticides. *J. Environ. Monit.* **2012**, *14*, 465−472.

(6) Garrison, A. W. Probing the enantioselectivity of chiral pesticides. *Environ. Sci. Technol.* **2006**, *40*, 16−23.

(7) Sekhon, B. S. Chiral pesticides. *J. Pestic. Sci.* **2009**, *34*, 1−12.

(8) Yang, L.; Li, S.; Li, Y.; Gao, R. Bioactivity of triazole fungicide enantiomers. *Chin. J. Pestic. Sci.* **2002**, *4*, 67−70.

(9) Dong, F.; Li, J.; Chankvetadze, B.; Cheng, Y.; Xu, J.; Liu, X.; Li, Y.; Chen, X.; Bertucci, C.; Tedesco, D. Chiral triazole fungicide difenoconazole: absolute stereochemistry, stereoselective bioactivity, aquatic toxicity, and environmental behavior in vegetables and soil. *Environ. Sci. Technol.* **2013**, *47*, 3386−3394.

(10) Kurihara, N.; Miyamoto, J.; Paulson, G.; Zeeh, B.; Skidmore, M.; Hollingworth, R.; Kuiper, H. Chirality in synthetic agrochemicals: bioactivity and safety consideration. *Pure Appl. Chem.* **1997**, *69*, 1335−1348.

(11) Burden, R. S.; Carter, G. A.; Clark, T.; Cooke, D. T.; Croker, S. J.; Deas, A. H.; Hedden, P.; James, C. S.; Lenton, J. R. Comparative activity of the enantiomers of triadimenol and paclobutrazol as inhibitors of fungal growth and plant sterol and gibberellin biosynthesis. *Pestic. Sci.* **1987**, *21*, 253−267.

(12) Huang, L.; Lu, D.; Zhang, P.; Diao, J.; Zhou, Z. Enantioselective toxic effects of hexaconazole enantiomers against scenedesmus obliquus. *Chirality* **2012**, *24*, 610−614.

(13) Cheng, C.; Huang, L.; Diao, J.; Zhou, Z. Enantioselective toxic effects and degradation of myclobutanil enantiomers in scenedesmus obliquus. *Chirality* **2013**, *25*, 858−864.

(14) Kenneke, J. F.; Mazur, C. S.; Kellock, K. A.; Overmyer, J. P. Mechanistic approach to understanding the toxicity of the azole fungicide triadimefon to a nontarget aquatic insect and implications for exposure assessment. *Environ. Sci. Technol.* **2009**, *43*, 5507−5513.

(15) Li, Z.; Zhang, Y.; Li, Q.; Wang, W.; Li, J. Enantioselective degradation, abiotic racemization, and chiral transformation of triadimefon in soils. *Environ. Sci. Technol.* **2011**, *45*, 2797−2803.

(16) Wang, X.; Wang, X.; Zhang, H.; Wu, C.; Wang, X.; Xu, H.; Wang, X.; Li, Z. Enantioselective degradation of tebuconazole in cabbage, cucumber, and soils. *Chirality* **2012**, *24*, 104−111.

(17) Li, J.; Dong, F.; Cheng, Y.; Liu, X.; Xu, J.; Li, Y.; Chen, X.; Kong, Z.; Zheng, Y. Simultaneous enantioselective determination of triazole fungicide difenoconazole and its main chiral metabolite in vegetables and soil by normal-phase high-performance liquid chromatography. *Anal. Bioanal. Chem.* **2012**, *404*, 2017−2031.

(18) Shen, Z.; Zhang, P.; Xu, X.; Wang, X.; Zhou, Z.; Liu, D. Gender-related differences in stereoselective degradation of flutriafol in rabbits. *J. Agric. Food Chem.* **2011**, *59*, 10071−10077.

(19) Buerge, I. J.; Poiger, T.; Mueller, M. D.; Buser, H.-R. Influence of pH on the stereoselective degradation of the fungicides epoxiconazole and cyproconazole in soils. *Environ. Sci. Technol.* **2006**, *40*, 5443−5450.

(20) Wang, X.; Zhang, H.; Xu, H.; Wang, X.; Wu, C.; Yang, H.; Li, Z.; Wang, Q. Enantioselective residue dissipation of hexaconazole in cucumber (Cucumis sativus L.), head cabbage (Brassica oleracea L. var. caulorapa DC.), and soils. *J. Agric. Food Chem.* **2012**, *60*, 2212−2218.

(21) Li, C.; Zhang, Y.; L, L.; W, W.; L, J. The seperation and transformation of triazole fungicides. *Chin. J. Anal. Chem.* **2010**, *38*, 37−40.

(22) Zhang, H.; Wang, X.; Qian, M.; Wang, X.; Xu, H.; Xu, M.; Wang, Q. Residue analysis and degradation studies of fenbuconazole and myclobutanil in strawberry by chiral high-performance liquid chromatography−tandem mass spectrometry. *J. Agric. Food Chem.* **2011**, *59*, 12012−12017.
(23) Dong, F.; Liu, X.; Zheng, Y.; Cao, Q.; Li, C. Stereoselective degradation of fungicide triadimenol in cucumber plants. *Chirality* **2010**, *22*, 292−298.
(24) Wang, Q.; Qiu, J.; Zhou, Z.; Cao, A.; Wang, X.; Zhu, W.; Dang, Z. Stereoselective pharmacokinetics of diniconazole enantiomers in rabbits. *Chirality* **2009**, *21*, 699−703.
(25) El-Sharkawy, E. E.; El-Nisr, N. A. Testicular dysfunction induced by penconazole fungicide on male albino rats. *Comp. Clin. Pathol.* **2013**, *22*, 475−480.
(26) Perdichizzi, S.; Mascolo, M. G.; Silingardi, P.; Morandi, E.; Rotondo, F.; Guerrini, A.; Prete, L.; Vaccari, M.; Colacci, A. Cancer-related genes transcriptionally induced by the fungicide penconazole. *Toxicol. In Vitro* **2014**, *28*, 125−130.
(27) Lehotay, S. J.; Mastovska, K.; Lightfield, A. T. Use of buffering and other means to improve results of problematic pesticides in fast and easy method for residue analysis of fruits and vegetables. *J. AOAC Int.* **2005**, *88*, 615−629.
(28) Wang, J.; Leung, D.; Chow, W. Applications of LC/ESI-MS/MS and UHPLC QqTOF MS for the determination of 148 pesticides in berries. *J. Agric. Food Chem.* **2010**, *58*, 5904−5925.
(29) Gosetti, F.; Mazzucco, E.; Zampieri, D.; Gennaro, C. M. Signal suppression/enhancement in high-performance liquid chromatography tandem mass spectrometry. *J. Chromatogr., A* **2010**, *1217*, 3929−3937.
(30) Martins, J. M.; Mermoud, A. Sorption and degradation of four nitro aromatic herbicides in mono- and multi-solute saturated/unsaturated soil batch systems. *J. Contam. Hydrol.* **1998**, *33*, 187−210.
(31) Garrison, A. W.; Schmitt, P.; Martens, D.; Kettup, A. Enantiomeric selectivity in the environmental degradation of dichlorprop as determined by high-performance capillary electrophoresis. *Environ. Sci. Technol.* **1996**, *30*, 2449−2455.
(32) Diao, J.; Xu, P.; Wang, P.; Lu, D.; Lu, Y.; Zhou, Z. Enantioselective degradation in the sediment and aquatic toxicity to daphnia magna of the herbicide lactofen enantiomers. *J. Agric. Food Chem.* **2010**, *58*, 2439−2445.
(33) Marucchini, C.; Zadra, C. Stereoselective degradation of metalaxyl and metalaxyl-M in soil and sunflower plants. *Chirality* **2002**, *14*, 32−38.
(34) Gu, X.; Wang, P.; Liu, Y.; Zhou, Z. Stereoselective degradation of diclofop-methyl in soil and Chinese cabbage. *Pestic. Biochem. Phys.* **2008**, *92*, 1−7.
(35) Wang, X. Q.; Jia, G. F.; Qiu, J.; Diao, J. L.; Zhu, W. T.; Lv, C. G.; Zhou, Z. Q. Stereoselective degradation of fungicide benalaxyl in soils and cucumber plants. *Chirality* **2007**, *19*, 300−306.
(36) Liu, D.; Wang, P.; Zhu, W.; Gu, X.; Zhou, W.; Zhou, Z. Enantioselective degradation of fipronil in Chinese cabbage (Brassica pekinensis). *Food Chem.* **2008**, *110*, 399−405.
(37) Lu, D.; Liu, D.; Gu, X.; Diao, J. L.; Zhou, Z. Stereoselective metabolism of fipronil in water hyacinth (Eichhornia crassipes). *Pestic. Biochem. Phys.* **2010**, *97*, 289−293.
(38) Dong, F.; Cheng, L.; Liu, X.; Xu, J.; Li, J.; Li, Y.; Kong, Z.; Jian, Q.; Zheng, Y. Enantioselective analysis of triazole fungicide myclobutanil in cucumber and soil under different application modes by chiral liquid chromatography/tandem mass spectrometry. *J. Agric. Food Chem.* **2015**, *60*, 1929−1936.

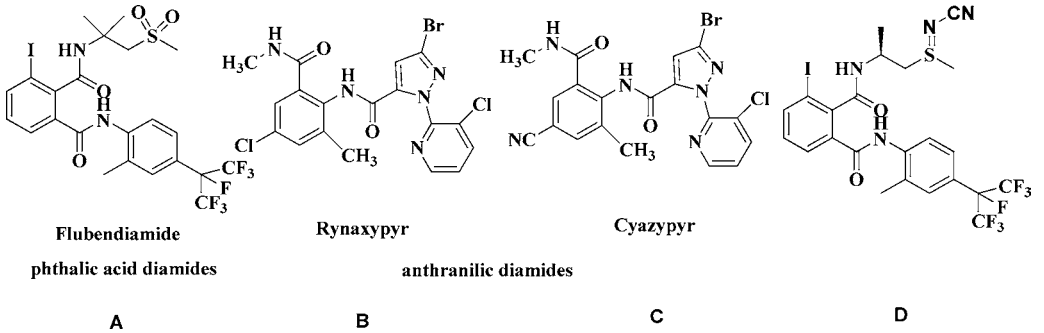


Figure 1.

**General Synthetic Procedures for Compounds 1a−g, 2a−f, 3a−c,e, and 4a−c,e.** These phthalamide intermediates **1a−d,f**, **2a−d,2f**, **3a−c**, **4a−c** were synthesized according to the method reported in our previous publication (Scheme 1) .[19]

(*S*,*R*)-$N^2$-(1-(*N*-Cyano-*S*-methylsulfinimidoyl)propan-2-yl)-$N^1$-(2-methyl-4-(perfluoropropan-2-yl)phenyl)phthalamide, **1e**: white solid; yield 68.3%, mp 107−109 °C; $^1$H NMR (300 MHz, DMSO-$d_6$) $\delta$ 10.00 (s, 1H), 8.74 (d, $J$ = 6.7 Hz, 1H), 7.81−7.79 (d, $J$ = 6.0 Hz, 1H), 7.68−7.54 (m, 6H), 4.32−4.24 (m, 1H), 3.25 (d, $J$ = 7.0 Hz, 1H), 2.80 (s, 3H), 2.39 (s, 3H), 1.28 (d, $J$ = 3.9 Hz, 3H). HRMS calcd for $C_{23}H_{21}F_7N_4O_2SH$ ([M + H]$^+$), 551.1346; found, 551.1349. $[\alpha]^{20}_D$ = −64.2 (*c* 10, MeOH).

(*S*,*S*)-$N^2$-(1-(*N*-Cyano-*S*-methylsulfinimidoyl)propan-2-yl)-$N^1$-(2-methyl-4-(perfluoropropan-2-yl)phenyl)phthalamide, **2e**: white solid; yield 31.7%; mp 114−116 °C; $^1$H NMR (400 MHz, DMSO-$d_6$) $\delta$ 10.01 (s, 1H), 8.59 (d, $J$ = 7.7 Hz, 1H), 7.80 (d, $J$ = 8.2 Hz, 1H), 7.67−7.53 (m, 6H), 4.33−4.25 (m, 1H), 3.28 (d, $J$ = 8.7 Hz, 2H), 2.80 (s, 3H), 2.38 (s, 3H), 1.28 (d, $J$ = 6.4 Hz, 3H). HRMS calcd for $C_{23}H_{21}F_7N_4O_2SH$ ([M + H]$^+$), 551.1346; found, 551.1349. $[\alpha]^{20}_D$ = +76.0 (*c* 10, MeOH).

(*R*,*S*)-$N^2$-(1-(*N*-Cyano-*S*-methylsulfinimidoyl)propan-2-yl)-$N^1$-(2-methyl-4-(perfluoropropan-2-yl)phenyl)phthalamide,**3e**: white solid; yield 70.4%, mp 106−108 °C; $^1$H NMR (300 MHz, DMSO-$d_6$) $\delta$ 10.00 (s, 1H), 8.74 (d, $J$ = 6.7 Hz, 1H), 7.81−7.79 (d, $J$ = 6.0 Hz, 1H), 7.68−7.54 (m, 6H), 4.32−4.24 (m, 1H), 3.25 (d, $J$ = 7.0 Hz, 1H), 2.80 (s, 3H), 2.39 (s, 3H), 1.28 (d, $J$ = 3.9 Hz, 3H). HRMS calcd for $C_{23}H_{21}F_7N_4O_2SH$ ([M + H]$^+$), 551.1346; found, 551.1349. $[\alpha]^{20}_D$ = +63.9 (*c* 10, MeOH).

(*R*,*R*)-$N^2$-(1-(*N*-Cyano-*S*-methylsulfinimidoyl)propan-2-yl)-$N^1$-(2-methyl-4-(perfluoropropan-2-yl)phenyl)phthalamide, **4e**: white solid; yield 29.6%; mp 115−116 °C; $^1$H NMR (400 MHz, DMSO-$d_6$) $\delta$ 10.01 (s, 1H), 8.59 (d, $J$ = 7.7 Hz, 1H), 7.80 (d, $J$ = 8.2 Hz, 1H), 7.67−7.53 (m, 6H), 4.33−4.25 (m, 1H), 3.28 (d, $J$ = 8.7 Hz, 2H), 2.80 (s, 3H), 2.38 (s, 3H), 1.28 (d, $J$ = 6.4 Hz, 3H). HRMS calcd for $C_{23}H_{21}F_7N_4O_2SH$ ([M + H]$^+$), 551.1346; found, 551.1349. $[\alpha]^{20}_D$ = −75.8 (*c* 10, MeOH).

(*S*,*R*)-$N^2$-(1-(*N*-Cyano-*S*-methylsulfinimidoyl)propan-2-yl)-$N^1$-(3-(trifluoromethyl)phenyl)phthalamide,**1g**: white solid; yield 72.9%; mp 194−195 °C; $^1$H NMR (400 MHz, DMSO-$d_6$) $\delta$ 10.64 (s, 1H), 8.81 (d, $J$ = 6.9 Hz, 1H), 8.15 (s, 1H), 8.05 (d, $J$ = 6.8 Hz, 1H), 7.93 (d, $J$ = 7.4 Hz, 1H), 7.75 (d, $J$ = 6.3 Hz, 1H), 7.59 (d, $J$ = 6.7, 13.2 Hz, 1H), 7.46 (d, $J$ = 6.6 Hz, 1H), 7.32 (d, $J$ = 5.9, 12.4 Hz, 1H), 4.27−4.25 (m, 1H), 3.29−3.27 (m, 1H), 3.24−3.19 (m, 1H), 2.81 (s, 3H), 1.27 (d, $J$ = 4.4 Hz, 3H). HRMS calcd for $C_{20}H_{18}F_3IN_4O_2SH$ ([M + H]$^+$), 563.0220; found, 563.0227. $[\alpha]^{20}_D$ = −13.2 (*c* 10, MeOH).

**General Synthetic Procedure for Compounds Ia−g, IIa−f, IIIa−c,e, and IVa−c,e.** To a solution of **1a−g**, **2a−f**, **3a−c,e**, or **4a−c,e** (1 mmol) in dichloromethane was added dropwise trifluoroacetic anhydride (TFAA) (0.630 g, 3 mmol) over 15 min at room temperature. Then the reaction mixture was stirred for another 0.5 h. The resulting mixture was washed with dilute hydrochloric acid, water, an aqueous sodium carbonate solution, and then water successively. The organic layer was dried ($MgSO_4$) and concentrated under reduced pressure to yield compounds **Ia−g**, **IIa−f**, **IIIa−c,e**, and **IVa−c,e**.[27]

Scheme 1

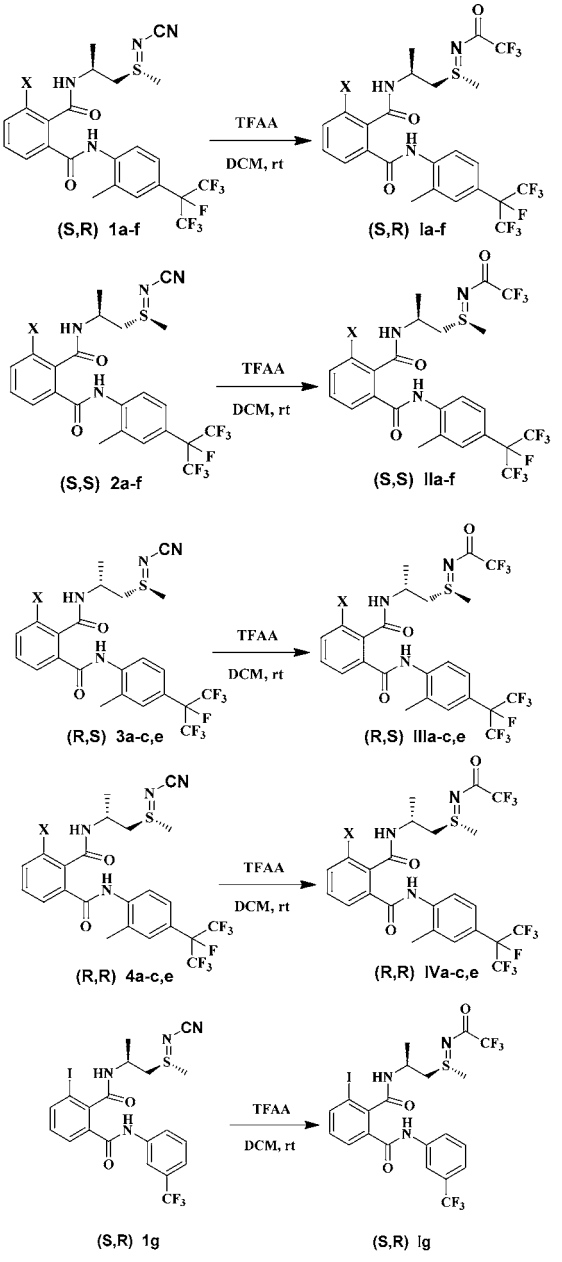


a: X=I, b: X=F, c: X=Cl, d: X=$NO_2$, e: X=H, f: X=Br.

(*S*,*R*)-3-Iodo-$N^2$-(1-(*N*-trifluoroacetyl-*S*-methylsulfinimidoyl)-propan-2-yl)-$N^1$-(2-methyl-4-(perfluoropropan-2-yl)phenyl)-

phthalamide, **Ia**: white solid; yield 90.3%; mp 185−186 °C; $^1$H NMR (400 MHz, $CDCl_3$-$d_6$) $\delta$ 8.68 (s, 1H, Ar-NH), 7.93 (t, $J$ = 9.3 Hz, 2H, Ar−H), 7.69 (d, $J$ = 7.8 Hz, 1H, Ar−H), 7.57 (d, $J$ = 7.6 Hz, 1H, −CNH), 7.44 (s, 1H, Ar−H), 7.31 (d, $J$ = 8.5 Hz, 1H, Ar−H), 7.07 (t, $J$ = 7.8 Hz, 1H, Ar−H), 4.53 (m, 1H, −N−CH), 3.38 (dd, $J$ = 13.0, 8.5 Hz, 1H, $-SCH_2$), 3.06 (dd, $J$ = 13.0, 4.0 Hz, 1H, $-SCH_2$), 2.37 (s, 3H, $-SCH_3$), 2.34 (s, 3H, $ArCH_3$), 1.32 (d, $J$ = 6.8 Hz, 3H, $-CCH_3$). Anal. calcd for $C_{24}H_{20}F_{10}IN_3O_3S$: C, 38.57; H, 2.70; N, 5.62. Found: C, 39.48; H, 2.79; N, 5.50. $[\alpha]^{20}_D$ = −21.2 ($c$ = 10, MeOH).

(*S*,*R*)-3-Fluoro-$N^2$-(1-(*N*-trifluoroacetyl-*S*-methylsulfinimidoyl)-propan-2-yl)-$N^1$-(2-methyl-4-(perfluoropropan-2-yl)phenyl)-phthalamide, **Ib**: white solid; yield 89.6%; mp 115−117 °C; $^1$H NMR (400 MHz, DMSO-$d_6$) $\delta$ 10.01 (s, 1H, Ar−NH), 8.67 (d, $J$ = 8.0 Hz, 1H, −CNH), 7.76 (d, $J$ = 8.3 Hz, 1H, Ar−H), 7.56 (m, 4H, Ar−H), 7.46 (d, $J$ = 8.5 Hz, 1H, Ar−H), 4.29 (m, 1H, −N−CH), 2.94−2.89 (m, 1H, $-SCH_2$), 2.77(dd, $J$ = 13.0, 4.5 Hz, 1H, $-SCH_2$), 2.47 (s, 3H, $-SCH_3$), 2.37 (s, 3H, $ArCH_3$), 1.23 (d, $J$ = 6.6 Hz, 3H, $-CCH_3$). HRMS calcd for $C_{24}H_{20}F_{11}N_3O_3SH$ ([M + H]$^+$), 640.1123; found, 640.1129. $[\alpha]^{20}_D$ = −4.4 ($c$ 0.05, EtOAc).

(*S*,*R*)-3-Chloro-$N^2$-(1-(*N*-trifluoroacetyl-*S*-methylsulfinimidoyl)-propan-2-yl)-$N^1$-(2-methyl-4-(perfluoropropan-2-yl)phenyl)-phthalamide, **Ic**: white solid; yield 92.3%; mp 103−105 °C; $^1$H NMR (400 MHz, DMSO-$d_6$) $\delta$ 10.06 (s, 1H, Ar−NH), 8.94 (d, $J$ = 8.0 Hz, 1H, −CNH), 7.77 (d, $J$ = 8.0 Hz, 2H, Ar−H), 7.70 (d, $J$ = 7.9 Hz, 1H, Ar−H), 7.61−7.50 (m, 4H, Ar−H), 4.32 (m, 1H, −N−CH), 3.39 (m, 1H, $-SCH_2$), 3.32−3.27 (m, 1H, $-SCH_2$), 2.79 (s, 3H, $-SCH_3$), 2.37 (s, 3H, $ArCH_3$), 1.23 (d, $J$ = 6.5 Hz, 3H, $-CCH_3$). Anal. calcd for $C_{24}H_{20}ClF_{10}N_3O_3S$: C, 43.95; H, 3.07; N, 6.41. Found: C, 44.05; H, 3.15; N, 6.63. $[\alpha]^{20}_D$ = −3.8 ($c$ 1, MeOH).

(*S*,*R*)-3-Nitro-$N^2$-(1-(*N*-trifluoroacetyl-*S*-methylsulfinimidoyl)-propan-2-yl)-$N^1$-(2-methyl-4-(perfluoropropan-2-yl)phenyl)-phthalamide, **Id**: white solid; yield 89.8%; mp 117−119 °C; $^1$H NMR (400 MHz, DMSO-$d_6$) $\delta$ 10.22 (s, 1H, Ar−NH), 9.05 (d, $J$ = 7.6 Hz, 1H, −CNH), 8.27 (d, $J$ = 6.9 Hz, 1H), 8.12 (d, $J$ = 7.4 Hz, 1H, Ar−H), 7.84 (m, 2H, Ar−H), 7.56 (m, 2H, Ar−H), 4.28 (m, 1H, −N−CH), 3.32−3.25 (m, 2H, $-SCH_2$), 2.78 (s, 3H, $-SCH_3$), 2.40 (s, 3H, $ArCH_3$), 1.21 (s, 3H, $-CCH_3$). Anal. calcd for $C_{24}H_{20}F_{10}N_4O_5S$: C, 43.25; H, 3.02; N, 8.48. Found: C, 43.09; H, 2.98; N, 8.48. $[\alpha]^{20}_D$ = −15.8 ($c$ 4.2, EtOAc).

(*S*,*R*)-$N^1$-(2-Methyl-4-(perfluoropropan-2-yl)phenyl)-$N^2$-(1-(*N*-trifluoroacetyl-*S*-methylsulfinimidoyl)propan-2-yl)phthalamide, **Ie**: white solid; yield 93.2%; mp 88−90 °C; $^1$H NMR (400 MHz, DMSO-$d_6$) $\delta$ 10.01 (s, 1H), 8.79 (d, $J$ = 8.3 Hz, 1H), 7.81 (d, $J$ = 8.8 Hz, 1H), 7.70−7.68 (m, 1H), 7.61−7.58 (m, 3H), 7.53−7.51 (m, 2H), 4.40−4.31 (m, 1H), 3.42 (dd, $J$ = 12.6, 8.8 Hz, 2H), 2.85 (s, 3H), 2.38 (s, 3H), 1.27 (d, $J$ = 6.7 Hz, 3H). HRMS calcd for $C_{24}H_{21}F_{10}N_3O_3SH$ ([M + H]$^+$), 622.1217; found, 622.1220. $[\alpha]^{20}_D$ = −15.6 ($c$ 10, MeOH).

(*S*,*R*)-3-Bromo-$N^2$-(1-(*N*-trifluoroacetyl-*S*-methylsulfinimidoyl)-propan-2-yl)-$N^1$-(2-methyl-4-(perfluoropropan-2-yl)phenyl)-phthalamide, **If**: white solid; yield 91.2%; mp 116−117 °C; $^1$H NMR (400 MHz, DMSO-$d_6$) $\delta$ 10.03 (d, $J$ = 13.6 Hz, 1H, Ar−NH), 8.92 (t, $J$ = 8.9 Hz, 1H, −CNH), 7.85 (d, $J$ = 7.9 Hz, 1H, Ar−H), 7.82−7.75 (m, 2H, Ar−H), 7.70 (d, $J$ = 7.9 Hz, 1H, Ar−H), 7.62−7.56 (m, 1H, Ar−H), 7.53 (d, $J$ = 14.0 Hz, 2H, Ar−H), 4.33 (m, 1H, −N−CH), 3.38 (d, $J$ = 12.7 Hz, 1H, $-SCH_2$), 3.32−3.27 (m, 1H, $-SCH_2$), 2.79 (s, 3H, $-SCH_3$), 2.37 (s, 3H, $ArCH_3$)), 1.24 (d, $J$ = 6.6 Hz, 3H, $-CCH_3$). HRMS calcd for $C_{24}H_{20}BrF_{10}N_3O_3SH$ ([M + H]$^+$), 700.0332; found, 700.0334. $[\alpha]^{20}_D$ = −2.4 ($c$ 1, MeOH).

(*S*,*R*)-$N^2$-(1-(*N*-Trifluoroacetyl-*S*-methylsulfinimidoyl)propan-2-yl)-$N^1$-(3-(trifluoromethyl)phenyl)phthalamide, **Ig**: white solid; yield 90.9%; mp 188−191 °C; $^1$H NMR (400 MHz, DMSO-$d_6$) $\delta$ 10.63 (s, 1H), 8.81 (d, $J$ = 8.0 Hz, 1H), 8.15 (s, 1H), 8.05 (d, $J$ = 7.8 Hz, 1H), 7.94 (d, $J$ = 7.9 Hz, 1H), 7.76 (d, $J$ = 7.5 Hz, 1H), 7.58 (t, $J$ = 7.8 Hz, 1H), 7.45 (d, $J$ = 7.3 Hz, 1H), 7.31 (t, $J$ = 7.7 Hz, 1H), 4.31 (d, $J$ = 6.2 Hz, 1H), 3.46−3.39 (m, 1H), 3.28 (dd, $J$ = 12.5, 5.2 Hz, 1H), 2.84 (s, 3H), 1.25 (d, $J$ = 6.3 Hz, 3H). HRMS calcd for $C_{21}H_{18}F_6IN_3O_3SH$ ([M + H]$^+$), 634.0081; found, 634.0081. $[\alpha]^{20}_D$ = +50.6 ($c$ 10, EtOA).

(*S*,*S*)-3-Iodo-$N^2$-(1-(*N*-trifluoroacetyl-*S*-methylsulfinimidoyl)-propan-2-yl)-$N^1$-(2-methyl-4-(perfluoropropan-2-yl)phenyl)-phthalamide, **IIa**: white solid, yield 89.7%; mp 142−144 °C; $^1$H NMR (400 MHz, DMSO-$d_6$) $\delta$ 9.99 (s, 1H, Ar−NH), 8.70 (d, $J$ = 7.8 Hz, 1H, −CNH), 8.04 (d, $J$ = 7.8 Hz, 1H, Ar−H), 7.78 (t, $J$ = 6.8 Hz, 2H, Ar−H), 7.52 (d, $J$ = 9.2 Hz, 2H, Ar−H), 7.31 (t, $J$ = 7.8 Hz, 1H, Ar−H), 4.32 (dt, $J$ = 13.8, 6.8 Hz, 1H, −N−CH), 3.32 (d, $J$ = 6.7 Hz, 2H, $-SCH_2$), 2.74 (s, 3H, $-SCH_3$), 2.36 (s, 3H, $ArCH_3$), 1.29 (d, $J$ = 6.7 Hz, 3H, $ArCH_3$). HRMS calcd for $C_{24}H_{20}F_{10}IN_3O_3SH$ ([M + H]$^+$), 748.0183; found, 748.0179. $[\alpha]^{20}_D$ = +9.8 ($c$ 1, MeOH).

(*S*,*S*)-3-Fluoro-$N^2$-(1-(*N*-trifluoroacetyl-*S*-methylsulfinimidoyl)-propan-2-yl)-$N^1$-(2-methyl-4-(perfluoropropan-2-yl)phenyl)-phthalamide, **IIb**: white solid; yield 90.4%; mp 101−102 °C; $^1$H NMR (400 MHz, DMSO-$d_6$) $\delta$ 10.06 (s, 1H, Ar−NH), 8.76 (d, $J$ = 7.8 Hz, 1H, −CNH), 7.75 (d, $J$ = 6.7 Hz, 2H, Ar−H), 7.68 (d, $J$ = 7.7 Hz, 1H, Ar−H), 7.55 (dd, $J$ = 21.9, 9.3 Hz, 3H, Ar−H), 4.33 (m, 1H, −N−CH), 3.32−3.30 (m, 2H, $-SCH_2$), 2.76 (s, 3H, $-SCH_3$), 2.36 (s, 3H, $ArCH_3$), 1.25 (d, $J$ = 6.3 Hz, 3H, $-CCH_3$). HRMS calcd for $C_{24}H_{20}F_{11}N_3O_3SH$ ([M + H]$^+$), 640.1123; found, 640.1129. $[\alpha]^{20}_D$ = +26.8 ($c$ 3, MeOH).

(*S*,*S*)-3-Chloro-$N^2$-(1-(*N*-trifluoroacetyl-*S*-methylsulfinimidoyl)-propan-2-yl)-$N^1$-(2-methyl-4-(perfluoropropan-2-yl)phenyl)-phthalamide, **IIc**: white solid, yield 88.8%; mp 112−114 °C; $^1$H NMR (400 MHz, DMSO-$d_6$) $\delta$ 10.07 (s, 1H, Ar−NH), 8.77 (d, $J$ = 7.9 Hz, 1H, −CNH), 7.75 (t, $J$ = 6.5 Hz, 2H), 7.69 (d, $J$ = 8.0 Hz, 1H, Ar−H), 7.56 (dd, $J$ = 21.8, 9.1 Hz, 4H, Ar−H), 4.33 (dd, $J$ = 13.2, 6.9 Hz, 1H, −N−CH), 3.36 (m, 2H, $-SCH_2$), 2.77 (s, 3H, $-SCH_3$), 2.37 (s, 3H, $ArCH_3$), 1.26 (d, $J$ = 6.6 Hz, 3H, $-CCH_3$). HRMS calcd for $C_{24}H_{20}ClF_{10}N_3O_3SH$ ([M + H]$^+$), 656.0827; found, 656.0835. $[\alpha]^{20}_D$ = +10.6 ($c$ 3, MeOH).

(*S*,*S*)-3-Nitro-$N^2$-(1-(*N*-trifluoroacetyl-*S*-methylsulfinimidoyl)-propan-2-yl)-$N^1$-(2-methyl-4-(perfluoropropan-2-yl)phenyl)-phthalamide, **IId**: white solid; yield 90.2%; mp 124−126 °C; $^1$H NMR (400 MHz, DMSO-$d_6$) $\delta$ 10.23 (s, 1H, Ar−NH), 8.89 (d, $J$ = 7.6 Hz, 1H, −CNH), 8.25 (d, $J$ = 8.1 Hz, 1H, Ar−H), 8.11 (d, $J$ = 7.4 Hz, 1H, Ar−H), 7.83 (t, $J$ = 8.0 Hz, 2H, Ar−H), 7.54 (d, $J$ = 8.2 Hz, 2H, Ar−H), 4.32−4.24 (m, 1H, −N−CH), 3.29 (d, $J$ = 6.7 Hz, 2H, $-SCH_2$), 2.74 (s, 3H, $-SCH_3$), 2.39 (s, 3H, $ArCH_3$), 1.24 (d, $J$ = 6.6 Hz, 3H, $-CCH_3$). Aanl. calcd for $C_{24}H_{20}F_{10}N_4O_5S$: C, 43.25; H, 3.02; N, 8.48. Found: C, 43.09; H, 2.98; N, 8.48. $[\alpha]^{20}_D$ = +30.2 ($c$ 2, MeOH).

(*S*,*S*)-$N^1$-(2-Methyl-4-(perfluoropropan-2-yl)phenyl)-$N^2$-(1-(*N*-trifluoroacetyl-*S*-methylsulfinimidoyl)propan-2-yl)phthalamide, **IIe**: white solid; yield 93.2%; mp 84−86 °C; $^1$H NMR (400 MHz, DMSO-$d_6$) $\delta$ 10.00 (s, 1H), 8.59 (d, $J$ = 8.0 Hz, 1H), 7.79 (d, $J$ = 8.5 Hz, 1H), 7.68−7.66 (m, 1H), 7.59 (d, $J$ = 5.7 Hz, 3H), 7.52−7.50 (m, 2H), 4.37−4.29 (m, 1H), 3.39 (d, $J$ = 6.2 Hz, 2H), 2.82 (s, 3H), 2.37 (s, 3H), 1.28 (d, $J$ = 6.7 Hz, 3H). HRMS calcd for $C_{24}H_{21}F_{10}N_3O_3SH$ ([M + H]$^+$), 622.1217; found, 622.1220. $[\alpha]^{20}_D$ = +41.2 ($c$ 2, MeOH).

(*S*,*S*)-3-Bromo-$N^2$-(1-(*N*-trifluoroacetyl-*S*-methylsulfinimidoyl)-propan-2-yl)-$N^1$-(2-methyl-4-(perfluoropropan-2-yl)phenyl)-phthalamide, **IIf**: white solid; yield 28.8%; mp 119−123 °C; $^1$H NMR (400 MHz, DMSO-$d_6$) $\delta$ 10.04 (d, $J$ = 10.7 Hz, 1H, Ar−NH), 8.75 (t, $J$ = 8.0 Hz, 1H, −CNH), 7.85−7.66 (m, 3H, Ar−H), 7.60−7.47 (m, 3H, Ar−H), 4.38−4.29 (m, 1H, −N−CH), 3.31 (d, $J$ = 13.5 Hz, 2H, $-SCH_2$), 2.77 (s, 3H, $-SCH_3$), 2.36 (s, 3H, $ArCH_3$), 1.26 (d, $J$ = 6.6 Hz, 3H, $-CCH_3$). HRMS calcd for $C_{24}H_{20}BrF_{10}N_3O_3SH$ ([M + H]$^+$), 700.0332; found, 700.0334. $[\alpha]^{20}_D$ = +10.0 ($c$ 1, MeOH).

(*R*,*S*)-3-Iodo-$N^2$-(1-(*N*-trifluoroacetyl-*S*-methylsulfinimidoyl)-propan-2-yl)-$N^1$-(2-methyl-4-(perfluoropropan-2-yl)phenyl)-phthalamide, **IIIa**: white solid; yield 89.7%; mp 184−186 °C; $^1$H NMR (400 MHz, $CDCl_3$-$d_6$) $\delta$ 8.68 (s, 1H, Ar−NH), 7.93 (t, $J$ = 9.3 Hz, 2H, Ar−H), 7.69 (d, $J$ = 7.8 Hz, 1H, −CNH), 7.57 (d, $J$ = 7.6 Hz, 1H, Ar−H), 7.44 (s, 1H, Ar−H), 7.31 (d, $J$ = 8.5 Hz, 1H, Ar−H), 7.07 (t, $J$ = 7.8 Hz, 1H, Ar−H), 4.53 (m, 1H, −N−CH), 3.38 (dd, $J$ = 13.0, 8.5 Hz, 1H, $-SCH_2$), 3.06 (dd, $J$ = 13.0, 4.0 Hz, 1H, $-SCH_2$), 2.37 (s, 3H, $-SCH_3$), 2.34 (s, 3H, $ArCH_3$), 1.32 (d, $J$ = 6.8 Hz, 3H, $-CCH_3$). Anal. calcd for $C_{24}H_{20}F_{10}IN_3O_3S$: C, 38.57; H, 2.70; N, 5.62. Found: C, 39.48; H, 2.79; N, 5.50. $[\alpha]^{20}_D$ = +20.8 ($c$ 5, MeOH).

(*R*,*S*)-3-Fluoro-$N^2$-(1-(*N*-trifluoroacetyl-*S*-methylsulfinimidoyl)-propan-2-yl)-$N^1$-(2-methyl-4-(perfluoropropan-2-yl)phenyl)-phthalamide, **IIIb**: white solid; yield 90.6%; mp 116−118 °C; $^1$H NMR (400 MHz, DMSO-$d_6$) $\delta$ 10.02 (s, 1H, Ar−NH), 8.68 (d, $J$ = 8.0 Hz, 1H, −CNH), 7.77 (d, $J$ = 8.3 Hz, 1H, Ar−H), 7.57 (m, 4H, Ar−

H), 7.47 (d, $J$ = 8.5 Hz, 1H, Ar−H), 4.30 (m, 1H, −N−CH), 2.95−2.90 (m, 1H, $-SCH_2$), 2.78 (dd, $J$ = 13.0, 4.5 Hz, 1H, $-SCH_2$), 2.48 (s, 3H, $-SCH_3$), 2.38 (s, 3H, $ArCH_3$), 1.23 (d, $J$ = 6.6 Hz, 3H, $-CCH_3$). HRMS calcd for $C_{24}H_{20}F_{11}N_3O_3SH$ ($[M + H]^+$), 640.1123; found, 640.1129. $[\alpha]^{20}_D$ = +4.6 ($c$ 0.05, EtOAc).

(*R,S*)-3-Chloro-$N^2$-(1-(*N*-trifluoroacetyl-*S*-methylsulfinimidoyl)-propan-2-yl)-$N^1$-(2-methyl-4-(perfluoropropan-2-yl)phenyl)-phthalamide, **IIIc**: white solid; yield 89.1%; mp 104−105 °C; $^1$H NMR (400 MHz, DMSO-$d_6$) $\delta$ 10.06 (s, 1H, Ar−NH), 8.94 (d, $J$ = 8.0 Hz, 1H, −CNH), 7.77 (d, $J$ = 8.0 Hz, 2H, Ar−H), 7.70 (d, $J$ = 7.9 Hz, 1H, Ar−H), 7.61−7.50 (m, 4H, Ar−H), 4.32 (m, 1H, −N−CH), 3.39 (m, 1H, $-SCH_2$), 3.32−3.27 (m, 1H, $-SCH_2$), 2.79 (s, 3H, $-SCH_3$), 2.37 (s, 3H, $ArCH_3$), 1.23 (d, $J$ = 6.5 Hz, 3H, $-CCH_3$). Anal. calcd for $C_{24}H_{20}ClF_{10}N_3O_3S$: C, 44.12; H, 3.17; N, 6.48. Found: C, 44.05; H, 3.15; N, 6.63. $[\alpha]^{20}_D$ = +3.6 ($c$ 1, MeOH).

(*R,S*)-$N^1$-(2-Methyl-4-(perfluoropropan-2-yl)phenyl)-$N^2$-(1-(*N*-trifluoroacetyl-*S*-methylsulfinimidoyl)propan-2-yl)phthalamide, **IIIe**: white solid; yield 92.8%; mp 87−88 °C; $^1$H NMR (400 MHz, DMSO-$d_6$) $\delta$ 10.01 (s, 1H), 8.79 (d, $J$ = 8.3 Hz, 1H), 7.81 (d, $J$ = 8.8 Hz, 1H), 7.70−7.68 (m, 1H), 7.61−7.58 (m, 3H), 7.53−7.51 (m, 2H), 4.40−4.31 (m, 1H), 3.42 (dd, $J$ = 12.6, 8.8 Hz, 2H), 2.85 (s, 3H), 2.38 (s, 3H), 1.27 (d, $J$ = 6.7 Hz, 3H). HRMS calcd for $C_{24}H_{21}F_{10}N_3O_3SH$ ($[M + H]^+$), 622.1217; found, 622.1220. $[\alpha]^{20}_D$ = +15.2 ($c$ 10, MeOH).

(*R,R*)-3-Iodo-$N^2$-(1-(*N*-trifluoroacetyl-*S*-methylsulfinimidoyl)-propan-2-yl)-$N^1$-(2-methyl-4-(perfluoropropan-2-yl)phenyl)-phthalamide, **IVa**: white solid; yield 91.7%; mp 140−142 °C; $^1$H NMR (400 MHz, $CDCl_3$-$d_6$) $\delta$ 8.43 (s, 1H, Ar−NH), 8.12 (d, $J$ = 8.4 Hz, 1H, Ar−H), 7.94 (d, $J$ = 7.4 Hz, 1H, −CNH), 7.69 (d, $J$ = 7.6 Hz, 1H, Ar−H), 7.44 (d, $J$ = 8.1 Hz, 2H, Ar−H), 7.33 (d, $J$ = 7.3 Hz, 1H, Ar−H), 7.18 (t, $J$ = 7.9 Hz, 1H, Ar−H), 4.19 (m, 1H, −N−CH), 3.48 (dd, $J$ = 12.9, 8.7 Hz, 1H, $-SCH_2$), 3.06 (dd, $J$ = 12.9, 3.5 Hz, 1H, $-SCH_2$), 2.40 (s, 3H, $-SCH_3$), 2.36 (s, 3H, $ArCH_3$), 1.50 (d, $J$ = 6.9 Hz, 3H, $-CCH_3$). HRMS calcd for $C_{24}H_{20}F_{10}IN_3O_3SH$ ($[M + H]^+$), 748.0183; found, 748.0179. $[\alpha]^{20}_D$ = −9.6 ($c$ 1, MeOH).

(*R,R*)-3-Fluoro-$N^2$-(1-(*N*-trifluoroacetyl-*S*-methylsulfinimidoyl)-propan-2-yl)-$N^1$-(2-methyl-4-(perfluoropropan-2-yl)phenyl)-phthalamide, **IVb**: white solid; yield 89.7%; mp 100−101 °C; $^1$H NMR (400 MHz, DMSO-$d_6$) $\delta$ 10.06 (s, 1H, Ar−NH), 8.76 (d, $J$ = 7.8 Hz, 1H, −CNH), 7.75 (d, $J$ = 6.7 Hz, 2H, Ar−H), 7.68 (d, $J$ = 7.7 Hz, 1H, Ar−H), 7.55 (dd, $J$ = 21.9, 9.3 Hz, 3H, Ar−H), 4.33 (m, 1H, −N−CH), 3.32−3.30 (m, 2H, $-SCH_2$), 2.76 (s, 3H, $-SCH_3$), 2.36 (s, 3H, $ArCH_3$), 1.25 (d, $J$ = 6.3 Hz, 3H, $-CCH_3$). HRMS calcd for $C_{24}H_{20}F_{11}N_3O_3SH$ ($[M + H]^+$), 640.1123; found, 640.1129. $[\alpha]^{20}_D$ = −26.4 ($c$ 3, MeOH).

(*R,R*)-3-Chloro-$N^2$-(1-(*N*-trifluoroacetyl-*S*-methylsulfinimidoyl)-propan-2-yl)-$N^1$-(2-methyl-4-(perfluoropropan-2-yl)phenyl)-phthalamide, **IVc**: white solid; yield 90.1%; mp 113−114 °C; $^1$H NMR (400 MHz, DMSO-$d_6$) $\delta$ 10.07 (s, 1H, Ar−NH), 8.77 (d, $J$ = 7.9 Hz, 1H, −CNH), 7.75 (t, $J$ = 6.5 Hz, 2H), 7.69 (d, $J$ = 8.0 Hz, 1H, Ar−H), 7.56 (dd, $J$ = 21.8, 9.1 Hz, 4H, Ar−H), 4.33 (dd, $J$ = 13.2, 6.9 Hz, 1H, −N−CH), 3.36 (m, 2H, $-SCH_2$), 2.77 (s, 3H, $-SCH_3$), 2.37 (s, 3H, $ArCH_3$), 1.26 (d, $J$ = 6.6 Hz, 3H, $-CCH_3$). HRMS calcd for $C_{24}H_{20}ClF_{10}N_3O_3SH$ ($[M + H]^+$), 656.0827; found, 656.0835. $[\alpha]^{20}_D$ = −10.4 ($c$ 3, MeOH).

(*R,R*)-$N^1$-(2-Methyl-4-(perfluoropropan-2-yl)phenyl)-$N^2$-(1-(*N*-trifluoroacetyl-*S*-methylsulfinimidoyl)propan-2-yl)phthalamide, **IVe**: white solid; yield 93.2%; mp 85−86 °C; $^1$H NMR (400 MHz, DMSO-$d_6$) $\delta$ 10.00 (s, 1H), 8.59 (d, $J$ = 8.0 Hz, 1H), 7.79 (d, $J$ = 8.5 Hz, 1H), 7.68−7.66 (m, 1H), 7.59 (d, $J$ = 5.7 Hz, 3H), 7.52−7.50 (m, 2H), 4.37−4.29 (m, 1H), 3.39 (d, $J$ = 6.2 Hz, 2H), 2.82 (s, 3H), 2.37 (s, 3H), 1.28 (d, $J$ = 6.7 Hz, 3H). HRMS calcd for $C_{24}H_{21}F_{10}N_3O_3SH$ ($[M + H]^+$), 622.1217; found, 622.1220. $[\alpha]^{20}_D$ = −40.8 ($c$ 10, MeOH).

**X-ray Diffraction.** A colorless crystal **Ig** suitable for X-ray diffraction study was cultivated in the test tube from DMSO by self-volatilization. A crystal with dimensions of 0.20 mm × 0.15 mm × 0.10 mm was mounted on a Bruker SMART 1000 CCD diffractometer equipped with a graphite-monochromatic Mo K$\alpha$ radiation ($\lambda$ = 0.71073 Å). Intensity data were collected at 293(2) K by using a multiscan mode in the range of 3.05° ≤ $\theta$ ≤ 25.50° with the following index ranges: −16 ≤ $h$ ≤ 16, −16 ≤ $k$ ≤ 16, and −27 ≤ $l$ ≤ 26. A total of 31784 reflections were collected, and 4768 were independent ($R_{int}$ = 0.0441), of which 4091 with $I > 2\sigma(I)$ were observed. X-ray single-crystal diffraction is shown in Figure 2 with the following

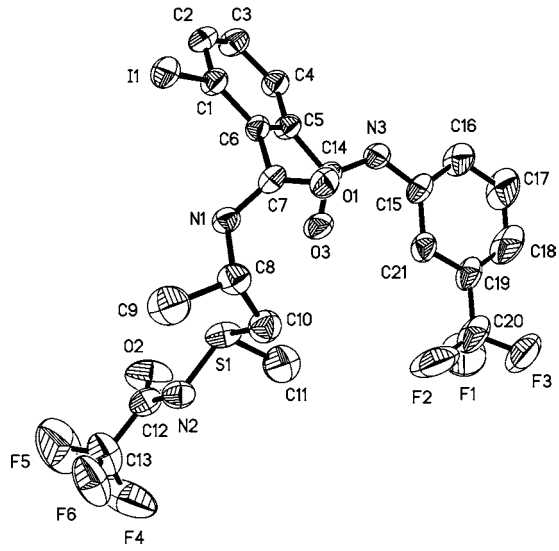


**Figure 2.** Crystal structure of compound **Ig**.

crystallographic parameters: $a$ = 13.998(2) Å, $b$ = 13.998 (2) Å, $c$ = 22.660(5) Å, $\alpha$ = 90°, $\beta$ = 90°, $\gamma$ = 120°, $V$ = 3845.4(11) Å$^3$, $Z$ = 4, $D_c$ = 1.644 mg m$^{-3}$, $\mu$ = 1.401 mm$^{-1}$, $F$ (000) = 1878, $R$ = 0.0539, $w_R$ = 0.1349, final $R$ factor = 4.54%, final $w_R$ factor = 12.87%, absolute structure parameter = −0.02 (3). The crystal structure was solved by direct methods with SHELXS-97[28] and refined by full-matrix least-squares refinements based on $F^2$ with SHELXL-97. All non-hydrogen atoms were refined anisotropically, and all hydrogen atoms were located in the calculated positions and refined with a riding model.

**Biological Assay.** All bioassays were performed on representative test organisms reared in the laboratory. The bioassay was repeated at 25 ± 1 °C according to the statistical requirements. Assessments were made on a dead/alive basis, and mortality rates were corrected using Abbott's formula.[29] Evaluations were based on a percentage scale of 0−100, in which 0 = no activity and 100 = total control. The standard deviations of the tested biological values were ±5%. $LC_{50}$ values were calculated by probit analysis.[30]

**Larvicidal Activity against Oriental Armyworm (*Pseudaletia separata* Walker).** The larvicidal activity of title compounds and the standard flubendiamide against oriental armyworm was tested according to the leaf-dip method using the reported procedure.[31] The insecticidal activity is summarized in Table 1. $LC_{50}$ values of compounds **Ia,b,d**, **IIb,d,f**, **IIIa,b**, **IVa**, and flubendiamide against oriental armyworm are listed in Table 2.

**Larvicidal Activity against Diamondback Moth (*Plutella xylostella* L.).** The larvicidal activity of title compounds and flubendiamide against diamondback moth was tested by the leaf-dip method using the reported procedure.[32,33] The insecticidal activity is summarized in Table 3.

## RESULTS AND DISCUSSION

**Synthesis.** The synthesis of *N*-trifluoroacetyl sulfilimines was achieved by the key intermediates *N*-cyano sulfilimines as shown in Scheme 1. The *N*-cyano group was proved to be easily cleaved upon treatment with TFAA at room temperature. Compared with *N*-cyano sulfilimines, these *N*-trifluoroacetyl sulfiliminyl derivatives displayed better solubility and improved hydrophobicity.

**Table 1. Insecticidal Activity of Compounds Ia−f, IIa−f, IIIa−c,e, IVa−c,e and Flubendiamide against Oriental Armyworm**

| | larvicidal activity (%) at concn of | | | | | | | | | | |
|---|---|---|---|---|---|---|---|---|---|---|---|
| compd | 200 mg $L^{-1}$ | 100 mg $L^{-1}$ | 50 mg $L^{-1}$ | 25 mg $L^{-1}$ | 10 mg $L^{-1}$ | 5 mg $L^{-1}$ | 2.5 mg $L^{-1}$ | 1 mg $L^{-1}$ | 0.5 mg $L^{-1}$ | 0.25 mg $L^{-1}$ | 0.1 mg $L^{-1}$ |
| **Ia** | 100 | 100 | 100 | 100 | 100 | 100 | 100 | 100 | 100 | 100 | 60 |
| **Ib** | 100 | 100 | 100 | 100 | 100 | 100 | 100 | 100 | 40 | | |
| **Ic** | 100 | 100 | 100 | 100 | 100 | 100 | 100 | 100 | 100 | 60 | |
| **Id** | 100 | 100 | 100 | 100 | 100 | 60 | | | | | |
| **Ie** | 100 | 100 | 100 | 100 | 100 | 60 | | | | | |
| **If** | 100 | 100 | 100 | 100 | 100 | 100 | 100 | 70 | | | |
| **IIa** | 100 | 100 | 100 | 100 | 100 | 100 | 100 | 100 | 100 | 100 | 60 |
| **IIb** | 100 | 100 | 100 | 100 | 100 | 100 | 100 | 100 | 70 | | |
| **IIc** | 100 | 100 | 100 | 100 | 100 | 100 | 100 | 100 | 100 | 60 | |
| **IId** | 100 | 100 | 100 | 100 | 100 | 100 | 100 | 100 | 20 | | |
| **IIe** | 100 | 100 | 100 | 60 | 40 | | | | | | |
| **IIf** | 100 | 100 | 100 | 100 | 100 | 100 | 100 | 100 | 100 | 100 | 30 |
| **IIIa** | 100 | 100 | 100 | 100 | 100 | 100 | 100 | 100 | 10 | | |
| **IIIb** | 100 | 100 | 100 | 100 | 40 | | | | | | |
| **IIIc** | 100 | 100 | 100 | 100 | 100 | 60 | | | | | |
| **IIIe** | 100 | 100 | 60 | | | | | | | | |
| **IVa** | 100 | 100 | 100 | 100 | 100 | 100 | 100 | 100 | 40 | 20 | 10 |
| **IVb** | 100 | 100 | 100 | 100 | 50 | | | | | | |
| **IVc** | 100 | 100 | 100 | 100 | 100 | 100 | 100 | 20 | | | |
| **IVe** | 100 | 100 | 60 | | | | | | | | |
| flubendiamide | | | 100 | 100 | 100 | 100 | 100 | 100 | 100 | 100 | 50 |

**Table 2. $LC_{50}$ Values of Compounds Ia,b,d, IIa,b,d,f, IIIa,b, IVa, and Flubendiamide against Oriental Armyworm**

| | $LC_{50}$(mg/L) | | | |
|---|---|---|---|---|
| compd | $y = a + bx$ | $R$ | $LC_{50}$ | $LC_{95}$ |
| **Ia** | $y = 14.4459 + 10.9593x$ | 0.9468 | 0.1374 | 0.1942 |
| **Ib** | $y = 6.1688 + 4.9956x$ | 0.9988 | 0.5835 | 1.2453 |
| **Id** | $y = 3.2828 + 3.0490x$ | 0.9399 | 3.6577 | 12.6672 |
| **IIa** | $y = 8.6832 + 3.7658x$ | 0.9914 | 0.1052 | 0.2876 |
| **IIb** | $y = 6.6165 + 3.4223x$ | 0.9735 | 0.3370 | 1.0193 |
| **IId** | $y = 6.4616 + 7.3125x$ | 0.9782 | 0.6311 | 1.0594 |
| **IIf** | $y = 11.0336 + 7.2617x$ | 0.9913 | 0.1476 | 0.2487 |
| **IIIa** | $y = 6.4647 + 8.6005x$ | 0.9875 | 0.6756 | 1.0494 |
| **IIIb** | $y = 2.6064 + 2.1918x$ | 0.9871 | 12.3621 | 69.5919 |
| **IVa** | $y = 5.5815 + 2.0234x$ | 0.9491 | 0.5160 | 3.3537 |
| flubendiamide | $y = 7.4237 + 2.6428x$ | 0.9945 | 0.1230 | 0.5160 |

**Table 3. Insecticidal Activity of Compounds Ia,f, IIa−c, and Flubendiamide against Diamondback Moth**

| | larvicidal activity (%) at concn of | | | | | | | |
|---|---|---|---|---|---|---|---|---|
| compd | 1 mg $L^{-1}$ | $10^{-1}$ mg $L^{-1}$ | $10^{-2}$ mg $L^{-1}$ | $10^{-3}$mg $L^{-1}$ | $10^{-4}$ mg $L^{-1}$ | $10^{-5}$ mg $L^{-1}$ | $10^{-6}$ mg $L^{-1}$ | $10^{-7}$ mg $L^{-1}$ |
| **Ia** | 100 | 100 | 90 | 40 | | | | |
| **If** | 100 | 100 | 100 | 100 | 100 | 100 | 100 | 70 |
| **IIa** | 100 | 100 | 100 | 100 | 100 | 40 | | |
| **IIb** | 100 | 100 | 100 | 40 | | | | |
| **IIc** | 100 | 100 | 100 | 100 | 100 | 100 | 80 | 20 |
| flubendiamide | | 100 | 100 | 50 | 0 | | | |

The novel structures of these title compounds were characterized by melting point, $^1$H NMR, elemental analysis (or high-resolution mass spectrometry), and optical polarimetry. The chemical shifts of the active proton signals in the anilide moiety were at 10.01−10.22 ppm in DMSO-$d_6$. However, the active proton signals of −NHCO− on the amide bridge in the aliphatic amide moiety were observed at $\delta$ 8.67−9.05 and $\delta$ 8.70−8.89 in DMSO-$d_6$, respectively.

**Crystal Structure Analysis.** The molecular structure of the title compound is shown in Figure 2. Generally, the average bond lengths and bond angles of the benzene ring, amide group, $CF_3$ group, or other bonds are within normal ranges.[34−38] The S(1)═N(2) bond [1.679(6)Å] is longer than the general C═N double-bond length of 1.27 Å. The torsion angle of N(2)−S(1)−C(10)−C(8) is −93.4(6)°. As shown in Figure 2, the two phenyl rings are nearly vertical with a quite small dihedral angle ($\theta$) of 40.8°. In the intermolecular face-to-face $\pi-\pi$ stacking pattern of the title compound, it is worth mentioning that the two molecules of each stacking unit (C15−C21) are cetro-symmetric, which can be proved by the

relative position of the two phenyl rings of the two molecules. The crystal packing structure demonstrates the existence of three intermolecular hydrogen bond and an intramolecular hydrogen bond: N−H---O and N−H---I. These interactions are estimated to play a role in stabilizing the crystal structure.

**Structure−Activity Relationship (SAR).** *Larvicidal Activity against Oriental Armyworm.* The larvicidal activity of compounds **Ia−f**, **IIa−f**, **IIIa−c**,**e**, and **IVa−c**,**e** against oriental armyworm are listed in Table 1. Most title compounds exhibited good to excellent activity against oriental armyworm. Generally speaking, these stereoisomers exhibited different impacts on biological activity following the sequence (Sc, Ss) ≥ (Sc, Rs) ≫ (Rc, Rs) > (Rc, Ss), which is not in accordance with *N*-cyano sulfiliminyl structures reported in our previous publication as ((Sc, Ss) ≥ (Sc, Rs) ≫ (Rc, Ss) > (Rc, Rs)).[19] As shown in Table 1, for example, **IIa** (Sc, Ss) showed 60% insecticidal activity at 0.1 mg $L^{-1}$, whereas **IIIa** (Rc, Ss) gave a death rate of 10% at only 0.5 mg $L^{-1}$. As seen in Rs configurations, **Ia** (Sc, Rs) (100%) showed better insecticidal activity than **IVa** (Rc, Rs) (20%) at a concentration of 0.25 mg $L^{-1}$. These observations indicated that activities varied significantly depending upon carbon and sulfur chirality. As seen in comparison with other structures in the four configurations, **II** (Sc, Ss) was most active, followed by **I** (Sc, Rs) and **IV** (Rc, Rs), whereas **III** (Rc, Ss) was almost inactive. It was further concluded that a reasonable coordination of both carbon and sulfur chirality accounted for the improvement of insecticidal activity and that a possible synergistic effect was involved.

In comparison, in some cases these diastereoisomers with Sc configurations (**Ia** vs **IIa**, **Ib** vs **IIb**, and **Ic** vs **IIc**), Rc configurations (**IIIb** vs **IVb** and **IIIe** vs **IVe**) showed similar activities. Whereas **IIf** (Sc, Ss) displayed 30% insecticidal activity at 0.1 mg $L^{-1}$, the larvicidal activity of **If** (Sc, Rs) was 70% at 1 mg $L^{-1}$, and **IId** (Sc, Ss) showed better activity than **Id** (Sc, Rs). These observations showed that Ss configurations gave higher activity than Rs counterparts in these Sc configurations. However, in other cases, Rs configurations showed better activity than Ss counterparts in these Rc configurations, such as **IVa** versus **IIIa**, **IVb** versus **IIIb**, and **IVc** versus **IIIc**. Carbon chirality has a stronger influence on the activity than sulfur, as shown in Rs configurations (**Ia** vs **IIIa**, **Ib** vs **IIIb**, **Ic** vs **IIIc**, and **Ie** vs **IIIe**) and in Ss configurations (**IIa** vs **IVa**, **IIb** vs **IVb**, **IIc** vs **IVc**, and **IIe** vs **IVe**).

As shown in Table 1, all compounds showed a mortality of 100% at 10 mg $L^{-1}$, except **IIe**, **IIIb**, **IIIe**, **IVb**, and **IVe**. Particularly, **Ia**, **Ic**, **IIa**, **IIc**, **IIf**, and **IVa** exhibited 100% larvicidal activities even at 1 mg $L^{-1}$. It is worth noting that **Ia**, **IIa**, and **IIf** showed activities as excellent as that of flubendiamide. Furthermore, the iodine substituent in each configuration showed the best larvicidal activity, which was consistent with the previous paper.[26] Br substituent as well as Cl, $NO_2$, F, and H possessed inferior insecticidal activity against oriental armyworm. Compared with *N*-cyanosulfilimines,[19] the results of larvicidal activity against oriental armyworm implied that the introduction of the *N*-trifluoroacetyl group was essential for improvement of larvicidal activity. This is probably due to these *N*-trifluoroacetyl sulfiliminyl derivatives displaying better solubility and improved hydrophobicites. In comparison with our previous research,[39] *N*-trifluoroacetyl sulfilimines with one methyl group in the aliphatic amido moiety gave better activity than those corresponding structures with two methyl groups, so it was concluded that the conventional second methyl group in the aliphatic amido side chain of dicarboxamide might not be requisite during our molecular design stragety.

From Table 2, it was found that the $LC_{50}$ value of **IIa** was 0.1052 mg $L^{-1}$, slightly lower than that of flubendiamide (0.1230 mg $L^{-1}$). In addition, the $LC_{50}$ values of compounds **Ia**, **IIb**, and **IIf** were 0.1374, 0.3374, and 0.1476 mg $L^{-1}$, respectively.

*Larvicidal Activity against Diamondback moth.* The larvicidal activities of compounds **Ia**, **If**, and **IIa−c** and flubendiamide against diamondback moth are listed in Table 3. From that table, we observed that most compounds exhibited excellent activities. Compared with different substituents I, F, and Cl in the phthaloyl moiety of the title compounds, Br revealed the best activity, a death rate of 100% at $10^{-6}$ mg $L^{-1}$, which is a much better activity than that of flubendiamide (0% at $10^{-4}$ mg $L^{-1}$) with a striking difference of >100-fold. Also, **IIa** and **IIc** gave higher activity than flubendiamide; the larvicidal activities of **IIa** and **IIc** were 40% at $10^{-5}$ mg $L^{-1}$ and 80% at $10^{-6}$ mg $L^{-1}$, respectively, better than that of flubendiamide. Whereas **Ia** and **IIb** reached the same activity level as flubendiamide. The bioassay results indicated that chiral dicarboxamide scaffolds containing *N*-trifluoroacetyl sulfiliminyl moiety were favorable to improve the larvicidal activity toward the diamondback moth.

**CoMFA Analysis by SYBYL.** The CoMFA method is widely used in drug design because it allows for rapid prediction of QSAR of newly designed molecules.[40−43] Using SYBYL,[44] a brief CoMFA is taken for two data sets. Compounds in data set 1 are **Ia**,**b**,**d**, **IIb**,**d**,**f**, **IIIa**,**b**, and **IVa**. In addition to compounds in data set 1, compounds with *N*-cyano sulfiliminyl substituted in the aliphatic amide moiety are included in data set 2. The conformations of all molecules are optimized with Tripos force field and Gasteiger−Hukel charges, whereas the activity data are reported as the negative logarithms of $LC_{50}$. Detailed CoMFA results for the two data sets are shown in Figures 3 and 4, respectively.

The result for data set 1 draws similar conclusions as in a previous paper.[19] The green area near the I substituent suggests that a bulkier group is favorable. The small yellow area indicates a less bulky substituent enhances activity. Thus, the molecules

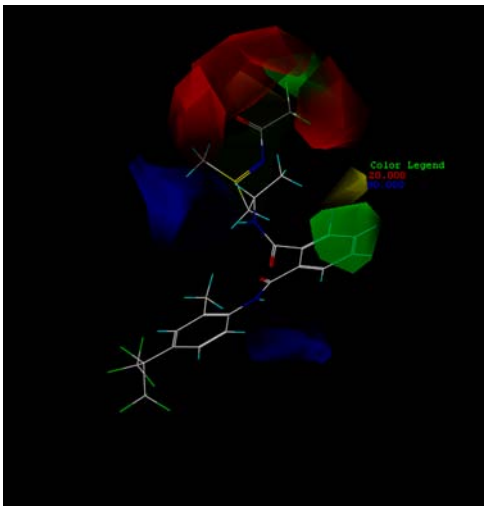


**Figure 3.** CoMFA results for data set 1. The molecule shown in this figure is **Ia**.

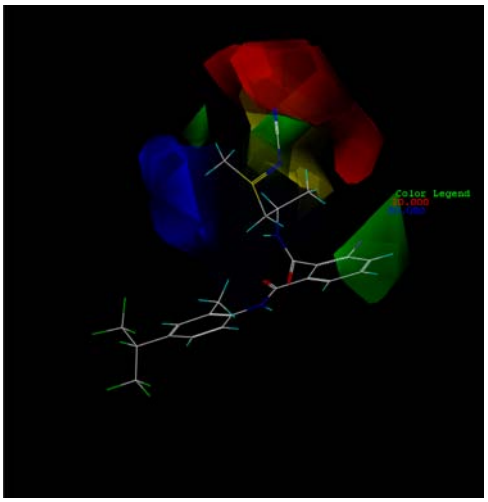


**Figure 4.** CoMFA results for data set 2. The molecule shown in this figure is the (Sc, Rs) configuration of **D** (Figure 1).

with Sc configurations (**I** and **II**) have a better activity than Rc configurations. Finally, the red area surrounding the $COCF_3$ group indicates that more electronegativity is favorable here.

Compared with the results from data set 2, molecules with a $COCF_3$ group in the aliphatic amide moiety give a similar conclusion. The similarity between Figures 3 and 4 indicates that the structure−activity relationship reported in a previous paper[19] is also suitable for these $COCF_3$-substitued molecules.

A partial least-square analysis gives an excellent linear relationship between predicted and actual activities ($R_2$ = 1.000), which indicates a valid CoMFA model.

In summary, this is the first report of chiral *N*-trifluoroacetyl sulfilimines. Four series of phthalamides were designed, synthesized, and evaluated against oriental armyworm and diamondback moth for insecticidal activity. These *N*-trifluoroacetyl sulfilimines exhibited a sequence of activity against oriental armyworm of (Sc, Ss) ≥ (Sc, Rs) ≫ (Rc, Rs) > (Rc, Ss), whereas carbon chirality influenced the activities more strongly than sulfur. For diamondback moth, compounds **If**, **IIa**, and **IIc** exhibited much stronger activity than flubendiamide. CoMFA calculation indicated that stereoisomers with Sc configurations containing more electronegative groups such as $COCF_3$ are favorable to attain their high activity. It was further concluded that the conventional second methyl group in the aliphatic amido side chain of dicarboxamide might not be a requisite in search of novel sulfiliminyl insecticides.

## AUTHOR INFORMATION

### Corresponding Author

*(Z.L.) Phone: +86-22-23503732. E-mail: nkzml@vip.163.com.

### Funding

This work was supported by the Project supported by the National Basic Research Program of China (No. 2010CB126106), the National Key Technologies R&D Program (No. 2011BAE06B05), and Syngenta Postgraduate Fellowship awarded to S. Zhou.

### Notes

The authors declare no competing financial interest.

## REFERENCES

(1) Katsuhira, T.; Furuya, T.; Gotoh, M.; Tohnishi, M.; Sakata, K.; Morimoto, M.; Seo, A. Preparation of heterocyclic dicarboxylic acid diamide derivatives as agricultural and horticultural insecticides. WO2001000575, 2001.

(2) Katsuhira, T.; Furuya, T.; Gotoh, M.; Tohnishi, M.; Takaishi, H.; Sakata, K.; Morimoto, M.; Seo, A. Preparation of heterocyclic dicarboxylic acid diamide derivatives as agricultural and horticultural insecticides. EP 1188745, 2000.

(3) Tohnishi, M.; Nakao, H.; Furuya, T.; Seo, A.; Kodama, H.; Tsubata, K.; Freudenberger, J. H.; Cordova, D.; Flexner, L.; Bellin, C. A.; Dubas, C. M.; Smith, B. K.; Hughes, K. A.; Hollingshaus, J. G.; Clark, C. E.; Benner, E. A. Flubendiamide, a novel insecticide highly active against lepidopterous insect pests. *J. Pestic. Sci.* **2005**, *30*, 354−360.

(4) Hamaguchi, H.; Hirooka, T. Insecticides affecting calcium homeostasis − flubendiamide. In *Modern Crop Protection Compounds*, 2nd ed.; Kŕamer, W., Schirmer, U., Jeschke, P., Witschel, M., Eds.; Wiley-VCH Verlag: Weinheim, Germany, 2012; Vol. 3, pp 1396−1409.

(5) Seo, A.; Tohnishi, M.; Nakao, H.; Furuya, T.; Kodama, H.; Tsubata, K.; Fujioka, S.; Kodama, H.; Nishimatsu, T.; Hirooka, T. Flubendiamide, a new insecticide characterized by its novel chemistry and biology. In *Pesticide Chemistry: Crop Protection, Public Health, Environmental Safety*; Ohkawa, H., Miyagawa, H., Lee, P. W., Eds.; Wiley-VCH Verlag: Weinheim, Germany, 2007; pp 127−135.

(6) Nakao, H.; Harayama, H.; Yamaguchi, M.; Tohnishi, M.; Morimoto, M.; Fujioka, S. Preparation of phthalamide derivatives as insecticides. WO 2002088074, 2002.

(7) Harayama, H.; Tohnishi, M.; Morimoto, M.; Fujioka, S. Preparation of phthalamide derivatives as insecticides. WO 2002088075, 2002.

(8) Mochizuki, K.; Inoue, S.; Hatanaka, T. Optically active phthalamide derivative, agricultural or horticultural insecticide, and method of using the same. U.S. 2008260440, 2008.

(9) Tohnishi, M.; Nakao, H.; Kohno, E.; Nishida, T.; Furuya, T.; Shimizu, T.; Seo, A.; Sakata, K.; Fujioka, S.; Kanno, H. Preparation of phthalic acid diamides as agricultural and horticultural insecticides. EP 0919542, 1999.

(10) Tohnishi, M.; Nakao, H.; Kohno, E.; Nishida, T.; Furuya, T.; Shimizu, T.; Seo, A.; Sakata, K.; Fujioka, S.; Kanno, H. Preparation of phthalamides as agrohorticultural insecticides. EP 1006107, 2000.

(11) Tozai, M.; Morimoto, M.; Fujioka, N.; Seo, A. Preparation of phthalicdiamides and insecticides for agriculture and horticulture. JP 2001335559, 2001.

(12) Wada, K.; Gomibuchi, T.; Yoneta, Y.; Otsu, Y.; Shibuya, K.; Matsuo, H.; Fischer, R. Preparation of phthalamide derivatives as insecticides. WO 2004000796, 2003.

(13) Wada, K.; Gomibuchi, T.; Yoneta, Y.; Otsu, Y.; Shibuya, K.; Nakakura, N.; Fischer, R. Preparation of $N^1$-(pyrazol-1-ymethyl)-2-methylphenyl) phthalamides and related compounds as insecticides. WO 2005095351, 2005.

(14) Lahm, G. P.; Selby, T. P.; Frendenberger, J. H.; Stevenson, T. M.; Myers, B. J.; Seburyamo, G.; Smith, B. K.; Flexner, L.; Clark, C. E.; Cordova, D. Insecticidal anthranilic diamides: a new class of potent ryanodine receptor activators. *Bioorg. Med. Chem. Lett.* **2005**, *15*, 4898−4906.

(15) Lahm, G. P.; Cordova, D.; Barry, J. D. New and selective ryanodinereceptor activators for insect control. *Bioorg. Med. Chem.* **2009**, *17*, 4127−4133.

(16) Lahm, G. P.; Stevenson, T. M.; Selby, T. P.; Freudenberger, J. H.; Cordova, D.; Flexner, L.; Bellin, C. A.; Dubas, C. M.; Smith, B. K.; Hughes, K. A.; Hollingshaus, J. G.; Clark, C. E.; Benner, E. A.; Rynaxypyr, T. M. A new insecticidal anthranilicdiamide that acts as a potent and selective ryanodine receptor activator. *Bioorg. Med. Chem. Lett.* **2007**, *17*, 6274−6279.

(17) Hughes, K. A.; Lahm, G. P.; Selby, T. P.; Stevenson, T. M. Cyanoanthranilamide insecticides. WO2004067528, 2004.

(18) DuPont Rynaxypyr Insect Control Technical Bulletin; http://www2.dupont.com/Production_Agriculture/en_US/assets/downloads/pdfs/Rynaxypyr_Tech_Bulletin.pdf.

(19) Zhou, S.; Jia, Z. H.; Xiong, L. X.; Yan, T.; Yang, N.; Wu, G. P.; Song, H. B.; Li, Z. M. Chiral dicarboxamide scaffolds containing sulfiliminyl moiety as potential ryanodine receptor activators. *J. Agric. Food Chem.* **2014**, *62* (27), 6269−6277.
(20) Li, Z. M.; Zhou, S.; Yan, T.; Zhou, Y. Y.; Xiong, L. X.; Li, Y. Q. Preparation of chiral bisamide derivatives and geometric isomers as insecticides. CN103420884A, 2013.
(21) Muller, K.; Faeh, C.; Diederich, F. Fluorine in pharmaceuticals: looking beyond intuition. *Science* **2007**, *317*, 1881−1887.
(22) Dobele, M.; Wiehn, M. S.; Brase, S. Traceless solide-phase synthesis of trifluoromethylarenes. *Angew. Chem., Int. Ed.* **2011**, *50*, 11533−11535.
(23) Singh, R. P.; Shreeve, J. M. Nucleophili trifluoromethylation reactions of organic compounds with (trifluoromethyl) trimethylsilane. *Tetrahedron* **2000**, *56*, 7613−7632.
(24) Wiehn, M. S.; Vinogradova, E. V.; Togni, A. Electrophilic trifluoromethylation of arenes and N-heteroarenes using hypervalent iodine reagents. *J. Fluorine Chem.* **2010**, *131*, 951−957.
(25) Fantasia, S.; Welch, J. M.; Togni, A. Reactivity of a hypervalent iodine trifluoromethylation reagent toward THF: ring opening and formation of trifluoromethyl ethers. *J. Org. Chem.* **2010**, *75*, 1779−1782.
(26) Zhou, S.; Yan, Tao.; Wang, B. L.; Li, Z. Design, synthesis, structure-activity relationship and insecticidal activities of trifluoromethyl-containing sulfiliminyl and sulfoximinyl phthalic acid diamide structures. *Chin. J. Chem.* **2014**, *32* (7), 567−562.
(27) García Mancheño, O.; Bistri, O.; Bolm, C. Iodine and metal-free synthesis of *N*-cyano sulfilimines: novel and easy access of NH-sulfoximines. *Org. Lett.* **2007**, *19*, 3809−3811.
(28) Sheldrick, G. M. *SHELXS97 and SHELXL97*; University of Göttingen, Germany, 1997.
(29) Abbott, W. S. A method of computing the effectiveness of an insecticide. *J. Econ. Entomol.* **1925**, *18*, 265−267.
(30) Raymond, M. Presentation d'un programme Basicd'analyse log-probit pour miero-ordinateur. *Cah. ORSTOM Ser. Ent. Med. Parasitol.* **1985**, *23*, 117−121.
(31) Wu, Y. D.; Shen, J. L.; Chen, J.; Lin, X. W.; Li, A. M. Evaluation of two resistance monitoring methods in *Helicoverpa armigera*: topical application method and leaf dipping method. *Plant Prot.* **1996**, *22* (5), 3−6.
(32) Ma, H.; Wang, K. Y.; Xia, X. M.; Zhang, Y.; Guo, Q. L. The toxicity testing of five insecticides to different instar larvae of *Spodoptera exigua*. *Mod. Agrochem.* **2006**, *5*, 44−46.
(33) Busivine, J. R. Recommended methods for measurement of pest resistance to pesticides. *FAO Plant Production and Protection Paper 21*; FAO: Rome, Italy, 1980; pp 3−13 and 119−122.
(34) Sun, N. B.; Liu, X. H.; Weng, J. Q.; Tan, C. X. An unexpected product *N*-(3-((2-fluorobenzyl)thio)-5-methyl-4*H*-1,2,4-triazol-4-yl)-acetimidamide: synthesis and structure analysis. *J. Chem. Soc. Pak.* **2013**, *35*, 499−502.
(35) Jin, J. C.; Sun, Z. H.; Yang, M. Y.; Wu, J.; Liu, X. H. Synthesis, crystal structure, and theoretical studies of *N*-(4-((4-chlorobenzyl)-oxy)phenyl)-4-(trifluoromethyl)pyrimidin-2-amine. *J. Chem.* **2013**, *2013*, No. 521757.
(36) Liu, X. H.; Weng, J. Q.; Tan, C. X. Synthesis, crystal structure, and fungicidal activity of 5-(4-cyclopropyl-5-((3-fluorobenzyl)thio)-4*H*-1,2,4-triazol-3-yl)-4-methyl-1,2,3-thiadiazole. *J. Chem.* **2013**, *2013*, No. 306361.
(37) Liu, X. H.; Tan, C. X.; Weng, J. Q.; Liu, H. J. (*E*)-(4-Bromobenzylidene)amino cyclopropanecarboxylate. *Acta Crystallogr. E* **2012**, *68*, O493.
(38) Tan, C. X.; Weng, J. Q.; Liu, Z. X.; Liu, X. H.; Zhao, W. G. Synthesis, crystal structure, and fungicidal activity of a novel 1,2,3-thiadiazole compound. *Phosphorus Sulfur Silicon Relat. Elem.* **2012**, *187*, 990−996.
(39) Zhou, S.; Yan, T.; Li, Y. X.; Jia, Z. H.; Wang, B. L.; Zhao, Y.; Qiao, Y. Y.; Xiong, L. X.; Li, Y. Q.; Li, Z. M. Novel phthalamides containing sulfiliminyl moieties and derivatives as potential ryanodine receptor modulators. *Org. Biomol Chem.* **2014**, *12* (34), 6643−6652.
(40) Liu, X. H.; Sun, Z. H.; Yang, M. Y.; Tan, C. X.; Weng, J. Q.; Zhang, Y. G.; Ma, Y. Microwave assistant one pot synthesis, crystal structure, antifungal activities and 3D-QSAR of novel 1,2,4-triazolo-[4,3-9*a*]pyridines. *Chem. Biol. Drug Des.* **2014**, *84*, 342−347.
(41) Sun, G. X.; Sun, Z. H.; Yang, M. Y.; Liu, X. H.; Ma, Y.; Wei, Y. Y. Design, synthesis, biological activities and 3D-QSAR of new *N*,*N*′-diacylhydrazines containing 2,4-dichlorophenoxy moieties. *Molecules* **2013**, *18*, 14876−14891.
(42) Sun, N. B.; Shi, Y. X.; Liu, X. H.; Ma, Y.; Tan, C. X.; Weng, J. Q.; Jin, J. Z.; Li, B. J. Design, synthesis, antifungal activities and 3D-QSAR of new *N*,*N*′-diacylhydrazines containing 2,4-dichlorophenoxy moiety. *Int. J. Mol. Sci.* **2013**, *14*, 21741−21756.
(43) Liu, X. H.; Xu, X. Y.; Tan, C. X.; Weng, J. Q.; Chen, J. Synthesis, crystal structure, herbicidal activities and 3D-QSAR study of some novel 1,2,4-triazolo[4,3-*a*]pyridine derivatives. *Pest Manag. Sci.* DOI: 10.1002/ps.3804.
(44) SYBYL 6.9, Tripos Associates, St. Louis, MO, USA.

Table 1. Physicochemical Properties of the Antibiotics Investigated in This Study[f]

| Compound | Molecular Formula | Structure | Molecular Weight | $pK_a$ | Log $K_{ow}$ | $K_{oc}$ (L/kg)[e] |
|---|---|---|---|---|---|---|
| Tetracycline (TC) | $C_{22}H_{24}N_2O_8$ | 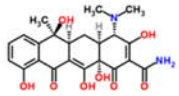 | 444.43 | 3.3; 7.68; 9.69[a] | -1.3 | $1.37\times10^5$ |
| Sulfamethazine (SMZ) | $C_{12}H_{14}N_4O_2S$ | 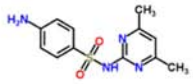 | 278.33 | 2.07; 7.49[a] | 0.76 | 165 |
| Norfloxacin (NOR) | $C_{16}H_{18}FN_3O_3$ | 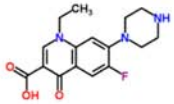 | 319.33 | 3.11; 6.1; 8.6[b] | -1.03 | $7.48\times10^4$ |
| Erythromycin (ERY) | $C_{37}H_{67}NO_{13}$ | 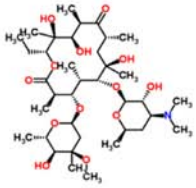 | 733.93 | 8.88; 12.91[c] | na* | $1.63\times10^4$ |
| Chloramphenicol (CAP) | $C_{11}H_{12}C_{l2}N_2O_5$ | 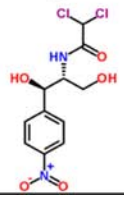 | 323.13 | 5.5; 9.61[d] | 0.92 | 127.63 |

[a]Sarmah et al., 2006. [b]Zhang et al., 2009. [c]Yang et al., 2009. [d]Yamanoto et al., 2005. [e]Measured in the sorption experiment. [f]*na: not available. Log $K_{ow}$: the logarithm of the octanol/water partition coefficient. $K_{oc}$: soil adsorption coefficient.

of antibiotics in various crops. Findings from this study would facilitate a better understanding of the transfer of antibiotics to the soil−plant system and the potential ecological and human risks through exposure to antibiotic contamination.

## MATERIALS AND METHODS

**Antibiotics and Chemicals.** Target antibiotic compounds were selected mainly based on their frequent usage in human and livestock in the PRD and other regions as well as their environmental behaviors.[25−27] Tetracycline (TC), sulfamethazine (SMZ), norfloxacin (NOR), erythromycin (ERY), and chloramphenicol (CAP), which belong to five different antibiotic types, were examined in this study (Table 1). All standards and some internal standards (SMZ-$d_4$, NOR-$d_5$, and ERY-$^{13}C_2$) were obtained from Sigma-Aldrich (USA), CAP-$d_5$ was purchased from Dr Ehrenstorfer GmbH (Germany), and TC-$d_6$ was obtained from Toronto Research Chemicals (Canada). Oasis HLB extraction cartridges (6 mL, 500 mg) (Waters Corporation, USA) were used for the extraction and purification of the target compounds. All the organic solvents used were of HPLC grade and purchased from Merck Corporation (Germany). Individual stock solutions and internal standards were prepared at 100 mg/L in methanol and stored in an amber glass vial at −20 °C.

**Sampling Sites.** Six locations (Huizhou, Foshan, Zhongshan, Guangzhou, Dongguan, and Shenzhen) in the PRD region were sampled. The region contains more than 11 million hectares of arable land, and the sampling sites were representative regarding farming practice and had long history (>20 y) of wastewater reuse. The irrigation water in Huizhou, Foshan, Zhongshan, and Guangzhou was mainly domestic wastewater that was largely untreated and discharged directly into open ditches or nearby rivers, while fishpond water was used for irrigation in Dongguan and Shenzhen (Figure 1).

Irrigation water, soil, and crops were sampled in July 2013. Water samples were collected in 1 L amber glass bottles, with 50 mL of methanol immediately added and pH adjusted to 3.0 using 4 M $H_2SO_4$ to preserve the aqueous samples (five replicates per sampling site). Soil and crop samples were collected from five random plots (100 × 100 $m^2$) on each sampling site. Soil samples were collected at two depths: 0−10 cm and 10−20 cm. An adjacent plot without cultivation served as the control with no antibiotic contamination. Soil samples were characterized, and their physicochemical properties are given in Table S1 in the Supporting Information. Chinese white cabbage, water spinach, Chinese radish, corn, and rice were harvested around the soil-sampling sites when the crops reached marketable size. Five whole crops were randomly collected from each plot, which were pooled to form a bulk sample to result in five replicates per site. Crops cultivated in a greenhouse without wastewater irrigation were used as control crops. Once in the laboratory, the water samples were passed through 0.7 μm glass fiber filters (Whatman GF/F, U.K.), and extraction was carried out within 3 days. Soil samples and fresh crops were rinsed

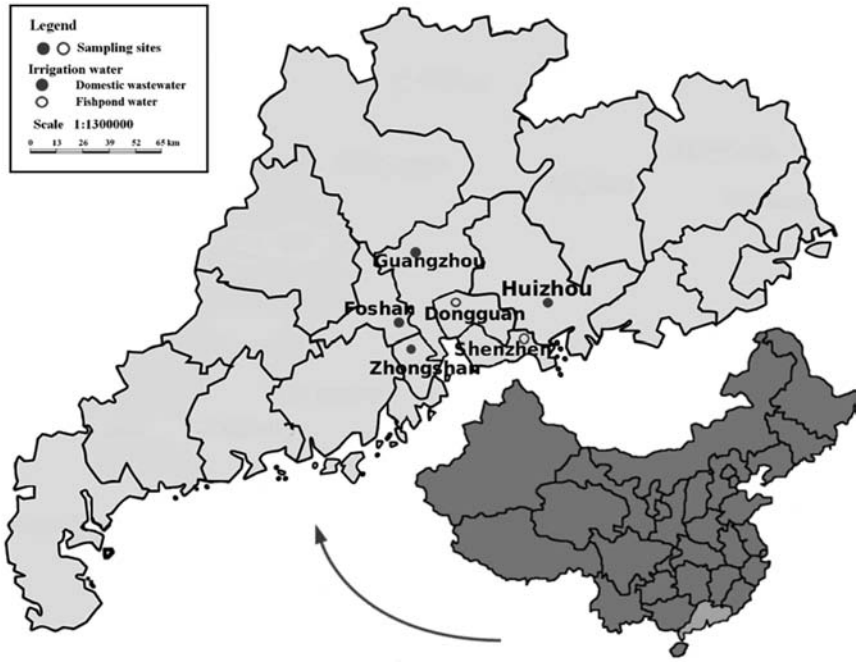


**Figure 1.** Information on the sampling sites in the Pearl River Delta, southern China.

with deionized water and freeze-dried. The dried samples were then ground to powder and stored at −20 °C until extraction.

**Extraction.** *Water Samples.* The target antibiotics in the water samples were extracted by solid phase extraction (SPE) using Oasis HLB cartridges. The internal standards (100 ng) and 0.2 g of disodium ethylenediaminetetraacetate ($Na_2EDTA$) were spiked into each water sample (1 L). The SPE cartridges were preconditioned with 10 mL of methanol and 10 mL of Milli-Q water, after which the water samples were passed through the cartridge at a flow rate of 10 mL/min. The analytes were eluted from the cartridge with 10 mL of methanol, concentrated under a gentle nitrogen stream, and then redissolved in 1 mL of methanol. The final extract was filtered through a nylon syringe filter into a 2 mL amber glass vial and stored at −18 °C before the LC−MS/MS analysis.

*Soil Samples.* One gram of freeze-dried soil was ground up and spiked with 100 μL of each internal standard (1.0 mg/L). The soil samples were extracted three times with 30 mL of acetonitrile and 0.2 M citric acid buffer (pH 4.4) (v:v = 1:1) by vortex (60 s each time) and ultrasonication (15 min each time). The mixture was centrifuged in air-cooled conditions at 1370 g for 10 min and concentrated; the extract for each soil sample was evaporated to near dryness, 0.2 g of $Na_2EDTA$ was added, and the mixture was diluted to 200 mL with Milli-Q water. Each cartridge was preconditioned with 10 mL of methanol and 10 mL of Milli-Q water, and the extracts were passed through HLB cartridges for purification. The analytes were eluted from the cartridge with 10 mL of methanol and dried under a gentle nitrogen stream. Finally, the residue was redissolved in 1 mL of methanol for analysis.

*Crop Samples.* One gram of each freeze-dried crop tissue was ground and spiked with 100 μL of each internal standard (1.0 mg/L). The crop samples were extracted three times with 30 mL of mixed solution of acidified acetonitrile (pH 3) and acetone (v:v = 1:1) by vortex mixing (60 s each time) and ultrasonication (15 min each), followed by centrifugation in air-cooled conditions at 12000*g* for 15 min. The combined extractions were pipetted into a 200 mL round-bottom flask and evaporated to remove the organic solvent; 0.2 g of $Na_2EDTA$ was added, and the mixture was diluted to 200 mL with Milli-Q water and passed through the preconditioned HLB cartridges for purification. The analytes were then eluted from the cartridge with 10 mL of methanol and dried under a gentle nitrogen stream. Finally, the residue was redissolved in 1 mL of methanol for analysis.

**Liquid Chromatography Mass Spectrometry Analysis.** The target antibiotic compounds were analyzed by HPLC−MS/MS (Agilent Liquid Chromatography 1100 series HPLC system coupled to an Agilent 6410 triple quadrupole MS) equipped with an electrospray ionization (ESI) source (Agilent, USA) in multiple-reaction monitoring (MRM) mode. The analyses were performed in negative mode for CAP and in positive mode for the other antibiotics. Nitrogen gas was used as the drying and collision gas. The chromatographic column was an Agilent Eclipse XDB-C18 (3.0 × 75 mm, 3.5 μm) column with a Poroshell 120 precolumn filter (3.0 mm, 0.2 μm). The column temperature was maintained at 40 °C for the analysis of the antibiotics.

For ESI+, 0.01% formic acid was used as mobile phase A and acetonitrile as mobile phase B. Gradient conditions were set as follows: 0 min, 20% B; 3 min, 40% B; 6 min, 60% B; 8 min, 80% B; 9 min, 95% B and 13 min, 20% B. For ESI−, Milli-Q water was used as mobile phase A and acetonitrile as mobile phase B (v:v = 15:85) with isocratic elution. The injection volume was 10 μL, and the flow rates of the mobile phases were 0.3 mL/min and 0.35 mL/min for the positive and negative modes, respectively.

Mass spectrometric conditions were optimized using Optimizer (Agilent, USA) for fine-tuning of the fragmentor voltage, collision energy (CE), and multiple reaction monitoring mode (MRM) transitions for each antibiotic (Table S2 in the Supporting Information). The following optimized parameters were selected: drying gas temperature 350 °C, drying gas flow rate 9 mL/min (ESI+), 11 mL/min (ESI−), capillary voltage 3500 V. The system was re-equilibrated for 5 min between runs.

**Estimation of the Bioconcentration Factor and Dietary Intake.** The ability of a plant to accumulate antibiotics from the soil was estimated using the bioconcentration factor (BCF), which was calculated as the ratio of the chemical concentration in the crop tissue to the chemical concentration in the soil (all based on dry weight):

$$\mathrm{BCF} = \frac{\text{concentration in crop tissue (μg/kg)}}{\text{concentration in soil (μg/kg)}}$$

An exploratory assessment of the potential human exposure to antibiotics through the consumption of edible crops was conducted. The level of human exposure was calculated as

$$\text{human exposure} = C \times D \times W \times T$$

where $C$ is the concentration of antibiotics in the edible tissue (ng/g wet weight), $D$ is the average daily consumption of edible crops (g wet weight/kg body weight day), $W$ is the body weight (kg) of the person consuming the crops, and $T$ is the exposure time (day). The concentrations of antibiotic in crop were converted to a fresh weight basis using the average water content of each crop (95.3% for Chinese white cabbage, 91.4% for water spinach, 95.3% for Chinese radish, 76.0% for corn, and 11.6% for rice).[28] The annual exposure of a 70 kg individual was estimated using the average daily consumption of edible crops (11.8, 0.6, 0.5, 9.2, and 24.0 g wet weight/kg body weight-day for Chinese white cabbage, water spinach, Chinese radish, corn, and rice, respectively).[29]

**Quantification and Quality Control.** To account for the potential analyte loss, a reagent blank, method blank, and spiked matrices were analyzed together with the water, soil, and crop samples. None of the analytes were detected in the blank controls for water, soil, and crop samples. Quantification of each antibiotic compound was obtained using the internal standard method. Analytical precision was measured by analyzing one sample in triplicate for every 10 samples, and the calculated relative standard deviation was less than 10%.[28] The recoveries of the target compounds ranged between 70% and 120% (Table S3 in the Supporting Information). Limit of detection (LOD) and limit of quantification (LOQ) of the antibiotics were calculated with signal/noise ratios (S/N) of 3 and 10, respectively. The S/N ratios were obtained by using the software Masshunter (Agilent, USA). The LOQ of the target compounds ranged from 0.40 to 1.13 ng/L for the water samples, 0.70 to 4.63 ng/g for the soil samples, and 0.80 to 4.40 ng/g for the crop samples (Table S3 in the Supporting Information). Ten concentrations (0.5, 1, 2, 5, 10, 20, 50, 100, 200, and 500 ng/L) of individual antibiotics were used to calculate the calibration curves ($r^2 > 0.999$). Recoveries of the study compounds were performed by spiking the standard solutions to DI water, soil, and crop tissue samples. Ion suppression and enhancement are considered as the major sources of inaccurate quantitative results in complex matrices.[22,30] Initial recovery was done using the internal standards and standard solutions to correct for matrix effects, spiking 100 $\mu$g/L of each standard into the sample extracts and comparing the obtained concentration in matrix to the concentration in solvent. Values of smaller or greater than 100% indicate signal suppression and enhancement, respectively.[31]

## RESULTS AND DISCUSSION

**Antibiotics in Irrigation Water.** The target antibiotics were detected at concentrations above the LOQ in the irrigation water samples (Figure 2). The highest concentration was 69.3−234.0 ng/L for TC, and the lowest was 4.0−58.2 ng/L for SMZ. These results were in general agreement with those for agricultural irrigation water.[32,33] The wastewaters in Dongguan and Shenzhen contained significantly higher concentrations of antibiotics (ranging 12.9−234.0 ng/L and 10.5−184.0 ng/L, respectively) than those in the other regions ($p < 0.05$). This can be attributed to the common practice of directly adding antibiotics to water or in medicated feeds to control bacterial diseases in farmed fish.[34] In the irrigation waters from Foshan, Zhongshan, and Guangzhou, TC and CAP were found at relatively high concentrations. The wastewater used for crop irrigation in Huizhou had the lowest concentrations of the various antibiotics. The cropland in Huizhou is located on the upper-middle reaches of the Danshui River and has less interference from human activities.

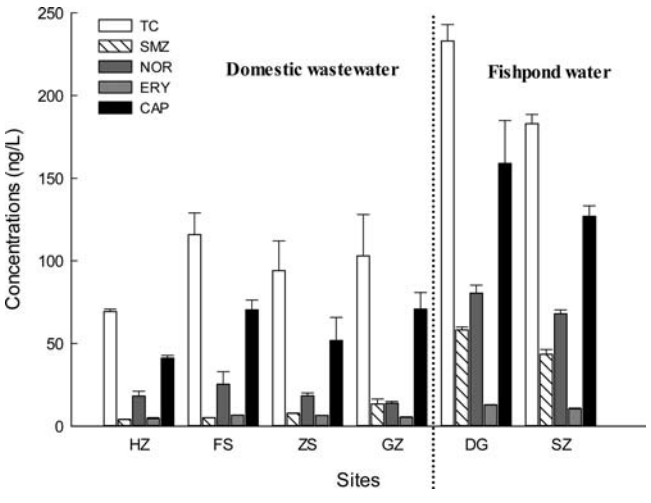


**Figure 2.** Concentrations (ng/L) of antibiotics in irrigation water in the Pearl River Delta, China (mean ± SD, $n = 5$).

**Antibiotics in Soils.** TC, SMZ, NOR, ERY, and CAP were all detected in the surface layer (0−10 cm) irrigated soil samples from the six sites (Table 2). TC, NOR, and CAP in most cases had significantly higher concentrations in soils irrigated by fishpond water than those by domestic wastewater ($p < 0.05$). TC, NOR, and CAP showed a similar trend in concentration in the corresponding irrigation waters ($r = 0.93$, $p < 0.05$). All five target antibiotics detected in the irrigation water could be found in the irrigated soils. Both the irrigation water and irrigated soil samples from Dongguan and Shenzhen had significantly higher concentrations than the other sampling sites, especially for TC and CAP ($p < 0.05$), suggesting that the irrigation water (domestic wastewater and fishpond water) was the major contributing source.

Antibiotics persist in the environment after they are released into the soil from irrigation water.[35] Although wastewater is also used for irrigation in other countries, few studies have examined the presence and accumulation of antibiotics in irrigated soils and crops.[5,36,37] Kinney et al. (2006)[36] detected ERY in reclaimed water and wastewater-irrigated soils at concentrations of 177−611 ng/L and 0.02−15 $\mu$g/kg, respectively. Chen et al. (2011)[5] found TC, NOR, and CAP in the soils of Hebei, China, under wastewater irrigation for approximately 50 years. The present study found that the concentrations of TC, SMZ, NOR, and CAP in soil samples were significantly higher in Dongguan than in the other sites ($p < 0.05$), which corresponded to their higher concentrations in the irrigation water. NOR was frequently found at concentrations as high as 66.7 $\mu$g/kg in the irrigated soils. NOR is one of the most frequently detected antibiotics in various environmental media including water, soil, and plants,[17,38] which could be related to its extensive medical and veterinary use. It may also come from animal manure,[39] which was commonly applied in these areas. It is not surprising that NOR was consistently found at high concentrations in wastewater irrigated soils in the PRD. TC (5.0−21.9 $\mu$g/kg), SMZ (1.3−4.2 $\mu$g/kg), ERY (1.1−4.4 $\mu$g/kg), and CAP (3.2−22.3 $\mu$g/kg) were also found in the six sampling sites. TC had higher concentrations in soil irrigated with fishpond water than that with domestic wastewater. TC was detected at higher concentrations in 0−10 cm soils than in 10−20 cm soils, which is in line with its strong tendency to sorb onto soils due to their high $K_{oc}$ values (Table 1). SMZ have similarly low concentrations in the two soil depths. Sorption of SMZ to soils was influenced by its physicochemical properties and soil pH. The average soil pH in the six sampling sites was 7.51. According to the p$K_a$ values of SMZ, the fraction of deprotonated species would be increased, which would have decreased its sorption to the soil.[33,40] Therefore, SMZ is very

Table 2. Concentrations ($\mu$g/kg dw) of Antibiotics Detected in the Irrigated Soils in the Pearl River Delta, China (Mean ± SD, $n$ = 5)

| | soil depth (cm) | TC | SMZ | NOR | ERY | CAP |
|---|---|---|---|---|---|---|
| HZ | 0−10 | 8.9 ± 0.2 | 1.4 ± 0.1 | 23.9 ± 2.5 | 1.1 ± 0.1 | 4.1 ± 0.9 |
| | 10−20 | <LOQ | 1.3 ± 0.1 | 20.5 ± 2.3 | <LOQ | <LOQ |
| FS | 0−10 | 17.1 ± 1.4 | 3.8 ± 0.6 | 36.8 ± 1.9 | 4.4 ± 0.2 | 10.1 ± 0.7 |
| | 10−20 | 10.3 ± 0.3 | 3.6 ± 0.4 | 34.9 ± 0.7 | 3.9 ± 0.2 | 8.1 ± 1.8 |
| ZS | 0−10 | 15.8 ± 1.1 | 2.8 ± 0.6 | 28.5 ± 0.7 | 3.6 ± 0.1 | 6.6 ± 1.3 |
| | 10−20 | 10.5 ± 0.1 | 2.5 ± 0.2 | 25.6 ± 0.6 | 2.3 ± 0.1 | 3.2 ± 0.3 |
| GZ | 0−10 | 13.0 ± 2.4 | 2.1 ± 0.1 | 25.5 ± 1.1 | 3.5 ± 0.1 | 5.5 ± 0.4 |
| | 10−20 | 5.0 ± 0.02 | 2.0 ± 0.1 | 21.1 ± 1.0 | <LOQ | <LOQ |
| DG | 0−10 | 21.9 ± 2.7 | 4.2 ± 0.2 | 66.7 ± 1.1 | 3.4 ± 0.3 | 22.3 ± 0.8 |
| | 10−20 | 19.7 ± 2.3 | 4.0 ± 0.1 | 60.8 ± 2.4 | 3.0 ± 0.1 | 19.3 ± 1.2 |
| SZ | 0−10 | 18.2 ± 1.5 | 2.2 ± 0.1 | 34.4 ± 1.8 | 3.7 ± 0.2 | 11.4 ± 1.2 |
| | 10−20 | 16.7 ± 0.3 | 2.3 ± 0.1 | 27.2 ± 8.8 | 2.2 ± 0.1 | 8.9 ± 0.8 |

mobile and its concentrations were similar in the two soil layers at all sampling sites. Although most of the antibiotics were found in the two soil layers, the concentrations were higher at 0−10 cm than 10−20 cm due to their sorption and migration upon continuous irrigation. Chen et al. (2011)[5] detected TC at higher concentrations in the upper layer soil in wastewater irrigated plot in Hebei Province. The distribution of the target antibiotics in the soil profiles indicates that they were preferably retained in soil, which may lead to further contamination of plants. Nevertheless, the concentrations of antibiotics in this study were significantly lower than those reported in other studies. For example, Hu et al. (2010)[41] detected TC in wastewater-irrigated soils at concentrations of 2.5−105 $\mu$g/kg, which could be attributed to the control of antibiotic use by the Chinese government in recent years.[38,41]

**Antibiotics in Crops.** NOR was consistently found at the highest concentrations (4.6−23.6 $\mu$g/kg) in crop tissues, followed by CAP (2.6−22.4 $\mu$g/kg) and TC (4.0−10.1 $\mu$g/kg) (Table S4 in the Supporting Information), which is similar to the results of Hu et al. (2010).[41] However, SMZ and ERY were not detected in most of the vegetable crops. The leaves of Chinese white cabbage and water spinach were found to contain a variety of antibiotics, e.g., three out of the five antibiotics with concentrations of 2.6−23.6 $\mu$g/kg in Chinese white cabbage. Three antibiotics were found in water spinach leaves, though mostly at a lower concentration (5.5−21.8 $\mu$g/kg). SMZ and ERY were only found in the roots of Chinese radish and Chinese white cabbage. SMZ was not liable to be retained in the surface soil and absorbed by crops as indicated by its small $K_d$ value, even though SMZ was present in most of the irrigated soil samples. Furthermore, ERY was rapidly adsorbed onto clay particles where protonation occurred.[42] It is difficult for ERY to be absorbed through the cellular membranes and translocate into crops as it has a greater molecular weight than the other compounds.[43] SMZ and ERY also have a shorter degradation time than the other three.[40] Therefore, these antibiotics are not easily absorbed by crops and tend not to accumulate in the plant tissues. Residue degradation, soil-binding, and leaching are other factors that can limit the availability of antibiotics for uptake by crops.[41]

**Bioconcentration Factor of Antibiotics in Crops.** The mean BCF values for different crops from the six sites are shown in Figure 3. The reported BCF values represent the minimum values due to biodegradation under the field conditions.

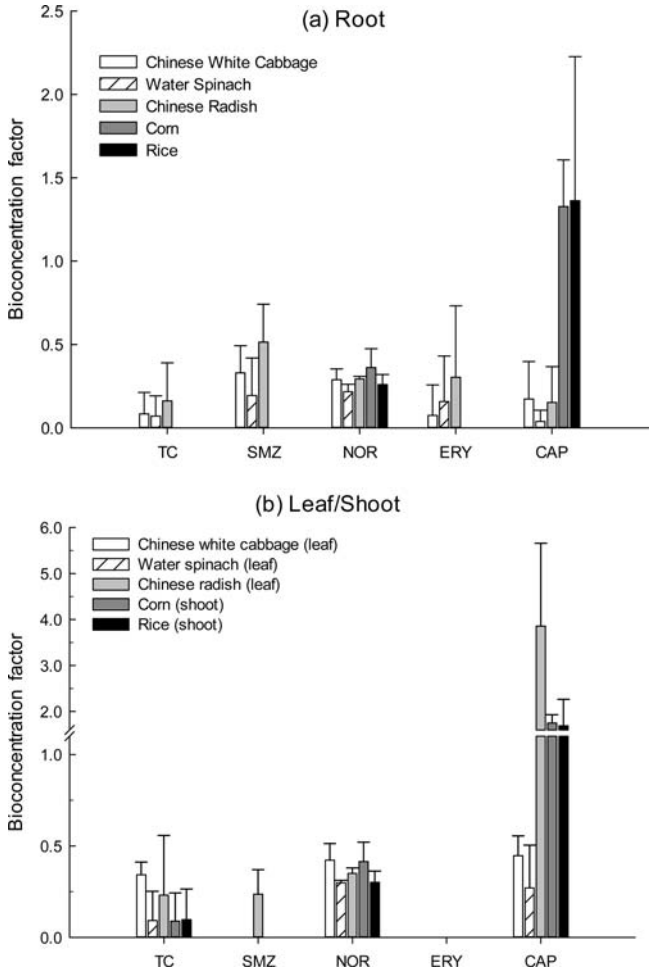


Figure 3. Bioconcentration factor (BCF) values of antibiotics in different crops (mean ± SD, $n$ = 5).

The $BCF_{root}$ values for CAP in the roots of corn and rice were 1.33 and 1.36, respectively, and the values for the other compounds were below one. CAP was also found in the shoots of Chinese radish, corn, and rice, which had $BCF_{leaf/shoot}$ values of 3.86, 1.75, and 1.69, respectively. In the five crops, the values of $BCF_{leaf/shoot}$ for TC, NOR, and CAP were larger than those for $BCF_{root}$. In contrast, the $BCF_{root}$ values for SMZ and ERY were larger than their $BCF_{leaf/shoot}$ because SMZ and ERY were not detected in most crop tissues. Moreover, the $BCF_{root}$ and $BCF_{leaf/shoot}$ values for TC, SMZ, NOR, and ERY were less than

one, indicating that they were not readily absorbed and the plants did not accumulate the antibiotics.

The uptake and translocation of antibiotics varied among the crop species. For example, although CAP was found in the roots of corn and rice ($BCF_{root}$ 1.33−1.36), it showed limited accumulation in the roots of Chinese white cabbage, water spinach, and Chinese radish ($BCF_{root}$ 0.03−0.17). In addition, all except ERY were present in the leaves of Chinese radish, and the $BCF_{leaf/shoot}$ of CAP in Chinese radish was the highest. Herklotz et al. (2010)[22] reported high concentration of sulfamethoxazole in cabbage (23.6−3200 ng/g, dry weight) under ideal hydroponics conditions. However, another study only found low concentrations of ionic compounds in crops, probably due to the repulsion of the anions by the negative electrical potential of the plant cell membrane.[44] The average soil pH was 7.5, and as SMZ existed primarily in anionic form, it was difficult for the crops to absorb. Therefore, SMZ showed limited accumulation in both roots and shoots, which is comparable to the findings of Wu et al.(2013).[7] In all, the differences in the uptake and accumulation of antibiotics are governed by the crop species, harvest time, and environmental conditions.

**Translocation of Antibiotics within Crops.** The distribution of TC, NOR, and CAP in Chinese white cabbage, water spinach, Chinese radish, corn, and rice was in the descending order of fruit > shoot/leaf > root, which suggests that the three antibiotics were transported in the transpiration stream within the xylem of the plants. In contrast, the concentrations of SMZ and ERY followed the order of root > shoot/leaf > fruit. The concentration of sulfamethoxazole in roots was about 10 times that in leaves of greenhouse grown vegetable (lettuce, cucumber, pepper, and spinach).[7] Migliore et al. (1998)[45] also found that the concentration of sulfonamides in roots was higher than that in leaves for wheat and corn. The translocation of antibiotics in crops depends on the physicochemical properties of antibiotics and crop species as well as the concentrations of antibiotics in soil.[46] The species type and the growth stage can affect the accumulation and distribution of antibiotics in crops.[15] According to the reported inhibitory concentrations of antibiotics on plants,[47] crop growth would not be significantly affected at the antibiotic concentrations detected in this study.

The translocation factor (TF) represents the translocation of antibiotics from the roots to the leaves and/or shoots, and is calculated simply as the ratio of the leaf to root concentration ([leaf]/[root]). The uptake by plants is considered to occur by passive transport. Once a chemical is taken up by roots, translocation driven by the transpiration process will distribute the chemical to other parts of the plant, and the ratio of root to leaf concentrations is dependent on the amount of water transpired and the growth rate of the plants.[48] In this study, all of the antibiotics were found in the leaves and/or shoots, except ERY, which was not detected in leaves and/or shoots. Thus, the TF for ERY cannot be calculated; TF for SMZ could only be calculated in Chinese radish.

The TF for NOR was generally larger than 1 in all five crops, indicating that NOR was preferentially transferred from the roots to the shoots (Table 3). The TFs for CAP in water spinach, rice, and corn were also larger than 1. Other antibiotics, especially ERY and SMZ, were found to accumulate in roots (TF < 1). The translocation of sulfonamides agreed with the findings of previous reports for cabbage, lettuce, cucumber, and pepper.[19,22] For example, Herklotz et al. (2010)[42] found that the concentration of sulfamethoxazole in roots was 135 times that in the leaves of cabbages grown in a nutrient solution, and the fraction of sulfamethoxazole in cabbage roots accounted for 98.4% of the total uptake. The translocation of organic compounds within plants is affected by several factors, e.g., hydrophilicity.[49] It was found that the TF was at a maximum for compounds having log $K_{ow}$ from −1.03 to 0.92, except for SMZ. Ionization could reduce the translocation of ionized organic compounds to shoots.[50] This may happen in SMZ under the present environmental conditions (existed predominantly as anion) coupled with their low root cell membrane permeability to ionized SMZ. Nonionic compounds that are highly hydrophilic were less able to cross the hydrophobic membranes, while highly lipophilic compounds were less likely to be transferred to shoots because they were retained in the root lipids.[50] In the present study, the five antibiotics have similar log $K_{ow}$ that could not distinguish the importance of hydrophilicity on the translocation and accumulation of organic compounds in crops. Moreover, uptake was species specific, even when the crops shared the same irrigated soil.[20,44] Therefore, antibiotics demonstrate different translocation behaviors in different plants according to their physicochemical properties as well as plant species, growth, and transpiration rates.

**Table 3. Translocation Factor (TF) Values of Antibiotics in Different Crops (Mean ± SD, $n$ = 5)[a]**

| | TC | SMZ | NOR | CAP |
|---|---|---|---|---|
| Chinese white cabbage | 0.5 ± 0.1 | | 1.5 ± 0.2 | 0.8 ± 0.2 |
| water spinach | 0.4 ± 0.2 | | 1.4 ± 0.4 | 1.2 ± 0.7 |
| Chinese radish | 0.7 ± 0.3 | 0.2 ± 0.1 | 1.2 ± 0.03 | 0.8 ± 0.2 |
| corn | | | 1.2 ± 0.1 | 1.4 ± 0.3 |
| rice | | | 1.2 ± 0.03 | 1.4 ± 0.5 |

[a]TF for ERY could not be calculated.

**Human Exposure Implications.** On average, the level of daily human exposure to the five antibiotics through the consumption of edible crops ranged from 0.003 to 21.8 μg (Table 4). SMZ and ERY were only detected in Chinese radish, indicating that there would be negligible risk associated with the consumption of these crops. However, the levels of TC, NOR, and CAP were relatively high, especially for corn and rice (daily human exposure was 0.34−2.77 and 11.0−21.8 μg, respectively). The annual human exposure has been estimated based on the daily consumption of these five edible crops (1.1 to 7950 μg). Moreover, the United Nations Food and Agriculture Organization has established acceptable daily intake (ADI) levels for TC (0−30 μg/kg bw) and ERY (0.0−0.7 μg/kg bw). Assuming that the body weight of an average adult is 70 kg, the maximum permissible intake of TC is 2100 μg/day while that for ERY is 49 μg/day. Although the estimated values of daily human exposure in this study were much lower than the minimum therapeutic doses (typically in the 20−200 mg range) and below the recommended ADI values, antibiotic-resistant bacteria or their corresponding resistance genes have been shown to spread to humans via the food chain.[51] Thus, further research is needed to assess the accumulation of these antibiotics in the food chain to determine the safe concentrations for human consumption.

The results of this study indicate that the use of wastewater and fishpond water to irrigate croplands could lead to the accumulation of antibiotics in soils and edible crops. However,

Table 4. Human Exposure to Antibiotics in Chinese White Cabbage, Water Spinach, Chinese Radish, Corn, and Rice, Calculated from the Concentrations of These Compounds in the Edible Tissues

| | TC | | SMZ | | NOR | | ERY | | CAP | |
|---|---|---|---|---|---|---|---|---|---|---|
| human exposure ($\mu$g) | daily | annual | daily | annual | daily | annual | daily | annual | daily | annual |
| Chinese white cabbage (leaf) | 0.23 | 84.6 | | | 0.59 | 216 | | | 0.21 | 75.2 |
| water spinach (leaf) | 0.01 | 2.8 | | | 0.05 | 18.5 | | | 0.02 | 6.8 |
| Chinese radish (root) | 0.01 | 2.0 | 0.01 | 1.9 | 0.02 | 6.8 | 0.003 | 1.1 | 0.004 | 1.6 |
| corn (fruit) | 0.34 | 125 | | | 2.27 | 830 | | | 2.77 | 1011 |
| rice (fruit) | 11 | 3998 | | | 17.2 | 6266 | | | 21.8 | 7955 |

significant disparities were observed in the potential root uptake and subsequent accumulation of the different antibiotics in relation to their physicochemical properties (e.g., ionization, degradation time, and molecular size) and the environmental conditions. SMZ and ERY preferentially accumulated in roots as they have difficulties in moving up the crops, while TC, NOR, and CAP were more prevalent in leaves/shoots and fruits. More experimental data on other types of antibiotics or organic compounds are needed for verification. Although the levels of antibiotics ingested through the consumption of edible crops were much lower than the minimum therapeutic doses or ADI levels, the findings from this study provide basic information on the accumulation of antibiotics in edible crops and help evaluate human exposure to antibiotics through crop consumption. Further research on the potential long-term health effects of ingesting different types of antibiotics through dietary uptake is necessary.

## ■ ASSOCIATED CONTENT

### Supporting Information

A detailed description of the properties of soils from the study sites (Table S1), the optimized MRM parameters for the analysis of antibiotics by HPLC-MS/MS (Table S2), and the extraction recoveries of antibiotics in different matrices (Table S3), as well as the concentrations ($\mu$g/kg dw) of antibiotics in different crop tissues (Table S4). This material is available free of charge via the Internet at http://pubs.acs.org.

## ■ AUTHOR INFORMATION

### Corresponding Author

*Phone: 852-39436378. Fax: 852-26037732. E-mail: leemanchu@cuhk.edu.hk.

### Notes

The authors declare no competing financial interest.

## ■ ACKNOWLEDGMENTS

We thank Ben Yeung (The Chinese University of Hong Kong) for his technical assistance and Dr. Yinge Zhao of the Croucher Institute for Environmental Sciences (Hong Kong Baptist University) for her support in laboratory analyses.

## ■ ABBREVIATIONS USED

PRD, Pearl River Delta; PPCPs, pharmaceuticals and personal care products; TC, tetracycline; SMZ, sulfamethazine; NOR, norfloxaxin; ERY, erythromycin; CAP, chloramphenicol; HZ, Huizhou; FS, Foshan; ZS, Zhongshan; GZ, Guangzhou; DG, Dongguan; SZ, Shenzhen; HLB, hydrophilic−lipophilic balanced; SPE, solid phase extraction; $Na_2EDTA$, disodium ethylenediaminetetraacetate; HPLC−MS/MS, high performance liquid chromatography double mass spectrometry; ESI, electrospray ionization; MRM, multiple-reaction monitoring; CE, collision energy; LOD, limit of detection; LOQ, limit of quantification; S/N, signal/noise; $K_{oc}$, soil adsorption coefficient; p$K_a$, a logarithmic measure of the acid dissociation constant; BCF, bioconcentration factor; TF, translocation factor

## ■ REFERENCES

(1) IPCC Intergovernmental Panel on Climate Change. http://www.ipcc.ch/s (16th July 2014).

(2) WWAP (World Water Assessment Programme). http://www.unesco.org/new/en/natural-sciences/environment/water/wwap/s (16th July 2014).

(3) Raschid-Sally, L.; Jayakody, P. *Drivers and Characteristics of Wastewater Agriculture in Developing Countries-Results From a Global Assessment*; International Water Management Institute: Colombo, Sri Lanka, 2008; pp 1−30.

(4) Shi, Y.; Gao, L.; Li, W.; Liu, J.; Cai, Y. Investigation of fluoroquinolones, sulfonamides and macrolides in long-term wastewater irrigation soil in Tianjin, China. *Bull. Environ. Contam. Toxicol.* **2012**, *89*, 857−861.

(5) Chen, F.; Ying, G. G.; Kong, L. X.; Wang, L.; Zhao, J. L.; Zhou, L. J.; Zhang, L. J. Distribution and accumulation of endocrine-disrupting chemicals and pharmaceuticals in wastewater irrigated soils in Hebei, China. *Environ. Pollut.* **2011**, *159*, 1490−1498.

(6) Papadopoulos, F.; Parissopoulos, G.; Papadopoulos, A.; Zdragas, A.; Ntanos, D.; Prochaska, C.; Metaxa, I. Assessment of reclaimed municipal wastewater application on rice cultivation. *Environ. Manage.* **2009**, *43*, 135−143.

(7) Yan, C. X.; Yang, Y.; Zhou, J. L.; Liu, M.; Nie, M. H.; Shi, H.; Gu, L. J. Antibiotics in the surface water of the Yangtze Estuary: occurrence, distribution and risk assessment. *Environ. Pollut.* **2013**, *175*, 22−29.

(8) USEPA. *Guidelines for Water Reuse*; U.S. Agency for International Development: Washington, DC, 2004; EPA/625/R-92/004.

(9) SAEPA. *South Australian Reclaimed Water Guidelines*; Department of Human Services and Environmental Protection Agency, Government of South Australia: Adelaide, Australia, 1999.

(10) WELL. *Guidelines for wastewater reuse in agriculture and aquaculture: recommended revisions based on new research evidence*; Water and Environmental Health: London, 2000; Task No.: 68 Part 1.

(11) Gao, L. H.; Shi, Y. L.; Li, W. H.; Niu, H. Y.; Liu, J. M.; Cai, Y. Q. Occurrence of antibiotics in eight sewage treatment plants in Beijing, China. *Chemosphere* **2012**, *86*, 665−671.

(12) Xu, W.; Zhang, G.; Li, X.; Zou, S.; Li, P.; Hu, Z.; Li, J. Occurrence and elimination of antibiotics at four sewage treatment plants in the Pearl River Delta (PRD), South China. *Water Res.* **2007**, *41*, 4526−4534.

(13) Yang, J. F.; Ying, G. G.; Zhao, J. L.; Tao, R.; Sua, H. C.; Liu, Y. S. Spatial and seasonal distribution of selected antibiotics in surface waters of the Pearl Rivers, China. *J. Environ. Sci. Health.* **2011**, *46*, 272−280.

(14) Malchi, T.; Maor, Y.; Tadmor, G.; Shenker, M.; Chefetz, B. Irrigation of root vegetables with treated wastewater: evaluating uptake of pharmaceuticals and the associated human health risks. *Environ. Sci. Technol.* **2014**, *48*, 9325−9333.

(15) Wu, X.; Conkle, J. L.; Ernst, F.; Gan, J. Treated wastewater irrigation: uptake of pharmaceutical and personal care products by common vegetables under field conditions. *Environ. Sci. Technol.* **2014**, *48*, 11286−11293.
(16) United States Environmental Protection Agency. *Pharmaceuticals and personal care products*. http://www.epa.gov/ppcp/basic2.html (16th July 2014).
(17) Yiruhan; Wang, Q. J.; Mo, C. H.; Li, Y. W.; Gao, P.; Tai, Y. P.; Zhang, Y.; Ruan, Z. L.; Xu, J. W. Determination of four fluoroquinolone antibiotics in tap water in Guangzhou and Macao. *Environ. Pollut.* **2010**, *158*, 2350−2358.
(18) Sabourin, L.; Duenk, P.; Bonte-Gelok, S.; Payne, M.; Lapen, D. R.; Topp, E. Uptake of pharmaceuticals, hormones and parabens into vegetables grown in soil fertilized with municipal biosolids. *Environ. Sci. Technol.* **2012**, *431*, 233−236.
(19) Wu, X.; Ernst, F.; Conkle, J. L.; Gan, J. Comparative uptake and translocation of pharmaceutical and personal care products (PPCPs) by common vegetables. *Environ. Int.* **2013**, *60*, 15−22.
(20) Kang, D. H.; Gupta, S.; Rosen, C.; Fritz, V.; Singh, A.; Chander, Y.; Murray, H.; Rohwer, C. Antibiotic uptake by vegetable crops from manure-applied soils. *J. Agric. Food Chem.* **2013**, *61*, 9992−10001.
(21) Watkinsona, A. J.; Murbyd, E. J.; Kolpine, D. W.; Costanzo, S. D. The occurrence of antibiotics in an urban watershed: From wastewater to drinking water. *Sci. Total Environ.* **2009**, *407*, 2711−2723.
(22) Herklotz, P. A.; Gurung, P.; Vanden Heuvel, B.; Kinney, C. A. Uptake of human pharmaceuticals by plants grown under hydroponic conditions. *Chemosphere* **2010**, *78*, 1416−1421.
(23) Agriculture, Fisheries and Conservation Department. *Agriculture in HK*. http://www.afcd.gov.hk/english/agriculture/agr_hk/agr_hk.html (16th July 2014).
(24) Department of Agriculture of GuangDong Province. http://www.gdagri.gov.cn/ (16th July 2014).
(25) Sarmah, A. K.; Meyer, M. T.; Boxall, A. B. A global perspective on the use, sales, exposure pathways, occurrence, fate and effects of veterinary antibiotics (VAs) in the environment. *Chemosphere* **2006**, *65*, 725−759.
(26) Zhou, L. J.; Ying, G. G.; Zhao, J. L.; Yang, J. F.; Wang, L.; Yang, B.; Liu, S. Trends in the occurrence of human and veterinary antibiotics in the sediments of the Yellow River, Hai River and Liao River in northern China. *Environ. Pollut.* **2011**, *159*, 1877−1885.
(27) Jiang, Y. H.; Li, M. X.; Guo, C. S.; An, D.; Xu, J.; Zhang, Y.; Xi, B. D. Distribution and ecological risk of antibiotics in a typical effluent - receiving river (Wangyang River) in north China. *Chemosphere* **2014**, *112*, 267−274.
(28) USEPA. *QA/QC guidance for sampling and analysis of sediments, water, and tissues for dredged material evaluations*; U.S. Agency for International Development: Washington, DC, 1995; EPA 823-B-95-001.
(29) USEPA. *Exposure factors handbook*; U.S. Agency for International Development: Washington, DC, 2011; EPA 600-R-090-052F.
(30) Hummel, D.; Loffler, D.; Fink, G.; Ternes, T. A. Simultaneous determination of psychoactive drugs and their metabolites in aqueous matrices by liquid chromatography mass spectrometry. *Environ. Sci. Technol.* **2006**, *40*, 7321−7328.
(31) Grujić, S.; Vasiljević, T.; Lausević, M. Determination of multiple pharmaceutical classes in surface and ground waters by liquid chromatography-ion trap-tandem mass spectrometry. *J. Chromatogr., A* **2009**, *1216*, 4989−5000.
(32) Kummerer, K. Antibiotics in the aquatic environment-a review-part I. *Chemosphere* **2009**, *75*, 417−434.
(33) Boxall, A. B. A.; Kolpin, D. W.; Halling-Sørensen, B.; Tolls, J. Are veterinary medicines causing environmental risks? *Environ. Sci. Technol.* **2003**, *37*, 286−294.
(34) Luo, Y.; Xu, L.; Rysz, M.; Wang, Y. Q.; Zhang, H.; Alvarez, P. J. J. Occurrence and transport of tetracycline, sulfonamide, quinolone, and macrolide antibiotics in the Haihe River Basin, China. *Environ. Sci. Technol.* **2011**, *45*, 1827−1833.
(35) Ternes, T. A.; Bonerz, M.; Herrmann, N.; Teiser, B.; Andersen, H. R. Irrigation of treated wastewater in Braunschweig, Germany: an option to remove pharmaceuticals and musk fragrances. *Chemosphere* **2007**, *66*, 894−904.
(36) Kinney, C. A.; Furlong, E. T.; Werner, S. L.; Cahill, J. D. Presence and distribution of wastewater-derived pharmaceuticals in soil irrigated with reclaimed water. *Environ. Toxicol. Chem.* **2006**, *25*, 317−326.
(37) Chefetz, B.; Mualem, T.; Ben-Ari, J. Sorption and mobility of pharmaceutical compounds in soil irrigated with reclaimed wastewater. *Chemosphere* **2008**, *73*, 1335−1343.
(38) Li, Y. W.; Wu, X. L.; Mo, C. H.; Tai, Y. P.; Huang, X. P.; Xiang, L. Investigation of sulfonamide, tetracycline, and quinolone antibiotics in vegetable farmland soil in the Pearl River Delta area, Southern China. *J. Agric. Food Chem.* **2011**, *59*, 7268−7276.
(39) Zhao, L.; Dong, Y. H.; Wang, H. Residues of veterinary antibiotics in manures from feedlot livestock in eight provinces of China. *Sci. Total Environ.* **2010**, *408*, 1069−1075.
(40) Thiele-Bruhn, S. Pharmaceutical antibiotic compounds in soils—a review. *J. Plant Nutr. Soil Sci.* **2003**, *166*, 145−167.
(41) Hu, X.; Zhou, Q.; Luo, Y. Occurrence and source analysis of typical veterinary antibiotics in manure, soil, vegetables and groundwater from organic vegetable bases, northern China. *Environ. Pollut.* **2010**, *158*, 2992−2998.
(42) Kim, Y. H.; Heinze, T. M.; Kim, S. J.; Cerniglia, C. E. Adsorption and clay-catalyzed degradation of erythromycin A on homoionic clays. *J. Environ. Qual.* **2004**, *33*, 257−264.
(43) Sanderson, H.; Brain, R. A.; Johnson, D. J.; Wilson, C. J.; Solomon, K. R. Toxicity classification and evaluation of four pharmaceuticals classes: antibiotics, antineoplastics, cardiovascular, and sex hormones. *Toxicology* **2004**, *203*, 27−40.
(44) Calderón-Preciado, D.; Matamoros, V.; Bayona, J. M. Occurrence and potential crop uptake of emerging contaminants and related compounds in an agricultural irrigation network. *Sci. Total Environ.* **2011**, *412*, 14−19.
(45) Migliore, L.; Civitareale, C.; Cozzolino, S.; Casoria, P.; Brambilla, G.; Gaudio, L. Laboratory models to evaluate phytotoxicity of sulphadimethoxine on terrestrial plants. *Chemosphere* **1998**, *37*, 2957−2961.
(46) Chiou, C. T.; Sheng, G. Y.; Manes, M. A partition-limited model for the plant uptake of organic contaminants from soil and water. *Environ. Sci. Technol.* **2001**, *35*, 1437−1444.
(47) Hillis, D. G.; Fletcher, J.; Solomon, K. R.; Sibley, P. K. Effects of ten antibiotics on seed germination and root elongation in three plant species. *Arch. Environ. Contam. Toxicol.* **2011**, *60*, 220−232.
(48) Simonich, S. L.; Hites, R. A. Organic pollutant accumulation in vegetation. *Environ. Sci. Technol.* **1995**, *29*, 2905−2914.
(49) Trapp, S.; Legind, C. N., Uptake of organic contaminants from soil into vegetables and fruits. In *Dealing with Contaminated Sites*; Swartjes, F. A., Ed.; Springer: New York, 2011; Vol. *9*, pp 369−408.
(50) Tanoue, R.; Sato, Y.; Motoyama, M.; Nakagawa, S.; Shinohara, R.; Nomiyama, K. Plant uptake of pharmaceutical chemicals detected in recycled organic manure and reclaimed wastewater. *J. Agric. Food Chem.* **2012**, *60*, 10203−10211.
(51) Boehme, S.; Werner, G.; Klare, I.; Reissbrodt, R.; Witte, W. Occurrence of antibiotic-resistant enterobacteria in agricultural foodstuffs. *Mol. Nutr. Food Res.* **2004**, *48*, 522−531.

**Scheme 1. Synthetic Routes of Compounds 1−37**

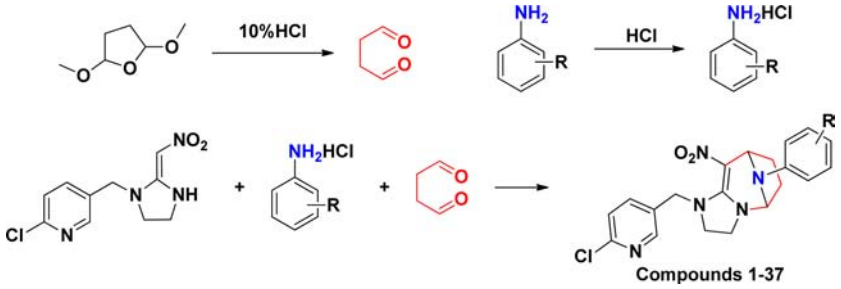


## MATERIALS AND METHODS

**Instruments.** All melting points were obtained with a Büchi Melting Point B540 and are uncorrected. Nuclear magnetic resonance spectra were recorded on a Bruker AM-400 spectrometer with $CDCl_3$ or DMSO-$d_6$ as the solvent ($^1$H at 400 MHz and $^{13}$C at 100 MHz) and TMS as the internal standard. Chemical shifts are reported in parts per million ($\delta$). Coupling constants ($J$) are reported in hertz (Hz). High-resolution electron mass spectra (ESI-TOF) were performed on a Micromass LC-TOF spectrometer. Analytical thin-layer chromatography (TLC) was carried out on precoated plates (silica gel 60 $F_{254}$), and spots were visualized with ultraviolet (UV) light.

**General Synthetic Procedure for the Substituted Aniline Hydrochloride.** The corresponding aniline (10 mmol) in ethyl acetate (15 mL) was cooled to 0 °C. A solution of concentrated HCl was dropwise added and the pH value of the reaction mixture adjusted to 1−2. After the addition was completed, precipitate was filtered and washed with less concentrated HCl and ethyl acetate. After drying under vacuum, the obtained corresponding aniline hydrochloride could be used without further purification.

**Preparation of the Solution of Succinaldehyde.** A mixture of 2,5-dimethoxydihydrofuran (0.290 g, 2.2 mmol) and 0.4 mL of 10% aqueous HCl was stirred at room temperature. After 12 h, the pH value of the mixture was adjusted to 2−3 by saturated aqueous $NaHCO_3$. The solution could be used directly in the next step.

**General Synthetic Procedure for Compounds 1−37.** A mixture of starting material **B** (2 mmol) and corresponding aniline hydrochloride (2.5 mmol) in acetonitrile (20 mL) was stirred at 0 °C. Then the solution of succinaldehyde was slowly added, and the reaction was monitored by TLC. After 1.5 h, the pH value of the mixture was adjusted to 7−8 by saturated aqueous $NaHCO_3$, and the solvent was removed under reduced pressure. Then, water was added, the mixture was extracted with dichloromethane (3 × 50 mL), and the organic layer was washed with brine, dried over anhydrous sodium sulfate, filtered, and concentrated. The residue was purified by silica gel column chromatography to afford the corresponding product.

*1-((6-Chloropyridin-3-yl)methyl)-9-nitro-10-phenyl-2,3,5,6,7,8-hexahydro-1H-5,8-epiminoimidazo[1,2-a]azepine (**1**):* yield, 44.8%; mp, 173−174 °C; $^1$H NMR (400 MHz, DMSO-$d_6$) $\delta$ 8.16 (d, $J$ = 2.0 Hz, 1H), 7.30−7.20 (m, 4H), 6.94 (d, $J$ = 8.0 Hz, 2H), 6.89 (t, $J$ = 7.2 Hz, 1H), 5.62 (s, 1H), 5.26 (s, 1H), 4.79 (d, $J$ = 15.6 Hz, 1H), 4.60 (d, $J$ = 15.6 Hz, 1H), 3.82−3.71 (m, 1H), 3.70−3.50 (m, 2H), 3.46−3.36 (m, 1H), 2.28−2.12 (m, 3H), 2.00−1.85 (m, 1H); $^{13}$C NMR (100 MHz, DMSO-$d_6$) $\delta$ 156.0, 149.6, 149.6, 145.0, 138.9, 132.4, 129.7, 124.5, 120.6, 117.7, 109.3, 71.5, 56.9, 50.7, 49.7, 47.4, 31.5, 31.4; HRMS (ES+) calcd for $C_{20}H_{20}{}^{35}ClN_5O_2Na$ (M + Na)$^+$ 420.1203, found 420.1195; calcd for $C_{20}H_{20}{}^{37}ClN_5O_2Na$ (M + Na)$^+$ 422.1174; found 422.1186.

*10-(4-Bromophenyl)-1-((6-chloropyridin-3-yl)methyl)-9-nitro-2,3,5,6,7,8-hexahydro-1H-5,8-epiminoimidazo[1,2-a]azepine (**2**):* yield, 84.0%; mp, 203−204 °C; $^1$H NMR (400 MHz, DMSO-$d_6$) $\delta$ 8.18 (d, $J$ = 2.0 Hz, 1H), 7.38 (d, $J$ = 8.0 Hz, 2H), 7.27 (s, 2H), 6.91 (d, $J$ = 8.4 Hz, 2H), 5.62 (s, 1H), 5.23 (s, 1H), 4.86 (d, $J$ = 15.6 Hz, 1H), 4.58 (d, $J$ = 15.6 Hz, 1H), 3.82−3.71 (m, 1H), 3.72−3.61 (m, 1H), 3.62−3.52 (m, 1H), 3.50−3.39 (m, 1H), 2.28−2.10 (m, 3H), 1.98−1.88 (m, 1H); $^{13}$C NMR (100 MHz, DMSO-$d_6$) $\delta$ 155.8, 149.7, 149.6, 144.5, 138.8, 132.3, 124.4, 119.9, 112.2, 109.0, 71.5, 57.1, 50.6, 49.8, 47.3, 31.6, 31.4; HRMS (ES+) calcd for $C_{20}H_{20}{}^{35}Cl^{79}BrN_5O_2$ (M + H)$^+$ 476.0489, found 476.0487; calcd for $C_{20}H_{20}{}^{37}Cl^{81}BrN_5O_2$ (M + H)$^+$ 480.0439, found 480.0447.

*1-((6-Chloropyridin-3-yl)methyl)-10-(4-methoxyphenyl)-9-nitro-2,3,5,6,7,8-hexahydro-1H-5,8-epiminoimidazo[1,2-a]azepine (**3**):* yield, 82.5%; mp, 177−178 °C; $^1$H NMR (400 MHz, DMSO-$d_6$) $\delta$ 8.13 (d, $J$ = 2.0 Hz, 1H), 7.28−7.20 (m, 2H), 6.88 (d, $J$ = 8.4 Hz, 2H), 6.82 (d, $J$ = 8.4 Hz, 2H), 5.53 (s, 1H), 5.17 (s, 1H), 4.87 (d, $J$ = 15.6 Hz, 1H), 4.57 (d, $J$ = 15.6 Hz, 1H), 3.84−3.75 (m, 1H), 3.74 (s, 3H), 3.71−3.58 (m, 2H), 3.58−3.48 (m, 1H), 2.26−2.05 (m, 3H), 1.95−1.83 (m, 1H); $^{13}$C NMR (100 MHz, DMSO-$d_6$) $\delta$ 155.9, 153.6, 149.6, 138.9, 138.5, 132.5, 124.5, 124.3, 118.9, 115.0, 109.2, 72.0, 55.5, 50.5, 49.5, 47.5, 31.6, 31.5, 15.6; HRMS (ES+) calcd for $C_{21}H_{22}{}^{35}ClN_5O_3Na$ (M + Na)$^+$ 450.1303, found 450.1324; calcd for $C_{21}H_{22}{}^{37}ClN_5O_3Na$ (M + Na)$^+$ 452.1279, found 452.1290.

*1-((6-Chloropyridin-3-yl)methyl)-10-(4-fluorophenyl)-9-nitro-2,3,5,6,7,8-hexahydro-1H-5,8-epiminoimidazo[1,2-a]azepine (**4**):* yield, 35.9%; mp, 165−166 °C; $^1$H NMR (400 MHz, DMSO-$d_6$) $\delta$ 8.15 (d, $J$ = 1.6 Hz, 1H), 7.37 (dd, $J$ = 8.4, 1.6 Hz, 1H), 7.28 (d, $J$ = 8.4 Hz, 1H), 7.05 (t, $J$ = 8.8 Hz, 2H), 6.98−6.89 (m, 2H), 5.58 (s, 1H), 5.22 (s, 1H), 4.81 (d, $J$ = 15.6 Hz, 1H), 4.61 (d, $J$ = 15.6 Hz, 1H), 3.82−3.71 (m, 1H), 3.70−3.61 (m, 1H), 3.61−3.51 (m, 1H), 3.50−3.39 (m, 1H), 2.29−2.07 (m, 3H), 1.97−1.87 (m, 1H); $^{13}$C NMR (100 MHz, DMSO-$d_6$) $\delta$ 156.9 (d, $J$ = 236.8 Hz), 155.8, 149.7, 149.6, 141.5 (d, $J$ = 2.0 Hz), 139.0, 132.3, 124.3, 119.1 (d, $J$ = 7.6 Hz), 116.1 (d, $J$ = 22.1 Hz), 109.1, 71.9, 57.4, 50.7, 49.8, 47.3, 31.7, 31.5; HRMS (ES+) calcd for $C_{20}H_{20}{}^{35}ClFN_5O_2$ (M + H)$^+$ 416.1290, found 416.1278; calcd for $C_{20}H_{20}{}^{37}ClFN_5O_2$ (M + H)$^+$ 418.1260, found 418.1265.

*1-((6-Chloropyridin-3-yl)methyl)-9-nitro-10-(p-tolyl)-2,3,5,6,7,8-hexahydro-1H-5,8-epiminoimidazo[1,2-a]azepine (**5**):* yield, 72.3%; mp, 183−184 °C; $^1$H NMR (400 MHz, DMSO-$d_6$) $\delta$ 8.11 (d, $J$ = 1.6 Hz, 1H), 7.29 (dd, $J$ = 8.4, 1.6 Hz, 1H), 7.23 (d, $J$ = 8.0 Hz, 1H), 7.02 (d, $J$ = 7.2 Hz, 2H), 6.82 (d, $J$ = 7.2 Hz, 2H), 5.57 (s, 1H), 5.20 (s, 1H), 4.86 (d, $J$ = 15.2 Hz, 1H), 4.56 (d, $J$ = 15.2 Hz, 1H), 3.84−3.70 (m, 1H), 3.72−3.59 (m, 1H), 3.58−3.47 (m, 1H), 3.47−3.36 (m, 1H), 2.24 (s, 3H), 2.23−2.03 (m, 3H), 1.97−1.83 (m, 1H); $^{13}$C NMR (100 MHz, DMSO-$d_6$) $\delta$ 155.8, 149.6, 149.6, 142.6, 139.0, 132.4, 130.1, 129.3, 124.4, 117.7, 109.3, 71.7, 57.0, 50.5, 49.7, 47.6, 31.5, 31.4, 20.6; HRMS (ES+) calcd for $C_{21}H_{23}{}^{35}ClN_5O_2$ (M + H)$^+$ 412.1540, found 412.1542; calcd for $C_{21}H_{23}{}^{37}ClN_5O_2$ (M + H)$^+$ 414.1511, found 414.1517.

*1-((6-Chloropyridin-3-yl)methyl)-9-nitro-10-(4-(trifluoromethyl)-phenyl)-2,3,5,6,7,8-hexahydro-1H-5,8-epiminoimidazo[1,2-a]-azepine (**6**):* yield, 46.2%; mp, 190−191 °C; $^1$H NMR (400 MHz, DMSO-$d_6$) $\delta$ 8.15 (d, $J$ = 1.6 Hz, 1H), 7.56 (d, $J$ = 8.0 Hz, 2H), 7.35 (dd, $J$ = 8.4, 1.6 Hz, 1H), 7.21 (d, $J$ = 8.4 Hz, 1H), 7.11 (d, $J$ = 8.0 Hz, 2H), 5.75 (s, 1H), 5.35 (s, 1H), 4.87 (d, $J$ = 15.6 Hz, 1H), 4.59 (d, $J$ = 15.6 Hz, 1H), 3.83−3.73 (m, 1H), 3.73−3.56 (m, 2H), 3.53−3.42 (m, 1H), 2.31−2.14 (m, 3H), 2.01−1.91 (m, 1H); $^{13}$C NMR (100 MHz, DMSO-$d_6$) $\delta$ 155.9, 149.7, 149.6, 148.4, 139.0, 132.3, 126.9 (d, $J$ = 3.6 Hz), 125.2 (d, $J$ = 270.9 Hz), 124.2, 120.6 (q, $J$ = 32.0 Hz), 117.7, 109.0, 71.2, 57.0, 50.7, 50.0, 47.2, 31.6, 31.3; HRMS (ES+) calcd for $C_{21}H_{20}{}^{35}ClN_5O_2F_3$ (M + H)$^+$ 466.1258, found 466.1252; calcd for $C_{21}H_{20}{}^{37}ClN_5O_2F_3$ (M + H)$^+$ 468.1228, found 468.1225.

*4-(1-((6-Chloropyridin-3-yl)methyl)-9-nitro-2,3,5,6,7,8-hexahydro-1H-5,8-epiminoimidazo[1,2-a]azepin-10-yl)benzonitrile (**7**):*

yield, 89.4%; mp, 220−221 °C; $^1$H NMR (400 MHz, DMSO-$d_6$) $\delta$ 8.11 (d, $J$ = 1.6 Hz, 1H), 7.64 (d, $J$ = 7.6 Hz, 2H), 7.40 (dd, $J$ = 8.0, 1.6 Hz, 1H), 7.28 (d, $J$ = 8.4 Hz, 1H), 7.06 (d, $J$ = 8.0 Hz, 2H), 5.75 (s, 1H), 5.36 (s, 1H), 4.81 (d, $J$ = 15.6 Hz, 1H), 4.59 (d, $J$ = 15.6 Hz, 1H), 3.82−3.43 (m, 4H), 2.31−2.10 (m, 3H), 2.01−1.89 (m, 1H); $^{13}$C NMR (100 MHz, DMSO-$d_6$) $\delta$ 160.6, 154.5, 154.2, 153.7, 143.9, 138.8, 137.0, 129.1, 124.6, 122.8, 113.9, 106.8, 75.9, 61.7, 55.5, 54.9, 51.9, 36.4, 36.0; HRMS (ES+) calcd for $C_{21}H_{20}{}^{35}ClN_6O_2$ (M + H)$^+$ 423.1336, found 423.1337; calcd for $C_{21}H_{20}{}^{37}ClN_6O_2$ (M + H)$^+$ 425.1307, found 425.1313.

*10-(4-Chlorophenyl)-1-((6-chloropyridin-3-yl)methyl)-9-nitro-2,3,5,6,7,8-hexahydro-1H-5,8-epiminoimidazo[1,2-a]azepine (**8**):* yield, 68.6%; mp, 200−201 °C; $^1$H NMR (400 MHz, DMSO-$d_6$) $\delta$ 8.13 (d, $J$ = 1.6 Hz, 1H), 7.30−7.18 (m, 4H), 6.91 (d, $J$ = 8.0 Hz, 2H), 5.57 (s, 1H), 5.19 (s, 1H), 4.80 (d, $J$ = 15.6 Hz, 1H), 4.54 (d, $J$ = 15.6 Hz, 1H), 3.79−3.67 (m, 1H), 3.67−3.57 (m, 1H), 3.57−3.47 (m, 1H), 3.47−3.34 (m, 1H), 2.25−2.06 (m, 3H), 1.95−1.83 (m, 1H); $^{13}$C NMR (100 MHz, DMSO-$d_6$) $\delta$ 160.6, 154.4, 154.4, 148.8, 143.7, 137.1, 134.2, 129.1, 129.1, 124.2, 113.8, 76.3, 62.0, 55.4, 54.6, 52.1, 36.4, 36.1; HRMS (ES+) calcd for $C_{20}H_{20}{}^{35}Cl_2N_5O_2$ (M + H)$^+$ 432.0994, found 432.0982; calcd for $C_{20}H_{20}{}^{37}Cl_2N_5O_2$ (M + H)$^+$ 436.0935, found 436.0940.

*1-((6-Chloropyridin-3-yl)methyl)-9-nitro-10-(4-nitrophenyl)-2,3,5,6,7,8-hexahydro-1H-5,8-epiminoimidazo[1,2-a]azepine (**9**):* yield, 65.7%; mp, 234−235 °C; $^1$H NMR (400 MHz, DMSO-$d_6$) $\delta$ 8.10 (d, $J$ = 9.2 Hz, 2H), 8.05 (d, $J$ = 2.0 Hz, 1H), 7.44 (dd, $J$ = 8.4, 2.4 Hz, 1H), 7.24 (d, $J$ = 8.4 Hz, 1H), 7.10 (d, $J$ = 9.2 Hz, 2H), 5.80 (s, 1H), 5.43 (d, $J$ = 5.6 Hz, 1H), 4.84 (d, $J$ = 15.6 Hz, 1H), 4.58 (d, $J$ = 15.6 Hz, 1H), 3.82−3.61 (m, 3H), 3.57−3.49 (m, 1H), 2.31−2.16 (m, 3H), 2.03−1.94 (m, 1H); $^{13}$C NMR (100 MHz, DMSO-$d_6$) $\delta$ 155.7, 151.0, 149.6, 149.3, 140.3, 139.3, 132.1, 126.0, 124.2, 117.3, 109.2, 71.2, 57.4, 50.7, 50.3, 47.1, 31.7, 31.2; HRMS (ES+) calcd for $C_{20}H_{20}{}^{35}ClN_6O_4$ (M + H)$^+$ 443.1235, found 443.1252; calcd for $C_{20}H_{20}{}^{37}ClN_6O_4$ (M + H)$^+$ 445.1205, found 445.1221.

*10-(2-Chlorophenyl)-1-((6-chloropyridin-3-yl)methyl)-9-nitro-2,3,5,6,7,8-hexahydro-1H-5,8-epiminoimidazo[1,2-a]azepine (**10**):* yield, 75.8%; mp, 181−182 °C; $^1$H NMR (400 MHz, DMSO-$d_6$) $\delta$ 8.28 (d, $J$ = 2.0 Hz, 1H), 7.69 (dd, $J$ = 8.4, 2.4 Hz, 1H), 7.48−7.40 (m, 2H), 7.19 (t, $J$ = 7.6 Hz, 1H), 7.05 (t, $J$ = 7.6 Hz, 1H), 6.93 (d, $J$ = 8.0 Hz, 1H), 5.47 (s, 1H), 5.20 (s, 1H), 4.81 (d, $J$ = 15.6 Hz, 1H), 4.74 (d, $J$ = 15.6 Hz, 1H), 3.80−3.61 (m, 2H), 3.59−3.40 (m, 2H), 2.26−2.06 (m, 3H), 1.98−1.85 (m, 1H); $^{13}$C NMR (100 MHz, DMSO-$d_6$) $\delta$ 155.9, 149.8, 149.7, 141.5, 139.7, 132.4, 131.3, 128.5, 126.0, 124.5, 124.4, 121.9, 108.5, 72.4, 58.7, 51.0, 49.9, 46.5, 31.7, 31.6; HRMS (ES+) calcd for $C_{20}H_{19}{}^{35}Cl_2N_5O_2Na$ (M + Na)$^+$ 454.0808, found 454.0819; calcd for $C_{20}H_{19}{}^{37}Cl_2N_5O_2Na$ (M + Na)$^+$ 458.0754, found 458.0745.

*10-(2-Bromophenyl)-1-((6-chloropyridin-3-yl)methyl)-9-nitro-2,3,5,6,7,8-hexahydro-1H-5,8-epiminoimidazo[1,2-a]azepine (**11**):* yield, 76.0%; mp, 181−182 °C; $^1$H NMR (400 MHz, DMSO-$d_6$) $\delta$ 8.30 (d, $J$ = 2.0 Hz, 1H), 7.71 (dd, $J$ = 8.0, 2.0 Hz, 1H), 7.60 (d, $J$ = 8.0 Hz, 1H), 7.46 (d, $J$ = 8.0 Hz, 1H), 7.24 (t, $J$ = 7.6 Hz, 1H), 7.03−6.90 (m, 2H), 5.44 (s, 1H), 5.21 (s, 1H), 4.82 (d, $J$ = 15.6 Hz, 1H), 4.75 (d, $J$ = 15.6 Hz, 1H), 3.81−3.62 (m, 2H), 3.62−3.51 (m, 1H), 3.52−3.42 (m, 1H), 2.26−2.05 (m, 3H), 1.97−1.85 (m, 1H); $^{13}$C NMR (100 MHz, DMSO-$d_6$) $\delta$ 156.0, 149.8, 149.8, 142.8, 139.8, 134.5, 132.4, 129.0, 125.1, 124.5, 122.3, 116.8, 108.4, 72.8, 59.0, 51.1, 50.0, 46.5, 31.7, 31.6; HRMS (ES+) calcd for $C_{20}H_{19}{}^{35}Cl^{79}BrN_5O_2Na$ (M + Na)$^+$ 498.0303, found 498.0321; calcd for $C_{20}H_{19}{}^{37}Cl^{81}BrN_5O_2Na$ (M + Na)$^+$ 502.0258, found 502.0267.

*1-((6-Chloropyridin-3-yl)methyl)-10-(2-fluorophenyl)-9-nitro-2,3,5,6,7,8-hexahydro-1H-5,8-epiminoimidazo[1,2-a]azepine (**12**):* yield, 42.1%; mp, 168−169 °C; $^1$H NMR (400 MHz, DMSO-$d_6$) $\delta$ 8.21 (d, $J$ = 1.6 Hz, 1H), 7.50 (dd, $J$ = 8.0, 1.6 Hz, 1H), 7.35 (d, $J$ = 8.4 Hz, 1H), 7.22−7.12 (m, 1H), 7.07−6.94 (m, 2H), 6.88−6.79 (m, 1H), 5.41 (s, 1H), 5.21 (s, 1H), 4.76 (d, $J$ = 15.2 Hz, 1H), 4.69 (d, $J$ = 15.2 Hz, 1H), 3.81−3.63 (m, 2H), 3.54−3.42 (m, 2H), 2.26−2.09 (m, 3H), 1.99−1.87 (m, 1H); $^{13}$C NMR (100 MHz, DMSO-$d_6$) $\delta$ 155.68, 154.09 (d, $J$ = 243.2 Hz), 149.7, 149.6, 139.3, 132.4 (d, $J$ = 9.0 Hz), 132.3, 125.5 (d, $J$ = 3.1 Hz), 124.5, 122.9 (d, $J$ = 8.0 Hz), 120.9 (d, $J$ = 3.0 Hz), 116.7 (d, $J$ = 20.9 Hz), 108.7, 72.5 (d, $J$ = 8.2 Hz), 58.2 (d, $J$ = 3.5 Hz), 50.9, 49.9, 46.8, 31.5, 31.2; HRMS (ES+) calcd for $C_{20}H_{20}{}^{35}ClFN_5O_2$ (M + H)$^+$ 416.1290, found 416.1293; calcd for $C_{20}H_{20}{}^{37}ClFN_5O_2$ (M + H)$^+$ 418.1260, found 418.1267.

*1-((6-Chloropyridin-3-yl)methyl)-9-nitro-10-(o-tolyl)-2,3,5,6,7,8-hexahydro-1H-5,8-epiminoimidazo[1,2-a]azepine (**13**):* yield, 40.8%; mp, 155−156 °C; $^1$H NMR (400 MHz, DMSO-$d_6$) $\delta$ 8.29 (d, $J$ = 1.6 Hz, 1H), 7.69 (dd, $J$ = 8.4, 2.0 Hz, 1H), 7.45 (d, $J$ = 8.0 Hz, 1H), 7.15 (d, $J$ = 7.2 Hz, 1H), 7.02 (t, $J$ = 7.6 Hz, 1H), 6.97−6.90 (m, 1H), 6.76 (d, $J$ = 8.0 Hz, 1H), 5.15 (s, 1H), 4.96 (s, 1H), 4.81 (d, $J$ = 15.6 Hz, 1H), 4.73 (d, $J$ = 15.6 Hz, 1H), 3.75−3.58 (m, 2H), 3.56−3.36 (m, 2H), 2.27 (s, 3H), 2.24−2.04 (m, 3H), 1.93−1.84 (m, 1H); $^{13}$C NMR (100 MHz, DMSO-$d_6$) $\delta$ 160.9, 154.6, 154.5, 147.9, 144.5, 137.2, 136.7, 135.0, 131.7, 129.3, 127.8, 124.4, 113.7, 77.5, 63.4, 55.7, 54.6, 51.4, 36.6, 36.3, 24.2; HRMS (ES+) calcd for $C_{21}H_{23}{}^{35}ClN_5O_2$ (M + H)$^+$ 412.1540, found 412.1535; calcd for $C_{21}H_{23}{}^{37}ClN_5O_2$ (M + H)$^+$ 414.1511, found 414.1513.

*1-((6-Chloropyridin-3-yl)methyl)-10-(2-methoxyphenyl)-9-nitro-2,3,5,6,7,8-hexahydro-1H-5,8-epiminoimidazo[1,2-a]azepine (**14**):* yield, 42.5%; mp, 120−121 °C; $^1$H NMR (400 MHz, DMSO-$d_6$) $\delta$ 8.22 (d, $J$ = 2.0 Hz, 1H), 7.52 (dd, $J$ = 8.4, 2.4 Hz, 1H), 7.37 (d, $J$ = 8.0 Hz, 1H), 7.01−6.92 (m, 2H), 6.82−6.75 (m, 1H), 6.66 (d, $J$ = 7.6 Hz, 1H), 5.58 (d, $J$ = 5.2 Hz, 1H), 5.10 (d, $J$ = 5.2 Hz, 1H), 4.74 (d, $J$ = 16.4 Hz, 1H), 4.68 (d, $J$ = 16.4 Hz, 1H), 3.83 (s, 3H), 3.78−3.57 (m, 2H), 3.40−3.36 (m, 1H), 3.30−3.23 (m, 1H), 2.26−1.99 (m, 3H), 1.96−1.84 (m, 1H); $^{13}$C NMR (100 MHz, DMSO-$d_6$) $\delta$ 155.8, 151.2, 149.8, 149.7, 139.4, 133.4, 132.4, 124.5, 122.9, 121.4, 119.6, 112.6, 108.9, 71.9, 58.0, 50.8, 49.7, 47.2, 31.6, 30.9, 15.6; HRMS (ES+) calcd for $C_{21}H_{23}{}^{35}ClN_5O_3$ (M + H)$^+$ 428.1489, found 428.1489; calcd for $C_{21}H_{23}{}^{37}ClN_5O_3$ (M + H)$^+$ 430.1460, found 430.1468.

*2-(1-((6-Chloropyridin-3-yl)methyl)-9-nitro-2,3,5,6,7,8-hexahydro-1H-5,8-epiminoimidazo[1,2-a]azepin-10-yl)benzonitrile (**15**):* yield, 52.6%; mp, 197−198 °C; $^1$H NMR (400 MHz, DMSO-$d_6$) $\delta$ 8.23 (d, $J$ = 2.4 Hz, 1H), 7.73 (dd, $J$ = 7.6, 1.6 Hz, 1H), 7.60 (dd, $J$ = 8.0, 2.4 Hz, 1H), 7.56−7.49 (m, 1H), 7.39 (d, $J$ = 8.0 Hz, 1H), 7.13 (t, $J$ = 7.2 Hz, 1H), 6.96 (d, $J$ = 8.4 Hz, 1H), 5.56 (s, 1H), 5.49 (d, $J$ = 5.2 Hz, 1H), 4.78 (d, $J$ = 15.6 Hz, 1H), 4.72 (d, $J$ = 15.6 Hz, 1H), 3.83−3.51 (m, 4H), 2.33−2.18 (m, 3H), 2.00−1.91 (m, 1H); $^{13}$C NMR (100 MHz, DMSO-$d_6$) $\delta$ 155.8, 149.8, 149.6, 147.6, 139.5, 135.2, 134.9, 132.3, 124.5, 122.8, 120.4, 118.7, 108.4, 103.2, 72.8, 59.1, 51.1, 50.1, 46.2, 31.9, 31.8; HRMS (ES+) calcd for $C_{21}H_{20}{}^{35}ClN_6O_2$ (M + H)$^+$ 423.1336, found 423.1338; calcd for $C_{21}H_{20}{}^{37}ClN_6O_2$ (M + H)$^+$ 425.1307, found 425.1299.

*1-((6-Chloropyridin-3-yl)methyl)-9-nitro-10-(m-tolyl)-2,3,5,6,7,8-hexahydro-1H-5,8-epiminoimidazo[1,2-a]azepine (**16**):* yield, 64.6%; mp, 199−200 °C; $^1$H NMR (400 MHz, DMSO-$d_6$) $\delta$ 8.16 (d, $J$ = 1.6 Hz, 1H), 7.24 (s, 2H), 7.15−7.07 (m, 1H), 6.78 (s, 1H), 6.76−6.68 (m, 2H), 5.60 (s, 1H), 5.24 (s, 1H), 4.81 (d, $J$ = 15.6 Hz, 1H), 4.59 (d, $J$ = 15.6 Hz, 1H), 3.84−3.71 (m, 1H), 3.70−3.51 (m, 2H), 3.49−3.36 (m, 1H), 2.25 (s, 3H), 2.21−2.07 (m, 3H), 1.96−1.87 (m, 1H); $^{13}$C NMR (100 MHz, DMSO-$d_6$) $\delta$ 156.1, 149.6, 149.6, 145.0, 138.9, 138.8, 132.5, 129.5, 124.4, 121.5, 118.3, 114.9, 109.3, 71.4, 56.9, 50.7, 49.6, 47.5, 31.5, 31.4, 21.9; HRMS (ES+) calcd for $C_{21}H_{23}{}^{35}ClN_5O_2$ (M + H)$^+$ 412.1540, found 412.1540; calcd for $C_{21}H_{23}{}^{37}ClN_5O_2$ (M + H)$^+$ 414.1511, found 414.1514.

*1-((6-Chloropyridin-3-yl)methyl)-9-nitro-10-(3-(trifluoromethyl)-phenyl)-2,3,5,6,7,8-hexahydro-1H-5,8-epiminoimidazo[1,2-a]-azepine (**17**):* yield, 69.8%; mp, 222−223 °C; $^1$H NMR (400 MHz, DMSO-$d_6$) $\delta$ 8.14 (d, $J$ = 1.6 Hz, 1H), 7.46 (t, $J$ = 8.0 Hz, 1H), 7.33 (d, $J$ = 8.4 Hz, 1H), 7.29−7.24 (m, 2H), 7.21 (d, $J$ = 8.0 Hz, 2H), 5.77 (s, 1H), 5.36 (s, 1H), 4.77 (d, $J$ = 15.6 Hz, 1H), 4.61 (d, $J$ = 15.6 Hz, 1H), 3.85−3.71 (m, 1H), 3.73−3.51 (m, 2H), 3.52−3.40 (m, 1H), 2.34−2.11 (m, 3H), 2.01−1.87 (m, 1H); $^{13}$C NMR (100 MHz, DMSO-$d_6$) $\delta$ 156.1, 149.7, 149.5, 145.8, 138.9, 132.3, 130.8, 130.5 (d, $J$ = 31.0 Hz), 126.0, 124.3, 121.5, 115.5 (dd, $J$ = 298.6, 4.3 Hz), 108.9, 71.4, 57.2, 50.8, 49.8, 47.2, 31.6, 31.3; HRMS (ES+) calcd for $C_{21}H_{20}{}^{35}ClF_3N_5O_2$ (M + H)$^+$ 466.1258, found 466.1258; calcd for $C_{21}H_{20}{}^{37}ClF_3N_5O_2$ (M + H)$^+$ 468.1228, found 468.1232.

*1-((6-Chloropyridin-3-yl)methyl)-10-(3-methoxyphenyl)-9-nitro-2,3,5,6,7,8-hexahydro-1H-5,8-epiminoimidazo[1,2-a]azepine (**18**):*

yield, 72.2%; mp, 204−205 °C; $^1$H NMR (400 MHz, DMSO-$d_6$) $\delta$ 8.17 (d, $J$ = 2.4 Hz, 1H), 7.31 (dd, $J$ = 8.0, 2.4 Hz, 1H), 7.27 (d, $J$ = 8.0 Hz, 1H), 7.14 (t, $J$ = 8.0 Hz, 1H), 6.53 (d, $J$ = 8.4 Hz, 1H), 6.51−6.45 (m, 2H), 5.63 (s, 1H), 5.24 (s, 1H), 4.83 (d, $J$ = 15.6 Hz, 1H), 4.60 (d, $J$ = 15.6 Hz, 1H), 3.86−3.72 (m, 1H), 3.71 (s, 3H), 3.69−3.51 (m, 2H), 3.50−3.39 (m, 1H), 2.29−2.10 (m, 3H), 1.96−1.85 (m, 1H); $^{13}$C NMR (100 MHz, DMSO-$d_6$) $\delta$ 160.7, 156.2, 149.6, 149.5, 146.4, 138.9, 132.5, 130.5, 124.4, 110.3, 109.2, 106.0, 103.9, 71.6, 57.0, 55.4, 50.8, 49.6, 47.4, 31.5; HRMS (ES+) calcd for $C_{21}H_{23}{}^{35}ClN_5O_3$ (M + H)$^+$ 428.1489, found 428.1489; calcd for $C_{21}H_{23}{}^{37}ClN_5O_3$ (M + H)$^+$ 430.1460, found 430.1465.

*10-(3-Chlorophenyl)-1-((6-chloropyridin-3-yl)methyl)-9-nitro-2,3,5,6,7,8-hexahydro-1H-5,8-epiminoimidazo[1,2-a]azepine* (**19**): yield, 59.6%; mp, 209−210 °C; $^1$H NMR (400 MHz, DMSO-$d_6$) $\delta$ 8.18 (d, $J$ = 2.4 Hz, 1H), 7.36 (dd, $J$ = 8.4, 2.4 Hz, 1H), 7.29 (d, $J$ = 8.0 Hz, 1H), 7.24 (t, $J$ = 8.0 Hz, 1H), 7.03 (t, $J$ = 2.0 Hz, 1H), 6.92 (dd, $J$ = 8.0, 1.2 Hz, 1H), 6.88 (dd, $J$ = 8.0, 1.6 Hz, 1H), 5.67 (s, 1H), 5.27 (s, 1H), 4.79 (d, $J$ = 15.6 Hz, 1H), 4.62 (d, $J$ = 15.6 Hz, 1H), 3.85−3.71 (m, 1H), 3.71−3.54 (m, 2H), 3.53−3.42 (m, 1H), 2.30−2.11 (m, 3H), 1.97−1.86 (m, 1H); $^{13}$C NMR (100 MHz, DMSO-$d_6$) $\delta$ 156.1, 149.7, 149.5, 146.7, 138.9, 134.3, 132.4, 131.3, 124.4, 120.4, 117.4, 116.3, 108.9, 71.4, 57.0, 50.9, 49.8, 47.2, 31.6, 31.3; HRMS (ES+) calcd for $C_{20}H_{20}{}^{35}Cl_2N_5O_2$ (M + H)$^+$ 432.0994, found 432.0990; calcd for $C_{20}H_{20}{}^{37}Cl_2N_5O_2$ (M + H)$^+$ 436.0935, found 436.0942.

*1-((6-Chloropyridin-3-yl)methyl)-9-nitro-10-(3-nitrophenyl)-2,3,5,6,7,8-hexahydro-1H-5,8-epiminoimidazo[1,2-a]azepine* (**20**): yield, 73.6%; mp, 221−222 °C; $^1$H NMR (400 MHz, DMSO-$d_6$) $\delta$ 8.06 (d, $J$ = 2.4 Hz, 1H), 7.75−7.70 (m, 2H), 7.53−7.46 (m, 1H), 7.43−7.35 (m, 2H), 7.26 (d, $J$ = 8.0 Hz, 1H), 5.79 (s, 1H), 5.37 (d, $J$ = 5.6 Hz, 1H), 4.79 (d, $J$ = 15.6 Hz, 1H), 4.59 (d, $J$ = 15.6 Hz, 1H), 3.84−3.74 (m, 1H), 3.73−3.58 (m, 2H), 3.54−3.46 (m, 1H), 2.31−2.14 (m, 3H), 2.01−1.92 (m, 1H); $^{13}$C NMR (100 MHz, DMSO-$d_6$) $\delta$ 155.8, 149.6, 149.4, 146.3, 143.3, 139.1, 132.2, 131.0, 124.2, 124.2, 115.3, 111.9, 108.8, 71.5, 57.4, 50.8, 50.2, 47.1, 31.7, 31.3; HRMS (ES+) calcd for $C_{20}H_{20}{}^{35}ClN_6O_4$ (M + H)$^+$ 443.1235, found 443.1237; calcd for $C_{20}H_{20}{}^{37}ClN_6O_4$ (M + H)$^+$ 445.1205, found 445.1202.

*1-((6-Chloropyridin-3-yl)methyl)-10-(3-fluorophenyl)-9-nitro-2,3,5,6,7,8-hexahydro-1H-5,8-epiminoimidazo[1,2-a]azepine* (**21**): yield, 47.7%; mp, 205−206 °C; $^1$H NMR (400 MHz, DMSO-$d_6$) $\delta$ 8.16 (d, $J$ = 2.0 Hz, 1H), 7.38 (dd, $J$ = 8.4, 2.4 Hz, 1H), 7.29 (d, $J$ = 8.0 Hz, 1H), 7.24 (dd, $J$ = 15.2, 8.0 Hz, 1H), 6.83−6.77 (m, 1H), 6.77−6.72 (m, 1H), 6.72−6.64 (m, 1H), 5.64 (s, 1H), 5.26 (d, $J$ = 5.6 Hz, 1H), 4.79 (d, $J$ = 15.6 Hz, 1H), 4.62 (d, $J$ = 15.6 Hz, 1H), 3.83−3.71 (m, 1H), 3.71−3.56 (m, 2H), 3.54−3.43 (m, 1H), 2.29−2.11 (m, 3H), 1.97−1.87 (m, 1H); $^{13}$C NMR (100 MHz, DMSO-$d_6$) $\delta$ 162.3, 156.1, 149.5, 148.4 (d, $J$ = 260.8 Hz), 147.2, 139.0, 132.4, 131.3 (d, $J$ = 9.9 Hz), 124.4, 113.6 (d, $J$ = 2.4 Hz), 109.1, 107.1 (d, $J$ = 21.1 Hz), 104.7 (d, $J$ = 25.3 Hz), 71.5, 57.1, 50.8, 49.9, 47.2, 31.6, 31.3; HRMS (ES+) calcd for $C_{20}H_{20}{}^{35}ClFN_5O_2$ (M + H)$^+$ 416.1290, found 416.1279; calcd for $C_{20}H_{20}{}^{37}ClFN_5O_2$ (M + H)$^+$ 418.1260, found 418.1269.

*1-((6-Chloropyridin-3-yl)methyl)-10-(3-fluoro-4-methoxyphenyl)-9-nitro-2,3,5,6,7,8-hexahydro-1H-5,8-epiminoimidazo[1,2-a]-azepine* (**22**): yield, 61.0%; mp, 195−196 °C; $^1$H NMR (400 MHz, DMSO-$d_6$) $\delta$ 8.12 (d, $J$ = 1.6 Hz, 1H), 7.38 (dd, $J$ = 8.4 Hz, 2.0 Hz, 1H), 7.28 (d, $J$ = 8.4 Hz, 1H), 7.01 (t, $J$ = 9.2 Hz, 1H), 6.93 (d, $J$ = 14.0 Hz, 1H), 6.61 (d, $J$ = 8.8 Hz, 1H), 5.54 (s, 1H), 5.17 (s, 1H), 4.86 (d, $J$ = 16.0 Hz, 1H), 4.60 (d, $J$ = 16.0 Hz, 1H), 3.81 (s, 3H), 3.79−3.71 (m, 1H), 3.70−3.53 (m, 2H), 3.51−3.40 (m, 1H), 2.30−2.05 (m, 3H), 1.97−1.81 (m, 1H); $^{13}$C NMR (100 MHz, DMSO-$d_6$) $\delta$ 155.9, 152.3 (d, $J$ = 242.3 Hz), 149.6, 149.5, 141.3 (d, $J$ = 11.0 Hz), 139.2 (d, $J$ = 8.7 Hz), 139.1, 132.4, 124.3, 115.3 (d, $J$ = 2.6 Hz), 113.2 (d, $J$ = 2.8 Hz), 109.0, 106.5 (d, $J$ = 21.7 Hz), 71.9, 57.4, 56.7, 50.7, 49.7, 47.3, 31.6, 31.4; HRMS (ES+) calcd for $C_{21}H_{22}{}^{35}ClFN_5O_3$ (M + H)$^+$ 446.1395, found 446.1389; calcd for $C_{21}H_{22}{}^{37}ClFN_5O_3$ (M + H)$^+$ 448.1366, found 448.1375.

*1-((6-Chloropyridin-3-yl)methyl)-10-(2-fluoro-4-methylphenyl)-9-nitro-2,3,5,6,7,8-hexahydro-1H-5,8-epiminoimidazo[1,2-a]azepine* (**23**): yield, 83.0%; mp, 174−175 °C; $^1$H NMR (400 MHz, DMSO-$d_6$) $\delta$ 8.17 (d, $J$ = 1.6 Hz, 1H), 7.52 (dd, $J$ = 8.0, 1.6 Hz, 1H), 7.35 (d, $J$ = 8.0 Hz, 1H), 6.99 (d, $J$ = 14.4 Hz, 1H), 6.81 (d, $J$ = 8.0 Hz, 1H), 6.73−6.64 (m, 1H), 5.35 (s, 1H), 5.15 (s, 1H), 4.81 (d, $J$ = 15.2 Hz, 1H), 4.66 (d, $J$ = 15.2 Hz, 1H), 3.81−3.59 (m, 2H), 3.57−3.38 (m, 2H), 2.26 (s, 3H), 2.23−2.03 (m, 3H), 1.97−1.84 (m, 1H); $^{13}$C NMR (100 MHz, DMSO-$d_6$) $\delta$ 155.5, 153.8 (d, $J$ = 243.1 Hz), 149.7, 149.6, 139.4, 132.5 (d, $J$ = 7.7 Hz), 132.3, 129.7 (d, $J$ = 8.9 Hz), 125.8, 124.4, 120.6, 117.2 (d, $J$ = 20.8 Hz), 108.8, 72.5 (d, $J$ = 8.0 Hz), 58.2, 50.7, 49.9, 46.9, 31.5, 31.2, 20.4; HRMS (ES+) calcd for $C_{21}H_{22}{}^{35}ClFN_5O_2$ (M + H)$^+$ 430.1446, found 430.1444; calcd for $C_{21}H_{22}{}^{37}ClFN_5O_2$ (M + H)$^+$ 432.1417, found 432.1416.

*1-((6-Chloropyridin-3-yl)methyl)-10-(2,6-difluorophenyl)-9-nitro-2,3,5,6,7,8-hexahydro-1H-5,8-epiminoimidazo[1,2-a]azepine* (**24**): yield, 34.2%; mp, 163−164 °C; $^1$H NMR (400 MHz, DMSO-$d_6$) $\delta$ 8.25 (d, $J$ = 2.4 Hz, 1H), 7.62 (dd, $J$ = 8.0, 2.4 Hz, 1H), 7.40 (d, $J$ = 8.0 Hz, 1H), 7.06−6.98 (m, 3H), 5.46−5.34 (m, 2H), 4.81 (d, $J$ = 15.6 Hz, 1H), 4.73 (d, $J$ = 15.6 Hz, 1H), 3.82−3.64 (m, 2H), 3.64−3.43 (m, 2H), 2.24−2.06 (m, 3H), 1.91−1.81 (m, 1H); $^{13}$C NMR (100 MHz, DMSO-$d_6$) $\delta$ 155.0 (d, $J$ = 244.6 Hz), 155.5, 154.9 (d, $J$ = 244.7 Hz), 149.7, 149.6, 139.4, 132.5, 124.5, 122.7 (t, $J$ = 10.5 Hz), 121.6 (t, $J$ = 12.5 Hz), 113.4 (d, $J$ = 25.8 Hz), 113.4 (d, $J$ = 11.7 Hz), 110.0, 73.2 (t, $J$ = 5.4 Hz), 59.6 (t, $J$ = 6.0 Hz), 51.0, 50.1, 46.4, 31.5, 31.1; HRMS (ES+) calcd for $C_{20}H_{19}{}^{35}ClF_2N_5O_2$ (M + H)$^+$ 434.1195, found 434.1196; calcd for $C_{20}H_{19}{}^{37}ClF_2N_5O_2$ (M + H)$^+$ 436.1166, found 436.1173.

*1-((6-Chloropyridin-3-yl)methyl)-10-(3,4-dichlorophenyl)-9-nitro-2,3,5,6,7,8-hexahydro-1H-5,8-epiminoimidazo[1,2-a]azepine* (**25**): yield, 64.7%; mp, 206−207 °C; $^1$H NMR (400 MHz, DMSO-$d_6$) $\delta$ 8.17 (d, $J$ = 1.6 Hz, 1H), 7.44 (d, $J$ = 8.8 Hz, 1H), 7.38 (dd, $J$ = 8.0, 1.6 Hz, 1H), 7.26 (d, $J$ = 8.0 Hz, 1H), 7.23 (d, $J$ = 2.0 Hz, 1H), 6.91 (dd, $J$ = 8.8, 2.0 Hz, 1H), 5.67 (s, 1H), 5.27 (d, $J$ = 5.2 Hz, 1H), 4.84 (d, $J$ = 15.6 Hz, 1H), 4.61 (d, $J$ = 15.6 Hz, 1H), 3.81−3.71 (m, 1H), 3.72−3.55 (m, 2H), 3.56−3.45 (m, 1H), 2.28−2.09 (m, 3H), 1.98−1.86 (m, 1H); $^{13}$C NMR (100 MHz, DMSO-$d_6$) $\delta$ 155.9, 149.7, 149.5, 145.4, 138.9, 132.3, 132.1, 131.4, 124.2, 122.2, 119.3, 118.1, 108.8, 71.5, 57.3, 50.8, 50.0, 47.1, 31.6, 31.3; HRMS (ES+) calcd for $C_{20}H_{19}{}^{35}Cl_3N_5O_2$ (M + H)$^+$ 466.0604, found 466.0599; calcd for $C_{20}H_{19}{}^{37}Cl_3N_5O_2$ (M + H)$^+$ 472.0516, found 472.0512.

*1-((6-Chloropyridin-3-yl)methyl)-10-(2,5-dimethoxyphenyl)-9-nitro-2,3,5,6,7,8-hexahydro-1H-5,8-epiminoimidazo[1,2-a]azepine* (**26**): yield, 41.2%; mp, 125−126 °C; $^1$H NMR (400 MHz, DMSO-$d_6$) $\delta$ 8.21 (d, $J$ = 2.4 Hz, 1H), 7.49 (dd, $J$ = 8.0, 2.4 Hz, 1H), 7.33 (d, $J$ = 8.0 Hz, 1H), 6.91 (d, $J$ = 8.8 Hz, 1H), 6.53 (dd, $J$ = 8.8, 2.8 Hz, 1H), 6.28 (d, $J$ = 2.8 Hz, 1H), 5.63 (d, $J$ = 4.8 Hz, 1H), 5.16 (d, $J$ = 4.8 Hz, 1H), 4.78 (d, $J$ = 15.6 Hz, 1H), 4.71 (d, $J$ = 15.6 Hz, 1H), 3.77 (s, 3H), 3.76−3.68 (m, 1H), 3.65 (s, 3H), 3.64−3.56 (m, 1H), 3.45−3.34 (m, 2H), 2.25−2.02 (m, 3H), 1.93−1.82 (m, 1H); $^{13}$C NMR (100 MHz, DMSO-$d_6$) $\delta$ 156.0, 154.0, 149.7, 149.5, 145.4, 139.2, 134.5, 132.5, 124.4, 113.8, 108.7, 107.1, 105.9, 71.9, 58.0, 56.6, 55.6, 50.8, 49.4, 47.0, 31.6, 30.9; HRMS (ES+) calcd for $C_{22}H_{25}{}^{35}ClN_5O_4$ (M + H)$^+$ 458.1595, found 458.1597; calcd for $C_{22}H_{25}{}^{37}ClN_5O_4$ (M + H)$^+$ 460.1566, found 460.1578.

*1-((6-Chloropyridin-3-yl)methyl)-10-(2,3-dimethylphenyl)-9-nitro-2,3,5,6,7,8-hexahydro-1H-5,8-epiminoimidazo[1,2-a]azepine* (**27**): yield, 41.1%; mp, 171−172 °C; $^1$H NMR (400 MHz, DMSO-$d_6$) $\delta$ 8.30 (d, $J$ = 2.0 Hz, 1H), 7.72 (dd, $J$ = 8.0, 2.4 Hz, 1H), 7.47 (d, $J$ = 8.0 Hz, 1H), 6.99−6.83 (m, 2H), 6.65 (d, $J$ = 7.6 Hz, 1H), 5.03 (d, $J$ = 4.4 Hz, 1H), 4.88 (d, $J$ = 4.4 Hz, 1H), 4.82 (d, $J$ = 15.2 Hz, 1H), 4.74 (d, $J$ = 15.2 Hz, 1H), 3.75−3.58 (m, 2H), 3.59−3.44 (m, 1H), 3.42−3.34 (m, 1H), 2.25−2.22 (m, 1H), 2.22 (s, 3H), 2.21−2.18 (m, 1H), 2.15 (s, 3H), 2.12−2.05 (m, 1H), 1.91−1.85 (m, 1H); $^{13}$C NMR (100 MHz, DMSO-$d_6$) $\delta$ 156.2, 149.9, 149.8, 143.2, 139.8, 138.0, 132.4, 129.2, 126.0, 125.1, 124.5, 117.6, 109.0, 73.5, 59.1, 51.0, 49.8, 46.6, 31.8, 31.7, 20.8, 15.1; HRMS (ES+) calcd for $C_{22}H_{25}{}^{35}ClN_5O_2$ (M + H)$^+$ 426.1697, found 426.1692; calcd for $C_{22}H_{25}{}^{37}ClN_5O_2$ (M + H)$^+$ 428.1667, found 428.1678.

*1-((6-Chloropyridin-3-yl)methyl)-10-(2,4-dimethylphenyl)-9-nitro-2,3,5,6,7,8-hexahydro-1H-5,8-epiminoimidazo[1,2-a]azepine* (**28**): yield, 31.9%; mp, 157−158 °C; $^1$H NMR (400 MHz, DMSO-$d_6$) $\delta$ 8.28 (d, $J$ = 2.0 Hz, 1H), 7.70 (dd, $J$ = 8.0, 2.0 Hz, 1H), 7.45 (d, $J$ = 8.0 Hz, 1H), 6.96 (s, 1H), 6.79 (d, $J$ = 8.0 Hz, 1H), 6.63 (d, $J$ = 8.4 Hz, 1H), 5.09 (d, $J$ = 3.6 Hz, 1H), 4.90 (d, $J$ = 3.6 Hz, 1H), 4.80 (d, $J$ = 15.6 Hz, 1H), 4.75 (d, $J$ = 15.6 Hz, 1H), 3.76−3.59 (m, 2H), 3.59−

3.46 (m, 1H), 3.45−3.37 (m, 1H), 2.23 (s, 3H), 2.21 (s, 3H), 2.19−2.00 (m, 3H), 1.93−1.83 (m, 1H); $^{13}$C NMR (100 MHz, DMSO-$d_6$) $\delta$ 156.1, 149.8, 149.8, 140.6, 139.8, 132.5, 132.4, 131.7, 130.0, 127.2, 124.5, 119.6, 109.0, 72.9, 58.7, 50.9, 49.8, 46.7, 31.8, 31.5, 20.7, 19.3; HRMS (ES+) calcd for $C_{22}H_{25}{}^{35}ClN_5O_2$ (M + H)$^+$ 426.1697, found 426.1693; calcd for $C_{22}H_{25}{}^{37}ClN_5O_2$ (M + H)$^+$ 428.1667, found 428.1660.

*1-((6-Chloropyridin-3-yl)methyl)-10-(2,5-dimethylphenyl)-9-nitro-2,3,5,6,7,8-hexahydro-1H-5,8-epiminoimidazo[1,2-a]azepine (**29**):* yield, 80.0%; mp, 157−158 °C; $^1$H NMR (400 MHz, DMSO-$d_6$) $\delta$ 8.29 (d, $J$ = 2.0 Hz, 1H), 7.67 (dd, $J$ = 8.0, 2.4 Hz, 1H), 7.42 (d, $J$ = 8.4 Hz, 1H), 7.04 (d, $J$ = 7.6 Hz, 1H), 6.76 (d, $J$ = 7.2 Hz, 1H), 6.64 (s, 1H), 5.15 (d, $J$ = 4.0 Hz, 1H), 4.99 (d, $J$ = 4.0 Hz, 1H), 4.86 (d, $J$ = 15.6 Hz, 1H), 4.68 (d, $J$ = 15.6 Hz, 1H), 3.79−3.67 (m, 1H), 3.67−3.56 (m, 1H), 3.52−3.35 (m, 2H), 2.23 (s, 3H), 2.22−2.20 (m, 1H), 2.20 (s, 3H), 2.19−2.15 (m, 1H), 2.13−2.03 (m, 1H), 1.93−1.86 (m, 1H); $^{13}$C NMR (100 MHz, DMSO-$d_6$) $\delta$ 156.4, 149.7, 149.6, 143.1, 139.5, 135.8, 132.5, 131.8, 126.9, 124.4, 123.7, 120.4, 108.9, 72.8, 58.6, 51.1, 49.5, 46.7, 31.8, 31.5, 21.5, 19.1; HRMS (ES+) calcd for $C_{22}H_{25}{}^{35}ClN_5O_2$ (M + H)$^+$ 426.1697, found 426.1690; calcd for $C_{22}H_{25}{}^{37}ClN_5O_2$ (M + H)$^+$ 428.1667, found 428.1679.

*1-((6-Chloropyridin-3-yl)methyl)-10-(2,5-dichlorophenyl)-9-nitro-2,3,5,6,7,8-hexahydro-1H-5,8-epiminoimidazo[1,2-a]azepine (**30**):* yield, 46.8%; mp, 157−158 °C; $^1$H NMR (400 MHz, DMSO-$d_6$) $\delta$ 8.28 (d, $J$ = 2.0 Hz, 1H), 7.67 (dd, $J$ = 8.4, 2.8 Hz, 1H), 7.47 (d, $J$ = 8.8 Hz, 1H), 7.42 (d, $J$ = 8.4 Hz, 1H), 7.13 (dd, $J$ = 8.4, 2.4 Hz, 1H), 6.92 (d, $J$ = 2.4 Hz, 1H), 5.54 (s, 1H), 5.32 (d, $J$ = 4.0 Hz, 1H), 4.83 (d, $J$ = 15.6 Hz, 1H), 4.75 (d, $J$ = 15.6 Hz, 1H), 3.80−3.61 (m, 2H), 3.61−3.49 (m, 2H), 2.28−2.13 (m, 3H), 1.96−1.85 (m, 1H); $^{13}$C NMR (100 MHz, DMSO-$d_6$) $\delta$ 156.1, 149.8, 149.6, 142.8, 139.4, 132.7, 132.6, 132.3, 124.6, 124.5, 124.0, 121.4, 107.9, 72.3, 58.7, 51.1, 49.8, 46.3, 31.6, 31.5; HRMS (ES+) calcd for $C_{20}H_{19}{}^{35}Cl_3N_5O_2$ (M + H)$^+$ 466.0604, found 466.0591; calcd for $C_{20}H_{19}{}^{37}Cl_3N_5O_2$ (M + H)$^+$ 472.0516, found 472.0529.

*1-((6-Chloropyridin-3-yl)methyl)-10-(3,4-dimethylphenyl)-9-nitro-2,3,5,6,7,8-hexahydro-1H-5,8-epiminoimidazo[1,2-a]azepine (**31**):* yield, 66.1%; mp, 196−197 °C; $^1$H NMR (400 MHz, DMSO-$d_6$) $\delta$ 8.08 (d, $J$ = 2.0 Hz, 1H), 7.26 (dd, $J$ = 8.4, 2.4 Hz, 1H), 7.18 (d, $J$ = 8.4 Hz, 1H), 6.96 (d, $J$ = 8.4 Hz, 1H), 6.75 (s, 1H), 6.67−6.61 (m, 1H), 5.55 (d, $J$ = 4.0 Hz, 1H), 5.20 (d, $J$ = 4.8 Hz, 1H), 4.87 (d, $J$ = 16.0 Hz, 1H), 4.56 (d, $J$ = 16.0 Hz, 1H), 3.84−3.71 (m, 1H), 3.68−3.50 (m, 2H), 3.45−3.36 (m, 1H), 2.23−2.17 (m, 2H), 2.16 (s, 3H), 2.15 (s, 3H), 2.13−2.05 (m, 2H), 1.95−1.85 (m, 1H); $^{13}$C NMR (100 MHz, DMSO-$d_6$) $\delta$ 155.9, 149.5, 149.5, 142.9, 138.9, 137.3, 132.4, 130.6, 128.2, 124.2, 119.0, 115.1, 109.4, 71.5, 57.0, 50.6, 49.5, 47.6, 31.5, 31.4, 20.3, 19.0; HRMS (ES-) calcd for $C_{22}H_{23}{}^{35}ClN_5O_2$ (M − H)$^+$ 424.1540, found 424.1543; calcd for $C_{22}H_{23}{}^{37}ClN_5O_2$ (M − H)$^+$ 426.1511, found 426.1516.

*1-((6-Chloropyridin-3-yl)methyl)-10-(3,5-dimethylphenyl)-9-nitro-2,3,5,6,7,8-hexahydro-1H-5,8-epiminoimidazo[1,2-a]azepine (**32**):* yield, 53.2%; mp, 214−215 °C; $^1$H NMR (400 MHz, DMSO-$d_6$) $\delta$ 8.15 (s, 1H), 7.26−7.18 (m, 2H), 6.57 (s, 2H), 6.54 (s, 1H), 5.57 (d, $J$ = 3.6 Hz, 1H), 5.22 (d, $J$ = 4.8 Hz, 1H), 4.82 (d, $J$ = 15.6 Hz, 1H), 4.59 (d, $J$ = 15.6 Hz, 1H), 3.82−3.73 (m, 1H), 3.69−3.52 (m, 2H), 3.47−3.37 (m, 1H), 2.20 (s, 6H), 2.18−2.03 (m, 3H), 1.95−1.85 (m, 1H); $^{13}$C NMR (100 MHz, DMSO-$d_6$) $\delta$ 156.1, 149.6, 149.5, 145.0, 138.8, 138.6, 132.5, 124.3, 122.5, 115.5, 109.3, 71.4, 57.0, 50.7, 49.6, 47.6, 31.5, 31.4, 21.8; HRMS (ES-) calcd for $C_{22}H_{23}{}^{35}ClN_5O_2$ (M − H)$^+$ 424.1540, found 424.1543; calcd for $C_{22}H_{23}{}^{37}ClN_5O_2$ (M − H)$^+$ 426.1511, found 426.1517.

*1-((6-Chloropyridin-3-yl)methyl)-10-(2,5-difluorophenyl)-9-nitro-2,3,5,6,7,8-hexahydro-1H-5,8-epiminoimidazo[1,2-a]azepine (**33**):* yield, 74.8%; mp, 195−196 °C; $^1$H NMR (400 MHz, DMSO-$d_6$) $\delta$ 8.20 (d, $J$ = 2.0 Hz, 1H), 7.53 (dd, $J$ = 8.0, 2.0 Hz, 1H), 7.35 (d, $J$ = 8.0 Hz, 1H), 7.27−7.16 (m, 1H), 6.84−6.74 (m, 1H), 6.68−6.58 (m, 1H), 5.44 (s, 1H), 5.27 (s, 1H), 4.79 (d, $J$ = 15.6 Hz, 1H), 4.69 (d, $J$ = 15.6 Hz, 1H), 3.79−3.65 (m, 2H), 3.62−3.50 (m, 2H), 2.25−2.11 (m, 3H), 1.96−1.83 (m, 1H); $^{13}$C NMR (101 MHz, DMSO-$d_6$) $\delta$158.8 (d, $J$ = 239.3 Hz), 155.8, 150.2 (d, $J$ = 238.9 Hz), 149.8, 149.5, 139.2, 132.3, 124.4, 117.9 (d, $J$ = 10.8 Hz), 117.7 (d, $J$ = 10.4 Hz), 108.6 (d, $J$ = 8.2 Hz), 108.5, 108.4 (d, $J$ = 8.1 Hz), 107.8 (d, $J$ = 27.7 Hz), 72.3 (d, $J$ = 8.0 Hz), 58.3, 51.0, 50.1, 46.5, 31.4, 31.2; $^{19}$F NMR (376 MHz, DMSO-$d_6$) $\delta$ −115.94 to −116.56 (m, 1F), −127.09 to −127.39 (m, 1F); HRMS (ES+) calcd for $C_{20}H_{18}{}^{35}ClF_2N_5O_2Na$ (M + Na)$^+$ 456.1015, found 456.1021; calcd for $C_{20}H_{18}{}^{37}ClF_2N_5O_2Na$ (M + Na)$^+$ 458.0985, found 458.0995.

*1-((6-Chloropyridin-3-yl)methyl)-9-nitro-10-(2,3,4,5-tetrafluorophenyl)-2,3,5,6,7,8-hexahydro-1H-5,8-epiminoimidazo[1,2-a]azepine (**34**):* yield, 51.3%; mp, 195−196 °C; $^1$H NMR (400 MHz, DMSO-$d_6$) $\delta$ 8.12 (d, $J$ = 2.4 Hz, 1H), 7.61 (dd, $J$ = 8.0, 2.4 Hz, 1H), 7.37 (d, $J$ = 8.0 Hz, 1H), 6.80−6.69 (m, 1H), 5.42 (s, 1H), 5.26 (d, $J$ = 4.8 Hz, 1H), 4.85 (d, $J$ = 15.6 Hz, 1H), 4.66 (d, $J$ = 15.6 Hz, 1H), 3.79−3.58 (m, 4H), 2.25−2.13 (m, 3H), 1.96−1.88 (m, 1H); $^{13}$C NMR (100 MHz, DMSO-$d_6$) $\delta$ 153.8, 148.2, 147.8, 137.9, 136.6, 130.6, 128.1, 125.5, 122.7, 117.0, 106.9, 101.4, 101.2, 70.7 (d, $J$ = 6.5 Hz), 57.1 (d, $J$ = 5.0 Hz), 49.3, 48.9, 44.7, 29.8, 29.6; $^{19}$F NMR (376 MHz, DMSO-$d_6$) $\delta$ −138.96 to −139.37 (m, 1F), −149.38 to −149.60 (m, 1F), −156.26 (t, $J$ = 21.3 Hz, 1F), −166.60 to −167.07 (m, 1F); HRMS (ES+) calcd for $C_{20}H_{16}{}^{35}ClF_4N_5O_2Na$ (M + Na)$^+$ 492.0826, found 492.0825; calcd for $C_{20}H_{16}{}^{37}ClF_4N_5O_2Na$ (M + Na)$^+$ 494.0797, found 494.0795.

*1-((6-Chloropyridin-3-yl)methyl)-10-(2,4-difluorophenyl)-9-nitro-2,3,5,6,7,8-hexahydro-1H-5,8-epiminoimidazo[1,2-a]azepine (**35**):* yield, 56.4%; mp, 189−190 °C; $^1$H NMR (400 MHz, DMSO-$d_6$) $\delta$ 8.20 (d, $J$ = 2.0 Hz, 1H), 7.57 (dd, $J$ = 8.0, 2.0 Hz, 1H), 7.38 (d, $J$ = 8.0 Hz, 1H), 7.29−7.19 (m, 1H), 6.95−6.87 (m, 1H), 6.87−6.79 (m, 1H), 5.34 (d, $J$ = 3.6 Hz, 1H), 5.16 (d, $J$ = 3.6 Hz, 1H), 4.76 (d, $J$ = 15.6 Hz, 1H), 4.70 (d, $J$ = 15.6 Hz, 1H), 3.81−3.62 (m, 2H), 3.57−3.43 (m, 2H), 2.26−2.06 (m, 3H), 1.98−1.85 (m, 1H); $^{13}$C NMR (100 MHz, DMSO-$d_6$) $\delta$ 156.8 (d, $J$ = 240.8 Hz), 156.6 (d, $J$ = 240.8 Hz), 155.1, 153.4 (d, $J$ = 246.9 Hz), 153.2 (d, $J$ = 246.6 Hz), 149.3, 149.1, 139.0, 131.8, 128.8 (d, $J$ = 3.4 Hz), 128.7 (d, $J$ = 3.3 Hz), 123.9, 120.9 (d, $J$ = 4.5 Hz), 120.8 (d, $J$ = 4.2 Hz), 111.4 (d, $J$ = 3.4 Hz), 111.2 (d, $J$ = 3.3 Hz), 108.0, 105.1, 104.9 (d, $J$ = 51.9 Hz), 72.0 (d, $J$ = 7.4 Hz), 57.9 (d, $J$ = 3.3 Hz), 50.4, 49.5, 46.2, 31.0, 30.8; $^{19}$F NMR (376 MHz, DMSO-$d_6$) $\delta$ −117.30 to −117.47 (m, 1F), −119.20 to −119.35 (m, 1F); HRMS (ES+) calcd for $C_{20}H_{19}{}^{35}ClF_2N_5O_2$ (M + H)$^+$ 434.1195, found 434.1195; calcd for $C_{20}H_{19}{}^{37}ClF_2N_5O_2$ (M + H)$^+$ 436.1166, found 436.1156.

*1-((6-Chloropyridin-3-yl)methyl)-10-(2,3-difluorophenyl)-9-nitro-2,3,5,6,7,8-hexahydro-1H-5,8-epiminoimidazo[1,2-a]azepine (**36**):* yield, 67.9%; mp, 193−194 °C; $^1$H NMR (400 MHz, DMSO-$d_6$) $\delta$ 8.20 (d, $J$ = 1.6 Hz, 1H), 7.53 (dd, $J$ = 8.0, 1.6 Hz, 1H), 7.36 (d, $J$ = 8.0 Hz, 1H), 7.09−6.94 (m, 2H), 6.75−6.59 (m, 1H), 5.44 (s, 1H), 5.25 (s, 1H), 4.78 (d, $J$ = 15.6 Hz, 1H), 4.69 (d, $J$ = 15.6 Hz, 1H), 3.81−3.64 (m, 2H), 3.61−3.47 (m, 2H), 2.26−2.10 (m, 3H), 1.99−1.86 (m, 1H); $^{13}$C NMR (100 MHz, DMSO-$d_6$) $\delta$ 155.1, 150.7 (d, $J$ = 243.7 Hz), 150.6 (d, $J$ = 243.6 Hz), 149.3, 149.1, 142.0 (d, $J$ = 245.1 Hz), 141.8 (d, $J$ = 244.9 Hz), 138.9, 133.9 (d, $J$ = 4.1 Hz), 131.8, 124.6 (dd, $J$ = 8.6, 4.3 Hz), 123.9, 115.7, 109.7 (d, $J$ = 17.3 Hz), 108.1, 72.0 (d, $J$ = 7.5 Hz), 58.0 (d, $J$ = 3.6 Hz), 50.4, 49.6, 46.1, 30.9, 30.8; $^{19}$F NMR (376 MHz, DMSO-$d_6$) $\delta$ −138.08 to −138.43 (m, 1F), −148.91 to −149.30 (m, 1F); HRMS (ES+) calcd for $C_{20}H_{19}{}^{35}ClF_2N_5O_2$ (M + H)$^+$ 434.1195, found 434.1185; calcd for $C_{20}H_{19}{}^{37}ClF_2N_5O_2$ (M + H)$^+$ 436.1166, found 436.1159.

*1-((6-Chloropyridin-3-yl)methyl)-9-nitro-10-(2,4,5-trifluorophenyl)-2,3,5,6,7,8-hexahydro-1H-5,8-epiminoimidazo[1,2-a]azepine (**37**):* yield, 77.9%; mp, 184−185 °C; $^1$H NMR (400 MHz, DMSO-$d_6$) $\delta$ 8.18 (d, $J$ = 2.0 Hz, 1H), 7.60 (dd, $J$ = 8.4, 2.0 Hz, 1H), 7.57−7.48 (m, 1H), 7.37 (d, $J$ = 8.4 Hz, 1H), 6.90−6.80 (m, 1H), 5.38 (s, 1H), 5.24 (d, $J$ = 4.8 Hz, 1H), 4.81 (d, $J$ = 15.6 Hz, 1H), 4.70 (d, $J$ = 15.6 Hz, 1H), 3.78−3.66 (m, 2H), 3.67−3.52 (m, 2H), 2.26−2.10 (m, 3H), 1.95−1.85 (m, 1H); $^{13}$C NMR (100 MHz, DMSO-$d_6$) $\delta$ 155.2, 149.3, 149.0, 138.9, 131.8, 123.8, 108.6 (d, $J$ = 4.6 Hz), 108.4 (d, $J$ = 4.6 Hz), 107.9, 106.9, 106.7 (d, $J$ = 6.2 Hz), 106.4, 71.8 (d, $J$ = 7.0 Hz), 58.0 (d, $J$ = 4.8 Hz), 50.4, 49.7, 45.9, 30.8, 30.7; $^{19}$F NMR (376 MHz, DMSO-$d_6$) $\delta$ −122.75 to −123.04 (m, 1F), −141.06 to −141.51 (m, 1F), −144.07 to −144.38 (m, 1F); HRMS (ES+) calcd for $C_{20}H_{18}{}^{35}ClF_3N_5O_2$ (M + H)$^+$ 452.1101, found 452.1091; calcd for $C_{20}H_{18}{}^{37}ClF_3N_5O_2$ (M + H)$^+$ 454.1072, found 454.1087.

**X-ray Diffraction Analysis.** Compound **1** was recrystallized by slow evaporation from a mixture of acetone, dichloromethane, and cyclohexane (1:1:1, v/v/v) to afford a suitable single crystal. Yellow blocks of compound **1** (0.29 mm × 0.21 mm × 0.14 mm) were mounted on a quartz fiber. Cell dimensions and intensities were measured at 293 K on a Bruker SMART CCD area detector diffractometer with graphite monochromated Mo K$\alpha$ radiation ($\lambda$ = 0.71073 Å); $\theta_{max}$ = 25.99°; 10716 measured reflections; 3627 independent reflections ($R_{int}$ = 0.0475). Data were corrected for Lorentz and polarization effects and for absorption ($t_{min}$ = 0.7050 and $t_{max}$ = 1.0000). The structure was solved by direct methods using SHELXS-97;[11] all other calculations were performed with a Bruker SAINT System and Bruker SMART programs.[12] Full-matrix least-squares refinement based on $F^2$ using the weight of $1/ [\sigma^2 (F_0^2) + (0.0613P)^2 + 0.0371P]$ gave final values of $R$ = 0.0542, $\omega R$ = 0.1462, and GOF ($F$) = 1.022 for 253 variables and 3627 contributing reflections. Maximum shift/error = 0.000(3) and max/min residual electron density = 0.530/−0.519 e Å$^{-3}$. Hydrogen atoms were observed and refined with a fixed value of their isotropic displacement parameter.

**Biological Assay.** All bioassays were performed on representative test organisms reared in the laboratory. The bioassay was repeated at 25 ± 1 °C according to statistical requirements. All compounds were dissolved in *N*,*N*-dimethylformamide (AP, Shanghai Chemical Reagent Co., Ltd., Shanghai, China) and diluted with distilled water containing Triton X-100 (0.1 mg L$^{-1}$) to obtain series concentrations of 20 and 4 mg L$^{-1}$ and others for bioassays. For comparative purposes, IMI and CYC were tested under the same conditions.

**Insecticidal Test for Cowpea Aphid (*A. craccivora*).** The insecticidal activity of synthetic compounds against cowpea aphid was tested by using the leaf-dip method.[13,14] Horsebean plant leaves with 30−40 apterous adults were dipped in diluted solutions of the chemicals containing Triton X-100 (0.1 mg L$^{-1}$) for 5 s, and the excess dilution was sucked out with filter paper; the burgeons were placed in the conditioned room (25 ± 1 °C, 50% realtive humidity). Water containing Triton X-100 (0.1 mg L$^{-1}$) was used as control. The mortality rates were evaluated 24 h after treatment. Each treatment had three repetitions, and the data were adjusted and subjected to probit analysis as before.

**Insecticidal Test for Armyworm (*Pseudaletia separata* Walker).** The insecticidal activity against armyworm was tested by foliar application.[15−17] Individual corn (*Zea mays*) leaves were placed on moistened pieces of filter paper in Petri dishes. The leaves were then sprayed with the compound solution and allowed to dry. The dishes were infested with 10 third-instar larvae and placed in the conditioned room. The mortality rates were evaluated 48 h after treatment. Each treatment had three repetitions, and the data were adjusted and subjected to probit analysis as before.

**Insecticidal Test for Brown Planthopper (*N. lugens*).** The insecticidal activity against brown planthopper was tested by foliar application. Rice seedlings were placed on moistened pieces of filter paper in Petri dishes. The dishes were infested with 30−40 third-instar larvae and then sprayed with the compound solutions (2.5 mL) using a Potter spray tower (pressure, 5 lb/in$^2$; settlement, 4.35 mg/cm$^2$). Samples were placed in the conditioned room. The mortality rates were evaluated 48 h after treatment. Each treatment had three repetitions, and the data were adjusted and subject to probit analysis as before.

## RESULTS AND DISCUSSION

**Synthesis.** To synthesize azabridged neonicotinoid compounds, the major obstacle was the synthetic methodology. Through comparison of the structures of the 1,3-dicarbonyl derivative and our starting material **B** (cyclic $\beta$-nitroenamine), similar nucleophilic centers were found in these two types of substances, which implied that the target compounds can be constructed in an intermolecular way involving primary amine hydrochlorides and dialdehydes.[10] Consequently, the commercialized glutaraldehyde was first chosen to synthesize eight-membered azabridged neonicotinoid analogues. Therefore, to obtain seven-membered azabridges, the preparation of succinaldehyde was the main task in this work.

Hitherto, various methods of acidic[17−23] and nonacidic hydrolysis[24] were reported to prepare succinaldehyde from commercially available and synthetic equivalent 2,5-dimethoxydihydrofuran (DMTHF). Furthermore, according to our previous study of eight-membered azabridges,[10] it was found that an acidic environment was conducive to the formation of azabridged neonicotinoid compounds. Thus, compound **3** was chosen to study the influence of the pH value, and the results are listed in Table 1.

**Table 1. Optimization of Compound 3**

| entry | hydrolyzed succinaldehyde | time (h) | yield[a] (%) |
|---|---|---|---|
| 1 | pH 1−2 | 1.5 | 66.0 |
| 2 | pH 2−3 | 1.5 | 82.5 |
| 3 | pH 6−7 | 1.5 | 44.2 |
| 4 | pH 8−9 | 1.5 | tr[b] |
| 5 | pH 2−3 | 0.5 | 45.5 |
| 6 | pH 2−3 | 5.0 | 26.2 |
| 7 | pH 2−3 | 10.0 | 20.0 |
| 8 | nonacidic[c] | 1.5 | 60.1 |

[a]Isolated yields. [b]tr, trace. [c]See ref 24.

To begin with, the solution of succinaldehyde was used immediately after acidic hydrolysis of DMTHF. The reaction was monitored by TLC, and the target compound **3** was successfully acquired in a good yield (Table 1, entry 1), which encouraged us to optimize the pH value of succinaldehyde solution before it was used in the next step. From the experimental data in Table 1, it was observed that the pH value below 2 or above 3 would display relatively low yields (Table 1, entries 1−4). These results demonstrated that the pH value at 2−3 was more suitable to synthesize seven-membered azabridged compounds.

On the basis of this optimal condition, the reaction time was also investigated. The corresponding yields were increased, but decreased with the extension of time (Table 1, entries 2 and 5−7). Therefore, the reaction was carried out in 1.5 h, because the decomposition rate of our target compound was more rapid than the formation rate after a period of time. Eventually, the nonacidic condition was also studied (Table 1, entry 8). The succinaldehyde was prepared following literature procedures;[24] however, the corresponding yield was still lower than that of acid condition.

**Crystal Structure Analysis.** To provide more evidence for the proposed molecular structure and establish the conformation of the target compounds, compound **1** was recrystallized by slow evaporation and its single-crystal structure was determined by X-ray crystallography as illustrated in Figure 3.

Unlikely eight-membered compounds, the pyridine ring, and benzene ring of compound **1** pointed to the same direction. Compared with the *trans*-configuration of nitro in the crystal structure of IMI,[26] the nitro groups of compound **1** was in *cis*-configuration as anticipated. There are some characteristics of the bond lengths. For example, the bond lengths of C(9)—N(2) (1.35 Å) and C(9)—N(3) (1.34 Å) were obviously shorter than the typical C—N single bond (1.47 Å) but close to that of C=N (1.33 Å), owing to the transfer of the lone-pair electrons on the amines to C(10)=C(9) and the delocalization of the electrons extended as far as the electron-withdrawing

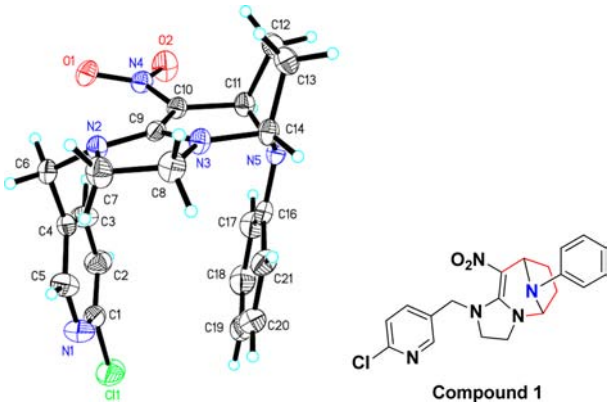


**Figure 3.** Crystal and chemical structures of compound **1**.

group ($-NO_2$), forming a coplanar olefin−amine $\pi$-electron network.[25,26] Moreover, it also made the bond lengths of C(10)═C(9) (1.41 Å) and C—$NO_2$ (C(10)—N(4); 1.36 Å) longer than that of normal C═C (1.34 Å) and shorter than that of typical C—$NO_2$ (C—N; 1.49 Å), respectively.

**Insecticidal Activity.** Table 2 lists the insecticidal activities of the title compounds against cowpea aphid (*A. craccivora*), brown planthopper (*N. lugens*), and armyworm (*P. separata* Walker). Most of the compounds exhibited significant insecticidal activities against these three species of pests. Compound **1** with no substituent on the phenyl group presented similar insecticidal activities against cowpea aphid and brown planthopper, but lower bioactivity against armyworm, compared with seven-membered oxabridged compound CYC (Table 3). Then, the substitution effect on insecticidal activities was investigated.

The compounds with various types of substitutions on position 4 of the phenyl group were first synthesized (**2**–**9**). The bioassay showed that introducing an electron-donating group (OMe and Me) (**3** and **5**) and a fluorine atom (**4**) could contribute to great improvement of activity against armyworm while presenting considerable activities against brown planthopper and cowpea aphid. Meanwhile, bringing in an electron-withdrawing group ($CF_3$, CN, $NO_2$) (**6**, **7**, and **9**), a bromine atom (**2**), or a chlorine atom (**8**) on the phenyl ring would decrease the activities against brown planthopper and cowpea aphid but increase the bioactivity against armyworm, compared with compound **1**.

On position 2 of the phenyl group, the compound with a cyano group (**15**) displayed relatively low insecticidal activities and the others (**10**–**14**) exhibited excellent bioactivities against the three species of pests, which confirmed that position 2 was the key substitution site for structural derivation to obtain high-activity molecules. Moreover, on the basis of the $LC_{50}$ value in Table 3, with the radius of the halogen atom increasing (**10**–**12**), the insecticidal activities showed decreasing tendency against armyworm, but still higher than that of CYC and IMI. Notably, compounds **12** and **13** demonstrated the relatively higher bioactivities among the structures with substitution on position 2.

The insecticidal activities of all the compounds with a substituent on position 3 (**16**–**21**) were lower than that of compound **1** against brown planthopper and cowpea aphid. However, among these, compounds **16** and **21** presented relatively high bioactivities against the three species of pests. Combined with the discussion above, we could preliminarily conclude that introducing a methyl group and a fluorine atom on any site of the phenyl group was favorable to increase the insecticidal activities and that position 2 was an important site for obtaining high-activity compounds.

**Table 2. Insecticidal Activities of Compounds 1−37**

| | | mortality[a] (%) | | | |
|---|---|---|---|---|---|
| | | *P. separata* Walker | | *A. craccivora* | |
| compd | R | 20 mg $L^{-1}$ | 4 mg $L^{-1}$ | 20 mg $L^{-1}$ | 4 mg $L^{-1}$ |
| **1** | H | 0 | 0 | 100 | 100 |
| **2** | 4-Br | 0 | 0 | 100 | 100 |
| **3** | 4-OMe | 80 | 10 | 100 | 100 |
| **4** | 4-F | 80 | 10 | 100 | 100 |
| **5** | 4-Me | 90 | 10 | 100 | 100 |
| **6** | 4-$CF_3$ | 60 | 0 | 100 | 80 |
| **7** | 4-CN | 50 | 0 | 100 | 80 |
| **8** | 4-Cl | 80 | 30 | 100 | 100 |
| **9** | 4-$NO_2$ | 0 | 0 | 0 | 0 |
| **10** | 2-Cl | 80 | 10 | 100 | 100 |
| **11** | 2-Br | 70 | 10 | 100 | 100 |
| **12** | 2-F | 90 | 30 | 100 | 100 |
| **13** | 2-Me | 80 | 30 | 100 | 100 |
| **14** | 2-OMe | 80 | 30 | 100 | 100 |
| **15** | 2-CN | 0 | 0 | 50 | 0 |
| **16** | 3-Me | 40 | 0 | 100 | 100 |
| **17** | 3-$CF_3$ | 0 | 0 | 0 | 0 |
| **18** | 3-OMe | 100 | 0 | 100 | 40 |
| **19** | 3-Cl | 100 | 0 | 100 | 30 |
| **20** | 3-$NO_2$ | 80 | 0 | 100 | 0 |
| **21** | 3-F | 50 | 0 | 100 | 70 |
| **22** | 3-F-4-OMe | 100 | 0 | 100 | 0 |
| **23** | 2-F-4-Me | 70 | 0 | 100 | 0 |
| **24** | 2,6-$(F)_2$ | 100 | 0 | 100 | 50 |
| **25** | 3,4-$(Cl)_2$ | 0 | 0 | 0 | 0 |
| **26** | 2,5-$(OMe)_2$ | 70 | 30 | 100 | 100 |
| **27** | 2,3-$(Me)_2$ | 80 | 20 | 100 | 100 |
| **28** | 2,4-$(Me)_2$ | 100 | 0 | 100 | 100 |
| **29** | 2,5-$(Me)_2$ | 90 | 50 | 100 | 100 |
| **30** | 2,5-$(Cl)_2$ | 70 | 0 | 100 | 90 |
| **31** | 3,4-$(Me)_2$ | 0 | 0 | 100 | 0 |
| **32** | 3,5-$(Me)_2$ | 80 | 10 | 100 | 80 |
| **33** | 2,5-$(F)_2$ | 80 | 0 | 90 | 70 |
| **34** | 2,3,4,5-$(F)_4$ | 0 | 0 | 0 | 0 |
| **35** | 2,4-$(F)_2$ | 30 | 0 | 100 | 95 |
| **36** | 2,3-$(F)_2$ | 90 | 30 | 100 | 95 |
| **37** | 2,4,5-$(F)_3$ | 80 | 0 | 100 | 90 |
| CYC | | 40 | 0 | 100 | 100 |
| IMI | | 40 | 0 | 100 | 100 |

[a]At 4 mg $L^{-1}$, the mortality of all compounds against brown planthopper (*Nilaparvata lugens*) was 100%.

Therefore, further SAR study of two substitutions on the phenyl group was carried out. Initially, the combinations of fluorine atom with methoxy group (**22**) and methyl (**23**) were carried out. Unfortunately, the insecticidal activities against cowpea aphid and armyworm were decreased dramatically, which was not a good result for exploring a potential neonicotinoid insecticide with superior bioactivities against the three species of pests. Then, we turned our attention to dimethyl substitution on the phenyl group.

2,3-Dimethyl (**27**), 2,4-dimethyl (**28**), and 2,5-dimethyl groups (**29**) were introduced into the phenyl group; owing to the sterically hindered effect of the substituent, the


dx.doi.org/10.1021/jf504014y | J. Agric. Food Chem. 2014, 62, 11070−11079

Table 3. $LC_{50}$ Values of Some Compounds against Three Species of Pests

| | | $LC_{50}$ (95% fiducial limits) (mg $L^{-1}$) | | |
|---|---|---|---|---|
| compd | R | *A. craccivora* | *N. lugens* | *P. separata* Walker |
| **1** | H | 0.342 (0.256−0.438) | 0.504 (0.427−0.597) | nt[a] |
| **2** | 4-Br | 0.574 (0.481−0.679) | 1.015 (0.870−1.181) | nt |
| **3** | 4-OMe | 0.172 (0.064−0.270) | 0.179 (0.140−0.221) | 10.937 (9.526−12.536) |
| **4** | 4-F | 0.403 (0.341−0.464) | 0.338 (0.239−0.450) | nt |
| **5** | 4-Me | 0.196 (0.158−0.233) | 0.511 (0.439−0.591) | nt |
| **6** | 4-$CF_3$ | 2.938 (2.433−3.602) | 0.860 (0.721−1.029) | nt |
| **7** | 4-CN | 2.718 (2.241−3.324) | 1.803 (1.544−2.111) | nt |
| **8** | 4-Cl | 2.469 (1.965−3.220) | 0.558 (0.451−0.671) | 7.550 (5.497−10.387) |
| **10** | 2-Cl | 0.412 (0.352−0.481) | 0.232 (0.193−0.277) | 10.984 (7.696−15.326) |
| **11** | 2-Br | 0.409 (0.343−0.487) | 0.151 (0.119−0.183) | 11.019 (9.436−12.845) |
| **12** | 2-F | 0.184 (0.149−0.219) | 0.338 (0.239−0.450) | 6.103 (4.590−7.823) |
| **13** | 2-Me | 0.396 (0.334−0.462) | 0.129 (0.047−0.231) | 6.762 (4.993−8.961) |
| **14** | 2-OMe | 0.419 (0.247−0.615) | 0.178 (0.134−0.222) | nt |
| **16** | 3-Me | 0.421 (0.357−0.491) | 0.831 (0.710−0.951) | nt |
| **18** | 3-OMe | nt | 0.418 (0.351−0.489) | nt |
| **19** | 3-Cl | nt | 0.429 (0.360−0.506) | nt |
| **24** | 2,6-$(F)_2$ | nt | 0.395 (0.327−0.469) | nt |
| **25** | 3,4-$(Cl)_2$ | nt | 0.859 (0.629−1.230) | nt |
| **26** | 2,5-$(OMe)_2$ | 0.490 (0.325−0.702) | 0.062 (0.041−0.082) | 8.421 (6.037−11.292) |
| **27** | 2,3-$(Me)_2$ | 0.864 (0.556−1.339) | 0.279 (0.133−0.473) | 9.549 (6.996−12.899) |
| **28** | 2,4-$(Me)_2$ | 0.450 (0.229−0.744) | 0.039 (0.006−0.077) | nt |
| **29** | 2,5-$(Me)_2$ | 0.426 (0.156−0.793) | 0.054 (0.033−0.077) | 4.756 (3.510−6.374) |
| **30** | 2,5-$(Cl)_2$ | 1.268 (0.855−1.982) | 0.072 (0.045−0.099) | nt |
| CYC | | 0.435 (0.168−0.748) | 0.383 (0.197−0.593) | 26.692 (22.904−31.123) |
| IMI | | 0.634 (0.458−0.838) | 1.089 (0.973−1.218) | 34.078 (26.087−49.535) |

[a]Not tested.

compound with a 2,6-dimethyl group could not be synthesized. Excitingly, compounds **28** ($LC_{50}$ = 0.039 mg $L^{-1}$) and **29** ($LC_{50}$ = 0.054 mg $L^{-1}$) displayed an improvement of about 1 order of magnitude over CYC ($LC_{50}$ = 0.383 mg $L^{-1}$) in insecticidal activity against brown planthopper and an activity similar to that of **13** against cowpea aphid. Furthermore, the insecticidal activity of compound **29** was 7-fold higher than that of IMI against armyworm. Thus, we replaced the 2,5-dimethyl with 2,5-dimethoxy (**26**), 2,5-dichloro (**30**), and 2,5-difluoro (**33**) to study the variations of bioactivities. Compounds **26**, **30**, and **33** showed comparable activity against brown planthopper, but lower activities against armyworm and cowpea aphid, respectively, which implied that introducing disubstitution on positions 2 and 5 of the phenyl group could obtain a molecule with high activity against brown planthopper.

Difluoro- and multifluoro-substituted compounds were also studied (**24**, **33**−**37**). Compared with compound **12**, introducing multiple fluorine atoms into the phenyl group could not lead to the increase of bioactivities against three species of pests. Therefore, the substitution of a methyl group on the phenyl group was more favorable for the improvement of insecticidal activities than that of fluorine atoms.

Table 4 lists the comparison of insecticidal activities between eight-membered[10] and seven-membered compounds. At low concentration (4 and 20 mg $L^{-1}$), most seven-membered azabridged compounds showed apparently higher bioactivities than eight-membered compounds against the three species of pests. These results indicated that the ring size played a very important role in increasing the insecticidal activities.

**Docking Study.** A docking study was performed to explore the binding modes of our compounds. The crystal structure of the *Aplysia californica* acetylcholine binding protein (*Ac*-AChBP) complexed with IMI (PDB code 3C79) was selected to construct the binding models,[27] which showed high affinity with neonicotinoids and was a good prototype for investigating the binding mode of neonicotinoids.[28] For comparison, compounds **1** and **29** were built, minimized, and docked into

Table 4. Comparison of Insecticidal Activities between Eight- and Seven-Membered Compounds

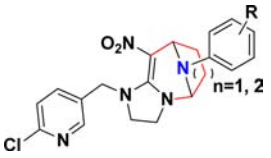


| | | mortality (%) | | | | | |
|---|---|---|---|---|---|---|---|
| | | *N. lugens*[a] | | *A. craccivora*[a] | | *P. separata* Walker[b] | |
| entry | R | *n* = 1 | *n* = 2 | *n* = 1 | *n* = 2 | *n* = 1 | *n* = 2 |
| 1 | H | 100 | 0 | 100 | 20 | 0 | 0 |
| 2 | 4-Me | 100 | 50 | 100 | 5 | 90 | 0 |
| 3 | 2-Me | 100 | 0 | 100 | 30 | 80 | 0 |
| 4 | 3-Me | 100 | 0 | 100 | 10 | 40 | 0 |
| 5 | 4-Br | 100 | 0 | 100 | 0 | 0 | 0 |
| 6 | 2-F | 100 | 0 | 100 | 20 | 90 | 0 |
| 7 | 2-Cl | 100 | 0 | 100 | 30 | 80 | 0 |
| 8 | 2-Br | 100 | 0 | 100 | 5 | 70 | 0 |
| 9 | 3-$NO_2$ | 100 | 0 | 0 | 15 | 80 | 0 |
| 10 | 4-$NO_2$ | 100 | 0 | 0 | 0 | 0 | 0 |
| 11 | 4-Cl | 100 | 0 | 100 | 0 | 80 | 0 |
| 12 | 2,5-$(OMe)_2$ | 100 | 20 | 100 | 20 | 70 | 0 |

[a]At 4 mg $L^{-1}$. [b]At 20 mg $L^{-1}$.


dx.doi.org/10.1021/jf504014y | J. Agric. Food Chem. 2014, 62, 11070−11079

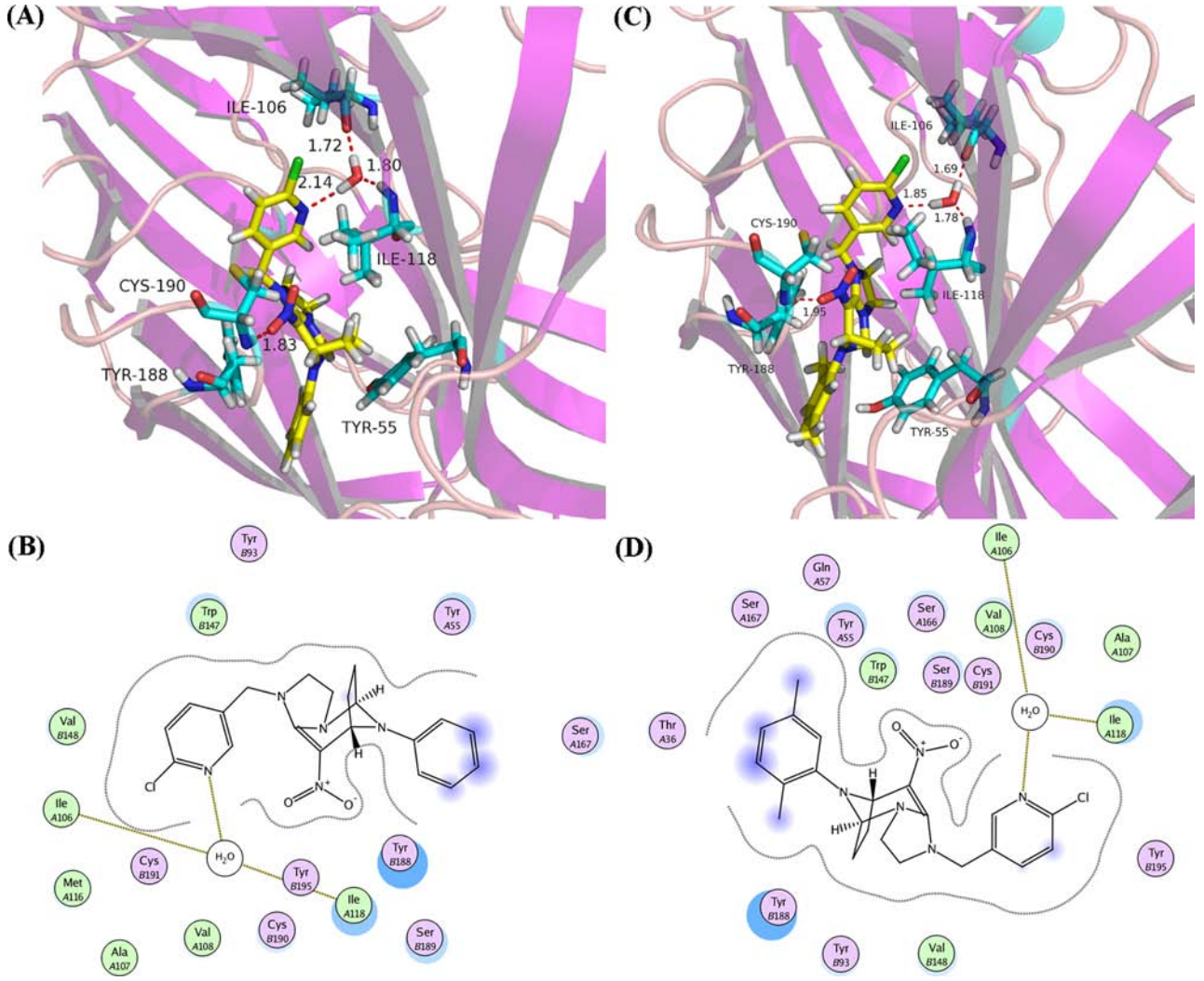


**Figure 4.** Binding modes of compounds **1** (A, B) and **29** (C, D).

the ligand binding pocket of *Ac*-AChBP by using the Induced Fit Docking approach, of which the IFDScore scoring function was selected to evaluate the docking results. All atoms within 20 Å around IMI in the 3C79 structure were selected as binding pocket and considered in the docking study. All computational studies were performed using Maestro 9.0 (Schrödinger, LLC, 2013).

The docking poses of compounds **1** and **29** were depicted in Figure 4. It was found that water bridged hydrogen bonding network played key roles for the ligands recognition, which has also been reported for the binding of IMI and other neonicotinoid compounds.[27,28] Also, N−H···O hydrogen bonds were observed between the peptide N−H of Cys190 and the nitro groups of compounds. The phenyl group inserted into the interspace between loop C and the adjacent subunit, and located between the Tyr188 and Tyr55. Comparing with compound **1**, the methyl group introduced into position 2 of phenyl group in compound **29** could improve the hydrophobic interactions with receptor (Figure 4B and 4D), which might be one of the reasons for the improvement of insecticidal activity.

In conclusion, 37 novel seven-membered azabridged neonicotinoid analogues were designed and synthesized. The pH value at 2−3 of hydrolyzed succinaldehyde solution was an optimized condition to synthesize target compounds in excellent yields. The bioassays showed that most of the compounds presented superior bioactivities to IMI and seven-membered oxabridged compound CYC against cowpea aphid, brown planthopper, and armyworm. Compared with IMI, compound **29** with 2,5-dimethyl group, displayed 7 fold and 20 fold higher activities against armyworm and brown planthopper, respectively. Moreover, seven-membered compounds showed much higher bioactivities against three species of pests than that of eight-membered azabridge neonicotinoids, which implied that the framework of a seven-membered azabridge could significantly improve the insecticidal activity of neonicotinoid analogues and was a very good lead structure to discover potential pesticides. Further studies on field testing of the title compounds are in progress.

## ■ ASSOCIATED CONTENT

### Supporting Information

Crystallographic information files (CIF) of compound **1**. This material is available free of charge via the Internet at http://pubs.acs.org.

## AUTHOR INFORMATION


### Corresponding Authors

*(Z.L.) Phone: +86-21-64253540. Fax: +86-21-64252603. E-mail: lizhong@ecust.edu.cn.

*(X.X.) E-mail: xyxu@ecust.edu.cn.



### Funding

This work was financially supported by the National High Technology Research and Development Program of China (863 Program, 2011AA10A207) and the National Natural Science Foundation of China (21272071, 21172070, and 21472046). This work was also partly supported by the National Key Technology R&D Program of China (2011BAE06B01) and the Fundamental Research Funds for the Central Universities.


### Notes

The authors declare no competing financial interest.

## REFERENCES


(1) Arthur, K. Emerging structure of the nicotinic acetylcholine receptors. *Nat. Rev. Neurosci.* **2002**, *3*, 102−114.

(2) Sher, E.; Chen, Y.; Sharples, T. J.; Broad, L. M.; Benedetti, G.; Zwart, R.; McPhie, G. I.; Pearson, K. H.; Baldwinson, T.; De Filippi, G. Physiological roles of neuronal nicotinic receptor subtypes: new insights on the nicotinic modulation of neurotransmitter release, synaptic transmission and plasticity. *Curr. Top. Med. Chem.* **2004**, *4*, 283−297.

(3) D'Hoedt, D.; Bertrand, D. Nicotinic acetylcholine receptors: an overview on drug discovery. *Expert Opin. Ther. Targets* **2009**, *13*, 395−411.

(4) Changeux, J. P. Nicotine addiction and nicotinic receptors: lessons from genetically modified mice. *Nat. Rev. Neurosci.* **2010**, *11*, 389−401.

(5) Tomizawa, M.; Casida, J. E. Molecular recognition of neonicotinoid insecticides: the determinants of life or death. *Acc. Chem. Res.* **2009**, *42*, 260−269.

(6) Badio, B.; Daly, J. W. Epibatidine, a potent analgetic and nicotinic agonist. *Mol. Pharmacol.* **1994**, *45*, 563−569.

(7) Xu, R.; Bai, D.; Chu, G.; Tao, J.; Zhu, X. Synthesis and analgesic activity of epibatidine analogues. *Bioorg. Med. Chem. Lett.* **1996**, *6*, 279−282.

(8) Wright, E.; Gallagher, T.; Sharples, C. G. V.; Wonnacott, S. Synthesis of UB-165: a novel nicotinic ligand and anatoxina/epibatidine hybrid. *Bioorg. Med. Chem. Lett.* **1997**, *7*, 2867−2870.

(9) Shao, X.; Fu, H.; Xu, X.; Xu, X.; Liu, Z.; Li, Z.; Qian, X. Divalent and oxabridged neonicotinoids constructed by dialdehydes and nitromethylene analogues of imidacloprid: design, synthesis, crystal structure, and insecticidal activities. *J. Agric. Food Chem.* **2010**, *58*, 2696−2702.

(10) Xu, R.; Xia, R.; Luo, M.; Xu, X.; Cheng, J.; Shao, X.; Li, Z. Design, synthesis, crystal structures, and insecticidal activities of eight-membered azabridge neonicotinoid analogues. *J. Agric. Food Chem.* **2014**, *62*, 381−390.

(11) Sheldrick, G. M. *SHELXTL*, version 5.0; University of Göttingen: Göttingen, Germany, 2001.

(12) Bruker. *SMART*, version 5.628; *SAINT*, version 6.45; and *SADABS*; Bruker AXS: Madison, WI, USA, 2001.

(13) Tian, Z.; Shao, X.; Li, Z.; Qian, X.; Huang, Q. Synthesis, insecticidal activity, and QSAR of novel nitromethylene neonicotinoids with tetrahydropyridine fixed *cis*-configuration and exo-ring ether modification. *J. Agric. Food Chem.* **2007**, *55*, 2288−2292.

(14) Tian, Z.; Jiang, Z.; Li, Z.; Song, G.; Huang, Q. Syntheses and biological activities of octahydro-1*H*-cyclopenta[*d*]pyrimidine derivatives. *J. Agric. Food Chem.* **2007**, *55*, 143−147.

(15) Wei, S.; Qian, X.; Zhang, R.; Song, G. Synthesis and quantitative structure-activity relationships of new 2,5-disubstituted-1,3,4-oxadiazoles. *J. Agric. Food Chem.* **2001**, *49*, 143−130.

(16) Li, C.; Wang, Q.; Huang, R.; Mao, C.; Shang, J.; Bi, F. Synthesis and insecticidal evalution of propesticides of benzoylphenylureas. *J. Agric. Food Chem.* **2005**, *49*, 38−41.

(17) Meltzer, P. C.; Wang, B.; Chen, Z.; Blundell, P.; Jayaraman, M.; Gonzalez, M. D.; George, C.; Madras, B. K. Synthesis of 6- and 7-hydroxy-8-azabicyclo[3.2.1]octanes and their binding affinity for the dopamine and serotonin transporters. *J. Med. Chem.* **2001**, *44*, 2619−2635.

(18) Mueller, R.; Yang, J.; Duan, C.; Pop, E.; Zhang, L.; Huang, T.; Denisenko, A.; Denisko, O. V.; Oniciu, D. C.; Bisgaier, C. L.; Pape, M. E.; Freiman, C. D.; Goetz, B.; Cramer, C. T.; Hopson, K. L.; Dasseux, J. H. Long hydrocarbon chain ether diols and ether diacids that favorably alter lipid disorders in vivo. *J. Med. Chem.* **2004**, *47*, 5183−5197.

(19) Enkisch, C.; Schneider, C. Sequential Mannich-aza-Michael reactions for the stereodivergent synthesis of highly substituted pyrrolidines. *Eur. J. Org. Chem.* **2009**, 5549−5564.

(20) Fournial, A.; Ranaivondrambola, T.; Mathé-Allainmat, M.; Robins, R. J.; Lebreton, J. A short and efficient synthesis of bridgehead mono- and dideuteriated tropinones. *Eur. J. Org. Chem.* **2010**, 152−156.

(21) Suzuki, M.; Ohuchi, Y.; Asanuma, H.; Kaneko, T.; Yokomori, S.; Ito, C.; Isobe, Y.; Muramatsu, M. Synthesis and evaluation of novel 2-oxo-1,2-dihydro-3-quinolinecarboxamide derivatives as potent and selective serotonin 5-$HT_4$ receptor agonists. *Chem. Pharm. Bull.* **2001**, *49*, 29−39.

(22) Hayashi, Y.; Umemiya, S. Pot economy in the synthesis of prostaglandin $A_1$ and $E_1$ methyl esters. *Angew. Chem., Int. Ed.* **2013**, *52*, 3450−3452.

(23) Ferris, G. E.; Hong, K.; Roundtree, I. A.; Morken, J. P. A catalytic enantioselective tandem allylation strategy for rapid terpene construction: application to the synthesis of pumilaside aglycon. *J. Am. Chem. Soc.* **2013**, *135*, 2501−2504.

(24) Coulthard, G.; Erb, W.; Aggarwal, V. K. Stereocontrolled organocatalytic synthesis of prostaglandin $PGF_{2\alpha}$ in seven steps. *Nature* **2012**, *489*, 278−281.

(25) Sasada, Y. Molecular and crystal structure. In *Chemistry Handbook*, 3rd ed.; The Chemical Society of Japan, Maruzen: Tokyo, 1984.

(26) Kagabu, S.; Matsuno, H. Chloronicotinyl insecticides. 8. Crystal and molecular structures of imidacloprid and analogous compounds. *J. Agric. Food Chem.* **1997**, *45*, 276−281.

(27) Talley, T. T.; Harel, M.; Hibbs, R. E.; Radic, Z.; Tomizawa, M.; Casida, J. E.; Taylor, P. Atomic interactions of neonicotinoids agonists with AChBP: molecular recognition of the distinctive electronegative pharmacophore. *Proc. Natl. Acad. Sci. U.S.A.* **2008**, *105*, 7606−7611.

(28) Xia, S.; Cheng, J.; Feng, Y.; Shao, X.; Luo, H.; Xu, Z.; Xu, X.; Li, Z. Computational investigations about the effects of hetero-molecular aggregation on bioactivities: a case of neonicotinoids and water. *Chin. J. Chem.* **2014**, *32*, 324−334.

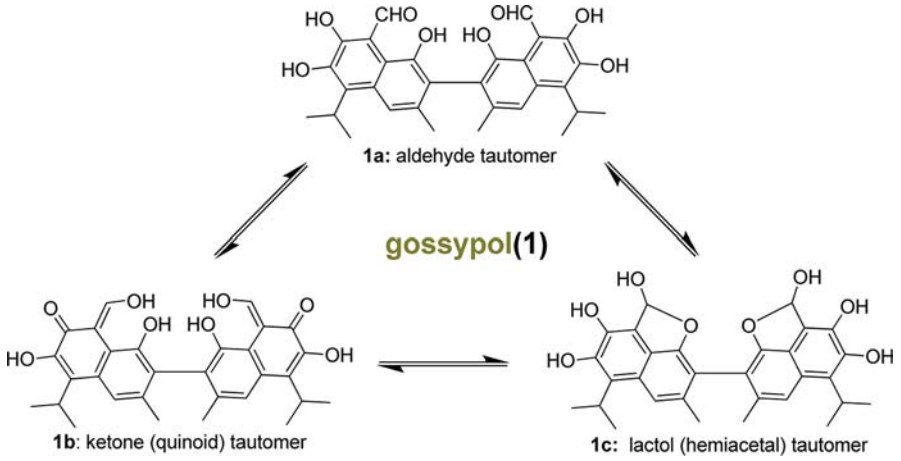


**Figure 1.** Structures of gossypol and its tautomeric forms.

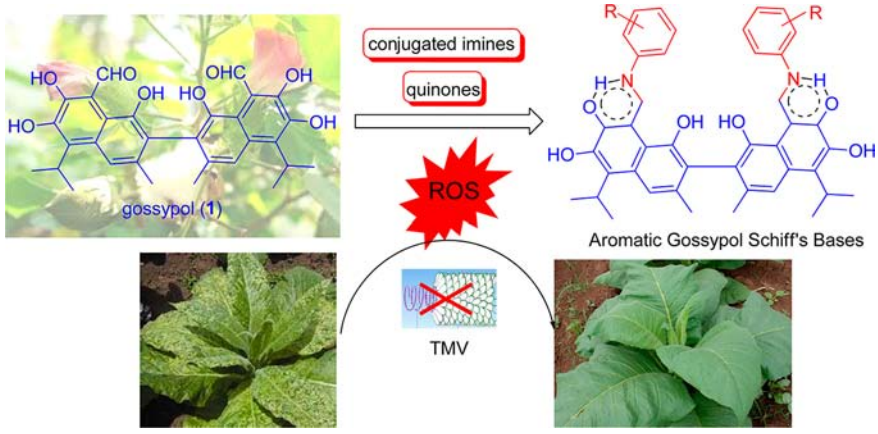


**Figure 2.** Design of compounds **3**–**25**.

gossypol and aromatic amines are expected to adjust gossypol to produce ROS and thus modulate the anti-TMV activity level. (Figure 2) In this contribution, a family of aromatic gossypol Schiff base derivatives has been synthesized and their anti-TMV activities have been determined using both in vitro and in vivo test methods. The structure–activity relationships of these derivatives were discussed as well. Field trial and toxicity evaluation were also conducted for the compound with high anti-TMV activity primarily to assess its potential as an antivirus candidate. Additionally, the synthesized derivatives were also investigated for their potential as fungicidal, insecticidal, or herbicidal reagents (see the Supporting Information).

## MATERIALS AND METHODS

**General.** Reagents were purchased from commercial sources and were used as received. All anhydrous solvents were dried and purified by standard techniques just before use. Reaction progress was monitored by thin-layer chromatography on silica gel GF-254 with detection by UV. Melting points were determined on an X-4 binocular microscope melting point apparatus and are uncorrected. $^{1}$H NMR and $^{13}$C NMR spectra were recorded on a Bruker Ascend 300/400 MHz spectrometer. Chemical shift values ($\delta$) are given in parts per million and downfield from internal tetramethylsilane. High-resolution mass spectra (HRMS) were recorded on FT-ICR MS (Ionspec, 7.0 T).

**General Procedure for the Synthesis of Aromatic Gossypol Schiff Bases 3–10, 12–14, 19, 21, 22, 24, and 25.** A solution of gossypol acetic acid (**2**, 0.50 g, 0.86 mmol) and aromatic amine (1.73 mmol) in ethanol (50 mL) was stirred and refluxed for 5 h, and then the reaction mixture was cooled to room temperature. The resulting solid was filtered, washed with ethanol, and recrystallized to give the desired gossypol derivatives.

**General Procedure for the Synthesis of Aromatic Gossypol Schiff Base Derivatives 11 and 23.** A mixture of aromatic amine (1.73 mmol), NaOH (2.59 mmol), and ethanol (50 mL) was stirred and refluxed for 1 h. Then gossypol acetic acid (**2**, 0.50 g, 0.86 mmol) was added, and the reaction liquid was refluxes for a further 5 h. The reaction mixture was cooled to room temperature, and then the resulting solid was filtered, washed with ethanol, and then recrystallized to give the desired gossypol derivatives.

**General Procedure for the Synthesis of Aromatic Gossypol Schiff Bases 15–18 and 20.** A solution of gossypol acetic acid (**2**, 0.50 g, 0.86 mmol) and aromatic amine (3.46 mmol) in ethanol (50 mL) was stirred and refluxed for 5 h and then the reaction mixture was cooled to room temperature. The resulting solid was filtered, washed with ethanol, and then recrystallized to give the desired gossypol derivatives.

*Data for* ***3****:* chocolate crystal recrystallized from benzene; yield, 95%; mp, 252–253 °C (lit.[17] 258–260 °C); $^{1}$H NMR (300 MHz, $CDCl_3$), $\delta$ 14.92 (d, $J$ = 12.3 Hz, 2H), 10.18 (d, $J$ = 12.3 Hz, 2H), 7.88 (s, 2H), 7.63 (s, 2H), 7.41–7.28 (m, 8H), 7.18 (t, $J$ = 7.1 Hz, 2H), 5.76 (s, 2H), 3.79–3.67 (m, 2H), 2.16 (s, 6H), 1.58–1.53 (m, 12H); $^{13}$C NMR (75 MHz, $CDCl_3$), $\delta$ 174.34, 154.14, 149.39, 147.00, 139.47, 132.76, 129.87, 129.78, 128.76, 125.88, 118.68, 118.21, 116.31, 114.46, 105.09, 27.57, 20.32, 20.29, 20.10; HRMS (ESI) calcd for $C_{42}H_{39}N_2O_6$ $(M - H)^-$ 667.2814, found 667.2812.

*Data for* ***4****:* orange crystal recrystallized from chloroform; yield, 95%; mp, 246–248 °C; $^{1}$H NMR (400 MHz, $CDCl_3$), $\delta$ 14.97 (d, $J$ = 12.4 Hz, 2H), 10.15 (d, $J$ = 12.4 Hz, 2H), 7.91 (s, 2H), 7.63 (s, 2H), 7.23–7.13 (m, 8H), 5.74 (s, 2H), 3.80–3.69 (m, 2H), 2.33 (s, 6H), 2.15 (s, 6H), 1.58–1.53 (m, 12H); $^{13}$C NMR (100 MHz, $CDCl_3$), $\delta$


dx.doi.org/10.1021/jf504411g | J. Agric. Food Chem. 2014, 62, 11080–11088

173.91, 154.21, 149.35, 147.03, 137.00, 135.95, 132.61, 130.42, 129.66, 128.49, 118.62, 118.14, 116.17, 114.49, 104.84, 27.55, 20.94, 20.35, 20.31, 20.13; HRMS (ESI) calcd for $C_{44}H_{43}N_2O_6$ $(M - H)^-$ 695.3127, found 695.3139.

*Data for* ***5:*** dark orange crystal recrystallized from tetrahydrofuran and ethanol; yield, 60%; mp, 272−274 °C (lit.[18] 287−289 °C); $^1$H NMR (400 MHz, $CDCl_3$), $\delta$ 15.08 (d, $J$ = 12.0 Hz, 2H), 10.09 (d, $J$ = 12.0 Hz, 2H), 7.90 (s, 2H), 7.63 (s, 2H), 7.24 (d, $J$ = 9.0 Hz, 4H), 6.89 (d, $J$ = 9.0 Hz, 4H), 5.75 (s, 2H), 3.79 (s, 6H), 3.77−3.70 (m, 2H), 2.15 (s, 6H), 1.57−1.54 (m, 12H); $^{13}$C NMR (100 MHz, $CDCl_3$), $\delta$ 173.44, 157.94, 154.43, 149.30, 147.03, 132.82, 132.48, 129.54, 128.31, 119.65, 118.56, 116.09, 115.09, 114.50, 104.74, 55.59, 27.54, 20.37, 20.33, 20.13; HRMS (ESI) calcd for $C_{44}H_{45}N_2O_8$ $(M + H)^+$ 729.3170, found 729.3163.

*Data for* ***6:*** orange crystal recrystallized from pyridine; yield, 79%; mp, 241−243 °C (lit.[19] 291 °C); $^1$H NMR (400 MHz, DMSO-$d_6$), $\delta$ 15.18 (d, $J$ = 11.8 Hz, 2H), 10.30 (d, $J$ = 11.8 Hz, 2H), 9.66 (s, 2H), 8.52 (s, 2H), 8.15 (s, 2H), 7.51 (s, 2H), 7.21 (d, $J$ = 8.8 Hz, 4H), 6.83 (d, $J$ = 8.8 Hz, 4H), 3.79−3.70 (m, 2H), 1.99 (s, 6H), 1.49−1.44 (m, 12H); $^{13}$C NMR (100 MHz, DMSO-$d_6$), $\delta$ 172.52, 155.74, 153.64, 149.98, 146.16, 132.00, 131.27, 127.99, 127.47, 120.75, 119.36, 116.90, 116.46, 115.49, 104.98, 26.56, 20.27, 20.24, 20.21; HRMS (ESI) calcd for $C_{42}H_{39}N_2O_8$ $(M - H)^-$ 699.2712, found 699.2712.

*Data for* ***7:*** yellow crystal recrystallized from pyridine and ethanol; yield, 78%; mp, 266 °C (dec) (lit.[20] 203−204 °C); $^1$H NMR (400 MHz, DMSO-$d_6$), $\delta$ 14.96 (d, $J$ = 11.6 Hz, 2H), 10.31 (d, $J$ = 11.6 Hz, 2H), 8.54 (s, 2H), 8.22 (s, 2H), 7.52 (s, 2H), 7.45−7.38 (m, 4H), 7.30 (t, $J$ = 8.5 Hz, 4H), 3.79−3.71 (m, 2H), 2.00 (s, 6H), 1.49−1.43 (m, 12H); $^{13}$C NMR (100 MHz, DMSO-$d_6$), $\delta$ 173.56, 160.93, 158.52, 153.87, 150.11, 146.10, 136.30, 132.46, 128.86, 127.77, 121.16, 119.83, 119.75, 117.10, 116.89, 116.66, 115.35, 105.61, 26.60, 20.22, 20.19; HRMS (ESI) calcd for $C_{42}H_{37}F_2N_2O_6$ (M -H)$^-$ 703.2625, found 703.2603.

*Data for* ***8:*** yellow crystal recrystallized from chloroform and ethanol; yield, 64%; mp, 286−287 °C (lit.[19] 302 °C); $^1$H NMR (400 MHz, $CDCl_3$), $\delta$ 14.95 (d, $J$ = 12.0 Hz, 2H), 10.09 (d, $J$ = 12.0 Hz, 2H), 7.82 (s, 2H), 7.63 (s, 2H), 7.33 (d, $J$ = 8.6 Hz, 4H), 7.23 (d, $J$ = 8.6 Hz, 4H), 5.75 (s, 2H), 3.80−3.64 (m, 2H), 2.15 (s, 6H), 1.56−1.53 (m, 12H); $^{13}$C NMR (100 MHz, $CDCl_3$), $\delta$ 174.65, 153.69, 149.37, 146.90, 138.13, 133.01, 131.13, 129.97, 129.91, 129.13, 119.29, 118.82, 116.29, 114.21, 105.30, 27.58, 20.28, 20.24, 20.10; HRMS (ESI) calcd for $C_{42}H_{37}Cl_2N_2O_6$ $(M - H)^-$ 735.2034, found 735.2034.

*Data for* ***9:*** orange-red crystal recrystallized from pyridine and ethanol; yield, 81%; mp, 284−286 °C (lit.[19] 305−306 °C); $^1$H NMR (400 MHz, $CDCl_3$), $\delta$ 14.84 (d, $J$ = 11.7 Hz, 2H), 10.12 (d, $J$ = 11.7 Hz, 2H), 8.24 (d, $J$ = 9.0 Hz, 4H), 7.69 (s, 2H), 7.64 (s, 2H), 7.36 (d, $J$ = 9.0 Hz, 4H), 5.82 (s, 2H), 3.75−3.66 (m, 2H), 2.17 (s, 6H), 1.58−1.52 (m, 12H); $^{13}$C NMR (100 MHz, $CDCl_3$), $\delta$ 176.46, 155.92, 151.73, 149.87, 149.67, 146.75, 137.66, 135.94, 134.01, 130.47, 125.94, 123.74, 117.51, 107.20, 106.02, 27.69, 20.19, 20.14, 20.12; HRMS (ESI) calcd for $C_{42}H_{38}N_4NaO_{10}$ $(M + Na)^+$ 781.2480, found 781.2486.

*Data for* ***10:*** gold crystal recrystallized from pyridine and ethanol; yield, 79%; mp, 261−263 °C; $^1$H NMR (400 MHz, $CDCl_3$), $\delta$ 14.89 (d, $J$ = 11.2 Hz, 2H), 10.15 (d, $J$ = 12.0 Hz, 2H), 7.77 (s, 2H), 7.65−7.55 (m, 6H), 7.37 (d, $J$ = 8.4 Hz, 4H), 5.75 (s, 2H), 3.78−3.68 (m, 2H), 2.16 (s, 6H), 1.58−1.55 (m, 12H); $^{13}$C NMR (100 MHz, $CDCl_3$), $\delta$ 175.51, 153.08, 149.89, 149.48, 146.85, 142.44, 140.87, 133.41, 130.20, 129.67, 127.21, 127.19, 127.15, 119.01, 117.90, 116.45, 105.87, 105.85, 27.62, 20.25, 20.19, 20.10; HRMS (ESI) calcd for $C_{44}H_{38}F_6N_2NaO_6$ $(M + Na)^+$ 827.2526, found 827.2520.

*Data for* ***11:*** purple solid; yield, 36%; mp, >300 °C; $^1$H NMR (400 MHz, DMSO-$d_6$), $\delta$ 14.94 (d, $J$ = 11.7 Hz, 2H), 10.41 (d, $J$ = 11.7 Hz, 2H), 8.58 (s, 2H), 8.34 (s, 2H), 7.64 (d, $J$ = 8.0 Hz, 4H), 7.52 (s, 2H), 7.29 (d, $J$ = 8.0 Hz, 4H), 3.80−3.70 (m, 2H), 2.00 (s, 6H), 1.52−1.43 (m, 12H); $^{13}$C NMR (100 MHz, DMSO-$d_6$), $\delta$ 174.71, 153.23, 146.68, 145.89, 139.81, 133.05, 129.55, 128.31, 127.85, 127.12, 121.85, 117.28, 115.75, 112.67, 106.31, 27.12, 20.72, 20.68; HRMS (ESI) calcd for $C_{42}H_{39}N_2O_{12}S_2$ $(M - 2Na + H)^-$ 827.1950, found 827.1928.

*Data for* ***12:*** yellow solid; yield, 72%; mp, 251−253 °C; $^1$H NMR (400 MHz, $CDCl_3$), $\delta$ 14.94 (d, $J$ = 12.0 Hz, 2H), 10.10 (d, $J$ = 12.0 Hz, 2H), 7.81 (s, 2H), 7.63 (s, 2H), 7.31 (d, $J$ = 8.6 Hz, 4H), 7.22 (d, $J$ = 8.6 Hz, 4H), 5.80 (s, 2H), 3.77−3.67 (m, 2H), 2.16 (s, 6H), 1.56−1.53 (m, 12H); $^{13}$C NMR (100 MHz, $CDCl_3$), $\delta$ 174.77, 153.99, 149.39, 146.89, 146.59, 138.27, 133.08, 129.97, 129.27, 122.66, 121.67, 119.30, 119.11, 118.84, 116.36, 114.22, 105.42, 27.59, 20.28, 20.24, 20.10; HRMS (ESI) calcd for $C_{44}H_{37}F_6N_2O_8$ $(M - H)^-$ 835.2460, found 835.2441.

*Data for* ***13:*** gold solid; yield, 91%; mp, 262−263 °C (lit.[19] 268−268 °C); $^1$H NMR (400 MHz, DMSO-$d_6$), $\delta$ 14.67 (d, $J$ = 12.7 Hz, 2H), 10.48 (s, 2H), 10.43 (d, $J$ = 12.7 Hz, 2H), 8.68 (s, 2H), 8.21 (s, 2H), 7.51 (s, 2H), 7.33 (d, $J$ = 8.1 Hz, 2H), 7.07−6.98 (m, 4H), 6.86 (t, $J$ = 7.3 Hz, 2H), 3.78−3.70 (m, 2H), 2.00 (s, 6H), 1.49−1.44 (m, 12H); $^{13}$C NMR (100 MHz, DMSO-$d_6$), $\delta$ 174.09, 150.90, 150.09, 147.37, 146.49, 132.15, 128.02, 127.73, 127.39, 125.84, 120.87, 119.94, 117.04, 115.99, 115.38, 114.71, 105.64, 26.56, 20.23, 20.21; HRMS (ESI) $m/z$ calcd for $C_{42}H_{39}N_2O_8$ $(M - H)^-$ 699.2712, found 699.2704.

*Data for* ***14:*** orange crystal recrystallized from pyridine; yield, 56%; mp, 259−262 °C (lit.[19] 287 °C); $^1$H NMR (400 MHz, DMSO-$d_6$), $\delta$ 14.86 (d, $J$ = 12.0 Hz, 2H), 10.34 (d, $J$ = 12.0 Hz, 2H), 9.82 (s, 2H), 8.57(s, 2H), 8.32 (s, 2H), 7.51 (s, 2H), 7.22 (t, $J$ = 8.1 Hz, 2H), 6.78−6.74 (m, 2H), 6.73 (t, $J$ = 1.9 Hz, 2H), 6.63 (dd, $J$ = 8.1, 1.9 Hz, 2H), 3.80−3.68 (m, 2H), 1.99 (s, 6H), 1.49−1.44 (m, 12H); $^{13}$C NMR (100 MHz, DMSO-$d_6$), $\delta$ 174.04, 158.87, 152.99, 150.23, 146.21, 140.50, 132.42, 130.91, 128.80, 127.75, 121.20, 117.08, 115.31, 112.80, 108.52, 105.50, 104.19, 26.61, 20.20, 20.18; HRMS (ESI) $m/z$ calcd for $C_{42}H_{39}N_2O_8$ $(M - H)^-$ 699.2712, found 699.2704.

*Data for* ***15:*** yellow solid; yield, 76%; mp, 252−254 °C; $^1$H NMR (400 MHz, $CDCl_3$), $\delta$ 14.75 (d, $J$ = 12.8 Hz, 2H), 10.20 (d, $J$ = 12.8 Hz, 2H), 7.97 (s, 2H), 7.63 (s, 2H), 7.37 (d, $J$ = 7.5 Hz, 2H), 7.14 (t, $J$ = 7.3 Hz, 2H), 6.98 (d, $J$ = 7.8 Hz, 2H), 6.93 (t, $J$ = 7.7 Hz, 2H), 5.76 (s, 2H), 4.03 (s, 6H), 3.78−3.69 (m, 2H), 2.15 (s, 6H), 1.58−1.52 (m, 12H); $^{13}$C NMR (100 MHz, $CDCl_3$), $\delta$ 174.31, 152.40, 149.78, 149.39, 147.18, 132.64, 129.78, 128.83, 128.29, 126.13, 121.27, 118.61, 116.20, 115.50, 114.52, 111.49, 105.41, 56.19, 27.53, 20.33, 20.28, 20.12; HRMS (ESI) calcd for $C_{44}H_{43}N_2O_8$ $(M - H)^-$ 727.3025, found 727.3002.

*Data for* ***16:*** yellow solid; yield, 83%; mp, 266−268 °C; $^1$H NMR (400 MHz, $CDCl_3$), $\delta$ 14.82 (d, $J$ = 12.2 Hz, 2H), 10.14 (d, $J$ = 12.2 Hz, 2H), 7.87 (s, 2H), 7.63 (s, 2H), 7.26−7.23 (t, $J$ = 8.0 Hz, 2H), 6.89 (dd, $J$ = 8.0, 1.4 Hz, 2H), 6.81 (s, 2H), 6.71 (dd, $J$ = 8.0, 1.4 Hz, 2H), 5.83 (s, 2H), 3.79 (s, 6H), 3.76−3.67 (m, 2H), 2.15 (s, 6H), 1.57−1.52 (m, 12H); $^{13}$C NMR (100 MHz, $CDCl_3$), $\delta$ 174.33, 160.83, 154.04, 149.42, 146.94, 140.61, 132.82, 130.69, 129.73, 128.86, 118.66, 116.38, 114.40, 111.27, 110.48, 105.07, 104.17, 55.45, 27.56, 20.29, 20.13; HRMS (ESI) calcd for $C_{44}H_{43}N_2O_8$ $(M - H)^-$ 727.3025, found 727.3009.

*Data for* ***17:*** orange solid; yield, 97%; mp, 255−257 °C; $^1$H NMR (400 MHz, $CDCl_3$), $\delta$ 14.89 (d, $J$ = 12.8 Hz, 2H), 10.13 (d, $J$ = 12.8 Hz, 2H), 7.99 (s, 2H), 7.63 (s, 2H), 7.27 (d, $J$ = 8.8 Hz, 2H), 6.54 (d, $J$ = 2.4 Hz, 2H), 6.44 (dd, $J$ = 8.8, 2.4 Hz, 2H), 5.76 (s, 2H), 3.99 (s, 6H), 3.79 (s, 6H), 3.77−3.69 (m, 2H), 2.15 (s, 6H), 1.57−1.52 (m, 12H); $^{13}$C NMR (100 MHz, $CDCl_3$), $\delta$ 173.35, 158.65, 152.58, 151.01, 149.33, 147.22, 132.35, 129.51, 127.85, 122.56, 118.46, 116.56, 116.06, 114.60, 105.06, 104.97, 99.27, 56.22, 55.63, 27.51, 20.38, 20.33, 20.14; HRMS (ESI) calcd for $C_{46}H_{47}N_2O_{10}$ $(M - H)^-$ 787.3236, found 787.3236.

*Data for* ***18:*** gold solid; yield, 89%; mp, 234−235 °C; $^1$H NMR (400 MHz, DMSO-$d_6$), $\delta$ 14.62 (d, $J$ = 11.6 Hz, 2H), 10.39 (d, $J$ = 11.6 Hz, 2H), 8.72 (s, 2H), 8.35 (s, 2H), 7.52 (s, 2H), 7.12 (d, $J$ = 6.8 Hz, 2H), 6.92 (s, 2H), 6.77 (d, $J$ = 6.8 Hz, 2H), 3.90 (s, 6H), 3.69 (br s, 8H), 1.98 (s, 6H), 1.46 (br s, 12H); $^{13}$C NMR (100 MHz, DMSO-$d_6$), $\delta$ 174.76, 154.00, 150.79, 150.35, 146.52, 143.23, 132.48, 129.00, 128.66, 128.00, 120.80, 117.14, 115.03, 113.19, 109.66, 106.21, 101.40, 56.49, 55.59, 26.61, 20.18; HRMS (ESI) calcd for $C_{46}H_{47}N_2O_{10}$ $(M - H)^-$ 787.3236, found 787.3219.

*Data for* ***19:*** chocolate solid; yield, 43%; mp, 251−253 °C; $^1$H NMR (400 MHz, $CDCl_3$), $\delta$ 15.21 (d, $J$ = 11.0 Hz, 2H), 10.10 (d, $J$ = 11.0 Hz, 2H), 7.74 (s, 2H), 7.68 (d, $J$ = 7.7 Hz, 2H), 7.62 (s, 2H), 7.53 (t, $J$ = 7.7 Hz, 2H), 7.46 (d, $J$ = 7.7 Hz, 2H), 7.26 (t, $J$ = 7.7 Hz, 2H),

**Scheme 1. General Synthetic Route for Target Compounds 3−25**

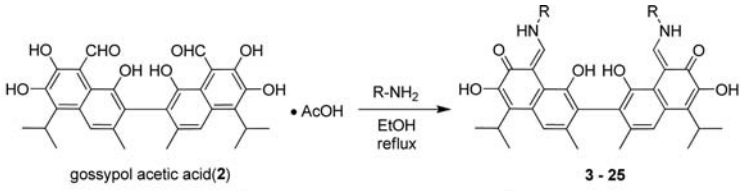


| Compd. | R | Compd. | R | Compd. | R |
|---|---|---|---|---|---|
| 3 | | 11 | 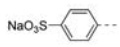 | 19 | |
| 4 | | 12 | 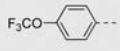 | 20 | |
| 5 | 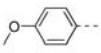 | 13 | | 21 | |
| 6 | 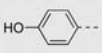 | 14 | | 22 | |
| 7 | 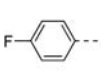 | 15 | | 23 | 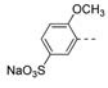 |
| 8 | 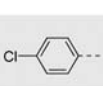 | 16 | | 24 | 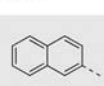 |
| 9 | 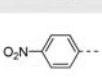 | 17 | | 25 | |
| 10 | 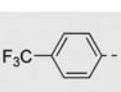 | 18 | 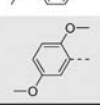 | | |

5.77 (s, 2H), 3.76−3.66 (m, 2H), 2.15 (s, 6H), 1.57−1.51 (m, 12H); $^{13}$C NMR (100 MHz, $CDCl_3$), $\delta$ 174.94, 154.82, 149.50, 146.83, 138.56, 133.50, 133.34, 130.21, 129.54, 127.10, 127.05, 126.99, 126.94, 125.26, 125.00, 122.28, 121.15, 120.85, 119.03, 118.92, 116.41, 114.15, 106.43, 27.59, 20.23, 20.19, 20.12; HRMS (ESI) calcd for $C_{44}H_{37}F_6N_2O_6$ $(M - H)^-$ 803.2561, found 803.2533.

*Data for **20**:* yellow solid; yield, 81%; mp, 262−264 °C (lit.[21] 216−217.5 °C); $^1$H NMR (400 MHz, $CDCl_3$), $\delta$ 15.02 (d, $J$ = 11.7 Hz, 2H), 10.14 (d, $J$ = 11.7 Hz, 2H), 7.79 (s, 2H), 7.65 (s, 2H), 7.54−7.41 (m, 8H), 5.79 (s, 2H), 3.77−3.69 (m, 2H), 2.16 (s, 6H), 1.58−1.53 (m, 12H); $^{13}$C NMR (100 MHz, $CDCl_3$), $\delta$ 175.19, 153.49, 149.49, 146.87, 140.23, 133.31, 133.11, 132.66, 132.32, 131.98, 130.54, 130.12, 129.55, 124.89, 122.18, 122.14, 122.10, 121.16, 118.97, 116.44, 114.91, 114.87, 114.11, 105.69, 27.63, 20.27, 20.24, 20.12; HRMS (ESI) calcd for $C_{44}H_{37}F_6N_2O_6$ $(M - H)^-$ 803.2561, found 903.2543.

*Data for **21**:* yellow crystal recrystallized from petroleum ether and ethyl acetate; yield, 49%; mp, 221−223 °C; $^1$H NMR (400 MHz, $CDCl_3$), $\delta$ 15.12 (d, $J$ = 11.6 Hz, 2H), 10.10 (d, $J$ = 11.6 Hz, 2H), 7.72−7.62 (m, 10H), 5.85 (s, 2H), 3.89−3.58 (m, 2H), 2.17 (s, 6H), 1.57−1.51 (m, 12H); $^{13}$C NMR (100 MHz, $CDCl_3$), $\delta$ 175.87, 152.50, 149.68, 146.72, 141.32, 133.99, 133.93, 133.66, 133.32, 130.49, 130.45, 124.15, 121.44, 119.22, 118.41, 117.71, 116.73, 113.77, 106.48, 27.71, 20.20, 20.17; HRMS (ESI) calcd for $C_{46}H_{35}F_{12}N_2O_6$ $(M - H)^-$ 939.2309, found 939.2283.

*Data for **22**:* orange-red crystal recrystallized from pyridine and ethanol; yield, 62%; mp, 269−270 °C (lit.[19] 280−282 °C); $^1$H NMR (400 MHz, $CDCl_3$), $\delta$ 15.03 (d, $J$ = 11.6 Hz, 2H), 10.16 (d, $J$ = 11.6 Hz, 2H), 8.15 (s, 2H), 8.00 (d, $J$ = 7.5 Hz, 2H), 7.73 (s, 2H), 7.66 (s, 2H), 7.62−7.50 (m, 4H), 5.79 (s, 2H), 3.76−3.70 (m, 2H), 2.17 (s, 6H), 1.56 (br s, 12H); $^{13}$C NMR (100 MHz, $CDCl_3$), $\delta$ 175.68, 152.92, 149.84, 149.57, 149.37, 146.75, 141.03, 133.63, 130.80, 130.32, 130.10, 124.12, 119.80, 119.13, 116.55, 112.09, 106.15, 27.65, 20.22, 20.20, 20.14.

*Data for **23**:* yellow solid; yield, 65%; mp, >300 °C; $^1$H NMR (400 MHz, DMSO-$d_6$), $\delta$ 14.93 (d, $J$ = 12.2 Hz, 2H), 10.42 (d, $J$ = 12.2 Hz, 2H), 8.66 (s, 2H), 8.62 (s, 2H), 7.69 (s, 2H), 7.48 (s, 2H), 7.43 (d, $J$ = 8.5 Hz, 2H), 7.14 (d, $J$ = 8.5 Hz, 2H), 3.97 (s, 6H), 3.80−3.68 (m, 2H), 1.97 (s, 6H), 1.51−1.41 (m, 12H); $^{13}$C NMR (100 MHz, DMSO-$d_6$), $\delta$ 174.48, 150.97, 150.68, 149.01, 146.23, 141.88, 132.34, 128.66, 127.72, 127.38, 123.09, 121.61, 116.97, 115.30, 112.34, 111.12, 106.29, 56.38, 26.61, 20.32, 20.22, 20.19; HRMS (ESI) calcd for $C_{44}H_{43}N_2O_{14}S_2$ $(M - 2Na + H)^-$ 887.2161, found 887.2121.

*Data for **24**:* orange-red crystal recrystallized from pyridine and ethanol; yield, 82%; mp, 281 °C (lit.[19] 302−303 °C); $^1$H NMR (400 MHz, $CDCl_3$), $\delta$ 15.17 (d, $J$ = 12.2 Hz, 2H), 10.32 (d, $J$ = 12.2 Hz, 2H), 7.92 (s, 2H), 7.84 (d, $J$ = 8.8 Hz, 2H), 7.78 (d, $J$ = 7.4 Hz, 4H), 7.69 (s, 2H), 7.67 (s, 2H), 7.51−7.38 (m, 6H), 5.85 (s, 2H), 3.82−3.70 (m, 2H), 2.19 (s, 6H), 1.59−1.55 (m, 12H); $^{13}$C NMR (100 MHz, $CDCl_3$), $\delta$ 174.36, 153.88, 149.81, 149.44, 147.01, 136.86, 133.82, 132.88, 131.46, 130.09, 129.82, 128.80, 127.85, 127.50, 127.25, 125.79, 118.74, 117.41, 116.31, 115.22, 105.33, 27.57, 20.33, 20.28, 20.14.

*Data for **25**:* orange-red solid; yield, 86%; mp, 280−281 °C (lit.[19] 283−285.5 °C); $^1$H NMR (400 MHz, $CDCl_3$), $\delta$ 15.88 (d, $J$ = 11.6 Hz, 2H), 10.36 (d, $J$ = 11.6 Hz, 2H), 8.36 (d, $J$ = 8.4 Hz, 2H), 7.99 (s, 2H), 7.91 (d, $J$ = 8.4 Hz, 2H), 7.75−7.70 (m, 4H), 7.68 (s, 2H), 7.60 (t, $J$ = 7.5 Hz, 2H), 7.52 (d, $J$ = 7.4 Hz, 2H), 7.44 (t, $J$ = 7.8 Hz, 2H), 5.86 (s, 2H), 3.85−3.73 (m, 2H), 2.20 (s, 6H), 1.60 (t, $J$ = 6.1 Hz, 12H); $^{13}$C NMR (100 MHz, $CDCl_3$), $\delta$ 174.30, 155.54, 149.84, 149.54, 147.03, 136.11, 135.94, 134.22, 132.86, 129.76, 128.93, 128.55, 127.34, 126.89, 126.38, 125.74, 125.59, 123.72, 121.22, 118.69, 116.31, 114.44, 113.69, 105.89, 27.59, 20.34, 20.29, 20.15.


dx.doi.org/10.1021/jf504411g | J. Agric. Food Chem. 2014, 62, 11080−11088

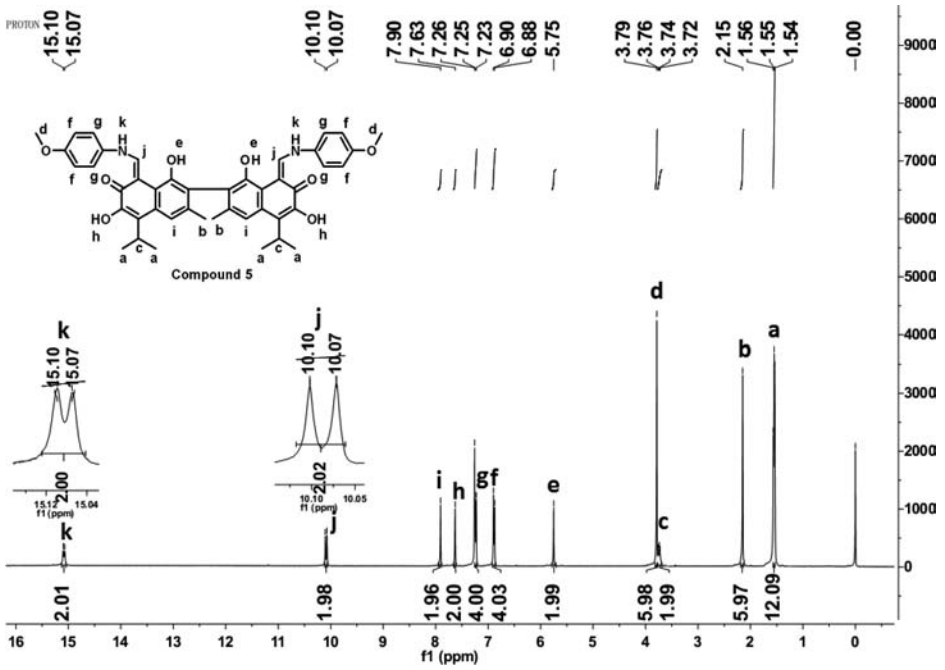


**Figure 3.** $^1$H NMR spectra of compound **5**.

**Biological Assay.** The anti-TMV activity of all compounds was tested using our previously reported methods.[22]

The field trials were carried out in the trial area of the Institute of Agricultural Environment and Resource, Yunnan Academy of Agricultural Sciences, Kunming City, China, between June and July 2014. The formulation of compound **19** (1% emulsifiable concentrates (EC)) was prepared in our research group. It was diluted to 750 L/ha before use.

The rat oral gavage acute toxicity of pesticides was performed in Xu He (Tianjin) Pharmaceutical Technology Co., Ltd. in May 2014. Sixteen rats, half males and half females, were divided randomly into four groups. The samples were respectively configured to 5 and 50 mg/mL.

## RESULTS AND DISCUSSION

**Chemistry.** Gossypol (**1**) was obtained using our previously reported method.[23] Gossypol acetic acid (**2**) was purchased from commercial sources. A series of Schiff bases of gossypol (**3**−**25**) were prepared by treating **2** with the corresponding amines in ethanol (Scheme 1). The Schiff bases had poor solubility in ethanol, so they were simply collected by filtration. Recrystallization of the products from suitable solvents could give purer samples. Unfortunately, recrystallization was not fit for compounds **15**−**18** and **20**. However, they were obtained via the employment of excess amine when the preparation was repeated. For compounds **11** and **23**, the sulfonic sodium salts of corresponding amines were prepared from homologous aminobenzenesulfonic acid and NaOH, for which were used 3 equiv of gossypol to ensure them a sodium sulfonate group. It is worth mentioning that if there are multiple electron withdrawing groups on the ortho and para positions of aromatic amine, such as 2,4-dinitroaniline and 2-nitro-4-(trifluoromethyl)aniline, the corresponding Schiff base of gossypol could not be achieved but the dehydration product of gossypol, anhydrogossypol,[24] was obtained. All of our synthetic gossypol Schiff bases exist in the enamine−enamine form[15,25] in solution as determined by $^1$H NMR. For compound **5**, for example, the structure can be interpreted by the $^1$H NMR spectrum (Figure 3). The signal peaks of symmetrical protons should appear at the same position and have identical coupling constants because of the axial symmetry of the structure. The presence of doublet peaks with the coupling constant of 12.0 Hz in the $^1$H NMR spectrum can be attributed to the signals of **H**—C═C proton (j) and **H**—NAr proton (k). This behavior can be rationally explained by the fact that two protons are adjacent and coupled with each other.

**Antiviral Biological Assay.** Compounds **1**−**25** were initially tested for their phytotoxic activities against the test plant, *Nicotiana tabacum* L. The results indicated that these natural product-based compounds showed no phytotoxic activity at 500 $\mu$g/mL. In other words, the compounds caused no harm to the test plant; therefore, there would be no interference with the determination of anti-TMV data.

The antiviral bioassay of the compounds against TMV was carried out, and the antiviral results are listed in Tables 1 and 2. To make a judgment on the antiviral potency of the synthesized compounds, the commercially available plant virucide ribavirin[24] was used as the control.

The in vitro anti-TMV activities of compounds **1**−**25** and the contrast compound ribavirin are shown in Table 1. The results indicate that these target compounds exhibit moderate to excellent activities against TMV. Among these compounds, gossypol (**1**) and gossypol acetic acid (**2**) displayed similar in vitro anti-TMV activities (**1**, 32%; **2**, 28%); however, they were less effective than ribavirin (38%) at 500 $\mu$g/mL. In contrast, except for **6**, **22**, and **24**, other aromatic gossypol Schiff bases of **3**−**25** showed equivalent or even higher antiviral activities than ribavirin (38%); especially compounds **5**, **9**, **10**, **12**, **15**, **17**, **19**, and **23** displayed obviously higher anti-TMV activities at a concentration of 500 $\mu$g/mL, and the antiviral activities of compounds **9** and **19** at 100 $\mu$g/mL even reach the level of ribavirin at 500 $\mu$g/mL.

On comparison with the parent dianilinogossypol (**3**), except for *p*-hydroxy compound **6**, the activities of Schiff bases **4**−**12** with different substituent groups on the para position of aniline are higher. However, they displayed distinctly different activity levels against TMV in vitro. Compounds with methoxy (**5**),

**Table 1. In Vitro Antiviral Activity of Compounds 1−25 and Ribavirin against TMV**

| compd | concn (μg/mL) | in vitro curative effect (%) | compd | concn (μg/mL) | in vitro curative effect (%) |
|---|---|---|---|---|---|
| **1** | 500 | 32 | **14** | 500 | 30 |
| | 100 | 0 | | 100 | 0 |
| **2** | 500 | 28 | **15** | 500 | 58 |
| | 100 | 0 | | 100 | 14 |
| **3** | 500 | 32 | **16** | 500 | 40 |
| | 100 | 0 | | 100 | 0 |
| **4** | 500 | 40 | **17** | 500 | 53 |
| | 100 | 0 | | 100 | 22 |
| **5** | 500 | 47 | **18** | 500 | 30 |
| | 100 | 10 | | 100 | 0 |
| **6** | 500 | 24 | **19** | 500 | 62 |
| | 100 | 0 | | 100 | 32 |
| **7** | 500 | 37 | **20** | 500 | 39 |
| | 100 | 6 | | 100 | 0 |
| **8** | 500 | 44 | **21** | 500 | 32 |
| | 100 | 0 | | 100 | 0 |
| **9** | 500 | 50 | **22** | 500 | 26 |
| | 100 | 39 | | 100 | 0 |
| **10** | 500 | 57 | **23** | 500 | 47 |
| | 100 | 20 | | 100 | 18 |
| **11** | 500 | 40 | **24** | 500 | 25 |
| | 100 | 0 | | 100 | 0 |
| **12** | 500 | 52 | **25** | 500 | 44 |
| | 100 | 20 | | 100 | 16 |
| **13** | 500 | 33 | ribavirin | 500 | 38 |
| | 100 | 0 | | 100 | 14 |

**Table 2. In Vivo Anti-TMV Activity of Compounds 1−25 and Ribavirin**

| | | in vivo activity | | |
|---|---|---|---|---|
| compd | concn (μg/mL) | inactivation effect (%) | curative effect (%) | protection effect (%) |
| **1** | 500 | 35 | 29 | 29 |
| | 100 | 8 | 0 | 0 |
| **2** | 500 | 32 | 30 | 33 |
| | 100 | 0 | 0 | 0 |
| **3** | 500 | 52 | 34 | 44 |
| | 100 | 27 | 0 | 27 |
| **4** | 500 | 8 | 37 | 50 |
| | 100 | 0 | 0 | 17 |
| **5** | 500 | 46 | 42 | 44 |
| | 100 | 19 | 20 | 21 |
| **6** | 500 | 20 | 17 | 23 |
| | 100 | 0 | 0 | 0 |
| **7** | 500 | 33 | 36 | 35 |
| | 100 | 11 | 0 | 9 |
| **8** | 500 | 36 | 41 | 43 |
| | 100 | 9 | 19 | 20 |
| **9** | 500 | 36 | 47 | 42 |
| | 100 | 12 | 40 | 22 |
| **10** | 500 | 35 | 51 | 42 |
| | 100 | 25 | 22 | 19 |
| **11** | 500 | 38 | 35 | 36 |
| | 100 | 0 | 0 | 9 |
| **12** | 500 | 54 | 50 | 56 |
| | 100 | 26 | 21 | 23 |
| **13** | 500 | 35 | 36 | 34 |
| | 100 | 10 | 0 | 9 |
| **14** | 500 | 40 | 34 | 38 |
| | 100 | 10 | 8 | 15 |
| **15** | 500 | 51 | 55 | 56 |
| | 100 | 16 | 20 | 27 |
| **16** | 500 | 46 | 43 | 48 |
| | 100 | 18 | 9 | 23 |
| **17** | 500 | 56 | 48 | 50 |
| | 100 | 28 | 19 | 23 |
| **18** | 500 | 36 | 33 | 36 |
| | 100 | 8 | 0 | 0 |
| **19** | 500 | 60 | 57 | 62 |
| | 100 | 23 | 30 | 26 |
| **20** | 500 | 52 | 35 | 48 |
| | 100 | 17 | 13 | 22 |
| **21** | 500 | 41 | 35 | 37 |
| | 100 | 12 | 0 | 9 |
| **22** | 500 | 26 | 23 | 34 |
| | 100 | 0 | 0 | 0 |
| **23** | 500 | 46 | 43 | 38 |
| | 100 | 17 | 13 | 15 |
| **24** | 500 | 37 | 28 | 30 |
| | 100 | 8 | 0 | 0 |
| **25** | 500 | 39 | 37 | 43 |
| | 100 | 10 | 19 | 16 |
| ribavirin | 500 | 38 | 37 | 40 |
| | 100 | 12 | 17 | 18 |

nitro (**9**), trifluoromethyl (**10**), and trifluoromethoxy (**12**) showed excellent activities (48, 50, 57, and 52%, respectively). To investigate the influence of the position and the number of substituents on the activities, **13**−**23** were synthesized. Compared with their para-substitutional substrates, corresponding substituent groups on the ortho position were beneficial to the increase of their anti-TMV activities, whereas the substituent groups on meta positions were unfavorable to the anti-TMV activities (MeO, **15** > **5** > **16**; $CF_3$, **19** > **10** >**20**; $NO_2$, **9** > **22**). However, the substituent group of the hydroxyl was an exception, as the *o*-hydroxyl compound **13** and *m*-hydroxyl compound **14** had higher activities than *p*-hydroxyl compound **6**. Furthermore, the level of the anti-TMV activities could not be improved by increasing the number of substituent groups. Among methoxy-substituted compounds **5** and **15**−**18**, **15** with only one substituent group on the ortho position displayed the best inhibitory effect. However, **23** (18%) with *o*-methoxy and *m*-sodium sulfonate substituent groups exhibited better inhibitory effect than **11** (0%) and **15** (14%) at 100 μg/mL. The Schiff bases of naphthylamines were synthesized as well, and their anti-TMV activities were performed. Compound **25** (44% at 500 μg/mL), obtained by the condensation of gossypol and 1-naphthylamine, displayed a better inhibitory


dx.doi.org/10.1021/jf504411g | J. Agric. Food Chem. 2014, 62, 11080−11088

effect than dianilinogossypol (**3**, 32% at 500 μg/mL). At variance with **25**, the activity of 2-naphthylamine Schiff base **24** (25% at 500 μg/mL) was relatively lower than that of **3**.

Due to their well-performed behaviors of in vitro antiviral activities against TMV, the in vivo antiviral activities of these compounds deserve to be exploited further. As shown in Table 2, the majority of the compounds also displayed equivalent or higher in vivo activities than the control ribavirin at a concentration of 500 μg/mL. In particular, Schiff bases **12**, **15**, **17**, and **19** exhibited obviously higher anti-TMV activities than ribavirin at 500 μg/mL, of which compound **19** with an *o*-trifluoromethyl group showed the best activity (inactivation activity, 60%/500 μg/mL and 23%/100 μg/mL; curative activity, 57%/500 μg/mL and 30%/100 μg/mL; and protection activity, 62%/500 μg/mL and 26%/100 μg/mL), confirmed by the in vivo inactivation tests, curative tests, and protection tests. Additionally, the in vivo curative activities of these compounds displayed structure−activity relationships similar to the activities in vitro. More importantly, compound **9** with a *p*-nitro group showed a better effect at 100 μg/mL (40%), which is even higher than that of ribavirin at 500 μg/mL (37%).

Interestingly, the in vivo inactivation and protection activities of dianilinogossypol (**3**) displayed excellent inhibitory effects (inactivation activity, 52%/500 μg/mL and 27%/100 μg/mL; protection activity, 44%/ 500 μg/mL and 27%/100 μg/mL). However, only **12**, **15**, **17**, **19**, and **20** exhibited obviously better in vivo curative and protection activities at 500 μg/mL than parent dianilinogossypol (**3**). These results indicated the introduction of trifluoromethoxy, methoxy, and trifluoromethyl on the aromatic ring of aniline could increase the anti-TMV activities level of parent dianilinogossypol. Further analysis of the relationship between the positions of substituents and anti-TMV activities indicated that the order of methoxy and trifluoromethyl is ortho > meta > para position (**15** > **16** > **5**, **19** > **20** > **10**). Other groups and the number of them displayed similar SAR to anti-TMV activities in vitro. The derivatives of naphthylamines (**24** and **25**) had lower inhibitory effect than dianilinogossypol (**3**), but 1-naphthylamine (**25**) is relatively higher than that of 2-naphthylamine (**24**).

**Evaluation of Anti-TMV Activity of 19 in the Field.** Compound **19**, which had exhibited the best anti-TMV activity both in vitro and in vivo in the laboratory, was employed to evaluate the antiviral activity in the field. A 1% EC solution of **19** was prepared and evaluated for the control of TMV in Tengchong county of Yunnan province (southern China). The results of the field trials are shown in Table 3, which indicated that **19** at the amount of 10 g ai/ha had the same control effect (about 66%) as 5% amino glycan at 100 g ai/ha and 20% moroxydine hydrochloride−cupric acetate at 600 g ai/ha at 10 days after spraying. Therefore, it was suggested that **19** could be considered as an alternative to the employed plant virus inhibitor for further development on the basis of the field trials.

**Table 3. Anti-TMV Effect in the Field in 2014**

| compd | amount (g ai/ha) | controlled effect (%) |
|---|---|---|
| **19** | 10 | 66.61 |
| | 50 | 83.88 |
| | 100 | 94.56 |
| 5% amino glycan | 100 | 65.70 |
| 20% moroxydine hydrochloride−cupric acetate | 600 | 66.57 |

**Rat Oral Gavage Acute Toxicity of Gossypol and 19.** To balance the toxicity versus efficacy of compound **19**, we next explored the tolerated dose of **19** and gossypol using a group of rats. They were treated with a single dose of 500 or 50 mg/kg and observed for a period of 14 days, monitoring morbidity (body weight loss) and mortality. All rats were alive after 14 days. The weight of the rats that were treated with gossypol at 500 mg/kg slightly declined over the first 6 days. There is no obvious weight difference between any other two groups (Figure 4). Therefore, gossypol and **19** display low toxicity to rats, but the toxicity of **19** is lower.

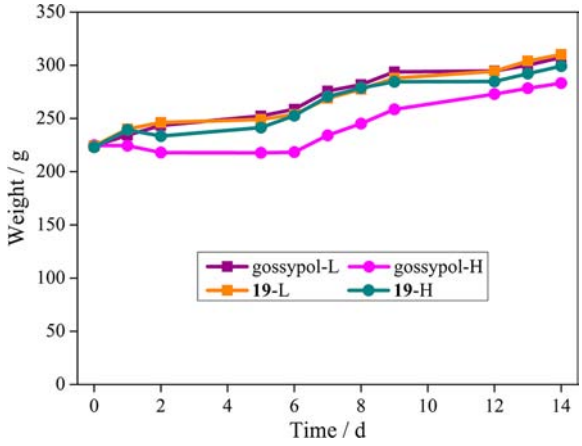


**Figure 4.** Average weight of rats. Gossypol-L, dosage of gossypol is 50 mg/kg; gossypol-H, dosage of gossypol is 500 mg/kg; **19**-L, dosage of **19** is 50 mg/kg; **19**-H, dosage of **19** is 500 mg/kg.

In summary, to eliminate the toxicity caused by the aldehyde group, retain the electron transfer functionalities to generate ROS, and adjust the anti-TMV activity level of gossypol, a series of aromatic gossypol Schiff bases **3**−**25** were prepared and investigated for their anti-TMV activity for the first time. The bioassay results indicated that most of these Schiff bases showed moderate to excellent activities against TMV and were more effective than gossypol (**1**) and gossypol acetic acid (**2**). The introduction of methoxy, trifluoromethyl, or trifluoromethoxy groups, positioned ortho to amine of enamine, could significantly increase the anti-TMV activity levels. Among all of the compounds, compound **19** with an *o*-trifluoromethyl group showed the best anti-TMV activities both in vitro and in vivo in the laboratory. Furthermore, the compound at 10 g ai/ha in the field trial had the same control effect as 5% amino glycan at 100 g ai/ha and 20% moroxydine hydrochloride−cupric acetate at 600 g ai/ha. More importantly, it showed lower toxicity to rats than gossypol. Because of the easy preparation, good anti-TMV activity, and low toxicity, the *o*-trifluoromethylaniline Schiff base (**19**) is expected to be developed as a promising candidate as an inhibitor of plant virus. Further studies on structural optimization and mechanism of action are currently underway in our laboratory.

## ■ ASSOCIATED CONTENT

### Ⓢ Supporting Information

Fungicidal, insecticidal, and herbicidal activities. This material is available free of charge via the Internet at http://pubs.acs.org.

## AUTHOR INFORMATION


### Corresponding Author

*(Q.W.) Phone: +86-(0)22-23503952. Fax: +86-(0)22-23503952. E-mail: wang98h@263.net or wangqm@nankai.edu.cn.



### Funding

We are grateful to the National Natural Science Foundation of China (21132003, 21121002, 21372131), the Specialized Research Fund for the Doctoral Program of Higher Education (20120031110010), and the Science Technology Plan Project of China Tobacco Yunnan Co. (2012YN08) for generous financial support for our programs.


### Notes

The authors declare no competing financial interest.

## REFERENCES


(1) (a) Vermel, E. M.; Kruglyak, S. A. Anticancer activity of some alkaloids. *Vopr. Onkol.* **1962**, *8*, 9−17. (b) Wang, G.; Nikolovska-Coleska, Z.; Yang, C. Y.; Wang, R.; Tang, G.; Guo, J.; Shangary, S.; Qiu, S.; Gao, W.; Yang, D.; Meagher, J.; Stuckey, J.; Krajewski, K.; Jiang, S.; Roller, P. P.; Abaan, H. O.; Tomita, Y.; Wang, S. Structure-based design of potent small-molecule inhibitors of anti-apoptotic Bcl-2 proteins. *J. Med. Chem.* **2006**, *49*, 6139−6142. (c) Meng, Y.; Tang, W.; Dai, Y.; Wu, X.; Liu, M.; Ji, Q.; Ji, M.; Pienta, K.; Lawrence, T.; Xu, L. Natural BH3 mimetic (−)-gossypol chemosensitizes human prostate cancer via Bcl-xL inhibition accompanied by increase of Puma and Noxa. *Mol. Cancer Ther.* **2008**, *7*, 2192−2202. (d) Wang, X.; Howell, C. P.; Chen, F.; Yin, J.; Jiang, Y. Gossypol − a polyphenolic compound from cotton plant. *Adv. Food Nutr. Res.* **2009**, *58*, 215−263.

(2) Campbell, K. N.; Morris, R. C.; Adams, R. The structure of gossypol. *J. Am. Chem. Soc.* **1937**, *59*, 1723−1728.

(3) (a) Abraham, K. J.; Pierce, M. L.; Essenberg, M. The phytoalexins desoxyhemigossypol and hemigossypol are elicited by *Xanthomonas* in *Gossypium* cotyledons. *Phytochemistry* **1999**, *52*, 829−836. (b) Liu, J.; Benedict, C. R.; Stipanovic, R. D.; Bell, A. A. Purification and characterization of *S*-adenosyl-L-methionine: desoxyhemigossypol-6-*O*-methyltransferase from cotton plants. *Plant Physiol.* **1999**, *121*, 1017−1024. (c) Puckhaber, L. S.; Dowd, M. K.; Stipanovic, R. D.; Howell, C. R. Toxicity of (+) and (−)-gossypol to the plant pathogen *Rhizoctonia solani*. *J. Agric. Food Chem.* **2002**, *50*, 7017−7021.

(4) Stipanovic, R. D.; Altman, D. W.; Begin, D. L.; Greenblatt, G. A.; Benedict, J. H. Terpenoid aldehydes in upland cottons: analysis by aniline and HPLC methods. *J. Agric. Food Chem.* **1988**, *36*, 509−515.

(5) (a) Yang, J.; Chen, G.; Li, L. L.; Pan, W.; Zhang, F.; Yang, J.; Wu, S.; Tien, P. Synthesis and anti-H5N1 activity of chiral gossypol derivatives and its analogs implicated by a viral entry blocking mechanism. *Bioorg. Med. Chem. Lett.* **2013**, *23*, 2619−2623. (b) Yang, J.; Zhang, F.; Li, J. R.; Chen, G.; Wu, S. W.; Ouyang, W. J.; Pan, W.; Yu, R.; Yang, J. X.; Tien, P. Synthesis and antiviral activities of novel gossypol derivatives. *Bioorg. Med. Chem. Lett.* **2012**, *22*, 1415−1420.

(6) (a) Wichmann, K.; Vaheri, A.; Luukkainen, T. Inhibiting herpes simplex virus type 2 infection in human epithelial cells by gossypol, a potent spermicidal and contraceptive agent. *Am. J. Obstet. Gynecol.* **1982**, *142*, 593−594. (b) Radloff, R. J.; Deck, L. M.; Royer, R. E.; Vander Jagt, D. L. Antiviral activities of gossypol and its derivatives against herpes simplex virus type II. *Pharmacol. Res. Commun.* **1986**, *18*, 1063−1067.

(7) Vichkanova, S. A.; Oifa, A. I.; Goryunova, L. V. Antiviral properties of gossypol in experimental influenza pneumonia. *Antibiotiki* **1970**, *15*, 1071−1073.

(8) Wu, Y. F. A mixture of polyhydroxy binaphthaldehyde and fatty acid used as a novel broad-spectrum agricultural antiviral agent and its preparation method. CN1489904A, 2004.

(9) Ritzenthaler, C. Resistance to plant viruses: old issue, news answers? *Curr. Opin. Biotechnol.* **2005**, *16*, 118−122.

(10) (a) Ouyang, G. P.; Cai, X. J.; Chen, Z.; Song, B. A.; Bhadury, P. S.; Yang, S.; Jin, L. H.; Xue, W.; Hu, D. Y.; Zeng, S. Synthesis and antiviral activities of pyrazole derivatives containing an oxime moiety. *J. Agric. Food Chem.* **2008**, *56*, 10160−10167. (b) Chen, M. H.; Chen, Z.; Song, B. A.; Bhadury, P. S.; Yang, S.; Cai, X. J.; Hu, D. Y.; Xue, W.; Zeng, S. Synthesis and antiviral activities of chiral thiourea derivatives containing an α-aminophosphonate moiety. *J. Agric. Food Chem.* **2009**, *57*, 1383−1388. (c) Li, Y. M.; Zhang, Z. K.; Jia, Y. T.; Shen, Y. M.; He, H. P.; Fang, R. X.; Chen, X. Y.; Hao, X. J. 3-Acetonyl-3-hydroxyoxindole: a new inducer of systemic acquired resistance in plants. *Plant Biotechnol. J.* **2008**, *6*, 301−308. (d) Bachrach, U. Antiviral activity of oxidized polyamines. *Amino Acids* **2007**, *33*, 267−272. (e) Su, B.; Chen, F.; Wang, L.; Wang, Q. Design, synthesis, antiviral activity, and structure−activity relationships (SARs) of two types of structurally novel phenanthroindo/quinolizidine analogues. *J. Agric. Food Chem.* **2014**, *62*, 1233−1239. (f) Song, H.; Liu, Y.; Liu, Y.; Wang, L.; Wang, Q. Synthesis and antiviral and fungicidal activity evaluation of β-carboline, dihydro-β-carboline, tetrahydro-β-carboline alkaloids, and their derivatives. *J. Agric. Food Chem.* **2014**, *62*, 1010−1018.

(11) Dodou, K. Investigations on gossypol: past and present developments. *Expert Opin. Invest. Drugs* **2005**, *14*, 1419−1434.

(12) Kovacic, P. Mechanism of drug and toxic actions of gossypol: focus on reactive oxygen species and electron transfer. *Curr. Med. Chem.* **2003**, *10*, 2711−2718.

(13) Bacsó, R. Y.; Hafez, M.; Király, Z.; Király, L. Inhibition of virus replication and symptom expression by reactive oxygen species in tobacco infected with tobacco mosaic virus. *Acta Phytopathol. Entomol.* **2011**, *46*, 1−10.

(14) Kenar, J. A. Reaction chemistry of gossypol and its derivatives. *J. Am. Oil Chem. Soc.* **2006**, *83*, 269−302.

(15) Przybylski, P.; Huczynski, A.; Pyta, K.; Brzezinski, B.; Bartl, F. Biological properties of Schiff bases and azo derivatives of phenols. *Curr. Org. Chem.* **2009**, *13*, 124−148.

(16) (a) Przybylski, P.; Pyta, K.; Remlein-Starosta, D.; Schroeder, G.; Brzezinski, B.; Bartl, F. Antifungal activity of alkyl and heterocyclic aza-derivatives of gossypol as well as their complexes with $NaClO_4$ against *Fusarium oxysporum* f. sp. *lupini*. *Bioorg. Med. Chem. Lett.* **2009**, *19*, 1996−2000. (b) Zhang, L.; Jiang, H.; Cao, X.; Zhao, H.; Wang, F.; Cui, Y.; Jiang, B. Chiral gossypol derivatives: evaluation of their anticancer activity and molecular modeling. *Eur. J. Med. Chem.* **2009**, *44*, 3961−3972. (c) Przybylski, P.; Pyta, K.; Stefanska, J.; Ratajczak-Sitarz, M.; Katrusiak, A.; Huczynski, A.; Brzezinski, B. Synthesis, crystal structures and antibacterial activity studies of aza-derivatives of phytoalexin from cotton plant − gossypol. *Eur. J. Med. Chem.* **2009**, *44*, 4393−4403.

(17) Baram, N. I.; Biktimirov, L.; Dzhurabekova, S. B.; Kamaev, F. G.; Ismailov, A. I. Imines of gossypol ethers. *Chem. Nat. Compd.* **1991**, *27*, 309−312.

(18) Przybylski, P.; Maluszynska, M.; Brzezinski, B. Spectroscopic and semiempirical studies of new Schiff base of gossypol with allylamine in solution. *J. Mol. Struct.* **2005**, *750*, 152−157.

(19) Dechary, J. M.; Brown, L. E. Substituted arylimino derivatives of gossypol. *J. Am. Oil Chem. Soc.* **1956**, *33*, 76−78.

(20) (a) That, Q. T.; Nguyen, K. P. P.; Hansen, P. E. Schiff bases of gossypol: an NMR and DFT study. *Magn. Reson. Chem.* **2005**, *43*, 302−308. (b) Zhou, X.; Wang, W.; Gu, J. NMR investigation of bis-4-fluoroaniline Schiff base of gossypol. *Acta Chim. Sinica* **1986**, *44*, 357−359.

(21) Zhou, X.; Wang, W.; Gu, J. Novel fluorine-containing derivatives of gossypol. *Acta Chim. Sinica* **1988**, *46*, 375−378.

(22) Wang, K. L.; Su, B.; Wang, Z. W.; Wu, M.; Li, Z.; Hu, Y. N.; Fan, Z. J.; Mi, N.; Wang, Q. M. Synthesis and antiviral activities of phenanthroindolizidine alkaloids and their derivatives. *J. Agric. Food Chem.* **2010**, *58*, 2703−2709.

(23) Li, L.; Liu, Y. X.; Wang, Q. M. Regioselective oxidative dehydrogenation in nonenzymatic condition: a synthetic route to gossypol. *Eur. J. Org. Chem.* **2013**, *2013*, 8014−8021.

(24) Structures of anhydrogossypol and ribavirin:

(25) (a) Matlin, S. A.; Roshdy, S.; Cass, Q. B.; Freitas, L. C. G.; Longo, R. L.; Malvestiti, I. Structural investigations of gossypol Schiff's bases. *J. Braz. Chem. Soc.* **1990**, *1*, 128−133. (b) Przybylski, P.; Pyta,

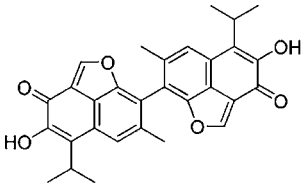


Anhydrogossypol

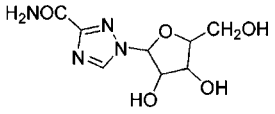


Ribavirin

K.; Ratajczak-Sitarz, M.; Katrusiak, A.; Brzezinski, B. Structure of a new Schiff base of gossypol with ethyl 4-amino-1-piperidine carboxylate in the solid and in the solution. *Polym. J. Chem.* **2009**, *83*, 747−759. (c) Przybylski, P.; Schilf, W.; Kamienski, B.; Brzezinski, B.; Bartl, F. CP/MAS spectroscopy in the determination of the tautomeric forms of gossypol, its Schiff bases and hydrazones in the solid state. *Magn. Reson. Chem.* **2008**, *46*, 534−544. (d) Ilkevych, N. S.; Schroeder, G.; Rybachenko, V. I.; Chotiy, K. Y.; Makarova, R. A. Vibrational spectra, structure and antioxidant activity of gossypol imine derivatives. *Spectrochim. Acta Part A* **2012**, *86*, 328−335.

## MATERIALS AND METHODS

**Samples and Irradiation.** Dried spices (turmeric, oregano, and cinnamon) packed in polyvinyl chloride (PVC) film were purchased from a local market in Daegu, South Korea, and stored in a refrigerator at 5 °C. These spices were handpicked from carefully selected crops and air-dried before being ground to the perfect texture by accurately calibrated machines during the process of manufacturing. The samples were $\gamma$-irradiated (1 and 10 kGy at a dose rate of 2.1 kGy/h) at room temperature using a Co-60 $\gamma$-ray source (AECL, IR-79, MDS Nordion International Co. Ltd., Ottawa, ON, Canada) at the Korean Atomic Energy Research Institute (KAERI), in Jeongeup, Korea. The absorbed doses were confirmed using alanine dosimeters with a diameter of 5 mm (Bruker Instruments, Rheinstetten, Germany). The free-radical signals were measured using a Bruker EMS 104 EPR analyzer (Bruker Instruments, Rheinstetten, Germany). After irradiation until EPR measurements the spice samples were stored at normal laboratory conditions, temperature (23 ± 3 °C), and relative humidity (58−64%) in the dark. However, the sample pretreatments were carried out in normal white fluorescent illumination of laboratory.

**Moisture Contents Determination.** The moisture contents of the spices samples were measured after various sample pretreatments. One gram of the powder sample was placed in an aluminum disc and kept in an electrically heated dry oven at 105 °C for 2−3 h under normal atmospheric pressure. The samples were then transferred to a desiccator for 30 min followed by weight measurements within 2 min time to cool to ambient temperature. Finally, the moisture content was calculated until their absolute differences did not exceed 0.002 g. For each sample, three determinations were carried out.

**EPR Spectroscopy.** To investigate the radiation-induced free radicals in the dried spice samples, three different sample pretreatments were conducted to decrease the moisture content of the spices prior to the EPR measurements:

(i) FD: Freeze-drying (Bondiro, Ilsin Bio Base, Yangju, Kyunggido, Korea) of the samples.[16]
(ii) OD: Oven-drying (HB-502M, Hanbaek Scientific Co., Bucheon, Kyunggido, Korea).[17]
(iii) AE: Alcoholic extraction of the samples was carried out as described by de Jesus et al.[19] Approximately 6 g of the spice samples was put into a beaker containing 40 mL of an 80% ethyl alcohol solution in deionized water. The samples were mixed adequately using a glass rod and kept for 30 min at ambient temperature (23 ± 3 °C). The solid fraction was then separated by filtration, pressed further to reduce the moisture, and then dried in air for 1 h at ambient temperature before being put into the EPR tube.
(iv) WAE: Washing of the finely chopped sample for 20 min with distilled water using a nylon sieve (150 mm). The residues were used after alcoholic extraction as described above.[20,21]

The sample (approximately 0.1 g after the pretreatments) was placed in a quartz EPR tube (5 mm diameter). The open end of the sample tube was then sealed with plastic film. EPR was performed after 15 days of irradiation in accordance with the European standard, EN 1787,[10] using a X-band EPR spectrometer (JES-TE200, Jeol Co., Tokyo, Japan) at room temperature under the following conditions: power, 0.4 mW; frequency, 9.10−9.21 GHz; center field, 324 ± 2 mT; sweep width, 10−25 mT; modulation frequency, 100 kHz; modulation width, 1−2 mT; amplitude, 50−400; sweep time, 30 s; and time constant, 0.03 s. All analyses were conducted in triplicate ($n$ = 3), and the mean values (±standard deviation) are reported. Microsoft Excel (Microsoft Office 2010 version) and Origin (version 8) software were used for data analysis and presentation. The EPR signal height was computed using ESPRIT-425 software (Jeol Co.) as the peak-to-peak amplitude of the first derivative spectrum, whereas the signal intensity was presented in arbitrary units per unit sample weight (AU/mg). The $g$-values were determined using an internal Mn(II) standard attached to the EPR cavity. In addition, $g$ values were also confirmed by calculation using the relation $g$ = 71.448 × microwave (GHz)/magnetic field (mT). This relation was obtained by substituting the values of Bohr magneton ($\beta_e$) and Planck's constant ($h$) in appropriate units into the EPR resonance equation.

## RESULTS AND DISCUSSION

**Spectral Features of the Nonirradiated Samples.** Figure 1 shows the EPR spectra of all of the nonirradiated spice samples subjected to different extraction techniques. The spectra were invariably characterized by a central line at $g_0$ = 2.006 with a line width ($\Delta B_{pp}$) of 0.63 mT as a native signal, plausibly attributable to the photooxodation of the existing polyphenols. Experimental parameters of the spectrometer were kept identical during

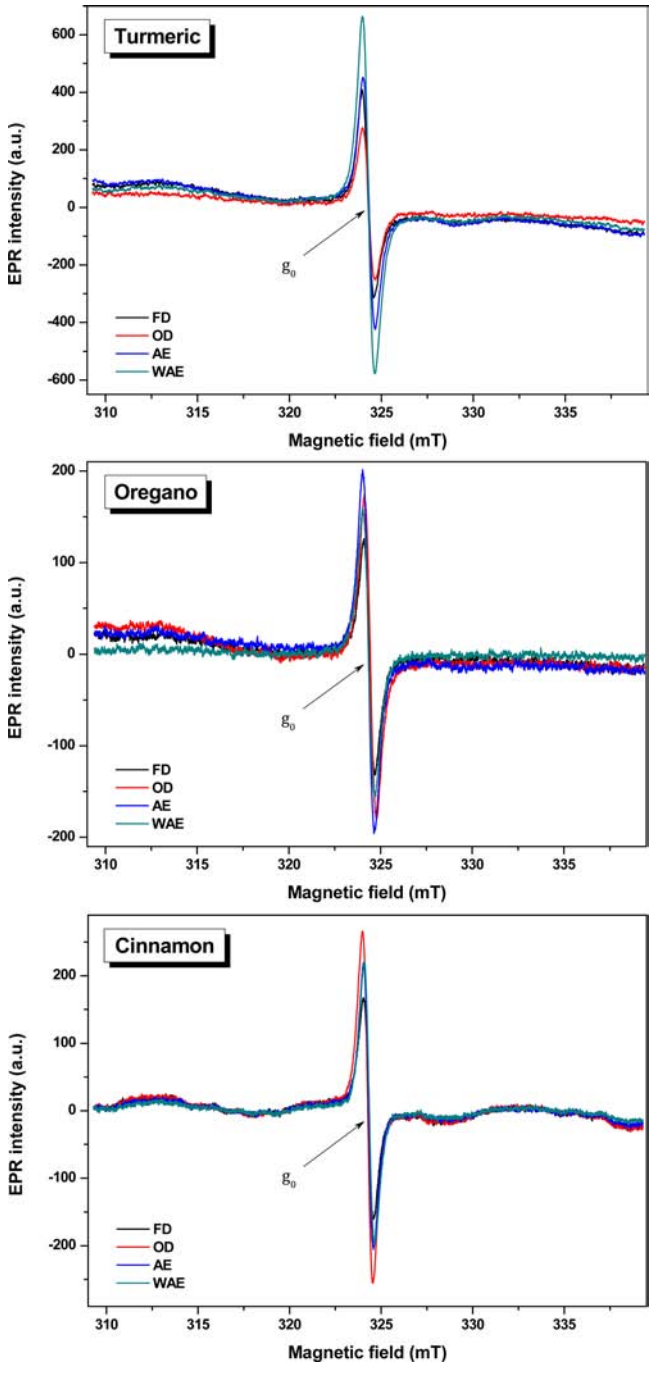


**Figure 1.** EPR spectra of the nonirradiated spices after different drying treatments. FD, freeze-drying; OD, oven-drying; AE, alcoholic extraction; and WAE, water washing alcoholic extraction.


dx.doi.org/10.1021/jf502258r | J. Agric. Food Chem. 2014, 62, 11089−11098

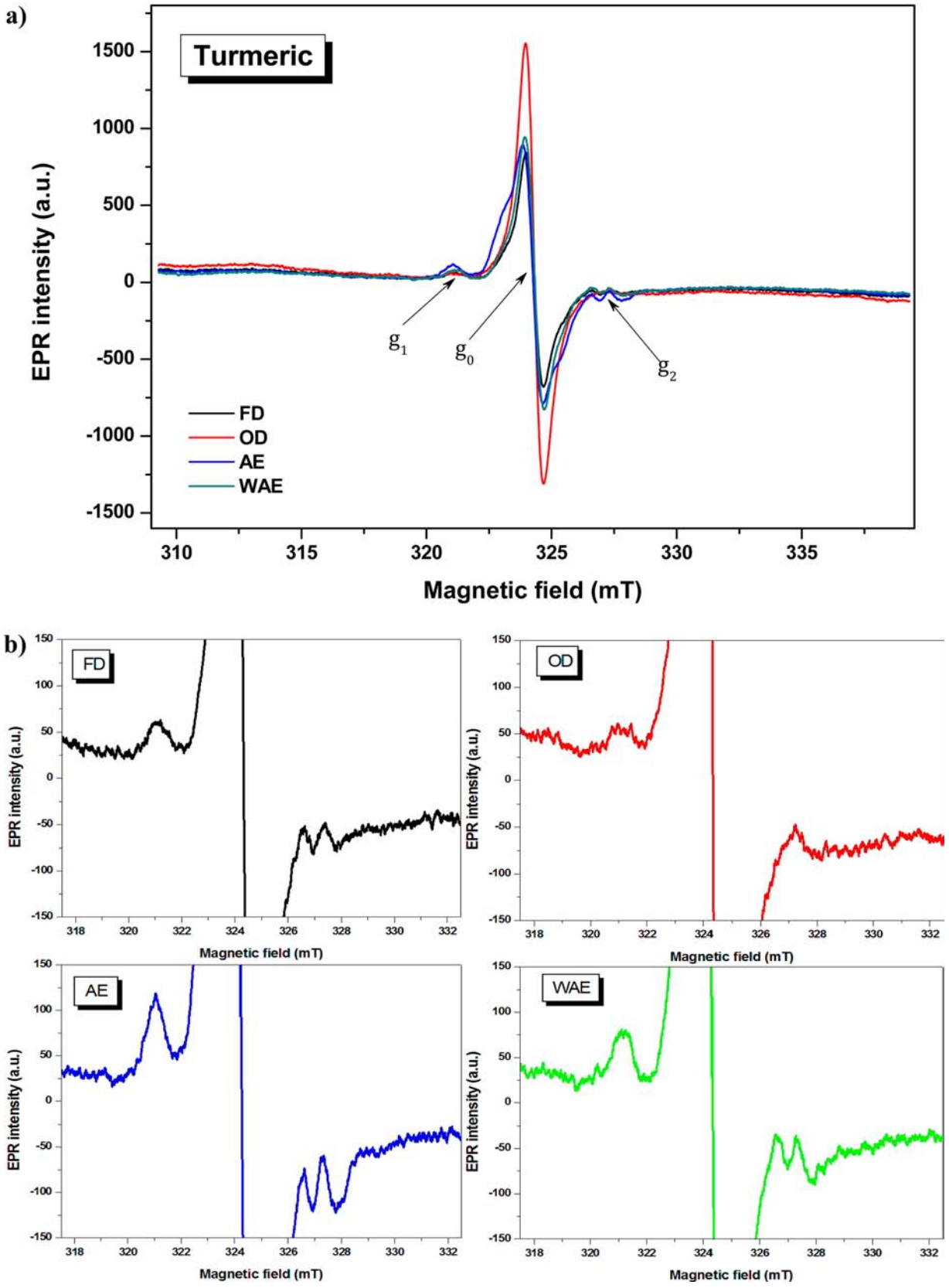


**Figure 2.** Radiation-induced EPR signals in 10 kGy-irradiated turmeric after different sample drying pretreatments (FD, freeze-drying; OD, oven-drying; AE, alcoholic extraction; WAE, water washing and alcoholic extraction): (a) superposed EPR spectra and (b) magnified spectra.

measurements of all of the samples. Several reports have suggested that these free radicals are semiquinone radicals produced by the oxidation of plant polyphenolics[22] or lignin.[23] The intensity of the singlet ($g_0$ = 2.006) was almost identical for the spice samples subjected to FD, OD, AE, and WAE. Recently, Akram et al. reported changes in the signal intensity of sauce


dx.doi.org/10.1021/jf502258r | J. Agric. Food Chem. 2014, 62, 11089−11098

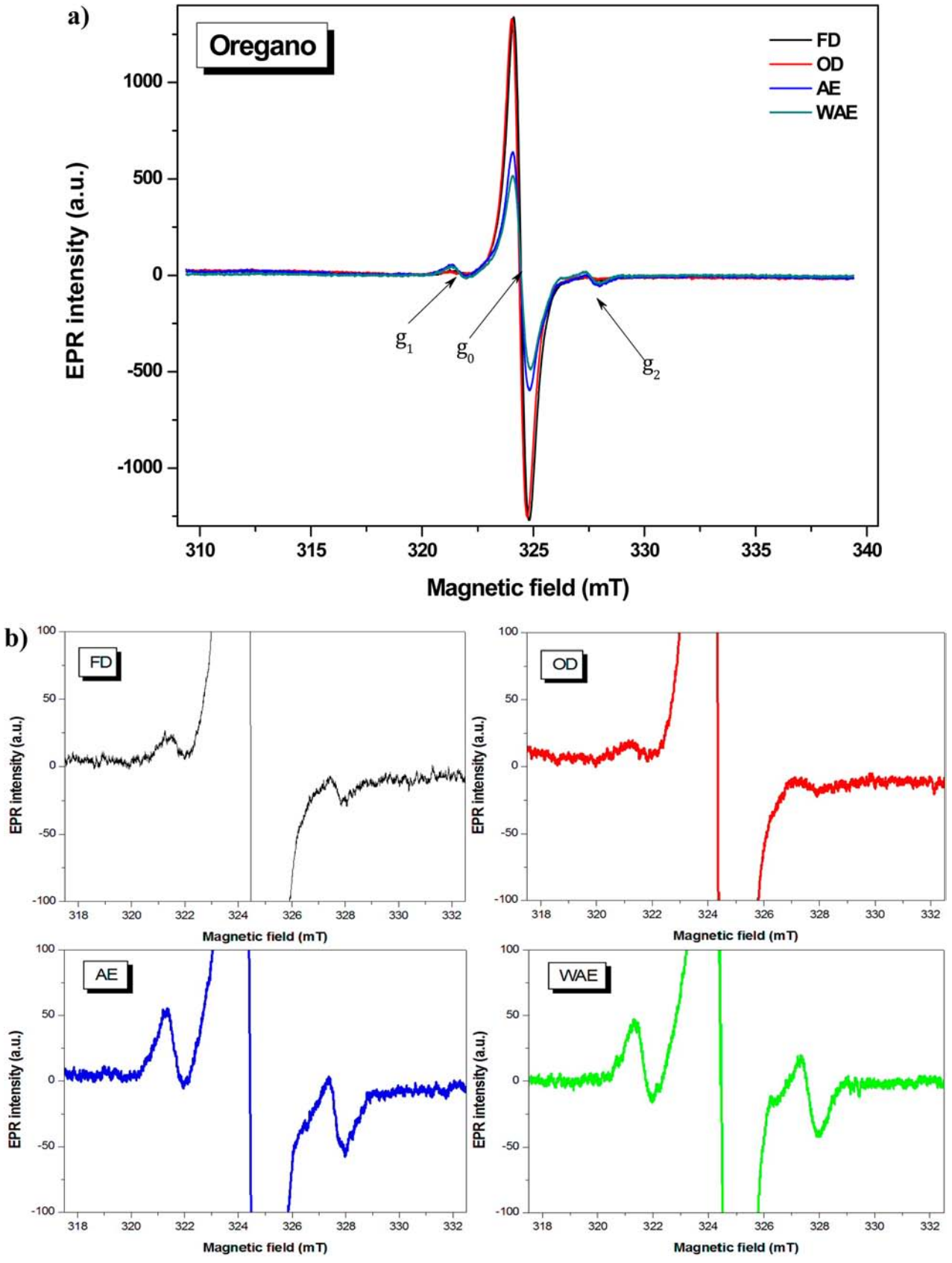


**Figure 3.** Radiation-induced EPR signals in 10 kGy-irradiated oregano after different sample drying pretreatments (FD, freeze-drying; OD, oven-drying; AE, alcoholic extraction; WAE, water washing and alcoholic extraction): (a) superposed EPR spectra and (b) magnified spectra.

samples subjected to different sample pretreatments.[21] However, no such effect was observed for the present spice samples, suggesting that the stability of the existing paramagnetic centers depends on the type of food. Thus, complex matrixes of all of the


dx.doi.org/10.1021/jf502258r | J. Agric. Food Chem. 2014, 62, 11089−11098

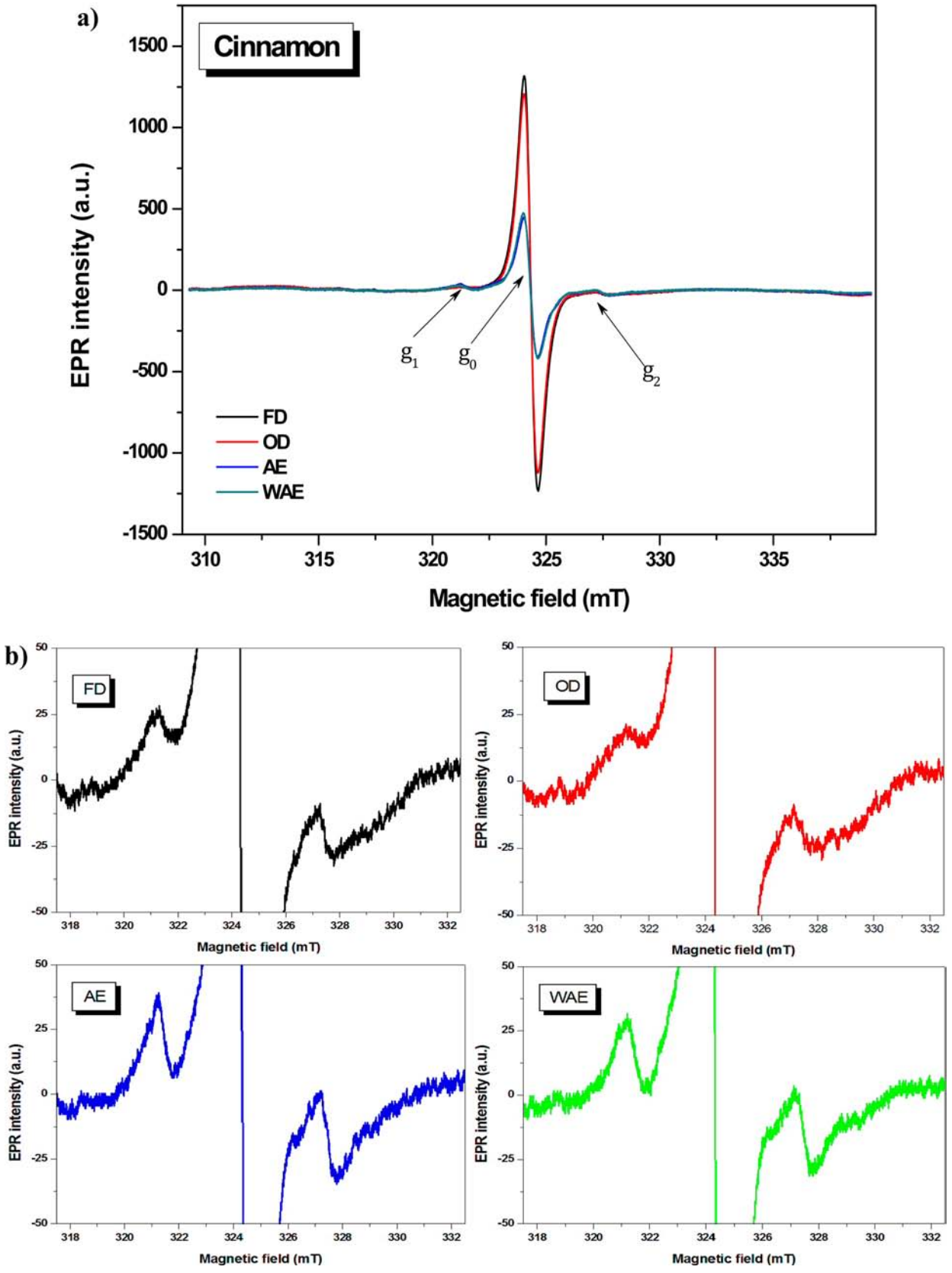


**Figure 4.** Radiation-induced EPR signals in 10 kGy-irradiated cinnamon after different sample drying pretreatments (FD, freeze-drying; OD, oven-drying; AE, alcoholic extraction; WAE, water washing and alcoholic extraction): (a) superposed EPR spectra and (b) magnified spectra.

spice samples with different moisture contents even after sample pretreatments could be responsible for the inconsistent manifestations of the signal intensities without any defined trend.

**Spectral Features of Irradiated Samples.** Figures 2, 3, and 4 show the spectral features of the three spice samples subjected to post irradiation sample pretreatments. Complex EPR spectra


dx.doi.org/10.1021/jf502258r | J. Agric. Food Chem. 2014, 62, 11089−11098

**Table 1. EPR Signal Information from Irradiated Spices with Different Drying Pretreatments**

| | | | g-value[b] | | | |
|---|---|---|---|---|---|---|
| sample | dose (kGy) | treatment[a] | $g_1$ | $g_0$ | $g_2$ | $g_1$–$g_2$ distance (mT) |
| tumeric | 0 | FD | | 2.006 ± 0.00015 | | |
| | | OD | | 2.007 ± 0.00012 | | |
| | | AE | | 2.007 ± 0.00007 | | |
| | | WAE | | 2.007 ± 0.00009 | | |
| | 1 | FD | 2.024 ± 0.00042 | 2.007 ± 0.00011 | 1.987 ± 0.00013 | 6.0 ± 0.1 |
| | | OD | 2.024 ± 0.00031 | 2.007 ± 0.00023 | 1.987 ± 0.00055 | 6.1 ± 0.0 |
| | | AE | 2.024 ± 0.00017 | 2.007 ± 0.00018 | 1.987 ± 0.00020 | 6.2 ± 0.2 |
| | | WAE | 2.024 ± 0.00042 | 2.007 ± 0.00012 | 1.987 ± 0.00027 | 6.1 ± 0.1 |
| | 10 | FD | 2.024 ± 0.00002 | 2.007 ± 0.00010 | 1.986 ± 0.00010 | 6.1 ± 0.1 |
| | | OD | 2.024 ± 0.00033 | 2.007 ± 0.00037 | 1.987 ± 0.00013 | 6.1 ± 0.1 |
| | | AE | 2.024 ± 0.00017 | 2.007 ± 0.00007 | 1.986 ± 0.00055 | 6.2 ± 0.1 |
| | | WAE | 2.024 ± 0.00042 | 2.007 ± 0.00012 | 1.986 ± 0.00053 | 6.2 ± 0.1 |
| oregano | 0 | FD | | 2.007 ± 0.00010 | | |
| | | OD | | 2.007 ± 0.00012 | | |
| | | AE | | 2.007 ± 0.00007 | | |
| | | WAE | | 2.007 ± 0.00006 | | |
| | 1 | FD | 2.024 ± 0.00017 | 2.007 ± 0.00017 | 1.987 ± 0.00051 | 6.0 ± 0.1 |
| | | OD | | 2.007 ± 0.00009 | | |
| | | AE | 2.024 ± 0.00023 | 2.007 ± 0.00015 | 1.987 ± 0.00026 | 6.1 ± 0.0 |
| | | WAE | 2.024 ± 0.00050 | 2.007 ± 0.00011 | 1.987 ± 0.00022 | 6.0 ± 0.1 |
| | 10 | FD | 2.025 ± 0.00027 | 2.006 ± 0.00027 | 1.987 ± 0.00062 | 6.1 ± 0.0 |
| | | OD | 2.024 ± 0.00025 | 2.007 ± 0.00025 | 1.987 ± 0.00051 | 6.0 ± 0.1 |
| | | AE | 2.024 ± 0.00028 | 2.007 ± 0.00028 | 1.987 ± 0.00019 | 6.1 ± 0.1 |
| | | WAE | 2.024 ± 0.00031 | 2.006 ± 0.00031 | 1.987 ± 0.00029 | 6.1 ± 0.1 |
| cinnamon | 0 | FD | | 2.007 ± 0.00004 | | |
| | | OD | | 2.007 ± 0.00019 | | |
| | | AE | | 2.007 ± 0.00016 | | |
| | | WAE | | 2.007 ± 0.00009 | | |
| | 1 | FD | 2.024 ± 0.00030 | 2.007 ± 0.00008 | 1.987 ± 0.00012 | 5.9 ± 0.0 |
| | | OD | 2.024 ± 0.00011 | 2.007 ± 0.00012 | 1.987 ± 0.00005 | 5.8 ± 0.1 |
| | | AE | 2.024 ± 0.00016 | 2.007 ± 0.00007 | 1.988 ± 0.00020 | 5.8 ± 0.1 |
| | | WAE | 2.024 ± 0.00013 | 2.007 ± 0.00015 | 1.987 ± 0.00017 | 5.9 ± 0.1 |
| | 10 | FD | 2.024 ± 0.00017 | 2.007 ± 0.00016 | 1.987 ± 0.00015 | 6.0 ± 0.0 |
| | | OD | 2.025 ± 0.00026 | 2.007 ± 0.00021 | 1.987 ± 0.00012 | 6.0 ± 0.1 |
| | | AE | 2.024 ± 0.00012 | 2.007 ± 0.00017 | 1.987 ± 0.00003 | 6.0 ± 0.1 |
| | | WAE | 2.024 ± 0.00023 | 2.007 ± 0.00011 | 1.987 ± 0.00012 | 6.0 ± 0.0 |

[a]FD = freeze-drying, OD = oven-drying, AE = alcoholic extraction, WAE = water-washing and alcoholic extraction. [b]$g$ value ($g_1$ = left, $g_0$ = central, $g_2$ = right) = 71.448 × microwave (GHz)/magnetic field (mT).

were observed, with an increase in the signal intensity of the existing weak singlet ($g$ = 2.006). Raffi et al. and Ahn et al. previously reported similar observations, where an intense signal was noticed in the spectrum of irradiated spice and vegetable; the relatively high intensity was attributed to irradiation treatment.[24,25] The line width ($\Delta B_{pp}$) of the EPR signal was observed to increase from 0.74 to 0.91 mT, and was possibly due to the induction of multiple paramagnetic centers in the matrix of the spice samples. In addition, a radiation specific triplet signal with a hyperfine coupling constant (hfcc) of 3 mT was observed for all samples and identified as originating from the cellulose radical. The triplet was characterized by $g_0$ (central line) at 2.006, $g_1$ (left line) at 2.024, and $g_2$ (right line) at 1.986. Deighton et al.[26] reported that the left line is strictly due to radiation-induced cellulose radicals, whereas the right line, induced by lignin radicals, is sensitive to irradiation as well as the drying processes.[27] The triplet signal of the cellulosic radical is a well-established signature of radiation processing of foods.[12] In case of the irradiated turmeric, an additional weak line at the extreme right of the central signal was observed after FD, AE, and WAE pretreatments as depicted in Figure 2. This signal was possibly because of the axially symmetric radiation-induced doublet of carbohydrate radicals and was masked in case of OD samples. A similar observation has recently been reported in case of the irradiated medicinal plant products where irradiated EPR spectra were the superposition of three paramagnetic centers of polyphenols, cellulose, and carbohydrate radicals.[7] Therefore, in case of turmeric, all three sample pretreatments, FD, AE, and WAE, were successful in identifying radiation-specific radicals beyond doubt.

**Characteristics of EPR Spectra of the Irradiated Spices after Drying Treatments.** To enhance the distinct visibility of the radiation-specific EPR lines for the spices, the samples were subjected to various pretreatments (OD, FD, AE, and WAE) prior to EPR analysis. The intensity of the central signal ($g_0$) of all of the irradiated spice samples was enhanced. The most prominent increase in intensities was observed for FD and OD samples (Figures 2, 3, and 4). However, in case of OD samples, the spectral profile changed minimally following irradiation, although the two radiation-induced side lines ($g_1$ = 2.024 and $g_2$ =

**Table 2. Moisture Contents (%) of Dried Spices at Different Drying Treatments**

| | | treatment[a] | | | |
|---|---|---|---|---|---|
| sample | dose (kGy) | FD | OD | AE | WAE |
| tumeric | 0 | 1.204 ± 0.063 | 1.692 ± 0.250 | 5.441 ± 0.234 | 4.738 ± 0.574 |
| | 1 | 1.072 ± 0.042 | 1.405 ± 0.085 | 5.922 ± 0.173 | 4.822 ± 0.486 |
| | 10 | 1.261 ± 0.191 | 1.757 ± 0.155 | 5.999 ± 0.320 | 5.363 ± 0.093 |
| oregano | 0 | 1.969 ± 0.249 | 2.011 ± 0.728 | 5.602 ± 0.384 | 5.831 ± 0.393 |
| | 1 | 1.546 ± 0.074 | 2.013 ± 0.050 | 5.798 ± 0.067 | 5.885 ± 0.372 |
| | 10 | 1.455 ± 0.266 | 2.369 ± 1.241 | 5.844 ± 0.403 | 6.164 ± 0.788 |
| cinnamon | 0 | 2.896 ± 0.164 | 2.614 ± 0.589 | 6.190 ± 0.231 | 6.844 ± 0.452 |
| | 1 | 2.516 ± 0.099 | 2.454 ± 0.395 | 6.418 ± 0.390 | 6.729 ± 0.511 |
| | 10 | 2.409 ± 0.268 | 3.197 ± 1.925 | 6.277 ± 0.337 | 7.296 ± 0.937 |

[a]FD = freeze-drying, OD = oven-drying, AE = alcoholic extraction, WAE = water-washing and alcoholic extraction.

**Table 3. EPR Signal Ratios (Intensity) of Irradiated Spices at Different Sample Drying Pretreatments**

| | | | signal ratio ($g_n$ intensity/$g_1$ intensity)[b] | | |
|---|---|---|---|---|---|
| sample | dose (kGy) | treatment[a] | left ($g_1$) | center ($g_0$) | right ($g_2$) |
| tumeric | 1 | FD | 1.0 ± 0.0 d | 41.2 ± 5.0 b | 1.1 ± 0.0 d |
| | | OD | 1.0 ± 0.0 d | 102.7 ± 20.9 a | 1.3 ± 0.4 d |
| | | AE | 1.0 ± 0.0 d | 16.1 ± 0.7 c | 1.0 ± 0.0 d |
| | | WAE | 1.0 ± 0.0 d | 21.0 ± 0.8 c | 1.0 ± 0.1 d |
| | 10 | FD | 1.0 ± 0.0 d | 41.3 ± 2.7 b | 1.0 ± 0.0 d |
| | | OD | 1.0 ± 0.0 d | 55.4 ± 4.6 a | 1.2 ± 0.1 d |
| | | AE | 1.0 ± 0.0 d | 13.9 ± 0.8 c | 1.0 ± 0.1 d |
| | | WAE | 1.0 ± 0.0 d | 14.9 ± 0.7 c | 1.0 ± 0.0 d |
| oregano | 1 | FD | 1.0 ± 0.0 c | 119.7 ± 45.8 a | 1.0 ± 0.0 c |
| | | OD | | | |
| | | AE | 1.0 ± 0.0 c | 16.6 ± 19.9 b | 1.0 ± 0.1 c |
| | | WAE | 1.0 ± 0.0 c | 18.6 ± 16.2 b | 1.1 ± 0.2 c |
| | 10 | FD | 1.0 ± 0.0 e | 45.8 ± 2.2 b | 1.0 ± 0.0 e |
| | | OD | 1.0 ± 0.0 e | 77.8 ± 1.9 a | 1.0 ± 0.0 e |
| | | AE | 1.0 ± 0.0 e | 19.9 ± 0.7 c | 1.0 ± 0.1 e |
| | | WAE | 1.0 ± 0.0 e | 16.2 ± 0.4 d | 1.0 ± 0.0 e |
| cinnamon | 1 | FD | 1.0 ± 0.0 d | 153.5 ± 15.4 b | 1.3 ± 0.0 d |
| | | OD | 1.0 ± 0.0 d | 368.9 ± 167.8 a | 2.8 ± 1.9 d |
| | | AE | 1.0 ± 0.0 d | 21.1 ± 3.3 c | 1.0 ± 0.1 d |
| | | WAE | 1.0 ± 0.0 d | 22.3 ± 1.2 c | 1.1 ± 0.1 d |
| | 10 | FD | 1.0 ± 0.0 d | 68.8 ± 2.6 b | 1.0 ± 0.0 d |
| | | OD | 1.0 ± 0.0 d | 95.7 ± 7.2 a | 1.2 ± 0.1 d |
| | | AE | 1.0 ± 0.0 d | 19.1 ± 1.2 c | 1.0 ± 0.1 d |
| | | WAE | 1.0 ± 0.0 d | 20.9 ± 1.6 c | 1.0 ± 0.1 d |

[a]Treatments: FD = freeze-drying, OD = oven-drying, AE = alcoholic extraction, WAE = water-washing and alcoholic extraction. [b]Values within a row followed by different letters are significantly different based on Duncan's multiple range test.

1.986) were still apparent for all of the samples at a radiation dose of 1 kGy. Table 1 shows that the $g$-values ($g_1$ = 2.024, $g_0$ = 2.006, and $g_2$ = 1.986) and the distance ($g_1-g_2$ = 6.0 ± 0.1 mT) between the two satellite lines did not vary significantly with variation of the samples and the pretreatments, which indicates that the radiation-induced free radicals remained unchanged following different pretreatments. In other words, the detection marker identified as cellulose radicals was apparent for all samples and indicated the irradiation history as per EN 1787.[12] However, the intensity of the signal varied detectably with different pretreatment procedures. The side lines were not prominent, especially for the 1 kGy-irradiated OD samples. The signal intensity of the side EPR lines of the cellulose radical increased significantly in the case of all of the AE samples (Figures 2, 3, and 4). However, no further enhancement in the signal intensity was observed after the incorporation of the water-washing step, as reported by Akram et al. in the case of sauce samples.[21] In the case of the irradiated sauce samples, an enhancement in the central line signal intensity after sample pretreatment has also been reported. However, in the present case of the spices, no such increase in the central line intensity was observed, probably because of the considerable differences in the moisture contents between the samples subjected to conventional drying methods (FD, OD) and alcohol assisted extraction treatments (AE and WAE) as shown in Table 2. After alcoholic extraction, both the nonirradiated and the irradiated samples showed an increase in moisture content enhancing the chance of recombination of the paramagnetic centers in the spice moiety. The low starch content (ca. 7−12%) may also influence the EPR spectral profile.[28] It has recently been reported that the presence of starch and the initial water content of a food sample are responsible for the observed differences between the initial and final spectra of the irradiated samples.[7] In the case of cereals, the water content was shown to affect the initial spectra, particularly during irradiation, but the

final spectra were independent of hydration.[29] Table 3 shows the ratio of the signal intensities of the central line ($g_0$) and right line ($g_2$) to the intensity of the left line ($g_1$). The signal ratios were also observed to vary with the irradiation doses and the sample types. The ratio of the intensity of the side signals (corresponding to radiation-induced cellulose radicals) to the total intensity of the central EPR signal was reported to be ca. 5% for irradiated *Foeniculi fructus* and 50% for irradiated citrus fruits.[30,31] In general, the signal intensity ratio of the OD and FD samples was 1:6:1 and 1:7:1, respectively. However, the ideal signal intensity ratio in case of radiation-induced cellulose radicals has been reported as 1:2:1.[32] The ratio of the signal intensity of the right line to that of the left line was observed to be higher for the OD samples in comparison with that of other pretreated samples, and the maximum value was obtained for cinnamon. However, the spectra of the OD and FD samples were not as clear as those of the AE and WAE samples, and thus identification was difficult for the 1 kGy-irradiated sample. The samples subjected to AE and WAE exhibited improved and distinct radiation-induced triplets, as shown in the cases of turmeric (Figure 2b), oregano (Figure 3b), and cinnamon (Figure 4b), possibly because of the removal of the short-lived polyphenolic radicals ($g$ = 2.006) during the sample pretreatments. Consequently, the intensity of the central lines for AE and WAE treated spice samples was found to be reduced, resulting in relative enhancement of the cellulosic triplet as depicted in Figures 2a, 3a, and 4a. The intensity ratio of the central signal to the left signal of all of the AE samples was observed to be less than that of the OD samples, confirming the aforementioned behavior of the EPR signals as demonstrated in Table 3. The behavior of the EPR lines ($g_1$ and $g_0$) with increase in dose from 1 to 10 kGy after different sample pretreatments was also studied. A dose-dependent increase in the radiation-induced cellulose radical signals in the flesh of irradiated vegetables after different sample pretreatments has already been reported by de Jesus et al.[33] In case of the spice samples, the signal intensities were measured by the peak to peak amplitude of the EPR lines. To take into account the variable sample quantities in EPR tubes, the signal intensities in arbitrary unit (AU) of each aliquot were divided by the respective sample weight. The percentage EPR signal intensity was then calculated by normalizing the intensities with respect to 100 as shown in Figure 5. In the case of the OD and FD spice samples, the percentage intensity of the $g_0$ line showed a sharp increase at 1 kGy, followed by a slower enhancement up to 10 kGy. On the contrary, in most of the irradiated food samples sharp enhancements in signal intensities have been observed with increasing dose because food samples have not been subjected to any postirradiation treatments prior to EPR measurements.[7,34] Therefore, in those food samples, the radiation-induced radicals at $g_0$ responsible for intensity enhancement have not been removed. In this study, the spice samples were subjected to postirradiation pretreatments (FD, AE, and WAE) to eliminate the radiation-induced paramagnetic centers at $g_0$ to enhance the signatures of the radiation-specific radicals in EPR spectra. In case of AE and WAE samples, the intensities of the $g_0$ line did not show any sharp enhancement with the increasing dose because the majority of the radiation-induced polyphenolic radicals were eliminated during chemical extraction processes as depicted in Figure 5. A similar observation of a slow increase in EPR signal intensity in case of irradiated sea vegetables after pretreatments has recently been reported in our earlier communication.[35] In addition, at very high dose the intensity normally showed saturation probably because of the increased recombination rate

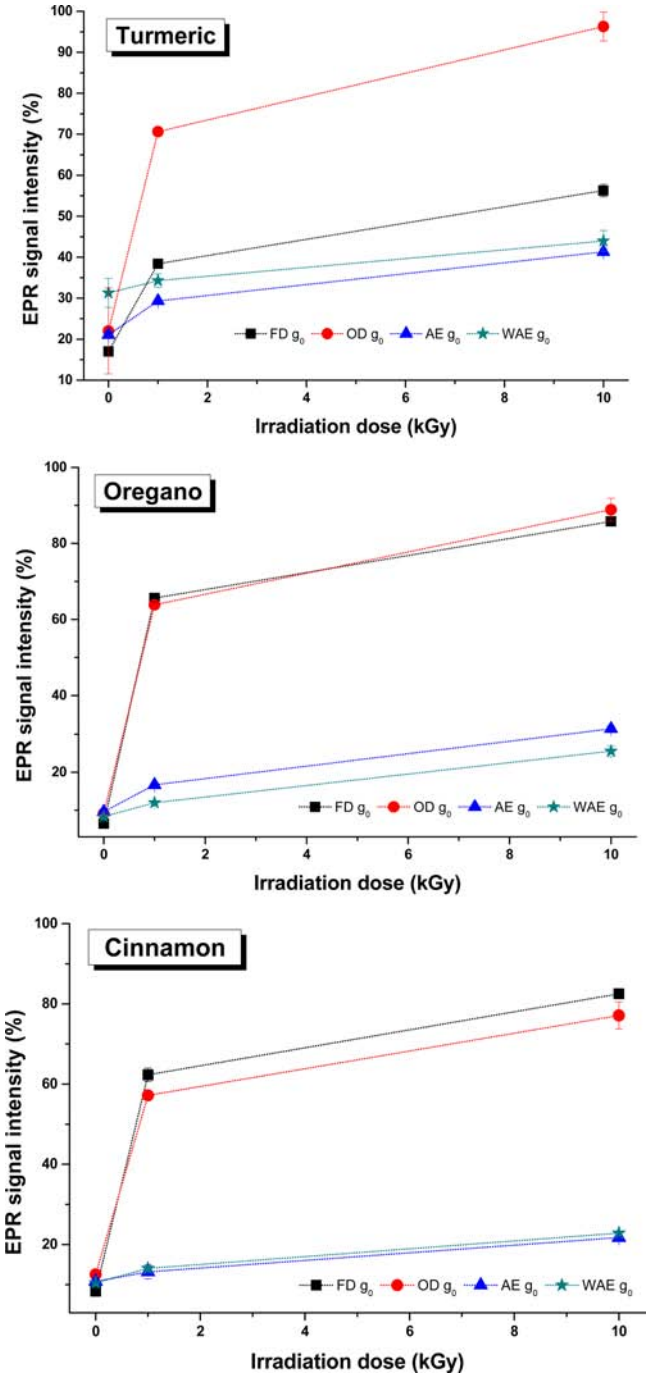


**Figure 5.** Response of the EPR signal intensity with increasing radiation dose for the spices (turmeric, oregano, and cinnamon) after different sample drying pretreatments (FD, freeze-drying; OD, oven-drying; AE, alcoholic extraction; WAE, water washing and alcoholic extraction). The percentage EPR signal intensity was calculated by dividing the weight normalized EPR intensities by 100.

of the radiation-induced radicals due to the enhanced spin density. A similar observation has been reported in the case of irradiated guar gum samples, where the EPR signal intensity did not exhibit any distinct trend with increasing dose, possibly because of the fast recombination of the induced free radicals.[36] However, the qualitative detection of irradiation features was possible for all of the irradiated spice samples on the basis of changes in EPR spectra, and the change was most prominent in the case of the samples subjected to AE pretreatment.


dx.doi.org/10.1021/jf502258r | J. Agric. Food Chem. 2014, 62, 11089−11098

In conclusion, an advanced approach to the EPR analysis of irradiated food samples incorporating the alcoholic-extraction process resulted in improvement in the identification of irradiation status for irradiated spice samples relative to samples pretreated with conventional oven and freeze-drying protocols. The alcoholic-extraction method gave rise to enhanced EPR spectral features, and particularly improved signal intensity, and thus enabled clear detection of irradiation. An addendum water-washing step (in addition to the alcoholic extraction) produced no further enhancement of the EPR spectra. These results suggest that the signature of the paramagnetic radicals in cellulose, produced by irradiation, can be enhanced by the alcoholic extraction process, and this protocol is useful for the identification of $\gamma$-irradiated spices.

## AUTHOR INFORMATION

### Corresponding Author

*Tel.: +82 53 950 5775. Fax: +82 53 950 6772. E-mail: jhkwon@knu.ac.kr.

### Funding

This work was supported by the National Research Foundation of Korea (NRF) grant funded by the Korean government (no. 2013R1A1A4A03006993).

### Notes

The authors declare no competing financial interest.

## REFERENCES

(1) Bendini, A.; Toschi, T. G.; Lercker, G. Influence of gamma irradiation and microwaves on the linear unsaturated hydrocarbon fraction in spices. *Z. Lebensm.-Unters. Forsch.* **1998**, *207*, 214−218.

(2) Tjaberg, T. B.; Underdal, B.; Lunde, G. The effect of ionizing radiation on the microbial content and volatile constituents of spices. *J. Appl. Bacteriol.* **1972**, *35*, 473−478.

(3) Loaharanu, P. Status and prospects of food irradiation. *Food Technol.* **1994**, *52*, 124−131.

(4) IAEA. Food authorization database, 2013; available from: http://nucleus.iaea.org/ifa/FoodAuthorisationDisplay.aspx.

(5) Loaharanu, P. Food irradiation: current status and future prospects. *New Methods of Food Preservation*; Springer: New York, 1995; pp 90−111.

(6) Chauhan, S. K.; Kumar, R.; Nadanasabapathy, S.; Bawa, A. S. Detection methods for irradiated foods. *Compr. Rev. Food Sci. Food Saf.* **2009**, *8*, 4−16.

(7) Sanyal, B.; Chatterjee, S.; Variyar, P. S.; Sharma, A. Application of EPR spectroscopy to identify irradiated Indian medicinal plant products. *J. Food Sci.* **2012**, *77*, C710−C718.

(8) Kwon, J. H.; Ahn, J. J.; Akram, K.; Son, I. J.; Lee, S. O. Characterization of radiation-induced luminescence properties and free radicals for the identification of different gamma-irradiated teas. *Anal. Bioanal. Chem.* **2013**, *405*, 4225−4234.

(9) Lee, J.; Kausar, T.; Kim, B. K.; Kwon, J. H. Detection of $\gamma$-Irradiated Sesame Seeds before and after Roasting by Analyzing Photostimulated Luminescence, Thermoluminescence, and Electron Spin Resonance. *J. Agric. Food Chem.* **2008**, *56*, 7184−7188.

(10) EN1786. *Foodstuffs - Detection of irradiated food containing bone − Method by ESR spectroscopy*; European Committee for Standardization: Brussels, Belgium, 1996.

(11) EN13708. *Foodstuffs - Detection of irradiated food containing crystalline sugar by ESR spectroscopy*; European Committee for Standardization: Brussels, Belgium, 2001.

(12) EN1787. *Foodstuffs-Detection of irradiated food containing cellulose by ESR spectroscopy*; European Committee for Standardization: Brussels, Belgium, 2000.

(13) Raffi, J.; Yordanov, N. D.; Chabane, S.; Douifi, L.; Gancheva, V.; Ivanova, S. Identification of irradiation treatment of aromatic herbs, spices and fruits by electron paramagnetic resonance and thermoluminescence. *Spectrochim. Acta, Part A* **2000**, *56*, 409−416.

(14) Yordanov, N. D.; Gancheva, V. A new approach for extension of the identification period of irradiated cellulose-containing foodstuffs by EPR spectroscopy. *Appl. Radiat. Isot.* **2000**, *5*, 195−198.

(15) Raffi, J.; Stocker, P. Electron paramagnetic resonance detection of irradiated foodstuffs. *Appl. Magn. Reson.* **1996**, *10*, 357−373.

(16) Yordanov, N. D.; Aleksieva, K.; Dimitrova, A.; Georgieva, L.; Tzvetkova, E. Multifrequency EPR study on freeze-dried fruits before and after X-ray irradiation. *Radiat. Phys. Chem.* **2006**, *75*, 1069−1074.

(17) Akram, K.; Ahn, J. J.; Yoon, S. R.; Kwon, J. H. Identification of irradiated spaghetti sauces sauces using different physical techniques. *J. Food Qual.* **2012**, *35*, 292−297.

(18) Kikuchi, M.; Hussain, M. S.; Morishita, N.; Ukai, M.; Kobayashi, Y.; Shimoyama, Y. ESR study of free radicals in mango. *Spectrochim. Acta, Part A* **2010**, *75*, 310−313.

(19) de Jesus, E. F. O.; Rossi, A. M.; Lopes, R. T. An ESR study on identification of gamma-irradiated kiwi, papaya and tomato using fruit pulp. *Int. J. Food Sci. Technol.* **1999**, *34*, 173−178.

(20) Ahn, J. J.; Akram, K.; Jo, D.; Kwon, J. H. Investigation of different factors affecting the electron spin resonance-based characterization of gamma-irradiated fresh, white, and red ginseng. *J. Ginseng Res.* **2012**, *36*, 308−313.

(21) Akram, K.; Ahn, J. J.; Kwon, J. H. Characterization of electron spin resonance spectroscopy of irradiated sauces with different sample pretreatment. *Food Chem.* **2013**, *138*, 1878−1883.

(22) Scewartz, H. M.; Bolton, J. R.; Brog, D. C. *Biological Applications of Electron Spin Resonance*; John Wiley & Sons Inc.: New York, 1972.

(23) Tabner, B. J.; Tabner, V. A. Electron spin resonance spectra of gamma-irradiated citrus fruits, skin, skin components and stalks. *Int. J. Food Sci. Technol.* **1994**, *29*, 143−152.

(24) Raffi, J.; Stevenson, M. H.; Kent, M.; Thiery, J. M.; Belliardo, J. J. Intercomparison on electron spin resonance identification of irradiated foodstuffs. *Int. J. Food Sci. Technol.* **1992**, *27*, 111−24.

(25) Ahn, J. J.; Akram, K.; Kim, H. K.; Kwon, J. H. Electron spin resonance spectroscopy for the identification of irradiated food with complex ESR signals. *Food Anal. Methods* **2013**, *6*, 301−308.

(26) Deighton, N.; Glidwell, S. M.; Goodman, B. A.; Morrison, I. M. Electron paramagnetic resonance of gamma-irradiated cellulose and lignocellulosic material. *Int. J. Food Sci. Technol.* **1993**, *28*, 45−55.

(27) de Jesus, E. F. O.; Rossi, A. M.; Lopes, R. T. Influence of sample treatment on ESR signal of irradiated citrus. *Appl. Radiat. Isot.* **1996**, *47*, 1647−1653.

(28) Dashak, D. A.; Dawang, M. L.; Lucas, N. B. An assessment of the proximate chemical composition of locally produced spices known as dadawa basso and dadawa kalwa from three markets in Plateau State of Nigeria. *Food Chem.* **2001**, *75*, 231−235.

(29) Raffi, J. J.; Agnel, J. P. L. Influence of the physical structure of irradiated starches on their electron spin resonance spectra kinetics. *J. Phys. Chem.* **1983**, *87*, 2369−2373.

(30) Tabner, B. J.; Tabner, V. A. An electron spin resonance study of gamma irradiated citrus fruits. *Radiat. Phys. Chem.* **1993**, *41*, 545−552.

(31) Yamaoki, R.; Tsujino, T.; Kimura, S.; Mino, Y.; Ohta, M. Detection of organic free radicals in irradiated *Foeniculi fructus* by electron spin resonance spectroscopy. *J. Nat. Med.* **2009**, *63*, 28−31.

(32) Sultanov, K.; Turaev, A. S. Mechanism of the radiolytic transformations of cellulose. *Chem. Nat. Compd.* **1996**, *32*, 570−576.

(33) de Jesus, E. F. O.; Rossi, A. M.; Lopes, R. T. Identification and dose determination using ESR measurements in the flesh of irradiated vegetal products. *Appl. Radiat. Isot.* **2000**, *52*, 1375−1383.

(34) Sanyal, B.; Sharma, A. A new electron paramagnetic resonance method to identify irradiated soybean. *J. Food Sci.* **2009**, *74*, N57−N64.

(35) Ahn, J. J.; Sanyal, B.; Park, E. J.; Lim, H. K.; Kwon, J. H. Effects of sample pretreatments on EPR spectral characteristics of irradiated sea algae − an advanced approach to identify irradiation status. *RSC Adv.* **2014**, *4*, 32312−32319.

(36) Gupta, S.; Shah, B.; Sanyal, B.; Variyar, P. S.; Sharma, A. Role of initial apparent viscosity and moisture content on post irradiation

rheological properties of guar gum. *Food Hydrocolloids* **2009**, *23*, 1785−1791.

analogues, which possess several characteristics that allow them to interact with analytes and serve as chiral selectors.[10−13] The most enantioselective separations of amino acids were carried out on teicoplanin or teicoplanin aglycone chiral stationary phases. The retention occurs when the teicoplanin ammonium group interacts with the carboxylate group of the amino acid or the ammonium group of the amino acid interacts with teicoplanin carboxylate, whereas chiral discrimination results from a complex interaction between analyte and tertiary teicoplanin structure.[13] The retention and chiral resolution can be optimized by changing the concentration and nature of the organic modifier in the mobile phase and enhancing steric conformation of the chiral stationary phase by adjusting pH, ionic strength of the mobile phase, and column temperature.[12−15]

Up to date, there are few papers dealing with the determination of amino acids in hydrolyzed protein fertilizers (HPFs).[16−18] Alarcón-Flores and co-workers[16] developed an ultrahigh-performance liquid chromatography−tandem mass spectrometry (UHPLC−MS/MS) method for the non-chiral determination of 19 underivatized protein amino acids in HPF samples. All amino acids were separated in 8 min by reversed phase, with the addition of the mobile-phase pentadecafluorooctanoic acid as the ion-pairing reagent. Cavani et al.[17] described the separation of protein amino acids derivatized with dansyl chloride by micellar electrokinetic chromatography and direct ultraviolet (UV) detection, employing $\beta$-cyclodextrin as the chiral selector. However, only one amino acid (dansylated D-/L-alanine) was considered, and its degree of racemization was calculated. More recently, Sánchez-Hernández et al.[18] have proposed a capillary electrophoresis−tandem mass spectrometry technique using cyclodextrins as chiral selectors to determine the degree of racemization of the free amino acids in HPFs. The enantiomeric separation of up to 14 amino acids was achieved in about 60 min with resolutions above 1.0.

In this study, a rapid and selective HPLC method based on chiral teicoplanin stationary phase and coupled with tandem mass spectrometry was developed and applied for the first time to the enantioselective determination of free amino acids in HPFs. Under optimized conditions, enantiomeric separation of 15 amino acids was achieved with a run time of 15 min. The method was validated and successfully applied to the analysis of five commercially available HPF samples.

## MATERIALS AND METHODS

**Chemicals and Reagents.** Amino acids L-alanine, L-arginine, L-asparagine, L-aspartic acid, L-cysteine, glycine, L-glutamine, L-glutamic acid, L-histidine, L-leucine, L-isoleucine, L-lysine, L-methionine, L-phenylalanine, L-proline, L-serine, L-threonine, L-tryptophan, L-tyrosine, and L-valine were purchased from Sigma-Aldrich (St. Louis, MO) as the L-amino acid kit. D-amino acids D-alanine, D-arginine, D-asparagine, D-aspartic acid, D-cysteine, D-glutamine, D-glutamic acid, D-histidine, D-leucine, D-lysine, D-methionine, D-phenylalanine, D-proline, D-serine, D-threonine, D-tryptophan, D-tyrosine, and D-valine were purchased separately also from Sigma-Aldrich (St. Louis, MO). Stock standard solution was made at 1 g/L concentration level in 1 mol/L aqueous formic acid solution and kept at 4 °C, in amber glass containers. Working standard solutions were made by appropriate dilution of stock standards in methanol/water solution (50:50, v/v) and kept at 4 °C temperature in amber glass vials prior to analysis. Ultra liquid chromatography−mass spectrometry (LC−MS) acetonitrile was purchased from Carl Roth GmbH & Co. (Karlsruhe, Germany), and ammonium acetate, formic acid, acetic acid, ethanol, and methanol (all LC−MS grade) were purchased from Sigma-Aldrich (St. Louis, MO). Purified water was obtained with a Milli-Q apparatus (Millipore, Bedford, MA).

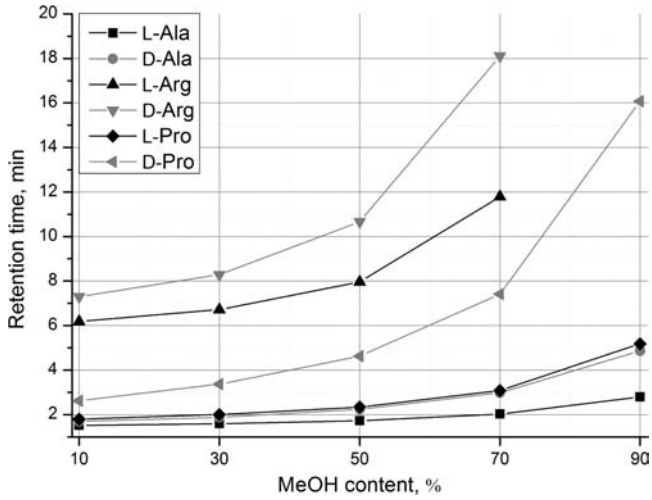


**Figure 1.** Effect of the methanol content in the mobile phase on the retention times of D-/L-Ala, D-/L-Arg, and D-/L-Pro enantiomers ($n$ = 2).

**HPLC−MS/MS Analyses.** Chromatographic separations were performed using an Agilent 1290 Infinity LC system coupled with a triple quadrupole 6410 tandem mass spectrometer equipped with an electrospray ionization (ESI) interface (Agilent Technologies, Santa Clara, CA). The column used was a 150 × 2.1 mm inner diameter, 5 $\mu$m, Astec CHIROBIOTIC T2 purchased from Sigma-Aldrich (St. Louis, MO). Data acquisition and processing were performed with Mass Hunter 5.0 software (Agilent Technologies, Santa Clara, CA). The mobile phase flow rate was 0.3 mL/min; the column was maintained at 15 °C temperature; and the sample volume was 2 $\mu$L. A binary mobile phase with gradient elution was used. Solvent A was water with 10 mmol/L ammonium acetate (pH 4.2), and solvent B was methanol/water (95:5, v/v) with 10 mmol/L ammonium acetate (pH 4.2). The gradient program was set as follows: 0−5 min, 5−50% A; 5−12 min, 50% A; and 12−13 min, 50−5% A. This was followed by a 2 min equilibration period prior to the injection of next sample. The total run time was 15 min.

MS/MS detection was performed in multiple reaction monitoring (MRM) mode. The ESI ion source was set for positive ionization at the following setup: capillary voltage, 4 kV; gas temperature, 300 °C; gas flow, 8 L/min; and nebulizer gas pressure, 30 psi. Cell accelerator voltage and dwell time were kept constant for all analytes and were set at 6 eV and 20 ms, respectively.

**Sample Preparation.** Five commercially available HPF products, namely, Aminocat 30% (sample A), Terra Sorb Complex (sample B), ILSA Drip Forte (sample C), Protifert LMW8 (sample D), and Rutter (sample E), were obtained from local suppliers. These HPF concentrates are viscous liquids containing free amino acids. All samples were prepared according to the procedure suggested by Alarcón-Flores et al.[16] An aliquot of fertilizer was weighed (100 mg), and 10 mL of water solution was adjusted to pH 1.5 with heptafluorobutyric acid. The mixture was thoroughly vortexed for 1 min and centrifuged for 15 min at 3000 rpm. After centrifugation, supernatant was filtered through a nylon 0.20 $\mu$m filter (Carl Roth GmbH & Co., Karlsruhe, Germany), 20 $\mu$L of the filtrate was transferred into the vial, 980 $\mu$L of initial mobile phase was added, and the final solution was taken for HPLC−MS/MS analysis. Because of the large amount of glutamic acid in sample A, the quantitation of D-/L-Glu in this sample was performed separately from 10 times extra-diluted extract.

## RESULTS AND DISCUSSION

**HPLC Separation Optimization.** Macrocyclic antibiotic-based chiral stationary phases are compatible with both organic and aqueous mobile phases. This makes Chirobiotic T2 the ideal stationary phase for resolving polar compounds, such as amino acids. Several parameters, such as nature and content of

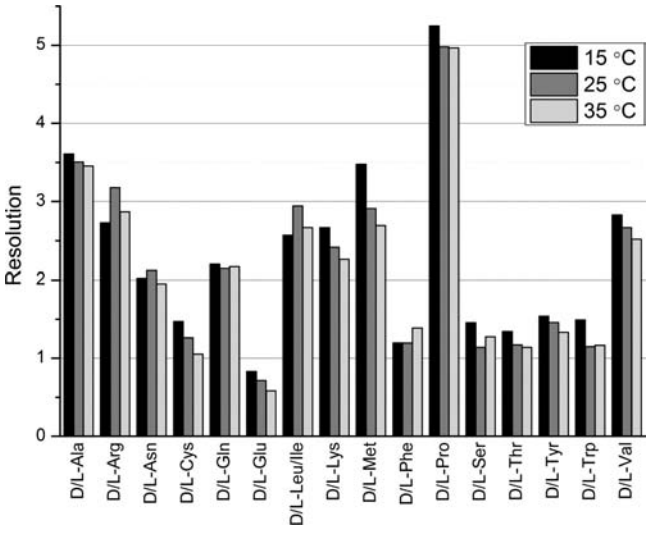


**Figure 2.** Effect of the temperature on the enatiomeric resolution of amino acids obtained in gradient elution mode ($n$ = 2).

the organic modifier in the mobile phase, mobile phase pH, and column temperature, were tested to find the optimum conditions allowing for the highest enantiomeric resolution of the analytes. Typically, the resolution of amino acids is influenced by the nature of organic modifier.[19,20] Three organic modifiers, namely, acetonitrile, ethanol, and methanol, were tested in the current study. Acetonitrile provided the best resolution for isobaric D-Leu/D-Iso and L-Leu/L-Iso pairs, but enantiomeric resolution of the rest of the D-/L-amino acids was reduced significantly. It was shown that the resolution can be improved with the increase of the organic modifier chain length.[21] However, the use of ethanol as the organic modifier increased the system back pressure and considerably decreased peak efficiency. Therefore, methanol was chosen for further optimization. For some analytes in reversed-phase separation mode, macrocyclic glycopeptide-based stationary phases exhibit U-shaped retention versus mobile-phase composition plots.[22−24] The increase in retention with decreasing the MeOH concentration at water-rich mobile-phase compositions is usually observed when hydrophobic interactions between analytes and stationary phase are dominant. At organic-rich mobile-phase compositions, an opposite trend is observed, which can be attributed to the lower solubility of the analytes in less polar mobile phases. The analytes therefore favored the stationary phase, which resulted in a stronger retention at a higher MeOH amount.[24] Figure 1 shows the plots of the retention times for three representative enantiomer pairs as a function of the MeOH concentration in the mobile phase. In this case, the gradually decreasing retention times with the decrease in the amount of MeOH in the mobile phase is not followed by a retention increase at water-rich mobile-phase compositions. The retention times are substantially unaffected by changes in mobile-phase composition for MeOH concentrations lower than 30% (v/v). Obtained results suggest that, for very hydrophilic compounds, such as amino acids, hydrophobic interactions are not the driven retention forces even at water-rich mobile phases.

It was reported earlier[21,25,26] that the discrimination of D-/L-amino acid enantiomers is also influenced by teicoplanin conformation, which can be affected by mobile-phase pH and temperature. Ammonium acetate, which exhibits adequate buffering capacity over the working pH range (3.8−6.8) of the stationary phase, was employed for mobile-phase pH adjustment. No significant effect on enantioselectivity within the pH range of 4−6 was observed, and only slightly better resolution was achieved at lower pH values. Teicoplanin contains a single primary amine ($pK_a \approx 9.2$) and a single carboxylic ($pK_a \approx 2.5$) group, which are mainly responsible for chiral recognition.[27] Thus, the variation of the pH between 4 and 6 does not change the charge state of the amino group and only slightly (at pH < 4.5) affects the charge state of the carboxylic

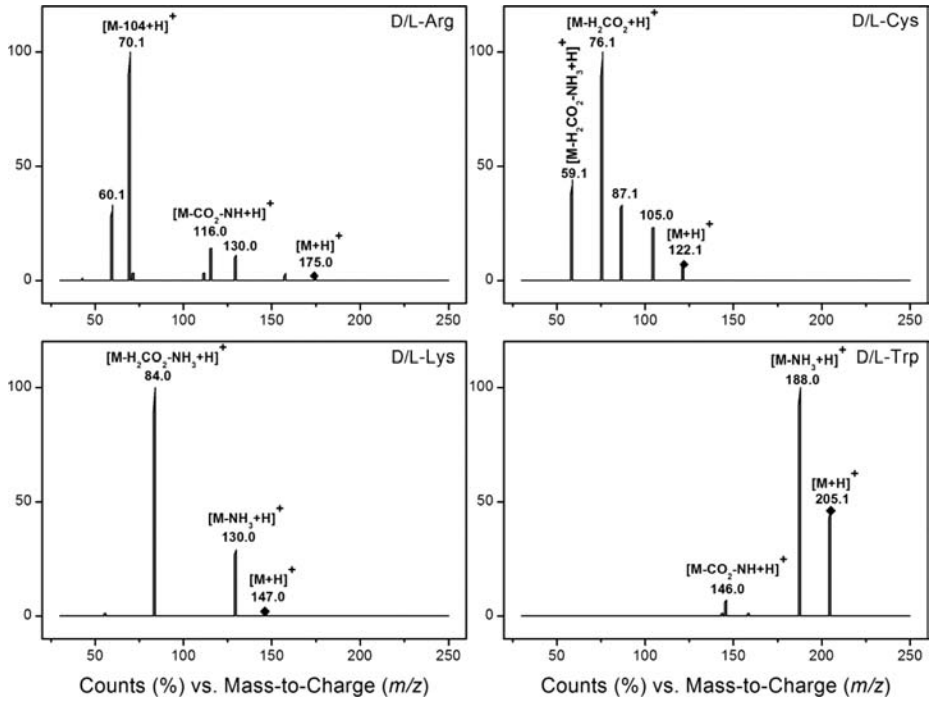


**Figure 3.** Product ion scan mass spectra of representative D-/L-amino acids (100 $\mu$g/L) obtained by direct infusion.


dx.doi.org/10.1021/jf5047333 | J. Agric. Food Chem. 2014, 62, 11099−11108

**Table 1. Optimized MRM Transition Parameters for Studied Amino Acids**

| amino acid | abbreviation | precursor ion | MRM transition[a] | fragmentor voltage (V) | collision energy (eV) |
|---|---|---|---|---|---|
| alanine | Ala | 90 | **90 → 44** | 70 | 10 |
| arginine | Arg | 175 | **175 → 70** | 90 | 25 |
| | | | 175 → 116 | | 11 |
| asparagine | Asn | 133 | **133 → 74** | 70 | 13 |
| | | | 133 → 87 | | 4 |
| aspartic acid | Asp | 134 | **134 → 74** | 70 | 12 |
| | | | 134 → 88 | | 5 |
| cysteine | Cys | 122 | **122 → 76** | 70 | 11 |
| | | | 122 → 59 | | 9 |
| glutamic acid | Glu | 148 | **148 → 84** | 70 | 14 |
| | | | 148 → 130 | | 4 |
| glutamine | Gln | 147 | **147 → 84** | 70 | 16 |
| | | | 147 → 130 | | 5 |
| glycine | Gly | 76 | **76 → 30** | 70 | 4 |
| | | | 76 → 48 | | 3 |
| histidine | His | 156 | **156 → 110** | 100 | 12 |
| | | | 156 → 95 | | 15 |
| isoleucine | Iso | 132 | **132 → 69** | 90 | 16 |
| | | | 132 → 86 | | 5 |
| leucine | Leu | 132 | **132 → 86** | 90 | 6 |
| | | | 132 → 69 | | 18 |
| lysine | Lys | 147 | **147 → 84** | 90 | 16 |
| | | | 147 → 130 | | 5 |
| methionine | Met | 150 | **150 → 104** | 80 | 6 |
| | | | 150 → 133 | | 4 |
| phenylalanine | Phe | 166 | **166 → 120** | 90 | 10 |
| | | | 166 → 103 | | 22 |
| proline | Pro | 116 | **116 → 70** | 60 | 14 |
| serine | Ser | 106 | **106 → 60** | 70 | 8 |
| | | | 106 → 42 | | 18 |
| threonine | Thr | 120 | **120 → 74** | 70 | 7 |
| | | | 120 → 102 | | 3 |
| tryptophan | Trp | 205 | **205 → 188** | 75 | 2 |
| | | | 205 → 146 | | 2 |
| tyrosine | Tyr | 182 | **182 → 136** | 60 | 8 |
| | | | 182 → 165 | | 3 |
| valine | Val | 118 | **118 → 72** | 50 | 7 |
| | | | 118 → 55 | | 23 |

[a]Quantitation transitions are in bold.

group. However, amino acids with pI values lower than 4, namely, D-/L-aspartic acid (pI = 2.98) and D-/L-glutamic acid (pI = 3.08) were only partially resolved under these conditions. Because of the limited stationary-phase pH working range, it was impossible to try to resolve them in their fully protonated form. On the basis of the obtained results, mobile phase with pH 4.2 was chosen for further experiments. It should be noted that more acidic mobile phase is favored over positive ESI ionization mode for better signal response.

From the temperature dependence obtained in gradient elution mode, it was observed that, for most amino acids at the lower temperature, the resolution of the enantiomers increases (Figure 2). A lower temperature generally results in better enantioselectivity ($\alpha$) on most macrocyclic glycopeptide-based chiral stationary phases employed in reversed-phase mode because of the negative enthalpy difference [$\Delta(\Delta H^\circ)$] for the transfer of enantiomers from the mobile phase to the stationary phase.[22,24] All investigated amino acid enantiomers, except for D-/L-Asn, gave negative $\Delta(\Delta H^\circ)$ values, with correlation coefficients higher than 0.98 (results not shown). However, resolution does not always follow the same trend of selectivity. As observed from Figure 2, some D-/L-amino acid pairs exhibited slight $R_s$ improvement with increase of the temperature. Raising the temperature most often is associated with an increase in peak efficiency. Thus, because the resolution factor combines both retention differences and efficiency, the higher contribution to the resolution for these acids most likely came from the increase in efficiency.

Several other parameters, such as buffer concentration, flow rate, and sample volume, were also briefly tested to improve chromatographic performance, but no obvious improvement in the enantiomeric resolution was observed.

**Tandem Mass Spectrometry.** Ion source and MS parameters were optimized manually via direct infusion of a standard solution of 100 $\mu$g/L of each amino acid at 3 $\mu$L/min flow rate. The standard solutions were prepared in water/MeOH (50:50, v/v) containing 10 mmol/L formic acid. Full-scan MS spectra showed the most abundant protonated $[M + H]^+$ molecular ion for all amino acids in positive ESI mode. First quadrupole was set to single ion monitoring mode

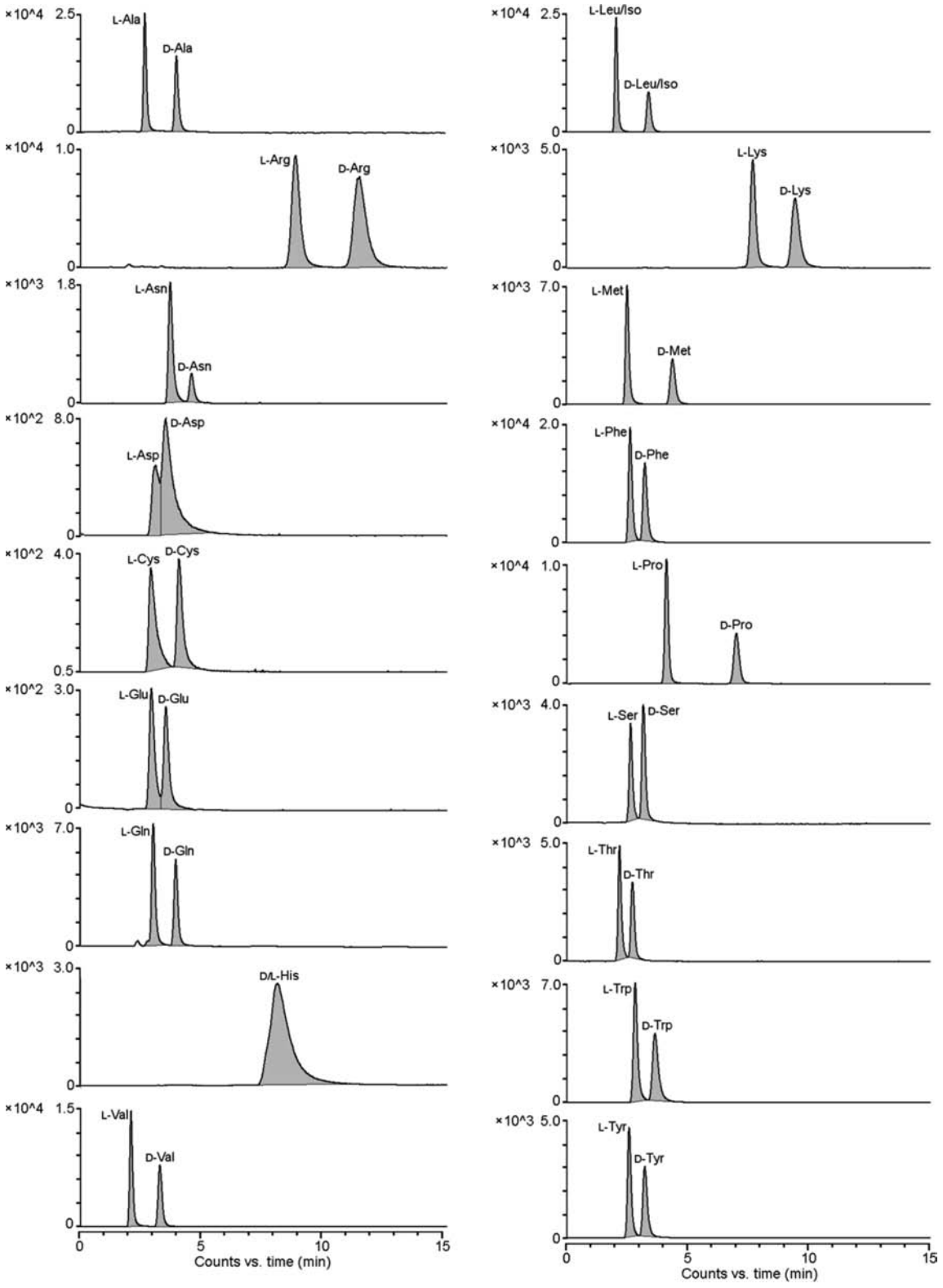


**Figure 4.** MRM chromatograms (transitions used for quantitation) of the amino acid standard mixture at the 50 $\mu$g/mL level obtained under optimized HPLC−MS/MS conditions.

for the selected protonated precursor ion, and the fragmentor voltages (from 50 to 150 V) were tuned individually to each amino acid. Then, product ion MS spectra were acquired, and from the collision-induced dissociation (CID) experiments, the most abundant transition ions were selected. Only one transition was monitored for alanine and proline because of their low molecular weights. The rest of the amino acids produced quantitative and qualitative MRM transitions each. Most of the amino acids gave quantitative MRM transitions corresponding to the loss of formic acid $[M - HCOOH + H]^+$ or formic acid and ammonia $[M - HCOOH - NH_3 + H]^+$, whereas Arg and Trp led to the formation of $[M - 104 + H]^+$


dx.doi.org/10.1021/jf5047333 | J. Agric. Food Chem. 2014, 62, 11099−11108

Table 2. Summary of the Recovery and Precision Data for Sample A ($n$ = 4)

| | | | intraday (RSD %) | | | interday (RSD %) | | |
|---|---|---|---|---|---|---|---|---|
| analyte | enantiomer | recovery (%) (RSD %) | sample A | spike level of 0.5 μg/mL | spike level of 5.0 μg/mL | sample A | spike level of 0.5 μg/mL | spike level of 5.0 μg/mL |
| alanine | D | 88.7 (18.7) | ND[a] | 5.9 | 2.3 | ND | 3.0 | 8.8 |
| | L | 93.5 (3.8) | 4.2 | 5.5 | 1.6 | 6.8 | 4.8 | 7.0 |
| arginine | D | 95.0 (13.2) | ND | 3.9 | 2.1 | ND | 13.9 | 5.6 |
| | L | 92.7 (11.9) | 7.4 | 2.0 | 2.6 | 6.2 | 1.9 | 7.3 |
| asparagine | D | 89.2 (19.6) | ND | 6.7 | 0.4 | ND | 3.5 | 18.0 |
| | L | 115.3 (16.7) | 3.9 | 4.6 | 1.3 | 7.4 | 3.4 | 7.1 |
| aspartic acid | D/L | 108.4 (23.1) | 2.8 | 8.5 | 2.2 | 11.9 | 1.3 | 8.9 |
| cysteine | D | 114.8 (3.3) | ND | 6.2 | 4.0 | ND | 3.4 | 11.7 |
| | L | 80.5 (20.2) | ND | 6.3 | 1.1 | ND | 3.6 | 6.4 |
| glutamic acid | D/L | 92.3 (6.0) | 3.9 | 7.1 | 6.5 | 8.4 | 1.5 | 0.8 |
| glutamine | D | 80.3 (15.9) | ND | 5.9 | 2.0 | ND | 1.7 | 13.4 |
| | L | 85.2 (3.8) | 0.9 | 10.5 | 1.3 | 13.8 | 19.7 | 11.6 |
| glycine | | 99.0 (19.1) | 2.9 | 5.4 | 3.2 | 0.7 | 0.5 | 2.7 |
| histidine | D/L | 97.2 (11.0) | 3.4 | 4.5 | 2.3 | 21.7 | 7.6 | 1.8 |
| leucine/isoleucine | D | 95.1 (13.0) | ND | 6.1 | 1.2 | ND | 1.3 | 5.1 |
| | L | 98.8 (6.6) | 5.9 | 5.8 | 1.5 | 8.9 | 1.8 | 8.8 |
| lysine | D | 78.4 (7.2) | ND | 5.6 | 2.1 | ND | 7.8 | 15.6 |
| | L | 101.3 (8.9) | 8.0 | 1.6 | 0.7 | 11.7 | 12.7 | 2.7 |
| methionine | D | 86.6 (10.9) | ND | 8.6 | 2.8 | ND | 8.6 | 7.7 |
| | L | 93.4 (21.7) | 4.3 | 10.1 | 3.0 | 12.4 | 1.1 | 12.3 |
| phenylalanine | D | 79.8 (15.1) | ND | 3.9 | 1.4 | ND | 4.6 | 6.4 |
| | L | 81.0 (6.5) | 7.3 | 7.6 | 2.8 | 0.6 | 6.7 | 9.4 |
| proline | D | 98.7 (6.0) | 8.3 | 10.9 | 2.7 | 6.7 | 13.4 | 14.0 |
| | L | 96.6 (15.5) | 6.9 | 5.7 | 1.2 | 13.8 | 1.0 | 9.8 |
| serine | D | 95.4 (7.1) | ND | 2.6 | 1.7 | ND | 5.2 | 18.1 |
| | L | 97.6 (19.0) | 7.4 | 7.0 | 2.4 | 10.0 | 0.0 | 2.7 |
| threonine | D | 73.4 (11.4) | ND | 4.9 | 1.7 | ND | 5.7 | 15.5 |
| | L | 102.0 (13.5) | 8.1 | 6.6 | 1.7 | 6.4 | 0.5 | 8.8 |
| tryptophan | D | 106.2 (16.0) | ND | 4.1 | 2.2 | ND | 5.6 | 9.8 |
| | L | 116 (6.0) | 7.6 | 7.9 | 6.6 | 8.1 | 8.7 | 5.0 |
| tyrosine | D | 98.7 (21.9) | ND | 16.4 | 3.8 | ND | 2.7 | 14.0 |
| | L | 97.0 (15.5) | 3.7 | 7.7 | 4.6 | 19.5 | 3.0 | 14.6 |
| valine | D | 91.1 (13.4) | ND | 5.4 | 0.9 | ND | 4.3 | 5.0 |
| | L | 99.4 (1.8) | 4.7 | 7.4 | 1.8 | 5.5 | 0.5 | 10.5 |

[a]ND = not detected.

and $[M - NH_3 + H]^+$ ions, respectively (Figure 3). The CID collision energies were also tuned manually by monitoring product ion intensity in MRM mode in the range from 2 to 30 eV. All optimal transitions as well as fragmentor voltages and collision energies for investigated amino acids are presented in Table 1.

MRM chromatograms (only transitions used for quantitation) of the amino acid standard mixture at the 50 μg/mL level obtained under optimized HPLC–MS/MS conditions are presented in Figure 4. As can be observed, complete enantiomeric separation of 15 amino acids was achieved in about 15 min. D-/L-Glu and D-/L-Asp pairs were partially resolved, and only for D-/L-His enantiomers was no resolution obtained.

**Method Validation.** The proposed method was validated in terms of linearity, limit of detection (LOD), limit of quantitation (LOQ), accuracy, and precision, following the ICH harmonized tripartite guideline.[28] All HPF samples from the point of composition (provided by the manufacturer) and brief visual evaluation looked similar, but preliminary investigations showed that sample A contains the highest total amount of free amino acids. Consequently, this sample was chosen as the model matrix for validation.

One significant drawback of ESI–MS is that the ionization process is greatly affected by the co-eluting matrix compounds.[29] The matrix effect typically results in the suppression or, less frequently, enhancement of the analyte signal. Isotopically labeled internal standards or matrix-matched calibration are the two common approaches that have been widely used to eliminate or correct matrix effects in LC–MS/MS analyses. However, neither the blank matrix of analyzed fertilizers nor isotopically labeled standards for all investigated amino acids are unavailable. Therefore, in this study, matrix effects were evaluated by the standard addition method. The signal suppression/enhancement observed with each analyte was calculated as the percentage difference in signal intensity measured in the sample extract versus that measured in the pure solvent

$$\text{percentage difference (\%)} = (A_{\text{spiked}} - A_{\text{unspiked}})/A_{\text{solv}} \times 100\%$$

where $A_{\text{spiked}}$ is the analyte peak area in the spiked sample, $A_{\text{unspiked}}$ is the peak area without spiking, and $A_{\text{solv}}$ is the peak area in pure solvent.

A value of 100% is indicative if no signal suppression/enhancement is observed. The aliquots of 10 μL sample extracts were spiked at two concentration levels (100 and 500 μg/mL),

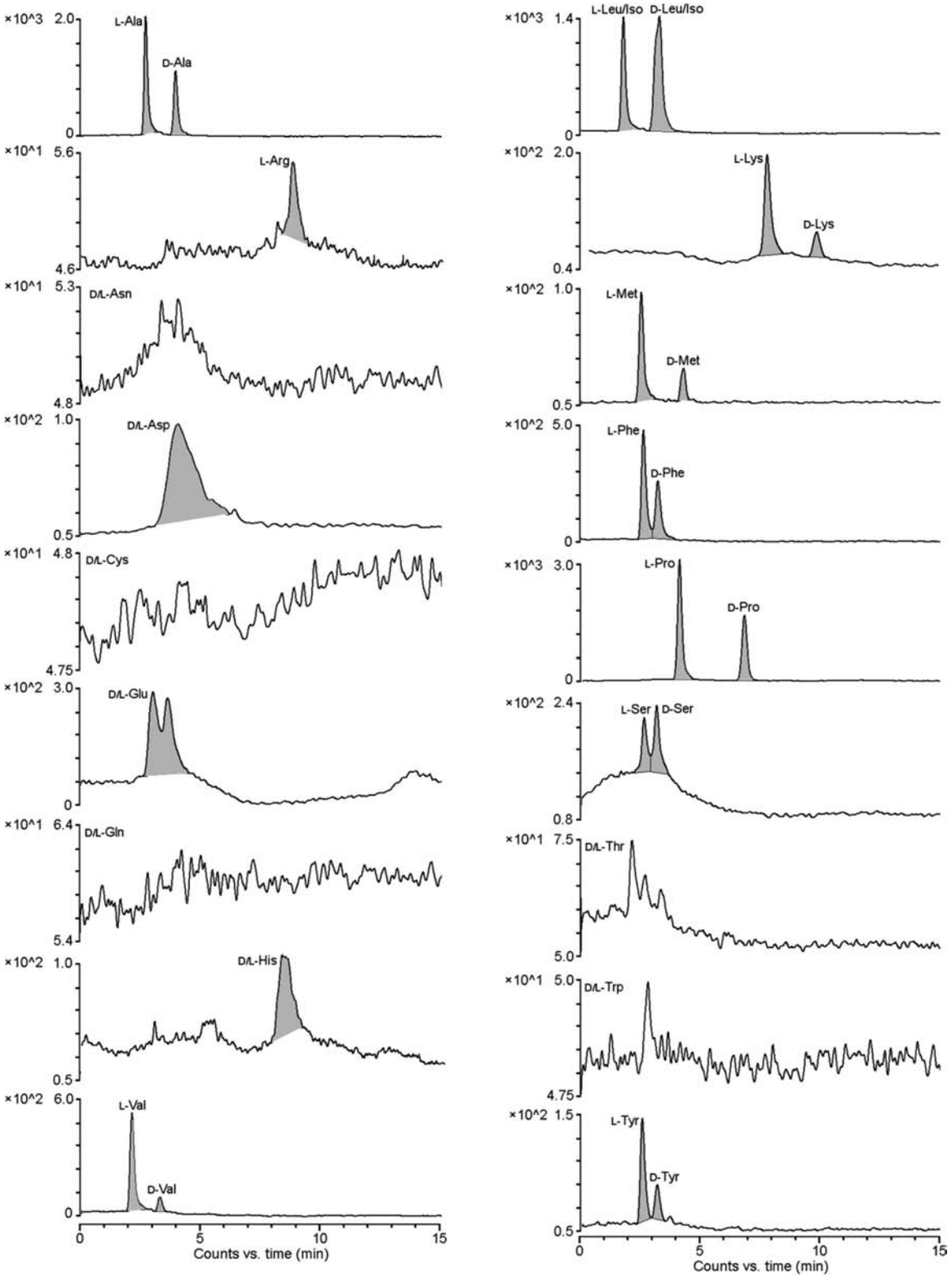


**Figure 5.** MRM chromatograms (transitions used for quantitation) obtained for sample D (Protifert LMW8).

diluted by a factor of 100, and analyzed. Because of high dilution factor of the extracts, signal suppression was not crucial and was in the range of 90.2−117.1% (see Table S1 of the Supporting Information). Nonetheless, to ensure bias-free results, the standard addition protocol was employed for quantitation.

LODs and LOQs were determined (see Table S1 of the Supporting Information) from standard addition experiments (for sample A) based on the standard deviation of the response and the slope, expressed as follows:

$$\text{LOD} = 3.3\sigma/S \quad \text{and} \quad \text{LOQ} = 10\sigma/S$$

where $\sigma$ is the standard deviation of $y$ intercepts of regression lines and $S$ is the slope estimated from the regression curve.


dx.doi.org/10.1021/jf5047333 | J. Agric. Food Chem. 2014, 62, 11099−11108

Table 3. Determined Concentrations of the D- and L-Amino Acids in the Commercial HPF Samples ($n$ = 3)

| analyte | enantiomer | determined amount (mg/g) (±SD) | | | | |
|---|---|---|---|---|---|---|
| | | sample A | sample B | sample C | sample D | sample E |
| alanine | D | ND[a] | 0.3 (0.1) | 1.7 (0.2) | 14.0 (0.3) | 2.1 (0.3) |
| | L | 9.2 (0.2) | 7.8 (0.7) | 2.7 (0.3) | 15.9 (0.4) | 3.9 (0.3) |
| arginine | D | ND | ND | ND | ND | ND |
| | L | 7.1 (1.4) | 9.5 (1.7) | 0.82 (0.01) | 1.1 (0.1) | 1.2 (0.3) |
| asparagine | D | ND | ND | ND | ND | ND |
| | L | 1.9 (0.5) | 1.8 (0.4) | 0.07 (0.02) | ND | ND |
| aspartic acid | D/L | 10.9 (0.8) | 14.9 (0.5) | 0.25 (0.05) | 12.5 (1.5) | ND |
| cysteine | D | ND | ND | ND | ND | ND |
| | L | ND | ND | ND | ND | ND |
| glutamic acid | D/L | 151.6 (5.5) | 34.4 (5.0) | 0.50 (0.1) | 11.5 (0.6) | 31.9 (1.5) |
| glutamine | D | ND | ND | ND | ND | ND |
| | L | 0.6 (0.1) | 2.8 (0.5) | 0.05 (0.02) | ND | 1.72 (0.5) |
| glycine | | 18.8 (0.6) | 38.0 (5.0) | 5.3 (0.2) | 68.2 (5.0) | 11.2 (1.5) |
| histidine | D/L | 5.7 (0.3) | 9.3 (2.0) | 0.30 (0.05) | 2.6 (0.1) | 1.49 (0.2) |
| leucine/isoleucine | D | ND | ND | ND | 5.5 (0.5) | 0.55 (0.1) |
| | L | 3.4 (0.7) | 2.7 (0.2) | 0.63 (0.04) | 2.0 (0.1) | 0.49 (0.05) |
| lysine | D | ND | ND | ND | 5.8 (0.5) | ND |
| | L | 27.7 (0.9) | 24.8 (1.3) | 0.52 (0.01) | 6.1 (1.0) | 2.4 (0.4) |
| methionine | D | ND | ND | ND | 0.62 (0.1) | ND |
| | L | 0.4 (0.1) | 0.4 (0.1) | 0.25 (0.1) | 0.63 (0.1) | 0.4 (0.2) |
| phenylalanine | D | N.D. | 0.6 (0.1) | 0.03 (0.01) | 1.5 (0.1) | 0.35 (0.1) |
| | L | 4.3 (0.4) | 4.6 (0.1) | 0.37 (0.1) | 1.7 (0.1) | 0.68 (0.2) |
| proline | D | 1.0 (0.2) | 2.1 (0.3) | 0.18 (0.03) | 10.8 (0.3) | 1.6 (0.3) |
| | L | 5.9 (1.0) | 6.6 (1.0) | 0.18 (0.04) | 11.4 (0.2) | 1.9 (0.3) |
| serine | D | ND | ND | ND | 1.5 (0.2) | ND |
| | L | 8.6 (0.1) | 7.3 (1.6) | 0.24 (0.1) | 0.56 (0.05) | 2.0 (0.2) |
| threonine | D | ND | ND | ND | ND | ND |
| | L | 7.7 (0.1) | 7.9 (0.4) | 0.8 (0.3) | ND | 0.6 (0.1) |
| tryptophan | D | ND | ND | ND | ND | ND |
| | L | 1.4 (0.4) | 1.4 (0.5) | 0.07 (0.01) | ND | 0.25 (0.03) |
| tyrosine | D | ND | ND | ND | 0.80 (0.1) | ND |
| | L | 3.0 (0.4) | 3.0 (0.4) | 0.20 (0.03) | 1.7 (0.1) | 0.70 (0.1) |
| valine | D | ND | ND | 0.02 (0.01) | 1.1 (0.1) | 0.03 (0.01) |
| | L | 2.0 (0.3) | 7.7 (0.4) | 0.61 (0.1) | 1.6 (0.2) | 0.42 (0.01) |

[a]ND = not detected.

Table 4. Declared and Determined Amounts of Free Amino Acids in Commercial HPF Samples ($n$ = 3)

| sample | brand | declared amount (w/w) of amino acids | determined amount[a] (w/w) of L-amino acids (%) (±SD) | determined amount (w/w) of D-amino acids (%) (±SD) |
|---|---|---|---|---|
| A | Aminocat 30% | contains 30% free L-amino acids + glycine | 27.0 (1.4) | <0.1 |
| B | Terra Sorb Complex | contains 20% free L-amino acids + glycine | 18.5 (2.2) | 0.3 |
| C | ILSA Drip Forte | total amino acids of >50%; contains free amino acids, mainly in the L form | 1.4 (0.2) | 0.2 |
| D | Protifert LMW8 | total amino acids of 50% and free amino acids of 15%; no information on polarization | 12.3 (0.2) | 4.2 (0.2) |
| E | Rutter | no information | 6.1 (0.6) | 0.5 (0.1) |

[a]Amounts of enantiomerically unresolved amino acids and glycine were included to L-amino acids.

Because of the high number of closely eluting analytes, the time segmentation for MRM analysis was not employed and the dwell time for each MRM transition was set to 20 ms. Although this led to reduced detectability and narrower linear ranges, obtained sensitivity was still acceptable for HPF samples.

Because of the absence of reference materials, method trueness was evaluated by spiking/recovery experiments. Fertilizer aliquots (100 mg) were spiked with an approximately 50 $\mu$g/mL standard of L- and D-amino acids, and the sample preparation procedure was applied. The recovery values ranged from 73.4% for D-threonine to 115.3% for D-asparagine, with relative standard deviations (RSDs) lower than 20%, except for L-methionine (21.7%) and D-tyrosine (21.9%). Precision was evaluated in terms of repeatability and reproducibility. Interday repeatability was evaluated for the sample without spiking and spiked at two concentration levels: 0.5 and 5.0 $\mu$g/mL. This procedure was also performed for interday precision experiments within 4 sequential days. Recovery and precision data are summarized in Table 2.

**Sample Analysis.** Five commercially available HPF samples were analyzed under optimized HPLC−MS/MS conditions.

As already mentioned above, samples were prepared according to the recently published procedure;[16] therefore, no additional optimization of this step was performed. Only stability of the analytes was checked, and no racemization during the extraction procedure was observed. Because of low or no enantiomeric resolution, aspartic acid, glutamic acid, and histidine were determined as the sum of D and L enantiomers, whereas for unresolved isobaric D-Iso/D-Leu and L-Iso/L-Leu, only the sum of L-Iso and L-Leu as well as D-Iso and D-Leu amounts was measured. As an example, MRM chromatograms of sample D are presented in Figure 5. Determined concentrations of the individual amino acid enantiomers are summarized in Table 3. Finally, the obtained total amounts of D- and L-amino acids were compared to those declared by the manufacturer (Table 4). Unfortunately, composition of sample E was not specified. As seen, for samples A, B, and D, the determined values agree well with the amounts provided by manufacturers. The majority of the amino acids in sample C most likely exist in bonded form. Samples A and B had the highest enantiomerical purity, whereas in sample D, at least one-fourth of the total amino acid amount was the D enantiomer.

## ■ ASSOCIATED CONTENT

### Supporting Information

Method performance data in terms of regression parameters, LODs, LOQs, and signal suppression (Table S1). This material is available free of charge via the Internet at http://pubs.acs.org.

## ■ AUTHOR INFORMATION


### Corresponding Author

*Telephone: +370-5-2193119. Fax: +370-5-2330987. E-mail: lukas.taujenis@chf.vu.lt.



### Funding

The study was funded from the European Community's Social Foundation under Grant Agreement VP1-3.1-SMM-08-K-01-004/KS-120000-1756.


### Notes

The authors declare no competing financial interest.

## ■ ABBREVIATIONS USED

CID, collision-induced dissociation; ESI, electrospray ionization; HPF, hydrolyzed protein fertilizer; LOD, limit of detection; LOQ, limit of quantitation; MRM, multiple reaction monitoring

## ■ REFERENCES


(1) Jie, M.; Raza, W.; Xu, Y. C.; Shen, Q.-R. Preparation and optimization of amino acid chelated micronutrient fertilizer by hydrolyzation of chicken waste feathers and the effects on growth of rice. *J. Plant Nutr.* **2008**, *31*, 571−582.

(2) Paleckiene, R.; Sviklas, A.; Šlinkšiene, R. Physicochemical properties of a microelement fertilizer with amino acids. *Russ. J. Appl. Chem.* **2007**, *80*, 352−357.

(3) Forsum, O.; Svennerstam, H.; Ganeteg, U.; Nasholm, T. Capacities and constraints of amino acid utilization in *Arabidopsis*. *New Phytol.* **2008**, *179*, 1058−1069.

(4) Svennerstam, H.; Ganeteg, U.; Bellini, C.; Nasholm, T. Comprehensive screening of *Arabidopsis* mutants suggests the lysine histidine transporter 1 to be involved in plant uptake of amino acids. *Plant Physiol.* **2007**, *143*, 1853−1860.

(5) Dołowy, M.; Pyka, A. Application of TLC, HPLC and GC methods to the study of amino acid and peptide enantiomers: A review. *Biomed. Chromatogr.* **2013**, *28*, 84−101.

(6) Ilisz, I.; Berkecz, R.; Peter, A. Application of chiral derivatizing agents in the high-performance liquid chromatographic separation of amino acid enantiomers: A review. *J. Pharm. Biomed. Anal.* **2008**, *47*, 1−15.

(7) Ilisz, I.; Aranyi, A.; Peter, A. Chiral derivatizations applied for the separation of unusual amino acid enantiomers by liquid chromatography and related techniques. *J. Chromatogr. A* **2013**, *1296*, 119−139.

(8) Lämmerhoffer, M. Chiral recognition by enantioselective liquid chromatography: Mechanisms and modern chiral stationary phases. *J. Chromatogr. A* **2010**, *1217*, 814−856.

(9) Armstrong, D. W.; Tang, Y.; Chen, S.; Zhou, Y.; Bagwill, C.; Chen, J. R. Macrocyclic antibiotics as a new class of chiral selectors for liquid chromatography. *Anal. Chem.* **1994**, *66*, 1473−1484.

(10) Armstrong, D. W.; Liu, Y. B.; Ekborg-Ott, K. H. Covalently bonded teicoplanin chiral stationary-phase for HPLC enantioseparations. *Chirality* **1995**, *7*, 474−497.

(11) Péter, A.; Török, G.; Armstrong, D. W. High-performance liquid chromatographic separation of enantiomers of unusual amino acids on a teicoplanin chiral stationary phase. *J. Chromatogr. A* **1998**, *793*, 283−296.

(12) Ilisz, I.; Berkecz, R.; Péter, A. HPLC separation of amino acid enantiomers and small peptides on macrocyclic antibiotic-based chiral stationary phases: A review. *J. Sep. Sci.* **2006**, *29*, 1305−1321.

(13) Ilisz, I.; Berkecz, R.; Péter, A. Retention mechanism of high-performance liquid chromatographic enantioseparation on macrocyclic glycopeptide-based chiral stationary phases. *J. Chromatogr. A* **2009**, *1216*, 1845−1860.

(14) Poplewska, I.; Kramarz, R.; Piatkowski, W.; Seidel-Morgenstern, A.; Antos, D. Behavior of adsorbed and fluid phases versus retention properties of amino acids on the teicoplanin chiral selector. *J. Chromatogr. A* **2008**, *1192*, 130−138.

(15) Beesley, T. E.; Lee, J. T. Method development strategy and applications update for CHIROBIOTIC chiral stationary phases. *J. Liq. Chromatogr. Relat. Technol.* **2009**, *32*, 1733−1767.

(16) Alarcón-Flores, M. I.; Romero-González, R.; Frenich, A. G.; Martínez Vidal, J. L.; Reyes, R. C. Rapid determination of underivatized amino acids in fertilizers by ultra high performance liquid chromatography coupled to tandem mass spectrometry. *Anal. Methods* **2010**, *2*, 1745−1751.

(17) Cavani, L.; Ciavatta, C.; Gessa, C. Determination of free L- and D-alanine in hydrolysed protein fertilisers by capillary electrophoresis. *J. Chromatogr. A* **2003**, *985*, 463−469.

(18) Sánchez-Hernández, L.; Serra, N. S.; Marina, M. L.; Crego, A. L. Enantiomeric separation of free L- and D-amino acids in hydrolyzed protein fertilizers by capillary electrophoresis tandem mass spectrometry. *J. Agric. Food Chem.* **2013**, *61*, 5022−5030.

(19) Jandera, P.; Skavrada, M.; Klemmova, K.; Backovska, V.; Guiochon, G. Effect of the mobile phase on the retention behaviour of optical isomers of carboxylic acids and amino acids in liquid chromatography on bonded teicoplanin columns. *J. Chromatogr. A* **2001**, *917*, 123−133.

(20) Poplewska, I.; Kramarz, R.; Piatkowski, W.; Seidel-Morgenstern, A.; Antos, D. Behavior of adsorbed and fluid phases versus retention properties of amino acids on the teicoplanin chiral selector. *J. Chromatogr. A* **2008**, *1192*, 130−138.

(21) Beesley, T. E.; Lee, J. T. Method development strategy and applications update for CHIROBIOTIC chiral stationary phases. *J. Liq. Chromatogr. Relat. Technol.* **2009**, *32*, 1733−1767.

(22) Tesarŏvá, E.; Bosáková, Z.; Pacáková, V. Comparison of enantioselective separation of *N-tert*-butyloxycarbonyl amino acids and their non-blocked analogues on teicoplanin-based chiral stationary phase. *J. Chromatogr. A* **1999**, *838*, 121−129.

(23) Schlauch, M.; Frahm, A. W. Enantiomeric and diastereomeric high-performance liquid chromatographic separation of cyclic *β*-substituted *α*-amino acids on a teicoplanin chiral stationary phase. *J. Chromatogr. A* **2000**, *868*, 197−207.

(24) Péter, A.; Vekes, E.; Armstrong, D. W. Effects of temperature on retention of chiral compounds on a ristocetin A chiral stationary phase. *J. Chromatogr. A* **2002**, *958*, 89−107.

(25) Schlauch, M.; Kos, O.; Frahm, A. W. Comparison of three chiral stationary phases with respect to their enantio- and diastereoselectivity

for cyclic β-substituted α-amino acids. *J. Pharm. Biomed. Anal.* **2002**, *27*, 409−419.
(26) Berthod, A.; He, B. L. F.; Beesley, T. E. Temperature and enantioseparation by macrocyclic glycopeptide chiral stationary phases. *J. Chromatogr. A* **2004**, *1060*, 205−214.
(27) Berthod, A.; Liu, Y.; Bagwill, C.; Armstrong, D. W. Facile liquid chromatographic enantioresolution of native amino acids and peptides using a teicoplanin chiral stationary phase. *J. Chromatogr. A* **1996**, *731*, 123−137.
(28) Thompson, M.; Ellison, S. L. R.; Wood, R. Harmonized guidelines for single-laboratory validation of methods of analysis. *Pure Appl. Chem.* **2002**, *74*, 835−855.
(29) Taylor, P. J. Matrix effects: The Achilles heel of quantitative high-performance liquid chromatography−electrospray−tandem mass spectrometry. *Clin. Biochem.* **2005**, *38*, 328−334.

luteolin, quercetin, apigenin, rutin, and kaempferol), which are the constituents responsible for its free radical scavenging activity.[16]

Resorcinol is known as a fluorescent compound (molar fluorescence coefficient, $\varepsilon = 1.59 \times 10^7$ $M^{-1}$ $cm^{-1}$), and its fluorescence intensity decreases as a result of its sequential chlorination with HOCl.[17] Heasley et al. reported that the non-fluorescent monochloro- to dichloro- and to trichlororesorcinol products are formed.[18] The HOCl scavenging activity of the tested polyphenols (as $IC_{25}$ values) is directly linked to the decrease in resorcinol fluorescence under HOCl attack in the presence of polyphenols. The scavenging activity of the polyphenols was also measured with the KI/taurine assay chosen as a reference method.[19]

In this study, the HOCl scavenging activities of polyphenols (flavonoids, simple hydroxybenzoic and hydroxycinnamic acids, etc.) individually and in mixtures (e.g., in herbal teas) were determined with the developed method for the first time. In the preparation of herbal teas for analysis, the method of microwave extraction was used, having distinct advantages of reduced cost and time and increased reproducibility over classical extraction methods (such as Soxhlet extraction, liquid−liquid extraction, column chromatography, and preconcentration techniques). The results obtained with the developed method for polyphenolic compounds and herbal teas were statistically compared [using the analysis of variance (ANOVA) test] to those found by the reference methods KI/taurine and HPLC. As a result, the advantages of the optimized sample preparation (microwave extraction) and fluorometric determination (HOCl scavenging activity measurement) procedures were clearly stated.

## MATERIALS AND METHODS

**Reagents and Apparatus.** The following chemical substances of analytical reagent grade were supplied from the corresponding sources: methanol (MeOH), ethanol (EtOH), quercetin (QR), kaempferol, myricetin, rutin (RT), chlorogenic acid (CHA), naringenin, luteolin (LT), apigenin, gallic acid, and taurine (2-aminoethanesulfonic acid) from Sigma (Taufkirchen, Germany), 4-chlororesorcinol, *p*-coumaric acid, chrysin, and rosmarinic acid from Aldrich (Taufkirchen, Germany), sodium hypochlorite (NaOCl) from Merck (Darmstadt, Germany), acetic acid and potassium iodide from Riedel-de Haën (Taufkirchen, Germany), and resorcinol, hesperetin, (+)-catechin (C), (−)-epicatechin (EC), (−)-epigallocatechin (EGC), (−)-epigallocatechin gallate (EGCG), and ellagic acid from Fluka (Buchs, Switzerland). Herbal material leaves (green tea, sage, yarrow, and alchemilla) were obtained from a local market.

The fluorescence intensity and absorption measurements were performed using a Varian (Mulgrave, Victoria, Australia) Cary Eclipse model spectrofluorometer and a Cary 100 model ultraviolet−visible (UV−vis) spectrophotometer, respectively. The ETHOS-One (Milestone, Shelton, CT) closed vessel oven system was used for microwave-assisted extraction (MAE). Distilled water was supplied from Simpak1 Synergy purification system (Millipore, Billerica, MA). A Waters Breeze 2 model HPLC system (Milford, MA) consisting of a 2998 photodiode array detector and Empower PRO software was used for chromatographic separation, detection, and data acquisition.

**Preparation of Solutions.** The HOCl solution was prepared daily from a commercial solution (0.5%, v/v) by acidification with diluted sulfuric acid to pH 6.2. This stock solution was diluted 10-fold, and its concentration was determined using constant molar absorptivity ($\varepsilon$ = 100 L $mol^{-1}$ $cm^{-1}$) at 235 nm.[20] The fluorogenic resorcinol probe, potassium iodide, and taurine solutions were prepared in distilled water at 50 $\mu$M, 2.0 M, and 0.15 M concentrations, respectively. The polyphenolic solutions were freshly prepared in absolute ethanol. Methanol and 1.0% (v/v) acetic acid were used as the mobile phase for HPLC analysis.

**MAE of Herbal Teas.** The ETHOS-One (Milestone, Shelton, CT) closed vessel oven system equipped with 12 Teflon [polytetrafluoroethylene (PTFE)] vessels and an automatic fiber optic temperature control system were used for MAEs. Extractions were performed at 500 W and 80 °C, and a magnetic stirring rod was added in each vessel. The cut herbal materials were extracted using the following method: a 10 mL ethanol (80%) solution was added to 0.5 g of dried sample powder placed in an inner vessel. The vessels were placed symmetrically in the oven system. The herbal material in EtOH was microwave-irradiated as follows: 3 min for heating to the desired temperature (80 °C), 3 min for balancing at 80 °C, and 5 min for cooling. All herbal extracts were diluted (1:100) with 80% ethanol. The ethanolic extracts were filtered through a filter paper and membrane media (0.45 $\mu$m) successively before analysis.

**Resorcinol Assay.** The fluorometric resorcinol assay was performed as described by Özyürek et al.,[21] with some modifications. The reaction mixture contained polyphenol solution or herbal extract at a proper concentration, 0.5 mL of 0.15 mM HOCl for starting the reaction, and water was added to make the final volume of 4.0 mL. After incubation for 10 min at 37 °C, 1.0 mL of resorcinol (50 $\mu$M) was added to the reaction mixture and incubated for 5 min. At the end of the incubation period, the fluorescence intensity of the remaining resorcinol was measured at 304 nm ($\lambda_{ex}$ = 277 nm). Maximal fluorescence reduction (i.e., intensity difference) of resorcinol took place under HOCl attack without antioxidants, and this difference was reduced in the presence of polyphenols, enabling the HOCl scavenging activity measurement. The HOCl scavenging activity was calculated with the aid of eq 1, where $I_o$ is the fluorescence intensity of the resorcinol probe initially (i.e., prior to HOCl attack) and $I_1$ and $I_2$ are the fluorescence intensities of the resorcinol probe after chlorination in the absence and presence of polyphenolic scavenger, respectively.

$$\text{inhibition ratio (\%)} = 100[(I_2 - I_1)/(I_0 - I_1)] \quad (1)$$

The $IC_{25}$ values of the polyphenols were calculated using a plot of inhibition percentage as a function of $C_{scavenger}$. Because the fluorescence intensity of the reaction mixture was derived from the resorcinol probe alone, possible interferences from scavenger compounds or real sample constituents were absent.

**KI/Taurine Assay.** HOCl scavenging activity of polyphenols and herbal materials was determined using the spectrophotometric KI/taurine reference method described by Soobrattee et al.[19] The reaction mixture contained 1.0 mL of pH 7.4 phosphate buffer, 0.5 mL of taurine, 0−2.0 mL of scavenger solution at a proper concentration, 0.2 mL of HOCl, and water added to make the final volume of 3.7 mL. After the formation of taurine chloramine, potassium iodide (0.5 mL) was added and absorbance was measured at 350 nm ($\varepsilon = 2.29 \times 10^4$ $M^{-1}$ $s^{-1}$).[22] The herbal tea extracts were used by diluting at a ratio of 1:100 so as not to yield any absorbance interference at 350 nm.

The HOCl scavenging activity was calculated with respect to eq 2, where $A_o$ and $A$ are the absorbances of the reaction mixture in the absence and presence of polyphenol, respectively.

$$\text{inhibition ratio (\%)} = 100[(A_o - A)/A_o] \quad (2)$$

**HPLC Assay.** A gradient elution system was used for the determination of the resorcinol probe. The initial composition of the mobile phase (50% A/50% B) was modified using a linear gradient to (slope of 1.0) 60% A/40% B at 5 min, 70% A/30% B at 8 min, 80% A/20% B at 11 min, and a final composition of 90% A/10% B at 14 min. The mobile phases A and B were methanol and 1% (v/v) acetic acid, respectively. The chromatograms were obtained using a reverse-phase Agilent Eclipse XDB C18 column (4.6 × 250 mm, 5 $\mu$m particle size), with the following parameters: $V_{sample}$, 20 $\mu$L; flow rate, 1.0 mL $min^{-1}$; and $\lambda_{resorcinol}$, 275 nm. The retention time of 4-chlororesorcinol, a chlorination product, was found with the aid of a standard.

**Statistical Analysis.** All data were entered in an Excel database and analyzed with SPSS software for Windows. The data obtained

from the resorcinol and KI/taurine assays were compared to the aid of the ANOVA test at a selected confidence level of 95%.[23]

## RESULTS AND DISCUSSION

The HOCl scavenging activity of polyphenols (i.e., flavonoids and simple hydroxybenzoic and hydroxycinnamic acids) individually and in mixtures was evaluated by our recently developed resorcinol fluorometric method.[21] In the preparation of herbal extracts for analysis, the method of microwave extraction was used, having distinct advantages of reduced cost and time and increased reproducibility over classical extraction methods (such as Soxhlet extraction, liquid–liquid extraction, column chromatography, and preconcentration techniques). While MAE enables the reduction of the extraction time (because of its fast and multiple extraction capability) and solvent volumes, sonication may require a longer time and larger solvent volumes and sometimes repeated extractions.[24] The scavenging activity measurements using the resorcinol method were statistically compared to those obtained with KI/taurine and HPLC.

The fluorescence intensity of resorcinol was followed between 0 and 20 min (Figure 1) with and without scavenger

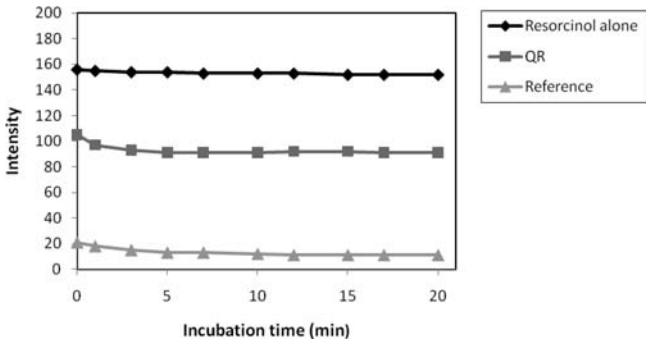


**Figure 1.** Fluorescence intensity as a function of time: (◆) resorcinol alone and resorcinol exposed to HOCl in the (▲) absence and (■) presence (3 $\mu$M QR) of a scavenger.

(i.e., QR). Standing under incubation conditions, the resorcinol probe did not lose its original fluorescence intensity, while upon HOCl oxidation, this intensity was greatly attenuated because of the formation of chlorination products. This fluorescence attenuation was decreased in the presence of an antioxidant polyphenol, such as QR, because of its competition with resorcinol for HOCl quenching. The optimal incubation time was chosen as 5 min, which was sufficient to reach a plateau in intensity (Figure 1).

Figure 2 shows the fluorescence spectra of resorcinol with varying QR concentrations. The maximal decrease in fluorescence intensity of resorcinol was observed under HOCl exposure in the absence of a scavenger as a result of conversion to non-fluorescent products. In comparison to the behavior of the resorcinol probe under HOCl exposure, the fluorescence intensity at 304 nm rose with increasing scavenger concentration (2.0–8.0 $\mu$M QR). This fluorescence increase is related to the scavenging activity of the scavenger. HOCl scavenging activity can be calculated using this intensity difference of resorcinol recorded in the presence and absence of a scavenger at varying concentrations.

**Optimization of MAE Conditions.** MAE conditions were optimized by measuring the HOCl scavenging activity (inhibition percentage) with the use of the resorcinol method

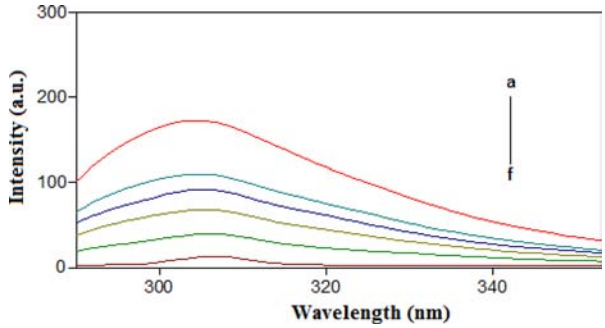


**Figure 2.** Fluorescence spectra of the resorcinol probe at varying scavenger (QR) concentrations [a, 10 $\mu$M resorcinol (alone); b, 8.0 $\mu$M QR; c, 6.0 $\mu$M QR; d, 4.0 $\mu$M QR; e, 2.0 $\mu$M QR; and f, 0 $\mu$M QR (reference)].

(Figure 3). Green tea was chosen as a representative sample for the optimization MAE technique. The effect of the extraction time (0–10 min), temperature (50–100 °C), type of solvent (ethanol, methanol, or water), composition of solvent (ethanol/water at 20, 40, 60, 80, and 100%), and liquid/solid ratio (10–40) on MAE efficiency were determined.

The effect of the extraction temperature and time are shown in Figure 3a. It can be observed that increasing the temperature of the solvent from 50 to 100 °C significantly increased the extraction efficiency up to 3 min, because of the increase in solubility with the temperature.[25] The inhibition percentage slightly decreased when the temperature and time were higher than 80 °C and 3 min, respectively. Therefore, 80 °C and 3 min were chosen as the optimal temperature and time for effective MAE.

Figure 3b shows that the extraction of green tea was greatly influenced by the ethanol concentration in water. The inhibition percentage of green tea extract increased with an increase in the ethanol concentration up to 80% (v/v), beyond which a decrease in HOCl scavenging activity was observed. The possible reasons are (i) highest solubility of lipophilic and hydrophilic antioxidants at this solvent composition and (ii) expansion of the contact surface area with some amount of water.[25] Therefore, 80% (v/v) ethanol concentration in water was chosen as optimal for effective MAE.

Figure 3c shows that the maximum extraction efficiency was obtained using methanol among the pure solvents tested. However, when water was added to pure solvents, 80% ethanol (v/v) was the most appropriate leachant solvent for effective MAE, probably because of the maintenance of a lipophilic/hydrophilic balance of dissolved antioxidants.

Figure 3d shows the effect of the liquid/solid ratio on the MAE of green tea. The HOCl scavenging activity of green tea increased with an increase in the liquid/solid ratio up to 20:1 (mL $g^{-1}$), beyond which the activity decreased because of unnecessary dilution of antioxidants. Therefore, the optimal liquid/solid ratio was determined as 20:1 (mL $g^{-1}$) to reach a high extraction efficiency.

**Testing of Incubation Reaction Products with the Resorcinol Assay.** It is apparent that neither QR nor chlorination products of QR (QR + HOCl) upon HOCl attack exhibit a fluorescence intensity at 350 nm (spectra e and f of Figure 4), meaning that QR competition with the resorcinol probe for HOCl can be followed simply by observing the changes in the resorcinol probe without interference from QR. In other words, the only constituent giving rise to a change

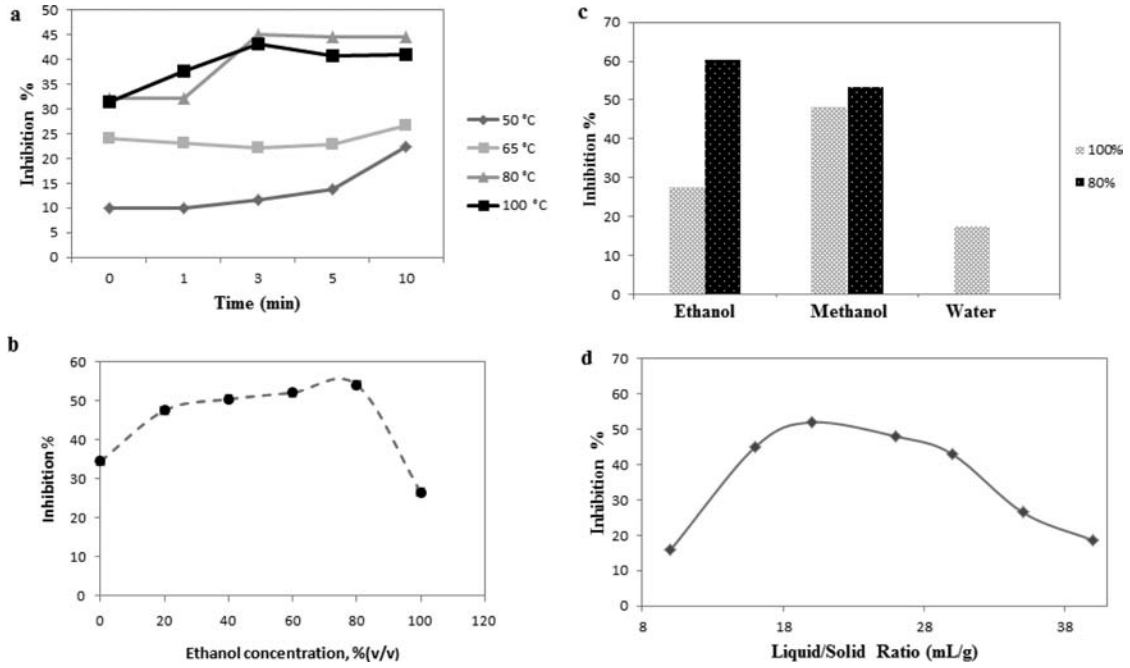


**Figure 3.** Effects of MAE conditions on the inhibition percentage of green tea extract: (a) effect of the extraction time and temperature, (b) effect of the ethanol composition, (c) effect of the solvent type, and (d) effect of the liquid/solid ratio (average of $N = 3$ measurements for each data point).

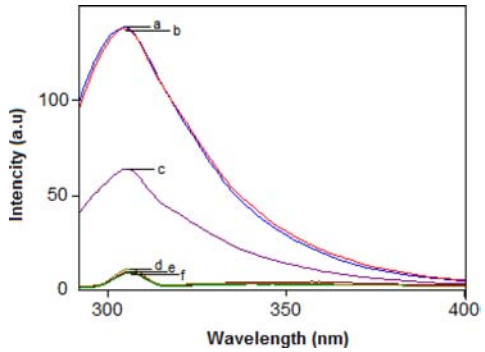


**Figure 4.** Fluorescence spectra of the resorcinol probe: (a) 0.5 mM resorcinol (initial concentration), (b) resorcinol + QR, (c) resorcinol + QR + HOCl, (d) resorcinol + HOCl, (e) QR + HOCl, and (f) QR ($\lambda_{ex}$ = 277 nm).

in fluorescence intensity in the system is the resorcinol probe (spectra a–d of Figure 4). Because QR scavenges some of the HOCl in the incubation system, the intensity increases (relative to that of the chlorinated probe) as a result of this competition with QR (spectra c of Figure 4).

**Analysis of the Results of Resorcinol and KI/Taurine Methods.** The scavenging activity of polyphenols was evaluated by a fluorometric resorcinol assay recently developed in our laboratory.[21] This method evaluates the activity of a scavenger to inhibit the hypochlorite-mediated chlorination of resorcinol, producing non-fluorescent products. The diminution of fluorescence intensity is related to the HOCl scavenging activity of the scavenger. The proposed method was compared to the spectrophotometric KI/taurine method in Table 1.

Quercetin exhibits a high antioxidant[26] and radical scavenging activity,[27] which depend upon the 5-hydroxy-4-keto substitution in the A ring, the 2,3 double bond promoting conjugation between the rings, and 3′,4′-dihydroxy catechol substitution in the B ring. Gomes et al.[28] reported that

**Table 1. HOCl Scavenging Activity of Polyphenols Determined by the Resorcinol and KI/Taurine Methods ($N$ = 4 or 5)[a]**

| HOCl scavenger | $IC_{25}$ value with respect to the resorcinol method ($\mu$M) | $IC_{25}$ value with respect to the KI/taurine method ($\mu$M) |
|---|---|---|
| | Phenolic Acids | |
| rosmarinic acid | 1.26 | ND[b] |
| gallic acid | 1.44 | 2.52 |
| 3-coumaric acid | 2.18 | ND |
| ellagic acid | 2.92 | 3.27 |
| chlorogenic acid | 7.20 | 5.79 |
| | Flavonoids | |
| (−)-epigallocatechin gallate | 0.10 | 0.14 |
| quercetin | 1.19 | 1.64 |
| apigenin | 1.22 | ND |
| chrysin | 1.36 | ND |
| (−)-epigallocatechin | 1.41 | 2.58 |
| hesperetin | 1.58 | 12.14 |
| naringenin | 1.73 | 12.19 |
| rutin | 2.05 | 4.69 |
| myricetin | 2.29 | 2.27 |
| (−)-epicatechin | 2.34 | 2.47 |
| (+)-catechin | 2.52 | 2.49 |
| kaempferol | 2.64 | 4.33 |
| luteolin | 3.56 | ND |

[a] $p = 0.05$; $F_{exp} = 3.788$; $F_{crit(table)} = 4.747$; and $F_{exp} < F_{crit(table)}$. [b] ND = $IC_{25}$ value within the studied concentration range could not be determined.

quercetin ($IC_{50}$ = 1.1 $\mu$M) was the most effective scavenger of HOCl, followed by apigenin and chrysin with an equal $IC_{50}$ ($IC_{50}$ = 3.9 $\mu$M) and luteolin ($IC_{50}$ = 7.1 $\mu$M). The $IC_{25}$ values found with the fluorometric resorcinol method concur with this order of activities (Table 1). The 5,7-dihydroxylated A ring and C3–OH substitution contribute significantly to the HOCl

scavenging activity.[28] When quercetin was subjected to HOCl, chlorination occurred only at two sites (C6 and C8) of the A ring. Binsack et al.[29] detected the chlorination products of quercetin as 6-chloroquercetin and 6,8-dichloroquercetin by HPLC and nuclear magnetic resonance (NMR) techniques.

The hierarchy for HOCl scavenging activity of the flavonol aglycones with respect to the resorcinol assay was quercetin > myricetin > kaempferol (Table 1). Soobrattee et al.[19] reported that the antioxidant capacity of these flavonols is also connected to the number of hydroxyl groups present. The presence of a third hydroxyl group in the B ring at the C-5 position does not contribute to an extra effectiveness of myricetin compared to that of quercetin simply having an *o*-diphenolic structure. Firuzi et al. reported that rutin (quercetin 3-rutinoside; $IC_{25}$ = 22.7 $\mu$M) has lower HOCl scavenging activity than its corresponding aglycone (quercetin; $IC_{25}$ = 8.8 $\mu$M).[30] This is supported by data in Table 1 that the glycosylation of flavonoids reduces their HOCl scavenging activity ($IC_{25}$ values of rutin and quercetin were 2.05 and 1.19 $\mu$M, respectively).

HOCl scavenging activities of flavan-3-ols using the resorcinol method were observed for epigallocatechin gallate (8 OH; 0.10 $\mu$M), epigallocatechin (6 OH; 1.41 $\mu$M), epicatechin (5 OH; 2.34 $\mu$M), and catechin (5 OH; 2.52 $\mu$M) in this order, with the values in parentheses showing the number of hydroxyl groups per molecule and the $IC_{25}$ value, respectively. An increase of HOCl scavenging activities of flavan-3-ols correlated with the number of hydroxyl groups. Similarly, Soobrattee et al.[19] reported that the antioxidant activities of flavan-3-ols decreased with a decrease in hydroxyl groups (EGCG > ECG > EGC > EC > C). Particularly, the three adjacent phenolic −OH groups on both the B ring (at 3′, 4′, and 5′ positions) and the gallate moiety of EGCG give a higher stability to the radical structure emerging from HOCl oxidation by increasing electron delocalization over the whole molecule.[31,32] In our study, EGCG ranked as the strongest HOCl scavenger in both the resorcinol and KI/taurine assays (Table 1), but Soobrattee et al. surprisingly reported close HOCl scavenging activities for EGCG and EC using the KI/taurine assay, despite the fact that epicatechin is devoid of *o*-dihydroxy substitution in the B ring.[19]

It has been reported in the literature that simultaneous light absorption of the probe and scavengers may give rise to problems in the KI/taurine spectrophotometric method. For example, the HOCl scavenging activity of the oxicam group non-steroidal anti-inflammatory drugs could not be determined with KI/taurine because of the strong absorption in the range of 200−420 nm.[33] Similarly, because flavones have a strong absorption band (apigenin, 337 nm; chrysin, 313 nm) in this range,[34] HOCl scavenging activity of flavones could not be evaluated by the KI/taurine method.

The two-way ANOVA test was used for statistical analysis.[23] ANOVA showed that the experimentally found results (consisting of 13 HOCl scavengers excluding the values for compounds that could not be evaluated by the KI/taurine method) with both methods were statistically alike at a 95% confidence level ($F_{exp}$ = 3.788; $F_{crit(table)}$ = 4.747; and $F_{exp} < F_{crit(table)}$ at $p$ = 0.05). Thus, the fluorometric resorcinol method was validated against the KI/taurine method for HOCl scavenging activity assessment of polyphenols.

**Analysis of the Results Obtained by Resorcinol and HPLC Methods.** The initial and remaining amounts of resorcinol probe undergoing HOCl attack were determined by fluorometric and HPLC methods in the presence and absence of a complex scavenger matrix (i.e., green tea extract). The retention times for resorcinol and its chlorination product 4-chlororesorcinol (detected at 275 nm) were 3.10 and 4.60 min, respectively. The chromatograms showed that more resorcinol remained in the reaction medium with increasing volumes of green tea extract because of less conversion to chlorination products. This situation can be clearly observed from the increasing peak heights of the resorcinol probe. For example, approximately 46.5% of resorcinol was converted into its chlorination products in the absence of a scavenger. In the presence of a potent scavenger solution, such as 0.5 and 1.0 mL volumes of green tea extract, the conversion ratio of resorcinol was considerably smaller (27.0 and 7.5%, respectively).

Table 2 shows the concentration of the remaining resorcinol probe in the incubation mixture with respect to the resorcinol and HPLC assays. The remaining resorcinol concentrations (mM) were calculated with the aid of the corresponding calibration curves and correlated well among themselves ($r$ = 0.9973).

**Table 2. Analysis of Resorcinol before and after Incubation with HOCl in the Presence and Absence of Green Tea Extract (Reference) Using Resorcinol and HPLC Methods ($N$ = 3)[a]**

| mixture | concentration of remaining resorcinol with respect to the resorcinol assay (mM) | concentration of remaining resorcinol with respect to the HPLC assay (mM) |
|---|---|---|
| reference | 1.03 ± 0.05 | 1.07 ± 0.05 |
| 0.3 mL of green tea extract | 1.10 ± 0.05 | 1.19 ± 0.03 |
| 0.5 mL of green tea extract | 1.38 ± 0.03 | 1.46 ± 0.02 |
| 0.8 mL of green tea extract | 1.57 ± 0.05 | 1.68 ± 0.04 |
| 1.0 mL of green tea extract | 1.78 ± 0.08 | 1.85 ± 0.06 |

[a] $[\text{Resorcinol}]_{FL} = 1.03[\text{resorcinol}]_{HPLC} + 0.03$ ($r$ = 0.9973).

**Application of the Resorcinol Method to Some Herbal Extracts.** The resorcinol assay was applied to herbal extracts, and the results were compared to the KI/taurine assay as inhibition percentage values. The obtained results demonstrate that green tea extract exhibited the highest HOCl scavenging activity by a large difference in both assays. This is not surprising in view of the fact that green tea is distinguished by its remarkable content of polyphenols, especially catechins, such as epicatechin, epigallocatechin, epicatechin gallate, and epigallocatechin gallate,[35] all of which exhibited high HOCl scavenging activities with respect of the spectroflorometric resorcinol assay (Table 1). The results are also in accordance with those reported by Valentão et al.,[36] indicating that green tea infusion exhibited higher HOCl scavenging activity than small centaury (*Centaurium erythraea* L.)-lyophilized infusion. The inhibition percentages measured with the resorcinol and KI/taurine methods are shown in a bar diagram (Figure 5). The hierarchy for HOCl scavenging activity of herbal teas with respect to the resorcinol assay was green tea > sage tea > yarrow > lady's mantle.

In comparison of the resorcinol and KI/taurine assays in the HOCl scavenging activity measurement, it was observed that the fluorometric resorcinol assay can be securely used without interference from polyphenols or herbal tea constituents, while real sample components or scavengers may show strong absorption in the 200−400 nm range, thereby potentially interfering with the KI/taurine assay.

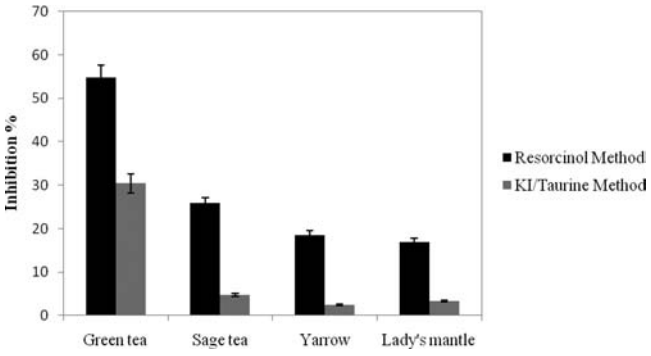


**Figure 5.** Inhibition percentage of some herbal teas (1:100 diluted extract) calculated with the resorcinol assay in comparison to the KI/taurine assay.

**Possible Advantages and Drawbacks.** In principle, the proposed resorcinol assay may be susceptible to interferences, arising from the fact that the excitation and emission wavelengths fall in the UV region. However, no such interference has experimentally been observed in this study, because the possible scavengers, taken for analysis at relatively small concentrations compared to the probe, did not cause any change in the fluorescence intensity of resorcinol. ROS scavenging methods using fluorogenic probes generally provide a superiority of simplicity, selectivity, and sensitivity over other similar spectroscopic methods.[37] The existing methods for quantifying HOCl scavenging activity have some limitations, such as possible UV absorption in the KI/taurine assay. The widely used TNB method, on the basis of the prevention of TNB oxidation in the presence of HOCl scavengers, may suffer from the extra capability of thiols to directly reduce 5,5′-dithiobis-(2-nitrobenzoic acid) (DTNB) to TNB without involvement of any scavenger. The fluorometric resorcinol assay overcomes all of these disadvantages by rendering the relatively specific detection of HOCl and is reliably applied to scavenging activity estimation of polyphenols and herbal materials.

In addition, the resorcinol probe is a right choice for the HOCl assay, because other common oxidants and radical species (except hydroxyl radicals) may not oxidize resorcinol by limitation of their standard redox potentials, thereby supporting selectivity of the proposed assay. This method has been successfully validated against reference assays (KI/taurine and HPLC).

## AUTHOR INFORMATION

### Corresponding Author

*Telephone: +90-212-473-7070. Fax: +90-212-473-7180. E-mail: mozyurek@istanbul.edu.tr.

### Funding

Nazan Durusoy thanks the Istanbul University Research Fund, Bilimsel Arastirma Projeleri (BAP) Yurutucu Sekreterligi, for the support given to her M.Sc. Thesis Project 29902 and the Institute of Pure and Applied Sciences, Istanbul University (Istanbul University Fen Bilimleri Enstitüsü), for the support given to her M.Sc. thesis work with the title "Development of a Novel Spectrofluorometric Method for the Hypochlorous Acid Scavenging Activity Measurement of Polyphenols". The authors also extend their gratitude to the Turkish Scientific and Technical Research Council (TUBITAK) for the Research Project 112T372.

### Notes

The authors declare no competing financial interest.

## REFERENCES

(1) Winterbourn, C. C.; Kettle, A. J. Biomarkers of myleperoxidase-derived hypochlorous acid. *Free Radical Biol. Med.* **2000**, *29*, 403−409.

(2) Magalhaes, L. M.; Segundo, M. A.; Reis, S.; Lima, J. L. F. C. Methodological aspects about in vitro evaluation of antioxidant properties. *Anal. Chim. Acta* **2008**, *613*, 1−19.

(3) Zhang, R.; Brennan, M. L.; Shen, Z.; MacPherson, J. C.; Schmitt, D.; Molenda, C. E.; Hazen, S. L. Myeloperoxidase functions as a major enzymatic catalyst for initiation of lipid peroxidation at sites of inflammation. *J. Biol. Chem.* **2002**, *277*, 46116−46122.

(4) Hawkins, C. L.; Davies, M. J. Degradation of hyaluronic acid, poly- and mono-saccharides, and model compounds by hypochlorite: evidence for radical intermediates and fragmentation. *Free Radical Biol. Med.* **1998**, *24*, 1396−1410.

(5) Magalhaes, L. M.; Segundo, M. A.; Reis, S.; Lima, J. L. F. C.; Estela, J. M.; Cerda, V. Automatic in vitro determination of hypochlorous acid scavenging capacity exploiting multisyringe flow injection analysis and chemiluminescence. *Anal. Chem.* **2007**, *79*, 3933−3939.

(6) Gatto, M. T.; Firuzi, O.; Agostino, R.; Grippa, E.; Borsò, A.; Spinelli, F.; Pavan, L.; Petrolati, M.; Petrucci, R.; Marrosu, G.; Saso, L. Development of a new assay for the screening of the hypochlorous acid scavengers based on reversed-phase high-performance liquid chromatography. *Biomed. Chromatogr.* **2002**, *16*, 404−411.

(7) Haenen, G. R.; Bast, A. Scavenging of hypochlorous acid by lipoic acid. *Biochem. Pharmacol.* **1991**, *42*, 2244−2246.

(8) Ching, T.-L.; de Jong, J.; Bast, A. A method for screening hypochlorous acid scavengers by inhibition of the oxidation of 5-thio-2-nitrobenzoic acid: Application to anti-asthmatic drugs. *Anal. Biochem.* **1994**, *218*, 377−381.

(9) Yan, L. J.; Traber, M. G.; Kobuchi, H.; Matsugo, S.; Tritschler, H. J.; Packer, L. Efficacy of hypochlorous acid scavengers in the prevention of protein carbonyl formation. *Arch. Biochem. Biophys.* **1996**, *327*, 330−334.

(10) Grippa, E.; Pavone, F.; Gatto, M. T.; Petrucci, R.; Marrosu, G.; Silvestrini, B.; Saso, L. In vitro evaluation of antioxidant activity by electrophoresis and high performance liquid chromatography. *Biochim. Biophys. Acta* **2000**, *1524*, 171−177.

(11) Bravo, L. Polyphenols: Chemistry, dietary sources, metabolism, and nutritional significance. *Nutr. Rev.* **1998**, *56*, 317−333.

(12) de Groot, H.; Rauen, U. Tissue injury by reactive oxygen species and the protective effects of flavonoids. *Fundam. Clin. Pharmacol.* **1998**, *12*, 249−255.

(13) Del Rio, D.; Stewart, A. J.; Mullen, W.; Burns, J.; Lean, M. E.; Brighenti, F.; Crozier, A. HPLC−MS$^n$ analysis of phenolic compounds and purine alkaloids in green and black tea. *J. Agric. Food Chem.* **2004**, *52*, 2807−2815.

(14) Zheng, W.; Wang, S. Y. Antioxidant activity and phenolic compounds in selected herbs. *J. Agric. Food Chem.* **2001**, *49*, 5165−5170.

(15) Wojdyło, A.; Oszmiański, J.; Czemerys, R. Antioxidant activity and phenolic compounds in 32 selected herbs. *Food Chem.* **2007**, *105*, 940−949.

(16) Smolyakova, I. M.; Andreeva, V. Yu.; Kalinkina, G. I.; Avdeenko, S. N.; Shchetinin, P. P. Development of extraction techniques and standardization methods for a common lady's mantle (*Alchemilla vulgaris*) extract. *Pharm. Chem. J.* **2012**, *45*, 675−678.

(17) Pistonesi, M. F.; Nezio, M. S. D.; Centurión, M. E.; Palomeque, M. E.; Lista, A. G.; Band, B. S. F. Determination of phenol, resorcinol and hydroquinone in air samples by synchronous fluorescence using partial least-squares (PLS). *Talanta* **2006**, *69*, 1265−1268.

(18) Heasley, V. L.; Burns, M. D.; Kemalyan, N. A.; McKee, T. C.; Schroeter, H.; Teegarden, B. R.; Whitney, S. E.; Wershaw, R. L. Aqueous chlorination of resorcinol. *Environ. Toxicol. Chem.* **1989**, *8*, 1159−1163.

(19) Soobrattee, M. A.; Neergheen, V. S.; Luximon-Ramma, A.; Aruoma, O. I.; Bahorun, T. Phenolics as potential antioxidant therapeutic agents: Mechanism and actions. *Mutat. Res.* **2005**, *579*, 200−213.
(20) Aruoma, O. I. Scavenging of hypochlorous acid by carvedilol and ebselen *in vitro*. *Gen. Pharmacol.* **1997**, *28*, 269−272.
(21) Özyürek, M.; Bekdeşer, B.; Güçlü, K.; Apak, R. Resorcinol as a spectrofluorometric probe for the hypochlorous acid scavenging activity assay of biological samples. *Anal. Chem.* **2012**, *84*, 9529−9536.
(22) Gressier, B.; Lebegue, N.; Brunet, C.; Luyckx, M.; Dine, T.; Cazin, M.; Cazin, J. C. Scavenging of reactive oxygen species by letosteine, a molecule with two blocked −SH groups. *Pharm. World Sci.* **1995**, *17*, 76−80.
(23) Miller, J. C.; Miller, J. N. *Statistics for Analytical Chemists*, 3rd ed.; Ellis Horwood and Prentice Hall: New York, 1993.
(24) Eskilsson, C. S.; Björklund, E. Analytical-scale microwave-assisted extraction. *J. Chromatogr. A* **2000**, *902*, 227−250.
(25) Hemwimon, S.; Pavasant, P.; Shotipruk, A. Microwave-assisted extraction of antioxidative anthraquinones from roots of *Morinda citrifolia*. *Sep. Purif. Technol.* **2007**, *54*, 44−50.
(26) Apak, R.; Güçlü, K.; Demirata, B.; Özyürek, M.; Çelik, S. E.; Bektaşoğlu, B.; Berker, K. I.; Özyurt, D. Comparative evaluation of total antioxidant capacity assays applied to phenolic compounds, and the CUPRAC assay. *Molecules* **2007**, *12*, 1496−1547.
(27) Seyoum, A.; Asres, K.; El-Fiky, F. K. Structure−radical scavenging activity relationships of flavonoids. *Phytochemistry* **2006**, *67*, 2058−2070.
(28) Gomes, A.; Fernandes, E.; Silva, A. M. S.; Santos, C. M. M.; Pinto, D. C. G. A.; Cavaleiro, J. A. S.; Lima, J. L. F. C. 2-Styrylchromones: Novel strong scavengers of reactive oxygen and nitrogen species. *Bioorg. Med. Chem.* **2007**, *15*, 6027−6036.
(29) Binsack, R.; Boersma, B. J.; Patel, R. P.; Kirk, M.; White, C. R.; Darley-Usmar, V.; Barnes, S.; Zhou, F.; Parks, D. A. Enhanced antioxidant activity after chlorination of quercetin by hypochlorous acid. *Alcohol.: Clin. Exp. Res.* **2001**, *25*, 434−443.
(30) Firuzi, O.; Mladěnka, P.; Petrucci, R.; Marrosu, G.; Saso, L. Hypochlorite scavenging activity of flavonoids. *J. Pharm. Pharmacol.* **2004**, *56*, 801−807.
(31) Bors, W.; Heller, W.; Michel, C.; Saran, M. Flavonoids as antioxidants: Determination of radical-scavenging efficiencies. *Methods Enzymol.* **1990**, *186*, 343−355.
(32) Plaza, M.; Pozzo, T.; Liu, J.; Ara, K. Z. G.; Turner, C.; Karlsson, E. N. Substituent effects on *in vitro* antioxidizing properties, stability, and solubility in flavonoids. *J. Agric. Food Chem.* **2014**, *62*, 3321−3333.
(33) Van Antwerpen, P.; Dubois, J.; Gelbcke, M.; Neve, J. The reactions of oxicam and sulfoanilide non steroidal anti-inflammatory drugs with hypochlorous acid: Determination of the rate constants with an assay based on the competition with *para*-aminobenzoic acid chlorination and identification of some oxidation products. *Free Radical Res.* **2004**, *38*, 251−258.
(34) Rice-Evans, C. A.; Miller, N. J.; Paganga, G. Structure−antioxidant activity relationships of flavonoids and phenolic acids. *Free Radical Biol. Med.* **1996**, *20*, 933−956.
(35) Graham, H. N. Green tea composition, consumption, and polyphenol chemistry. *Prev. Med.* **1992**, *21*, 334−350.
(36) Valentão, P.; Fernandes, E.; Carvalho, F.; Andrade, P. B.; Seabra, R. M.; Bastos, M. L. Hydroxyl radical and hypochlorous acid scavenging activity of small centaury (*Centaurium erythraea*) infusion. A comparative study with green tea (*Camellia sinensis*). *Phytomedicine* **2003**, *10*, 517−522.
(37) Gomes, A.; Fernandes, E.; Lima, J. L. F. C. Fluorescence probes used for detection of reactive oxygen species. *J. Biochem. Biophys. Methods* **2005**, *65*, 45−80.

very important significance to the fast and exact detection of ZEN. Recently, immunogen was obtained by coupling 5-aminozearalenone with bovine serum albumin (BSA) through the amino group at the C-5 position of the compound and conjugated to carrier protein by the Mannich reaction.[16−18] Although the specificity of the antibody had been improved somewhat, the sensitivity with ZEN was not as good as those with antibodies produced using CMO-ZEN as immunogen.

In the current study, a highly specific anti-ZEN monoclonal antibody of high titer was produced using a new immunogen, which was made using a different method of conjugating the hapten to protein carrier. The monoclonal antibody-based competitive ELISA test (microwell plate) and colloidal gold immunoassay (membrane-based) was developed to analyze ZEN in corn samples.

## MATERIALS AND METHODS

**Chemicals and Materials.** ZEN, ZAN, α-ZOL, β-ZOL, α-ZAL, β-ZAL, Freund's incomplete adjuvant (FIA), Freund's complete adjuvant (FCA), gold chloride trihydrate, 1,4-butanediol diglycidyl ether, RPMI-1640, hypoxanthine aminopterin thymidine (HAT), hypoxanthine thymidine (HT), 1-(3-(dimethylamino)propyl)-3-ethylcarbodiimide hydrochloricde (EDC), and a mouse monoclonal antibody isotyping kit were purchased from Sigma (St. Louis, MO, USA). BSA and ovalbumin (OVA) were bought from BDH (VWR International Ltd.). Goat anti-mouse IgG antibody (whole molecule) was from Sino-American Biotechnology Co. (Luoyang, China). PEG1500 was from Roche (Mannheim, Germany). Ninety-six-well culture plates were bought from Nunc (Roskilde, Denmark). Protein G affinity columns were bought from Amersham Biosciences. Nitrocellulose membrane, filter membrane, glass fiber, and absorbent pad were purchased from Millipore (Bedford, MA, USA). Eight-week-old female BALB/c mice were obtained from the Laboratory Animal Center, Zhengzhou University, China, and raised under strictly controlled conditions. The other reagents and solvents were of analytical grade or higher. Murine myeloma $NS_0$ cells were kindly provided by Dr. Howard, Institute for Animal Health, UK, and maintained in RPMI-1640 medium (Invitrogen, Carlsbad, CA, USA) supplemented with 10% (v/v) fetal bovine serum (Invitrogen) in our laboratory.

**Apparatus.** The Microplate Reader 550 was from Bio-Rad (Richmond, CA, USA). Milli-Q water was obtained from Millipore (Bedford, MA, USA). An XYZ Biostrip Dispenser, CM 4000 Cutter, and TSR3000 membrane strip reader were all purchased from Bio-Dot (Richmond, CA, USA).

**Preparation of Immunogens and Coating Antigens.** The hapten of ZEN was coupled to the carrier proteins BSA or OVA by 1,4-butanediol diglycidyl ether to generate ZEA−BSA or ZEN−OVAconjugates.[19−21] ZEN−BSA conjugate was used as immunogen, and ZEN−OVA conjugate was employed as coating antigen in ELISA. The procedure included two steps, which are shown in Figure 1. First, 7 mg of BSA/OVA was dissolved in 1 mL of DDW, and 1 mol/L sodium hydroxide was used to adjuste the pH to 10.8. Butane-1,4-diol diglycidyl ether (6 μL) was added, and the solution was placed at room temperature under a nitrogen atmosphere for 20 h; 1.5 mL of 0.5 mol/L sodium hydroxide was degassed using nitrogen, in which 5 mg of ZEN was dissolved, and then added to the epoxy-activated BSA/OVA solution. The reaction mixture was placed at room temperature under a nitrogen atmosphere for 20 h. The conjugates were purified by dialysis against 0.01 mol/L phosphate-buffered saline (PBS, pH 7.4), and the immunogen was stored at −20 °C.

**Immunization.** Six female 8-week-old BALB/c mice were injected subcutaneously four times with ZEN−BSA conjugate. The first dose consisted of 10 μg of immunogen as an emulsion of PBS and FCA. The three subsequent injections were given at 3 week intervals with the same dosage of immunogen emulsified in FIA. Sera were collected 2 weeks after the fourth immunization and screened for anti-ZEN activity by ELISA.[22] One mouse that produced a high titer of antibodies and showed competitive inhibition with ZEN was used for fusion. The mouse selected as the spleen donor for hybridoma production received a final intraperitoneal injection of 50 μg of conjugate in PBS 4 days before cell fusion.[23,24]

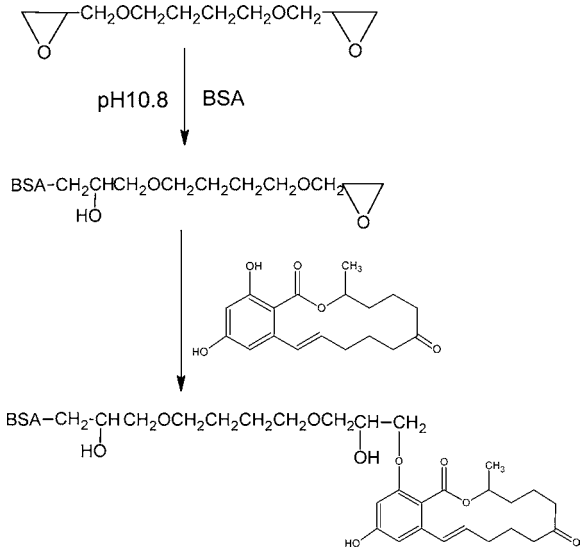


**Figure 1.** Synthetic scheme of ZEN immunogen.

**Cell Fusion and Hybridoma Screening.** Spleen cells from the immunized mouse were fused with NS0 cell using PEG1500.[25] Ten days after fusion, supernatants of hybridoma colonies were recovered and screened by ELISA antibody binding to ZEN. The selected wells were subcloned by limiting dilution. Ascites fluids were produced in paraffin-primed BALB/c mice and the mAbs purified using a protein A affinity column.

**Monitoring of Antibody Titers.** Antibody titer was monitored by ELISA. Microplates were coated with 50 μL/well of ZEN−OVA (2 μg/mL) in 0.05 M carbonate−bicarbonate buffer (pH 9.6) and then incubated at 37 °C for 2 h. After a washing with PBST [PBS containing 0.05% Tween 20 (v/v), pH 7.4], the wells were blocked with 200 μL of 5% normal swine serum in PBST (blocking buffer) and then incubated at 37 °C for 1 h. After another washing step, 50 μL/well with 2-fold serially diluted antibody in blocking buffer was added and incubated for 15 min at 37 °C. Following a washing step, goat anti-mouse−HRP conjugate (1:1000 in PBST, 50 μL/well) was added and incubated for 30 min at 37 °C. The plates were washed again, and 50 μL/well of TMB in chromogen buffer was added; color development was stopped after 10 min with 2 mol/L $H_2SO_4$ (50 μL/well). The optical densities (OD) were measured at 450 nm with an ELISA plate reader.

**Competitive ELISA.** Microplates were coated with ZEN−OVA as above, then 50 μL/well of ZEN serially diluted in PBS at 0, 0.625, 1.25, 2.5, 5, 10, or 20 ng/mL (for the ZEN analogues higher concentrations were used) was added, with 50 μL/well ant-ZEN mAbs (50000-fold diluted in PBS) and incubated for 15 min at 37 °C. Following a washing step, goat anti-mouse−HRP conjugate (1:1000 in PBST, 50 μL/well) was added, and plates were incubated for 30 min at 37 °C. The plates were washed again, and 50 μL/well of HRP substrate was added; color development stopped after 10 min with 2 mol/L $H_2SO_4$ (50 μL/well). The optical densities (OD) were measured at 450 nm with an ELISA plate reader. From the titration curve, the concentration of ZEN giving half-maximal inhibition ($IC_{50}$) was obtained and used for the calculation of cross-reactivity.[26]

To determine the specificity of the antibody inhibition of binding of the anti-ZEN antibody with zearalanone, α-zearalenol, β-zearalenol, α-zearalanol, and β-zearalanol were determined. Cross-reactivity was determined according to the following formula:[27]

Table 1. Immunological Properties of ZEN mAb Detected by ELISA

| mAb | titer | $IC_{50}$(ng/mL) | $K_a$ (L/mol) | eq of linear regression | $R^2$ |
|---|---|---|---|---|---|
| 3G10 | $1:1.28 \times 10^5$ | 1.297 | $4.5 \times 10^{10}$ | $y = -0.5636x + 2.2545$ | 0.9919 |
| 4A3-A10 | $1:1.024 \times 10^6$ | 1.165 | $9 \times 10^{10}$ | $y = -0.5058x + 2.0413$ | 0.9920 |
| 4A3-F9 | $1:5.12 \times 10^5$ | 1.115 | $3 \times 10^{11}$ | $y = -0.53x + 2.1253$ | 0.9946 |
| 4F11-H5 | $1:1.024 \times 10^6$ | 1.309 | $6.5 \times 10^{10}$ | $y = -0.5258x + 2.1389$ | 0.9946 |

$$\text{cross-reactivity}(\%) = \frac{\text{concn of standard ZEN inhibiting 50\% of antibody binding}}{\text{concn of other compounds inhibiting 50\% of antibody binding}} \times 100\%$$

**Preparation of Colloidal Gold Conjugate of the Anti-ZEN Monoclonal Antibody.** Gold chloride was reducted by 1% sodium citrate to produce colloidal gold, of which the mean particle diameter was 24 nm.[28,29] $K_2CO_3$ (0.2 mol/L) was used to adjust the colloidal gold solution to pH 8.2. Thirty microliters of anti-ZEN mAb solution was 2-fold serially diluted in DDW and then mixed with 125 μL of colloidal gold solution to determine the most appropriate protein concentration for conjugation; 125 μL of a 10% NaCl solution was added following incubation for 5 min at room temperature. As the concentration of mAb decreased, the color of samples changed from brilliant red to blue. The most appropriate concentration of mAb for colloidal gold labeling was the lowest concentration of mAb solution that produced a change in color.[30]

One hundred microliters of mAb solution at 0.1 mg/mL in DDW (optimum protein concentration)was dripped into 100 mL of colloidal gold solution (pH 8.2). After 70 min of gentle mixing, 10 mL of 10% BSA solution was added, and after 10 min, the mixture was centrifuged at 12000*g* for 30 min at 4 °C. The supernatant was discarded, and the pellet was washed two times with 20 mmol/L borate buffer (pH 9.0) containing 1% BSA. The final pellets were suspended in 50 mL of TB [20 mmol/L borate buffer (pH 9.0) containing 1% BSA, 3% sucrose, and 0.03% sodium azide] and stored at 4 °C.[30]

**Preparation of Immunochromatographic Test Strips.** Generally, an immunochromatographic test strip consisted of a nitrocellulose (NC) membrane and three pads (sample, conjugate, and absorbent pads). The NC membrane was pasted at the center of a semirigid polyethylene sheet, and the conjugate pad and the absorbent pad were attached with overlaps of 2 and 3 mm, respectively, with the NC membrane. The sample pad was pasted with a 3 mm overlap on the conjugate pad.[31] The test strip was prepared by applying ZEN−OVA (0.3 mg/mL) and Protein A (0.5 mg/mL) to the nitrocellulose membrane (NC) as the test and control lines, respectively, situated 0.5 cm apart at the center of the membrane. The reagents were applied as dots at 1 μL/cm. After drying for 4 h at 50 °C, the prepared membrane was stored under dry conditions. The conjugate pad was saturated with 5 μL/cm of mAb−gold conjugate and dried at 37 °C for 40 min. The sample pad (40 × 300 mm) was treated with 100 mmol/L PB (pH 7.4) containing 1% BSA, 0.3% Tween 20, 5% sucrose, and 0.05% sodium azide and then dried at 45 °C for 4 h.

**Test Procedure and Principle.** One hundred and twenty microliters of ZEN standard solution or sample extract was applied to the sample pad, which was allowed to flow toward the absorbent pad. After 5−10 min, ZEN was nonexistent in the sample, and all of the mAb−gold conjugate would be trapped by the capture reagents to form a test line, which was vivid red to be seen obviously (negative). When ZEN existed in the sample, it would compete with the immobilized capture reagents for the limited amount of mAb−gold conjugate. Hence, the more ZEN existed, the more shallow the test line colored. If there was more than enough ZEN, there would be no visible test line because the reaction of mAb−gold conjugate and the capture reagents was blocked completely. The control line was colored red to ensure that the strip and the test procedure were correct. If no color appeared at the control line, it would mean that the test procedure was either improperly conducted or the strip was invalid, and the sample should be tested again using a new strip.[14]

**Preparation of Cereal and Feed Samples.** For corn, barley, oat, rice, and wheat, 5 g samples were mixed with 2 mL of 1 N HCl and extracted for 5 min, then 5 mL of methylene chloride was added, and the mixture was violently shaken for 15 min. After filtering, the upper water phase was abandoned, and the lower phase was mixed with an equal volume of 0.13 mol/L $NaHCO_3$ and violently shaken for 15 min. After centrifugation for 10 min at 6000 rpm, the upper clear liquid was used directly for analysis without further cleanup. Before the spiking and recovery studies, it was verified by HPLC that each test sample did not contain ZEN.

**Identification of the Test Strip Performance.** ZEN-free corn extracts spiked with ZEN (0, 1, 2, 5, 10, and 20 ng/mL) were presented to the test strip to estimate the sensitivity of the assay. As the method described above, three replicates of each sample were tested. A TSR3000 membrane strip reader (Bio-Dot) was used to measure the relative optical density (ROD) of the test line. The standard curve was constructed by plotting the G/D×A-ROD (pixel) values obtained from the standard samples against its logarithm concentrations. The linearity was assessed by the coefficient of determination ($R^2$). The lower detection limit (LDL) of the test strip using the instrumental measurement was defined as the amount of ZEN in the standard sample solution that caused a 10% decrease of the peak−ROD or G/D×A of that produced by the 0 ng/mL ZEN sample. The sensitivity with the naked eye was set at the lowest concentration of ZEN presenting no color at the test line.

To determine the accuracy, corn samples containing 2, 5, and 10 μg/kg of ZEN were tested. Three replicates of each sample were tested with the same batch of test strips. The optical density of the test line was measured using the test strip reader, and sample values were calculated from the standard curve.

**HPLC Analysis.** Twenty gram samples of cereals or feed were finely ground in a mortar with sodium chloride (2 g). For the method validation, ZEN at 25, 50, 100, 200, 400, 600, and 800 μg/kg was added to 20 g of ground corn samples. The sample was extracted with 50.0 mL of acetonitrile/water (90:10 (v/v)) and shaking for 30 min on a horizontal shaker before filtration through an Ederol folded filter paper. A 10.0 mL sample of the extract was diluted with 40.0 mL of water and filtered through a 0.2 μm filter membrane before HPLC analysis. The excitation wavelength ($\lambda_{ex}$) and emission wavelength ($\lambda_{em}$) were set at 274 and 440 nm, respectively.[32]

## RESULTS AND DISCUSSION

**mAb Production.** Twelve days after fusion, a total of 120 hybridomas secreting specific mAb against ZEN were obtained by ELISA screening with ZEN−OVA antigen. Eight of these hybridomas were cloned by limiting dilution and further expanded for characterization, and four of these clones, identified as 3G10, 4A3-A10, 4A3-F9, and 4F11-H5 were used for the preparation of ascites fluid. The interaction of each mAb with ZEN was analyzed by ELISA. Isotyping showed that all of them belonged to the IgG1 subclass. The immunological properties of the four monoclonal antibodies detected by ELISA are shown in Table 1.

All of the mAbs were highly specific for ZEN with 4A3-F9 as marginally the most sensitive hybridoma, and this antibody was selected for developing the test strip. To determine the specificity of the optimized competitive ELISA and the mAb 4A3-F9, testing for cross-reactivity with a number of closely related compounds was undertaken. As shown in Table 2, the

Table 2. Cross-Reaction of Monoclonal Antibody 4A3-F9 with ZEN and Its Analogues

| Ag | Structures | $IC_{50}$ (ng/mL) | Cross-reactivity (%) |
|---|---|---|---|
| Zearalenone | 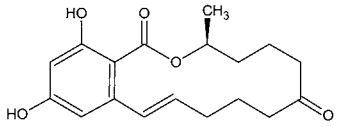 | 1.115 | 100 |
| Zearalanone | 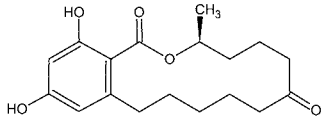 | 2.099 | 53.121 |
| α-zearalenol | 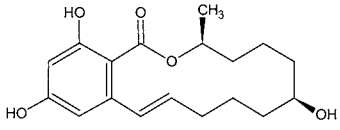 | 44.618 | 2.499 |
| β-zearalenol | 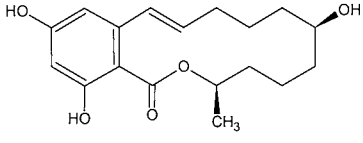 | 39.827 | 2.800 |
| α-zearalanol | 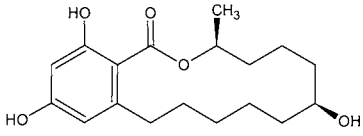 | 28.933 | 3.854 |
| β-zearalanol | 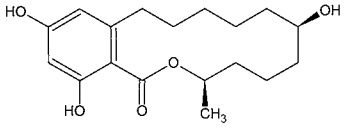 | 65.259 | 1.709 |

highest cross-reactivity was 53.121%, obtained for zearalanone; the other test compounds gave a cross-reactivity of <4%.

**Sensitivity of the Test Strip.** As shown in Figure 2, the sensitivity of the test strip was confirmed to be 20 ng/mL by unaided visual assessment, which could be understood to indicate that if the test strip was assumed positive, the ZEN concentration of corn was ≥20 μg/kg. Test line measurements using a Bio-Dot TSR3000 Membrane Strip Reader gave G/peak and G/D×A (area) of the relative optical density (ROD) decreasing as the ZEN concentration in the standard samples increased. The sigmoidal dose−response curve produced by the concentration of standard ZEN and the G/D×A ROD showed good linearity ($y = -0.6536x + 0.8526$, $R^2 = 0.9898$) in the range of 0−20 ng/mL of ZEN with the $IC_{50}$ calculated as 3.4 ng/mL. The LDL of the test strip was 0.84 μg/kg by the test strip reader and was 1 μg/kg by unaided visual assessment (Figure 2).

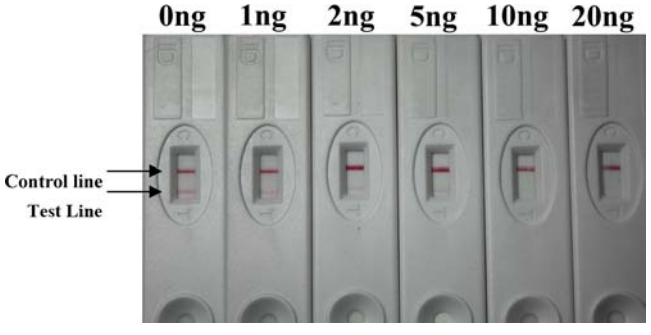


Figure 2. Standard ZEN corn samples were tested using the test strips and the test lines with the naked eye.

**Recovery of ZEN in Corn Samples.** Recoveries for intra-assay reproducibility ranged from 91.30 to 95.27%, and the highest coefficient of variation (CV) was 5.32%. For interassay reproducibility, the test strips of three different batches were used for three replicate testings of the samples, and recoveries ranged from 92.73 to 97.07%. The highest CV was 4.84%. The results are shown in Table 3.


dx.doi.org/10.1021/jf503092j | J. Agric. Food Chem. 2014, 62, 11116−11121

Table 3. Recovery and Intra-assay and Interassay Precision of the Test Strips for ZEN Spiked in Corn Samples[a]

| | intra-assay | | | interassay | | |
|---|---|---|---|---|---|---|
| spiked ZEN (μg/kg) | mean ± SD (μg/kg) | recovery (%) | CV (%) | mean ± SD (μg/kg) | recovery (%) | CV (%) |
| 2 | 1.88 ± 0.10 | 94.16 ± 4.75 | 5.32 | 1.85 ± 0.06 | 96.17 ± 1.26 | 3.24 |
| 5 | 4.76 ± 0.07 | 95.27 ± 1.47 | 1.47 | 4.75 ± 0.23 | 97.07 ± 1.10 | 4.84 |
| 10 | 9.13 ± 0.06 | 91.30 ± 0.62 | 0.66 | 9.27 ± 0.16 | 92.73 ± 1.61 | 1.73 |

[a]Extracts of corn spiked with ZEN at 2, 5, and 10 μg/kg were tested using the strips, the optical density of the test line was measured using the strip reader, and the sample values were calculated from the standard curve. Intra-assay precision was estimated by using one batch of the test strips ($n$ = 3). For interassay precision, three batches of the test strips were used to detect the given samples. The recoveries and coefficients of variation are calculated from triplicate assays in all cases.

**Simultaneous Detection of ZEN in Natural Samples.** The ZEN concentrations of 50 corn samples were analyzed by the test strips, competitive indirect ELISA, and HPLC, and the results were compared. Table 4 shows the summarized results

Table 4. Results of Positive Corn Sample Analyzed with Different Methods

| | ZEN positive samples by | | | |
|---|---|---|---|---|
| | test strip | | ELISA | HPLC |
| corn sample | unaided visual[a] | strip reader (μg/kg) | (μg/kg) | (μg/kg) |
| 1 | − − − | 3.4 ± 0.5 | 4.0 ± 0.9 | 3.6 |
| 6 | + + + | 231.1 ± 49.8 | 190.7 ± 20.9 | 217.2 |
| 18 | + − − | 20.8 ± 2.8 | 14.3 ± 1.6 | 18.8 |
| 23 | + + + | 1691.3 ± 73.2 | 1089.4 ± 50.9 | 1589.4 |
| 25 | + + + | 210.0 ± 34.2 | 189.7 ± 20.8 | 193.6 |
| 32 | + + + | 4168.4 ± 782.6 | 3982.1 ± 590.3 | 3218.6 |
| 38 | + + + | 90.7 ± 17.1 | 89.9 ± 12.3 | 78.5 |
| 43 | + + + | 364.7 ± 41.3 | 293.4 ± 31.2 | 310.5 |
| 47 | + + + | 757.8 ± 79.5 | 589.0 ± 41.6 | 893.3 |
| 49 | + + + | 854.3 ± 103.2 | 683.3 ± 30.2 | 829.6 |

[a]+, positive, ZEN content in the sample is >20 μg/kg; −, negative, ZEN content in the sample is <20 μg/kg.

of the three analytical methods. The three methods showed the same 10 of 50 corn samples to be contaminated with ZEN. Most of the remaining corn samples were also contaminated with ZEN but at levels of mycotoxin of <0.1 μg/kg. The samples that showed positive by competitive indirect ELISA and test strips were confirmed for the accurate quantity by HPLC. The results of ZEN determination in naturally contaminated corn samples by the competitive indirect ELISA and the test strips were consistent with those by HPLC (Table 4).[31] To guarantee the accuracy of the result, analysis by test strips with unaided visual assessment should be done three times at least. The testing time and procedures of the test strips were shorter and more convenient than other methods, and the determination of inspection results were obtained by unaided visual assessment; the test strip is going to be a significant method for on-site and rapid detection of ZEN in corn samples.

**Conclusions.** Our results have demonstrated a methodology for the preparation of rapidly induced antibodies of high specificity and titer against ZEN by using a ZEN−BSA conjugate prepared using 1,4-butanediol diglycidyl ether as the linker,[33] which ensured the preservation of the 7-oxo substituent characteristic of ZEN as an antigenic determinant. The selected anti-ZEN monoclonal antibody showed lower cross-reactivity with the five ZEN analogues. A competitive ELISA and an immunochromatographic test strip for the determination of ZEN contamination in corn samples has been developed using this specific mAb. In summary, the antibody specificity for a ZEN epitope resulting in a very low reactivity with the five ZEN analogues has overcome previous problems in the immunodetection of this contaminant. The competitive indirect ELISA and an immunochromatographic test strip developed in this study are ideally suited for the specific quantitative detection of ZEN contamination in corn.

## AUTHOR INFORMATION


### Corresponding Author

*(G.Z.) Phone: +86-371-65723778. E-mail: zhanggaiping2003@163.com.

### Author Contributions

‖Y.S. and X.H. contributed equally to this work.



### Funding

This research was supported by the National Science & Technology Pillar Program of "12th Five-Year Plan" (2014BAD13B05) and the Science-Technology Foundation for Outstanding Young Scientists of Henan Academy of Agricultural Sciences (2013YQ29).


### Notes

The authors declare no competing financial interest.

## ACKNOWLEDGMENTS

We thank Norman A. Gregson, London University, for grammatical and editorial assistance.

## REFERENCES


(1) Grernmels, J. F. Mycotoxins: their implications for human and animal health. *Vet. Q.* **1999**, *21*, 115−120.

(2) Newberne, P. M. The new world of mycotoxins − animal and human health. *Clin. Toxicol.* **1974**, *7*, 161−177.

(3) Weidenbörner, M. *Encyclopedia of Food Mycotoxins*; Springer: Berlin, Germany, 2001.

(4) Tiemann, U.; Dänicke, S. In vivo and in vitro effects of the mycotoxins zearalenone and deoxynivalenol on different non-reproductive and reproductive organs in female pigs. *Food Addit. Contam.* **2007**, *24*, 306−314.

(5) Kuiper-Goodman, T.; Scott, P. M.; Watanabe, H. Risk assessment of the mycotoxin zearalenone. *Regul. Toxicol. Pharmacol.* **1987**, *7*, 253−306.

(6) Minervini, F.; Dell Aquila, M. E. Zearalenone and reproductive function in farm animals. *Int. J. Mol. Sci.* **2008**, *9* (12), 2570−2584.

(7) Kiang, D. T.; Kennedy, B. J.; Pathre, S. V.; Mirocha, C. J. Binding characteristics of zearalenone analogs to estrogen receptors. *Cancer Res.* **1978**, *38*, 3611−3615.

(8) Schoevers, E. J.; Santos, R. R.; Colenbrander, B.; Fink-Gremmels, J.; Roelen, B. A. Transgenerational toxicity of zearalenone in pigs. *Reprod. Toxicol.* **2012**, *34*, 110−119.

(9) European Commission. Commission Regulation (EC) No. 1881/2006 of 19 December 2006 setting maximum levels for certain contaminants in foodstuffs. *Off. J. Eur. Union* **2006**, 364.
(10) Egmond, H. V.; Jonker, M. A. *Worldwide Regulations for Mycotoxins in Food and Feed in 2003*; Food and Agriculture Organization of the United Nations: Rome, Italy, 2004.
(11) Songsermsakul, P.; Sontag, G.; Cichna-Markl, M.; Zentek, J.; Razzazi-Fazeli, E. Determination of zearalenone and its metabolites in urine, plasma and faeces of horses by HPLC-APCI-MS. *J. Chromatogr., B* **2006**, *843*, 252−261.
(12) Urraca, J. L.; Benito-Peña, E.; Pérez-Conde, C.; Moreno-Bondi, M. C.; Pestka, J. J. Analysis of zearalenone in cereal and swine feed samples using an automated flow-through immunosensor. *J. Agric. Food Chem.* **2005**, *53*, 3338−3344.
(13) Scott, P. M.; Panalaks, T.; Kanhere, S.; Miles, W. F. Determination of zearalenone in cornflakes and other corn-based foods by thin layer chromatography, high pressure liquid chromatography, and gas-liquid chromatography/high resolution mass spectrometry. *J. Assoc. Off. Anal Chem.* **1978**, *61*, 593−600.
(14) Zhao, Y.; Zhang, G.; Liu, Q.; Teng, M.; Yang, J.; Wang, J. Development of a lateral flow colloidal gold immunoassay strip for the rapid detection of enrofloxacin residues. *J. Agric. Food Chem.* **2008**, *56*, 12138−12142.
(15) Shim, W. B.; Eremin, S. A. One-step simultaneous immunochromatographic strip test for multianalysis of ochratoxin A and zearalenone. *J. Microbiol. Biotechnol.* **2009**, *19*, 83−92.
(16) Morgan, A. C., Jr; Galloway, D. R.; Reisfeld, R. A. Production and characterization of monoclonal antibody to a melanoma specific glycoprotein. *Hybridoma* **1981**, *1*, 27−36.
(17) Gao, Y.; Yang, M.; Peng, C.; Li, X.; Cai, R.; Qi, Y. Preparation of highly specific anti-zearalenone antibodies by using the cationic protein conjugate and development of an indirect competitive enzyme-linked immunosorbent assay. *Analyst* **2012**, *137*, 229−236.
(18) Tanaka, T.; Teshima, R.; Ikebuchi, H.; Sawada, J.; Ichinoe, M. Sensitive enzyme-linked immunosorbent assay for the mycotoxin zearalenone in barley and Job's-tears. *J. Agric. Food Chem.* **1995**, *43*, 946−950.
(19) Shelver, W. L.; Smith, D. J. Development of an immunoassay for the $\beta$-adrenergic agonist ractopamine. *J. Immunoassay* **2000**, *21*, 1−23.
(20) Li, M.; Chen, Z.; Zhu, Q. Development and identification of monoclonal antibodies against ractopamine. *Hybridoma* **2007**, *26*, 148−154.
(21) Hermanson, G. T. *Bioconjugate Techniques*; Academic Press: New York, 1996.
(22) Tijssen, P. *Practice and Theory of Enzyme Immunoassays*; Elsevier Science: Amsterdam, The Netherlands, 1985.
(23) Kabat, E. A.; Mayer, M. M. *Experimental Immunochemistry*; Thomas: New York, 1948
(24) Harlow, E.; Lane, D. *Using Antibodies: A Laboratory Manual*; Cold Spring Harbor Laboratory Press: Cold Spring Harbor, NY, USA, 1999.
(25) Köhler, G.; Milstein, C. Continuous cultures of fused cells secreting antibody of predefined specificity. *Nature* **1975**, *256*, 495−497.
(26) Qian, G.; Wang, L.; Wu, Y.; Zhang, Q.; Sun, Q.; Liu, Y.; Liu, F. A monoclonal antibody-based sensitive enzyme-linked immunosorbent assay (ELISA) for the analysis of the organophosphorous pesticides chlorpyrifos-methyl in real samples. *Food Chem.* **2009**, *117*, 364−370.
(27) Wang, X. H.; Liu, T.; Xu, N.; Zhang, Y.; Wang, S. Enzyme-linked immunosorbent assay and colloidal gold immunoassay for ochratoxin A: investigation of analytical conditions and sample matrix on assay performance. *Anal. Bioanal. Chem.* **2007**, *389*, 903−911.
(28) Hayat, M. A., Ed. *Colloidal Gold. Principles, Methods, and Applications*; Academic Press: San Diego, CA, USA, 1989; Vol. 2.
(29) Bassab, C.; Syamal, R. Manufacturing high-quality gold sol. *IVD Technol.* **2001**, *8*, 46−54.
(30) Zhang, G.; Wang, X.; Zhi, A.; Bao, Y.; Yang, Y.; Qu, M.; Luo, J.; Li, Q.; Guo, J.; Wang, Z.; Yang, J.; Xing, G.; Chai, S.; Shi, T.; Liu, Q. Development of a lateral flow immunoassay strip for screening of sulfamonomethoxine residues. *Food Addit. Contam. Part A: Chem. Anal. Control Expo. Risk Assess.* **2008**, *25*, 413−423.
(31) Shim, W. B.; Kim, K. Y.; Chung, D. H. Development and validation of a gold nanoparticle immunochromatographic assay (ICG) for the detection of zearalenone. *J. Agric. Food Chem.* **2009**, *57*, 4035−4041.
(32) De Saeger, S.; Sibanda, L.; Van Peteghem, C. Analysis of zearalenone and $\alpha$-zearalenol in animal feed using high-performance liquid chromatography. *Anal. Chim. Acta* **2003**, *487*, 137−143.
(33) Burkin, A. A.; Kononenko, G. P.; Soboleva, N. A. Group-specific antibodies against zearalenone and its metabolites and synthetic analogs. *Appl. Biochem. Microbiol.* **2002**, *38*, 169−176.

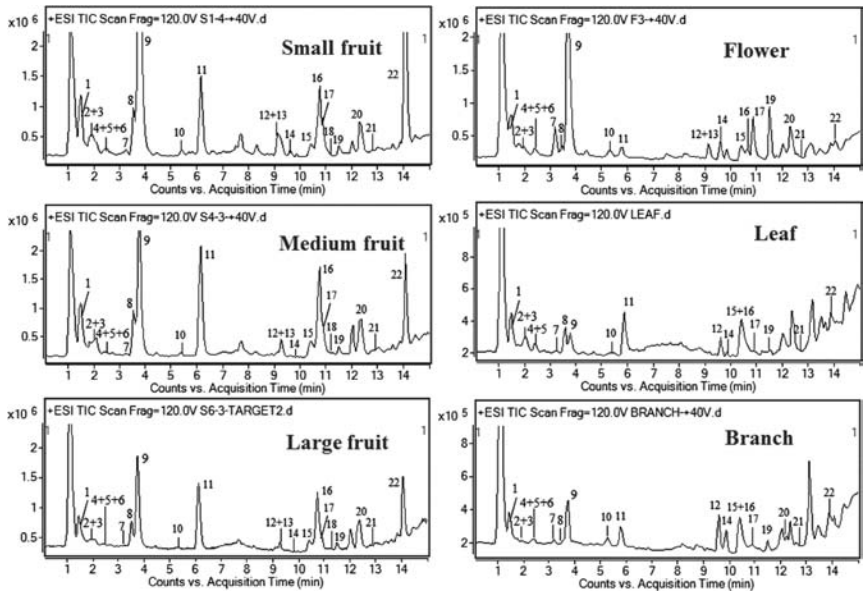


**Figure 1.** Total ion chromatograms (TIC) of different parts (fruit, flower, leaf, and branch) of CGT by RRLC-MS in positive ion mode. Detection was set in positive ion mode with a 120 V fragmentor. Peak numbers of compounds are in accordance with those in Table 1.

30 min at 100 Hz. The supernatants were centrifuged at room temperature for 10 min at 16200*g*, and different samples were diluted different times (6 times for small fruits and flowers and 3 times for medium and large fruits) with methanol before use. An aliquot of 2 $\mu$L of the filtrate was injected for RRLC analysis and 1 $\mu$L for MS analysis.

Standard stock solutions of naringin, rhoifolin, meranzin hydrate, and isoimperatorin were prepared at concentrations of 1000, 800, 200, and 200 $\mu$g/mL, respectively, and stored at −20 °C. Prior to injection, stock solutions were appropriately diluted with methanol to a series of appropriate concentrations used as working solutions.

**RRLC-ESI-MS/MS Analysis.** Analysis was performed on an Agilent 1260 series HPLC system coupled with a 6530 Accurate-Mass Q-TOF system with a Dual AJS ESI source (Agilent Technologies, Palo Alto, CA, USA). Samples were separated on an Agilent ZORBAX SB-C18 column (4.6 mm × 50 mm, 1.8 $\mu$m) at 25 °C. The mobile phase consisted of 0.1% aqueous formic acid (A) and acetonitrile (B) using a gradient program of 25% B in 0−3 min, 25−90% B in 3−14 min, and 90−100% B in 14−15 min. The flow rate was 0.5 mL/min.

The conditions of the ion source were as follows: nebulizer gas setting at 45 psig, capillary voltage at 3000 V, fragmentor voltage at 120 V, drying gas ($N_2$) flow rate and temperature at 10 L/min and 325 °C, and sheath gas flow rate and temperature at 11 L/min and 350 °C. MS acquisition was performed by using electrospray inonization (ESI) in positive ion mode. Collision energy was set at 20 V. All of the data were acquired using the extended dynamic range mode (2 GHz), and the mass range was set at 100−1000 Da in centroid mode. The TOF was calibrated every day before sample analysis and, subsequently, used reference masses at $m/z$ 121.0508 and 922.0098 to obtain high-accuracy mass measurements.

**RRLC-DAD Analysis.** *Instrument and Chromatographic Conditions.* Quantitative analysis was performed on an Agilent 1260 Infinity LC system equipped with a photodiode array detector. Samples were separated on an Agilent ZORBAX SB-C18 column (4.6 × 50 mm$^2$, 1.8 $\mu$m) at 25 °C. Mobile phase consisted of 0.1% aqueous formic acid (A) and methanol (B) using a gradient program of 35−39% B in 0−3 min, 39−39% B in 3−5 min, 39−55% B in 5−12 min, 55−90% B in 12−21 min, and 90−100% B in 21−23 min. The flow rate was 0.5 mL/min. Different detection wavelengths were performed for different periods of time: 283 nm for 0−9 min, 330 nm for 9−18 min, and 310 nm for 18−23 min.

*Method Validation.* An aliquot of 2 $\mu$L of working solutions were injected into RRLC for analysis; the calibration curves were constructed by plotting the peak areas versus the concentration of each analyte. The limit of detection (LOD) and limit of quantification (LOQ) for each analyte were defined by the concentrations that generated peaks with signal-to-noise values ($S/N$) of 3 and 10, respectively.

The precision of the developed method was determined by the intra- and interday variations. For the intraday test, the samples were analyzed six times within the same day, while for the interday test, the samples were examined in duplicates for 3 consecutive days.

To confirm the repeatability, six replicates of the same samples were extracted and analyzed. For the stability test, the same sample was stored at room temperature and analyzed by replicate injection at 0, 2, 4, 8, 16, and 24 h. The RSDs were used to evaluate the method repeatability and stability. Accuracy was calculated as the percentage of recovery. Recovery tests were performed by spiking a known amount of the four standards to 0.25 g of powder and then extracted and analyzed with the same procedures. Six replicates were performed for the test.

**Determination of Total Phenolics.** Total phenolic contents (TPC) of each sample were determined by using the Folin−Ciocalteu reagent according to Singleton and Rossi with slight modifications.[15,16] Gallic acid was used to prepare a standard curve, and final values were expressed in milligrams of gallic acid equivalents (mg of GAE/g). Diluted CGT extracts were incubated with Folin−Ciocalteu phenol reagent. The color was developed by adding sodium carbonate (10%), and absorbance was measured at 765 nm.

**Antioxidant Assays.** *Free Radical Scavenging Capacity.* The free radical scavenging capacity was analyzed by the DPPH assay.[17,18] DPPH is a stable organic nitrogen radical with purple color. Upon reduction by an antioxidant, the solution color faded and the reaction could be monitored by a spectrophotometer at 517 nm. The decrease in absorbance was proportional to the antioxidant capacity and could be measured in comparison to Trolox as standard. All samples and standard were diluted in methanol. A 100 $\mu$L aliquot of CGT extracts was mixed with 100 $\mu$L of DPPH (0.2 mM) in methanol, and the change in optical density (517 nm) was monitored after 30 min using a microplate reader. Results were expressed as $\mu$M Trolox equivalents (TE)/g.

*Ferric Reducing Antioxidant Power Assay.* The FRAP assay was carried out by a commercial kit (Beyotime) following the instruction manual.[19,20] Under acidic conditions, antioxidants can restore ferric tripyridyltriazine ($Fe^{3+}$-TPTZ) into blue $Fe^{2+}$-TPTZ. The total antioxidant activity of antioxidants can be reflected by the absorbance of $Fe^{2+}$-TPTZ at 593 nm. Absorbance was measured at 593 nm using a

**Table 1. Characterization of Chemical Constituents in Different Parts of CGT by LC-QTOF-MS/MS Analysis in Positive Ion Mode**

| no. | $t_R$ (min) | $[M + H]^+$ | diff (ppm) | formula | $\lambda_{max}$ (nm) | identification | large fruit | med fruit | small fruit | leaf | branch | flower | class |
|---|---|---|---|---|---|---|---|---|---|---|---|---|---|
| 1 | 1.416 | 595.1656 | 0.19 | $C_{27}H_{30}O_{15}$ | 270 | vicenin-2 | ++[c] | ++ | ++ | ++ | + | ++ | a[d] |
| 2 | 1.927 | 565.1555 | −0.53 | $C_{26}H_{28}O_{14}$ | *a* | apigenin-8-*C*-glucoside-*O*-arabinoside or apigenin-6-*C*-glucoside-*O*-arabinoside | ++ | ++ | ++ | ++ | + | + | a |
| 3 | 2.020 | 579.1712 | −0.64 | $C_{27}H_{30}O_{14}$ | *a* | apigenin-8-*C*-glucoside-*O*-rhamnoside or apigenin-6-*C*-glucoside-*O*-rhamnoside | ++ | ++ | ++ | ++ | + | + | a |
| 4 | 2.401 | 595.1668 | −2.74 | $C_{27}H_{30}O_{15}$ | 255 | luteolin-7-O-rutinoside | + | + | + | ++ | ++ | + | b |
| 5 | 2.430 | 433.1139 | −2.64 | $C_{21}H_{20}O_{10}$ | 270 | apigenin-8-C-glucoside | ++ | ++ | ++ | + | + | + | a |
| 6 | 2.627 | 597.1825 | −2.69 | $C_{27}H_{32}O_{15}$ | 283 | eriocitrin | + | + | + | - | + | ++ | c |
| 7 | 3.238 | 581.1855 | 2.24 | $C_{27}H_{32}O_{14}$ | 283 | narirutin[b] | + | ++ | ++ | + | + | +++ | c |
| 8 | 3.576 | 579.1716 | −0.91 | $C_{27}H_{30}O_{14}$ | 330 | rhiofolin[b] | +++ | +++ | +++ | +++ | ++ | +++ | b |
| 9 | 3.778 | 581.1876 | −1.74 | $C_{27}H_{32}O_{14}$ | 283 | naringin[b] | +++ | +++ | +++ | ++ | ++ | +++ | c |
| 10 | 5.733 | 725.2273 | 1.62 | $C_{33}H_{40}O_{18}$ | 280 | melitidin | + | + | + | + | + | + | c |
| 11 | 6.208 | 279.1228 | −0.49 | $C_{15}H_{18}O_5$ | 330 | meranzin hydrate[b] | +++ | +++ | +++ | + | + | + | d |
| 12 | 9.111 | 273.0756 | 0.39 | $C_{15}H_{12}O_5$ | 283 | naringenin | ++ | ++ | +++ | + | + | +++ | e |
| 13 | 9.246 | 261.1119 | 1.17 | $C_{15}H_{16}O_4$ | 330 | meranzin | ++ | ++ | ++ | - | - | + | d |
| 14 | 9.584 | 333.1699 | −1.66 | $C_{19}H_{24}O_5$ | 320 | marmin | + | + | + | + | + | + | d |
| 15 | 10.596 | 217.0495 | 0.21 | $C_{12}H_8O_4$ | 320 | bergaptan[b] | ++ | ++ | + | + | + | + | d |
| 16 | 10.664 | 261.1126 | −1.70 | $C_{15}H_{16}O_4$ | 320 | isomaranzin | +++ | +++ | +++ | + | + | ++ | d |
| 17 | 10.934 | 471.2017 | −2.28 | $C_{26}H_{30}O_8$ | 210 | limonin[b] | ++ | ++ | +++ | + | ++ | +++ | f |
| 18 | 11.140 | 473.2156 | 1.19 | $C_{26}H_{32}O_8$ | 210 | isoobacunoic acid | + | ++ | + | − | − | − | f |
| 19 | 11.474 | 515.227 | 0.45 | $C_{28}H_{34}O_9$ | 210 | nomilin[b] | ++ | ++ | ++ | + | + | +++ | f |
| 20 | 12.284 | 455.2074 | −1.87 | $C_{26}H_{30}O_7$ | 210 | obacunone[b] | +++ | +++ | +++ | − | + | +++ | f |
| 21 | 12.962 | 271.0965 | 0.02 | $C_{16}H_{14}O_4$ | 310 | imperatorin | ++ | ++ | ++ | + | ++ | ++ | d |
| 22 | 14.039 | 271.0965 | 0.02 | $C_{16}H_{14}O_4$ | 310 | isoimperatorin[b] | +++ | +++ | +++ | + | ++ | ++ | d |

[a]Unknown. [b]Confirmed by standard compounds. [c]The criteria of the grading levels were defined according to the peak areas after reconstructing extracted ion chromatograms of the target compounds: −, not detected; peak area in the range of $(0-1) \times 10^5$ defined as "+", meaning low-level; $(1-10) \times 10^5$ defined as "++", meaning moderate-level; peak area > $10 \times 10^5$ defined as "+++", meaning high-abundance. [d]Different letters represent different classes of compounds: a, flavone *C*-glycosides; b, flavone *O*-glycosides; c, flavanone *O*-glycosides; d, coumarins; e, flavanone aglycone; f, limonoids.



dx.doi.org/10.1021/jf5036355 | J. Agric. Food Chem. 2014, 62, 11122−11129

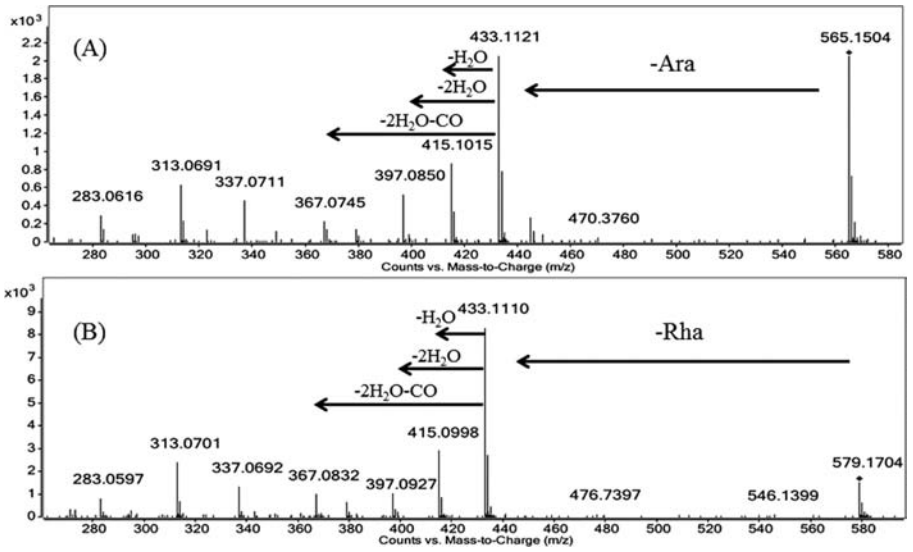


**Figure 2.** MS/MS spectra of (A) compound **2** and (B) compound **3** in positive ion mode with 20 V collision energy.

microplate reader, with $FeSO_4$ as the antioxidant standard. The results of the FRAP assay were calculated as mM $FeSO_4$/(g of powder).

*ABTS Radical Scavenging Activity Assay.* The ABTS assay was performed by a commercial kit (Beyotime) following the instruction manual.[21,22] With the appropriate oxidants, ABTS can be oxidized into green $ABTS^{\cdot+}$, while antioxidants can inhibit this process. The total antioxidant activity of antioxidants can be reflected by the absorbance of $ABTS^{\cdot+}$ at 734 nm. Absorbance was measured at 734 nm using a microplate reader, with Trolox as an antioxidant standard. The results were calculated as $\mu$M TE/(g of powder).

**Statistical Analysis.** All determinations of antioxidant capacity were conducted in triplicates. The values expressed were the mean of three measurements. Statistical comparisons of the results were performed by one-way ANOVA using SPSS 11.5 (Chicago, IL). Significant differences ($p < 0.05$) between the different kinds of samples were analyzed by Duncan's multiple range test.

## RESULTS AND DISCUSSION

**Comparison of Chemical Constituents of Different Parts of CGT.** The profiling of CGT chemical constituents was analyzed by RRLC-ESI-QTOF/MS method (Figure 1). Based on their retention time and MS fragmentation behavior, a total of 22 compounds, including flavanone *O*-glycosides (peaks 6, 7, 9, and 10), flavanone aglycone (peak 12), flavone *C*- (peaks 1, 2, 3, and 5) and *O*-glycosides (peaks 4 and 8), coumarins (peaks 11, 13−16, 21, and 22), and limonoids (peaks17−20) were identified or tentatively characterized (Table 1).

Flavonoid glycosides are divided into two categories: flavonoid *O*- and *C*-glycosides. Favonoid *O*-glycosides ruptures are easily induced by loss of the sugar moiety, while fragmentations in *C*-glycosides focus preferentially on the glycidic moiety.[23,24] At low collision energies, the main fragments of flavonoid *C*-glycosides were due to the loss of water ($[M + H - nH_2O]^+$), and loss of the glucosidic methylol group as formaldehyde ($[M + H - CH_2O - 2H_2O]^+$).[25] In this work, 10 compounds were elucidated as flavonoid glycosides in CGT. Noteworthily, compounds **2** and **3** were identified in CGT for the first time. Figure 2 shows the MS/MS spectra of compounds **2** and **3** in positive ion mode with 120 V fragmentor voltage and 20 V collision energy. Compound **3** yielded a $[M + H]^+$ at $m/z$ 579.1704 and a predominant fragment ion at $m/z$ 433, corresponding to the loss of a terminal rhamnose from the protonated molecule. The product ion at $m/z$ 433 further undertook an inner sugar cleavage to yield the following fragments at $m/z$ 415 ($[M + H\text{-}145 - H_2O]^+$), 397 ($[M + H\text{-}145 - 2H_2O]^+$), 379 ($[M + H\text{-}145 - 3H_2O]^+$), and 367 ($[M + H\text{-}145 - 2H_2O - CH_2O]^+$). The preceding typical fragments were in agreement with 8-*C*-glucosyl apigenin (vitexin) or 6-*C*-glucosyl apigenin (isovitexin).[25] Therefore, compound **3** was proposed to be *O*-pentosylvitexin or -isovitexin. According to the literature data, the possible chemical structure of compound **3** was apigenin-8-*C*-glucoside-*O*-rhamnoside or apigenin-6-*C*-glucoside-*O*-rhamnoside, which has been detected in citrus species.[26−28] Compound **2** exhibited a $[M + H]^+$ at $m/z$ 565.1504, showing a similar MS/MS fragmentation pattern with compound 3. The same ion at $m/z$ 433 due to the loss of a terminal arabinose from precursor ion was also observed. Compared with compound **3**, compound **2** was plausibly identified as apigenin-8-*C*-glucoside-*O*-arabinoside or apigenin-6-*C*-glucoside-*O*-arabinoside.

Coumarin compounds are generally distributed throughout the *Citrus* species.[10] In the present work, a total of seven coumarins were detected and elucidated in CGT. Most coumarins exhibited quasi-molecular ions $[M + H]^+$, $[M + Na]^+$, and fragment ions $[M - CO + H]^+$, $[M - 2CO + H]^+$, $[M - CO_2 + H]^+$, and $[M - CO_2 - CO + H]^+$.

Citrus limonoids have attracted much more attention in recent years because of their health benefits.[29,30] By comparing their quasi-molecular weights, fragment ions, and chromatographic properties with the reported compounds in citrus fruits, we tentatively elucidated four limonoids in CGT, namely, limonin, nomilin, isoobacunoic acid, and obacunone.[31,32]

It has been widely reported that chemical constituents of Citrus species were dominated by flavonoids and limonoids.[31] However, our results showed that CGT contained various courmarins, such as meranzin hydrate, bergaptan, imperatorin, and isoimperatorin. We also observed that chemical constituents were more abundant in fruits and flowers than in leaves and branches. Different sizes of fruits had almost the same chemical constituents profile and yet varied in contents (Table 1), indicating that the harvesting time had no significant effect on the composition of chemical constituents. Isoobacunoic acid was only detected in fruits but not in other parts of CGT. The

compound obacunone was not detected in leaves, but we found abundant obacunone in fruits and flowers.

In summary, the composition and content of chemical constituents varied in different parts of CGT. The most abundant constituents in CGT, calculated by peak area in the MS spectrum, were rhiofolin, naringin, meranzin hydrate, and isoimperatorin.

**Quantitative Evaluation of Chemical Constituents Contents.** In order to develop a feasible and rapid method for quantitative analysis, different mobile phase systems (ACN−-water and methanol−water) were examined and compared. It was shown that a good separation can be obtained in the methanol−water system; however, rhiofolin and naringin were not satisfactorily separated (resolution < 1.5) in the ACN−water system. Finally the methanol−water system was used for the following experiment, considering the appropriate resolution.

To further and truly understand the content of chemical constituents in different tissues of CGT plants (fruits, leaves, flowers, and branches), four major compounds in CGT were quantified by RRLC combined with segmental monitoring strategy, including two flavonoids (rhiofolin and naringin) and two coumarins (meranzin hydrate and isoimperatorin). The naringin showed distinct maximal UV absorption at 283 nm, the rhiofolin and meranzin hydrate had maximal absorptions at 330 nm, and the isoimperatorin had maximal absorptions at 310 nm. To analyze them at one run, we divided the chromatographic fingerprinting into three segments according to the retention time of the four target compounds and set a specific detection wavelength for each segment. Therefore, the UV detector was monitored at 283 nm for 0−9 min, 330 nm for 9−18 min, and 310 nm for 18−23 min.

*Method Validation.* As the results summarized in Supporting Information (Table S1 and Table S2) show, all of the calibration curves exhibited good linearity ($r^2 \geq 0.9998$) within the test range. The LODs and LOQs were less than 0.19 μg/mL and 0.52 μg/mL, respectively. The intra- and interday variations (RSDs) of peak area for four analytes were less than 1.38 and 1.95%, respectively. The repeatability presented as RSDs were in the range from 1.36 to 2.20%. The stability presented as RSDs were less than 1.97%. The recoveries varied between 96.93% and 103.46%. The preceding data were considered to be satisfactory for subsequent analysis of all of the samples.

*Comparison of Main Chemical Constituents in Different Parts of CGT.* The RRLC-DAD assay method was subsequently applied to the simultaneous determination of the two flavonoids and two coumarins (Figure 3) in different parts (fruits, leaves, flowers, and branches) of CGT. The representative RRLC chromatograms of different parts of CGT are shown in Figure 4, and their contents are summarized in Table 2. Values are expressed as mean ± SD ($n$ = 3) in mg/(g of dried weight).

All of the fruit samples tested showed similar phytochemical profiles, but the content levels of the main compounds varied significantly. Among these parts, the small fruits had the highest contents of naringin, rhifolin, and isoimpertorin (256.48, 12.76, and 2.18 mg/g on average, respectively) except meranzin hydrate. Significant differences in contents of the main constituents among different sizes of fruits suggested that the ripening process may influence the quality of the fruits. It was clearly observed that the flower, an alternative source of flavonoids, had high amounts of naringin (135.75 mg/g on

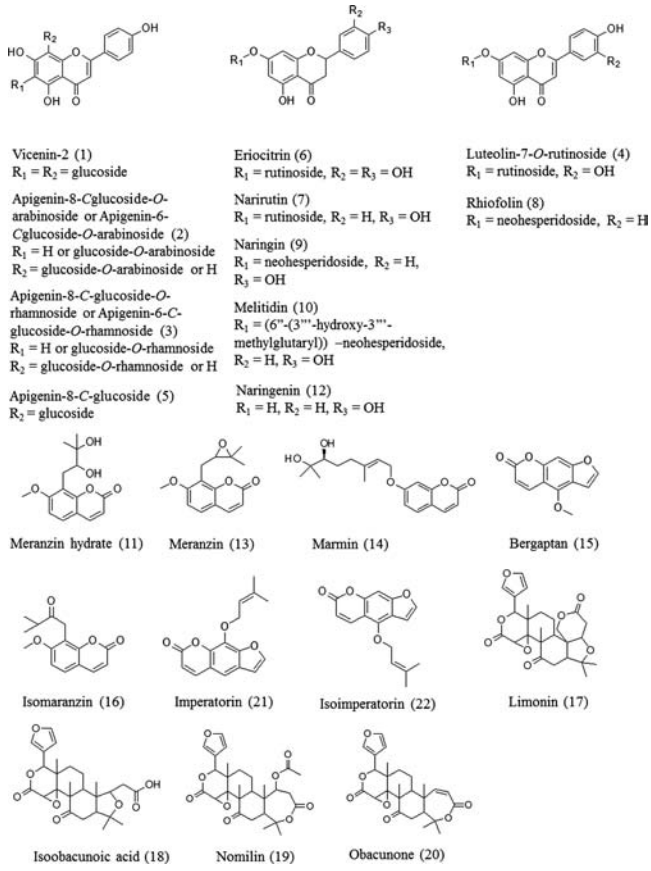


**Figure 3.** Chemical structures of the four quantitative analytes.

average). On the whole, naringin was found to be the predominant compound in different sizes of fruits and other parts of CGT. CGT leaves were found to have almost the same amount of naringin and rhoifolin, with the amount at 1.93 and 1.87 mg/g, respectively. Interestingly, the concentration of naringin in branches was nearly 2 times greater than that in leaves. The two coumarins were not detected in CGT leaves, isoimperatorin was present in a low content, and meranzin hydrate was not detected in CGT branches.

**Determination of Total Phenolic Contents.** Phenolic compounds are considered as the most important antioxidative components of herbs and other plant materials. In the present study; TPC of fruits, flowers, leaves, and branches in CGT, determined by Folin−Ciocalteu reagent, are shown in Figure 5a. The phenolic content of small fruits was significantly higher ($p$ < 0.05) than those of other parts (1.9−9.4-fold). The content of total phenolic varied widely in different parts of CGT and ranged from 11 (for branch) to 123 (for small fruit) mg of GAE/g. Flowers also contained relatively high content of total phenolic, following small fruits. No significant differences were found between medium fruits and large fruits, neither between leaves and branches.

**Determination of Antioxidant Activity.** The antioxidant activity of plant samples can be analyzed using a variety of *in vitro* assays. In the present study, the antioxidant activities of different parts of CGT were determined by DPPH, ABTS, and FRAP assay. It is quite clear that, as shown in Figure 5b−d, small fruit extracts showed the highest antioxidant capacity on average. The antioxidant activity values in three assays showed a similar tendency: small fruit > flower ∼ medium fruit > large fruit > leaf ∼ branch. Phenolic compounds were usually

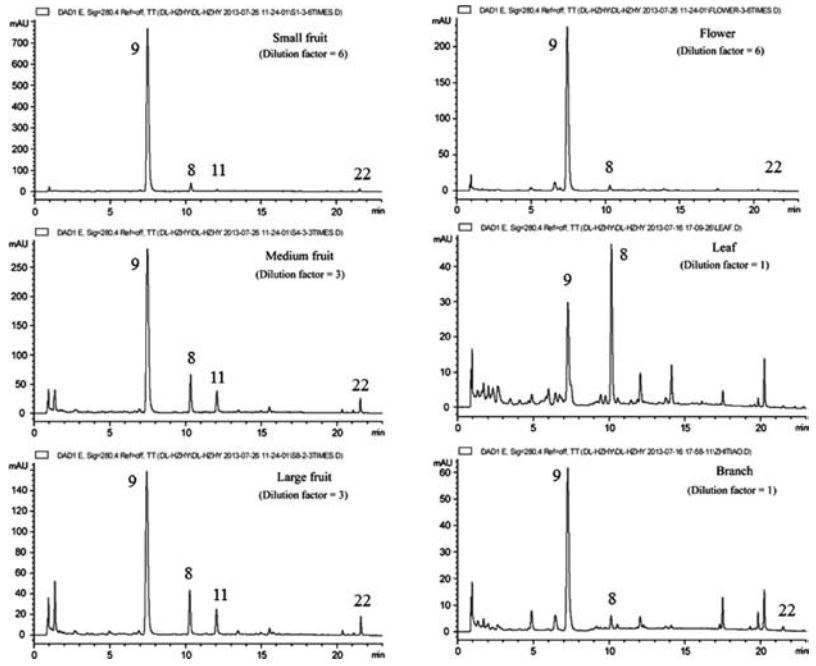


**Figure 4.** Representative RRLC chromatograms of different parts of CGT. Peak numbers of compounds are in accordance with those in Table 1.

**Table 2. Comparisons of Four Main Compounds in the Fruit, Flower, Leaf, and Branch of CGT**

| sample[a] | naringin | rhoifolin | meranzin hydrate | isoimperatorin |
|---|---|---|---|---|
| S1 | 284.35 ± 1.52[b] | 4.81 ± 0.07 | 1.25 ± 0.03 | 2.08 ± 0.02 |
| S2 | 257.06 ± 2.04 | 8.21 ± 0.12 | 1.14 ± 0.01 | 3.96 ± 0.06 |
| S3 | 251.46 ± 1.87 | 5.20 ± 0.08 | 1.20 ± 0.02 | 1.54 ± 0.01 |
| S4 | 269.21 ± 1.99 | 15.04 ± 0.23 | 0.90 ± 0.01 | 1.38 ± 0.01 |
| S5 | 222.01 ± 2.22 | 20.52 ± 0.21 | 1.82 ± 0.01 | 2.69 ± 0.05 |
| S6 | 258.56 ± 2.16 | 15.11 ± 0.27 | 1.37 ± 0.01 | 1.37 ± 0.01 |
| S7 | 262.88 ± 3.70 | 16.14 ± 0.20 | 1.42 ± 0.01 | 3.13 ± 0.04 |
| S8 | 246.30 ± 1.75 | 17.06 ± 0.19 | 1.74 ± 0.01 | 1.27 ± 0.01 |
| M1 | 57.41 ± 0.59 | 4.78 ± 0.05 | 2.17 ± 0.03 | 1.80 ± 0.03 |
| M2 | 78.44 ± 1.01 | 8.13 ± 0.06 | 1.53 ± 0.01 | 1.64 ± 0.02 |
| M3 | 79.81 ± 0.77 | 7.90 ± 0.05 | 1.98 ± 0.01 | 1.63 ± 0.02 |
| M4 | 62.06 ± 0.80 | 5.64 ± 0.08 | 1.76 ± 0.01 | 1.38 ± 0.02 |
| M5 | 75.46 ± 1.33 | 9.27 ± 0.10 | 1.01 ± 0.01 | 0.89 ± 0.01 |
| M6 | 86.09 ± 0.88 | 9.22 ± 0.16 | 2.07 ± 0.02 | 1.40 ± 0.01 |
| L1 | 36.07 ± 0.17 | 3.26 ± 0.06 | 1.57 ± 0.01 | 1.12 ± 0.02 |
| L2 | 49.88 ± 0.59 | 5.25 ± 0.04 | 1.29 ± 0.01 | 1.07 ± 0.01 |
| L3 | 39.64 ± 0.41 | 4.99 ± 0.06 | 0.73 ± 0.01 | 0.71 ± 0.005 |
| L4 | 45.12 ± 0.73 | 4.96 ± 0.08 | 1.53 ± 0.01 | 0.64 ± 0.004 |
| L5 | 43.24 ± 0.55 | 5.19 ± 0.04 | 1.25 ± 0.02 | 1.16 ± 0.01 |
| L6 | 44.32 ± 0.71 | 4.92 ± 0.02 | 0.95 ± 0.01 | 1.91 ± 0.02 |
| F1 | 167.38 ± 0.92 | 1.30 ± 0.01 | *c* | 0.13 ± 0.01 |
| F2 | 117.94 ± 1.56 | 1.08 ± 0.01 | *c* | 0.11 ± 0.00 |
| F3 | 121.94 ± 1.30 | 1.12 ± 0.02 | *c* | 0.11 ± 0.00 |
| leaf | 1.93 ± 0.01 | 1.87 ± 0.02 | *c* | *c* |
| branch | 5.24 ± 0.05 | 0.10 ± 0.00 | *c* | 0.03 ± 0.00 |

[a]S1−8 represent small fruit; M1−6 represent medium fruit; L1−6 represent large fruit; F1−3 represent flowers. [b]Values are expressed as mean ± SD ($n$ = 3) in mg/(g of dried weight). [c]Less than the limit of quantitation.

considered as the basis of antioxidant activity due to their hydroxyl group.[33] Similarly, our results revealed a positive relationship between contents of total phenolic and antioxidant activity. In the market, only fruits of CGT were consumed as food and health supplement. However, our study showed that other parts of CGT, especially flowers, might be used as an alternative dietary supplement.

In conclusion, we compared the chemical constituents profiles of different parts of CGT by RRLC-ESI-QTOF/MS and 22 compounds were identified or tentatively characterized. Of these, two *C*-glucosyl flavones (compounds **2** and **3**) were found, to our best knowledge, for the first time in CGT. This may give us some new insights into CGT, especially leaves and branches which have not been studied before. The

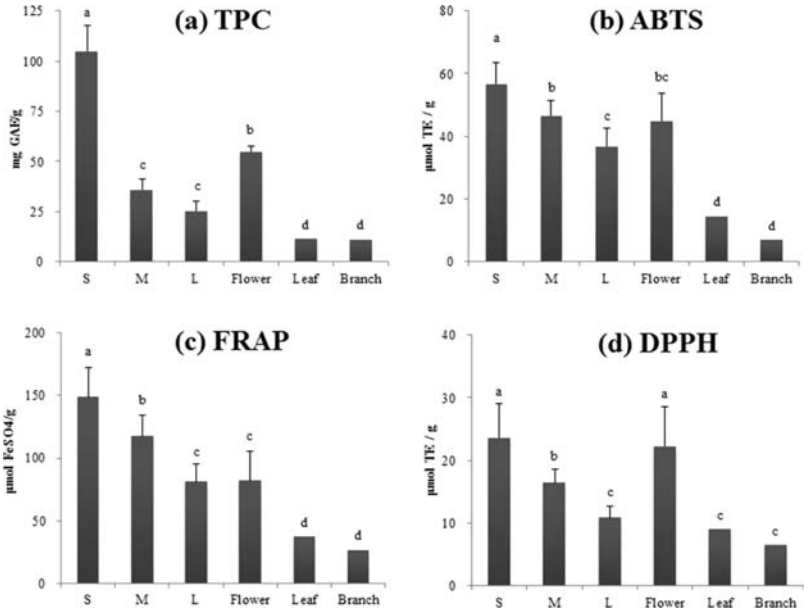


**Figure 5.** (a) Total phenolic contents (TPC) and (b) ABTS, (c) FRAP, and (d) DPPH, antioxidant activity of fruits, flowers, leaves, and branches of CGT. Values of fruits and flowers represent means ± SD (small fruits (S), $n = 8$; medium fruits (M), $n = 6$; large fruits (L), $n = 6$; flower, $n = 3$), while values of leaves and branches represent the antioxidant activity of only the one batch we collected.

quantification of four major compounds by RRLC combined with segmental monitoring strategy demonstrated that the contents of these compounds decreased with ripening of fruits. Fruits and flowers were found to be rich in phenolic compounds and had strong antioxidant activities. In particular, the discarded parts of CGT, leaves and branches, also contained some bioactive compounds and might be used as an alternative dietary supplement. We hope the results may provide useful information for future utilization of CGT.

## ■ ASSOCIATED CONTENT

### Supporting Information

RRLC method validation results (Tables S1 and S2). This material is available free of charge via the Internet at http://pubs.acs.org.

## ■ AUTHOR INFORMATION

### Corresponding Authors

*(E-H.L.) E-mail: liuehu2011@163.com. Phone: +86 25 83271379.

*(P.L.) E-mail: liping2004@126.com. Phone: +86 25 83271379.

### Funding

This work was supported by the National Natural Science Foundation of China (Grant 81473343), New Century Excellent Talents in University (Grant NCET-13-1034), Fundamental Research Funds for the Central Universities (Grant ZD2014YW0033), Talent Work Leading Group of Jiangsu Province (333 High-Level Talents Training Project, Grant BRA2012128), Priority Academic Program Development of Jiangsu Higher Education Institutions and "Six Talent Peaks Program" of Jiangsu Province of China (Grant 2013-YY-001).

### Notes

The authors declare no competing financial interest.

## ■ ABBREVIATIONS USED

CGT, *Citrus grandis* "Tomentosa"; Q-TOF, quadrupole time-of-flight; MS, mass spectrometry; RRLC, rapid resolution liquid chromatography; ESI, electrospray inonization; DPPH, 2,2-diphenyl-1-picrylhydrazyl; ABTS, 2,2′-azinobis(3-ethylbenzthiazolinesulfonic acid) diammonium salt; FRAP, ferric reducing antioxidant power; TPTZ, ferric tripyridyltriazine; TPC, total phenolic contents; GAE, gallic acid equivalents; ANOVA, analysis of variance; DAD, diode array detector; RSD, relative standard deviation; TE, Trolox equivalent

## ■ REFERENCES

(1) Zhang, M.; Duan, C.; Zang, Y.; Huang, Z.; Liu, G. The flavonoid composition of flavedo and juice from the pummelo cultivar (*Citrus grandis* (L.) Osbeck) and the grapefruit cultivar (*Citrus paradisi*) from China. *Food Chem.* **2011**, *129*, 1530−1536.

(2) Wen, B.; Cai, C. T.; Wang, R. L.; Tan, Y. H.; Lan, Q. Y. Critical moisture content windows differ for the cryopreservation of pomelo (*Citrus Grandis*) seeds and embryonicaxes. *CryoLetters* **2010**, *31*, 29−39.

(3) *Chinese Pharmacopeia Commission, Citri Grandis Exocarpium (Huajuhong), Pharmacopeia of the People's Republic of China*, 2010 ed.; China Medical Science: Beijing, 2010; Vol. *1*, pp 69−70.

(4) Yu, J.; Wang, L.; Walzem, R. L.; Miller, E. G.; Pike, L. M.; Patil, B. S. Antioxidant activity of Citrus limonoids, flavonoids, and coumarins. *J. Agric. Food Chem.* **2005**, *53*, 2009−2014.

(5) Jayaraman, J.; Jesudoss, V. A. S.; Menon, V. P.; Namasivayam, N. Anti-inflammatory role of naringenin in rats with ethanol induced liver injury. *Toxicol. Mech. Methods* **2012**, *22*, 568−576.

(6) Li, P. B.; Ma, Y.; Wang, Y. G.; Su, W. W. Experimental studies on antitussive, expectorant and antiasthmatic effects of extract from *Citrus grandis* var. tomentosa. *Zhongguo Zhongyao Zazhi.* **2006**, *31*, 1350−1352.

(7) Nogata, Y.; Sakamoto, K.; Shiratsuchi, H.; Ishii, T.; Yano, M.; Ohta, H. Flavonoid Composition of Fruit Tissues of Citrus Species. *Biosci., Biotechnol., Biochem.* **2006**, *70*, 178−192.

(8) Gattuso, G.; Barreca, D.; Gargiulli, C.; Leuzzi, U.; Caristi, C. Flavonoid Composition of Citrus Juices. *Molecules* **2007**, *12*, 1641−1673.

(9) Breksa Iii, A. P.; Hidalgo, M. B.; Yuen, M. L. Liquid chromatography−electrospray ionisation mass spectrometry method for the rapid identification of citrus limonoid glucosides in citrus juices and extracts. *Food Chem.* **2009**, *117*, 739−744.
(10) Dugrand, A.; Olry, A.; Duval, T.; Hehn, A.; Froelicher, Y.; Bourgaud, F. Coumarin and furanocoumarin quantitation in citrus peel via ultraperformance liquid chromatography coupled with mass spectrometry (UPLC-MS). *J. Agric. Food Chem.* **2013**, *61*, 10677−10684.
(11) Li, P. L.; Liu, M. H.; Hu, J. H.; Su, W. W. Systematic chemical profiling of *Citrus grandis* 'Tomentosa' by ultra-fast liquid chromatography/diode-array detector/quadrupole time-of-flight tandem mass spectrometry. *J. Pharm. Biomed. Anal.* **2014**, *90*, 167−179.
(12) Han, H. B.; Li, H.; Hao, R. L.; Chen, Y. F.; Ni, H.; Li, H. H. One-step column chromatographic extraction with gradient elution followed by automatic separation of volatiles, flavonoids and polysaccharides from *Citrus grandis*. *Food Chem.* **2014**, *145*, 542−548.
(13) Xu, G.; Feng, C.; Zhou, Y.; Han, Q. B.; Qiao, C. F.; Huang, S. X.; Chang, D. C.; Zhao, Q. S.; Luo, K. Q.; Xu, H. X. Bioassay and Ultraperformance Liquid Chromatography/Mass Spectrometry Guided Isolation of Apoptosis-Inducing Benzophenones and Xanthone from the Pericarp of *Garcinia yunnanensis* Hu. *J. Agric. Food Chem.* **2008**, *56*, 11144−11150.
(14) Xia, B.; Zhou, Y.; Tan, H. S.; Ding, L. S.; Xu, H. X. Advanced ultra-performance liquid chromatography-photodiode array-quadrupole time-of-flight mass spectrometric methods for simultaneous screening and quantification of triterpenoids in *Poria cocos*. *Food Chem.* **2014**, *152*, 237−244.
(15) Singleton, V. L.; Rossi, J. A. Colorimetry of total phenolics with phosphomolybdic−phosphotungstic acid reagents. *Am. J. Enol. Vitic.* **1965**, *16*, 144−158.
(16) Shao, Y.; Tang, F.; Huang, Y.; Xu, F.; Chen, Y.; Tong, C.; Chen, H.; Bao, J. Analysis of genotype environment interactions for polyphenols and antioxidant capacity of rice by association mapping. *J. Agric. Food Chem.* **2014**, *62*, 5361−5368.
(17) Seeram, N. P.; Aviram, M.; Zhang, Y.; Henning, S. M.; Feng, L.; Dreher, M.; Heber, D. Comparison of antioxidant potency of commonly consumed polyphenol-rich beverages in the United States. *J. Agric. Food Chem.* **2008**, *56*, 1415−1422.
(18) Liang, X. L.; Wang, X. L.; Li, Z.; Hao, Q. H.; Wang, S. Y. Improved in vitro assays of superoxide anion and 1,1-diphenyl-2-picrylhydrazyl (DPPH) radical-scavenging activity of isoflavones and isoflavone metabolites. *J. Agric. Food Chem.* **2010**, *58*, 11548−11552.
(19) Chen, T. S.; Liou, S. Y.; Wu, H. C.; Tsai, F. J.; Tsai, C. H.; Huang, C. Y.; Chang, Y. L. New analytical method for investigating the antioxidant power of food extracts on the basis of their electron-donating ability: comparison to the ferric reducing/antioxidant power (FRAP) assay. *J. Agric. Food Chem.* **2010**, *58*, 8477−8480.
(20) Dudonne, S.; Vitrac, X.; Coutiere, P.; Woillez, M.; Mérillon, J. M. Comparative study of antioxidant properties and total phenolic content of 30 plant extracts of industrial interest using DPPH, ABTS, FRAP, SOD, and ORAC assays. *J. Agric. Food Chem.* **2009**, *57*, 1768−1774.
(21) Tao, B.; Ye, F.; Li, H.; Hu, Q.; Xue, S.; Zhao, G. Phenolic Profile and in Vitro Antioxidant Capacity of Insoluble Dietary Fiber Powders from Citrus (Citrus junosSieb. ex Tanaka) Pomace as Affected by Ultrafine Grinding. *J. Agric. Food Chem.* **2014**, *62*, 7166−7173.
(22) Li, S. Y.; Yu, Y.; Li, S. P. Identification of Antioxidants in Essential Oil of Radix Angelicae Sinensis Using HPLC Coupled with DAD-MS and ABTS-Based Assay. *J. Agric. Food Chem.* **2007**, *55*, 3358−3362.
(23) Zheng, G. D.; Zhou, P.; Yang, H.; Li, Y. S.; Li, P.; Liu, E. H. Rapid resolution liquid chromatography-electrospray ionisation tandem mass spectrometry method for identification of chemical constituents in Citri Reticulatae Pericarpium. *Food Chem.* **2013**, *136*, 604−611.
(24) Cuyckens, F.; Rozenberg, R.; de Hoffmann, E.; Claeys, M. Structure characterization of flavonoid O-diglycosides by positive and negative nano-electrospray ionization ion trap mass spectrometry. *J. Mass Spectrom.* **2001**, *36*, 1203−1210.
(25) Abad-Garcia, B.; Garmon-Lobato, S.; Berrueta, L. A.; Gallo, B.; Vicente, F. New features on the fragmentation and differentiation of C-glycosidic flavone isomers by positive electrospray ionization and triple quadrupole mass spectrometry. *Rapid Commun. Mass Spectrom.* **2008**, *22*, 1834−1842.
(26) Li, W.; Qiu, Y.; Patterson, C. A.; Beta, T. The analysis of phenolic constituents in glabrous canaryseed groats. *Food Chem.* **2011**, *127*, 10−20.
(27) Roowi, S.; Crozier, A. Flavonoids in tropical citrus species. *J. Agric. Food Chem.* **2011**, *59*, 12217−12225.
(28) Piccinelli, A. L.; García, M. M.; Armenteros, D. M.; Alfonso, M. A.; Arevalo, A. C.; Campone, L.; Rastrelli, L. HPLC-PDA-MS and NMR characterization of C-glycosyl flavones in a hydroalcoholic extract of Citrus aurantifolia leaves with antiplatelet activity. *J. Agric. Food Chem.* **2008**, *56*, 1574−1581.
(29) Tundis, R.; Loizzo, M. R.; Menichini, F. An overview on chemical aspects and potential health benefits of limonoids and their derivatives. *Crit. Rev. Food Sci. Nutr.* **2014**, *54*, 225−250.
(30) Chidambara Murthy, K. N.; Jayaprakasha, G. K.; Patil, B. S. Citrus limonoids and curcumin additively inhibit human colon cancer cells. *Food Funct.* **2013**, *4*, 803−810.
(31) Duan, L.; Guo, L.; Liu, K.; Liu, E. H.; Li, P. Characterization and classification of seven citrus herbs by liquid chromatography-quadrupole time-of-flight mass spectrometry and genetic algorithm optimized support vector machines. *J. Chromatogr. A* **2014**, *1339*, 118−127.
(32) Tian, Q.; Li, D.; Barbacci, D.; Schwartz, S. J.; Patil, B. S. Electron ionization mass spectrometry of citrus limonoids. *Rapid Commun. Mass Spectrom.* **2003**, *17*, 2517−2522.
(33) Zheng, W.; Wang, S. Y. Antioxidant Activity and Phenolic Compounds in Selected Herbs. *J. Agric. Food Chem.* **2001**, *49*, 5165−5170.

number of studies using SPE pretreatment in cooperation with liquid chromatography coupled to triple-quadruple tandem mass spectrometry (LC−MS/MS) to quantify BPs in foodstuffs because this method is highly sensitive, has a wide range of applicability, and consumes less solvent. However, the traditional SPE sorbents generally retain analytes by nonselective hydrophobic or polar interactions that lead to partial coextraction of interferences, resulting in suppression of the analyte signal.[19,20] In order to enhance the selectivity of the extraction, molecularly imprinted polymers (MIPs), based on specific recognition of the template molecule, allowing a selective extraction of a target molecule or its structural analogues, were developed.[21−23] In the past few years, MIPs were widely used as a new selective sorbent for cleaning up SPE and for extracting trace levels of compounds from complex matrices.[24−26] Several approaches have been used to prepare BPA imprinted polymers and have been applied to analyze foodstuffs.[27,28] However, the application of MIP for the determination of structurally related BP analogues in foodstuffs has been limited to date.

In this study, we aim to develop a method for the group-selective extraction of seven BPs (BPS, BPF, BPA, BPB, BPAF, TCBPA, and TBBPA) in beverage and canned food samples based on MIP-SPE with LC−MS/MS analysis. The high selectivity of MIP-SPE was compared with the selectivity of the traditional HLB SPE cartridge. In addition, the validated method was used to determine the target compound concentrations in beverage and canned food samples that were collected from a supermarket in Beijing. To our knowledge, this is the first study in which seven bisphenols were included together as target compounds in the development of an analytical method based on MIP-SPE for analyzing foodstuffs.

## MATERIALS AND METHODS

**Reagents and Chemicals.** For this experiment, BPS (purity >98%), BPF (purity >99%), BPA (purity 98.5%), BPA-$d_4$ (purity >97.8%), BPB (purity >98%), and BPAF (purity 98%) were purchased from Tokyo Chemical Industry Co. Ltd. (Tokyo, Japan). BPF-$d_{10}$ and BPS-$^{13}C_{12}$ (purity >99%) were purchased from Toronto Research Chemical Inc. (Ontario, Canada), and BPAF-$d_4$ was purchased from CDN Isotopes Inc. (Quebec, Canada). TCBPA (purity >99%), TCBPA-$^{13}C_{12}$ (purity >99%), TBBPA (purity >99%), and TBBPA-$^{13}C_{12}$ (purity >99%) were obtained from Cambridge Isotope Laboratories Inc. (Andover, MA). In addition, water, acetonitrile (MeCN, water <0.01%), and methanol (MeOH, water <0.01%) were purchased from Sigma−Aldrich (LC−MS-grade, St. Louis, MO). Furthermore, the formic acid and ammonium hydroxide for analysis (28−30 wt % solution of $NH_3$ in water) were supplied by Acros Organics (Morris Plains, NJ). The molecularly imprinted polymers (product code AFFINIMIP SPE bisphenol A cartridges) were provided by Polyintell (Val de Reuil, France). Oasis HLB cartridges (200 mg, 6 mL) were purchased from Waters (Milford, MA), and the stock standard solutions (1000 mg/L) were individually prepared by dissolving in MeOH and were stored at −20 °C. Working solutions were prepared by serial dilution of stock solutions with MeOH/water (50:50 v/v).

**Sample Collection.** Fourteen beverage samples [7 pairs; in each pair one is packed in cans and another in poly(ethylene terephthalate) (PET) or Tetra Pak] and four canned foods from different brands, commonly consumed by the local population, were purchased from a supermarket in Beijing, China. They contained soda, tea drink, juice, vegetable, and meat. Purchasing of the samples was carried out in February 2014. All samples were stored at room temperature and opened only at the moment of analysis.

**Sample Preparation and Solid-Phase Extraction Procedure.** After the samples had been opened, the carbonated beverage samples were degassed by sonication for 30 min to form the loading solution for SPE procedures. Juice and milk samples were centrifuged at 9000$g$ for 5 min to avoid blocking of the cartridges. Regarding the canned food, a total of 1 g of each homogenized sample was added to 5 mL of MeCN for extraction. Following sonication for 20 min, the mixtures were centrifuged at 9000$g$ for 5 min, and the supernatants were collected. Subsequently, 5 mL of hexane was added to remove the fat by liquid−liquid extraction. The MeCN layer was collected and evaporated to 1 mL under a gentle nitrogen stream, which was diluted to 10 mL with LC−MS-grade water to form the loading solution.

A diagram of the MIP-SPE procedure is shown in Figure 1. Briefly, the pretreated loading solutions were loaded onto the MIP-SPE

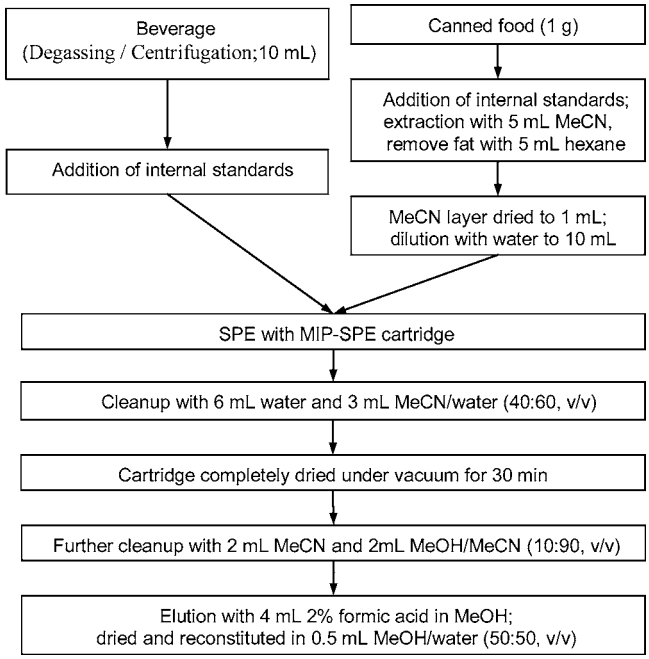


**Figure 1.** Diagram of MIP-SPE procedure for analysis of target BPs in beverage and canned food.

cartridges at a flow rate of 1 mL/min. The MIP-SPE cartridges had been previously conditioned with 3 mL of MeOH, 3 mL of MeCN, and 3 mL of water. After the loading step, the sorbents were cleaned up with water and MeCN/water (40:60 v/v). Next, the sorbents were completely dried and further washed with MeCN and MeOH/MeCN (10:90 v/v). After elution, the eluates were evaporated to dryness and the residues were reconstructed in 500 $\mu$L of a MeOH/water (50:50 v/v) solution for LC−MS analysis.

The protocol for HLB cartridges was conducted according to our previous report.[29] Briefly, the HLB cartridges were conditioned with 6 mL of MeOH and 6 mL of water. After loading of the samples, the cartridges were washed with 6 mL of MeOH/water (50:50 v/v) to remove interference. In addition, the extracts were eluted with 6 mL of 2% ammonia in 100% MeOH. The eluates were evaporated and reconstructed in 500 $\mu$L of a MeOH/water (50:50 v/v) mixture before LC−MS analysis.

**LC−MS Analysis.** The target analytes were separated with an Acquity ultraperformance liquid chromatography system (Waters, Milford, MA). The analytical column was an Acquity ethylene bridged hybrid (BEH) C18 column (2.1 mm × 100 mm; 1.7 $\mu$m; Waters). The mobile phase consisted of a MeOH−water isocratic mixture (40:60 v/v), which was held for 1 min, and a linear gradient from 40% to 80% MeOH that was held for 5 min. The MeOH content was increased to 100% at 6.1 min, held for 2.0 min, and returned to the initial conditions for equilibration. The flow rate was 0.3 mL/min and the injection volume was 5 $\mu$L.

A Xevo TQ-S triple-quadrupole mass spectrometer (Waters, Milford, MA) was used to determine the analyte concentrations. The MS/MS acquisition was operated in negative-ion mode with multiple reaction monitoring (MRM). The source operating conditions were as follows: a capillary voltage of 2.9 kV; source and desolvation temperatures of 150 and 400 °C, respectively; and a desolvation gas flow rate of 1000 L/h. For each analyte, identification was based on the retention time of the quantification and conformation ions. The corresponding cone voltage and collision energies were optimized for maximum intensity (see Supporting Information for optimized MS/MS parameters).

**Method Validation.** Three types of foodstuffs (orange juice, red wine, and canned fish) were used to evaluate the analytical characteristics of the procedure based on the use of MIP-SPE as a selective sorbent prior to chromatographic analysis. This method was evaluated in terms of linearity, accuracy, precision, and sensitivity. In the present study, isotopic internal standards were employed to compensate for the matrix effects and the loss during analysis. Calibration curves were constructed by plotting the peak area ratios of the pure analytes to the internal standards against the analyte concentrations (linearity ranges for BPF, BPB, and TBBPA were 0.2, 0.5, 1, 2, 5, 10, and 20 ng/mL; for BPA and TCBPA, 0.1, 0.25, 0.5, 1, 2.5, 5, and 10 ng/mL; and for BPS and BPAF, 0.02, 0.05, 0.1, 0.2, 0.5, 1, and 2 ng/mL). BPA-$d_4$ was selected as an internal standard for BPB because no commercially labeled standards are available. For assessment of accuracy and precision, the whole MIP-SPE procedures were applied to orange juice, red wine, and canned fish samples spiked with seven BPs at three fortification levels. Analyses of six replicates were conducted to evaluate the precision of the method (expressed as the relative standard deviation, RSD %) and to evaluate the accuracy (expressed as absolute recovery).

The limits of quantification (LOQ) and the limits of detection (LOD), through the proposed method, were determined on the basis of the signal-to-noise (S/N) ratio of the actual analyte peak and the baseline close to the peak. This procedure was performed by successive analyses of spiked noncontaminated samples with decreasing amounts of the analytes until an S/N ratio of 10:1 (LOQ) or 3:1 (LOD) was reached.[13,15] LOQ of BPA in canned food could not be measured because of high background levels in all of these samples, and the corresponding LOQ was estimated by BPA-$d_4$ in the present study.

**Quality Assurance and Quality Control (QA/QC).** Different authors have reviewed the challenge of accurately detecting BPA at ultralow concentrations.[18,30] Background contamination can easily occur at trace levels because the target analytes are inherently ubiquitous in the laboratory environment. In this study, heat-treated glassware, LC−MS-grade solvents, and solvent-washed materials were used to prevent background contamination. In addition, one key problem associated with the development of an MIP-SPE method occurs because the residual template is not completely removed from the polymeric matrix and leaking occurs during the SPE procedure, which results in a false-positive result when the same molecule is used as the template. The template of the MIP sorbent that was used in this experiment is a dummy template that was synthesized commercially and contains two aromatic rings that are similar to BPA, one of which is a phenol. The template is removed by thoroughly washing and does not interfere with the target analytes. Furthermore, a procedural blank containing LC−MS water in place of the foodstuff samples was subjected to the same extraction protocol as the actual samples and was analyzed to evaluate the contamination levels for the entire procedure. Only trace levels of BPA (S/N < 5) and BPS (S/N < 2) were found in the procedural blank (see Supporting Information). The corresponding peak areas were deducted from the analysis results. Quantification was based on the internal calibration curves constructed by injection of seven calibration standards. A midpoint calibration standard was injected to check instrumental drift in sensitivity, and pure MeOH was injected to monitor sample carryover after every 10th sample analysis.

## RESULTS AND DISCUSSION

**Development of the Molecularly Imprinted Polymer Solid-Phase Extraction Procedure.** In this study, the MIP-SPE procedure was optimized on the basis of the manufacturer's instructions (AFFINIMIP SPE bisphenol A cartridges) to develop an MIP-SPE method that was suitable for simultaneous extraction of related BP analogues in beverage and canned food samples. First, the loading solutions were kept in an aqueous environment with less than 10% organic solvent, which resulted in complete retention of the analytes on the MIP-SPE through nonspecific interactions, such as hydrophobic or ion-exchange interactions. For the washing step, 6 mL of pure water was used to eliminate salts and hydrophilic interference. Next, 3 mL aliquots of the different MeCN/water solvent compositions (40:60, 50:50, and 60:40 v/v) were assessed to select a suitable solvent for removing the nonselectively bound polar matrix interference. A washing solvent consisting of 3 mL of MeCN/water (40:60 v/v) was optimal for cleaning and did not compromise recovery of the analytes.

To enable the polymer to selectively interact with the analytes, a complete drying step was necessary for the sorbents to shift from the aqueous to the nonaqueous washing step. After the drying step, 2 mL of MeCN (a polar nonprotic solvent) was used to induce the formation of specific interactions through hydrogen bonds between the analytes and the MIP monomers. Next, 2 mL of a MeOH/MeCN (10:90 v/v) mixture was applied to the cartridges to elute nonspecifically bound apolar matrix interference. As shown in Figure 2, recovery was closely associated with MeOH content

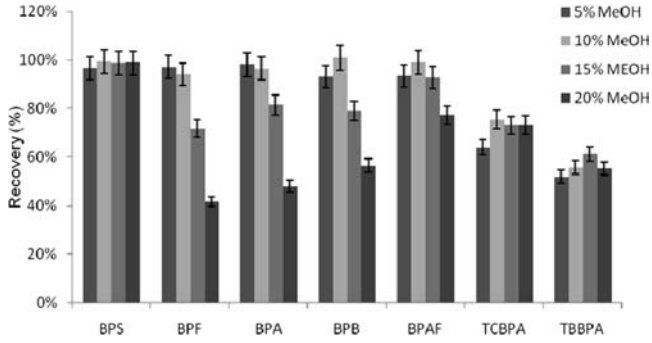


**Figure 2.** Comparison of analyte recoveries for use of different MeOH concentrations in MeCN during the washing step ($n$ = 3).

in the MeCN that was used in the washing step, and more than 10% MeOH in the MeCN resulted in significant losses of BPF, BPA, and BPB but not the other BPs. The presence of a higher portion of protic solvent, such as MeOH, would break the specific interactions, and these compounds with lower affinities for MIP were more easily removed during the washing step. When optimizing the elution conditions, we found that TCBPA and TBBPA were difficult to elute from the cartridge when 100% MeOH was used as the solvent. The desorption of these two compounds was achieved by percolating 100% MeOH with the addition of 2% formic acid, which was effective for disrupting the interactions between analytes and sorbents and for obtaining satisfactory recoveries.

During the SPE process, breakthrough potentially occurred due to the large loading sample volume or the high analyte concentration, which would decrease the recovery of the

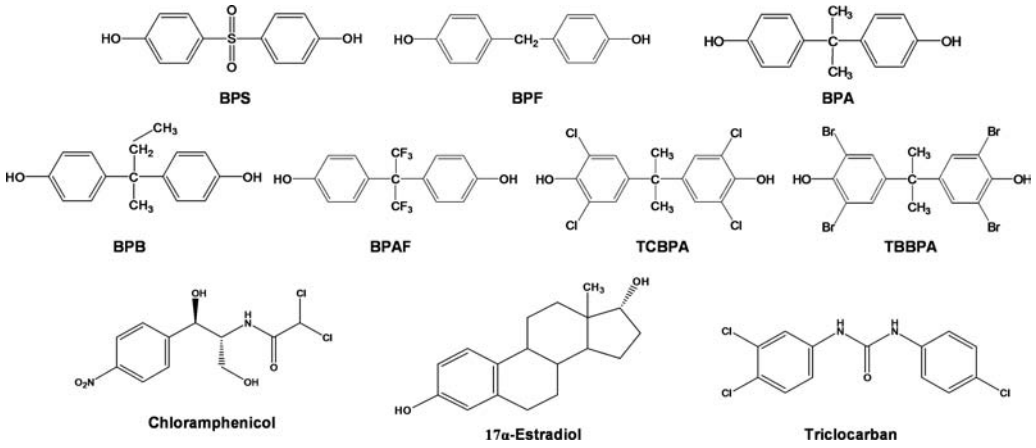


**Figure 3.** Structures of the seven analytes and the other three compounds used in selectivity binding tests.

method. Therefore, the breakthrough was assessed by extracting spiked orange juice (BPF, BPB, and TBBPA, 0.5 ng/mL; BPA and TCBPA, 0.25 ng/mL; BPS and BPAF, 0.05 ng/mL) with different sample loading volumes (5, 10, 20, 40, and 80 mL). No breakthrough occurred in these tests, and all analytes maintained a stable recovery as the sample volume increased from 5 to 80 mL, which indicated the preconcentration potential of the MIP-SPE. In this study, a 10 mL sample volume was selected because lower preconcentration times were needed, lower matrix interferences were introduced, and the sensitivity was sufficient for routine analysis.

**Selectivity of Molecularly Imprinted Polymer Solid-Phase Extraction.** To evaluate the selectivity of the MIP-SPE method, a comparison with the hydrophobic−lipophilic balance (Oasis HLB) SPE cartridge, which is one of the most widely employed reverse-phase cartridges for determining BPA concentrations in foodstuffs,[31−33] was conducted. The group-selective potential of the MIP-SPE procedure was tested by spiking the water with analytes and three other compounds (chloramphenicol, 17$\alpha$-estradiol, and triclocarban) belonging to the same range of polarity as the target analytes (Figure 3). The results obtained by the MIP-SPE procedure were compared with those obtained by the Oasis HLB. As shown in Figure 4, less than 10% of the chloramphenicol was retained by the MIP-SPE cartridge because its chemical structure shared less similarity with the bisphenols and was removed by the washing step. In addition, the lack of retention for triclocarban on the MIP-SPE was observed in the test even if it was a more hydrophobic compound. However, 17$\alpha$-estradiol was an exception to this behavior; it presented an extraction recovery of approximately 50% on the MIP-SPE cartridge. This recovery is explained by the similar arrangement of phenolic hydroxyl groups to the BP analogues. In contrast, the HLB was expected to be less selective than MIP-SPE because all of the compounds with a wide range of polarities were well retained after the loading and rinsing steps.

On the basis of the comparison above, it was shown that the presence of cavities in the MIP occurred. However, this result was not sufficient for demonstrating the real selectivity of the MIP for its application to real samples. Optimal selectivity necessitates the presence of a cleaner baseline or less matrix suppression for real sample analysis. In this study, two types of matrices (orange juice and canned fish) were spiked at the same concentrations and were passed through the MIP-SPE and HLB cartridges for analysis. After extraction and purification by

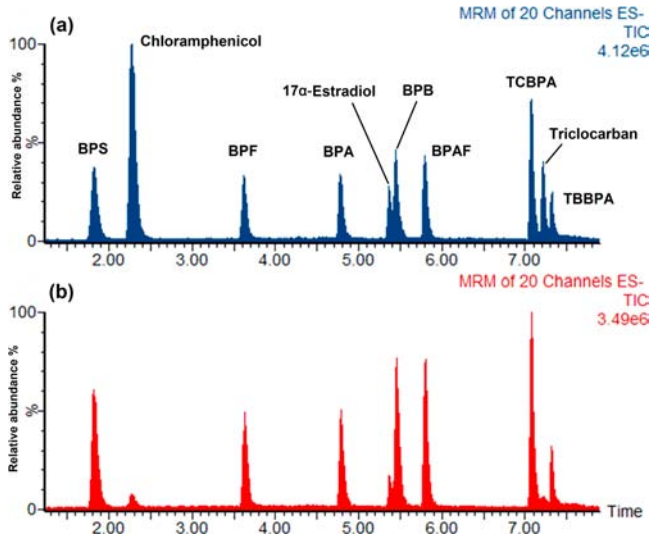


**Figure 4.** Chromatograms obtained from selectivity tests between (a) Oasis HLB and (b) MIP-SPE. The lack of chloramphenicol, 17$\alpha$-estradiol, and triclocarban retention on MIP demonstrates the selectivity of the extraction procedure on MIP-SPE.

the MIP-SPE and HLB cartridges, the chromatograms that corresponded to each analyte are shown in Figure 5. Using the MIP-SPE instead of the Oasis HLB for the extraction and purification process resulted in a cleaner baseline and in less matrix suppression for most of the analytes. In addition, another advantage of MIP-SPE is its ability to remove the majority of the pigment from the sample matrix to obtain cleaner extracts (see Supporting Information).

**Validation of Molecularly Imprinted Polymer Solid-Phase Extraction Method.** The calibration curves were constructed from the peak area ratio of the analyte to the internal standards (BPA-$d_4$, TCBPA-$^{13}C_{12}$, TBBPA-$^{13}C_{12}$, and BPF-$d_{10}$, 5 ng/mL; BPS-$^{13}C_{12}$ and BPAF-$d_4$, 0.5 ng/mL) versus the analyte concentrations and were linear with a correlation coefficient of >0.99 in the concentration ranges evaluated. Table 1 illustrates the recoveries and the RSDs of the analytes in the spiked orange juice, red wine, and canned fish. The results showed that the recoveries were in the 50−103% range, with RSD values of less than 15% for all of the analytes. The LOQ, obtained after the MIP-SPE procedures of 10 mL beverage samples or 1 g canned food samples, varied from 0.002 to 0.15 ng/mL in the beverage samples and from 0.03 to


dx.doi.org/10.1021/jf5037933 | J. Agric. Food Chem. 2014, 62, 11130−11137

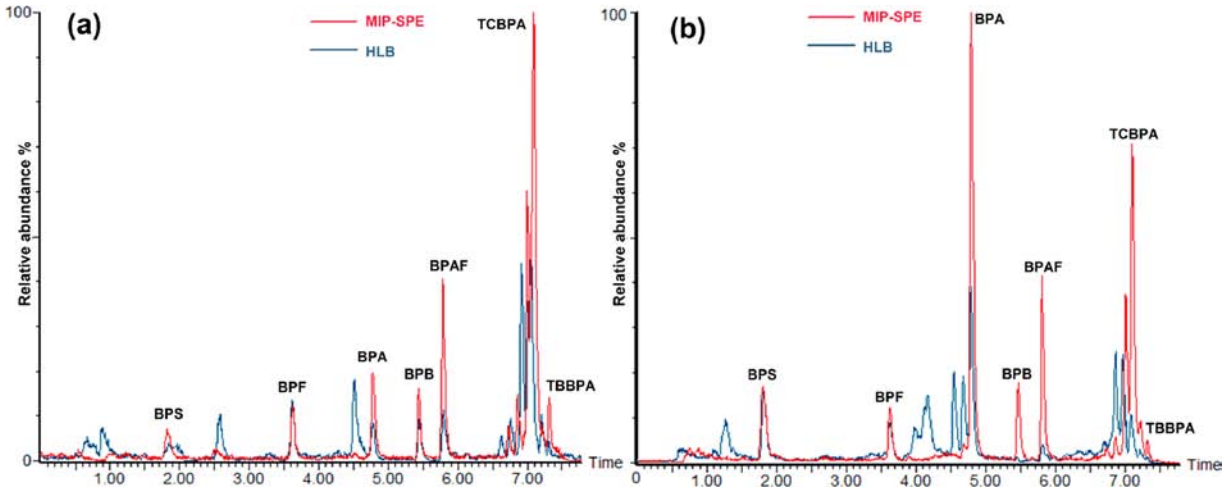


**Figure 5.** Comparison of purification performance of Oasis HLB and MIP-SPE for (a) spiked orange juice and (b) spiked canned fish samples. Samples were spiked with 2.5 ng of BPF, BPB, and TBBPA; 1.25 ng of BPA and TCBPA; and 0.25 ng of BPS and BPAF.

**Table 1. Recoveries, Relative Standard Deviations, and Limits of Quantification of Target Compounds in Food Samples ($n$ = 6)**

| orange juice | | | | red wine | | | | canned fish | | | |
|---|---|---|---|---|---|---|---|---|---|---|---|
| spike (ng/mL) | recovery (%) | RSD (%) | LOQ (ng/mL) | spike (ng/mL) | recovery (%) | RSD (%) | LOQ (ng/mL) | spike (ng/g) | recovery (%) | RSD (%) | LOQ (ng/g) |
| Bisphenol S | | | | | | | | | | | |
| 0.005 | 82 | 9 | 0.006 | 0.005 | 88 | 13 | 0.007 | 0.1 | 73 | 3 | 0.07 |
| 0.02 | 100 | 6 | | 0.02 | 78 | 11 | | 0.2 | 80 | 9 | |
| 0.05 | 98 | 5 | | 0.05 | 87 | 8 | | 0.5 | 82 | 4 | |
| Bisphenol F | | | | | | | | | | | |
| 0.05 | 82 | 7 | 0.054 | 0.05 | 78 | 9 | 0.029 | 1 | 78 | 10 | 0.5 |
| 0.2 | 82 | 8 | | 0.2 | 96 | 4 | | 2 | 74 | 3 | |
| 0.5 | 82 | 4 | | 0.5 | 81 | 6 | | 5 | 73 | 6 | |
| Bisphenol A | | | | | | | | | | | |
| 0.025 | 86 | 9 | 0.013 | 0.025 | 95 | 6 | 0.01 | 0.5 | 81 | 14 | 0.12 |
| 0.1 | 91 | 7 | | 0.1 | 99 | 5 | | 1 | 88 | 6 | |
| 0.25 | 92 | 4 | | 0.25 | 99 | 5 | | 2.5 | 89 | 8 | |
| Bisphenol B | | | | | | | | | | | |
| 0.05 | 83 | 8 | 0.15 | 0.05 | 86 | 9 | 0.04 | 1 | 79 | 9 | 1.5 |
| 0.2 | 93 | 9 | | 0.2 | 97 | 5 | | 2 | 80 | 12 | |
| 0.5 | 92 | 9 | | 0.5 | 92 | 5 | | 5 | 82 | 3 | |
| Bisphenol AF | | | | | | | | | | | |
| 0.005 | 93 | 10 | 0.003 | 0.005 | 91 | 6 | 0.002 | 0.1 | 81 | 9 | 0.03 |
| 0.02 | 85 | 4 | | 0.02 | 89 | 5 | | 0.2 | 79 | 7 | |
| 0.05 | 103 | 6 | | 0.05 | 98 | 4 | | 0.5 | 79 | 3 | |
| Tetrachlorobisphenol A | | | | | | | | | | | |
| 0.025 | 68 | 8 | 0.005 | 0.025 | 82 | 11 | 0.005 | 0.5 | 72 | 15 | 0.28 |
| 0.1 | 73 | 5 | | 0.1 | 72 | 2 | | 1 | 74 | 11 | |
| 0.25 | 84 | 4 | | 0.25 | 76 | 4 | | 2.5 | 78 | 9 | |
| Tetrabromobisphenol A | | | | | | | | | | | |
| 0.05 | 50 | 10 | 0.012 | 0.05 | 60 | 12 | 0.032 | 1 | 57 | 14 | 0.6 |
| 0.2 | 53 | 5 | | 0.2 | 65 | 7 | | 2 | 61 | 11 | |
| 0.5 | 61 | 10 | | 0.5 | 63 | 5 | | 5 | 67 | 8 | |

1.5 ng/g in the canned food samples. These results provided lower LOQs for BPA and its analogues relative to the LOQs reported in previously published methods[33−37] (see Supporting Information for comparison with other methods).

**Application of the Method.** To demonstrate the applicability of the developed method, several beverage samples and canned foods were randomly purchased from local supermarkets in Beijing. Figure 6 shows the typical LC−MS/MS chromatograms that corresponded to canned pork luncheon meat, in which BPS, BPF, and BPA were detected. The analyte concentrations are summarized in Table 2. BPB, TCBPA, and TBBPA were not detected in any of the samples, and the concentrations of the other BPs in the beverage products were generally low. BPA and BPF were the most frequently detected BPs in the beverage samples and varied from ND to 12 ng/mL and from ND to 0.39 ng/mL, respectively. These levels are similar to the levels that were observed in beverages by Geens et al.[33] (BPA, <LOQ−8.1 ng/


dx.doi.org/10.1021/jf5037933 | J. Agric. Food Chem. 2014, 62, 11130−11137

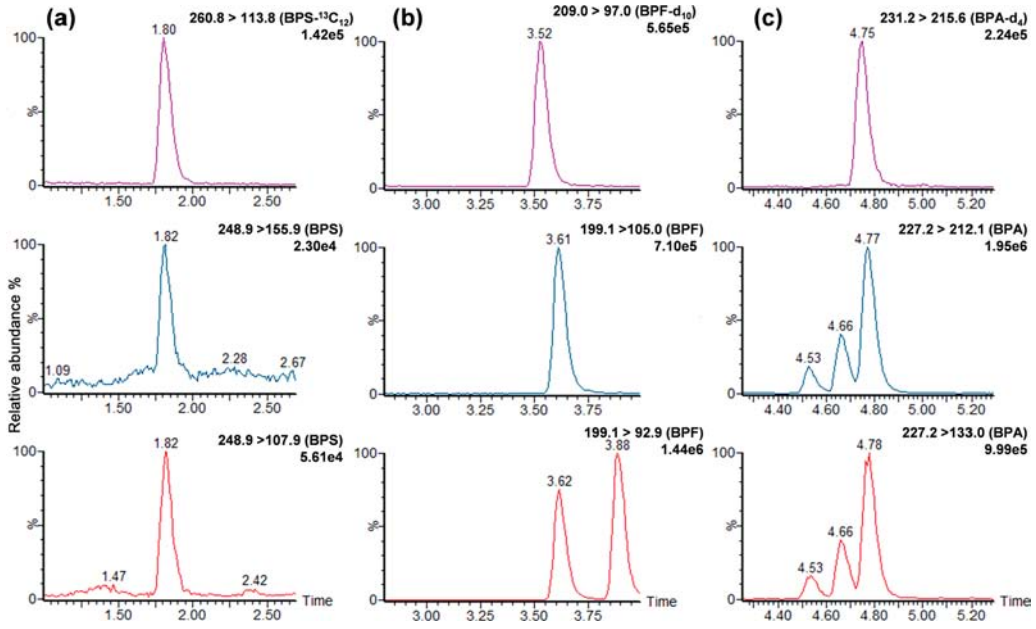


**Figure 6.** Typical LC−MS/MS chromatograms obtained from a canned pork luncheon meat sample: (a) BPS (0.22 ng/g), (b) BPF (35 ng/g), and (c) BPA (30 ng/g) were detected.

**Table 2. Concentrations of Bisphenols in Beverage and Canned Food Samples[a]**

| Beverages | | | | | |
|---|---|---|---|---|---|
| | | concn (ng/mL) | | | |
| volume (mL) | packaging type | BPS | BPF | BPA | BPAF |
| Soda (lemon flavored) | | | | | |
| 600 | PET | ND | ND | ND | ND |
| 330 | can | ND | ND | 0.063 | ND |
| Soda (orange flavored) | | | | | |
| 600 | PET | ND | ND | ND | ND |
| 330 | can | ND | <LOQ | <LOQ | ND |
| Soda (apple flavored) | | | | | |
| 600 | PET | ND | ND | ND | ND |
| 330 | can | ND | <LOQ | 0.083 | ND |
| Tea Drinks | | | | | |
| 600 | PET | ND | ND | 0.27 | <LOQ |
| 330 | can | ND | <LOQ | 9.7 | ND |
| Vitamin Drinks | | | | | |
| 600 | PET | ND | ND | ND | ND |
| 330 | can | ND | <LOQ | 0.067 | ND |
| Coconut Juice | | | | | |
| 245 | Tetra Pak | 0.036 | ND | 0.23 | 0.052 |
| 245 | can | 0.019 | 0.39 | 12 | 0.013 |
| Milk | | | | | |
| 125 | Tetra Pak | ND | ND | 0.019 | ND |
| 245 | can | ND | 0.36 | 8.8 | ND |
| Canned Foods | | | | | |
| | | concn (ng/g) | | | |
| sample | weight (g) | BPS | BPF | BPA | BPAF |
| corn (filling liquid) | 425 | ND | <LOQ | <LOQ | ND |
| corn (solid content) | | 0.26 | 4.3 | 6.5 | 0.070 |
| pork luncheon meat | 340 | 0.22 | 35 | 30 | ND |
| fish (tuna) | 185 | <LOQ | ND | 17 | ND |
| fish (fried dace) | 227 | ND | 2.2 | 58 | ND |

[a]BPB, TCBPA, and TBBPA were not detected in any of the samples.

mL), Cao et al.[34] (BPA, 0.032−4.5 ng/mL), Cacho et al.[14] (BPF, ND−0.26 ng/mL), and Gallart-Ayala et al.[35] (BPF: ND−0.22 ng/mL). Compared with BPA and BPF, less than 25% of the samples contained BPS and BPAF above the LOQ in the beverages, which indicated their minor use in food contact materials.

Influences of the packaging materials were evaluated by comparing the BP concentrations in seven paired beverage samples. The only difference in each pairs is that one was packed in cans and the other in PET or Tetra Pak. As shown in Table 2, beverages in the packing materials with PET or Tetra Pak had lower BPA and BPF contamination or detection rates relative to the same beverages packed in cans. This result indicated that the BPA and BPF in these types of foods primarily originated from the can's inner coating.

For the canned food samples, BPS, BPA and BPF concentrations were comparable to the BP concentrations that were recently reported for canned food[13,33,36,37](see Supporting Information) and were approximately 1 order of magnitude greater than those in the canned beverages. The higher concentrations in canned food most likely occurred because the chemicals preferred a more lipophilic environment than the aqueous phase or resulted from differences in sterilization conditions and coating types.[33]

In conclusion, the above-mentioned applications proved that this MIP-SPE method is a powerful method to make group-selective extraction and purification in a single step and provide cleaner extracts. The method offers many advantages such as high selectivity, low solvent consumption, and ease of use, which make it possible to replace traditional SPE methods for the analysis of bisphenol analogues in complex matrices.

## ■ ASSOCIATED CONTENT

### Ⓢ Supporting Information

Three tables listing optimized MS/MS parameters, reported method parameters, and reported concentrations of BPs in beverage and canned food samples; two figures showing chromatograms of analytes in the procedural blank and


dx.doi.org/10.1021/jf5037933 | J. Agric. Food Chem. 2014, 62, 11130−11137

comparison of final extracts from MIP-SPE and HLB cartridges. This material is available free of charge via the Internet at http://pubs.acs.org.

## AUTHOR INFORMATION


### Corresponding Author

*Telephone +86 10 64407191; e-mail shaobingch@sina.com.

### Author Contributions

‡Y.Y. and J.Y. contributed equally to this work.



### Funding

We gratefully acknowledge financial support from National Natural Science Foundation of China (41273132 and No. 21307006) and National Key Technology R&D Program (Grant 2012BAK17B01).


### Notes

The authors declare no competing financial interest.

## REFERENCES


(1) Chen, M. Y.; Ike, M.; Fujita, M. Acute toxicity, mutagenicity, and estrogenicity of bisphenol-A and other bisphenols. *Environ. Toxicol.* **2002**, *17*, 80−86.

(2) Vandenberg, L. N.; Hauser, R.; Marcus, M.; Olea, N.; Welshons, W. V. Human exposure to bisphenol A (BPA). *Reprod. Toxicol.* **2007**, *24*, 139−177.

(3) Birnbaum, L. S.; Bucher, J. R.; Collman, G. W.; Zeldin, D. C.; Johnson, A. F.; Schug, T. T.; Heindel, J. J. Consortium-based science: The NIEHS's multipronged, collaborative approach to assessing the health effects of bisphenol A. *Environ. Health Perspect.* **2012**, *120*, 1640−1644.

(4) Liao, C.; Liu, F.; Kannan, K. Bisphenol S, a new bisphenol analogue, in paper products and currency bills and its association with bisphenol A residues. *Environ. Sci. Technol.* **2012**, *46*, 6515−6522.

(5) Satoh, K.; Ohyama, K.; Aoki, N.; Iida, M.; Nagai, F. Study on anti-androgenic effects of bisphenol A diglycidyl ether (BADGE), bisphenol F diglycidyl ether (BFDGE) and their derivatives using cells stably transfected with human androgen receptor, AR-EcoScreen. *Food Chem. Toxicol.* **2004**, *42*, 983−993.

(6) Liao, C.; Kannan, K. Concentrations and profiles of bisphenol A and other bisphenol analogues in foodstuffs from the United States and their implications for human exposure. *J. Agric. Food Chem.* **2013**, *61*, 4655−4662.

(7) Matsushima, A.; Liu, X.; Okada, H.; Shimohigashi, M.; Shimohigashi, Y. Bisphenol AF is a full agonist for the estrogen receptor ER$\alpha$ but a highly specific antagonist for ER$\beta$. *Environ. Health Perspect.* **2010**, *118*, 1267−1272.

(8) Li, Y.; Burns, K. A.; Arao, Y.; Luh, C. J.; Korach, K. S. Differential estrogenic actions of endocrine-disrupting chemicals bisphenol A, bisphenol AF, and zearalenone through estrogen receptor $\alpha$ and $\beta$ in vitro. *Environ. Health Perspect.* **2012**, *120*, 1029−1035.

(9) Grignard, E.; Lapenna, S.; Bremer, S. Weak estrogenic transcriptional activities of bisphenol A and bisphenol S. *Toxicol. In Vitro* **2012**, *26*, 727−731.

(10) Cabaton, N.; Dumont, C.; Severin, I.; Perdu, E.; Zalko, D.; Cherkaoui-Malki, M.; Chagnon, M. C. Genotoxic and endocrine activities of bis(hydroxyphenyl)methane (bisphenol F) and its derivatives in the HepG2 cell line. *Toxicology* **2009**, *255*, 15−24.

(11) Kitamura, S.; Jinno, N.; Ohta, S.; Kuroki, H.; Fujimoto, N. Thyroid hormonal activity of the flame retardants tetrabromobisphenol A and tetrachlorobisphenol A. *Biochem. Biophys. Res. Commun.* **2002**, *293*, 554−559.

(12) Geens, T.; Aerts, D.; Berthot, C.; Bourguignon, J. P.; Goeyens, L.; Lecomte, P.; Maghuin-Rogister, G.; Pironnet, A. M.; Pussemier, L.; Scippo, M. L.; Van, L. J.; Covaci, A. A review of dietary and non-dietary exposure to bisphenol-A. *Food Chem. Toxicol.* **2012**, *50*, 3725−3740.

(13) Viñas, P.; Campillo, N.; Martínez-Castillo, N.; Hernández-Córdoba, M. Comparison of two derivatization-based methods for solid-phase microextraction-gas chromatography-mass spectrometric determination of bisphenol A, bisphenol S and biphenol migrated from food cans. *Anal. Bioanal. Chem.* **2010**, *397*, 115−125.

(14) Cacho, J. I.; Campillo, N.; Viñas, P.; Hernández-Córdoba, M. Stir bar sorptive extraction coupled to gas chromatography-mass spectrometry for the determination of bisphenols in canned beverages and filling liquids of canned vegetables. *J. Chromatogr. A* **2012**, *1247*, 146−153.

(15) Cunha, S. C.; Almeida, C.; Mendes, E.; Fernandes, J. O. Simultaneous determination of bisphenol A and bisphenol B in beverages and powdered infant formula by dispersive liquid-liquid micro-extraction and heart-cutting multidimensional gas chromatography-mass spectrometry. *Food Addit. Contam., Part A* **2011**, *28*, 513−526.

(16) Shi, Z. X.; Wu, Y. N.; Li, J. G.; Zhao, Y. F.; Feng, J. F. Dietary exposure assessment of Chinese adults and nursing infants to tetrabromobisphenol-A and hexabromocyclododecanes: Occurrence measurements in foods and human milk. *Environ. Sci. Technol.* **2009**, *43*, 4314−4319.

(17) Liao, C.; Kannan, K. A survey of bisphenol A and other bisphenol analogues in foodstuffs from nine cities in China. *Food Addit. Contam., Part A* **2014**, *31*, 319−329.

(18) Ballesteros-Gómez, A.; Rubio, S.; Pérez-Bendito, D. Analytical methods for the determination of bisphenol A in food. *J. Chromatogr. A* **2009**, *1216*, 449−469.

(19) Baggiani, C.; Anfossi, L.; Giovannoli, C. Solid phase extraction of food contaminants using molecular imprinted polymers. *Anal. Chim. Acta* **2007**, *591*, 29−39.

(20) Gros, M.; Pizzolato, T. M.; Petrovic, M.; de Alda, M. J.; Barcelo, D. Trace level determination of beta-blockers in waste waters by highly selective molecularly imprinted polymers extraction followed by liquid chromatography-quadrupole-linear ion trap mass spectrometry. *J. Chromatogr. A* **2008**, *1189*, 374−384.

(21) Lofgreen, J. E.; Moudrakovski, I. L.; Ozin, G. A. Molecularly imprinted mesoporous organosilica. *ACS Nano* **2011**, *5*, 2277−2287.

(22) Pichon, V.; Haupt, K. Affinity separations on molecularly imprinted polymers with special emphasis on solid-phase extraction. *J. Liq. Chromatogr. Relat. Technol.* **2006**, *29*, 989−1023.

(23) Pichon, V.; Chapuis-Hugon, F. Role of molecularly imprinted polymers for selective determination of environmental pollutants: A review. *Anal. Chim. Acta* **2008**, *622*, 48−61.

(24) Lucci, P.; Derrien, D.; Alix, F.; Pérollier, C.; Bayoudh, S. Molecularly imprinted polymer solid-phase extraction for detection of zearalenone in cereal sample extracts. *Anal. Chim. Acta* **2010**, *672*, 15−19.

(25) Sun, Z.; Schüssler, W.; Sengl, M.; Niessner, R.; Knopp, D. Selective trace analysis of diclofenac in surface and wastewater samples using solid-phase extraction with a new molecularly imprinted polymer. *Anal. Chim. Acta* **2008**, *620*, 73−81.

(26) Lucci, P.; Núñez, O.; Galceran, M. T. Solid-phase extraction using molecularly imprinted polymer for selective extraction of natural and synthetic estrogens from aqueous samples. *J. Chromatogr. A* **2011**, *1218*, 4828−4833.

(27) Herrero-Hernández, E.; Carabias-Martínez, R.; Rodríguez-Gonzalo, E. Use of a bisphenol-A imprinted polymer as a selective sorbent for the determination of phenols and phenoxyacids in honey by liquid chromatography with diode array and tandem mass spectrometric detection. *Anal. Chim. Acta* **2009**, *650*, 195−201.

(28) O'Mahony, J.; Moloney, M.; McCormack, M.; Nicholls, I. A.; Mizaikoff, B.; Danaher, M. Design and implementation of an imprinted material for the extraction of the endocrine disruptor bisphenol A from milk. *J. Chromatogr. B* **2013**, *931*, 164−169.

(29) Yang, Y.; Lu, L.; Zhang, J.; Yang, Y.; Wu, Y.; Shao, B. Simultaneous determination of seven bisphenols in environmental water and solid samples by liquid chromatography-electrospray tandem mass spectrometry. *J. Chromatogr. A* **2014**, *1328*, 26−34.

(30) Gallart-Ayala, H.; Moyano, E.; Galceran, M. T. *Bisphenol A and Phthalates: Uses, Health Effects and Environmental Risks*; Nova Science Publishers: Hauppauge, NY, 2009; p 187.
(31) Sun, C.; Leong, L. P.; Barlow, P. J.; Chan, S. H.; Bloodworth, B. C. Single laboratory validation of a method for the determination of bisphenol A, bisphenol A diglycidyl ether and its derivatives in canned foods by reversed-phase liquid chromatography. *J. Chromatogr. A* **2006**, *1129*, 145−148.
(32) Shao, B.; Han, H.; Hu, J.; Zhao, J.; Wu, G.; Xue, Y.; Ma, Y.; Zhang, S. Determination of alkylphenol and bisphenol A in beverages using liquid chromatography/electrospray ionization tandem mass spectrometry. *Anal. Chim. Acta* **2005**, *530*, 245−252.
(33) Geens, T.; Apelbaum, T. Z.; Goeyens, L.; Neels, H.; Covaci, A. Intake of bisphenol A from canned beverages and foods on the Belgian market. *Food Addit. Contam., Part A* **2010**, *27*, 1627−1637.
(34) Cao, X. L.; Corriveau, J.; Popovic, S. Levels of bisphenol A in canned soft drink products in Canadian markets. *J. Agric. Food Chem.* **2009**, *57*, 1307−1311.
(35) Gallart-Ayala, H.; Moyano, E.; Galceran, M. T. Analysis of bisphenols in soft drinks by on-line solid phase extraction fast liquid chromatography-tandem mass spectrometry. *Anal. Chim. Acta* **2011**, *683*, 227−233.
(36) Noonan, G. O.; Ackerman, L. K.; Begley, T. H. Concentration of bisphenol A in highly consumed canned foods on the U.S. market. *J. Agric. Food Chem.* **2011**, *59*, 7178−7185.
(37) Grumetto, L.; Montesano, D.; Seccia, S.; Albrizio, S.; Barbato, F. Determination of bisphenol A and bisphenol B residues in canned peeled tomatoes by reversed-phase liquid chromatography. *J. Agric. Food Chem.* **2008**, *56*, 10633−10637.

neous internal distribution of binding sites, the mass transfer of target molecules from solution to cavities is obstructed by the adsorption of the template on the surface of MIPs, which causes low binding affinity.

To overcome these problems, a surface-imprinting technique combined with magnetic nanoparticles [superparamagnetic MIPs (M-MIPs)] has been applied recently,[19−21] in which most of the binding sites on the surface of polymers are exposed to facilitate the recognition and removal of the template. In addition, magnetic support can be easily isolated from the real samples using a magnet. However, traditional polymerization processes of MIPs are conducted in organic phase, thereby restricting its application in aqueous systems. In recent years, water-compatible MIPs have been developed. For example, tramadol-imprinted polymers embedding $SiO_2$−$Fe_3O_4$ nanoparticles were prepared in double-distilled water and then used to separate tramadol from human urine samples. The obtained MMIPNPs exhibit high sensitivity and low detection limits.[22] Tao Jing et al.[23] prepared lysozyme-imprinted magnetic nanoparticles immersed in phosphate buffer (0.2 mol $L^{-1}$, pH 6.2) and reused them 5 times. The high adsorption capability and high saturation magnetization of the lysozyme-imprinted magnetic nanoparticles enable their efficient separation from the crude sample. However, to the best of our knowledge, only a few studies on M-MIPs of vanillin have been conducted.

In this paper, we report the use of a simple method to prepare core−shell M-MIPs in a methanol−water reaction system. The obtained M-MIPs were used for the separation and pre-concentration of vanillin. The $Fe_3O_4$ nanoparticles were synthesized by the alkaline co-precipitation method and then coated by a $SiO_2$ layer, in which the surface was modified by 3-methacryloxypropyltrimethoxysilane (MPS) to form end vinyl bonds that provided reaction sites to induce the occurrence of imprinted polymerization on the surface of the $Fe_3O_4$@$SiO_2$@MPS. Finally, M-MIP particles were prepared for the separation and enrichment of vanillin from the aqueous solution before further HPLC−UV analysis. These M-MIPs are water-compatible and highly selective, and they exhibit fast binding kinetics and can be rapidly separated.

## EXPERIMENTAL SECTION

**Reagents and Materials.** Vanillin, methyl vanillin, ethyl vanillin, ferrous sulfate heptahydrate ($FeSO_4·7H_2O$), anhydrous ferric chloride ($FeCl_3$), ammonia ($NH_3·H_2O$), ethanol, methanol, and acetic acid were all purchased from Sinopharm Chemical Reagent Co., Ltd. (Shanghai, China). Methacrylic acid (MAA), ethylene glycol dimethacrylamide (EGDMA), 2,2-azobis(isobutyronitrile) (AIBN), and MPS were obtained from Sigma (Shanghai, China). Tetraethoxysilane (TEOS) was obtained from Aladdin (Shanghai, China). All of these chemicals were of analytical reagent grade.

**Preparation of $Fe_3O_4$@$SiO_2$ Nanoparticles.** The $Fe_3O_4$ magnetic nanoparticles were synthesized via the alkaline co-precipitation method. Briefly, 1.63 g of $FeCl_3$ and 1.45 g of $FeSO_4·7H_2O$ were dissolved in 100 mL of distilled water with vigorous stirring for 20 min under a nitrogen atmosphere. When the temperature was increased to 60 °C, 5 mL of $NH_3·H_2O$ (25−28%, w/w) was injected into the mixture rapidly, and then the solution immediately turned black. The reaction was allowed to proceed for 60 min under a nitrogen atmosphere. The black product was separated from the liquid using a permanent magnet and then washed with distilled water several times until the pH of the washing water was neutral.

The obtained $Fe_3O_4$ nanoparticles were dispersed homogeneously into 100 mL of distilled water by sonication for 20 min. The magnetic dispersion (10 mL) was mixed with 80 mL of ethanol, followed by the addition of 5 mL of ammonia (25−28%, w/w). Subsequently, 1 mL of TEOS was added drop by drop, and the reaction was maintained for 6 h at 40 °C. The obtained $Fe_3O_4$@$SiO_2$ particles were collected using a magnet, rinsed alternately with ethanol and water 3 times, and then dried under vacuum for 24 h.

MPS, a silane coupling agent, was used to modify the silica surface to enhance the binding capacity between the magnetic particles and the MIPs. In this procedure, 500 mg of $Fe_3O_4$@$SiO_2$ particles was dispersed in 50 mL of anhydrous toluene by sonication for 20 min, followed by the addition of 10 mL of MPS. The reaction was conducted with reflux for 24 h at 50 °C under a nitrogen atmosphere. The resulting $Fe_3O_4$@$SiO_2$−MPS was thoroughly washed with toluene and dried under vacuum.

**Preparation of M-MIPs.** The M-MIPs were synthesized by dissolving 0.68 mmol of vanillin (as template) and 2.72 mmol of MAA (as a functional monomer) in 30 mL of methanol/water (9:1, v/v) solution. After vortex oscillation, the mixture was stored under refrigeration at 4 °C overnight to form hydrogen bonds between vanillin and MAA. Subsequently, 100 mg of modified $Fe_3O_4$@$SiO_2$, 6.8 mmol of EGDMA (as a cross-linker), and 30 mg of AIBN (as an initiator) were dispersed in 20 mL of methanol/water (9:1, v/v) by sonication for 25 min, followed by the addition of the vanillin−MAA mixture. After nitrogen gas injection, the solution was mixed at 50 °C for 8 h, then kept at 60 °C for 24 h, and further aged for 6 h at 80 °C. The polymer products were eluted with methanol/acetic acid (9:1, v/v) in a Soxhlet extractor for 48 h to remove the templates. Finally, the obtained M-MIPs were dried under vacuum for 24 h. Superparamagnetic non-MIPs (M-NIPs, as a control) were prepared using the method described previously without the addition of vanillin.

**Characterization.** Fourier transform infrared (FTIR) spectra were recorded using the FTIR spectrophotometer (Nicolet 5700, Thermo Electron Corporation, Waltham, MA). X-ray powder diffraction (XRD) patterns were recorded using an XRD analyzer (D8-FOCUS, Bruker, Karlsruhe, Germany). Transmission electron microscopy (TEM) images were obtained on a JEOL (JEM-2010HR, Japan) transmission electron microscope. The magnetic properties were examined by vibrating sample magnetometry (VSM, 7407, Lakeshore, Westerville, OH). The amounts of analytes were determined by a HPLC−UV (Agilent Technologies 1260 Infinity) method. The ZORBAX SB-C18 column with a 250 × 4.6 mm inner diameter was used as the analytical column. HPLC−UV conditions employed were as follows: mobile phase, methanol/water/acetic acid (3:7:0.05, v/v/v); flow rate, 0.3 mL $min^{-1}$; and detection wavelength, 279 nm, under room temperature.

**Binding Experiment.** To evaluate the adsorption capacity of M-MIPs or M-NIPs, 10 mg of particles was dispersed in 5 mL of vanillin solution with concentrations from 0.04 to 0.15 mmol $L^{-1}$. The mixture was incubated at room temperature for 24 h and then separated by a magnet to determine the concentration of vanillin in supernatant solution.

The M-MIPs or M-NIPs (20 mg) were added to 30 mL of 0.08 mmol $L^{-1}$ vanillin solution to investigate their kinetic adsorption properties. The mixture was incubated in a shaker at room temperature, and samples were obtained at different times. The microspheres were then separated by a magnet to determine the residual concentration of vanillin using a UV spectrophotometer at 279 nm.

Selectivity experiments were conducted using vanillin, methyl vanillin, and ethyl vanillin as structural analogues. M-MIPs (20 mg) or M-NIPs (20 mg) were dispersed into 2.0 mL methanol−water solutions containing 0.08 mmol $L^{-1}$ vanillin, methyl vanillin, and ethyl vanillin. The amount of vanillin, methyl vanillin, and ethyl vanillin in the supernatant were determined by UV after shaking for 12 h at room temperature. The recognition ability of M-MIPs was evaluated using the imprinting factor ($\alpha$), which is defined in the following equation:

$$\alpha = Q_{MIP}/Q_{NIP}$$

where $Q_{MIP}$ and $Q_{NIP}$ are the adsorption amounts of the templates or analogues on M-MIPs and M-NIPs, respectively.

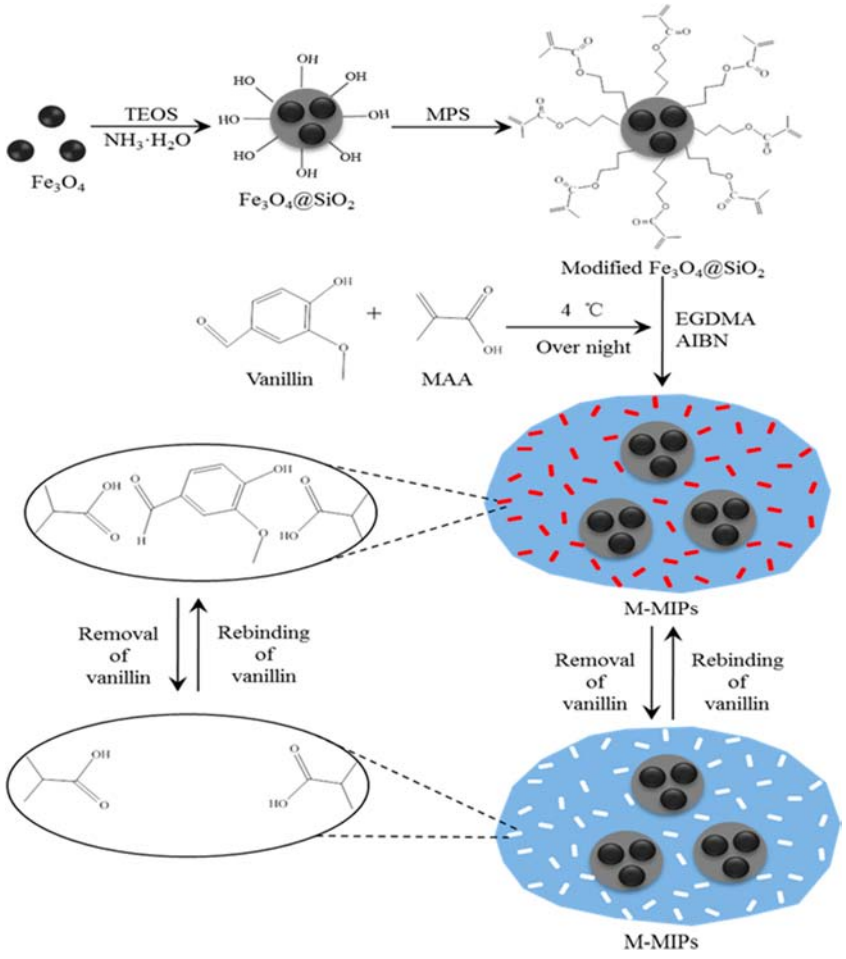


**Figure 1.** Synthesis schematic of M-MIPs.

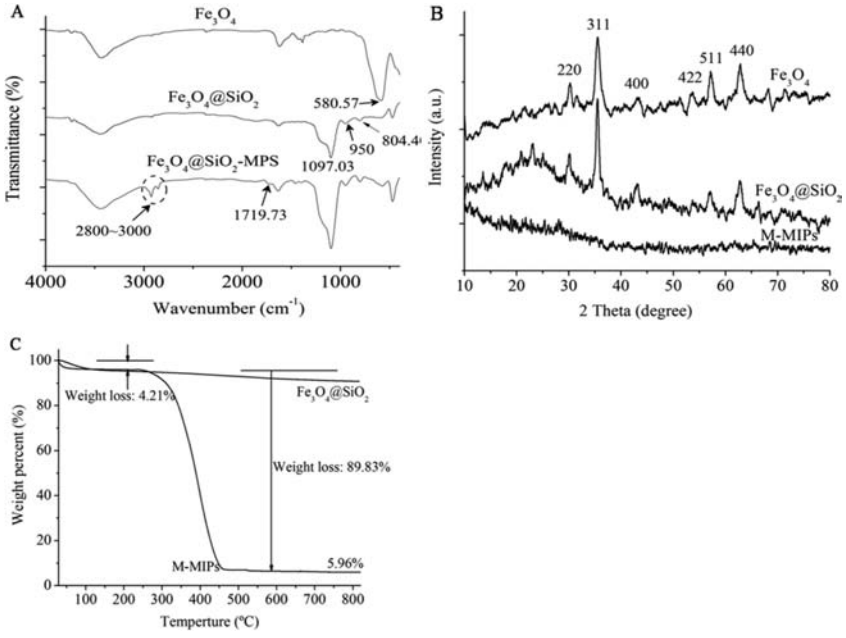


**Figure 2.** (A) FTIR spectra of $Fe_3O_4@SiO_2$, MPS, and $Fe_3O_4@SiO_2$–MPS, (B) XRD of $Fe_3O_4$, $Fe_3O_4@SiO_2$, and M-MIPs, and (C) thermogravimetric curves of $Fe_3O_4@SiO_2$ and M-MIPs.

**Analysis of Vanillin in Real Samples.** Several commercial food samples (bread, milk powder, biscuit, and chocolate) were purchased from the local market in Nanchang. The food samples were ground to a fine powder using a mortar and pestle. Food samples (2 g) unspiked or spiked with different concentrations of vanillin standard solutions (2 mL or 0.01, 0.04, or 0.08 mmol $L^{-1}$) and using water (20 mL) were

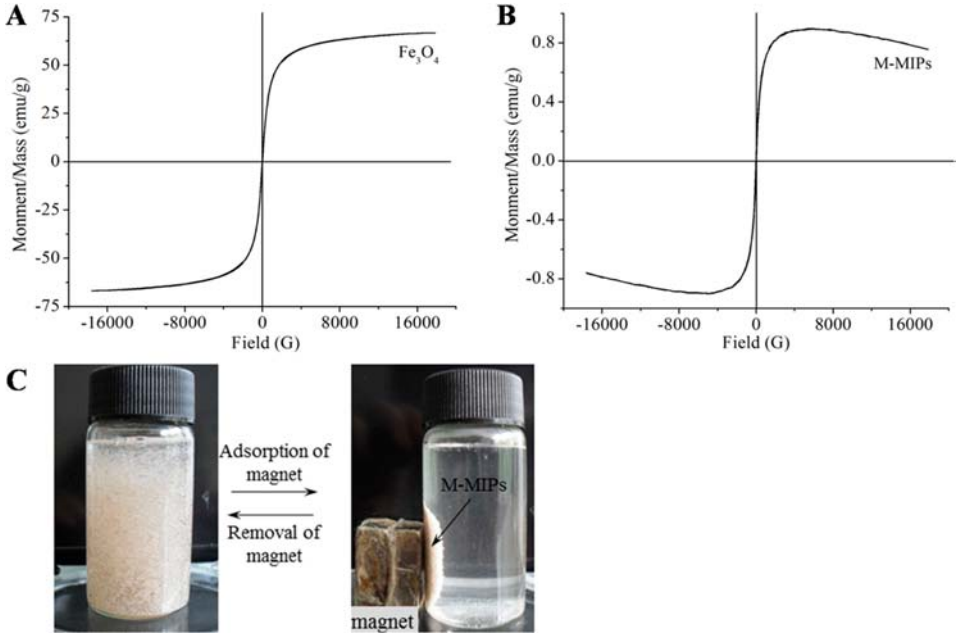


**Figure 3.** Hysteresis loops of the (A) $Fe_3O_4$ nanoparticle and (B) M-MIPs and (C) magnetic separation picture of M-MIPs.

extracted for 30 min. The solutions were then centrifuged and filtered to obtain the extract solution. The M-MIP particles (20 mg) were added to the extract solution, which was then shaken at room temperature for 1 h. A magnet ($N_{35}$ model) was used to separate the M-MIP particles from the solution. The supernatant was measured by HPLC−UV and determined the amount of vanillin. The food sample without spiking was used as a control group. Thus, the recovery of food samples with spiking has been subtracted by the level of vanillin in the control group. The vanillin adsorbed onto the M-MIP sorbent was subsequently eluted with 2 mL of methanol/acetic acid (9:1, v/v). After desorption for 2 h, the template molecule vanillin and adsorbent were easily and rapidly separated using a magnet. The solution containing the template molecule vanillin was dissolved in 2 mL of acetonitrile solvent. The recovery amounts of vanillin in food samples were then determined by HPLC−UV. All of the tests were conducted in triplicate, and the data were reported as the mean values. In addition, matrix interferences could be excluded using selective M-MIPs as the extracting agent. The absorbance values were measured by deducting the absorbance of blank samples.

## RESULTS AND DISCUSSION

**Preparation of M-MIPs.** The water-compatible M-MIPs of vanillin were synthesized via a multi-step polymerization method, as illustrated in Figure 1. Superparamagnetic $Fe_3O_4$ nanoparticles were produced using the co-precipitation method[24] and then coated with a thin film of silica to enhance the dispersibility of magnetic particles and prevent oxidation. MPS was then allowed to react with the hydroxyl of $Fe_3O_4$@$SiO_2$ to introduce vinyl groups, which induced the copolymerization of MIPs to occur on the surface of the microspheres upon the addition of MAA. On the other hand, TEOS has a lot of −OH groups, which can make MPS graft easily onto the $Fe_3O_4$−$SiO_2$ surface. Finally, the M-MIPs were prepared after the templates were eluted with methanol/acetic acid solution. The obtained M-MIPs enabled the easy recognition, separation, and enrichment of the template from complex food sample samples.

**FTIR Spectroscopy.** Figure 2A shows the FTIR spectra of $Fe_3O_4$, $Fe_3O_4$@$SiO_2$, and $Fe_3O_4$@$SiO_2$−MPS. The characteristic peak of $Fe_3O_4$ was observed at 580.57 $cm^{-1}$. The peaks at

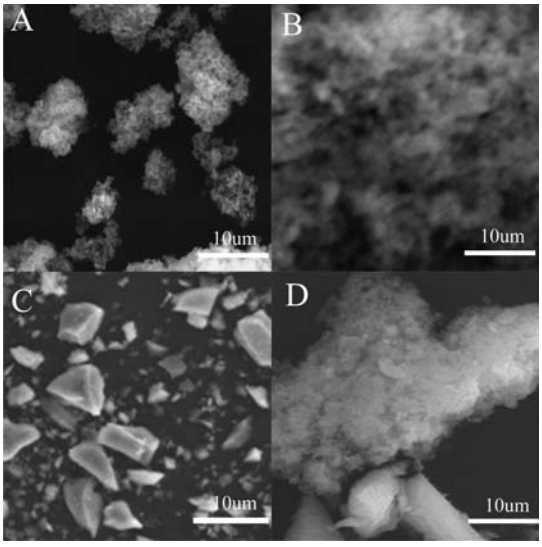


**Figure 4.** SEM images of (A and B) M-MIPs and (C and D) M-NIPs.

1097.03, 950.00, and 804.40 $cm^{-1}$ were attributed to the stretching vibrations of Si−O−Si, Si−O−H, and Si−O, respectively, indicating the formation of the silica shell. The absorbance peaks from 2800 to 3000 $cm^{-1}$ were attributed to the stretching vibrations of the C−H bond from the methyl and methylene groups. The peak at 1719.73 $cm^{-1}$ was attributed to the stretching vibration of the carbonyl group, which indicated the successful modification of MPS.

**Crystalline Structure Analysis.** Figure 2B shows the XRD patterns of $Fe_3O_4$, $Fe_3O_4$@$SiO_2$, and M-MIPs. A series of characteristic peaks for $Fe_3O_4$ in the $2\theta$ range of 10−80° were observed at $2\theta$ = 30.32°, 35.42°, 43.39°, 53.60°, 57.22°, and 62.79°. These peaks were indexed to the (220), (311), (400), (422), (511), and (440) crystalline planes, respectively, which matched well with the data for magnetite [Joint Committee on Powder Diffraction Standards (JCPDS) card 19-629]. However, a few $\gamma$-$Fe_2O_3$ particles were obtained because of the


dx.doi.org/10.1021/jf504144g | J. Agric. Food Chem. 2014, 62, 11138−11145

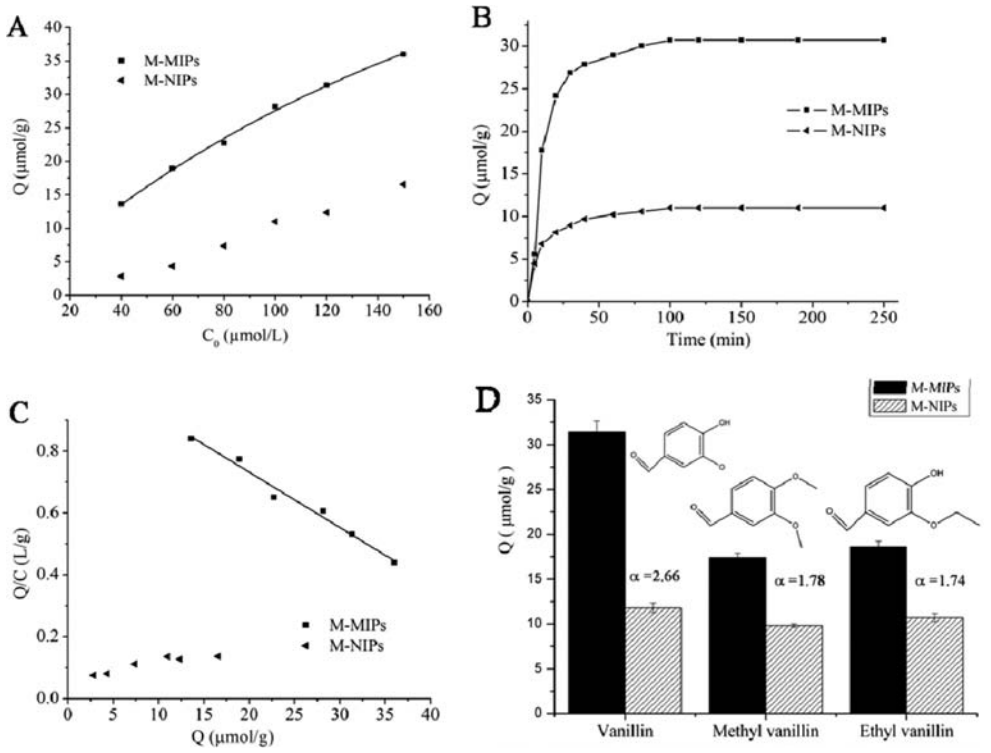


**Figure 5.** (A) Static adsorption isotherms of M-MIPs and M-NIPs, (B) adsorption kinetic behavior of M-MIPs and M-NIPs, (C) Scatchard analysis plots of M-MIPs and M-NIPs, and (D) competitive binding of vanillin, methyl vanillin, and ethyl vanillin on M-MIPs and M-NIPs.

**Table 1. M-MIP Recoveries (%) and Relative Standard Deviations (RSD %) Obtained from Analysis of Four Different Samples Spiked with Vanillin**

| | spiked concentration (mmol $L^{-1}$) | | | | | |
|---|---|---|---|---|---|---|
| | 0.01 | | 0.04 | | 0.08 | |
| sample | M-MIPs | M-NIPs | M-MIPs | M-NIPs | M-MIPs | M-NIPs |
| bread | 83.39[a] ± 4.27[b] | 42.37 ± 4.21 | 92.52 ± 3.56 | 38.76 ± 2.91 | 91.27 ± 3.45 | 36.48 ± 4.25 |
| milk powder | 86.23 ± 5.17 | 33.41 ± 3.48 | 85.35 ± 3.98 | 32.84 ± 4.12 | 89. 97 ± 4.79 | 44.96 ± 3.58 |
| biscuit | 91.46 ± 3.49 | 37.72 ± 4.33 | 89.37 ± 2.72 | 39.57 ± 4.38 | 95.58 ± 2.48 | 47.39 ± 2.94 |
| chocolate | 89.27 ± 3.13 | 41.45 ± 3.72 | 92.37 ± 3.28 | 32.49 ± 4.79 | 92.37 ± 4.18 | 47.32 ± 3.68 |

[a]Average value from three individual experiments. The recovery of the food sample with spiking has been subtracted by the level of vanillin in the control group. [b]$n$ = 3.

oxidation of $Fe_3O_4$ during the co-precipitation and silanization processes.[25−27] This finding was not considered in this study, because these particles exhibited similar magnetic properties and either phase allows for the growth of the silica shell on its surface.[28] Furthermore, by comparing the XRD patterns of $Fe_3O_4$ and $Fe_3O_4$@$SiO_2$, some other characteristic peaks for $SiO_2$ were observed in the $2\theta$ range of 10−35°. Meanwhile, a few peaks could be observed in the M-MIP curve for thick MIPs, which significantly decreased the content of $Fe_3O_4$@$SiO_2$ in all of the samples. This inference can be validated by the results of thermogravimetric analysis (TGA) and VSM.

**TGA.** The thermogravimetric curves of $Fe_3O_4$@$SiO_2$ and M-MIPs are shown in Figure 2C, which quantified the encapsulation efficiency of the $Fe_3O_4$@$SiO_2$ particles that were covered with the M-MIPs. When the temperature increased to 200 °C, the weight of both samples decreased by approximately 4.21%, because of dehydration of the physically adsorbed water or solvent residues. A flat curve of $Fe_3O_4$@$SiO_2$ was then observed from 200 to 800 °C. However, the MIPs decomposed rapidly at temperatures of >800 °C. The decrease in mass was 89.83%, especially from 300 to 500 °C. The residual weight (5.96%) was attributed to the thermostable $Fe_3O_4$@$SiO_2$.

**Magnetic Properties of $Fe_3O_4$ and M-MIPs.** The magnetic properties of $Fe_3O_4$ and M-MIPs were determined using VSM at room temperature. The magnetic hysteresis loop of the dried samples is shown in Figure 3. The saturation magnetization ($M_s$) value of the M-MIPs was significantly decreased to 0.90 emu $g^{-1}$, in comparison to pure $Fe_3O_4$ (66.80 emu $g^{-1}$). The decrease in the magnetization value was due to the formation of thick polymers that covered the M-MIP particles. Moreover, hysteresis did not occur, and remanence and coercivity were zero; thus, both samples were superparamagnetic. As such, the M-MIPs with low $M_s$ values could be easily attracted to an external magnetic field at the wall of the vial (Figure 3C). When the magnet was removed, the M-MIPs were re-dispersed into the solution.

**Morphology Analysis.** Figure 4 shows the SEM images of the M-MIPs and M-NIPs. In comparison to the irregular and compact structure of the M-NIPs, the structure of the M-MIPs

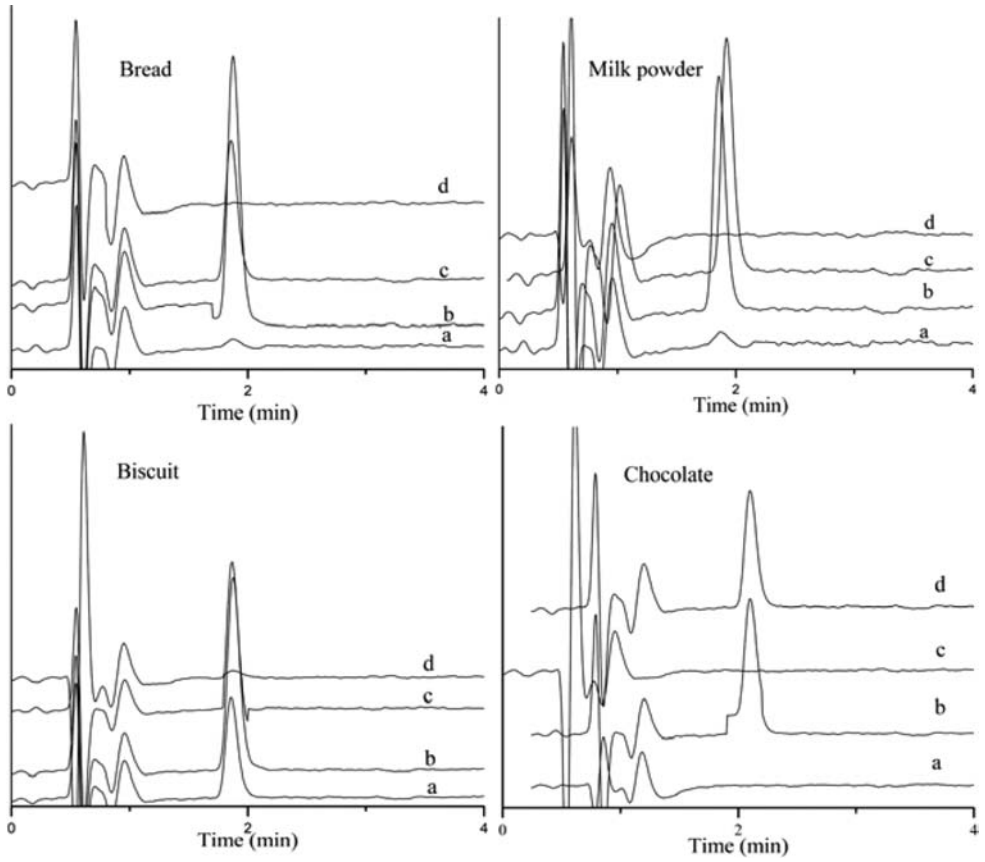


**Figure 6.** HPLC–UV chromatograms of bread, milk powder, biscuit, and chocolate samples. The samples were (a) not spiked, (b) spiked with 0.01 mmol $L^{-1}$ vanillin and without extraction, (c) spiked with 0.01 mmol $L^{-1}$ vanillin and with M-MIP extraction, and (d) spiked with 0.01 mmol $L^{-1}$ vanillin and the remaining solution after extraction.

was loose and porous with many cavities, which facilitated the mass transport and binding kinetics of the template molecules.

**Binding Properties of the M-MIPs.** To estimate the adsorption capability of the M-MIPs and M-NIPs, static adsorption experiments were conducted using different initial concentrations of vanillin solution. Figure 5A shows that the binding amount of the M-MIPs and M-NIPs for vanillin was increased with the increase in the vanillin concentration. Moreover, the amount of vanillin bound to the M-MIPs was much higher than that bound to the M-NIPs. The Scatchard equation was adopted to evaluate the binding ability of the M-MIPs and M-NIPs.[29] The Scatchard equation is expressed as follows:

$$\frac{Q}{C} = \frac{Q_{max}}{K_d} - \frac{Q}{K_d}$$

where $Q$ is the amount of vanillin bound to M-MIPs at equilibrium, $Q_{max}$ is the apparent maximum binding amount, $C_0$ is the initial concentration of vanillin, $C$ is the concentration of the supernatant at equilibrium, and $K_d$ is the dissociation constant.

As shown in Figure 5C, the Scatchard plot for the M-MIPs was a single straight line with a good linear relationship ($R^2$ = 0.981), which indicated that the binding sites in the M-MIPs were almost homogeneous. As a control, the M-NIPs with nonlinear correlation possessed fewer homogeneous binding sites. The linear regression equation for the M-MIPs was $Q/C = 1.090 - 0.017Q$. The $Q_{max}$ and $K_d$ were calculated to be 64.12 $\mu$mol $g^{-1}$ and 58.82 $\mu$mol $L^{-1}$, respectively, on the basis of the slope and intercept of the Scatchard plot. These values confirmed the high affinity of the M-MIPs to vanillin.

Kinetic adsorption experiments for M-MIPs and M-NIPs were carried out to investigate the binding process. As shown in Figure 5B, the adsorption capacity of M-MIPs was much higher than that of M-NIPs. The adsorption amount of M-MIPs increased rapidly in the first 30 min, and the curve became relatively flat until reaching equilibrium after approximately 100 min. A similar behavior was observed for the M-NIPs in Figure 5B. Cavities with recognition sites on the surface of the M-MIPs were occupied rapidly by template molecules, which increased the difficulty of transferring vanillin into the inner sites. Given that no specific recognition sites matched vanillin in terms of shape, size, and functional groups in the M-NIPs, the binding amount of the M-NIPs was obviously lower than that of the M-MIPs.

To investigate the binding specificity of the M-MIPs, a selectivity test was conducted using structural analogues of vanillin, methyl vanillin, and ethyl vanillin as control compounds. As shown in Figure 5D, the adsorption capacity of the M-NIPs is similar and non-selective for the three compounds because selective recognition sites are absent in the M-NIPs. However, the M-MIPs showed a significantly higher binding capacity for vanillin than methyl vanillin and ethyl vanillin. The binding capacities of the M-MIPs for vanillin, methyl vanillin, and ethyl vanillin were 31.4, 17.4, and 18.6 $\mu$mol $g^{-1}$, respectively. Accordingly, the imprinting factor values ($\alpha$) of the M-MIPs for vanillin, methyl vanillin, and ethyl vanillin were 2.66, 1.78, and 1.74, respectively. These results

indicated that the M-MIPs exhibited highly specific recognition ability for vanillin. The high selectivity for vanillin may be based on two factors: (1) the first factor is the difference in chemical structures between vanillin, methyl vanillin, and ethyl vanillin, and (2) only vanillin can specifically match the binding sites of the template in terms of size and shape.

**Method Validation and Application to the Analysis of Vanillin in Food Samples.** To assess the practical applicability of the M-MIPs, four food samples (bread, milk powder, biscuit, and chocolate) were used as real samples in the analysis. At the three spiked vanillin concentrations of 0.01, 0.04, and 0.08 mmol $L^{-1}$, the extraction recoveries of the M-MIPs were 83.39−95.58% with relative standard deviations of 2.48−5.17% (Table 1.). The determined limits of detection and quantification were 2.67 and 8.0 $\mu$mol $L^{-1}$ at signal-to-noise ratios of 3 and 10, respectively. The regression equation was attained, $A_{(279\ nm)} = 8.33021x + 2.77378$ ($R^2 = 0.9996$) within 0.1−5.0 mmol $L^{-1}$. Moreover, the separation process was finished within 10 s when a magnet was used. The results of HPLC−UV chromatograms (Figure 6) also indicated that M-MIPs had high selectivity and enrichment ability.

In summary, novel superparamagnetic particles coated with vanillin-imprinted polymer were synthesized using MAA as the functional monomer and EGDMA as the cross-linker. The resultant M-MIPs showed some attractive characteristics, such as higher binding capacity, faster binding kinetics, and quicker separation. The analytical method based on M-MIPs was successfully applied to vanillin analysis in spiked food samples with higher selectivity and concentration. Thus, the approach offers a simple and straightforward technique for selective separation and fast enrichment of vanillin from complicated food matrices.

## AUTHOR INFORMATION

### Corresponding Authors

*Telephone/Fax: +86-791-86634810. E-mail: peng_hailong@aliyun.com.

*Telephone/Fax: +86-791-86634810. E-mail: huaxiong100@126.com.

### Funding

This work was funded by the National Natural Science Foundation of China (21201098, 51102131, 31160317, 21275158, and 21105117), the Jiangxi Department of Education Fund (GJJ13039), and the Specialized Research Fund for the Doctoral Program of Higher Education (20113601110004).

### Notes

The authors declare no competing financial interest.

## REFERENCES

(1) Zabkova, M.; Otero, M.; Minceva, M.; Zabka, M.; Rodrigues, A. E. Separation of synthetic vanillin at different pH onto polymeric adsorbent Sephabeads SP206. *Chem. Eng. Process.* **2006**, *45*, 598−607.

(2) Walton, N. J.; Narbad, A.; Faulds, C.; Williamson, G. Novel approaches to the biosynthesis of vanillin. *Curr. Opin. Biotechnol.* **2000**, *11*, 490−496.

(3) Nadiah, M. Y.; Eri, T.; Takaomi, K. Molecularly imprinted polymer particles having coordinated hydrogen bonding in covalent-imprinting for efficient recognition towards vanillin. *Sep. Purif. Technol.* **2014**, *122*, 341−349.

(4) Peng, H. L.; Wang, S. Q.; Zhang, Z.; Xiong, X.; Li, J. H.; Chen, L. X.; Li, Y. B. Molecularly imprinted photonic hydrogels as colorimetric sensors for rapid and label-free detection of vanillin. *J. Agric. Food Chem.* **2012**, *60*, 1921−1928.

(5) Zhang, G. W.; Ni, Y. N. Simultaneous spectrophotometric determination of vanillin and ethyl maltol in food by multivariate calibration approach. *J. Anal. Sci.* **2005**, *01*, 20−23.

(6) Su, L. Q.; Guo, X. L.; Han, S. A. Preparation and evaluation of vanilli molecularly imprinted polymer microspheres by reversible addition−fragmentation chain transfer precipitation polymerization. *Anal. Methods* **2014**, *6*, 2512−2517.

(7) Dong, Z. Z.; Gu, F. L.; Xu, F.; Wang, Q. H. Comparison of four kinds of extraction techniques and kinetics of microwave-assisted extraction of vanillin from *Vanilla planifolia* Andrews. *Food Chem.* **2014**, *143*, 54−61.

(8) Waliszewski, K. N.; Pardio, V. T.; Ovando, S. L. A simple and rapid HPLC technique for vanillin determination in alcohol extract. *Food Chem.* **2007**, *101*, 1059−1062.

(9) DeJager, L. S.; Perfetti, G. A.; Diachenko, G. W. Comparison of headspace−SPME−GC−MS and LC−MS for the detection and quantification of coumarin, vanillin, and ethyl vanillin in vanilla extract products. *Food Chem.* **2008**, *107*, 1701−1709.

(10) Trenholm, R. A.; Vanderford, B. J.; Drewes, J. E.; Snyder, S. A. Determination of household chemicals using gas chromatography and liquid chromatography with tandem mass spectrometry. *J. Chromatogr. A* **2008**, *1190*, 253−262.

(11) Sostaric, T.; Boyce, M. C.; Spickett, E. E. Analysis of the volatile components in vanilla extracts and flavorings by solid-phase microextraction and gas chromatography. *J. Agric. Food Chem.* **2000**, *48*, 5802−5807.

(12) Shen, Y.; Han, C.; Liu, B.; Lin, Z. F.; Zhou, X. J.; Wang, C. J.; Zhu, Z. N. Determination of vanillin, ethyl vanillin, and coumarin in infant formula by liquid chromatography−quadrupole linear ion trap mass spectrometry. *J. Dairy Sci.* **2014**, *97*, 679−686.

(13) Song, X. L.; Xu, S. F.; Chen, L. X.; Wei, Y. Q.; Xiong, H. Recent advances in molecularly imprinted polymers in food analysis. *J. Appl. Polym. Sci.* **2014**, *131*, 40766.

(14) Jiang, T.; Zhao, L.; Chu, B.; Feng, Q.; Yan, W.; Lin, J. M. Molecularly imprinted solid-phase extraction for the selective determination of 17$\beta$-estradiol in fishery samples with high performance liquid chromatography. *Talanta* **2009**, *78*, 442−447.

(15) Byun, H. S.; Youn, Y. N.; Yun, Y. H.; Yoon, S. D. Selective separation of aspirin using molecularly imprinted polymers. *Sep. Purif. Technol.* **2010**, *74*, 144−153.

(16) Guo, Y.; Wang, R. Y.; Chi, W. H.; Liu, S. A.; Shi, H. G.; Guo, T. Y. One-step synthesis of reactant-product-dual-template imprinted capsules as phosphotriesterase mimetic enzymes for pesticide elimination. *RSC Adv.* **2014**, *4*, 7881−7884.

(17) Wang, S.; Peng, H.; Xiong, H.; Ruan, X.; Huang, S.; Dong, L. Preparation and recognition mechanism of vanillin molecularly imprinted polymer microspheres. *Food Sci.* **2012**, *33*, 1−7.

(18) Wang, G. S.; Cao, Q. E.; Xiong, J.; Zhu, X. F.; Hou, N. B.; Ding, Z. T. Preparation and recognition properties of vanillin-imprinted polymers. *Helv. Chim. Acta* **2006**, *89*, 3032−3040.

(19) Kong, X.; Gao, R.; He, X.; Chen, L.; Zhang, Y. Synthesis and characterization of the core−shell magnetic molecularly imprinted polymers ($Fe_3O_4$@MIPs) adsorbents for effective extraction and determination of sulfonamides in the poultry feed. *J. Chromatogr. A* **2012**, *1245*, 8−16.

(20) Lin, Z.; Cheng, W.; Li, Y.; Liu, Z.; Chen, X.; Huang, C. A novel superparamagnetic surface molecularly imprinted nanoparticle adopting dummy template: An efficient solid-phase extraction adsorbent for bisphenol A. *Anal. Chim. Acta* **2012**, *720*, 71−76.

(21) Luo, X.; Zhan, Y.; Huang, Y.; Yang, L.; Tu, X.; Luo, S. Removal of water-soluble acid dyes from water environment using a novel magnetic molecularly imprinted polymer. *J. Hazard. Mater.* **2011**, *187*, 274−282.

(22) Madrakian, T.; Afkhami, A.; Mahmood-Kashani, H.; Ahmadi, M. Superparamagnetic surface molecularly imprinted nanoparticles for sensitive solid-phase extraction of tramadol from urine samples. *Talanta* **2013**, *105*, 255−261.

(23) Jing, T.; Du, H.; Dai, Q.; Xia, H.; Niu, J.; Hao, Q.; Mei, S.; Zhou, Y. Magnetic molecularly imprinted nanoparticles for recognition of lysozyme. *Biosens. Bioelectron.* **2010**, *26*, 301−306.
(24) Dong, L. L.; Peng, H. L.; Wang, S. Q.; Zhang, Z.; Li, J. H.; Ai, F. R.; Zhao, Q.; Luo, M.; Xiong, H.; Chen, L. X. Thermally and magnetically dual-responsive mesoporous silica nanospheres: Preparation, characterization, and properties for the controlled release of sophoridine. *J. Appl. Polym. Sci.* **2014**, *131*, 40477.
(25) Ning, F. J.; Peng, H. L.; Li, J. H.; Chen, L. X.; Xiong, H. Molecularly imprinted polymer on magnetic graphene oxide for fast and selective extraction of 17$\beta$-estradiol. *J. Agric. Food Chem.* **2014**, *62*, 7436−7443.
(26) Liu, B.; Han, M.; Guan, G.; Wang, S.; Liu, R.; Zhang, Z. Highly controllable molecular imprinting at superparamagnetic iron oxide nanoparticles for ultrafast enrichment and separation. *J. Phys. Chem. C* **2011**, *115*, 17320−1732.
(27) Li, X. Y.; Huang, X. L.; Liu, D. P.; Wang, X.; Song, S. Y.; Zhou, L.; Zhang, H. J. Synthesis of 3D hierarchical $Fe_3O_4$/graphene composites with high lithium storage capacity and for controlled drug delivery. *J. Phys. Chem. C* **2011**, *115*, 21567−21573.
(28) Wang, X.; Wang, L.; He, X.; Zhang, Y.; Chen, L. A molecularly imprinted polymer-coated nanocomposite of magnetic nanoparticles for estrone recognition. *Talanta* **2009**, *78*, 327−332.
(29) Fan, J.; Wei, Y.; Wang, J.; Wu, C.; Shi, H. Study of molecularly imprinted solid-phase extraction of diphenylguanidine and its structural analogs. *Anal. Chim. Acta* **2009**, *639*, 42−50.

**Table 1. Major Spoilage Bacteria in Fresh Chilled Fish and Lamb[22−25]**

| | occurrence/spoilage potential | | | | | | |
|---|---|---|---|---|---|---|---|
| | NZ[a] salmon | | | white fish (Atlantic cod) | | | |
| bacterium | vacuum or $N_2$ | MAP ($CO_2$) | air | vacuum or $N_2$ | MAP ($CO_2$) | air | NZ lamb |
| *Shewanella putrefaciens* | occas[b]/very high | occas/very high | occas/very high | freq[c]/very high | freq/very high | freq/very high | occas/very high |
| *Pseudomonas fluorescens* | freq/high | occas/high | dom[d,e]/high | | | freq/high | freq/high |
| *Photobacterium phosphoreum* | | | | | freq/high | | |
| *Serratia liquefaciens* | dom/high | | infreq[f]/high | | | | |
| *Serratia proteomaculans* | | | | | | | freq/high |
| *Rahnella aquatilis* | | | occas/high | | | | freq/high |
| *Brochothrix thermosphacta* | | | | | | | occas/high |
| *Clostridia* spp. | occas/high | | | occas/high | occas/high | | occas/high |
| *Hafnia alvei* | dom/mod[g] | freq/mod | | | | | |
| *Lactobacillus* spp. | freq/low | dom/mod | | | | | freq/low |

[a]New Zealand. [b]Occasional. [c]Frequent. [d]Other *Pseudomonas* spp. also significant. [e]Dominant. [f]Infrequent. [g]Moderate.

**Table 2. Extracts and Reference Compounds Used in This Study**

| | species information | | extraction | |
|---|---|---|---|---|
| | common name | scientific name | extracted material | yield, % of dm |
| | Skin and Seed Extracts | | | |
| ApSk | apple (Braeburn) | *Malus domestica* | skin powder | 34 |
| AvPu | avocado (Hass) | *Persea americana* | pulp (waterless) | 13 |
| AvSd | avocado (Hass) | *Persea americana* | seed powder | 11 |
| AvSk | avocado (Hass) | *Persea americana* | skin powder | 13 |
| BaSk | banana | *Musa* sp. | skin powder | 22 |
| FeSk | feijoa | *Feijoa sellowiana* | skin powder | 37 |
| GrSd | grape (Sauvignon blanc) | *Vitis vinifera* | seed powder | n/a |
| KiSk | kiwifruit (Green) | *Actinidia deliciosa* | skin powder | 34 |
| LeSk | lemon | *Citrus limon* | skin powder | 35 |
| MaSd | mango (Tommy Atkins) | *Mangifera indica* | seed (incl endocarp) powder | 19 |
| MaSk | mango (Tommy Atkins) | *Mangifera indica* | skin powder | 40 |
| MdSk | mandarin | *Citrus reticulata* | skin powder | 37 |
| MnSk | mangosteen | *Garcinia mangostana* | skin (pericarp) powder | 37 |
| OrSk | orange | *Citrus sinensis* | skin powder | 33 |
| PaSk | passionfruit | *Passiflora edulis* | skin powder | 22 |
| PiSk | pineapple | *Ananas comosus* | skin powder | 28 |
| PwSk | pawpaw | *Asimina triloba* | skin powder | 22 |
| | Extracts of Fruit Juicing Residues | | | |
| BlaJu | blackberry | *Rubus fruticosus* | whole fruit juicing residue | 25 |
| BlcJu | blackcurrant | *Ribes nigrum* | whole fruit juicing residue | 34 |
| BoJu | boysenberry | *Rubus ursinus* × *Rubus idaeus* | whole fruit juicing residue | 15 |
| BluJu | blueberry | *Vaccinium* sp. | whole fruit juicing residue | 45 |
| RaJu | raspberry | *Rubus idaeus* | whole fruit juicing residue | 25 |
| StJu | strawberry | *Fragaria* sp. | whole fruit juicing residue | 16 |
| ToJu | tomato | *Solanum lycopersicum* | whole fruit juicing residue | 16 |
| | full name | scientific name | extracted material | |
| | Tannins | | | |
| CaTa | cationic mimosa tannin | *Acacia* spp. | bark | |
| MiTa | mimosa | *Acacia* spp. | bark | |
| PiTa | pine | *Pinus radiata* | bark | |
| mTaAc | modified tannic acid | *Acacia* spp. | see TaAc | |
| TaAc | tannic acid | *Caesalpinia spinosa*, *Rhus coriaria*, *Rhus semialata*, *Rhus typhina*, *Quercus infectoria* | *C. spinosa* pods, *R. semialata* and *R. typhina* gallnuts, *Q. infectoria* and *R. coriaria* leaves | |

| ref compds | full name | ref compds | full name |
|---|---|---|---|
| ascorbic acid | ascorbic acid | gallic acid | gallic acid |
| catechin[a] | (+)-catechin | Trolox | Trolox |

[a]Anhydrous (+)-catechin was used for antioxidant capacity tests and (+)-catechin hydrate for ZI studies.

Thus, although spices and herbs are typically rich in bioactive essential oils containing simple phenols, terpenoids, and other bioactive compounds,[16] such volatile compounds were excluded from the scope of the present work because of their strong flavors and odors.

In the present study a major goal was to identify natural extracts that could be used for shelf-life extension of fresh (refrigerated/chilled) fish and lamb by controlling their spoilage bacteria. Extracts from different materials have heterogeneous compositions and thus tend to differ in regard to their abilities to inhibit different bacteria. We focused on nonvolatile extracts from natural products in order to minimize cost and toxicology compliance issues as well as to mitigate any possible changes in the organoleptic properties (the effects on organoleptic properties of different extracts will depend on the amount migrating to the food and the type of food item and

should be tested as part of shelf-life trials). The search was narrowed down to extracts from byproducts of fruit processing industries[2,3,5−8] and tannins derived from different wood components that could be made readily available in New Zealand. The wider bioeconomy would benefit from adding value to agricultural byproducts while health-conscious consumers also tend to prefer natural antioxidants and antibacterial agents.

The major spoilage organisms of chilled fish and lamb are psychrotolerant bacteria. *Shewanella putrefaciens* is a major white fish and chilled lamb spoilage bacterium; very low numbers produce enough $H_2S$ and other sulfur volatiles for a highly offensive rotten-egg odor, as well as trimethylamine and other off-flavor compounds.[18] *Photobacterium phosphoreum* and *Pseudomonas fluorescens* are also able to rapidly spoil fish and/or lamb, when present. The facultative anaerobe *Brochothrix thermosphacta* is a concern for aerobically stored, vacuum-packed or MAP chilled red meats. In anaerobic conditions psychrotrophic Clostridia spp. such as *Clostridium estertheticum* can spoil these products as well.[19] Lactobacilli typically produce a fermentative yeasty odor, but their impact on sensory properties depends also on the food. In some cases lactobacilli may be considered beneficial if they inhibit other, more potent bacteria such as Clostridia. The main spoilage bacteria for fresh New Zealand fish[18,20,21] and lamb[22] are summarized in Table 1. In addition to the bacteria already mentioned, they include several Enterobacteriaceae species, and all were included in the current study except for *Rahnella*. In selecting the target bacteria we aimed to include the food-borne bacteria that are mostly linked to outbreaks worldwide, as well as those associated with spoilage of different sources of food and having different phenotypic characteristics which might be expected to have differences in susceptibility (e.g., Gram-positive and Gram-negative bacteria).

A second goal of the study was to determine the potential suitability of the natural extracts for use in dietary antioxidant supplements. Manufacturers typically claim that antioxidant dietary supplements possess antiaging properties and offer protection against various diseases. The potential benefits of such supplements are uncertain, and high doses of some antioxidant supplements such as vitamin A, vitamin E, and beta-carotene have even been linked to increased all-cause mortality.[23] On the other hand, the many health-promoting effects of fruits are seldom contested and are largely attributed to the antioxidant properties of their phenolic compounds.[24,25]

In this study we evaluated the antibacterial and antioxidant properties of nonvolatile extracts from byproducts of fruit processing industries[2,3,5−8] and tannins derived from trees. To assist with future regulatory acceptance, we have also identified the main phenolic compounds in eight of the most promising extracts.

## MATERIALS AND METHODS

**Materials.** The raw materials and reference compounds used for this study are listed in Table 2. Most of the fruit skins and seeds came from ripe fresh whole fruits obtained from local fruit vendors. The berry fruits were purchased frozen from a local supermarket. Avocado skins and seeds were recovered from fresh avocado processing residue supplied by Fressure Foods, NZ, and processed in-house to generate the extracts used in the study. Reference and standard compounds (ascorbic acid, (+)-catechin, gallic acid, and Trolox), solvents, and reagents were of analytical grade and from Sigma-Aldrich except for acetone, which was from Merck, Darmstadt, Germany. Tannic acid (TaAc) was purchased from BDH Laboratory Supplies, Poole, England. Grape seed extract was obtained from NZ Extracts Ltd., NZ. African mango seed extract (not the mango seed extract in Table 2, which was produced by the authors and used for antibacterial and antioxidant tests) came from Hanzhong TRG Biotech Co. Ltd., Hanzhong City, China. Mimosa tannin and cationic mimosa tannin were supplied by Christian D. Markmann GmbH, Hamburg, Germany. Pine tannin was an in-house product of Scion, NZ (see Processing).

**Processing.** For most of the fruits, skins and seeds were separated from pulp manually, then scraped, and rinsed clean of most pulp and juice/oil residues. Berry fruits (frozen) and tomatoes were juiced at room temperature with a low-temperature Ultem auger juicer (Oscar DA1000, Oscar Juicers, NZ); the juicing residues consisted of the skins and seeds of the fruits. After segregation of the fruit components, the parts to be extracted were immediately frozen at −82 °C, then lyophilized, and ground into powder through a 1 mm mesh using a Wiley mill. Tannic acid is extracted from the leaves, gallnuts, and pods of a range of wood species (Table 2) using water, organic solvents, or their mixtures; the grape seed extract originated from a water-based extraction process; mimosa tannin is commercially extracted from the bark of various acacia species; cationic tannin is a flocculant for pulp mill effluents produced from mimosa tannin by the Mannich reaction; pine tannin originated from alkali extraction of radiata pine (*Pinus radiata*) bark.

**Extraction.** A portion (12−100 g) of fruit skin or seed powder was placed in a Schott bottle (0.5 or 1 L) and extracted with acetone−water (80:20, v/v) at a consistency of 10% for 90 min at 50 °C while the bottle was shaken at 180 rpm. The mixture was then centrifuged (3000 rpm, 5 min) and the supernatant collected by decanting and/or pipetting. The particle residue was washed twice with water, and all the supernatants were combined. The acetone was evaporated from the supernatant under reduced pressure at room temperature, after which the water phase was frozen at −82 °C and lyophilized. The particle residue from the extraction was then re-extracted as described above, and the lyophilized extract powders from both extractions were combined to give the final extract. The extracts were stored in a freezer at −20 °C pending use.

**Thermal Modification of Tannic Acid (TaAc).** For the thermal modification of TaAc,[26] 10.0 g of TaAc was dissolved in 90.0 g of deionized water. The solution was decanted into the Teflon insert of a calorimetric bomb, which was then halfway immersed into an oil bath at 200 °C. After 260 min, the bomb was removed from the bath and allowed to cool overnight. The minor amount of insoluble material found at the bottom of the inset was discarded, and the solution was lyophilized, yielding a brown powder similar in appearance to the starting material.

**Chemical Assays.** *Total Phenol Content (TPC).* Total phenol content of extracts was determined by the Folin−Ciocalteu method according to Kähkonen et al.[27] Absorption was measured at 765 nm using a Cary 300 Bio UV−visible spectrophotometer. A calibration curve (linear fit $R^2$ = 0.9985; 0.005−0.018 mg/mL gallic acid; $A_{765}$ = 0.5−1.6) was constructed with gallic acid, and the sample TPCs (mean of three or more replicates) were expressed as gallic acid equivalents (mg GAE/g) on dry extract weight basis. Anhydrous (+)-catechin was used to check the accuracy of the method.

*Total Flavonoid Content (TFC).* Total flavonoid content was determined using the colorimetric assay described by Dewanto et al.[28] A Cary 300 Bio UV−visible spectrophotometer was used to measure the absorbance at 510 nm. (+)-Catechin hydrate was used for the calibration curve (linear fit $R^2$ = 0.9995; 0.01−0.04 mg/mL catechin; $A_{510}$ = 0.34−0.92), and the results were expressed as catechin equivalents (mg CE/g) on dry extract weight basis. Samples were analyzed in three or more replicates and the results averaged.

*Identifying Phenolic Compounds.* Eight of the extracts with the highest phenol content, excluding CaTa, were also analyzed by LCMS. To extract the phenolic compounds, 1.0 mL of ethanol/Milli-Q water/formic acid (80/20/1, v/v/v) was added to approximately 50 mg of extract, and the mixtures were vigorously agitated using a vortex mixer. Samples were then stored overnight at 4 °C, centrifuged, and diluted 10-fold with methanol before analysis by ultrahigh performance liquid chromatography−high resolution mass spectrometry (LCMS) using a

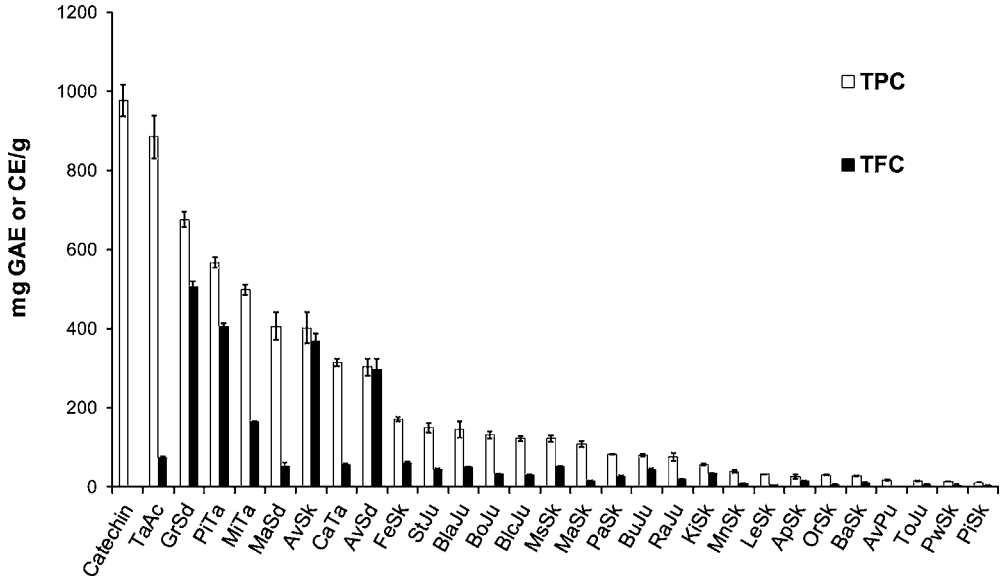


**Figure 1.** Total phenol content (TPC as gallic acid equivalents) and total flavonoid content (TFC as catechin equivalents) of extracts and catechin (external standard). See Table 2 for abbreviations.

Dionex Ultimate 3000 Rapid Separation LC and a micrOTOF QII mass spectrometer (Bruker Daltonics, Bremen, Germany) fitted with an electrospray ion source. Component separation by LC was achieved using two UHPLC Zorbax SB-C18 2.1 × 100 mm, 1.8 μm columns (Agilent, Melbourne, Australia) connected in series. The columns were maintained at 60 °C with a mobile phase flow rate of 350 μL/min. The solvents were A, 100% acetonitrile, and B, 0.2% formic acid, with a solvent gradient of 10% A, 90% B, 0−0.5 min; linear gradient to 45% A, 45% B, 0.5−18 min; linear gradient to 100% A, 18−25 min; 100% A, 25−28 min; linear gradient to 10% A, 90% B, 28−28.2 min; 10% A, 90% B until the next sample injection at 31 min. Injection volumes were 1 μL. The micrOTOF QII parameters were 225 °C; drying $N_2$ 6 L/min; nebulizer $N_2$ 1.5 bar, end plate offset −500 V, mass range 100−1500 Da, acquisition rate 2 scans/s. Negative ion electrospray was used with a capillary voltage of +3500 V. Postacquisition internal mass calibration used sodium formate clusters with the sodium formate delivered by a syringe pump at the start of each chromatographic analysis. Each sample was analyzed in standard HRMS mode and then reanalyzed in HR/MS/MS mode to obtain information about the molecular fragments. mSigma values were calculated to compare measured isotope ratio matches with expected ratios. An automated MS/MS routine was used where the most intense ion present in a survey scan was isolated and then fragmented in the collision chamber in subsequent scans.

*Antioxidant Capacity Assays.* The antioxidant capacity of samples was determined by the DPPH (2,2-diphenyl-1-picrylhydrazyl) radical scavenging method. The steady state measurement variant of the method, based on different dilutions of the sample, was used as described by Buthkup et al.[29] with some modifications: 80% acetone was used as the solvent for DPPH samples and as the blank, and the control was 3.9 mL of DPPH solution + 0.1 mL of 80% acetone. A Cary 300 Bio UV−visible spectrophotometer was used to measure the absorbance at 517 nm; the maximum time before absorption measurement was 120 min. The results were expressed as the effective concentration $EC_{50}$, defined as the amount of antioxidant necessary to decrease DPPH radical absorbance by 50%. A more powerful antioxidant will thus have a lower $EC_{50}$ value. The assays were performed in triplicate and the results averaged.

**Antibacterial Assays.** *Bacterial Strains.* *Listeria monocytogenes* ScottA, *Staphylococcus aureus* ATCC 25923, *P. fluorescens*, *Serratia liquefaciens*, *Salmonella* Enteritidis, *P. phosphoreum*, *Hafnia alvei*, *Salmonella* Typhimurium, *S. putrefaciens*, *Yersinia enterocolitica*, and *Lactobacillus* sp. were obtained from The NZ Institute for Plant & Food Research Limited culture collection, NZ. *Escherichia coli* O157:H7, methicillin-resistant *S. aureus*, and *B. thermosphacta* were purchased from the Environmental Science & Research Centre, NZ. *C. estertheticum* and *Serratia proteomaculans* were kindly supplied by AgResearch, NZ. Bacterial strains were recovered in Brain Heart Infusion (BHI, Difco, NZ) and kept in blood agar plates (Fort Richard, NZ) at 4 °C for storage until the experimental day. Bacteria were grown in Mueller−Hinton broth (MHB, Difco) except for *L. monocytogenes* (grown in Trypticase Soya Broth supplemented with 0.6% of yeast extract, TSBYE, Difco) for 24−48 h prior to the experiments. Each bacterium was incubated at its optimal growth temperature to achieve $1 \times 10^8$ to $1 \times 10^9$ colony-forming units/mL (CFU/mL).

*Preparation of Compounds for Antibacterial Assays.* Extracts were weighed in sterile vials and kept at −20 °C. On the experimental day appropriate dilutions were performed to achieve the final concentration desired. Most of the compounds (Table 2) were diluted in sterile water, while PiTa, gallic acid, catechin, and CaTa were diluted in 80% acetone (ECP, NZ) to facilitate their dissolution.

*Gel Diffusion Assays.* The gel diffusion assays were carried out according to Eseifeka et al.[30] with some modifications. Compounds tested were solubilized as described above and prepared at a final concentration of 10 mg/mL. Bacteria were grown as described above and then centrifuged for 5 min at 4,000 rpm, washed twice with phosphate buffered saline solution, and resuspended in 10 mL of 1% salt peptone water (SPW: 1% NaCl, 0.1% Difco peptone) to achieve a final concentration of $1 \times 10^5$ to $1 \times 10^6$ CFU/mL. An aliquot (1 mL) of each bacterium suspension was placed into a Petri dish and immediately mixed with 18 mL of melted Mueller−Hinton agar (MHA) or Trypticase soya agar supplemented with 0.6% yeast extract (TSAYE, Difco) for *L. monocytogenes*. The plate was then gently swirled and the agar left to solidify in the laminar flow for ca. 30 min. Using a sterile 6 mm core borer, wells were made into the agar, and 35 μL of test compound solution was deposited into them. Appropriate diluent controls were included in all plates. Each of the bacteria was incubated at its optimum growth temperature (from 20 to 37 °C) for 24 to 48 h. The zones of (growth) inhibition (ZIs) surrounding the wells were measured with a digital caliper. A control disk containing 35 μL of 80% acetone was included in each tested plate. Three independent experiments were conducted in triplicate.

*Minimum Inhibitory Concentration (MIC) (NCCLS, 1993).*[31] The determination of MIC was only performed for some of the compounds, the selection being mainly based on the results of the ZI assays. The bacterial strains were prepared as described above with minor modifications. Bacteria were grown in MHB or TSBYE for 24−

**Table 3. Compounds Identified in Extracts**

| retention time (min) | peak area | measd mass to charge ratio ($m/z$) | formula $(M - H)^-$ | $\delta$ (mDa)[a] | mSigma[b] | proposed compd ID[c] | ID level[d] |
|---|---|---|---|---|---|---|---|
| TaAc | | | | | | | |
| 11.45 | 6375389 | 773.0755[e] | $C_{69}H_{46}O_{42}$ | 3.7 | 14.6 | nonagalloyl glucose | 3 |
| 10.93 | 6263395 | 697.0688[e] | $C_{62}H_{42}O_{38}$ | 1.5 | 5.7 | octagalloyl glucose | 3 |
| 11.89 | 5411294 | 1132.7814 | no match | | | | 5 |
| 10.31 | 5243978 | 621.0628[e] | $C_{55}H_{38}O_{34}$ | 0.0 | 18.8 | heptagalloyl glucose | 3 |
| 11.74 | 4814487 | 1132.7812 | no match | | | | 5 |
| 9.57 | 4253607 | 545.0557[e] | $C_{48}H_{34}O_{30}$ | −1.6 | 20.9 | hexagalloyl glucose | 3 |
| 12.34 | 4157982 | 1234.4550 | no match | | | | 5 |
| 4.69 | 3322599 | 321.0251 | $C_{14}H_9O_9$ | −0.1 | 15.9 | digallic acid | 2 |
| 12.19 | 3270636 | 1183.4513 | no match | | | | 5 |
| 12.72 | 2607683 | 1335.7923 | no match | | | | 5 |
| 8.79 | 1973555 | 939.1125 | $C_{41}H_{32}O_{26}$ | −1.6 | 17.5 | pentagalloyl glucose | 3 |
| MaSd | | | | | | | |
| 10.32 | 6161114 | 621.0630[e] | $C_{55}H_{38}O_{34}$ | −0.2 | 18.0 | heptagalloyl glucose | 3 |
| 9.52 | 3025594 | 545.0557[e] | $C_{48}H_{36}O_{30}$ | 1.6 | 17.4 | hexagalloyl glucose | 3 |
| 10.79 | 2946321 | 697.0688[e] | $C_{62}H_{42}O_{38}$ | 0.5 | 7.3 | octagalloyl glucose | 3 |
| 8.79 | 1759565 | 939.1114 | $C_{41}H_{31}O_{26}$ | 0.5 | 26.4 | pentagalloyl glucose | 3 |
| 8.42 | 551348 | 300.9986 | $C_{14}H_5O_8$ | −0.4 | 11.0 | ellagic acid | 3 |
| 2.49 | 450380 | 343.0669 | $C_{14}H_{15}O_{10}$ | −0.2 | 13.1 | galloylquinic acid | 3 |
| 10.03 | 295294 | 387.1662 | $C_{18}H_{27}O_9$ | −0.2 | 18.5 | unknown | 4 |
| 2.43 | 287535 | 331.0665 | $C_{13}H_{15}O_{10}$ | 0.5 | 17.2 | galloylglucose | 3 |
| 9.92 | 283156 | 545.0557 | $C_{48}H_{34}O_{30}$ | −1.6 | 8.7 | hexagalloyl glucose | 4 |
| 6.04 | 282024 | 421.0759 | $C_{19}H_{17}O_{11}$ | −1.8 | 16.4 | tetrahydroxyxanthone glucoside | 3 |
| PiTa | | | | | | | |
| 9 | 1967402 | 303.0515 | $C_{15}H_{11}O_7$ | −0.5 | 2.4 | dihydroquercetin | 2 |
| 4.9 | 751612 | 289.0713 | $C_{15}H_{13}O_6$ | −0.5 | 13.4 | catechin | 1 |
| 13.54 | 644914 | 301.0355 | $C_{15}H_9O_7$ | −0.1 | 16.1 | quercetin | 1 |
| 4.61 | 469483 | 577.1330 | $C_{30}H_{25}O_{12}$ | −2.2 | 13.6 | procyanidin dimer | 2 |
| 9.46 | 193960 | 243.0661 | $C_{14}H_{11}O_4$ | 0.2 | 9.9 | piceatannol | 3 |
| 4.11 | 185973 | 577.1330 | $C_{30}H_{25}O_{12}$ | 2.1 | 28.8 | procyanidin B1 | 1 |
| 4.76 | 134849 | 865.1981 | $C_{45}H_{37}O_{18}$ | 0.4 | 41.8 | procyanidin trimer | 2 |
| MiTa | | | | | | | |
| 6.61 | 1770118 | 881.1965 | $C_{45}H_{37}O_{19}$ | 3.0 | 11.7 | catechin > catechin > gallocatechin | 2 |
| 4.32 | 1755201 | 593.1303 | $C_{30}H_{25}O_{13}$ | −0.3 | 16.8 | catechin > gallocatechin | 1 |
| 7.68 | 1225781 | 865.2020 | $C_{45}H_{37}O_{18}$ | −3.5 | 14.6 | prorobinetinidin trimer | 1 |
| 5.68 | 1090680 | 577.1358 | $C_{30}H_{25}O_{12}$ | 0.6 | 14.4 | prorobinetinidin dimer | 2 |
| 6.8 | 636396 | 577.1341 | $C_{30}H_{25}O_{12}$ | 1.0 | 34.4 | prorobinetinidin dimer | 3 |
| 5.33 | 615076 | 289.0715 | $C_{15}H_{13}O_6$ | 0.3 | 13.4 | robinetinidin | 1 |
| 5 | 583533 | 511.1452 | $C_{23}H_{27}O_{13}$ | 0.5 | 23.9 | unknown | 2 |
| 4.9 | 451913 | 289.0713 | $C_{15}H_{13}O_6$ | 0.4 | 14.6 | catechin | 2 |
| 5.45 | 372797 | 577.1352 | $C_{30}H_{25}O_{12}$ | 0.1 | 8.2 | prorobinetinidin dimer | 1 |
| 6.72 | 361332 | 561.1403 | $C_{30}H_{25}O_{11}$ | 0.0 | 11.3 | fisetinidol-4 > 8-catechin | 3 |
| 2.63 | 335443 | 339.0361 | $C_{14}H_{11}O_{10}$ | 0.3 | 11.5 | unknown | 4 |
| GrSd | | | | | | | |
| 4.92 | 3293050 | 289.0733 | $C_{15}H_{13}O_6$ | 1.5 | 4.6 | catechin | 1 |
| 6.13 | 2954710 | 289.0743 | $C_{15}H_{13}O_6$ | 2.5 | 16.2 | epicatechin | 1 |
| 5.47 | 907789 | 577.1394 | $C_{30}H_{25}O_{12}$ | −4.3 | 9.4 | procyanidin B2 | 1 |
| 4.14 | 863849 | 577.1357 | $C_{30}H_{25}O_{12}$ | −0.6 | 17.5 | procyanidin B1 | 1 |
| 4.76 | 476798 | 865.2017 | $C_{45}H_{37}O_{18}$ | 3.2 | 10.3 | procyanidin trimer | 3 |
| 4.62 | 457356 | 577.1360 | $C_{30}H_{25}O_{12}$ | −0.8 | 11.8 | procyanidin dimer | 2 |
| 6.41 | 384381 | 865.2063 | $C_{45}H_{37}O_{18}$ | 7.7 | 15.5 | procyanidin trimer | 3 |
| 2.63 | 335443 | 169.013 | $C_7H_5O_5$ | −0.6 | 39.8 | gallic acid | 3 |
| 6.33 | 316940 | 291.0900 | $C_{15}H_{15}O_6$ | 2.6 | 13.4 | unknown | 4 |
| 6.72 | 213246 | 576.1303 | $C_{60}H_{49}O_{24}$ | −3.0 | 74.8 | procyanidin tetramer | 3 |
| 13.57 | 146856 | 301.0370 | $C_{15}H_9O_7$ | −1.5 | 6.0 | quercetin | 1 |
| 2.43 | 287535 | 331.0665 | $C_{13}H_{15}O_{10}$ | 0.5 | 17.2 | galloylglucose | 3 |
| 6.04 | 282024 | 421.0759 | $C_{19}H_{17}O_{11}$ | −1.8 | 16.4 | tetrahydroxyxanthone glucoside | 3 |
| AvSk | | | | | | | |
| 6.12 | 2490173 | 289.0722 | $C_{15}H_{13}O_6$ | 0.4 | 16.9 | epicatechin | 1 |
| 5.46 | 2074746 | 577.1359 | $C_{30}H_{25}O_{12}$ | 0.8 | 9.1 | procyanidin B2 | 1 |


dx.doi.org/10.1021/jf503819t | J. Agric. Food Chem. 2014, 62, 11146−11156

**Table 3. continued**

| retention time (min) | peak area | measd mass to charge ratio ($m/z$) | formula $(M - H)^-$ | $\delta$ (mDa)[a] | mSigma[b] | proposed compd ID[c] | ID level[d] |
|---|---|---|---|---|---|---|---|
| 6.4 | 1039617 | 865.2019 | $C_{45}H_{37}O_{18}$ | 3.4 | 10.2 | procyanidin trimer | 2 |
| 5.14 | 953374 | 353.0870 | $C_{16}H_{17}O_9$ | 0.8 | 15.4 | chlorogenic acid | 1 |
| 6.72 | 663401 | 576.1260 | $C_{60}H_{49}O_{24}$ | −1.3 | 14.8 | procyanidin tetramer | 3 |
| 4.98 | 424041 | 443.1910 | $C_{21}H_{31}O_{10}$ | −1.3 | 22.8 | unknown | 4 |
| 5.66 | 334857 | 576.1251 | $C_{60}H_{49}O_{24}$ | −2.2 | 52.5 | procyanidin tetramer | 3 |
| 8.4 | 289662 | 577.1347 | $C_{30}H_{25}O_{12}$ | 0.5 | 11.9 | procyanidin dimer | 2 |
| 5.37 | 256002 | 865.1987 | $C_{45}H_{37}O_{18}$ | 0.2 | 10.6 | procyanidin trimer | 3 |
| 7.52 | 228052 | 595.1299 | $C_{26}H_{27}O_{16}$ | 0.6 | 28.8 | quercetin 3-arabinoglucoside | 2 |
| AvSd | | | | | | | |
| 3.79 | 1445056 | 353.0876 | $C_{16}H_{17}O_9$ | −0.2 | 8.2 | neochlorogenic acid | 2 |
| 6.13 | 940333 | 289.0722 | $C_{15}H_{13}O_6$ | −0.4 | 17.7 | epicatechin | 1 |
| 6.4 | 765748 | 863.1842 | $C_{45}H_{35}O_{18}$ | 1.3 | 18.0 | procyanidin trimer A-linkage | 4 |
| 4.93 | 736750 | 337.0931 | $C_{16}H_{17}O_8$ | 0.2 | 13.8 | coumaryl quinic acid | 1 |
| 3.18 | 633272 | 315.1080 | $C_{14}H_{19}O_8$ | 0.5 | 15.3 | unknown | 4 |
| 5.99 | 499408 | 863.1821 | $C_{45}H_{35}O_{18}$ | −0.8 | 23.0 | procyanidin trimer A-linkage | 4 |
| 8.9 | 472840 | 441.1775 | $C_{21}H_{29}O_{10}$ | −0.8 | 3.5 | unknown | 4 |
| 4.33 | 433427 | 345.1189 | $C_{15}H_{21}O_9$ | 0.2 | 16.7 | unknown | 4 |
| 5.3 | 293381 | 575.1169 | $C_{60}H_{47}O_{24}$ | 2.6 | 111.4 | procyanidin tetramer A2 | 3 |
| 5.18 | 222293 | 353.0869 | $C_{16}H_{17}O_9$ | −0.9 | 13.8 | chlorogenic acid | 1 |
| FeSk | | | | | | | |
| 4.91 | 670167 | 289.0718 | $C_{15}H_{13}O_6$ | 0.0 | 16.6 | catechin | 1 |
| 2.9 | 631225 | 783.0693 | $C_{34}H_{23}O_{22}$ | 0.6 | 11.2 | bis(HHDP)glucose | 2 |
| 6.54 | 309894 | 329.0872 | $C_{14}H_{17}O_9$ | −0.6 | 14.8 | vanillic acid glucoside | 3 |
| 3.04 | 264788 | 305.0666 | $C_{15}H_{13}O_7$ | 0.1 | 16.1 | gallocatechin | 3 |
| 12.82 | 242912 | 551.1022 | $C_{24}H_{23}O_{15}$ | −2.0 | 21.9 | unknown | 4 |
| 2.47 | 199363 | 466.0261 | $C_{41}H_{24}O_{26}$ | 2.2 | 4.2 | castalagin (ET) | 2 |
| 7.64 | 187079 | 433.0386 | $C_{19}H_{13}O_{12}$ | −2.6 | 14.9 | ellagic acid pentoside | 2 |
| 8.66 | 186096 | 463.0864 | $C_{21}H_{19}O_{12}$ | −1.8 | 20.5 | quercetin 3-galactoside | 1 |
| 4.26 | 180061 | 603.0672 | $C_{56}H_{38}O_{31}$ | −3.2 | 12.6 | ChemSpider ID: 10197386 | 3 |
| 9.4 | 178821 | 491.0812 | $C_{22}H_{19}O_{13}$ | −1.9 | 19.7 | methylquercetin glucuronide | 3 |

[a]Delta (mDa) difference between the measured and calculated $m/z$ values for the assigned formula. [b]mSigma: numerical expression for the difference in the measured and calculated isotope pattern of a compound; low values indicate a good match. [c]Identification. [d]1. Positive identification: retention time, calculated elemental composition, mSigma value, and fragment ion masses all correspond to an authentic standard. 2. Tentative identification: elemental formula calculated with mSigma value support; possible structure identified in chemical databases (e.g., ChemSpider); fragment ion mass data supports the proposed molecular structure. 3. Possible identification: elemental formula calculated with mSigma value support; possible structure identified in chemical databases, but no support from fragment ion mass data. 4. Elemental identification: elemental formula calculated with mSigma values support but no suitable compound found in chemical database. 5. No identification: no reasonable calculated elemental formula fits the measured mass data. [e]Double charged ion [2−].

48 h. The cultures were then centrifuged for 5 min at 4,000 rpm, washed twice with phosphate buffered saline solution, and resuspended in 10 mL of 1% SPW. The test compounds were prepared as described previously to obtain a final concentration of 20 mg/mL. In a 96-well plate, an aliquot (120 $\mu$L) of MHB or TSBYE broth was distributed. Each bacterium was inoculated (5 $\mu$L) in duplicate into the wells. After that, compounds were 2-fold serially diluted (10 to 0.078 mg/mL) and added to the inoculated wells (125 $\mu$L). Absorbance measurements (OD 595 nm) were taken once the dilution was completed ($T_0$). Plates were incubated at the optimum growth temperatures of each bacterium. Final absorbance readings were taken after 24 h, and the level of growth inhibition was determined by comparing them with the readings at $T_0$ and subtracting control backgrounds. The MIC values were taken as the lowest concentration of compounds that completely inhibited the growth of the microorganisms after 24 h of incubation. Four independent experiments were conducted in duplicate. If a given replicate did not prevent growth at 10 mg/mL, a value of 20 mg/mL for the MIC was used to calculate means and standard errors.

## RESULTS AND DISCUSSION

**Phenolic Composition of Extracts.** The TPC and TFC of extracts are shown in Figure 1. The extracts contain some moisture (typically 5−10%), which was not considered in the TPC and TFC results. Anhydrous (+)-catechin, the external standard for checking the accuracy of the TPC assay, yielded the expected result of ∼1000 mg GAE/g. The extracts with high TPC values (>300 mg GAE/g) were either tannins or seed extracts, AvSk being the only exception. The mass data and identification attempts for the most abundant compounds (with retention times of 2−18 min) in each extract are shown in Table 3 (see Table 3 footnote for the definition of the different levels of identification).

The phenols of AvSk and AvSd consisted mostly of flavonoids, as shown by their high TFC/TPC ratios. Their TPC values were much higher than those reported by Rodríguez-Carpena et al.,[32] who extracted fresh avocado skins and seeds with 70% acetone. This may be due to differences in material preparation and extraction methods. The base peak chromatographs (BPCs) of AvSk and AvSd showed that these extracts contained a large number of compounds. Many of the compounds detected in these extracts were identified at levels 1−3 as procyanidin monomers, dimers, or oligomers. Phenolic acids were also detected in the avocado extracts. These results

are in agreement with the work of Rodríguez-Carpena et al.,[32] who found that the phenolic compounds in Hass avocado skins and seeds were predominantly procyanidins.

The condensed tannins (PiTa, MiTa, and CaTa) showed quite different TFC/TPC ratios. For PiTa it was high, which is supported by the LCMS results. Its BPC was relatively simple with only seven compounds. Dihydroquercetin and five procyanidins were identified with a high level of certainty (level 1 or 2). A much lower TPC of 363 mg GAE/g was reported for a commercial pine bark extract from *Pinus maritima*.[37] Regarding MiTa, its tannin content of ca. 77% of the dry matter (according to its technical datasheet) is somewhat higher than expected based on its TPC, even allowing for a moisture content of 10%. Since condensed tannins are proanthocyanidins, the rather low TFC/TPC ratio of MiTa is also surprising. However, the LCMS analysis showed that its main components are flavonoids. Cationic tannin is produced from mimosa tannin by the Mannich reaction, which introduces quaternary amino groups into the tannin. Based on the TPC and TFC values of CaTa and MiTa, this reaction reduces both TPC and the TFC/TPC ratio.

The high TPC and low TFC/TPC ratio of TaAc and MaSd are consistent with gallotannins. This is supported by the LCMS data showing the presence of polygalloyl glucoses containing 5−9 (TaAc) or 5−8 (MaSd) galloyl units, identified at level 3. The BPCs of the two extracts also had many similarities. Aragbo[1] found ca. 75% of tannin-related substances in mango seed to be gallotannins and 25% related to condensed tannins, while Kabuki et al.[34] found mango seeds to contain 79.5% of unspecified polyphenols. Engels et al.,[35] who extracted mango seeds with 80% acetone, found the seed extracts to contain galloyl glucoses with 4−12 galloyl groups.

Grape seed extracts have high TPC,[5] which was also the case for the one used in this investigation (GrSd). According to Nakamura et al.,[36] the phenolic substances in grape seed extracts are mainly oligomeric and polymeric proanthocyanidins with minor amounts of low molecular weight procyanidins and gallic acid. Our LCMS results gave similar results, although the most prominent components were identified as catechin and epicatechin at level 1. The BPC of GrSd resembled that of AvSk; some of their identified major components were also the same.

The extracts from berry juicing residues and some of the fruit skin extracts had moderate TPCs (57−172 mg GAE/g), their TFC/TPC ratios ranging from 0.24 to 0.61. The LCMS data show that FeSk phenols comprised flavonoids, ellagitannins, and phenolic acids. They often contained a pentoside or hexoside moiety and were identified at level 1 or 2. Earlier reports have shown that commonly eaten berries such as those included in this study contain the same types of phenols.[37]

The skins of most other fruits and AvPu gave low TPC values (<40 mg GAE/g), a result that agrees with earlier studies.[5,38] In the case of citrus fruit skin extracts, they have been reported to contain low amounts of flavonoids (glycosylated flavanones, flavones, and bound flavonols) and bound phenolic acids.[38]

**Antioxidant Capacity of Samples.** The $EC_{50}$ values of some reference compounds (Table 4), derived from the DPPH radical assay, were somewhat higher than those reported with methanol as the solvent by Mishra et al.[39] This could be due to the different solvents used in the studies. To enable comparison of reference compounds and extracts the $EC_{50}$ values were expressed as μg/mL in Figure 2. Only the extracts that yielded

**Table 4. Antioxidant Capacity of Reference Compounds**

| | $EC_{50}$, μmol of compound/μmol of DPPH | |
|---|---|---|
| compound | this study | Mishra et al. (2012)[39] |
| ascorbic acid | 0.29 ± 0.02 | 0.17 ± 0.01 |
| gallic acid | 0.09 ± 0.01 | 0.07 ± 0.01 |
| (+)-catechin, anhydrous | 0.25 ± 0.02 | n/a |
| (+)-catechin hydrate | 0.29 ± 0.02 | n/a |
| ferulic acid | 0.57 ± 0.05 | 0.36 ± 0.04 |
| Trolox | 0.32 ± 0.00 | n/a |

$EC_{50}$ values <50 μg/mL are included in Figure 2; the other extracts in Table 2 showed relatively weak antioxidant properties ($EC_{50}$ from 130 to 600 μg/mL). The ten extracts with the lowest $EC_{50}$ values and the highest TPCs are the same, showing that TPC is a good predictor of antioxidant capacity.[33] In fact, the Folin−Ciocalteu method used for TPC determination is also an antioxidant assay. Any nonphenolic antioxidants such as ascorbic acid, if present, would thus also contribute to the TPC value. The large variability of the TFC/TPC ratios between these extracts implies that, for the majority of them, it is the quantity rather than the type (flavonoid vs nonflavonoid) of phenols that matters for antioxidant capacity. However, the antioxidant capacity of the mainly nonflavonoid extract MaSd was higher than those of the mainly flavonoid-type GrSd and PiTa, which had higher TPCs. Flavonoid-type phenols are known to possess significant antioxidant activity.[40] Arogba's finding[1] of more tannin-related compounds in mango seed meal than condensed tannins suggests that gallic acid units (three hydroxyls per aromatic ring), which may be free (gallic acid) or esterified (e.g., polygalloyl glucoses in TaAc), contribute more to antioxidant capacity than catechin, epicatechin, or other flavonoid units (typically 1−2 phenolic hydroxyls per aromatic ring). This hypothesis is corroborated by the very high antioxidant capacity of TaAc and a comparison of the antioxidant capacities of gallic acid and catechin (Table 4), representing gallotannins and condensed (flavonoid-type) tannins, respectively. The high antioxidant capacities of TaAc and MaSd can thus be traced back to their similar phenolic structures and high TPCs. The antioxidant capacity of TaAc exceeded those of the nonphenolic antioxidants ascorbic acid and Trolox (a synthetic, water-soluble variant of vitamin E).

The extract from mango (MaSd) also compares favorably with the commercial grape seed extract (GrSd), a dietary supplement, and the other berry extracts. Avocado extracts (AvSk and AvSd) also performed well, better than the berry extracts. As mentioned earlier, the phenolic profiles of GrSd and AvSk are rather similar. Condensed tannins and kiwifruit extracts are also found in some dietary supplements. African mango seed extract is commercially available; however, a sample obtained for the present study showed a very low TPC of 23 ± 2 mg/g GAE. No commercial avocado skin or seed based dietary supplements seem to be available. Since mango seeds and avocado skins/seeds are produced in large quantities as byproducts of the mango juice and avocado oil[4] industries, respectively, these fruit parts could potentially be exploited to a greater extent for dietary supplement production in a similar fashion to the grape seed extracts currently used.

**Antibacterial Activity of Extracts.** ZI assays were carried out on 18 extracts with high TPCs, and the results are shown in Table 5. Thermally modified TaAc (mTaAc) proved to have the highest antibacterial activity in terms of ZI diameter and range of bacteria affected. The purpose of the thermal

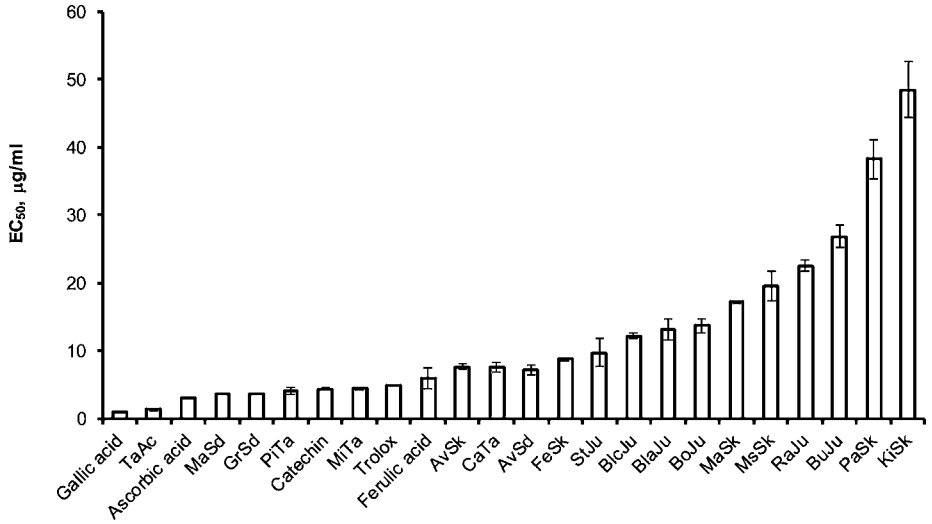


**Figure 2.** Antioxidant capacity of extracts and reference compounds as effective concentration ($EC_{50}$).

**Table 5. Zones of Inhibition (cm, ± Standard Error) of Extracts and Reference Compounds (10 mg/mL) with Different Bacteria**

| bacterium | mTaAc | TaAc | MaSd | FeSk | MaSk | MiTa | GrSd | MsSk | AvSk |
|---|---|---|---|---|---|---|---|---|---|
| *S. putrefaciens* | 9.4 ± 10.3 | 13.2 ± 1.6 | 13.6 ± 0.6 | 7.8 ± 3.9 | 4.4 ± 4.8 | 10.9 ± 1.0 | 12.8 ± 0.7 | 14.4 ± 0.4 | 11.6 ± 1.3 |
| *P. phosphoreum* | 19.6 ± 5.5 | 13.5 ± 0.5 | 12.9 ± 0.7 | 11.5 ± 0.5 | 5.0 ± 5.5 | 11.1 ± 0.1.0 | 11.3 ± 0.3 | 6.8 ± 7.5 | 5.5 ± 6.0 |
| *P. fluorescens* | 17.8 ± 2.8 | 16.2 ± 1.5 | 14.9 ± 0.6 | 16.0 ± 1.8 | 10.4 ± 0.4 | 6.1 ± 6.7 | 5.7 ± 6.3 | 0 | 0 |
| *S. liquefíciens* | 18.2 ± 2.3 | 15.8 ± 1.6 | 15.0 ± 0.4 | 15.3 ± 0.7 | 10.0 ± 0.7 | 3.3 ± 5.1 | 3.1 ± 4.8 | 0 | 0 |
| *S. proteomaculans* | 16.1 ± 1.2 | 15.4 ± 0.8 | 15.3 ± 1.7 | 15.7 ± 1.1 | 10.5 ± 0.9 | 4.9 ± 5.4 | 4.6 ± 5.0 | 0 | 0 |
| *B. thermosphacta* | 20.6 ± 3.9 | 14.4 ± 1.1 | 12.0 ± 5.9 | 10.5 ± 1.7 | 10.5 ± 0.8 | 11.2 ± 0.7 | 13.3 ± 0.9 | 15.0 ± 0.3 | 10.4 ± 5.1 |
| *C. esterthearum* | 9.3 ± 10.2 | 16.7 ± 1.6 | 12.7 ± 6.3 | 2.5 ± 6.1 | 0 | 6.7 ± 7.4 | 6.8 ± 7.4 | 13.5 ± 0.8 | 12.5 ± 0.4 |
| *H. alvei* | 10.2 ± 8.0 | 15.2 ± 0.7 | 14.1 ± 0.7 | 16.2 ± 0.9 | 10.1 ± 0.7 | 10.8 ± 2.9 | 10.7 ± 0.4 | 5.0 ± 5.5 | 4.9 ± 5.4 |
| *Lactobacillus* sp. | 19.9 ± 1.8 | 14.0 ± 1.6 | 12.7 ± 1.0 | 6.6 ± 7.3 | 4.5 ± 5.0 | 5.2 ± 5.7 | 0 | 0 | 0 |
| *L. monocytogenes* | 14.6 ± 1.3 | 4.9 ± 5.3 | 9.7 ± 0.6 | 9.0 ± 0.3 | 3.2 ± 5.0 | 4.5 ± 4.9 | 9.0 ± 0.5 | 13.2 ± 0.7 | 4.2 ± 4.6 |
| *E. coli* | 14.0 ± 3.0 | 17.8 ± 3.0 | 16.4 ± 0.5 | 18.5 ± 2.0 | 11.0 ± 1.1 | 0 | 0 | 0 | 0 |
| *S.* Enteriditis | 15.2 ± 0.9 | 15.8 ± 7.9 | 16.2 ± 0.4 | 16.9 ± 1.5 | 10.5 ± 0.4 | 5.5 ± 6.0 | 2.4 ± 6.0 | 0 | 0 |
| *S.* Typhimurium | 14.5 ± 0.8 | 16.6 ± 1.9 | 16.5 ± 1.7 | 17.6 ± 1.4 | 10.0 ± 0.4 | 0 | 5.8 ± 6.3 | 0 | 0 |
| *S. aureus* MRSA | 31.6 ± 1.8 | 18.3 ± 0.7 | 16.0 ± 0.9 | 12.2 ± 0.4 | 12.0 ± 0.8 | 17.1 ± 1.2 | 15.2 ± 0.5 | 12.9 ± 0.6 | 14.6 ± 0.5 |
| *S. aureus* ATCC | 33.1 ± 1.7 | 18.2 ± 0.8 | 16.5 ± 0.5 | 13.1 ± 2.5 | 12.1 ± 0.5 | 18.6 ± 1.7 | 15.5 ± 1.0 | 14.0 ± 0.6 | 14.8 ± 0.7 |
| *Y. enterocolitica* | 25.2 ± 0.8 | 18.0 ± 0.9 | 16.7 ± 1.5 | 15.0 ± 1.4 | 11.7 ± 1.4 | 12.8 ± 1.3 | 11.3 ± 0.7 | 0 | 0 |

| bacterium | AvSd | gallic acid | PiTa | KiSk | BluB | catechin | PaSk | CaTa | ApSk |
|---|---|---|---|---|---|---|---|---|---|
| *S. putrefaciens* | 11.4 ± 0.5 | 8.6 ± 0.7 | 10.1 ± 1.0 | 8.9 ± 0.4 | 4.2 ± 4.6 | 8.4 ± 0.5 | 4.6 ± 5.0 | 2.9 ± 4.5 | 4.7 ± 5.2 |
| *P. phosphoreum* | 5.5 ± 6.1 | 3.0 ± 4.7 | 3.0 ± 1.7 | 3.0 ± 4.7 | 4.3 ± 0.6 | 0 | 0 | 0 | 0 |
| *P. fluorescens* | 0 | 7.2 ± 4.5 | 0 | 0 | 0 | 0 | 0 | 0 | 0 |
| *S. liquefíciens* | 0 | 6.6 ± 5.1 | 0 | 0 | 0 | 0 | 0 | 0 | 0 |
| *S. proteomaculans* | 0 | 7.8 ± 3.9 | 0 | 0 | 0 | 0 | 1.6 ± 3.9 | 0 | 0 |
| *B. thermosphacta* | 8.2 ± 6.4 | 0 | 5.0 ± 5.5 | 6.0 ± 4.6 | 1.5 ± 3.6 | 4.3 ± 4.7 | | | |
| *C. esterthearum* | 10.6 ± 5.3 | 0 | 0 | 2.9 ± 4.5 | 4.2 ± 4.7 | 0 | 3.1 ± 4.7 | 3.6 ± 5.5 | 0 |
| *H. alvei* | 0 | 9.0 ± 0.7 | 0 | 0 | 3.2 ± 4.9 | 1.6 ± 3.8 | 0 | 0 | 0 |
| *Lactobacillus* sp. | 0 | 9.7 ± 0.6 | 0 | 0 | 0 | 0 | 0 | 0 | 0 |
| *L. monocytogenes* | 4.9 ± 5.3 | 0 | 0 | 0 | 0 | 0 | 0 | 0 | 0 |
| *E. coli* | 0 | 0 | 0 | 0 | 0 | 0 | 0 | 0 | 0 |
| *S.* Enteriditis | 0 | 10.0 ± 1.1 | 0 | 5.4 ± 5.9 | 6.0 ± 5.5 | 0 | 0 | 0 | 0 |
| *S.* Typhimurium | 0 | 10.0 ± 1.0 | 0 | 4.7 ± 5.1 | 9.2 ± 1.2 | 3.0 ± 4.6 | 0 | 0 | 0 |
| *S. aureus* MRSA | 14.7 ± 1.8 | 0 | 13.3 ± 0.8 | 8.8 ± 4.3 | 8.9 ± 0.5 | 0 | 5.6 ± 4.5 | 0 | 6.0 ± 4.7 |
| *S. aureus* ATCC | 15.5 ± 2.0 | 0 | 13.7 ± 0.6 | 9.3 ± 0.3 | 4.2 ± 4.6 | 5.0 ± 5.5 | 0 | 0 | 1.3 ± 3.2 |
| *Y. enterocolitica* | 5.6 ± 6.1 | 4.2 ± 4.6 | 10.0 ± 1.8 | 0. | 0 | 0 | 0 | 8.9 ± 0.5 | 0 |

modification was to find out whether compounds such as pyrogallol, produced during the treatment, would enhance the antibacterial activity of TaAc.[26] According to Kim et al.,[26] the antibacterial activity measured by the formation of zone of growth inhibition ZI data of mTaAc against several Gram-positive and Gram-negative bacteria increased with an increase in treatment temperature. The increase was attributed to production of gallic acid and pyrogallol, which were found to have greater antibacterial activity than unmodified tannic acid. The product obtained at the highest treatment temperature


dx.doi.org/10.1021/jf503819t | J. Agric. Food Chem. 2014, 62, 11146−11156

Table 6. Minimum Inhibitory Concentration (mg/mL, ± Standard Error) of Extracts and Reference Compounds for Different Bacteria

| bacterium | MaSd | TaAc | mTaAc | FeSk | AvSd | MiTa | GrSd | AvSk |
|---|---|---|---|---|---|---|---|---|
| *S. putrefaciens* | 0.47 ± 1.56 | 0.16 ± 2.60 | 3.13 ± 2.39 | 2.50 ± 1.23 | 0.94 ± 0.14 | 12.50 ± 3.39 | 2.50 ± 2.50 | 2.50 ± 2.32 |
| *P. phosphoreum* | 1.56 ± 3.09 | 0.94 ± 0.71 | 0.63 ± 1.55 | 2.50 ± 3.26 | 20.00 ± 2.11 | 12.50 ± 3.16 | 20.00 ± 2.78 | 20.00 ± 0.00 |
| *P. fluorescens* | 1.56 ± 2.34 | 3.75 ± 3.33 | 10.00 ± 2.63 | 2.50 ± 2.70 | 5.00 ± 1.25 | 11.25 ± 3.37 | 20.00 ± 3.15 | 10.00 ± 2.10 |
| *S. liquefaciens* | 1.56 ± 0.78 | 10.63 ± 3.65 | 15.00 ± 3.05 | 20.00 ± 3.48 | 20.00 ± 3.07 | 1.88 ± 3.45 | 11.25 ± 3.43 | 20.00 ± 3.07 |
| *S. proteomaculans* | 1.25 ± 0.29 | 5.00 ± 2.59 | 15.00 ± 2.66 | 20.00 ± 1.43 | 20.00 ± 2.67 | 20.00 ± 0.00 | 20.00 ± 0.00 | 20.00 ± 1.25 |
| *B. thermosphacta* | 0.47 ± 1.20 | 0.31 ± 1.57 | 3.13 ± 1.14 | 1.25 ± 0.13 | 0.63 ± 0.74 | 3.75 ± 3.75 | 7.50 ± 3.09 | 0.63 ± 1.21 |
| *C. esterthearum* | 0.12 ± 0.04 | 0.18 ± 0.19 | 0.06 ± 0.01 | 1.25 ± 0.30 | 0.47 ± 0.34 | 0.47 ± 0.75 | 0.31 ± 3.23 | 0.94 ± 2.39 |
| *H. alvei* | 1.88 ± 1.42 | 1.88 ± 3.05 | 10.00 ± 2.32 | 10.00 ± 3.26 | 20.00 ± 0.00 | 20.00 ± 2.67 | 20.00 ± 2.19 | 20.00 ± 0.00 |
| *Lactobacillus* sp. | 7.50 ± 1.44 | 15.00 ± 1.94 | 7.50 ± 0.97 | 20.00 ± 2.96 | 0.31 ± 0.08 | 20.00 ± 2.65 | 15.00 ± 2.66 | 0.31 ± 0.08 |
| *L. monocytogenes* | 1.88 ± 0.28 | 0.63 ± 0.16 | 5.00 ± 1.12 | 3.75 ± 3.58 | 2.50 ± 0.21 | 7.50 ± 3.01 | 5.00 ± 3.46 | 5.00 ± 2.62 |
| *E. coli* O157:H7 | 1.56 ± 0.69 | 1.88 ± 0.67 | 1.88 ± 0.58 | 2.50 ± 1.38 | 10.00 ± 1.83 | 7.50 ± 2.63 | 20.00 ± 2.75 | 20.00 ± 0.00 |
| *S.* Enteriditis | 0.94 ± 3.11 | 0.78 ± 3.17 | 2.50 ± 2.97 | 2.50 ± 1.53 | 20.00 ± 1.25 | 6.25 ± 2.71 | 20.00 ± 0.00 | 20.00 ± 0.00 |
| *S.* Typhimurium | 5.00 ± 2.74 | 5.00 ± 2.50 | 3.75 ± 1.22 | 10.00 ± 2.70 | 20.00 ± 1.83 | 20.00 ± 1.64 | 20.00 ± 0.00 | 20.00 ± 0.00 |
| *S. aureus* MRSA | 0.16 ± 0.14 | 0.06 ± 0.16 | 0.12 ± 0.19 | 1.25 ± 2.81 | 1.88 ± 3.09 | 1.56 ± 3.08 | 0.63 ± 0.10 | 12.50 ± 3.34 |
| *S. aureus* ATCC | 0.31 ± 0.08 | 1.29 ± 0.77 | 0.20 ± 0.19 | 1.25 ± 0.12 | 5.63 ± 3.04 | 1.88 ± 3.01 | 0.63 ± 0.05 | 2.50 ± 2.97 |
| *Y. enterocolitica* | 5.63 ± 8.52 | 1.88 ± 2.44 | 20.00 ± 1.64 | 20.00 ± 3.38 | 5.00 ± 1.30 | 20.00 ± 2.19 | 2.50 ± 3.37 | 20.00 ± 2.20 |

(200 °C) also showed greater antibacterial activity than gallic acid but not as great as pyrogallol. The results of our ZI assay (mTaAc > TaAc > gallic acid; pyrogallol was not investigated) are partly in line with Kim's findings.[26] In general, the extracts with a high or moderately high antioxidant capacity produced large ZIs with most bacteria. The monomeric reference compounds gallic acid and catechin, however, had much lower antibacterial activity than the extracts rich in polygalloyl glucoses (TaAc, MaSd) or procyanidins of different sizes and monomeric flavanols (PiTa, GrSd). Our findings agree with those of Chung et al.,[41] who reported tannic acid to be a more potent antibacterial agent than gallic acid against food-borne bacteria.

The MIC assays were only carried out for selected extracts (Table 6) based on their performance in the ZI assays and potential availability as byproducts. The best-performing extracts in the ZI and MIC assays were clearly MaSd and TaAc, followed by mTaAc and FeSk. According to Engels et al.,[35,42] the antibacterial activity of mango seed extracts is due to the iron-chelating ability of the gallotannins with steric effects making the smaller gallotannins somewhat more effective than the larger ones. Other antibacterial chelating compounds such as mangiferin[43] (a tetrahydroxyxanthone glucoside) worked synergistically with the gallotannins. A tetrahydroxyxanthone glucoside was also identified in MaSd at level 3. The fact that MaSd and TaAc exhibited similar antibacterial activities despite the large difference in their TPC could thus be largely due to the presence of mangiferin (and/or other chelating compounds). Their different gallotannin size distributions, resulting in different degrees of steric hindrance, could also affect their relative antibacterial activities.[42] The weak antibacterial effects of gallic acid compared to TaAc and MaSd are likely due to the fact that the iron ($Fe^{3+}$) chelates formed by the extracts are able to form lattices by coordinating with up to three *o*-dihydroxyphenyl moieties, possibly from different molecules, until the complexes get large enough to precipitate out of the solution.[42] In general, the highest levels of antibacterial activity were seen against the Gram-positive bacteria: *S. aureus*, *C. estertheticum*, *B. thermosphacta*, and *L. monocytogenes*. The Gram-negative bacterium *S. putrefaciens* and *Lactobacillus* sp. (Gram-positive) were more difficult to inhibit than Gram-positive bacteria as only AvSk and AvSd showed low MICs against them. Gram-negative bacteria are usually more resistant to antibacterial agents than Gram-positive because of their protective polysaccharide layer,[44] as it was also observed in the present study. This becomes important as many pathogenic and spoilage bacteria are Gram-negative.

A comparison of the MIC values with the spoilage bacteria information in Table 1 shows that MaSd and TaAc in particular are able to provide significant inhibition of several major fish and lamb spoilage bacteria while also inhibiting many pathogenic bacteria. Kabuki et al.[34] found that the MIC profile of ethanolic mango seed extract was different from those of flavonoid-based ethanolic extracts (tea catechins and theaflavins). Also FeSk and mTaAc gave relatively low MIC values against several of the bacteria tested. Based on the MIC and ZI results, these four extracts proved the most promising candidates for antibacterial packaging films able to extend the shelf life of chilled fish and lamb. As for the other compounds, their MIC values may be too high for such applications despite their ZI activity at the dose investigated. This is the case especially when activity against a broad range of bacteria is desired. Before any packaging materials containing these compounds may be used for food transport, however, the migrating compounds and the packaging material (at least its food contact layer) must comply with strict toxicity criteria. These depend on the type of compound and the expected level of migration. For any novel compounds or packaging materials, nontoxicity must be demonstrated unless exclusion from toxicity testing has been granted. Migration limits include compound-specific limits and maximum limits applying to all compounds (e.g., 60 mg/kg food in the EU) regardless of toxicity. Compliance with these issues should be an integral part of antimicrobial packaging design from the outset. Using compounds (of natural origin where possible) and packaging materials approved for food contact by European Food Safety Authority (EFSA), the US Food and Drug Administration (FDA), and other food safety authorities can significantly reduce testing requirements and improve the chances of finding feasible antibacterial packaging solutions.

To sum up, based on our in vitro assays, the most promising natural extracts for antibacterial packaging films were MaSd and TaAc, i.e., the extracts rich in polygalloyl glucoses and with the highest antioxidant capacity. However, the TPC and LCMS

analyses indicate that TaAc is higher in polygalloyl glucoses than MaSd, whose antibacterial activity was somewhat higher. This could be due to the different polygalloyl (penta- to nonagalloyl) glucose size distributions in the two extracts or other components in MaSd working synergistically with polygalloyl glucoses and/or showing high antibacterial activity on their own. Extracts rich in flavonoid type phenols showed a moderate level of antibacterial activity while those with low total phenol content displayed low activity. Further work should be carried out on the extracts based on polygalloyl glucoses, particularly relating to the economics of using them in supplement and packaging applications and in relation to their safety for human consumption.

## AUTHOR INFORMATION

### Corresponding Author

*Tel: + 64 7 343 5899. Fax: +64 7 348 0952. E-mail: petri.widsten@scionresearch.com.

### Notes

The authors declare no competing financial interest.

## ACKNOWLEDGMENTS

The authors wish to thank Fressure Foods, NZ, for supplying the avocado processing residue.

## REFERENCES

(1) Arogba, S. S. Mango (*Mangifera indica*) kernel: chromatographic analysis of the tannin, and stability study of the associated polyphenol oxidase activity. *J. Food. Compos. Anal.* **2000**, *13*, 149−156.

(2) Ayala-Zavala, J. F.; Rosas-Domínguez, C.; Vega-Vega, V.; González-Aguilar, G. A. Antioxidant enrichment and antimicrobial protection of fresh-cut fruits using their own byproducts: Looking for integral exploitation. *J. Food Sci.* **2010**, *75*, R175−R181.

(3) Balasundram, N.; Sundram, K.; Samman, S. Phenolic compounds in plants and agri-industrial by-products: Antioxidant activity, occurrence, and potential uses. *Food Chem.* **2006**, *99*, 191−203.

(4) Kosińska, A.; Karamać, M.; Estrella, I.; Hernández, T.; Bartolomé, B.; Dykes, G. A. Phenolic compound profiles and antioxidant capacity of *Persea americana* Mill. peels and seeds of two varieties. *J. Agric. Food Chem.* **2012**, *60*, 4613−4619.

(5) Peschel, W.; Sanchez-Rabaneda, F.; Diekmann, W.; Plescher, A.; Gartzia, I.; Jimenez, D.; Lamuela-Raventos, R.; Buxaderas, S.; Codina, C. An industrial approach in the search of natural antioxidants from vegetable and fruit wastes. *Food Chem.* **2006**, *97*, 137−150.

(6) Schieber, A.; Stintzing, F. C.; Carle, R. By-products of plant food processing as a source of functional compounds-recent developments. *Trends Food Sci. Technol.* **2001**, *12*, 401−413.

(7) Sun-Waterhouse, D.; Wen, I.; Wibisono, R.; Melton, L. D.; Wadhwa, S. Evaluation of the extraction efficiency for polyphenol extracts from by-products of green kiwifruit juicing. *Int. J. Food Sci. Technol.* **2009**, *44*, 2644−2652.

(8) Wijngaard, H. H.; Rößle, C.; Brunton, N. A survey of Irish fruit and vegetable waste and by-products as a source of polyphenolic antioxidants. *Food Chem.* **2009**, *116*, 202−207.

(9) Laks, P. E. An overview of condensed tannin structure. In *Chemistry and Significance of Condensed Tannins*; Hemingway, R. W., Karchesy, J. J., Branham, S. J., Eds.; Plenum Press: New York, 1989; pp 131−136.

(10) Haddock, E. A.; Gupta, R. J.; Al-Shafi, S. M. K.; Haslam, E.; Magnolato, D. The metabolism of gallic acid and hexahydroxydiphenic acid in plants. Part 1. Introduction. Naturally occurring galloyl esters. *J. Chem. Soc., Perkin Trans. 1* **1982**, 2515−2524.

(11) Salminen, J. P.; Ossipov, V.; Haukioja, E.; Pihlaja, K. Seasonal variation in the content of hydrolysable tannins in leaves of *Betula pubescens*. *Phytochemistry* **2001**, *57*, 15−22.

(12) Floros, J. D.; Dock, L. L.; Han, J. H. Active packaging technologies and applications. *Food, Cosmet. Drug Packag.* **1997**, *20*, 10−17.

(13) Suppakul, P.; Miltz, J.; Sonnevel, K.; Bigger, S. W. Active packaging technologies with an emphasis on antimicrobial packaging and its applications. *J. Food Sci.* **2003**, *68*, 408−420.

(14) Vermeiren, L.; Devlieghere, F.; Beest, M.; Kruijf, N.; Debevere, J. Developments in the active packaging of foods. *Trends Food Sci. Technol.* **1999**, *10*, 77−86.

(15) Zagory, D. Ethylene-removing packaging. In *Active Food Packaging*; Rooney, M. L., Ed.; Blackie Academic and Professional: London, 1995; pp 38−54.

(16) Kuorwel, K. K.; Cran, M. J.; Sonneveld, K.; Miltz, J.; Bigger, S. W. Essential oils and their principal constituents as antimicrobial agents for synthetic packaging films. *J. Food Sci.* **2011**, *76*, R164−R177.

(17) Maqsood, S.; Benjakul, S.; Shahidi, F. Emerging role of phenolic compounds as natural food additives in fish and fish products. *Crit. Rev. Food Sci. Nutr.* **2013**, *53*, 162−179.

(18) Gram, L.; Dalgaard, P. Fish spoilage bacteria—problems and solutions. *Curr. Opin. Biotechnol.* **2002**, *13*, 262−266.

(19) Adam, K. H.; Flint, S. H.; Brightwell, G. Psychrophilic and psychrotrophic clostridia: sporulation and germination processes and their role in the spoilage of chilled, vacuum-packaged beef, lamb and venison. *Int. J. Food Sci. Technol.* **2010**, *45*, 1539−1544.

(20) Johanson, M. R.; Fletcher, G. C. Response of microbial flora in modified atmosphere packaging in salmon fillets. In *Proc. Microbes and Molecules 2002 conference: Physiology, Health and the Environment*; University of Canterbury: Christchurch, New Zealand, 2002; p 218.

(21) Shaw, B. G.; Shewan, J. M. Psychrophilic spoilage bacteria of fish. *J. Appl. Bacteriol.* **1968**, *31*, 89−96.

(22) Mills, J.; Gribble, A. Chilled lamb storage—new findings. AgResearch Meat Industry Workshop, 5 March 2013, Hamilton, New Zealand. http://www.agresearch.co.nz/our-science/meat-dairy-foods/food-quality/meat-industry-workshop/2013workshop/Food%20Assurance%20Speaker%204%20-%20Mills.pdf.

(23) Bjelakovic, G.; Nikolova, D.; Gluud, L. L.; Simonetti, R. G.; Gluud, C. Mortality in randomized trials of antioxidant supplements for primary and secondary prevention: systematic review and meta-analysis. *JAMA, J. Am. Med. Assoc.* **2007**, *297*, 842−857.

(24) Craig, W. J. Phytochemicals: guardians of our health. *J. Am. Diet. Assoc.* **1997**, *97* (Suppl.), S199−204.

(25) Heim, K. E.; Tagliaferro, A. R.; Bobilya, D. J. Flavonoid antioxidants: chemistry, metabolism and structure−activity relationships. *J. Nutr. Biochem.* **2002**, *13*, 572−584.

(26) Kim, T. J.; Silva, J. L.; Jung, Y. S. Enhanced functional properties of tannic acid after thermal hydrolysis. *Food Chem.* **2011**, *126*, 116−120.

(27) Kähkönen, M. P.; Hopia, A. I.; Vuorela, H. J.; Rauha, J.-P.; Pihlaja, K.; Kujala, T. S.; Heinonen, M. Antioxidant activity of plant extracts containing phenolic compounds. *J. Agric. Food Chem.* **1999**, *47*, 3954−3962.

(28) Dewanto, V.; Wu, X.; Adom, K. K.; Liu, R. H. Thermal processing enhances the nutritional value of tomatoes by increasing total antioxidant activity. *J. Agric. Food Chem.* **2002**, *50*, 3010−3014.

(29) Butkhup, L.; Chowtivannakul, S.; Gaensakoo, R.; Prathepha, P.; Samappito, S. Study of the phenolic composition of Shiraz red grape cultivar (*Vitis vinifera* L.) cultivated in north-eastern Thailand and its antioxidant and antimicrobial activity. *S. Afr. J. Enol. Vitic.* **2010**, *31*, 89−98.

(30) Ezeifeka, G. O.; Orji, M. U.; Mbata, T. I.; Patrick, A. O. Antimicrobial activities of *Cajanus cajan*, *Garcinia kola* and *Xylopia aethiopica* on pathogenic microorganisms. *Biotechnology* **2004**, *3*, 41−43.

(31) National Committee for Clinical Laboratory Standards (NCCLS). *Methods for dilution antimicrobial susceptibility tests for bacteria that grow aerobically*, 3rd ed.; Clinical and Laboratory Standards Institute (CLSI): Villanova, PA, USA; approved standard NCCLS document M7-A3, Vol. *13*, No. 25, December 1993.

(32) Rodríguez-Carpena, J. G.; Morcuende, D.; Andrade, M. J.; Kylli, P.; Estévez, M. Avocado (*Persea americana* Mill.) phenolics, in vitro antioxidant and antimicrobial activities, and inhibition of lipid and protein oxidation in porcine patties. *J. Agric. Food Chem.* **2011**, *59*, 5625−5635.
(33) Dudonné, S.; Vitrac, X.; Coutière, P.; Woillez, M.; Mérillon, J.-M. Comparative study of antioxidant properties and total phenolic content of 30 plant extracts of industrial interest using DPPH, ABTS, FRAP, SOD, and ORAC assays. *J. Agric. Food Chem.* **2009**, *57*, 1768−1774.
(34) Kabuki, T.; Nakajima, H.; Arai, M.; Ueda, S.; Kuwabara, Y.; Dosako, S. Characterization of novel antimicrobial compounds from mango (*Mangifera indica* L.) kernel seeds. *Food Chem.* **2000**, *71*, 61−66.
(35) Engels, C.; Knödler, M.; Zhao, Y.-Y.; Carle, R.; Gäzle, M. G.; Schieber, A. Antimicrobial activity of gallotannins isolated from mango (*Mangifera indica* L.) kernels. *J. Agric. Food Chem.* **2009**, *57*, 7712−7718.
(36) Nakamura, Y.; Tsuji, S.; Tonogai, Y. Analysis of proanthocyanidins in grape seed extracts, health foods and grape seed oils. *J. Health Sci.* **2003**, *49*, 45−54.
(37) Puupponen-Pimiä, R.; Nohynek, L.; Alakomi, H.-L.; Oksman-Caldentey, K.-J. Bioactive berry compounds—novel tools against human pathogens. *Appl. Microbiol. Biotechnol.* **2005**, *67*, 8−18.
(38) Bocco, A.; Cuvelier, M. E.; Richard, H.; Berset, C. Anti-oxidant activity and phenolic composition of citrus peel and seed extracts. *J. Agric. Food Chem.* **1998**, *46*, 2123−2129.
(39) Mishra, K.; Ojha, H.; Chaudhury, N. K. Estimation of antiradical properties of antioxidants using DPPH assay: A critical review and results. *Food Chem.* **2012**, *130*, 1036−1043.
(40) Colón, M.; Nerín, C. Role of catechins in the antioxidant capacity of an active film containing green tea, green coffee, and grapefruit extracts. *J. Agric. Food Chem.* **2012**, *60*, 9842−9849.
(41) Chung, K.-T.; Stevens, S. E., Jr.; Lin, W.-F.; Wei, C. I. Growth inhibition of selected food-borne bacteria by tannic acid, propyl gallate and related compounds. *Lett. Appl. Microbiol.* **1993**, *17*, 29−32.
(42) Engels, C.; Gäzle, M. G.; Schieber, A. Fractionation of gallotannins from mango (*Mangifera indica* L.) kernels by high-speed counter-current chromatography and determination of their antibacterial activity. *J. Agric. Food Chem.* **2010**, *58*, 775−780.
(43) Matkowsi, A.; Kus, P.; Goralska, E.; Wozniak, D. Mangiferin - a bioactive xanthonoid, not only from mango and not just antioxidant. *Mini-Rev. Med. Chem.* **2013**, *13*, 439−455.
(44) Stevens, K. A.; Sheldon, B. W.; Klapes, N. A.; Klaenhammer, T. R. Nisin treatment for inactivation of Salmonella species and other Gram-negative bacteria. *Appl. Environ. Microbiol.* **1991**, *57*, 3613−3615.

evaluated. The primary structure−activity relationship of the MGDGs was also discussed.

## MATERIALS AND METHODS

**Chemicals.** Spectral-grade solvents for spectroscopic measurements were obtained from Sigma-Aldrich. High-performance liquid chromatography (HPLC)-grade solvents were obtained from Merck, Inc. (Merck KgaA, Darmstadt, Germany). All of the other solvents were of analytical grade (Yuwang Reagent Company, Shandong, China).

Cell culture materials, such as Dulbecco's modified Eagle's medium (DMEM), fetal bovine serum (FBS), trypsin, glutamine, and penicillin/streptomycin (PES), were obtained from Gibco. Dexamethasone, 3-isobutyl-methylxanthine, insulin, and dimethyl sulfoxide (DMSO) were obtained from Sigma-Aldrich. The TG kit was purchased from BioSino Biotechnology and Science, Inc., China, and the NEFA-C kit was purchased from NEFA C-test Wako, Japan.

**General Experimental Procedures.** Optical rotation was measured on a PerkinElmer model 241 polarimeter (Norwalk, CT). $^1$H and $^{13}$C nuclear magnetic resonance (NMR) spectra were recorded on JEOL JNM-ECP 600 spectrometers using tetramethylsilane (TMS) as the internal standard, and chemical shifts were recorded as $\delta$ values. Silica gel (100−200 and 200−300 mesh, Qingdao Haiyang Chemical Co., Ltd., Qingdao, China) and Sephadex LH-20 (GE Healthcare Bio-Sciences AB, Uppsala, Sweden) were used for column chromatography. Thin-layer chromatography (TLC) silica gel $GF_{254}$ plates (Yantai Zi Fu Chemical Co., Ltd., Yantai, China) were used for TLC analysis.

**Plant Material.** Fronds of *S. horneri* (Turner) C. Agardh were collected from Changdao in Shandong, China, in October 2010. The original seaweed was identified by Prof. Xiaoqi Zeng (College of Fisheries, Ocean University of China), and a voucher specimen was deposited at the School of Medicine and Pharmacy, Ocean University of China. The alga was washed using water after its collection, dried thoroughly, and stored at room temperature.

**Extraction and Isolation.** *S. horneri* (1170.8 g) was powdered and repeatedly refluxed 3 times with 70% alcohol to obtain a hydroalcoholic solution. The solution obtained was concentrated under reduced pressure, and the remaining aqueous suspension was extracted with the same volume of ethyl acetate (EtOAc) to obtain an EtOAc extract.

The EtOAc extract (4.25 g) was fractionated using vacuum liquid chromatography (VLC) over silica gel by gradient elution using $CH_2Cl_2$/MeOH. The sixth fraction (95:5 $CH_2Cl_2$/MeOH, 853.6 mg) was subsequently separated over Sephadex LH-20 with $CH_2Cl_2$/MeOH (1:1), followed by flash silica gel column chromatography with $CH_2Cl_2$/MeOH (96:4) to obtain a mixture of MGDGs (white powder, 153.4 mg).

The purity of the MGDGs was analyzed using TLC developed with three solvent systems (I, 93:7 $CH_2Cl_2$/MeOH; II, 1:2 $CH_2Cl_2$/EtOAc; and III, 1:1 $CH_2Cl_2$/$Me_2CO$). Only one purplish pink spot was visualized using a 5% methanolic sulfuric acid spray, followed by heating at 115 °C.

**Structure Elucidation of MGDGs.** White amorphous powder. $^1$H NMR (600 MHz, $CDCl_3$) $\delta$: 4.39 (1H, dd, $J$ = 3.1 and 12.0 Hz, H-1), 5.29 (1H, m, H-2), 3.91 (2H, dd, $J$ = 5.4 and 11.1 Hz, H-3), 4.26 (1H, d, $J$ = 7.6 Hz, H-1′), 3.66 (1H, m, H-2′), 3.59 (1H, m, H-3′), 3.69 (1H, m, H-4′), 3.54 (1H, t, $J$ = 5.3 Hz, H-5′), 3.84 (1H, dd, $J$ = 4.4 and 11.8 Hz, H-6′), 3.71 (1H, m, H-6′), 1.25−1.35 [brs, $(CH_2)_n$], 0.87 (6H, t, $J$ = 7.0 Hz, $CH_3$). $^{13}$C NMR (150 MHz, $CDCl_3$) $\delta$: 63.0 (C-1), 70.3 (C-2), 68.2 (C-3), 104.2 (C-1′), 71.4 (C-2′), 73.6 (C-3′), 69.2 (C-4′), 74.7 (C-5′), 62.0 (C-6′), 174.0 and 173.6 (−CO−), 27.3−34.4 [$(CH_2)_n$], 14.3 ($CH_3$). This powder was identified to be 1,2-*O*-diacyl-3-*O*-$\beta$-D-galactopyranosylglycerol (MGDG) by comparing NMR data to the literature.[14]

**Alkaline Hydrolysis.**[15−17] A solution of the total MGDGs (35 mg) in MeOH (3.5 mL) was treated with 5% NaOMe/MeOH (3.5 mL) under stirring at room temperature for 10 min. The mixture was extracted with hexane 3 times. The hexane layer was washed with $H_2O$, dried over anhydrous $Na_2SO_4$, and evaporated to yield a mixture of fatty acid methyl esters (FAMEs). The MeOH layer was neutralized with 2 N HCl/MeOH and evaporated to give a solid residue, which was purified using flash silica gel column chromatography with $CH_2Cl_2$/MeOH (16:9) to obtain monogalactosylglycerol. The optical rotation of the monogalactosylglycerol was then measured to resolve the absolute configuration of glycerol.

**Gas Chromatography−Flame Ionization Detector (GC−FID) Analysis.** GC analysis was performed using a HP 5890 series II chromatograph (Hewlett-Packard, Avondale, PA) equipped with a flame ionization detector (FID), and a SGE 30QC3/AC 20-0.5 capillary column (30 m × 0.32 mm, 0.5 $\mu$m, SGE Analytical Science, Ringwood, Australia) was used for separation. Nitrogen was used as the carrier gas at a flow rate of 1.0 mL/min. The oven temperature was held at 150 °C for 1 min, increased by 15 °C/min to 200 °C, and then increased by 2 °C/min to 250 °C. The injector temperature was set at 270 °C, and the detector temperature was 270 °C. The injection volume was 0.6 $\mu$L.

**Identification of the Molecular Species in MGDGs.** High-performance liquid chromatography−tandem mass spectrometry (HPLC−MS/MS) analysis was performed using a Waters ACQUITY liquid chromatography system (Waters Corp., Milford, MA) coupled with a diode array detector (DAD) and an Amazon SL mass spectrometer (Bruker Daltonics, Bremen, Germany). The HPLC separation used a YMC ODS Pack-A C18 column (250 × 4.6 mm inner diameter, 5 $\mu$m, Tokyo, Japan). The mobile phase was a mixture of water (A) and methanol (B) as follows: 0−40 min, 96 → 100% B; and 40−50 min, 100% B. A flow rate of 1.0 mL/min with detection at 203 nm was used. The injection volume was 10 $\mu$L, and injections were performed using the autosampler.

Electrospray ionization−quadrupole ion trap mass spectrometry (ESI−QITMS) in positive-ion mode was used. The parameters of the ESI interface were as follows: high-voltage (HV) capillary, 4500 V; HV end plate offset, −500 V; MS/MS isolation width, 4.0 units; and collision gas, helium. All skimmer collisionally activated dissociation (CAD) and MS/MS spectra represent averages of five scans. In the MS/MS experiment, the data-dependent MS/MS scan mode was used. The scan mass range was $m/z$ 100−1000.

**Preparation of Major MGDG Molecular Species.** Semi-preparative HPLC was performed on a Shimadzu LC-6AD (Tokyo, Japan) coupled to a photodiode array detector (SPD-M20A). The semi-preparative HPLC column (250 × 10 mm inner diameter, 5 $\mu$m) was prefilled with C18 (YMC ODS Pack-A, Tokyo, Japan), and a linear gradient of $H_2O$ (A) and MeOH (B) was used at a flow rate of 4.0 mL/min. The following elution program was used for separation: 0−40 min, 96 → 100% B; 40−50 min, 100% B; and 50−55 min, 100 → 96% B. The detection wavelength was 203 nm. This preparation yielded compounds **1** (3.1 mg), **3** (1.7 mg), **5** (3.4 mg), **9** (6.4 mg), and **10** (26.2 mg) as well as a mixture of compounds **7** and **8** (12.1 mg).

**Bioassay.** The inhibitory effect on lipid accumulation was assessed in 3T3-L1 adipocytes by measuring the intracellular contents of TG and FFAs. 3T3-L1 preadipocytes were cultured and induced to differentiate into adipocytes as previously described.[18−20] Briefly, confluent 3T3-L1 preadipocytes after 1 day were treated with 1 $\mu$mol/L dexamethasone, 0.5 mmol/L 3-isobutyl-methylxanthine, and 10 $\mu$g/mL (270 munits/mL) insulin for 3 days in high-glucose DMEM containing 10% FBS. At the same time, cells of compound-treated groups were treated with 10 $\mu$M MGDGs **1**, **3**, **5**, **7** + **8**, **9**, or **10** dissolved in DMSO (final DMSO concentration of 0.5%, v/v), respectively. While for the control group, cells were cultured without compounds. Cells were then switched to 10% FBS/DMEM containing only 5 $\mu$g/mL (135 munits/mL) insulin for 3 more days and then switched to 10% FBS/DMEM without insulin. In a normal group, cells were cultured without induction medium or any compounds.

At 14 days after induction of differentiation, 3T3-L1 cells in 48-well plates were lysed and analyzed using the TG kit and the NEFA-C kit according to the protocols provided by the manufacturers. The TG and NEFA values were corrected by their protein content.

**Statistical Analysis.** Values are expressed as the mean ± standard deviation (SD). Statistical analysis was performed with SPSS 11.0. Significant differences between means were evaluated by one-way analysis of variance (ANOVA), and Tukey's studentized range test was used for post-hoc evaluations. $p < 0.05$ was considered to indicate statistical significance.

## RESULTS

**Isolation and Structure Elucidation of MGDGs.** The EtOAc extract of *S. horneri* was chromatographed repeatedly over silica gel and Sephadex LH-20 to obtain a mixture of MGDGs as white powder (Figure 1). The $^1$H NMR spectrum

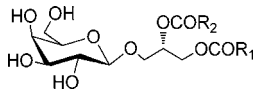


**Figure 1.** Structure of MGDGs.

showed the following characteristic signal pattern because of glycoglycerolipid: a triplet at $\delta_H$ 0.87 (6H, t, $J$ = 7.0 Hz, terminal methyl in fatty acyl), a broad signal centered at $\delta_H$ 1.27 (methylene in the fatty acyl), a mass of signals between $\delta_H$ 3.5 and 5.3 (12H, sugar and glycerol moiety), and a doublet signal at $\delta_H$ 4.26 (1H, d, $J$ = 7.6 Hz, anomeric proton). The $^{13}$C NMR spectrum revealed one anomeric carbon at $\delta_C$ 104.2 and two carbonyl carbons at $\delta_C$ 174.0 and 173.6. The spectrum was identified as MGDGs by comparison of the NMR spectra to previously reported data.[14] To determine the absolute configuration of C-2 in the glycerol moiety, an alkaline hydrolysis experiment was performed. The monogalactosylglycerol from the MeOH layer was identified as (2*R*)-1-*O*-*β*-D-galactopyranosylglycerol with $[\alpha]_D^{25}$ 7.7° (*c* 0.8, $H_2O$) (9.0°,[15] 10.1°,[16] or 7.9°[21]). The optical rotation of (2*S*)-1-*O*-*β*-D-galactopyranosylglycerol was reported to be +6.2°.[17]

The composition of fatty acids was identified through GC–FID analysis for FAMEs, which was derived from an alkaline hydrolysis experiment. The following composition was identified: a mixture of myristate (14:0), palmitate (16:0), palmitoleate [16:1(*ω*-7)], oleate [18:1(*ω*-9)], linoleate [18:2(*ω*-6)], and linolenate [18:3(*ω*-3)] in the ratio of 21.1:29.3:8.0:9.4:12.5:19.6.

**Identification of the MGDG Molecular Species.** The composition of molecular species of MGDGs in *S. horneri* was clarified through HPLC–MS/MS. A total of 10 MGDGs were found under the optimized HPLC condition (Figure 2), and their identities are shown in Table 1 (MS/MS spectrum; see the Supporting Information). The molecular weight of each MGDG was determined by $[M + Na]^+$ and $[M + NH_4]^+$ ions in positive ESI–MS. In the following MS/MS, the precursor $[M + NH_4]^+$ ions produced fragment ions, namely, $[M + H - 180]^+$ and $[M + H - 162]^+$, because of the loss of a galactosyl moiety, and the precursor also produced $[R_xCO + 74]^+$ ions because of the loss of the neutral fatty acid. In addition, the precursor $[M + Na]^+$ ions yielded a pair of abundant fragment ions, namely, $[M + Na-R_xCOOH]^+$, which were derived from the neutral loss of free fatty acid from the *sn*-1 ($x$ = 1) or *sn*-2 ($x$ = 2) position. These two ions were easy to distinguish in MS/MS spectra because of their high peak intensity. Most importantly, the peak intensity of $[M + Na-R_1COOH]^+$ was always greater than that of $[M + Na-R_2COOH]^+$,[22−24] which was used to determine the fatty acyl attachments in each MGDG.

For example, MGDG **10** (Figure 3) had a molecular formula of $C_{43}H_{80}O_{10}$ and was assigned on the basis of $m/z$ 779 (100%, $[M + Na]^+$) and 774 (35%, $[M + NH_4]^+$) as well as relevant ions $m/z$ 595 (11%, $[M + H - 162]^+$) and 577 (19%, $[M + H - 180]^+$). The base peak at $m/z$ 523 (100%, $[M + Na-R_1COOH]^+$) and the minor peak at $m/z$ 497 (37%, $[M + Na-R_2COOH]^+$) in the MS/MS spectra indicated that hexadecanoyl (palmityl, 16:0) was linked to the *sn*-1 position and that octadecadienoyl (18:1) was linked to the *sn*-2 position. In combination with the GC analysis results, the 18:1 fatty acyl was determined as oleoyl [18:1(*ω*-9)].

On the basis of the above findings, 10 molecular species of MGDGs were identified (Figure 1 and Table 1).

**Preparation of Major MGDG Molecular Species.** The major MGDGs (**1**, **3**, **5**, **9**, and **10** as well as a mixture of **7** and **8**) were subsequently obtained using semi-preparative HPLC. This study was the first report on the MGDG molecular species **3**, **5**, **9** and **10** isolated from *S. horneri*.

**Effect of MGDG Molecular Species on TG and FFA Levels in Mature 3T3-L1 Adipocytes.** 3T3-L1 preadipocytes were treated with compounds **1**, **3**, **5**, **9**, and **10** as well as the mixture of compounds **7** and **8** at a concentration of 10 $\mu$M.

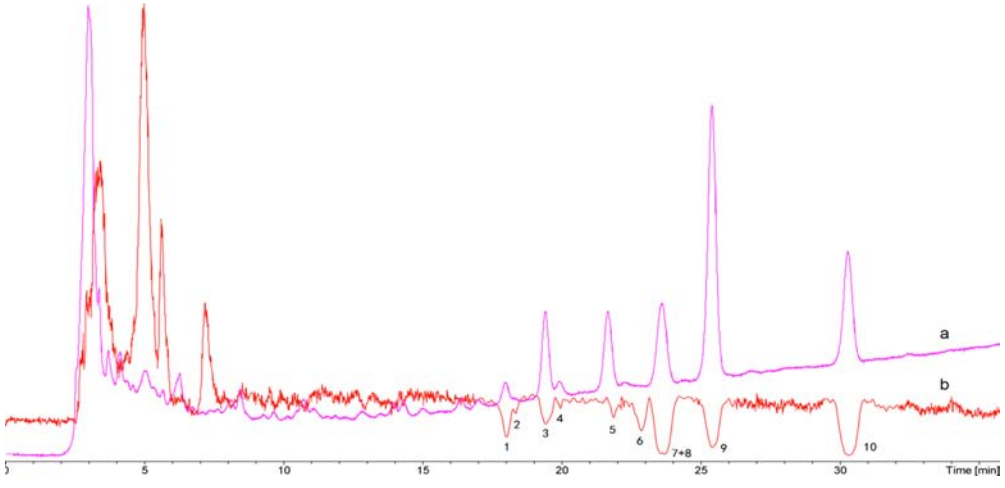


**Figure 2.** HPLC–MS analysis of MGDGs from *S. horneri*: (a) high-performance liquid chromatography–diode array detection (HPLC–DAD) chromatogram at 203 nm and (b) total ion chromatogram (TIC).

**Table 1. HPLC−MS/MS Analysis of MGDGs 1−10**

| MGDG | *sn*-1/*sn*-2 | molecular formula | molecular weight | MS data $[M + Na]^+$ | MS/MS data $[M + Na-RCOOH]^+$ | retention time (min) |
|---|---|---|---|---|---|---|
| **1**[a] | 14:0/16:1 | $C_{39}H_{72}O_{10}$ | 700 | 723 (100) | 495 (100), 469 (38) | 17.9 |
| **2** | 16:0/14:1 | $C_{39}H_{72}O_{10}$ | 700 | 723 (100) | 467 (100), 497 (41) | 18.4 |
| **3**[a] | 14:0/18:2 | $C_{41}H_{74}O_{10}$ | 726 | 749 (100) | 521 (100), 469 (42) | 19.5 |
| **4** | 16:0/16:2 | $C_{41}H_{74}O_{10}$ | 726 | 749 (100) | 493 (100), 497 (39) | 20.0 |
| **5**[a] | 16:0/18:3 | $C_{43}H_{76}O_{10}$ | 752 | 775 (100) | 519 (100), 497 (40) | 21.4 |
| **6** | 14:0/16:0 | $C_{39}H_{74}O_{10}$ | 702 | 725 (100) | 497 (100), 469 (52) | 22.8 |
| **7**[a,b] | 14:0/18:1 | $C_{41}H_{76}O_{10}$ | 728 | 751 (100) | 523 (100), 469 (41) | 23.3 |
| **8**[a,b] | 16:0/16:1 | $C_{41}H_{76}O_{10}$ | 728 | 751 (100) | 495 (100), 497 (32) | 23.9 |
| **9**[a] | 16:0/18:2 | $C_{43}H_{78}O_{10}$ | 754 | 777 (100) | 521 (100), 497 (42) | 25.4 |
| **10**[a] | 16:0/18:1 | $C_{43}H_{80}O_{10}$ | 756 | 779 (100) | 523 (100), 497 (36) | 30.5 |

[a]Obtained using semi-preparative HPLC. [b]Obtained as a mixture of compounds **7** and **8**.

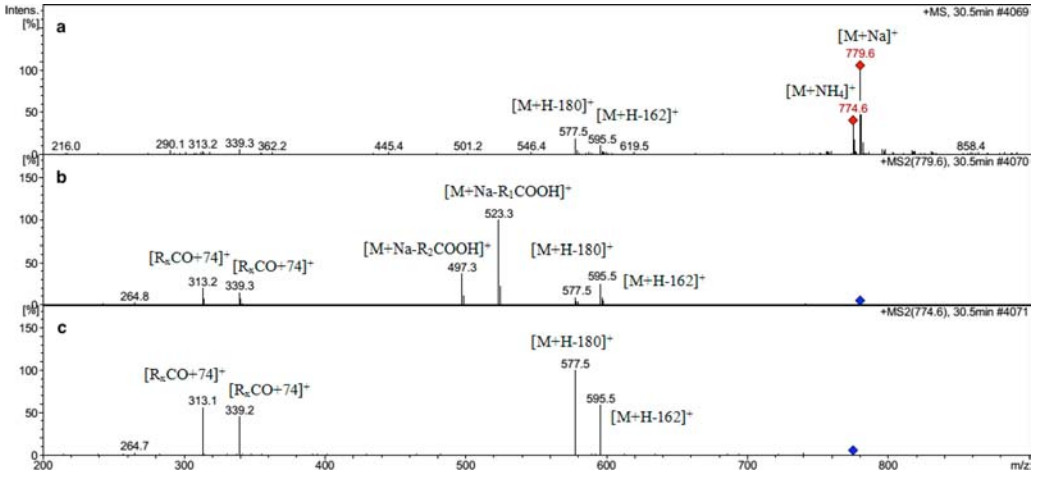


**Figure 3.** (a) Full-scan LC/ESI−MS spectrum of MGDG **10** in positive-ion mode, (b) $MS^2$ spectrum of the trapped $[M + Na]^+$ ion at *m/z* 779, and (c) $MS^2$ spectrum of the trapped $[M + NH_4]^+$ ion at *m/z* 774.

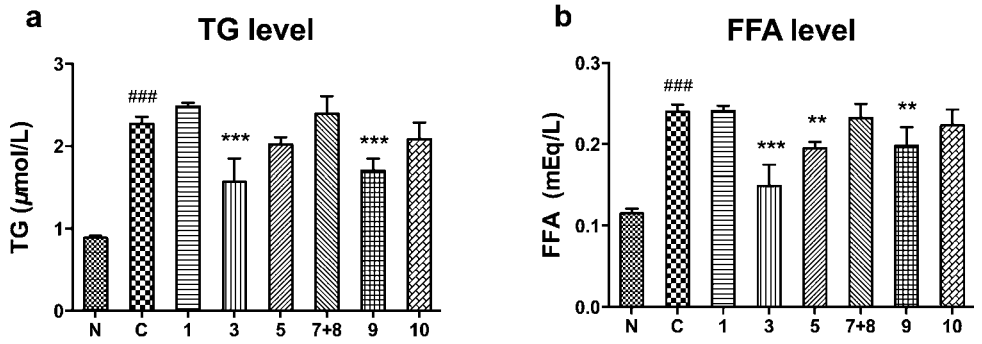


**Figure 4.** Effects of MGDGs on TG and FFA levels in 3T3-L1 adipocytes. The following groups were analyzed: N, normal groups, cells were cultured without induction medium or any samples; C, control groups, cells were cultured with induction medium for 14 days; compound-treated groups, cells were cultured with induction medium and treated with 10 μM MGDGs **1**, **3**, **5**, **7** + **8**, **9**, and **10** for 14 days. At 14 days after induction of differentiation, the cells were lysed using an Omni Ruptor and analyzed using the TG and NEFA kits according to the protocols provided by the manufacturers. Data represent the means ± SD of six determinations. (###) $p < 0.001$ versus the normal group. (**) $p < 0.01$ and (***) $p < 0.001$ versus the control group.

At this concentration, there were no treatment-related changes in cell viability [3-(4,5-dimethylthiazol-2-yl)-2,5-diphenyltetrazolium bromide (MTT) method; data not shown].

In comparison to untreated cells (Figure 4), compounds **3** [*sn*-1/*sn*-2 14:0/18:2(ω-6)] and **9** [*sn*-1/*sn*-2 16:0/18:2(ω-6)] significantly suppressed the accumulation of TGs in mature 3T3-L1 cells with TG levels of 1.568 ± 0.2808 and 1.701 ± 0.1460 μmol/L, respectively. In contrast, compounds **1** [*sn*-1/*sn*-2 14:0/16:1(ω-7)], **7** [*sn*-1/*sn*-2 14:0/18:1(ω-9)] and **8** [*sn*-1/*sn*-2 16:0/16:1(ω-7)], and **10** [*sn*-1/*sn*-2 16:0/18:1(ω-9)] did not effectively suppress the accumulation of TG levels, with TG levels of 2.484 ± 0.0460, 2.395 ± 0.2148, and 2.084 ± 0.2015 μmol/L, respectively (Figure 4a). The FFA content in mature 3T3-L1 cells was also determined. Compounds **3**, **5**, and **9** showed inhibitory effects on FFA accumulation, with FFA levels of 0.149 ± 0.0258, 0.195 ± 0.0079, and 0.198 ± 0.0229 mequiv/L, respectively (Figure 4b). As a result, the pattern of inhibitory effects on FFA levels was similar to that on TG accumulation. These results indicated that some MGDG molecular species from *S. horneri* reduced the TG and FFA

levels in lipid metabolism, and these results also indicated that linoleyl [18:2(ω-6)] at the *sn*-2 position was an essential group for these activities.

## DISCUSSION

The present study showed that palmitic acid (16:0) was the most abundant fatty acid (FA) in the MGDGs of *S. horneri*. This result agreed with Terasaki et al.[25] and Airanthi et al.,[26] who reported that 16:0 is the major FA in the total lipids of the same species. The major unsaturated fatty acids (UFAs) found in our study were $C_{18}$ UFAs [including 18:3(ω-3), 18:2(ω-6), and 18:1(ω-9)], which differed from the study by Hossain et al.,[27] who reported that $C_{20}$ UFAs are the major UFAs in this species. The FA composition is influenced by species[28,29] and environmental factors.[29−31] Seasonal variation is an important factor for the difference in polyunsaturated fatty acid (PUFA) species. Sanina et al.[30] reported that partial substitution of $C_{20}$ by $C_{18}$ PUFAs in glycolipids occurs from summer to winter in marine macrophytes. Our results supported this view because the seaweed used in the present study was collected in October, but $C_{20}$ UFAs were not detected. This result was due to the extraction and isolation process, which is often used for studies on chemical constituents of traditional Chinese medicine (TCM). Procedures using classic lipid extraction methods[32,33] as well as anti-enzyme and antioxidant measures should be used in future studies.

MGDGs identified in the present study contained mainly $C_{14}$ and $C_{16}$ saturated FAs at the *sn*-1 position as well as $C_{18}$ and $C_{16}$ unsaturated FAs at the *sn*-2 position of the glycerol backbone. The eukaryotic pathway consists of two reactions involving glycoglycerolipid synthetase in the plastid and endoplasmic reticulum (ER). The synthetase in the plastid mainly generates glycoglycerolipids containing 16 carbon atoms at the *sn*-2 position, and the synthetase in the ER generates glycoglycerolipids containing 18 carbon atoms at the *sn*-2 position.[34,35] Our data suggested that the glycoglycerolipid synthetase in *S. horneri* exists in both the plastid and ER.

Compounds **3** and **9** with linoleyl [18:2(ω-6)] at the *sn*-2 position of the glycerol backbone showed stronger inhibitory effects on TG and FFA accumulation than the other compounds. Saturated fatty acyl (14:0 and 16:0) at the *sn*-1 position contributed to the inhibitory effect. As a well-known essential fatty acid, linoleic acid [18:2(ω-6)] functions as a precursor of arachidonic acid [20:4(ω-6)] and a series of pro-inflammatory eicosanoids. Linoleic acid can regulate low-density lipoprotein cholesterol (LDL-C) metabolism by downregulating LDL-C production and enhancing its clearance.[36] Studies have demonstrated that linoleic acid also suppresses sterol regulatory element-binding protein 1c (SREBP-1c) expression[37] and activates peroxisome proliferator-activated receptor (PPAR) α and γ,[38,39] thus leading to lipid degradation.

Metabolic disorders, such as obesity, type-2 diabetes, and metabolic syndrome, can occur when TG and FFA accumulate in adipocytes.[19] Our results introduced a new chemical structure type of MGDGs with linoleyl in the *sn*-2 position that can reduce the levels of TG and FFA in adipocytes, which might be beneficial for lipid metabolism improvement. Because lipid metabolism disorders are an important risk factor of CVDs, our findings also indicated that MGDGs in *S. horneri* might be important effective components associated with the anti-CVD function of this edible seaweed.

## ASSOCIATED CONTENT

### Supporting Information

MS data of MGDGs **1**−**10**. This material is available free of charge via the Internet at http://pubs.acs.org.

## AUTHOR INFORMATION


### Corresponding Author

*Telephone: +86-532-82031823. Fax: +86-532-82033054. E-mail: liuhongb@ouc.edu.cn.

### Author Contributions

†Ai-Cui Ma and Zhen Chen contributed equally to this work.



### Funding

Financial support by the National Natural Science Foundation of China (NSFC, 31271845) to Hong-Bing Liu is gratefully acknowledged.

### Notes

The authors declare no competing financial interest.

## ACKNOWLEDGMENTS

The authors thank Prof. Yuan-hong Wang (Laboratory of Chemical Analysis, Ocean University of China) for providing standards and assisting in FAME identification.


## ABBREVIATIONS USED

MGDG, monogalactosyldiacylglycerol; DGDG, digalactosyldiacylglycerol; SQDG, sulfoquinovosyldiacylglycerol; TG, triglyceride; FFA, free fatty acid; FA, fatty acid; FAME, fatty acid methyl ester; CVD, cardiovascular disease; DMEM, Dulbecco's modified Eagle's medium; TCM, traditional Chinese medicine; ER, endoplasmic reticulum; LDL-C, low-density lipoprotein cholesterol; SREBP-1c, sterol regulatory element-binding protein 1c; PPAR, peroxisome proliferator-activated receptor

## REFERENCES


(1) Zeng, C. K.; Lu, B. R. *Flora Algarum Marinarum Sinicarum, Tomus 3: Phaeophyta (No. 2) Fucales*; Science Press: Beijing, China, 2000.

(2) Zeng, Q. K. *Zhong Guo Jing Ji Hai Zao Zhi*; Science Press: Beijing, China, 1962.

(3) Guan, H. S.; Wang, S. G. *Chinese Marine Materia Medica*, 1st ed.; Shanghai Scientific and Technical Publishers, China Ocean Press, and Chemical Industry Press: Shanghai and Beijing, China, 2009.

(4) Chen, Z.; Liu, H. B. Research progress in chemical components and biological activity of *Sargassum*. *Chin. J. Mar. Drugs* **2012**, *31*, 41−51.

(5) Ermakova, S.; Sokolova, R.; Kim, S. M.; Um, B. H.; Isakov, V.; Zvyagintseva, T. Fucoidans from brown seaweeds *Sargassum hornery*, *Eclonia cava*, *Costaria costata*: Structural characteristics and anticancer activity. *Appl. Biochem. Biotechnol.* **2011**, *164*, 841−850.

(6) Liu, Q. Y.; Meng, Q. Y.; Liu, Z. H. Extraction and measurement of two kinds of seaweed polysaccharides and their antitumor effect *in vitro*. *Guangdong Yaoxueyuan Xuebao* **2003**, *19*, 336−337.

(7) Nakazawa, S.; Abe, F.; Kuroda, H.; Kohno, K.; Higashi, T.; Umezaki, I. Antitumor effect of water extracts from marine algae (II). *Sargassum horneri* (Turner) C. Agardh. *Chemotherapy* **1976**, *24*, 443−447.

(8) Preeprame, S.; Hayashi, K.; Lee, J. B.; Sankawa, U.; Hayashi, T. A novel antivirally active fucan sulfate derived from an edible brown alga, *Sargassum horneri*. *Chem. Pharm. Bull.* **2001**, *49*, 484−485.

(9) Athukorala, Y.; Jung, W. K.; Vasanthan, T.; Jeon, Y. J. Ananticoagulative polysaccharide from an enzymatic hydrolysate of *Ecklonia cava*. *Carbohydr. Polym.* **2006**, *66*, 184−191.

(10) Kim, Y. A.; Kong, C. S.; Um, Y. R.; Lee, J. I.; Nam, T. J.; Seo, Y. Antioxidant efficacy of extracts from a variety of seaweeds in a cellular system. *Ocean Sci. J.* **2008**, *43*, 31−37.
(11) Uchiyama, S.; Yamaguchi, M. Anabolic effect of marine alga *Sargassum horneri* extract on bone components in the femoral-diaphyseal and -metaphyseal tissues of young and aged rats *in vivo*. *J. Health Sci.* **2002**, *48*, 325−330.
(12) Uchiyama, S.; Yamaguchi, M. Inhibitory effect of marine alga *Sargassum horneri* extract on bone resorption in tissue culture *in vitro*. *J. Health Sci.* **2002**, *48*, 154−160.
(13) Yunoki, K.; Sato, M.; Seki, K.; Ohkubo, T.; Tanaka, Y.; Ohnishi, M. Simultaneous quantification of plant glyceroglycolipids including sulfoquinovosyldiacylglycerol by HPLC−ELSD with binary gradient elution. *Lipids* **2009**, *44*, 77−83.
(14) Sakano, Y.; Mutsuga, M.; Tanaka, R.; Suganuma, H.; Inakuma, T.; Toyoda, M.; Goda, Y.; Shibuya, M.; Ebizuka, Y. Inhibition of human lanosterol synthase by the constituents of *Colocasia esculenta* (taro). *Biol. Pharm. Bull.* **2005**, *28*, 299−304.
(15) Oshima, Y.; Yamada, S.; Matsunaga, K.; Moriya, T.; Ohizumi, Y. A monogalactosyl diacylglycerol from a cultured marine dinoflagellate, *Scrippsiella trochoidea*. *J. Nat. Prod.* **1994**, *57*, 534−536.
(16) Tang, H. F.; Yi, Y. H.; Yao, X. S. Studies on the chemical constituents from marine brown alga *Ishige okamurai* (III). *China J. Chin. Mater. Med.* **2002**, *27*, 269−273.
(17) Tuntiwachwuttikul, P.; Pootaeng-On, Y.; Phansa, P.; Taylor, W. C. Cerebrosides and a monoacylmonogalactosylglycerol from *Clinacanthus nutans*. *Chem. Pharm. Bull.* **2004**, *52*, 27−32.
(18) Zhang, Y.; Qian, Q.; Ge, D.; Li, Y.; Wang, X.; Chen, Q.; Gao, X.; Wang, T. Identification of benzophenone C-glucosides from mango tree leaves and their inhibitory effect on triglyceride accumulation in 3T3-L1 adipocytes. *J. Agric. Food Chem.* **2011**, *59*, 11526−11533.
(19) Zhang, Y.; Han, L.; Ge, D.; Liu, X.; Liu, E.; Wu, C.; Gao, X.; Wang, T. Isolation, Structural elucidation, MS profiling, and evaluation of triglyceride accumulation inhibitory effects of benzophenone C-glucosides from leaves of *Mangifera indica* L. *J. Agric. Food Chem.* **2013**, *61*, 1884−1195.
(20) Pinent, M.; Bladé, M. C.; Salvadó, M. J.; Arola, L.; Ardévol, A. Intracellular mediators of procyanidin-induced lipolysis in 3T3-L1 adipocytes. *J. Agric. Food Chem.* **2005**, *53*, 262−266.
(21) Son, B. W.; Cho, Y. J.; Kim, N. K.; Choi, H. D. New glyceroglycolipids from the brown alga *Sargassum thunbergii*. *Bull. Korean Chem. Soc.* **1992**, *13*, 584−586.
(22) Guella, G.; Frassanito, R.; Mancini, I. A new solution for an old problem: The regiochemical distribution of the acyl chains in galactolipids can be established by electrospray ionization tandem mass spectrometry. *Rapid Commun. Mass Spectrom.* **2003**, *17*, 1982−1994.
(23) Gray, C. G.; Lasiter, A. D.; Li, C.; Leblond, J. D. Mono- and digalactosyldiacylglycerol composition of dinoflagellates. I. Peridinin-containing taxa. *Eur. J. Phycol.* **2009**, *44*, 191−197.
(24) Esch, S. W.; Tamura, P.; Sparks, A. A.; Roth, M. R.; Devaiah, S. P.; Heinz, E.; Wang, X. M.; Williams, T. D.; Welti, R. Rapid characterization of the fatty acyl composition of complex lipids by collision-induced dissociation time-of-flight mass spectrometry. *J. Lipid Res.* **2007**, *48*, 235−241.
(25) Terasaki, M.; Hirose, A.; Narayan, B.; Baba, Y.; Kawagoe, C.; Yasui, H.; Saga, N.; Hosokawa, M.; Miyashita, K. Evaluation of recoverable functional lipid components of several brown seaweeds (Phaeophyta) from Japan with special reference to fucoxanthin and fucosterol contents. *J. Phycol.* **2009**, *45*, 974−980.
(26) Airanthi, M. K. W. A.; Sasaki, N.; Iwasaki, S.; Baba, N.; Abe, M.; Hosokawa, M.; Miyashita, K. Effect of brown seaweed lipids on fatty acid composition and lipid hydroperoxide levels of mouse liver. *J. Agric. Food Chem.* **2011**, *59*, 4156−4163.
(27) Hossain, Z.; Kurihara, H.; Takahashi, K. Biochemical composition and lipid compositional properties of the brown alga *Sargassum horneri*. *Pak. J. Biol. Sci.* **2003**, *6*, 1497−1500.
(28) Sanina, N. M.; Goncharova, S. N.; Kostetsky, E. Y. Fatty acid composition of individual polar lipid classes from marine macrophytes. *Phytochemistry* **2004**, *65*, 721−730.
(29) Silva, G.; Pereira, R. B.; Valentão, P.; Andrade, P. B.; Sousa, C. Distinct fatty acid profile of ten brown macroalgae. *Rev. Bras. Farmacogn.* **2013**, *23*, 608−613.
(30) Sanina, N. M.; Goncharova, S. N.; Kostetsky, E. Y. Seasonal changes of fatty acid composition and thermotropic behavior of polar lipids from marine macrophytes. *Phytochemistry* **2008**, *69*, 1517−1527.
(31) Murakami, K.; Yamaguchi, Y.; Noda, K.; Fujii, T.; Shinohara, N.; Ushirokawa, T.; Sugawa-Katayama, Y.; Katayama, M. Seasonal variation in the chemical composition of a marine brown alga, *Sargassum horneri* (Turner) C. Agardh. *J. Food Compos. Anal.* **2011**, *24*, 231−236.
(32) Bligh, E. G.; Dyer, W. J. A rapid method of total lipid extraction and purification. *Can. J. Biochem. Physiol.* **1959**, *37*, 911−917.
(33) Folch, J.; Lees, M.; Sloane-Stanley, G. A simple method for the isolation and purification of total lipides from animal tissues. *J. Biol. Chem.* **1957**, *226*, 497−509.
(34) Klaus, D.; Härtel, H.; Fitzpatrick, L. M.; Froehlich, J. E.; Hubert, J.; Benning, C.; Dörmann, P. Digalactosyldiacylglycerol synthesis in chloroplasts of the *Arabidopsis dgd1* mutant. *Plant Physiol.* **2002**, *128*, 885−895.
(35) Heinz, E.; Roughan, P. G. Similarities and differences in lipid metabolism of chloroplasts isolated from 18:3 and 16:3 plants. *Plant Physiol.* **1983**, *72*, 273−279.
(36) Wijendran, V.; Hayes, K. C. Dietary $\omega$-6 and $\omega$-3 fatty acid balance and cardiovascular health. *Annu. Rev. Nutr.* **2004**, *24*, 597−615.
(37) Yoshikawa, T.; Shimano, H.; Yahagi, N.; Ide, T.; Amemiya-Kudo, M.; Matsuzaka, T.; Nakakuki, M.; Tomita, S.; Okazaki, H.; Tamura, Y.; Iizuka, Y.; Ohashi, K.; Takahashi, A.; Sone, H.; Osuga, J.-i.; Gotoda, T.; Ishibashi, S.; Yamada, N. Polyunsaturated fatty acids suppress sterol regulatory element-binding protein 1c promoter activity by inhibition of liver X receptor (LXR) binding to LXR response elements. *J. Biol. Chem.* **2002**, *277*, 1705−1711.
(38) Issemann, I.; Prince, R. A.; Tugwood, J. D.; Green, S. The peroxisome proliferator-activated receptor: retinoid X receptor heterodimer is activated by fatty acids and fibrate hypolipidaemic drugs. *J. Mol. Endocrinol.* **1993**, *11*, 37−47.
(39) Desvergne, B.; Wahli, W. Peroxisome proliferator-activated receptors: Nuclear control of metabolism. *Endocr. Rev.* **1999**, *20*, 649−688.

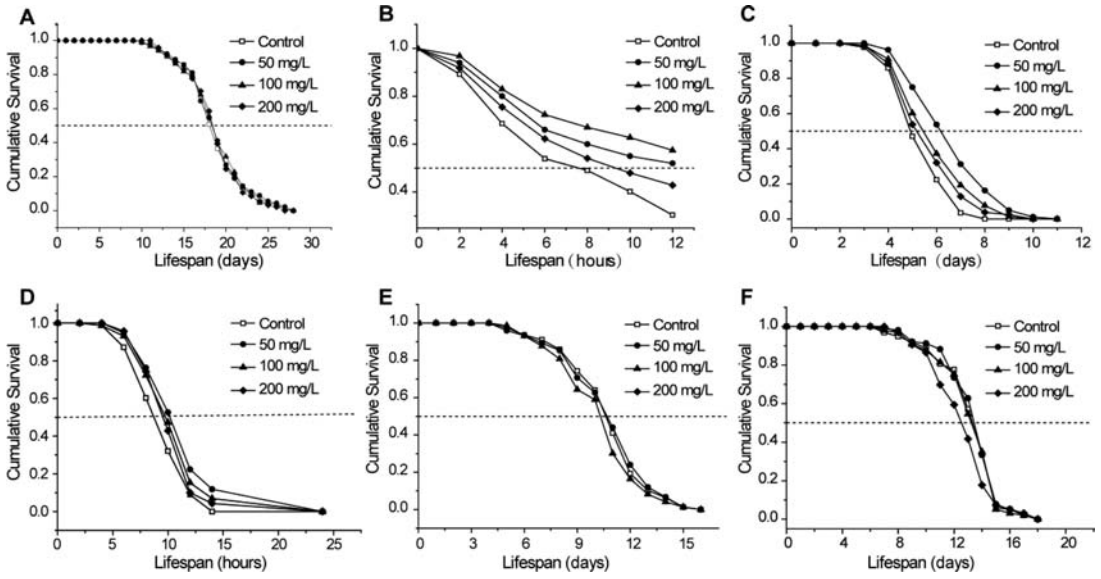


**Figure 1.** BTE treatment results in the alterations of stress response to specific environmental stimuli. (A) Effect of BTE on the lifespan of wild type N2 nematodes under normal culture conditions at 25 °C. (B) Survival of wild type N2 nematodes during 12 h of exposure in 500 mM NaCl. (C) BTE effects of UV irradiation at a dose of 2000 J/m$^2$. (D) Survival of wild type N2 nematodes at 35 °C until all worms are dead. (E) BTE-pretreatment effects on acute $MnCl_2$-induced toxicity. (F) BTE-post-treatment effects on acute $MnCl_2$-induced toxicity.

adding 0.5 L of boiling deionized water to the black tea for 30 min, and subsequently filtering through cotton wool. Each infusion was mixed and freeze-dried. BTE was stored at −20 °C and dissolved in water before use. The composition of BTE was shown in Table S1.

***Caenorhabditis elegans* strains and maintenance.** Wild type N2, TK22 (*mev-1(kn1)*), and VC199 (*sir-2.1 (ok434)*) strains were used in the experiments. The University of Minnesota *C. elegans* Genetics Center (CGC) provided all strains. Strains were maintained at 20 °C on standard nematode growth medium (NGM) with dead *E. coli* OP50 (killed by UV, 9999 J/m$^2$) (as shown in Figure S1) as food source. Age-synchronized nematodes were propagated using the sodium hypochlorite/NaOH method,[10] and cultured on Ø60 mm Petri dishes at 20 °C. All assays were performed at 25 °C unless otherwise stated, and plates in stress resistance assays contained 50 $\mu$M 5-fluoro-2′-deoxyuridine (FUDR) (Sigma-Aldrich, St. Louis, MO, USA). All tested *C. elegans* strains were assessed in triplicate, and three replicates of all trials were performed. BTE (50, 100, or 200 mg/L) was diluted into a suspension of dead *E. coli* OP50, which corresponded to the BTE concentrations we evaluated, and then added to the surface of the NGM plates to the final indicated concentrations. All lifespan and stress assays were conducted in a double-blind manner.

**Lifespan assays.** All lifespan assays were performed according to standard protocols.[11] In brief, age-synchronized wild type N2 (4 days old) nematodes were transferred to NGM plates with BTE or controls to establish the entire nematode lifespan. The number of individuals alive was counted every day, and mortality was recorded until 100% mortality was achieved. Lifespan assay of *mev-1* nematodes (5 days old) was conducted under the same culture conditions.

**Stress assays.** For stress assays, age-synchronized wild type N2 and VC199 (4 days old) nematodes were treated with BTE for 2 d, or controls in the absence of BTE; then nematodes were subsequently transferred to high-salt plates containing 500 mM NaCl (Sinopharm Chemical Reagent, CO, Shanghai, China), 35 °C, UV irradiated in a UVP CL-1000 Ultraviolet Cross-linker (Cambridge, UK) with a dose of 2000 J/m$^2$ and acutely exposed for 30 min to 35 mM manganese chloride ($MnCl_2$) (Sinopharm Chemical Reagent, CO. Shanghai, China), which corresponded to LD25 for $MnCl_2$.[12] The mortality rate was determined by recording the number of dead nematodes over a 1 or 2 h period in heat shock and osmotic stress assays. The survival rate was scored for 1 or 2 h until the controls reached approximately 50% mortality, and once per day in UV and $MnCl_2$ stress assays by touch-provoked movement; animals that failed to respond were considered dead.

The acute $MnCl_2$ treatments assay was also conducted as below; age-synchronized N2 (4 days old) nematodes were acutely exposed for 30 min at 25 °C to 35 mM $MnCl_2$.[12] Then the nematodes were subsequently washed and placed on the control or BTE plates.

**Measurement of reactive oxygen species.** Intracellular reactive oxygen species (ROS) in *C. elegans* were determined by dichloro-fluorescin diacetate (DCF-DA). Nematodes were collected and lysed in 48 h of treatment. Samples were analyzed immediately after lysis. The analysis was performed according to a commercially available kit (Beyotime Institute of Biotechnology, China) as previously described.[13−15] Samples were read every 20 min for 2 h at excitation 488 nm and emission 525 nm.

**Activities of superoxide dismutase (SOD), catalase (CAT), and glutathione peroxidase (GSH-PX).** SOD, CAT, and GSH-PX activities were measured spectrophotometrically using commercially available kits (Nanjing Jiancheng Bioengineering Institute, China) according to the manufacturer's instructions, respectively. The protein contents were determined by a commercially BCA kit (Auragene, China).

**Quantitative RT-PCR.** Total RNA was isolated using Trizol (Invitrogen, USA), and cDNA was synthesized using a cDNA synthesis kit (Takara, Dalian, China). qRT-PCR was carried out using SYBR Premix Ex Taq (Takara, Japan) and the Rotor Gene Q (Qiagen, Germany). qRT-PCR was performed for *sod-3*, *daf-16*, *sir-2.1*, *osr-1*, *skn-1*, *hsf-1*, and *sek-1* and normalization of transcript quantity was carried out using the *actin* genes. Samples were run in triplicate ($n$ = 3), and the primers were shown in Table S2.

**Statistical analyses.** Data were expressed as means ± SD (standard deviation). Lifespan assays were processed using the Kaplan-Meir test, and the log rank test was applied to determine significant differences among group scored data using SPSS 18.0 (Demo version, Armonk, NY). One-way Analysis of Variance (ANOVA), followed by $t$-tests, was used to ascertain significant differences between the controls and BTE treated groups in the Origin 8.0 software (Demo version, Northampton, MA). Differences were considered significant at the $P \leq 0.05$ level.

## RESULTS

### BTE increased resistance of the wild type N2 to high osmotic stress, severe heat shock, and UV irradiation,

**but did not affect lifespan and attenuated $MnCl_2$-induced toxicity.** BTE did not affect the worm lifespan. Compared with the control (the mean lifespan (ML) = 18.7 d, $N$ = 85), the BTE-treatment groups at 50 mg/L (ML = 18.9 d, $N$ = 90), 100 mg/L (ML = 18.8 d, $N$ = 88), and 200 mg/L (ML = 18.8 d, $N$ = 94) showed no effects in the worms' mean lifespan (Figure 1A).

BTE protected N2 nematodes against high NaCl toxicity compared to untreated controls (Figure 1B). Following 12 h of exposure to 500 mM NaCl, the surviving control population reduced to 30.4% ($N$ = 102) of the initial study population; however, 52.0% (50 mg/L, $N$ = 100), 57.4% (100 mg/L, $N$ = 94), and 42.9% (200 mg/L, $N$ = 98) of the initial BTE treated nematode population survived ($P < 0.01$).

N2 nematodes were incubated in BTE under UV irradiation, and the mean lifespan was 6.7 d (50 mg/L, $P < 0.01$, $N$ = 80), 6.2 d (100 mg/L, $P < 0.01$, $N$ = 78), and 6.0 d (200 mg/L, $P$ = 0.05, $N$ = 78) instead of 5.6 days in the control group ($N$ = 85), which represented a significant resistance and reparation (Figure 1C). The nematode lifespan was significantly extended by 21.6%, 10.7%, and 7.1%.

Results showed BTE increased survival rates of *C. elegans* exposed to thermal stress (Figure 1D). The data showed that the mean lifespan pretreated with BTE was 12.1 h (50 mg/L, $P < 0.01$, $N$ = 77), 11.2 h (100 mg/L, $P$ = 0.01, $N$ = 72), and 10.8 h (200 mg/L, $P < 0.05$, $N$ = 70) instead of 9.7 h in the control group ($N$ = 78), indicating enhanced capacity to tolerate heat shock, resulting in increased survival rate based on BTE.

BTE pretreatment did not increase lifespan under $MnCl_2$ stress. The mean lifespan was 10.9 d (50 mg/L, $N$ = 75), 10.4 d (100 mg/L, $N$ = 73), 10.5 d (200 mg/L, $N$ = 79), and 10.8 d (control, $N$ = 78) (Figure 1E). Also, BTE post-treatment at 50 and 100 mg/L did not decrease mortality induced by $MnCl_2$. The mean lifespan under $MnCl_2$ conditions was 13.5 d (50 mg/L, $N$ = 102) and 13.2 d (100 mg/L, $N$ = 97). While the higher BTE concentration significantly accelerated their nematode mortality, with a mean lifespan of 12.8 d (200 mg/L, $P < 0.05$, $N$ = 95). The control group mean lifespan was 13.3 d ($N$ = 98) (Figure 1F).

**BTE diminished ROS levels dependent on concentration in *C. elegans*.** Dose-dependent attenuation of ROS levels in the wild type nematodes fed with BTE is shown in Figure 2. Significant differences were observed for BTE treatments compared with control (50 mg/L, $p < 0.01$; 100 mg/L, $P < 0.001$ and 200 mg/L, $P < 0.001$ at 100 min).

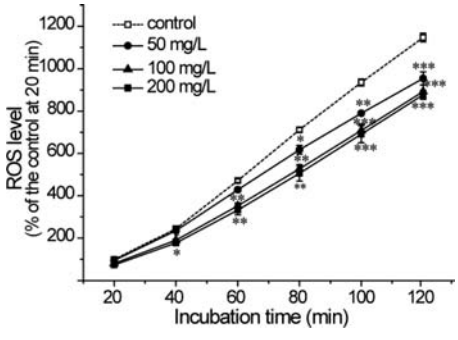


**Figure 2.** BTE decreased ROS accumulation in *C. elegans* under normal culture conditions, detected in a 120 min course. *$P < 0.05$; **$P < 0.01$; ***$P < 0.001$.

**BTE increased GSH-PX activity but not CAT and SOD activity.** The activities of various antioxidant enzymes were analyzed in control and pretreated batches of *C. elegans*. Our results showed that with increasing concentration of BTE (50 mg/L, 100 mg/L, or 200 mg/L), as shown in Figure 3, GSH-PX activity was significantly increased by 55.9% ($P < 0.05$), 98.7% ($P < 0.01$), and 87.3% ($P < 0.01$) (Figure 3A). Interestingly, CAT activity was significantly decreased by 30.0% ($P < 0.05$), 80.4% ($P < 0.01$), and 75.1% ($P < 0.01$) (Figure 3B). In addition, the BTE pretreatment did not induce the activity of SOD compared to the control (Figure 3C).

**BTE up-regulated the mRNA levels of stress-responsive genes.** We first measured changes of the mRNA levels of several stress-responsive transcription factors, including *daf-16*, *hsf-1*, and *skn-1*. BTE did not affect the three genes expression compared with controls. Then, we tested some other regulators of lifespan and stress markers, such as *sir-2.1*, *sod-3*, and *gsh-px*. The expressions of *sir-2.1* were enhanced by 2.19- (50 mg/L), 2.35- (100 mg/L), and 2.69-fold (200 mg/L) (both $P < 0.001$). The *sod-3* expression was up-regulated 2.14- (50 mg/L) ($P < 0.001$) and 1.87-fold (100 mg/L) ($P < 0.01$). The *gsh-px* expression was up-regulated 1.57- (50 mg/L) ($P < 0.01$) and 1.87-fold (100 mg/L) ($P < 0.001$). 200 mg/L BTE did not significantly regulate the *sod-3* and *gsh-px* expression (Figure 4).

Osmotic stress might have independent pathways to other stress in *C. elegans*.[9] So we measured the mRNA levels of *osr-1* and *sek-1* in the osmotic stress response pathway.[16,17] Our results indicated that BTE up-regulated *sek-1* expression by 2.36- (50 mg/L) ($P < 0.001$), 2.20- (100 mg/L) ($P < 0.001$), and 1.57-fold (200 mg/L) ($P < 0.01$). However, BTE did not affect the expression of *osr-1* (Figure 4).

**BTE slightly reduced internal oxidative stress and increased mean lifespan in mev-1 mutant under normal culture conditions without significance.** The BTE treated group survival rate showed a slightly increased trend without significant extent in the hypersensitive mutant *mev-1* at 25 °C compared to the control, demonstrating the following increased mean lifespan due to BTE treatment: 13.6 d (control), 14.0 d (50 mg/L), 14.4 d (100 mg/L), and 14.5 d (200 mg/L) (Figure 5).

**BTE did not affect the survival rate of the sir-2.1 mutant under heat and UV stress, but increased the survival rate under osmotic stress.** BTE protected *sir-2.1* mutants against 500 mM NaCl stress compared to controls (Figure 6A). Following 12 h of exposure to high NaCl, the surviving control population was reduced to 30.7% ($N$ = 114) of the initial study population; however, 42.7% (50 mg/L, $N$ = 110), 52.4% (100 mg/L, $N$ = 103), and 44.2% (200 mg/L, $N$ = 104) of the initial BTE treated nematode population survived ($P < 0.01$).

BTE pretreatment did not increase lifespan under UV and heat stress. The mean lifespan was 5.6 d (50 mg/L, $N$ = 87), 5.7 d (100 mg/L, $N$ = 85), 5.5 d (200 mg/L, $N$ = 71), and 5.6 d (control, $N$ = 96) under UV stress (Figure 6B). The mean lifespan was 9.9 h (50 mg/L, $N$ = 84), 9.8 h (100 mg/L, $N$ = 90), 9.7 h (200 mg/L, $N$ = 79), and 9.6 h (control, $N$ = 84) under heat stress (Figure 6C).

## DISCUSSION

In the present study, we observed that BTE increased *C. elegans* survival during high NaCl, UV, and acute heat stress. However, BTE had no effects on lifespan-extension under normal culture

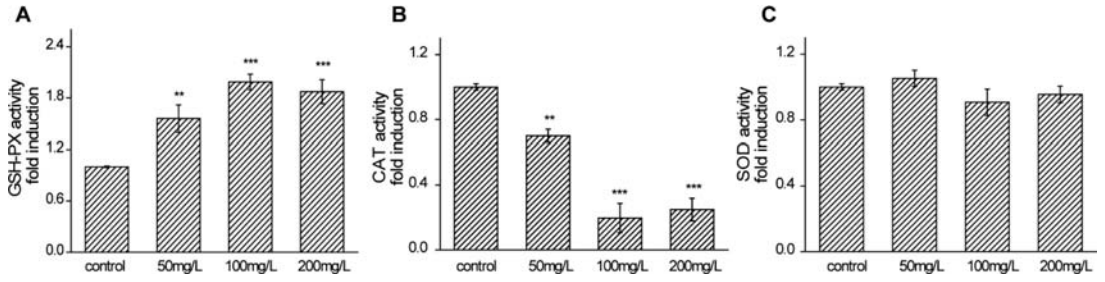


**Figure 3.** Effects of BTE treatment on the activities of GSH-PX (A), CAT (B), and SOD (C) in wild type N2 nematodes. *$P < 0.05$; **$P < 0.01$; ***$P < 0.001$.

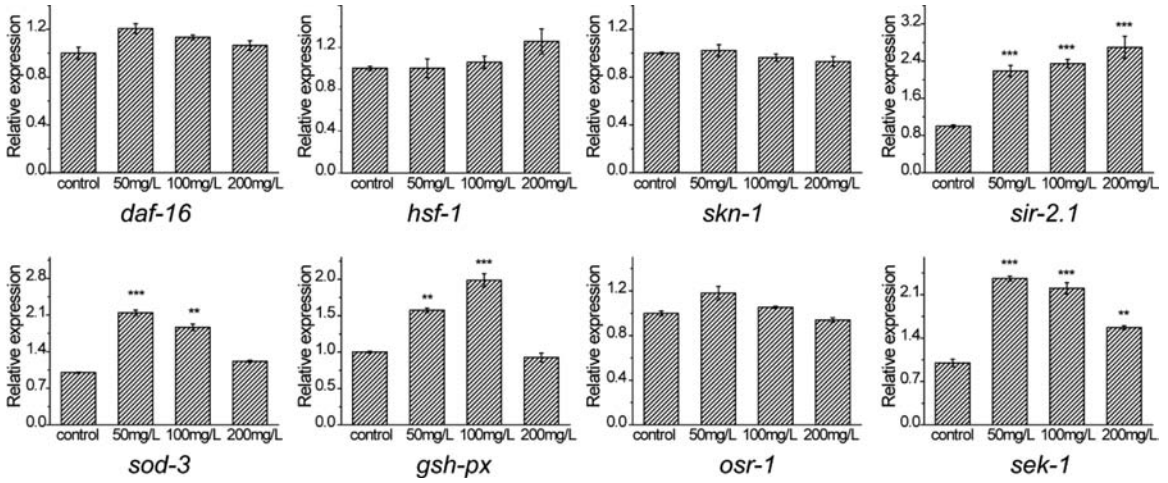


**Figure 4.** Relative mRNA level of *daf-16*, *hsf-1*, *skn-1*, *sir-2.1*, *sod-3*, *gsh-px*, *osr-1*, and *sek-1* after 48 h of BTE treatment. *$P < 0.05$; **$P < 0.01$; ***$P < 0.001$.

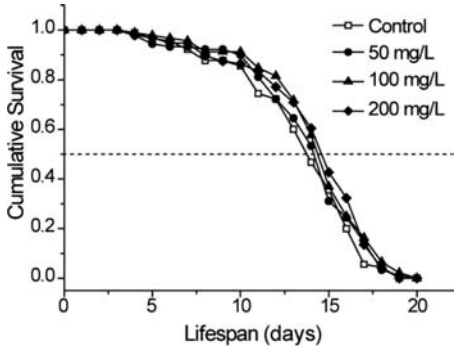


**Figure 5.** Effects of BTE on mutant *C. elegans* strain *mev-1* lifespan.

conditions and prolonging nematode survival from $MnCl_2$ treatment at the concentrations we used. These results suggest that BTE treatment selectively enhances nematodes' resistance to environmental stresses, which notably broadens our knowledge of the biological effects of black tea. The results of this study showed *C. elegans* treated with BTE were resistant to some stressors; therefore, it is conceivable that BTE elicited the response of the stress resistant system.

Multiple studies have demonstrated that polyphenol-rich botanical extracts have been shown to have differential stress resistance in nematodes.[17−20] Blueberry extract increases thermotolerance but is not protective against paraquat-induced oxidative stress.[17] Cranberry extract containing abundant flavonoids promotes survival of *C. elegans* to heat shock and does not improve nematodes' resistance to oxidative stress or

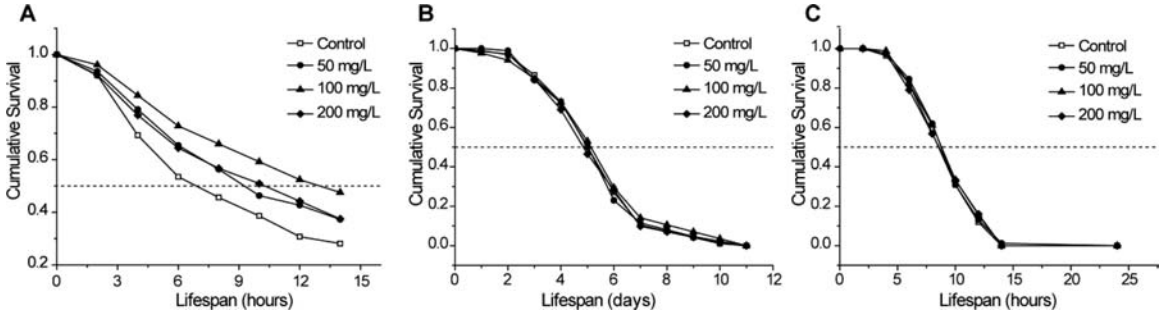


**Figure 6.** Effects of BTE on *sir-2.1* mutants under stress resistance. (A) Survival of VC199 worms during 12 h of exposure in 500 mM NaCl. (B) BTE effects on VC199 worms under UV irradiation at 2000 J/m$^2$. (C) Survival of VC199 worms at 35 °C.

UV irradiation and even renders them more sensitive to osmotic stresses of *C. elegans*.[20] Similarly, BTE contains a high number of polyphenols, which might be one of the most important contributors to the stress resistance of *C. elegans*. Black tea polyphenol has been shown to promote longevity and stress resistance in Drosophila,[6] and a large number of polyphenols in tea have demonstrated beneficial effects to *C. elegans*.[13−15,21−25] In addition, BTE contains a high level of caffeine, which is the main component (Table S1). Caffeine extends lifespan, improves healthspan, and delays age-associated pathology in *C. elegans* up to 97.1 mg/L (500 $\mu$M),[26] which is a relatively high bioactive concentration compared to polyphenols. However, postirradiation exposure to 19.4−1942 mg/L (0.1−10 mM) of caffeine did not create a modifying effect in *C. elegans*.[27] Moreover, the other phytochemicals in black tea may contribute to increased ability of *C. elegans* to stress resistance, such as theanine,[28] organic acids, and metals. A number of experiments have shown that different phytochemicals may interact and synergize to exert their biological functions.[29] Considering complex bioactive constituents, BTE-induced stress resistance may be due to the synergistic effects generated by the interaction of unique black tea phytochemicals.

We further observed that despite the fact that BTE could protect *C. elegans* against stress challenge, concentration is an important factor. Our findings indicated that BTE increased survival in a negative dose-dependent manner under heat and UV stress. The most effective concentration was 100 mg/L under osmotic stress. Also, toxic effects were observed at 200 mg/L under $MnCl_2$ post-treatment. Similarly, the concentration of whole apple extracts played an important role in increasing the resistance to different stresses in *C. elegans*.[18] Tannic-, gallic-, and ellagic-acids, and catechin, which are phytochemicals, exhibited variable effects on stress resistance based on concentration.[30] Compounds such as myricetin, quercetin, kaempferol, and naringenin are accumulated in a concentration-dependent manner in *C. elegans*.[23] Therefore, different concentrations of BTE exerted different effects under different environmental stresses. However, we did not exclude the possibility of the hormetic mechanisms on the dose−response curves for BTE. Multiple studies have found many plant extracts or phytochemicals exerted hormetic effects.[19,26,30−33] By acting as a moderate stress-stimulus, it can be hypothesized that compounds in BTE at lower levels, such as caffeine,[26] quercetin,[33] and tannic acid,[30] modulated an adaptive response, leading to an enhancement in stress resistance. It is therefore important to evaluate the possible effects of BTE at higher concentrations for future study.

Multiple studies have found an inverse relationship between black tea consumption and the risk of age-related diseases in mammals, including in human.[1,5] To exert any effects, absorption and biotransformation of chemical ingredients in BTE were taken into account. Some compounds contained in both green tea and black tea, such as catechins, were relatively well established in mammals, including in human.[5] Absorption and biotransformation of epicatechin and quercetin have already been evaluated in *C. elegans*.[24,34] Differential uptake and biotransformation of quercetin and quercetin-3-*O*-glucoside (Q3Glc) produced different effects to the lifespan of *C. elegans*, because Q3Glc was taken up to a greater extent than quercetin.[35] Therefore, the effects of absorption and biotransformation of compounds in BTE on the stress resistance in *C. elegans* should be considered. However, little information about the uptake and metabolism of unique polyphenols in black tea is available due to difficulties in determination of specific constituents of black tea—theaflavins or thearubigins.[5]

Black tea is known to have antioxidant capacity.[1] Also, ROS are generated by environmental threats such as UV, heat, and metal ions.[9] To understand whether BTE increased stress resistance by its antioxidant activity, we measured the ROS levels in *C. elegans* after 48 h of BTE-treatment. Our results indicated that BTE indeed decreased ROS in *C. elegans*. To see whether this inhibition of ROS formation due to BTE treatment might affect antioxidant systems, we quantified the activities of SOD, CAT, and GSH-PX and the mRNA levels of *sod-3* and *gsh-px*. While no induction of SOD activity was observed at the concentrations we evaluated, the GSH-PX activity was found to be significantly increased in *C. elegans* treated by BTE. However, CAT activity was decreased significantly after BTE treatment, which surprised us. A previous study found that EGb761, an extract of *Ginkgo biolba*, reduced catalase transcripts.[36] Resveratrol also reduced the total catalase activity in MRC-5 cells.[37] Future experiments are needed to investigate why and how BTE reduced CAT activity. Then we found that *gsh-px* and *sod-3* expression was up-regulated by BTE. Superoxide dismutase (SOD) is one important antioxidant enzyme, responsible for the conversion (dismutation) of superoxide detoxification.[38] *C. elegans* has two isoforms of mitochondrial SOD (encoded by *sod-2* and *sod-3*), two cytosolic SODs (*sod-1* and *sod-5*), and one extracellular SOD (*sod-4*).[38] *sod-1* contributes most of the SOD activity, and the relative contribution of *sod-3* was very small.[39] So this might be the reason for the inconformity between the mRNA level of *sod-3* and the SOD activity.

To further identify the antioxidant capacity of BTE, we performed the lifespan assay of *mev-1* mutants. *mev-1* nematodes, which possess a mutation in the Cytochrome *b* large subunit of the mitochondrial complex II, have been used to examine whether plant extracts protect against chronic oxidative stress.[40,41] ROS accumulation was 2-fold greater in *mev-1* nematodes relative to the wild type; consequently, *mev-1* individuals showed increased oxidative stress, accelerated aging, and reduced lifespan.[9] Our results showed that BTE only slightly extended the mean lifespan of *mev-1* mutants. In addition, BTE could not increase lifespan under normal conditions at the concentrations we used. Our finding indicated antioxidant capacity was not predictive of lifespan benefits,[31] even in a mutant containing high ROS levels. The causal relationship between antioxidant and antiaging has been long debated in the field. Many medicinal plant studies in *C. elegans* showed no clear and direct correlation between antioxidant capacity and longevity.[32] Based on these results, the antioxidant activity of BTE might be necessary but not sufficient to protect against aging to *C. elegans*.[42]

*C. elegans sir-2.1* can regulate lifespan and stress responses.[43] Nematodes overexpressing SIR-2.1 were resistance to stress, and *sir-2.1* loss-of-function mutants were stress sensitive.[44] We found that BTE could up-regulate expression of *sir-2.1*. Confirming the crucial role of *sir-2.1*, we observed that the protective effects induced by BTE were dependent on the expression of *sir-2.1* under UV and heat stress, not osmotic stress. *C. elegans* SIR-2.1 protein can function in a stress-response pathway of longevity,[44] and this effect is dependent on *daf-16*.[43] BTE did not affect the *daf-16* gene expression but increased expression of the *daf-16* target *sod-3*. Components in BTE, such as epigallocatechingallate (EGCG) and quercetin,

have been identified to induce a translocation of DAF-16 from the cytoplasm to the nucleus.[21,45] So BTE might induce translocation of DAF-16 to the nucleus to modulate an adaptive response to environmental changes.[46] Therefore, BTE might increase stress resistance through a *sir-2.1/daf-16/sod-3* signaling pathway.

Osmotic regulatory genes controlled osmotic stress resistance independent of temperature and oxidative stress response mechanisms.[47] OSR-1 coupled with SEK-1/MAPKK regulates the resistance of *C. elegans* to hyperosmotic stress.[16] Blueberry extracts increased longevity through the OSR-1/SEK-1 pathway in *C. elegans*,[17] while SEK-1, but not OSR-1, are required for quercetin-induced lifespan-extending in *C. elegans*.[48] Our results showed that BTE significantly up-regulated the expression of *sek-1*, not *osr-1*, which partly indicated how BTE increased survival of *C. elegans* under an osmotic environment. To get a mechanistic insight, further systematic studies are warranted to identify the underlying mechanisms of BTE's differential effects on stress resistance in *C. elegans*.

Here we provide a report of the efficacy in BTE to increased osmotic stress, heat shock, and UV irradiation resistance in *C. elegans*. However, BTE did not attenuate $MnCl_2$-induced mortality and increased lifespan under normal cultural conditions. Our results suggested BTE improved heat and UV stress resistance, not osmotic stress, in a *sir-2.1* dependent manner. In addition, BTE concentration is very important for nematode stress resistance. It is important to elucidate the mechanisms of black tea extracts to further clarify the understanding of stress response processes, and evaluate the health benefit of this worldwide beverage.

## ■ ASSOCIATED CONTENT

### Supporting Information

Detailed description of materials and methods; table showing the composition of black tea extracts; table listing the primers used for the quantitative real-time reverse transcription-polymerase chain reaction; and figure showing the growth characteristics of *E. coil* OP50 in LB after UV irradiation (9999 J/m$^2$). This material is available free of charge via the Internet at http://pubs.acs.org.

## ■ AUTHOR INFORMATION


### Corresponding Authors

*E-mail: gongyushun@hunau.net. Phone: 086-15874184082. Fax: 086-731-84635304 (Yu-Shun Gong).

*E-mail: larkin-liu@163.com. Phone: 086-13807492258. Fax: 086-731-84635304 (Zhong-Hua Liu).



### Funding

The authors acknowledge the National Natural Science Foundation of China (No. 31270733), the Project of Education Department in Hunan (12W005), and the Graduate Student Innovative Research Projects in Hunan (CX2014B301) for financial support.


### Notes

The authors declare no competing financial interest.

## ■ ACKNOWLEDGMENTS


Some *C. elegans* strains were provided by CGC, which is funded by the NIH Office of Research Infrastructure Programs (P40 OD010440).


## ■ REFERENCES


(1) Pan, M. H.; Lai, C. S.; Wang, H.; Lo, C. Y.; Ho, C. T.; Li, S. Black tea in chemo-prevention of cancer and other human diseases. *Food Sci. Human Wellness* **2013**, *2*, 12−21.

(2) Yang, J.; Liu, R. H. The phenolic profiles and antioxidant activity in different types of tea. *Int. J. Food. Sci. Technol.* **2013**, *48*, 163−171.

(3) Oliveira, P.; Silva, B.; Dias, T.; Tomás, G.; Teixeira, N.; Alves, M.; Silva, B. M.; Oliveira, P. F. White Tea (*Camellia Sinensis* (L.)): Antioxidant Properties and Beneficial Health Effects. *Int. J. Food. Sci. Nutrition Dietetics* **2013**, *101*, 1−15.

(4) Li, S.; Lo, C. Y.; Pan, M. H.; Lai, C. S.; Ho, C. T. Black tea: chemical analysis and stability. *Food. Funct.* **2013**, *4*, 10−18.

(5) Łuczaj, W.; Skrzydlewska, E. Antioxidative properties of black tea. *Prev. Med.* **2005**, *40*, 910−918.

(6) Peng, C.; Chan, H. Y. E.; Li, Y. M.; Huang, Y.; Chen, Z. Y. Black tea theaflavins extend the lifespan of fruit flies. *Exp. Gerontol.* **2009**, *44*, 773−783.

(7) Baruah, A. M.; Mahanta, P. K. Fermentation characteristics of some assamica clones and process optimization of black tea manufacturing. *J. Agric. Food. Chem.* **2003**, *51*, 6578−6588.

(8) Bartwal, A.; Mall, R.; Lohani, P.; Guru, S.; Arora, S. Role of secondary metabolites and brassinosteroids in plant defense against environmental stresses. *J. Plant. Growth. Regul.* **2013**, *32*, 216−232.

(9) Rodriguez, M.; Snoek, L. B.; De Bono, M.; Kammenga, J. E. Worms under stress: *C. elegans* stress response and its relevance to complex human disease and aging. *Trends Genet.* **2013**, *29*, 367−374.

(10) Stiernagle, T. Maintenance of *C. elegans*. *WormBook* **2006**, DOI: 10.1895/wormbook.1.101.1.

(11) Kenyon, C.; Chang, J.; Gensch, E.; Rudner, A.; Tabtiang, R. A C. elegans mutant that lives twice as long as wild type. *Nature* **1993**, *366*, 461−464.

(12) Benedetto, A.; Au, C.; Avila, D. S.; Milatovic, D.; Aschner, M. Extracellular Dopamine Potentiates Mn-Induced Oxidative Stress, Lifespan Reduction, and Dopaminergic Neurodegeneration in a BLI-3-Dependent Manner in Caenorhabditis elegans. *PLoS Genet.* **2010**, *6*, e1001084.

(13) Brown, M. K.; Evans, J. L.; Luo, Y. Beneficial effects of natural antioxidants EGCG and $\alpha$-lipoic acid on lifespan and age-dependent behavioral declines in *Caenorhabditis elegans*. *Pharmacol. Biochem. Behav.* **2006**, *85*, 620−628.

(14) Abbas, S.; Wink, M. Epigallocatechin gallate from green tea (*Camellia sinensis*) increases lifespan and stress resistance in *Caenorhabditis elegans*. *Planta Med.* **2009**, *75*, 216−221.

(15) Zhang, L.; Jie, G.; Zhang, J.; Zhao, B. Significant longevity-extending effects of EGCG on *Caenorhabditis elegans* under stress. *Free Rad. Biol. Med.* **2009**, *46*, 414−421.

(16) Solomon, A.; Bandhakavi, S.; Jabbar, S.; Shah, R.; Beitel, G. J.; Morimoto, R. I. *Caenorhabditis elegans* OSR-1 regulates behavioral and physiological responses to hyperosmotic environments. *Genetics* **2004**, *167*, 161−170.

(17) Wilson, M. A.; Shukitt-Hale, B.; Kalt, W.; Ingram, D. K.; Joseph, J. A.; Wolkow, C. A. Blueberry polyphenols increase lifespan and thermotolerance in *Caenorhabditis elegans*. *Aging cell* **2006**, *5*, 59−68.

(18) Vayndorf, E. M.; L, S. S.; Liu, R. H. Whole apple extracts increase lifespan, healthspan and resistance to stress in *Caenorhabditis elegans*. *J. Funct. Foods* **2013**, *5*, 1235−1243.

(19) Wiegant, F. A.; Surinova, S.; Ytsma, E.; Langelaar-Makkinje, M.; Wikman, G.; Post, J. Plant adaptogens increase lifespan and stress resistance in *C.elegans*. *Biogerontology* **2009**, *10*, 27−42.

(20) Guha, S.; Cao, M.; Kane, R. M.; Savino, A. M.; Zou, S.; Dong, Y. The longevity effect of cranberry extract in *Caenorhabditis elegans* is modulated by *daf-16* and *osr-1*. *Age* **2013**, *35*, 1559−1574.

(21) Bartholome, A.; Kampkötter, A.; Tanner, S.; Sies, H.; Klotz, L. O. Epigallocatechin gallate-induced modulation of FoxO signaling in mammalian cells and *C.elegans*: FoxO stimulation is masked via PI3K/Akt activation by hydrogen peroxide formed in cell culture. *Arch. Biochem. Biophys.* **2010**, *501*, 58−64.

(22) Saul, N.; Pietsch, K.; Menzel, R.; Stürzenbaum, S. R.; Steinberg, C. E. Catechin induced longevity in *C. elegans*: From key regulator genes to disposable soma. *Mech. Ageing Dev.* **2009**, *130*, 477−486.
(23) Grünz, G.; Haas, K.; Soukup, S.; Klingenspor, M.; Kulling, S. E.; Daniel, H.; Spanier, B. Structural features and bioavailability of four flavonoids and their implications for lifespan-extending and antioxidant actions in *C. elegans*. *Mech. Ageing Dev.* **2012**, *133*, 1−10.
(24) Surco-Laos, F.; Dueñas, M.; González-Manzano, S.; Cabello, J.; Santos-Buelga, C.; González-Paramás, A. M. Influence of catechins and their methylated metabolites on lifespan and resistance to oxidative and thermal stress of *Caenorhabditis elegans* and epicatechin uptake. *Food Res. Int.* **2012**, *46*, 514−521.
(25) Saul, N.; Pietsch, K.; Menzel, R.; Stürzenbaum, S. R.; Steinberg, C. E. The longevity effect of tannic acid in *Caenorhabditis elegans*: disposable soma meets hormesis. *J. Gerontol. A: Biol.* **2010**, *65*, 626−635.
(26) Sutphin, G. L.; Bishop, E.; Yanos, M. E.; M?ller, R. M.; Kaeberlein, M. Caffeine extends life span, improves healthspan, and delays age-associated pathology in *Caenorhabditis elegans*. *Longevity Healthspan* **2012**, *1*, 1−12.
(27) Keller, C. I.; Calkins, J.; Hartman, P. S.; Rupert, C. S. UV photobiology of the nematode Caenorhabditis elegans: action spectra, absence of photoreactivation and effects of caffeine. *Photochem. Photobiol.* **1987**, *46*, 483−488.
(28) Gong, Y.; Luo, Y.; Huang, J.-a.; Zhang, J.; Peng, Y.; Liu, Z.; Baolu, Z. Theanine improves stress resistance in *Caenorhabditis elegans*. *J. Funct. Foods* **2012**, *4*, 988−993.
(29) Liu, R. H. Potential synergy of phytochemicals in cancer prevention: mechanism of action. *J. Nutr.* **2004**, *134*, 3479S−3485S.
(30) Saul, N.; Pietsch, K.; Stürzenbaum, S. R.; Menzel, R.; Steinberg, C. E. Diversity of polyphenol action in Caenorhabditis elegans: between toxicity and longevity. *J. Nat. Prod.* **2011**, *74*, 1713−1720.
(31) Pun, P. B. L.; Gruber, J.; Tang, S. Y.; Schaffer, S.; Ong, R. L. S.; Fong, S.; Ng, L. F.; Cheah, I.; Halliwell, B. Ageing in nematodes: do antioxidants extend lifespan in *Caenorhabditis elegans*? *Biogerontology* **2010**, *11*, 17−30.
(32) Tang, S. Y.; Halliwell, B. Medicinal plants and antioxidants: What do we learn from cell culture and *Caenorhabditis elegans* studies? *Biochem. Biophys. Res. Commun.* **2010**, *394*, 1−5.
(33) Pietsch, K.; Saul, N.; Chakrabarti, S.; Stürzenbaum, S. R.; Menzel, R.; Steinberg, C. E. Hormetins, antioxidants and prooxidants: defining quercetin-, caffeic acid-and rosmarinic acid-mediated life extension in *C. elegans*. *Biogerontology* **2011**, *12*, 329−347.
(34) Surco-Laos, F.; Cabello, J.; Gómez-Orte, E.; González-Manzano, S.; González-Paramás, A. M.; Santos-Buelga, C.; Dueñas, M. Effects of O-methylated metabolites of quercetin on oxidative stress, thermotolerance, lifespan and bioavailability on *Caenorhabditis elegans*. *Food Funct.* **2011**, *2*, 445−456.
(35) Dueñas, M.; Surco-Laos, F.; González-Manzano, S.; González-Paramás, A. M.; Gómez-Orte, E.; Cabello, J.; Santos-Buelga, C. Deglycosylation is a key step in biotransformation and lifespan effects of quercetin-3-*O*-glucoside in *Caenorhabditis elegans*. *Pharmacol. Res.* **2013**, *76*, 41−48.
(36) Kampkötter, A.; Pielarski, T.; Rohrig, R.; Timpel, C.; Chovolou, Y.; Wätjen, W.; Kahl, R. The *Ginkgo biloba* extract EGb761 reduces stress sensitivity, ROS accumulation and expression of catalase and glutathione *S*-transferase 4 in *Caenorhabditis elegans*. *Pharmacol. Res.* **2007**, *55*, 139−147.
(37) Robb, E. L.; Page, M. M.; Wiens, B. E.; Stuart, J. A. Molecular mechanisms of oxidative stress resistance induced by resveratrol: Specific and progressive induction of MnSOD. *Biochem. Biophys. Res. Commun.* **2008**, *367*, 406−412.
(38) Gruber, J.; Ng, L. F.; Fong, S.; Wong, Y. T.; Koh, S. A.; Chen, C. B.; Shui, G.; Cheong, W. F.; Schaffer, S.; Wenk, M. R. Mitochondrial changes in ageing *Caenorhabditis elegans*—what do we learn from superoxide dismutase knockouts? *PloS one* **2011**, *6*, e19444.
(39) Doonan, R.; McElwee, J. J.; Matthijssens, F.; Walker, G. A.; Houthoofd, K.; Back, P.; Matscheski, A.; Vanfleteren, J. R.; Gems, D. Against the oxidative damage theory of aging: superoxide dismutases protect against oxidative stress but have little or no effect on life span in *Caenorhabditis elegans*. *Gene. Dev.* **2008**, *22*, 3236−3241.
(40) Ishii, N.; Fujii, M.; Hartman, P. S.; Tsuda, M.; Yasuda, K.; Senoo-Matsuda, N.; Yanase, S.; Ayusawa, D.; Suzuki, K. A mutation in succinate dehydrogenase cytochrome b causes oxidative stress and ageing in nematodes. *Nature* **1998**, *394*, 694−697.
(41) Gruber, J.; Ng, L. F.; Poovathingal, S. K.; Halliwell, B. Deceptively simple but simply deceptive−*Caenorhabditis elegans* lifespan studies: Considerations for aging and antioxidant effects. *FEBS Lett.* **2009**, *583*, 3377−3387.
(42) Gems, D.; Doonan, R. Antioxidant defense and aging in C. elegans: is the oxidative damage theory of aging wrong? *Cell Cycle* **2009**, *8*, 1681−1687.
(43) Tissenbaum, H. A.; Guarente, L. Increased dosage of a *sir-2* gene extends lifespan in *Caenorhabditis elegans*. *Nature* **2001**, *410*, 227−230.
(44) Berdichevsky, A.; Viswanathan, M.; Horvitz, H. R.; Guarente, L. *C. elegans* SIR-2.1 Interacts with 14−3-3 Proteins to Activate DAF-16 and Extend Life Span. *Cell* **2006**, *125*, 1165−1177.
(45) Kampkötter, A.; Nkwonkam, C. G.; Zurawski, R. F.; Timpel, C.; Chovolou, Y.; Wätjen, W.; Kahl, R. Investigations of protective effects of the flavonoids quercetin and rutin on stress resistance in the model organism *Caenorhabditis elegans*. *Toxicology* **2007**, *234*, 113−123.
(46) Henderson, S. T.; Johnson, T. E. *daf-16* integrates developmental and environmental inputs to mediate aging in the nematode *Caenorhabditis elegans*. *Curr. Biol.* **2001**, *11*, 1975−1980.
(47) Mazzeo, L. E. M.; Dersh, D.; Boccitto, M.; Kalb, R. G.; Lamitina, T. Stress and aging induce distinct polyQ protein aggregation states. *P. Natl. Acad. Sci.USA* **2012**, *109*, 10587−10592.
(48) Pietsch, K.; Saul, N.; Menzel, R.; Stürzenbaum, S. R. Quercetin mediated lifespan extension in *Caenorhabditis elegans* is modulated by *age-1*, *daf-2*, *sek-1* and *unc-43*. *Biogerontology* **2009**, *10*, 565−578.

Table 1. Total Polyphenol and Flavonoid Content and Their Bioaccessibility in Wheat as Influenced by Domestic Processing

| type of processing | total polyphenol content[a] (mg/g) | bioaccessible polyphenol content[a] (mg/g) | percent bioaccessibility | total flavonoid content[b] (mg/g) | bioaccessible flavonoid content[b] (mg/g) | percent bioaccessibility | tannins (mg/g) |
|---|---|---|---|---|---|---|---|
| native | 1.20 ± 0.09 | 0.96 ± 0.07 | 80.0 | 0.84 ± 0.14 | 0.04 ± 0.01 | 4.80 | 0.45 ± 0.03 |
| sprouting | 1.43 ± 0.02[c] | 0.92 ± 0.13 | 64.3 | 0.96 ± 0.12 | 0.04 ± 0.01 | 4.20 | 0.60 ± 0.02[c] |
| cooking | | | | | | | |
| roasting | 1.44 ± 0.07[c] | 0.71 ± 0.12[c] | 49.3 | 1.30 ± 0.48[c] | 0.03 ± 0.01 | 1.30 | 0.78 ± 0.08[c] |
| pressure-cooking | 0.76 ± 0.06[c] | 0.76 ± 0.12[c] | 100 | 0.53 ± 0.10 | 0.02 ± 0.00 | 3.77 | 0.17 ± 0.06[c] |
| open-pan boiling | 0.98 ± 0.09[c] | 0.84 ± 0.09 | 85.7 | 0.20 ± 0.06[c] | 0.04 ± 0.01 | 20.0 | |
| microwave heating | 0.79 ± 0.10[c] | 0.77 ± 0.08[c] | 97.5 | 0.22 ± 0.09[c] | 0.03 ± 0.00 | 13.6 | |

[a]Gallic acid equivalents. [b]Catechin equivalents. Values are mean ± SD of triplicates. [c]Significantly different from native grain ($P < 0.05$).

*glaucum*).[15] The most common forms of domestic processing are sprouting, roasting, pressure-cooking, open-pan boiling, and microwave heating, which may bring about several changes in the nutritional quality of food. Hence, the present investigation was carried out to determine the extent to which domestic processing influences phenolic profile and bioaccessibility of polyphenols from commonly consumed cereals (wheat and sorghum) and legumes (green gram and chickpea).

## MATERIALS AND METHODS

**Materials.** Sorghum (*Sorghum bicolor L. Moench*), wheat (*Triticum aestivum L.*), green gram (*Vigna radiata L.*), and chickpea (*Cicer arietinum L.*) were procured from the National Seeds Corporation (Mysore, Karnataka, India). Standard phenolic compounds, pepsin, pancreatin, and bile extract (porcine origin), were procured from Sigma-Aldrich Chemical Co. (St. Louis, MO, USA). HPLC-grade solvents were from Qualigens Chem. Co. (Mumbai, India). All other chemicals and reagents used were of analytical grade.

**Processing of Grain Samples.** A known amount of grain samples was subjected to various types of domestic processing in triplicates as described below.

*Sprouting.* After soaking the grains overnight (30 g in 90 mL), water was decanted, and samples were allowed to germinate for a period of 48 h under ambient conditions (25 °C), while keeping them wet by intermittently spraying water. The sprouted grains were dried under shade, powdered, and used for extraction.

*Heat Processing.* (i) Pressure-cooking: Powdered grain samples were pressure-cooked (15 p.s.i.) in triple-distilled water (10 g in 30 mL) for 15 min. (ii) Open-pan boiling: Powdered grain samples were boiled in triple-distilled water (10 g in 50 mL) on a hot plate for 10 min. (iii) Microwave heating: Powdered grain samples were microwave heated in triple-distilled water (10 g in 50 mL) for 4 min in a household microwave system (SAMSUNG Trio, Combi-CE1031LAT; Samsung Electronics Co. Ltd., Suwon, Korea) at 450 W. Cooked samples were used for further studies. (iv) Roasting: Known quantity of each sample (30 g) was roasted on preheated acid-washed sand at 150 °C ± 2 °C for 5 min (until the sample gave a characteristic aroma and color). Roasted sample was cooled to room temperature, powdered, and stored in airtight pouches in dark at 4 °C until future studies.

**Analysis of Polyphenols.** *Extraction of Polyphenols.* Extraction of polyphenols was carried out by refluxing the grain samples (2 g) in acidified methanol for 2 h.[16] Total polyphenols, total flavonoids, and tannins were analyzed in the filtered extracts as described below.

*Total Polyphenols.* Total polyphenol content was estimated by Folin−Ciocalteu method as described by Singleton et al.,[17] with slight modifications. Briefly, an aliquot of acidified methanolic extract was appropriately diluted with water to 3.0 mL, mixed with 1 mL each of 1N Folin−Ciocalteu reagent and 20% sodium carbonate, and incubated for 30 min at room temperature. The absorbance was recorded in a spectrophotometer (UV-1800, Shimadzu Corporation, Kyoto, Japan) and compared with those of known standard gallic acid concentrations ($R^2$ = 0.999). The total polyphenol content was computed as mg equivalent gallic acid per g of sample.

*Total Flavonoids.* Total flavonoid content was determined according to the method of Zhishen et al.[18] Acidified methanolic extract (0.1 mL) was diluted with 4.9 mL of distilled water and mixed with 0.3 mL of (5% w/v) $NaNO_2$. After 5 min, 0.3 mL of (10% w/v) $AlCl_3$ and 2 mL of 1 M NaOH were added. The sample was then diluted with distilled water to a total volume of 10 mL. The mixture was vortexed and the absorbance was read at 510 nm. Standard catechin was used to prepare a calibration curve ($R^2$ = 0.999). The flavonoid concentration was expressed as mg catechin equivalents per g of sample.

*Tannins.* Tannin content was determined by the modified vanillin−HCl method.[19] An aliquot of acidified methanolic extract was appropriately diluted to 1 mL with distilled water and was mixed with 5 mL of vanillin−HCl reagent. The samples were allowed to stand at room temperature for 20 min and the color developed was recorded at 500 nm. The absorbance was also recorded for standard catechin solution ($R^2$ = 0.998) and the tannin concentration was expressed as mg catechin equivalents per g of sample.

*HPLC Analysis.* Phenolic extracts of native and processed samples were analyzed by HPLC to obtain a profile of individual phenolic compounds.[20] Analysis was carried out in an HPLC system (Agilent 1200 Series; Agilent Technologies Inc., Santa Clara, CA, USA) equipped with a diode array detector. Filtered samples (20 μL) were analyzed for polyphenols using a C18 analytical column (250 × 4.6 mm; 5 μm; Agilent Technologies Inc., USA) with the mobile phase consisting of 0.1% trifluoroacetic acid as solvent A and 100% methanol as solvent B. The total run time was 60 min with a flow rate of 1.0 mL/min with the gradient program as follows: initial B concentration of 20% to 40% in 40 min which was maintained for 10 min and then again to 20% B in the next five min and 5 min of postrun for reconditioning. Peaks were recorded simultaneously at 280 and 320 nm.

**Bioaccessibility of Polyphenols.** Bioaccessibility of polyphenols was determined by an in vitro method as described by Luten et al.,[21] involving simulated gastrointestinal digestion with suitable modifications. Initially, simulated gastric digestion was carried out by incubating the powdered samples (10 g) with pepsin at pH 2.0 and a temperature of 37 °C for 2 h. At the end of gastric digestion, titratable acidity was determined in an aliquot of gastric digest as the amount of 0.2 M sodium hydroxide required to attain a pH of 7.5 in the presence of a mixture of pancreatin and bile extract dissolved in 0.1 M sodium bicarbonate (4 g of pancreatin and 25 g of bile extract per L).

Subsequently, intestinal digestion was simulated by suspending segments of dialysis tubing (molecular mass cutoff: 10 kDa) containing 25-mL aliquots of sodium bicarbonate solution, being equivalent in moles to the titratable acidity (sodium hydroxide needed to neutralize the gastric digest), in Erlenmeyer flasks containing the gastric digest and incubated at 37 °C with shaking until the pH of the digest reached 5.0. Pancreatin−bile extract mixture (5 mL) was then added and

**Table 2. Total Polyphenol and Flavonoid Content and Their Bioaccessibility in Sorghum as Influenced by Domestic Processing**

| type of processing | total polyphenol content[a] (mg/g) | bioaccessible polyphenol content[a] (mg/g) | percent bioaccessibility | total flavonoid content[b] (mg/g) | bioaccessible flavonoid content[b] (mg/g) | percent bioaccessibility | tannins (mg/g) |
|---|---|---|---|---|---|---|---|
| native | 1.12 ± 0.05 | 0.60 ± 0.09 | 53.6 | 0.89 ± 0.33 | 0.09 ± 0.03 | 2.50 | 0.62 ± 0.06 |
| sprouting | 1.18 ± 0.16 | 0.64 ± 0.05 | 54.2 | 0.56 ± 0.81[c] | 0.10 ± 0.01 | 3.90 | 1.26 ± 0.44[c] |
| cooking | | | | | | | |
| roasting | 1.67 ± 0.22[c] | 0.51 ± 0.09[c] | 30.5 | 0.65 ± 0.61[c] | 0.10 ± 0.03 | 3.77 | 1.85 ± 0.16[c] |
| pressure-cooking | 0.55 ± 0.05[c] | 0.55 ± 0.07 | 100 | 0.43 ± 0.14[c] | 0.09 ± 0.01 | 10.8 | 0.48 ± 0.11 |
| open-pan boiling | 0.64 ± 0.06[c] | 0.53 ± 0.06[c] | 82.8 | 0.48 ± 0.07[c] | 0.08 ± 0.03 | 16.7 | 0.28 ± 0.07[c] |
| microwave heating | 0.60 ± 0.04[c] | 0.46 ± 0.08[c] | 76.7 | 0.43 ± 0.11[c] | 0.04 ± 0.01[c] | 9.30 | 0.44 ± 0.09 |

[a]Gallic acid equivalents. [b]Catechin equivalents. Values are mean ± SD of triplicates. [c]Significantly different from native grain ($P < 0.05$).

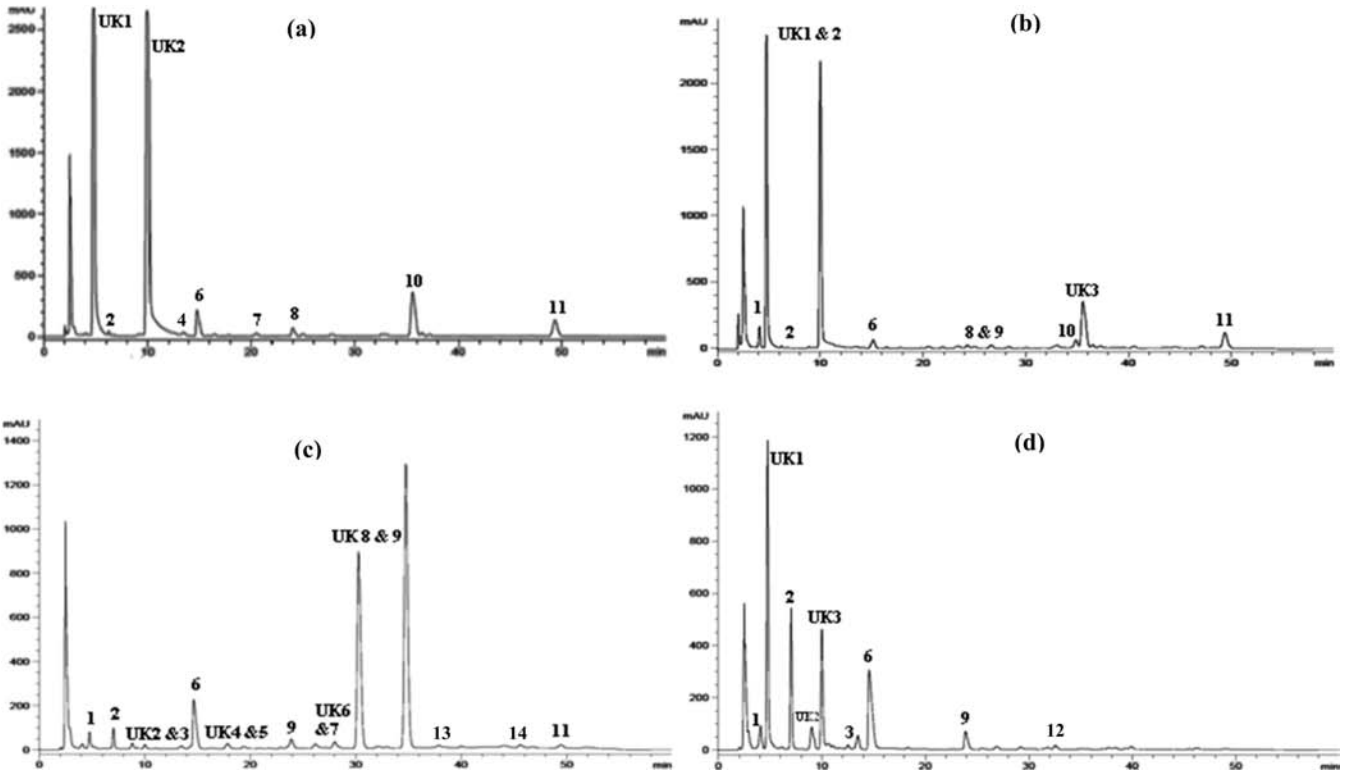


**Figure 1.** HPLC profiles of polyphenols from (a) wheat, (b) sorghum, (c) green gram, and (d) chickpea. 1: Gallic acid; 2: protocatechuic acid; 3: *p*-hydroxy benzoic acid; 4: vanillic acid; 6: syringic acid; 7: *p*-coumaric acid; 8: ferulic acid; 9: sinapic acid; 10: salicylic acid; 11: *t*-cinnamic acid; 12: luteolin; 13: rutin; 14: quercetin; UK: unknown phenolic compound.

incubation was continued for 2 h or longer until the pH of the digest reached 7.0. At the end of this simulated gastrointestinal digestion, the dialyzate was analyzed for polyphenols by both spectrophotometry and HPLC as described in previous paragraphs. The bioaccessible polyphenol present in the grain sample is the dialyzable portion of the total polyphenol, which is expressed as percent bioaccessibility.

**Statistical Analysis.** All determinations were made in three replicates, and the average values are reported. Statistical analysis was carried out using Graphpad INSTAT, Version 3.06, Graphpad software. Data were analyzed by applying one-way analysis of variance (ANOVA) and the differences between means were assessed by Dunnet's test and considered significant when $P < 0.05$.

## RESULTS

Phenolic extracts of native and variously processed cereals and legumes, as well as of dialysates obtained after simulated gastric digestion of these samples, were analyzed for total polyphenols, flavonoids, tannins, and individual polyphenol profile.

**Total Polyphenol, Flavonoid, and Tannin Content of Cereal Grains.** Total polyphenol content, total flavonoid content, and tannin content of wheat are given in Table 1. Total polyphenol content of unprocessed wheat was 1.20 mg/g, which significantly increased on sprouting (by 19%) and roasting (by 20%) ($P < 0.05$). Drastic reduction in polyphenol content was observed on pressure-cooking (by 27%), open-pan boiling (by 18%), and microwave heating (by 34%) ($P < 0.05$). Total flavonoid in native wheat was 0.84 mg/g, which increased by 50% on roasting. Open-pan boiling and microwave heating had deleterious effect (4-fold decrease) on total flavonoid content of wheat, whereas pressure-cooking and sprouting did not alter this much. Native wheat had a total tannin content of 0.45 mg/g which increased significantly on sprouting and roasting (by 33% and 73%, respectively) ($P < 0.05$). Pressure-cooking reduced tannin content of wheat to 0.17 mg/g, while open-pan boiling and microwave heating had even higher

Table 3. Concentrations ($\mu$g/g) of Identified Phenolic Compounds in Native and Processed Wheat[a]

| | | | | heat processing | | | |
|---|---|---|---|---|---|---|---|
| sl no. | compound | native | sprouting | roasting | pressure-cooking | open-pan boiling | microwave heating |
| 1 | gallic acid | | | | 2.97 | 4.58 | 7.63 |
| 2 | protocatechuic acid | 7.86 | 6.00 | 11.9 | | | |
| 3 | gentisic acid | | | | 2.04 | 1.34 | 1.12 |
| 4 | vanillic acid | 13.3 | 16.2 | 123.6 | 4.67 | 6.74 | 5.09 |
| 5 | syringic acid | 58.5 | 69.8 | 41.3 | 89.2 | 58.9 | 68.5 |
| 6 | *p*-coumaric acid | 13.8 | 18.9 | 15.4 | 35.5 | 51.6 | 40.2 |
| 7 | ferulic acid | 11.6 | 13.2 | 14.1 | 12.2 | 10.4 | 9.99 |
| 8 | sinapic acid | | | | 1.07 | 0.79 | 1.48 |
| 9 | salicylic acid | 459.3 | 452.5 | 664.1 | 109.5 | 67.2 | 80.8 |
| 10 | *t*-cinnamic acid | 27.4 | 23.4 | 34.1 | 4.04 | 2.73 | 2.92 |
| total identified phenolic compounds ($\mu$g/g) | | 591.8 | 600.0 | 904.5 | 261.2 | 204.3 | 217.7 |

[a]Values are means of triplicates.

Table 4. Concentrations ($\mu$g/g) of Identified Phenolic Compounds in Native and Processed Sorghum[a]

| | | | | heat processing | | | |
|---|---|---|---|---|---|---|---|
| sl no. | compound | native | sprouting | roasting | pressure-cooking | open-pan boiling | microwave heating |
| 1 | gallic acid | 45.8 | | 5.43 | | 2.02 | 8.23 |
| 2 | protocatechuic acid | 3.59 | 7.57 | 22.7 | 1.49 | | 3.11 |
| 3 | *p*-hydroxy benzoic acid | | 11.5 | | 3.62 | 3.45 | 6.20 |
| 4 | gentisic acid | | 2.17 | | 1.62 | 2.04 | 4.83 |
| 5 | vanillic acid | | | 278.3 | | | |
| 6 | caffeic acid | 1.91 | 1.88 | 3.39 | 7.62 | 7.18 | 18.3 |
| 7 | syringic acid | 15.6 | 14.0 | 22.5 | 19.2 | 10.9 | 44.1 |
| 8 | *p*-coumaric acid | 3.77 | 2.07 | 7.32 | 3.08 | 5.32 | 9.78 |
| 9 | ferulic acid | 6.25 | 7.49 | 20.5 | 8.95 | 7.97 | 17.6 |
| 10 | sinapic acid | 8.22 | 8.12 | 10.2 | 4.52 | 5.81 | 11.6 |
| 11 | salicylic acid | 63.4 | 69.9 | 187.4 | 18.4 | 10.7 | 13.4 |
| 12 | *t*-cinnamic acid | 21.8 | 20.0 | 72.9 | | 1.94 | 10.3 |
| 13 | hesperitin | | | | 0.36 | | 0.53 |
| total identified phenolic compound ($\mu$g/g) | | 170.3 | 144.7 | 630.6 | 68.9 | 57.3 | 148.0 |

[a]Values are means of triplicates.

deleterious effect, making tannin content below detectable limits.

Total polyphenol, total flavonoid, and tannin content of native and processed sorghum are presented in Table 2. Total polyphenol content of native sorghum was 1.12 mg/g which significantly reduced (by 43−51%) ($P < 0.05$) on heat treatment except roasting, where there was a significant increase (49%) ($P < 0.05$). Sprouting did not cause any significant change in the total phenol content. Significant reduction of total flavonoid content (0.89 mg/g) was observed after sprouting (38%) and heat treatments (27−52%) ($P < 0.05$). Tannin content of unprocessed sorghum was 0.62 mg/g which significantly increased on sprouting (2-fold increase) and roasting (3-fold increase) the cereal ($P < 0.05$). Open-pan boiling drastically reduced (55%) the tannin content ($P < 0.05$).

**HPLC Profile of Phenols of Cereal Grains.** The profile of individual phenolic compounds of wheat is shown in Figure 1a. About 17 compounds have been detected in native form and two unidentified compounds are the major phenolics (Supporting Information (SI) Table 1). The identified compounds found in native wheat are protocatechuic acid, vanillic acid, syringic acid, *p*-coumaric acid, ferulic acid, salicylic acid, and *t*-cinnamic acid. Concentrations of individual identified phenolic compounds are given in Table 3. Among the identified compounds, concentration of salicylic acid (459 $\mu$g/g) was highest followed by syringic acid (58 $\mu$g/g). No significant effect was seen after sprouting the wheat, while there was an increase after roasting (592−904 $\mu$g/g) ($p < 0.05$). Pressure-cooking, open-pan boiling, and microwave heating reduced the concentration of identified compounds to about 50%. Interestingly, protocatechuic acid appeared in profiles of native, sprouted, and roasted samples, while sinapic acid was observed only in pressure-cooked, open-pan boiled, and microwave heated samples.

The profile of individual polyphenolic compounds in native sorghum is shown in Figure 1b. Native sorghum contained a total of 16 compounds out of which 9 compounds are identified as gallic acid, protocatechuic acid, caffeic acid, syringic acid, *p*-coumaric acid, ferulic acid, sinapic acid, salicylic acid, and *t*-cinnamic acid (SI Table 2). Concentrations of various phenolic compounds in native and processed sorghum are given in Table 4. Two unidentified phenolic compounds were major compounds in native sorghum, equally contributing together to more than 75% of the total peak area. They are probably hydroxybenzoic acids since they showed maximum absorbance at 280 nm. Unidentified phenol (UK2) was affected significantly by pressure-cooking, open-pan boiling, and

Table 5. Concentrations ($\mu$g/g) of Identified Phenolic Compounds in Native and Processed Wheat Dialysate Samples[a]

| | | | | heat processing | | | |
|---|---|---|---|---|---|---|---|
| sl no. | compound | native | sprouting | roasting | pressure-cooking | open-pan boiling | microwave heating |
| 1 | gallic acid | | 15.8 | 210.0 | 13.37 | | |
| 2 | syringic acid | | | 11.4 | 16.9 | | 14.3 |

[a]Values are means of triplicates.

Table 6. Concentrations ($\mu$g/g) of Identified Phenolic Compounds in Native and Processed Sorghum Dialysate Samples[a]

| | | | | heat processing | | | |
|---|---|---|---|---|---|---|---|
| sl no. | compound | native | sprouting | roasting | pressure-cooking | open-pan boiling | microwave heating |
| 1 | protocatechuic acid | | | 54.5 | | | |
| 2 | *p*-hydroxy benzoic acid | 6.32 | | | 1.9 | 2.85 | 5.02 |
| 3 | vanillic acid | | 28.6 | 29.3 | 23.6 | 19.3 | |
| 4 | caffeic acid | | | 28.1 | 37.0 | 9.80 | |
| 5 | *p*-coumaric acid | 6.52 | 21.4 | 13.1 | 5.10 | 17.3 | 18.8 |
| 6 | ferulic acid | 3.21 | 10.7 | 10.2 | 3.60 | | 12.8 |
| 7 | sinapic acid | 1.56 | | 5.56 | 5.50 | | 1.11 |
| 8 | salicylic acid | 30.7 | 51.9 | 35.3 | | | |
| total identified phenolic compound ($\mu$g/g) | | 48.3 | 112.6 | 176.0 | 66.7 | 49.3 | 37.7 |

[a]Values are means of triplicates.

Table 7. Total Polyphenol and Flavonoid Content and Their Bioaccessibility in Green Gram As Influenced by Domestic Processing

| type of processing | total polyphenol content[a] (mg/g) | bioaccessible polyphenol content[a] (mg/g) | percent bioaccessibility | total flavonoid content[b] (mg/g) | bioaccessible flavonoid content[b] (mg/g) | percent bioaccessibility | tannins (mg/g) |
|---|---|---|---|---|---|---|---|
| native | 4.03 ± 0.51 | 2.71 ± 0.12 | 67.2 | 1.56 ± 0.20 | 0.21 ± 0.02 | 13.5 | 4.05 ± 1.4 |
| sprouting | 2.81 ± 0.51[c] | 2.80 ± 0.21 | 99.6 | 1.64 ± 0.52 | 0.28 ± 0.04[c] | 17.1 | 1.41 ± 0.63[c] |
| cooking | | | | | | | |
| roasting | 5.00 ± 0.35[c] | 3.01 ± 0.08[c] | 60.2 | 1.92 ± 0.20 | 0.21 ± 0.02 | 10.9 | 3.28 ± 0.59 |
| pressure-cooking | 4.65 ± 0.74 | 2.70 ± 0.27 | 58.1 | 1.84 ± 0.30 | 0.25 ± 0.05 | 13.6 | 7.58 ± 0.83[c] |
| open-pan boiling | 4.40 ± 0.37 | 2.85 ± 0.25 | 64.8 | 1.08 ± 0.30[c] | 0.22 ± 0.03 | 20.4 | 7.14 ± 3.21 |
| microwave heating | 3.04 ± 0.48[c] | 2.26 ± 0.41[c] | 74.3 | 1.06 ± 0.12[c] | 0.22 ± 0.07 | 20.7 | 4.69 ± 2.10 |

[a]Gallic acid equivalents. [b]Catechin equivalents. Values are mean ± SD of triplicates. [c]Significantly different from native grain ($P < 0.05$).

microwave heating, which reduced from 38.5 to 6.1, 1.1, and 6.7% respectively. Concentration of salicylic acid (64 $\mu$g/g) was highest among identified phenolics of sorghum followed by gallic acid (46 $\mu$g/g). Roasting (630 to 170 $\mu$g/g) showed extremely higher concentrations of identified phenolic compounds. Sprouting (170 to 144 $\mu$g/g) reduced the concentration of identified phenolics significantly. Drastic reduction of identified compounds was observed on pressure-cooking (170 to 69 $\mu$g/g), open-pan boiling (170 to 57 $\mu$g/g), and microwave heating (170 to 148 $\mu$g/g). Gallic acid concentration was much affected by all forms of processing especially sprouting and pressure-cooking, wherein concentration was either below detectable limit or there was a complete absence of gallic acid. Significant increase of salicylic acid concentration (3-fold) was seen in the roasted sample.

**Bioaccessibility of Polyphenols from Cereal Grains.** Bioaccessible polyphenol content from native wheat was 0.96 mg/g (Table 1). Roasting (26%), pressure-cooking (21%), and microwave heating (20%) reduced bioaccessible flavonoid content significantly ($P < 0.05$), whereas no significant change was noticed on sprouting and open-pan boiling. Bioaccessible flavonoid content of native wheat was only 0.04 mg/g, which did not alter much by any of the domestic cooking processes.

Bioaccessible total polyphenol and total flavonoid in native and processed sorghum is given in Table 2. Bioaccessible polyphenol content from native grain was 0.60 mg/g, which reduced significantly ($P < 0.05$) on roasting, open-pan boiling, and microwave heating (15, 12, and 23%, respectively). Sprouting and pressure-cooking did not show any significant effect on total bioaccessible polyphenol. Total bioaccessible flavonoid content from native grain was 0.09 mg/g, which constituted only about 2.5% of total flavonoid content. No significant changes in bioaccessible flavonoid content were observed in any forms of processing except microwave heating (56% reduction).

*HPLC Profile of Bioaccessible Polyphenols of Cereal Grains.* The profile of bioaccessible polyphenols from native wheat showed that not all compounds were bioaccessible; out of 17 compounds, only 4 phenolic compounds were found to be bioaccessible (chromatogram not shown). The major bioaccessible phenolic compound was an unidentified polyphenol constituting about 90% of the total area percentage of the native grain. Concentrations of identified phenolics are

**Table 8. Total Polyphenol and Flavonoid Content and Their Bioaccessibility in Chickpea As Influenced by Domestic Processing**

| type of processing | total polyphenol content[a] (mg/g) | bioaccessible polyphenol content[a] (mg/g) | percent bioaccessibility | total flavonoid content[b] (mg/g) | bioaccessible flavonoid content[b] (mg/g) | percent bioaccessibility | tannins (mg/g) |
|---|---|---|---|---|---|---|---|
| native | 1.54 ± 0.28 | 1.49 ± 0.28 | 96.7 | 1.47 ± 0.21 | 0.10 ± 0.03 | 6.80 | 0.68 ± 0.22 |
| sprouting | 1.86 ± 0.29 | 1.62 ± 0.20 | 87.1 | 1.75 ± 0.42 | 0.13 ± 0.05 | 7.43 | 0.44 ± 0.09 |
| cooking | | | | | | | |
| roasting | 1.75 ± 0.14 | 1.75 ± 0.22[c] | 100 | 1.43 ± 0.24 | 0.10 ± 0.01 | 6.99 | 0.26 ± 0.33[c] |
| pressure-cooking | 2.36 ± 0.22[c] | 1.33 ± 0.29[c] | 56.3 | 0.29 ± 0.07[c] | 0.11 ± 0.03 | 37.9 | 1.90 ± 0.63[c] |
| open-pan boiling | 2.53 ± 0.61[c] | 1.35 ± 0.13[c] | 53.4 | 0.24 ± 0.07[c] | 0.10 ± 0.01 | 41.7 | 2.67 ± 0.55[c] |
| microwave heating | 3.43 ± 0.48[c] | 1.40 ± 0.22 | 40.8 | 0.33 ± 0.04[c] | 0.09 ± 0.01 | 2.97 | 2.36 ± 0.49[c] |

[a]Gallic acid equivalents. [b]Catechin equivalents. Values are mean ± SD of triplicates. [c]Significantly different from native grain ($P < 0.05$).

**Table 9. Concentrations (μg/g) of Identified Phenolic Compounds in Native and Processed Green Gram[a]**

| | | | | heat processing | | | |
|---|---|---|---|---|---|---|---|
| sl no. | compound | native | sprouting | roasting | pressure-cooking | open-pan boiling | microwave heating |
| 1 | gallic acid | 3.47 | 15.5 | 10.1 | 3.93 | 4.34 | 13.8 |
| 2 | protocatechuic acid | 57.6 | 93.1 | 41.5 | 33.2 | 21.7 | 39.0 |
| 3 | *p*-hydroxy benzoic acid | | | | 17.2 | 8.38 | 0.23 |
| 4 | gentisic acid | | | 8.71 | | | |
| 5 | vanillic acid | 23.1 | 27.5 | 60.7 | | | |
| 6 | caffeic acid | 3.46 | | | | | 1.52 |
| 7 | syringic acid | 123.3 | 113.8 | 123.7 | 158.1 | 107.8 | 140.4 |
| 8 | sinapic acid | 19.2 | 12.9 | 17.4 | 20.5 | 7.6 | 17.9 |
| 9 | *t*-cinnamic acid | 5.91 | 3.03 | 10.3 | 6.17 | 1.39 | 3.26 |
| 10 | rutin | 3.62 | | 1.22 | | | |
| 11 | quercetin | 7.16 | | 23.6 | | | |
| total identified phenolic compound (μg/g) | | 252.5 | 265.8 | 290.5 | 239.1 | 151.2 | 216.1 |

[a]Values are means of triplicates.

given in Table 5. Gallic acid, which was not bioaccessible from the native grain, was bioaccessible from sprouted, roasted, and pressure-cooked samples. Similarly, syringic was bioaccessible from roasted, pressure-cooked, and microwave heated samples.

The HPLC profile of dialysate of native sorghum showed that not all compounds are bioaccessible; out of 16 compounds, only 5 compounds were bioaccessible (chromatogram not shown). The major compound in native and processed samples was an unidentified compound, while the identified compounds were *p*-hydroxy benzoic acid, *p*-coumaric acid, ferulic acid, sinapic acid, and salicylic acid. Concentrations of identified phenolic compounds are given in Table 6. Among the identified phenolic compounds, salicylic acid was the major compound in native grain. Sprouting and roasting significantly increased the concentration of identified compounds (48 to 112 and 176 μg/g, respectively) ($P < 0.05$), while pressure-cooking, open-pan boiling, and microwave heating did not make any significant difference. The concentration of vanillic acid (which was originally not present in this grain) was particularly increased on processing, except microwave heating.

**Total Polyphenol, Flavonoid, and Tannin Content of Legumes.** Total polyphenol, total flavonoid, and tannin content of native and processed green gram are given in Table 7. Total polyphenol content of native green gram was 4.03 mg/g. Significant reduction of total polyphenol content was observed on sprouting (30% decrease) and microwave heating (25% decrease). Pressure-cooking and open-pan boiling of green gram did not alter the polyphenol content. Total flavonoid content of native green gram was 1.56 mg/g, which reduced significantly on open-pan boiling and microwave heating (about 30% decrease in each case). Sprouted, roasted, and pressure-cooked samples did not show any significant difference in total flavonoid content. Tannin content was reduced from 4.05 to 1.41 mg/g on sprouting, while roasting (87%) and open-pan boiling (76%) increased the same which correlated with the increase in total polyphenol content.

Total polyphenol content of native chickpea was 1.54 mg/g, which increased on pressure-cooking (53%), open-pan boiling (64%), and microwave heating (by >2-fold increase) (Table 8). Total flavonoid content of native legume was 1.47 mg/g, which drastically reduced on pressure-cooking (80%), open-pan boiling (84%), and microwave heating (78%). Sprouted and roasted samples did not show any difference in total polyphenol or total flavonoid content. Tannin content of native chickpea was 0.68 mg/g, which reduced significantly on roasting (62%). Pressure-cooking (>2-fold), open-pan boiling, and microwave heating (both >3-fold) increased total tannin to a large extent.

**HPLC Profile of Phenols of Legumes.** Native green gram showed a total of 20 polyphenols on HPLC, out of which 9 were identified (SI Table 3). HPLC profile showed gallic acid, protocatechuic acid, vanillic acid, caffeic acid, syringic acid, sinapic acid, *t*-cinnamic acid, rutin, and quercetin among identified phenolic compounds (Figure 1c), while the two major phenolics were not identified. Concentrations of

Table 10. Concentrations ($\mu$g/g) of Identified Phenolic Compounds in Native and Processed Chickpea[a]

| | | | | heat processing | | | |
|---|---|---|---|---|---|---|---|
| sl no. | compound | native | sprouting | roasting | pressure-cooking | open-pan boiling | microwave heating |
| 1 | gallic acid | 40.2 | 14.7 | | 12.6 | 15.7 | 20.8 |
| 2 | protocatechuic acid | 358.9 | 22.7 | 514.2 | 466.8 | 283.9 | 312.1 |
| 3 | *p*-hydroxy benzoic acid | 10.5 | 9.84 | 14.9 | | 57.6 | 53.3 |
| 4 | gentisic acid | 26.0 | 15.1 | 34.4 | 13.6 | 15.2 | 18.5 |
| 5 | vanillic acid | 80.8 | 74.2 | 70.2 | 7.54 | 34.4 | 45.1 |
| 6 | syringic acid | 222.1 | 206.6 | 186.9 | 222.1 | 270.2 | 354.9 |
| 7 | *p*-coumaric acid | | | | 0.33 | 0.51 | 0.46 |
| 8 | ferulic acid | 0.90 | | | 0.97 | 0.84 | 0.84 |
| 9 | sinapic acid | 7.81 | | | 0.47 | 0.53 | 0.49 |
| 10 | salicylic acid | | 29.2 | | 76.6 | 37.5 | 6.57 |
| 11 | luteolin | 1.56 | | | 6.55 | 8.31 | 10.2 |
| 12 | *t*-cinnamic acid | | | | | | 2.93 |
| total identified phenolic compound ($\mu$g/g) | | 748.8 | 372.3 | 820.6 | 807.6 | 724.7 | 825.7 |

[a]Values are means of triplicates.

Table 11. Concentrations ($\mu$g/g) of Identified Phenolic Compounds in Native and Processed Green Gram Dialysate Samples[a]

| | | | | heat processing | | | |
|---|---|---|---|---|---|---|---|
| sl no. | compound | native | sprouting | roasting | pressure-cooking | open-pan boiling | microwave heating |
| 1 | gallic acid | 58.4 | 57.0 | | 16.1 | 43.6 | 55.9 |
| 2 | protocatechuic acid | 17.6 | 80.3 | 63.1 | 33.2 | 30.9 | 21.5 |
| 3 | *p*-hydroxy benzoic acid | | 2.61 | | | | |
| 4 | syringic acid | | 66.5 | 35.3 | 15.7 | 33.8 | |
| 5 | *p*-coumaric acid | 12.7 | 77.8 | 26.7 | 2.68 | 11.0 | |
| 6 | ferulic acid | | 1.4 | | | | |
| 7 | sinapic acid | 25.8 | 13.7 | 31.8 | 20.5 | 32.2 | 24.6 |
| 8 | *t*-cinnamic acid | | | 1.17 | 0.38 | | |
| 9 | hesperitin | | | | 6.88 | 6.62 | |
| total identified phenolic compound ($\mu$g/g) | | 114.5 | 252.3 | 158.1 | 95.4 | 147.4 | 102.0 |

[a]Values are means of triplicates.

identified compounds are represented in Table 9. Total concentration of identified phenolic compounds in native green gram was 252 $\mu$g/g. Open-pan boiling drastically reduced the concentration of identified phenolic compounds (from 252 to 151 $\mu$g/g). No significant difference was observed in other types of processing.

Phenolic compounds identified from the HPLC profile of native chickpea were gallic acid, protocatechuic acid, *p*-hydroxy benzoic acid, gentisic acid, vanillic acid, syringic acid, and luteolin (Figure 1d). The major phenolic of chickpea could not be identified, while among identified compounds, syringic acid followed by protocatechuic acid were major compounds (SI Table 4). Concentration of identified compounds in native legume was 748 $\mu$g/g, which drastically reduced to about 50% upon sprouting (Table 10). Other processing methods did not significantly influence the concentration of identified polyphenol compounds.

**Bioaccessibility of Polyphenols from Legumes.** Bioaccessible portion of total polyphenols, total flavonoids, and tannins from native and processed green gram are given in Table 7. Total bioaccessible polyphenol content in native green gram was 2.71 mg/g, which did not alter significantly on sprouting, pressure-cooking, or open-pan boiling. Roasted green gram showed higher (11%) total bioaccessible content while microwave-heated sample showed decreased content (16%) compared to native grain. Total bioaccessible flavonoid content from native green gram was 0.21 mg/g and an increase of 33% of the same was observed in sprouted sample. Heat processing generally did not change the total bioaccessible flavonoid content of green gram.

Bioaccessible polyphenol content of native chickpea was 1.49 mg/g (Table 8). Significant increase in bioaccessible total polyphenol content was seen in roasted samples (17%), while reduction of the same was observed in pressure-cooked (11%) and open-pan boiled samples (10%). Bioaccessible total flavonoid content of native legume was only 100 $\mu$g/g, which remained unaltered in all the processed samples.

*HPLC Profile of Bioaccessible Polyphenols of Legumes.* HPLC profile of bioaccessible polyphenols of native green gram (not shown) revealed a total of 11 compounds, out of which identified ones are gallic acid, protocatechuic acid, *p*-coumaric acid, and sinapic acid. Three major unidentified compounds constituted about 96% of the total bioaccessible phenolics. As given in Table 11, concentration-wise, gallic acid was highest (58 $\mu$g/g) followed by sinapic acid (26 $\mu$g/g). Concentration of total identified bioaccessible polyphenols increased >2-fold on sprouting. Significant reduction of identified polyphenols was seen on pressure-cooking (17%) ($P < 0.05$).

Bioaccessible polyphenols from native chickpea consisted of 9 compounds, out of which 4 were identified as gallic acid, protocatechuic acid, salicylic acid, and rutin. Not all compounds found in the native grain were bioaccessible (HPLC profile not

Table 12. Concentrations ($\mu$g/g) of Identified Phenolic Compounds in Native and Processed Chickpea Dialysate Samples[a]

| | | | | heat processing | | | |
|---|---|---|---|---|---|---|---|
| sl no. | compound | native | sprouting | roasting | pressure-cooking | open-pan boiling | microwave heating |
| 1 | gallic acid | 78.5 | 81.9 | 88.9 | 55.3 | 79.2 | 99.9 |
| 2 | protocatechuic acid | 45.7 | 50.3 | 186.6 | 187.2 | 74.1 | 169.4 |
| 3 | salicylic acid | 322.6 | 118.1 | 234.7 | 322.8 | 277.9 | 320.9 |
| 4 | *t*-cinnamic acid | | | 153.3 | | | |
| 5 | rutin | 29.8 | 13.5 | 30.3 | 32.1 | 40.1 | 32.6 |
| total identified phenolic compound ($\mu$g/g) | | 476.6 | 263.8 | 693.8 | 597.4 | 471.3 | 622.8 |

[a]Values are means of triplicates.

shown). Concentrations of different phenolic compounds bioaccessible from native and processed chickpea are given in Table 12. Concentration of total bioaccessible identified polyphenol from native sample was 477 $\mu$g/g, which reduced to about 55% on sprouting. On the other hand, significant increase of the same was noticed after roasting (45%), pressure-cooking (25%,) and microwave heating (30%) ($P < 0.05$), while open-pan boiling produced no significant change.

## DISCUSSION

Cereals and legumes are important food components in vegetarian populations because of their high nutritional quality, and these are generally consumed after some form of processing. It is well-known that processing may affect the composition of cereals and legumes to a significant extent. Knowledge on the bioaccessibility of polyphenols as influenced by domestic processing is limiting. The present investigation was aimed to assess the total and bioaccessible polyphenol content of the common cereals (wheat and sorghum) and legumes (green gram and chickpea) as influenced by various domestic processing methods.

Total polyphenol content of native sorghum observed in the present study viz., 1.12 mg/g, is similar to the value reported in literature.[22] Sorghum showed higher amount of total flavonoid content in both native and processed forms compared to wheat. Sprouting increased total polyphenol content in wheat. It is reported that sprouted waxy wheat variety has better nutritional composition, with higher total phenolic content along with higher dietary fiber and free amino acids, than the unsprouted wheat.[23,24] As seen in the earlier reports, our study also showed higher amount of tannins in sorghum when compared to wheat, which increased considerably on sprouting and roasting. There is evidence of possible health benefits of tannins, which has led to the research on sorghum tannins.[25,26] Pressure-cooking, open-pan boiling, and microwave heating significantly reduced total polyphenol, total flavonoid, and tannin content in both sorghum and wheat.

Green gram provides appreciable amounts of total polyphenol compared to chickpea (4.03 vs 1.54 mg/g) among the two legumes studied, however, these values are higher than those reported by Shweta et al.[27] The observed reduction in total polyphenol content during sprouting agrees with the report of Antu and Sudesh.[28] Interestingly, total polyphenol content increased significantly after pressure-cooking, open-pan boiling, and microwave heating in chickpea. This may be due to the disruption of matrix of legume in the presence of excess of water and temperature. This is interesting in the context of antihyperglycemic activity along with antioxidant properties of chickpea being attributable to its polyphenols.[29] Sprouting caused a significant reduction in total polyphenols of green gram, but not in the case of chickpea. It may also be noted that germinated chickpea is reported to be effective in reducing cholesterol levels in rats,[30] and diets containing roasted chickpea had a beneficial effect on both triglyceride and cholesterol levels in rats.[31] The effect of pressure-cooking, open-pan boiling, and microwave heating on the total flavonoid content was more in the case of chickpea as compared to green gram. Total tannin content of green gram was comparatively higher than in chickpea.

The number of phenolic compounds present in chickpea was found to be more when compared to green gram, wheat, and sorghum. As observed in our previous study,[15] roasting increased the concentration of phenolic compounds irrespective of the grains studied. In the case of sprouting, the concentration of identified polyphenols increased significantly in sorghum and chickpea. When individual phenolic compounds were considered, concentration of vanillic acid and ferulic acid increased in sprouted wheat, as observed by Yang et al.[32] Vanillic acid concentration increased significantly after roasting of all the grains except chickpea. Syringic acid concentration increased significantly in all the grains on microwave heating. Reduction in the concentration of phenolic compounds was observed after pressure-cooking, open-pan boiling, and microwave heating in wheat, sorghum, and green gram.

Wheat provided comparatively more bioaccessible polyphenols than sorghum. Roasting and microwave heating decreased total bioaccessible polyphenol content from both sorghum and wheat. Total bioaccessible flavonoid content from both these cereals was very low (1−20% bioaccessible) compared to bioaccessible total polyphenol content. Bioaccessible polyphenol content from legumes was more than that found from the cereals. However, bioaccessible polyphenol from green gram was comparatively more than the bioaccessible total polyphenol from chickpea. Similar trend was seen in the case of bioaccessible flavonoid content from green gram and chickpea. Domestic processing methods did not show any effect (except sprouting and microwave heating) on the bioaccessible flavonoid content from both the legumes and cereals. Although there was a seemingly increase in the total polyphenol content after pressure-cooking, open-pan boiling, and microwave heating in chickpea, this was not consequent in the total bioaccessible polyphenol content.

Phenolic acids, both hydroxybenzoic and hydroxycinnamic acids, were most common polyphenolic compounds detected in all the grains analyzed. Generally, not all the phenolic compounds (revealed by HPLC), were bioaccessible from the grains analyzed. An unidentified phenolic compound which constituted about 38% of native sorghum was less than 2% bioaccessible. The number of phenolic compounds bioacces-

sible from green gram was more than that from all other grains. Wheat showed comparatively lesser number of bioaccessible polyphenols than sorghum. Roasting had a notable effect on the polyphenol content in wheat as compared to any other processing methods. Sprouting increased the concentration of bioaccessible polyphenols especially in sorghum and green gram. It has been shown that cereals which fulfill the nutritional principles of whole grains, on sprouting become more nutritious in terms of phenolic compounds, vitamins, and minerals when compared to their native form as grain's mobilized energy reservoir becomes readily available in its active form.[33] Concentration of bioaccessible ferulic acid was particularly increased on sprouting, roasting, and microwave heating of sorghum. Ferulic acid, a common phenolic acid has been reported to elevate the activities of detoxifying enzymes, namely glutathione-*S*-transferase, and lower the incidence of colonic carcinomas induced by azoxymethane in vivo.[34] Concentration of protocatechuic acid increased significantly after domestic processing in green gram and chickpea. Protocatechuic acid, which is structurally similar to gallic acid, has been associated with a large number of pharmacological properties.[35]

As reported earlier in finger millet and pearl millet, it appears that polyphenols present at higher concentration in the grain are not necessarily more bioaccessible.[15] Composition of bioaccessible phenolic compounds varied among wheat and sorghum when compared to finger millet and pearl millet. Sprouting and roasting had a beneficial effect on the concentration of polyphenols in all the grains as observed in the case of finger millet and pearl millet. Among the cereals studied, wheat stands next to pearl millet in terms of bioaccessible polyphenols.

Significant difference was observed in the polyphenol content among the grains studied. Even though cereals and legumes possessed appreciable amounts of polyphenols, the amount of bioaccessible polyphenols was considerably low. Domestic processing had a marked effect on the phenolic profiles of cereals and legumes studied, with the effect depending mainly on the food matrix. Typically, sprouting, which increased the concentration of bioaccessible polyphenols in green gram, drastically reduced the same in the case of chickpea. Sprouting and roasting had a more advantageous effect over other domestic processing methods. Use of sprouted and roasted grains as ingredients in the functional foods could provide a higher amount of bioaccessible polyphenols/flavonoids in order to maximize the potential health benefits from them.

## ■ ASSOCIATED CONTENT

### Ⓢ Supporting Information

Additional data tables as mentioned in the text. This material is available free of charge via the Internet at http://pubs.acs.org.

## ■ AUTHOR INFORMATION


### Corresponding Author

*E-mail: ksri.cftri@gmail.com. Fax: +91-821-2517233. Tel: +91-821-2514876.


### Notes

The authors declare no competing financial interest.

## ■ ACKNOWLEDGMENTS

G.H. is thankful to the Indian Council of Medical Research, New Delhi for the award of Senior Research Fellowship.

## ■ REFERENCES


(1) Singh, M.; Arseneault, M.; Sanderson, T.; Murthy, V.; Ramassamy, C. Challenges for research on polyphenols from foods in alzheimer's disease: bioavailability, metabolism, and cellular and molecular mechanisms. *J. Agric. Food Chem.* **2008**, *56*, 4855−4873.

(2) Abdul-Hamid, A.; Luan, Y. S. Functional properties of dietary fibre prepared from defatted rice bran. *Food Chem.* **2000**, *68*, 15−19.

(3) Truswell, A. S. Cereal grains and coronary heart disease. *Eur. J. Clin. Nutr.* **2003**, *56*, 1−14.

(4) Food and Agriculture Organization of the United Nations. *FAOSTAT*. http://faostat.fao.org/default.aspx.

(5) Adom, K. K.; Sorrells, M. E.; Liu, R. H. Phytochemical profiles and antioxidant activity of wheat varieties. *J. Agric. Food Chem.* **2003**, *51*, 7825−7834.

(6) Dykes, L.; Rooney, L. W.; Waniska, R. D.; Rooney, W. L. Phenolic compounds and antioxidant activity of sorghum grains of varying genotypes. *J. Agric. Food Chem.* **2005**, *53*, 6813−6818.

(7) Awika, J. M.; Rooney, L. W.; Wu, X.; Prior, R. L.; Cisneros-Zevallos, L. Screening methods to measure antioxidant activity of sorghum (*Sorghum bicolor*) and sorghum products. *J. Agric. Food Chem.* **2003**, *51*, 6657−6662.

(8) Fardet, A. New hypotheses for the health-protective mechanisms of whole-grain cereals: what is beyond fibre? *Nutr. Res. Rev.* **2010**, *23*, 65−134.

(9) de Munter, J. S.; Hu, F. B.; Spiegelman, D.; Franz, M.; van Dam, R. M. Whole grain, bran, and germ intake and risk of type 2 diabetes: a prospective cohort study and systematic review. *PLoS Med.* **2007**, *4*, 1385−1395.

(10) Jensen, M. K.; Koh-Banerjee, P.; Hu, F. B.; Franz, M.; Sampson, L.; Gronbaek, M.; Rimm, E. B. Intakes of whole grains, bran, and germ and the risk of coronary heart disease in men. *Am. J. Clin. Nutr.* **2004**, *80*, 1492−1499.

(11) Aparicio-Fernández, X.; García-Gasca, T.; Yousef, G. G.; Lila, M. A.; González de Mejia, E.; Loarca-Piña, G. Chemopreventive activity of polyphenolics from black Jamapa bean (*Phaseolus vulgaris* L.) on HeLa and HaCaT cells. *J. Agric. Food Chem.* **2006**, *54*, 2116−2122.

(12) Aparicio-Fernández, X.; Reynoso-Camacho, R.; Castaño-Tostado, E.; García-Gasca, T.; González de Mejía, E.; et al. Antiradical capacity and induction of apoptosis in HeLa cells by a *Phaseolus vulgaris* extract. *Plant Foods Hum. Nutr.* **2008**, *63*, 35−40.

(13) Dong, M.; He, X.; Liu, R. H. Phytochemicals of black bean seed coats: isolation, structure elucidation, and their antiproliferative and antioxidative activities. *J. Agric. Food Chem.* **2007**, *55*, 6044−6051.

(14) Tagliazucchi, D.; Verzelloni, E.; Bertolini, D.; Conte, A. *In vitro* bioaccessibility and antioxidant activity of grape polyphenols. *Food Chem.* **2010**, *120*, 599−606.

(15) Hithamani, G.; Srinivasan, K. Effect of domestic processing on the polyphenol content and bioaccessibility in finger millet (*Eleusine coracana*) and pearl millet (*Pennisetum glaucum*). *Food Chem.* **2014**, *164*, 55−62.

(16) Chetan, S.; Malleshi, N. G. Finger millet polyphenols: Optimization of extraction and the effect of pH on their stability. *Food Chem.* **2007**, *105*, 860−870.

(17) Singleton, V. L.; Rossi, J. A. Colorimetry of total phenolics with phosphomolybdic-phosphotungstic acid reagents. *Am. J. Enol. Vitic.* **1965**, *16*, 144−158.

(18) Zhishen, J.; Mengcheng, T.; Jianming, W. Determination of flavonoid contents in mulberry and their scavenging effects on superoxide radicals. *Food Chem.* **1999**, *64*, 555−559.

(19) Price, M. L.; Van Scoyoc, S.; Butler, L. G. A critical evaluation of the vanillin reaction as an assay for tannin in sorghum grain. *J. Agric. Food Chem.* **1978**, *26*, 1214−1218.

(20) Court, W. A. High-performance reversed-phase liquid chromatography of naturally occurring phenolic compounds. *J. Chromatogr.* **1977**, *130*, 287−291.

(21) Luten, J.; Crews, H.; Flynn, A.; Van Dael, P.; Kastenmayer, P.; et al. Inter-laboratory trial on the determination of the *in vitro* iron dialyzability from food. *J. Sci. Food Agric.* **1996**, *72*, 415−424.

(22) Afify, A. E.-M. M. R.; El-Batagi, H. S.; El-Salam, S. M. A.; Omran, A. A. Biochemical changes in phenols, flavonoids, tannins, vitamin E, β-carotene and antioxidant activity during soaking of three white sorghum varieties. *Asian Pac. J. Trop. Biomed.* **2012**, *2*, 203−209.
(23) Hung, P. V.; Hatcher, D. W.; Barker, W. Phenolic acid composition of sprouted wheats by ultra-performance liquid chromatography (UPLC) and their antioxidant activities. *Food Chem.* **2011**, *126*, 1896−1901.
(24) Hung, P. V.; Maeda, T.; Yamamoto, S.; Morita, N. Effects of germination on nutritional composition of waxy wheat. *J. Sci. Food Agric.* **2012**, *92*, 667−672.
(25) Prior, R. L.; Gu, L. Occurrence and biological significance of proanthocyanidins in the American diet. *Phytochemistry* **2005**, *66*, 2264−2280.
(26) Henley, E. C.; Taylor, J. R.; Obukosia, S. D. The importance of dietary protein in human health: combating protein deficiency in sub-Saharan Africa through transgenic biofortified sorghum. *Adv. Food Nutr. Res.* **2010**, *60*, 21−52.
(27) Shweta, K.; Shobha, A. U.; Padmini, G. Polyphenols and tannins in Indian pulses: Effect of soaking, germination and pressure cooking. *Food Res. Int.* **2010**, *43*, 526−530.
(28) Antu, G.; Sudesh, J. Effect of processing treatments on nutritional and antinutritional contents of green gram. *J. Food Biochem.* **2006**, *30*, 535−546.
(29) Tiwari, A. K.; Swapna, M.; Ayesha, S. B.; Zehra, A.; Agawane, S. B.; Madhusudana, K. Identification of proglycemic and antihyperglycemic activity in antioxidant rich fraction of some common food grains. *Int. Food Res. J.* **2011**, *18*, 915−923.
(30) Jaya, T. V.; Venkataraman, L. V.; Murthy, K. S. K. Influence of germinated legumes on hypercholesteremic rats: influence of ungerminated or germinated chickpea and green gram. *Nutr. Rep. Int.* **1979**, *20*, 371−381.
(31) Chandrasekhar, T. M. U.; Geetha, G.; Shanthi, V. Effect of raw and roasted chickpea on some physiological parameters in albino rats. *Indian J. Nutr. Diet.* **1983**, *20*, 40−45.
(32) Yang, F.; Basu, T. K.; Ooraikul, B. Studies on germination conditions and antioxidant contents of wheat grain. *Int. J. Food Sci. Nutr.* **2001**, *52*, 319−330.
(33) Plaza, L.; de Ancos, B.; Cano, P. M. Nutritional and health-related compounds in sprouts and seeds of soybean (*Glycine max*), wheat (*Triticum aestivum*.L) and alfalfa (*Medicago sativa*) treated by a new drying method. *Eur. Food Res. Technol.* **2003**, *216*, 138−144.
(34) Kawabata, K.; Yamamoto, T.; Hara, A.; Shimizu, M.; Yamada, Y.; Matsunaga, K.; Tanaka, T.; Mori, H. Modifying effects of ferulic acid on azoxymethane-induced colon carcinogenesis in F344 rats. *Cancer Lett.* **2000**, *157*, 15−21.
(35) Kakkar, S.; Bais, S. A review on protocatechuic acid and its pharmacological potential. *ISRN Pharmacol.* **2014**, *2014*, 1−9.

times.[21] Several ANCs could be detected in the whole eyeball of pigs[1] fed 2.4−12 mg ANC/kg body weight in blueberries for up to 8 weeks and where the concentration in the whole eye appeared to be correlated with blueberry dose. Human intake of ANC is estimated at approximately 200 mg daily in the North American population[22] or approximately 2.7 mg/kg body weight for a 72 kg person.

Despite the volume of research surrounding ANC effects on vision and their ability to become localized in ocular tissues, there is still a paucity of solid clinical evidence to support existing commercial claims of improvement in night vision to normal-sighted individuals associated with the consumption of blueberries and other ANC-containing foods. This paper describes the results of two placebo-controlled, randomized crossover studies that tested a normal-sighted middle-aged human population for blueberry ANC effects on dark adaptation, scotopic vision, and recovery from photobleaching of the retina.

## MATERIALS AND METHODS

**Study Design and Participants.** Two prospective, placebo-controlled, double-blind, crossover studies, S2 (short duration, two products) and L1 (long duration, one product), were conducted to examine human visual function after intake of blueberry products. Vision testing was conducted under reduced light at specific intervals after the consumption of blueberry products, placebo, or nothing (washout). In S2 the assignment of the 72 subjects to two crossover groups was balanced between testing sites (2), gender (2) and age (3) (Table 1). Similarly, in L1 the assignment of the 59 subjects to two crossover groups was balanced between testing sites (2), gender (2), and age (2) (Table 1). There were no drop-outs from S2, whereas in L1 there were two. Partial results of drop-outs were removed from the L1 analysis. Both studies were approved by the research ethics review board of Dalhousie University (Canada) and were in accordance with the tenets of the Declaration of Helsinki. The Clinicaltrials.gov identifier for both S2 and L1 is NCT01942746.

One hundred and twenty individuals were recruited using printed advertisements posted in two rural communities of Nova Scotia, Canada. Inclusion criteria were male or female, age 35−65 years, with no ocular history other than refractive glasses. The minimum criteria for visual function required for inclusion were (1) visual acuity better than 6/7.5 on EDTRS acuity chart (VectorVision, Greenville, OH, USA) at 2.5 m, (2) contrast sensitivity within normal range to all spatial frequencies tested on Visteck 3000 (VectorVision) at 2.5 m, (3) stereoacuity better than 80 s of arc on Frisby stereoacuity test (Clement Clarke International Ltd., Essex, UK), and (4) intraocular pressure lower than 21 mmHg from the average of three measures using a Mentor tonopen-XL (Innova Medical Ophthalmics, Toronto, Canada).

In the process of eliminating amblyopia (dimness in vision), candidates were examined for manifest strabismus (unable to focus both eyes on one spot) and anisotropia (nonuniform responsiveness between both eyes). Ophthalmologic examination also included direct retinoscopic assessment of retinal pigment epithelium and retina as well as a slit lamp examination of anterior segment. Family and medical history excluded subjects with family history of retinal degeneration, glaucoma, diabetes, hypertension, cataract, and amblyopia. On the basis of these criteria, 72 and 59 subjects were recruited for S2 and L1, respectively, and were assigned to groups that were age and gender-matched (Table 1). All 59 participants of L1 had previously participated in S2. The S2 was completed approximately 7 months before the commencement of L1.

During the intervention and the washout period of both S2 and L1, subjects were instructed to abstain from ANC-containing foods and were provided with a list of alternative fruit choices, such as melons, green grapes, kiwi fruit, green-peeled apples. Compliance to the dietary restriction was assessed using a questionnaire. All subjects were considered to be well-nourished before and during the study. During the study their diet was modified only by the restriction on intake of nonapproved ANC-containing products.

**Table 1. Summary of Two Clinical Trials, S2 and L1, That Examine Blueberry Anthocyanin Effects on Dark Vision**

| | | clinical trial | |
|---|---|---|---|
| | | short trial with two blueberry products (S2) | long trial with one blueberry product (L1) |
| study design | randomized, double-blind | double crossover | single crossover |
| vision testing | sites | 2 | 2 |
| | testers | 2 | 1 |
| vision testing schedule | after products | 3 weeks | 8 weeks |
| | | | 12 weeks |
| | after washout | 3 weeks | 4 weeks |
| | | | 8 weeks |
| test products and daily dose | placebo | red beet powder, 3 capsules | placebo juice (300 mL) |
| | blueberry juice | 300 mL containing 271 mg C3g eq[a] | 300 mL containing 346 mg C3g eq |
| | other products | blueberry powder, 3 capsules, 7.11 mg C3g eq | none |
| study population | no. of subjects | 72 | 59 |
| | age and gender | age 35−47 years; M = 11; F = 16 | age 35−50 years; M = 8; F = 14 |
| | | age 48−55 years; M = 9; F = 17 | age 51−65 years; M = 14; F = 24 |
| | | age 56−65 years; M = 7; F = 12 | |
| | drop out | 0 | 2 |

[a]C3g eq, cyanidin 3 glucoside equivalents.

**Test Products.** In both S2 and L1 blueberry intake was standardized for ANC content, which was consumed in the form of single-strength blueberry juice (BJ) and in S2 also as a freeze-dried BJ powder. BJ was produced using a commercial process (VanDyks Health Products, Caledonia Nova Scotia, www.vandykblueberries.ca) using previously frozen blueberries that were equal proportions of the cultivars 'Tifblue' (*V. asheii* Reade) and 'Rubel' (*V. corymbosum* L.). The composition of these blueberry cultivars has been reported.[23] Pasteurized juice was stored in 350 mL clear glass bottles, kept refrigerated, and stored in the dark until delivery to subjects and for no longer than 3 months.

In S2 colorimetric analysis of ANCs[24] at the time of BJ production indicated an ANC concentration of 6.04 (SD = 0.18) mg of C3g eq/g dry weight. In L1, BJ had an ANC concentration of 6.83 (SD = 0.20) mg C3g eq/g dry weight at the time of production that declined by 19% to 5.52 (SD = 0.09) mg C3g eq/g dry weight by the end of 3 months of refrigerated storage. In both S2 and L1, 300 mL of BJ and in L1 300 mL of placebo juice composed of food grade ingredients (Table 2) were consumed daily. The BJ provided subjects in S2 with a daily ANC dose of 271 mg C3g eq and in L1 with 346 mg C3g eq (Table 1). The BJ powder used in S2 was produced from freeze-dried BJ and packaged in gelatin capsules. Each capsule contained 2.37 mg C3g eq per capsule; three capsules were consumed for a total daily ANC intake of 7.11 C3g eq. In S2 the placebo was freeze-dried red beet powder in gelatin capsules. Red beet color is due to betalain pigments. Red beets do not contain ANCs; their nutrient composition

**Table 2. Composition of Blueberry Juice Placebo Used in Trial with Long Intervention and One Blueberry Test Product (L1)**

| ingredient | percent (w/w) |
|---|---|
| water | 88.37 |
| fructose | 4.0 |
| glucose | 4.0 |
| ascorbic acid | 0.5 |
| citric acid | 0.5 |
| sodium citrate | 0.3 |
| malic acid | 0.3 |
| red color | 0.70 |
| blue color | 0.02 |
| cranberry flavor | 0.60 |
| blueberry flavor | 0.70 |
| xanthum gum | 0.015 |
| total | 100.00 |

has been described.[25] Subjects were instructed to consume their test product before noon.

Dietary compliance was assessed in L1 using a questionnaire where full compliance for test product consumption was defined as having taken a total 300 mL of BJ or placebo at least 5 days per week. Full compliance to the ANC-free dietary restriction was defined as two or fewer servings of ANC-containing food per week. No adjustment was made to account for missed doses of product or noncompliance to the ANC-free diet.

**Product Intake and Vision Testing.** In S2 vision was tested two times and in L1 vision was tested three times before the diet intervention commenced so that subjects could become accustomed to the way in which the vision tests were conducted. In S2 after this pretreatment testing, subjects consumed BJ products or placebo daily for 3 weeks. Randomization was carried out to assign the order of dietary treatment to each subject. In S2 each subject had their vision tested after 3 weeks of product intake and then again after 3 weeks of washout until all three products (BJ, BJ capsule, placebo) were tested. This 3 week cycle to test three products each took 18 weeks. In L1 after pretreatment testing and randomization, vision was tested after 8 and 12 weeks of daily BJ or placebo intake and after 4 and 8 weeks of washout. In L1 this cycle of two products and two washouts took 40 weeks. Vision was tested at the same time of the day (±2 h) within an individual to avoid possible diurnal effects on vision. No attempt was made to schedule vision testing at a fixed period after consumption of BJ, BJ capsules, or placebos. Vision was always tested by the same person and at the same location (Table 1).

A vision testing session lasted <90 min. The vision tests were always performed in the same order, starting with dark adaptation (DA) followed by scotopic visual acuity (VA), contrast sensitivity (CS), and finally the test for macular stress recovery (MSR) time. The tests were generated by computerized systems (VPixx v.3.0, VPIXX Technologies, St. Bruno, Canada) on a Macintosh computer and displayed on a high-resolution (1960 × 1280 pixels) calibrated CRT monitor (model G90f, ViewSonic, Walnut, CA, USA) using custom-made protocols. Calibration (LS-110 photometer, Minolta, Ramsey, NJ, USA) of the CRT monitor for each workstation was carried out at the start of the study, and the calibration results were verified at the end of the study to ensure stability of the monitor output.

**Vision Testing.** *Dark Adaptation (DA) Testing.* In S2, subjects were first asked to look at a diffuse light of 12000 lx for 120 s to achieve controlled photobleaching of their retinal pigment. Room lights were then turned off and the 30 min DA test was performed in the dark. A red fixation target was presented on the right-hand side of the computer monitor. For the right eye, a dim white stimulus light was randomly presented in the upper or lower part of the left side of the monitor, at a distance of 15° nasal to the fixation point. The intensity of the light stimulus was increased until the subject could identify the position of the light stimulus. Up to 20 s was allowed for the subject to determine the position of the light stimulus on the monitor (upper or lower portion). This task was repeated once every minute for 30 min. To compensate for the limitations of the monitor's range of light intensities as subjects became dark adapted, subjects wore neutral density filtered goggles as their DA progressed in both S2 and L1. Goggles were applied when the monitor's intensity was close to the minimum range, where linearity in luminosity was more variable.

In L1 standard retinal photobleaching before DA testing employed a light intensity of 25000 lx for 120 s. In contrast to S2 DA testing, in the L1 the intensity of the dim light was decreased until it could no longer be perceived. Although these two strategies (increasing vs decreasing light intensity) yielded different absolute threshold values between S2 and L1, there was no impact on the DA dynamic changes.

*Visual Acuity (VA) Testing.* To test scotopic VA after the 30 min DA test, subjects continued to wear the light attenuation goggles while single black optotypes of varying size with crowding bars against a white background were presented to them. There were eight different optotypes (letters) of similar discrimination difficulties.[26] Optotype light intensity was 100 cd/m$^2$ for the background and 0.316 cd/m$^2$ for the black letters. Optotypes were first shown at a small size and then their size was increased until the subject could correctly identify the letter. The VA values were measured as the minimum size of the optotype that was correctly perceived through a staircase threshold approach with the third to the sixth reversals averaged for a final value. With this method the threshold scotopic VA was measured 12 times per session.

*Contrast Sensitivity (CS) Testing.* While still in darkness and with the subject wearing the light attenuation goggles, sine wave gratings of three spatial frequencies (1, 3, and 10 cycles/degree) were presented at various levels of contrast, starting at 50% of full black/white contrast using the Michaelson contrast equation.[27] A staircase method was used to determine the minimum contrast discernible. The three spatial frequencies were randomized, and the subject had to correctly determine the orientation of the grating on the monitor (−30, 0, or 30°). Following a correct answer the tester decreased the contrast, whereas after an incorrect answer, the tester increased the contrast. The mean of eight final reversals was considered as the CS threshold for each of the spatial frequencies. In our statistical analysis, we retained only the CS threshold, expressed in percent contrast, for one of the three spatial frequencies used (3 cycles/degree).

*Macular Stress Recovery (MSR) Testing.* For the MSR test, the light attenuation goggles were removed. Then VA was measured as the smallest readable optotype from a computerized five-line, five-letter chart similar to EDTRS charts with a white background intensity set at 100 cd/m$^2$. After VA was established in those conditions, retinal photobleaching was achieved when one eye was exposed to a diffuse light of $3.5 \times 10^4$ cd/m$^2$ (intensity measured at the cornea) for 20 s in S2 or, in L1, to $8.0 \times 10^4$ cd/m$^2$ for 20 s. After this bleaching exposure, the subject was presented again with the EDTRS chart, and the time was measured to recover VA to one line above the smallest optotype before retinal photobleaching. To ensure minimal bias, EDTRS charts presented after bleaching were different from those presented before bleaching, however, with letters of the same reading difficulty level. Due to the nature of the bleaching process, the test could be conducted only once during a vision testing session.

**Statistical Analysis.** *Experimental Design.* Data were analyzed using the ANOVA procedure in GenStat.[28] S2 and L1 employed a crossover design that was balanced between testing sites, age, and dietary treatment. In both trials all participants were tested with every dietary treatment and with washout periods between each treatment.

In both S2 and L1 all data were evaluated for normality and, when necessary, data were converted to $\log_{10}$ to achieve normal distribution of variation. In S2 the analysis model was product (i.e., placebo, BJ, and BJ capsule) for fixed effects and test site, week, and age for random effects. In L1 the analysis model was product (i.e., BJ and placebo) for fixed effects and week and age for random effects. In both S2 and L1 covariation for each subject's performance on vision tests before the study began (pretreatment) was identified and corrected. In S2 the

second pretreatment test results were used for this correction, whereas in L1 the third pretreatment test results were used. Covariate correction was also applied to adjust for possible carry-over effects due to the order of the products taken. In S2 this was the specific order of BJ, BJ capsule, or placebo capsule, whereas in L1 it was the order of BJ or placebo.

*DA Curve Fitting and Variates.* For DA measurements in S2 and L1 raw data were first corrected for the discrepancy point(s) created by the use of neutral density filter goggles that subjects wore once the minimum monitor intensity was too great. Once corrected, the resulting scatterplot was fitted with two exponential functions (Figure 1). The first curve corresponded to the sensitivity gain of the cone photoreceptors, whereas the second curve corresponded to the sensitivity gain of the rod photoreceptors. The time (min) at the intersection of the two curves was defined as the cone−rod transition ($DA_{CRT}$) (Tables 3 and 4).

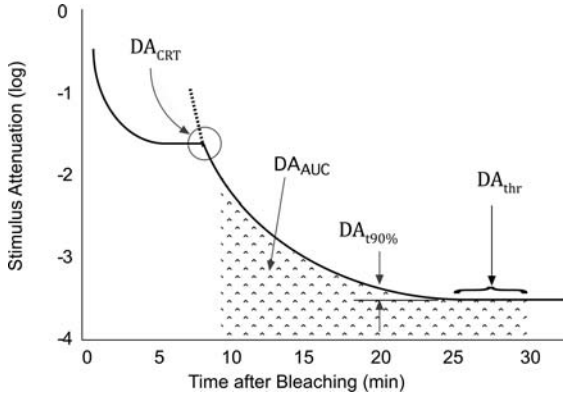


**Figure 1.** Exponentially fitted curves for the early (cone) and late (rod) portion of the dark adaptometry function. The intersection of the two curves indicates the time (min) of the rod/cone transition, $DA_{CRT}$. Measures of dark adaptation included (1) the area under the curve between 9 and 30 min ($DA_{AUC}$), (2) time (min) at 90% of the asymptote ($DA_{t90\%}$) on the second curve, and (3) the final dark threshold ($DA_{thr}$) as defined by $log_{10}$ light intensity during the last 5 min of the 30 min test.

From the second curve two measures were developed to assess the rate of DA. First the area under the DA curve between 9 and 30 min was calculated ($DA_{AUC}$). A lower $DA_{AUC}$ reflects more rapid and more complete dark adaptation. Another measure of DA was the time (min) to reach 90% of the asymptote of the 9−30 min curve, which was defined as $DA_{t90\%}$. Fewer minutes to reach $DA_{t90\%}$ indicated more rapid dark adaptation. To determine the lowest level of light perceived, that is, the dark threshold ($DA_{thr}$), the mean light intensity during the last 5 min of the DA test (25−30 min) was determined from the second fitted curve.

MSR test results were log transformed to normalize variation for ANOVA, whereas their back-transformed decimal values are reported on a log scale for ease of presentation (Figures 2 and 3).

Results of selected vision tests including ($DA_{thr}$), scotopic CS, scotopic VA, and the MSR time were used to investigate their possible relationships with dietary treatments using a principal component analysis (PCA). A correlation matrix was used to identify relationships and is presented as a two-dimensional biplot for S2 (Figure 4A) and L1 (Figure 4B).

## RESULTS

In S2 and L1 there were no reports about adverse effects related to the treatment products. Dietary compliance, where full compliance was ≥5 full doses of study products per week, was reported by 89% of the respondents. Full compliance to diet restrictions, which was ≤2 servings of other ANC-containing food per week, was 60%. Overall response to the compliance questionnaire was 80%.

**Table 3. Dark Adaptation Results Calculated from Fitted Curves from the Trial with a 3 Week Intervention Period and Examining Two Blueberry Test Products (S2)**

| treatment | $DA_{CRT}$[a] (min) | $DA_{AUC}$[b] | $DA_{t90\%}$[c] (min) | $DA_{thr}$[d] ($10^{-2}$ cd/m$^2$[e]) |
|---|---|---|---|---|
| **Mean, 3 Week Treatment** | | | | |
| juice | 6.18 | 55.61 | 31.49 | −0.51 |
| capsule | 6.52 | 55.32 | 34.98 | −0.53 |
| placebo | 8.29 | 55.97 | 29.16 | −0.47 |
| grand mean | 6.700 | 55.64 | 31.88 | −0.50 |
| SEM | 0.574 | 0.238 | 1.888 | 0.014 |
| *F* prob, treatment | ns | ns | ns | 0.000 |
| effect size | 0.43 | 0.32 | 0.36 | 0.51 |
| *F* prob, capsule vs juice | | | | ns |
| *F* prob, placebo vs (capsule and juice) | | | | 0.004 |
| **Mean, 3 Week Washout** | | | | |
| juice | 7.80 | 53.85 | 31.31 | −0.59 |
| capsule | 8.91 | 53.91 | 31.64 | −0.58 |
| placebo | 5.25 | 54.39 | 30.60 | −0.56 |
| grand mean | 7.32 | 54.05 | 31.19 | −0.58 |
| SEM | 0.757 | 0.271 | 2.109 | 0.014 |
| *F* prob, washout | 0.002 | ns | ns | ns |
| effect size | 0.39 | 0.23 | 0.06 | 0.25 |
| *F* prob, capsule vs juice | 0.021 | | | |
| *F* prob, placebo vs (capsule and juice) | 0.008 | | | |

[a]$DA_{CRT}$, dark adaptation cone rod transition. [b]$DA_{AUC}$, area under the curve, 9−30 min. [c]$DA_{t90\%}$, time to reach 90% of asymptote. [d]$DA_{thr}$, final dark threshold, last 5 min. [e]cd/m$^2$ candela per square meter.

**Vision Test Results.** In general, ANC had no effect on measures of DA or night vision in either S2 or L1. In neither S2 nor L1 was there an effect of blueberry ANC intake on the time (min) to the rod cone conversion, that is, $DA_{CRT}$ (Tables 3 and 4). In S2 there was no effect of dietary treatment on the $DA_{AUC}$ or the $DA_{t90\%}$ (Table 3). In S2, however, the threshold light intensity, that is, the average $DA_{thr}$, was greater in the placebo group (i.e., required a higher light intensity) than either the BJ or the BJ capsule ($P = 0.004$) group (Table 3). In L1 there were no treatment effects (BJ vs placebo) on any of the four measures of DA including $DA_{RCT}$, $DA_{AUC}$, $DA_{t90\%}$, or $DA_{thr}$ (Table 4). In S2 and L1 there were no effects of blueberry product intake on VA or CS in the dark-adapted subjects (Tables 5 and 6).

The MSR test that measured the time (s) to recover visual acuity after exposure of the retina to bright light showed significantly shorter recovery times after BJ versus placebo in both S2 (Figure 2) and L1 (Figure 3). In S2, which employed a 3 week intervention, blueberry-fed subjects had a reduced MSR time compared to placebo ($P = 0.033$). Also, there was no statistical difference between the two ANC daily doses (271 and 7.11 mg C3g eq) employed in S2; both doses reduced MSR time compared to the placebo ($P = 0.014$). In S2 after 3 weeks of washout, there was no significant difference between BJ and placebo, although the trend for a shorter MSR time was still apparent (Figure 2). In L1 the daily consumption of 346 mg C3g eq in BJ reduced the recovery time after photobleaching of the macula; this effect was observed at 8 weeks ($P = 0.027$) and 12 weeks ($P = 0.030$). Whereas the trend for a reduced MSR time persisted after 4 weeks of washout, neither

**Table 4. Dark Adaptation Test Results Calculated from Fitted Curves Obtained from Trial (LI) with Long Intervention Period Examining One Blueberry Test Product**

| | $DA_{CRT}$[a] (min) | $DA_{AUC}$[b] | $DA_{t90\%}$[c] (min) | $DA_{thr}$[d] ($10^{-2}$cd/m$^2$)[e] |
|---|---|---|---|---|
| **Mean, 8 Week Treatment** | | | | |
| juice | 6.24 | 37.90 | 22.22 | −1.49 |
| placebo | 6.53 | 37.61 | 22.46 | −1.52 |
| grand mean | 6.38 | 37.76 | 22.34 | −1.50 |
| SEM | 0.189 | 0.556 | 0.818 | 0.024 |
| *F* prob, treatment | ns | ns | ns | ns |
| effect size | 0.20 | 0.07 | 0.04 | 0.16 |
| **Mean, 16 Week Treatment** | | | | |
| juice | 6.55 | 36.66 | 20.82 | −1.54 |
| placebo | 6.97 | 36.34 | 20.63 | −1.54 |
| grand mean | 6.76 | 36.50 | 20.72 | −1.54 |
| SEM | 0.236 | 0.485 | 0.562 | 0.024 |
| *F* prob, treatment | ns | ns | ns | ns |
| effect size | 0.23 | 0.09 | 0.04 | 0.00 |
| **Mean, 4 Week Washout** | | | | |
| juice | 6.44 | 37.10 | 22.23 | −1.53 |
| placebo | 6.59 | 37.79 | 22.22 | −1.55 |
| grand mean | 6.51 | 36.95 | 22.22 | −1.54 |
| SEM | 0.454 | 0.539 | 0.871 | 0.026 |
| *F* prob, washout | ns | ns | ns | ns |
| effect size | 0.04 | 0.20 | 0.00 | 0.10 |
| **Mean, 8 Week Washout** | | | | |
| juice | 6.50 | 37.04 | 21.29 | −1.51 |
| placebo | 7.21 | 37.08 | 20.84 | −1.50 |
| grand mean | 6.85 | 37.06 | 21.07 | −1.51 |
| SEM | 0.526 | 0.477 | 0.599 | 0.024 |
| *F* prob, washout | ns | ns | ns | ns |
| effect size | 0.18 | 0.01 | 0.08 | 0.05 |

[a]$DA_{CRT}$, dark adaptation cone rod transition. [b]$DA_{AUC}$, area under the curve, 9−30 min. [c]$DA_{t90\%}$, time to reach 90% of asymptote. [d]$DA_{thr}$, final dark threshold, last 5 min. [e]cd/m$^2$, candela per square meter.

the 4 or 8 week washout was significantly different from the placebo (Figure 3).

PCA biplots were used to collectively illustrate possible relationships among the vision test results and dietary treatments. The S2 biplot accounted for 93% of the total variation (Figure 4A) with 63% in the first score (vertical axis) and 30% in the second score (horizontal axis). The L1 biplot accounted for 81% of the variation with 52% in the first score and 29% in the second score (Figure 4B). In both S2 and L1 the vector distances from each vision test (CS, $DA_{thr}$, MSR, and VA) to the origin were quite similar, indicating that each of the four vision tests contributed roughly equally to the total variation illustrated by the biplots.

In S2 the Euclidian distances between the dietary treatments distinguished the low-dose blueberry capsule (C) and the high-dose BJ (B) from the placebo (P) along the MSR axis (Figure 4 A; solid line ellipse for blueberry products and washouts, dashed line ellipse for placebo treatment and washout). The capsule washout ($C_w$) and BJ washout ($B_w$) were also associated with low MSR values, suggesting a persistence of the effect during the washout. In the L1 biplot, the BJ and placebo treatments were well separated along the MSR axis (Figure 4A; solid line ellipse for BJ and BJ washout results, dashed line for placebo and placebo washout results). In both S2 and L1 the blueberry-related coordinates occurred in the negative quadrant of the biplot because improved MSR was due to a more negative (lower) recovery time. In S2 especially, but also in L1, the placebo and placebo washout coordinates occurred on the periphery of the biplot, indicating high variation because these treatments were inactive.

In both S2 and L1 the angle created by the CS and MSR vectors was smaller than the angle created by other pairs of vision test vectors (Figure 4). This suggests that, among the four vision tests included in the plot, MSR and CS were more strongly and positively correlated to each other. Also, the MSR and CS vector angles were similar in S2 and L1 despite the fact that the position of the CS coordinates differed by >90° between the two trials. The perpendicular line segment distances for the blueberry products were shorter in S2 than in L1, suggesting a closer relationship between CS and blueberry intake in S2, which used a shorter intervention.

The effect of blueberry ANC on DA is of great interest to the field, and in this paper DA performance is indicated in the biplot as $DA_{thr}$, the final dark threshold. In both S2 and L1 $DA_{thr}$ was strongly associated with the first PCA score, because its cosine angle was small in relation to score 1. Score 1 contributed the greatest percentage (63% in S2; 52% in L1) of the variation illustrated by the biplot, indicating that the $DA_{thr}$ was associated with high variation (Figure 4). The length of the perpendicular line segments from the dietary treatments to the $DA_{thr}$ vector varied, suggesting no real pattern in the $DA_{thr}$ response in relation to the diet treatment. VA also contributed strongly to score 1, particularly in L1. VA and $DA_{thr}$ were strongly and negatively correlated.

## DISCUSSION

Results of the S2 and L1 trials contribute to a body of research investigating the action of ANC in vision physiology (for a review, see Tremblay and Kalt[29]) and especially in relation to night vision and bilberry ANC (for a review, see Canter and Ernst[2]). Although S2 and L1 employed nonpurified blueberry products, the hypothesis underlying the design of the trials was that ANC was the blueberry component that could affect human vision because other abundant BJ components, including organic acids, simple sugars, and polysaccharides, have no demonstrated effect on vision.

**Dose and Treatment Regimen.** Together the S2 and L1 studies spanned a wide range of exposure to ANCs. The S2 trial delivered in BJ 5.69 g C3g eq of ANC in 21 days, whereas the capsule delivered 199 mg C3g eq (or 3.4% of BJ dose) in the same period. In L1, BJ delivered a total of 29.1 g of ANCs in 84 days. The high daily dose of BJ in S2 and L1 (Table 1) is comparable to ANC doses used in other studies.[30,31] The design of S2 and L1 did not test for acute effects because the time between product ingestion and vision testing was not controlled.

Whether subjects were aware of the test product identity should be considered, because vision testing is psychophysical and can be susceptible to bias. In S2, subjects were informed that the BJ and the BJ powder capsule were the same product in two formulations and doses. Also in S2, the BJ powder in the capsule was deemed indistinguishable from the red beet powder capsule placebo. Many subjects in S2 and L1 had never previously consumed single-strength BJ and were not familiar with its sensory qualities. There was at least 8 weeks between when subjects consumed BJ or the placebo juice. Subjects had no opportunity to consume BJ and placebo juice at the same time.

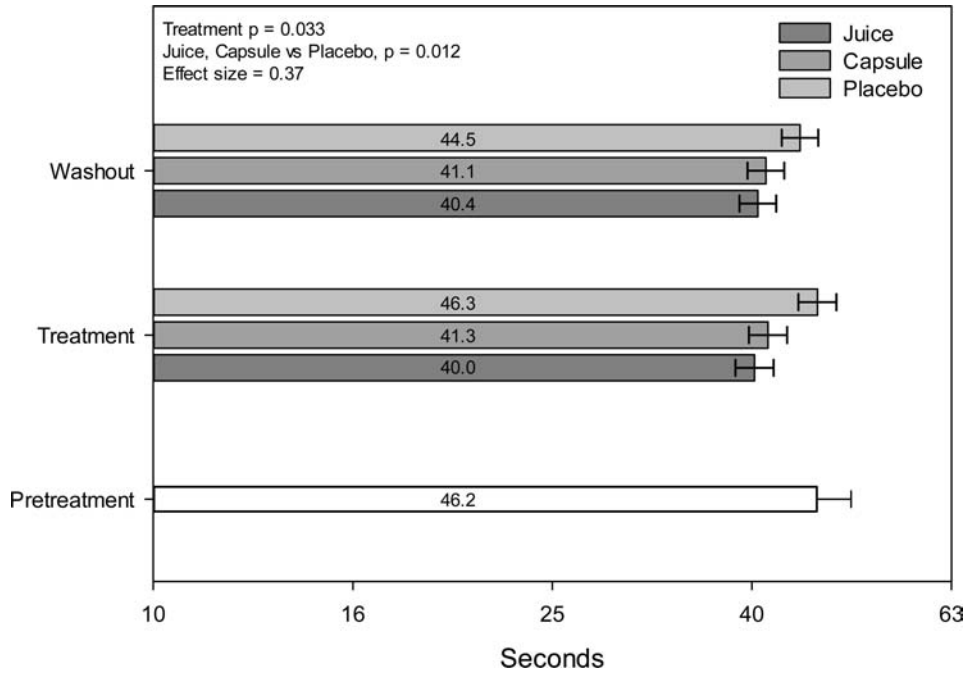


**Figure 2.** Macular stress recovery (MSR) test results defined as time (s) to recover visual acuity after retinal photobleaching in a short trial testing two blueberry products and placebo (S2) with $n = 72$. Mean MSR times ± SEM are shown for the pretreatment (no dietary products) and then after 3 weeks of dietary intervention and 3 weeks of washout. Means are back-transformed from log values which were used for ANOVA. These back-transformed values are plotted on a log scale with back transformed values shown.

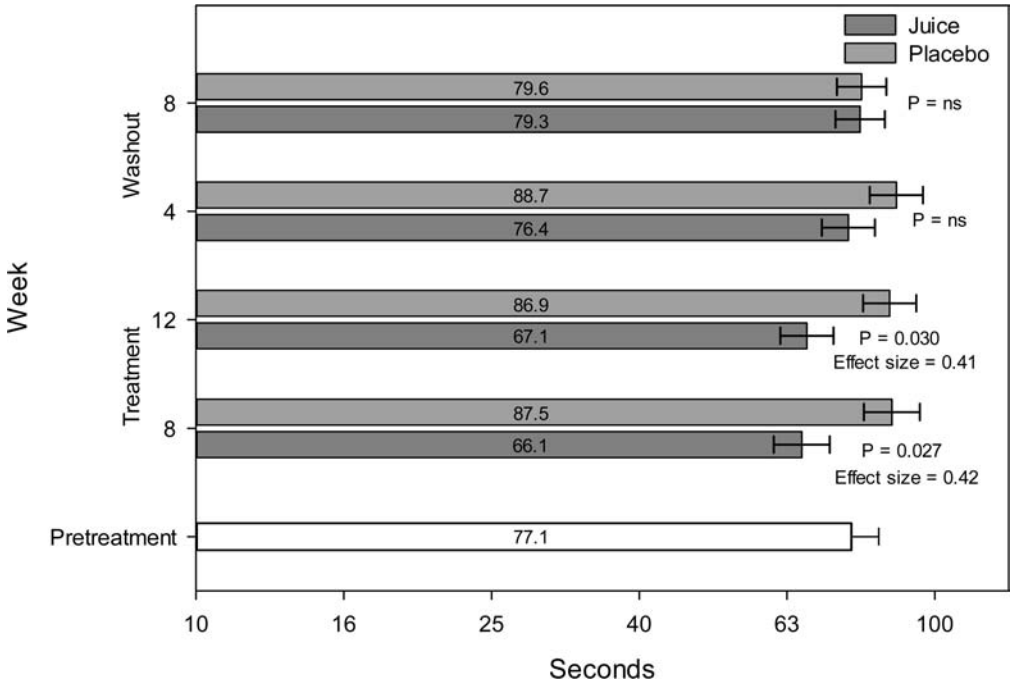


**Figure 3.** Macular stress recovery (MSR) test results defined as time (s) to recover visual acuity after retinal photobleaching in a long trial testing one blueberry product and placebo (L1) with $n = 59$. Mean MSR times ± SEM are shown for the pretreatment (no dietary products) and then after 8 and 12 weeks of dietary intervention and 4 and 8 weeks of washout. Means are back-transformed from log values which were used for ANOVA. These back-transformed values are plotted on a log scale with back transformed values shown.

**Vision Tests.** *DA.* There was no evidence of improved DA with ANC intake in either S2 or L1. In S2 however, a significant treatment effect on $DA_{thr}$ (Table 3) supported some previous studies[11,32−34] wherein ANC intake reduced the final dark threshold light intensity. Although not significant, the 3 week washout in S2 also supported this trend (Table 3). Whereas this suggests that ANC improved the sensitivity of the dark-adapted retina, the effect size (0.5 for treatment period; 0.25 for washout) was moderate. Also, there were no improvements in any other correlated measures of DA ($DA_{RCT}$, $DA_{AUC}$, $DA_{t90\%}$). Furthermore, the L1 trial failed to show a similar trend for $DA_{thr}$, despite a longer intervention with a high ANC dose. It is

**Table 5. Visual Acuity and Contrast Sensitivity in the Dark after 30 min of Dark Adaptation in a Trial (S2) with a Short (3 Week) Intervention with a High Dose (Juice) and a Low Dose (Capsule) of Anthocyanins in Blueberry Products**

| | visual acuity (log minimal angle of resolution) | contrast sensitivity (%) |
|---|---|---|
| **Mean, 3 Week Treatment** | | |
| juice | 0.41 | 3.03 |
| capsule | 0.41 | 3.03 |
| placebo | 0.41 | 3.17 |
| grand mean | 0.41 | 3.08 |
| SEM | 0.005 | 0.060 |
| *F* prob, treatment | ns | ns |
| effect size | 0.00 | 0.27 |
| *F* prob, capsule vs juice | | |
| *F* prob, placebo vs capsule and juice | | |
| **Mean, 3 Week Washout** | | |
| juice | 0.39 | 2.89 |
| capsule | 0.40 | 2.76 |
| placebo | 0.41 | 2.82 |
| grand mean | 0.40 | 2.82 |
| SEM | 0.004 | 0.060 |
| *F* prob, washout | 0.014 | ns |
| effect size | 0.58 | 0.25 |
| *F* prob, capsule vs juice | 0.022 | |
| *F* prob, placebo vs capsule and juice | 0.042 | |

**Table 6. Visual Acuity and Contrast Sensitivity in the Dark after 30 min Dark Adaptation in a Trial (L1) with a Long Intervention Testing Blueberry Juice with a Juice Placebo**

| | visual acuity (log minimal angle of resolution) | contrast sensitivity (%) |
|---|---|---|
| **8 Week Treatment** | | |
| juice | 0.47 | 3.03 |
| placebo | 0.45 | 3.36 |
| grand mean | 0.46 | 3.20 |
| SEM | 0.011 | 0.174 |
| treatment | ns | ns |
| effect size | 0.23 | 0.25 |
| **12 Week Treatment** | | |
| juice | 0.45 | 2.78 |
| placebo | 0.44 | 2.97 |
| grand mean | 0.44 | 2.88 |
| SEM | 0.011 | 0.143 |
| treatment | ns | ns |
| effect size | 0.00 | 0.17 |
| **4 Week Washout** | | |
| juice | 0.44 | 2.66 |
| placebo | 0.43 | 2.65 |
| grand mean | 0.43 | 2.65 |
| SEM | 0.011 | 0.112 |
| treatment | NS | NS |
| effect size | 0.12 | 0.01 |
| **8 Week Washout** | | |
| juice | 0.43 | 2.73 |
| placebo | 0.43 | 2.51 |
| grand mean | 0.43 | 2.62 |
| SEM | 0.011 | 0.139 |
| treatment | ns | ns |
| effect size | 0.00 | 0.20 |

worth noting that this improvement in the $DA_{thr}$ in S2 was approximately 0.05 $log_{10}$ cd/$m^2$ (Tables 3 and 4) and is a difference that can be detected only under controlled conditions and would be imperceptible in real life. Variation in the $DA_{thr}$ means in S2 (SEM = 0.014) and L1 (SEM = 0.024) was of the same order of magnitude, suggesting that differences in the DA testing method were not a factor in the difference in $DA_{thr}$ values between the two trials (Tables 3 and 4).

Together the S2 and L1 $DA_{thr}$ results do not support the early European literature that report improvement in DA parameters with ANCs,[11,32−34] results which Canter and Ernst[2] suggest may be influenced by weak experimental design. When Levy[5] used double-blinded, crossover, randomized control protocols, they failed to show improvement in DA among young normal-sighted men in a study using different ANC doses and durations. Muth et al.[7] also used rigorous protocols and found no effects among young normal-sighted men in other attributes of scotopic vision (VA and CS), but they did not test DA specifically. The S2 and L1 trials were designed to test for ANC effects on DA, CS, and VA in a population spanning 30 years in age (35−65, Table 1) across both genders. Subjects older than 65 years were not included in the study because the incidence of confounding vision health conditions such as subclinical cataracts and retinal dysfunctions is more common in this population group.

*CS and VA.* The lack of an ANC effect on either CS or VA in both S2 and L1 may not be surprising because both of these tests rely more on the photoreceptor density and their underlying synaptic circuitry and less on mechanisms where ANC have been shown to be influential.[35,36] A few studies have proposed an effect of ANCs on VA and CS,[17,37] whereas randomized controlled design studies report negative results for ANC effects on CS[6−8] and on VA.[7] Notably, symptoms of asthenopia (visual fatigue) that can relate to changes in VA and CS were reported to be reduced, on the basis of a subjective assessment.[3]

*MSR.* The MSR test, which measured the recovery time of visual acuity after controlled photoreceptor bleaching, depends heavily on the regeneration of rhodopsin[38] in a way that is similar to DA. The degree of photoreceptor bleaching for the MSR test was greater than for DA testing in both S2 and L1. The MSR test measures the recovery of prebleaching acuity involving cone photoreceptors, whereas the DA test assesses the sensitivity of rod photoreceptors. Although photostress recovery time increases with subject age, it is independent of pupil size, ametropia (refractive error), and VA.[38] The MSR test, which is also known as the retinal dazzling or blinding test, has been used clinically to discriminate retinal diseases from conditions of the optic nerve.[39−41]

In S2 and L1 ANC intake significantly reduced the MSR time; however, the effect size was moderate, ranging between 0.37 and 0.42. In S2 the improvement in MSR was observed in just 3 weeks, and this trend persisted during the 3 week washout. MSR improvement in S2 was found with both the high (271 mg C3g eq daily) and a low (7.11 mg C3g eq daily) ANC dose (Table 1; Figure 2). In L1, which used a high ANC dose (346 mg C3g daily), a similar reduction in MSR time was seen at 8 weeks ($P$ = 0.027) and at 12 weeks ($P$ = 0.03) and with a nonsignificant trend persisting at 4 weeks of washout.

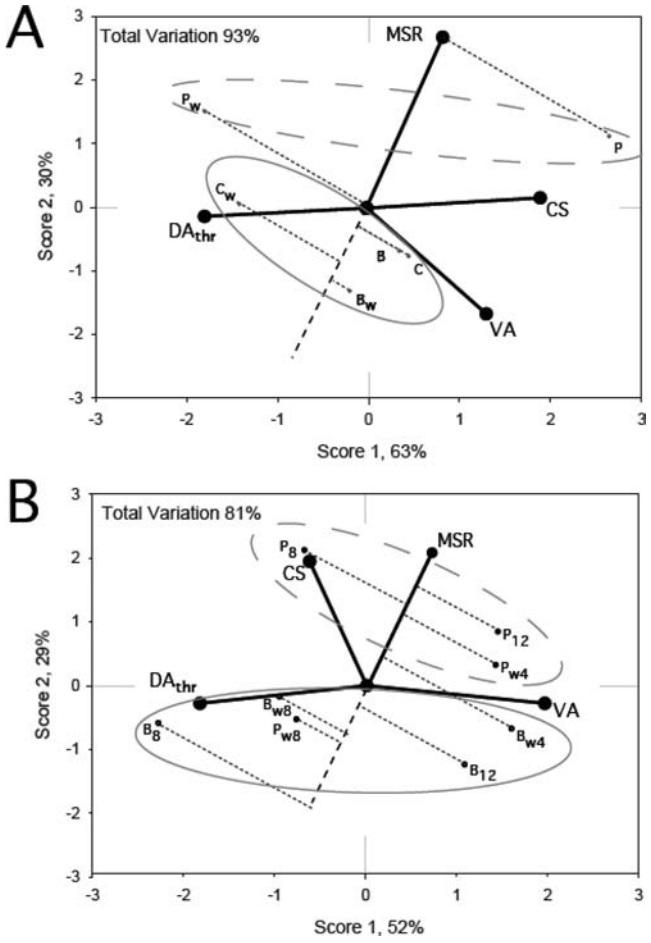


**Figure 4.** Principal component analyses for two clinical trials comparing results for measures of night vision. One trial used a short (3 weeks) intervention and tested two blueberry products (S2) (A); the other trial used a longer intervention (up to 12 weeks) and tested one blueberry product (L1) (B). Panel A and B abbreviations for vision tests: $DA_{thr}$, dark threshold; CS, contrast sensitivity; MSR, macular stress recovery; VA, visual acuity. Panel A interventions: B, blueberry juice, 3 weeks; $B_W$, blueberry juice, 3 week washout; C, blueberry capsule, 3 weeks; $C_W$, blueberry capsule, 3 week washout; P, placebo, 3 weeks; $P_W$, placebo, 3 week washout. Panel B interventions: $B_8$, blueberry juice, 8 weeks; $B_{12}$, blueberry juice, 12 weeks; $B_{w4}$, blueberry juice, 4 week washout; $B_{w8}$, blueberry juice, 8 week washout; $P_8$, placebo juice, 8 weeks; $P_{12}$, placebo juice, 12 weeks; $P_{w4}$, placebo juice, 4 week washout; $P_{w8}$, placebo juice, 8 week washout.

Together the results suggest that ongoing exposure to even a small ANC dose improved MSR time and that the effect persisted for a time after the cessation of ANC intake. This result may be related to the occurrence of ANC glycosides in tissues[42] including eye tissues[1,21] and the persistence of ANC metabolites in enteric circulation.[43] A diverse array of phase II metabolites of ANC have recently been reported to persist in urine.[43] It is not known whether phase II metabolites of ANC affect MSR.

**Multivariate PCA.** The multivariate PCA explained the MSR test results with respect to the variation accounted for in S2 (Figure 4A) and L1 (Figure 4B). The MSR vector correlated poorly with the other three vision test vectors that together contributed to a large proportion of the total variation. Whereas all four vision tests ($DA_{thr}$, MSR, VA, and CS) were poorly correlated, the coordinates of the blueberry treatment groups (solid line ellipse) were clustered along the MSR axis in both S2 and L1. Furthermore, the quite random positioning of the blueberry treatment groups along the $DA_{thr}$, VA, or CS vectors in both S2 and L1 suggests that the absence of statistical significance for these three vision tests is not due to an unpowered study but rather to the absence of correlation between these three vision tests and the intake of ANC.

**Study Design.** Canter and Ernst[2] cited the need for rigorous clinical research designs and controls to examine possible ANC effects on vision, which the S2 and L1 trials attempted to do. Study volunteers were middle-aged and had undergone detailed prescreening prior to enrollment to ensure that the study population was made up of normal-sighted individuals who were free of vision conditions or pathologies that could influence the vision testing. Rigor in the S2 and L1 study designs included double-blinding by vision testers (to the current usage) and subjects (to the identity) of test products or washouts. The use of a complete crossover and the use of a placebo also contributed to the strength of the study design. Conducting vision testing before the start of the dietary intervention (pretreatment) mitigated any effect of the subject learning the new vision tests, and in L1 subjects were already familiar with the tests due to their prior participation in S2. Covariate correction addressed possible effects unrelated to the dietary intervention that may have affected vision test performance.

A challenge in investigating phytochemical interventions is that beneficial effects may not occur in healthy well-nourished populations who have access to a variety of plant-based foods, whereas effects may be still be demonstrable in a phytochemically deficient population. And within the well-nourished Western population, volunteers for nutritional studies are more likely to be nutrition-conscious and consuming a diet containing fruits and vegetables. Results of our study thus contribute to the evidence that nutritional studies related to vision should either target more vulnerable populations or utilize other investigational strategies. ANC intervention studies that target a population with an existing vision pathology may yield more positive outcomes; examples can already be found in relation to glaucoma symptoms[44,45] and vascular pathologies.[46,47] The notion that suboptimal vision may be improved by dietary ANCs has been proposed recently by Shin et al.[48] We are currently investigating ANC intake effects in individuals with impaired vision. Also, large-scale epidemiological studies have associated ANC intake with risk reduction for cardiovascular factors[49,50] and type 2 diabetes,[51] and therefore such an approach is warranted to examine vision health and performance.

Although S2 and L1 failed to demonstrate functional ANC benefits, we have recently reported a potent action of ANC in protecting rats from retinal injury created by exposure to intense light.[19] In this study retinal damage, which was measured objectively by electroretinography and retinal tissue histology, was reduced from 60% in the placebo-fed rats to 20% in BJ-enriched diet. Animal studies benefit significantly from their control of genetics, lifestyle, diet, and the availability of many more research models. Furthermore, laboratory animals that have had limited or no previous exposure to ANCs may be predisposed to greater ANC action compared to humans, where ANC may be consumed regularly and persist in vivo for a long period.[42,43]

The S2 and L1 trials were rigorously designed to test for ANC effects on the performance of subjects in common

psychophysical tests that measure visual function in the dark. ANC intervention had, at best, a moderate effect on the rate of recovery after retinal photobleaching. The magnitude of the effect would not likely translate into subjectively detectable improvement in everyday visual performance. There was no effect of ANC intake on dark adaptation and scotopic vision. At this juncture, with the limited positive results from well-designed human interventional studies in normal populations, it may be useful to investigate the role of ANC in vision using an epidemiological approach or in interventional studies that target specific pathologies or experimental models.

## AUTHOR INFORMATION

### Corresponding Author

*(W.K.) Phone: (902) 365-8561. Fax: (902) 365-8455. E-mail: wilhelmina.kalt@agr.gc.ca.

### Author Contributions

W.Kalt, J.E.M., and F.T. contributed to the project concept and study design, development of the overall research plan, and oversight in data analysis. F.T. developed the psychophysical tests. J.E.M. was study coordinator with activities in hands-on data collection, coordination with vision testers, and data analysis. S.A.E.F. was responsible for the statistical design and analysis. W.K. wrote the paper. W.K. and F.T. had primary responsibility for the final content. All authors read and approved the final manuscript.

### Funding

This research was funded by Agriculture and Agri-Food Canada and the U.S. Highbush Blueberry Council.

### Notes

The authors declare no competing financial interest.

## ACKNOWLEDGMENTS

Vision testers: S2, Jane Carver, Peter Wightman; L1, Bradley Monro. Clinical screening for enrollment: Joan Parkinson, Darren Behn. Technical support: Melinda Vinqvist-Tymchuk.

## ABBREVIATIONS USED

ANC, anthocyanin; BJ, blueberry juice; cd/m$^2$, candela per meter squared; CS, contrast sensitivity; C3g eq, cyanidin 3-glucoside equivalents; DA, dark adaptometry; $DA_{AUC}$, area under the curve 9−30 min; $DA_{CRT}$, cone rod transition; $DA_{t90\%}$, time to reach 90% of asymptote; $DA_{thr}$, final threshold, last 5 min; L1, long trial, one blueberry product; MSR, macular stress recovery; PCA, principle component analysis; S2, short trial, two blueberry products; VA, visual acuity

## REFERENCES

(1) Kalt, W.; Hanneken, A.; Milbury, P.; Tremblay, F. Recent research on polyphenolics in vision and eye health. *J. Agric. Food Chem.* **2010**, *58*, 4001−4007.

(2) Canter, P. H.; Ernst, E. Anthocyanosides of *Vaccinium myrtillus* (bilberry) for night vision − a systematic review of placebo-controlled trials. *Surv. Ophthalmol.* **2004**, *49*, 38−50.

(3) Nakaishi, H.; Matsumoto, H.; Tominaga, S.; Hirayama, M. Effects of black current anthocyanoside intake on dark adaptation and VDT work-induced transient refractive alteration in healthy humans. *Altern. Med. Rev.* **2000**, *5*, 553−562.

(4) Matsumoto, H.; Nakamura, Y.; Tachibanaki, S.; Kawamura, S.; Hirayama, M. Stimulatory effect of cyanidin 3-glycosides on the regeneration of rhodopsin. *J. Agric. Food Chem.* **2003**, *51*, 3560−3563.

(5) Levy, Y.; Glovinsky, Y. The effect of anthocyanosides on night vision. *Eye* **1998**, *12*, 967−969.

(6) Mayser, H.; Wilhelm, H. Effects of anthocyanosides on contrast vision [abstract]. *Invest. Ophth. Vis. Sci.* **2001**, *42*, 348.

(7) Muth, E.; Laurent, J.; Jasper, P. The effect of bilberry nutritional supplementation on night visual acuity and contrast sensitivity. *Altern. Med. Rev.* **2000**, *5*, 164−173.

(8) Zadok, D.; Levy, Y.; Glovinsky, Y. The effect of anthocyanosides in a multiple oral dose on night vision. *Eye* **1999**, *13* (Pt 6), 734−736.

(9) Jayle, G.; Aubert, L. Action of anthocyanin glycosides on the scotopic and mesopic vision of the normal subject. *Therapie* **1964**, *19*, 171−185.

(10) Alfieri, R.; Sole, P. Influence of anthocyanosides, in oral-perilingual administration, on the adapto-electroretinogram (AERG) in red light in humans. *C. R. Seances Soc. Biol. Fil.* **1966**, *160*, 1590−1593.

(11) Belleoud, L.; Leluan, D.; Boyer, Y. Etude des effets des glucosides d'anthocyan sur la vision nocturne des controleurs d'aerodrome. *Rev. Med. Aeronautique Spatiale* **1966**, *18*, 3−7.

(12) Jayle, G.; Aubry, M.; Gavini, H.; Braccini, G.; Baume, C. D. I. Study concerning the action of anthocyanoside extracts of *Vaccinium myrtillus* on night vision. *Ann. Ocul.* **1965**, *198*, 556−562.

(13) Ponte, F.; Lauricella, M. Effect of *Vaccinium myrtillus* total extract on the recovery in the dark of the human electroretinogram. *Atti VII Simposio*; ISCERG: Istanbul, Turkey, 1969; pp 335−336.

(14) Sala, D.; Rossi, P.; Rolando, S. Effetto degli antocianosidi sulle "performances" visive alle basse luminanze. *Minerva Ophtalmol.* **1979**, *21*, 283−285.

(15) Sbrozzi, F.; Landini, J.; Zago, M. Night vision affected by anthocyanosides. An electoretinographic test. *Minerva Ophtalmol.* **1983**, *24*, 189−193.

(16) Magnasco, A.; Zingirian, M. Influenza degli antocianosidi sulla soglia retinica differnziale mesopica [Influence of anthocyanosides on the mesopic differential threshold of the retina]. *Ann. Ottamol. Clin. Ocul.* **1966**, *92*, 188−193.

(17) Lee, J.; Lee, H.; Kim, C.; Hong, Y.; Choe, C.; You, T.; Seong, G. Purified high-dose anthocyanoside oligomer administration improves nocturnal vision and clinical symptoms in myopia subjects. *Br. J. Nutr.* **2005**, *93*, 895−899.

(18) Milbury, P.; Graf, B.; Curran-Celentano, J.; Blumberg, J. Bilberry (*Vaccinium myrtillus*) anthocyanins modulate heme oxygenase-1 and glutathione S-transferase-pi expression in ARPE-19 cells. *Invest. Ophth. Vis. Sci.* **2007**, *48*, 2343−2349.

(19) Tremblay, F.; Waterhouse, J.; Nason, J.; Kalt, W. Prophylactic neuroprotection by blueberry-enriched diet in a rat model of light-induced retinopathy. *J. Nutr. Biochem.* **2013**, *24*, 647−655.

(20) Liu, Y.; Song, X.; Han, Y.; Zhou, F.; Zhang, D.; Ji, B.; Hu, J.; Lv, Y.; Cai, S.; Wei, Y.; Gao, F.; Jia, X. Identification of anthocyanin components of wild Chinese blueberries and amelioration of light-induced retinal damage in pigmented rabbit using whole berries. *J. Agric. Food Chem.* **2010**, *59*, 356−363.

(21) Matsumoto, H.; Nakamura, Y.; Iida, H.; Ito, K.; Ohguro, H. Comparative assessment of distribution of blackcurrant anthocyanins in rabbit and rat ocular tissues. *Exp. Eye Res.* **2006**, *83*, 348−356.

(22) Clifford, M. N. Review: Anthocyanins − nature, occurrence and dietary burden. *J. Sci. Food Agric.* **2000**, *80*, 1063−1072.

(23) Forney, C. F.; Kalt, W.; Jordan, M. A.; Vinqvist-Tymchuk, M. R.; Fillmore, S. A. E. Compositional changes in blueberry and cranberry fruit during ripening. *Acta Hortic. (ISHS)* **2012**, *926*, 331−337.

(24) Wrolstad, R.; Durst, R.; Lee, J. Tracking color and pigment changes in anthocyanin products. *Trends Food Sci. Technol.* **2005**, *16*, 423−428.

(25) U.S. Department of Agriculture. National Nutrient Database for Standard Reference, release 25, 2012.

(26) Ferris, F. L., 3rd; Freidlin, V.; Kassoff, A.; Green, S. B.; Milton, R.C. Relative letter and position difficulty on visual acuity charts from the Early Treatment Diabetic Retinopathy Study. *Am. J. Ophthalmol.* **1993**, *116*, 735−740.

(27) Ginsburg, A. P. Contrast sensitivity and functional vision. *Int. Ophthalmol. Clin.* **2003**, *43*, 5−15.

(28) Payne, R. W.; Murray, D. A.; Harding, S. A.; Baird, D. B.; Soutar, D. M. *Genstat for Windows Introduction*, 12th ed.; VSN International: Hemel Hempstead, UK, 2009.
(29) Tremblay, F.; Kalt, W. Anthocyanins in visual performance and ocular diseases. In *Anthocyanins in Health and Disease*; Wallace, T. C., Giusti, M. M., Eds.; CRC Press: Boca Raton, FL, USA, 2013; pp 245−278.
(30) Manach, C.; Williamson, G.; Morand, C.; Scalbert, A.; Remesy, C. Bioavailability and bioefficacy of polyphenols in humans. I. Review of 97 bioavailability studies. *Am. J. Clin. Nutr.* **2005**, *81*, 230S−242S.
(31) Manach, C.; Donovan, J. L. Pharmacokinetics and metabolism of dietary flavonoids in humans. *Free Radical Res.* **2004**, *38*, 771−785.
(32) Urso, G. Azione degli antocianosidi del *Vaccinium myrtillus* associati a betacarotene sulla sensibilità luminosa. *Ann. Ottalmol. Clin. Ocul.* **1967**, *93*, 931−938.
(33) Zavarise, G. Sull'effetto del trattamento prolungato con antocianusidi sul senso luminoso. *Ann. Ottalmol. Clin. Ocul.* **1968**, *94*, 209−214.
(34) Fiorini, G.; Biancacci, A.; Graziano, F. Modificazioni perimetriche ed adattometriche dopo ingestione di mirtillina associata a beta-carotene. *Ann. Ottalmol. Clin. Ocul.* **1965**, *91*, 371−386.
(35) Matsumoto, H.; Yoshizawa, T. Rhodopsin regeneration is accelerated via noncovalent 11-cis retinal-opsin complex − a role of retinal binding pocket of opsin. *Photochem. Photobiol.* **2008**, *84*, 985−989.
(36) Tirupula, K.; Balem, F.; Yanamala, N.; Klein-Seetharaman, J. pH-Dependent interaction of rhodopsin with cyanidin-3-glucoside. 2. Functional aspects. *Photochem. Photobiol.* **2009**, *85*, 463−470.
(37) Sole, P.; Rigal, D.; Peyresblanques, J. Effects of cyaninoside chloride and Heleniene on mesopic and scotopic vision in myopia and night blindness. *J. Fr. Ophtalmol.* **1984**, *7*, 35−39.
(38) Margrain, T. H.; Thomson, D. Sources of variability in the clinical photostress test. *Ophthal. Physiol. Optics* **2002**, *22*, 61−67.
(39) Dimitrov, P. N.; Robman, L. D.; Varsamidis, M.; Aung, K. Z.; Makeyeva, G. A.; Guymer, R. H.; Vingrys, A. J. Visual function tests as potential biomarkers in age-related macular degeneration. *Invest. Ophthalmol. Vis. Sci.* **2011**, *52*, 9457−9469.
(40) Newsome, D. A.; Negreiro, M. Reproducible measurement of macular light flash recovery time using a novel device can indicate the presence and worsening of macular diseases. *Curr. Eye Res.* **2009**, *34*, 162−170.
(41) Wolffsohn, J. S.; Anderson, S. J.; Mitchell, J.; Woodcock, A.; Rubinstein, M.; Ffytche, T.; Browning, A.; Willbond, K.; Amoaku, W. M.; Bradley, C. Effect of age related macular degeneration on the Eger macular stressometer photostress recovery time. *Br. J. Ophthalmol.* **2006**, *90*, 432−434.
(42) Kalt, W.; Blumberg, J.; McDonald, J.; Vinqvist-Tymchuk, M.; Fillmore, S.; Graf, B.; O'Leary, J.; Milbury, P. Identification of anthocyanins in the liver, eye, and brain of blueberry-fed pigs. *J. Agric. Food Chem.* **2008**, *56*, 705−712.
(43) Kalt, W.; Liu, Y.; McDonald, J. E.; Vinqvist-Tymchuk, M. R.; Fillmore, S. A. E. Anthocyanin metabolites are abundant and persistent in human urine. *J. Agric. Food Chem.* **2014**, *62*, 3926−3934.
(44) Ohguro, H.; Ohguro, I.; Katai, M.; Tanaka, S. Two-year randomized, placebo-controlled study of black currant anthocyanins on visual field in glaucoma. *Ophthalmologica* **2012**, *228*, 26−35.
(45) Steigerwalt, R. D.; Belcaro, G.; Morazzoni, P.; Bombardelli, E.; Burki, C.; Schönlau, F. Mirtogenol® potentiates latanoprost in lowering intraocular pressure and improves ocular blood flow in asymptomatic subjects. *Clin. Ophthalmol.* **2010**, *4*, 471−476.
(46) Kim, E. S.; Yu, S. Y.; Kwon, S. J.; Kwon, O. W.; Kim, S. Y.; Kim, T. W.; Ahn, J. K.; Oum, B. S.; Lew, Y. J.; Lee, J. E.; Chung, H.; Kwak, H. W. Clinical evaluation of patients with nonproliferative diabetic retinopathy following medication of anthocyanoside: multicenter study. *J. Korean Ophthalmol. Soc.* **2008**, *49*, 1629−1633.
(47) Huismans, H. Traitment medicamenteux de la retinopathie diabetique en practique ophthalmologique. *Der Augenspiegel* **1988**, *34*, 16−21.
(48) Shin, J. Y.; Yu, H. G. Chlorogenic acid supplementation improves multifocal electroretinography in patients with retinitis pigmentosa. *J. Korean Med. Sci.* **2014**, *29*, 117−121.
(49) Cassidy, A.; Mukamal, K. J.; Liu, L.; Franz, M.; Eliassen, A. H.; Rimm, E. B. High anthocyanin intake is associated with a reduced risk of myocardial infarction in young and middle-aged women. *Circulation* **2013**, *127*, 188−196.
(50) Jennings, A.; Welch, A. A.; Fairweather-Tait, S. J.; Kay, C.; Minihane, A.-M.; Chowienczyk, P.; Jiang, B.; Cecelja, M.; Spector, T.; Macgregor, A.; Cassidy, A. Higher anthocyanin intake is associated with lower arterial stiffness and central blood pressure in women. *Am. J. Clin. Nutr.* **2012**, *96*, 781−788.
(51) Wedick, N. M.; Pan, A.; Cassidy, A.; Rimm, E. B.; Sampson, L.; Rosner, B.; Willett, W.; Hu, F. B.; Sun, Q.; van Dam, R. M. Dietary flavonoid intakes and risk of type 2 diabetes in US men and women. *Am. J. Clin. Nutr.* **2012**, *95*, 925−933.

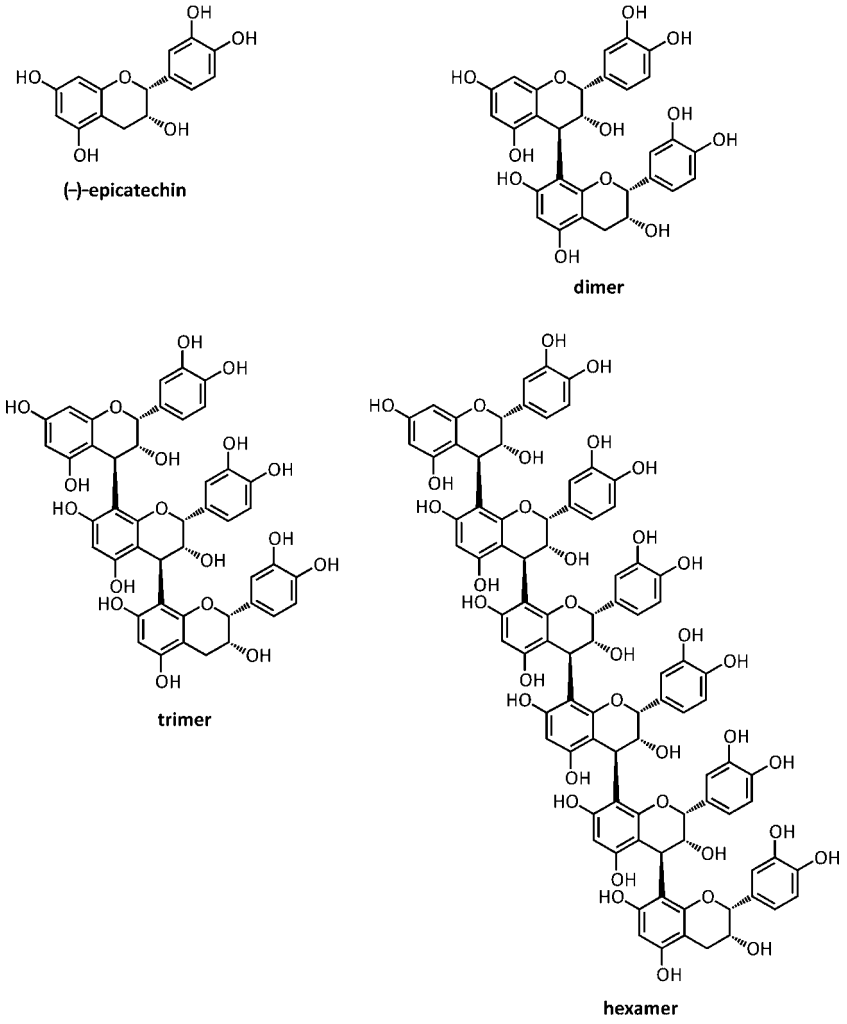


**Figure 1.** Structures of (−)-epicatechin and a representative (−)-epicatechin dimer, trimer, and hexamer.

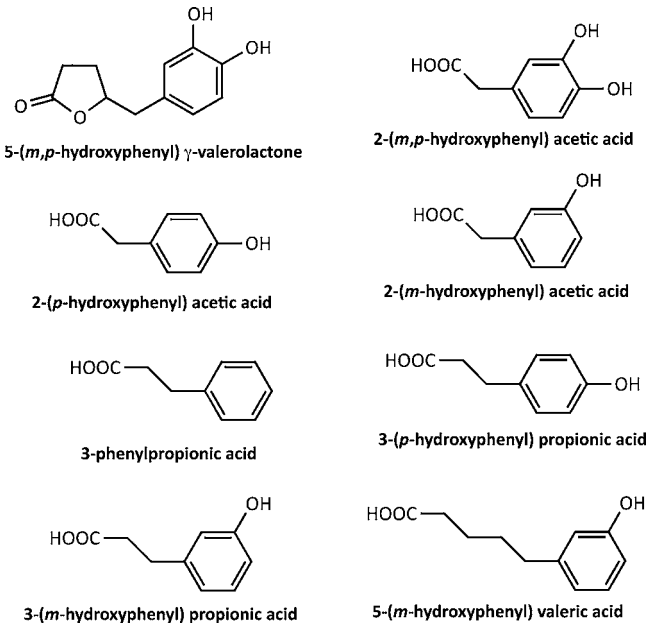


**Figure 2.** Structures of selected representative metabolites produced by microbial metabolism of native catechins and procyanidins in the colon.

accumulation of native flavanols and microbial metabolites. Flavanol monomers and PCs (as well as other classes of flavonoids) appear to be metabolized to a small pool of a few dozen common microbial metabolites.[15,35] This raises the question of whether the qualitative profile of native flavanols is relevant for modulating the profile of metabolites accumulated in the colon. Very few studies have compared the colonic tissue accumulation of native flavanols and microbial metabolites from distinct dietary profiles of native flavanols;[36] the majority of studies focus on metabolism and accumulation of single compounds or a single flavanol-rich food. Furthermore, the majority of the data on microbial metabolism of flavanols pertains to catechin monomers and small PCs (dimers, trimers, etc.). Very little is known about the metabolism of larger PCs, as these compounds have been studied in matrices that are also rich in smaller compounds (cocoa, apples, GSE, etc.) but have not yet been studied individually. Due to this lack of data, the metabolic fate of large PCs in the gut remains largely unknown.

The objectives of this study were to (1) determine the quantitative and qualitative profile of flavanols and their microbial metabolites accumulated in the colon during habitual exposure to flavanol-rich cocoa extract and (2) compare profiles accumulated in the colon during habitual exposure to distinct profiles of dietary flavanols (monomer-rich, oligomer-rich, and polymer-rich fractions). We hypothesize that administration of equal amounts of flavanols with distinct qualitative profiles to


dx.doi.org/10.1021/jf503838q | J. Agric. Food Chem. 2014, 62, 11190−11199

**Table 1. Levels of Native Flavanol Monomers and Procyanidins in Cocoa Extract and Individual Cocoa Fractions**

| class | composition[a] (mg compound/g dried fraction) | | | |
|---|---|---|---|---|
| | CE[b] | M[c] | O[d] | P[e] |
| catechin monomers | 7.59 ± 0.0806 b | 40.2 ± 0.682 c | 0.806 ± 0.0129 a | 0.0899 ± 0.0146 a |
| PC dimers | 8.48 ± 0.155 b | 15.0 ± 0.394 c | 24.7 ± 0.267 d | 0.347 ± 0.0408 a |
| PC trimers−hexamers | 18.0 ± 0.763 c | 10.3 ± 0.422 b | 50.4 ± 1.08 d | 5.04 ± 0.231 a |
| PC heptamers−decamers | 4.65 ± 0.208 b | 0.338 ± 0.153 a | 6.83 ± 0.141 b | 5.82 ± 1.45 b |

[a]Treatments with different letters in the same row are significantly different ($P < 0.05$). Data are reported as mean ± SEM from $n = 3$ replicate analyses. [b]Cocoa flavanol extract. [c]Monomer-rich fraction. [d]Oligomer-rich fraction. [e]Polymer-rich fraction.

mice would result in colonic tissue accumulation of distinct qualitative and quantitative profiles of both native flavanols and their microbial metabolites in the colon tissue. Specifically, we hypothesize that (1) administration of cocoa flavanols will increase colonic tissue levels of flavanols and metabolites compared to a low-flavanols control diet and (2) administration of cocoa oligomers and polymers will result in reduced colonic tissue levels of monomeric flavanols and metabolites compared to cocoa extract or cocoa monomers.

## MATERIALS AND METHODS

**Chemicals and Standards.** Milli-Q water was prepared using a Millipore Milli-Q Gradient system (Billerica, MA, USA). Ascorbic acid, (+)-catechin hydrate (C), (−)-EC, epigallocatechin [(−)-(EGC)], epicatechin gallate [(−)-ECG], epigallocatechin gallate [(−)-(EGCG)], *p*-coumaric acid, *m*-coumaric acid, ferulic acid, isoferulic acid, caffeic acid, protocatechuic acid, 3-hydroxybenzoic acid, 4-hydroxybenzoic acid, vanillic acid, homovanillic acid, gallic acid, 4-hydroxymandelic acid, pyrogallol, catechol, phenylacetic acid, 2-(3′-hydroxyphenyl)acetic acid, 2-(4′-hydroxyphenyl)acetic acid, 3-(3′,4′-dihrdroxyphenyl)acetic acid, 3-phenylpropionic acid, 3-(4′-hydroxyphenyl)propionic acid, 5-phenyl-valeric acid, phloretin, hippuric acid, 3-(3′-hydroxyphenyl)propionic acid, and 3-(3′,4′-dihydroxyphenyl)propionic acid were obtained from Sigma (St. Louis, MO, USA). PC dimer $B_2$ and trimer $C_1$ were obtained from ChromaDex (Irvine, CA, USA). Purified PC dimer $B_1$, dimer $B_2$-gallate, dimer $B_5$, trimer $T_2$, tetramer $A_2$, and pentamers (DP 5) through decamers (DP 10) were obtained from Planta Analytica (Danbury, CT, USA). Solvents for extraction, fractionation, and normal-phase HPLC were of ACS grade or better (Fisher, Pittsburgh, PA, USA,or VWR, Radnor, PA, USA). Solvents for UPLC-MS/MS were of LC-MS grade (VWR).

**Cocoa Flavanols.** A flavanol-rich cocoa extract (CE) was produced and separated into fractions with distinct flavanol compositions (monomer-, oligomer-, and polymer-rich fractions). Procedures for extraction, fractionation, and characterization of CE and the fractions were described previously.[23] The levels of total flavanol monomers, dimers, and larger PCs in the CE and cocoa monomer, oligomer, and polymer fractions are presented in Table 1. The levels of individual compounds are presented in the Supporting Information (Table S1). Compared to CE, the monomer-rich fraction is highly enriched for monomers, slightly enriched for dimers, reduced in PCs DP 3−6, and depleted of PCs DP 7−10. The oligomer-rich fraction is highly depleted of monomers, greatly enriched for dimers and PCs DP 3−6, and slightly enriched for DP 7−10. The polymer-rich fraction is highly depleted for monomers, dimers, and PCs DP 3−6 and slightly enriched for PCs DP 7−10. It should be noted that these values are from reverse-phase UPLC analysis that quantified PCs only up to DP 10; the composition of larger PCs that make up a large portion of CE and the majority of the polymer fraction (see Figure S1) are not reflected in the total composition values in Table 1. The normal-phase HPLC flavanol profiles of CE and cocoa PC fractions are shown in Figure S1. By comparing relative peak heights and retention times (retention time roughly correlates to degree of polymerization in normal-phase analysis of flavanols) within each chromatogram, the monomer-, oligomer-, and polymer-rich fractions were indeed relatively enriched for flavanol monomers, oligomers, and polymers, respectively, compared to CE and each other.

**Animals.** Animal experiments were approved by the Institutional Animal Care and Use Committee (IACUC) at Virginia Polytechnic Institute and State University (protocol 13-099-FST). Male C57BL/6J mice ($N = 54$, ∼25 g) were obtained from Jackson (Bar Harbor, ME, USA). Following arrival, mice were maintained on standard rodent chow for 2 weeks under standard conditions (3 mice/cage, 12 h light/dark cycle, 30−70% relative humidity, 20−26 °C) to acclimatize to the vivarium. To reduce coprophagy, bedding was changed twice per week throughout the study. Mice were provided food and water ad libitum unless otherwise specified.

**Diets.** Mice were assigned to one of five diet/treatment combinations ($n = 9$/group). Animals were fed a basal high-fat diet (60% kcal from fat) from the diet-induced obesity model series (D12492, Research Diets, Inc., New Brunswick, NJ, USA). This a semipurified diet with the minimal polyphenol or phenolic background level that is practically attainable; the composition of this basal diet was reported previously[23] and is presented in Table S4 in the Supporting Information. The diet was provided alone (control) or supplemented with CE or one of the three cocoa fractions. The diets containing CE or cocoa fractions were formulated (262.53 mg/kg diet) to provide doses of 25 mg/kg body weight (BW)/day based on an estimated daily food consumption of 95.23 g food/kg BW/day for male C57BL/6J mice from previous studies in our laboratory (data not shown). Diets were maintained at −20 °C throughout the study to prevent degradation of lipids or cocoa compounds. To maintain freshness and prevent degradation of fat or cocoa compounds, food was replaced twice per week for all cages. Animals were maintained on diets for 12 weeks. Food intake for each cage was measured twice per week by weighing food provided and weighing leftover food prior to replacement with fresh food. Food intake did not differ between treatment groups (data not shown).[23]

**Animal Procedures.** Animal body weights (weekly), body composition (weeks 1, 5, 8, and 11), glucose tolerance (week 10), and insulin tolerance (week 11) were measured. These results have been described previously.[23]

**Euthanasia and Necropsy.** At the end of week 12, mice were fasted overnight and euthanized by $CO_2$ (following AVMA Guidelines on Euthanasia) followed by bilateral pneumothorax. Following euthanasia, the abdominal cavity was opened ventrally, and the intestines were removed by cutting through the rectum and gently removing the intestinal tract from the distal end. The colon (between the cecum and rectum) was excised and thoroughly flushed with prechilled 1× phosphate-buffered saline (PBS, VWR) and immediately snap-frozen in liquid $N_2$. Samples were stored at −80 °C prior to sample preparation.

**Extraction of Flavanols and Microbial Metabolites.** Sample preparation and extraction was performed using our previously published method with modifications.[30] Tissue samples were freeze-dried for >24 h using a FreeZone 1 L freeze-dryer (Labconco, Kansas City, MO, USA). Zirconium oxide tissue homogenization beads (∼100 mg, 0.5−1 mm, Next Advance, Averill Park, NY, USA) were added to each sample (25−35 mg dry tissue) along with 50 μL of Milli-Q water and 50 μL of a 1% (w/v) aqueous ascorbic acid solution. Samples were homogenized in a Bullet Blender (Next Advance, speed 7, 1 min, 4 °C). Liquid−liquid extraction was performed by adding 1 mL of ethyl acetate and blending in a Bullet Blender (5 min, speed 9, 4 °C, Next Advance). Samples were centrifuged (5 min, 17000*g*, room temperature), and the organic supernatant was collected. The extraction was repeated on the resulting pellet, and the supernatants were pooled for each sample and dried under a gentle stream of $N_2$ (35 °C). Following liquid−liquid

extraction, solid-phase extraction (SPE) was performed on the remaining pellet. An extraction solution (1 mL acetone/water/glacial acetic acid, 70:28:2 v/v/v) was added to each sample along with 100 $\mu$L of 4% aqueous phosphoric acid. Samples were homogenized in a Bullet Blender (5 min, speed 9, 4 °C) and centrifuged (5 min, 17000*g*, room temperature), and the supernatant was collected. The extraction was repeated, and the supernatants were pooled for each sample. The pooled extracts were diluted with 12 mL of water. Oasis HLB SPE cartridges (1 $cm^3$, 30 mg sorbent, Waters, Milford, MA, USA) were preconditioned with 1 mL of methanol (MeOH) followed by 1 mL of water. The diluted samples (2 mL of pooled extracts + 12 mL of water) were loaded onto the cartridges using a vacuum manifold. Cartridges were washed sequentially with 1 mL of acidified water (0.1% formic acid, v/v) followed by 0.5 mL of 5% (v/v) aqueous MeOH containing 0.1% formic acid (v/v). Cartridges were eluted sequentially with 2 mL of acidified MeOH (0.1% formic acid, v/v) followed by 2 mL of acetone/water/glacial acetic acid (70:28:2) and collected into the tubes containing the dried ethyl acetate extracts from the same sample. Samples were dried under vacuum in a Speed-Vac (45 °C) to remove acetone and MeOH, then frozen on dry ice and freeze-dried for >24 h to remove water and acetic acid. Dried samples were resolubilized in 1 mL of 0.1% formic acid in water/0.1% formic acid in acetonitrile (ACN) (95:5 v/v), sonicated in ice water (25 min), and then filtered into certified LC-MS vials (Waters) using a Samplicity filtration system (0.2 $\mu$m PTFE Philic Millex Samplicity filters, Millipore). Filtered samples were analyzed immediately. The extraction recovery of native flavanols and metabolites by this method was validated in our previous method paper.[30]

For extraction of the diet, 3 g samples of each diet were weighed in triplicate and defatted using hexane. Samples were vortexed with 20 mL of hexane, sonicated on ice (10 min), and centrifuged (5 min, 3500*g*, room temperature), the supernatant was discarded, and the procedure was repeated. An extraction solution (10 mL of acetone/water/glacial acetic acid, 70:28:2 v/v/v) was added to each sample. Samples were then vortexed for 30 s and sonicated on ice for 10 min. Samples were centrifuged (5 min, 3500*g*, room temperature), and the supernatant was collected. The extraction was repeated. The supernatants were pooled for each sample, and 2 mL was diluted with 12 mL of water. Oasis HLB SPE cartridges (1 $cm^3$, 30 mg sorbent, Waters) were preconditioned as described above. The diluted samples (2 mL of pooled extracts + 12 mL of water) were loaded onto the cartridges using a vacuum manifold. Cartridges were washed and eluted as described above into tubes containing the dried ethyl acetate extracts from the same sample. Samples were dried under vacuum in a Speed-Vac (45 °C) to remove acetone and methanol, then frozen on dry ice and freeze-dried for >24 h to remove water and acetic acid. Dried samples were resolubilized, sonicated, and filtered into LC-MS vials as described above. Filtered samples were analyzed immediately.

**UPLC-MS/MS Analysis of Flavanols and Microbial Metabolites.** UPLC-MS/MS analysis was performed using our previously published method with modifications.[30] Details of the methodology are found in the Supporting Information.

**Folin−Ciocalteu Assay.** To extract phenolics from the diet, samples of each diet were weighed in triplicate, defatted twice, and extracted twice as described above. For the Folin assay, 200 $\mu$L of each sample was combined with 2.5 mL of 0.2 N Folin−Ciocalteau reagent. Then, 2.0 mL of saturated aqueous $Na_2CO_3$ was added to each sample, and samples were incubated at room temperature for 2 h. The absorbance was then read at 765 nm. The standard curve was prepared using gallic acid, and total phenolics were calculated as milligrams of gallic acid equivalents (GAE) per gram of material.

**Data and Statistical Analysis.** Outliers were identified and removed using Dixon's *Q* test at the $\alpha = 0.05$ level if necessary. Data were analyzed by one-way ANOVA to determine overall significance of treatment. If significance was detected, Tukey's HSD post hoc test was then performed to compare all treatment means. Significance was defined as $P < 0.05$.

## RESULTS AND DISCUSSION

**Dietary Levels of Native Flavanols.** Levels of native cocoa catechins and PCs in the diet are presented in Figure S2 in the Supporting Information. UPLC-MS/MS analysis of the diets showed that the profile of native flavanols in the diet matched those of the pure extracts. As seen in Figure S2A, the amount of total native flavanols (catechins and PCs) in the control diet is negligible, including an undetectable level of oligomers. This demonstrates that there is essentially no background contribution of catechins or PCs (that can be measured by our UPLC-MS/MS method, i.e., DP 1−10) in the basal control diet and that the only source of catechins and PCs in each diet is the CE or the cocoa fraction added to the basal diet. Panels B−D of Figure S2 show that the monomer- and oligomer-supplemented diets were enriched with monomeric and oligomeric flavanols, respectively, at levels that are significantly higher than those in the other fractions. Overall, the total amount of native flavanols that can be measured by our UPLC-MS/MS method (DP 1−10) found in the polymer diet was lower than in the diets supplemented with CE, monomers, or oligomers, as seen in Figure S2A. This is due to the fact that the larger PC compounds (DP > 10) that make up a large portion of the polymer fraction (see Figure S1) are not resolved or detected with this method as previously shown. Therefore, the measured levels are not reflective of all compounds present in the polymer fraction, but rather those that can be accurately measured using the present UPLC-MS/MS method. These data demonstrate that the vast majority of native flavanols in the diet are from the cocoa fractions and not the basal diet itself.

**Dietary Levels of Metabolites.** Background levels of metabolite compounds (compounds that we identified as microbial metabolites of catechins and PCs but that were present in the diets before being administrated to mice) present in the diets are shown in Figure S3 in the Supporting Information. There was a significant concentration of these compounds in the basal control diet (1.13 ± 0.0273 mg/g, Figure S3A); supplementation of the basal diet with CE or cocoa fractions did not significantly alter the levels present in the diet (1.23 ± 0.0402−1.71 ± 0.292 mg/g). The majority of the metabolites present in the diets are compounds other than the phenylalkyl and benzoic acid derivatives (Figure S3D), such as ferulic acid. These compounds are common in plant materials[37] and are likely introduced from plant-based ingredients in the semipurified diet (Table S4). There were somewhat higher (but not statistically different) levels of phenylalkyl and benzoic acid derivatives in the monomer-supplemented diet (Figure S3B−C). This is potentially due to fractionation, which may cause phenylalkyl and benzoic acids occurring in cocoa to elute with the monomer fraction during SPE. It should be noted that we have previously observed appreciable levels of these metabolites in intestines of rats fed a semipurified basal control diet;[30] these compounds appear to be unavoidable background components in plant-based rodent diets. Overall, these data show that there is no significant contribution of metabolite compounds by the CE or cocoa fractions above levels present in the basal diet alone and that levels of metabolites present in the diets are similar across treatment groups.

On the basis of analysis of the diets, differences in the levels of native flavanols (catechins and PCs) and their microbial metabolites in the colon of mice fed these diets would be expected to be due solely to the composition of the CE or fraction with which each diet was supplemented.

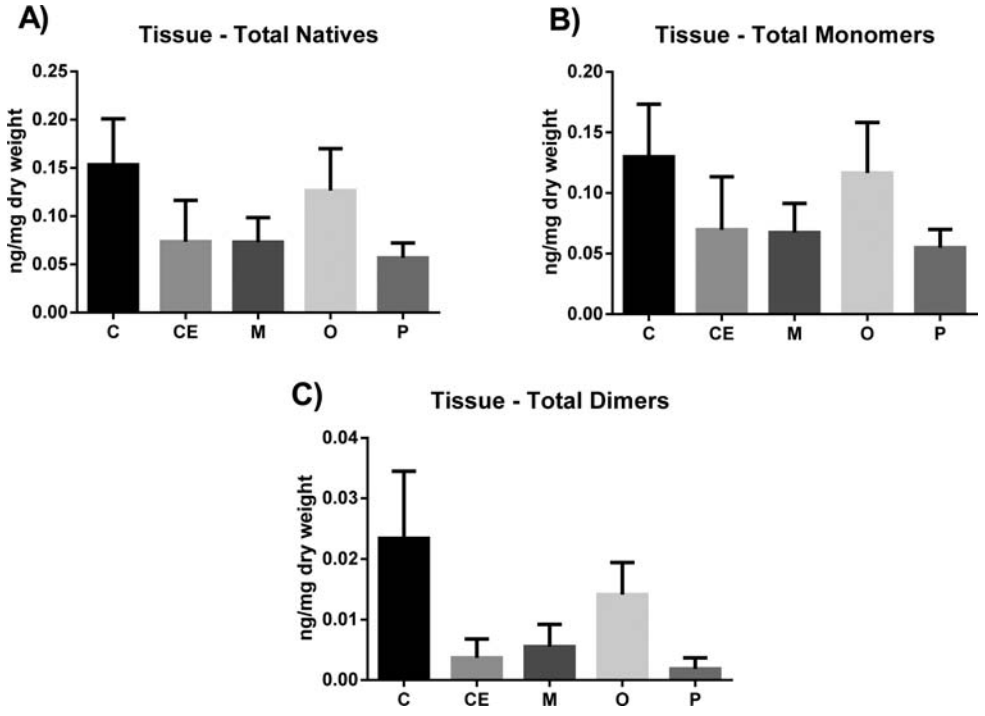


**Figure 3.** Tissue levels of total native compounds (A), total monomers (B), and total dimers (C) in mouse colon tissue following 12 weeks of exposure to the experimental diets. Mice were fasted for 12 h prior to euthanasia and collection of colon tissue. Data are presented as the mean ± SEM from $n = 9$ animals. No significant differences were detected between treatments for total native compounds, total monomers, or total dimers (one-way ANOVA with Tukey's HSD post hoc test, significance defined as $P < 0.05$). Treatments: mice fed basal control diet (C), mice fed control diet supplemented with cocoa extract (CE), mice fed control diet supplemented with cocoa monomers (M), mice fed control diet supplemented with cocoa oligomers (O), and mice fed control diet supplemented with cocoa polymers (P).

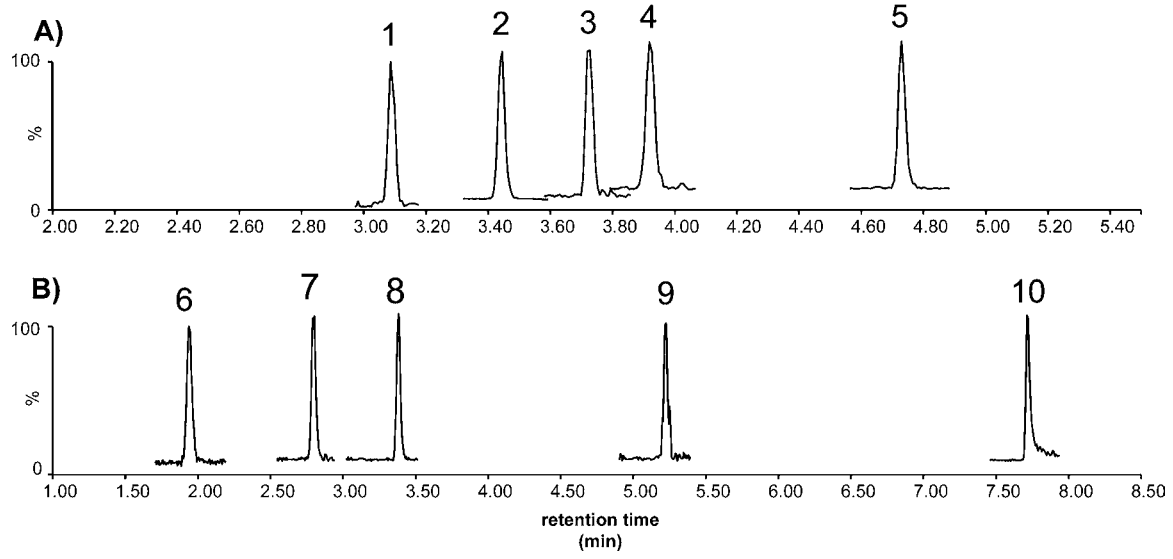


**Figure 4.** Representative UPLC-MS/MS multireaction monitoring (MRM) chromatograms of detected native flavanols (A) and microbial metabolites (B) in the colon tissue of a mouse fed a basal diet supplemented with cocoa oligomers for 12 weeks. All chromatograms are normalized to equal height (100% relative intensity). All chromatograms are from the same animal. Compound identities: (1) catechin; (2) PC $B_2$; (3) (−)-epicatechin; (4) PC $C_1$; (5) PC $B_5$; (6) 3,4-dihydroxybenzoic acid; (7) 4-hydroxybenzoic acid; (8) 3-hydroxybenzoic acid; (9) phenylacetic acid; (10) unknown metabolite [an isomer of 5-(3′,4′-dihydroxyphenyl)valeric acid].

**Colon Tissue Levels of Native Flavanols.** The levels of native flavanols detected in mouse colons are shown in Figure 3. Supplementation of the basal control diet with flavanols did not increase the colonic tissue accumulation of these compounds compared to the basal control diet alone. Whereas tissue accumulation levels of native flavanols were extremely low, the chromatograms shown in Figure 4A demonstrate that the peaks are large, accurately measurable peaks, as opposed to very small peaks and/or baseline noise. Furthermore, quantified peaks were found to be above the signal-to-noise ratio limit of 10:1 for lower limit of quantification. These data suggest that there was very little tissue accumulation of native flavanols in the colon during


dx.doi.org/10.1021/jf503838q | J. Agric. Food Chem. 2014, 62, 11190−11199

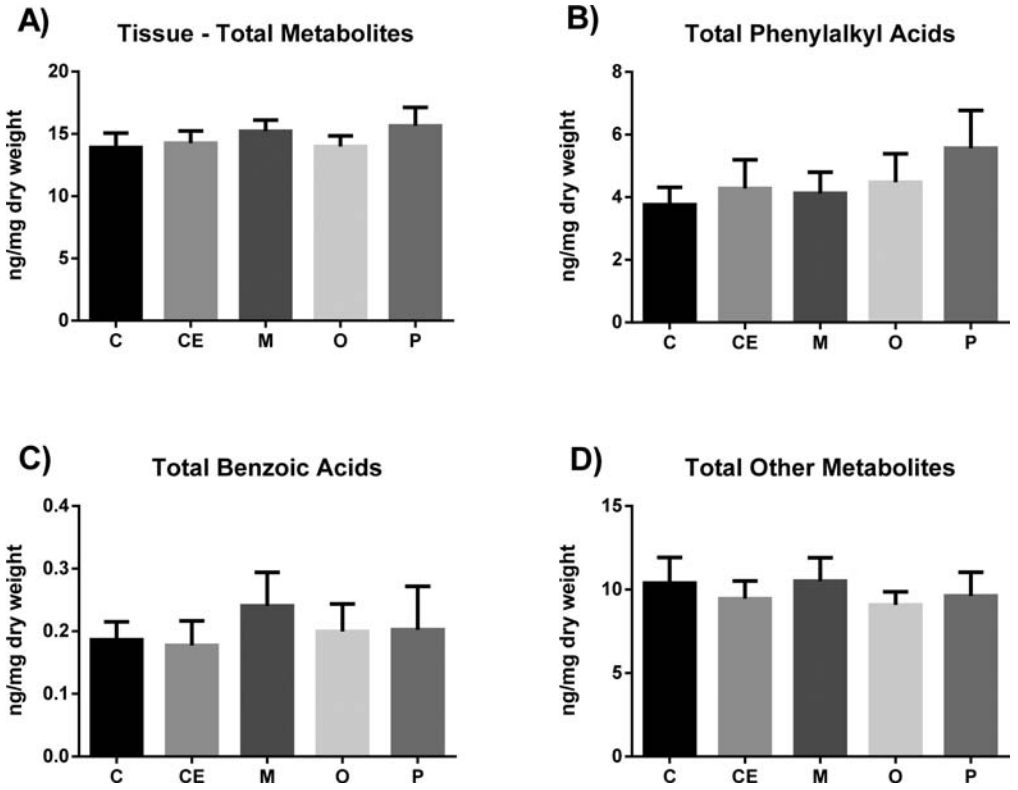


**Figure 5.** Tissue levels of total metabolites (A), total phenylalkyl (phenylacetic, phenylpropionic, and phenylvaleric) acid derivatives (B), total benzoic acid derivatives (C), and total other metabolites (D) in mouse colon tissue following 12 weeks of exposure to the experimental diets. Mice were fasted for 12 h prior to euthanasia and collection of colon tissue. Data are presented as the mean ± SEM from $n = 9$ animals. No significant differences were detected between treatments for total native compounds, total monomers, or total dimers (one-way ANOVA with Tukey's HSD post hoc test, significance defined as $P < 0.05$). Treatments: mice fed basal control diet (C), mice fed control diet supplemented with cocoa extract (CE), mice fed control diet supplemented with cocoa monomers (M), mice fed control diet supplemented with cocoa oligomers (O), and mice fed control diet supplemented with cocoa polymers (P).

the 12 week feeding period, but tissue accumulation was measurable. Our data differ from the results of previous studies of colonic tissue accumulation that have used much higher doses (125−1000 mg/kg) and found significant colonic tissue accumulation of flavanols.[11,29,30] This finding could be due to the comparatively low dose (25 mg/kg) or the 12 h fast before euthanasia. Both of those factors contribute to the accumulation and retention of these native flavanols in coloninc tissues. However, the 12 h fast alone would not result in significant depletion of ingested native flavanolss and their metabolites, partly due to the gastrointestinal (GI) transit time required to reach the colon [a portion of food ingested in the hours prior to fasting would still be in the lower GI tract at 12 h, as reflected by the fact that about half of the mouse colons contained fecal matter at the time of sacrifice in the present study (data not shown)]. Furthermore, acute studies have shown appreciable levels of native flavanols and their metabolites in the colon at from 8 to 18 h postadministration of flavanols,[11,28,30] albeit with much higher doses administered.

The finding that chronic feeding of flavanols did not elevate levels of intact flavanols in the colon was completely unexpected, due to the fact that the basal diet had roughly $10^5$−$10^6$-fold lower levels of native flavanols than any of the cocoa-supplemented diets (Supporting Information Figure S2A). One possible explanation for this is that the 12 week feeding of the cocoa-supplemented diet may have stimulated the gut microbiota in these animals to adapt and become extremely efficient at metabolizing native flavanols; the gut microbiota in animals fed the basal control diet would have had little stimulus to increase their metabolism of the native flavanols. The net effect of a 12 week feeding of flavanols would be to accumulate less of the native flavanols in the colon, despite higher dietary levels. Another possibility is that chronic exposure to flavanols could have unregulated detoxification pathways in the gut epithelium (phase-I/II enzymes and apical efflux transporters such as multidrug-resistant proteins (MRPs) and P-glycoprotein (Pgp)].[38,39] Similar to the first possibility, the gut epithelium in animals fed a semipurified (and largely polyphenol-free) diet would have had little stimulus to increase their metabolism of the native flavanols. Phase-I/II metabolites were not analyzed in the present study due to the sheer number of compounds measured. Provocative data have shown that chronic dosing of grape flavanols for 10 days up-regulates both phase-II metabolism of catechins and depolymerization of procyanidins (likely by the gut microflora) from an acute dose compared to an acute dose without prior chronic dosing, although this study reported only blood levels.[40] This suggests that both mechanisms may be responsible for our data. Future studies could employ various strategies to quantify phase-I/II metabolites of flavanols.[41] For example, parallel analyses could be performed on the same tissue, with one sample first incubated in $\beta$-glucuronidase/sulfatase prior to extraction and the other sample extracted without enzymatic deconjugation, with the difference in measured native flavanols between the two assays representing the extent of glucuronidation and sulfation. Assessment of *O*-methylated metabolites is more challenging, as enzymatic deconjugation is

not feasible and *O*-methyl derivatives must be measured directly, doubling or tripling the number of compounds to monitor.

Interestingly, no PCs larger than trimers (DP 3) were detected above the lower limit of detection (LLOD) in the colon tissue, despite the fact that these larger compounds made up significant portions of the oligomer- and polymer-supplemented diets (Table 1; Figures S1 and S2D) and were easily detectable using our UPLC-MS/MS method. Therefore, it appears that larger PCs are particularly affected by alterations to colonic metabolism occurring during chronic flavanol exposure.

**Colon Tissue Levels of Metabolites.** The levels of microbial metabolites detected in mouse colons are shown in Figure 5. Similar to the native flavanols, the UPLC-MS/MS peaks for the predominant metabolites (Figure 4B) were sizable and not merely "noise", confirming the accuracy and reliability of these data. Mean tissue accumulation levels of microbial metabolites were notably greater than accumulation of native flavanols (13.9−15.2 vs 0.0568−0.153 ng/mg tissue, respectively). However, there were no statistically significant differences in the accumulated levels of total metabolites or in any subclass of metabolites (Figure 5B−D) between treatments. Considering only the four treatments supplemented with CE or cocoa fractions, the data suggest that no matter the source or size (DP) of flavanols, they are all metabolized into similar qualitative and quantitative profiles of compounds during chronic exposure. The finding that the levels of microbial metabolites were not elevated in the flavanol-supplemented diets compared to control was quite surprising, given the differences in dietary levels of flavanols between the diets (Supporting Information Figure S2). Our hypothesis that extensive microbial metabolism of native flavanols potentially led to their low tissue levels (Figure 3) would suggest that extremely high levels of the resulting metabolites should be found in the colon of flavanol-fed mice compared to basal control; clearly this was not the case. Therefore, the reason for the similarity in colonic levels of native flavanols and microbial metabolites between basal control and flavanol-fed mice remains unclear.

**Folin−Ciocalteu Assay.** The surprising finding that total levels of accumulated metabolites were similar for the basal control diet and diets supplemented with cocoa flavanols suggested the possibility that the basal diet contained other phenolics that were not detected by the UPLC-MS/MS assay. UPLC-MS/MS was specific for common catechin monomers and B-type PCs; the presence of other phenolics in the diets that could be metabolized to the few dozen common metabolites could explain the data in Figure 5. Therefore, the Folin−Ciocalteu assay was performed on the diets to determine the total concentration of phenolics that could have been metabolized to the common metabolites measured by UPLC-MS/MS. As shown in Figure S4 in the Supporting Inforamtion, the concentrations of total phenolics in all diets supplemented with CE or the cocoa fractions were significantly higher than that of the basal control diet. These data are in agreement with UPLC-MS/MS data showing that supplementation of the basal control diet with cocoa flavanols significantly increased the phenolic content of the diet and the available substrates for microbial metabolism. However, the magnitude of the differences in levels of phenolic compounds between basal control and supplemented diets differed greatly for the two assays (~2.2-fold for the Folin assay vs $\sim 10^5-10^6$-fold for the UPLC-MS/MS assay). It should be noted that the Folin assay more accurately represents the total antioxidant activity, including nonphenolic constituents[42]). Nevertheless, both measures confirm significantly greater levels of phenolics available for microbial metabolism in flavanol-supplemented diets compared to control, but these differences are not reflected in tissue accumulation of microbial metabolites in the colon tissue (Figure 5). Therefore, similarities in colon metabolite levels between control and flavanol-supplemented mice are not due to large levels of undetected phenolics in the background diet but rather due to colonic metabolism and clearance of native flavanols in flavanol-supplemented mice. Lignins are a potential source of the same metabolites that are produced by metabolism of flavanols, but which may not have been accounted for by the Folin assay. Lignins are found in virtually all plant materials used for animal feeds,[43] as well as cacao beans.[44] However, lignins in the diets used for the present study would likely be almost exclusively from the basal control diet, as lignin would not be appreciably extracted from the cocoa (efficient lignin extraction generally requires high heat, whereas our extractions were performed at room temperature).[45−47] These compounds were not measured by our specific UPLC-MS/MS method, and therefore would not be accounted for in our analysis of native flavanols. It is unknown if the levels of lignins present in the basal control diet contributed to the measured Folin values. Lignins have Folin activity,[48,49] but it is inversely proportional to lignin DP.[50] Therefore, large lignins would have contributed little to observed Folin values. Anaerobic microbial metabolism of lignins results in the formation of several phenolic metabolites also formed by metabolism of flavanols,[51] including phenylacetic acid, benzoic acid, 3-phenylpropionic acid, acid, vanillic acid, ferulic acid, caffeic acid, and catechol. Therefore, the presence of high levels of large lignins in the basal control diet could partly explain why this diet produced similar levels of phenolic metabolites compared to flavanol-supplemented diets (assuming that supplementation with flavanols did not significantly increase the level of precursor compounds above that present in the basal diet).

One limitation of the present study is that the mice were fed a high-fat, low-carbohydrate diet (60 and 20% kcal from fat and carbohydrates, respectively; Supporting Information Table S4).[23] It is unknown how the high-fat diet affected gut microflora composition and subsequent metabolism and tissue accumulation of flavanols. Future work is required to examine the colon tissue accumulation during low-fat (~10% kcal from fat) feeding. However, the present data are relevant, as there is interest in using cocoa flavanols to combat obesity and type-2 diabetes,[22,23] which typically occur in the context of a high-fat diet.

To the best of our knowledge, the present study represents the longest known chronic flavanol feeding study for which colonic tissue accumulation data are reported. Although colonic tissue accumulation levels may be transient (compounds present in the tissue may be metabolized inside cells and/or effluxed into circulation or back into the lumen over time), these levels represent the typical profile of flavanols and their metabolites to which the colon tissue is exposed during chronic flavanol intake.

Our findings, and those of Wang et al.,[40] highlight the pronounced differences observed between single acute doses in animals not previously exposed to flavanols[11] and chronic low doses to which the gut microbiota and epithelium adapt. The results from the present study indicate that we do not yet fully understand the fate of ingested flavanols in the colon during chronic dietary exposure to these compounds. There have been comparatively few studies that characterize the fate of flavanols during long-term chronic exposure to these compounds. Our data demonstrate that these factors (time and dose) warrant further consideration in future studies comparing various doses

and various exposure times. The rationale for these studies is that chronic, low-dose exposure to flavanols is more relevant to human health than high-dose, acute exposure in animals not previously exposed to flavanols.

Additionally, due to the unexpected findings of this study, little is still known regarding the metabolism of larger PCs. We hoped that feeding oligomeric and polymeric PCs would provide data regarding their metabolism. It is known that PC dimers can be metabolized by microflora to dimeric ring-opening intermediates without depolymerization.[13] This key discovery suggests that larger PCs may also be incrementally metabolized from the ends inward and are not necessarily depolymerized prior to ring-opening and other reactions. However, it is still unknown how the dimeric intermediates are further metabolized. Potential metabolic fates of larger PCs include formation of similar intermediates by ring opening (trimers → trimeric intermediates, tetramers → tetrameric intermediates, etc.) and depolymerization to smaller PCs and monomers (this has been shown to be minimal in the stomach and small intestine, but occurrence in the colon remains unknown) prior to further metabolism;[40] alternatively, these larger PCs compounds may remain largely intact and unmetabolized.

Therefore, studies are warranted to compare colonic metabolism and tissue accumulation of flavanols, as well as blood pharmacokinetics,[40] during acute versus chronic exposure. Such studies should compare the quantitative and qualitative profiles of native flavanols and their microbial metabolites in the colon at relevant time points of dietary flavanol exposure. Relevant time points for such studies would likely follow a single acute dose without prior exposure, 1 week chronic exposure, 1 month chronic exposure, and so forth. Such studies are necessary to generate data relevant to human use, where flavanols are typically ingested throughout the lifespan from foods as well as dietary supplements. Additionally, the correlation between colonic tissue accumulation profiles and colonic activity resulting from distinct dietary flavanol profiles warrants further consideration. We have previously shown that distinct flavanol profiles result in distinct biological activities, but the impact of small versus large PCs on colon health remains poorly understood. This study suggests that differences in colon tissue activities would not be predicted by differences in accumulation profiles.

## ■ ASSOCIATED CONTENT

### Supporting Information

Individual compound composition of cocoa extract and cocoa fractions; UPLC-MS/MS methodology and MRM parameters for all native flavanols and microbial metabolites; normal-phase HPLC profiles of cocoa extract and cocoa fractions. This material is available free of charge via the Internet at http://pubs.acs.org.

## ■ AUTHOR INFORMATION


### Corresponding Author

*(A.P.N.) Phone: (540) 231-8391. Fax: (540) 231-9293. E-mail: andrewn@vt.edu.

### Present Address

[§]Flavorseal, 35179 Avon Commerce Parkway, Avon, OH 44011, USA.



### Funding

Start-up research funding for A.P.N. from the Department of Food Science and Technology and the College of Agriculture and Life Sciences at Virginia Polytechnic Institute and State University was used to support this research.

### Notes

The authors declare no competing financial interest.

## ■ ACKNOWLEDGMENTS

We acknowledge Laura Griffin and Dr. Katherine Thompson-Witrick for assistance with characterization of cocoa extract and fractions, Dr. Hengjian Wang for assistance with the Folin assay, and Gabrielle Fundaro, Dr. Joseph Stevens, Mostafa Ali, Karen Strat, Pamela Suroski, Charles Nwaihesie, Benjamin Furrow, and Julie Holdridge for assistance with the animal experiments.


## ■ ABBREVIATIONS USED

ACN, acetonitrile; C, catechin; CE, cocoa extract; DP, degrees of polymerization; EC, epicatechin; ECG, epicatechin gallate; EGC, epigallocatechin; EGCG, epigallocatechin gallate; GAE, gallic acid equivalents; IACUC, Institutional Animal Care and Use Committee; LLOD, lower limit of detection; MeOH, methanol; MRPs, multidrug-resistant proteins; Pgp, P-glycoprotein; PBS, phosphate-buffered saline; PC, procyanidin

## ■ REFERENCES


(1) Hammerstone, J. F. Procyanidin content and variation in some commonly consumed foods. *J. Nutr.* **2000**, *130*, 2086S.

(2) Lee, K. W. Cocoa has more phenolic phytochemicals and a higher antioxidant capacity than teas and red wine. *J. Agric. Food Chem.* **2003**, *51*, 7292−7295.

(3) Crozier, S. J.; Preston, A. G.; Hurst, J. W.; Payne, M. J.; Mann, J.; Hainly, L.; Miller, D. L. Cacao seeds are a "Super Fruit": a comparative analysis of various fruit powders and products. *Chem. Cent. J.* **2011**, 510.1186/1752-153X-5-5.

(4) Shoji, T.; Masumoto, S.; Moriichi, N.; Akiyama, H.; Kanda, T.; Ohtake, Y.; Goda, Y. Apple procyanidin oligomers absorption in rats after oral administration: analysis of procyanidins in plasma using the Porter method and high-performance liquid chromatography/tandem mass spectrometry. *J. Agric. Food Chem.* **2006**, *54*, 884−892.

(5) Serra, A.; Macia, A.; Romero, M. P.; Valls, J.; Blade, C.; Arola, L.; Motilva, M. J. Bioavailability of procyanidin dimers and trimers and matrix food effects in in vitro and in vivo models. *Br. J. Nutr.* **2010**, *103*, 944−952.

(6) Donovan, J. L.; Manach, C.; Rios, L.; Morand, C.; Scalbert, A.; Remesy, C. Procyanidins are not bioavailable in rats fed a single meal containing a grapeseed extract or the procyanidin dimer B-3. *Br. J. Nutr.* **2002**, *87*, 299−306.

(7) Stoupi, S.; Williamson, G.; Viton, F.; Barron, D.; King, L. J.; Brown, J. E.; Clifford, M. N. *In vivo* bioavailability, absorption, excretion, and pharmacokinetics of [$^{14}$C]procyanidin B2 in male rats. *Drug Metab. Dispos.* **2010**, *38*, 287−291.

(8) Urpi-Sarda, M.; Monagas, M.; Khan, N.; Lamuela-Raventos, R. M.; Santos-Buelga, C.; Sacanella, E.; Castell, M.; Permanyer, J.; Andres-Lacueva, C. Epicatechin, procyanidins, and phenolic microbial metabolites after cocoa intake in humans and rats. *Anal. Bioanal. Chem.* **2009**, *394*, 1545−1556.

(9) Aura, A. M.; Mattila, I.; Seppanen-Laakso, T.; Miettinen, J.; Oksman-Caldentey, K. M.; Oresic, M. Microbial metabolism of catechin stereoisomers by human faecal microbiota: comparison of targeted analysis and a non-targeted metabolomics method. *Phytochem. Lett.* **2008**, *1*, 18−22.

(10) Deprez, S.; Brezillon, C.; Rabot, S.; Philippe, C.; Mila, I.; Lapierre, C.; Scalbert, A. Polymeric proanthocyanidins are catabolized by human colonic microflora into low-molecular-weight phenolic acids. *J. Nutr.* **2000**, *130*, 2733−2738.

(11) Tsang, C.; Auger, C.; Mullen, W.; Bornet, A.; Rouanet, J. M.; Crozier, A.; Teissedre, P. L. The absorption, metabolism and excretion of flavan-3-ols and procyanidins following the ingestion of a grape seed extract by rats. *Br. J. Nutr.* **2005**, *94*, 170−181.

(12) Stoupi, S.; Williamson, G.; Drynan, J. W.; Barron, D.; Clifford, M. N. A comparison of the *in vitro* biotransformation of (−)-epicatechin

and procyanidin B2 by human faecal microbiota. *Mol. Nutr. Food Res.* **2010**, *54*, 747−759.
(13) Stoupi, S.; Williamson, G.; Drynan, J. W.; Barron, D.; Clifford, M. N. Procyanidin B2 catabolism by human fecal microflora: partial characterization of "dimeric" intermediates. *Arch. Biochem. Biophys.* **2010**, *501*, 73−78.
(14) Gonthier, M. P.; Donovan, J. L.; Texier, O.; Felgines, C.; Remesy, C.; Scalbert, A. Metabolism of dietary procyanidins in rats. *Free Radical Biol. Med.* **2003**, *35*, 837−844.
(15) Appeldoorn, M. M.; Vincken, J.-P.; Aura, A.-M.; Hollman, P. C. H.; Gruppen, H. Procyanidin dimers are metabolized by human microbiota with 2-(3,4-dihydroxyphenyl)acetic acid and 5-(3,4-dihydroxyphenyl)-γ-valerolactone as the major metabolites. *J. Agric. Food Chem.* **2009**, *57*, 1084−1092.
(16) Wang, D. J.; Williams, B. A.; Ferruzzi, M. G.; D'Arcy, B. R. Microbial metabolites, but not other phenolics derived from grape seed phenolic extract, are transported through differentiated Caco-2 cell monolayers. *Food Chem.* **2013**, *138*, 1564−1573.
(17) Miene, C.; Weise, A.; Glei, M. Impact of polyphenol metabolites produced by colonic microbiota on expression of COX-2 and GSTT2 in human colon cells (LT97). *Nutr. Cancer* **2011**, *63*, 653−662.
(18) Larrosa, M.; Luceri, C.; Vivoli, E.; Pagliuca, C.; Lodovici, M.; Moneti, G.; Dolara, P. Polyphenol metabolites from colonic microbiota exert anti-inflammatory activity on different inflammation models. *Mol. Nutr. Food Res.* **2009**, *53*, 1044−1054.
(19) Cheah, K.; Bastian, S. P.; Acott, T. V.; Abimosleh, S.; Lymn, K.; Howarth, G. Grape seed extract reduces the severity of selected disease markers in the proximal colon of dextran sulphate sodium-induced colitis in rats. *Dig. Dis. Sci.* **2013**, *58*, 970−977.
(20) Derry, M. M.; Raina, K.; Balaiya, V.; Jain, A. K.; Shrotriya, S.; Huber, K. M.; Serkova, N. J.; Agarwal, R.; Agarwal, C. Grape seed extract efficacy against azoxymethane-induced colon tumorigenesis in A/J mice: interlinking miRNA with cytokine signaling and inflammation. *Cancer Prev. Res.* **2013**, *6*, 625−633.
(21) Song, P.; Zhang, R.; Wang, X.; He, P.; Tan, L.; Ma, X. Dietary grape-seed procyanidins decreased postweaning diarrhea by modulating intestinal permeability and suppressing oxidative stress in rats. *J. Agric. Food Chem.* **2011**, *59*, 6227−6232.
(22) Gu, Y.; Yu, S.; Park, J. Y.; Harvatine, K.; Lambert, J. D. Dietary cocoa reduces metabolic endotoxemia and adipose tissue inflammation in high-fat fed mice. *J. Nutr. Biochem.* **2013**, 439−445.
(23) Dorenkott, M. R.; Griffin, L. E.; Goodrich, K. M.; Thompson-Witrick, K. A.; Fundaro, G.; Ye, L.; Stevens, J. R.; Ali, M.; O'Keefe, S. F.; Hulver, M. W.; Neilson, A. P. Oligomeric cocoa procyanidins possess enhanced bioactivity compared to monomeric and polymeric cocoa procyanidins for preventing the development of obesity, insulin resistance, and impaired glucose tolerance during high-fat feeding. *J. Agric. Food Chem.* **2014**, *62*, 2216−2227.
(24) Espley, R. V.; Butts, C. A.; Laing, W. A.; Martell, S.; Smith, H.; McGhie, T. K.; Zhang, J.; Paturi, G.; Hedderley, D.; Bovy, A.; Schouten, H. J.; Putterill, J.; Allan, A. C.; Hellens, R. P. Dietary flavonoids from modified apple reduce inflammation markers and modulate gut microbiota in mice. *J. Nutr.* **2014**, *144*, 146−154.
(25) Massot-Cladera, M.; Perez-Berezo, T.; Franch, A.; Castell, M.; Perez-Cano, F. J. Cocoa modulatory effect on rat faecal microbiota and colonic crosstalk. *Arch. Biochem. Biophys.* **2012**, *527*, 105−112.
(26) Kahle, K.; Kraus, M.; Scheppach, W.; Richling, E. Colonic availability of apple polyphenols − a study in ileostomy subjects. *Mol. Nutr. Food Res.* **2005**, *49*, 1143−1150.
(27) Hagl, S.; Deusser, H.; Soyalan, B.; Janzowski, C.; Will, F.; Dietrich, H.; Albert, F. W.; Rohner, S.; Richling, E. Colonic availability of polyphenols and D-(−)-quinic acid after apple smoothie consumption. *Mol. Nutr. Food Res.* **2011**, *55*, 368−377.
(28) Abia, R.; Fry, S. C. Degradation and metabolism of C-14-labelled proanthocyanidins from carob (*Ceratonia siliqua*) pods in the gastrointestinal tract of the rat. *J. Sci. Food Agric.* **2001**, *81*, 1156−1165.
(29) Choy, Y. Y.; Jaggers, G. K.; Oteiza, P. I.; Waterhouse, A. L. Bioavailability of intact proanthocyanidins in the rat colon after ingestion of grape seed extract. *J. Agric. Food Chem.* **2013**, *61*, 121−127.
(30) Goodrich, K. M.; Neilson, A. P. Simultaneous UPLC−MS/MS analysis of native catechins and procyanidins and their microbial metabolites in intestinal contents and tissues of male Wistar Furth inbred rats. *J. Chromatogr., B* **2014**, *958*, 63−74.
(31) Turnbaugh, P. J.; Ridaura, V. K.; Faith, J. J.; Rey, F. E.; Knight, R.; Gordon, J. I. The effect of diet on the human gut microbiome: a metagenomic analysis in humanized gnotobiotic mice. *Sci. Transl. Med.* **2009**, *1*10.1126/scitranslmed.3000322.
(32) Le Blay, G.; Michel, C.; Blottière, H. M.; Cherbut, C. Prolonged intake of fructo-oligosaccharides induces a short-term elevation of lactic acid-producing bacteria and a persistent increase in cecal butyrate in rats. *J. Nutr.* **1999**, *129*, 2231−2235.
(33) Hidalgo, M.; Oruna-Concha, M. J.; Kolida, S.; Walton, G. E.; Kallithraka, S.; Spencer, J. P. E.; Gibson, G. R.; de Pascual-Teresa, S. Metabolism of anthocyanins by human gut microflora and their influence on gut bacterial growth. *J. Agric. Food Chem.* **2012**, *60*, 3882−3890.
(34) Sánchez-Patán, F.; Cueva, C.; Monagas, M.; Walton, G. E.; Gibson M, G. R.; Quintanilla-López, J. E.; Lebrón-Aguilar, R.; Martín-Álvarez, P. J.; Moreno-Arribas, M. V.; Bartolomé, B. In vitro fermentation of a red wine extract by human gut microbiota: changes in microbial groups and formation of phenolic metabolites. *J. Agric. Food Chem.* **2012**, *60*, 2136−2147.
(35) van't Slot, G.; Humpf, H. U. Degradation and metabolism of catechin, epigallocatechin-3-gallate (EGCG), and related compounds by the intestinal microbiota in the pig cecum model. *J. Agric. Food Chem.* **2009**, *57*, 8041−8048.
(36) van Dorsten, F. A.; Peters, S.; Gross, G.; Gomez-Roldan, V.; Klinkenberg, M.; de Vos, R. C.; Vaughan, E. E.; van Duynhoven, J. P.; Possemiers, S.; van de Wiele, T.; Jacobs, D. M. Gut microbial metabolism of polyphenols from black tea and red wine/grape juice is source-specific and colon-region dependent. *J. Agric. Food Chem.* **2012**, *60*, 11331−11342.
(37) Zhao, Z.; Egashira, Y.; Sanada, H. Phenolic antioxidants richly contained in corn bran are slightly bioavailable in rats. *J. Agric. Food Chem.* **2005**, *53*, 5030−5035.
(38) Jiang, W.; Hu, M. Mutual interactions between flavonoids and enzymatic and transporter elements responsible for flavonoid disposition via phase II metabolic pathways. *RSC Adv.* **2012**, *2*, 7948−7963.
(39) Hong, J.; Lambert, J. D.; Lee, S. H.; Sinko, P. J.; Yang, C. S. Involvement of multidrug resistance-associated proteins in regulating cellular levels of (−)-epigallocatechin-3-gallate and its methyl metabolites. *Biochem. Biophys. Res. Commun.* **2003**, *310*, 222−227.
(40) Wang, J.; Ferruzzi, M. G.; Ho, L.; Blount, J.; Janle, E. M.; Gong, B.; Pan, Y.; Gowda, G. A. N.; Raftery, D.; Arrieta-Cruz, I.; Sharma, V.; Cooper, B.; Lobo, J.; Simon, J. E.; Zhang, C. F.; Cheng, A.; Qian, X. J.; Ono, K.; Teplow, D. B.; Pavlides, C.; Dixon, R. A.; Pasinetti, G. M. Brain-targeted proanthocyanidin metabolites for Alzheimer's disease treatment. *J. Neurosci.* **2012**, *32*, 5144−5150.
(41) Neilson, A. P.; Sapper, T. N.; Janle, E. M.; Rudolph, R.; Matusheski, N. V.; Ferruzzi, M. G. Chocolate matrix factors modulate the pharmacokinetic behavior of cocoa flavan-3-ol phase II metabolites following oral consumption by Sprague−Dawley rats. *J. Agric. Food Chem.* **2010**, *58*, 6685−6691.
(42) Everette, J. D.; Bryant, Q. M.; Green, A. M.; Abbey, Y. A.; Wangila, G. W.; Walker, R. B. Thorough study of reactivity of various compound classes toward the Folin−Ciocalteu reagent. *J. Agric. Food Chem.* **2010**, *58*, 8139−8144.
(43) Knudsen, K. E. B. Carbohydrate and lignin contents of plant materials used in animal feeding. *Anim. Feed Sci. Technol.* **1997**, *67*, 319−338.
(44) Lecumberri, E.; Mateos, R.; Izquierdo-Pulido, M.; Rupérez, P.; Goya, L.; Bravo, L. Dietary fibre composition, antioxidant capacity and physico-chemical properties of a fibre-rich product from cocoa (*Theobroma cacao* L.). *Food Chem.* **2007**, *104*, 948−954.
(45) Ye, Y.; Zhang, Y.; Fan, J.; Chang, J. Novel method for production of phenolics by combining lignin extraction with lignin depolymerization in aqueous ethanol. *Ind. Eng. Chem. Res.* **2011**, *51*, 103−110.

(46) Lee, S. H.; Doherty, T. V.; Linhardt, R. J.; Dordick, J. S. Ionic liquid-mediated selective extraction of lignin from wood leading to enhanced enzymatic cellulose hydrolysis. *Biotechnol. Bioeng.* **2009**, *102*, 1368−1376.
(47) Pang, Z.; Chen, J.; Dong, C.; Yang, G. Highly selective and efficient extraction of lignin in kraft pulp by aqueous ionic liquids for enhanced bleaching properties. *RSC Adv.* **2014**, *4*, 29897−29900.
(48) García, A.; González Alriols, M.; Spigno, G.; Labidi, J. Lignin as natural radical scavenger. Effect of the obtaining and purification processes on the antioxidant behaviour of lignin. *Biochem. Eng. J.* **2012**, *67*, 173−185.
(49) Salanti, A.; Zoia, L.; Orlandi, M.; Zanini, F.; Elegir, G. Structural characterization and antioxidant activity evaluation of lignins from rice husk. *J. Agric. Food Chem.* **2010**, *58*, 10049−10055.
(50) Dizhbite, T.; Telysheva, G.; Jurkjane, V.; Viesturs, U. Characterization of the radical scavenging activity of lignins−−natural antioxidants. *Bioresour. Technol.* **2004**, *95*, 309−317.
(51) Colberg, P. J.; Young, L. Y. Aromatic and volatile acid intermediates observed during anaerobic metabolism of lignin-derived oligomers. *Appl. Environ. Microb.* **1985**, *49*, 350−358.

BBCH (Biologische Bundesanstalt, Bundessortenamt and Chemical Industry) scale (system for a uniform coding of phonologically similar growth stages of all monodicotyledonous plant species).

**Sample Preparation.** The aerial parts of winter wheat, *T. aestivum* L. var. Legenda, voucher specimen 4 (BBCH 47), were harvested at principal growth stage in July 2012. The plant material directly after harvesting was frozen in the laboratory freezer (−18 °C), and then lyophilized using freeze-dryer Gamma 2-16 LSC from Martin Christ Gefriertrocknungsanlagen GmbH, Germany (time, 3 days; pressure, 1 mbar). *T. aestivum* L. aerial parts were powdered using an Ultra Centrifugal Mill ZM 200 (Retsch), a modern grinder, which does not cause sample warmup (12-tooth rotor; sieve size, 0.50 mm), and defatted in a Soxhlet extractor with chloroform. The plant material was then used for extraction.

**Chemical Reagents.** Solvents used in the study (methanol, acetonitrile, formic acid, toluene, chloroform, ethyl acetate, 85% orthophosphoric acid, and acetic acid) were of the analytical purity grade, purchased from J. T. Baker (Deventher, The Netherlands). D-Glucose, D-glucuronic acid, D-ribose, L-cystein methyl ester hydrochloride, *o*-toryl isothiocyanate, and 2,2-diphenyl-1-picrylhydrazyl radical (DPPH$^{\bullet}$) were obtained from Sigma-Aldrich Chemical Co. (St. Louis, MO, USA). Fractions were analyzed by TLC (25DC, Alufilien, 20 cm × 20 cm cellulose, Merck, Darmstadt, Germany). The TLC-DPPH$^{\bullet}$ test was performed on the surface of aluminum-backed silica gel 60 $F_{254}$ plates (Merck). Other chemicals were obtained from POCH S.A. (Gliwice, Poland). Phenolic standard solutions were prepared at a concentration of 1 mg/mL.

**Extraction and Fractionation of Crude Wheat Extract.** Defatted aerial parts of winter *T. aestivum* L. var. Legenda (250 g) were subjected to triple extraction with boiling 70% aqueous methanol solution (v/v; 2.5 L; 1 h) under reflux. The collected extracts were combined and filtered through a filter funnel, concentrated using a rotary evaporator (Heidolph), and freeze-dried. The crude extract (40 g) was fractionated using vacuum liquid chromatography; it was suspended in water, and the solution was applied to a 6 cm × 10 cm, 40−63 μm, LiChroprep RP-18 (Merck) preparative column, previously preconditioned with water. The column was washed first with water to remove sugars and then with 40% methanol to elute phenolics. The fraction washed out with 40% methanol was used in the next step of the purification procedure, because it was shown by UHPLC-PDA-ESI-MS/MS analyses to contain numerous phenolic compounds, mainly phenolic acids and flavonoids. Ultrahigh-performance chromatographic separations were performed on an Acquity UPLC System chromatograph (Waters Corp., Milford, MA, USA), equipped with a PDA and a triple-quadrupole mass detector (Acquity TQD, Waters). The crude wheat extract and phenolic fraction were separated on an Acquity HSS C18 (100 × 2.1 mm, 1.8 μm; Waters) column, maintained at 40 °C. The elution (400 μL/min) was carried out with a gradient of solvent B (acetonitrile with 0.1% formic acid) in solvent A (water with 0.1% formic acid): 0−4 min, 7% B; 4−22 min, 7−17% B; 22−24.95 min, 17−45% B; 24.95−25 min, 45−95% B; 25−27 min, 95% B; 27−27.05 min, 95−7% B; 27.05−30 min, 7% B. One microliter of a sample was injected for analysis. The PDA was operated in the range of 220−480 nm (3.6 nm resolution). Mass analyses were performed in the negative ionization mode, using the following conditions: capillary voltage, 2.8 kV; cone voltage, 35 V; source temperature, 140 °C; desolvation temperature, 350 °C; cone gas flow (nitrogen), 100 L/h; desolvation gas flow, 800 L/h; collision gas (argon) flow, 0.1 mL/min. All data were acquired and processed using Waters MassLynx 4.1 software.

**Purification of Phenolic Compounds.** The fraction washed out with 40% methanol was used for isolation of phenolics according to a previously used protocol but with slight modifications.[16] In short, the 40% methanol fraction was condensed nearly to dryness in vacuo, redissolved in distilled water, and loaded onto a preparative column (4 cm × 50 cm, 40−63 μm, LiChroprep RP-18, Merck). The column was washed with water and then with increasing concentrations of methanol in water (5% increments from 0 to 100% methanol). Ten milliliter fractions were collected and checked by TLC on cellulose plates (15:85 acetic acid/water; 25DC, Alufilien, 20 cm × 20 cm cellulose; Merck), and spots were visualized under UV at 366 nm. Fractions showing similar TLC patterns (41 fractions) were combined, evaporated, dissolved in water, freeze-dried, and further analyzed by HPLC. HPLC analyses were performed on a Waters system equipped with a model 616 pump, a model 600s controller, and a model 996 PAD detector. Millenium Chromatography Manager software (Waters Corp.) was used to monitor chromatographic parameters and to process the data. Twenty microliters of each fraction was injected for analysis. Fractions were applied to a Eurospher-100 C18 column (Knauer, Germany) (0.4 cm × 25 cm i.d., 5 μm) and eluted at 1 mL/min with a linear gradient of 1% $H_3PO_4$ in water/60% methanol in 1% aqueous $H_3PO_4$ (80:20%), increasing to 0:100% over 60 min. The column was maintained at 50 °C. Fractions possessing one compound were combined and evaporated to dryness. Fractions containing more than one compound were further purified on a C18 glass column (2 cm × 50 cm, 25−40 μm, Merck) using an isocratic system (methanol/1% $H_3PO_4$).

Semipreparative HPLC was used for purification in the case of fractions obtained in small amounts. This system was equipped with Gilson 321 pump, a liquid handler Gilson GX-271 with a 2 mL sample loop, a Gilson Prep ELSTM II detector, and a semipreparative reserved phase Atlantis Prep T3 (250 mm × 10 mm i.d., 5 μm) column and an Agilent Eclipse Plus C18, (150 mm × 4.6 mm i.d., 3.5 μm) analytical column. The choice of the column depended on the amount of purified fraction. Solvent system (A, $H_2O$ containing 0.2% HCOOH; B, $CH_3CN$ containing 0.2% HCOOH) was optimized individually for each fraction. The column temperature was maintained at 30 °C.

In this way 14 pure phenolic compounds were isolated.

**Mass Analyses of Purified Compounds.** Exact masses of wheat phenolics were determined by direct infusion electrospray high-resolution (Q-TOF) mass spectrometry (HRESI-MS), using a SYNAPT G2-S HDMS mass spectrometer (Waters, Manchester, UK).

Fragmentation analyses were performed by direct infusion electrospray mass spectrometry, using an Acquity TQD mass spectrometer (Waters Corp., Milford, MA, USA).

**NMR Analysis.** NMR spectra were acquired in 650 μL of methanol-$d_4$ at 25 °C or DMSO-$d_6$ at 70 °C on a Bruker Avance III HD 500 MHz instrument (Bruker BioSpin GmbH, Rheinstetten, Germany) equipped with a 5 mm probe ($^1$H, 500.18 MHz; $^{13}$C, 125.79 MHz). Standard pulse sequences and parameters were used to obtain 1D $^1$H, 1D selective TOCSY, 1D selective ROESY, 1D $^{13}$C, and DEPT-135, gCOSY, ROESY (mixing time = 250 ms), gHSQC, gHSQC-TOCSY (mixing time = 80 ms), gHMBC spectra. Chemical shift referencing was carried out using the internal solvent resonances at $\delta_H$ 3.31 and $\delta_C$ 49.0 for methanol-$d_4$ and at $\delta_H$ 2.50 and $\delta_C$ 39.51 for DMSO-$d_6$ (calibrated to TMS at 0.00 ppm).

**Determination of the Absolute Configuration of Sugars.** The absolute configuration of sugars was determined according to a modified method of Tanaka et al.[17] Flavonoids were subjected to acid hydrolysis (1 mL of 2 M HCl, 2 h, 100 °C). Aglycones or partially hydrolyzed *C*-glycosides were then extracted with ethyl acetate (3 × 1 mL), and sugar-containing aqueous layers were neutralized with Amberlite IRA-400 (OH− form). After drying, the samples were used to determine the absolute configuration of the constituent monosaccharides. Samples of monosaccharides obtained after acid hydrolysis of flavonoids were dissolved in 100 μL of anhydrous pyridine, containing 0.5 mg of L-cysteine methyl ester hydrochloride, and heated at 60 °C for 1 h. Then 100 μL of *o*-toryl isothiocyanate (0.5 mg) solution in pyridine was added, and the mixture was heated for another hour, at 60 °C. After cooling, samples were analyzed by UPLC-ESI-MS/MS. Chromatographic separations were carried out on an Acquity BEH C18 column (100 × 2.1 mm, 1.7 μm; Waters). Mass spectrometry analyses were performed in positive ionization mode, using the SRM method. Details of the analysis can be found in the work of Pérez et al.[18] D-Glucose (Glc), D-glucuronic acid (GlcA), and D-ribose (Rib) were identified on the basis of retention time and $m/z$ values of authentic standards, derivatized in the same way.

**TLC-DPPH$^{\bullet}$ Test.** The ability of isolated wheat phenolic compounds to scavenge DPPH$^{\bullet}$ radicals was determined using a

TLC rapid test. Briefly, standard solutions (1 mg/mL) of the purified phenolic acids, flavonoids, and rutin (positive control) were prepared. Aliquots of the standard solutions (5 μL) were applied to aluminum-backed silica gel chromatographic plates by means of a micropipet with a scale. All of the samples were applied bandwise (5 mm wide), with a distance of 10 mm between them, and a 10 mm distance from both the left and low edge of the plate. The plates were developed in vertical chambers presaturated for 15 min with the optimized mobile phase: acetonitrile/water/chloroform/formic acid (60:15:10:5, v/v/v/v). The plates were developed to a distance of 90 mm and dried in a hood for 10 min before derivatization. TLC plates were immersed for 5 s in freshly prepared 0.2% (w/v) methanolic DPPH• solution. After removal of excess DPPH•, plates were kept in the dark for 30 min and then scanned by means of flatbed scanner. The test was performed in triplicate.

**Image Processing Procedure.** Videoscans saved as JPG files were processed by means of a Sorbfil TLC Videodensitometer, a program elaborated by Sorbpolymer JSC (Sorbpolymer JSC, Krasnodar, Russian Federation, 2006; http://www.sorbfil.com). A detailed description of the procedure can be found in a previous publication.[19] First the background was corrected using the option "Background approximation"; for this purpose 50 marker points were placed on the brightness map generated after choosing the aforementioned option. Then the "Correct background" option was chosen to obtain uniform background brightness required to correctly evaluate the free radical scavenging activity of the isolated compounds. As the bands of active polyphenols appear as bright zones against a darker background, it is crucial to chose "Bright spots" option from the program toolbar. Finally, the tracks were assigned, each track corresponding to a given compound. There were 15 tracks, in total, 14 corresponding to all of the isolated polyphenols and one for rutin, which was used as a standard, with well recognized free radical scavenging activity. The bands of active compounds were converted to corresponding peaks, as also seen in Figure 3. The area under the peak of each individual compound was related to the area under the peak of rutin, developed and derivatized under the same conditions.

**Quantification of Wheat Phenolics.** Phenolic compounds were quantified in crude extract prepared at a concentration of 1 mg/mL using chromatographic conditions presented under Extraction and Fractionation of Crude Wheat Extract. These determinations were carried out using the external standard method. Phenolic acids were quantified using 5-caffeoylquinic acid (chlorogenic acid) as a group standard, and UV detection was performed at 325 nm. Flavonoids were quantified using rutin as a group standard, and UV detection was performed at 255 nm.

**Chemical Data of New Wheat Flavonoids. 15**: luteolin 6-*C*-[$6_{Glc''}$-*O*-*E*-caffeoyl-*β*-D-glucopyranosyl(1″→2)-*β*-glucopyranoside] (2 mg), yellow solid; UV (UPLC-PDA) $\lambda_{max}$ (nm) 271, 335; HRESI-MS (Q-TOF), *m*/*z* 771.1770 $[M - H]^-$ (calcd for $C_{36}H_{35}O_{19}^-$ = 771.1778); ESI-MS/MS (TQ), *m*/*z* 773 $[M + H]^+$, 611 $[M + H - 162]^+$, 449 $[M + H - 162 - 162]^+$, 329 $[M + H - 162 - 162 - 120]^+$, 287 $[Y^0 + H]^+ = [M + H - 162 - 162 - 162]$, 325 $[Caf + H + 162 - 18]^+$, 163 $[Caf + H - 18]^+$ (NMR data are presented in Table 1).

**17**: luteolin 6-*C*-[$5_{Rib''}$-*O*-*E*-feruoyl-*β*-D-ribofuranosyl(1″→2)-*β*-glucopyranoside] (4 mg), yellow solid; UV (UPLC-PDA) $\lambda_{max}$ (nm) 271, 335; HRESI-MS (Q-TOF), *m*/*z* 755.1827 $[M - H]^-$ (calcd for $C_{36}H_{35}O_{18}^-$ = 755.1829); ESI-MS/MS (TQ), *m*/*z* 757 $[M + H]^+$, 449 $[M + H - 176 - 132]^+$, 287 $[Y^0 + H]^+ = [M + H - 176 - 132 - 162]^+$, 309 $[Fer + H + 132 - 18]^+$, 177 $[Fer + H - 18]^+$.

**19**: 3′,4′,5′-*O*-trimethyltricetin 7-*O*-[*β*-D-glucuropyranosyl(1″→2)-*β*-D-glucopyranoside] (9 mg), yellow solid; UV (UPLC-PDA) $\lambda_{max}$ (nm) 270, 328; HRESI-MS (Q-TOF), *m*/*z* 681.1670 $[M - H]^-$ (calcd for $C_{30}H_{33}O_{18}^-$ = 681.1672); ESI-MS/MS (TQ), *m*/*z* 683 $[M + H]^+$, 507 $[M + H - 176]^+$, 345 $[Y^0 + H]^+ = [M + H - 176 - 162]^+$ (NMR data are presented in Table 2).

**Statistical Analysis.** Each calibration curve was constructed by running standards of six different concentrations, in triplicate. All samples were prepared in triplicate, and chromatographic analyses were also performed in triplicate.

**Table 1. NMR Spectroscopic Data (DMSO-$d_6$, 70 °C, 500 MHz) for Compounds 15 and 17**

| | 15 | | 17 | |
|---|---|---|---|---|
| | $\delta_H$ (*J* in Hz) | $\delta_C$ | $\delta_H$ (*J* in Hz) | $\delta_C$ |
| 2 | | 163.5 | | 163.5 |
| 3 | 6.42, s | 102.5 | 6.51, s | 102.6 |
| 4 | | 181.4 | | 181.4 |
| 5 | | 160.5 | | 160.0 |
| 6 | | 107.7 | | 108.2 |
| 7 | | 162.9 | | 162.6 |
| 8 | 6.39, s | 93.1 | 6.47, s | 93.2 |
| 9 | | 156.1 | | 156.1 |
| 10 | | 103.0 | | 103.2 |
| 1′ | | 121.5 | | 121.5 |
| 2′ | 7.33, d (2.2) | 113.2 | 7.36, d (2.1) | 113.2 |
| 3′ | | 145.3 | | 145.4 |
| 4′ | | 149.1 | | 149.2 |
| 5′ | 6.85, d (8.4) | 115.6 | 6.85, d (8.4) | 115.7 |
| 6′ | 7.25, dd (8.4, 2.2) | 118.5 | 7.30, dd (8.4, 2.0) | 118.5 |
| | 6-*C*-*β*-Glc | | 6-*C*-*β*-Glc | |
| 1 | 4.74, d (9.9) | 71.0 | 4.72, d (9.9) | 71.2 |
| 2 | 4.34, br s | 80.8 | 4.27, br s | 74.4 |
| 3 | 3.50, t (8.3) | 78.1 | 3.46, t (8.3) | 78.8 |
| 4 | 3.27[a] | 70.0 | 3.25[a] | 70.3 |
| 5 | 3.26, m | 81.0 | 3.26[a] | 80.8 |
| 6 | 3.71, dd (12.0, 2.0) | 61.1 | 3.72, dd (11.6, 1.5) | 61.1 |
| | 3.48[a] | | 3.48, dd (12.0, 5.9) | |
| | $2^{Glc}$-*O*-*β*-Glc″ | | $2^{Glc}$-*O*-*β*-Rib″ | |
| 1 | 4.28, d (7.9) | 104.8 | 5.16, s | 107.6 |
| 2 | 2.96, t (9.2) | 74.2 | 3.77, d (3.1) | 81.2 |
| 3 | 3.12, t (9.0) | 76.1 | 3.53, dd (5.9, 3.3) | 77.5 |
| 4 | 3.05, t (8.5) | 69.0 | 2.93, q (5.0) | 80.5 |
| 5 | 2.98, m | 73.3 | 3.82, ddd (11.6, 5.4, 5.4) | 62.7 |
| 6 | 3.85, br d (12.0) | 62.1 | | |
| | 3.74, br d (12.0) | | | |
| | $6^{Glc}$-*O*-Caf | | $5^{Rib}$-*O*-Fer | |
| 1 | | 125.4 | | 125.4 |
| 2 | 6.97, d (1.9) | 114.5 | 7.22, d (2.2) | 111.5 |
| 3 | | 147.7 | | 147.7 |
| 4 | | 145.1 | | 149.1 |
| 5 | 6.76, d (8.1) | 115.4 | 6.81, d (8.1) | 115.4 |
| 6 | 6.83, dd (8.2, 1.7) | 120.7 | 7.01 dd (8.2, 1.6) | 122.5 |
| 7 | 7.22, d (15.9) | 144.2 | 7.41, d (15.9) | 144.5 |
| 8 | 6.03, d (15.9) | 113.6 | 6.27, d (15.9) | 114.0 |
| 9 | | 165.6 | | 165.7 |
| $OCH_3$ | | | 3.84, s | 55.6 |

[a]Overlapping signal.

## RESULTS AND DISCUSSION

**Analysis of Phenolics.** UHPLC analysis of the methanol extract from wheat green aerial parts revealed the presence of numerous phenolic compounds (Figure 1). Separation of the compounds by low-pressure liquid chromatography followed by purification of fractions on a semipreparative C18 column afforded 14 single isolated compounds (**2**, **3**, **5**, **6**, **9**, **11**–**19**), for which structures were determined by spectrometric and spectroscopic techniques. Additionally, compounds **1**, **4**, **7**, **8**, and **10** were identified on the basis of the obtained UV spectra and fragmentation pathways. To the best of our knowledge, flavonoids **15**, **17**, and **19** are novel structures and have never been reported in the plant kingdom.

**Table 2. NMR Spectroscopic Data (Methanol-$d_4$, 25 °C, 500 MHz) for Compound 19**

| | 19 | |
|---|---|---|
| | $\delta_H$ ($J$ in Hz) | $\delta_C$ |
| 2 | | 165.9 |
| 3 | 6.76, s | 106.1 |
| 4 | | 184.2 |
| 5 | | 162.9 |
| 6 | 6.54, d (2.0) | 101.3 |
| 7 | | 164.8 |
| 8 | 6.90, d (1.9) | 96.9 |
| 9 | | 158.9 |
| 10 | | 107.2 |
| 1′ | | 127.9 |
| 2′ | 7.30, s | 105.4 |
| 3′ | | 155.0 |
| 4′ | | 142.7 |
| 5′ | | 155.0 |
| 6′ | 7.30, s | 105.4 |
| 4′-*O*-$CH_3$ | 3.85, s | 61.2 |
| 3′,5′-di-*O*-$CH_3$ | 3.96, s | 57.0 |
| | 7-*O*-$\beta$-Glc | |
| 1 | 5.33, d (7.1) | 100.2 |
| 2 | 3.75, t (8.1) | 83.5 |
| 3 | 3.72, t (8.8) | 77.5 |
| 4 | 3.46, dd (9.6, 8.2) | 71.0 |
| 5 | 3.55, ddd (9.6, 6.2, 2.6) | 78.2 |
| 6 | 3.93, dd (12.4, 2.1) | 62.4 |
| | 3.71[a] | |
| | $2^{Glc}$-*O*-$\beta$-GlcA″ | |
| 1 | 4.71, d (7.8) | 104.9 |
| 2 | 3.30, m | 75.6 |
| 3 | 3.44[a] | 77.5 |
| 4 | 3.44[a] | 73.5 |
| 5 | 3.69, d (7.8) | 76.8 |
| 6 | | 174.8 |

[a]Overlapping signal.

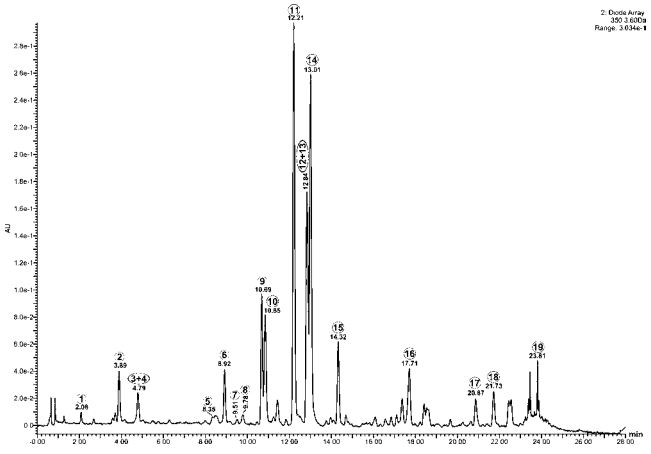

**Figure 1.** UPLC-UV (350 nm) chromatogram of the crude extract from the aerial parts of wheat (*Triticum aestivum* L.). Peak numbers correspond to the numbering of compounds in the text.

Six compounds visible in the UV chromatogram displayed maximum absorption typical for caffeic acid derivatives ($\lambda_{max}$ = 325 nm) and were identified on the basis of their ESI-MS/MS fragmentation patterns as 3-*O*-caffeoylquinic acid (**1**), 5-*O*-caffeoylquinic acid (**2**), 4-*O*-caffeoylquinic acid (**3**), 3-*O*-feruoylquinic acid (**4**), 5-*O*-feruoylquinic acid (**7**), and 4-*O*-feruoylquinic acid (**8**).[20] Compound **5** possessed a UV spectrum ($\lambda_{max}$ = 310 nm) and mass to charge ratio ($m/z$ 163) characteristic for *p*-coumaric acid. The remaining 12 compounds showed UV spectra typical for flavones. Hydrolysis of the purified flavonoids, followed by determination of absolute configuration of monosaccharides, showed that these were D-Glc, D-Xyl, D-GlcA, D-Rib, L-Ara, and L-Rha. Chromatographic separation of the extract afforded numerous flavonoids, including five known flavonoid glycosides, identified on the basis of their ESI-MS/MS and NMR analyses, namely, isoorientin 6″-*O*-$\beta$-D-xylopyranoside (**10**), isoorientin (luteolin 6-*C*-$\beta$-glucopyranoside) (**11**), isoschaftoside (apigenin 6-*C*-$\alpha$-arabinopyranoside 8-*C*-$\beta$-glucopyranoside) (**13**), isoscoparin 2″-*O*-$\alpha$-L-rhamnopyranoside (**16**), and tricin 7-*O*-rutinoside (**18**) (Figure 2).[21−24] NMR spectroscopy data included various 1D [$^1$H, proton-decoupled $^{13}$C and DEPT-135, selective excitation 1D-TOCSY and 1D-ROESY (mixing times of 120 and 250 ms, respectively) and 2D [$^1$H−$^1$H *g*COSY (magnitude mode), $^1$H−$^1$H TOCSY, $^1$H−$^1$H ROESY, $^1$H−$^{13}$C *g*HSQC, $^1$H−$^{13}$C *g*HSQC-TOCSY (mixing time of 80 ms), and $^1$H−$^{13}$C *g*HMBC ($^nJ_{CH}$ = 8 Hz)] spectra. Peaks 6, 9, 12, and 14 visible in the UV chromatogram were tentatively identified on the basis of their UV spectra and ESI-MS/MS fragmentation patterns as luteolin *C*-hexoside *O*-hexoside, luteolin *C*-(pentosyl-hexoside), apigenin *C*-hexoside *C*-pentoside, and luteolin *C*-hexoside *O*-deoxyhexoside, respectively.[25]

Compounds **15** and **17** had UV spectra typical for flavones, and positive ESI-MS analyses showed that their protonated molecules had $m/z$ values of 773 and 757, respectively. The collision-induced dissociation (CID) of these precursor ions revealed their monodesmosidic character. The MS/MS spectrum of **15** showed the presence of a fragment ion of $m/z$ 611 $[M + H - 162]^+$, suggesting the loss of caffeic acid, which is supported by dehydrated protonated caffeic acid ions at $m/z$ 163 $[Caf + H - 18]^+$ and 325 $[Caf + H + 162 - 18]^+$. Further fragment ions at $m/z$ 449 $[M + H - 162 - 162]^+$ and 287 $[M + H - 162 - 162 - 162]$ corresponded with the loss of two consecutive hexoses. Likewise, the MS/MS spectrum of **17** showed the presence of a fragment ion of 449 $[M + H - 176 - 132]^+$, suggesting the loss of pentose and ferulic acid, which is supported by dehydrated protonated ferulic acid ions at $m/z$ 177 $[Fer + H - 18]^+$ and intensive 309 $[Fer + H + 132 - 18]^+$. Further fragment ion at $m/z$ 287 $[M + H - 176 - 132 - 162]^+$ corresponds with luteolin $[Y^0 + H]^+$ and the loss of a hexose unit. A precise structure elucidation was possible after 1D and 2D NMR analyses of these compounds. $^1$H NMR spectra of **15** and **17** performed at 25 °C showed the presence of duplicated signals, corresponding with two rotameric conformers. Therefore, all of the 1D and 2D spectra were performed at 70 °C. The $^{13}$C NMR spectrum of **15** showed 36 signals, sorted by $^{13}$C and DEPT-135 experiments into 2 $CH_2$, 20 CH, and 14 quaternary carbon atoms. The $^1$H NMR spectrum revealed the presence of a 6-*C* substituted luteolin as characterized by signals at $\delta$ 7.33 (d, $J$ = 2.2 Hz; H-2′), 7.25 (dd, $J$ = 8.4, 2.2 Hz; H-6′), and 6.85 (d, $J$ = 8.4 Hz; H-5′) in accordance with the AMX system and two singlets at $\delta$ 6.42 (H-3) and $\delta$ 6.39 (H-8) and the absence of an H-6 signal. The carbohydrate region showed the presence of two anomeric proton signals at $\delta$ 4.74 (d, $J$ = 9.9 Hz; H-$1_{Glc}$) and 4.28 (d, $J$ = 7.9 Hz; H-$1_{Glc''}$), characterizing the presence of two sugar units. On the basis of the values of coupling constants ($J$ > 7 Hz) and the analysis of $^1$H, and $^{13}$C


dx.doi.org/10.1021/jf5038689 | J. Agric. Food Chem. 2014, 62, 11200−11208

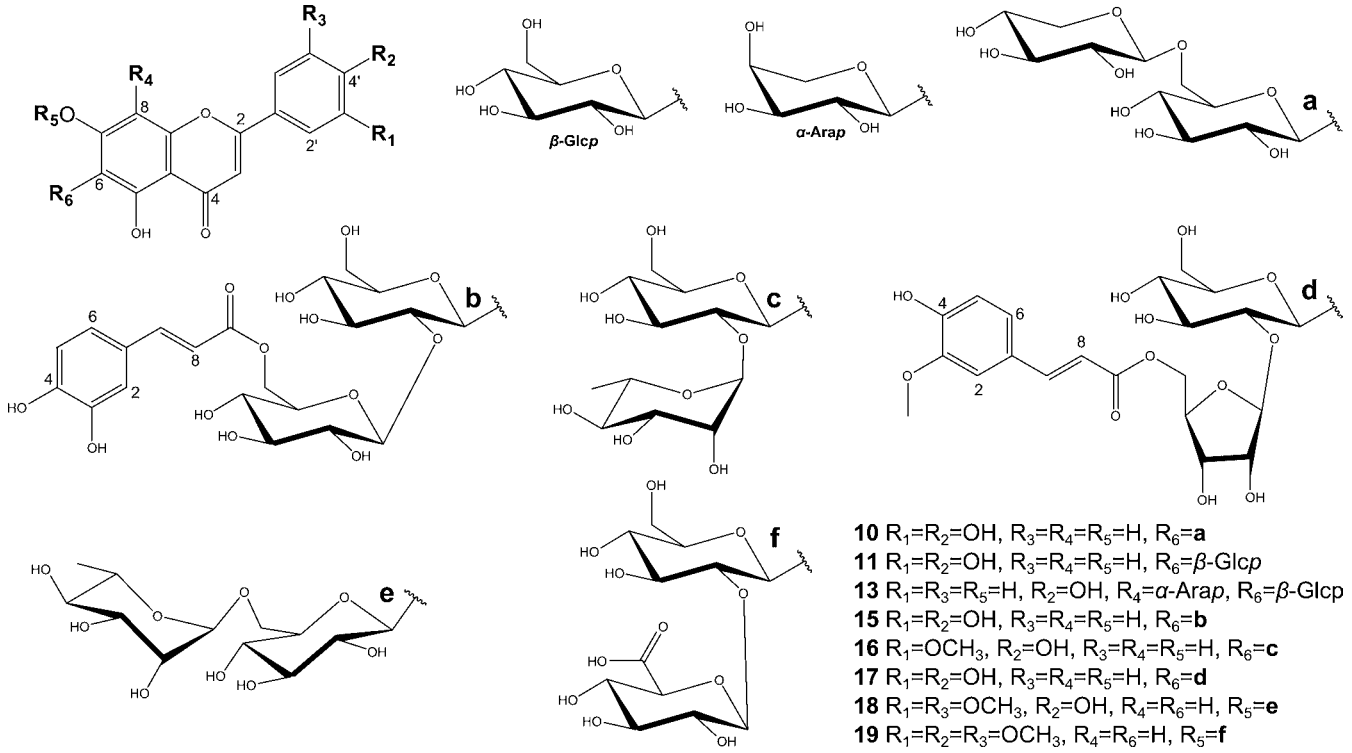


**Figure 2.** Structures of flavone glycosides isolated from the aerial parts of wheat (*T. aestivum* L.).

NMR spectra and 1D TOCSY, COSY, HSQC, HSQC-TOCSY, and HMBC data, the two sugar units were elucidated as *β*-glucopyranoside $\delta_{H/C}$ 4.74 (H-$1_{Glc}$)/71.0 (C-$1_{Glc}$) and *β*-glucopyranoside $\delta_{H/C}$ 4.28 (H-$1_{Glc''}$)/104.8 (C-$1_{Glc''}$) (Table 1). The long-range correlations observed in the HMBC spectrum between the anomeric proton of the glucose ($\delta_H$ 4.28, H-$1_{Glc''}$) and C-2 of glucose ($\delta_C$ 80.8) indicated the presence of interglycosidic linkage between these hexosyl units (1→2). This was further supported by the NOE effect detected in the rotating frame nuclear Overhauser effect spectroscopy spectrum (ROESY) between H-$1_{Glc''}$ and H-$2_{Glc}$. The 6-*C* glycosidation site was determined by the correlation observed in the HMBC spectrum from anomeric proton at $\delta_H$ 4.74 (H-$1_{Glc}$) to carbon C-6 ($\delta_C$ 107.7). Additionally, the aromatic region of the $^1$H and COSY spectra of **15** contained sets of resonances characteristic for an *E*-($J_{\alpha,\beta}$ = 15.9 Hz) olefinic moiety, and the AMX system corresponded to a 3,4-dihydroxyphenyl group at $\delta_H$ 6.97 (d, *J* = 1.9 Hz, H-$2_{Caf}$), 6.76 (d, *J* = 8.1 Hz, H-$5_{Caf}$), and 6.83 (dd, *J* = 8.2, 1.7 Hz, H-$6_{Caf}$); it was identified as an *E*-caffeoyl group. Protons H-$6_{Glc''}$ in compound **15** were downfield shifted to $\delta_H$ 3.85 (br d, *J* = 12.0 Hz) and 3.74 (br d, *J* = 12.0 Hz) and exhibited correlations in the HMBC spectra with the carbonyl carbon resonating at $\delta_C$ 165.6, corresponding with C-$9_{Caf}$. Therefore, **15** was luteolin 6-*C*-[$6_{Glc''}$-*O*-*E*-caffeoyl-*β*-D-glucopyranosyl(1″→2)-*β*-glucopyranoside], a new acylated flavonoid.

Compound **17**, according to the ESI-MS/MS fragmentation pattern, similar to **15**, was acylated with phenolic acid, and $^1$H and $^{13}$C NMR spectra were in agreement with a 6-*C* substituted luteolin nucleus. The carbohydrate region showed the presence of two anomeric proton signals at *δ* 4.72 (d, *J* = 9.9 Hz; H-$1_{Glc}$) and singlet at *δ* 5.16 (H-$1_{Rib''}$), characterizing the presence of two sugar units. On the basis of the analysis of $^1$H and $^{13}$C NMR spectra and 1D TOCSY, COSY, HSQC, HSQC-TOCSY, and HMBC data, the two sugar units were elucidated as *β*-glucopyranoside $\delta_{H/C}$ 4.72 (H-$1_{Glc}$)/71.2 (C-$1_{Glc}$) and *β*-ribofuranoside $\delta_{H/C}$ 5.16 (H-$1_{Rib''}$)/107.6 (C-$1_{Rib''}$), which is reported for the first time as a constituent in glycosylated flavonoids. The long-range correlations observed in the HMBC spectrum between the anomeric proton of the ribose ($\delta_H$ 5.16, H-$1_{Rib''}$) and C-2 of glucose ($\delta_C$ 74.4) indicated the presence of an interglycosidic linkage between these units (1→2). This was further supported by the NOE effect detected in the rotating frame nuclear Overhauser effect spectroscopy spectrum (ROESY) between H-$1_{Rib''}$ and H-$2_{Glc}$. The 6-*C* glycosidation site was determined by the correlation observed in the HMBC spectrum from the anomeric proton at $\delta_H$ 4.72 (H-$1_{Glc}$) to carbon C-6 ($\delta_C$ 108.2). The aromatic region of the $^1$H and COSY spectra of **17**, similar to **15**, contained sets of resonances characteristic for an *E*- ($J_{\alpha,\beta}$ = 15.9 Hz) olefinic moiety and an AMX system at $\delta_H$ 7.22 (d, *J* = 2.2 Hz, H-$2_{Fer}$), 6.81 (d, *J* = 8.1 Hz, H-$5_{Fer}$), and 7.01 (dd, *J* = 8.2, 1.6 Hz, H-$6_{Fer}$), and it was identified as an *E*-feruoyl group. Protons H-$5_{Rib''}$ in compound **17** were downfield shifted to $\delta_H$ 3.82 (ddd, *J* = 11.6, 5.4, 5.4 Hz; 2H) and exhibited correlations in the HMBC spectra with the carbonyl carbon resonated at $\delta_C$ 165.7, corresponding with C-$9_{Fer}$. Therefore, **17** was luteolin 6-*C*-[$5_{Rib''}$-*O*-*E*-feruoyl-*β*-D-ribofuranosyl(1″→2)-*β*-glucopyranoside], a new acylated flavonoid.

Compound **19** presented a UV spectrum corresponding with a 5,7-dihydroxy-3′,4′,5′-trimethoxyflavone skeleton at $\lambda_{max}$ 270 and 328 nm.[26] ESI-MS analysis showed that its protonated molecule had an *m*/*z* value of 683. The collision-induced dissociation (CID) of this precursor ion revealed its monodesmosidic character. The MS/MS spectrum of **19** showed the presence of a fragment ion of *m*/*z* 507 $[M + H - 176]^+$, suggesting the loss of a hexuronic acid, and *m*/*z* 345 $[M + H - 176 - 162]^+$, corresponding to the 3′,4′,5′-*O*-trimethyltricetin ion $[Y^0 + H]^+$. The $^{13}$C NMR spectrum of **19** showed 30 signals, sorted by $^{13}$C and DEPT-135 experiments


dx.doi.org/10.1021/jf5038689 | J. Agric. Food Chem. 2014, 62, 11200−11208

into 3 $CH_3$, 1 $CH_2$, 15 CH, and 11 quaternary carbon atoms. The $^1$H NMR spectrum revealed the presence of a 7-*O* substituted 3′,4′,5′-*O*-trimethyltricetin as characterized by two doublets at $\delta$ 6.90 ($J$ = 1.9 Hz; H-8) and 6.54 ($J$ = 2.0 Hz; H-6), and four singlets at $\delta$ 6.76 (H-3), $\delta$ 7.30 (2H, H-2′/6′), $\delta$ 3.96 (6H, 3′,5′-di-*O*-$CH_3$) and $\delta$ 3.85 (3H, 4′-$OCH_3$). The carbohydrate region of the $^1$H NMR spectrum showed the presence of the oxymethine protons in the range $\delta$ 3.30−3.93. Moreover, two anomeric proton signals at $\delta_H$ 5.33 (d, $J$ = 7.1 Hz; H-$1_{Glc}$) and 4.71 (d, $J$ = 7.8 Hz; H-$1_{GlcA''}$) were also observed, indicating the presence of two sugar units. On the basis of the values of coupling constants ($J$ > 7 Hz), and the analysis of $^1$H and $^{13}$C NMR spectra and 1D TOCSY, COSY, HSQC, HSQC-TOCSY, and HMBC data, the two sugar units were elucidated as $\beta$-glucopyranoside $\delta_{H/C}$ 5.33 (H-$1_{Glc}$)/100.2 (C-$1_{Glc}$) and $\beta$-glucuropyranoside $\delta_{H/C}$ 4.71 (H-$1_{GlcA''}$)/104.9 (C-$1_{GlcA''}$) (Table 2). The long-range correlations observed in the HMBC spectrum between the anomeric proton of the glucuronic acid ($\delta_H$ 4.71, H-$1_{GlcA''}$) and C-2 of glucose ($\delta_C$ 83.5) indicated the presence of an interglycosidic linkage between these hexosyl units (1→2). This was further supported by the NOE effect detected in the ROESY spectrum between H-$1_{GlcA''}$ and H-$2_{Glc}$. The 7-*O* glycosidation site was determined by the correlation observed in the HMBC spectrum from the anomeric proton at $\delta_H$ 5.33 (H-$1_{Glc}$) to carbon C-7 ($\delta_C$ 164.8) and the NOE effect visible in the ROESY spectrum between H-$1_{Glc}$ and H-6/8. Therefore, compound **19** was identified as 3′,4′,5′-*O*-trimethyltricetin 7-*O*-[$\beta$-D-glucuropyranosyl(1″→2)-$\beta$-D-glucopyranoside], a new flavonoid. Among the newly isolated compounds, flavonoids **15** and **17** were acylated with hydroxycinnamic acids. As acylation influences the spectroscopic characteristics of flavones, by increasing their UV-B-absorbing capacity, it is important in shielding plants against UV-B radiation.[27,28]

Flavones, in particular the C-glycosyl-flavones, are the most common type of flavonoids found in grasses. The first flavone to be characterized in wheat was tricin, which was identified as a rust resistance factor in wheat leaves. Flavonoid research on the Poaceae reported the presence of flavone-*C*-glycosides, tricin 5-glucoside, tricin 7-glucoside, isovitexin, iso-orientin glycosides, and lucenin 7-methyl ether.[29] Moreover, the soluble phenolic compounds including flavonols were considered in *T. aestivum* L.[30] Two new flavonoid-*C*-glycosides named triticuside A and triticuside B were isolated from the bran of this species.[31] Olenichenko et al.[32] reported 15 phenolic compounds, most of them (90%) being flavonoids and their derivatives, mainly *C*-glycosides of two flavones (apigenin and luteolin) and their *O*-derivatives. The major component of the phenolic complex in winter wheat leaves (cv. Moskovskaya 39) was isoorientin, identified also in our study (compound **11**).

**Phytochemical Analysis.** Qualitative study revealed that *T. aestivum* L. contained large amounts of flavones. The concentration of particular phenolics in *T. aestivum* L. was determined in this study. 5-Caffeoylquinic acid for phenolic acids and rutin for flavones were used as standards for quantitative determination. The total phenolics concentration in wheat determined with UPLC was 181.71 ± 11.18 mg/g of aerial part dry matter (isolated compounds: 162.78 ± 10.01 mg/g dry weight) (Table 3). Most of them (86.6%) were flavonoids and their derivatives. Luteolin and its derivatives represented 68.4% of total phenolics content in *T. aestivum* L. aerial parts. The predominant compound was flavone **11**, the content of which was 39.41 ± 2.66 mg/g dry weight (dw). Also,

**Table 3. Concentration of Identified Phenolics in *Triticum aestivum* L. Extract**

| retention time (min) | compd | concn (mg/g dw ± SD, $n$ = 3) |
|---|---|---|
| | **Phenolic Acids** | |
| 2.08 | **1** | 1.24 ± 0.19 |
| 3.89 | **2** | 8.43 ± 0.33 |
| 4.79 | **3** + **4** | 6.46 ± 0.34 |
| 8.35 | **5** | 5.49 ± 0.23 |
| 9.51 | **7** | 0.84 ± 0.15 |
| 9.78 | **8** | 1.86 ± 0.10 |
| | **Flavonoids** | |
| 8.92 | **6** | 17.56 ± 1.01 |
| 10.69 | **9** | 11.20 ± 0.76 |
| 10.85 | **10** | 11.74 ± 0.73 |
| 12.21 | **11** | 39.41 ± 2.66 |
| 12.84 | **12** + **13** | 19.61 ± 1.11 |
| 13.01 | **14** | 32.90 ± 2.21 |
| 14.32 | **15** | 7.95 ± 0.67 |
| 17.71 | **16** | 7.17 ± 0.41 |
| 20.87 | **17** | 3.53 ± 0.17 |
| 21.73 | **18** | 3.69 ± 0.15 |
| 23.81 | **19** | 2.61 ± 0.14 |
| total | | 181.71 ± 11.18 |

phenolic **14** was present in high amount (32.90 ± 2.21 mg/g dw). Concentrations and profiles of these compounds may be affected by many factors, such as environment, cultivar, soil conditions, cropping year, growth location, species, and plant organs used in the analysis. According to Zagoskina et al.,[33] winter wheat leaves contained higher amounts of soluble phenolic compounds than crowns and roots. In general, phenolic compounds play an important role in winter wheat adaptation to low temperature. Changes in phenolic compound metabolism, manifested in the accumulation of phenylpropanoids and flavonoids (predominantly flavones) in plant leaves, can contribute to plant resistance to cold stress.[32]

**DPPH• Scavenging Activity of Isolated Compounds.** Plant polyphenols are known for their antioxidant properties and beneficial effects on human health. Several papers have been published reporting on the antioxidant effect of the whole *T. aestivum* L. extract, indicating its beneficial effect in some pathological processes.[34,35] The free radical scavenging activity of polyphenols strongly depends on their chemical structure; the amount and position of free hydroxyl groups influence the observed activity.[36,37] The compounds isolated from *T. aestivum* L. can be classified into one of the following groups of polyphenols: phenolic acids, flavone glycosides, or acylated flavone glycosides. The free radical scavenging activity of these compounds was tested in a simple and rapid TLC-DPPH• test with image processing (Figure 3). The analyzed plant species contains two common hydroxycinnamic acids, caffeic and ferulic acid, esterified with quinic acid, which were proved to be more potent free radical scavengers when compared to rutin (Figure 3a). Caffeic acid derivatives can be considered as the main free radical scavenging polyphenols present in *T. aestivum* L. and responsible for terminating radical chain reactions. All of the isolated and active phenolic acids were present in esterified form, but with free hydroxyl groups responsible for free radical scavenging activity. This is in accordance with a review by Rice-Evans et al.,[37] who stated that hydroxycinnamic acids are usually present in plants as simple esters but not glycosylated at the

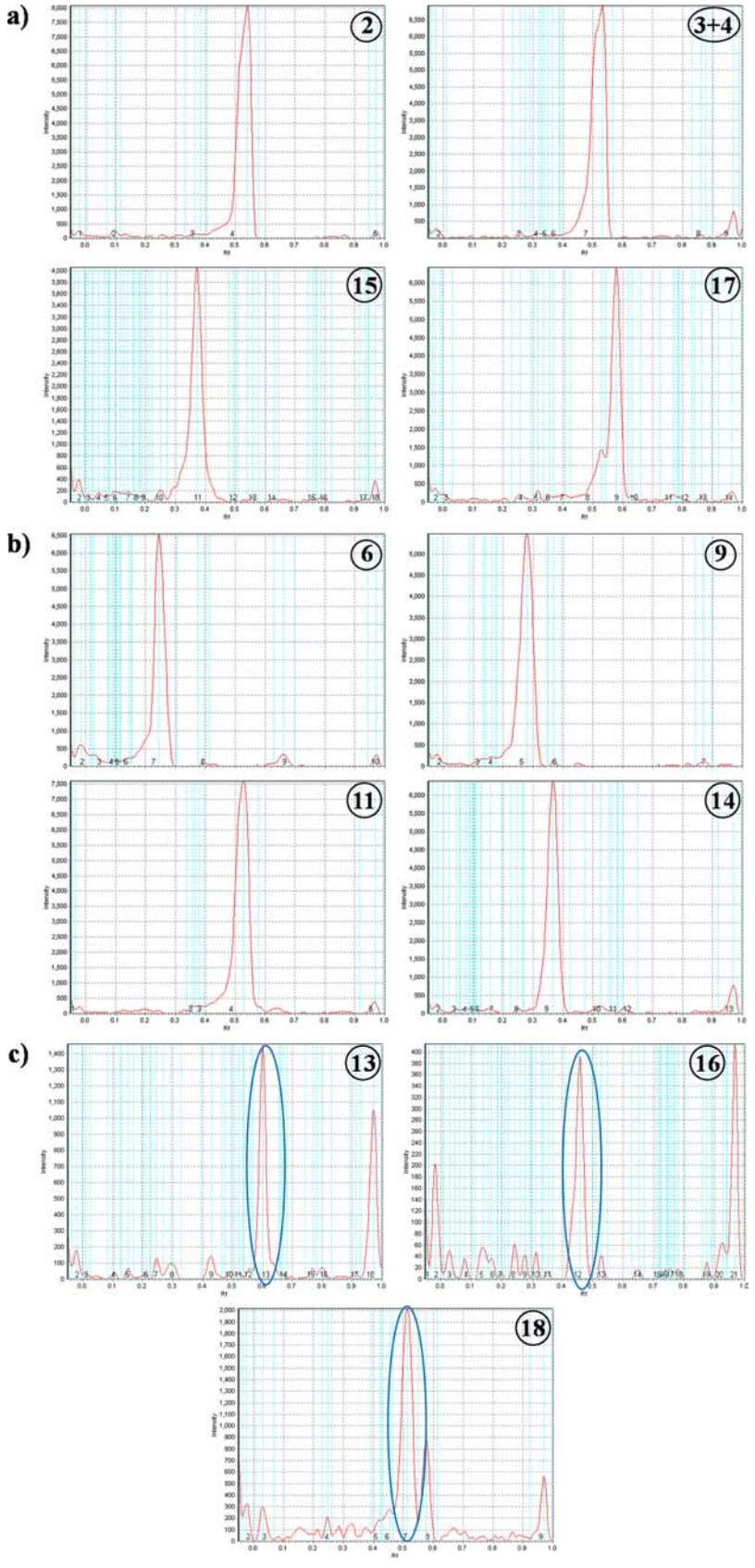


**Figure 3.** Line profile plots, obtained with the use of the image processing procedure, for isolated compounds with free radical scavenging activity: (a) phenolic acids and acylated flavone glycosides; (b) luteolin glycosides; (c) flavone glycosides characterized with relatively weak activity.

phenolic hydroxyl groups. These acids were also identified as acylating agents (compounds **15** and **17**).

*T. aestivum* L. was found to be rich in flavones, especially in luteolin derivatives. No flavonols were identified in the analyzed


dx.doi.org/10.1021/jf5038689 | *J. Agric. Food Chem.* 2014, 62, 11200−11208

species, which confirms that there is a mutual exclusion between flavones and flavonols in many plant species.[37] Flavonols have been proven to be more potent free radical scavengers when compared to flavones, due to the presence of a hydroxyl group at the C3 position in the former group of polyphenols. In the present study all of the isolated luteolin derivatives were found to be potent free radical scavengers (Figure 3b). Noteworthy is the fact that all of the isolated luteolin derivatives were not glycosylated at position C7. Musialik et al. proved that a hydroxyl group at this position is the most acidic site in flavonoids.[38] Due to the acidic properties, this group participates in radical reactions via the SPLET (sequential proton-loss electron-transfer) mechanism, in polar solvents, enabling fast scavenging of the DPPH• radical.[38] Luteolin derivatives glycosylated at the C7 position were found to be weak free radical scavengers.[37] Relatively high free radical scavenging activity of luteolin glycosides can be ascribed not only to the presence of free hydroxyl group at the C7 position but also to the catechol moiety in the B ring. All other isolated flavones were less active, or the activity was not observed even in the presence of free hydroxyl group at the C7 position, for example, apigenin *C*-hexoside *C*-pentoside (not active; **12**), isoschaftoside (weak activity; **13**), or isoscoparin 2″-*O*-α-L-rhamnopyranoside (weak activity; **16**). All of these compounds lack two free hydroxyl groups in the ortho position in the B ring. Tricin 7-*O*-rutinoside (**18**) was also found to be less active than rutin and luteolin derivatives (Figure 3c).

To sum up it can be underscored that caffeic acid derivatives and luteolin glycosides, with a free hydroxyl group in the C7 position, are mainly responsible for the free radical scavenging activity of *T. aestivum* L. phenolic fraction. This species, although not synthesizing potent flavonol antioxidants, as the products of secondary metabolism, may use flavone *C*-glycosides with a free acidic hydroxyl group to terminate radical reactions.

## AUTHOR INFORMATION


### Corresponding Author

*(I.K.) Phone: +48 81 8863421, ext. 391. Fax: +48 81 8864547. E-mail: ikowalska@iung.pulawy.pl.



### Funding

This work was supported by the National Science Center in Poland (Project 2011/01/D/NZ9/04684).

### Notes

The authors declare no competing financial interest.


## ACKNOWLEDGMENTS

Special thanks go to Dr. Krzysztof Jonczyk (Department of Systems and Economics of Crop Production of Institute of Soil Science and Plant Cultivation, State Research Institute in Pulawy) for plant materials.

## REFERENCES


(1) Dinelli, G.; Carretero, A. S.; Di Silvestro, R.; Marotti, I.; Fu, S.; Benedettelli, S.; Ghiselli, L.; Gutierrez, A. F. Determination of phenolic compounds in modern and old varieties of durum wheat using liquid chromatography coupled with time-of-flight mass spectrometry. *J. Chromatogr., A* **2009**, *1216*, 7229−7240.

(2) Adom, K. K.; Sorrells, M. E.; Liu, R. H. Phytochemical profiles and antioxidant activity of wheat varieties. *J. Agric. Food Chem.* **2003**, *51*, 7825−7834.

(3) Adom, K. K.; Sorrells, M. E.; Liu, R. H. Phytochemicals and antioxidant activity of milled fractions of different wheat varieties. *J. Agric. Food Chem.* **2005**, *53*, 2297−2306.

(4) Ward, J. L.; Poutanen, K.; Gebruers, K.; Piironen, V.; Lampi, A. M.; Nyström, L.; Andersson, A. A. M.; Aman, P.; Boros, D.; Rakszegie, M.; Bedõ, Z.; Shewry, P. R. The HEALTHGRAIN cereal diversity screen: concept, results and prospects. *J. Agric. Food Chem.* **2008**, *56*, 9699−9709.

(5) Yu, L.; Haley, S.; Perret, J.; Harrys, M. Comparison of wheat flours grown at different locations for their antioxidant properties. *Food Chem.* **2004**, *86* (1), 11−16.

(6) Carbone, K.; Giannini, B.; Picchi, V.; Lo Scalzo, R.; Cecchini, F. Phenolic composition and free radical scavenging activity of different apple varieties in relation to the cultivar, tissue type and storage. *Food Chem.* **2011**, *127* (2), 493−500.

(7) Shahidi, F.; Chandrasekara, A.; Zhong, Y. Bioactive phytochemicals in vegetables. In *Handbook of Vegetables and Vegetable Processing*; Singha, N. K., Ed.; Wiley: Ames, IA, USA, 2011; pp 125−158.

(8) Winkel-Shirley, B. Flavonoid biosynthesis. A colorful model for genetics, biochemistry, cell biology, and biotechnology. *Plant Physiol.* **2001**, *126*, 485−493.

(9) Stalikas, C. D. Extraction, separation, and detection methods for phenolic acids and flavonoids. *J. Sep. Sci.* **2007**, *30*, 3268−3295.

(10) Rice-Evans, C. A.; Miller, N. J.; Paganga, G. Antioxidant properties of phenolic compounds. *Trends Plant Sci.* **1997**, *2*, 152−159.

(11) Haig, T. Application of hyphenated chromatography-mass spectrometry techniques to plant allelopathy research. *J. Chem. Ecol.* **2001**, *27* (12), 2363−2396.

(12) Zielinski, H.; Kozlowska, H. Antioxidant activity and total phenolics in selected cereal grains and their different morphological fractions. *J. Agric. Food Chem.* **2000**, *48*, 2008−2016.

(13) Naczk, M.; Shahidi, F. Phenolics in cereals, fruits and vegetables: occurrence, extraction and analysis. *J. Pharm. Biomed. Anal.* **2006**, *41*, 1523−1542.

(14) Zuchowski, J.; Jonczyk, K.; Kapusta, I.; Szajwaj, B.; Oleszek, W. Phenolic acid content of organic and conventionally grown winter wheat. *Cereal Res. Commun.* **2009**, *37* (2), 189−197.

(15) Zuchowski, J.; Jonczyk, K.; Pecio, L.; Oleszek, W. Phenolic acid concentrations in organically and conventionally cultivated spring and winter wheat. *J. Sci. Food Agric.* **2011**, *91* (6), 1089−1095.

(16) Kowalska, I.; Stochmal, A.; Kapusta, I.; Janda, B.; Pizza, C.; Piacente, S.; Oleszek, W. Flavonoids from barrel medic (*Medicago truncatula*) aerial parts. *J. Agric. Food Chem.* **2007**, *55*, 2645−2652.

(17) Tanaka, T.; Nakashima, T.; Ueda, T.; Tomii, K.; Kouno, I. Facile discrimination of aldose enantiomers by reversed-phase HPLC. *Chem. Pharm. Bull.* **2007**, *55*, 899−901.

(18) Pérez, A. J.; Simonet, A. M.; Calle, J. M.; Pecio, L.; Guerra, J. O.; Stochmal, A.; Macías, F. A. Phytotoxic steroidal saponins from *Agave offoyana* leaves. *Phytochemistry* **2014**, *105*, 92−100.

(19) Kowalska, I.; Ciesla, Ł.; Oniszczuk, T.; Waksmundzka-Hajnos, M.; Oleszek, W.; Stochmal, A. Comparison of two TLC-DPPH•-image processing procedures for studying free radical scavenging activity of compounds from selected varieties of *Medicago sativa*. *J. Liq. Chromatogr. Relat. Technol.* **2013**, *36*, 2387−2394.

(20) Clifford, M. N.; Johnston, K. L.; Knight, S.; Kuhnert, N. Hierarchical scheme for LC-MS$^n$ identification of chlorogenic acids. *J. Agric. Food Chem.* **2003**, *51*, 2900−2911.

(21) Estiartea, M.; Penuelas, J.; Kimball, B. A.; Hendrix, D. L.; Pinter, P. J., Jr.; Wall, G. W.; LaMorte, R. L.; Hunsaker, D. J. Free-air $CO_2$ enrichment of wheat: leaf flavonoid concentration throughout the growth cycle. *Physiol. Plant.* **1999**, *105*, 423−433.

(22) Dinelli, G.; Segura-Carretero, A.; Di Silvestro, A.; Marotti, I.; Arráez-Román, D.; Benedettelli, S.; Ghiselli, L.; Fernadez-Gutierrez, A. Profiles of phenolic compounds in modern and old common wheat varieties determined by liquid chromatography coupled with time-of-flight mass spectrometry. *J. Chromatogr., A* **2011**, *1218*, 7670−7681.

(23) Cummins, I.; Brazier-Hicks, M.; Stobiecki, M.; Franski, R.; Edwards, R. Selective disruption of wheat secondary metabolism by herbicide safeners. *Phytochemistry* **2006**, *67*, 1722−1730.

(24) de Olivieira, D. M.; Siqueira, E. P.; Nunes, Y. R. F.; Cota, B. B. Flavonoids from leaves of *Mauritia flexuosa*. *Rev. Bras. Farm.* **2013**, *23*, 614−620.
(25) Cavaliere, C.; Foglia, P.; Pastorini, E.; Samperi, R.; Lagana, A. Identification and mass spectrometric characterization of glycosylated flavonoids in *Triticum durum* plants by high-performance liquid chromatography with tandem mass spectrometry. *Rapid Commun. Mass Spectrom.* **2005**, *19*, 3143−3158.
(26) Mabry, T. J.; Markham, K. R.; Thomas, M. B. *The Systematic Identification of Flavonoids*; Springer-Verlag: Berlin, Germany, 1970; p 105.
(27) Stochmal, A.; Oleszek, W. Effect of acylation of flavones with hydroxycinnamic acids on their spectral characteristics. *Nat. Prod. Commun.* **2007**, 571−574.
(28) Stochmal, A.; Oleszek, W. Seasonal and structural changes of flavones in alfalfa (*Medicago sativa*) aerial parts. *J. Food Agric. Environ.* **2007**, *5*, 170.
(29) Harborne, J. B.; Boardley, M.; Fröst, S.; Holm, G. The flavonoids in leaves of diploid *Triticum* species (Gramineae). *Plant System. Evol.* **1986**, *154*, 251−257.
(30) Zagoskina, N. V.; Olenichenko, N. A.; Iun'véĭ, Ch.; Zhivukhina, E. A. Formation of phenol compounds in various cultivars of wheat (*Triticum aestivum* L.). *Priklad. Biokhim. Mikrobiol.* **2005**, *41*, 113−116.
(31) Feng, X.; Jiang, D.; Shan, Y.; Dai, T.; Dong, Y.; Cao, W. New flavonoid-*C*-glycosides from *Triticum aestivum*. *Chem. Nat. Compd.* **2008**, *44*, 171−173.
(32) Olenichenko, N. A.; Ossipov, V. I.; Zagoskina, N. V. Effect of cold hardening on the phenolic complex of winter wheat leaves. *Russ. J. Plant Physiol.* **2006**, *53*, 495−500.
(33) Zagoskina, N. V.; Olenichenko, N. A.; Klimov, S. V.; Astakhova, N. V.; Zhivukhina, E. A.; Trunova, T. I. The effects of cold acclimation of winter wheat plants on changes in $CO_2$ exchange and phenolic compound formation. *Russ. J. Plant Physiol.* **2005**, *52*, 320−325.
(34) Khan, G. M.; Ansari, S. H.; Ahmad, F. Pharmacognostic standardization, antioxidant and free radical scavenging activity of the seeds of *Triticum aestivum* L. − a dietary staple. *J. Young Pharm.* **2013**, *5*, 54−59.
(35) Mohan, Y.; Jesuthankaraj, G. N.; Thangavelu, N. R. Antidiabetic and antioxidant properties of *Triticum aestivum* in streptozotocin-induced diabetic rats. *Adv. Pharm. Sci.* **2013**, article ID 716073, 9 pages, DOI: 10.1155/2013/716073.
(36) Burda, S.; Oleszek, W. Antioxidant and antiradical activities of flavonoids. *J. Agric. Food Chem.* **2001**, *49*, 2774−2779.
(37) Rice-Evans, C. A.; Miller, N. J.; Paganga, G. Structure-antioxidant activity relationships of flavonoids and phenolic acids. *Free Radical Biol. Med.* **1996**, *20*, 933−956.
(38) Musialik, M.; Kuzmicz, R.; Pawłowski, T. S.; Litwinienko, G. Acidity of hydroxyl groups: an overlooked influence on antiradical properties of flavonoids. *J. Org. Chem.* **2009**, *74*, 2699−2709.

**Site-Directed Mutagenesis.** Site-directed mutagenesis was performed using a one-step PCR method with plasmid *cgt*/pST as the template and a pair of complementary primers (Table 1). The PCR products were treated with *Dpn*I and then used to transform *E. coli* JM109 cells. The intended mutations were confirmed by DNA sequencing. To generate expression strains, the resulting (mutant) plasmids were used to transformed *B. subtilis* WB600 competent cells.

**Table 1. Primers Used for Site-Directed Mutagenesis**

| desired mutation | primer sequence (5′−3′)[a] | DNA template |
|---|---|---|
| D577E | GCAATGTGTATGAAAACTTCGAG | *cgt*/pST |
| | CTCGAAGTTTTCATACACATTGC | |
| D577R | GCAATGTGTATCGTAACTTCGAG | *cgt*/pST |
| | CTCGAAGTTACGATACACATTGC | |
| D577K | GCAATGTGTATAAGAACTTCGAG | *cgt*/pST |
| | CTCGAAGTTCTTATACACATTGC | |
| D577H | GCAATGTGTATCATAACTTCGAG | *cgt*/pST |
| | CTCGAAGTTATGATACACATTGC | |

[a]Nucleotide sequences corresponding to the mutated amino acids are underlined.

**Production and Purification of CGTase Proteins.** A single colony of *B. subtilis* WB600 harboring *cgt*/pST (wild type or mutant) was inoculated into 50 mL of Luria−Bertani medium containing 5 μg/mL kanamycin and grown at 37 °C overnight. A 2 mL portion of this overnight culture was then diluted into 50 mL of terrific broth containing 5 μg/mL kanamycin and incubated on a rotary shaker (200 rpm) at 37 °C for 48 h. The CGTase present in the supernatant was purified to homogeneity, as previously described.[11] The purified enzymes were aliquoted and stored at −80 °C. The protein concentration was determined using the Bradford assay,[16] with reagents obtained from the Bio-Rad protein assay reagent kit (Bio-Rad, Hercules, CA). Bovine serum albumin was used as the standard.

**Enzyme Assays.** All assays were measured by incubating 0.1 mL of appropriately diluted purified CGTase with 0.9 mL of 1% (w/v) maltodextrin (DE = 3, Roquette Frères, Lestrem, France) in 10 mM phosphate buffer (pH 6.5) at 50 °C for 10 min. The concentrations of α-, β-, and γ-cyclodextrin formed were determined using the methyl orange,[17] phenolphthalein,[18] and bromocresol green[19] methods, respectively. One unit of each activity was defined as the amount of enzyme that produced 1 μmol of the corresponding cyclodextrin per minute.

**High-Performance Liquid Chromatography (HPLC) Product Analysis.** The formation of cyclodextrins under conditions resembling an industrial production process was performed by incubating 0.1 unit/mL CGTase (β-cyclization activity) with 5% (wet basis, w/v) soluble starch solution in 10 mM phosphate buffer (pH 6.5) at 45 °C for 24 h. At regular time intervals, samples were taken and boiled for 20 min. The concentrations of α-, β-, and γ-cyclodextrin in the reaction mixture were determined by HPLC, as described in previous reports.[12,20,21]

**Structure Modeling of the (Mutant) CGTase.** The X-ray crystal structure of the wild-type CGTase from *B. circulans* was obtained from the Research Collaboratory for Structural Bioinformatics (RCSB) Protein Data Bank (PDB accession code 1CXI).[22] Homology models of the mutant CGTases were constructed using the SWISS-MODEL protein-modeling server (http://www.expasy.ch/swissmod/SWISS-MODEL.html).[23] The PyMol molecular graphics system (http://www.pymol.org) was used to visualize and analyze the model structure.

## RESULTS

**Expression and Purification of the Wild-Type and Mutant CGTases.** *B. circulans* β-CGTase mutants D577E, D577R, D577K, and D577H were successfully constructed using site-directed mutagenesis. The wild-type and mutant CGTases were expressed in *B. subtilis* WB600, and the secreted proteins were isolated from the culture medium. There were no obvious differences in the levels of expression among the recombinant wild-type and mutant CGTases, with 20−25 mg of each of the CGTase proteins produced per liter in shake-flask cultures. The mutant CGTase proteins were purified to apparent homogeneity using a combination of anion-exchange and hydrophobic chromatographies. The purity and molecular weight of the wild-type and mutant CGTase proteins were verified using sodium dodecyl sulfate−polyacrylamide gel electrophoresis (SDS−PAGE) (data not shown).

**Cyclization Activities of Wild-Type and Mutant CGTases.** The CGTase enzymes were assayed to determine α-, β- and γ-cyclization activities (Table 2). None of the mutations had a substantial effect upon the ratio of β-cyclization activity to total cyclization activity. These ratios varied from 74.6% (D577E) to 76.6% (D577K), with D577H, D577R, and the wild type having intermediate values, in that order. However, the D577E mutant displayed a 14.0% increase in total cyclization activity and an 11.2% overall increase in the β-cyclization activity when compared to the wild-type CGTase. More interesting, the D577R mutant displayed an even larger enhancement of total cyclization activity (32.5%), resulting in a 30.7% overall increase in β-cyclization activity, compared to that of the wild-type CGTase. In contrast, the D577K mutant showed only a 1.3% increase in the total cyclization activity and a 1.5% increase in β-cyclization activity. Finally, the D577H mutant displayed slight decreases in the total cyclization activity and β-cyclization activity compared to wild-type CGTase.

**Starch Conversions of the Wild-Type and Mutant CGTases under Conditions Resembling Industrial Production Processes.** To assess the performance of the mutant CGTases under conditions resembling those used in the industrial production of β-cyclodextrin, each enzyme was assayed in a reaction mixture containing CGTase protein (0.1 unit/mL β-cyclization activity) and 5% (wet basis, w/v) soluble starch. The reaction mixtures were incubated at 45 °C and sampled over a 24 h time course. Although small amounts of α- and γ-cyclodextrin were produced, β-cyclodextrin was the main product for all CGTases (Figure 1). After 24 h of incubation, the wild-type enzyme converted 45.4% of the starch into cyclodextrins, of which the majority (69.2%) was β-cyclodextrin (Table 3).

**Table 2. Cyclization Activities of the Wild-Type and Mutant CGTases from *B. circulans* STB01[a]**

| CGTase | α-cyclization activity (units/mg) | β-cyclization activity (units/mg) | γ-cyclization activity (units/mg) | total (units/mg) |
|---|---|---|---|---|
| wild type | 31.6 ± 0.3 ab (10.4) | 231.6 ± 1.9 b (76.5) | 39.6 ± 0.8 a (13.1) | 302.8 b |
| D577E | 36.9 ± 0.5 d (10.7) | 257.6 ± 2.6 c (74.6) | 50.7 ± 0.7 b (14.7) | 345.2 c |
| D577R | 31.1 ± 0.3 a (7.7) | 302.8 ± 2.3 d (75.5) | 67.4 ± 0.9 c (16.8) | 401.3 d |
| D577K | 32.2 ± 0.4 b (10.5) | 235.0 ± 2.2 b (76.6) | 39.6 ± 0.4 a (12.9) | 306.8 b |
| D577H | 33.2 ± 0.4 c (11.2) | 222.3 ± 1.8 a (75.0) | 41.0 ± 0.3 a (13.8) | 296.5 a |

[a]Numbers in parentheses indicate the ratio in specific activities for the formation of the different cyclodextrins. Each value represents the mean of three independent measurements, and means with different letters within the same column are significantly different ($p < 0.05$).

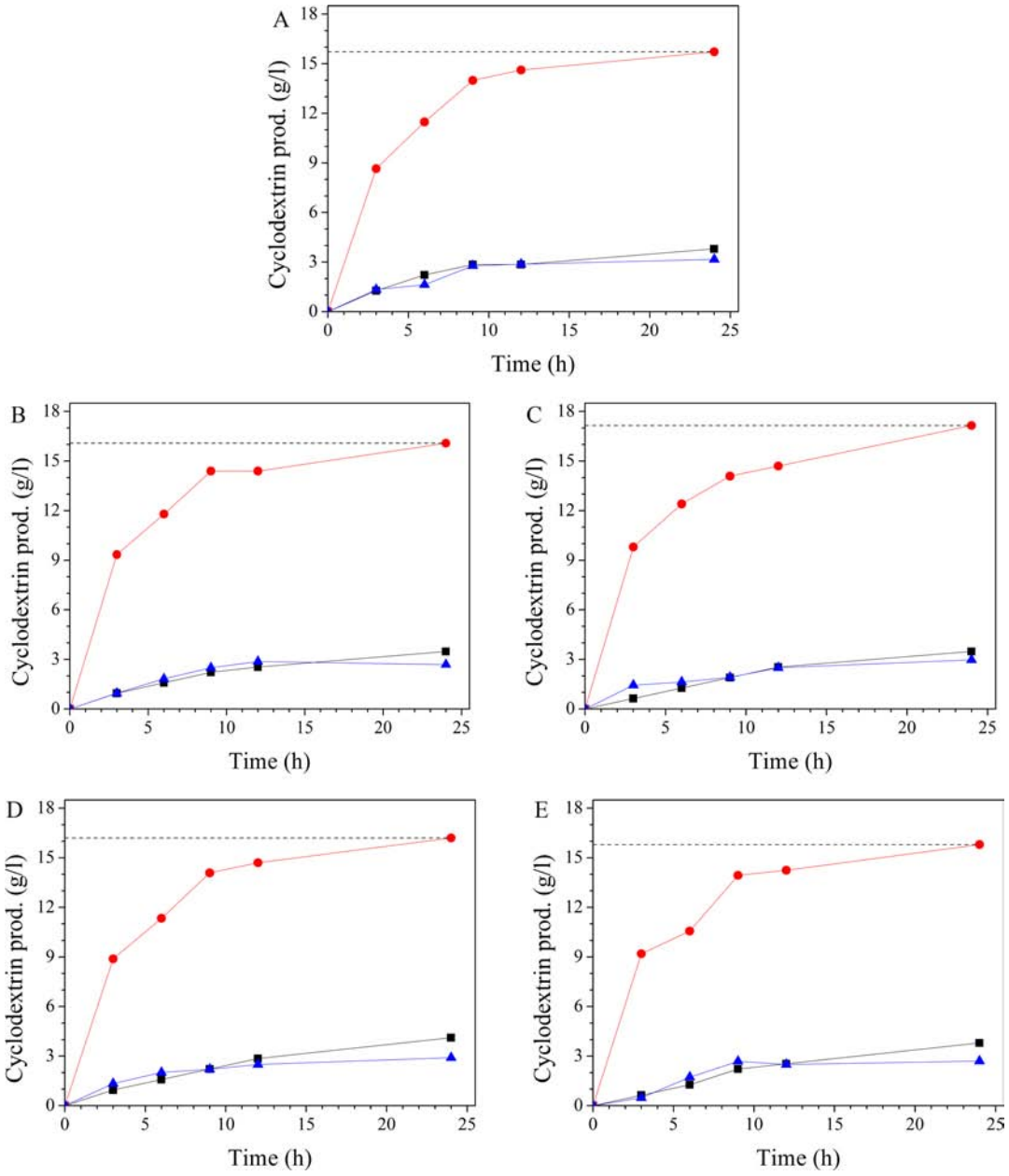


**Figure 1.** Cyclodextrins formed during incubation of the (mutant) CGTases from *B. circulans* STB01 (0.1 unit/mL $\beta$-cyclization activity) with 5% (wet basis, w/v) soluble starch solution in 10 mM phosphate buffer (pH 6.5) at 45 °C for 24 h: (black line) $\alpha$-cyclodextrin, (red line) $\beta$-cyclodextrin, and (blue line) $\gamma$-cyclodextrin for (A) wild-type CGTase, (B) mutant D577E, (C) mutant D577R, (D) mutant D577K, and (E) mutant D577H.

**Table 3. Starch Conversions of the Wild-Type and Mutant CGTases from *B. circulans* STB01**[a]

| | | product (g/L) | | |
|---|---|---|---|---|
| CGTase | conversion of starch into cyclodextrins (%) | $\alpha$ | $\beta$ | $\gamma$ |
| wild type | 45.4 | 3.8 ± 0.1 ab (16.7) | 15.7 ± 0.2 a (69.2) | 3.2 ± 0.1 b (14.1) |
| D577E | 44.6 | 3.5 ± 0.2 a (15.7) | 16.1 ± 0.1 b (72.2) | 2.7 ± 0.1 a (12.1) |
| D577R | 47.4 | 3.5 ± 0.1 a (14.8) | 17.2 ± 0.1 c (72.6) | 3.0 ± 0.2 ab (12.6) |
| D577K | 46.4 | 4.1 ± 0.1 b (17.7) | 16.2 ± 0.2 b (69.8) | 2.9 ± 0.1 a (12.5) |
| D577H | 44.6 | 3.8 ± 0.2 ab (17.0) | 15.8 ± 0.1 a (70.9) | 2.7 ± 0.1 a (12.1) |

[a]CGTase proteins (0.1 unit/mL $\beta$-cyclization activity) were incubated with 5% (wet basis, w/v) soluble starch solution at pH 6.5 and 45 °C for 24 h. Numbers in parentheses indicate the percentage of each cyclodextrin present in the product mixture. Each value represents the mean of three independent measurements, and means with different letters within the same column are significantly different ($p < 0.05$).

The mutant CGTases produced somewhat more $\beta$-cyclodextrin under the same reaction conditions (Figure 1 and Table 3). The D577R mutant showed the greatest enhancement in $\beta$-cyclodextrin production, converting 47.4% of the starch into cyclodextrins, of which 72.6% was $\beta$-cyclodextrin. This represents a 9.5% enhancement in $\beta$-cyclodextrin production.


dx.doi.org/10.1021/jf503523z | J. Agric. Food Chem. 2014, 62, 11209−11214

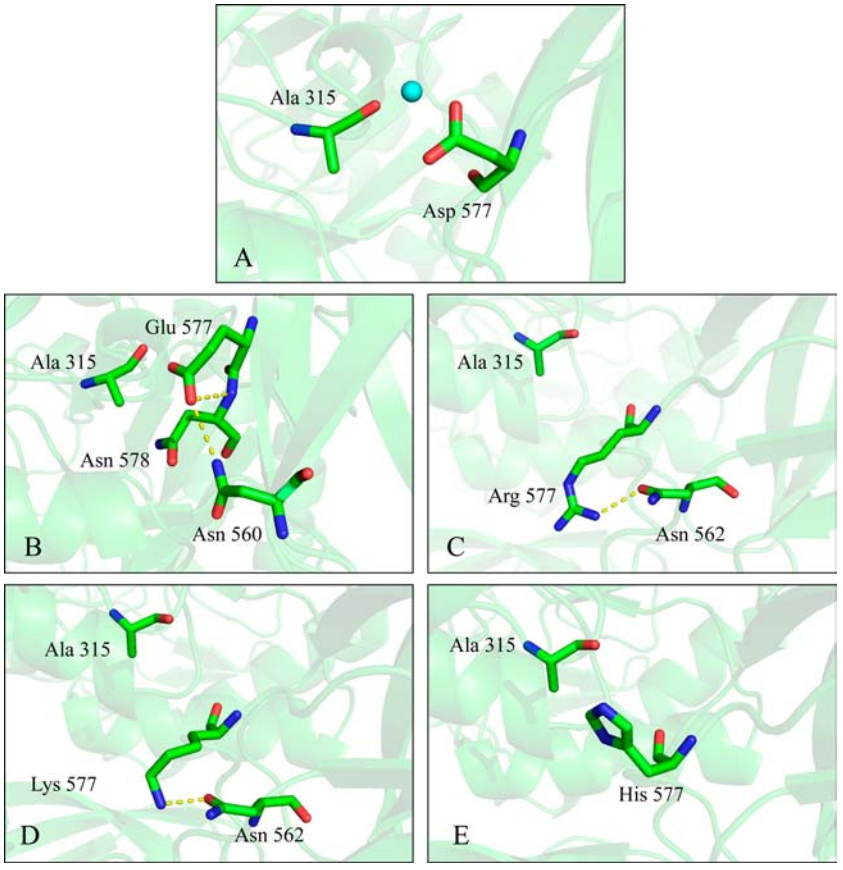


**Figure 2.** Models of the (mutant) CGTases from *B. circulans* STB01: (yellow dashed line) hydrogen bond, (cyan ball) $Ca^{2+}$ in site CaIII, (green) carbon, (red) oxygen, and (blue) nitrogen for (A) wild-type CGTases, (B) mutant D577E, (C) mutant D577R, (D) mutant D577K, and (E) mutant D577H.

The D577K mutant showed a 3.1% increase in $\beta$-cyclodextrin production, converting 46.4% of the starch to cyclodextrins, of which 69.8% was $\beta$-cyclodextrin. Although the D577E mutant showed a slight decline in starch conversion, the mutation resulted in a 2.5% increase in $\beta$-cyclodextrin production, which came at the expense of $\alpha$-cyclodextrin and $\gamma$-cyclodextrin production. The D577H mutant had a slightly lower starch conversion and almost the same $\beta$-cyclodextrin production when compared to the wild-type CGTase.

**Homology Modeling of the Mutant $\beta$-CGTases.** A structural model of each of the mutant CGTases was prepared using the SWISS-MODEL protein-modeling server (Figure 2).[23] Substitution of aspartate for glutamate conserves the negative charge but adds an additional aliphatic carbon and increases the chain length. Comparing the homology model of D577E (Figure 2B) to the structure of the wild-type $\beta$-CGTase (Figure 2A) suggests that the glutamate residue forms additional hydrogen bonds with residues Asn560 and Asn578. Substitution of the negatively charged aspartate with a positively charged residue, such as arginine (Figure 2C) or lysine (Figure 2D), changes the ionic character of this residue and may also introduce a hydrogen bond with Asn562. Substitution of aspartate by histidine (Figure 2E) also changes the ionic character of the residue, but in this case, no additional hydrogen bonds are predicted.

## DISCUSSION

Biochemical studies have revealed calcium-binding sites in the protein molecules of this family.[24,25] Previous reports about calcium-binding sites had showed that the amino acid residues within these regions related to the catalytic activity and thermal stability of $\alpha$-amylase.[26−28] Although there are some differences between CGTase and $\alpha$-amylase in these regions, it was also indicated that the mutation of the amino acid residues at calcium-binding sites could affect the CGTase activities.[29,30] This suggested that the calcium-binding sites might have a critical function to CGTase. The results supported this hypothesis, demonstrating that mutations at the site CaIII of $\beta$-CGTase from *B. circulans* strain STB01, specifically replacement of Asp 577 with glutamate, arginine, or lysine, could have a beneficial effect on $\beta$-cyclization activity; the mutants enhanced the $\beta$-cyclization activity in the order D577R > D577E > D577K.

The homology modeling results appeared to support the hypothesis that the enhancement in $\beta$-cyclization activity of $\beta$-CGTase was related to a conformational stabilizing effect, because all of the mutants with a newly introduced hydrogen bond by mutations of Asp577 showed higher $\beta$-cyclization activities (Figure 2 and Table 2). A possible explanation was that the increase of enzyme stability was more conducive to the synthesis of the main product in the enzyme-catalyzed reaction. However, the enhancement in the $\beta$-cyclization activity might not completely depend upon the conformational stabilizing effect. The structural changes suggested that D577E gave the greatest increase in the number of interactions between the side chain at residue 577 and the other residues in domain D, followed by D577R and D577K. The order in which the substitutions enhanced the $\beta$-cyclization activity did not correlate with the changes in structure predicted by homology modeling. Previous studies have shown that domain D might be involved in positioning domain E in the correct orientation.[31] Furthermore, domain E has an important role in adsorbing starch granules.[32]

Therefore, to identify the molecular bases for the effects seen here, future studies must resort to more sophisticated modeling approaches.

In addition, under the same reaction conditions resembling industrial production processes, the mutants with enhanced $\beta$-cyclization activities could produce more $\beta$-cyclodextrin in the order D577R > D577K > D577E. The D577R mutant demonstrated a substantial enhancement in $\beta$-cyclodextrin production. More importantly, because of a higher $\beta$-cyclization activity, the amount of D577R protein in the reaction mixture could be reduced by 30.7% when compared to the wild-type CGTase. Although the D577E mutant showed only a 2.5% increase in $\beta$-cyclodextrin production, the amount of mutant protein was also reduced by 11.2%. Thus, these mutations of Asp577 resulted in the increased $\beta$-cyclodextrin production and reduced amount of CGTase required during the reaction process.

In conclusion, Asp577, which is located on the periphery of domain D and is a key residue within calcium-binding site CaIII, played an important role in cyclization activity. The mutations D577R and D577E could obviously enhance the total cyclization activity and $\beta$-cyclization activity. Furthermore, under conditions resembling industrial production processes, the D577R and D577E mutants displayed increased $\beta$-cyclodextrin production; the higher $\beta$-cyclization activities resulted in the significant reduction in the amount of mutant protein required during the process. Thus, the two mutants were much more suitable for the industrial production of $\beta$-cyclodextrin than the wild-type enzyme.

## AUTHOR INFORMATION


### Corresponding Author

*Telephone/Fax: 86-510-85329237. E-mail: zfli@jiangnan.edu.cn.



### Funding

Financial support for this work was obtained from the National Natural Science Foundation of China (31101228), the Natural Science Foundation of Jiangsu Province (BK2011152), and the Fok Ying-Tong Education Foundation, China (131069).

### Notes

The authors declare no competing financial interest.


## REFERENCES


(1) Szejtli, J. Introduction and general overview of cyclodextrin chemistry. *Chem. Rev.* **1998**, *98*, 1743−1753.

(2) Saenger, W. Cyclodextrin inclusion compounds in research and industry. *Angew. Chem.* **1980**, *19*, 344−362.

(3) Del Valle, E. M. M. Cyclodextrins and their uses: A review. *Process Biochem.* **2004**, *39*, 1033−1046.

(4) Li, Z.; Wang, M.; Wang, F.; Gu, Z.; Du, G.; Wu, J.; Chen, J. $\gamma$-Cyclodextrin: A review on enzymatic production and applications. *Appl. Microbiol. Biot.* **2007**, *77*, 245−255.

(5) Li, Z.; Chen, S.; Gu, Z.; Chen, J.; Wu, J. $\alpha$-Cyclodextrin: Enzymatic production and food applications. *Trends Food Sci. Technol.* **2014**, *35*, 151−160.

(6) Penninga, D.; Strokopytov, B.; Rozeboom, H. J.; Lawson, C. L.; Dijkstra, B. W.; Bergsma, J.; Dijkhuizen, L. Site-directed mutations in tyrosine 195 of cyclodextrin glycosyltransferase from *Bacillus circulans* strain 251 affect activity and product specificity. *Biochemistry* **1995**, *34*, 3368−3376.

(7) van der Veen, B. A.; Uitdehaag, J. C.; Dijkstra, B. W.; Dijkhuizen, L. Engineering of cyclodextrin glycosyltransferase reaction and product specificity. *Biochim. Biophys. Acta, Protein Struct. Mol. Enzymol.* **2000**, *1543*, 336−360.

(8) Leemhuis, H.; Kelly, R. M.; Dijkhuizen, L. Engineering of cyclodextrin glucanotransferases and the impact for biotechnological applications. *Appl. Microbiol. Biotechnol.* **2010**, *85*, 823−835.

(9) Ban, X. F.; Li, C. M.; Bao, C. H.; Gu, Z. B.; Li, Z. F. Structure and function analysis of calcium binding sites in cyclodextrin glucanotransferase. *Prog. Biochem. Biophys.* **2013**, *40*, 1239−1246.

(10) Li, C. M.; Ban, X. F.; Gu, Z. B.; Li, Z. F. Calcium ion contribution to thermostability of cyclodextrin glycosyltransferase is closely related to calcium-binding site CaIII. *J. Agric. Food Chem.* **2013**, *61*, 8836−8841.

(11) Yanisch-Perron, C.; Vieira, J.; Messing, J. Improved M13 phage cloning vectors and host strains: Nucleotide sequences of the M13mp18 and pUC19 vectors. *Gene* **1985**, *33*, 103−119.

(12) Li, Z. F.; Ban, X. F.; Gu, Z. B.; Li, C. M.; Huang, M.; Hong, Y.; Cheng, L. Mutations enhance $\beta$-cyclodextrin specificity of cyclodextrin glycosyltransferase from *Bacillus circulans*. *Carbohydr. Polym.* **2014**, *108*, 112−117.

(13) Wu, X. C.; Lee, W.; Tran, L.; Wong, S. L. Engineering a *Bacillus subtilis* expression−secretion system with a strain deficient in 6 extracellular proteases. *J. Bacteriol.* **1991**, *173*, 4952−4958.

(14) Joseph, S.; David, W. *Molecular Cloning: A Laboratory Manual*; Cold Spring Harbor Laboratory Press: New York, 2001; Vol. 2.

(15) Spizizen, J. Transformation of biochemically deficient strains of *Bacillus subtilis* by deoxyribonucleate. *Proc. Natl. Acad. Sci. U. S. A.* **1958**, *44*, 1072−1078.

(16) Bradford, M. M. A rapid and sensitive method for the quantitation of microgram quantities of protein utilizing the principle of protein−dye binding. *Anal. Biochem.* **1976**, *72*, 248−254.

(17) Lejeune, A.; Sakaguchi, K.; Imanaka, T. A spectrophotometric assay for the cyclization activity of cyclomaltohexaose ($\alpha$-cyclodextrin) glucanotransferase. *Anal. Biochem.* **1989**, *181*, 6−11.

(18) Makela, M.; Korpela, T.; Laakso, S. Colorimetric determination of $\beta$-cyclodextrin: Two assay modifications based on molecular complexation of phenolphtalein. *J. Biochem. Biophys. Methods* **1987**, *14*, 85−92.

(19) Kato, T.; Horikoshi, K. Colorimetric determination of $\gamma$-cyclodextrin. *Anal. Chem.* **1984**, *56*, 1738−1740.

(20) Li, Z. F.; Zhang, J. Y.; Wang, M.; Gu, Z. B.; Du, G. C.; Li, J. K.; Wu, J.; Chen, J. Mutations at subsite-3 in cyclodextrin glycosyltransferase from *Paenibacillus macerans* enhancing $\alpha$-cyclodextrin specificity. *Appl. Microbiol. Biotechnol.* **2009**, *83*, 483−490.

(21) Li, Z. F.; Zhang, J. Y.; Sun, Q.; Wang, M.; Gu, Z. B.; Du, G. C.; Wu, J.; Chen, J. Mutations of lysine 47 in cyclodextrin glycosyltransferase from *Paenibacillus macerans* enhance $\beta$-cyclodextrin specificity. *J. Agric. Food Chem.* **2009**, *57*, 8386−8391.

(22) Knegtel, R. M.; Strokopytov, B.; Penninga, D.; Faber, O. G.; Rozeboom, H. J.; Kalk, K. H.; Dijkhuizen, L.; Dijkstra, B. W. Crystallographic studies of the interaction of cyclodextrin glycosyltransferase from *Bacillus circulans* strain 251 with natural substrates and products. *J. Biol. Chem.* **1995**, *270*, 29256−29264.

(23) Arnold, K.; Bordoli, L.; Kopp, J.; Schwede, T. The SWISS-MODEL workspace: A web-based environment for protein structure homology modelling. *Bioinformatics* **2006**, *22*, 195−201.

(24) Janecek, S. $\alpha$-Amylase family: Molecular biology and evolution. *Prog. Biophys. Mol. Biol.* **1997**, *67*, 67−97.

(25) Buisson, G.; Duee, E.; Haser, R.; Payan, F. Three dimensional structure of porcine pancreatic $\alpha$-amylase at 2.9 Å resolution. Role of calcium in structure and activity. *EMBO J.* **1987**, *6*, 3909−3916.

(26) Sajedi, R. H.; Taghdir, M.; Naderi-Manesh, H.; Khajeh, K.; Ranjbar, B. Nucleotide sequence, structural investigation and homology modeling studies of a $Ca^{2+}$-independent $\alpha$-amylase with acidic pH-profile. *J. Biochem. Mol. Biol.* **2007**, *40*, 315−324.

(27) Yadav, J. K. A differential behavior of $\alpha$-amylase, in terms of catalytic activity and thermal stability, in response to higher concentration $CaCl_2$. *Int. J. Biol. Macromol.* **2012**, *51*, 146−152.

(28) Igarashi, K.; Hatada, Y.; Ikawa, K.; Araki, H.; Ozawa, T.; Kobayashi, T.; Ozaki, K.; Ito, S. Improved thermostability of a *Bacillus* $\alpha$-amylase by deletion of an arginine-glycine residue is caused by enhanced calcium binding. *Biochem. Biophys. Res. Commun.* **1998**, *248*, 372−377.

(29) Goh, P. H.; Illias, R. M.; Goh, K. M. Rational mutagenesis of cyclodextrin glucanotransferase at the calcium binding regions for enhancement of thermostability. *Int. J. Mol. Sci.* **2012**, *13*, 5307−5323.
(30) Nakamura, A.; Haga, K.; Yamane, K. Three histidine residues in the active center of cyclodextrin glucanotransferase from alkalophilic *Bacillus* sp. 1011—Effects of the replacement on pH dependence and transition-state stabilization. *Biochemistry* **1993**, *32*, 6624−6631.
(31) Rimphanitchayakit, V.; Tonozuka, T.; Sakano, Y. Construction of chimeric cyclodextrin glucanotransferases from *Bacillius circulans* A11 and *Paenibacillus macerans* IAM1243 and analysis of their product specificity. *Carbohydr. Res.* **2005**, *340*, 2279−2289.
(32) Penninga, D.; vanderVeen, B. A.; Knegtel, R. M. A.; vanHijum, S.; Rozeboom, H. J.; Kalk, K. H.; Dijkstra, B. W.; Dijkhuizen, L. The raw starch binding domain of cyclodextrin glycosyltransferase from *Bacillus circulans* strain 251. *J. Biol. Chem.* **1996**, *271*, 32777−32784.

molecule (noncovalent approach). The spatial assembly of these interaction sites is subsequently fixed through polymerization in the presence of a cross-linking agent. After removal of the template, binding cavities capable of recognizing and rebinding the template molecules are obtained. The binding pockets are more or less complementary to the template regarding size, shape, and arrangement of the functionalities within the cavity.[22−24] Molecularly imprinted materials offer an interesting alternative as controlled release systems; some examples are described in the bibliography, although the majority of them are focused on pharmaceutical applications.[25,26] In the present study the molecularly imprinted polymer (MIP) technology was applied to develop active food packaging for the controlled release of ferulic acid.

Ferulic acid is a phenolic acid that belongs to the hydroxycinnamic acids and occurs widely in the plant kingdom. It is a strong antioxidant, excellent at neutralizing free radicals, especially the free radicals known as "superoxide", "hydroxyl radical", and "nitric oxide". It also acts synergistically with other antioxidants to increase their efficacy.[27] In addition to its low toxicity, this phenolic acid presents biological properties such as antimicrobial, antioxidant, and anti-inflammatory activities among others. Besides, it has been used by the food industry in many applications (e.g., production of vanillin, as a cross-linking agent, as a preservative, etc.).[28,29]

The kinetic release of ferulic acid from the ferulic acid-imprinted polymers developed into food simulants and into real food samples was studied. A mathematical modeling based on Fick's second law was used to determine the key parameters of the diffusion process and the partition and diffusion coefficients.

## MATERIALS AND METHODS

**Chemicals and Standard Solutions.** All reagents used were of chromatographic grade and used without further purification. Ultrapure water from a Milli-Q water purification system (Millipore, Bedford, MA, USA) was used. Ferulic acid (FA, 99%), 2-hydroxyethyl methacrylate (HEMA, 97%), ethylene glycol dimethacrylate (EDMA, 98%), 2-(dimethylamino)ethyl methacrylate (DMAEMA, 99%), and dimethyldichlorosilane (99.0%) were all from Sigma-Aldrich (St. Louis, MO, USA). Methanol (MeOH, gradient grade for liquid chromatography and hypergrade for LC-MS), ethanol (EtOH, absolute for analysis), and isooctane (for analysis) were obtained from Merck (Darmstadt, Germany). Acetic acid solution (puriss, p.a. for HPLC) was obtained from Sigma-Aldrich (Steinheim, Germany).

The chemical structure and the physicochemical characteristics of ferulic acid (CAS Registry No. 1135-24-6) are presented in Table 1. Data were acquired from the Scifinder database.

A stock solution of ferulic acid was prepared in MeOH, with a known concentration of 1000 $\mu$g/mL. From this stock solution an intermediate solution of 100 $\mu$g/mL was prepared. Calibration standard solutions of ferulic acid were prepared by carrying out diverse dilutions with MeOH. The concentrations of these solutions ranged from 0.05 to 10 $\mu$g/mL. Solutions were stored at 4 °C and protected from light.

**Table 1. Chemical Structure and Physicochemical Properties of Ferulic Acid**

| Chemical structure | Physico-chemical properties |
|---|---|
| 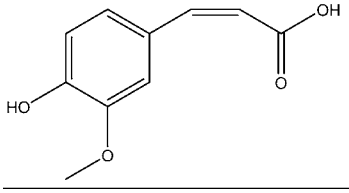 | Molecular weight (MW) 194.185<br>Boiling point (BP) 372.3±27.0 °C<br>log P (octanol-water) 1.51 |

**Molecularly Imprinted Hydrogel Preparation.** Molecularly imprinted hydrogels were prepared according to the method of Benito-Peña et al.[30] Briefly, to obtain the imprinted hydrogel, the template hydroferulic acid (200 mM) and the functional monomers DMAEMA (400 mM) and HEMA (7400 mM) were mixed and placed in a 5 mL glass vial. The mixture was left in contact for several minutes and then, after the addition of EDMA (530 mM) and ABDV (10 mM), cooled and purged with nitrogen for 15 min to remove dissolved oxygen. The prepolymerization mixture solution was injected into molds constituted by two glass plates pretreated with dimethyldichlorosilane and separated by a 0.9 mm thick silicone frame. The molds were placed in an oven at 50 °C for 12 h and later at 70 °C for 24 h more. The hydrogels were removed from the molds and immersed in boiling water for 15 min to remove unreacted components and subsequently rinsed with EtOH 96%, and supernatants were monitored by HPLC-DAD until the removal of the template (HFA) was 99.9%. Finally, the hydrogels were dried and stored.

**Foodstuff.** Chicken roast samples stuffed with ham and cheese were kindly supplied by Nutreco (Nutreco, España, S.A.). The nutritional composition according the supplier was protein, 20.4%; total fat, 6.2%; and total carbohydrate, 0.6%.

**Migration Test: Overall Migration.** Ferulic acid-imprinted polymers were cut in pieces of 2 × 5 cm$^2$ and accurately weighed. These materials were put in contact with the selected food simulants (10% EtOH (v/v), 50% EtOH (v/v), 3% acetic acid (w/v)) and substitutes (95% EtOH (v/v) and isooctane). According to the current legislation,[31] food simulants can be replaced by substitute food simulants if there is scientific evidence that the substitute food simulants overestimate migration compared to the regulated food simulants. Isooctane and 95% ethanol (v/v) are substitutes for fat foods, widely used under the previous legislation and with extensive usage as food simulants. All of the materials were placed so that the whole surface remained in contact with the solvent. The volume used was 20 mL, and all assays were done in triplicate.

Time and temperature conditions were 10 days at 40 °C for 10% EtOH (v/v) 50% EtOH (v/v), 95% EtOH (v/v), and 3% acetic acid (w/v) and 2 days at 20 °C for isooctane. After this time, solvents were placed in glass Petri plates, previously dried and weighed a minimum of five times, and evaporated to dryness using a bath. The residue was determined gravimetrically using the weight difference of the Petri plates, and all of the values were expressed in mg/dm$^2$.

**Release Studies.** *Release Assay in Food Simulants.* Ferulic acid-imprinted polymers were cut in pieces of 1 × 1 cm$^2$. These polymer samples were placed in 60 mL amber flasks in contact with 50 mL of the selected simulants and substitutes (10% EtOH (v/v), 20% EtOH (v/v), 50% EtOH (v/v), 3% acetic acid (w/v), 95% EtOH (v/v), and isooctane), representatives of the main foods that may be intended this antioxidant. All assays were done in triplicate. Likewise, the migration tests in vegetable oil were performed by total immersion.

The time−temperature conditions for each simulant are presented in Table 2. The kinetics release of ferulic acid into 20% EtOH (v/v) and 3% acetic acid (w/v) was only conducted at 25 °C. Aliquots of 0.5 mL were removed at selected time intervals. In the case of isooctane, it was evaporated under a nitrogen vapor stream, and then the residue was dissolved in 0.5 mL of MeOH. After that, all samples were filtered through a 0.45 $\mu$m PTFE membrane filter (Advanted, Toyo Roshi Kaisha, Ltd., Japan).

*Release Assay in Food Samples.* Chicken samples were halved in two pieces, one of them containing the stuffing and the other one the chicken breast. Ferulic acid-imprinted polymers were cut in pieces of 0.5 × 3 cm$^2$. All of them, food samples and the polymeric materials, were accurately weighed. In each piece of chicken, a precise incision was done in the most homogeneous area and ferulic acid-imprinted polymer MIP was incorporated in it. Then, the set was wrapped in aluminum foil, packed in plastic bags, and sealed.

**Table 2. Time−Temperature Conditions for Migration Assays in Food Simulants and Real Food**

| food simulant/real food | temperature (°C) | time (h) |
|---|---|---|
| 10% EtOH (v/v) | 4 | 3, 6, 9, 12, 24, 48, 72, 144, 192, 240, 312, 384, 480, 528, 576, 672, 840 |
| | 20 | 3, 6, 9, 12, 24, 48, 72, 144, 192, 240, 312, 384, 480, 528, 576, 672, 840 |
| 3% acetic acid (w/v) | 25 | 1, 7, 17, 41, 53, 70, 91, 114, 138, 158, 264, 370, 476, |
| 20% EtOH (v/v) | 25 | 1.8, 7.8, −, −, 53.8, 70.8, 91.8, 114.8, −, 158.8, 264.8, 370.8, 476.8 |
| 50% EtOH(v/v) | 4 | 3, 6, 9, 12, 24, 48, 72, 144, 192, 240, 312, 384, 480, 528, 576, 672, 840 |
| | 20 | 3, 6, 9, 12, 24, 48, 72, 144, 192, 240, 312, 384, 480, 528, 576, 672, 840 |
| 95% EtOH (v/v) | 4 | 3, 6, 9, 12, 24, 48, 72, 96, 168, 240, 336, 528 |
| | 20 | 3, 6, 9, 12, 24, 48, 72, 96, 168, 240, 336, 528 |
| isooctane | 4 | 3, 6, 9, 12, 24, 48, 72, 96, 168, 240, 336, 528 |
| | 20 | 3, 6, 9, 12, 24, 48, 72, 96, 168, 240, 336, 528 |
| chicken roti | 4 | 24, 48, 120, 168, 216, 312, 360, 504, 576, 660 |

The samples were stored at 4 °C, and at each selected time the samples were withdrawn. Packages were carefully unwrapped, and the polymeric material was removed, cleaned, and extracted. The time−temperature conditions for the assay are presented in Table 2.

*Extraction Procedure of Ferulic Acid from the Polymeric Materials.* Ferulic acid was extracted from MIPs by placing them in amber flasks of 60 mL hermetically closed with 50 mL of pure MeOH. Then, they were stored at 40 °C during 24 h. After the extraction time, an aliquot was taken, filtered through a 0.45 μm PTFE membrane filter (Advanted, Toyo Roshi Kaisha, Ltd., Japan), and analyzed by HPLC.

In migration studies, the quantification of migrants transferred is usually measured in the food. However, due to the fact that foods are complex matrices, the extraction processes are difficult and lead to very laborious and time-consuming methods and losses related to the existence of several steps. For this reason, to avoid all of these problems, instead of determining the quantity of migrants in the foodstuff, the migrant that remained in the polymer was determined and it was assumed that all of the missing migrant was in the food.

In this case, the concentration of the ferulic acid released was indirectly calculated as the difference between the initial concentration and the concentrations at selected time intervals in the polymer.

To verify if the extraction had been complete, the MIP hydrogel was cleaned with MeOH to remove any remaining migrant that came from the methanolic extraction solution, and it was submitted to a second extraction under the same conditions.

**Equipment and Chromatographic Conditions.** *HPLC-DAD.* Chromatographic analyses were performed on a HP1100 system (Hewlett-Packard, Waldbronn, Germany) consisting of a quaternary pump, a degassing device, an autosampler, a column thermostating system, a diode array detector (DAD), and an Agilent Chemstation for LC and LC/MS system software. A Kromasil ODS (C18) (150 × 3.20 mm i.d., 5 μm) column thermostated at 35 °C was used. The mobile phases consisted of A (MeOH) and B (0.1% acetic acid (v/v) water). The gradient elution program was as follows: 0−2 min, mobile phase isocratic at 10% A; 2−10 min, linear gradient from 10 to 100% A followed by washing (10−18 min 100% A); and finally re-equilibration of the column. The flow rate was 0.5 mL/min and the injection volume 20 μL. The ferulic acid retention time was ($t_R$ = 9.343 min). Chromatograms were registered at 325 nm.

Identification of ferulic acid was made by comparison of the retention time and UV spectrum with those of a pure standard.

Quantification was performed on the basis of linear calibration plots of peak area against concentration. A calibration line was constructed based on six concentration levels of standard solutions within the 0.1−10 mg/L range, and it was fitted to a linear equation $y = 214.88x - 9.6896$ ($R^2 = 0.99995$).

The limits of detection and quantification (defined as a signal 3 and 10 times, respectively, the height of the noise level), determined in accordance with American Chemical Society (ACS) guidelines,[32] were 0.05 and 0.1 mg/L, respectively.

*HPLC-MS as a Confirmatory Technique.* For confirmation purposes a LC-MS/MS system comprising an Accela autosampler and an Accela 1250 pump fitted with a degasser and a column oven coupled to a triple-quadrupole mass spectrometer TSQ Quantum Access max controlled by Xcalibur was used (Thermo Fisher Scientific, San Jose, CA, USA). Mass data were acquired in the negative ion mode employing electrospray ionization (ESI). Mass spectra were monitored in the mass range $m/z$ 150−225. Nitrogen was used as sheath gas (pressure = 35 psi) and as auxiliary gas (pressure = 10 arbitrary units), and argon was used as the collision gas (1.5 mTorr). Optimized MS/MS detector settings were as follows: spray voltage, 2500 V; vaporizer temperature, 340 °C; and capillary temperature, 350 °C.

With regard to LC-MS chromatographic conditions, the mobile phase consisted of A (MeOH) and B (Milli-Q water), whereas the column and the gradient elution system were the same as for HPLC-DAD analysis.

*Identification of Monomers by GC-MS.* The monomers and starting substances used in the fabrication of MIPs were identified by GC-MS (FisonsGC8000 series gas chromatograph, mass selective detector MD800, Manchester, UK). Briefly, approximately 300 mg of material was place in a glass container with 20 mL of methanol and extracted for 24 h at 40 °C. After that, the material was separated from the solution, and an aliquot of 1 μL was removed, filtered, and injected into the GC-MS. A ZB-5 MS (Zebron Capillary GC column from Phenomenex, USA) (30 m × 0.25 mm i.d. × 1 μm film thickness) column was used. Helium was used as carrier gas at a flow rate of 1 mL/min. The ramp temperature was initially set at 40 °C for 4 min, then raised at the rate of 15 °C/min to 150 °C, then increased at 30 °C/min until 200 °C, and held for 10 min. The injector temperature and the split ratio were 175 °C and 1:30, respectively. The MS detector was operated in the full scan mode with an acquisition range of $m/z$ 33−300.

**Mathematical Model.** *Calculation of Partition Coefficients MIP/Food (Food Simulant/Substitute) ($K_{P/S}$).* Partition coefficients between MIP and food or food simulants were calculated according to the equation

$$K_{P/S} = \frac{C_P}{C_S}$$

where $K_{P/S}$ is the partition coefficient between the MIP and the food, food simulant, or substitute. $C_P$ is the concentration of substance in the MIP at equilibrium, in μg/g. $C_S$ is the concentration of substance in the simulant at equilibrium, in μg/g.

*Calculation of Diffusion Coefficients.* A mathematical model based on Fick's second law to assess ferulic acid release from MIPs into the food and food simulants was employed.

$$\frac{\partial C_P}{\partial t} = D\frac{\partial^2 C_P}{\partial x^2}$$

$C_p$ is the concentration of the migrant in the polymer at time $t$ (s) and position $x$, and $D$ is the diffusion coefficient in P ($cm^2/s$).

An analytical solution of this differential equation, proposed by Crank,[33] is usually employed to determine the diffusion coefficient; after a small modification, it can be expressed by the equation[34]

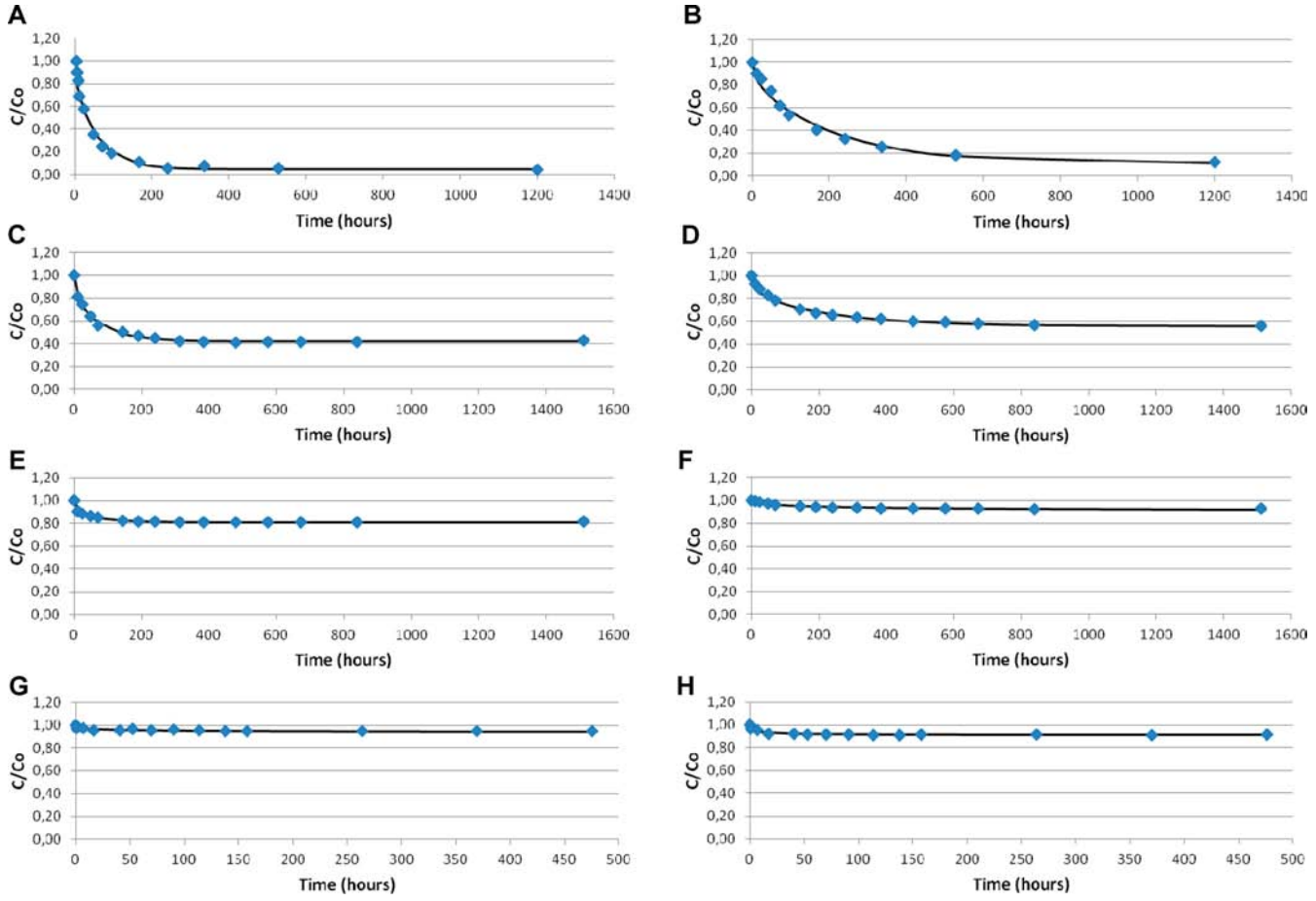


**Figure 1.** Diffusion of ferulic acid from MIP into 95% EtOH (v/v) food substitute at 20 °C (A), into 95% EtOH (v/v) food substitute at 4 °C (B), into 50% EtOH (v/v) food simulant at 20 °C (C), into 50% EtOH (v/v) food simulant at 4 °C (D), into 10% EtOH (v/v) food simulant at 20 °C (E), into 10% EtOH (v/v) food simulant at 4 °C (F), into 20% EtOH (v/v) food simulant at 25 °C (G), and into 3% acetic acid (w/v) food simulant at 25 °C (H).

$$\frac{m_{F,t}}{A} = C_{P,0}\rho_P d_P\left(\frac{\alpha}{1+\alpha}\right)\times\left[1-\sum_{n=1}^{\alpha}\frac{2\alpha(1+\alpha)}{1+\alpha+\alpha^2 q_n^2}\exp\left(-D_P t\frac{q_n^2}{d_P^2}\right)\right]$$

$$\alpha = \frac{1}{K_{P/F}}\frac{V_F}{V_P}$$

where $m_{F,t}$ is the mass of the migrant transferred from P into F after time $t$ ($\mu$g); $A$ is the area of P in contact with F (cm$^2$); $C_{P,0}$ is the initial concentration of the migrant in P (mg/kg); $\rho_P$ is the density of P (g/cm$^3$); $t$ is the migration time (s); $d_P$ is the thickness of P (cm); $V_P$ is the volume of P (cm$^3$); $V_F$ is the volume of F (cm$^3$); $q_n$ is the positive roots of the equation $\tan q_n = -\alpha q_n$; $D_P$ is the diffusion coefficient of the migrant in the polymer (cm$^2$/s); and $K_{P/F}$ is the partition coefficient of the migrant between P and F.

## RESULTS AND DISCUSSION

Ferulic acid molecularly imprinted polymers (MIPs) were developed as a novel controlled release system to be applied as an active food packaging.

To assess the safety and suitability of the active materials developed for use as food contact materials, overall migration tests were conducted. The overall migration assays evaluate the total amount of nonvolatile substances released from the material into food simulants. The migration tests were performed under the time−temperature conditions that represent the worst possible scenario for the intended applications, namely, any long-term storage at room temperature or below. After migration tests, no physical changes were observed in the materials, and all overall migration results were lower than the limit (<10 mg/dm$^2$) established by Commission Regulation (EU) No. 10/2011;[31] thus, the ferulic acid-imprinted polymers (MIPs) comply with food contact materials legislation regarding this limit.

The release behavior of ferulic acid from the new active system into food simulants and food was investigated. High-performance liquid chromatography with diode array detector (HPLC-DAD) was used to quantify ferulic acid. HPLC-MS was used for confirmatory purposes, and the characteristic mass corresponding to the deprotonated molecular ion $[M-H]^-$ was detected.

The monomers used in the molecularly imprinted hydrogel preparation were successfully identified by GC-MS by means of comparison of their mass spectra with the Wiley mass spectrum library.

For these release studies it is crucial to establish the initial concentration of the active compound that is present in the developed material. Thus, the determined concentration of the antioxidant in the developed MIPs before the release studies was 30.8 mg/g (RSD 5%, $n$ = 6).

Table 3. Diffusion and Partition Coefficients and RMSE Values for the Food Simulants and Real Food Samples

| food simulant/real food | temperature (°C) | $K_{P/F}$ exp | $K_{P/F}$ est | $D$ ($cm^2/s$) | RMSE % |
|---|---|---|---|---|---|
| 10% EtOH (v/v) | 4 | $4.2 \times 10^3$ | $3.2 \times 10^3$ | $1.8 \times 10^{-11}$ | 0.60 |
| | 20 | $2.1 \times 10^3$ | $1.5 \times 10^3$ | $8.0 \times 10^{-10}$ | 0.28 |
| 50% EtOH (v/v) | 4 | $3.4 \times 10^2$ | $4.4 \times 10^2$ | $5.0 \times 10^{-10}$ | 1.33 |
| | 20 | $1.9 \times 10^2$ | $2.5 \times 10^2$ | $1.8 \times 10^{-9}$ | 1.10 |
| 95% EtOH (v/v) | 4 | $3.6 \times 10^1$ | $4.4 \times 10^1$ | $9.3 \times 10^{-10}$ | 3.93 |
| | 20 | $1.4 \times 10^1$ | $3.5 \times 10^1$ | $4.2 \times 10^{-9}$ | 1.37 |
| 20% EtOH (v/v) | 25 | | $1.9 \times 10^3$ | $1.6 \times 10^{-10}$ | 0.43 |
| 3% acetic acid (w/v) | 25 | | $1.1 \times 10^3$ | $8.7 \times 10^{-10}$ | 0.47 |
| chicken roti | 4 | $6.1 \times 10^1$ | $1.0 \times 10^2$ | $5.1 \times 10^{-10}$ | 8.6 |

With regard to the release studies, Figure 1A−G shows the relative amount ($C/C_0$) of ferulic acid in the ethanolic food simulants at different temperatures. For the ferulic acid MIP−95% EtOH (v/v) system, the percentages of release at 4 and 20 °C were 82.0 and 85.9%, respectively, after equilibrium was reached.

In general, a decrease in the EtOH content in food simulants resulted in lower amounts of the antioxidant released; thus, in the food simulant 50% EtOH (v/v), the release of ferulic acid was 38.6 and 44.9% at 4 and 20 °C, respectively. In the case of 10% EtOH (v/v), the percentages of release were 6.5% at 4 °C and 10% at 20 °C. For the 20% EtOH (v/v) the delivery kinetics was only carried out at 25 °C.

The delivery of ferulic acid into the food simulant 3% acetic acid (w/v) at 25 °C is illustrated in Figure 1H. The percentage of release (8.7%) was higher than that obtained in simulant EtOH (20% v/v) at the same temperature.

No release of the antioxidant was observed at the quantification level in the vegetable oil and isooctane (LOQ = 0.1 μg/mL). This fact could be explained because of the scarce solubility of ferulic acid in these food simulants.

To characterize the kinetic release process, the partition coefficient ($K_{P/F}$) and the diffusion coefficient ($D$) were determined.

The partition coefficient ($K_{P/F}$) indicates the relative solubility of the active compound between the MIP and the food simulant or food when the equilibrium is reached. Values of $K_{P/F} > 1$ indicate that the active compound is found in greater concentration in the polymer (MIP) than in the food or food simulant.[35−40] The experimental and estimated $K_{P/F}$ values of ferulic acid in food simulants are presented in Table 3. The lower values at the temperatures studied correspond with the food simulant 95% EtOH (v/v), which are in good agreement with the higher percentages the release of the antioxidant. On the contrary, the highest values correspond to 10% EtOH (v/v), indicating the tendency of ferulic acid to remain in the polymer (MIP) rather than be delivered into the food simulant. As can be seen in Table 3 there was a good correlation between the $K_{P/F}$ values calculated from experimental data and those theoretically estimated. The diffusion coefficients of ferulic acid determined in the MIP−food simulant systems are presented in Table 3. The values obtained ranged between $1.8 \times 10^{-11}$ and $4.2 \times 10^{-9}$ $cm^2/s$. As expected, $D$ increased with the temperature, and for the ethanolic simulants $D$ also increased with the percentage of EtOH in the food simulant; therefore, the faster diffusion occurred in 95% EtOH (v/v). Because no migration occurred in isooctane and vegetable oil, $D$ was not calculated.

López-de-Dicastillo et al.[41] found values within the range from $1 \times 10^{-14}$ to $1 \times 10^{-13}$ for the diffusion of ferulic acid from an active antioxidant packaging films based on an ethylene vinyl alcohol copolymer (EVOH) matrix into water, 10% EtOH, and 95% EtOH at 37 °C.

When compared to the diffusion of other antioxidants, the $D$ values obtained in the present work were within the same range as those obtained in a study conducted by Ortiz-Vázquez et al.,[42] in which they investigated the release of BHT from poly(lactic acid) (PLA) films into 95% EtOH at different temperatures ($(0.295−19.04) \times 10^{-10}$ $cm^2/s$). Manzanarez-López et al.[43] studied the migration kinetics of α-tocopherol from PLA films in EtOH and reported values between $3.16 \times 10^{-11}$ and $38.00 \times 10^{-11}$ $cm^2/s$. Lower $D$ values ($4.60 \times 10^{-10}$−$6.58 \times 10^{-12}$ $cm^2/s$) for α-tocopherol in a low-density polyethylene (LDPE)/polypropylene blend films−95% EtOH system were reported by Zhu et al.[44]

Iñiguez-Franco et al.[35] determined the diffusion of two polyphenols, catechin and epicatechin, from PLA films into different ethanolic simulants; the $D$ values obtained were between $0.49 \times 10^{-11}$ and $51.2 \times 10^{-11}$ $cm^2/s$. Higher $D$ values were found for resveratrol from PLA films into EtOH ($(3.06−82.60) \times 10^{-11}$ $cm^2/s$[45]). These values were in general lower than those obtained in this study for ferulic acid.

The results indicate that using MIP hydrogels as active packaging systems enables controlled release through extended periods (4−6 days) compared with EVOH films,[41] so it is possible to prolong the shelf life of the food over more time. This advantage is related to the strong binding of the FA toward the active sites of the MIP films, which is in concordance with the higher binding properties that MIP polymers display.[30]

A wide range of diffusivities ($(0.19−176.1) \times 10^{-10} cm^2/s$) were reported by Jamshidian et al.,[46] who evaluated the release of synthetic phenolic antioxidants from extruded poly(lactic acid) (PLA) films into food simulants at 20 and 40 °C. Similar values of diffusivity were obtained for solvent-cast PLA films.[47]

The release kinetics of ferulic acid from the active system developed in real samples was also studied; for that purpose a stuffed chicken roast was selected as foodstuff. The release tests were conducted as described under Materials and Methods. As has been pointed out earlier, the ferulic acid remaining in the MIP was quantified instead of the antioxidant delivered into the food to avoid the analytical problems associated with the extraction of the compound in the food matrix. Figure 2 illustrates the delivery of ferulic acid from the MIP into the food sample; the percentage of release was 98% at equilibrium. The key parameters of the release process and partition and diffusion coefficients are listed in Table 3. A middle rate of release was obtained, so the active system developed could be useful for the intermediate-term protection of packed foods against lipid oxidation and consequently extend their shelf life.

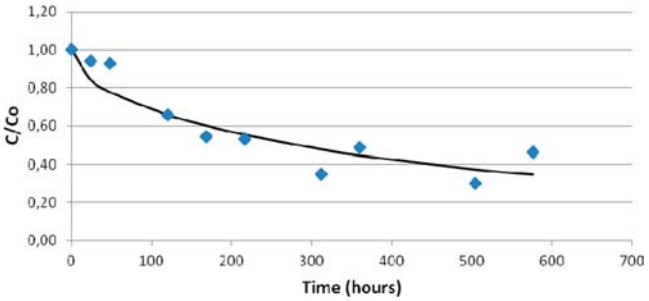


**Figure 2.** Diffusion of ferulic acid from MIP into chicken roti.

For the ferulic acid release studies, the food simulant that represents most appropriately the behavior of stuffed chicken roast samples seems to be 50% ethanol (v/v).

The Arrhenius equation was used to study the effect of the temperature on the diffusion of ferulic acid from the MIP into ethanolic food simulants.

$$D = D_0\, e^{-E_A/RT}$$

$D$ is the diffusion coefficient ($cm^2/s$), $D_0$ is the preexponential factor ($cm^2/s$), $E_A$ is the activation energy (kJ/mol), $R$ is the gas constant (kJ/mol K), and $T$ is the temperature (K).

The $E_A$ was determined from the slope by representing the $1/T$ versus the logarithm of $D$. The determination was performed using the data obtained in this work (two temperatures) and assuming a linear behavior within this range. The $E_A$ is the energy necessary for a given compound to move through the polymeric matrix.[48,49] The $E_A$ and $D_0$ values for the systems studied are presented in Table 4. Higher values

**Table 4. $E_A$ and $D_0$ Values for the Systems Studied**

| food simulant | $D_0$ | $E_A$ |
|---|---|---|
| 10% EtOH (v/v) | $2.23 \times 10^{19}$ | 159.6 |
| 50% EtOH (v/v) | 8.23 | 54.20 |
| 95% EtOH (v/v) | $7.58 \times 10^{2}$ | 63.20 |

of $E_A$, 175−177 and 164.7 ± 27.7 kJ/mol, were obtained for other antioxidants (resveratrol and butylated hydroxytoluene (BHT)) incorporated into poly(lactic acid) matrices[42,45]). This indicates that less energy is required for the diffusion of ferulic acid from the MIP hydrogels into the food simulants studied compared to resveratrol and BHT from PLA into EtOH.

With the aim of measuring the fit between the experimental and estimated data, the root of mean-square error percent (RMSE (%)) was calculated according the following equation:

$$\text{RMSE (\%)} = \frac{1}{M_{P,0}}\sqrt{\frac{1}{n}\sum_{i=1}^{n}((M_{F,t})_{exp,i} - (M_{F,t})_{pred,i})^2} \times 100$$

$n$ is the number of experimental points per migration/release curve, $i$ is the number of observations, and $M_{P,0}$ is the initial amount of the migrant in the polymer ($\mu g$).

RMSE (%) values <4 were obtained in all food simulants, indicating that there was a very good fit between the experimental and estimated data. A low RMSE value (8.6%) was also obtained for the real food chicken roti. This means that this model can be used to predict the release of ferulic acid into food simulants and food matrices.

In brief, an active system based on molecularly imprinted polymers for the sustained delivery of ferulic acid was developed. The release kinetics of ferulic acid into food simulants and one real sample were studied. The diffusion coefficients were calculated by using a mathematical model based on Fick's second law, and the values obtained ranged between $1.8 \times 10^{-11}$ and $4.2 \times 10^{-9}$ $cm^2/s$. Both the temperature and the percentage of EtOH of the simulant affected the diffusion. The proposed system could be used as an antioxidant controlled release packaging to inhibit or delay lipid oxidation.

## AUTHOR INFORMATION


### Corresponding Author

*(A.R.-B.Q.) Phone: +34 881 814965. E-mail: ana.rodriguez.bernaldo@usc.es.



### Funding

The study was financially supported by the Directorate General for Technology Transfer and Business Development (National R&D&I Plan 2008-2011; INNPACTO 2010 Call) of the Ministry of Economy and Competitiveness of the Spanish government, ref no. IPT-060000-2010-014 "MIPFOOD". R.S. is grateful to the "Parga Pondal" Program financed by "Consellería de Innovación e Industria, Xunta de Galicia" for her postdoctoral contract.


### Notes

The authors declare no competing financial interest.

## ACKNOWLEDGMENTS


We are grateful to C. Casal, P. Blanco, and G. Hermelo for their excellent technical assistance.


## REFERENCES


(1) Barriuso, B.; Astiasarán, I.; Ansorena, D. A review of analytical methods measuring lipid oxidation status in foods: a challenging task. *Eur. Food Res. Technol.* **2013**, *236*, 1−15.

(2) Nerín, C.; Tovar, L.; Salafranca, J. Behaviour of a new antioxidant active film versus oxidizable model compounds. *J. Food Eng.* **2008**, *84*, 313−320.

(3) Camo, J.; Beltrán, J. A.; Roncalés, P. Extension of the display life of lamb with an antioxidant active packaging. *Meat Sci.* **2008**, *80*, 1086−1091.

(4) López-de-Dicastillo, C.; Pezo, D.; Nerín, C.; López-Carballo, G.; Catalá, R.; Gavara, R.; Hernández-Muñoz, P. Reducing oxidation of foods through antioxidant active packaging based on ethyl vinyl alcohol and natural flavonoids. *Packag. Technol. Sci.* **2012**, *25*, 457−466.

(5) Barbosa-Pereira, L.; Cruz, J. M.; Sendón, R.; Rodríguez- Bernaldo de Quirós, A.; Ares, A.; Castro-López, M.; Abad, M. J.; Maroto, J.; Paseiro-Losada, P. Development of antioxidant active films containing tocopherols to extend the shelf life of fish. *Food Control* **2013**, *31*, 236−243.

(6) Mastromatteo, M.; Mastromatteo, M.; Conte, A.; Del Nobile, A. M. Advances in controlled release devices for food packaging applications. *Trends Food Sci. Technol.* **2010**, *21*, 591−598.

(7) Imran, M.; Revol-Junelles, A. M.; Martyn, A.; Tehrany, E. A.; Jacquot, M.; Linder; Desobry, S. Active food packaging evolution: transformation from micro- to nanotechnology. *Crit. Rev. Food Sci. Nutr.* **2010**, *50*, 799−821.

(8) De Kruijf, N.; van Beest, M.; Rijk, R.; Sipilainen-Malm, T.; Paseiro Losada, P.; DeMeulenaer, B. Active and intelligent packaging: applications and regulatory aspects. *Food Addit. Contam.* **2002**, *19*, 144−162.

(9) LaCoste, A.; Schaich, K. M.; Zumbrunnen, D.; Yam, K. L. Advancing controlled release packaging through smart blending. *Packag. Technol. Sci.* **2005**, *18*, 77−87.

(10) Koontz, J. L.; Moffitt, R. D.; Marcy, J. E.; O'Keefe, S. F.; Duncan, S. E.; Long, T. E. Controlled release of α-tocopherol, quercetin, and their cyclodextrin inclusion complexes from linear low-density polyethylene (LLDPE) films into a coconut oil model food system. *Food Addit. Contam.* **2010**, *27*, 1598−1607.
(11) Gemili, S.; Yemenicioğlu, A.; Altınkaya, S. A. Development of antioxidant food packaging materials with controlled release properties. *J. Food Eng.* **2010**, *96*, 325−332.
(12) Mastromatteo, M.; Barbuzzi, B.; Conte, A.; Del Nobile, A. M. Controlled release of thymol from zein based film. *Innovative Food Sci. Emerging Technol.* **2009**, *10*, 222−227.
(13) Chen, X.; Lee, D. S.; Zhu, X.; Yam, K. L. Release kinetics of tocopherol and quercetin from binary antioxidant controlled-release packaging films. *J. Agric. Food Chem.* **2012**, *60*, 3492−3497.
(14) Pothakamury, U. R.; Barbosa-Cánovas, G. V. Fundamental aspects of controlled release in foods. *Trends Food Sci. Technol.* **1995**, *6*, 397−406.
(15) Frascareli, E. C.; Silva, V. M.; Tonona, R. V.; Hubinger, M. D. Effect of process conditions on the microencapsulation of coffee oil by spray drying. *Food Bioprod. Process.* **2012**, *90*, 413−424.
(16) Koontz, J. L.; Marcy, J. E.; O'Keefe, S. F.; Duncan, S. E. Cyclodextrin inclusion complex formation and solid state characterization of the natural antioxidants α-tocopherol and quercetin. *J. Agric. Food Chem.* **2009**, *57*, 1162−1171.
(17) Wan, J.; Gordon, J. B.; Muirhead, K.; Hickey, M. W.; Coventry, M. J. Incorporation of nisin in micro-particles of calcium alginate. *Lett. Appl. Microbiol.* **1997**, *24*, 153−158.
(18) Donsì, F.; Annunziata, M.; Sessa, M.; Ferrari, G. Nanoencapsulation of essential oils to enhance their antimicrobial activity in foods. *LWT−Food Sci. Technol.* **2011**, *44*, 1908−1914.
(19) Buonocore, G. G.; Conte, A.; Corbo, M. R.; Sinigaglia, M.; Del Nobile, M. A. Mono- and multilayer active films containing lysozyme as antimicrobial agent. *Innovative Food Sci. Emerging Technol.* **2005**, *6*, 459−464.
(20) Ha, J. U.; Kim, Y. M.; Lee, D. S. Multilayered antimicrobial polyethylene films applied to the packaging of ground beef. *Packag. Technol. Sci.* **2001**, *15*, 55−62.
(21) Granda-Restrepo, D. M.; Soto-Valdez, H.; Peralta, E.; Troncoso-Rojas, R.; Vallejo-Córdoba, B.; Gámez-Meza, N.; Graciano-Verdugo, A. Z. Migration of α-tocopherol from an active multilayer film into whole milk powder. *Food Res. Int.* **2009**, *42*, 1396−1402.
(22) Mayes, A. G.; Mosbach, K. Molecularly imprinted polymers: useful materials for analytical chemistry? *TrAC, Trends Anal Chem.* **1997**, *16* (6), 321−332.
(23) Sellergren, B. Noncovalent molecular imprinting: antibody-like molecular recognition in polymeric network materials. *TrAC, Trends Anal Chem.* **1997**, *16* (6), 310−320.
(24) Takeuchi, T.; Haginaka, J. Separation and sensing based on molecular recognition using molecularly imprinted polymers. *J. Chromatogr., B* **1999**, *728*, 1−20.
(25) Puoci, F.; Iemma, F.; Cirillo, G.; Picci, N.; Matricardi, P.; Alhaique, F. Molecularly imprinted polymers for 5-fluorouracil release in biological fluids. *Molecules* **2007**, *12*, 805−814.
(26) Mirzaei, M.; Hassani Najafabadi, S. A. H.; Abdouss, M.; Azodi-Deilami, S.; Asadi, E.; Hosseini, M. R. M.; Piramoon, M. Preparation and utilization of microporous molecularly imprinted polymer for sustained release of tetracycline. *J. Appl. Polym. Sci.* **2013**, DOI: 10.1002/APP.38311.
(27) Trombino, S.; Serini, S.; Di Nicuolo, F.; Celleno, L.; Andò, S.; Picci, N.; Calviello, G.; Palozza, P. Antioxidant effect of ferulic acid in isolated membranes and intact cells: synergistic interactions with α-tocopherol, β-carotene, and ascorbic acid. *J. Agric. Food Chem.* **2004**, *52*, 2411−2420.
(28) Ou, S.; Kwok, K. C. Ferulic acid: pharmaceutical functions, preparation and applications in foods. *J. Sci. Food Agric.* **2004**, *84*, 1261−1269.
(29) El-Seedi, H. R.; El-Said, A. M. A.; Khalifa, S. A. M.; Göransson, U.; Bohlin, L.; Borg-Karlson, A. K.; Verpoorte, R. Biosynthesis, natural sources, dietary intake, pharmacokinetic properties, and biological activities of hydroxycinnamic acids. *J. Agric. Food Chem.* **2012**, *60*, 10877−10895.
(30) Benito-Peña, E.; González-Vallejo, V.; Rico-Yuste, A.; Barbosa-Pereira, L.; Cruz, J. M.; Bilbao, A.; Alvarez-Lorenzo, C.; Moreno-Bondi, M. C. Molecularly imprinted hydrogels as functional active packaging materials. *Chem.−Eur. J.* **2014** (submitted for publication).
(31) Commission Regulation (EU) No. 10/2011 of 14 January 2011 on plastic materials and articles intended to come into contact with food. *Off. J. Eur. Communities* **2011**, *L12*, 1−132.
(32) American Chemical Society (ACS). Subcommittee of environmental analytical chemistry. *Anal. Chem.* **1980**, *52*, 2242−2280.
(33) Crank, J. *The Mathematics of Diffusion*, 2nd ed.; Clarendon: Oxford, UK, 1975; pp 44−68.
(34) Simoneau, C. Applicability of generally recognised diffusion models for the estimation of specific migration in support of EU Directive 2002/72/EC, 2010; retrieved from http://publications.jrc.ec.europa.eu/repository/bitstream/111111111/14935/1/reqno_jrc59476_mathmod_v10_cs_2010_09_24_final.pdf%5B1%5D.pdf.
(35) Iñiguez-Franco, F.; Soto-Valdez, H.; Peralta, E.; Ayala-Zavala, J. F.; Auras, R.; Gámez-Meza, N. Antioxidant activity and diffusion of catechin and epicatechin from antioxidant active films made of poly(L-lactic acid). *J. Agric. Food Chem.* **2012**, *60*, 6515−6523.
(36) Sanches Silva, A.; Cruz Freire, J. M.; Sendón García, R.; Franz, R.; Paseiro Losada, P. Time−temperature study of the kinetics of migration of DPBD from plastics into chocolate, chocolate spread and margarine. *Food Res. Int.* **2007**, *40*, 679−686.
(37) Sanches-Silva, A.; Cruz, J. M.; Sendón, R.; Franz, R.; Paseiro-Losada, P. Kinetic migration studies from packaging films into meat products. *Meat Sci.* **2007**, *77*, 238−245.
(38) Sanches-Silva, A.; Pastorelli, S.; Cruz, J. M.; Simoneau, C.; Castanheira, I.; Paseiro-Losada, P. Development of a method to study the migration of six photoinitiators into powdered milk. *J. Agric. Food Chem.* **2008**, *56*, 2722−2726.
(39) Sanches-Silva, A.; Andre, C.; Castanheira, I.; Cruz, J. M.; Pastorelli, S.; Simoneau, C.; Paseiro-Losada, P. Study of the migration of photoinitiators used in printed food-packaging materials into food simulants. *J. Agric. Food Chem.* **2009**, *57*, 9516−9523.
(40) Sanches-Silva, A.; Cruz, J. M.; Sendón, R.; Franz, R.; Paseiro-Losada, P. Migration and diffusion of diphenylbutadiene from packages into foods. *J. Agric. Food Chem.* **2009**, *57*, 10225−10230.
(41) López-de-Dicastillo, C.; Gómez-Estaca, J.; Catalá, R.; Gavara, R.; Hernández-Muñoz, P. Active antioxidant packaging films: development and effect on lipid stability of brined sardines. *Food Chem.* **2012**, *131*, 1376−1384.
(42) Ortiz-Vazquez, H.; Shin, J.; Soto-Valdez, H.; Auras, R. Release of butylated hydroxytoluene (BHT) from poly(lactic acid) films. *Polym. Test.* **2011**, *30*, 463−471.
(43) Manzanarez-López, F.; Soto-Valdez, H.; Auras, R.; Peralta, E. Release of α-tocopherol from poly(lactic acid) films, and its effect on the oxidative stability of soybean oil. *J. Food Eng.* **2011**, *104*, 508−517.
(44) Zhu, X.; Lee, D. S.; Yam, K. L. Release property and antioxidant effectiveness of tocopherol-incorporated LDPE/PP blend films. *Food Addit. Contam.* **2012**, *29* (3), 461−468.
(45) Soto-Valdez, H.; Auras, R.; Peralta, E. Fabrication of poly(lactic acid) films with resveratrol and the diffusion of resveratrol into ethanol. *J. Appl. Polym. Sci.* **2011**, *121* (2), 970−978.
(46) Jamshidian, M.; Tehrany, E. A.; Desobry, S. Release of synthetic phenolic antioxidants from extruded poly lactic acid (PLA) film. *Food Control* **2012**, *28*, 445−455.
(47) Jamshidian, M.; Tehrany, E. A.; Desobry, S. Antioxidants release from solvent-cast PLA film: investigation of PLA antioxidant-active packaging. *Food Bioprocess Technol.* **2013**, *6* (6), 1450−1463.
(48) Limm, W.; Hollifield, H. C. Modelling of additive diffusion in polyolefins. *Food Addit. Contam.* **1996**, *13* (8), 949−967.
(49) Graciano-Verdugo, A. Z.; Soto-Valdez, H.; Peralta, E.; Cruz-Zárate, P.; Islas-Rubio, A. R.; Sánchez-Valdes, S.; Sánchez-Escalante, A.; González-Méndez, N.; González-Ríos, H. Migration of α-tocopherol from LDPE films to corn oil and its effect on the oxidative stability. *Food Res. Int.* **2010**, *43*, 1073−1078.

Table 1. Mineral Concentrations in Wheat Samples[a]

| wheat fractions | minerals (mg/100 g dry weight) | | | | | |
|---|---|---|---|---|---|---|
| | Fe | Mn | Zn | Ca | Mg | Cu |
| aleurone | 14.0 ± 0.36 | 9.50 ± 0.29 | 10.02 ± 0.29 | 102 ± 1.13 | 792 ± 6.7 | 1.53 ± 0.11 |
| aleurone (micromilled) | 12.7 ± 0.05 | 6.81 ± 0.11 | 8.15 ± 0.18 | 91.0 ± 0.09 | 660.1 ± 0.41 | 1.30 ± 0.04 |
| whole wheat | 3.5 ± 0.05 | 4.71 ± 0.55 | 3.18 ± 0.09 | 40.4 ± 0.47 | 139.6 ± 3.4 | 0.47 ± 0.02 |
| whole wheat (micromilled) | 3.5 ± 0.10 | 4.02 ± 0.07 | 2.99 ± 0.03 | 39.5 ± 0.63 | 129.3 ± 2.2 | 0.36 ± 0.04 |

[a]Values are means ± SEM ($n$ = 4).

charred over a Bunsen burner flame at a low heat to eliminate smoke before placing in a muffle furnace at 525 °C for 3 h hours during which all the organic matter was oxidized leaving remnants of clean white ash. Samples were oven-dried for 48 h, cooled in a desiccator, and reweighed. Fe, Mg, Zn, Ca, and Mn concentrations in the samples were analyzed using inductively coupled plasma optical emission spectrometry (ICP-OES, Thermo-Fisher). Plasma parameters and sample aspiration methods were performed according to the manufacturer's recommendations. Mineral concentrations were extrapolated from the standard curve in the range of 0.1−10 μg/mL. The internal standard, yttrium (Merck Millipore), was added to each sample according to manufacturer's specification to correct for sample losses due to volatility and evaporation.

**In Vitro Peptic−Pancreatic Digestion.** Samples were digested by simulated peptic−pancreatic digestion.[13] Enzymes and bile extract were demineralized with Chelex-100 (Bio-Rad Laboratories Ltd., Hercules, CA) before performing the experiments. The weight of samples used for experiment was calculated according to iron content in different samples to ensure that equal amounts of iron (150 μg) were used for digestion experiments. Following this, known weights of samples (in quadruplicate) were added to 10 mL of isotonic saline solution (140 mM NaCl and 5 mM KCl) and were adjusted to pH 2.0 with HCl (1 M). During peptic digestion, 0.5 mL pepsin (16 mg/mL) was added, and the mixture was incubated at 37 °C for 75 min followed by pH adjustment to 5.5 with $NaHCO_3$ (1 M) to stop peptic digestion. Afterward, 2.5 mL of bile−pancreatin extract (8.5 mg/mL bile extract and 1.4 mg/mL pancreatin) was added and pH was adjusted to 7.0 with $NaHCO_3$ (1 M) to start pancreatin−bile digestion. The volume was brought to 15 mL by adding isotonic saline solution, and the mixture was incubated at 37 °C for 120 min. Following digestion, tubes were centrifuged at 3000$g$ for 5 min and of the digests supernatant of digests was retained for experiment.

**Cell Culture.** Caco-2 cells (ATCC; HTB-37) at passage 28 were used for the experiments. Cells were grown in Dulbecco's modified Eagle's medium (DMEM, Gibco, Life Technologies, U.K.), which contained 1% antibiotic/antimycotic solution, 25 mM HEPES, and 10% fetal bovine serum. For the experiment, cells were trypsinized and seeded into 6-well plates at a density of 50 000 cells in 2.5 mL of DMEM. Cells were incubated at 37 °C with 5% $CO_2$ and 95% air for 14 days while the medium was changed every 2 days.

The day before experiments, DMEM was replaced with minimum essential medium (MEM, Gibco Life Technologies, U.K.) containing 10 mmol/L PIPES, 1% penicillin and streptomycin, 11 μM dexamethasone, and 0.87 μM insulin, and the cells were incubated at 37 °C for 24 h. Afterward fresh MEM (2 mL) was added to the cells. An amount of 1.5 mL of each digest was pipetted into cellulose dialysis tubing (15 000 Da molecular weight cutoff dialysis membranes (Tubing Spectra/Por 7 dialysis membrane, Fisher Scientific) that were exposed to the medium bathing the cells. Cells were then incubated at 37 °C for 2 h for iron uptake. The baseline control was incubated with only MEM medium. Following that, the digest was removed, 1 mL of supplemented MEM was added to the cells, and these were incubated for a further 22 h. Following this incubation period, cells were washed with PBS and lysed with mammalian protein extraction reagent (MPER, Thermo Fisher Scientific, Cramlington, U.K.). The cell lysate was centrifuged (5 min, 16 000$g$) to remove cell debris, and the supernatant used for ferritin and protein analysis. Thereafter, cells were harvested in 200 mL of PER protein lysate solution (Thermo Scientific) and analyzed for ferritin content using a commercially available ELISA (Ramco Laboratories, TX, U.S.A.). Experiments were carried out in triplicate and data expressed as nanograms of ferritin per milligram of cell protein.

**In Vitro Digestion with Driselase.** Wholegrain wheat flour was digested with Driselase (EC286-055-3), an enzyme mixture containing laminarinase, xylanase, and cellulase activity that hydrolyses cell walls of plants. Two milliliters of enzyme solution (1 unit/mL) was made by mixing 100 μL of 2% Driselase (w/v) with 1.9 mL of buffer (1.33 mL of 50 mM sodium acetate and 0.57 mL of 50 mM acetic acid, pH 2.5). An amount of 100 mg of wholegrain wheat flour was added to 2 mL of enzyme solution, and this was incubated at 37 °C for 6 h. The control group was incubated with the buffer without Driselase. After digestion, tubes were centrifuged at 3000$g$ for 5 min and the supernatant was saved for measurement of soluble iron afterward.

**Iron Solubility from Wheat Samples.** The amount of soluble iron was analyzed using the ferrozine assay.[14] The blank solution consisted of enzymes without the wheat samples. One milliliter of supernatant from each of the digests, the blank, and the standards was added to microfuge tubes (Figure 2). To this was added 0.1 mL of solution containing 10% HCl (v/v) and 5% hydroxylamine hydrochloride (w/v), mixed, and incubated at room temperature for 30 min. Afterward, 0.1 mL of a solution containing 5 mg/mL ferrozine and 1 M 4-(2-hydroxyethyl)-1-piperazineethanesulfonic acid (HEPES) buffer was added, mixed, and allowed to stand at room temperature for 1 h. Finally, the absorbance of the solutions was measured in a spectrophotometer (Camspec M330 UV−vis) at 562 nm. Standard solutions containing 0.015−0.5 μg/mL $FeCl_3$ were prepared and treated as with the samples.

**Microscopic Localization of Iron in Wheat Aleurone Layer.** The localization of iron and the structure of AL observed under the microscope after staining with Perl's Prussian blue according to a protocol described by Wang and Cuschieri.[15] The stain used was a mixture of 2.5% potassium ferrocyanide (w/v) in 2.5% HCl (v/v). Approximately 50 mg of wheat sample and 500 μL of Perl's Prussian blue solution were placed in 1.5 mL microfuge tubes and incubated at room temperature for 30 min before examination with a light microscope (Axioskop 2 mot plus, Car-Zeiss, U.K.) to reveal tissue structure and iron deposits in the AL.

**Animal Studies.** Changes to the structure of AL and the iron content of the aleurone cells in different regions of the gastrointestinal tract and in feces were also determined. Eight male 6 weeks old C57BL/6 mice (Charles Rivers, Kent, U.K.) were used for the studies. Mice were fasted overnight and then fed in two groups of four mice, wholegrain wheat flour or aleurone flour ad libitum for 24 h to allow complete transit through the gastrointestinal tract. Mice were housed in a light- and temperature-controlled room with ad libitum access to deionized water.

Following the feeding of flour for 24 h, mice were anaesthetized, and sacrificed by cervical dislocation and contents of the stomach, duodenum, jejunum, ileum, and colon contents as well as feces from the mice were removed and placed in tubes for microscopic examination. Perl's Prussian blue staining and light microscopic examination in each sample was performed as described above. All procedures were conducted in accordance with methods approved by the United Kingdom Animals (Scientific Procedures) Act 1986.

**Statistical Analysis.** Data were analyzed with Microsoft Office Excel 2010 and SPSS software 20.0.0 (SPSS Inc., U.S.A.). Data are shown as mean ± SEM. Comparison of means was analyzed either by Student's unpaired $t$ test or one-way analysis of variance (ANOVA)

with Turkey's post-test for multiple comparisons. Significant differences were considered at $P < 0.05$.

## RESULTS

**Mineral Analysis in Wheat Samples.** Table 1 shows the mineral content of wholegrain wheat and aleurone samples. Mineral concentrations were significantly enriched in the aleurone fraction compared with the whole wheat samples, with iron in particular being some 3−4-fold enriched. The mineral content of wholegrain and aleurone flour was not significantly altered following micromilling.

**Microscopic Localization of Iron in Wheat Products.** Light microscopy revealed the localization of iron in the aleurone layer of whole wheat (Figure 1). Aleurone cells were largely resistant to in vivo digestion during transit along the gastrointestinal tract. Microscopic examination of digests from mice that were fed aleurone flour overnight revealed iron-stained globules encased within aleurone cells obtained from different regions of the gastrointestinal tract (Figure 2A−E) and also in fecal contents (Figure 2F).

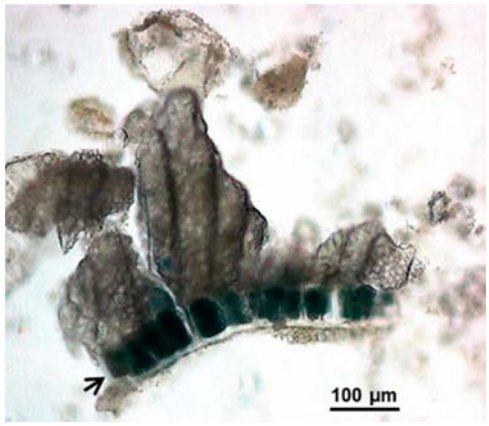


**Figure 1.** Localization of iron in the aleurone layer of whole grain wheat flour. Wheat flour treated with Perl's Prussian blue solution and visualized under the microscope revealed a single blue-stained aleurone layer (arrow).

**In Vitro Iron Solubility from Aleurone Samples.** The aleurone cell walls were disrupted by enzymatic digestion with Driselase (Figure 3, parts A and B) and by micromilling (Figure 3, parts C and D). Next we investigated whether enzymatic or mechanical disruption of aleurone cells would alter bioaccessibility of iron. Following Driselase treatment (Figure 4A) and mechanical disruption through micromilling there was a significant increase in iron solubility in aleurone and whole wheat samples (Figure 4B).

**Micromilling and Iron Availability in Wheat Aleurone.** To determine whether mechanical disruption of the aleurone cell layer increased iron solubility and in turn led to increased iron bioaccessibility, we employed a model of in vitro digestion/cell iron uptake.[13] Micromilling of purified aleurone flour and wholegrain wheat flour (Figure 5) significantly enhanced iron bioaccessibility after peptic−pancreatin digestion of the samples and iron uptake in Caco-2 cells, using cell ferritin protein content as a surrogate marker.

## DISCUSSION

Fortification of staple crops with iron is recommended for alleviation of the high prevalence of ID and IDA in population groups in many countries.[16] Well-established strategies employ ferrous (II) salts, ferric (III) salts, ferric (III) chelates, or elemental Fe powders as the primary fortificants.[17] Moreover, iron supplementation poses inherently difficult issues such as solubility, bioavailability, toxicity, or tolerability in the gastrointestinal (GI) tract.[18,19] Consequently, transgenic transformation of cereals and other food crops became an attractive option for improving iron nutrition in human populations.[20,21] Plants have been genetically modified to yield grains that express ferritin,[22] phytase,[23,24] hemoglobin,[25,26] or coexpression of ferritin and phytase in an attempt to improve iron nutrition.[27] Biofortification is still in its developmental phase and is beset by numerous challenges both technical and emotive. Thus, if a simple food processing technique could increase iron bioaccessibility, or a naturally iron-rich food component could be modified to provide a bioaccessible and bioavailable source of iron for food fortification, this would represent a major advance in human nutrition.

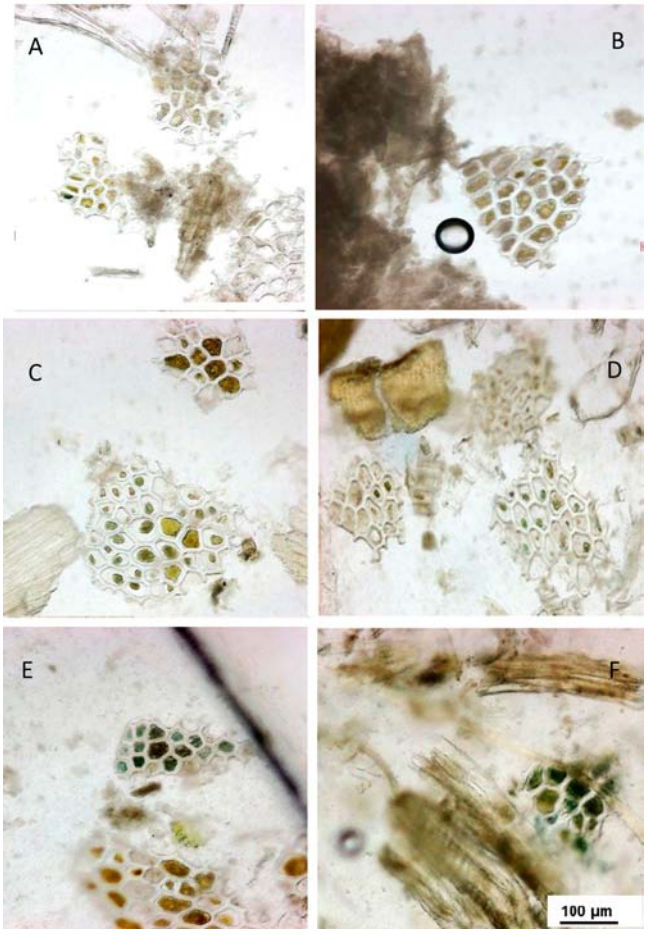


**Figure 2.** Structure and localization of iron in aleurone flour after passing through gastrointestinal tract of mice. Mice were fed aleurone flour overnight, and food contents were obtained from different parts of the gastrointestinal (GI) tract for microscopic observation. Samples were obtained from stomach (A), duodenum (B), jejunum (C), ileum (D), colon (E), and feces (F).

Here we have investigated whether wheat aleurone might provide a bioaccessible source of iron. One immediate obstacle to the use of aleurone is that the cell walls, which are composed of mainly nonstarch polysaccharides (dietary fiber), are highly resistant to digestion in the upper GI tract of humans and many experimental animals. Microscopic examination of the lumenal

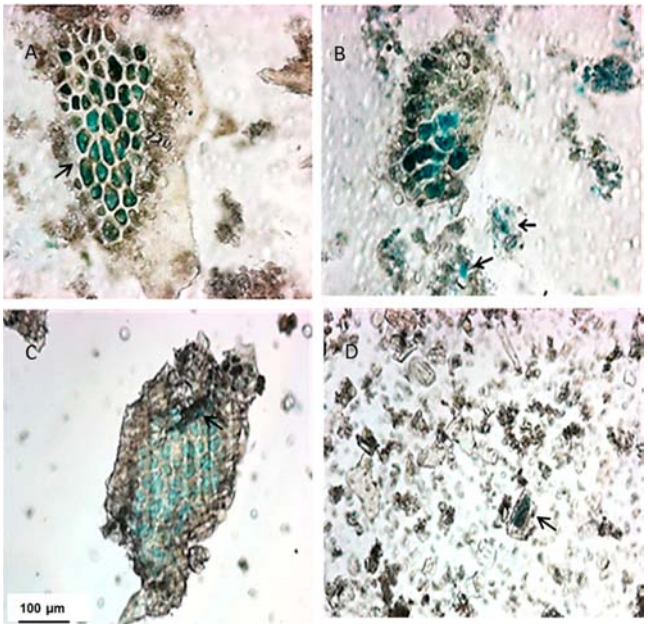


**Figure 3.** Location of iron in wheat flour before (A) and after (B) digestion by Driselase. Wholegrain wheat flour was digested by Driselase (final concentration of 0.1%) at 37 °C for 6 h. Structure and localization of iron in whole aleurone flour (C) and micromilled aleurone flour (D). Samples were treated with Perl's Prussian blue solution and observed under microscope. Iron staining in intact aleurone in wholegrain and aleurone flour and in diffuse particle globules in digested wholegrain and micromilled aleurone (arrows).

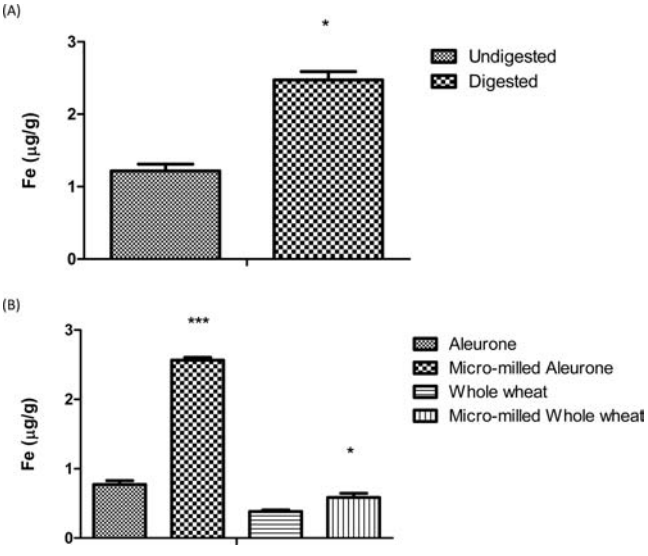


**Figure 4.** Iron solubility in whole grain wheat flour after digestion with Driselase (A). Iron solubility from standard and micromilled aleurone and whole grain wheat flour (B). Data are means ± SEM, $n$ = 4−6. Comparison of means was analyzed by Student's $t$ test. * $P < 0.0001$ (aleurone), and $P < 0.05$ (whole grain wheat).

contents from different segments of mouse (GI) tract and even from fecal samples revealed encapsulated iron in intact aleurone cells (Figure 2). This suggests that iron in aleurone cells is partly inaccessible even after transit throughout the entire length of the GI tract. It has been reported that plant cell walls are resistant to digestion in the upper GI tract of humans[28] with only 60% of the aleurone cell walls degraded in this region in the pig.[29] Colonic fermentation could lead to further

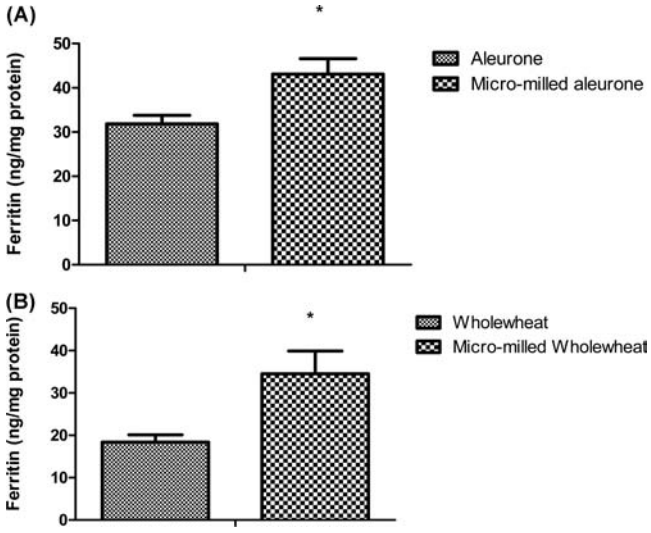


**Figure 5.** Iron bioaccessibility from standard and micromilled aleurone flour (A) and whole grain wheat flour (B) expressed in terms of Caco-2 cell ferritin synthesis. Data are means ± SEM, $n$ = 6. Comparison of means was analyzed using Student's $t$ test. * $P < 0.01$.

degradation of cell walls and the release of nutrients in the distal segment of the GI tract. A study using animal models demonstrated that 45% and 24% of aleurone was degraded during fermentation in the colon of rats and cockerels, respectively.[30] Moreover, partial degradation of the aleurone cell walls was evident in fecal samples from rats[31] fed wheat fractions. However, for iron at least, little or no absorption takes place in the colon.[32,33]

Clearly to be of use as a food fortificant the aleurone cell walls would need to be disrupted to provide increased access to the iron contained within. Our first approach was to use an enzymatic digest with Driselase. Following a 6 h digest with Driselase there was a significant increase in the release of soluble iron (Figure 4A). While this approach increases iron release from aleurone cells, its use would be limited to situations where predigested aleurone could be added as a food fortificant. We therefore also used a nonenzymatic approach by mechanically disrupting aleurone through micromilling. Micromilling of the AL was found to significantly increase iron solubility and bioaccessibility (Figures 4B and 5). The increase in bioaccessibility might be due to increased digestibility and degradability by grinding, which in ruminants increases the surface area of the samples for enhanced enzymatic digestion.[34] Furthermore, there is evidence that phytic acid, a resident component of the AL, is decreased during ball milling.[35] Phytic acid is a potent inhibitor of non-heme iron bioavailability.[13,36] It is possible that changes in phytate species and concentration as a result of micromilling may influence iron bioaccessibility from aleurone flour, and this is currently under investigation. Moreover, particle size reduction increased redistribution of cellulose-rich fiber fractions (another potent resident inhibitor of iron absorption) in favor of water-soluble fiber components as well as increased gastrointestinal function.[37]

An advantage of the mechanical approach to iron release from wheat aleurone is that the bioaccessibility of the endogenous aleurone iron reservoir could be increased through modified food processing technique. Potentially this could enhance the bioaccessibility of iron from wholegrain flour. Furthermore, micromilled aleurone could offer a natural, stable,

bioavailable iron fortificant or complement in foods. While our study has focused on iron, micromilled aleurone could potentially provide a bioavailable source of a number of other minerals (e.g., calcium) and vitamins (e.g., thiamine, nicotinic acid, and folate), all of which are commonly added as fortificants to white wheat flour.[38−40] Indeed, aleurone has been studied previously as a potential folate source for incorporation into bread. This approach would also be feasible for iron fortification. Published data already shows that wheat bread made with white flour enriched with 20% aleurone has a flavor similar to standard white bread and contains comparable levels of nutrients to wholegrain bread.[41] Subsequent studies will address the optimal particle size and relative proportions of micromilled aleurone enrichment required to achieve comparable or improved iron absorption efficacy to standard inorganic iron fortificants. This strategy might contribute to an improvement of the management of iron status in vulnerable groups in different countries. While our in vitro data support the notion that micromilled aleurone might be useful as an iron fortificant, it will be important to validate our findings in vivo by assessing the bioavailability of iron from aleurone-enriched wheat products in human volunteers, both in single-meal studies and also as part of more complex diets.

## AUTHOR INFORMATION


### Corresponding Author

*(G.O.L.-D.) Mail: Diabetes and Nutrtional Sciences Division, Faculty of Life Sciences and Medicine, King's College London, Franklin-Wilkins Building, 150 Stamford Street, London SE1 9NH, UK. Phone: +44(0)2078484256. Fax: +44(0) 2078484500. E-mail: yemisi.latunde-dada@kcl.ac.uk.


### Notes

The authors declare no competing financial interest.

## ACKNOWLEDGMENTS

C.H.E. was in receipt of a BBSRC CASE studentship award with Premier Foods (U.K.) as an industrial partner. We thank Walter von Redding (Bühler AG) for supplying the wheat samples used in this study.

## REFERENCES


(1) De Benoist, B.; McLean, E.; Egli, I.; Cogswell, M. *Worldwide Prevalence of 507 Anaemia. 18 1993−2005*; World Health Organization: Geneva, Switzerland, 2008; pp 508−512.

(2) Zimmermann, M. B.; Biebinger, R.; Egli, I.; Zeder, C.; Hurrell, R. F. Iron deficiency up-regulates iron absorption from ferrous sulphate but not ferric pyrophosphate and consequently food fortification with ferrous sulphate has relatively greater efficacy in iron-deficient individuals. *Br. J. Nutr.* **2011**, *105* (8), 1245−1250.

(3) Orozco, M. N.; Solomons, N. W.; Schumann, K.; Friel, J. K.; de Montenegro, A. L. Antioxidant-rich oral supplements attenuate the effects of oral iron on in situ oxidation susceptibility of human feces. *J. Nutr.* **2010**, *140* (6), 1105−1110.

(4) *National Diet and Nutrition Survey. Results from Years 1−4 (combined) of the Rolling Programme (2008/2009−2011/12)*; Bates, B., Lennox, A., Prentice, A., Bates, C. S., Pape, P., Nicholson, S., Swan, G., Eds.; Public Health England: London, U.K., May 2014; PHE publications gateway no. 2014051.

(5) Antoine, C.; Peyron, S.; Mabille, F.; Lapierre, C.; Bouchet, B.; Abecassis, J.; Rouau, X. Individual contribution of grain outer layers and their cell wall structure to the mechanical properties of wheat bran. *J. Agric. Food Chem.* **2003**, *51* (7), 2026−2033.

(6) Hurrell, R. F. Fortification: overcoming technical and practical barriers. *J. Nutr.* **2002**, *132* (4 Suppl), 806S−812S.

(7) Latunde-Dada, G. O. Biochemical determinants of food iron availability: soya fibre and iron interactions. *Biochem. Soc. Trans.* **1996**, *24* (3), 506S.

(8) Wu, B.; Andersch, F.; Weschke, W.; Weber, H.; Becker, J. S. Diverse accumulation and distribution of nutrient elements in developing wheat grain studied by laser ablation inductively coupled plasma mass spectrometry imaging. *Metallomics* **2013**, *5* (9), 1276−1284.

(9) Hilty, F. M.; Arnold, M.; Hilbe, M.; Teleki, A.; Knijnenburg, J. T.; Ehrensperger, F.; Hurrell, R. F.; Pratsinis, S. E.; Langhans, W.; Zimmermann, M. B. Iron from nanocompounds containing iron and zinc is highly bioavailable in rats without tissue accumulation. *Nat. Nanotechnol.* **2010**, *5* (5), 374−380.

(10) Swain, J. H.; Newman, S. M.; Hunt, J. R. Bioavailability of elemental iron powders to rats is less than bakery-grade ferrous sulfate and predicted by iron solubility and particle surface area. *J. Nutr.* **2003**, *133* (11), 3546−3552.

(11) Buttrose, M. S. Submicroscopic development and structure of starch granules in cereal endosperms. *J. Ultrastruct. Res.* **1960**, *4*, 231−257.

(12) Buttrose, M. S. Ultrastructure of barley aleurone cells as shown by freeze-etching. *Planta* **1971**, *96* (1), 13−26.

(13) Glahn, R. P.; Wortley, G. M.; South, P. K.; Miller, D. D. Inhibition of iron uptake by phytic acid, tannic acid, and ZnCl2: studies using an in vitro digestion/Caco-2 cell model. *J. Agric. Food Chem.* **2002**, *50* (2), 390−395.

(14) Sanz-Penella, J. M.; Laparra, J. M.; Sanz, Y.; Haros, M. Assessment of iron bioavailability in whole wheat bread by addition of phytase-producing bifidobacteria. *J. Agric. Food Chem.* **2012**, *60* (12), 3190−3195.

(15) Wang, Z.; Cuschieri, A. Tumour cell labelling by magnetic nanoparticles with determination of intracellular iron content and spatial distribution of the intracellular iron. *Int. J. Mol. Sci.* **2013**, *14* (5), 9111−9125.

(16) Zimmermann, M. B.; Winichagoon, P.; Gowachirapant, S.; Hess, S. Y.; Harrington, M.; Chavasit, V.; Lynch, S. R.; Hurrell, R. F. Comparison of the efficacy of wheat-based snacks fortified with ferrous sulfate, electrolytic iron, or hydrogen-reduced elemental iron: randomized, double-blind, controlled trial in Thai women. *Am. J. Clin. Nutr.* **2005**, *82* (6), 1276−1282.

(17) Gera, T.; Sachdev, H. S.; Boy, E. Effect of iron-fortified foods on hematologic and biological outcomes: systematic review of randomized controlled trials. *Am. J. Clin. Nutr.* **2012**, *96* (2), 309−324.

(18) Lund, E. K.; Wharf, S. G.; Fairweather-Tait, S. J.; Johnson, I. T. Increases in the concentrations of available iron in response to dietary iron supplementation are associated with changes in crypt cell proliferation in rat large intestine. *J. Nutr.* **1998**, *128* (2), 175−179.

(19) Lund, E. K.; Wharf, S. G.; Fairweather-Tait, S. J.; Johnson, I. T. Oral ferrous sulfate supplements increase the free radical-generating capacity of feces from healthy volunteers. *Am. J. Clin. Nutr.* **1999**, *69* (2), 250−255.

(20) Ali, N.; Paul, S.; Gayen, D.; Sarkar, S. N.; Datta, K.; Datta, S. K. Development of low phytate rice by RNAi mediated seed-specific silencing of inositol 1,3,4,5,6-pentakisphosphate 2-kinase gene (IPK1). *PLoS One* **2013**, *8* (7), e68161.

(21) Kanobe, M. N.; Rodermel, S. R.; Bailey, T.; Scott, M. P. Changes in endogenous gene transcript and protein levels in maize plants expressing the soybean ferritin transgene. *Front. Plant Sci.* **2013**, *4*, 196.

(22) Liu, Q. Q.; Yao, Q. H.; Wang, H. M.; Gu, M. H. [Endosperm-specific expression of the ferritin gene in transgenic rice (Oryza sativa L.) results in increased iron content of milling rice]. *Yichuan Xuebao* **2004**, *31* (5), 518−524.

(23) Ma, X. F.; Tudor, S.; Butler, T.; Ge, Y.; Xi, Y.; Bouton, J.; Harrison, M.; Wang, Z. Y. Transgenic expression of phytase and acid phosphatase genes in alfalfa (Medicagosativa) leads to improved phosphate uptake in natural soils. *Mol. Breed.* **2012**, *30* (1), 377−391.

(24) Holm, P. B.; Kristiansen, K. N.; Pedersen, H. B. Transgenic approaches in commonly consumed cereals to improve iron and zinc content and bioavailability. *J. Nutr.* **2002**, *132* (3), 514S−516S.
(25) Bodnar, A. L.; Proulx, A. K.; Scott, M. P.; Beavers, A.; Reddy, M. B. Iron bioavailability of maize hemoglobin in a Caco-2 cell culture model. *J. Agric. Food Chem.* **2013**, *61* (30), 7349−7356.
(26) Hebelstrup, K. H.; Shah, J. K.; Simpson, C.; Schjoerring, J. K.; Mandon, J.; Cristescu, S. M.; Harren, F. J.; Christiansen, M. W.; Mur, L. A.; Igamberdiev, A. U. An assessment of the biotechnological use of hemoglobin modulation in cereals. *Physiol. Plant.* **2014**, *150* (4), 593−603.
(27) Drakakaki, G.; Marcel, S.; Glahn, R. P.; Lund, E. K.; Pariagh, S.; Fischer, R.; Christou, P.; Stoger, E. Endosperm-specific co-expression of recombinant soybean ferritin and Aspergillus phytase in maize results in significant increases in the levels of bioavailable iron. *Plant Mol. Biol.* **2005**, *59* (6), 869−880.
(28) Flint, H. J.; Bayer, E. A.; Rincon, M. T.; Lamed, R.; White, B. A. Polysaccharide utilization by gut bacteria: potential for new insights from genomic analysis. *Nat. Rev. Microbiol.* **2008**, *6* (2), 121−131.
(29) Le, G. M.; Serena, A.; Jorgensen, H.; Theil, P. K.; Bach Knudsen, K. E. The role of whole-wheat grain and wheat and rye ingredients on the digestion and fermentation processes in the gut—a model experiment with pigs. *Br. J. Nutr.* **2009**, *102* (11), 1590−1600.
(30) Bach Knudsen, K. E.; Wolstrup, J.; Eggum, B. O. The nutritive value of botanically defined mill fractions of barley. 2. The influence of hind-gut microflora in rats on digestibility of protein and energy of endosperm and husk of Bomi and M-1508. *Z. Tierphysiol., Tierernaehr. Futtermittelkd.* **1982**, *48* (5), 276−287.
(31) Harris, P. J.; Chavan, R. R.; Ferguson, L. R. Production and characterisation of two wheat-bran fractions: an aleurone-rich and a pericarp-rich fraction. *Mol. Nutr. Food Res.* **2005**, *49* (6), 536−545.
(32) Johnston, K. L.; Johnson, D. M.; Marks, J.; Srai, S. K.; Debnam, E. S.; Sharp, P. A. Non-haem iron transport in the rat proximal colon. *Eur. J. Clin. Invest.* **2006**, *36* (1), 35−40.
(33) Takeuchi, K.; Bjarnason, I.; Laftah, A. H.; Latunde-Dada, G. O.; Simpson, R. J.; McKie, A. T. Expression of iron absorption genes in mouse large intestine. *Scand. J. Gastroenterol.* **2005**, *40* (2), 169−177.
(34) Fiems, L. O.; Cottyn, B. G.; Boucque, C. V.; Vanacker, J. M.; Buysse, F. X. Effect of grain processing on in sacco digestibility and degradability in the rumen. *Arch. Tierernaehr.* **1990**, *40* (8), 713−721.
(35) Cheryan, M. Phytic acid interactions in food systems. *Crit. Rev. Food Sci. Nutr.* **1980**, *13* (4), 297−335.
(36) Sharp, P. A. Intestinal iron absorption: regulation by dietary and systemic factors. *Int. J. Vitam. Nutr. Res.* **2010**, *80*, 231−242.
(37) Tovey, F. I.; Hobsley, M. Milling of wheat, maize and rice: effects on fibre and lipid content and health. *World J. Gastroenterol.* **2004**, *10* (12), 1695−1696.
(38) Fenech, M.; Noakes, M.; Clifton, P.; Topping, D. Aleurone flour is a rich source of bioavailable folate in humans. *J. Nutr.* **1999**, *129* (6), 1114−1119.
(39) Fenech, M.; Noakes, M.; Clifton, P.; Topping, D. Aleurone flour increases red-cell folate and lowers plasma homocyst(e)ine substantially in man. *Br. J. Nutr.* **2005**, *93* (3), 353−360.
(40) Zaupa, M.; Scazzina, F.; Dall'Asta, M.; Calani, L.; Del, R. D.; Bianchi, M. A.; Melegari, C.; De, A. P.; Tribuzio, G.; Pellegrini, N.; Brighenti, F. In vitro bioaccessibility of phenolics and vitamins from durum wheat aleurone fractions. *J. Agric. Food Chem.* **2014**, *62* (7), 1543−1549.
(41) Brouns, F.; Adam-Perrot, A.; Atwell, B.; Reding, W. V. Nutritional and technological aspects of wheat aleurone fiber: Implications for use in food. In *Dietary Fiber: New Frontiers for Food and Health*; van der Kamp, J. W. M., Jones, J., McCleary, B., Topping, D., Eds.; Wageningen Academic Publishers: Wageningen, The Netherlands, 2010; pp 395−413.

content, antioxidant activity, phenolic profile (HPLC-DAD-ESI-$MS^n$), and sensory acceptability.

## MATERIALS AND METHODS

Dry-blanched peanut skin (cv. Runner IAC 886) samples were kindly donated by CAP—Agroindustrial, Dumont, São Paulo, Brazil. White sugar, vanilla, wheat flour, baking powder, margarine, eggs, salt, brown sugar, oatmeal, sodium bicarbonate, and bittersweet chocolate were procured from a local market in São Paulo, Brazil. Folin—Ciocalteu's reagent, DPPH, ABTS, mono- and dibasic potassium phosphates, hydrogen peroxide, 5,5-dimethyl-1-pyrroline-*N*-oxide (DMPO), ferrous sulfate, protocatechuic acid, *p*-coumaric acid, (+)-catechin, and (−)-epicatechin were purchased from Sigma-Aldrich Canada (Oakville, ON, Canada). Sodium carbonate, sodium hydroxide, potassium persulfate, hexane, methanol, acetonitrile, formic acid, and sodium hydroxide were purchased from Fisher Scientific (Ottawa, ON, Canada).

**Cookie Making.** The cookie formulation was developed by our research group. Control and fortified formulations are shown in Table 1.

**Table 1. Formulation of Control and Fortified Cookies**

| ingredient | wet basis (%) | | | |
|---|---|---|---|---|
| white sugar | 8.96 | 8.84 | 8.80 | 8.73 |
| vanilla | 0.15 | 0.15 | 0.15 | 0.15 |
| wheat flour | 22.5 | 22.2 | 22.1 | 21.9 |
| baking powder | 0.15 | 0.15 | 0.15 | 0.15 |
| margarine | 8.96 | 8.84 | 8.80 | 8.73 |
| eggs | 6.41 | 6.33 | 6.29 | 6.25 |
| salt | 0.15 | 0.15 | 0.15 | 0.15 |
| brown sugar | 7.72 | 7.62 | 7.58 | 7.53 |
| oatmeal | 12.8 | 12.7 | 12.6 | 12.5 |
| sodium bicarbonate | 0.15 | 0.15 | 0.15 | 0.15 |
| bittersweet chocolate | 32.0 | 31.6 | 31.5 | 31.2 |
| peanut skins | | 1.30 | 1.80 | 2.50 |

The process was carried out in two steps. In a first bowl, margarine, brown sugar, and white sugar were homogenized in a mixer (Mondial, Barueri, SP, Brazil), which was followed by the addition of eggs and vanilla, a further mixing step for 5 min, and the addition of wheat flour. In a second bowl, oatmeal, salt, baking powder, and sodium bicarbonate were homogenized. Both mixtures were then blended with chocolate chips and fractionated in four parts to which different amounts of peanut skins (excluding control) were mixed. Each cookie weighed 32 g. Cookies were baked for 15 min at 280 °C using an Esmaltec oven (Esmaltec, Fortaleza, CE, Brazil). The samples were stored at room temperature (25 °C) until checked for their microbiological safety (within 2 days) followed by sensory analyses on the third day. The remaining samples (chemical analyses) were immediately frozen (−20 °C) for further analysis, within 1 month.

**Proximate Composition.** The ash, lipid, protein, and fiber contents of the sample were determined using AOAC[14] methods. Total carbohydrates were calculated by difference, and results are reported as percentage of the sample on a dry weight basis.

**Extraction of Phenolic Compounds.** Cookies were ground using a coffee bean grinder (model CBG5 series, Black & Decker Canada Inc., Brockville, ON, Canada), and the powder so obtained was passed through a mesh 16 (sieve opening 1 mm, Tyler test sieve, Mentor, OH, USA) sieve. The samples were defatted three times using hexane (solid/solvent, 1:5, w/v) in a Waring blender (model 33BL73, Waring Products Division Dynamics Co. of America, New Hartford, CT, USA). Defatted samples were immediately used for the extraction of phenolic compounds.

Defatted cookies were extracted with 70% acetone in a gyratory water bath shaker (model G76, New Brunswick Scientific Co. Inc., New Brunswick, NJ, USA) at 30 °C for 20 min, at a solid to solvent ratio of 2.5% (w/v). After centrifugation at 4000*g* (IEC Centra MP4, International Equipament Co., Needham Heights, MA, USA), the upper layer was collected and extraction was repeated twice. The combined supernatant was evaporated to remove the organic solvent in vacuo at 40 °C (Buchi, Flawil, Switzerland), and the residue containing soluble phenolics (free plus soluble esters) was stored at −20 °C until used for further analysis, within 1 month.

**Total Phenolic Contents (TPC).** TPC were evaluated using the Folin—Ciocalteu method[15] with minor modifications.[16] Phenolic extracts were diluted to 5 mg/mL, and the solution so obtained (0.5 mL) was mixed with distilled water (4.0 mL) and Folin—Ciocalteu reagent (2.5 mL). After 3 min, 1 mL of a saturated solution (30%, w/v) of $Na_2CO_3$ was added, and the mixture was kept in the dark at room temperature (23 °C) for 2 h. The absorbance was read at 760 nm using an Agilent UV—visible spectrophotometer (Agilent 8453, Agilent Technologies, Palo Alto, CA, USA). The results were expressed as milligram catechin equivalents (CE) per gram dry weight of cookies.

**DPPH Radical Scavenging Activity.** The DPPH assay was carried out using a slightly modified version of the method previously explained.[17,18] The phenolic extracts were diluted in methanol (20 mg/mL), and 1 mL of the solution so obtained was mixed with 250 $\mu$L of a methanolic solution of DPPH (0.5 mM). The mixture was kept in the dark at room temperature (23 °C) for 10 min, after which it was injected onto the capillary tubing that guides the sample through the sample cavity of a Bruker e-scan EPR spectrophotometer (Bruker E-Scan, Bruker Biospin Co., Billercia, MA, USA). The spectrum was recorded with the following parameters: $5.02 \times 10^2$ receiver gain, 1.93 G modulation amplitude, 2.62 s sweep time, 8 scans, 100.000 G sweep width, 3495.258 G center field, 5.12 ms time constant, 9.793220 GHz microwave frequency, and 86.00 kHz modulation frequency. The DPPH scavenging activity of the extracts was calculated using the equation

$$\text{DPPH scavenging activity (\%)} = [(\text{EPR}_{\text{control}} - \text{EPR}_{\text{sample}})/(\text{EPR}_{\text{control}})] \times 100$$

where $\text{EPR}_{\text{control}}$ is the signal intensity of DPPH radical + methanol and $\text{EPR}_{\text{sample}}$ is the signal intensity of DPPH radical + phenolic extract or catechin. The results were expressed as catechin equivalents per gram dry weight of cookies.

**ABTS Radical Cation Scavenging Activity.** The ABTS assay[19] was performed using a modified version of the method described by de Camargo et al.[16] The ABTS radical (7.00 mM) was generated in 100 mM phosphate buffer saline solution (PBS) (pH 7.4, 0.15 M sodium chloride) via potassium persulfate oxidation (2.45 mM). Prior to analysis, the stock solution of ABTS was diluted with PBS to reach an absorbance value of 0.70 (734 nm). Phenolic extracts were diluted in PBS (30 mg/mL), and 20 $\mu$L of the extract so obtained was added to 2 mL of the ABTS radical cation solution. The absorbance was read at 734 nm after 6 min using an Agilent UV—visible spectrophotometer (Agilent 8453). ABTS radical cation scavenging activity was calculated using the equation

$$\text{ABTS radical scavenging activity (\%)} = [(\text{Abs}_{\text{control}} - \text{Abs}_{\text{sample}})/(\text{Abs}_{\text{control}})] \times 100$$

where $\text{Abs}_{\text{control}}$ is the absorbance of the ABTS radical + PBS and $\text{Abs}_{\text{sample}}$ is the absorbance of ABTS radical cation + phenolic extract or trolox. The results were expressed as micromoles of trolox equivalent (TE) per gram dry weight of cookies.

**Hydrogen Peroxide Scavenging Activity.** The hydrogen peroxide scavenging activity of phenolic extracts was evaluated as previously explained.[20] Phenolic extracts (10 mg/mL) and 0.4 mM hydrogen peroxide solution were prepared in 0.1 M phosphate buffer (pH 7.4). The extracts (0.4 mL) were mixed with hydrogen peroxide solution (0.6 mL), and the final volume was made to 2.0 mL with the same buffer. The samples were kept in a gyrotory water bath shaker (model G76, New Brunswick Scientific Co. Inc.) for 40 min, and the absorbance was read at 230 nm in an Agilent UV—visible spectrophotometer (Agilent 8453). Blanks devoid of hydrogen peroxide (in phosphate buffer) were prepared for background corrections. The hydrogen peroxide scavenging activity was calculated using the equation

Table 2. Proximate Composition Cookies with Different Levels of Peanut Skins[a]

| component | control | 1.3% | 1.8% | 2.5% | peanut skins |
|---|---|---|---|---|---|
| ash | 1.78 ± 0.01b | 2.08 ± 0.09b | 1.89 ± 0.35b | 1.92 ± 0.06b | 2.89 ± 0.38a |
| lipid | 19.1 ± 1.28a | 21.3 ± 1.11a | 20.7 ± 1.26a | 21.6 ± 0.76a | 11.2 ± 0.31b |
| protein | 4.10 ± 0.05b | 4.21 ± 0.01b | 4.19 ± 0.11b | 4.30 ± 0.04b | 4.66 ± 0.04a |
| insoluble fiber | 6.40 ± 0.91c | 7.54 ± 0.04bc | 7.81 ± 0.88bc | 9.70 ± 0.96b | 76.6 ± 1.48a |
| soluble fiber | 2.17 ± 0.30b | 1.99 ± 0.03b | 2.43 ± 0.10b | 2.00 ± 0.33b | 4.11 ± 0.25a |
| carbohydrate | 66.3 | 63.3 | 63.2 | 60.0 | 0.31 |

[a]Data represent mean values for each sample ± standard deviation ($n = 3$). Means with the same letters within a row are not statistically ($p > 0.05$) different. Carbohydrates were calculated by difference. Results are expressed on a dry weight basis of cookies.

$$\text{hydrogen peroxide scavenging activity (\%)} = [(\text{Abs}_{\text{control}} - \text{Abs}_{\text{sample}})/(\text{Abs}_{\text{control}})] \times 100$$

where $\text{Abs}_{\text{control}}$ is the absorbance of $H_2O_2$ + phosphate buffer and $\text{Abs}_{\text{sample}}$ is the absorbance of $H_2O_2$ + phenolic extract or catechin. The results were expressed as catechin equivalents per gram dry weight of cookies.

**Reducing Power.** The reducing power assay was performed according to a method described by Alasalvar et al.[21] The extracts (6 mg/mL) were prepared in phosphate buffer (pH 6.6, 0.2 mM). Extracts (1.0 mL) were then mixed with phosphate buffer (2.5 mL) and 1% (w/v) potassium ferricyanide solution (2.5 mL), followed by their incubation at 50 °C for 20 min in a gyrotory water bath shaker (model G76, New Brunswick Scientific Co. Inc.), and subsequently a 10% (w/v) solution of trichloroacetic acid (2.5 mL) was added to it. The mixture was centrifuged at 1750*g* for 10 min, and the supernatant (2.5 mL) was added to distilled water (2.5 mL) and 0.1% (w/v) ferric chloride solution (0.5 mL). The absorbance was read at 700 nm, as before. The results were expressed as micromoles of trolox equivalents per gram dry weight of cookies.

**Hydroxyl Radical Scavenging Activity.** The ability of phenolic compounds in scavenging hydroxyl radicals generated by Fenton reaction was evaluated by electron paramagnetic resonance (EPR) spectroscopy using a slightly modified version of a method previously reported.[20] Extracts were prepared in 0.1 M phosphate buffer (pH 7.4). A 0.2 mL portion of the solution so obtained was mixed with 0.2 mL of $H_2O_2$ (10 mM), 0.4 mL of 17.6 mM DMPO, and 0.2 mL of $FeSO_4$ (10 mM). After 3 min, the EPR spectrum was recorded using a Bruker e-scan EPR spectrophotometer (Bruker E-Scan, Bruker Biospin Co.) The spectrum was recorded with the same parameters as for DPPH. The hydroxyl radical scavenging activity of the extracts was calculated using the equation

$$\text{hydroxyl radical scavenging activity (\%)} = [(\text{EPR}_{\text{control}} - \text{EPR}_{\text{sample}})/(\text{EPR}_{\text{control}})] \times 100$$

where $\text{EPR}_{\text{control}}$ is the signal intensity of hydroxyl radical + phosphate buffer and $\text{EPR}_{\text{sample}}$ is the signal intensity of hydroxyl radical + phenolic extract or catechin. The results were expressed as micromoles of catechin equivalents per gram dry weight of cookies.

**HPLC-DAD-ESI- $MS^n$ Analysis.** The identification of the major soluble phenolics (free plus soluble esters) was performed using an Agilent 1100 system (Agilent) equipped with a G1311A quaternary pump, a G1379A degasser, a G1329A ALS automatic sampler, a G1130B ALS Therm, a G1316 Colcom column compartment, a G1315B diode array detector, and a system controller linked to Chem Station Data handling system (Agilent). Separations were performed with a SUPELCOSIL LC-18 column (4.6 × 250 mm × 5 μm, Merck, Darmstadt, Germany). The binary mobile phase consisted of 0.1% formic acid (A) and 0.1% formic acid in acetonitrile (B). The flow rate of mobile phase was 0.5 mL/min, and the elution gradient used was as follows: 0 min, 100% A; 5 min, 90% A; 35 min, 85% A; 45 min, 60% A; held at 60% A from 45 to 50 min; afterward, mobile phase A was increased to 100% at 55 min, followed by column equilibration from 55 to 65 min. The compounds were detected at 280 nm, and the samples were filtered before injection using a 0.45 μm PTFE membrane syringe filter (Thermo Scientific, Rockwood, TN, USA).

HPLC-ESI-$MS^n$ analysis was carried out using the same conditions as described above in an Agilent 1100 series capillary liquid chromatography−mass selective detector (LC-MSD) ion trap system in electrospray ionization (ESI) in the negative mode. The data were acquired and analyzed with Agilent LC-MSD software (Agilent). The scan range was from $m/z$ 50 to 1200, using smart parameter setting, drying nitrogen gas at 350 °C, flow 12 L/min, and nebulizer gas pressure of 70 psi. Protocatechuic acid, (+)-catechin, and (−)-epicatechin were identified by comparing their retention times and ion fragmentation with coded and authentic standard and the same conditions as the samples. Dimers, trimers, and tetramers of proanthocyanidins were tentatively identified using tandem mass spectrometry ($MS^n$), UV spectral, and literature data.[8]

**Sensory Evaluation.** The present study was approved by the ethics committee of "Luiz de Queiroz" College of Agriculture, University of São Paulo, Brazil. Sensory analyses were performed using the acceptability test. Sixty volunteers, students and employees, from "Luiz de Queiroz" College of Agriculture (ESALQ/USP), aged between 18 and 60 years, participated in the acceptability test. The panel was composed by 72% women, with no history of allergy to peanuts or other ingredients of the formulation. Samples were placed in white ceramic plates coded with three-digit random numbers and delivered to the panel. The members received a set of four samples (control and cookies with added 1.3, 1.8, and 2.5% peanut skins) and water (25 °C). Participants were requested to rinse their mouths between each sample and evaluate color, odor, taste, texture, and overall impression. Scores were recorded on a paper ballot using a five-point hedonic scale (5 = extremely like, 4 = like, 3 = neither like nor dislike, 2 = dislike, and 1 = extremely dislike). Acceptable scores were ≥3 points.

**Statistical Analysis.** Unless stated otherwise, the experimental design was randomized with three replications, and the results were analyzed using Tukey's test ($p < 0.05$) and SAS software.

## RESULTS AND DISCUSSION

**Proximate Composition.** A cookie formulation (Table 1) was developed by a gastronomy professional from our research group for different addition levels of peanut skins. Such concentrations were decided on the basis of the saturation point, at which an increase in peanut skin concentration would result in a loss of pasting properties. Chocolate flavor was chosen to avoid or mask potential bitterness and astringent mouthfeel due to the presence of peanut skins, which was reported by the sensory panel in a first formulation developed (data not shown).

The proximate composition of the cookies and peanut skins, reported on a dry weight basis, is summarized in Table 2. The moisture content is shown in Figure 1. Industrial and homemade cookies have several differences, and one of them is the moisture content. Homemade cookies tend to be softer, mainly because of the moisture content and freshness. In the present study, the addition of peanut skins increased the moisture retention of cookies in a concentration-dependent manner upon addition of up to 1.8% peanut skins, from which no difference was found,

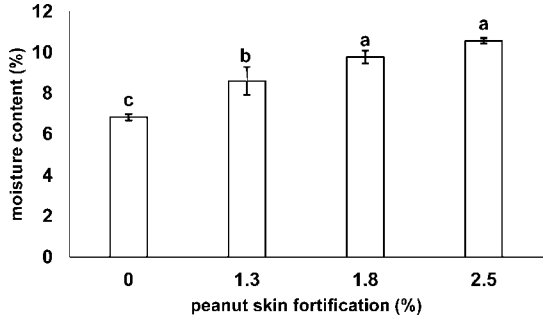


**Figure 1.** Moisture content of cookies fortified with peanut skins. Data represent the mean ± standard deviation of each sample ($n = 3$). Means with different letters indicate significant differences ($p < 0.05$).

suggesting that the saturation point for moisture retention was achieved.

The addition of 2.5% peanut skins resulted in a 50% increase of insoluble fiber content. These data are supported by the high content of insoluble fiber in peanut skins. Dietary fiber intake has been recognized for the reduction of cardiovascular disease risk and colorectal cancer,[22,23] management of diabetes, and body weight gain.[24,25] The insoluble fiber increase is in good agreement with a previous study reporting the use of peanut skins to fortify peanut butter.[9] A negative correlation existed between the addition of peanut skins and the carbohydrate content ($r = -0.9663$); a 10% reduction in total carbohydrates was noted. According to a randomized intervention study,[26] a low-carbohydrate Mediterranean diet improved cardiovascular disease risk factors and diabetes control in overweight patients with type 2 diabetes mellitus. In the present study, the addition of peanut skins to cookies increased the content of insoluble fiber and moisture retention and decreased the total carbohydrate content.

**Total Phenolic Content.** Phenolic compounds are secondary metabolites found in nuts, vegetables, cereals, legumes, and certain vegetable oils as well as in alcoholic and nonalcoholic beverages.[17,27−31] The TPC of peanut skins used in the present study as well as their contribution to the TPC of whole peanuts has already been reported.[16,32] Although their contribution as a weight percentage of peanuts was very low, around 2.6%,[33] the same does not apply for their contribution to the TPC in whole peanuts as their removal during the blanching process induced a reduction of 45% in TPC.[32]

Most peanuts for industrial purposes, such as production of candies, chocolates, and stuffing, are subjected to a blanching process that removes their skins, and these become a byproduct. In the current study, cookies were fortified with peanut skins, and their contribution to the TPC is summarized in Table 3. Food ingredients such as wheat flour, oatmeal, and chocolate, which have been used in the present study, also have polyphenols;[34−36] however, they have a different qualitative and quantitative polyphenol composition when compared to peanut skins. The addition of 2.5% peanut skins to cookies increased the TPC of the product by almost 50%. Although no recommended daily intake has been established for polyphenols, the extensive literature available lends support for the consumption of dietary sources of polyphenols.

**DPPH Radical Scavenging Activity Using Electron Paramagnetic Resonance (EPR).** The radical scavenging activity results are given in Table 3 and Figure 2A, showing a decrease of the EPR signal. Although TPC displayed an increase of around 50%, DPPH radical scavenging activity increased by up to 250% upon addition of peanut skins. The increase of both TPC and DPPH scavenging activity demonstrates the potential enhancement of beneficial health effect of the product due to increase in the content of bioactives present. Furthermore, the data suggest that the heating process did not have any detrimental effect on either TPC or scavenging activity. In fact, the phenolic content and antioxidant activity of food products may be increased upon heating.[18]

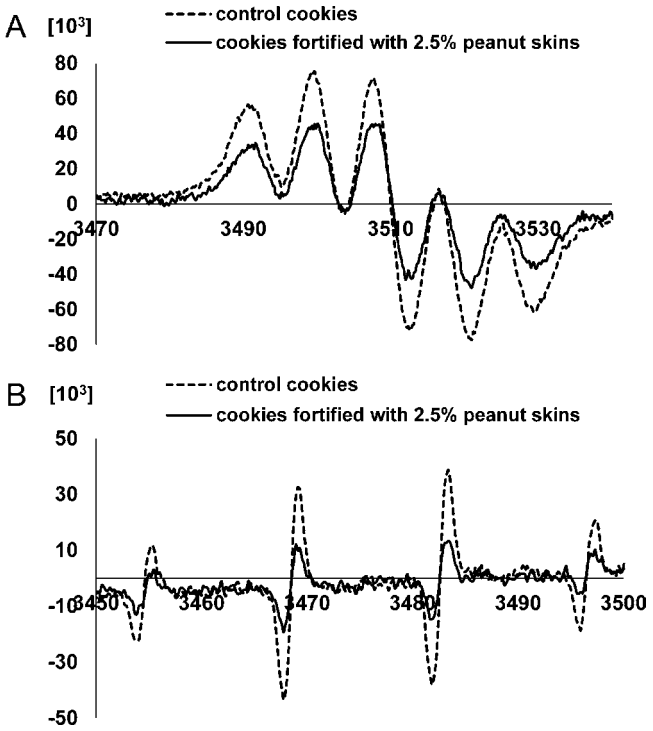


**Figure 2.** Electron paramagnetic resonance signals of phenolics of control cookies and cookies fortified with 2.5% peanut skins as evaluated by DPPH (A) and DMPO-OH (B) assays.

**Table 3. Total Phenolic Content (TPC), Antioxidant Activity, and Reducing Power (RP) of Cookies Fortified with Peanut Skins[a]**

| addition level (%) | TPC (mg CE/g) | DPPH (μmol CE/g) | ABTS (μmol TE/g) | $H_2O_2$ (μmol CE/g) | RP (μmol TE/g) | HRSA (μmol CE/g) |
|---|---|---|---|---|---|---|
| control, 0 | 61.2 ± 3.1d | 1028 ± 119d | 1119 ± 81.0c | 372.0 ± 14.3d | 57.14 ± 5.34d | 563 ± 46c |
| 1.3 | 68.5 ± 1.2c | 1715 ± 13.2c | 1769 ± 40.3b | 520.6 ± 19.8c | 97.18 ± 7.59c | 657 ± 6.7b |
| 1.8 | 78.5 ± 2.8b | 2437 ± 190b | 1986 ± 229b | 692.3 ± 12.3b | 113.3 ± 5.23b | 706 ± 2.9ab |
| 2.5 | 91.4 ± 2.0a | 3607 ± 169a | 2579 ± 176a | 997.5 ± 22.4a | 134.9 ± 3.25a | 766 ± 6.8a |

[a]Data represent mean values for each sample ± standard deviation ($n = 3$). Means followed by the same letters within a column are not significantly ($p > 0.05$) different. CE, catechin equivalents; TE, trolox equivalents. HRSA, hydroxyl radical scavenging activity. Results are expressed on a dry weight basis of cookies.


dx.doi.org/10.1021/jf503625p | J. Agric. Food Chem. 2014, 62, 11228−11235

Table 4. Content of Soluble Polyphenols (Micrograms per Gram Dry Weight) of Cookies Fortified with Peanut Skins[a,b]

| compound | addition level | | | |
|---|---|---|---|---|
| phenolic compounds | control, 0% | 1.3% | 1.8% | 2.5% |
| protocatechuic acid[c] | 56.94 ± 2.03a | 55.96 ± 0.83a | 56.61 ± 0.25a | 58.14 ± 1.69a |
| (+)-catechin[c] | 219.2 ± 3.78a | 219.2 ± 8.90a | 220.1 ± 16.8a | 241.7 ± 13.3a |
| (−)-epicatechin[c] | 340.3 ± 19.4b | 355.6 ± 11.1ab | 385.1 ± 4.78ab | 426.0 ± 58.4a |
| procyanidin dimer A[d] | 118.5 ± 2.05b | 131.8 ± 2.23a | 129.6 ± 2.56a | 132.7 ± 2.43a |
| procyanidin dimer B[d] | 2708 ± 64.4bc | 2688 ± 35.0c | 2826 ± 33.2ab | 2859 ± 68.0a |
| procyanidin trimer A[d] | nd | 108.3 ± 1.33c | 318.9 ± 6.36b | 601.4 ± 22.7a |
| procyanidin tetramer A[d] | nd | 42.48 ± 0.44c | 55.97 ± 4.94b | 173.0 ± 4.98a |
| total | 3443 | 3601 | 3992 | 4492 |

[a]Data represent mean values for each sample ± standard deviation ($n = 3$). Means followed by the same letters within a row are not significantly ($p > 0.05$) different. [b]The contents (μg/g) of soluble phenolics in the original peanut skins were 118.9 ± 1.09 (protocatechuic acid); 1211 ± 49.0 ((+)-catechin); 450.7 ± 15.5 ((−)-epicatechin); 3623 ± 60.1 (procyanidin dimer A); 1477 ± 27.5 (procyanidin dimer B); 6494 ± 296 (procyanidin trimer A); 827.6 ± 51.7 (procyanidin tetramer A). [c]Identified with authentic standards. [d]Values are given as catechin equivalents.

**ABTS Radical Cation Scavenging Activity.** The antioxidant evaluation carried out using the ABTS method demonstrated the same trend as that from the DPPH assay (Table 3). The total antioxidant activity, which comprises hydrophilic and lipophilic antioxidants, was increased from 1119 to 2579 μmol TE/g. As demonstrated by the proximate composition, peanut skins still have a lipid content of 11%. Tocopherol, which is found in the lipid fraction of peanuts,[37] renders antioxidant properties. However, in the present study, the samples were defatted prior to the analysis for phenolics and antioxidant activity; thus, tocopherol is not affecting the assay results. According to Francisco and Resurreccion,[10] infusions prepared with Runner type peanut skins had the highest antioxidant activity as evaluated by the ABTS assay when compared to other preparations using Virginia or Spanish cultivars. It is interesting to note that peanut skins have been reported to possess a higher antioxidant activity than green tea.[38]

**Hydrogen Peroxide Scavenging Activity.** Hydrogen peroxide in the presence of ferrous ion generates hydroxyl radicals via Fenton's reaction, which makes the hydrogen peroxide scavenging assay a biologically relevant one. Hydroxyl radicals are highly reactive, leading to changes in DNA[39] and inactivating enzymes.[40] Furthermore, hydrogen peroxide induces cell damage.[41] Data from the present study (Table 3) demonstrated that control cookies already had scavenging activity against hydrogen peroxide, which, as mentioned before, is due to the presence of antioxidant compounds from its ingredients such as wheat flour, oatmeal, and chocolate. Furthermore, the baking process generates Maillard reaction products; these are produced in the presence of reducing sugars and amino acids. Such compounds also have antioxidant properties and may influence the evaluation. However, there was a clear concentration-dependent increase in the ability of phenolic groups in scavenging hydrogen peroxide, which was significant upon addition of peanut skins at 1.3, 1.8, and 2.5%.

**Reducing Power.** The reducing power measures the ability of phenolic compounds to reduce ferric to ferrous ion. As already mentioned, ferrous ions participate in Fenton's reaction, as well as in the oxidation of proteins and lipids. Phenolic compounds demonstrated the ability to scavenge hydrogen peroxide to different extents. Thus, evaluating the ability of phenolic compounds in preventing oxidative damages through other mechanisms provides useful information to anticipate additional protective effects of the bioactive compounds.

The reducing power of cookies fortified with 2.5% peanut skins rose by 136% (Table 3). The reducing power has been correlated with the degree of hydroxylation and conjugation in the phenolic compounds.[42] Peanut skins have a high content of proanthocyanidins, which possess several hydroxyl groups; this may explain the increase in reducing power despite the low addition level of peanut skins. The addition of 2.5% peanut skins in peanut butter[9] induced an increase of 747% in reducing power as evaluated by ferric reducing antioxidant power assay (FRAP); however, a direct comparison with the present study is not possible due to the different starting material (peanut butter) and method used by these authors. Whereas the FRAP assay is evaluated in acidic medium (pH 3.6), the method applied in the present study was carried out at pH 6.6. In fact, the antioxidant/reducing power of phenolic compounds has been demonstrated to be dependent on the pH of the medium.[43]

**Hydroxyl Radical Scavenging Activity.** Reactive oxygen species (ROS) are involved in several pathologies and the aging process; among them, hydroxyl radicals are of special concern and, although short-lived, they play an important role in the development of chronic diseases. They can be produced by Fenton's reaction in the presence of ferrous ions, via decomposition of hydroperoxides, which are intermediate in lipid oxidation process, and UV light. In the present study, the Fenton's reaction was carried out to produce hydroxyl radicals, and DMPO was used in the reaction medium as a spin trap to enable the study of scavenging activity of phenolics as evaluated by EPR.

The addition of peanut skins increased the hydroxyl scavenging activity of cookies (Table 3), which can also be seen by the decrease in the intensity of the EPR signals (Figure 2B). As monomeric flavonoids and proanthocyanidins are the major phenolic compounds in peanut skins, the results were expressed as catechin equivalents. No difference was found between 1.8 and 2.5% addition levels; however, in other experiments, a significant difference was observed, which suggests that the addition of 2.5% would provide more potential health benefits to consumers.

The control cookies and those fortified with 2.5% peanut skins had scavenging activities in the range of 563 and 766 μmol CE/g, respectively. Peanut butter fortified with peanut skins also exhibited higher ORAC values. According to Ma et al.,[9] peanut butter fortified with dry-blanched peanut skins was more effective in neutralizing peroxyl radicals than that fortified with roasted peanut skins. Another study[11] reported similar results

**Table 5. Sensory Acceptability of Cookies Fortified with Peanut Skins**[a]

| addition level (%) | color | odor | taste | texture | overall impression |
|---|---|---|---|---|---|
| control, 0 | 3.7 ± 1.0a | 3.9 ± 0.9a | 4.1 ± 1.0a | 3.9 ± 1.1a | 4.0 ± 1.1a |
| 1.3 | 4.1 ± 0.8a | 4.0 ± 0.9a | 4.2 ± 1.0a | 3.9 ± 1.0a | 4.1 ± 0.8a |
| 1.8 | 3.9 ± 0.7a | 4.0 ± 0.9a | 4.1 ± 0.8a | 4.0 ± 0.9a | 4.2 ± 1.0a |
| 2.5 | 4.2 ± 0.8a | 3.9 ± 1.0a | 3.9 ± 1.1a | 3.6 ± 1.0a | 3.9 ± 1.0a |

[a]Data represent the mean scores for each sample ± standard deviation ($n$ = 60); means with the same letters within a row are not significantly ($p$ > 0.05) different from each other; 5 = extremely liked, 4 = liked, 3 = neither liked nor disliked, 2 = disliked, and 1 = extremely disliked). Acceptable scores were ≥3 points.

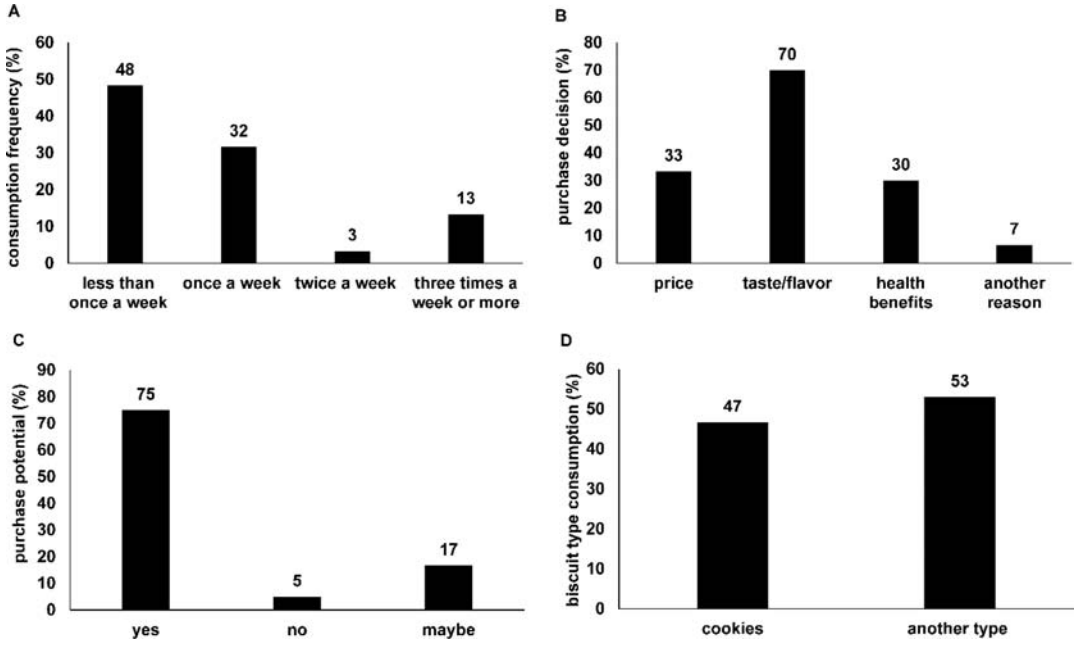


**Figure 3.** Complementary information collected during sensory evaluation of cookies fortified with peanut skins: (A) how often do you consume cookies? (B) what influences your cookie purchase decision? (C) would you increase your cookie consumption in the case of having additional health benefits?; (D) which kind of cookie do you consume more often?

using the ORAC assay for peanut butter and peanut paste with added peanut skins. The present study demonstrated increases in the antioxidant activity of cookies in the range of 36−251%, depending on the assay, and all results were statistically significant ($p$ < 0.05), which suggests that cookies with added peanut skins have potential health benefits, yet to be fully substantiated and exploited.

**HPLC-DAD-ESI-MS$^n$ Analysis.** The data presented so far have evidenced improvement in the potential health benefits of cookies fortified with peanut skins. Peanut skins have several phenolic compounds, namely, phenolic acids, stilbenes, monomeric flavonoids, and dimeric to oligomeric proanthocyanidins. However, in the present study the major phenolic compounds were evaluated as biomarkers to explain the potential functionality of cookies with added peanut skins (Table 4).

Here, we also focused only on the soluble phenolic as they accounted for >90% of total phenolic compounds in peanut skins (data not shown). Protocatechuic acid was positively identified by comparison of its retention time and fragmentation pattern with those of authentic standard. The MS and MS$^2$ spectra of protocatechuic acid gave ions at $m/z$ 153 and 109, respectively. The deprotonated molecular ion $[M - H]^-$ of both (+)-catechin and (−)-epicatechin exhibited an $m/z$ signal at 289 and MS$^2$ spectra at $m/z$ 245, and their identities were confirmed according to their different retention times by comparison with those of authentic standards. In accordance with the literature,[17,28] protocatechuic acid, (+)-catechin, and (−)-epicatechin showed loss of $CO_2$, giving $[M - H - 44]^-$ as their characteristic ion in MS$^2$. The major procyanidins, which consist exclusively of (epi)catechin units, were tentatively identified according to the literature.[8,44] Procyanidin dimer A showed a deprotonated molecular ion at $m/z$ 575 and at $m/z$ 449, 423, 407, 289, and 285 in MS$^2$. Procyanidin dimer B exhibited an $m/z$ at 577 and in MS$^2$ at $m/z$ 451, 425, 407, 289, and 287. The MS fragmentation of procyanidin trimer A gave deprotonated ion at $m/z$ 863 and at $m/z$ 737, 711, 693, 575, 559, and 449 in MS$^2$. Procyanidin tetramer A showed an $m/z$ signal at 1149 in MS and at $m/z$ 861, 737, and 575 in MS$^2$. The mass spectra of the most representative compound tentatively identified as procyanidin dimer B is provided as Supporting Information. Prodelphinidins, which have (epi)gallocatechin in their structures, were also present in peanut skins; however, their concentration was very low and had no effect on their concentration in cookies fortified with peanut skins.

Protocatechuic acid and (+)-catechin did not show any significant increase ($p$ > 0.05). Protocatechuic acid and (+)-catechin were present at less than 1 and 2% in the free nonconjugated phenolic fraction of peanut skins in the present study (data not shown), which may explain the lack of increase for such compounds in cookies fortified with peanut skins. On the other hand, the content of (−)-epicatechin increased upon

addition of peanut skins, and a small, but significant, increase was found for procyanidin dimers A and B.

The formulation used in the present study included a high proportion of chocolate, which also has a high content of (−)-epicatechin and procyanidins;[36] this may explain why the threshold for the increase of (−)-epicatechin and procyanidins B was achieved only with 2.5 and 1.8%, respectively, in comparison with the control. However, procyanidin dimer A, which is the major one in peanut skins, also increased with the lowest addition (1.3%). Furthermore, procyanidin trimers and tetramers were not found in the control sample, but were gradually increased with increasing addition levels of peanut skins.

The addition of peanut skins to cookies rendered an increase of up to 30% in major phenolics as evaluated by HPLC-DAD-ESI-MS$^n$. Data from the present study demonstrated that proanthocyanidins accounted for the highest increase in phenolics of cookies fortified with peanut skins. The degree of polymerization of proanthocyanidins has an effect on their absorption. According to Ou and Gu,[45] proanthocyanidins with a degree of polymerization of <5 are absorbable, which lends support to the potential health benefits of the product formulated in this study.

**Sensory Evaluation.** To ensure the safety of cookies prepared here, coagulase-positive *Staphylococcus aureus*, yeasts and molds, *Salmonella* spp., total coliform, *Escherichia coli*, and aflatoxins were investigated (data not shown). The heating process and storage may influence the color of polyphenol-rich source material, which has been demonstrated by sensory evaluation. An unexpected food color may be the first attribute related to consumers' rejection. The peanut skins used in the present study were a byproduct of the dry blanching process, which involved heating at 70−90 °C for 2 h. This process and long-term storage may have some influence on the color of the skins. Furthermore, the peanut skin color might change the final color of the peanut skins fortified cookie. However, the present study revealed no humanly perceptible changes in the final product (Table 5). The color of dry-blanched peanut skins (cv. Runner IAC 886) is light brown. The combination of this color, low peanut skin concentration, and the chocolate flavor of the cookie produced here may be the reason for imperceptible color changes. Furthermore, no change in the remaining sensory attributes were found among samples (Table 5), all of which received scores ≥3, which was considered acceptable. Figure 3 shows additional results collected during the sensory evaluation. Results from the consumption frequency demonstrate a potential to be exploited for increasing cookie consumption by 48% as noted by the volunteers that consumed cookies only once a week or less. Taste/flavor is a factor that mainly influences their purchase decision (70%). This demonstrates the importance of sensory evaluation in the development of new products. According to their responses, a cookie with higher health benefit would have a positive impact on their future purchase decision. Additionally, 47% of the panel mentioned cookies as the most consumed kind of biscuits, which demonstrates their preference for this kind of biscuit in comparison with others available on the market.

In summary, physical and chemical properties of cookies were influenced by the addition of peanut skins. Carbohydrate content decreased, whereas the contents of insoluble fiber, moisture, total polyphenol, and antioxidant activity increased. Protocatechuic acid and (+)-catechin were identified and quantified, but only the contents of (−)-epicatechin and procyanidin dimers A and B increased. Procyanidin trimers and tetramers, which were not found in the control samples, were also increased. Sensory evaluation demonstrated no significant difference among the control and the remaining samples; thus, cookies fortified with peanut skins offer promise for possible commercialization.

## ■ ASSOCIATED CONTENT

### Ⓢ Supporting Information

Figure S1. This material is available free of charge via the Internet at http://pubs.acs.org.

## ■ AUTHOR INFORMATION

### Corresponding Author

*(F.S.) E-mail: fshahidi@gmail.com or fshahidi@mun.ca.

### Funding

A.D.C. acknowledges CNPq (National Council for Scientific and Technological Development − Brazil) for granting an international Ph.D. internship through the Science without Borders program (Process 242589/2012-0). This research was also supported by the doctoral scholarship granted by FAPESP (São Paulo Research Foundation) to the first author in Brazil (Process 2012/17683-0). F.S. thanks the Natural Science and Engineering Research Council (NSERC) of Canada for partial financial support in the form of a Discovery Grant.

### Notes

The authors declare no competing financial interest.

## ■ REFERENCES

(1) Sarnoski, P. J.; Boyer, R. R.; O'Keefe, S. F. Application of proanthocyanidins from peanut skins as a natural yeast inhibitory agent. *J. Food Sci.* **2012**, *77*, M242−M249.

(2) Lewis, W. E.; Harris, G. K.; Sanders, T. H.; White, B. L.; Dean, L. L. Antioxidant and anti-inflammatory effects of peanut skin extracts. *Food Nutr. Sci.* **2013**, *4*, 22−32.

(3) Rossi, M.; Negri, E.; Parpinel, M.; Lagiou, P.; Bosetti, C.; Talamini, R.; Montella, M.; Giacosa, A.; Franceschi, S.; La Vecchia, C. Proanthocyanidins and the risk of colorectal cancer in Italy. *Cancer Causes Control* **2010**, *21*, 243−250.

(4) Chandrasekara, N.; Shahidi, F. Antioxidative potential of cashew phenolics in food and biological model systems as affected by roasting. *Food Chem.* **2011**, *129*, 1388−1396.

(5) Phan-Thien, K.-Y.; Wright, G. C.; Lee, N. A. Peanut antioxidants: part 2. Quantitation of free and matrix-bound phytochemicals in five selected genotypes with diverse antioxidant capacity by high performance liquid chromatography (HPLC). *LWT−Food Sci. Technol.* **2014**, *57*, 312−319.

(6) Monagas, M.; Garrido, I.; Lebron-Aguilar, R.; Gomez-Cordoves, M.; Rybarczyk, A.; Amarowicz, R.; Bartolome, B. Comparative flavan-3-ol profile and antioxidant capacity of roasted peanut, hazelnut, and almond skins. *J. Agric. Food Chem.* **2009**, *57*, 10590−10599.

(7) Francisco, M. L. D.; Resurreccion, A. V. A. Development of a reversed-phase high performance liquid chromatography (RP-HPLC) procedure for the simultaneous determination of phenolic compounds in peanut skin extracts. *Food Chem.* **2009**, *117*, 356−363.

(8) Sarnoski, P. J.; Johnson, J. V.; Reed, K. A.; Tanko, J. M.; O'Keefe, S. F. Separation and characterisation of proanthocyanidins in Virginia type peanut skins by LC-MS$^n$. *Food Chem.* **2012**, *131*, 927−939.

(9) Ma, Y. Y.; Kerr, W. L.; Swanson, R. B.; Hargrove, J. L.; Pegg, R. B. Peanut skins-fortified peanut butters: Effect of processing on the phenolics content, fibre content and antioxidant activity. *Food Chem.* **2014**, *145*, 883−891.

(10) Francisco, M. L. D.; Resurreccion, A. V. A. Antioxidant capacity and sensory profiles of peanut skin infusions. *LWT−Food Sci. Technol.* **2012**, *47*, 189−198.

(11) Hathorn, C. S.; Sanders, T. H. Flavor and antioxidant capacity of peanut paste and peanut butter supplemented with peanut skins. *J. Food Sci.* **2012**, *77*, S407−S411.

(12) Sharma, P.; Gujral, H. S. Cookie making behavior of wheat−barley flour blends and effects on antioxidant properties. *LWT−Food Sci. Technol.* **2014**, *55*, 301−307.
(13) Bilgiçli, N.; İbanoğlu, Ş.; Herken, E. N. Effect of dietary fibre addition on the selected nutritional properties of cookies. *J. Food Eng.* **2007**, *78*, 86−89.
(14) AOAC. *Official Methods of Analysis of AOAC International*, 18th ed.; AOAC International: Gaithersburg, MD, USA, 2006.
(15) Swain, T.; Hillis, W. E. The phenolic constituents of *Prunus domestica*. I.—The quantitative analysis of phenolic constituents. *J. Sci. Food Agric.* **1959**, *10*, 63−68.
(16) de Camargo, A.; Vieira, T.; Regitano-D'Arce, M.; Calori-Domingues, M.; Canniatti-Brazaca, S. Gamma radiation effects on peanut skin antioxidants. *Int. J. Mol. Sci.* **2012**, *13*, 3073−3084.
(17) John, J. A.; Shahidi, F. Phenolic compounds and antioxidant activity of Brazil nut (*Bertholletia excelsa*). *J. Funct. Foods* **2010**, *2*, 196−209.
(18) Chandrasekara, N.; Shahidi, F. Effect of roasting on phenolic content and antioxidant activities of whole cashew nuts, kernels, and testa. *J. Agric. Food Chem.* **2011**, *59*, 5006−5014.
(19) Re, R.; Pellegrini, N.; Proteggente, A.; Pannala, A.; Yang, M.; Rice-Evans, C. Antioxidant activity applying an improved ABTS radical cation decolorization assay. *Free Radical Biol. Med.* **1999**, *26*, 1231−1237.
(20) Wettasinghe, M.; Shahidi, F. Scavenging of reactive-oxygen species and DPPH free radicals by extracts of borage and evening primrose meals. *Food Chem.* **2000**, *70*, 17−26.
(21) Alasalvar, C.; Karamac, M.; Kosinska, A.; Rybarczyk, A.; Shahidi, F.; Amarowicz, R. Antioxidant activity of hazelnut skin phenolics. *J. Agric. Food Chem.* **2009**, *57*, 4645−4650.
(22) Bingham, S. A.; Day, N. E.; Luben, R.; Ferrari, P.; Slimani, N.; Norat, T.; Clavel-Chapelon, F.; Kesse, E.; Nieters, A.; Boeing, H.; Tjonneland, A.; Overvad, K.; Martinez, C.; Dorronsoro, M.; Gonzalez, C. A.; Key, T. J.; Trichopoulou, A.; Naska, A.; Vineis, P.; Tumino, R.; Krogh, V.; Bueno-de-Mesquita, H. B.; Peeters, P. H. M.; Berglund, G.; Hallmans, G.; Lund, E.; Skeie, G.; Kaaks, R.; Riboli, E. Dietary fibre in food and protection against colorectal cancer in the European prospective investigation into cancer and nutrition (EPIC): an observational study. *Lancet* **2003**, *361*, 1496−1501.
(23) Eshak, E. S.; Iso, H.; Date, C.; Kikuchi, S.; Watanabe, Y.; Wada, Y.; Wakai, K.; Tamakoshi, A.; JACC Study Group.. Dietary fiber intake is associated with reduced risk of mortality from cardiovascular disease among Japanese men and women. *J. Nutr.* **2010**, *140*, 1445−1453.
(24) Post, R. E.; Mainous, A. G.; King, D. E.; Simpson, K. N. Dietary fiber for the treatment of type 2 diabetes mellitus: a meta-analysis. *J. Am. Board Family Med.* **2012**, *25*, 16−23.
(25) Du, H.; van der A, D. L.; Boshuizen, H. C.; Forouhi, N. G.; Wareham, N. J.; Halkjær, J.; Tjønneland, A.; Overvad, K.; Jakobsen, M. U.; Boeing, H.; Buijsse, B.; Masala, G.; Palli, D.; Sørensen, T. I. A.; Saris, W. H. M.; Feskens, E. J. M. Dietary fiber and subsequent changes in body weight and waist circumference in European men and women. *Am. J. Clin. Nutr.* **2010**, *91*, 329−336.
(26) Elhayany, A.; Lustman, A.; Abel, R.; Attal-Singer, J.; Vinker, S. A low carbohydrate Mediterranean diet improves cardiovascular risk factors and diabetes control among overweight patients with type 2 diabetes mellitus: a 1-year prospective randomized intervention study. *Diabetes, Obes. Metab.* **2010**, *12*, 204−209.
(27) Tiveron, A. P.; Melo, P. S.; Bergamaschi, K. B.; Vieira, T. M. F. S.; Regitano-d'Arce, M. A. B.; Alencar, S. M. Antioxidant activity of Brazilian vegetables and its relation with phenolic composition. *Int. J. Mol. Sci.* **2012**, *13*, 8943−8957.
(28) Chandrasekara, A.; Shahidi, F. Determination of antioxidant activity in free and hydrolyzed fractions of millet grains and characterization of their phenolic profiles by HPLC-DAD-ESI-MS$^n$. *J. Funct. Foods* **2011**, *3*, 144−158.
(29) de Toledo, N. M. V.; Rocha, L. C.; da Silva, A. G.; Brazaca, S. G. C. Interaction and digestibility of phaseolin/polyphenol in the common bean. *Food Chem.* **2013**, *138*, 776−780.
(30) Miraliakbari, H.; Shahidi, F. Antioxidant activity of minor components of tree nut oils. *Food Chem.* **2008**, *111*, 421−427.
(31) Fracassetti, D.; Lawrence, N.; Tredoux, A. G. J.; Tirelli, A.; Nieuwoudt, H. H.; Du Toit, W. J. Quantification of glutathione, catechin and caffeic acid in grape juice and wine by a novel ultra-performance liquid chromatography method. *Food Chem.* **2011**, *128*, 1136−1142.
(32) de Camargo, A. C.; Vieira, T. M. F. S.; Regitano-d'Arce, M. A. B.; de Alencar, S. M.; Calori-Domingues, M. A.; Spoto, M. H. F.; Canniatti-Brazaca, S. G. Gamma irradiation of in-shell and blanched peanuts protects against mycotoxic fungi and retains their nutraceutical components during long-term storage. *Int. J. Mol. Sci.* **2012**, *13*, 10935−10958.
(33) Sobolev, V. S.; Cole, R. J. Note on utilisation of peanut seed testa. *J. Sci. Food Agric.* **2004**, *84*, 105−111.
(34) Liyana-Pathirana, C. M.; Shahidi, F. Antioxidant activity of commercial soft and hard wheat (*Triticum aestivum* L.) as affected by gastric pH conditions. *J. Agric. Food Chem.* **2005**, *53*, 2433−2440.
(35) Rakić, S.; Janković, S.; Marčetić, M.; Živković, D.; Kuzevski, J. The impact of storage on the primary and secondary metabolites, antioxidant activity and digestibility of oat grains (*Avena sativa*). *J. Funct. Foods* **2014**, *7*, 373−380.
(36) Gu, L. W.; House, S. E.; Wu, X. L.; Ou, B. X.; Prior, R. L. Procyanidin and catechin contents and antioxidant capacity of cocoa and chocolate products. *J. Agric. Food Chem.* **2006**, *54*, 4057−4061.
(37) de Camargo, A. C.; Vieira, T. M. F. S.; Regitano-D'Arce, M. A. B.; de Alencar, S. M.; Calori-Domingues, M. A.; Canniatti-Brazaca, S. G. Gamma radiation induced oxidation and tocopherols decrease in in-shell, peeled and blanched peanuts. *Int. J. Mol. Sci.* **2012**, *13*, 2827−2845.
(38) Yu, J.; Ahmedna, M.; Goktepe, P. Effects of processing methods and extraction solvents on concentration and antioxidant activity of peanut skin phenolics. *Food Chem.* **2005**, *90*, 199−206.
(39) Shahidi, F.; Alasalvar, C.; Liyana-Pathirana, C. M. Antioxidant phytochemicals in hazelnut kernel (*Corylus avellana* L.) and hazelnut byproducts. *J. Agric. Food Chem.* **2007**, *55*, 1212−1220.
(40) Fernandes, S. P.; Dringen, R.; Lawen, A.; Robinson, S. R. Inactivation of astrocytic glutamine synthetase by hydrogen peroxide requires iron. *Neurosci. Lett.* **2011**, *490*, 27−30.
(41) Chen, M.-c.; Ye, Y.-y.; Ji, G.; Liu, J.-w. Hesperidin upregulates heme oxygenase-1 to attenuate hydrogen peroxide-induced cell damage in hepatic L02 cells. *J. Agric. Food Chem.* **2010**, *58*, 3330−3335.
(42) Pulido, R.; Bravo, L.; Saura-Calixto, F. Antioxidant activity of dietary polyphenols as determined by a modified ferric reducing/antioxidant power assay. *J. Agric. Food Chem.* **2000**, *48*, 3396−3402.
(43) Paiva-Martins, F.; Gordon, M. H. Effects of pH and ferric ions on the antioxidant activity of olive polyphenols in oil-in-water emulsions. *J. Am. Oil Chem. Soc.* **2002**, *79*, 571−576.
(44) Appeldoorn, M. M.; Sanders, M.; Vincken, J. P.; Cheynier, V.; Le Guerneve, C.; Hollman, P. C. H.; Gruppen, H. Efficient isolation of major procyanidin A-type dimers from peanut skins and B-type dimers from grape seeds. *Food Chem.* **2009**, *117*, 713−720.
(45) Ou, K.; Gu, L. Absorption and metabolism of proanthocyanidins. *J. Funct. Foods* **2014**, *7*, 43−53.

**Table 1. Identified Volatiles in Raw, Freshly Roasted, or Stored Roasted Almonds (cv. Butte/Padre)[a]**

| PCA code | volatile compound | $t_R$[b] of unknown | standard KI | unknown KI | literature KI[c] | extracted ion[d] | internal standard | compounds newly produced during storage |
|---|---|---|---|---|---|---|---|---|
| | **aldehydes and ketones (28)** | | | | | | | |
| X1 | butanal[e] | 3.44 | 784 | 784 | 822 | 72 | octanal-$d_{16}$ | |
| X2 | 2-methylbutanal | 3.91 | | 887 | 910 | 57 | octanal-$d_{16}$ | |
| X3 | 3-methylbutanal | 3.97 | | 900 | 912 | 44 | octanal-$d_{16}$ | |
| X4 | 2,3-butanedione[e] | 4.94 | 960 | 961 | 970 | 86 | octanal-$d_{16}$ | |
| X5 | pentanal | 4.98 | | 963 | 935 | 58 | octanal-$d_{16}$ | |
| X6 | hexanal[e] | 7.13 | 1073 | 1073 | 1084 | 72 | octanal-$d_{16}$ | |
| X7 | 2-heptanone[e] | 9.72 | 1189 | 1179 | 1170 | 58 | octanal-$d_{16}$ | |
| X8 | heptanal[e] | 9.78 | 1184 | 1182 | 1174 | 70 | octanal-$d_{16}$ | |
| X9 | 2-hexenal | 10.64 | | 1215 | 1204 | 69 | octanal-$d_{16}$ | |
| X10 | 2-methyloxolan-3-one[e] | 11.85 | 1261 | 1261 | 1266 | 43 | octanal-$d_{16}$ | |
| X11 | 3-hydroxybutan-2-one[e] | 12.40 | 1281 | 1282 | 1287 | 88 | octanal-$d_{16}$ | |
| X12 | 2-octanone | 12.41 | | | 1285 | 58 | octanal-$d_{16}$ | new |
| X13 | octanal[e] | 12.57 | 1288 | 1288 | 1280 | 84 | octanal-$d_{16}$ | |
| X14 | 1-hydroxypropan-2-one | 12.76 | | 1295 | 1291 | 74 | octanal-$d_{16}$ | |
| X15 | (*Z*)-2-heptenal | 13.49 | | 1326 | 1299 | 83 | octanal-$d_{16}$ | |
| X16 | 2-nonanone | 14.98 | | | 1388 | 58 | octanal-$d_{16}$ | new |
| X17 | nonanal[e] | 15.11 | 1395 | 1396 | 1385 | 98 | octanal-$d_{16}$ | |
| X18 | 3-octen-2-one | 15.30 | | | 1323 | 111 | octanal-$d_{16}$ | new |
| X19 | (*E*)-2-octenal[e] | 15.70 | 1436 | 1435 | 1442 | 83 | octanal-$d_{16}$ | |
| X20 | furfural[e] | 16.12 | 1464 | 1465 | 1455 | 96 | octanal-$d_{16}$ | |
| X21 | 2-decanone | 16.47 | | | 1484 | 58 | octanal-$d_{16}$ | new |
| X22 | decanal[e] | 16.63 | 1503 | 1502 | 1484 | 82 | octanal-$d_{16}$ | |
| X23 | benzaldehyde[e] | 16.90 | 1527 | 1528 | 1495 | 106 | octanal-$d_{16}$ | |
| X24 | (*Z*)-2-nonenal[e] | 17.01 | 1537 | 1539 | 1510 | 83 | octanal-$d_{16}$ | |
| X25 | 2-phenylacetaldehyde[e] | 18.04 | 1639 | 1640 | 1640 | 91 | octanal-$d_{16}$ | |
| X26 | (*E*)-2-decenal | 18.11 | | | 1760 | 41 | octanal-$d_{16}$ | new |
| X27 | 2,4-nonadienal | 18.50 | | | 1709 | 81 | octanal-$d_{16}$ | new |
| X28 | 2-undecenal | 18.86 | | | 1712 | 83 | octanal-$d_{16}$ | new |
| | **pyrazines (7)** | | | | | | | |
| X29 | 2-methylpyrazine[e] | 11.97 | 1266 | 1265 | 1239 | 94 | 2-methylpyrazine-$d_6$ | |
| X30 | 2,5-dimethylpyrazine[e] | 13.51 | 1327 | 1326 | 1320 | 108 | 2-methylpyrazine-$d_6$ | |
| X31 | 2,6-dimethylpyrazine | 13.66 | | 1334 | 1308 | 108 | 2-methylpyrazine-$d_6$ | |
| X32 | 2-ethylpyrazine | 13.81 | | 1340 | 1354 | 107 | 2-methylpyrazine-$d_6$ | |
| X33 | 2,3-dimethylpyrazine | 14.12 | | 1353 | 1324 | 108 | 2-methylpyrazine-$d_6$ | |
| X34 | 2-ethyl-6-methylpyrazine | 15.00 | | 1391 | 1381 | 121 | 2-methylpyrazine-$d_6$ | |
| X35 | trimethylpyrazine | 15.34 | | 1409 | 1395 | 122 | 2-methylpyrazine-$d_6$ | |
| | **alcohols (18)** | | | | | | | |
| X36 | 2-methyl-1-propanol[e] | 7.54 | 1096 | 1092 | 1099 | 74 | hexyl-$d_{13}$ alcohol | |
| X37 | 3-pentanol[e] | 7.92 | 1111 | 1108 | 1107 | 59 | hexyl-$d_{13}$ alcohol | |
| X38 | 2-propenol[e] | 7.98 | | 1111 | 1136 | 57 | hexyl-$d_{13}$ alcohol | |
| X39 | 1-butanol[e] | 8.82 | 1143 | 1144 | 1145 | 56 | hexyl-$d_{13}$ alcohol | |
| X40 | 3-methyl-1-butanol[e] | 10.46 | 1209 | 1208 | 1205 | 70 | hexyl-$d_{13}$ alcohol | |
| X41 | 1-pentanol[e] | 11.61 | 1251 | 1252 | 1255 | 70 | hexyl-$d_{13}$ alcohol | |
| X42 | 1-chloro-2-propanol[e] | 13.23 | 1314 | 1315 | | 79 | hexyl-$d_{13}$ alcohol | |
| X43 | 1-hexanol[e] | 14.33 | 1360 | 1362 | 1360 | 69 | hexyl-$d_{13}$ alcohol | |
| X44 | 2-chloro-1-propanol | 14.54 | | 1371 | | 31 | hexyl-$d_{13}$ alcohol | |
| X45 | 1-octen-3-ol | 15.95 | | | 1395 | 57 | hexyl-$d_{13}$ alcohol | new |
| X46 | 1-methylthio-2-propanol[e] | 15.96 | 1454 | 1454 | | 106 | hexyl-$d_{13}$ alcohol | |
| X47 | 1-heptanol[e] | 16.09 | 1467 | 1463 | 1467 | 70 | hexyl-$d_{13}$ alcohol | |
| X48 | 2-ethylthioethanol[e] | 16.98 | 1597 | 1536 | | 75 | hexyl-$d_{13}$ alcohol | |
| X49 | 1-octanol[e] | 17.26 | 1563 | 1564 | 1553 | 84 | hexyl-$d_{13}$ alcohol | |
| X50 | 1,2-propanediol | 17.54 | | 1591 | 1603 | 45 | hexyl-$d_{13}$ alcohol | |
| X51 | nonanol | 18.11 | | | 1619 | 56 | hexyl-$d_{13}$ alcohol | new |
| X52 | furfuryl alcohol[e] | 18.13 | 1661 | 1663 | 1661 | 98 | hexyl-$d_{13}$ alcohol | |
| X53 | 2-phenylethyl alcohol[e] | 19.90 | 1929 | 1930 | 1925 | 91 | hexyl-$d_{13}$ alcohol | |
| | **additional compounds (18)** | | | | | | | |
| X54 | ethyl acetate[e] | 3.58 | 874 | 876 | 885 | 61 | 2-methylpyrazine-$d_6$ | |
| X55 | $\alpha$-pinene[e] | 5.82 | 1014 | 1013 | 1032 | 93 | 2-methylpyrazine-$d_6$ | |
| X56 | methylsulfanylmethane[e] | 6.88 | 1062 | 1062 | 1071 | 94 | 2-methylpyrazine-$d_6$ | |


dx.doi.org/10.1021/jf503817g | J. Agric. Food Chem. 2014, 62, 11236−11245

**Table 1. continued**

| PCA code | volatile compound | $t_R$[b] of unknown | standard KI | unknown KI | literature KI[c] | extracted ion[d] | internal standard | compounds newly produced during storage |
|---|---|---|---|---|---|---|---|---|
| X57 | pentyl oxirane | 8.66 | | | | 71 | octanal-$d_{16}$ | new |
| X58 | hexyl oxirane | 11.54 | | | | 71 | octanal-$d_{16}$ | new |
| X59 | limonene[e] | 10.10 | 1197 | 1195 | 1201 | 68 | 2-methylpyrazine-$d_6$ | |
| X60 | 2-pentylfuran | 11.01 | | 1229 | 1221 | 81 | 2-methylpyrazine-$d_6$ | |
| X61 | acetic acid | 15.91 | | | 1450 | 43 | hexyl-$d_{13}$ alcohol | new |
| X62 | pyrrole[e] | 16.76 | 1514 | 1515 | 1509 | 67 | hexyl-$d_{13}$ alcohol | |
| X63 | $\gamma$-dihydrofuran-2(3*H*)-one | 17.95 | | 1640 | 1635 | 86 | hexyl-$d_{13}$ alcohol | |
| X64 | vinyl hexanoate | 18.16 | | | | 99 | hexyl-$d_{13}$ alcohol | new |
| X65 | $\gamma$-oxepan-2-one[e] | 18.57 | 1719 | 1720 | 1694 | 85 | hexyl-$d_{13}$ alcohol | |
| X66 | pentanoic acid | 18.77 | | | 1720 | 60 | hexyl-$d_{13}$ alcohol | new |
| X67 | caproic acid[e] | 19.47 | 1859 | 1857 | 1829 | 60 | hexyl-$d_{13}$ alcohol | |
| X68 | heptanoic acid | 20.08 | | | 1990 | 60 | hexyl-$d_{13}$ alcohol | new |
| X69 | 2-acetylpyrrole | 20.24 | | 1991 | 1950 | 94 | hexyl-$d_{13}$ alcohol | |
| X70 | octanoic acid | 20.66 | | | 2083 | 60 | hexyl-$d_{13}$ alcohol | new |
| X71 | nonanoic acid | 21.23 | | | 2202 | 60 | hexyl-$d_{13}$ alcohol | new |

[a]Volatiles were identified in freshly roasted almonds and in stored almonds after roasting. DB-Wax was used as the analytical column. [b]$t_R$, retention time. [c]KI, Kovats' index; and values were obtained from http://flavornet.org or www.pherobase.com. [d]Extracted ion from total ion scan used for quantitation. [e]Compounds verified with authentic standards.

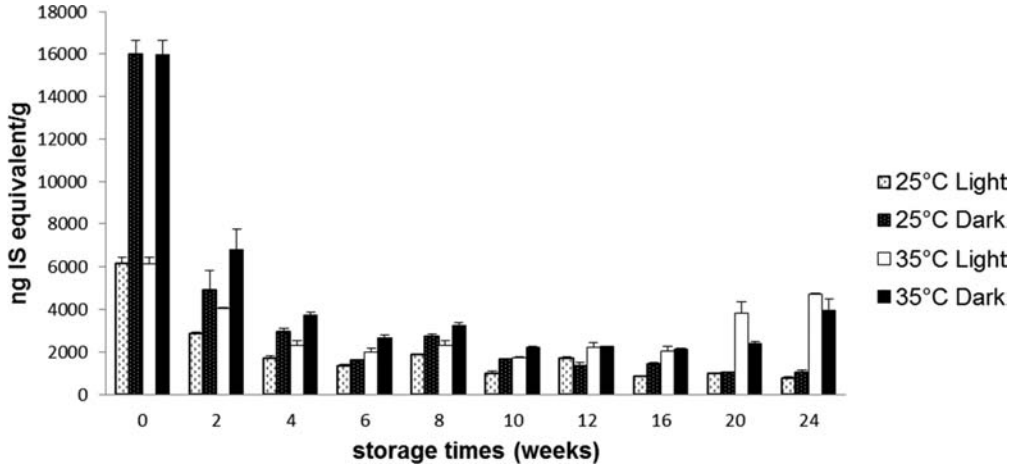


**Figure 1.** Sum of almond volatile compounds for different roastings, storage temperatures, and storage times.

are not static, and moderate values may reflect depletion rather than low levels of oxidation. The TBA assay can be used to monitor the formation of malondialdehyde, a product of lipid oxidation.[13] However, low TBA values are not absolute indicators of oxidation as malondialdehyde may not be a good marker for other lipid-derived aldehydes and artifacts can easily form during the analysis procedure.[13] Hexanal, the most commonly used marker of lipid oxidation, exists in raw almonds and is generated during heat processing.[14,15] During the initial stages of storage, the hexanal, formed during thermal processing, volatilizes, and levels decrease.[16] As lipids oxidize during storage, the levels of hexanal increase.[17]

Numerous volatile compounds are generated through the Maillard reaction and via lipid oxidation during roasting and are important to flavor.[18,19] These include ketones, aldehydes, pyrazines, alcohols, aromatic hydrocarbons, furans, and pyrroles. Pyrazines, furans, and pyrroles are key components of toasted almond aroma.[18] Pyrazines, which have nutty and roasted aromas, are formed during heating via Maillard sugar–amine reactions and Strecker degradation.[20] The thermal degradation of sugars such as fructose and glucose produce furan-containing compounds (e.g., furfural).[18] Linoleic acid is a precursor to many aldehydes and alcohols[21] including (*E*)-2-heptenal and nonanal.[22] (*E*)-2-Heptenal is responsible for pungent and green aromas,[18] and nonanal is responsible for tallow and fruity aromas.[23] Thermal decomposition of methyl linoleate hydroperoxide generates 1-octen-3-ol,[22] which contributes to an herbaceous aroma in almonds.[18] The oxidation of linolenic acid produces (*Z*)-3-hexen-1-ol (a green leaf aroma)[24] and 1-butanol (an unripe apple aroma).[22,25] Other lipid oxidation volatiles such as lactones, including butyrolactone, contribute to milky and creamy aromas in foods[26]

Roasted almonds often display inconsistent shelf life stability and can develop rancidity during storage, which is usually detected only after nuts develop considerable off-flavors. The inconsistent identification of the presence and extent of rancidity leads to considerable product loss. At the same time, the levels of the desirable aromas that arise from roasting tend to decrease during storage. To address this, we used HS-SPME GC-MS to (1) evaluate changes in volatile profiles of roasted almonds during 6 months of storage, (2) identify possible early markers of rancidity development in roasted almonds, and (3) gain a better understanding of the time line

**Table 2. Volatiles Detected in Almond Samples: Raw, Freshly Roasted, or Stored Roasted at 35 °C for 24 Weeks (Nanograms per Gram)**

| | | light roast (28 min at 138 °C) | | | dark roast (38 min at 138 °C) | | |
|---|---|---|---|---|---|---|---|
| volatile compound | raw | 0 weeks | 10 weeks | 24 weeks | 0 weeks | 10 weeks | 24 weeks |
| **aldehydes and ketones** | | | | | | | |
| butanal | 19.6 ± 2.7 | 27.6 ± 1.5 | ND[a] | 12.6 ± 1.2 | 40.8 ± 2.1 | ND | 25.4 ± 2.3 |
| 2-methylbutanal | 14.3 ± 0.3 | 1468.6 ± 25.7 | 119.9 ± 3.4 | 76.6 ± 0.4 | 6573.7 ± 275.0 | 325.1 ± 58.1 | 137.6 ± 17.3 |
| 3-methylbutanal | 32.4 ± 0.5 | 911.4 ± 50.9 | 146.8 ± 3.6 | 89.0 ± 0.9 | 4268.9 ± 381.8 | 231.6 ± 45.2 | 117.3 ± 10.3 |
| 2,3-butanedione | 8.0 ± 0.3 | 100.3 ± 0.8 | 3.4 ± 4.8 | 10.6 ± 1.3 | 226.3 ± 13.7 | 7.3 ± 0.3 | 16.8 ± 1.7 |
| pentanal | 50.4 ± 5.7 | 223.0 ± 8.6 | 44.7 ± 1.2 | 221.8 ± 15.6 | 264.1 ± 15.9 | 33.2 ± 4.2 | 369.3 ± 53.6 |
| hexanal | 422.6 ± 97.9 | 983.0 ± 133.7 | 441.4 ± 1.9 | 1631.8 ± 75.1 | 1140.8 ± 3.8 | 377.8 ± 45.8 | 1565.4 ± 251.2 |
| 2-heptanone | 50.0 ± 4.7 | 72.0 ± 7.3 | 65.7 ± 1.6 | 237.3 ± 0.9 | 123.6 ± 3.0 | 40.1 ± 2.6 | 351.7 ± 38.6 |
| heptanal | 40.5 ± 8.9 | 75.2 ± 16.2 | 90.0 ± 1.4 | 306.0 ± 3.9 | 114.8 ± 3.0 | 60.6 ± 2.8 | 214.6 ± 33.0 |
| 2-hexenal | ND | 14.6 ± 2.7 | ND | 5.1 ± 0.3 | 14.1 ± 2.7 | ND | 4.1 ± 0.0 |
| 2-methyloxolan-3-one | ND | 15.4 ± 1.3 | 24.4 ± 1.5 | 8.7 ± 0.9 | 128.1 ± 11.0 | 57.9 ± 6.8 | 25.1 ± 2.5 |
| 3-hydroxybutan-2-one | ND | 2.2 ± 0.2 | ND | ND | 3.8 ± 0.6 | 0.3 ± 0.1 | ND |
| 2-octanone | ND | ND | ND | 33.3 ± 0.1 | ND | ND | 34.2 ± 4.0 |
| octanal | 25.2 ± 4.7 | 31.1 ± 7.3 | 53.5 ± 1.5 | 265.1 ± 6.2 | 42.0 ± 3.0 | 36.2 ± 2.0 | 155.6 ± 27.5 |
| 1-hydroxypropan-2-one | 1.3 ± 0.0 | 9.0 ± 0.9 | 0.4 ± 0.0 | 0.2 ± 0.0 | 13.7 ± 3.0 | 0.8 ± 0.1 | 0.5 ± 0.1 |
| (*Z*)-2-heptenal | 19.1 ± 0.9 | 65.6 ± 13.2 | 9.7 ± 0.2 | 43.9 ± 0.6 | 61.9 ± 1.6 | 9.5 ± 0.5 | 32.1 ± 4.4 |
| 2-nonanone | ND | ND | ND | 31.2 ± 0.2 | ND | ND | 28.6 ± 4.3 |
| nonanal | 36.6 ± 4.9 | 55.9 ± 13.3 | 46.1 ± 0.3 | 112.5 ± 8.1 | 70.5 ± 18.9 | 50.6 ± 2.5 | 59.9 ± 10.3 |
| 3-octen-2-one | ND | ND | ND | 45.4 ± 0.9 | ND | ND | 33.6 ± 4.5 |
| (*E*)-2-octenal | 7.3 ± 0.9 | 12.5 ± 2.1 | 5.7 ± 0.1 | 42.0 ± 0.3 | 15.9 ± 2.0 | 6.8 ± 0.6 | 34.5 ± 5.3 |
| furfural | ND | 103.2 ± 8.7 | 11.2 ± 1.0 | 4.9 ± 0.1 | 460.0 ± 21.4 | 31.5 ± 2.0 | 8.9 ± 0.8 |
| 2-decanone | ND | ND | ND | 10.3 ± 0.4 | ND | ND | 7.6 ± 1.3 |
| decanal | ND | 6.9 ± 2.3 | 2.5 ± 0.4 | 8.3 ± 0.6 | 4.6 ± 1.0 | 2.4 ± 0.3 | 3.8 ± 0.5 |
| benzaldehyde | 2934.6 ± 272.5 | 368.8 ± 41.2 | 431.7 ± 20.5 | 1048.6 ± 81.5 | 331.9 ± 65.4 | 724.8 ± 173.5 | 180.3 ± 5.8 |
| (*Z*)-2-nonenal | ND | ND | ND | 5.7 ± 0.5 | 5.3 ± 1.7 | ND | 2.9 ± 0.3 |
| 2-phenylacetaldehyde | ND | 107.5 ± 20.3 | 20.2 ± 0.8 | 14.2 ± 0.8 | 491.3 ± 45.4 | 27.0 ± 3.6 | 8.8 ± 1.7 |
| (*E*)-2-decenal | ND | ND | ND | 10.9 ± 0.9 | ND | ND | 6.6 ± 1.4 |
| 2,4-nonadienal | ND | ND | ND | 15.4 ± 1.1 | ND | ND | 10.4 ± 1.6 |
| 2-undecenal | ND | ND | ND | 3.4 ± 0.3 | ND | ND | 1.8 ± 0.3 |
| **pyrazines** | | | | | | | |
| 2-methylpyrazine | ND | 4.1 ± 0.3 | 4.1 ± 0.2 | 2.6 ± 0.2 | 26.5 ± 1.8 | 9.1 ± 0.8 | 7.3 ± 0.7 |
| 2,5-dimethylpyrazine | 11.4 ± 0.5 | 16.2 ± 0.6 | 21.0 ± 1.5 | 7.3 ± 0.6 | 66.5 ± 0.4 | 47.5 ± 2.0 | 28.2 ± 2.2 |
| 2,6-dimethylpyrazine | ND | ND | 1.3 ± 0.1 | 0.8 ± 0.1 | 4.2 ± 0.6 | 4.0 ± 0.2 | 2.9 ± 0.3 |
| 2-ethylpyrazine | ND | ND | ND | ND | 3.2 ± 0.1 | 1.8 ± 0.1 | 1.4 ± 0.1 |
| 2,3-dimethylpyrazine | ND | ND | ND | ND | 1.4 ± 0.1 | 0.8 ± 0.0 | 0.6 ± 0.0 |
| 2-ethyl-6-methylpyrazine | ND | ND | 0.6 ± 0.1 | 0.6 ± 0.1 | 2.2 ± 0.0 | 2.2 ± 0.0 | 2.2 ± 0.2 |
| trimethylpyrazine | ND | ND | 1.8 ± 0.1 | 1.0 ± 0.0 | 6.1 ± 0.2 | 6.5 ± 0.1 | 5.3 ± 0.6 |
| **alcohols** | | | | | | | |
| 2-methyl-1-propanol | 3.6 ± 0.3 | 1.3 ± 0.1 | 0.5 ± 0.0 | 0.4 ± 0.0 | 1.1 ± 0.1 | 0.3 ± 0.0 | 0.3 ± 0.0 |
| 3-pentanol | ND | 0.8 ± 0.1 | ND | ND | 2.7 ± 0.3 | 0.6 ± 0.0 | ND |
| 2-propenol | ND | 2.0 ± 0.0 | ND | ND | 2.2 ± 0.1 | ND | 0.1 ± 0.1 |
| 1-butanol | 8.4 ± 2.3 | 11.2 ± 1.1 | 5.1 ± 1.9 | 4.5 ± 0.1 | 10.7 ± 0.4 | 4.3 ± 0.3 | 11.6 ± 1.3 |
| 3-methyl-1-butanol | 86.4 ± 3.3 | 19.1 ± 0.3 | 13.7 ± 0.6 | 15.0 ± 1.0 | 17.2 ± 0.6 | 10.6 ± 0.7 | 8.1 ± 0.6 |
| 1-pentanol | 30.3 ± 4.4 | 45.6 ± 2.9 | 29.3 ± 1.2 | 52.1 ± 0.0 | 54.3 ± 1.3 | 14.4 ± 1.8 | 101.1 ± 11.2 |
| 1-chloro-2-propanol | 106.2 ± 5.4 | 161.9 ± 2.8 | 12.9 ± 0.8 | 1.6 ± 0.0 | 149.6 ± 7.6 | 11.3 ± 1.2 | 2.0 ± 0.3 |
| 1-hexanol | 47.0 ± 1.1 | 53.1 ± 5.5 | 50.6 ± 2.1 | 48.0 ± 1.1 | 70.1 ± 0.7 | 21.8 ± 1.2 | 23.1 ± 2.3 |
| 2-chloro-1-propanol | 41.9 ± 3.5 | 59.5 ± 0.3 | 5.9 ± 0.2 | 1.1 ± 0.3 | 53.4 ± 2.2 | 5.5 ± 0.3 | 1.1 ± 0.2 |
| 1-octen-3-ol | ND | ND | ND | 6.9 ± 0.1 | ND | ND | 8.9 ± 1.3 |
| 1-methylthio-2-propanol | 12.8 ± 1.3 | 247.2 ± 23.9 | 38.9 ± 2.4 | 7.2 ± 0.8 | 325.0 ± 53.1 | 19.4 ± 1.5 | 4.5 ± 0.8 |
| 1-heptanol | 3.2 ± 0.4 | 3.8 ± 1.0 | 8.7 ± 0.5 | 36.7 ± 1.1 | 6.0 ± 0.4 | 5.0 ± 0.1 | 33.5 ± 4.6 |
| 2-ethyl thioethanol | 1.0 ± 0.0 | 20.5 ± 3.1 | 4.7 ± 0.3 | 1.1 ± 0.0 | 29.2 ± 3.9 | 3.0 ± 0.2 | 0.9 ± 0.1 |
| 1-octanol | 0.8 ± 0.0 | 1.2 ± 0.2 | 2.0 ± 0.1 | 7.6 ± 0.2 | 1.6 ± 0.1 | 1.2 ± 0.0 | 5.9 ± 1.0 |
| 1,2-propanediol | 269.1 ± 2.5 | 789.4 ± 72.3 | 210.6 ± 5.5 | 139.3 ± 3.5 | 647.0 ± 73.8 | 208.4 ± 35.2 | 258.5 ± 51.1 |
| nonanol | ND | ND | ND | 2.0 ± 0.1 | ND | ND | 1.0 ± 0.1 |
| furfuryl alcohol | 0.6 ± 0.0 | 1.2 ± 0.1 | 0.8 ± 0.1 | 0.6 ± 0.0 | 5.2 ± 0.4 | 1.1 ± 0.1 | 0.4 ± 0.0 |
| 2-phenylethyl alcohol | 6.2 ± 0.6 | 0.9 ± 0.0 | 1.5 ± 0.1 | 1.9 ± 0.1 | 0.9 ± 0.2 | 1.5 ± 0.0 | 1.6 ± 0.1 |
| **additional compounds** | | | | | | | |
| ethyl acetate | ND | 12.0 ± 1.2 | ND | ND | 9.9 ± 0.8 | ND | ND |


dx.doi.org/10.1021/jf503817g | *J. Agric. Food Chem.* 2014, 62, 11236−11245

**Table 2. continued**

| volatile compound | raw | light roast (28 min at 138 °C) | | | dark roast (38 min at 138 °C) | | |
|---|---|---|---|---|---|---|---|
| | | 0 weeks | 10 weeks | 24 weeks | 0 weeks | 10 weeks | 24 weeks |
| α-pinene | 15.0 ± 0.1 | 16.5 ± 1.5 | 5.3 ± 0.4 | 2.3 ± 0.2 | 14.6 ± 0.9 | 5.1 ± 0.3 | 2.8 ± 0.5 |
| methylsulfanylmethane | ND | 4.5 ± 0.7 | ND | ND | 6.1 ± 2.0 | ND | ND |
| pentyl oxirane | ND | ND | ND | 27.8 ± 0.9 | ND | ND | 97.5 ± 9.3 |
| hexyl oxirane | ND | ND | ND | 42.1 ± 0.2 | ND | ND | 2.9 ± 0.3 |
| limonene | 16.6 ± 0.5 | 14.5 ± 1.4 | 6.5 ± 0.2 | 3.3 ± 0.2 | 13.0 ± 0.5 | 5.1 ± 0.1 | 3.0 ± 0.2 |
| 2-pentylfuran | 2.4 ± 0.8 | 16.6 ± 1.2 | 12.8 ± 0.8 | 49.8 ± 3.1 | 30.0 ± 0.2 | 14.7 ± 0.2 | 27.2 ± 1.0 |
| acetic acid | ND | ND | ND | 45.2 ± 2.3 | ND | ND | 60.2 ± 16.1 |
| pyrrole | ND | 0.6 ± 0.1 | 0.2 ± 0.0 | 0.4 ± 0.0 | 2.1 ± 0.3 | 0.2 ± 0.0 | 0.4 ± 0.1 |
| γ-dihydrofuran-2(3*H*)-one | 0.7 ± 0.0 | 1.8 ± 0.2 | 0.9 ± 0.1 | 0.9 ± 0.1 | 2.2 ± 0.1 | 0.9 ± 0.1 | 1.1 ± 0.2 |
| vinyl hexanoate | ND | ND | ND | 4.9 ± 0.2 | ND | ND | 8.1 ± 1.3 |
| γ-oxepan-2-one | 1.2 ± 0.3 | 1.6 ± 0.2 | 2.8 ± 0.1 | 8.0 ± 0.1 | 2.4 ± 0.3 | 1.7 ± 0.1 | 7.1 ± 1.0 |
| pentanoic acid | ND | ND | ND | 2.5 ± 0.2 | ND | ND | 5.9 ± 1.9 |
| caproic acid | 1.8 ± 0.6 | 5.7 ± 1.3 | 9.2 ± 0.6 | 42.4 ± 4.3 | 6.7 ± 0.1 | 10.7 ± 0.7 | 52.0 ± 15.8 |
| heptanoic acid | ND | ND | ND | 4.6 ± 0.4 | ND | ND | 2.7 ± 0.6 |
| 2-acetylpyrrole | ND | 0.2 ± 0.0 | 0.4 ± 0.0 | 0.5 ± 0.0 | 0.7 ± 0.1 | 0.7 ± 0.0 | 0.8 ± 0.1 |
| octanoic acid | ND | ND | ND | 5.1 ± 0.7 | ND | ND | 2.0 ± 0.3 |
| nonanoic acid | ND | ND | ND | 2.5 ± 0.2 | ND | ND | 0.4 ± 0.0 |

[a]ND, not detected.

for fading of aromas and the point when oxidation products start to dominate volatile profiles.

## MATERIALS AND METHODS

**Reagents.** C7−C40 saturated alkanes standard (1000 μg/mL in hexane), ethanol (HPLC/spectrophotometric grade), and 36 other standards were purchased from either Sigma-Aldrich (St. Louis, MO, USA) or Fisher Scientific (Pittsburgh, PA, USA) (Table 1). The exceptions were decanal (Eastman, Rochester, NY, USA), 2-ethylthioethanol (Alfa Aesar, Ward Hill, MA, USA), 3-hydroxybutan-2-one (Supelco, Bellefonte, PA, USA), and 1-methylthio-2-propanol (Ryan Scientific, Inc., Mount Pleasant, SC, USA). Octanal-$d_{16}$, 2-methylpyrazine-$d_6$, and *n*-hexyl-$d_{13}$ alcohol were purchased from C/D/N Isotopes Inc. (Quebec, Canada). The stable isotopes were used as stable isotope internal standards for three major categories of identified compounds (i.e., aldehydes, pyrazines, and alcohols).

**Almond Samples and Roasting.** Raw almond kernels (cv. Butte/Padre) were obtained from Hughson Nut Co. (Hughson, CA, USA) and had been in storage at ambient warehouse temperatures for 7 months since harvest. Kernels were commercially dry roasted using a Revent baking rotary roaster (Ready Roast, Madera, CA, USA). Almonds were roasted in triplicate batches (4.5−5.4 kg each) at 138 °C using different roasting times to achieve light (28 min) and dark roast (38 min). The almonds were stored in two E7/2 Conviron chambers (Manitoba, Canada) with controlled environments of 25 or 35 °C and at 65% relative humidity. The almonds were placed in a single layer on trays in the dark by covering the trays with aluminum foil to simulate dark storage. All almonds were evaluated at 0, 2, 4, 6, 8, 10, 12, 16, 20, and 24 weeks of storage.

To prepare samples for analysis, a random 50 g sample was removed from each tray and ground for 5 s at low speed with a Waring laboratory blender (Torrington, CT, USA). The ground samples were passed through a Tyler standard sieve (16 mesh; Mentor, OH, USA) to collect almond powder of a uniform particle size. For HS-SPME analysis, 5 g (±1%) of the powder was transferred into a 22.5 × 75 mm (20 mL) glass headspace vial (Sigma-Aldrich). Samples were prepared in duplicate ($n$ = 2).

**HS-SPME Sampling and Gas Chromatography Analysis.** Volatile extraction was carried out as described previously.[27] Briefly, a 1 cm 50/30 μm SPME fiber assembly coated with divinylbenzene/carboxen/polydimethylsiloxane (Supelco, Inc.) was used for headspace analyses of almond sample volatiles. A mixed internal standard solution (octanal-$d_{16}$, 2-methylpyrazine-$d_6$, and *n*-hexyl-$d_{13}$ alcohol) was added to each headspace vial containing a 5 g sample of ground almond (10 ng/g). Equilibration time was 40 min, and the SPME fiber extraction time was 30 min in the headspace of the vials at room temperature (24 ± 1 °C). Following headspace extraction, SPME fibers were injected into the GC and remained in the GC inlet for 10 min.

**GC-MS Analysis.** Volatile analysis was determined using GC-MS analysis on an HP 6890 coupled to an Agilent 5973 mass selective detector (Agilent, Palo Alto, CA, USA) as previously described.[27] Compounds were separated on a DB-Wax column (30 m × 0.25 mm i.d., 0.25 μm film thickness, Agilent Technologies) by applying 35 °C for 1 min, 5 °C/min to 100 °C, and 20 °C/min to a final temperature of 250 °C, with a final holding time of 5 min. The injection was performed in splitless mode (0.7 mm splitless inlet liner, Supelco), and the injector temperature was 220 °C. The purge valve was opened at 0.5 min at a 50 mL/min flow rate. Carrier gas was helium (99.999%) with a constant starting flow rate at 0.7 mL/min. The detector was fitted with an electron impact ionization source set at 230 °C. The quadrupole temperature was set to 150 °C, and the transfer line temperature was kept at 250 °C. The solvent delay was set to 3 min. Total ion chromatograms were collected by scanning from $m/z$ 30 to 150 at a rate of 3.06 scans/s.

**Identification and Relative Quantification of Volatile Compounds.** Volatile compounds were identified by comparison of their mass spectra and retention times with those of authentic standards. Volatile compounds without authentic standards were tentatively identified by comparing the Kovats' retention indices (KI) and/or mass spectrum with those reported in the NIST Mass Spectral Search Program (version 2.0 a) with <80% as a cutoff to match compounds. The KIs were calculated from the retention times of $C_6$−$C_{40}$ *n*-alkanes.

The full spectrum was scanned in total ion chromatogram (TIC) mode. Relative quantification of each volatile compound was performed using a unique extracted ion peak area at its respective retention time and comparing to the extracted ion peak area of one of three internal standards (i.e., octanal-$d_{16}$, 2-methylpyrazine-$d_6$, and *n*-hexyl-$d_{13}$ alcohol, for aldehydes, pyrazines, and alcohols, respectively) as described previously.[27] Concentration was calculated using the following equation according to Baek and Cadwallader:[28]

$$\text{concentration}\left(\frac{\text{ng}}{\text{g}}\right) = \frac{\text{extracted ion peak area}}{\text{extracted ion peak area of IS}} \times \left(\text{IS} \times \frac{10\ \text{ng}}{\text{g}}\right)$$

The peak area of each extracted ion for each analyte was divided by the peak area of extracted ion for the respective internal standard. The area ratio obtained was subsequently converted to relative

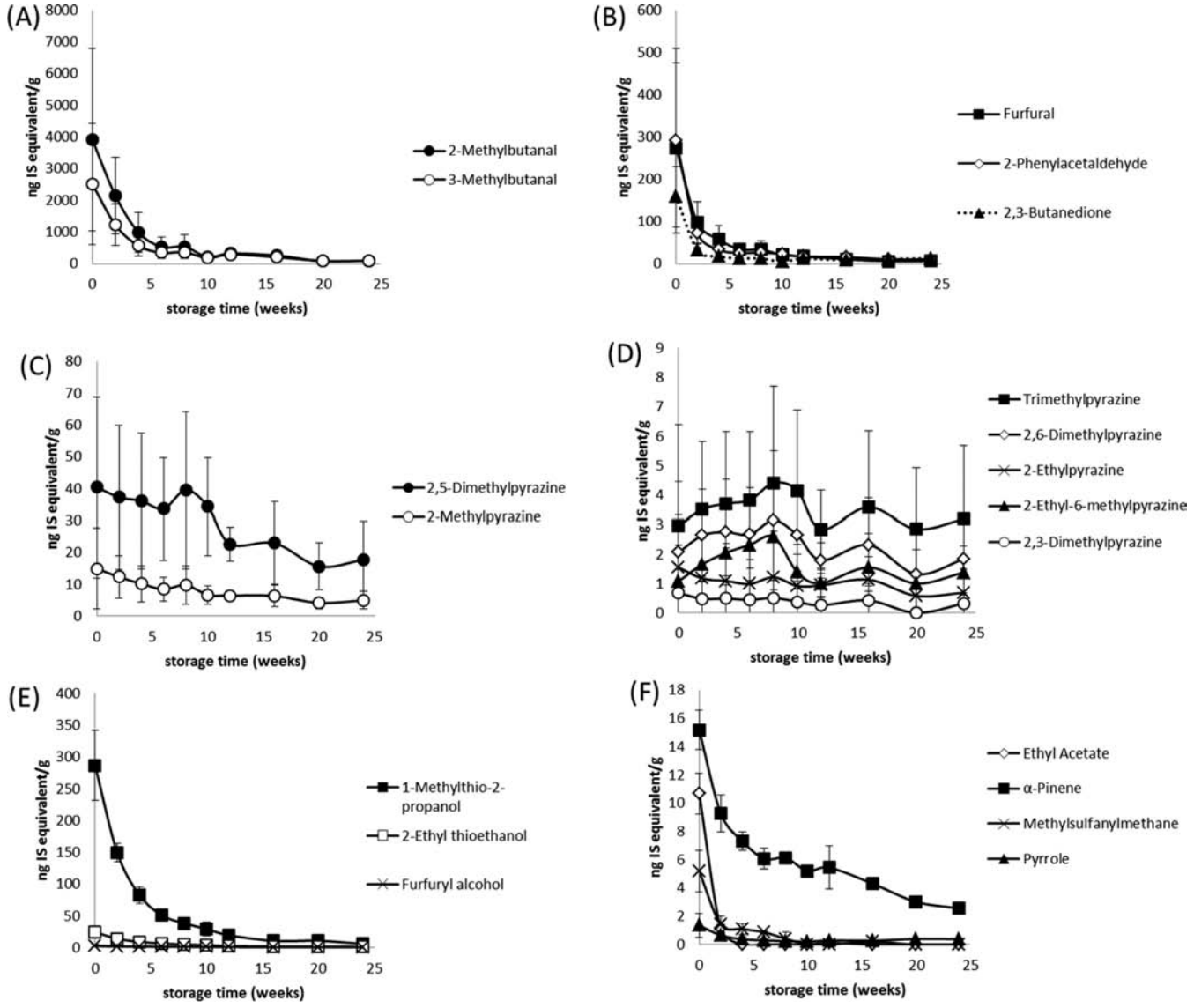


**Figure 2.** Roasted almond volatile compounds that decreased during almond storage: (A, B) carbonyls; (C, D) pyrazines; (E) alcohols; (F) additional volatiles. Concentrations are the average concentrations across the roasting treatments evaluated (i.e., light- and dark-roasted samples) and stored at 35 °C over 24 weeks.

concentration of the analyte in a 5 g sample based on the concentration of the appropriate IS (10 ng IS/g almond). The obtained relative concentration was used to compare the difference in volatile profiles among raw and roasted almonds.

**Statistical Analysis.** Principal component analysis (PCA) was performed to visualize clustering formation of different conditions (roasting time and storage time) and the relationship between volatile compounds and samples. Before PCA was performed, a one-way analysis of variance (ANOVA) was used to determine the volatile compounds significantly different in volatile concentrations across the whole data set. XLSTAT (version 2013.05.06) was employed for this analysis. The data were then normalized by log transformation for normal distribution and autoscaling for unit scaling. MetaboAnalyst (www.metaboanalyst.ca) was used for PCA.

## ■ RESULTS AND DISCUSSION

Seventy-one volatile compounds were identified using NIST libraries and the Kovats index, in freshly roasted and roasted stored almonds.[27] These include 28 aldehydes and ketones, 7 pyrazines, 18 alcohols, and 18 additional compounds (Table 1). The identities of 38 of these compounds were confirmed with authentic standards. Raw almonds contained the fewest volatiles, whereas levels increased in freshly roasted and roasted stored almonds. Some volatiles were specifically unique to the raw,[27] roasted, or roasted stored almonds (Table 1). Seventeen new volatiles were formed during storage and include ketones (2-octanone, 2-nonanone, 3-octen-2-one, and 2-decanone), aldehydes ((*E*)-2-decenal, 2,4-nonadienal, and 2-undecenal), alcohols (1-octen-3-ol and nonanol), oxiranes (pentyl oxirane and hexyl oxirane), and short-chain acids (acetic acid, pentanoic acid, heptanoic acid, and octanoic acid). Higher levels of 1-octen-3-ol, acetic acid, and pentanoic acid were found in the dark-roast almonds as compared to the light-roast almonds. Lower levels of 3-oceten-2-one, 2-decanone, (*E*)-2-decenal, 2,4-nonadienal, and 2-undecenal were found in the dark-roast almonds as compared to the light-roast almonds.

The roasted almonds were stored in dark controlled environments at 25 or 35 °C with 65% relative humidity. Storage studies evaluated the influence of storage temperature and storage time on total volatile compounds in light- and dark-roast almonds over 24 weeks. The dark-roast almonds had

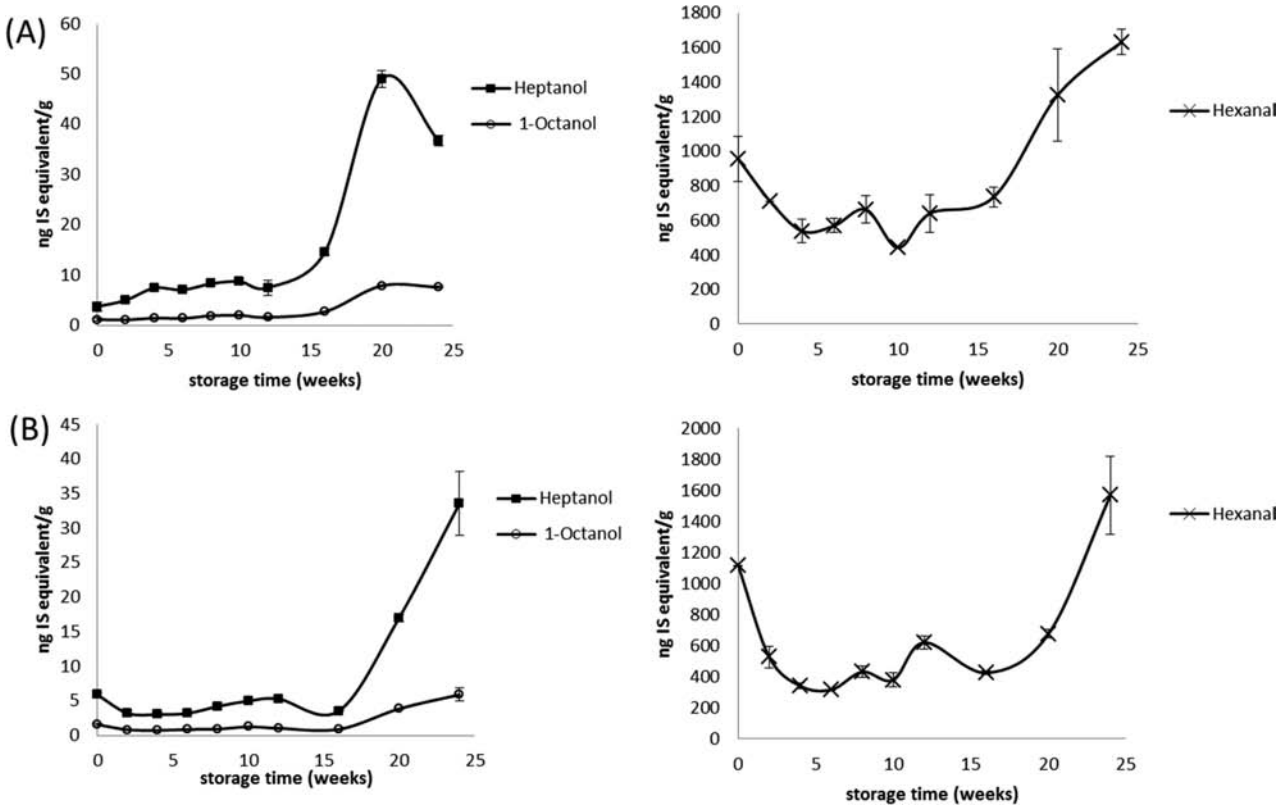


**Figure 3.** Roasted almond volatile compounds that increased with storage time: 1-heptanol, 1-octanol, and hexanal (a traditional indicator for oxidation in almonds) in (A) light-roasted and (B) dark-roasted samples stored at 35 °C over 24 weeks.

**Table 3. Volatiles Formed during the Storage of Almonds at 35°C (Nanograms per Gram)**

| | light roast (28 min at 138 °C) | | | dark roast (38 min at 138 °C) | | |
|---|---|---|---|---|---|---|
| volatile compound | 16 weeks | 20 weeks | 24 weeks | 16 weeks | 20 weeks | 24 weeks |
| 2-octanone | 13.4 ± 1.4 | 52.3 ± 2.9 | 33.3 ± 0.1 | 6.4 ± 0.2 | 15.4 ± 0.9 | 34.2 ± 4.0 |
| 2-nonanone | 9.8 ± 1.4 | 47.5 ± 0.9 | 31.2 ± 0.2 | 4.8 ± 0.3 | 16.4 ± 0.4 | 28.6 ± 4.3 |
| 3-octen-2-one | 18.1 ± 1.8 | 41.1 ± 2.0 | 45.4 ± 0.9 | 9.1 ± 0.4 | 19.7 ± 0.6 | 33.6 ± 4.5 |
| 2-decanone | 2.8 ± 0.2 | 13.4 ± 0.2 | 10.3 ± 0.4 | ND[a] | 7.2 ± 1.4 | 7.6 ± 1.3 |
| (*E*)-2-decenal | 2.9 ± 0.1 | 7.1 ± 1.1 | 10.9 ± 0.9 | 2.4 ± 0.8 | 5.6 ± 0.4 | 6.6 ± 1.4 |
| 2,4-nonadienal | 10.5 ± 0.9 | 14.2 ± 1.2 | 15.4 ± 1.1 | 7.5 ± 0.1 | 10.9 ± 0.5 | 10.4 ± 1.6 |
| 2-undecenal | ND | 2.1 ± 0.7 | 3.4 ± 0.3 | ND | 1.5 ± 0.1 | 1.8 ± 0.3 |
| 1-octen-3-ol | 2.2 ± 0.2 | 7.4 ± 0.4 | 6.9 ± 0.1 | 1.4 ± 0.0 | 4.1 ± 0.0 | 8.9 ± 1.3 |
| nonanol | 0.8 ± 0.1 | 2.2 ± 0.1 | 2.0 ± 0.1 | 0.5 ± 0.1 | 1.1 ± 0.3 | 1.0 ± 0.1 |
| pentyl oxirane | 9.9 ± 0.8 | 55.8 ± 11.1 | 27.8 ± 0.9 | 5.0 ± 0.8 | 9.5 ± 0.4 | 97.5 ± 9.3 |
| hexyl oxirane | 31.0 ± 3.1 | 1.7 ± 0.7 | 42.1 ± 0.2 | 9.7 ± 1.5 | 12.2 ± 0.6 | 2.9 ± 0.3 |
| acetic acid | 35.8 ± 2.7 | 60.8 ± 3.0 | 45.2 ± 2.3 | 43.5 ± 5.4 | 57.9 ± 1.5 | 60.2 ± 16.1 |
| vinyl hexanoate | 1.5 ± 0.2 | 6.8 ± 0.1 | 4.9 ± 0.2 | 1.2 ± 0.0 | 4.1 ± 0.4 | 8.1 ± 1.3 |
| pentanoic acid | 0.9 ± 0.1 | 6.1 ± 0.2 | 2.5 ± 0.2 | 0.5 ± 0.1 | 3.3 ± 0.0 | 5.9 ± 1.9 |
| heptanoic acid | 0.6 ± 0.0 | 5.4 ± 2.3 | 4.6 ± 0.4 | 0.5 ± 0.1 | 4.1 ± 0.7 | 2.7 ± 0.6 |
| octanoic acid | 0.4 ± 0.1 | 5.2 ± 2.3 | 5.1 ± 0.7 | 0.2 ± 0.0 | 3.6 ± 0.7 | 2.0 ± 0.3 |
| nonanoic acid | ND | 1.3 ± 0.8 | 2.5 ± 0.2 | ND | 0.6 ± 0.2 | 0.4 ± 0.0 |

[a]ND, not detected.

higher levels of total volatiles as compared to the light-roast almonds (Figure 1). Regardless of the degree of roasting or storage temperature, total volatiles decreased significantly during the first 4 weeks of storage. Volatiles continued to decrease at a slower rate between 6 and 24 weeks. The decrease in total volatiles was due to the loss of volatile compounds that were formed during the roasting process (Table 2). The almonds stored at 35 °C demonstrated increases in total volatiles after 20 weeks of storage, whereas no increases were observed in almonds stored at 25 °C.

The decreases in volatile compounds in the light- and dark-roast almonds stored at 25 or 35 °C were similar. In general, roasting increases the concentration of branch-chain aldehydes, alcohols, pyrazines, heterocyclic, and sulfur-containing compounds.[27] Herein, we found that the majority of these compounds decreased significantly with storage and could not be detected after 8−10 weeks of storage.

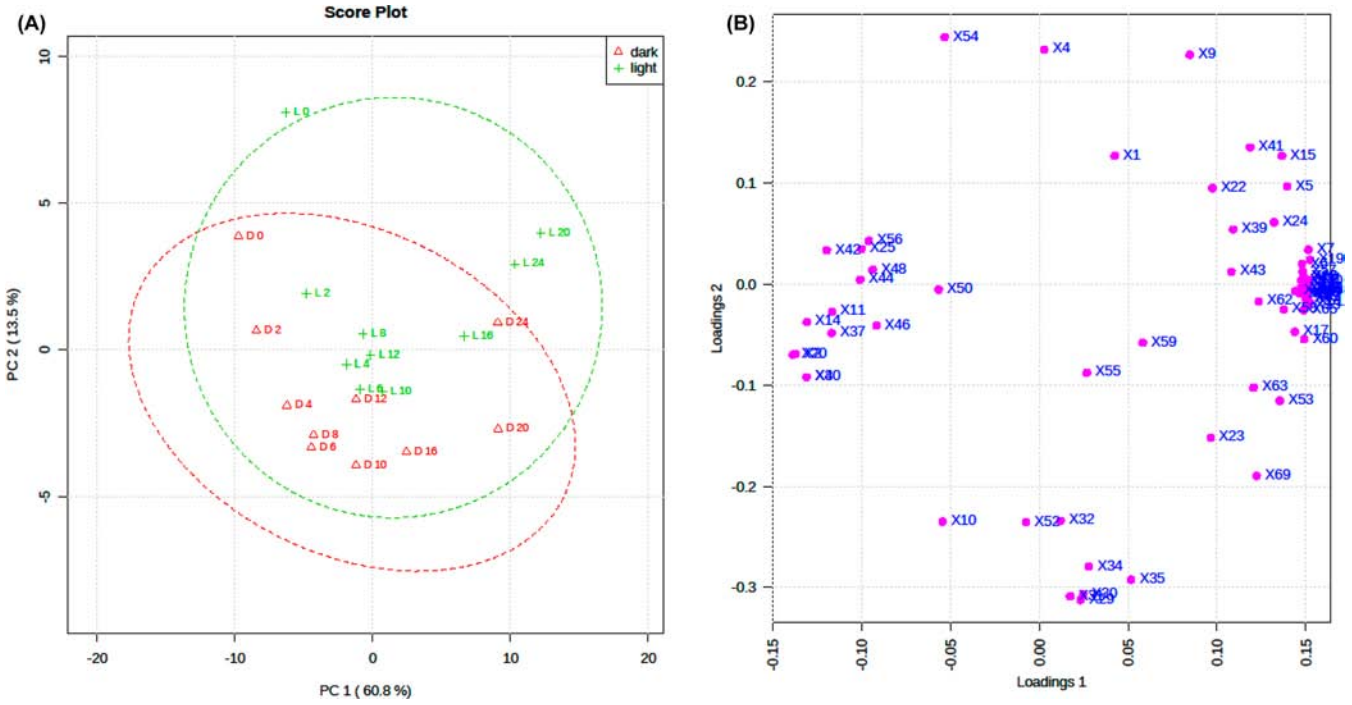


**Figure 4.** Principal component analysis on 68 volatile compounds determined by HS-SPME-GC-MS for different roasting and storage times: (A) PCA score plot with sample labeling; (B) PCA loading plot with compound codes. Compound codes are explained in Table 1.

The volatile carbonyl compounds detected in roasted almonds include 2-methylbutanal, 3-methylbutanal (Figure 2A), 2,3-butanedione, furfural, and 2-phenylacetaladehyde (Figure 2B). The concentrations of these volatiles decreased by 75−89% in the first month of storage and remained low through the remainder of the 6 month study. 2-Methylbutanal and 2-phenylacetaldehyde are produced through the Strecker reaction.[29] The concentration of these compounds decreased by 45−75% in the first 2 weeks of storage and remained low through the remainder of the 24 week study.

Pyrazines are key components of toasted almond aroma[18] and are formed in almonds during roasting.[27] Herein, most pyrazines did not show significant decrease during storage ($p < 0.05$) (Figure 2C,D). This result is consistent with Warner et al.'s study on roasted peanuts.[30] By 24 weeks of storage the concentrations of trimethylpyrazine and 2,6-dimethylpyrazine remained at initial levels (Figure 2D).

Roasting promoted the formation of Maillard reaction products including furfuryl alcohol and two branched-chain ketones (1-hydroxypropan-2-one and 3-hydroxybutan-2-one). These volatiles decreased significantly (>90%) by 10 weeks of storage regardless of the degree of roast (Table 2). The two sulfur-containing volatiles (1-methylthio-2-propanol and 2-ethylthio-ethanol) formed during roasting decreased significantly with storage time (Figure 2E). The majority of additional volatiles that were detected, such as ethyl acetate, $\alpha$-pinene, methylsulfanylmethane, and pyrrole, also decreased during storage (Figure 2F).

Levels of straight-chain aldehydes (e.g., butanal, pentanal, hexanal, heptanal, octanal, and nonanal) were significantly higher in the roasted almonds immediately after roasting. Straight-chain aldehydes and alcohols are products of lipid oxidation, generated in response to thermal processing.[18,27] The levels of straight-chain aldehydes decreased over the first 6−10 weeks of storage. After 20 weeks of storage, the levels of these aldehydes increased again, reflecting lipid oxidation (Table 2). The levels of heptanal increased 2−4-fold as compared to its original concentration after 24 weeks of storage. Heptanal is a common oxidation product of oleic acid.[31] The levels of caproic acid (hexanoic acid) began to increase at ∼16 weeks, increasing by 7-fold at 24 weeks. Caporic acid can be generated by the oxidation of lipids.[32]

Hexanal is commonly used as a volatile marker of oxidation in foods.[12] Hexanal is an abundant oxidation product and therefore is more easily detected than are other oxidation products.[12] However, the concentration of hexanal in nuts is affected by numerous factors including kernel maturity,[33] roasting conditions,[15] fat content,[12] and variety.[8] Significant oxidation has generally occurred when substantial increases in hexanal are measurable, and the quality of the almonds may no longer be acceptable.

During initial stages of storage, we found that the levels of hexanal decreased. Levels then increased at ∼20−24 weeks of storage regardless of the degree of roasting (Figure 3A,B). This is similar to results shown by García-Llatas et al.[16] The levels of 1-heptanol increased more significantly between 16 and 20 weeks of storage regardless of the degree of roast (Figure 3A,B), and the response was more sensitive than the response of hexanal. Additionally, unlike hexanal, the levels of 1-heptanol did not show a decrease during the initial 16 weeks of storage. A similar trend was observed for 1-octanol; however, the response of 1-octanol was not as sensitive as that of 1-heptanol.

Additional potential markers of oxidative events include compounds that were initially absent in the roasted almonds but detectable ∼16−20 weeks of storage (i.e., 2-octanone, 2-nonanone, 3-octen-2-one, 2-decanone, (*E*)-2-decenal, 2,4-nonadienal, 2-undecenal, 1-octen-3-ol, nonanol, pentyl oxirane, hexyl oxirane, acetic acid, vinyl hexanoate, pentanoic acid, heptanoic acid, octanoic acid, and nonanoic acid). At 16 weeks of storage, the levels of 2-octanone, 3-octen-2-one, and acetic

acid showed significant increases (Table 3), whereas hexanal levels (the traditional marker) were not significantly increased. At 24 weeks of storage, 2-octanone, 3-octen-2-one, and acetic acid levels increased between 1.2- and 5.3-fold as compared with their levels at 16 weeks. Thus, 2-octanone, 3-octen-2-one, and acetic acid may be more sensitive indicators of early oxidation development in roasted almonds than hexanal.

A PCA was performed on the data. ANOVA indicated that 2,3-dimethylpyrazine, 2-methyl-1-propanol, and 2-propenol were not significant compounds ($p < 0.001$), and so these compounds were excluded from the PCA. In the PCA score plot, 74.3% of the variance could be explained within the first two dimensions (Figure 4A). Almond samples were separated on the basis of storage periods; volatile profiles in late storage periods (16−24 weeks) separated from volitle profiles from early storage periods (0−12 weeks). PC1 explains 60.8% of the total variance. Along the PC1, early storage periods clustered on the left side, whereas late storage periods clustered on the right side. PC2 explains 13.5% of the total variance. Light-roast samples clustered in the bottom right quadrant, whereas dark-roast samples clustered in the top right.

The PCA loading plot (Figure 4B) indicates that compounds formed during storage drive the separation (i.e., 2-octanone (X12), 2-nonanone (X16), 3-octen-2-one (X18), 2-decanone (X21), (*E*)-2-decenal (X26), 2,4-nonadienal (X27), 2-undecenal (X28), 1-octen-3-ol (X45), nonanol (X51), pentyl oxirane (X57), hexyl oxirane (X58), acetic acid (X61), vinyl hexanoate (X64), pentanoic acid (X66), heptanoic acid (X68), octanoic acid (X70), and nonanoic acid (X71)).

In conclusion, improved sensitivity of oxidation may be achieved by evaluating the levels of two groups of volatile compounds. The first are those that are absent from raw and freshly roasted almonds but detectable around 16 weeks of storage and include certain oxiranes, carbonyls, and short-chain acids. The second includes heptanol and 1-octanol as these correlate to early stages of oxidation and are observed before hexanal levels rise. Together these markers can be used to probe early changes in product quality, improve the sensitivity of detection for oxidation, and help to prevent the loss from significant oxidation in almonds at later stages.

In addition, we found significant decreases in roasting-related aroma volatiles at 4 weeks of storage, independent of the degree of roast or storage temperature. In general, a low volatile stage occurs around the fourth week of storage. This is followed by increasing levels of volatiles associated with lipid oxidation. At a storage temperature of 35 °C, oxidation-related volatiles begin to dominate the volatile profile at 20 weeks.

## AUTHOR INFORMATION


### Corresponding Author

*(A.E.M.) Mail: Department of Food Science and Technology, Robert Mondavi Institute, South Building, University of California, Davis, One Shields Avenue, Davis, CA 95616, USA. Phone: (530) 752-7926. Fax: (530) 752-4759. E-mail: aemitchell@ucdavis.edu.



### Funding

The Almond Board of California provided financial support for this study.


### Notes

The authors declare no competing financial interest.

## ACKNOWLEDGMENTS

We especially thank Guangwei Huang for numerous thoughtful discussions and Sylvia Yada for editorial support. Additionally, we thank Anna Hjelmeland for analytical support.

## ABBREVIATIONS USED

HS, headspace; SPME, solid phase microextraction; GC-MS, gas chromatography−mass spectrometry; TBA, thiobarbituric acid; PV, peroxide value; KI, Kovats' retention index; TIC, total ion chromatogram

## REFERENCES


(1) California Almond Board. Almond Almanac, 2012; http://almondboard.com/AboutTheAlmondBoard/Documents/2012%20Almond%20Almanac_FINAL.pdf.

(2) Senesi, E.; Rizzolo, A.; Colombo, C.; Testoni, A. Influence of pre-processing storage conditions on peeled almond quality. *Ital. J. Food Sci.* **1996**, *2*, 115−125.

(3) Kader, A. A. In-plant storage. In *Almond Production Manual*; Micke, C. W., Ed.; Publication 3364; University of California, Division of Agriculture and Natural Resources: Davis, CA, USA, 1996; pp 274−277.

(4) Almond Board of California. *Guidelines for Validation of Dry Roasting Processes*, 2007; http://www.almondboard.com.

(5) Abdallah, A.; Ahumada, M. H.; Gradziel, T. M. Oil content and fatty acid composition of almond kernels from different genotypes and California production regions. *J. Am. Soc. Hortic. Sci.* **1998**, *123*, 1029−1033.

(6) Kodad, O.; Socias i Company, R. Variability of oil content and of major fatty acid composition in almond (*Prunus amygdalus* Batsch) and its relationship with kernel quality. *J. Agric. Food Chem.* **2008**, *56*, 4096−4101.

(7) Buransompob, A.; Tang, J.; Mao, R.; Swanson, B. G. Rancidity of walnuts and almonds affected by short time heat treatments for insect control. *J. Food Process. Preserv.* **2003**, *27*, 445−464.

(8) Zacheo, G.; Cappello, M. S.; Gallo, A.; Santino, A.; Cappello, A. R. Changes associated with post-harvest ageing in almond seeds. *LWT−Food Sci. Technol.* **2000**, *33*, 415−423.

(9) Agila, A.; Barringer, S. Effect of roasting conditions on color and volatile profile including HMF level in sweet almonds (*Prunus dulcis*). *J. Food Sci.* **2012**, *77*, C461−C468.

(10) Severini, C.; De Pilli, T.; Baiano, A.; Gomes, T. Autoxidation of packed roasted almonds as affected by two packaging films. *J. Food Process. Preserv.* **2003**, *27*, 321−335.

(11) Zacheo, G.; Cappello, A. R.; Perrone, L. M.; Gnoni, G. V. Analysis of factors influencing lipid oxidation of almond seeds during accelerated ageing. *LWT−Food Sci. Technol.* **1998**, *31*, 6−9.

(12) Laguerre, M.; Lecomte, J.; Villeneuve, P. Evaluation of the ability of antioxidants to counteract lipid oxidation: existing methods, new trends and challenges. *Prog. Lipid Res.* **2007**, *46*, 244−282.

(13) Guillén-Sans, R.; Guzmán-Chozas, M. The thiobarbituric acid (TBA) reaction in foods: a review. *Crit. Rev. Food Sci. Nutr.* **1998**, *38*, 315−350.

(14) Beck, J. J.; Mahoney, N. E.; Cook, D.; Gee, W. S. Volatile analysis of ground almonds contaminated with naturally occurring fungi. *J. Agric. Food Chem.* **2011**, *59*, 6180−6187.

(15) Siegmund, B.; Murkovic, M. Changes in chemical composition of pumpkin seeds during the roasting process for production of pumpkin seed oil (part 2: volatile compounds). *Food Chem.* **2004**, *84*, 367−374.

(16) García-Llatas, G.; Lagarda, M. J.; Clemente, G.; Farré, R. Monitoring of headspace volatiles in milk-cereal-based liquid infant foods during storage. *Eur. J. Lipid Sci. Technol.* **2006**, *108*, 1028−1036.

(17) Mexis, S. F.; Badeka, A. V.; Kontominas, M. G. Quality evaluation of raw ground almond kernels (*Prunus dulcis*): effect of active and modified atmosphere packaging, container oxygen barrier

and storage conditions. *Innovative Food Sci. Emerging Technol.* **2009**, *10*, 580−589.
(18) Vázquez-Araújo, L.; Enguix, L.; Verdú, A.; García-García, E.; Carbonell-Barrachina, A. A. Investigation of aromatic compounds in toasted almonds used for the manufacture of *turrón*. *Eur. Food Res. Technol.* **2008**, *227*, 243−254.
(19) Vázquez-Araújo, L.; Verdú, A.; Navarro, P.; Martínez-Sánchez, F.; Carbonell-Barrachina, A. A. Changes in volatile compounds and sensory quality during toasting of Spanish almonds. *Int. J. Food Sci. Technol.* **2009**, *44*, 2225−2233.
(20) Alasalvar, C.; Shahidi, F.; Cadwallader, K. R. Comparison of natural and roasted Turkish Tombul hazelnut (*Corylus avellana* L.) volatiles and flavor by DHA/GC/MS and descriptive sensory analysis. *J. Agric. Food Chem.* **2003**, *51*, 5067−5072.
(21) Peréz, A. G.; Sanz, C.; Olías, R.; Olías, J. M. Lipoxygenase and hydroperoxide lyase activities in ripening strawberry fruits. *J. Agric. Food Chem.* **1999**, *47*, 249−253.
(22) Frankel, E. N. Chemistry of autoxidation: mechanism, products and flavor significance. In *Flavor Chemistry of Fats and Oils*; Min, D. B., Smouse, T. H., Eds.; American Oil Chemists' Society: Champaign, IL, USA, 1985; pp 1−38.
(23) Lasekan, O.; Abbas, K. Investigation of the roasting conditions with minimal acrylamide generation in tropical almond (*Terminalia catappa*) nuts by response surface methodology. *Food Chem.* **2011**, *125*, 713−718.
(24) Stone, E. J.; Hall, R. M.; Kazeniac, S. J. Formation of aldehydes and alcohols in tomato fruit from U-14 C-labeled linolenic and linoleic acids. *J. Food Sci.* **1975**, *40*, 1138−1141.
(25) Nykänen, L.; Suomalainen, H. *Aroma of Beer, Wine and Distilled Alcoholic Beverages*, 1st ed.; D. Riedel Publishing: Boston, MA, USA, 1983; p 27.
(26) Burdock, G. A. *Fenaroli's Handbook of Flavor Ingredients*, 5th ed.; CRC Press: Boca Raton, FL, USA, 2004; 223 pp.
(27) Xiao, L.; Lee, J.; Zhang, G.; Ebeler, S. E.; Wickramasinghe, Y.; Seiber, J.; Mitchell, A. E. HS-SPME GC/MS characterization of volatiles in raw and dry-roasted almonds (*Prunus dulcis*). *Food Chem.* **2014**, *151*, 31−39.
(28) Baek, H. H.; Cadwallader, K. R. Volatile compounds in flavor concentrates produced from crayfish-processing byproducts with and without protease treatment. *J. Agric. Food Chem.* **1996**, *44*, 3262−3267.
(29) Pripis-Nicolau, L.; Bertrand, A.; Maujean, A. Formation of flavor components by the reaction of amino acid and carbonyl compounds in mild conditions. *J. Agric. Food Chem.* **2000**, *48*, 3761−3766.
(30) Warner, K. J. H.; Dimick, P. S.; Ziegler, G. R.; Mumma, R. O.; Hollender, R. 'Flavor-fade' and off-flavors in ground roasted peanuts as related to selected pyrazines and aldehydes. *J. Food Sci.* **1996**, *61*, 469−472.
(31) Frankel, E. *Lipid Oxidation*; The Oily Press: Dundee, UK, 1998; pp 63−69.
(32) Snyder, J. M.; Frankel, E. N.; Selke, E. Capillary gas chromatographic analyses of headspace volatiles from vegetable oils. *J. Am. Oil Chem. Soc.* **1985**, *62*, 1675−1679.
(33) Pattee, H. E.; Singleton, J. A.; Johns, E. B.; Mullin, B. C. Changes in the volatile profile of peanuts and their relation to enzyme activity levels during maturation. *J. Agric. Food Chem.* **1970**, *18* (3), 353−356.

droplets.[21] Furthermore, it has been reported that the storage stability of emulsions stabilized by nonionic surfactants is strongly dependent upon their PIT,[22−24] which depends on salt concentration. Many previous studies on the impact of salt on nanoemulsion formation have utilized simple organic solvents or liquids as the oil phase. In this study, we utilized an oil phase that is more representative of those that might be used in the food industry, that is, vitamin E acetate dissolved in medium-chain triglycerides (MCT).

Recently, we demonstrated that stable vitamin E-enriched emulsions containing very fine droplets ($d$ < 60 nm) could be produced by spontaneous emulsification.[25] We also showed that addition of cosolvents to the aqueous phase of these emulsions had an appreciable influence on their formation and stability.[26,27] The purpose of the present study was to investigate the influence of two salts commonly used in industrial applications (NaCl and $CaCl_2$) on the formation and stability of vitamin E emulsions produced using spontaneous emulsification. The knowledge gained from this study will be useful for the successful incorporation of emulsion-based delivery systems into commercial products.

## MATERIALS AND METHODS

**Materials.** Vitamin E acetate (VE) was kindly donated by BASF (Ludwigshafen, Germany). MCT oil (MIGLYOL 812) was purchased from Warner Graham Co. (Sasol Germany GmbH). Nonionic surfactant (Tween 80), sodium chloride, calcium chloride anhydrous, citric acid, and sodium benzoate were purchased from Sigma-Aldrich Co. (St. Louis, MO, USA). Double-distilled water was used in the preparation of all solutions and emulsions.

**Emulsion Preparation.** Emulsion formation was carried out using the spontaneous emulsification procedure described in our previous study.[27] In brief, spontaneous emulsification was performed by the addition of an organic phase to an aqueous phase with constant magnetic stirring (600 rpm) at 25 °C. The organic phase consisted of VE, MCT, and surfactant, whereas the aqueous phase consisted of a buffer solution containing 0.8 wt % citric acid, 0.08 wt % sodium benzoate, and different levels of NaCl or $CaCl_2$ (pH 3.0). On the basis of the results of our previous studies, we prepared emulsions with the following composition: 8% vitamin E acetate; 2% MCT; 10% Tween 80; and 80% buffer solution (pH 3). The oil (8 g VE + 2 g MCT) and surfactant (10 g) were first mixed together to form an organic phase, which was then slowly poured into 80 g of aqueous phase over a 15 min period with continuous stirring.

Emulsions were diluted in three different ways to contain final systems with different droplet concentrations and aqueous phase compositions: (i) with buffer solution (pH 3); (ii) with salt solutions (NaCl or $CaCl_2$) with similar salt concentrations as the emulsions (pH 3); and (iii) with salt solutions containing various salt concentrations.

**Particle Size Measurements.** Particle size distributions were measured using a dynamic light scattering instrument (Zetasizer Nano ZS, Malvern Instruments, Malvern, UK). This instrument determines the particle size from intensity−time fluctuations of a laser beam (633 nm) scattered from a sample at an angle of 173°. Each individual measurement was an average of 13 runs. To avoid multiple scattering effects, samples were diluted (500 times) before the particle size measurements using buffer solution (pH 3.0). The mean droplet radius ($Z$-average) was calculated from the particle size distribution. All measurements were conducted at ambient temperature.

**Turbidity Measurements and Cloud Point Calculation.** The influence of temperature on emulsion turbidity was determined using a UV−visible spectrophotometer with temperature scanning capabilities (Evolution Array, Thermo Scientific). The absorbance ($A$) at 600 nm was measured as the temperature was increased from 20 to 95 °C at 1 °C/min. The cloud point was empirically defined as the temperature at which the slope of the turbidity−temperature profile ($d\tau/dT$) first reached a maximum value during heating.

**Statistical Analysis.** All experiments were carried out two or three times using two freshly prepared samples, and the results are reported as the calculated mean and standard deviation of these measurements. Differences between group means were determined by analysis of variance (ANOVA) using statistical software (version 12.0; SPSS, Inc., Chicago, IL, USA). Means were subjected to Duncan's test, and a $P$ value of <0.05 was considered statistically significant.

## RESULTS AND DISCUSSION

**Effect of Salts on Initial Particle Size.** Initially, the influence of salt type and concentration on the size of the oil droplets formed in vitamin E emulsions produced by spontaneous emulsification was determined. The oil phase contained 80% vitamin E and 20% MCT. This composition produced the smallest particle size as shown in a previous study,[25] and so we used this oil phase composition in the present study. The aqueous phase contained either 0−1 N NaCl or 0−0.5 N $CaCl_2$. The influence of different salt concentrations on the initial mean droplet diameter of the emulsions was measured. The mean droplet diameter remained relatively constant at all salt levels used: ≈52 nm from 0 to 1 N NaCl and ≈51 nm from 0 to 0.5 N $CaCl_2$. Therefore, the addition of salt did not have an appreciable effect on the mean droplet diameter of the emulsions at any of the levels tested. The particle size distributions of all these emulsions were also similar, that is,, monomodal with similar modes and widths (data not shown).

In principle, one might expect the presence of salts to affect the size of the droplets produced by spontaneous emulsification by altering the bulk physicochemical properties of the aqueous phase (e.g., density, refractive index, viscosity, and interfacial tension) or by altering its molecular properties (e.g., structural organization). Changes in the viscosity of an aqueous solution would be expected to affect the mass transport kinetics of surfactant and oil molecules at the boundary between the organic and aqueous phases, which could influence the spontaneous formation of small droplets at the phase boundary.[28] Changes in oil/water interfacial tension would also be expected to influence spontaneous droplet formation by altering the dynamics of the phase boundary. Having said this, the addition of NaCl and $CaCl_2$ to aqueous solutions at the highest levels used in this study (1 and 0.5 N, respectively) should only slightly increase their interfacial tension, viscosity, density, and refractive index (Table 1). Consequently, the influence of salts on the physicochemical properties of the

**Table 1. Effect of Salt Concentration (N Salts in Aqueous Phase) on the Relative Viscosity, Refractive Index, Relative Density, and Excess Interfacial Tension**

| | relative viscosity $\eta/\eta_o$[a] | refractive index | relative density (kg/L) | excess interfacial tension[b] (mN/m) |
|---|---|---|---|---|
| water | 1.000[c] | 1.333[c] | 1.000[c] | 0.0[e] |
| NaCl solution (1 N) | 1.090[c] | 1.343[c] | 1.038[c] | 0.9[e] |
| $CaCl_2$ solution (0.5 N) | 1.070[d] | 1.346[c] | 1.044[c] | 1.9[e] |

[a]Ratio of the absolute viscosity of solution at 20 °C to the ratio of the absolute viscosity of water at 20 °C. [b]Excess interfacial tension is defined as the difference between interfacial tension of hydrocarbon/salts solution and interfacial tension of hydrocarbon/water. [c]Reference 50. [d]Reference 51. [e]Reference 52.

aqueous phase might be expected to be relatively small. Previous studies have shown that changes in the solubility and optimum curvature of surfactants in surfactant−oil−water (SOW) mixtures play a crucial role in the spontaneous formation of oil droplets using low-energy methods.[8,29,30] The fact that we observed no influence of salts on the initial particle size in this study (Table 1 and Figure 1) suggests that the salts did not have an appreciable influence on surfactant solubility or optimum curvature under the conditions used. Nevertheless, this is likely to be highly dependent on the nature of the surfactant used to form the emulsions.

**Effect of Salts on Thermal Stability.** Emulsion-based delivery systems are usually exposed to elevated temperatures during their manufacture, storage, or utilization, for example, hot filling, pasteurization, or cooking. Therefore, information about the thermal stability of emulsions is of particular importance for many commercial applications. We therefore investigated the impact of salt type and concentration on the thermal stability of the vitamin E emulsions using a spectrophotometric method. The turbidity of emulsions containing different NaCl and $CaCl_2$ concentrations was measured as they were subjected to a temperature increase from 20 to 95 °C. The turbidity profiles in the presence of NaCl and $CaCl_2$ were qualitatively similar, and therefore we show only the results for the emulsion containing NaCl (Figure 1a).

The turbidity of the emulsions remained relatively low and constant during heating from 0 to 75 °C in the absence of NaCl, then increased sharply around 75−80 °C, and then remained high upon further heating from 80 to 95 °C (Figure 1a). This steep rise in turbidity can be ascribed to an increase in droplet size during heating. As the temperature increased, there would be progressive dehydration of the polar headgroups of the nonionic surfactant molecules (Tween 80), which would reduce the hydration repulsion between the droplets, thereby promoting droplet coalescence.[31,32] Furthermore, dehydration of the surfactant headgroups changes the optimum curvature of the surfactant monolayer toward unity, which favors ultralow interfacial tension, high interfacial flexibility, and droplet coalescence.[3,33] The turbidity−temperature profiles of emulsions containing salt were more complex than those containing no salt (Figure 1a). For instance, for the emulsions containing 0.15 N NaCl, the turbidity remained low and constant from 20 to 74 °C, increased steeply from 74 to 78 °C, and remained high from 78 to 88 °C, which was qualitatively similar as the turbidity−temperature profile measured in the absence of salt. However, upon increasing the temperature further, there was a sharp drop in the turbidity from 88 to 90 °C, followed by another steep increase from 90 to 93 °C, after which the turbidity remained high from 93 to 95 °C (Figure 1a). The turbidity−temperature profiles observed for the emulsions containing salt can be related to a transitional phase inversion of the SOW system around the PIT. The phase inversion temperature is governed by changes in the optimum curvature and relative solubility of nonionic surfactants with temperature.[29,34] The molecular geometry of a surfactant can be defined by a packing parameter, $p$[35]

$$p = \frac{a_T}{a_H}$$

where $a_T$ and $a_H$ are the cross-sectional areas of the lipophilic tail-group and hydrophilic headgroup, respectively. Initially, the emulsions had relatively low turbidities at room temperature

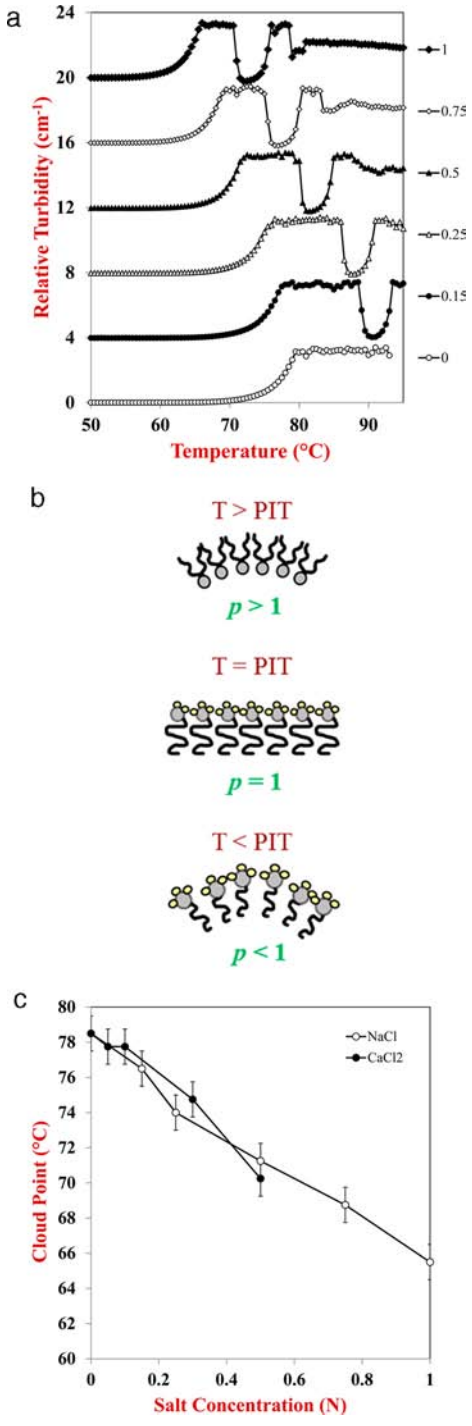


**Figure 1.** (a) Influence of temperature on the relative turbidity of vitamin E-enriched mini-emulsion produced using 10% oil phase (vitamin E/MCT, 8:2), 10% surfactant phase (Tween 80), and 80% aqueous phase with different concentrations (N) of NaCl. To prevent overlap of the graphs, the unit values of 4, 8, 12, 16, and 20 were added to the turbidity data obtained for the emulsion with aqueous phase containing 0.15, 0.25, 0.5, 0.75, and 1 N NaCl, respectively, and the corresponding turbidities were reported as relative turbidity. (b) Packing parameter ($p$) and optimum curvature of Tween 80 at different temperatures. (c) Influence of salt concentration on the cloud point of vitamin E-enriched mini-emulsion produced using 10% oil phase (vitamin E/MCT, 8:2), 10% surfactant phase (Tween 80), and 80% aqueous phase.

because they contained very small droplets that did not scatter light strongly.[36] At these low temperatures the surfactant is relatively hydrophilic, and the corresponding optimum curvature ($p < 1$) favors the formation of oil-in-water emulsions. As temperature increases, the headgroup of the nonionic surfactant (Tween 80) undergoes progressive dehydration, causing the packing parameter to increase (Figure 1b). As a result, the rate of droplet coalescence increases because of the reduced hydration repulsion between droplets and the increase in interfacial flexibility, and so there is a corresponding increase in turbidity. However, when the temperature reaches the PIT, the surfactant monolayer has zero curvature, the packing parameter is close to unity ($p = 1$), and the interfacial tension becomes ultralow (Figure 1b). These changes favor the formation of a bicontinuous microemulsion phase containing very small structures that do not scatter light strongly, thereby leading to a reduction in turbidity. Increasing the temperature above the PIT further dehydrates the headgroups of the surfactant molecules, which increases their lipophilicity, increases the packing parameter ($p > 1$), and changes the optimum curvature so that it favors the formation of water-in-oil emulsions (Figure 1b). The water droplets in the water-in-oil emulsions formed above the PIT are relatively large and therefore scatter light strongly, leading to increased turbidity.[3,29]

The impact of salt on the turbidity−temperature profiles of the emulsions can be attributed to the fact that salt decreases the PIT of the emulsions. In the absence of salt, the PIT is relatively high, and therefore we observed only the initial droplet coalescence regimen. In the presence of sufficient salt, the PIT moved into the experimental temperature range, and we could observe droplet coalescence, microemulsion formation, and phase inversion. A similar behavior was observed in the turbidity−temperature profiles of vitamin E-enriched emulsions in the absence and presence of glycerol; that is, glycerol reduced the PIT.[26]

The turbidity versus temperature profiles were used to determine the cloud points of the emulsions so that we could establish the influence of salt type and concentration on their thermal behavior. The cloud point of the emulsions decreased from around 78 to 65 °C when the NaCl concentration was increased from 0 to 1 M and decreased from around 78 to 70 °C when the $CaCl_2$ concentration was increased from 0 to 0.5 N (Figure 1c). The ability of NaCl[14,15,20,37] and $CaCl_2$[14,15,37] to decrease the cloud points of nonionic surfactant has been reported previously. Our results are also in agreement with previous studies that have reported that the cloud point and/or PIT of nonionic surfactants is a linear function of their salt concentration.[15,38,39] The decrease in thermal stability (cloud point) of emulsions in the presence of NaCl and $CaCl_2$ can be attributed to the effect of these salts on the solubility and packing characteristics of nonionic surfactants.

Specific anionic[19,40,41] and cationic[12,16,19,40] salt ions may either increase (salting in) or decrease (salting out) the solubility of nonionic surfactants due to their effects on the structural organization of water molecules. Ions can be classified as either "structure-makers" (salting out) or "structure-breakers" (salting in) according to their position in the Hofmeister series.[42,43] The presence of mineral ions in an aqueous solution may alter the PIT of a nonionic surfactant by altering the solubility and packing characteristics of the surfactant molecules. In particular, salts may affect the optimum curvature of the surfactants by altering the hydration of their hydrophilic headgroups. In this study, we found that both NaCl and $CaCl_2$ reduced the PIT of the emulsions, which suggests that they increased the packing parameter ($p$) by promoting headgroup dehydration. Previously, this affect has been attributed to the fact that these ions promote structure formation of bulk water around the ions, thereby reducing the amount of water molecules available to hydrate the surfactant headgroups.[18] In an alternative interpretation of the Hofmeister series, Kabalnov et al.[44] suggested that the salting-in and salting-out phenomena have an interfacial origin driven by preferential adsorption/desorption of salt ions at the hydrophilic headgroup of the nonionic surfactant monolayers. Adding NaCl as a nonadsorbing salt dehydrates the hydrophilic headgroups through an osmotic effect associated with preferential ion exclusion, [44] thereby altering the optimum curvature and decreasing the PIT.

The fact that salt addition did not strongly influence the size of droplets during emulsion formation, but did influence their thermal stability (Figure 2), may have been due to their influence on the dehydration of the hydrophilic headgroups at different temperatures. Emulsion formation was carried out at low (room) temperature, and therefore the surfactant molecules would have been highly hydrated. Presumably, headgroup hydration was still sufficient in the presence of salt to generate a strong steric repulsion between the droplets and to have a high surfactant curvature. However, once the emulsions were heated, the effects of salts became more pronounced because the surfactants were already partially dehydrated, and any further change due to salt addition was sufficient to promote instability.

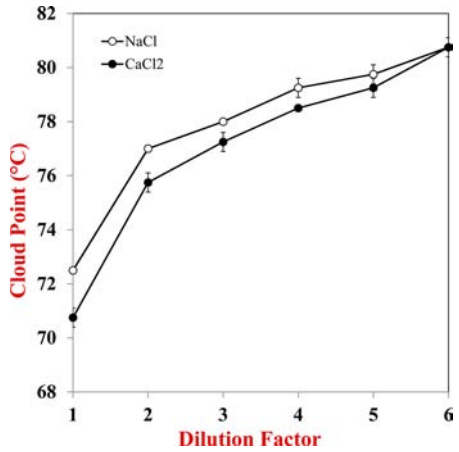


**Figure 2.** Influence of dilution on the cloud point of vitamin E-enriched mini-emulsion produced using 10% oil phase (vitamin E/MCT, 8:2), 10% surfactant phase (Tween 80), and 80% aqueous phase (0.5 M salt). Oil phase concentrations were 10, 5, 3.33, 2.5, and 1.67, and salt concentrations were 0.4, 0.2, 0.13, 0.1, 0.08, and 0.067 N for the emulsion diluted with dilution factors of 1, 2, 3, 4, 5, and 6, respectively.

**Influence of Dilution on Thermal Stability.** Emulsions are diluted when they are incorporated into functional food and beverage products. Our previous studies have shown that emulsion dilution may have an appreciable influence on emulsion thermal stability.[26,27,45] We therefore examined the influence of dilution with buffer solution on the thermal stability of vitamin E emulsions initially containing 0.5 N NaCl or $CaCl_2$ in the aqueous phase. Qualitatively, all of the diluted

emulsions had similar turbidity−temperature profiles as the undiluted emulsions (Figure 1a): upon increasing the temperature from 20 to 95 °C, the turbidity initially remained low, then steeply increased, then sharply decreased to a minimum, then steeply increased again, and then remained high (data not shown). The cloud points determined from these profiles increased from 73 to 81 °C for NaCl and from 70 to 81 °C $CaCl_2$ as the emulsion dilution factor (DF) increased from 1 to 6 (Figure 2). As these samples were diluted with buffer solution, the observed results may have been due to a decrease in salt concentration in the aqueous phase or due to a decrease in oil droplet concentration.

We therefore carried out additional experiments in which the emulsions were diluted with various salt solutions so as to obtain samples where (i) the droplet concentration was kept constant, but the salt concentration varied (Figure 3) or (ii) the droplet concentration varied, but the salt concentration was kept constant (Figure 4). In the diluted emulsions with fixed droplet concentration, the cloud point increased from around 73 to 77 °C for NaCl and from around 72 to 77 °C for $CaCl_2$ as the salt content decreased from 0.4 to 0.2 N, respectively (Figure 3). These results suggest that at least part of the increase in cloud point observed upon emulsion dilution (Figure 2) was related to a reduction in salt concentration in the aqueous phase. In the diluted emulsions with fixed salt concentration, the cloud point initially increased and then decreased as the droplet content was reduced from 10 to 1% (Figure 4a). This effect may have been an artifact of the cloud point measurement at high droplet concentration. As the droplet concentration increased, there was an increase in the overall turbidity of the samples due to an increase in light scattering by the droplets (Figure 4b). In the emulsions with the highest droplet concentrations, the turbidity was so great (>3 $cm^{-1}$) that it was not possible to observe the entire region where rapid droplet coalescence occurred. Consequently, it was not possible to accurately measure the cloud points for these samples. In the more dilute emulsions (≤3% oil), the cloud point decreased with increasing dilution (decreasing droplet concentration), which may have been due to changes in the nature of the microemulsion phase formed around the PIT when the SOW ratio was changed. Taken together, these results suggest that the increase in cloud point observed when salt-containing emulsions were diluted with buffer solution was primarily due to the reduced salt concentration in the aqueous phase, rather than the reduced droplet concentration.

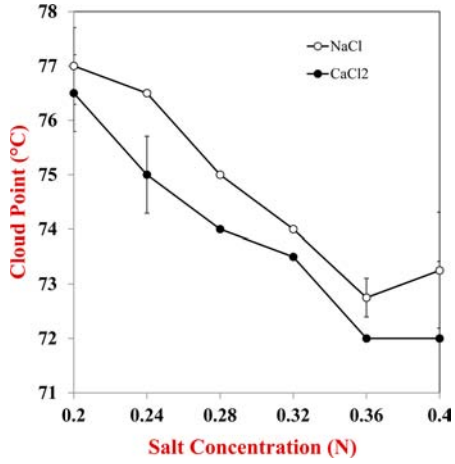


**Figure 3.** Influence of salt concentration on the cloud point of vitamin E-enriched mini-emulsions containing 5% oil phase. The initial emulsion was produced using 10% oil phase (vitamin E/MCT, 8:2), 10% surfactant phase (Tween 80), and 0.4 N salt.

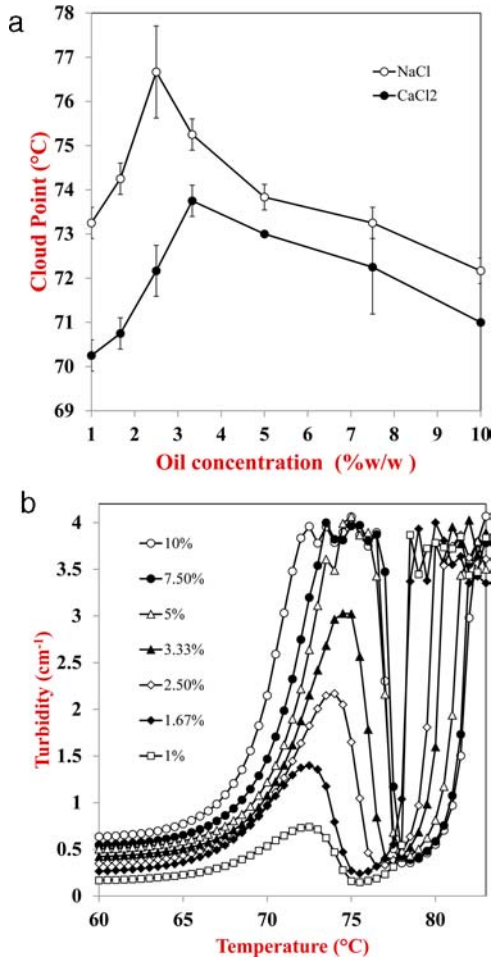


**Figure 4.** (a) Influence of oil phase concentration on the cloud point of diluted vitamin E-enriched mini-emulsions containing 0.4 N salts. The initial emulsion was produced using 10% oil phase (vitamin E/MCT, 8:2), 10% surfactant phase (Tween 80), and 0.4 N NaCl. (b) Influence of temperature on the turbidity of vitamin E-enriched miniemulsions containing 0.4 N $CaCl_2$ and different oil phase concentrations. The initial emulsion was produced using 10% oil phase (vitamin E/MCT, 8/2), 10% surfactant phase (Tween 80), and 0.4 N $CaCl_2$.

**Influence of Salts and Dilution on Isothermal Stability.** Physical stability of emulsion-based delivery systems during storage, transport, and utilization is required for most commercial applications. Emulsions may become unstable through a number of different physicochemical processes, including flocculation, coalescence, Ostwald ripening, and gravitational separation.[10,33] The mechanism and rate of breakdown depend on emulsion composition and microstructure, as well as the environmental conditions experienced during its lifetime. We therefore examined the influence of salt addition and dilution on the storage stability of vitamin E emulsions. A series of emulsions was fabricated with different droplet concentrations (2.5 or 10 wt %) and salt concentrations (0, 0.2, and 0.4 N NaCl or $CaCl_2$) by diluting an initial emulsion with different types and amounts of salt solution. After preparation, the resulting emulsions were stored for 1

month at three storage temperatures representing refrigeration conditions (5 °C), ambient storage in mild climates (20 °C), and ambient storage in hot climates (37 °C).

The initial emulsion formed by spontaneous emulsification contained 0% salt and 10% oil and was therefore designated "0/10". The extent of droplet growth in this emulsion after 1 month of storage was appreciable and increased with increasing storage temperature: ~15% at 5 °C, 19% at 20 °C, and 54% at 37 °C (Figure 5). The droplet size distribution of these

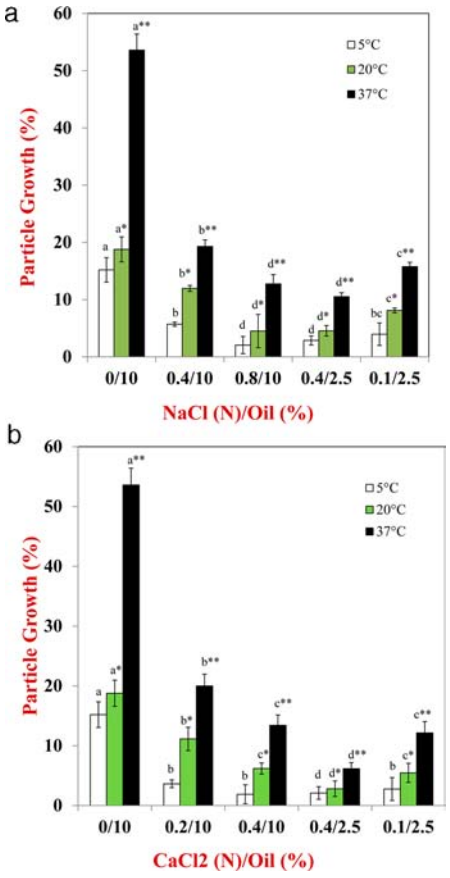


**Figure 5.** (a) Influence of storage time and temperature on the particle growth (%) of vitamin E-enriched mini-emulsions containing different ratios of NaCl (N)/oil phase. The initial emulsions were produced using 10% oil phase (vitamin E/MCT, 8:2), 10% surfactant phase (Tween 80), and different NaCl concentrations (0, 0.4, and 0.8 N). Means within different letters and the same number of stars are significantly ($P < 0.05$) different. (b) Influence of storage time and temperature on the particle growth (%) of vitamin E-enriched mini-emulsions containing different ratios of $CaCl_2$ (M)/oil phase. The initial emulsions were produced using 10% oil phase (vitamin E/MCT, 8:2), 10% surfactant phase (Tween 80), and different $CaCl_2$ concentrations (0, 0.2, and 0.4 N). Means within different letters and the same number of stars are significantly ($P < 0.05$) different.

emulsions remained monomodal throughout storage at all temperatures (data not shown). The stability of the emulsions to droplet growth improved significantly ($P < 0.05$) as the level of NaCl or $CaCl_2$ added was increased, especially at the elevated temperatures (Figure 5). In addition, reducing the droplet concentration from 10 to 2.5% also led to a significant ($P < 0.05$) inhibition of droplet growth for emulsions containing both types of salt (Figure 5). Overall, these results suggest that the addition of NaCl or $CaCl_2$ improved the isothermal storage stability of the emulsions, even though it decreased their thermal stability by reducing the cloud point (Figure 2). This independence of thermal and isothermal stability of vitamin E emulsions has also been reported upon posthomogenization addition of cosurfactants.[46]

There are a number of possible mechanisms that might be responsible for the observed instability of the emulsions during storage: flocculation, coalescence, and Ostwald ripening.[4,33] We do not believe that flocculation played an important role in emulsion instability as we did not observe any flocs using an optical microscope. We therefore postulated that the observed instability was due to either coalescence or Oswald ripening. It is often difficult to distinguish between these two mechanisms because they both lead to a net increase in mean droplet diameter over time.[33,47] An increase in droplet growth rate with increasing temperature could be attributed to the effects of temperature on coalescence and/or Ostwald ripening. Increasing temperature can dehydrate the surfactant headgroups and thereby increase droplet coalescence by (i) decreasing the hydration repulsion between droplets and (ii) by changing the optimum curvature of the surfactant monolayer toward unity.[3,31,48] A temperature rise may also increase the rate of Ostwald ripening by increasing the diffusion rate or solubility of the oil molecules in the aqueous phase.[49]

Inorganic salts might influence the isothermal storage stability of oil-in-water emulsions stabilized by nonionic surfactant through a number of mechanisms:

*Effect of Salts on Surfactant Headgroup Dehydration.* Previous studies have reported that salts that decrease the cloud point of emulsions stabilized by nonionic surfactant also increase droplet coalescence.[11,20] This effect was attributed to the ability of the salts to promote dehydration of the surfactant headgroup, thereby reducing the hydration repulsion between droplets and altering the surfactant monolayer curvature. However, the fact that we actually observed a decrease in droplet growth during storage in the presence of NaCl and $CaCl_2$ suggested that this mechanism was not prominent under the conditions used.

*Effect of Salts on van der Waals Interactions.* van der Waals interactions are attractive forces that almost always act between oil droplets suspended in water and, therefore, promote droplet aggregation. The addition of salts to an aqueous solution appreciably decreases the magnitude of the van der Waals interaction due to an electrostatic screening effect.[33] This mechanism may therefore account for the increased storage stability of the emulsions in the presence of salt, because there would have been a reduction in the attractive forces acting between the oil droplets. It should be noted that salt can also decrease the electrostatic interaction between the droplets through electrostatic screening, thereby increasing droplet coalescence.

*Effect of Salts on Oil Solubility.* One of the major factors influencing the rate of Ostwald ripening in oil-in-water emulsions is the solubility of the oil phase in the aqueous phase.[33] The addition of salts to the aqueous phase changes the structural organization of the water molecules, which will alter the equilibrium solubility of oil molecules. Salt addition causes an increase in interfacial tension (Table 1), which would increase the free energy associated with introducing a nonpolar molecule into water, thereby decreasing its water solubility. Consequently, addition of salt to the emulsions may have reduced the rate of Ostwald ripening, which is consistent with the reduction in droplet growth rate observed in the presence of salt observed in this study.

In summary, the addition of salt may have improved the storage stability of the emulsions by decreasing the attractive interactions between them (thereby decreasing coalescence) or by reducing the water solubility of the oil phase (thereby decreasing Ostwald ripening). Further studies are required to establish the relative importance of these two different physicochemical mechanisms. The improved stability of the emulsions to droplet growth when the droplet concentration was reduced can simply be attributed to the reduction in droplet collision frequency in the more dilute system.

**Conclusions.** In this study, we examined the influence of salts on the formation, properties, and stability of vitamin E-enriched emulsions prepared by spontaneous emulsification. We have shown that the addition of salts (NaCl and $CaCl_2$) to the aqueous phase of the emulsions did not change the initial droplet size produced. However, the ability of salts to modulate surfactant properties had an appreciable effect on their thermal stability: the cloud point decreased with increasing salt concentration. This effect was attributed to the ability of salts to promote dehydration of the surfactant headgroup, which alters the optimum curvature of the surfactant monolayer. The isothermal stability of the emulsions was influenced by storage temperature, with the droplet growth rate increasing with increasing temperature. This effect was attributed to the impact of temperature on the rate of droplet coalescence and Ostwald ripening. Addition of salts to the emulsions decreased the rate of droplet growth during isothermal storage. This effect was attributed to the ability of salts to reduce the attractive van der Waals interactions between droplets (thereby reducing coalescence) or to reduce the solubility of the oil molecules in water (thereby reducing Ostwald ripening). These results have important implications for the development of emulsion-based delivery systems for application in products containing salts.

## AUTHOR INFORMATION


### Corresponding Author

*(D.J.M.) Phone: (413) 545-1019. Fax: (413) 545-1262. E-mail: mcclements@foodsci.umass.edu.



### Funding

This material is based upon work supported by the Cooperative State Research, Extension, Education Service, U.S. Department of Agriculture, Massachusetts Agricultural Experiment Station (Project 831), and by the U.S. Department of Agriculture, NRI Grants (2011-03539 and 2013-03795).


### Notes

The opinions expressed in this paper are those of the authors and do not represent statements of position, intention, or strategy of PepsiCo Inc.

The authors declare no competing financial interest.

## ACKNOWLEDGMENTS

We thank William Mutilangi of PepsiCo for useful advice and discussions on this research.

## REFERENCES


(1) McClements, D. J. Emulsion design to improve the delivery of functional lipophilic components. In *Annual Review of Food Science and Technology*; Annual Reviews: Palo Alto, CA, USA, 2010; Vol. 1, pp 241−269.

(2) McClements, D. J. Advances in fabrication of emulsions with enhanced functionality using structural design principles. *Curr. Opin. Colloid Interface Sci.* **2012**, *17*, 234−245.

(3) McClements, D. J.; Rao, J. Food-grade nanoemulsions: formulation, fabrication, properties, performance, biological fate, and potential toxicity. *Crit. Rev. Food Sci. Nutr.* **2011**, *51*, 285−330.

(4) Tadros, T.; Izquierdo, P.; Esquena, J.; Solans, C. Formation and stability of nano-emulsions. *Adv. Colloid Interface Sci.* **2004**, *108−109*, 303−318.

(5) McClements, D. J. Nanoemulsion-based oral delivery systems for lipophilic bioactive components: nutraceuticals and pharmaceuticals. *Ther. Delivery* **2013**, *4*, 841−57.

(6) Anton, N.; Benoit, J. P.; Saulnier, P. Design and production of nanoparticles formulated from nano-emulsion templates − a review. *J. Controlled Release* **2008**, *128*, 185−199.

(7) Solans, C.; Esquena, J.; Forgiarini, A. M.; Uson, N.; Morales, D.; Izquierdo, P.; Azemar, N.; Garcia-Celma, M. J. Nano-emulsions: formation, properties, and applications. In *Adsorption and Aggregation of Surfactants in Solution*; Mittal, K. L., Shah, D. O., Eds.; CRC Press: Boca Raton, FL, USA, 2003; Vol. 109, pp 525−554.

(8) Solans, C.; Solé, I. Nano-emulsions: formation by low-energy methods. *Curr. Opin. Colloid Interface Sci.* **2012**, *17*, 246−254.

(9) Anton, N.; Benoit, J.-P.; Saulnier, P. Design and production of nanoparticles formulated from nano-emulsion templates − a review. *J. Controlled Release* **2008**, *128*, 185−199.

(10) McClements, D. J. Edible nanoemulsions: fabrication, properties, and functional performance. *Soft Matter* **2011**, *7*, 2297−2316.

(11) Schott, H.; Royce, A. E. Effect of inorganic additives on solutions of non-ionic surfactants V: emulsion stability. *J. Pharm. Sci.* **1983**, *72*, 1427−1436.

(12) Schott, H. Salting in of nonionic surfactants by complexation with inorganic salts. *J. Colloid Interface Sci.* **1973**, *43*, 150−155.

(13) Schott, H.; Han, S. K. Effect of inorganic additives on solutions of nonionic surfactants. 2. *J. Pharm. Sci.* **1975**, *64*, 658−664.

(14) Shinoda, K.; Takeda, H. The effect of added salts in water on the hydrophile-lipophile balance of nonionic surfactants: the effect of added salts on the phase inversion temperature of emulsions. *J. Colloid Interface Sci.* **1970**, *32*, 642−646.

(15) Sunderland, V. B.; Enever, R. P. The influence of formulation variables on phase inversion temperatures of emulsions as determined by a programmed viscometric technique. *J. Pharm. Pharmacol.* **1972**, *24*, 804−814.

(16) Schott, H.; Han, S. K. Interaction of inorganic additives with solutions of nonionic surfactants. 3. Effect on critical micelle concentrations and krafft points. *Abstr. Papers Am. Chem. Soc.* **1975**, 26−26.

(17) Schott, H.; Han, S. K. Effect of inorganic additives on solutions of nonionic surfactants. 3. Cmcs and surface properties. *J. Pharm. Sci.* **1976**, *65*, 975−978.

(18) Anton, N.; Saulnier, P.; Béduneau, A.; Benoit, J. P. Salting-out effect induced by temperature cycling on a water/nonionic surfactant/oil system. *J. Phys. Chem. B* **2007**, *111*, 3651−3657.

(19) Mei, Z.; Xu, J.; Sun, D. O/W nano-emulsions with tunable PIT induced by inorganic salts. *Colloids Surf., A* **2011**, *375*, 102−108.

(20) Florence, A. T.; Madsen, F.; Puisieux, F. Emulsion stabilization by nonionic surfactants − relevance of surfactant cloud point. *J. Pharm. Pharmacol.* **1975**, *27*, 385−394.

(21) Iwanaga, T.; Suzuki, M.; Kunieda, H. Effect of added salts or polyols on the liquid crystalline structures of polyoxyethylene-type nonionic surfactants. *Langmuir* **1998**, *14*, 5775−5781.

(22) Shinoda, K.; Saito, H. Stability of O/W type emulsions as functions of temperature and HLB of emulsifiers − emulsification by PIT-method. *J. Colloid Interface Sci.* **1969**, *30*, 258−263.

(23) Rao, J.; McClements, D. J. Stabilization of phase inversion temperature nanoemulsions by surfactant displacement. *J. Agric. Food Chem.* **2010**, *58*, 7059−7066.

(24) Ee, S. L.; Duan, X.; Liew, J.; Nguyen, Q. D. Droplet size and stability of nano-emulsions produced by the temperature phase inversion method. *Chem. Eng. J.* **2008**, *140*, 626−631.

(25) Saberi, A. H.; Fang, Y.; McClements, D. J. Fabrication of vitamin E-enriched nanoemulsions: factors affecting particle size using spontaneous emulsification. *J. Colloid Interface Sci.* **2013**, *391*, 95−102.

(26) Saberi, A. H.; Fang, Y.; McClements, D. J. Effect of glycerol on formation, stability, and properties of vitamin-E enriched nanoemulsions produced using spontaneous emulsification. *J. Colloid Interface Sci.* **2013**, *411*, 105−113.
(27) Saberi, A. H.; Fang, Y.; McClements, D. J. Fabrication of vitamin E-enriched nanoemulsions by spontaneous emulsification: effect of propylene glycol and ethanol on formation, stability, and properties. *Food Res. Int.* **2013**, *54*, 812−820.
(28) Solans, C.; Esquena, J.; Forgiarini, A. M.; Uson, N.; Morales, D.; Izquierdo, P.; Azemar, N.; Garcia-Celma, M. J. In *Adsorption and Aggregation of Surfactants in Solution*; Mittal, K. L., Shah, D. O., Eds.; CRC Press: Boca Raton, FL, USA, 2002; p 525.
(29) Anton, N.; Vandamme, T. F. The universality of low-energy nano-emulsification. *Int. J. Pharm.* **2009**, *377*, 142−147.
(30) Bouchemal, K.; Briançon, S.; Perrier, E.; Fessi, H. Nano-emulsion formulation using spontaneous emulsification: solvent, oil and surfactant optimization. *Int. J. Pharm.* **2004**, *280*, 241−251.
(31) Israelachvili, J. *Intermolecular and Surface Forces*, 3rd ed.; Academic Press: London, UK, 2011.
(32) Shinoda, K.; Friberg, S. *Emulsions and Solubilization*; Wiley Interscience: New York, 1986.
(33) McClements, D. J. *Food Emulsions: Principles, Practice, and Techniques*, 2nd ed.; CRC Press: Boca Raton, FL, USA, 2005.
(34) Anton, N.; Gayet, P.; Benoit, J.-P.; Saulnier, P. Nano-emulsions and nanocapsules by the PIT method: an investigation on the role of the temperature cycling on the emulsion phase inversion. *Int. J. Pharm.* **2007**, *344*, 44−52.
(35) Israelachvili, J. *Intermolecular and Surface Forces*, 2nd ed.; Academic Press: London, UK, 1992.
(36) McClements, D. J. Theoretical prediction of emulsion color. *Adv. Colloid Interface Sci.* **2002**, *97*, 63−89.
(37) Yoshihara, K.; Ohshima, H.; Momozawa, N.; Sakai, H.; Abe, M. Binding constants of symmetrical or antisymmetric electrolytes and aggregation numbers of oil-in-water type microemulsions with a nonionic surfactant. *Langmuir* **1995**, *11*, 2979−2984.
(38) Lin, X. L.; Xu, J.; Hou, W. G.; Sun, D. J. Effect of additives on the cloud points of two tri-block copolymers in aqueous solution. *Colloid Surf. A* **2004**, *237*, 1−6.
(39) Maclay, W. N. Factors affecting the solubility of nonionic emulsifiers. *J. Colloid Sci.* **1956**, *11*, 272−285.
(40) Schott, H.; Royce, A. E. Effect of inorganic additives on solutions of nonionic surfactants VI: further cloud point relations. *J. Pharm. Sci.* **1984**, *73*, 793−799.
(41) Leontidis, E. Hofmeister anion effects on surfactant self-assembly and the formation of mesoporous solids. *Curr. Opin. Colloid Interface Sci.* **2002**, *7*, 81−91.
(42) Collins, K. D.; Washabaugh, M. W. The Hofmeister effect and the behavior of water at interfaces. *Q. Rev. Biophys.* **1985**, *18*, 323−422.
(43) Franks, F. In *Water − A Comprehensive Treatise*; Franks, F., Ed.; Plenum Press: New York, 1973; Vol. 2.
(44) Kabalnov, A.; Olsson, U.; Wennerstroem, H. Salt effects on nonionic microemulsions are driven by adsorption/depletion at the surfactant monolayer. *J. Phys. Chem.* **1995**, *99*, 6220−6230.
(45) Saberi, A. H.; Fang, Y.; McClements, D. J. Stabilization of vitamin E-enriched mini-emulsions: influence of organic and aqueous phase composition. *Colloids Surf., A* **2014**, *449*, 65−73.
(46) Saberi, A. H.; Fang, Y.; McClements, D. J. Stabilization of vitamin E-enriched nanoemulsions: influence of post-homogenization cosurfactant addition. *J. Agric. Food Chem.* **2014**, *62*, 1625−1633.
(47) Nazarzadeh, E.; Anthonypillai, T.; Sajjadi, S. On the growth mechanisms of nanoemulsions. *J. Colloid Interface Sci.* **2013**, *397*, 154−162.
(48) Kabalnov, A. S.; Wennerström, H. Macroemulsion stability: the oriented wedge theory revisited. *Langmuir* **1996**, *12*, 276−292.
(49) Taylor, P. Ostwald ripening in emulsions. *Adv. Colloid Interface Sci.* **1998**, *75*, 107−163.
(50) Weast, R. C. *Handbook of Chemistry and Physics*; CRC Press: Boca Raton, FL, USA, 1986.
(51) *Calcium Chloride Handbook*; Dow Chemical Co., http://www.prog-univers.com/IMG/pdf/CalciumChloridHandbook-2.pdf.
(52) Lima, E. R. A.; de Melo, B. M.; Baptista, L. T.; Paredes, M. L. L. Specific ion effects on the interfacial tension of water/hydrocarbon systems. *Braz. J. Chem. Eng.* **2013**, *30*, 55−62.

between the central region and the surrounding subaleurone layer.[22] However, it is not clear whether these heterogeneous starch granules have different structures.

In this study, heterogeneous starch granules were separated from the kernels of TRS, and their structures were investigated. The objective of this study was to compare the structures of heterogeneous starch granules from high-amylose rice. The results could add to our understanding of the structures of different morphology starch granules from high-amylose cereal crops.

## MATERIALS AND METHODS

**Plant Materials.** An *indica* rice cultivar Te-qing (TQ) and its transgenic resistant starch rice line (TRS) with high amylose content were used in this study. TRS was generated from TQ after transgenic inhibition of both SBE I and SBE IIb through an antisense RNA technique and was homozygous for the transgene.[13] TQ and TRS were cultivated in the transgenic close experiment field of Yangzhou University, Yangzhou, China. Mature kernels were used to isolate starches.

**Total Starch Isolation.** Total starches were isolated from TQ and TRS mature kernels according to the method of Wei et al.[21] with some modifications. Brown kernels were steeped in deionized water overnight at 4 °C, and homogenized with ice-cold water in a home blender. The homogenate was squeezed through five layers of cotton cloth. The residue was homogenized and squeezed twice more in a mortar with a pestle to facilitate the release of starch granules. The combined extract was filtered with 150, 75, and 38 $\mu$m sieves and centrifuged at 5000*g* for 10 min. The yellow gel-like layer on top of the packed white starch precipitate was carefully scraped off and discarded. The process of centrifugation separation was repeated several times until no dirty material existed. The precipitated starch was dehydrated with anhydrous ethanol two times, dried at 40 °C, ground into powders, and passed through a 38 $\mu$m sieve.

**Separation of Heterogeneous Starch Granules.** TRS polygonal, aggregate, elongated, and hollow starch granules were separated from the different regions of the mature kernels referring to the methods of Ao et al.,[2] Peng et al.,[23] Naguleswarana et al.,[24] and Dhital et al.,[25] and combining with the regional distribution of heterogeneous starch granules in endosperm. The detailed separation methods were as described below.

**Separation of TRS Polygonal Starch Granules.** The central regions of the kernels were cut with a stainless razor blade, and used to isolate the crude starch as total starch isolation from kernels. The crude starch was suspended in deionized water and centrifuged at 100*g* for 5 min. The precipitate was repeatedly suspended and centrifuged ten times. Finally, the precipitate was again suspended with 40 mL of deionized water in a 50 mL centrifuge tube and settled for 1 h. The upper 30 mL of starch suspension was collected, and the residual starch suspension was repeatedly made up to 40 mL with deionized water and settled ten times. After that, the collected starch suspension was centrifuged at 5000*g* for 10 min, and the starch precipitate was dehydrated and dried to obtain the TRS polygonal starch granules.

**Separation of TRS Hollow Starch Granules.** The kernels were steeped in deionized water overnight at 4 °C. The peripheral regions (about 0.3 mm thickness) of kernels were cut with a stainless razor blade and used to isolate the crude starch as total starch isolation from kernels. The crude starch was suspended in 50% (v/v) glycerol aqueous solution and centrifuged at 100*g* for 5 min. The supernatant was collected, and the precipitate was repeatedly suspended and centrifuged ten times. After that, the collected supernatant was centrifuged at 5000*g* for 10 min to obtain the starch precipitate. The starch precipitate was suspended in 30% (v/v) glycerol aqueous solution and centrifuged at 100*g* for 5 min. The starch precipitate was repeatedly suspended and centrifuged ten times. Finally, the starch precipitate was washed with deionized water three times to remove the glycerol, dehydrated, and dried to obtain the TRS hollow starch granules.

**Separation of TRS Elongated and Aggregate Starch Granules.** The middle regions between the central region and the surrounding subaleurone layer of the kernels were cut with a stainless razor blade and used to isolate the crude starch as total starch isolation from kernels. The crude starch was suspended in deionized water and centrifuged at 100*g* for 5 min. The precipitate was repeatedly suspended and centrifuged ten times. After that, the precipitate was suspended in 30% (v/v) glycerol aqueous solution and centrifuged at 100*g* for 5 min. The supernatant was collected, and the precipitate was repeatedly suspended and centrifuged ten times. The collected supernatant was centrifuged at 5000*g* for 10 min, and the starch precipitate was washed with deionized water three times, dehydrated, and dried to obtain the TRS elongated starch granules. The precipitate obtained from starch suspension in 30% glycerol was again suspended with 40 mL of deionized water in a 50 mL centrifuge tube and settled for 30 min. The supernatant was discarded, and the starch precipitate was repeatedly suspended and settled ten times. Finally, the starch precipitate was dehydrated and dried to obtain the TRS aggregate starch granules.

**Morphology Observation.** A starch suspension (1%, w/v) was prepared with 50% glycerol aqueous solution. Ten microliters of starch suspension was placed on the microscope slide and covered with a coverslip. The starch granule morphology and Maltese cross were viewed under an Olympus BX 53 polarizing microscope equipped with a CCD camera.

**Measurements of Iodine Absorption Spectrum, Iodine Blue Value, and Amylose Content.** Iodine absorption spectrum, iodine blue value, and amylose content of starch were determined according to the method of Man et al.[26] with some modifications. Ten milligrams of dry starch was dispersed in 5 mL of dimethyl sulfoxide (DMSO) containing 10% 6.0 M urea. Dissolution was obtained by incubating the mixture at 95 °C for 1 h with intermittent vortexing. A 1.0 mL aliquot of the starch−DMSO solution was then placed in a 50 mL volumetric flask along with 45 mL of deionized water, and 1.0 mL of iodine solution (0.2% $I_2$ and 2% KI, w/v) was added. The mixture was made up to 50 mL with deionized water, mixed immediately, and placed in darkness for 20 min. Control solution was made in the same way but without sample. All samples were scanned from 400 to 900 nm with a spectrophotometer (Ultrospec 6300 pro, Amershan Biosciences). The $\lambda_{max}$ was the wavelength (in nm) at which the absorbance was the highest over the range of the wavelengths. Iodine blue value was measured at 680 nm under the above experimental conditions. Apparent amylose content (AAC) was evaluated from absorbance at 620 nm. The recorded values were converted to percent of amylose by reference to a standard curve prepared with amylopectin from corn (Sigma-Aldrich 10120) and amylose from potato. The experiments were performed in triplicate.

**Gel-Permeation Chromatography (GPC) Analysis.** Starch was deproteinized with protease and sodium bisulfite, and debranched with isoamylase following the methods of Tran et al.[27] and Li et al.[28] The molecular weight distribution of debranched starch was analyzed using a PL-GPC 220 high temperature chromatograph (Agilent Technologies UK Limited, Shropshire, U.K.) with three columns (PL110-6100, 6300, 6525) and a differential refractive index detector according to the method of Cai et al.[29] The areas of peaks were integrated, and their relative peak area was expressed as a percentage of the total area of all peaks. The experiments were performed two times.

**X-ray Powder Diffraction (XRD) Analysis.** XRD analysis of starch was carried out on an XRD (D8, Bruker, Germany) as described by Wei et al.[30] All the specimens were stored in a desiccator where a saturated solution of NaCl maintained a constant humidity for 1 week before measurements. The relative crystallinity (%) was measured following the method of Wei et al.[30] A smooth curve that connected peak baselines was computer-plotted on the diffractogram. The areas of peaks at 5.6°, 15°, 17°, 18°, 20°, and 23° at 2$\theta$ above the smooth curve were taken as the crystalline portion. The ratio of diffraction peak area to total diffraction area over the diffraction angle 4−30° at 2$\theta$ was taken as the relative crystallinity. The relative crystallinity was quantitatively analyzed three times.

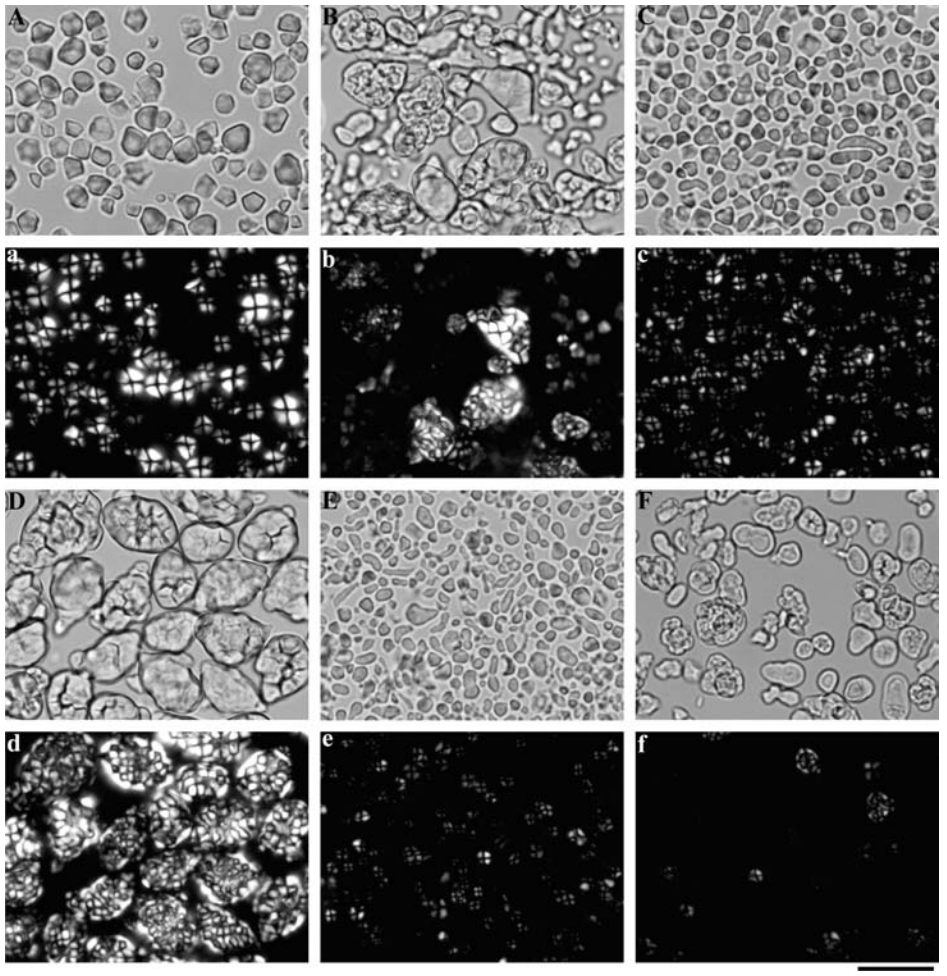


**Figure 1.** Microphotographs of starch granules under normal light (A–F) and polarizing light (a–f). (A, a), TQ total starch granules; (B, b), TRS total starch granules; (C, c), TRS polygonal starch granules; (D, d), TRS aggregate starch granules; (E, e), TRS elongated starch granules; (F, f), TRS hollow starch granules. Scale bar = 20 $\mu$m.

**Attenuated Total Reflectance Fourier Transform Infrared (ATR-FTIR) Analysis.** ATR-FTIR analysis of starch was carried out on a Varian 7000 FTIR spectrometer with a DTGS detector equipped with an ATR single-reflectance cell containing a germanium crystal (45° incidence angle) (PIKE Technologies, USA) as previously described by Wei et al.[30] The spectra were quantitatively analyzed three times.

**Solid-State $^{13}$C Cross-Polarization Magic-Angle Spinning Nuclear Magnetic Resonance ($^{13}$C CP/MAS NMR) Analysis.** High-resolution solid-state $^{13}$C CP/MAS NMR analysis of starch was carried out at B0 = 9.4 T on a Bruker AVANCE III 400 WB spectrometer as previously described by Man et al.[31] Amorphous starch was prepared by gelatinizing native starch following the method of Wei et al.[30] The spectrum of amorphous starch was matched to the intensity of native starch at 84 ppm and subtracted to produce the ordered subspectrum. The $^{13}$C CP/MAS NMR original spectrum and ordered subspectrum were peak fitted by using PeakFit version 4.12. The quantitative analyses of double-helix, single-helix, and amorphous conformational features within starch were carried out according to the method described by Tan et al.[32] The spectra were quantitatively analyzed three times.

**Small-Angle X-ray Scattering (SAXS) Analysis.** SAXS measurement of starch was carried out on a Bruker NanoStar SAXS instrument equipped with Vantec 2000 detector and pinhole collimation for point focus geometry as previously described by Cai et al.[33] SAXS data sets were analyzed using DIFFRAC$^{plus}$ NanoFit software. Parameters of the SAXS spectrum were determined according to the simple graphical method.[33] The experiments were performed two times.

**Differential Scanning Calorimetry (DSC) Analysis.** The thermal properties of starch were determined using DSC (200-F3, Netzsch, Germany). Three milligrams of starch was mixed with 9 $\mu$L of deionized water and hermetically sealed in an aluminum pan overnight at 4 °C. After equilibrating for 1 h at room temperature, the sample was scanned against a blank (empty pan) at a heating rate of 10 °C/min from 25 to 130 °C. The major parameters of the DSC profile were described as onset temperature ($T_o$), peak temperature ($T_p$), conclusion temperature ($T_c$), gelatinization range ($\Delta T$), and gelatinization enthalpy ($\Delta H$). The experiments were performed two times.

**Statistical Analysis.** The data reported in all of the tables were mean values and standard deviation. One-way analysis of variance (ANOVA) and Tukey's test ($p < 0.05$) were evaluated using the SPSS 16.0 Statistical Software Program.

## RESULTS AND DISCUSSION

**Separations and Morphologies of TRS Heterogeneous Starch Granules.** TRS starch contained heterogeneous starch granules.[16] These heterogeneous granules were distributed in different regions of the endosperm.[22] According to the distribution regions of heterogeneous starch granules, we separated these heterogeneous starch granules using different methods in this study. Figure 1 showed the morphology and the separation effectiveness of heterogeneous starch granules. TQ total starch granules isolated from kernels were homogeneous in morphological structure, showed polygonal

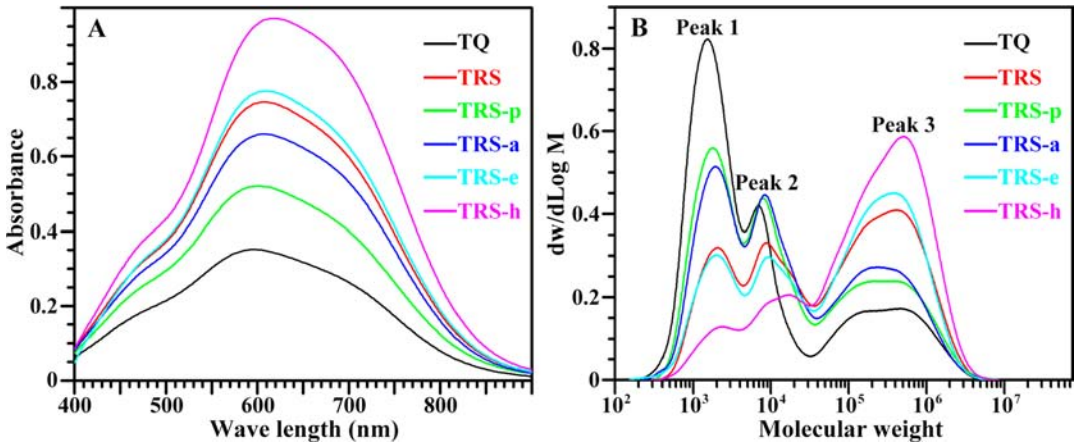


**Figure 2.** Absorbance spectra of starch–iodine complex (A) and GPC profiles of isoamylase-debranched starches (B). TQ, TRS, TRS-p, TRS-a, TRS-e, and TRS-h are TQ total starch, TRS total starch, TRS polygonal starch granules, TRS aggregate starch granules, TRS elongated starch granules, and TRS hollow starch granules, respectively.

**Table 1. Iodine Absorbance, Amylose Content, and Molecular Weight Distribution of Starch[a]**

| | | | | peak area[d] (%) | | | |
|---|---|---|---|---|---|---|---|
| starches | $\lambda_{max}$[b] (nm) | BV[b] | AAC[c] (%) | peak 1 | peak 2 | peak 3 | peak1/peak2[d] |
| TQ total starch | 597.3 ± 1.5 a | 0.294 ± 0.007 a | 25.5 ± 0.6 a | 55.3 ± 0.2 e | 19.4 ± 0.5 b | 25.3 ± 0.3 a | 2.84 ± 0.08 e |
| TRS total starch | 608.0 ± 0.0 c | 0.650 ± 0.001 d | 60.0 ± 0.1 d | 20.9 ± 0.8 b | 23.9 ± 0.2 d | 55.2 ± 0.6 c | 0.88 ± 0.04 b |
| TRS polygonal granule | 601.3 ± 0.6 b | 0.438 ± 0.001 b | 39.8 ± 0.1 b | 37.0 ± 0.8 d | 27.1 ± 0.1 e | 35.9 ± 0.7 b | 1.36 ± 0.04 d |
| TRS aggregate granule | 607.3 ± 0.6 c | 0.579 ± 0.007 c | 52.6 ± 0.5 c | 34.2 ± 0.1 c | 28.9 ± 0.0 f | 36.9 ± 0.0 b | 1.18 ± 0.00 c |
| TRS elongated granule | 608.7 ± 1.2 c | 0.681 ± 0.001 e | 62.6 ± 0.1 e | 20.3 ± 0.2 b | 22.1 ± 1.1 c | 57.5 ± 0.9 d | 0.92 ± 0.06 b |
| TRS hollow granule | 618.7 ± 0.6 d | 0.893 ± 0.002 f | 80.2 ± 0.2 f | 7.7 ± 0.3 a | 16.5 ± 0.2 a | 75.8 ± 0.5 e | 0.47 ± 0.01 a |

[a]Data are means ± standard deviations, $n = 3$ for $\lambda_{max}$, BV, and AAC, $n = 2$ for peak area and peak1/peak2. Values in the same column with different letters are significantly different ($P < 0.05$). [b]Maximum absorption wavelength ($\lambda_{max}$) and the absorbance at 680 nm (iodine blue value, BV) of starch–iodine complex. [c]Apparent amylose content (AAC) determined by iodine colorimetric method from the absorbance at 620 nm. [d]GPC parameters of isoamylase-debranched starch. Peak1/peak2 is the area ratio of peak 1 and peak 2.

morphology, and had a typical Maltese cross in one granule (Figures 1A, 1a). Normal rice starch is compound starch, which means that many starch granules individually form and develop in one amyloplast. These separate starch granules (in fact they are subgranules of compound starch) are freely released from the amyloplast when starch is isolated from mature endosperm.[16,34] TRS total starch granules isolated from kernels were significantly heterogeneous in morphological structures and birefringent patterns (Figures 1B, 1b). These heterogeneous starch granules could be classified into four types: polygonal, aggregate, elongated, and hollow starch granules according to their morphological structures and birefringent patterns. TRS polygonal starch granules showed polygonal morphology, had a typical Maltese cross in one granule, and were essentially similar to the TQ polygonal starch granule (Figures 1 C, 1c). According to the morphological structure of TRS polygonal starch granule, we thought that it was compound starch. TRS aggregate starch granules consisted of many subgranules, showed large voluminous, nonangular rounded bodies, and had many Maltese crosses in one granule. In fact, each subgranule of aggregate starch had only one Maltese cross. There was a thick band or wall encircling the entire exterior of the aggregate starch granule (Figures 1D, 1d). The morphological structure of TRS aggregate starch had been reported in high-amylose rice by Kim et al.[12] and Wei et al.,[16] and the exterior band or wall prevented the release of subgranules during starch isolation.[12,16] That meant that the isolated starch was still the aggregate body of many subgranules, and was therefore designated as aggregate starch. At the early stage of TRS aggregate starch development, starch subgranules individually form and develop in one amyloplast. At the middle stage of starch development, adjacent subgranules start fusion. At the late stage of starch development, the subgranules located at the periphery of the aggregate starch fuse together and form a continuous outer band or wall.[34] Starch granule is considered as elongated granule when the ratio of long axis and short axis is larger than 1.3.[8,35] TRS elongated starch granules contained some small spherical granules. The spherical granule had one typical Maltese cross, and the elongated granule consisted of several small granules and showed very weak Maltese cross (Figures 1E, 1e). The elongated starch granules in high-amylose maize are formed from fusion of several small granules.[35] TRS hollow starch granules were similar to TRS aggregate starch granule in surface shape, but their interiors lacked subgranules and had no birefringence (Figures 1F, 1f). The hollow starch granule has been reported in high-amylose wheat and barley endosperm,[9−11] but its formation is not unclear until now. Among the four types of heterogeneous starch granules, the purity of aggregate starch granules was the highest (Figures 1D, 1d), but the polygonal starch granules contained some small spherical and elongated starch granules (Figures 1C, 1c), the elongated starch granules had some polygonal and small aggregate starch granules (Figures 1E, 1e), and the hollow starch granules contaminated some small aggregate starch granules (Figures 1F, 1f).

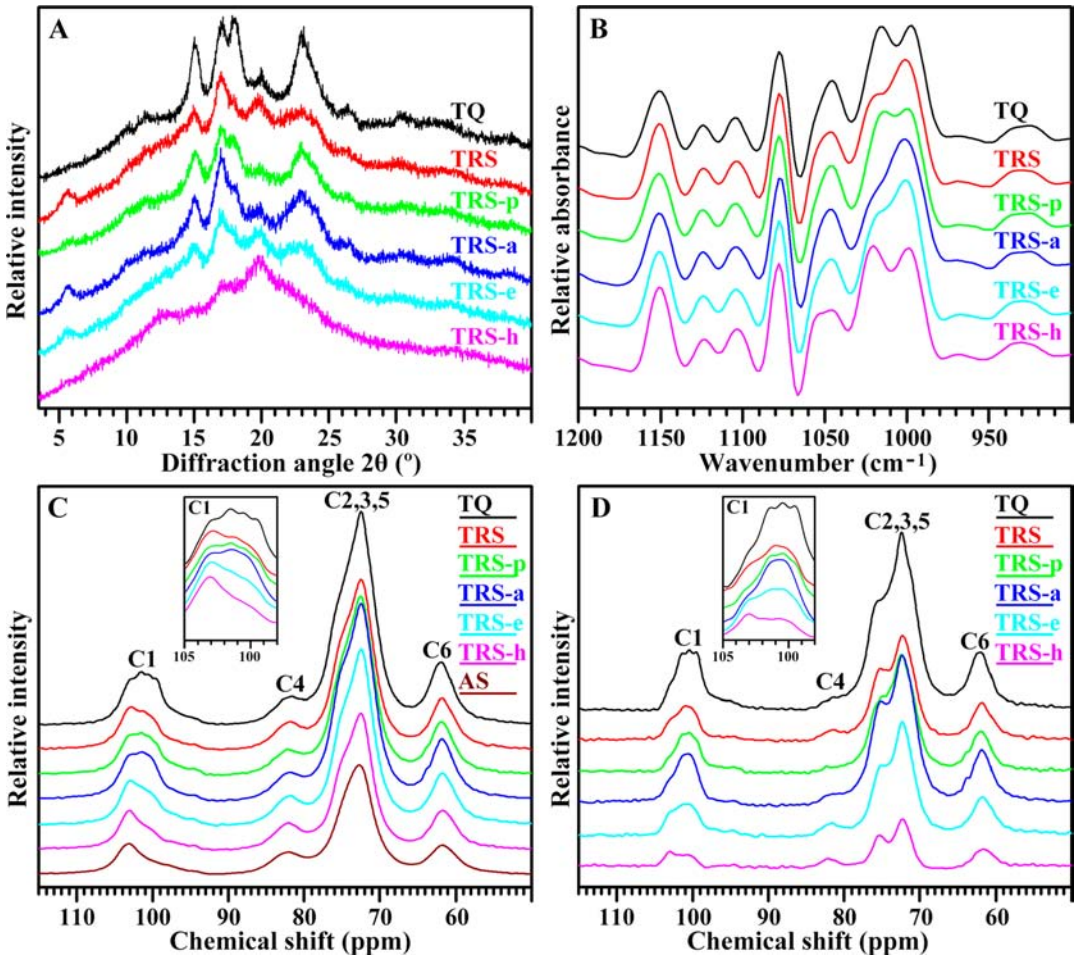


**Figure 3.** XRD spectra (A), ATR-FTIR spectra (B), and $^{13}C$ CP/MAS NMR original spectra (C) and ordered subspectra (D) of starches. AS is amorphous starch. TQ, TRS, TRS-p, TRS-a, TRS-e, and TRS-h are TQ total starch, TRS total starch, TRS polygonal starch granules, TRS aggregate starch granules, TRS elongated starch granules, and TRS hollow starch granules, respectively.

**Iodine Absorption Spectra and Amylose Contents of TRS Heterogeneous Starch Granules.** The iodine absorption spectra of TQ total starch, TRS total starch, and TRS heterogeneous starch granules are presented in Figure 2A, and they showed significant difference. The maximum absorption wavelength ($\lambda_{max}$), iodine blue value (BV), and AAC of starch were summarized in Table 1. The $\lambda_{max}$, BV, and AAC of starches had significantly positive relationships for each other. The correlation coefficients were 0.989, 0.983, and 0.999 between $\lambda_{max}$ and BV, $\lambda_{max}$ and AAC, and BV and AAC, respectively ($P < 0.001$). The AAC of TRS total starch was 60.0%, and was markedly higher than that of TQ total starch (25.5%), which was in agreement with the previous report.[21] TRS heterogeneous starch granules showed significantly different AAC. The hollow starch granules had the highest AAC (80.2%), and the polygonal starch granules showed the lowest AAC (39.8%). The significantly different AACs of TRS heterogeneous starch granules indicated that these heterogeneous starch granules significantly differed in not only the morphology but also the structure.

**Molecular Weight Distributions of TRS Heterogeneous Starch Granules.** The molecular weight distributions of isoamylase-debranched starches as determined by GPC are shown in Figure 2B. A trimodal distribution of low, middle, and high molecular weight peaks, designated peak 1, peak 2, and peak 3, respectively, was observed. Peak 1 and peak 2 consist of short (A and short B chains) and long (long B chains) branch-chains of amylopectin, respectively. The area ratio of peak 1 to peak 2 might be used as an index of the extent of branching of amylopectin; the higher the ratio, the higher the branching degree.[36] Peak 3 mainly includes amylose.[37] The GPC parameters are summarized in Table 1. The AC determined based on iodine and starch affinity is described as AAC, which overestimates AC if there are branched molecules with long side chains that bind iodine.[38] The present results showed that the ACs of TRS total starch and TRS heterogeneous starch granules determined by GPC were significantly lower than AACs obtained by iodine colorimetric method (Table 1), which was in agreement with the report of Shi et al.[38] and indicated that the intermediate chain and amylopectin long branch-chain could bind iodine to increase the value of AAC. In the present study, the correlation coefficient between AAC obtained by iodine colorimetric method and AC determined by GPC was 0.963 ($P < 0.002$), indicating that the AAC and AC had a significantly positive relationship though the AC was lower than the AAC. The molecular weight distributions and the branching degrees were significantly different among TRS heterogeneous starch granules, indicating that these heterogeneous starch granules had different molecular structures.

**XRD Patterns of TRS Heterogeneous Starch Granules.** Native starches can be divided into A-, B-, and C-type crystallinity according to their XRD patterns.[39] XRD patterns of

Table 2. Relative Crystallinity, IR Ratio, and the Proportions of Single Helix, Double Helix, and Amorphous Conformation of Starch[a]

| | | IR ratio[c] | | rel proportion[d] (%) | | |
|---|---|---|---|---|---|---|
| starches | rel crystallinity[b] (%) | 1045/1022 $cm^{-1}$ | 1022/995 $cm^{-1}$ | single helix | double helix | amorphous conformation |
| TQ total starch | 25.6 ± 0.1 f | 0.57 ± 0.02 b | 0.99 ± 0.00 d | 5.6 ± 0.2 b | 40.8 ± 1.4 e | 53.7 ± 1.6 a |
| TRS total starch | 14.2 ± 0.2 c | 0.62 ± 0.02 b | 0.74 ± 0.01 b | 4.6 ± 0.2 a | 28.9 ± 1.1 bc | 66.5 ± 1.3 c |
| TRS polygonal granule | 18.9 ± 0.5 d | 0.57 ± 0.02 b | 0.98 ± 0.00 d | 4.7 ± 0.2 a | 30.9 ± 1.2 c | 64.4 ± 1.4 c |
| TRS aggregate granule | 20.1 ± 0.6 e | 0.74 ± 0.02 c | 0.67 ± 0.02 a | 6.9 ± 0.2 d | 35.4 ± 1.1 d | 57.6 ± 1.3 b |
| TRS elongated granule | 11.8 ± 0.4 b | 0.57 ± 0.02 b | 0.77 ± 0.01 c | 6.2 ± 0.3 c | 26.7 ± 1.2 b | 67.0 ± 1.5 c |
| TRS hollow granule | 1.1 ± 0.0 a | 0.46 ± 0.03 a | 1.02 ± 0.00 e | 6.6 ± 0.3 cd | 8.0 ± 0.4 a | 85.4 ± 0.7 d |

[a]Data are means ± standard deviations, $n = 3$. Values in the same column with different letters are significantly different ($P < 0.05$). [b]Relative crystallinity determined by XRD. [c]IR ratio determined by ATR-FTIR. [d]Relative proportion determined by $^{13}C$ CP/MAS NMR.

TQ total starch, TRS total starch, and TRS heterogeneous starch granules are presented in Figure 3A, and their relative crystallinities are shown in Table 2. TQ total starch showed strong reflection at about 15° and 23° 2$\theta$ and an unresolved doublet at 17° and 18° 2$\theta$, indicating that it had a typical A-type XRD pattern, and was similar to that of normal cereal starches.[39] TRS total starch showed strong reflection at about 15°, 17°, and 23° 2$\theta$ and a small peak at about 5.6° 2$\theta$, indicating that TRS total starch was C-type crystallinity, which was in agreement with our previous report.[21] It was very interesting that TRS heterogeneous starch granules had different XRD patterns. The polygonal starch granules exhibited A-type crystallinity, the aggregate and elongated starch granules showed C-type crystallinity, and the hollow starch granules had no crystallinity. The different crystalline structures might result from the different ACs. Cheetham and Tao[39] thought that the crystalline type of maize starch could be varied from A- to B- via C-type when AC increased. The TQ total starch had the highest relative crystallinity, which was in agreement with the lowest amylose content. The elongated starch granules had very low crystalline peak intensities, resulting in low relative crystallinity. The hollow starch granules did not show birefringence under polarizing light, which was in agreement with an absence of crystallinity measured by XRD. The absence of crystallinity has also been reported in wheat hollow starch granules.[40]

**ATR-FTIR Spectra of TRS Heterogeneous Starch Granules.** The ATR-FTIR spectrum of starch is sensitive to the short-range ordered structure. The variations in spectra among different starches can be interpreted in terms of the short-range ordered structure present in the external region of starch granule.[41] The ATR-FTIR spectra of TQ total starch, TRS total starch, and TRS heterogeneous starch granules in the 1200−900 $cm^{-1}$ region are shown in Figure 3B. The bands at 1045 and 1022 $cm^{-1}$ are associated with ordered/crystalline and amorphous regions in starch, respectively. The ratio of absorbance 1045/1022 $cm^{-1}$ is used to quantify the degree of order, and that of 1022/995 $cm^{-1}$ can be used as a measure of the proportion of amorphous to ordered carbohydrate structure in the starch.[41] The ratios for 1045/1022 and 1022/995 $cm^{-1}$ of TQ total starch, TRS total starch, and TRS heterogeneous starch granules are shown in Table 2. On the basis of both the spectra and calculated data, the ATR-FTIR characteristics were significantly different among TRS heterogeneous starch granules, indicating that TRS heterogeneous starch granules had different short-range ordered structures in the external region of granule.

**$^{13}C$ CP/MAS NMR Spectra of TRS Heterogeneous Starch Granules.** The solid-state $^{13}C$ CP/MAS NMR spectra of TQ total starch, TRS total starch, and TRS heterogeneous starch granules are shown in Figure 3C. The resonances at different ppm were assigned according to the data reported in the literature.[42,43] The C1 resonance, which gives information about both the crystalline nature and the noncrystalline (but rigid) chains, has been used to examine the crystallinity of starches. A-type starch is a triplet at the C1 region; B-type starch shows a doublet. C-type starch has an inconspicuous triplet or doublet according to the proportions of A- and B-type allomorph.[42,43] Amorphous starch has one peak at 103 ppm, which arises from the amorphous domain for C1, and the peak intensity is positively relative with AC.[32] TQ total starch had a clear triplet at 99.5, 100.5, and 101.5 ppm, and TRS total starch showed an inconspicuous doublet at the C1 region and a strong peak at 103 ppm, indicating that TQ total starch had A-type crystallinity, and TRS total starch had C-type crystallinity and high AC. This result was in agreement with our previous report.[21] TRS polygonal starch granules showed a triplet at the C1 region, TRS aggregate and elongated starch granules had an inconspicuous doublet, and TRS hollow starch granules exhibited no peak except the amorphous peak at 103 ppm. These results indicated that TRS polygonal starch granules had A-type crystallinity, TRS aggregate and elongated starch granules had C-type crystallinity, and TRS hollow starch granules had no crystallinity, and were in agreement with the XRD patterns of TRS heterogeneous starch granules.

Figure 3D shows the ordered subspectra of starches. In this analysis, the standard amorphous starch spectrum was subtracted from the test spectrum until there was no residual intensity at 84 ppm (a region of the spectrum with intensity due solely to amorphous conformations).[32] The ordered subspectra were similar to the original spectra, but they had clearer crystalline peaks of C1 resonances than the original spectra. The ordered subspectra were peak-fitted. A combination (50/50) of Lorentzian and Gaussian profiles gave an acceptable fit (data not shown). The proportions of single helixes, double helixes, and amorphous components are listed in Table 2, and showed significant difference among TRS heterogeneous starch granules. The amylopectin side chains can form two types of helices in starch granule. Helices that are packed in the short-range order are defined as the double helical order, and helices that are packed in long-range order are related to the packing of double helices forming crystallinity. That means that the double helices at a short-range level would be prerequisite for occurrence of the crystallinity but the crystallinity would not necessarily be present when short-range order exists.[41] The double helices in the short- and long-range distance can both be detected by $^{13}C$ CP/MAS NMR, but only the double helices in the long-range

distance can be detected by XRD.[42] Therefore, the double helix content of starch was generally higher than its relative crystallinity, especially for high-amylose starch (Table 2). In the present study, the double helix contents of the elongated and hollow starch granules were markedly higher than their relative crystallinities, indicating that most of the double helices did not form the crystallinity in these starches, which was in agreement with their very high amylose contents (Table 1).

**SAXS Spectra of TRS Heterogeneous Starch Granules.** A comparison of the SAXS spectra of starches is shown in Figure 4. All starches were scaled to equal intensity at high $q$ ($q$ = 0.2 Å$^{-1}$) to account for variations in sample concentrations.[44] The SAXS patterns were at the same relative scale and therefore directly comparable. The well-resolved main scattering peak around scattering vector ($q_0$) of about 0.07 Å$^{-1}$ is thought to arise from the periodic arrangement of alternating crystalline and amorphous lamellae of amylopectin, and corresponds to the lamellar repeat distance or Bragg spacing. The peak intensity depends mainly on the degree of order in semicrystalline regions.[45] The parameters of the SAXS peak were determined using the simple graphical method[33] and are presented in Table 3. The peak position and Bragg spacing were not significantly different among TQ total starch, TRS total starch, and TRS heterogeneous starch granules. However, the scattering peak intensity and peak full width at half-maximum were significantly different among TRS heterogeneous starch granules. The scattering peak could not be detected in TRS hollow starch granules, which might result from the high AC and was in agreement with the finding that no crystallinity was detected by XRD and NMR. In native starches, the intensity of the scattering peak decreases with increasing AC, which might result from the decrease in the electron density difference between crystalline and amorphous regions of the lamellae.[45] This in turn may be caused by several factors: cocrystallization of amylose macromolecules with amylopectin side chains within crystalline lamellae, accumulation of amylose chains oriented transverse to the lamellar stack within amorphous lamellae, and accumulation of amylose tie-chains inside both crystalline and amorphous lamellae.[45,46]

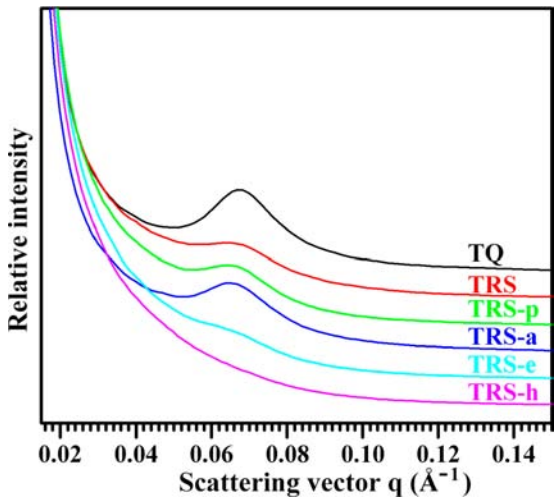


**Figure 4.** SAXS patterns of starches. TQ, TRS, TRS-p, TRS-a, TRS-e, and TRS-h are TQ total starch, TRS total starch, TRS polygonal starch granules, TRS aggregate starch granules, TRS elongated starch granules, and TRS hollow starch granules, respectively.

**Thermal Properties of TRS Heterogeneous Starch Granules.** DSC thermograms of TQ total starch, TRS total starch, and TRS heterogeneous starch granules are shown in Figure 5, and the thermal properties are summarized in Table 4.

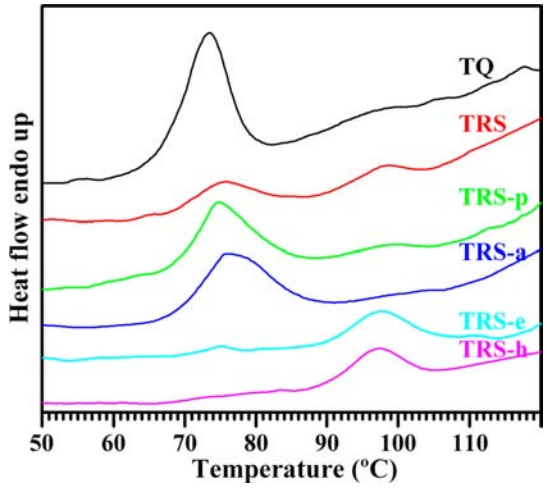


**Figure 5.** DSC thermograms of starches. TQ, TRS, TRS-p, TRS-a, TRS-e, and TRS-h are TQ total starch, TRS total starch, TRS polygonal starch granules, TRS aggregate starch granules, TRS elongated starch granules, and TRS hollow starch granules, respectively.

TRS total starch had significantly higher gelatinization temperature and lower gelatinization enthalpy than TQ total starch, which might result from the high AC in TRS total starch and was in agreement with our previous report.[47] TRS heterogeneous starch granules showed significantly different thermal properties. TQ total starch, TRS polygonal starch granules, and TRS aggregate starch granules had one clear peak with $T_p$ from 73.6 to 76.2 °C. TRS total starch and TRS elongated starch granules had two peaks with $T_p$ at about 76 and 98 °C, but the first peak was very weak in TRS elongated

**Table 3. SAXS Parameters of Starch**[a]

| starches | $I_{max}$[b] (counts) | $S_{max}$[b] (Å$^{-1}$) | $\Delta S$[b] (Å$^{-1}$) | $D$[b] (nm) |
|---|---|---|---|---|
| TQ total starch | 187.4 ± 0.0 d | 0.068 ± 0.001 a | 0.017 ± 0.000 c | 9.3 ± 0.1 a |
| TRS total starch | 53.7 ± 0.0 b | 0.068 ± 0.001 a | 0.015 ± 0.000 b | 9.3 ± 0.1 a |
| TRS polygonal granule | 65.7 ± 11.5 b | 0.068 ± 0.001 a | 0.015 ± 0.000 b | 9.3 ± 0.1 a |
| TRS aggregate granule | 109.4 ± 2.7 c | 0.067 ± 0.001 a | 0.016 ± 0.001 c | 9.4 ± 0.1 a |
| TRS elongated granule | 16.4 ± 0.3 a | 0.067 ± 0.001 a | 0.011 ± 0.000 a | 9.4 ± 0.1 a |
| TRS hollow granule | –[c] | – | – | – |

[a]Data are means ± standard deviations, $n$ = 2. Values in the same column with different letters are significantly different ($P$ < 0.05). [b]$I_{max}$, peak intensity; $S_{max}$, peak position; $\Delta S$, peak full width at half-maximum; $D$, Bragg spacing ($2\pi/S_{max}$). [c]Data are not detected.


dx.doi.org/10.1021/jf503999r | J. Agric. Food Chem. 2014, 62, 11254−11263

Table 4. DSC Parameters of Starch[a]

| starches | peak 1 | | | | | peak 2 | | | | |
|---|---|---|---|---|---|---|---|---|---|---|
| | $T_o$[b] (°C) | $T_p$[b] (°C) | $T_c$[b] (°C) | $\Delta T$[b] (°C) | $\Delta H$[b] (J/g) | $T_o$ (°C) | $T_p$ (°C) | $T_c$ (°C) | $\Delta T$ (°C) | $\Delta H$ (J/g) |
| TQ total starch | 66.9 ± 0.3 a | 73.6 ± 0.0 a | 78.9 ± 0.3 b | 12.0 ± 0.6 b | 12.4 ± 0.2 d | –[c] | – | – | – | – |
| TRS total starch | 69.1 ± 0.1 c | 76.3 ± 0.4 c | 83.6 ± 0.3 c | 14.5 ± 0.1 c | 2.8 ± 0.3 b | 90.4 ± 0.1 a | 97.6 ± 0.4 a | 103.2 ± 0.4 a | 12.8 ± 0.4 a | 1.6 ± 0.4 a |
| TRS polygonal granule | 68.3 ± 0.1 b | 75.2 ± 0.4 b | 84.8 ± 0.3 d | 16.6 ± 0.4 d | 8.9 ± 0.1 c | – | – | – | – | – |
| TRS aggregate granule | 68.5 ± 0.2 bc | 76.2 ± 0.1 bc | 86.9 ± 0.1 e | 18.4 ± 0.1 e | 8.9 ± 0.2 c | – | – | – | – | – |
| TRS elongated granule | 70.6 ± 0.3 d | 75.4 ± 0.1 bc | 78.2 ± 0.1 a | 7.6 ± 0.2 a | 0.4 ± 0.1 a | 90.1 ± 0.1 a | 97.9 ± 0.3 a | 105.2 ± 0.3 b | 15.1 ± 0.4 b | 3.5 ± 0.3 b |
| TRS hollow granule | – | – | – | – | – | 90.3 ± 0.4 a | 97.7 ± 0.2 a | 103.9 ± 0.1 a | 13.7 ± 0.5 ab | 3.2 ± 0.1 b |

[a]Data are means ± standard deviations, $n = 2$. Values in the same column with different letters are significantly different ($P < 0.05$). [b]$T_o$, onset temperature; $T_p$, peak temperature; $T_c$, conclusion temperature; $\Delta T$, gelatinization range; $\Delta H$, enthalpy of gelatinization. [c]Data are not detected.

starch granules. TRS hollow starch granules had one clear peak with $T_p$ at 98 °C. After immediate rescan of the gelatinized TRS total starch, elongated starch, and hollow starch, the peaks with $T_p$ at about 76 °C disappeared, but the peaks with $T_p$ at about 98 °C still existed on rescanned DSC thermograms (data not shown). The peaks with $T_p$ at about 98 °C disappeared after removal of lipids from high-amylose maize starch.[48] Therefore, the peak with $T_p$ from 73.6 to 76.3 °C was due to the dissociation of double-helical crystallites of the amylopectin molecules, and the peaks with $T_p$ at about 98 °C corresponded to the melting of the amorphous amylose−lipid complex, which had a lower thermal transition temperature than the crystalline amylose−lipid complex ($T_p$, about 120 °C).[48] In the present study, no V-type crystalline pattern was found in TQ total starch, TRS total starch, and TRS heterogeneous starch granules. Therefore, the peaks with $T_p$ at 98 °C were the melting of the amorphous amylose−lipid complex. It was noteworthy that TQ total starch, TRS polygonal granules, and TRS aggregate granules also had very weak amylose−lipid dissociation peak for their low amylose contents. This result was in agreement with XRD patterns that the amylose−lipid complex diffraction peak of $2\theta$ 20° was very prominent in TRS total starch, TRS elongated starch granules, and TRS hollow starch granules, especially for TRS hollow starch granules. The low relative crystallinity and double helix content and weak birefringence in TRS elongated starch granules were in agreement with the weak DSC peak of melting double-helical crystallites of the amylopectin molecules. The very low relative crystallinity and double helix content, no birefringence, and very high proportion of amorphous conformation in TRS hollow starch granules were also in agreement with the only DSC peak of melting the amorphous amylose−lipid complex. Though TRS total starch had similar double helix content to TRS elongated granules, their DSC parameters were significantly different. The main reason might be attributed to the difference in amylose content, granule morphology and size distribution, crystalline type, and molecular ordered structure in short- and long-range distance.[49] In addition, TRS total starch was a mixture of polygonal, aggregate, elongated, and hollow granules, which added the complication of analyzing DSC parameters for TRS total starch.

In conclusion, TRS polygonal, aggregate, elongated, and hollow starch granules were separated from the different regions of the mature kernels of high-amylose rice. These heterogeneous starch granules were essentially different in structures, including morphology, birefringence, iodine maximum absorption wavelength, iodine blue value, AC, molecular weight distribution, crystalline type, relative crystallinity, short-range ordered structure, relative proportions of single helix, double helix, and amorphous conformation, and scattering peak intensity and peak full width at half-maximum of SAXS. The different structures of TRS heterogeneous starch granules resulted in significantly different thermal properties.

## AUTHOR INFORMATION

### Corresponding Authors

*C.W.: College of Bioscience and Biotechnology, Yangzhou University, Yangzhou 225009, China. Tel: +86 514 87997217. E-mail: cxwei@yzu.edu.cn.

*Q.L.: Agricultural College, Yangzhou University, Yangzhou 225009, China. Tel: +86 514 87996648. E-mail: qqliu@yzu.edu.cn.

### Funding

This study was financially supported by grants from the National Natural Science Foundation of China (31270221), the Qing Lan Project of Jiangsu Province, the Talent Project of Yangzhou University, the Doctoral Program of Yangzhou University, and the Priority Academic Program Development of Jiangsu Higher Education Institutions.

### Notes

The authors declare no competing financial interest.

## ■ ACKNOWLEDGMENTS

The authors are grateful to Prof. Robert G. Gilbert (Huazhong University of Science and Technology, China) and Prof. Chengjun Zhu (Wuhan Ausinorigin High Tech Co., Ltd., China) for kindly providing technical assistance of GPC analysis.

## ■ ABBREVIATIONS USED

AC, amylose content; AAC, apparent amylose content; ATR-FTIR, attenuated total reflectance Fourier transform infrared; $^{13}$C CP/MAS NMR, solid-state $^{13}$C cross-polarization magic-angle spinning nuclear magnetic resonance; DSC, differential scanning calorimetry; GPC, gel-permeation chromatography; SAXS, small-angle X-ray scattering; TQ, Te-qing (wild type rice cultivar); TRS, transgenic resistant starch rice line; XRD, X-ray powder diffraction

## ■ REFERENCES

(1) Tester, R. F.; Karkalas, J.; Qi, X. Starch structure and digestibility enzyme-substrate relationship. *World's Poultry Sci. J.* **2004**, *60*, 186–195.

(2) Ao, Z.; Jane, J. L. Characterization and modeling of the A- and B-granule starches of wheat, triticale, and barley. *Carbohydr. Polym.* **2007**, *67*, 46–55.

(3) Lindeboom, N.; Chang, P. R.; Tyler, R. T. Analytical, biochemical and physicochemical aspects of starch granule size, with emphasis on small granule starches: a review. *Starch* **2004**, *56*, 89–99.

(4) Li, W.; Shan, Y.; Xiao, X.; Luo, Q.; Zheng, J.; Ouyang, S.; Zhang, G. Physicochemical properties of A- and B-starch granules isolated from hard red and soft red winter wheat. *J. Agric. Food Chem.* **2013**, *61*, 6477–6484.

(5) Dhital, S.; Shrestha, A. K.; Hasjim, J.; Gidley, M. J. Physicochemical and structural properties of maize and potato starches as a function of granule size. *J. Agric. Food Chem.* **2011**, *59*, 10151–10161.

(6) Kaur, L.; Singh, J.; McCarthy, O. J.; Singh, H. Physico-chemical, rheological and structural properties of fractionated potato starches. *J. Food Eng.* **2007**, *82*, 383–394.

(7) Singh, N.; Kaur, L. Morphological, thermal, rheological and retrogradation properties of potato starch fractions varying in granule size. *J. Sci. Food Agric.* **2004**, *84*, 1241–1252.

(8) Jiang, H. X.; Campbell, M.; Blanco, M.; Jane, J. L. Characterization of maize amylose-extender (*ae*) mutant starches: Part II. structures and properties of starch residues remaining after enzymatic hydrolysis at boiling-water temperature. *Carbohydr. Polym.* **2010**, *80*, 1–12.

(9) Regina, A.; Bird, A.; Topping, D.; Bowden, S.; Freeman, J.; Barsby, T.; Kosar-Hashemi, B.; Li, Z. Y.; Rahman, S.; Morell, M. High-amylose wheat generated by RNA interference improves indices of large-bowel health in rats. *Proc. Natl. Acad. Sci. U.S.A.* **2006**, *103*, 3546–3551.

(10) Regina, A.; Kosar-Hashemi, B.; Ling, S.; Li, Z. Y.; Rahman, S.; Morell, M. Control of starch branching in barley defined through differential RNAi suppression of starch branching enzyme IIa and IIb. *J. Exp. Bot.* **2010**, *61*, 1469–1482.

(11) Slade, A. J.; McGuire, C.; Loeffler, D.; Mullenberg, J.; Skinner, W.; Fazio, G.; Holm, A.; Brandt, K. M.; Steine, M. N.; Goodstal, J. F.; Knauf, V. Development of high amylose wheat through TILLING. *BMC Plant Biol.* **2012**, *12*, 69.

(12) Kim, K. S.; Hwang, H. G.; Kang, H. J.; Hwang, I. K.; Lee, Y. T.; Choi, H. C. Ultrastructure of individual and compound starch granules in isolation preparation from a high-quality, low-amylose rice, Ilpumbyeo, and its mutant, G2, a high-dietary fiber, high-amylose rice. *J. Agric. Food Chem.* **2005**, *53*, 8745–8751.

(13) Zhu, L. J.; Gu, M. H.; Meng, X. L.; Cheung, S. C. K.; Yu, H. X.; Huang, J.; Sun, Y.; Shi, Y. C.; Liu, Q. Q. High-amylose rice improves indices of animal health in normal and diabetic rats. *Plant Biotechnol. J.* **2012**, *10*, 353–362.

(14) Carciofi, M.; Blennow, A.; Jensen, S. L.; Shaik, S. S.; Henriksen, A.; Buléon, A.; Holm, P. B.; Hebelstrup, K. H. Concerted suppression of all starch branching enzyme genes in barley produces amylose-only starch granules. *BMC Plant Biol.* **2012**, *12*, 223.

(15) Chen, P.; Yu, L.; Simon, G.; Petinakis, E.; Dean, K.; Chen, L. Morphologies and microstructures of corn starches with different amylose-amylopectin ratios studied by confocal laser scanning microscope. *J. Cereal Sci.* **2009**, *50*, 241–247.

(16) Wei, C. X.; Qin, F. L.; Zhu, L. J.; Zhou, W. D.; Chen, Y. F.; Wang, Y. P.; Gu, M. H.; Liu, Q. Q. Microstructure and ultrastructure of high-amylose rice resistant starch granules modified by antisense RNA inhibition of starch branching enzyme. *J. Agric. Food Chem.* **2010**, *58*, 1224–1232.

(17) Wellner, N.; Georget, D. M. R.; Parker, M. L.; Morris, V. J. In situ Raman microscopy of starch granule structures in wild type and *ae* mutant maize kernels. *Starch* **2011**, *63*, 128–138.

(18) Liu, D.; Parker, M. L.; Wellner, N.; Kirby, A. R.; Cross, K.; Morris, V. J.; Cheng, F. Structural variability between starch granules in wild type and in *ae* high-amylose mutant maize kernels. *Carbohydr. Polym.* **2013**, *97*, 458–468.

(19) Dhital, S.; Shelat, K. J.; Shrestha, A. K.; Gidley, M. J. Heterogeneity in maize starch granule internal architecture deduced from diffusion of fluorescent dextran probes. *Carbohydr. Polym.* **2013**, *93*, 365–373.

(20) Cai, C. H.; Zhao, L. X.; Huang, J.; Chen, Y. F.; Wei, C. X. Morphology, structure and gelatinization properties of heterogeneous starch granules from high-amylose maize. *Carbohydr. Polym.* **2014**, *102*, 606–614.

(21) Wei, C. X.; Xu, B.; Qin, F. L.; Yu, H. G.; Chen, C.; Meng, X. L.; Zhu, L. J.; Wang, Y. P.; Gu, M. H.; Liu, Q. Q. C-type starch from high-amylose rice resistant starch granules modified by antisense RNA inhibition of starch branching enzyme. *J. Agric. Food Chem.* **2010**, *58*, 7383–7388.

(22) Cai, C. H.; Huang, J.; Zhao, L. X.; Liu, Q. Q.; Zhang, C. Q.; Wei, C. X. Heterogeneous structure and spatial distribution in endosperm of high-amylose rice starch granules with different morphologies. *J. Agric. Food Chem.* **2014**, *62*, 10143–10152.

(23) Peng, M.; Gao, M.; Abdel-Aal, E. S. M.; Hucl, P.; Chibbar, R. N. Separation and characterization of A- and B-type starch granules in wheat endosperm. *Cereal Chem.* **1999**, *76*, 375–379.

(24) Naguleswaran, S.; Li, J.; Vasanthan, T.; Bressler, D.; Hoover, R. Amylolysis of large and small granules of native triticale, wheat and corn starches using a mixture of $\alpha$-amylase and glucoamylase. *Carbohydr. Polym.* **2012**, *88*, 864–874.

(25) Dhital, S.; Shrestha, A. K.; Gidley, M. J. Relationship between granule size and *in vitro* digestibility of maize and potato starches. *Carbohydr. Polym.* **2010**, *82*, 480–488.

(26) Man, J. M.; Yang, Y.; Zhang, C. Q.; Zhou, X. H.; Dong, Y.; Zhang, F. M.; Liu, Q. Q.; Wei, C. X. Structural changes of high-amylose rice starch residues following in vitro and in vivo digestion. *J. Agric. Food Chem.* **2012**, *60*, 9332–9341.

(27) Tran, T. T. B.; Shelat, K. J.; Tang, D.; Li, E.; Gilbert, R. G.; Hasjim, J. Milling of rice grains. The degradation on three structural levels of starch in rice flour can be independently controlled during grinding. *J. Agric. Food Chem.* **2011**, *59*, 3964–3973.

(28) Li, E.; Hasjim, J.; Dhital, S.; Godwin, I. D.; Gilbert, R. G. Effect of a gibberellin-biosynthesis inhibitor treatment on the physicochemical properties of sorghum starch. *J. Cereal Sci.* **2011**, *53*, 328−334.
(29) Cai, J. W.; Cai, C. H.; Man, J. M.; Zhou, W. D.; Wei, C. X. Structural and functional properties of C-type starches. *Carbohydr. Polym.* **2014**, *101*, 289−300.
(30) Wei, C. X.; Qin, F. L.; Zhou, W. D.; Yu, H. G.; Xu, B.; Chen, C.; Zhu, L. J.; Wang, Y. P.; Gu, M. H.; Liu, Q. Q. Granule structure and distribution of allomorphs in C-type high-amylose rice starch granule modified by antisense RNA inhibition of starch branching enzyme. *J. Agric. Food Chem.* **2010**, *58*, 11946−11954.
(31) Man, J. M.; Yang, Y.; Huang, J.; Zhang, C. Q.; Chen, Y. F.; Wang, Y. P.; Gu, M. H.; Liu, Q. Q.; Wei, C. X. Effect of simultaneous inhibition of starch branching enzymes I and IIb on the crystalline structure of rice starches with different amylose contents. *J. Agric. Food Chem.* **2013**, *61*, 9930−9937.
(32) Tan, I.; Flanagan, B. M.; Halley, P. J.; Whittaker, A. K.; Gidley, M. J. A method for estimating the nature and relative proportions of amorphous, single, and double-helical components in starch granules by $^{13}$C CP/MAS NMR. *Biomacromolecules* **2007**, *8*, 885−891.
(33) Cai, C. H.; Cai, J. W.; Man, J. M.; Yang, Y.; Wang, Z. F.; Wei, C. X. Allomorph distribution and granule structure of lotus rhizome C-type starch during gelatinization. *Food Chem.* **2014**, *142*, 408−415.
(34) Wei, C. X.; Qin, F. L.; Zhou, W. D.; Chen, Y. F.; Xu, B.; Wang, Y. P.; Gu, M. H.; Liu, Q. Q. Formation of semi-compound C-type starch granule in high-amylose rice developed by antisense RNA inhibition of starch-branching enzyme. *J. Agric. Food Chem.* **2010**, *58*, 11097−11104.
(35) Jiang, H. X.; Horner, H. T.; Pepper, T. M.; Blanco, M.; Campbell, M.; Jane, J. L. Formation of elongated starch granules in high-amylose maize. *Carbohydr. Polym.* **2010**, *80*, 533−538.
(36) Wang, Y. J.; White, P.; Pollak, L.; Jane, J. Characterization of starch structures of 17 maize endosperm mutant genotypes with Oh43 inbred line background. *Cereal Chem.* **1993**, *70*, 171−179.
(37) Song, Y.; Jane, J. Characterization of barley starches of waxy, normal, and high amylose varieties. *Carbohydr. Polym.* **2000**, *41*, 365−377.
(38) Shi, Y. C.; Capitani, T.; Trzasko, P.; Jeffcoat, R. Molecular structure of a low-amylopectin starch and other high-amylose maize starches. *J. Cereal Sci.* **1998**, *27*, 289−299.
(39) Cheetham, N. W. H.; Tao, L. Variation in crystalline type with amylose content in maize starch granules: an X-ray powder diffraction study. *Carbohydr. Polym.* **1998**, *36*, 277−284.
(40) Yamamori, M.; Fujita, S.; Hayakawa, K.; Matsuki, J. Genetic elimination of a starch granule protein, SGP-1, of wheat generates an altered starch with apparent high amylose. *Theor. Appl. Genet.* **2000**, *101*, 21−29.
(41) Sevenou, O.; Hill, S. E.; Farhat, I. A.; Mitchell, J. R. Organisation of the external region of the starch granule as determined by infrared spectroscopy. *Int. J. Biol. Macromol.* **2002**, *31*, 79−85.
(42) Atichokudomchai, N.; Varavinit, S.; Chinachoti, P. A study of ordered structure in acid-modified tapioca starch by $^{13}$C CP/MAS solid-state NMR. *Carbohydr. Polym.* **2004**, *58*, 383−389.
(43) Bogracheva, T. Y.; Wang, Y. L.; Hedley, C. L. The effect of water content on the ordered/disordered structures in starches. *Biopolymers* **2001**, *58*, 247−259.
(44) Sanderson, J. S.; Daniels, R. D.; Donald, A. M.; Blennow, A.; Engelsen, S. B. Exploratory SAXS and HPAEC-PAD studies of starches from diverse plant genotypes. *Carbohydr. Polym.* **2006**, *64*, 433−443.
(45) Blazek, J.; Gilbert, E. P. Application of small-angle X-ray and neutron scattering techniques to the characterisation of starch structure: a review. *Carbohydr. Polym.* **2011**, *85*, 281−293.
(46) Yuryev, V. P.; Krivandin, A. V.; Kiseleva, V. I.; Wasserman, L. A.; Genkina, N. K.; Fornal, J.; Blaszczak, W.; Schiraldi, A. Structural parameters of amylopectin clusters and semi-crystalline growth rings in wheat starches with different amylose content. *Carbohydr. Res.* **2004**, *339*, 2683−2691.
(47) Wei, C. X.; Qin, F. L.; Zhou, W. D.; Xu, B.; Chen, C.; Chen, Y. F.; Wang, Y. P.; Gu, M. H.; Liu, Q. Q. Comparison of the crystalline properties and structural changes of starches from high-amylose transgenic rice and its wild type during heating. *Food Chem.* **2011**, *128*, 645−652.
(48) Jiang, H. X.; Lio, J.; Blanco, M.; Campbell, M.; Jane, J. L. Resistant-starch formation in high-amylose maize starch during kernel development. *J. Agric. Food Chem.* **2010**, *58*, 8043−8047.
(49) Miao, M.; Zhang, T.; Mu, W. M.; Jiang, B. Structural characterizations of waxy maize starch residue following in vitro pancreatin and amyloglucosidase synergistic hydrolysis. *Food Hydrocolloids* **2011**, *25*, 214−220.

Table 1. Composition of Model Solutions To Study the Interactions between Steviol Glycosides and Anthocyanins[a]

| symbol | C3G (mg $L^{-1}$) | P3G (mg $L^{-1}$) | Ste (mg $L^{-1}$) | RebA (mg $L^{-1}$) | Suc (g $L^{-1}$) | Glu (g $L^{-1}$) | Fru (g $L^{-1}$) | BA (mg $L^{-1}$) |
|---|---|---|---|---|---|---|---|---|
| C3G/C | 100 | | | | | | | 150 |
| C3G/Ste200 | 100 | | 200 | | | | | 150 |
| C3G/Ste125 | 100 | | 125 | | | | | 150 |
| C3G/Ste50 | 100 | | 50 | | | | | 150 |
| C3G/RebA200 | 100 | | | 200 | | | | 150 |
| C3G/RebA125 | 100 | | | 125 | | | | 150 |
| C3G/RebA50 | 100 | | | 50 | | | | 150 |
| C3G/Suc | 100 | | | | 100 | | | 150 |
| C3G/GF | 100 | | | | | 50 | 50 | 150 |
| C3G/Mix | 100 | | 100 | 100 | 100 | | | 150 |
| P3G/C | | 100 | | | | | | 150 |
| P3G/Ste200 | | 100 | 200 | | | | | 150 |
| P3G/Ste125 | | 100 | 125 | | | | | 150 |
| P3G/Ste50 | | 100 | 50 | | | | | 150 |
| P3G/RebA200 | | 100 | | 200 | | | | 150 |
| P3G/RebA125 | | 100 | | 125 | | | | 150 |
| P3G/RebA50 | | 100 | | 50 | | | | 150 |
| P3G/Suc | | 100 | | | 100 | | | 150 |
| P3G/GF | | 100 | | | | 50 | 50 | 150 |
| P3G/Mix | | 100 | 100 | 100 | 100 | | | 150 |

[a]The acidity of all solutions was pH 3.6 and was set using citric acid−sodium phosphate buffer prepared according to the method of Ruzin.[20] Abbreviations: BA, benzoic acid; C3G, cyanidin-3-glucoside; Fru, fructose; Glu, glucose; P3G, pelargonidin-3-glucoside; RebA, rebaudioside A; Ste, stevioside; Suc, sucrose.

carbonated drinks,[11−14] dairy products and pastries,[15,16] and hot beverages, model solutions, and solid sweetener.[9,10] All of the cited publications show that the stability of glycosides decreases with increasing acidity (significant decomposition at room temperature occurred only in solutions with a pH <2). The thermal degradation of sweetener in solutions and solid form occurred above 80 and 140 °C, respectively.

The present study reports the interactions between steviol glycosides and selected food antioxidants: vitamin C and anthocyanins. These compounds can be found mainly in fruits and fruit products, accounting for their health-promoting properties and, in the case of anthocyanins, their sensory quality. The impact on the stability of steviol glycosides during storage was also determined, and the results were compared to those obtained by other research teams. All of the tests were performed on model solutions in conditions similar to those prevailing in fruit juices and beverages.

## MATERIALS AND METHODS

**Materials.** Highly purified steviol glycosides, rebaudioside A (RebA, 96.2%) and stevioside (Ste, 98.5%), were obtained from ChromaDex (Irvine, CA, USA). Certified standards of anthocyanins, cyanidin-3-*O*-glucoside (C3G, 98.79%) and pelargonidin-3-*O*-glucoside (P3G, 99.22%), were purchased from Extrasynthese (Genay, France). L-Ascorbic acid (99%) was obtained from POCh (Gliwice, Poland). Acetonitrile for chromatography (HPLC grade) was acquired from Sigma-Aldrich (St. Louis, MO, USA). Other chemicals were of analytical grade and came from various suppliers.

**Instrumentation.** All chromatographic analyses were performed using Waters (Milford, MA, USA) equipment: 2695 Separations Module, 2995 Photodiode Array Detector, and 2414 Refractive Index Detector. During preparation of the sample an ME235S analytical balance (Sartorius AG, Göttingen, Germany) and an HI 211 pH meter (Hanna Instruments, Woonsocket, RI, USA) were used.

**Analytical Methods.** Steviol glycosides were determined using a method proposed by Bergs et al. with modifications.[17] For the analysis a Sunfire C8, 5 $\mu$m, 4.6 mm × 250 mm analytical column with a Sunfire C8 Sentry guard cartridge, 5 $\mu$m, 4.6 mm × 20 mm (both Waters) was used. Separation of the 10 $\mu$L samples was performed within 12 min at a flow rate of 1 mL $min^{-1}$ and a column temperature of 40 °C. Samples were eluted using a gradient of 1.8 mM hydrochloric acid (solvent A) and acetonitrile (solvent B), as follows (time, corresponding composition): 0 min, 65% A; 3 min, 65% A; 5 min, 60% A; 7 min, 60% A; 9 min, 65% A; 12 min, 65% A. Compounds were quantified using UV absorption at 210 nm.

The L-ascorbic (AA) and L-dehydroascorbic acid (DHAA) contents were measured according to the a method proposed by Odriozola-Serrano et al.[18] Before analysis, 1 mL of the sample was diluted with 1 mL of 0.01% phosphoric acid (determination of AA) or 1 mL of 1 g $L^{-1}$ solution of dithiothreitol (DTT) in 0.01% phosphoric acid (determination of AA and DHAA sum). The samples with DTT were kept in the cold (4 °C) for at least 1 h before injection. Separation was done on a Sunfire C18, 5 $\mu$m, 4.6 mm × 250 mm analytical column with a Sunfire C18 Sentry guard cartridge, 5 $\mu$m, 4.6 mm × 20 mm (both Waters). Analysis of the 10 $\mu$L samples was performed within 10 min at a flow rate 1 mL $min^{-1}$ and a column temperature of 25 °C. The samples were eluted isocratically using 0.01% phosphoric acid. The compounds were quantified using UV absorption at 245 nm.

Anthocyanin concentrations were determined using a method proposed by Oszmiański[19] using the same analytical column and guard column as described above. Separation of the 10 $\mu$L samples was performed within 26 min at a flow rate of 1 mL $min^{-1}$ and a column temperature of 25 °C. The samples were eluted using a gradient of 80% solution of acetonitrile in 4.5% formic acid (solvent A) and 4.5% formic acid (solvent B), as follows (time, corresponding composition): 0 min, 0% A; 7 min, 15% A; 15 min, 15% A; 21 min, 100% A; 26 min, 0% A. Compounds were quantified using vis absorption at 520 nm.

Glucose, fructose, and sucrose were determined according to EN 12630:1999 standard. For the analysis a Sugar-Pak I, 10 $\mu$m, 6.5 mm × 300 mm analytical column with a Sugar-Pak Guard-Pak insert, 10 $\mu$m (both Waters), was used. Separation of the 10 $\mu$L samples was performed within 18 min at a flow rate 0.5 mL $min^{-1}$ and a column temperature of 90 °C. Samples were eluted isocratically using 0.1 mM calcium disodium EDTA. The compounds were quantified using a refractive index detector.

**Model Solutions.** During research work, two series of experiments were conducted. The first investigated the interactions between steviol glycosides and two anthocyanins, cyanidin-3-glucoside and pelargoni-

din-3-glucoside (Table 1); the second series investigated interactions between stevioside and ascorbic acid (Table 2). The component

**Table 2. Composition of Model Solutions To Study the Interactions between Steviol Glycosides and Vitamin C[a]**

| symbol | AA (mg $L^{-1}$) | Ste (mg $L^{-1}$) | Suc (g $L^{-1}$) | BA (mg $L^{-1}$) | buffer |
|---|---|---|---|---|---|
| pH4.0/C | 500 | | | 150 | 4.0 |
| pH4.0/Ste200 | 500 | 200 | | 150 | 4.0 |
| pH4.0/Ste125 | 500 | 125 | | 150 | 4.0 |
| pH4.0/Ste50 | 500 | 50 | | 150 | 4.0 |
| pH4.0/Suc | 500 | | 100 | 150 | 4.0 |
| pH3.6/C | 500 | | | 150 | 3.6 |
| pH3.6/Ste200 | 500 | 200 | | 150 | 3.6 |
| pH3.6/Ste125 | 500 | 125 | | 150 | 3.6 |
| pH3.6/Ste50 | 500 | 50 | | 150 | 3.6 |
| pH3.6/Suc | 500 | | 100 | 150 | 3.6 |
| pH3.2/C | 500 | | | 150 | 3.2 |
| pH3.2/Ste200 | 500 | 200 | | 150 | 3.2 |
| pH3.2/Ste125 | 500 | 125 | | 150 | 3.2 |
| pH3.2/Ste50 | 500 | 50 | | 150 | 3.2 |
| pH3.2/Suc | 500 | | 100 | 150 | 3.2 |

[a]The acidity of solutions has been set using citric acid−sodium phosphate buffers prepared according to the method of Ruzin.[20] Abbreviations: AA, ascorbic acid; BA, benzoic acid; Ste, stevioside; Suc, sucrose.

concentrations and pH were set taking into account the values typical for fruit juices and the legal requirements for steviol glycoside concentration in beverages (applicable in the European Union).[21] Samples were kept in the dark at ambient temperature for up to 60 and 7 days for the first and second series, respectively.

**Statistical Analysis.** Data were analyzed using Statistica 7.1 software (StatSoft, Tulsa, OK, USA). The statistical significance of the differences in mean values was determined using an ANOVA test at $\alpha = 0.05$, and when significant differences existed, a Tukey test was performed. The kinetic parameters of degradation reactions were found using linear (C3G, P3G, AA) and nonlinear regression (DHAA). All of the results were obtained from duplicate analyses of two independent samples.

## RESULTS AND DISCUSSION

**Stability of Steviol Glycosides.** Concentrations of stevioside and rebaudioside in all of the model solutions investigated in the study were measured on the first and last days of each experiment (data not shown). The Tukey test did not reveal statistically significant differences between the initial and final concentrations of glycosides in any sample. These results are consistent with previous studies. Chang and Cook[11] found that steviol glycosides in carbonated drinks are stable at room temperature. These results were later confirmed by many authors examining various food matrices.[9,10,12−16]

**Kinetics of Anthocyanin Degradation.** Anthocyanins are a group of flavylium cation based glycosides that act as pigments and antioxidants in plant tissues. The main route of their degradation leads through deglycosylation and cleavage to aldehyde and benzoic acid derivatives.[22,23] The kinetics of anthocyanin (ACN) decrease is often described as a first-order reaction with results expressed as half-life time values (eq 1−3).[24−27]

$$\mathrm{ACN} \xrightarrow{k_1} \text{product} \quad (1)$$

$$c_{\mathrm{ACN}} = c_{\mathrm{ACN},0} \exp(-k_1 t) \quad (2)$$

$$t_{1/2} = \ln 2/k_1 \quad (3)$$

$c_{\mathrm{ACN}}$ = concentration of ACN, $c_{\mathrm{ACN},0}$ = initial concentration of ACN, $k_1$ = rate of reaction, $t$ = time, and $t_{1/2}$ = half-life time.

The rates of this reaction were determined using linear regression. The influence of the type of sweetener and its concentration on the C3G and P3G half-life time is shown in Figure 1. Detailed data can be found in Table S1 in the Supporting Information.

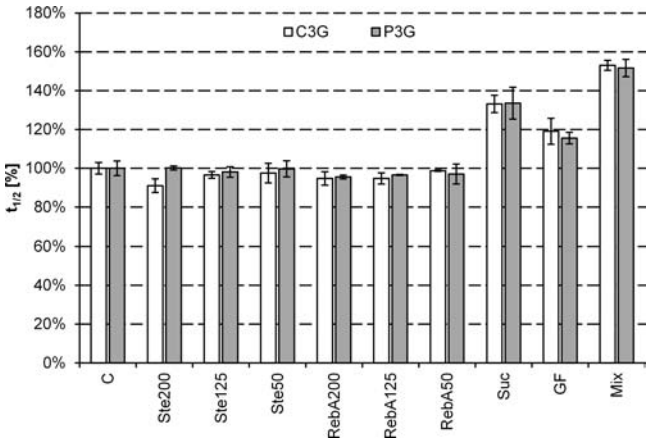


**Figure 1.** Influence of sweetener type and concentration on anthocyanin half-life times. Symbols and composition of model solutions are described in Table 1. Error bars represent standard deviation. Results were obtained from a duplicate analysis of two independent samples.

The addition of steviol glycosides, even at the highest concentration of 200 mg $L^{-1}$, did not affect the anthocyanin degradation rate. Regardless of the glycoside used and its concentration, the differences between the sample and control were statistically insignificant. The addition of sugars at a concentration of 100 g $L^{-1}$ significantly increased the stability of both anthocyanins by ca. 15% for a glucose−fructose mixture and by ca. 33% for sucrose. The simultaneous use of both sucrose and steviol glycosides turned out to be optimal with respect to anthocyanin stabilization: the half-life values of C3G and P3G were >50% higher than those observed in the control samples. Pelargonidin-3-glucoside was more stable than cyanidin-3-glucoside. This fact is consistent with the principle that increased hydroxylation of the flavylium cation decreases the stability of anthocyanins.[28] The effect of sweeteners was similar for both anthocyanins.

The influence of sugar on the stability of anthocyanin in water solutions is dependent to a large extent on the temperature, concentration, and type of sugar. Low concentrations, below 20%, of most carbohydrates stabilize pigments during storage in cold and ambient temperatures; an exception is fructose, which shows a destabilizing effect.[29−31] The results obtained in this study are consistent with these conclusions: anthocyanins were more stable in solutions containing sugars, and sucrose was also a better stabilizer than a mixture of glucose and fructose. Steviol glycosides did not affect the stability of anthocyanins, although they enhanced the protective properties of carbohydrates. The mechanism of this process is not yet known and should be examined in further research.

**Kinetics of Vitamin C Degradation.** The mechanism of AA degradation is specific, as it depends on several factors, whether it follows an aerobic or anaerobic pathway. The first

step of both pathways leads to the formation of DHAA, through ascorbic radical as intermediate in the anaerobic pathway or the multistage aerobic pathway catalyzed by metal ions. The second step is the irreversible hydrolysis to 2,3-diketogulonic acid (DKGA). DHAA retains part of the antioxidant and health-promoting activities of AA, although DKGA and further metabolites do not have such properites.[32]

Reduction of DHAA to AA occurs in the presence of reducing agents or enzymes such as dehydroascorbate reductase. Lack of such compounds in model solutions allows the above-mentioned reaction to be considered irreversible, so the degradation of ascorbic acid can be regarded as two consecutive first-order reactions (eq 4).[33]

$$\mathrm{AA} \xrightarrow{k_1} \mathrm{DHAA} \xrightarrow{k_2} \mathrm{DKGA} \tag{4}$$

Changes in the concentration of compounds can be described with differential equations. Their solutions (eqs 5 and 6) can be used to determine the kinetic parameters of the reaction.

$$c_{\mathrm{AA}} = c_{\mathrm{AA},0} \exp(-k_1 t) \tag{5}$$

$$c_{\mathrm{DHAA}} = \frac{k_1 c_{\mathrm{AA},0}}{k_2 - k_1}[\exp(-k_1 t) - \exp(-k_2 t)] \tag{6}$$

$c_{\mathrm{AA}}$ = concentration of AA, $c_{\mathrm{AA},0}$ = initial concentration of AA, $c_{\mathrm{DHAA}}$ = concentration of DHAA, $k_1$ = rate of first reaction, $k_2$ = rate of second reaction, and $t$ = time.

Rates of reaction were found using linear (AA) and nonlinear regression (DHAA). The fit of the model kinetics to experimental data is shown in Figure 2. The experimental data are highly consistent with the assumed model of the kinetics; for each sample the coefficient of determination was >0.95 (significant at $\alpha = 0.05$).

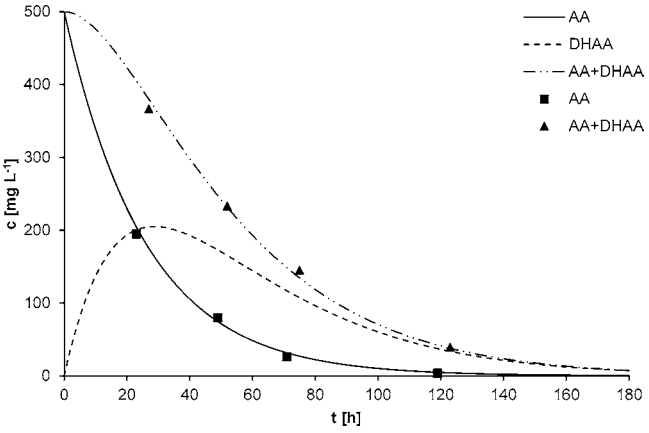


**Figure 2.** Fit between changes of ascorbic (AA) and dehydroascorbic (DHAA) acid concentration computed using kinetic equations (eqs 5 and 6; lines) and experimental data (dots) in sample pH4.0/Ste200 (composition of sample in Table 2).

A graphical representation of the influence of the type of sweetener and its concentration on the stability of vitamin C (AA and DHAA) at various pH values is shown in Figure 3 (AA) and Figure 4 (DHAA). Detailed data can be found in Table S2 in the Supporting Information.

The addition of steviol glycosides significantly increased the stability of both ascorbic and dehydroascorbic acid. The rate of degradation of ascorbic acid decreased by 4.0−22.3%, depending on the conditions. In the case of DHAA the protective

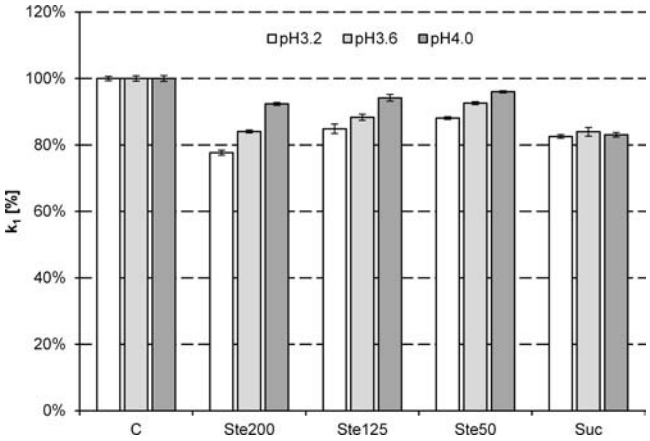


**Figure 3.** Influence of sweetener type, concentration, and acidity of solution on ascorbic acid degradation rate. Symbols and composition of model solutions are described in Table 2. Error bars represent standard deviation. Results were obtained from a duplicate analysis of two independent samples.

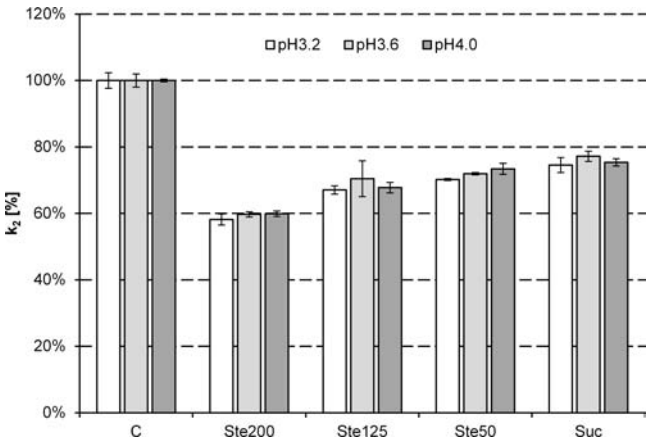


**Figure 4.** Influence of sweetener type, concentration, and acidity of solution on dehydroascorbic acid degradation rate. Symbols and composition of model solutions are described in Table 2. Error bars represent standard deviation. Results were obtained from a duplicate analysis of two independent samples.

effect was stronger: the rate of degradation was 26.6−41.9% lower than in the control sample. Higher concentrations of sweetener strengthened the protective effect; however, this relationship was not linearly proportional.

The acidity of the solution influenced the stability of vitamin C and the stabilizing effect of glycosides from *S. rebaudiana*. Higher acidity of the solutions significantly improved the protective effect of steviol glycosides on AA stability and, to a lesser extent, on DHAA stability. In general, ascorbic acid degradation is fastest in a pH close to 4.0 due to the maximum occurrence of hydrogen ascorbate ions.[32,34]

Control samples containing sucrose (100 g $L^{-1}$) were also examined. The protective effect of this carbohydrate was observed. Its strength did not depend on the acidity of the solution.

The protective effect of steviol glycosides on the stability of ascorbic acid was observed by Kroyer; however, his experiments were very limited.[9,10] Our research confirmed and expanded these results: the protective effect applied to both vitamin C forms, and it depended on the concentration of the sweetener

and acidity of the sample. The protective effect of sucrose on ascorbic acid is consistent with earlier publications.[35,36]

To our best knowledge this is the first study concerning the influence of steviol glycosides on anthocyanin stability. It also considerably expanded earlier experiments regarding interactions between stevioside and vitamin C.

The presented data demonstrate that the addition of glycosides from *S. rebaudiana* can increase the stability of vitamin C in water solutions of an acidic pH to a greater extent than sucrose used in sensory equivalent amounts. The addition of steviol glycosides also enhanced the protective effect of sucrose on anthocyanins. This fact may be of practical importance, indicating the additional benefits of using this natural noncaloric sweetener for fruit beverages.

Our research was conducted on model solutions, which, on the one hand, simplifies following the changes occurring in the sample, but, on the other hand, eliminates the influence of other constituents of real matrices, for example, radicals and metal ions, which might significantly change the degradation pattern through Fenton or Haber−Weiss reactions. The observed phenomena should be further investigated in complex food samples.[37]

## ■ ASSOCIATED CONTENT

### Supporting Information

Anthocyanin half-lives and ascorbic acid and dehydroascorbic acid degradation rates. This material is available free of charge via the Internet at http://pubs.acs.org.

## ■ AUTHOR INFORMATION


### Corresponding Author

*(L.W.) E-mail: lukasz.wozniak@ibprs.pl. Phone: (+48) 22 6063604. Fax: (+48) 22 8490426.


### Notes

The authors declare no competing financial interest.

## ■ ABBREVIATIONS USED

AA, ascorbic acid; ACN, anthocyanin (in general); BA, benzoic acid; C3G, cyanidin-3-glucoside; DHAA, dehydroascorbic acid; DTT, dithiothreitol; EDTA, ethylenediaminetetraacetic acid; HPLC, high-performance liquid chromatography; P3G, pelargonidin-3-glucoside; RebA, rebaudioside A; Ste, stevioside

## ■ REFERENCES


(1) Pawar, R. S.; Krynitsky, A. J.; Rader, J. I. Sweeteners from plants − with emphasis on *Stevia rebaudiana* (Bertoni) and *Siraitia grosvenorii* (Swingle). *Anal. Bioanal. Chem.* **2013**, *405*, 4397−4407.

(2) Ceunen, S.; Geuns, J. M. C. Steviol glycosides: chemical diversity, metabolism and function. *J. Nat. Prod.* **2013**, *76*, 1201−1228.

(3) Misra, H.; Soni, M.; Silawat, N.; Mehta, D.; Mehta, B. H.; Jain, D. C. Antidiabetic activity of medium-polar extract from the leaves of *Stevia rebaudiana* Bert. (Bertoni) on alloxan-induced diabetic rats. *J. Pharm. BioAllied Sci.* **2011**, *3*, 242−248.

(4) *Alternative Sweeteners*, 4th ed.; O'Brien Nabors, L., Ed.; CRC Press: Boca Raton, FL, USA, 2012; pp 159−180.

(5) Chatsudthipong, V.; Muanprasat, C. Stevioside and related compounds. Therapeutic benefits beyond sweetness. *Pharmacol. Ther.* **2009**, *121*, 41−54.

(6) Lemus-Mondaca, R.; Vega-Gálvez, A.; Zura-Bravo, L.; Ah-Hen, K. *Stevia rebaudiana* Bertoni, source of a high-potency natural sweetener: a comprehensive review on the biochemical, nutritional and functional aspects. *Food Chem.* **2012**, *132*, 1121−1132.

(7) Stoyanova, S.; Geuns, J. M. C.; Hideg, É.; Van Den Ende, W. The food additives inulin and stevioside counteract oxidative stress. *Int. J. Food Sci. Nutr.* **2011**, *62*, 207−214.

(8) Geuns, J. M. C.; Hajihashemi, S.; Claes, A. In *Stevia: Six Months Beyond Authorisation. Proceedings of the 6th EUSTAS Stevia Symposium*; Geuns, J. M. C., Ed.; Euprint: Heverlee, Belgium, 2012; pp 157−180.

(9) Kroyer, G. T. The low calorie sweetener stevioside: stability and interaction with food ingredients. *LWT−Food Sci. Technol.* **1999**, *32*, 509−512.

(10) Kroyer, G. T. Stevioside and stevia-sweetener in food: application, stability and interaction with food ingredients. *J. Verbrauch. Lebensm.* **2010**, *5*, 225−229.

(11) Chang, S. S.; Cook, J. M. Stability studies of stevioside and rebaudioside-A in carbonated beverages. *J. Agric. Food Chem.* **1983**, *31*, 409−412.

(12) Clos, J. F.; DuBois, G. E.; Prakash, I. Photostability of rebaudioside A and stevioside in beverages. *J. Agric. Food Chem.* **2008**, *56*, 8507−8513.

(13) Wölwer-Rieck, U.; Tomberg, W.; Wawrzun, A. Investigations on the stability of stevioside and rebaudioside A in soft drinks. *J. Agric. Food Chem.* **2010**, *58*, 12216−12220.

(14) Prakash, I.; Clos, J. F.; Chaturvedula, V. S. P. Stability of rebaudioside A under acidic conditions and its degradation products. *Food Res. Int.* **2012**, *48*, 65−75.

(15) Prakash, I.; DuBois, G. E.; Clos, J. F.; Wilkens, K. L.; Fosdick, L. E. Development of rebiana, a natural, non-caloric sweetener. *Food Chem. Toxicol.* **2008**, *46*, S75−S82.

(16) Jooken, E.; Amery, R.; Struyf, T.; Duquenne, B.; Geuns, J. M. C.; Meesschaert, B. Stability of steviol glycosides in several food matrices. *J. Agric. Food Chem.* **2012**, *60*, 10606−10612.

(17) Bergs, G.; Burghoff, B.; Joehnck, M.; Martin, G.; Schembecker, G. Fast and isocratic HPLC-method for steviol glycosides analysis from *Stevia rebaudiana* leaves. *J. Verbr. Lebensm.* **2012**, *7*, 147−154.

(18) Odriozola-Serrano, I.; Hernández-Jover, T.; Martín-Belloso, O. Comparative evaluation of UV-HPLC methods and reducing agents to determine vitamin C in fruits. *Food Chem.* **2007**, *105*, 1151−1158.

(19) Oszmiański, J. Stabilization and application of anthocyanin chokeberry dye to colouring of beverages. *ACTA Sci. Polym. Technol. Aliment.* **2002**, *1*, 37−45.

(20) Ruzin, S. E. Appendix II: Buffers. In *Plant Microtechnique and Microscopy*; Oxford University Press: New York, 1999; pp 223−234.

(21) EU Comission. Commission Regulation (EU) No. 1131/2011. *Off. J. Eur. Union* **2011**, *L295*, 205−211.

(22) Sadilova, E.; Stintzing, F. C.; Carle, R. Thermal degradation of acylated and nonacylated anthocyanins. *J. Food Sci.* **2006**, *71*, C504−C512.

(23) Seeram, N. P.; Bourquin, L. D.; Nair, M. G. Degradation products of cyanidin glycosides from tart cherries and their bioactivities. *J. Agric. Food Chem.* **2001**, *49*, 4924−4929.

(24) West, M. E.; Mauer, L. J. Color and chemical stability of a variety of anthocyanins and ascorbic acid in solution and powder forms. *J. Agric. Food Chem.* **2013**, *61*, 4169−4179.

(25) Patras, A.; Brunton, N. B.; O'Donnell, C.; Tiwari, B. K. Effect of thermal processing on anthocyanin stability in foods; mechanisms and kinetics of degradation. *Trends Food Sci. Technol.* **2010**, *21*, 3−11.

(26) Song, B. J.; Sapper, T. N.; Burtch, C. E.; Brimmer, K.; Goldschmidt, M.; Feruzzi, M. G. Photo and thermodegradation of anthocyanins from grape and purple sweet potato in model beverage systems. *J. Agric. Food Chem.* **2013**, *61*, 1364−1372.

(27) Hernández-Herrero, J. A.; Frutos, J. M. Degradation kinetics of pigments, colour and stability of the antioxidant capacity in juice model systems from six anthocyanin sources. *Int. J. Food Sci. Technol.* **2011**, *46*, 2550−2557.

(28) Bąkowska-Barczak, A. Acylated anthocyanins as stable, natural food colorants − a review. *Polym. J. Food Nutr. Sci.* **2005**, *14/55*, 107−116.

(29) Rubinskiene, M.; Viskelis, P.; Jasutiene, I.; Viskeline, R.; Bobinas, C. Impact of various factors on the composition and stability of black currant anthocyanins. *Food Res. Int.* **2005**, *38*, 867−871.

(30) Nikkhah, E.; Khayamy, M.; Heidari, R.; Jamee, R. Effect of sugar treatment on stability of anthocyanin pigments in berries. *J. Biol. Sci.* **2007**, *7*, 1412−1417.
(31) Cavalcanti, R. N.; Santos, D. T.; Meireles, M. A. A. Non-thermal stabilization mechanisms of anthocyanins in model and food systems − an overview. *Food Res. Int.* **2011**, *44*, 499−509.
(32) *Handbook of Food Engineering*, 2nd ed.; Heldman, D. R., Lund, D. B., Ed.; CRC Press: Boca Raton, FL, USA, 2007.
(33) Vieira, M. C.; Teixeira, A. A.; Silva, C. L. M. Mathematical modeling of the thermal degradation kinetics of vitamin C in cupuaçu (*Theobroma grandiflorum*) nectar. *J. Food Eng.* **2000**, *43*, 1−7.
(34) Finholt, P.; Paulssen, R. B.; Higuchi, T. Rate of anaerobic degradation of ascorbic acid in aqueous solution. *J. Pharm. Sci.* **1963**, *52*, 948−954.
(35) Rojas, A. M.; Gerschenson, L. N. Ascorbic acid destruction in sweet aqueous model systems. *Lebensm. Wiss. Technol.* **1997**, *30*, 567−572.
(36) Rojas, A. M.; Gerschenson, L. N. Ascorbic acid destruction in aqueous model systems: an additional discussion. *J. Sci. Food Agric.* **2001**, *81*, 1433−1439.
(37) Yin, J.-J.; Fu, P. P.; Lutterodt, H.; Zhou, Y.-T.; Antholine, W. E.; Wamer, W. Dual role of selected antioxidants found in dietary supplements: crossover between anti- and pro-oxidant activities in presence of copper. *J. Agric. Food Chem.* **2012**, *60*, 2554−2561.

milk after 12 weeks are highly important for further understanding of the shelf life of lactose-hydrolyzed UHT milk.

## MATERIAL AND METHODS

**Chemical Reagents.** Bis-Tris, $D_2O$ containing 0.025% sodium trimethylsilyl-[2,2,3,3-$_2H_4$]-1-propionate (TSP), 1,4-dithioerythritol, guanidine hydrochloride, sodium citrate dehydrate, and trifluoroacetic acid were obtained from Sigma-Aldrich Inc. (Steinheim, Germany). Acetonitrile was purchased from Mikrolab RA 1016 (Rathburn Chemicals, Ltd. Walkerburn, UK).

**Milk Samples.** Four types of milk (conventional indirect UHT, lactose-hydrolyzed direct UHT, lactose-hydrolyzed indirect UHT, and filtered (lactose-reduced) indirect UHT) were produced at a commercial Danish dairy plant (Arla Foods, Esbjerg, Denmark) (Table 1). The milk contained 1.5% (w/w) fat and 3.5% (w/w) protein. All milks were UHT heated using indirect heat treatment, where a tubular heat exchanger was used to heat the milk, followed by cooling with a plate heat exchanger.[16] An additional lactose-hydrolyzed milk batch was heat-treated using direct heat treatment, where steam was injected into the milk, followed by flash cooling.[16] The UHT temperature range is 140−145 °C for 4−6 s, and the direct heating temperature is generally 2−3 °C higher than the indirect heating temperature; however, the overall heat load is considerably lower.[16] Ultra- and nanofiltrations (cutoff was 10000 and 250 Da for the UF and NF filters, respectively)[17] were applied to reduce the lactose content to approximately 60% in the lactose-hydrolyzed and the filtered milk before heat treatment. The remaining lactose was enzymatically hydrolyzed after heat treatment, by addition of $\beta$-galactosidase (Maxilact LAG 5000, DSM, Heerlen, The Netherlands). The enzyme was dosed in an appropriate concentration to obtain total lactose hydrolysis (<1% of original lactose level) after 7 days of storage at 21 °C. All milk samples were packaged aseptically in 1 L Tetra Brik cartons. The milk samples were stored in an air-conditioned room at 22 °C. After 14, 21, 28, 45, 60, 90, 120, 150, 180, 210, 240, and 270 days of storage, one carton of each milk type was opened for analyses. Milk samples for $^1$H NMR spectroscopic analysis were filtered using Amicon Ultra 0.5 mL 10 kDa (Millipore, Bedford, MA, USA) spin filters at 10000*g* for 15 min, and the supernatant was subsequently frozen at −80 °C in 2 mL tubes. Milk samples for RP-HPLC-MS analysis were skimmed by centrifugation (Sorvall RC 5B plus, Thermo, Waltham, MA, USA) at 12800*g* for 30 min at 4 °C, and the skim milk was subsequently frozen at −80 °C in 2 mL tubes.

**Table 1. Overview of Milk Types, Heat Treatment, and Lactose Level Included in the Study[a]**

| milk | enzymatic hydrolysis | heat treatment | filtration | level of lactose (% of original level) | amount of lactose (% w/w) |
|---|---|---|---|---|---|
| conventional indirect UHT | − | indirect | − | 100 | 5 |
| lactose-hydrolyzed direct UHT | + | direct | + | <1 | 0.01 |
| lactose-hydrolyzed indirect UHT | + | indirect | + | <1 | 0.01 |
| filtered indirect UHT | − | indirect | + | 60 | 3 |

[a]All milk contained 1.5% (w/w) fat and 3.5% (w/w) protein.

**Aroma Profiling by Dynamic Headspace Sampling (DHS) and GC-MS.** DHS GC-MS was used to extract and analyze the volatile compounds in the fresh, unfrozen milk according to the procedure described by Jansson et al.[18] Adsorbent traps (Tenax TA, 200 g Tenax TA, 35/60 mesh, Markes International Limited, Llantrisant, UK) were used to isolate the volatile compounds, which were then desorbed (250 °C, 15 min) onto a cold trap (U-TIIGCP, Markes International Limited) using a thermal desorption system (ultra-UNITY, Markes International Limited). Subsequently, the volatiles were injected into a gas chromatograph (Finnigan trace GC ultra, Thermo, Waltham, MA, USA) and separated using a CP-Wax 52CB column (50 m × 0.25 mm, film thickness 0.25 $\mu$m, Varian, Palo Alto, CA, USA). The separated volatile compounds were detected using a single-quadrupole mass spectrometer (Finnigan Trace dual-stage quadrupole (DSQ), Thermo). The mass spectrometer scanned over a mass to charge ($m/z$) range of 45−650 (4.46 scans/s) in TIC mode. In total, 28 compounds were identified using the NIST mass spectral library (NIST MS search 2.0, 2011) and external standards. Dimethyl disulfide (DMDS), dimethyl trisulfide (DMTS), 2-ethylfuran, and 2-pentylfuran were quantified using external standard curves as previously described.[1]

**Metabolite Profiling by $^1$H NMR Spectroscopy.** Prior to proton nuclear magnetic resonance ($^1$H NMR) spectroscopy, the milk filtrates were thawed in randomized order and analyzed as described previously by Jansson et al.:[1] Four hundred microliters of milk was mixed with 200 $\mu$L of $D_2O$ containing 0.025% TSP as an internal standard. The samples were analyzed on a Bruker Avance III 600 spectrometer (Bruker Biospin, Rheinstetten, Germany) equipped with a 5 mm triple-resonance (TXI) probe. From a single 90° pulse experiment with a relaxation delay of 5 s standard one-dimensional spectra were obtained. The water peak was suppressed by irradiation during the relaxation delay, and a total of 64 scans were collected into 32K data points, scanning with a spectral width of 12.15 ppm. The data were multiplied by a 0.3 Hz line-broadening function and subsequently Fourier transformed. The TSP signal at 0 ppm was used as a reference, and all of the $^1$H spectra were manually baseline and phase corrected using Topspin 3.2 (Bruker Biospin). The sugar regions at 5.29−5.22, 5.0−4.49, and 4.11−3.32 ppm and the region with citrate at 2.74−2.47 ppm were removed from the data to facilitate the interpretation of the other metabolites. Metabolite concentrations were calculated for alanine, isoleucine, leucine, lysine, methionine, tryptophan, tyrosine, valine, formate lactose, glucose, and galactose, using Chenomx NMR suite 7.7 (Chenomx, Edmonton, Canada).

**Protein Profiling and Determination of Glycation by RP-HPLC-MS.** The RP-HPLC-MS procedure used in the present study was modified according to Jensen et al., and the procedures for sample preparation, settings for the HPLC, ESI source, and the mass selective detector were as described by Frederiksen et al.[19,20] Proteins were separated by reversed phase chromatography using an Agilent 1100 system (Agilent Technologies, Santa Clara, CA, USA) with a Jupiter C4 column (250 mm × 2 mm, 5 $\mu$M particle size, 300 Å pores; Phenomenex, Torrance, CA, USA) operated at 40 °C and a G1315A diode array detector with ultraviolet (UV) detection at 214 nm coupled to a mass selective detector for identification and relative quantification. The ESI source and the mass selective detector settings were as follows: ion mode was positive, the capillary exit voltage for the fragmentor was 200 V, the capillary voltage was 4500 V, and the nitrogen drying gas flow and temperature were 10 mL/min and 300 °C, respectively. Average molecular masses ($M_w$) of the milk proteins were obtained using the deconvolution algorithm of the ChemStation software (rev. B.04.01 SP [650], Agilent Technologies). All milk samples were analyzed in technical duplicates. The relative protein content of the intact milk proteins was calculated as the integrated area of each intact protein normalized with total integrated peak area in each LC chromatogram (Figure 2). "Total CN" comprised the sum of relative amounts of $\alpha_{s1}$-CN, $\alpha_{s2}$-CN, $\beta$-CN, and $\kappa$-CN.

**Statistical Analysis.** Prior to multivariate data analysis, $^1$H NMR spectroscopic data were mean-centered and Pareto-scaled. Principal component analysis (PCA) was applied to the centered and scaled data to elucidate differences between the milk types. A partial least-squares (PLS) regression model was used to predict the storage time, and a corresponding variable important in projection (VIP) plot was applied to identify the metabolites correlating strongest with the storage-induced changes. The PLS model was cross-validated (CV) using segmented CV with nine splits, where it was ensured that each sample replicate was in the same split. The root-mean-square error of cross-validation (RMSECV) was used as a measure of model performance. PCA was performed using SIMCA P+ 13.0 (Umetrics,

**Table 2. Overview of the Chemical Changes in Carbohydrates, Proteins, Free Amino Acids, and Strecker Degradation Compounds during Storage of Conventional, Lactose-Hydrolyzed, and Filtered UHT Milk**

| | changes during storage | | | | |
|---|---|---|---|---|---|
| chemical compound | conventional indirect UHT | lactose-hydrolyzed direct UHT | lactose-hydrolyzed indirect UHT | filtered indirect UHT | method |
| lactose[a] | NS[b] (54.18−54.31)a | NS (0.278−0.214)b | NS (0.249−0.207)b | NS (27.30−39.19)c | $^1$H NMR |
| galactose[a] | NS (0.356−0.407)b | NS (34.53−27.94)a | NS (24.56−27.88)a | NS (0.208−0.275)b | $^1$H NMR |
| glucose[a] | ND[c] | NS (41.43−32.66)a | NS (29.17−32.84)a | NS (0.136−0.148)a | $^1$H NMR |
| formate[a] | (↑)[d] $p$ = 0.025 (0.02−0.034)a | (↑) $p$ = 0.001 (0.007−0.022)a | (↑) $p$ = 0.001 (0.008−0.02)a | NS (0.009−0.019)a | $^1$H NMR |
| alanine[a] | NS (0.019−0.018)b | (↑) $p$ < 0.001 (0.018−0.026)a | (↑) $p$ < 0.001 (0.015−0.027)a | NS (0.016−0.016)b | $^1$H NMR |
| isoleucine[a] | NS (0.003−0.003)b | (↑) $p$ = 0.007 (0.007−0.129)a | (↑) $p$ < 0.001 (0.067−0.154)a | NS(0.004−0.003)b | $^1$H NMR |
| leucine[a] | NS (0.001−0.001)b | (↑) $p$ = 0.015 (0.003−0.033)a | (↑) $p$ = 0.003 (0.003−0.033)a | NS (0.001−0.006)b | $^1$H NMR |
| lysine[a] | NS(0.007−0.016)a | (↑) $p$ = 0.012 (0.007−0.018)a | (↑) $p$ = 0.026 (0.007−0.023)a | NS(0.005−0.021)a | $^1$H NMR |
| methionine[a] | NS (0.004−0.007)a | NS (0.002−0.005)a | NS (0.003−0.003)a | NS (0.002−0.004)a | $^1$H NMR |
| phenylalanine[a] | ND | (↑) $p$ = 0.006 (0.002−0.007)a | (↑) $p$ = 0.001 (0.001−0.009)a | ND | $^1$H NMR |
| tryptophan[a] | ND | (↑) $p$ = 0.063 (0.002−0.027)a | (↑) $p$ = 0.023 (0.002−0.036)a | ND | $^1$H NMR |
| tyrosine[a] | ND | (↑) $p$ = 0.002 (0.002−0.005)a | (↑) $p$ < 0.001 (0.002−0.006)a | ND | $^1$H NMR |
| valine[a] | NS (0.006−0.006)b | (↑) $p$ = 0.007 (0.012−0.118)a | (↑) $p$ = 0.001 (0.011−0.132)a | NS (0.007−0.005)b | $^1$H NMR |
| total CN[e] | (↓)[f] $p$ < 0.001 (65.3−54.9)b | (↓) $p$ < 0.001 (64.1−24.9)a | (↓) $p$ < 0.001 (64.4−28.5)a | (↓) $p$ < 0.001 (65.6−55.7)b | HPLC-MS |
| glycoprotein[e] | (↑) $p$ = 0.002 (3.3−4.8)b | (↑) $p$ < 0.001 (2.3−4.3)b | (↑) $p$ < 0.001 (3.1−6.5)a | (↑) $p$ = 0.001 (3.0−4.9)a | HPLC-MS |
| κ-CN[e] | (↓) $p$ < 0.001 (2.3−1.0)b | (↓) $p$ < 0.001 (3.4−0.6)a | (↓) $p$ < 0.001 (3.6−0.6)a | (↓) $p$ < 0.001 (2.7−1.3)b | HPLC-MS |
| $\alpha_{s1}$-CN[e] | NS (25.5−21.5)b | (↓) $p$ = 0.001 (22.8−12.6)a | (↓) $p$ < 0.001 (24.3−14.1)a | NS (25.4−21.0)b | HPLC-MS |
| $\alpha_{s2}$-CN[e] | NS (3.5−2.6)b | (↓) $p$ = 0.004 (4.1−2.0)a | (↓) $p$ = 0.004 (3.7−1.7)a | (↓) $p$ = 0.003 (4.3−2.2)a | HPLC-MS |
| β-CN[e] | (↓) $p$ = 0.001 (30.8−25.0)b | (↓) $p$ < 0.001 (31.5−5.4)a | (↓) $p$ < 0.001 (29.6−5.6)a | (↓) $p$ < 0.003 (30.3−26.3)b | HPLC-MS |
| β-LG[e] | (↓) $p$ < 0.001 (3.8−1.5)b | (↓) $p$ < 0.001 (4.8−0.7)a | (↓) $p$ < 0.001 (5.6−1.3)a | (↓) $p$ < 0.001 (4.5−2.5)b | HPLC-MS |
| benzaldehyde[g] | NS (2.31−3.38)a | NS (1.88−1.76)a | NS (2.28−2.87)a | NS (2.36−2.05)a | GC-MS |
| DMDS[g,h] | NS (0.49−0.11)a | NS (0.44−0.12)a | NS (0.60−0.07)a | NS (0.27−0.49)a | GC-MS |
| DMTS[g,i] | NS (1.75−0.17)a | NS (1.42−0.21)a | NS (1.89−0.20)a | NS (1.36−0.24)a | GC-MS |
| 2-ethylfuran[g] | (↑) $p$ = 0.005 (0.64−0.77)a | NS (0.60−0.79)a | NS (0.59−0.68)a | (↑) $p$ = 0.002 (0.62−0.76)a | GC-MS |
| 2-pentylfuran[g] | NS ((↑)$p$ = 0.053) (0.99−1.07)a | NS (0.86−1.04)a | NS (0.88−0.94)a | NS (1.04−1.07)a | GC-MS |
| 2-methylfuran[g] | ND | ND | ND | ND | GC-MS |

[a]Average start and end concentration (mM), based on three batches of conventional and lactose-hydrolyzed UHT milk, and two batches of filtered UHT milk. The samples were analyzed as technical triplicates. Lower case letters (a−c) indicate a significant difference in concentration between the milk types at storage day 270, $p < 0.05$. [b]Not significant. [c]Not detected. [d]Indicates a significant increase during storage determined from the slope of the curve. [e]Average start and end concentration, % intact protein, based on one batch (technical triplicates) of each milk type. [f]Indicates a significant decrease during storage determined from the slope of the curve. [g]Average start and end concentration (μg/kg), based on three batches of conventional and lactose-hydrolyzed UHT milk, and two batches of filtered UHT milk. The samples were made in technical triplicates. [h]Dimethyl disulfide. [i]Dimethyl trisulfide.



dx.doi.org/10.1021/jf5041044 | J. Agric. Food Chem. 2014, 62, 11270−11278

Umeå, Sweden) and PLS was performed using PLS Toolbox 6.71 (eigenvector Research Inc. Wenatchee, WA, USA) in MATLAB 7.11 (Mathworks, Natick, MA, USA).

To test the effect of milk type and storage time on the quantified proteins, amino acids, formate, carbohydrates, and the Strecker degradation compound linear mixed models (LME), least-squares means (LSMEANS), and Tukey's honest significant differences test ($\alpha$ = 0.05) were calculated in R (version 3.0.2, R Foundation for Statistical Computing, Vienna, Austria).

## RESULTS

Chemical changes in UHT-heated milk stored at 22 °C were followed over a period of 9 months. $^1$H NMR spectroscopy was applied to follow proteolysis through the detection of free amino acids. In total, nine free amino acids could be quantified (Table 2), and most of them increased significantly in the lactose-hydrolyzed milk during storage, for example, isoleucine (Figure 1), whereas they remained constant or were not

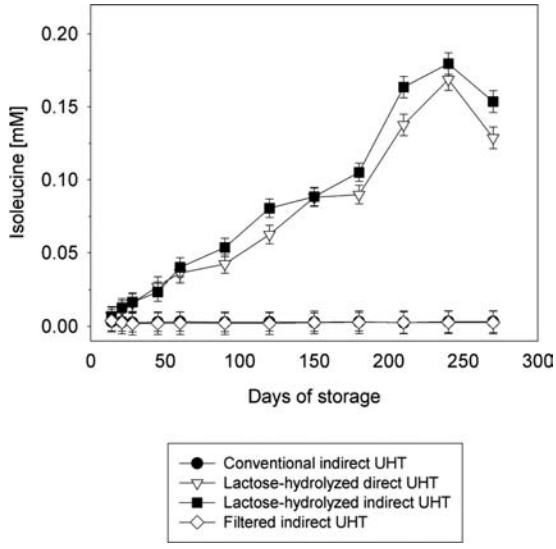


**Figure 1.** Concentration of isoleucine in conventional, lactose-hydrolyzed, and filtered UHT milk, quantified by $^1$H NMR spectroscopy.

detected (phenylalanine, tryptophan, and tyrosine) in the filtered and conventional UHT milk (Figure 1; Table 2). The only exceptions were methionine, which was constant throughout the storage period, and lysine, which increased in all milk types.

To investigate which proteins gave rise to the increased level of amino acids in the lactose-hydrolyzed UHT milk, the intact proteins in the milk were separated using RP-HPLC and detected with an UV detector at 214 nm, resulting in the chromatogram shown in Figure 2. Proteolysis was measured as a decrease in content of intact protein, and proteolysis was observed for all proteins in all milk types during storage. However, the level of proteolysis was significantly higher in the lactose-hydrolyzed UHT milk compared to the filtered and conventional UHT milk (Table 2). The relative amount of total intact CN was reduced by 56% for lactose-hydrolyzed indirect UHT-heated milk and by 61% for lactose-hydrolyzed direct UHT-heated milk during the storage period, as compared to 15% for conventional and filtered indirect UHT-heated milk (Table 2). The two most extensively hydrolyzed proteins during storage were $\beta$-CN and $\alpha_{s1}$-CN (Figure 3), which were reduced by approximately 80 and 45%, respectively (Table 2),

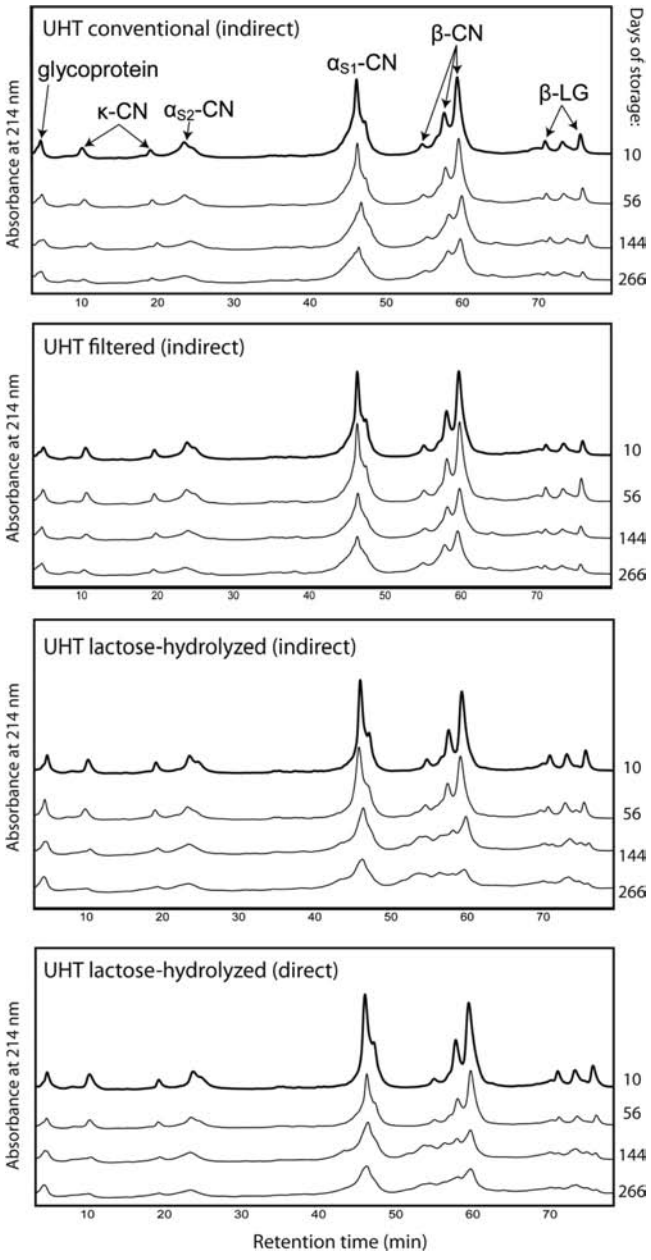


**Figure 2.** RP-HPLC chromatogram with UV detection at 214 nm of proteins in conventional, filtered, and lactose-hydrolyzed UHT milk at four storage times.

in lactose-hydrolyzed milk compared to a more moderate reduction for conventional and filtered milk. The content of intact $\kappa$-CN and intact $\beta$-LG decreased in all milk types, (Table 2), whereas $\alpha_{s2}$-CN content decreased only in the filtered and lactose-hydrolyzed UHT milk.

The identified amino acids and their involvement in Strecker degradation product formation are summarized in the Supporting Information. Five putative Strecker degradation products were identified; however, no clear connection between the volatile compounds and the increased levels of free amino acids could be observed. Likewise, no clear effects of lactose hydrolysis, filtration, or heat treatment on volatile compound formation were revealed (Table 2).

Exploring the MS, we detected glycation of all major milk proteins in the four milk types at all storage times as N-linked glycans with mass addition of 162 and 324 Da, indicating that

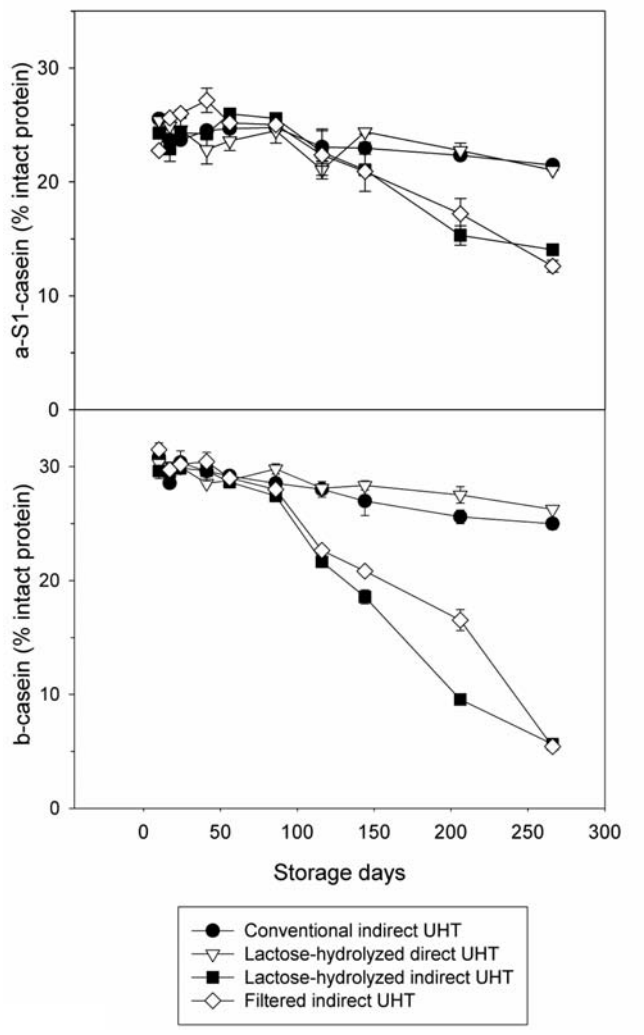


**Figure 3.** Relative quantification of $\alpha_{s1}$-casein and $\beta$-casein in conventional, lactose-hydrolyzed, and filtered UHT milk as a function of storage.

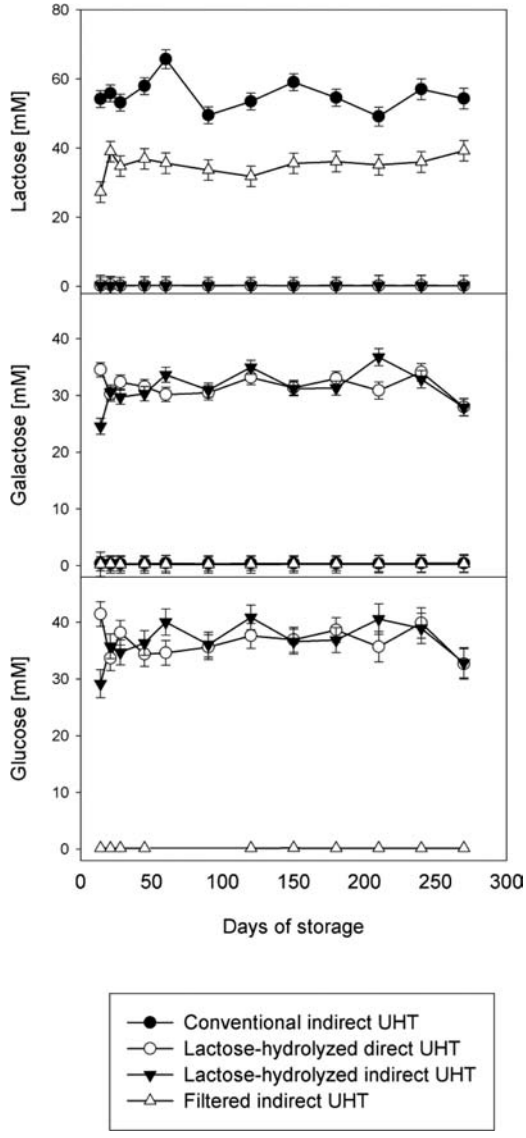


**Figure 4.** Concentration of lactose, galactose, and glucose in conventional, lactose-hydrolyzed, and filtered UHT milk, quantified by $^1$H NMR spectroscopy.

hexose and lactose molecules, respectively, were attached to the proteins. The level and type of glycation could not be revealed from the method used. Furthermore, another indicator for protein glycation is the hydrophilic protein fraction in the UV chromatograms, denoted glycoproteins, identified as the first peak eluting from the RP-HPLC column (Figure 2). The glycoprotein has previously been identified as glycosylated $\kappa$-CN and must also be considered to contain glycated peptides.[19] This peak increased significantly during storage in all milk samples, although being significantly highest in indirect heated lactose-hydrolyzed milk (Table 2). Even though protein glycation was observed, the level of free carbohydrates analyzed with $^1$H NMR spectroscopy was constant during the storage time, although after 240 days of storage, a decrease in glucose and galactose content was observed in all lactose-hydrolyzed milk samples (Figure 4), which is consistent with a decrease in the concentration of free amino acids, as shown in Figure 1 for isoleucine.

Finally, formate can be formed from the deoxyosones and may therefore be an indicator of the Maillard reaction. It was found that initial formate concentrations were highest in conventional milk; however, during storage similar formation rates were observed for all milk types, except for the filtered milk (Table 2).

Furthermore, the $^1$H NMR spectroscopic data were analyzed using an untargeted approach to elucidate how storage affected overall metabolite composition. In Figure 5 a PCA of $^1$H NMR spectroscopic data showed a separation along PC1 and PC2 between the lactose-removed (lactose-hydrolyzed and filtered UHT milk) and non-lactose-removed (conventional UHT milk) samples, probably due to the dilution (removal of 40% lactose) occurring in this step. In fresh samples (<50 days old), no clear separation between lactose-hydrolyzed milk and filtered milk could be observed. On the other hand, along PC1 a pronounced effect of storage was observed for lactose-hydrolyzed milk, whereas for the conventional and filtered milks the storage effect was much smaller. A PLS regression model with $^1$H NMR spectroscopic variables as $X$ and storage time as $Y$ was generated for each milk type (Figure 6A,C,E). The models revealed that the storage time of lactose-hydrolyzed and filtered milk could be predicted within a variance of 11 days ($R^2$ CV was 0.99 and 0.98, respectively;

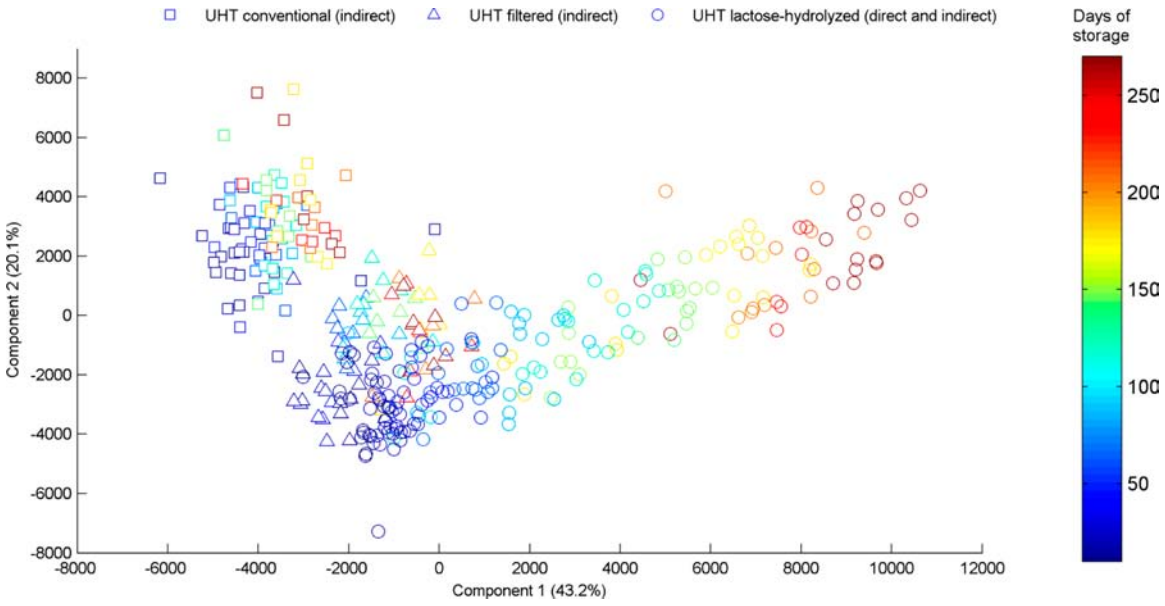


**Figure 5.** PCA score plot of $^{1}$H NMR spectroscopic data of conventional, filtered, and lactose-hydrolyzed UHT milk during storage. Samples are colored according to days of storage. The first principal component explains 43.2% of the variation, and the second principal component explains 20.1% of the variation.

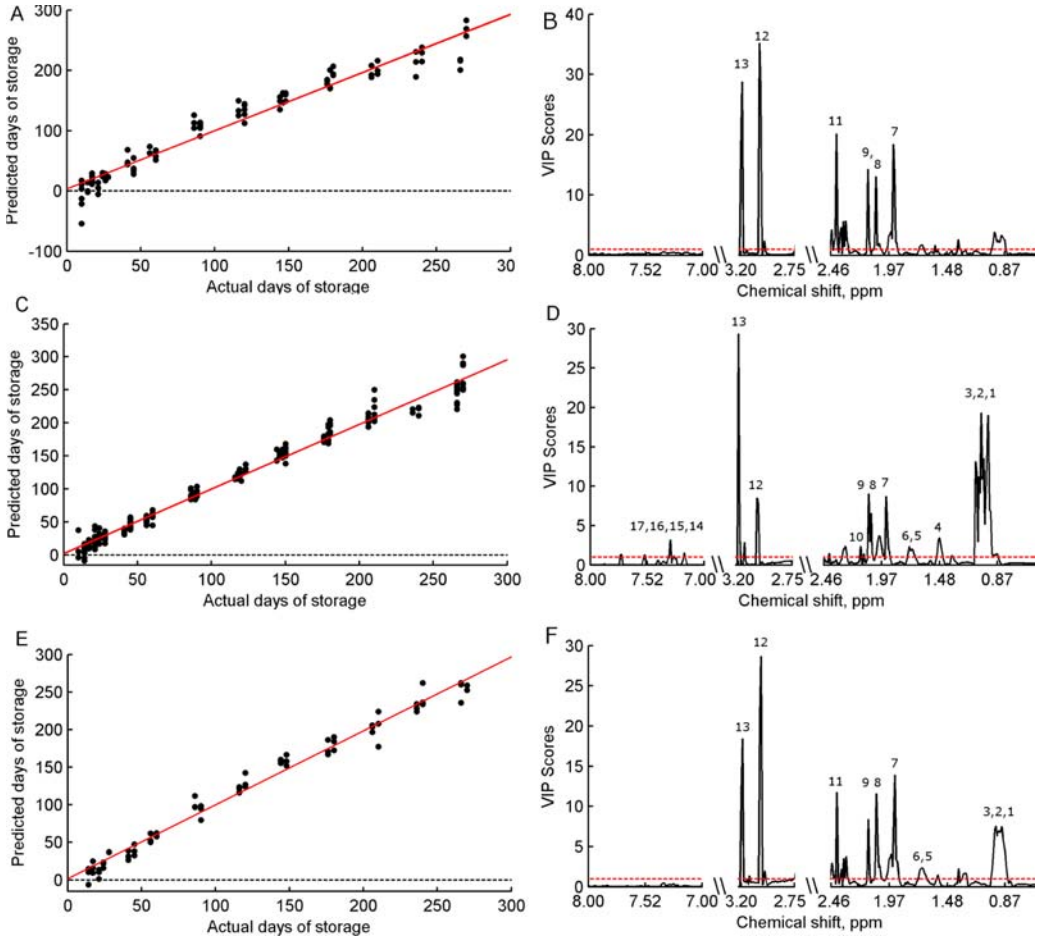


**Figure 6.** PLS regression plots from $^{1}$H NMR spectroscopic data with predicted versus actual and corresponding VIP plot for model based on (A, B) conventional UHT milk ($n$ = 33), $R^2$ CV = 0.95, RMSECV = 18.59 days; (C, D) lactose-hydrolyzed UHT milk ($n$ = 65), $R^2$ CV = 0.98, RMSECV = 11.23 days; and (E, F) filtered UHT milk ($n$ = 23), $R^2$ CV = 0.98, RMSECV = 11.45 days. Peak numbers indicate the metabolites important for the regression: 1, 2, 3, leucine, isoleucine, valine; 4, alanine; 5, 6, lysine, leucine; 7, acetate; 8, *N*-acetyl carbohydrates; 9, 10, methionine; 11, not identified; 12, 13, creatine/creatinine, choline; 14, 15, 16, 17, hippurate, tyrosine, tryptophan, phenylalanine.


dx.doi.org/10.1021/jf504104q | *J. Agric. Food Chem.* 2014, 62, 11270−11278

RMSECV was 11.23 and 11.45 days, respectively), and the storage time of conventional milk could be predicted within a variance of 19 days ($R^2$ CV was 0.95 and RMSECV was 18.59 days). To find the metabolites responsible for the changes during storage, VIP scores were plotted for each PLS model (Figure 6B,D,F). Choline was significant in all milk types, whereas amino acids (leucine, isoleucine, valine, alanine, phenylalanine), as expected, were much more important in lactose-hydrolyzed milk as compared to the other milk types. In the unhydrolyzed milk samples hippurate, creatine/creatinine, *N*-acetyl carbohydrates, and acetate were identified as significant.

## DISCUSSION

Storage stability is of importance in UHT milk to maintain consumer acceptability of the milk. In the present study, chemical changes that could be detrimental to milk quality were investigated in UHT milk produced with and without lactose hydrolysis during a storage period of 9 months. Furthermore, filtered indirectly heated UHT milk was included to follow the effect of the $\beta$-galactosidase added to the milk. The two different heat treatments (direct and indirect) applied to the lactose-hydrolyzed milk were included to investigate the effect of severity of heat treatment. The indirect lactose-hydrolyzed UHT milk had a significantly higher level of glycoprotein compared to the direct lactose-hydrolyzed UHT milk. However, the type of heat treatment did not have any effect on volatile compounds, metabolite profile, or proteolytic activity, and therefore the term lactose-hydrolyzed milk refers to both milk types.

**Proteolysis Has Major Effect in Lactose-Hydrolyzed Milk.** $^1$H NMR spectroscopy was used to identify metabolites in the milk, and PCA of $^1$H NMR spectroscopic data revealed much more severe storage-induced changes in lactose-hydrolyzed milk than in the conventional and filtered UHT milk (Figure 5). This result shows that major chemical changes are not induced by the filtration but rather they can be attributed to the addition of the $\beta$-galactosidase preparation. The PLS models calculated (Figure 6) could predict the time of storage of each milk with a high precision, as reflected in the low RMSECV values (11−19 days). However, the prediction was considerably better for lactose-hydrolyzed UHT milk than conventional UHT milk, which supports the more severe storage-induced changes in the lactose-hydrolyzed UHT milk shown in the PCA. In the present study proteolysis was the major chemical change observed. Lysine was the only amino acid that increased in all milk types during storage; however, the increase was only significant in the lactose-hydrolyzed milk, which likely can be ascribed to the presence of heat-stable endogenous proteases that cleave proteins after lysine and arginine (Lys or Arg in $P^1$ position).[21−24] A decrease in lysine could be expected due to its involvement in the Maillard reaction. However, the binding of carbohydrates to lysine seems to be of minor importance compared to the proteolytic activity. No significant changes were observed in methionine during storage, which is different from a previous study[1] in which a decrease of methionine was observed during storage in the conventional and lactose-hydrolyzed UHT milk. This difference suggests that methionine is affected by batch variations.[18]

The increased proteolytic activity was further elucidated by RP HPLS-MS by investigating the content of intact protein during storage. Our study showed that the caseins present in the lactose-hydrolyzed UHT milk were considerably affected by the proteolytic activity, whereas in the conventional UHT milk only a moderate proteolytic activity could be observed during storage. The proteolytic activity in the filtered milk did not deviate from the conventional UHT milk, which indicates that no proteolysis originated from the filtration step. The most hydrolyzed proteins in the lactose-hydrolyzed UHT milk were $\beta$-CN and $\alpha_{s1}$-CN, which significantly decreased after 90 days of storage (Table 2; Figure 2). This was an important pattern depicting differences between the lactose-hydrolyzed and conventional UHT milks during storage. The results are in agreement with the results from Tossavainen and Kallioinen, who investigated lactose-hydrolyzed and conventional UHT milks stored at different temperatures (5, 22, 30, and 45 °C) for 12 weeks.[6] In addition, Tossavainen and Kallioinen found that the $\alpha_{s1}$-, $\alpha_{s2}$-, and $\beta$-CN were the most extensively degraded proteins, whereas $\beta$-LG, $\alpha$-LA, and $\kappa$-casein were less affected.[14] Another interesting observation was that the free amino acids increased immediately during storage, whereas the reduction in $\beta$-CN and $\alpha_{s1}$-CN was not observed until after 90 days in the lactose-hydrolyzed milk. These findings could indicate that a low degree of hydrolysis of proteins gives rise to an increase in the level of free amino acids but does not affect the proteins sufficiently to be detectable by RP HPLC-MS.

The decrease in $\beta$-CN and $\alpha_{s1}$-CN after approximately 90 days of storage (Figure 2) seems to relate to the development of an off-flavor, which typically develops after 90 days. Casein contains a high amount of hydrophobic amino acids, which are highly correlated to bitterness,[25,26] and a proteolysis of casein and especially $\beta$-CN and $\alpha_{s1}$-CN would consequently result in a bitter taste.[27−30] McKellar et al. investigated proteolysis and bitterness in UHT milk during 8 months storage at ambient temperature and observed a high correlation between storage time, proteolysis, and bitterness.[8]

**Maillard Reaction in the Lactose-Hydrolyzed Milk.** The Maillard reaction is dependent on the reaction between amines (primarily protein-bound lysine and N-terminals) and reducing carbohydrates, and the type and concentration of these substrates are highly important for the level of Maillard reaction product formation.[1,2] In the present study protein glycation, formate, and Strecker degradation product formation were investigated in filtered, lactose-hydrolyzed, and conventional UHT milks. The relative estimate of identified glycopeptides and -protein increased during storage for all milk types (Table 2), although the absolute degree of glycation could not be quantified on the basis of the RP HPLC-MS method applied. This is in contrast to the study by Carulli et al., who observed a higher degree of glycation of $\alpha$-LA and $\beta$-LG in the presence of glucose and galactose compared to lactose.[5] Likewise, we were not able to detect a significant difference in the degree of formate or in the Strecker degradation product formation analyzed (2-pentylfuran, 2-methylfuran, DMDS, DMTS, and benzaldehyde) during storage.

Strecker aldehydes have been shown to affect the milk aroma,[31,32] and both lactose hydrolysis and proteolysis were expected to promote the formation of Strecker aldehydes in lactose-hydrolyzed milk as compared to conventional UHT milk. However, the lack of significant differences could indicate that the Maillard reaction may not be the most important pathway for their formation.[33,34] For instance, benzaldehyde was observed in all milk types, whereas its precursor, phenylalanine,[35] was detected only in lactose-hydrolyzed milk (Table 2). Valero et al. observed an increase of benzaldehyde in

skim milk during storage.[34] However, the present study could not support this observation.

We previously observed a striking correlation between 2-methylbutanal, isoleucine, and furosine formation in lactose-hydrolyzed UHT milk after approximately 90 days of storage.[1] This seems to be closely connected to the decrease in intact casein concentrations observed here. Hence, a possible link between proteolysis, glycation, and Strecker aldehyde formation seems likely, although we cannot prove causality.

A final aspect that might affect the quality of lactose-hydrolyzed milk is the dilution that occurs during the filtration step; thus, the lactose-hydrolyzed and filtered UHT milk were heat-treated with a 40% lower level of lactose compared to the conventional milk. This was reflected by a lower formate level in fresh lactose-hydrolyzed and filtered milk (Table 2), but did not result in different rates of formate formation during storage. The most significant pathway for formate generation is through $\alpha$-dicarbonyls generated in the Maillard reaction,[36,37] but our results indicate that the type of sugar and proteolysis are not decisive factors for the formation of formate in milk. However, a lower level of lactose during heating could be reflected in the lower initial concentration of the Maillard reaction compounds furosine and 2-methylbutanal in the lactose-hydrolyzed milk compared to the conventional milk in a previous study by Jansson et al.[1] In addition, the type of sugar was decisive for the formation rate of furosine and 2-methylbutanal in the lactose-hydrolyzed UHT milk.

The present study shows that the side effects of the added $\beta$-galactosidase are highly relevant for the chemical reactions taking place in the lactose-hydrolyzed milk during storage. Tossavainen and Kallioinen[6] investigated how heat treatment before and after the addition of $\beta$-galactosidase to lactose-hydrolyzed milk affects the proteolytic activity, but no significant difference was observed between the different enzymatic treatments. In milk hydrolyzed prior to the heat treatment, a higher concentration of $\beta$-galactosidase is added compared to the milk hydrolyzed after the heat treatment to obtain the same hydrolytic effect. However, the implication of higher enzyme addition may be additional enzyme activity after heat treatment as a result of an incomplete inactivation during heating. Although an increased heating temperature would increase inactivation of enzyme activity, it would also affect the nutritional value of the milk.[6]

The generation of free amino acids during storage of lactose-hydrolyzed milk originates most likely from either enzymatic impurity in the used $\beta$-galactosidase preparation and/or side activities of the $\beta$-galactosidase. Higher levels of proteolytic activity contribute to the flavor of the milk through formation of flavor-active amino acids/peptides and/or through formation of additional Maillard reaction products, for example, Strecker aldehydes. The reactivity of glucose and galactose determines the rate of the Maillard reaction. In addition, our results indicate that a sufficient level of free amino acids is required to accelerate the Maillard reaction. To gain an improved understanding of the chemical changes observed in lactose-hydrolyzed milk, it would be relevant to focus on the proteins $\beta$-CN and $\alpha_{s1}$-CN, which are most affected by the proteolytic activity.

## ■ ASSOCIATED CONTENT

### Supporting Information

Table with overview of amino acids identified using $^1$H NMR spectroscopy and their involvement in formation of Strecker degradation aldehydes identified using GCMS. This material is available free of charge via the Internet at http://pubs.acs.org.

## ■ AUTHOR INFORMATION


### Corresponding Author

*(H.C.B.) E-mail: HanneC.Bertram@agrsci.dk. Phone: +45 871 58353.



### Funding

The present study was financially supported by Arla Foods Amba, Food Future Innovation (FFI), Danish Dairy Research Foundation, and Aarhus University.


### Notes

The authors declare no competing financial interest.

## ■ ACKNOWLEDGMENTS


We are thankful for the excellent technical assistance of Birgitte Foged and Hanne S. Møller. The present study is part of the Ph.D. work of T. Jansson.


## ■ ABBREVIATIONS USED

CN, casein; CV, cross-validated; Da, dalton; DMDS, dimethyl disulfide; DMTS, dimethyl trisulfide; DSQ, dual-stage quadrupole; RP HPLC, reversed phase high-pressure liquid chromatography; GC-MS, gas chromatography−mass spectrometry; LA, lactalbumin; LG, lactoglobulin; LME, linear mixed model; LSMEANS, least square means; MS, mass spectrometry; NMR, nuclear magnetic resonance; PC, principal component; PCA, principal component analysis; PLS, partial least-squares; RMSECV, root mean square error of cross validation; TIC, total ion current; TSP, sodium trimethylsilyl-[2,2,3,3-$_2$H$_4$]-1-propionate; UHT, ultrahigh temperature; UV, ultraviolet; VIP, variable importance in projection

## ■ REFERENCES


(1) Jansson, T.; Clausen, M. R.; Sundekilde, U. K.; Eggers, N.; Nyegaard, S.; Larsen, L. B.; Ray, C.; Sundgren, A.; Andersen, H. J.; Bertram, H. C. Lactose-hydrolyzed milk is more prone to chemical changes than conventional ultra-high-temperature (UHT) milk. *J. Agric. Food Chem.* **2014**, *62*, 7886−7896.

(2) Messia, M. C.; Candigliota, T.; Marconi, E. Assessment of quality and technological characterization of lactose-hydrolyzed milk. *Food Chem.* **2007**, *104*, 910−917.

(3) Tossavainen, O.; Kallioinen, H. Effect of lactose-hydrolysis on furosine and available lysine in UHT skim milk. *Milchwissenschaft* **2008**, *63*, 22−26.

(4) Kato, Y.; Matsuda, T.; Kato, N.; Nakamura, R. Browning and protein polymerization induced by amino-carbonyl reaction of ovalbumin with glucose and galactose. *J. Agric. Food Chem.* **1988**, *36*, 806−809.

(5) Carulli, S.; Calvano, C. D.; Palmisano, F.; Pischetsrieder, M. MALDI-TOF MS characterization of glycation products of whey proteins in a glucose/galactose model system and lactose-free milk. *J. Agric. Food Chem.* **2011**, *59*, 1793−1803.

(6) Tossavainen, O.; Kallioinen, H. Proteolytic changes in lactose hydrolyzed UHT milks during storage. *Milchwissenschaft−Milk Sci. Int.* **2007**, *62*, 410−415.

(7) Evangelisti, F.; Calcagno, C.; Nardi, S.; Zunin, P. Deterioration of protein fraction by Maillard reaction in dietetic milks. *J. Dairy Res.* **1999**, *66*, 237−243.

(8) McKellar, R. C.; Froehlich, D. A.; Butler, G.; Cholette, H.; Campbell, C. The effect of uncooled storage on proteolysis bitterness and apparent viscosity in ultra high temperature milk. *Can. Inst. Food Sci. Technol. J.* **1984**, *17*, 14−17.

(9) Van Boekel, M. A. J. S. Formation of flavor compounds in the Maillard reaction. *Biotechnol. Adv.* **2006**, *24*, 230−233.

(10) Rerkrai, S.; Jeon, I. J.; Bassette, R. Effect of various direct ultra-high temperature heat treatments on flavor of commercially prepared milks. *J. Dairy Sci.* **1987**, *70*, 2046−2054.
(11) Kokkinidou, S.; Peterson, D. G. Control of Maillard-type off-flavor development in ultrahigh-temperature-processed bovine milk by phenolic chemistry. *J. Agric. Food Chem.* **2014**, *62*, 8023−8033.
(12) Enright, E.; Bland, A. P.; Needs, E. C.; Kelly, A. L. Proteolysis and physicochemical changes in milk on storage as affected by UHT treatment, plasmin activity and $KIO_3$ addition. *Int. Dairy J.* **1999**, *9*, 581−591.
(13) Rauh, V. M.; Johansen, L. B.; Ipsen, R.; Paulsson, M.; Larsen, L. B.; Hammershøj, M. Plasmin activity in UHT milk: relationship between proteolysis, age gelation, and bitterness. *J. Agric. Food Chem.* **2014**, *62*, 6852−6860.
(14) Tossavainen, O.; Kallioinen, H. Furosine formation and proteolytic changes in carbohydrate reduced UHT milks. *Milchwissenschaft* **2008**, *63*, 254−258.
(15) Mittal, S. B.; Newell, G.; Hourigan, J. A.; Zadow, J. G. The effect of protease contaminations in lactase in the flavour of lactose-hydrolyzed milks. *Aust. J. Dairy Technol.* **1991**, *46*, 46−47.
(16) Tetra Pak. *Dairy Processing Handbook*, 2nd ed.; Tetra Pak Processing Systems AB: Malmö, Sweden, 2003; pp 227−246.
(17) Holst, H. H.; Lauritzen, K. Process for producing lactose-free milk. Patent U.S. 8,445,052 B2, 2013.
(18) Jansson, T.; Jensen, S.; Eggers, N.; Clausen, M. R.; Larsen, L. B.; Ray, C.; Sundgren, A.; Andersen, H. J.; Bertram, H. C. Volatile component profiles of conventional and lactose-hydrolyzed UHT milk − a dynamic headspace gas chromatography-mass spectrometry study. *Dairy Sci. Technol.* **2014**, *94*, 311−325.
(19) Jensen, H. B.; Poulsen, N. A.; Andersen, K. K.; Hammershøj, M.; Poulsen, H. D.; Larsen, L. B. Distinct composition of bovine milk from Jersey and Holstein-Friesian cows with good, poor or non-coagulation properties as reflected in protein genetic variants and isoforms. *J. Dairy Sci.* **2012**, *95*, 6905−6917.
(20) Frederiksen, P. D.; Andersen, K. K.; Hammershøj, M.; Poulsen, H. D.; Sørensen, J.; Bakman, M.; Qvist, K. B.; Larsen, L. B. Composition and effect of blending of noncoagulating, poorly coagulating, and well-coagulating bovine milk from individual Danish Holstein cows. *J. Dairy Sci.* **2011**, *94*, 4787−4799.
(21) Sørhaug, T.; Stepaniak, L. Psychrotrophs and their enzymes in milk and dairy products: quality aspects. *Trends Food Sci. Technol.* **1997**, *8*, 35−41.
(22) Hinz, K.; Larsen, L. B.; Wellnitz, O.; Bruckmaier, R. M.; Kelly, A. L. Proteolytic and proteomic changes in milk at quarter level following infusion with *Escherichia coli* lipopolysaccharide. *J. Dairy Sci.* **2012**, *95*, 1655−1666.
(23) Wedholm, A.; Møller, H. S.; Lindmark-Månsson, H.; Rasmussen, M. D.; Andrén, A.; Larsen, L. B. Identification of peptides in milk as a result of proteolysis at different levels of somatic cell counts using LC MALDI MS/MS detection. *J. Dairy Res.* **2008**, *75*, 76−83.
(24) Crudden, A.; Fox, F.; Kelly, A. L. Factors affecting the hydrolytic action of plasmin in milk. *Int. Dairy J.* **2005**, *15*, 305−313.
(25) Guigoz, Y.; Solms, J. Bitter peptides, occurrence and structure. *Chem. Senses* **1976**, *2*, 71−84.
(26) Ney, K. H. Bitterness of peptides: amino acid composition and chain length. *ACS Symp. Ser.* **1979**, *No. 115*, 149−173.
(27) Kilara, A.; Panyam, D. Peptides from milk proteins and their properties. *Crit. Rev. Food Sci. Nutr.* **2003**, *43*, 607−633.
(28) Gomez, B. M. J.; Garde, S.; Gaya, P.; Medina, M.; Nun, M. Relationship between level of hydrophobic peptides and bitterness in cheese made from pasteurized and raw milk. *J. Dairy Res.* **1997**, *64*, 289−297.
(29) Harwalkar, V. R.; Cholette, H.; McKellar, R. C.; Emmons, D. B. Relation between proteolysis and astringent off-flavor in milk. *J. Dairy Sci.* **1993**, *76*, 2521−2527.
(30) Karametsi, K.; Kokkinidou, S.; Ronningen, I.; Peterson, D. G. Identification of bitter peptides in aged cheddar cheese. *J. Agric. Food Chem.* **2014**, *62*, 8034−8041.
(31) Pripis-Nicolau, L.; de Revel, G.; Bertrand, A.; Maujean, A. Formation of flavor components by the reaction of amino acid and carbonyl compounds in mild conditions. *J. Agric. Food Chem.* **2000**, *48*, 3761−3766.
(32) Hofmann, T.; Schieberle, P. Formation of aroma-active Strecker-aldehydes by a direct oxidative degradation of Amadori compounds. *J. Agric. Food Chem.* **2000**, *48*, 4301−4305.
(33) Hougaard, A. B.; Vestergaard, J. S.; Varming, C.; Bredie, W. L. P.; Ipsen, R. H. Composition of volatile compounds in bovine milk heat treated by instant infusion pasteurisation and their correlation to sensory analysis. *Int. J. Dairy Technol.* **2011**, *64*, 34−44.
(34) Valero, E.; Villamiel, M.; Miralles, B.; Sanz, J.; Martinéz-Castro, I. Changes in flavour and volatile components during storage of whole and skimmed UHT milk. *Food Chem.* **2001**, *72*, 51−58.
(35) Adamiec, J.; Rössner, J.; Velíšek, J. Minor Strecker degradation products of phenylalanine and phenylglycine. *Eur. Food Res. Technol.* **2001**, *212*, 135−140.
(36) Smuda, M.; Glomb, M. A. Fragmentation pathways during Maillard-induced carbohydrate degradation. *J. Agric. Food Chem.* **2013**, *61*, 10198−10208.
(37) Brands, C. M.; van Boekel, M. A. J. S. Reaction of monosaccharides during heating of sugar-casein systems: building of a reaction network model. *J. Agric. Food Chem.* **2001**, *49*, 4667−4675.

concentrations required for protection (i.e., dose-dependency of the phenolic antioxidants) are a critical issue. It has been suggested that protein-to-protein radical transfer may occur at a faster rate than protein-to-phenol radical transfer, especially when the antioxidant concentration is low.[9] In a model system with 1% phenol relative to protein (w/w), Jongberg, Lund, Østdal, and Skibsted[22] demonstrated that a green tea extract could limit radical transfer from perferrylmyoglobin to myosin by scavenging the hypervalent myoglobin species.

In the present study the dose-dependent reduction of perferrylmyoglobin radicals by myofibrillar proteins (MPI) and bovine serum albumin (BSA), plant extracts from green tea (GTE), maté (ME), and rosemary (RE), and three phenolic compounds characteristic of those extracts, namely catechin, caffeic acid, and carnosic acid, has been investigated. The reduction of perferrylmyoglobin radical by these proteins, plant extracts, and phenols was monitored directly by electron paramagnetic resonance (EPR) spectroscopy to obtain quantitative information on the concentrations of well-defined phenols and plant extracts required to afford protection against protein oxidation. The role of thiols in perferrylmyoglobin radical reduction was also investigated for MPI and BSA using *N*-ethylmaleimide, a modifying agent with a high degree of specificity for thiols.[23]

## MATERIALS AND METHODS

**Chemicals and reagents.** Myoglobin from equine heart (MbFe(III)) of >90% purity and bovine serum albumin (BSA) of >96% purity were obtained from Sigma-Aldrich, Steinheim, Germany. Guardian Green Tea extract 20 M (GTE) and Guardian Rosemary extract 202 (RE) were obtained from DuPont Nutrition and Biosciences ApS (formerly Danisco A/S), Brabrand, Denmark. Dried maté leaves (*Ilex paraguariensis*) of the Brazilian trade mark Tertúlia (Ervateria Marca Ltd.a., Jaborá, Santa Catarina) were obtained from a local market in Brasilia, Brazil. Carnosic acid, caffeic acid, and catechin were obtained from Sigma-Aldrich, St. Louis, MO. All other reagents were of analytical grade. Double-deionized water (Milipore, Bedford, MA) was used throughout.

**Extraction of phenolics from maté leaves.** An aliquot of 0.5 g maté leaves was mixed with 50 mL of double-deionized water in an ultrasonic bath for 15 min, centrifuged for 10 min at 936 g, and filtered through Whatman 589/3 filter paper (GE Healthcare Life Sciences, Buckinghamshire, UK). These extracts were used on the day of preparation. The phenolic concentration was determined by Folin Ciocalteu's method as described by Singleton and Rossi.[24] In brief, maté extract was dissolved in double-deionized water and left to react with Folin–Ciocalteu phenol reagent for 8 min. Subsequently, 20% sodium carbonate was added and the reaction mixture was left to incubate at 20 °C for 2 h. The phenol concentration was determined spectrophotometrically at 765 nm against a standard curve prepared from gallic acid. The concentrations are given in gallic acid equivalents (g/100 g dry extract; % w/w), $n = 5$.

**Isolation of myofibrillar proteins.** Myofibrillar protein isolates (MPI) were prepared from pork *Longissimus dorsi* muscle according to Park and Xiong[25] with slight modifications as described by Koutina, Jongberg, and Skibsted.[26]

**Protein identification by gel-electrophoresis (SDS-page).** Freeze-dried MPI was mixed with 0.1 M Tris buffer (pH 7.4, $I = 1.0$) and stirred for 30 min at 20 °C. The protein suspension was centrifuged at 12100*g* for 1 min, and the supernatant was collected. Total protein concentration was determined spectrophotometrically by measuring absorbance at 280 nm. The molar extinction coefficient of myosin, $A_{280(1g/l)}$ 0.496 and the molar mass of myosin (520000) were used to calculate the molar concentration of MPI in μM myosin equivalents. Dissolved MPI was analyzed with or without prior addition of 5% SDS by SDS-PAGE using NuPAGE Novex 3–8% TRIS-Acetate Gels with or without addition of dithiotreitol (DTT) as reducing agent (Invitrogen, Carlsbad, CA) as described by Jongberg et al.[22]

**Blocking of protein thiol groups with NEM.** Thiol groups in 10 mg/mL MPI or BSA were blocked by reaction with 100 μM *N*-ethylmaleimide (NEM) in 0.1 M Tris buffer (pH 7.4, $I = 1.0$) for 90 min at 4 °C.[12] NEM-blocked samples (MPI-NEM, BSA-NEM) were used on the day of preparation.

**Quantification of thiol groups.** Protein thiols were quantified by reaction with 5,5′-dithiobis(2-nitrobenzoic acid) (DTNB)[27] according to Jongberg, Terkelsen, Miklos, Lund[28] with slight modifications. In brief, an aliquot of 835 μL of dissolved protein (MPI, MPI-NEM, BSA, or BSA-NEM) was mixed with 165 μL of 10 mM DTNB dissolved in 0.10 M Tris buffer (pH 7.4, $I = 1.0$) and left to react for 30 min, protected from light at 20 °C. The absorbance at 412 nm was obtained before ($ABS_{412\text{-before}}$) and after reaction with DTNB ($ABS_{412\text{-after}}$) for both samples and blanks containing Tris buffer. Thiol concentrations were calculated based on a 5-point standard curve (0.4–83.3 μM) of L-cysteine diluted in Tris buffer. Thiol concentrations are reported as nmol thiol/mg protein.

**Preparation of freeze-quenched samples.** Myoglobin (30 mg) was dissolved in 1.0 mL of 0.1 M Tris buffer (pH 7.4, $I = 1.0$) and purified on a Sephadex PD10 column preconditioned with 25 mL of 0.1 M Tris buffer. Myoglobin concentrations were determined spectrophotometrically at 525 nm using $\varepsilon = 7.700\ M^{-1}\ cm^{-1}$.[29] Myoglobin (100 μM final concentration) was mixed with proteins, phenols, or plant extracts (for concentrations see text and figure legends) in a total volume of 270 μL in a 1.5 mL Eppendorf tube and transferred to an EPR tube (5 mm outside diameter, 227 mm length (Wilmad, NJ) using a syringe with a needle and long plastic tubing. Thirty microliters of $H_2O_2$ (100 μM final concentration) was then added in a similar manner, and the samples were vortex mixed and frozen in liquid nitrogen 15 s after $H_2O_2$ addition. BSA was dissolved in Tris buffer, and MPI was applied as a suspension in Tris buffer. A stock solution of RE (120 mg/mL) was dissolved in ethanol and subsequently diluted in Tris buffer. GTE and ME were dissolved and diluted directly in Tris buffer. Aqueous stock solutions of caffeic acid (61 mM) and catechin (55 mM) were prepared in Tris buffer/ethanol (1:1, v/v). Stock solutions of carnosic acid (107 mM) were made up in acetonitrile and subsequently diluted with Tris buffer.

**Radical detection by Electron Paramagnetic Resonance (EPR) spectroscopy.** Freeze-quenched samples were mounted in the cavity of an ECS 106 or EMX X-band spectrometer (Bruker, Rheinstetten, Germany) equipped with a quartz liquid nitrogen finger dewar flask filled with liquid nitrogen. Radical spectra were obtained using identical settings with four acquisitions averaged. The peak intensity (PI) of the Trp-radical signal was determined by the maximum intensity of the detected peak after baseline subtraction using WINEPR software.

$$PI_{Sample} = Intensity_{max.peak} - Intensity_{Baseline}$$

The peak intensity was normalized to gain the relative peak intensity (Rel.PI) by using the mean PI of the control samples without any oxidation substrate, indicated as the peak intensity normalization factor ($PI_{Norm}$).

$$Rel.PI = \frac{PI_{Sample}}{PI_{Norm}} \times 100\%$$

**Dose–response analysis and calculation of $IC_{50}$ values.** Dose–response analysis was performed by calculating the $IC_{50}$ values (concentration of reductant to obtain 50% inhibition of the perferrylmyoglobin radical signal) using Origin Pro 9.1.0 (OriginLab Coperation, Northampton, MA).[30] The relative peak intensity was fitted as a function of the logarithm of molecular concentration using Sigmoidal fitting and the DoseResp function.

$$y = A1 + \frac{A2 - A1}{1 + 10^{(\log x0 - x)p}}$$

The $x$ values are the logarithm of dose, and the log$x$0 is the center of the curve, meaning the concentration for half response. Global fit

was used to fix the upper (A2) and lower (A1) limits to 100 and 0%, respectively.

**Statistical data analysis.** All experiments were conducted in triplicates as a minimum unless otherwise stated, and data are expressed as mean ± standard deviation (sd). Statistical analysis were performed using R version 2.12.1, The R Foundation for Statistical Computing (ISBN 3-900051-07-0). Data were analyzed by analysis of variance (ANOVA) using a linear model with mixed effects, where replicates were included as random effects and concentration was included as a systematic effect. Student's $t$ test using Microsoft Excel was applied for statistical analysis of the $IC_{50}$ values and variation in relative peak intensity. Significance for all data analysis was assumed at $P < 0.05$

## RESULTS

**Characterization of protein radicals.** MPI was isolated from pork *longissimus dorsi* muscle, and the proteins were identified by the molecular mass after separation by SDS-PAGE (Figure 1). MPI consists of primarily myosin heavy chain

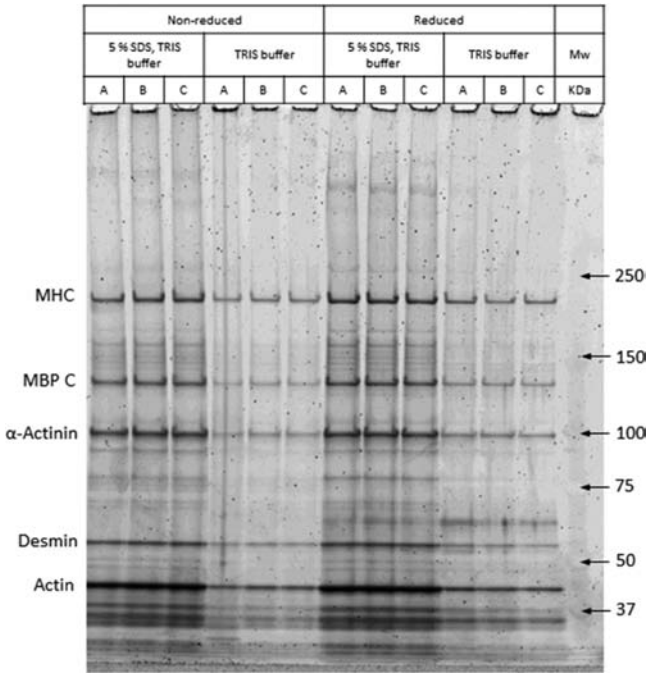


**Figure 1.** SDS-PAGE analysis of porcine myofibrillar protein isolate (MPI) suspended in 0.1 M Tris buffer (pH 7.4, $I$ = 1.0) with or without addition of 5% sodium dodecyl sulfate (SDS). Reduced samples were treated with dithiothreitol (DTT) prior to running the gel. A, B, and C represent triplicate suspensions, and $M_w$ indicates a mixed protein standard with known molecular masses indicated on the figure. Myosin heavy chain (MHC), myosin binding protein C (MBP C), α-actinin, desmin, and actin were identified based on their molecular masses.

(MHC, ~220 kDa), myosin binding protein C (MBP C, ~130 kDa), α-actinin (~100 kDa), desmin (~55 kDa), and actin (~42 kDa) according to Lametsch et al.[31] These proteins were found to dissolve in the 0.1 M Tris buffer (pH 7.4, $I$ = 1.0) both with and without 5% SDS. Although the presence of SDS increased protein solubility, as indicated by the increased protein band intensities, the protein compositions of the solutions with and without SDS were the same, and Tris buffer without SDS was therefore used throughout the study.

Reaction between MbFe(III) and hydrogen peroxide (1:1 molar ratio) for 15 s before freeze-quenching in liquid nitrogen at 77 K resulted in the detection of a protein radical by EPR spectroscopy (Figure 2, upper spectra in A, B, C, and D). No signals were observed when any one of the components of the reaction mixture was omitted (data not shown). The observed spectra are interpreted in terms of the presence of a mixture of Trp-derived peroxyl and Tyr-derived phenoxyl radicals with hyperfine coupling constant and $g$-values as reported previously,[9] with the major EPR absorptions of each species indicated by TRP and TYR.

The presence of increasing concentrations of MPI in the reaction mixture of MbFe(III) and hydrogen peroxide reduced the intensity of the features assigned to the Trp-peroxyl radical, with this being most noticeable with the low field component (i.e., the left-hand feature) due to the presence of significant overlap of the other components of this signal with features from the Tyr phenoxyl radical. The Trp-peroxyl radical was almost fully extinguished with a concentration of MPI of 14.8 μM (Figure 2A). The intensity of the EPR absorptions assigned to the Tyr-phenoxyl radical also decreased in the presence of increasing concentrations of MPI (Figure 2A). These data are interpreted in terms of subsequent reaction of the Mb-derived Trp and Tyr radicals with the MPI protein, rather than interference with the initial formation of these species on the Mb protein.

In order to assess whether this process was specific to MPI, similar experiments were carried out in which increasing concentrations of BSA were added to the Mb/hydrogen peroxide system. This resulted in a concentration-dependent decrease in the Trp-peroxyl radical signal (Figure 2B). Modification of the Mb-derived Tyr-radical signal was also detected, with increasing concentrations of BSA resulting in the detection of a broad signal with increased intensity at an identical $g$ value. This change is interpreted in terms of radical transfer from the perferrylmyglobin species to BSA, with the formation of a mixture of different radical species on the BSA; these are likely to be predominantly Tyr-derived phenoxyl radicals (as the $g$ value remains unchanged) in different environments, with the latter resulting in the loss of spectral resolution (i.e., a broad absorption envelope rather than distinct spectral features).[32] As no additional protein radicals were observed in the experiments in which MPI was added to the reaction mixture, it is proposed that the radicals formed on the MPI must be located on residues/sites which do not give rise to EPR-detectable absorptions, or are too short-lived to be detected under the conditions employed. As one potential target residue on the MPI with which the Mb-derived radicals might react is the Cys residues (cf. previous reports on the reaction of Mb-derived radicals with thiols),[9] further experiments were carried out with MPI and BSA with blocked Cys residues.

**Role of Cys residues on MPI and BSA and concentration dependency in perferrylmyoglobin radical transfer.** The average number of thiol groups per molecule present in the MPI preparations was found to be 15 (Table 1). As MHC contains 16 Cys residues, whereas other myofibrillar proteins contain fewer (e.g., 6 in actin), this value represents a mean thiol concentration of all proteins combined in the MPI. In contrast, the average number of thiol groups was found to be 0.2 for BSA (Table 1). The sequence of native BSA contains one free Cys, but it is well established that a considerable proportion of these residues are present in modified or derivatized forms in plasma,[33] so this value of <1 is not surprising. The protein thiol groups of MPI and BSA

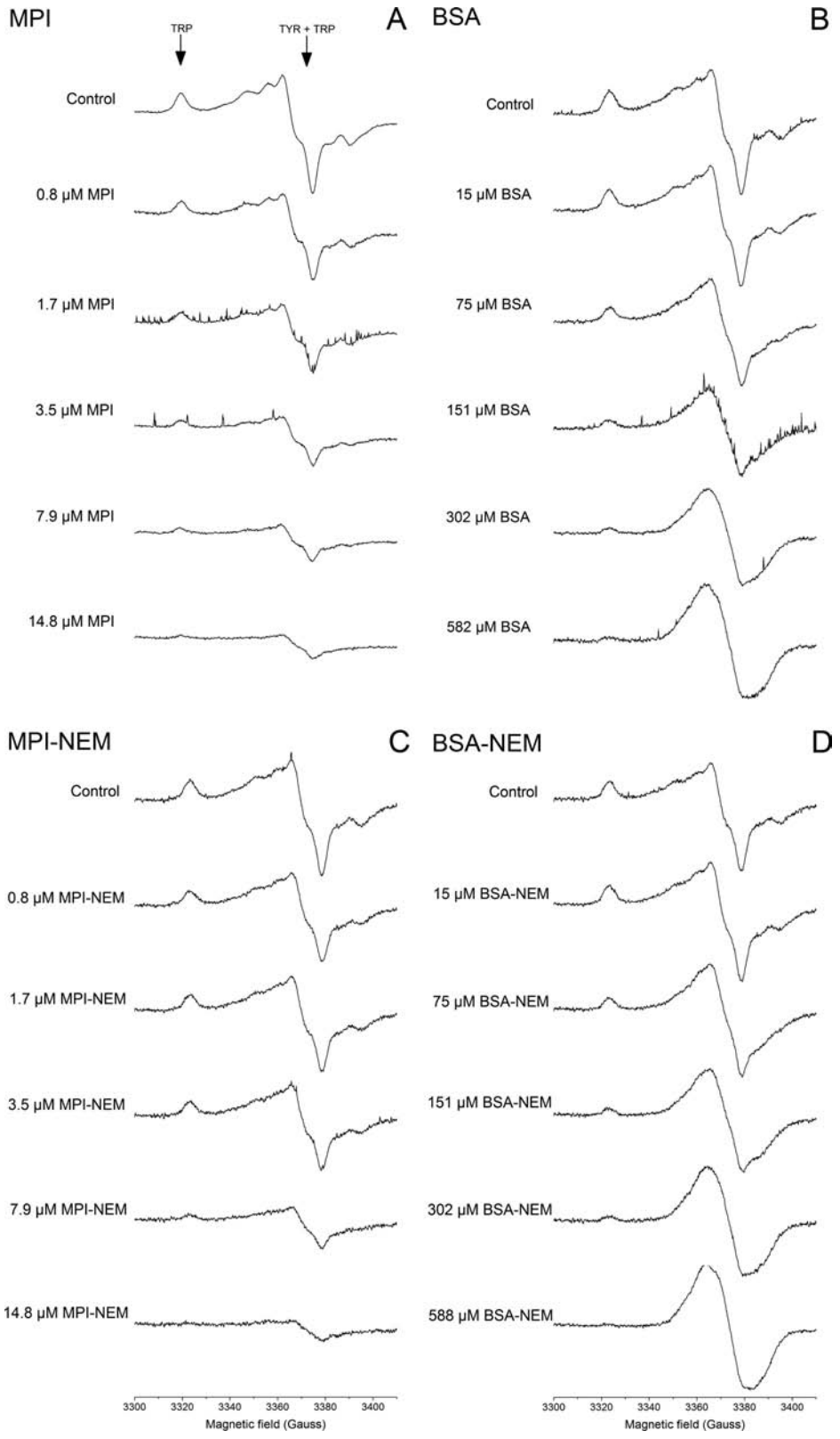


**Figure 2.** EPR spectra of perferrylmyoglobin radicals generated by reaction with hydrogen peroxide in a 1:1 molar ratio (100 $\mu$M) alone or in the presence of (A) MPI, (B) BSA, (C) MPI-NEM, or (D) BSA-NEM in increasing concentrations. The signals assigned to the Trp-peroxyl radical and the Tyr-phenoxyl radical are indicated by arrows in the Control−MPI EPR spectra (upper left panel). The spiking observed on some spectra is experimental artifacts caused by gas bubbles.

were blocked by *N*-ethylmaleimide (NEM) as described in the Materials and Methods to obtain MPI-NEM and BSA-NEM. The efficiency of thiol-blocking was calculated to be 90 and 75% for MPI and BSA, respectively (Table 1). The low blocking percentage for BSA may be ascribed to the constrained location of the Cys-34 residue in a cleft in the


dx.doi.org/10.1021/jf5041433 | *J. Agric. Food Chem.* 2014, 62, 11279−11288

**Table 1. Concentration of Thiol Groups in Proteins Presented as Mean ± sd ($n$ = 3) and Efficiency of Thiol-Blocking by *N*-Ethylmaleimide (NEM)**

| protein | [thiols] nmol/mg protein | thiols per protein molecule[a] | efficiency of thiol blocking |
|---|---|---|---|
| MPI | 29.0 ± 2.8 | 15.1 ± 1.2 | |
| MPI-NEM | 3.1 ± 0.9 | 1.6 ± 0.4 | 90% |
| BSA | 3.6 ± 1.0 | 0.2 ± 0.1 | |
| BSA-NEM | 0.9 ± 1.0 | 0.1 ± 0.1 | 75% |

[a]Thiols per molecule are calculated from the concentration of thiols divided by the molecular mass of BSA or MPI using myosin as reference.

BSA structure. Higher concentrations of NEM which might result in a greater extent of reaction at the Cys-34 residue were not employed, in order to avoid reaction at other (less reactive, nucleophilic) sites such as Lys residues.[23]

These NEM-blocked proteins were subsequently employed in EPR experiments as outlined above for the nonblocked proteins. While blocking of the Cys-34 residues on BSA did not give rise to any noticeable effect on the EPR spectra obtained for the BSA system (Figure 2D), increasing concentrations of MPI-NEM resulted in the detection of EPR signals from the Mb-derived radicals of diminished intensity (Figure 2C). These data are interpreted in terms of a key role for the Cys residues of MPI in reaction with the perferrylmyglobin radicals, with subsequent formation of thiyl radicals on the MPI proteins when the Cys residues are not blocked.

Dose−response curves were generated by plotting the relative peak intensity of the Trp-peroxyl radical signal against the concentration of MPI, BSA, or their NEM-blocked counterparts as a function of their molecular (primary $x$-axis) or mass-based (secondary $x$-axis) concentrations (Figure 3). As the half-life of the perferrylmyoglobin radical is short, reactions were stopped after 15 s by freeze-quenching, such that the reactions did not reach equilibrium. The same concentrations of myoglobin and hydrogen peroxide were used in all experiments. Hence, the dose−response curves represent titration curves of the Mb-derived Trp-peroxyl radical by the added reactive agents, which provide information on the stoichiometry of these reactions.

The dose−response curve for native MPI was found to be steeper than that for MPI-NEM (Figure 3), and the relative peak intensity at 3.5 $\mu$M MPI or MPI-NEM was found to be significantly ($P$ = 0.014) different. This confirms that blocking the Cys thiol groups dramatically affects the rate of reaction of MPI with the Mb-derived Trp-peroxyl radicals. In contrast, the effect of blocking the Cys-34 residue of BSA observed in these dose−response curves was less dramatic. This may arise from steric interactions due to the partly buried nature of the BSA Cys-34 residue.

$IC_{50}$ values were estimated for comparison of the titration data obtained with MPI and BSA, and they indicate that 114 $\mu$M BSA is required to reduce the Trp-signal by 50% whereas only 1.1 $\mu$M is required for MPI (Table 2). This suggests that

**Table 2. $IC_{50}$ Values for the Reduction of Perferrylmyoglobin Radical by Proteins, Extracts, and Phenols Presented as Mean ± sd ($n \geq 3$)[a]**

| sample | $IC_{50}$ ($\mu$M) |
|---|---|
| MPI | 1.1 ± 0.2 c |
| MPI-NEM | 4.5 ± 2.8 bc |
| BSA | 114 ± 12 a |
| BSA-NEM | 94 ± 40 a |
| Green Tea extract | 11.0 ± 4.3 b |
| Maté extract | 15.0 ± 8.3 b |
| Rosemary extract | 14.0 ± 5.9 b |
| Catechin | 2.2 ± 1.2 c |
| Caffeic acid | 0.3 ± 0.1 d |
| Carnosic acid | 58 ± 43 ab |

[a]Letters (a−d) denote significant difference ($P$ < 0.05) between samples.

MPI is a 100-fold more efficient reducing agent compared to BSA based on the molecular concentration. When considering the size of the protein and comparing by mass-based concentrations, only a ∼10-fold higher BSA concentration was necessary to reduce the Trp-signal by 50% as compared to MPI. This indicates that the amino acid composition of the

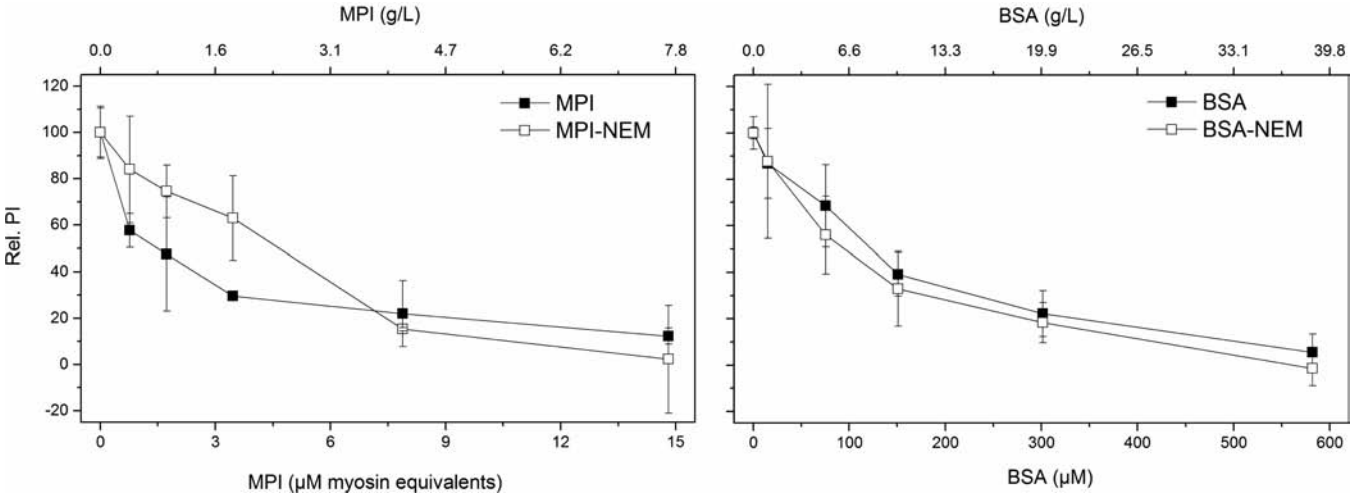


**Figure 3.** Dose−response curves of the relative peak intensity (Rel.PI, mean ± standard deviation, $n \geq 3$) of the Trp-peroxyl radical as a function of the molar concentrations of MPI and MPI-NEM (left panel), and BSA and BSA-NEM (right panel). The secondary (top) $x$-axis presents the mass-based concentration of the proteins.

target protein is a major factor in the observed reducing capacity. Expressing the $IC_{50}$ value of MPI or BSA based on the thiol concentration in each protein gives 17 ± 3 or 23 ± 3 μM thiols, respectively (calculated e.g. for MPI as 15.1 thiols per molecule × 1.1 ± 0.2 μM MPI). As the two numbers are not significantly different, this indicates that the thiol reactivities of the two proteins are comparable despite the steric hindrance for the BSA thiol. This may arise from the different reaction times used for the two proteins.

**Characterization of green tea, maté, and rosemary extracts.** The total phenolic content of the three plant extracts from green tea (GTE), maté (ME), and rosemary (RE) varied with the highest concentration (determined in gallic acid equivalents by the Folin−Ciocalteau assay) for GTE followed by ME and then RE (Table 3). The total phenolic content determined for ME corresponds well with the average total phenolic content of 8.4 g/100 g dry matter reported for three commercial maté brands.[34]

**Table 3. Total Phenolic Content in Extracts Presented as Mean ± sd ($n$ = 3)**

| extract | total phenolic content (% w/w)[a] |
|---|---|
| Green tea extract | 23.8 ± 1.3[b] |
| Maté extract | 7.7 ± 0.9 |
| Rosemary extract | 4.8 ± 0.1[b] |

[a]g of gallic acid equivalents/100 g of extract. [b]Jongberg, Lund, Østdal, and Skibsted.[23]

The phenolic composition of green tea (*Camellia sinensis*) extract consists primarily of flavonoids, such as catechin, epicatechin, epicatechin gallate, epigallocatechin gallate, and quercetin, with lower levels of hydrocinnamic acids, caffeic, coumaric, and ferulic acid.[35] Maté (*Ilex paraguariensis*) extract consists primarily of caffeoyl derivatives, including caffeic acid, chlorogenic acid, 3,4-dicaffeoylquinic acid, 3,5-dicaffeoylquinic acid, and 4,5-dicaffeoylquinic acid.[36] Rosemary (*Rosemarinus officialis*) extract consists primarily of phenolic diterpenes, such as carnosic acid, carnosol, rosmanol, rosmadial, 12-methoxycarnosic acid, epi- and iso-rosmanol, and the phenolic acids rosmarinic and caffeic acid.[35]

**Perferrylmyoglobin radical scavenging by green tea, maté, and rosemary extracts.** Addition of the plant extracts to the reaction mixture of MbFe(III) and hydrogen peroxide showed that all plant extracts were able to reduce the perferrylmyoglobin radicals (Figure 4). The EPR spectra demonstrated that both the Tyr-phenoxyl and Trp-peroxyl radicals were reduced in the presence of increasing concentrations of these extracts. This is presumed to result in the generation of phenoxyl-/catechol-derived radicals on the phenols present in the extracts, though these transients were not detected. The absence of EPR signals from such extract-derived radicals is not surprising, as both a number of species are likely to be formed from such complex mixtures and these species are likely to undergo rapid subsequent reaction (dimerization or disproportionation) due to their low molecular mass and unhindered nature.

The relative capability of the different extracts to reduce the Mb Trp-peroxyl radical was examined by determining dose−response curves based on the concentration of gallic acid equivalents in the extracts (Figure 4, left lower panel) or the mass of extract used (Figure 4, right lower panel). Full reduction of the Trp-peroxyl radical signal was detected with each extract, and there was no significant difference in the gallic acid equivalents between the three extracts required to achieve this (Figure 4, left lower panel). In contrast, when the reducing capacity of the extracts was assessed based on the amount of extract added, much lower levels of GTE (∼10 mg/L) were necessary to reduce the radical signal by 50% compared to ME and RE, where ∼40 mg/L and ∼60 mg/L, respectively, were necessary (Figure 4, right lower panel). These data indicate that the total phenolic content has a more marked impact on the reducing capacity of these extracts against the perferrylmyoglobin radicals than the specific composition of the phenolic compounds present in each extract.

**Perferrylmyoglobin radical scavenging by catechin, caffeic acid, and carnosic acid.** In light of the above data, further experiments were carried out with a number of specific phenolic compounds (catechin, caffeic acid, and carnosic acid) to determine their relative efficacies with regard to reaction with Mb radicals. The EPR spectra obtained from reaction mixtures containing these three phenolic compounds showed that all of them were able to scavenge perferrylmyoglobin radicals (Figure 5). The spectra obtained indicate that no additional phenoxyl radicals from the added compounds were formed as a result of radical transfer, as no additional EPR signals were observed. However, significant reductions in the intensity of the Mb-derived radicals were observed, indicating that reaction had occurred. Even at the highest phenol concentrations, a weak residual signal was detected (Figure 5, upper panels). However, as identical signals were observed at elevated concentrations (up to 100 μM catechin, data not shown), the modifications are more likely to be an artifact rather than a secondary phenoxyl radical.[9,37]

Dose−response curves obtained for increasing concentrations of these plant phenols, presented in molar concentration of the phenolic compounds, showed that the phenols had markedly different reducing capacities (Figure 5, lower panel). Caffeic acid was a far more efficient scavenger of the perferrylmyoglobin radicals as compared to catechin, and carnosic acid was least efficient. These phenols were selected as representatives of the extracts, GTE, MA, and RE, as they are the dominant phenol in each extract. However, while the reducing capacity of the extracts was shown to be primarily dependent on the total phenolic content, and showed little variation with regard to phenol composition, these phenols when present alone showed marked variations.

## DISCUSSION

**Protection against meat protein oxidation by phenol-rich extracts.** The reducing capacity of the proteins, plant extracts, and phenols was quantified by their $IC_{50}$ values (Table 2) and may be used to predict whether a specific phenol-rich extract may protect against protein oxidation. Comparing the $IC_{50}$ values between the two proteins showed that the proteins in the MPI are ∼100-fold more efficient as compared to BSA, and after blocking the thiol groups by NEM this ratio dropped to ∼20, indicating that the thiol groups are highly significant for the reducing capacity. No significant differences were observed between the plant extracts, indicating that the exact phenolic composition of these extracts is not the most important factor with regard to the overall reducing capacity and that the total amount of phenol is important for these extracts where several phenols are present in mixtures. In fact, other constituents of the extracts, such as fillers or fibers, may be of higher importance, facilitating radical transfer processes in the extract.

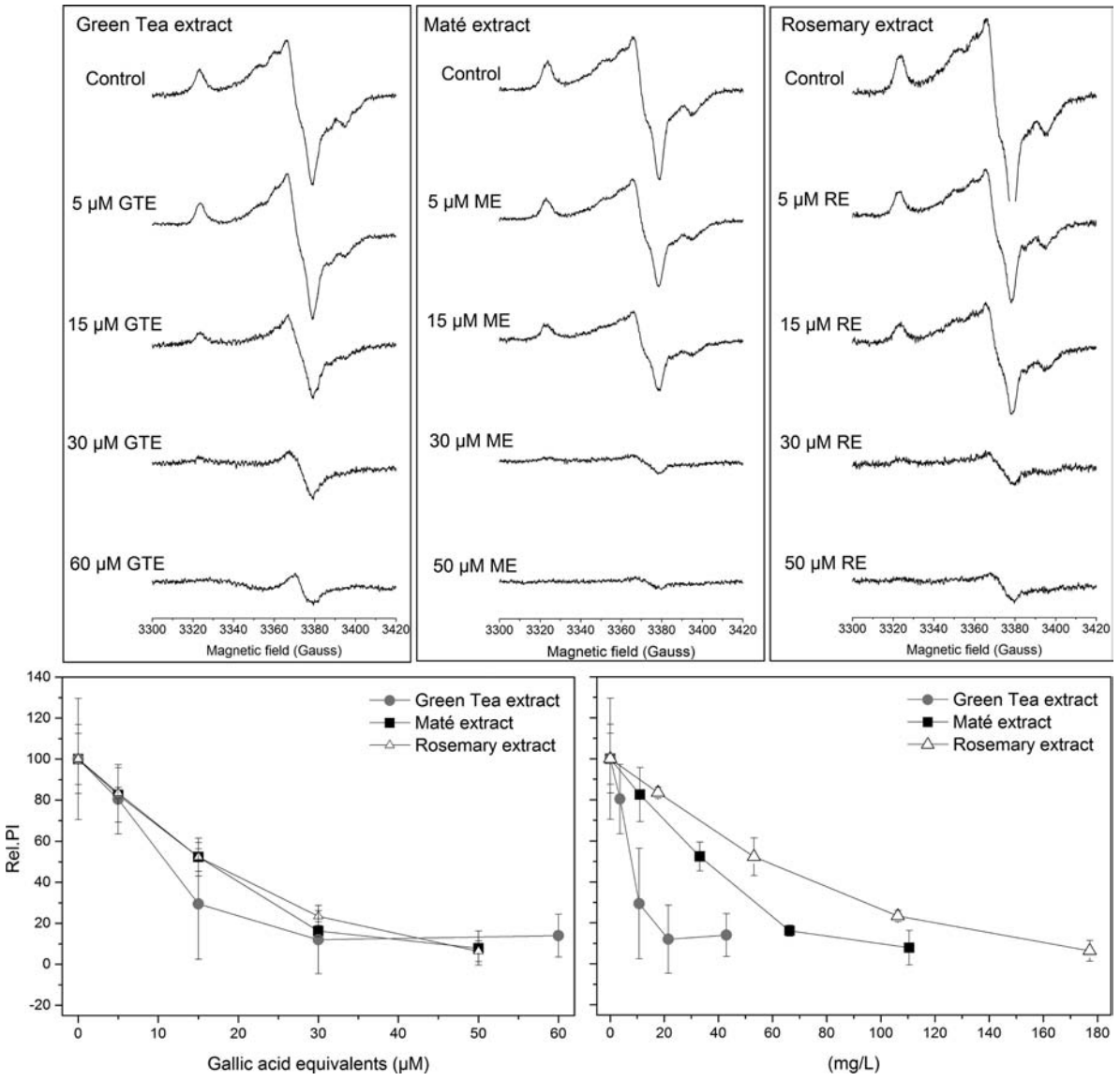


**Figure 4.** Upper panels: EPR spectra of perferrylmyoglobin radicals generated by reaction with hydrogen peroxide in a 1:1 molar ratio (100 $\mu$M) alone or in the presence of green tea (GTE), maté (ME), or rosemary (RE) extracts in increasing concentrations. Lower panels: Dose−response curves of the relative peak intensity (Rel.PI, mean ± standard deviation, $n \geq 3$) of the Trp-peroxyl radical as a function of the molar- (left panel) or mass-based (right) concentrations of green tea, maté, or rosemary extract.

A study including the same GTE and RE extracts was recently presented by Jongberg et al.[22] Phenoxyl radicals are stabilized when coordinated to divalent metal ions, such as $Zn^{2+}$, hereby preventing the dimerization reaction and enhancing the radical signals.[38,39] The results of Jongberg et al.[22] showed increased phenoxyl radical intensities of RE as compared to GTE after reaction with the perferrylmyglobin radical in the presence of Zn(II), and this increase was explained by more efficient radical-derived polymerization reaction of the phenols contained in the GTE as compared to the RE. This is of major significance for the application of such extracts to foods, as the addition of "antioxidative" ingredients may add flavors or aromas to the given food product. In order to minimize any off-flavors derived from the extract, a high total phenolic content and high ability to terminate radical processes by polymerization is beneficial, and radical transfer processes in the extract are of importance in this respect.

In the present study, it was shown that with the isolated, specific phenols there is considerable variation in $IC_{50}$ values, with caffeic acid being significantly more efficient than catechin, which in turn was significantly more efficient than carnosic acid. All three phenols examined contain catechol moieties (Figure 6), which are important for their radical scavenging activity.[35] Caffeic acid, which contains a single catechol moiety with two hydroxyl groups, showed the most efficient reducing capacity toward perferrylmyoglobin radicals when compared with catechin, which contains four hydroxyl groups. Hence, the *number* of hydroxyl groups in the aromatic structure may not be the most significant contributor to the reducing capacity observed, and other properties may be important for effective Mb radical scavenging. The carboxylate groups of caffeic and carnosic acids are powerful electron delocalizing groups that affect the $pK_a$ values of the neighboring phenolic hydroxyl groups. The carboxylic acids are deprotonated in the reaction mixture (pH 7.4), as the $pK_{a1c}$ values of caffeic acid and


dx.doi.org/10.1021/jf5041433 | J. Agric. Food Chem. 2014, 62, 11279−11288

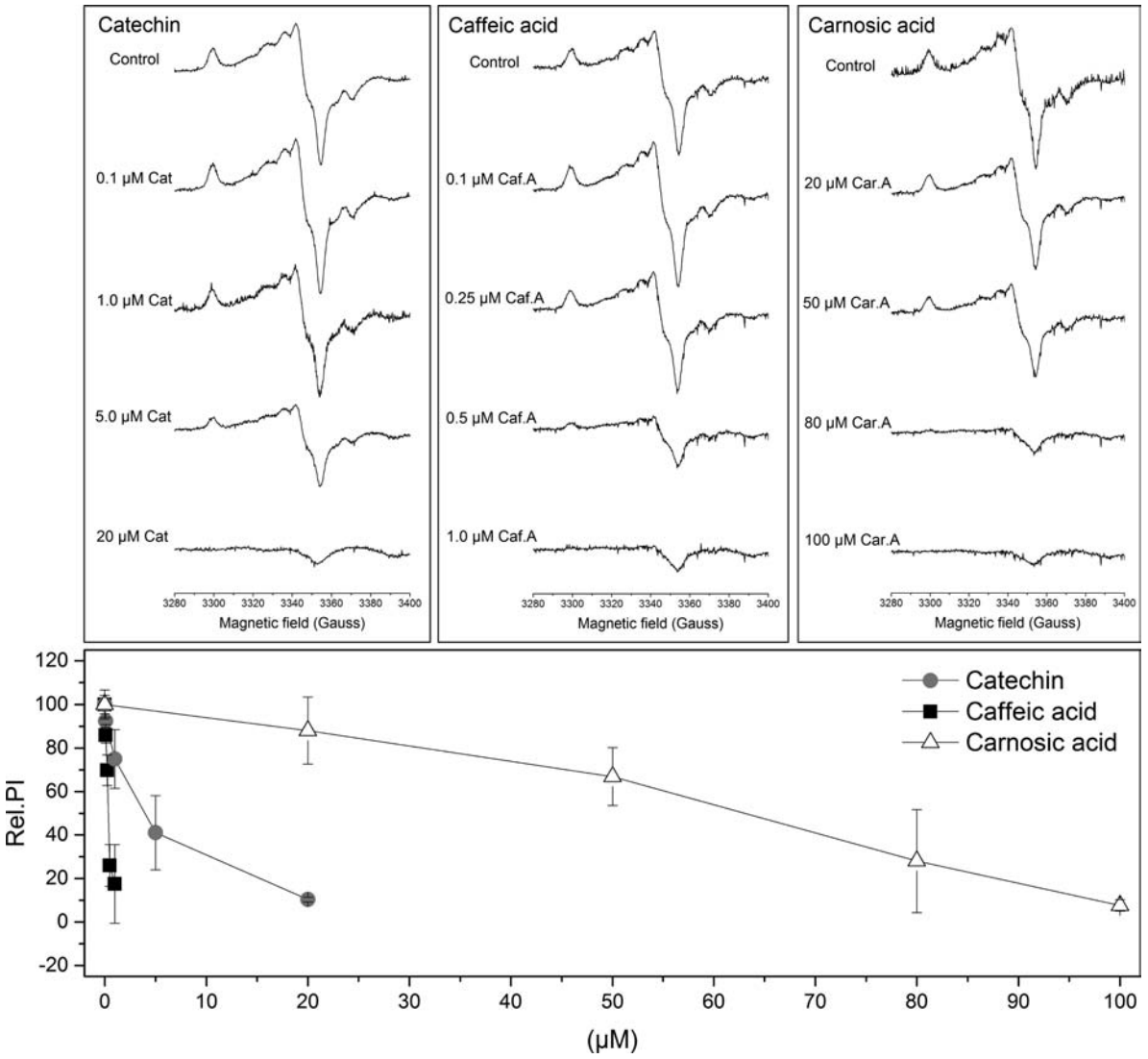


**Figure 5.** Upper panels: EPR spectra of perferrylmyoglobin radicals generated by reaction with hydrogen peroxide in a 1:1 molar ratio (100 $\mu$M) alone or in the presence of catechin (Cat), caffeic acid (Caf.A), or carnosic caid (Car.A) in increasing concentrations. Lower panel: Dose–response curves of relative peak intensity (Re.PI, mean ± standard deviation, $n \geq 3$) of the Trp-peroxyl radical as a function of the molar concentration of catechin, caffeic acid, or carnosic acid.

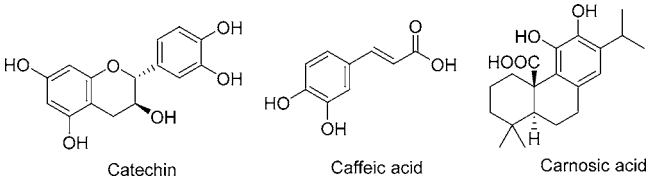


**Figure 6.** Chemical structures of catechin, caffeic acid, and carnosic acid.

carnosic acid are 4.36 and 4.9, respectively.[40,41] In contrast, catechin is protonated in the reaction mixture, as the p$K_a$ values of the most acidic groups, the catechol and phloroglucinol moieties, are 8.7 and 9.7 for the B-ring and A-ring, respectively.[42] The presence of the ionized form of the phenol enhanced the reducing capacity, as an increased electron density enhances the ability of the molecule to donate electrons. Nevertheless, Silva et al.[40] found that structural modification of the ethylenic side-chain on the aromatic ring of caffeic acid to yield alkyl esters actually increased the radical scavenging activity toward DPPH$^{\bullet}$ (2,2-diphenyl-1-picrylhydrazyl radical). The same authors concluded that no relationship between the radical scavenging activity and p$K_a$ exists, and they suggested that other physicochemical properties, such as the redox potential, could be of major importance for the radical scavenging capacities.[40]

A third factor to consider with regard to the reducing capacity is the size and three-dimensional structure of the phenols (Figure 6). Caffeic acid has a planar structure, which may allow it to react at protein sites that are inaccessible to larger more bulky molecules. An example of this could be catechin, in which the C-ring allows the B-ring to be in the pseudoaxial position, which may decrease the reactivity of the phenol with the protein radical due to steric hindrance. Similarly, the carboxylic group of carnosic acid is also in an axial position, and this may reduce the reactivity toward the protein radicals. A final factor to consider is the radical–radical interactions resulting in the polymerization of phenolic compounds that terminate radicals and regenerate the hydroxyl groups to regenerate their radical scavenging activity. Carnosic acid contains only one unsubstituted carbon atom in the

aromatic ring and may not polymerize to the same extent as catechin and caffeic acid, which both contain multiple unsubstituted carbons. Hence, the low reducing capacity of carnosic acid may be due to the limited ability to regenerate the phenolic moiety. However, in extracts multiple components are present and other radical transfer mechanisms may be active.

Overall, the results based on the $IC_{50}$ values indicate that MPI is 15-fold more efficient as a scavenger of the perferrylmyoglobin radical as compared to GTE or RE based on the molecular concentration of the components. This may reflect the different chemical reactivity of a thiol compared to a phenol, and it suggests that the molar ratio between GTE and MPI needs to be >15 in order to obtain efficient protection against protein-to-protein radical transfer.

Polyphenols have been shown, based on kinetic experiments and modeling, to protect lipids against oxidation by meat pigments in the gastric tract.[43] In other complex systems, such as meat emulsions, 100 ppm GTE, corresponding to 1.6% GTE per MPI, has been found to protect against protein thiol loss.[28] In the present study, the mass-based concentrations of MPI and GTE needed to reduce the Trp-radical signal by 50% were 0.6 g/L (Figure 3) and 8 mg/L (Figure 4), respectively. Calculation of the mass to mass percentage of GTE per MPI gives 1.3%, which is within the concentration range of GTE per MPI in the meat emulsion study mentioned above. This indicates that the model system applied may allow an effective preliminary evaluation of the amounts of plant extracts needed to inhibit protein oxidation in meat and meat products.

## AUTHOR INFORMATION


### Corresponding Author

*E-mail: jongberg@food.ku.dk. Tel.: +4535332181. Fax.: +4535333344.

### Present Address

§(M.J.D.) Department of Biomedical Sciences, Building 4.5, Panum Institute, University of Copenhagen, Blegdamsvej 3, Copenhagen, 2200 Denmark.



### Funding

The authors thank The Danish Council for Independent Research | Technology and Production within The Danish Agency for Science Technology and Innovation for granting the project entitled: "Antioxidant mechanisms of natural phenolic compounds against protein cross-link formation in meat and meat systems" (11-117033).


### Notes

The authors declare no competing financial interest.

## ACKNOWLEDGMENTS

The authors are grateful for the technical assistance of Bente Danielsen from the Faculty of Science, University of Copenhagen.

## REFERENCES


(1) George, P.; Irvine, D. H. The reaction between metmyoglobin and hydrogen peroxide. *Biochem. J.* **1952**, *52*, 511−517.

(2) Gibson, J. F.; Ingram, D. J. E.; Nicholls, P. Free Radical Produced in the Reaction of Metmyoglobin with Hydrogen Peroxide. *Nature* **1958**, *181*, 1398−1399.

(3) Kroger-Ohlsen, M.; Carlsen, C. U.; Andersen, M. L.; Skibsted, L. H. Pseudoperoxidase activity of myoglobin: Pigment catalyzed formation of radicals in meat systems. In *ACS symposium series 807, Free Radicals in Food*; Morelle, M., Shahidi, F., Ho, C., Eds.; American Chemical Society: Washington, DC, 2002; pp 138−150.

(4) Davies, M. J. Identification of a globin-free radical in equine myoglobin treated with peroxides. *Biochim. Biophys. Acta, Bioenerg.* **1991**, *1077*, 86−90.

(5) Gunther, M. R.; Kelman, D. J.; Corbett, J. T.; Mason, R. P. Self-peroxidation of Metmyoglobin Results in Formation of an Oxygen-reactive Tryptophan-centered Radical. *J. Biol. Chem.* **1995**, *270*, 16075−16081.

(6) Libardi, S. H.; Skibsted, L. H.; Cardoso, D. R. Oxidation of carbon monoxide by perferrylmyoglobin. *J. Agric. Food Chem.* **2014**, *62*, 1950−1955.

(7) Witting, P. K.; Douglas, D. J.; Mauk, A. G. Reaction of human myoglobin and $H_2O_2$. Involvement of a thiyl radical produced at cysteine 110. *J. Biol. Chem.* **2000**, *275*, 20391−20398.

(8) DeGray, J. A.; Gunther, M. R.; Tschirret-Guth, R. A.; Ortiz de Montellano, P. R.; Mason, R. P. Peroxidation of a specific tryptophan of metmyoglobin by hydrogen peroxide. *J. Biol. Chem.* **1997**, *272*, 2359−2362.

(9) Irwin, J. A.; Østdal, H.; Davies, M. J. Myoglobin-Induced Oxidative Damage: Evidence for Radical Transfer from Oxidized Myoglobin to Other Proteins and Antioxidants. *Arch. Biochem. Biophys.* **1999**, *362*, 94−104.

(10) Kelman, D. J.; DeGray, J. A.; Mason, R. P. Reaction of Myoglobin with Hydrogen Peroxide Forms a Peroxyl Radical Which Oxidizes Substrates. *J. Biol. Chem.* **1994**, *269*, 7458−7463.

(11) Davies, M. J.; Dean, R. T. *Radical-mediated protein oxidation*; Oxford Science Publications: Oxford, 2003.

(12) Lund, M. N.; Luxford, C.; Skibsted, L. H.; Davies, M. J. Oxidation of myosin by heme proteins generates myosin radicals and protein cross-links. *Biochem. J.* **2008**, *410*, 565−574.

(13) Frederiksen, A. M.; Lund, M. N.; Andersen, M. L.; Skibsted, L. H. Oxidation of porcine myosin by hypervalent myoglobin: The role of thiol groups. *J. Agric. Food Chem.* **2008**, *56*, 3297−3304.

(14) Uniprot Consortium, Myosin heavy chain 2b, MYH4_PIG. URL: http://www.uniprot.org/uniprot/Q9TV62 (2014, July 7).

(15) Xiong, Y. L.; Park, D.; Ooizumi, T. Variation in the cross-linking pattern of porcine myofibrillar protein exposed to three different oxidative environments. *J. Agric. Food Chem.* **2009**, *57*, 153−159.

(16) Lund, M. N.; Lametsch, R.; Hviid, M. S.; Jensen, O. N.; Skibsted, L. H. High-Oxygen Packaging Atmosphere Influences Protein Oxidation and Tenderness of Porcine longissimus dorsi during Chill Storage. *Meat Sci.* **2007**, *77*, 295−303.

(17) Shah, M. A.; Bosco, S. J. D.; Mir, S. A. Plant extracts as natural antioxidants in meat and meat products. *Meat Sci.* **2014**, *98*, 21−33.

(18) Rodríguez-Carpena, J. G.; Morcuende, D.; Estévez, M. Avocado by-products as inhibitors of color deterioration and lipid and protein oxidation in raw porcine patties subjected to chilled storage. *Meat Sci.* **2011**, *89*, 166−173.

(19) Rababah, T.; Hettiarachchy, N.; Horax, R.; Eswaranandam, S.; Mauromoustakos, A.; Dickson, J.; Niebuhr, S. Effect of electron beam irradiation and storage at 5C on thiobarbituric acid reactive substances and carbonyl content in chicken breast meat infused with antioxidants and selected plant extracts. *J. Agric. Food Chem.* **2004**, *52*, 8236−8241.

(20) Lara, M. S.; Gutierrez, J. I.; Timón, M.; Andrés, A. I. Evaluation of two natural extracts (*Rosmarinus officinalis* L. and *Melissa officinalis* L.) as antioxidants in cooked pork patties packed in MAP. *Meat Sci.* **2011**, *88*, 481−488.

(21) Jongberg, S.; Tørngren, M. A.; Gunvig, A.; Skibsted, L. H.; Lund, M. N. Effect of green tea or rosemary extract on protein oxidation in Bologna type sausages prepared from oxidatively stressed pork. *Meat Sci.* **2013**, *93*, 538−546.

(22) Jongberg, S.; Lund, M. N.; Ostdal, H.; Skibsted, L. H. Phenolic antioxidant scavenging of myosin radicals generated by hypervalent myoglobin. *J. Agric. Food Chem.* **2012**, *60*, 12020−12028.

(23) Lundblad, R. L. *Techniques in protein modification*; CRC Press: Boca Raton, FL, 1995.

(24) Singleton, V. L.; Rossi, J. A. Colorimetry of total phenolics with phosphomolybdic-phosphotungstic acid reagents. *Am. J. Enol. Vitic.* **1965**, *16*, 144−158.

(25) Park, D.; Xiong, Y. L. Oxidative modification of amino acids in porcine myofibrillar protein isolates exposed to three oxidizing systems. *Food Chem.* **2007**, *103*, 607−616.
(26) Koutina, G.; Jongberg, S.; Skibsted, L. H. Protein and lipid oxidation in Parma ham during production. *J. Agric. Food Chem.* **2012**, *60*, 9737−9745.
(27) Ellman, G. L. Tissue Sulfhydryl Groups. *Arch. Biochem. Biophys.* **1959**, *82*, 70−77.
(28) Jongberg, S.; Terkelsen, L. S.; Miklos, R.; Lund, M. N. Green tea extract impair meat emulsion properties by disturbing protein disulfide cross-linking. *Meat Sci.* **2015**, *100*, 2−9.
(29) Andersen, H. J.; Skibsted, L. H. Kinetics and Mechanism of Thermal Oxidation and Photooxidation of Nitrosylmyoglobin in Aqueous Solution. *J. Agric. Food Chem.* **1992**, *40*, 1741−1750.
(30) Kajer, T. B.; Fairfull-Smith, K. E.; Yamasaki, T.; Yamada, K.; Fu, S.; Bottle, S. E.; Hawkins, C. L.; Davies, M. J. Inhibition of myeloperoxidase- and neutrophil-mediated oxidant production by tetraethyl and tetramethyl nitroxides. *Free Radical Biol. Med.* **2014**, *70*, 96−105.
(31) Lametsch, R.; Larsen, M. R.; Essén-Gustavsson, B.; Jensen-Waern, M.; Lundstrom, K.; Lindahl, G. Postmortem changes in pork muscle protein phosphorylation in relation to RN genotype. *J. Agric. Food Chem.* **2011**, *59*, 11608−11615.
(32) Østdal, H.; Skibsted, L. H.; Andersen, H. J. Formation of long-lived protein radicals in the reaction between $H_2O_2$-activated metmyoglobin and other proteins. *Free Radical Biol. Med.* **1997**, *23*, 754−761.
(33) Turell, L.; Radi, R.; Alvarez, B. The thiol pool in human plasma: The central contribution of albumin to redox processes. *Free Radical Biol. Med.* **2013**, *65*, 244−253.
(34) Bravo, L.; Goya, L.; Lecumberri, E. LC/MS characterization of phenolic constituents of mate (*Ilex paraguariensis*, St. Hil.) and its antioxidant activity compared to commonly consumed beverages. *Food Res. Int.* **2007**, *40*, 393−405.
(35) Brewer, M. S. Natural antioxidants: Sources, compounds, mechanisms of action, and potential applications. *Comp. Rev. Food Sci. Food Saf.* **2011**, *10*, 221−247.
(36) Heck, C. I.; De Mejia, E. G. Yerba mate tea (*Ilex paraguariensis*): A comprehensive review on chemistry, health implications, and technological considerations. *J. Food Sci.* **2007**, *72*, R138−R151.
(37) Østdal, H.; Andersen, H. J.; Davies, M. J. Formation of long-lived radicals on proteins by radical transfer from heme enzymes—A common process? *Arch. Biochem. Biophys.* **1999**, *362*, 105−112.
(38) Chen, Y. R.; Chen, C. L.; Chen, W.; Zweier, J. L.; Augusto, O.; Radi, R.; Mason, R. P. Formation of protein tyrosine ortho-semiquinone radical and nitrotyrosine from cytochrome c-derived tyrosyl radical. *J. Biol. Chem.* **2004**, *279*, 18054−18062.
(39) Dalsgaard, T. K.; Nielsen, J. H.; Brown, B. E.; Stadler, N.; Davies, M. J. Dityrosine, 3,4-dihydroxyphenylalanine (DOPA), and radical formation from tyrosine residues on milk proteins with globular and flexible structures as a result of riboflavin-mediated photo-oxidation. *J. Agric. Food Chem.* **2011**, *59*, 7939−7947.
(40) Silva, F. A. M.; Borges, F.; Guimarães, C.; Lima, J. L. F. C.; Matos, C.; Reis, S. Phenolic acids and derivatives: Studies on the relationship among structure, radical scavenging activity, and physicochemical parameters. *J. Agric. Food Chem.* **2000**, *48*, 2122−2126.
(41) Bentayeb, K.; Rubio, C.; Batlle, R.; Nerín, C. Direct determination of carnosic acid in a new active packaging based on natural extract of rosemary. *Anal. Bioanal. Chem.* **2007**, *389*, 1989−1996.
(42) Herrero-Martínez, J. M.; Sanmartin, M.; Rosés, M.; Bosch, E.; Ráfols, C. Determination of dissociation constants of flavonoids by capillary electrophoresis. *Electrophoresis* **2005**, *26*, 1886−1895.
(43) Lorrain, B.; Dangles, O.; Genot, C.; Dufour, C. Chemical modeling of heme-induced lipid oxidation in gastric conditions and inhibition by dietary polyphenols. *J. Agric. Food Chem.* **2010**, *58*, 676−683.

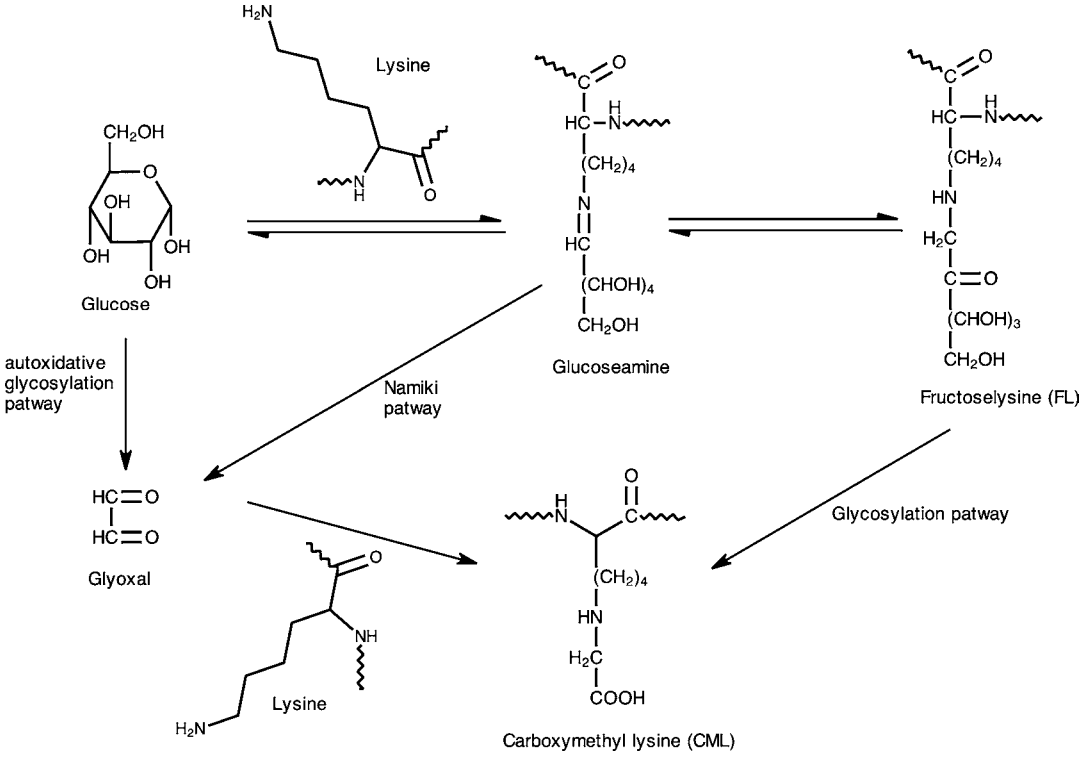


**Figure 1.** Pathways of CML formation (adapted from Han et al.[30]).

was interacted with calcium chloride and epicatechin to form casein−calcium and casein−epicatechin complexes. These complexes were heated in the presence of glucose at temperatures ranging from 70 to 150 °C, covering food processing conditions. FL and CML were determined in the heated mixtures as early and advanced glycation products, respectively.

## MATERIALS AND METHODS

**Chemicals.** Casein from bovine milk, glucose, (−)-epicatechin, sodium borohydride (Fluka), and CML standard were purchased from Sigma-Aldrich Chemie Gmbh (Germany), whereas calcium chloride, disodium hydrogen phosphate, potassium dihydrogen phosphate, and boric acid were from Merck (Germany). Furosine standard was purchased from Neosystem Laboratoire (Strasbourg, France). Hydrochloric acid and formic acid were also purchased from Sigma-Aldrich (Germany) and were of HPLC grade.

**Consumables.** Syringe filters (nylon, 0.45 μm), Oasis HLB (1 mL, 30 mg) solid-phase extraction cartridges, Acquity UPLC HSS T3 column (4.6 × 150 mm, 3 μm), and Atlantis dC18 column (250 × 4.6 mm, 5 μm) were supplied by Waters (Millford, MA).

**Preparation of Casein Complexes.** Casein was suspended in 50 mM phosphate buffer (pH 6.8) at a concentration of 5%. The suspension was continuously stirred for 20 min using a magnetic stirrer. Next, 0.1% of calcium chloride was added to promote ionic interaction between casein molecules and calcium ions, or 0.1% of epicatechin was added to promote hydrophobic interaction between casein and epicatechin molecules. The contents were continuously stirred for 20 min to maintain the casein−calcium or casein−epicatechin complexes. Afterward, 5% of glucose was added onto these complexes and stirred for further 20 min to obtain final mixtures of casein−glucose−calcium (CN-G-Ca) and casein−glucose−epicatechin (CN-G-EC). The control (CN-G) was a mixture of 5% casein and 5% glucose. Finally, the mixtures were glycated in solution state or in dry state after freeze-drying. The glycation reactions were performed in tightly closed test tubes containing the mixtures (in solution or dry states) prepared as described above. The tubes were placed in an oil bath and heated at 70, 90, 110, 130, and 150 °C for 10 min. A set of samples was also heated at 70 °C for 6 h.

To see the effect of protein conformation on glycation potential of casein, high shear microfluidization was applied to cause physical modification of the casein micelles. The casein suspension (5%) was treated under 30 000 psi for 5 min using a high-shear microfluidizer device (M110P, Microfluidics, Newton, MA). High-shear treated casein was dried by freeze-drying and kept at −20 °C. It was used to prepare the mixtures of high-shear treated casein−glucose−calcium (hsCN-G-Ca) and high-shear treated casein−glucose−epicatechin (hsCN-G-EC) complexes as described above. In this case, the control (hsCN-G) was a mixture of 5% high-shear treated casein and 5% glucose. The mixtures were glycated in dry state after freeze-drying by heating at 70 °C for 6 h.

The concentrations of FL and CML were determined as early and advanced glycation products in the heated mixtures. To see the effect of storage on the concentrations of FL and CML concentrations, the samples were incubated at 37 °C for 7 days after heat treatment.

**Analysis of Furosine by HPLC.** Analysis of furosine was performed according to Gökmen et al.[17] 30 mg of sample was weighed into a glass tube, and 10 mL of hydrochloric acid (8 N) was added. The tubes were flushed with nitrogen and tightly closed. They were hydrolyzed for 23 h at 110 °C. The hydrolyzates were filtered through filter paper, and then 100 μL was put into a glass vial. It was evaporated to dryness under nitrogen gas. The content then was washed with 1 mL of deionized water and passed through OASIS HLB cartridges. Ten microliters was injected into the HPLC system. Chromatographic separation was performed on an Atlantis HILIC column (250 × 4.6 mm, 5 μm) at 40 °C with a mobile phase of 1% formic acid at a flow rate of 1 mL/min. Data acquisition was performed acquiring chromatograms at the detection wavelength of 280 nm. Quantification was based on the calibration curve prepared using calibration solutions of furosine (1−10 mg/L), and was expressed as mg/g protein.

**Analysis of CML by LC−MS/MS.** Analysis of CML was performed according to Palermo et al.[18] with some modifications. A total of 20 mg of sample was mixed with 100 μL of deionized water in a glass tube. 450 μL of sodium borate buffer (0.2 M, pH 9.2) and 500

μL of sodium borohydride (1 M solution prepared in 0.1 M NaOH) were added. They were incubated at room temperature for 4 h to reduce fructoselysine into hexitol lysine. Afterward, 2 mL of hydrochloric acid (8 N) was added, and the tubes were closed under nitrogen flush. They were hydrolyzed for 24 h at 110 °C. Twenty microliters of hydrolyzate was evaporated with nitrogen. After the content was washed with 1 mL of deionized water, it was passed through a preconditioned Oasis HLB cartridge for cleanup. The first 8 drops of the eluent were discarded, and the rest was collected and diluted properly prior to LC−MS/MS analysis. The sample was injected into an Acquity UPLC HSS T3 column (4.6 × 150 mm, 3 μm) at 40 °C coupled to a Waters LC−MS/MS system operated in positive ionization mode using the following interface parameters: source temperature of 120 °C, desolvation temperature of 450 °C, collision gas flow of 0.20 mL/min, desolvation gas flow of 900 L/min, capillary voltage of 3 kV, cone voltage of 25 V, and extractor voltage of 2 V. Chromatographic separation was performed by using a mobile phase consisting of 0.1% formic acid in water:0.1% formic acid in acetonitrile (90:10, v/v) at a flow rate of 0.50 mL/min. Acquisition was performed by monitoring $m/z$ ratio of 205.10 for CML, 84.10 and 130.10 for its product ions. Quantification was performed by means of a matrix-matched calibration curve. Hydrolyzate of unheated protein was used as blank matrix. Calibration solutions of CML were prepared in the blank matrix at concentrations of 0, 1, 2.5, 5.0, and 10 μg/mL. They then were subjected to the lengthy extraction procedure that was used for actual samples, and analyzed as described above.

**Statistical Analysis.** The samples were analyzed at least in triplicate. Statistical analyses were performed by using IBM SPSS Statistics 19. Differences between mean values of samples were evaluated by analysis of variance (ANOVA), and the Duncan test was applied to determine significant differences at $p < 0.05$ level. Determination of significant differences between samples before and after incubation was performed with independent samples $t$ test.

## RESULTS AND DISCUSSION

**Effects of Complex Formation on Glycation of Casein.** Exogenous glycation of proteins that takes place during food processing may occur in a wide range of temperatures. In this study, glycation behavior of casein was investigated by forming hydrophobic or ionic interactions prior to heating. In the presence of glucose, casein−calcium and casein−epicatechin complexes were heated at temperatures of 70, 90, 110, 130, and 150 °C for 10 min to monitor glycation under aqueous and dry conditions.

Furosine is a good marker of early glycation especially for monitoring modification of proteins rich in lysine like casein. Figure 2 shows furosine concentrations of casein complexes heated at different temperatures in solution and dry state conditions. In solution state, furosine concentrations of all samples gradually increased as the temperature increased from 70 to 130 °C during heating. Further increase of temperature from 130 to 150 °C did not cause a remarkable increase in furosine concentrations. There were statistically significant differences ($p < 0.05$) in furosine concentrations of the samples heated at 70, 90, 110, and 130 °C. In comparison to the control, there were no significant differences ($p > 0.05$) in furosine levels for casein complexes formed with calcium and epicatechin at all temperatures studied except 130 and 150 °C.

The effect of temperature on furosine concentrations was different for the samples heated in dry state than in solution state. Furosine levels increased when the temperature was raised from 70 to 110 °C. With an exception for 150 °C, furosine concentrations of the samples glycated in dry state were higher than those of the samples glycated in solution state at all temperatures studied. This indicates a higher glycation potential of casein in dry conditions. It is known that the first

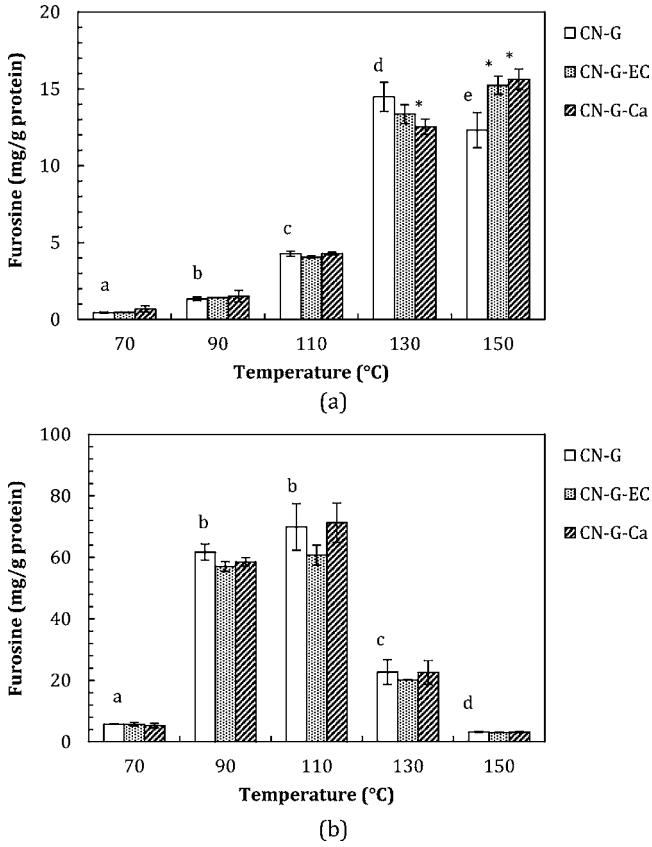


**Figure 2.** Effects of complex formation on furosine concentration of samples heated at different temperatures in (a) solution state, and (b) dry state. Bars with different letters indicate significant difference for control (CN-G) at $p < 0.05$ level. Bars with an asterisk indicate significant differences of complexes from control (CN-G) within the same temperature ($p < 0.05$).

stage of the glycation reaction is a condensation between the amino group of casein and the carbonyl group of glucose, yielding one molecule of water. Hence, the presence of water in the medium might be suppressing the reaction.

The peak levels of furosine were observed for the samples heated at 110 °C for 10 min in dry state that were significantly higher ($p < 0.05$) than the levels observed for the samples heated in solution state. Increasing the temperature in the dry state from 110 to 130 and to 150 °C caused a gradual decrease in furosine levels. It is a fact that furosine, an acid derivative of FL, is the indicator of early glycation. As an intermediate compound, FL can be converted faster to advanced glycation products at higher temperatures. So, the furosine concentration decreases as glycation progresses. FL is considered as the main precursor of CML.[19] It was shown that decomposition of FL leads to formation of CML.[20] Similar to the results observed in solution state, there were no significant differences ($p > 0.05$) in furosine levels for casein complexes formed with calcium and epicatechin.

Figure 3 shows CML concentrations of casein complexes heated at different temperatures in solution and dry state conditions. In solution state, there was a gradual increase in CML concentrations of the samples as the temperature increased from 70 to 150 °C (Figure 3a). For the control (CN-G), the CML level increased by a factor of 114 when the temperature was increased from 70 to 150 °C during heating. However, this increase was limited to 39 and 60 times for


dx.doi.org/10.1021/jf5038954 | J. Agric. Food Chem. 2014, 62, 11289−11295

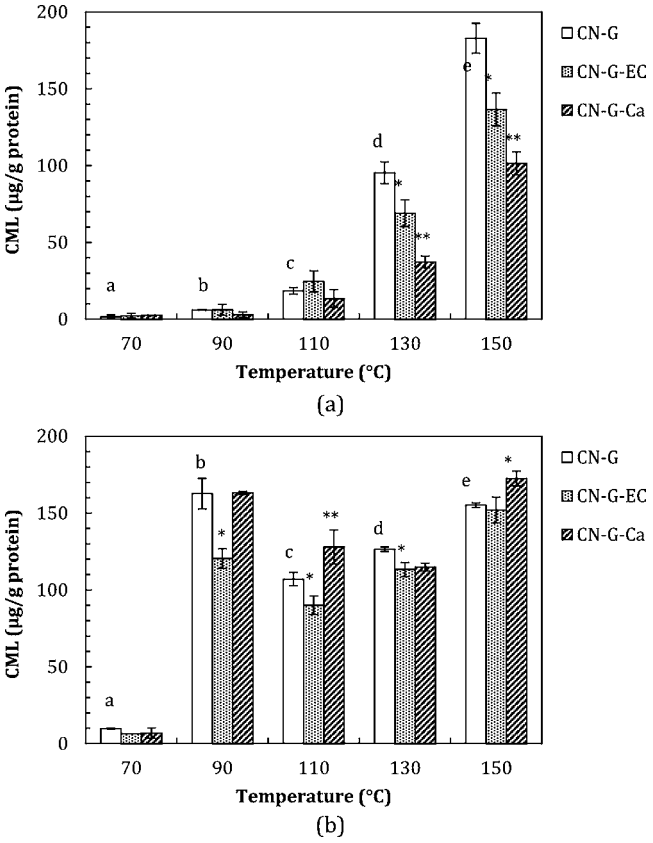


**Figure 3.** Effects of complex formation on CML concentration of samples heated at different temperatures in (a) solution state, and (b) dry state. Bars with different letters indicate significant difference for control (CN-G) at $p < 0.05$ level. Bars with an asterisk indicate significant differences of complexes from control (CN-G) within the same temperature ($p < 0.05$).

casein complexes formed with calcium and epicatechin, respectively. This revealed that formation of casein−calcium and casein−epicatechin complexes before heat treatment has a potential to limit the formation of advanced glycation end products during heating under certain conditions. At 130 and 150 °C, the amounts of CML formed during heating in the samples of casein complexes (CN-G-Ca and CN-G-EC) were found significantly lower ($p < 0.05$) than those formed in the control (CN-G). It is known that calcium ions act as a cross-linker forming bridges between casein micelles.[21] Formation of the casein−calcium complex through ionic interaction makes it difficult for glucose to bind amine groups of casein. On the other hand, there are different possible mechanisms for epicatechin to limit glycation. Protein−phenol interactions are known so far by taking place between hydrophobic residues of protein and polyphenols, mainly flavonoids. Noncovalent interaction between protein molecules and polyphenols results in bridges that make protein molecules hold together.[22] Hence, the first mechanism of epicatechin is to form a complex with casein, which is sterically hindered for glucose molecules. Because polyphenols are known to have carbonyl-trapping activity,[23,24] the second mechanism of epicatechin might be trapping glucose derived dicarbonyl compounds like glyoxal. CML may be formed from FL or from the reaction between glyoxal and lysine residues of protein (Figure 1). Hence, the decreased CML level besides the undiminished FL level indicates that epicatechin may have trapped glyoxal, and therefore have inhibited advanced glycation of casein. In our experiments, epicatechin did not cause a significant reduction in early glycation as stated earlier; however, the CML level significantly decreased ($p < 0.05$). There is another potential mechanism for epicatechin to limit glycation; Yin et al.[25] reported that epicatechin inhibited formation of intermediary radicals during the Maillard reaction. It was explained that autoxidation of epicatechin yielded formation of quinones that reacted with lysine through either a Michael-type addition or a Strecker-like reaction. There is additional evidence that supports such a reaction happening at 110 °C in semi dry mixtures; the reaction of glycine and the oxidized form of catechin leads to the formation of single- and double-addition products.[26] However, that kind of mechanism is favorable at alkaline conditions in which polyphenols may readily oxidize to respective quinones.[27] Therefore, this mechanism should occur to a limited extent at the conditions applied in this study.

In dry state, there was a remarkable increase in the amounts of CML formed in the samples when the temperature was increased from 70 to 90 °C (Figure 3b). In general, the CML levels were comparable to each other for all samples heated at 90, 110, 130, and 150 °C. In detail, the casein−epicatechin complex had significantly lower amounts of CML during heating at 90, 110, and 130 °C ($p < 0.05$). The casein−calcium complex had a lower amount of CML during heating only at 130 °C ($p < 0.05$). It is thought that the thermal impact suppressed molecular interactions because the treatment was harsh during heating casein complexes in dry state. Calcium ion accelerates dehydration of sugar molecules as do all mono-, di-, and trivalent cations.[28] Dehydration of glucose causes ian ncrease in the formation of CML through the glyoxal pathway, as explained in Figure 1. This is the most probable reason for higher amounts of CML found in heated casein−calcium complexes in dry state.

**Effects of Protein Conformation on Glycation of Casein.** In the second part, the complexes were formed using high-shear treated casein to understand the effects of physical modifications on the glycation tendency of casein. High-shear application was performed by treatment of casein suspension using a microfluidizer at 30 000 psi for 5 min.

As mentioned before, formation of casein complexes with calcium and epicatechin before heat treatment did not cause a change in the formation of early glycation products measured as furosine in the samples (Figure 4). However, heating the complexes prepared from high-shear treated casein formed lower amounts of furosine than the complexes prepared from native casein ($p < 0.05$). This indicated that physical modification has an effect on complex formation, and therefore on protein glycation. Among others, high-shear treated casein−epicatechin complex (hsCN-G-EC) had the lowest amount of furosine ($p < 0.05$).

It is thought that more hydrophobic and ionic interaction sites might become available for epicatechin and calcium to bind when casein micelle was dissociated. This consequence could have yielded a decrease in glycation reaction. Altuner et al.[29] showed that high hydrostatic pressure affected noncovalent interactions and especially hydrophobic bonds in milk. It was reported that as the pressure applied increased, the casein micelles decomposed into submicelles and the embedded hydrophobic areas inside the micelles repositioned in such a way that they readily interfered with the fluorescent marker, 1,8-naphthaleresulfonic acid (ANS).

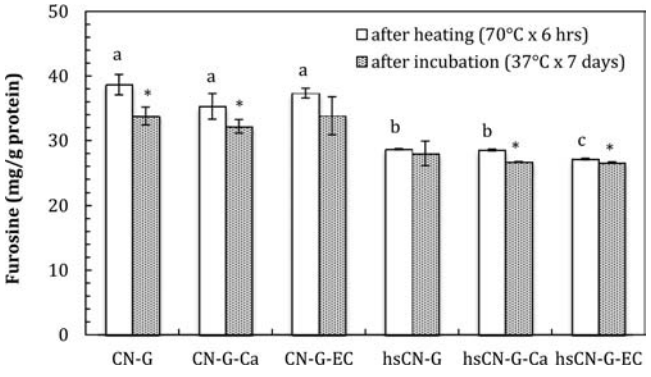


**Figure 4.** Furosine levels of native and high-shear treated casein complexes heated at 70 °C for 6 h. Bars with different letters indicate significant difference between complexes at $p < 0.05$ level. Bars with an asterisk indicate significant differences between samples before and after incubation ($p < 0.05$).

To see the progression of glycation during storage, the heated mixtures of casein complexes were incubated at 37 °C for 7 days. As shown in Figure 4, furosine concentrations decreased slightly during incubation. This is not surprising because FL being an intermediate compound formed in the Maillard reaction would decrease as glycation further developed under the stated conditions. Ahmed et al.[20] reported that FL content decreased during 15 days of reaction at 37 °C. Also, Han et al.[30] reported a decrease in FL and its simultaneous conversion to CML in the lysine−glucose−lipid model system during 4 h of incubation at 100 °C.

Figure 5 shows the amounts of CML formed in the mixtures of native and high-shear treated casein complexes during

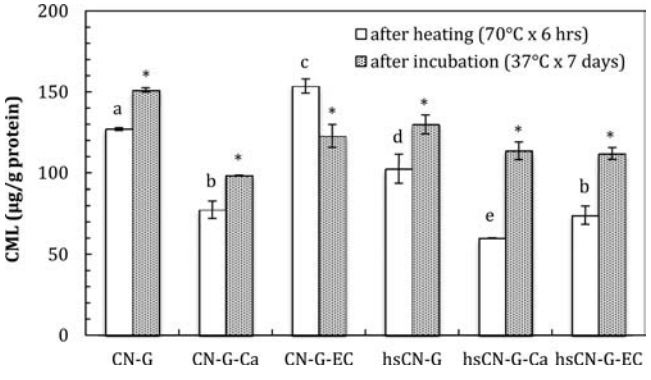


**Figure 5.** CML levels of native and high-shear treated casein complexes heated at 70 °C for 6 h. Bars with different letters indicate significant difference between complexes at $p < 0.05$ level. Bars with an asterisk indicate significant differences between samples before and after incubation ($p < 0.05$).

heating at 70 °C for 6 h. Interestingly, the presence of calcium ions showed a distinct antiglycation effect on native casein in terms of the formation of CML as the indicator of advanced glycation, whereas epicatechin caused an increase in CML level during heating. During incubation at 37 °C for 7 days, CML levels increased in all samples with an exception for the heated mixture of casein−epicatechin complex (CN-G-EC). It is a fact that calcium ions act as a cross-linking agent, forming bridges between casein micelles.[21] The results of the present study bring evidence that forming casein−calcium complex makes it difficult for glucose to bind amine groups of casein. There are conflicting reports about epicatechin; some reported an antiglycation effect,[23−26,31] while others reported an increased glycation.[32,33] Epicatechin was found to be an effective agent for the inhibition of thermally developed Maillard reaction products and reduced the cooked flavor in UHT milk.[31] Some reported antiglycation effect of epicatechin by carbonyl trapping,[23,24] while others explained the mechanism through quinone formation reacting with amines[25,26] as mentioned above. Also, Zhang et al.[34] reported that polyphenols reduce glyoxal generation by inhibiting lipid peroxidation. However, in a recent review, it was stated that epicatechin could both inhibit and enhance glycation.[33] It was explained by Fujiwara et al.[32] that catechol group containing polyphenols generates hydrogen peroxide during autoxidation of catechol structure, then hydrogen peroxide may generate hydroxyl radicals, and finally CML is generated by the reaction of hydroxyl radicals and Amadori products. So, the increased CML level of the complex prepared from the native casein in this study could be explained by the oxidation triggering effect of epicatechin. However, the CML level could be decreased if the complex was prepared using high-shear treated casein (Figure 5). It is thought that epicatechin can bind to casein structure more easily when it is treated using high-shear microfluidizer because the hidden hydrophobic sites within intact protein are exposed to interaction. Epicatechin has the ability to make weak hydrophobic interactions through hydrophobic amino acids of protein such as proline, tryptophan, tyrosine, and phenylalanine.[35]

So far, several methods have been proposed to inhibit protein glycation during food processing. The main thought is the blockage of carbonyl attachment to proteins, preventing oxidative stress or breaking down formed AGE cross-links. As exemplified for casein, this study proposes ionic and weak hydrophobic interactions as a strategy to limit advanced glycation of proteins during heating in a wide range of temperatures in both solution and dry states. It is certain that epicatechin or calcium ions do not block free amine groups of proteins, but they form steric hindrance that makes it difficult for carbonyl compounds to bind to amine groups on protein molecule. Casein micelle has a hydrophobic core and a hydrophilic surface. High shear treatment of casein allows more interaction sites, causing exposure of embedded hydrophobic regions within the intact molecule. So if the hydrophobic complex is to be formed to reduce glycation, physical modification of protein prior to complexation seems advantageous. Under the stated conditions, antiglycation effects of epicatechin molecules and calcium ions as hydrophobic and ionic interaction agents are remarkable in the advanced state. However, these interactions do not make significant differences in the early stage of glycation.

In conclusion, calcium ions and epicatechin molecules may inhibit the glycation of casein during heating under aqueous and dry conditions as follows:

- In aqueous solution state, calcium ions act as cross-linking agent forming bridges between casein micelles that make it difficult for carbonyl compounds to bind to glycation sites on protein.
- In dry state, calcium ions accelerate dehydration of glucose that may enhance advanced glycation of casein through the formation of glyoxal at high temperatures.
- Epicatechin forms a complex with casein through a well-known protein−phenolic interaction phenomenon that

may cause reduction in the accessibility of glycation sites on protein.

- Epicatechin may limit early glycation of protein through the formation of quinones that further react with amine residues on protein. However, this effect is more favorable under strong alkaline and oxidizing conditions.
- Epicatechin may limit advanced glycation by trapping glyoxal formed from the degradation of glucose. The reduced CML concentrations despite undiminished furosine levels indicate that mechanism is dominating in our experimental conditions.

The above-mentioned effects of calcium and epicatechin observed in the model system can be useful to prevent casein glycation in actual food systems such as pasteurized or sterilized milk and spray dried milk powder. Inhibition of Maillard reaction during milk processing not only improves the nutritional value of milk products, but also brings some sensorial advantages such as prevention of off-flavor. However, it should be kept in mind that the ingredient profile has substantial effects on advanced glycation.

## AUTHOR INFORMATION

### Corresponding Author

*Tel.: +90-312-2977108. Fax: +90-312-2992123. E-mail: vgokmen@hacettepe.edu.tr.

### Notes

The authors declare no competing financial interest.

## REFERENCES

(1) Reddy, V. P.; Beyaz, A. Inhibitors of the Maillard reaction and AGE breakers as therapeutics for multiple diseases. *Drug Discovery Today* **2006**, *11*, 646−654.

(2) Henle, T. Protein-bound advanced glycation endproducts (AGEs) as bioactive amino acid derivatives in foods. *Amino Acids* **2005**, *29*, 313−322.

(3) Šebeková, K.; Somoza, V. Dietary advanced glycation end-products (AGEs) and their health effects − PRO. *Mol. Nutr. Food Res.* **2007**, *51*, 1079−1084.

(4) Wang, Z.; Jiang, Y.; Liu, N.; Ren, L.; Zhu, Y.; An, Y.; Chen, D. Advanced glycation end-product Nε-carboxymethyl-Lysine accelerates progression of atherosclerotic calcification in diabetes. *Atherosclerosis* **2012**, *221*, 387−396.

(5) Li, J.; Liu, D.; Sun, L.; Lu, Y.; Zhang, Z. Advanced glycation end products and neurodegenerative diseases: Mechanisms and perspective. *J. Neurol. Sci.* **2012**, *317*, 1−5.

(6) Baynes, J. W. The role of AGEs in aging: causation or correlation. *Exp. Gerontol.* **2001**, *36*, 1527−1537.

(7) Vlassara, H. Advanced glycation in health and disease role of the modern environment. *Ann. N. Y. Acad. Sci.* **2005**, *1043*, 452−460.

(8) He, J.; Zeng, M.; Zheng, Z.; He, Z.; Chen, J. Simultaneous determination of $N^{\varepsilon}$-(carboxymethyl) lysine and $N^{\varepsilon}$-(carboxyethyl) lysine in cereal foods by LC−MS/MS. *Eur. Food Res. Technol.* **2014**, *238*, 367−374.

(9) Poulsen, M. W.; Hedegaard, R. V.; Andersen, J. M.; de Courten, B.; Bügel, S.; Nielsen, J.; Skibsted, L. H.; Dragsted, L. O. Advanced glycation endproducts in food and their effects on health. *Food Chem. Toxicol.* **2013**, *60*, 10−37.

(10) Zeng, J.; Davies, M. J. Evidence for the formation of adducts and S-(carboxymethyl)cysteine on reaction of α-dicarbonyl compounds with thiol groups on amino acids, peptides, and proteins. *Chem. Res. Toxicol.* **2005**, *18*, 1232−1241.

(11) Ames, J. M. Determination of $N^{\varepsilon}$-(carboxymethyl)lysine in foods and related systems. *Ann. N. Y. Acad. Sci.* **2008**, *1126*, 20−24.

(12) Yazdi, S. Y.; Corredig, M.; Dalgleish, D. G. Studying the structure of β-casein-depleted bovine casein micelles using electron microscopy and fluorescent polyphenols. *Food Hydrocolloids* **2014**, DOI: 10.1016/j.foodhyd.2014.03.022.

(13) Jindal, S.; Naeem, A. Consequential secondary structure alterations and aggregation during prolonged casein glycation. *J. Fluoresc.* **2013**, *23*, 367−374.

(14) Jing, H.; Kitts, D. D. Chemical and biochemical properties of casein−sugar Maillard reaction products. *Food Chem. Toxicol.* **2002**, *40*, 1007−1015.

(15) Peng, X.; Ma, J.; Chen, F.; Wang, M. Naturally occurring inhibitors against the formation of advanced glycation end-products. *Food Funct.* **2011**, *2*, 289−301.

(16) Mesías, M.; Navarro, M.; Gökmen, V.; Morales, F. J. Antiglycative effect of fruit and vegetable seed extracts: inhibition of AGE formation and carbonyl-trapping abilities. *J. Sci. Food Agric.* **2013**, *93*, 2037−2044.

(17) Gökmen, V.; Serpen, A.; Morales, F. J. Determination of furosine in thermally processed foods by hydrophilic interaction liquid chromatography. *J. AOAC Int.* **2009**, *92*, 1460−1463.

(18) Palermo, M.; Fiore, A.; Fogliano, V. Okara promoted acrylamide and carboxymethyl-lysine formation in bakery products. *J. Agric. Food Chem.* **2012**, *60*, 10141−10146.

(19) Lima, M.; Assar, S. H.; Ames, J. M. Formation of $N^{\varepsilon}$-(carboxymethyl)lysine and loss of lysine in casein glucose-fatty acid model systems. *J. Agric. Food Chem.* **2010**, *58*, 1954−1958.

(20) Ahmed, M. U.; Thorpe, S. R.; Baynes, J. W. Identification of $N^{\varepsilon}$-carboxymethyllysine as a degradation product of fructoselysine in glycated protein. *J. Biol. Chem.* **1986**, *261*, 4889−4894.

(21) Nair, P. K. Colloidal behaviour of casein micelles with concentration. Ph.D. Thesis, Canada, 2012; pp 7−12; https://atrium.lib.uoguelph.ca/xmlui/handle/10214/3997.

(22) Siebert, K. J.; Troukhanova, N. V.; Lynn, P. Y. Nature of polyphenol-protein interactions. *J. Agric. Food Chem.* **1996**, *44*, 80−85.

(23) Totlani, V. M.; Peterson, D. G. Influence of epicatechin reactions on the mechanisms of Maillard product formation in low moisture model systems. *J. Agric. Food Chem.* **2007**, *55*, 414−420.

(24) Sang, S.; Shao, X.; Bai, N.; Lo, C. Y.; Yang, C. S.; Ho, C. T. Tea polyphenol (−)- epigallocatechin-3-gallate: A new trapping agent of reactive dicarbonyl species. *Chem. Res. Toxicol.* **2007**, *20*, 1862−1870.

(25) Yin, J.; Hedegaard, R. V.; Skibsted, L. H.; Andersen, M. L. Epicatechin and epigallocatechin gallate inhibit formation of intermediary radicals during heating of lysine and glucose. *Food Chem.* **2014**, *146*, 48−55.

(26) Guerra, P. V.; Yaylayan, V. A. Interaction of flavanols with amino acids: Postoxidative reactivity of the B-ring of catechin with glycine. *J. Agric. Food Chem.* **2014**, *62*, 3831−3836.

(27) Rawel, H. M.; Kroll, J.; Rohn, S. Reactions of phenolic substances with lysozyme-physicochemical characterisation and proteolytic digestion of the derivatives. *Food Chem.* **2001**, *72*, 59−71.

(28) Gökmen, V.; Şenyuva, H. Z. Effects of some cations on the formation of acrylamide and furfurals in glucose-asparagine model system. *Eur. Food Res. Technol.* **2007**, *225*, 815−820.

(29) Altuner, E. M.; Alpas, H.; Erdem, Y. K.; Bozoglu, F. Effect of high hydrostatic pressure on physicochemical and biochemical properties of milk. *Eur. Food Res. Technol.* **2006**, *222*, 392−396.

(30) Han, L.; Li, L.; Li, B.; Zhao, D.; Li, Y.; Xu, Z.; Liu, G. Hydroxyl radical induced by lipid in Maillard reaction model system promotes diet-derived Ne-carboxymethyllysine formation. *Food Chem. Toxicol.* **2013**, *60*, 536−541.

(31) Colahan-Sederstrom, P. M.; Peterson, D. G. Inhibition of key aroma compound generated during ultrahigh-temperature processing of bovine milk via epicatechin addition. *J. Agric. Food Chem.* **2005**, *53*, 398−402.

(32) Fujiwara, Y.; Kiyota, N.; Tsurushima, K.; Yoshitomi, M.; Mera, K.; Sakashita, N.; Takeya, M.; Ikeda, T.; Araki, T.; Nohara, T.; Nagai, R. Natural compounds containing a catechol group enhance the formation of $N^{\varepsilon}$-(carboxymethyl)lysine of the Maillard reaction. *Free Radical Biol. Med.* **2011**, *50*, 883−891.

(33) Nagai, R.; Shirakawa, J.; Ohno, R.; Moroishi, N.; Nagai, M. Inhibition of AGEs formation by natural products. *Amino Acids* **2014**, *46*, 261−266.
(34) Zhang, X.; Chen, F.; Wang, M. Antioxidant and antiglycation activity of selected dietary polyphenols in a cookie model. *J. Agric. Food Chem.* **2014**, *62*, 1643−1648.
(35) Bartolomé, B.; Estrella, I.; Hernández, M. T. Interaction of low molecular weight phenolics with proteins (BSA). *J. Food Sci.* **2000**, *65*, 617−621.

**Table 1. Experimental Conditions for CYP Enzyme Assays**

| enzyme (protein content in reaction buffer) | probe substrate (test concn) | reaction buffer (salt concn) | reaction time (min) | stop solution |
|---|---|---|---|---|
| CYP1A2 (0.13 mg protein/mL) | phenacetin (94 $\mu$M) | potassium phosphate (100 mM) | 20 | acetonitrile |
| CYP2C9 (0.046 mg protein/mL) | tolbutamide (106 $\mu$M) | Tris-HCl (100 mM) | 30 | 6% acetic acid in acetonitrile |
| CYP2C19 (0.37 mg protein/mL) | (*S*)-mephenytoin (30 $\mu$M) | potassium phosphate (50 mM) | 20 | dichloromethane |
| CYP2D6 (0.079 mg protein/mL) | dextromethorphan (2 $\mu$M) | potassium phosphate (100 mM) | 30 | 70% perchloric acid |
| CYP3A4 (0.16 mg protein/mL) | testosterone (61 $\mu$M) | potassium phosphate (100 mM) | 10 | 50% methanol in acetonitrile |

**Table 2. Analytical Conditions for CYP Enzyme Assays**

| | mobile phase | | | |
|---|---|---|---|---|
| | solvent A | solvent B | gradient B | detected wavelength (nm) |
| CYP1A2 | ultrapure water with 0.1% TFA | methanol with 0.1% TFA | 5−15% (5 min, liner gradient) 15−40% (5 min, liner gradient) 40−100% (1 min, liner gradient) 100% (3 min, isocratic) | 244 |
| CYP2C9 | 10 mM sodium acetate buffer (pH 3.4) | methanol | 30% (8 min, isocratic) 30−50% (4 min, liner gradient) 50% (5 min, isocratic) | 228 |
| CYP2C19 | 20 mM sodium perchlorate | acetonitrile | 5−20% (10 min, liner gradient) 20% (5 min, isocratic) | 228 |
| CYP2D6 | ultrapure water with 0.1% TFA | methanol with 0.1% TFA | 5−50% (30 min, liner gradient) 50% (10 min, isocratic) 50−100% (5 min, liner gradient) 100% (10 min, isocratic) | excitation: 280; fluorescence: 310 |
| CYP3A4 | ultrapure water with 0.1% acetic acid | methanol with 0.1% acetic acid | 30−80% (22 min, liner gradient) 80−100% (1 min, liner gradient) 100% (10 min, isocratic) | 240 |

Aldrich, MO, U.S.A.) by CYP2C9, respectively, were measured by the Waters AQCUITY UPLC H-Class system (MA, U.S.A.) with an ACQUITY UPLC BEH C18 column (Waters, MA, U.S.A.) at a flow rate of 0.4 mL/min at 40 °C. (±)-4′-Hydroxymephenytoin, a metabolite of (*S*)-mephenytoin (BD Gentest, MA, U.S.A.) by CYP2C19, was measured using the above UPLC system as described above at a flow rate of 0.5 mL/min at 40 °C. Dextromethorphan, a metabolite of dextrorphan (Wako Pure Chemicals Industries Ltd., Osaka, Japan) by CYP2D6, was measured by the Shimadzu LC Solution system (Kyoto, Japan) with an Ascentis Express C18 column (Sigma-Aldrich, MO, U.S.A.) at a flow rate of 0.8 mL/min at 40 °C. 6$\beta$-Hydroxytestosterone, a metabolite of testosterone (Nacalai Tesque Inc., Kyoto, Japan) by CYP3A4, was measured by the Waters Alliance HPLC system (Waters, MA, U.S.A.) with an Ascentis Express C18 column (Sigma-Aldrich, MO, U.S.A.) at a flow rate of 0.8 mL/min at 40 °C. Other analytical conditions such as mobile phase, gradient condition, and detected wavelength are presented in Table 2.

First, the inhibitory effects of EEP-B55 on the various enzymatic activities of CYPs were examined, and the $IC_{50}$ values for each CYP activity were calculated using GraphPad Prism software version 5.02 (Graphpad Software, Inc., La Jolla, U.S.A.). The test concentrations ($\mu$g/mL) of EEP-B55 used in each CYP enzyme assay were as follows: 0.8 to 67.2 for CYP1A2, 0.105 to 65.6 for CYP2C9, 0.617 to 50.0 for CYP2C19, 4.06 to 130.0 for CYP2D6, and 0.794 to 193.0 for CYP3A4. Each assay was performed in duplicate. Second, the inhibitory effects of the major ingredients of EEP-B55, the quantities of which are shown in Table 3, on the enzymatic activities of CYP were measured at a concentration of 50 $\mu$M in screening. Each assay was performed in duplicate. Then, the relative contributions of artepillin C, baccharin, kaempferide, dihydrokaempferide, isosakuranetin, and kaempferol to the inhibitory effect of EEP-B55 on each CYP activity were obtained in duplicate. In this study, the test concentrations of these compounds were individually determined by calculating the quantities of them in EEP-B55 that caused 70% inhibition for each of 5 CYP enzymatic activities. Artepillin C, kaempferide, dihydrokaempferide, isosakuranetin, and kaempferol, the contributions of which were each more than 5%, were further evaluated by calculating their $IC_{50}$ values in each CYP enzyme assay. This assay was performed in triplicate.

**Table 3. Major Ingredients and Their Respective Contents in EEP-B55**

| ingredients | ($\mu$g/mg of solid content) |
|---|---|
| artepillin C | 170.4 |
| baccharin | 50.3 |
| kaempferide | 29.4 |
| drupanin | 25.3 |
| *p*-coumaric acid | 19.3 |
| dihydrokaempferide | 16.5 |
| betuletol | 15.6 |
| isosakuranetin | 3.7 |
| kaempferol | 1.2 |

**In Vivo Assay.** Male Wistar/ST rats (7 weeks old) were purchased from Japan SLC Inc. (Shizuoka, Japan), fed on a standard diet (CE-2; Clea Japan Inc., Tokyo, Japan) ad libitum, and allowed free access to tap water. After acclimatization for 7 days, the animals were orally administered EEP-B55 at 100 mg/kg or 250 mg/kg (20 mL/kg) under fasting conditions for approximately 16 h. EEP-B55 was mixed with dextrin to prepare a powder formulation comprising 40% EEP-B55 content and suspended in a 0.5% methylcellulose solution. Blood samples were collected from the jugular vein under ether anesthesia before and at 10, 20, 30, and 60 min after administration. After a 2-week wash out period, blood samples were collected from the portal vein at 10 min after administration of the same dose of EEP-B55 as described above. After centrifugation at 1118*g* for 10 min at 4 °C, serum samples were collected, deproteinized by adding an equal volume of methanol/acetonitrile mixed solution containing 2% acetic acid, and then centrifuged at 6439*g* for 10 min at 4 °C. The supernatant was collected and filtered, and it was used for measuring the concentrations of artepillin C detected at 315 nm, kaempferide at 360 nm, dihydrokaempferide at 290 nm,

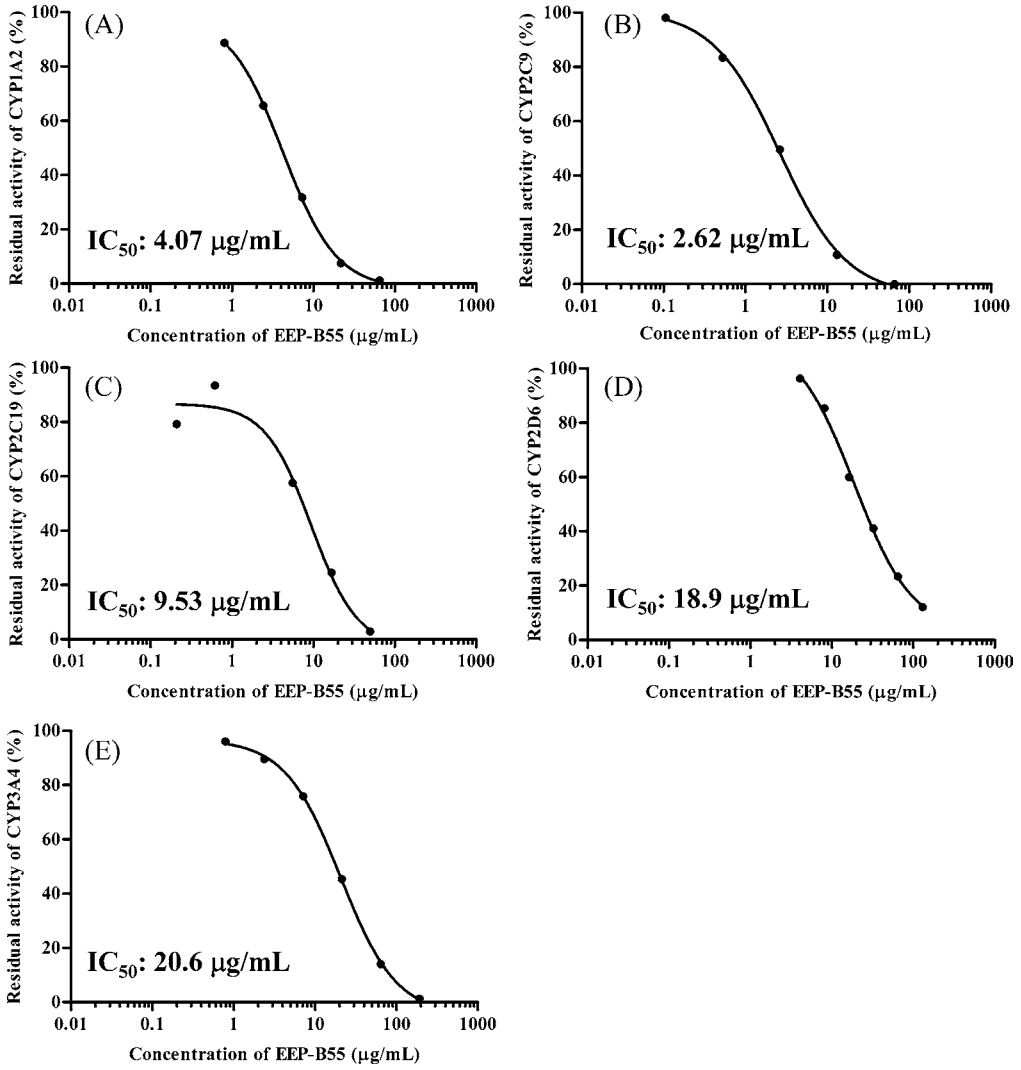


**Figure 1.** Effects of EEP-B55 on the activity of (A) CYP1A2, (B) CYP2C9, (C) CYP2C19, (D) CYP2D6, and (E) CYP3A4. Each value represents the average of duplicate assays, and the $IC_{50}$ values were calculated by nonlinear regression analysis using the GraphPad Prism software version 5.02.

**Table 4. Inhibition Ratio (%) of Major Ingredients of EEP-B55 at a Concentration of 50 $\mu$M**

| ingredients | CYP1A2 | CYP2C9 | CYP2C19 | CYP2D6 | CYP3A4 |
|---|---|---|---|---|---|
| artepillin C | 86.3 | 50.7 | 60.4 | 13.3 | 31.2 |
| baccharin | 17.4 | 60.7 | 13.9 | 0.6 | 30.9 |
| kaempferide[a] | 60.7 | 28.0 | 9.8 | 19.0 | 12.7 |
| drupanin | 16.7 | 7.6 | 3.1 | 1.2 | 7.1 |
| *p*-coumaric acid | 1.8 | 0.0 | 0.0 | 0.7 | 1.9 |
| dihydrokaempferide | 28.2 | 0.0 | 96.7 | 10.7 | 88.9 |
| betuletol[a] | 3.1 | 1.4 | 1.0 | 0.9 | 5.7 |
| isosakuranetin | 86.6 | 94.9 | 100.0 | 30.3 | 91.8 |
| kaempferol | 100.0 | 83.7 | 77.9 | 37.7 | 82.4 |

[a]Kaempferide and betuletol were each dissolved in the reaction buffer at 50 $\mu$M.

isosakuranetin at 290 nm, and kaempferol at 360 nm by a Shimadzu LC Solution system with photodiode array detector. These compounds were separated with an Ascentis Express C18 column using ultrapure water with 0.1% trifluoroacetic acid (TFA, solvent A) and methanol with 0.1% TFA (solvent B) and linear gradient conditions at 40−90% of solvent B for 50 min with a flow rate of 0.5 mL/min at 40 °C. The animal study was handled according to our company's regulations based on the Standards Relating to the Care and Management of Laboratory Animals and Relief of Pain (Notice No. 88 of the Ministry of Environment dated April 28, 2006), and the protocol of the animal study was approved by the Animal Ethics Committee of API Co., Ltd. (protocol 41-010).

## RESULTS

**Effect of EEP-B55 on the Activity of Human Recombinant CYPs.** First, we found that EEP-B55 inhibited all the CYP enzymatic activities tested in a concentration-

dependent manner (Figure 1). Second, in screening of EEP-B55's ingredients at a concentration of 50 $\mu$M, the following ingredients exhibited the inhibition ratio of 50% or more: artepillin C for CYP1A2, CYP2C9, and CYP2C19, baccharin for CYP2C9, kaempferide for CYP1A2, dihydrokaempferide for CYP2C19 and CYP3A4, isosakuranetin for CYP1A2, CYP2C9, CYP2C19, and CYP3A4, and kaempferol for CYP1A2, CYP2C9, CYP2C19, and CYP3A4. No ingredients inhibited CYP2D6 enzyme activity by more than 50%. Conversely, drupanin, *p*-coumaric acid, and betuletol did not cause the inhibition of more than 20% for all the CYP enzymes tested (Table 4). We examined a contribution of EEP-B55 ingredients to inhibition of each CYP activity and found that artepillin C, kaempferide, and isosakuranetin were effective for CYP1A2 activity; artepillin C was for CYP2C9 activity; artepillin C, dihydrokaempferide, isosakuranetin, and kaempferol were for CYP2C19 activity; artepillin C and kaempferide were for CYP2D6 activity; and artepillin C, dihydrokaempferide, and isosakuranetin were for CYP3A4 activity (Table 5). In addition, the $IC_{50}$ values of these ingredients were as follows: 16.1 $\mu$M for artepillin C, 6.0 $\mu$M for kaempferide, and 15.9 $\mu$M for isosakuranetin in the CYP1A2 enzyme assay; 34.9 $\mu$M for artepillin C in the CYP2C9 enzyme assay; 37.0 $\mu$M for artepillin C, 2.0 $\mu$M for dihydrokaempferide, 1.7 $\mu$M for isosakuranetin, and 31.9 $\mu$M for kaempferol in the CYP2C19 enzyme assay; 427.4 $\mu$M for artepillin C and 14.6 $\mu$M for kaempferide in the CYP2D6 enzyme assay; and 268.9 $\mu$M for artepillin C, 10.5 $\mu$M for dihydrokaempferide, and 4.3 $\mu$M for isosakuranetin in the CYP3A4 enzyme assay (Table 5).

**Pharmacokinetic Study on EEP-B55 Ingredients in Rats.** In the peripheral blood, maximum serum concentrations (Cmax; mean ± SD) of artepillin C reached 415 ± 360 nM and 487 ± 307 nM at doses of 100 mg/kg and 250 mg/kg, respectively, at 10 min (Tmax) after administration. The area under the curve (AUC; mean ± SD) of artepillin C was 9551 ± 6729 nmol·min/L and 9991 ± 4037 nmol·min/L at doses of 100 mg/kg and 250 mg/kg, respectively. At 10 min after administration, serum concentrations (mean ± SD) of artepillin C in portal blood were 2794 ± 955 nM and 7142 ± 5044 nM at doses of 100 mg/kg and 250 mg/kg, respectively. In contrast, kaempferide, dihydrokaempferide, isosakuranetin, and kaempferol in serum were not detected and their lower limits of detection (LLD) were as follows: 4.97, 7.15, 4.87, and 5.97 nM, respectively.

**Table 5. Relative Contribution and $IC_{50}$ Values of Major Ingredients of EEP-B55**

| | contribution ratio[a] (%) | $IC_{50}$ values[b] ($\mu$M) |
|---|---|---|
| **CYP1A2** | | |
| artepillin C | 55.3 | 16.1 |
| kaempferide | 47.1 | 6.0 |
| isosakuranetin | 5.1 | 15.9 |
| kaempferol | 1.9 | – |
| **CYP2C9** | | |
| artepillin C | 58.6 | 34.9 |
| baccharin | 3.7 | – |
| isosakuranetin | 0.9 | – |
| kaempferol | 1.8 | – |
| **CYP2C19** | | |
| artepillin C | 21.2 | 37.0 |
| dihydrokaempferide | 29.9 | 2.0 |
| isosakuranetin | 16.8 | 1.7 |
| kaempferol | 12.2 | 31.9 |
| **CYP2D6** | | |
| artepillin C | 11.2 | 427.4 |
| kaempferide | 47.0 | 14.6 |
| isosakuranetin | 4.5 | – |
| kaempferol | 0.2 | – |
| **CYP3A4** | | |
| artepillin C | 21.8 | 268.9 |
| dihydrokaempferide | 21.5 | 10.5 |
| isosakuranetin | 23.0 | 4.3 |
| kaempferol | 0.0 | – |

[a]The final concentrations of the test materials were as follows: EEP-B55 16.9 $\mu$g/mL, artepillin C 9.6 $\mu$M, kaempferide 1.7 $\mu$M, isosakuranetin 0.22 $\mu$M, and kaempferol 0.07 $\mu$M in the CYP1A2 assay; EEP-B55 5.3 $\mu$g/mL, artepillin C 3.0 $\mu$M, baccharin 0.74 $\mu$M, isosakuranetin 0.069 $\mu$M, and kaempferol 0.022 $\mu$M in the CYP2C9 assay; EEP-B55 12.8 $\mu$g/mL, artepillin C 7.3 $\mu$M, dihydrokaempferide 0.7 $\mu$M, isosakuranetin 0.17 $\mu$M, and kaempferol 0.053 $\mu$M in the CYP2C19 assay; EEP-B55 36.9 $\mu$g/mL, artepillin C 20.9 $\mu$M, kaempferide 3.6 $\mu$M, isosakuranetin 0.48 $\mu$M, and kaempferol 0.15 $\mu$M in the CYP2D6 assay; EEP-B55 34.6 $\mu$g/mL, artepillin C 19.6 $\mu$M, dihydrokaempferide 1.9 $\mu$M, isosakuranetin 0.45 $\mu$M, and kaempferol 0.14 $\mu$M in the CYP3A4 assay. [b]Artepillin C, kaempferide, and isosakuranetin were tested at concentrations of 0.78 to 100.0 $\mu$M, 0.063 to 16.0 $\mu$M, and 0.78 to 100.0 $\mu$M, respectively, in the CYP1A2 assay. Artepillin C was tested at concentrations of 0.66 to 1000.0 $\mu$M in the CYP2C9 assay. Artepillin C, dihydrokaempferide, isosakuranetin, and kaempferol were tested at concentrations of 0.33 to 200.0 $\mu$M, 0.046 to 100.0 $\mu$M, 0.082 to 50.0 $\mu$M, and 0.016 to 100.0 $\mu$M, respectively, in the CYP2C19 assay. Artepillin C and kaempferide were tested at concentrations of 39.0 to 1000.0 $\mu$M and 0.62 to 16.0 $\mu$M, respectively, in the CYP2D6 assay. Artepillin C, dihydrokaempferide, and isosakuranetin were tested at concentrations of 15.6 to 1000.0 $\mu$M, 0.78 to 100.0 $\mu$M, and 0.16 to 100.0 $\mu$M, respectively, in the CYP3A4 assay.

## DISCUSSION

In general, changes in pharmacokinetics and pharmacodynamic responses are thought to be caused by drug–drug or drug–food interactions. In pharmacokinetic interactions, approximately 65% of drug–drug interactions occur in metabolic sites, and drug metabolic enzymes are considered to be the most important interactive sites.[18] A large number of drugs are metabolized by CYP enzymes in the liver, and more than 90% of drug–drug interactions occur at the CYP-catalyzed step.[18] Similarly, supplement–drug interactions involving CYP activity are occasionally found to cause considerable adverse events. For these reasons, we evaluated the effects of an ethanol extract of Brazilian green propolis and its major ingredients on the activity of CYP enzymes in vitro. We selected CYP isoforms CYP1A2, CYP2C9, CYP2C19, CYP2D6, and CYP3A4 because more than 90% of drugs are known to be metabolized by these 5 CYP enzymes.[19] In addition, CYP2 and CYP3 families are known to be largely different between human and rat in genome sequences.[20] We therefore used human recombinant CYPs in the present study.

It is difficult to estimate the risk of interactions between drugs and a natural product such as propolis extract because natural products include multiple chemical substances. In the present study, we tried to estimate the risk of an interaction with EEP-B55 in the following steps. First, we evaluated the effects of EEP-B55 and its major ingredients on the activities of CYP enzymes, and calculated the $IC_{50}$ value of each ingredient showing a contribution of more than 5% in vitro CYP enzyme assays. Second, to extrapolate the risk of a propolis–drug

interaction in humans, we measured blood concentrations of the ingredients after oral administration of EEP-B55 in rats and compared them with their $IC_{50}$ values obtained in the in vitro assay.

EEP-B55 reduced the activity of CYP1A2, CYP2C9, CYP2C19, CYP2D6, and CYP3A4 in a concentration-dependent manner, and it was shown that artepillin C, kaempferide, dihydrokaempferide, isosakuranetin, and kaempferol made a major contribution to the inhibitory activity of EEP-B55. Among these compounds, kaempferol, a flavonoid found in fruits and vegetables, is known to inhibit CYP1A2,[21,22] CYP2C9,[23,24] and CYP3A/CYP3A4[25−27] activities in vitro and in vivo. In accordance with the previous reports, kaempferol was found to inhibit these CYP enzyme activities by more than 80% at a concentration of 50 $\mu$M in our in vitro assay (Table 4).

Recently, the number of adverse events caused by the interaction of dietary supplements with drugs has increased, and it has generally been reported that dietary supplements ingredients which possibly cause the interaction with drugs exhibit the $IC_{50}$ values almost less than 50 $\mu$M for CYP enzyme inhibition in vitro. This is the reason for the concentration of 50 $\mu$M used in the in vitro screening test. For example, black cohosh (*Actaea racemosa L.*) has been reported to inhibit CYP2D6 activity in a clinical trial,[28] and the ingredients of black cohosh, fukinolic acid ($IC_{50}$ value: 5.4 $\mu$M), cimicifugic acid A ($IC_{50}$ value: 9.0 $\mu$M), and cimicifugic acid B ($IC_{50}$ value: 12.6 $\mu$M) have been suggested to be responsible for this clinical event in vitro.[29,30] Goldenseal (*Hydrastis Canadensis L.*) exhibits inhibition of human CYP2D6 and CYP3A4 activities,[28,31,32] and these activities are affected by its ingredients of berberine ($IC_{50}$ value: 45 $\mu$M) and hydrastine isomer ($IC_{50}$ values: (+) isomer is 25 $\mu$M and (−) isomer is 30 $\mu$M), respectively, in vitro.[33] Piperine, a major ingredient of black pepper (*Piper nigrum L.*), inhibits human CYP2C9 and CYP1A2 activities in clinical trial,[34,35] and $IC_{50}$ values of piperine were 40.7 $\mu$M and 29.8 $\mu$M for CYP2C9 and CYP1A2, respectively, in vitro.[36] Thus, the $IC_{50}$ value of effective ingredients in a supplement which has been reported the interaction with drug in clinical are always below 50 $\mu$M for the inhibition of CYP enzyme activity. In our in vitro assay, artepillin C was found to reduce all 5 tested CYP enzyme activities, whereas its $IC_{50}$ values for CYP2D6 and CYP3A4 enzymes were greater than 200 $\mu$M, suggesting that the inhibitory activity of artepillin C against these CYPs is relatively weak.

To inhibit CYP enzyme activity in vivo, artepillin C, kaempferide, dihydrokaempferide, isosakuranetin, and/or kaempferol need to be absorbed after ingestion of EEP-B55, and the CYP enzymes in hepatocytes need to be exposed to them at the concentration of their $IC_{50}$ value or more. When EEP-B55 was orally administered at doses of 100 mg/kg and 250 mg/kg in rats, artepillin C was detected in peripheral blood as well as in portal blood. However, the other compounds (i.e., kaempferide, dihydrokaempferide, isosakuranetin, and kaempferol) were not detected in either the peripheral or portal blood even at a dose of 250 mg/kg. The dose of 250 mg/kg is estimated to be equivalent to 5-fold of the recommended daily intake, 500 mg/day, when converting animal doses to human equivalent doses based on their body surface area. This dose corresponds to a dose of 42.5 mg/kg for artepillin C. The bioavailability of artepillin C is known to be low, and the reason is thought to be clearance by the liver.[37] When a free-form compound in blood permeates the cell membrane in the liver by transcellular passive diffusion, its concentration is held in equilibrium between the blood and the hepatocytes. Because artepillin C is transported by transcellular passive diffusion,[38] the concentration of this compound in hepatocytes is thought to be equal to that in peripheral blood. Shimizu et al. have indicated that artepillin C is absorbed as a free-form through the intestinal tract and approximately 5% of them are incorporated into hepatocytes in vitro experiments using Caco-2 and HepG2 cells.[39] The concentration of artepillin C was 7142 ± 5044 nM in portal blood at 10 min after a single oral administration of EEP-B55 (250 mg/kg), and its exposure concentration on hepatocytes is roughly estimated at 400 nM. This predicted concentration is similar to the peripheral blood concentration (Cmax: 487 ± 307 nM). The $IC_{50}$ values of artepillin C for CYP1A2, CYP2C9, and CYP2C19 were approximately 33-, 70-, and 75-fold, respectively, higher than the Cmax value in peripheral blood. The blood concentrations of the other potent compounds, kaempferide, dihydrokaempferide, isosakuranetin, and kaempferol, were below their LLD concentration, and their minimum $IC_{50}$ values (Table 5) for the CYP enzymes tested were 1200-, 280-, 350-, and 5300-fold, respectively, higher than the concentration of their LLD. Thus, it is conceivable that the activities of liver CYP enzymes are not markedly affected by artepillin C at the recommended daily intake of EEP-B55.

An inhibitory effect of a given compound on CYP's enzymatic activity in vitro is not necessarily related to its influence on the pharmacokinetics of drugs in human. For example, silybin, an active constituent of milk thistle (*Silybum marianum L.*), has been found to be a potent mechanism-based inhibitor of CYP3A4 and CYP2C9 enzymes[40] but not to cause a clinically significant interaction with drugs because there are large differences between the blood silybin concentration after ingestion of silybin-containing supplements and its $IC_{50}$ values for CYP activities.[41,42] It has also been reported that kavalactones, active ingredients in kavakava (*Piper methysticum G.*), inhibit the activity of CYP1A2 and CYP3A4[43] but do not induce a clinically significant interaction with drugs for the same reason as described for silybin.[28] These findings seem to support our conclusion that EEP-B55 hardly affects interactions with drugs in the case of the recommended daily intake even though compounds such as artepillin C have inhibitory effects on CYP enzymes in vitro. However, it is necessary to consider species differences between rats and humans in the pharmacokinetics of drugs. Oral absorption is often more rapid, and the hepatic first-pass effect is also often greater in rodents than in humans. Thus, the blood concentrations of major EEP-B55 ingredients will be much higher in humans than in rats. In general, the extent of absorption is thought not to differ substantially because the diffusion of drugs through the small intestine epithelium is similar in most species.[44] It is therefore likely that the concentration of artepillin C found in rat portal blood corresponds to the human blood concentration of it after oral ingestion of EEP-B55. If so, the $IC_{50}$ value of artepillin C for CYP1A2, which was the lowest such value, was approximately 2.3-fold higher than the concentration in rat portal blood (16.1 $\mu$M vs 7.14 $\mu$M) after oral administration of EEP-B55 at a dose of 250 mg/kg, which is estimated to be equivalent to 5-fold the amount of the recommended daily intake. Poor bioavailability of flavonoids is well-known in human[45] and also in rat.[46] The present study also showed extremely low blood concentrations (blow LLD) of the inhibitory flavonoids, kaempferide, dihydrokaempferide, iso-

sakuranetin, and kaempferol, after oral administration of EEP-B55.

This is the first report on an investigation of the interaction of propolis extract with drugs, and the present results indicate that ethanol extract of Brazilian green propolis is unlikely to attenuate the hepatic metabolism of drugs under dosing condition comparable to daily intake. This expectation can be supported by the fact that no undesirable interactions between propolis extracts and drugs have been reported. Meanwhile, further investigations on whether administration of EEP-B55 alter expression of CYP enzymes would give us valuable information regarding the interactions of EEP-B55 with drugs because induction of drug metabolizing enzyme reduces the efficacy of drugs.

## AUTHOR INFORMATION

### Corresponding Author

*E-mail: ichihara-kenji@api3838.co.jp. Fax: +81-58-294-8388.

### Notes

The authors declare no competing financial interest.

## ACKNOWLEDGMENTS

We thank Mr. Kenji Kato, a staff member of our laboratory, for extraction and purification of artepillin C, dihydrokaempferide, betuletol, and kaempferide.

## ABBREVIATIONS USED

CYP, cytochrome P450; $K_i$, inhibition constant; EEP-B55, ethanol extract of Brazilian green propolis; LC, liquid chromatography; $IC_{50}$, fifty percent inhibitory concentration; TFA, trifluoroacetic acid; Cmax, maximum serum concentration; AUC, area under the curve; LLD, lower limit of detection

## REFERENCES

(1) Schmidt, L. E.; Dalhoff, K. Food-drug interactions. *Drugs* **2002**, *62*, 1481−1502.

(2) Bailey, D. G.; Malcolm, J.; Arnold, O.; Spence, J. D. Grapefruit juice-drug interactions. *Br. J. Clin. Pharmacol.* **1998**, *46*, 101−110.

(3) Hamann, G. L.; Campbell, J. D.; George, C. M. Warfarin-cranberry juice interaction. *Ann. Pharmacother.* **2011**, *45*, e17.

(4) Wang, Z.; Gorski, J. C.; Hamman, M. A.; Huang, S. M.; Lesko, L. J.; Hall, S. D. The effects of St John's wort (Hypericum perforatum) on human cytochrome P450 activity. *Clin. Pharmacol. Ther.* **2001**, *70*, 317−326.

(5) Hall, S. D.; Wang, Z.; Huang, S. M.; Hamman, M. A.; Vasavada, N.; Adigun, A. Q.; Hilligoss, J. K.; Miller, M.; Gorski, J. C. The interaction between St John's wort and an oral contraceptive. *Clin. Pharmacol. Ther.* **2003**, *74*, 525−535.

(6) EFSA Panel on Dietetic Products, Nutrition and Allergies (NDA). Statement on the safety of glucosamine for patients receiving coumarin anticoagulants. *EFSA J.* **2011**, *9*, 2473−2480.

(7) Kumazawa, S.; Shimoi, K.; Hayashi, K.; Ishii, T.; Hamasaka, T.; Nakayama, T. Identification of metabolites in plasma and urine of Uruguayan propolis-treated rats. *J. Agric. Food Chem.* **2004**, *52*, 3083−3088.

(8) Ahn, M. R.; Kunimasa, K.; Kumazawa, S.; Nakayama, T.; Kaji, K.; Uto, Y.; Hori, H.; Nagasawa, H.; Ohta, T. Correlation between antiangiogenic activity and antioxidant activity of various components from propolis. *Mol. Nutr Food Res.* **2009**, *53*, 643−651.

(9) Kartal, M.; Yildiz, S.; Kaya, S.; Kurucu, S.; Topçu, G. Antimicrobial activity of propolis samples from two different regions of Anatolia. *J. Ethnopharmacol.* **2003**, *86*, 69−73.

(10) Amoros, M.; Lurton, E.; Boustie, J.; Girre, L.; Sauvager, F.; Cormier, M. Comparison of the anti-herpes simplex virus activities of propolis and 3-methyl-but-2-enyl caffeate. *J. Nat. Prod.* **1994**, *57*, 644−647.

(11) Paulino, N.; Teixeira, C.; Martins, R.; Scremin, A.; Dirsch, V. M.; Vollmar, A. M.; Abreu, S. R.; de Castro, S. L.; Marcucci, M. C. Evaluation of the analgesic and anti-inflammatory effects of a Brazilian green propolis. *Planta Med.* **2006**, *72*, 899−906.

(12) Ozkul, Y.; Silici, S.; Eroğlu, E. The anticarcinogenic effect of propolis in human lymphocytes culture. *Phytomedicine* **2005**, *12*, 742−747.

(13) El-khawaga, O. A.; Salem, T. A.; Elshal, M. F. Protective role of Egyptian propolis against tumor in mice. *Clin. Chim. Acta* **2003**, *338*, 11−16.

(14) Ghisalberti, E. L. Propolis: A review. *Bee World* **1979**, *60*, 59−84.

(15) Hata, T.; Tazawa, S.; Ohta, S.; Rhyu, M. R.; Misaka, T.; Ichihara, K. Artepillin C, a major ingredient of Brazilian propolis, induces a pungent taste by activating TRPA1 channels. *PLoS One* **2012**, *7*, e48072.

(16) Righi, A. A.; Negri, G.; Salatino, A. Comparative chemistry of propolis from eight brazilian localities. *J. Evidence-Based Complementary Altern. Med.* **2013**, *2013*, 267878.

(17) U.S. Department of Health and Human Services Food and Drug Administration. Guidance for Industry: Drug Interaction Studies-Study Design, Data Analysis, and Implications for Dosing and Labeling. 2006.

(18) Hirata-Koizumi, M.; Saito, M.; Urano, T.; Miyake, S.; Hasegawa, R. Improvement of package insert CYP information for prescription drugs marketed in Japan. *Bull. Natl. Inst. Health Sci. (in Japanese)* **2005**, *123*, 12−18.

(19) Wrighton, S. A.; Stevens, J. C. The human hepatic cytochromes P450 involved in drug metabolism. *Crit Rev. Toxicol.* **1992**, *22*, 1−21.

(20) Mugford, C. A.; Kedderis, G. L. Sex-dependent metabolism of xenobiotics. *Drug Metab Rev.* **1998**, *30*, 441−498.

(21) Chang, T. K.; Chen, J.; Yeung, E. Y. Effect of Ginkgo biloba extract on procarcinogen-bioactivating human CYP1 enzymes: identification of isorhamnetin, kaempferol, and quercetin as potent inhibitors of CYP1B1. *Toxicol. Appl. Pharmacol.* **2006**, *213*, 18−26.

(22) von Moltke, L. L.; Weemhoff, J. L.; Bedir, E.; Khan, I. A.; Harmatz, J. S.; Goldman, P.; Greenblatt, D. J. Inhibition of human cytochromes P450 by components of Ginkgo biloba. *J. Pharm. Pharmacol.* **2004**, *56*, 1039−1044.

(23) Si, D.; Wang, Y.; Zhou, Y. H.; Guo, Y.; Wang, J.; Zhou, H.; Li, Z. S.; Fawcett, J. P. Mechanism of CYP2C9 inhibition by flavones and flavonols. *Drug Metab. Dispos.* **2009**, *37*, 629−634.

(24) Kimura, Y.; Ito, H.; Ohnishi, R.; Hatano, T. Inhibitory effects of polyphenols on human cytochrome P450 3A4 and 2C9 activity. *Food Chem. Toxicol.* **2010**, *48*, 429−435.

(25) Pal, D.; Mitra, A. K. MDR- and CYP3A4-mediated drug-herbal interactions. *Life Sci.* **2006**, *78*, 2131−2145.

(26) Ha, H. R.; Chen, J.; Leuenberger, P. M.; Freiburghaus, A. U.; Follath, F. In vitro inhibition of midazolam and quinidine metabolism by flavonoids. *Eur. J. Clin Pharmacol.* **1995**, *48*, 367−371.

(27) Li, C.; Li, X.; Choi, J. S. Enhanced bioavailability of etoposide after oral or intravenous administration of etoposide with kaempferol in rats. *Arch Pharm. Res.* **2009**, *32*, 133−138.

(28) Gurley, B. J.; Gardner, S. F.; Hubbard, M. A.; Williams, D. K.; Gentry, W. B.; Khan, I. A.; Shah, A. In vivo effects of goldenseal, kava kava, black cohosh, and valerian on human cytochrome P450 1A2, 2D6, 2E1, and 3A4/5 phenotypes. *Clin Pharmacol Ther.* **2005**, *77*, 415−426.

(29) Huang, Y.; Jiang, B.; Nuntanakorn, P.; Kennelly, E. J.; Shord, S.; Lawal, T. O.; Mahady, G. B. Fukinolic acid derivatives and triterpene glycosides from black cohosh inhibit CYP isozymes, but are not cytotoxic to Hep-G2 cells in vitro. *Curr. Drug Saf.* **2010**, *5*, 118−124.

(30) Gurley, B. J.; Fifer, E. K.; Gardner, Z. Pharmacokinetic herb-drug interactions (part 2): drug interactions involving popular botanical dietary supplements and their clinical relevance. *Planta Med.* **2012**, *78*, 1490−1514.

(31) Gurley, B. J.; Swain, A.; Hubbard, M. A.; Williams, D. K.; Barone, G.; Hartsfield, F.; Tong, Y.; Carrier, D. J.; Cheboyina, S.; Battu, S. K. Clinical assessment of CYP2D6-mediated herb-drug interactions in humans: effects of milk thistle, black cohosh, goldenseal, kava kava, St. John's wort, and Echinacea. *Mol. Nutr. Food Res.* **2008**, *52*, 755−763.
(32) Gurley, B. J.; Swain, A.; Hubbard, M. A.; Hartsfield, F.; Thaden, J.; Williams, D. K.; Gentry, W. B.; Tong, Y. Supplementation with goldenseal (Hydrastis canadensis), but not kava kava (Piper methysticum), inhibits human CYP3A activity in vivo. *Clin. Pharmacol. Ther.* **2008**, *83*, 61−69.
(33) Chatterjee, P.; Franklin, M. R. Human cytochrome p450 inhibition and metabolic-intermediate complex formation by goldenseal extract and its methylenedioxyphenyl components. *Drug Metab. Dispos.* **2003**, *31*, 1391−1397.
(34) Velpandian, T.; Jasuja, R.; Bhardwaj, R. K.; Jaiswal, J.; Gupta, S. K. Piperine in food: interference in the pharmacokinetics of phenytoin. *Eur. J. Drug Metab Pharmacokinet.* **2001**, *26*, 241−247.
(35) Bano, G.; Raina, R. K.; Zutshi, U.; Bedi, K. L.; Johri, R. K.; Sharma, S. C. Effect of piperine on bioavailability and pharmacokinetics of propranolol and theophylline in healthy volunteers. *Eur. J. Clin Pharmacol.* **1991**, *41*, 615−617.
(36) Volak, L. P.; Ghirmai, S.; Cashman, J. R.; Court, M. H. Curcuminoids inhibit multiple human cytochromes P450, UDP-glucuronosyltransferase, and sulfotransferase enzymes, whereas piperine is a relatively selective CYP3A4 inhibitor. *Drug Metab. Dispos.* **2008**, *36*, 1594−1605.
(37) Konishi, Y.; Hitomi, Y.; Yoshida, M.; Yoshioka, E. Absorption and bioavailability of artepillin C in rats after oral administration. *J. Agric. Food Chem.* **2005**, *53*, 9928−9933.
(38) Konishi, Y. Transepithelial transport of artepillin C in intestinal Caco-2 cell monolayers. *Biochim. Biophys. Acta* **2005**, *1713*, 138−144.
(39) Shimizu, K.; Ashida, H.; Matsuura, Y.; Kanazawa, K. Antioxidative bioavailability of artepillin C in Brazilian propolis. *Arch. Biochem. Biophys.* **2004**, *424*, 181−188.
(40) Sridar, C.; Goosen, T. C.; Kent, U. M.; Williams, J. A.; Hollenberg, P. F. Silybin inactivates cytochromes P450 3A4 and 2C9 and inhibits major hepatic glucuronosyltransferases. *Drug Metab. Dispos.* **2004**, *32*, 587−594.
(41) Zuber, R.; Modrianský, M.; Dvorák, Z.; Rohovský, P.; Ulrichová, J.; Simánek, V.; Anzenbacher, P. Effect of silybin and its congeners on human liver microsomal cytochrome P450 activities. *Phytother. Res.* **2002**, *16*, 632−638.
(42) Doehmer, J.; Tewes, B.; Klein, K. U.; Gritzko, K.; Muschick, H.; Mengs, U. Assessment of drug-drug interaction for silymarin. *Toxicol In Vitro.* **2008**, *22*, 610−617.
(43) Zou, L.; Henderson, G. L.; Harkey, M. R.; Sakai, Y.; Li, A. Effects of kava (Kava-kava, 'Awa, Yaqona, Piper methysticum) on c-DNA-expressed cytochrome P450 enzymes and human cryopreserved hepatocytes. *Phytomedicine* **2004**, *11*, 285−294.
(44) Nau, H. Species differences in pharmacokinetics and drug teratogenesis. *Environ. Health Perspect.* **1986**, *70*, 113−129.
(45) Thilakarathna, S. H.; Rupasinghe, H. P. Flavonoid bioavailability and attempts for bioavailability enhancement. *Nutrients* **2013**, *5*, 3367−3387.
(46) Gao, S.; Hu, M. Bioavailability challenges associated with development of anti-cancer phenolics. *Mini Rev. Med. Chem.* **2010**, *10*, 550−567.

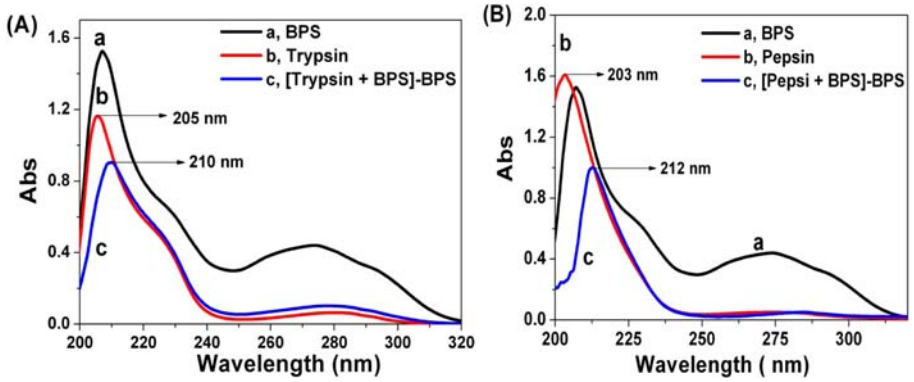


**Figure 1.** (A) Absorption spectra of trypsin, BPS, and trypsin−BPS. (B) Absorption spectra of pepsin, BPS, and pepsin−BPS. The concentrations of trypsin and pepsin were $2.0 \times 10^{-5}$ mol·L$^{-1}$; the concentrations of BPS were $4.0 \times 10^{-5}$ mol·L$^{-1}$.

BPS enters the human digestive system such as stomach and duodenum, digestive proteases may be the indirect binding targets. Both pepsin and trypsin are principal protein-degrading or proteolytic enzymes in the digestive system. The former is released by the chief cells in the stomach, while the latter is produced in the pancreas as the inactive proenzyme trypsinogen in the duodenum. During the process of digestion, each of these two enzymes is specialized in cleaving links between particular types of amino acids, leading to the breakdown of dietary proteins into their components.[15,16] Due to the importance of pepsin and trypsin in the digestive system of human, they are often selected as binding model proteins to investigate the effects on their activities and conformational structures of small molecules that are found in food and medicinal herbs.[17−26] However, little is known about the binding interactions of BPS with pepsin and trypsin and the effects of BPS on their activities.

Herein, pepsin and trypsin were selected as the investigated digestion enzyme models to study the binding interactions of BPS. The effects of BPS on the activities and conformations of pepsin and trypsin were investigated by means of multispectroscopic techniques and molecular modeling method in order to cast some light on the future study of the toxicity of BPS.

## MATERIALS AND METHODS

**Materials.** Trypsin (from porcine pancreas), pepsin (from porcine stomach mucosa), bovine hemoglobin (from bovine erythrocyte), and *N*-benzoyl-D,L-arginine-*p*-nitroanilide (BApNA) were purchased from Sigma-Aldrich Company (St. Louis, MO) and were used without further purification. Analytical standard of BPS (≥98%) was obtained from Aladdin Industrial Corporation (Kaplan Ave, City of Industry, CA). The other reagents were all of analytical purity. Pepsin solution was prepared in pH 2.00 citric acid buffer (0.025 M, 0.1 M NaCl). Trypsin solution was prepared in a phosphate buffer (0.01 M) of pH 7.40. The 0.5 wt % solution of bovine hemoglobin was prepared in pH 2.00 citric acid buffer. Muriatic acid (reagent grade, 37%) was used to adjust the pH of buffer solution. The 10% of trichloroacetic acid was prepared in water. BApNA (3.0 mM) was dissolved in DMSO and was stored at 0−4 °C. Water was purified with a Milli-Q purification system (Barnstead, Dubuque, IA, USA).

**UV−Vis Spectroscopy.** A SPECORD S600 (Germany, Jena) equipped with 1.0 cm quartz cells was used to record the UV−vis spectra of trypsin or pepsin in the absence and presence of BPS. During the assay of enzyme activity, BApNA and bovine hemoglobin were used as substrates for trypsin and pepsin, respectively.[27,28] Each experiment was repeated three times in order to take the mean. The activity of trypsin was determined by BApNA degradation into *p*-nitroaniline, which is detected by spectrophotometer based on the increase in absorbance at 410 nm in a phosphate buffer (pH 7.40, 0.01 M$^{-1}$) in the absence and presence of trypsin ($5.0 \times 10^{-6}$ mol·L$^{-1}$). In addition, the Anson method was used to detect pepsin activity.[28] First, 1 mL of pepsin (30.0 $\mu$M) and different volumes of BPS were mixed in a 10 mL centrifuge tube, and then different volumes of citric acid buffer were dropped into the above solution and made up to a constant volume of 3 mL. Second, the pepsin−BPS systems were set at 37 °C for 20 min, and then 2 mL of bovine hemoglobin (0.5 wt %) solution was added to the above solution. Third, 2 mL of 10% trichloroacetic acid was used to terminate the above reactions after 20 min. The supernatant was obtained by centrifuging at 12,000 rpm for 20 min twice and was measured via OD 275 nm. The original activity of pepsin is 3000 NFU/mg, and the activity of pepsin in the presence of BPS was obtained by eq 1:

$$\text{activity}/_{(\text{NFU/mg})} = 3000 \times \frac{\text{OD275(pepsin−BPS)}}{\text{OD275(original pepsin)}} \quad (1)$$

**Fluorescence Spectroscopy.** An LS-50B spectrofluorimeter (Waltham, MA, USA) equipped with 1.0 cm quartz cells and a thermostat bath was used to record the steady-state fluorescence and synchronous fluorescence spectra of trypsin ($2 \times 10^{-5}$ mol·L$^{-1}$) and pepsin ($2 \times 10^{-5}$ mol·L$^{-1}$) in the absence and presence of BPS (from 0 to $5.0 \times 10^{-5}$ mol·L$^{-1}$). As for steady-state fluorescence spectral experiments, the excitation wavelength was selected as 280 nm and the scan range of emission wavelengths was from 300 to 500 nm. The scan speed and the slit widths of emission and excitation were set at 500 nm/min, 5.0 nm, and 5.0 nm, respectively. In addition, the wavelength intervals $\Delta\lambda$ ($\lambda_{em} - \lambda_{ex}$) were set at 15 and 60 nm to obtain the synchronous fluorescence spectra of trypsin and pepsin in the same experimental conditions as the steady-state fluorescence emission spectra.

**Circular Dichroism Spectroscopy.** A Chirascan spectrometer (Applied Photophyysics Ltd., Leatherhead, Surrey, U.K.) equipped with a temperature control quantum were used to measure the circular dichroism (CD) spectra of trypsin ($2.5 \times 10^{-5}$ mol·L$^{-1}$) and pepsin ($2.5 \times 10^{-5}$ mol·L$^{-1}$) in the absence and presence of BPS. The CD spectra were recorded from 190 to 260 nm with a scan speed of 20 nm/min and a bandwidth of 1 nm using 0.1 cm quartz cells.

**Molecular Modeling.** The molecular docking program Autodock 4.2.3 and Autodock tools v 1.5.4 were used to study the binding models of trypsin and pepsin with BPS at the molecular level.[29] The geometry of BPS was optimized using density functional theory (DFT) at the level of B3LYP/6-311G by the program Gaussian 09.[30] The molecular structures of trypsin (PDB ID 2ZQ1) and pepsin (PDB ID 5PEP) were obtained from RCSB Protein Data Bank, http://www.rcsb.org/pdb.[31,32] During molecular calculation studies, all water molecules and ligands were removed from the molecular structures of trypsin and pepsin, and essential hydrogen atoms, Kollman united atom type charges, and salvation parameters were also added in the protein model.[19,33] The Gasteiger partial charges were added to atoms

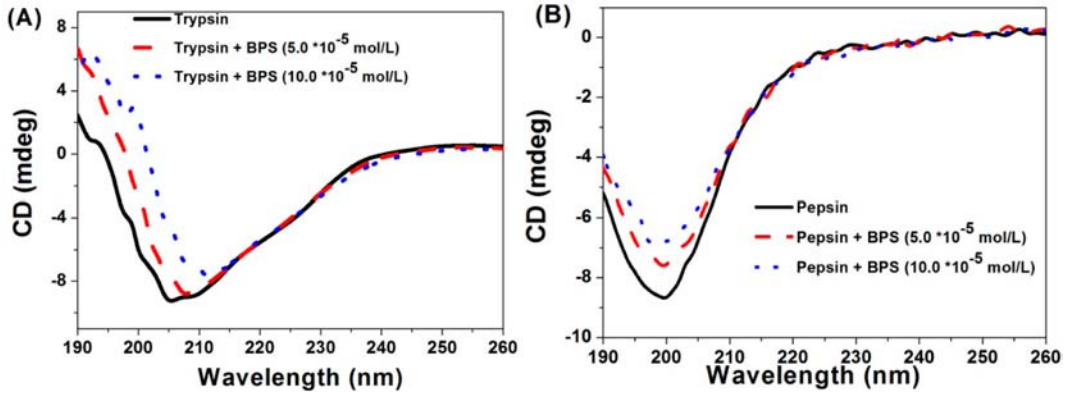


**Figure 2.** Far-UV CD spectra of trypsin (A) and pepsin (B) ($2.5 \times 10^{-5}$ mol·L$^{-1}$) in the absence and presence of BPS.

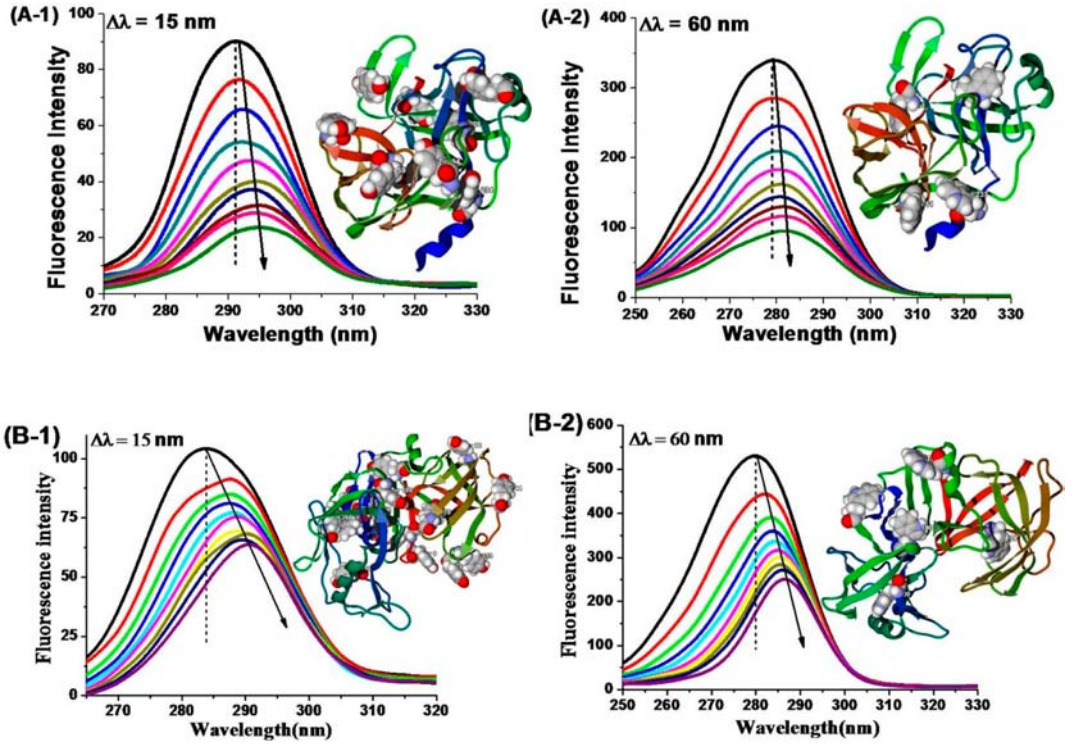


**Figure 3.** Effects of BPS on the synchronous fluorescence spectra of trypsin (A) and pepsin (B), $c$ (trypsin) = $c$ (pepsin) = $2.0 \times 10^{-5}$ mol·L$^{-1}$. $c$ (BPS) ($\times 10^{-5}$ mol·L$^{-1}$) (from top to bottom), 0, 0.5, 1.0, 1.5, 2.0, 2.5, 3.0, 3.5, 4.0, and 5.0, respectively. The insets show the positions of Trp residues and Tyr residues in the three-dimensional structures of trypsin and pepsin.

of BPS, and rotatable bonds were defined. In addition, the grid box sizes of BPS−trypsin/pepsin systems were 126 Å × 126 Å × 126 Å, with grid spacing of 0.375 Å, while the GA population size was set at 150, the maximum number of energy evaluation was set at 2500000, the number of GA runs was set at 100, and others used were default parameters. When the docking calculation finished, Molegro Molecular Viewer software (Molegro—A CLC bio company, Aarhus, Denmark) was used to analyze the predicted binding mode with the lowest binding free energy and the hydrogen bond interactions of BPS with trypsin and pepsin.[34]

## RESULTS AND DISCUSSION

**Effect of BPS on the Secondary Structure of Trypsin and Pepsin.** Absorption spectroscopy is a simple and excellent technique for determining the conformational transitions in proteins, which are presented by the changes of wavelength of absorption and the strength of their absorbance.[35] The UV−vis absorption spectra of trypsin and pepsin in the absence and presence of BPS are shown in Figure 1A,B. Both trypsin and pepsin show two main absorption bands. The strong one is from 200 to 230 nm and reflects the secondary structures of trypsin and pepsin.[36] The weak one between 260 and 290 nm is caused by the absorbance of the main two aromatic amino acids tryptophan (Trp) and tyrosine (Tyr) and indicates the transformation of the microenvironment of their chromophores.[37] It can be seen from Figure 1A,B that the absorbance intensities of the former peak decrease with a red shift in the presence of BPS. This peak that comes from the n−$\pi^*$ transitions reflects the conformations of protein backbone.[36] Upon BPS binding, the peak was red-shifted by 5 and 9 nm for trypsin and pepsin, respectively. These changes are related to the alterations in the secondary structures of trypsin and pepsin.[36,38] In addition, the absorption spectra of the aromatic amino acids in trypsin and pepsin also change. The absorbance intensity at about 278 nm of trypsin increases in the presence of

BPS, indicating that the unfolding of trypsin induced by BPS results in exposing aromatic amino acids to the aqueous solvent. For pepsin, the maximum of the absorption of aromatic amino acids is shifted to long wavelength. Therefore, the binding interactions of BPS with trypsin and pepsin not only induce the secondary structure changes of these two enzymes but also partly affect the tertiary structure of enzymes.

The far-UV CD spectra from 190 to 260 nm coming from electronic transitions between molecular orbitals in ground and excited states of proteins provide another well-studied method for determining the secondary structure of proteins.[39] Herein, the influences of BPS on the CD spectra of trypsin and pepsin are shown in Figure 2A,B. It is observed that a strong negative band at about 200 nm coming from the n−$\pi^*$ transitions is changed obviously. First, the intensities of CD spectra of trypsin and pepsin display obvious decreases in the presence of BPS, indicating the significant variations of the secondary structural components of enzymes. In addition, the red shift of maximum peak also implies that the interactions of BPS with trypsin and pepsin induce a change of the proteins' secondary structure and loosen the skeleton of trypsin and pepsin.[40] These results are consistent with the above conclusion of UV−vis measurement.

**Effect of BPS on the Tertiary Structure of Trypsin and Pepsin.** There are multiple Trp residues and Tyr residues in trypsin and pepsin. The intrinsic fluorescence of these two kinds of aromatic amino acid residues was used to evaluate the changes in the tertiary structure of trypsin and pepsin caused by BPS.[41] As shown in the insets of Figure 3A-1,A-2, there are ten Tyr residues (Tyr-20, 29, 39, 59, 94, 151, 172, 184, 228, 234) and four Trp residues (Trp-51, 141, 215, 237) in trypsin.[42] In addition, it can be seen from the insets of Figure 3B-1,B-2 that pepsin contains 13 Tyr residues (Tyr-9, 14, 44, 75, 86, 113, 114, 175, 189, 268, 275, 310, 311) and five Trp residues (Trp-39, 141, 181, 190, 300).[43] Herein, the synchronous fluorescence spectroscopy was used to evaluate the effects of BPS on the microenvironment of Trp and Tyr residues of trypsin and pepsin. When $\Delta\lambda$ is fixed at 15 and 60 nm, the synchronous fluorescence can give spectral information on Tyr residues and Trp residues, respectively.[44] Figure 3A,B shows the effects of BPS on the synchronous fluorescence spectra of trypsin and pepsin. As shown in Figure 3, the addition of BPS in enzyme solution resulted in strong fluorescence quenching of Trp residues and Tyr residues in trypsin and pepsin. The polarity of their microenvironment can be presented by the $\lambda_{max}$ of Tyr and Trp residues.[45] Figure 3A-1,A-2 shows, upon the gradual addition of BPS to trypsin, red shifts around 4 and 2 nm of the maximum emission wavelength of Tyr and Trp residues, indicating that the conformation of trypsin changed, BPS binding resulted in a more polar environment for Tyr residues and Trp residues, and the fluorophores of enzymes have easy contact with solvent molecules. The vicinities of Trp residues and Tyr residues are rearranged. In addition, the results of Figure 3B-1,B-2 show that the interactions of BPS with pepsin induce more obvious changes of the environment of Trp residues and Tyr residues than those of trypsin, since the maximum emission wavelength of Tyr and Trp residues in pepsin shifted 7 and 8 nm, respectively. In a word, the tertiary structure of pepsin is more easily changed by BPS binding than that of trypsin.

**Effects of BPS on the Activities of Trypsin and Pepsin.** According to the UV−vis, CD, and fluorescence spectral results, it was found that BPS not only affected the secondary structure of these two enzymes but also partly affected their tertiary structure. Therefore, it is necessary to study the effects of BPS on the enzymatic activities of trypsin and pepsin. The activity of trypsin or pepsin in the presence of BPS was obtained by setting the relative activity of trypsin or pepsin as 100% in the absence of BPS. As shown in Figure 4, the activity

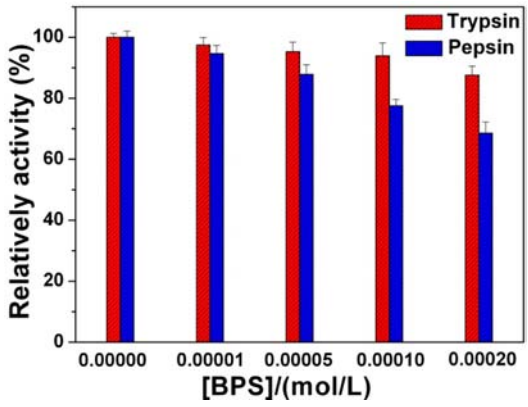


**Figure 4.** Trypsin and pepsin activities in the absence and presence of BPS at different concentrations, $c$ (trypsin) = $c$ (pepsin) = $1.0 \times 10^{-5}$ mol·L$^{-1}$.

of pepsin decreases obviously with the increasing concentration of BPS, while the activity of trypsin does not change remarkably. The interaction probably occurs near the active site of pepsin. Therefore, these results indicated that when BPS enters human stomach and duodenum, it can probably inhibit pepsin activity, but not trypsin activity. Using these activity experiments, it is difficult to obtain information about the binding sites of BPS in pepsin or trypsin. The binding nature of BPS with these two enzymes should be further investigated.

**The Putative Binding Sites of BPS in Trypsin and Pepsin.** Herein, molecular docking-based calculation was used to find the preferable binding sites of BPS in trypsin and pepsin. If BPS enters the active pocket of trypsin or pepsin and locates near the key amino acids, it may affect the enzyme activity. In trypsin, His-57, Asp-102, and Ser-195 are mainly catalytic residues.[45] In addition, Asp-189, Ser-190, and Gly-219 can play important roles in the trypsin activity.[46] As for pepsin, Asp-32 and Asp-215 are the main two catalytic residues.[47] The predicted binding models of BPS with trypsin and pepsin with the lowest docking energy are shown in Figure 5A,B. It was indicated that there were many amino acid residues taking part in the binding interactions of enzymes with BPS. As for trypsin, Asn-97, 100, Gln-175, Gly-174, 216, 219, Ile-176, Leu-99, Met-180, Ser-214, Thr-98, 177, Trp-215, and Val-227 form the binding pocket of BPS; while in pepsin, Asp-32, 215, Asn-37, Ala-130, Gly-34, 76, 217, Ile-73, 128, Ser-35, 36, 129, Thr-74, 218, and Tyr-75, 189 take part in binding with BPS. It can be seen in Figure 5A that there are no directly binding interactions between BPS and catalytic residues (His-57, Asp-102, and Ser-195) of trypsin. On the contrary, for pepsin it can be seen from Figure 5B that hydrogen bonding interactions exist between the two catalytic residues (Asp-32 and Asp-215) of pepsin and BPS. Therefore, it is deduced that BPS binds into the primary substrate-binding pocket and occupyies the active site of pepsin, leading to the enzyme inhibition. These calculation results well explained the in vitro data that BPS binding affected the activity of pepsin and did not obviously affect that of trypsin. Besides the conformation changes induced by BPS

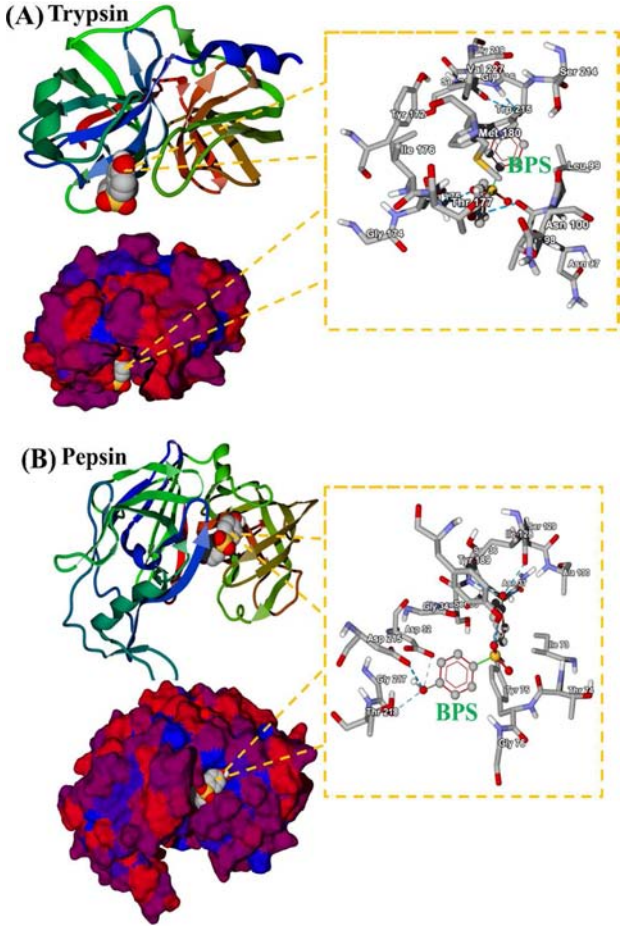


**Figure 5.** Predicted orientations of the lowest docking energy conformations of BPS with trypsin (A) and pepsin (B).

binding, the direct interactions between BPS and catalytic amino acid residues were another main reason resulting in the decrease of enzyme activity.

**Binding Nature of BPS with Trypsin and Pepsin.** Seen from the molecular docking-based calculations, the interactions of BPS with trypsin and pepsin are not presumed to be only one kind of force. First, many hydrogen bonding interactions exist in their binding processes. There are four hydrogen bonds (Gln-175, −S═O, 2.802 Å; Ile-176, −OH, 2.739 Å; Gly-216, −OH, 2.675 Å, 3.024 Å) in the binding interaction of BPS with trypsin. In addition, seven hydrogen bonds (Asp-215, −OH, 3.067 Å; Asp-32, −OH, 3.446 Å; Gly-217, −OH, 2.954 Å; Asn-37, −OH, 2.908 Å; Ile-128, −OH, 3.249 Å; Ser-36, −OH, 3.510 Å; Tyr-189, −S═O, 2.665 Å) exist between BPS and pepsin. Therefore, hydrogen bonding interactions play a key role in stabilizing BPS−trypsin/pepsin complexes. Second, many polar and nonpolar amino acid residues take part in the binding of trypsin and pepsin with BPS, so other binding forces including hydrophobic and electrostatic forces should not be excluded.

In order to provide convincing evidence for the binding energies of BPS with trypsin and pepsin, the best binding site with minimum binding energy is selected from the minimum energy conformers from 100 runs. The results given are in the form of the estimated free energy of binding, $E_{\text{intermol}}$ (the final intermolecular energy), $E_{\text{VHD}}$ (VDW + Hbond + desolvo energy), $E_{\text{elec}}$ (the electrostatic energy), $E_{\text{total}}$ (the final total internal energy), and $E_{\text{torsional}}$ (the torsional free energy). The docking summaries of BPS−trypsin and BPS−pepsin are listed in Tables 1 and 2, respectively. As data show, the negative values of the estimated free energy of binding indicate the spontaneity of the binding of trypsin and pepsin with BPS. In addition, $E_{\text{VHD}}$ energy including van der Waals energy ($E_{\text{VDW}}$), $E_{\text{Hbond}}$, and $E_{\text{desolvo}}$ are the main part of binding free energy, which imply that hydrogen bonds along with hydrophobic interactions play a crucial role in complexation processes of BPS with trypsin and pepsin. Although $E_{\text{elec}}$ force is also involved in the binding interactions of BPS with trypsin and pepsin, it is not the mainly driving force.

Apart from the molecular modeling, the fluorescence quenching method was also used to obtain the binding parameters including fluorescence quenching mechanism, binding constants, binding sites, and thermodynamic parameters ($\Delta H^\circ$, $\Delta G^\circ$, $\Delta S^\circ$). The fluorescence emission spectra of trypsin and pepsin in the absence and presence of BPS are shown in Figure 6A,B.

When excited at 280 nm, trypsin and pepsin produced their fluorescence spectra in the wavelength range of 300−500 nm with the emission maxima at 337 and 345 nm, respectively, which come from Trp and Tyr residues. At the same concentration, the fluorescence emission intensity of pepsin was stronger than that of trypsin. The main reason is that the number of Trp and Tyr residues in pepsin is more than that of trypsin. In addition, the difference in the emission maximum of trypsin and pepsin implies that the microenvironment of Trp and Tyr residues in trypsin is more hydrophobic than for those residues in pepsin, which probably affects their ability in binding with BPS. As the data show, additions of BPS result in fluorescence quenching of the intrinsic fluorescence of trypsin and pepsin. The fluorescence quenching intensity of trypsin induced by BPS was stronger than that of pepsin. In addition, the fluorescence quenching data were analyzed by the Stern−Volmer eq 2:[48]

$$\frac{F_0}{F_{\text{cor}}} = 1 + K_{\text{sv}}[Q] \tag{2}$$

where $F_0$ and $F_{\text{cor}}$ are the corrected fluorescence intensities of trypsin and pepsin in the absence and presence of BPS, respectively.[49] $K_{\text{sv}}$ is the Stern−Volmer dynamic quenching constant, and $[Q]$ is the concentration of BPS. Figure 7A,B displayed the Stern−Volmer plots for the fluorescence quenching of teypsin and pepsin by BPS at 298 and 310 K. The nature of the fluorescence quenching process can be determined by evaluating its dependence on temperature. Dynamic quenching is increased with an increase of system temperature; on the contrary, static quenching decreases at higher temperature.[50] Thus, it can be seen from Figure 7A,B that the rise in temperature did decrease the $K_{\text{sv}}$ values, indicating that the fluorescence quenching of trypsin and pepsin induced by BPS was not initiated from dynamic collision but from the complex formation between BPS and trypsin or pepsin. In addition, the UV−vis spectral changes of trypsin and pepsin induced by BPS binding also confirmed that the fluorescence quenching of trypsin and pepsin by BPS was static quenching because the UV−vis spectra of trypsin and pepsin would have no detectable changes if the quenching was a dynamic mechanism.[51]

Results from fluorescence quenching data can also be used to estimate the binding constants ($K_{\text{A}}$) and binding sites ($n$) of the BPS−trypsin/pepsin system by eq 3.[52,54]

**Table 1. Docking Results of BPS with Trypsin**

| rank | run | estimated free energy of binding (kcal/mol) | $E_{intermol}$ (kcal/mol) | $E_{VHD}$ (kcal/mol) | $E_{elec}$ (kcal/mol) | $E_{total}$ (kcal/mol) | $E_{torsional}$ (kcal/mol) | no. in cluster |
|---|---|---|---|---|---|---|---|---|
| 1 | 7 | −5.05 | −6.24 | −6.00 | −0.25 | −0.23 | +1.19 | 24 |
| 2 | 56 | −4.66 | −5.85 | −5.62 | −0.23 | −0.20 | +1.19 | 11 |
| 3 | 5 | −4.64 | −5.83 | −5.73 | −0.10 | −0.25 | +1.19 | 11 |
| 4 | 76 | −4.38 | −5.57 | −5.53 | −0.04 | −0.21 | +1.19 | 3 |
| 5 | 86 | −4.34 | −5.53 | −5.31 | −0.22 | −0.28 | +1.19 | 4 |
| 6 | 35 | −4.31 | −5.50 | −5.21 | −0.30 | −0.21 | +1.19 | 4 |
| 7 | 27 | −4.31 | −5.50 | −5.19 | −0.32 | −0.08 | +1.19 | 2 |
| 8 | 97 | −4.25 | −5.44 | −5.16 | −0.28 | −0.22 | +1.19 | 2 |
| 9 | 44 | −4.17 | −5.36 | −5.15 | −0.21 | −0.23 | +1.19 | 1 |
| 10 | 92 | −4.13 | −5.32 | −5.08 | −0.24 | −0.28 | +1.19 | 3 |
| 11 | 19 | −4.12 | −5.32 | −5.12 | −0.19 | −0.22 | +1.19 | 2 |
| 12 | 72 | −4.12 | −5.32 | −4.81 | −0.50 | −0.28 | +1.19 | 4 |
| 13 | 85 | −4.12 | −5.32 | −4.95 | −0.36 | −0.28 | +1.19 | 3 |
| 14 | 74 | −4.07 | −5.26 | −5.07 | −0.19 | −0.28 | +1.19 | 2 |
| 15 | 1 | −3.99 | −5.19 | −5.05 | −0.13 | −0.17 | +1.19 | 1 |
| 16 | 66 | −3.94 | −5.13 | −4.93 | −0.20 | −0.31 | +1.19 | 6 |
| 17 | 21 | −3.93 | −5.13 | −5.04 | −0.09 | −0.30 | +1.19 | 3 |
| 18 | 77 | −3.91 | −5.11 | −4.68 | −0.42 | −0.25 | +1.19 | 1 |
| 19 | 88 | −3.90 | −5.09 | −4.85 | −0.24 | −0.21 | +1.19 | 1 |
| 20 | 82 | −3.87 | −5.06 | −4.89 | −0.17 | −0.28 | +1.19 | 1 |
| 21 | 38 | −3.86 | −5.05 | −4.76 | −0.29 | −0.27 | +1.19 | 3 |
| 22 | 75 | −3.79 | −4.98 | −4.74 | −0.24 | −0.30 | +1.19 | 1 |
| 23 | 54 | −3.74 | −4.93 | −4.62 | −0.31 | −0.30 | +1.19 | 1 |
| 24 | 79 | −3.71 | −4.91 | −4.62 | −0.28 | −0.26 | +1.19 | 1 |
| 25 | 11 | −3.67 | −4.87 | −4.57 | −0.29 | −0.31 | +1.19 | 4 |
| 26 | 50 | −3.48 | −4.68 | −4.63 | −0.05 | −0.32 | +1.19 | 1 |

**Table 2. Docking Results of BPS with Pepsin**

| rank | run | estimated free energy of binding kcal/mol) | $E_{intermol}$ (kcal/mol) | $E_{VHD}$ (kcal/mol) | $E_{elec}$ (kcal/mol) | $E_{total}$ (kcal/mol) | $E_{torsional}$ (kcal/mol) | no. in cluster |
|---|---|---|---|---|---|---|---|---|
| 1 | 13 | −6.61 | −7.80 | −7.36 | −0.44 | −0.29 | +1.19 | 22 |
| 2 | 5 | −6.14 | −7.34 | −7.02 | −0.31 | −0.31 | +1.19 | 10 |
| 3 | 99 | −6.11 | −7.30 | −7.08 | −0.22 | −0.20 | +1.19 | 3 |
| 4 | 81 | −6.02 | −7.21 | −6.95 | −0.26 | −0.27 | +1.19 | 1 |
| 5 | 51 | −5.82 | −7.01 | −6.79 | −0.22 | −0.30 | +1.19 | 6 |
| 6 | 17 | −5.76 | −6.96 | −6.75 | −0.21 | −0.25 | +1.19 | 18 |
| 7 | 85 | −5.60 | −6.80 | −6.45 | −0.34 | −0.27 | +1.19 | 2 |
| 8 | 41 | −5.58 | −6.78 | −6.57 | −0.20 | −0.21 | +1.19 | 6 |
| 9 | 55 | −5.56 | −6.76 | −6.58 | −0.17 | −0.29 | +1.19 | 10 |
| 10 | 12 | −5.53 | −6.72 | −6.49 | −0.23 | −0.27 | +1.19 | 2 |
| 11 | 54 | −5.43 | −6.63 | −6.30 | −0.32 | −0.27 | +1.19 | 3 |
| 12 | 77 | −5.38 | −6.57 | −6.36 | −0.21 | −0.21 | +1.19 | 1 |
| 13 | 89 | −5.37 | −6.56 | −5.94 | −0.62 | −0.27 | +1.19 | 3 |
| 14 | 76 | −5.31 | −6.50 | −6.22 | −0.29 | −0.31 | +1.19 | 3 |
| 15 | 6 | −5.28 | −6.47 | −6.31 | −0.16 | −0.19 | +1.19 | 1 |
| 16 | 16 | −5.24 | −6.43 | −6.28 | −0.15 | −0.28 | +1.19 | 1 |
| 17 | 26 | −5.20 | −6.39 | −6.14 | −0.25 | −0.27 | +1.19 | 1 |
| 18 | 68 | −5.11 | −6.31 | −6.17 | −0.14 | −0.28 | +1.19 | 3 |
| 19 | 38 | −5.10 | −6.29 | −6.16 | −0.13 | −0.20 | +1.19 | 1 |
| 20 | 52 | −5.10 | −6.29 | −6.11 | −0.18 | −0.28 | +1.19 | 1 |
| 21 | 27 | −4.95 | −6.14 | −5.61 | −0.53 | −0.30 | +1.19 | 1 |
| 22 | 1 | −4.92 | −6.12 | −5.49 | −0.62 | −0.29 | +1.19 | 1 |

$$\log \frac{F_0 - F_{cor}}{F_{cor}} = n \log K_A - n \log\left(\frac{1}{[Q_t] - (F_0 - F_{cor})[P_t]/F_0}\right) \quad (3)$$

where $F_0$ and $F_{cor}$ are the corrected fluorescence intensities of enzymes in the absence and presence of BPS, respectively.[49] $[P_t]$ and $[Q_t]$ are the total concentration of enzymes and BPS, respectively. $K_A$ is the binding constant, and $n$ is the number of binding sites. According to eq 3, the plots of $\log[(F_0 - F_{cor})/F_{cor}]$ vs $\log(1/([Q_t] - (F_0 - F_{cor})[P_t]/F_0))$ are shown in Figure 8A,B. As depicted in Figure 8A,B, the plots give straight lines. The values of $n$ and $K_A$ are summarized in Table 3. The computed binding site ($n$) values clearly indicate the existence

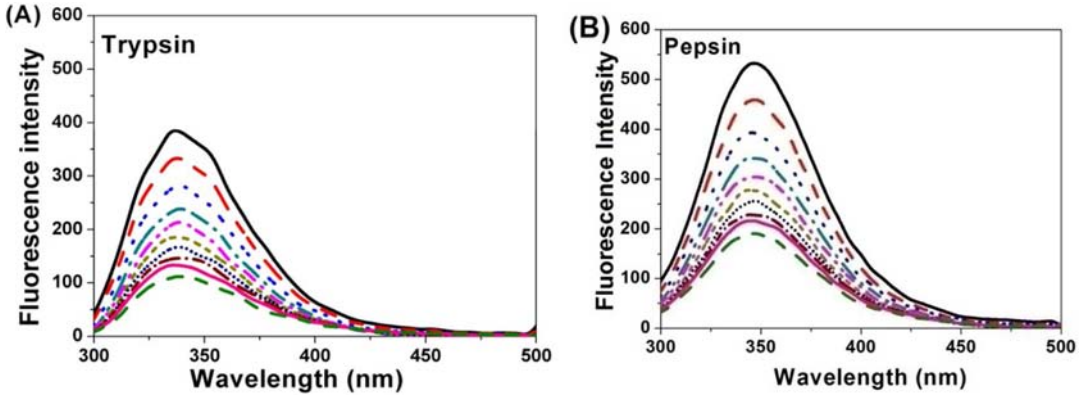


**Figure 6.** Fluorescence emission spectra of trypsin (A) and pepsin (B) in the absence and presence of BPS, $c$ (trypsin) = $c$ (pepsin) = $2.0 \times 10^{-5}$ mol·L$^{-1}$. $c$ (BPS) ($\times 10^{-5}$ mol·L$^{-1}$) (from top to bottom), 0, 0.5, 1.0, 1.5, 2.0, 2.5, 3.0, 3.5, 4.0, and 5.0, respectively.

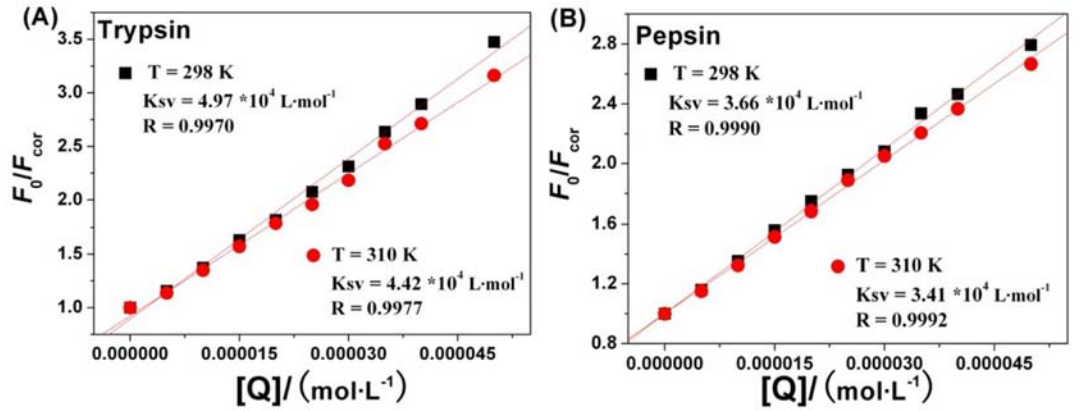


**Figure 7.** Stern–Volmer plots for the quenching of trypsin (A) and pepsin (B) by BPS. $\lambda_{ex}$ = 280 nm, $\lambda_{em}$ (trypsin) = 336 nm, $\lambda_{em}$ (pepsin) = 345 nm.

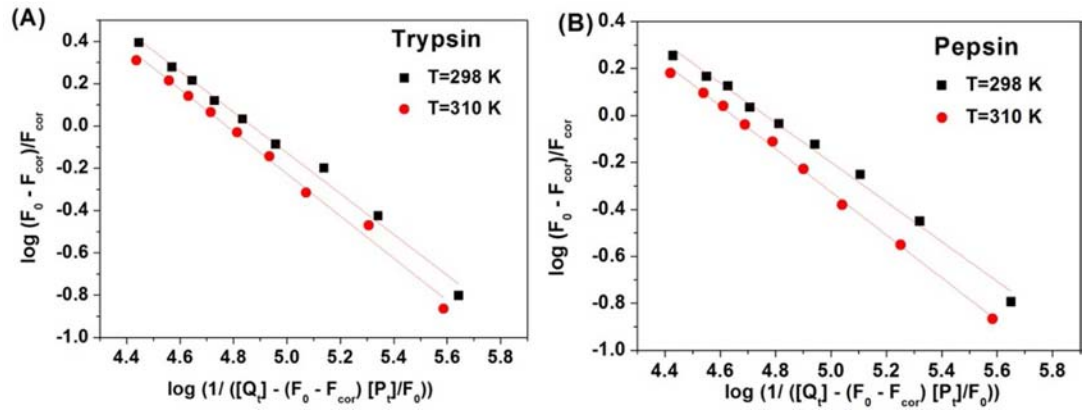


**Figure 8.** Plots of $\log(F_0 - F_{cor})/F_{cor}$ as a function of $\log(1/([Q_t] - (F_0 - F_{cor})[P_t]/F_0))$ of BPS with trypsin (A) and pepsin (B). $\lambda_{ex}$ = 280 nm, $\lambda_{em}$ (trypsin) = 336 nm, $\lambda_{em}$ (pepsin) = 345 nm.

**Table 3. Association Parameters of Trypsin and Pepsin with BPS at Different Temperatures**

| enzyme | $T$ (K) | $K_A$ (L·mol$^{-1}$) | $n$ | $\Delta H°$ (kJ·mol$^{-1}$) | $\Delta G°$ (kJ·mol$^{-1}$) | $\Delta S°$ (J·mol$^{-1}$·K$^{-1}$) |
|---|---|---|---|---|---|---|
| trypsin | 298 | $7.42 \times 10^4$ | 0.96 | −14.56 | −27.78 | 44.36 |
| | 310 | $5.91 \times 10^4$ | 0.99 | | −28.32 | |
| pepsin | 298 | $5.78 \times 10^4$ | 0.85 | −16.88 | −27.16 | 34.50 |
| | 310 | $4.44 \times 10^4$ | 0.91 | | −27.58 | |

of mainly one kind of binding site for trypsin and pepsin with BPS and the formation of the molar ratio 1:1 complex, respectively. In addition, the factor of the order of binding constants of BPS with trypsin and pepsin is $10^4$, which is lower than that of antibody–antigen complex ($10^9$–$10^{10}$).[55] These results imply that the binding of BPS with these two enzymes is


dx.doi.org/10.1021/jf504347w | J. Agric. Food Chem. 2014, 62, 11303–11311

of moderate intensity. Except for the binding constant $K_A$ and the number of binding sites $n$, thermodynamic parameters ($\Delta H^\circ$, $\Delta G^\circ$, $\Delta S^\circ$) are also obtained by using eqs 4−6.

$$\ln \frac{(K_A)_2}{(K_A)_1} = \frac{\Delta H^\circ}{R}\left(\frac{1}{T_1} - \frac{1}{T_2}\right) \quad (4)$$

$$\Delta G^\circ = -RT \ln K_A \quad (5)$$

$$\Delta S = \frac{\Delta H^\circ - \Delta G^\circ}{T} \quad (6)$$

As shown in Table 3, $\Delta G^\circ < 0$, $\Delta H^\circ < 0$, and $\Delta S^\circ > 0$ of BPS−trypsin and BPS−pepsin systems. As for trypsin and pepsin binding BPS, there are many similarities. First, the negative values of $\Delta G^\circ$ indicated the spontaneity of the binding of trypsin and pepsin with BPS. Second, the positive values of $\Delta S^\circ$ are 44.36 J·mol$^{-1}$·K$^{-1}$ and 34.50 J·mol$^{-1}$·K$^{-1}$ for trypsin and pepsin, indicating that hydrophobic forces are involved in the BPS−trypsin and BPS−pepsin binding processes.[53] Third, the values of $\Delta H^\circ$ are negative and are not about zero, which indicate that hydrogen bonds also play important roles in their binding processes. Analyzing from the molecular structure of BPS, the benzene rings of BPS having hydrophobic property enhance the possibility of their hydrophobic interactions with the hydrophobic amino acid residues in trypsin and pepsin. The $\pi-\pi$ stacking interactions of BPS with aromatic amino acids of enzymes might be involved. The two −OH on aromatic rings and −S═O linking two benzene rings might make BPS bind with trypsin and pepsin by hydrogen bonds. In addition, the molecular modeling results also support the above conclusion that hydrophobic and hydrogen bonding forces are the main driving forces stabilizing BPS−trypsin/pepsin complex.

**Conclusions.** This is the first study that offers a detailed binding mechanism of BPS with trypsin and pepsin and its effects on the structures and activities of these two digestion enzymes. The results showed that the binding interactions existed between BPS and enzymes. The secondary and tertiary structures of trypsin and pepsin are affected upon BPS binding. Moreover, the binding of BPS to pepsin did cause an obvious decrease of enzyme activity. However, the interaction of BPS with trypsin did not inhibit the activity remarkably. The present study could provide some important biophysical insights on the binding mechanisms of bisphenol analogues with digestive proteases from the point of view of food security.

## AUTHOR INFORMATION


### Corresponding Author

*Tel: +86 515 88233188. Fax: +86 515 88233188. E-mail: wyqing76@126.com.



### Funding

We gratefully acknowledge financial support of the Fund for the National Natural Science Foundation of China (Project No. 21201147), the Natural Science Foundation of Jiangsu Province (Grant No. BK2012671), the Natural Science Foundation of Education Department of Jiangsu Province (Grant No. 12KJA180009), the Jiangsu Fundament of "Qilan Project" and "333 Project", and the sponsorship of Jiangsu Overseas Research & Training Program for University Prominent Young & Middle-aged Teachers and Presidents.


### Notes

The authors declare no competing financial interest.

## REFERENCES


(1) Arnich, N.; Canivenc-Lavier, M.; Kolf-Clauw, M.; Coffigny, H.; Cravedi, J.; Grob, K.; Macherey, A.; Masset, D.; Maximilien, R.; Narbonne, J.; Nesslany, F.; Stadler, J.; Tulliez, J. Conclusions of the french food safety agency on the toxicity of bisphenol A. *Int. J. Hyg. Environ. Health* **2011**, *214*, 271−275.

(2) Sun, C.; Leong, L. P.; Barlow, P. J.; Chan, S. H.; Bloodworth, B. C. Single laboratory validation of a method for the determination of Bisphenol A, Bisphenol A diglycidyl ether and its derivatives in canned foods by reversed-phase liquid chromatography. *J. Chromatogr. A* **2006**, *1129*, 145−148.

(3) Biles, J. E.; McNeal, T. P.; Begley, T. H.; Hollifield, H. C. Determination of bisphenol A in reusable polycarbonate food-constact plastics and migration to food-simulating liquids. *J. Agric. Food. Chem.* **1997**, *45*, 3541−3544.

(4) European Community Directive 2004/19/EC of 1 March 2004 amending Directive 2002/72/EC relating to plastic materials and articles intended to come into contact with foodstuffs. *Off. J. Eur. Commun.* **2004**, *L71*, 8−21.

(5) Munguia-Lopez, E. M.; Peralta, E.; Gonzalez-Leon, A.; Vargas-Requena, V.; Soto-Valdez, H. Migration of bisphenol A (BPA) from epoxy can coatings to jalapeño peppers and an acid food simulant. *J. Agric. Food. Chem.* **2002**, *50*, 7299−7302.

(6) Michałowicz, J. Bisphenol A—Sources, toxicity and biotransformation. *Environ. Toxicol. Pharmacol.* **2014**, *37*, 738−758.

(7) Migeot, V.; Dupuis, A.; Cariot, A.; Albouy-Llaty, M.; Pierre, F.; Rabouan, S. Bisphenol A and its chlorinated derivatives in human colostrums. *Environ. Sci. Technol.* **2013**, *47*, 13791−13797.

(8) Mathew, M.; Sreedhanya, S.; Manoj, P.; Aravindakumar, C. T.; Aravind, U. K. Exploring the interaction of bisphenol-S with serum albumins: A better or worse alternative for bisphenol A? *J. Phys. Chem. B* **2014**, *118*, 3832−3843.

(9) Liao, C.; Liu, F.; Kannan, K. Bisphenol S, a new bisphenol analogue, in paper products and currency bills and its association with bisphenol a residues. *Environ. Sci. Technol.* **2012**, *46*, 6515−6522.

(10) Liao, C.; Liu, F.; Guo, Y.; Moon, H. B.; Nakata, H.; Wu, Q.; Kannan, K. Occurrence of eight bisphenol analogues in indoor dust from the United States and several Asian countries: Implications for human exposure. *Environ. Sci. Technol.* **2012**, *46*, 9138−9145.

(11) Ike, M.; Chen, M. Y.; Danzl, E.; Sei, K.; Fujita, M. Biodegradation of a variety of bisphenols under aerobic and anaerobic conditions. *Water Sci. Technol.* **2006**, *53*, 153−159.

(12) Vandenberg, L. N.; Chahoud, I.; Heindel, J. J.; Padmanabhan, V.; Paumgartten, F. J. R.; Schoenfelder, G. Urinary, circulating, and tissue biomonitoring studies indicate widespread exposure to bisphenol A. *Environ. Health Perspect.* **2010**, *118* (8), 1055−1070.

(13) Pirard, C.; Sagot, C.; Deville, M.; Dubois, N.; Charlier, C. Urinary levels of bisphenol A, triclosan and 4-nonylphenol in a general Belgian population. *Environ. Int.* **2012**, *48*, 78−83.

(14) Calafat, A.; Ye, X.; Wong, L.; Reidy, J.; Needham, L. Exporsure of the US population to bisphenol A and 4-tertiary-octylphenol: 2003−2004. *Environ. Health Perspect.* **2008**, *116*, 39−44.

(15) Gole, A.; Dash, C.; Rao, M.; Sastry, M. Encapsulation and biocatalytic activity of the enzyme pepsin in fatty lipid films by selective electrostatic interactions. *Chem. Commun.* **2000**, *16*, 297−298.

(16) Khaldi, N.; Vijayakumar, V.; Duallas, D. C.; Guerrero, A.; Wickramasinghe, S.; Smilowitz, J. T.; Medrano, J. F.; Lebrilla, C. B.; Shields, D. C.; German, J. B. Predicting the important enzymes in human breast milk digestion. *J. Agric. Food Chem.* **2014**, *62*, 7225−7232.

(17) Zhang, H. J.; You, J.; Liang, H. L.; Qi, T. T.; Yang, R.; Qu, L. B. Investigation on the binding interaction between silybin and pepsin by spectral and molecular docking. *Int. J. Biol. Macromol.* **2014**, *67*, 105−111.

(18) Wang, R. Y.; Xie, Y. Z.; Zhang, Y. H.; Kang, X. H.; Wang, X. G.; Ge, B. Y.; Chang, J. B. Comparative study of the binding of pepsin to four alkaloids by spectrofluorimetry. *Spectrochim. Acta, Part A* **2013**, *108*, 62−74.

(19) Wang, Y. Q.; Zhang, H. M. Comparative studies of the binding of six phthalate plasticizers to pepsin by multispectroscopic approach and molecular modeling. *J. Agric. Food Chem.* **2013**, *61*, 11191−11200.
(20) Gonçalves, R.; Mateus, N.; De Freitas, V. Influence of carbohydrates on the interaction of procyanidin B3 with trypsin. *J. Agric. Food Chem.* **2011**, *59*, 11794−11802.
(21) Gonçalves, R.; Mateus, N.; De Freitas, V. Biological relevance of the interaction between procyanidins and trypsin: a multitechnique approach. *J. Agric. Food Chem.* **2010**, *58*, 11924−11932.
(22) Goncalves, R.; Mateus, N.; Pianet, I.; Laguerre, M.; Freitas, V. Mechanisms of tannin-induced trypsin inhibition: A molecular approach. *Langmuir* **2011**, *21*, 13122−13129.
(23) Wu, X. L.; He, W. Y.; Wang, W. P.; Luo, X. P.; Cao, H. Y.; Lin, L. X.; Feng, K. Q.; Liu, Z. G. Investigation of the interaction between (−)-epigallocatechin-3-gallate with trypsin and alpha-chymotrypsin. *Int. J. Food Sci. Technol.* **2013**, *48*, 2340−2347.
(24) Li, Q.; Wei, Q. Y.; Yuan, E.; Yang, J. G.; Ning, Z. X. Interaction between four flavonoids and trypsin: effect of the characteristics of trypsin and antioxidant activity of flavonoids. *Int. J. Food Sci. Technol.* **2014**, *49*, 1063−1069.
(25) Mu, Y.; Lin, J.; Liu, R. T. Interaction of sodium benzoate with trypsin by spectroscopic techniques. *Spectrochim. Acta, Part A* **2011**, *83*, 130−135.
(26) Bandyopadhy, P.; Ghosh, A. K.; Ghhosh, C. Recent developments on polyphenol-protein interactions: effects on tea and coffee taste, antioxidant properties and the digestive system. *Food Funct.* **2012**, *3*, 592−605.
(27) Alves, R. G.; Soares, S.; Mateus, N.; Freits, V. D. Inhibition of trypsin by condensed tannins and wine. *J. Agric. Food Chem.* **2007**, *55*, 7596−7601.
(28) Anson, D. L. The estimation of pepsin, trypsin, papain, and cathepsin with haemoglobin. *J. Gen. Physiol.* **1938**, *22*, 79−89.
(29) Morris, G. M.; Huey, R.; Lindstrom, W.; Sanner, M. F.; Belew, R. K.; Goodsell, D. S.; Olson, A. J. Autocock4 and AutodockTool4: automated docking with selective receptor flexibility. *J. Comput. Chem.* **2009**, *16*, 2785−2791.
(30) Frisch, M. J.; Trucks, G. W.; Schlegel, H. B.; Scuseria, G. E.; Robb, M. A.; Cheeseman, J. R.; Scalmani, G.; Barone, V.; Mennucci, B.; Petersson, G. A.; Nakatsuji, H.; Caricato, M.; Li, X.; Hratchian, H. P.; Izmaylov, A. F.; Bloino, J.; Zheng, G.; Sonnenberg, J. L.; Hada, M.; Ehara, M.; Toyota, K.; Fukuda, R.; Hasegawa, J.; Ishida, M.; Nakajima, T.; Honda, Y.; Kitao, O.; Nakai, H.; Vreven, T.; Montgomery, J. A., Jr.; Peralta, J. E.; Ogliaro, F.; Bearpark, M.; Heyd, J. J.; Brothers, E.; Kudin, K. N.; Staroverov, V. N.; Kobayashi, R.; Normand, J.; Raghavachari, K.; Rendell, A.; Burant, J. C.; Iyengar, S. S.; Tomasi, J.; Cossi, M.; Rega, N.; Millam, J. M.; Klene, M.; Knox, J. E.; Cross, J. B.; Bakken, V.; Adamo, C.; Jaramillo, J.; Gomperts, R.; Stratmann, R. E.; Yazyev, O.; Austin, A. J.; Cammi, R.; Pomelli, C.; Ochterski, J. W.; Martin, R. L.; Morokuma, K.; Zakrzewski, V. G.; Voth, G. A.; Salvador, P.; Dannenberg, J. J.; Dapprich, S.; Daniels, A. D.; Farkas, Ö.; Foresman, J. B.; Ortiz, J. V.; Cioslowski, J.; Fox, D. J. *Gaussian 09 Revision D.01. 2009*; Gaussian Inc.: Wallingford, CT, 2013.
(31) Brandt, T.; Holzmann, N.; Muley, L.; Khayat, M.; Wegscheid-Gerlach, C.; Baum, B.; Heine, A.; Hangauer, D.; Klebe, G. Congeneric but still distinct: how closely related trypsin ligands exhibit different thermodynamic and structural properties. *J. Mol. Biol.* **2011**, *405*, 1170−1187.
(32) Cooper, J. B.; Khan, G.; Taylor, G.; Tickle, I. J.; Blundell, T. L. X-ray analyses of aspartic proteinases. II. Three-dimensional structure of the hexagonal crystal form of porcine pepsin at 2.3 Å resolution. *J. Mol. Biol.* **1990**, *214*, 199−222.
(33) Zeng, H. J.; You, J.; Liang, H. L.; Qi, T. T.; Yang, R.; Qu, L. B. Investigation of the binding interaction between silybin and pepsin by spectral and molecular docking. *Int. J. Biol. Macromol.* **2014**, *67*, 105−111.
(34) http://www.clcbio.com/products/molegro.
(35) Schmid, F.-X. Biological macromolecules: UV-visible spectrophotometry. *eLS* **2001**, 1−4.
(36) Rosenheck, K.; Doty, P. The far ultraviolet absorption spectra of polypeptide and protein solution and their dependence on conformation. *Proc. Natl. Acad. Sci. U.S.A.* **1961**, *47*, 1775−1785.
(37) Shanmugaraj, K.; Anandakumar, S.; Ilanchelian, M. Probing the binding interaction of thionine with lysozyme: A spectroscopic and molecular docking investigation. *Dyes Pigments* **2015**, *112*, 210−219.
(38) Wang, Y. Q.; Zhang, H. M. Comprehensive studies on the nature of interaction between catalase and $SiO_2$ nanoparticle. *Mater. Res. Bull.* **2014**, *60*, 51−56.
(39) Greenfield, N. J. Using circular dichroism spectra to estimate protein secondary structure. *Nat. Protoc.* **2007**, *1*, 2876−2890.
(40) Wang, Y. Q.; Tan, C. Y.; Zhuang, S. L.; Zhai, P. Z.; Cui, Y.; Zhou, Q. H.; Zhang, H. M.; Fei, Z. H. In vitro and in silico investigations of the binding interactions between chlorophenols and trypsin. *J. Hazard. Mater.* **2014**, *278*, 55−65.
(41) Wei, X. L.; Ge, Z. Q. Effect of grapheme oxide on conformation and activity of catalase. *Carbon* **2013**, *60*, 401−409.
(42) Brandt, T.; Holzmann, N.; Muley, L.; Khayat, M.; Wegscheid-Gerlach, C.; Baum, B.; Heine, A.; Hangauer, D.; Klebe, G. Congeneric but still distinct: how closely related trypsin ligands exhibit different thermodynamic and structural properties. *J. Mol. Biol.* **2011**, *405*, 1170−1187.
(43) Cooper, J. B.; Khan, G.; Taylor, G.; Tickle, I. J.; Blundell, T. L. X-ray analyses of aspartic proteinases. II. Three-dimensional structure of the hexagonal crystal forms of porcine pepsin at 2.3 Å resolution. *J. Mol. Biol.* **1990**, *214*, 199−222.
(44) Abert, W. C.; Gregory, W. M.; Allan, G. S. The binding interaction of coomassie blue with proteins. *Anal. Biochem.* **1993**, *213*, 407−413.
(45) Higaki, J. N.; Gibson, B. W.; Craik, C. S. Evolution of catalysis in the serine proteases. *Cold Spring Harbor Symp. Quant. Biol.* **1987**, *52*, 615−621.
(46) Maliar, T.; Jedinák, A.; Kadrabová, J.; Šturdík, E. Anticonvulsant properties of various acetylhydrazones, oxamoylhydrazones and semicarbazones derived from aromatic and unsaturated carbonyl compounds. *Eur. J. Med. Chem.* **2004**, *39*, 241−248.
(47) Sielecki, A. R.; Fedorov, A. A.; Boodhoo, A.; Andreeva, N. S.; James, M. N. G. Molecular and crystal structures of monoclinic porcine pepsin refined at 1.8 A resolution. *J. Mol. Biol.* **1990**, *214*, 143−170.
(48) Lakowicz, J. R. *Principles of fluorescence spectroscopy*; Plenum Press: New York; 1999; p 237.
(49) Gayen, A.; Chatterjee, C.; Mukhopadhyay, C. GM1-induced structural changes of bovine serum albumin. *Biomacromolecules* **2008**, *9*, 974−983.
(50) Rehman, M. T.; Shamsi, H.; Khan, U. Insight into the binding mechanism of imipenem to human serum albumin by spectroscopic and computational approaches. *Mol. Pharmaceutics* **2014**, *11*, 1785−1797.
(51) Shahabadi, N.; Maghsudi, M. Multi-spectroscopic and molecular modeling studies on the interaction of antihypertensive drug; methyldopa with calf thymus DNA. *Mol. BioSyst.* **2014**, *10*, 338−347.
(52) Bi, S. Y.; Ding, L.; Tian, Y.; Song, D. Q.; Zhou, X.; Liu, X.; Zhang, H. Q. Investigation of the interaction between flavonoids and human serum albumin. *J. Mol. Struct.* **2004**, *703*, 37−45.
(53) Zhang, H. M.; Lou, K.; Cao, J.; Wang, Y. Q. Interaction of a hydrophobic-functionalized PAMAM dendrimer with bovine serum albumin: Thermodynamic and structural changes. *Langmuir* **2014**, *30*, 5536−5544.
(54) Pierce, M. M.; Raman, C. S.; Nall, B. T. Isothermal titration calorimetry of protein-protein interactions. *Methods* **1999**, *19*, 213−221.
(55) Ross, P. D.; Subramanian, S. Thermodynamics of protein association reactions: forces contributing to stability. *Biochemistry* **1981**, *20*, 3096−3102.

two hybrids, FxCh77 and FxCh90 (fourth week of February), in 2009. In all cases, three biological replicates per genotype were obtained, all representing at least four different fruits each. Juice was obtained using a hand extractor to avoid squeezing the flavedo and to prevent juice becoming contaminated with peel components. Juice samples of 10 mL aliquots each were placed in 22 mL crimp cap headspace vials and kept frozen at −20 °C until analyzed. Two 10 mL aliquots corresponding to technical replicates of each sample were analyzed. The total number of analysis was 24 (3 biological samples × 2 technical replicates for all 4 genotypes).

Eleven fruit quality traits were also evaluated, as usual, in the *Citrus* breeding program: fruit weight (FW, g); fruit diameter (FD, mm), measured in the transversal section including flavedo and albedo; rind thickness (RT, mm), including albedo; juice volume (JV, mL), quantified as the volume of juice without pulp; number of seeds per fruit (SN); juice content (JC) as JV% of FW; total soluble solids (TSS, degrees Brix), measured with a digital refractometer (PR-101$\alpha$; Palette, Atago; Tokyo, Japan); acidity (*A*), determined by titration with 0.4 N NaOH and a phenolphthalein indicator; maturation index as the ratio between TSS and *A* (Brix/*A*); and color of rind and juice (Rcol and Jcol, respectively), evaluated by visual comparisons with the chromatic circle (from red, 1, to yellow, 20). All of these traits were used for the principal component analysis (see Figure 2).

**HS-SPME Extraction Conditions.** Immediately before the analysis, samples were thawed at 20 °C for 10 min and were then subjected to headspace solid phase microextraction (HS-SPME). Extraction was carried out using 10 mL of sample placed into a 22 mL crimp cap headspace vial. A 50/30 $\mu$m DVB/CAR/PDMS (Supelco, Bellefonte, PA, USA) fiber was used in all cases. Samples were preincubated for 10 min at 50 °C, and volatiles were extracted from the vial headspace for an additional 20 min period at the same temperature, as previously described.[13] Desorption was performed for 1 min at 250 °C in the splitless mode.

**Gas Chromatography−Mass Spectrometry Conditions.** VOCs were analyzed by GC-MS using a COMBI-PAL autosampler (CTC Analytics, Zwingen, Switzerland), and a 6890N gas chromatograph coupled to a 5975B mass spectrometer (Agilent Technologies, Santa Clara, CA, USA), equipped with a J&W Scientific DB-5 ms fused silica capillary column (5−95 phenyl−dimethylpolysiloxane as the stationary phase; 60 m length; 0.25 mm i.d.; 1 $\mu$m film thickness) (Folsom, CA, USA). Oven temperature conditions were 40 °C for 2 min, with 5 °C/min ramp until 250 °C, and were then held isothermally at 250 °C for 5 min. Helium was used as the carrier gas at 1.2 mL/min constant flow. Detection was performed by an Agilent mass spectrometer in the EI mode (ionization energy, 70 eV; source temperature, 230 °C). Acquisition was performed in the scan mode (mass range, $m/z$ 35−220; 7 scans/s). Considering that the molecular weight of the identified compound with the highest mass (nootkatone) was 218 Da, a wider $m/z$ range was not necessary. Chromatograms and spectra were recorded and processed using the Enhanced ChemStation for GC-MS software (Agilent). For the unequivocal identification of volatile compounds, both standards and samples were also injected into a 6890N gas chromatograph (Agilent) coupled to a Pegasus 4D time-of-flight (TOF) mass spectrometer (LECO, St. Joseph, MI, USA) under the following chromatographic conditions: BPX35 column (30 m, 0.32 mm, 0.25 $\mu$m), helium (1.5 mL/min) constant flow, and the same oven temperature ramp as previously described. Ionization was performed by EI (ionization energy, 70 eV; source temperature, 200 °C), and acquisition was performed within the mass range $m/z$ 35−300.

**Compound Identification.** Compound identification in each sample was based on the comparison of both mass spectrum and retention time in two columns of different polarity with those of pure standards. The retention times of the identified compounds in each column are detailed in Supporting Information (SI) Table S1. From 113 compounds, 103 compounds were identified in the *Citrus* samples when analyzed with each of the two columns. The other 10 volatiles were overlapped by more abundant compounds in the BPX35 column chromatograms, and therefore their identity could not be confirmed. The identification of these 10 compounds was based on the similarity of mass spectrum and retention time in only one column, and should therefore be considered tentative, as indicated in Table 1. The compounds used as a reference were of analytical grade and purchased from Sigma-Aldrich Química (Madrid, Spain), except for 2-carene, which was obtained from Extrasynthese (Genay, France). In addition to the commercial compounds, four esters (ethyl heptanoate, methyl octanoate, methyl nonanoate, and ethyl nonanoate) were synthesized by acid-catalyzed esterification, according to González-Mas et al.[13] For relative quantification, one specific ion for each compound was selected, and the corresponding peak from the extracted ion chromatogram was integrated. The ion selected for the integration of each peak was that with the highest signal-to-noise ratio and one that was specific enough to provide good peak integration for that particular region of the chromatogram. An admixture reference sample was prepared by mixing equal amounts of each sample corresponding to the four analyzed genotypes. This admixture was aliquoted (10 mL in 22 mL headspace vials), stored, and further treated as any other sample. This admixture contained all of the compounds identified in any of the samples at an intermediate concentration between those in the individual samples. The admixture aliquots were injected regularly (one admixture for every five to six samples) as part of the injection series and were used as a reference to normalize for temporal variation and fiber aging. All of the samples were analyzed using the same SPME fiber. Finally, the normalized results (corrected for temporal variation and fiber aging) for each compound were expressed as the relative levels to the average levels present in the Chandler juice. If a compound was not detected in Chandler, the ratio was calculated to the levels in a genotype that contained it, as indicated (Table 1).

**Statistical Analysis.** A principal component analysis (PCA) and a hierarchical cluster analysis (HCA) were done to analyze the volatile data set, which included all of the replicates and samples. In them both, the ratio of the levels of each volatile in a sample to the average of the four genotypes was $\log_2$-transformed. For the PCA, SIMCA-P version 11 (Umetrics, Umea, Sweden) was used with Pareto normalization. For the HCA, Acuity 4.0 (Axon Instruments, Union City, CA, USA) was used with the distance metrics based on the Pearson correlation.

To represent the phenotypic traits (either volatile levels or quality traits) that were intermediate or significantly under or over the parental levels, the *Z*-scores of the average values for each genotype were calculated. Data were expressed as the values relative to the corresponding level in Chandler, $\log_2$-transformed ($\log R_{Fortune}$ or $\log R_{hybrid}$), and then *Z*-score standardization was performed for each metabolite in all the samples. To calculate the fold change between hybrids and Fortune, the *Z*-score for the difference was calculated using $ZD = \log R_{hybrid} - \log R_{Fortune}/(SE^2_{hybrid} + SE^2_{Fortune})^{1/2}$, where $SE^2$ is the squared standard error of the mean. The *Z*-score for each phenotypic trait (volatile level or other) in both of the two hybrids was plotted against the corresponding *Z*-scores in Fortune (Figure 1 and SI Figure S2). The between, under, or over parental sectors were defined by the *X* and *Y* axes, and the slope 1 diagonal, where the phenotypic traits with the *Z*-score hybrid > 0 ($y > 0$) and ZD > 0 were in the *overparent* sector and the phenotypic traits with the *Z*-score hybrid < 0 and ZD < 0 in the *underparent* sector. To determine the significance of the differences relating to both Chandler and Fortune, the *p*-value associated with each *Z*-score and ZD was calculated. The metabolites and physiological parameters in each sector were considered statistically significant with a *p*-value < 0.05 (SI Table S2).

## RESULTS AND DISCUSSION

Table 1 lists the VOCs detected by the HS-SPME-GC-MS technique and the relative volatile levels in hybrids FxCh90 and FxCh77 as compared to those in the parental genotypes: Fortune mandarin and Chandler pummelo. In all, 113 compounds were identified: 31 esters (22 aliphatic and 9 monoterpene acetates), 23 aldehydes (18 aliphatic, 4 monoterpene, and 1 norisoprenoid), 20 alcohols (11 aliphatic and 9 monoterpene), 14 monoterpene hydrocarbons, 13

**Table 1. Relative Levels (Fold Changes) of the VOCs Detected in the Juices of Two *Citrus* Hybrids and Their Parental Varieties[a]**

| code | cluster | volatile organic compound | family code[b]/no. | retention time (min) | specific ion ($m/z$) | Chandler | FxCh90 | FxCh77 | Fortune |
|---|---|---|---|---|---|---|---|---|---|
| 1 | A1 | linalool[c] | Alc/1 | 27.15 | 93 | 1 ± 0.69 a | 37.57 ± 2.12 c | 131.14 ± 18.44 d | 26.77 ± 1.66 b |
| 2 | A1 | $\beta$-citronellol[c] | Alc/2 | 31.15 | 81 | 1 ± 0.53 a | 6.32 ± 0.27 c | 16.57 ± 0.64 d | 4.53 ± 0.45 b |
| 3 | A1 | perillaldehyde[c] | Ald/1 | 33.43 | 68 | 1 ± 0.29 a | 5.58 ± 1.18 b | 22.44 ± 10.67 d | 15.19 ± 5.28 c |
| 4 | A1 | $\alpha$-terpineol[c] | Alc/3 | 30.75 | 59 | 1 ± 0.59 a | 4.07 ± 0.81 b | 8.14 ± 2.06 d | 5.67 ± 0.69 c |
| 5 | A1 | $\beta$-citronellal[c,d] | Ald/2 | 28.92 | 69 | | | 1 ± 0.23 | |
| 6 | A1 | hexyl acetate[e] | Est/1 | 23.86 | 56 | 1 ± 0.86 a | 32.96 ± 11.01 c | 17.91 ± 3.96 b | 0.98 ± 0.22 a |
| 7 | A1 | geraniol[c] | Alc/4 | 31.95 | 69 | 1 ± 0.63 a | 4.02 ± 0.50 b | 7.47 ± 1.05 c | 1.50 ± 0.47 a |
| 8 | A1 | nerol[c] | Alc/5 | 31.28 | 93 | 1 ± 0.47 a | 2.79 ± 0.20 b | 3.98 ± 0.71 c | 1.86 ± 2.07 b |
| 9 | A2 | heptyl acetate[d] | Est/2 | 27.27 | 43 | | 8.67 ± 2.44 b | 1 ± 0.77 a | |
| 10 | A2 | 1-decanol[d] | Alc/6 | 32.50 | 115 | | 15.23 ± 3.47 b | 1 ± 0.20 a | traces |
| 11 | A2 | 1-nonanol | Alc/7 | 29.36 | 70 | 1 ± 0.37 a | 8.23 ± 0.90 c | 1.89 ± 0.37 b | 0.82 ± 0.30 a |
| 12 | A2 | sabinene | Mt hd/1 | 23.09 | 93 | 1 ± 0.53 a | 8.42 ± 4.11 c | 4.76 ± 2.35 bc | 1.34 ± 0.82 ab |
| 13 | A2 | $\alpha$-terpinyl acetate[c,f] | Est/3 | 35.10 | 121 | | 38.06 ± 11.68 b | 1.19 ± 0.57 a | 1 ± 0.23 a |
| 14 | A2 | nonyl acetate | Est/4 | 33.47 | 98 | 1 ± 2.35 a | 487.1 ± 147.7 c | 22.58 ± 8.53 b | 22.54 ± 6.43 b |
| 15 | A2 | linalyl acetate | Est/5 | 31.82 | 93 | 1 ± 0.47 a | 217.92 ± 60.01 c | 22.38 ± 1.43 b | 7.29 ± 0.92 ab |
| 16 | A2 | neral[e] | Ald/3 | 31.81 | 84 | 1 ± 0.55 a | 46.90 ± 10.02 c | 6.23 ± 0.98 b | 6.21 ± 0.69 b |
| 17 | A2 | 1-octanol | Alc/8 | 26.00 | 56 | 1 ± 0.33 a | 37.82 ± 1.14 b | 2.18 ± 0.95 a | 2.18 ± 0.26 a |
| 18 | A2 | methyl decanoate | Est/6 | 33.94 | 74 | 1 ± 0.82 a | 9.23 ± 1.03 d | 1.98 ± 0.85 b | 3.14 ± 0.92 c |
| 19 | A2 | octyl acetate | Est/7 | 30.47 | 70 | 1 ± 0.53 a | 574.5 ± 171.6 c | 16.72 ± 0.93 ab | 64.08 ± 0.30 b |
| 20 | A2 | decyl acetate | Est/8 | 36.29 | 70 | 1 ± 1.51 a | 727.3 ± 219.4 c | 43.00 ± 8.12 ab | 68.70 ± 11.4 b |
| 21 | A2 | terpinen-4-ol[c] | Alc/9 | 30.38 | 93 | 1 ± 0.77 a | 34.86 ± 7.42 d | 5.35 ± 1.63 b | 15.86 ± 2.59 c |
| 22 | A2 | $\gamma$-terpinene | Mt hd/2 | 26.03 | 93 | 1 ± 0.61 a | 16.56 ± 3.96 d | 3.53 ± 1.09 b | 5.16 ± 0.85 c |
| 23 | A2 | ($E$)-carvyl acetate[c] | Est/9 | 35.30 | 84 | 1 ± 1.17 a | 43.19 ± 18.72 b | 3.72 ± 1.20 a | 7.36 ± 4.56 a |
| 24 | A2 | dodecanal | Ald/4 | 36.55 | 57 | 1 ± 2.35 a | 78.60 ± 24.86 c | 22.92 ± 9.32 b | 20.38 ± 8.79 b |
| 25 | A2 | geranyl acetate[c] | Est/10 | 35.50 | 69 | 1 ± 0.96 a | 41.21 ± 22.00 c | 18.59 ± 8.14 b | 14.09 ± 1.39 b |
| 26 | A2 | terpinolene | Mt hd/3 | 27.05 | 121 | 1 ± 0.40 a | 6.84 ± 1.30 c | 5.21 ± 1.33 b | 4.78 ± 0.33 b |
| 27 | A2 | $\alpha$-terpinene | Mt hd/4 | 24.65 | 121 | 1 ± 0.52 a | 12.26 ± 4.37 c | 5.11 ± 1.65 b | 4.75 ± 1.80 b |
| 28 | A2 | citronellyl acetate[c] | Est/11 | 34.69 | 95 | 1 ± 0.62 a | 95.15 ± 29.37 c | 91.39 ± 37.02 c | 47.41 ± 4.01 b |
| 29 | A2 | $\alpha$-pinene | Mt hd/5 | 21.67 | 93 | 1 ± 0.41 a | 11.09 ± 2.41 b | 15.50 ± 5.37 c | 9.17 ± 1.18 b |
| 30 | A2 | limonene | Mt hd/6 | 25.11 | 108 | 1 ± 0.25 a | 2.66 ± 0.21 bc | 2.89 ± 0.28 c | 2.46 ± 0.10 b |
| 31 | A2 | $\alpha$-phellandrene | Mt hd/7 | 24.29 | 93 | 1 ± 0.41 a | 8.62 ± 1.63 c | 11.15 ± 3.15 d | 5.64 ± 0.58 b |
| 32 | A2 | myrcene | Mt hd/8 | 23.28 | 91 | 1 ± 0.42 a | 4.42 ± 0.50 c | 5.20 ± 0.96 d | 3.21 ± 0.28 b |
| 33 | A2 | ($Z$)-carvyl acetate[c] | Est/12 | 34.50 | 84 | 1 ± 0.46 a | 4.47 ± 1.37 b | 5.32 ± 1.90 b | 4.27 ± 1.58 b |
| 34 | A2 | neryl acetate[c] | Est/13 | 34.97 | 69 | 1 ± 0.55 a | 4.80 ± 1.25 c | 4.57 ± 2.04 c | 1.90 ± 0.19 b |
| 35 | A2 | camphene | Mt hd/9 | 22.44 | 93 | 1 ± 1.04 a | 2.99 ± 0.62 bc | 3.41 ± 1.00 c | 1.95 ± 0.20 b |
| 36 | A2 | 3-carene | Mt hd/10 | 24.43 | 93 | 1 ± 0.56 a | 2.47 ± 0.19 b | 1.40 ± 0.54 a | 1.39 ± 0.64 a |
| 37 | A2 | eucalyptol (1,8-cineole)[e] | Mt cyc ether/1 | 25.38 | 154 | 1 ± 0.62 a | 2.19 ± 0.36 b | 3.08 ± 0.07 b | 0.30 ± 0.06 a |
| 38 | A2 | ($Z$)-3-hexenal | Ald/5 | 15.92 | 69 | 1 ± 0.89 a | 1.44 ± 0.47 a | 0.95 ± 0.26 a | 0.44 ± 0.14 a |
| 39 | A2 | bornyl acetate[c] | Est/14 | 33.66 | 121 | 1 ± 1.17 a | 5.59 ± 1.57 c | 3.82 ± 1.63 b | |
| 40 | A2 | $\beta$-pinene | Mt hd/11 | 23.46 | 93 | 1 ± 0.88 b | 1.04 ± 0.35 b | 1.25 ± 0.34 b | 0.17 ± 0.03 a |
| 41 | A2 | $\alpha$-copaene | Sqt/1 | 36.41 | 119 | 1 ± 0.58 b | 1.21 ± 0.37 b | 1.15 ± 0.43 b | 0.35 ± 0.02 a |
| 42 | A2 | decanal | Ald/6 | 30.59 | 57 | 1 ± 0.19 a | 3.65 ± 2.44 b | 0.90 ± 0.98 a | 0.78 ± 0.22 a |
| 43 | A2 | undecanal | Ald/7 | 33.67 | 57 | 1 ± 0.18 b | 1.62 ± 0.59 c | 0.65 ± 0.12 a | 0.76 ± 0.09 ab |
| 44 | B | ($Z$)-limonene oxide[g] | Mt cyc ether/2 | 28.77 | 67 | 1 ± 1.15 a | 2.87 ± 0.64 b | 4.75 ± 0.53 c | 3.47 ± 0.14 b |
| 45 | B | 1-penten-3-one | Ket/1 | 11.57 | 55 | 1 ± 0.52 a | 0.60 ± 0.04 a | 2.98 ± 1.94 b | 2.45 ± 0.59 b |
| 46 | B | ($E$)-2-hexenal | Ald/8 | 18.17 | 83 | 1 ± 0.70 a | 0.64 ± 0.06 a | 1.27 ± 0.58 a | 1.02 ± 0.16 a |
| 47 | B | ($E$)-2-pentenal | Ald/9 | 14.30 | 83 | 1 ± 0.45 b | 0.35 ± 0.05 a | 1.44 ± 0.83 b | 1.45 ± 0.25 b |
| 48 | B | ($E$)-limonene oxide[g] | Mt cyc ether/3 | 28.84 | 94 | 1 ± 0.77 a | 3.54 ± 0.70 b | 6.11 ± 1.11 c | 6.81 ± 4.59 bc |
| 49 | B | ($Z$)-carveol[c] | Alc/10 | 31.83 | 109 | 1 ± 0.49 a | 6.32 ± 3.50 c | 2.89 ± 0.34b | 6.91 ± 0.85 c |
| 50 | B | carvone[c] | Ket/2 | 32.31 | 82 | 1 ± 0.68 a | 5.10 ± 1.01 b | 5.64 ± 1.17 b | 20.89 ± 1.02 c |
| 51 | B | ($E$)-carveol[c] | Alc/11 | 31.41 | 109 | 1 ± 0.36 a | 2.00 ± 0.08 b | 2.46 ± 0.32 b | 5.35 ± 0.71 c |
| 52 | B | dihydrocarvone[c] | Ket/3 | 30.89 | 95 | 1 ± 0.40 a | 3.06 ± 0.50 b | 5.76 ± 1.11 c | 10.25 ± 0.38 d |
| 53 | B | ethyl decanoate | Est/15 | 35.91 | 88 | 1 ± 0.78 a | 3.09 ± 0.25 b | 2.96 ± 1.31 b | 16.43 ± 3.04 c |
| 54 | B | acetaldehyde | Ald/10 | 4.77 | 43 | 1 ± 0.25 a | 1.57 ± 0.25 b | 1.55 ± 0.40 b | 2.75 ± 0.22 c |
| 55 | B | ethanol | Alc/12 | 5.64 | 45 | 1 ± 0.59 a | 2.39 ± 0.67 b | 1.66 ± 0.59 ab | 6.05 ± 1.64 c |
| 56 | B | ($E$)-2-decenal | Ald/11 | 32.43 | 70 | 1 ± 0.37 a | 1.44 ± 0.34 b | 0.87 ± 0.29 a | 2.15 ± 0.38 c |
| 57 | B | ethyl butanoate | Est/16 | 15.88 | 88 | 1 ± 2.04 a | 3.58 ± 1.14 a | 2.92 ± 2.79 a | 27.11 ± 5.07 b |
| 58 | B | ethyl octanoate | Est/17 | 30.04 | 88 | 1 ± 0.55 a | 0.96 ± 0.06 a | 1.46 ± 1.20 a | 4.05 ± 0.81 b |
| 59 | B | ethyl propanoate | Est/18 | 12.47 | 57 | 1 ± 1.08 a | 1.52 ± 0.38 a | 0.31 ± 0.48 a | 22.36 ± 7.40 b |
| 60 | B | propyl acetate[e,f] | Est/19 | 12.52 | 61 | | | | 1 ± 0.53 |
| 61 | B | ethyl 2-methylbutanoate[f] | Est/20 | 17.87 | 102 | | | | 1 ± 0.25 |


dx.doi.org/10.1021/jf5043079 | J. Agric. Food Chem. 2014, 62, 11312−11322

**Table 1. continued**

| code | cluster | volatile organic compound | family code[b]/no. | retention time (min) | specific ion ($m/z$) | Chandler | FxCh90 | FxCh77 | Fortune |
|---|---|---|---|---|---|---|---|---|---|
| 62 | B | ethyl acetate | Est/21 | 9.18 | 61 | 1 ± 0.42 a | 0.44 ± 0.12 a | 0.19 ± 0.02 a | 40.71 ± 7.12 b |
| 63 | B | 3-methylfuran | Fur/1 | 9.16 | 82 | 1 ± 0.32 a | 0.78 ± 0.17 a | 1.10 ± 0.28 a | 2.91 ± 0.94 b |
| 64 | B | ethyl nonanoate | Est/22 | 33.05 | 88 | 1 ± 0.91 a | 0.36 ± 0.13 a | 1.13 ± 0.53 a | 5.59 ± 1.51 b |
| 65 | C1 | geranylacetone[h] | Ket/4 | 37.62 | 43 | 1 ± 0.26 b | 0.60 ± 0.11 a | 1.33 ± 0.57 c | 0.58 ± 0.14 a |
| 66 | C1 | (*Z*)-3-hexen-1-ol | Alc/13 | 18.16 | 82 | 1 ± 0.92 b | 0.10 ± 0.06 a | 1.20 ± 1.09 b | 0.33 ± 0.09 ab |
| 67 | C1 | geranial[c,e] | Ald/12 | 32.60 | 69 | 1 ± 0.41 b | 0.44 ± 0.23 a | 1.10 ± 0.63 b | 0.39 ± 0.11 a |
| 68 | C1 | (*E*,*E*)-2,4-decadienal | Ald/13 | 34.17 | 81 | 1 ± 0.68 b | 0.32 ± 0.30 a | 0.79 ± 0.54 ab | 0.24 ± 0.08 a |
| 69 | C1 | 1-penten-3-ol | Alc/14 | 11.46 | 57 | 1 ± 0.64 b | 0.28 ± 0.01 a | 0.54 ± 0.11 ab | 0.54 ± 0.14 ab |
| 70 | C1 | β-cyclocitral[e,h] | Ald/14 | 31.63 | 137 | 1 ± 0.42 c | 0.27 ± 0.05 a | 0.58 ± 0.17 ab | 0.78 ± 0.13 bc |
| 71 | C1 | β-ionone[h] | Ket/5 | 38.90 | 177 | 1 ± 0.44 b | 0.20 ± 0.03 a | 0.92 ± 0.50 b | 0.88 ± 0.18 b |
| 72 | C1 | 3-pentanone | Ket/6 | 11.97 | 57 | 1 ± 0.63 b | 0.11 ± 0.04 a | 0.55 ± 0.21 b | 0.59 ± 0.19 ab |
| 73 | C1 | hexyl butanoate | Est/23 | 29.94 | 89 | 1 ± 0.71 b | 0.57 ± 0.15 ab | 1.05 ± 0.23 b | 0.31 ± 0.07 a |
| 74 | C1 | hexyl hexanoate[I] | Est/24 | 35.72 | 117 | 1 ± 0.45 b | 0.33 ± 0.08 a | 0.59 ± 0.15 a | 0.22 ± 0.06 a |
| 75 | C1 | butyl hexanoate[I] | Est/25 | 29.92 | 117 | 1 ± 1.10 b | 0.54 ± 0.16 ab | 0.73 ± 0.24 ab | 0.45 ± 0.06 a |
| 76 | C1 | nootkatone[j] | Ket/7 | 47.87 | 121 | 1 ± 0.33 b | 0.14 ± 0.01 ab | 0.43 ± 0.15 ab | 0.02 ± 0.01 a |
| 77 | C1 | α-humulene (α-caryophyllene) | Sqt/2 | 38.82 | 80 | 1 ± 0.64 b | 0.14 ± 0.03 a | 0.10 ± 0.05 a | 0.04 ± 0.01 a |
| 78 | C1 | β-caryophyllene | Sqt/3 | 37.87 | 133 | 1 ± 0.57 b | 0.04 ± 0.01 a | 0.04 ± 0.02 a | |
| 79 | C1 | (*Z*)-linalool oxide[c,k] | Alc/15 | 26.47 | 111 | 1 ± 0.24 b | 0.03 ± 0.01 a | 0.03 ± 0.01 a | traces |
| 80 | C2 | methyl nonanoate | Est/26 | 30.91 | 74 | 1 ± 0.51 a | 1.09 ± 0.14 a | 0.64 ± 0.18 a | 1.02 ± 0.11 a |
| 81 | C2 | isobornyl acetate[c,e] | Est/27 | 33.48 | 121 | 1 ± 0.87 a | 0.91 ± 0.07 a | 0.56 ± 0.21 a | 0.73 ± 0.13 a |
| 82 | C2 | valencene | Sqt/4 | 39.69 | 133 | 1 ± 0.56 b | 0.39 ± 0.04 a | 0.29 ± 0.07 a | 1.16 ± 0.32 b |
| 83 | C2 | 2-methylfuran | Fur/2 | 8.84 | 82 | 1 ± 0.25 b | 0.25 ± 0.06 a | 0.51 ± 0.18 a | 1.13 ± 0.29 b |
| 84 | C2 | 2-ethylfuran | Fur/3 | 12.17 | 81 | 1 ± 0.21 b | 0.14 ± 0.04 a | 0.30 ± 0.09 a | 1.22 ± 0.24 b |
| 85 | C2 | (*E*)-2-octenal | Ald/15 | 25.79 | 70 | 1 ± 0.24 c | 0.11 ± 0.02 a | 0.24 ± 0.11 a | 0.51 ± 0.15 b |
| 86 | C2 | ethyl heptanoate | Est/28 | 26.82 | 88 | 1 ± 0.67 b | | 0.13 ± 0.20 a | 1.76 ± 0.31 b |
| 87 | C2 | pseudocumene | Ar/1 | 23.85 | 105 | 1 ± 0.18 b | 0.18 ± 0.09 a | 0.12 ± 0.05 a | 0.24 ± 0.01 a |
| 88 | C2 | 1-hexanol | Alc/16 | 18.59 | 56 | 1 ± 0.70 b | 0.06 ± 0.01 a | 0.17 ± 0.13 a | 0.22 ± 0.18 a |
| 89 | C2 | hexanal | Ald/16 | 16.01 | 56 | 1 ± 0.22 b | 0.09 ± 0.02 a | 0.12 ± 0.02 a | 0.23 ± 0.02 a |
| 90 | C2 | pentanal | Ald/17 | 12.04 | 58 | 1 ± 0.24 b | 0.09 ± 0.01 a | 0.13 ± 0.04 a | 0.23 ± 0.04 a |
| 91 | C2 | 2-pentylfuran | Fur/4 | 23.36 | 138 | 1 ± 0.19 c | 0.08 ± 0.02 a | 0.16 ± 0.07 ab | 0.29 ± 0.05 b |
| 92 | C2 | 1-octen-3-ol | Alc/17 | 22.85 | 57 | 1 ± 0.32 b | 0.06 ± 0.05 a | 0.04 ± 0.03 a | 0.14 ± 0.03 a |
| 93 | C2 | 3-octanone[I] | Ket/8 | 23.10 | 99 | 1 ± 0.41 b | 0.03 ± 0.01 a | 0.04 ± 0.02 a | 0.10 ± 0.05 a |
| 94 | C2 | nonanal | Ald/18 | 27.30 | 57 | 1 ± 0.15 c | 0.25 ± 0.02 a | 0.17 ± 0.05 a | 0.60 ± 0.06 b |
| 95 | C2 | (*E*)-2-nonenal | Ald/19 | 29.21 | 70 | 1 ± 0.28 b | 0.15 ± 0.01 a | 0.14 ± 0.04 a | 0.98 ± 0.20 b |
| 96 | C2 | 2-nonanone[I] | Ket/9 | 26.79 | 58 | 1 ± 0.38 c | 0.09 ± 0.01 a | 0.09 ± 0.02 a | 0.49 ± 0.08 b |
| 97 | C2 | heptanal | Ald/20 | 20.00 | 70 | 1 ± 0.26 c | 0.06 ± 0.01 a | 0.07 ± 0.03 a | 0.42 ± 0.01 b |
| 98 | C2 | 2,3-pentanedione | Ket/10 | 11.91 | 100 | 1 ± 0.28 c | 0.03 ± 0.02 a | 0.03 ± 0.02 a | 0.53 ± 0.16 b |
| 99 | C2 | 1-heptanol | Alc/18 | 22.44 | 70 | 1 ± 0.55 b | 0.24 ± 0.04 a | 0.17 ± 0.05 a | 0.58 ± 0.32 a |
| 100 | C2 | 6-methyl-5-hepten-2-one[e,h] | Ket/11 | 23.03 | 108 | 1 ± 0.40 b | 0.03 ± 0.01 a | | 0.12 ± 0.02 a |
| 101 | C2 | 1-pentanol | Alc/19 | 14.60 | 41 | 1 ± 0.48 b | 0.03 ± 0.05 a | | 0.11 ± 0.02 a |
| 102 | C2 | ethyl hexanoate | Est/29 | 23.37 | 88 | 1 ± 0.66 b | 0.08 ± 0.01 a | 0.28 ± 0.33 a | 0.62 ± 0.11 ab |
| 103 | C2 | methyl hexanoate | Est/30 | 20.68 | 74 | 1 ± 0.46 b | 0.02 ± 0.02 a | 0.06 ± 0.05 a | 0.07 ± 0.02 a |
| 104 | C2 | methyl octanoate | Est/31 | 27.74 | 74 | 1 ± 0.49 b | 0.64 ± 0.15 ab | 0.51 ± 0.23 a | 0.44 ± 0.08 a |
| 105 | C2 | octanal | Ald/21 | 23.77 | 57 | 1 ± 0.22 b | 0.42 ± 0.20 a | 0.19 ± 0.13 a | 0.39 ± 0.05 a |
| 106 | C2 | 1-octen-3-one | Ket/12 | 22.82 | 70 | 1 ± 0.46 b | 0.22 ± 0.01 a | 0.12 ± 0.01 a | 0.19 ± 0.07 a |
| 107 | C2 | (*E*)-2-heptenal[e] | Ald/22 | 22.14 | 83 | 1 ± 0.26 b | 0.15 ± 0.01 a | 0.19 ± 0.09 a | 0.23 ± 0.05 a |
| 108 | C2 | *p*-cymene | Mt hd/12 | 24.91 | 119 | 1 ± 0.85 b | | 0.02 ± 0.01 a | |
| 109 | C2 | (*Z*)-ocimene | Mt hd/13 | 24.87 | 93 | 1 ± 0.61 | | | |
| 110 | C2 | (*E*,*E*)-2,4-nonadienal | Ald/23 | 31.10 | 81 | 1 ± 0.31 | | | |
| 111 | C2 | (*E*)-linalool oxide[c,k] | Alc/20 | 27.00 | 111 | 1 ± 0.22 | | | |
| 112 | C2 | 2-carene[e] | Mt hd/14 | 24.05 | 93 | 1 ± 0.25 | | | traces |
| 113 | C2 | γ-dodecalactone | Ket/13 | 43.71 | 85 | traces | | | |

[a]Data are normalized to the mean response values in the Chandler variety, unless otherwise indicated. Mean corresponding to $n = 6$ values. Means followed by different letters in the same row are significantly different ($p < 0.05$) in the Duncan's text. [b]Code family: Ald, aldehyde; Ket, ketone; Alc, alcohol; Est, ester; Fur, furane; Mt hd, monoterpene hydrocarbon; Sqt, sesquiterpene; Ar, aromatic hydrocarbon; Mt cyc ether, monoterpene cyclic ether. [c]Monoterpene-derived compounds. [d]Data are normalized to the mean response calculated for FxCh77 since this compound was not present in the Chandler variety. [e]Tentative identification based on coincidence of mass spectrum and retention time in only one capillary column. [f]Data are normalized to the mean response calculated for the Fortune variety. [g]In addition to the alcohol group, it has a tetrahydrofuran group. [h]Norisoprenoid compounds. [I]New compounds reported for the first time in *Citrus* juices. [j]Sesquiterpene compounds. [k]Its cyclic ether group is an epoxy group.


dx.doi.org/10.1021/jf5043079 | J. Agric. Food Chem. 2014, 62, 11312−11322

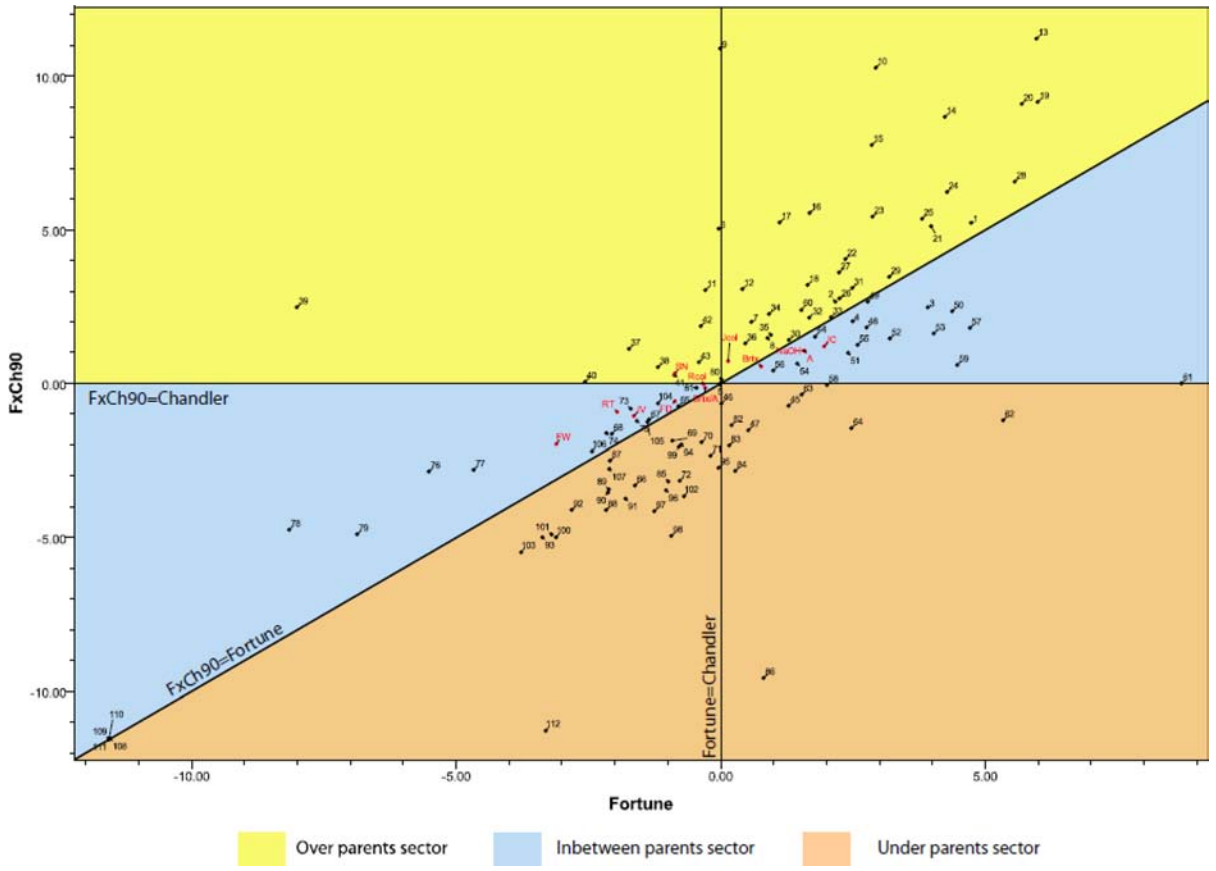


**Figure 1.** Values for the different metabolites and phenotype traits in hybrid FxCh90 in relation to the values in Fortune. Values are expressed as standardized *Z*-score values of $\log_2$ relative to Chandler (value = 0). The blue sector defines those traits whose value in the hybrid fell between the values of the parents. The pale orange and pale yellow sectors correspond to the *underparent* sector and the *overparent* sector, respectively. Volatile compounds are represented in black; phenotypic traits are represented in red.

ketones (7 aliphatic, 2 norisoprenoid, 3 monoterpene, and 1 sesquiterpene), 4 sesquiterpene hydrocarbons, 3 monoterpene cyclic ethers, 4 furans, and 1 aromatic hydrocarbon. Although more than 300 VOCs have been reported in other *Citrus* juice,[9,15,17−19] some were identified only tentatively.[9,11,20−22] To assign chemical names to our data set, in this work we used the actual compounds to verify the identification of the VOCs analyzed by confirming and expanding the power of our volatile profiling platform.[13] All of these compounds were unequivocally identified based on the coincidence of both mass spectrum and retention time with those of pure standards in two capillary columns of different polarity, with the only exception of 10 compounds not identified in the second column (Table 1). A representative chromatogram is shown in SI Figure S1.

The majority of the identified compounds were described in our previous *Citrus* juice studies, which included Chandler pummelo, Fortune and Clemenules mandarins, and Powell orange.[13] In this work, eight new compounds were identified in hybrids FxCh90 and FxCh77 and their parental genotypes: (*E*)-2-decenal (*m* 56), isobornyl acetate (*m* 81), dihydrocarvone (*m* 52), hexyl butanoate (*m* 73), butyl hexanoate (*m* 75), hexyl hexanoate (*m* 74), 3-octanone (*m* 93), and 2-nonanone (*m* 96). The first four compounds have been previously identified in other *Citrus* genotypes: (*E*)-2-decenal in tangerine hybrids juices and in pummelo, lime, orange, and tangerine peel oils,[9,23,24] isobornyl acetate in pummelo peel,[25] dihydrocarvone in orange and mandarin juices,[9,20,26] and hexyl butanoate in orange and tangerine hybrids juices and mandarin peel.[9,11,27] The other four compounds are described here for the first time in the juice of a *Citrus* species (Table 1). Hexyl butanoate and butyl hexanoate are typical apple fruit volatile compounds that can be used as a maturity index in this fruit; butyl hexanoate is also an insect attractant.[28,29] Regarding 3-octanone, it has been described as having a mushroom odor, similar to 1-octen-3-one, this being another aliphatic ketone identified frequently in *Citrus* juice.[3,9,30] The other new ketone, 2-nonanone, has been identified in several matrixes such as kiwifruit juices, in the essential oil of several Rutaceae species, in yellowfin tuna, or even as a component of cheese aroma.[31−35] The compound 2-nonanone has been described to have nematicidal and antifungal properties.[36,37] In fact an active packaging system based on the release of 2-nonanone is used to increase the postharvest shelf life of fresh wild strawberries in the marketing stage; excessive levels of this volatile can, however, affect the taste of berries and lead consumers to reject the product.[38]

As seen in Table 1, almost all of the identified compounds were detected in the four genotypes. Only four compounds were identified exclusively in the Chandler parental genotype ((*Z*)-ocimene, (*E*,*E*)-2,4-nonadienal, (*E*)-linalool oxide, and γ-dodecalactone; *m* 109, *m* 110, *m* 111, and *m* 113, respectively). Similarly, propyl acetate (*m* 60) and ethyl 2-methylbutanoate (*m* 61) were compounds identified exclusively in the parental Fortune genotype. Regarding hybrids, β-citronellal (*m* 5) was the only exclusive compound identified in the FxCh77 hybrid,

while no exclusive compound was detected in the FxCh90 hybrid.

The relative levels of each compound for all of the genotypes are shown in relation to the level of each compound in the Chandler genotype, because this is the genotype where the largest number of compounds was identified (107 compounds, with γ-dodecalactone, *m* 113, only detected in trace amounts). The relative levels of those compounds not detected in Chandler are expressed in relation to a genotype containing it (Table 1). Although very few qualitative differences were observed in any of the four genotypes, differences in the levels of accumulation were observed for almost all of the compounds, indicating that the characteristic volatile profile of each genotype relies on quantitative rather than qualitative differences.

Although it seemed reasonable to expect that hybrids would show that the levels of most volatiles are intermediate between those of the two parents, the results revealed that 56 of the 113 compounds were present at transgressive levels in at least one of the hybrids. Indeed, 40 compounds in the hybrids presented significantly higher levels than in any of their parents, and 16 compounds were present at statistically significantly lower levels. The remaining 57 volatiles were present at levels that were either intermediate or not significantly different from one of the parentals. The most extreme behavior was shown by ester compounds hexyl acetate (*m* 6), α-terpinyl acetate (*m* 13), or linalyl acetate (*m* 15), present in hybrid FxCh90 at levels of 30-fold or higher than in any of their parentals. Compounds such as ethyl heptanoate (*m* 86), 6-methyl-5-hepten-2-one (*m* 100), and 1-pentanol (*m* 101), which were present at different levels well above the threshold levels in both parentals, were not be detected in at least one of the hybrids, while 2,3-pentanedione (*m* 98) was reduced 17-fold in the hybrids (Table 1). This transgressive behavior can be observed graphically for FxCh90 and FxCh77 in Figure 1 and SI Figure S2, respectively, where the volatiles that over- or underaccumulated in the hybrids if compared to their parents are shown in the three defined areas (overaccumulating zone, underaccumulating zone, and interparents zone). The statistical significance of these differences is shown in Table 1 and SI Figure S3. However, the transgressive behavior described for the levels of volatile compounds in these hybrids was not observed for other fruit quality traits (see those traits in the interparental zone in the plots, in Figure 2 and in SI Figure S4). A similar transgressive behavior in the volatile profile has been observed in a number of peach siblings derived from a cross also involving one hybrid as a parent[39] and also in apple,[40] which probably indicates that volatile traits are especially prone to this type of transgressive behavior.

To globally verify whether the volatile profiles can be used to differentiate both hybrids from the parental genotypes and to identify the volatiles that contributed the most to the separation between the new materials generated by breeding and the parental genotypes, a PCA was performed using the complete data set. Based on the volatile profile, Figure 3 shows that all four genotypes are completely separated from each other. Principal component 1 accounts for the majority of total variance (53.6% of variance), and mainly separates the parent Chandler pummelo from the other three genotypes, and also the parent Fortune from their derived hybrids to a lesser extent. The relative position of the samples in the PCA space is not consistent with any of the hybrids, with a volatile phenotype intermediate shown between the two parentals. In fact,

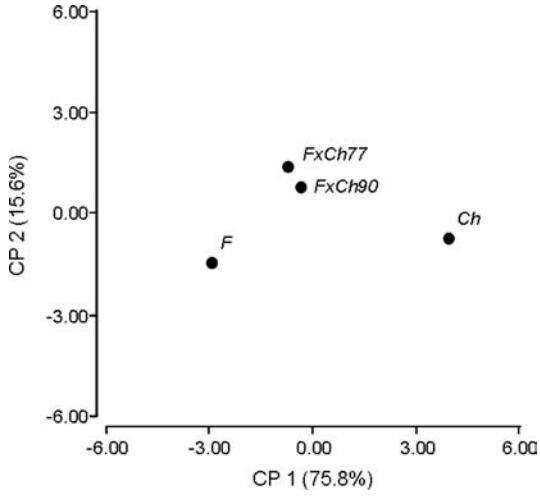


**Figure 2.** Principal component analysis score plot based on a data set of 11 fruit quality traits. Principal components 1 and 2 are represented.

principal component 1 confirmed that both hybrids showed rather transgressive behavior, with a volatile profile opposed to that of the male parental Chandler pummelo, which was even more distant to Chandler than the other parental, Fortune mandarin. Of the two hybrids, FxCh90 was seen to be slightly more transgressive than FxCh77. An analysis of the loading plot revealed the compounds to be responsible for the separation between samples (Figure 4). The volatile compounds that most contributed to the first component were a group of monoterpenoid compounds (*p*-cymene, (*Z*)-ocimene, (*E*)-linalool oxide, 2-carene; *m* 108, *m* 109, *m* 111, *m* 112, respectively) and (*E,E*)-2,4-nonadienal (*m* 110), which are almost exclusive of Chandler pummelo. This group of compounds also differentiated Chandler pummelo from Clemenules mandarin and Powell orange, as previously reported,[13] and some have also been identified in the other few pummelo juice and flavedo studies.[14,15,25,41] According to the literature, 2-carene has never been detected in orange and mandarin aroma juices, and (*Z*)-ocimene, linalool oxides, and (*E,E*)-2,4-nonadienal have been detected only very occasionally.[1,11,14,21,22,42] In contrast, *p*-cymene has been frequently isolated in these juices.[6,9,11,12,18,19,43] Fortune mandarin, and the two hybrids in particular, show higher levels of acetic esters octyl acetate (*m* 19), nonyl acetate (*m* 14), decyl acetate (*m* 20), α-terpinyl acetate (*m* 13), linalyl acetate (*m* 15), geranyl acetate (*m* 25), and citronellyl acetate (*m* 28), the monoterpene alcohol linalool (*m* 1), and long-chain lipid derivatives 1-decanol (*m* 10) and dodecanal (*m* 24).

Principal component 2 explained about 22.4% of variance and clearly separated Fortune from the other three genotypes (SI Figure S5). What differentiated Fortune from the rest was mainly the higher levels of propyl acetate (*m* 60) and a series of ethyl esters: ethyl 2-methylbutanoate (*m* 61), ethyl acetate (*m* 62), ethyl propanoate (*m* 59), ethyl butanoate (*m* 57), and ethyl nonanoate (*m* 64) (SI Figure S6). Principal component 3, accounting for only 10.2% of variance, revealed that it is possible to distinguish the two hybrids from each another in accordance with specific volatiles (Figure 3). According to the loading plot corresponding to PC3, hybrid FxCh90 was characterized by higher levels of acetate compounds heptyl acetate (*m* 9), octyl acetate (*m* 19), nonyl acetate (*m* 14), decyl acetate (*m* 20), methyl decanoate (*m* 18), α-terpinyl acetate (*m* 13) and (*E*)-carvyl acetate (*m* 23), and also long-chain lipid

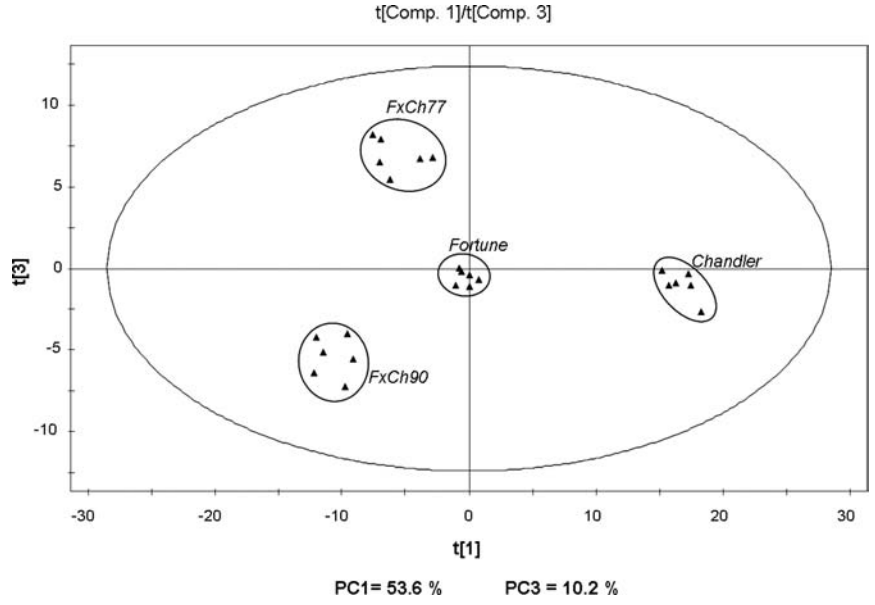


**Figure 3.** Principal component analysis score plot based on 113 volatile compounds. Principal components 1 and 3 are represented.

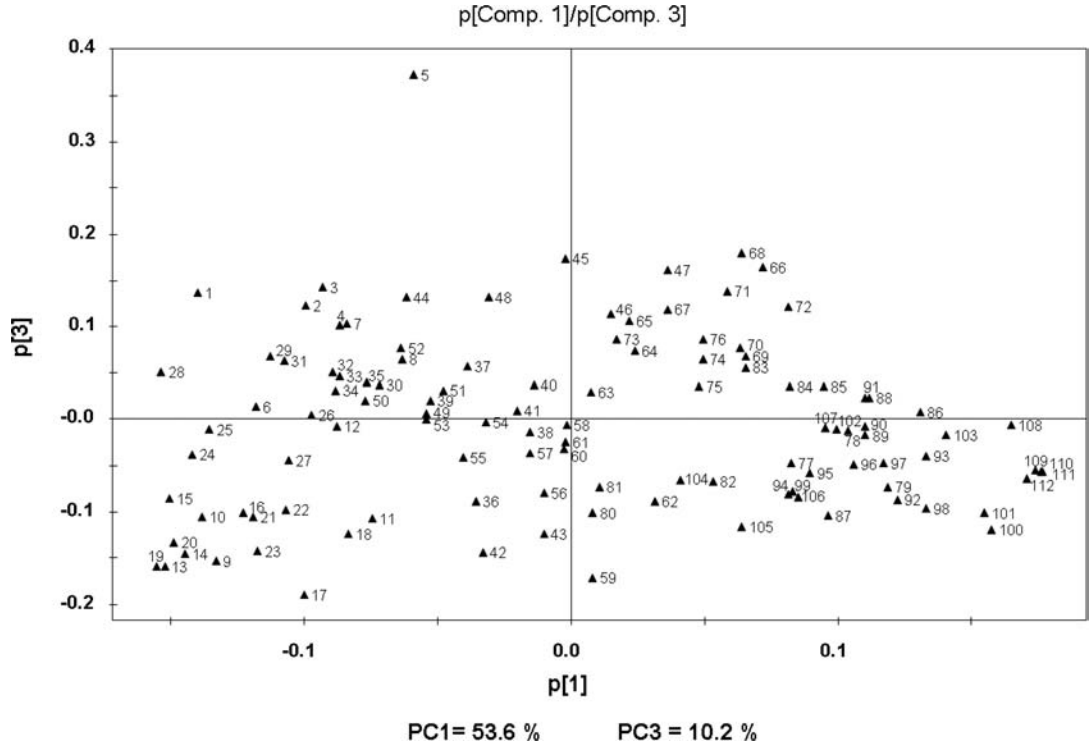


**Figure 4.** Principal component analysis loading plot based on volatile composition for principal components 1 and 3. Each number corresponds to a particular volatile compound, as indicated in Table 1.

derivatives 1-octanol (*m* 17), decanal (*m* 42), and undecanal (*m* 43) (Figure 4). Hybrid FxCh77, however, was characterized by lower levels of these compounds, together with higher levels of monoterpenoids linalool (*m* 1), *β*-citronellol (*m* 2), perillaldehyde (*m* 3), *α*-terpineol (*m* 4), *β*-citronellal (*m* 5), geraniol (*m* 7), (*Z*)- and (*E*)-limonene oxides (*m* 44 and *m* 48, respectively), and geranial (*m* 67), norisoprenoids geranylacetone (*m* 65), and *β*-ionone (*m* 71), $C_5$ and $C_6$ lipid derivatives 1-penten-3-one (*m* 45), (*E*)-2-pentenal (*m* 47), 3-pentanone (*m* 72), and (*Z*)-3-hexen-1-ol (*m* 66) (Figure 4).

When the complete data set of fruit quality traits was used (Figure 2), the PCA showed that both hybrids displayed mostly an intermediate behavior between their parental genotypes for these traits, as revealed by principal component 1, which accounted for most of the total variability (75.8%).

The HCA done over the same volatile data set confirmed that FxCh90 and FxCh77 shared the most similar volatile profile (Figure 5). Consistently with the PCA results, the volatile profile of the Fortune genotype in HCA clustering also fell between Chandler and the hybrids. HCA also allowed us to analyze the compounds to check if clustering revealed any

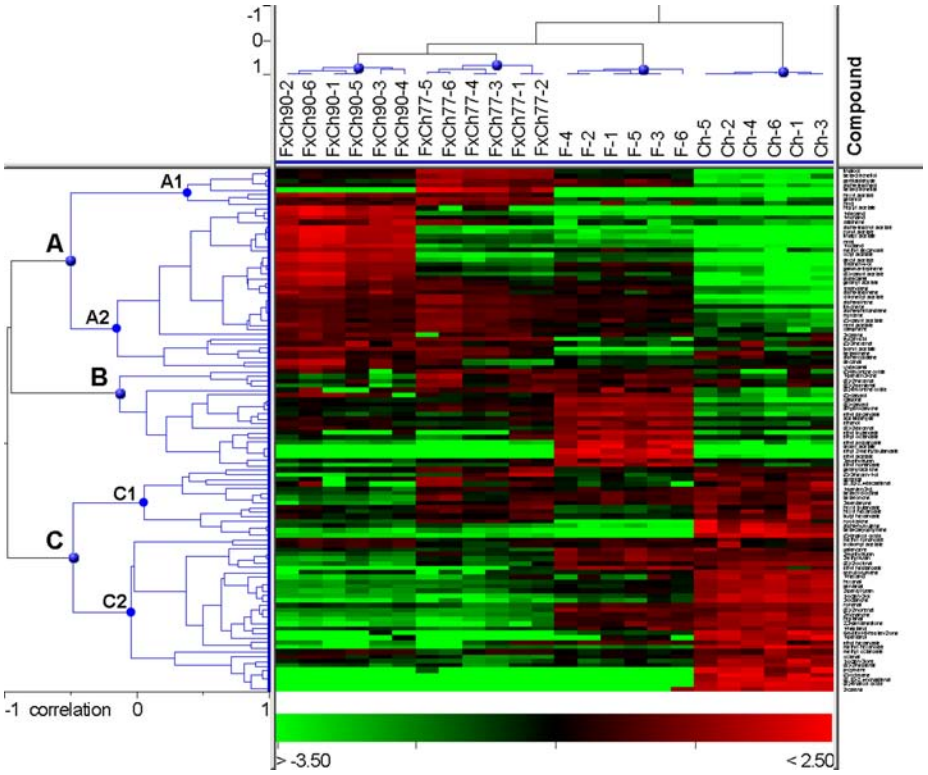


**Figure 5.** Hierarchical cluster analysis of both samples and volatile compounds. Samples grouped according to varieties: Ch, Chandler; F, Fortune; FxCh90 and FxCh77 hybrids. Volatiles grouped into clusters A, B, and C, and subclusters A1, A2, C1, and C2. Colors in the heatmap are related to fold change, in accordance with the scale shown at the bottom: red for higher levels; green for lower levels.

underlying relationship between them. Compounds were organized by HCA into three clusters, namely, A, B, and C, with some subclusters (named A1, A2, C1, and C2), as shown in Table 1. The compounds in cluster A were generally present with higher values in the hybrids than in their parentals. All of these compounds have been generally described in *Citrus* juices.[13,18] Subcluster A1 included the compounds generally present at the highest levels in hybrid FxCh77. These compounds are principally several monoterpene alcohols such as linalool (*m* 1), *β*-citronellol (*m* 2), or geraniol (*m* 7), and monoterpene aldehydes such as *β*-citronellal (*m* 5). Actually this latter compound is exclusive for the FxCh77 genotype and has been identified only in very few mandarins, orange, or hybrids juices.[13,19,43,44] Subcluster A2 mainly included the compounds that accumulated preferentially in the FxCh90 genotype and included *α*-terpinyl acetate (*m* 13), nonyl acetate (*m* 14), neral (*m* 16), *α*-terpinene (*m* 27), 3-carene (*m* 36), or decanal (*m* 42). Interestingly, most of these compounds are aliphatic and monoterpene acetates and monoterpene hydrocarbons. The results from the compounds in cluster A indicated that the two hybrids showed higher levels than their parental genotypes of many monoterpenoid compounds, such as linalool (*m* 1), *β*-citronellol (*m* 2), geraniol (*m* 7), citronelly acetate (*m* 28), or *α*-phellandrene (*m* 31). The odor of these last compounds has been described as floral, fruity, or citrus,[15] which are positive aromatic notes that can make these two hybrids more appealing to consumers. Nevertheless, a taste panel will be necessary to confirm this term.

Cluster B was defined principally by the compounds found more abundantly in Fortune than in the other three genotypes. These include compounds such as propyl acetate (*m* 60), which has never been described in other *Citrus* genotypes in the literature,[13] (*E*)-2-decenal (*m* 56), 3-methylfuran (*m* 63), and ketones carvone (*m* 50) and dihydrocarvone (*m* 52). Seven ethyl esters, e.g., ethyl octanoate (*m* 58), ethyl 2-methylbutanoate (*m* 61), or ethyl acetate (*m* 62), were more abundant in the Fortune genotype, which is consistent with the results of the loading plots for PC2. According to the literature, these ethyl esters have been frequently identified in many *Citrus* juices.[3,11,17,18,20,24,45] It should be noted that the Fortune samples analyzed herein were relatively rich in ethanol as compared to the other genotypes. This observation might explain the high levels of ethyl esters as they can be produced by esterification of ethanol with the acyl groups derived from fatty acid and amino acid metabolism.[46]

Finally, cluster C included the compounds that were more abundant in Chandler than in the other three genotypes. Subcluster C1 included the compounds found more abundantly in Chandler but also in hybrid FxCh77 (the most similar hybrid to Chandler), such as geranylacetone (*m* 65) or geranial (*m* 67). Subcluster C2 included the compounds that were more abundant in the Chandler genotype than in the other three genotypes. A number of aliphatic aldehydes (pentanal to nonanal, *m* 90, *m* 89, *m* 97, *m* 105, and *m* 94, respectively) and olefins (*E*)-2-heptenal, (*E*)-2-octenal, and (*E*,*E*)-2,4-nonadienal; *m* 107, *m* 85, and *m* 110, respectively), several aliphatic alcohols (1-pentanol, 1-hexanol, 1-heptanol, and 1-octen-3-ol; *m* 101, *m* 88, *m* 99, and *m* 92, respectively), and some aliphatic ketones (3-octanone, 2-nonanone, 2,3-pentanedione, 6-methyl-5-hepten-2-one, and 1-octen-3-one; *m* 93, *m* 96, *m* 98, *m* 100, and *m* 106, respectively) abounded in this genotype if compared to the other three genotypes. The higher levels of aliphatic aldehydes (octanal, nonanal) can, in part, be responsible for peely and fatty notes of pummelo juices.[15]

The higher levels of both 3-octanone and 1-octen-3-one can confer a hint of mushroom to the characteristic pummelo juice aroma.[30] These compounds were detected in Fortune and in hybrids FxCh90 and FxCh77 at almost trace levels. Several esters, such as some alkyl hexanoates (*m* 74, *m* 103), and compound 2-pentylfuran (*m* 91), were also present in larger quantities in Chandler than in Fortune or the hybrids. Moreover, as we noted in the analysis of the loading plots, some monoterpene compounds, such as *p*-cymene (*m* 108), (*Z*)-ocimene (*m* 109), 2-carene (*m* 112), or (*Z*)- and (*E*)-linalool oxide (*m* 79 and *m* 111, respectively), were also more abundant in Chandler juices, and some were not even detected in the hybrids. Nevertheless, Chandler juice generally showed lower levels of monoterpene compounds than the other three genotypes. Regarding sesquiterpenes, α-humulene (*m* 77) and β-caryophyllene (*m* 78) (subcluster C1) were much more profuse in the Chandler genotype than in any of the other three genotypes here studied or in Powell orange and Clemenules mandarin, according to a previous study.[13] However, sesquiterpene compounds α-copaene (*m* 41) and nootkatone (*m* 76), which served to differentiate Chandler from Powell orange, Clemenules mandarin, or Fortune juices in a previous study,[13] were herein found at similar levels in their hybrids FxCh90 and FxCh77. Therefore, these compounds are unsuitable to differentiate Chandler from their hybrids. The differential terpene profile can explain, at least partially, why pummelo juices exhibit the most differential volatile profile as compared to orange and mandarine juices, and a more similar profile to that of grapefruit.[13,25,41] It is interesting to note that some volatile compounds described in the only other previous study into pummelo juice[15] were not detected in our study (2-ethylhexanol, dimethylsulfone, and (*E*)-2-dodecenal). This might be due to biological variability, differences in growth conditions, or the chemical nature of the fiber used for volatile extraction, among other causes.

This study basically indicates that the differences in the volatile profile between the juice of the two *Citrus* parental genotypes (Chandler pummelo and Fortune mandarin) and their two hybrids are mainly quantitative. Each genotype exhibited a specific volatile profile that can be used for classification or identification purposes. As also noted in our previous study into *Citrus* aroma, there seems to be only a small number of *Citrus* genotype-specific compounds.[13] Most remarkably, the two hybrids characterized herein showed a transgressive (i.e., not intermediate) volatile profile when compared to those of the parents, which completely differed from that of Chandler pummelo and was more similar to that of Fortune mandarin. FxCh90 is especially rich in aliphatic and monoterpene acetates, while FxCh77 contains higher levels of monoterpene hydrocarbons and monoterpene alcohols than any of their parents. In our case the most characteristic VOCs of the Fortune genotype are 3-methylfuran (*m* 63), (*E*)-2-decenal (*m* 56), carvone (*m* 50), and dihydrocarvone (*m* 52), and some ethyl esters (*m* 53, *m* 57, *m* 58, *m* 59, *m* 61, *m* 62, and *m* 64). Finally, the juice of the Chandler genotype is more abundant in aliphatic compounds (aldehydes, alcohols, and ketones), some monoterpene hydrocarbons (*p*-cymene, (*Z*)-ocimene, and 2-carene; *m* 108, *m* 109, and *m* 112, respectively), and sesquiterpenes, such as α-humulene (*m* 77) and β-caryophyllene (*m* 78).

In conclusion, the volatile analysis platform used has allowed us to identify genotypes with differences in the aromatic profile that either enhance or inhibit some of the volatile characteristics of their parents, which the genetic analysis neither predicted nor anticipated. The HS-SPME-GC-MS analysis of *Citrus* juice has proven to be a tool that allows genotype differentiation that can be used in the assessment of *Citrus* breeding programs.

## ■ ASSOCIATED CONTENT

### Supporting Information

Figures showing the total ion count chromatogram of hybrid FxCh90(Figure S1), values for the different metabolites and phenotype traits in hybrid FxCh77 in relation to the values in Fortune (Figure S2), *Z*-score plots showing the traits with transgressive behavior above and below the Fortune range (Figure S3), fruit quality traits for the four genotypes (Figure S4), principal component analysis score plot based on volatile composition for principal components 1 and 2 (Figure S5), and principal component analysis loading plot based on volatile composition for principal components 1 and 2 (Figure S6) and tables listing retention times of the identified compounds under the two different chromatographic conditions used (Table S1) and statistical significance and values of the *Z*-scores shown in Figure 1 and Figure S2 (Table S2). This material is available free of charge via the Internet at http://pubs.acs.org.

## ■ AUTHOR INFORMATION


### Corresponding Author

*Tel.: + 34 96 3424000. Fax: + 34 96 3424001. E-mail: gonzalez_mde@gva.es.

### Present Address

[⊥]Instituto de Biología Molecular y Celular de Plantas, CSIC—Universidad Politécnica de Valencia, Ciudad Politécnica de la Innovación, Edificio 8 E, Ingeniero Fausto Elio, 46022 Valencia, Spain.

### Author Contributions

[‖]J.L.R. and M.C.G.-M. contributed equally to this work.



### Funding

This work has been supported by Projects GVPRE/2008/164 of Conselleria d'Educació of the Valencian Community and RTA2011-00132-C02 of INIA. M.C.G.-M. is contracted by the Fundación Agroalimed (Conselleria d'Agricultura of VC).


### Notes

The authors declare no competing financial interest.

## ■ ACKNOWLEDGMENTS


We thank I. Herrero and T. Caballero for laboratory assistance. We also thank A. Gutiérrez for networking activities. Volatile profiling was performed at the Metabolomic facilities of the *Instituto de Biología Molecular y Celular de Plantas*, CSIC (Spain).


## ■ ABBREVIATIONS USED

VOCs, volatile organic compounds; HS-SPME, headspace solid phase microextraction; DVB/CAR/PDMS, divinylbenzene/carboxen/poly(dimethylsiloxane); *m*, metabolite; PCA, principal component analysis (PC2, principal component 2; PC3, principal component 3); HCA, hierarchical cluster analysis

## ■ REFERENCES


(1) Moshonas, G. P.; Shaw, P. E. Quantitation of volatile constituents in mandarin juices and its use for comparison with orange juices by multivariate analysis. *J. Agric. Food Chem.* **1997**, *45*, 3968−3972.

(2) Buettner, A.; Schieberle, P. Evaluation of key aroma compounds in hand-squeezed grapefruit juice (*Citrus paradisi* Macfayden) by quantitation and flavor reconstitution experiments. *J. Agric. Food Chem.* **2001**, *49*, 1358−1363.
(3) Buettner, A.; Schieberle, P. Evaluation of aroma differences between hand-squeezed juices from Valencia Late and Navel oranges by quantitation of key odorants and flavor reconstitution experiments. *J. Agric. Food Chem.* **2001**, *49*, 2387−2394.
(4) Rouseff, R. L.; Perez-Cacho, P. R.; Jabalpurwala, F. Historical review of Citrus flavor research during the past 100 years. *J. Agric. Food Chem.* **2009**, *57*, 8115−8124.
(5) Arena, E.; Guarrera, N.; Campisi, S.; Asmundo, C. N. Comparison of odour active compounds detected by gas-chromatography-olfactometry between hand-squeezed juices from different orange varieties. *Food Chem.* **2006**, *98*, 59−63.
(6) Barboni, T.; Luro, F.; Chiaramonti, N.; Desjobert, J.-M.; Muselli, A.; Costa, J. Volatile composition of hybrids *Citrus* juices by headspace solid-phase micro extraction/gas chromatography/mass spectrometry. *Food Chem.* **2009**, *116*, 382−390.
(7) Barboni, T.; Muselli, A.; Luro, F.; Desjobert, J.-M.; Costa, J. Influence of processing steps and fruit maturity on volatile concentrations in juices from clementine, mandarin and their hybrids. *Eur. Food Res. Technol.* **2010**, *231*, 379−386.
(8) Tietel, Z.; Porat, R.; Weiss, K.; Ulrich, D. Identification of aroma-active compounds in fresh and stored 'Mor' mandarins. *Int. J. Food Sci. Technol.* **2011**, *46*, 2225−2231.
(9) Miyazaki, T.; Plotto, A.; Goodner, K.; Gmitter, F. G., Jr. Distribution of aroma volatile compounds in tangerine hybrids and proposed inheritance. *J. Sci. Food Agric.* **2011**, *91*, 449−460.
(10) Jordan, M. J.; Tillman, T. N.; Mucci, B.; Laencina, J. Using HS-SPME to determine the effects of reducing insoluble solids on aromatic composition of orange juice. *LWT−Food Sci. Technol.* **2001**, *34*, 244−250.
(11) Brat, P.; Rega, B.; Alter, P.; Reynes, M.; Brillouet, J.-M. Distribution of volatile compounds in the pulp, cloud, and serum of freshly squeezed orange juice. *J. Agric. Food Chem.* **2003**, *51*, 3442−3447.
(12) Pérez-López, A. J.; Carbonell-Barrachina, A. A. Volatile odour components and sensory quality of fresh and processed mandarin juices. *J. Sci. Food Agric.* **2006**, *86*, 2404−2411.
(13) González-Mas, M. C.; Rambla, J. L.; Alamar, M. C.; Gutiérrez, A.; Granell, A. Comparative analysis of the volatile fraction of fruit juice from different *Citrus* species. *PLoS One* **2011**, *6*, No. e22016.
(14) Shaw, P. E.; Goodner, K. L.; Moshonas, M. G.; Hearn, C. J. Comparison of grapefruit hybrid fruit with parent fruit based on composition of volatile components. *Sci. Hortic. (Amsterdam, Neth.)* **2001**, *91*, 71−80.
(15) Cheong, M. W.; Liu, S. Q.; Zhou, W.; Curran, P.; Yu, B. Chemical composition and sensory profile of pomelo (*Citrus grandis* (L.) Osbeck) juice. *Food Chem.* **2012**, *135*, 2505−2513.
(16) Bernet, G. P.; Fernandez-Ribacoba, J.; Carbonell, E. A.; Asins, M. J. Comparative genome-wide segregation analysis and map construction using a reciprocal cross design to facilitate citrus germplasm utilization. *Mol. Breed.* **2010**, *25*, 659−673.
(17) Bylaite, E.; Meyer, A. S. Characterisation of volatile aroma compounds of orange juices by three dynamic and static headspace gas chromatography techniques. *Eur. Food Res. Technol.* **2006**, *222*, 176−184.
(18) Ruiz Perez-Cacho, P.; Rouseff, R. L. Fresh squeezed orange juice odor: A review. *Crit. Rev. Food Sci.* **2008**, *48*, 681−695.
(19) Tomiyama, K.; Aoki, H.; Oikawa, T.; Sakurai, K.; Kasahara, Y.; Kawakami, Y. Characteristic volatile components of Japanese sour citrus fruits: Yuzu, Sudachi and Kabosu. *Flavour Fragrance J.* **2012**, *27*, 341−355.
(20) Selli, S.; Cabaroglu, T.; Canbas, A. Volatile flavour components of orange juice obtained from the cv. Kozan of Turkey. *J. Food Compos. Anal.* **2004**, *17*, 789−796.
(21) Mahattanatawee, K.; Rouseff, R.; Valim, M. F.; Naim, M. Identification and aroma impact of norisoprenoids in orange juice. *J. Agric. Food Chem.* **2005**, *53*, 393−397.
(22) Qiao, Y.; Xie, B. J.; Zhang, Y.; Fan, G.; Yao, X. L.; Pan, S. Y. Characterization of aroma active compounds in fruit juice and peel oil of Jinchen sweet orange fruit (*Citrus sinensis* (L.) Osbeck) by GC-MS and GC-O. *Molecules* **2008**, *13*, 1333−1344.
(23) Minh Tu, N. T.; Thanh, L. X.; Une, A.; Ukeda, H.; Sawamura, M. Volatile constituents of Vietnamese pummelo, orange, tangerine and lime peel oils. *Flavour Fragrance J.* **2002**, *17*, 169−174.
(24) Miyazaki, T.; Plotto, A.; Baldwin, E. A.; Reyes-De-Corcuera, J. I.; Gmitter, F. G., Jr. Aroma characterization of tangerine hybrids by gas-chromatography-olfactometry and sensory evaluation. *J. Sci. Food Agric.* **2012**, *92*, 727−735.
(25) Cheong, M.-W.; Liu, S.-Q.; Yeo, J.; Chionh, H.-K.; Pramudya, K.; Curran, P.; Yu, B. Identification of aroma-active compounds in Malaysian pomelo (*Citrus grandis* (L.) Osbeck) peel by gas chromatography-olfactometry. *J. Essent. Oil Res.* **2011**, *23*, 34−42.
(26) Elmaci, Y.; Altug, T. Flavor characterization of three mandarin cultivars (Satsuma, Bodrum, Clemantine) by using GC/MS and flavour profile analysis techniques. *J. Food Qual.* **2005**, *28*, 163−170.
(27) Liu, C.; Cheng, Y.; Zhang, H.; Deng, X.; Chen, F.; Xu, J. Volatile constituents of wild Citrus Mangshanyegan (*Citrus nobilis* Lauriro) Peel oil. *J. Agric. Food Chem.* **2012**, *60*, 2617−2628.
(28) Natale, D.; Mattiacci, L.; Pasqualini, E.; Dorn, S. Apple and peach fruit volatiles and the apple constituent butyl hexanoate attract female oriental fruit moth, *Cydia molesta*, in the laboratory. *J. Appl. Entomol.* **2004**, *128*, 22−27.
(29) Villatoro, C.; Altisent, R.; Echeverría, G.; Graell, J.; López, M. L.; Lara, I. Changes in biosynthesis of aroma volatile compounds during on-tree maturation of 'Pink Lady®' apples. *Postharvest Biol. Technol.* **2008**, *47*, 286−297.
(30) Cho, I. H.; Lee, S. M.; Kim, S. Y.; Choi, H.-K.; Kim, K.-O.; Kim, Y.-S. Differentiation of aroma characteristics of pine-mushrooms (*Tricholoma matsutake* Sing.) of different grades using Gas Chromatography-Olfactometry and sensory analysis. *J. Agric. Food Chem.* **2007**, *55*, 2323−2328.
(31) Wan, X. M.; Stevenson, R. J.; Chen, X. D.; Melton, L. D. Application of headspace solid-phase microextraction to volatile flavour profile development during storage and ripening of kiwifruit. *Food Res. Int.* **1999**, *32*, 175−183.
(32) Biniyaz, T.; Habibi, Z.; Masoudi, S.; Rustaiyan, A. Composition of the essential oils of *Haplophyllum furfuraceum* Bge. ex Boiss. and *Haplophyllum virgatum* Spach. from Iran. *J. Essent. Oil Res.* **2007**, *19*, 49−51.
(33) Edirisinghe, R. K. B.; Graham, A. J.; Taylor, S. J. Characterisation of the volatiles of yellowfin tuna (*Thummus albacares*) during storage by solid phase microextraction and GC-MS and their relationship to fish quality parameters. *Int. J. Food Sci. Technol.* **2007**, *42*, 1139−1147.
(34) Dob, T.; Dahmane, D.; Gauriat-Desrdy, B.; Daligault, V. Volatile constituents of the essential oil of *Ruta chalepensis* L. subsp. Angustifolia (Pers.) P. Cout. *J. Essent. Oil Res.* **2008**, *20*, 306−309.
(35) Poveda, J. M.; Sánchez-Palomo, E.; Pérez-Coello, M. S.; Cabezas, L. Volatile composition, olfactometry profile and sensory evaluation of semi-hard Spanish goat cheeses. *Dairy Sci. Technol.* **2008**, *88*, 355−367.
(36) Gu, Y. Q.; Mo, M. H.; Zhou, J. P.; Zou, C. S.; Zhang, K. Q. Evaluation and identification of potential organic nematicidal volatiles from soil bacteria. *Soil Biol. Biochem.* **2007**, *39*, 2567−2575.
(37) Neri, F.; Mari, M.; Brigati, S.; Bertolini, P. Fungicidal activity of plant volatile compounds for controlling *Monilinia laxa* in some fruit. *Plant Dis.* **2007**, *91*, 30−35.
(38) Almenar, E.; Catalá, R.; Hernández-Muñoz, P.; Gavara, R. Optimization of an active package for wild strawberries bases on the release of 2-nonanone. *LWT−Food Sci. Technol.* **2009**, *42*, 587−593.
(39) Sánchez, G.; Martínez, J.; Romeu, J.; García, J.; Monforte, A. J.; Badenes, M. L.; Granell, A. The peach volatilome modularity is

reflected at the genetic and environmental response level in a QTL mapping population. *BMC Plant Biol.* **2014**, *14*, 137.
(40) Dunemann, F.; Ulrich, D.; Boudichevskaia, A.; Grafe, C.; Weber, W. E. QTL mapping of aroma compounds analysed by headspace solid-phase microextraction gas chromatography in the apple progeny 'Discovery' x 'Prima'. *Mol. Breed.* **2009**, *23*, 501−521.
(41) Sawamura, M.; Kuriyama, T. Quantitative determination of volatile constituents in the pummelo (*Citrus grandis* Osbeck forma Tosa-buntan). *J. Agric. Food Chem.* **1988**, *36*, 567−569.
(42) Rinaldi, M.; Gindro, R.; Barbeni, M.; Allegrone, G. Pattern recognition and genetic algorithms for discrimination of orange juices and reduction of significant components from headspace solid-phase microextraction. *Phytochem. Anal.* **2009**, *20*, 402−407.
(43) Tounsi, M. S.; Wannes, W. A.; Ouerghemmi, I.; Jegham, S.; Njima, Y. B.; Hamdaoui, G.; Zemni, H.; Marzouk, B. Juice components and antioxidant capacity of four Tunisian Citrus varieties. *J. Sci. Food Agric.* **2011**, *91*, 142−151.
(44) Jordán, M. J.; Goodner, K. L.; Castillo, M.; Laencina, J. Comparison of two headspace solid phase microextraction fibres for the detection of volatile chemical concentration changes due to industrial processing of orange juice. *J. Sci. Food Agric.* **2005**, *85*, 1065−1071.
(45) Plotto, A.; Margaría, C. A.; Goodner, K. L.; Baldwin, E. A. Odour and flavour thresholds for key aroma components in an orange juice matrix: Esters and miscellaneous compounds. *Flavour Fragrance J.* **2008**, *23*, 398−406.
(46) Tietel, Z.; Lewinsohn, E.; Fallik, E.; Porat, R. Elucidating the roles of ethanol fermentation metabolism in causing off-flavors in mandarins. *J. Agric. Food Chem.* **2011**, *59*, 11779−11785.

## NOTE ADDED AFTER ASAP PUBLICATION

An additional Supporting Information file has posted for this paper on November 10, 2014.

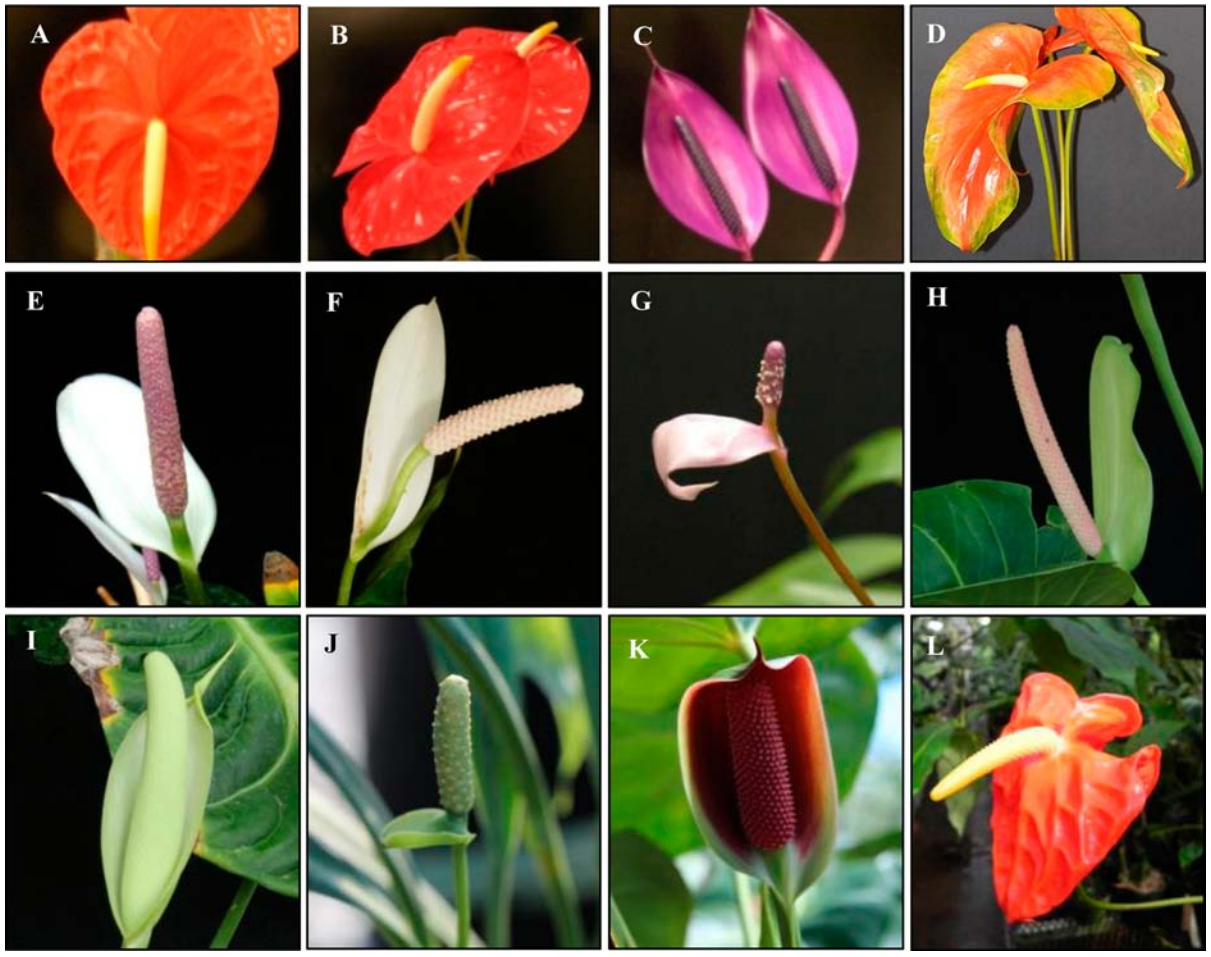


**Figure 1.** *Anthurium* spathes from commercial varieties (A–D) and species (E–L): (A) standard commercial cultivar 'Nitta', (B) standard commercial cultivar 'New Pahoa Red', (C) tulip commercial cultivar 'ARCS', (D) Obake commercial cultivar 'Tropic Sunrise', (E) *A. antioquiense*, (F) *A. armeniense*, (G) *A. amnicola*, (H) *A. hoffmannii*, (I) *A. veitchii*, (J) *A. bakeri*, (K) *A. kamemotoanum*, and (L) *A. andraeanum*.

larger study of the Araceae.[5] Iwata et al.[4] noted the presence of a major flavone component in several commercial *Anthurium* cultivars, which they suggested might be an acacetin derivative, but the structure was not determined. A 2001 study described the isolation of four new flavone C-glycosides from an *Anthurium versicolor* sample,[13] while in 2012 three additional examples were reported from the commercial *Anthurium* cultivar 'New Pahoa Red'.[14] Contemporary with this study, additional flavonoids from a range of commercial *Anthurium* cultivars were identified, largely on the basis of MS/MS data.[15]

Flavonoids have proved useful as chemotaxonomic markers in a range of agriculturally important plants, being used to categorize plants as diverse as plums,[16] grapes,[17] nettles,[18] and yew (*Taxus* spp.).[19] Modern analytical methods, in particular hyphenated mass spectrometry techniques combined with high-performance liquid chromatography (HPLC-MS) and gas chromatography (GC-MS), have proved invaluable in carrying out chemotaxonomic analyses. These methods have the capability to monitor and quantitate hundreds or even thousands of metabolites, while simultaneously providing high-resolution mass or fragmentation data that can be used to identify key compounds, allowing a much more rigorous analysis of the total metabolite content of the organism. Statistical techniques such as principal component analysis (PCA), hierarchical cluster analysis (HCA), and partial least squares discriminant analysis (PLS-DA) can be used to simplify the dimensionality of the data and compare different samples and classes.

In this study, we performed HPLC-MS analysis of the flavonoid components of 28 commercial cultivars of *Anthurium* grown in Hawaii, in addition to eight species sampled from living collections. Analysis of these data by HCA, PCA, and PLS-DA revealed distinctive differences in the various commercial cultivars and identified key anthocyanins (**1**–**3**), flavone glycosides (**4**–**8**), and other phenolics (**9**) that can be used in differentiating the cultivars and their ancestry.

## MATERIALS AND METHODS

**General Experimental Procedures.** NMR spectra were recorded on an Avance DRX 400 (Bruker, Billerica, MA) with the solvent used as an internal standard; MS analyses were conducted on an Accurate Mass 6530 qTOF HPLC-MS (Agilent, Santa Clara, CA) attached to an 1260 Infinity HPLC system (Agilent, Santa Clara, CA); preparative HPLC separations were carried out on a Dionex Ultimate 3000 HPLC system (Thermo-Fisher, Waltham, MA). All solvents were HPLC-grade and used without further purification.

**Biological Material.** Plant tissues of commercial cultivars of *Anthurium* were provided by Grayson Inouye, Keaau, HI, member of the Hawaiian Anthurium Industry Association; by *Anthurium* breeder and grower Stanley Oishi, Pahoa, HI; or from cultivars maintained at the greenhouses of Daniel K. Inouye U.S. Pacific Basin Agricultural Research Center facilities in Hilo, HI. Fresh, fully expanded spathes of anthurium cut flowers harvested at marketable stage were used in

these analyses. Anthuriums are market-ready when the tiny flowers on the spadix, which mature from the bottom up, have begun to open, associated with a change of color and appearance. Market-ready anthuriums have at least one-quarter but less than one-third of the flowers on the distal tip of the spadix tightly closed, typically with a contrasting color to the remainder of the spadix. The "nose" of the spadix is approximately $^1/_2$ to $^3/_4$ in. long. The spathe tissue from bicolored (Obake) cultivars was separated by color and processed separately. All commercial cultivars and most species were analyzed in triplicate, with the exception of *A. andraeanum* ABG 19931433, *A. armeniense*, and *Anthurium veitchii* (two spathes each), in addition to *A. andraeanum* ABG19911368, *A. amnicola* Selby 1976-0053-002, and *A. amnicola* MBG Croat 84952 (one spathe each); peak areas shown are average values. Species sampled were obtained from the University of Hawaii at Manoa (*Anthurium bakeri* and *A. kamemotoanum*), the Atlanta Botanical Garden (*A. amnicola* and *A. andraeanum*), Marie Selby Botanical Gardens (*A. amnicola*, *A. antioquiense*, *A. armeniense*, *A. hoffmannii*, and *A. veitchii*) and the Missouri Botanical Garden (*A. amnicola*). Pedigree data for some commercial cultivars were available from historical records: these included 'ARCS',[1] 'Lavender Lady',[1] 'Lady Jane',[1] 'Tropic Sunrise',[20] 'Hokuloa',[21] 'Centennial',[22] 'Tropic Mist',[23] 'Kalapana',[23] 'Tropic Fire',[24] 'Jasmine',[25] 'Marian Seefurth',[26] 'Tropic Lime' (T. Amore, personal communication), and 'Princess Aiko'.[27]

**Analytical HPLC-MS.** Spathes (spadix was not included) were chopped and extracted in methanol−HCl (0.5%) overnight at room temperature at a ratio of 10 mL of solvent per 1 g of tissue. An Inertsil ODS-4 150 mm × 2.1 mm i.d., 3 μm column (GL Sciences) was used for all analytical HPLC separations, and 0.5% formic acid was added to both solvents in order to improve peak shape for anthocyanin components. A complex gradient was employed with a flow rate of 0.4 mL/min, starting at 100% $H_2O$ and ramping to 9% acetonitrile (MeCN) over 10 min, holding for 20 min, before ramping to 24% MeCN over 30 min, holding for 5 min, then ramping to 40% over 13 min. The column was then ramped to 100% MeCN over 5 min, before reverting to initial conditions for the next analysis. Peak areas were obtained for each compound at either 525 nm (anthocyanins), 330 nm (flavones), or 280 nm (other phenolics). In total, 315 compounds were analyzed.

An Agilent Jetstream source in positive mode was used for mass analysis, with a capillary voltage of 3500 V and a fragmenter voltage of 175 V. Gas temperature was 300 °C at a flow rate of 8 L/min; sheath gas was at 350 °C at 11 L/min. Masses were detected from $m/z$ 100 to 2000, with internal calibration carried out by use of internal standards at $m/z$ 121.0509 and 922.0098.

**Statistical and Multivariate Data Analyses.** Statistical analysis was conducted by use of Massprofiler Professional software (Agilent, Santa Clara, CA). Three sample sets were used for statistical analyses. For initial hierarchical clustering analysis (HCA) and the first principal component analysis (PCA), the full set of 28 commerical cultivars and eight species was used, with a total of 315 metabolites. For the second PCA and PLS-DA analyses, a reduced sample set of 27 commercial cultivars and four species was used, with a total of 196 metabolites. Finally, for the Heatmap analysis, a reduced sample set of 27 cultivars and four species was used, with 42 metabolites (Tables 2 and 3) used for analysis. For HCA, Euclidean distances were used with complete clustering. For PCA, raw compound integration values were baselined to the median across all samples. They were transformed via log2 prior to analysis, and eight principal components were used. For PLS-DA analysis, two components were used, with auto-scaling and 3-fold validation. Validation with confusion matrices confirmed the assigned groupings.

**Large-Scale Extractions and Isolation of Selected Metabolites.** Spathes from the 'ARCS' cultivar (40 g) were extracted twice with methanol−HCl (0.1%, 400 mL) at room temperature. The crude extract was reduced under vacuum, dissolved in methanol, and passed through Amberlite XAD-4 resin (50 g) to remove nonpolar metabolites. This extract was then fractionated by reversed-phase (RP) HPLC on a 250 × 20 mm i.d., 5 μm, Sunrise C-18 column (Shimadzu) under isocratic conditions (20% MeCN−$H_2O$, 10 mL/min), with peaks monitored by online UV detection, to yield compound **7** (18.7 mg). High-resolution mass spectrometry data were consistent with the proposed structure, and NMR data matched well with literature values.[29]

The isolation of flavonoids **4**−**6** has been reported previously.[14] Neobudofficide **8** and epicatechin **9** were isolated from the same extraction. Briefly, leaves (39 g) from the 'New Pahoa Red' cultivar of *A. andraeanum* were obtained from Pacific Floral Exchange (Keaau, HI) and extracted and passed through a resin as described above. This extract was then fractionated by reversed-phase HPLC on a 250 × 20 mm i.d., 5 μm, Sunrise C-18 column (Shimadzu), under isocratic conditions (18% MeCN−$H_2O$, 10 mL/min), to yield **8** (11.1 mg) and **9** (14.6 mg). High-resolution electrospray ionization (ESI) MS data were consistent with the proposed structures, and NMR data matched well with literature values.[30,31]

## RESULTS AND DISCUSSION

**General.** Twenty-eight Hawaiian *Anthurium* cultivars were selected for analysis, including a variety of colors and encompassing standard-shaped, tulip-shaped, and Obake cultivars. In addition, in order to provide a baseline against which to compare the commercial cultivars, a small suite of species were sampled from living collections (Table 1). Specimens were extracted with methanol−HCl and the extracts were analyzed via HPLC-MS (Figure 2). Analyses were carried out at three wavelengths, 525, 330, and 280 nm, and peak areas for a total of 315 compounds were obtained. Compounds absorbing at 525 nm possessed UV/vis spectra consistent with anthocyanin pigments, while compounds absorbing at 330 nm had UV/vis spectra characteristic of flavonols, with mass spectrometry data suggesting that most were present as glycosides or similarly decorated species. Compounds absorbing primarily at 280 nm were more heterogeneous, but UV and MS data suggested the presence of other phenolic metabolites. While 315 compounds were detected overall, only 161 were found in commercial cultivars; the remaining metabolites were found only in *Anthurium* species. Of the 161 compounds detected in commercial cultivars, 12 were exclusive to the standard varieties and 70 to tulip varieties, with the remaining 79 metabolites found in both standard and tulip-shaped cultivars.

Positive identifications were not made for the majority of metabolites; however, several key compounds (Figure 3) were identified by comparison with standards, including the pelargonidin, cyanidin, and peonidin 3-rutinosides (**1**−**3**). Previous analyses conducted by thin-layer chromatography (TLC) had detected only peonidin 3-rutinoside (**3**) in purple cultivars such as 'ARCS';[6,7] however, using HPLC-MS, we were able to detect **3** in a number of red-spathed cultivars, as also reported in a 2013 study on anthurium spathe color.[15] When detected, peonidin 3-rutinoside (**3**) always co-occurred with cyanidin 3-rutinoside (**2**), a biosynthetic precursor (Tables 2 and 3). In purple spathes, the ratios of peak areas (525 nm) of peonidin to cyanidin rutinosides were much higher than those in red cultivars. For example, 'ARCS' and *A. amnicola* had percentage ratios of 19.1% and 19.8%, respectively, while the bright red cultivars 'Kozohara' and 'New Pahoa Red', despite containing significant quantities of **3**, possessed much lower ratios of **3**:**2** (0.3% and 2.9%, respectively). Thus, we propose that this ratio is a contributing factor in determining the observed color of the spathe, though other factors such as vacuolar pH and the presence of copigments may also have an effect.[8]

Accessions of *A. amnicola* and *A. kamemotoanum* species sampled (Figures 1G,K) accumulated higher levels of cyanidin rutinosides compared to pelargonidin 3-rutinoside, **1**, as did

Table 1. *Anthurium* Cultivars and Species Used for Analysis[a]

| Variety[a] | Code | Icon[b] | Form | Color | Ancestry (if known) |
|---|---|---|---|---|---|
| 'ARCS' | ARC | | tulip | purple | *A. amn.*, *A. formosum*, *A. kam.*, *A. and.*[1] |
| 'Princess Aiko' UH1299 | Aik | | tulip | pink | *A. antioquiense* x 'Tatsuta Pink Obake' |
| 'Ami' | Ami | | tulip | white | - |
| 'Calypso' | Cal | | tulip | red | - |
| 'Centennial' UH1272 | Cen | | tulip | white | *A. and.*, *A. lindenianum*, *A. amn.*, *A. ant.*[22] |
| 'Hokuloa' UH1349 | Hok | | tulip | white | 'Tropic Mist', 'Marian Seefurth', *A. ant.*[21] |
| 'Jasmine' | Jas | | standard | green | 'Starlight' (female) x 'Midori' (male)[25] |
| 'Kalapana' UH1016 | Kal | | standard | red/green | 'Diamond Jubilee' x 'Paradise Pink'[23] |
| 'Kozohara' | Koz | | standard | red | - |
| 'Lady Jane' | LaJ | | tulip | red | *A. ant.*[1] |
| 'Lavender Lady' | LaL | | tulip | purple | *A. amn.*, *A. formosum*, *A. kam.*, *A. and.*[1] |
| 'Tropic Lime' UH1181 | LiT | | tulip | green | *A. and.*, *A. lindenianum*, *A. kam.* |
| 'Marian Seefurth' H33 | MaS | | standard | pink | 'Haga White' x pink clone[26] |
| 'Maile' | Mai | | standard | white | - |
| 'Midori' | Mid | | standard | green | - |
| 'Momohara' | Mom | | standard | orange | - |
| 'New Pahoa Red' | NPR | | standard | red | - |
| 'New Pahoa Obake' | NPO | | standard | red/green | Sport of 'New Pahoa Red' |
| 'New Pahoa Salmon' | NPS | | standard | salmon | Sport of 'New Pahoa Red' |
| 'New Pahoa White' | NPW | | standard | white | Sport of 'New Pahoa Red' |
| 'Nitta' | Nit | | standard | orange | - |
| 'Oishi Orange Obake' | OrO | | standard | orange/green | - |
| 'Ozaki Red' | OzR | | standard | red | - |
| 'Princess Lily' | PrL | | standard | red | - |
| 'Snowball' | Sno | | standard[c] | white | - |
| 'Tropic Fire' UH1245 | TrF | | standard[c] | red | 'Kalapana', *A. antioquiense*[24] |
| 'Tropic Mist' UH780 | TrM | | standard | white | 'Manoa Mist' x coral accession[23] |
| 'Tropic Sunrise' UH1071 | TrS | | standard | orange/green | 'Anuenue' x 'Soga Orange Obake'[20] |
| **Species** | **Code** | | | **Color** | **Accession** |
| *A. amnicola* | AmU | | tulip | Purple | UH A667 |
| *A. amnicola* | AmS | | tulip | Purple | Selby 1976-0053-002 |
| *A. amnicola* | AmA | | tulip | Purple | ABG 19911372 |
| *A. amnicola* | AmM | | tulip | Purple | MBG Croat 84952 |
| *A. andraeanum* | AdA | | standard | Orange | ABG 19931433 |
| *A. andraeanum* | AdB | | standard | Orange | ABG 19911368 |
| *A. antioquiense* | Ant | | tulip | White | Selby 1989-0038 |
| *A. armeniense* | Arm | | tulip | White | Selby 1979-1055 |
| *A. bakeri* | Bak | | N/A | Green | UH A116 |
| *A. hoffmannii* | Hof | | tulip | Green | Selby 1993-0176 |
| *A. kamemotoanum* | Kam | | tulip | Red | UH A288 |
| *A. veitchii* | Vei | | tulip | Green | Selby 199300178 |

[a]UH accession numbers are given where known. [b]For Obake cultivars, the colored portion is indicated by a rectangular icon and the green portion with an oval icon. [c]'Snowball' and 'Tropic Fire' possess intermediate shapes; chemically they are closer to standard varieties and have been classified as such.

red-spathed standard and tulip cultivars. In comparison, both accessions of the *A. andraeanum* species (Figure 1L) examined displayed lower cyanidin rutinoside levels (compared to pelargonidin rutinoside) and no peonidin rutinoside, a pattern also found in commercial orange-spathed cultivars. Kamemoto and Kuehnle[1] previously described the wild-type *A. andraeanum* spathe as "orange-red". Thus, it is interesting to speculate that factors increasing cyanidin levels in modern cultivars, including activity of the flavonoid 3′-hydroxylase,[9,10,12] may have been acquired through hybridization with other species.

In addition to anthocyanins, a number of other flavonoid components were identified: embinin (**4**) and its two derivatives 4‴-(3,4-dimethoxycinnamoyl)embinin (**5**) and 4‴-ferruloylembinin (**6**);[14] two additional flavone glycosides, isocytisoside 7-glucoside (**7**)[28] and neobudofficide (**8**);[29] and the flavanol epicatechin (**9**),[30] which were isolated by HPLC and characterized by standard spectroscopic techniques. Peak areas for a selection of metabolites from commercial cultivars and species are given in Tables 2 and 3, respectively.

In their 2013 report, Li et al.[15] characterized several flavonoid components of commercial *Anthurium* cultivars on the basis of MS/MS data. Of particular interest was a metabolite designated f11, which gave a strong $[M + H]^+$ ion at $m/z$ 607.1 and was identified by the authors as methyleucalyptin (benzoyl)glucoside. Given the prominence of embinin (**4**) in all of the standard *Anthurium* cultivars that were analyzed, it seemed possible that this had been misidentified in the prior study, as **4** also gives a strong pseudomolecular ion at $m/z$ 607. Literature MS/MS data for compound f11 showed fragments at $m/z$ 461, 443, 395, 365, and 341. MS/MS analysis was conducted on an authentic sample of embinin, revealing a very similar fragmentation pattern to those reported by Li et al.;[15] these match well with those of other flavonoid C-glycosides.[31,32] As such, we suggest that compound f11 reported by Li et al. was instead embinin (**4**). Likewise, the reported metabolites f5 and f4, which have pseudomolecular ions at $m/z$ 593 and 579 (both $[M + H]^+$), respectively, and possess very similar fragmentation patterns, are most likely demethylated embinin derivatives.

**Hierarchical Cluster Analysis.** The data were subjected to hierarchical cluster analysis, revealing a wide range of different chemotypes that we have separated into nine classes (Figure 4). All standard (including Obake) cultivars fell into a single

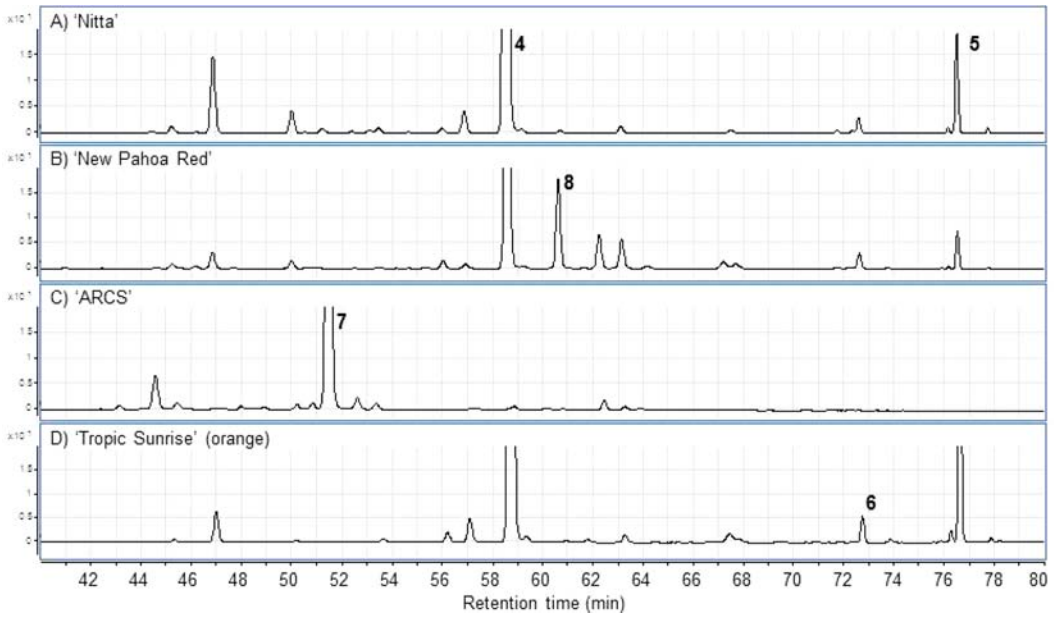


**Figure 2.** HPLC-MS analysis of representative *Anthurium* cultivars. UV absorbance at 330 nm is shown. (A) Standard commercial cultivar 'Nitta'; (B) 'New Pahoa' cultivar Standard, 'New Pahoa Red'; (C) Tulip-shaped commercial cultivar 'ARCS'; (D) Obake cultivar 'Tropic Sunrise' (orange portion). Numbered peaks reference flavonols described in Tables 2 and 3 and illustrated in Figure 3.

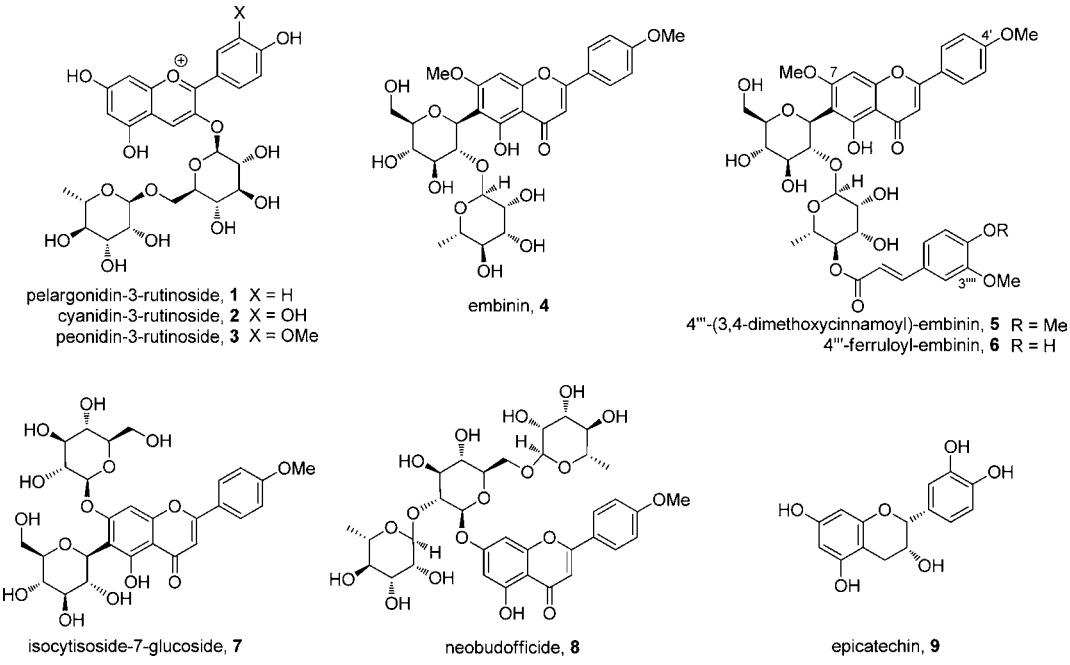


**Figure 3.** Compounds identified from commercial *Anthurium* cultivars.

supergroup, designated D. This low chemical diversity is probably due to the fact that most commercial standard cultivars derive primarily from *A. andraeanum*, with less if any genetic contributions from other *Anthurium* species. For ease of analysis we have separated them into three separate subcategories: D1, 'New Pahoa' cultivars; D2; and D3, which included both accessions of *A. andraeanum*. Of particular interest were the relationships between the recently developed 'New Pahoa' cultivars. These 'New Pahoa' cultivars derive from sports that arose from tissue culture clones, and they possess vibrant colors and a long vase life (S. Oishi, personal communication). The cultivars cluster very tightly together; 'New Pahoa' cultivars are extremely similar chemically, and changes in pigment levels are one of the very few changes observed among them, a finding that supports their clonal origins.

In contrast, tulip-shaped cultivars exhibited a much greater range of chemical diversity, separating into seven chemotypes (Figure 4). The irregularly-shaped *A. bakeri* was the single member of chemotype A and is distantly related phylogenetically to all other species and cultivars used in this study.[2] Chemotype B consisted of the 'Tropic Lime' and 'Princess Aiko' cultivars, while chemotype C consisted of 'Hokuloa', 'Lady Jane', 'Ami', and the intermediate-shaped 'Snowball' cultivar.


dx.doi.org/10.1021/jf502187c | J. Agric. Food Chem. 2014, 62, 11323−11334

**Table 2. Peak Areas for Selected Metabolites for *Anthurium* Commercial Cultivars**

| Cmp No[a] | RT | Mass | $\lambda_{max}$ | ARC | Aik | Ami | Cal | Cen | Hok | Jas | Kal G | Kal R | Koz | LaJ | LaL | LiT | Mai | MaS | Mid | Mom | Nit | NPO G | NPO R | NPR | NPS | NPW | OrO G | OrO O | OzR | PrL | Sno | TrF | TrM | TrS G | TrS O |
|---|---|---|---|---|---|---|---|---|---|---|---|---|---|---|---|---|---|---|---|---|---|---|---|---|---|---|---|---|---|---|---|---|---|---|
| *525nm (anthocyanins)* | | | | | | | | | | | | | | | | | | | | | | | | | | | | | | | | | | |
| **1** | 34.4 | 579.1692 | 277, 502 | 30.4 | 3.4 | 0 | 103 | 0 | 0 | 0 | 15.3 | 100 | 259 | 20.3 | 0 | 0 | 0 | 4.8 | 0 | 238 | 506 | 4.7 | 106 | 89.2 | 181 | 0 | 5.2 | 591 | 129 | 84.9 | 0 | 248 | 0 | 15.3 | 326 |
| **2** | 26.4 | 595.1644 | 280, 518 | 505 | 73.4 | 7.5 | 1108 | 0 | 0 | 0 | 88.7 | 1462 | 3851 | 593 | 52.0 | 0 | 0 | 106 | 0 | 21.8 | 13.6 | 9.9 | 754 | 605 | 19.1 | 0 | 0 | 15.1 | 859 | 605 | 0 | 2410 | 0 | 0 | 12.8 |
| **3** | 39.2 | 609.1798 | 278, 517 | 97.0 | 0 | 0 | 8.4 | 0 | 0 | 0 | 0 | 2.4 | 10.8 | 9.2 | 2.7 | 0 | 0 | 0 | 0 | 0 | 0 | 0 | 20.3 | 17.6 | 0 | 0 | 0 | 0 | 16.3 | 4.1 | 0 | 11.1 | 0 | 0 | 0 |
| *330nm (flavones)* | | | | | | | | | | | | | | | | | | | | | | | | | | | | | | | | | | |
| **4** | 58.7 | 607.2011 | 271, 336 | 6.1 | 492 | 2173 | 13.6 | 15.0 | 1535 | 3140 | 3720 | 3219 | 2135 | 2094 | 4.0 | 70.4 | 468 | 3010 | 4515 | 1864 | 3103 | 2755 | 2648 | 1898 | 2748 | 2174 | 4590 | 3209 | 2079 | 2171 | 2114 | 2131 | 4413 | 3547 | 2756 |
| **5** | 76.6 | 797.2630 | 274, 326 | 0 | 1.3 | 6.0 | 0 | 0 | 0 | 17.1 | 388 | 97 | 77.2 | 6.3 | 0 | 0 | 95.5 | 18.3 | 23.3 | 27.9 | 224 | 122 | 73.2 | 51.6 | 29.0 | 91.3 | 127 | 54.3 | 109 | 60.6 | 55.2 | 4.8 | 49.7 | 664 | 434 |
| **6** | 72.7 | 783.2462 | 273, 328 | 0 | 0 | 16.5 | 0 | 0 | 0 | 8.3 | 545 | 50.8 | 50.1 | 15.5 | 0 | 0 | 113 | 15.2 | 3.3 | 160 | 43.5 | 224.5 | 51.2 | 24.5 | 31.3 | 26.5 | 91.1 | 27.8 | 150. | 13.3 | 51.3 | 24.2 | 27.0 | 44.3 | 54.0 |
| **7** | 51.4 | 609.1794 | 270, 333 | 1732 | 221 | 1274 | 3.1 | 240 | 461 | 9.0 | 13.1 | 10.5 | 14.6 | 1105 | 1505 | 8.8 | 5.1 | 2.9 | 6.8 | 6.1 | 15.1 | 0.3 | 0.3 | 0.3 | 0.2 | 0.7 | 1.7 | 1.2 | 1.0 | 5.5 | 1496 | 413 | 2.6 | 2.1 | 4.3 |
| **8** | 60.7 | 739.2411 | 266, 334 | 1.0 | 253 | 0 | 0 | 0 | 10.8 | 0 | 0 | 0 | 0 | 0 | 2.5 | 45.6 | 0 | 13.4 | 0 | 5.2 | 0 | 508 | 459 | 332 | 472 | 400 | 0 | 0 | 11.3 | 0 | 0 | 0 | 22.4 | 0 | 0 |
| **10** | 12.6 | 247.0586 | 288, 340 | 1.1 | 39.8 | 34.1 | 0 | 7.6 | 11.4 | 0 | 0 | 0 | 1.1 | 52.3 | 1.7 | 1.1 | 0 | 0 | 0.7 | 0 | 0 | 0 | 0 | 0 | 0 | 0 | 0 | 0 | 0 | 1.2 | 0 | 0 | 0 | 1.0 | 1.3 |
| **11** | 15.5 | 147.0785 | 283[b], 310 | 0 | 0 | 0 | 0 | 0 | 0 | 0 | 0 | 0 | 0 | 0 | 0 | 0 | 0 | 0 | 0 | 0 | 0 | 0 | 0 | 0 | 0 | 0 | 0 | 0 | 0 | 0 | 0 | 0 | 0 | 0 | 0 |
| **12** | 22.0 | 423.0905 | 317, 367 | 0 | 0 | 0 | 0 | 0 | 1.4 | 0 | 0 | 0 | 0 | 6.8 | 75.0 | 0 | 0 | 0 | 0 | 0 | 0 | 0 | 0 | 0 | 0 | 0 | 0 | 0 | 0 | 0 | 0 | 0 | 0 | 0 | 0 |
| **13** | 23.1 | 313.1306 | 291[b], 329 | 0 | 0 | 0 | 0 | 0 | 0 | 0 | 0 | 0 | 0 | 0 | 0 | 0 | 0 | 0 | 0 | 0 | 0 | 0 | 0 | 0 | 0 | 0 | 0 | 0 | 0 | 0 | 0 | 0 | 0 | 0 | 0 |
| **14** | 29.5 | 367.1006 | 285, 384 | 8.3 | 0 | 0 | 0 | 0 | 0 | 0 | 0 | 0 | 0 | 0 | 0 | 0 | 0 | 0 | 0 | 0 | 0 | 0 | 0 | 0 | 0 | 0 | 0 | 0 | 0 | 0 | 0 | 0 | 0 | 0 | 0 |
| **15** | 34.5 | 595.1630 | 270, 335 | 45.1 | 2.1 | 31.2 | 8.4 | 11.0 | 1.1 | 0 | 0 | 0 | 0 | 25.1 | 19.2 | 0 | 0 | 0 | 0 | 0 | 0 | 0 | 0 | 0 | 0 | 0 | 0 | 0 | 0 | 0 | 12.7 | 0 | 0 | 0 | 0 |
| **16** | 38.8 | 565.1536 | 270, 335 | 94.5 | 242 | 0 | 70.9 | 0 | 0 | 0 | 0 | 0 | 0 | 0 | 0 | 34.7 | 0 | 0 | 0 | 0 | 0 | 0 | 0 | 0 | 0 | 0 | 0 | 0 | 0 | 0 | 0 | 0 | 0 | 0 | 0 |
| **17** | 41.4 | 433.1114 | 268, 337 | 0 | 0 | 0 | 169 | 0 | 0 | 0 | 0 | 0 | 0 | 0 | 0 | 0 | 0 | 0 | 0 | 0 | 0 | 0 | 0 | 0 | 0 | 0 | 0 | 0 | 0 | 0 | 0 | 0 | 0 | 0 | 0 |
| **18** | 41.6 | 437.1063 | 318, 363 | 0 | 8.9 | 29.7 | 0 | 0 | 45.1 | 0 | 0 | 0 | 0 | 47.7 | 0 | 0 | 0 | 0 | 0 | 0 | 0 | 0 | 0 | 0 | 0 | 0 | 0 | 0 | 0.7 | 0 | 0 | 0 | 0 | 0 | 0 |
| **19** | 44.6 | 433.1119 | 269, 339 | 124 | 7.4 | 29.6 | 559 | 13.1 | 5.6 | 3.5 | 1.3 | 1.5 | 6.2 | 26.1 | 128 | 6.2 | 1.1 | 0.9 | 4.0 | 5.0 | 6.2 | 1.1 | 0.5 | 1.7 | 2.2 | 0.4 | 1.1 | 0.8 | 4.1 | 3.8 | 17.8 | 3.5 | 2.3 | 0.6 | 0.8 |
| **20** | 45.1 | 741.2208 | 268, 345 | 0 | 0 | 0 | 0 | 0 | 0 | 0 | 0 | 0 | 0 | 0 | 0 | 0 | 0 | 0 | 0 | 0 | 0 | 0 | 0 | 0 | 0 | 0 | 0 | 0 | 0 | 0 | 30 | 6.2 | 0 | 0 | 0 |
| **21** | 45.2 | 579.1687 | 269, 338 | 0 | 0 | 0 | 507 | 59.7 | 0 | 19.7 | 0 | 0 | 0 | 0 | 0 | 0 | 39.2 | 0 | 0 | 0 | 0 | 0 | 0 | 0 | 1.7 | 0 | 0 | 0 | 0 | 0 | 0 | 0 | 0 | 0 | 0 |
| **22** | 45.4 | 477.2077 | 263, 345 | 0 | 0 | 0 | 0 | 0 | 0 | 0 | 0 | 0 | 0 | 0 | 0 | 0 | 0 | 0 | 0 | 0 | 0 | 0 | 0 | 0 | 0 | 0 | 0 | 0 | 0 | 0 | 0 | 0 | 0 | 0 | 0 |
| **23** | 46.1 | 727.2035 | 265, 345 | 0 | 0 | 7.5 | 1.7 | 48.0 | 0 | 11.6 | 10.6 | 5.1 | 4.6 | 7.3 | 0 | 0 | 3.3 | 0 | 18.4 | 4.0 | 4.7 | 8.5 | 6.6 | 8.5 | 11.6 | 3.5 | 9.1 | 11.6 | 5.4 | 4.8 | 11.0 | 0 | 4.2 | 3.3 | 3.3 |
| **24** | 46.8 | 579.1690 | 269, 352 | 0 | 21.0 | 0 | 0 | 0 | 0 | 0 | 0 | 0 | 0 | 0 | 0 | 0 | 0 | 0 | 0 | 0 | 0 | 0 | 0 | 0 | 0 | 0 | 0 | 0 | 0 | 0 | 0 | 0 | 0 | 0 | 0 |
| **25** | 46.9 | 593.1855 | 270, 337 | 0 | 73.0 | 220 | 0 | 0 | 74.1 | 178 | 97.1 | 75.1 | 91.8 | 182 | 0 | 6.3 | 130 | 100 | 230 | 96.6 | 212 | 103 | 100 | 72.3 | 104 | 85.1 | 171 | 151 | 93.7 | 95.8 | 88.7 | 131 | 242 | 107 | 78.1 |
| **26** | 50.8 | 579.1682 | 272, 334 | 32.6 | 90.1 | 0 | 0 | 0 | 0 | 0 | 0 | 0 | 0 | 0 | 0 | 30.9 | 0 | 0 | 0 | 0 | 0 | 0 | 0 | 0 | 0 | 0 | 0 | 0 | 0 | 0 | 0 | 0 | 0 | 0 | 0 |
| **27** | 51.3 | 725.2272 | 279, 338 | 0 | 41.1 | 0 | 0 | 0 | 2.7 | 0 | 0 | 0 | 0 | 0 | 0 | 0 | 0 | 1.7 | 0 | 0 | 0 | 13.4 | 8.6 | 5.8 | 9.5 | 5.1 | 0 | 0 | 0.3 | 0 | 0 | 0 | 5.1 | 0 | 0 |
| **28** | 53.4 | 607.2001 | 280, 329 | 0 | 16.5 | 28.4 | 0 | 0 | 4.4 | 15.2 | 11.5 | 9.8 | 7.6 | 27.1 | 0 | 2.6 | 13.7 | 7.5 | 15.0 | 12.7 | 19.7 | 14.7 | 12.9 | 9.7 | 14.7 | 10.7 | 16.0 | 12.4 | 9.7 | 2.7 | 17.0 | 8.3 | 11.2 | 18.2 | 10.9 |
| **29** | 54.8 | 609.1785 | 274, 338 | 0 | 0 | 6.2 | 0 | 21.0 | 4.1 | 4.1 | 5.5 | 4.6 | 3.0 | 1.7 | 0 | 16.4 | 4.8 | 5.2 | 5.7 | 4.1 | 3.7 | 3.8 | 3.7 | 2.6 | 3.5 | 4.2 | 4.3 | 4.1 | 2.6 | 3.0 | 7.6 | 2.1 | 4.8 | 6.0 | 4.4 |
| **30** | 56.2 | 577.1886 | 264, 331 | 0 | 0 | 0 | 0 | 0 | 0 | 8.5 | 5.1 | 12.7 | 0 | 0 | 0 | 0 | 40 | 0 | 0 | 13.9 | 11.1 | 27.1 | 15.0 | 17.4 | 21.7 | 27.4 | 41.4 | 28.1 | 10.5 | 0 | 0 | 11.7 | 0 | 24.2 | 17.0 |
| **31** | 56.9 | 593.1845 | 271, 335 | 4.9 | 11.3 | 44.8 | 0 | 243 | 36.0 | 73.0 | 68.5 | 43.1 | 30.9 | 40.4 | 0 | 0 | 84.0 | 66.3 | 132 | 26.7 | 65.8 | 41.4 | 35.9 | 23.2 | 36.0 | 25.6 | 96.6 | 59.7 | 21.2 | 28.6 | 43.5 | 45.5 | 61.5 | 81.3 | 55.8 |
| **32** | 58.8 | 447.1260 | 270, 338 | 12.7 | 1.0 | 1.1 | 0 | 19.5 | 3.6 | 1.9 | 0 | 0 | 0 | 1.2 | 9.1 | 13.9 | 0 | 0 | 1.5 | 1.0 | 1.0 | 0 | 0 | 0 | 0 | 0 | 0 | 0 | 0 | 1.3 | 10.9 | 1.2 | 0 | 0 | 0 |
| **33** | 59.2 | 593.1854 | 275, 338 | 0 | 7.3 | 14.1 | 2.9 | 0 | 8.6 | 20.2 | 29.6 | 28.5 | 12.2 | 14.0 | 0 | 4.7 | 33.2 | 22.8 | 25.4 | 13.5 | 15.2 | 27.6 | 39.7 | 13.7 | 23.7 | 17.0 | 38.1 | 23.8 | 12.3 | 14.4 | 19.1 | 9.9 | 34.2 | 22.9 | 19.6 |
| **34** | 60.1 | 815.2345 | 275, 333 | 5.4 | 1.6 | 5.3 | 0 | 4.0 | 11.6 | 0 | 0 | 0 | 0 | 4.7 | 5.7 | 0 | 0 | 0 | 0 | 0 | 0 | 0 | 0 | 0 | 0 | 0 | 0 | 0 | 0 | 0 | 1.2 | 0 | 0 | 0 | 0 |
| **35** | 61.5 | 729.2000 | 271, 336 | 0 | 0 | 0 | 0 | 0 | 0 | 0 | 0 | 0 | 0 | 0 | 67.1 | 0 | 0 | 0 | 0 | 0 | 0 | 0 | 0 | 0 | 0 | 0 | 0 | 0 | 0 | 0 | 0 | 0 | 0 | 0 | 0 |
| **36** | 62.2 | 593.1856 | 267, 334 | 0 | 130 | 0 | 5.8 | 0 | 4.0 | 0 | 0 | 0 | 0 | 0 | 4.1 | 0 | 0 | 5.0 | 0 | 0 | 0 | 267 | 190 | 136 | 203 | 143 | 0 | 0 | 2.0 | 0 | 0 | 0 | 5.1 | 0 | 0 |
| **37** | 64.2 | 447.1270 | 270, 330 | 0 | 14.0 | 1.6 | 19.0 | 0 | 0 | 0 | 0 | 0 | 0 | 3.0 | 0 | 6.8 | 0 | 0 | 0 | 0 | 0 | 19.3 | 17.3 | 12.6 | 25.2 | 10.7 | 0 | 0 | 0 | 0 | 0 | 0 | 0 | 0.9 | 0.8 |
| **38** | 65.6 | 393.1248 | 325 | 0 | 0 | 0 | 0 | 0 | 0 | 0 | 0 | 0 | 0 | 0 | 0 | 0 | 0 | 0 | 0 | 0 | 0 | 0 | 0 | 0 | 0 | 0 | 0 | 0 | 0 | 0 | 0 | 0 | 0 | 0 | 0 |
| **39** | 67.2 | 591.2050 | 271, 337 | 0 | 0 | 0 | 0 | 0 | 0 | 0 | 0 | 0 | 15.8 | 0 | 0 | 0 | 21.3 | 0 | 0 | 18.8 | 0 | 61.7 | 34.7 | 33.4 | 35.4 | 38.8 | 98.7 | 52.5 | 52.7 | 0 | 12.5 | 9.9 | 22.5 | 37.5 | 27.1 |
| *280nm (other phenolics)* | | | | | | | | | | | | | | | | | | | | | | | | | | | | | | | | | | |
| **9** | 18.4 | 291.0851 | 278 | 571 | 714 | 896 | 1123 | 560 | 617 | 600 | 513 | 669 | 1207 | 934 | 286 | 187 | 115 | 740 | 505 | 1469 | 1290 | 850 | 1066 | 919 | 1432 | 669 | 1130 | 2264 | 894 | 937 | 887 | 1142 | 742 | 807 | 1270 |
| **40** | 17.7 | 579.1477 | 279 | 377 | 423 | 472 | 538 | 334 | 346 | 381 | 350 | 344 | 592 | 514 | 177 | 200 | 707 | 413 | 296 | 408 | 497 | 538 | 560 | 502 | 722 | 412 | 761 | 1098 | 473 | 452 | 536 | 561 | 461 | 561 | 670 |
| **41** | 28.3 | 867.2095 | 278 | 211 | 259 | 192 | 220 | 157 | 155 | 223 | 174 | 152 | 221 | 251 | 85.4 | 64.2 | 349. | 189 | 143 | 90.2 | 151 | 329 | 207 | 214 | 357 | 228 | 495 | 488 | 201 | 192 | 271 | 243 | 235 | 329 | 268 |
| **42** | 41.4 | 851.2041 | 279 | 57.5 | 77.2 | 75.2 | 29 | 41.9 | 83.7 | 80.2 | 96.9 | 49.8 | 43.9 | 96.1 | 42.4 | 34.6 | 91.8 | 51.6 | 62.4 | 52.6 | 31.5 | 115 | 57.2 | 57.4 | 97.8 | 75.7 | 169 | 111 | 57.8 | 35.2 | 76.4 | 58.4 | 81.1 | 122 | 58.1 |

[a]Compounds **1**–**9** correspond to structures **1**–**9** in Figure 3. Numbers **10**–**42** are numerical designations only. [b]Shoulder.

**Table 3. Peak Areas for Selected Metabolites for *Anthurium* Species**

| compd[a] | RT | mass | AdA | AdB | AmU | AmA | AmS | AmM | Ant | Arm | Bak | Hof | Kam | Vei |
|---|---|---|---|---|---|---|---|---|---|---|---|---|---|---|
| | | | | | | 525 nm (Anthocyanins) | | | | | | | | |
| **1** | 34.4 | 579.1692 | 625 | 615 | 1.3 | 0.7 | 0.5 | 1.8 | 0 | 0 | 0 | 0 | 9.0 | 0 |
| **2** | 26.4 | 595.1644 | 13.4 | 15.6 | 283 | 150 | 136 | 68.4 | 5.8 | 0 | 0 | 0 | 921 | 0 |
| **3** | 39.2 | 609.1798 | 0 | 0 | 47.9 | 22.3 | 20.8 | 32.8 | 1.8 | 0 | 0 | 0 | 6.8 | 0 |
| | | | | | | 330 nm (Flavones) | | | | | | | | |
| **4** | 58.7 | 607.2011 | 3689 | 3338 | 0 | 1.0 | 0 | 0 | 3.3 | 1.5 | 0 | 0 | 0 | 0 |
| **5** | 76.6 | 797.2630 | 0 | 0 | 0 | 0 | 0 | 0 | 0 | 0 | 0 | 0 | 0 | 0 |
| **6** | 72.7 | 783.2462 | 39.4 | 1.4 | 0 | 0 | 0 | 0 | 0 | 0 | 0 | 0 | 0 | 0 |
| **7** | 51.4 | 609.1794 | 0 | 0 | 1626 | 427 | 824 | 183 | 719 | 0 | 0 | 0 | 0 | 0 |
| **8** | 60.7 | 739.2411 | 8.7 | 7.7 | 0 | 0 | 0 | 0 | 0 | 19.6 | 0 | 0 | 0 | 0 |
| **10** | 12.6 | 247.0586 | 0 | 0 | 0 | 0 | 0 | 0 | 84.4 | 0 | 0 | 0 | 0 | 0 |
| **11** | 15.5 | 147.0785 | 0 | 0 | 38.7 | 5.5 | 17.8 | 3.7 | 0 | 0 | 0 | 0 | 0 | 0 |
| **12** | 22.0 | 423.0905 | 0 | 0 | 0 | 0 | 0 | 0 | 71.8 | 0 | 0 | 0 | 0 | 0 |
| **13** | 23.1 | 313.1306 | 0 | 0 | 0 | 0 | 0 | 0 | 0 | 0 | 407 | 0 | 0 | 0 |
| **14** | 29.5 | 367.1006 | 0 | 0 | 21.4 | 12.3 | 6.8 | 10.8 | 0 | 0 | 0 | 0 | 0 | 0 |
| **15** | 34.5 | 595.1630 | 0 | 0 | 0 | 0 | 0 | 0 | 6.9 | 0 | 0 | 0 | 0 | 0 |
| **16** | 38.8 | 565.1536 | 0 | 0 | 0 | 0 | 0 | 189 | 33.6 | 0 | 0 | 69.5 | 0 | 0 |
| **17** | 41.4 | 433.1114 | 0 | 0 | 0 | 0 | 0 | 0 | 0 | 0 | 0 | 0 | 0 | 0 |
| **18** | 41.6 | 437.1063 | 0 | 0 | 0 | 0 | 0 | 0 | 33.1 | 0 | 0 | 0 | 0 | 0 |
| **19** | 44.6 | 433.1119 | 0 | 0 | 62.4 | 17.8 | 17.9 | 34.9 | 14.1 | 0.7 | 0 | 4.2 | 92.5 | 4.0 |
| **20** | 45.1 | 741.2208 | 0 | 0 | 0 | 0 | 0 | 0 | 0 | 25.5 | 0 | 0 | 0 | 0 |
| **21** | 45.2 | 579.1687 | 0 | 0 | 0 | 0 | 0 | 0 | 0 | 8.1 | 0 | 115 | 0 | 0 |
| **22** | 45.4 | 477.2077 | 0 | 0 | 0 | 0 | 0 | 0 | 0 | 0 | 0 | 0 | 468 | 0 |
| **23** | 46.1 | 727.2035 | 4.4 | 6.3 | 0 | 0 | 0 | 0 | 0 | 0 | 0 | 0 | 0 | 0 |
| **24** | 46.8 | 579.1690 | 0 | 0 | 16.1 | 4.9 | 7.8 | 17.6 | 0 | 0 | 0 | 0 | 0 | 0 |
| **25** | 46.9 | 593.1855 | 143 | 59.4 | 0 | 0 | 0 | 0 | 0 | 0 | 0 | 0 | 0 | 0 |
| **26** | 50.8 | 579.1682 | 0 | 0 | 0 | 0 | 0 | 0 | 11.9 | 12.8 | 0 | 0 | 0 | 0 |
| **27** | 51.3 | 725.2272 | 0 | 0 | 0 | 0 | 0 | 0 | 0 | 2.2 | 0 | 0 | 0 | 0 |
| **28** | 53.4 | 607.2001 | 5.6 | 4.9 | 0 | 0 | 0 | 0 | 0 | 0 | 0 | 0 | 0 | 0 |
| **29** | 54.8 | 609.1785 | 5.7 | 7.0 | 0 | 0 | 0 | 0 | 0 | 2.1 | 0 | 0 | 13.1 | 6.6 |
| **30** | 56.2 | 433.1101 | 22.0 | 18.1 | 0 | 0 | 0 | 0 | 0 | 0 | 0.9 | 0 | 0 | 0 |
| **31** | 56.9 | 593.1845 | 58.8 | 64.9 | 0 | 0 | 0 | 0 | 1.2 | 65.7 | 0 | 0 | 0 | 0 |
| **32** | 58.8 | 447.1260 | 1.0 | 0.5 | 138 | 2.9 | 0.2 | 9.2 | 0 | 0 | 0 | 0 | 0 | 0 |
| **33** | 59.2 | 593.1854 | 24.2 | 21.4 | 0 | 0 | 0 | 0 | 4.0 | 0 | 0 | 0 | 0 | 0 |
| **34** | 60.1 | 815.2345 | 0 | 0 | 0 | 0 | 0 | 0 | 2.9 | 0 | 0 | 0 | 0 | 0 |
| **35** | 61.5 | 729.2000 | 0 | 0 | 0 | 0 | 0 | 0 | 9.6 | 0 | 0 | 0 | 0 | 0 |
| **36** | 62.2 | 593.1856 | 2.1 | 0.5 | 1.6 | 0 | 0 | 0 | 0 | 405 | 0 | 0 | 0 | 0 |
| **37** | 64.2 | 447.1270 | 1.7 | 0.9 | 0 | 0 | 0 | 0 | 0 | 27.8 | 0 | 0 | 0 | 0 |
| **38** | 65.6 | 393.1248 | 0 | 0 | 0 | 0 | 0 | 0 | 26.3 | 0 | 0 | 0 | 0 | 70.7 |
| **39** | 67.2 | 591.2050 | 51.2 | 9.5 | 0 | 0 | 0 | 0 | 0 | 0 | 0 | 0 | 0 | 0 |
| | | | | | | 280 nm (Other Phenolics) | | | | | | | | |
| **9** | 18.4 | 291.0851 | 1900 | 1720 | 323 | 197 | 244 | 244 | 112 | 348 | 88.8 | 438 | 252 | 334 |
| **40** | 17.7 | 579.1477 | 723 | 689 | 166 | 113 | 138 | 133 | 67.0 | 204 | 36.6 | 265 | 126 | 214 |
| **41** | 28.3 | 867.2095 | 234 | 237 | 74.0 | 55.8 | 64.4 | 55.5 | 26.4 | 98.2 | 1.5 | 135 | 95.4 | 104 |
| **42** | 41.4 | 851.2041 | 103 | 88.8 | 9 | 2.5 | 11.8 | 3.6 | 35.0 | 42.9 | 5.5 | 27.9 | 28.3 | 11.7 |

[a]Compounds **1**−**9** correspond to structures **1**−**9** in Figure 3. Numbers **10**−**42** are numerical designations only.

*A. armeniense* is the sole member of chemotype E, while *A. kamemotoanum* and 'Calypso' are likewise the sole members of chemotypes F and G. Chemotype H consisted of *A. hoffmannii*, *A. veitchii*, and the commercial 'Centennial' cultivar. Finally, chemotype I contained the species *A. antioquiense* and *A. amnicola* in addition to the 'ARCS' and 'Lavender Lady' cultivars, which share *A. amnicola* as pollen parent. The multiple accessions sampled of *A. amnicola* and *A. andraeanum* clustered together in chemotypes I and D, respectively.

The greater heterogeneity among the tulip samples was expected, given that while all of the standard samples analyzed have been bred largely from *A. andraeanum*, tulip cultivars have a much wider range of ancestry, including *A. amnicola*, *A. antioquiense*, *A. armeniense*, *A. hoffmannii*, *A. formosum*, and *A. kamemotoanum*, as well as others not tested in this study such as *A. lindenianum* and *A. nymphaeifolium*. Relationships between the species analyzed were similar to those obtained by genetic analysis,[2] indicating that chemometric analysis may be a valid tool for investigating the phylogenetic relationships among these species.

**Principal Component Analysis.** HCA offers a powerful tool for analysis and differentiation of *Anthurium* species. However, for commercial cultivars, particularly hybrid cultivars that have ancestry from multiple species, complicating factors can arise. Such cultivars may contain flavonoids derived from the biosynthetic pathways of multiple ancestral species, and as

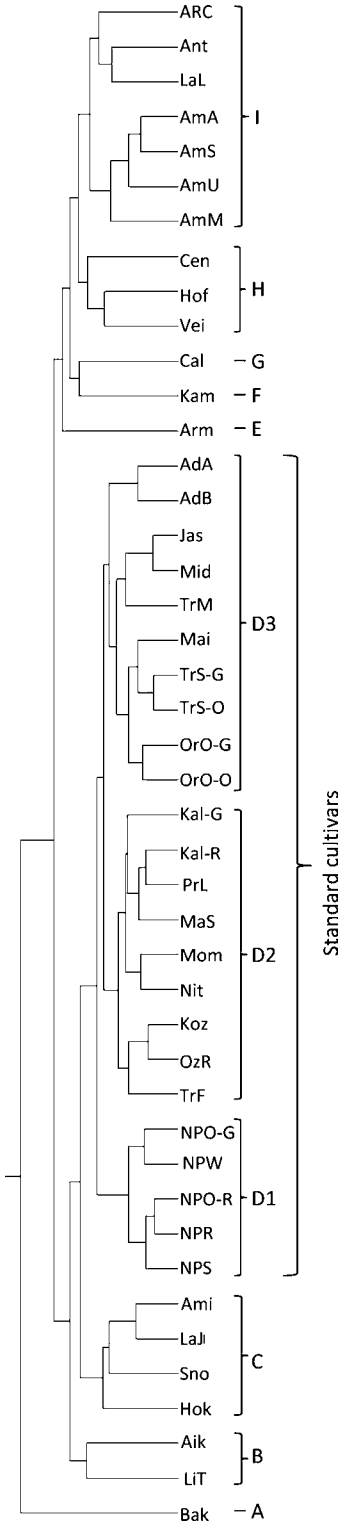


**Figure 4.** Hierarchical cluster analysis of *Anthurium* cultivars and species. Cultivars have been categorized into nine chemotypes (A–I), as indicated, with chemotype D (standard cultivars) further subdivided.

such the position of such cultivars in the dendrogram can change dramatically, depending on the specific quantities of flavonoid components and the clustering algorithm and distance measures used in the analysis. Principal component analysis (PCA) offers a multidimensional display of results, which can reveal additional differentiating factors and better separate cultivars with multiple species in their ancestry; PCA was used to expand upon the results obtained through HCA.

Initial PCA of commercial *Anthurium* cultivars and species showed separation of the various commercial cultivars based on spathe shape, with standard (including Obake) samples scoring higher in PC2 than tulip cultivars (Figure 5). However, while

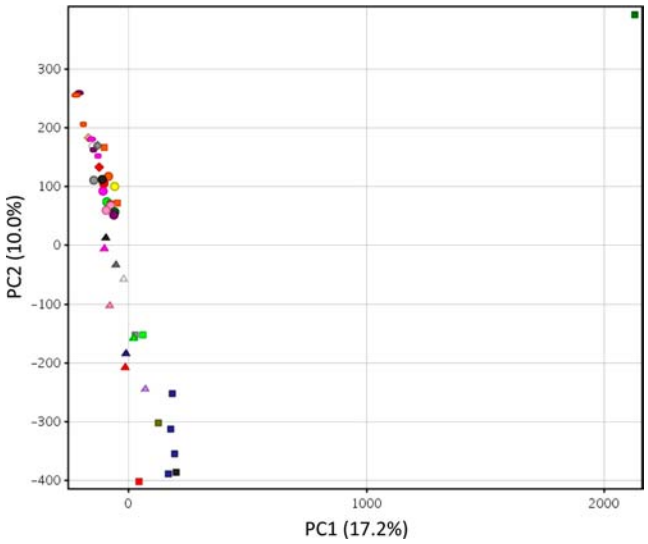


**Figure 5.** Principal component analysis of commercial *Anthurium* cultivars and species, displaying principal components 1 and 2. Full set of samples and 315 metabolites were used. Contribution to overall variation were PC1 17.2% and PC2 10.0%. See Table 1 for cultivar identities. *A. bakeri* can be seen as an outlier at the top right.

some separation was observed along PC2, the majority of the remaining principal components were not useful for the differentiation of commercial cultivars, as they were dominated by the more outlying species and cultivars, in particular *A. bakeri* and *A. kamemotoanum*, but also *A. armeniense* and *A. veitchii*. The chemical profiles of these four species are very different from most of the commercially available *Anthurium* cultivars and they share only a few chemical constituents in common. Likewise, the commercial cultivar 'Calypso' is also chemically very distinct from most of the other commercial varieties. Inclusion of such outlying varieties leads to reduced differentiation of the cultivars of interest and requires the use of large number of principal components to account for the observed differences. In order to focus more specifically on the majority of commercial cultivars, the analysis was repeated with 'Calypso' and the outlying species listed above omitted, with a total of 196 metabolites used.

For this new analysis, eight principal components were used, which accounted for a total of 63% of the total variation in the samples. The requirement for such a large number of components may be due to the very high chemical diversity and degree of variation between the samples. PC1 accounted for 18.7% of the observed variance between the species and cultivars analyzed, separating standard cultivars from tulip-shaped cultivars and species (Figure 6A). PC2 (9.5%) separated the majority of commercial cultivars from *A. amnicola*, which scored very high in this component, and from *A. antioquiense* and the commercial varieties 'Tropic Lime' and 'Princess Aiko', which had very low PC2 scores. Principal component 3 (6.9%) differentiated 'Tropic Lime', 'Lavender Lady', and *A. antioquiense* from others. 'New Pahoa' and Obake cultivars clustered close to


dx.doi.org/10.1021/jf502187c | J. Agric. Food Chem. 2014, 62, 11323−11334

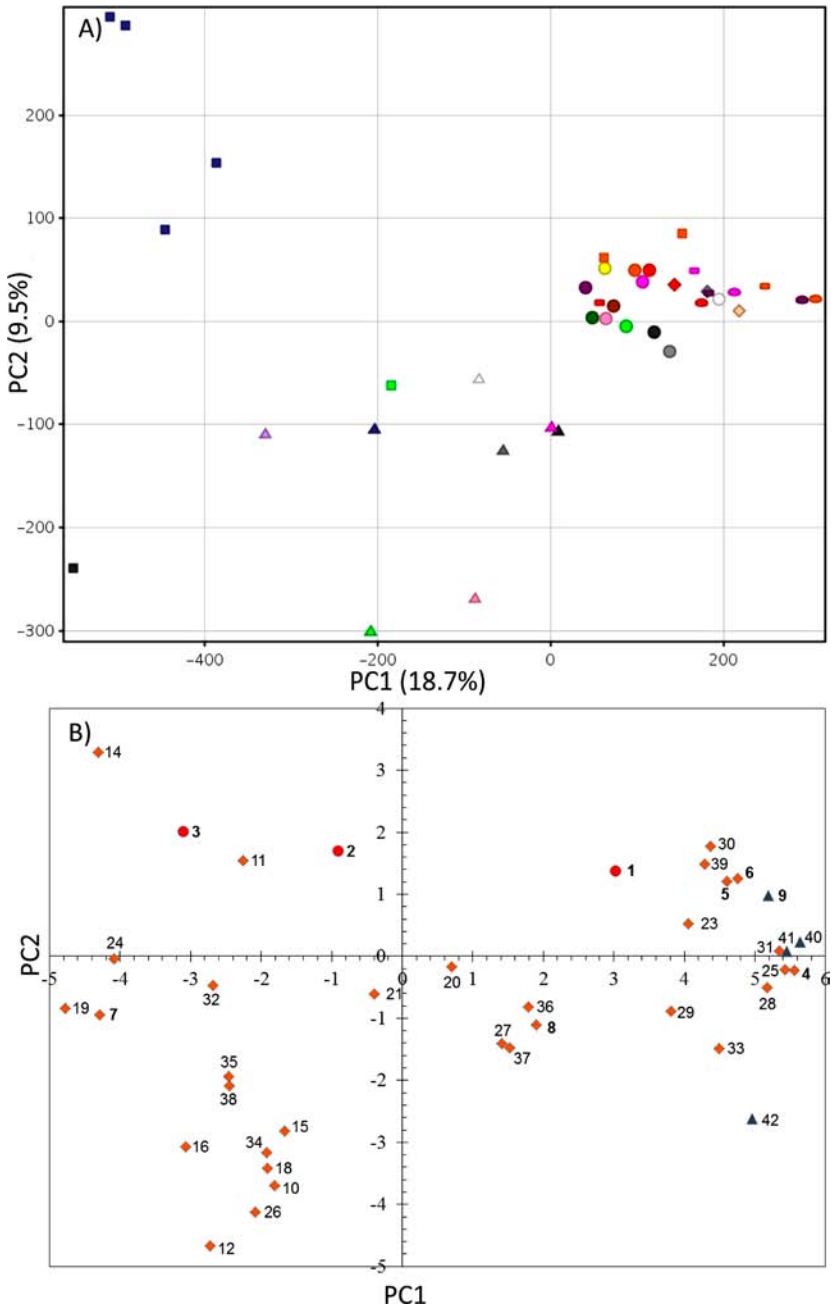


**Figure 6.** Principal component analysis of selected *Anthurium* cultivars for reduced sample set of 196 metabolites. Contribution to overall variation: PC1, 17.2%; PC2, 10.0%; PC3, 8.1%; PC4, 6.5%; PC5, 6.0%; PC6, 5.4%; PC7, 4.9%; and PC8, 4.0%. (A) Score plot of PC1 and PC2 scores; see Table 1 for cultivar identities. (B) Loading plot for selected metabolites contributing to PC1 and PC2. Red circles indicate anthocyanins, orange diamonds show flavones, and gray triangles represent other phenolics. Labels correspond to metabolites as defined in Tables 2 and 3.

the other standard varieties, with characteristic high values in PC1 and moderate values in PC2. Commercial tulip cultivars clustered less tightly, but tended to low PC2 values and moderate PC1 values (Figure 6A). The 'Tropic Fire' and 'Snowball' cultivars have a shape intermediate between a classic standard and tulip shape; these clustered with standard cultivars, suggestive of a pedigree with significant contributions from *A. andraeanum*. Another characteristic pattern was the predictable difference observed between the green and colored portions of the bicolored Obake spathes, with the green portion of all Obake spathes scoring higher in PC1, which may be associated with reduced concentrations of pelargonidin 3-rutinoside (**1**) in green tissue.

These results mirrored those from the HCA and highlighted the difference between standard and tulip cultivars. Analysis of the loading plot (Figure 6B) highlighted key metabolites responsible for differentiation of principal components. Several of these metabolites could be found in the species sampled; their presence in commercial cultivars may reflect the presence of a particular species in their pedigree. Metabolites with high loading values for PC1 were found in the majority of standard cultivars. In particular, **6**, **25**, **28**, and **39** were found in all commercial standard cultivars and also in the parent species *A. andraeanum*, consistent with ancestry from this species. The modified embinin derivatives **5** and **6** were found in particularly


dx.doi.org/10.1021/jf502187c | *J. Agric. Food Chem.* 2014, 62, 11323−11334

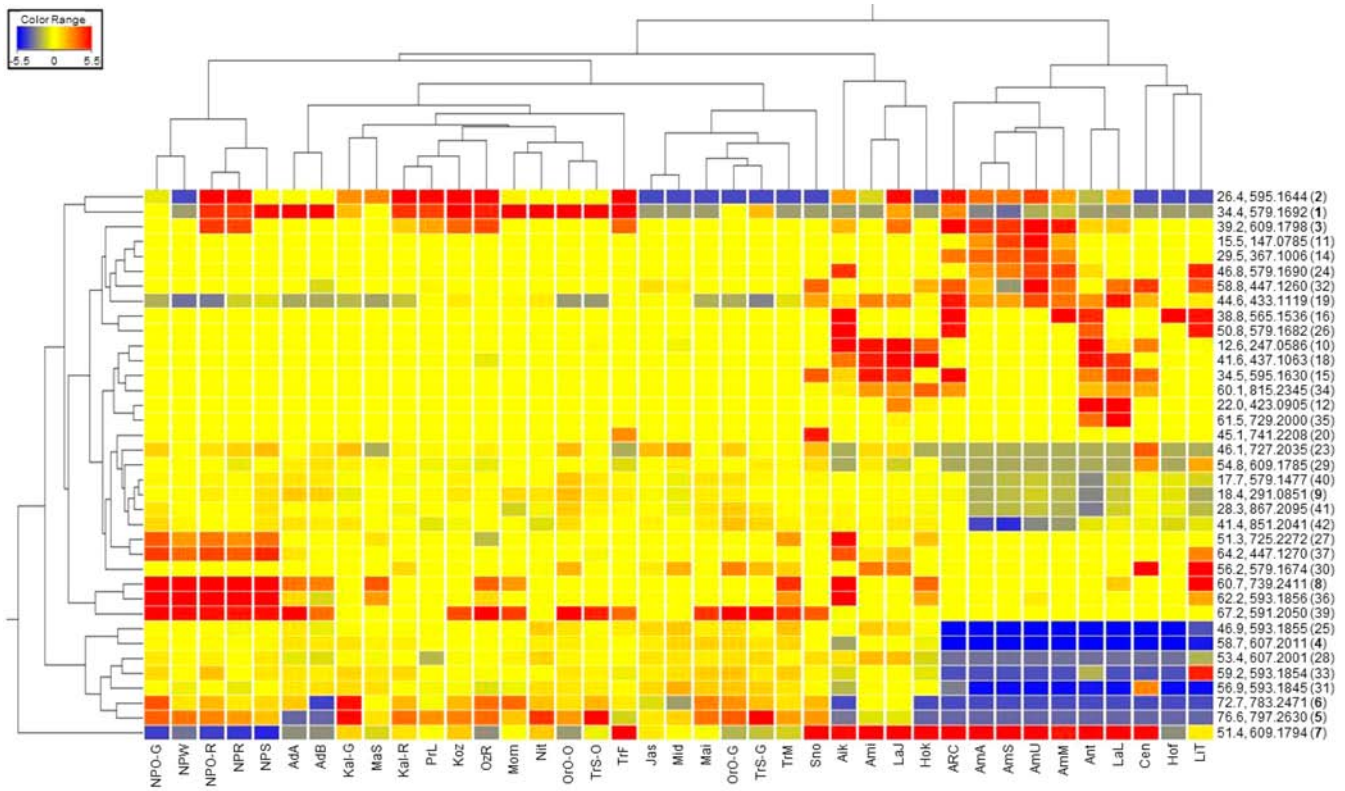


**Figure 7.** Heatmap from hierarchical cluster analysis of *Anthurium* species and commercial cultivars, using metabolites listed in Tables 2 and 3. The dendrogram at the top shows clustering of cultivars, while the dendrogram at the left displays clustering of individual compounds, with Euclidean distances and complete clustering. Normalized levels of selected metabolites are shown in the central portion of the figure.

high levels in both 'New Pahoa' and Obake cultivars. Additionally, the phenolic compounds **9**, **40**, **41**, and **42** had very high loading values for PC1: while these metabolites were found in all *Anthurium* cultivars and species, the levels were much higher in standard than in tulip cultivars.

Several metabolites scoring low in PC1 and high in PC2 (e.g., **11** and **14**) (Figure 6B) were characteristic of *A. amnicola* but were found only in the species itself and not in any commercial cultivars, while peonidin 3-rutinoside (**3**) was also found in *A. kamemotoanum* and in all red and purple commercial cultivars. In contrast, compounds scoring low in PC1 and moderately in PC2 were found in both *A. amnicola* and a range of commercial cultivars. Compound **32** proved a particularly useful marker: it was found in the commercial cultivars 'ARCS', 'Centennial', and 'Lavender Lady', and all three have confirmed pedigrees including *A. amnicola*. However, the 'Tropic Lime' cultivar, which lacks any known *A. amnicola* ancestry, also contains this metabolite. We suggest that in 'Tropic Lime' this metabolite may derive from the contribution of *A. lindenianum* to the pedigree, though we were unable to obtain samples of this species for analysis. Two additional metabolites scoring low in PC1 and moderately in PC2, **7** and **19**, were found in both *A. amnicola* and *A. antioquiense*, with the latter also found in *A. kamemotoanum*, and could represent ancestry from any of these species. All surveyed commercial tulip cultivars, except for 'Calypso' and 'Tropic Lime', contained high levels of isocytisoside 7-glucoside (**7**). A subset of tulip cultivars, including 'Tropic Fire', 'Lady Jane', 'Ami', 'Snowball', and 'Hokuloa', contained significant quantities of both embinin (**4**) and isocytisoside 7-glucoside (**7**), reflecting their known or probable ('Ami' and 'Snowball') mixed pedigrees from *A. andraeanum* as well as *A. amnicola* and/or *A. antioquiense*, the latter two being closely related tulip species.[1]

Similarly, compounds scoring low in PC2 and low to moderate in PC1 were indicative of *A. antioquiense* ancestry (Figure 6B). Two in particular were good markers for *A. antioquiense* ancestry in commercial cultivars. Compound **10** was present in high abundance in 'Princess Aiko', 'Centennial', and 'Hokuloa', all of which have confirmed *A. antioquiense* ancestry, and in 'Lady Jane' or 'Ami' with probable *A. antioquiense* ancestry; while **18** was present in all of these except 'Centennial'. On the other hand, 'Tropic Fire', which also has *A. antioquiense* ancestry, does not contain either of these metabolites. Thus, while the presence of a metabolite may be indicative of a particular *Anthurium* species in the lineage of a given commercial cultivar, the absence of such a metabolite does not necessarily indicate that the species is not a progenitor, as cultivar development involves selecting for and excluding traits over multiple generations of selective breeding. Compound **16** was similarly widespread in these cultivars, but as it is also found in *A. hoffmannii*, and some accessions of *A. amnicola*, this metabolite was not a unique marker of *A. antioquiense* ancestry.

Similar analyses were conducted for other species, but characteristic metabolites indicating ancestry from *A. kamemotoanum*, *A. hoffmannii*, *A. bakeri*, or *A. veitchii* could not be identified. The latter two species are not commonly used in breeding commercial *Anthurium* cultivars in Hawaii, but *A. kamemotoanum* is an ancestor of both 'ARCS' and 'Lavender Lady'. As discussed earlier, *A. kamemotoanum* shares several metabolites in common with *A. amnicola*, including **19** and **3**.

Both of these species are involved in the pedigree of 'ARCS' and 'Lavender Lady', which may be why unique identifying metabolites cannot be identified for *A. kamemotoanum*.

Additional clustering analysis was conducted on the reduced sample list, using the metabolites displayed in Tables 2 and 3, and the results are displayed as a heatmap (Figure 7). This analysis displays cultivar clustering horizontally and metabolite clustering vertically, while the central portion of the figure displays normalized metabolite quantities. Metabolites that cluster closely together likely share a common ancestry and/or biochemical origin and thus can suggest metabolic pathways associated with complex compound mixtures. For example, the anthocyanins pelargonidin 3-rutinoside (**1**) and cyanidin 3-rutinoside (**2**) cluster tightly together, consistent with their production from precursors originating from a common biosynthetic pathway. Likewise, embinin (**4**) clustered tightly with the two derivatives **5** and **6**, in addition to the two unidentified compounds **25** and **33**. On the basis of this tight clustering, we propose that these two unidentified metabolites are biosynthetically related to embinin **4**. They possess masses of 593.1855 and 593.1854 respectively, consistent with a molecular formula of $C_{28}H_{32}O_{14}$, and as such we suggest that they are demethylated embinin derivatives. Clustering was also observed between **3**, **11**, **14**, **19**, and **32**, described previously as compounds found in species *A. amnicola*, *A. antioquiense*, or *A. kamemotoanum*, among others.

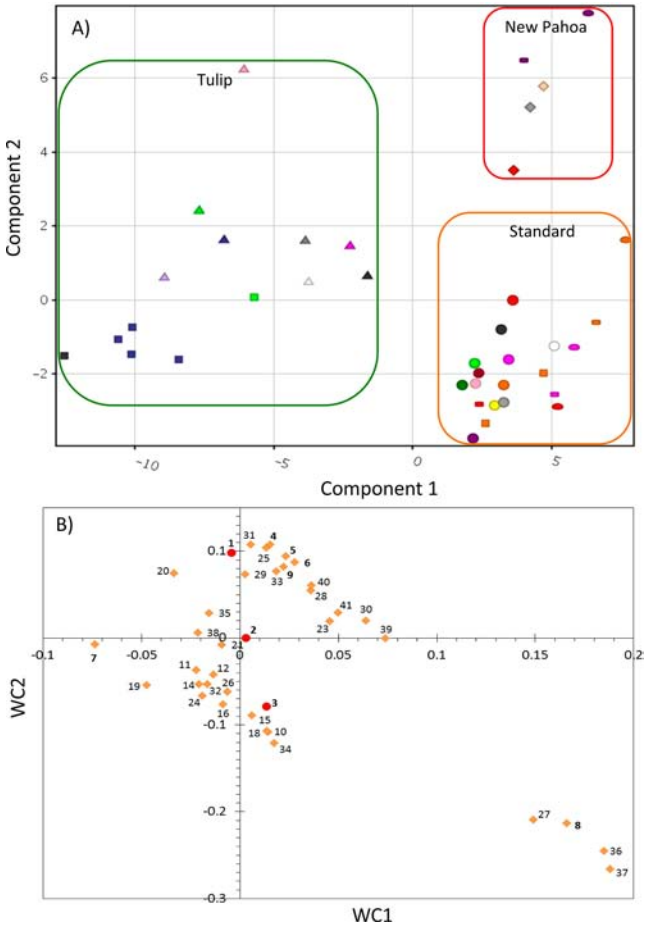


**Figure 8.** Partial least squares discriminant analysis (PLS-DA) of selected *Anthurium* cultivars for a reduced sample set of 196 metabolites. (A) Score plot of component 1 and component 2 scores; see Table 1 for cultivar identities. Highlighting around classes is for clarity only. (B) Loading plot for selected metabolites that contribute to classifying 'New Pahoa' (WC0) and "standard" (WC1) cultivars. Red circles indicate anthocyanins, orange diamonds show flavones, and gray triangles represent other flavonoids. Labels correspond to metabolites as defined in Tables 2 and 3.

Partial least squares discriminant analysis (PLS-DA) was conducted on the reduced data set in order to confirm the results obtained by PCA. PLS-DA offers an excellent tool for discrimination of classes in analyses requiring dimensional reduction.[33] PLS-DA was carried out for three designated classes: standard, tulip, and 'New Pahoa' cultivars. Visualization by use of components 1 and 2 (Figure 8A), showed clear differentiation between the three classes. As this PLS-DA analysis had been optimized to differentiate between 'New Pahoa' and other standard (including Obake) cultivars, it gave much better separation between these two categories than the PCA. In contrast to other standard cultivars, 'New Pahoa' cultivars all scored very highly in component 2, highlighting the fact that there are characteristic chemical differences between the two groups. Analysis of loading plots for the data revealed key metabolites involved in discrimination of 'New Pahoa' from other standard varieties (Figure 8B). Two of these metabolites, **36** and **37**, were characteristic of 'New Pahoa' cultivars, though they were also found in 'Princess Aiko' and in *A. armeniense* (Tables 2 and 3). This may indicate that 'New Pahoa' and 'Princess Aiko' cultivars contain *A. armeniense*, or a closely related species, in their pedigrees. However, ancestry data for 'New Pahoa' varieties is not publicly available, and only the immediate progenitors for 'Princess Aiko' are known.[28] Co-occurrence of these metabolites in different cultivars might also be due to interaction of biosynthetic pathways contributed by multiple ancestral species or to variations arising de novo during cultivar development.

Overall, this research displays the utility of chemotaxonomic analysis in classification of the *Anthurium* genus, both for species and for commercial cultivars. This study lays the groundwork for future work on the identification of key metabolites indicative of a particular ancestry and for identification of the key biosynthetic pathways involved in their biosynthesis.

## ■ ASSOCIATED CONTENT

### Supporting Information

Nine figures illustrating MS/MS fragmentation of embinin **4**, additional PLS-DA loading plot, and NMR spectra for **7**–**9** (pdf); one table giving peak areas for all 315 analyzed metabolites in all commercial cultivars and species (xls). This material is available free of charge via the Internet at http://pubs.acs.org.

## ■ AUTHOR INFORMATION

### Corresponding Author

*Telephone (808) 981-8001; fax (808) 981-4520; e-mail borris@hawaii.edu.

### Notes

The authors declare no competing financial interest.

## ■ ACKNOWLEDGMENTS

We thank Dr. Teresita Amore, University of Hawaii at Manoa, for information on the pedigree of University of Hawaii cultivars and her generosity in providing *Anthurium* species for analysis, and Joanne Lichty of the University of Hawaii for help in *A. kamemotoanum* and *A. amnicola* species sampling and acquisition, respectively. Many thanks to Grayson Inouye for

his generosity in providing cultivar spathe samples; Stanley Oishi for providing New Pahoa Salmon, New Pahoa Obake, and Orange Obake; Lynne Kuwabara of the Hawaii Anthurium Industry Association for *Anthurium* cultivars; Dr. Thomas Croat and Andrew Wyatt of Missouri Botanical Garden; Laurie Birch and Dr. Bruce Holst of Marie Selby Botanical Gardens; and Michael Wenzel of the Atlanta Botanical Garden for species. Photos provided courtesy of Michael Wenzel, Atlanta Botanical Garden (*A. andraeanum*); Dr. Phil Nelson, Marie Selby Botanical Gardens (*A. amnicola*, *A. antioquiense*, *A. armeniense*, *A. hoffmannii*, and *A. veitchii*); Dr. Jon Suzuki, USDA (*A. bakeri* and *A. kamemotoanum*); and Dr. Barbara Bliss, USDA (commercial cultivars). This project is supported in part by the NSF Hawaii EPSCoR Program under National Science Foundation Award EPS-0903833 and by the College of Pharmacy, University of Hawaii at Hilo.

## ■ ABBREVIATIONS

HCA, hierarchical cluster analysis; PCA, principal component analysis; PLS-DA, partial least squares discriminant analysis

## ■ REFERENCES

(1) Kamemoto, H.; Kuehnle, A. R. *Breeding Anthuriums in Hawaii*; University of Hawaii Press: Honolulu, 1997; p 168.
(2) Carlsen, M. M.; Croat, T. B. A molecular phylogeny of the species-rich neotropical genus *Anthurium* (Araceae) based on combined chloroplast and nuclear DNA. *Syst. Bot.* **2013**, *38*, 576−588.
(3) Iwata, R. Y.; Tang, C. S.; Kamemoto, H. Anthocyanins of *Anthurium andreanum* Lind. *J. Am. Soc. Hortic. Sci.* **1979**, *104*, 464−466.
(4) Iwata, R. Y.; Tang, C. S.; Kamemoto, H. Concentration of anthocyanins affecting spathe color in anthuriums. *J. Am. Soc. Hortic. Sci.* **1985**, *110*, 383−385.
(5) Williams, C. A.; Harborne, J. B.; Mayo, S. J. Anthocyanin pigments and leaf flavonoids in the family Araceae. *Phytochemistry* **1981**, *20*, 217−234.
(6) Marutani, M.; Tang, C. S.; Paull, R. Anthocyanins in the lavender anthurium. *HortScience* **1987**, *22*, 620−622.
(7) Wannakrairoj, S.; Kamemoto, H. Histological distribution of anthocyanins in *Anthurium* spathes. *HortScience* **1990**, *25*, 809.
(8) Avila-Rostant, O.; Lennon, A. M.; Umaharan, P. Spathe color variation in *Anthurium andraeanum* Hort. and its relationship to vacuolar pH. *HortScience* **2010**, *45*, 1768−1772.
(9) Elibox, W.; Umaharan, P. Inheritance of major spathe colors in *Anthurium andraeanum* Hort. is determined by three major genes. *HortScience* **2008**, *43*, 787−791.
(10) Kamemoto, H.; Iwata, R. Y.; Marutani, M. Genetics of the major spathe colors in anthuriums. *Hawaii Inst. Trop. Agric. Hum. Resour. Res. Ext. Ser.* **1988**, *056*, 8−88.
(11) Collette, V. E.; Jameson, P. E.; Schwinn, K. E.; et al. Temporal and spatial expression of flavonoid biosynthetic genes in flowers of *Anthurium andraeanum*. *Physiol. Plant.* **2004**, *122*, 297−304.
(12) Gopaulchan, D.; Umaharan, P.; Lennon, A. M. A molecular assessment of the genetic model of spathe color inheritance in *Anthurium andraeanum* (Hort.). *Planta* **2014**, *239*, 695−705.
(13) Aquino, R.; Morelli, S.; Lauro, M. R.; Abdo, S.; Saija, A.; Tomaino, A. Phenolic constituents and antioxidant activity of an extract of *Anthurium versicolor* leaves. *J. Nat. Prod.* **2001**, *64*, 1019−1023.
(14) Clark, B. R.; Suzuki, J. Y.; Bliss, B. J.; Borris, R. P. Flavone C-glycosides from *Anthurium andraeanum*. *Nat. Prod. Commun.* **2012**, *7*, 747−748.
(15) Li, C.; Yang, G.; Huang, S.; Lu, D.; Wang, C.; Chen, J.; Yin, J. Characterization of flavonoids in anthurium spathes and their contribution to spathe coloration. *J. Hortic. Sci. Biotechnol.* **2013**, *88*, 208−215.
(16) Treutter, D.; Wang, D.; Farag, M. A.; et al. Diversity of phenolic profiles in the fruit skin of *Prunus domestica* plums and related species. *J. Agric. Food Chem.* **2012**, *60*, 12011−12019.
(17) Ferrandino, A.; Guidoni, S. Anthocyanins, flavonols and hydroxycinnamates: an attempt to use them to discriminate *Vitis vinifera* L. cv 'Barbera' clones. *Eur. Food Res. Technol.* **2010**, *230*, 417−427.
(18) Farag, M. A.; Weigend, M.; Luebert, F.; Brokamp, G.; Wessjohann, L. A. Phytochemical, phylogenetic, and anti-inflammatory evaluation of 43 *Urtica* accessions (stinging nettle) based on UPLC-Q-TOF-MS metabolomic profiles. *Phytochemistry* **2013**, *96*, 170−183.
(19) Truus, K.; Vaher, M.; Borissova, M.; et al. Characterization of yew tree (*Taxus*) varieties by fingerprint and principal component analyses. *Nat. Prod. Commun.* **2012**, *7*, 1143−1146.
(20) Kuehnle, A. R.; Amore, T. D.; Kamemoto. H.; Kunisaki, J. T.; Lichty, J. S.; Uchida, J. Y. 'Tropic Sunrise' anthurium. *New Plants for Hawaii*, NPH-A-3; University of Hawaii: Honolulu, 2000.
(21) Kuehnle, A. R.; Amore, T. D.; Kamemoto. H.; Kunisaki, J. T.; Lichty, J. S.; Uchida, J. Y. 'Hokuloa' and 'Hilo Moon' anthuriums. *New Plants for Hawaii*, NPH-A-5; University of Hawaii: Honolulu, 2002.
(22) Kuehnle, A. R.; Amore, T. D.; Kamemoto. H.; Kunisaki, J. T.; Lichty, J. S.; Uchida, J. Y. 'Centennial' anthurium. *New Plants for Hawaii*, NPH-A-11; University of Hawaii: Honolulu, 2007.
(23) Kamemoto, H.; Kuehnle, A. R.; Kunisaki, J. T.; Aragaki, M.; Lichty, J. S.; Amore, T. D. 'Kalapana', 'Tropic Ice', and 'Tropic Mist' Anthurium. *Hawaii Cooperative Extension Service, Horticulture Digest 104*; University of Hawaii: Honolulu, 1995.
(24) Kamemoto, H.; Kuehnle, A. R. Anthurium plant named Tropic Fire. U.S. Plant Patent 9797 P, February 4, 1997.
(25) Hayashi, C. K. Anthurium plant named Jasmine. U.S. Plant Patent 9880 P, April 29, 1997.
(26) Kamemoto, H.; Nakasone, H. Y. Evaluation and improvement of anthurium clones. *Hawaii Agric. Exp. Stn., Tech. Bull.* **1963**, *58*, 28.
(27) Kuehnle, A. R.; Amore, T. D.; Kamemoto. H.; Kunisaki, J. T.; Lichty, J. S.; Uchida, J. Y. 'Princess Aiko' ('Imperial') and 'Regina', two novelty anthuriums. *New Plants for Hawaii*, NPH-A-7; University of Hawaii: Honolulu, 2004.
(28) Ohtsuki, T.; Miyagawa, T.; Koyano, T.; Kowithayakorn, T.; Ishibashi, M. Isolation and structure elucidation of flavonoid glycosides from *Solanum verbascifolium*. *Phytochem. Lett.* **2010**, *3*, 88−92.
(29) Neretina, O. V.; Gromova, A. S.; Lutskii, V. I.; Semenov, A. A.; Ushakov, I. A.; Makar'eva, T. N.; Owen, N. I. Secondary metabolites from *Hedysarum setigerum*. *Chem. Nat. Compd.* **2004**, *40*, 91−92.
(30) Harborne, J. B. *The Flavonoids: Advances in Research since 1986*; Chapman and Hall/CRC Press: London, 1994; p 676.
(31) Abranko, L.; Garcia-Reyes, J. F.; Molina-Diaz, A. In-source fragmentation and accurate mass analysis of multiclass flavonoid conjugates by electrospray ionization time-of-flight mass spectrometry. *J. Mass Spectrom.* **2011**, *46*, 478−488.
(32) Guo, X.; Yue, Y.; Tang, F.; Wang, J.; Yao, X.; Sun, J. A comparison of C-glycoside flavonoid isomers by electrospray ionization quadropole time-of-flight tandem mass spectrometry in negative and positive ion mode. *Int. J. Mass Spectrom.* **2013**, *333*, 59−66.
(33) Barker, M.; Rayens, W. Partial least squares for discrimination. *J. Chemometr.* **2003**, *17*, 166−173.

**Table 1. Xenobiotics of the Targeted Analysis**

| ID | name of molecule | formula | classification |
|---|---|---|---|
| 1 | 5-hydroxythiabendazole | $C_{10}H_7N_3OS$ | antibiotic |
| 2 | acetamiprid | $C_{10}H_{11}ClN_4$ | pesticide |
| 3 | albendazole | $C_{12}H_{15}N_3O_2S$ | antibiotic |
| 4 | aldicarb | $C_7H_{14}N_2O_2S$ | pesticide |
| 5 | amitraz | $C_{19}H_{23}N_3$ | pesticide |
| 6 | atrazine | $C_8H_{14}ClN_5$ | pesticide |
| 7 | azoxystrobin | $C_{22}H_{17}N_3O_5$ | pesticide |
| 8 | boscalid | $C_{18}H_{12}Cl_2N_2O$ | pesticide |
| 9 | carbaryl | $C_{12}H_{11}NO_2$ | pesticide |
| 10 | carbendazim | $C_9H_9N_3O_2$ | pesticide |
| 11 | carbofuran | $C_{12}H_{15}NO_3$ | pesticide |
| 12 | carfentrazone-ethyl | $C_{15}H_{14}Cl_2F_3N_3O_3$ | pesticide |
| 13 | chlorfenvinphos | $C_{12}H_{14}Cl_3O_4P$ | pesticide |
| 14 | clothianidin | $C_6H_8ClN_5O_2S$ | pesticide |
| 15 | coumaphos | $C_{14}H_{16}ClO_5PS$ | pesticide |
| 16 | cyproconazol | $C_{15}H_{18}ClN_3O$ | pesticide |
| 17 | cyprodinil | $C_{14}H_{15}N_3$ | pesticide |
| 18 | diazinon | $C_{12}H_{21}N_2O_3PS$ | pesticide |
| 19 | dichlorvos | $C_4H_7Cl_2O_4P$ | pesticide |
| 20 | difenoconazol | $C_{19}H_{17}Cl_2N_3O_3$ | pesticide |
| 21 | diflubenzuron | $C_{14}H_9ClF_2N_2O_2$ | pesticide |
| 22 | dimethoate | $C_5H_{12}NO_3PS_2$ | pesticide |
| 23 | dimethomorph | $C_{21}H_{22}ClNO_4$ | pesticide |
| 24 | dimetridazole | $C_5H_7N_3O_2$ | antibiotic |
| 25 | diphenylamine | $C_{12}H_{11}N$ | pesticide |
| 26 | febantel | $C_{20}H_{22}N_4O_6S$ | antibiotic |
| 27 | fenbendazole | $C_{15}H_{13}N_3O_2S$ | antibiotic |
| 28 | fenoxycarb | $C_{17}H_{19}NO_4$ | pesticide |
| 29 | flubendazole | $C_{16}H_{12}FN_3O_3$ | antibiotic |
| 30 | flusilazole | $C_{16}H_{15}F_2N_3Si$ | pesticide |
| 31 | fluvalinate | $C_{26}H_{22}ClF_3N_2O_3$ | pesticide |
| 32 | furazolidone | $C_8H_7N_3O_5$ | antibiotic |
| 33 | hexaconazol | $C_{14}H_{17}Cl_2N_3O$ | pesticide |
| 34 | imidacloprid | $C_9H_{10}ClN_5O_2$ | pesticide |
| 35 | indoxacarb | $C_{22}H_{17}ClF_3N_3O_7$ | pesticide |
| 36 | iprodione | $C_{13}H_{13}Cl_2N_3O_3$ | pesticide |
| 37 | malathion | $C_{10}H_{19}O_6PS_2$ | pesticide |
| 38 | mebendazole | $C_{16}H_{13}N_3O_3$ | antibiotic |
| 39 | metalaxyl | $C_{15}H_{21}NO_4$ | pesticide |
| 40 | methoxyfenozide | $C_{22}H_{28}N_2O_3$ | pesticide |
| 41 | metolachlor | $C_{15}H_{22}ClNO_2$ | pesticide |
| 42 | metronidazole | $C_6H_9N_3O_3$ | antibiotic |
| 43 | myclobutanil | $C_{15}H_{17}ClN_4$ | pesticide |
| 44 | nifuroxazide | $C_{12}H_9N_3O_5$ | antibiotic |
| 45 | oxfendazole | $C_{15}H_{13}N_3O_3S$ | antibiotic |
| 46 | oxibendazole | $C_{12}H_{15}N_3O_3$ | antibiotic |
| 47 | penconazol | $C_{13}H_{15}Cl_2N_3$ | pesticide |
| 48 | pendimethalin | $C_{13}H_{19}N_3O_4$ | pesticide |
| 49 | piperonyl-butoxide | $C_{19}H_{30}O_5$ | pesticide |
| 50 | pirimiphos-ethyl | $C_{13}H_{24}N_3O_3PS$ | pesticide |
| 51 | pirimiphos-methyl | $C_{11}H_{20}N_3O_3PS$ | pesticide |
| 52 | prochloraz | $C_{15}H_{16}Cl_3N_3O_2$ | pesticide |
| 53 | propiconazole | $C_{15}H_{17}Cl_2N_3O_2$ | pesticide |
| 54 | pyraclostrobin | $C_{19}H_{18}ClN_3O_4$ | pesticide |
| 55 | pyrimethanil | $C_{12}H_{13}N_3$ | pesticide |
| 56 | pyriproxifen | $C_{20}H_{19}NO_3$ | pesticide |
| 57 | ronidazole | $C_6H_8N_4O_4$ | antibiotic |
| 58 | simazine | $C_7H_{12}ClN_5$ | pesticide |
| 59 | spinosad | $C_{41}H_{65}NO_{10}$ | pesticide |
| 60 | spirodiclofen | $C_{21}H_{24}Cl_2O_4$ | pesticide |
| 61 | sulfachloropyridazine | $C_{10}H_9ClN_4O_2S$ | antibiotic |
| 62 | sulfadiazine | $C_{10}H_{10}N_4O_2S$ | antibiotic |
| 63 | sulfadimethoxine | $C_{12}H_{14}N_4O_4S$ | antibiotic |
| 64 | sulfamerazine | $C_{11}H_{12}N_4O_2S$ | antibiotic |
| 65 | sulfamethazine | $C_{12}H_{14}N_4O_2S$ | antibiotic |
| 66 | sulfamethizole | $C_9H_{10}N_4O_2S_2$ | antibiotic |
| 67 | sulfamethoxazole | $C_{10}H_{11}N_3O_3S$ | antibiotic |
| 68 | sulfamethoxypyridazine | $C_{11}H_{12}N_4O_3S$ | antibiotic |
| 69 | sulfamonomethoxine | $C_{11}H_{12}N_4O_3S$ | antibiotic |
| 70 | sulfaphenazole | $C_{15}H_{14}N_4O_2S$ | antibiotic |
| 71 | sulfapyridine | $C_{11}H_{11}N_3O_2S$ | antibiotic |
| 72 | sulfaquinoxaline | $C_{14}H_{12}N_4O_2S$ | antibiotic |
| 73 | sulfathiazole | $C_9H_9N_3O_2S_2$ | antibiotic |
| 74 | sulfisoxazole | $C_{11}H1_3N_3O_3S$ | antibiotic |
| 75 | tebuconazole | $C_{16}H_{22}ClN_3O$ | pesticide |
| 76 | tebufenozide | $C_{22}H_{28}N_2O_2$ | pesticide |
| 77 | tebuthiuron | $C_9H_{16}N_4OS$ | pesticide |
| 78 | tetramethrin | $C_{19}H_{25}NO_4$ | pesticide |
| 79 | thiabendazole | $C_{10}H_7N_3S$ | pesticide |
| 80 | thiacloprid | $C_{10}H_9ClN_4S$ | pesticide |
| 81 | thiamethoxam | $C_8H_{10}ClN_5O_3S$ | pesticide |
| 82 | trifloxystrobin | $C_{20}H_{19}F_3N_2O_4$ | pesticide |
| 83 | trimethoprim | $C_{14}H_{18}N_4O_3$ | antibiotic |

HCD in the LTQ/Orbitrap) or by resonance (radial excitation with LTQ and SORI-CID Qh/ICR). Although the recorded CID spectra are instrument-dependent, they are a very useful tool for confirming metabolite structure, especially when the product ions from CID are analyzed under high-resolution conditions yielding their respective elemental composition.[27]

Beside improvements brought in the fields of screening and multiplexed quantification of pollutants in various matrices, LC-HRMS methods have also been coupled to untargeted data processing approaches[28] or to effect directed analysis studies[29] to highlight untargeted chemical contaminants in wastewater effluents and river sediments. Furthermore, HRMS is nowadays the tool most used for metabolomics, which deals with the large-scale detection and quantification of metabolites in biological media. Metabolomics is an interdisciplinary approach,[30] which combines analytical chemistry, mathematics, statistics, and bioinformatics. In this context, the main objective of the present study is to demonstrate that LC-HRMS combined with a metabolomics data treatment workflow, which is mostly used for systems biology and biomarker discovery studies, is highly relevant to the field of food control by enabling the monitoring and identification of emerging pollutants and also by improving the chemical characterization of food matrices.

We chose to focus on the analysis of honey as a proof-of-concept study. Honey is a complex matrix obtained from bees during the harvest of nectar and pollen. Bees also play a major role in biodiversity as well as in the pollination[31,32] of plants, which is very important in agriculture. However, they are exposed to pesticides sprayed on fields and fruit trees. The European Union has established maximum residue levels (MRLs) for some pesticides in honey, the lowest of them being 10 $\mu$g/kg.[33] Three types of collateral damage may occur: (i) pollution of harvests and hence honey; (ii) poisoning of the

bees and decimation of their colonies; and (iii) chronic intoxication of consumers. The decline in the number of bee colonies in Europe in general and France in particular has considerably reduced honey production, whereas consumption has remained stable. As a consequence, most of the honey consumed in France is imported from around the world, and advanced methods are required to improve the chemical characterization of honey to highlight adulteration or contamination.

We report here the development, validation, and application of an LC-HRMS approach enabling the detection of 83 pollutants known to occur in honey samples and indicating whether or not their concentrations are above or below regulatory limits. We show that the same raw data can be processed using metabolomics like workflow, including automatic peak detection and alignment software, data mining, and multivariate statistical analysis tools to highlight untargeted and unknown chlorinated chemical contaminants and also to discriminate honey samples according to their floral origin.

## MATERIALS AND METHODS

**Chemicals and Reagents.** All standards (see Table 1, 28 antibiotics and 55 pesticides, >95% purity), magnesium sulfate salt ($MgSO_4$, >99%), sodium acetate ($CH_3COONa$, >97%), and glycine (>99% purity) were from Sigma-Aldrich (Saint-Quentin Fallavier, France). HPLC grade acetonitrile (ACN), formic acid (HCOOH, content >99%), dichloromethane ($CH_2Cl_2$), methyl *tert*-butyl ether (MTBE), sterile Falcon tubes (50 mL), and propylene tubes (5 mL) were from VWR International (Fontenay-sous-Bois, France). HPLC grade methanol (MeOH) was from Carlo Erba reagents (Val de Reuil, France). HPLC grade water was obtained by purifying demineralized water in a Milli-Q system (Millipore, Molsheim, France). The standard mixtures used for the external calibration of the MS instrument (Calmix-positive, for the positive ion mode, consisting of caffeine, L-methionylarginyl-phenylalanyl-alanine acetate, and Ultramark 1621; and Calmix-negative, for the negative ion mode, consisting of the same mixture plus sodium dodecyl sulfate and sodium taurocholate) were from Thermo Fisher Scientific (Les Ulis, France).

**Preparation of Stock Solutions.** Stock solution (1 mg/mL when possible) of each standard was prepared by dissolving 1 mg of each substance in 1 mL of an appropriate solvent consisting of $H_2O$, ACN, MeOH, $H_2O$/ACN, or $H_2O$/MeOH (50:50, v/v. containing or not 0.1% formic acid). A working mixed standard solution (1 $\mu$g/mL) was prepared by diluting each standard stock solution by a factor of 1000 with water. To minimize degradation of standards, stock and working standard solutions were stored at −20 °C immediately after preparation.

**Honey Samples.** A panel of 76 honeys was purchased by Institut National de la Consommation (INC, which is the French national institute for consumer protection) from different stores in the Paris region (France). These honeys were produced from around the world and from different types of flowers (multifloral, lavender, acacia, mountain, orange tree, and eucalyptus). They were of various prices and quality, ranging from discount, private label, handmade, to luxury, and of different kinds of label (i.e., none, organic farming, red label, and protected environmental indication (IGP)).

**Sample Preparation.** Honey samples were processed by liquid−liquid extraction with acetonitrile solvent, by adapting the protocol developed by Pizzuti et al.[34] to extract pesticides from soybeans to honey samples. Each honey sample (5 g) was weighed into a 50 mL polypropylene Falcon tube with a screw cap, and 4 mL of water was added to homogenize the samples of various consistencies (liquid, solid, or creamy). Each sample was then prepared in six replicates. Three of six replicates were spiked with an appropriate volume of working solution (1 $\mu$g/mL) to obtain a concentration of 10 ng/g for each targeted pollutant. Samples were then extracted with 10 mL of ACN with 2 g of magnesium sulfate and 2.5 g of sodium acetate added. The 50 mL Falcon tubes were rotated end-over-end for 1 h. After centrifugation at 3500 rpm for 5 min, an aliquot of 4 mL of the upper layer extract (acetonitrile) was transferred into a 5 mL propylene tube. The eluents were evaporated to dryness under nitrogen. Samples were then reconstituted to 200 $\mu$L of $H_2O$/ACN (95:5, v/v) before injection into the LC-HRMS system.

**Liquid Chromatography and Mass Spectrometry.** Analyses were performed using a Nexera LC-30AD liquid chromatographic system (Shimadzu, Marne-la-Vallée, France) coupled to an Exactive mass spectrometer (Thermo Fisher Scientific, Les Ulis, France) fitted with an electrospray source operated in the positive ionization mode. The software interface was Xcalibur (version 2.1) (Thermo Fisher Scientific). To ensure the accuracy of the mass measurements, the instrument was calibrated every week in both polarities with a homemade modified Calmix solution (Thermo Fisher Scientific) with the addition of 100 $\mu$L of glycine solution (10 $\mu$g/mL) to 150 $\mu$L of Calmix. For singly charged ions, the mass resolution power of the analyzer was set to 25 000 ($m/\Delta m$, full width at half-maximum at $m/z$ 200) and the mass accuracy over the range of $m/z$ 70−1000 was below 5 ppm. The AGC target and the maximum injection time were set to $10^6$ and 50 ms, respectively. The high-performance liquid chromatographic (HPLC) separation was performed on an Xterra C18 (5 $\mu$m, 150 mm × 2.1 mm) column (Waters, Guyancourt, France) with a Javelin column filter 0.5 $\mu$m (Thermo Fisher Scientific). The mobile phases were composed of water (A) and acetonitrile (B), both containing 0.1% formic acid. The elution consisted of an isocratic step of 2 min at 5% phase B, followed by a linear gradient from 5 to 100% of phase B from 2 to 22 min. These proportions were kept constant for 4 min before returning to 5% B from 26.1 to 30 min. The flow rate of the mobile phase was 0.3 mL/min, and the injection volume was 10 $\mu$L. The column and the automatic sample injector were kept at 30 and 4 °C, respectively. For the ESI source, the capillary voltage was set to 4800 V. For droplet evaporation, the sheath and auxiliary gas ($N_2$) flows were fixed at 28 and 9 arbitrary units, respectively. The capillary temperature was set to 280 °C. For MS/MS experiments, a Q-Exactive (Thermo Fisher Scientific) was used with the same source parameters and chromatography conditions as previously described. Two scan events were used: (i) an MS scan with a mass resolution power, AGC target, and maximum injection time set to 70 000 ($m/\Delta m$, full width at half-maximum at 200 u), $10^6$, and 50 ms, respectively; and (ii) an MS/MS scan (in HCD mode without LMCO limit) at normalized collision energies of 20 and 40%, with a mass resolution power, AGC target, maximum injection time, isolation width set to 17500 ($m/\Delta m$, full width at half-maximum at 200 u), $10^6$, 250 ms, and 0.4 $m/z$, respectively.

**Experimental Design.** Samples were randomized and analyzed in three batches of 152 samples (76 spiked and nonspiked samples). Within each batch, nonspiked samples were injected first. A blank and a pool of the 83 compounds of interest (in buffer at 100 ng/mL) were injected every 5 and 10 biological samples, respectively.

**Data Processing.** *Targeted Data Processing.* All raw data were processed with two application managers of Xcalibur 2.1 software: Qualbrowser (for peak detection) and Quanbrowser (for peak integration). The identification of the xenobiotics of interest from raw data was based on four criteria: (1) retention time of the expected molecule compared with the retention time of standard compound in a time window of ±0.15 min; (2) accurate mass measurement of the analyte (mass tolerance ±5 ppm); (3) reliability of the isotopic pattern compared with that of the reference compound; and (4) increase of the chromatographic peaks area in honey spiked with xenobiotics.

*Data Processing for the Nontargeted Approach.* Peak detection, alignment, and integration were performed with the XCMS software package. Raw files were first converted to mzXML format with MSconvert (ProteoWizard[35]). Data were processed using XCMS version 1.30.3 running under R version 3.0.0. The R software was installed on a Lenovo ThinkStation C20X 24 core Intel Xeon E5645 2.4 GHz with 24 Go RAM running Linux (Centos release 6.4 Final x86_64). The CentWave algorithm was used.[36] The list of the parameters used is available as Supporting Information (Table 3s). The resulting peak table was then processed as described below. First,

features were quantile normalized.[37] Features were then kept if they were detected with the same trend (i.e., present or absent) in the three replicates of 90% of honeys, with a coefficient of variation below 30% and with a sample to blank concentration ratio above a factor of 10. Finally, features were annotated by matching their mass accurate measured mass at ±10 ppm with theoretical ones contained in the KEGG,[38] HMDB,[39] and Metlin[40] databases by using an informatics tool developed in R language.

*Identification of Chlorinated Xenobiotics in Honey Samples.* A script was written in R language to highlight the chlorinated molecules thanks to the specific isotopic patterns provided by chlorine atoms. This script uses the peak table generated by XCMS. It groups two variables with the same retention time (±5 s) and differing by 1.9970 ± 0.0010 $m/z$, which corresponds to the accurate $m/z$ difference between the two natural chlorine isotope masses (i.e., $^{35}Cl$ and $^{37}Cl$).

*Statistical Analyses. (a) Multivariate Statistical Analyses.* The data resulting from the XCMS process were mean-centered and logarithm-scaled and then analyzed using SIMCA-P11 software (Umetrics, Umea, Sweden) for multivariate analyses using principal component analysis (PCA) and projection to latent structure discriminant analysis (PLS-DA). This software returns a variable importance in projection (VIP) score, which reflects the contribution of the variables to the model. A variable is considered as important for the model when its VIP is above 1. The PLS-DA models were validated using the cross-validation function of SIMCA-P11 and by permutation tests ($k$ = 100).

*(b) Univariate Statistical Analyses.* For each VIP feature, the normality assumption was checked (Shapiro–Wilk test, $\alpha$ = 5%). Then, the Wilcoxon test was used with $\alpha$ = 5% to determine the significance ($p$ value) between the two groups.

## RESULTS AND DISCUSSION

**Screening of Emerging Pollutants in Honey Samples Using a Targeted Approach.** *Method Development and Validation.* An HRMS-based metabolomic approach was first developed and implemented with honey samples as a proof-of-concept study. A list of 83 pollutants (55 pesticides and 28 antibiotics) of interest was drawn up (Table 1). A liquid–liquid extraction method and a UHPLC-HRMS method were developed and validated to (i) detect these 83 pollutants, (ii) indicate whether their concentrations in honeys are above or below regulatory limits, and (iii) detect a wide range of chemicals present in honeys.

Method development and validation are detailed in the Supporting Information. Briefly, a spectral database including chromatographic retention times and MS information (i.e., protonated, adduct, isotope, and in-source fragment ions for each molecule of interest) was built to select the ions to be extracted from raw data. Table 1s displays retention times and ions used for detection and quantification. Metabolite extraction from honey samples was achieved using acetonitrile supplemented with magnesium sulfate and sodium acetate (please refer to Materials and Methods for additional information), and an LC-HRMS method was optimized to achieve chromatographic separation of the 83 xenobiotics of interest within 30 min. This method was validated by studies of linearity, matrix effect, and intra-assay precision and by determination of the limit of detection (LOD), which corresponds in our case to the lowest concentration for which the coefficient of variation of the areas of triplicates was <15%. Intra-assay precision was satisfactory with RSD below 15%. Linearity was evaluated in the range from 0.01 to 1000 $\mu$g/kg and the determination coefficient ($r^2$) was >0.99 for all compounds. LOD values ranged from 0.1 to 10 $\mu$g/kg.

Finally, the sensitivity achieved with our method is comparable to[12] or even better[1,34] than that achieved with triple-quadrupole instruments operated in the MRM mode. In addition, all LOD values determined are below the regulatory values imposed by the European Union, when available (Table 2s).

*Targeted Analysis of Honey Samples.* Seventy-six honey samples from different countries and of different floral origins were selected. The results of the targeted analysis indicate that 74 of 76 honeys are contaminated with at least one molecule of the 83 selected xenobiotics. Figure 1a displays the number of molecules detected in each honey. A bimodal distribution seems to emerge with maximum points corresponding to two and seven molecules per honey. Classifications of the number of molecules per honey were made by country, floral origin, and organic farming, but did not show significant correlation (data not shown). Two honeys, in which no pollutants were found, came from organic farming in Australia and Mexico.

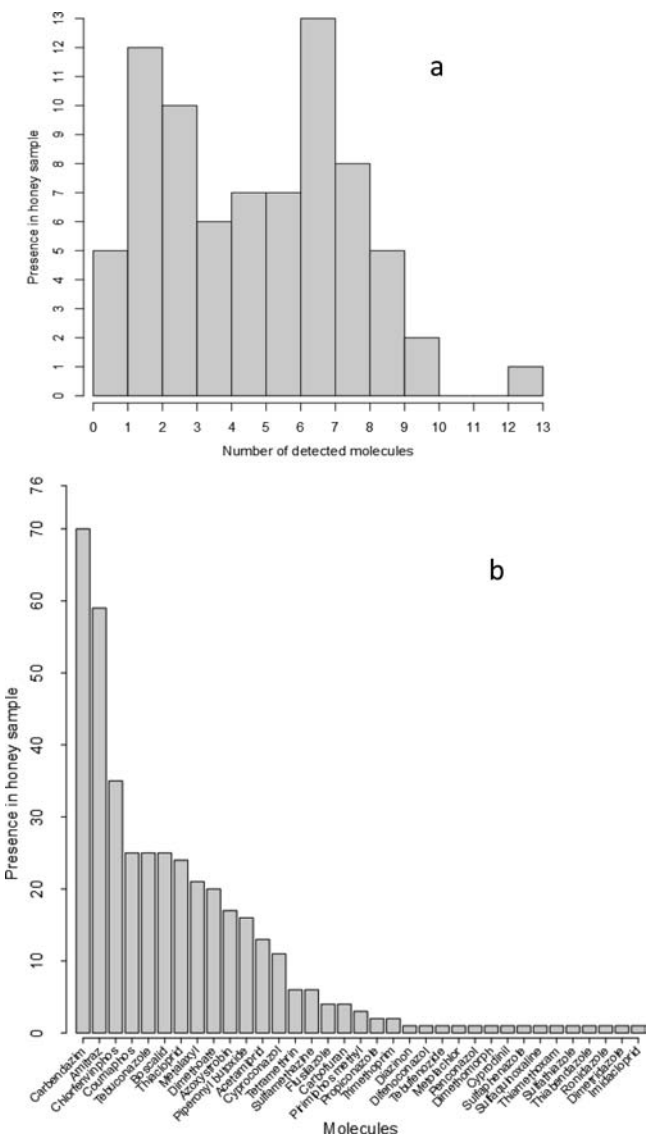


**Figure 1.** Targeted analysis of xenobiotics in honey samples: (a) histogram representing the number of molecules found in honey; (b) representation of the number of honey samples in which each molecule was found.

Figure 1b displays the number of xenobiotics detected and their presence in honey samples. It indicates that 35 of 83

**Table 2. Xenobiotics Detected in Honey Samples**

| ID | *m/z* | RT (min) | interpretation | occurrence in honey samples (floral origin) | ID status[a] |
|---|---|---|---|---|---|
| 1 | 189.9817 | 7.9 | 2,6-dichlorobenzamide ($C_7H_5ONCl_2$) | 6 (lavender) | identified (a, b, c) |
| 2 | 236.1407 | 12.5 | $C_{11}H_{22}NO_2Cl$ | 70 (miscellaneous) | a, e |
| 3 | 243.0971 | 2.9 | $C_5H_{15}N_6O_3Cl$ | 15 (miscellaneous) | a, e |
| 4 | 253.0308 | 11.2 | thiacloprid ($C_{10}H_9N_4SCl$) | 20 (miscellaneous) | identified (a, b, c) |
| 5 | 256.0598 | 9.6 | imidacloprid ($C_9H_{10}N_5O_2Cl$) | 1 (orange tree) | identified (a, b, c) |
| 6 | 277.1069 | 13.7 | $C_{10}H_{17}N_4O_3Cl$ | 1 (multifloral) | a, e |
| 7 | 277.2158 | 12.5 | $C_{13}H_{29}\ N_4Cl$ | 13 (miscellaneous) | a, e |
| 8 | 284.0834 | 6.0 | $C_{11}H_{19}NO_3Cl_2$ | 38 (miscellaneous) | a, e |
| 9 | 292.1204 | 15.3 | cyproconazole ($C_{15}H_{18}N_3OCl$) | 9 (miscellaneous) | identified (a, b, c) |
| 10 | 308.1520 | 16.3 | tebuconazole ($C_{16}H_{22}N_3OCl$) | 30 (miscellaneous) | identified (a, b, c) |
| 11 | 325.1255 | 9.4 | $C_{17}H_{22}N_2\ Cl_2$ | 39 (miscellaneous) | a, e |
| 12 | 341.0610 | 12.7 | $C_{11}H_{18}N_4O_2S\ Cl_2$ | 56 (miscellaneous) | a, e |
| 13 | 347.1973 | 16.5 | $C_{18}H_{31}O_4Cl$ | 48 (miscellaneous) | a, e |
| 14 | 357.1520 | 8.5 | $C_{12}H_{25}N_4O_6Cl$ | 38 (miscellaneous) | a, e |
| 15 | 369.1526 | 9.7 | U50488[b] ($C_{19}H_{26}N_2OCl_2$) | 15 (miscellaneous) | a, e |
| 16 | 387.1622 | 9.9 | $C_{17}H_{27}N_4O_2SCl$ | 47 (miscellaneous) | a, e |

[a]a, elemental composition; b, retention times matching with that of a standard; c, MS/MS matching with that of a standard; d, MS/MS matching with a structural hypothesis; e, MS/MS experiment available. [b]Structural hypothesis obtained from the Scifinder database (elemental composition).

targeted molecules were detected. The three most frequently recovered compounds were carbendazim, amitraz, and chlorfenvinphos (i.e., 70, 59, and 35 times in 76). Carbendazim is a fungicide belonging to the carbamate family, which is commonly used in cereal and fruit crops. It has been banned in the European Union (EU) since 2009.[41] Amitraz is an acaricide belonging to the family of formamidines. It is commonly used by beekeepers to protect their hives against the parasite *Varroa destructor*.[42] Finally, chlorfenvinphos is an insecticide and an acaricide belonging to the family of organophosphates. It was mainly used against fly larvae in farmed chicken or beef.[43] Because of its toxicity, it was banned in the EU in 2007. Some beekeepers may still use it to combat *Varroa* because it is more effective than amitraz.[44] However, our results, which provide an order of magnitude of concentration, indicate that no xenobiotics were found at concentrations above the regulatory threshold levels of the EU.

**Data Mining from LC-HRMS Fingerprints.** Unlike data acquired on a triple-quadrupole mass spectrometer operated in the MRM mode, HRMS-based data can be subjected to subsequent data mining procedures to highlight unanticipated information, as already performed with metabolomics in systems biology or for biomarker discovery. Proof-of-concept studies detailed below emphasize the relevance of such an approach for the detection of unexpected xenobiotics and for an improved chemical characterization of honeys.

To this end, raw data were processed using XCMS software, a collection of algorithms written in R language for the detection and alignment of peaks. XCMS output is a data matrix that can thus be processed by data mining algorithms and can also be subjected to multivariate statistical analyses.

*Detection of Unexpected Xenobiotics.* How to discriminate between signals related to metabolites (i.e., all organic substances naturally occurring from the metabolism of the living organism studied) or xenobiotics and contained in LC-HRMS fingerprints is a key question. It was addressed at the beginning of the 2000s by chemoinformatic analysis that describes metabolites present in the *Escherichia coli* bacteria listed in the EcoCyc and KEGG databases in terms of fragment-based fingerprints and descriptors based on physicochemical properties.[45] Other studies, such as those of Gupta et al.,[46] Dobson et al.,[47] and Peironcely et al.,[48] were subsequently published. Peironcely et al., for example, found some discrimination trends between metabolites and nonmetabolites on a PCA score plot on the basis that metabolites tend to have a higher water solubility, lower molecular mass, fewer C, N, and S atoms, and a lower number of cycles and rotatable bonds than nonmetabolites.[48]

However, from the analysis of these studies, it is difficult to establish rules to discriminate between signals related to either metabolites or xenobiotics in LC-HRMS data sets. The fact that xenobiotics can be metabolized by living organisms or degraded by the environment, and also the difficulty of automatically generating relevant elemental compositions from accurate measured mass despite the availability of chemical and empirical rules,[49] further complicates this task. Thus, we decided to focus on chlorine-containing compounds for this proof-of-concept study.

As chlorine atoms mainly occur in biological media as sodium chloride, chlorine-containing organic compounds are assumed to be, or at least to come from, xenobiotics produced by human industrial activity. Note that 35% of our 83 targeted xenobiotics contain at least one chlorine atom. In addition, chlorinated compounds can be easily and selectively detected in biological media using HRMS-based instruments thanks to their particular natural isotopic signature consisting of two stable isotopes, $^{35}Cl$ and $^{37}Cl$, the latter having a relative abundance of 33% of the first one and these two isotope masses being separated by 1.9970 u. We therefore developed an algorithm written in R language that highlights features differing by 1.9970 ± 0.0010 u (for singly charged ions) and occurring at the same retention time (±5 s) from peak tables produced by an automatic peak detection and alignment software.

First, 76 XCMS peak tables (see Supporting Information for the XCMS parameters, Table 3s) were produced on triplicates of each honey sample to improve the accuracy of RT and measured masses when compared with a single peak table containing 228 samples. These peak tables were then annotated with public databases (see Materials and Methods) and processed by our algorithm. Features highlighted by this algorithm in all 76 peak tables were then merged, leading to a

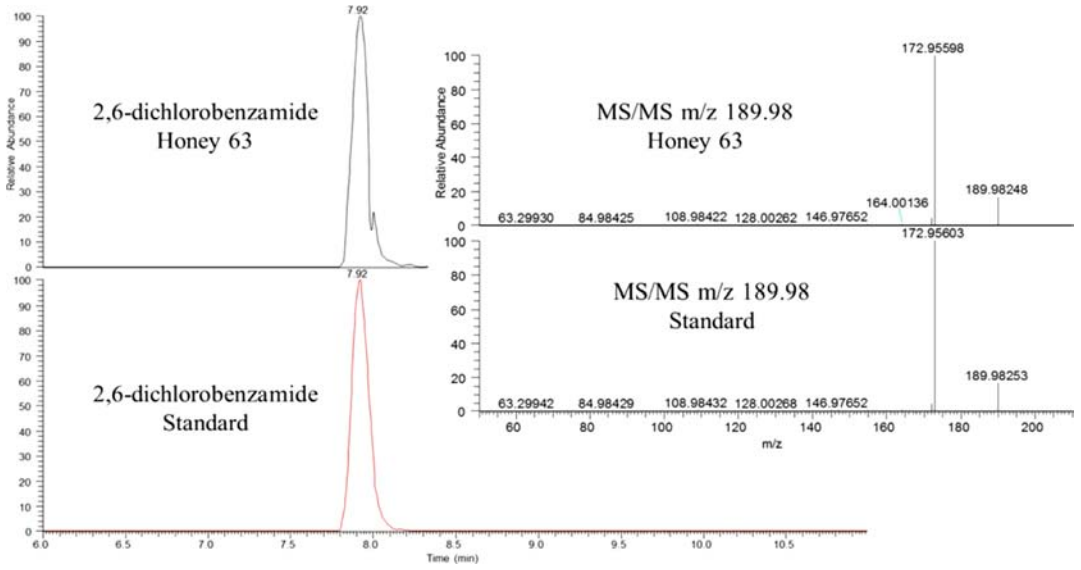


**Figure 2.** Identification of 2,6-dichlorobenzamide in honey ($[M + H]^+$ = 189.9821, $m/z \pm 8$ ppm).

peak table containing 25000 features. First, it is of note that 97% of the chlorinated molecules previously monitored in the course of the targeted approach were present in this peak table. Then, due to the high number of features, manual inspection was limited to the 1300 most represented features, which were sorted by increasing $m/z$ values. Features corresponding to a unique molecule were then merged in 143 clusters corresponding to couples of potential $^{35}$Cl- and $^{37}$Cl-containing ions and which were manually inspected. Only 28 of them were confirmed to correspond to chlorinated ions, among which 13 chlorinated compounds were detected in honeys (i.e., the others features were artifacts generated by the automatic peak detection process). The inspection of a fraction of the peak table shows that too many false positives are selected using only the criteria retention time and $m/z$ difference.

Additional criteria were then applied: (i) the relative abundance the $^{37}$Cl ion had to be between 20 and 120% of the $^{35}$Cl, which ensures the detection of ions bearing one to four chlorine atoms; (ii) the retention time had to be above 90 s (to avoid false positives due to the huge number of molecules present in the void volume); (iii) the area of the chromatographic peak related to the monoisotopic ion should be above $10^6$ AU; and (iv) sample (i.e., mean of the three replicates per honey) to blank concentration ratio should be above a factor of 3. By these means, only 4 chlorinated molecules of 35 previously detected in the targeted analysis (i.e., thiacloprid, imidacloprid, cyproconazole, tebuconazole) were detected, but the number of clusters generated was much smaller, thus allowing manual inspection. Moreover, this led to the detection of 18 new chlorinated compounds that are present in at least one honey sample, in addition to the 4 chlorinated compounds that were part of our list.

An XCMS peak table including the 228 samples (i.e., 76 honeys analyzed in triplicate) was generated without any specific criteria (see the Supporting Information for the XCMS parameters, Table 4s) to confirm the presence of these new chlorinated compounds. This led to the confirmation of 12 chlorinated molecules of the 18 initial ones, and 10 of them were present in at least 10 kinds of honey samples (Table 2).

MS/MS information, elemental composition, and isotope pattern regarding the number of Cl atoms were obtained successfully for these 12 compounds. However, only two structures were proposed on the basis of the MS/MS interpretation. The CID spectrum of compound **15** matched with U50488, a compound present in the Scifinder database (Table 2), whereas compound **1** was identified as 2,6-dichlorobenzamide by matching its retention time, accurate measured mass, isotopic pattern, and CID spectrum to those of the purchased compound (Figure 2), and it was found in 6 of 11 French lavender honeys (Table 2). Interestingly, this molecule is the metabolite of dichlobenil, a herbicide that was not part on our list of xenobiotics and which was widely used in lavender and lavendin plantations until it was banned in France in 2010.

*Honey Typing.* Besides the detection of chemical contaminants and/or their metabolites, we would also like to show that LC-HRMS and associated data mining could be relevant to improving the chemical characterization of honey samples. Here we focus on the discovery of biomarkers of floral origin that could help to detect fraud and provide a preliminary experiment. To this end, we used the XCMS peak table previously produced on the 76 kinds of honey samples (see Table 4s for XCMS parameters). This peak table contained 121,000 features and 300 samples (i.e., 76 honeys analyzed in triplicate and 72 analytical blanks). It was filtered out (see Materials and Methods for more detail), and 42500 analytically relevant signals were kept for multivariate statistical analyses.

The PCA score plot displayed in Figure 3a shows a clear discrimination between single-flower (acacia, lavender and orange) and multifloral (multiple flowers and mountain) honeys, except for eucalyptus honey samples for which the sampling was too small (four honey samples only). It also indicates that acacia honey samples are well separated of orange and lavender honey samples. We then focused on the discrimination between single and multifloral honey samples and used PLS-DA, the score plot of which is shown in Figure 3b, to confirm these results. This PLS-DA model was validated using the cross-validation function of the SIMCA P11 software and by permutation tests ($k$ = 500), which dramatically reduced the performances of the model, thus confirming its validity (Figure 3c).

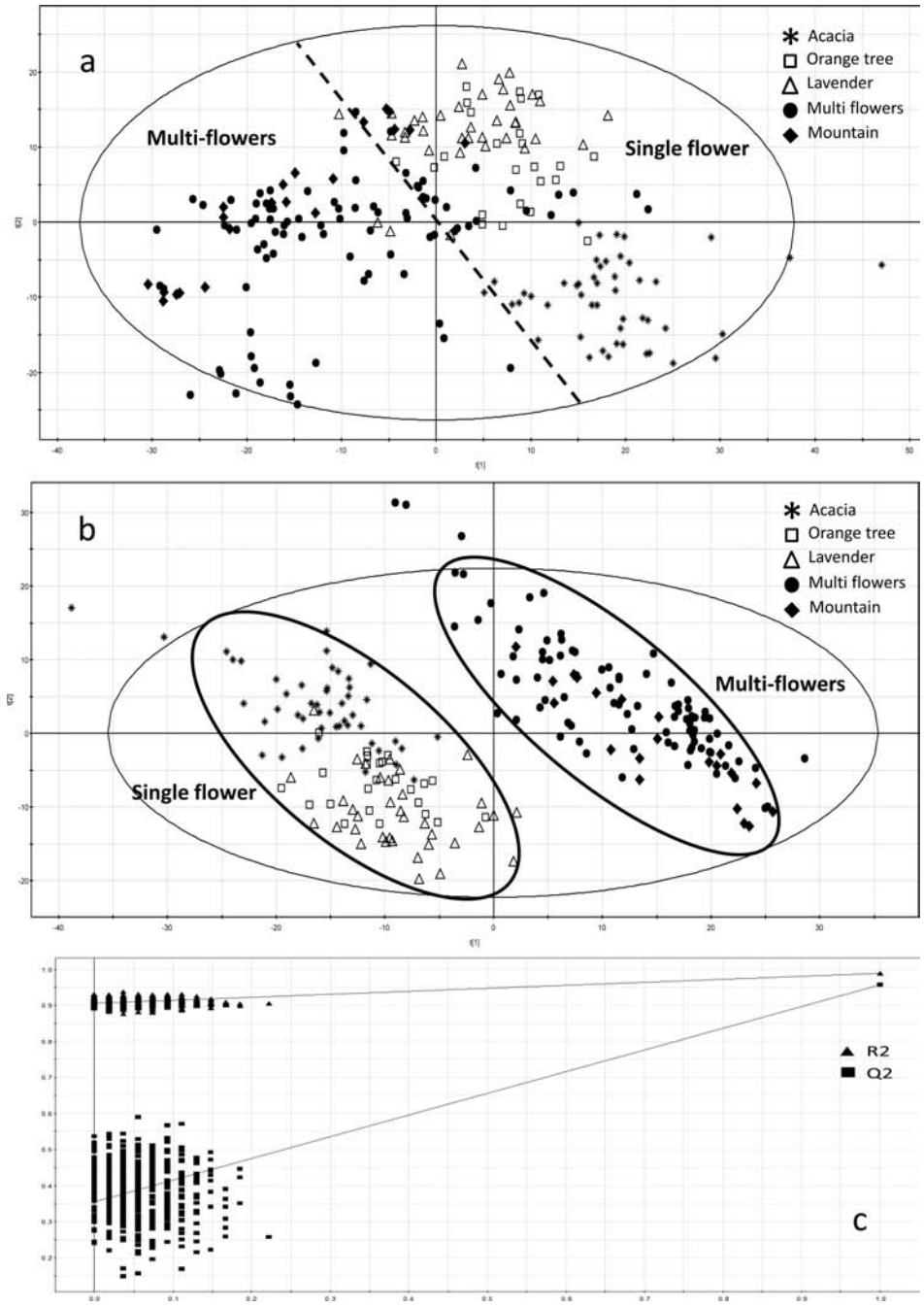


**Figure 3.** Multivariate statistical analyses of the data set of 76 honey samples. Multifloral (●), mountain (◆), acacia (*), orange tree (□), and lavender (△) honey samples. (a) PCA score plot of honey samples (excluding eucalyptus). Data were log-transformed and centered before multivariate statistical analysis. (b) PLSDA score plot of honey samples. (c) Validation model of PLSDA by permutation tests ($k$ = 500) on the first component. R2(Y) corresponds to the proportion of the variance of the response variable that is explained by the model, and Q2 (cum) expresses the cumulative proportion of the variance of the variables that can be predicted by the model. Permutation of data from multifloral samples related to data from single-flower samples dramatically decreased the performance of the model, thus confirming its validity.

Variables exhibiting a VIP score (please refer to the Materials and Methods for more details) above a value of 2 were then annotated using public databases such as KEGG,[38] HMDB,[39] and METLIN.[40] Six of the most significant annotated variables (VIP > 2) were selected. Their significance was confirmed by the Wilcoxon test with $\alpha$ = 5% (after verification of the normality assumption with the Shapiro−Wilk test; see Materials and Methods for more details), and their box and whisker plots are displayed in Figure 4.

Five of these six variables were putatively identified and exhibited MS spectra compatible with the proposed structure; a flavone-like structure was proposed for the last one (Table 3). CID spectra (in HCD mode) are available as Supporting Information. Figure 5 displays CID spectra of $m/z$ 438 (i.e., X84952) and a proposed fragmentation scheme suggesting that the precursor ion could be lunarine, an alkaloid occurring in plants of the *Lunaria* genus, native to central and southern Europe. A complete fragmentation scheme of lunarine is provided as Supporting Information (Figure 6s).

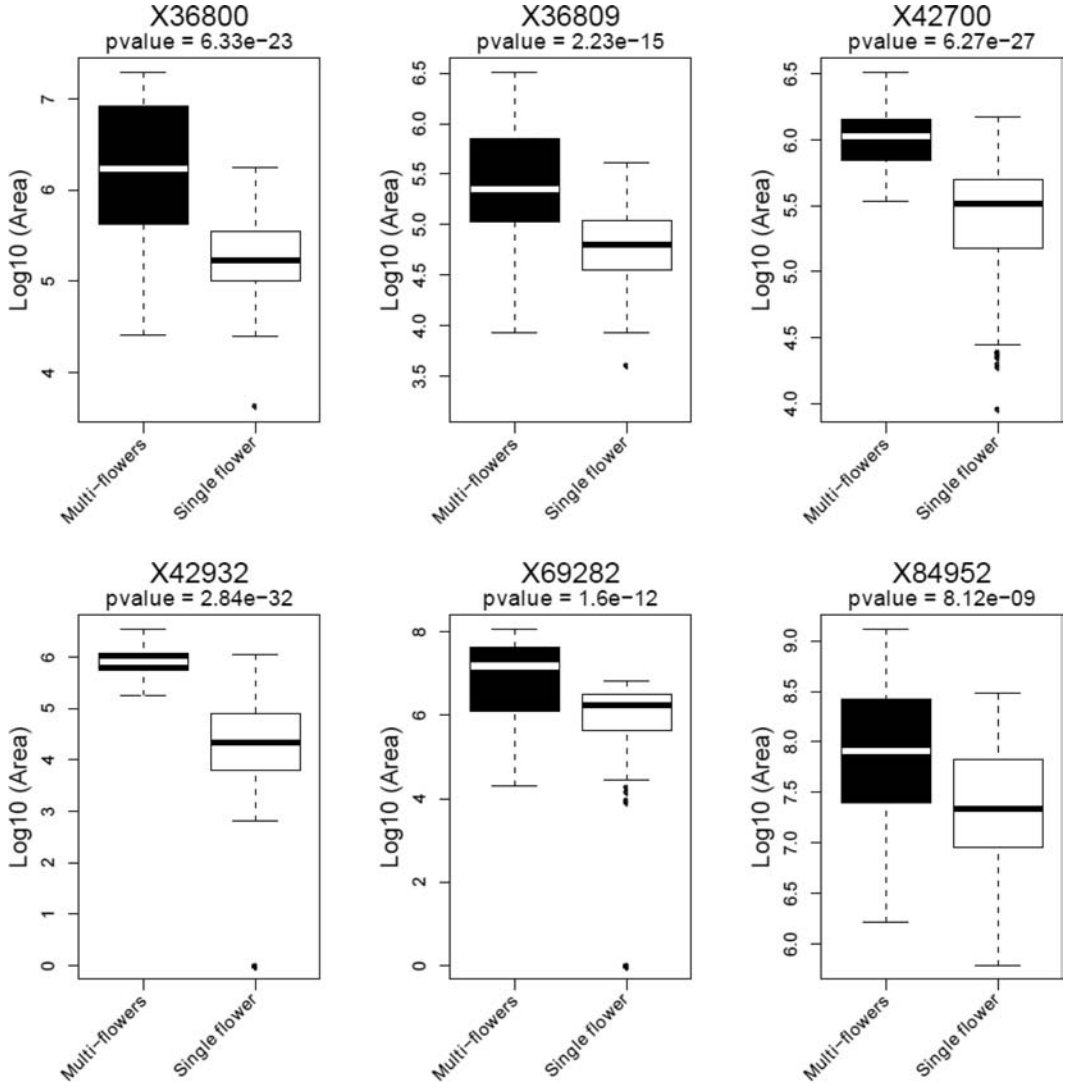


**Figure 4.** Box-plot of the six features of the most significance from PLS-DA. The thick line corresponds to the median. The box corresponds to the first and third quartiles. The whiskers represent 1.5 times the interquartile range. The outliers are marked by dots. Names of molecules putatively identified: X36800, methyl 2-(2-ethoxyacetamido)-4-methylpentanoate; X36809, methyl 2-(2-ethoxyacetamido)-2-methylpentanoate; X42700, *N*-D-glucosylarylamine; X42932, piscidic acid; X69282, flavone with ramification C18H16O8; X84952, lunarine.

**Table 3. Significant Features for the Discrimination between Single-Flower and Multifloral Honey Samples**

| feature | *m/z* | RT (min) | interpretation | ID status[a] |
|---|---|---|---|---|
| X36800 | 232.15433 | 5.5 | methyl 2-(2-ethoxyacetamido)-2-methylpentanoate or methyl 2-(2-ethoxyacetamido)-4-methylpentanoate | a, d |
| X36809 | 232.15433 | 5.7 | methyl 2-(2-ethoxyacetamido)-2-methylpentanoate or methyl 2-(2-ethoxyacetamido)-4-methylpentanoate | a, d |
| X42700 | 256.11795 | 1.6 | *N*-D-glucosylarylamine | a, d |
| X42932 | 257.0654 | 3.8 | piscidic acid | a, d |
| X69282 | 361.09179 | 11 | flavone with ramification $C_{18}H_{16}O_8$ | a, d |
| X84952 | 438.23873 | 7.9 | lunarine | a, d |

[a]a, *m/z* matching structure; b, retention times matching with that of a standard; c, CID spectrum matching with that of a standard; d, CID spectrum experiment available.

These molecules enable discrimination between multifloral and single-flower honeys and could be used for fraud detection (i.e., selling of multifloral honeys instead of single-flower honeys) after confirmation studies. Indeed, these are preliminary results based on information indicated on labels. Additional data mining procedures should be developed to improve these results, and confirmatory studies have to be undertaken, based on confirmation of floral origins of honey by melissopalinological, sensory, or chemical analyses.

In conclusion, this study demonstrates that LC-HRMS and LC-HRMS/MS associated with "metabolomics like" data mining tools are versatile tools allowing both target and global analyses for a better characterization of food matrices by enabling (i) conventional multiplexed and targeted analyses of xenobiotics, (ii) the detection of untargeted and unknown chemical contaminants, and (iii) the detection of metabolites useful for the characterization of food matrices. This was achieved by performing a proof-of-concept study on honey samples. Our results for a panel of 76 honeys showed that at least 1 of the 83 targeted pollutants was detected in 74 of the 76 honeys and that an average of 5 xenobiotics were found per

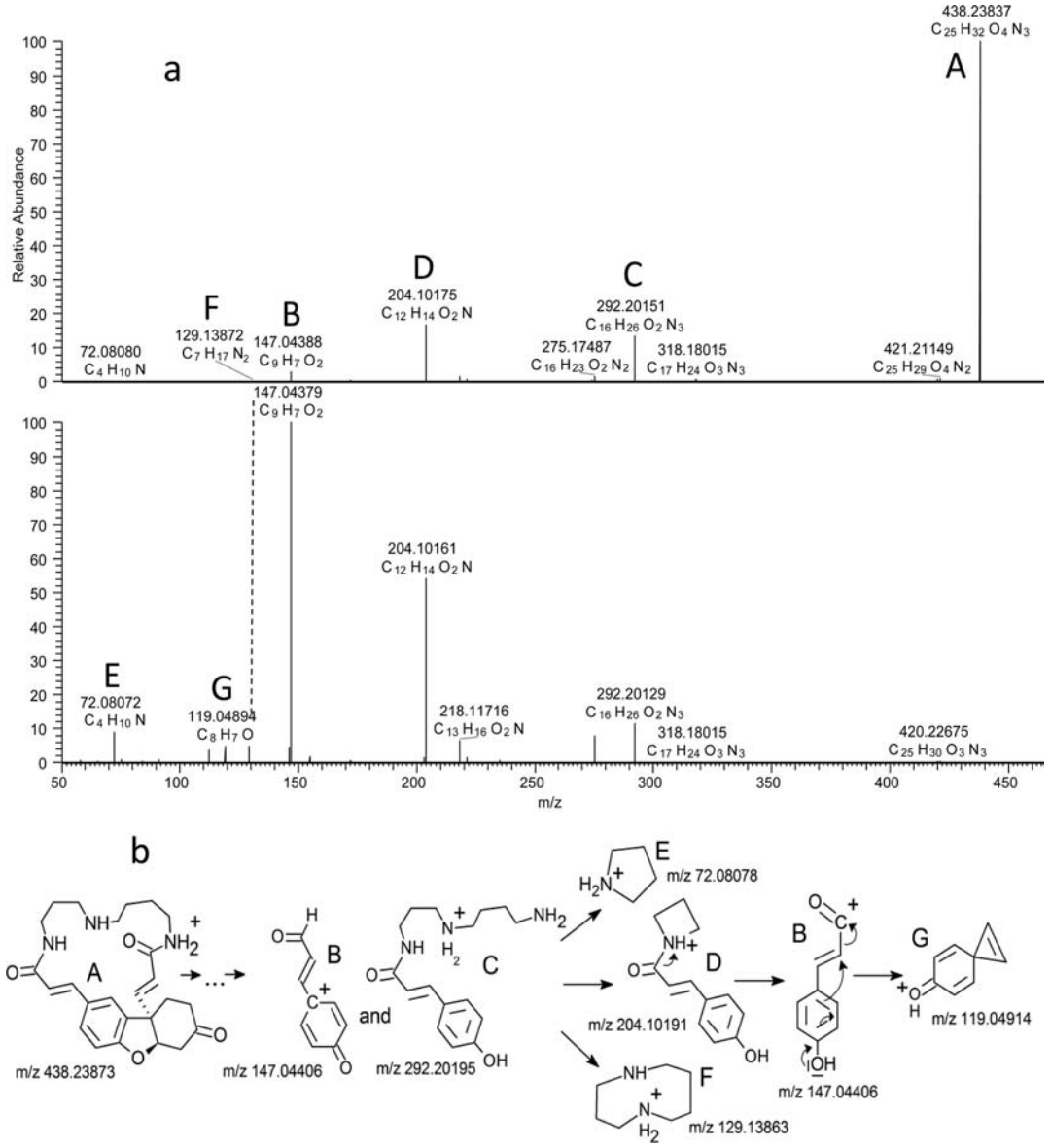


**Figure 5.** Characterization of lunarine from a honey sample: (a) CID spectrum of protonated variable X84952 annotated as lunarine recorded in HCD mode under (a) 20% and (b) 40% normalized collision energies; (b) summary of the proposed formal mechanism of fragmentations for lunarine (a complete scheme is available as Supporting Information, Figure 6s).

honey, with concentrations below the regulatory limits. Multivariate statistical analyses performed on analytically relevant features discriminated honey samples according to their floral origin. The data mining procedure also highlighted the presence of 12 unknown chlorinated chemicals in honey samples. One of these compounds was present in 4 lavender honeys and was formally identified as 2,6-dichlorobenzamide (a metabolite of dichlobenil, a herbicide that was widely used in lavender plantations before 2010).

Such an approach could be applied to any other food matrix to build (i) spectral databases of metabolites and pollutants to improve data set annotation and compound identification and (ii) metabolite fingerprint databases related to any given food matrix that could be coupled with data mining tools to highlight the presence of unexpected compounds. However, this requires the development of standardization and normalization tools to handle batch-to-batch variations of signal intensities and chromatographic retention times and also the analysis of a large number of samples to build a robust model. Furthermore, and as emphasized by our results, the characterization of untargeted and unknown chemicals by using MS and CID information remains highly challenging, but informatics tools such as in silico fragmenters and software for fragment ion prediction[50−53] that could be combined with other physical−chemical properties such as retention time index or octanol−water partitioning coefficients[54] could be of value to address this issue.

## ■ ASSOCIATED CONTENT

### Ⓢ Supporting Information

Building of the spectral database, the choice of chromatographic conditions, metabolite extraction, validation of the developed method, and detailed scheme for lunarine fragmentation; table with information about the molecules present in the spectral database (name, formula, detected ions, extracted masses, retention time and log $K_{o/w}$), table with


dx.doi.org/10.1021/jf504400c | J. Agric. Food Chem. 2014, 62, 11335−11345

information about the validation parameters (i.e., recovery (%), RSD (%), LOD ($\mu$g/kg)) and EU MLR ($\mu$g/kg), two tables that list the two sets of XCMS parameters used for the detection of features in honey samples, and $MS^2$ spectra of the six features that discriminate between floral origins. This material is available free of charge via the Internet at http://pubs.acs.org.

## AUTHOR INFORMATION


### Corresponding Author

*(C.J.) Phone: +33 1 69 08 43 66. Fax: +33 1 69 08 59 07. E-mail: christophe.junot@cea.fr.



### Funding

This work was funded by the French National Institutes of Consumers (INC) and by Bpi France as part of the Agrifood GPS collaborative project. J.C. is supported by a grant from Association Nationale de Recherche et de Technologie.


### Notes

The authors declare no competing financial interest.

## ACKNOWLEDGMENTS

We thank Dr. François Fenaille for helpful discussion.

## ABBREVIATIONS USED

EU MRL, European maximal residue level; HCD, higher collision-induced dissociation; LC-HRMS, liquid chromatography coupled to high-resolution mass spectrometry; LOD, limit of detection; MRM, multiple reaction monitoring; PCA, principal component analysis; PLS-DA, projection on latent structures-discriminant analysis; QqQ, triple quadrupole; QuEChERS, quick, easy, cheap, effective, rugged, and safe; RSD, relative standard deviation; VIP, variable importance in projections

## REFERENCES


(1) Gomez-Perez, M. L.; Plaza-Bolanos, P.; Romero-Gonzalez, R.; Martinez-Vidal, J. L.; Garrido-Frenich, A. *J. Chromatogr., A* **2012**, *1248*, 130−138.

(2) Jackson, R. J.; Minjares, R.; Naumoff, K. S.; Shrimali, B. P.; Martin, L. K. *J. Hunger Environ. Nutr.* **2009**, *4*, 393−408.

(3) Bohm, D. A.; Stachel, C. S.; Gowik, P. *Anal. Bioanal. Chem.* **2012**, *403*, 2943−2953.

(4) Cherta, L.; Portoles, T.; Beltran, J.; Pitarch, E.; Mol, J. G. J.; Hernandez, F. *J. Chromatogr., A* **2013**, *1314*, 224−240.

(5) Feo, M. L.; Eljarrat, E.; Barcelo, D. *Rapid Commun. Mass Spectrom.* **2011**, *25*, 869−876.

(6) Gros, M.; Petrovic, M.; Barcelo, D. *Anal. Bioanal. Chem.* **2006**, *386*, 941−952.

(7) Herrmann, A.; Rosen, J.; Jansson, D.; Hellenas, K. E. *J. Chromatogr., A* **2012**, *1235*, 115−124.

(8) Ho, Y. B.; Zakaria, M. P.; Latif, P. A.; Saari, N. *J. Chromatogr., A* **2012**, *1262*, 160−168.

(9) Wiest, L.; Bulete, A.; Giroud, B.; Fratta, C.; Amic, S.; Lambert, O.; Pouliquen, H.; Arnaudguilhem, C. *J. Chromatogr., A* **2011**, *1218*, 5743−5756.

(10) Cannon, W. R.; Jarman, K. H.; Webb-Robertson, B. J.; Baxter, D. J.; Oehmen, C. S.; Jarman, K. D.; Heredia-Langner, A.; Auberry, K. J.; Anderson, G. A. *J. Proteome Res.* **2005**, *4*, 1687−1698.

(11) Kapp, E. A.; Schutz, F.; Connolly, L. M.; Chakel, J. A.; Meza, J. E.; Miller, C. A.; Fenyo, D.; Eng, J. K.; Adkins, J. N.; Omenn, G. S.; Simpson, R. J. *Proteomics* **2005**, *5*, 3475−3490.

(12) Kmellar, B.; Fodor, P.; Pareja, L.; Ferrer, C.; Martinez-Uroz, M. A.; Valverde, A.; Fernandez-Alba, A. R. *J. Chromatogr., A* **2008**, *1215*, 37−50.

(13) Lehotay, S. J.; de Kok, A.; Hiemstra, M.; Van, B. P. *J. AOAC Int.* **2005**, *88*, 595−614.

(14) Schenck, F. J.; Hobbs, J. E. *Bull. Environ. Contam. Toxicol.* **2004**, *73*, 24−30.

(15) Wang, J.; Chow, W.; Leung, D.; Chang, J. *J. Agric. Food Chem.* **2012**, *60*, 12088−12104.

(16) Masia, A.; Ibanez, M.; Blasco, C.; Sancho, J. V.; Pico, Y.; Hernandez, F. *Anal. Chim. Acta* **2013**, *761*, 117−127.

(17) De, D. E.; Commissati, I.; Suman, M. *J. Mass Spectrom.* **2012**, *47*, 1232−1241.

(18) Kaufmann, A.; Butcher, P.; Maden, K.; Walker, S.; Widmer, M. *Anal. Chim. Acta* **2011**, *700*, 86−94.

(19) Peters, R. J.; Bolck, Y. J.; Rutgers, P.; Stolker, A. A.; Nielen, M. W. *J. Chromatogr., A* **2009**, *1216*, 8206−8216.

(20) Petrovic, M.; Gros, M.; Barcelo, D. *J. Chromatogr., A* **2006**, *1124*, 68−81.

(21) Polgar, L.; Garcia-Reyes, J. F.; Fodor, P.; Gyepes, A.; Dernovics, M.; Abranko, L.; Gilbert-Lopez, B.; Molina-Diaz, A. *J. Chromatogr., A* **2012**, *1249*, 83−91.

(22) Kaufmann, A.; Butcher, P.; Maden, K.; Walker, S.; Widmer, M. *Analyst* **2011**, *136*, 1898−1909.

(23) Leon, N.; Roca, M.; Igualada, C.; Martins, C. P.; Pastor, A.; Yusa, V. *J. Chromatogr., A* **2012**, *1258*, 55−65.

(24) Masia, A.; Campo, J.; Blasco, C.; Pico, Y. *J. Chromatogr., A* **2014**, *1345*, 86−97.

(25) Farre, M.; Pico, Y.; Barcelo, D. *J. Chromatogr., A* **2014**, *1328*, 66−79.

(26) Hernandez, F.; Sancho, J. V.; Ibanez, M.; Abad, E.; Portoles, T.; Mattioli, L. *Anal. Bioanal. Chem.* **2012**, *403*, 1251−1264.

(27) Junot, C.; Madalinski, G.; Tabet, J. C.; Ezan, E. *Analyst* **2010**, *135*, 2203−2219.

(28) Schymanski, E. L.; Jeon, J.; Gulde, R.; Fenner, K.; Ruff, M.; Singer, H. P.; Hollender, J. *Environ. Sci. Technol.* **2014**, *48*, 2097−2098.

(29) Weiss, J. M.; Simon, E.; Stroomberg, G. J.; de, B. R.; de, B. J.; van der Linden, S. C.; Leonards, P. E.; Lamoree, M. H. *Anal. Bioanal. Chem.* **2011**, *400*, 3141−3149.

(30) Junot, C.; Fenaille, F.; Colsch, B.; Bécher, F. *Mass Spectrom. Rev.* **2013**, *33*, 471−500.

(31) Klein, A. M.; Vaissiere, B. E.; Cane, J. H.; Steffan-Dewenter, I.; Cunningham, S. A.; Kremen, C.; Tscharntke, T. *Proc. Biol. Sci.* **2007**, *274*, 303−313.

(32) Steffan-Dewenter, I.; Potts, S. G.; Packer, L. *Trends Ecol. Evol.* **2005**, *20*, 651−652.

(33) Regulation (EC) No. 396/2005 of the European Parliament and of the Council of 23 February 2005 on maximum residue levels of pesticides in or on food and feed of plant and animal origin and amending Council Directive 91/414/EEC; http://ec.europa.eu/sanco_pesticides/public/?event=homepage (accessed April 18, 2014); *Off. J. Eur. Communities* **2005**, *L 70* (1).

(34) Pizzutti, I. R.; de Kok, A.; Hiemstra, M.; Wickert, C.; Prestes, O. D. *J. Chromatogr., A* **2009**, *1216*, 4539−4552.

(35) Kessner, D.; Chambers, M.; Burke, R.; Agus, D.; Mallick, P. *Bioinformatics* **2008**, *24*, 2534−2536.

(36) Tautenhahn, R.; Bottcher, C.; Neumann, S. *BMC Bioinformatics* **2008**, *9*, 504.

(37) Lee, J.; Park, J.; Lim, M. S.; Seong, S. J.; Seo, J. J.; Park, S. M.; Lee, H. W.; Yoon, Y. R. *Anal. Sci.* **2012**, *28*, 801−805.

(38) Kanehisa, M. *Novartis Found. Symp.* **2002**, *247*, 91−101.

(39) Wishart, D. S.; Jewison, T.; Guo, A. C.; Wilson, M.; Knox, C.; Liu, Y.; Djoumbou, Y.; Mandal, R.; Aziat, F.; Dong, E.; Bouatra, S.; Sinelnikov, I.; Arndt, D.; Xia, J.; Liu, P.; Yallou, F.; Bjorndahl, T.; Perez-Pineiro, R.; Eisner, R.; Allen, F.; Neveu, V.; Greiner, R.; Scalbert, A. *Nucleic Acids Res.* **2013**, *41*, D801−D807.

(40) Smith, C. A.; O'Maille, G.; Want, E. J.; Qin, C.; Trauger, S. A.; Brandon, T. R.; Custodio, D. E.; Abagyan, R.; Siuzdak, G. *Ther. Drug Monit.* **2005**, *27*, 747−751.

(41) Regulation (EC) No. 1107/2009 of the European Parliament and of the Council of 21 October 2009 concerning the placing of plant

protection products on the market and repealing Council Directives 79/117/EEC and 91/414/EEC; *Off. J. Eur. Communities* **2009**.
(42) The European Agency for the Evaluation of Medicinal Products (EMEA). Commitee for veterinary medicinal products: Amitraz (Bees); EMEA/MRL/572/99-FINAL, 1999.
(43) Agency for Toxic Substances and Disease Registry (ATSDR). *Toxicological Profile for Chlorfenvinphos*; U.S. Department of Health and Human Services: Public Health Service: Washington, DC, USA, 1997.
(44) Higes, M.; Martin-Hernandez, R.; Martinez-Salvador, A.; Garrido-Bailon, E.; Gonzalez-Porto, A. V.; Meana, A.; Bernal, J. L.; Del Nozal, M. J.; Bernal, J. *Environ. Microbiol. Rep.* **2010**, *2*, 243−250.
(45) Nobeli, I.; Ponstingl, H.; Krissinel, E. B.; Thornton, J. M. *J. Mol. Biol.* **2003**, *334*, 697−719.
(46) Gupta, S.; ires-de-Sousa, J. *Mol. Divers.* **2007**, *11*, 23−36.
(47) Dobson, P. D.; Patel, Y.; Kell, D. B. *Drug Discovery Today* **2009**, *14*, 31−40.
(48) Peironcely, J. E.; Reijmers, T.; Coulier, L.; Bender, A.; Hankemeier, T. *PLoS One* **2011**, *6*, No. e28966.
(49) Kind, T.; Fiehn, O. *BMC Bioinformatics* **2007**, *8*, 105.
(50) Wolf, S.; Schmidt, S.; Muller-Hannemann, M.; Neumann, S. *BMC Bioinformatics* **2010**, *11*, 148.
(51) Gerlich, M.; Neumann, S. *J. Mass Spectrom.* **2013**, *48*, 291−298.
(52) Allen, F.; Pon, A.; Wilson, M.; Greiner, R.; Wishart, D. *Nucleic Acids Res.* **2014**, *42*, W94−W99.
(53) Wang, Y.; Kora, G.; Bowen, B. P.; Pan, C. *Anal. Chem.* **2014**, *86*, 9496−9503.
(54) Schymanski, E. L.; Meringer, M.; Brack, W. *Anal. Chem.* **2011**, *83*, 903−912.

The products selected to implement the pesticide impurities detection program in Greece include both solid and liquid formulations. Initial screening of formulated pesticide products revealed the presence of carbaryl in copper oxide formulation. Carbaryl (1-naphthyl-*N*-methylcarbamate) is a widely used highly effective carbamate insecticide, with both agricultural and residential/domestic uses. However, it poses a potential hazard for health due to its relatively high acute toxicity.[12]

For the quantitative determination of carbaryl residues in plant matrices, soil, and water, several sample preparation methods have been developed, depending on the matrix used. For pesticide formulations liquid−liquid extraction (LLE) is the easiest and most common procedure followed by many pesticide laboratories. Conventional high-performance liquid chromatographic methods (HPLC) using reversed phase C18 columns have been extensively used with aqueous−organic mobile phases containing various proportions of acetonitrile, methanol, and methanol/acetonitrile in isocratic or gradient elution and UV, electrochemical, and fluorescence detection. Liquid chromatography with ion trap mass spectrometry and GC-MS were also used in multiresidue methods for quantitation of carbaryl in fresh fruit and vegetable samples. The typical limits of detection achieved were 0.01−0.02 mg/kg in plant matrices,[13,14] 0.2−5 μg/L in water,[15−17] and 0.15−0.64 μg/kg in soil[18−20]

Nowadays, the online combination of high-performance liquid chromatography and mass spectrometry (LC-MS) or tandem mass spectrometry (LC-MS/MS) holds a significant position in the analysis of contaminants and pesticides, in particular, because these methods provide unambiguous identification of thermally labile and polar pesticides at trace levels. Interfaces for LC-MS such as electrospray ionization (ESI) and atmospheric pressure chemical ionization (APCI) have been important tools in environmental analytical chemistry, especially in the area of pesticide analyses in soil and water. Recent developments in instrumentation made more readily available the high-resolution mass spectrometer (e.g., QTOF-UHPLC systems) with ≥10000 resolution. These instruments are ideal for the detection and identification of unknown substances and will have wide application in pesticide formulation control in the future.

Thus, a logical strategy is first to inject a diluted solution of the pesticide formulation to the GC-MS system, because the number of peaks eluting from the system can be assessed and possibly identified with existing libraries and then ideally confirmed. The next step is to use HPLC analysis coupled with mass spectrometry to incorporate thermally labile compounds that are not stable under GC conditions.

The aim of this work is to illustrate our testing strategy using as an example the determination of a trace amount of carbaryl (organic contaminant) in copper oxychloride solid pesticide formulation including the development and full validation of the method based on HPLC-DAD and confirmation of the identity of the compound with HPLC-PDA-ESI-MS.

## MATERIALS AND METHODS

**Working Standard Solutions and Sample Preparation.** An analytical standard of carbaryl (99.8%) was purchased from Sigma-Aldrich (Steinheim, Germany). HPLC grade water, acetone, and methanol were obtained from Fischer Scientific (USA) and LC-MS water and methanol from Merck (Germany). The stock solution of carbaryl (1000 μg/mL) was prepared in acetone. For GC-MS all solutions used for verification purposes were prepared in acetone as well. All working solutions used for method validation in the HPLC part were prepared in methanol (HPLC grade). Samples of two different inorganic copper oxychlorides formulated as wettable powder were obtained from the Greek market.

The GC-MS analysis was performed on a Chromtech Evolution MS/MS triple-quadrupole mass spectrometer built on an Agilent 5975 B inert XL EI/CI MSD system. Samples were injected with a Gerstel MPS-2 autosampler using a 10 μL syringe. Separations were performed on a DB-5MS 30 m × 0.25 mm × 1.0 μm column (J&W, Folsom, CA, USA). Helium was used as the carrier gas at a flow rate of 1.2 mL $min^{-1}$. Briefly, the oven temperature was initially programmed to 45 °C. The temperature was increased to 130 °C at 25 °C/min and held for 2 min. The temperature was further increased to 180 °C at 12 °C/min, to 240 °C at 7 °C/min, and finally to 320 °C at 10 °C/min, which was held for 2 min. The injector, MS transfer line, and MS heater temperatures were maintained at 250 °C. The mass spectrometer was operated in the full scan data acquisition mode. The transfer line, manifold, and source of ionization temperatures were 250, 40, and 230 °C, respectively. The electron multiplier voltage was set at 2000 V. The total GC analysis time was 44.85 min, and carbaryl eluted at 11.05 min.

For the HPLC-DAD method 10 matrix-matched solutions were freshly prepared by spiking copper formulation product (with no organic impurities present at the retention time of carbaryl) performed in such way to obtain concentrations of 0.2, 0.4, 1, 2, 4, 8, 12, 16, 20, and 200 μg/g formulated product. A similar 10 solutions were prepared for the HPLC-MS method, at a concentration range from 0.1 to 20 μg/g formulated product.

A representative pesticide formulation subsample of 5 g was placed into a 100 mL glass volumetric flask with methanol. The sample was pretreated in an ultrasonic bath, to ensure complete dissolution of organic components, for 15 min. The sample solution was filtered through a 0.45 μm nylon filter membrane and/or centrifuged (Heraeus Labofuge 400R Thermo Electron Corp., 5 min, 2000 rpm) prior to injection of the solution into the HPLC column.

**High-Performance Liquid Chromatography.** The HPLC system used was a Shimadzu UFLC instrument, equipped with a column oven (CTO-20A), a diode array detection system (SPD-M20A), a degasser (DGU-20As), and an autosampler (Sil-20AC) and connected to a reverse-phase Nucleosil C18 column (250 mm × 4 mm × 5 μm, Macherey-Nagel). The analysis was carried out using, as mobile phase, an isocratic mixture of methanol/water 70:30. The mobile phase was filtered and degassed prior to use. The detection wavelength was set at 220 nm. The flow rate of the mobile phase was maintained at 1.0 mL $min^{-1}$, which provided a pressure of 148 bar. System control and data analysis were carried out using LC LabSolution software (Shimadzu). The temperature of the column was maintained at 40 °C during all runs, and the injection volume was 10 μL. The total run time was 10 min. The retention time of carbaryl was 4.9 min.

**Liquid Chromatography Coupled with Diode Array and Mass Spectrometry.** Carbaryl presence was confirmed using HPLC-DAD-ESI-MS. A Shimadzu LCMS-2010 EV liquid chromatograph−mass spectrometer together with a SIL-20A prominence autosampler and an SPD-M20A diode array detector was used with LC-MS solution version 3.0 software. The latter was coupled in series with a mass selective detector equipped with an atmospheric pressure ionization source usable as either ESI interface. The LC separation was achieved on a Shim-Pack XR-ODS 2.2 μm, 100 × 4.6 mm i.d.. chromatographic column using the isocratic mobile phase of methanol/water 70:30 with the addition of formic acid (0.1%) in the aqueous phase to promote ionization of carbaryl molecule. The flow rate was 0.5 mL $min^{-1}$. The identification of carbaryl (4.20 min, retention time) was achieved by the HPLC-ESI-MS system functioning in the positive ionization mode. Full scan and selected ion monitoring mode (SIM mode) were applied, and the characteristic ions at 145 and 202 amu were observed (Figure 2).

## RESULTS AND DISCUSSION

In the presented work, the first step of the screening procedure revealed the presence of carbaryl in the copper oxychloride formulation (see full scan MS chromatogram, Figure 1).

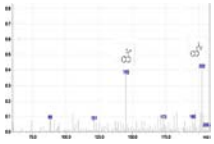

**Figure 1.** Full scan mass spectrum peak eluting at 4.2 min attributed to carbaryl (diluted pesticide formulation).

Because carbaryl is thermally labile[21] and decomposes to α-naphthol either in the injector or additionally during elution, it was decided to determine its concentration in the formulations by HPLC under the conditions described above (Figures 2−4). Additionally, maximum information was gained through the use of HPLC coupled with mass spectrometry (Figures 5 and 6) and PDA (Figure 7).

If a potential carbaryl peak was detected in the copper oxide pesticide formulations analyzed with the optimum chromatographic conditions described under High-Performance Liquid Chromatography (Figure 1), that peak was then identified by full scan mass spectrometry with HPLC-PDA-ESI-MS (Figures 5 and 7) and further quantified with the use of both techniques.

The only peak that was assessed with regard to its mass spectrometry profile was the peak eluting at 4.9 min in the HPLC (or at 4.2 min in LC-MS method) because the other two eluting peaks (1.6 and 2.3 min) are lower than the 2.91 min void time of the column.

With regard to the sample preparation step and its impact on analyte retention, the critical step is purification of the sample prior to injection. In this context both nylon filtering and centrifugation showed similar GC-MS chromatograms, indicating that for GC-amenable compounds no significant alteration of their composition was evidenced.

**Validation of the HPLC LC-PDA-ESI-MS Procedure.** For the validation of the method, the following parameters were determined: linearity, repeatability, reproducibility, limit of detection (LOD) and limit of quantification (LOQ), recoveries, and matrix-dependent variations as is established by the EU guidelines for HPLC-UV and LC-MS methods.[22,23] Linearity and matrix effect were assessed by analyzing standard solutions and matrix-matched standards to cover the expected range of carbaryl concentrations as an impurity in commercial formulations. The results are presented in Table 1. Both HPLC and HPLC-MS provided linear responses over the mentioned concentration ranges with excellent correlation coefficient ($r^2$) values. No matrix effect was observed.

Accuracy was assessed after performing a recovery study with both methods. Recoveries and repeatability relative standard deviations ($RSD_r$) with the HPLC method were, respectively, in the range of 89.2−102.1% and 5.10, 3.13, and 2.45% at the three concentration levels of 2, 16, and 200 μg/kg. In the case of LC-MS the recoveries and RSD values were in the range of 91.1−102.9% and 3.12, 4.11, and 4.77%, respectively, at 0.4, 4, and 16 μg/g spike levels. The Dixon test revealed that there was no outlier in the recovery values obtained by both methods.

For reproducibility studies with both methods, five replicate determinations were performed on five different days at three standard concentration levels (2, 16, and 200 μg/g, HPLC method and 0.4, 4, and 16 μg/g, LC-MS method) on one pesticide lot. The $RSD_r$ values for reproducibility were 2.38, 4.1, and 4.34%, respectively. In the LC-MS method, the $RSD_r$ values for reproducibility were 4.05, 3.65, and 2.48%, respectively. To calculate the homogeneity of the variances of the repeatability and reproducibility RSDs, the Cochran test was applied, which indicated no outliers. The LOD and LOQ were determined as 3 times the standard deviation of the blank (matrix without analyte) and 10 times the standard deviation of the blank (formulation sample not containing carbaryl). LOD and LOQ values are presented in Table 1, and the respective chromatograms at LOQ level are shown in Figures 4 and 6.

The above results demonstrate the reliability and accuracy of the measurement of carbaryl in commercial pesticide formulations and indicate an absence of systematic error.

**Chromatographic Peak Confirmation.** It is important to point out that the same sample solutions were used for both HPLC-DAD and LC-PDA-MS systems, simultaneously, to ensure the presence of carbaryl in the samples analyzed.

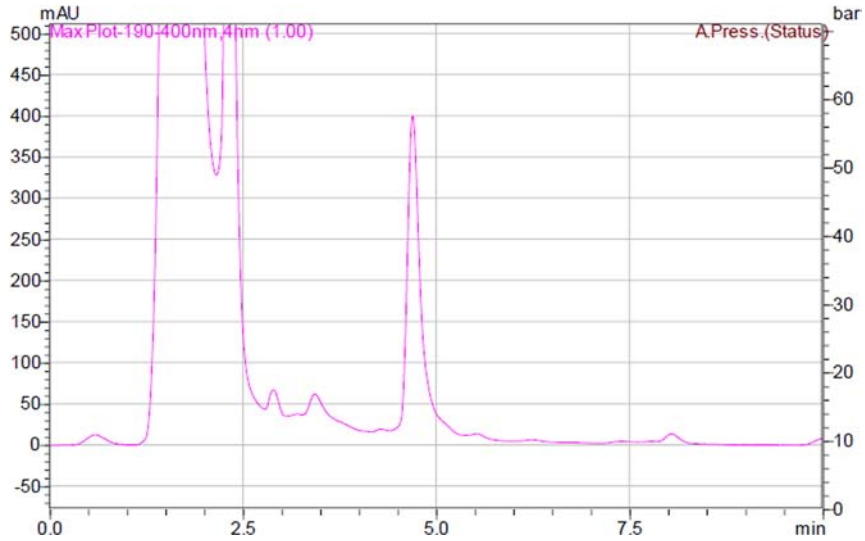


**Figure 2.** HPLC-PDA maximum plot chromatogram of the diluted pesticide formulation.


dx.doi.org/10.1021/jf504729g | J. Agric. Food Chem. 2014, 62, 11347−11352

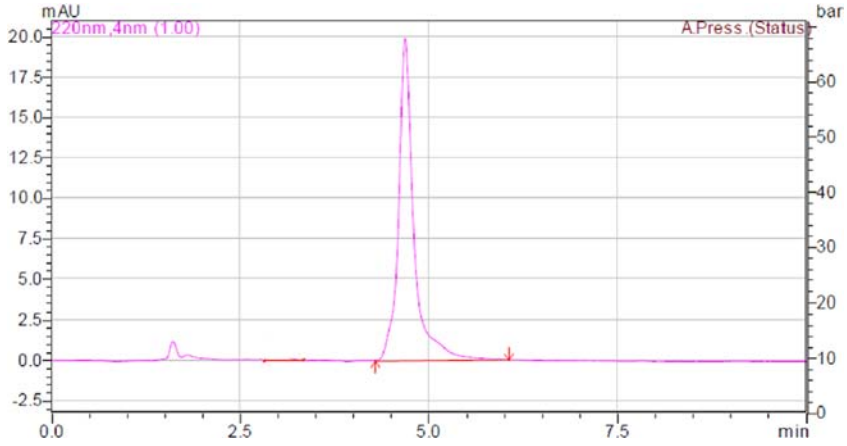


**Figure 3.** HPLC-UV chromatogram of carbaryl analytical standard.

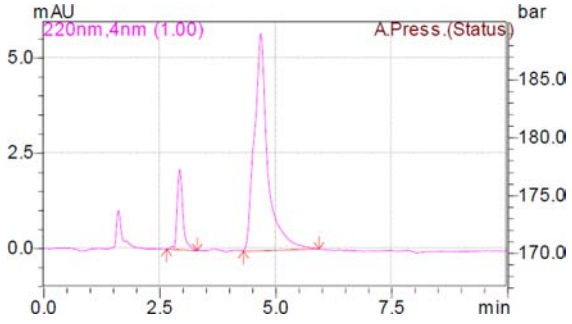


**Figure 4.** HPLC-UV chromatogram of carbaryl in a sample extract spiked at LOQ level.

Specificity is a measurement of the degree of interference in the analysis of pesticide formulation. The chromatographic peak was identified/confirmed according to molecular masses obtained by LC-ESI-MS in the positive ionization mode. The SIM chromatogram at 4.2 min verified the presence of two specific anions that characterize the molecule.

The ions obtained by this method are typical and previously reported by other research teams.[13,24] Thus, $m/z$ 202 corresponds to $[M + H]^+$, whereas $m/z$ 145 corresponds to $[M - 56]^+$.

**Comparison with Other Analytical Studies.** The advantage of the proposed methodology is the quantitative and sensitive determination of carbaryl in pesticide formulations. The extraction of the analyte from a formulation product assisted with ultrasonication resulted in repeatable and reproducible results. Considering the need to test for organic impurities in inorganic formulations, the presented method is an efficient solution for the analysis of carbaryl in such formulations. The principle of the stepwise procedure developed can be applied for testing other formulations as well.

Another sensitive and selective way to detect carbaryl would be using a fluorescence detector. An indicative work in this field was published in 2011.[18] However, the fluorescence method

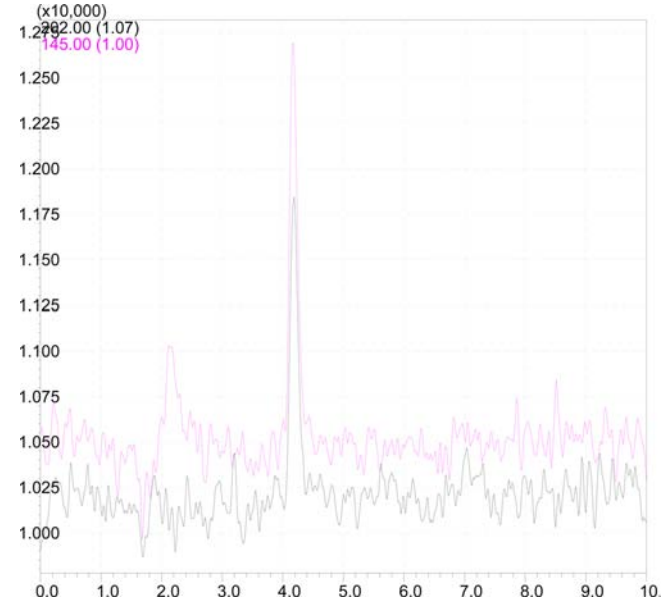


**Figure 6.** SIM chromatogram of carbaryl in sample extract spiked at LOQ level.

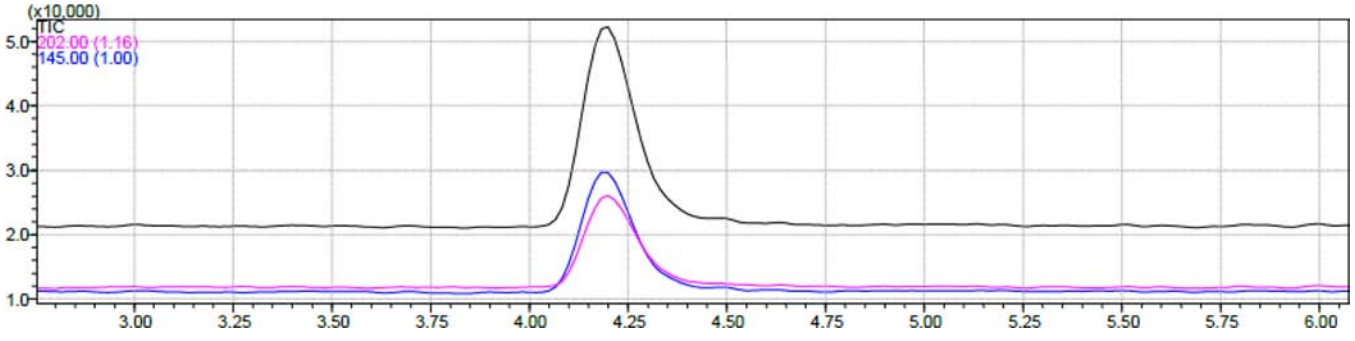


**Figure 5.** SIM chromatogram of carbaryl standard solution at 1 $\mu$g mL$^{-1}$.


dx.doi.org/10.1021/jf504729g | J. Agric. Food Chem. 2014, 62, 11347−11352

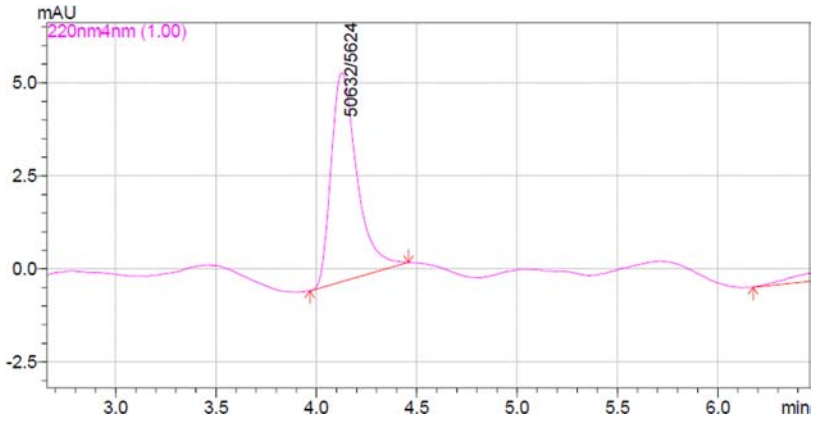


**Figure 7.** UV chromatogram of carbaryl of sample extract spiked at 220 nm using LC-PDA-ESI-MS.

**Table 1. Analytical Performance of HPLC and HPLC-MS Methods**

| method | linear range ($\mu g/g_{form}$) | LOD ($\mu g/g_{form}$) | LOQ ($\mu g/g_{form}$) | calibration equation | correlation coefficient, $r^2$ |
|---|---|---|---|---|---|
| HPLC-DAD | 0.2−200 | 0.13 | 0.42 | $y = 211948x + 47423$ | 0.9974 |
| HPLC-ESI-MS | 0.1−20 | 0.05 | 0.18 | $y = 371278x - 1921.1$ | 0.9995 |

has some drawbacks related to (1) time-consuming postcolumn derivatization, (2) time-consuming sample preparation, and (3) the lack of confirmatory information from the analytical results.

The testing strategy proposed in this paper is a novel and logical combination of existing chromatographic techniques, which were fully validated for this particular purpose. Therefore, it could be used to monitor the purity profile of pesticide formulations.

**Contamination of Real Samples and Preliminary Risk Assessment.** Our procedure was applied for the determination of the concentration of carbaryl in formulations. Specifically, two formulations of copper oxychloride from the Greek market were received and analyzed for the presence of carbaryl, and one of them contained carbaryl at a concentration of 12.4 mg/kg formulation. This concentration clearly demonstrates that cross-contamination occurred probably in the production−assembly line, because it is far below the usual concentration of carbaryl in formulations with copper oxychloride.[25]

In the presented case carbaryl's concentration was determined at 12.4 mg/kg formulation. The MRL of carbaryl varies between 0.01 and 0.8 mg/kg.[26] Assuming the worst scenario of copper oxychloride being applied at double the suggested rate (8 kg/ha) and all pesticide being deposited on grape bunches harvested with a yield of 10 tons/ha on the day of treatment, the resulting carbaryl residue would be 0.0012 mg/kg. It would not be detectable and would not cause any risk for consumers or result in MRL violation. However, there might be some adverse health effects for the pesticide applicators. The latter scenario is of importance considering that users of plant protection products tend to be less careful with inorganic pesticides, and thus unintended exposure to an acute toxic substance (carbaryl in this case) could take place.

In this case study the presence of carbaryl was verified in an inorganic pesticide formulation, indicating cross-contamination in the production. In this regard, it is evident that the combination of various chromatographic techniques and detection methods should be employed in the portfolio of analytical laboratories aiming to detect impurities and ensure the quality of pesticide products.

Unexpected impurities or contaminations in pesticides might constitute a hazardous threat to the environment and human health. In this regard authorities should encompass regular monitoring applying specific techniques to detect the presence of harmful impurities. It is expected that the presented procedure will be used as a routine approach in laboratories involved in pesticide formulation analyses. This strategy will be strengthened by a complementary LC-MS screening approach that is currently being pursued in our laboratories. Regular monitoring of contaminants in pesticide formulations followed by appropriate regulatory actions could ideally prevent or substantially reduce counterfeiting and would ensure proper quality of plant protection products, minimize the risk for pesticide applicators and residents, and protect human health and the environment.

## AUTHOR INFORMATION

### Corresponding Authors

*(H.K.) Mail: Research Associate, Laboratory of Chemical Control of Pesticides, Department of Pesticides Control and Phytopharmacy, Benaki Phytopathological Institute, 8 St. Delta Street, Kifissia, 14561 Athens, Greece. E-mail: E.Karassali@bpi.gr.

*(K.M.K.) Mail: Research Assistant, Laboratory of Pesticides Toxicology, Department of Pesticides Control and Phytopharmacy, Benaki Phytopathological Institute, 8 St. Delta Street, Kifissia, 14561 Athens, Greece. E-mail: K.Kasiotis@bpi.gr.

### Author Contributions

‖H.K. and K.M.K made equal contributions to this work.

### Notes

The authors declare no competing financial interest.

## REFERENCES

(1) ECPA. http://www.ecpa.eu/files/gavin/15020_15020.pdf (accessed July 3, 2014).

(2) Counterfeit-Pesticides. http://www.chem.unep.ch/unepsaicm/prague_nov06/meeting_docs/ecpa.pdf.

(3) Baker, E. L., Jr.; Warren, M.; Zack, M.; Dobbin, R. D.; Miles, J. W.; Miller, S.; Alderman, L.; Teeters, W. R. Epidemic malathion poisoning in Pakistan malaria workers. *Lancet* **1978**, *1*, 31−34.

(4) Josse, R.; Sharanek, A.; Savary, C. C.; Guillouzo, A. Impact of isomalathion on malathion cytotoxicity and genotoxicity in human HepaRG cells. *Chem.−Biol. Interactions* **2014**, *209*, 68−76.
(5) Ambrus, A.; Hamilton, D. J.; Kuiper, H. A.; Racke, K. D. Significance of impurities in the safety evaluation of crop protection products (IUPAC technical report). *Pure Appl. Chem.* **2003**, *75*, 937−973.
(6) Burger, J.; de Mol, F.; Gerowitt, B. The "necessary extent" of pesticide use − thoughts about a key term in German pesticide policy. *Crop Prot.* **2008**, *27*, 343−351.
(7) European Commission, Regulation (EC) No. 1107/09 of the European Parliament and of the Council of 21 October 2009 concerning the placement of plant protection products and repealing Council Directives 79/117/EEC and 91/414/EEC. *Off. J. Eur. Union* **2009**, *L 309/1*.
(8) FAO/WHO-Panel. http://www.fao.org/agriculture/crops/thematic-sitemap/theme/pests/jmps/en/ (accessed July 15, 2014).
(9) Ahuja, S. Assuring quality of drugs by monitoring impurities. *Adv. Drug Delivery Rev.* **2007**, *59*, 3−11.
(10) Argentine, M. D.; Owens, P. K.; Olsen, B. A. Strategies for the investigation and control of process-related impurities in drug substances. *Adv. Drug Delivery Rev.* **2007**, *59*, 12−28.
(11) Gallart-Mateu, D.; Armenta, S.; de la Guardia, M. Implementing the contamination prevention programs in the pesticide industry by infrared spectroscopy. *Talanta* **2014**, *119*, 312−319.
(12) EFSA Scientific Report (2006) 80, 1−71, conclusion on the peer review of carbaryl, 2006.
(13) Radisic, M. M.; Vasiljevic, T. M.; Dujakovic, N. N.; Lausevic, M. D. Application of matrix solid-phase dispersion and liquid chromatography-ion trap mass spectrometry for the analysis of pesticide residues in fruits. *Food Anal. Methods* **2013**, *6*, 648−657.
(14) Chowdhury, M. A. Z.; Fakhruddin, A. N. M.; Islam, M. N.; Moniruzzaman, M.; Gan, S. H.; Alam, M. K. Detection of the residues of nineteen pesticides in fresh vegetable samples using gas chromatography-mass spectrometry. *Food Control* **2013**, *34*, 457−465.
(15) Goulart, S. M.; Alves, R. D.; Neves, A. A.; de Queiroz, J. H.; de Assis, T. C.; de Queiroz, M. E. L. R. Optimization and validation of liquid-liquid extraction with low temperature partitioning for determination of carbamates in water. *Anal. Chim. Acta* **2010**, *671*, 41−47.
(16) Driss, M. R.; Hennion, M. C.; Bouguerra, M. L. Determination of carbaryl and some organophosphorus pesticides in drinking-water using online liquid-chromatographic preconcentration techniques. *J. Chromatogr.* **1993**, *639*, 352−358.
(17) He, L. J.; Wang, C. J.; Sun, Y. J.; Luo, X. L.; Zhang, J.; Lu, K. Dispersive liquid-liquid microextraction followed by high-performance liquid chromatography for the determination of three carbamate pesticides in water samples. *Int. J. Environ. Chem.* **2009**, *89*, 439−448.
(18) Asensio-Ramos, M.; Hernandez-Borges, J.; Borges-Miquel, T. M.; Rodriguez-Delgado, M. A. Ionic liquid-dispersive liquid-liquid microextraction for the simultaneous determination of pesticides and metabolites in soils using high-performance liquid chromatography and fluorescence detection. *J. Chromatogr., A* **2011**, *1218*, 4808−4816.
(19) Zhang, T.; Ma, C.; Wu, M.; Ye, Y.; Chen, H. X.; Huang, J. L. Selective microextraction of carbaryl and naproxen using organic-inorganic monolithic columns containing a double molecular imprint. *Microchim. Acta* **2013**, *180*, 695−702.
(20) Asensio-Ramos, M.; Hernandez-Borges, J.; Gonzalez-Hernandez, G.; Rodriguez-Delgado, M. A. Hollow-fiber liquid-phase microextraction for the determination of pesticides and metabolites in soils and water samples using HPLC and fluorescence detection. *Electrophoresis* **2012**, *33*, 2184−2191.
(21) Song, X. L.; McNair, H. M. Fast gas chromatography analysis of N-carbamates with cold on-column injection. *J. Chromatogr Sci.* **2002**, *40*, 321−325.
(22) ICH. Validation of Analytical Procedures: Text and Methodology Q2(R1), http://www.ich.org/fileadmin/Public_Web_Site/ICH_Products/Guidelines/Quality/Q2_R1/Step4/Q2_R1__Guideline.pdf, 2005.
(23) Validation, Bioanalytical Method Validation "Guidance for Industry", http://www.fda.gov/downloads/Drugs/Guidances/ucm070107.pdf.
(24) Nogueira, J. M. F.; Sandra, T.; Sandra, P. Multiresidue screening of neutral pesticides in water samples by high performance liquid chromatography−electrospray mass spectrometry. *Anal. Chim. Acta* **2004**, *505*, 209−215.
(25) Carbaryl-Copper-Oxychloride, http://www.epa.govt.nz/Publications/Organophosphate%20and%20carbamate%20supporting%20information.pdf.
(26) EU-Pesticides, http://ec.europa.eu/sanco_pesticides/public/?event=homepage.

## RESULTS AND DISCUSSION

**Photoisomerization with Various Sensitizers.** To isomerize (*all-E*)-carotenoids to *Z*-isomers, heat treatment has been the typical method used so far.[3,7,11] Very recently, we reported a detailed study on the thermal isomerization of high-purity (*all-E*)-lycopene (≥99%), which showed that heating (*all-E*)-lycopene at 50 °C in hexane produced ca. 30% (5*Z*)-lycopene as a main product, whereas the use of benzene generated ca. 20% (13*Z*)-lycopene.[12] On the other hand, there are some reports on the photosensitized *E*/*Z* isomerization of carotenoids, an alternative method to thermal processing, which has been confined to (*all-E*)-*β*-carotene.[13,14] Under these circumstances, we performed the photoisomerization of (*all-E*)-lycopene to the corresponding *Z*-forms in acetone in the presence of four kinds of sensitizers using filtered light. After irradiation with 480−600 nm light for 60 min, the concentrations of undecomposed lycopene remaining in solution were determined to be $1.5 \times 10^{-5}$ mol/L (with MB), $1.7 \times 10^{-5}$ mol/L (with chlorophyll *a*), and $1.7 \times 10^{-5}$ mol/L (without sensitizer) under ≥600 nm light irradiation; $0.7 \times 10^{-5}$ mol/L (with erythrosine), $1.0 \times 10^{-5}$ mol/L (with RB), and $1.9 \times 10^{-5}$ mol/L (without sensitizer) by the HPLC analysis; typical chromatograms are shown in Figure 1. The total amounts of *Z*-isomers relative to the remaining lycopene after the reaction were 57.4, 51.3, 47.7, and 46.4% with MB, chlorophyll *a*, erythrosine, and RB, respectively (Table 1). On the other hand, the blank tests irradiated at the light regions more than 600 nm and between 480 and 600 nm without sensitizer resulted in *Z*-isomer contents of only 7.4 and 7.7%, respectively. To the best of our knowledge, photoisomerization of (*all-E*)-lycopene was previously conducted by Stahl et al.[15] and Lee and Chen.[16] However, Stahl et al.[15] performed the iodine-catalyzed isomerization; the iodine is inedible, and the reaction mechanism would contain a radical process principally.[17] Then, Lee and Chen[16] carried out the isomerization of (*all-E*)-lycopene by direct light irradiation for 60 min, obtaining only a few percent of *Z*-isomers. Our results obviously indicated that the use of sensitizer and filtered light resulted in an accelerated isomerization of (*all-E*)-lycopene to *Z*-isomers. MB was the most efficient sensitizer for the isomerization among the reagents tested; however, it is not approved for use in food processing. In contrast, chlorophyll *a*, erythrosine, and RB are usable in such industrial fields, and therefore erythrosine appears to be the most suitable sensitizer for (*all-E*)-lycopene isomerization.

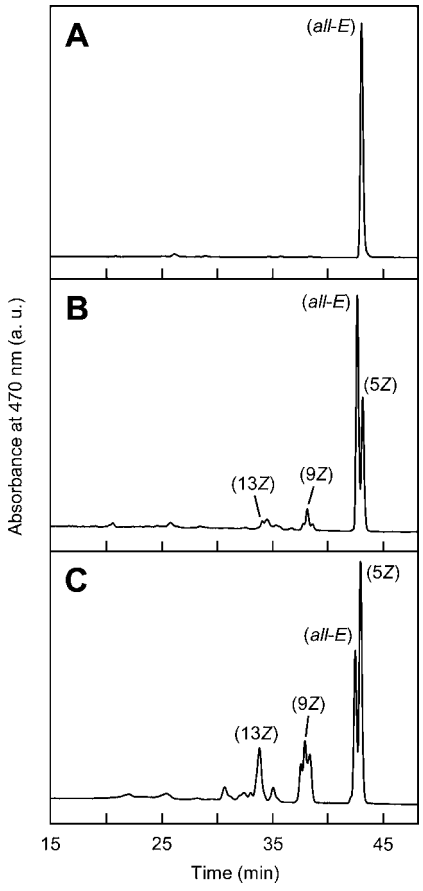


**Figure 1.** Reversed-phase HPLC charts of (A) (*all-E*)-lycopene and photoirradiated lycopene with rose bengal (RB) as a sensitizer in (B) acetone and (C) hexane at 32 °C for 60 min. Unidentified peaks contain multi-(*Z*)-isomers as well as other mono-(*Z*)-isomers.

As for the individual *Z*-isomers generated, several *Z*-isomers of lycopene were observed in the HPLC chart in addition to (5*Z*)-, (9*Z*)-, and (13*Z*)-lycopene (Figure 1B), which are predominantly contained in processed food.[7] In all cases with the above sensitizers after 60 min of irradiation, (5*Z*)-lycopene showed the greatest increases to 39.9, 31.7, 37.7, and 29.9% relative to the remaining lycopene with MB, chlorophyll *a*, erythrosine, and RB, respectively (Table 1). On the other hand, (9*Z*)-, (13*Z*)-, and other *Z*-isomers increased to <10% with each sensitizer under the same irradiation duration. (5*Z*)-Lycopene exhibits higher bioavailability[7] and antioxidant activity[10] compared to (*all-E*)-lycopene and possibly to (9*Z*)- and (13*Z*)-lycopene. In addition, (5*Z*)-lycopene is estimated to be thermodynamically more stable than (9*Z*)- and (13*Z*)-lycopene according to the results of quantum chemistry calculations.[18] Therefore, we believe that photosensitized isomerization is an effective method to produce lycopene isomers with sophisticated functionalities and greater storage stability among the *Z*-isomers.

**Time Course of the Photosensitized Isomerization of Lycopene and Solvent Effects on the Content of *Z*-Isomers.** To determine the optimum conditions for photosensitized isomerization of (*all-E*)-lycopene, the sensitizers erythrosine and RB, which are approved for use in food processing and have good isomerization efficiency, as mentioned above, were used. The time course examinations of photosensitized isomerization of lycopene were carried out with the sensitizers in acetone (Figure 2A,B). The total amount of *Z*-isomers of lycopene with erythrosine was slightly greater than with RB, and (5*Z*)-lycopene constituted the majority of *Z*-isomers with both sensitizers. Using erythrosine, (9*Z*)-lycopene, a kinetically preferable isomer, initially emerged and likely reversed to the (*all-E*)-form with time.

Next, solvent effects on isomerization with the two sensitizers were investigated using ethyl acetate (Figure 2C,D) and hexane (Figure 2E,F), both of which are approved for use in the food, drink, and dietary supplement manufacturing industries. After irradiation in ethyl acetate for 60 min, the concentrations of lycopene remaining in solutions were $0.6 \times 10^{-5}$ mol/L with both erythrosine and RB; on the other hand, relatively higher levels of lycopene were obtained in hexane: $1.7 \times 10^{-5}$ mol/L with erythrosine and $1.4 \times 10^{-5}$ mol/L with RB. The total amounts of *Z*-isomers relative to the remaining lycopene after 60 min irradiation were 80.4, 67.6, and 47.7% in hexane, ethyl

**Table 1. Photoisomerization of (*all-E*)-Lycopene to Individual *Z*-Isomers with Methylene Blue (MB), Chlorophyll *a*, Erythrosine, and Rose Bengal (RB) as Sensitizers**

| | | content[a] (%) | | | | |
|---|---|---|---|---|---|---|
| sensitizer | irradiation (nm) | total *Z*-isomers[b] | 5*Z* | 9*Z* | 13*Z* | other *Z*[c] |
| MB | ≥600 | 57.4 ± 3.8 | 39.9 ± 3.3 | 7.1 ± 0.6 | 3.6 ± 0.2 | 6.8 ± 1.3 |
| chlorophyll *a* | ≥600 | 51.3 ± 5.9 | 31.7 ± 2.8 | 7.1 ± 1.3 | 3.4 ± 0.6 | 9.1 ± 3.8 |
| no sensitizer | ≥600 | 7.4 ± 0.6 | nd[d] | 3.2 ± 1.2 | 3.2 ± 0.7 | 0.9 ± 0.5 |
| erythrosine | 480−600 | 47.7 ± 1.7 | 37.7 ± 1.2 | 7.6 ± 0.3 | 1.2 ± 1.2 | 1.2 ± 1.2 |
| RB | 480−600 | 46.4 ± 0.7 | 29.9 ± 1.0 | 6.8 ± 0.02 | 3.3 ± 0.5 | 6.4 ± 1.0 |
| no sensitizer | 480−600 | 7.7 ± 2.0 | nd | 1.2 ± 1.0 | 4.4 ± 0.9 | 2.1 ± 0.5 |

[a]Percentage content of *Z*-isomers of lycopene isomerized from (*all-E*)-form by photoirradiation for 60 min in acetone. Values are represented as mean ± standard error ($n$ = 3). [b]Total amount of *Z*-isomers of lycopene. [c]Sum of *Z*-isomers of lycopene other than (5*Z*)-, (9*Z*)-, and (13*Z*)-forms. [d]Not detected.

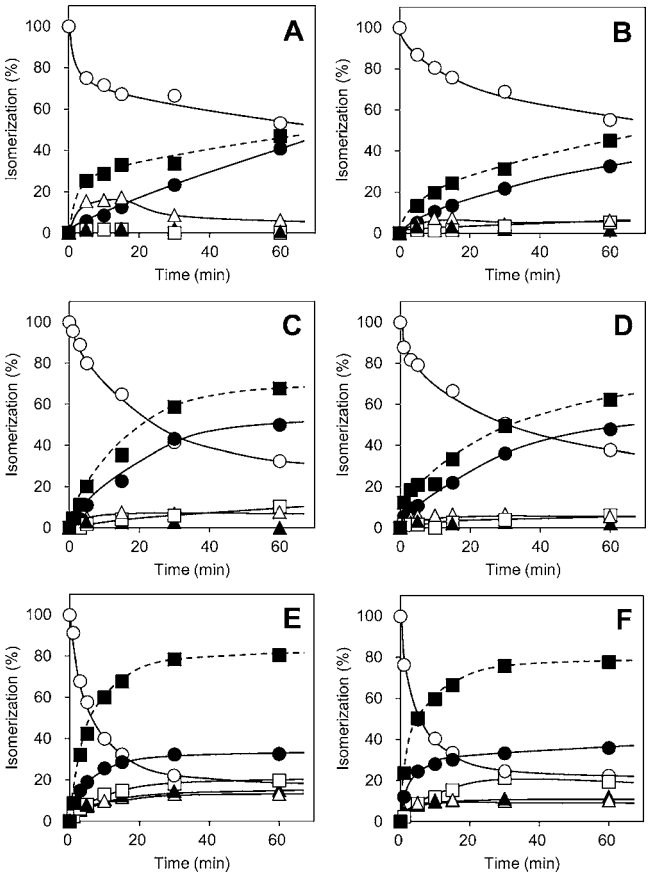


**Figure 2.** Photoisomerization of (*all-E*)-lycopene to individual *Z*-isomers in (A, B) acetone, (C, D) ethyl acetate, and (E, F) hexane with (A, C, E) erythrosine and (B, D, F) RB as a sensitizer under 480−600 nm light irradiation. Changes in the isomer content are presented relative to the total amount of lycopene isomers at each sampling point: (○) (*all-E*)-lycopene; (●) (5*Z*)-lycopene; (△ (9*Z*)-lycopene; (▲) (13*Z*)-lycopene; (□) other *Z*-isomers including those unidentified; (■) total amount of *Z*-isomers.

acetate, and acetone, respectively (Figure 2E,C,A), and a similar tendency was also observed with RB (Figure 2F,D,B). As for the individual *Z*-isomers, (5*Z*)-lycopene was again predominantly produced in each condition and both (9*Z*)-lycopene and (13*Z*)-lycopene exceeded 10% by content after 60 min of irradiation with erythrosine (Figure 2E) or RB (Figures 1C and 2F) in hexane. In addition, the total amount of other *Z*-isomers except for (5*Z*)-, (9*Z*)- and (13*Z*)-lycopenes was also markedly increased in hexane, 19.7 and 19.4% with erythrosine and RB, respectively. These results demonstrate that the use of a less polar solvent not only accelerated *Z*-isomerization but also was effective in suppressing the degradation of lycopene. To explain the higher rate of the photosensitized isomerization of (*all-E*)-lycopene to the *Z*-isomers, it could be reasonable to investigate the energy gap between the photosensitizer in an excited triplet state and the (*all-E*)-lycopene in a triplet state.[13,14,19]

In conclusion, the photoisomerization of (*all-E*)-lycopene to *Z*-isomers with sensitizer and filtered light has proven to be more effective than thermal isomerization. In particular, the reaction condition with erythrosine in hexane under 60 min of irradiation at wavelengths between 480 and 600 nm was the best method to enrich the content of *Z*-isomers and suppress the degradation of lycopene. These findings will contribute to the development of facile isomerization of (*all-E*)-lycopene to *Z*-isomers in the fields of food, drink, and dietary supplement manufacturing.

**Masaki Honda*,[†]**
**Haruyuki Igami[†]**
**Takahiro Kawana[†]**
**Kento Hayashi[‡]**
**Munenori Takehara[‡]**
**Yoshinori Inoue[‡]**
**Chitoshi Kitamura[‡]**

[†]Research and Development Division, Kagome Company, Ltd., Nishitomiyama, Nasushiobara 329-2762, Japan

[‡]Department of Materials Science, The University of Shiga Prefecture, Hassaka, Hikone 522-8533, Japan

## AUTHOR INFORMATION

### Corresponding Author

*(M.H.) Phone: +81-287-36-2935. Fax: +81-287-39-1038. E-mail: Masaki_Honda2@kagome.co.jp.

### Notes

The authors declare no competing financial interest.

## REFERENCES

(1) Holden, J. M.; Eldridge, A. L.; Beecher, G. R.; Buzzard, I. M.; Bhagwat, S.; Davis, C. S.; Douglass, L. W.; Gebhardt, S.; Haytowitz, D.; Schakel, S. Carotenoid content of U.S. foods: an update of the database. *J. Food Compos. Anal.* **1999**, *12*, 169−196.

(2) Khoo, H.-E.; Prasad, K. N.; Kong, K.-W.; Jiang, Y.; Ismail, A. Carotenoids and their isomers: color pigments in fruits and vegetables. *Molecules* **2011**, *16*, 1710−1738.

(3) Schieber, A.; Carle, R. Occurrence of carotenoid *cis*-isomers in food: technological, analytical, and nutritional implications. *Trends Food Sci. Technol.* **2005**, *16*, 416−422.

(4) Stahl, W.; Schwarz, W.; Sundquist, A. R.; Sies, H. *cis–trans* isomers of lycopene and β-carotene in human serum and tissues. *Arch. Biochem. Biophys.* **1992**, *294*, 173–177.
(5) Boileau, A. C.; Merchen, N. R.; Wasson, K.; Atkinson, C. A.; Erdman, J. W., Jr. *cis*-Lycopene is more bioavailable than *trans*-lycopene in vitro and in vivo in lymph-cannulated ferrets. *J. Nutr.* **1999**, *129*, 1176–1181.
(6) Richelle, M.; Sanchez, B.; Tavazzi, I.; Lambelet, P.; Bortlik, K.; Williamson, G. Lycopene isomerisation takes place within enterocytes during absorption in human subjects. *Br. J. Nutr.* **2010**, *103*, 1800–1807.
(7) Richelle, M.; Lambelet, P.; Rytz, A.; Tavazzi, I.; Mermoud, A.-F.; Juhel, C.; Borel, P.; Bortlik, K. The proportion of lycopene isomers in human plasma is modulated by lycopene isomer profile in the meal but not by lycopene preparation. *Br. J. Nutr.* **2012**, *107*, 1482–1488.
(8) Failla, M. L.; Chitchumroonchokchai, C.; Ishida, B. K. In vitro micellarization and intestinal cell uptake of *cis* isomers of lycopene exceed those of all-*trans* lycopene. *J. Nutr.* **2008**, *138*, 482–486.
(9) Unlu, N. Z.; Bohn, T.; Francis, D. M.; Nagaraja, H. N.; Clinton, S. K.; Schwartz, S. J. Lycopene from heat-induced *cis*-isomer-rich tomato sauce is more bioavailable than from all-*trans*-rich tomato sauce in human subjects. *Br. J. Nutr.* **2007**, *98*, 140–146.
(10) Müller, L.; Goupy, P.; Fröhlich, K.; Dangles, O.; Caris-Veyrat, C.; Böhm, V. Comparative study on antioxidant activity of lycopene (*Z*)-isomers in different assays. *J. Agric. Food Chem.* **2011**, *59*, 4504–4511.
(11) Honda, M.; Takahashi, N.; Kuwa, T.; Takehara, M.; Inoue, Y.; Kumagai, T. Spectral characterization of *Z*-isomers of lycopene formed during heat treatment and solvent effects on the *E*/*Z* isomerization process. *Food Chem.* **2015**, *171*, 323–329.
(12) Takehara, M.; Nishimura, M.; Kuwa, T.; Inoue, Y.; Kitamura, C.; Kumagai, T.; Honda, M. Characterization and thermal isomerization of (*all-E*)-lycopene. *J. Agric. Food Chem.* **2014**, *62*, 264–269.
(13) Jensen, N. H.; Nielsen, A. B.; Wilbrandt, R. Chlorophyll *a* sensitized trans–cis photoisomerization of *all-trans*-β-carotene. *J. Am. Chem. Soc.* **1982**, *104*, 6117–6119.
(14) Kuki, M.; Koyama, Y.; Nagae, H. Triplet-sensitized and thermal isomerization of all-trans, 7-cis, 9-cis, 13-cis and 15-cis isomers of β-carotene: configurational dependence of the quantum yield of isomerization via the $T_1$ state. *J. Phys. Chem.* **1991**, *95*, 7171–7180.
(15) Stahl, W.; Sundquist, A. R.; Hanusch, M.; Schwarz, W.; Sies, H. Separation of β-carotene and lycopene geometrical isomers in biological samples. *Clin. Chem.* **1993**, *39*, 810–814.
(16) Lee, M. T.; Chen, B. H. Stability of lycopene during heating and illumination in a model system. *Food Chem.* **2002**, *78*, 425–431.
(17) Ideses, R.; Shani, A. Study of the radical mechanism of iodine-catalyzed isomerization of conjugated diene systems. *J. Am. Oil Chem. Soc.* **1989**, *66*, 948–952.
(18) Guo, W.-H.; Tu, C.-Y.; Hu, C.-H. cis–trans isomerizations of β-carotene and lycopene: a theoretical study. *J. Phys. Chem. B* **2008**, *112*, 12158–12167.
(19) DeRosa, M. C.; Crutchley, R. J. Photosensitized singlet oxygen and its applications. *Coord. Chem. Rev.* **2002**, *233–234*, 351–371.

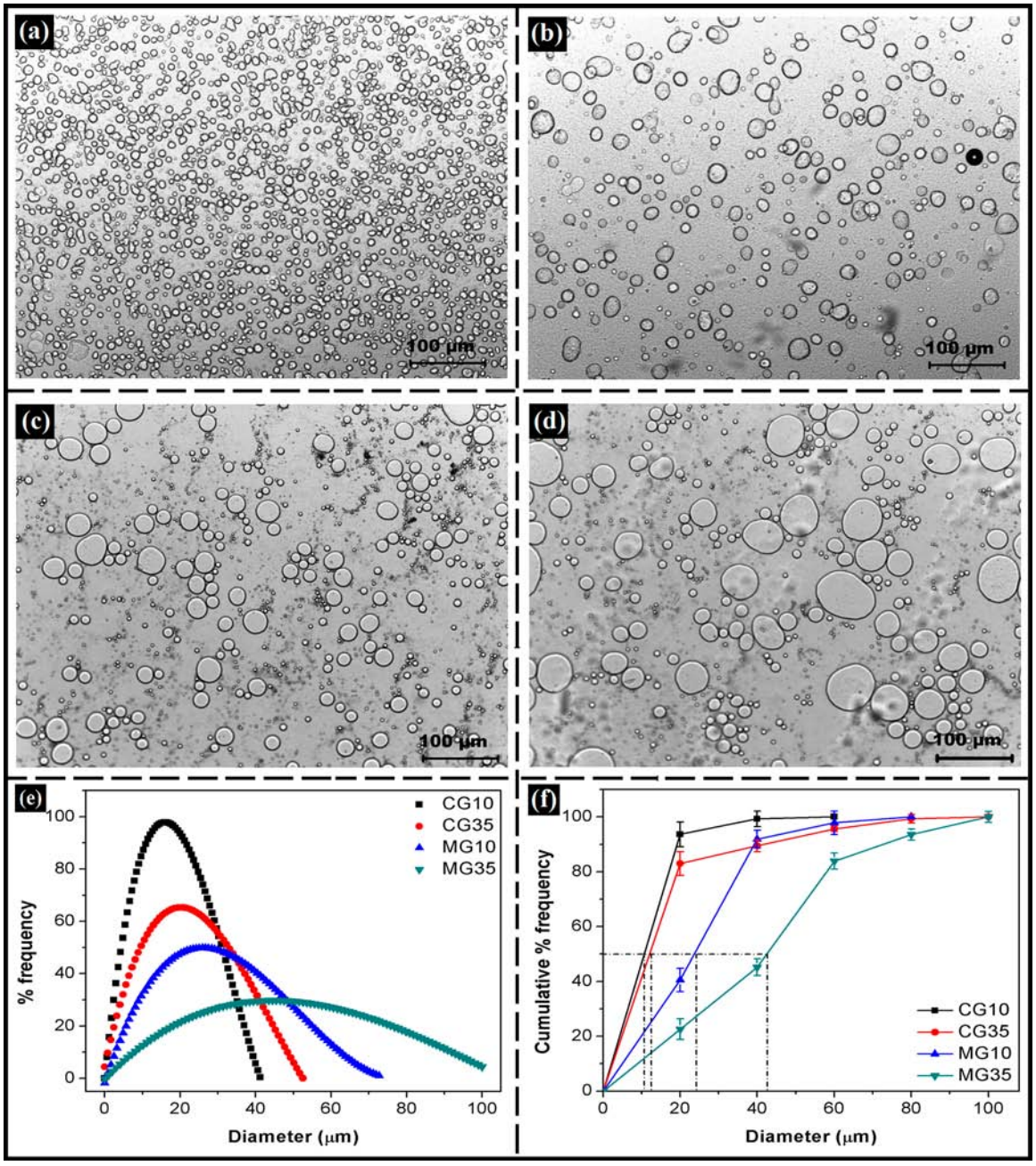


**Figure 1.** Microscopic images of (a) CG10, (b) CG35, (c) MG10, and (d) MG35 and size distribution analysis: (e) % frequency and (f) cumulative percentage frequency of the droplets of the emulsion gels.

obsogenic nature of the foods.[8] To reduce the high calorie content, researchers have been trying to develop water-in-oil (cocoa butter) emulsion gels.[9] These emulsion gels can be used as chocolates or suppositories. Gelatin is a good emulsifying and gelling agent, often used in the preparation of emulsion gels. Gelatin improves the processing of the emulsion when low fat or high aqueous phase volume is needed.[10] Gelatin improves the stability of the emulsions by preventing coalescence of the dispersed aqueous phase. In addition to these properties, gelatin gel has a similar "melt in the mouth" behavior (melting point of ~32 °C) as that of fats.[10] Yet limited research has been carried using gelatin-based cocoa butter emulsion gels.[10,11] On the other hand, to the best of our knowledge, gelatin-based mango butter-based emulsion gels as the cocoa butter equivalents have not been investigated.

The aim of this work is to check the usage of mango butter emulsion gels as cocoa butter equivalents. The emulsion gels were critically evaluated by performing microscopy, XRD, DSC, and mechanical studies.

## MATERIALS AND METHODS

**Materials.** Cocoa butter and mango butter were procured from NV Organics (P) Ltd., New Delhi, India. Span 80 (Sorbitan monooleate) was purchased from Himedia, Mumbai, India. Metronidazole (MZ) was a kind gift from Aarthi drugs, Mumbai, India. Double distilled water (DW) was used throughout the study. All of the experiments were performed in triplicate.

**Preparation of Emulsion Gels.** Emulsions of cocoa butter and mango butter were prepared by the hot emulsification method.[12] Span 80 was chosen as the emulsifier as it is a FDA (Food and Drug Administration, US) approved nonionic and biocompatible surfac-

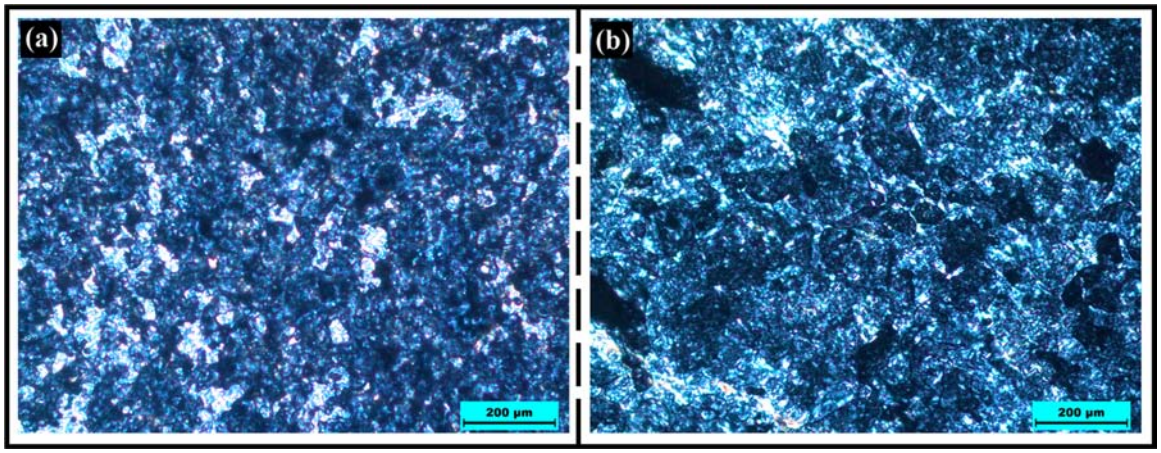


**Figure 2.** Polarized micrographs of (a) CG10 and (b) MG10.

tant.[13] Accurately weighed cocoa butter and span 80 were melted at 45 °C using a temperature-controlled water bath. The above mixture was homogenized for 5 min at 1200 rpm (45 °C) using an overhead stirrer (RQ-126/D, Remi Motors Ltd., India). Gelatin solution (20% w/w, 45 °C) was added drop-by-drop to the mixture and homogenized for another 15 min at the same temperature. The hot homogenized emulsion was poured into culture bottles (10 mL) and incubated at room temperature (25 °C) for 30 min to induce gelation. Mango butter-based formulations were also prepared in a similar fashion.

**Microscopic Studies.** Microstructure of the emulsion gels was observed using an upright bright-field microscope (Leica DM750 equipped with ICC50 HD camera, Germany) and polarized microscope (Leica DMLP attached with Leica DFC 295 camera, Germany). For bright field microscopy, molten emulsion gels were taken on a glass slide and visualized under the microscope. On the other hand, emulsion gels were made into a thin smear and visualized under the polarized microscope. Size distribution of the emulsion droplets was performed by image processing using National instrument vision assistant (NI vision assistant-2010, US) software.

**XRD Studies.** The physical nature of the emulsion gels was studied by X-ray diffraction (XRD) studies. A Philips X-ray diffractometer (Pananalytical, X-Pert Pro; Almelo, Netherlands) was used to study the polymorphism of the emulsion gels in their native state. Gels were spread over a glass plate and then subjected to X-ray analysis. X-rays of 1.54 Å were generated by a Cu K$\alpha$ source. The diffraction was measured in the 2$\theta$ range of 5−50°.

**DSC Studies.** The thermal properties, solid fat content (SFC), and crystallization behavior of the emulsion gels were examined by DSC studies using a differential scanning calorimeter (DSC-200 F3MAIA, Netzsch, Germany). Accurately weighed 10−15 mg of the formulations was taken in pure aluminum (Al) crucibles and hermetically sealed with pierced Al lids. The formulations were heated from 20 to 60 °C at 2 K/min and kept at 60 °C for 10 min to remove the crystal memory. The formulations then were cooled from 60 to 10 °C at 2 K/min, and the formulations were incubated at 10 °C for 1.0 h to allow isothermal crystallization. The analysis was performed under inert atmosphere using $N_2$ gas. The results were analyzed using the Netzsch-proteus software.

**Mechanical Analysis.** Mechanical properties of the emulsion gels were determined using a static mechanical tester (Stable Micro-systems, TA-HD plus, U.K.). To determine the strength, viscoelastic nature, and spreadability of the emulsion gels, uniaxial compression, stress relaxation, and spreadability experiments were conducted, respectively. Supporting Information Table S1 summarizes the details of the mechanical studies.

## ■ RESULTS AND DISCUSSION

**Preparation of the Emulsion Gels.** The molten fats appeared as pale yellow translucent liquids. Addition of gelatin solution resulted in the formation of milky white emulsions. Appearance of milky white color without any phase separation is an indication to the formation of emulsions.[14] After incubation at room temperature, the emulsions that failed to flow under gravity, upon inversion of the vials, were regarded as emulsion gels.[15] The stability of the emulsion gels was dependent on the type of the vegetable fat used. During preparation, cocoa butter emulsion gels were able to accommodate 70% (w/w) aqueous gelatin solution. On the other hand, only 35% (w/w) gelatin solution was accommodated within the mango butter-based emulsion gels. An increase in the aqueous proportion beyond 70% and 35% for cocoa butter and mango butter formulations, respectively, resulted in the phase separation. The pictographs of the cocoa butter and mango butter emulsion gels have been shown in Supporting Information Figures S1 and S2, respectively. The difference in the gelation properties of the vegetable fats can be attributed to the variation in the fatty acid compositions. The total unsaturated fatty acid content in cocoa butter is in the range of 36−43%, whereas in mango butter it is in the range of 43−59%.[6] Literature suggests that the crystallization efficiency of the fats depends on the proportion of the unsaturated fatty acids present.[16] This may be associated with the molecular geometry of the fatty acids. The tetrahedran bond angles of carbon enable the saturated fatty acids to arrange in linear and stack-wise fashion. On the other hand, the presence of double bonds (unsaturation) in carbon linkages leads to the bending of the fatty acyl molecules.[16] These molecules do not stack well and lead to weak intermolecular interactions, which, in turn, affect the crystallization process. As mango butter possesses a higher amount of unsaturated fatty acids than cocoa butter, the crystallization efficiency was found to be lower. The emulsion gels were stored at 4 °C and were stable for more than 12 months. Because mango butter formed stable emulsion gels up to MG35, we chose CG10, MG10, CG35, and MG35 as the representative formulations for further characterization.

**Microscopic Studies.** The microstructure of the emulsion gels showed evenly dispersed circular droplets of aqueous phase in the fat matrix (Figure 1). An increase in the droplet size was noticed with increase in the aqueous phase. Prevention of the droplets coalescence was responsible for the formation of such spatially arranged distinct droplets. Similar kinds of microstructures have been previously reported.[11,17] At higher water to fat ratio in cocoa butter emulsion gels (>70% (w/w) aqueous phase) and mango butter emulsion gels (>35% (w/w)

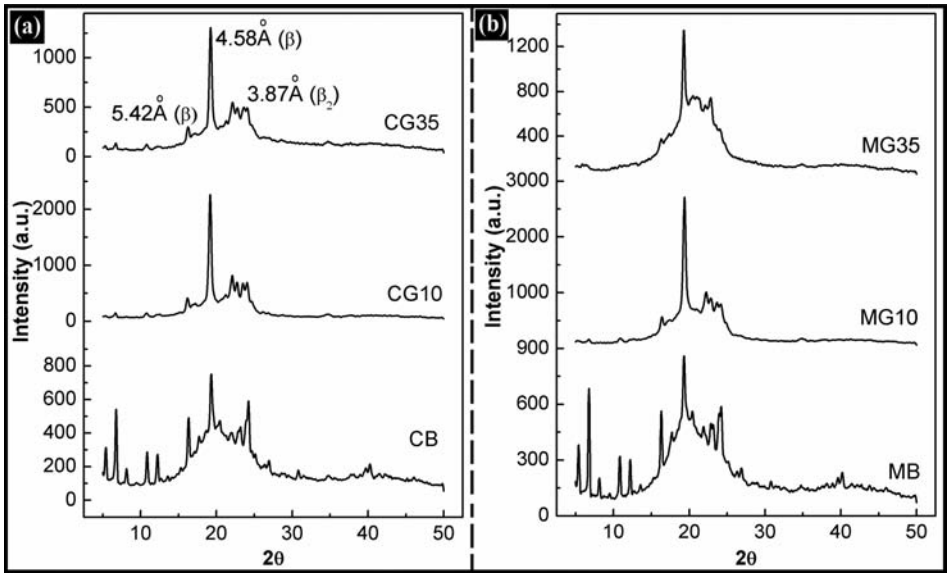


**Figure 3.** XRD profiles of (a) CB, CB-based gels and (b) MB, MB-based gels.

aqueous phase), crystallization of fats was not sufficient to prevent droplet coalescence. Hence, larger and nonuniform droplets were observed in the unstable emulsion gels (Supporting Information Figure S3). Formation of water-in-oil emulsion was confirmed by dilution test.[18] Both kinds of emulsion gels showed uniform dispersion within the oil phase and showed phase separation in water (Supporting Information Figure S4). This indicated the formation of water-in-oil type of emulsions.

Polarized light micrographs of the emulsion gels showed the presence of continuous crystalline network (Figure 2). Aqueous phase was dispersed as dark circles in the bright colored fat matrices of CG10 and MG10 (representative emulsion gels). The continuous crystalline network stabilized the emulsion by physically locking the dispersed phase.[11,18] Bright field micrographs of the molten emulsion gels showed dispersed water droplets within the fat continuous phase (Figure 1). Light micrographs of cocoa butter emulsions showed by Norton et al. (2012) also contained a similar kind of microstructure.[10] The presence of fat around the water droplets imparts microbiological and physical stability to the emulsion gels. The probability of microbial growth within the water droplets is minimized by completely isolating the aqueous phase from the environment. This helps in imparting microbial stability to the emulsion gels. The presence of emulsifiers affects the network crystallization. Hence, a high percentage of gelatin (20% (w/w)) solution was used in the study. High gelatin concentration enhances the rate of adsorption of the gelatin at the newly formed fat−droplet interface. Rapid gelatin adsorption enhances the gelatin membrane formation, thereby resulting in the decrease of the interfacial tension.[9] Lower interfacial tension prevented the coalescence of the droplets during the homogenization process and resulted in the formation of smaller droplets. In general, a narrow size distribution was observed in the formulations with lower aqueous proportion as compared to the formulations with higher proportions of the aqueous phase (Figure 1e). CG10 and MG10 had a narrow size distribution as compared to CG35 and MG35, respectively. The mean size of the droplets ($d_{32}$) was calculated using the following equation:

$$d_{32} = \sum n_i d_i^3 / \sum n_i d_i^2 \quad (1)$$

where $n_i$ is the number of droplets with diameter $d_i$.

The mean size of the droplets varied in the order of CG10 (15.2 $\mu$m) < CG35 (17.5 $\mu$m) < MG10 (19.63 $\mu$m) < MG35 (41.05 $\mu$m). The differences in the mean droplet size of the emulsion gels with the same water to fat ratio can be explained by the differences in the fatty acid composition of cocoa butter and mango butter. In general, long chain saturated fatty acids behave as solid at the fat−droplet interface, and the unsaturated fatty acids behave as liquid. Because the rate of crystallization of the unsaturated fatty acids at the fat−droplet interface is slower as compared to the rate of crystallization of the saturated fatty acids,[19] coalescence of the droplets might have led to the formation of the larger droplets in mango butter-based emulsion gels. Stearic hindrances associated with the unsaturated fatty acids slows the crystallization rate.[19] The average diameter ($d_{avg}$) of the droplets was calculated from Figure 1f (shown as dotted lines). The diameter of the 50% population of the droplets was considered as $d_{avg}$. The $d_{avg}$ values were in close proximity of the $d_{32}$ values.

**XRD Studies.** The XRD profiles of the emulsion gels and the vegetable fats have been shown in Figure 3. Literature suggests that cocoa butter and mango butter exist in four to six polymorphic forms.[6,20] The characteristic peaks ($d$-values: 3.79, 4.2 Å) corresponding to $\alpha$ polymeric state were not found in the XRD profiles of the vegetable fats and their corresponding emulsion gels.[21] Four characteristic $d$-values (3.7, 3.94, 4.58, and 5.42 Å), corresponding to the $\beta$ polymorphic state of the fatty acids, were observed both in the vegetable fats and in their emulsion gels.[21] Peaks at 19.3° and 16.3° 2$\theta$ corresponded to the $d$-values of 4.58 and 5.42 Å, respectively.[21,22] These peaks were conserved in both kinds of emulsion gels. This indicated that the stable polymorphic state ($\beta$) was retained by the emulsion gels. But their peak intensity was lowered as compared to the peaks of pure cocoa butter and mango butter. This suggested that the number of fatty acids present in $\beta$ polymorphic state might have been reduced and transformed to the other polymorphic states. The presence of a peak at 2$\theta$ 23.2° ($d$-value: 3.83 Å) indicated the presence of $\beta'_2$ and $\beta'_1$ polymorphic forms.[21] These peaks were retained in all of the

emulsion gels, and their intensity was not significantly changed. In general, $\beta'_2$ and $\beta'_1$ polymorphic states are intermediary polymorphic states during the conversion of $\alpha$ polymorphic fatty acids to the stable $\beta$ polymorphic fatty acids.[23,24] Because wide-angle X-ray scattering was performed, the peaks below 5° 2$\theta$ were not observed. Hence, confirmation for the existence of $\alpha$ polymorphic state could not be established. In general, tempering of the fats at high temperature leads to the polymorphic transition.[25] Keeping this in mind, emulsion gels were prepared by melting the fats at 45 °C, so as to minimize the tempering effects. As a result, minimal changes in the polymorphic state of the emulsion gels were observed.

Although the position of the peaks and the $d$-value of the $\beta$ polymorphic state were not significantly changed, the full width half-maximum (FWHM) values of the emulsion gels were altered (Table 2). The change in the fwhm values can be correlated to the change in the crystallinity of the emulsion gels. The change in the crystallinity was determined by calculating the crystal size ($D$) using the Debye−Scherrer equation:[26]

**Table 2. XRD Parameters of the Cocoa Butter, Mango Butter, and Emulsion Gels**

| sample | FWHM of peak at 19.3° 2$\theta$ | crystal size ($D$), nm |
|---|---|---|
| cocoa butter | 0.14 | 61.11 |
| CG10 | 0.22 | 38.9 |
| CG35 | 0.25 | 33.68 |
| mango butter | 0.16 | 53.5 |
| MG10 | 0.22 | 38.9 |
| MG35 | 0.26 | 32.71 |

$$D = \frac{K\lambda}{\beta \cos\theta} \tag{2}$$

where $K$ is the Scherrer constant or shape factor, 0.89 (as shape of the crystallite is unknown); $\lambda$ is the Cu K$\alpha$ wavelength, that is, 1.54 Å; $\beta$ is the full width at half-maximum (fwhm) of the diffraction peak in radians; and $\theta$ is the Braggs diffraction angle.

The crystal size was determined using the $\beta$ polymorphic peak (19.3° 2$\theta$), because it had the maximum intensity. The crystal size of cocoa butter was reduced with the incorporation of gelatin solution within the emulsion gels (Table 2). The decrease in the crystal size can be attributed to the presence of a heterogeneous system (fat and water mixture) within the emulsion gels.[27] During crystallization, the crystal growth of cocoa butter might have been hindered by the presence of a heterogeneous system.[27] This led to the formation of smaller crystal sizes in the emulsion gels. The changes in crystal size suggested that the crystallinity of the emulsion gels was also changed. XRD patterns of the cocoa butter, mango butter, and their corresponding emulsion gels (hump-like structures at ∼20°) suggested predominantly amorphous nature. Amorphousity of the emulsion gels was dependent on the proportion of the aqueous gelatin solution and liquid triacylglycerols. Change in the crystal size of the fats can be correlated to the amorphousity of the gels.[28] Crystallinity of the cocoa butter and the mango butter gels was found to be in the order of cocoa butter > CG10 > CG35 and mango butter > MG10 > MG35, respectively. Higher crystallinity of the cocoa butter-based emulsion gels was due to the presence of a higher amount of saturated fatty acids in cocoa butter as compared to mango butter.

**DSC Studies.** Heating DSC curves showed four and five endotherms in cocoa butter and mango butter-based emulsion gels over the temperature range of 10−40 °C, respectively (Figure 4a and b). The presence of more than one endotherm indicated the existence of the fats in different polymorphic states. Pure cocoa butter and mango butter yielded a sharp endotherm at 36.7 and 38.4 °C, respectively, corresponding to the $\beta$ polymorphic state.[29] The peak intensity of the $\beta$ state's endotherm was decreased with the addition of aqueous phase. Simultaneously, considerable enhancement in the peak intensities of the other polymorphic forms ($\alpha$ and $\beta'$) was noticed. The presence of peaks at ∼20 °C indicated the existence of $\alpha$ polymorphic state of triacylglycerols in the emulsion gels.[29] Next to the $\alpha$-polymorphic peaks, a peak corresponding to the $\beta'$ polymorphism was observed. Pure fats showed a broad endotherm of $\beta'$ polymorphic triacylglycerols with two overlapping endothermic peaks ($\beta'_2$ and $\beta'_1$ states) (indicated by arrows in Figure 4a and b).[21] Incorporation of water showed distinct endothermic $\beta'_2$ and $\beta'_1$ polymorphic peaks in the emulsion gels. This indicated that the presence of water might have slowed the polymorphic transformation (from $\alpha$ to $\beta$) of fats. The extent of overlapping of $\beta'_2$ and $\beta'_1$ states was higher in cocoa butter-based emulsion gels, whereas separate endotherms were noticed in mango butter-based emulsion gels. Thermal profiles of CG10 and CG35 showed overlapping endotherms of $\beta'_2$ and $\beta'_1$ (as that of cocoa butter) and an extra peak of $\alpha$ polymorphic state (unlike cocoa butter). On the contrary, MG10 and MG35 showed separate endotherms of $\alpha$, $\beta'_2$, and $\beta'_1$ polymorphic states (unlike mango butter). The melting endotherm of $\beta$ was not prominent in the emulsion gels as compared to the pure fats. In addition to the aforementioned peaks (corresponding to $\alpha$, $\beta'$, and $\beta$ polymorphic states), an additional peak at very low temperatures (<15 °C) was noticed in pure mango butter and its corresponding emulsion gels. This peak was due to the sub-$\alpha$ or $\gamma$ polymorphic triacylglycerols.[21] The cocoa butter-based emulsion gels did not show any such a peak. This may be explained by the merging of the endotherms of $\gamma$ and $\alpha$ polymorphic triacylglycerols.

Because different polymorphic states were existing, the amount of fat (cocoa butter and mango butter) present in those forms was calculated as solid fat content (SFC) in the emulsion gels.[6]

$$\%\mathrm{SFC} = \frac{\Delta H_t}{\Delta H_m} * 100 \tag{3}$$

where $\Delta H_t$ is the change in enthalpy at time $t$ and $\Delta H_m$ is the change in enthalpy during total melting.

The change in the enthalpy during the endothermic events was calculated by integrating the area under the peak.[30,31] The peak temperatures ($T$) of the endotherms, change in enthalpies ($\Delta H$), and SFC associated with the corresponding endotherms (polymorphic states) have been tabulated in Table 3. SFC of the $\beta$ polymorphic state was higher in pure cocoa butter and mango butter, whereas SFC of the $\alpha$ and $\beta'$ polymorphic states was increased in the emulsion gels. Figure 4c shows the SFC profiles of the emulsion gels at different temperatures. Melting points of $\alpha$ and $\beta'$ polymorphic states of mango butter were found to be lower than that of cocoa butter, whereas the melting point of the $\beta$ polymorphic state was found to be higher than that of cocoa butter. This suggested that the pure mango butter was softer than cocoa butter at low temperatures

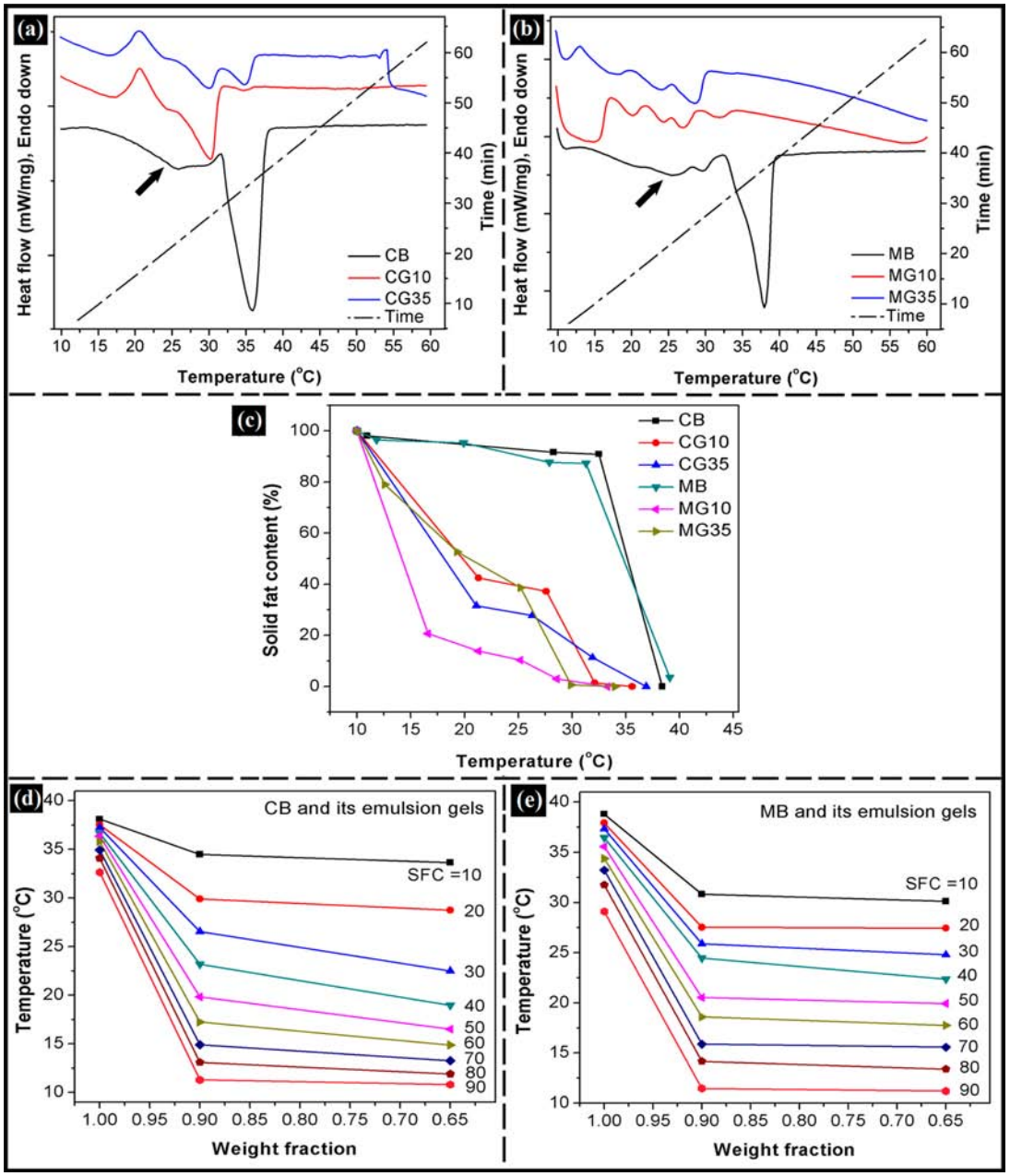


**Figure 4.** Melting endotherms of (a) CB, CB emulsion gels and (b) MB, MB emulsion gels; (c) SFC of the emulsion gels; and isosolid diagrams of (d) CB, CB emulsion gels and (e) MB, MB emulsion gels.

**Table 3. Melting Analysis of Cocoa Butter, Mango Butter, and Emulsion Gels**

| | polymorphic state | | | | | | | | | | | |
|---|---|---|---|---|---|---|---|---|---|---|---|---|
| | $\alpha$ | | | $\beta'_2$ | | | $\beta'_1$ | | | $\beta$ | | |
| sample | $T$ (°C) | $\Delta H$ (J/g) | SFC | $T$ (°C) | $\Delta H$ (J/g) | SFC | $T$ (°C) | $\Delta H$ (J/g) | SFC | $T$ (°C) | $\Delta H$ (J/g) | SFC |
| CB | 10.9 | 1.5 | 2.0 | 26.8 | 4.7 | 6.4 | 30.9 | 0.53 | 0.71 | 36.7 | 66.7 | 90.8 |
| CG10 | 18.2 | 36.3 | 45.2 | 25.1 | 3.3 | 5.2 | 31.1 | 12.6 | 25.8 | 35.3 | 9.1 | 11.4 |
| CG35 | 17.3 | 31.8 | 68.4 | 25.2 | 1.8 | 3.8 | 30.8 | 7.6 | 16.4 | 35.6 | 5.3 | 11.3 |
| | polymorphic state | | | | | | | | | | | |
| | 1 ~ sub $\alpha$ or $\gamma$ | | | 2 ~ $\alpha$ | | | 3 ~ $\beta'_2$ | | | 4 ~ $\beta'_1$ | | | 5 ~ $\beta$ | | |
| sample | $T$ (°C) | $\Delta H$ (J/g) | SFC | $T$ (°C) | $\Delta H$ (J/g) | SFC | $T$ (°C) | $\Delta H$ (J/g) | SFC | $T$ (°C) | $\Delta H$ (J/g) | SFC | $T$ (°C) | $\Delta H$ (J/g) | SFC |
| MB | 11.1 | 5.4 | 3.5 | 19.9 | 0.6 | 1.2 | 25.5 | 3.8 | 7.6 | 29.6 | 1.4 | 0.4 | 38.0 | 41.4 | 83.7 |
| MG10 | 15 | 37.1 | 79.3 | 20.1 | 3.2 | 6.9 | 24.4 | 1.6 | 3.5 | 27.0 | 3.5 | 7.4 | 31.9 | 1.4 | 2.9 |
| MG35 | 11.1 | 5.3 | 20.9 | 18.3 | 6.7 | 26.4 | 24.0 | 3.6 | 13.9 | 28.6 | 9.7 | 38.1 | 33.4 | 0.2 | 0.6 |


dx.doi.org/10.1021/jf502658y | J. Agric. Food Chem. 2014, 62, 11357−11368

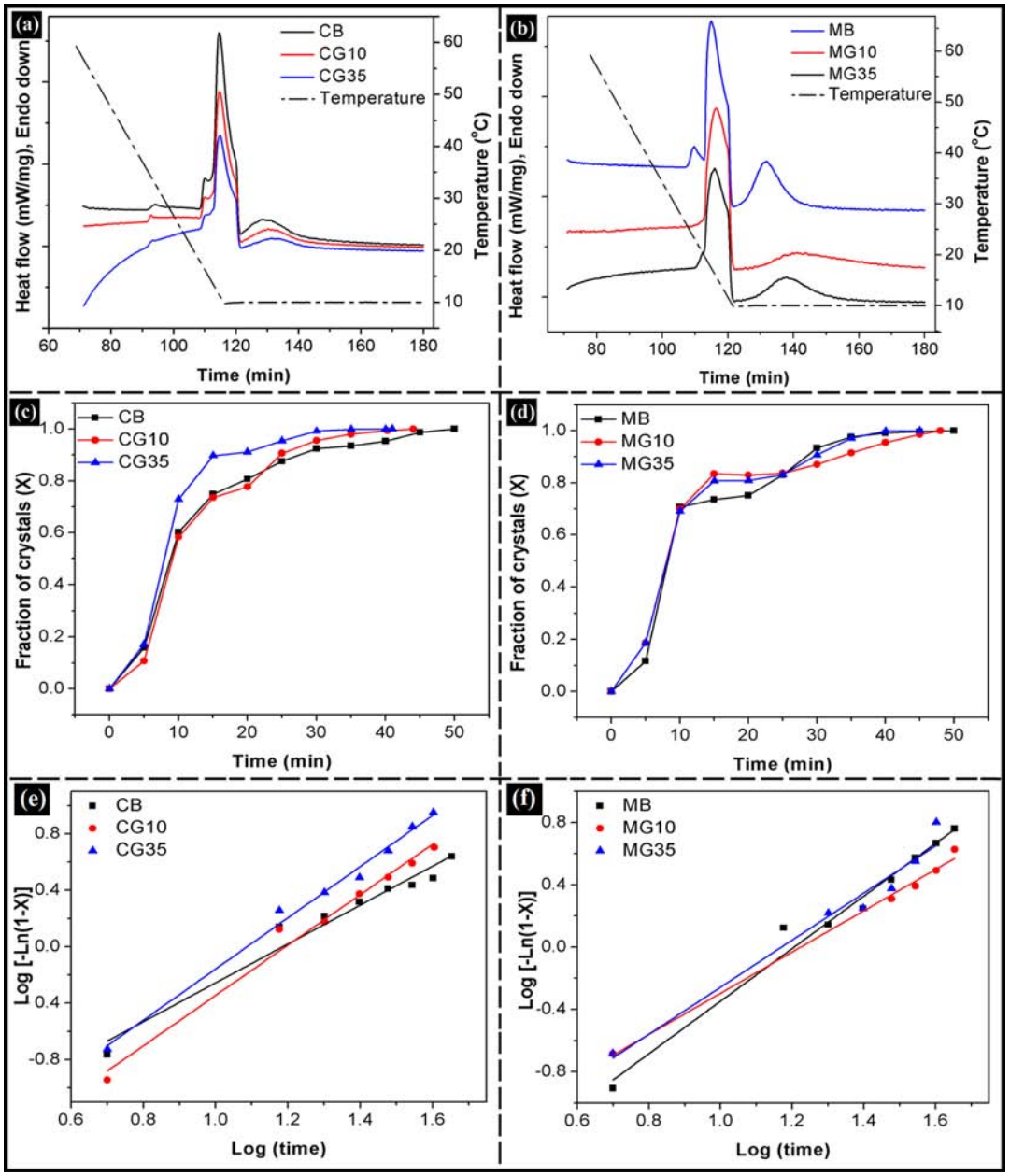


**Figure 5.** Crystallization exotherms of (a) CB, CB emulsion gels and (b) MB, MB emulsion gels; crystal fraction of (c) CB, CB emulsion gels and (d) MB, MB emulsion gels; and Avrami analysis of (e) CB, CB emulsion gels and (f) MB, MB emulsion gels.

but retained a higher number of solids at higher temperatures. This was due to the presence of the higher oleic acid content, which might have a "dilution effect" on the saturated fatty acids, thereby increasing the softness of mango butter.[6] On the other hand, mango butter contains longer chain fatty acids such as behenic and lignoceric acids. These fatty acids contributed to the induction of the stable $\beta$ polymorphic state, which resulted in the higher melting point of mango butter.

SFC content of cocoa butter and mango butter was drastically decreased when water was added. There was no significant difference in the rate of decrease in SFC of CG10 and CG35, but it was significant in MG10 and MG35. MG35 lost almost ~80% of the SFC below 15 °C. This may be the reason that mango butter could not form stable emulsion gels beyond 35% (w/w) aqueous phase. This indicated that the emulsion gels became softer than the pure fats and their thermal stability was greatly influenced. To measure the compatibility of the emulsion gel components and their effects on the gel softening, isosolid diagrams were drawn (Figure 4d and e).

In general, isosolid diagrams links the points of different samples with equal solid content in weight fraction−temperature graphs. As a matter of fact, if the isosolid lines are parallel and approximately horizontal to each other, then the components are said to be compatible with each other.[6] Isosolid diagrams suggested that the mango butter emulsion gels were softer than the cocoa butter emulsion gels. This may be explained by the lower melting points of the mango butter emulsion gels than the cocoa butter emulsion gels at the equal SFC. A sudden decrease in the melting points of the isosolid lines was observed when 10% (w/w) of gelatin solution was added to either cocoa butter or mango butter. The decrease in


dx.doi.org/10.1021/jf502658y | J. Agric. Food Chem. 2014, 62, 11357−11368

the melting temperature indicated softening of the emulsion gels. The results suggested that the softening effect was more pronounced when 10% (w/w) aqueous phase was added to cocoa butter and mango butter. Upon further addition of aqueous phase (35% w/w), no significant softening effect was observed, which resulted in almost parallel lines. The isosolid lines of the mango butter emulsion gels were more parallel to each other than the cocoa butter emulsion gels. This indicated that the softening was continuing in cocoa butter emulsion gels, but a plateau phase was reached in mango butter emulsion gels. Because the isosolid lines were not horizontal and parallel to each other up to the 90% solid fraction, the gel components (butter and gelatin solution) seemed to be not compatible with each other. Yet the compatibility was improved when the aqueous portion was raised to 35% (w/w). 100% compatibility among the fat (cocoa butter and mango butter) and aqueous phase cannot be expected due to the thermodynamic instability among them. Yet the compatibility of the fat and the aqueous phase was improved when a higher amount of gelatin (20% w/w) solution was added. Comparatively, the components of the mango butter emulsion gels were more compatible than the cocoa butter emulsion gels. This can be explained by the fact that the isosolid lines were more parallel and horizontal to each other in mango butter emulsion gels. This may be due to the presence of the higher amount of unsaturated fatty acids in mango butter. Disordered packing of unsaturated fatty acids might have allowed the incorporation of the aqueous phase in the emulsion gels and subsequent improvement of the compatibility of the fat and the aqueous phases.

**Crystallization Studies.** Isothermal crystallization studies of the emulsion gels were performed by holding them at 60 °C for 10 min (to eliminate the crystal memory of the fats) and subsequently cooling to 10 °C at 1 °C/min, followed by holding at 10 °C for 1 h. The crystallization exotherms of cocoa butter and mango butter emulsion gels can be divided into three exothermal events (Figure 5a and b). The first exotherm (~19 °C) was not distinctly separated but exists as a shoulder peak of the second exotherm at ~22.5 °C. The intensity of the shoulder peak was reduced when water was added to the fats. The third exotherm was recorded during the isothermal stage that spans over a wide time range. These kind of exothermic events were similar to the fat mixtures of cocoa butter.[29,31] Crystallization of the fats started at 22.5 °C and continued up to 10 °C, leading to a broad exotherm. Evolution of this kind of exotherm is a characteristic feature of hexagonal packing of triacylglycerol chains in $\alpha$ form.[29] Literature suggests that the progressive crystallization of triacylglycerides arranges from liquid crystalline to double-chain length ($2L$) organization in $\alpha$ form.[29] The first exothermic peak (shoulder peak) corresponded to the crystallization of the high-melting saturated fatty acids.[29] The second (major) exothermic event was due to the transformation of monounsaturated fatty acids.[29] During crystallization, a steep increase of the second exotherm at 15.4 and 15.1 °C was noticed in cocoa butter and mango butter emulsion gels, respectively. On the basis of these events, it can be inferred that the saturated fatty acids acted like seed crystals for the transformation of the liquid crystalline fat. Because the crystal growth of the saturated fatty acids was coinciding with the transformation of the unsaturated fatty acids, the first exotherm in DSC thermogram existed as the shoulder peak. The transformation of the fatty acids continued even during the isothermal stage. Crystallization at 10 °C suggested the transformation of the liquid crystalline fatty acids into $\alpha$ polymorphic state.[21] Because the crystallization at 10 °C resulted in a broad exotherm, it was expected that some of the $\alpha$ polymorphic fatty acids might have converted to $\beta'$ polymorphic state (found in DSC melting and XRD profiles as well).[21,29] Overall, the peak positions did not change, but the enthalpies associated with the exotherms of emulsion gels were changed due to the difference in the peak intensities. The overall crystallization enthalpies of the pure fats and the emulsion gels have been provided in Table 4. On the basis of the difference in crystallization enthalpies, the Avrami equation (eq 4) was used to predict the nucleation and crystal growth in emulsion gels.[30]

**Table 4. Avrami Analysis of the DSC Exotherms**

| sample | $\Delta H_c$ (J/g) | $n$ | $k \times 10^{-3}$ (min) | $t_{1/2}$ (min) |
|---|---|---|---|---|
| cocoa butter | 2.28 | 0.94 | 103.0 | 7.56 |
| CG10 | 1.55 | 1.26 | 42.7 | 9.10 |
| CG35 | 0.96 | 1.63 | 19.5 | 8.88 |
| mango butter | 1.94 | 1.05 | 82.0 | 7.65 |
| MG10 | 1.41 | 1.32 | 24.1 | 12.68 |
| MG35 | 0.94 | 1.45 | 17.1 | 12.85 |

$$\ln[\ln(1/(1 - X_t))] = \ln k + n \ln t \quad (4)$$

where $X$ is the fraction of the crystals formed at time $t$ during crystallization, $k$ is the crystallization rate constant (measure of crystallization), which depends on the crystallization temperature, and $n$ is the Avrami exponent. The Avrami exponent determines the dimensionality of crystallization. Crystal fraction ($X$) at a given time was calculated by the ratio of partial enthalpy ($\Delta H_x$) to the total crystallization enthalpy ($\Delta H_c$).

Figure 5c and d indicates that the crystal formation was very rapid during the early stages of the crystallization. Subsequently, the rate of formation was slowed and ultimately reached a stationary phase. The shape of the curves ($X$ vs $t$) illustrates the crystallization mechanism of the substance.[32] The shape of the curves did not change, indicating that the crystallization mechanism was not affected by the incorporation of the aqueous phase.[32] To better understand the crystallization mechanism, the crystal fraction ($X$) was used to calculate the Avrami parameters ($n$ and $k$). Crystallization data of the emulsion gels showed good fitting ($R^2 > 0.95$) to the Avrami equation (Figure 5e and f). The Avrami parameters calculated from the fit curves have been given in Table 4. $n$ values were found to be in the range of 0.9−1.5. This suggested the occurrence of instantaneous nucleation during the crystallization process.[21] $n$ values below 2 suggest that the nucleation rate was very rapid at the beginning, but decreased as the time progressed (as predicted by $X$ vs $t$ curves).[30] $n$ values indicated needle-like growth of the crystals along one or two dimensions. Formation of the spherulitic crystals was reported by the growth of the small needle like crystals during suspension crystallization with agitation.[33] Because static crystallization (no agitation) was studied in DSC, needle-like crystals might have not aggregated to spherulites.

On the other hand, high $k$ values (Table 4) suggested rapid crystallization in cocoa butter, followed by mango butter and the emulsion gels, respectively. The rate of crystallization was influenced by the presence of water. CG10 and MG10 had a higher rate of crystallization as compared to CG35 and MG35, respectively. The presence of aqueous phase might have prevented the growth of the crystals in quick time. Increase

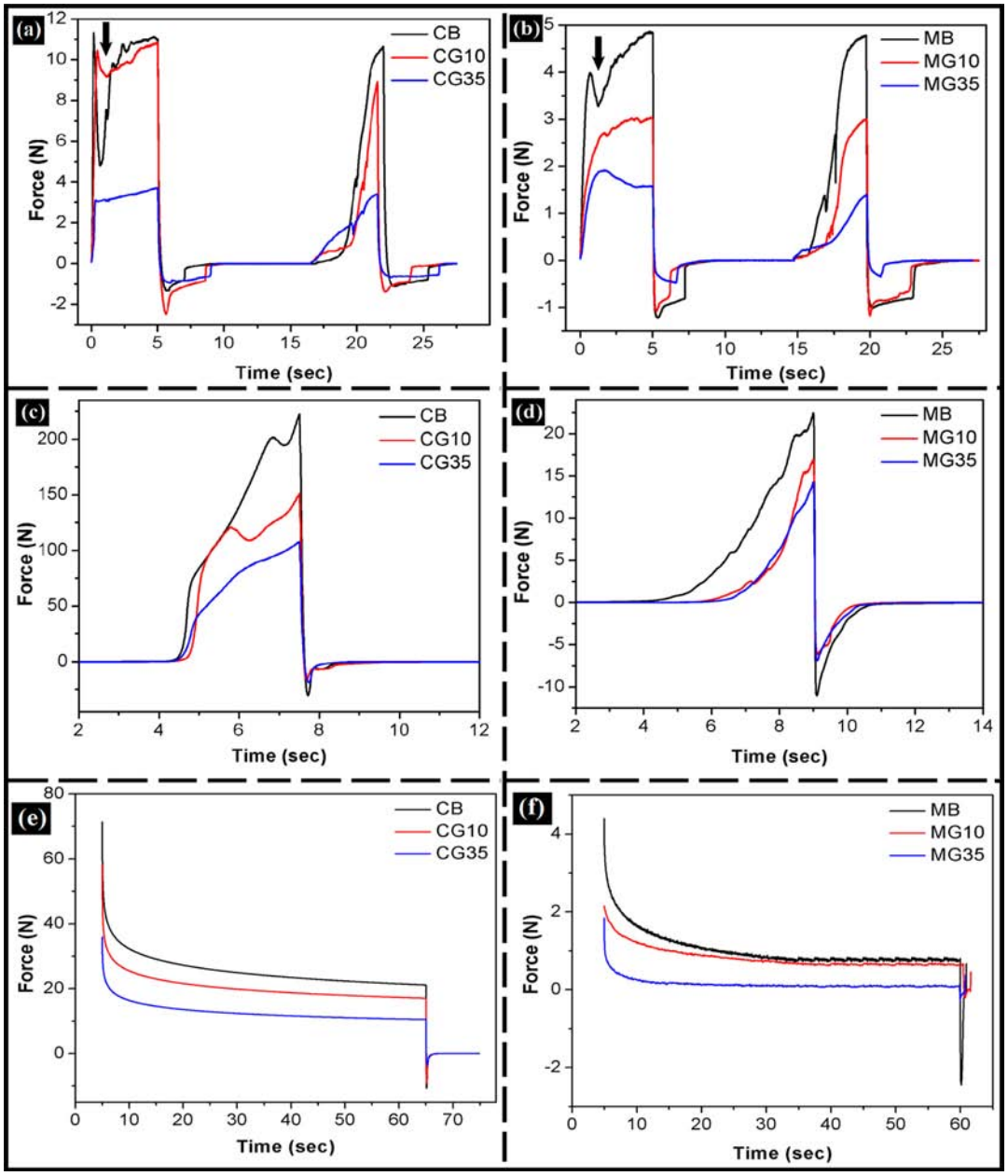


**Figure 6.** Mechanical analysis of the emulsion gels. Compression studies of (a) CB, CB emulsion gels and (b) MB, MB emulsion gels; stress relaxation studies of (c) CB, CB emulsion gels and (d) MB, MB emulsion gels; and spreadability of (e) CB, CB emulsion gels and (f) MB, MB emulsion gels.

in the crystallization time might also have led to the change in dimensionality of the growing crystals.[30] Hence, $n$ values suggested the possibility of two-dimensional growth of the crystals. Change in the crystallization times was determined by calculating the half-time of the crystallization ($t_{1/2}$). Because $k$ is dependent on nucleation, crystal growth, and temperature, it can be directly related to the half-time of crystallization ($t_{1/2}$).

$$(t_{1/2})^n = 0.693/k \quad (5)$$

$t_{1/2}$ is a function of both $n$ and $k$. It provides information about the time taken to form 50% of the crystals. The $t_{1/2}$ values were lower in pure fats as compared to the emulsion gels (Table 4). This indicated that the rate of crystallization was highest in cocoa butter and mango butter followed by CG10, CG35, MG10, and MG35 under the experimental conditions. As the rate of fat crystallization was slower in emulsion gels with higher water proportions, water droplets coalescence has led to the formation of unstable emulsion gels. Higher crystallization rates in cocoa butter emulsion gels facilitated the cocoa butter to tolerate high amounts of water. Because the rate of crystallization was slower in mango butter emulsion gels, the water droplets might have coalesced prior to the fat crystallization. Hence, stable cocoa butter emulsion gels were formed even at high proportion of water (70% (w/w)) as compared to the mango butter emulsion gels (35% (w/w)).

**Mechanical Analysis.** During the two-cycle uniaxial compression test, fracturing of pure cocoa butter and mango butter (shown by an arrow in Figure 6a and b) indicated the brittle nature of the pure fats. Fracture points were also seen during the second cycle of compression in the pure fats. Emulsion gels, except CG10, did not show fracture points. This

indicated a decrease in the brittleness with the addition of the aqueous phase. Higher brittleness can be attributed to the higher cohesive strength of the pure fats (Supporting Information Table S2). The triacylglycerols in pure fats are tightly packed either in double or in triple chain length structures.[34] This kind of orientation favors ordered arrangement of the triacylglycerols and imparts higher cohesive strength.[34] The presence of aqueous phase might have disturbed the orientation of the triacylglycerols, which resulted in the decrease in the cohesiveness, hardness, and gumminess of the emulsion gels (Supporting Information Table S2). This indicated that the emulsion gels became softer with the incorporation of the aqueous phase (as predicted during melting studies). Increase in the softness might have enhanced the adhesive nature and spreadability of the emulsion gels. Interestingly, adhesiveness of the cocoa butter and mango butter emulsion gels was enhanced when a lower amount of aqueous phase was added, but a reverse trend was observed when a higher amount of aqueous phase was added. The presence of gelatin in the aqueous phase might be responsible for the enhancement in the adhesive nature of the emulsion gels, but at higher amounts of gelatin, the intermolecular attraction (cohesive interactions) between the gelatin molecules might have dominated the adhesive forces.[35] Increase in the spreadable nature of the emulsion gels was confirmed by spreadability studies (Figure 6c and d). Application of force during the spreadability test did not result in the syneresis of water. Because the water droplets were physically locked within the fat continuous phase (evident from the microscopic studies), syneresis did not occur, which in turn imparted physical stability to the emulsion gels. CG35 and MG35 showed higher spreadability than CG10, MG10 followed by cocoa butter and mango butter. Increase in the softness may be associated with the spreadability of the emulsion gels. During cyclic compression studies, springiness of the emulsion gels did not vary significantly. This suggested that the elastic nature of the pure fats was not altered in the emulsion gels. To confirm this and to critically evaluate the viscoelastic properties of the emulsion gels, stress relaxation studies were conducted.

The stress relaxation profiles of the emulsion gels have been shown in Figure 6e and f. The firmness ($F_0$) and the residual force ($F_r$) were higher in cocoa butter and mango butter as compared to the emulsion gels. $F_0$ and $F_r$ decreased with the increase in the aqueous phase. This was due to the decrease in the SFC of the emulsion gels. The stress relaxation profiles of the emulsion gels followed an exponential decay function. The force decay with respect to time ($F(t)$) during the relaxation of the emulsion gels was analyzed by fitting the data in modified Peleg's equation.[36]

$$\frac{(F_0 - F(t))t}{F_0} = k_1 + k_2 t \tag{6}$$

where $F_0$ is the maximum force attained after loading; $k_1$ and $k_2$ represent the initial rate and extent of the relaxation, respectively.

Normalized stress relaxation data from modified Peleg's equation yielded a straight line with good fitting ($R^2 > 0.995$) (Supporting Information Figure S5). Curve analysis indicated that the initial rate of relaxation ($k_1$) was decreased with the increase in the proportion of the aqueous phase, but the extent of relaxation ($k_2$) did not vary significantly in both kinds of emulsion gels (Table 5). Although $k_2$ (slope) represents the total relaxation behavior of the formulations, almost similar values were obtained. To find the viscoelastic nature and to know the stress relaxation behavior, asymptotic residual force was calculated from the stress relaxation curve ($F^*$):[37]

**Table 5. Viscoelastic Parameters of CB, MB, and Emulsion Gels from Stress Relaxation Studies**

| samples | $F_0$ (N) | $F_r$ (N) | $k_1$ | $k_2$ | $F^*$ | % relaxation |
|---|---|---|---|---|---|---|
| CB | 71.37 | 21.09 | 0.036 | 0.001 | 0.29 | 70.45 |
| CG10 | 58.17 | 15.03 | 0.031 | 0.016 | 0.26 | 74.16 |
| CG35 | 35.98 | 8.42 | 0.015 | 0.001 | 0.24 | 76.60 |
| MB | 4.39 | 0.74 | 0.041 | 0.017 | 0.17 | 83.14 |
| MG10 | 2.15 | 0.26 | 0.013 | 0.017 | 0.12 | 87.90 |
| MG35 | 1.85 | 0.08 | 0.005 | 0.017 | 0.04 | 95.67 |

$$F^* = \frac{F_r}{F_0} \tag{7}$$

where $F_r$ is the residual force after relaxation and $F_0$ is the maximum force attained prior to the relaxation.

For viscoelastic materials, $F^*$ lies in the range of 0−1. "$F^*$" value close to 1.0 indicates that the material is an elastic material. There was a reduction in the $F^*$ values with the decrease in the SFC of the emulsion gels. This indicated that the elastic nature of the cocoa butter and mango butter decreased with the increase in the aqueous phase. Cocoa butter and mango butter emulsion gels have shown $F^*$ values in the range of 0−1, suggesting that the developed emulsion gels were viscoelastic in nature. % relaxation was calculated using eq 8:

$$\%\text{relaxation} = \left(\frac{F_0 - F_r}{F_0}\right)*100 \tag{8}$$

Mango butter emulsion gels showed more relaxation than cocoa butter emulsion gels (Table 5). Because mango butter emulsion gels were more amorphous than the cocoa butter emulsion gels (as per XRD studies), relaxation of the mango butter emulsion gels was more than that of the cocoa butter emulsion gels.

In conclusion, this study is intended to develop mango butter emulsion gels as the cocoa butter equivalents. Stable gelatin-based cocoa butter and mango butter emulsion gels were formed by a simple hot emulsification method. Cocoa butter incorporated high amounts of aqueous fraction (70% (w/w)) as compared to mango butter (35% (w/w)). The water droplets were dispersed within the fat continuous matrix. In general, physical and microbiological stabilities are the major concerns in the usage of water containing products in confectionaries. The presence of fat around the water droplets imparted physical stability to the emulsion gels. Because water droplets were locked within the crystallized fats, microbial contamination can be arrested. Avrami analysis indicated that the rate of fat crystallization was higher in cocoa butter and it was decreasing with the increase in water proportion. A high fat crystallization rate in cocoa butter might be responsible for the high tolerance capacity of the water as compared to mango butter. X-ray diffractograms indicated the fats present in the emulsion gels had a stable $\beta$ polymorphic state even after tempering. The effect of tempering was lowered as the emulsion gels were prepared by melting the fats at lower temperature (45 °C). DSC results suggested that the emulsion gels showed a high percentage of SFC as $\beta$ polymorphic form and intermediary polymorphic forms ($\beta'_1$ and $\beta'_2$). As $\beta'_1$ and

$\beta'_2$ possess the melting point at ~30 °C, the emulsion gels may have high chances of consumer acceptance if employed in the preparation of chocolates and/or other confectionaries. Increase in softness and spreading nature of the emulsion gels with respect to the pure fats also will favor the consumer acceptance. Mango butter emulsion gels are found to be softer than the cocoa butter emulsion gels, which may be due to the presence of high amounts of liquid-like unsaturated fatty acids. On the basis of the observations, it was suggested that the mango butter emulsion gels may have potential to be used as cocoa butter equivalents in food and pharmaceutical industries. Yet, prior to the use of mango butter emulsion gels as the cocoa butter equivalents, the emulsion gels need to be tested for the microsafety issues and compared to the existing marketed formulations.

## ■ ASSOCIATED CONTENT

### Supporting Information

Supplementary figures and tables. This material is available free of charge via the Internet at http://pubs.acs.org.

## ■ AUTHOR INFORMATION


### Corresponding Author

*Tel.: +91-876-3366085. E-mail: pal.kunal@yahoo.com, kpal.nitrkl@gmail.com.



### Funding

The funds leveraged from the project (SR/FT/LS-171/2009), sanctioned by the Science and Engineering Research Board (SERB), Government of India, are hereby acknowledged. The leading author is thankful for the scholarship provided by the National Institute of Technology, Rourkela (NIT-R), India, for the completion of his Ph.D. degree.


### Notes

The authors declare no competing financial interest.

## ■ ACKNOWLEDGMENTS


We acknowledge the logistical support from the National Institute of Technology, Rourkela, India.


## ■ ABBREVIATIONS

CB, cocoa butter; DSC, differential scanning calorimeter; MB, mango butter; NI, National Instruments; SFC, solid fat content; XRD, X-ray diffraction

## ■ REFERENCES


(1) Jahurul, M. H. A.; Zaidul, I. S. M.; Norulaini, N. A. N.; Sahena, F.; Jinap, S.; Azmir, J.; Sharif, K. M.; Omar, A. K. M. Cocoa butter fats and possibilities of substitution in food products concerning cocoa varieties, alternative sources, extraction methods, composition, and characteristics. *J. Food Eng.* **2013**, *117*, 467−476.

(2) Yanus, R. L.; Sela, H.; Borojovich, E. J. C.; Zakon, Y.; Saphier, M.; Nikolski, A.; Gutflais, E.; Lorber, A.; Karpas, Z. Trace elements in cocoa solids and chocolate: An ICPMS study. *Talanta* **2014**, *119*, 1−4.

(3) Lipp, M.; Anklam, E. Review of cocoa butter and alternative fats for use in chocolate−Part A. Compositional data. *Food Chem.* **1998**, *62*, 73−97.

(4) Sonwai, S.; Kaphueakngam, P.; Flood, A. Blending of mango kernel fat and palm oil mid-fraction to obtain cocoa butter equivalent. *J. Food Sci. Technol.* **2012**, 1−13.

(5) Metzger, J.; Bornscheuer, U. Lipids as renewable resources: current state of chemical and biotechnological conversion and diversification. *Appl. Microbiol. Biotechnol.* **2006**, *71*, 13−22.

(6) Solís-Fuentes, J. A.; Durán-de-Bazúa, M. C. Mango seed uses: thermal behaviour of mango seed almond fat and its mixtures with cocoa butter. *Bioresour. Technol.* **2004**, *92*, 71−78.

(7) Kabuki, T.; Nakajima, H.; Arai, M.; Ueda, S.; Kuwabara, Y.; Dosako, S. i. Characterization of novel antimicrobial compounds from mango (Mangifera indica L.) kernel seeds. *Food Chem.* **2000**, *71*, 61−66.

(8) Le Révérend, B. J.; Norton, I. T.; Cox, P. W.; Spyropoulos, F. Colloidal aspects of eating. *Curr. Opin. Colloid Interface Sci.* **2010**, *15*, 84−89.

(9) Boutin, C.; Giroux, H. J.; Paquin, P.; Britten, M. Characterization and acid-induced gelation of butter oil emulsions produced from heated whey protein dispersions. *Int. Dairy J.* **2007**, *17*, 696−703.

(10) Norton, J. E.; Fryer, P. J. Investigation of changes in formulation and processing parameters on the physical properties of cocoa butter emulsions. *J. Food Eng.* **2012**, *113*, 329−336.

(11) di Bari, V.; Norton, J. E.; Norton, I. T. Effect of processing on the microstructural properties of water-in-cocoa butter emulsions. *J. Food Eng.* **2014**, *122*, 8−14.

(12) Sagiri, S. S.; Behera, B.; Pal, K.; Basak, P. Lanolin-based organogels as a matrix for topical drug delivery. *J. Appl. Polym. Sci.* **2013**, *128*, 3831−3839.

(13) Cottrell, T.; van Peij, J. 7 Sorbitan esters and polysorbates. *Emulsifiers Food Technol.* **2004**, 162.

(14) Ibrahim, M. M.; Hafez, S. A.; Mahdy, M. M. Organogels, hydrogels and bigels as transdermal delivery systems for diltiazem hydrochloride. *Asian J. Pharm. Sci.* **2013**, *8*, 48−57.

(15) Satapathy, D.; Biswas, D.; Behera, B.; Sagiri, S. S.; Pal, K.; Pramanik, K. Sunflower-oil-based lecithin organogels as matrices for controlled drug delivery. *J. Appl. Polym. Sci.* **2013**, *129*, 585−594.

(16) Ghotra, B. S.; Dyal, S. D.; Narine, S. S. Lipid shortenings: a review. *Food Res. Int.* **2002**, *35*, 1015−1048.

(17) Norton, J. E.; Fryer, P. J.; Parkinson, J.; Cox, P. W. Development and characterisation of tempered cocoa butter emulsions containing up to 60% water. *J. Food Eng.* **2009**, *95*, 172−178.

(18) Ghosh, S.; Rousseau, D. Fat crystals and water-in-oil emulsion stability. *Curr. Opin. Colloid Interface Sci.* **2011**, *16*, 421−431.

(19) Himawan, C.; Starov, V.; Stapley, A. Thermodynamic and kinetic aspects of fat crystallization. *Adv. Colloid Interface Sci.* **2006**, *122*, 3−33.

(20) MacMillan, S. D.; Roberts, K. J.; Rossi, A.; Wells, M. A.; Polgreen, M. C.; Smith, I. H. In situ small angle x-ray scattering (SAXS) studies of polymorphism with the associated crystallization of cocoa butter fat using shearing conditions. *Cryst. Growth Des.* **2002**, *2*, 221−226.

(21) Marangoni, A. G.; McGauley, S. E. Relationship between crystallization behavior and structure in cocoa butter. *Cryst. Growth Des.* **2002**, *3*, 95−108.

(22) Campos, R.; Ollivon, M.; Marangoni, A. G. Molecular composition dynamics and structure of cocoa butter. *Cryst. Growth Des.* **2009**, *10*, 205−217.

(23) Hindle, S.; Povey, M. W.; Smith, K. Characterizing cocoa butter seed crystals by the oil-in-water emulsion crystallization method. *J. Am. Oil Chem. Soc.* **2002**, *79*, 993−1002.

(24) Fredrick, E.; Van de Walle, D.; Walstra, P.; Zijtveld, J. H.; Fischer, S.; Van der Meeren, P.; Dewettinck, K. Isothermal crystallization behaviour of milk fat in bulk and emulsified state. *Int. Dairy J.* **2011**, *21*, 685−695.

(25) Bricknell, J.; Hartel, R. Relation of fat bloom in chocolate to polymorphic transition of cocoa butter. *J. Am. Oil Chem. Soc.* **1998**, *75*, 1609−1615.

(26) Ramananarivo, H. R.; Abdelouahdi, K.; Amer, W.; Zahouily, M.; Clark, J.; Solhy, A. Tunable structure of zirconia nanoparticles by biopolymer gelation: Design, synthesis and characterization. *Eur. J. Inorg. Chem.* **2012**, *2012*, 5465−5469.

(27) Hodate, Y.; Ueno, S.; Yano, J.; Katsuragi, T.; Tezuka, Y.; Tagawa, T.; Yoshimoto, N.; Sato, K. Ultrasonic velocity measurement of crystallization rates of palm oil in oil-water emulsions. *Colloids Surf., A* **1997**, *128*, 217−224.

(28) Niu, H. J.; Hampshire, D. P. Fabrication of nanocrystalline and amorphous Chevrel phase PbMo6S8 powder by ball milling. *Phys. C (Amsterdam, Neth.)* **2002**, *372*−*376*, 1145−1147.
(29) Lopez, C.; Riaublanc, A.; Lesieur, P.; Bourgaux, C.; Keller, G.; Ollivon, M. Definition of a model fat for crystallization-in-emulsion studies. *J. Am. Oil Chem. Soc.* **2001**, *78*, 1233−1244.
(30) Metin, S.; Hartel, R. Thermal analysis of isothermal crystallization kinetics in blends of cocoa butter with milk fat or milk fat fractions. *J. Am. Oil Chem. Soc.* **1998**, *75*, 1617−1624.
(31) Foubert, I.; Vanrolleghem, P. A.; Thas, O.; Dewettinck, K. Influence of chemical composition on the isothermal cocoa butter crystallization. *J. Food Sci.* **2004**, *69*, E478−E487.
(32) Sharples, A. *Introduction to Polymer Crystallization*; St. Martin's Press: London, 1966
(33) Ahza, A. B. *Kinetics of Milk Fat Crystallization in a Continuous Crystallizer*; University of Wisconsin-Madison: Madison, WI, 1995.
(34) Smith, K. W. Cocoa butter and cocoa butter equivalents. *Structured and Modified Lipids*; Marcel Dekker: New York, 2001; pp 401−422.
(35) Abruzzo, A.; Bigucci, F.; Cerchiara, T.; Cruciani, F.; Vitali, B.; Luppi, B. Mucoadhesive chitosan/gelatin films for buccal delivery of propranolol hydrochloride. *Carbohydr. Polym.* **2012**, *87*, 581−588.
(36) Peleg, M. Characterization of the stress relaxation curves of solid foods. *J. Food Sci.* **1979**, *44*, 277−281.
(37) Bellido, G. G.; Hatcher, D. W. Asian noodles: Revisiting Peleg's analysis for presenting stress relaxation data in soft solid foods. *J. Food Eng.* **2009**, *92*, 29−36.

**Table 1. Primer Sequences for the *Waxy* Gene Amplification and Q-PCR Analysis of the *Waxy* Gene**

| primer pair[a] | forward and reverse PCR primer sequences | annealing temperature (°C) | amplified region[b] |
|---|---|---|---|
| GB1 | F: 5′-CGCAGAAACGAACAAACAGA-3<br>R: 5′-TTCAGTCAGGTTTTGTCGACTTT-3′ | 55 | 543−1499 |
| GB2 | F: 5′-CCGGACAAAACCGTGTACTT-3<br>R: 5′-GATCGATCGACGACGAGAAT-3′ | 60 | 1434−2290 |
| GB3 | F: 5′-ACCGCGTGTTCATCG-3′<br>R: 5′-CTTGTCGTAGCCGTCAA-3′ | 55 | 2223−3002 |
| GB4 | F: 5′-ACGACTGGCACACGGGCCTTC-3′<br>R: 5′-TCACTCAATCATCCATCCAT-3′ | 60 | 2701−3587 |
| GB5 | F: 5′-GGCCAAGGCGCTGAACAAG-3′<br>R: 5′-GAGGCAAGCGGCACAACAAAAC-3′ | 60 | 3338−4524 |
| EF | F: 5′-AAGGATCTCAAGCGTGGG-3′<br>R: 5′-GTGGGATGTGTGGCAGTC-3′ | 60 | |
| C5 | F: 5′-CTCCAGGGAATGCGCTATGGAAC-3′<br>R: 5′-AGTTCTTGGCAGGTCCCTTCCAG-3′ | 60 | |

[a]GB1, GB2, GB3, GB4, and GB5 were used to amplify the full-length DNA sequence of the *Waxy* gene. [b]Position in the amplified region refers to the nucleotide sequence Genbank X07931.

are relatively fewer than those on wheat, rice, and maize, but some molecular information could be documented. Barley *Waxy* gene consists of 12 exons and 11 introns and codes 603 amino acids with a transit peptide of 72 amino acid residues.[19] A high level of variations is also found in the barley *Waxy* gene sequence, and some important nucleotide changes can greatly affect the amylose synthesis and further alter starch properties. It has been demonstrated that a 400 bp (approximately) deletion in the 5′ untranslated region (5′UTR) led to a significant decrease of the mRNA transcript level and the GBSS I protein level and thus low-amylose trait.[20−24] Three SNP mutations in the *Waxy* gene produce amylose-free traits.[20,22,25] Like wheat or rice, low-amylose or amylose-free barley has special starch properties and thus can expand the use of barley grain. However, in previous studies, investigations of the full-length sequence of the *Waxy* gene were conducted only on several barley accessions,[20,25,26] and only a few studies were carried out with the combination of nucleotide differences, the mRNA expression level, the GBSS I protein level, the amylose content, and starch properties.[20,25,26] Therefore, further comprehensive study on the *Waxy* locus with a larger population should be useful for understanding the genes controlling amylose synthesis and starch properties and improving barley starch quality.

Hull-less barley is also called naked barley and has advantages over hulled barley, such as easy processing and higher content of functional components. The Qinghai-Tibet plateau (QTB) in China has the most abundant hull-less barley resources in the world and is also the only region where hull-less barley serves as the first food crop, accounting for 60% of total crop planting area and 55% of tonnage harvested.[27] Hull-less barley is respectfully called "Qingke" by Tibetans and is always an important economic and cultural carrier for the Tibetan people. To date, hull-less barley has attracted more and more attention in the world due to its potential health benefits.[28−30] Barley flour, alone or as a mixture with wheat, has been processed into various types of food products, such as biscuits, noodles, steam buns, and breads. With the increase of processed products of hull-less barley, more and more attention has been paid to starch properties and the screening of germplasm resources for starch traits. We have determined the amylose content of about 300 hull-less barley accessions mainly from QTB in China and found the amylose content was widely variable with a range of 0−40%. This indicates the *Waxy* gene responsible for amylose synthesis may have rich variations, and a further study of the *Waxy* gene in hull-less barley from QTB could be useful for producing various types of barley with more variable amylose contents. Therefore, in this study, we selected 34 of 300 barley accessions that we had analyzed before, with different amylose contents from QTB in China, to conduct the characterization of DNA sequence variations of the full length of the *Waxy* gene and to determine the expression differences of *Waxy* alleles at both RNA and protein levels and to characterize the starch properties to understand how sequence polymorphisms in the *Waxy* gene affect amylose synthesis and starch properties in hull-less barley from QTB in China.

## MATERIALS AND METHODS

**Plant Material.** A total of 34 hull-less barley (*Hordeum vulgare* L. var. *nudum* Hook. F.) accessions with different amylose contents were used in this study, comprising 13 indigenous varieties and 21 cultivars or breeding lines. Among these accessions, breeding lines Z999, Z1191, and Z1979 were derived from the crosses of local varieties × overseas introduced lines. All barley accessions were collected from QTB in China and planted in Shuangliu, Chengdu, Sichuan, China. All accessions and breeding lines were planted as three replicates in three blocks in the same field. Within each block, each of the accessions and breeding lines was planted in one plot using a randomized block design. Barley grains from the same accession or breeding line were mixed at an equal grain number or weight from three plots in three blocks. The mixed samples were used to conduct further analyses.

**Determination of Amylose Content, Swelling Power, and Starch Pasting Properties.** Starch was isolated with a proteinase extraction method.[31] Amylose content was measured using an iodine adsorption method.[7] Swelling power was measured according to the method reported by Konik-Rose et al.[32] Pasting properties were

**Table 2. Variations of DNA Sequences of the *Waxy* Gene among Barley Haplotypes[a]**

| | | | nucleotide | | amino acid | | | |
|---|---|---|---|---|---|---|---|---|
| region | position[b] | category | *Waxy* I DNA group | *Waxy* II DNA group | Wx A1 | Wx A2 | Wx B1 | Wx B2 |
| 5′UTR | 589−590 | INDEL | **TAGC (I-1, I-2)**/—— | —— | | | | |
| | 621−1023 | INDEL | ——/403 bp deletion (I-3) | —— | | | | |
| | 636−637 | INDEL | TTGCT | ——/TTGCT (II-3) | | | | |
| | 680 | SNP | A | **G**/A (II-4, II-5) | | | | |
| | 698 | SNP | G/**A (I-1, I-2)** | G | | | | |
| | 718−719 | SSR | ——/AGCGG (I-1, I-2) | ——/AGCGG (II-1, II-2)/ **AGCGGAGCGGAGCGG (II-3)** | | | | |
| | 756−757 | SSR | ——/CGAG (I-4, I-5, I-6) | —— | | | | |
| | 794 | SNP | C | C/**A (II-3)** | | | | |
| | 882−883 | SSR | TCAC | TCAC/—— (II-1, II-3)/ **CCAC (II-5)** | | | | |
| | 955 | SNP | G | G/C (II-4, II-5) | | | | |
| | 964 | SNP | G | G/C (II-4, II-5) | | | | |
| | 974−975 | SSR | —— | ——/**AGA (II-3)** | | | | |
| intron 1 within 5′ UTR | 1007 | SNP | C | C/A (II-1, II-2) | | | | |
| | 1026−1036 | INDEL | GCAGCCGGCCG | GCAGCCGGCCG/—— (II-4, II-5) | | | | |
| | 1084−1085 | INDEL | GATTC | ——/GATTC (II-4, II-5) | | | | |
| | 1087 | SNP | G | G/C (II-1, II-2) | | | | |
| | 1102−1103 | INDEL | AT/—— **(I-1, I-2)** | AT | | | | |
| | 1109 | SNP | T/**A (I-1, I-2)** | T | | | | |
| | 1132 | SNP | T/**A (I-1, I-2)** | T/**A (II-3)** | | | | |
| | 1139 | SNP | T/**A (I-1, I−2)** | T/**A (II-3)** | | | | |
| | 1240 | SNP | G | G/**C (II-3)** | | | | |
| | 1291 | INDEL | G | G/C (II-1, II-2) | | | | |
| | 1325−1326 | INDEL | 191 bp insertion (I-3, I-4, I-5, I-6)/**187 bp insertion (I-1, I-2)** | —— | | | | |
| | 1326 | SNP | A | G | | | | |
| | 1327 | SNP | C | A | | | | |
| | 1377 | SNP | G/**C (I-1, I-2)** | G | | | | |
| | 1389 | SNP | C | T | | | | |
| | 1390 | SNP | C | T | | | | |
| | 1392 | SNP | T | A | | | | |
| | 1415 | SNP | T | C | | | | |
| | 1418 | SNP | C | T | | | | |
| | 1424 | SNP | T | G | | | | |
| | 1433 | SNP | A | G | | | | |
| | 1446 | SNP | A/G (I-1, I-2) | G | | | | |
| | 1586 | SNP | C/**T (I-1, I-2)** | C | A | **V** | A | A |
| exon 2 | 1652 | SNP | G | A | R | R | R | R |
| | 1653−1654 | INDEL | TCGGCGCC | —— | S, A | P, S, M | —— | —— |
| | | | GTCCATG | | S, A | P, S, M | | |
| | 1660 | SNP | A | G | H | H | R | R |
| | 1662 | SNP | G | C | A | A | P | P |
| | 1664 | SNP | T | A | F | F | F | F |
| | 1679 | SNP | G | C | L | L | L | L |
| | 1691 | SNP | G | C | K | K | N | N |
| | 1694 | SNP | C | G | P | P | P | P |
| | 1697 | SNP | A | G | A | A | A | A |
| | 1702 | SNP | G | C | G | G | A | A |
| | 1704 | SNP | A | G | T | T | A | A |
| | 1707 | SNP | T | C | F | F | L | L |
| | 1718 | SNP | G | G/**A (II-3)** | R | R | R | R |
| | 1722 | SNP | G | A | V | V | I | I |
| | 1771 | SNP | A | G | N | N | S | S |
| | 1797 | SNP | C | C/A (II-1, II-2) | R | R | S | R |
| | 1799 | SNP | T | C | | | | |
| | 1877 | SNP | C | T | D | D | D | D |
| | 1892 | SNP | T | C | L | L | L | L |


dx.doi.org/10.1021/jf5026746 | J. Agric. Food Chem. 2014, 62, 11369−11385

**Table 2. continued**

| region | position[b] | category | nucleotide | | amino acid | | | |
|---|---|---|---|---|---|---|---|---|
| | | | *Waxy* I DNA group | *Waxy* II DNA group | Wx A1 | Wx A2 | Wx B1 | Wx B2 |
| | 1895 | SNP | A | C | P | P | P | P |
| | 1898 | SNP | A | G | P | P | P | P |
| intron 2 | 1919 | SNP | C | T | | | | |
| | 1920 | SNP | A | C | | | | |
| | 1922 | SNP | T | C | | | | |
| | 1924 | SNP | C | A | | | | |
| | 1929 | SNP | A | C | | | | |
| | 1981 | SNP | T | C | | | | |
| intron 3 | 2153 | SNP | G/A (I-1, I-2) | A | | | | |
| exon 4 | 2167 | SNP | G | G/A (II-4, II-5) | K | K | K | K |
| intron 4 | 2275 | SNP | G/C (I-1) | C | | | | |
| | 2284 | SNP | G | G/**C (II-3)** | | | | |
| | 2302 | SNP | T/**G (I-2)** | T | | | | |
| | 2308 | SNP | T/**C (I-2)** | T | | | | |
| | 2310 | SNP | T/**C (I-2)** | T | | | | |
| | 2312 | SNP | C/**A (I-2)** | C | | | | |
| | 2323 | SNP | A/**T (I-2)** | A | | | | |
| | 2328 | SNP | C/**G (I-2)** | C | | | | |
| | 2329 | INDEL | ——/**T (I-2)** | —— | | | | |
| | 2330 | INDEL | ——/**C (I-2)** | —— | | | | |
| | 2332 | SNP | G/**C (I-2)** | G | | | | |
| | 2333 | SNP | G/**A (I-2)** | G | | | | |
| exon 5 | 2434 | SNP | G | A | T | T | T | T |
| | 2440 | SNP | C | T | Y | Y | Y | Y |
| | 2453 | SNP | C/T (I-5) | C | E/stop codon (I-5)[M] | E/stop codon (I-5)[M] | E | E |
| | 2482 | SNP | G/A (I-1) | A | A | A | A | A |
| intron 5 | 2667 | SNP | C | T/C (II-3) | | | | |
| intron 6 | 2780 | SNP | T/**C (I-1)** | T | | | | |
| | 2798 | INDEL | T/—— **(I-1)** | T | | | | |
| | 2799 | INDEL | G/—— **(I-1)** | G | | | | |
| | 2836 | SNP | C | A | | | | |
| exon 7 | 3077 | SNP | C/**T (I-6)** | C | P/L (I-6)[M] | P/L (I-6)[M] | P | P |
| | 3078 | SNP | C/**T (I-6)** | C | | | | |
| | 3118 | SNP | T/**C (I-6)** | T | C/R (I-6)[M] | C/R (I-6)[M] | C | C |
| | 3159 | SNP | A | A/C (II-4, II-5) | G | G | G | G |
| intron 7 | 3249 | SNP | G/**C (I-1)** | C | | | | |
| | 3252 | INDEL | —— | ——/**C (II-3)** | | | | |
| | 3267 | SNP | T | T/**C (II-3)** | | | | |
| | 3268 | SNP | T | T/**C (II-3)** | | | | |
| exon 8 | 3362 | SNP | A/G (I-1) | G | A | A | A | A |
| intron 8 | 3521 | SNP | G | G/**C (II-3)** | | | | |
| | 3537 | SNP | A | T/A (II-1,II-2) | | | | |
| | 3546 | SNP | T | C/T (II-1,II-2) | | | | |
| | 3560 | SNP | C | G/C (II-1,II-2) | | | | |
| intron 9 | 3818 | SNP | G/C (I-1, I-2) | C | | | | |
| | 3822 | SNP | T | T/A (II-1,II-2) | | | | |
| | 3823 | SNP | C | C/A (II-1,II-2) | | | | |
| | 3847 | SNP | T/G (I-1, I-2) | G | | | | |


dx.doi.org/10.1021/jf5026746 | J. Agric. Food Chem. 2014, 62, 11369−11385

**Table 2. continued**

| region | position[b] | category | nucleotide | | amino acid | | | |
|---|---|---|---|---|---|---|---|---|
| | | | *Waxy* I DNA group | *Waxy* II DNA group | Wx A1 | Wx A2 | Wx B1 | Wx B2 |
| | 3871 | SNP | T/**A (I-1, I-2)** | T/**A (II-3)** | | | | |
| | 3874 | SNP | T/**C (I-1, I-2)** | T/**C (II-3)** | | | | |
| exon 10 | 3935 | SNP | G | G/**T (II-2)** | G | G | G/W (II-2)$^{M}$ | G |
| intron 10 | 3992 | SNP | A | A/T (II-1, II-2) | | | | |
| | 4015 | SNP | T/C (I-1, I-2) | C | | | | |
| intron 11 | 4204 | SNP | C/T (I-1, I-2) | T | | | | |
| | 4208 | SNP | T/G (I-1, I-2) | G | | | | |
| | 4210−4211 | INDEL | AATGGTGA/—— (I-1, I-2) | —— | | | | |
| | 4212 | SNP | T/C (I-1, I-2) | C | | | | |
| | 4213 | SNP | T/A (I-1, I-2) | A | | | | |
| | 4215 | SNP | A/G (I-1, I-2) | G | | | | |
| | 4317 | SNP | G | G/A (II-3) | | | | |
| 3′UTR | 4390 | INDEL | A | A/—— (II-1, II-2) | | | | |
| | 4391 | INDEL | A | A/—— (II-1, II-2) | | | | |

[a]A superscript "M" indicates the alteration of the amino acid residue in the mature protein region. Nucleotides and amino acids bolded and underlined are newly identified nucleotide sequence variations. The sequence of the 187 insertion was TGCATACACGTTTCTGTTTCCA-ACCAAGCCTTTGATTCTATGCAATTCCAAAAAAAAACATTTCATATTTTTGTCATGGAATTCGACTGCACGCTACAAGAAAAACA-CCAGTATGGAGTATATTTTACCCTCACTGCAGTTCCCCCTCTGTACACGCGATTTAACCGACTGTTTTGCTACTACCCGTAC. [b]Position refers to the nucleotide position in Genbank accession no. X07931.

measured by using a Micro Visco-Amylo-Graph (A. W. Brabender Instruments, South Hackensack, NJ, USA) and followed the procedure given: starch (10 g) was suspended with distilled water (98 mL) and 10% (m/v) $AgNO_3$ (2 mL), then the starch suspension was heated from 50 to 92 °C at the rate of 7.5 °C/min, held at 92 °C for 5 min, cooled to 50 °C at 7.5 °C/min, and held at 50 °C for 1 min, and the rotation speed was 250 rpm. All determinations were performed in triplicate with the mixed grains (equal weight of grains) of three plots from three blocks for each accession.

**PCR and Sequencing.** DNA was extracted from young hull-less barley leaves according to the CTAB procedure.[33] Five primer pairs[23,26] were used to amplify the full length of *Waxy* genes (Table 1). The PCR was carried out in a 20 μL volume containing 100 ng of DNA template, 0.1 μM of each primer, 200 μM of each dNTP, 1.5 mM $MgCl_2$, 1× PCR reaction buffer, and 1 unit of Taq DNA polymerase (TaKaRa Inc., Dalian, China). The PCR procedure consisted of a pre-incubation at 94 °C for 4 min, followed by 35 cycles of 94 °C for 40 s, 60 or 55 °C for 50 s, 72 °C for 50 s, and a final extension at 72 °C for 6 min.

PCR products were separated with 1% agarose gels, and the target band was purified with a Universal DNA Purification Kit (Tiangen, China). The purified band was then ligated into the pMD19-T vector (TaKaRa Inc.) and transformed into the competent cells of *Escherichia coli* (JM109). Purified plasmid DNAs from at least three colonies from each PCR DNA band were sequenced by Invitrogen (Shanghai, China).

**Transcript Level Analysis Using Q-PCR.** Total RNA was extracted from developing endosperms, which were obtained from the 8th, 13th, 18th, 23rd, and 28th day post anthesis (dpa) using RNAiso Plus (TaKaRa Inc.) and Fruit-mate purification kits (TaKaRa Inc.). A total of 15 endosperms from three plots (randomly collected five endosperms from each plot) were mixed and ground and then used for RNA extraction for each developmental stage of each accession. cDNA was synthesized from total RNAs using oligo $(dT)_{18}$ primer and M-MLV reverse transcriptase (TaKaRa Inc.). The gene-specific Q-PCR primer (C5) was designed according to a barley *Waxy* mRNA sequence (X07932). The Q-PCR procedure consisted of a pre-incubation at 94 °C for 5 min, followed by 40 cycles of 95 °C for 15 s, 60 °C for 15 s, and extension at 72 °C for 15 s. All reactions were performed in the Chromo4 real-time PCR detector system (Bio-Rad, Hercules, CA, USA) using iQ SYBR green supermix (Bio-Rad). To normalize the cDNA templates, a housekeeping gene encoding elongation factor 1α (EF) was co-amplified as a control.[34] All primers (Table 1) were synthesized by Invitrogen. Each accession was analyzed with three replicates.

**Separation of GBSS I Protein by SDS-PAGE.** Extraction of GBSS I protein was mainly based on the reports by Pan et al.[35] and Yamamori et al.[36] The developing endosperms without pericarp and embryo were collected at the 8th, 13th, 18th, 23rd, and 28th dpa, then homogenized in washing extraction buffer (55 mmol $L^{-1}$ Tris-HCl, pH 6.8; 23 g $L^{-1}$ SDS; 5% (v/v) β-mercaptoethanol; and 10% (v/v) glycerol) with a mortar. The extraction of GBSS I protein was performed from mixed endosperms of 15 seeds from three plots for each developmental stage of each barley accession or breeding line. The mixture was incubated at 25 °C with shaking at a speed of 150 rpm for 2 h and then centrifuged (CP100-WX; Hitachi, Japan) at 12000 rpm for 4 min. The supernatant was discarded, and the sediment was washed twice with each of the SDS washing buffer, distilled water, and acetone, and finally dried overnight. GBSS I protein was released by boiling starch (5 mg) in 400 μL of protein extraction buffer (containing 62 mmol $L^{-1}$ Tris-HCl, pH 6.8; 23 g $L^{-1}$ SDS; 5% (v/v) β-mercaptoethanol; 10% (v/v) glycerol; 0.05 g $L^{-1}$ bromophenol blue) for 15 min and centrifuged (with CP100-WX) at 12000 rpm for 10 min at 4 °C. Protein supernatant (20 μL) was separated with 10% SDS-PAGE gels, which contained acrylamide/Bis at a ratio of 30:0.135, and protein gels were then stained with silver staining solutions.

**Data Analysis.** The deduced amino acid sequence of GBSS I protein was predicted using BioEdit. Multiple alignments of nucleotide and amino acid sequences were performed by Clustalx1.83 and further adjusted manually. A phylogenetic tree based on nucleotide sequence differences was constructed by MEGA 4.0 with the UPGMA method. Cis-acting regulatory DNA elements were searched using Plant Care[37] and PLACE.[38] Transcript levels of *Waxy* gene were calculated using Gene Expression Analysis for iCycler iQ Real-Time PCR Detection System. Significant difference was determined by the least significant difference (LSD) test using Tukey's test (SPSS package, version 17.0).

## RESULTS

**DNA Sequence Variations of the Barley *Waxy* Gene.** A total of 116 polymorphic variations were detected in the 34 barley accessions; 39 of them were not reported in previous studies. These 116 polymorphic variations comprised 4 simple sequence repeats (SSRs), 18 insertions and deletions (INDELs), and 94 single-nucleotide polymorphisms (SNPs) (Table 2). Furthermore, these polymorphic sites were mainly distributed in 5′UTR (untranslated region), intron 1, and exons 1 and 2. No polymorphic variations were found in exons 3, 6, 9, 11, and 12, and only 33 polymorphic variations were located in coding regions.

A phylogenetic tree (Figure 1) was constructed on the basis of the multiple alignment of *Waxy* gene sequences of a total of 42 barley accessions, including the 34 accessions in this study, plus another 8 sequences downloaded from NCBI. All accessions were divided into two DNA groups: the *Waxy* I DNA group containing 25 barley accessions and the *Waxy* II DNA group containing another 17 accessions. Considering the 34 accessions sequenced in this study, *Waxy* I and *Waxy* II DNA groups can be further classified into six (HP I-1−I-6) and five (HP II-1−II-5) haplotypes, respectively. Haplotype (HP) I-4, including 13 accessions, was the representative haplotype for the *Waxy* I DNA group, and HP II-4 with 9 accessions was the major haplotype for the *Waxy* II DNA group. Detailed sequence variations among haplotypes are listed in Table 2 and Figure 2A. The *Waxy* I DNA group was different from the *Waxy* II DNA group mainly because the *Waxy* I DNA group had an insertion of about 190 bp in the first intron 1 and a 15 bp insertion within the second exon. Among the *Waxy* I DNA group, HP I-1 and I-2 were distinguished from the others mainly due to a newly found 187 bp insertion in intron 1 instead of the specific 191 bp insertion. In addition, HP I-1 and I-2 contained a transversion of a C-to-T base, which was first identified in the second exon of barley *Waxy* gene. HP I-3 (Z1979) was peculiar due to a large deletion of a 403 bp in the promoter region. In the phylogenetic tree, GU599883, GSHO 1828, MMD, and GSHO 908C and HP I-3 were clustered into a small single clade because all of them had the 403 bp fragment deletion in the promoter region. HP I-5 was similar to I-4 except for the substitution of a T for $C^{2453}$ base in the fifth exon that was also identified in barley cv. SH97 and Yon M Kei. HP I-6 was also the same as I-4, with the exception of a T instead of $C^{3077}$, a T instead of $C^{3078}$, and a C instead of $T^{3118}$ in the seventh exon, and all three of these SNPs were first identified in barley *Waxy* gene. For the *Waxy* II DNA group, HP II-2 was almost identical to II-1 except for the substitution of a T for $G^{3935}$ in the 10th exon. HP II-3 formed a single clade in the phylogenetic tree because it contained some unique SSRs and many other newly found SNPs in introns and 5′UTR. HP II-5 was the same as II-4 with the exception of a single base change of a C to a T between positions 882 and 883 in 5′UTR.

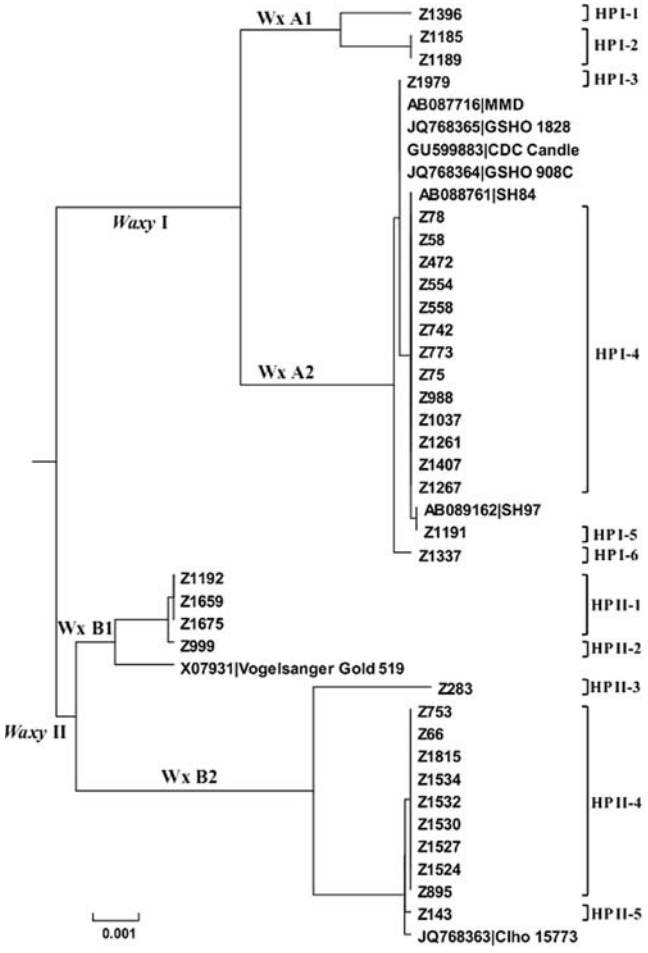


**Figure 1.** Phylogenetic tree of barley *Waxy* gene nucleotide sequences constructed using the multiple alignment. Nucleotide sequences were from 34 QTB barley accessions and breeding lines and 8 down-loaded sequences. HP is the abbreviation of haplotype. Genomic DNA sequences (AB087716|MMD, AB088761|SH84, GU599883|CDC Candle, JQ768365|GSHO 1828, JQ768364|GSHO 908C, AB089162|SH97, JQ768363|CIho 15773, X07931|Vogelsanger Gold519) were downloaded from NCBI. The format is Genbank number|Strain.

**Differential Expression of mRNA Transcripts of *Waxy* Gene.** To investigate mRNA differential transcript expression among haplotypes, a total of 26 of the 34 barley accessions, representing different haplotypes, were used for analysis. To reduce the number of samples, six and two accessions, belonging to HP I-4 and II-4, respectively, were randomly excluded, due to more accessions being present within HP I-4 and HP II-4. As shown in Figure 3A, the transcript level of the barley *Waxy* gene generally showed a wide range of variations during endosperm development, starting with a very low level at the 8th dpa, increasing rapidly, and peaking at the 13th or 18th dpa, then declining. Moreover, significant difference of transcript level was observed among *Waxy* DNA groups or haplotypes. The average transcript level of the *Waxy* I DNA group or HP I-4 was significantly higher than that of the *Waxy* II DNA group or HP II-4 haplotype (Figure 3B). Among different haplotypes, the order sorted by the average transcript level was HP II-2 > I-4 > I-6 > I-1 > II-4 > II-3 > I-2 > II-1 > II-5 > I-3 > I-5. Additionally, attention was paid to some special accessions. The transcript level of Z773 in HP I-4 was the highest and that of Z1191 in HP I-5 was the lowest, which contained a single nucleotide change in the fifth exon compared to Z773. The level of the differential transcript expression between them was up to 99-fold. HP I-3 with a 403 bp deletion also had an extremely low transcript level. However, HP I-6 with three base substitutions in the seventh exon, displayed a normal level of *Waxy* gene transcript, and HP II-2 with a single base mutation in the 10th exon had relatively higher transcript level.

**Analysis of Cis-Acting Regulatory DNA Elements in 5′UTR.** The number of putative cis-acting regulatory DNA

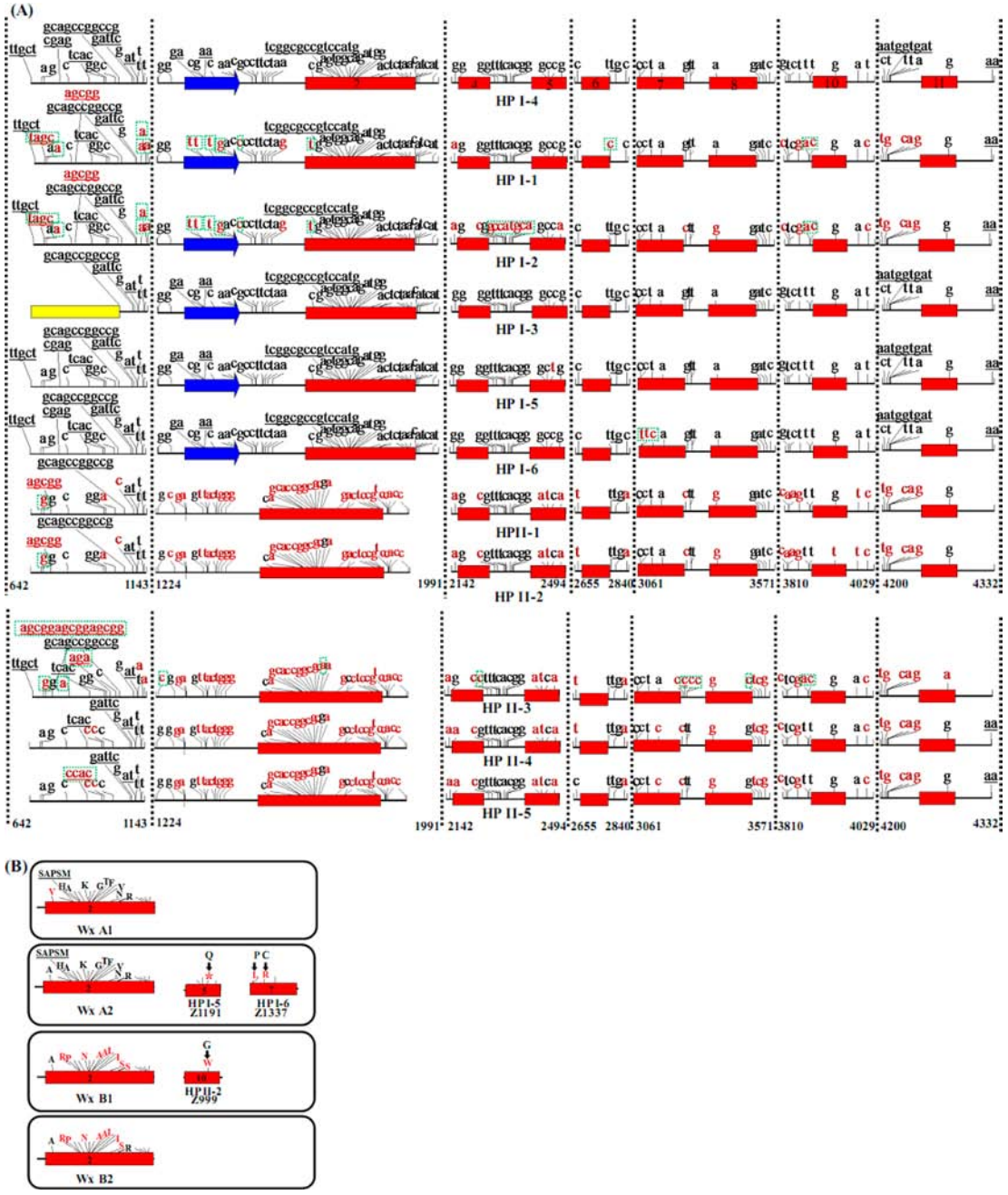


**Figure 2.** Variations of DNA and amino acid sequences of the *Waxy* gene among barley haplotypes and *Waxy* DNA groups. Red boxes represent exons. Lines between exons represent introns. SNPs underlined represent insertion. (A) Variations of DNA sequences of the waxy gene among barley haplotypes. The numbers at the bottom of the figure indicate the nucleotide positions referred to the nucleotide sequence Genbank No. X07931. The blue arrow represents the 191 or 187 bp insertion in intron 1. The yellow box represents the 403 bp deletion. The red bases mean different nucleotides from those accessions compared to HP I-4 at the same position. The green boxes represent the locations of newly identified SNPs. The DNA sequence variations of 11 haplotypes were distributed among seven nucleotide sequence regions, indicated as 642−1143, 1224−1991, 2142−2494, 2655−2840, 3061−3571, 3810−4029, and 4200−4332 at the bottom of the figure. (B) Variations of deduced amino acid sequences of the *Waxy* gene among four haplotypes and the altered amino acid residues within four Wx types labeled with one-letter amino acid abbreviations. Synonymous mutation is not shown. Amino acids are listed at the same position corresponding to nucleotides. ∗ represents the stop codon. The red SNPs indicate different SNPs from those haplotypes compared to the type of Wx A2 at the same position. The numbers inside the red boxes are exon numbers.

elements was different in 5′UTRs of the *Waxy* gene among 11 haplotypes with differential transcript expression. We tried to identify putative cis-acting regulatory DNA elements in the 5′UTRs to understand whether regulatory element divergences were associated with the transcription efficiency of *Waxy* genes. Up to 174 DNA regulatory elements were found in HP I-4, I-5, and I-6. In contrast, HP I-3 contained only 73 DNA regulatory elements because of the 403 bp deletion. The 403 bp deletion contained −300 element, RYREPEAT motif, and some other elements required for seed- and endosperm-specific expression.[24] Meanwhile, there might be about 49 cis-acting motifs in the 191 bp (187 bp) insertion, and most of them might be


dx.doi.org/10.1021/jf5026746 | J. Agric. Food Chem. 2014, 62, 11369−11385

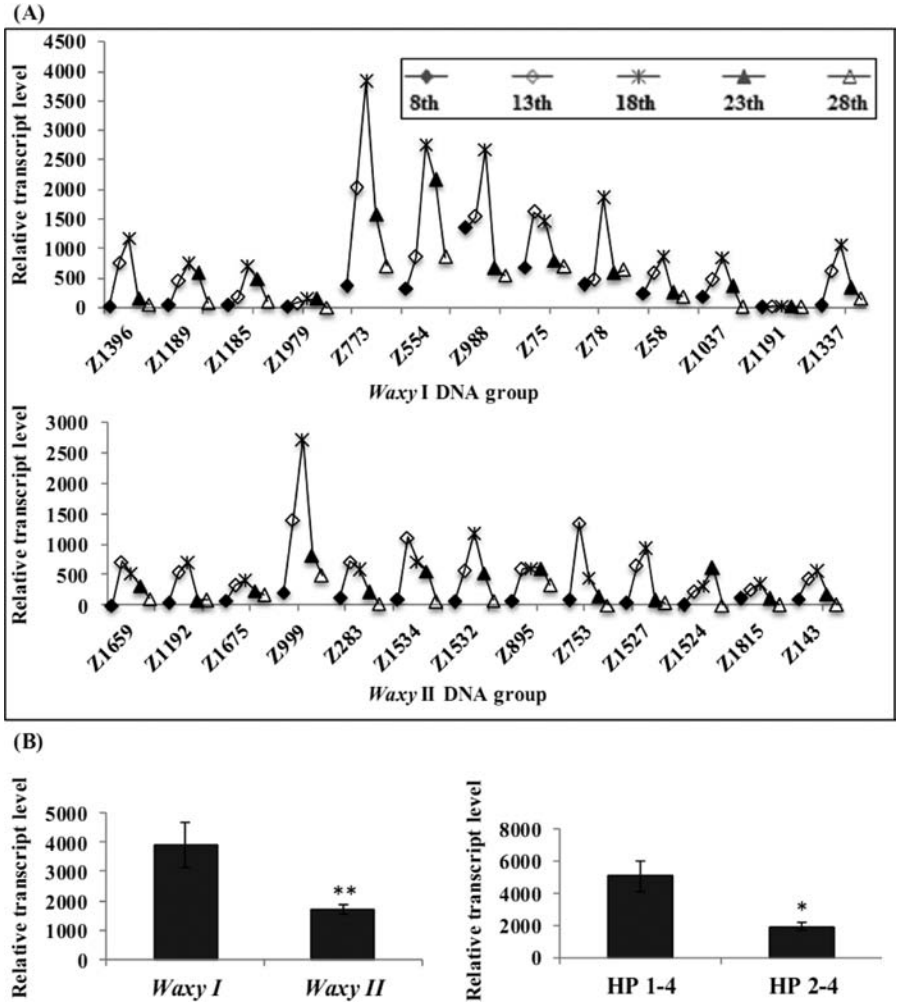


**Figure 3.** mRNA expression pattern of the barley *Waxy* gene: (A) relative transcript levels during five endosperm development stages of 26 barley accessions; (B) average transcript levels of barley *Waxy* DNA groups and haplotypes. Average transcript levels were calculated by total values of five endosperm development stages for each *Waxy* DNA group or haplotype divided by the number of accessions used for each *Waxy* DNA group or haplotype. (∗) Difference is significant at the $p < 0.05$ level; (∗∗) difference is significant at the $p < 0.01$ level.

involved in light responsiveness and stress tolerance.[24] In addition, we found the *Waxy* gene in HP I-1, I-2, I-3, II-1, and II-3, with relatively lower mRNA levels, also lacked either seven or eight RYREPEAT elements due to the single-base substitution of $A^{684}$ or $G^{698}$ (Table 3). RYREPEAT elements were believed to be involved in seed-specific regulation.[39] In addition, by comparison with HP II-4, the single base-substitution of T to C between positions 882 and 883 in HP II-5 resulted in the absence of putative SORLIP5AT that was thought to be involved in light responsiveness (Table 3).

**Variation of Deduced GBSS I Protein Sequences.** Fifteen amino acid alterations were identified in the deduced GBSS I protein sequences, due to a total of 33 polymorphic sites in coding regions, including 11 amino acid changes in the transit peptide and 4 of them within the mature protein regions.

According to these variations in the transit peptide, the 34 accessions in this study could be obviously divided into four protein groups of Wx A1, Wx A2, Wx B1, and Wx B2. As shown in Figure 1, except that HP I-1 and I-2 belonged to Wx A1, the rest of the accessions in the *Waxy* I DNA group were classified into protein group Wx A2. The difference among the four protein groups Wx A1, Wx A2, Wx B1, and Wx B2 was that Wx A1 and Wx A2 contained a five amino acid insertion of serine (Ser)−alanine (Ala)−proline (Pro)−Ser−methionine (Met) and some other amino acid alterations in the transit peptide (Table 2 and Figure 2B). Protein group Wx B1 was completely identical with Wx B2 except for the substitution of Ser for the 70th Arg (Table 2 and Figure 2B) that was caused by one SNP in the second exon.

The sequences of mature protein within the four protein groups were identical with the exceptions of HP I-5 (Z1191) and HP I-6 (Z1337) of protein group Wx A2 and HP II-2 (Z999) of group Wx B1. For Z1191, the 189th glutamine (Gln) was mutated to a stop codon because of the substitution of T for $C^{2453}$ in the 5th exon (Table 2 and Figure 2B). For Z1337, the 321th Pro and the 335th cysteine (Cys) were replaced by a leucine (Leu) and an arginine (Arg), respectively, because of the three newly found SNPs in the 7th exon (Table 2 and Figure 2B). As shown in Figure 4A, the two amino acids substituted were conserved in most cereal crops. For Z999, a tryptophan (Trp) was substituted for the 513th glycine (Gly) due to the mutation of $G^{3935}$ to T in the 10th exon (Table 2 and Figure 2B). From the result of a CDD Search on NCBI, the 513th Gly was highly conserved in the GBSS I protein of the grass family and even in glycogen synthase of various bacteria (Figure 4B).

Table 3. Variations of Cis-Acting Regulatory Elements of the *Waxy* Gene among Barley Haplotypes

| position[b] | nucleotide | haplotype and DNA group | cis-acting DNA regulatory element[a] | |
|---|---|---|---|---|
| | | | name | function |
| 589−590 | AGC | II-1, II-2 | ANAERO2CONSENSUS[a] | fermentative pathway |
| 621−1023 | 403 deletion | I-3 | total of 101 regulatory elements | |
| 636−637 | —— | I-3, II-1, II-2, II-4, II-5 | DOFCOREZM | binding of Dof proteins |
| 684 | G | II-1, II-2, II-3, I-3 | INTRONLOWER | 3′ intron−exon splice junctions |
| | | | total of 6 RY-REPEAT elements | seed-specific expression |
| 698 | A | I-1, I-2 | total of 8 RY-REPEAT elements | seed-specific expression |
| 794 | A | II-1 | MYBCOREATCYCB1 | cell cycle phase-independent activation |
| 882−883 | —— | II-1, II-2 | SORLIP5AT | light-induced expression |
| | | | SORLIP5AT(−) | light-induced expression |
| | | | GTGANTG10 | pollen gene expression |
| | | | CACTFTPPCA1 | mesophyll-specific and phosphoenolpyruvate carboxylase expression |
| | CCAC | II-5 | SORLIP5AT | light-induced expression |
| 1007 | A | II-1, II-2 | WBOXNTERF3[a] | stress resistance |
| | | | WRKY71OS*α* | stress resistance |
| 1084−1085 | —— | II-1, II-2, II-3 | ARR1AT | environmental stimuli |
| 1087 | C | II-1, II-2 | CURECORECR | coordinate copper and oxygen-responsive expression |
| 1102−1103 | —— | I-1, I-2 | P1BS | phosphate starvation |
| | | | P1BS(−) | phosphate starvation |
| 1109 | A | I-1, I-2 | GATABOX | light regulation and tissue-specific expression |
| | | | MYBST1 | core motif of MybSt1 binding site |
| | | | REBETALGLHCB21 | phytochrome regulation |
| 1132 | A | I-1, I-2, II-3 | CACTFTPPCA1 | mesophyll-specific and phosphoenolpyruvate carboxylase expression |
| 1325−1326 | 187 bp insertion | I-1, I-2 | total of 49 regulatory elements | |
| | 191 bp insertion | I-3, I-4, I-5, I-6 | total of 41 regulatory elements | |
| 1326 | A | *Waxy* I DNA group | POLLEN1LELAT52 | pollen-specific activation |
| | | | GT1CONSENSUS | light regulation |
| 1390 | C | *Waxy* I DNA group | HDZIP2ATATHB2 | light regulation |
| 1392 | T | *Waxy* I DNA group | POLASIG3 | plant polyadenylation signal |
| 1415 | T | *Waxy* I DNA group | POLLEN1LELAT52*α* | pollen-specific activation |
| | C | *Waxy* II DNA group | GT1CONSENSUS[a] | light regulation |
| | | | MYBCOREATCYCB1[a] | cell cycle phase−independent activation |
| 1424 | G | *Waxy* II DNA group | MYB2CONSENSUSAT | dehydration |
| | | | MYBCORE | water stress and regulation of flavonoid biosynthesis |
| 1433 | A | *Waxy* I DNA group | GT1CONSENSUS[a] | light regulation |
| | G | *Waxy* II DNA group | DOFCOREZM[a] | binding of Dof proteins |
| 1446 | G | I-1, I-2, *Waxy* II DNA group | MYB1AT | responsible for dehydration |

[a]Cis-acting DNA regulatory elements without a superscript "a" indicated that they were missing because of nucleotide variations of haplotypes listed in this table. [b]Position refers to the nucleotide position in Genbank accession no. X07931. "(-)" means this regulatory element is located in the antisense strand.

**Differing Levels of GBSS I Protein among Haplotypes.** GBSS I protein was also extracted from the developing endosperms at the 8th, 13th, 18th, 23rd, and 28th dpa and separated by SDS-PAGE. The level of GBSS I protein was estimated visually. As shown in Figure 5, GBSS I was detected as a band of about 60 kDa by SDS-PAGE analysis of proteins extracted from starch granules and identified on the basis of the known molecular markers. The level of GBSS I protein expressed was related to the variations at DNA and transcript levels. GBSS I protein expressed with a very low level at the 8th dpa and then remained stable with a high level from the 13th dpa (Figure 5). It was found that the GBSS I protein concentration for each barley accession was largely consistent with the level of total mRNA expression (Figure 6). Additionally, special attention was paid to HP I-5, I-6, and II-2 because there were some mutations in their mature GBSS I protein. Hardly any GBSS I protein was detected for HP I-5, which carried a stop codon to terminate the extending polypeptide chain. The GBSS I protein level of HP I-6, with two amino acid alterations, was moderate and did not change sharply in comparison with normal types of barley accessions. HP II-2 presented a relatively high GBSS I protein level. We also focused our attention on HP I-3, because it contained a 403 bp deletion in the 5′UTR. HP I-3 had a very low level of GBSS I protein during the entire development of the endosperm.

**Difference in Starch Properties.** The starch properties, including amylose content, swelling power, and pasting properties, were determined. Tables 4 and 5 show the results of statistical analysis for the starch properties of different *Waxy*

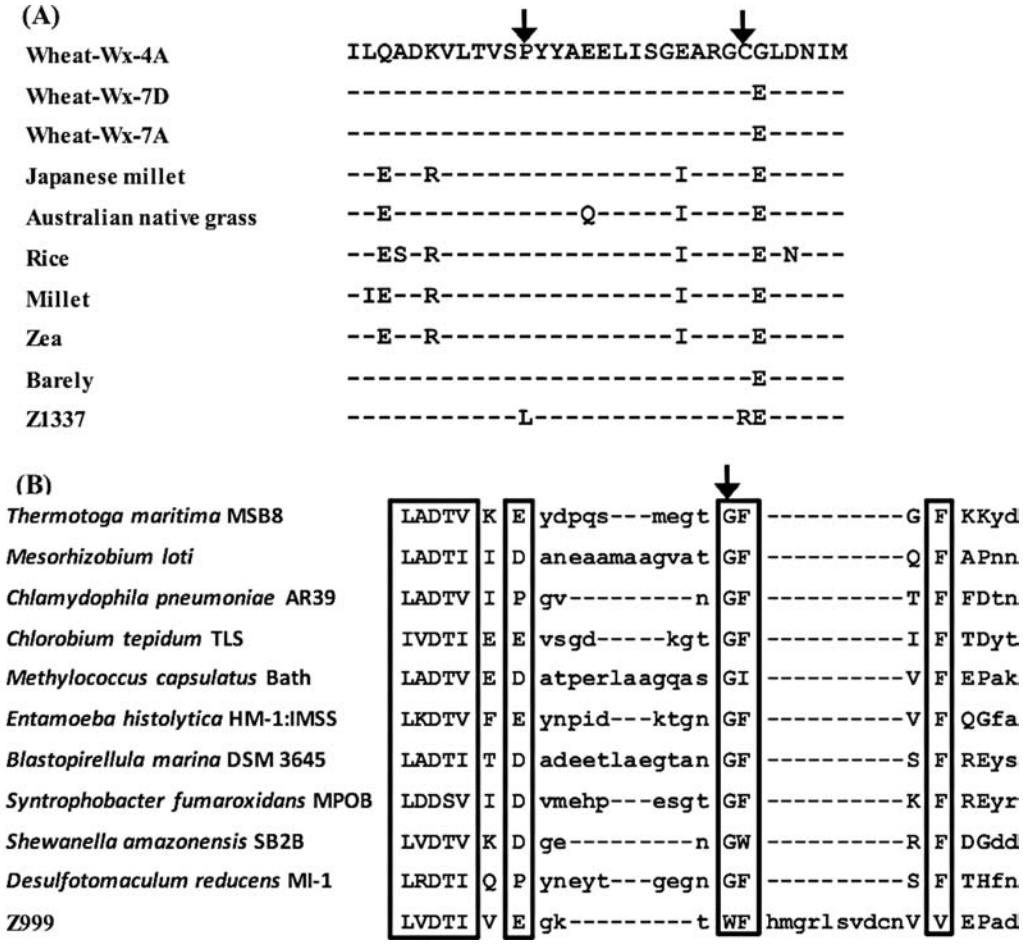


**Figure 4.** Conservation of amino acid residues of *Waxy* proteins and glycogen synthases. (A) Conservation of the amino acid residues at the 321th Pro and the 335th Cys in the GBSS I protein of most cereal crops. These two conserved amino acids at similar positions are indicated by arrows on the top of the figure. Short-dash lines indicate the same residues as that of wheat-Wx-4A. Genbank accession numbers of these crops are listed in order as BAA88509, BAA88512, HQ338724, BAM38099, EF600044, EF600036, NP_001267750, HQ423234, and X07931. (B) Conservation of the amino acid residues at the 513th Gly in GBSS I proteins or glycogen synthases. The top 10 most diverse members from the cluster of sequences are used to create a domain model. Short-dash lines indicate the deletion of amino acid residues; lower case letter indicates unconserved amino acid residues. The boxed residues indicate that they are highly conserved. The 513th Gly at a similar position is pointed out by arrows. Genbank accession numbers in order are AAD35976, AAK58596, NP_445448, NP_662888, YP_113933, XP_653076, ZP_01093037, YP_846231, YP_928323, and ZP_01665840.

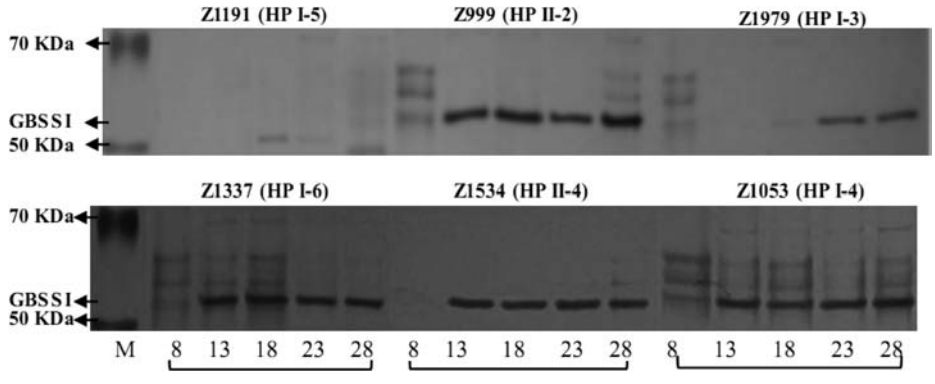


**Figure 5.** Separation of GBSS I proteins during five endosperm developmental stages of barley by SDS-PAGE. M, marker, ProteinRuler IV (Trans). Numbers 8, 13, 18, 23, and 28 represent the developmental endosperms at the 8th, 13th, 18th, 23rd, and 28th dpa, respectively. The GBSS I protein band of hull-less barley (about 60 kDa) and molecular markers are indicated on the left side.

DNA groups or haplotypes. Significant differences in some starch properties were found between HP I-4 and II-4, the representative types for *Waxy* I and *Waxy* II DNA groups, respectively. Amylose content, pasting temperature, time to peak viscosity, peak temperature, final viscosity, and setback viscosity of HP I-4 were significantly higher than those of HP II-4, but HP I-4 showed significantly lower swelling power, lower peak viscosity, and lower breakdown viscosity compared

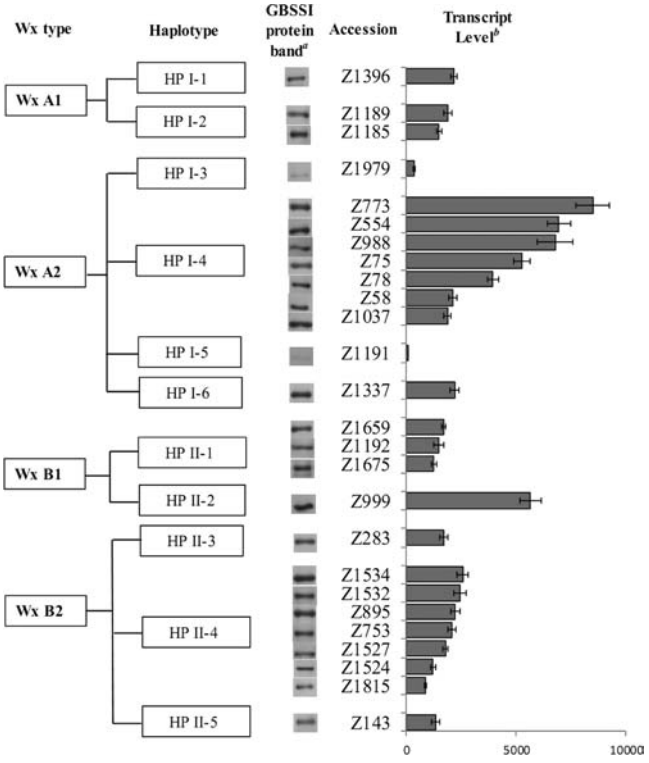


**Figure 6.** Alignment of deduced amino acid sequence types (Wx), expression levels of GBSS I proteins, and their transcript levels from different barley haplotypes. [a]Protein bands show GBSS I level of endosperm developmental stage at the 28th dpa. The GBSS I protein band of barley was about 60 kDa. [b]Total transcript level contains transcript levels from all five endosperm developmental stages.

to HP II-4. These results indicated that HP I-4 had lower hot-pasting stability, higher cold-pasting viscosity, and better gel-forming performance than those of HP II-4. Except for three low-amylose or amylose-free haplotypes (HP I-3, I-5, and II-2), the difference in starch properties between *Waxy* I and *Waxy* II DNA groups resembled the difference between HP I-4 and II-4. In addition, significant differences for trough viscosity were observed between *Waxy* I and *Waxy* II DNA groups. The starch properties of low-amylose and amylose-free accessions and Z1337 (HP I-6) containing mutations in mature protein regions are highlighted in Figure 7 and Table 6. HP I-6 (Z1337), with two amino acid mutations in the mature protein region, showed higher peak time and lower breakdown viscosity value (Figure 7 and Table 6). HP I-5 (Z1191), HP II-2 (Z999), and HP I-3 (Z1979) were of low or zero amylose content, and they had much higher swelling power value (about 20) than the representative types (Tables 4 and 6). Their starch also presented the typical pasting characteristics of lower pasting temperature, shorter peak time, higher peak viscosity, lower peak temperature, lower final viscosity, and higher breakdown viscosity than other types (Figure 7 and Table 6), which was consistent with previous findings.[40] To a large extent, the change in starch pasting properties and swelling power values was derived from the alteration of amylose/amylopectin ratio, and low amylose content usually caused high swelling power value, high peak pasting viscosity, and low peak temperature.[4,40,41] The differences in starch properties presented in this study were consistent with the differences in amylose content.

**Table 4. Difference in Starch Properties between HP I-4 and HP II-4[a]**

| type | no. of accessions | AC[b] (%) | SP[c] | PT[c] (°C) | TTP[c] (min) | PV[c] (BU) | PVT[b] (°C) | FV[b] (BU) | BD[b] (BU) | SB[b] (BU) |
|---|---|---|---|---|---|---|---|---|---|---|
| HP I-4 | 13 | 32.70 ± 0.94 | 13.53 ± 0.74 | 73.15 ± 1.27 | 6.20 ± 0.10 | 584.95 ± 13.70 | 92.59 ± 0.14 | 751.60 ± 13.13 | 164.10 ± 10.56 | 330.75 ± 7.04 |
| HP II-4 | 9 | 27.75 ± 1.46 | 16.00 ± 0.49 | 68.39 ± 4.91 | 5.68 ± 0.03 | 660.00 ± 10.54 | 91.20 ± 0.19 | 674.71 ± 15.13 | 263.14 ± 5.52 | 277.86 ± 8.16 |

[a]AC, amylose content; SP, swelling power; PT, pasting temperature; TTP, time to peak viscosity; PV, peak viscosity; PVT, peak viscosity temperature; FV, final viscosity; BD, breakdown viscosity; SB, setback viscosity. [b]Difference is significant at the 0.01 level. [c]Difference is significant at the 0.05 level.


dx.doi.org/10.1021/jf5026746 | J. Agric. Food Chem. 2014, 62, 11369−11385

Table 5. Difference in Starch Properties between the *Waxy* I and *Waxy* II DNA Groups[a]

| group | no. of accessions | AC[b] (%) | SP[b] | PT[b] (°C) | TTP[b] (min) | PV[b] (BU) | PVT[c] (°C) | TV[b] (BU) | FV[c] (BU) | BD[c] (BU) | SB[c] (BU) |
|---|---|---|---|---|---|---|---|---|---|---|---|
| *Waxy* I | 19 | 32.29 ± 0.96 | 13.48 ± 0.67 | 73.86 ± 1.10 | 6.31 ± 0.10 | 573.67 ± 61.41 | 92.50 ± 0.13 | 421.38 ± 6.42 | 752.54 ± 11.69 | 152.30 ± 10.45 | 331.17 ± 6.45 |
| *Waxy* II | 15 | 27.96 ± 1.30 | 15.75 ± 0.50 | 70.02 ± 1.30 | 5.82 ± 0.09 | 632.06 ± 67.47 | 91.33 ± 0.17 | 387.72 ± 9.59 | 659.94 ± 16.45 | 244.33 ± 13.14 | 272.22 ± 9.50 |

[a]AC, amylose content; SP, swelling power; PT, pasting temperature; TTP, time to peak viscosity; PV, peak viscosity; PVT, peak viscosity temperature; TV, trough viscosity; FV, final viscosity; BD, breakdown viscosity; SB, setback viscosity. Three amylose-free or low-amylose accessions, Z1191 (HP I-5), Z999 (HP II-2), Z1979 (HP I-3), were not included. [b]Difference is significant at the 0.05 level. [c]Difference is significant at the 0.01 level.

## DISCUSSION

**Wide Variations of DNA Sequences of the *Waxy* Alleles Have Different Effects on Amylose Content in Barley.** Tibet is the center of Oriental barley,[42] and barley accessions collected from QTB are indeed highly variable.[27,43,44] In this study, a total of 116 polymorphic sites were identified from the *Waxy* genes of the 34 barley accessions. Particularly, 39 new nucleotide variations were found for the first time. For example, a 187 bp instead of a 191 bp insertion was found in intron 1 of HP I-1 and HP I-2 haplotypes, and three SNPs were found in HP 1-6 (Z1337), resulting in two amino acid residue alterations within the mature protein region. All accessions were obviously divided into two DNA groups or 11 haplotypes according to the sequence differences. These results indicate that the *Waxy* genes from different hull-less barley accessions from QTB are highly variable in genetic backgrounds, which may be a major factor responsible for the wide range of amylose content of QTB barley accessions used in this study. Although the deficiency of SSIIa or SBE activity has also been proven to greatly elevate the amylose content of the induced cereal crop grains,[2,4,8,45] SSIIa and SBE were not candidate enzymes in the determination of amylose content change for those 34 barley accessions because no obvious changes in the intensity of SSIIa and SBE on the SDS-PAGE gel were observed in our work. Extensive genetic diversity of the *Waxy* gene may be due to the wide range of geographic origin of these accessions as well as the low level of domestic selection of these indigenous barley accessions. Due to the wide variations of the *Waxy* gene nucleotide sequences, significant differences in the expression of *Waxy* gene transcripts and GBSS I proteins and in some starch properties were observed among different *Waxy* DNA groups or haplotypes. The *Waxy* I DNA group had an average transcript level significantly higher than that of the *Waxy* II DNA group and had significantly different starch properties. HP I-5 with a SNP, a T for $C^{2453}$ change in the fifth exon, presented very low transcript level and undetectable GBSS I protein on SDS-PAGE gel and the amylose-free type. HP II-2 with a T for $G^{3935}$ change in the 10th exon, had relatively high transcript level and normal GBSS I protein level on the SDS-PAGE gel, but showed no amylose content. HP I-3 with a 403 bp deletion gave an extremely low level of *Waxy* transcript, undetectable GBSS I protein, and low amylose content. These differences in the amylose content correspond to the variation of the *Waxy* gene at the nucleotide level. The changes of nucleotides in the coding and noncoding regions greatly influence the expression of the *Waxy* gene.

**Effect of Polymorphic Sites in the Coding Region on the Function of *Waxy* Gene.** Four amino acid alterations were identified in the mature protein region of the *Waxy* protein due to five SNPs. One SNP, a T for $G^{3935}$ in the 10th exon, was identified only in Z999 (HP II-2) and resulted in the change of $Gly^{513}$ to Trp in the mature region of GBSS I protein and was the only difference of both nucleotides and deduced amino acids of *Waxy* gene between HP II-1 and II-2. However, the expression of *Waxy* gene and starch properties of Z999 (HP II-2) presented significant differences from that of HP II-1. The level of transcript and GBSS I protein in accession Z999 was obviously higher than that of HP II-1. Interestingly, accession Z999 with high GBSS I protein level displayed amylose-free phenotype and the resulting special starch pasting characteristics, whereas HP II-1 showed normal transcription, amylose content, and starch properties. The 513th Gly was located in

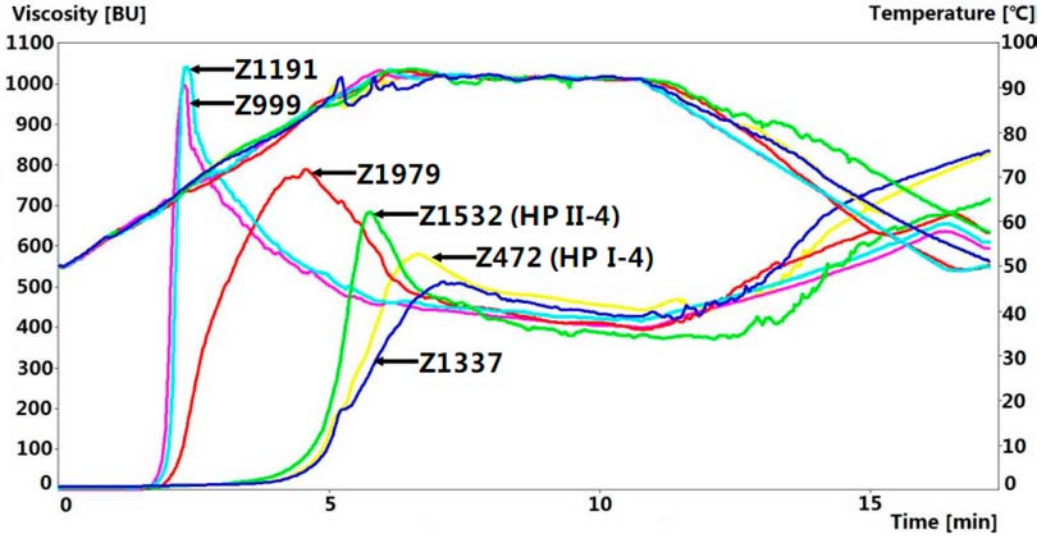


**Figure 7.** Starch pasting profiles of selected barley accessions. Z1191 (HP 1-5) and Z999 (HP 2-2) are amylose-free barley, Z1979 (HP 1-3) is a low-amylose barley, Z1337 (HP I-6) contains two amino acid mutations in the mature protein region. Z1532 (HP II-4) and Z472 (HP I-4) are used as controls due to their normal starch properties compared with anylose-free or low-amylose ones.

the conserved glycosyltranferase domain (GT-1) that transfers UDP-, ADP-, GDP-, or CMP-linked sugars to fructose-6-phosphate, glycogen, and many other substrates.[46] The 513th Gly was not located within the region of conserved motifs I–VIII or not involved in the formation of $\alpha$-helices and $\beta$-sheets.[46] However, multiple alignment analysis found the 513th Gly was highly conserved in GBSS I proteins of cereal crops and even in glycogen synthases of various bacteria. Therefore, a single amino acid residue substitution may completely deactivate the function of the GBSS I protein, which causes amylose-free characteristics. This demonstrates that the 513th Gly may be a very critical site for maintaining the functional activity of the GBSS I protein. The similar high expression pattern of the *Waxy* gene coexisting with no amylose characteristic was also reported in another amylose-free barley cultivar, CDC Alamo,[47] which contained the substitution of Val for the 287th Asp, an essential conserved amino acid in the conserved starch catalytic domain (GT-5) within the catalytic core, which was found in many starch synthases and glycosyltransferases that use only ADPglucose as substrate.[46,47] Moreover, the 287th Asp participates in the formation of 380s loop,[48,49] which was important in determining the specificity of many starch synthases.[46] However, it is still hard to explain why a single amino acid change occurring in these two special sites would increase the transcript level to a large extent. Possibly, the enhancers located further upstream of the *Waxy* gene or other genes affect the transcription of the *Waxy* gene.

The other SNP alteration of $C^{2453}$ to T in the fifth exon was detected in accession Z1191 (HP I-5). This SNP was also the only difference between accessions HP I-5 and HP I-4 that was one of the major haplotypes of QTB hull-less barley, but the expression level of *Waxy* transcript and amylose content of Z1191 (HP I-5) was almost undetected, whereas HP I-4 presented a much higher mRNA transcript level and amylose content. These results indicate the alteration of $C^{2453}$ to T in the fifth exon of barley *Waxy* gene can greatly affect the function of the *Waxy* gene. Actually, the same SNP mutation was earlier reported in barley cultivars SH97 and Yon M Kei.[20,22] Similarly, both of them also presented undetectable GBSS I protein and amylose-free characteristics. The alteration of $C^{2453}$ to T in the fifth exon of barley *Waxy* gene brings about a pre-existing terminator in extending the polypeptide chain and probably results in premature termination of the GBSS I protein or limits the combination of amyloplast to incomplete peptide, thus blocking amylose synthesis. However, Yon M Kei showed slightly normal transcript level,[22] which was inconsistent with the result of HP I-5 haplotype. We aligned the *Waxy* gene sequences from these two accessions and found they were not completely identical. Therefore, other base alterations in the *Waxy* sequence may cause different levels of transcription, or different genetic background changed the mRNA expression profiles even if both of them contained the same critical mutation site.

In this study, another three SNPs were identified for the first time, and all of them were located in the seventh exon of Z1337 (HP I-6), an indigenous hull-less QTB barley. The three SNPs resulted in Leu and Arg instead of the 321st Pro and the 335th Cys. The two substituted residues were located in the starch catalytic domain (GT-5) within the catalytic core, and the 321st Pro was in motif II and located between an $\alpha$-helix and a $\beta$-sheet.[46] Both the 321st Pro and the 335th Cys were very conserved in most cereal crops. Except for the lowest breakdown value of starch viscosity and higher peak time, Z1337 showed no obvious changes for the transcription of the *Waxy* gene, GBSS I protein level, and most of the starch properties. This indicates that the change of these amino acid residues has little effect on the function of *Waxy* gene.

High conservation in the mature region of the *Waxy* protein is essential for ensuring the normal function of the GBSS I protein. Compared with only 4 amino acid alterations in the mature protein region, a total of 11 mutations were found in the transit peptide. In particular, a 15 bp insertion in the second exon resulted in five additional residues in the transit peptides, which classified barley accessions in this study into Wx A1, Wx A2, Wx B1, and Wx B2 protein groups. Significant difference in GBSS I protein level among Wx A1, Wx A2, Wx B1, and Wx B2 protein groups (except for a few accessions) could not be observed visually on SDS-PAGE gel, but transcript level and starch properties of Wx A1, Wx A2, Wx B1, and Wx B2 protein groups displayed significant differences. Therefore, it was

Table 6. Difference in Starch Properties among Four Special Accessions and Normal Barley Accessions[a]

| type | AC (%) | SP | PT (°C) | TTP (min) | PV (BU) | PVT (°C) | TV (BU) | FV (BU) | BD (BU) | SB (BU) |
|---|---|---|---|---|---|---|---|---|---|---|
| Z1191 (HP I-5) | 0 ± 0.15 | 20.01 ± 0.85 | 61.50 ± 0.54 | 2.37 ± 0.11 | 1042.00 ± 33.27 | 67.5 ± 0.57 | 402.00 ± 14.27 | 649.00 ± 17.83 | 622.00 ± 13.77 | 229.00 ± 15.24 |
| Z999 (HP II-2) | 0 ± 0.08 | 20.79 ± 0.79 | 62.20 ± 0.52 | 2.3 ± 0.08 | 995.00 ± 25.91 | 67.1 ± 0.51 | 401.00 ± 12.72 | 632.00 ± 21.60 | 594.00 ± 19.46 | 231.00 ± 16.41 |
| Z1979 (HP I-3) | 6.63 ± 0.18 | 21.03 ± 0.68 | 63.20 ± 0.61 | 4.57 ± 0.15 | 790.00 ± 26.35 | 83.7 ± 0.66 | 398.00 ± 12.24 | 664.00 ± 15.90 | 392.00 ± 11.46 | 266.00 ± 14.27 |
| Z1337 (HP I-6) | 33.76 ± 0.05 | 17.65 ± 0.58 | 77.65 ± 0.63 | 7.00 ± 0.14 | 519.00 ± 8.49 | 92.55 ± 0.21 | 440.00 ± 16.97 | 804.50 ± 20.51 | 79.00 ± 8.49 | 364.50 ± 3.53 |
| Z472 (HPI-4) | 32.30 ± 0.10 | 11.52 ± 0.34 | 74.50 ± 1.69 | 6.60 ± 0.00 | 573.00 ± 2.83 | 92.80 ± 0.29 | 435.00 ± 14.14 | 748.50 ± 7.78 | 138.00 ± 16.97 | 313.50 ± 6.36 |
| Z1532 (HP II-4) | 27.23 ± 0.08 | 16.97 ± 0.55 | 75.05 ± 0.50 | 5.77 ± 0.07 | 679.00 ± 5.66 | 91.50 ± 0.14 | 385.00 ± 9.90 | 684.50 ± 14.85 | 294.00. ± 15.56 | 259.50 ± 4.95 |

[a]AC, amylose content; SP, swelling power; PT, pasting temperature; TTP, time to peak viscosity; PV, peak viscosity; PVT, peak temperature; TV, trough viscosity; FV, final viscosity; BD, breakdown viscosity; SB, setback viscosity. Z472 (HPI-4) and Z1532 (HP II-4) were served as control, here we defined them as normal types because of their common starch properties.

thought that the 15 bp insertion might have an impact on GBSS I protein level and starch properties.

**Effect of Polymorphic Sites in Noncoding Region on the Function of Barley *Waxy* Gene.** The effects of variations in the noncoding region on gene expression have attracted more and more attention. Especially, the variations in the 5′UTR usually play an important role in the transcription level. A number of cis-acting DNA regulatory elements and trans-acting protein impacting transcription have been characterized in the 5′UTR of the *Waxy* gene.[50−58] Fragment deletion or just a single SNP could disturb the combination of cis-acting motif and protein and, thus, drastically influence the expression level of transcripts. It has been reported that a large deletion in the 5′UTR had a negative effect on the transcription of the *Waxy* gene. For example, a 140 bp deletion in 5′UTR of the *Waxy* gene significantly decreased the transcript level, GBSS I activity, and amylose content in potato.[59] In this study, a total of 84 polymorphic sites were found in the noncoding region, making up nearly 77% of all polymorphisms. First, we analyzed the effect of two large fragment deletions on the function of the *Waxy* gene. The 403 bp deletion in 5′UTR was found in accession Z1979 (HP I-3), including the transcription start site, TATA box, exon 1 and partial intron 1. Z1979 also had low transcript level, low GBSS I protein content and low amylose content, which was consistent with previous studies. This suggests that the large deletion in the 5′UTR negatively affects transcription of the *Waxy* gene. It was further found that there might be up to about 100 cis-acting regulatory DNA elements in the 403 bp deleted fragment, many of which are involved in seed-specific regulation and light responsiveness.[24]

All accessions in this study were divided into two *Waxy* DNA groups mainly according to the 191 bp insertion in intron 1 within the 5′UTR: the *Waxy* I DNA group containing such an insertion and the *Waxy* II DNA group without the corresponding insertion. The average transcript level of the *Waxy* I DNA group (or haplotype I-4) was significantly higher than that of the *Waxy* II DNA group (or haplotype II-4), and the amylose content of the *Waxy* I DNA group (or haplotype I-4) was significantly higher than that of the *Waxy* II DNA group (or haplotype II-4). This result indicates that the 191 bp insertion probably has a positive effect on the function of barley *Waxy* gene. It has been reported that cis-acting motifs in the first intron within the 5′UTR of rice *Waxy* gene usually play a positive role in the transcript level.[60] A total of 49 additional putative cis-acting motifs were found in the 191 bp insertion, most of them involved in light responsiveness and stress tolerance and some responsible for embryo-specific expression.[24] Therefore, these additional cis-acting motifs might have positive effects on enhancing the *Waxy* gene transcription, which finally affects amylose content, swelling power, and starch pasting characteristics of hull-less barley. The insertion of approximately 190 bp has been reported previously; however, its role was always neglected due to two possible reasons. First, this insertion was found in both waxy and wild phenotypes, which make its role less obvious. Second, it was difficult to assess its role when the studies were carried out on only several barley accessions.[20,22] Our study investigated a population of 34 barley accessions and breeding lines, making it possible to compare the groups with a number of accessions having the presence/absence of the 191 bp fragment.

Besides such large fragments as 403 bp or 191 bp INDELs, some other SNPs, SSRs, and short INDELs were found in 5′UTR, which may affect DNA regulatory elements, which

finally affect the function of barley *Waxy* gene. HP I-1, I-2, II-1, and II-3 expressed relatively low transcript level, possibly due to the lack of seven or eight putative RYREPEAT elements that were conserved in many seed-specific promoters. It has been reported that increasing the copy number of a cis-acting element likely improved the gene expression level.[61,62] Therefore, the reduction of RYREPEAT copies was probably relevant to the decrease in *Waxy* gene expression. Likewise, the transcript level of HP II-5 was much lower than the average transcript level of the HP II-4 haplotype, probably because HP II-5 lacked the putative SORLIP5AT, which was involved in light responsiveness, due to the single base difference.

**Effect of GBSS I on the Starch Properties of Hull-less Barley from QTB.** This study particularly indicates that the specific variations of the *Waxy* genes of hull-less barley from Qinghai-Tibet play an important role on amylose synthesis, and the starch properties are strongly influenced by the change of amylose content. Actually, starch biosynthesis and the resulting starch properties are influenced by multiple concerted biosynthetic enzymes, rather than a single biosynthetic enzyme. Amylose contents in cereal grains were not only changed by the *Waxy* gene but also highly elevated when the activity of SBE or SSIIa was drastically reduced.[2,4,8,45] However, to our knowledge, in a normal case, when other starch biosynthetic enzymes do not suffer from significant change, GBSS I is the main target enzyme responsible for amylose formation.[9−13,63] As the genes encoding those starch biosynthetic enzymes locate on different chromosomes in cereals, it is unlikely that the changed activities of those enzymes cosegregated with the *Waxy* gene in a large population. In this study, the hull-less population was mainly composed of indigenous varieties or breeding lines through crossing among indigenous varieties, so GBSS I should be the target enzyme controlling amylose content.

Except for the amylose content, starch properties were also modified with the alteration of amylopectin properties.[64] The high percentage of long chains (degree of polymerization > 35) in amylopectin displayed elevated swelling power.[65] GBSS I was also thought to be responsible for the synthesis of the extra-long-chain fraction of amylopectin.[14,15] However, previous studies on waxy rice and wheat showed that when GBSS I was deactivated, carbon was mainly allocated to amylopectin, and thus low-amylose or amylose-free mutants were produced, whereas no significant changes were observed for chain length distribution of amylopectin and starch granules.[14,66−68] Therefore, it is indicated that amylose content change might be the main cause of alterations in starch properties of the accessions in this study.

## AUTHOR INFORMATION


### Corresponding Authors

*(Z.P.) E-mail: Panzf@cib.ac.cn.

*(M.Y.) E-mail: Yumq@cib.ac.cn.



### Funding

This work was financially supported by the National Natural Science Foundation of China (31101150), West Light Foundation of the Chinese Academy of Sciences, and the National Science and Technology Supporting Programs of China (2012BAD03B01).


### Notes

The authors declare no competing financial interest.

## REFERENCES


(1) Clarke, B.; Liang, R.; Morell, M. K.; Bird, A. R.; Jenkins, C. L.; Li, Z. Y. Gene expression in a starch synthase IIa mutant of barley: changes in the level of gene transcription and grain composition. *Funct. Integr. Genomics* **2008**, *8*, 211−221.

(2) Morell, M. K.; Kosar-Hashemi, B.; Cmiel, M.; Samuel, M. S.; Chandler, P.; Rahman, S.; Buleon, A.; Batey, I. L.; Li, Z. Y. Barley *sex6* mutants lack starch synthase IIa activity and contain a starch with novel properties. *Plant J.* **2003**, *34*, 173−185.

(3) Bird, A. R.; Flory, C.; Davies, D. A.; Usher, S.; Topping, D. L. A novel barley cultivar (Himalaya 292) with a specific gene mutation in starch synthase IIa raises large bowel starch and short-chain fatty acids in rats. *J. Nutr.* **2004**, *134*, 831−835.

(4) Carciofi, M.; Blennow, A.; Jensen, S. L.; Shaik, S. S.; Henriksen, A.; Buléon, A.; Holm, P. B.; Hebelstrup, K. H. Concerted suppression of all starch branching enzyme genes in barley produces amylose-only starch granules. *BMC Plant Biol.* **2012**, *12*, 223.

(5) Fredriksson, H.; Silverio, J.; Andersson, R.; Eliasson, A.-C.; Åman, P. The influence of amylose and amylopectin characteristics on gelatinization and retrogradation properties of different starches. *Carbohydr. Polym.* **1998**, *35*, 119−134.

(6) Yamamori, M.; Quynh, N. T. Differential effects of Wx-A1, -B1 and -D1 protein deficiencies on apparent amylose content and starch pasting properties in common wheat. *Theor. Appl. Genet.* **2000**, *100*, 32−38.

(7) Konik-Rose, C.; Thistleton, J.; Chanvrier, H.; Tan, I.; Halley, P.; Gidley, M.; Kosar-Hashemi, B.; Wang, H.; Larroque, O.; Ikea, J. Effects of starch synthase IIa gene dosage on grain, protein and starch in endosperm of wheat. *Theor. Appl. Genet.* **2007**, *115*, 1053−1065.

(8) Regina, A.; Bird, A.; Topping, D.; Bowden, S.; Freeman, J.; Barsby, T.; Kosar-Hashemi, B.; Li, Z. Y.; Rahman, S.; Morell, M. High-amylose wheat generated by RNA interference improves indices of large-bowel health in rats. *Proc. Natl. Acad. Sci. U.S.A.* **2006**, *103*, 3546−3451.

(9) Nakamura, T.; Yamamori, M.; Hirano, H.; Hidaka, S. Decrease of waxy (Wx) protein in two common wheat cultivars with low amylose content. *Plant Breed.* **1993**, *111*, 99−105.

(10) Denyer, K.; Johnson, P.; Zeeman, S.; Smith, A. M. The control of amylose synthesis. *J. Plant Physiol.* **2001**, *158*, 479−487.

(11) Nelson, O. E.; Rines, H. W. The enzymatic deficiency in the waxy mutant of maize. *Biochem. Biophys. Res. Commun.* **1962**, *9*, 297−300.

(12) Wang, Z. Y.; Zheng, F. Q.; Shen, G. Z.; Gao, J. P.; Snustad, D. P.; Li, M. G.; Zhang, J. L.; Hong, M. M. The amylose content in rice endosperm is related to the post-transcriptional regulation of the Waxy gene. *Plant J.* **1995**, *7*, 613−622.

(13) Yanagisawa, T.; Kiribuchi-Otobe, C.; Yoshida, H. An alanine to threonine change in the Wx-D1 protein reduces GBSS I activity in waxy mutant wheat. *Euphytica* **2001**, *121*, 209−214.

(14) Hanashiro, I.; Itoh, K.; Kuratomi, Y.; Yamazaki, M.; Igarashi, T.; Matsugasako, J.; Takeda, Y. Granule-bound starch synthase I is responsible for biosynthesis of extra-long unit chains of amylopectin in rice. *Plant Cell Physiol.* **2008**, *49*, 925−933.

(15) Ral, J. P.; Colleoni, C.; Wattebled, F.; Dauvillee, D.; Nempont, C.; Deschamps, P.; Li, Z.; Morell, M. K.; Chibbar, R.; Purton, S.; d'Hulst, C.; Ball, S. G. Circadian clock regulation of starch metabolism establishes GBSS I as a major contributor to amylopectin synthesis in *Chlamydomonas reinhardtii*. *Plant Physiol.* **2006**, *142*, 305−317.

(16) Hanyu, Y.; Jiang, H.; Blanco, M.; Jane, J. L. Characterization of normal and waxy corn starch for bioethanol production. *J. Agric. Food Chem.* **2012**, *61*, 379−386.

(17) Ibáñez, A. M.; Wood, D. F.; Yokoyama, W. H.; Park, I.; Tinoco, M. A.; Hudson, C. A.; McKenzie, K. S.; Shoemaker, C. F. Viscoelastic properties of waxy and nonwaxy rice flours, their fat and protein-free starch, and the microstructure of their cooked kernels. *J. Agric. Food Chem.* **2007**, *55*, 6761−6771.

(18) Sang, Y.; Bean, S.; Seib, P. A.; Pedersen, J.; Shi, Y.-C. Structure and functional properties of sorghum starches differing in amylose content. *J. Agric. Food Chem.* **2008**, *56*, 6680−6685.

(19) Rohde, W.; Becker, D.; Salamini, F. Structural analysis of the waxy locus from *Hordeum vulgare*. *Nucleic Acids Res.* **1988**, *16*, 7185−7185.
(20) Domon, E.; Saito, A.; Takeda, K. Comparison of the *waxy* locus sequence from a non-waxy strain and two waxy mutants of spontaneous and artificial origins in barley. *Genes Genet. Syst.* **2002**, *77*, 351−360.
(21) Domon, E.; Fuijita, M.; Ishikawa, N. The insertion/deletion polymorphisms in the *waxy* gene of barley genetic resources from East Asia. *Theor. Appl. Genet.* **2002**, *104*, 132−138.
(22) Patron, N. J.; Smith, A. M.; Fahy, B. F.; Hylton, C. M.; Naldrett, M. J.; Rossnagel, B. G.; Denyer, K. The altered pattern of amylose accumulation in the endosperm of low-amylose barley cultivars is attributable to a single mutant allele of granule-bound starch synthase I with a deletion in the 5′-non-coding region. *Plant Physiol.* **2002**, *130*, 190−198.
(23) Ma, J.; Jiang, Q. T.; Wei, Y. M.; Andre, L.; Lu, Z. X.; Chen, G. Y.; Liu, Y. X.; Zheng, Y. L. Molecular characterization and comparative analysis of two waxy alleles in barley. *Genes Genomics* **2010**, *32*, 513−520.
(24) Ma, J.; Jiang, Q. T.; Zhao, Q. Z.; Zhao, S.; Lan, X. J.; Dai, S. F.; Lu, Z. X.; Liu, C. J.; Wei, Y. M.; Zheng, Y. L. Characterization and expression analysis of waxy alleles in barley accessions. *Genetica* **2013**, *141*, 227−238.
(25) Asare, E. K.; Baga, M.; Rossnagel, B. G.; Chibbar, R. N. Polymorphism in the barley granule bound starch synthase 1 (gbss1) gene associated with grain starch variant amylose concentration. *J. Agric. Food Chem.* **2012**, *60*, 10082−10092.
(26) Zhu, C. M.; Zhang, J. Single nucleotide polymorphism of Wx gene associated with amylose content in barley germplasm. *Sci. Agric. Sinica* **2010**, *43*, 889−898.
(27) Pan, Z.; Deng, G.; Zhai, X.; Wu, F.; Yu, M. Genetic diversity of Acid-PAGE monomeric prolamins in cultivated hulless barley (*Hordeum vulgare* L.) from Qinghai−Tibet plateau in China. *Genet. Res. Crop Evol.* **2007**, *54*, 1691−1699.
(28) Wood, P. J. Relationships between solution properties of cereal $\beta$-glucans and physiological effects − a review. *Trends Food Sci. Technol.* **2004**, *15*, 313−320.
(29) Foster-Powell, K.; Holt, S. H.; Brand-Miller, J. C. International table of glycemic index and glycemic load values: 2002. *Am. J. Clin. Nutr.* **2002**, *76*, 5−56.
(30) Dickin, E.; Steele, K.; Edwards-Jones, G.; Wright, D. Agronomic diversity of naked barley (*Hordeum vulgare* L.): a potential resource for breeding new food barley for Europe. *Euphytica* **2012**, *184*, 85−99.
(31) Morrison, W.; Milligan, T.; Azudin, M. A relationship between the amylose and lipid contents of starches from diploid cereals. *J. Cereal Sci.* **1984**, *2*, 257−271.
(32) Konik-Rose, C. M.; Moss, R.; Rahman, S.; Appels, R.; Stoddard, F.; McMaster, G.; Li, Z. Y. Evaluation of the 40 mg swelling test for measuring starch functionality. *Starch/Staerke* **2001**, *53*, 14−20.
(33) Wang, G. L. *Principle of Plant Gene Engineering*; Science Press: Beijing, China, 1997.
(34) Liang, J. J.; Deng, G. B.; Long, H.; Pan, Z. F.; Wang, C. P.; Cai, P.; Xu, D. L.; Nima, Z. X.; Yu, M. Q. Virus-induced silencing of genes encoding LEA protein in Tibetan hulless barley (*Hordeum vulgare* ssp. *vulgare*) and their relationship to drought tolerance. *Mol. Breed.* **2012**, *30*, 441−451.
(35) Pan, Z. F.; Deng, G. B.; Wang, T.; Yu, M. Q. An improved 1D-SDS-PAGE method for identification of wheat Waxy protein. *Chinese J. Appl. Environ. Biol.* **2000**, *6*, 487−489.
(36) Yamamori, M.; Endo, T. R. Variation of starch granule proteins and chromosome mapping of their coding genes in common wheat. *Theor. Appl. Genet.* **1996**, *93*, 275−281.
(37) Lescot, M.; Déhais, P.; Thijs, G.; Marchal, K.; Moreau, Y.; Van de Peer, Y.; Rouzé, P.; Rombauts, S. PlantCARE, a database of plant cis-acting regulatory elements and a portal to tools for in silico analysis of promoter sequences. *Nucleic Acids Res.* **2002**, *30*, 325−327.
(38) Higo, K.; Ugawa, Y.; Iwamoto, M.; Korenaga, T. Plant cis-acting regulatory DNA elements (PLACE) database: 1999. *Nucleic Acids Res.* **1999**, *27*, 297−300.
(39) Bäumlein, H.; Villarroel, R.; Inzé, D.; Wobus, U. Cis-analysis of a seed protein gene promoter: the conservative RY repeat CATGCATG within the legumin box is essential for tissue-specific expression of a legumin gene. *Plant J.* **1992**, *2*, 233−239.
(40) Blazek, J.; Copeland, L. Pasting and swelling properties of wheat flour and starch in relation to amylose content. *Carbohydr. Polym.* **2008**, *71*, 380−387.
(41) Gujral, H. S.; Sharma, P.; Kaur, H.; Singh, J. Physiochemical, pasting, and thermal properties of starch isolated from different barley cultivars. *Int. J. Food Prop.* **2013**, *16*, 1494−1506.
(42) Zhang, Q.; Maroof, M. S.; Yang, P. Ribosomal DNA polymorphisms and the Oriental-Occidental genetic differentiation in cultivated barley. *Theor. Appl. Genet.* **1992**, *84*, 682−687.
(43) Yang, P.; Liu, X. J.; Liu, X. C.; Yang, W. Y.; Feng, Z. Y. Diversity analysis of the developed qingke (hulless barley) cultivars representing different growing regions of the Qinghai-Tibet Plateau in China using sequence-related amplified polymorphism (SRAP) markers. *Afr. J. Biotechnol.* **2010**, *9*, 8530−8538.
(44) Wang, C. P.; Pan, Z. F.; Nima, Z. X.; Tang, Y. W.; Cai, P.; Liang, J. J.; Deng, G. B.; Long, H.; Yu, M. Q. Starch granule-associated proteins of hull-less barley (*Hordeum vulgare* L.) from the Qinghai-Tibet Plateau in China. *J. Sci. Food Agric.* **2011**, *91*, 616−624.
(45) Regina, A.; Kosar-Hashemi, B.; Ling, S.; Li, Z. Y.; Rahman, S.; Morell, M. Control of starch branching in barley defined through differential RNAi suppression of starch branching enzyme IIa and IIb. *J. Exp. Bot.* **2010**, *61*, 1469−1482.
(46) Leterrier, M.; Holappa, L. D.; Broglie, K. E.; Beckles, D. M. Cloning, characterisation and comparative analysis of a starch synthase IV gene in wheat: functional and evolutionary implications. *BMC Plant Biol.* **2008**, *8*, 98.
(47) Tarbouriech, N.; Charnock, S. J.; Davies, G. J. Three-dimensional structures of the Mn and Mg dTDP complexes of the family GT-2 glycosyltransferase SpsA: a comparison with related NDP-sugar glycosyltransferases. *J. Mol. Biol.* **2001**, *314*, 655−661.
(48) Buschiazzo, A.; Ugalde, J. E.; Guerin, M. E.; Shepard, W.; Ugalde, R. A.; Alzari, P. M. Crystal structure of glycogen synthase: homologous enzymes catalyze glycogen synthesis and degradation. *EMBO J.* **2004**, *23*, 3196−3205.
(49) Busi, M. V.; Palopoli, N.; Valdez, H. A.; Fornasari, M. S.; Wayllace, N. Z.; Gomez-Casati, D. F.; Parisi, G.; Ugalde, R. A. Functional and structural characterization of the catalytic domain of the starch synthase III from *Arabidopsis thaliana*. *Proteins* **2008**, *70*, 31−40.
(50) Chen, L.; Wang, Z. Y. Nuclear protein binding sites in 5′-upstream region of the rice *Waxy* gene. *Acta Phytophysiol. Sinica* **1996**, *22*, 349−356.
(51) Yao, C. P.; Wang, Z. Y. Effects of 5′ upstream region deletion on rice *Waxy* gene expression. *Acta Phytophysiol. Sinica* **1996**, *22*, 431−436.
(52) Kreis, M. Structure and evolution of seed storage proteins and their genes with particular reference to those of wheat, barley and rye. *Oxford Surv. Plant Mol. Cell Biol.* **1985**, *2*, 253−317.
(53) Albani, D.; Hammond-Kosack, M.; Smith, C.; Conlan, S.; Colot, V.; Holdsworth, M.; Bevan, M. W. The wheat transcriptional activator SPA: a seed-specific bZIP protein that recognizes the GCN4-like motif in the bifactorial endosperm box of prolamin genes. *Plant Cell* **1997**, *9*, 171−184.
(54) Diaz, I.; Carbonero, P. Barley BLZ1: a bZIP transcriptional activator that interacts with endosperm-specific gene promoters. *Plant J.* **1998**, *13*, 629−640.
(55) Cheng, S. J.; Wang, Z. Y.; Hong, M. M. Rice bZIP protein, REB, interacts with GCN4 motif in promoter of *Waxy* gene. *Sci. China Ser. C: Life Sci.* **2002**, *45*, 352−360.
(56) Reidt, W.; Wohlfarth, T.; Ellerström, M.; Czihal, A.; Tewes, A.; Ezcurra, I.; Rask, L.; Bäumlein, H. Gene regulation during late

embryogenesis: the RY motif of maturation-specific gene promoters is a direct target of the FUS3 gene product. *Plant J.* **2000**, *21*, 401−408.
(57) Zhu, Y.; Cai, X. L.; Wang, Z. Y.; Hong, M. M. An interaction between a MYC protein and an EREBP protein is involved in transcriptional regulation of the rice Wx gene. *J. Biol. Chem.* **2003**, *278*, 47803−47811.
(58) Wang, J. C.; Xu, H.; Zhu, Y.; Liu, Q. Q.; Cai, X. L. OsbZIP58, a basic leucine zipper transcription factor, regulates starch biosynthesis in rice endosperm. *J. Exp. Bot.* **2013**, *64*, 3453−3466.
(59) Kluth, A.; Sprunck, S.; Becker, D.; Lörz, H.; Lütticke, S. 5′ deletion of a gbss1 promoter region from wheat leads to changes in tissue and developmental specificities. *Plant Mol. Biol.* **2002**, *49*, 665−678.
(60) Barrett, L. W.; Fletcher, S.; Wilton, S. D. Regulation of eukaryotic gene expression by the untranslated gene regions and other non-coding elements. *Cell. Mol. Life Sci.: CMLS* **2012**, *69*, 3613−3634.
(61) Rushton, P. J.; Reinstädler, A.; Lipka, V.; Lippok, B.; Somssich, I. E. Synthetic plant promoters containing defined regulatory elements provide novel insights into pathogen-and wound-induced signaling. *Plant Cell* **2002**, *14*, 749−762.
(62) Rogers, H.; Bate, N.; Combe, J.; Sullivan, J.; Sweetman, J.; Swan, C.; Lonsdale, D.; Twell, D. Functional analysis of cis-regulatory elements within the promoter of the tobacco late pollen gene g10. *Plant Mol. Biol.* **2001**, *45*, 577−585.
(63) Li, J. R.; Zhao, W.; Li, Q. Z.; Ye, X. G.; An, B. Y.; Li, X.; Zhang, X. RNA silencing of *waxy* gene results in low levels of amylose in the seeds of transgenic wheat (*Triticum aestivum* L.). *Acta Genet. Sinica* **2005**, *32*, 846−854.
(64) Tester, R. F.; Morrison, W. R. Swelling and gelatinisation of cereal starches. I. Effects of amylopectin, amylose and lipids. *Cereal Chem.* **1990**, *67*, 551−557.
(65) Sasaki, T.; Matsuki, J. Effect of wheat starch structure on swelling power. *Cereal Chem.* **1998**, *75*, 525−529.
(66) Kim, W.; Johnson, J. W.; Graybosch, R. A.; Gaine, C. S. Physicochemical properties and end-use quality of wheat starch as a function of waxy protein alleles. *J. Cereal Sci.* **2007**, *37*, 195−204.
(67) Miura, H.; Wickramasinghe, M. H. A.; Subasinghe, R. M.; Araki, E.; Komae, K. Development of near-isogenic lines of wheat carrying different null *Wx* alleles and their starch properties. *Euphytica* **2002**, *123*, 353−359.
(68) Zhang, M. Z.; Fang, J. H.; Yan, X.; Liu, J.; Bao, J. S.; Fransson, G.; Andersson, R.; Jansson, C.; Aman, P.; Sun, C. Molecular insights into how a deficiency of amylose affects carbon allocation − carbohydrate and oil analyses and gene expression profiling in the seeds of a rice waxy mutant. *BMC Plant Biol.* **2012**, *12*, 230.

## NOTE ADDED AFTER ASAP PUBLICATION

This article published November 7, 2014 with errors in the amino acids columns of Table 2. The corrected version posted November 14, 2014.

**Table 1. Fertilizer Treatments and Application Rates**

| | application rate | |
|---|---|---|
| treatments ($n$ = 3) | low dose (75 kg N ha$^{-1}$) | high dose (150 kg N ha$^{-1}$) |
| composted chicken manure | 18.7 g/pot (coded L−M) | 37.4 g/pot (coded H−M) |
| chemical fertilizer | urea 0.72 g, $Ca(H_2PO_4)_2{\cdot}H_2O$ 1.39 g, $K_2SO_4$ 0.33g/pot (coded L−C) | urea 1.45 g, $Ca(H_2PO_4)_2{\cdot}H_2O$ 2.78 g, $K_2SO_4$ 0.67 g/pot (coded H−C) |
| compost−chemical fertilizer (1:1) | chicken manure 9.35 g + urea 0.36 g, $Ca(H_2PO_4)_2{\cdot}H_2O$ 0.70 g, $K_2SO_4$ 0.16 g/pot (coded L−M+C) | chicken manure 18.7 g + urea 0.72 g, $Ca(H_2PO_4)_2{\cdot}H_2O$ 1.39 g, $K_2SO_4$ 0.33 g/pot (coded H−M+C) |
| control | no fertilizer application (coded CK) | |

had different N isotope ratios, with a range from −3.9‰ to 0.5‰ for synthetic fertilizers, 5.3‰ to 7.2‰ for animal manure, and 9.3‰ to 20.9‰ for compost manure,[12] and the mean value of $\delta^{15}$N was 0.2‰ for synthetic fertilizers and 8‰ for organic manure.[13] The $\delta^{15}$N value of plants is affected by many factors such as the timing of application and the chemical form of synthetic fertilizer,[14] form of manure,[15,16] growth stages,[14,17] and irrigation water.[13]

The $\delta^{15}$N values in different plants were significantly different between organic and conventional production and may vary with growth periods. The mean $\delta^{15}$N values of products from organic and conventional agriculture vary with mean values 8.1‰ and −0.1‰ for tomatoes, 7.6‰ and 2.9‰ for lettuces, and 5.1‰ and 4.7‰ for carrots.[18] The $\delta^{15}$N values of leaves and grains of maize grown with composted pig manure were also significantly ($P < 0.05$) higher than those grown with urea even after 70 days of growth,[14] and the $\delta^{15}$N of maize increased for urea or decreased for composted manure with time, probably because of isotope fractionation accompanied by N losses and an increased uptake of soil-derived N by the maize.[14] Cabbage treated with compost had a higher $\delta^{15}$N value (>9.0%) than that treated with urea (<1.0%). Further, specific $\delta^{15}$N signals of basal N inputs were detected in the outer parts of cabbage formed in the early growth stage, while those of additional N inputs were detected in the inner parts of cabbage formed in the latter growth stage.[19] Different parts of the plant also had different $\delta^{15}$N values, such as roots, stems, leaves, and grains for maize;[14] root, shoot, unpolished grain, and polished grain for rice;[20] and fruits and leaves for cucumber.[21] Thus, for these reasons it could be difficult to identify a certain value to discriminate organic food from conventional ones.

Although some reports indicated that the $\delta^{15}$N of vegetables or crops differed between organic and conventional agriculture, the conclusions were drawn either from the results of a single cultivating experiment for carrots, tomatoes, lettuces,[13,22,23] maize,[14] Chinese cabbage,[19,22] cabbage, and onions,[22] or from statistical data on commercial products such as paprika,[22] tomatoes,[18,22] lettuces, and carrots,[18] or from a crop rotation experiment for canola, barley, and wheat for four years[15] and lettuces, onions, and cabbages for three years.[24] Particularly, as far as we know, no study has been published on investigating the variations of the $\delta^{15}$N value of a single crop in different seasons.

The $\delta^{15}$N values between organic crops and conventional crops overlapped, most probably due to $^{15}$N enrichment of plant-available N derived from synthetic fertilizer through N loss via $NH_3$ volatilization and denitrification with time after fertilization in soil.[17,18,22,23] In our previous study, the overlapped $\delta^{15}$N values were observed in *Brassica campestris* with combined application of organic and synthetic fertilizers.[17] Some reports drew a conclusion that $^{15}$N isotope analysis could only be used to determine whether chemical fertilizer had been singly applied.[18,23] The chemical fertilizer combined with composted manure as the basal application was very common in practice, but there are relatively limited reports on the application of $^{15}$N isotope analysis to identify the use of synthetic fertilizers in organic farming, so the $^{15}$N technique is worth being further studied under the fact that there are currently no other better and reliable techniques available.

Because of the increasing demand on food in China, natural soils such as pasture and forest are converting to agricultural soils. Up to now, most of the relevant studies have been conducted with agricultural soils cultivated for a long time with chemical fertilization, which may have severe effects on the $\delta^{15}$N of plants. It is very common for conventional agriculture to apply chemical fertilizer and composted manure as basal fertilizer, which could increase the $\delta^{15}$N of plant.[17] It is difficult to discriminate if a vegetable with a high $\delta^{15}$N value was really organic, because chemical fertilizer could be used during 2 years of organic conversion. Through a well-schemed experiment, the purpose of this study is to investigate the dynamics of the $\delta^{15}$N value in a single crop with Chinese cabbage (*B. chinensis*) in different seasons with different fertilizer treatments in an uncultivated soil. This result would explore the potential of applying $^{15}$N isotope analysis to discriminate the authenticity of organic food, and further contribute to the $\delta^{15}$N database developed.

## MATERIALS AND METHODS

**Soil and Fertilizers.** A brown soil without any fertilization history was collected from a site of Laoshan Mountain, China (120°53′13″ E, 36°22′10″ N), with temperate marine climate. The soil has a pH in distilled water (1:1) of 6.8, soil organic matter of 7.4 g kg$^{-1}$, total N of 0.676 g kg$^{-1}$, available N of 65.4 mg kg$^{-1}$, available P of 8.9 mg kg$^{-1}$, available K of 75.0 mg kg$^{-1}$, and a total $\delta^{15}$N value of 6.9‰. Because there is no available standard for NPK content evaluation in organic soil in China, instead we referred to the Green food standard−Environmental quality for production area issued by Ministry of Agriculture, China, for the evaluation.[28] The result showed that the NPK content of the soil is low (high, median, and low).

Two types of fertilizer were chosen for this experiment. The organic fertilizer was chicken manure with high-temperature compost treatment (total N of 20.4 g kg$^{-1}$, $P_2O_5$ of 40.0 g kg$^{-1}$, $K_2O$ of 24 g kg$^{-1}$, $\delta^{15}$N of 13.0‰). The chemical fertilizers contained urea (total N of 460 g kg$^{-1}$, $\delta^{15}$N of −1.2‰), calcium superphosphate ($P_2O_5$ of 120 g kg$^{-1}$) and potassium sulfate ($K_2O$ of 500 g kg$^{-1}$).

**Pot Experiment.** A pot experiment with *B. chinensis*, which has a short and fast growing period and can be planted for 2−3 seasons with continual harvest during its entire growing process, was successively conducted in the spring of 2011, the autumn of 2011,and the spring of 2012 at an erimental field of Qingdao Academy of Agricultural Sciences, China. Three treatments with two levels were conducted: for organic treatment, composted chicken manure (code L−M for low dose and H−M for high dose); for chemical treatment, urea application combined with calcium superphosphate and potassium sulfate (N/P/K = 2:1:1) (code L−C for low dose and H−C for high

dose); for compost−chemical treatment, equal parts organic N, chemical N, and potassium sulfate (code L−M+C for low dose and H−M+C for high dose). The control was given no additional fertilizer (code CK). Fertilizer applications equivalent to 75 and 150 kg N $ha^{-1}$ were made for each fertilizer type. Three treatments were employed in a completely randomized factorial design in triplicate.

The spring experiments of 2011 and 2012 were conducted according to the application rates shown in Table 1. After the spring experiment, the autumn experiment of 2011 was conducted in the same pot without any further application to explore the effect of previously added fertilizer in the soil. The soil was air-dried and griddled through a 50 mm sieve, and then 10 kg was thoroughly mixed with fertilizer as a basal application then placed into each plastic pot (200 mm bottom diameter × 300 mm top diameter × 220 mm height, ∼44 L in volume). Sixty-three pots were prepared 5 days before the spring and autumn experiments of 2011 and the spring experiment of 2012, and 20 seeds were planted in each pot on May 23 and August 25, 2011, and May 8, 2012. During the experiment, the vegetables were watered on demand with tap water containing $NO_3^-$ of 33.0 mg $L^{-1}$.

**Sample Collection and Preparation.** Composted chicken manure sample and chemical fertilizer sample were taken before the start of the experiment. The above-ground parts of *B. chinensis* of each treatment were sampled from three pots at the seedling stage (∼20 plants per pot), middle stage (∼10 plants), and terminal stage (∼6 plants), which were conducted on the dates of June 14 (25 days after seeding, DAS 25), June 23 (DAS 31), and June 30 (DAS 38) for the spring experiment of 2011; September 19 (DAS 26), September 29 (DAS 36), and October 9 (DAS 46) for the autumn experiment of 2011; and June 4 (DAS 26), June 15 (DAS 37), and June 27 (DAS 49) for the spring experiment of 2012, respectively. To investigate the relationship between $\delta^{15}N$ of soil and plant, a portion of the soil sample was collected during the spring experiment of 2011 as the vegetable sampling time.

The urea fertilizer sample was directly crushed into powder and sieved. The compost sample was first dried at 60 °C in an oven and then crushed and sieved. The soil samples were air-dried and then homogenized and passed through a 100-mesh sieve. The *B. chinensis* samples were heated at 105 °C in an oven for 30 min to inactivate all enzymes and then dried at 70 °C, homogenized, and passed through a 100-mesh sieve. All the prepared samples were kept in desiccators before analysis.

**Analytical Procedures.** Samples of fertilizer or vegetable containing ∼200−400 μg of N were weighed into tin capsules and then automatically analyzed for their $\delta^{15}N$ and %N values using elemental analyzer−isotope ratio mass spectrometry (EA-IRMS, Elementar Vario PYRO cube equipped with Isoprime100, Isoprime Ltd., England). The EA-IRMS conditions were as follows: the temperature of the oxidation furnace and the reduction furnace were set at 1020 and 650 °C, respectively, and the rate of carrier gas flow was set at 230 mL $min^{-1}$. The nitrogen isotope composition was calculated as

$$\delta^{15}N_{sample}\ (‰) = [(R_{sample}/R_{standard}) - 1] \times 1000 \quad (1)$$

where $R$ is the ratio of $^{15}N/^{14}N$ and standard refers to the ratio for atmospheric $N_2$. Pure $N_2$ ($\delta^{15}N$ = 0‰) served as the reference gas. IAEA-$N_1$ (ammonium sulfate, $\delta^{15}N$ = 0.4‰ ± 0.2‰) was used as the standard reference material. The analytical precision and reproducibility of the measurements for $\delta^{15}N$ were better than ±0.2‰.

**Statistical Analysis.** For statistical analysis, data were first tested for homogeneity of variance and normality of distribution. Analysis of variance (ANOVA) was performed on all experimental variables using the general linear models procedure of the SPSS 10.0 package (SPSS Inc., Chicago, IL, USA) to assess treatment effects. When treatment effects were significant, means were separated by Duncan's multiple range test.

## RESULTS AND DISCUSSION

**Variations in $\delta^{15}N$ Value of *B. chinensis* with Different N Source and Rate in Spring of 2011.** For the spring experiment of 2011 (as shown in Figure 1), the $\delta^{15}N$ values of

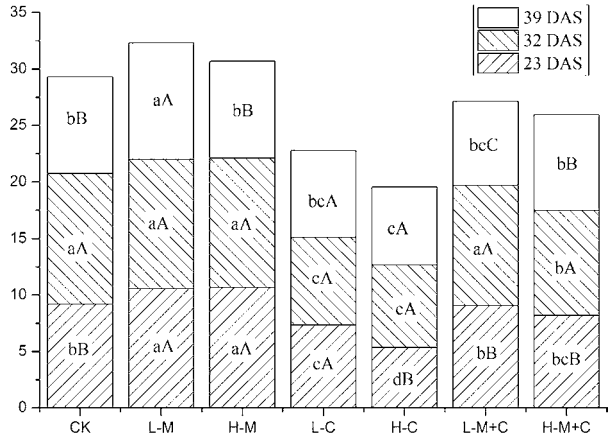


**Figure 1.** Variation in $\delta^{15}N$ of *B. chinensis* for the spring experiment of 2011. Treatment codes are described in Table 1. The same lowercase letter in the bars indicate no significant difference between different treatments at the same stage, and the same capital letters indicate no significant difference between different stages for the same treatment ($\alpha$ = 0.05 level).

*B. chinensis* receiving compost manure at 23 DAS were 10.6‰−10.7‰, significantly higher ($p < 0.05$) than that of the treatment L−C and H−C (5.4‰−7.4‰), L−M+C and H−M+C (8.2‰−9.1‰), and CK (9.2‰), which reflected the $\delta^{15}N$ of chicken compost manure (13.0‰), chemical fertilizer (−1.2‰), and soil N of CK (2.5‰). Temporal variations of $\delta^{15}N$ in the plant could be partially attributed to changes in the concentration and $\delta^{15}N$ value of soil inorganic N that is available for plant uptake. Figure 1 shows that the $\delta^{15}N$ values of *B. chinensis* became higher at DAS 32 for compost treatment (14.4‰), for chemical treatment (7.3‰−7.7‰), for compost−chemical treatment (9.3‰−10.6‰), and for CK (11.5‰). The $\delta^{15}N$ value of the vegetable increased during the later stage of growth, attributable to a decrease in the availability of the synthetic fertilizer over time and an increasing contribution of natural soil nitrogen to plant total nitrogen.[13] However, the value became lower at 39 DAS for compost treatment (8.6‰−10.3‰), for chemical treatment (6.9‰−7.7‰), for compost−chemical treatment (7.4‰−8.5‰), and for CK (8.6‰). There was also a similar report that the $\delta^{15}N$ value of *Brassica campestris* became lower at harvest time (60 DAT) for all treatments except for split additional manure.[19] A previous report also indicated the trend that the $\delta^{15}N$ of corn growing from 30 to 70 days varied from 7.7‰ to 6.7‰ for compost treatment, from 1.0 to 6.0‰ for chemical treatment, and from 4.5‰ to 6.1‰ for compost−chemical treatment.[14] A possible reason for this was that $NO_3^-$ is the most abundant N for plant uptake when compost with enriched $^{15}N$ was added in upland soils,[25] and more $^{15}N$-enriched $NH_4^+$ and $NO_3^-$ produced by nitrification were assimilated with time.[19] The $\delta^{15}N$ values of *B. chinensis* for the same treatment generally did not significantly differ between the low and high doses. The possible reasons for this were that when excess compost or chemical fertilizers were added in the soil, the mineralized N would be the dominant source for plant-N. It is possible that

this source exceeds the uptake ability of the plant, so the $\delta^{15}$N would not be changed even though more N was still available for the plant.[26] However, we also observed exceptions for L−C (mean value of 7.4‰) and H−C (5.4‰) at 23 DAS, L−M+C (10.6‰) and H−M+C (9.3‰) at 32 DAS, and L−M (10.3‰) and H−M (8.6‰) at 39 DAS, and the $\delta^{15}$N of *B. chinensis* for the compost−chemical treatment (8.2‰−9.1‰) was similar to that of CK. Reasons for this could be that the varied microbial immobilization ability of N leads to different mineralizations of fertilizers in soil, but this hypothesis needs to be further studied. There was a significant difference ($p < 0.05$) between the composted manure and the chemical fertilizer for three growth times with the exception of H−M and L−C at 39 DAS; the reasons could be that more N was lost and mineralization at 39 DAS resulted in the small difference of $\delta^{15}$N between H−M and L−C. The difference of different treatments was large at 23 DAS but became smaller at 39 DAS, which is a trend that was similar to the previous reports.[14,19,20,23,26] The results of this experiment indicated that the $\delta^{15}$N values of *B. chinensis* were affected by the addition of fertilizers, and that *B. chinesis* has a higher $\delta^{15}$N value than that of the N source for chemical treatment and for CK but not for compost treatment.

There was an overlap value without a significant difference between H−M (11.4‰) or L−M (11.4‰) and L−M+C (10.6‰) at 32 DAS, and between H−M (8.6‰) and L−M+C (7.4‰) or L−M+C(8.5‰) at 39 DAS, which was also confirmed by the previous reports for vegetables of *Brassica campestris*,[17] tomatoes,[18] lettuces,[18,22,23] onions, cabbages, and Chinese cabbages.[22] Thus, $\delta^{15}$N value could be used as a rough organic marker only in the case of single fertilizer application.[23] It is necessary to employ a statistical methodology to classify a randomly analyzed "off the shelf" sample as organic/conventional.[22]

**Variations in $\delta^{15}$N of *B. chinensis* without Fertilizer Application in Autumn of 2011.** In the autumn experiment of 2011, no additional fertilizer was applied to any pot after the spring experiment. Although the $\delta^{15}$N of the crop may be more affected by the presence of fertilizers, the value could also increase without the addition of fertilizer due to fractionation of N in previous fertilizers.[15] Compared with the results of the spring experiment of 2011, the $\delta^{15}$N value of *B. chinensis* rose especially for CK, L−C, H−C, and H−M+C due to more N mineralized dominantly in soil with a similar amount of $\delta^{15}$N for plant uptake. However, no significant difference was observed between the compost treatment and the chemical treatment (shown in Figure 2). For the autumn experiment of 2011, the $\delta^{15}$N mean value for CK increased significantly to 13.4‰ at 26 DAS, which was higher than that of the spring experiment of 2011 with a 45.6% increase. The $\delta^{15}$N mean values for the L−C (11.5‰), H−C (10.7‰), and H−M+C (10.6‰) were also higher than those of the same treatment in spring 2011 with increases of 55.4%, 98.1%, and 51.4%, respectively. However, the $\delta^{15}$N mean values for L−M (11.2‰), H−M (13.4‰), and L−M+C (11.9‰) at 26 DAS increased slightly with increases of 6.7%, 25.2%, and 14.4%, respectively. Our result was in agreement with the previously reported canola case, where the $\delta^{15}$N of canola was about 5.5‰ in the first year, 6.6‰ in the third year with hog manure, and 8.5‰ in the fourth year without hog manure application.[15] This could be explained by the fact that more $^{15}$N were enriched due to N lost or fractionation in soil after the spring

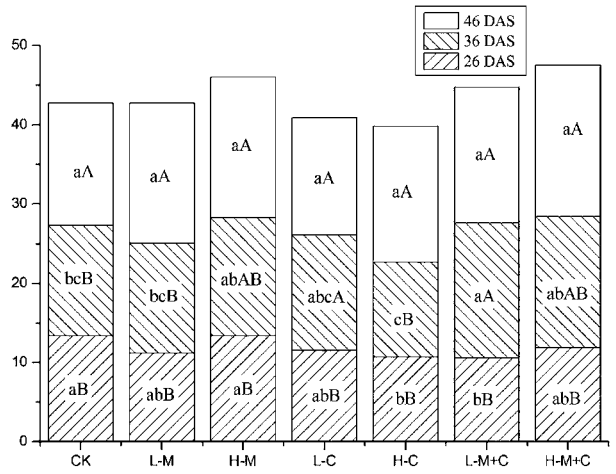


**Figure 2.** Variation in $\delta^{15}$N of *B. chinensis* for the autumn experiment of 2011. Treatment codes are described in Table 1. The same lowercase letter in the bars indicate no significant difference between different treatments at the same stage, and the same capital letters indicate no significant difference between different stages for the same treatment ($\alpha$ = 0.05 level).

experiment and were absorbed by the vegetable in the autumn experiment.

With the growth of *B. chinensis*, the $\delta^{15}$N mean value continued to be higher and was maintained at a high level with a range of 12.0−17.0‰ at 36 DAS and 14.8‰−19.1‰ at 46 DAS for all treatments (shown in Figure 2) due to high uptake of $\delta^{15}$N with the help of microbial nitrification effects. The maximum value of $\delta^{15}$N in *B. chinensis* was 17.7‰ for H−M, which was higher than that of organic tomato (16.6‰), lettuce (17.2‰), carrot (11.2‰),[12,17] cabbage (16.0‰),[18] and rice at harvest (<9.0‰),[19] as well as lettuce (<9.0‰),[22] and it extended the known database of the $\delta^{15}$N value in organic food. The large variation of $\delta^{15}$N in *B. chinensis* for most treatments between the terminal stage (46 DAS) and the seedling stage (26 DAS) was also observed, which was >6.0‰ for the treatment of L−M, H−C, L−M+C, and H−M+C. The mean values of $\delta^{15}$N for the treatments L−C and H−C were lower than those of the treatments L−M and H−M at the terminal stage (46 DAS). However, there were no significant differences among the various treatments, except for H−C (12.0‰) compared with L−M+C (17.0‰) and H−M+C (16.5‰). These findings indicated that the $\delta^{15}$N value of *B. chinensis* without chemical fertilizer application (such as in organic conversion) may also be higher than that of organic vegetable as other studies reported and proved that the vegetable with chemical fertilizer history within organic conversion would possibly be mislabeled as "organic food" if only judging on its high $\delta^{15}$N value.

**Variations in $\delta^{15}$N Values of *B. chinensis* with Further Fertilizer Application in Spring of 2012.** For the spring experiment of 2012, the same dose fertilizer as the 2011 spring experiment was employed to the corresponding treatment after the autumn experiment. As shown in Figure 3, the $\delta^{15}$N values for *B. chinensis* at 26 DAS decreased compared with that of the autumn experiment. Compared with the 2011 autumn experiment, we observed a sharp decrease in chemical fertilizer treatment. The mean $\delta^{15}$N values of L−C and H−C were significantly lower at 72.2% and 72.9%, respectively. This finding could result from additional urea-N application with more available $^{14}$N to plants, and it is in good agreement with

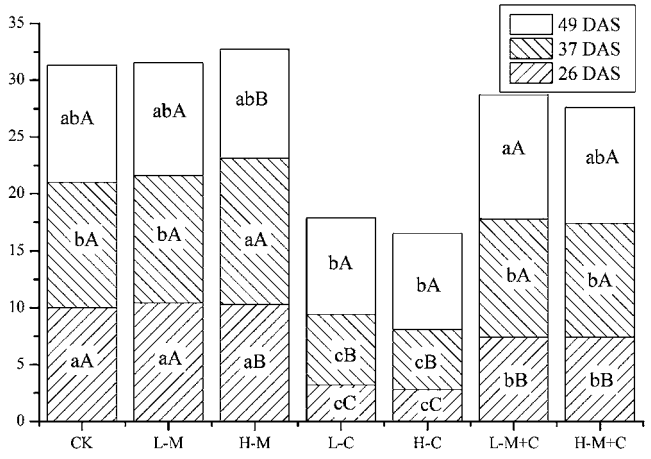


**Figure 3.** Variation in $\delta^{15}$N of *B. chinensis* for the spring experiment of 2012. Treatment codes are described in Table 1. The same lowercase letter in the bars indicate no significant difference between different treatments at the same stage, and the same capital letters indicate no significant difference between different stages for the same treatment ($\alpha$ = 0.05 level).

previous reports depicting the fast response and sharp decline in $\delta^{15}$N values with additional chemical fertilization in Chinese cabbage[19] and lettuce.[23] The results in the 2012 experiment at 26 DAS had a similar trend as those from the spring experiment of 2011, with the range of 10.0‰ for CK, 10.3‰−10.4 ‰ for L−M and H−M, 2.8‰−3.2‰ for L−C and H−C, and 7.4‰ for L−M+C and H−M+C. The values observed in this experiment for the treatment L−C and H−C were also lower than those of the 2011 spring experiment at 55.4% and 48.1%, respectively, which may result from two applications of urea-N. The $\delta^{15}$N value of the vegetable reflected the isotopic composition and historical fertilization of N sources and changed remarkably when isotopically different N sources were added.[19] For treatments of L−M+C and H−M+C, the mean $\delta^{15}$N values were much lower than those of the autumn experiment at 29.2% and 37.3%, respectively. The results were slightly lower than those from the 2011 spring experiment at 17.6% and 9.8%, respectively. However, results from treatments of CK, L−M, and H−M were similar to those of the spring experiment and lower than those of the autumn experiment in 2011. These results indicated that the types of fertilizers directly affected the $\delta^{15}$N value of the vegetable as previously reported.[14] Different manures may have different temporal effect patterns, for instance, the grain $\delta^{15}$N of barley in hog manure plots showed an increase tendency with time, but the phenomenon was not observed in the cattle manure treatment.[15] In our study, there was also a tendency observed that the $\delta^{15}$N values of *B. chinensis* receiving chemical fertilizer treatment were significantly lower ($p$ < 0.05) than those receiving compost manure at the early growth stages. The difference became narrower during the later stage, possibly due to a decrease in the availability of the chemical fertilizer over time (plant uptake, loss and immobilization, etc.) and contribution of natural soil nitrogen to plant total $\delta^{15}$N.[13] At 49 DAS, the $\delta^{15}$N value for L−M and H−M decreased compared with that at 37 DAS, from 11.2 to 9.9‰ and from 12.8‰ to +9.6‰, respectively, which may be explained by uptake of mineralized N from the organic pool decreasing the value during the later period.[14] The $\delta^{15}$N value for treatment H−C (8.4‰) has significant differences ($p$ < 0.05) with that of CK (10.3‰) and L−M+C (10.9‰), and there were no significant differences observed among other treatments. Although the $\delta^{15}$N of *B. chinensis* may be increased by compost application or decreased by chemical application, the results of this season experiment also showed that no significant differences ($p$ > 0.05) were observed between high dose and low dose for the same treatment, except for L−M and H−M at 37 DAS. This result corroborated that fertilizer quantity was not a key factor effecting $\delta^{15}$N of carrot[13] and cabbage.[26] The $\delta^{15}$N value of the vegetable may vary depending on the vegetable variety and the fertilizer type. The $\delta^{15}$N values of *B. chinensis* observed in this experiment were different from those for cabbage that were 7.7‰ for CK, 3.2‰ for urea, and 11.9−13.2‰ for liquid manure-A and 13.0‰−14.9‰ for liquid manure-B.[16] Another example was that the $\delta^{15}$N values for strawberry fruits grown in the presence of inorganic and organic fertilizers were −0.4 ± 1.5‰ and 9.2 ± 1.7‰, respectively.[27] This may be because of different manures with different $\delta^{15}$N values and variations in the uptake rates of different vegetables.

As a summary of the pot experiments of three continuous seasons at middle stage, the $\delta^{15}$N value of *B. chinensis* for the spring experiment of 2011 at 32 DAS has a similar value to that of 2012 at 37 DAS (shown in Figure 4), which was mostly

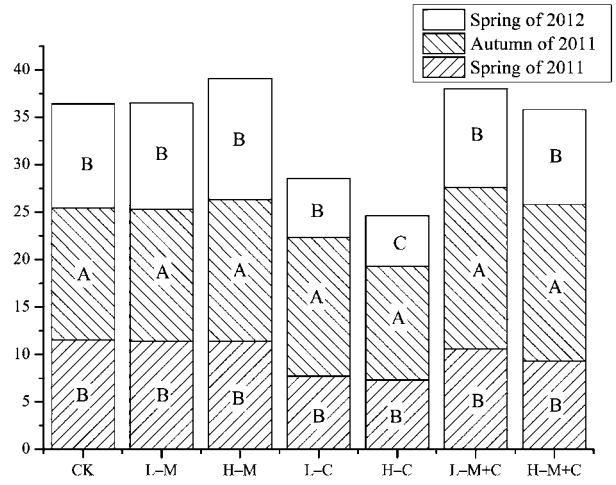


**Figure 4.** Variation in $\delta^{15}$N of *B. chinensis* for the middle stage of three experiments. Treatment codes are described in Table 1. The same capital letter in the bars indicate no significant difference between different seasons at the middle stage ($\alpha$ = 0.05 level).

affected by the types of fertilizers. Both experiments had a similar tendency, which is that there was a significant difference between the compost treatment and the chemical treatment. However, there was an apparent overlap in $\delta^{15}$N value for the combined application of chemical and compost fertilizer. The $\delta^{15}$N value of *B. chinensis* for the autumn of 2011 without any additional fertilizer at 36 DAS increased (shown in Figure 2), and was higher than those of the spring of 2011 and 2012, but there was no significant difference between the compost treatment and the chemical treatment.

**Variation in $\delta^{15}$N Value of Soil with Different N Source and Rate.** The total $\delta^{15}$N of soil was determined only for the spring experiment of 2011 to investigate the variation in $\delta^{15}$N of soil affected by different fertilizers and the relationship of $\delta^{15}$N between soil and plant. The $\delta^{15}$N mean value of soil (no fertilizer application) before this experiment was 6.9‰, which

was very close to the previous report[20] with 6.4‰. After fertilization and uptake by vegetables, the $\delta^{15}$N mean value range of soil at 23 DAS was 2.5‰ for CK, 5.3‰−6.3‰ for L−M and H−M, 2.2‰−2.4‰ for H−C and L−C, and 2.7‰−4.5‰ for L−M+C and H−M+C, as shown in Figure 5. The

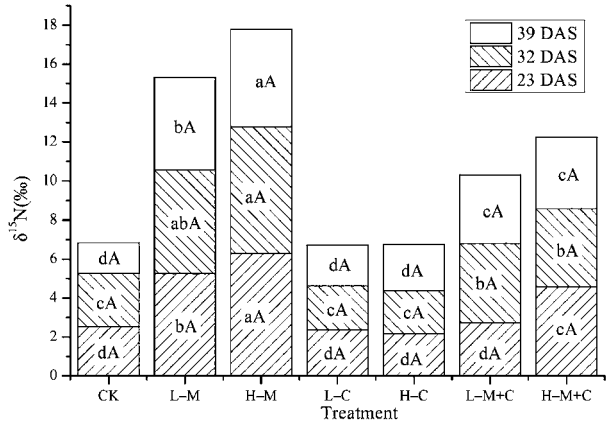


**Figure 5.** Variation in $\delta^{15}$N of soil for the spring experiment of 2011. Treatment codes are described in Table 1. The same lowercase letter in the bars indicate no significant difference between different treatments at the same stage, and the same capital letters indicate no significant difference between different stages for the same treatment ($\alpha$ = 0.05 level).

total $\delta^{15}$N mean value of soil was lower for chemical treatment than that for compost treatment, which may be explained by the fact that the $\delta^{15}$N of soil was more affected by the chemical fertilizer than by the compost fertilizer. There was a significant difference ($p < 0.05$) between the compost treatment (L−M, H−M) and CK as well as other treatments. There was also a report[25] that the total $\delta^{15}$N value of soil was significantly higher for compost-applied (8.8‰) than for fertilizer-applied (5.9‰), which corroborated that the $\delta^{15}$N value of upland-grown plants receiving compost would be higher than those treated with chemical fertilizer because $NO_3^-$ is the most abundant N for plant uptake. However, another report showed that there was no difference between the organic production and the integrated production for total $\delta^{15}$N of soil, because the quantity of fertilizer application added was only ∼1/100 of the total soil N-pool.[24] As shown in Figure 5, the $\delta^{15}$N mean value of soil from 32 DAS to 39 DAS varied over time from 2.7‰ to 1.6‰ for CK, and also had a tendency to go from higher to lower for other treatments. Although the total $\delta^{15}$N values slightly varied with the growing stage for all treatments, there were no significant differences ($p > 0.05$) among three stages. The total $\delta^{15}$N values of the treatment L−M (5.3‰) and H−M (6.3‰) were higher than those of L−C (2.4‰) and H−C (2.2‰) at 23 DAS, which were also significantly different ($p < 0.05$) at 32 DAS and 39 DAS. The $\delta^{15}$N values of soil were affected by the different fertilizer treatments found in this experiment, and the $\delta^{15}$N values of *B. chinensis* were also affected by that of soil, as per the previous report that the $\delta^{15}$N of upland-grown plants receiving compost would be higher than for those treated with chemical fertilizer.[16]

Figure 6 shows that the $\delta^{15}$N of *B. chinensis* were all higher than that of soil during the spring experiment of 2011, which has a positive correlation to that of soil at the seedling stage ($R^2$ = 0.537, $p$ = 0.0656). As *B. chinensis* grew, the positive correlation became minor at the middle stage ($R^2$ = 0.485, $p$ =

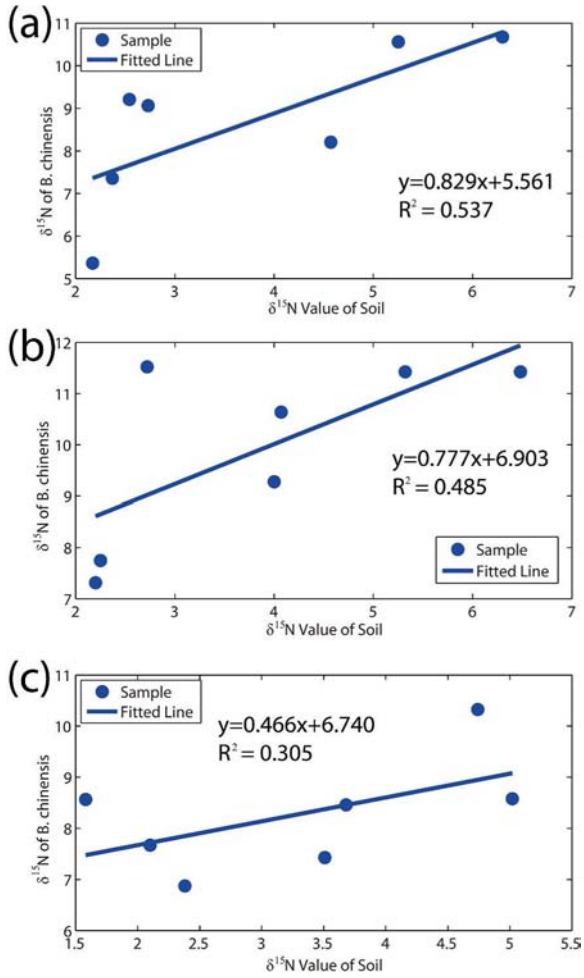


**Figure 6.** Relationship of $\delta^{15}$N between *B. chinensis* and soil in the spring experiment of 2011 at the seedling stage (a), the middle stage (b), or the terminal stage (c).

0.0848) and the terminal stage ($R^2$ = 0.305, $p$ = 0.2102). The results also confirmed that total $\delta^{15}$N value of *B. chinensis* was greatly affected by N derived from compost or fertilizer rather than indigenous soil-N during the early growth season as previously reported.[25] The results demonstrate that there was no strong correlation ($p > 0.05$) between *B. chinensis* and soil in terms of $\delta^{15}$N value, which was in agreement with the previous study.[25]

Finally, the results of this experiment confirmed that the $\delta^{15}$N value of *B. chinensis* increased when organic manure fertilizer was applied and was significantly different fromthose for manure treatment and chemical treatment. With the growth, the $\delta^{15}$N value of *B. chinensis* varied depending on the fertilizer application. There was no fixed cutoff value for $\delta^{15}$N in organic discrimination. The $\delta^{15}$N value of *B. chinensis* in the autumn of 2011 without any fertilizer application was higher than those for the spring experiments of 2011 and 2012. This may be the result of the fact that more soil-$^{15}$N from N lost or fractionation in soil after the spring experiment was absorbed by the vegetable, which confirmed that using uncultivated soil in the pot experiment could eliminate the effect of background interference on the $\delta^{15}$N of plant. The $\delta^{15}$N value of soil was slightly affected by fertilizers and varied without significant difference among three growing stages of *B. chinensis*. Thus, the $\delta^{15}$N value may be useful to discriminate whether a particular


dx.doi.org/10.1021/jf502627c | J. Agric. Food Chem. 2014, 62, 11386−11392

vegetable was grown in the presence of a chemical fertilizer (a low value, ~3.0‰) or in the presence of compost manure or a chemical−compost fertilizer (a high value, ~10.0‰). Once again, it was difficult to discriminate if a labeled organic vegetable was really grown without chemical fertilizer just using the $\delta^{15}$N value, especially for the overlap value of those planted with chemical−compost fertilizer. However, the results also indicated that the $\delta^{15}$N value of *B. chinensis* grown with compost manure or chemical−compost treatment has a higher value compared to vegetables previously reported, which could be useful for the development of the $\delta^{15}$N value database for organic food discrimination.

## AUTHOR INFORMATION

### Corresponding Author

*Institute of Quality and Standards for Agricultural Products, Zhejiang Academy of Agricultural Sciences, Shiqiao Road 198, Hangzhou 310021, P.R. China. Tel.: +86-571-8640-6862. Fax: +86-571-8640-1834. E-mail: ywytea@163.com.

### Notes

The authors declare no competing financial interest.

## ACKNOWLEDGMENTS

This work was funded by the Zhejiang Key team of Science and Technology Innovation (2010R50028), Zhejiang Academy of Agricultural Sciences (2011R19Y01E01), and International Scientific and Technological Cooperation Award of the People's Republic of China (2012DFA31140). We also thank Master Shengzhi Shao for the help of figure revision.

## REFERENCES

(1) Willer, H., Lukas, K., Eds. *The World of Organic Agriculture—Statistics and Emerging Trends 2012*; Research Institute of Organic Agriculture (FiBL) and International Federation of Organic Agriculture Movements (IFOAM): Frick, Switzerland, and Bonn, Germany, 2012.

(2) Batte, M. T.; Hooker, N. H.; Haab, T. C.; Beaverson, J. Putting their money where their mouths are: Consumer willingness to pay for multi-ingredient, processed organic food products. *Food Policy* **2007**, *32* (2), 145−149.

(3) Lundegårdh, B.; Mårensson, A. Organically Produced Plant Foods—Evidence of Health Benefits. *Acta Agric. Scand., Sect. B* **2003**, *53* (1), 3−15.

(4) Lin, B. H.; Huang, C. L.; Smith, T. A. Organic premiums of US fresh produce. *Renew. Agric. Food Sys.* **2008**, *23*, 208−216.

(5) FAO/ITC/CTA. Requirements for producing and exporting organic products to major markets (Chapter 1). *World Markets for Organic Fruit and Vegetables—Opportunities for Developing Countries in the Production and Export of Organic Horticultural Products*; http://www.fao.org/docrep/004/y1669e/y1669e00.htm#Contents (accessed Jan 2,2013).

(6) Tranter, R. B.; Bennett, R. M.; Costa, L.; Cowan, C.; Holt, G. C.; Jones, P. J.; Miele, M.; Sottomayor, M.; Vestergaard, J. Consumers' willingness-to-pay for organic conversion-grade food: Evidence from five EU countries. *Food Policy* **2009**, *34* (3), 287−294.

(7) Sheng, J. P.; Qiao, Y. H.; Yu, M. M.; Fan, B. Market trends and accreditation systems for organic food in China. *Trends Food Sci. Technol.* **2009**, *20* (9), 396−401.

(8) Anonymous. Food safety concerns boost organic food sales in China. *Meat Int.* **2007**, *17* (6), 33−34.

(9) Chen, J.; Lobo, A. Organic food products in China: Determinants of consumers' purchase intentions. *Int. Rev. Retail, Distrib. Consum. Res.* **2012**, *22* (3), 293−314.

(10) Siderer, Y.; Maquet, A.; Anklam, E. Need for research to support consumer confidence in the growing organic food market. *Trends Food Sci. Technol.* **2005**, *16* (8), 332−343.

(11) Bateman, A. S.; Kelly, S. M. Fertilizer nitrogen isotope signatures. *Isot. Environ. Health Stud.* **2007**, *43* (3), 237−247.

(12) Lim, S. S.; Lee, S. M.; Lee, S. H.; Choi, W. J. Nitrogen isotope composition of synthetic fertilizer, raw livestock manure slurry, and composted livestock manure. *Korean J. Soil Sci. Fert.* **2010**, *43* (4), 453−457.

(13) Bateman, A. S.; Kelly, S. D.; Jickells, T. D. Nitrogen isotope relationships between crops and fertilizer: Implications for using nitrogen isotope analysis as an indicator of agricultural regime. *J. Agric. Food Chem.* **2005**, *53*, 5760−5765.

(14) Choi, W. J.; Lee, S. M.; Ro, H. M.; Kim, K. C.; Yoo, S. H. Natural $^{15}$N abundances of maize and soil amended with urea and composted pig manure. *Plant Soil* **2002**, *245*, 223−232.

(15) Choi, W. J.; Arshad, M. A.; Chang, S. X.; Kim, T. H. Grain $^{15}$N of crops applied with organic and chemical fertilizers in a four-year rotation. *Plant Soil* **2006**, *284*, 165−174.

(16) Lim, S. S.; Choi, W. J.; Kwak, J. H.; Jung, J. W.; Chang, S. X.; Kim, H. Y.; Yoon, K. S.; Choi, S. M. Nitrogen and carbon isotope responses of Chinese cabbage and chrysanthemum to the application of liquid pig manure. *Plant Soil* **2007**, *295*, 67−77.

(17) Yuan, Y. W.; Zhao, M.; Zhang, Z. H.; Chen, T. J.; Yang, G. L.; Wang, Q. Effect of different fertilizers on nitrogen isotope composition and nitrate content of *Brassica campestris*. *J. Agric. Food Chem.* **2012**, *60*, 1456−1460.

(18) Bateman, A. S.; Kelly, S. D.; Woolfe, M. Nitrogen isotope composition of organically and conventionally grown crops. *J. Agric. Food Chem.* **2007**, *55*, 2664−2670.

(19) Yun, S. I.; Ro, H. M.; Choi, W. J.; Chang, S. X. Interactive effects of N fertilizer source and timing of fertilization leave specific N isotopic signatures in Chinese cabbage and soil. *Soil Biol. Biochem.* **2006**, *38*, 1682−1689.

(20) Yun, S. I.; Lim, S. S.; Lee, G. S.; Lee, S. M.; Kim, H. Y.; Ro, H. M.; Choi, W. J. Natural $^{15}$N abundance of paddy rice (*Oryza sativa* L.) grown with synthetic fertilizer, livestock manure compost, and hairy vetch. *Biol. Fert. Soils* **2011**, *47* (6), 607−617.

(21) Yuan, Y. W.; Zhang, Z. H.; Zhao, M.; Xu, M. F.; Yang, G. L.; Zheng, J. C.; Wang, Q. Study on the effect of different fertilizer on the stable nitrogen isotope of soil, leaf and cucumber. *J. Nucl. Agric. Sci.* **2010**, *24* (1), 108−113 (in Chinese with English abstract).

(22) Schmidt, H. L.; Roßmann, A.; Voerkelius, S.; Schnitzler, W. H.; Georgi, M.; Grassmann, J.; Zimmermann, G.; Winkler, R. Isotope characteristics of vegetables and wheat from conventional and organic production. *Isot. Environ. Health Stud.* **2005**, *41*, 223−228.

(23) Šturm, M.; Maršić, N. K.; Lojen, S. Can $\delta^{15}$N in lettuce tissues reveal the use of synthetic nitrogen fertiliser in organic production? *J. Sci. Food Agric.* **2010**, *91*, 262−267.

(24) Georgi, M.; Voerkelius, S.; Rossmann, A.; Graβmann, J.; Schnitzler, W. H. Multi-element isotope ratios of vegetables from integrated and organic production. *Plant Soil* **2005**, *275*, 93−100.

(25) Choi, W. J.; Ro, H. M.; Lee, S. M. Natural $^{15}$N abundances of inorganic nitrogen in soil treated with fertilizer and compost under changing soil moisture regimes. *Soil Biol. Biochem.* **2003**, *35*, 1289−1298.

(26) Yun, S. I.; Ro, H. M. Natural $\delta^{15}$N abundance of plant and soil inorganic-N as evidence for over-fertilization with compost. *Soil Biol. Biochem.* **2009**, *41*, 1541−1547.

(27) Nakano, A.; Uehara, Y. Effect of fertilizer and soil nitrogen on delta $^{15}$N values of strawberry. *Bull. Natl. Inst. Veg. Tea Sci.* **2006**, *5*, 7−13.

(28) *Green food—Environmental quality for production area*; NY/T 391-2013; The Agriculture Industry Standard of Ministry of Agriculture: China, 2013 (in Chinese) .

**Table 1. Effects of Available Nitrogen and Cultivar on Yield and Nutrients in Curly Kale Cultivars HAT, Reflex, and TIARA**

| N (kg ha$^{-1}$) | cv. | total yield[a] | edible yield[a] | stalk weight[a] | stalk height[b] | leaf N[c] | leaf S[c] | stalk N[c] | stalk S[c] | total N uptake[d] | total S uptake[d] |
|---|---|---|---|---|---|---|---|---|---|---|---|
| 90 | HAT | 50.1 ± 2.6[e] | 13.7 ± 1.3 | 19.4 ± 1.9 | 77 ± 6.7 | 23.6 ± 0.8 | 7.7 ± 0.4 | 9.9 ± 1.8 | 3.9 ± 0.3 | 168 ± 22.9 | 57 ± 10.6 |
| 230 | | 75.4 ± 2.7 | 18.3 ± 2.7 | 34.7 ± 4.8 | 104 ± 14.9 | 26.2 ± 0.9 | 7.2 ± 0.5 | 14.8 ± 3.9 | 3.4 ± 0.4 | 264 ± 35.6 | 69 ± 10.0 |
| N effect | | ***[f] | NS | ** | * | * | NS | NS | NS | * | NS |
| 90 | Reflex | 50.6 ± 3.6 | 17.1 ± 1.1 | 19.0 ± 1.3 | 70 ± 5.1 | 23.9 ± 1.3 | 6.7 ± 0.6 | 9.7 ± 1.1 | 4.4 ± 0.4 | 169 ± 13.5 | 53 ± 7.4 |
| 135 | | 59.1 ± 1.5 | 22.2 ± 1.1 | 22.2 ± 2.3 | 75 ± 2.6 | 25.2 ± 2.4 | 6.6 ± 1.1 | 11.7 ± 0.8 | 4.2 ± 1.0 | 223 ± 28.0 | 63 ± 11.0 |
| 185 | | 66.3 ± 1.4 | 22.6 ± 0.7 | 24.6 ± 1.0 | 79 ± 3.8 | 27.9 ± 0.2 | 7.2 ± 0.7 | 12.7 ± 1.0 | 4.2 ± 0.3 | 254 ± 29.0 | 69 ± 11.3 |
| 230 | | 68.3 ± 6.7 | 23.7 ± 1.3 | 27.6 ± 1.3 | 90 ± 4.0 | 26.5 ± 2.9 | 6.3 ± 1.2 | 13.6 ± 1.6 | 3.5 ± 0.8 | 271 ± 27.3 | 66 ± 7.6 |
| N effect | | ** | *** | *** | ** | NS | NS | * | NS | ** | NS |
| 90 | TIARA | 45.1 ± 4.4 | 14.2 ± 0.5 | 16.9 ± 3.2 | 69 ± 2.7 | 27.6 ± 3.1 | 8.8 ± 0.2 | 15.0 ± 0.9 | 5.7 ± 0.2 | 203 ± 31.6 | 68 ± 4.5 |
| 135 | | 50.2 ± 5.5 | 14.1 ± 3.3 | 21.1 ± 1.6 | 75 ± 4.9 | 32.0 ± 9.5 | 9.5 ± 2.1 | 17.9 ± 3.2 | 6.2 ± 0.7 | 238 ± 47.0 | 74 ± 11.5 |
| 185 | | 54.0 ± 2.2 | 15.3 ± 0.3 | 21.3 ± 0.9 | 80 ± 3.6 | 27.7 ± 1.5 | 8.5 ± 1.7 | 19.6 ± 0.8 | 5.7 ± 0.4 | 237 ± 5.9 | 71 ± 11.5 |
| 230 | | 56.7 ± 3.1 | 15.8 ± 2.7 | 25.4 ± 3.8 | 83 ± 8.3 | 32.1 ± 1.8 | 7.9 ± 0.4 | 17.7 ± 2.4 | 5.0 ± 0.8 | 300 ± 60.8 | 77 ± 16.5 |
| N effect | | * | NS | * | * | NS | NS | NS | NS | NS | NS |
| significance | | | | | | | | | | | |
| N | | *** | *** | *** | *** | NS | NS | ** | * | *** | NS |
| CV | | *** | *** | *** | *** | NS | ** | *** | *** | NS | NS |
| N × CV | | NS | NS | NS | NS | NS | NS | NS | NS | NS | NS |

[a]Tonne ha$^{-1}$, [b]cm. [c]g kg$^{-1}$dry matter. [d]kg ha$^{-1}$. [e]± standard deviation. [f]*, $p \leq 0.05$; **, $p < 0.01$; ***, $p < 0.001$ in a general linear model among N level and cultivar means ($n = 3$) within each column. NS, not significant.

relationship between N availability and flavonol or total phenolic concentrations in leaf mustard (*Brassica juncea*), tomato (*Lycopersicon esculentum*), and *Arabidopsis thaliana*.[26,27] Moreover, a report on eight different field-grown curly kale cultivars showed relatively high flavonoid concentrations in traditional old cultivars in contrast to lower concentrations in hybrids.[5]

However, the influence of the genetic variation on flavonoid glycoside and GLS concentrations associated with fertilizer strategies, agronomic characteristic, and biomass allocation in traditional and F1 hybrid cultivars of curly kale has not been reported. Trials conducted under field growth conditions with less control over biogeochemical environments compared to, for example, greenhouse experiments are necessary in the testing of agronomic practices, particularly when a crop stand is examined with relevance to growers and consumers.

On the basis of testing genetic variation between traditional and F1 hybrid kale cultivars to optimize fertilizer management based on genotype, the objectives of this study were as follows: (i) investigate whether GLS and flavonoid glycoside concentration and composition differed markedly among cultivars; (ii) determine if varying N supplies in relationship to agronomic characteristic and biomass allocation modified GLS and flavonoid glycoside composition and concentration; and (iii) investigate field S and N application effects on GLS concentration and composition.

## MATERIALS AND METHODS

**Chemicals.** Glucoiberin, progoitrin, glucoraphanin, gluconapin, sinigrin, 4-hydroxyglucobrassicin, glucobrassicin, 4-methoxyglucobrassicin, and neoglucobrassicin were obtained from C2 Bioengineering ApS (Karlslunde, Denmark); glucotropaeolin was from PhytoLab GmbH & Co. KG (Vestenbergsgreuth, Germany); and acetic acid, barium acetate, calcium glycerophosphate hydrate, methanol, sulfatase, and sodium hydroxide were obtained from Sigma-Aldrich (Steinheim, Germany).

**Field Experiment.** The field site was located at the Department of Food Science in Aarslev, Denmark (55°18′N, 10°27′E) on a sandy loam (Typic Agrudalf) soil containing 1.35% organic C, 33% coarse sand, 38.8% fine sand, 12.6% silt, and 13.4% clay. Inorganic N and S levels in the field before planting were 10 and <4 kg ha$^{-1}$, respectively. Seeds of the F1 hybrid 'Reflex' (SeedCom A/S, Denmark) and the traditional cultivars 'Halvhøj Ekstra Moskruset Tiara' (TIARA) accession 1833 and 'Høj Amager Toftø' (HAT) accession 4085 (both NordGen germplasm collection)[28] were sown on April 4, 2011, and propagated in an unheated greenhouse. Plants were transferred to the field on May 5, 2011, with a row/plant distance of 50/60 cm, respectively. Plots of 3 × 5 m$^2$ with the two outermost rows as guard rows to eliminate border effects were arranged in a complete randomized block design with three replication of plots ($n = 3$) per fertilizer level and cultivar (see below). An insect net was applied over the plots and used for pest management to reduce herbivory until August 16, 2011. Weeding was conducted manually and mechanically once during the experimental trial. The trials included two separate experimental regimes. Experiments were performed as follows: In experiment I, Reflex, HAT, and TIARA were grown under 30 kg S ha$^{-1}$ with 90, 135, 185, or 230 kg N ha$^{-1}$ available in the field (36 plots in total with 30 kg S and 185 kg N ha$^{-1}$ being standard conditions); and under experiment II, Reflex had either 4 or 30 kg S ha$^{-1}$ available combined with 90, 135, or 185 kg N ha$^{-1}$ accessible in the field (18 plots in total). Fertilizer levels applied were adjusted according to the levels in the field measured before planting. S fertilizer was dispersed just prior to planting, and approximately half the total N fertilizer dose was distributed just after planting. The other half was given 6 weeks later. Granulate kieserite ($MgSO_4$, 20% S, K+S Kali GmbH, Germany) and granulate calcium ammonium nitrate ($NH_4NO_3$+Ca, 27% N, Hydro Agri Danmark A/S, Denmark) were used as S and N sources, respectively. On October 10, 2011, 10 plants from each replicate plot were harvested, including the entire stalk and leaves (corresponding to 3.1 m$^2$), and total yield was assessed. Four of 10 plants from each plot were evaluated with respect to stalk height from plant base at soil surface to the plant top. Yield characteristics were estimated as follows: edible yield as usable leaf weight (stem diameter < 7 mm) and stalk weight without leaves, stems, and top. Entire plants were maintained at a temperature of 1 °C and 100% relative humidity in black plastic bags until further analysis within 4 days. The plants were handled carefully to avoid tissue disruption and thereby loss of GLSs. The described experiments correspond to analyses 2, 3, and 4 reported by Jensen et al.[10] from which sensory evaluation of the different fertilization approaches was assessed.

**Plant Analyses.** Representative samples of approximately 200 g of separated leaves and stalks from each plot were oven-dried at 80 °C to a constant weight, and dry matter content (DM) was calculated. Total leaf and stalk N and S concentrations were analyzed from the oven-dried material. VDLUFA methods were used to determine plant N and S.[29,30]

**Glucosinolate Analysis.** Three of the 10 harvested plants per replication plot ($n$ = 3) were randomly selected, and nine evenly distributed leaves per plant with a stem width at the widest point of approximately 7 mm were removed from the primary stem. Curly kale leaves were rinsed in cold tap water, chopped fine, immediately frozen in liquid nitrogen, and stored at −24 °C until freeze-drying in a CHRIST freeze-dryer, Gamma 1-20 (Osterode am Harz, Germany). After freeze-drying, the samples were ground in an Ultra Centrifugal Mill, ZM 200 (Retsch, Haan, Germany). GLS concentration was determined as described by Beck et al.[31]

**Flavonoid Glycoside and Hydroxycinnamic Acid Analysis.** Twenty milligrams of the freeze-dried ground leaves was extracted with 600 μL of 60% methanol (MeOH) (Roth, Karlsruhe, Germany) and shaken for 40 min in a Thermomixer (Eppendorf, Thermo Fischer Scientific Inc., Wesseling-Berzdorf, Germany) at 1400 rpm and 20 °C. Hereafter, extracts were centrifuged at 12000 rpm for 10 min. The supernatant was transferred to a new sterile test tube. The procedure was repeated twice with 400 μL of 60% MeOH, for 20 min, and with 200 μL of 60% MeOH, for 10 min. The combined supernatants were filtered through a Spin-X (Sigma-Aldrich Chemical Co., St. Louis, MO, USA) tube by centrifugation at 3000 rpm for 5 min and dry evaporated in a vacuum centrifuge. The residue was dissolved in 200 μL of distilled water. Flavonoid glycosides and hydroxycinnamic acid derivatives were qualified by HPLC-DAD-MS$^n$ according to their parent ions and fragmentation patterns as described by Schmidt et al.[23] and quantified as equivalents of caffoylquinic acid and 3-*O*-glycosides of quercetin, kaempferol, and isorhamnetin as described by Neugart et al.[32] Analyses were done for experiment I but not experiment II as influences of S on flavonoid glycosides and hydroxycinnamic acid derivatives were not expected.

**Statistical Analyses.** All univariate statistical analyses were performed in SAS (SAS Institute Inc., Cary, NC, USA; release 9.2, 2000). The general linear model and general linear mixed model procedures were applied for comparison of least-squares (LS) means ($p \leq 0.05$). GLS, flavonoid glycoside, and hydroxycinnamic acid derivative analyses (this study) and sensory analyses (reported in Jensen et al.[10]) were made from all treatments in experiment I except HAT grown under 135 and 185 kg N ha$^{-1}$. Therefore, each of the 10 cultivar and N level combinations in experiment I were grouped as one factor to compare data analysis results using statistical contrasts. All linear relationships were investigated using a simple linear regression.

## RESULTS AND DISCUSSION

**Agronomic Characteristics and Glucosinolate Concentrations.** *Experiment I: N Level and Cultivar Effects.* The three cultivars showed distinct differences in agronomic characteristic parameters, which consisted of total and edible yield, stalk weight and height, and leaf and stalk N and S content as well as total N and S uptake. The HAT cultivar exhibited the highest total yield, but Reflex generated the highest edible yield (Table 1). The shift in highest total and edible yield between HAT and Reflex, respectively, corresponded to stalk data. Likewise, higher leaf S and stalk N and S concentrations corresponded to lower yields of TIARA, opposite Reflex. Similar to our findings, Padilla et al.[33] identified different morphologic and agronomic traits of 148 kale landraces (*acephala* group) resulting in 5 clusters based on these trait differences. The higher stalk N concentration in TIARA indicated that TIARA growth was not limited by N availability at increased N applications, which was consistent with the capacity of cabbage to take up more N than required for growth.[34] Total S uptake did not respond to increased application of N, whereas total N uptake increased continuously from 90 to 230 kg N ha$^{-1}$ applied (Table 1). This result does not support the close association in plant N and S assimilation, where adenosine 5′-phosphosulfate (APS) plays a special role in relationship to S assimilation[35] and APS reductase activity, which is controlled by N availability.[36] Possibly *B. oleracea*, with the capacity to accumulate nitrate, does not apply strictly to this hypothesis as similar findings of less N and S interaction in relation to plant N and S concentration have been reported in other field studies.[14,15,34] Thus, increasing N application resulted in increased edible yield of Reflex, whereas TIARA showed no response in biomass despite elevated stalk N concentrations (Table 1). The response of HAT to N was mainly found in increased stalk biomass and total yield.

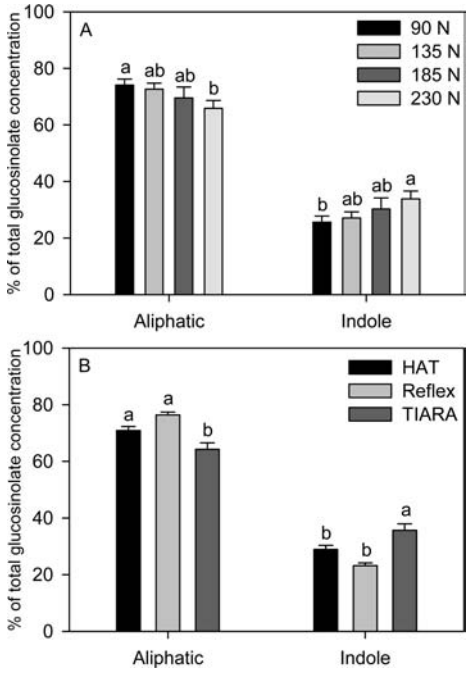


**Figure 1.** Effects of available nitrogen (kg ha$^{-1}$) on aliphatic and indole percentage of total GLS concentration in curly kale cultivars HAT, Reflex, and TIARA. Different letters indicate significant differences ($p \leq 0.05$) among cultivars or N levels ($n$ = 3) within the glucosinolate groups. There were no statistical interactions between N and cultivar. Bars represent standard errors.

Different agronomic characteristics were associated with a diverse GLS composition observed among the three cultivars. The following GLSs were identified: the aliphatic GLSs, including glucoiberin (3-methylsulfinylpropyl GLS), sinigrin (2-propenyl GLS), glucoraphanin (4-methylsulfinylbutyl GLS), gluconapin (3-butenyl GLS), and progoitrin ((*R*)-2-hydroxy-3-butenyl GLS); the indole GLSs, including glucobrassicin (3-indolymethyl GLS), 4-hydroxy glucobrassicin (4-hydroxy-3-indolylmethyl GLS), 4-methoxy glucobrassicin (4-methoxy-3-indolylmethyl GLS), and neoglucobrassicin (1-methoxy-3-indolylmethyl GLS); and the aromatic gluconasturtiin (2-phenylethyl GLS). Cultivars differed in total GLS concentration (TIARA, 3503 μg g$^{-1}$ DM; HAT, 2799 μg g$^{-1}$ DM; Reflex, 2454 μg g$^{-1}$ DM; cultivar, $p < 0.01$; N × cultivar, not significant). Increased N application resulted in a decreased percentage of the aliphatic GLS group and a corresponding increase in indole GLS percentage (Figure 1A, $p < 0.0001$). Studies in broccoli and green cabbage were congruent with our results, but the present study is the first documented in field-grown curly kale.[13−15] However, wild-type Col-0 *Arabidopsis* studies found $NO_3^-$ addition repressed the shikimate pathway, responsible for the synthesis of flavonols and the indole GLS amino acid precursor tryptophan.[19,37] A negative linear relationship was detected for Reflex, between edible yield and aliphatic or total GLS concentration, respectively ($p$ = 0.0193, $R^2$ = 0.44; and $p$ =


dx.doi.org/10.1021/jf503096p | J. Agric. Food Chem. 2014, 62, 11393−11402

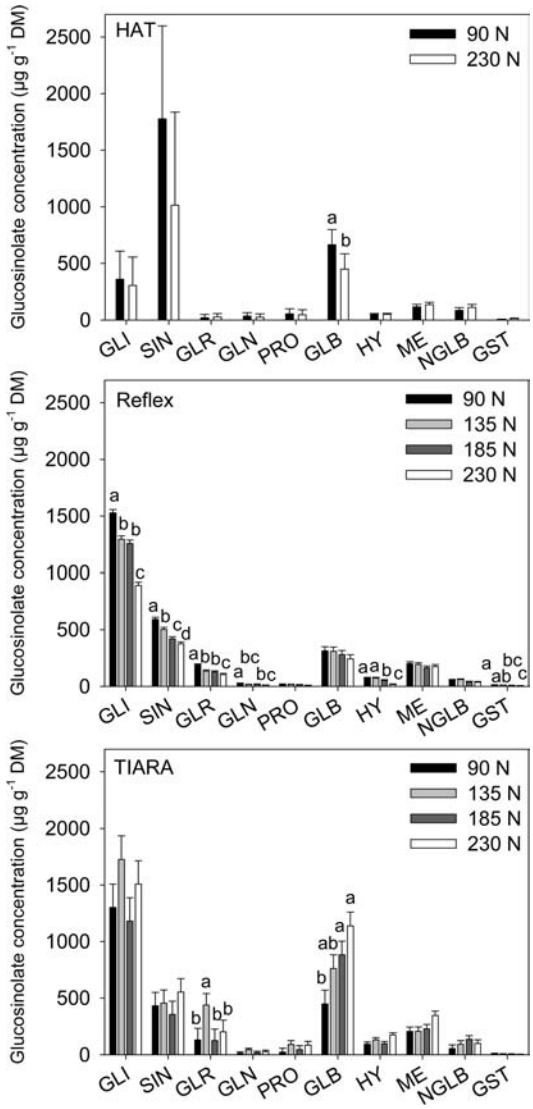


**Figure 2.** Effects of nitrogen (N) available (kg $ha^{-1}$) on individual glucosinolate concentrations ($\mu g\ g^{-1}$ DM) in the edible plant material of curly kale cultivars HAT, Reflex, and TIARA. Different letters indicate significant differences ($p \leq 0.05$) in a general linear mixed model among N level means ($n = 3$) within glucosinolate. Bars represent standard errors. GLI, glucoiberin; SIN, sinigrin; GLR, glucoraphanin; GLN, gluconapin; PRO, progoitrin; GLB, glucobrassicin; HY, 4-hydroxyglucobrassicin; ME, 4-methoxyglucobrassicin; NGLB, neoglucobrassicin; GST, gluconasturtiin.

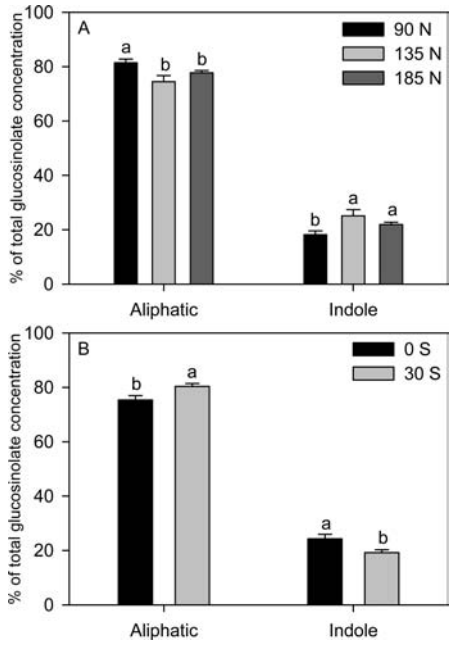


**Figure 3.** Effects of nitrogen and sulfur available (kg $ha^{-1}$) on aliphatic and indole percentages of the total GLS concentration in the edible plant material of curly kale cultivar Reflex. Different letters indicate significant differences ($p \leq 0.05$) between N or S level means ($n = 3$) within the glucosinolate group. Bars represent standard errors.

0.0023, $R^2 = 0.62$, respectively), while TIARA showed a positive linear relationship between indole GLS concentration and edible yield ($p = 0.0395$, $R^2 = 0.36$). Suggestions on increased biosynthesis of C-, N-, and S-containing phytochemicals in cases of limited availability to one or more of the compounds have been put forward.[18−20] For example, increased N availability under normal $CO_2$ conditions might increase N-containing phytochemicals such as GLSs as C limits growth. Likewise, growth limitation by less N availability might shift to metabolism of phytochemicals containing much C, such as flavonoids. Partly contradicting our results, studies on GLS content of Chinese kale (*Brassica alboglabra* L.) grown under increasing N levels showed reduced aliphatic GLS but enhanced indole GLS concentrations with both ambient and elevated $CO_2$ levels.[38] In this study the increased indole GLS concentration response in TIARA reflected limited growth by factors other than N and, to some extent, aliphatic and total GLS decrease in Reflex, where N but not C was presumably scarce. However, GLSs also contain C, and the biosynthetic pathways for N- and C-containing phytochemicals cannot be fully distinguished, as indicated above. This was further documented by Sønderby et al.,[39] who reported an epistatic effect of aliphatic myeloblastosis (MYB) transcription factor on total indole GLS concentration. Moreover, aliphatic GLSs also contain N, although less than indole GLSs. Controlled crop improvement is very often aimed at higher yield, which was demonstrated in our results, where the modern F1 hybrid Reflex showed increased edible yield (Table 1). Therefore, reduced growth and higher N concentration in TIARA might be associated with increased indole GLS percentage, and total GLS concentration, compared with HAT and Reflex, which exhibited higher yield, lower N concentrations, and variable ratios between leaf and stalk growth.

Notable differences between individual GLS concentrations of the cultivars were detected (Figure 2). These differences reflected the diverse growing patterns as a result of increasing N application where the homomethionine-derived aliphatic GLSs glucoiberin and sinigrin concentrations decreased in Reflex opposite no response in TIARA. Further cultivar differences were revealed for the dihomomethionine-derived aliphatic GLSs glucoraphanin and gluconapin with concentration decreases in Reflex in contrast to an optimum of glucoraphanin concentration at 135 kg N $ha^{-1}$ in TIARA. Possibly the activity of methylthioalkylmalate synthase 1 (MAM) and MAM3, which catalyzes condensations in the chain elongation process of homomethionine- and dihomomethionine-derived aliphatic GLSs,[37] responds differently to N and S, dependent on the cultivar. A S-dependent response in MAM activity due to more substrate in the chain elongation process has previously been suggested,[40] whereas our results propose genetically determined diverse N sensitivity. N effects on the indole glucobrassicin

**Table 2. Effects of Nitrogen and Sulfur Available on Glucosinolate Concentrations in the Edible Plant Material of Curly Kale Cultivar Reflex[a]**

| | | aliphatic ($\mu$g g$^{-1}$ DM) | | | | | indole ($\mu$g g$^{-1}$ DM) | | | | aromatic ($\mu$g g$^{-1}$ DM) |
|---|---|---|---|---|---|---|---|---|---|---|---|
| N (kg ha$^{-1}$) | S (kg ha$^{-1}$) | GLI | SIN | GLR | GLN | PRO | GLB | HY | ME | NGLB | GST |
| 90 | 4 | 1041 ± 290[b] | 350 ± 120 | 122 ± 39 | 10 ± 4 | 12 ± 4 | 150 ± 62 | 62 ± 11 | 147 ± 47 | 51 ± 26 | 7 ± 2 |
| | 30 | 2214 ± 176 | 860 ± 204 | 279 ± 37 | 40 ± 8 | 30 ± 8 | 260 ± 61 | 112 ± 24 | 199 ± 4 | 59 ± 6 | 20 ± 5 |
| 135 | 4 | 519 ± 146 | 229 ± 95 | 53 ± 12 | 5 ± 2 | 5 ± 2 | 119 ± 65 | 45 ± 8 | 136 ± 51 | 38 ± 7 | 3 ± 2 |
| | 30 | 1384 ± 227 | 534 ± 17 | 171 ± 35 | 21 ± 4 | 19 ± 5 | 264 ± 5 | 72 ± 21 | 160 ± 2 | 68 ± 24 | 12 ± 1 |
| 185 | 4 | 1094 ± 204 | 406 ± 10 | 125 ± 39 | 11 ± 3 | 15 ± 8 | 246 ± 64 | 62 ± 7 | 129 ± 28 | 48 ± 9 | 8 ± 1 |
| | 30 | 1912 ± 467 | 637 ± 95 | 260 ± 74 | 27 ± 9 | 30 ± 2 | 448 ± 79 | 83 ± 29 | 171 ± 20 | 61 ± 6 | 11 ± 1 |
| significance | | | | | | | | | | | |
| N | | **[c] | * | ** | * | * | NS | NS | NS | NS | ** |
| S | | *** | *** | *** | *** | *** | ** | ** | NS | NS | *** |
| N × S | | NS | NS | NS | NS | NS | NS | NS | NS | NS | * |

[a]For abbreviations please consult Figure 2. [b]± standard deviation. [c]*, $p \leq 0.05$; **, $p < 0.01$; ***, $p < 0.001$ in a general linear model between S and N level means ($n = 3$). NS, not significant.

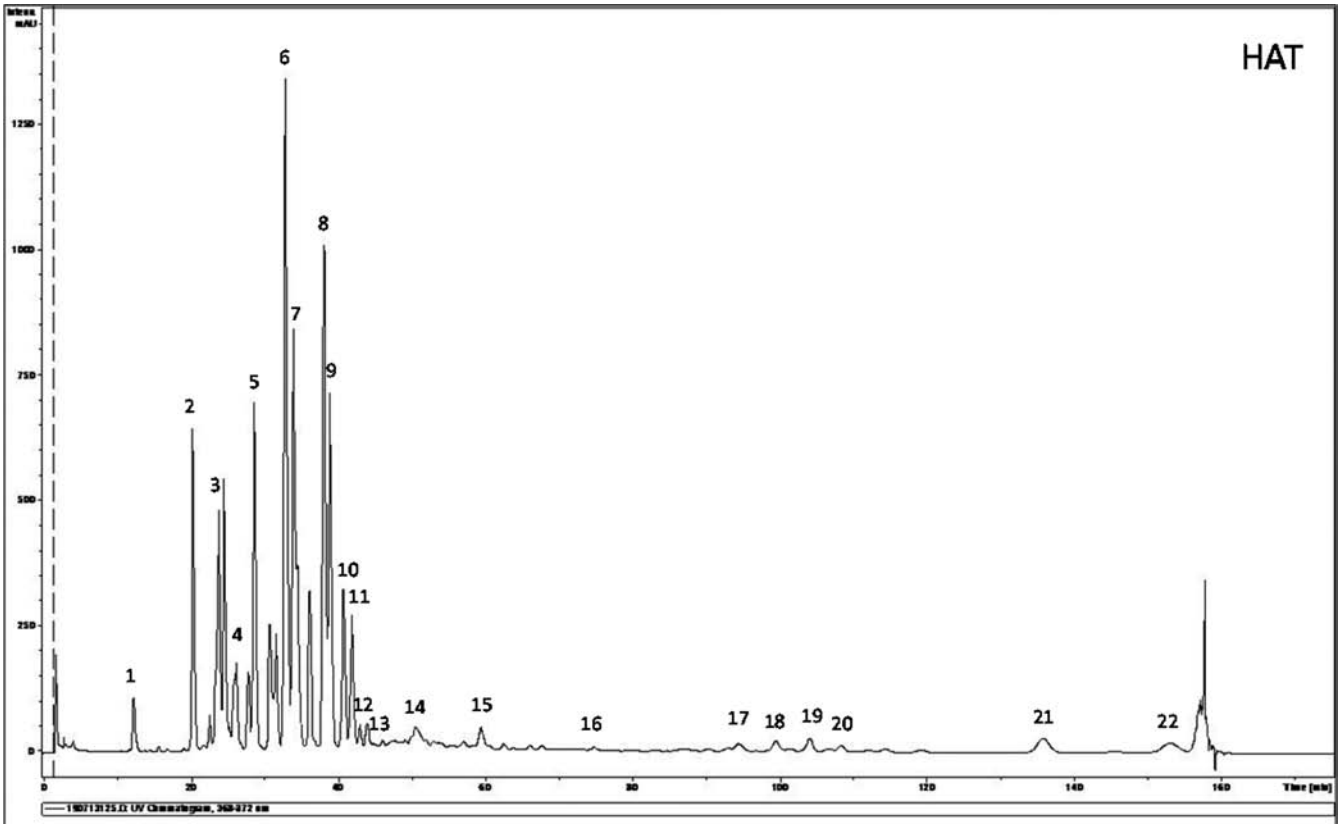


**Figure 4.** Chromatogram of a kale extract at 370 nm measured by HPLC-MS$^n$. For compound names please refer to Table 3.

differed between all cultivars with increasing concentrations in TIARA and no response in Reflex. Furthermore, a trend of more glucobrassicin hydroxylation and methoxylation with increasing N application in TIARA is suggested. Higher susceptibility of indole GLSs to environmental influences[11] supports the diverse responses of indole GLSs among cultivars in contrast to uniform and possibly genetically determined responses to N of aliphatic GLSs within cultivar. In a study of 148 kale landraces (*acephala* group), 5 clusters based on morphologic and agronomic traits differed in total GLS concentration and all individual GLSs except sinigrin.[4] Calculated from the agronomic traits described, the cluster with the highest edible yield contained the highest total GLS concentration, opposite TIARA in our study. The cluster constituted by the tallest plants and lower edible yields had lowest total GLS concentration but highest concentration of glucoiberin. The results suggested a similar relationship between agronomic traits and GLS content, but the agronomic characteristics and GLS concentrations were not comparable. Stalk S status might be important to GLS concentration; internal sulfate pools in *Arabidopsis thaliana* have been documented mobile under S deficiencies due to high vacuolar transporter expression.[41] However, the three cultivars showed no visible signs of S deficiency, that is, uniform chlorosis, and stalk S concentration level was positively related to leaf GLS


dx.doi.org/10.1021/jf503096p | J. Agric. Food Chem. 2014, 62, 11393−11402

**Table 3. Selected Flavonoid Glycosides and Hydroxycinnamic Acid Derivatives in the Edible Plant Material of Curly Kale Cultivars HAT, Reflex, and TIARA (See Figure 4)**

| | |
|---|---|
| nonacylated monoglycoside | isorhamnetin-3-*O*-D-glucoside (peak 19) |
| nonacylated diglycosides | kaempferol-3-*O*-sophoroside (peak 15) |
| | isorhamnetin-3-*O*-D-glucoside-7-*O*-D-glucoside (peak 12) |
| nonacylated triglycosides | quercetin-3-*O*-sophoroside-7-*O*-D-glucoside (peak 2) |
| | kaempferol-3-*O*-sophoroside-7-*O*-D-glucoside (peak 3) |
| | isorhamnetin-3-*O*-sophoroside-7-*O*-D-glucoside (peak 4) |
| | isorhamnetin-3-*O*-triglucoside (peak 14) |
| monoacylated diglycosides | kaempferol-3-*O*-sinapoyl-sophoroside (peak 16) |
| | kaempferol-3-*O*-feruloyl-sophoroside (peak 17) |
| monoacylated triglycosides | kaempferol-3-*O*-hydroxyferuoyl-sophoroside-7-*O*-D-glucoside (peak 5) |
| | quercetin-3-*O*-sinapoyl-sophoroside-7-*O*-D-glucoside (peak 6) |
| | kaempferol-3-*O*-sinapoyl-sophoroside-7-*O*-D-glucoside (peak 8) |
| | kaempferol-3-*O*-feruloyl-sophoroside-7-*O*-D-glucoside (peak 10) |
| | kaempferol-3-*O*-coumaroyl-sophoroside-7-*O*-D-glucoside (peak 13) |
| monoacylated tetraglycosides | kaempferol-3-*O*-sinapoyl-sophoroside-7-*O*-diglucoside (peak 9) |
| | kaempferol-3-*O*-feruloyl-sophoroside-7-*O*-diglucoside (peak 11) |
| | quercetin-3-*O*-sophoroside-7-*O*-sinapoyl-diglucoside (peak 7) |
| diacylated tetraglycosides | quercetin-3-*O*-disinapoyl-triglucoside-7-*O*-D-glucoside (peak 18) |
| | kaempferol-3-*O*-disinapoyl-triglucoside-7-*O*-D-glucoside (peak 20) |
| hydroxycinnamic acid derivatives | caffeoylquinic acid (peak 1) |
| | disinapoylgentiobiose (peak 21) |
| | sinapoyl-feruloyl-gentiobiose (peak 22) |

concentration level rather than exhibiting an inverse relationship. These results indicated the necessity to examine agronomic characteristic and biomass allocation of traditional and F1 hybrid curly kale cultivars to assess altered GLS composition in future research.

*Experiment II: N and S Level Effects.* The GLSs identified were similar to those resolved in experiment I. S application increased the total GLS concentration substantially, besides the percentage of the aliphatic GLS group within total GLS concentration, and decreased indole GLS percentage correspondingly (Figure 3B, $p = 0.00911$; Table 2). Similarly, Stavridou et al.[14] and Rosen et al.[15] showed a comparable response to S fertilization in field studies of broccoli and cabbage, but diverse effects were observed from N supplies. In the current study, an interaction between N and S levels was only found for gluconasturtiin (Table 2). Earlier investigations in other *Brassica* species grown in pots have demonstrated higher level interactions between N and S applications in relationship to GLS concentration.[12,17] Our results obtained under less constricted field conditions showed relatively higher total N uptake at low N fertilizer levels and total S uptake in experiment II (40 kg S $ha^{-1}$ on average when no S was applied; data not included). This reflects influence from other soil properties under field conditions contra, for example, pots or hydroponics, such as N and S mineralization of soil organic matter. These observations might explain the reduced number of interactions between N and S as the N and S soil pool is influenced by other factors in addition to fertilizers applied.[15] They emphasize the challenges in transfer of management methods to manipulate GLS biosynthesis from highly controlled environments to large-scale production under field conditions. Closely related N and S assimilation in plants often causes an interaction between N and S fertilizers in relationship to plant N and S concentrations. APS reductase regulates the balance between S partitioning in primary or secondary metabolism and controls 90% of the primary sulfate reduction, which leads to cysteine and glutathione, which both donate S in core GLS biosynthesis.[37,42] However, Mugford et al.[20] reported that even though APS reductase capacity was reduced and resulted in sulfate accumulation, the GLS pathway end-products showed no decrease in a mutant *Arabidopsis thaliana*. Therefore, although a close relationship existed between N and S assimilation and between primary and secondary S metabolism with respect to GLS biosynthesis, enzyme and substrate levels were under more complex regulation,[20] which was consolidated by multifaceted soil properties in the present study.

**Agronomic Characteristics, Flavonoid Glycosides, and Hydroxycinnamic Acid Derivatives.** *Experiment I: N Level and Cultivar Effects.* Schmidt et al.[23] and Neugart et al.[32] identified 71 flavonoid glycosides and 3 main hydroxycinnamic acid derivatives, which were also detected in HAT, Reflex, and TIARA. We selected 19 structurally different flavonoid glycosides, including the main flavonol glycosides and related structures in kale, and the three main hydroxycinnamic acid derivatives to examine cultivar and N level effects on these phytochemicals (Figure 4; Table 3). Kaempferol glycosides were the main constituent in the three kale cultivars, followed by hydroxycinnamic acid derivatives, and quercetin glycosides (Table 4). Quercetin and total flavonoid glycosides decreased with increasing N application in Reflex. This was in line with the results of Stewart et al.,[26] who found decreasing concentrations of quercetin and total flavonoid aglycones as well as kaempferol and isorhamnetin in *Arabidopsis thaliana* when increasing N levels were applied. Furthermore, another *Arabidopsis* study revealed a broad and clear coordinated response to $NO_3^-$ addition in genes controlling phenylpropanoid and flavonoid metabolism, as well as primary metabolism, suggesting a shift away from C-rich phytochemicals, such as flavonols.[19] This corresponded to the balance between N and C in relationship to primary and secondary metabolism as discussed in connection to GLSs.

Higher quercetin glycoside and lower isorhamnetin glycoside concentrations in Reflex, as compared to HAT ($p < 0.0001$ and $p < 0.01$, respectively), indicated decreased quercetin to isorhamnetin conversion in Reflex, possibly due to the reduced activity of the responsible enzyme, quercetin-3-*O*-methyltransferase, which is suggested not to be affected by N concentration.[40] Cultivar differences in our study do not support this as Reflex seemed to be more responsive to N fertilization with respect to phytochemical modulation as well as biomass production. A study on two F1 kale hybrids revealed no changes

**Table 4. Effects of Available Nitrogen and Cultivar on Flavonoid Glycoside and Total Hydroxycinnamic Acid Derivative Concentrations in the Edible Plant Material of Curly Kale Cultivars HAT, Reflex, and TIARA**

| N ($kg\ ha^{-1}$) | cv. | kaempferol glycosides ($mg\ g^{-1}$ DM) | quercetin glycosides ($mg\ g^{-1}$ DM) | isorhamnetin glycosides ($mg\ g^{-1}$ DM) | total flavonoid glycosides ($mg\ g^{-1}$ DM) | total hydroxycinnamic acid derivatives ($mg\ g^{-1}$ DM) |
|---|---|---|---|---|---|---|
| 90 | HAT | 6.43 ± 0.69[a] | 1.89 ± 0.58 | 1.05 ± 0.69 | 9.37 ± 0.60 | 2.39 ± 0.09 |
| 230 | | 5.60 ± 0.96 | 1.37 ± 0.23 | 0.62 ± 0.11 | 7.58 ± 0.97 | 2.20 ± 0.38 |
| N effect | | NS[b] | NS | NS | NS | NS |
| 90 | Reflex | 5.39 ± 0.08 | 3.52 ± 0.34 | 0.20 ± 0.02 | 9.12 ± 0.44 | 2.15 ± 0.02 |
| 135 | | 4.98 ± 0.28 | 2.99 ± 0.20 | 0.19 ± 0.01 | 8.16 ± 0.33 | 2.12 ± 0.17 |
| 185 | | 5.32 ± 0.18 | 2.74 ± 0.34 | 0.21 ± 0 | 8.27 ± 0.49 | 2.08 ± 0.15 |
| 230 | | 5.22 ± 0.35 | 2.36 ± 0.26 | 0.21 ± 0.02 | 7.79 ± 0.57 | 1.90 ± 0.11 |
| N effect | | NS | ** | NS | * | NS |
| 90 | TIARA | 6.71 ± 2.34 | 2.87 ± 0.76 | 0.67 ± 0.14 | 10.26 ± 2.39 | 3.51 ± 1.08 |
| 135 | | 6.87 ± 0.72 | 3.21 ± 1.55 | 0.64 ± 0.08 | 10.72 ± 2.34 | 3.48 ± 0.52 |
| 185 | | 6.47 ± 1.39 | 1.68 ± 0.57 | 0.82 ± 0.21 | 8.97 ± 2.03 | 4.09 ± 1.05 |
| 230 | | 5.43 ± 1.20 | 1.67 ± 0.55 | 0.60 ± 0.18 | 7.70 ± 1.83 | 3.52 ± 0.12 |
| N effect | | NS | NS | NS | NS | NS |
| | | | | | | |
| significance | | | | | | |
| N | | NS | ** | NS | NS | NS |
| CV | | NS | ** | *** | NS | *** |
| N × CV | | NS | NS | NS | NS | NS |

[a] ± standard deviation. [b] *, $p \leq 0.05$; **, $p < 0.01$; ***, $p < 0.001$ in a general linear model among N level and cultivar means ($n = 3$) within chemical group. NS, not significant.

in phenolic compound concentrations when application of N increased, although yield increased in one of the cultivars.[43] Kaempferol is a precursor to quercetin, and isorhamnetin is a methylated product of quercetin; therefore, the lack of response of kaempferol and isorhamnetin to increased N levels might be due to the absence of a catechol structure in the B-ring and, consequently, a lower antioxidant activity.[44] However, both increases and decreases in concentrations of individual kaempferol flavonoids were revealed in tronchuda cabbage (*B. oleracea* L. var. *costata* DC.) grown under moderate and high N levels.[45] Variations were due to harvest time and plant part, with no consistency, suggesting additional ontogenetic and environmental influences. The above-mentioned indicates that the F1 hybrid Reflex was more responsive to N fertilization compared to TIARA and HAT. This could be explained by breeding focusing on increased biomass production, which strictly relates to N responsiveness and possibly corresponds to the clear response to N fertilization as the agronomic characteristics revealed in the present study.

N level had no effect on total hydroxycinnamic acid derivatives (Table 4). TIARA had the highest concentration of hydroxycinnamic acid derivatives, as well as isorhamnetin glycosides compared to Reflex ($p < 0.0001$). This might reflect different cultivar yields, like for the GLSs. However, cinnamic acid is the flavonoid and hydroxycinnamic acid precursor, and its biosynthesis is controlled by phenylalanine ammonia-lyase (PAL) activity, which is responsible for phenylalanine conversion into cinnamic acid in flavonol biosynthesis.[46] Increased N levels have been found to reduce PAL activity.[47] Therefore, elevated N concentration in TIARA does not support our results. Furthermore, high N concentration and reduced plant growth might shift secondary metabolism toward N-containing phytochemicals, as argued earlier. Simple linear regression results between flavonoid glycoside groups or total hydroxycinnamic acid derivatives and either leaf N concentration or total N uptake revealed no relationships between these parameters for any of the cultivars (data not included). Inconsistent with our results, Fallovo et al.[40] found a negative linear relationship between quercetin and kaempferol as well as total flavonoids and N concentration in *Brassica rapa* and *Brassica juncea* leaves. However, in Reflex a negative linear relationship between edible yield and kaempferol, quercetin, and total flavonoid glycosides was detected ($p = 0.0345$, $R^2 = 0.18$; $p < 0.0001$, $R^2 = 0.52$ and $p < 0.0001$, $R^2 = 0.58$, respectively). These results support the effects of N application and agronomic characteristic on flavonoid glycosides and hydroxycinnamic acid derivatives if we assume Reflex was N but not C limited at high edible yield levels.

Distinct agronomic characteristics among the three kale cultivars were associated with a diverse non-, mono-, and diacylated mono-, di-, or tetraglycosylated flavonoid composition ($p < 0.001$). Whereas the nonacylated monoglycoside (isorhamnetin-3-*O*-D-glucoside) was detected only in HAT, the nonacylated diglycosides were comparable in the traditional cultivars HAT and TIARA. Lower concentrations were resolved in the F1 hybrid Reflex ($p < 0.001$), possibly due to higher edible yield. The main kale flavonoid glycosides, the monoacylated tri- and tetraglycosides, decreased in concentration with increasing N application in Reflex (Figure 5). Likewise, the minor monoacylated diglycosides decreased in TIARA. Schmidt et al.[5] reported similar cultivar effects on flavonoid glycosides in kale as a response to changing temperature and radiation. The different responses to N application of Reflex and TIARA might therefore explain the variable effects on monoacylated diglycosides and monoacylated tri- and tetraglycosides. A study in cauliflower showed a higher kaempferol-3-diglucoside-7-diglucoside concentration with mineral fertilizer application containing less total N due to a high share of compost compared to the other cultivation methods.[48] Diacylated tetraglycoside concentrations in TIARA seemed to follow elevated leaf N level patterns at 135 and 230 kg N $ha^{-1}$ applications. This was inconsistent with the results of Scheible et al.,[19] suggesting less C-rich phytochemicals under high $NO_3^-$ levels. We propose a different response to excess N uptake in TIARA, because glucose molecules, as a result of primary metabolism, possibly lead to glycosylation resulting in

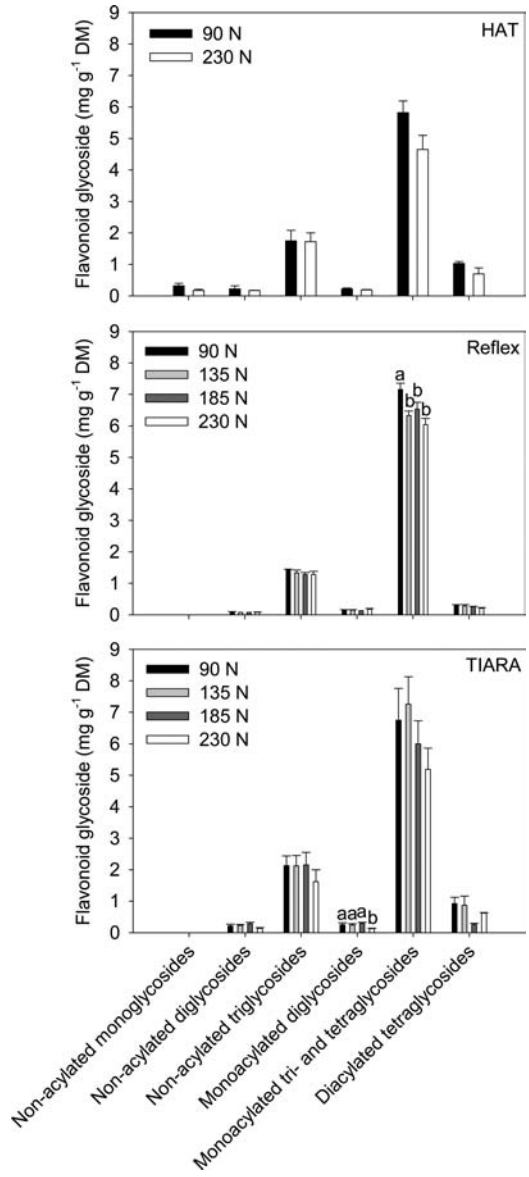


**Figure 5.** Effects of nitrogen (N) available (kg $ha^{-1}$) on flavonoid glycoside concentration (mg $g^{-1}$ DM) in the edible plant material of curly kale cultivars HAT, Reflex, and TIARA. Different letters indicate significant differences ($p \leq 0.05$) in a general linear model among N level means ($n = 3$) within flavonoid glycoside group. Bars represent standard errors.

higher diacylated tetraglycoside concentrations. Fritz et al.[49] found elevated glucose concentration in N-replete compared to N-deficient tobacco plants (*Nicotiana tabacum* L.), supporting our suggestion. Results did not reveal differences in free glucose levels among cultivars and N levels (0.82 mg $g^{-1}$ DM on average, data not included), which indicates all cultivars had the same threshold for free glucose, in contrast to the moiety levels in GLS or flavonoid glycoside molecules, which differed between cultivars. In summary, monoacylated diglycosides and monoacylated tri- and tetraglycosides decreased with increasing N application in TIARA and Reflex, respectively. The main kale glycosides, that is, nonacylated triglycosides, were not affected.

In conclusion, genetic differences between traditional and F1 hybrid cultivars were reflected in cultivar agronomic characteristics and N responses and could be associated with phytochemical composition and concentration. Our results emphasize that N and S fertilizer management and cultivar selection can be used as a tool for optimization of GLS and flavonoid concentrations as well as edible yield. However, the target of interest subsequently defines the choice of cultivar and fertilizer strategy. Furthermore, it points to the positive perspective of reintroduction of traditional kale cultivars with health beneficial compounds and, additionally, the potential role of phytochemicals related to sensory properties, as reported by Jensen et al.[10]

## AUTHOR INFORMATION

### Corresponding Author

*(M.G.) Phone: +45 87158327. Fax: +45 87154891. E-mail: Marie.Gronbaek@agrsci.dk.

### Funding

This work was a part of the "MaxVeg" project financed by The Danish Council for Strategic Researchs Programme Commission on Health, Food and Welfare.

### Notes

The authors declare no competing financial interest.

## ACKNOWLEDGMENTS

We are grateful to Astrid Bergmann, Jens Barfod, and Knud Erik Pedersen for performing the field experiments and to Birgitte Foged and Antje Bamberg for contributing to the chemical analyses.

## ABBREVIATIONS USED

APS, adenosine 5′-phosphosulfate; DM, dry matter; GLB, glucobrassicin; GLI, glucoiberin; GLN, gluconapin; GLR, glucoraphanin; GLS, glucosinolate; GST, gluconasturtiin; HAT, Høj Amager Toftø; HY, 4-hydroxyglucobrassicin; LS, least-squares; MAM, methylthioalkylmalate synthase; ME, 4-methoxyglucobrassicin; MeOH, methanol; MYB, myeloblastosis; NGLB, neoglucobrassicin; PAL, phenylalanine ammonia-lyase; PRO, progoitrin; SIN, sinigrin; TIARA, Halvhøj Ekstra Moskruset TIARA

## REFERENCES

(1) Fahey, J. W.; Zalcmann, A. T.; Talalay, P. The chemical diversity and distribution of glucosinolates and isothiocyanates among plants. *Phytochemistry* **2001**, *56*, 5−51.

(2) Christensen, S.; Bothmer, R.; Poulsen, G.; Maggioni, L.; Phillip, M.; Andersen, B. A.; Jørgensen, R. B. AFLP analysis of genetic diversity in leafy kale (*Brassica oleracea* L. convar. *acephala* (DC.) Alef.) landraces, cultivars and wild populations in Europe. *Genet. Resour. Crop Evol.* **2011**, *58*, 657−666.

(3) Kopsell, D. A.; Kopsell, D. E.; Curran-Celentano, J. Carotenoid pigments in kale are influenced by nitrogen concentration and form. *J. Sci. Food Agric.* **2007**, *87*, 900−907.

(4) Cartea, M.; Velasco, P.; Obregon, S.; Padilla, G.; Haro, A. Seasonal variation in glucosinolate content in *Brassica oleracea* crops grown in northwestern Spain. *Phytochemistry* **2008**, *69*, 403−410.

(5) Schmidt, S.; Zietz, M.; Schreiner, M.; Rohn, S.; Kroh, L. W.; Krumbein, A. Genotypic and climatic influences on the concentration and composition of flavonoids in kale (*Brassica oleracea* var. *sabellica*). *Food Chem.* **2010**, *119*, 1293−1299.

(6) Kushad, M. M.; Brown, A. F.; Kurilich, A. C.; Juvik, J. A.; Klein, B. P.; Wallig, M. A.; Jeffery, E. H. Variation of glucosinolates in vegetable crops of *Brassica oleracea*. *J. Agric. Food Chem.* **1999**, *47*, 1541−1548.

(7) Nilsson, J.; Olsson, K.; Engqvist, G.; Ekvall, J.; Olsson, M.; Nyman, M.; Akesson, B. Variation in the content of glucosinolates, hydroxycinnamic acids, carotenoids, total antioxidant capacity and

low-molecular-weight carbohydrates in *Brassica* vegetables. *J. Sci. Food Agric.* **2006**, *86*, 528−538.
(8) Verhoeven, D. T. H.; Verhagen, H.; Goldbohm, R. A.; van den Brandt, P. A.; van Poppel, G. A review of mechanisms underlying anticarcinogenicity by brassica vegetables. *Chem.−Biol. Interact.* **1997**, *103*, 79−129.
(9) Williams, D. J.; Pun, S. Glucosinolates in *Brassica* vegetables: role in bitterness and hence significance. *Food Aust.* **2011**, *63*, 407−412.
(10) Jensen, S.; Groenbaek, M.; Beck, T. K.; Kristensen, H. L.; Kidmose, U. Influence of cultivar and fertilizer approach on curly kale (*Brassica oleracea* L. var. *sabellica*). 2. Variations in the content of phytochemicals and how it is reflected in the sensory properties. *J. Agric. Food Chem.* **2014**, submitted.
(11) Brown, P. D.; Tokuhisa, J. G.; Reichelt, M.; Gershenzon, J. Variation of glucosinolate accumulation among different organs and developmental stages of *Arabidopsis thaliana*. *Phytochemistry* **2003**, *62*, 471−481.
(12) Groenbaek, M.; Kristensen, H. L. Split dose fertilization with urea increases glucosinolate contents in white cabbage (*Brassica oleracea* L. var. *capitata*) under experimental pot conditions. *Sci. Hortic.* **2014**, *168*, 64−72.
(13) Jones, R. B.; Imsic, M.; Franz, P.; Hale, G.; Tomkins, R. B. High nitrogen during growth reduced glucoraphanin and flavonol content in broccoli (*Brassica oleracea* var. *italica*) heads. *Aust. J. Exp. Agric.* **2007**, *47*, 1498−1505.
(14) Stavridou, E.; Kristensen, H. L.; Krumbein, A.; Schreiner, M.; Thorup-Kristensen, K. Effect of differential N and S competition in inter- and sole cropping of *Brassica* species and lettuce on glucosinolate concentration. *J. Agric. Food Chem.* **2012**, *60*, 6268−6278.
(15) Rosen, C. J.; Fritz, V. A.; Gardner, G. M.; Hecht, S. S.; Carmella, S. G.; Kenney, P. M. Cabbage yield and glucosinolate concentrations as affected by nitrogen and sulfur fertility. *HortScience* **2005**, *40*, 1493−1498.
(16) Omirou, M. D.; Papadopoulou, K. K.; Papastylianou, I.; Constantinou, M.; Karpouzas, D. G.; Asimakopoulos, I.; Ehaliotis, C. Impact of nitrogen and sulfur fertilization on the composition of glucosinolates in relation to sulfur assimilation in different plant organs of broccoli. *J. Agric. Food Chem.* **2009**, *57*, 9408−9417.
(17) Schonhof, I.; Blankenburg, D.; Muller, S.; Krumbein, A. Sulfur and nitrogen supply influence growth, product appearance, and glucosinolate concentration of broccoli. *J. Plant Nutr. Soil Sci.* **2007**, *170*, 65−72.
(18) Bryant, J. P.; Chapin, F. S.; Klein, D. R. Carbon nutrient balance of boreal plants in relation to vertebrate herbivory. *Oikos* **1983**, *40*, 357−368.
(19) Scheible, W. R. d.; Morcuende, R.; Czechowski, T.; Fritz, C.; Osuna, D.; Palacios-Rojas, N.; Schindelasch, D.; Thimm, O.; Udvardi, M. K.; Stitt, M. Genome-wide reprogramming of primary and secondary metabolism, protein synthesis, cellular growth processes, and the regulatory infrastructure of *Arabidopsis* in response to nitrogen. *Plant Physiol.* **2004**, *136*, 2483−2499.
(20) Mugford, S. G.; Lee, B. R.; Koprivova, A.; Matthewman, C.; Kopriva, S. Control of sulfur partitioning between primary and secondary metabolism. *Plant J.* **2011**, *65*, 96−105.
(21) Manach, C.; Williamson, G.; Morand, C.; Scalbert, A.; Remesy, C. Bioavailability and bioefficacy of polyphenols in humans. I. Review of 97 bioavailability studies. *Am. J. Clin. Nutr.* **2005**, *81*, 230−242.
(22) Zietz, M.; Weckmuller, A.; Schmidt, S.; Rohn, S.; Schreiner, M.; Krumbein, A.; Kroh, L. W. Genotypic and climatic influence on the antioxidant activity of flavonoids in kale (*Brassica oleracea* var. *sabellica*). *J. Agric. Food Chem.* **2010**, *58*, 2123−2130.
(23) Schmidt, S.; Zietz, M.; Schreiner, M.; Rohn, S.; Kroh, L. W.; Krumbein, A. Identification of complex, naturally occurring flavonoid glycosides in kale (*Brassica oleracea* var. *sabellica*) by high-performance liquid chromatography diode-array detection/electrospray ionization multi-stage mass spectrometry. *Rapid Commun. Mass Spectrom.* **2010**, *24*, 2009−2022.
(24) Hämäläinen, M.; Nieminen, R.; Vuorela, P.; Heinonen, M.; Moilanen, E. Anti-inflammatory effects of flavonoids: genistein, kaempferol, quercetin, and daidzein inhibit STAT-1 and NF-κB activations, whereas flavone, isorhamnetin, naringenin, and pelargonidin inhibit only NF-κB activation along with their inhibitory effect on iNOS expression and NO production in activated macrophages. *Mediators Inflamm.* **2007**, *58*, 657−666.
(25) Hollman, P. C. H.; Devries, J. H. M.; Vanleeuwen, S. D.; Mengelers, M. J. B.; Katan, M. B. Absorption of dietary quercetin glycosides and quercetin in healthy ileostomy volunteers. *Am. J. Clin. Nutr.* **1995**, *62*, 1276−1282.
(26) Stewart, A. J.; Chapman, W.; Jenkins, G. I.; Graham, I.; Martin, T.; Crozier, A. The effect of nitrogen and phosphorus deficiency on flavonol accumulation in plant tissues. *Plant Cell Environ.* **2001**, *24*, 1189−1197.
(27) Li, J.; Zhu, Z.; Gerendas, J. Effects of nitrogen and sulfur on total phenolics and antioxidant activity in two genotypes of leaf mustard. *J. Plant Nutr.* **2008**, *31*, 1642−1655.
(28) NordGen germplasm collection. http://www.nordgen.org/index.php/en/content/view/full/2/ (accessed June 27, 2014).
(29) VDLUFA. *Stickstoffverbindungen, Band III, Die chemische Untersuchung von Futtermitteln*, 3rd ed.; VDLUFA-Verlag: Darmstadt, Germany, 1976; Vol. 4.
(30) VDLUFA. *Mengenelemente, Methodenbuch*, 3rd ed.; VDLUFA-Verlag: Darmstadt, Germany, 1976; Vol. 10.
(31) Beck, T. K.; Jensen, S.; Bjoern, G. K.; Kidmose, U. The masking effect of sucrose on perception of bitter compounds in *Brassica* vegetables. *J. Sens. Stud.* **2014**, *29*, 190−200.
(32) Neugart, S.; Zietz, M.; Schreiner, M.; Rohn, S.; Kroh, L. W.; Krumbein, A. Structurally different flavonol glycosides and hydroxycinnamic acid derivatives respond differently to moderate UV-B radiation exposure. *Physiol. Plant.* **2012**, *145*, 582−593.
(33) Padilla, G.; Cartea, M. E.; Ordas, A. Comparison of several clustering methods in grouping kale landraces. *J. Am. Soc. Hortic. Sci.* **2007**, *132*, 387−395.
(34) Maynard, D. N.; Barker, A. V.; Minotti, P. L.; Peck, N. H. Nitrate accumulation in vegetables. *Adv. Agron.* **1976**, *28*, 71−118.
(35) Reuveny, Z.; Dougall, D. K.; Trinity, P. M. Regulatory coupling of nitrate and sulfate assimilation pathways in cultured tobacco cells. *Proc. Natl. Acad. Sci. U.S.A.* **1980**, *77*, 6670−6672.
(36) Koprivova, A.; Suter, M.; den Camp, R. O.; Brunold, C.; Kopriva, S. Regulation of sulfate assimilation by nitrogen in *Arabidopsis*. *Plant Physiol.* **2000**, *122*, 737−746.
(37) Sønderby, I. E.; Geu-Flores, F.; Halkier, B. A. Biosynthesis of glucosinolates − gene discovery and beyond. *Trends Plant Sci.* **2010**, *15*, 283−290.
(38) La, G. X.; Fang, P.; Teng, Y. B.; Li, Y. J.; Lin, X. Y. Effect of CO2 enrichment on the glucosinolate contents under different nitrogen levels in bolting stem of Chinese kale (*Brassica alboglabra* L.). *J. Zhejiang Univ. Sci. B* **2009**, *10*, 454−464.
(39) Sønderby, I. E.; Burow, M.; Rowe, H. C.; Kliebenstein, D. J.; Halkier, B. A. A complex interplay of three R2R3MYB transcription factors determines the profile of aliphatic glucosinolates in *Arabidopsis*. *Plant Physiol.* **2010**, *153*, 348−363.
(40) Fallovo, C.; Schreiner, M.; Schwarz, D.; Colla, G.; Krumbein, A. Phytochemical changes induced by different nitrogen supply forms and radiation levels in two leafy *Brassica* species. *J. Agric. Food Chem.* **2011**, *59*, 4198−4207.
(41) Kataoka, T.; Watanabe-Takahashi, A.; Hayashi, N.; Ohnishi, M.; Mimura, T.; Buchner, P.; Hawkesford, M. J.; Yamaya, T.; Takahashi, H. Vacuolar sulfate transporters are essential determinants controlling internal distribution of sulfate in *Arabidopsis*. *Plant Cell* **2004**, *16*, 2693−2704.
(42) Vauclare, P.; Kopriva, S.; Fell, D.; Suter, M.; Sticher, L.; von Ballmoos, P.; Krahenbuhl, U.; den Camp, R. O.; Brunold, C. Flux control of sulphate assimilation in *Arabidopsis thaliana*: adenosine 5′-phosphosulphate reductase is more susceptible than ATP sulphurylase to negative control by thiols. *Plant J.* **2002**, *31*, 729−740.
(43) Lata, B. Variability in enzymatic and non-enzymatic antioxidants in red and green-leafy kale in relation to soil type and N-level. *Sci. Hortic.* **2014**, *168*, 38−45.
(44) Fiol, M.; Adermann, S.; Neugart, S.; Rohn, S.; Mugge, C.; Schreiner, M.; Krumbein, A.; Kroh, L. W. Highly glycosylated and

acylated flavonols isolated from kale (*Brassica oleracea* var. *sabellica*) – structure-antioxidant activity relationship. *Food Res. Int.* **2012**, *47*, 80–89.

(45) Sousa, C.; Pereira, D. M.; Pereira, J. A.; Bento, A.; Rodrigues, M. A.; Dopico-Garcia, S.; Valentao, P.; Lopes, G.; Ferreres, F.; Seabra, R. M.; Andrade, P. B. Multivariate analysis of tronchuda cabbage (*Brassica oleracea* L. var. *costata* DC) phenolics: influence of fertilizers. *J. Agric. Food Chem.* **2008**, *56*, 2231–2239.

(46) Hahlbrock, K.; Grisebach, H. Enzymic controls in the biosynthesis of lignin and flavonoids. *Annu. Rev. Plant Physiol. Plant Mol. Biol.* **1979**, *30*, 105–130.

(47) Ibrahim, M. H.; Jaafar, H. Z. E.; Rahmat, A.; Rahman, Z. A. Effects of nitrogen fertilization on synthesis of primary and secondary metabolites in three varieties of kacip fatimah (*Labisia pumila* Blume). *Int. J. Mol. Sci.* **2011**, *12*, 5238–5254.

(48) Martinez-Blanco, J.; Anton, A.; Rieradevall, J.; Castellari, M.; Munoz, P. Comparing nutritional value and yield as functional units in the environmental assessment of horticultural production with organic or mineral fertilization. *Int. J. Life Cycle Assess.* **2011**, *16*, 12–26.

(49) Fritz, C.; Palacios-Rojas, N.; Feil, R.; Stitt, M. Regulation of secondary metabolism by the carbon-nitrogen status in tobacco: nitrate inhibits large sectors of phenylpropanoid metabolism. *Plant J.* **2006**, *46*, 533–548.

**Table 1. Characteristics of Compounds Used in the Study**

| Code | Commercial name | Active ingredient (concentration) | | General use | Concentration used* |
|---|---|---|---|---|---|
| A | Aliette® Flash | Fosetyl-Aluminium (80% w/w) | 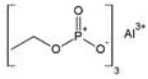 | Fungicide and/or PRI | 3 g/L |
| B | Amid Thin® W | 1-Naphthaleneacetamide (8.4% w/w) | | Thinning agent | 0.6 g/L |
| C | Bion® 50 WG | Acibenzolar-*S*-methyl (50% w/w) | | PRI | 0.4 g/L |
| D | Iodus®2 CS | Laminarin (4.5% w/v) | 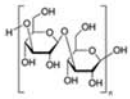 | PRI | 7.5 mL/L |
| E | MaxCel® | 6-benzyladenine (1.9% w/v) | 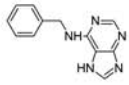 | Thinning agent | 7.5 mL/L |
| F | PRM 12® RP | Etephon (12% w/v) | 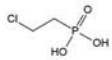 | Thinning agent | 3 mL/L |
| G | Regalis® | Prohexadione-Ca (10% w/w) | | Growth regulator | 2.5 g/L |
| H | Rhodofix® | Naphthalene acetic acid (1% w/w) | | Thinning agent | 1.5 g/L |
| I | Stifenia® | Fen 560 (Fenugrec 100% w/w) | | PRI | 10 g/L |
| J | V-Plaask® | Organic mixture, K, Ca, Mg, B + salicylic acid derivatives (concentration not given) | | Fertilizer + PRI | 10 mL/L |
| K | Agrimycin® 17 | Streptomycin (17% w/w) | | Bactericide | 0.1 g/L |

*Concentration of commercial product.

costly in terms of time and price. Protection assays in field conditions also require infrastructures and regulatory agreements to manipulate pathogen inocula or rely on natural infections that may fluctuate from year to year. In addition, the number of candidate preparations regularly increases, and recent results suggest that new PRIs will soon be identified with the design of miniaturized cultivation systems involving the model plant *Arabidopsis* to test many compounds in <2 days.[16,17] However, because of the specificity of plant responsiveness to a given compound, it is obvious that ultimate assays must use the pathosystem of interest. In addition, it is noteworthy that the cuticle, a physical barrier that may prevent foliar-sprayed PRIs from reaching cellular targets, differs in thickness and composition between plant species.

In the present study we developed a methodology for the upstream screening of PRIs against the causative agent of fire blight, *Erwinia amylovora*, on young apple (*Malus* × *domestica*) plants. Fire blight is a devastating disease affecting apples, pears, and more generally members of the *Malinae* (ex *Maloideae*) tribe of the family *Rosaceae*.[18] Its control is far from optimal due to the limited number of efficient bactericidal chemicals and because it occurs very sporadically, with outbreaks difficult to forecast. Furthermore, the obvious long-term breeding programs for resistance do not allow quick response to spatiotemporally limited attacks.[18] All of these specificities explain why fire blight is still expanding around the world with regular outbreaks[19] and why it has been classified as a quarantine disease in most countries. The use of PRIs to confer protection against *E. amylovora* is an attractive strategy to prevent or reduce incidence of fire blight to an acceptable level. Our methodology to screen PRIs relies on the ability of a given PRI to trigger activation of defenses in conditions that favor resistance development without the use of the pathogen even for the evaluation of priming agents. It includes (i) the foliar spraying of candidate preparations on plantlets in greenhouse assays, (ii) the possible subsequent foliar spraying of hydrogen peroxide ($H_2O_2$) to simulate a pathogen attack and to discriminate compounds that directly activate defense genes from those that prime immunity, and (iii) the monitoring of transcription levels of 28 carefully selected defense genes that are part of the plant defense system[4] including PR-proteins, secondary metabolic pathways, cell wall modifications, antioxidant mechanisms, and signaling pathways in apple tissue after PRI application. The 28 defense genes were chosen to represent the widest diversity of known defense mechanisms but in a user-friendly format (96-well qPCR). Using this methodology, we compared the ability of several PRI candidates and plant growth regulators to induce apple defenses as well as to protect against fire blight in semicontrolled conditions. Our aim

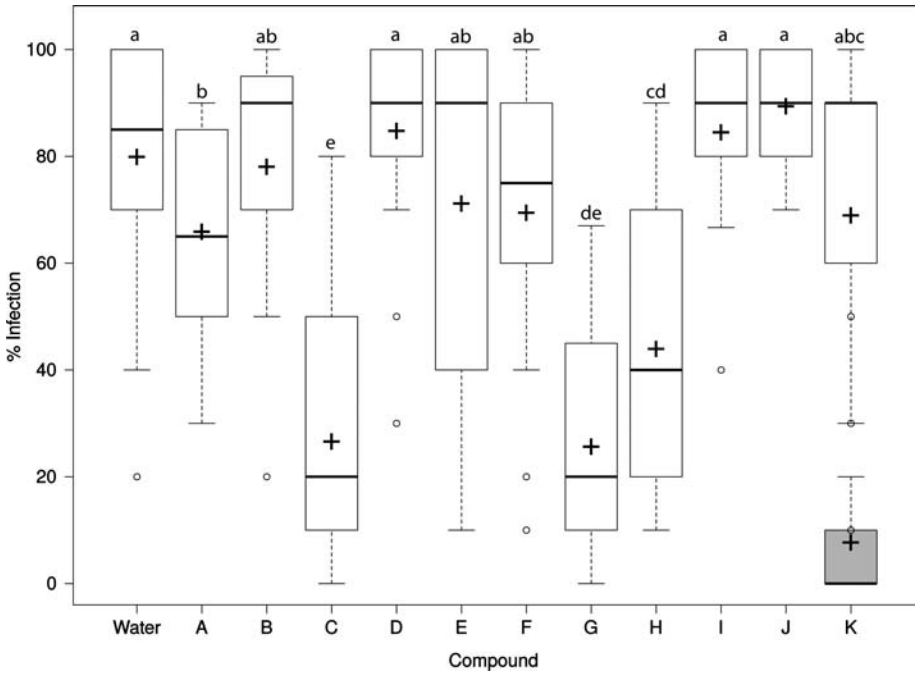


**Figure 1.** Efficacy of 10 candidate PRIs (A–J) against fire blight on apple seedlings. PRIs were applied 4 days before leaf inoculation with *E. amylovora*. Water (applied 4 days before inoculation) and product K (applied 4 days before inoculation, white box) were used as negative controls. Product K applied 4 h before inoculation (gray box) was used as a positive biocidal control. Data are percentages of plants exhibiting a progressive necrosis on stem per plot of 10 plants ($n \geq 15$, i.e., 3 plots per experiment × 5 independent experiments at least). Medians are represented by black horizontal segments in each box and means by "+" symbols. Boxes with the same letters represent means that are not significantly different.

was to demonstrate that monitoring the expression of a few genes may be of great usefulness to discriminate active from nonactive compounds on apple tissues and reduce their number included in further tests.

## MATERIAL AND METHODS

**Materials and General Methodologies.** Experiments were conducted on apple seedlings (4–6 leaves) from open-pollinated cv. Golden Delicious grown in a greenhouse under semicontrolled conditions (natural photoperiod supplemented with artificial light if needed, 17 °C night, 23–30 °C day, according to the sunlight). A virulent French standard strain CFBP1430 of *E. amylovora* was used for the inoculations.[20] Bacteria were grown for 24 h at 27 °C on King's medium B, allowing bacterial cells to reach the exponential growth phase.[21] Bacterial suspensions were prepared in reverse osmosis water to yield a concentration of $10^8$ colony-forming units (CFU)/mL and sprayed on entire seedlings to runoff with the help of a pressurized hand sprayer. The compounds tested in this study were the following: (A) Aliette Flash (Bayer CropScience, France), (B) Amid Thin W (Nufarm SAS, France), (C) Bion 50 WG (Syngenta, Switzerland), (D) Iodus 2 CS (Goëmar, France), (E) MaxCel (Philagro, France), (F) PRM 12 RP (Bayer CropScience, France), (G) Regalis (BASF, Germany), (H) Rhodofix (Nufarm SAS, France), (I) Stifenia (SOFT, France), (J) V-Plaask (Plaaskem, Italy), and (K) Agrimycin 17 (Nufarm SAS, France). Their known characteristics are given in Table 1. They were prepared in reverse osmosis water and sprayed on entire seedlings to runoff with the help of an electric airless spray painter.

**Testing of the Protective Efficiency.** In each experiment, the experimental design was a randomized block of 3 plots of 10 seedlings per treatment. Compounds (or water) were sprayed 4 days before inoculation. On the morning of the day of inoculation, the youngest nearly expanded leaf of each plant was wounded by a double incision perpendicular to the midrib near the petiole, and the bacterial suspension was sprayed 4 h later. As biocidal control, untreated plants were sprayed with product K immediately after wounding and allowed to dry for 4 h before inoculation. Symptoms were assessed 3 weeks later. Disease incidence (DI), that is, the percentage of plants exhibiting a progressive necrosis on stem, was calculated per plot. The protection rate in each plot $X$ was also set as follows: % protection = $[(\mu DI_{water} - DI_X)/\mu DI_{water})] \times 100$, where $\mu DI_{water}$ is the mean of DI of the three plots of water control and where negative values are treated as if they were zero. Each treatment was repeated in five independent biological experiments at least, and all experiments contained the two controls, water, and the biocidal reference.

**Defenses Analyses.** The experimental design was a randomized block of 5 plots of 5 seedlings per treatment. One day after application of compounds, the five youngest expanded leaves of one plot per block were collected, pooled, frozen in liquid nitrogen, and kept at −80 °C until extraction. Then 2 of the 4 remaining plots per block were sprayed with 40 mM $H_2O_2$ to runoff with a trigger sprayer. The five youngest expanded leaves per plot (treated with $H_2O_2$ or not) were sampled on days 2 and 3 as on day 1. RNA extraction, reverse-transcription, and quantitative real-time PCR were performed as previously described,[22] using the same set of primers of 28 defense genes and of 3 reference genes.[23] Relative changes in defense gene expression were calculated using the $2^{-\Delta\Delta Ct}$ method[24] and the 3 internal reference genes for normalization[25] and relative to water control plants at every sampling date. Three independent biological experiments were performed.

**Data Analyses.** The statistical programming environment R[26] was used for all data analyses. To compare protection efficiency, a nonparametric rank-based statistical test was used. Means of disease incidence were pairwise compared with a Wilcoxon test, and corresponding $p$ values were adjusted using the Benjamini–Hochberg correction. Treatments were declared to significantly differ for a corrected $p$ value <0.05. Clustering of gene expression in the heatmap representation was performed using dissimilarity distance (1 − cor($X$,$Y$)). In the principal component analysis (PCA), plots and correlation coefficients of each variable (gene) versus each dimension were obtained using the FactoMineR R package.[27] Statistical evaluation of treatment effects on defense response was done with multivariate ANOVA.

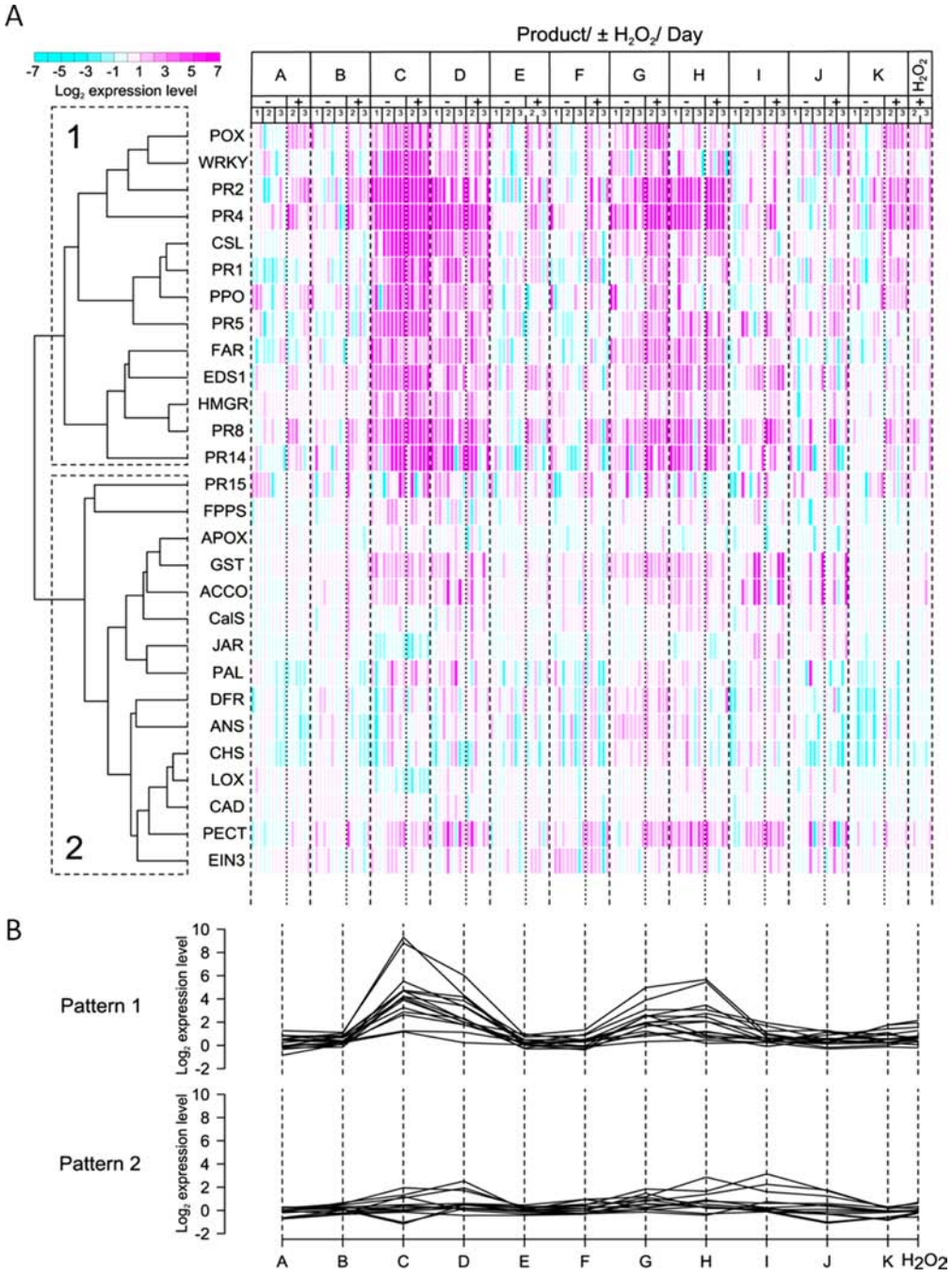


**Figure 2.** Defense gene expression profiles obtained after product application on apple seedlings. (A) Heatmap profiling across all experimental conditions (product, day, ± $H_2O_2$) with hierarchical clustering of genes: ACCO, 1-aminocyclopropene-1-carboxylate oxidase; ANS, anthocyanidin synthase; APOX, ascorbate peroxidase; CalS, callose synthase; CHS, chalcone synthase; CAD, cinnamyl-alcohol dehydrogenase; CSL, cysteine sulfoxide lyase; DFR, dihydroflavonol reductase; EIN3, EIN3-binding F box protein 1; EDS1, enhanced disease susceptibility 1; Far, (*E*,*E*)-α-farnesene synthase; FPPS, farnesyl pyrophosphate synthase; GST, glutathione *S*-transferase; HMGR, hydroxymethyl glutarate-CoA reductase; JAR, jasmonate resistant 1; LOX, 13-lipoxygenase; PAL, phenylalanine ammonia-lyase; Pect, pectin methyl esterase; PR, pathogenesis-related protein; PPO, polyphenol oxidase; POX, peroxidase; WRKY, WRKY transcription factor 30. (B) Expression patterns of genes from the two main clusters and for each compound averaged over all experimental conditions ($n$ = 15, i.e., 5 experimental conditions (days and ± $H_2O_2$) × 3 independent experiments).

## RESULTS AND DISCUSSION

**Protective Efficiency against *E. amylovora*.** The 10 commercially released products (Table 1) were first tested for their protective efficiency against *E. amylovora* when applied 4 days before inoculation (Figure 1). They were compared to water applied also 4 days before inoculation and to product K (biocidal reference) applied 4 days or 4 h before inoculation. Disease incidence obtained with water control shows that a stringent testing procedure was applied. However, great differences in disease incidence after the different treatments were observed.

Resulting values of protection rate ranging from >70% for compounds C and G to <10% for compounds A, B, D, E, F, I, and J and the biocide K applied 4 days before inoculation were observed (Figure 1). Those values are in the range of a previous observation with PRIs.[5] Compound H displayed intermediate-to-high protection efficiency. Although not as efficient as the

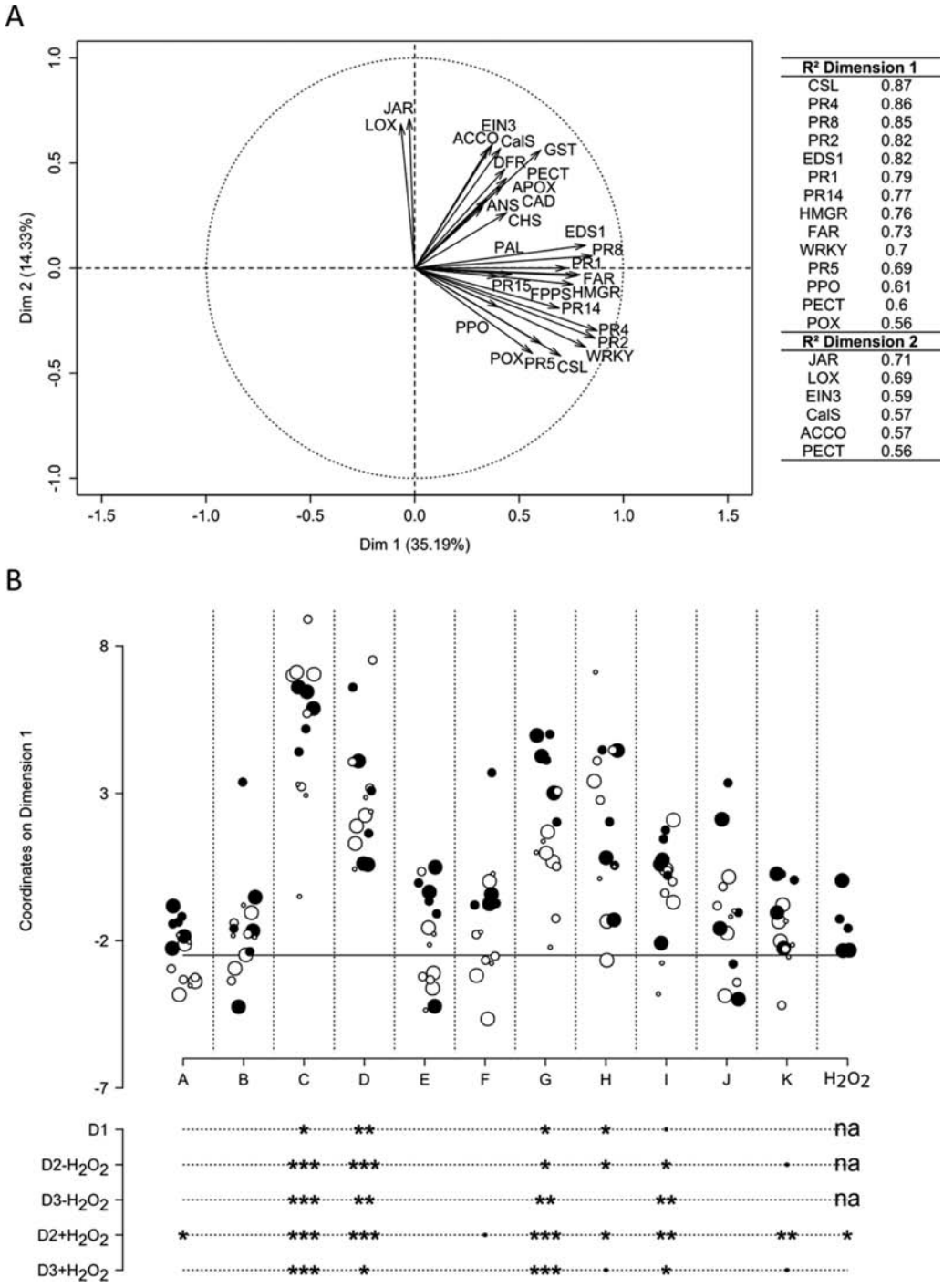


| R² Dimension 1 | |
|---|---|
| CSL | 0.87 |
| PR4 | 0.86 |
| PR8 | 0.85 |
| PR2 | 0.82 |
| EDS1 | 0.82 |
| PR1 | 0.79 |
| PR14 | 0.77 |
| HMGR | 0.76 |
| FAR | 0.73 |
| WRKY | 0.7 |
| PR5 | 0.69 |
| PPO | 0.61 |
| PECT | 0.6 |
| POX | 0.56 |
| **R² Dimension 2** | |
| JAR | 0.71 |
| LOX | 0.69 |
| EIN3 | 0.59 |
| CalS | 0.57 |
| ACCO | 0.57 |
| PECT | 0.56 |

**Figure 3.** Principal component analysis (PCA) of gene expression among experimental conditions. (A) Variables (genes) projected on the dimension 1/dimension 2 map and list of most correlated variables (genes) ($r^2 > 0.5$) with each of the two dimensions. All correlation coefficient ($r^2$) were significant at $p < 10^{-15}$. Dim, dimension; ACCO, 1-aminocyclopropene-1-carboxylate oxidase; ANS, anthocyanidin synthase; APOX, ascorbate peroxidase; CalS, callose synthase; CHS, chalcone synthase; CAD, cinnamyl-alcohol dehydrogenase; CSL, cysteine sulfoxide lyase; DFR, dihydroflavonol reductase; EIN3, EIN3-binding F box protein 1; EDS1, enhanced disease susceptibility 1; Far, (*E*,*E*)-α-farnesene synthase; FPPS, farnesyl pyrophosphate synthase; GST, glutathione *S*-transferase; HMGR, hydroxymethyl glutarate-CoA reductase; JAR, jasmonate resistant 1; LOX, 13-lipoxygenase; PAL, phenylalanine ammonia-lyase; Pect, pectin methyl esterase; PR, pathogenesis-related protein; PPO, polyphenol oxidase; POX, peroxidase; WRKY, WRKY transcription factor 30. (B) Coordinates of samples on dimension 1. Different sampling days are indicated by circles of increasing size: white dots, no $H_2O_2$ application; black dots, $H_2O_2$ application. A small amount of jittering was added to improve visualization. The horizontal line indicates the position of the calibrator sample (water treatment at each sampling date, the expression levels of which set the 0 value). (Bottom) Result of a linear model constructed with the dimension 1 coordinates as the response vector and the factors day/$H_2O_2$ treatment showing significant differences between a given compound and water treatment (one-way ANOVA; ∗, $p < 0.05$; ∗∗, $p < 0.01$; ∗∗∗, $p < 0.001$). na, not applicable.

biocide K applied 4 h before inoculation, the three compounds C, G, and H allowed significant protection when compared to water control and all other products. The lack of effectiveness with product K applied 4 days before inoculation highly suggests that


dx.doi.org/10.1021/jf504221x | J. Agric. Food Chem. 2014, 62, 11403−11411

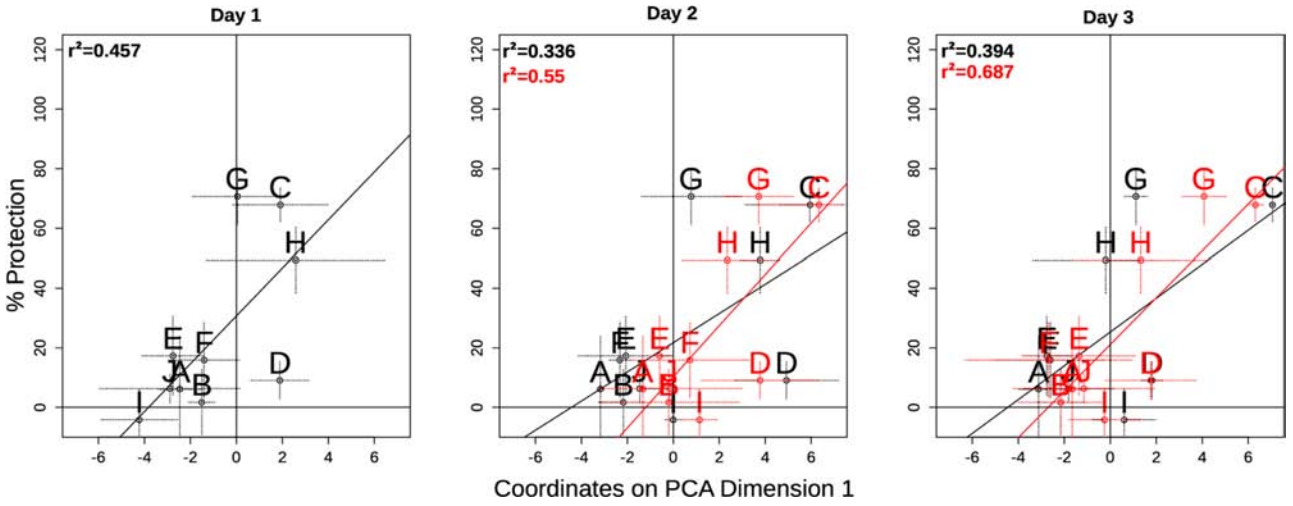


**Figure 4.** Relationships between defense gene expression and protective effects at each analysis date. Coordinates on dimension 1 of the previous PCA averaged across biological replicates were used as a measure of gene expression induction activity. $H_2O_2$ application for priming activity assay: black, without; red, with. Bars correspond to standard deviation ($n = 3$ for PCA coordinates and $n \geq 15$ for the protection assays). Correlation coefficients of linear models are indicated in each plot.

reduction of disease incidence with compounds C, G, and H is unlikely to be due to a bactericidal effect. Lack of direct antibacterial activity was therefore verified in vitro (data not shown) and allows us to assume that the high protection efficiency of these three compounds indeed relies on a PRI effect. In addition, applying these candidate PRIs only 4 h before inoculation was less efficient in protection, especially for G and H (Supporting Information Figure s1).

These results indicate that time is needed for the plant to activate its defense system. This is in accordance with previous works; for example, 3 days were described to be necessary for acibenzolar-*S*-methyl-treated tomato seedlings to develop a successful resistance against *Clavibacter michiganensis* ssp. *michiganensis*.[28] Next we focused on the defense stimulating activities of these compounds to determine how much induction of a given set of defense genes and the protection efficiency are correlated.

**Defense Gene Expression Monitoring.** As protective effects were mostly observed when inoculation was performed 4 days after candidate treatments, activation of defense responses at the transcriptional level is expected to be visible within 3 days following product application. Expressions of 28 marker genes[22,23] were therefore monitored 1, 2, and 3 days after spraying. Global overview of the data set clearly indicated a differential ability of the compounds to modulate gene expression (Figure 2). Clustering the genes according to their expression levels gave two main patterns. The first one included genes encoding PR-proteins, terpenoid biosynthetic enzymes, and salicylic acid-related markers, and those were strongly up-regulated in several samples (C, D, G, and H) but not in the others. The remaining genes including flavonoid and jasmonic acid marker genes were found to be weakly influenced by treatments. Contrasted activation of salicylate and jasmonate pathways probably relies on the common antagonism reported between these two pathways.[8] However, given the diversity of compounds assayed here, it was quite unexpected to mobilize only salicylate-related defenses.

A PCA performed using genes as variables and samples as individuals (Figure 3) revealed that the first dimension (35% of the initial variation) was the only one to correctly separate the samples while coherently taking into account the strength of biological measurements ($r^2 > 0.6$, $p < 10^{-6}$ between biological repeats). Dimension 1 clearly clustered two groups of genes, and those that strongly correlated with it ($r^2 > 0.5$, $p < 10^{-15}$) (Figure 3A) corresponded to those having the first expression pattern described above (Figure 2B). This indicated that the data set could be correctly summarized by using dimension 1 as a new variable. By comparing values of samples projected on this dimension, we observed three intensities of gene induction, according to the product applied, ranging from high (compound C) to intermediate (D, G, H, I) and low (A, B, E, F, J, K) (Figure 3B). For this last group of compounds, gene expression levels did not significantly change in most cases in comparison to water treatment. The expression pattern for compound C, which contained acibenzolar-*S*-methyl, a well-known SAR inducer,[6,29] was expected. In addition, previous studies already reported the induction of PR-protein encoding genes by acibenzolar-*S*-methyl in apple trees.[13,30] Concerning compounds that efficiently activate apple defenses, we found a strong interactive effect between compound and day factors (MANOVA, $p < 10^{-7}$). Only four compounds, C, D, G, and H, significantly activated expression of genes belonging to the first cluster 1 day after application (smaller symbols) (Figure 3B). Significant inductions at day 2 were observed for compounds C and D, as well as G, H, and I to a lesser extent ($p < 0.05$). A transient effect could be attributed to compounds D and H because intensities at 2 days were always stronger than at 3 days. Interestingly, laminarin (compound D) was reported to induce both salicylic acid- and jasmonic acid-related defenses in grapevine and tobacco,[31,32] whereas in apple only salicylic acid-related markers were induced. This difference of results might reveal specificities in the perception/signaling systems between plant species; however, both previous studies dealt with cell suspension cultures and favored laminarin in reaching its targets. Our data also showed that compound G triggered a priming effect, because expression levels of pattern 1 genes without $H_2O_2$ application were significantly lower (Student's *t* test, $p < 0.05$) than after $H_2O_2$ application on days 2 and 3 (Figure 3B). Our results are in agreement with a previous study on prohexadione-Ca (compound G), which reported stronger activation of defense genes in

prohexadione-Ca-treated apple trees challenged with *Venturia inaequalis*, the causative agent of apple scab.[33] Interestingly, this study also indicated that defense genes primed with prohexadione-Ca were related to salicylic acid signaling, as observed here. Another study showed that this plant growth regulator altered flavonoid metabolism by activation of the expression of genes encoding chalcone synthase (CHS) and flavanone 3-hydroxylase (FHT).[34,35] However, in our conditions, this compound only slightly induced the expression of the flavonoid related genes *CHS*, *DFR* (dihydroflavonol reductase), and *ANS* (anthocyanidin synthase), in comparison to genes encoding PR-proteins. It was quite surprising that PRIs, which triggered defense activation in our study, did not display specificities in the set of induced genes, as has been previously shown for other plant species. For example, acibenzolar-*S*-methyl, the active molecule of product C, and chitosan triggered specific responses in strawberry, in particular concerning the flavonoid biosynthetic pathway.[35]

In the light of the present results and data found in the literature, it seems that the same PRI is able to trigger specific responses in distinct hosts. Although differences in treatment application (time, concentration, method of spraying, plant material) could be the source of such discrepancies, this specificity could also reflect specific abilities of plant species to respond to elicitors.

**Correlation between Intensity of Gene Induction and Protection Efficiency.** We next investigated to what extent the protective effect was correlated with defense induction levels (estimated with values of projected individuals on dimension 1) for the apple/*E. amylovora* pathosystem. To establish such a correlation, we plotted at each analysis date the protection data obtained for compounds applied 4 days before inoculation (data resulting from Figure 1) vs PCA abscissa (Figure 3B).

On the whole, positive correlations between protection efficiency and defense induction were obtained at the three sampling dates, although not always significant ($p$ values of 0.03, 0.07, and 0.05 for days 1, 2, and 3, respectively) (Figure 4). However, correlations were stronger and more significant with samples corresponding to $H_2O_2$-treated leaves ($r^2 = 0.55$, $p = 0.01$; and $r^2 = 0.687$, $p = 0.003$ at days 2 and 3, respectively). This increase could be explained by the priming effect of compound G, which therefore contributed more to the model when defense induction was revealed by spraying $H_2O_2$. Our results show that the higher the coordinates were on dimension 1, the higher the protective effect, with the exception of compound D. Using coordinates on dimension 2 (which represented only 14% of the initial variance) in a similar way gave only low correlation coefficients (Supporting Information Figure s2). This reinforces that defense genes represented by this dimension are not related to active defense against *E. amylovora*. Taken together, our results were able to discriminate compounds with no effects by testing a relatively low number of genes.

It is noteworthy that the most efficient products (C, G, and H) displaying protective effects together with defense elicitation are synthetic inputs dealing with phytohormone signaling pathway. Although the effects of product C (acibenzolar-*S*-methyl) and G (prohexadione-Ca) were expected,[13,36] the activity of product H gave interesting prospects. This preparation is an auxin analogue (naphthaleneacetic acid) used as a thinning agent in apple orchards. Its effect contrasted with the antagonistic interactions between the salicylic acid and auxin signaling pathways usually reported.[37] Indeed, those three compounds, C, G, and H, triggered similar responses in our case. The fact that compound H had a high protection efficiency together with high induction activity suggests that new disease managements could take into account the property of particular growth regulators to induce plant defenses. Activities of compounds D and H displayed contrasting profiles. Whereas both triggered moderate and transient activation of defenses in a similar way, their protection efficacies strongly differed. Indeed, compound H was able to confer a significant protection against *E. amylovora*, whereas compound D did not. Our hypothesis is that compound H may either induce the expression of defenses not assayed here or alter plant development in a way that reduces susceptibility of treated plants to *E. amylovora*. However, no particular macroscopic phenotype was seen on our apple seedlings during the time of experiment. Synergism between auxin and jasmonate signaling pathways has been reported several times.[38] Because methyl jasmonate treatments were shown to protect apple seedlings against *E. amylovora*,[39] it is possible that a set of defense commonly regulated by auxin and jasmonates is involved in the responses of apple to this bacterial pathogen. As far as compound D is concerned, it could be interesting to try to correlate the transient defense induction with a protective effect 2 days after spraying. However, and from a practical point of view, the lack of protective effectiveness observed 4 days after treatment would suggest a difficult integration in orchard disease management with the requirement of a high treatment frequency.

It is interesting to point out that product A does not protect against *E. amylovora* or stimulate defense responses in our experimental conditions. This product belongs to the phosphite family and is registered for the control of various diseases including fire blight on apple and pear. Its mode of action is known to be complex with both direct and indirect effects.[5] According to our results, it does not appear to be a PRI in apple. However, for this compound as well as for other inactive compounds in our experimental conditions, we cannot exclude dose rate effects, which were not tested here and which have been reported in several works.[32,40,41]

Another interesting finding to further improve the use of PRIs is that strong marker genes among the 28 assayed here were identified. In particular, PR-protein encoding genes and several secondary metabolism genes strongly responded to PRI treatments. It is known that field-grown plants often exhibit high expression levels of PR-proteins.[5] However, an appropriate combination of those markers might help to uncover how plants respond to PRIs and, for example, to determine periods or organs of maximum responsiveness.

Taken together, our results show that compounds failing to activate specific defense genes (and with no direct antimicrobial activity) are most unlikely to confer protection against *E. amylovora*. The molecular tool and the associated methodology developed in this work could therefore be proposed to agribusiness to facilitate the screening of PRIs, which are efficient against fire blight without the difficult handling of the pathogen. The strong marker genes highlighted by the screening may also be further used to test the influence of different experimental factors on PRI activity and to improve their integration into disease management programs.

## ■ ASSOCIATED CONTENT

### Supporting Information

Figures s1 and s2 (which completes Figure 4). This material is available free of charge via the Internet at http://pubs.acs.org.

## AUTHOR INFORMATION


### Corresponding Author

*(M.-N.B.) Phone: +33 2-41-22-57-13. Fax: +33 2-41-22-57-05. E-mail: marie-noelle.brisset@angers.inra.fr.

### Present Addresses

§(T.D.B.) Université François Rabelais de Tours, EA2106 Biomolécules et Biotechnologies Végétales, F-37200 Tours, France.

⊗(J.S.) INRA, UMR1128 Génétique et Microbiologie, F-54506 Nancy, France.


### Notes

The authors declare no competing financial interest.

## ACKNOWLEDGMENTS

We thank Roland Chartier, Martine Devaux, Christelle Heintz, Arnaud Indiana, and Clément Gravouil for excellent technical assistance. We are grateful to the INEM team of IRHS Angers for apple seedling production and plant maintenance.

## REFERENCES


(1) Dangl, J. L.; Horvath, D. M.; Staskawicz, B. J. Pivoting the plant immune system from dissection to deployment. *Science* **2013**, *341*, 746−751.

(2) Boller, T.; Felix, G. A renaissance of elicitors: perception of microbe-associated molecular patterns and danger signals by pattern-recognition receptors. *Annu. Rev. Plant Biol.* **2009**, *60*, 379−406.

(3) Henry, G.; Thonart, P.; Ongena, M. PAMPs, MAMPs, DAMPs and others: an update on the diversity of plant immunity elicitors. *Biotechnol. Agron. Soc. Environ.* **2012**, *16*, 257−268.

(4) Spoel, S. H.; Dong, X. How do plants achieve immunity? Defence without specialized immune cells. *Nat. Rev. Immunol.* **2012**, *12*, 89−100.

(5) Walters, D. R.; Ratsep, J.; Havis, N. D. Controlling crop diseases using induced resistance: challenges for the future. *J. Exp. Bot.* **2013**, *64*, 1263−1280.

(6) Gozzo, F.; Faoro, F. Systemic acquired resistance (50 years after discovery): moving from the lab to the field. *J. Agric. Food Chem.* **2013**, *61*, 12473−12491.

(7) Da Rocha, A.; Hammerschmidt, R. History and perspectives on the use of disease resistance inducers in horticultural crops. *HortTechnology* **2005**, *15*, 518−529.

(8) Pieterse, C. M. J.; Van der Does, D.; Zamioudis, C.; Leon-Reyes, A.; Van Wees, S. C. M. Hormonal modulation of plant immunity. *Annu. Rev. Cell Dev. Biol.* **2012**, *28*, 489−521.

(9) Conrath, U. Priming of induced plant defense responses. *Adv. Bot. Res.* **2009**, *51*, 361−395.

(10) Conrath, U. Molecular aspects of defence priming. *Trends Plant Sci.* **2011**, *16*, 524−531.

(11) Fu, Z. Q.; Dong, X. Systemic acquired resistance: turning local infection into global defense. *Annu. Rev. Plant Biol.* **2013**, *64*, 839−863.

(12) Csinos, A. S.; Pappu, H. R.; McPherson, R. M.; Stephenson, M. G. Management of tomato spotted wilt virus in flue-cured tobacco with acibenzolar-*S*-methyl and imidacloprid. *Plant Dis.* **2001**, *85*, 292−296.

(13) Brisset, M.-N.; Cesbron, S.; Thomson, S. V.; Paulin, J.-P. Acibenzolar-*S*-methyl induces the accumulation of defense-related enzymes in apple and protects from fire blight. *Eur. J. Plant Pathol.* **2000**, *106*, 529−536.

(14) Matheron, M. E.; Porchas, M. Suppression of *Phytophthora* root and crown rot on pepper plants treated with acibenzolar-*S*-methyl. *Plant Dis.* **2002**, *86*, 292−297.

(15) Walters, D.; Walsh, D.; Newton, A.; Lyon, G. Induced resistance for plant disease control: maximizing the efficacy of resistance elicitors. *Phytopathology* **2005**, *95*, 1368−1373.

(16) Noutoshi, Y.; Okazaki, M.; Kida, T.; Nishina, Y.; Morishita, Y.; Ogawa, T.; Suzuki, H.; Shibata, D.; Jikumaru, Y.; Hanada, A.; Kamiya, Y.; Shirasu, K. Novel plant immune-priming compounds identified via high-throughput chemical screening target salicylic acid glucosyltransferases in *Arabidopsis*. *Plant Cell* **2012**, *24*, 3795−3804.

(17) Schreiber, K. J.; Nasmith, C. G.; Allard, G.; Singh, J.; Subramaniam, R.; Desveaux, D. Found in translation: high-throughput chemical screening in *Arabidopsis thaliana* identifies small molecules that reduce Fusarium head blight disease in wheat. *Mol. Plant−Microbe Interact.* **2011**, *24*, 640−648.

(18) Vanneste, J. L. *Fire Blight: The Disease and Its Causative Agent, Erwinia amylovora*; Vanneste, J. L., Ed.; CABI: Wallingford, UK, 2000.

(19) Jock, S.; Wensing, A.; Pulawska, J.; Drenova, N.; Dreo, T.; Geider, K. Molecular analyses of *Erwinia amylovora* strains isolated in Russia, Poland, Slovenia and Austria describing further spread of fire blight in Europe. *Microbiol. Res.* **2013**, *168*, 447−454.

(20) Paulin, J. P.; Samson, R. Le feu bacterien en France. II. Caractères des souches d'*Erwinia amylovora* (Burrill) Winslow et al., 1920, isolées du foyer franco-belge. *Ann. Phytopathol.* **1973**, *5*, 389−397.

(21) King, E. O.; Ward, M. K.; Raney, D. E. Two simple media for the demonstration of pyocyanin and fluorescin. *J. Lab. Clin. Med.* **1954**, *44*, 301−307.

(22) Vergne, E.; Dugé de Bernonville, T.; Dupuis, F.; Sourice, S.; Cournol, R.; Berthelot, P.; Barny, M. A.; Brisset, M. N.; Chevreau, E. Membrane-targeted $HrpN_{Ea}$ can modulate apple defense gene expression. *Mol. Plant−Microbe Interact.* **2014**, *27*, 125−135.

(23) Brisset, M. N.; Dugé de Bernonville, T. Device for determining or studying the state of stimulation of the natural defences of plants or portions of plants. U.S. Patent US20130090261, 2013.

(24) Schmittgen, T. D.; Livak, K. J. Analyzing real-time PCR data by the comparative $C_T$ method. *Nat. Protoc.* **2008**, *3*, 1101−1108.

(25) Vandesompele, J.; De Preter, K.; Pattyn, F.; Poppe, B.; Van Roy, N.; De Paepe, A.; Speleman, F. Accurate normalization of real-time quantitative RT-PCR data by geometric averaging of multiple internal control genes. *Genome Biol.* **2002**, *3*, RESEARCH0034.

(26) R Core Team. *R: A Language and Environment for Statistical Computing*; R Foundation for Statistical Computing: Vienna, Austria, 2013; http://www.R-project.org/.

(27) Lê, S.; Josse, J.; Husson, F. FactoMineR: An R package for multivariate analysis. *J. Stat. Softw.* **2008**, *25*, 1−18.

(28) Baysal, O.; Soylu, E. M.; Soylu, S. Induction of defence-related enzymes and resistance by the plant activator acibenzolar-*S*-methyl in tomato seedlings against bacterial canker caused by *Clavibacter michiganensis* ssp. *michiganensis*. *Plant Pathol.* **2003**, *52*, 747−753.

(29) Oostendorp, M.; Kunz, W.; Dietrich, B.; Staub, T. Induced disease resistance in plants by chemicals. *Eur. J. Plant Pathol.* **2001**, *107*, 19−28.

(30) Maxson-Stein, K.; He, S. Y.; Hammerschmidt, R.; Jones, A. L. Effect of treating apple trees with acibenzolar-*S*-methyl on fire blight and expression of pathogenesis-related protein genes. *Plant Dis.* **2002**, *86*, 785−790.

(31) Aziz, A.; Poinssot, B.; Daire, X.; Adrian, M.; Bézier, A.; Lambert, B.; Joubert, J. M.; Pugin, A. Laminarin elicits defense responses in grapevine and induces protection against *Botrytis cinerea* and *Plasmopara viticola*. *Mol. Plant−Microbe Interact.* **2003**, *16*, 1118−1128.

(32) Klarzynski, O.; Plesse, B.; Joubert, J. M.; Yvin, J. C.; Kopp, M.; Kloareg, B.; Fritig, B. Linear $\beta$-1,3 glucans are elicitors of defense responses in tobacco. *Plant Physiol.* **2000**, *124*, 1027−1038.

(33) Bini, F.; Ragaini, A.; Bazzi, C. Resistance responses induced by the plant growth retardant prohexadione-Ca in apple against scab infections. *Ann. Appl. Biol.* **2008**, *152*, 19−27.

(34) Fischer, T. C.; Halbwirth, H.; Roemmelt, S.; Sabatini, E.; Schlangen, K.; Andreotti, C.; Spinelli, F.; Costa, G.; Forkmann, G.; Treutter, D.; Stich, K. Induction of polyphenol gene expression in apple (*Malus* × *domestica*) after the application of a dioxygenase inhibitor. *Physiol. Plant.* **2006**, *128*, 604−617.

(35) Landi, L.; Feliziani, E.; Romanazzi, G. Expression of defense genes in strawberry fruits treated with different resistance inducers. *J. Agric. Food Chem.* **2014**, *62*, 3047−3056.

(36) Buban, T.; Földes, L.; Fekete, Z.; Rademacher, W. Effectiveness of the resistance inducer prohexadione-Ca against fire blight in shoots of apple trees inoculated with *Erwinia amylovora*. *Bull. OEPP/EPPO Bull.* **2004**, *34*, 369−376.

(37) Robert-Seilaniantz, A.; Grant, M.; Jones, J. D. G. Hormone crosstalk in plant disease and defense: more than just jasmonate-salicylate antagonism. *Annu. Rev. Phytopathol.* **2011**, *49*, 317−343.
(38) Kazan, K.; Manners, J. M. Linking development to defense: auxin in plant-pathogen interactions. *Trends Plant Sci.* **2009**, *14*, 373−382.
(39) Dugé De Bernonville, T.; Gaucher, M.; Flors, V.; Gaillard, S.; Paulin, J. P.; Dat, J. F.; Brisset, M. N. T3SS-dependent differential modulations of the jasmonic acid pathway in susceptible and resistant genotypes of *Malus* spp. challenged with *Erwinia amylovora*. *Plant Sci.* **2012**, *188*−*189*, 1−9.
(40) Kauss, H.; Theisinger-Hinkel, E.; Conrath, U. Dichloroisonicotinic and salicylic acid, inducers of systemic acquired resistance, enhance fungal elicitor responses. *Plant J.* **1991**, *2*, 655−660.
(41) Durango, D.; Pulgarin, N.; Echeverri, F.; Escobar, G.; Quiñones, W. Effect of salicylic acid and structurally related compounds in the accumulation of phytoalexins in cotyledons of common bean (*Phaseolus vulgaris* L.) cultivars. *Molecules* **2013**, *18*, 10609−10628.

lignin moieties, found at 56, 124, 148, and 153 ppm, as well as to COOH groups at 174 ppm.[22]

Complementary molecular characterization of complex matrices may be obtained by the combination of NMR spectra with structural information provided by thermally assisted hydrolysis and methylation reactions (thermochemolysis) followed by gas chromatography−mass spectrometry (GC-MS).[24,25] Pyrolysis in the presence of tetramethylammonium hydroxide involves the controlled partial cleavage of chemical bonds with the simultaneous solvolysis and methylation of ester and ether bonds present in natural organic materials, thereby enhancing both thermal stability and chromatographic detection of different polar functional groups.[26] Moreover, the off-line technique allows the analysis of large quantities of solid material and thus a more representative sample and more effective qualitative and quantitative measurements of structural components and their relationship with biological activity.[27] The aim of this study was to evaluate by $^{13}C$ NMR spectroscopy and thermochemolysis the molecular characteristics of HAs isolated from five mature vermicomposts of different composition and to measure their bioactivity by the emergence of lateral roots in maize seedlings.

## MATERIALS AND METHODS

**Preparation of Vermicomposts.** Five different vermicomposts were prepared using the following different substrates: (1) cattle manure; (2) cattle manure and sugar cane bagasse (1:1 w/w as dry mass); (3) cattle manure and sunflower cake (1:1 w/w as dry mass); (4) cattle manure, sugar cane bagasse, and sunflower cake (1:1:1 w/w/w as dry mass); and (5) filter cake from a sugar cane factory. Each organic residue was placed on a concrete cylinder (100 cm internal diameter) with a 150 L capacity using two replicates (two cylinders per treatment). The humidity was maintained at 65−70% by weekly addition of water followed by mixing. After approximately 1 month of composting, the earthworm *Eisenia fetida* was introduced at a ratio of 5 kg of worms per cubic meter of organic residue. At the end of the transformation process, the worms were removed by attracting them to a pile of fresh organic residue (cattle manure) in a corner of the container. The VCs were air-dried, powdered with a ball mill, and sieved through a 500 $\mu$m mesh. Total organic carbon (OC) and total nitrogen (TN) contents were determined by dry combustion using an automatic CHN analyzer (PerkinElmer 2400 series, Norwalk, CT, USA).

**Extraction of Humic Acids.** The humic acids were extracted and purified as reported previously.[5] Briefly, 10 volumes of 0.5 M NaOH was mixed with 1 volume of earthworm compost under a $N_2$ atmosphere and shaken overnight. After 12 h, the suspension was centrifuged at 5000*g* and acidified (pH 1.5) using 6 M HCl. This suspension was allowed to settle overnight, the precipitated humic acids were recovered by centrifugation at 5000*g*, resolubilized in 0.5 M NaOH, and precipitated by acidification (pH 1.5) with 6 M HCl, and the resulting pellet after centrifugation at 5000*g* was mixed with 10 volumes of a 0.1 M HCl and 0.3 M HF. After centrifugation at 5000*g* for 15 min, the precipitate was repeatedly washed with water until a negative test against $AgNO_3$ was obtained. The pH of the final suspension was adjusted to pH 7.0 with 0.01 M KOH and then dialyzed against deionized water using a 1 kDa cutoff membrane (Thomas Scientific, Swedesboro, NJ, USA), and lyophilized. Five humic acids (HA1, HA2, HA3, HA4, and HA5) were obtained from the respective vermicomposts (1−5) described above.

**Characterization of HA.** *Offline Thermochemolysis and GC-MS Analysis.* About 100 mg of purified humic acid was placed in a quartz boat and moistened with 0.5 mL of tetramethylammonium hydroxide (25% in methanol) solution. After the mixture had dried under a gentle stream of nitrogen for about 10 min, the sample was introduced into a Pyrex tubular reactor (50 cm × 3.5 cm i.d.) and heated at 400 °C for 30 min in a furnace. The products released by thermochemolysis were continuously transferred by a flow of helium (20 mL/min) into two successive chloroform (50 mL) traps kept in an iced salt bath. The chloroform solutions were combined in a round flask and concentrated by rotoevaporation under reduced pressure. The residue was redissolved in 1 mL of chloroform and transferred to a glass vial for GC-MS analysis. Two thermochemolysis replicates were carried out for each humic acid sample. The products of thermochemolysis were analyzed by GC-MS. Chromatographic separations were carried out with a GC-MS QP2010 Plus instrument (Shimadzu, Tokyo, Japan). The column used was a 30 m × 0.25 mm id, 0.25 $\mu$m, Rtx-5MS WCOT. Chromatographic separation was achieved with the following temperature program: 60 °C for 1 min (isothermal), raised at 7 °C/min to 100 °C and then at 4 °C/min to 320 °C, followed by 10 min at 320 °C (isothermal). The carrier gas was helium at 1.90 mL/min, the injector temperature was 250 °C, and the split injection mode had a split flow at 30 mL/min. Mass spectra were obtained in EI mode (70 eV), and scanning was in the range $m/z$ 45−850 with a cycle time of 1 s. Compound identification was based on comparison of mass spectra with the NIST library database, published spectra, and real standards. For quantitative analysis, due to the large variety of detected compounds with different chromatographic responses, external calibration curves were built by mixing methyl esters and/or methyl ethers of the following molecular standards: tridecanoic acid, octadecanol, 16-hydroxyhexadecanoic acid, docosanoic acid, $\beta$-sitosterol, and cinnamic acid. Increasing amounts of standard mixtures were placed in a quartz boat and moistened with 0.5 mL of tetramethylammonium hydroxide (25% in methanol) solution. The same thermochemolysis conditions as for compost samples were applied to the standards. The lignin transformation was estimated using specific thermochemolysis products in the following indices:[26,28]

**Ad/AlP** (P6/P4): benzoic acid, 4-methoxy-, methyl ester/benzaldehyde, 4-methoxy

**Ad/AlS** (S6/S4): benzoic acid, 3,4,5-trimethoxy-, methyl ester/benzaldehyde, 3,4,5-trimethoxy

**Ad/AlG** (G6/G4): benzoic acid, 3, 4-dimethoxy-, methyl ester/benzaldehyde, 3,4-dimethoxy

$\Gamma_G$ [G6/(G14 + G15)]: benzoic acid, 3,4-dimethoxy-, methyl ester/1,2-dimethoxy-4(1,2,3-trimethoxypropyl)benzene

*Solid-State CP-MAS $^{13}C$ NMR Spectroscopy.* The C functionality distributions of the humic acid samples were determined by solid-state CP-MAS $^{13}C$ NMR spectroscopy. The spectra were acquired with an Avance 500 MHz (Bruker, Karlsruhe, Germany) spectrometer equipped with a 4 mm wide-bore MAS probe and operating at $^{13}C$ and $^{1}H$ frequencies of 125 and 500 MHz, respectively. The samples (100−200 mg) were packed in 4 mm zirconia rotors with Kel−F caps, which were spun at 13 ± 1 kHz. The spectra were acquired by the ramped CP-MAS method, with linear amplitude variation of the $^{1}H$ pulse. The experiments were carried out using a cross-polarization time of 1.0 ms, an acquisition time of 25 ms, a cycle delay of 2 s, and a high-power two-pulse phase modulation (TPPM) proton decoupling of 70 kHz. Bruker Topspin 1.3 software (Bruker Biospin, Karlsruhe, Germany) was used to collect and process the spectra. All of the free induction decays (FIDs) were transformed by applying a 4K zero filling and a line broadening of 75 Hz. The spectra were normalized by area and integrated in the following $^{13}C$ chemical shift intervals: 190−160 ppm (carbonyls of ketones, quinones, aldehydes, and carboxyls), 160−140 ppm (phenols and O-substituted aromatic C), 140−110 ppm (unsubstituted aromatic C and olefinic C), 110−95 ppm (anomeric C), 95−65 ppm (O-alkyl systems), 65−45 ppm (methoxy substituent; *N*-alkyl groups), and 45−0 ppm (alkyl C, mainly $CH_2$ and $CH_3$). The relative areas of the alkyl (45−0 ppm) and aromatic (160−110 ppm) components were summed to represent the proportion of hydrophobic C in the humic samples (degree of hydrophobicity, HB). Similarly, the summation of the relative areas in intervals related to polar groups (190−160 and 110−45 ppm) indicates the degree of C hydrophilicity (HI); the HB/HI ratio was then calculated. The ratio between the signal areas in the 45−65 ppm interval (methoxyl-C) over those in the 140−160 ppm range (O-aromatic-C), denoted the lignin ratio, was used to discriminate the contribution of lignin components.[21]

*Bioactivity of HA.* Detailed experimental protocols for lateral root emergence and acidification of the growth medium for the maize seedling have been reported.[21] Briefly, maize seedlings with homogeneous root length (1 ± 0.2 cm) were treated or not (control) for 48 h with different humic acids applied at a concentration of 2 mM C and adjusted to pH 7.00 with diluted HCl or NaOH. Next, seedlings were washed abundantly with deionized water and transferred to a 2 mM $CaCl_2$ solution at pH 7.00 ± 0.01. After 48 h, the seedlings were collected. Then, the seedling roots were digitized, and the number of lateral roots was counted. We used five pots as replicates ($n$ = 5) with five seedlings in each pot.

## RESULTS AND DISCUSSION

The total ion chromatograms derived from the thermochemolysis products obtained from the different humic acids extracted from the vermicomposted plant biomass residues and from cattle manure are shown in Figures 1 and 2.

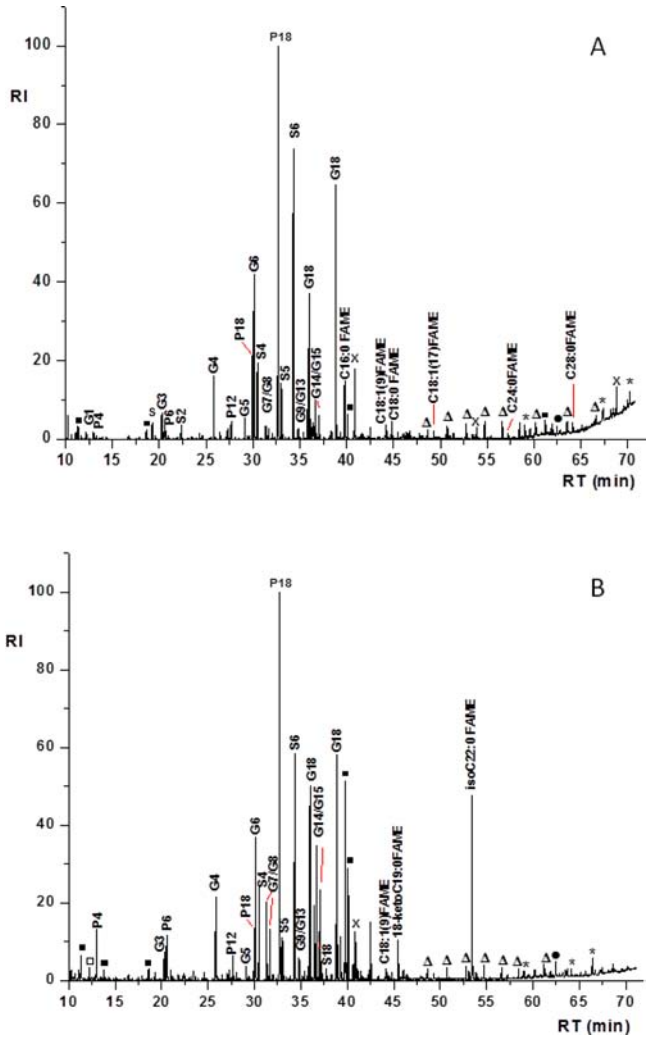


**Figure 1.** Total ion current (TIC) obtained from offline pyrolysis GC-MS of humic acids isolated from vermicompost of (A) cattle manure and (B) sugar cane bagasse.

Thermochemolysis of humic acids released more than 200 different molecules, which were identified as methyl ethers and esters of natural compounds. The list of compounds identified in different pyrograms is shown in the Supporting Information, whereas the data in Table 1 summarize the amount and distribution of the major compound classes. Most of the humic

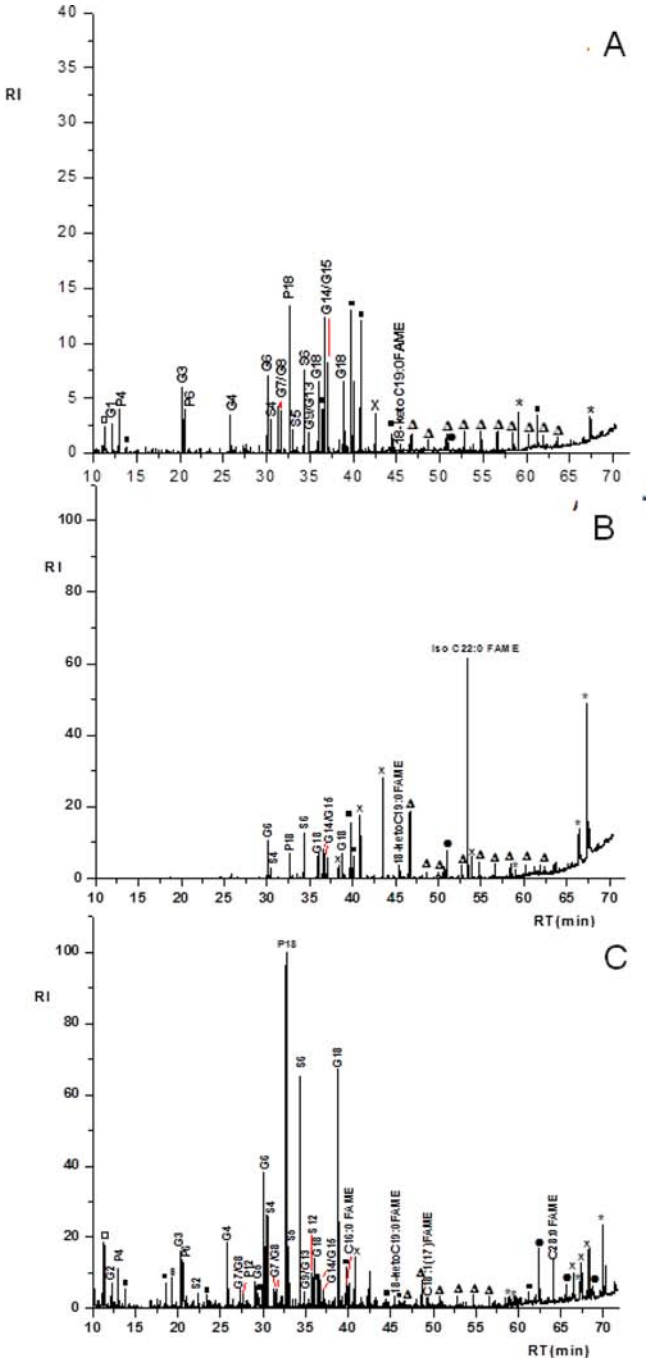


**Figure 2.** Total ion current (TIC) obtained from offline pyrolysis GC-MS of humic acids isolated from vermicompost of (A) sunflower cake, (B) a mixture of cattle manure, sugar cane bagasse, and sunflower cake, and (C) sugar cane filter cake.

components originated from higher plant residues that had been biostabilized by microbial activity and were represented by lignin, alkyl biopolymers, nitrogenous compounds, terpenes, and sterol products. The thermochemolysis revealed noticeable differences in humic acid composition, presumably reflecting the variable sources of organic residues for vermicompost production. HA2 and HA3 showed the largest amount of lignins and nitrogenous compounds, whereas HA1 and HA4 were characterized by a large presence of C-alkyl compounds, and HA5 was characterized by terpenes and sterol derivatives.

**Table 1. Yields (Milligrams per Kilogram) and Composition of Main Thermochemolysis Products Released from Humic Acids of Different Vermicomposts**

| compound class[a] | HA1[b] | HA2[b] | HA3[b] | HA4[b] | HA5[b] |
|---|---|---|---|---|---|
| total lignins | 950 ± 66.5 | 4271 ± 213.5 | 870 ± 69.6 | 65 ± 3.2 | 2976 ± 208.3 |
| P | 223 ± 8.9 | 1067 ± 74.7 | 196 ± 5.8 | 8 ± 0.2 | 799 ± 33.9 |
| G | 406 ± 8.1 | 2179 ± 87.2 | 532 ± 21.3 | 41 ± 1.6 | 1228 ± 98.2 |
| S | 242 ± 9.4 | 775 ± 62.0 | 107 ± 2.1 | 16 ± 0.3 | 708 ± 63.7 |
| P6/P4 | 2.3 ± 0.07 | 0.9 ± 0.02 | 1.1 ± 0.02 | nd | 1.4 ± 0.04 |
| G6/G4 | 2.6 ± 0.29 | 1.6 ± 0.05 | 2.1 ± 0.04 | nd | 1.9 ± 0.06 |
| S6/S4 | 4.7 ± 0.4 | 2.7 ± 0.08 | 2.7 ± 0.08 | 4.7 ± 0.1 | 2.2 ± 0.04 |
| $\Gamma_G$ | 2.8 ± 0.1 | 0.6 ± 0.05 | 0.4 ± 0.02 | 0.8 ± 0.02 | 2.3 ± 0.05 |
| alkyl-C (fatty acids as methyl esters, alcohols, alkanes, alkenes) | 291 ± 8.7 | 1274 ± 25.5 | 239 ± 19.1 | 228 ± 9.1 | 942 ± 47.1 |
| terpenes and steroids | 40 ± 11.8 | 130 ± 3.9 | 118 ± 2.4 | 212 ± 17.0 | 305 ± 12.7 |
| nitrogenous compounds | 148 ± 2.6 | 1618 ± 113.3 | 409 ± 28.6 | 49 ± 2.4 | 818 ± 57.3 |
| carbohydrate derivatives | 12 ± 0.2 | 136 ± 5.4 | 46 ± 2.3 | nd | 218 ± 15.3 |

[a]P, *p*-hydroxyphenyl; G, guaiacyl; S, syringyl; P6/P4, G6/G4, S6/S4, and $\Gamma_G$ are indices to evaluate lignin transformation using specific thermochemolysis products as described under Materials and Methods. The values represent the means from two chromatograms followed by standard deviation. [b]HA1, HA2, HA3, HA4, and HA5 are the humic acids isolated from vermicomposts produced with cattle manure, sugar cane bagasse, sunflower cake, a mixture of cattle manure, bagasse, and sunflower cake, and sugar cane filter cake residue, respectively.

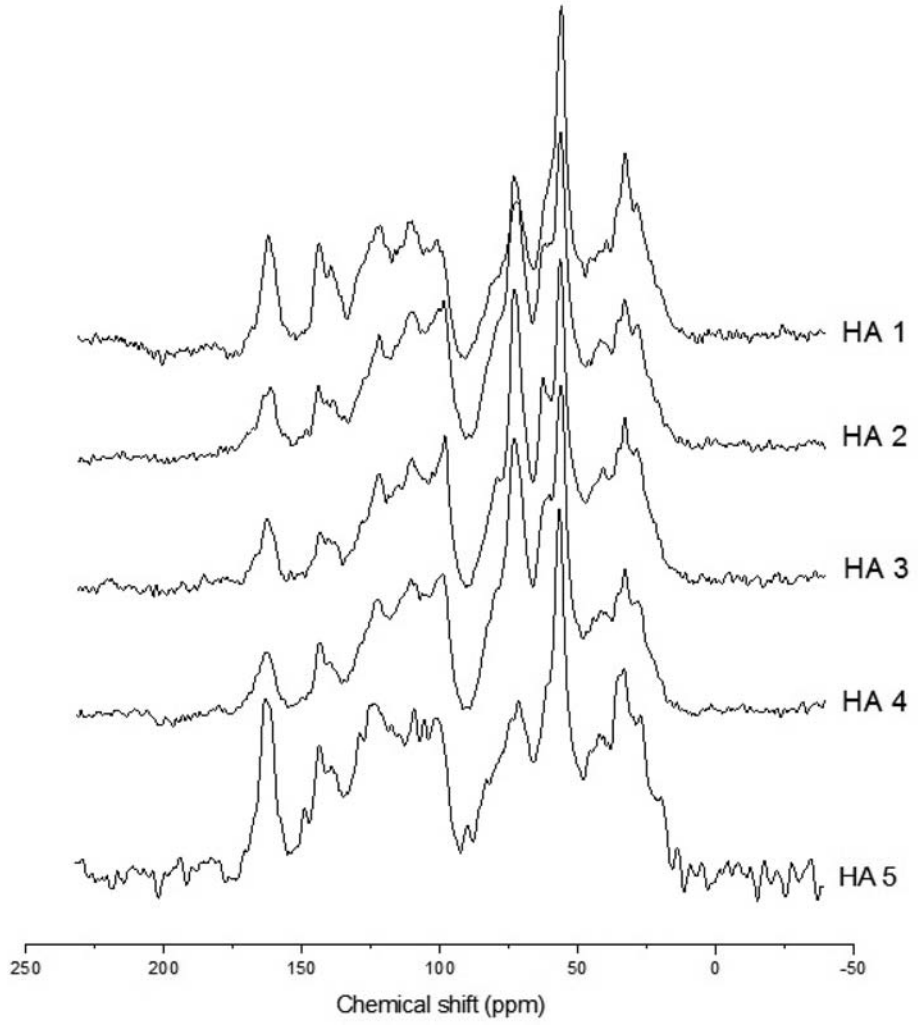


**Figure 3.** CP-MAS $^{13}C$ NMR spectra of humic acids from different vermicomposts: (HA1) cattle manure; (HA2) sugar cane bagasse; (HA3) sunflower cake; (HA4) mixture of cattle manure, sugar cane bagasse, and sunflower cake; (HA5) sugar cane filter cake.

The various lignin components released by thermochemolysis from humic acids were associated with the current symbolism for basic lignin structures used in thermochemolysis analysis: P, *p*-hydroxyphenyl; G, guaiacyl (3-methoxy-4-hydroxyphenyl); and S, syringyl (3,5-dimethoxy-4-hydroxyphenyl).[26] As expected, the most representative lignin

Table 2. Integration Area of $^{13}C$ CPMAS-NMR Spectra from Different Humic Acids (HAs): (HA1) Cattle Manure; (HA2) Cattle Manure and Sugar Cane Bagasse; (HA3) Cattle Manure and Sunflower Cake Obtained after Oil Extraction; (HA4) Cattle Manure, Sugar Cane Bagasse, and Sunflower Cake; (HA5) Filter Cake at 90 Days of Vermicomposting Time

| | chemical shift (ppm) | | | | | | | |
|---|---|---|---|---|---|---|---|---|
| humic acid | 0−45 | 45−65 | 65−95 | 95−110 | 110−140 | 140−160 | 160−190 | HB/HI |
| HA1 | 25.25 | 23.07 | 12.38 | 6.53 | 20.15 | 7.22 | 5.41 | 1.79 |
| HA2 | 20.77 | 21.31 | 19.61 | 9.53 | 17.62 | 5.86 | 5.30 | 0.79 |
| HA3 | 22.68 | 22.24 | 18.96 | 8.87 | 17.31 | 5.13 | 4.81 | 0.82 |
| HA4 | 19.08 | 22.81 | 20.46 | 8.96 | 18.53 | 5.51 | 4.65 | 0.76 |
| HA5 | 21.91 | 17.94 | 14.64 | 9.35 | 20.39 | 7.48 | 8.30 | 0.99 |

compound found among the pyrolyzed products for all humic acids was a propenoic acid derivative (2-propenoic acid, 3-(4-methoxyphenyl)-methyl ester, P18), which is a basic component of lignified tissues of herbaceous crops and grasses. The lignin compounds decrease in the following manner: HA2 > HA5 > HA1 > HA3 > HA4. HA2 obtained from sugar cane bagasse and cattle manure showed 65.7 times more lignin than HA4 obtained from the mixture of bagasse, cattle manure, and sunflower cake (Table 1). A large range of methylated guaiacyl derivatives were found in all HAs, although at lower concentration with respect to the propenoic acid monomer, whereas limited distribution and lower abundance were shown by syringyl units. Useful specific components found in all humic extracts may be associated with the presence of either microbially processed organic materials or undecomposed plant debris. The extent of lignin decomposition may be estimated by structural indices that are based on the relative amount of specific thermochemolysis products.[26−28] Whereas the aldehydic (G4 and S4) and acidic (G6 and S6) forms of lignin structures result from progressive degradation of lignin polymer, involving the ongoing oxidation of propyl chain, the corresponding homologues with integral hydroxylated side chains (G14/15, S14/15) are indicative of unaltered lignin components, which retain the typical $\beta$-O-4 ether intermolecular linkages. Therefore, the indices are obtained (Table 1) by dividing the amount found for the acidic structures by that of, respectively, G4 and S4 aldehydes (Ad/AlG = G6/G4, Ad/AlS = S6/S4) and for the global yield of threo/erythro isomers (ΓG = G6/[G14 + G15]) currently used as indicators of the bio-oxidative transformation of lignin polymers. The larger the values of dimensionless indices, the wider the decomposition process of lignin substrates. The largest amount of fatty acids identified as methyl ester derivatives was observed in HA2 isolated from sugar cane bagasse followed by HA5 from filter cake. However, a larger diversity of methyl esters of fatty acids was found in HA1. The main methyl ester derivatives were even- and odd-numbered long chains from plant and bacterial origin, respectively. HA5 was characterized by the presence of docosanol, a long-chain alcohol from carbohydrate enzymatic reactions. Squalene was found in all humic acids, whereas 15-hydroxydehydroabietic acid was found only in HA2 and $\beta$-sitosterol only in HA3. Large amounts of cholest-7-ene-3-ol acetate were found in HA5 and lanost-8-ene-3,7-dione in HA2.

The most common nitrogenous compounds found in all humic acids, and in larger amounts in HA3, were 2,4-dimethoxyphenylamine, *N*-methoxycarbonyl, and benzenamine. Proline derivatives were found only in HA1 and HA5, whereas pyrrolidone and pyrimidone derivatives were found only in HA2 and HA3. Few compounds derived directly from carbohydrates were found in the samples and only as furan derivatives.

The $^{13}C$ NMR spectra were characterized by a sharp resonance in the 45−65 ppm range for all humic acids (Figure 3). The main signal centered around 55 ppm, associated with the methoxy substituents in the aromatic ring of guaiacyl and syringyl components of lignified tissues of plants, which clearly indicate the incorporation of lignin derivatives in mature vermicomposts. The broad and strong signals found in the alkyl-C region (0−45 ppm) region revealed the large incorporation of alkyl chains pertaining to different components. The peaks at 16 and 23 ppm may be derived mainly from $CH_3-$ and $CH_2-$ groups of various lipid compounds, such as waxes, polyesters, and phospholipids. In addition to the peaks between 0 and 30 ppm, many distinct signals were shown in the broad alkyl-C region around 30−45 ppm with signals at 30, 32, 39, and 44 ppm, which indicate the simultaneous presence of different alkyl chains from linear and branched fatty acid and peptide derivatives. The inclusion of N-containing organic compounds was stressed by the peaks positioned at 40−44 ppm, which were assigned to both $C_\alpha$ and $C_\beta$ in amino acids.[20] Moreover, a different preservation of nitrogen components in the humic extracts was also suggested by the comparison of the intense peak at 55 ppm, with a less pronounced intensity of the O-aromatic functional groups in the 140−160 ppm interval, found in the $^{13}C$ NMR spectra of HA2, HA3, and HA4 (Figure 3 and Table 2). Besides the lignin structures, the signals included in the 45−60 ppm chemical shift range may also result from the C−N bonds in amino acid moieties. In this respect the comparison of signal intensity in the 45−60 ppm interval over that in the 140−160 ppm range may be helpful for a more accurate assignment of methoxyl and phenolic resonances. This dimensionless index, hereby denoted the lignin ratio, has been used to improve discrimination between signals from lignin units characteristic of other phenolic components or peptidic moieties.[20] Whereas a sharply lower ratio of <1 is usually associated with the inclusion of tannin and polyphenol constituents to the global O-aromatic-C signals, the opposite prevalence of the upper fractional part indicates the contribution of C−N bonds in the 45−60 ppm area. Therefore, the discrepancy between methoxyl-C and phenolic-C signals, summarized by the larger lignin ratio found in HA2, HA3, and HA4 humic extracts (Table 2), suggests a greater incorporation of peptidic moieties and a lesser preservation of lignin derivatives in the stabilized organic fractions of sugar cane bagasse, sunflower cake, and mixed mature vermicompost.

The different resonances in the O-alkyl-C region (65−110 ppm) are currently assigned to monomeric units in oligo- and polysaccharide chains of plant tissue. The intense signal around 72 ppm corresponds to the overlapping resonances of carbons 2, 3, and 5 in the pyranoside structure in cellulose and some hemicelluloses, whereas the signal at 104 ppm is assigned to the anomeric carbon 1 of the glucose unit in cellulose. The

shoulders localized around 62−65 and 84−88 ppm result from carbons 6 and 4 of monomeric units, respectively. The low-field resonances (higher chemical shift) of each couple indicate the presence of crystalline forms of cellulose, whereas the high-field resonances are assigned to either amorphous cellulose or hemicellulose structures. Besides the signals usually assigned to cellulose, the spectra of different HAs revealed three additional resonances around 93, 106, and 110 ppm. These signals may be related, respectively, to the di-O-alkyl-C of monomeric units of simple carbohydrates and to the C1 of either hemicellulose or pectic polysaccharides chains contained in cell walls of plants, such as $\alpha$-1,5 arabinan, $\beta$-1,4 galactan, and $\alpha$-1,4 galacturonan.

In the aromatic/olefinic-C region (110−145 ppm), the different resonances around 120 and 123 ppm are related to unsubstituted and C-substituted aryl carbon pertaining to both lignin monomers and ring components of polyphenols. The signal intensity shown by the specific O-aromatic region (145−160 ppm) in HAs confirms the incorporation of O-substituted ring carbon derived from different lignin structures. The evident resonances shown at 152 (sharp) and 158 ppm chemical shift ranges are usually assigned to carbons 3, 4, and 5 in the aromatic ring of lignin components, with carbon 3 and 5 being coupled to the corresponding methoxyl substituents. Finally, the intense signal in the carbonyl region (160−190 ppm) at 174 ppm suggests the contribution of carbonyl groups of peptide bonds of amino acid moieties in all of the humic materials. The relative distribution of organic functional groups and the hydrophobic index indicate that the HAs from cattle manure and filter cake underwent a more advanced humification process, with a final large preservation of recalcitrant hydrophobic components. Conversely, the lignin ratio and the larger amount of polysaccharides found in HA2, HA3, and HA4 (Figure 3) revealed a steady maintenance of biolabile compounds in the final mature vermicompost, with the mixed vermicompost showing a lower hydrophobic character (Table 2).

The results of the root growth biological assay represented by humic acid application are shown in Figure 4. All of the humic acids from mature vermicomposts showed an improvement in the number of lateral roots ranging from 36 to 135% with respect to control plants. However, HA4 showed no significant differences related to the control by the mean test applied. The lowest and no significant effect was found for HA4 extracted from the mixture of cattle manure, bagasse, and sunflower cake. Among those humic acids that produced significant bioactivity effect, we have humic acids re-isolated from bagasse (HA2) and sunflower cake (HA3), which enhanced the emergence of lateral roots in a very similar range from 51 to 58%, respectively. HA1 extracted from cattle manure revealed an increase of 98%, whereas the larger promotion was associated with HA5 from filter cake vermicompost.

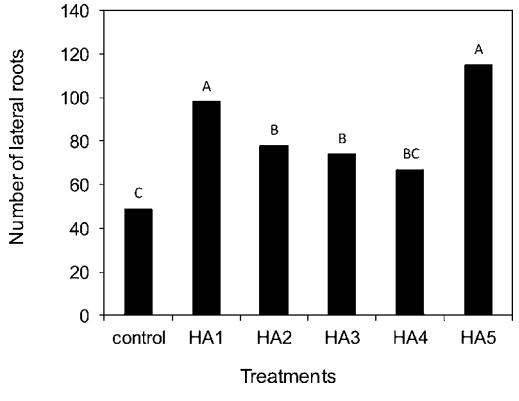


**Figure 4.** Number of lateral roots in maize seedlings treated with humic acids from different vermicomposts: (HA1) cattle manure; (HA2) sugar cane bagasse; (HA3) sunflower cake; (HA4) mixture of cattle manure, sugar cane bagasse, and sunflower cake; (HA5) sugar cane filter cake. Different letters represent a significant difference by means of Duncan's test ($p < 0.01$). The coefficient of variation was 13.37%.

Vermicomposting technology, using earthworms as versatile natural bioreactors for effective recycling of organic wastes to the soil, is an environmentally suitable method to convert residual biomass into nutrient-rich composts for crop production.[29] Considerable work has been carried out on vermicomposting processes of various organic materials such as animal manures, agricultural wastes, forestry wastes, city leaf litter and food residues, sewage sludge, and industrial wastes such as paper pulp and distillery wastes. Vermicomposting represents an important environmental service for waste recycling coupled with the generation of valuable products.[29] The results of $^{13}$C NMR spectroscopy and offline thermochemolysis GC-MS indicate that despite the intense biochemical transformation process of accelerated humification by earthworms, the final humic products retained the chemical features inherited from the original organic source. Contrary to the indications of $^{13}$C NMR spectra, a relatively low yield of carbohydrates was detected among the pyrolysis products. The lack of polysaccharide compounds was already noted in applications of thermochemolysis on plant woody tissues and soil organic matter.[24,26] These authors pointed out that the large amount of thermally unstable hydroxyl functional groups in polysaccharide chains makes the pyrolysis technique less suitable for the effective detection of carbohydrates in complex geochemical matrices. It is thus conceivable that for compost samples the setup of thermochemolysis parameters may be highly selective for lignin and alkyl components and may reduce the simultaneous identification of carbohydrate units from cellulose. Such selective detection reinforces the use of different approaches for a more complete compound inventory associated with the supramolecular structure of humic substances.

The different humic acids showed a variable effect on the emergence of lateral roots (Figure 4) and were characterized by an uneven incorporation of alkyl and aromatic hydrophobic components (Tables 1 and 2). To date, the most hydrophobic humic acids were isolated from cattle manure and filter cake biomasses, and they provided the best stimulation of lateral root emergence (Figure 4). In contrast, the root biostimulation effect was decreased by humic acids from sugar cane bagasse, sunflower cake, and mixed materials, which were characterized by the progressive lowering of hydrophobic character (Table 2). These results are consistent with the previous findings that humic fractions with a larger hydrophobicity provide a steady and high bioactivity, and the presence of aromatic and aliphatic components, such as lignin compounds and methyl esteres derivatives, is closely related to the ability of humic acids to induce lateral root emergence.[23,27,30,31] An apparent inconsistency with these previous findings was presented in the current thermochemolysis results, which showed that the largest lignin content was for HAs from sugar cane bagasse (Table 1). However, the most abundant aromatic monomers

found in the pyrograms of HA2 were 3-(4-methoxyphenyl)-2-propenoic (P18) and 3-(4,5-dimethoxyphenyl)-2-propenoic (G18) derivatives, which accounted for about 40% of the total lignin content (Table 1). These molecules originated either from the side-chain oxidation of lignin units or from the aromatic domains of plant biopolymers, the important relative contribution of which in herbaceous plants may have exaggerated the total content of lignin in the HAs from sugar cane, compared to those from cattle manure and filter cake. Moreover, the higher values of lignin structural index found in the pyrograms of HA2 and HA5 (Table 1) suggest the occurrence of an intense decomposition process of lignin biopolymers in the humic fraction from cattle manure and filter cake. Therefore, the most advanced humification may have promoted a preferential accumulation of small and active aromatic fragments bound to the supramolecular humic acids structure, which should allow a more prompt physiological response compared to the partial undecomposed and rigid lignin residues.[16]

In addition to the content of specific molecules, the ratio of hydrophobic to hydrophilic moieties is considered an important characteristic for the bioactivity of humic extracts. The role of humic hydrophobicity may be explained by the selective preservation, in humic recalcitrant compartments, of active biofragments that may be successively released by conformational changes of humic associations in solution.[8,19,21] The reduced microbial and enzymatic activity provided by the hydrophobic domains is assumed to contribute to the protection of biolabile hydrophilic compounds, which may become available to the plant root system by means of cell exudation in the rhizosphere.[28,32] For example, plants treated with humic substances showed enhanced exudation of organic acids, thereby leading to a modification of structural arrangement and to a release of active molecules in the rhizosphere.[22]

The present results confirm that mature vermicompost is a viable way to recycle agricultural biomass and to demonstrate that, acting as a source of bioactivity, humic extracts represent an additional valuable biological product for a wide range of agricultural practices.[18] Notwithstanding the modification by the composting processes, the final humic substances retained a chemical composition strongly related to the composition of the initial biomass. Although the role of hydrophobic humic components needs further evaluation to gain a deeper insight into the structure−activity relationship, the association of detailed molecular characterization and bioactivity assays are unavoidable requirements for a more accurate and valuable utilization of humic material as plant growth promoters and for a comprehensive understanding of the interaction between plant and soil organic matter.

## ■ ASSOCIATED CONTENT

### Ⓢ Supporting Information

Compounds obtained by GC-MS analysis from different humic acids extracted from vermicomposts. This material is available free of charge via the Internet at http://pubs.acs.org.

## ■ AUTHOR INFORMATION

### Corresponding Author

*(L.P.C.) Phone/fax: +55 22 27397198. E-mail: canellas@uenf.br.

### Funding

The work was supported by Conselho Nacional de Desenvolvimento Científico e Tecnológico (CNPq), Fundação de Amparo à Pesquisa do Estado do Rio de Janeiro (FAPERJ), Instituto Nacional de Ciência e Tecnologia (INCT) para a Fixação Biológica de Nitrogênio, Internacional Foundation of Science (IFS), and OCWP.

### Notes

The authors declare no competing financial interest.

## ■ REFERENCES

(1) Valdrighi, M. M.; Pera, A.; Agnolucci, M.; Frassinetti, S.; Lunardi, D.; Vallini, G. Effects of compost-derived humic acids on vegetable biomass production and microbial growth within a plant (*Cichorium intybus*)−soil system: a comparative study. *Agric., Ecosyst. Environ.* **1996**, *58*, 133−144.

(2) Edwards, C. A.; Arancon, N. Q.; Sherman, R. L. *Vermiculture Technology: Earthworms, Organic Wastes, And Environmental Management*; CRC Press: Boca Raton, FL, USA, 2010; p 601.

(3) Ali, M.; Griffiths, A. J.; Williams, K. P.; Jones, D. L. Evaluating the growth characteristics of lettuce in vermicompost and green waste compost. *Eur. J. Soil Biol.* **2007**, *43*, S316−S319.

(4) Muscolo, A.; Bovalo, F.; Giomfriddo, F.; Nardi, S. Earthworm humi matter produces auxin-like effects on *Daucus carota* cell growth and nitrate metabolism. *Soil Biol. Biochem.* **1999**, *31*, 1303−1311.

(5) Canellas, L. P.; Okorokova-Façanha, A.; Olivares, F. L.; Façanha, A. R. Humic acids isolated from earthworm compost enhance root elongation, lateral root emergence, and plasma membrane $H^+$-ATPase activity in maize roots. *Plant Physiol.* **2002**, *130*, 1951−1957.

(6) Arancon, N. Q.; Lee, S.; Edwards, C. A.; Atiyeh, R. M. Effects of humic acids and aqueous extracts derived from cattle, food and paper-waste vermicomposts on growth of greenhouse plants. *Pedobiologia* **2003**, *47*, 741−744.

(7) Arancon, N. Q.; Edwards, C. A.; Atiyeh, R.; Metzger, J. D. Effects of vermicomposts produced from food waste on the growth and yields of greenhouse peppers. *Bioresour. Technol.* **2004**, *93*, 139−144.

(8) Canellas, L. P.; Piccolo, A.; Dobbss, L. B.; Spaccini, R.; Olivares, F. L.; Zandonadi, D. B.; Façanha, A. R. Chemical composition and bioactivity properties of size-fractions separated from a vermicompost humic acid. *Chemosphere* **2010**, *78*, 457−466.

(9) Warman, P. R.; Anglopez, M. J. Vermicompost derived from different feedstocks as a plant growth medium. *Bioresour. Technol.* **2010**, *101*, 4479−4483.

(10) Nardi, S.; Concheri, G.; Dell'agnola, G. Biological activity of humus. In *Humic Substances in Terrestrial Ecosystems*; Piccolo, A., Ed.; Elsevier: Amsterdam, The Netherlands, 1996; pp 361−40.

(11) Masciandaro, G.; Ceccanti, B.; Garcia, C. Soil agroecological management: fertirrigation and vermicompost treatments. *Bioresour. Technol.* **1999**, *59*, 199−206.

(12) Dell'Agnola, G., Nardi, S. On overview of earthworm activity in the soil. In *On Earthworms Selected Symposia and Monographs*, Part 2; Bonvicini Pagliai, A. M., Omodeo, P., Eds.; Mucchi Ed.e: Modena, Italy, 1987; pp 103−112.

(13) Muscolo, A.; Nardi, S. Auxin or auxin-like activity of humic matter. In *The Role of Humic Substances in the Ecosystems and Environmental Protection*; Drozd, J., Gonet, S. S., Senesi, N., Weber, J., Eds.; Polish Society of Humic Substances: Wroclaw, Poland, 1997; pp 987−992.

(14) Canellas, L. P.; Martinez-Balmori, D.; Médici, L. O.; Aguiar, N. O.; Campostrini, E.; Rosa, R. C. C.; Façanha, A. R.; Olivares, F. L. A combination of humic substances and *Herbaspirillum seropedicae* inoculation enhances the growth of maize (*Zea mays* L.). *Plant Soil* **2013**, *366*, 119−132.

(15) Atiyeh, R. M.; Lee, S.; Edwards, C. A.; Arancon, N. Q.; Metzger, J. D. The influence of humic acids derived from earthworm-processed organic wastes on plant growth. *Bioresour. Technol.* **2002**, *84*, 7−14.

(16) Quaggiotti, S.; Ruperti, B.; Pizzeghello, D.; Francioso, O.; Tugnoli, V.; Nardi, S. Effect of low molecular size humic substances on

nitrate uptake and expression of genes involved in nitrate transport in maize (*Zea mays* L.). *J. Exp. Bot.* **2004**, *55*, 803−813.
(17) Zandonadi, D. B.; Canellas, L. P.; Façanha, A. R. Indoleacetic and humic acids induce lateral root development through a concerted plasmalemma and tonoplast $H^+$ pumps activation. *Planta* **2007**, *225*, 1583−1595.
(18) Canellas, L. P.; Olivares, F. L. Physiological responses to humic substances as plant growth promoter. *Chem. Biol. Technol. Agric.* **2014**, *1*, 3.
(19) Dobbss, L. B.; Canellas, L. P.; Olivares, F. L.; Aguiar, N. O.; Peres, L. E. P.; Azevedo, M.; Spaccini, R.; Piccolo, A.; Facanha, A. R. Bioactivity of chemically transformed humic matter from vermicompost on plant root growth. *J. Agric. Food Chem.* **2010**, *58*, 3681−3688.
(20) De Marco, A.; Spaccini, R.; Vittozzi, P.; Esposito, F.; Berg, B.; Virzo De Santo, A. Decomposition of black locust and black pine leaf litter in two coeval forest stands on Mount Vesuvius and dynamics of organic components analyzed through conventional chemical methods and NMR spectroscopy. *Soil Biol. Biochem.* **2012**, *51*, 1−15.
(21) Aguiar, N. O.; Novotny, E. H.; Oliveira, A. L.; Rumjanek, V. M.; Olivares, F. L.; Canellas, L.P. Prediction of humic acids bioactivity using spectroscopy and multivariate analysis. *J. Geochem. Explor.* **2013**, *129*, 95−102.
(22) Canellas, L. P.; Dobbss, L. B.; Oliveira, A. L.; Chagas, J. G.; Aguiar, N. O.; Rumjanek, V. M.; Novotny, E. H.; Olivares, F. L.; Spaccini, R.; Piccolo, A. Chemical properties of humic matter as related to induction of plant lateral roots. *Eur. J. Soil Sci.* **2012**, *63*, 315−324.
(23) Aguiar, N. O.; Olivares, F. L.; Novotny, E. H.; Dobbss, L. B.; Balmori, D. M.; Santos-Júnior, L. G.; Chagas, J. G.; Façanha, A. R.; Canellas, L. P. Bioactivity of humic acids isolated from vermicomposts at different maturation stages. *Plant Soil* **2013**, *362*, 161−174.
(24) Spaccini, R.; Sannino, D.; Piccolo, A.; Fagnano, M. Molecular changes in organic matter of a compost-amended soil. *Eur. J. Soil Sci.* **2009**, *60*, 287−296.
(25) Zhou, P.; Pan, G. X.; Spaccini, R.; Piccolo, A. Molecular changes in particulate organic matter (POM) in a typical Chinese paddy soil under different long-term fertilizer treatments. *Eur. J. Soil Sci.* **2010**, *61*, 231−242.
(26) Spaccini, R.; Song, X. Y.; Cozzolino, V.; Piccolo, A. Molecular evaluation of soil organic matter characteristics in three agricultural soils by improved off-line thermochemolysis: the effect of hydrofluoric acid demineralisation treatment. *Anal. Chim. Acta* **2013**, *802*, 46−55.
(27) Martinez-Balmori, D.; Olivares, F. L.; Spaccini, R.; Aguiar, K. P.; Araújo, M. F.; Aguiar, N. O.; Guridi, F.; Canellas, L. P. Molecular characteristics of vermicompost and their relationship to preservation of inoculated nitrogen-fixing bacteria. *J. Anal. Appl. Pyrolysis* **2013**, *104*, 540−550.
(28) Song, X. Y.; Spaccini, R.; Pan, G.; Piccolo, A. Stabilization by hydrophobic protection as a molecular mechanism for organic carbon sequestration in maize-amended rice paddy soils. *Sci. Total Environ.* **2013**, *458*−*460*, 319−330.
(29) Padmavathiamma, P. K.; Li, L. Y.; Kumari, U. R. An experimental study of vermi-biowaste composting for agricultural soil improvement. *Bioresour. Technol.* **2008**, *99*, 1672−1681.
(30) Canellas, L. P.; Zandonadi, D. B.; Busato, J. G.; Baldotto, M. A.; Simões, M. L.; Martin-Neto, L.; Façanha, A. R.; Spaccini, R.; Piccolo, A. Bioactivity and chemical characteristics of humic acids from tropical soils sequence. *Soil Sci.* **2008**, *173*, 624−637.
(31) Canellas, L. P.; Spaccini, R.; Piccolo, A.; Dobbss, L. B.; Okorokova-Façanha, A. L.; Santos, G. A.; Olivares, F. L.; Façanha, A. R. Relationships between chemical characteristics and root growth promotion of humic acids isolated from Brazilian Oxisols. *Soil Sci.* **2009**, *174*, 611−624.
(32) Spaccini, R.; Piccolo, A.; Conte, P.; Haberhauer, G.; Gerzabek, M. H. Increased soil organic carbon sequestration through hydrophobic protection by humic substances. *Soil Biol. Biochem.* **2002**, *34*, 1839−1851.

release in functional foods, for example, low-fat, low-sugar food. Previous studies either on pure gels (e.g., pectin gels, protein gels, carrageenan gels) or mixed gels (e.g., starch-carrageenan gels, pectin-gelatin gels) have shown that the gel structure affects volatile release from food,[14,16−18] and gels with stronger texture had weakened volatile profile.[14] In EFP gels, oil droplets are immobilized in a viscoelastic gel network, with slowed rates of diffusion and mass transfer of volatile molecules. When the gel network collapses under mechanical forces (e.g., chewing), volatile release can be accelerated.[17] Therefore, EFP gels can behave as volatile carriers to control volatile release and target delivery. Although biopolymer gels have long been used as delivery systems for bioactives, they differ from EFP gels in physicochemical properties and functional values. Among the few studies conducted, Lee et al.[19] reported that volatile retention ranged from 60 to 100% in EFP gels and from 5 to 25% in emulsions when stored at 37 °C for 72 h.

In the current study, cold-set EFP gels were prepared through acidification by glucono-$\delta$-lactone (GDL), and different volatile compounds were incorporated into the gels. The main objective of the study was to understand the release behavior of volatiles in EFP gels with different rheological properties by adjusting the protein and oil content. Because protein gels are sometimes used as fat replacers in food,[20] another goal was to explore the possibility of slowing volatile release in oil-reduced systems by creating stronger EFP gels.

## MATERIALS AND METHODS

**Materials.** WPI (BiPro), which contained >90% w/w total protein (5% moisture, 1% fat, 3% ash, 1% lactose), was bought from Davisco Food International (Le Sueur, MN, USA). Sunflower oil was purchased from a local supermarket and used without further purification.

**Chemicals.** Glucono-$\delta$-lactone (GDL), sodium azide, 1-propanol (>99.5% purity), diacetyl (>99.5% purity), 2-pentanone (>99% purity), hexanal (>99% purity), 2-heptanone (>99% purity), Nile red, and fast green were all products of Sigma-Aldrich (St. Louis, MO, USA).

**Preparation of EFP Gels.** EFP gels were prepared following the method described by Sok Line et al.[21] with some modifications. Briefly, WPI suspension was prepared by dispersing the powdered WPI in deionized water, and the mixture was stirred overnight to ensure complete dissolution. Sodium azide (0.01% w/w) was added to inhibit microbial growth. The solution was then heated at 85 °C for 30 min in a water bath, followed by rapid cooling to room temperature (~23 °C) with an ice−water mixture. An oil-in-water emulsion was prepared by mixing the heated WPI solution and sunflower oil at 10 000 rpm for 1 min using an Ultra-Turrax (IKA, Staufen, Germany), followed by high-pressure homogenization (M110-EH Microfluidizer, Microfluidics International Corp., Newton, MA, USA) at 50 MPa for three passes. The emulsions were immediately cooled to room temperature (~23 °C) with tap water and stored in an incubator for further use. The droplet sizes of the emulsions were determined by dynamic light scattering using a Zetasizer Nano-ZS90 (Malvern Instruments Ltd., Malvern, UK) at a fixed detector angle of 90°. The refractive indices of the particle and water were set at 1.45 and 1.33, respectively. To minimize multiple scattering effects, emulsions were diluted with deionized water to an oil concentration of ~0.005% w/w prior to each measurement. The intensity mean diameter (nm) based on three repeats was reported.

To induce cold gelation, GDL (0.5% w/w) was added into the emulsions and incubated at 25 °C for 16 h. The evolution of the pH of the emulsions during gelation was recorded by Cinac (Ysebaert Dairy Division, Frepillon, France). In the measurement, the sample tubes with one pH probe in each tube were kept in a water bath (25 °C), and the pH values of the samples were recorded every 5 min for 16 h.

For comparison purposes, an ungelled emulsion (no GDL, 20% oil, 5% WPI, w/w) and an emulsion with unheated WPI solution (20% oil, 5% WPI, 0.5% GDL, w/w) were also prepared using the above method.

**Characterization of EFP Gels.** *Viscoelastic Properties.* After the addition of GDL, emulsions (~15 mL) were allowed to form gels in a AR 2000ex rheometer (TA Instruments, Crawley, UK) using a concentric cylinder geometry (cup radius = 15 mm, rotor radius = 14 mm). To avoid water evaporation, a thin layer of tetradecane oil was added to the surface of the samples. The samples were oscillated at a strain of 0.5% and a frequency of 1 Hz to ensure the linear behavior and measurements were taken every 10 s for 16 h. The measurement was performed at 25 ± 0.05 °C, controlled by a Grant GD 120 stirred thermostatic circulator (Grant Instruments, Cambridge, UK). The evolution of the storage and loss moduli ($G'$ and $G''$) of the samples during oscillation was recorded. Dynamic strain sweep measurement (strain 0.1−300%, frequency 1 Hz) was previously carried out to determine the linear viscoelastic range of the gels. Gelation time ($T_{gel}$), defined as the time point at which the $G'$ time curve and $G''$ time curve crossed over, was also reported. The pH value of the emulsions at $T_{gel}$ was defined as gelation pH ($pH_{gel}$).

*Mechanical Properties.* A large deformation rheological test was applied to evaluate the mechanical properties of EFP gels. The gels were formed in cylindrical plastic beakers (20 mm internal diameter × 35 mm height) for 16 h at 25 °C. The test was performed on a TA-HDi Texture Analyzer (Stable Micro System, Godalming, UK) with a cylindrical plunger (diameter = 5 mm) and a 5 kg load, operating at a test speed of 1 mm/s to a total penetration distance of 10 mm. Three parameters were recorded: force at breaking (N), defined as the first significant inflection point in the force−distance curve; strain at breaking (mm), defined as the penetration distance at which the force at breaking was recorded; and stiffness (N/mm), defined as the initial slope of the force−distance curve.[22] The reported results were the mean value of eight replicates.

*Water-Holding Capacity (WHC).* For WHC determination, EFP gels were formed in Nalgene centrifuge tubes (Sigma-Aldrich). The gels were centrifuged at 20 000$g$ (Sorval RC 5B Plus, DuPont Instruments, Connecticut, US) for 30 min at 4 °C, and the water released was then drained, and the amount of water was calculated. WHC was determined as

$$\mathrm{WHC} = \frac{W_T - W_F}{W_T} \times 100\%$$

where $W_T$ was the total amount (g) of water in the gel and $W_F$ was the quantity of water (g) released. The mean of three repeats was reported.[23]

*Microstructure.* Confocal scanning laser microscopy was used to observe the microstructure of the EFP gels. A thin layer (~2 mm) of the gel was transferred to a glass slide and stained with a mixture of Nile red (0.1%, w/v, in distilled water) and fast green (0.1%, w/v, in distilled water) at a ratio of 3:1. Confocal observation was performed after 5 h of labeling using a Leica TCS SP5 microscope (Leica Microsystems GmbH, Wetzlar, Germany). Images of representative areas of each sample were taken using a 63× oil immersion objective (numerical aperture = 1.4) at an excitation wavelength of 633 nm, provided by a He−Ne laser.

**Emulsion Flavoring.** Emulsion flavoring was achieved before the addition of GDL, and the procedure was described in a previous study.[27] Briefly, a volatile-ethanol solution (5% v/v for each volatile) was added into emulsions in gastight glass vials (20 mL, silicone/PTFE seals) (La-pha-pack GmbH, Langerwehe, Germany) to reach a concentration of 500 mg/L for each volatile, and the solution was equilibrated for 1 h. Two grams of the flavored emulsion was rapidly transferred to a headspace vial (20 mL, silicone/PTFE seals) (La-pha-pack GmbH) containing 0.01 g of GDL. The vials were stored at 25 °C for 16 h before GC headspace analysis.

**GC Headspace Analysis.** Headspace concentrations of the volatiles at different time points (0.5,1, 2, 4, 6, 10, 20 min) were measured using a Varian CP-3800 gas chromatograph (Varian Inc.,

Palo Alto, CA, USA) equipped with a ZB-5MSi capillary column (60 m, 0.25 mm i.d., film thickness = 0.25 $\mu$m) and coupled with a FID detector. Headspace vials containing EFP gels were incubated at 37 °C for different times in a Combi PAL autosampler (CTC Analytics AG, Switzerland). Injections of the headspace (1 mL) were performed using a preheated (42 °C) 2.5 mL thermostated gastight syringe (Hamilton, Switzerland) under split mode (1:10). Only one sampling was made in each vial. Injector and FID temperatures were 225 and 230 °C, respectively. The helium carrier gas flow rate was 1 mL/min. The temperature program was as follows: 50 °C (4 min), 200 °C at 10 °C/min rate, 240 °C at 40 °C/min rate (2 min).

To quantify the concentrations of the volatiles in the headspace, calibration curves of the tested five volatiles were plotted using peak areas obtained from GC analysis against six known concentrations of each volatile in ethanol. The completely vaporized volatile-ethanol solution (2.0 $\mu$L solution in a 20 mL vial, incubated at 37 °C for 1 h) was analyzed according to the above GC methods. Results were based on triple analysis.[24]

**Statistical Analysis.** Statistical analysis was performed using OriginPro 7.5. All of the measurements were repeated at least three times. A one-way analysis of variance (ANOVA), followed by Tukey's test, was applied to determine significant differences between the mean values of each test. A significance level of $p < 0.05$ was used throughout the study.

## RESULTS AND DISCUSSION

**Characterization of EFP Gels.** Storage modulus ($G'$) is an indicator of the energy reserved every cycle of deformation, and its value reflects the elastic or solid-like properties of the tested sample, whereas loss modulus ($G''$) is a measure of the energy dissipated by the sample and is connected with the viscous or liquid-like properties of the sample. Figure 1 shows the evolution of $G'$ and $G''$ as the gelation process went on after the addition of GDL. A change in the pH of the emulsion was also recorded. As the graph indicates, when the pH of the emulsion decreased to about pH 5.9, $G'$ and $G''$ increased dramatically, and the $G'$ value dominated the $G''$ value thereafter, indicating onset of gelation in the emulsion.[12] The $G'$ values increased further with a decrease in the pH of the emulsion, reaching a plateau at around pH 4.7, indicating the formation of an elastic gel at pH values below pH 5. The increase in the $G'$ over time was attributed to structure rearrangements within the emulsion, and a compact gel network was gradually formed.[25] The gelation process took place mainly in the first 16 h, as the storage modulus increased slowly after that.

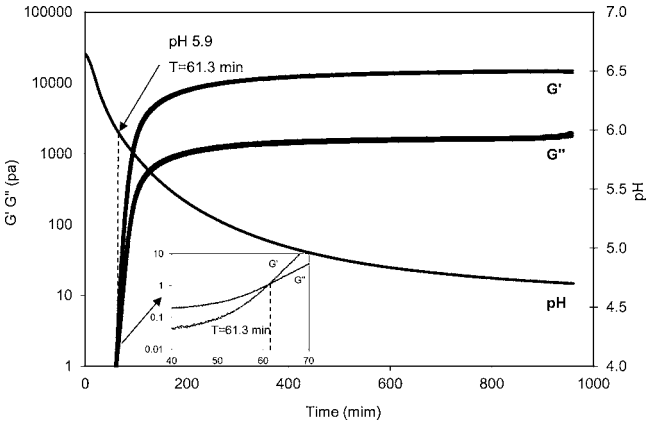


**Figure 1.** Evolution of storage modulus ($G'$), loss modulus ($G''$), and pH during the cold-gelation of emulsion filled protein gel (5% WPI, 20% oil, 0.5% GDL, w/w). The protein solution was preheated at 85 °C for 30 min. The inset image highlights the intersection of $G'$ and $G''$.

WPI contributed to the majority of the gel network, and the change in the WPI content allowed great variation in the physicochemical properties of the EFP gels. Particle size analysis showed that the increase in the WPI content coincided with an increase in the droplet size, and all the emulsions had droplet sizes < 300 nm, with a fine droplet distribution. The size difference could be attributed to depletion flocculation and bridge flocculation induced by the denatured protein in the continuous phase.[26] No significant difference in $T_{gel}$ was observed in gels with a WPI content from 4 to 6%. Because the evolution of the pH was induced by GDL, all of the emulsions started gelation at the same $pH_{gel}$ ($p > 0.05$) (Table 1). During gelation, the presence of GDL allowed a pH decrease to a value below the isoelectric point of the WPI, which resulted in a reduced repulsion force between protein aggregates and then association of the aggregates through noncovalent interactions.[27] In gels with a higher WPI content, protein interactions and the packing density increased, leading to a strengthened gel matrix with a higher $G'$ (Figure 2). It was also observed that an increase in the WPI content from 3 to 6% led to ~3-fold enhancement of the storage modulus. The relationship between the protein concentration and the gel storage modulus follows a power law, $G' = f(c^x)$,[28] and the exponent $x$ is calculated from the slope of the log−log relationship between the storage modulus and the protein concentration. The exponent is dependent on the gel microstructure and gelation conditions (e.g., pH, salt composition).[28,29] For heat-set protein gels (WPI 0.1−10% w/w), the constant could reach >4.[30,31] In the current cold-set EFP gels with 20% oil, the power law constant decreased to 2.6. This change indicated that in EFP gels, the contribution of the protein concentration to the storage modulus was reduced, which could be a sign of the active role of oil droplets in the gel.[31]

Visual observation found that the gel with 3% WPI was pourable, reflecting a weak network. Gels with higher WPI content presented soft solid-like properties with a smooth surface and homogeneous cross section. The mechanical properties of the gels were determined by a texture analyzer under a penetration test. For all of the gels, an increase in the WPI content induced an increase in both the force and the strain at breaking, suggesting that more rigid gels were formed with a higher WPI content (Table 1). This finding was in agreement with published data for cold-set protein gels.[32] The resistance against the deformation of a protein network and dispersed oil droplets was measured as a force.[8] In the more rigid gels, a closer proximity among the protein chains allowed a more even distribution of applied force against breaking down of the gel network. It was also found that the force increased more than proportionally with the strain value with an increase in the WPI content, suggesting that the gels with a higher WPI content became more strain-hardening.[8] Stiffness calculation reconfirmed the findings because the value increased with the WPI content. In line with the visual observation, the gel with 3% WPI presented poor mechanical properties (the lowest force at breaking and stiffness). Determination of the WHC showed that a higher WPI content also contributed to a higher WHC, although only a slight difference was found for gels with WPI ≥ 4%. In the gel with 3% WPI, about 1/3 of the water was lost after a centrifuge test, suggesting a weak water−protein gel interaction and a less compact gel structure. The above result

Table 1. Effect of WPI Content (w/w) on the Properties of EFP Gels (20% w/w oil)[a]

| | 3% WPI | 4% WPI | 5% WPI | 6% WPI |
|---|---|---|---|---|
| size (nm) | 200.4 ± 6.7a | 209.7 ± 7.8a | 223.6 ± 6.8b | 267.0 ± 8.9c |
| $T_{gel}$ (min) | 46.1 ± 1.5a | 59.4 ± 1.6b | 61.3 ± 2.1b | 59.4 ± 1.8b |
| $pH_{gel}$ | 5.91 ± 0.13a | 5.80 ± 0.14a | 6.02 ± 0.21a | 5.94 ± 0.19a |
| force at breaking (N) | 0.16 ± 0.01a | 0.60 ± 0.02b | 1.44 ± 0.08c | 2.36 ± 0.16d |
| strain at breaking (mm) | 2.57 ± 0.09a | 3.42 ± 0.17b | 4.88 ± 0.27c | 5.51 ± 0.47d |
| stiffness (N/mm) | 0.08 ± 0.00a | 0.17 ± 0.01b | 0.29 ± 0.01c | 0.42 ± 0.01d |
| WHC[b] (%) | 67.79 ± 1.50a | 95.16 ± 1.74b | 97.89 ± 1.2b | 100 ± 0.02c |

[a]Gelation was induced with the addition of 0.5% w/w GDL. Within each row, values with different letters are significantly different ($p < 0.05$). [b]WHC, water holding capacity.

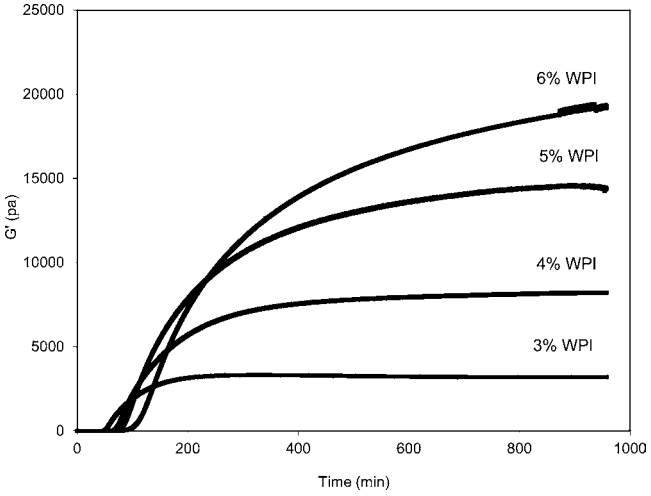


Figure 2. Effect of WPI content (w/w) on the evolution of the storage modulus ($G'$) during the cold-gelation of emulsion-filled protein gels (20% oil, 0.5% GDL, w/w). The protein solution was preheated at 85 °C for 30 min.

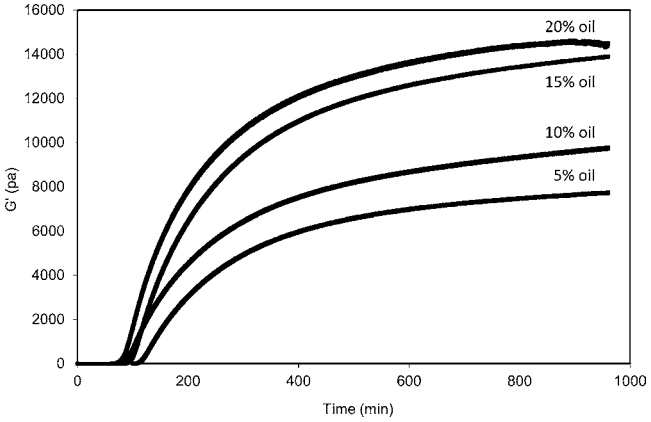


Figure 3. Effect of oil content (w/w) on the evolution of storage modulus ($G'$) during the cold gelation of emulsion-filled protein gels (5% WPI, 0.5% GDL, w/w). Protein solution was preheated at 85 °C for 30 min.

also showed that WPI content ≥4% was essential to obtain gels with suitable mechanical properties.

Because oil droplets behaved as active fillers in EFP gels, the oil content showed large effects on the gel properties (Table 2). First, a higher oil content greatly shortened the gelation process. For example, with 5% oil, the gelation took place 104.3 min after the addition of GDL, but with 20% oil, the gelation was observed much earlier (61.3 min after GDL addition) (Table 2). In gels with a higher oil droplet concentration, more droplet−droplet and droplet−matrix interactions were expected, and the emulsion presented elastic properties ($G' > G''$) at a much earlier stage.

Second, the maximum rate of increase in $G'$ and the final $G'$ were higher for gels with a higher oil content (Figure 3). Similar results were reported by Sok Line et al.,[21] who found that the presence of 30% oil in the protein network enhanced about 10-fold of the storage modulus. The findings reconfirmed that oil droplets were acting as space fillers in the gels, and they helped to build a gel matrix structure through the interaction between the protein covering the droplets and the protein in the bulk phase.[11]

Third, gels with a higher oil content had a higher value of force at breaking and stiffness, although the effect was much smaller than that of the WPI content. According to Kim et al.,[8] the increase in the force at breaking with the oil content was more significant in gels containing smaller droplets. However, such an increase in force was not observed in the current study, probably because of the slight deviation in the droplet size of emulsions with different oil contents. Furthermore, the increased WPI concentration in the water phase (reduced water content due to the increase in the oil content) could also contribute to the enhancement of the gel texture. The decrease in the strain at breaking indicated that the gels became more

Table 2. Effect of Oil Content (w/w) on the Properties of EFP gels (5% w/w WPI)[a]

| | 5% oil | 10% oil | 15% oil | 20% oil |
|---|---|---|---|---|
| size (nm) | 179.4 ± 7.4a | 195.0 ± 4.4b | 211.3 ± 5.2c | 223.6 ± 6.8d |
| $T_{gel}$ (min) | 104.3 ± 2.4a | 77 ± 1.7b | 74.3 ± 1.9b | 61.3 ± 2.1c |
| force at breaking (N) | 1.19 ± 0.07a | 1.25 ± 0.06ab | 1.32 ± 0.06bc | 1.44 ± 0.08cd |
| strain at breaking (mm) | 8.37 ± 0.61a | 7.13 ± 0.52b | 5.88 ± 0.52c | 4.88 ± 0.27d |
| stiffness (N/mm) | 0.13 ± 0.01a | 0.16 ± 0.01b | 0.21 ± 0.01c | 0.29 ± 0.01d |
| WHC[b] (%) | 96.66 ± 0.47a | 98.31 ± 0.30b | 99.16 ± 0.42b | 97.89 ± 1.20ab |

[a]Gelation was induced with the addition of 0.5% w/w GDL. Within each row, values with different letters are significantly different ($p < 0.05$). [b]WHC, water holding capacity.

brittle with the increase in the oil content. The finding was also reported in previous studies.[8,32,33] The minor effect of the oil content on the WHC was probably due to the fact that the water was mostly bound to the protein, and the slight increase in the rigidity or compactness of the gel did not present a profound enhancement of the WHC.

From a theoretical point of view, an increase in the oil content would result in a decrease in both the force and strain at breaking for gels with foreign droplets , as a result of stress concentration. Stress concentration can be induced by structure defects in the structure, for example, oil droplets in the protein gel network. Becauise of the inhomogeneity in the gel, the gel between droplets is deformed at a higher level than the gel at the surface of the droplets under large deformation. The stress concentration between droplets triggers gel fracture due to dissociation of gel from the droplets or fracture of the gel matrix.[34,35] Therefore, protein gels with a higher oil content were more likely to break down at lower stress and strain. However, a slight increase rather than a decrease in the breaking force with the oil content was observed in the current study, which could be attributed to the viscous properties of the EFP gels. In these gels, viscous flow arose as a result of local yielding in the area where the stress was concentrated, and energy was dissipated. Furthermore, the viscous nature of the interfacial layer of the oil droplets in the gels can dissipate energy, as well.[11] Therefore, more force was required to break the EFP gels with the higher oil content. Another possible reason responsible for the slight increase in the breaking force was that the slip between droplets and the gel matrix took place at the expense of additional force.[36]

Figure 4 shows representative confocal microscopy images of EFP gels with different WPI contents and oil contents. As the pictures indicate, all of the oil droplets (green) had a regular spherical shape, and they were evenly distributed, with no clear droplet aggregation being observed. The images did not present large difference in droplet size of different systems, and the droplet size obtained was in good agreement with that determined by dynamic light scattering, suggesting that little or no coalescence occurred upon gelation. Careful observation of the protein network (red) showed variation in gel structures in gels with different compositions. Gel A (5% WPI, 20% oil) presented a continuous network with evenly distributed small pores, whereas in gel B (5% WPI, 10% oil), the pores became rather big, and they broke the network. By contrast, gel C (3% WPI, 20% oil) did not show a typical gel network but, rather, a network containing only some protein clumps, and individual oil droplets were observed. This observation supported the previous finding that both WPI and oil contributed to form the gel network, and increase in WPI content or oil content could result in gels with higher compactness.

**Volatile Release from EFP Gels.** Five volatile compounds, that is, propanol (C3), diacetyl (C4), pentanone (C5), hexanal (C6), and heptanone (C7), were incorporated into the EFP gels, and their release behaviors were evaluated. The selection of these compounds was mostly based on the carbon numbers and polarity of the different compounds. Diacetyl is the most hydrophilic one (log $P$ = −1.43), whereas heptanone is the most lipophilic one (log $P$ = 1.98), with propanol (log $P$ = 0.25), pentanone (log $P$ = 0.91), and hexanal (log $P$ = 1.78) in between them.[37] Volatile release from food is mainly controlled by two factors: the volatility of volatile compounds (thermodynamic factor) and the resistance to mass transfer from a food matrix to the air phase (kinetic factor).[38] The

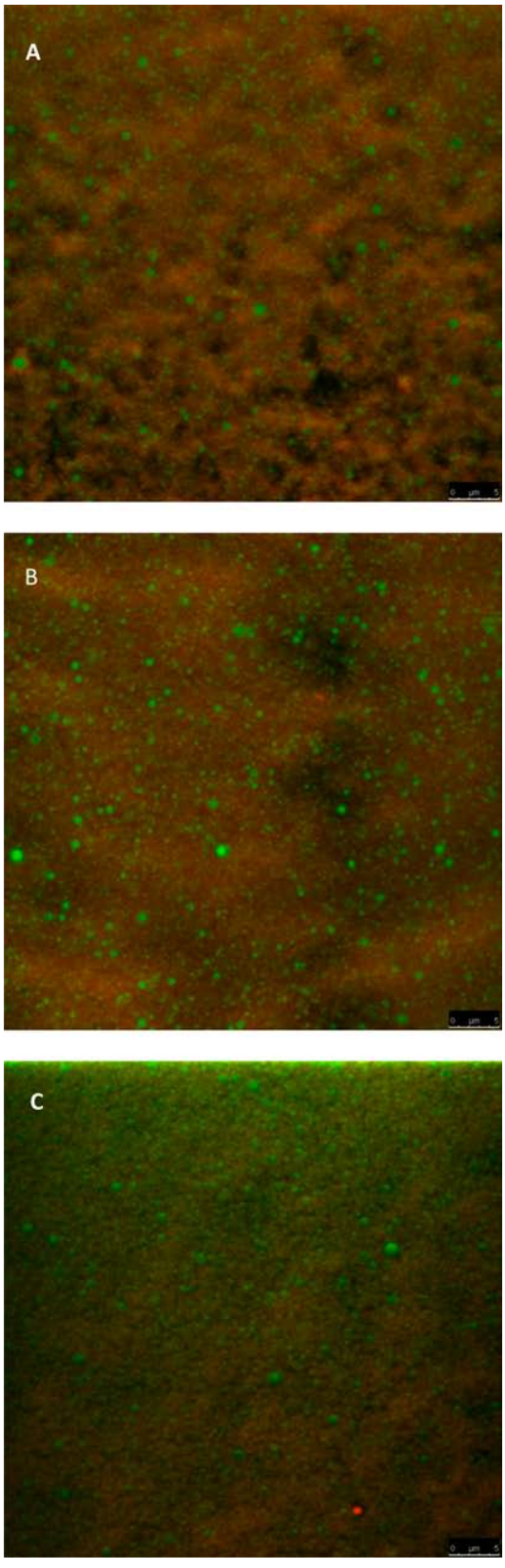


**Figure 4.** Confocal microscopy images of cold-set emulsion filled protein gels with different WPI contents and oil contents: A (5% WPI, 20% oil, w/w), B (5% WPI, 10% oil, w/w), and C (3% WPI, 20% oil, w/w). Green represents the oil; red, the protein. Gelation was induced with the addition of 0.5% w/w GDL. Gels were labeled for 5 h before confocal observation. The bars indicate 5 $\mu$m in length.

thermodynamic factor determines the retention or partition of volatiles in the matrix at equilibrium, and the kinetic factor mainly affects the release rate of volatiles from the foods. The rationale of encapsulating emulsion droplets within a protein gel network was to reduce the rate of volatile diffusion from oil droplets to the continuous phase and to the external environment (e.g., headspace, saliva) and mass transfer inside aqueous phase by creating physical barriers in the oil–water interface and aqueous phase. Pre-experiments (using the same GC method described in Material and Methods) indicated that volatile compounds had linear releases ($r^2$ ranging from 0.96 to 0.99) in the initial stage from 0.5 to 6 or 10 min, and release equilibrium was reached within 20 min. The slope of the linear curve was regarded as the release rate of each volatile compound. Headspace concentrations at equilibrium were used to calculate partition coefficients $K_{A/E}$ ($K_{A/E} = C_A/C_E$, $C_A$, $C_E$ were the volatile concentrations in the headspace and bulk emulsions, respectively).

Figure 5 shows the release rates of the volatile compounds in EFP gels (with GDL) or ungelled emulsions (no GDL). In the

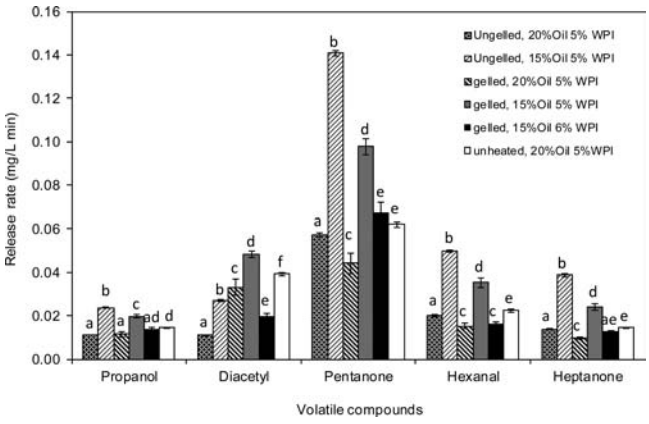


**Figure 5.** Release rates of the volatiles in EFP gels (with GDL) and ungelled emulsions (no GDL) varying in WPI content (w/w), oil content (w/w), and in the emulsion with unheated WPI solution (with 0.5% w/w GDL). Gelation was induced with the addition of 0.5% w/w GDL. Samples were incubated at 37 °C before each measuring point.

systems with 20 or 15% oil, most volatiles had lower release rates in EFP gels than those in the corresponding ungelled emulsions. For example, in the EFP gel with 15% oil and 5% WPI, pentanone had a release rate of 0.098 ± 0.004 mg/L min, whereas in the ungelled emulsion, the release rate was 0.141 ± 0.001 mg/L min. Similarly, most volatile compounds had a lower $K_{A/E}$ in the EFP gels than in the ungelled counterparts (Table 3). Therefore, in the EFP gels, volatile release was at a lower rate and of lower intensity. Similar findings were also reported in other gel systems. Boland et al.[14] compared volatile release from gelatin gel, pectin gel, and starch gel and found that increasing gel hardness could reduce the amount of volatiles released to the headspace. Guinard and Marty[39] reported that firm gels made with gelatin and carrageenan had volatiles released with a lower intensity than soft gels made with the same gelling agents.

The effect of the gel network on the volatile release could work through two different mechanisms. One was the physical entrapment of volatile compounds in the gel matrix. It was reported that the presence of an entangled polymer network in a gel system could inhibit diffusion and reduce the mobility of small molecules, for example, volatile compounds.[40] One may argue that the open space in the gel network (e.g., pores) could provide channels for the movement of small molecules, and the release of volatiles may not be blocked by the gel. In fact, Juteau-Vigier et al.[16] concluded in their study that the structure level of carrageenan gel did not show a big influence (<20%) on diffusion properties of ethyl hexanoate, but they admitted that the mobility of the volatile compounds was limited by the matrix organization. In the same study, it was also observed that addition of 1% carrageenan induced a 5.3-fold reduction in the diffusion coefficient of the volatiles. In EFP gels, volatile compounds, especially the more hydrophobic ones, were mostly distributed inside oil droplets, which were covered by compact protein films. The movement of volatiles across the interface could be inhibited to a higher level when the protein film gelled and cross-linked with the gel matrix. The gel matrix may provide additional force to retard the movement of both hydrophobic and hydrophilic compounds.

The second mechanism involved interactions between volatile compounds and gel components, which was also responsible for the reduced partition coefficients of ethyl hexanoate in the study conducted by Juteau-Vigier et al.[16] The interactions between the volatiles and protein in the current system could be due to adsorption, complexation, and entrapment.[15] WPI (or β-lactoglobulin) can attract ketones and esters through hydrophobic interaction or covalent binding.[41,42] The former attraction occurs in the hydrophobic pocket (the central calyx) of the protein,[41] whereas the latter could happen at a protein surface.[43]

According to Harrison and Hills,[44] binding reduced the concentration of free volatile compounds in the aqueous phase and, consequently, the released volatiles into the headspace. Protein adsorbed at the interface can act as a barrier to slow mass transfer of volatiles, leading to reduced release rate.[45] For example, the presence of β-lactoglobulin at the miglyol–water interface increased resistance to the transfer of benzaldehyde across the lipid layer.[46] In EFP gels, the interaction between the volatiles and protein was strengthened when the protein was

**Table 3. Air–Gel Partition Coefficients ($K_{A/E} \times 10^4$) of the Volatiles in EFP Gels (with GDL) and Ungelled Emulsions (no GDL) Varying in WPI Content (w/w), Oil Content (w/w), and in the Emulsion with Unheated WPI Solution (with GDL)[a]**

| gelled or ungelled | oil content (w/w) | WPI content (w/w) | propanol | diacetyl | pentanone | hexanal | heptanone |
|---|---|---|---|---|---|---|---|
| ungelled | 20 | 5 | 0.78 ± 0.02a | 1.07 ± 0.06a | 3.71 ± 0.13a | 1.36 ± 0.06a | 0.85 ± 0.03a |
| ungelled | 15 | 5 | 0.82 ± 0.02a | 0.84 ± 0.02b | 4.59 ± 0.11b | 1.54 ± 0.05b | 1.26 ± 0.06b |
| gelled | 20 | 5 | 0.72 ± 0.02b | 1.43 ± 0.05c | 3.18 ± 0.12c | 1.16 ± 0.07c | 0.73 ± 0.04c |
| gelled | 15 | 5 | 0.74 ± 0.02b | 1.33 ± 0.04d | 3.82 ± 0.13a | 1.54 ± 0.05b | 1.05 ± 0.03d |
| gelled | 15 | 6 | 0.67 ± 0.04b | 0.70 ± 0.05e | 3.31 ± 0.25c | 1.00 ± 0.06e | 0.88 ± 0.06a |
| not heat-treated | 20 | 5 | 0.84 ± 0.01d | 1.75 ± 0.01f | 3.86 ± 0.07a | 1.36 ± 0.03a | 0.90 ± 0.02a |

[a]Gelation was induced with the addition of 0.5% w/w GDL. Within each column, values with different letters are significantly different ($p < 0.05$).

Table 4. Air−Gel Partition Coefficients ($K_{A/E} \times 10^4$) of the Volatiles in EFP Gels (20% w/w oil) with Different WPI Contents[a]

| WPI content (%, w/w) | propanol | diacetyl | pentanone | hexanal | heptanone |
|---|---|---|---|---|---|
| 3 | 0.82 ± 0.02a | 1.19 ± 0.02a | 3.91 ± 0.10a | 1.35 ± 0.03a | 0.93 ± 0.01a |
| 4 | 0.81 ± 0.01a | 1.58 ± 0.01b | 3.95 ± 0.06a | 1.48 ± 0.04b | 0.96 ± 0.03a |
| 5 | 0.72 ± 0.02b | 1.43 ± 0.05c | 3.18 ± 0.12b | 1.16 ± 0.07c | 0.73 ± 0.04b |
| 6 | 0.68 ± 0.03b | 0.69 ± 0.03d | 2.97 ± 0.17b | 0.81 ± 0.04d | 0.68 ± 0.03b |

[a]Gelation was induced with the addition of 0.5% w/w GDL. Within each column, values with different letters are significantly different ($p < 0.05$).

heat-denatured. It was reported that in the heating stage, the selected temperature and time must yield >95% of the protein to be aggregated so as to produce a gel with appropriate mechanical properties.[47] Therefore, in EFP gels, more hydrophobic sites could be present,[3,4] and they were able to bind volatile compounds. In an emulsion with unheated protein (with GDL, weak gel), the release rates and partition coefficients of the volatiles were significantly higher than those in the EFP gel and the ungelled emulsion (heat-treated protein, no GDL) with the same compositions (Table 3). This finding could be associated with the newly exposed hydrophobic area in the protein structure during heat treatment, which provides additional binding sites for the hydrophobic volatile compounds. This deduction contradicted the conclusion made by O'Neill and Kinsella,[48] who argued that unfolding of the protein structure (chemically modified by urea, sulfate, or ethanol) would result in a reduced binding affinity for hydrophobic compounds. The disagreement could be due to the different denaturation methods applied. In fact, O'Neill and Kinsella[48] found that the number of binding sites remained unchanged during denaturation, whereas the binding sites were believed to increase in the current study. For the more hydrophilic compounds, interaction with the protein was induced mainly by hydrogen bonding.

It is well accepted that a reduction in the oil content can accelerate the release of hydrophobic volatile compounds.[49] In the gelled system, the acceleration was of a much lower level than that in the ungelled system (Figure 5). For example, the release rate of heptanone increased from 0.0138 ± 0.0002 to 0.0388 ± 0.0008 mg/L min in the ungelled systems (181% increase) by reducing the oil content from 20 to 15%, whereas it increased from 0.0097 ± 0.0006 to 0.0239 ± 0.0014 mg/L min in the gelled systems (146% increase). Therefore, the EFP gel has the potential to slow the volatile release in an oil-reduced system. To verify this hypothesis, an EFP gel with a lower oil content (15% oil) but stronger gel network (higher WPI content, 6%) was made. Static headspace analysis revealed that four out of five volatiles in the low-oil content gel had either a lower or an unaffected release rate in comparison with those in the high-oil content gel system (20% oil, 5% WPI) (Figure 5). In terms of partition coefficients, a similar conclusion was made. Propanol and pentanone had unchanged $K_{A/E}$ values as those in the high-oil content gel, and diacetyl and hexanal had lower $K_{A/E}$ values (Table 3).

To better correlate the gel structure and volatile release, further studies were conducted on the effects of the WPI and oil contents on volatile release in EFP gels. Figure 6 shows the release rates of volatiles in EFP gels with different WPI contents. The expected decrease in the release rate with the increase in the WPI content was observed when the WPI content was ≥4%, and in the 3% WPI EFP gel, the volatiles presented lower release rates than those in the 4% WPI EFP gel. The effect of the WPI content on the partition coefficients of the volatiles followed a similar trend (Table 4), as reduced

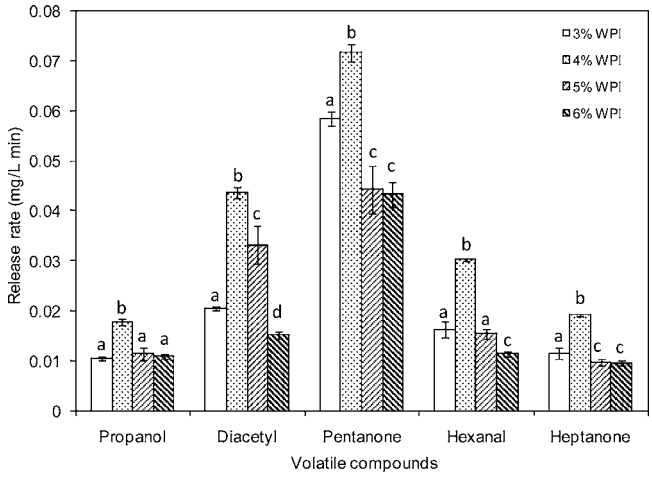


Figure 6. Release rates of the volatiles in EFP gels varying in WPI content (20% w/w oil).Gelation was induced with the addition of 0.5% w/w GDL. Samples were incubated at 37 °C before each measuring point.

$K_{A/E}$ values were obtained with the increase in the WPI content from 4 to 5 and 6%. Similar results were reported in gelatin gels and pectin gels, in which the increase in the gelling agent concentration resulted in more rigid gels and lower partition coefficients of the volatiles.[14]

Along with the strengthened volatile-protein interaction, the gel with the higher protein content provided a more compact network and smaller pores to slow volatile release. Spotti et al.[50] found that an increase in the WPI content from 12 to 16% could reduce the pore size of the WPI gel from 157 to 63 nm; however, only a slight or no significant difference in the $K_{A/E}$ values was observed for volatiles in gels containing 3 and 4% WPI. The relatively lower release of volatile in the 3% WPI system could be the result of the earlier commencement of the gelation (Table 1), and more volatiles were trapped in the gel network before headspace analysis. Although volatiles in the EFP gel with 6% WPI showed the lowest release rates and partition coefficients, the difference was rather small compared with the release in the 5% WPI system. The result indicated that both the steric hindrance and volatile-protein bindings in the EFP gels reached a maximum level in the 5% WPI system, and they were not linearly increased with a further increase in the WPI content. An exception to the above discussion was diacetyl, whose release was significantly inhibited in the 6% WPI system. It could be related to its high hydrophilic characteristic, and it was mostly distributed in the continuous aqueous phase. In a system with a higher protein content, almost all the water was trapped in the network.

Oils can act as volatile precursors, as solvents for volatile compounds, and as volatile release modulators. Changes in oil property or oil content can lead to a significantly different volatile releasing profile.[49] The result obtained in this study was

Table 5. Air−Gel Partition Coefficients ($K_{A/E} \times 10^4$) of the Volatiles in EFP Gels (20% w/w WPI) with Different Oil Contents[a]

| oil content (%, w/w) | propanol | diacetyl | pentanone | hexanal | heptanone |
|---|---|---|---|---|---|
| 5 | 0.74 ± 0.01a | 1.39 ± 0.02a | 5.85 ± 0.04a | 2.66 ± 0.12a | 2.68 ± 0.03a |
| 10 | 0.80 ± 0.01b | 1.00 ± 0.02b | 4.82 ± 0.08b | 1.92 ± 0.02b | 1.71 ± 0.02b |
| 15 | 0.74 ± 0.02a | 1.33 ± 0.04a | 3.82 ± 0.13c | 1.54 ± 0.05c | 1.05 ± 0.03c |
| 20 | 0.72 ± 0.02a | 1.43 ± 0.05a | 3.18 ± 0.12d | 1.16 ± 0.07d | 0.73 ± 0.04d |

[a]Gelation was induced with the addition of 0.5% w/w GDL. Within each column, values with different letters are significantly different ($p < 0.05$).

in agreement with previous findings that an increase in the oil content can result in a decreased release of lipophilic volatile compounds[49] because volatiles would have reduced concentration in the oil droplets. In EFP gels, increased stiffness with a higher oil content in the gels also contributed to inhibit volatile release. Significantly reduced partition coefficients of pentanone, hexanal, and heptanone with an increase in the oil content were observed in the current gels (Table 5). However, the effect on the release rates of pentanone and hexanal was rather small or even insignificant when the oil content was reduced to 5−15% (Figure 7). The finding suggested that the barrier function of the gel network worked better in a low-oil-content system, but in gels with a higher oil content, the slowed release by the gel network could not compensate the quick release induced by a reduction in the oil content. The decreased release rate of heptanone could be due to its high lipophilic characteristic (log $P$ = 1.98), and it had a strong affinity for the oil phase. For the hydrophilic volatile compounds, that is, propanol and diacetyl, a change in the oil content did not show a consistent effect on the release rates and partition coefficients, and sometimes the effect was insignificant.

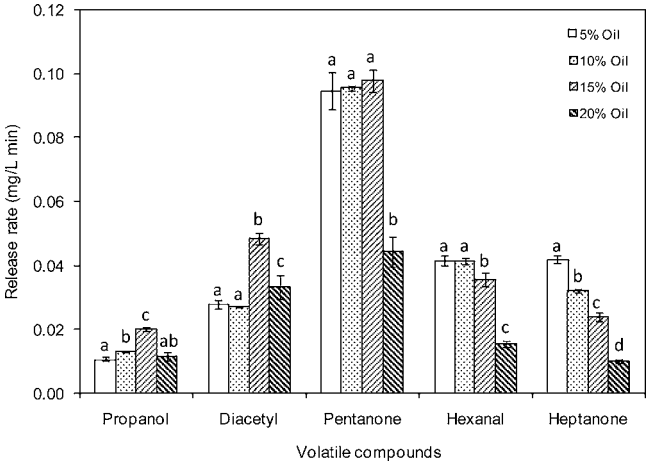


**Figure 7.** Release rates of the volatiles in EFP gels varying in oil content (5% w/w WPI). Gelation was induced with the addition of 0.5% w/w GDL. Samples were incubated at 37 °C before each measuring point.

This work presents the application of EFP gels as delivery systems for volatile compounds. The results have demonstrated that EFP gels can slow volatile release from the gels and reduce the air−gel partition coefficients at equilibrium. Because WPI content showed a dominant effect on the rheological properties (both small deformation and large deformation properties) of EFP gels, and oil content gave a bigger effect on volatile release, producing more rigid EFP gels by increasing the WPI content provided a novel means to inhibit volatile release in oil-reduced gels. Therefore, EFP gels could find applications in fat-reduced foods with improved flavor profile. However, flavor perception is influenced not only by the released volatile but also by the food texture, and both of them vary significantly during oral processing. To better apply EFP gels to real food systems, further attempts can be made to understand the effect of gel breakdown on volatile release and volatile−texture interaction on flavor perception, either in vivo or in vitro.

## AUTHOR INFORMATION

### Corresponding Author

*Tel.: +353 25 42468. Fax: +353 25 42340. E-mail: song.miao@teagasc.ie.

### Notes

The authors declare no competing financial interest.

## REFERENCES

(1) Dickinson, E. Emulsion gels: the structuring of soft solid with protein-stabilized oil droplets. *Food Hydrocolloids* **2012**, *28*, 224−241.
(2) Aguilera, J. M.; Kinsella, J. E.; Liboff, M. Structure-compressive stress relationships in mixed dairy gels. *Food Struct.* **1993**, *12*, 469−474.
(3) Twomey, M.; Keogh, M. K.; Mehra, R.; O'Kennedy, B. T. Gel characteristics of β-lactoglobulin, whey protein concentrate and whey protein isolate. *J. Texture Stud.* **1997**, *28*, 387−403.
(4) Raikos, V. Effect of heat treatment on milk protein functionality at emulsion interfaces. A review. *Food Hydrocolloids* **2010**, *24*, 259−265.
(5) Alting, A. C.; Weijers, M.; de Hoog, E. H. A.; van de Pijpekamp, A. M.; Cohen Stuart, M. A.; Hamer, R. J.; de Kruif, C. G.; Visschers, R. W. Acid-induced cold gelation of globular proteins: effects of protein aggregate characteristics and disulfide bonding on rheological properties. *J. Agric. Food Chem.* **2004**, *52*, 623−631.
(6) Kuhn, K. R.; Cavallieri, A. L. F; Cunha, R. L. Cold-set whey protein−flaxseed gum gels induced by mono or divalent salt addition. *Food Hydrocolloids* **2011**, *25*, 1302−1310.
(7) Dickinson, E.; Yamamoto, Y. Rheology of milk protein gels and protein-stabilized emulsion gels cross-linked with transglutaminase. *J. Agric. Food Chem.* **1996**, *44*, 1371−1377.
(8) Kim, K. H.; Renkenma, J. M. S.; van Vliet, T. Rheological properties of soybean protein isolate gels containing emulsion droplets. *Food Hydrocolloids* **2001**, *15*, 295−302.
(9) Sala, G.; van Vliet, T.; Cohen Stuart, M. A.; van Aken, G. A.; van de Velde, F. Deformation and fracture of emulsion-filled gels: effect of oil content and deformation speed. *Food Hydrocolloids* **2009**, *23*, 1381−1393.
(10) van der Poel, C. On the rheology of concentrated dispersions. *Rheol. Acta* **1958**, *1*, 198−205.
(11) van Vliet, T. Rheological properties of filled gels. Influence of filler matrix interaction. *Colloid Polym. Sci.* **1988**, *266*, 518−524.
(12) Ye, A.; Taylor, S. Characterization of cold-set gels produced from heated emulsions stabilized by whey protein. *Int. Dairy J.* **2009**, *19*, 721−727.
(13) Foegeding, E. A.; Bowland, E. L.; Hardin, C. C. Factors that determine the fracture properties and microstructure of globular protein gels. *Food Hydrocolloids* **1995**, *9*, 237−249.
(14) Boland, A. B.; Delahunty, C. M.; van Ruth, S. M. Influence of the texture of gelatin gels and pectin gels on strawberry flavour release and perception. *Food Chem.* **2006**, *96*, 452−460.

(15) Guichard, E. Interactions between flavor compounds and food ingredients and their influence on flavor perception. *Food Rev. Int.* **2002**, *18*, 49−70.
(16) Juteau-Vigier, A.; Atlan, S.; Deleris, I.; Guichard, E.; Souchon, I.; Trelea, I. C. Ethyl hexanoate transfer modeling in carrageenan matrices for determination of diffusion and partition properties. *J. Agric. Food Chem.* **2007**, *55*, 3577−3584.
(17) Hansson, A.; Giannouli, P.; van Ruth, S. The influence of gel strength on aroma release from pectin gels in a model mouth and in vivo, monitored with proton-transfer-reaction mass spectrometry. *J. Agric. Food Chem.* **2003**, *51*, 4732−4740.
(18) Linforth, R. S. T.; Pearson, K. S. K.; Taylor, A. J. In vivo flavor release from gelatin-sucrose gels containing droplets of flavor compounds. *J. Agric. Food Chem.* **2007**, *55*, 7859−7863.
(19) Lee, H. A.; Choi, S. J.; Woon, T. W. Characteristics of sodium caseinate- and soy protein isolate-stabilized emulsion-gels formed by microbial transglutaminase. *J. Food Sci.* **2006**, *71*, C352−C357.
(20) Sandoval-Castilla, O.; Lobato-Calleros, C.; Aguirre-Mandujano, E.; Vernon-Carter, E. J. Microstructure and texture of yogurt as influenced by fat replacers. *Int. Dairy J.* **2004**, *14*, 151−159.
(21) Sok Line, V. L.; Remondetto, G. E.; Subirade, M. Cold gelation of β-lactoglobulin oil-in-water emulsions. *Food Hydrocolloids* **2005**, *19*, 269−278.
(22) Fiszman, S. M.; Salvador, A. Effect of gelatin on the texture of yoghurt and of acid-heat-induced milk gels. *Eur. Food Res. Technol.* **1999**, *208*, 100−105.
(23) Yang, M.; Liu, F.; Tang, C. Properties and microstructure of transglutaminase-set soy protein-stabilized emulsion gels. *Food Res. Int.* **2013**, *52*, 409−418.
(24) Mao, L.; Roos, Y. H.; Miao, S. Volatile release from self-assembly structured emulsions: effect of monoglyceride contents, oil contents and oil types. *J. Agric. Food Chem.* **2013**, *61*, 1427−1434.
(25) Mellema, M.; van Opheusden, J. H. J.; van Vliet, T. Categorization of rheological scaling models for particle gels applied to casein gels. *J. Rheol.* **2002**, *46*, 11−29.
(26) Euston, S. R.; Finnigan, S. R.; Hirst, R. L. Aggregation kinetics of heated whey protein-stabilized emulsions. *Food Hydrocolloids* **2000**, *14*, 155−161.
(27) Alting, A. C.; Hamer, R. J.; de Kruif, C. G.; Visschers, R. W. Formation of disulphide bonds in acid-induced gels of pre-heated whey protein isolate. *J. Agric. Food Chem.* **2000**, *48*, 5001−5007.
(28) Clark, A. H. Gels and gelling. In *Physical Chemistry of Foods*; Schwartzberg, H. G., Hartel, R. W., Eds.; Dekker: New York, 1992; pp 263−306.
(29) Renkema, J. M. S.; van Vliet, T. Concentration dependence of dynamic moduli of heat-induced soy protein gels. *Food Hydrocolloids* **2004**, *18*, 483−487.
(30) Vreeker, R.; Hoeskstra, L. L.; den Boer, D. C.; Agterof, W. G. M. Fractal aggregation of whey proteins. *Food Hydrocolloids* **1992**, *6*, 423−435.
(31) Boutin, C.; Giroux, H. J.; Paquin, P.; Britten, M. Characterization and acid-induced gelation of butter oil emulsions produced from heated whey protein dispersions. *Int. Dairy J.* **2007**, *17*, 696−703.
(32) Rosa, P.; Sala, G.; van Vliet, T.; van de Velde, F. Cold gelation of whey protein emulsions. *J. Texture Stud.* **2006**, *37*, 516−537.
(33) Sala, G.; van Aken, G. A.; Cohen Stuart, M. A.; van de Velde, F. Effect of droplet-matrix interaction on large deformation properties of emulsion-filled gels. *J. Texture Stud.* **2007**, *38*, 511−535.
(34) van Vliet, T.; Luyten, H.; Walstra, P. Time dependent fracture behaviour of foods. In *Food Colloids and Polymer, Stability and Mechanical Properties*; Dickinson, E., Walstra, P., Eds.; Royal Society of Chemistry: Cambridge, UK, 1993; pp 175−190.
(35) van Vliet, T.; Walstra, P. Large deformation and fracture behaviour of gels. *Faraday Discuss.* **1995**, *101*, 359−370.
(36) Brownsey, G. J.; Ellis, H. S.; Ridout, M. J.; Ring, S. G. Elasticity and failure in composite gels. *J. Rheol.* **1987**, *31*, 635−649.
(37) Haynes, W. M. *CRC Handbook of Chemistry and Physics*, 92nd ed.; CRC Press, Boca Raton, FL, 2011.
(38) de Roos, K. B. Physicochemical models of flavor release from foods. In *Flavor Research*; Roberts, D. D., Taylor, A. J., Eds.; American Chemical Society: Washington, DC, 2000; pp 126−141.
(39) Guinard, J.-X.; Marty, C. Time-intensity measurement of flavor release from a model gel system: effect of gelling agent type and concentration. *J. Food Sci.* **1995**, *60*, 727−730.
(40) Perreault, V.; Britten, M.; Turgeon, S. L.; Seuvre, A.-M.; Cayot, P.; Voilley, A. Effects of heat treatment and acid-induced gelation on aroma release from flavoured skim milk. *Food Chem.* **2010**, *118*, 90−95.
(41) Wu, S. Y.; Pérez, M. D.; Puyol, P.; Sawyer, L. β-Lactoglobulin binds palmitate within its central cavity. *J. Biol. Chem.* **1999**, *274*, 170−174.
(42) Tavel, L.; Andriot, I.; Moreau, C.; Guichard, E. Interactions between β-lactoglobulin and aroma compounds: different binding behaviors as a function of ligand structure. *J. Agric. Food Chem.* **2008**, *56*, 10208−10217.
(43) Lübke, M.; Guichard, E.; Le Quéré, J. L. Infrared spectroscopic study of β-lactoglobulin interactions with flavor compounds. In *Flavor Release*; Roberts, D. D., Taylor, A. J., Eds.; American Chemical Society: Washington, DC, 2000; pp 282−292.
(44) Harrison, M.; Hills, B. P. Mathematical model of flavor release from liquids containing aroma-binding macromolecules. *J. Agric. Food Chem.* **1997**, *45*, 1883−1890.
(45) Harvey, B.; Druaux, C.; Voilley, A. Effect of protein on the retention and transfer of aroma compounds at the lipid−water interface. In *Food Macromolecules and Colloids*; Dickinson, E., Lorient, D., Eds.; The Royal Society of Chemistry: Cambridge, UK, 1995; pp 154−163.
(46) Rogacheva, S.; Espinosa-Diaz, M. A.; Voilley, A. Transfer of aroma compounds in water−lipid systems: binding tendency of β-lactoglobulin. *J. Agric. Food Chem.* **1999**, *47*, 259−263.
(47) Alting, A. C., Hamer, R. J., de Kruif, C. G., de Jongh, H. H. J., Simons, J. W. F. A., Visschers, R. W. Physical and chemical interactions in pH-induced aggregation and gelation of whey proteins. In *Food Colloids, Biopolymers and Materials*; Dickinson, E., Van Vliet, T., Eds.; Royal Society of Chemistry: Cambridge, UK, 2003; pp 49−57.
(48) O'Neill, T. E.; Kinsella, J. E. Binding of alkanone flavors to β-lactoglobulin: effects of conformational and chemical modification. *J. Agric. Food Chem.* **1987**, *35*, 770−774.
(49) de Roos, K. B. How lipids influence food flavor. *Food Technol.* **1997**, *7* (51), 60−62.
(50) Spotti, M. J.; Santiago, L. G.; Rubiolo, A. C.; Carrara, C. R. Mechanical and microstructural properties of milk whey protein/espina corona gum mixed gels. *LWT−Food Sci. Technol.* **2012**, *48*, 69−74.

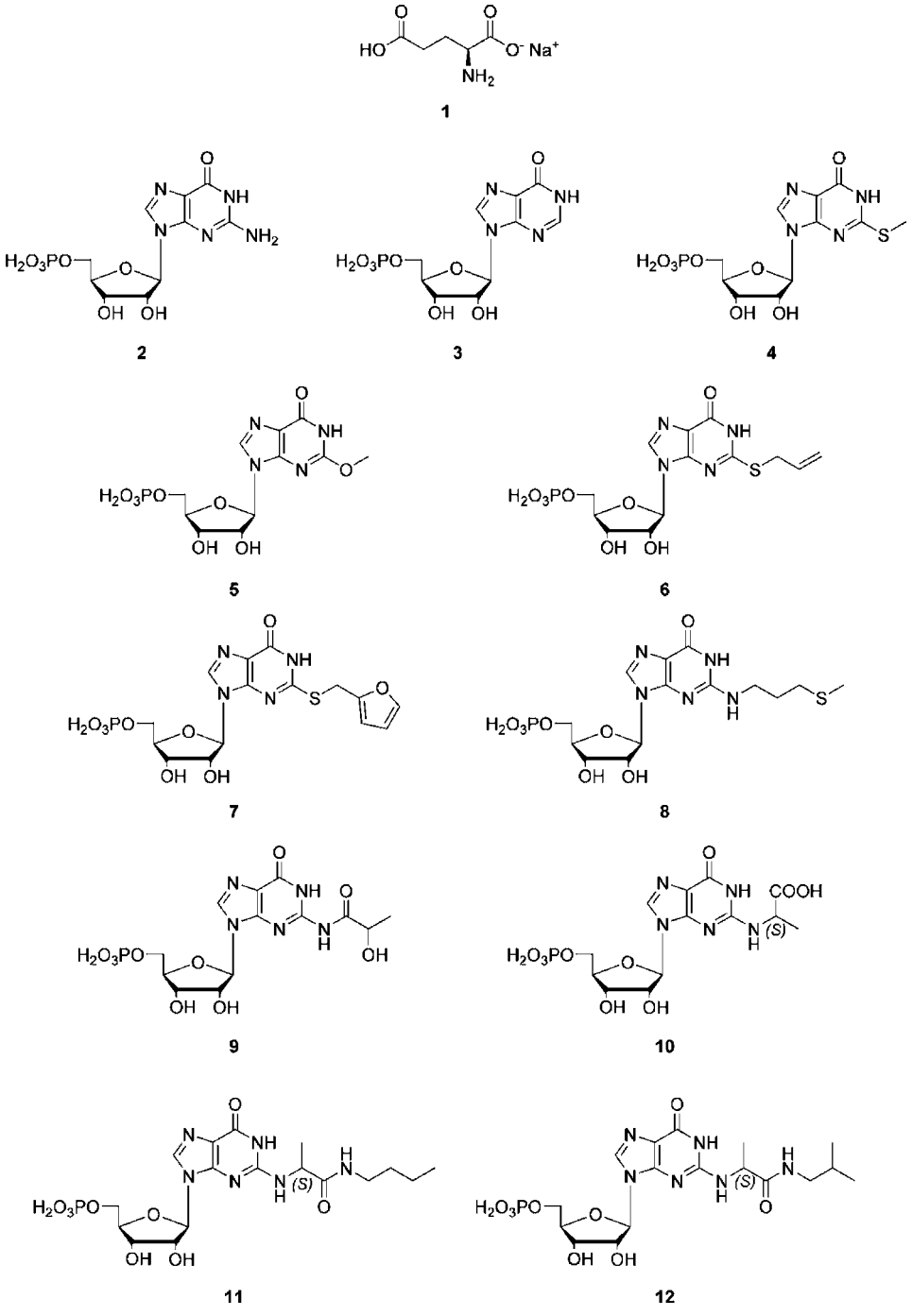


**Figure 1.** Chemical structures of umami-tasting and umami-modulating molecules: monosodium L-glutamate (**1**), guanosine 5′-monophosphate (**2**), inosine 5′-monophosphate (**3**), 2-methylthioinosine 5′-monophosphate (**4**), 2-methoxyinosine 5′-monophosphate (**5**), 2-allylthioinosine 5′-monophosphate (**6**), 2-furfurylthioinosine 5′-monophosphate (**7**), $N^2$-(3-methylthiopropyl)guanosine 5′-monophosphate (**8**), $N^2$-lactoylguanosine 5′-monophosphate (**9**), (*S*)-$N^2$-(1-carboxyethyl)guanosine 5′-monophosphate (**10**), (*S*)-$N^2$-{[1-(*N*-butylamino)carbonyl]ethyl}guanosine 5′-monophosphate (**11**), and (*S*)-$N^2$-{[1-(*N*-isobutylamino)carbonyl]ethyl}guanosine 5′-monophosphate (**12**).

Despite these achievements in the synthesis of umami taste-enhancing nucleotides, the growing aversion of alienated consumers toward nonnatural chemicals added to foods is creating an increasing request for flavor molecules of biological origin or made by "greener" or "kitchen-type" chemistry.[4] This inspired initiatives targeting the discovery of previously unknown, naturally occurring chemosensorica in processed food. Among those sharing a guanosine 5′-monophosphate scaffold, $N^2$-lactoylguanosine 5′-monophosphate, **9** (Figure 1), has been identified in fermented tuna fish, while (*S*)-$N^2$-(1-carboxyethyl)guanosine 5′-phosphate (**10**) was isolated from yeast extracts.[11,12] Accompanied by its corresponding (*R*)-configured isomer, the latter nucleotide has been reported to be generated by Maillard-type reactions of nucleotide **2** with dihydroxyacetone, glyceraldehyde, and hexoses, respectively.[12] Intriguingly, only the (*S*)-configured nucleotide **10** showed a high $\beta$-value of 7.0 while the corresponding (*R*)-isomer showed only marginal sensory activity,[12] again demonstrating that small structural changes impact on the umami taste-enhancing activity of this molecule. To further widen the portfolio of


dx.doi.org/10.1021/jf504686s | J. Agric. Food Chem. 2014, 62, 11429−11440

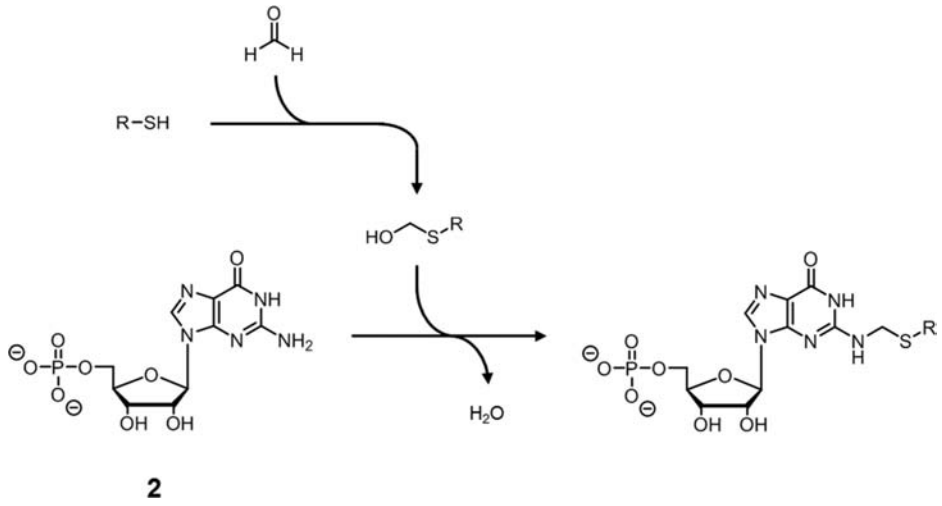


**Figure 2.** $N^2$-Alkyl- and $N^2$-arylthiomethylation of guanosine 5′-monophosphates by Maillard-type reaction of guanosine 5′-monophosphate (**2**), formaldehyde, and organic thiols.

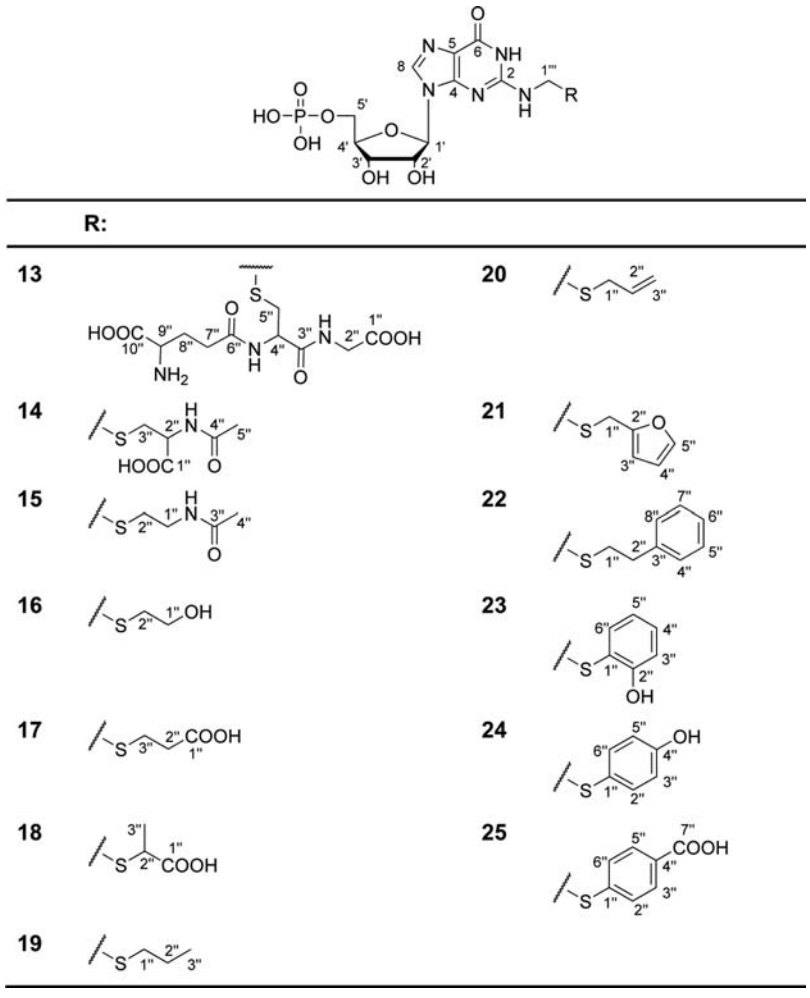


**Figure 3.** Chemical structures of $N^2$-(alkylthiomethyl)guanosine 5′-monophosphates **13**−**20** and $N^2$-(arylthiomethyl)guanosine 5′-monophosphates **21**−**25**.

Maillard-type modified derivatives of nucleotide **2**, the $N^2$-(1-carboxyethyl)guanosine 5′-phosphate scaffold was further altered by amidation of the side chain's carboxy group, thus leading to butylated (**11**) and isobutylated ribonucleotides (**12**) with an increased $\beta$-value of 7.6.[13,14] These results were verified both by human psychophysical as well as cell-based T1R1/T1R3 receptor assays.[14]

Inspired by the reported beneficial effect of a sulfur atom in $N^2$-alkylated ribonucleotides,[9] the objective of the present study was to prepare sulfur-containing guanosine 5′-monophosphates


dx.doi.org/10.1021/jf504686s | J. Agric. Food Chem. 2014, 62, 11429−11440

by means of Maillard-type reactions of nucleotide **2** with glycine's Strecker aldehyde formaldehyde and organic thiols, as depicted in Figure 2, and to evaluate their umami taste-enhancing potential of these chemosensorica in vivo by means of human sensory studies and in vitro by means of T1R1/T1R3 taste receptor experiments.

## MATERIALS AND METHODS

**Chemicals and Materials.** The following chemicals were obtained commercially: dipotassium hydrogen phosphate, formic acid, glycine, mercaptoethanol, monosodium L-glutamate monohydrate, orthophosphoric acid, potassium dihydrogen phosphate, and 1-propanethiol (Merck KGaA, Darmstadt, Germany); formaldehyde, D-glucose, L-glutathione (reduced), and 2-propen-1-thiol (Fluka, Buchs, Switzerland); 2-furanmethanethiol, inosine 5′-monophosphate disodium salt, 2-mercaptophenol, 2-mercaptobenzoic acid, 2-mercaptopropionic acid, 3-mercaptopropionic acid, 4-mercaptophenol, *N*-acetylcysteamine, and *N*-acetyl-L-cysteine (Sigma−Aldrich, Steinheim, Germany); guanosine 5′-monophosphate disodium salt and 2-phenethylthiol (Acros Organics, Geel, Belgium); and HPLC-grade solvents (J. T. Baker, Deventer, Netherlands). Deionized water used for chromatography was purified by means of a Milli-Q gradient A10 system (Millipore, Molsheim, France). Deuterated solvents and 3-trimethylsilyl-2,2,3,3-$d_4$-propionic acid sodium salt were supplied by Euriso-Top (Gif-Sur-Yvette, France). For medium-pressure liquid chromatography, RP-18-bulk material (LiChroprep RP-18, 25−40 μm, Merck KGaA, Darmstadt, Germany) was used. Sensory analyses were performed with Evian bottled water (Danone Waters Deutschland, Frankfurt, Germany).

**Preparation of $N^2$-(Alkylthiomethyl)guanosine and $N^2$-(Arythiomethyl)guanosine 5′-Monophosphate Derivatives.** Following a literature protocol[15] with some modifications, formaldehyde (2 mmol; 50 μL of a 36% solution in water) was added to a solution of potassium phosphate buffer (40 mL, pH 7.0; 30 mmol/L) containing one of the mercaptans (15 mmol/L), namely, L-glutathione, *N*-acetyl-L-cysteine, *N*-acetylcysteamine, 2-mercaptophenol, 2- and 3-mercaptopropionic acid, 1-propanethiol, 2-propen-1-thiol, 2-furanmethanethiol, 2-phenethylthiol, 2- and 4-mercaptophenol, and 2-mercaptobenzoic acid, respectively. After the mixture was stirred for 4 h at 40 °C in a closed vessel, guanosine 5′-monophosphate (0.6 mmol) was added and stirring was continued at 40 °C for another 16 h. Subsequently, the reaction product was isolated by means of reversed-phase medium-pressure liquid chromatography (RP-MPLC) on a Buechi-Sepacore system (Flawil, Switzerland) equipped with a 150 × 40 mm column filled with 25−40 μm LiChroprep RP-18 material (Merck KGaA Darmstadt, Germany). The effluent was monitored at 260 nm, and chromatography was performed at a flow rate of 40 mL/min with 1% aqueous formic acid (solvent A) and methanol (solvent B) as eluents. *S*-[1-($N^2$-guanosinyl)methyl]-glutathione 5′-monophosphate, **13** (Figure 3), $N^2$-(2-acetylaminoethylthiomethyl)guanosine 5′-monophosphate (**15**), and $N^2$-(phenethylthiomethyl)guanosine 5′-monophosphate (**22**) were isolated by eluting with 100% solvent A for 2 min, then increasing solvent B from 0 to 40% within 3 min, and finally increasing to 100% solvent B within an additional 16 min. 100% organic solvent was maintained for an additional 5 min. For isolation of nucleotide derivatives $N^2$-(2-hydroxyethylthiomethyl)guanosine 5′-monophosphate (**16**), $N^2$-(2-carboxyethylthiomethyl)guanosine 5′-monophosphate (**17**), $N^2$-(1-carboxyethylthiomethyl)guanosine 5′-monophosphate (**18**), $N^2$-(furfurylthiomethyl)guanosine 5′-monophosphate (**21**), $N^2$-(2-hydroxyphenylthiomethyl)guanosine 5′-monophosphate (**23**), $N^2$-(4-hydroxyphenylthiomethyl)guanosine 5′-monophosphate (**24**), and $N^2$-(4-carboxyphenylthiomethyl)guanosine 5′-monophosphate (**25**), elution was started isocratically with 100% solvent A for 5 min, and then the content of solvent B was linearly increased to 100% during 35 min and maintained for an additional 5 min. Purification of $N^2$-(propylthiomethyl)guanosine 5′-monophosphate (**19**) and $N^2$-(prop-2-enylthiomethyl)guanosine 5′-monophosphate (**20**) was achieved by isocratic elution with 100% eluent A for 2 min and then increasing the content of eluent B to 45% within 8 min, to 80% in 20 min, and finally to 100% in 1 min. Elution with 100% solvent B was continued for 5 min. $N^2$-[(2-Acetylamino-2-carboxyethyl)thiomethyl]-guanosine 5′-monophosphate (**14**) was isolated by increasing the content of solvent B from 0% to 15% within 10 min, then to 30% within 20 min, and finally within 10 min to 100%, with continued elution with 100% organic solvent for 5 min. Fractions showing UV absorbance at 260 nm were collected individually with an automated fraction collector, freed from organic solvents in vacuum, and lyophilized three times.

*S-[1-($N^2$-Guanosinyl)methyl]glutathione 5′-Monophosphate (**13**).* UV/vis (1% formic acid in water/methanol, 60/40 v/v) $\lambda_{max}$ = 260 nm. UPLC-TOF-MS (ESI$^-$) *m/z* 681.1357 ([M − H]$^-$, meas); *m/z* 681.1340 ([M − H]$^-$, calcd for $C_{21}H_{30}N_8O_{14}PS$). $^1$H NMR (500 MHz, $D_2O$, COSY) δ (ppm) 2.05 [q, 2H, *J* = 7.2, 14.3 Hz, H−C(8″)], 2.43 [t, 2H, *J* = 7.5 Hz, H−C(7″)], 2.95 [dd, 1H, *J* = 8.7, 14.3 Hz, H−C(5″$_A$)], 3.15 [dd, 1H, *J* = 8.7, 14.3 Hz, H−C(5″$_B$)], 3.80 [t, 1H, *J* = 6.3 Hz, H−C(9″)], 3.89 [s, 2H, H−C(2″)], 4.05 [m, 1H, H−C(5′$_A$)], 4.13 [m, 1H, H−C(5′$_B$)], 4.30 [m, 1H, H−C(4′)], 4.41 [t, 1H, *J* = 5.1 Hz, H−C(3′)], 4.51 [d, 1H, *J* = 14.2 Hz, H−C(1‴$_A$)], 4.62 [dd, 1H, *J* = 5.7, 8.8 Hz, H−C(4″)], 4.70 [t, 1H, *J* = 7.8 Hz, H−C(2′)], 4.71 [d, 1H, *J* = 14.2 Hz, H−C(1‴$_B$)], 6.02 [d, 1H, *J* = 4.3 Hz, H−C(1′)], 8.52 [s, 1H, H−C(8)]. $^{13}$C NMR (125 MHz, $D_2O$, HMBC, HSQC) δ (ppm) 25.8 [$CH_2$, C(8″)], 30.8 [$CH_2$, C(7″)], 32.3 [$CH_2$, C(5″)], 41.2 [$CH_2$, C(2″)], 43.5 [$CH_2$, C(1‴)], 53.1 [CH, C(4″)], 53.2 [CH, C(9″)], 64.0 [d, $CH_2$, $^2J_{C,P}$ = 4.3 Hz, C(5′)], 69.8 [CH, C(3′)], 74.3 [CH, C(2′)], 83.8 [d, CH, $^3J_{C,P}$ = 8.7 Hz, C(4′)], 88.6 [CH, C(1′)], 112.4 [C, C(5)], 137.0 [CH, C(8)], 150.2 [C, C(4)], 152.7 [C, C(2)], 156.4 [C, C(6)], 172.6 [C, C(10″)], 172.8 [C, C(3″)], 173.0 [C, C(1″)], 174.8 [C, C(6″)].

*$N^2$-[(2-Acetylamino-2-carboxyethyl)thiomethyl]guanosine 5′-Monophosphate (**14**).* UV/vis (1% formic acid in water/methanol, 80/20 v/v) $\lambda_{max}$ = 260 nm. UPLC-TOF-MS (ESI$^-$) *m/z* 537.0809 ([M − H]$^-$, meas); *m/z* 537.0805; ([M − H]$^-$, calcd for $C_{16}H_{22}N_6O_{11}PS$). $^1$H NMR (500 MHz, $D_2O$, COSY) δ (ppm) 2.00 [s, 3H, H−C(5″)], 3.04 [dd, 1H, *J* = 8.1, 14.0 Hz, H−C(3″$_A$)], 3.23 [dd, 1H, *J* = 4.5 Hz, 14.0 Hz, H−C(3″$_B$)], 4.11 [m, 2H, H−C(5′)], 4.32 [m, 1H, H−C(4′)], 4.47 [dd, 1H, *J* = 4.5, 8.1 Hz, H−C(2″)], 4.51 [t, 1H, *J* = 4.9 Hz, H−C(3′)], 4.62 [d, 1H, *J* = 14.3 Hz, H−C(1‴$_A$)], 4.66 [d, 1H, *J* = 14.3 Hz, H−C(1‴$_B$)], 4.80 [t, 1H, *J* = 4.4 Hz, H−C(2′)], 6.04 [d, 1H, *J* = 3.7 Hz, H−C(1′)], 8.16 [s, 1H, H−C(8)]. $^{13}$C NMR (125 MHz, $D_2O$, HMBC, HSQC) δ (ppm) 24.8 [C(5″)], 36.2 [$CH_2$, C(3″)], 46.7 [$CH_2$, C(1‴)], 57.3 [CH, C(2″)], 67.5 [d, $CH_2$, $^2J_{C,P}$ = 5.2 Hz, C(5′)], 73.2 [CH, C(3′)], 76.7 [CH, C(2′)], 86.4 [d, CH, $^3J_{C,P}$ = 8.8 Hz, C(4′)], 90.7 [CH, C(1′)], 119.2 [C, C(5)], 140.9 [CH, C(8)], 154.2 [C, C(4)], 154.7 [C, C(2)], 161.9 [C, C(6)], 176.4 [C, C(4″)], 179.3 [C(1″)].

*$N^2$-(2-Acetylaminoethylthiomethyl)guanosine 5′-Monophosphate (**15**).* UV/vis (1% formic acid in water/methanol, 60/40 v/v) $\lambda_{max}$ = 260 nm. UPLC-TOF-MS (ESI$^-$) *m/z* 493.0904 ([M − H]$^-$, meas); *m/z* 493.0824 ([M − H]$^-$, calcd for $C_{15}H_{23}N_6O_9PS$). $^1$H NMR (500 MHz, $D_2O$, COSY) δ (ppm) 1.94 [s, 3H, H−C(4″)], 2.86 [t, 2H, *J* = 6.6 Hz, H−C(2″)], 3.42 [dt, 2H, *J* = 1.7, 6.5 Hz, H−C(1″)], 4.10 [ddd, 2H, *J* = 3.6, 5.6, 11.6 Hz, H−C(5′$_A$)], 4.18 [ddd, 2H, *J* = 3.6, 5.6, 11.6 Hz, H−C(5′$_B$)], 4.33 [m, 1H, H−C(4′)], 4.49 [t, 1H, *J* = 4.9 Hz, H−C(3′)], 4.62 [d, 1H, *J* = 14.3 Hz, H−C(1‴$_A$)], 4.68 [d, 1H, *J* = 14.2 Hz, H−C(1‴$_B$)], 4.76 [t, 1H, *J* = 4.9 Hz, H−C(2′)], 6.07 [d, 1H, *J* = 4.6 Hz, H−C(1′)], 8.48 [s, 1H, H−C(8)]. $^{13}$C NMR (125 MHz, $D_2O$, HMBC, HSQC) δ (ppm) 24.5 [C(4″)], 32.8 [$CH_2$, C(2″)], 41.7 [$CH_2$, C(1″)], 45.8 [$CH_2$, C(1‴)], 66.9 [d, $CH_2$, $^2J_{C,P}$ = 5.6 Hz, C(5′)], 72.6 [CH, C(3′)], 76.8 [CH, C(2′)], 86.3 [d, CH, $^3J_{C,P}$ = 8.5 Hz, C(4′)], 90.1 [CH, C(1′)], 116.0 [C, C(5)], 139.7 [CH, C(8)], 153.4 [C, C(4)], 155.1 [C, C(2)], 160.1 [C, C(6)], 176.9 [C, C(3″)].

*$N^2$-(2-Hydroxyethylthiomethyl)guanosine 5′-Monophosphate (**16**).* UV/vis (1% formic acid in water/methanol, 60/40 v/v) $\lambda_{max}$ = 260 nm. UPLC-TOF-MS (ESI$^-$) *m/z* 452.0630 ([M − H]$^-$, meas); *m/z* 452.0642 ([M − H]$^-$, calcd for $C_{13}H_{19}N_5O_9PS$). $^1$H NMR (500 MHz, $D_2O$, COSY) δ (ppm) 2.91 [t, 2H, *J* = 6.2 Hz, H−C(1″)], 3.73 [t, 2H, *J* = 6.2 Hz, H−C(2″)], 4.13 [m, 1H, H−C(5′$_A$)], 4.27 [m, 1H,

H−C(5′$_B$)], 4.39 [m, 1H, H−C(4′)], 4.52 [t, $J$ = 5.3 Hz, 1H, H−C(3′)], 4.59 [d, 1H, $J$ = 14.3 Hz, H−C(1‴$_A$)], 4.63 [d, 1H, $J$ = 14.3 Hz, H−C(1‴$_B$)], 4.78 [m, 1H, H−C(2′)], 6.05 [d, $J$ = 3.5 Hz, 1H, H−C(1′)], 8.77 [s, 1H, H−C(8)]. $^{13}$C NMR (125 MHz, $D_2O$, HSQC, HMBC) $\delta$ (ppm) 32.9 [$CH_2$, C(1″)], 43.2 [$CH_2$, C(1‴)], 60.7 [$CH_2$, C(2″)], 63.8 [d, $CH_2$, $^2J_{C,P}$ = 4.8 Hz, C(5′)], 69.4 [CH, C(3′)], 74.4 [CH, C(2′)], 83.6 [d, CH, $^3J_{C,P}$ = 8.5 Hz, C(4′)], 89.3 [CH, C(1′)], 110.4 [C, C(5)], 136.2 [CH, C(8)], 149.7 [C, C(4)], 153.0 [C, C(2)], 156.0 [C, C(6)].

*$N^2$-(2-Carboxyethylthiomethyl)guanosine 5′-Monophosphate (**17**).* UV/vis (1% formic acid in water/methanol, 60/40 v/v) $\lambda_{max}$ = 260 nm. UPLC-TOF-MS (ESI$^-$) $m/z$ 480.0591 ([M − H]$^-$, meas); $m/z$ 480.0590 ([M − H]$^-$, calcd for $C_{14}H_{19}N_5O_{10}PS$). $^1$H NMR (500 MHz, $D_2O$, COSY) $\delta$ (ppm) 2.63 [m, 2H, H−C(2″)], 2.84 [m, 2H, H−C(3″)], 4.03 [m, 2H, H−C(5′)], 4.24 [m, 1H H−C(4′)], 4.43 [t, 1H, $J$ = 4.7 Hz, H−C(3′)], 4.57 [d, 1H, $J$ = 14.0 Hz, H−C(1‴$_A$)], 4.65 [d, 1H, $J$ = 14.1 Hz, H−C(1‴$_B$)], 4.70−4.77 [m, 1H, H−C(2′)], 5.93 [d, 2H, $J$ = 4.2 Hz, H−C(1′)], 8.01 [s, 1H, H−C(8)]. $^{13}$C NMR (125 MHz, $D_2O$, HMBC, HSQC) $\delta$ (ppm) 28.7 [$CH_2$, C(3″)], 38.0 [$CH_2$, C(2″)], 46.2 [$CH_2$, C(1‴)], 67.5 [d, $CH_2$, $^2J_{C,P}$ = 4.8 Hz, C(5′)], 73.2 [CH, C(3′)], 76.7 [CH, C(2′)], 86.6 [d, CH, $^3J_{C,P}$ = 7.5 Hz, C(4′)], 90.4 [CH, C(1′)], 119.3 [C, C(5)], 140.7 [CH, C(8)], 149.9 [C, C(4)], 154.5 [C, C(2)], 155.0 [C, C(6)], 180.4 [C, C(1″)].

*$N^2$-(1-Carboxyethylthiomethyl)guanosine 5′-Monophosphate (**18**).* UV/vis (1% formic acid in water/methanol, 60/40 v/v) $\lambda_{max}$ = 260 nm. UPLC-TOF-MS (ESI$^-$) $m/z$ 480.0591 ([M − H]$^-$, meas); $m/z$ 480.0590 ([M − H]$^-$, calcd for $C_{14}H_{19}N_5O_{10}PS$). $^1$H NMR (500 MHz, $D_2O$, COSY) $\delta$ (ppm) 1.49 [d, 3H, $J$ = 7.1 Hz, H−C(3″)], 3.83 [m, 1H, H−C(2″)], 4.14 [m, 1H, H−C(5′$_A$)], 4.25 [m, 1H, H−C(5′$_B$)], 4.38 [m, 1H, H−C(4′)], 4.51 [m, 1H, H−C(3′)], 4.71 [m, 1H, H−C(2′)], 4.73 [d, 1H, $J$ = 13.3 Hz, H−C(1‴$_A$)], 4.83 [d, 1H, $J$ = 13.0 Hz, H−C(1‴$_B$)], 6.14 [d, 2H, $J$ = 4.2 Hz, H−C(1′)], 8.87 [s, 1H, H−C(8)]. $^{13}$C NMR (125 MHz, $D_2O$, HMBC, HSQC) $\delta$ (ppm) 16.9 [$CH_3$, C(3″)], 41.4 [CH, C(2″)], 43.1 [$CH_2$, C(1‴)], 63.9 [d, $CH_2$, $^2J_{C,P}$ = 4.6 Hz, C(5′)], 69.5 [CH, C(3′)], 74.3 [CH, C(2′)], 83.6 [d, CH, $^3J_{C,P}$ = 8.1 Hz, C(4′)], 89.0 [CH, C(1′)], 111.3 [C, C(5)], 136.5 [CH, C(8)], 149.9 [C, C(4)], 152.7 [C, C(2)], 156.6 [C, C(6)], 177.9 [C, C(1″)].

*$N^2$-(Propylthiomethyl)guanosine 5′-Monophosphate (**19**).* UV/vis (1% formic acid in water/methanol, 40/60 v/v) $\lambda_{max}$ = 260 nm. UPLC-TOF-MS (ESI$^-$) $m/z$ 450.0843 ([M − H]$^-$, meas); $m/z$ 450.0848 ([M − H]$^-$, calcd for $C_{14}H_{21}N_5O_8PS$). $^1$H NMR (500 MHz, $D_2O$, COSY) $\delta$ (ppm) 0.95 [t, 3H, $J$ = 7.4 Hz, H−C(3″)], 1.65 [m, 2H, H−C(2″)], 2.69 [t, 2H, $J$ = 7.4 Hz, H−C(1″)], 4.07 [m, 2H, H−C(5′)], 4.31 [m, 1H, H−C(4′)], 4.48 [t, 1H, $J$ = 4.4 Hz, H−C(3′)], 4.57 [d, 1H, $J$ = 14.1 Hz, H−C(1‴$_A$)], 4.67 [d, 1H, $J$ = 14.2 Hz, H−C(1‴$_B$)], 4.75 [t, 1H, $J$ = 5.7 Hz, H−C(2′)], 5.96 [d, 1H, $J$ = 5.3 Hz, H−C(1′)], 8.12 [s, 1H, H−C(8)]. $^{13}$C NMR (125 MHz, $D_2O$, HMBC, HSQC) $\delta$ (ppm) 15.6 [$CH_3$, C(3″)], 25.8 [$CH_2$, C(2″)], 35.9 [$CH_2$, C(1″)], 46.0 [$CH_2$, C(1‴)], 67.6 [d, CH, $^3J_{C,P}$ = 4.7 Hz, C(5′)], 73.6 [CH, C(3′)], 76.6 [CH, C(2′)], 86.8 [d, $CH_2$, $^2J_{C,P}$ = 8.4 Hz, C(4′)], 90.2 [CH, C(1′)], 119.3 [C, C(5)], 140.7 [CH, C(8)], 154.5 [C, C(4)], 154.9 [C, C(2)], 161.7 [C, C(6)].

*$N^2$-(Prop-2-enylthiomethyl)guanosine 5′-Monophosphate (**20**).* UV/vis (1% formic acid in water/methanol, 40/60 v/v) $\lambda_{max}$ = 260 nm. UPLC-TOF-MS (ESI$^-$) $m/z$ 448.0684 ([M − H]$^-$, meas); $m/z$ 448.0692 ([M − H]$^-$, calcd for $C_{14}H_{19}N_5O_8PS$). $^1$H NMR (500 MHz, $D_2O$, COSY) $\delta$ (ppm) 3.34 [d, 2H, $J$ = 8.1 Hz, H−C(1″)], 4.12 [ddd, 1H, $J$ = 3.5, 5.2, 11.7 Hz, H−C(5′$_A$)], 4.21 [ddd, 1H, $J$ = 3.4, 4.2, 11.8 Hz, H−C(5′$_B$)], 4.36 [m, 1H, H−C(4′)], 4.49 [t, 1H, $J$ = 5.0 Hz, H−C(3′)], 4.58 [d, 1H, $J$ = 14.2 Hz, H−C(1‴$_A$)], 4.62 [d, 1H, $J$ = 14.2 Hz, H−C(1‴$_B$)], 4.78 [t, 1H, $J$ = 4.4 Hz, H−C(2′)], 5.16 [d, 1H, $J$ = 10.0 Hz, H−C(3″$_A$)], 5.21 [d, 1H, $J$ = 17.0 Hz, H−C(3″$_B$)], 5.91 [m, 1H, H−C(2″)], 6.09 [d, 1H, $J$ = 4.2 Hz, H−C(1′)], 8.66 [s, 1H, H−C(8)]. $^{13}$C NMR (125 MHz, $D_2O$, HMBC, HSQC) $\delta$ (ppm) 36.4 [$CH_2$, C(1″)], 45.5 [$CH_2$, C(1‴)], 67.0 [d, $CH_2$, $^2J_{C,P}$ = 5.1 Hz, C(5′)], 72.6 [CH, C(3′)], 77.2 [CH, C(2′)], 86.6 [d, CH, $^3J_{C,P}$ = 8.0 Hz, C(4′)], 91.9 [CH, C(1′)], 114.8 [C, C(5)], 120.5 [$CH_2$, C(3″)], 137.4 [CH, C(2″)], 139.7 [C−H, C(8)], 153.1 [C, C(4)], 155.7 [C, C(2)], 159.5 [C, C(6)].

*$N^2$-(Furfurylthiomethyl)guanosine 5′-Monophosphate (**21**).* UV/vis (1% formic acid in water/methanol, 50/50 v/v) $\lambda_{max}$ = 260 nm. UPLC-TOF-MS (ESI$^-$) $m/z$ 488.0634 ([M − H]$^-$, meas); $m/z$ 488.0641 ([M − H]$^-$, calcd for $C_{16}H_{19}N_5O_9PS$). $^1$H NMR (500 MHz, $D_2O$, COSY) $\delta$ (ppm) 3.97 [d, 2H, $J$ = 2.0 Hz, H−C(1″)], 4.10 [m, 2H, H−C(5′)], 4.32 [m, 1H, H−C(4′)], 4.51 [t, 1H, $J$ = 4.6 Hz, H−C(3′)], 4.65 [d, 1H, $J$ = 14.3 Hz, H−C(1‴$_A$)], 4.71 [d, 1H, $J$ = 14.3 Hz, H−C(1‴$_B$)], 4.81 [t, 1H, $J$ = 5.5 Hz, H−C(2′)], 6.02 [d, 1H, $J$ = 5.6 Hz, H−C(1′)], 6.26 [d, 1H, $J$ = 3.3 Hz, H−C(5″)], 6.34 [dd, 1H, $J$ = 1.9, 3.0 Hz, H−C(4″)], 7.41 [d, 1H, $J$ = 1.8 Hz, H−C(3″)], 8.11 [s, 1H, H−C(8)]. $^{13}$C NMR (125 MHz, $D_2O$, HMBC, HSQC) $\delta$ (ppm) 30.2 [$CH_2$, C(1″)], 46.4 [$CH_2$, C(1‴)], 67.5 [d, $CH_2$, $^2J_{C,P}$ = 5.1 Hz, C(5′)], 73.3 [CH, C(3′)], 76.6 [CH, C(2′)], 86.6 [d, $CH_2$, $^3J_{C,P}$ = 8.2 Hz, C(4′)] 90.1 [CH, C(1′)], 110.4 [CH, C(4″)], 113.5 [CH, C(5″)], 119.2 [C, C(5)], 140.9 [CH, C(8)], 145.5 [CH, C(3″)], 154.3 [C, C(4)], 154.62 [C, C(2″)/C(2)], 154.64 [C, C(2″)/C(2)], 161.9 [C, C(6)].

*$N^2$-(Phenethylthiomethyl)guanosine 5′-Monophosphate (**22**).* UV/vis (1% formic acid in water/methanol, 40/60 v/v) $\lambda_{max}$ = 260 nm. UPLC-TOF-MS (ESI$^-$) $m/z$ 512.1019 ([M − H]$^-$, meas); $m/z$ 512.1005 ([M − H]$^-$, calcd for $C_{19}H_{23}N_5O_8PS$). $^1$H NMR (500 MHz, $D_2O$/methanol-$d_4$, COSY) $\delta$ (ppm) 2.88 [t, 2H, $J$ = 7.0 Hz, H−C(2″)], 3.03 [t, 2H, $J$ = 7.0 Hz, H−C(1″)], 4.10 [m, 2H, H−C(5′)], 4.26 [m, 1H, H−C(4′)], 4.47 [t, 1H, $J$ = 5.2 Hz, H−C(3′)], 4.51 [d, 1H, $J$ = 14.2 Hz, H−C(1‴$_A$)], 4.56 [d, 1H, $J$ = 14.2 Hz, H−C(1‴$_B$)], 4.70 [d, 1H, $J$ = 5.2 Hz, H−C(2′)], 5.95 [d, 1H, $J$ = 5.1 Hz, H−C(1′)], 7.14 [t, 1H, $J$ = 7.0 Hz, H−C(6″)], 7.16−7.25 [m, 4H, H−C(4″,5″,7″,8″)], 8.08 [s, 1H, H−C(8)]. $^{13}$C NMR (125 MHz, $D_2O$/methanol-$d_4$, HMBC, HSQC) $\delta$ (ppm) 35.1 [$CH_2$, C(1″)], 38.3 [$CH_2$, C(2″)], 46.3 [$CH_2$, C(1‴)], 67.5 [d, $CH_2$, $^2J_{C,P}$ = 4.8 Hz, C(5′)], 73.2 [CH, C(3′)], 76.7 [CH, C(2′)], 86.3 [d, CH, $^3J_{C,P}$ = 8.2 Hz, C(4′)], 90.5 [CH, C(1′)], 119.5 [C, C(5)], 129.2 [CH, C(6″)], 131.2/131.7 [CH, C(4″,5″,7″,8″)], 140.8 [C, C(3″)], 143.4 [C, C(8)], 154.2 [C, C(4)], 154.5 [C, C(2)], 161.8 [C, C(6)].

*$N^2$-(2-Hydroxyphenylthiomethyl)guanosine 5′-Monophosphate (**23**).* UV/vis (1% formic acid in water/methanol, 60/40 v/v) $\lambda_{max}$ = 260 nm. UPLC-TOF-MS (ESI$^-$) $m/z$ 500.0640 ([M − H]$^-$, meas); $m/z$ 500.0641 ([M − H]$^-$, calcd for $C_{17}H_{19}N_5O_9PS$). $^1$H NMR (500 MHz, methanol-$d_4$) $\delta$ (ppm) 4.15 [ddd, 1H, $J$ = 3.2, 5.5, 11.8 Hz, H−C(5′$_A$)], 4.25 [ddd, 1H, $J$ = 2.8, 4.4, 11.8 Hz, H−C(5′$_B$)], 4.39 [m, 1H, H−C(4′)], 4.48 [t, 1H, $J$ = 5.2 Hz, H−C(3′)], 4.64 [t, 1H, $J$ = 5.2 Hz, H−C(2′)], 4.76 [d, 1H, $J$ = 13.4 Hz, H−C(1‴$_A$)], 5.02 [d, 1H, $J$ = 13.4 Hz, H−C(1‴$_B$)], 5.88 [d, 1H, $J$ = 4.0 Hz, H−C(1′)], 6.84 [td, 1H, $J$ = 1.1, 7.5 Hz, H−C(5″)], 6.88 [dd, 1H, $J$ = 1.0, 8.2 Hz, H−C(3″)], 7.18 [td, 1H, $J$ = 1.6, 8.1 Hz, H−C(4″)], 7.51 [dd, 1H, $J$ = 1.6, 7.7 Hz, H−C(6″)], 8.63 [s, 1H, H−C(8)]. $^{13}$C NMR (125 MHz, methanol-$d_4$, HMBC) $\delta$ (ppm) 46.1 [$CH_2$, C(1‴)], 63.8 [d, $CH_2$, $^2J_{C,P}$ = 4.7 Hz, C(5′)], 69.4 [CH, C(3′)], 74.3 [CH, C(2′)], 83.5 [d, CH, $^3J_{C,P}$ = 8.9 Hz, C(4′)], 88.7 [CH, C(1′)], 115.2 [CH, C(3″)], 117.2 [C, C(1″)], 117.8 [C, C(5)], 120.8 [CH, C(5″)], 131.2 [CH, C(4″)], 136.4 [C, C(2″)], 137.5 [CH, C(8)], 149.7 [C, C(2)], 153.0 [C, C(4)], 156.4 [C, C(6)], 157.0 [C, C(6″)].

*$N^2$-(4-Hydroxyphenylthiomethyl)guanosine 5′-Monophosphate (**24**).* UV/vis (1% formic acid in water/methanol, 60/40 v/v) $\lambda_{max}$ = 260 nm. UPLC-TOF-MS (ESI$^-$) $m/z$ 500.0640 ([M − H]$^-$, meas); $m/z$ 500.0641 ([M − H]$^-$, calcd for $C_{17}H_{19}N_5O_9PS$). $^1$H NMR (500 MHz, DMSO-$d_6$) $\delta$ (ppm) 3.93 [m, 1H, H−C(5′$_A$)], 4.05 [m, 1H, H−C(5′$_B$)], 4.07 [m, 1H, H−C(4′)], 4.15 [dd, $J$ = 3.9, 4.9 Hz, H−C(3′)], 4.50 [t, $J$ = 5.3 Hz, H−C(2′)], 4.62−4.78 [m, 2H, H−C(1‴)], 5.77 [d, $J$ = 5.7 Hz, H−C(1′)], 6.75 [d, 2H, $J$ = 8.7 Hz H−C(3″/5″)], 7.31 [d, 2H, $J$ = 8.7 Hz, H−C(2″/6″)], 7.95 [s, 1H, H−C(8)]. $^{13}$C NMR (125 MHz, DMSO-$d_6$, HMBC) $\delta$ (ppm) 47.7 [$CH_2$, C(1‴)], 66.1 [d, $CH_2$, $^2J_{C,P}$ = 5.4 Hz, C(5′)], 71.0 [CH, C(3′)], 73.5 [CH, C(2′)], 83.4 [d, CH, $^3J_{C,P}$ = 7.8 Hz, C(4′)], 87.3 [CH, C(1′)], 116.7 [CH, C(3″)/C(5″)], 117.8 [C, C(5)], 122.5 [C, C(1″)], 134.9 [CH, C(2″)/C(6″)], 136.7 [CH, C(8)], 150.9 [C, C(4)], 151.9 [C, C(2)], 156.7 [C, C(6)], 157.9 [C, C(4″)].

*$N^2$-(4-Carboxyphenylthiomethyl)guanosine 5′-Monophosphate (**25**).* UV/vis (1% formic acid in water/methanol, 60/40 v/v) $\lambda_{max}$ = 260 nm. LC-MS (ESI$^-$) $m/z$ (%) 528 (85, [M − H]$^-$), 362 (75, [M −

$C_8H_7O_2S]^-$). MS/MS (ESI$^-$) $m/z$ (%) 528 (100, [M − H]$^-$), 362 (10, [M − $C_8H_7O_2S]^-$). $^1$H NMR (500 MHz, DMSO-$d_6$) $\delta$ (ppm) 3.94 [m, 1H, H−C(5′$_A$)], 4.01 [m, 1H, H−C(5′$_B$)], 4.08 [m, 1H, H−C(4′)], 4.15 [dd, $J$ = 3.7, 4.8 Hz, H−C(3′)], 5.03 [m, 2H, H−C(1‴)], 5.78 [d, $J$ = 5.5 Hz, H−C(1′)], 7.53 [t, 2H, $J$ = 8.5 Hz, H−C(3″/ 5″)], 7.86 [d, 2H, $J$ = 8.5 Hz, H−C(2″/6″)], 7.96 [s, 1H, H−C(8)]. $^{13}$C NMR (125 MHz, DMSO-$d_6$, HMBC) $\delta$ (ppm) 44.1 [$CH_2$, C(1‴)], 65.9 [d, $CH_2$, $^2J_{C,P}$ = 5.1 Hz, C(5′)], 77.1 [CH, C(3′)], 73.9 [CH, C(2′)], 83.9 [d, CH, $^3J_{C,P}$ = 8.2 Hz, C(4′)], 87.6 [CH, C(1′)], 117.9 [C, C(5)], 128.0 [C, C(4″)], 128.3 [CH, C(3″)/C(5″)], 130.3 [CH, C(2″)/C(6″)], 136.9 [CH, C(8)], 142.1 [C, C(1″)], 150.8 [C, C(4)], 151.8 [C, C(2)], 157.0 [C, C(6)], 167.4 [C, C(7″)].

**Hydrolytic Stability of Nucleotide 21 in Aqueous Solution.** A solution of $N^2$-(furfurylthiomethyl)guanosine 5′-monophosphate (**21**; 1.0 mg) in potassium phosphate buffer (1 mL, pH 4.0/6.0/8.0) was stored at 22 °C and analyzed by means of RP-HPLC with diode array detection (DAD) after 7 h. To evaluate the stability over a longer period of time, the samples dissolved at pH 6.0 and 8.0 were stored at room temperature and analyzed daily by RP-HPLC-DAD.

**Sensory Analyses.** *Precautions Taken for Sensory Analysis.* Prior to sensory analysis, the isolated compounds were suspended in water and, after removal of volatiles in high vacuum (<5 mPa), were freeze-dried three times and analytically confirmed to be essentially free of solvents and buffer compounds used. Formic acid, which is considered "generally recognized as safe" (GRAS) as a flavoring agent for food and feed applications, was used to adjust the pH value of solutions that should be sensorially analyzed to pH 6.0, because trace amounts of this acid do not influence the sensory profile of the test solution. In order to minimize the ingestion of test compounds, the "sip and spit" method was applied, meaning that the test solutions were expectorated. During sensory analyses, the oral cavity was frequently rinsed with water.

*Training of the Sensory Panel.* Thirteen subjects (8 women and 5 men, aged 22−30 years), who gave informed consent to participate in the sensory tests of the present investigation and have no history of known taste disorders, were trained to evaluate the taste of aqueous solutions of the following standard taste compounds in bottled water (pH 6.0): sucrose (50 mmol/L) for sweet taste, lactic acid (20 mmol/L) for sour taste, NaCl (20 mmol/L) for salty taste, caffeine (1 mmol/L) for bitter taste, and monosodium L-glutamate (3 mmol/L) for umami taste. Additionally, the panel was familiarized to differentiate several umami taste qualities by tasting solutions of monosodium L-glutamate (3 mmol/L), a binary mixture of monosodium L-glutamate (3 mmol/L) and guanosine 5′-monophosphate (0.1 mmol/L), and a disodium succinate solution (5 mmol/L). The assessors had participated earlier at regular intervals for at least 18 months in sensory experiments (triangle tests, isointensity testings, scale training) and were, therefore, familiar with the techniques applied. To prevent any cross-modal interactions with olfactory inputs, the panelists wore nose clips.

*Determination of Taste-Enhancing Activity and Calculation of $\beta$-Values.* To evaluate the taste-enhancing potential of nucleotide derivatives, a paired comparison test was performed as reported earlier.[6,12] Briefly, a solution of the test nucleotide (50 $\mu$mol/L) was compared to solutions containing ascending concentrations (in 30% steps) of inosine 5′-monophosphate (**3**), all compounds being dissolved in an aqueous monosodium L-glutamate matrix (3 mmol/L; pH 6). The solutions were presented to the panel in randomly coded cups in a series of five duo tests. Under forced-choice conditions, panelists were asked to determine the sample possessing the stronger umami taste. Subsequently, the percentage of panelists rating the solution containing the test nucleotide to exhibit a more intense umami taste was calculated, subjected to a Probit transformation, and plotted against the logarithm of the corresponding inosine 5′-monophosphate concentrations. By means of linear regression, the inosine 5′-monophosphate concentration was calculated at which panelists were unable to distinguish between test and reference solution. The $\beta$-value of the test compound was calculated according to $v = \beta v'$, wherein $v$ represents the inosine 5′-monophosphate concentration at the point of umami taste equality (micromoles per liter) and $v'$ is the concentration of the test nucleotide (micromoles per liter).

**Cell-Based hT1R1/rT1r3 Umami Taste Receptor Experiments.** Functional experiments were carried out in the human embryonic kidney cell line PEAK$^{Rapid}$ (American Type Culture Collection, Manassas, VA) stably expressing the umami receptor subunit hTAS1R1 and the G protein subunit mG$\alpha$15. Cells were cultured under regular conditions at 37 °C, 5% $CO_2$, and 95% humidity in Dulbecco's modified Eagle medium (D-MEM) high-glucose GlutaMAX (Invitrogen, Karlsruhe, Germany) supplied with fetal calf serum (FCS; 10%, tetracycline-free), penicillin G (10 000 units/mL), and streptomycin (10 mg/mL) and selected for stable expression of hT1R1 and mG$\alpha$15 with G418 (50 $\mu$g/mL), zeocin (100 $\mu$g/$\mu$L), hygromycin (100 $\mu$g/mL, all Invitrogen), and puromycin (1.0 $\mu$g/mL, Sigma−Aldrich, Schnelldorf, Germany).

For functional experiments, cells were seeded into 96-well plates (Greiner Bio-One, Frickenhausen, Germany) coated with poly-D-lysine (10 $\mu$g/mL) to improve cell adhesion. To enable expression of a functional umami receptor, cells were transfected with rTas1r3 (in pcDNA3, Invitrogen) by use of Lipofectamine2000 (Invitrogen) in serum-free D-MEM low-glucose GlutaMAX (Invitrogen). After transfection, cells were cultured in D-MEM low-glucose GlutaMAX with dialyzed FCS for about 24 h. Prior to the experiment, cells were incubated for 1 h with Fluo4-AM (2 $\mu$mol/L, Molecular Probes) in serum-free D-MEM low-glucose GlutaMAX containing 2.5 mM probenecide to block leakage of the fluorescent dye. Cells were washed with bath solution [130 mmol/L NaCl, 5 mmol/L KCl, 10 mmol/L $N$-(2-hydroxyethyl)piperazine-$N'$-ethanesulfonic acid (HEPES), 2 mmol/L $CaCl_2$, and 10 mmol/L glucose, pH 7.4] three times and incubated at room temperature for ∼40 min to allow complete de-esterification of the fluorescent dye. Test substances were dissolved in bath solution. For coapplication experiments, the individual substances were premixed prior to application. Intracellular calcium levels were recorded during automated application of test solutions on a fluorometric imaging plate reader (FLIPR$^{384}$, Molecular Devices, Munich, Germany). To control for cell number and vitality, isoproterenol was applied subsequent to test compounds. Cells transfected with empty vector stimulated with the same test solution served as control for unspecific responses of the cellular background. Data were collected from two independent experiments carried out in quadruplicate. Raw fluorescence signals of hT1R1/rT1r3-expressing cells were corrected for fluorescence signals of mock-transfected cells (software FLIPR$^{384}$, Molecular Devices, Munich, Germany) and normalized to baseline fluorescence ($\Delta F/F$, SigmaPlot 9.01, Systat Software GmbH, Erkrath, Germany).

Fluorescence signals after coapplication of test compounds with L-glutamic acid were analyzed for statistical significance compared to those induced by sole application of L-glutamic acid in the presence and absence of the allosteric enhancer inosine 5′-monophosphate by one-way analysis of variance followed by a Tukey's posthoc means comparison test with 5% $\alpha$-risk level (GraphPad Prism 4.03, GraphPad Software, Inc., La Jolla, CA).

**Generation of $N^2$-(Propylthiomethyl)guanosine 5′-Monophosphate (19) by Maillard Reaction from Guanosine 5′-Monophosphate (2), Glucose, Glycine, and 1-Propylthiol.** Ternary solutions of glucose (0.1, 1.0, 10, 100, 200, 500, or 1000 mmol/L), glycine (1 mol/L), and 1-propanethiol (5, 10, 20, or 50 mmol/L) in potassium phosphate buffer (2 mL, 2 mol/L, pH 7) were heated at 40 °C for 4 h. Then a solution (400 $\mu$L) of a guanosine 5′-monophosphate (25 mmol/L) in potassium phosphate buffer (2 mol/L, pH 7) was added, and incubation was continued for additional 16 h at 40 °C. The reaction solutions were made up to 10 mL with 1% aqueous formic acid and directly used for HPLC-MS/MS analysis of $N^2$-(propylthiomethyl)guanosine 5′-monophosphate (**19**). Quantitation was performed by six-point external calibration using an analyte-free matrix solution of glucose and glycine treated like the ternary reaction systems described above but in the absence of **2**. Solutions containing defined amounts of **19** in concentrations ranging from 0.005 to 0.170 $\mu$mol/L were prepared. The calibration curve, obtained

by linear regression analysis of the peak area versus concentration, showed a linear response with a correlation coefficient of $R^2 > 0.99$.

**Medium-Pressure Liquid Chromatography.** Medium-pressure liquid chromatography (MPLC) was performed on a Sepacore chromatography system (Buechi, Flawil, Switzerland) consisting of two C-605 pumps with C-615 pump manager, manual rheodyne injection port (20 mL loop), C-635 UV/vis detector, and C-660 fraction collector. Chromatography was performed at a flow rate of 40 mL/min on a self-packed 150 × 40 mm i.d. polypropylene cartridge filled with 25−40 μm LiChroprep RP-18 Material (Merck KGaA, Darmstadt, Germany).

**High-Performance Liquid Chromatography.** Analytical HPLC was carried out on an HPLC apparatus (Jasco, Groß-Umstadt, Germany), consisting of two PU-2087 Plus pumps, M800 gradient mixer, DG-2080−53 degasser, auto sampler (AS-2055 Plus) and diode array detector (MD-2010 Plus). Chrompass software was used for data acquisition. With a flow rate of 0.8 mL/min, chromatography was performed on a 250 × 4.6 mm i.d., 5 μm, Microsorb-MW 100−5 C18 column (Varian, Darmstadt, Germany). The output was monitored at 220 and 260 nm; 1% aqueous formic acid (solvent A) and methanol (solvent B) were used as eluents. After sample injection (10 μL), isocratic elution with 100% solvent A was performed for 5 min. Subsequently, the content of organic solvent was linearly increased to 100% within 25 min, and 100% solvent B was maintained for an additional 5 min.

**High-Performance Liquid Chromatography/Tandem Mass Spectroscopy.** For HPLC-ESI-MS/MS analysis, a Dionex UHPLC UltiMate 3000 HPLC system (Dionex, Idstein), consisting of HPG-3400SD type binary pump, SRD-3400 type degasser, WSP-3000TSL type autosampler, and TCC-3000SD type column compartment and operated with the DC MS Link 2.8.0.2633 software, was linked to an API 4000 QTRAP mass spectrometer (AB Sciex Instruments, Darmstadt, Germany), which was equipped with an electrospray ionization (ESI) source and operated in negative ionization mode. Nitrogen served as nebulizer gas (50 psi), and heated at 400 °C as turbo gas for solvent drying (60 psi). Nitrogen also served as curtain (20 psi) and collision gas ($4.5 \times 10^{-5}$ Torr). For the detection of **19**, the following transition reactions were optimized prior to analyses and monitored for a duration of 100 ms each. Declustering potential (DP), collision energy (CE), and collision cell exit potential (CXP) are given in parentheses: $m/z$ 450 → 374 (DP −65 V, CE −24 V, CXP −11 V), $m/z$ 450 → 161 (DP −65 V, CE −50 V, CXP −11 V), and $m/z$ 450 → 374 (DP −65 V, CE −36 V, CXP −1 V). Both quadrupoles were set at unit resolution.

For HPLC-ESI-MS/MS analysis, data acquisition and integration were carried out with Analyst 1.5.1 software (Applied Biosystems). After sample injection (5 μL), chromatographic separation was performed on a 150 × 2.0 mm i.d., 3 μm, Phenomenex Luna PFP column (Phenomenex, Aschaffenburg, Germany) by use of a linear binary gradient with a flow rate of 200 μL/min. Eluent A was 1% formic acid in acetonitrile, and eluent B was 1% formic acid in water. Chromatographic separation was performed as follows: After isocratic elution with 100% solvent B for 5 min, the content of solvent A increased to 50% within 10 min and then to 100% within 2 min. The organic solvent was finally maintained at 100% for an additional 5 min. With help of a Valco valve, the effluent was directed into the mass spectrometer during minutes 12 and 22 of each chromatographic run, while the remaining effluent was split into the waste. To determine the effect of matrix components on the LC-MS/MS analysis, 5 μL of analyte-free matrix solutions were injected into the LC-MS/MS system described above, but in addition, a constant flow (10 μL/min) of a solution of **19** (0.19 μmol/L) was introduced by means of a PHD 4400 Hpsi type syringe pump (Harvard Apparatus, Holliston, MA) connected to the solvent flow via a three-way valve.

**Ultraperformance Liquid Chromatography/Time-of-Flight Mass Spectrometry.** Mass spectra of the compounds were measured on a Waters Synapt G2 HDMS mass spectrometer (Waters, Manchester, U.K.) coupled to an Acquity UPLC core system (Waters) consisting of a binary solvent manager, sample manager and column oven. The compounds were dissolved in 1 mL of methanol ,and aliquots (1−5 μL) were injected into the UPLC-TOF-MS system equipped with a 150 × 2 mm, 1.7 μm, BEH C18 column (Waters). Operated with a flow rate of 0.3 mL/min at a temperature of 40 °C, the following gradient was used for chromatography: starting with a mixture (5/95 v/v) of acetonitrile and aqueous formic acid (0.1%, pH 2.5), the acetonitrile content was increased to 95% within 3 min and held at 95% for 1 min. Calibration of the Synapt G2 was performed with a solution of sodium formate (0.5 mmol/L) in 2-propanol/water (9/1 v/v). Data were processed by use of MassLynx 4.1 (Waters) and the tool elemental composition. All data were lock mass (leucine enkephalin) corrected ($[M + H]^+$, $m/z$ 556.2771, $[M - H]^-$, $m/z$ 554.2615). Measurements were performed with negative ESI and the resolution mode consisting of the following parameters: capillary voltage (+2.5 or −3.0 kV), sampling cone (30 V), extraction cone (4.0 V), source temperature (150 °C), desolvation temperature (450 °C), cone gas (30 L/h), and desolvation gas (850 L/h).

**Nuclear Magnetic Resonance Spectroscopy.** The $^1$H, $^{13}$C, and two-dimensional (2D) NMR spectroscopic experiments were performed on a 500 MHz Avance III NMR spectrometer from Bruker (Rheinstetten, Germany), equipped with a TCI cryoprobe and operating at 500 and 125 MHz for $^1$H and $^{13}$C, respectively. Unless stated otherwise, all experiments were performed at 300 K. Samples were dissolved in $D_2O$ with 3-(trimethylsilyl)propionic-2,2,3,3-$d_4$ acid sodium salt (TMSP) used as reference. In methanol-$d_4$, tetramethylsilane (TMS) served as reference. For accurate NMR signal assignment, correlation (COSY), heteronuclear single quantum coherence (HSQC), and heteronuclear multiple-bond correlation (HMBC) spectroscopic experiments were carried out by use of pulse sequences from the Bruker software library. While data processing was performed with Topspin version 1.3 (Bruker, Rheinstetten, Germany), the individual data interpretation was done with MestReNova 5.1.0−2940 (Mestrelab Research S.L., Santiago de Compostela, Spain).

## RESULTS AND DISCUSSION

Recent investigations revealed that $N^2$-1-carboxyalkylation of guanosine 5′-monophosphate by Maillard-type reactions with reducing carbohydrates increased the umami-enhancing potential of the nucleotide; for example, (*S*)-$N^2$-(1-carboxyethyl)guanosine 5′-phosphate (**10**) was isolated as a high-potency umami enhancer from yeast extracts.[12,13] Furthermore, amidation of the side chain's carboxy group induced a further increase of sensory activity of **10**; for example, butylation revealed the high-potency umami enhancer **11**.[14] Since the presence of sulfur atoms in synthetic $N^2$-alkylated nucleotides was described to be beneficial for sensory activity,[6−10] the following experiments targeted the substitution of the exocyclic amino function of guanosine 5′-monophosphate (**2**) with formaldehyde, the Strecker aldehyde of glycine, and alkyl- and arylmercaptans, respectively, by means of Maillard-type reaction chemistry following the scheme depicted in Figure 2.

**Preparation of $N^2$-(Alkylthiomethyl)guanosine and $N^2$-(Arylthiomethyl)guanosine 5′-Monophosphates 13−25.** In a first set of experiments, the umami-enhancing guanosine 5′-monophosphate (**2**) was reacted for 16 h at 40 °C with a binary mixture of formaldehyde and the kokumi-active glutathione, which was preincubated for 4 h at the same temperature. Reaction product **13** was isolated by means of RP-MPLC in a purity of >98% [$^1$H NMR, HPLC with evaporative light-scattering detector (ELSD)] and its structure was determined by means of UPLC-TOF-MS and 1D/2D-NMR experiments. UPLC-TOF-MS revealed $m/z$ 681.1357 as a pseudo-molecular ion ($[M - H]^-$), which is in accordance with the calculated mass of 681.1340 ($C_{21}H_{30}N_8O_{14}PS$). COSY, HSQC, and HMBC spectra allowed us to assign the proton signals at 2.05, 2.43, and 3.80 ppm to H−C(8″), H−C(7″), and

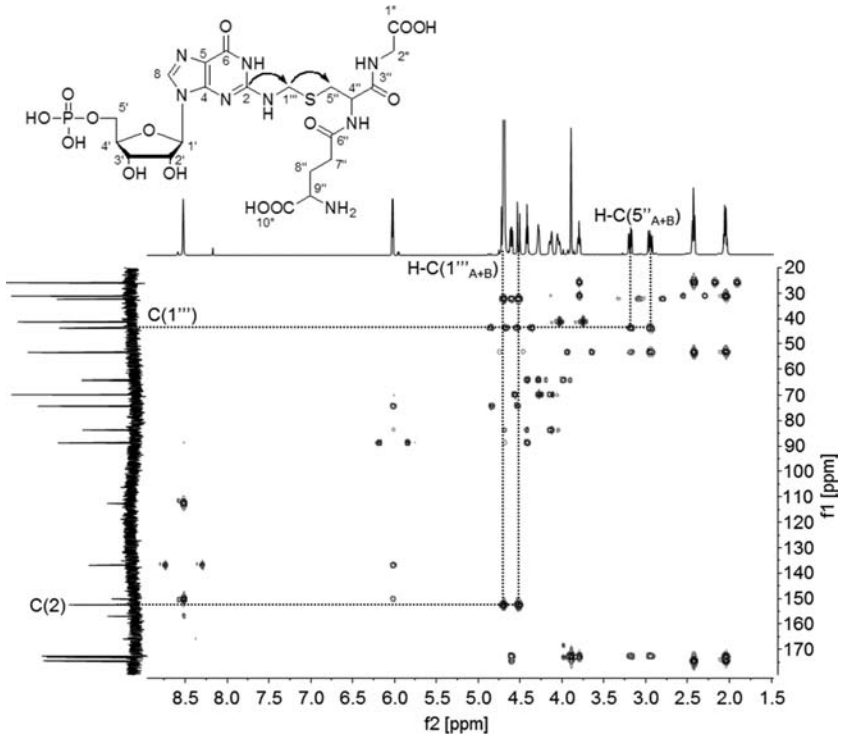


**Figure 4.** Excerpt of HMBC spectrum (500 MHz, $D_2O$) of *S*-[1-($N^2$-guanosinyl)methyl]glutathione 5′-monophosphate (**13**) generated from guanosine 5′-monophosphate (**2**), formaldehyde, and glutathione.

H−C(9″) of the glutamyl residue. $^1J_{C,H}$ couplings observed in the HSQC spectrum identified carbon signals resonating at 25.8, 30.8, and 53.2 parts per million (ppm) to correspond to the carbon atoms C(8″), C(7″), and C(9″), respectively. The two quaternary carbon atoms C(10″) and C(6″) resonated at 172.6 and 174.8 ppm and showed the expected $^{2,3}J_{C,H}$-couplings in the HMBC spectrum. The cysteine moiety showed proton signals at 2.95 [H−C(5″$_A$)], 3.07 [H−C(5″$_B$)], and 4.62 ppm [H−C(4″))] and the corresponding carbon resonances at 32.3 [C(5″)] and 53.1 ppm [C(4″)]. The signal at 172.8 ppm was assigned to the carbon atom C(3″), showing heteronuclear $^{2,3}J$-coupling with the protons H−C(2″), H−C(4″), and H−C(5″). The singlet at 3.89 ppm in the $^1$H NMR spectrum and at 41.2 ppm in the $^{13}$C NMR spectrum were attributed to methylene group of the glycine moiety. In addition, the HMBC experiment led to the identification of the carbon signal at 173.0 ppm as the glycine carboxy carbon C(1″). Moreover, the singlet at 8.52 ppm in the $^1$H NMR spectrum and the signal at 137.0 ppm in the $^{13}$C NMR spectrum were assigned to position C(8) of the purine scaffold. Due to heteronuclear $^3J$- and $^4J$-coupling detectable in the HMBC, the signals resonating at 112.4, 150.2, and 156.4 ppm were assigned as the quaternary carbon atoms C(5), C(4), and C(6) of the nucleotide moiety. The proton signals at 4.05, 4.13, 4.30, 4.41, 4.70, and 6.02 ppm in the $^1$H NMR spectrum and at 64.0, 83.8, 69.8, 74.3, and 88.6 ppm in the $^{13}$C NMR spectrum were attributed to the positions 5′$_{A+B}$, 4′, 3′, 2′, and 1′ of the nucleotide's ribose moiety. The presence of the phosphate group in the molecule was confirmed by coupling of the $^{31}$P nucleus with the carbon atoms C(5′) and C(4′); for example, coupling constants of 4.3 and 8.7 Hz were observed for $^2J$- and $^3J$-coupling of the phosphate group with C(5′) and C(4′), respectively. Two doublets recorded in the $^1$H NMR spectrum at 4.51 and 4.71 ppm were assigned as protons of the methylene group C(1‴), and with help of the HSQC spectrum, the carbon atom resonating at 43.5 ppm was assigned to this methylene group. This carbon atom showed heteronuclear $^3J$-coupling with diastereotopic methylene protons H−C(5″$_{A+B}$) of the cysteine residue. Connection to the nucleotide scaffold was verified by heteronuclear $^3J$-coupling of the quaternary carbon atom C(2) at 152.7 ppm to two proton signals of the methylene group H−C(1‴) (Figure 4). With all these spectroscopic data taken into consideration, the reaction product **13** was unequivocally identified as *S*-[1-($N^2$-guanosinyl)methyl]glutathione 5′-monophosphate (Figure 3).

By a straightforward synthetic approach, a series of $N^2$-(alkylthiomethyl)guanosine and $N^2$-(arylthiomethyl)guanosine 5′-monophosphates, **14**−**25**, was successfully generated by reacting guanosine 5′-monophosphate (**2**) with formaldehyde and *N*-acetyl-L-cysteine, *N*-acetylcysteamine, 2-mercaptophenol, 2- and 3-mercaptopropionic acid, 1-propanethiol, 2-propen-1-thiol, 2-furanmethanethiol, 2-phenethylthiol, 2- and 4-mercaptophenol, and 2-mercaptobenzoic acid, respectively (Figure 3).

To investigate the hydrolytic stability of such $N^2$-(alkylthiomethyl)guanosine 5′-monophosphates in aqueous solution, solutions of **21** in phosphate buffer were kept at pH 4.0, 6.0, and 8.0 at room temperature and repeatedly analyzed by RP-HPLC-DAD. While the target nucleotide remained rather stable at pH 4.0 and 6.0, storage under alkaline conditions induced rapid degradation with a half-life time of 8 days (data not shown).

**Sensory Evaluation of $N^2$-(Alkylthiomethyl)guanosine and $N^2$-(Arylthiomethyl)guanosine 5′-Monophosphates.** In order to study the umami taste-enhancing properties of ribonucleotides **13**−**25**, the highly purified substances were presented to a panel of trained assessors in a series of forced-choice comparison tests described earlier (Table 1).[6,13] To evaluate the umami taste synergism between L-glutamic acid

**Table 1. Umami-Enhancing Activity ($\beta$-Value) of Reference Nucleotides (2 and 3) and $N^2$-(Methylene-*S*-alkyl/aryl)guanosine 5′-Monophosphate Derivatives (13−25)**

| nucleotide derivative[a] | $\beta$-value |
|---|---|
| inosine 5′-monophosphate, disodium salt (**3**) | 1.0 |
| guanosine 5′-monophosphate, disodium salt (**2**) | 2.4 |
| *S*-[1-($N^2$-guanosinyl)methyl]glutathione 5′-monophosphate (**13**) | 1.1 |
| $N^2$-[(2-acetylamino-2-carboxyethyl)thiomethyl]guanosine 5′-monophosphate (**14**) | 2.3 |
| $N^2$-(2-acetylaminoethylthiomethyl)guanosine 5′-monophosphate (**15**) | 2.8 |
| $N^2$-(2-hydroxyethylthiomethyl)guanosine 5′-monophosphate (**16**) | 2.8 |
| $N^2$-(2-carboxyethylthiomethyl)guanosine 5′-monophosphate (**17**) | 2.5 |
| $N^2$-(1-carboxyethylthiomethyl)guanosine 5′-monophosphate (**18**) | 3.1 |
| $N^2$-(propylthiomethyl)guanosine 5′-monophosphate (**19**) | 5.1 |
| $N^2$-(prop-2-enylthiomethyl)guanosine 5′-monophosphate (**20**) | 4.1 |
| $N^2$-(furfurylthiomethyl)guanosine 5′-monophosphate (**21**) | 3.1 |
| $N^2$-(phenethylthiomethyl)guanosine 5′-monophosphate (**22**) | 2.7 |
| $N^2$-(2-hydroxyphenylthiomethyl)guanosine 5′-monophosphate (**23**) | 2.1 |
| $N^2$-(4-hydroxyphenylthiomethyl)guanosine 5′-monophosphate (**24**) | 3.0 |
| $N^2$-(4-carboxyphenylthiomethyl)guanosine 5′-monophosphate (**25**) | 3.6 |

[a]Chemical structures and numbering of the compounds refer to Figures 1 and 4.

and ribonucleotides, each target ribonucleotide (50 $\mu$mol/L) was dissolved in a matrix of monosodium glutamate (3 mmol/L; pH 6). In five duo tests, panelists had to evaluate this solution for umami taste intensity in comparison with reference solutions containing increasing concentrations (in 30% steps) of inosine 5′-monophosphate (**3**) dissolved in the monosodium glutamate matrix. The percent of panelists judging the test solution to exhibit more intense umami taste was calculated and, after Probit transformation, related to the logarithm of the corresponding inosine 5′-monophosphate reference solutions. By means of linear regression, the concentration of inosine 5′-monophosphate was calculated at which panelists were unable to distinguish between test and reference solutions. Subsequently, the $\beta$-value was calculated as the ratio of the inosine 5′-monophosphate concentration perceived as isointense to test solution and the concentration of the target ribonucleotide applied in this sensory test. Reference nucleotide **2** was evaluated with a $\beta$-value of 2.4, thus being well in line with literature data.[6,13]

Sensory analysis of the 5′-GMP/glutathione conjugate **13** revealed umami enhancement with a $\beta$-value of 1.1, which is close to that of the reference inosine 5′-monophosphate, **3** (Table 1). To evaluate the influence of mercaptan structure on the taste-enhancing properties of the nucleotide conjugate, the tripeptide glutathione was substituted by *N*-acetylcysteine to give nucleotide **14**. Sensory evaluation revealed a $\beta$-value of 2.3, thus demonstrating that ribonucleotide **14** possessed taste-modifying properties equivalent to its mother nucleotide **3**. Removal of the carboxy group from the *N*-acetylcysteine moiety showed an additional increase of the umami-enhancing potential ($\beta$-value 2.8) of the *N*-acetylcysteamine conjugate **15**, while substituting the acetylated amino by an hydroxyl group to give **16** did not alter the sensory properties of the target nucleotide. Removal of the *N*-acetylamino group from *N*-acetylcysteine revealed a slightly lower $\beta$-value of 2.5 for the corresponding 3-mercaptopropionic acid conjugate **17**. Shifting the carboxyl group from the $\alpha$- into the $\beta$-position induced an increase in sensory activity from a $\beta$-value of 2.5 (**17**) to 3.1 (**18**). Complete absence of all functional groups in the mercaptan structure revealed the 5′-GMP/propanethiol conjugate **19** with a remarkably higher taste-enhancing potential ($\beta$-value 5.1) than the molecules evaluated before. Substitution of the propyl residue in **19** by an allyl residue (**20**) slightly decreased the $\beta$-value of the nucleotide to 4.1. These data confirm earlier observations,[13,14] that the incorporation of small and nonpolar *N*-substituents in **2** evoke more pronounced umami-enhancement activity than large and hydrophilic substituents.

A second set of experiments focused on the activity of $N^2$-(arylthiomethyl)guanosine 5′-monophosphates, exhibiting an

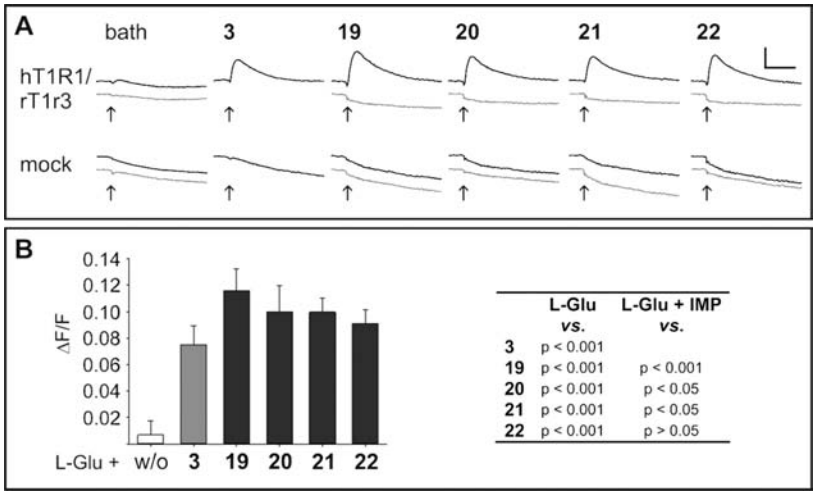


**Figure 5.** Umami-enhancing activity of selected $N^2$-(alkylthiomethyl)guanosine 5′-monophosphates (**19**, **20**) and $N^2$-(arylthiomethyl)guanosine 5′-monophosphates (**21**, **22**) assessed in umami receptor assay. (A) Calcium fluorescence traces from PEAK Rapid/G$\alpha$15 cells expressing the umami receptor heteromer hT1R1/rT1r3 (upper row) and control cells (lower row) to application (↑) of **19** (0.05 mmol/L), **20** (0.05 mol/L), **21** (0.05 mmol/L), **22** (0.05 mol/L), and 5′-IMP (**3**; 0.5 mmol/L), in the absence (gray) and presence (black) of L-glutamate (0.5 mM). Control cells were transfected with empty vector. Scale: *y*-axis, 1050 counts; *x*-axis, 2 min. (B) Fluorescence ratios of cells expressing hT1R1/rT1r3 to L-glutamate (0.5 mM) in the absence (white bar) and presence of 5′-IMP (**3**; 0.5 mM; light gray bar) and nucleotides **19**−**22** (each 0.05 mmol/L; dark gray bars) ($N$ = 2).

aromatic ring in the mercaptan moiety. Conjugates of guanosine 5′-monophosphate with the key food odorants 2-furfurylthiol and 2-phenethylthiol,[16] respectively, showed only slightly increased umami-enhancement activity with $\beta$-values of 3.1 (**21**) and 2.7 (**22**) when compared to the reference nucleotide **2** (Table 1). While $N^2$-(2-hydroxyphenylthiomethyl)guanosine 5′-monophosphate (**23**) showed an even lower $\beta$-value of 2.1, shifting the hydroxy group at the phenyl ring from the ortho into the para position resulted in ribonucleotide **24**, evaluated with an increased $\beta$-value of 3.0. However, replacement of the hydroxyl group in **24** by a carboxy function induced a further increase in the taste-enhancing potential of the target nucleotide **25** to reach a $\beta$-value of 3.6. Intriguingly, substitution of the exocyclic amino group of **3** with $N^2$-(arylthiomethyl) groups followed a different structure–activity relationship than substitution with $N^2$-(alkylthiomethyl) groups. The sensory activity of $N^2$-(arylthiomethyl) derivatives seems to depend on the substitution pattern of the aromatic moiety rather than on the size of the substituent.

**Enhancing Effect of Nucleotides on Functionally Expressed hT1R1/rT1r3 Umami Receptor.** Although the candidate umami taste receptors in humans were identified almost a decade ago,[4] only a few studies have combined human psychophysical experiments with functional expression of T1 receptors so far.[14,17] As the human sensory data obtained for $N^2$-(alkylthiomethyl)guanosine and $N^2$-(arylthiomethyl)-guanosine 5′-monophosphates implied high chemoselectivity of the umami receptor binding site, the enhancing effect of the most efficient compounds **19**–**22** on the L-glutamate-induced response of functionally expressed T1R1/T1r3 umami receptor was investigated (Figure 5).

In human embryonic kidney PEAK$^{Rapid}$ cells that stably express the G protein subunit mG$\alpha$15, activation of the heteromeric umami receptor combination of hT1R1 and rT1r3 is coupled to release of calcium from the endoplasmatic reticulum that can be detected by fluorescent dyes. Since L-glutamate and nucleotide enhancer are known to interact with the T1R1 subunit of the umami receptor heteromer, the functional expression system is likely to resemble the detection of umami compounds in human taste receptor cells.[5,14,18] With regard to its sensitivity to L-glutamate, the pharmacological characteristics of our umami functional expression system were well in accordance with previously published in vitro data.[5]

Calcium traces of T1R1/T1r3-expressing cells and mock-transfected cells (control) upon bath application of $N^2$-(alkylthiomethyl)guanosine 5′-monophosphates (**19** and **20**; 0.05 mmol/L each), $N^2$-(arylthiomethyl)guanosine 5′-monophosphates (**21** and **22**; 0.05 mmol/L each), and reference nucleotide **3** (0.5 mmol/L each) in the presence or absence of L-glutamic acid (0.5 mmol/L) are depicted in Figure 5A. In the absence of L-glutamate, none of the compounds elicited calcium fluorescence responses from T1R1/R3-expressing cells nor from mock-transfected cells (Figure 5A, gray traces). These data propose that the $N^2$-(alkylthiomethyl)guanosine and $N^2$-(arylthiomethyl)guanosine 5′-monophosphates do not exhibit intrinsic umami taste activity. However, the receptor-dependent fluorescence signal to L-glutamate (0.5 mmol/L) was strongly enhanced by 0.05 mM **19**, **20**, **21**, and **22** (Figure 5A, black traces).

Each of the tested ribonucleotides **19**–**22** increased receptor responses in a more pronounced manner than 5′-IMP did (**3**), thus confirming the human sensory data shown above. The average normalized fluorescence ratios of T1R1/R3-expressing cells upon coapplication of L-glutamate (0.5 mM) and the target compounds **19**, **20**, and **21** (0.05 mM), respectively, significantly exceeded those induced by L-glutamate (0.5 mM) and 5′-IMP (**3**), even though **3** was employed at a 10-fold higher concentration (Figure 5B).

Interestingly, the rank order of the compound's in vitro efficacy in modulating the T1R1/R3 receptor (**19** > **20** = **21** > **22**) resembles that of the human sensory data, although the differences were less pronounced at the cellular level. For example, **19** ($\beta$-value 5.1) showed almost twice the activity of **22** ($\beta$ value 2.7) in the human sensory experiment, but the fluorescence ratio of 0.116 ± 0.017 measured for **19** elicited an only 27% higher signal than **22** (0.091 ± 0.010). These differences between human sensory and taste receptor data may be explained either by response differences of the cells expressing the hT1R1-rT1r3 receptor construct when compared to human umami taste receptor cells or by assuming that the umami-enhancing activity of the modified nucleotides is only partially mediated by the T1R1/R3 umami receptor.

**Maillard-type Generation of $N^2$-(Propylthiomethyl)-guanosine 5′-monophosphate (19).** Apart from the formation of volatile odorants,[16] the generation of taste modulators by the Maillard reaction gained increasing attention during recent decades.[12−14,19−25] As the Strecker aldehyde formaldehyde is released from the amino acid glycine upon thermal processing in the presence of reducing carbohydrates, the following experiments were done to investigate the generation of target nucleotide **19** by food-related Maillard-type reactions involving glycine, glucose, and 1-propanethiol, known as a key odorant released from freshly cut onions.[26] After thermal reaction in phosphate buffer (pH 7.0), the reaction mixture was analyzed by means of HPLC-MS/MS (ESI$^-$) analysis in the multiple reaction monitoring (MRM) mode. As depicted in Figure 6, the target molecule **19**, eluted after 14.1 min, was detected at the same retention time in the Maillard reaction system and was further verified by means of cochromatography. External quantitation of **19** by means of HPLC-MS/MS in reaction systems varying the molar carbohydrate/amino acid ratio between 1 and 1000 revealed that the generation of **19** went through a maximum of 6.5 $\mu$g/

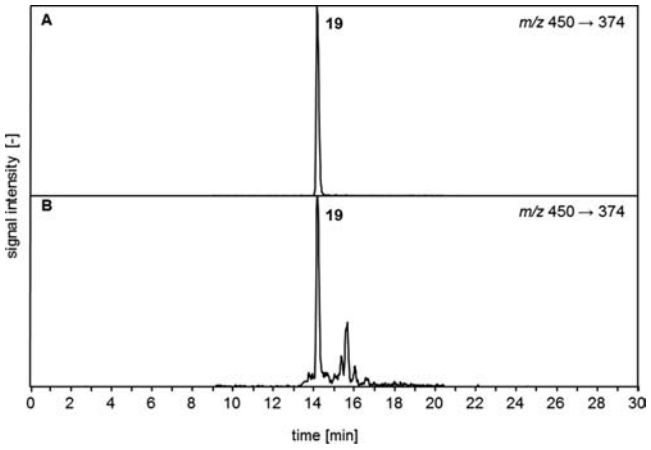


**Figure 6.** HPLC-MS/MS (ESI$^-$) analysis of (A) purified sample of $N^2$-(propylthiomethyl)guanosine 5′-monophosphate (**19**) and (B) nucleotide **19** in a Maillard-type reaction mixture of guanosine 5′-monophosphate (**2**), glucose, glycine, and 1-propanethiol. Signal intensity of the mass chromatograms is normalized.

100 mL at a glucose/glycine ratio of 10 (Figure 7). Furthermore, varying the amount of 1-propanethiol between

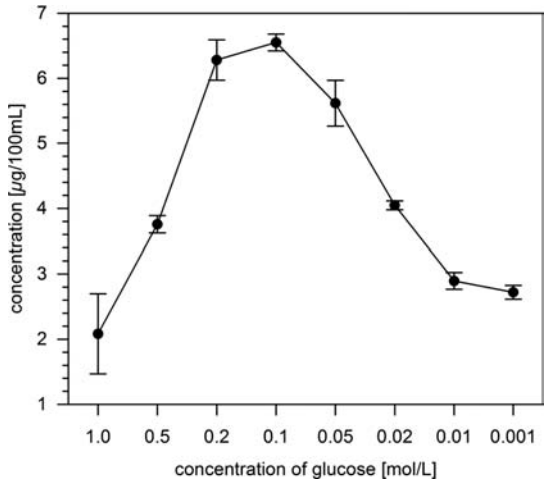


**Figure 7.** Influence of glucose (0.001−1.0 mmol/L) on the formation of $N^2$-(propylthiomethyl)guanosine 5′-monophosphate (**19**) from **2** (25 mmol/L), glycine (1 mol/L), and 1-propanethiol (5 mmol/L) in potassium phosphate buffer (2 mol/L, pH 7).

5 and 50 mmol/L at a glucose/glycine ratio of 10 revealed almost the same concentration of **19** varying between 5.8 and 7.1 µg/100 mL (data not shown), thus demonstrating the presence of formaldehyde rather than the thiol to be a limiting factor in the generation of **19**.

In summary, structurally versatile $N^2$-(alkylthiomethyl)-guanosine and $N^2$-(arylthiomethyl)guanosine 5′-monophosphates were preparatively generated and evaluated in their activity to enhance the umami taste of monosodium L-glutamate in vivo (human sensory experiments) and in vitro (T1R1/T1r3 taste receptor assay). The most active umami enhancer, $N^2$-(propylthiomethyl)guanosine 5′-monophosphate (**19**), showing a $\beta$-value of 5.1, was generated by Maillard-type reactions from guanosine 5′-monophosphate (**2**), glucose, glycine, and 1-propanethiol. Future studies are needed to fully exploit the potential of the exocyclic amino group of guanosine 5′-monophosphate as an effective anchor group to chemically fix small and hydrophobic food-derived molecules. This strategy opens a valuable avenue to produce high-potential chemosensorica from food-derived natural products by kitchen-type chemistry.

## AUTHOR INFORMATION

### Corresponding Author

*Phone +49-8161/71-2902; fax +49-8161/71-2949; e-mail thomas.hofmann@tum.de.

### Notes

The authors declare no competing financial interest.

## REFERENCES

(1) Ikeda, K. New seasonings. *Chem. Senses* **2002**, *27*, 847−849.
(2) Li, X.; Staszewski, L.; Xu, H.; Durick, K.; Zoller, M.; Adler, E. Human receptors for sweet and umami taste. *Proc. Natl. Acad. Sci. U.S.A.* **2002**, *99*, 4692−4696.
(3) Nelson, G.; Chandrashekar, J.; Hoon, M. A.; Feng, L.; Zhao, G.; Ryba, N. J. P.; Zuker, C. S. An amino acid taste receptor. *Nature* **2002**, *416*, 199.
(4) Behrens, M.; Meyerhof, W.; Hellfritsch, C.; Hofmann, T. Sweet and umami taste: Natural products, their chemosensory targets, and beyond. *Angew. Chem., Int. Ed.* **2011**, *50*, 2220−2242.
(5) Zhang, F.; Klebansky, B.; Fine, R. M.; Xu, H.; Pronin, A.; Liu, H.; Tachdijian, C.; Li, X. Molecular mechanism for the umami taste synergism. *Proc. Natl. Acad. Sci. U.S.A.* **2008**, *105*, 20930−20934.
(6) Yamaguchi, S.; Yoshikawa, T.; Ikeda, S.; Ninomiya, T. Measurement of the relative taste intensity of some L-α-amino acids and 5′-nucleotides. *J. Food Sci.* **1971**, *36*, 846−849.
(7) Imai, K.-I.; Marumoto, R.; Kobayashi, K.; Yoshioka, Y.; Toda, J.; Honjo, M. Synthesis of compounds related to inosine 5′-phosphate and their flavor enhancing activity. IV. 2-Substituted inosine 5′-phosphates. *Chem. Pharm. Bull.* **1971**, *19*, 576−586.
(8) Mizuta, E.; Toda, J.; Suzuki, N.; Sugibayashi, H.-M.; Imai, K.-I.; Nishikawa, M. Structure-activity relationship in the taste effect of ribonucleotide derivatives. *Chem. Pharm. Bull.* **1972**, *20*, 1114−1124.
(9) Cairoli, P.; Pieraccini, S.; Sironi, M.; Morelli, C. F.; Speranza, G.; Manitto, P. Studies on umami taste. Synthesis of new guanosine 5′-phosphate derivatives and their synergistic effect with monosodium glutamate. *J. Agric. Food Chem.* **2008**, *56*, 1043−1050.
(10) Morelli, C. F.; Manitto, P.; Speranza, G. Study on umami taste: the MSG taste-enhancing activity of $N^2$-alkyl and $N^2$-alkanoyl-5′-guanylic acids having a sulfoxide group inside the $N^2$-substituent. *Flavour Fragrance J.* **2011**, *26*, 279−281.
(11) De Rijke, E.; Ruisch, B.; Bakker, J.; Visser, J.; Leene, J.; Haiber, S.; de Klerk, A.; Winkel, C.; König, Th. LC-MS study to reduce ion suppression and to identify *N*-lactoylguanosine 5′-monophosphate in bonito: a new umami molecule? *J. Agric. Food Chem.* **2007**, *55*, 6417−6423.
(12) Festring, D.; Hofmann, T. Discovery of $N^2$-(1-carboxyethyl)-guanosine 5′-monophosphate as an umami-enhancing Maillard-modified nucleotide in yeast extracts. *J. Agric. Food Chem.* **2010**, *58*, 10614−10622.
(13) Festring, D.; Hofmann, T. Systematic studies on the chemical structure and umami enhancing activity of Maillard-modified guanosine 5′-monophosphates. *J. Agric. Food Chem.* **2011**, *59*, 665−676.
(14) Festring, D.; Brockhoff, A.; Meyerhof, W.; Hofmann, T. Stereoselective synthesis of amides sharing the guanosine 5′-monophosphate scaffold and umami enhancement studies using human sensory and hT1R1/rT1R3 receptor assays. *J. Agric. Food Chem.* **2011**, *59*, 8875−8885.
(15) Lu, K.; Ye, W.; Gold, A.; Ball, L. M.; Swenberg, J. Formation of *S*-[1-($N^2$-Deoxyguanosinyl)methyl]glutathione between glutathione and DNA induced by formaldehyde. *J. Am. Chem. Soc.* **2009**, *131*, 3414−3415.
(16) Dunkel, A.; Steinhaus, M.; Kotthoff, M.; Nowak, B.; Krautwurst, D.; Schieberle, P.; Hofmann, T. Nature's chemical signatures in human olfaction: A foodborne perspective for future biotechnology. *Angew. Chem., Int. Ed.* **2014**, *53*, 7124−7143.
(17) Dewis, M. L.; Phan, T.-H. T.; Ren, Z.; Meng, X.; Cui, M.; Mummalaneni, S.; Rhyu, M.-R.; DeSimone, J. A.; Lyall, V. N-Geranyl cyclopropyl-carboximide modulates salty and umami taste in humans and animal models. *J. Neurophysiol.* **2013**, *109*, 1078−1090.
(18) Xu, H.; Staszewski, L.; Tang, H.; Adler, E.; Zoller, M.; Li, X. Different functional roles of T1R subunits in the heteromeric taste receptors. *Proc. Natl. Acad. Sci. U.S.A.* **2004**, *101*, 14258−14263.
(19) Intelmann, D.; Batram, C.; Kuhn, Ch.; Haseleu, G.; Meyerhof, M.; Hofmann, T. Three TAS2R bitter taste receptors mediate the psychophysical responses to bitter compounds of hops (*Humulus lupulus* L.) and beer. *Chem. Percept.* **2009**, *2*, 118−132.
(20) Ottinger, H.; Hofmann, T. Identification of the taste enhancer alapyridaine in beef broth and evaluation of its sensory impact by taste reconstitution experiments. *J. Agric. Food Chem.* **2003**, *51*, 6791−6796.
(21) Ottinger, H.; Soldo, T.; Hofmann, T. Discovery and structure determination of a novel Maillard-derived sweetness enhancer by application of the comparative taste dilution analysis (cTDA). *J. Agric. Food Chem.* **2003**, *51*, 1035−1041.

(22) Soldo, T.; Blank, I.; Hofmann, T. (+)-(S)-Alapyridaine: A general taste enhancer? *Chem. Senses* **2003**, *28*, 371−379.
(23) Beksan, E.; Schieberle, P.; Robert, F.; Blank, I.; Fay, L. B.; Schlichtherle-Cerny, H.; Hofmann, T. Synthesis and sensory characterization of novel umami-tasting glutamate glycoconjugates. *J. Agric. Food Chem.* **2003**, *51*, 5428−5436.
(24) Sonntag, T.; Kunert, C.; Dunkel, A.; Hofmann, T. Sensory-guided identification of *N*-(1-methyl-4-oxoimidazolidin-2-ylidene)-α-amino acids as contributors to the thick-sour and mouth-drying orosensation of stewed beef juice. *J. Agric. Food Chem.* **2010**, *58*, 6341−6350.
(25) Kunert, C.; Walker, A.; Hofmann, T. Taste modulating *N*-(1-methyl-4-oxoimidazolidin-2-ylidene) α-amino acids formed from creatinine and reducing carbohydrates. *J. Agric. Food Chem.* **2011**, *59*, 8366−8376.
(26) Løkke, M. M.; Edelenbos, M.; Larsen, E.; Feilberg, A. Investigation of volatiles emitted from freshly cut onions (*Allium cepa* L.) by real time proton-transfer reaction-mass spectrometry (PTR-MS). *Sensors* **2012**, *12*, 16060−16076.

Table 1. Relative Amounts (MS Response) of Diosmetin-7-*O*-glucoside Metabolites from Each Colony (Mean ± SD, $n$ = 3)

| no. | bacterial strain | metabolite M1 | metabolite M2 | metabolite M3 |
|---|---|---|---|---|
| 1 | *Escherichia* sp. 4 | $(1.94 \pm 0.21) \times 10^4$ | $(5.36 \pm 0.72) \times 10^3$ | $(7.91 \pm 1.98) \times 10^3$ |
| 2 | *Escherichia* sp. 33 | $(1.77 \pm 0.11) \times 10^4$ | $(4.58 \pm 0.84) \times 10^3$ | $(5.29 \pm 1.20) \times 10^3$ |
| 3 | *Escherichia* sp. 34 | $(1.85 \pm 0.73) \times 10^4$ | $(5.58 \pm 1.34) \times 10^3$ | $(5.63 \pm 0.27) \times 10^3$ |
| 4 | *Enterococcus* sp. 30 | $(1.91 \pm 1.24) \times 10^4$ | $(6.21 \pm 1.59) \times 10^3$ | $(7.60 \pm 1.73) \times 10^3$ |
| 5 | *Enterococcus* sp. 41−2 | $(1.98 \pm 1.67) \times 10^4$ | $(5.86 \pm 0.51) \times 10^3$ | $(4.75 \pm 0.92) \times 10^3$ |
| 6 | *Bacillus* sp. 46 | $(1.93 \pm 1.08) \times 10^4$ | $(7.40 \pm 1.81) \times 10^3$ | $(2.36 \pm 0.49) \times 10^3$ |

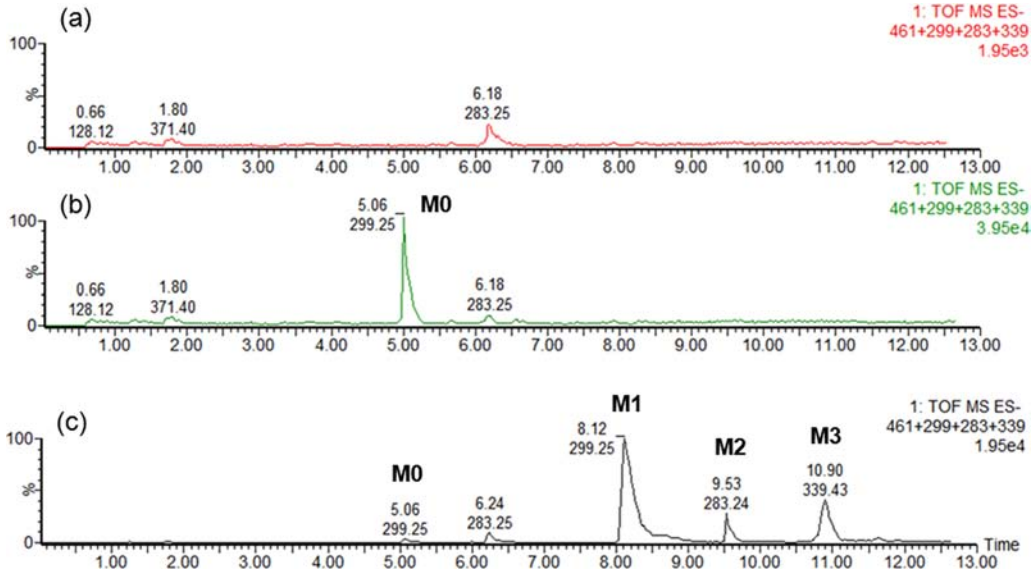


**Figure 1.** UPLC-MS chromatograms of diosmetin-7-*O*-glucoside and its metabolites: (a) blank sample (containing GAM only); (b) GAM with standard solution of diosmetin-7-*O*-glucoside sample; (c) *Escherichia* sp. 4 sample.

## MATERIALS AND METHODS

**Chemicals and Media.** The HPLC grade acetonitrile was purchased from TEDIA Co. Inc. (Fairfield, OH, USA). The distilled water was purified by an EPED super purification system (Nanjing, China). The formic acid was obtained from Merck KGaA (Darmstadt, Germany). Other reagents were all of analytical grade. AnaeroPack rectangular jars were purchased from Mitsubishi Gas Chemical Co. Inc. (Japan). Diosmetin-7-*O*-glucoside, diosmetin, and acacetin standard substances (purity > 98%) were purchased from Chengdu Preferred Biotechnology Co., Ltd. (Chengdu, China).

The general anaerobic medium (GAM) used in the fermentation experiment contained the following compounds per liter: 5.0 g of yeast extract, 3.0 g of glucose, 2.2 g of beef extract, 2.5 g of $KH_2PO_4$, 0.3 g of sodium thioglycolate, 13.5 g fo digestive serum powder, 10.0 g of proteose peptone, 3.0 g of soy peptone, 10.0 g of tryptone, 5.0 g of soluble starch, 1.2 g of beef liver extract powder, 3.0 g of NaCl, 0.3 g of L-cysteine hydrochloride, and about 1000 mL of distilled water. After the above were well mixed, the pH was adjusted to approximately 7.3 with NaOH aqueous solution. Then, the GAM was autoclaved at 121 °C for 20 min.

**Collection and Incubation of Fecal Samples.** Fresh human feces (4.0 g) were weighed and suspended in a centrifuge tube covered with 20 mL of sterile physiological saline and then homogenized adequately by a vortex-mixer. The mixture was centrifuged at 2000*g* for 10 min, and the suspension was used as the bacterial mixture.

The bacterial mixture was diluted serially in sterile water, and each of the dilutions was spread on the GAM agar plates, which were incubated under anaerobic condition in anaerobic jars for 48 h at 37 °C. Each bacterium picked up from the GAM agar plate was inoculated into 1.0 mL of GAM broth and anaerobically incubated at 37 °C for 24 h.

**16S rRNA Gene Sequencing and Phylogenetic Analysis.** The bacterial genomic DNA was extracted from the isolates using a Karroten Genomic DNA Purification Kit (Beijing, China). Their 16S rRNA sequences were amplified with two universal primers. The Gram-negative bacteria were 16S-2F (CATGCAAGTCGARCG) and 16S-2R (GGTGTGACGGGCGGT), whereas the Gram-positive bacteria were 16S-1F (AGAGTTTGATCCTGGCTCAG) and 16S-1R (AGAAAGGAGGTGATCC). The polymerase chain reaction (PCR) program used for amplification was as follows: 94 °C for 1 min, followed by 29 cycles consisting of 94 °C for 30 s, 55 °C for 30 s, and 72 °C for 2 min, and a single final extension step consisting of 72 °C for 10 min. The PCR products were purified from the agarose gel using a Karroten gel purification kit. Sequencing of the 16S rRNA fragments was performed by Majorbio (Shanghai, China). The homology search of the 16S rRNA gene sequence was performed by EzBioCloud server. The phylogenetic tree was constructed using the neighbor-joining method of the CLUSTAL W program and MEGA (ver 5.0) software.[26]

**Sample Preparation for Analysis.** The diosmetin-7-*O*-glucoside standard solution was prepared by dissolving accurately diosmetin-7-*O*-glucoside in methanol to give a final concentration of 3.0 mg/mL. The 0.1 mM standard solution was inoculated into 0.9 mL of GAM broth with 0.1 mL of precultured bacteria prepared from the culture stock and then anaerobically incubated at 37 °C for 24 h. The samples were extracted three times with ethyl acetate, and the ethyl acetate layer was dried under vacuum. Before UPLC-MS analysis, the samples were dissolved with 0.3 mL of methanol and centrifuged at 12000*g* for 10 min, and then the supernatant was filtered through a 0.22 μm membrane. To exclude the deviation deriving from one time test, each bacterial strain was prepared to be three samples for incubation with the diosmetin-7-*O*-glucoside standard, and the processed sample was tested three times.

**UPLC-MS Analysis.** The flavonoids were separated on a Waters Acquity UPLC system (Waters Corp., Milford, MA, USA) fitted with a Syncronis C 18 column (100 mm × 2.1 mm i.d., 1.7 μm; Thermo,

**Table 2. Diosmetin-7-*O*-glucoside and Its Metabolites Identified in Different Human Intestinal Bacterial Samples Using UPLC-MS/MS**

| peak | $t_R$[a](min) | exptl mass ($m/z$) | formula | $MS^2$ fragment ions | mass change | formula change |
|---|---|---|---|---|---|---|
| M0 | 5.06 | 462.1162 | $C_{22}H_{22}O_{11}$ | 461, 299, 284, 255, 151 | 0 | null |
| M1 | 8.10 | 300.0634 | $C_{16}H_{12}O_6$ | 299, 284, 256, 151 | −162.0528 | -Glc |
| M2 | 9.53 | 284.0685 | $C_{16}H_{12}O_5$ | 283, 268, 240, 151 | −178.0504 | -Glc − OH |
| M3 | 10.90 | 340.0947 | $C_{19}H_{16}O_6$ | 339, 283, 268, 240, 151 | −122.0215 | -Glc − OH + $CH_3$ + $C_2H_2O$ |

[a] $t_R$, retention time.

USA) by gradient elution using acetonitrile (solvent A) and 0.1% formic acid in distilled water (solvent B). The gradient profile was as follows: 0−7.5 min, from 10 to 30% solvent A; 10 min, 70% solvent A; 11 min, 95% solvent A; held for 1 min. The gradient was recycled back to 10% in 1 min for the next run. The injection volume was 5 μL. The temperature of the column oven was set to 35 °C.

Mass spectrometry was carried out using a Waters Acquity Synapt mass spectrometer (Waters Corp., Manchester, UK) connected to the UPLC system via an electrospray ionization (ESI) interface. Ionization took place in the negative ion mode. The conditions for the MS analysis were designed as follows: capillary voltage, 3.0 kV; cone gas flow rate, 50 L/h; source temperature, 120 °C; desolvation gas flow rate, 60 L/h at a temperature of 350 °C. All data in the centroid mode were acquired by using Masslynx$^{NT4.1}$ software (Waters Corp., Milford, MA, USA).

## RESULTS

**Characterization of the Human Intestinal Bacteria.** On the basis of the colony morphology, micromorphology, and comparative 16S rRNA gene sequence analysis, 67 *Escherichia*, 16 *Enterococcus*, and 16 *Bacillus* strains were identified. Due to the stronger bioconversion ability (Table 1), Gram-negative strain 4 was picked as a representative example for analysis. The PCR amplified 16S rRNA of strain 4 was 1298 bp, and its nucleotide sequence has been registered in GenBank under accession no. KC819112. After comparison of the 16S rRNA gene sequence with the CLUSTAL W program, the phylogenetic affiliation of strain 4 was determined. The phylogenetic tree also showed that the isolated strain 4 was in the same cluster with *Escherichia* species. It is closely related to *Escherichia coli* O157 EC4115 CP001164 with 99.15% similarity. Thus, we identified it as one species of the genus *Escherichia* and named it *Escherichia* sp. 4.

**Metabolic Profile of Diosmetin-7-*O*-glucoside by the Different Human Intestinal Bacteria.** According to the retention behaviors, changes of molecular weights and MS/MS fragment patterns, the prototype, and its metabolites could be tentatively identified. Compared with blank sample (Figure 1 and Table 2), parent compound diosmetin-7-*O*-glucoside (M0) and its three metabolites were detected in different human intestinal bacterial samples. Three metabolites were likely to be diosmetin-7-*O*-glucoside aglycone diosmetin (M1), acacetin (M2), and methylated and acetylated acacetin (M3). Considerable amounts of M1 and minor amounts of M2 were produced by the majority of the isolated intestinal bacterial strains such as *Escherichia* sp. 4. A small amount of M3 existed in the minority of the bacterial samples.

**Identification of the Diosmetin-7-*O*-glucoside Metabolites.** The retention time of diosmetin-7-*O*-glucoside (M0) was at 5.06 min, and its fragment ion was at $m/z$ 461 (Figure 2a). The precursor ion $[M - H]^-$ $m/z$ 461 afforded the diosmetin product ion at $m/z$ 299 by loss of the glucuronide group. Then, the $m/z$ 299 lost $CH_3$ to be $m/z$ 284. The $m/z$ 255 was generated from $m/z$ 284 by elimination of CO. The product ion at $m/z$ 151 was formed from the aglycone at $m/z$ 299 by the retro-Diels−Alder (RDA) cleavage (Figure 3a).

Metabolite M1 was detected as deprotonated molecular ion $[M - H]^-$ at $m/z$ 299 with the retention time at 8.10 min, which was 162 Da lower than that of M0 diosmetin-7-*O*-glucoside. It gave signals at $m/z$ 299, 284, 256, and 151. In the MS/MS spectrum of M1 are displayed similar product ions as M0 diosmetin-7-*O*-glucoside (Figure 2b). According to the MS/MS spectrum and the fragmentation regularity with standard diosmetin (Figure 3b), M1 was identified as the aglycone of diosmetin-7-*O*-glucoside, diosmetin.

The fragment ion of M2 (retention time, 9.53 min) was at $m/z$ 283 $[M - H]^-$. As illustrated in Figures 2c and 3c, the $m/z$ 283 lost $CH_3$ to give $m/z$ 268. The $m/z$ 268 was further fragmented to be $m/z$ 240 by the loss of CO. The $m/z$ 151 was obtained from $m/z$ 283 by RDA cleavage. Becausee M1 was 16 Da higher than M2, M2 was tentatively identified as dehydroxylated aglycone. Additionally, M2 was confirmed on the basis of its retention time and MS/MS spectrum compared with the standard of acacetin. Therefore, we concluded M2 was acacetin.

The characteristic fragment ion of M3 (Figure 2d) was at $m/z$ 339 $[M - H]^-$, which was 56 Da higher than that of M2, indicating the chemical structure of M3 could be the methylated and acetylated product of M2. According to the fragmentation pathway (Figure 3d), M3 lost $CH_2$ and $C_2H_2O$ to form $m/z$ 283. Then, $m/z$ 268 and 240 were obtained from $m/z$ 283 by the loss of $CH_3$ and $C_2H_3O$, respectively. The $m/z$ 151 was also obtained by RDA cleavage from $m/z$ 283. Thus, M3 was identified as the methylated and acetylated acacetin.

## DISCUSSION

The commercially available UPLC has proved to be one of the most promising recent developments in fast chromatographic separations. There has been substantial focus on UPLC separations with the objective of reducing analysis times while maintaining good efficiency. Additionally, the UPLC-Q-TOF/MS plays a crucial role in the study of drug metabolism because it can not only provide accurate masses of ions but also give valuable structural information from the MS/MS spectra.[24,25] According to the retention behaviors, changes of molecular weights, and MS/MS fragment patterns, the prototype and its metabolites can be tentatively identified.[27,28] Compared with the HPLC-MS technology, UPLC-MS significantly improves the repeatability and reliability of quantitative analysis as well as the accuracy of qualitative analysis.

On the basis of our experimental results, the metabolic pathways of diosmetin-7-*O*-glucoside by the isolated *Enterococci*, *Escherichia*, and *Bacillus* strains in vitro were proposed as shown in Figure 4. Diosmetin-7-*O*-glucoside in the human intestine might initially be involved in deglycosylation of the flavonoid glycoside by intestinal bacteria with β-D-glucosidase,

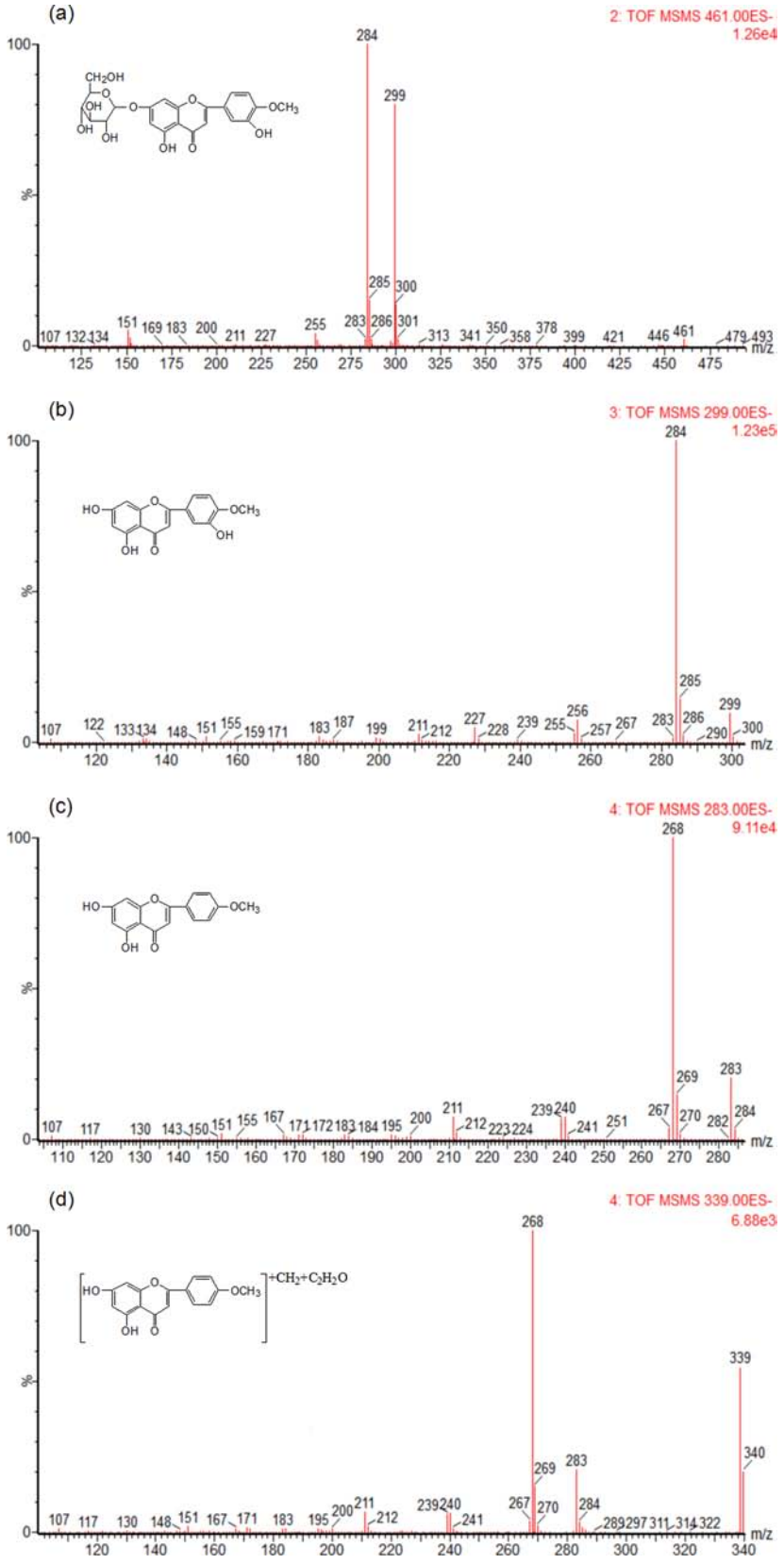


**Figure 2.** UPLC-MS/MS spectra: (a) M0 (*m*/*z* 461); (b) M1 (*m*/*z* 299); (c) M2 (*m*/*z* 283); (d) M3 (*m*/*z* 339).

and it was almost totally bioconverted to diosmetin, which thereafter could be further biocoverted to acacetin (M2). However, only a few intestinal bacteria such as *Escherichia* sp. 4 could produce methylated and acetylated acacetin (M3). An early study indicated that diosmetin could be reduced to its flavanone analogue hesperetin through reduction of the 2,3 double bond of the C-ring by intestinal bacterial enzymes.[29] However, the course of polyphenol degradation depended on


dx.doi.org/10.1021/jf502676j | *J. Agric. Food Chem.* 2014, 62, 11441−11448

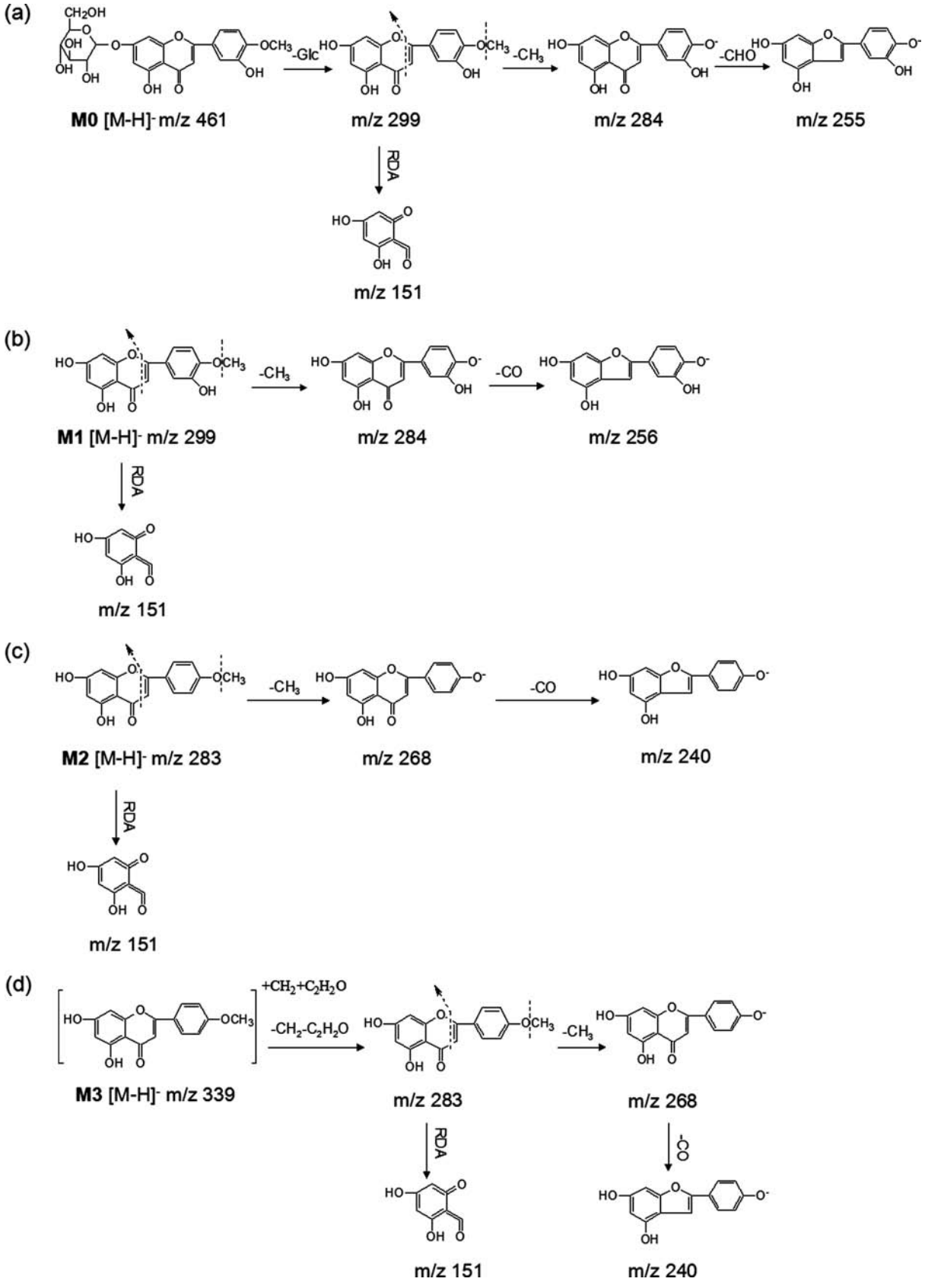


**Figure 3.** Proposed fragmentation pathways of M0−M3.

the type of bacteria in the gut,[30] and hydrogenation might not be a general feature of the intestinal microflora even though the bacteria were from the same strain. For example, quercetin could be hydrogenated to taxifolin by a *Clostridium orbiscindens* strain.[31] *Escherichia coli* HGH21 could bioconvert the isoflavone daidzin to daidzein and further metabolize the


dx.doi.org/10.1021/jf502676j | *J. Agric. Food Chem.* 2014, 62, 11441−11448

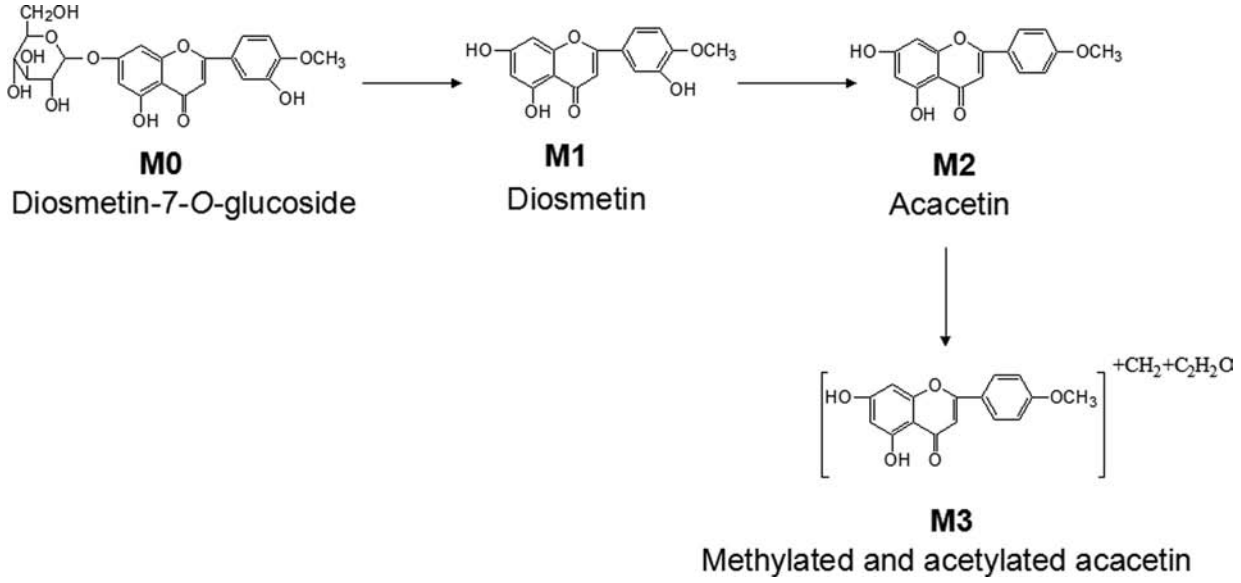


**Figure 4.** Proposed metabolic pathways of diosmetin-7-*O*-glucoside by the human intestinal bacteria.

isoflavone daidzein to dihydrodaidzein.[32] However, *Escherichia coli* JCM5491 did not convert daidzin to daidzein.[33] Therefore, it was speculated that the release of diosmetin improved diosmetin-7-*O*-glucoside bioavailability for absorption by colonic mucosa and/or further biotransformation to hesperetin by other human intestinal microorganisms. The removal of hydroxyl groups from aromatic rings and the acetylation of phenolic compounds might be exceptional metabolic activities. However, the conversion of phenolic compounds has been widely described in recent years.[34,35]

The human intestinal bacteria, classified as resident and transient flora, comprise a diversity of bacterial species and have excellent enzymatic systems contributing to their enormous catalytic and hydrolytic potential.[36] The factors influencing the flavonoids absorption in the gastrointestinal tract include deglycosylation before absorption, conjugation in the small intestine through glucuronidation, sulpfation or methylation, etc., and metabolism and degradation in the colon to smaller phenolic molecules by intestinal bacteria. The forms in which they circulate in vivo will influence their polarity and, thus, their localization and bioactivities.[37] Diosmetin commonly occurs in citrus species and olive leaves, shows significant antibacterial activity against drug-resistant *Staphylococcus aureus*,[38,39] and has the potential to suppress stem cell factor-/ultraviolet B-induced melanogenesis. Thus, it can be developed as an antipigmentation agent.[40] Diosmetin exhibits anticancer activity. It can inhibit tumor growth and protect tumor-induced apoptosis of the thymus[41] and shows significant cytotoxicities against colon cancer cell Colo205.[42] Additionally, diosmetin slightly inhibits superoxide anion generation or elastase release by human neutrophils, indicating moderate anti-inflammatory activity.[43] It can induce osteoblastic differentiation and is a promising agent for treating osteoporosis.[44] Diosmetin is one of the main active ingredients of some medications.[45] The metabolite acacetin can exert anti-inflammatory, anticancer, and antihypertension activities.[46,47] Deglycosylation is an important step in the absorption and metabolism of glycosides.[48−53] The absorption rate of aglycones is higher than that of their corresponding glycosides due to their higher lipophilicities and smaller molecular sizes.[54−56] Hence, the human intestinal bacteria play an important role in the pharmacological effects of diosmetin-7-*O*-glucoside in vivo.

As we know, the polarity of a compound might significantly affect its bioavailability. The polarity of flavonoid aglycones highly depends on the substitution of the three rings in their chemical structures. Flavonoids with methoxy groups on ring A or B are relatively nonpolar, which can protect them from extensive bacterial degradation.[57] The methoxy group is beneficial for the absorption if the dissolution is satisfactory.[58] Because the other intestinal bacteria might be also able to demeth(ox)ylate phenolic compunds, we speculated that the clinical effects of diosmetin-7-*O*-glucoside mainly resulted from diosmetin, which displayed stronger bioactivities and higher absorption rate than those of the parent compound in vivo. Although the metabolism results from our work might not fully reflect the interaction between human intestinal bacteria and medicines, it still could provide a good reference to study and understand the mechanism of the interaction.

## AUTHOR INFORMATION

### Corresponding Authors

*(S.J.) Phone/fax:+86 25 85811516. E-mail: jiangshu2000@163.com.

*(J.D.) Phone/fax: +86 25 85811116. E-mail: dja@njutcm.edu.cn.

### Funding

This work was financially supported by the National Basic Research Program of China (973 Program) (2011CB505300, 2011CB505303), the Nature Science Foundation of China (81072996, 81102743), Jiangsu Collaborative Innovation Center of Chinese Medicinal Resources Industrialization (ZDXM-1-10), and Construction Project for Jiangsu Key Laboratory for High Technology of TCM Formulae Research (BM2010576).

### Notes

The authors declare no competing financial interest.

## REFERENCES


(1) Patel, K.; Gadewar, M.; Tahilyani, V.; Patel, D. K. A review on pharmacological and analytical aspects of diosmetin: a concise report. *Chin. J. Integr. Med.* **2013**, *19*, 792−800.

(2) Gonzalez-Molina, E.; Moreno, D. A.; Garcia-Viguera, C. Genotype and harvest time influence the phytochemical quality of Fino lemon juice (*Citrus limon* (L.) Burm. F.) for industrial use. *J. Agric. Food Chem.* **2008**, *56*, 1669−1675.

(3) Lin, L. Z.; Chen, P.; Harnly, J. M. New phenolic components and chromatographic profiles of green and fermented teas. *J. Agric. Food Chem.* **2008**, *56*, 8130−8140.

(4) Cai, S. L.; Wu, Z.; Wu, J.; Wang, Q.; Shan, Y. Synthesis and biological activities of natural flavonoid diosmetin and its derivatives. *Chin. J. Org. Chem.* **2012**, *32*, 560−566.

(5) Chen, Z. J.; Kong, S. S.; Song, F. F.; Li, L. P.; Jiang, H. D. Pharmacokinetic study of luteolin, apigenin, chrysoeriol and diosmetin after oral administration of Flos Chrysanthemi extract in rats. *Fitoterapia* **2012**, *83*, 1616−1622.

(6) Jiang, H. D.; Cai, J.; Xu, J. H.; Zhou, X. M.; Xia, Q. Endothelium-dependent and direct relaxation induced by ethyl acetate extract from Flos Chrysanthemi in rat thoracic aorta. *J. Ethnopharmacol.* **2005**, *101*, 221−226.

(7) Rusu, M. A.; Tamas, M.; Puica, C.; Roman, I.; Sabadas, M. The hepatoprotective action of ten herbal extracts in CCl4 intoxicated liver. *Phytother. Res.* **2005**, *19*, 744−749.

(8) Bor, J. Y.; Chen, H. Y.; Yen, G. C. Evaluation of antioxidant activity and inhibitory effect on nitric oxide production of some common vegetables. *J. Agric. Food Chem.* **2006**, *54*, 1680−1686.

(9) Lii, C. K.; Lei, Y. P.; Yao, H. T.; Hsieh, Y. S.; Tsai, C. W.; Liu, K. L.; Chen, H. W. *Chrysanthemum morifolium* Ramat. reduces the oxidized LDL-induced expression of intercellular adhesion molecule-1 and E-selectin in human umbilical vein endothelial cells. *J. Ethnopharmacol.* **2010**, *128*, 213−220.

(10) Zhang, T.; Chen, D. Anticomplementary principles of a Chinese multiherb remedy for the treatment and prevention of SARS. *J. Ethnopharmacol.* **2008**, *117*, 351−361.

(11) Schmidt, M.; Scholz, C. J.; Gavril, G. L.; Otto, C.; Polednik, C.; Roller, J.; Hagen, R. Effect of *Galium verum* aqueous extract on growth, motility and gene expression in drug-sensitive and -resistant laryngeal carcinoma cell lines. *Int. J. Oncol.* **2014**, *44*, 745−760.

(12) Kim, D. H. Herbal medicines are activated by intestinal microflora. *Nat. Prod Sci.* **2002**, *8*, 35−43.

(13) Ley, R. E.; Hamady, M.; Lozupone, C.; Turnbaugh, P. J.; Ramey, R. R.; Bircher, J. S. Evolution of mammals and their gut microbes. *Science* **2008**, *320*, 1647−1651.

(14) Ley, R. E.; Peterson, D. A.; Gordon, J. I. Ecological and evolutionary forces shaping microbial diversity in the human intestine. *Cell* **2006**, *124*, 837−848.

(15) Xu, J.; Gordon, J. I. Honor thy symbionts. *Proc. Natl. Acad. Sci. U.S.A.* **2003**, *100*, 10452−10459.

(16) O'Hara, A. M.; Shanahan, F. The gut flora as a forgotten organ. *EMBO Rep.* **2006**, *7*, 688−693.

(17) Possemiers, S.; Bolca, S.; Verstraete, W.; Heyerick, A. The intestinal microbiome: a separate organ inside the body with the metabolic potential to influence the bioactivity of botanicals. *Fitoterapia* **2010**, *82*, 53−66.

(18) Serra, H.; Mendes, T.; Bronze, M. R.; Simplicio, A. L. Prediction of intestinal absorption and metabolism of pharmacologically active flavones and flavanones. *Bioorg. Med. Chem.* **2008**, *16*, 4009−4018.

(19) Wan, J. Y.; Liu, P.; Wang, H. Y.; Qi, L. W.; Wang, C. Z.; Li, P.; Yuan, C. S. Biotransformation and metabolic profile of American ginseng saponins with human intestinal microflora by liquid chromatography quadrupole time-of-flight mass spectrometry. *J. Chromatogr., A* **2013**, *1286*, 83−92.

(20) Chen, K. I.; Erh, M. H.; Su, N. W.; Liu, W. H.; Chou, C. C.; Cheng, K. C. Soyfoods and soybean products: from traditional use to modern applications. *Appl. Microbiol. Biotechnol.* **2012**, *96*, 9−22.

(21) Mei, M.; Ruan, J. Q.; Wu, W. J.; Zhou, R. N.; Lei, J. P.; Zhao, H. Y.; Yan, R.; Wang, Y. T. In vitro pharmacokinetic characterization of mulberroside A, the main polyhydroxylated stilbene in mulberry (*Morus alba* L.), and its bacterial metabolite oxyresveratrol in traditional oral use. *J. Agric. Food Chem.* **2012**, *60*, 2299−2308.

(22) Ruan, J. Q.; Leong, W. I.; Yan, R.; Wang, Y. T. Characterization of metabolism and in vitro permeability study of notoginsenoside R1 from Radix notoginseng. *J. Agric. Food Chem.* **2010**, *58*, 5770−5776.

(23) Guo, J. M.; Xue, C. F.; Shang, E. X.; Duan, J. A.; Tang, Y. P.; Qian, D. W. Identification of hyperoside metabolites in rat using ultra performance liquid chromatography/quadrupole-time-of-flight mass spectrometry. *J. Chromatogr., B* **2011**, *879*, 1987−1992.

(24) Han, H.; Yang, L.; Xu, Y.; Ding, Y.; Annie Bligh, S. W.; Zhang, T.; Wang, Z. T. Identification of metabolites of geniposide in rat urine using ultra-performance liquid chromatography time-of-flight tandem mass spectrometry. *Rapid Commun. Mass Spectrom.* **2011**, *25*, 3339−3350.

(25) Shen, J. Z.; Yang, C. Y.; Wu, C. M.; Feng, P. S.; Wang, Z. H.; Li, Y.; Li, Y. S.; Zhang, S. X. Identification of the major metabolites of quinocetone in swine urine using ultra-performance liquid chromatography/electrospray ionization quadrupole time-of-flight tandem mass spectrometry. *Rapid Commun. Mass Spectrom.* **2010**, *24*, 375−383.

(26) Yokoyama, S.; Niwa, T.; Osawa, T.; Suzuki, T. Characterization of an *O*-desmethylangolensin-producing bacterium isolated from human feces. *Arch. Microbiol.* **2010**, *192*, 15−22.

(27) Bourdon, F.; Lecoeur, M.; Verones, V.; Vaccher, C.; Lebegue, N.; Dine, T.; Kambia, N.; Goossens, J. F. *In vitro* pharmacokinetic profile of a benzopyridooxathiazepine derivative using rat microsomes and hepatocytes: identification of phases I and II metabolites. *J. Pharm. Biomed. Anal.* **2013**, *80*, 69−78.

(28) Brozinski, J. M.; Lahti, M.; Oikari, A.; Kronberg, L. Identification and dose dependency of ibuprofen biliary metabolites in rainbow trout. *Chemosphere* **2013**, *93*, 1789−1795.

(29) Spanakis, M.; Kasmas, S.; Niopas, I. Simultaneous determination of the flavonoid aglycones diosmetin and hesperetin in human plasma and urine by a validated GC/MS method: in vivo metabolic reduction of diosmetin to hesperetin. *Biomed. Chromatogr.* **2009**, *23*, 124−131.

(30) Bolca, S.; Van de Wiele, T.; Possemiers, S. Gut metabotypes govern health effects of dietary polyphenols. *Curr. Opin. Biotechnol.* **2013**, *24*, 220−225.

(31) Schoefer, L.; Mohan, R.; Schwiertz, A.; Braune, A.; Blaut, M. Anaerobic degradation of flavonoids by *Clostridium orbiscindens*. *Appl. Environ. Microbiol.* **2003**, *69*, 5849−5854.

(32) Hur, H. G.; Lay, J. O.; Beger, R. D.; Freeman, J. P.; Rafii, F. Isolation of human intestinal bacteria metabolizing the natural isoflavone glycosides daidzin and genistin. *Arch. Microbiol.* **2000**, *174*, 422−428.

(33) Ryota, T.; Seiichi, S.; Mitsuru, K.; Toshihiro, N.; Junei, K. Microbial metabolism of soy isoflavones by human intestinal bacterial strains. *J. Nat. Med.* **2008**, *62*, 456−460.

(34) Xue, C.; Jiang, S.; Guo, J.; Qian, D.; Duan, J. A.; Shang, E. Screening for *in vitro* metabolites of *Abelmoschus manihot* extract in intestinal bacteria by ultra-performance liquid chromatography/quadrupole time-of-flight mass spectrometry. *J. Chromatogr., B* **2011**, *879*, 3901−3908.

(35) Lu, L.; Qian, D.; Yang, J.; Jiang, S.; Guo, J.; Shang, E. X.; Duan, J. A. Identification of isoquercitrin metabolites produced by human intestinal bacteria using UPLC-Q-TOF/MS. *Biomed. Chromatogr.* **2013**, *27*, 509−514.

(36) Lee, J. E. S.; Sung, J.; Kol, G. Analysis of human and animal fecal microbiota for microbial source tracking. *ISME J.* **2011**, *5*, 362−365.

(37) Clavel, T.; Henderson, G.; Alpert, C. A.; Philippe, C.; Rigottier-Gois, L.; Dore, J.; Blaut, M. Intestinal bacterial communities that produce active estrogen-like compounds enterodiol and enterolactone in humans. *Appl. Environ. Microbiol.* **2005**, *71*, 6077−6085.

(38) Wang, S. Y.; Sun, Z. L.; Liu, T.; Gibbons, S.; Zhang, W. J.; Qing, M. Flavonoids from *Sophora moorcroftiana* and their synergistic antibacterial effects on MRSA. *Phytother. Res.* **2013**, DOI: 10.1002/ptr.5098.

(39) Chan, B. C.; Ip, M.; Gong, H.; Lui, S. L.; See, R. H.; Jolivalt, C.; Fung, K. P.; Leung, P. C.; Reiner, N. E.; Lau, C. B. Synergistic effects

of diosmetin with erythromycin against ABC transporter overexpressed methicillin-resistant *Staphylococcus aureus* (MRSA) RN4220/pUL5054 and inhibition of MRSA pyruvate kinase. *Phytomedicine* **2013**, *20*, 611−614.
(40) Lee, S. J.; Jung, T. H.; Kim, H.; Jeong, D.; Choi, G.; Park, W. K.; Kong, J. Y.; Jin, M. H.; Cho, H. Inhibition of c-Kit signaling by diosmetin isolated from *Chrysanthemum morifolium*. *Arch. Pharm. Res.* **2014**, *37*, 175−185.
(41) Zhao, R.; Chen, Z.; Jia, G.; Li, J.; Cai, Y.; Shao, X. Protective effects of diosmetin extracted from *Galium verum* L. on the thymus of U14-bearing mice. *Can. J. Physiol. Pharmacol.* **2011**, *89*, 665−673.
(42) Xie, Y. Y.; Yuan, D.; Yang, J. Y.; Wang, L. H.; Wu, C. F. Cytotoxic activity of flavonoids from the flowers of *Chrysanthemum morifolium* on human colon cancer Colo205 cells. *J. Asian Nat. Prod. Res.* **2009**, *11*, 771−778.
(43) Lin, A. S.; Lin, C. R.; Du, Y. C.; Lubken, T.; Chiang, M. Y.; Chen, I. H.; Wu, C. C.; Hwang, T. L.; Chen, S. L.; Yen, M. H.; Chang, F. R.; Wu, Y. C. Acasiane A and B and farnesirane A and B, diterpene derivatives from the roots of *Acacia farnesiana*. *Planta Med.* **2009**, *75*, 256−261.
(44) Hsu, Y. L.; Kuo, P. L. Diosmetin induces human osteoblastic differentiation through the protein kinase C/p38 and extracellular signal-regulated kinase 1/2 pathway. *J. Bone Miner. Res.* **2008**, *23*, 949−960.
(45) Poor, M.; Veres, B.; Jakus, P. B.; Antus, C.; Montsko, G.; Zrinyi, Z.; Vladimir-Knezevic, S.; Petrik, J.; Koszegi, T. Flavonoid diosmetin increases ATP levels in kidney cells and relieves ATP depleting effect of ochratoxin A. *J. Photochem. Photobiol. B* **2014**, *132*, 1−9.
(46) Kim, C.; Kim, M. C.; Kim, S. M.; Nam, D.; Choi, S. H.; Kim, S. H.; Ahn, K. S.; Lee, E. H.; Jung, S. H.; Ahn, K. S. *Chrysanthemum indicum* L. extract induces apoptosis through suppression of constitutive STAT3 activation in human prostate cancer DU145 cells. *Phytother. Res.* **2013**, *27*, 30−38.
(47) Senejoux, F.; Demougeot, C.; Kerram, P.; Aisa, H. A.; Berthelot, A.; Bevalot, F.; Girard-Thernier, C. Bioassay-guided isolation of vasorelaxant compounds from *Ziziphora clinopodioides* Lam. (Lamiaceae). *Fitoterapia* **2012**, *83*, 377−382.
(48) Nemeth, K.; Plumb, G. W.; Berrin, J. G.; Juge, N.; Jacob, R.; Naim, H. Y.; Williamson, G.; Swallow, D. M.; Kroon, P. A. Deglycosylation by small intestinal epithelial cell $\beta$-glucosidases is a critical step in the absorption and metabolism of dietary flavonoid glycosides in humans. *Eur. J. Nutr.* **2003**, *42*, 29−42.
(49) Tarko, T.; Duda-Chodak, A.; Zajac, N. Digestion and absorption of phenolic compounds assessed by in vitro simulation methods. A review. *Rocz. Panstw. Zakl. Hig.* **2013**, *64*, 79−84.
(50) Chen, Z.; Zheng, S.; Li, L.; Jiang, H. Metabolism of flavonoids in human: a comprehensive review. *Curr. Drug Metab.* **2014**, *15*, 48−61.
(51) Makarova, N. M. Bioavailability and metabolism of flavonoids. *Eksp. Klin. Farmakol.* **2011**, *74*, 33−40.
(52) Walle, T. Absorption and metabolism of flavonoids. *Free Radical Biol. Med.* **2004**, *36*, 829−837.
(53) Walle, T.; Browning, A. M.; Steed, L. L.; Reed, S. G.; Walle, U. K. Flavonoid glucosides are hydrolyzed and thus activated in the oral cavity in humans. *J. Nutr.* **2005**, *135*, 48−52.
(54) Izumi, T.; Piskula, M. K.; Osawa, S.; Obata, A.; Tobe, K.; Saito, M.; Kataoka, S.; Kubota, Y.; Kikuchi, M. Soy isoflavone aglycones are absorbed faster and in higher amounts than their glucosides in humans. *J. Nutr.* **2000**, *130*, 1695−1699.
(55) Wiczkowski, W.; Romaszko, J.; Bucinski, A.; Szawara-Nowak, D.; Honke, J.; Zielinski, H.; Piskula, M. K. Quercetin from shallots (*Alliumcepa* L. var. *aggregatum*) is more bioavailable than its glucosides. *J. Nutr.* **2008**, *138*, 885−888.
(56) Xue, C. F.; Guo, J. M.; Qian, D. W.; Duan, J. A.; Shu, Y. Absorption of flavonoids from Abelmoschus manihot extract by in situ intestinal perfusion. *Acta Pharm. Sinica* **2011**, *46*, 454−459.
(57) Wen, X.; Walle, T. Methylated flavonoids have greatly improved intestinal absorption and metabolic stability. *Drug Metab. Dispos.* **2006**, *34*, 1786−1792.
(58) Lin, Y. T.; Hsiu, S. L.; Hou, Y. C.; Chen, H. Y.; Chao, P. D. L. Degradation of flavonoid aglycones by rabbit, rat and human fecal flora. *Biol. Pharm. Bull.* **2003**, *26*, 747−751.

efficiency, smaller volume of organic solvents, simplicity of operation, simple and convenient equipment, and low cost per sample.[14] In recent years, modified QuEChERS methods for sample preparation with LC−MS/MS or GC−MS detection obtained high recoveries and reproducibility.[1,5,15−17] The above methods were approved and mainly employed in governments, food industry, and related laboratories, and much time was consumed because of complex procedures as well as the expensive cost. In the case of vegetables, the pesticide residue analysis was more different and difficult, corresponding to complex components in the matrix, and the pesticides sprayed were unknown during cultivation.

In this paper, different cleanup methods [primary secondary amine (PSA), multi-walled carbon nanotubes (MWCNTs), and polystyrene (PLS) as sorbents] based on QuEChERS sample preparation were evaluated for Chinese cabbage and cucumber. The analysis was carried out by tandem mass spectrometry within 10 min. The aim of this study was to develop rapid and robust analytical methods for the simultaneous extraction and determination of 238 pesticides in Chinese cabbage and cucumber.

## MATERIALS AND METHODS

**Chemicals and Reagents.** Most of the pesticide standards used in this work were purchased from Dr. Ehrenstorfer (Augsburg, Germany), Chem Service (West Chester, PA), and Fluka (Buchs, Germany), with the highest available purity. Some pesticide standards were generously provided by the Korean Food and Drug Administration. HPLC-grade acetonitrile, acetone, and methanol were obtained from Honeywell (Morristown, NJ). LC−MS-grade formic acid and ammonium formate were ordered from Fluka (Buchs, Germany). The DisQuE QuEChERS pouch as in the EN method 15662 sample preparation kit, was acquired from Waters (Milford, MA) and contained 4 g of anhydrous $MgSO_4$, 1 g of NaCl, 1.5 g of sodium citrate dehydrate, and 0.5 g of disodium citrate sesquihydrate. Dispersive solid-phase extraction (D-SPE) 5982-5021 was purchased from Agilent Technologies (Santa Clara, CA) and contained 25 mg of PSA and 150 mg of anhydrous $MgSO_4$. The 30 mg PSA cartridge column and 20 mg PLS cartridge column were purchased from Aisti Science (Wakayama, Japan). MWCNTs (15−20 nm) were purchased from Hanwha Nanotech (Seoul, Korea).

**Preparation of Standard Solutions.** Individual standard solutions were prepared in acetone, acetonitrile, or methanol with a concentration of approximately 1000 mg/L and stored at −20 °C. A working standard mixture was prepared by diluting each individual standard solution with methanol, to obtain a concentration of 10 mg/L for each compound. The linearity in the response was studied with standard solution prepared in both blank matrix extra and acetonitrile solvent.

**Sample Preparation.** Chinese cabbage (*Brassica rapa*) and cucumber (*Cucumis sativus*) were obtained as organic products from a Seoul local market in Korea, and no pesticide residue was detected in the vegetables. An approximately 200 g portion of sample was weighed and homogenized at 10 000 rpm for 1 min. A 10 g sample of homogenized Chinese cabbage (or cucumber) was weighed into a 50 mL Teflon centrifuge tube, followed by the addition of 10 mL of acetonitrile, and the tube was vigorously shaken for 1 min manually. A DisQuE QuEChERS pouch was added to each sample, which was then shaken again. The tube was centrifuged at 3500 rpm for 5 min at 4 °C after cooling on ice. Finally, the acetonitrile layer was prepared for the cleanup step.

**Sample Purification.** A total of 1 mL of the acetonitrile layer was transferred to a 2 mL microcentrifuge tube containing different sorbents, including D-SPE 5982-5021 containing 25 mg of PSA and 150 mg of $MgSO_4$ for method "A". A total of 2.5 mg of MWCNTs was added to the sorbent of method "A" as method "B". Only 10 mg of MWCNTs was used as the cleanup sorbent with D-SPE for method "C". The mixture was shaken vigorously for 2 min and centrifuged at 13 000 rpm for 2 min. Then, 400 μL of supernatant was transferred to an autosampler vial, followed by the addition of 100 μL of acetonitrile [0.5% (v/v) formic acid], and this was then filtered through a 0.2 μm polytetrafluoroethylene (PTFE) filter.

Moreover, the 30 mg PSA mini-cartridge column for method "D" and the 20 mg PLS mini-cartridge column for method "E" were also used for sample purification. The columns were preconditioned with 2 mL of acetone and activated with 2 mL of acetonitrile. After loading 1 mL of acetonitrile layer, the column was eluted with 1 mL of methanol [0.1% (v/v) formic acid] as the elution solvent. Then, the sample was dissolved in 1 mL of acetonitrile after evaporating the methanol, and 400 μL of solution was transferred to an autosample vial, to which 100 μL of acetonitrile [containing 0.5% (v/v) formic acid] was added for analysis.

**LC−MS/MS Analysis.** Triple quadrupole LC−MS/MS was a Shimadzu LCMS-8030 (Japan) equipped with an electrospray ionization (ESI) source, operating in positive and negative ionization modes. LC was carried out with two Shimadzu LC-30AD pumps (Japan), a Sil-30AC autosampler, a CTO-30AC column oven, and a CBM-20A controller. A Phenomenex Kinetex $C_{18}$ column (Phenomenex, Torrance, CA), 2.6 μm, 100 × 2.1 mm, was used. Nitrogen was used in the ion source and as the collision gas.

The LC−MS/MS system parameters were set as follows: flow rate, 0.5 mL/min; interface voltage, 4.5 kV; desolvation line temperature, 250 °C; nebulizing gas flow, 3 L/min; heat block temperature, 400 °C; performed gas flow, 15 L/min; and collision-induced ionization (CID) gas, 230 kPa. The temperature of the column was 40 °C, and a 10 μL amount of the sample extract was injected in each run.

**Mobile Phase.** Mobile phase A was water, and mobile phase B was methanol, both containing 5 mM ammonium formate and 0.1% (v/v) formic acid. The gradient program was as follows: 100% A (0% B) for 0.5 min from the start, ramped to 55% B linearly for 0.5 min, followed by a linear gradient up to 95% B over 7 min, and maintained for 2 min at 95% B. A constant flow rate of 0.5 mL/min was used, and the total running time was 10 min.

**Optimization of MS/MS Parameters.** The optimization of MS conditions was performed for each pesticide by introducing individual standard solutions directly into MS. The two most intense precursor ion−fragment ion transitions of each pesticide were chosen, and the optimal MS/MS parameters for all transitions were recorded. The final method was constructed on the basis of these data (see Table S1 of the Supporting Information).

**Matrix Effect Study.** Change of ionization efficiency in the presence of other compounds is call the matrix effect. An average matrix effect exceeding 25% is generally considered to significantly affect quantitative analytical results,[17,18] depending upon the relative standard deviation (RSD) values.

To an aliquot of blank extract in methanol, a pesticide mixture, 78% of the extract volume, was added. Matrix effect values were calculated for all samples using matrix-matched calibration and a methanol calibration slope with the following formula: ME (%) = $100 \times ((S_m/S_s) - 1)$, where ME is the matrix effect and $S_m$ and $S_s$ are the slopes of the calibration curves obtained in the matrix and methanol, respectively.

**Recovery Experiments.** A recovery study was performed by spiking each sample with a mixture of a working standard solution (10 mg/L) containing 238 pesticides to reach a final concentration of 8 and 40 μg/kg, and each spike level was repeated 3 times.

## RESULTS AND DISCUSSION

**LC−MS/MS Method Validation Using Standard Solutions.** The linearity of each pesticide in Chinese cabbage and cucumber samples was studied in the range of 1−200 μg/L with seven calibration points (1, 5, 10, 20, 50, 100, and 200 μg/L) by a matrix-matched standard calibration. Summary results are presented in Table S1 of the Supporting Information. These data indicated that the LC−MS/MS procedure had good linearity and high sensitivity. Approximately 96% of the

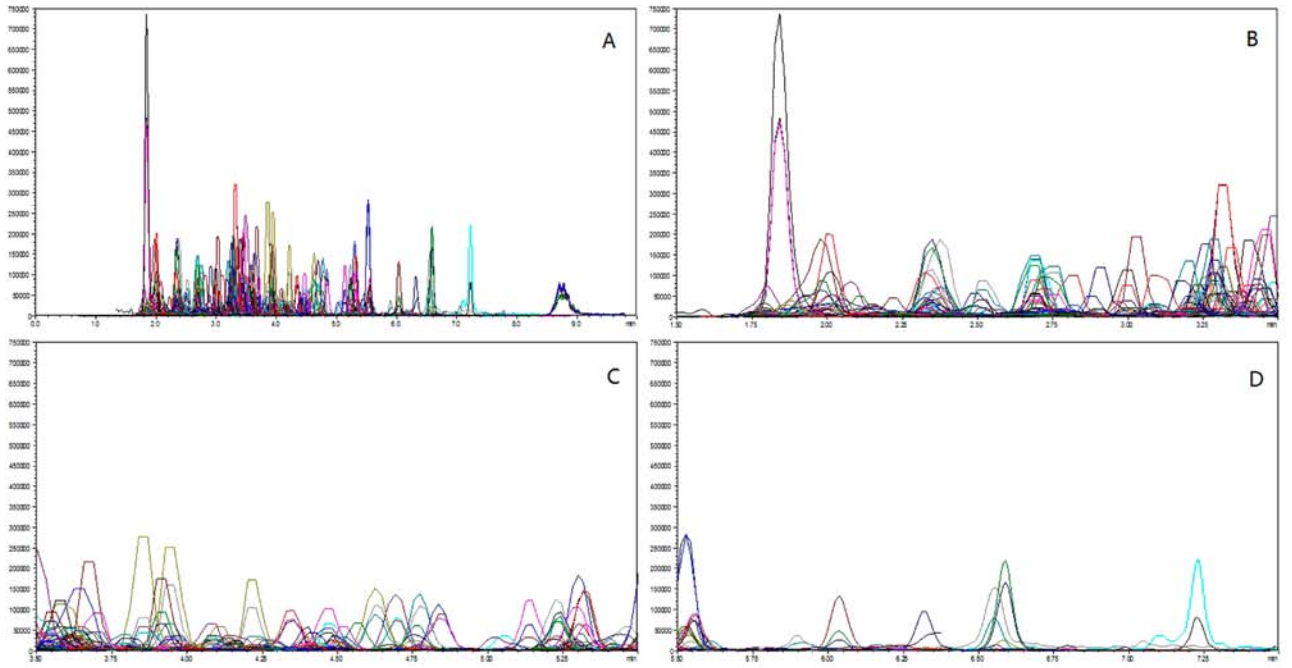


**Figure 1.** Chromatogram of 238 pesticides at a spiked level of 8 μg/kg in Chinese cabbage samples. The original chromatogram (A) was divided into panels B (1.5−3.5 min), C (3.5−5.5 min), and D (5.5−7.5 min) by running time.

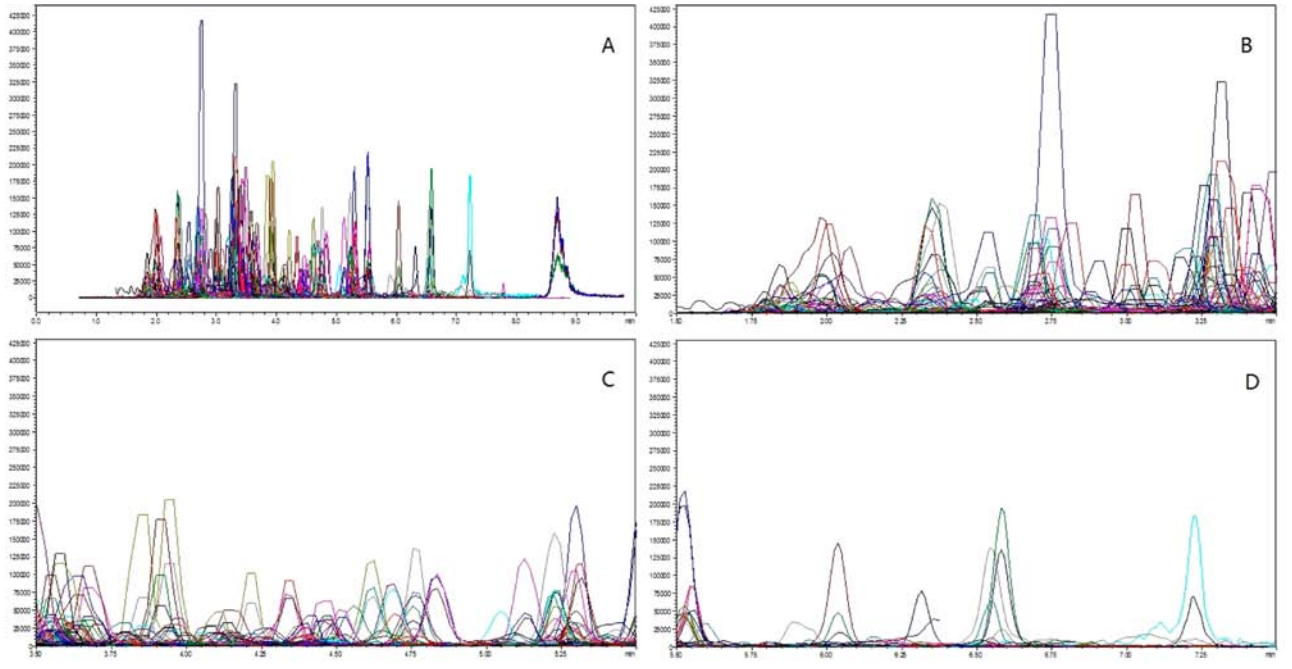


**Figure 2.** Chromatogram of 238 pesticides at a spiked level of 8 μg/kg in cucumber samples. The original chromatogram (A) was divided into panels B (1.5−3.5 min), C (3.5−5.5 min), and D (5.5−7.5 min) by running time.

pesticides (238 pesticides), in either the methanol or the matrix, analyzed by ESI in positive or negative mode, exhibited $r^2 \geq 0.99$ and a linear range from 1 to 200 μg/kg. For three pesticides, bentazone, fluoroxypyr, and trichlorfon, $r^2$ was less than 0.99 in both the methanol standard solution and the matrix solution. Seven pesticides, including boscalid, bromacil, cyazofamid, diafenthiuron, formothion, terbuthylazine, and triflumuron, showed $r^2 < 0.99$ in the Chinese cabbage matrix solution. In cucumber, seven pesticides, including bromacil, clothianidin, diafenthiuron, ethoxyquin, fludioxonil, formothion, and isoprothidane, had $r^2 < 0.99$ in the cucumber matrix solution.

In Chinese cabbage (see Table S2 of the Supporting Information), the limits of detection (LODs) for 211 of 238 pesticides were below 1 μg/kg, the LODs for 20 pesticides ranged between 1 and 2 μg/kg, and seven pesticides had LOD values above 2 μg/kg, including benthiavalicarb-isopropyl (2.15 μg/kg), fenpiclnoil (2.02 μg/kg), hexythiazox (2.92 μg/kg), malathion (2.02 μg/kg), orthosulfamuron (2.40 μg/kg), pyrazosulfuron-ethyl (2.00 μg/kg), and pyrazoxyfen (3.06 μg/


dx.doi.org/10.1021/jf504570b | J. Agric. Food Chem. 2014, 62, 11449−11456

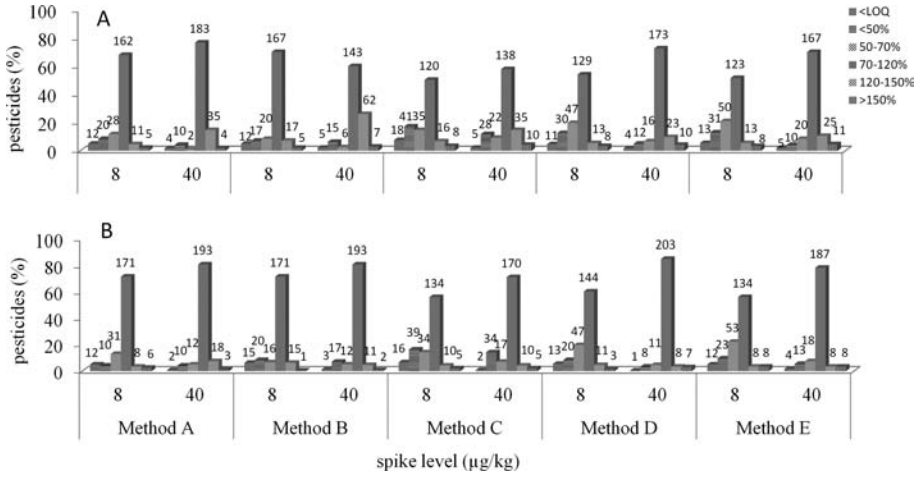


**Figure 3.** Percentage of pesticides within each recovery range with four different cleanup procedures by LC−MS/MS for the (A) Chinese cabbage and (B) cucumber samples. The number of pesticides is depicted above the bars.

kg). In the case of cucumber (see Table S3 of the Supporting Information), the LODs for 209 of 238 pesticides were below 1 μg/kg, the LODs for 17 pesticides ranged between 1 and 2 μg/kg, and 12 pesticides had LOD values above 2 μg/kg, containing bifenazate (4.69 μg/kg), boscalid (2.15 μg/kg), carbaryl (2.36 μg/kg), famoxadone (2.02 μg/kg), fipronil (2.30 μg/kg), hexythiazox (2.75 μg/kg), MCPA (2.04 μg/kg), mecarbam (2.02 μg/kg), metconazole (3.34 μg/kg), pyrazosulfuron-ethyl (4.04 μg/kg), tebuconazole (3.76 μg/kg), and triflumuron (6.32 μg/kg). There were no significant differences among the estimated instrument LOD values, which were calculated from the results obtained with standard solutions prepared with the matrix extract and solvent.

**Matrix Effect.** The matrix effect is very compound-dependent, often probably because of co-eluting matrix components, which interact with the pesticide in the ionization step in the interface.[6] Decreasing or increasing of the ion amount formed results in a corresponding positive or negative matrix effect, respectively.

The matrix effects were determined for 238 pesticides in two vegetables using five different cleanup methods at two concentration levels (8 and 40 μg/kg). The observed matrix effect values are presented in Table S1 of the Supporting Information. It could be concluded that the mean values of the matrix effect for 238 pesticides were 14.89 and 20.5% in Chinese cabbage and cucumber, respectively, which were less than 25%. However, 92 and 42 pesticides of the matrix effect values were still greater than 25% in two vegetables; it meant that there was a significant influence on quantitative detection that could not be ignored. Therefore, matrix-matched calibration curves were used for decreasing the influence of the matrix.

**Optimization of the Purification Procedure.** The recoveries and repeatability of the spiking experiments at the spiked levels of 8 and 40 μg/kg are listed in Tables S1 and S2 of the Supporting Information. The chromatograms are presented in Figures 1 and 2. Relevant histograms by five different cleanup steps with LC−MS/MS are shown in Figure 3.

Considerably higher recoveries were obtained when PSA D-SPE was applied in method "A". Recoveries of 183 and 193 of pesticides were in the range of 70−120% at a spiked level of 40 μg/kg in Chinese cabbage and cucumber, respectively (Table 1). The results were consistent with those presented in a former study, in which adequate recoveries were reported with the use of this method.[5,19−22] When PSA mini-cartridge column (method "D") replaced PSA D-SPE, as observed, the performance of method "D" reached the highest recoveries in cucumber; there was 203 pesticide recoveries in range of 70−120% (Table 2). In the case of Chinese cabbage, recoveries of method "D" were lower than those obtained in method "A"; 173 pesticide recoveries were in the range of 70−120% at a spiked level of 40 μg/kg.

The effect of MWCNTs (methods "B" and "C") for cleanup was investigated in target vegetables. 143 and 138 pesticide recoveries ranged from 70 to 120% at a spiked level of 40 μg/kg for Chinese cabbage, whereas 193 and 170 pesticide recoveries ranged from 70 to 120% at the same spiked level for cucumber. It meant that the lowest recoveries were achieved in method "C" (PSA sorbent was excluded) at a spiked level of 40 μg/kg in Chinese cabbage. Less acceptable recoveries were obtained using a PLS mini-cartridge column (method "E"); just 167 and 187 of the detected pesticide recoveries were in the acceptable range (70−120%) at a spiked level of 40 μg/kg in Chinese cabbage and cucumber, respectively.

On the basis of the above results in the recovery test, it could be concluded that the PSA D-SPE was the most suitable for Chinese cabbage and the PSA-mini cartridge column was the most suitable for cucumber out of the five investigated methods.

**Accuracy and Reproducibility Using Spiked Samples.** Both retention time and the presence of all ions in the correct ratio were necessary (see Table S1 of the Supporting Information)[23] for identification. In this study, there was no interference observed; the retention time and ion ratio should correspond to those obtained from a standard; and it showed good stability of relative selected reaction monitoring (SRM) responses.

From the recovery study, PSA D-SPE and PSA mini-cartridge column were selected as the best methods for matrix purification of Chinese cabbage and cucumber, respectively. The RSD results demonstrated that the methods were repeatable. In Chinese cabbage, 162 and 183 of the 238 pesticides in method "A" had recoveries in the range of 70−120% at the spiked levels of 8 and 40 μg/kg; the number of RSDs less than or equal to 10% was 84 and 139 pesticides; and

**Table 1. List of Pesticide Groups by Their Overall Recoveries with Method "A" at a Spiked Level of 40 μg/kg in Chinese Cabbage Samples**

| recovery | RSD | pesticides |
|---|---|---|
| <70% | | azimsulfuron, bifenazate, bioresmethrin, carboxin, ethaboxam (EBX), ethiofencarb, ethoxyquin, MCPA, mecoprop-*p*, nicosulfuron, quinmerac, penoxsulam, pyridalyl, sethoxydim, thifensulfuron-methyl, thiophanate-methyl (16) |
| 70−120% | <10% | acephate, alachlor, allethrin, atrazine, azinphos-ethyl, azoxystrobin, benthiavalicarb-isopropyl, benzoximate, bromobutide, buprofezin, butachlor, butocarboxim, cadusafos, carbendazim, carbofuran, carpropamid, chlorantraniliprole, chlorfenvinphos, chlorfluazuron, chlorpyrifos, chromafenozide, clofentezine, clomazone, clothianidin, cyflufenamid, cyproconazole, demeton-*S*-methyl, diazinon, diethofencarb, difenoconazole, dimepiperate, dimethametryn, dimethenamid, dimethoate, diniconazole, dinotefuran, diphenamid, disulfoton, emamectin benzoate, esprocarb, ethion, etofenprox, etoxazole, etrimfos, famoxadone, fenamidone, fenarimol, fenazaquin, fenothiocarb, fenoxanil, fenoxycarb, fenpiclnoil, fenpyroximate, fenthion, fentrazamide, fipronil, flonicamid, fluacrypyrim, fluazifop-butyl, flufenacet, flufenoxuron, fluopicolide, flusilazole, fosthiazate, furathiocarb, haloxyfop-*p*-methyl, hexazinore, hexythiazox, hydroxycarbofuran (3), imazalil, indoxacarb, iprobenfos, iprovalicarb, isofenphos, isoprothiolane, isoproturon, malathion, mepanipyrim, metalaxyl, metamifop, metconazole, methacrifos, methoxyfenozide, metolachlor, metrafenone, metribuzin, milbemectin-A3, monocrotophos, napropamide, norflurazon, omethoate, orysastrobin, oxadiazon, oxaziclomefone, pencycuron, permethrin, phosalone, piperophos, pirimiphos-ethyl, pirimiphos-methyl, prochloraz, propamocarb, propoxur, pymetrozine, pyraclofos, pyrazosulfuron-ethyl, pyrazoxyfen, pyrethrins, pyributicarb, pyridaben, pyriftalid, pyrimethanil, pyrimidifen, pyriproxyfen, quinoclamine, quizalofop-ethyl, simazine, simetryn, spinosad, tebufenozide, tebupirimfos, terbufos, terbutryn, thenylchlor, thiabendazole, thiacloprid, thiazopyr, thidiazuron, thiobencarb, thiodicarb, thiometon, triadimenol, triazophos, tricyclazole, triflumizole, triforine, 2,3,5-trimethacarb,3,4,5-trimethacarb, vamidothion (139) |
| | 10−20% | azinphos-methyl, bitertanol, bensulfuron-methyl, carbaryl, cyclosulfamuron, cymoxanil, cyprodinil, cyromazine, dichlofluanid, diphenylamine, ethoprophos, fenamiphos, fenbuconazole, fenobucarb, fenoxaprop-*p*-ethyl, fluazinam, flusulfamide, forchlorfenuron, halosulfuron-methyl, hexaconazole, imazosulfuron, imibenconazole, kresoxim-methyl, linuron, mandipropamid, mecarbam, mefenacet, methiocarb, metobromuron, mevinphos, ofurace, orthosulfamuron, pendimethalin, phenthoate, phorate, phosphamidone, phoxim, pirimicarb, probenazole, propanil, pyrazophos, pyriminobac-methyl (E.), tebuconazole, tebufenpyrad (44) |
| >120% | | acetochlor, anilofos, bendiocarb, bupirimate, cafenstrole, captan, coumaphos, dymron, diflubenzuron, dimethylvinphos, diuron, edifenphos, ethychlozate, fludioxonil, flutolanil, iprodione, isazofos, isoprocarb, lufenuron, mepronil, methabenzthiazuron, methidathion, methomyl, paclobutrazole, penconazole, procymidone, promecarb, prometryn, propachlor, pyraclostrobin, pyridaphenthion, pyroquilon, quinalphos, simeconazole, spirodiclofen, tetraconazole, thiamethoxam, triadimefon, zoxamide (39) |

**Table 2. List of Pesticide Groups by Their Overall Recoveries with Method "D" at a Spiked Level of 40 μg/kg in Cucumber Samples**

| recovery | RSD | pesticides |
|---|---|---|
| <70% | | bifenazate, bioresmethrin, barboxin, byromazine, demeton-*S*-methyl, dichlofluanid, diphenylamine, disulfoton, ethiofencarb, monocrotophos, phorate, propamocarb, propanil, pymetrozine, pyridalyl, pyrimethanil, sethoxydim, terbufos, thiophanate-methyl, thiometon (20) |
| 70−120% | <10% | acephate, acetochlor, alachlor, allethrin, anilofos, azinphos-ethyl, azinphos-methyl, bendiocarb, benthiavalicarb-isopropyl, bitertanol, bromobutide, bupirimate, butachlor, cadusafos, carbaryl, carbendazim, carbofuran, chlorantraniliprole, chlorfenvinphos, chlorfluazuron, chlorpyrifos, clofentezine, clomazone, coumaphos, cyproconazole, diethofencarb, difenoconazole, dimepiperate, dimethametryn, dimethenamid, dimethoate, dimethylvinphos, dinotefuran, diuron, dymron,edifenphos, esprocarb, ethion, ethoprophos, ethychlozate, etofenprox, etoxazole, etrimfos, fenamidone, fenamiphos, fenarimol, fenazaquin, fenobucarb, fenothiocarb, fenoxanil, fenoxaprop-*p*-ethyl, fenoxycarb, fenpyroximate, fipronil, fluacrypyrim, flufenoxuron, fluopicolide, forchlorfenuron, fosthiazate, halosulfuron-methyl, haloxyfop-*p*-methyl, hexazinore, hexythiazox, hydroxycarbofuran (3), imibenconazole, iprobenfos, iprodione, iprovalicarb, isazofos, isoproturon, kresoxim-methyl, linuron, malathion, mandipropamid, mefenacet, mepanipyrim, mepronil, metalaxyl, metamifop, metconazole, methabenzthiazuron, methacrifos, methidathion, methiocarb, methomyl, metobromuron, metolachlor, metrafenone, milbemectin-A3, omethoate, orysastrobin, oxadiazon, oxaziclomefone, paclobutrazole, penconazole, pencycuron, permethrin, phosalone, pirimicarb, pirimiphos-ethyl, probenazole, procymidone, promecarb, prometryn, propachlor, propoxur, pyraclofos, pyraclostrobin, pyrazophos, pyrazosulfuron-ethyl, pyrethrins, pyributicarb, pyridaben, pyridaphenthion, pyriftalid, pyrimidifen, pyriproxyfen, pyroquilon, quinmerac, quinoclamine, quizalofop-ethyl, simazine, simeconazole, simetryn, spinosad, tebufenozide, tebupirimfos, terbuthylazine, terbutryn, thenylchlor, thiabendazole, thiacloprid, thiamethoxam, thiazopyr, thidiazuron, thiobencarb, triadimenol, triazophos, triflumizole, 2,3,5-trimethacarb, 3,4,5-trimethacarb, vamidothion (142) |
| | 10−20% | atrazine, azoxystrobin, benzoximate, buprofezin, butocarboxim, cafenstrole, carpropamid, chromafenozide, cyflufenamid, cymoxanil, cyprodinil, diazinon, diflubenzuron, diniconazole, diphenamid, emamectin benzoate, ethaboxam (EBX), famoxadone, fenbuconazole, fenpiclnoil, fenthion, fentrazamide, flonicamid, fluazifop-butyl, fluazinam, flufenacet, flusilazole, flusulfamide, flutolanil, furathiocarb, hexaconazole, imazalil, indoxacarb, isofenphos, isoprocarb, lufenuron, MCPA, mecarbam, mecoprop-*p*, metribuzin, mevinphos, norflurazon, ofurace, pendimethalin, phenthoate, phosphamidone, phoxim, piperophos, pirimiphos-methyl, prochloraz, pyriminobac-methyl (E.), quinalphos, spirodiclofen, tebuconazole, tebufenpyrad, thiodicarb, napropamide, tricyclazole, triflumuron, triforine, zoxamide (61) |
| >120% | | azimsulfuron, bensulfuron-methyl, boscalid, captan, cyazofamid, cyclosulfamuron, imazosulfuron, methoxyfenozide, nicosulfuron, orthosulfamuron, penoxsulam, pyrazoxyfen, tetraconazole, thifensulfuron-methyl, triadimefon (15) |



dx.doi.org/10.1021/jf504570b | J. Agric. Food Chem. 2014, 62, 11449−11456

RSDs between 10 and 20% were 70 and 44 pesticides at the two spiked levels (Figure 4).

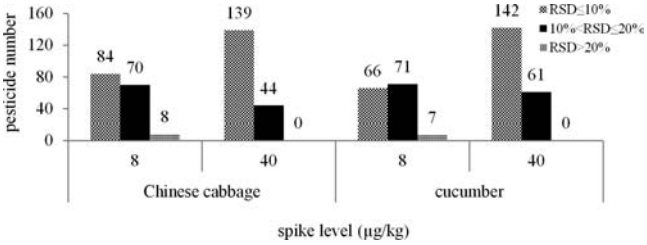


**Figure 4.** Repeatability of the optimization methods with a recovery in the range of 70−120%.

In the case of cucumber, 144 and 203 pesticides had acceptable recoveries at the spiked levels of 8 and 40 μg/kg in method "D", respectively, in which RSDs were less than or equal to 10% for 66 and 142 pesticides and RSDs of ≤20% were 137 and 203 pesticides at the two spiked levels. The results were satisfied with the selected purification method.

The limit of quantitation (LOQ), which is the lowest validated spike level with acceptable precision and sensitivity for all ions chosen for quantitation and identification, was between 0.16 and 10.20 μg/kg in Chinese cabbage and between 0.06 and 21.06 μg/kg in cucumber for the 238 pesticides.

The suitable methods were developed and validated using standards dissolved in methanol and proven to be rugged using matrix-matched standards of two samples. In general, Chinese cabbage and cucumber provided high matrix effects, showing greater dependence upon the cleanup procedure. During validation, the matrix effects were remarkable, although they could be compensated by the use of the matrix-matched calibration curves. In the case of Chinese cabbage, acceptable recoveries were achieved, except the methods containing MWCNTs. D-SPE using PSA removes acidic components, certain pigments, and to some extent sugars.[12,24] At the same time, freezing out removes most of the lipids, waxes, and sugars as well as other components with low solubility in acetonitrile that may negatively affect the robustness of the LC analysis.[12]

With regard to recovery values, the method containing excess MWCNTs (10 g) provided the lowest results. It can be ascertained that this sorbent combination was less efficient for the extraction of the selected pesticides from the investigated matrices. MWCNTs were used as the sorbent and obtained good results contributed to its high surface area, mechanical strength, and chemical stability.[25,26] The sorbent could adsorb many matrix components, such as primarily chlorophyll. It not only adsorbed the co-extractive matrix components but also the pesticides, especially those exhibiting planar ring structures. Therefore, when the matrix contained little pigment, MWCNTs could adsorb more analytes, resulting in low recoveries.

In cucumber, the percentage of pesticides ranging between 70 and 120% was higher than that in Chinese cabbage. It may be attributed to the different fatty acid contents of the vegetable, and the content of pigment in Chinese cabbage was more than that in cucumber.

In Chinese cabbage, method "A" was the best sorbent for purification, while method "D" was the most efficient for cucumber matrix purification. The validation results have shown acceptable recoveries and precision (RSDs of ≤20%) for most pesticides in the study. In general, when many pesticides were mixed together, they would influence each other and reduce the sensitivity. In this study, 238 pesticides were mixed, and acceptable results were obtained at a spiked level of 8 μg/kg, which was lower than others.[27,28] In recent years, pesticide residue limits were lower; the selected methods could meet the requirement of low multi-residue pesticide determination; and the high-resolution capacity of LC combined with the extremely short analysis time (10 min) offered a significant benefit for the determination of pesticide residues in vegetables.

The establishment of rapid and high-throughput detection methods for multi-residue pesticides in Chinese cabbage and cucumber samples solved the problem of complex pretreatment for grouping hundreds of pesticides and analyzing with different instruments; the procedure of sample preparation was reduced as well as the time and cost.

**Application of Real Chinese Cabbage and Cucumber Samples.** The developed methods were applied in routine analysis to Chinese cabbage and cucumber samples collected from local markets in Seoul. Among 15 Chinese cabbage samples, 3 have been proven to be chlorantraniliprole, of which the content was 0.21−0.31 mg/kg; methoxyfenozide was detected in 2 samples with the concentration ranging from 0.14 to 0.23 mg/kg; and iprovalicarb (0.22−0.36 mg/kg) and fluopicolide (0.04−0.12 mg/kg) were detected in 5 Chinese cabbage samples, as shown in Table 3. Among 14 cucumber samples, 2 have been proven to be thiacloprid, of which the content was 0.11−0.19 mg/kg, and ethaboxam was detected in 3 samples with the concentration ranging from 0.24 to 0.65 mg/kg (Table 3). Six of the detected pesticides, which were registered in Korea, were lower than their regulatory levels.

Two rapid and simple methods have been developed for the analyses of 238 pesticides in Chinese cabbage and cucumber prior to LC−MS/MS performance. Best recoveries were achieved with PSA D-SPE for cleanup in Chinese cabbage,

**Table 3. Analytical Results of Chinese Cabbage and Cucumber Real Samples**

| pesticide | number of samples | concentration range (mg/kg) | | LOD (μg/kg) | maximum residue limit (MRL) (mg/kg) |
|---|---|---|---|---|---|
| | | minimum | maximum | | |
| | | | Chinese Cabbage | | |
| chlorantraniliprole | 3 | 0.21 | 0.31 | 0.76 | 1.0 |
| methoxyfenozide | 2 | 0.14 | 0.23 | 0.36 | 2.0 |
| iprovalicarb | 2 | 0.22 | 0.36 | 0.19 | 0.7 |
| fluopicolide | 3 | 0.04 | 0.12 | 0.44 | 0.3 |
| | | | Cucumber | | |
| thiacloprid | 2 | 0.11 | 0.19 | 0.25 | 0.3 |
| ethaboxam | 3 | 0.24 | 0.65 | 0.42 | 2.0 |

and acceptable results were obtained by PSA mini-cartridge column in cucumber. The proposed methods have the advantage of detecting a large amount of pesticides in one single extraction and detection system, which is suitable for routine analysis and monitoring pesticides in Chinese cabbage and cucumber samples.

## ■ ASSOCIATED CONTENT

### Supporting Information

LC−MS/MS parameters, $r^2$, and matrix effects for the determination of 248 pesticides (Table S1) and LOD, average recoveries, and RSD obtained by LC−MS/MS in Chinese cabbage (Table S2) and cucumber (Table S3) samples. This material is available free of charge via the Internet at http://pubs.acs.org.

## ■ AUTHOR INFORMATION

### Corresponding Author

*Telephone: +86-532-8608-0523. Fax: +86-532-8608-0640. E-mail: zhuyzh@qau.edu.cn.

### Author Contributions

§Mei-Ai Zhao and Ya-Nan Feng contributed equally to this work.

### Funding

This study was carried out with the support from the Qingdao Municipal Science and Technology Commisson (Project 11-2-3-55-nsh), the Shandong National Science Foundation (Project ZR2011BM020), and the Initiating Fund of Qingdao Agricultural University (Project 630608), People's Republic of China.

### Notes

The authors declare no competing financial interest.

## ■ REFERENCES

(1) Pizzutti, I. R.; de Kok, A.; Zanella, R.; Adaimea, M. B.; Hiemstra, M.; Wickert, C.; Prestes, O. D. Method validation for the analysis of 169 pesticides in soya grain, without clean up, by liquid chromatography−tandem mass spectrometry using positive and negative electrospray ionization. *J. Chromatogr. A* **2007**, *1142*, 123−136.

(2) Sinha, S. N.; Rao, M. V. V.; Vasudev, K.; Odetokun, M. A liquid chromatography mass spectrometry-based method to measure organophosphorous insecticide, herbicide and non-organophosphorous pesticide in grape and apple samples. *Food Control* **2012**, *25*, 636−646.

(3) Hernández, F.; Pozo, O. J.; Sancho, J. V.; Bijlsma, L.; Barreda, M.; Pitarch, E. Multiresidue liquid chromatography tandem mass spectrometry determination of 52 non gas chromatography-amenable pesticides and metabolites in different food commodities. *J. Chromatogr. A* **2006**, *1109*, 242−252.

(4) Hetherton, C. L.; Sykes, M. D.; Fussell, R. J.; Goodall, D. M. A multi-residue screening method for the determination of 73 pesticides and metabolites in fruit and vegetables using high-performance liquid chromatography/tandem mass spectrometry. *Rapid Commun. Mass Spectrom.* **2004**, *18* (20), 2443−2450.

(5) Hiemstra, M.; Kok, A. Comprehensive multi-residue method for the target analysis of pesticides in crops using liquid chromatography−tandem mass spectrometry. *J. Chromatogr. A* **2007**, *1154*, 3−25.

(6) Jansson, C.; pihlstrom, T.; Osterdahl, B. G.; Markides, K. E. A new multi-residue method for analysis of pesticide residues in fruit and vegetables using liquid chromatography with tandem mass spectrometric detection. *J. Chromatogr. A* **2004**, *1023*, 93−104.

(7) Alder, L.; Greulich, K.; Kempe, G.; Vieth, B. Residue analysis of 500 high priority pesticides: Better by GC−MS or LC−MS/MS. *Mass Spectrom. Rev.* **2006**, *25*, 838−865.

(8) Pang, G. F.; Fan, C. L.; Liu, Y. M.; Cao, Y. Z.; Zhang, J. J.; Li, X. M.; Li, Z. Y.; Wu, Y. P.; Guo, T. T. Determination of residues of 446 pesticides in fruits and vegetables by three-cartridge solid-phase extraction/gas chromatography−mass spectrometry and liquid chromatography−tandem mass spectrometry. *J. AOAC Int.* **2006**, *89* (3), 740−771.

(9) Pang, G. F.; Fan, C. L.; Liu, Y. M.; Cao, Y. Z.; Zhang, J. J.; Fu, B. L.; Li, X. M.; Li, Z. Y.; Wu, Y. P. Multi-residue method for the determination of 450 pesticide residues in honey, fruit juice and wine by double-cartridge solid-phase extraction/gas chromatography−mass spectrometry and liquid chromatography−tandem mass spectrometry. *Food Addit. Contam.* **2006**, *23* (8), 777−810.

(10) Fuentes, E.; Baez, M. E.; Quinones, A. A suitability of microwave-assisted extraction coupled with solid-phase extraction for organo-phosphorus pesticide determination in olive oil. *J. Chromatogr. A* **2008**, *1207*, 38−45.

(11) Jiang, Y.; Li, Y.; Jiang, Y.; Li, J.; Pan, C. Determination of multiresidues in rapeseed, rapeseed oil, and rapeseed meal by acetonitrile extraction, low-temperature cleanup, and detection by liquid chromatography with tandem mass spectrometry. *J. Agric. Food Chem.* **2012**, *60*, 5089−5098.

(12) Anastassiades, M.; Lehotay, S. J.; Stajnbaher, D.; Schenck, F. J. Fast and easy multiresidue method employing acetonitrile extraction/partitioning and "dispersive solid-phase extraction" for the determination of pesticide residues in produce. *J. AOAC Int.* **2003**, *86*, 412−431.

(13) Anastassiades, M.; Maštovská, K.; Lehotay, S. J. Evaluation of analyte protectants to improve gas chromatographic analysis of pesticides. *J. Chromatogr. A* **2003**, *1015*, 163−184.

(14) Lehotay, S. J.; Son, K. A.; Kwon, H.; Koesukwiwat, U.; Fu, W. S.; Mastovska, K.; Hoh, E. Comparison of QuEChERS sample preparation methods for the analysis of pesticide residues in fruits and vegetables. *J. Chromatogr. A* **2010**, *1217*, 2548−2560.

(15) Hayward, D. G.; Wong, J. W.; Zhang, K.; Chang, J.; Shi, F.; Banerjee, K.; Yang, P. Multiresidue pesticide analysis in ginseng and spinach by nontargeted and targeted screening procedures. *J. AOAC Int.* **2011**, *94*, 1741−1751.

(16) Morales, A.; Ruiz, I.; Oliva, J.; Barba, A. Determination of sixteen pesticides in peppers using high-performance liquid chromatography/mass spectrometry. *J. Environ. Sci. Health, Part B* **2011**, *46*, 525−529.

(17) Polgár, L.; Kmellár, B.; García-Reyesb, J. F.; Fodor, P. Comprehensive evaluation of the clean-up step in QuEChERS procedure for the multi-residue determination of pesticides in different vegetable oils using LC−MS/MS. *Anal. Methods* **2012**, *4*, 1142−1148.

(18) Zrostlíková, J.; Hajšlová, J.; Godula, M.; Maštovská, K. Performance of programmed temperature vaporizer, pulsed splitless and on-column injection techniques in analysis of pesticide residues in plant matrices. *J. Chromatogr. A* **2001**, *937*, 73−86.

(19) Takatori, S.; Okihashi, M.; Okamoto, Y.; Kitagawa, Y.; Kakimoto, S.; Murata, H.; Sumimono, T.; Tanaka, Y. A rapid and easy multiresidue method for the determination of pesticide residues in vegetables, fruits, and cereals using liquid chromatography/tandem mass spectrometry. *J. AOAC Int.* **2008**, *91*, 871−883.

(20) Tian, Y. Y.; Liu, X. G.; Dong, F. S.; Xu, J.; Lu, C. H.; Kong, Z. Q. Simultaneous determination of aminopyralid, clopyralid, and picloram residues in vegetables and fruits using ultra-performance liquid chromatography/tandem mass spectrometry. *J. AOAC Int.* **2012**, *95*, 554−559.

(21) Zhang, F. Z.; Li, Y. J.; Yu, C. S.; Pan, C. P. Determination of six neonicotinoid insecticides residues in spinach, cucumber, apple and pomelo by QuEChERS method and LC−MS/MS. *Bull. Environ. Contam. Toxicol.* **2012**, *88*, 885−890.

(22) Zhang, K.; Wong, J. W.; Yang, O. P.; Tech, O. K.; DiBenedetto, A. L.; Lee, N. S. Multiresidue pesticide analysis of agricultural commodities using acetonitrile salt-out extraction, dispersive solid-phase sample clean-up, and high-performance liquid chromatography−tandem mass spectrometry. *J. Agric. Food Chem.* **2011**, *59*, 7636−7646.

(23) Stajnbaher, D.; Zupancic-Kralj, L. Multiresidue method for determination of 90 pesticides in fresh fruits and vegetables using solid-phase extraction and gas chromatography−mass spectrometry. *J. Chromatogr. A* **2003**, *1015*, 185−198.
(24) Rai, S.; Mukherjee, K.; Mal, M.; Wahile, A.; Saha, B. P.; Mukherjee, P. K. Determination of 6-gingerol in ginger (*Zingiber officinale*) using high-performance thin-layer chromatography. *J. Sep. Sci.* **2006**, *29*, 2292−2295.
(25) Zhao, P. Y.; Wang, L.; Jiang, Y. P.; Zhang, F. Z.; Pan, C. P. Dispersive cleanup of acetonitrile extracts of tea samples by mixed multiwalled carbon nanotubes, primary secondary amine, and graphitized carbon black sorbents. *J. Agric. Food Chem.* **2012**, *60*, 4026−4033.
(26) Zhao, P. Y.; Wang, L.; Luo, J. H.; Li, J. G.; Pan, C. P. Determination of pesticide residues in complex matrices using multiwalled carbon nanotubes as reversed-dispersive solid-phase extraction sorbent. *J. Sep. Sci.* **2012**, *35*, 153−158.
(27) Lee, S. W.; Choi, J. H.; Cho, S. K.; Yu, H. A.; El-Aty, A. M. A.; Shim, J. H. Development of a new QuEChERS method based on dry ice for the determination of 168 pesticides in paprika using tandem mass spectrometry. *J. Chromatogr. A* **2011**, *1218*, 4366−4377.
(28) Nguyen, T. D.; Yu, J. E.; Lee, D. M.; Lee, G. H. A multiresidue method for the determination of 107 pesticides in cabbage and radish using QuEChERS sample preparation method and gas chromatography mass spectrometry. *Food Chem.* **2008**, *110*, 207−213.

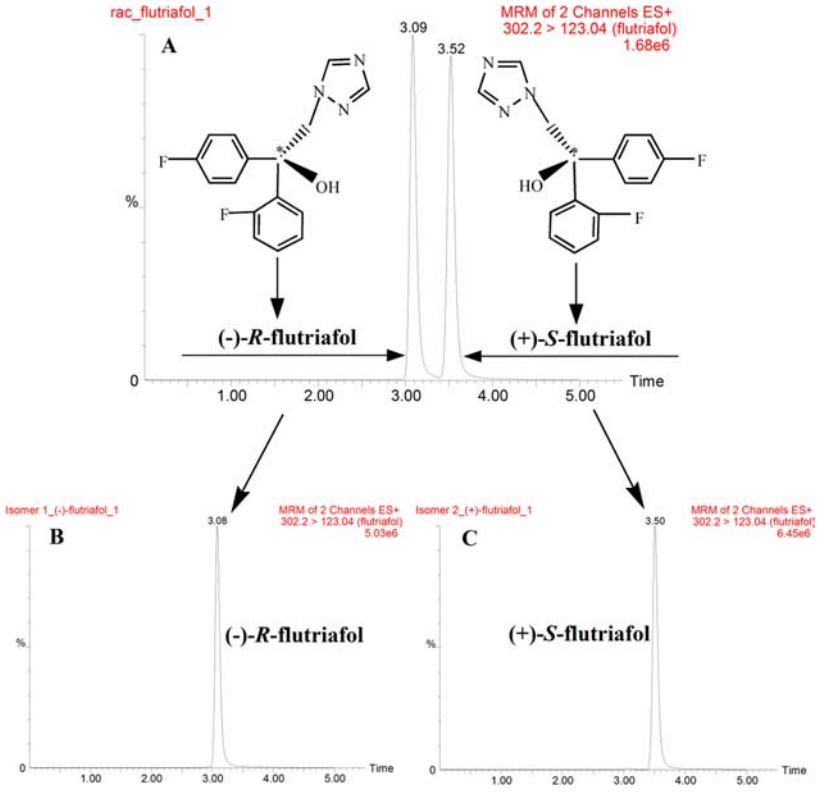


**Figure 1.** SFC-MS/MS chromatograms for the separation of flutriafol enantiomers on an IA-3 chiral column: (A) structures of the enantiomers of flutriafol and chromatogram of racemic flutriafol; (B) SFC-MS/MS chromatogram of (−)-*R*-flutriafol; (C) SFC-MS/MS chromatogram of (+)-*S*-flutriafol. ∗, chiral center.

residue analytical method for the accurate monitoring of trace information on flutriafol at the enantiomer level.

In this paper, the supercritical fluid (carbon dioxide, $CO_2$), which is nontoxic and nonreactive, exhibits various advantages. Featured by its low viscosity and high diffusivity, $CO_2$ contributes greatly to improve the separation efficiency, shorten the analysis time, and save labor cost. Moreover, the study adopted a postcolumn polar solvent compensation technology, which turned out to be a good solution to low ionization efficiency existing in the combination of supercritical fluid chromatography (SFC) with mass spectrometry (MS). Meanwhile, the influences of different parameters on the resolution and sensitivity were investigated and optimized. Besides, the adoption of QuEChERS (quick, easy, cheap, effective, rugged, and safe) methodology greatly simplified the sample preparation procedure. Therefore, a green, rapid, and sensitive analytical method for the determination of flutriafol enantiomers in vegetables, fruits, and soil was successfully established based on the SFC-MS/MS technique. In comparison with a previous paper,[23] the established method exerted obvious advantages in terms of solvent consumption, analysis time, and sensitivity. Furthermore, it had been used for the determination of flutriafol enantiomers in authentic samples. The result confirms that the proposed effective analytical method is environmentally friendly, convenient, and reliable in the detection of flutriafol enantiomers in food and environmental samples, which will facilitate further studies on the difference of individual enantiomers in toxicity, metabolism, and environmental fate.

## MATERIALS AND METHODS

**Chemicals and Reagents.** Racemic flutriafol (98.2% purity) was obtained from China Standard Material Center (Beijing, China). HPLC grade acetonitrile (ACN) was purchased from Sigma-Aldrich (Steinheim, Germany). Analytical grade NaCl, $MgSO_4$, and ACN were purchased from Beihua Fine-Chemicals Co. (Beijing, China). Ultrapure water was obtained from a Milli-Q system (Bedford, MA, USA). Sorbents including PSA (40 μm), C18 (40 μm), and GCB (40 μm) were obtained from Agela Technologies Inc. (Beijing, China). The mobile phase solvents were distilled and filtered through a 0.22 μm pore size filter membrane (Tengda, Tianjin, China) before use.

Standard stock solutions (100 mg/L) of racemic flutriafol were prepared in pure ACN and serially diluted to 5, 10, 50, 100, 500, and 1000 μg/L for flutriafol (2.5, 5, 25, 50, 250, and 500 μg/L of each enantiomer) with ACN. All solutions were wrapped with aluminum foil and stored in a refrigerator in the dark at −20 °C. The working standard solutions underwent no degradation for 3 months.

**SFC-MS/MS.** A Waters Acquity UPC$^2$ system (Milford, MA, USA) consisting of the Acquity UPC$^2$ binary solvent manager, the Acquity UPC$^2$ sample manager, the Acquity UPC$^2$ PDA detector, the auto back pressure regulator (ABPR), and the Waters compensation pump, was used for the separation of analytes. A Chiralpak IA-3 (150 mm × 4.6 mm i.d., Daicel, Japan) column with 3 μm particle size was used for the separation of the enantiomers of chiral flutriafol.

The enantiomeric analysis of flutriafol was performed using the Chiralpak IA-3 column after injection of a 1 μL volume standard working solution. The separation was carried out isocratically using solvent A ($CO_2$) and solvent B (methanol) in an 88:12 (v/v) ratio and at a 2.2 mL/min flow rate for 5 min. The temperatures of the column and sample manager were kept at 30 and 25 °C, respectively. The ABPR 2200 psi was selected, and the flow rate of compensation solution was 0.1 mL/min.

The parameters, including capacity factor ($k$), separation factor ($\alpha$), and resolution (Rs), were calculated from the formula $k = (t - t_0)/t_0$, $\alpha = k_2/k_1$, Rs $= 2(t_2 - t_1)/(W_1 + W_2)$, where $t_0$ is the void time at


dx.doi.org/10.1021/jf504324t | J. Agric. Food Chem. 2014, 62, 11457−11464

given conditions ($t_0$ = 0.85 min, determined using 1,3,5-yri*tert*-butylbenzene), $t$ is the retention time, $k$ is the retention factor, and $W$ is the baseline peak width.

The qualitative and quantitative analysis of flutriafol was conducted on a Xevo triple-quadrupole (Xevo-TQD) mass spectrometer (Waters Corp.) equipped with an electrospray ionization (ESI) source. The analyses were performed in the positive mode with a 3.5 kV capillary voltage, 150 °C source temperature, and 500 °C desolvation temperature. A 50 L/h cone gas flow and a 900 L/h desolvation gas flow were used. The nebulizer gas was 99.95% nitrogen, and the collision gas was 99.99% argon with a pressure of $2 \times 10^{-3}$ mbar in the T-Wave cell. MassLynx NT v. 4.1 (Waters, USA) software was used to collect and analyze the data obtained.

MS analyses were performed in the multiple reaction monitoring (MRM) mode, measuring the fragmentation of the protonated pseudomolecular ions of flutriafol. The monitoring conditions were optimized for flutriafol. A dwell time of 130 ms per ion pair was used to maintain the high sensitivity of the analysis, and a number of data points across the chromatographic peak were required. Typical conditions were as follows: the cone voltage of flutriafol was 24 V; $m/z$ 302.2 was selected as the precursor ion for flutriafol, $m/z$ 123.04 for its product quantitative ion, and $m/z$ 70.05 for its qualitative ion when the collision energy was set at 28 and 58 V. Under the conditions above, the retention times of (−)-*R*-flutriafol and (+)-*S*-flutriafol were approximately 3.08 and 3.50 min, respectively (Figure 1). These settings were utilized for all subsequent studies.

**Sample Preparation.** Tomato, cucumber, apple, grape, and soil (sandy loam) samples from trial plots were obtained from the Institute of Plant Protection (Haidian region, Beijing). These five matrices were not contaminated by the target analyte. The food samples were placed in polyethylene bags, then transported to the laboratory and stored in the dark at −20 °C until analysis. The soil samples were collected at depths of 0−30 cm at 15 randomly selected points. Afterward, the soil samples were air-dried at room temperature, homogenized, and passed through a 2 mm sieve. The treated samples were kept in the dark until analysis.

Approximately 300 g of blank samples (tomato, cucumber, apple, and grape) were homogenized in an Ultra-Turrax homogenizer (IKA-Werke, Staufen, Germany). Next, 10 g aliquots of the homogenized samples including soil (dry weight) were placed into 50 mL polypropylene centrifuge tubes with screw caps. Appropriate amounts of the working standard solutions were added to the blank samples to perform recovery studies. Then the samples were vortexed for 30 s and allowed to stand for 2 h at room temperature to be evenly distributed. Afterward, 10 mL of ACN (additional 5 mL $H_2O$ for soil) was added. After the tubes were vortexed for 3 min, 1 g of NaCl and 4 g of anhydrous $MgSO_4$ were added to the mixtures. These mixtures were vortexed for another 3 min. Subsequently, the tubes were centrifuged for 5 min at a relative centrifugal force (RCF) of 2811*g* with an effective radius of 13.5 cm. Then, 1.5 mL of the upper layer (ACN) was transferred to a single-use centrifuge tube containing 40 mg of PSA and 10 mg of GCB (whereas a single sorbent of 50 mg of C18 was used for the soil matrix) and 150 mg of anhydrous $MgSO_4$. The tubes were vortexed again for 30 s and centrifuged for 5 min at RCF of 2400*g* with an effective radius of 6.5 cm. The resulting supernatant was filtered using a 0.22 μm nylon syringe filter into an autosampler vial for chromatography injection. The comparative analysis of different sorbents will be discussed in a later section.

**Method Validation.** The developed method was validated according to a conventional validation procedure that included the following parameters: specificity, linearity, limits of detection (LODs) and quantification (LOQs), matrix effect, accuracy, precision, and stability.

For each matrix, 10 g of the blank samples was extracted and analyzed to verify the absence of any interfering species at retention times similar to the target analytes. The standard solutions and different matrix-matched standard solutions were analyzed in triplicate with the concentrations ranging from 5.0 to 1000 μg/L to determine the linearity of the method. The parameters of the linear regression equations, including the slopes, intercepts, standard deviations, and correlation coefficients ($R^2$), were calculated. The matrix-induced signal suppression/enhancement (SSE) was expressed as the slope ratio of the matrix-matched calibration curve/pure solvent calibration curve.

The LODs and LOQs were defined as the concentrations that produced signal-to-noise (S/N) ratios of 3 and 10, respectively. The matrix-dependent LOD and LOQ of the developed method were estimated using spiked samples (tomato, cucumber, apple, grape, and soil) at the lowest fortification level (10 μg/kg).

The accuracy and precision of the method were investigated by performing recovery assays. Five replicates of the spiked samples (tomato, cucumber, apple, grape, and soil) at three levels (10, 100, and 500 μg/kg) were prepared on three different days. The precision in the repeatability and reproducibility, expressed as the relative standard deviation (RSD), were determined from the intraday and interday assays.

The stability of the stock solutions (both in the solvent and in the matrix) was determined monthly by injecting a freshly prepared working solution. The stabilities of the spiked samples (100 μg/kg) with flutriafol were evaluated monthly. All of the samples used for stability detection were stored at −20 °C. The results of the stability tests were compared with those obtained from the freshly prepared sample using Student's $t$ test ($P < 0.05$).

## RESULTS AND DISCUSSION

**Optimization of Enantioseparation Conditions.** *Composition of the Mobile Phase.* To achieve excellent separation for flutriafol enantiomers on the IA-3 chiral column, different compositions of mobile phases were investigated. Comparative analysis assays were conducted, selecting methanol, ACN, 2-propanol, and mixtures of ACN and 2-propanol in varied proportions as modifier. Results showed that flutriafol enantiomers gave worse peak shape when ACN was selected as modifier, whereas the retention times for flutriafol enantiomers were all delayed, the first peak exceeding 5.5 min with the existence of 2-propanol. The reason is that methanol is a hydrogen-bond donor and acceptor, but ACN is just a weak hydrogen-bond acceptor. The chiral recognition process might be the joint interactions including hydrogen bonding between −OH on flutriafol and −NH on chiral stationary phase (CSP);[5,22] thus, with methanol as modifier, it exhibited stronger interactions and better peak shape than ACN. As for 2-propanol, there might be two aspects accounting for the delay of retention of flutriafol enantiomers. On the one hand, the polarity of 2-propanol is less than that of methanol, so the latter has stronger interactions with the polar action sites on CSP and was more easily recognized by CSP. On the other hand, 2-propanol possesses larger spatial volume than methanol, which is frustrated in the process of being recognized by CSP. Comparatively, methanol was more capable of separating flutriafol enantiomers. The effects of percentage of methanol on the retention and resolution are shown in Table 1. When methanol content increased from 6 to 15%, the retention time (RT) of flutriafol enantiomers was gradually shortened, and Rs was gradually decreased, whereas $\alpha$ remained almost unchanged. Thus, $CO_2$/methanol (88:12, v/v) was chosen as the mobile phase because of the relatively better resolution (2.40) and shorter retention (2.95, 3.32 min) (Figure 2). It exhibits an approximately 6-fold reduction in the retention time compared with a previous study.[23]

*Flow Rate of the Mobile Phase.* On the basis of the mobile phase of $CO_2$/methanol (88:12, v/v), the effects of flow rate of the mobile phase became another consideration. It was found that different flow rates of mobile phase gave rise to the change of retention time and resolution. As shown in Figure 2A, the

**Table 1. Effects of Percentage of $CO_2$ and Methanol on the Enantioseparation of Flutriafol, Concerning the Retention Time (RT), Separation Factor ($\alpha$), and Resolution (Rs)[a]**

| percentage in mobile phase (%) | | | RT | | | |
|---|---|---|---|---|---|---|
| $CO_2$ | methanol | total | (−)-*R*-flutriafol | (+)-*S*-flutriafol | $\alpha$ | Rs |
| 85 | 15 | 100 | 2.37 | 2.65 | 1.18 | 2.06 |
| 88 | 12 | 100 | 2.95 | 3.32 | 1.18 | 2.40 |
| 90 | 10 | 100 | 3.50 | 3.98 | 1.18 | 2.61 |
| 92 | 8 | 100 | 4.61 | | | |
| 94 | 6 | 100 | | | | |

[a]Flow rate, 2.2 mL/min; temperature, 30 °C; ABPR, 2200 psi; flow rate of compensation solvent (1% formic acid/methanol), 0.1 mL/min.

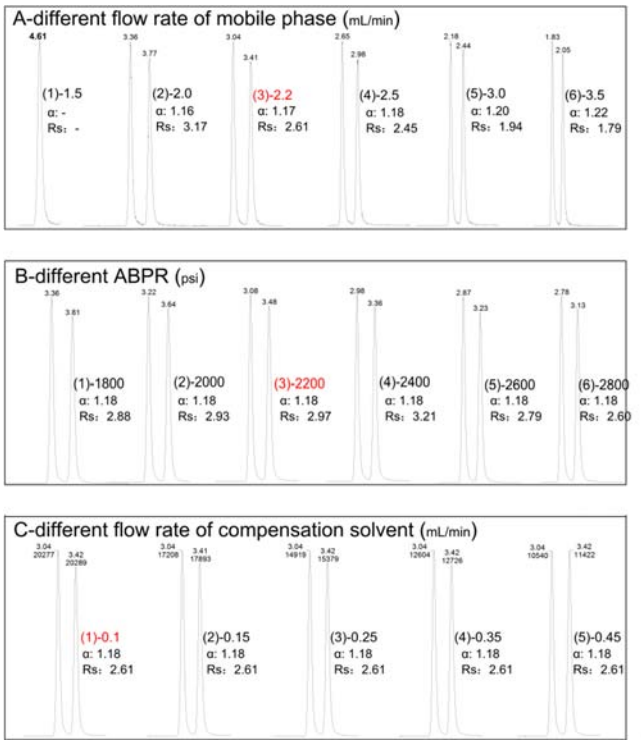


**Figure 2.** Comparison of effects of different parameters (A, flow rate of mobile phase; B, ABPR; and C, flow rate of compensation solvent) on the enantioseparation of flutriafol enantiomers, concerning the retention time (RT), separation factor ($\alpha$), resolution (Rs), and peak areas.

RT for flutriafol enantiomers was gradually shortened; meanwhile, Rs was lowered as the flow rate of the mobile phase increased from 1.5 to 3.5 mL/min. The effect of the flow rate of the mobile phase on resolution is due to changes in efficiency. That is relatively complicated in the SFC system because of the density gradient of the mobile phase along the column, which changes a lot as the flow rate varies. With better resolution (2.61) and relatively centered retention time (3.04, 3.41 min), the flow rate of 2.2 mL/min was selected for further study.

*ABPR Pressure.* The ABPR settings affect retention time by changing the density of the mobile phase before the release of pressure. To evaluate the effect of pressure on chromatographic separation for flutriafol enantiomers, ABPR was stepwise increased from 1800 (124 bar) to 2800 psi (193 bar) with 200 psi increments. The increase in ABPR resulted in a decrease in retention time and an increase in resolution, especially when it was below 2400 psi, but it had no impact on separation factor (Figure 2B). However, higher pressure is of no benefit to the usage lifetime of the chiral columns according to the instructions. Comprehensive consideration, 2200 psi, resulting in shorter retention and better resolution, was selected.

*Flow Rate of the Compensation Pump Solvent.* The pump was provided with compensation solution, commonly used 1% formic acid/methanol, which could improve ionization intensity to some extent. Efforts were made to investigate the effects of different flow rates of the compensation pump solvent in the range of 0.1−0.45 mL/min on resolution, retention, and peak area. Figure 2C shows that an increase in the flow rate had no influence on the retention and resolution of flutriafol enantiomers, but the peak areas for flutriafol enantiomers gradually decreased as the flow rate increased. That is because increased flow rate of compensation solvent results in a decrease of the amount of active ingredients that entered into the mass spectrum. Hence, for those compounds with low sensitivity, it is better to appropriately lower the flow rate to obtain higher signal response values. Less organic solvent and higher peak area made 0.1 mL/min the obvious choice in this experiment.

*Column Temperature.* Column temperature has been one of the important factors for optimization of chiral separations.[5,22,24,25] In this study, the chiral separation for flutriafol enantiomers was conducted with stepwise increases of column temperature from 30 to 40 °C under supercritical fluid state with 5 °C increments. The influence of temperature on the chiral separation of flutriafol enantiomers was relatively slight. It turned out that an increase in column temperature resulted in long retention and better resolution, which is the opposite of what was found in a previous HPLC study.[26] That is ascribed to the fact that as the column temperature increases, followed by decreases in the mobile phase density and reductions in the solvating power of mobile phase, the retention of analytes increases.[27] Therefore, the supercritical fluid can never be treated as normal state, such as liquid or gas, and should be given further investigation in later study. Considering the short retention time and relatively better separation, 30 °C was selected as the optimal temperature in this experiment.

**Elution Order of Flutriafol Enantiomers.** The two optically pure isomers of flutriafol were methodically collected by preparative chromatography. Then optical rotation of each isomer was determined on the basis of the same instrument conditions as in a previous study.[22] Each single isomer and racemic flutriafol were individually subjected to SFC-MS/MS determination under the same chromatographic conditions as mentioned in the above section. It turned out that the elution order of flutriafol was (−)-*R*-flutriafol and (+)-*S*-flutriafol in this study, respectively (Figure 1), which is exactly the same as in previous research using normal-phase liquid chromatography (NPLC).[8]

**Optimization of Cleanup Sorbents.** QuEChERS methodology, involving a streamlined procedure prior to sample analysis, has been widely employed because of its outstanding merits including simplicity, high throughput, and lower costs.[28−31] In this work, the effects of different types of sorbents on recovery and purification in different matrices were evaluated. Five types of sorbents for vegetables and fruits were investigated, including PSA (50 mg), C18 (50 mg), GCB (30 mg), and two kinds of sorbent mixtures (40 mg of PSA + 10

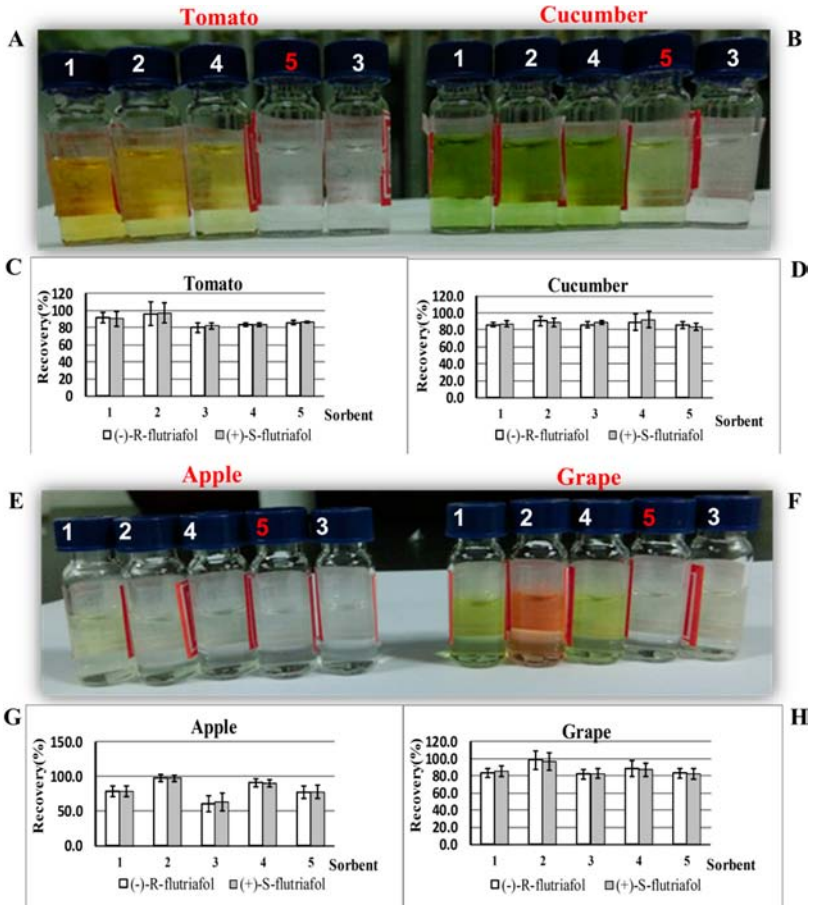


**Figure 3.** Effects of different sorbents on recoveries for flutriafol enantiomers (C, tomato; D, cucumber; G, apple; and H, grape) and purification performances in different matrices (A, tomato; B, cucumber; E, apple; and F, grape) at 100 $\mu$g/kg level ($n$ = 5). Sorbents 1, 2, 3, 4, 5, and 6 refer to 50 mg of PSA, 50 mg of C18, 30 mg of GCB, 40 mg of PSA + 10 mg of C18, and 40 mg of PSA + 10 mg of GCB, respectively. The number on the cap of each vial represents the corresponding sorbent.

**Table 2. Comparison of Matrix-Matched Calibration and Solvent Calibration with All of the Ranges at 2.5−500 $\mu$g/L for Each Enantiomer**

| enantiomer | matrix | regression equation | $R^2$ | slope ratio[a] (matrix/ACN) | matrix effect[b] (%) | LOD ($\mu$g/kg) | LOQ ($\mu$g/kg) |
|---|---|---|---|---|---|---|---|
| (−)-*R*-flutriafol | acetonitrile | $Y = 99.6X - 911.7$ | 0.999 | | | 0.35 | 1.18 |
| | tomato | $Y = 161.2X + 1418$ | 0.999 | 1.62 | 61.8 | 0.23 | 0.76 |
| | cucumber | $Y = 173.1X + 1056$ | 0.999 | 1.74 | 73.7 | 0.16 | 0.53 |
| | apple | $Y = 177.2X + 101.5$ | 1.000 | 1.78 | 77.8 | 0.12 | 0.41 |
| | grape | $Y = 194.2X + 736.3$ | 0.999 | 1.95 | 94.9 | 0.20 | 0.66 |
| | soil | $Y = 191.3X + 9096$ | 1.000 | 1.92 | 92.0 | 0.22 | 0.73 |
| (+)-*S*-flutriafol | acetonitrile | $Y = 97.5X - 852.4$ | 0.999 | | | 0.27 | 0.91 |
| | tomato | $Y = 176.8X + 1437.3$ | 0.999 | 1.81 | 81.4 | 0.18 | 0.58 |
| | cucumber | $Y = 201.8X + 1497.7$ | 0.999 | 2.07 | 107.1 | 0.17 | 0.56 |
| | apple | $Y = 173.1X + 1056$ | 1.000 | 1.78 | 77.6 | 0.16 | 0.52 |
| | grape | $Y = 166.5X + 342.5$ | 0.999 | 1.71 | 70.8 | 0.25 | 0.83 |
| | soil | $Y = 196.2X + 307.7$ | 0.999 | 2.01 | 101.3 | 0.18 | 0.61 |

[a]Slope ratio = matrix/ACN. [b]Matrix effect (%) = ((slope matrix − slope solvent)/slope solvent) × 100.

mg of C18 and 40 mg of PSA + 10 mg of GCB). Considering the particular characteristics of soil, four types of sorbents were made for a comparison, 40 mg PSA, 50 mg PSA, 50 mg C18, and 20 mg GCB. The influence of different sorbents on recoveries for flutriafol enantiomers and purification effects is shown in Figure 3.

As illustrated in Figure 3C,D,G,H, for vegetables and fruits, almost all tested types of sorbents exhibited satisfactory recoveries except for sorbent 3 (30 mg of GCB) applied to apple (G) with a recovery of approximately 60%. However, from Figure 3A,B,E,F, the purifying performance visually observed by the color varied with sorbents, and sorbents 5 (40 mg of PSA + 10 mg of GCB) and 3 (30 mg of GCB) exerted better cleanup effects compared with other sorbents for tomato, cucumber, and grape. Although treatment with sorbent 2 showed best recoveries, the purifying performance was not so


dx.doi.org/10.1021/jf504324t | J. Agric. Food Chem. 2014, 62, 11457−11464

**Table 3. Intraday and Interday Precision and Accuracy Results**

| | | intraday ($n$ = 5) | | | | interday ($n$ = 3) | | | |
|---|---|---|---|---|---|---|---|---|---|
| | | (−)-*R*-flutriafol | | (+)-*S*-flutriafol | | (−)-*R*-flutriafol | | (+)-*S*-flutriafol | |
| matrix | spike level ($\mu$g/kg) | recovery (%) | RSD[a,b] (%) | recovery (%) | RSD[a,b] (%) | recovery (%) | RSD[b,c] (%) | recovery (%) | RSD[b,c] (%) |
| tomato | 5 | 86.9 | 3.5 | 87.0 | 3.3 | 89.2 | 7.8 | 90.8 | 8.5 |
| | 50 | 85.5 | 2.6 | 86.3 | 0.9 | 83.9 | 4.3 | 85.0 | 2.7 |
| | 250 | 84.6 | 2.4 | 84.3 | 2.1 | 86.0 | 5.6 | 88.4 | 6.5 |
| cucumber | 5 | 90.2 | 2.6 | 92.7 | 2.9 | 87.6 | 7.1 | 86.8 | 8.6 |
| | 50 | 85.7 | 4.0 | 83.7 | 3.9 | 89.5 | 6.3 | 87.6 | 8.2 |
| | 250 | 88.6 | 6.9 | 90.4 | 7.6 | 94.6 | 3.7 | 86.9 | 7.7 |
| apple | 5 | 83.7 | 6.2 | 86.0 | 5.7 | 84.5 | 3.3 | 89.1 | 3.8 |
| | 50 | 77.2 | 9.6 | 77.8 | 9.5 | 81.1 | 6.4 | 83.2 | 4.8 |
| | 250 | 86.7 | 2.0 | 84.9 | 2.2 | 92.2 | 8.2 | 87.7 | 3.7 |
| grape | 5 | 82.1 | 5.9 | 80.3 | 6.6 | 93.9 | 7.6 | 80.0 | 5.3 |
| | 50 | 83.1 | 5.4 | 82.2 | 6.4 | 85.9 | 2.8 | 78.0 | 8.3 |
| | 250 | 84.8 | 2.1 | 87.5 | 4.1 | 86.1 | 2.3 | 85.9 | 5.1 |
| soil | 5 | 89.9 | 3.1 | 89.3 | 2.1 | 92.2 | 5.0 | 86.2 | 1.6 |
| | 50 | 87.8 | 3.8 | 87.2 | 2.6 | 96.4 | 7.3 | 85.8 | 2.4 |
| | 250 | 91.8 | 6.9 | 91.4 | 6.3 | 98.9 | 4.2 | 90.6 | 4.1 |

[a]RSD, relative standard deviation. [b]Intraday ($n$ = 5). [c]Interday ($n$ = 3).

good. Sorbent 3 exhibited an excellent cleanup effect, but poor recovery appeared in the treatment of apple matrix. Taking all of the factors into consideration, sorbent 5 (both satisfactory recoveries and purifying effect) was selected for vegetables and fruits. As for soil, all four tested types of sorbents exhibited satisfactory recoveries (78.9−95.8%). Comparatively, 50 mg of C18, the cheapest one, was chosen as the optimal sorbent. Compared with a previous paper,[23] it exhibits an approximately 6-fold reduction in terms of organic solvent consumption in the sample pretreatment procedure.

**Method Validation.** *Specificity and Linearity.* Blank samples of different matrices were applied to evaluate the specificity of the presented method, and no interference occurred at the retention time. Linear regression analysis was performed with the concentration range at 2.5−500 $\mu$g/L for each enantiomer. The standard solution and matrix-matched calibration curves (acetonitrile, tomato, cucumber, apple, grape, and soil) for each enantiomer are summarized in Table 2, including the slopes, intercepts, and coefficients of determination ($R^2$). Excellent linearities were observed for two enantiomers ($R^2 \geq 0.9990$ in all cases).

*LODs, LOQs, and Matrix Effect.* In this work, the LODs for both enantiomers were estimated at 0.12−0.35 $\mu$g/kg, whereas the corresponding LOQs were 0.41−1.18 $\mu$g/kg based on five replicated extractions and analyses of five spiked samples at low concentration levels. More than 40-fold sensitivity enhancement of the method was obtained compared with a previous study.[23] As is well-known, the occurrence of matrix effects is regarded as a major drawback in the analysis of pesticide residues in complex samples by liquid chromatography−mass spectrometry (LC-MS).[32] In the present study, the matrix effect was investigated in tomato, cucumber, apple, grape, and soil by comparing the standards in the solvent with the matrix-matched standards. It was considered to be a strong effect of signal suppression or enhancement when the values of matrix effects were below −50% or above +50%.[33] Data in Table 2 indicate strong signal enhancement for flutriafol enantiomers in five matrices with the slope ratios of matrix/ACN in a range of 1.62−2.07, and the matrix effects were between 61.8 and 107.1%. In this study, a calibration was performed for flutriafol enantiomers using external matrix-matched standards to eliminate the matrix effect to obtain more accurate and realistic results for all samples.

*Accuracy, Precision, and Stability.* Each blank sample matrix was spiked with racemic flutriafol at three concentration levels (10, 100, and 500 $\mu$g/kg) and then analyzed in quintuplicate. The precision and accuracy were expressed by the RSD (%) and the recovery (%) of spiked samples, respectively. The repeatability RSD[a] was calculated by comparing the standard deviation of recoveries of spiked samples injected on the same day (intraday). The reproducibility RSD[b] was measured by analyzing the standard deviation of recoveries of spiked samples injected on three different days (interday). As shown in Table 3, the method presented satisfactory recoveries (77.2−98.9%) and precision, with all RSDs below 9.6% at the three spiked concentration levels. For (+)-*S*-flutriafol, the intraday and interday recoveries for all five samples were 77.8−92.7 and 78.0−90.8%, with 0.9−9.5% RSD[a] (intraday RSD) and 1.6−8.6% RSD[b] (interday RSD), respectively, whereas they were 77.2−91.8% with 2.0−9.6% RSD[a] (intraday RSD) and 81.8−98.9% with 2.3−12.6% RSD[b] (interday) for (−)-*R*-flutriafol. In general, RSD[a] ($n$ = 5) ranged from 0.9 to 9.6% and RSD[b] ($n$ = 3) from 1.6 to 8.2%. Therefore, it is concluded that the proposed method and the SFC-MS/MS enantioselective analysis can achieve satisfactory accuracy and precision for the enantiomeric analysis in tomato, cucumber, apple, grape, and soil.

The stability of the stock solutions was tested monthly by injection of a newly prepared working standard solution. The spiked samples (tomato, cucumber, apple, grape, and soil, 100 $\mu$g/kg) for flutriafol were evaluated monthly, and all of the samples used in the stability test were stored at −20 °C. The

final results of the stability tests showed that no significant difference was observed ($P > 0.05$) during the solvent and matrix storage treatment as described under Materials and Methods.

*Application to Real Samples.* To ascertain its applicability, the validated SFC-MS/MS method was applied to analyze five kinds of matrix samples obtained from our residual trial field (Langfang, China, collected at 2 h after spaying commercial flutriafol formulation (25% flutriafol suspending agent at the dose of 225 g ai/hm$^2$) and local market (Beijing, China). Neither enantiomer of flutriafol was detected in all samples from the local market. (−)-*R*-Flutriafol and (+)-*S*-flutriafol in tomato, cucumber, apple, grape, and soil samples from the trial field were detected in the concentrations of 56.3 ± 3.1 and 57.4 ± 4.0, 86.5 ± 5.2 and 86.8 ± 3.9, 101.2 ± 6.7 and 102.1 ± 5.9, 130.4 ± 9.0 and 131.1 ± 8.4, and 109.8 ± 8.6 and 109.3 ± 7.8 μg/kg, respectively.

In this work, upon the primary evaluation of the SFC-MS/MS technique, a novel and rapid quantitative method for flutriafol enantiomers in tomato, cucumber, apple, grape, and soil has been established and validated. On the basis of the QuEChERS method, target compounds were extracted and purified and then analyzed using the chiral SFC-MS/MS in the ESI$^+$ mode. This work provides a novel and green chiral analytical method for the determination of flutriafol enantiomers in plants and environmental matrices. Importantly, the combination of SFC with MS greatly improves the sensitivity compared with previous research on flutriafol enantiomers. With good mean recoveries, excellent linearities, and satisfactory accuracy and precision, it could be selected as a suitable qualitative and quantitative alternative compared to existing complex and time-consuming methods. This rapid method facilitates further studies of the environmental behavior of each enantiomer of flutriafol and will finally help minimize the risks posed by this fungicide to humans, animals, and the environment.

## AUTHOR INFORMATION


### Corresponding Authors

*(F.D.) Phone: +86 10 62815938. Fax: +86 10 62815938. E-mail: dongfengshou@caas.cn.

*(Y.Z.) E-mail: zhengyongquan@ippcaas.cn.



### Funding

This work was financially supported by the National Natural Science Foundation of China (31272071).


### Notes

The authors declare no competing financial interest.

## ABBREVIATIONS USED

PSA, primary−secondary amine; GCB, graphitized carbon black; SSE, signal suppression/enhancement; RT, retention time; ABPR, auto back pressure regulator; UPC$^2$, ultra-performance convergence chromatography; SFC, supercritical fluid chromatography; MRM, multiple reaction monitoring; MS, mass spectrometry; ESI, electrospray ionization; CSP, chiral stationary phase

## REFERENCES


(1) Manclús, J. J.; Moreno, M. J.; Plana, E.; Montoya, Á. Development of monoclonal immunoassays for the determination of triazole fungicides in fruit juices. *J. Agric. Food Chem.* **2008**, *56*, 8793−8800.

(2) Sanagi, M. M.; See, H. H.; Ibrahim, W. A. W.; Naim, A. A. High temperature liquid chromatography of triazole fungicides on polybutadiene-coated zirconia stationary phase. *J. Chromatogr., A* **2004**, *1059*, 95−101.

(3) Konwick, B. J.; Garrison, A. W.; Avants, J. K.; Fisk, A. T. Bioaccumulation and biotransformation of chiral triazole fungicides in rainbow trout (*Oncorhynchus mykiss*). *Aquat. Toxicol.* **2006**, *80*, 372−381.

(4) Wu, Y. S.; Lee, H. K.; Li, S. F. Y. High-performance chiral separation of fourteen triazole fungicides by sulfated β-cyclodextrin-mediated capillary electrophoresis. *J. Chromatogr., A* **2001**, *912*, 171−179.

(5) Zhou, Y.; Li, L.; Lin, K. D.; Zhu, X. P.; Liu, W. P. Enantiomer separation of triazole fungicides by high-performance liquid chromatography. *Chirality* **2009**, *21*, 421−427.

(6) Crofton, K. M. A structure-activity relationship for the neurotoxicity of triazole fungicides. *Toxicol. Lett.* **1996**, *84*, 155−159.

(7) Ghauch, A. Rapid removal of flutriafol in water by zero-valent iron powder. *Chemosphere* **2008**, *71*, 816−826.

(8) Shen, Z. G.; Zhang, P.; Xu, X. Y.; Wang, X. R.; Zhou, Z. Q.; Liu, D. H. Gender-related differences in stereoselective degradation of flutriafol in rabbits. *J. Agric. Food Chem.* **2011**, *59*, 10071−10077.

(9) Yang, L. P.; Li, S. Z.; Li, Y. C.; Gao, R. Y. Bioactivity investigation of triazole fungicide enantiomers. *Chin. J. Pest Sci.* **2002**, *4*, 67−70.

(10) U.S. Environmental Protection Agency. Pesticide Monitoring, Phase II Fact Sheet Series 7 (of 14); Washington, DC, USA, 1991.

(11) http://www.fao.org/fileadmin/templates/agphome/documents/Pests_Pesticides/JMPR/Report11/Flutriafol.pdf.

(12) Bicchi, C.; Cordero, C.; Rubiolo, P.; Occelli, A. Simultaneous determination of six triazolic pesticide residues in apple and pear pulps by liquid chromatography with ultraviolet diode array detection. *J. AOAC Int.* **2001**, *84*, 1543−1550.

(13) Blasco, C.; Pico, Y.; Manes, J.; Font, G. Determination of fungicide residues in fruits and vegetables by liquid chromatography-atmospheric pressure chemical ionization mass spectrometry. *J. Chromatogr., A* **2002**, *947*, 227−235.

(14) Juan-Garcia, A.; Manes, J.; Font, G.; Pico, Y. Evaluation of solid-phase extraction and stir-bar sorptive extraction for the determination of fungicide residues at low-μg kg$^{-1}$ levels in grapes by liquid chromatography-mass spectrometry. *J. Chromatogr., A* **2004**, *1050*, 119−127.

(15) Li, J. G.; Wang, Y. F.; Yao, X. P.; Shi, J. W.; Fang, L. Y.; Jiang, L. Determination of 11 triazole fungicides in fruits using solid phase extraction and gas chromatography-tandem mass spectrometry. *Chin. J. Chromatogr.* **2012**, *30*, 262−266.

(16) Yang, Z. H.; Wei, C. J.; Jia, L. F.; Liang, D.; Zhao, J. Z. Simultaneous determination of the residue of seven commonly-used pesticides in strawberry with solid-phase extraction and gas chromatography. *J. Agro-Environ. Sci.* **2012**, *31*, 2304−2308.

(17) Huang, C. Q.; Ding, H. Y.; Zhu, X. Y.; Chen, L. L.; Li, B.; Lou, C. J. Simultaneous determination of 7 triazole alcohol fungicides in vegetables by liquid chromatography—tandem mass spectrometry. *J. Instrum. Anal.* **2011**, *30*, 656−660.

(18) Hu, Y. L.; Li, J. W.; Li, G. K. Synthesis and application of a novel molecularly imprinted polymer-coated stir bar for microextraction of triazole fungicides in soil. *J. Sep. Sci.* **2011**, *34*, 1190−1197.

(19) Wang, P.; Jiang, S. R.; Jiang, W.; Zhou, W. J.; Wang, Q. X.; Wang, P.; Zhou, Z. Q. Enantiomeric separation of flutriafol by HPLC. *Chin. J. Appl. Chem.* **2005**, *22*, 445−447.

(20) Wang, P.; Jiang, S. R.; Liu, D. H.; Wang, P.; Zhou, Z. Q. Direct enantiomeric resolutions of chiral triazole pesticides by high-performance liquid chromatography. *J. Biochem. Biophys. Methods* **2005**, *62*, 219−230.

(21) Tian, Q.; Ren, L. P.; Lv, C. G.; Zhou, Z. Q. Chiral resolution of eight triazole pestioioles by high performance liquid chromatography under reversed phase conditions. *Chin. J. Anal. Chem.* **2010**, *38*, 688−692.

(22) Qiu, J.; Dai, S. H.; Zheng, C. M.; Yang, S. M.; Chai, T. T.; Bie, M. Enantiomeric separation of triazole fungicides with 3-μm and 5-μm

particle chiral columns by reverse-phase high-performance liquid chromatography. *Chirality* **2011**, *23*, 479−486.
(23) Zhang, Q.; Tian, M. M.; Wang, M. Y.; Shi, H. Y.; Wang, M. H. Simultaneous enantioselective determination of triazole fungicide flutriafol in vegetables, fruits, wheat, soil and water by reversed-phase high-performance liquid chromatography. *J. Agric. Food Chem.* **2014**, *62*, 2809−2815.
(24) Zhang, H.; Wang, X. Q.; Zhuang, S. L.; Qian, M. R.; Jiang, K. Z.; Wang, X. Y.; Xu, H.; Qi, P. P.; Wang, Q. Enantioselective separation and simultaneous determination of fenarimol and nuarimol in fruits, vegetables, and soil by liquid chromatography−tandem mass spectrometry. *Anal. Bioanal. Chem.* **2012**, *404*, 1983−1991.
(25) Ellington, J. J.; Evans, J. J.; Prickett, K. B.; Champion, W. L., Jr. High-performance liquid chromatographic separation of the enantiomers of organophosphorus pesticides on polysaccharide chiral stationary phases. *J. Chromatogr., A* **2001**, *928*, 145−154.
(26) Liu, D. H.; Wang, P.; Zhu, W. D.; Gu, X.; Zhou, W. F.; Zhou, Z. Q. Enantioselective degradation of fipronil in Chinese cabbage (*Brassica pekinensis*). *Food Chem.* **2008**, *110*, 399−405.
(27) Zhang, C.; Jin, L. X.; Zhou, S. S.; Zhang, Y. F.; Feng, S. L.; Zhou, Q. Y. Chiral separation of neonicotinoid insecticides by polysaccharide-type stationary phases using high-performance liquid chromatography and supercritical fluid chromatography. *Chirality* **2011**, *23*, 215−221.
(28) Chen, G. Q.; Cao, P. Y.; Liu, R. J. A multi-residue method for fast determination of pesticides in tea by ultra performance liquid chromatography−electrospray tandem mass spectrometry combined with modified QuEChERS sample preparation procedure. *Food Chem.* **2011**, *125*, 1406−1411.
(29) Frenich, A. G.; Romero-González, R.; Gómez-Pérez, M. L.; Vidal, J. L. M. Multi-mycotoxin analysis in eggs using a QuEChERS-based extraction procedure and ultra-high-pressure liquid chromatography coupled to triple quadrupole mass spectrometry. *J. Chromatogr., A* **2011**, *1218*, 4349−4356.
(30) Wilkowska, A.; Biziuk, M. Determination of pesticide residues in food matrices using the QuEChERS methodology. *Food Chem.* **2011**, *125*, 803−812.
(31) Zhao, P. Y.; Wang, L.; Zhou, L.; Zhang, F. Z.; Kang, S.; Pan, C. P. Multi-walled carbon nanotubes as alternative reversed-dispersive solid phase extraction materials in pesticide multi-residue analysis with QuEChERS method. *J. Chromatogr., A* **2012**, *1225*, 17−25.
(32) Famiglini, G.; Palma, P.; Pierini, E.; Trufelli, H.; Cappiello, A. Organochlorine pesticides by LC-MS. *Anal. Chem.* **2008**, *80*, 3445−3449.
(33) Li, M. M.; Liu, X. G.; Dong, F. S.; Xu, J.; Kong, Z. Q.; Li, Y. B.; Zheng, Y. Q. Simultaneous determination of cyflumetofen and its main metabolite residues in samples of plant and animal origin using multi-walled carbon nanotubes in dispersive solid-phase extraction and ultrahigh performance liquid chromatography−tandem mass spectrometry. *J. Chromatogr., A* **2013**, *1300*, 95−103.

oxidase-A inhibitors,[11] antioxidants,[12−14] fungal membrane $H^+$ ATPase inhibitors,[15] and α-glucosidase inhibitors[16,17] direct from crude extracts of medicinal plants, endophytic fungi, and food.

For high-resolution α-amylase inhibition profiling of plant extracts, a sensitive, stable, and cheap assay that can be performed in microplates is needed. Most studies reported so far have been based on colorimetric measurements of reducing sugars by reaction with dinitrosalicylic acid (DNS method) or blue starch−iodine complexes formed between iodine and starch polymers.[18,19] Both methods use cheap reagents but are experimentally time-consuming and rely on secondary chemical processes to occur (i.e., reaction with DNS and formation of starch−iodine complexes). Direct assessment of α-amylase activity can be performed by colorimetric measurement of the formation of chromophores like 2-chloro-4-nitrophenolate and *p*-nitrophenolate by cleavage of substrates like 2-chloro-4-nitrophenyl-α-maltotrioside (CNP-G3) and *p*-nitrophenyl-α-D-maltoheptaoside (PNP-G7), respectively.[19,20] The 2-chloro-4-nitrophenyl chromophore hydrolyzes 10 times faster than the corresponding 4-nitrophenyl group, and α-amylase assays based on the former are therefore more sensitive.[20,21] In this work the development of a high-resolution microplate-based α-amylase inhibition assay using 2-chloro-4-nitrophenyl-α-D-maltotrioside as substrate is described. The aim is to implement a stable, cheap, and sensitive α-amylase assay suitable for fast and efficient high-resolution α-amylase profiling in combination with HPLC−SPE−NMR for analysis of α-amylase inhibitors in plant extracts with presumed anti-diabetic effect.

## EXPERIMENTAL SECTION

**Chemicals.** α-Amylase type VI-B (E.C. 3.2.1.1, from porcine pancreas, lyophilized powder), 2-chloro-4-nitrophenyl-α-D-maltotrioside (CNP-G3), sodium chloride, sodium azide, dimethyl sulfoxide (DMSO, ≥99.5%), acarbose, (−)-epicatechin, brucine, luteolin, myricetin, coumarin, trolox, and HPLC-grade acetonitrile were purchased from Sigma-Aldrich (St. Louis, MO). Calcium acetate and formic acid were purchased from Merck (Darmstadt, Germany), HPLC-grade methanol for extraction of cinnamon was from Fischer Scientific (Leicester, UK), and methanol-$d_4$ (99.80% D, less than 0.03% water) was from Euriso-top (Saint-Aubin Cedex, France). Cinnamon (*Cinnamomum verum* Presl) was purchased from Urtekram (Mariager, Denmark). Water was purified by 0.22 μm membrane filtration and deionization (Millipore, Billerica, MA).

**Extraction and Sample Preparation.** The stock solution of the artificial mixture consisted of 5 g/L brucine, 5 g/L coumarin, 2.5 g/L trolox, 0.875 g/L luteolin, 0.875 g/L myricetin, and 1.25 g/L (−)-epicatechin in a 1:1 mixture of HPLC solvents A and B, *vide infra*. Crude methanol extract of cinnamon was prepared by extracting 1 g of ground material with 10 mL of solvent at room temperature overnight. The extract was filtered (45 μm filter fitted to a 10 mL syringe) and evaporated to dryness. The dry extracts were reconstituted in phosphate buffer (pH 6.0) containing 10% DMSO to a concentration of 20 mg/mL. Ten-fold dilutions were performed 12 times for $IC_{50}$ determinations.

**Development of α-Amylase Assay.** The α-amylase assay was performed in 96-well microplates using a final volume of 200 μL. Unless otherwise stated, experiments were performed with phosphate buffer (0.1 mM) containing 0.02% $NaN_3$ and adjusted to pH 6.0 with 2.0 M phosphoric acid. Stock solutions of α-amylase and CNP-G3 in phosphate buffer were prepared at concentrations of 2.0 U/mL and 10.0 mM, respectively. To all wells were added 175 μL of buffer and 5 μL of enzyme solution (final well concentration 0.05 U/mL), and the microplate was subsequently incubated for 10 min. The reaction was started by addition of 20 μL of substrate solution (final well concentration 1.0 mM), whereafter the absorbance was measured at 405 nm every third minute for 30 min. Preincubation, incubation, and absorbance measurements were performed with a Multiscan FC microplate photometer with built-in incubator (Thermo Scientific, Waltham, MA) coupled to SkanIt version 2.5.1 software for data acquisition. Cleavage rates were obtained by plotting the absorbance values as a function of time using Microsoft Excel 2010 for slope calculations. Optimal concentrations of $Ca^{2+}$, $Cl^-$, and DMSO as well as optimal pH and temperature were assessed by measuring enzyme activities for the following array of parameter changes (in addition to above-described protocol): sodium chloride = 0, 10, 20, 30, 40, 50, 60, 70, 80, 90, and 100 mM; calcium acetate (using 60 mM sodium chloride) = 0, 0.5, 1.0, 2.0, and 2.5 mM; DMSO (using 60 mM sodium chloride and 1 mM calcium acetate) = 0, 2, 4, 6, 8, 10, 12, 14, 16, 18, and 20% v/v; temperature = 25, 28, 31, 34, 37, and 40 °C; pH = 5.0, 5.5, 5.7, 6.0, 6.3, 6.7, 7.0, and 7.5 (using 2.0 M phosphoric acid or 2.0 M NaOH for adjustment of buffer). Stability of the α-amylase enzyme was assessed for a period of 8 weeks. Stock solution of 20 U/mL enzyme in buffer (60 mM sodium chloride, 1 mM calcium acetate, pH 6.0) was dispersed in 600 μL aliquots and stored at −18 °C. The first measurement at day 0 was performed on a non-frozen enzyme solution; the remaining measurements were performed using thawed stock solutions diluted to 2.0 U/mL as above. Enzymatic activity of α-amylase was subsequently assessed three times per week for 2 weeks and then once a week for an additional 6 weeks. For comparison of kinetic vs end point measurements (using 5% DMSO, 60 mM sodium chloride, 1 mM calcium acetate, and pH 6.0), absorbance was measured at 405 nm every third minute for 30 min after addition of substrate. Subsequently the pH was adjusted to 12 by addition of 13 μL of 4 M NaOH solution, and the absorbance was measured for an additional 30 min.

**HPLC Separations and High-Resolution α-Amylase Inhibition Chromatograms.** HPLC separations were performed on an Aglient 1200 series instrument (Santa Clara, CA) consisting of a G1311A quaternary pump, a G1322A degasser, a G1316A thermostated column compartment, a G1315C photodiode-array detector, a G1367C high-performance auto sampler, and a G1364C fraction collector, all controlled by Agilent ChemStation version B.03.02 software. Analyses were performed at 40 °C on a 150 × 4.6 mm i.d. Phenomenex Luna $C_{18}(2)$ reversed-phase column (3 μm particle size, 100 Å pore size) with a flow rate of 0.5 mL/min. HPLC solvent A consisted of water−acetonitrile 95:5 added 0.1% formic acid, and solvent B consisted of acetonitrile−water 95:5 added 0.1% formic acid. For high-resolution α-amylase inhibition profiling, 10 μL of the artificial mixture was separated using the following gradient elution profile: 0 min, 5% B; 20 min, 70% B; 23 min, 70% B; 24 min, 5% B; 35 min, 5% B. The column eluate from 7.5 to 20 min was fractionated into one 96-well microplate (Sterilin Limited, Aberbargoed Caerphilly, United Kingdom) using the eight wells in column 12 as blank controls, yielding a resolution of 7 points per min. The microplates were subsequently evaporated to dryness using a SPD121P Savant SpeedVac concentrator (Thermo Scientific, Waltham, MA) equipped with an OFP400 oil-free pump and a RVT400 refrigerated vapor trap. α-Amylase cleavage rates (kinetic measurements) were measured for each well as described above (using 10% DMSO, 60 mM sodium chloride, 1 mM calcium acetate, pH 6.0), and inhibition was calculated using the formula

$$\%\ \text{inhibition} = \left(\frac{\text{slope}_{\text{blank}} - \text{slope}_{\text{sample}}}{\text{slope}_{\text{blank}}}\right) \times 100\%$$

Inhibition for each well was plotted at its respective retention time as an α-amylase inhibition profile underneath the HPLC chromatogram.

**Validation of HPLC Method for Separation of Artificial Mixture.** The HPLC method described above was used for the quantification of individual constituents in the artificial mixture and validation of linearity, sensitivity (limit of detection, LOD, and limit of quantification, LOQ), and precision (intra- and inter-day). The linearity was assessed using regression analysis of standard curves (254 nm) obtained from injection of 10 μL of a complex mixture containing brucine, coumarin, trolox, luteolin, myricetin, and epicatechin. Thus, a

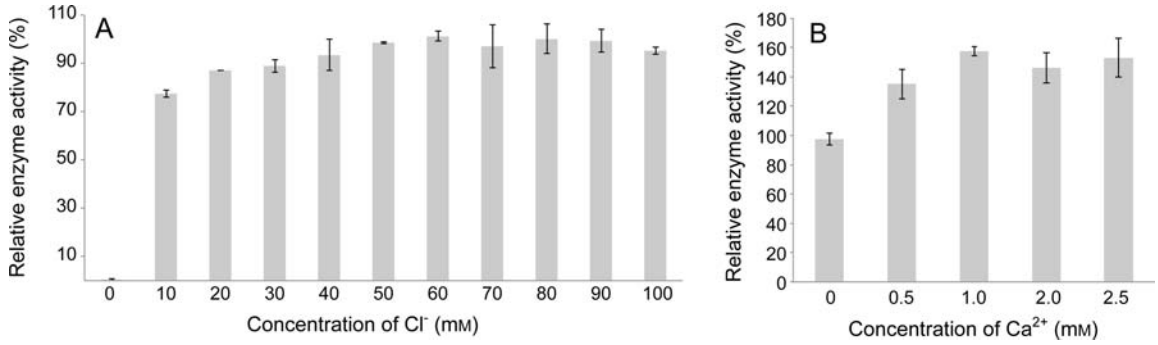


**Figure 1.** (A) Relative enzyme activity at different chloride ion concentrations. The enzyme activity in buffer containing 60 mM $Cl^-$ is normalized to 100%. (B) Relative enzyme activities at calcium ion concentrations in the range 0−2.5 mM. Data represent mean ± standard deviation of three replicate measurements.

stock solution containing 5 g/L brucine, 5 g/L coumarin, 2.5 g/L trolox, 0.875 g/L luteolin, 0.875 g/L myricetin, and 1.25 g/L (−)-epicatechin in a 1:1 mixture of HPLC solvents A and B was diluted two-fold 12 times with the same solvent mixture. The HPLC calibration curves were constructed by plotting the peak area ($A$) against the concentration of each standard solution ($c$) of each compound. The data were used for determining LOD (S/N = 3) and LOQ (S/N = 10). Precision of the method was determined after injection of 10 $\mu$L of the artificial mixture containing 200, 150, and 100 mg/L of each compound. The analysis was performed in quadruplicate on day 1 (intra-day precision) and for five additional days (inter-day precision). Results are expressed in %RSD (= SD/average) of the instruments.

**HPLC−HRMS−SPE−NMR Analysis.** Chromatographic separation of a 19.8 mg/mL solution of crude extract of cinnamon was performed using an Agilent 1200 system (Santa Clara, CA) comprising a photodiode-array detector, an autosampler, a quaternary pump, a degasser, and a thermostated column compartment, using the same column, solvent composition, temperature, and gradient profile as described above. A small proportion (1%) of the HPLC eluate was directed to a micrOTOF-Q II mass spectrometer (Bruker Daltonik GmbH, Bremen, Germany) equipped with an electrospray ionization interface. Mass spectra were acquired in positive-ion mode, using a drying temperature of 200 °C, capillary voltage of 4100 V, nebulizer pressure of 2.0 bar, and drying gas flow of 7 L/min. A solution of sodium formate clusters was automatically injected at the beginning of each run to enable internal mass calibration. The rest of the HPLC eluate was directed to the photodiode array detector and subsequently to a Prospekt 2 SPE unit (Spark Holland, Emmen, The Netherlands). Cumulative SPE trappings of individual analytes were performed for five consecutive injections (10 $\mu$L/injection) using absorption threshold at 254 nm to trigger analyte trapping. Chromatography, peak trapping, and analyte transfer from the SPE unit were controlled with HyStar version 3.2 software (Bruker Biospin GmbH, Rheinstetten, Germany). The HPLC eluate was diluted with Milli-Q water at a flow rate of 1.0 mL/min prior to trapping on 10 × 2 mm i.d. resin GP (general purpose, 5−15 $\mu$m, spherical shape, polydivinylbenzene phase) SPE cartridges from Spark Holland (Emmen, The Netherlands). After being dried for 45 min with pressurized nitrogen gas, analytes were automatically eluted into 1.7 mm o.d. NMR tubes (96 position tube racks) with methanol-$d_4$ using a Gilson liquid handler controlled by PrepGilson version 1.2 software (Bruker Biospin). NMR experiments were performed with a Bruker Avance III system ($^1$H operating frequency of 600.13 MHz) equipped with a Bruker SampleJet sample changer and a cryogenically cooled gradient inverse triple-resonance 1.7 mm TCI probe-head (Bruker Biospin) optimized for $^1$H and $^{13}$C observation. Icon NMR version 4.2 software (Bruker Biospin) was used for controlling automated acquisition of NMR data, and processing of NMR data was performed using Topspin version 3.0 software (Bruker Biospin). All NMR spectra were recorded in methanol-$d_4$ at 300 K. $^1$H and $^{13}$C chemical shifts were referenced to the residual solvent signal ($\delta$ 3.31 and $\delta$ 49.00, respectively). A one-dimensional $^1$H NMR spectrum was acquired in automation (temperature equilibration to 300 K, optimization of lock parameters, gradient shimming, and setting of receiver gain) with 30° pulses, 3.66 s inter-pulse intervals, 64k data points, and multiplied with an exponential function corresponding to line-broadening of 0.3 Hz prior to Fourier transform. Phase-sensitive DQF-COSY and NOESY spectra were recorded using a gradient-based pulse sequence with a 20 ppm spectral width and 2k × 512 data points (processed with forward linear prediction to 1k data points). A multiplicity-edited HSQC spectrum was acquired with the following parameters: spectral width 20 ppm for $^1$H and 200 ppm for $^{13}$C, 2k × 256 data points (processed with forward linear prediction to 1k data points), and 1.0 s relaxation delay. HMBC spectrum was optimized for $^nJ_{C,H}$ = 8 Hz and acquired using the following parameters: spectral width 20 ppm for $^1$H and 240 ppm for $^{13}$C, 2k × 128 data points (processed with forward linear prediction to 1k data points), and 1.0 s relaxation delay.

## RESULTS AND DISCUSSION

This work describes development and optimization of a direct colorimetric $\alpha$-amylase inhibitory assay based on cleavage of 2-chloro-4-nitrophenyl-$\alpha$-D-maltotrioside (CNP-G3), its implementation in microplates for high-resolution inhibition profiling, and its combination with HPLC−HRMS−SPE−NMR for fast and efficient identification of $\alpha$-amylase inhibitors in medicinal plant and functional food extracts with a presumed anti-diabetic effect. Porcine pancreatic $\alpha$-amylase and CNP-G3 were chosen as enzyme and substrate, respectively, in the current work because they are relatively cheap compared to human $\alpha$-amylase and maltopentaoside/maltoheptaoside substrates—an important factor for the use of high-resolution $\alpha$-amylase inhibition assays as a routine method in natural products and functional food research.

**Development and Optimization of $\alpha$-Amylase Bioassay with 2-Chloro-4-nitrophenyl-$\alpha$-D-maltotrioside Substrate.** Development and optimization of the $\alpha$-amylase inhibition assay using 2-chloro-4-nitrophenyl-$\alpha$-D-maltotrioside as substrate were based on the assay previously described.[20,21] The optimization and microplate-based adaptation ensure a sensitive, robust, and reproducible setup that is suitable for high-resolution $\alpha$-amylase inhibition profiling and further coupling with HPLC−HRMS−SPE−NMR. Initial experiments were performed with 0.1 mM phosphate buffer (pH 6.0) containing 0.02% $NaN_3$ and 0.05 U/mL $\alpha$-amylase (final well concentration). $NaN_3$ was added as a preservative it has been reported that $NaN_3$ in the buffer contributes to improvement of the enzyme activity as well.[20] After 10 min incubation, CNP-G3 (1.0 mM) was added to start the reaction, whereafter the absorbance was measured at 405 nm every third minute for 30

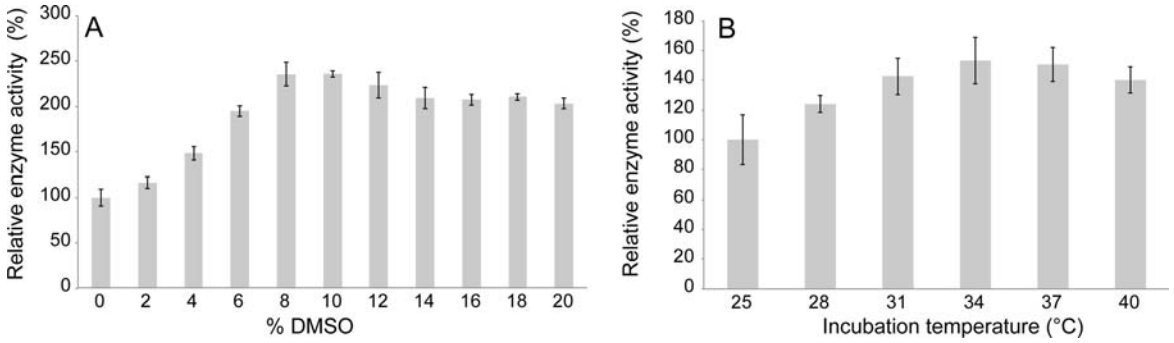


**Figure 2.** (A) Relative enzyme activities at different DMSO concentrations. The enzyme activity in buffer containing 0% DMSO is normalized to 100%. (B) Relative enzyme activities at different temperatures. The enzyme activity at 25 °C normalized to 100%. Data represent mean ± standard deviation of three replicate measurements.

**Table 1. Parameters for Validation of the HPLC Method for the Reference Compounds**

| | | precision (%RSD)[a] | | | sensitivity ($\mu$g) | |
|---|---|---|---|---|---|---|
| compound | amount on-column ($\mu$g) | intra-day | inter-day | linearity[b] | LOD | LOQ |
| brucine | 2.00 | 0.10 | 2.46 | $A = 1987.2c + 395.11$ $r = 0.997$ | 0.37 | 1.22 |
| (−)-epicatechin | | 0.28 | 1.29 | $A = 442.38c - 5.4712$ $r = 0.9998$ | 0.15 | 0.49 |
| myricetin | | 0.099 | 1.41 | $A = 6198.5c + 182.56$ $r = 0.9968$ | 0.012 | 0.040 |
| luteolin | | 0.076 | 1.92 | $A = 7168.5c + 10.307$ $r = 0.9999$ | 0.0053 | 0.018 |
| coumarin | | 0.71 | 1.10 | $A = 4266.7c - 8.6232$ $r = 0.9999$ | 0.039 | 0.13 |
| trolox | | 0.21 | 5.45 | $A = 221.02c + 51.112$ $r = 0.999$ | 0.79 | 2.64 |
| brucine | 1.50 | 0.45 | 5.24 | | | |
| (−)-epicatechin | | 0.32 | 2.55 | | | |
| myricetin | | 0.51 | 3.05 | | | |
| luteolin | | 0.34 | 2.78 | | | |
| coumarin | | 0.041 | 1.65 | | | |
| trolox | | 0.45 | 3.79 | | | |
| brucine | 1.00 | 0.99 | 2.75 | | | |
| (−)-epicatechin | | 0.23 | 1.09 | | | |
| myricetin | | 0.27 | 1.12 | | | |
| luteolin | | 0.27 | 0.78 | | | |
| coumarin | | 0.60 | 1.12 | | | |
| trolox | | 1.64 | 3.12 | | | |

[a] $n = 4$. [b] $A$ = peak area; $c$ = concentration of reference compound; $r$ = correlation coefficient.

min to obtain cleavage rates. Chloride ions are necessary for activation of the enzyme's hydrolyzing property,[22] and sodium chloride was therefore added to the phosphate buffer in concentrations of 0−100 mM. As seen in Figure 1A, the maximal enzyme activity was reached at 60 mM NaCl, and no further increase in enzyme activity was observed at higher concentrations. Likewise, calcium is required to stabilize and activate the enzyme,[23] and therefore calcium acetate was added to the buffer in concentrations of 0−2.5 mM. As seen in Figure 1B, maximal enzyme activity was achieved at a calcium acetate concentration of 1.0 mM. Thus, further experiments were performed with 0.1 mM phosphate buffer containing 60 mM sodium chloride, 1.0 mM calcium acetate, and 0.02% $NaN_3$.

The microplate-based $\alpha$-amylase inhibition assay used in a HPLC microfractionation setting requires subsequent evaporation of the HPLC solvent to allow use of high amount of organic solvent in the elution solvent. Subsequent dissolution in the above-described buffer containing DMSO improves dissolution of lipophilic constituents, but high amounts of DMSO are known to interfere with enzymes. Thus, the activity of $\alpha$-amylase was assessed with DMSO concentrations in the range 0−20%, as seen in Figure 2A. Maximum enzyme activity was achieved at 10% DMSO, i.e., a 2-fold increase in activity compared to that with no DMSO in the buffer DMSO did not decrease enzyme activity of porcine pancreatic $\alpha$-amylase dramatically at the tested concentrations. This confirms the robustness of porcine pancreatic $\alpha$-amylase in the presence of DMSO as previously described.[24]

The enzyme activities at different temperatures were assessed to determine the optimal incubation temperature, but also to

ensure enzyme stability during preincubation as well as incubation. As seen in Figure 2B, enzyme activity increased significantly from 25 to 34 °C, with only a slight decrease at 37 and 40 °C. The enzymatic cleavage rate at 37 °C remained constant during the 30 min of incubation, and 37 °C was therefore chosen as the optimal temperature for all further experiments.

The highest cleavage rate of CNP-G3 with porcine α-amylase was observed at pH 6 (Figure S1, Supporting Information), which is comparable with previous findings of pH optimum for pancreatic and salivary human α-amylase.[20] All results are based on cleavage rates, i.e., the slopes of the absorbance values plotted against measurement times, which (i) makes it possible to monitor the linearity of the reaction during the entire incubation time, and (ii) prevents the need for subtracting background absorbance for analytes that absorbs at 405 nm. However, we also explored the use of end point measurements after 30 min, especially because the increased absorbance of 2-chlorophenol under alkaline conditions might increase the sensitivity of the assay. In Figure S2 in the Supporting Information, the end point measurements at pH 5−7.5, i.e., absorbance measurements at 30 min, are compared with absorbance measurements after basifying all wells to pH 12 after 30 min. It is clear that adjusting the pH to 12 yields an increase in absorbance, with the relative increase being highest at incubation performed at low pH values. For pH 6 the adjustment to pH 12 gives an increase of approximately 20%, but given the potential problems with background absorbance of analytes from HPLC microfractionation, the use of cleavage rates is preferred, and that is what we used for the remainder of this work. A further warning about using end point measurements after adjusting to pH 12 is the autohydrolysis of CNP-G3, as shown in Figure S3 in the Supporting Information. Finally, the stability of α-amylase stored at −18 °C as ready-to-use aliquots of enzyme solution was assessed as a means of avoiding repeated freeze−thaw cycles of crude enzyme. Thus, aliquots corresponding to the amount of enzyme needed for one 96-well microplate were prepared, and the enzyme activity of each of these aliquots was measured for 8 weeks. Figure S4 in the Supporting Information shows that the enzyme had maximum activity within the first 2 weeks, whereafter the enzyme activity decreased. Thus, it is unfortunately not advisable to store porcine α-amylase in solution. With the above-described conditions, (−)-epicatechin, myricetin, and luteolin showed $IC_{50}$ values of 2300 ± 45, 37 ± 4.7, and 33 ± 8.9 μM, respectively.

**Validation of HPLC Method.** A mixture of three compounds with α-amylase inhibitory activity, i.e., (−)-epicatechin (**2**), myricetin (**3**), and luteolin (**4**), and three compounds without α-amylase inhibitory activity, i.e., brucine (**1**), coumarin (**5**), and trolox (**6**), was prepared. A reversed-phase HPLC separation that allowed baseline separation of **1**−**6** in the retention time ($R_t$) range 7.5−20 min was developed. The HPLC method was validated by determining linearity, sensitivity (LOD and LOQ), and precision (intra- and inter-day). The data are given in Table 1 and demonstrate a satisfactory performance of the HPLC method to be used for high-resolution α-amylase inhibition profiling.

**Microplate-Based High-Resolution α-Amylase Inhibition Profiles: Proof-of-Concept with Artificial Mixture.** Using the above-described HPLC method for separation of **1**−**6** (see Figure 3), the HPLC eluate from 7.5 to 20 min was fractionated into 88 wells of a 96-well microplate. The HPLC

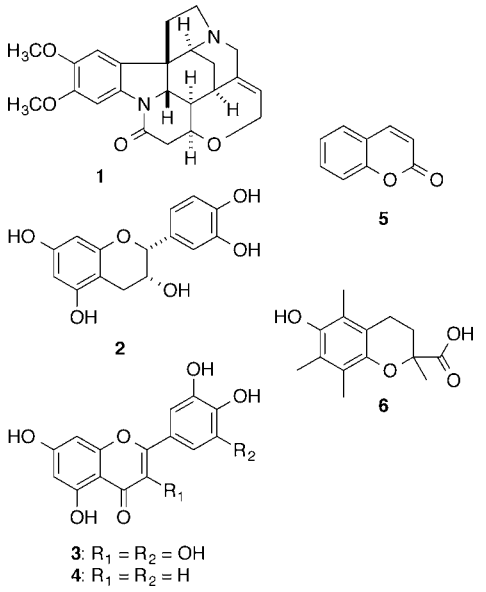


**Figure 3.** Structures of α-amylase inhibitors (−)-epicatechin (**2**), myricetin (**3**), and luteolin (**4**), and inactive constituents brucine (**1**), coumarin (**5**), and trolox (**6**), used for proof-of-concept of the microplate-based high-resolution α-amylase inhibition profiling developed in this work.

solvent was subsequently evaporated, and the α-amylase inhibition assay was performed for all wells as described above. The α-amylase cleavage rate of each well was calculated as percent inhibition (using the average of the last column of the microplate as blank control), and the results were plotted underneath the HPLC trace at 254 nm as well as the trace at 230 nm. The resulting high-resolution biochromatogram with a resolution of 7 data points per minute is shown in Figure 4.

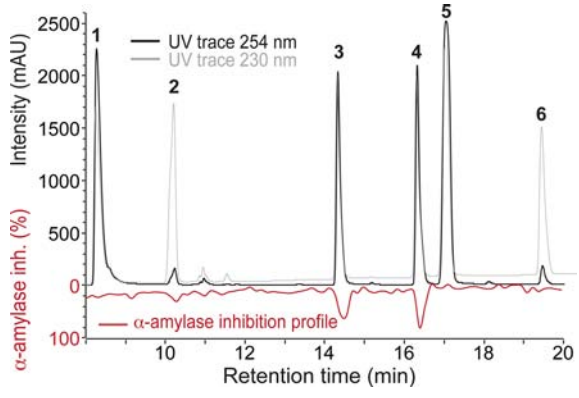


**Figure 4.** High-resolution biochromatogram of α-amylase inhibitors (−)-epicatechin (**2**), myricetin (**3**), and luteolin (**4**), as well as inactive constituents brucine (**1**), coumarin (**5**), and trolox (**6**). Black line: UV trace at 254 nm. Gray line: UV trace at 230 nm. Red line: high-resolution α-amylase inhibition profile.

From the figure it is evident that there is a perfect retention time match between the peaks of (−)-epicatechin (**2**), myricetin (**3**), and luteolin (**4**) in the HPLC chromatogram and the bioactivity peaks in the high-resolution α-amylase inhibition profile—in agreement with these compounds possessing α-amylase inhibitory activity. The weak peak for (−)-epicatechin in the biochromatogram is in agreement with the high $IC_{50}$ value of 2300 μM for **2** compared to the $IC_{50}$


dx.doi.org/10.1021/jf5047283 | J. Agric. Food Chem. 2014, 62, 11465−11471

values of 37 and 33 $\mu$M for **3** and **4**, respectively. Likewise, there are no observable bioactivity peaks corresponding with peaks for brucine (**1**), coumarin (**5**), and trolox (**6**) in the HPLC chromatogram. Thus, this proof-of-concept experiment shows that the high-resolution $\alpha$-amylase inhibition profile is an excellent tool for pinpointing individual constituents with $\alpha$-amylase inhibitory activity—and thereby focusing subsequent dereplication or full-structure elucidation on only the bioactive peaks. The peaks in the high-resolution $\alpha$-amylase inhibition profile are marginally broader than the corresponding peaks in the HPLC chromatogram, which might cause problems with closely eluting peaks. However, if needed, the resolution of the biochromatogram can be increased by fractionating into two 96-well plates and subsequently combining the results from $\alpha$-amylase inhibition assaying of both microplates. However, one should be aware of the lower sensitivity of the $\alpha$-amylase inhibition assay that evidently will follow from fractionating one HPLC peak into more wells in the microplate.

**High-Resolution $\alpha$-Amylase Inhibition Coupled with HPLC−HRMS−SPE−NMR for Analysis of Cinnamon Extract.** Cinnamon has previously been shown to reduce serum glucose, triglyceride, LDL cholesterol, and total cholesterol for type 2 diabetics,[25] and successive extraction with polar to nonpolar solvent showed 50% inhibition of the relative activity of porcine pancreatic $\alpha$-amylase *in vitro* at a concentration of 0.06 mg/mL isopropanol extract.[26] The fractionation might, however, concentrate the active constituent(s), and we therefore wanted to investigate crude extract of cinnamon. A crude methanol extract was prepared, and the $IC_{50}$ value of the crude extract was 0.200 ± 0.061 mg/mL. A total of 25 $\mu$g of crude methanol extract was subjected to analytical-scale reversed-phase HPLC, and the eluate from 11 to 27 min was fractionated into 88 wells (resolution = 5.5 data points per minute). After evaporation to dryness, the $\alpha$-amylase inhibition of each well was determined and plotted at their respective retention times to give the high-resolution biochromatogram shown in Figure 5. It is clearly seen that only the major peak at $R_t$ = 22 min showed $\alpha$-amylase inhibitory activity. Subsequent HPLC−HRMS−SPE−NMR analysis showed the major peak to be cinnamaldehyde (see Supporting Information Table S1 for $^1$H NMR data assignment and Figure S5−S10 for annotated MS, $^1$H NMR, and 2D COSY, NOESY, HSQC, and HMBC spectra obtained in the HPLC−HRMS−SPE−NMR mode).

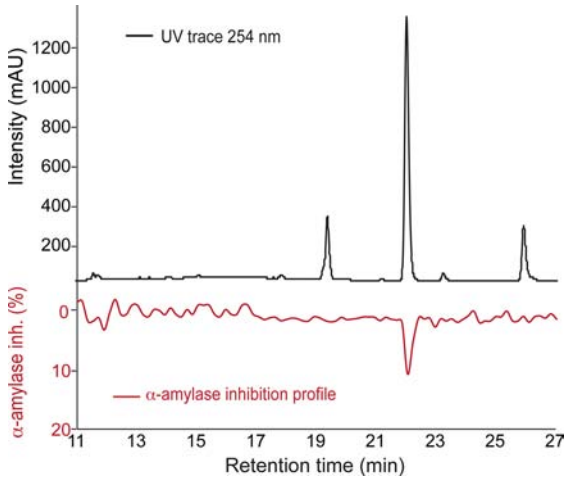


**Figure 5.** High-resolution biochromatogram of crude methanol extract of cinnamon. Black line: UV trace at 254 nm. Red line: high-resolution $\alpha$-amylase inhibition profile.

In conclusion, a microplate-based high-resolution $\alpha$-amylase inhibition assay that is compatible with HPLC−HRMS−SPE−NMR was developed. The proof-of-concept study with an artificial mixture as well as the investigation of crude methanol extract allowed direct identification of $\alpha$-amylase inhibitors by observing correlations between peaks in the high-resolution $\alpha$-amylase inhibition profile and the HPLC chromatogram.

## ■ ASSOCIATED CONTENT

### Supporting Information

Figure S1−S4 showing details from bioassay optimization, Figure S5−S10 showing annotated MS, $^1$H NMR, and 2D COSY, NOESY, HSQC, and HMBC spectra of cinnamaldehyde, and Table S1 showing $^1$H NMR data of cinnamaldehyde. This material is available free of charge via the Internet at http://pubs.acs.org.

## ■ AUTHOR INFORMATION

### Corresponding Author

*Tel.: +45 3533 6177. Fax: +45 3533 6001. E-mail: ds@sund.ku.dk.

### Funding

HPLC equipment used for high-resolution bioassay profiles was obtained via a grant from The Carlsberg Foundation. The 600 MHz HPLC−HRMS−SPE−NMR system used in this work was acquired through a grant from "Apotekerfonden af 1991", The Carlsberg Foundation, and the Danish Agency for Science, Technology and Innovation via the National Research Infrastructure funds.

### Notes

The authors declare no competing financial interest.

## ■ REFERENCES

(1) International Diabetes Federation. *IDF Diabetes Atlas*, 6th ed.; IDF: Brussels, 2013; ISBN 2-930229-85-3, online version at www.idf.org/diabetesatlas (accessed July 24, 2014).

(2) Marcovecchio, M. L.; Lucantoni, M.; Chiarelli, F. Role of chronic and acute hyperglycemia in the development of diabetes complications. *Diabetes Technol. Ther.* **2011**, *13*, 389−394.

(3) Whitcomb, D. C.; Lowe, M. E. Human pancreatic digestive enzymes. *Dig. Dis. Sci.* **2007**, *52*, 1−17.

(4) Eichler, H. G.; Korn, A.; Gasic, S.; Pirson, W.; Businger, J. The effect of a new specific $\alpha$-amylase inhibitor on post-prandial glucose and insulin excursions in normal subjects and Type 2 (non-insulin-dependent) diabetic patients. *Diabetologia* **1984**, *26*, 278−281.

(5) Fujisawa, T.; Ikegami, H.; Inoue, K.; Kawabata, Y.; Ogihara, T. Effect of two alpha-glucosidase inhibitors, voglibose and acarbose, on postprandial hyperglycemia correlates with subjective abdominal symptoms. *Metab., Clin. Exp.* **2005**, *54*, 387−390.

(6) Clissold, S. P.; Edwards, C. Acarbose. A preliminary review of its pharmacodynamics and pharmacokinetic properties and therapeutic potential. *Drugs* **1988**, *3*, 214−243.

(7) Etxeberria, U.; de la Garza, A. L.; Campión, J.; Martínez, J. A.; Milagro, F. I. Antidiabetic effects of natural plant extracts via inhibition of carbohydrate hydrolysis enzymes with emphasis on pancreatic alpha amylase. *Expert Opin. Ther. Targets* **2012**, *16*, 269−297.

(8) Giera, M.; Heus, F.; Janssen, L.; Kool, J.; Lingeman, H.; Irth, H. Microfractionation revisited: A 1536 well high resolution screening assay. *Anal. Chem.* **2009**, *81*, 5460−5466.

(9) Sprogøe, K.; Stærk, D.; Jäger, A. K.; Adsersen, A.; Hansen, S. H.; Witt, M.; Landbo, A.-K. R.; Meyer, A. S.; Jaroszewski, J. W. Targeted natural product isolation guided by HPLC-SPE-NMR: constituents of *Hubertia* species. *J. Nat. Prod.* **2007**, *70*, 1472−1477.

(10) Sprogøe, K.; Stærk, D.; Ziegler, H. L.; Jensen, T. H.; Holm-Møller, S. B.; Jaroszewski, J. W. Combining HPLC-PDA-MS-SPE-NMR with circular dichroism for complete natural product characterization in crude extracts: levorotatory gossypol in *Thespesia danis*. *J. Nat. Prod.* **2008**, *71*, 516−519.
(11) Grosso, C.; Jäger, A. K.; Staerk, D. Coupling of a high-resolution monoamine oxidase-A inhibitor assay and HPLC-SPE-NMR for advanced bioactivity profiling of plant extracts. *Phytochem. Anal.* **2013**, *24*, 141−147.
(12) Agnolet, S.; Wiese, S.; Verpoorte, R.; Staerk, D. Comprehensive analysis of commercial willow bark extracts by new technology platform: Combined use of metabolomics, high-performance liquid chromatography-solid-phase extraction-nuclear magnetic resonance spectroscopy and high-resolution radical scavenging assay. *J. Chromatogr., A* **2012**, *1262*, 130−137.
(13) Wiese, S.; Wubshet, S. G.; Nielsen, J.; Staerk, D. Coupling HPLC-SPE-NMR with a microplate-based high-resolution antioxidant assay for efficient analysis of antioxidants in food—Validation and proof-of-concept study with caper buds. *Food Chem.* **2013**, *141*, 4010−4018.
(14) Wubshet, S. G.; Nyberg, N. T.; Tejesvi, M. V.; Pirttilä, A. M.; Kajula, M.; Mattila, S.; Staerk, D. Targeting high-performance liquid chromatography-high-resolution mass spectrometry-solid-phase extraction-nuclear magnetic resonance analysis with high-resolution radical scavenging profiles—Bioactive secondary metabolites from the endophytic fungus *Penicillium namyslowskii*. *J. Chromatogr., A* **2013**, *1302*, 34−39.
(15) Kongstad, K. T.; Wubshet, S. G.; Johannesen, A.; Kjellerup, L.; Winther, A.-M. L.; Jäger, A. K.; Staerk, D. High-resolution screening combined with HPLC−HRMS−SPE−NMR for identification of fungal plasma membrane $H^+$-ATPase inhibitors from plants. *J. Agric. Food Chem.* **2014**, *62*, 5595−5602.
(16) Schmidt, J. S.; Lauridsen, M. B.; Dragsted, L. O.; Nielsen, J.; Staerk, D. Development of a bioassay-coupled HPLC-SPE-*tt*NMR platform for identification of α-glucosidase inhibitors in apple peel (*Malus* × *domestica* Borkh.). *Food Chem.* **2012**, *135*, 1692−1699.
(17) Wubshet, S. G.; Schmidt, J. S.; Wiese, S.; Staerk, D. High-Resolution Screening Combined with HPLC-HRMS-SPE-NMR for Identification of Potential Health-Promoting Constituents in Sea Aster and Searocket—New Nordic Food Ingredients. *J. Agric. Food Chem.* **2013**, *61*, 8616−8623.
(18) Xiao, Z.; Storms, R.; Tsang, A. A quantitative starch-iodine method for measuring alpha-amylase and glucoamylase activities. *Anal. Biochem.* **2006**, *351*, 146−148.
(19) Soor, S. K.; Hincke, M. T. Microplate reader-based kinetic determination of α-amylase activity: Application to quantitation of secretion from rat parotid acini. *Anal. Biochem.* **1990**, *188*, 187−191.
(20) Winn-Deen, E. S.; David, H.; Sigler, G.; Chavez, R. Development of a direct assay for α-amylase. *Clin. Chem.* **1988**, *34*, 2005−2008.
(21) Gella, F. J.; Gubern, G.; Vidal, R.; Canalias, F. Determination of total and pancreatic α-amylase in human serum with 2-chloro-4-nitrophenyl-α-D-maltotrioside as substrate. *Clin. Chim. Acta* **1997**, *259*, 147−160.
(22) Wakim, J.; Robinson, M.; Thoma, J. A. The active site of porcine-pancreatic alpha-amylase: Factors contributing to catalysis. *Carbohydr. Res.* **1969**, *10*, 487−503.
(23) Buisson, G.; Duée, E.; Haser, R.; Payan, F. Three dimensional structure of porcine pancreatic alfa-amylase at 2.9 Å resolution. Role of calcium in structure and acticity. *EMBO J.* **1987**, *6*, 3909−3916.
(24) Tao, B. Y.; Reilly, P. J.; Robyt, J. F. Detection of a covalent intermediate in the mechanism of action of porcine pancreatic alpha-amylase by using $^{13}C$ nuclear magnetic resonance. *Biochim. Biophys. Acta* **1989**, *995*, 214−220.
(25) Khan, A.; Safdar, M.; Khan, M. M. A.; Khattak, K. N.; Anderson, R. A. Cinnamon improves glucose and lipids of people with type 2 diabetes. *Diabetes Care* **2003**, *26*, 3215−3218.
(26) Ponnusamy, S.; Ravindran, R.; Zinjarde, S.; Bhargava, S.; Kumar, A. R. Evaluation of traditional Indian antidiabetic medicinal plants for human pancreatic amylase inhibitory effect *in vitro*. *J. Evidence-Based Complementary Altern. Med.* **2010**, *2011*, 1−10.

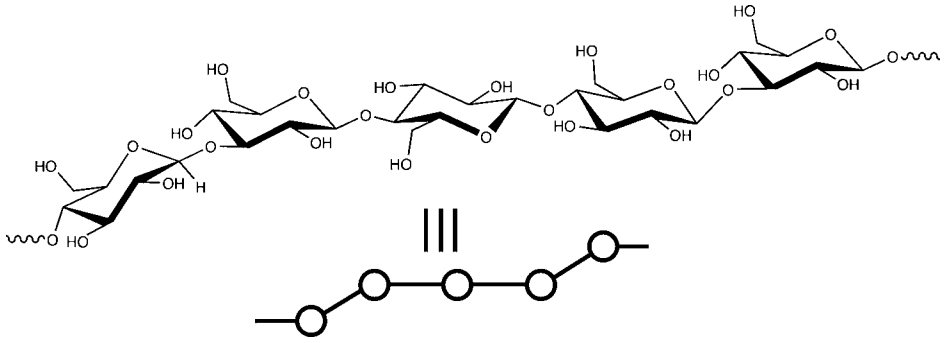

**Figure 1.** Schematic representation of (1→3)(1→4)-$\beta$-glucan with horizontal lines indicating $\beta$(1→4) linkages and diagonal lines indicating $\beta$(1→3) linkages.

stronger at pH 5.3 than at pH 6.5. The data are consistent with a stabilization of bile salt micelles in the presence of $\beta$-glucan due to a stronger multivalent binding of the $\beta$-glucan to bile salt micelles than to the monomers. $^{1}H-^{13}C$ NMR assays thus provide a rapid means for probing interactions between $\beta$-glucan and bile salts with atomic-level resolution.

## EXPERIMENTAL SECTION

**Materials.** Low and medium viscosity barley $\beta$-glucans (Figure 1) were obtained from Megazyme International Ltd. (Bray, Ireland), and these samples have previously been characterized by various physicochemical methods.[13] Briefly, low viscosity $\beta$-glucan had a molecular mass of 140 kDa as determined by high performance size-exclusion chromatography and a calibration curve using five $\beta$-glucan molar mass standard samples. Upon extensive hydrolysis with lichenase, a block structure ($\beta$-(1→4) linked glucopyranoses between $\beta$-(1→3) branches) of approximately 77% DP3, 19% DP4, and 3% DP5 (molar ratio) was derived. Medium viscosity $\beta$-glucan had a molecular mass of 200 kDa and a block structure of approximately 76% DP3, 19% DP4, and 4% DP5. Samples contained less than 1% each of protein or starch. Low viscosity barley $\beta$-glucan was chosen for the experiments monitoring $\beta$-glucan signals in order to improve spectral quality at lower sample viscosity (at high viscosity molecular tumbling rates decrease and NMR signals might become broad due to rapid relaxation). Signal appearance is less of an issue when monitoring the bile salt sample due to the higher achievable concentration, and medium viscosity barley $\beta$-glucan was used in these experiments due to the reportedly higher retention of bile salts by $\beta$-glucan of higher viscosity.[14] Bile salts, glycolate (GC) and taurochenodeoxycholate (TCDC) (Figure 2), along with buffer materials, sodium phosphate and sodium acetate, were obtained from Sigma-Aldrich (St. Louis, MO, USA). Buffers prepared at 100 mM concentration were sodium phosphate buffer of pH 6.5 and sodium acetate buffer of pH 5.3. Buffers were lyophilized and redissolved in $D_2O$ (Cambridge Isotope Laboratories, Tewksbury, MA, USA).

**Sample Preparation.** Low viscosity and medium viscosity barley $\beta$-glucan were dissolved in buffer to concentrations of 0.5, 1, 1.5, or 2% (w/v) and hydrated at 80 °C for 30 min. Stock solutions of bile salt were prepared in buffer, and bile salt was added to $\beta$-glucan samples at the concentrations indicated (3, 7, 10, 14, or 28 mM). Samples containing $\beta$-glucan and bile salts were incubated at 37 °C for 120 min under continuous shaking, and pure bile salt and $\beta$-glucan reference samples, in the absence of the potential interaction partner, were treated identically.

**NMR Spectroscopy.** Upon incubation at 37 °C for 120 min, the samples were directly transferred to 5 mm NMR sample tubes and analyzed by sensitivity-enhanced $^{1}H-^{13}C$ heteronuclear single-quantum correlation[15] (HSQC) experiments with a spectral width in the indirect ($^{13}C$) dimension that was reduced to permit rapid sampling of the $^{13}C$ dimension at high resolution. Experiments treating $\beta$-glucan as the host were recorded with a spectral width of 5 ppm and an offset in the $^{13}C$ dimension of 80 ppm. A total of 75 complex points

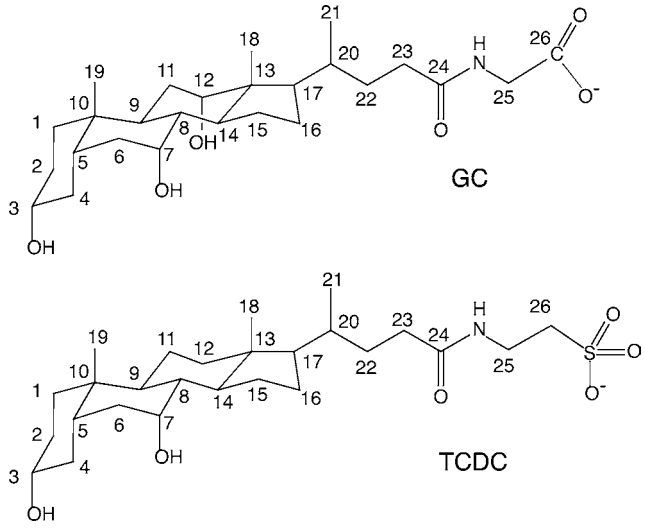


**Figure 2.** Structure of the bile salt molecules glycocholate (GC) and taurochendeoxycholate (TCDC) including their atom numbering.

were recorded in the $^{13}C$ dimension to sample an indirect acquisition time of 75 ms. Experiments treating bile salt as the host were recorded with a spectral width of 20 ppm centered around a spectral offset of 32 ppm. A total of 400 complex points were recorded in the $^{13}C$ dimension to sample an indirect acquisition time of 100 ms. The proton dimension was sampled with 1024 complex data points sampling 160 ms in both instances. Experiment times were 25 min for $^{1}H-^{13}C$ HSQC experiments with $\beta$-glucan as the host and 16 min for $^{1}H-^{13}C$ HSQC experiments with bile salt as the host. A recycle delay of 1 s was employed in each instance. For reference samples of bile salts and $\beta$-glucan, additional $^{1}H-^{13}C$ HSQC experiments were recorded sampling 60 ppm to yield the chemical shift values of the aliased spectral signals. All NMR spectra were recorded on an 800 MHz Bruker (Fällanden, Switzerland) Avance spectrometer equipped with a TCI Z-gradient CryoProbe and an 18.7 T magnet (Oxford Magnet Technology, Oxford, U.K.).

**Data Processing, Assignments, and Analysis.** All spectra were processed in Topspin 2.1 (Bruker) with extensive zero filling in both dimensions. Projections of $^{1}H-^{13}C$ HSQC experiments onto the $^{13}C$ dimension were created as projected spectra between $^{1}H$ chemical shifts of 3.4 and 3.8 ppm. Spectral assignments were obtained from the literature as full chemical shift assignments have been previously reported both for bile salts and for $\beta$-glucan.[16,17] In the fitting of titrations, the NMR signal changes in $\beta$-glucan upon addition of bile salt were treated as a chemical shift difference between individual $\beta$-glucan signals as shown in Figure 4. This treatment provides an internal reference and renders very small chemical shift changes detectable without the need for adding potentially interfering reference compounds. Due to the plethora of equivalent potential binding sites

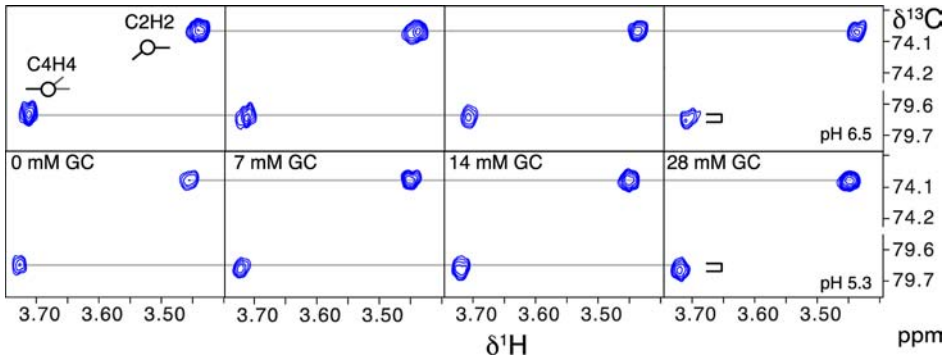


**Figure 3.** $^{1}H-^{13}C$ HSQC spectral region of 2% (w/v) low viscosity $\beta$-glucan (140 kDa) in the presence of increasing concentrations of glycocholate in 100 mM sodium phosphate buffer of pH 6.5 (top) and 100 mM sodium acetate buffer of pH 5.3 (bottom). The two resonances are of a C4H4 in a glycosidic bond and of a C2H2 in a glucopyranosyl unit that has a glycosidic bond at $O_3$. Chemical shift changes are highlighted by horizontal lines.

in $\beta$-glucan, adsorption of bile salts to $\beta$-glucan was treated as a Langmuir adsorption isotherm according to

$$\Delta\delta = \Delta\delta_0 + \Delta\Delta\delta_{max}\frac{c}{K_d + c} \quad (1)$$

where $\Delta\delta$ is the chemical shift difference between two select $\beta$-glucan signals, $\Delta\delta_0$ is the given chemical shift difference in the absence of bile salt, $\Delta\Delta\delta_{max}$ is the maximum change in this chemical shift difference upon saturation with bile salt, $c$ is the concentration of the bile salt, and $K_d$ is the dissociation constant. Fitting to the Langmuir adsorption isotherm was used to qualitatively probe the effect of weakly acidic pH on interactions between $\beta$-glucan and bile salt.

## RESULTS

In the current study, we attempt to probe interactions between $\beta$-glucan (Figure 1) and bile salts (using GC and TCDC as examples, see Figure 2) by $^{1}H-^{13}C$ NMR spectroscopic experiments on the time scale of minutes. The current study is thus aimed at establishing rapid binding assays for polysaccharide–host interactions and at improving the molecular understanding of interactions between $\beta$-glucans and bile salts.

In vitro binding assays were conducted using low viscosity $\beta$-glucan at a concentration of 2% (w/v) as the host and adding glycocholate of varying concentrations (0, 7, 14, and 28 mM). The detection of molecular interactions by probing carbohydrate signals has remained somewhat underexplored, presumably due to the congestion of carbohydrate signals in the $^{1}H$ dimension and the poor sensitivity of $^{13}C$ NMR spectroscopy at natural abundance. This sensitivity restriction is ameliorated by recent generations of NMR spectrometers employing cryogenically cooled detection electronics, by rapid pulsing techniques, or by $^{1}H$ homodecoupling.[18,19] Highly resolved $^{1}H-^{13}C$ spectra of carbohydrates can thus be obtained even at low millimolar concentrations on time scales of minutes or even seconds, especially when using narrow sweep widths in the $^{13}C$ dimension.[20−22] Resultant $\beta$-glucan $^{1}H-^{13}C$ HSQC spectra provided a signal-to-noise ratio above 20 for 2% (w/v) $\beta$-glucan samples within 25 min of experiment time. This signal-to-noise ratio proves sufficient for accurate measurements of $\beta$-glucan signal positions during the titrations with bile salts (Figure 3).

Titration of low viscosity $\beta$-glucan with bile salts yields systematic signal changes in the $\beta$-glucan $^{1}H-^{13}C$ HSQC spectra. Two well-separated signals showing different systematic changes were monitored to probe the interaction of $\beta$-glucan with bile salts (Figures 3, 4). Differences in chemical shift were obtained by peak picking of signals in the two-

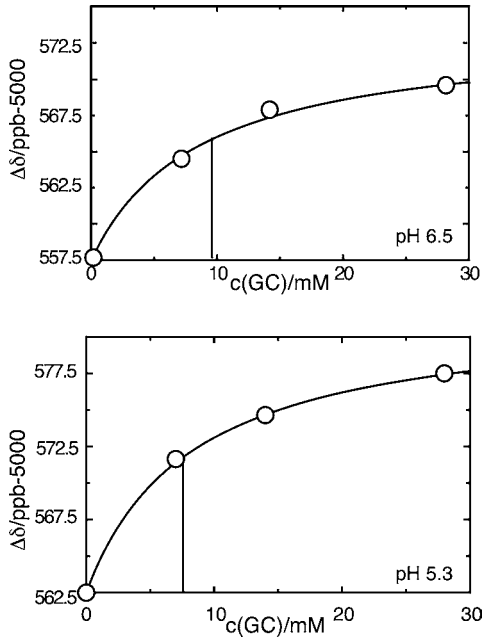


**Figure 4.** Chemical shift change ($\Delta\delta$) between the two $\beta$-glucan resonances displayed in Figure 3 upon addition of increasing glycocholate (GC) concentrations (0, 7, 14, 28 mM) at pH 6.5 (top) and pH 5.3 (bottom). Similar chemical shift trends at pH 5.3 and 6.5 indicate systematic and titration-responsive effects on the $\beta$-glucan signals upon addition of glycocholate. The chemical shift changes are consistent with a lower $K_d$ at pH 5.3.

dimensional experiments. In order to exclude systematic effects due to instabilities of the deuterium lock signal or temperature, the anticipated small chemical shift changes in the titration were measured as the chemical shift difference ($\Delta\delta$) between the two $\beta$-glucan signals. Changes in $\Delta\delta$ up to 15 parts per billion (3 Hz at a $^{13}C$ frequency of 201 MHz) were detected in experiments of 25 min duration. Titrations were conducted at 2 different pH values, 6.5 and 5.3 (Figure 4). Similar trends are observed in the titrations conducted at different pH values, and NMR determinations are consistent with previous in vitro studies with HPLC analysis indicating that the retention of bile salts by $\beta$-glucan-rich oat extrudates is higher near pH 5 than near pH 6.5.[23]

$^{1}H-^{13}C$ HSQC supports the notion of interactions between bile salts and $\beta$-glucan using reasonably rapid assays. The observation of the carbohydrate signal in monitoring guest

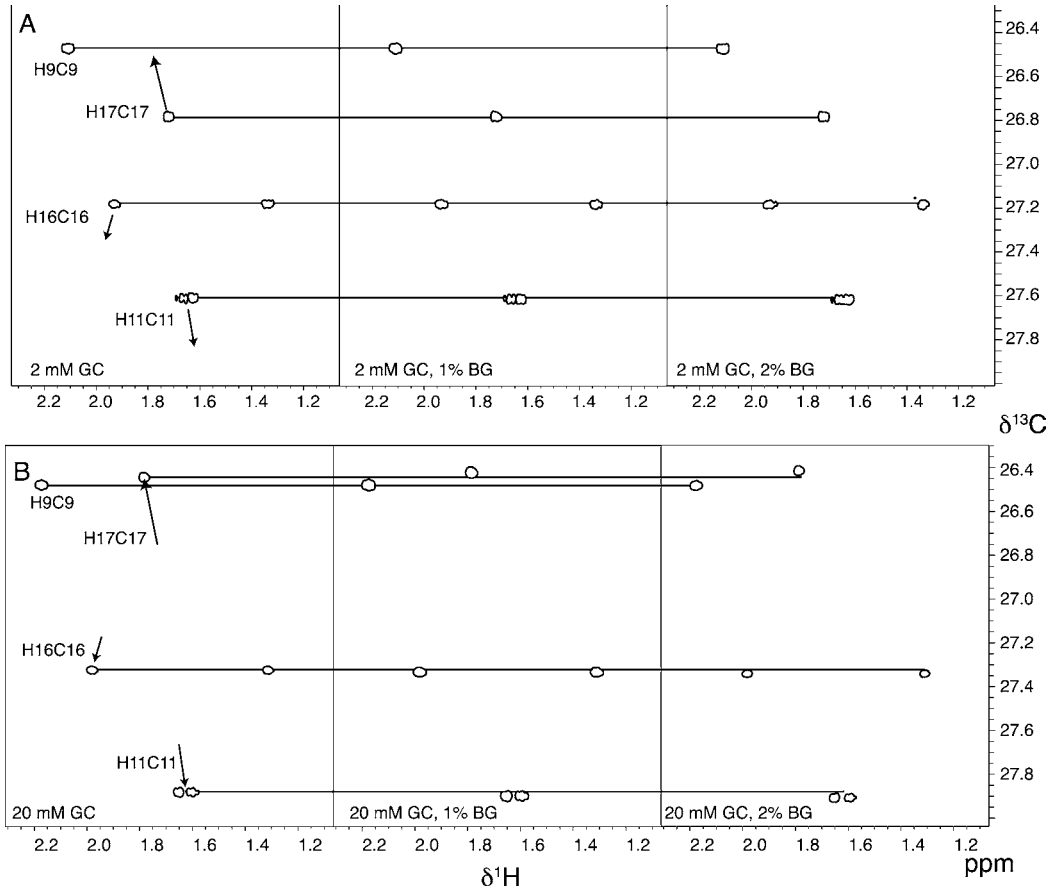


**Figure 5.** $^{1}H-^{13}C$ HSQC spectral region of glycocholate (2 mM in A and 20 mM in B) in the presence of increasing concentrations of medium viscosity $\beta$-glucan (200 kDa). Arrows indicate the change in GC signal when increasing the concentration from 2 mM to 20 mM. The addition of $\beta$-glucan induces small chemical shift changes of bile salt signals with the same trend as chemical shift changes upon the addition of bile salt itself. In the displayed spectral region, H11C11 and H16C16 resonances experience $^{13}C$ signal changes toward higher chemical shift, upon addition of $\beta$-glucan and of bile salt, while the H9C9 resonance remains unchanged and H17C17 shows a $^{13}C$ resonance change toward lower chemical shift, upon addition of $\beta$-glucan and of bile salt. These changes are more pronounced at 20 mM GC, above the critical micelle concentration of GC (7−11 mM).[28]

absorption onto functional polysaccharides or onto fragments thereof has practical advantages. The polysaccharide signals are intrinsically more robust to inaccuracies in sample pH or concentration, for instance due to the absence of easily ionizable groups in carbohydrates. Interactions between the bile salt and $\beta$-glucan were likewise probed by titrating medium viscosity $\beta$-glucan into samples containing a constant bile salt concentration, as previously described.[9] Chemical shift changes were monitored using $^{1}H-^{13}C$ HSQC experiments of 16 min duration, to yield the titration of glycocholate with $\beta$-glucan shown in Figure 5. Notably, rapid $^{1}H-^{13}C$ HSQC experiments can be conducted at concentrations near or below the critical micelle concentration of bile salts (low millimolar). Consequently, binding of $\beta$-glucan to glycocholate was monitored at 2 mM and at 20 mM bile salt concentration. Due to the aggregation into micelles, the glycocholate signals are strongly concentration dependent. Addition of up to 2% (w/v) medium viscosity $\beta$-glucan induces only small chemical shift changes at 2 mM bile salt and more pronounced chemical shift changes at 20 mM bile salt concentration. The bile salt signals are generally found to move upon $\beta$-glucan addition into the same direction that results from a concentration increase of the bile salt itself (Figure 5, Figure S1 in the Supporting Information). The presence of $\beta$-glucan therefore appears to stabilize micelle formation or lateral self-aggregation in the bile salt. Changes in bile salt signals themselves could be a consequence of increased local bile salt concentrations through confinement or excluded volume effects, thus underlining the usefulness of detecting signal changes in the binding partner to validate interactions.

Even using high-resolution spectroscopy, the chemical shift changes are at the edge of what is detectable. Hence, experiments were repeated using a different bile salt, taurochenodeoxycholate (TCDC) in order to validate the above findings. As for the titration with glycocholate, a downfield shift of the $^{13}C4$ signal in a glycosidic bond is detected upon addition of 7, 14, and 28 mM TCDC (Figure 6A). A titration of TCDC with $\beta$-glucan was conducted at a TCDC concentration of 3 mM to validate the viability of rapid $^{1}H-^{13}C$ HSQC assays at low millimolar bile salt concentrations. Chemical shift changes are again consistent with a stabilization of bile salt aggregation in the presence of $\beta$-glucan, as the addition of $\beta$-glucan consistently induces chemical shift changes in the bile salt that resemble chemical shift changes due to an increase in bile salt concentration (Figure 6B).

## ■ DISCUSSION

Polysaccharides play central roles as functional components of supramolecular assemblies in biology and technology. We find that $^{1}H-^{13}C$ HSQC NMR spectroscopy provides sufficient

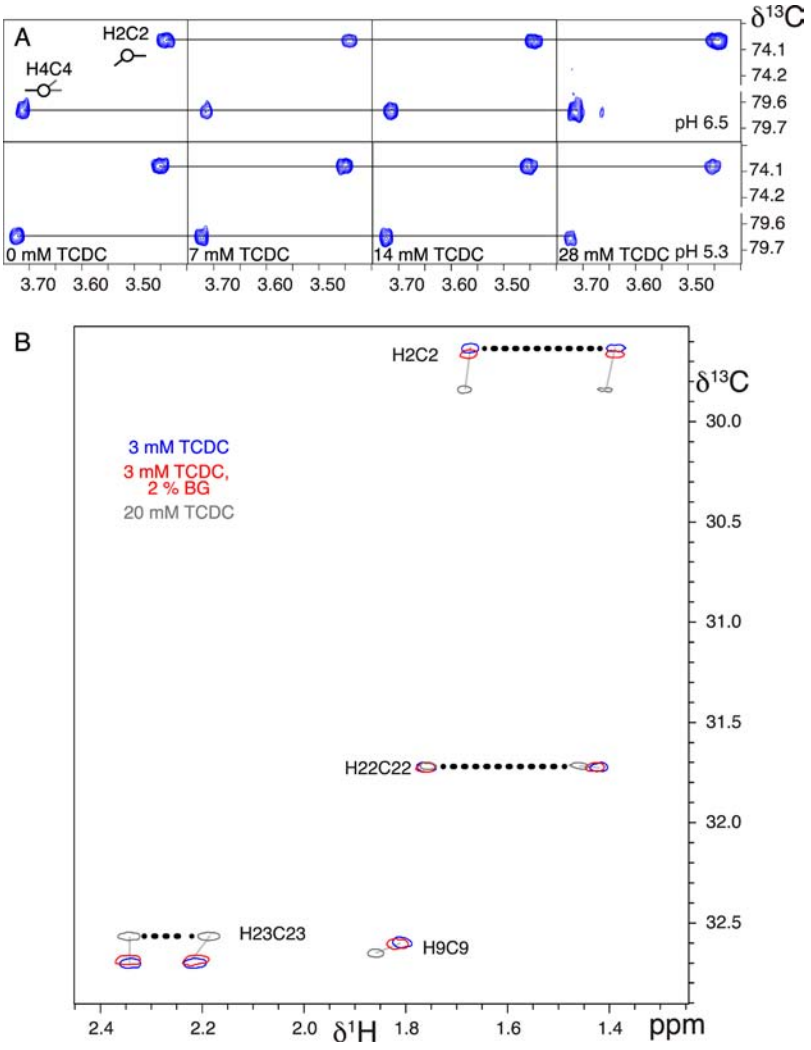


**Figure 6.** Titrations of $\beta$-glucan with TCDC (A; top pH 6.5, bottom pH 5.3) and of TCDC with $\beta$-glucan (B) support small chemical shift changes in the $\beta$-glucan and signal changes in the bile salt consistent with a stabilization of the micellar form.

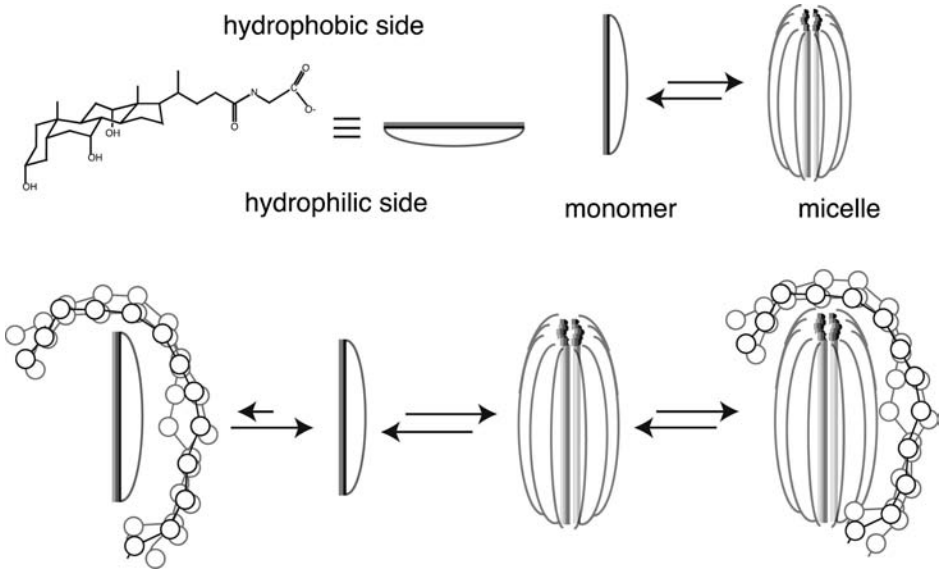


**Figure 7.** Model of $\beta$-glucan interaction with bile salts. The higher affinity between multivalent host and guest favors binding of $\beta$-glucan to the bile salt micelle relative to the monomer, thus stabilizing the micellar form, overall.


dx.doi.org/10.1021/jf504352w | J. Agric. Food Chem. 2014, 62, 11472−11478

sensitivity to enable rapid observations of molecular interactions involving polysaccharides and guest molecules at molecular detail. Such observations are feasible for probing interactions of β-glucan and bile salts, even though the interactions are dynamic and result in chemical shift changes in viscous polysaccharide solutions on the order of only 0.01 ppm. Interactions involving carbohydrates are commonly probed by NMR spectroscopy through the detection of signals from the non-carbohydrate binding partner,[9,24−26] as the carbohydrate $^{1}H$ spectral region usually is crowded and overlaps with the water signal. The observation of well-separated carbohydrate signals in aliased $^{1}H-^{13}C$ HSQC spectra enables the use of both binding partners as host and guest molecules in titrations. The detection of chemical shift changes in both binding partners then supports direct interactions with the carbohydrate.

Many attempts have been made to clarify how β-glucans might interact with bile salts in the small intestine, preventing their reabsorption and leading to excess excretion via the feces. Collectively, there are three main hypotheses: (a) increase, by β-glucans, of the intestinal viscosity whereby reabsorption of bile salts may be prevented by a potential β-glucan barrier layer; (b) entrapment of bile salt micelles in β-glucan molecular networks or aggregates; and (c) binding of bile salt monomers or micelles to β-glucans at a molecular level.[5,10] Here, we obtain $^{1}H-^{13}C$ HSQC titrations of bile salts and β-glucan that are consistent with direct molecular interactions between bile salts and all used β-glucans. The interaction results in a stabilization of bile salt micelles in the presence of β-glucan, presumably due to a stronger interaction of the β-glucan with the micelle than with the bile salt monomer (Figure 7), and influences β-glucan signals, primarily at the sites of glycosidic linkages (Figure S3 in the Supporting Information). An increased interaction between bile salt micelles and β-glucan is not surprising given the repetitive structure of the β-glucan and the resultant possibility for multivalent interactions between micelle and polymer. The minute chemical shift changes observed in the β-glucan argue against a cooperative structural transition of β-glucans upon addition of the bile salt host and against highly specific binding, opposite to the formation of hydrophobic inclusion complexes between amphiphilic hosts and α(1−4)-glucans.[24] Notably, the use of $^{1}H-^{13}C$ HSQC NMR at high magnetic field provides sufficient selectivity and sensitivity to examine polysaccharide−guest interactions within a time frame of minutes, making the screening of various host and guest molecules practical. We finally note that cholic acid based receptors have been devised as biomimetic receptors for carbohydrates, including β-glucosides.[27] These receptors exhibit multivalent interactions between the carbohydrate and the hydrophilic face of the cholic acid building blocks, thus exploiting similar interactions as those indicated in the model of Figure 7.

In conclusion, this study shows that $^{1}H-^{13}C$ NMR assays on the time scale of minutes detect signal changes in both bile salts and β-glucans, thus arguing for direct dynamic interactions, without inducing cooperative conformational changes in the β-glucans. Titrations are consistent with stronger interactions at pH 5.3 than at pH 6.5 in this in vitro assay. The changes in bile salt and β-glucan signals suggest a stabilization of bile salt micelles through transient, multivalent interactions with β-glucans.

## ■ ASSOCIATED CONTENT

### Supporting Information

An overview figure of bile acid signal changes upon concentration increase of the bile acid itself and upon addition of β-glucan is provided. These changes are mapped onto the bile acid structure. Interaction studies using laminaribiose as a model saccharide are demonstrated, indicating transient interactions with low specificity and weak effect on molecular tumbling, but exerting some small changes in glycosidic linkage conformation. This material is available free of charge via the Internet at http://pubs.acs.org.

## ■ AUTHOR INFORMATION

### Corresponding Author

*Technical University of Denmark, Kemitorvet, Building 201, DK-2800 Kgs. Lyngby, Denmark. E-mail: semei@kemi.dtu.dk.

### Funding

The authors gratefully acknowledge The Danish National Advanced Technology Foundation for financial support to the LIQFUN-project and funding by the Carlsberg Foundation Grant 2013_01_0709.

### Notes

The authors declare no competing financial interest.

## ■ ACKNOWLEDGMENTS

NMR spectra were recorded with the 800 MHz spectrometer of the Danish National Instrument Center for NMR Spectroscopy of Biological Macromolecules at the Technical University of Denmark.

## ■ REFERENCES

(1) Davidson, M. H.; Dugan, L. D.; Burns, J. H.; Bova, J.; Story, K.; Drennan, K. B. The hypocholesterolemic effects of beta-glucan in oatmeal and oat bran. A dose-controlled study. *JAMA, J. Am. Med. Assoc.* **1991**, *265*, 1833−1839.

(2) Lia, A.; Hallmans, G.; Sandberg, A. S.; Sundberg, B.; Aman, P.; Andersson, H. Oat β-glucan increases bile acid excretion and a fiber-rich barley fraction increases cholesterol excretion in ileostomy subjects. *Am. J. Clin. Nutr.* **1995**, *62*, 1245−1251.

(3) Truswell, A. S. Cereal grains and coronary heart disease. *Eur. J. Clin. Nutr.* **2002**, *56*, 1−14.

(4) Wood, P. J. Cereal β-glucans in diet and health. *J. Cereal Sci.* **2007**, *46*, 230−238.

(5) Theuwissen, E.; Mensink, R. P. Water-soluble dietary fibers and cardiovascular disease. *Physiol. Behav.* **2008**, *94*, 285−292.

(6) Bowles, R. K.; Morgan, K. R.; Furneaux, R. H.; Coles, G. D. 13C CP/MAS NMR study of the interaction of bile acids with barley β-d-glucan. *Carbohydr. Polym.* **1996**, *29*, 7−10.

(7) Simonsen, H. T.; Nielsen, M. S.; Christensen, N. J.; Christensen, U.; La Cour, T. V.; Motawia, M. S.; Jespersen, B. P.; Engelsen, S. B.; M?ller, B. L. Molecular interactions between barley and oat beta-glucans and phenolic derivatives. *J. Agric. Food Chem.* **2009**, *57*, 2056−2064.

(8) Story, J. A.; Kritchevsky, D. Comparison of the binding of various bile acids and bile salts in vitro by several types of fiber. *J. Nutr.* **1976**, *106*, 1292−1294.

(9) Gunness, P.; Flanagan, B. M.; Gidley, M. J. Molecular interactions between cereal soluble dietary fibre polymers and a model bile salt deduced from $^{13}C$ NMR titration. *J. Cereal Sci.* **2010**, *52*, 444−449.

(10) Gunness, P.; Gidley, M. J. Mechanisms underlying the cholesterol-lowering properties of soluble dietary fibre polysaccharides. *Food Funct.* **2010**, *1*, 149−155.

(11) Kim, H. J.; White, P. J. Interactional Effects of β-Glucan, Starch, and Protein in Heated Oat Slurries on Viscosity and In Vitro Bile Acid Binding. *J. Agric. Food Chem.* **2012**, *60*, 6217−6222.

(12) Northfield, T. C.; McColl, I. Postprandial concentrations of free and conjugated bile acids down the length of the normal human small intestine. *Gut* **1973**, *14*, 513−518.
(13) Mikkelsen, M. S.; Jespersen, B. M.; Larsen, F. H.; Blennow, A.; Engelsen, S. B. Molecular structure of large-scale extracted beta-glucan from barley and oat: Identification of a significantly changed block structure in a high beta-glucan barley mutant. *Food Chem.* **2013**, *136*, 130−138.
(14) Hyun, J. K.; White, P. J. In vitro bile-acid binding and fermentation of high, medium, and low molecular weight *β*-glucan. *J. Agric. Food Chem.* **2010**, *58*, 628−634.
(15) Kay, L.; Keifer, P.; Saarinen, T. Pure absorption gradient enhanced heteronuclear single quantum correlation spectroscopy with improved sensitivity. *J. Am. Chem. Soc.* **1992**, *114*, 10663−10665.
(16) Ijare, O.; Somashekar, B. S.; Jadegoud, Y.; Nagana Gowda, G. A. $^{1}$H and $^{13}$C NMR characterization and stereochemical assignments of bile acids in aqueous media. *Lipids* **2005**, *40*, 1031−1041.
(17) Petersen, B. O.; Olsen, O.; Beeren, S. R.; Hindsgaul, O.; Meier, S. Monitoring pathways of beta-glucan degradation by enzyme mixtures in situ. *Carbohydr. Res.* **2013**, *368*, 47−51.
(18) Schulze-Sunninghausen, D.; Becker, J.; Luy, B. Rapid heteronuclear single quantum correlation NMR spectra at natural abundance. *J. Am. Chem. Soc.* **2014**, *136*, 1242−1245.
(19) Paudel, L.; Adams, R. W.; Kiraly, P.; Aguilar, J. A.; Foroozandeh, M.; Cliff, M. J.; Nilsson, M.; Sandor, P.; Waltho, J. P.; Morris, G. A. Simultaneously enhancing spectral resolution and sensitivity in heteronuclear correlation NMR spectroscopy. *Angew. Chem.* **2013**, *52*, 11616−11619.
(20) Jeannerat, D. Computer optimized spectral aliasing in the indirect dimension of $^{1}$H-$^{13}$C heteronuclear 2D NMR experiments. A new algorithm and examples of applications to small molecules. *J. Magn. Reson.* **2007**, *186*, 112−122.
(21) Bojstrup, M.; Petersen, B. O.; Beeren, S. R.; Hindsgaul, O.; Meier, S. Fast and accurate quantitation of glucans in complex mixtures by optimized heteronuclear NMR spectroscopy. *Anal. Chem.* **2013**, *85*, 8802−8808.
(22) Petersen, B. O.; Hindsgaul, O.; Meier, S. Profiling of carbohydrate mixtures at unprecedented resolution using high-precision $^{1}$H-$^{13}$C chemical shift measurements and a reference library. *Analyst* **2014**, *139*, 401−406.
(23) Drzikova, B.; Dongowski, G.; Gebhardt, E.; Habel, A. The composition of dietary fibre-rich extrudates from oat affects bile acid binding and fermentation in vitro. *Food Chem.* **2005**, *90*, 181−192.
(24) Beeren, S. R.; Meier, S.; Hindsgaul, O. Probing helical hydrophobic binding sites in branched starch polysaccharides using NMR spectroscopy. *Chem.—Eur. J.* **2013**, *19*, 16314−16320.
(25) Ferrand, Y.; Crump, M. P.; Davis, A. P. A synthetic lectin analog for biomimetic disaccharide recognition. *Science* **2007**, *318*, 619−622.
(26) Klein, E.; Crump, M. P.; Davis, A. P. Carbohydrate recognition in water by a tricyclic polyamide receptor. *Angew. Chem.* **2004**, *44*, 298−302.
(27) Davis, A. P.; Wareham, R. S. Carbohydrate Recognition through Noncovalent Interactions: A Challenge for Biomimetic and Supramolecular Chemistry. *Angew. Chem.* **1999**, *38*, 2978−2996.
(28) Gouin, S.; Zhu, X. X. Fluorescence and NMR Studies of the Effect of a Bile Acid Dimer on the Micellation of Bile Salts. *Langmuir* **1998**, *14*, 4025−4029.

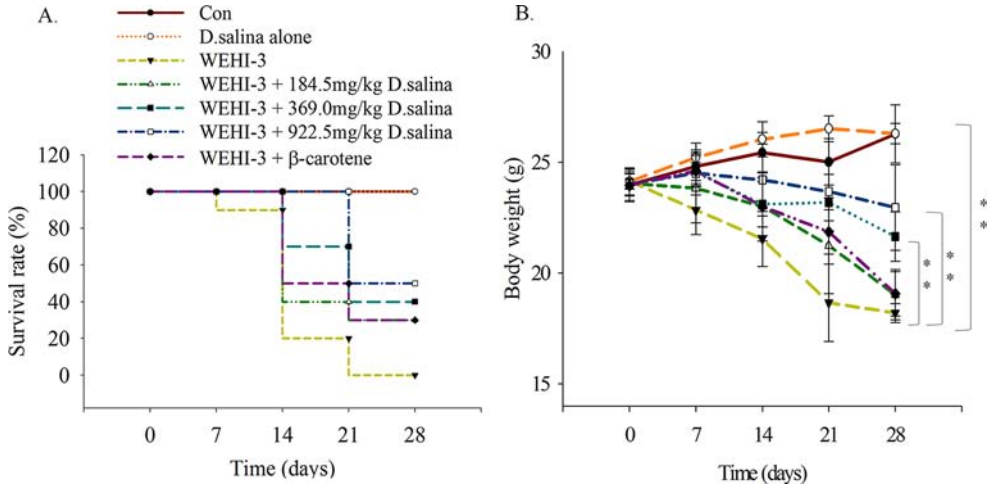


**Figure 1.** Effects of *D. salina* on survival rate and body weight. BALB/c mice were iv injected with WEHI-3 cells ($1 \times 10^5$ cells/mice) and treated with *D. salina* by oral administration for 4 weeks. ($n = 10$, mean ± SD.) *, **, and *** indicate significant difference between two groups at $p < 0.05$, $p < 0.01$, and $p < 0.001$, respectively.

contents in the *D. salina* of *all-trans*-*β*-carotene, 9- or 9′-*cis*-*β*-carotene, *all-trans*-zeaxanthin, *all-trans*-lutein, 13- or 13′-*cis*-*β*-carotene, *all-trans*-*α*-carotene, and 9- or 9′-*cis*-*β*-carotene were 138.25, 124.65, 11.27, 6.55, 4.95, 2.69, and 2.41 mg/g algae, respectively, measured by HPLC as described previously.[5,15] The ratio of *all-trans*- and *cis*-*β*-carotene, the major carotenoids in the algae, was 53:47. RPMI-1640 medium was obtained from Hyclone (South Logan, UT, USA). Fetal bovine serum (FBS) was obtained from Biological Industries (Kibbutz Beit Haemek, Israel). Penicillin−streptomycin and glutamine were obtain from Gibco BRL (Grrand Island, NY, USA). *β*-Carotene was obtained from Sigma (St. Louis, MO, USA).

**Animals.** A total of 140 male BALB/c mice, each at the age of 6 weeks and about 22−28 g in weight, were purchased from the Animal Department of BioLASCO Taiwan Co., Ltd. (Taipei City, Taiwan, ROC). The animals were maintained under a 12 h light/dark cycle in a humidity- and temperature-controlled room under standard laboratory conditions. Mice were housed five in each cage and allowed food and water ad libitum. They were acclimated and quarantined for a week prior to experimentation. The protocol for the animal study was approved by the Institutional Animal Care and Committee (IACUC no. 1074), and all mice were cared for following the institutional ethical guideline.[6,16]

**Cell Culture.** The WEHI-3 murine myelomonocytic leukemia cell line and YAC-1 murine lymphoma cell line were purchased from the Bioresource Collection and Research Center (Hsinchu, Taiwan). The cells were cultured onto 10 $cm^2$ dishes and maintained in RPMI-1640 medium supplemented with 10% fetal bovine serum, 100 $\mu$g/mL streptomycin, 100 U/mL penicillin, and 2 mM L-glutamine at 37 °C in a 5% $CO_2$ incubator.

**Experimental Designs.** The experiment was made up of two parts. In part I, over a period of 4 weeks, the effect of *D. salina* on the survival rate in WEHI-3 leukemic mice was investigated. In part II, over a period of 2 weeks, the immunomodulatory effects of *D. salina* on WEHI-3 leukemic mice were investigated. Seventy BALB/c mice were randomly divided into 7 groups with 10 animals in each group. *D. salina* was suspended in distilled water before use and administered by oral gauge. The dosages of *D. salina* used in this study were calculated from the commercial product's suggestion for daily intake (i.e., 15 mg/kg bw/human equals 184.5 mg/kg bw/mice). Group I was the control and group II was treated with *D. salina* only. Groups III−VII were intravenously injected via the tail vein with WEHI-3 cells ($1 \times 10^5$ cells/100 $\mu$L PBS) only. Group IV−VI were cotreated with *D. salina* at doses of 184.5, 369, and 922.5 mg/kg, respectively. Group VII was cotreated with 922.5 mg/kg *β*-carotene as the positive control.

**Cell Surface Markers Examination.** The mice were euthanized by $CO_2$, and whole blood was collected via heart puncture after injection of WEHI-3 cells for 2 weeks. The blood samples were immediately lysed with BD Pharm Lyse (BD Biosciences) and then centrifuged at 1500 rpm (1000*g*) for 15 min at 4 °C. The collected white blood cells evaluated for cell surface markers including T-cells, B-cells, monocytes, and macrophages were respectively stained with anti-CD3-FITC, anti-CD19-PE, anti-CD11b-PE, and anti-Mac-3-FITC antibodies (SouthernBiotech Inc.) and then were analyzed by flow cytometry (FACS Calibur, Becton Dickinson, NJ, USA) as previously described.[20]

**Organ Weight and Pathological Examination.** A necropsy was performed on each mouse, and the spleen was weighed after dissection. Then, it was examined grossly and fixed in 10% formalin buffer. A transverse section in the hilus was made at the largest extension of the spleen; red and white pulps of spleen were trimmed and embedded in paraffin, sectioned to a thickness of 2 $\mu$m, and stained with hematoxylin and eosin for the microscopic examination. For semiquantitative grading, the severity of the lesions was graded on the basis of the criteria of Shackelford et al.[21] with five grades of severity of lesions specified: 1 = minimal (<1%); 2 = slight (2−25%); 3 = moderate (26−50%); 4 = moderate/severe (51−75%); and 5 = severe/high (76−100%).

**Splenocyte Proliferation Examination.** About $1 \times 10^5$ splenocytes/mL isolated from the spleen in each group were individually cultured with RPMI-1640 medium in 24-well culture plates. Con A (5 $\mu$g/mL) and LPS (5 $\mu$g/mL) were added to activate T- and B-cells, respectively. The treated and untreated cells were incubated for 72 h in a $CO_2$ incubator. The proliferation of T- and B-cells was determined by MTT assay.[17]

**Cytokine Examination.** About $2 \times 10^5$ splenocytes/mL isolated from the spleen in each group were individually cultured with RPMI-1640 medium in 24-well culture plates. After stimulation of splenocytes with Con A (5 $\mu$g/mL) and incubating for 24 h, the plates were centrifuged for 4 min at 500*g*, and the supernatants were collected before use.[17,22] The contents of IFN-*γ*, IL-2, IL4, and IL-10 were quantified using commercial ELISA kits (Enzo Life Sciences, Vinci-Biochem, Vinci, Firenze, Italy). The procedurse followed in accordance with the manufacturer's protocols.

**Phagocytosis Examination.** The phagocytosis of macrophages in the PBMCs was measured by using the Phagotest kit (Orpegen Pharma, Heidelberg, Germany). The assay procedures followed in accordance with the manufacturer's instructions. Briefly, isolated cells from each mouse were individually incubated with the FITC-labeled *Escherichia coli* bacteria (20 $\mu$L) at 37 °C for 1 h. Next, 100 $\mu$L of ice-cold quenching solution was added to stop the reaction. Then, the macrophages/monocytes were fixed and stained with PI solution. The samples were analyzed by using a flow cytometer with Cellquest software.[22,23]

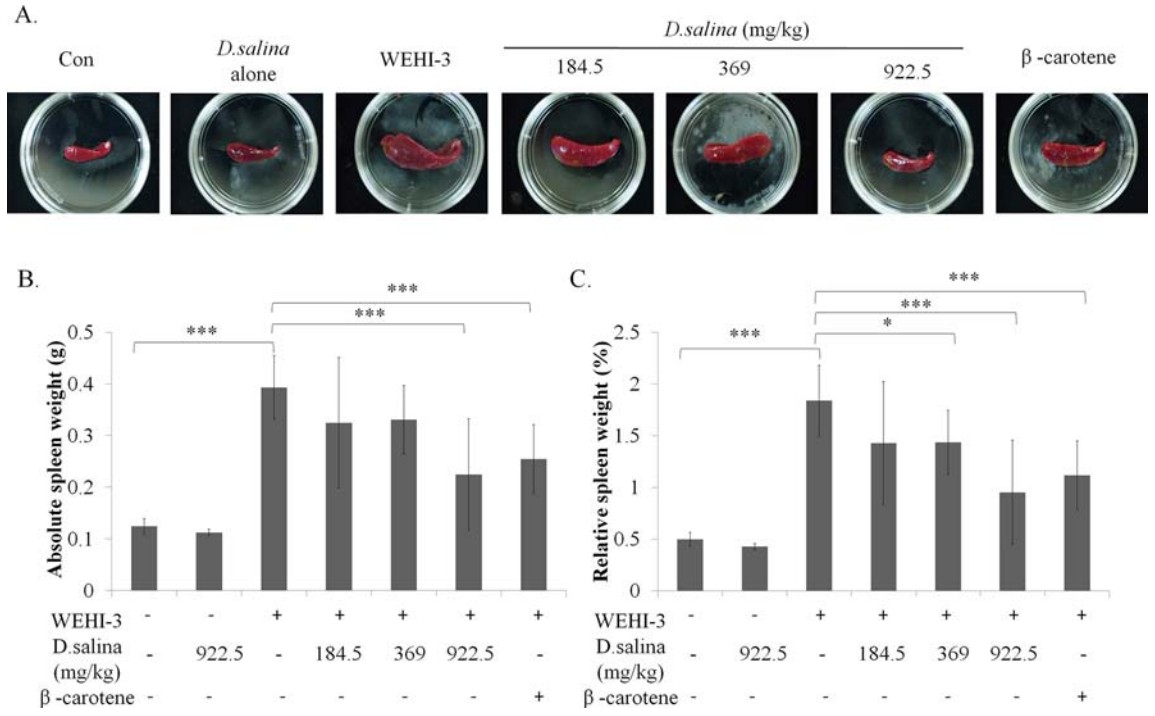


**Figure 2.** Change of spleen in the WEHI-3-induced leukemic mice. BALB/c mice were iv injected with WEHI-3 cells ($1 \times 10^5$ cells/mice) and treated with *D. salina* by oral administration for 2 weeks. Animals were sacrificed for examinations of gross (A) and spleen weights (B). ($n$ = 10, mean ± SD.) ∗, ∗∗, and ∗∗∗ indicate significant difference between two groups at $p < 0.05$, $p < 0.01$, and $p < 0.001$, respectively.

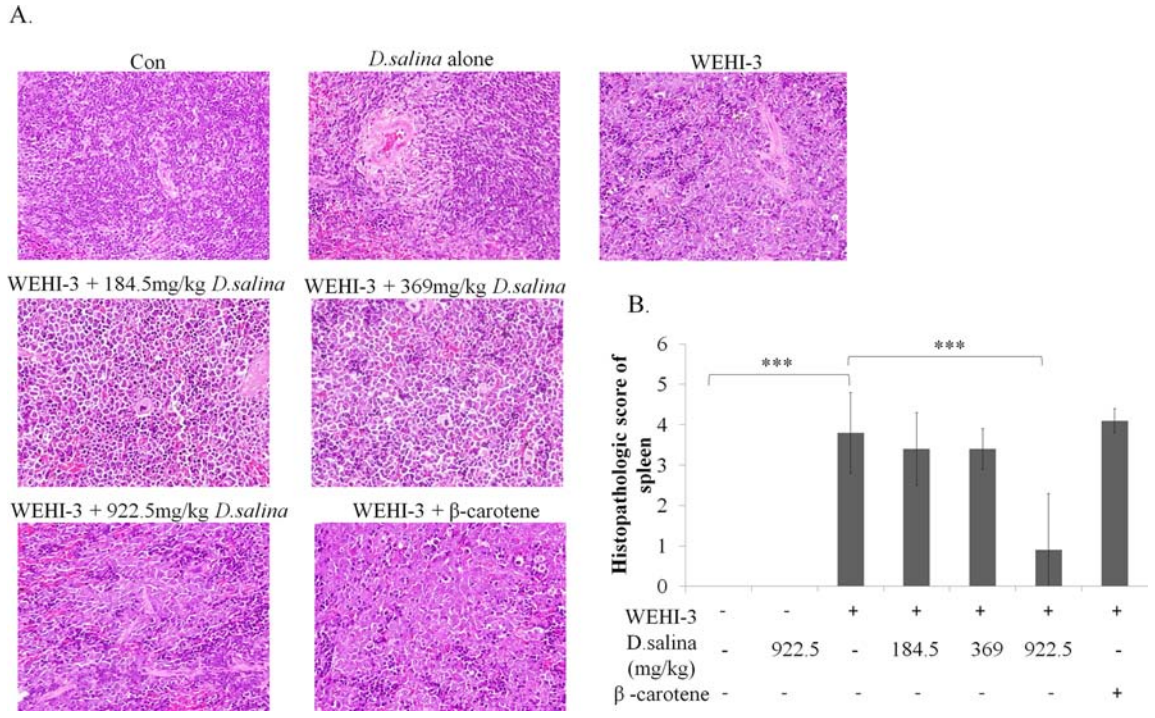


**Figure 3.** Hisopathological photographs and scores of spleen in the WEHI-3-induced leukemic mice. BALB/c mice were iv injected with WEHI-3 cells ($1 \times 10^5$ cells/mice) and treated with *D. salina* for 2 weeks. Spleens were sectioned, stained with hematoxylin eosin (400×) (A) and scored (B). The severity of the lesions was graded with five grades of severity of lesions specified: 1 = minimal (<1%); 2 = slight (2−25%); 3 = moderate (26−50%); 4 = moderate/severe (51−75%); and 5 = severe high (76−100%). ($n$ = 10, mean ± SD.) ∗, ∗∗, and ∗∗∗ indicate significant difference between two groups at $p < 0.05$, $p < 0.01$, and $p < 0.001$, respectively.

**NK Cell Cytotoxicity Examination.** Splenocytes isolated from spleens in each group were used as effector cells. YAC-1 cells sensitized to NK cell cytotoxicity were used as target cells. Target cell killing was determined with a lactic dehydrogenase (LDH) release assay by using the LDH-Cytotoxicity Assay Kit II (Biovision, Inc.). YAC-1 ($1 \times 10^5$) was cocultured with splenocytes at a final effector/target (E:T) ratio of 50:1 and incubated in 24-well culture plates for 6 h in an incubator. Ten microliters of supernatants was transferred into


dx.doi.org/10.1021/jf503564b | J. Agric. Food Chem. 2014, 62, 11479−11487

**Table 1. Effect of *D. salina* on Hematological Analysis in BALB/c Mice after Injection with WEHI-3 Cells for 2 Weeks[a]**

| group | WBC ($10^3/\mu L$) | RBC ($10^6/\mu L$) | Hb (g/dL) |
|---|---|---|---|
| control | 7.83 ± 2.29 | 10.52 ± 0.18 | 16.17 ± 0.15 |
| *D. salina* alone | 11.65 ± 2.38** | 10.72 ± 0.24 | 16.29 ± 0.4 |
| WEHI-3 | 14.45 ± 4.76** | 10.03 ± 0.62 | 15.56 ± 1.02 |
| WEHI-3 + 184.5 mg/kg *D. salina* | 10.81 ± 4.35 | 10.51 ± 0.47 | 16.3 ± 0.69 |
| WEHI-3 + 369.0 mg/kg *D. salina* | 6.96 ± 1.38### | 10.46 ± 0.28 | 16.24 ± 0.49 |
| WEHI-3 + 922.5 mg/kg *D. salina* | 9.86 ± 2.40# | 10.54 ± 0.4 | 16.31 ± 0.63 |
| WEHI-3 + $\beta$-carotene | 11 ± 3.61 | 10.78 ± 0.29 | 16.47 ± 0.47 |

[a]Each value represents the mean ± SD of 10 animals. *, **, and *** indicate significant difference from control groups ($p < 0.05$, $p < 0.01$, and $p < 0.001$, respectively). #, ##, and ### indicate significant difference from WEHI-3 groups ($p < 0.05$, $p < 0.01$, and $p < 0.001$, respectively).

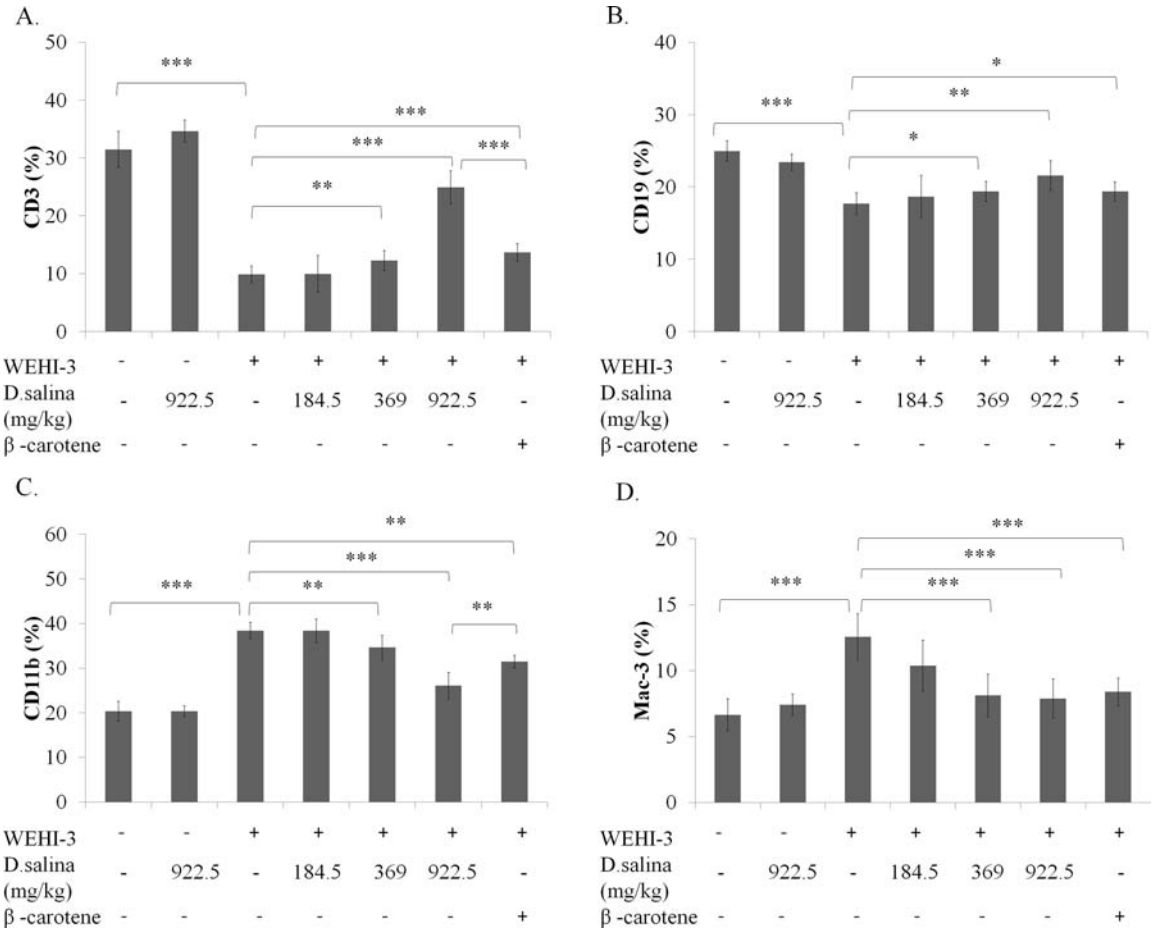


**Figure 4.** Effect of *D. salina* on cell markers of white blood cells from BALB/c mice. BALB/c mice were injected with WEHI-3 cells ($1 \times 10^5$ cells/mice) and treated with *D. salina* for 2 weeks. Blood was collected from individual animals and analyzed for cell markers (A) CD3, (B) CD19, (C) CD11b, and (D) Mac-3 by flow cytometry. ($n = 10$, mean ± SD.) *, **, and *** indicate significant difference between two groups at $p < 0.05$, $p < 0.01$, and $p < 0.001$, respectively.

a 96-well plate, followed by centrifuging for 4 min at 500*g*. One hundred microliters of LDH of substrate was added and incubated at room temperature. After 20 min, 10 $\mu$L of stop solution was added immediately, and then the absorbance was measured by microplate reader at OD450 nm. The NK cell cytotoxicity was calculated using the formula cytotoxicity % = (experimental OD − effector cell spontaneous OD − target cell spontaneous OD)/(target cell lysis OD − target cell spontaneous OD) × 100.[24]

**Statistical Analysis.** The data were expressed as mean ± SD, and the differences between any two groups were performed using one-way analysis of variance (ANOVA) followed by Dunnett's multiple-comparison tests using the statistical software SPSS (DR Marketing Co., Ltd., New Taipei City, Taiwan, ROC). Values of $p < 0.05$, $p < 0.01$, and $p < 0.001$ were used as the levels of significance.

## RESULTS

**Survival Rate and Body Weight Change in WEHI-3 Leukemic Mice.** Over a period of 4 weeks, the effects of *D. salina* on the survival rate and body weight in mice were recorded. As shown in Figure 1A, there was no significant difference between control and *D. salina* only treated group on the survival rate. *D. salina* (184.5, 369, and 922.5 mg/kg) prolonged the survival rate in WEHI-3 leukemic mice in a dose-dependent manner. Treatment with $\beta$-carotene, as a positive control group, showed the 30% survival rate when compared to the WEHI-3 only group at the fourth week. As shown in Figure 1B, *D. salina* (369 and 922.5 mg/kg) significantly restored the body weight when compared to WEHI-3 only group during 4

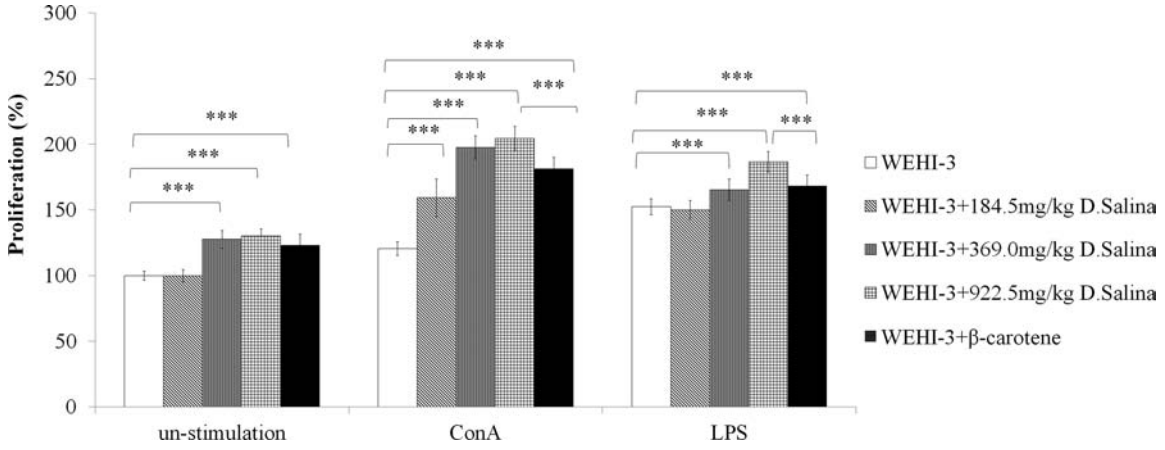


**Figure 5.** Effect of *D. salina* on the proliferation of T- and B-cells from BALB/c mice. Splenocytes were isolated from each group of BALB/c mice following *D. salina* treatment and then Con A and LPS stimulated for 3 days for examinations of T- and B-cell proliferation, respectively. ($n$ = 10, mean ± SD.) ∗, ∗∗, and ∗∗∗ indicate significant difference between two groups at $p < 0.05$, $p < 0.01$, and $p < 0.001$, respectively.

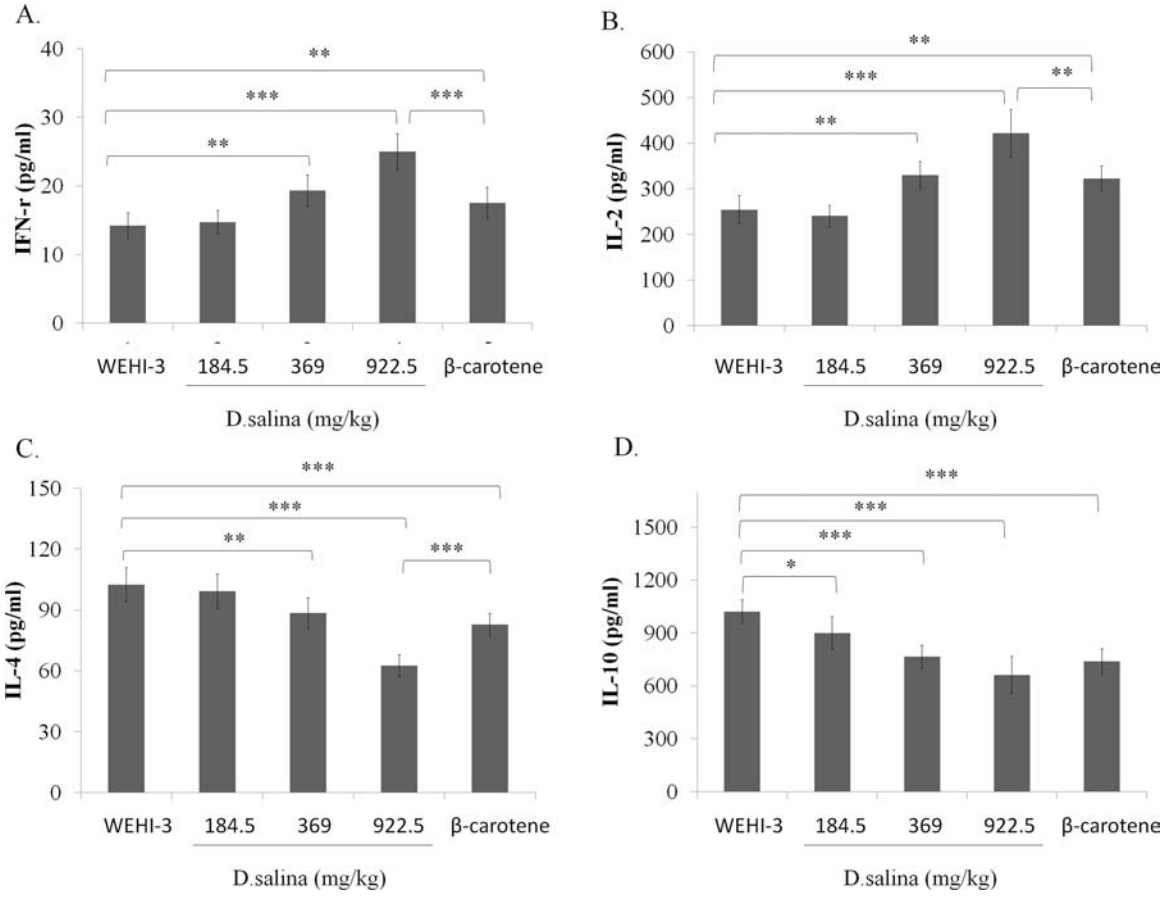


**Figure 6.** Effect of *D. salina* on the levels of cytokine after Con A stimulation of splenocytes from BALB/c mice. About $2 \times 10^5$ splenocyte cells in medium from WEHI-3 cells were injected into BALB/c mice following *D. salina* treatment for 2 weeks and then were stimulated with Con A (5 μg/mL). Levels of IFN-γ (A), IL-2 (B), IL-4 (C), and IL-10 (D) were determined by ELISA kit. ($n$ = 10, mean ± SD.) ∗, ∗∗, and ∗∗∗ indicate significant difference between two groups at $p < 0.05$, $p < 0.01$, and $p < 0.001$, respectively.

weeks ($p < 0.01$). *D. salina* treatment showed more beneficial effects than β-carotene in both the survival rate and body weight.

**Change of Spleen Weight in WEHI-3 Leukemic Mice.** Over a period of 2 weeks, the animals were euthanized, whole blood was collected, and spleen was isolated and weighed. The spleen size and weight are presented in Figure 2. There was no significant difference between control and *D. salina* only treated groups (Figure 2A). The treatment of WEHI-3 cells in group III had increased the absolute and relative organ weights ($p < 0.001$) (Figure 2B,C). The high dose of *D. salina* (922.5 mg/kg) and β-carotene treatment significantly decreased the absolute and relative weights of spleen when compared to the WEHI-3 only group ($p < 0.001$).

**Histopathological Examination of Spleen in WEHI-3 Leukemic Mice.** As shown in Figure 3A, no significant


dx.doi.org/10.1021/jf503564b | J. Agric. Food Chem. 2014, 62, 11479−11487

changes of spleen were found in the control and *D. salina* only group. However, numerous leukemia cells had infiltrated into the spleen of the WEHI-3 leukemic mice. The neoplastic cells showed round with enlarged nuclei, high nucleonic/cytoplasm ratios with highly mitosis, and increased megakaryocytes in the red pulp area of the spleen. The treatment of WEHI-3 cells in group III has increased the leukemia score in spleen ($p < 0.001$) (Figure 3B). The high dose of *D. salina* (922.5 mg/kg) group had significantly decreased leukemia scores of spleen when compared to the WEHI-3 only group ($p < 0.001$). None of the above effect was found in the $\beta$-carotene group.

**Hematology and Cell Surface Markers in WEHI-3 Leukemic Mice.** The results of hematological analysis in BALB/c mice following *D. salina* treatment are presented in Table 1. *D. salina* groups (369 and 922.5 mg/kg) showed decreased levels of WBC compared to the WEHI-3 only group ($p < 0.05$). There was no significant difference between the $\beta$-carotene and WEHI-3 only groups ($p > 0.05$). The cell surface markers of WBC from BALB/c mice following *D. salina* treatment are presented in Figure 4, which indicated that *D. salina* (369 and 922.5 mg/kg) and $\beta$-carotene increased the percentages of CD3 (Figure 4A) and CD19 (Figure 4B) compared to the WEHI-3 only group in a dose-dependent manner but decreased the percentages of CD11b (Figure 4C) and Mac-3 (Figure 4D).

**Proliferation of Splenocytes in WEHI-3 Leukemic Mice.** Splenic lymphocyte proliferation was stimulated by Con A and LPS in vitro as methods to evaluate T- and B-lymphocyte activities, respectively.[25] As shown in Figure 5, *D. salina* (369 and 922.5 mg/kg) enhanced the significant proliferation of splenocytes under untreated Con A and LPS conditions ($p < 0.001$). Especially, Con A-induced T-cell proliferation was significantly enhanced by *D. salina* (184.5, 369, and 922.5 mg/kg) ($p < 0.001$), and the proliferation rates of the treatment groups were increased nearly 38, 77, and 84% as compared with the WEHI-3 only group. Similarly, LPS-induced B-cell proliferation was significantly enhanced by *D. salina* (369 and 922.5 mg/kg), increasing nearly 13 and 34% as compared with the WEHI-3 only group. Also, both Con A- and LPS-induced T- and B-cell proliferations in the *D.salina*-treated group were higher than those of the $\beta$-carotene-treated group ($p < 0.001$).

**Levels of Cytokine after Con A Stimulation of Splenocytes in WEHI-3 Leukemic Mice.** The splenocytes from mice following Con A treatment were separated, and the levels of IFN-$\gamma$, IL-2, IL-4, and IL-10 were determined. As shown in Figure 6, *D. salina* significantly increased the levels of IFN-$\gamma$ (Figure 6A) and IL-2 (Figure 6B) in a dose-dependent manner. However, *D. salina* significantly reduced the levels of IL-4 (Figure 6C) and IL-10 (Figure 6D) when compared to the WEHI-3 only group. Additionally, *D. salina* (922.5 mg/kg) significantly enhanced the levels of IFN-$\gamma$ and IL-2 but decreased the level of IL-4 when compared to the $\beta$-carotene-treated group ($p < 0.01$).

**Activity of NK Cells in WEHI-3 Leukemic Mice.** YAC-1 as target cells could be killed by NK cells isolated from spleens of the mice at an effector/target ratio of 50:1. As shown in Figure 7, treatment with *D. salina* alone increased the activity of NK cells when compared to the control group ($p < 0.05$). However, there was significantly reduced NK cell activity in the WEHI-3 only group ($p < 0.001$). As compared to the WEHI-3 only group, the doses of 369 and 922.5 mg/kg *D. salina* treatment exhibited high activity of NK cells. Additionally, *D. salina* (922.5 mg/kg) treatment showed better activity than $\beta$-carotene treatment ($p < 0.0.5$).

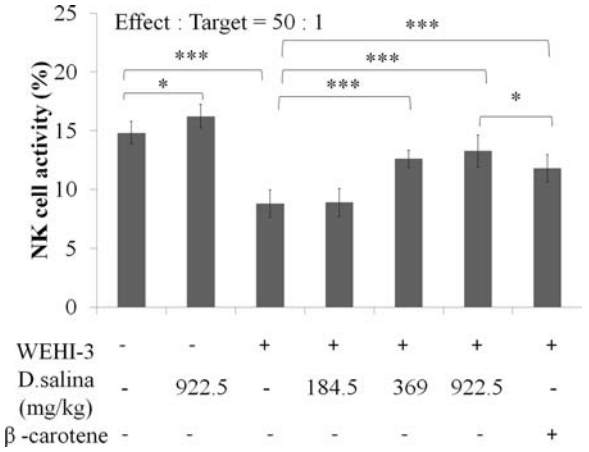


**Figure 7.** Effect of *D. salina* on the natural killer (NK) cell cytotoxic activity from BALB/c leukemic mice. The effects of *D. salina* on the YAC-1 target cells which were killed by NK cells from the mice following *D. salina* treatment in target cell ratio of 50:1 were analyzed for NK cell cytotoxic activity by LDH assay kit. ($n = 10$, mean ± SD.) *, **, and *** indicate significant difference between two groups at $p < 0.05$, $p < 0.01$, and $p < 0.001$, respectively.

**Macrophage Activity in WEHI-3 Leukemic Mice.** The phagocytosis from PBMC of the control and treated groups is presented in Figure 8. Treatment with *D. salina* alone increased

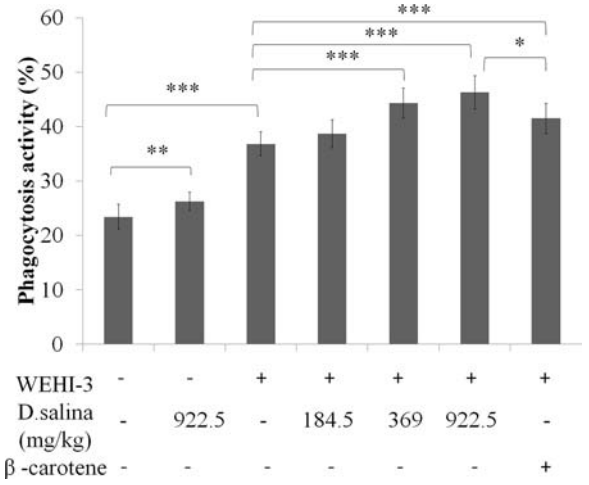


**Figure 8.** Effect of *D. salina* on the phagocytic activity by macrophages in WEHI-3-induced leukemic mice. Mice were injected without or with WEHI-3 cells ($1 \times 10^5$ cells/mice) and then orally treated with or without *D. salina* for 2 weeks. Cells were collected from animals of PBMC, and they were analyzed for phagocytic activity by flow cytometry. ($n = 10$, mean ± SD.) *, **, and *** indicate significant difference between two groups at $p < 0.05$, $p < 0.01$, and $p < 0.001$, respectively.

the phagocytosis rate when compared to the control group ($p < 0.01$) *D. salina* elevated the phagocytic rate compared to the WEHI-3 only group in a dose-dependent manner. At doses of 369 and 922.5 mg/kg, the effects enhanced the value from 36.8 to 44.3 and 46.3%, whereas increasing the dose to 184.5 mg/kg showed very little additional effect when compared to the WEHI-3 only group. These results indicated *D. salina*

promoted the activities of phagocytosis and showed stronger activity than that in mice treated by $\beta$-carotene ($p < 0.05$).

## DISCUSSION

In recent years, immunomodulation has become a promising direction in health food development in complementary and alternative medicine, especially for cancer. As $\beta$-carotene induced cytotoxicity in leukemia cells in vitro[10] and our pilot studies showed that *D. salina* inhibited the proliferation of leukemia cell lines including HL-60, KG-1, MOLT-4 and Jurkat cells, these raised the possibility that *D. salina* could be useful in complementary and alternative medicine against human leukemia. Thus, in the present study, we investigated the potential of *D. salina* in leukemia therapy in vivo. Our results showed that *D. salina* increased NK cell activity and phagocytosis and expression levels of IFN-$\gamma$ and IL-2 but reduced the levels of IL-4 and IL-10. These results provided strong support that the antileukemia immunity of *D. salina* was important in anti-WEHI3 leukemia in mice.

*D. salina*, which contains significant amounts of *all-trans*-$\beta$-carotene and 9- or 9′-*cis*-$\beta$-carotene, has excellent antioxidant activity. Also, 9- or 9′-*cis*-$\beta$-carotene has been implied to have better potential against the development of cardiovascular disease and malignant cancer as compared with the *all-trans* isomer.[5,13,26] This finding had been confirmed in our earlier studies, which suggested that *D. salina* enhanced the antioxidant enzyme activities against $CCl_4$- and UV-B-induced hepatotoxicity and corneal oxidative damage in mice.[6,16] Also, previous studies in vivo demonstrated that *D. salina* induced antioxidant enzyme activities against carcinogen-induced fibrosarcoma in rats as well as cisplatin combined vitamin E treatment[11] and that *D. bardawile* promoted the normal cell growth, but suppressed the tumor progression in mice.[12] Additionally, *D. salina* reduced LPS-induced inflammation via NF-$\kappa$B and MAPK pathways.[15] In the current study, *D. salina* promoted the immune response against leukemia in mice, therefore indicating that *D. salina* exhibited multiple biological functions including antioxidation, anti-inflammation, immunomodulation, and anticancer properties in vitro and in vivo.

The well-established WEHI-3 leukemic murine model has been used to show the increase in immature WBC, which consequently metastasized to the spleen, resulting in infiltration and enlargement.[20,27−29] The present study showed that *D. salina* (922.5 mg/kg) inhibited splenic tumor growth in leukemic mice (Figures 2 and 3). Results similar to ours can be found in combined treatment with chemotherapeutic drugs, arsenic trioxide, and *all-trans*-retinoic acid, which revealed that neoplastic cells appeared less in the splenic red pulp in leukemic mice following the drug treatment.[27]

In the current study, treatment with *D. salina* alone increased WBC (Table 1), with the increase still within the normal range. Also, the treatment showed no significant adverse effect (Figure 3). Following WEHI-3 cell injection, there was a significant increase in WBC, indicating that the increase was from the leukemia cells. This could be confirmed through the spleen pathology, indicating that leukemic cells were metastasized to the spleen tissue. This study showed *D. salina* caused an inhibitory effect on WEHI-3-induced WBC increase, which was probably due to *D. salina* inducing cell cycle arrest and apoptosis in neoplastic cells but not in normal cells.[8,9,12,30] In terms of lymphocyte population, there were similarity and corroboration between the significant increase in percentages of T- and B-cells in the blood by *D. salina* (Figure 4A,B) with the proliferation of T- and B- cells stimulated by Con A and LPS in the splenocytes (Figure 5). On the basis of the increment of T- and B-cells, it is suggested that the effects of *D. salina* in leukemic mice may involve activating a cascade of cellular and humoral immune responses.

IFN-$\gamma$, IL-2, IL-4, and IL-10 are immunity-related cytokines. Th1 cytokines such as IFN-$\gamma$ and IL-2 stimulate lymphocytes and macrophages to destroy pathogens and activate NK cells against viruses and tumors.[19] IL-4 can regulate Th2 cell differentiation and antibody formation. IL-4 not only suppresses Th1 and Th17 cell response via inducing IFN-$\gamma$ production, it also promotes tumor metastasis.[18] There is cross-inhibition between Th1 and Th2 cells. IL-10 is an immunosuppressive cytokine, which is produced and released from tumor cells and tumor-associated macrophages. Also, IL-10 is involved in STAT-mediated tumor progression.[31] Therefore, as the cytokines play a vital role in the development of immune response and antitumor property, we investigated the effects of *D. salina* on those targets. The results revealed that the levels of IFN-$\gamma$ and IL-2 were significantly increased, whereas the levels of IL-4 and IL-10 were significantly decreased following *D. salina* treatment compared with those of leukemic mice (Figure 6). This implied that the antileukemia property of *D. salina* might be achieved by regulating the Th1/Th2 balance and blocking STAT-mediated signal cascades, which attracted pro-inflammation to tumor development.

NK cells can release many kinds of cytokines and chemokines, which have a direct effect on tumors.[32] NK cells are known to be an early source of IFN-$\gamma$, which can decrease tumor proliferation and suppress angiogenesis.[32,33] Also, NF-$\kappa$B can induce target cell apoptosis via granule exocytosis and the death receptor activation.[34] It had been reported that spirulina increased the activity of tumoricidal NK cells via MyD88 signal transduction. Also, when cotreated with BCG-cell wall skeleton in melanoma, spirulina exerted a synergistic antitumor activity.[35] The present study revealed that *D. salina* treatment promoted NK cell activity when compared to the leukemia group (Figures 6A and 7), implying that *D. salina* might elicit MyD88 signal cascades to activate NK cell cytotoxicity.

Tumor-associated macrophages have been considered as an important source of tumor-promoting inflammation, and they consistently promote tumor growth and metastasis.[18] The present study revealed that WEHI-3 cell injection resulted in myelomonocytic leukemia, which had the characteristic of elevated monocytes coupled with increased macrophage population leading to splenic metastasis. Following *D. salina* treatment these effects, especially macrophage toward pro-inflammation induced by leukemia, could be inhibited (Figures 4D and 6D). This suggested that *D. salina* could prevent carcinogenesis via anti-inflammation by reducing macrophage production. Moreover, the proportions of phagocytosis by macrophage were significantly enhanced following *D. salina* treatment in leukemic mice (Figure 8). Phagocytosis is a process with antigen presentation for digesting dead cells and debris and killing microbes by phagocytes such as macrophages and dendritic cells. This indicated that *D. salina* might initiate an anticancer immune response resulting in phagocytosis of cancer by macrophages.

It is noted that following WEHI-3 cell injection, there were significant increases in the population and activity of macrophages (Figures 4D and 8), indicating that the increase stemmed from the leukemia cells. *D. salina* decreased the percentages of CD11b and Mac-3 cells in the blood, but the

phagocytosis of macrophage activity increased from PBMC in WEHI-3 leukemic mice. This suggested that *D. salina* probably induced differentiation, apoptosis, and anti-inflammation in leukemia cells and activated phagocytosis in normal cells. This could be confirmed through the increase of WBC and phagocytosis when treated with *D. salina* alone, as compared to control animals. Thus, *D. salina* could not only increase the immune response via promoting T- and B-cells proliferation and enhancing NK cells and macrophages activities but also induce cancer cell death via promoting differentiation, apoptosis, and altering tumor microenvironment, especially following *D. salina* treatment in leukemic mice.

The mechanisms of antileukemia include oxidative stress, inflammation, cell cycle arrest, apoptosis, autophagy, differentiation, immunomodulation, etc.[7,20,31,32] Previous studies showed that *D. salina* had antioxidative and anti-inflammatory activities via NF-$\kappa$B and JNK inactivation in vitro and in vivo[5,6,14,15] and that it induced cancer cell death coupled with cell cycle G0/G1 arrest and apoptosis through p53 and p21 up-regulation of Fas and FasL expression.[8,9] Three doses of *D. salina* were used in this study, and the results in the survival rate indicated the beneficial effects of these three doses. However, only one or two doses were found to have beneficial effects in the other experiments. From the above evidence, it is suggested that the modulating immune responses induced by *D. salina* might exert partial contribution in prolonging the biological life in leukemic mice.

Additionally, unlike *D. salina*, $\beta$-carotene did not show significant beneficial effects on body weight and splenic infiltration. This suggested that the efficacy of $\beta$-carotene in chemical synthesis was not as evident as in biological production. In support of this finding, previous studies revealed that the carotenoids extracted from *D. salina* showed more antioxidant enzyme activities against $CCl_4$-induced hepatotoxicity in rat[36] and induced higher apoptotic rate in prostate cancer cell line[8] as compared to synthetic $\beta$-carotene. In the current study, *D. salina* promoted the immune response against leukemia in mice better than $\beta$-carotene. It was also proposed that the combined antioxidant supplementation could be a useful chemopreventive approach against oxidative damage and carcinogenesis.[5,9,37] As *D. salina* has been a commercial product that contains *all-trans*-$\beta$-carotene, 9- or 9′-*cis*-$\beta$-carotene, and other carotenoids, the whole alga should show more powerful antileukemic effects as compared to those specific materials from *D. salina* itself.

In conclusion, the results showed that *D. salina* prolonged the survival rate and reduced the enlargement of the spleen in the leukemic mice. *D. salina* increased the population of T- and B-cells but decreased the population of monocytes and macrophages in the blood. *D. salina* improved immunomodulation by increasing the proliferation of T- and B-cells, enhancing the cytotoxicity of NK cells, and activating the phagocytosis of macrophages in leukemic mice. Therefore, we suggest that *D. salina* might be able to promote antileukemic properties partially through modulating immune responses in leukemic mice. However, these mechanisms of immunomodulation for antileukemic activity need to be clarified.

## AUTHOR INFORMATION

### Corresponding Authors

*(F.-J.L.) Mail: Institute of Medicine, Chung Shan Medical University, No. 110, Section 1, Jian-Guo N Road, Taichung 402, Taiwan. Phone: +886-4-24730022, ext. 12223. Fax: +886-4-23248189. E-mail: fjlu@csmu.edu.tw.

*(J.-W.L.) Mail: Graduate Institute of Veterinary Pathobiology, National Chung-Hsing University, No. 250 Kuo-Kung Road, Taichung 402, Taiwan. Phone: +886-4-22840894, ext 406. Fax: +886-4-22862073. E-mail: jwliao@dragon.nchu.edu.tw

### Funding

This work was supported by Grant CSMU101-108 from the Chung Shan Medical University and GONG BIH Enterprise Co. Ltd., Yunlin, Taiwan.

### Notes

The authors declare no competing financial interest.

## ACKNOWLEDGMENTS

We thank Dr. Jing-Gung Chung (Department of Biological Science and Technology, China Medical University, Taichung, Taiwan) for the help provided with the technique of cell surface marker by flow cytometry examinations. Flow cytometry was performed at the Instrument Center of Chung-Shan Medical University.

## REFERENCES

(1) Oren, A. A hundred years of *Dunaliella* research: 1905−2005. *Saline Syst.* **2005**, *1*, 2.

(2) Garcia-Gonzalez, M.; Moreno, J.; Manzano, J. C.; Florencio, F. J.; Guerrero, M. G. Production of *Dunaliella salina* biomass rich in 9-*cis*-$\beta$-carotene and lutein in a closed tubular photobioreactor. *J. Biotechnol.* **2005**, *115*, 81−90.

(3) Mokady, S.; Abramovici, A.; Cogan, U. The safety evaluation of *Dunaliella bardawil* as a potential food supplement. *Food Chem. Toxicol.* **1989**, *27*, 221−226.

(4) Kuroiwa, Y.; Nishikawa, A.; Imazawa, T.; Kitamura, Y.; Kanki, K.; Ishii, Y.; Umemura, T.; Hirose, M. A subchronic toxicity study of dunaliella carotene in F344 rats. *Food Chem. Toxicol.* **2006**, *44*, 138−145.

(5) Hu, C. C.; Lin, J. T.; Lu, F. J.; Chou, F. P.; Yang, D. J. Determination of carotenoids in *Dunaliella salina* cultivated in Taiwan and antioxidant capacity of the algal carotenoid extract. *Food Chem.* **2008**, *109*, 439−446.

(6) Hsu, Y. W.; Tsai, C. F.; Chang, W. H.; Ho, Y. C.; Chen, W. K.; Lu, F. J. Protective effects of *Dunaliella salina* − a carotenoids-rich alga, against carbon tetrachloride-induced hepatotoxicity in mice. *Food Chem. Toxicol.* **2008**, *46*, 3311−3317.

(7) Ma, B. Micro-algae as sources of fine chemicals. *Microbiol. Sci.* **1986**, *3*, 372−375.

(8) Jayappriyan, K. R.; Rajkumar, R.; Venkatakrishnan, V.; Nagaraj, S.; Rengasamy, R. In vitro anticancer activity of natural $\beta$-carotene from *Dunaliella salina* EU5891199 in PC-3 cells. *Biomed. Prev. Nutr.* **2013**, *3*, 99−105.

(9) Sheu, M. J.; Huang, G. J.; Wu, C. H.; Chen, J. S.; Chang, H. Y.; Chang, S. J.; Chung, J. G. Ethanol extract of *Dunaliella salina* induces cell cycle arrest and apoptosis in A549 human non-small cell lung cancer cells. *In Vivo* **2008**, *22*, 369−378.

(10) Upadhyaya, K. R.; Radha, K. S.; Madhyastha, H. K. Cell cycle regulation and induction of apoptosis by $\beta$-carotene in U937 and HL-60 leukemia cells. *J. Biochem. Mol. Biol.* **2007**, *40*, 1009−1015.

(11) Raja, R.; Hemaiswarya, S.; Balasubramanyam, D.; Rengasamy, R. Protective effect of *Dunaliella salina* (Volvocales, Chlorophyta) against experimentally induced fibrosarcoma on Wistar rats. *Microbiol. Res.* **2007**, *162*, 177−184.

(12) Fujii, Y.; Sakamoto, S.; Ben-Amotz, A.; Nagasawa, H. Effects of $\beta$-carotene-rich algae *Dunaliella bardawil* on the dynamic changes of normal and neoplastic mammary cells and general metabolism in mice. *Anticancer Res.* **1993**, *13*, 389−393.

(13) Levin, G.; Mokady, S. Antioxidant activity of 9-*cis* compared to *all-trans* $\beta$-carotene in vitro. *Free Radical Biol. Med.* **1994**, *17*, 77−82.

(14) Bitterman, N.; Melamed, Y.; Ben-Amotz, A. β-Carotene and CNS oxygen toxicity in rats. *J. Appl. Physiol.* **1994**, *76*, 1073−1076.
(15) Yang, D.-J.; Lin, J.-T.; Chen, Y.-C.; Liu, S.-C.; Lu, F.-J.; Chang, T.-J.; Wang, M.; Lin, H.-W.; Chang, Y.-Y. Suppressive effect of carotenoid extract of *Dunaliella salina* alga on production of LPS-stimulated pro-inflammatory mediators in RAW264.7 cells via NF-κB and JNK inactivation. *J. Funct. Foods* **2013**, *5*, 607−615.
(16) Tsai, C. F.; Lu, F. J.; Hsu, Y. W. Protective effects of *Dunaliella salina* − a carotenoids-rich alga − against ultraviolet B-induced corneal oxidative damage in mice. *Mol. Vision* **2012**, *18*, 1540−1547.
(17) Tang, X. H.; Yan, L. F.; Gao, J.; Yang, X. L.; Xu, Y. X.; Ge, H. Y.; Yang, H. D. Antitumor and immunomodulatory activity of polysaccharides from the root of *Limonium sinense* Kuntze. *Int. J. Biol. Macromol.* **2012**, *51*, 1134−1139.
(18) Mantovani, A.; Sica, A. Macrophages, innate immunity and cancer: balance, tolerance, and diversity. *Curr. Opin. Immunol.* **2010**, *22*, 231−237.
(19) Grivennikov, S. I.; Greten, F. R.; Karin, M. Immunity, inflammation, and cancer. *Cell* **2010**, *140*, 883−99.
(20) Lin, J. P.; Yang, J. S.; Lu, C. C.; Chiang, J. H.; Wu, C. L.; Lin, J. J.; Lin, H. L.; Yang, M. D.; Liu, K. C.; Chiu, T. H.; Chung, J. G. Rutin inhibits the proliferation of murine leukemia WEHI-3 cells in vivo and promotes immune response in vivo. *Leukemia Res.* **2009**, *33*, 823−828.
(21) Shackelford, C.; Long, G.; Wolf, J.; Okerberg, C.; Herbert, R. Qualitative and quantitative analysis of nonneoplastic lesions in toxicology studies. *Toxicol. Pathol.* **2002**, *30*, 93−96.
(22) Tang, N. Y.; Yang, J. S.; Chang, Y. H.; Lu, H. F.; Hsia, T. C.; Lin, W. C.; Chung, J. G. Effects of wogonin on the levels of cytokines and functions of leukocytes associated with NF-κB expression in Sprague-Dawley rats. *In Vivo* **2006**, *20*, 527−532.
(23) Stachowska, E.; Baskiewicz-Masiuk, M.; Dziedziejko, V.; Adler, G.; Bober, J.; Machalinski, B.; Chlubek, D. Conjugated linoleic acids can change phagocytosis of human monocytes/macrophages by reduction in Cox-2 expression. *Lipids* **2007**, *42*, 707−716.
(24) Zheng, M. H.; Feng, B.; Li, J. W.; Lu, A. G.; Wang, M. L.; Hu, W. G.; Sun, J. Y.; Hu, Y. Y.; Ma, J. J.; Yu, B. M. Effects and possible anti-tumor immunity of electrochemotherapy with bleomycin on human colon cancer xenografts in nude mice. *World J. Gastroenterol.* **2005**, *11*, 2426−2430.
(25) Han, S. B.; Kim, Y. H.; Lee, C. W.; Park, S. M.; Lee, H. Y.; Ahn, K. S.; Kim, I. H.; Kim, H. M. Characteristic immunostimulation by angelan isolated from *Angelica gigas* Nakai. *Immunopharmacology* **1998**, *40*, 39−48.
(26) Levin, G.; Yeshurun, M.; Mokady, S. In vivo antiperoxidative effect of 9-cis β-carotene compared with that of the all-trans isomer. *Nutr. Cancer* **1997**, *27*, 293−297.
(27) Lai, T. Y.; Lin, J. J.; Huang, W. W.; Kuo, S. C.; Wen, Y. F.; Lai, I. C.; Lin, C. C.; Yang, J. S.; Chung, J. G. Arsenic trioxide (As(2)O(3)) inhibits murine WEHI-3 leukemia in BALB/c mice in vivo. *Environ. Toxicol.* **2012**, *27*, 364−371.
(28) He, Q.; Na, X. The effects and mechanisms of a novel 2-aminosteroid on murine WEHI-3B leukemia cells in vitro and in vivo. *Leukemia Res.* **2001**, *25*, 455−461.
(29) Funk, R. K.; Maxwell, T. J.; Izumi, M.; Edwin, D.; Kreisel, F.; Ley, T. J.; Cheverud, J. M.; Graubert, T. A. Quantitative trait loci associated with susceptibility to therapy-related acute murine promyelocytic leukemia in hCG-PML/RARA transgenic mice. *Blood* **2008**, *112*, 1434−1442.
(30) Bechelli, J.; Coppage, M.; Rosell, K.; Liesveld, J. Cytotoxicity of algae extracts on normal and malignant cells. *Leukemia Res. Treat.* **2011**, DOI: 10.4061/2011/373519.
(31) Sica, A.; Allavena, P.; Mantovani, A. Cancer related inflammation: the macrophage connection. *Cancer Lett.* **2008**, *267*, 204−215.
(32) Malmberg, K. J.; Bryceson, Y. T.; Carlsten, M.; Andersson, S.; Bjorklund, A.; Bjorkstrom, N. K.; Baumann, B. C.; Fauriat, C.; Alici, E.; Dilber, M. S.; Ljunggren, H. G. NK cell-mediated targeting of human cancer and possibilities for new means of immunotherapy. *Cancer Immunol., Immunother.* **2008**, *57*, 1541−1552.
(33) Smyth, M. J.; Crowe, N. Y.; Pellicci, D. G.; Kyparissoudis, K.; Kelly, J. M.; Takeda, K.; Yagita, H.; Godfrey, D. I. Sequential production of interferon-γ by NK1.1(+) T cells and natural killer cells is essential for the antimetastatic effect of α-galactosylceramide. *Blood* **2002**, *99*, 1259−1266.
(34) Smyth, M. J.; Cretney, E.; Kelly, J. M.; Westwood, J. A.; Street, S. E.; Yagita, H.; Takeda, K.; van Dommelen, S. L.; Degli-Esposti, M. A.; Hayakawa, Y. Activation of NK cell cytotoxicity. *Mol. Immunol.* **2005**, *42*, 501−510.
(35) Akao, Y.; Ebihara, T.; Masuda, H.; Saeki, Y.; Akazawa, T.; Hazeki, K.; Hazeki, O.; Matsumoto, M.; Seya, T. Enhancement of antitumor natural killer cell activation by orally administered *Spirulina* extract in mice. *Cancer Sci.* **2009**, *100*, 1494−1501.
(36) Chidambara Murthy, K. N.; Vanitha, A.; Rajesha, J.; Mahadeva Swamy, M.; Sowmya, P. R.; Ravishankar, G. A. In vivo antioxidant activity of carotenoids from *Dunaliella salina* − a green microalga. *Life Sci.* **2005**, *76*, 1381−1390.
(37) Kim, Y.; Chongviriyaphan, N.; Liu, C.; Russell, R. M.; Wang, X. D. Combined antioxidant (β-carotene, α-tocopherol and ascorbic acid) supplementation increases the levels of lung retinoic acid and inhibits the activation of mitogen-activated protein kinase in the ferret lung cancer model. *Carcinogenesis* **2006**, *27*, 1410−1419.

extracts obtained by conventional extraction protocols are usually resuspended in acidified water (e.g., pH 2 with HCl), and the released free phenolic compounds are amassed with an organic solvent such as diethyl ether. Alkaline hydrolysis of phenolic extracts with NaOH under a nitrogen headspace yields phenolic compounds liberated from soluble esters, if present, whereas phenolic compounds bound to sugars are released by a subsequent acid hydrolysis involving 6 M HCl.[10−12] The liberated aglycones are easily identified by HPLC with UV diode array detection (DAD). For instance, Krygier et al.[13] successfully extracted free and soluble esterified phenolic acids in oilseeds from a methanol/acetone/water (7:7:6, v/v/v) extraction supernate. Their fractionation involved extracting the free phenolic compounds from an acidified aqueous suspension (pH 2 with HCl) of the supernate into a solvent mixture of diethyl ether and ethyl acetate. The aqueous residue was then subjected to alkaline hydrolysis to liberate soluble esterified phenolic compounds.

The determination of individual flavonoid glycosides present in foods is a formidable task, due to the numerous varieties that exist.[14] Therefore, to simply the situation, flavonoids are often analyzed after hydrolysis of their glycosides. The resulting aglycones are typically then separated by HPLC and identified using UV DAD detection or mass spectrometry.[5,14,15] Hertog et al.[14] acidified methanolic fruit and vegetable extracts with 6 M HCl, and the hydrolysis of flavonoid glycosides was performed under nitrogen at 90 °C for 2 h. The resultant aglycones were then identified by HPLC. Wang's research group[16] described the HPLC analysis of flavonoids in peanuts and other legume seeds with acid hydrolysis, in which the extraction was conducted on mixed ground seeds using 80% $CH_3OH$ containing 1.2 M HCl.

A certain percentage of phenolics, including some PACs, are "unextractable" or "insoluble" because, as aforementioned, they are bound to cell-wall material such as polysaccharides via covalent and hydrogen bonds as well as hydrophobic interactions.[3,7,8] Consequently, the phenolics content in any analytical determination is underestimated because of the bound phenolic cell-wall material that is not released by normal extraction protocols. To liberate bound phenolic derivatives, acid or base hydrolysis is applied to the plant sample prior to conventional extraction or to residual sediments resulting from conventional extraction procedures. According to Krygier et al.,[13] the residues from a methanol/acetone/water (7:7:6, v/v/v) extraction were hydrolyzed with alkali, and this effectively released insoluble bound phenolics. Similarly, Arranz et al.[7] treated a methanol/water extraction residue with $CH_3OH$/$H_2SO_4$ 90:10 (v/v) at 80 °C for 20 h to unfetter bound polyphenols, whereas the unextractable PACs were then released by mixing the aqueous acetonic residue with butanol/HCl (97.5:2.5, v/v) and $FeCl_3$ at 100 °C for 1 h. Furthermore, to liberate bound PAC derivatives, base hydrolysis was employed to treat cranberry pomace prior to conventional extraction protocols.[8] Caution must be exercised because severe alkaline conditions can, nonetheless, lead to cleavage of C−C interflavan bonds between the monomeric flavan-3-ol constituents. This may explain why alkaline-hydrolyzed PACs typically exist as monomers, dimers, trimers, and other low-molecular-weight oligomers. The A-ring of flavan-3-ols can also be broken by prolonged alkaline treatment.[8]

As previously reported, phenolic compounds of PS include simple phenolic acids (e.g., caffeic, ferulic, and coumaric acids), flavan-3-ols (e.g., (epi)catechin, epigallocatechin, catechin gallate, and epicatechin gallate), stilbenes (e.g., *trans*-resveratrol), and polymerized PACs,[17−19] but limited information is available concerning the soluble esterified and glycoside-bound phenolics and PACs of PS. Therefore, the objectives of this study were to liberate such soluble phenolic compounds from dry-blanched peanut skins (PS) extracts using alkaline and acid hydrolyses and then to characterize them by RP-HPLC-ESI-$MS^n$.

## MATERIALS AND METHODS

**Materials.** In a peanut processing plant, dry blanching of raw peanuts was performed to remove the seed coat (i.e., testa) from the kernel by transporting redskin peanuts on a conveyer belt through a low-temperature heating zone (at a maximum of 96 °C) for ∼45 min. The resultant dry-blanched PS were provided for this study by Universal Blanchers, LLC (Sylvester, GA, USA). After receipt of the PS, they were placed in a 4 °C refrigerator and analyzed within a month. All solvents and reagents were of analytical (ACS) grade, unless otherwise specified. Methanol, ethanol (95%), and hexanes were purchased from VWR International (Suwanee, GA, USA). (−)-Epiafzelechin was acquired from BOC Science (Shirley, NJ, USA), whereas all other phenolic standards were bought from either VWR International or the Sigma-Aldrich Chemical Co. (St. Louis, MO, USA).

**Phenolic Extraction.** Extraction of phenolics from PS was carried out in triplicate according to the method of Amarowicz et al.[20] with slight modifications. In brief, samples were first placed in Whatman cellulose extraction thimbles (43 mm i.d. × 123 mm e.l., VWR International), covered with a plug of glass wool, and defatted in a Soxhlet extraction apparatus under reflux for 12 h with hexanes. Defatted PS were transferred to 125 mL Erlenmeyer flasks at a mass-to-solvent ratio of 1:10 (w/v) with 80% (v/v) acetone. Extractions were performed in a gyrotary water bath shaker (model G76, New Brunswick Scientific Co., Inc., New Brunswick, NJ, USA) set at 150 rpm and a temperature of 45 °C for 30 min. The slurry was then filtered by gravity through fluted P8 filter paper (Fisher Scientific). The extraction process was repeated two more times as described above. All filtrates were pooled, and acetone was evaporated with a Büchi Rotavapor R-210 using a V-700 vacuum pump connected to a V-850 vacuum controller (Büchi Corp., New Castle, DE, USA) at 45 °C. The aqueous residue was frozen and then lyophilized in a FreeZone 2.5 L benchtop freeze-dryer (Labconco Corp., Kansas City, MO, USA) to ensure all traces of moisture were removed. The powder obtained was referred to as CE and stored in amber glass bottles at −20 °C until further analyzed.

**Hydrolysis of Phenolic Compounds from Crude Extracts.** Phenolic compounds from the acetonic PS extracts were fractionated into three classes (i.e., free, esterified, and glycoside-bound) from the acetonic PS extracts according to the method described by Dr. Amarowicz's laboratory[10,11] with slight modifications. Briefly, a 400 mg portion of each crude extract was dissolved in 20 mL of deionized water followed by acidification to pH 2 with 6 M HCl. Using a separatory funnel, free phenolic compounds were then extracted into 20 mL of diethyl ether. The extraction process was repeated four more times; the ether layers were transferred intermittently to a 100 mL round-bottom flask and the solvent was removed with a Büchi Rotavapor R-210 using a V-700 vacuum pump connected to a V-850 vacuum controller (Büchi Corp.) at 30 °C. Traces of water, when present, were removed from the contents in the round-bottom flask by a nitrogen evaporator (N-EVAP 111 with an aluminum bead dry bath set at ∼50 °C, Organomation Associates, Inc., Berlin, MA, USA). This sediment is referred to as F1 and was characterized by Ma et al.[19] The aqueous-phase residue in the separatory funnel was then mixed with 20 mL of 2 M NaOH, hydrolyzed under a $N_2$ atmosphere for 4 h at room temperature, and then acidified to pH 2 with 6 M HCl. Using 30 mL aliquots of diethyl ether, liberated phenolic compounds from soluble esters were extracted a total of five times. The ether layers were

**Table 1. Tentative Identification of Phenolic Compounds in Dry-Blanched Peanut Skins Crude Extracts (CE) by $C_{18}$ RP-HPLC-ESI-MS$^2$**

| compound no. | tentative identification[a] | $t_R$[b] (min) | $[M-H]^-$ | $[M-H]^{2-}/2$ | product ions[c] |
|---|---|---|---|---|---|
| **CE-1-1** | PAC A-type trimer [(E)C→B→(E)C→A→(E)C] | 3.6 | 863 | | 737, 711, 693, **575**, 559, 449, 287 |
| **CE-1-2** | PAC A-type trimer [(E)C→B→(E)C→B→(E)C] | 3.7 | 865 | | 739, 713, **695**, 577, 575, 451, 287 |
| **CE-1-3** | PAC A-type trimer [(E)C→B→(E)C→A→(E)C] | 3.8 | 863 | | 711, 693, 575, 559, 287 |
| **CE-1-4** | PAC A-type trimer [(E)C→A→(E)C→B→(E)C] | 3.8 | 863 | | 711, 693, 573, 451, 411, 289 |
| **CE-1-5** | PAC A-type pentamer [(E)C→B→(E)C→B→(E)C→A→(E)C→B→(E)C] | 3.9 | 1439 | 719 | 863, 575, 573 |
| **CE-1-6** | PAC B-type dimer [(E)C→B→(E)C] | 11.6 | 577 | | 559, 451, **425**, 407, 289, 287 |
| **CE-1-7** | PAC A-type trimer [(E)C→B→(E)C→A→(E)C] | 14.6 | 863 | | 845, 711, 693, **575**, 559, 449, 287 |
| **CE-1-8** | PAC A-type trimer [(E)C→A→(E)C→B→(E)C] | 14.6 | 863 | | 711, 693, 451, 411, 289 |
| **CE-1-9** | PAC A-type trimer [(E)C→A→(E)C→B→(E)C] | 16.2 | 863 | | **711**, 693, 573, 531, 451, 411, 289 |
| **CE-1-10** | PAC B-type dimer [(E)C→B→(E)C] | 19.3 | 577 | | 559, 451, **425**, 407, 289, 287 |
| **CE-1-11** | PAC A-type trimer [(E)C→B→(E)C→A→(E)C] | 20.9 | 863 | | 845, 737, 711, 693, 575, 559, 449, 287 |
| **CE-1-12** | PAC A-type trimer [(E)C→A→(E)C→B→(E)C] | 20.9 | 863 | | 737, **711**, 693, 573, 411, 289 |
| **CE-1-13** | PAC A-type dimer [(E)C→A→(E)C] | 21.0 | 575 | | 557, 539, **449**, 423, 407, 289, 285 |
| **CE-1-14** | PAC A-type pentamer [(E)C→B→(E)C→B→(E)C→A→(E)C→B→(E)C] | 21.2 | 1439 | 719 | 863, 575, 573, 287 |
| **CE-1-15** | PAC A-type pentamer [(E)C→B→(E)C→A→(E)C→B→(E)C→B→(E)C] | 21.3 | 1439 | 719 | 861, 577, 575, 287 |
| **CE-1-16** | PAC A-type tetramer [(E)C→A→(E)C→A→(E)C→B→(E)C] | 21.5 | 1149 | 574 | 997, 859 |
| **CE-1-17** | PAC A-type dimer [(E)C→A→(E)C] | 22.1 | 575 | | 557, 539, **449**, 423, 407, 289, 285 |
| **CE-1-18** | PAC A-type trimer [(E)C→B→(E)C→A→(E)C] | 22.5 | 863 | | 711, 693, 575, 559, 449, 287 |
| **CE-1-19** | PAC A-type trimer [(E)C→A→(E)C→B→(E)C] | 22.5 | 863 | | **711**, 693, 573, 531, 451, 411, 289 |
| **CE-1-20** | PAC A-type tetramer [(E)C→B→(E)C→A→(E)C→A→(E)C] | 24.7 | 1149 | 574 | 997, 861 |
| **CE-1-21** | PAC A-type dimer [(E)C→A→(E)C] | 25.2 | 575 | | 557, 539, **449**, 423, 289, 285 |
| **CE-1-22** | PAC A-type trimer [(E)C→B→(E)C→A→(E)C] | 25.7 | 863 | | 737, 711, 693, **575**, 559, 449, 287 |
| **CE-1-23** | PAC A-type trimer [(E)C→A→(E)C→B→(E)C] | 26.1 | 863 | | 737, **711**, 693, 573, 531, 451, 411, 289 |
| **CE-1-24** | PAC A-type dimer [(E)C→A→(E)C] | 27.4 | 575 | | **449**, 423, 289, 285 |
| **CE-1-25** | 316 Da flavonoid such as isorhamnetin + rutinoside sugar side-group | 27.7 | 623 | | 356, **315**, 300, 271, 255 $MS^3$ [315→300]: **300**, 271, 151 |
| **CE-1-26** | PAC A-type dimer [(E)C→A→(E)C] | 28.4 | 575 | | 557, 539, **449**, 423, 407, 289, 285 |
| **CE-1-27** | PAC A-type dimer [(E)C→A→(E)C] | 29.6 | 575 | | 557, 539, **449**, 423, 407, 289, 285 |

[a]A represents an A-type bond with both (C4→C8) and (C2→O→C7) linkages or (C4→C6) and (C2→O→C7) linkages; B represents a B-type bond, which can be (C4→C8) or (C4→C6) linkage; (E)C represents (epi)catechin. [b]Retention times ($t_R$) of the total ion chromatograms. [c]The most abundant ions observed in the mass spectra are indicated in bold; quinone methide (QM) fission diagnostic ions are underlined.

transferred intermittently to a 100 mL round-bottom flask and the solvent was removed with the Rotavapor. Traces of water, when present, were removed from the contents in the round-bottom flask by the N-EVAP. This sediment is referred to as F2. The aqueous-phase residue was then finally combined with 15 mL of 6 M HCl and hydrolyzed under a $N_2$ atmosphere for 1 h at 100 °C in a forced-air convection oven. Using 45 mL aliquots of diethyl ether, liberated phenolic compounds from soluble glycosides were extracted a total of five times. The ether layers were transferred intermittently to a 100 mL round-bottom flask and the solvent was removed with the Rotavapor. Traces of water, when present, were removed from the contents in the round-bottom flask by the N-EVAP. This sediment is referred to as F3.

**Reversed-Phase High-Performance Liquid Chromatography–Electrospray Ionization Mass Spectrometry (RP-HPLC-ESI-MS$^n$).** An Agilent 1200 series HPLC system consisting of a quaternary pump with a degasser, autosampler, thermostated column compartment, UV–vis diode array detection with standard flow cell, and 3D ChemStation software (Agilent Technologies, Santa Clara, CA, USA) was employed for the chromatography. A reversed-phase Luna $C_{18}(2)$ column (4.6 × 250 mm, 5 μm particle size; Phenomenex, Torrance, CA, USA) was utilized. A gradient elution consisting of mobile phase A ($H_2O/CH_3CN/CH_3COOH$, 93:5:2, v/v/v) and mobile phase B ($H_2O/CH_3CN/CH_3COOH$, 58:40:2, v/v/v) from 0 to 100% B over a 50 min period at a flow rate of 1 mL/min was employed. Before subsequent injections, the system was re-equilibrated for 30 min using 100% A. A 10 mg portion of the PS CE, F2, and F3, were dissolved in 5, 4, and 2 mL of 80% (v/v) methanol, respectively, and then passed through a Phenex-RC, 15 mm, nonsterile, 0.2 μm syringe filter (Phenomenex Inc.) before determination of their phenolics; the injection volume was 20 μL. Detection wavelengths employed were $\lambda$ = 255 and 260 nm (hydroxybenzoic acids, as well as ellagic acid and ellagic acid derivatives), 280 nm ((+)-catechin, (−)-epicatechin, and PACs), 320 nm (phenolic acids notably of the *trans*-cinnamic acid family), and 360 nm (flavonols and general flavonoids). Tentative identification of separated components was made by matching UV–vis spectra and retention time ($t_R$) mapping with commercial standards. For quantification, calibration curves were constructed for each standard to confirm linearity on the basis of the UV–vis signal as well as for the determination of response factors.

RP-HPLC-ESI-MS$^n$ analyses of the phenolics were performed on an Agilent 1100 HPLC system, with the same chromatography conditions as described above, coupled with a Bruker Esquire 3000$^{plus}$ ion-trap mass spectrometer (Bruker Daltonics Inc., Billerica, MA, USA), which was equipped with an ESI source. Instrument control and data acquisition were performed with Bruker Daltonics Esquire 5.3 software. The HPLC eluent flowed directly into the mass spectrometer via a flow splitter delivering roughly 100 μL/min. Mass spectra were acquired in the negative-ion mode with smart settings for a target mass at an $m/z$ of 800, compound stability at 100%, and trap drive level at 100%. The voltage applied to the capillary was 4.0 kV with an end plate offset of −500 V. Nitrogen was used as the nebulizing gas at a pressure of 10 psi, a dry gas flow rate of 6 L/min, and a dry gas temperature of 280 °C. The phenolic compounds were fragmented using the auto-MS$^2$ mode with the following precursor-ion selection

parameters: two precursor ions, threshold absorbance of 10000, threshold relativity of 5.0%, ion excluded after two spectra, and exclusion release after 0.5 min. All collision-induced dissociation mass spectra were obtained with He as the collision gas at a fragmentation voltage of 1 V after isolation of the desired precursor ion. A full scan was performed over the mass range of $m/z$ 100−1000 at a rate of $m/z$ 13000 per second under standard−normal scan mode. The ion current control target was 50000 with a maximum accumulation time of 50 ms. Each mass spectrum generated was based on an average of 10 scans. Precursor ions of interest were further subjected to auto-$MS^n$ under the same conditions as described above.

**Statistical Analysis.** For each quantified phenolic compound, the mean and standard deviation were calculated from the measurements of triplicate extractions.

## RESULTS AND DISCUSSION

Alkaline and acid hydrolyses of the PS crude extracts were performed prior to chromatographic analysis to liberate phenolic aglycones from soluble esters and glycosides, respectively. Even though the HPLC profile of hydrolyzed samples may not reflect the actual structure of each phenolic ester and glycoside present in PS, hydrolysis does simplify the identification of phenolic compounds and provides important information concerning the profile of the individual aglycones. Moreover, it allowed further compounds to be detected via chromatography. In the present study few phenolic species were isolated from the PS crude phenolic extracts (Table 1), unlike those first liberated via base and acid hydrolyses followed by RP-HPLC separation and detection by ESI-$MS^n$ (Tables 2 and 3).

**Identification of Phenolic Compounds Using RP-HPLC-ESI-$MS^n$.** Only PACs and rutin were detectable in the PS crude phenolic extracts. However, many phenolics were identified in the free phenolics fraction (F1) after acidification of the extract and then extraction of these compounds with ether. Characterization of F1 is reported elsewhere.[19] A large variety of phenolic compounds, including PACs (monomer to pentamer), hydroxybenzoic acids, *trans*-cinnamic acids, stilbenes, and flavonoids, were eluted in fractions F2 (i.e., phenolics liberated from soluble esters) and F3 (i.e., phenolics liberated from soluble glycosides). Noteworthy is that flavonoids were liberated primarily from glycosides and recovered in F3.

Phenolic acids and flavonoids show characteristic UV range absorbance patterns from 190 to 380 nm.[9,15] From UV−vis DAD, four groups of phenolic compounds were characterized, namely, hydroxybenzoic acids (255 and 260 nm), (+)-catechin, (−)-epicatechin, and their polymers (280 nm), hydroxycinnamic acids (320 nm), and flavonols (360 nm). These compounds was subsequently introduced to the ESI mass spectrometer and analyzed on the basis of their $m/z$ values. Tentative identification of separated compounds was based on mass spectrometry alone; positive identification was achieved by the matching of $t_R$ values and spectral data with those of commercial standards, when available. Possible misinterpretations of spectra are due to the presence of stereoisomers, which are impossible to distinguish by mass spectra. Typically, the cleavage of a distinctive moiety from a compound in $MS^n$ analysis brings about a corresponding change in mass. To illustrate, rutinoside possesses a characteristic mass of 308 Da, so loss of 18 and 15 Da typically indicates the cleavage of a $H_2O$ molecule and a $CH_3^\bullet$ group, respectively. A-type PACs ($m/z$ 575, 861, 863, 1151, 1149, 1437, 1725, etc.) display a 2 Da difference in $[M - H]^-$ from B-type polymers ($m/z$ 577, 865, 1153, 1441, 1729, etc.). Quinone methide fission (QM), retro-Diels−Alder fission (RDA), and heterocyclic ring fission (HRF) are three major fragmentation routes of PACs well-described in the literature.[21]

$^{ij}A^-$ and $^{ij}B^-$ ions are diagnostic fragments for flavonoid identification and produced by the RDA cleavage in the C-ring. $A^-$ and $B^-$ are product ions in the negative-ion mode consisting of intact A- and B-rings, whereas the superscript *i* and *j* indicate the positions in the C-ring where two C−C bonds have been broken. Besides RDA cleavage in the C-ring, losses of neutral molecules such as $H_2O$ (18 Da), CO (28 Da), $CO_2$ (44 Da), $C_2H_2O$ (42 Da), and $C_3O_2$ (68 Da) can be characteristic in the negative-ion mode. The fragmentations of flavone, flavonol, and flavanone aglycones in the negative-ion mode by ESI trap mass spectrometry are well-demonstrated by Fabre et al.[22] The successive loss of $CH_3^\bullet$ and then CO (28 Da) or $CHO^\bullet$ (29 Da) were characteristic in methoxylated flavonoids.[23] However, the position of the methoxy group must be identified by the comparison with standards or by NMR analysis.[24] A similar nomenclature of fragmentation was adopted as for flavonoids. $^{ij}A^-$ and $^{ij}B^-$ ions are RDA fragments produced by cleavage of two C−C bonds in the C-ring. The flavonoid having a C-ring attached to the A-ring of the other flavonoid is denoted "part I", and the other flavonoid is referred to as "part II". Identification of compounds detected in both PS crude extracts and each base- and acid-hydrolytic fraction is discussed as follows.

**PS Crude Extracts.** *Proanthocyanidins (PACs).* Compounds providing a molecular ion $[M - H]^-$ at $m/z$ 575 (compounds **CE-1-13**, **-17**, **-21**, **-24**, **-26**, and **-27**) and 577 (compounds **CE-1-6** and **-10**) are likely PAC A- and B-type dimers, respectively. In the negative-ion mode, A-type dimers yield product ions at $m/z$ 449 $[M - H - 126\ (C_6H_6O_3)]^-$ and 423 $[M - H - 152\ (C_8H_8O_3)]^-$ via HRF fragmentation at the top unit and RDA fragmentation at the base unit, respectively. Generally, the top unit is the favored site for RDA, but fission can occur at the base unit when blocked by A-type bonds.[21] QM ions were present at $m/z$ 289 $[M_T - H\ (290 - H)]^-$ (QM cleavage at the terminal (T) unit) and $m/z$ 285 $[M_E - 5H\ (290 - 5H)]^-$ (QM cleavage at the extension (E) unit). Likewise, product ions at $m/z$ 451 $[M - H - 126\ (C_6H_6O_3)]^-$, 425 $[M - H - 152\ (C_8H_8O_3)]^-$, 289 $[M_T - H\ (290 - H)]^-$, and 287 $[M_E - 3H\ (290 - 3H)]^-$ were present in the $MS^2$ fragmentation of B-type dimers. The fragment ion at $m/z$ 407 was generated by further loss of a $-H_2O$ moiety from the ion at $m/z$ 425. These data and characteristic MS fragmentation patterns are consistent with the findings of previous studies.[21,25,26]

Molecular ions present at $m/z$ 863 (compounds **CE-1-1**, **-3**, **-4**, **-7**, **-8**, **-9**, **-11**, **-12**, **-18**, **-19**, **-22**, and **-23**) and 865 (compound **CE-1-2**) were likely produced by PAC A- and B-type trimers, respectively. Theoretically, PAC trimers dissociate in a similar way to dimers: there are two types of A-type trimers both possessing a molecular ion at $m/z$ 863, but with different QM diagnostic ions caused by varied positions of the A-bond. QM cleavage between the top and middle units produced ions at $m/z$ 575 $[M_T - H\ (576 - H)]^-$ and 287 $[M_E - 3H\ (290 - 3H)]^-$, indicating that the A-type linkage is located between the middle and base units (compounds **CE-1-1**, **-3**, **-7**, **-11**, **-18**, and **-22**). The HRF and RDA fragmentation of the top unit yielded product ions at $m/z$ 737 $[M - H - 126\ (C_6H_6O_3)]^-$ and 711 $[M - H - 152\ (C_8H_8O_3)]^-$, respectively. The HRF fragmentation of the middle unit gave a product ion at $m/z$

**Table 2. Tentative Identification of Esterified Phenolic Compounds in Dry-Blanched Peanut Skins Crude Extracts by $C_{18}$ RP-HPLC-ESI-$MS^2$**

| compound no. | tentative identification[a] | UV $\lambda_{max}$[b] (nm) | $t_R$[c] (min) | $[M-H]^-$ | $[M-H]^{2-}/2$ | product ions[d] |
|---|---|---|---|---|---|---|
| **F-2-1** | gallocatechin | | 3.2 | 305 | | 261, 219, **179**, 125 |
| **F-2-2** | unknown (likely a gallocatechin derivative) | | 5.8 | 305 | | 261, 219, **179**, 125 |
| **F-2-3** | 3,4-dihydroxyphenylacetic acid (DOPAC) | | 8.2 | 167 | | **123** |
| **F-2-4** | ethyl protocatechuate | | 8.7 | 181 | | 163, **153**, 137, 109 |
| **F-2-5** | protocatechuic acid | 260, 294 | 9.7 | 153 | | **109** |
| **F-2-6** | unknown DOPAC derivative | | 10.5 | 357 | | 315, 273, 249, **189**, 167, 123 |
| **F-2-7** | DL-3-(4-hydroxyphenyl)lactic acid | | 11.9 | 181 | | 163, **137** |
| **F-2-8** | (−)-catechin | 234, 280 | 12.5 | 289 | | **245**, 205, 179, 125 |
| **F-2-9** | *p*-hydroxybenzoic acid | | 13.5 | 137 | | |
| **F-2-10** | (+)-catechin | 234, 280 | 13.9 | 289 | | **245**, 205, 179, 125 |
| **F-2-11** | *trans*-caffeic acid | | 17.3 | 179 | | **135** |
| **F-2-12** | (−)-epicatechin | 234, 280 | 17.7 | 289 | | **245**, 205,179, 125 |
| **F-2-13** | (−)-epiafzelechin | | 19.3 | 273 | | 255, **229**, 187, 166, 137, 123 |
| **F-2-14** | PAC A-type trimer [(E)C→B→(E)C→A→(E)C] | 234, 280 | 19.6 | 863 | | 737, 711, 693, **575**, 559, 449, 287 |
| **F-2-15** | PAC A-type trimer [(E)C→A→(E)C→B→(E)C] | | 19.9 | 863 | | 737, **711**, 693, 573, 531, 451, 411, 289 |
| **F-2-16** | prodelphinidin B-type dimer [(E)GC→B→(E)C] | | 20.4 | 593 | | 575, 467, **425**, 407, 303, 289 |
| **F-2-17** | prodelphinidin A-type dimer [(E)GC→A→(E)C] | | 20.8 | 591 | | 573, **465**, 439, 423, 301, 289 |
| **F-2-18** | prodelphinidin A-type dimer [(E)C→A→5-*O*-methyl (E)GC] | 230, 282 | 21.6 | 605 | | 587, 571, **479**, 451, 353, 319, 301, 285 |
| **F-2-19** | PAC A-type dimer [(E)C→A→(E)C] | 234, 280 | 22.2 | 575 | | 557, 539, **449**, 423, 407, 289, 285 |
| **F-2-20** | PAC B-type dimer [(E)C→B→(E)C] | | 22.6 | 577 | | 559, **451**, 425, 407, 289, 287 |
| **F-2-21** | PAC A-type dimer [(E)C→A→(E)C] | 234, 280 | 22.9 | 575 | | 557, 539, **449**, 423, 407, 289, 285 |
| **F-2-22** | *p*-coumaric acid | 234, 310 | 23.2 | 163 | | **119** |
| **F-2-23** | prodelphinidin A-type dimer [(E)C→A→(E)GC] | | 23.2 | 591 | | 573, **465**, 423, 305, 285 |
| **F-2-24** | *trans*-piceatannol | | 24.2 | 243 | | 243, 215, **225**, 201, 199, 175, 173, 159 |
| **F-2-25** | ferulic acid | 238, 292sh, 322 | 26.0 | 193 | | 178, 149, **134** |
| **F-2-26** | PAC A-type dimer [(E)C→A→(E)C] | 234, 280 | 26.3 | 575 | | 557, 539, **449**, 423, 407, 289, 285 |
| **F-2-27** | PAC A-type dimer [(E)C→A→(E)C] | 234, 280 | 27.6 | 575 | | 557, 539, **449**, 423, 407, 289, 285 |
| **F-2-28** | PAC A-type dimer [(E)C→A→(E)C] | 234, 280 | 28.3 | 575 | | 557, 539, **449**, 423, 407, 289, 285 |
| **F-2-29** | PAC A-type trimer [(E)C→B→(E)C→A→(E)C] | 234, 280 | 28.8 | 863 | | 737, 711, 693, **575**, 559, 449, 287 |
| **F-2-30** | PAC A-type dimer [(E)C→A→(E)C] | 234, 280 | 28.9 | 575 | | 557, 539, **449**, 423, 407, 289, 285 |
| **F-2-31** | PAC A-type dimer [(E)C→A→(E)C] | 234, 280 | 29.7 | 575 | | 557, 539, **449**, 423, 407, 289, 285 |
| **F-2-32** | PAC A-type tetramer [1B, 2A] | 234, 280 | 30.9 | 1149 | 574 | |
| **F-2-33** | PAC A-type trimer [(E)C→B→(E)C→A→(E)C] | 234, 280 | 31.8 | 863 | | 845, 737, 711, 693, **575**, 449, 287 |
| **F-2-34** | prodelphinidin A-type trimer [(E)GC→A→(E)C→A→(E)C] | | 32.1 | 877 | | 859, 841, **751**, 725, 599, 587, 575, 559, 461, 449, 301, 289 |
| **F-2-35** | propelargonidin A-type dimer [(E)C→A→(E)Afz] | | 32.1 | 559 | | 541, **433**, 423, 391, 285, 273 |
| **F-2-36** | PAC A-type trimer [(E)C→B→(E)C→A→(E)C] | 234, 280 | 32.2 | 863 | | 737, 711, 693, **575**, 559, 449, 287 |
| **F-2-37** | myricetin | | 32.3 | 317 | | 317, 271, 243, 227, **179**, 151, 137, 109 |
| **F-2-38** | PAC A-type tetramer [1B, 2A] | 234, 280 | 33.2 | 1149 | 574 | |
| **F-2-39** | PAC A-type tetramer [1B, 2A] | 234, 280 | 34.2 | 1149 | 574 | |
| **F-2-40** | prodelphinidin A-type trimer [(E)C→B→(E)GC→A→luteolin or kaempferol] | | 34.2 | 875 | | 857, 749, **723**, 597, 555, 301 |



dx.doi.org/10.1021/jf503836n | J. Agric. Food Chem. 2014, 62, 11488−11504

Table 2. continued

| compound no. | tentative identification[a] | UV $\lambda_{max}$ [b] (nm) | $t_R$ [c] (min) | $[M - H]^-$ | $[M - H]^{2-}/2$ | product ions[d] |
|---|---|---|---|---|---|---|
| **F-2-41** | prodelphinidin dimer [(E)C→B→methyl (E)GC] or [(E)GC→A→(E)GC] | | 34.3 | 607 | | |
| **F-2-42** | PAC A-type trimer [(E)C→A→(E)C→A→(E)C] | 234, 280 | 34.5 | 861 | | 843, 825, **735**, 709, 693, 575, 571, 449, 289, 285 |
| **F-2-43** | PAC A-type tetramer [1B, 2A] | | 34.6 | 1149 | 574 | |
| **F-2-44** | PAC A-type trimer [(E)C→B→(E)C→A→(E)C] | | 34.9 | 863 | | 737, 711, 693, 575, 559, 449, 287 |
| **F-2-45** | PAC A-type trimer [(E)C→A→(E)C→B→(E)C] | | 35.0 | 863 | | 737, **711**, 693, 573, 531, 451, 411, 289 |
| **F-2-46** | PAC A-type tetramer [1B, 2A] | 234, 280 | 35.4 | 1149 | 574 | |
| **F-2-47** | PAC A-type trimer [(E)C→A→(E)C→A→(E)CG] | | 35.6 | 1015 | 507 | |
| **F-2-48** | prodelphinidin A-type tetramer [(E)C→A→(E)GC→A→(E)C→A→(E)C] | 234, 280 | 37.4 | 1163 | 581 | 877, 873, 751, 575, 449, 411, 289, 285 |

[a]A represents an A-type bond with both (C4→C8) and (C2→O→C7) linkages or (C4→C6) and (C2→O→C7) linkages; B represents a B-type bond which can be (C4→C8) or (C4→C6) linkage; (E)C represents (epi)catechin, (E)GC represents (epi)gallocatechin, (E)CG represents (epi)catechin gallate, and (E)Afz represents (epi)afzelechin. [b]sh, shoulder in the spectrum. [c]Retention times ($t_R$) of the total ion chromatograms. [d]The most abundant ions observed in the mass spectra are indicated in bold; quinone methide (QM) fission diagnostic ions are underlined.

449. When the A-type linkage is located between the top and middle units (compounds **CE-1-4**, **-8**, **-9**, **-12**, **-19**, and **-23**), QM cleavage ions are present at $m/z$ 573 $[M_E - 3H\ (576 - 3H)]^-$ and 289 $[M_T - H\ (290 - H)]^-$. In this case, the product ion at $m/z$ 711 was formed by RDA fragmentation of the middle unit. The HRF fragmentation of the middle unit yielded product ions at $m/z$ 451 and 411. However, these two types of trimer, containing the same number of A-type bonds, were not well resolved by HPLC. Two series of fragments were observed in one mass spectrum. HRF and RDA fragmentation of the B-type trimer gave rise to dissociation ions at $m/z$ 739 $[M - H - 126\ (C_6H_6O_3)]^-$ and 713 $[M - H - 152\ (C_8H_8O_3)]^-$, respectively. The HRF fragmentation of the middle unit resulted in a product ion at $m/z$ 451. The prominent fragment ion at $m/z$ 695 was generated by further loss of a $-H_2O$ moiety from the RDA ion at $m/z$ 713. QM diagnostic ions were present at $m/z$ 577 $[M_T - H\ (578 - H)]^-$, 575 $[M_E - 3H\ (578 - 3H)]^-$, and 287 $[M_E - 3H\ (290 - 3H)]^-$.

$[M - 2H]^{2-}$ at $m/z$ 719 (compounds **CE-1-5**, **-14**, and **-15**) and 574 (compounds **CE-1-16** and **-20**) are doubly charged ions generated from a PAC A-type pentamer ($m/z$ 1439) and a PAC A-type tetramer ($m/z$ 1149), respectively. Apropos the pentamer (**CE-1-5** and **-14**), the diagnostic QM ions present at $m/z$ 863 $[M_T - H\ (864 - H)]^-$, 575 $[M_E - 3H\ (578 - 3H)]^-$, and 573 $[M_E - 3H\ (576 - 3H)]^-$ indicate a connection sequence such as (epi)catechin→B→(epi)catechin→B→(epi)-catechin→A→(epi)catechin→B→(epi)catechin, where A and B represent A- and B-type linkages, respectively. The A-type pentamer (**CE-1-15**) gave rise to QM cleavage fragments at $m/z$ 861 $[M_E - 3H\ (864 - 3H)]^-$, 577 $[M_T - H\ (578 - H)]^-$, and 575 $[M_T - H\ (576 - H)]^-$, being assigned to a sequence such as (epi)catechin→B→(epi)catechin→A→(epi)catechin→B→(epi)catechin→B→(epi)catechin. Vis-à-vis the tetramer, the QM fragment at $m/z$ 859 $[M_E - 3H\ (862 - 3H)]^-$ were observed when the B-type linkage is located between the base and its upper unit (**CE-1-16**). The production of a QM fragment at $m/z$ 861 $[M_T - H\ (862 - H)]^-$ indicates that the B-type linkage is located between the top and its subsequent unit, whereas the remaining units are linked by A-type bonds (compound **CE-1-20**).

*Flavonoid.* A 316 Da *O*-methylated flavonoid with a rutinoside attached was determined as compound **CE-1-25**. It yielded a $[M - H]^-$ at $m/z$ 623 and fragment ions at $m/z$ 315 $[M - H - 308]^-$ by loss of a rutinoside moiety and $m/z$ 300 $[M - H - 308 - 15]^-$ by further loss of a $CH_3^\bullet$ group from the deprotonated flavonoid aglycone. Although there is a wide range of candidates for 316 Da *O*-methylated flavonoids such as rhamnetin, isorhamnetin, tamarixetin, and neptin, the compound is likely to be isorhamnetin according to an NMR study reported by Lou's group.[27]

**Esterified Phenolics.** *Phenylacetic Acid.* Compound **F-2-3** yielded a molecular ion at $m/z$ 167 and a fragment ion at $m/z$ 123 by loss of a $-CO_2$ group from the carboxylic acid moiety. Among several candidates such as 3,4-dihydroxyphenylacetic acid (DOPAC), vanillic acid, orsellinic acid, and homogentisic acid, the most likely compound is DOPAC, as evidenced by $t_R$ matching with a commercial standard. Compound **F-2-6** is likely a derivative of DOPAC because of the fragment ion at $m/z$ 167 corresponding to the deprotonated form of DOPAC and its decarboxylated ion at $m/z$ 123.

*Hydroxycinnamic Acids.* Compound **F-2-11** yielded a molecular ion at $m/z$ 179 and its decarboxylated ion at $m/z$

**Table 3. Tentative Identification of Glycoside-bound Phenolic Compounds in Dry-blanched Peanut Skins Crude Extracts by $C_{18}$ RP-HPLC-ESI-MS$^n$**

| compound no. | tentative identification[a] | UV $\lambda_{max}$[b] (nm) | $t_R$[c] (min) | $[M-H]^-$ | product ions[d] |
|---|---|---|---|---|---|
| **F-3-1** | gallocatechin | | 3.2 | 305 | 261, 219, **179**, 125 |
| **F-3-2** | unknown (likely a gallocatechin derivative) | | 5.8 | 305 | 261, 219, **179**, 125 |
| **F-3-3** | 3,4-dihydroxyphenylacetic acid (DOPAC) | | 8.2 | 167 | **123** |
| **F-3-4** | methyl gallate | | 9.4 | 183 | **124** |
| **F-3-5** | protocatechuic acid | 260, 294 | 9.7 | 153 | **109** |
| **F-3-6** | protocatechuic acid derivative | | 9.8 | 233 | 213, 203, 167, **153**, 123, 109 |
| **F-3-7** | robinetin | | 12.8 | 301 | 301, 283, **257**, 229, 163, 137 |
| **F-3-8** | *p*-hydroxybenzoic acid | 256 | 13.1 | 137 | |
| **F-3-9** | (+)-catechin | 234, 280 | 13.8 | 289 | **245**, 205, 179, 125 |
| **F-3-10** | PAC A-type dimer [(E)C→A→(E)C→phloroglucinol] | | 15.9 | 699 | 681, 573, 547, 531, 453, **411**, 287, 285<br>MS$^3$[699→411]: 411, 349, 301, **285**, 257, 243, 215, 189, 163, 149, 125 |
| **F-3-11** | vanillic acid | 260, 292 | 16.1 | 167 | 152, **123**, 108 |
| **F-3-12** | PAC A-type dimer [(E)C→A→(E)C→phloroglucinol] | 238, 278 | 16.7 | 699 | 681, 573, 547, 531, 453, **411**, 285, 245 |
| **F-3-13** | PAC B-type dimer [(E)C→B→(E)C→phloroglucinol] | | 17.1 | 701 | **411**, 289, 245<br>MS$^3$[701→411]: 393, 383, 341, 307, **283**, 242 |
| **F-3-14** | (−)-epicatechin | | 17.3 | 289 | **245**, 205, 179, 125 |
| **F-3-15** | PAC A-type dimer [(E)C→A→(E)C→phloroglucinol] | 238, 278 | 17.6 | 699 | 681, 573, 531, 453, **411**, 287, 285, 245 |
| **F-3-16** | PAC B-type dimer [(E)C→B→(E)C→phloroglucinol] | | 17.9 | 701 | **411**, 289, 245 |
| **F-3-17** | PAC A-type dimer [(E)C→A→(E)C→phloroglucinol] | 238, 278 | 18.6 | 699 | 681, 573, 531, 453, **411**, 287, 285, 245 |
| **F-3-18** | PAC A-type dimer [(E)C→A→(E)C→phloroglucinol] | 238, 278 | 19.5 | 699 | 681, 573, 531, 453, **411**, 287, 285, 245 |
| **F-3-19** | PAC B-type dimer [(E)C→B→(E)C→phloroglucinol] | | 20.3 | 701 | **411**, 289, 245 |
| **F-3-20** | PAC A-type dimer [(E)C→A→(E)C→phloroglucinol] | 238, 278 | 20.6 | 699 | 681, 573, 531, 453, **411**, 287, 285, 245 |
| **F-3-21** | PAC A-type dimer [(E)C→A→(E)C] | 234, 280 | 20.8 | 575 | 557, 539, **449**, 423, 407, 289, 285 |
| **F-3-22** | homovanillic acid | | 20.8 | 181 | 137, **122** |
| **F-3-23** | PAC A-type dimer [(E)C→A→(E)C] | 234, 280 | 21.7 | 575 | 557, 539, **449**, 423, 407, 289, 285 |
| **F-3-24** | propelargonidin A-type trimer [(E)C→A→(E)Afz→B→(E)C] | | 22.2 | 847 | 711, 557, 435, **411**, 289 |
| **F-3-25** | PAC A-type dimer [(E)C→A→(E)C→phloroglucinol] | 238, 278 | 24.3 | 699 | 681, 573, 531, 453, **411**, 287, 285, 245 |
| **F-3-26** | PAC A-type dimer [(E)C→A→(E)C→phloroglucinol] | 238, 278 | 24.9 | 699 | 681, 573, 531, 453, **411**, 287, 285, 245 |
| **F-3-27** | PAC A-type dimer [(E)C→A→(E)C] | | 25 | 575 | 557, 539, **449**, 423, 407, 289, 285 |
| **F-3-28** | PAC A-type dimer [(E)C→A→(E)C→phloroglucinol] − $C_2H_2O$ (42 Da) | | 25.2 | 657 | 597, 547, 531, 411, 285, **245** |
| **F-3-29** | PAC A-type dimer [(E)C→A→(E)C→phloroglucinol] − $C_2H_2O$ (42 Da) | | 25.8 | 657 | 597, 547, 531, 411, 285, **245** |
| **F-3-30** | taxifolin | | 26.2 | 303 | 303, **285**, 257, 177, 125 |
| **F-3-31** | PAC A-type dimer [(E)C→A→(E)C→phloroglucinol] − $C_2H_2O$ (42 Da) | | 26.3 | 657 | 597, 547, 531, 411, **245** |
| **F-3-32** | PAC A-type dimer [(E)C→A→(E)C] | 234, 280 | 26.5 | 575 | 557, 539, **449**, 423, 407, 289, 285 |
| **F-3-33** | PAC A-type dimer [(E)C→A→(E)C→phloroglucinol] − $C_8H_8O_3$ (152 Da) | | 26.6 | 547 | 531, **437**, 423, 411, 285, 245 |
| **F-3-34** | PAC A-type dimer [(E)C→A→(E)Afz→phloroglucinol] | | 27.0 | 683 | 665, 647, **557**, 515, 423, 411, 397, 285<br>MS$^3$[683→557]: 539, 421, 395, **285**, 271 |
| **F-3-35** | PAC A-type dimer [(E)C→A→(E)C] | 234, 280 | 27.5 | 575 | 557, 539, **449**, 423, 407, 289, 285 |
| **F-3-36** | PAC A-type dimer [(E)C→A→(E)C] | 234, 280 | 28.2 | 575 | 557, 539, **449**, 423, 407, 289, 285 |
| **F-3-37** | PAC A-type dimer [(E)C→A→(E)C→phloroglucinol] | 238, 278 | 28.4 | 699 | 681, 573, 531, 453, **411**, 287, 285, 245 |
| **F-3-38** | PAC A-type dimer [(E)C→A→a novel flavan-3-ol] | | 28.5 | 589 | 571, 553, 463, **453**, 409, 303, 285<br>MS$^3$[589→453]: 409, 367, 344, **327**, 303, 176, 165 |
| **F-3-39** | PAC A-type dimer [(E)C→A→(E)C→phloroglucinol] − $C_8H_8O_4$ (168 Da) | | 30.1 | 531 | 513, 499, **405**, 393, 363, 309, 285, 245 |
| **F-3-40** | PAC A-type dimer [(E)C→A→(E)C] | 234, 280 | 30.3 | 575 | 557, 539, **449**, 423, 407, 289, 285 |
| **F-3-41** | PAC A-type dimer [(E)C→A→(E)Afz→phloroglucinol] | | 31.1 | 683 | 665, 647, **557**, 515, 423, 411, 397, 285 |
| **F-3-42** | PAC B-type dimer [(E)C→B→(E)C→phloroglucinol] − $C_8H_8O_3$ (152 Da) | | 32.2 | 549 | 531, 489, 423, **411**, 285 |
| **F-3-43** | fisetin | 248, 362 | 32.2 | 285 | 285, 257, 241, 229, 213, 177, **163**, 135, 121 |
| **F-3-44** | PAC A-type dimer [(E)C→A→(E)C→phloroglucinol] − $C_8H_8O_4$ (168 Da) | | 32.4 | 531 | 513, 499, **405**, 393, 363, 309, 285, 245 |
| **F-3-45** | PAC A-type dimer [(E)C→A→(E)Afz→phloroglucinol] − $C_6H_6O_3$ (126 Da) | | 32.6 | 557 | 539, **431**, 389, 285 |
| **F-3-46** | biflavonoid [eriodictyol→C-methyl robinetinidol] | | 33.4 | 587 | 569, **461**, 419, 301, 285<br>MS$^3$[587→461]: **443**, 339, 324, 301, 285, 293, 198 |
| **F-3-47** | PAC B-type dimer [(E)C→B→(E)C→phloroglucinol] − $C_8H_8O_3$ (152 Da) | | 33.5 | 549 | 531, 489, 423, **411**, 285 |
| **F-3-48** | PAC A-type dimer [(E)C→A→(E)C→phloroglucinol] − $C_8H_8O_4$ (168 Da) | | 33.9 | 531 | 513, 499, **405**, 393, 363, 309, 285, 245 |
| **F-3-49** | myricetin | | 34.1 | 317 | 317, 289, 271, 191, 179, **151**, 137, 125 |
| **F-3-50** | PAC A-type dimer [(E)C→A→(E)C→phloroglucinol] − $C_8H_8O_3$ (152 Da) | | 34.2 | 547 | 527, 489, 437, **421**, 360, 302, 245, 177 |
| **F-3-51** | PAC A-type dimer [(E)C→A→(E)C→phloroglucinol] − $C_8H_8O_4$ (168 Da) | | 34.3 | 531 | 469, **405**, 393, 363, 309, 285, 245 |
| **F-3-52** | propelargonidin A-type trimer [(E)Afz→A→(E)C→A→(E)C] | | 34.4 | 845 | **719**, 693, 575, 555, 449, 433, 289, 269 |


dx.doi.org/10.1021/jf503836n | J. Agric. Food Chem. 2014, 62, 11488−11504

**Table 3. continued**

| compound no. | tentative identification[a] | UV $\lambda_{max}$[b] (nm) | $t_R$[c] (min) | $[M - H]^-$ | product ions[d] |
|---|---|---|---|---|---|
| **F-3-53** | 3′,4′,5,6-tetrahydroxy-7-methoxyflavone | | 35.6 | 315 | 315, **300**, 232, 191 |
| **F-3-54** | genkwanin | 338 | 37.2 | 283 | **268**, 151 |
| **F-3-55** | prorobinetidin A-type dimer [(E)C→A→C-methyl (epi)robinetinidol] | | 37.5 | 589 | 571, 553, **463**, 421, 303, 285<br>$MS^3$[589→463]: 445, **435**, 341, 301, 295, 285, 198 |
| **F-3-56** | biflavonoid [eriodictyol→C-methyl robinetinidol] | | 37.7 | 587 | 569, 551, **461**, 447, 419, 301, 285<br>$MS^3$[587→461]: **443**, 301, 285, 293, 198 |
| **F-3-57** | prorobinetidin A-type dimer [(E)C→A→C-methyl (epi)robinetinidol] | | 38.1 | 589 | 571, 553, **463**, 421, 303, 285 |
| **F-3-58** | prodelphinidin dimer [(E)C→B→methyl (E)GC] or [(E)GC→A→(E)GC] | | 38.2 | 607 | |
| **F-3-59** | biflavonoid [eriodictyol→C-methyl robinetinidol] | | 38.3 | 587 | 569, 551, **461**, 421, 301, 285 |
| **F-3-60** | biochanin A | | 38.5 | 283 | **268**<br>$MS^3$[283→268]: 267, **239**, 224, 135 |
| **F-3-61** | isosakuranetin | | 38.9 | 285 | 285, **270**, 243, 226, 199, 164, 136 |
| **F-3-62** | prorobinetidin A-type dimer [(E)C→A→C-methyl (epi)robinetinidol] | | 39.0 | 589 | 571, 553, **463**, 421, 303, 285 |
| **F-3-63** | quercetin | 256, 370 | 39 | 301 | 301, 273, 257, 229, **179**, 151, 107 |
| **F-3-64** | prorobinetidin A-type dimer [(E)C→A→C-methyl (epi)robinetinidol] | | 39.7 | 589 | 571, 553, **463**, 421, 303, 285 |
| **F-3-65** | hesperetin | | 40.4 | 301 | **301**, 286, 283, 257, 242, 215, 164, 151, 125, 107 |
| **F-3-66** | PAC A-type dimer [(E)C→A→(E)Afz→phloroglucinol] − $C_6H_6O_3$ (126 Da) | | 41.1 | 557 | 539, 521, **431**, 389, 285 |
| **F-3-67** | biflavonoid [eriodictyol→C-methyl robinetinidol] | | 41.4 | 587 | 569, 551, **461**, 419, 301, 285 |
| **F-3-68** | prorobinetidin A-type dimer [(E)C→A→C-methyl (epi)robinetinidol] | | 41.7 | 589 | 571, 553, **463**, 421, 303, 285 |
| **F-3-69** | PAC A-type dimer [(E)C→A→(E)Afz→phloroglucinol] − $C_6H_6O_3$ (126 Da) | | 42.7 | 557 | 539, 521, **431**, 389, 285 |
| **F-3-70** | *trans*-3,3′,5,5′-tetrahydroxy-4′-methoxystilbene | | 43.9 | 273 | **258**, 163, 136, 109 |
| **F-3-71** | homoeriodictyol | | 44.4 | 301 | **301**, 286, 151 |
| **F-3-72** | pratensein | | 45.6 | 299 | **284**, 255, 177, 151, 122 |
| **F-3-73** | unknown | | 45.6 | 567 | 549, 505, **441**, 399, 325, 285 |
| **F-3-74** | 3′,5,6-trihydroxy-4′,7-dimethoxyflavone | | 46 | 329 | **314**, 299, 191 |
| **F-3-75** | kaempferol | 266, 326sh, 368 | 46.7 | 285 | **285**, 257, 241, 229, 213, 199, 151 |
| **F-3-76** | luteolin methyl ether (diosmetin) | 254sh, 266, 348 | 47.1 | 299 | 299, **284**, 217<br>$MS^3$ [299→284]: **284**, 256, 216, 151 |
| **F-3-77** | quercetin methyl ether (isorhamnetin) | 256, 370 | 47.3 | 315 | **315**, 300<br>$MS^3$ [315→300]: **300**, 271, 256, 151 |
| **F-3-78** | 3′,4′,5′-trimethylrobinetin | | 49 | 343 | 328, **313**, 299, 285, 135 |

[a] A represents an A-type bond with both (C4→C8) and (C2→O→C7) linkages or (C4→C6) and (C2→O→C7) linkages; B represents a B-type bond which can be (C4→C8) or (C4→C6) linkage; (E)C represents (epi)catechin, (E)GC represents (epi)gallocatechin, and (E)Afz represents (epi)afzelechin. [b] sh, shoulder in the spectrum. [c] Retention times ($t_R$) of the total ion chromatograms. [d] The most abundant ions observed in mass spectra are indicated in bold; quinone methide (QM) fission diagnostic ions are underlined.

135. It is further confirmed as *trans*-caffeic acid by $t_R$ matching with a commercial standard. Compound **F-2-22** was identified as *p*-coumaric acid by the standard ($\lambda_{max}$ = 310 nm), resulting in a $[M - H]^-$ at *m/z* 163 and a classic fragment at *m/z* 119 through neutral loss of $CO_2$. Compound **F-2-25** displayed a maximum UV absorption band at 322 nm and was further confirmed as ferulic acid by a commercial standard. It gave a $[M - H]^-$ at *m/z* 193 together with fragment ions at *m/z* 178 $[M - H - 15\ (CH_3)]^{\bullet -}$, 149 $[M - H - 44\ (CO_2)]^-$, and 134 $[M - H - 44\ (CO_2) - 15\ (CH_3)]^{\bullet -}$.

*Hydroxybenzoic Acids, Their Esters, and Phenyllactic Acid.* Compounds **F-2-4** and **-7** both yielded a molecular ion at *m/z* 181. Further dissociation ions of compound **F-2-4** were present at *m/z* 163 $[M - H - 18\ (H_2O)]^-$, 153 $[M - H - 28\ (CH_2CH_2)]^-$, 137 $[M - H - 44\ (C_2H_4O)]^-$, and 109 $[M - H - 72\ (COOCH_2CH_2)]^-$. The tentative candidate was ethyl protocatechuate. This compound in peanut seed testa was identified by NMR analysis performed by Huang et al.[28] Compound **F-2-7** gave fragment ions at *m/z* 163 $[M - H - 18\ (H_2O)]^-$ and 137 $[M - H - 44\ (CO_2)]^-$ and is likely DL-3-(4-hydroxyphenyl)lactic acid. Compound **F-2-5** was confirmed by a commercial standard to be protocatechuic acid ($\lambda_{max}$ = 260 nm), producing a molecular ion at *m/z* 153 and a fragment ion at *m/z* 109 by loss of $CO_2$ from the carboxylic acid moiety. *p*-Hydroxybenzoic acid (compound **F-2-9**) was recovered in F2 and showed a molecular ion at *m/z* 137. Although no significant $MS^2$ fragments were observed, this compound's identity was further confirmed by $t_R$ matching with a commercial standard.

*Procyanidins (Monomers to Tetramers).* Compounds **F-2-1** and **-2** are likely gallocatechin and a derivative, respectively. The molecular ion $[M - H]^-$ of gallocatechin was present at *m/z* 305, which further fragmented to product ions at *m/z* 261 $[M - H - 44]^-$ by loss of a $-CH_2-CHOH-$ group or neutral loss of $CO_2$, 219 $[M - H - 86]^-$ by loss of a $C_4H_4O_2$ from the A-ring plus 2H, and 179 $[M - H - 126]^-$ attributed to a $^{1,4}B^-$ ion. The conjugate $^{1,4}A^-$ fragment at *m/z* 125 represents the intact A-ring with two phenolic groups and is formed through a pathway as demonstrated by Miketova et al.[29] Compounds **F-2-8**, **-10**, and **-12** are stereoisomers with the same molecular ions at *m/z* 289. Classic fragments were observed at *m/z* 245 $[M - H - 44]^-$ by loss of a $-CH_2-CHOH-$ group or neutral loss of $CO_2$, 205 $[M - H - 84]^-$ by loss of $C_4H_4O_2$ from the A-ring, and 179 $[M - H - 110]^-$ by loss of $C_6H_6O_2$ (B-ring). The

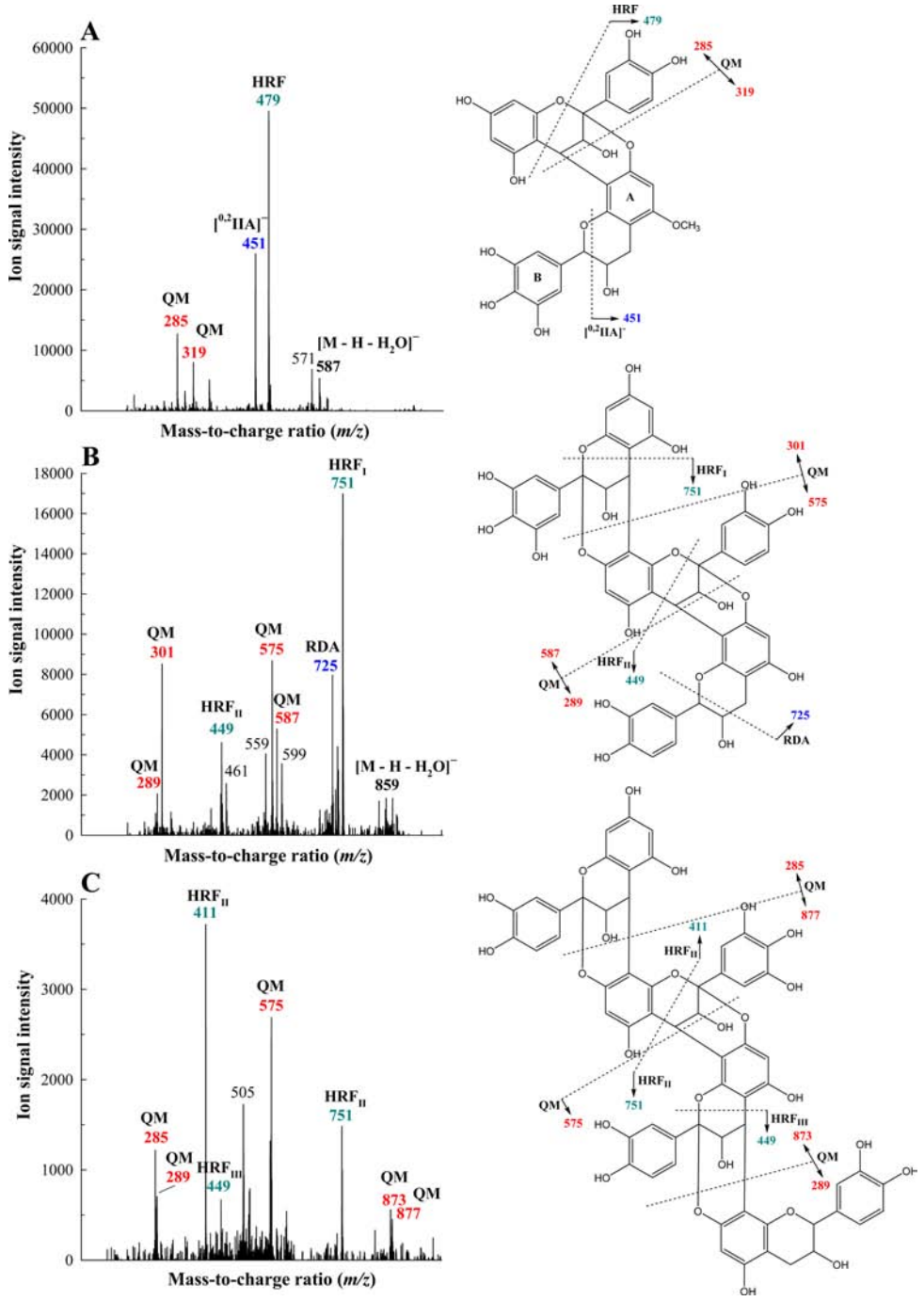


**Figure 1.** Tentative structures and fragmentation schemes of (A) prodelphinidin A-type dimer [(E)C→A→6-*O*-methyl (E)GC] (**F-2-18**, *m/z* 605), (B) prodelphinidin A-type trimer [(E)GC→A→(E)C→A→(E)C] (**F-2-34**, *m/z* 877), and (C) prodelphinidin A-type tetramer [(E)C→A→(E)GC→A→(E)C→A→(E)C] (**F-2-48**, *m/z* 1163). See Table 3 for formal designations.

fragmentation mechanisms of (epi)catechin were described by Bravo et al.[30] The compounds were further confirmed by standards as (−)-catechin (compound **F-2-8**), (+)-catechin (compound **F-2-10**), and (−)-epicatechin (compound **F-2-12**), respectively. Compound **F-2-13** was found to be (−)-epiafzelechin with a $[M - H]^-$ at *m/z* 273, which dissociated further into ions at *m/z* 229 $[M - H - 44]^-$ by loss of a $-CH_2-CHOH-$ group or neutral loss of $CO_2$, 187 $[M - H - 86]^-$ by loss of $C_4H_4O_2$ from the A-ring plus 2H, and 137 $[M - H - 136]^-$ attributed to a $^{1,3}A^-$ ion. The identification was confirmed by $t_R$ matching with a commercial standard.

Compounds **F-2-19**, **-21**, **-26**, **-27**, **-28**, **-30**, and **-31** are probably PAC A-type dimers, yielding molecular ions at *m/z* 575, whereas compound **F-2-20** is likely a PAC B-type dimer with a $[M - H]^-$ at *m/z* 577. As aforementioned, PAC A-type trimers (*m/z* 863) can further be divided into two categories according to the location of the A-bond. Compounds **F-2-14**, **-29**, **-33**, **-36**, and **-44** are likely PAC A-type trimers with an A-type linkage between the middle and bottom units. Trimers with an A-type linkage between the top and middle units are candidates for compounds **F-2-15** and **-45**. Compound **F-2-42**, yielding a $[M - H]^-$ at *m/z* 861, is likely a PAC trimer with


dx.doi.org/10.1021/jf503836n | J. Agric. Food Chem. 2014, 62, 11488−11504

two A-type linkages. The HRF fragment ions of the top unit were present at $m/z$ 735, whereas the RDA fragmentation of the base unit generated an ion at $m/z$ 709. The QM cleavage between the top and middle units gave ions at $m/z$ 575 $[M_T - H\ (576 - H)]^-$ and 285 $[M_E - 5H\ (290 - 5H)]^-$. The QM cleavage between the middle and base units produced ions at $m/z$ 289 $[M_T - H\ (290 - H)]^-$ and 571 $[M_E - 5H\ (576 - 5H)]^-$. The fragment at $m/z$ 449 was generated by fragmentation of the QM ion at $m/z$ 575 and HRF ion at $m/z$ 735 via the mechanism of HRF.[21]

Compounds **F-2-32**, **-38**, **-39**, **-43**, and **-46** are PAC A-type tetramers, displaying doubly charged ions $[M - 2H]^{2-}$ at $m/z$ 574. Noteworthy is that no significant fragments were observed for the determination of the flavan-3-ol connection sequence. Compound **F-2-47** yielded a $[M - 2H]^{2-}$ at $m/z$ 507. Although no significant $MS^2$ fragments were evident, the proposed candidate is a PAC A-type trimer with (epi)catechin gallate as its base unit.

*Propelargonidin.* Compound **F-2-35** ($m/z$ 559) is tentatively identified as a propelargonidin A-type dimer with (epi)afzelechin as its base unit. HRF fragmentation of the (epi)catechin top unit and the RDA fragmentation of the (epi)afzelechin base unit gave product ions at $m/z$ 433 $[M - H - 126\ (C_6H_6O_3)]^-$ and 423 $[M - H - 136\ (C_8H_8O_2)]^-$, respectively. Diagnostic ions at $m/z$ 273 $[M_T - H\ (274 - H)]^-$ and 285 $[M_E - 5H\ (290 - 5H)]^-$ were produced by QM fission. The fragmentation pathways of a similar propelargonidin A-type dimer, only with an (epi)afzelechin as its top unit, was well described by Appeldoorn et al.[25]

*Prodelphinidins.* Compound **F-2-16** is likely a prodelphinidin dimer containing a B-bond linked to (epi)gallocatechin (top) and (epi)catechin (base) units. It yielded a $[M - H]^-$ of $m/z$ 593 and further fragments at $m/z$ 467 $[M - H - 126\ (C_6H_6O_3)]^-$ by HRF at the top unit, 425 $[M - H - 168\ (C_8H_8O_4)]^-$ by RDA at the top unit, 303 $[M_E - 3H\ (306 - 3H)]^-$, and 289 $[M_T - H\ (290 - H)]^-$. The fragmentation scheme of this B-type prodelphinidin dimer has been documented.[31] Compound **F-2-17** showed a $[M - H]^-$ at $m/z$ 591 and is tentatively identified as a prodelphinidin dimer containing an A-bond linked to (epi)gallocatechin (top) and (epi)catechin (base) units. The HRF fragmentation of the (epi)gallocatechin unit and RDA fragmentation of the (epi)-catechin unit yielded product ions at $m/z$ 465 $[M - H - 126\ (C_6H_6O_3)]^-$ and 439 $[M - H - 152\ (C_8H_8O_3)]^-$, respectively. The QM cleavage ions were present at $m/z$ 289 $[M_T - H\ (290 - H)]^-$ and 301 $[M_E - 5H\ (306 - 5H)]^-$. On the other hand, compound **F-2-23** is a similar A-type prodelphinidin dimer but with (epi)catechin as its top unit and (epi)gallocatechin as its base unit. QM diagnostic ions were present at $m/z$ 305 $[M_T - H\ (306 - H)]^-$ and 285 $[M_E - 5H\ (289 - 5H)]^-$. A product ion at $m/z$ 423 $[M - H - 168\ (C_8H_8O_4)]^-$ was generated by the RDA fragment of the base (epi)gallocatechin unit.

A molecular ion $[M - H]^-$ at $m/z$ 605 was provided by compound **F-2-18**. It is likely a prodelphinidin A-type dimer with a (epi)catechin top unit connected to a 5-*O*-methyl (epi)gallocatechin. The HRF fragmentation of top (epi)-catechin unit gave an anion at $m/z$ 479 $[M - H - 126\ (C_6H_6O_3)]^-$. The $^{0,2}IIA^-$ fragment from the base methyl (epi)gallocatechin was present at $m/z$ 451 $[M - H - 154\ (C_7H_6O_4)]^-$, which indicates that the methoxy group is attached to the 5-position on the A-ring. QM diagnostic ions were found at $m/z$ 319 $[M_T - H\ (320 - H)]^-$ and 285 $[M_E - 5H\ (290 - 5H)]^-$. The tentative structure and fragmentation pathways for compound **F-2-18** are depicted in Figure 1A. Similarly, the proposed candidates for compound **F-2-41**, which yielded a $[M - H]^-$ at $m/z$ 607, are a prodelphinidin B-type dimer containing an (epi)catechin unit and a methyl (epi)-gallocatechin unit or a prodelphinidin A-type dimer with two (epi)gallocatechin units. Unfortunately, the identification cannot be unequivocally assigned because of the lack of significant $MS^2$ fragments.

Compound **F-2-34** yielded a $[M - H]^-$ at $m/z$ 877, which was tentatively identified as a prodelphinidin trimer with a connection sequence of (epi)gallocatechin→A→(epi)-catechin→A→(epi)catechin; here, A represents an A-type linkage. The HRF fragment from the (epi)gallocatechin top unit and the RDA fragment from the base (epi)catechin unit were present at $m/z$ 751 $[M - H - 126\ (C_6H_6O_3)]^-$ and 725 $[M - H - 152\ (C_8H_8O_3)]^-$, respectively. An ion at $m/z$ 599 was generated by RDA fragmentation of the HRF ion at $m/z$ 751. QM diagnostic ions were present at $m/z$ 575 $[M_T - H\ (576 - H)]^-$, 289 $[M_T - H\ (290 - H)]^-$, 301 $[M_E - 5H\ (306 - 5H)]^-$, and 587 $[M_E - H\ (592 - 5H)]^-$. HRF fragmentation of QM cleavage ions at $m/z$ 587 and 575 yielded anions at $m/z$ 461 and 449, respectively. The tentative structure and fragmentation pathways for compound **F-2-34** are depicted in Figure 1B. The tentative candidate for compound **F-2-40** is likely a prodelphinidin trimer containing a luteolin or kaempferol base unit. Further fragmentation of $[M - H]^-$ at $m/z$ 875 yielded ions at $m/z$ 749 $[M - H - 126\ (C_6H_6O_3)]^-$ and 723 $[M - H - 152\ (C_8H_8O_3)]^-$ by HRF and RDA fragmentation, respectively, indicating a top (epi)catechin unit with a B-type linkage to the following (epi)gallocatechin unit. Unfortunately, no significant diagnostic QM ions were observed in the mass spectra to further support the assignment. The $[M - 2H]^{2-}$ at $m/z$ 581 (compound **F-2-48**) was a doubly charged ion yielded by a prodelphinidin tetramer with a molecular mass of 1164 Da. The diagnostic QM fragments were present at $m/z$ 877 $[M_T - H\ (878 - H)]^-$, 575 $[M_T - H\ (576 - H)]^-$, 289 $[M_T - H\ (290 - H)]^-$, 873 $[M_E - 5H\ (878 - 5H)]^-$, and 285 $[M_E - 5H\ (290 - 5H)]^-$, indicating a connection sequence of (epi)catechin→A→(epi)-gallocatechin→A→(epi)catechin→A→(epi)catechin. HRF fragmentation of the QM ions at $m/z$ 877 and 575 gave further dissociation ions at $m/z$ 751 and 449, respectively. The proposed structure and fragmentation pathways for compound **F-2-48** are shown in Figure 1C.

*Flavonoid.* The proposed candidate for compound **F-2-37** is myricetin, which was further confirmed by $t_R$ matching with a commercial standard. Its $[M - H]^-$ at $m/z$ 317 dissociated into fragments at $m/z$ 271 $[M - H - 18\ (H_2O) - 28\ (CO)]^-$, 243 $[M - H - 18\ (H_2O) - 56\ (2CO)]^-$, and 227 $[M - H - 18\ (H_2O) - 28\ (CO) - 44\ (CO_2)]^-$. RDA diagnostic ions at $m/z$ 179, 151, and 137 were noted as $^{1,2}A^-$, $^{1,3}A^-$, and $^{1,2}B^-$, respectively.

*Stilbene.* Compound **F-2-24** was tentatively identified as *trans*-piceatannol by a molecular ion $[M - H]^-$ at $m/z$ 243. Further fragment ions were present at $m/z$ 225 $[M - H - 18\ (H_2O)]^-$, 201 $[M - H - 42\ (CHCOH)]^-$, 199 $[M - H - 42\ (CHCOH) - 2H]^-$, 175 $[M - H - 68\ (C_3O_2)]^-$, 173 $[M - H - 42\ (CHCOH) - 28\ (CO)]^-$, and 159 $[M - H - 42\ (CHCOH) - 42\ (C_2H_2O)$ or $M - H - 42\ (CHCOH) - 2H - 40\ (C_2O)]^-$. This is the CID fragmentation of $[M - H]^-$ when the deprotonation reaction occurs on the catechol moiety of *trans*-piceatannol. These fragmentation mechanisms have been elucidated and described by Stella et al.[32] Similar $MS^2$

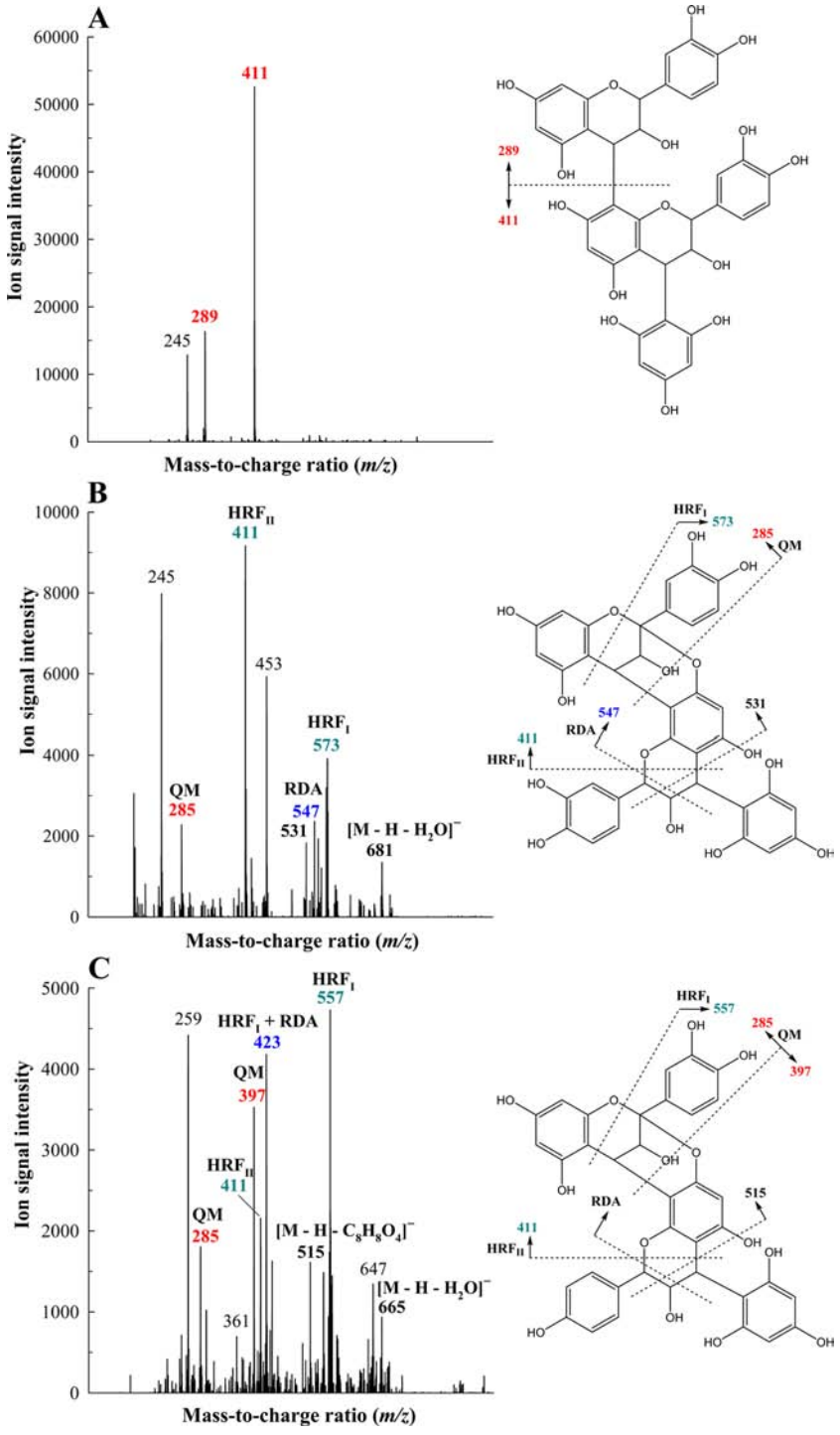


**Figure 2.** Tentative structures and fragmentation schemes of (A) PAC B-type dimer [(E)C→B→(E)C→phloroglucinol] (**F-3-13**, **-16**, and **-19**, *m/z* 701); (B) PAC A-type dimer [(E)C→A→(E)C→phloroglucinol] (**F-3-10**, **-12**, **-15**, **-17**, **-18**, **-20**, **-25**, **-26**, and **-38**, *m/z* 699); and (C) PAC A-type dimer [(E)C→A→(E)Afz→phloroglucinol] (**F-3-34** and **-43**, *m/z* 683). See Table 3 for formal designations.

fragments for *trans*-piceatannol in peanuts were reported by Ku et al.[33]

**Glycoside-Bound Phenolics.** *Phenolic Acids.* Compound **F-3-3** with a molecular ion $[M - H]^-$ at *m/z* 167 and a fragment ion at *m/z* 123 is likely DOPAC, as discussed for F2. Compound **F-3-5** was identified as protocatechuic acid by its $[M - H]^-$ at *m/z* 153 and the decarboxylated ion at *m/z* 109 $[M - H - 44\ (CO_2)]^-$. Compound **F-3-6** may be a protocatechuic acid derivative: it yielded a $[M - H]^-$ at *m/z* 233 and a prominent fragment ion at *m/z* 153, corresponding to deprotonated protocatechuic acid. Compound **F-3-8**, giving a molecular ion at *m/z* 137, was identified as *p*-hydroxybenzoic acid by UV spectra ($\lambda_{max}$ = 256 nm) and $t_R$ matching with a commercial standard.

Compound **F-3-11** is confirmed as vanillic acid by UV spectra ($\lambda_{max}$ = 260 nm) and $t_R$ matching with a commercial standard. It yielded a $[M - H]^-$ at *m/z* 167 and a fragment ion at *m/z* 123 by loss of $CO_2$ from the carboxylic acid moiety.

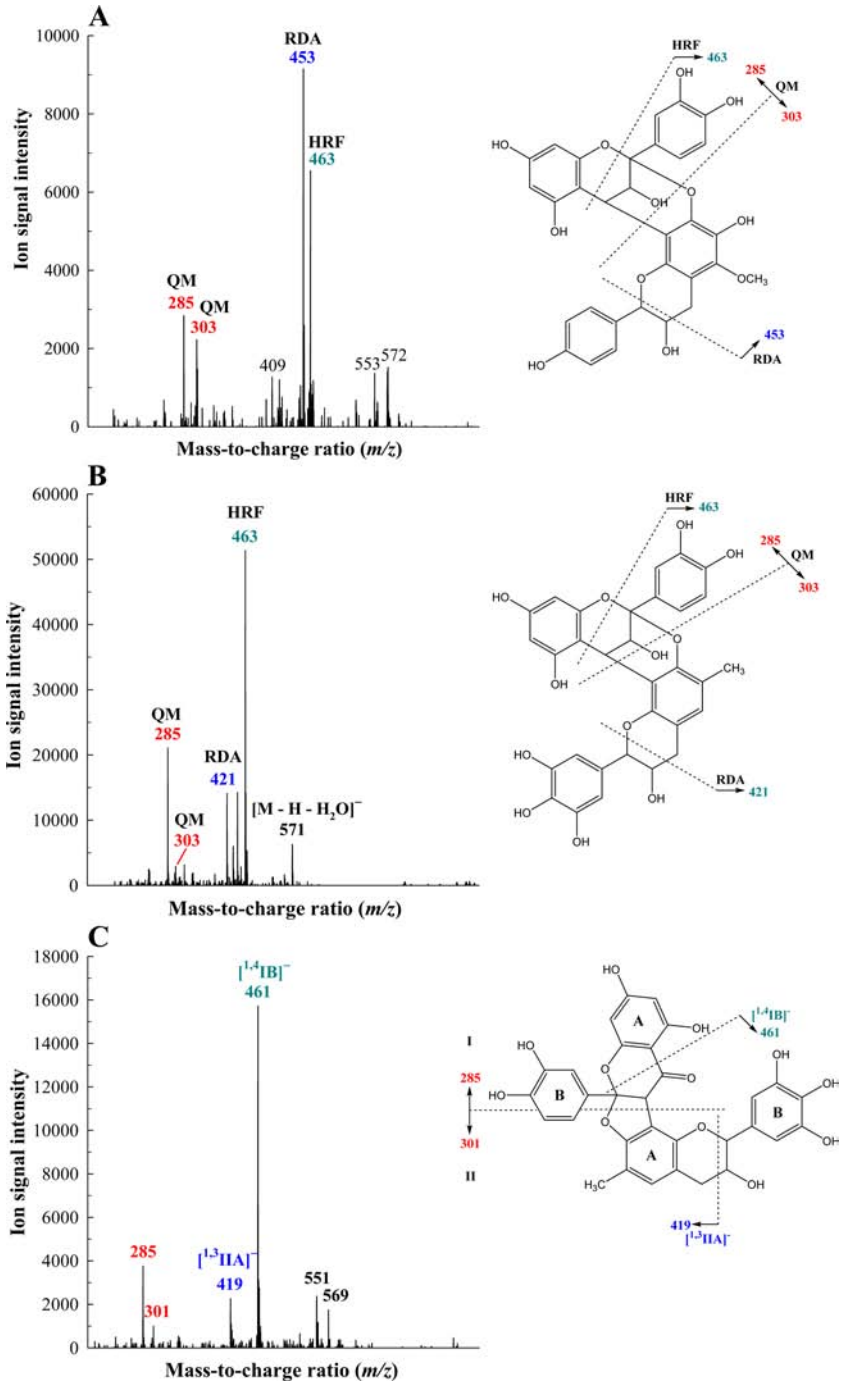


**Figure 3.** Tentative structures and fragmentation schemes of (A) PAC A-type dimer [(E)C→A→dihydroscutellarein] (**F-3-39**, *m/z* 589), (B) prorobinetidin A-type dimer [(E)C→A→C-methyl (epi)robinetinidol] (**F-3-56**, **-62**, **-64**, and **-68**, *m/z* 589), and (C) biflavanoid [eriodictyol→C-methyl robinetinidol] (**F-3-48**, **-57** and **-67**, *m/z* 587). See Table 3 for formal designations.

Other dissociation ions were present at *m/z* 152 [M − H − 15 $(CH_3)$]$^{\bullet-}$ and 108 [M − H − 44 $(CO_2)$ − 15 $(CH_3)$]$^{\bullet-}$. **F-3-22** is likely homovanillic acid with a [M − H]$^-$ at *m/z* 181, which dissociated further into fragments at *m/z* 137 [M − H − 44 $(CO_2)$]$^-$ and 122 [M − H − 44 $(CO_2)$ − 15 $(CH_3)$]$^{\bullet-}$.

*Procyanidins (Monomers to Dimers).* Compounds **F-3-1** and **F-3-2** are identified as gallocatechin and a derivative, as in F2. Compound **F-3-4** is likely methyl gallate, yielding a [M − H]$^-$ at *m/z* 183 and a fragment ion at 124 [M − H − 44 $(CO_2)$ − 15 $(CH_3)$]$^{\bullet-}$. Compounds **F-3-9** and **F-3-14** are (+)-catechin and (−)-epicatechin, respectively, as described for F2 and further confirmed by $t_R$ matching with commercial standards. Compounds **F-3-21**, **-23**, **-27**, **-32**, **-35**, **-36**, and **-40** are likely PAC A-type dimers with molecular ions at *m/z* 575 and QM ions at *m/z* 289 [$M_T$ − H (290 − H)]$^-$ and 285 [$M_E$ − 5H (290 − 5H)]$^-$.

*Propelargonidins.* Compound **F-3-24** (*m/z* 847) is likely a propelargonidin A-type trimer with an (epi)afzelechin middle unit. QM cleavage ions were present at *m/z* 289 [$M_T$ − H (290 − H)]$^-$ and 557 [$M_E$ − 3H (560 − 3H)]$^-$, indicating the presence of a B-type linkage between the middle (epi)-afzelechin unit and the base (epi)catechin unit. Compound **F-**


dx.doi.org/10.1021/jf503836n | *J. Agric. Food Chem.* 2014, 62, 11488−11504

**3-52** yielded a $[M - H]^-$ at *m/z* 845 and was tentatively identified as a propelargonidin trimer with one (epi)afzelechin top unit and two A-type linkages. QM cleavage of this trimer resulted in fragments at *m/z* 289 $[M_T - H\ (290 - H)]^-$, 575 $[M_T - H\ (576 - H)]^-$, and 269 $[M_E - 5H\ (273 - 5H)]^-$, 555 $[M_E - 5H\ (560 - 5H)]^-$. The fragmentation pathways for these two propelargonidin oligomers are well documented.[21,25]

*Proanthocyanidins (PACs) Containing an Additional Phloroglucinol Unit.* Compounds **F-3-10**, **-12**, **-15**, **-17**, **-18**, **-20**, **-25**, **-26**, and **-37** are likely A-type PAC dimers containing an additional phloroglucinol unit, which was reported in cranberry by Foo et al.[34] These compounds yielded molecular ions at *m/z* 699, which dissociated further into fragments at *m/z* 573 $[M - H - 126]^-$ by losing a phloroglucinol moiety ($C_6H_6O_3$) from the top (epi)catechin unit via the HRF function, 547 $[M - H - 152]^-$ by losing $C_8H_8O_3$ from the base (epi)catechin-phloroglucinol unit via the RDA function, and 531 $[M - H - 168]^-$ by losing $C_8H_8O_4$ from the base (epi)catechin-phloroglucinol unit. Product ions at *m/z* 411 and 287 were generated by HRF fragmentation at the base (epi)catechin-phloroglucinol unit. A QM diagnostic ion was present at *m/z* 285 $[M_E - 5H\ (290 - 5H)]^-$. It is interesting that the conjugate ion at *m/z* 413 was not observed. Our identification is further supported by the $MS^3$ experiment. Compounds **F-3-28**, **-29**, and **-31** (*m/z* 657) appear to be generated by losing a $C_2H_2O$ group (42 Da) from the additional phloroglucinol unit of the above-described PAC dimers. Compounds **F-3-33** and **-50** (*m/z* 547) are also likely fragments from the aforementioned dimers by RDA at the base (epi)catechin-phloroglucinol unit. Furthermore, compounds **F-3-39**, **-44**, **-48**, and **-51** (*m/z* 531) are tentatively identified as fragments from this dimer after loss of $C_8H_8O_4$ from the base (epi)catechin-phloroglucinol unit. Such cleavages can be induced by heat or acid hydrolysis applied to release phenolics bound to glycosides.

Compounds **F-3-13**, **-16**, and **-19** are tentatively identified as a similar PAC dimer, but the top (epi)catechin and the base (epi)catechin-phloroglucinol units are connected by a B-type linkage. The $[M - H]^-$ was present at *m/z* 701. Diagnostic ions were evident at *m/z* 289 $[M_T - H\ (290 - H)]^-$ and 411 $[M_B - 3H\ (414 - 3H)]^-$, indicating a fragmentation pathway as described by Sarnoski et al.[26] whereby QM cleavage is blocked by a carbonyl group on the C-ring of the base luteolin or kaempferol group. In the present study, the presence of an additional phloroglucinol unit, which is connected to the C-ring of the base (epi)catechin unit, inhibits QM fission. Our identification is further supported by the $MS^3$ experiment. Compounds **F-3-42** and **-47** (*m/z* 549) are likely fragments from the aforementioned B-type dimers by RDA at the base (epi)catechin-phloroglucinol unit.

The proposed candidate for compounds **F-3-34** and **-41** (*m/z* 683) is a PAC dimer with an (epi)catechin unit connected to an (epi)afzelechin-phloroglucinol unit through an A-type bond. HRF fragmentation ions of this dimer were present at *m/z* 557 $[M - H - 126\ (C_6H_6O_3)]^-$ and 411 $[M - H - 272\ (C_{15}H_{12}O_5)]^-$, which were assigned to HRF at the top (epi)catechin unit and the base (epi)afzelechin-phloroglucinol unit, respectively. Other product ions were observed at *m/z* 515 $[M - H - 168]^-$ by loss of $C_8H_8O_4$ from the base (epi)afzelechin-phloroglucinol unit and 423 $[M - H - 126\ (C_6H_6O_3) - 136\ (C_8H_8O_2)]^- + 2H$ by combination of HRF (at the top (epi)catechin unit) and RDA (at the base (epi)afzelechin-phloroglucinol unit) fragmentations. QM fission resulted in fragments at *m/z* 397 $[M_T - H\ (398 - H)]^-$ and 285 $[M_E - 5H\ (290 - 5H)]^-$. Our assignment is further supported by the $MS^3$ experiment. Compounds **F-3-45**, **-66**, and **-69** (*m/z* 557) are likely fragments from the aforementioned dimers by HRF at the top (epi)catechin unit. Further dissociation ions were present at *m/z* 431 $[M - H - 126\ (C_6H_6O_3)]^-$ by loss of the additional phloroglucinol group, 389 $[M - H - 168\ (C_8H_8O_4)]^-$, and 285 $[M - H - 272\ (C_{15}H_{12}O_5)]^-$ by HRF at the base (epi)afzelechin-phloroglucinol unit. These types of fragments can be caused by heat or acid applied in deglycosylation. The proposed structures and fragmentation pathways of the above three types of PACs containing an additional phloroglucinol unit are depicted in Figure 2, panels A, B, and C, respectively.

*Proanthocyanidin (PAC) Containing a Novel Flavan-3-ol Unit.* Compound **F-3-38** is likely a PAC dimer with a catechin connected to a novel flavan-3-ol unit through an A-type linkage. It yielded a $[M - H]^-$ at *m/z* 589, which further dissociated into ions at *m/z* 463 $[M - H - 126\ (C_6H_6O_3)]^-$ by HRF at the top catechin unit and 453 $[M - H - 136\ (C_8H_8O_2)]^-$ by RDA at the base unit. QM diagnostic ions were present at *m/z* 303 $[M_T - H\ (304 - H)]^-$ and 285 $[M_E - 5H\ (290 - 5H)]^-$. Our identification is further supported by the $MS^3$ experiment; nevertheless, further analyses are necessary to support the assignment. The tentative structure and fragmentation scheme are shown in Figure 3A. Compound **F-3-73** is probably a PAC derivative due to the product ions at *m/z* 441 and 285, which can be assigned to an HRF and a QM ion, respectively.

*Prorobinetidin and Prodelphinidin.* As shown in Figure 3B, compounds **F-3-55**, **-57**, **-62**, **-64**, and **-68** (*m/z* 589) are tentatively identified as a prorobinetidin dimer with a base unit most likely being a C-methyl (epi)robinetinidol A-linked to an (epi)catechin top unit. The HRF fragment ion of the (epi)catechin unit and RDA fragment ion of the C-methyl (epi)robinetinidol unit were present at *m/z* 463 $[M - H - 126\ (C_6H_6O_3)]^-$ and 421 $[M - H - 168\ (C_8H_8O_4)]^-$, respectively. QM cleavage gave rise to diagnostic ions at *m/z* 303 $[M_T - H\ (304 - H)]^-$ and 285 $[M_E - H\ (290 - 5H)]^-$, corresponding to C-methyl (epi)robinetinidol and (epi)catechin units, respectively. Our identification was further supported by the $MS^3$ experiment. The proposed candidate for compound **F-3-58** is a prodelphinidin dimer, as discussed in F2.

*Flavonols and Flavanonols.* Compound **F-3-7** yielded a molecular ion $[M - H]^-$ at *m/z* 301 and fragments at *m/z* 283 $[M - H - 18\ (H_2O)]^-$, 257 $[M - H - 44\ (CO_2)]^-$, and 229 $[M - H - 44\ (CO_2) - 28\ (CO)]^-$. $^{1,2}B^-$ and $^{1,2}A^-$ ions were present at *m/z* 163 and 137, respectively. The likely candidate is robinetin. Compound **F-3-78** yielded a $[M - H]^-$ at *m/z* 343, which further dissociated into ions at *m/z* 328 $[M - H - 15\ (CH_3)]^{\bullet -}$, 313 $[M - H - 30\ (2CH_3)]^-$, 299 $[M - H - 15\ (CH_3) - 29\ (HCO)]^-$, 285 $[M - H - 30\ (2CH_3) - 28\ (CO)]^-$, and 135 attributed to a $^{1,3}A^-$ fragment. The proposed candidate is 3′,4′,5′-trimethylrobinetin.

Compound **F-3-63** is identified as quercetin with a $[M - H]^-$ at *m/z* 301 that fragmented into ions at *m/z* 273 $[M - H - 28\ (CO)]^-$, 257 $[M - H - 44\ (CO_2)]^-$, and 229 $[M - H - 44\ (CO_2) - 28\ (CO)]^-$. The $^{1,2}A^-$ ion at *m/z* 179 further yielded ions at *m/z* 151 noted as $^{1,2}A^- - CO$ and 107 noted as $^{1,2}A^- - CO - CO_2$. This compound was further confirmed by UV spectra ($\lambda_{max}$ = 256 and 370 nm) and $t_R$ matching with a commercial standard. Compound **F-3-77** is likely a quercetin methyl ether such as isorhamnetin with a molecular ion $[M - H]^-$ at *m/z* 315 and a fragment at *m/z* 300 $[M - H - 15$

Table 4. Content of Selected Phenolics Quantified[a] in Dry-Blanched Peanut Skins by $C_{18}$ RP-HPLC

| phenolic compound | quantification UV $\lambda$ (nm) | content[b] (mg/100 g) |
|---|---|---|
| **esterified** | | |
| protocatechuic acid | 260 | 41.4 ± 1.72 |
| (+)-catechin | 280 | 52.0 ± 2.66 |
| (−)-epicatechin | 280 | 8.33 ± 0.40 |
| prodelphinidin A-type dimer [(E)C→A→5-*O*-methyl (E)GC] | 280 | 22.2 ± 0.58 |
| PAC A-type dimer [(E)C→A→(E)C] | 280 | 74.9 ± 2.84 |
| *p*-coumaric acid | 320 | 6.88 ± 0.22 |
| ferulic acid | 320 | 2.03 ± 0.12 |
| PAC A-type dimer [(E)C→A→(E)C] | 280 | 44.3 ± 3.32 |
| PAC A-type dimer [(E)C→A→(E)C] | 280 | 152 ± 7.09 |
| PAC A-type dimer [(E)C→A→(E)C] | 280 | 81.2 ± 1.74 |
| PAC A-type tetramer [1B, 2A] | 280 | 32.1 ± 2.03 |
| PAC A-type tetramer [1B, 2A] | 280 | 29.5 ± 0.86 |
| PAC A-type trimer [(E)C→B→(E)C→A→(E)C] | 280 | 15.2 ± 0.37 |
| PAC A-type tetramer [1B, 2A] | 280 | 10.2 ± 0.13 |
| PAC A-type tetramer [1B, 2A] | 280 | 15.1 ± 0.35 |
| PAC A-type trimer [(E)C→A→(E)C→A→(E)C] | 280 | 24.8 ± 0.75 |
| PAC A-type tetramer [1B, 2A] | 280 | 8.96 ± 0.56 |
| prodelphinidin tetramer [(E)C→A→(E)GC→A→(E)C→A→(E)C] | 280 | 3.66 ± 0.13 |
| **glycoside-bound** | | |
| protocatechuic acid | 260 | 21.5 ± 0.66 |
| (+)-catechin | 280 | 105 ± 4.57 |
| *p*-hydroxybenzoic acid | 255 | 1.72 ± 0.00 |
| vanillic acid | 260 | 2.38 ± 0.10 |
| PAC A-type dimer [(E)C→A→(E)C→phloroglucinol] | 280 | 86.2 ± 6.55 |
| PAC A-type dimer [(E)C→A→(E)C] | 280 | 110 ± 1.27 |
| kaempferol | 360 | 0.89 ± 0.67 |
| fisetin | 360 | 0.75 ± 0.03 |
| genkwanin | 320 | 0.08 ± 0.00 |
| quercetin | 360 | 1.62 ± 0.12 |
| diosmetin | 360 | 0.46 ± 0.00 |
| isorhamnetin | 360 | 1.29 ± 0.00 |

[a]PACs are quantified as (+)-catechin equivalents. Fisetin, genkwanin, isorhamnetin, and diosmetin are quantified using corresponding flavonoid aglycone equivalents. [b]Values are means of triplicate analyses ± standard deviation. Findings are reported as mg respective phenolic/100 g dry weight (dw) of dry-blanched peanut skins.

$(CH_3)]^{\bullet-}$. The $MS^3$ fragments of the ion at $m/z$ 315 were present at $m/z$ 300 $[M - H - 15\ (CH_3)]^{\bullet-}$, 271 $[M - H - 15\ (CH_3) - 29\ (HCO)]^-$, and 256 $[M - H - 44\ (CO_2) - 15\ (CH_3)]^{\bullet-}$. The $^{1,3}A^-$ ion at $m/z$ 151 is a diagnostic ion observed in CID fragmentation of isorhamnetin by ESI-MS.[23,35]

Compound **F-3-75** is kaempferol, which gave a $[M - H]^-$ at $m/z$ 285 and fragments at $m/z$ 257 $[M - H - 28\ (CO)]^-$, 241 $[M - H - 44\ (CO_2)]^-$, 229 $[M - H - 56\ (2CO)]^-$, 213 $[M - H - 44\ (CO_2) - 28\ (CO)]^-$, 199 $[M - H - 42\ (C_2H_2O) - 44\ (CO_2)]^-$, and 151 assigned to a $^{1,3}A^-$ fragment. Identification of kaempferol was confirmed by its UV absorption spectrum and $t_R$ matching with a commercial standard. Fabre et al.[22] described the fragmentation pathways of kaempferol by ESI-MS. Compound **F-3-43** is tentatively identified as fisetin. Fragments produced from $[M - H]^-$ at $m/z$ 285 were present at $m/z$ 257 $[M - H - 28\ (CO)]^-$, 241 $[M - H - 44\ (CO_2)]^-$, 229 $[M - H - 56\ (2CO)]^-$, 213 $[M - H - 44\ (CO_2) - 28\ (CO)]^-$, and 177 $[M - H - \text{ring B}]^-$. RDA cleavage at the 1/2-position on the C-ring generated ions $^{1,2}A^-$ ($m/z$ 163) and $^{1,2}B^-$ ($m/z$ 121), which are highly consistent with the dissociation routes described by Fabre et al.[22] The loss of a CO molecule from $^{1,2}A^-$ ion leads to a fragment at $m/z$ 135 noted as $^{1,2}A^- - CO$. Compound **F-3-49** yielded a $[M - H]^-$ at $m/z$ 317 and was identified as myricetin as described in F2.

Compound **F-3-30** yielded a $[M - H]^-$ at $m/z$ 303 that further fragmented into ions at $m/z$ 285 $[M - H - 18\ (H_2O)]^-$, 259 $[M - H - 44\ (CO_2)]^-$, 241 $[M - H - 18\ (H_2O) - 44\ (CO_2)]^-$, and 217 $[M - H - 18\ (H_2O) - 68\ (C_3O_2)]^-$. RDA cleavage at the 1/4-position on the C-ring gave rise to ions $^{1,4}B^-$ ($m/z$ 177) and $^{1,4}A^-$ ($m/z$ 125). The proposed candidate is taxifolin.

*Flavanones, Flavones, and Isoflavones.* Compound **F-3-65** is tentatively identified as hesperetin. It yielded a $[M - H]^-$ at $m/z$ 301 and further dissociation fragments at $m/z$ 286 $[M - H - 15\ (CH_3)]^{\bullet-}$, 283 $[M - H - 18\ (H_2O)]^-$, 257 $[M - H - 15\ (CH_3) - 29\ (HCO)]^-$, 242 $[M - H - 44\ (CO_2) - 15\ (CH_3)]^{\bullet-}$, and 215 $[M - H - 42\ (C_2H_2O) - 44\ (CO_2)]^-$. RDA diagnostic ions were present at $m/z$ 164, 151, and 125, which were ascribed to $^{1,2}A^-$, $^{1,3}A^-$, and $^{1,4}A^-$, respectively. Further loss of $CO_2$ from $^{1,3}A^-$ generated an ion at $m/z$ 107, noted as $^{1,3}A^- - CO_2$. It undergoes the similar fragmentation route of hesperetin as reported by Justesen.[35] Compound **F-3-71** ($m/z$ 301) is likely homoeriodictyol, producing RDA diagnostic ions at $m/z$ 151 assigned to $^{1,3}A^-$. Compound **F-3-**

**61** is likely isosakuranetin with a $[M - H]^-$ at $m/z$ 285 and further dissociation ions at $m/z$ 270 $[M - H - 15\ (CH_3)]^{\bullet -}$, 243 $[M - H - 42\ (C_2H_2O)]^-$, 226 $[M - H - 44\ (CO_2) - 15\ (CH_3)]^{\bullet -}$, and 199 $[M - H - 42\ (C_2H_2O) - 44\ (CO_2)]^-$. RDA cleavage at the 0/4-position of the C-ring after loss of $CH_3^{\bullet}$ gave a diagnostic ion at $m/z$ 164. This $-CH_3{}^{0,4}B^{\bullet -}$ ion lost a further CO molecule, leading to a fragment noted as $-CH_3{}^{0,4}B^{\bullet -} - CO$ ($m/z$ 136).

The proposed candidate of compound **F-3-53** is 3′,4′,5,6-tetrahydroxy-7-methoxyflavone. It yielded a $[M - H]^-$ at $m/z$ 315 that dissociated further into fragments at 300 $[M - H - 15\ (CH_3)]^{\bullet -}$ and 191 $[M - H - 109\ (B\text{-ring}) - 15\ (CH_3)]^{\bullet -}$. Compound **F-3-74** is likely a flavone dimethyl ether such as 3′,5,6-trihydroxy-4′,7-dimethoxyflavone, which gave a $[M - H]^-$ at $m/z$ 329. It dissociated further into fragments at $m/z$ 314 $[M - H - 15\ (CH_3)]^{\bullet -}$, 299 $[M - H - 30\ (2CH_3)]^-$, and 191 $[M - H - 15\ (CH_3) - 123\ (B\text{-ring})]^-$. Unfortunately, the actual position of the methoxy group for the above two compounds can not be confirmed without a commercial standard or NMR analysis. Compound **F-3-54** yielded a $[M - H]^-$ at $m/z$ 283 and a prominent fragment at $m/z$ 268 $[M - H - 15\ (CH_3)]^{\bullet -}$. The proposed candidate is genkwanin. An RDA diagnostic ion $-CH_3{}^{1,3}A^{\bullet -}$ was present at $m/z$ 151, with the identification being further confirmed by a UV $\lambda_{max}$ at 338 nm.[36] Compound **F-3-76** is likely a luteolin methyl ether such as diosmetin with a $[M - H]^-$ at $m/z$ 299 and a prominent fragment $m/z$ 284 $[M - H - 15\ (CH_3)]^{\bullet -}$. $MS^3$ [299→284] fragments were observed at $m/z$ 256 $[M - H - 15\ (CH_3) - 28\ (CO)]^{\bullet -}$, 240 $[M - H - 15\ (CH_3) - 44\ (CO_2)]^{\bullet -}$, 216 $[M - H - 15\ (CH_3) - 68\ (C_3O_2)]^{\bullet -}$, and 151 attributed to a $^{1,3}A^-$ fragment. The identification is supported by its UV spectra of 254(sh), 266, and 348 nm.[37] The fragmentation pathways for diosmetin were described by Justesen.[23]

Compound **F-3-60** is likely biochanin A. It yielded a $[M - H]^-$ at $m/z$ 283 and a prominent fragment at $m/z$ 268 $[M - H - 15\ (CH_3)]^{\bullet -}$. Further $MS^3$ [283→268] fragmentation generated ions at $m/z$ 267 $[M - H - 15\ (CH_3) - H]^{\bullet -}$, 239 $[M - H - 15\ (CH_3) - H - 28\ (CO)]^-$, 224 $[M - H - 15\ (CH_3) - H - 44\ (CO_2)]^-$, and 135 [A-ring fragment]$^-$, which are consistent with the $MS^3$ spectra of biochanin A obtained by Kang et al.[38] Biochanin A is an *O*-methylated isoflavone, and it has long been reported in peanuts.[39] Compound **F-3-72** exhibited a $[M - H]^-$ at $m/z$ 299. Further fragment ions were observed at $m/z$ 284 $[M - H - 15\ (CH_3)]^{\bullet -}$, 255 $[M - H - 15\ (CH_3) - 29\ (CHO)]^-$, 177 $[M - H - B\text{-ring}]^-$, and 151 attributed to a $^{1,3}A^-$ ion. The proposed candidate is pratensein, that is, 3′,5,7-trihydroxyisoflavone-4′-methoxy-3′-*O*-*β*-glucopyranoside, which has been found in peanut skin according to NMR.[27]

*Biflavonoids.* Compounds **F-3-46**, **-56**, **-59**, and **-67** are likely daphnodorin H-type biflavonoids composed of eriodictyol (part I) and C-methyl (epi)robinetinidol (part II) units. They gave a $[M - H]^-$ at $m/z$ 587 and fragment ions at $m/z$ 569 $[M - H - 18\ (H_2O)]^-$, 461 assigned to a $^{1,4}IB^-$ fragment, and 419 attributed to a $^{1,3}IIA^-$ fragment. The direct cleavage of the interflavan bond generated fragments at $m/z$ 285 [eriodictyol unit $(288 - 3H)]^-$ and 301 [C-methyl (epi)-robinetinidol unit $(304 - 3H)]^-$. This identification is further supported by the $MS^3$ experiment; however, NMR analysis is required to support the assignment. The tentative structure and fragmentation are present in Figure 3C.

*Stilbene.* Compound **F-3-70** is tentatively identified as *trans*-3,3′,5,5′-tetrahydroxy-4′-methoxystilbene. It yielded a $[M - H]^-$ at $m/z$ 273 and further dissociation ions at $m/z$ 258 $[M - H - 15\ (CH_3)]^{\bullet -}$, 163 $[M - H - 68\ (C_3O_2) - 42\ (C_2H_2O)]^-$, 136 $[M - H - 137\ (C_7H_5O_3)]^-$, and 109 $[M - H - 165\ (C_9H_9O_3)]^-$.

**Quantification.** Phenolic compounds were quantified on the basis of peak areas of the observed UV signals from the HPLC chromatograms and calibration curves of commercial standards. Mean phenolic contents for the identified compounds are reported in Table 4. All values are expressed in milligrams of respective phenolic compound per 100 g of dry weight (dw) of PS.

Protocatechuic acid was determined to be the most dominant in the non-PAC phenolics profile and comprised 6.62 and 6.48% of the esterified and glycoside-bound phenolic compounds, respectively. Kaempferol, fisetin, quercetin, isorhamnetin (flavonols), genkwanin, and dosmetin (flavones) are quantifiable flavonoid aglycones liberated from glycosides and account for 1.54% of the total glycoside-bound phenolic compounds. Quercetin and its methyl ether (isorhamnetin) are primary flavonoid aglycones and constituted 57.1% of the total recovered flavonoid aglycones. As aforementioned, PACs possess the lion's share of the phenolics in PS[19] and are the major phenolics released from esters and glycosides. PAC monomers ((+)-catechin and (−)-epicatechin), dimers, trimers, and tetramers constituted 9.65, 60.0, 6.38, and 15.9% of esterified phenolic compounds, respectively. The PAC monomer ((+)-catechin) and dimers are primary phenolics released from glycosides and account for 31.7 and 59.1% of total glycoside-bound phenolic compounds.

It should be noted that the quantification can be easily affected by many factors involved in the details of the extraction and fractionation protocols selected. As for flavonoids, strong acid hydrolysis may degrade unstable aglycones, whereas, on the other hand, some of the cell wall-bound glycosides may not be hydrolyzed completely, yielding inconsistent results.[14,40] The cleavage of the C−C interflavan bond between monomeric flavan-3-ol constituents can result from severe alkaline conditions.[8] This may possibly explain why a large portion of PAC monomers and dimers were found in the profile of esterified and glycoside-bound phenolic compounds. According to our MS data, there are also a number of fragments resulting from PACs containing an additional phloroglucinol unit due to heat or acid treatment, which would lead to underestimation of their quantity. PACs can be modified by thermal treatment. Yu et al.[18] reported a significant influence of the skin removal methods on the PACs content of PS. Dry heat, like that imparted during blanching of redskin peanuts, would increase A-type dimers and B-type trimers compared to directly peeled PS due to monomeric polymerization or the degradation of trimers and tetramers.

In conclusion, analysis of the crude extract gave a simple-looking HPLC chromatogram where only PACs and rutin were determined. In contrast, a large variety of soluble phenolic compounds were liberated from esters and glycosides in PS. They were further separated and detected by HPLC-ESI-$MS^n$. Compounds identified included PACs (monomers to tetramers), free phenolic acids (e.g., hydroxybenzoic acids and *trans*-cinnamic acids), stilbenes, and flavonoids. Free phenolic acids such as *p*-coumaric acid, ferulic acid, and caffeic acid were most likely released from their tartaric acid esters, which were revealed in our previous study.[19] Epicatechin was liberated from the soluble esters, whereas catechin was released from both soluble esters and glycosides. The increased sums of

phenolic aglycones (e.g., *p*-coumaric acid and catechin) was also quantified due to such liberation from esters and glycosides. To our knowledge this is the first report of PACs in PS containing an additional phloroglucinol unit. Although further analytical techniques are required for the final confirmation of some of the compounds identified, our data enrich the phenolic database of PS and perhaps provide a justification as to why PS might be considered as a valuable functional food ingredient.

## AUTHOR INFORMATION


### Corresponding Author

*(R.B.P.) Phone: (706) 542-1099. Fax: (706) 542-1050. E-mail: rpegg@uga.edu.



### Funding

This research was supported by a grant funded by the Georgia Food Industry Partnership, which is greatly appreciated.


### Notes

The authors declare no competing financial interest.

## ACKNOWLEDGMENTS

Use of the Proteomics and Mass Spectrometry (PAMS) core facility under the direction of Dr. Dennis Phillips of UGA's Department of Chemistry is acknowledged. Thanks are also extended to Bill Paulk at Sylvester Blanching, a division of Universal Blanchers, LLC, for the dry-blanched PS and to John T. Powell, President of the Peanut Institute Inc., Albany, GA, USA.

## REFERENCES


(1) Bravo, L. Polyphenols: chemistry, dietary sources, metabolism, and nutritional significance. *Nutr. Rev.* **1998**, *56*, 317−333.

(2) Naczk, M.; Shahidi, F. Extraction and analysis of phenolics in food. *J. Chromatogr., A* **2004**, *1054*, 95−111.

(3) Pinelo, M.; Arnous, A.; Meyer, A. Upgrading of grape skins: significance of plant cell-wall structural components and extraction techniques for phenol release. *Trends Food Sci. Technol.* **2006**, *17*, 579−590.

(4) Hartley, R. D.; Morrison, W. H., III; Himmelsbach, D. S.; Borneman, W. S. Cross-linking of cell wall phenolic arabinoxylans in graminaceous plants. *Phytochemistry* **1990**, *29*, 3705−3709.

(5) Hollman, P. C. H.; Arts, I. C. W. Flavonols, flavones and flavanols − nature, occurrence and dietary burden. *J. Sci. Food Agric.* **2000**, *80*, 1081−1093.

(6) Crozier, A.; Jaganath, I. B.; Clifford, M. N. Dietary phenolics: chemistry, bioavailability and effects on health. *Nat. Prod. Rep.* **2009**, *26*, 1001−1043.

(7) Arranz, S.; Saura-Calixto, F.; Shaha, S.; Kroon, P. A. High contents of nonextractable polyphenols in fruits suggest that polyphenol contents of plant foods have been underestimated. *J. Agric. Food Chem.* **2009**, *57*, 7298−7303.

(8) White, B. L.; Howard, R. L.; Prior, R. L. Release of bound procyanidins from cranberry pomace by alkaline hydrolysis. *J. Agric. Food Chem.* **2010**, *58*, 7572−7579.

(9) Robbins, R. J. Phenolic acids in foods: an overview of analytical methodology. *J. Agric. Food Chem.* **2003**, *51*, 2866−2887.

(10) Weidner, S.; Amarowicz, R.; Karamać, M.; Dąbrowski, G. Phenolic acids in caryopses of two cultivars of wheat, rye and triticale that display different resistance to pre-harvest sprouting. *Eur. Food Res. Technol.* **1999**, *210*, 109−113.

(11) Amarowicz, R.; Weidner, S. Content of phenolic acids in rye caryopses determined using DAD-HPLC method. *Czech. J. Food Sci.* **2001**, *19*, 201−205.

(12) Kim, K.-H.; Tsao, R.; Yang, R.; Cui, S. W. Phenolic acid profiles and antioxidant activities of wheat bran extracts and the effect of hydrolysis conditions. *Food Chem.* **2006**, *95*, 466−473.

(13) Krygier, K.; Sosulski, F.; Hogge, L. Free, esterified, and insoluble-bound phenolic acids. 1. Extraction and purification procedure. *J. Agric. Food Chem.* **1982**, *30*, 330−334.

(14) Hertog, M. G. L.; Hollman, P. C. H.; Venema, D. P. Optimization of a quantitative HPLC determination of potentially anticarcinogenic flavonoids in vegetables and fruits. *J. Agric. Food Chem.* **1992**, *40*, 1591−1598.

(15) Merken, H. M.; Beecher, G. R. Measurement of food flavonoids by high-performance liquid chromatography: a review. *J. Agric. Food Chem.* **2000**, *48*, 577−599.

(16) Wang, M. I.; Gillaspie, A. G.; Morris, J. B.; Pittman, R. N.; Davis, J.; Pederson, G. A. Flavonoid content in different legume germplasm seeds quantified by HPLC. *Plant Genet. Resour.* **2008**, *6*, 62−69.

(17) Yu, J.; Ahmedna, M.; Goktepe, I. Effects of processing methods and extraction solvents on concentration and antioxidant activity of peanut skin phenolics. *Food Chem.* **2005**, *90*, 199−206.

(18) Yu, J.; Ahmedna, M.; Goktepe, I.; Dai, J. Peanut skin procyanidins: composition and antioxidant activities as affected by processing. *J. Food Compos. Anal.* **2006**, *19*, 364−371.

(19) Ma, Y.; Kosińska-Cagnazzo, A.; Kerr, W. L.; Amarowicz, R.; Swanson, R. B.; Pegg, R. B. Separation and characterization of phenolic compounds from dry-blanched peanut skins by liquid chromatography−electrospray ionization mass spectrometry. *J. Chromatogr., A* **2014**, *1356*, 64−81.

(20) Amarowicz, R.; Troszyńska, A.; Baryłko-Pikielna, N.; Shahidi, F. Polyphenolics extracts from legume seeds: correlations between total antioxidant activity, total phenolics content, tannins content and astringency. *J. Food Lipids* **2004**, *11*, 278−286.

(21) Gu, L.; Kelm, M. A.; Hammerstone, J. F.; Zhang, Z.; Beecher, G.; Holden, J.; Haytowitz, D.; Prior, R. L. Liquid chromatographic/electrospray ionization mass spectrometric studies of proanthocyanidins in foods. *J. Mass Spectrom.* **2003**, *38*, 1272−1280.

(22) Fabre, N.; Rustan, I.; de Hoffmann, E.; Quetin-Leclercq, J. Determination of flavone, flavonol, and flavanone aglycones by negative ion liquid chromatography electrospray ion trap mass spectrometry. *J. Am. Soc. Mass Spectrom.* **2001**, *12*, 707−715.

(23) Justesen, U. Collision-induced fragmentation of deprotonated methoxylated flavonoids, obtained by electrospray ionization mass spectrometry. *J. Mass Spectrom.* **2001**, *36*, 169−178.

(24) Cuyckens, F.; Claeys, M. Mass spectrometry in the structural analysis of flavonoids. *J. Mass Spectrom.* **2004**, *39*, 1−15.

(25) Appeldoorn, M. M.; Vincken, J.-P.; Sanders, M.; Hollman, P. C. H.; Gruppen, H. Combined normal-phase and reversed-phase liquid chromatography/ESI-MS as a tool to determine the molecular diversity of A-type procyanidins in peanut skins. *J. Agric. Food Chem.* **2009**, *57*, 6007−6013.

(26) Sarnoski, P. J.; Johnson, J. V.; Reed, K. A.; Tanko, J. M.; O'Keefe, S. F. Separation and characterisation of proanthocyanidins in Virginia type peanut skins by LC-MS$^n$. *Food Chem.* **2012**, *131*, 927−939.

(27) Lou, H.; Yuan, H.; Yamazaki, Y.; Sasaki, T.; Oka, S. Alkaloids and flavonoids from peanut skins. *Planta Med.* **2001**, *67*, 345−349.

(28) Huang, S. C.; Yen, G.-C.; Chang, L.-W.; Yen, W.-J.; Duh, P.-D. Identification of an antioxidant, ethyl protocatechuate, in peanut seed testa. *J. Agric. Food Chem.* **2003**, *51*, 2380−2383.

(29) Miketova, P.; Schram, K. H.; Whitney, J.; Li, M.; Huang, R.; Kerns, E.; Valcic, S.; Timmermann, B. N.; Rourick, R.; Klohr, S. Tandem mass spectrometry studies of green tea catechins. Identification of three minor components in the polyphenolic extract of green tea. *J. Mass Spectrom.* **2000**, *35*, 860−869.

(30) Bravo, M. N.; Silva, S.; Coelho, A. V.; Vilas Boas, L.; Bronze, M. R. Analysis of phenolic compounds in Muscatel wines produced in Portugal. *Anal. Chim. Acta* **2006**, *563*, 84−92.

(31) Gu, L.; Kelm, M. A.; Hammerstone, J. F.; Beecher, G.; Holden, J.; Haytowitz, D.; Prior, R. L. Screening of foods containing proanthocyanidins and their structural characterization using LC-

MS/MS and thiolytic degradation. *J. Agric. Food Chem.* **2003**, *51*, 7513−7521.
(32) Stella, L.; De Rosso, M.; Panighel, A.; Vedova, A. D.; Flamini, R.; Traldi, P. Collisionally induced fragmentation of $[M-H]^-$ species of resveratrol and piceatannol investigated by deuterium labelling and accurate mass measurements. *Rapid Commun. Mass Spectrom.* **2008**, *22*, 3867−3872.
(33) Ku, K.-L.; Chang, P.-S.; Cheng, Y.-C.; Lien, C.-Y. Production of stilbenoids from the callus of *Arachis hypogaea*: a novel source of the anticancer compound piceatannol. *J. Agric. Food Chem.* **2005**, *53*, 3877−3881.
(34) Foo, L. Y.; Lu, Y.; Howell, A. B.; Vorsa, N. The structure of cranberry proanthocyanidins which inhibit adherence of uropathogenic P-fimbriated *Escherichia coli* in vitro. *Phytochemistry* **2000**, *54*, 173−181.
(35) Justesen, U. Negative atmospheric pressure chemical ionization low-energy collision activation mass spectrometry for the characterisation of flavonoids in extracts of fresh herbs. *J. Chromatogr., A* **2000**, *902*, 369−379.
(36) Skoula, M.; Grayer, R. J.; Kite, G. C.; Veitch, N. C. Exudate flavones and flavanones in *Origanum* species and their interspecific variation. *Biochem. Syst. Ecol.* **2008**, *36*, 646−654.
(37) Brad, K.; Chen, C. Physicochemical properties of diosmetin and lecithin complex. *Trop. J. Pharm. Res.* **2013**, *12*, 453−456.
(38) Kang, J.; Hick, L. A.; Price, W. E. A fragmentation study of isoflavones in negative electrospray ionization by $MS^n$ ion trap mass spectrometry and triple quadrupole mass spectrometry. *Rapid Commun. Mass Spectrom.* **2007**, *21*, 857−868.
(39) Chukwumah, Y. C.; Walker, L. T.; Verghese, M.; Bokanga, M.; Ogutu, S.; Alphonse, K. Comparison of extraction methods for the quantification of selected phytochemicals in peanuts (*Arachis hypogaea*). *J. Agric. Food Chem.* **2007**, *55*, 285−290.
(40) Nuutila, A. M.; Kammiovirta, K.; Oksman-Caldentey, K.-M. Comparison of methods for the hydrolysis of flavonoids and phenolic acids from onion and spinach for HPLC analysis. *Food Chem.* **2002**, *76*, 519−525.

## MATERIALS AND METHODS

**Materials.** 10-Undecenoic acid was obtained from Jayant Oil Mills (Mumbai, India). Methanol, propan-2-ol, butan-1-ol, 2-methylpropan-1-ol, hexan-1-ol, 2-ethylhexan-1-ol, hexane, and ethyl acetate were procured from Qualigens Fine Chemicals (Mumbai, India). Dichloromethane, *m*-chloroperbenzoic acid (m-CPBA), aniline, butylated hydroxytoluene (BHT), paraffin oil, ammonium thiocyanate, 1-methylimidazole, and HBf4 were purchased from Sigma-Aldrich (St. Louis, MO, USA). Hydrogen peroxide (30% aqueous solution), xylene, and *p*-toluenesulfonic acid (p-TSA) were purchased from M/s sd fine-chem Ltd., Mumbai, India. Formic acid solution (85%) and sulfuric acid (AR grade) were purchased from M/s Rankhem, New Delhi, India. Sebacic acid was procured from Sisco Research Laboratories (Mumbai, India). Jatropha oil was obtained from a local company. LZ 1359 and tricresyl phosphate (TCP) was used as control in antiwear and extreme pressure analyses, respectively. All of the chemicals were of analytical reagent grade and used as received.

**Methods.** The analytical determinations of the sebacic acid and jatropha oil derivatives were accomplished according to the official methods of the American Oil Chemists' Society (AOCS) as follows: acid value (AOCS Cd 63), iodine value (IV, AOCS Da 15-48), and oxirane value (OO, AOCS Cd 9-57). The base oil lubricant properties such as density, viscosity, and viscosity index were evaluated per methods described previously.[20] $^1$H NMR and $^{13}$C NMR spectra were recorded on Bruker AR X 400 spectrometer (400 MHz) and a Varian spectrometer at 75 MHz, respectively, and TMS was used as an internal standard. IR spectra were recorded in chloroform on a PerkinElmer Fourier transform (model Spectrum BX; Shelton, CT, USA) FT-IR spectrometer neat as thin film. The spectrum was recorded in absorbance mode.

A gas chromatograph Agilent 6890N series was employed to analyze the fatty acid composition using an HP-1 column (30 m × 0.25 mm × 0.5 $\mu$m). The flame ionization detector and injector were at 300 °C. The oven temperature was programmed at 150 °C for 2 min and then increased to 300 °C at 10 °C/min. The carrier gas used was nitrogen at a flow rate of 1.5 mL/min. The GC-MS analysis was carried out using an Agilent 6890 gas chromatograph connected to an Agilent 5973 mass spectrophotometer at 70 eV ($m/z$ 50−600; source at 230 °C and quadruple at 150 °C) in the EI mode using an HP-1 MS capillary column (30 m × 0.25 mm × 0.5 $\mu$m). The oven temperature was programmed at 150 °C for 2 min, 10 °C/min to 300 °C, and 20 min at 300 °C. The carrier gas used was helium at a flow rate of 1.0 mL/min.

The antioxidant activity of the synthesized epithio derivatives in three base oils was evaluated using a differential scanning calorimeter (DSC Q 2000, TA Instruments) under oxygen atmosphere. The oxidative onset temperature (OOT) was measured for base oils with and without added additives in dynamic mode. The temperature programming was set at 25−300 °C, ramped at 10 °C/min, and purified oxygen was passed through the sample enclosure at 50 mL/min. The oxidative onset temperature was determined from the start of the exothermic reaction peak in the DSC thermogram.

The load-carrying capacity and antiwear properties of synthesized additives were investigated using a Stanhope SETA four-ball tester. All of the wear tests were conducted at a rotating speed of 1200 rpm under a load of 40 kg, with a duration of 60 min. An optical microscope was used to determine the wear scar diameters (WSD) of the three lower balls with an accuracy of ±0.01 mm, and these diameters were averaged and cited as the WSD reported in this paper. The extreme pressure tests were run at 1475 rpm, ambient temperature at variable load, and test duration for 1 min or until the balls welded, whichever occurred first. The extreme pressure properties of three base oils with and without added additive at different concentrations were evaluated as weld point loads and are reproducible to within one loading increment (±10 kg for 10 kg loading increments).

The surface analysis of wear scar developed on the steel balls during the antiwear analysis was studied using a Hitachi S-3000N scanning electron microscope (SEM) with energy/wavelength dispersion, at a voltage of 20 kV.

**Synthesis of Di-2-ethylhexyl Sebacate.** Sebacic acid (200 g, 0.99 mol), 2-ethylhexanol (465 mL, 2.97 mol), *p*-toluenesulfonic acid (2 g, 1 wt % of KFA), and xylene, 100 mL, were taken in a four-necked round-bottom flask and stirred at 130−140 °C for a period of 8 h. The reaction was monitored by TLC. The crude product was distilled at 180 °C temperature and 5 mmHg to remove excess alcohol and xylene. The distilled product was extracted with hexane and washed with water until it was acid free, passed through $Na_2SO_4$, concentrated, and dried under vacuum. The product was further purified using basic alumina column chromatography by elution with hexane to obtain di-2-ethylhexyl sebacate with an acid value of <0.1. The yield of the product was found to be 95%. The structure of the product was characterized by FT-IR, EI-MS, and $^1$H NMR spectral studies.

**Synthesis of Epoxy Jatropha Fatty Acid *n*-Butyl Esters (EJB).** *n*-Butyl esters of jatropha fatty acids[21] (125 g, 0.385 mol), formic acid (26.6 g, 0.577 mol), and sulfuric acid (1.7 mL, 2 wt % of HCOOH and hydrogen peroxide) were taken in a three-necked round-bottom flask equipped with an overhead stirrer. A 30% aqueous hydrogen peroxide solution (117.9 mL, 1.155 mol) was added slowly to the contents under strong mechanical stirring at 15−20 °C over a duration of 1 h. After addition, the temperature was raised to 55−60 °C for 5 h. The product was extracted with ethyl acetate and washed with water until it was acid free, then passed through anhydrous sodium sulfate, and dried under reduced pressure to yield the product with oxirane oxygen content of 4.4%. The yield of the epoxy jatropha fatty acid *n*-butyl esters was found to be 95%. The structure of the product was characterized by FT-IR and $^1$H NMR spectral studies.

$^1$H NMR (400 MHz, $CDCl_3$) $\delta$ 0.85−0.95 (t, $-CH_2-CH_3$), 1.2−1.4 (m, $-CH_2-CH_3$), 1.4−1.5 (m, $CH_2-CHOCH-$), 1.6−1.7 (m, $CH_2-CH_2-CO-$), 2.8−3.1 (m, $-CHOCH-$), 2.3 (t, $-CH_2-C=O$), 4.05 (t, $-CH_2-O-C=O$); IR (neat, cm$^{-1}$) 2927 (C—H), 1740 (C=O), 826 (epoxy ring), 1172 (C—C (=O)—O).

**Preparation of Ionic Liquid [HMIM]$BF_4$.** 1-Methylimidazole (6 g, 0.0738 mol) was taken into a three-necked round-bottom flask. The temperature of the medium was sustained at 0 °C, and 48% tetrafluoroboric acid (9.54 mL, 0.0738 mol) was added slowly to it for 40 min, and then the reaction was further continued at room temperature for 2 h. After completion of the reaction, the contents were kept under high vacuum to remove moisture at 80−90 °C. The product was subjected to ethyl acetate washings to remove excess imidazole followed by drying under reduced pressure to obtain a light yellow viscous liquid.

**Synthesis of Alkyl 10-Undecenoates (2a-f).** 10-Undecenoic acid was esterified with different alcohols, namely, methanol, propan-2-ol, butan-1-ol, 2-methylpropan-1-ol, hexan-1-ol, and 2-ethylhexan-1-ol, in the presence of p-TSA (1 wt % of the acid) for a duration of 4−5 h to yield alkyl 10-undecenoates **2a−f**). The synthetic procedure is reported elsewhere.[22]

**Synthesis of Alkyl 10-Epoxyundecanoates (3a−f).** Alkyl 10-undecenoates were epoxidized using *m*-chloroperbenzoic acid to yield alkyl epoxy undecanoates. The synthetic procedure is reported elsewhere.[22]

**Typical Procedure for the Preparation of Butyl 10-Epithioundecanoate (4a−f).** *n*-Butyl 10-epoxyundecanoate (2 g, 0.0078 mol) and ammonium thiocyanate (0.594 g, 0.0078 mol) were taken into a round-bottom flask. Ionic liquid [HMIM]$BF_4$ (4 g) and water (2 g) in a 2:1 ratio were added to the contents, and the resultant reaction mixture was stirred at 60 °C for a period of 23 h. The progress of the reaction was monitored by TLC using hexane/ethyl acetate (90:10 v/v). After completion of the reaction, the crude product was extracted using ether, and the ethereal solution was washed with water and dried over sodium sulfate. The combined ether extracts were concentrated using a rotary evaporator. The structure of the product was established by GC-MS and GC (90%). The crude product was purified using silica gel column chromatography using hexane and ethyl acetate (80/20) to afford *n*-butyl 10-epithioundecanoate (1.44 g, 68% of isolated yield). The product was characterized by $^1$H NMR, IR, GC, and GC-MS spectral data.

**Methyl 10-Epithioundecanoate (ESUME, 4a):** 1.29 g, 60%; $^1$H NMR (400 MHz, $CDCl_3$) $\delta$ (TMS) 1.2−1.40 (m, 12 H, $-CH_2$), 1.4−1.65 (m, 2H, $CH2-CH2-C=O$), 1.75−1.85 (m, 2H, $H_2CSCH-CH_2$), 2.15−2.18 (d, 2H, $H_2CSCH$), 2.25−2.35 (t, 2H, $-CO-CH_2$),


dx.doi.org/10.1021/jf5033558 | J. Agric. Food Chem. 2014, 62, 11505−11511

2.48−2.52 (d, $H_2$CSCH), 3.6−3.65 (t, 2H −O—$CH_3$); $^{13}$C NMR (75 MHz, $CDCl_3$) δ 24.5−30.0 (−$CH_2$−), 25.8 (−$CH_2$—CH—S—$CH_2$), 29.5 (−$CH_2$—CH—S—$CH_2$), 34.0 (−$CH_2$—C═O), 51.0 ($CH_3$—O—C═O), 36.2 (−$CH_2$—CH—S—$CH_2$), 174.5 (−COO−); IR (neat, $cm^{-1}$) 2929 (−C—H stretching), 1736 (−C═O), 612 (−C—S− stretching), 1042 (−C—S− asymmetric stretching), 1172 (C—C(═O)—O); EIMS *m/z* 230 $[M]^+$, 215, 173, 199.

**2-Propyl 10-Epithioundecanoate (ESIPUES, 4b):** 1.29 g; 60%; $^1$H NMR (400 MHz, $CDCl_3$) δ (TMS) 1.20−1.36 (q, 6H, −CH—($CH_3$)$_2$), 1.42−1.66 (m, 14 H, −$CH_2$), 1.75−1.85 (m, 2H, $H_2$CSCH—$CH_2$), 2.15−2.18 (d, 2H, $H_2$CSCH), 2.2−2.3 (t, 2H, −CO—$CH_2$), 2.48−2.52 (d, $H_2$CSCH), 3.14−3.18 (d, 2H, O—$CH_2$); $^{13}$C NMR (75 MHz, $CDCl_3$) δ 14 ($CH_3$—$CH_2$−), 21.7 (($CH_3$)$_2$—CH−), 22.6−32.2 (−$CH_2$−), 34.3 (−$CH_2$—C═O), 36.5 (−$CH_2$—CH—S—$CH_2$), 30.5 (−$CH_2$—CH—S—$CH_2$), 174.5 (−COO−); IR (neat, $cm^{-1}$) 2927 (−C—H stretching), 1736 (−C═O), 612 (−C—S− stretching), 1042 (−C—S− asymmetric stretching), 1174 (C—C(═O)—O); EIMS *m/z* 281 $[M + Na]^+$, 259, 199, 181.

**2-Methyl-1-propyl 10-epithioundecanoate (ESC-4UES, 4c):** 1.20 g; 57%; $^1$H NMR (400 MHz, $CDCl_3$) δ (TMS) 0.86−0.95 (t, 3H, −$CH_3$), 1.18−1.65 (m, 18 H, −$CH_2$), 2.2−2.3 (t, 2H, −CO—$CH_2$), 1.72−1.8 (m, 2H, $H_2$CSCH—$CH_2$), 2.12−2.17 (d, 2H, $H_2$CSCH), 2.28−2.32 (t, 2H, −CO—$CH_2$), 2.42−2.48 (d, $U_2$CSCH), 3.85−3.95 (t, 2H −O—$CH_2$—($CH_2$)$_2$); $^{13}$C NMR (75 MHz, $CDCl_3$) 14 ($CH_3$—CH−), 19 (($CH_3$)$_2$—CH−), 21.7 (($CH_3$)$_2$—CH−), 22.6−32.2 (−$CH_2$−), 34.5 (−$CH_2$—C═O), 36.5 (−$CH_2$—CH—S—$CH_2$), 30.5 (−$CH_2$—CH—S—$CH_2$), 70.3 (−CH—O—C═O), 173.5 (−COO−); IR (neat, $cm^{-1}$) 2929 (−C—H stretching), 1736 (−C═O), 619 (−C—S−), 1042 (−C—S− asymmetric stretching), 1163 (C—C(═O)—O); EIMS *m/z* 295 [M + Na], 216, 199.

**Butyl 10-Epithioundecanoate (ESnBU-UES, 4d):** 1.44 g; 68%; $^1$H NMR (400 MHz, $CDCl_3$) δ (TMS) 0.9−1.0 (d, 3H, −$CH_3$), 1.2−1.40 (m, 14 H, −$CH_2$), 1.4−1.45 (m, 2H, CH2—$CH_2$—C═O), 1.75−1.85 (m, 2H, $H_2$CSCH—$CH_2$), 2.1−2.15 (d, 2H, $H_2$CSCH), 2.2−2.3 (t, 2H, −CO—$CH_2$), 2.45−2.5 (d, $H_2$CSCH), 4.0−4.1 (t, 2H, −O—$CH_2$—($CH_2$)$_2$); $^{13}$C NMR (75 MHz, $CDCl_3$) 13.5 ($CH_3$—$CH_2$−), 19.0 ($CH_3$—$CH_2$−), 25.0−30.5 (−$CH_2$−), 34.2 (−$CH_2$—C═O), 36.5 (−$CH_2$—CH—S—$CH_2$), 31.0 (−$CH_2$—CH—S—$CH_2$), 26.0 (−$CH_2$—CH—S—$CH_2$), 64.1 (−CHO—C═O), 173.8 (−COO−); IR (neat, $cm^{-1}$) 2929 (−C—H stretching), 1736 (−C═O), 619 (−C—S−), 1163 (−C—C(═O)—O); EIMS *m/z* 295 [M + Na], 216, 199.

**Hexyl 10-Epithioundecanoate (ESnHE-UES, 4e):** 1.37 g; 66.5%; $^1$H NMR (400 MHz, $CDCl_3$) δ (TMS) 0.95−1.0 (d, 3H, −$CH_3$), 1.3−1.50 (m, 18 H, −$CH_2$), 1.45−1.5 (m, 2H, CH2—$CH_2$—C═O), 1.8−1.85 (m, 2H, $H_2$CSCH—$CH_2$), 2.1−2.15 (d, 2H, $H_2$CSCH), 2.25−2.3 (t, 2H, −CO—$CH_2$), 2.45−2.5 (d, $H_2$CSCH), 4.05−4.1(t, 2H, −O—$CH_2$—($CH_2$)$_2$); $^{13}$C NMR (75 MHz, $CDCl_3$) δ 14.1 ($CH_3$—$CH_2$−), 22.5 ($CH_3$—$CH_2$−), 28.5−29.4 (−$CH_2$−), 25.5−26 (−$CH_2$—CH—S—$CH_2$), 31.5 (−$CH_2$—CH—S—$CH_2$), 34−34.2 (−$CH_2$—C═O), 36.0 (−$CH_2$—CH—S—$CH_2$), 64.5 (−CHO—C═O), 174 (−COO−); IR (neat, $cm^{-1}$) 2929 (−C—H stretching), 1738 (−C═O), 615 (−C—S−), 1163 (−C—C(═O)—O); EIMS *m/z* 323 $[M + Na]^+$, 199.

**2-Ethylhexyl 10-epithioundecanoate (ES2ET-HE-UES, 4f):** 1.3 g; 64%; $^1$H NMR (400 MHz, $CDCl_3$) δ (TMS) 0.8−0.95 (t, 6H, −($CH_3$)$_2$), 1.20−1.50 (m, 21 H, −$CH_2$), 1.75−1.85 (m, 2H, $H_2$CSCH—$CH_2$), 2.12−2.17 (d, 2H, $H_2$CSCH), 2.25−2.35 (t, 2H, −CO—$CH_2$), 2.48−2.52 (d, $H_2$CSCH), 3.95−4.0 (t, 2H −O—$CH_2$—($CH_2$)$_2$); $^{13}$C NMR (75 MHz, $CDCl_3$) δ 10.8 ($CH_3$—$CH_2$−), 14 ($CH_3$—$CH_2$−), 22.1−32.4 (−$CH_2$−), 30.5 (−$CH_2$—CH—S—$CH_2$), 36.5 (−$CH_2$—CH—S—$CH_2$), 38.5 (−$CH_2$—C═O), 66.5 (−CHO—C═O), 174 (−COO−); IR (neat, $cm^{-1}$) 2929 (−C—H stretching), 1732 (−C═O), 619 (−C—S−), 1042 (−C—S− asymmetric stretching), 1171 (−C—C(═O)—O); EIMS *m/z* 351 $[M + Na]^+$, 199.

## RESULTS AND DISCUSSION

In the present study epithio undecanoates were synthesized from epoxy undecanoates in a green reaction medium, ionic liquid. The use of ionic liquid for the synthesis of epithio compounds helps in carrying out the reaction under mild and neutral conditions to afford epithio undecanoates in high yields. The performance of the epithio derivative as multifunctional additives was evaluated in three base oils: epoxy jatropha *n*-butyl esters (EJB), di-2-ethylhexyl sebacate (DOS), and paraffin (S-105) base oil.

The epoxy undecanoates were used as starting material to synthesize epithio undecanoates using ammonium thiocyanate in stoichiometric ratio (Scheme 1). All of the reactions were

**Scheme 1. Synthesis of Epithio Undecanoates**

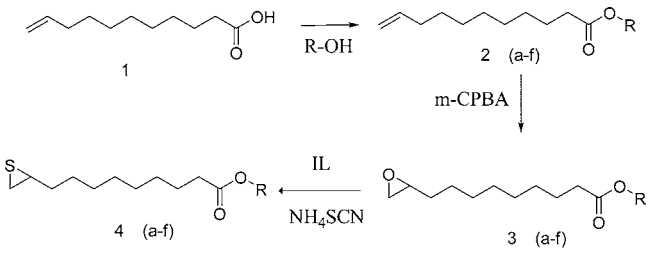


R= a, -$CH_3$; b, -CH-($CH_3$)$_2$; c, -$CH_2$-CH-($CH_3$)$_2$; d, -($CH_2$)$_3$-$CH_3$; e, -($CH_2$)$_5$-$CH_3$; f, -($CH_2$)$_5$-CH-($CH_3$)$_2$.

completed within 20−24 h, affording high yields of alkyl 10-epithioundecanoates as revealed by GC analysis (85−96%). The products were purified using silica gel column chromatography using hexane and ethyl acetate (80:20) to afford pure alkyl 10-epithioundecanoates with an isolated yield of 60−68%. The FT-IR spectra of the epoxy undecanoate derivatives are characterized by a stretching vibration frequency at 835 $cm^{-1}$, which is attributable to the epoxy stretching vibration frequency and asymmetric ring deformation at 916 $cm^{-1}$. In contrast, the IR spectral feature observed in epithio derivatives is the disappearance of these peaks, indicating complete conversion of epoxy to epithio group in the synthesized products. Two new peaks appeared at 619 and 1011 $cm^{-1}$, which are attributable to the symmetric and asymmetric epithio ring deformation,[23−25] proving the successful conversion of epoxide to epithio group. The FT-IR spectra also exhibited the characteristic absorptions of aliphatic carbons around 2987 and 2865 $cm^{-1}$ and an ester group (−COO−) around 1735 $cm^{-1}$.

In $^1$H NMR spectra of alkyl 10-epithioundecanoates, signals at 2.2 and 2.5 ppm corresponding to methylene and methine protons, respectively, confirmed the epithio ring introduction into the molecule, respectively. In epithio undecanoate derivatives the disappearance of peaks at 2.8−2.9 ppm corresponding to −CH− protons of the epoxy carbon confirmed the epithio ring formation. Both the infrared spectra and NMR spectra of these epithio derivatives indicated the absence of an epoxy group in the epithio derivatives. The GC-MS and GC chromatograms also indicated the absence of an epoxy group, indicating complete conversion into an epithio group. Signals in $^{13}$C NMR at 31.0 and 26.0 ppm confirm the presence of an epithio ring in the synthesized products. The adjacent methylene group of the epithio system was shifted to 36.0 ppm due to a β effect from the sulfur atom, also confirming the product formation.

**Performance Evaluation of the Epithio Derivatives as Antioxidants.** The antioxidant activity of the synthesized epithio derivatives and commercial antioxidant BHT were


dx.doi.org/10.1021/jf5033558 | J. Agric. Food Chem. 2014, 62, 11505−11511

evaluated using three base oils, EJB, DOS, and S-105. The oxidative onset temperature (OOT) of the pure base oils was found to be 164.4, 180.2, and 193.6 °C, respectively. The fatty acid composition of synthesized biolubricant base oil EJB revealed that almost all of the unsaturation converted to epoxy group as follows: C18:1 epoxy, 44.1%; C18:2 mono epoxy, 3%; and C18:2 di epoxy, 26%. The basic lubricant properties such as viscosity, viscosity index, and density exhibited by the three base oils are shown in Table 1. The additive percentage in base oils

**Table 1. Physicochemical Properties of Base Oils**

| property | | EJB | DOS | S-105 |
|---|---|---|---|---|
| density 15 °C (g/cm$^3$) | | 0.915 | 0.920 | 0.835 |
| viscosity | 40 °C, cSt | 11.15 | 12.38 | 10.28 |
| | 100 °C, cSt | 3.09 | 3.26 | 3.36 |
| viscosity index | | 126 | 126 | 117 |

was optimized using base oil (DOS) spiked with additive butyl 10-epithioundecanoate (**4d**) ranging from 0.5 to 4% and their OOTs are 181.8, 188.1, 229.2, 230.5, and 232.5 °C, respectively. The maximum antioxidant activity was observed at 2 wt % concentration, and even though the additive dosage was increased to 3 and 4%, a negligible increase in antioxidant activity was observed. Hence, the antioxidant efficacies of synthesized epithio derivatives and commercial antioxidant, BHT, were evaluated at 2 wt % concentration in the base oils. All of the epithio undecanoates exhibited superior performance compared to BHT in DOS base oil, whereas **4d** exhibited comparable performance with BHT in EJB and S-105 base oils. The nature of the ester alkyl group of the epithio undecanoate derivatives displayed different antioxidant activities in the three base oils tested. Products prepared from short-chain alcohols (methyl and *n*-butyl) exhibited better performance, and as the chain length increased (2-ethylhexyl), the antioxidant activity decreased. There is a clear effect of the length of the alkyl chain of the ester moiety of epithio derivatives on antioxidant potency, resulting in products (**4a** and **4d**) with greater antioxidant ability to stabilize base oil than their corresponding epithio derivative, **4e**. Similar results have been published earlier for ether derivatives of hydroxytyrosol and amino alcohols,[21,25] and in which the shorter alkyl side chains improved the scavenger activity and the reducing ability of hydroxytyrosol, and the presence of longer linear chains ($C_7$−$C_9$) decreased such antioxidant effects.[26] A cutoff effect in the antioxidant efficacy in relation to the alkyl chain length was also reported by Sorensen et al. on alkyl ferulates. The most efficient alkyl ferulates were methyl and butyl ferulate, whereas octyl ferulate was pro-oxidative, and the pro-oxidative effect increased further with an increment in the alkyl chain length from $C_8$ to $C_{12}$. Further elongation of the alkyl chain length to $C_{16}$ and $C_{20}$ resulted in weak pro-oxidative effects to weak antioxidative effects.[27] This might be also due to readily available sites for oxidation, making them more sensitive to cleavage than shorter ester chain lengths.[28−31] The three epithio derivatives prepared with iso alkyl epoxy undecanoates exhibited less antioxidant activity compared to straight-chain epithio derivatives. This could be related to the steric effect of side chains present in the ester chain of isoalkyl epithio derivatives.

Epithio derivatives with methyl and butyl ester chain lengths exhibited comparable antioxidant activities in base oil EJB. The same trend was observed in DOS and S-105 base oils, and the results are summarized in Table 2. The optimum chain length $C_4$ exhibited superior OOT of 229 °C among the synthesized

**Table 2. Antioxidant Property of the Synthesized Additives (2 wt %) in Three Lubricant Base Stocks**

| | oxidative onset temperature (OOT) (°C) | | |
|---|---|---|---|
| sample name[a] | EJB | DOS | S-105 |
| no additive | 164.4 | 180.2 | 193.6 |
| ESUME | 177.6 | 195.1 | 216.5 |
| ESIPAUES | 162.7 | 206.2 | 214.4 |
| ESC-4UES | 156.1 | 200.1 | 215.9 |
| ESnBU-UES | 180.6 | 229.2 | 242.0 |
| ES-2ET-HE-UES | 169.7 | 199.5 | 199.2 |
| BHT | 180.3 | 193.8 | 243.3 |

[a]ESUME, methyl 10-epithoundecanoate; ESIPAUES, 1-(2-propyl) 10-epithoundecanoate; ESC-4UES, 2-methyl-1-propyl 10-epithoundecanoate; ESnBU-UES, 1-butyl 10-epithoundecanoate; ES-2ET-HE-UES, 2-ethylhexyl 10-epithoundecanoate; BHT, butylated hydroxytoluene.

additives in DOS base oil. In the case of S-105 base oil, as the chain length increased from $C_1$ to $C_4$, an increase in activity, and on further increase in chain length ($C_8$), a decrease in activity were observed. Butyl 10-epithioundecanoate exhibited excellent antioxidant activity among all of the synthesized additives in the three base oils EJB, DOS, and S-105 with OOTs of 180.6, 229.2, and 242 °C, respectively, followed by **4a**. A typical dynamic DSC curve is given in Figure 1, showing the dynamic curve of a base oil without any additive and of a base oil with **4d** at 2 wt % concentration in EJB and S-105 base oil.

**Performance Evaluation of the Synthesized Epithio Derivatives as Extreme Pressure Additives.** The weld point (WP) in extreme pressure property can be defined as the load at which welding of the balls due to the friction between the stationary three balls and the rotating top ball is high enough to weld. The WP of a test sample can be evaluated within ±10 kg by increasing the smaller load close to the weld point. Higher WP indicates the better EP properties of the test sample. Compounds containing certain elements such as sulfur, phosphorus, and halogens are known to be capable of participating in tribochemical reactions with the friction surfaces and generating in situ tribofilms that reduce friction under extreme pressure conditions.[32] Therefore, the synthesized alkyl epithio undecanoates were evaluated for their EP activity using three base oils, EJB, DOS, and S-105, and the results were compared with those of commercial EP additive, TCP. In the absence of EP additives the three base oils displayed weld points of 160, 120, and 120 kg, respectively. The base oil doped with the additives was stirred under magnetic stirring for 30 min at 40 °C to attain the homogeneity of the sample. Butyl epithio undecanoate and base oil DOS were used for optimization of additive concentration. The improvement in weld point of the base oil was analyzed at different concentrations ranging from 0.5 to 4%, and their weld points were 130, 140, 170, 160, and 150 kg, respectively. From the results 2 wt % was the optimum concentration at which the maximum weld point was observed. Even though the concentration was increased further to 3 and 4%, a decrease in weld point was observed. The blending of EP additives with the base oils resulted in increased weld point of three base oils as shown in Table 3. As the chain length of the ester moiety of the episulfide undecanoate increased from $C_1$ to $C_4$, the weld point of the base oil EJB increased from 160 to 210 kg. Surprisingly, methyl and butyl ester chains of episulfide undecanoate exhibited similar weld points of 210 kg. In the case of the 2-ethyhexyl ester of episulfide undecanoate the decrease in weld load of 180 kg was observed. The same trend was observed in base oils DOS and

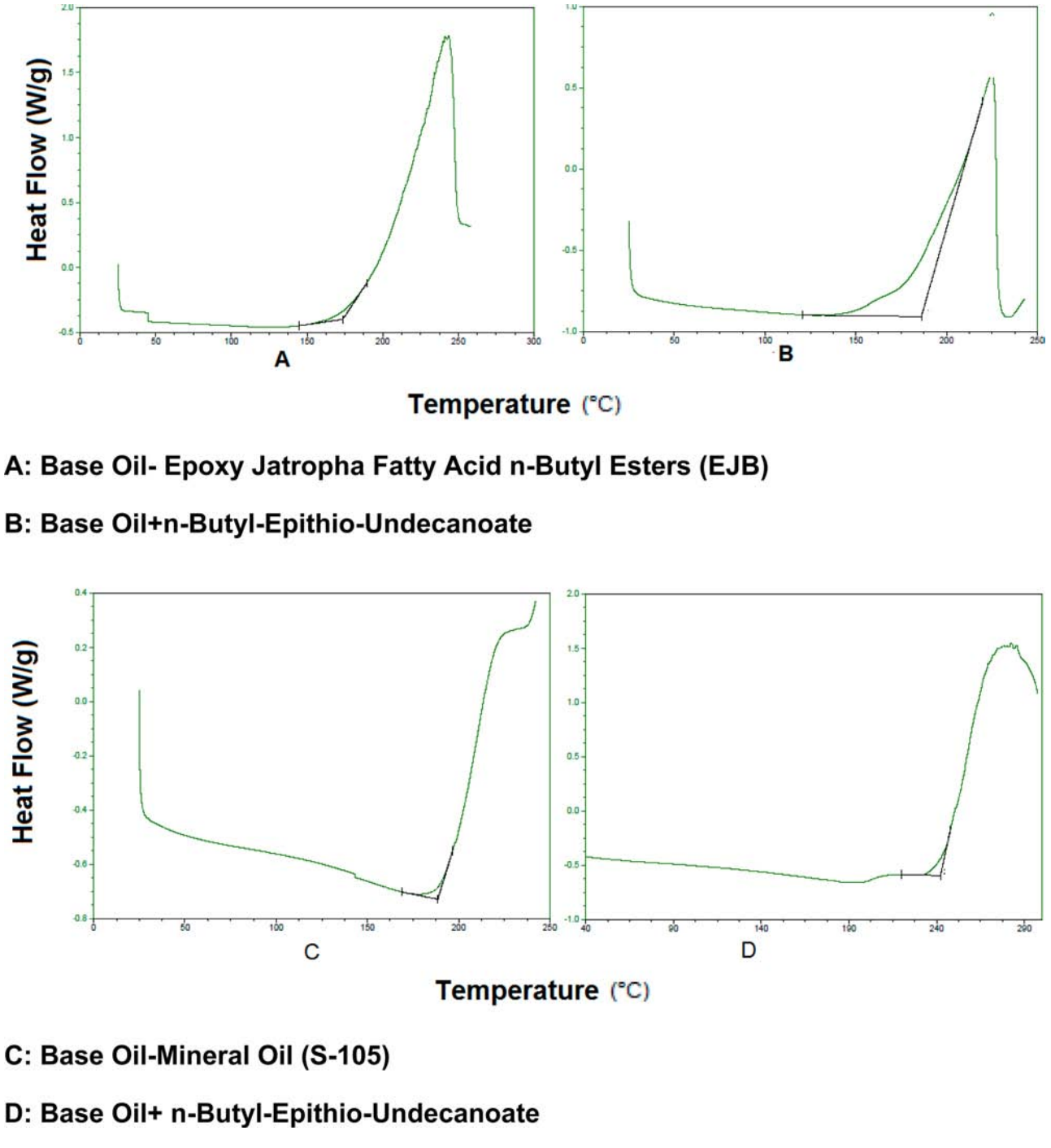


**Figure 1.** Nonisothermal DSC curves of base oil with and without antioxidant.

S-105. This shows a decrease in load-carrying capacity with increasing chain length of the alcohol moiety of the fatty acid ester of epithio derivatives. These results demonstrate the effects of molecular structure on lubricity property. This is in good agreement with the general observation that shorter chain lengths reduce molecular interactions and decrease the temperature stability of a protective lubricant film.[33] *n*-Butyl 10-epithioundecanoate exhibited comparable performance with commercial additive TCP in both base oils EJB and DOS and inferior performance in S-105. The synthesized additives exhibited better compatibility with biolubricant base oil (EJB) and synthetic ester (DOS) compared to mineral base oil (S-105), which indicates a better synergistic effect of the epithio derivatives with these two oils than with mineral oil. Similar enhancements of load-carrying capacity in biobased base stocks relative to mineral oil have been reported.[34] Results indicate that the prepared compounds exhibited improved EP activity, and they can be effectively used as EP additives for biobased lubricant basestocks.

**Performance Evaluation of Epithio Derivatives as Antiwear Additives.** The investigation of the antiwear ability of methyl and butyl epithio undecanoates was done by varying their concentration in base oil DOS. Figure 2 shows the variation of the WSD of the lower steel balls with different additive concentrations. It is observed from the figure that the addition of additives in base stock, even at small concentrations, can


dx.doi.org/10.1021/jf5033558 | J. Agric. Food Chem. 2014, 62, 11505−11511

**Table 3. Effect of 2 wt % Concentration of the Extreme Pressure Additive on Three Base Oils**

| | weld load (kg) | | |
|---|---|---|---|
| sample name | EJB | DOS | S-105 |
| no additive | 160 | 120 | 120 |
| ESUME | 210 | 170 | 160 |
| ESIPAUES | 180 | 140 | 130 |
| ESC-4UES | 180 | 140 | 130 |
| ESnBU-UES | 210 | 170 | 160 |
| ESnHE-UES | 170 | 130 | 120 |
| ES-2ET-HE-UES | 180 | 140 | 130 |
| TCP | 210 | 160 | 200 |

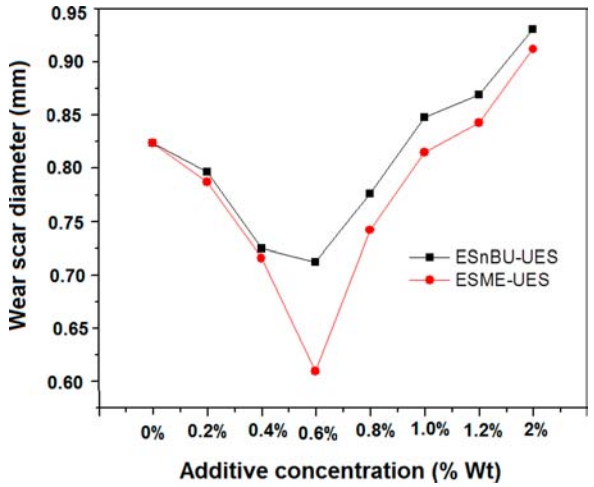


**Figure 2.** Wear scar diameter of the synthesized antiwear additive at different concentrations. ESnBU-UES, butyl epithio undecanoate; ESME-UES, methyl epithio undecanoate.

significantly reduce the WSD of the system. In particular, the introduction of 0.6 wt % methyl epithio undecanoate led to a decrease of the WSD by >26%. The addition of commercial antiwear additive LZ1359 also improved the AW property of the base fluid by 30%. The WSD decreased gradually with further increase of the additive concentration, implying that the AW property of the additive is dependent on its concentration in the base stock. When the additive concentration was below 0.6%, the WSD was smaller, indicating that additives demonstrated better AW property at a low concentration of 0.6%. This may be attributed to the formation of a more effective AW film by the additives through competing adsorption with base oil at a low concentration. The slight increase in the WSD with increasing additive concentration has also been reported in the literature.[35,36] This might be ascribed to corrosion of metal caused by the sulfur element present in the additives.

**Worn Surface Analysis.** Figure 3 shows the SEM images of the worn surface of steel balls lubricated with base oil DOS alone and with **4a** added oil at 0.6% concentration. The wear scar obtained from the test lubricated with base oil alone exhibited more scratches and deeper furrows compared with the scar produced with base oil with 0.6 wt % epithio derivative (**4a**). It can also be observed that the worn surface of steel balls lubricated by base oil with **4a** is shallower and smoother than that lubricated by base oil alone. This result further verifies that **4a** possesses good AW ability.

In conclusion, we have synthesized a series of novel epithio derivatives from 10-undecenoic acid. The addition of epithio derivatives as multifunctional additives to the base oils resulted in the enhancement of antioxidant, extreme pressure, and antiwear properties. Among the reported products, butyl 10-epithioundecanoate exhibited superior antioxidant and extreme pressure properties.

## AUTHOR INFORMATION


### Corresponding Author

*(R.B.N.P.) Phone: +91 040 27193370. Fax: +9140 27193370. E-mail: rbnprasad@iict.res.in.


### Notes

The authors declare no competing financial interest.

## REFERENCES


(1) Choi, U. S.; Ahn, B. G.; Kwon, O. K.; Chnat, Y. J. Tribological behavior of some antiwear additives in vegetable oils. *Tribol. Int.* **1997**, *37*, 677−683.

(2) Biermann, U.; Friedt, W.; Luhs, W.; Machmuller, G.; Metzger, J. O.; Klaas, M. R.; Schafer, H. J.; Schneider, M. P. New synthesis with oils and fats as renewable raw materials for the chemical industry. *Angew. Chem., Int. Ed.* **2000**, *39*, 2206−2224.

(3) Gunderson, R. J.; Hart, A. H. *Synthetic Lubricants*; Reinhold Publishing: New York, 1962; p 388.

(4) Mod, R. A.; Magne, F. C.; Sumrell, G.; Koos, R. E. Lubricants and lubricant additives: III. Performance characteristics of some thioacetate, phosphorodithioate, and hexachlorocyclopentadiene derivatives of stearic acid amides and esters. *J. Am. Oil Chem. Soc.* **1977**, *54*, 589−591.

(5) Magne, F. C.; Mod, R. R.; Sumrell, G.; Koos, R. E.; Parker, W. E. Lubricants and lubricant additives: II. Performance characteristics of some substituted fatty acid esters. *J. Am. Oil Chem. Soc.* **1975**, *52*, 494−497.


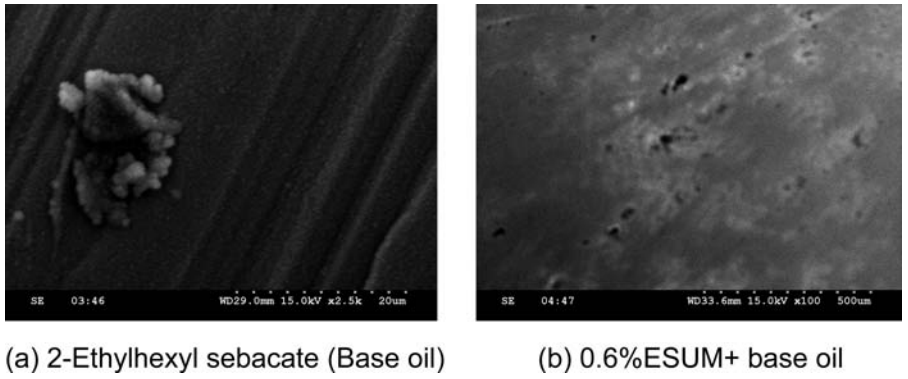


**Figure 3.** SEM morphologies of worn surfaces of base oil (a) and additive-doped base oil (b).

(6) Mod, R. R.; Magne, F. C.; Sumrell, G.; Koos, R. E. Lubricants and lubricant additives: III. Performance characteristics of some thioacetate, phosphoro dithioate and hexachlorocyclopentadiene derivatives of stearic acid amides and esters. *J. Am. Oil Chem. Soc.* **1977**, 589−591.
(7) Chibber, V. K.; Chuadhary, R. B.; Tyagi, O. S.; Anand, O. N. Antiwear and antifriction characteristics of tribochemical films of alkyl octa-decenoates and their derivatives. *Lubri. Sci.* **2006**, *18*, 63−76.
(8) Forbes, E. S.; Reid, A. J. D. Liquid phase adsorption/reaction studies of organo-sulfur compounds and their load carrying mechanism. *ASLE Trans.* **1973**, *16*, 50−60.
(9) Allum, K. G.; Ford, J. F. The influence of chemical structure on the load-carrying properties of certain organo-sulphur compounds. *J. Inst. Petrol.* **1965**, *51*, 145−161.
(10) Davey, W.; Edwards, E. D. The extreme-pressure lubricating properties of some sulphides and disulphides, in mineral oil, as assessed by the four-ball machine. *Wear* **1958**, *1* (4), 291−304.
(11) Allum, K. G.; Forbes, E. S. The influence of chemical structure on antiwear properties of organic disulfides. *J. Inst. Petrol.* **1967**, *53*, 173−185.
(12) Wakim, J. M. Cosulfurized products of high iodine valve triglyceride and nonwax ester of monoethenoid fatty acid as lubricant additives. U.S. Patent 3,986,966, 1976.
(13) Sharma, B. K.; Adhvaryu, A.; Erhan, S. Z. Synthesis of hydroxy thio-ether derivatives of vegetable oil. *J. Agric. Food Chem.* **2006**, *54*, 9866−9872.
(14) Michaelis, P. Epithio compounds as additives for lubricants. U.S. Patent 4,217,233, 1980.
(15) Gunstone, F. D.; Hussain, M. G.; Smith, D. M. Fatty acids, part 42. The preparation and properties of methyl monomercapto stearates, some related thiols and some methyl epithiostearates. *Chem. Phys. Lipids* **1974**, *13*, 71−91.
(16) Marcel, S. F.; Lie Ken, Jie.; Zheng, Y. F. Synthesis and physical properties of some 2,3- and 2,2[1]-epithio $C_{18}$ fatty acid derivatives. *Chem. Phys. Lipids* **1988**, *49*, 167−178.
(17) Gupta, R.; Ahmad, S. M., Jr.; Ahmad, F.; Osmin, S. M. *Indian J. Chem. B* **1978**, *25*, 429−431.
(18) Kuranova, I. L.; Snetkova, E. V. *J. Org. Chem.* **1978**, *43*, 2923−2925.
(19) Iranpoor, N.; Kazemi, F. Stereospecific formation of *S*-styrene sulfide: efficient conversion of epoxides to thiiranes catalysed with Ru. *Tetrahedron* **1997**, *53*, 11377−11382.
(20) Geethanjali, G.; Sony, M. K.; Padmaja, K. V.; Karuna, M. S. L.; Prasad, R. B. N. Preparation and properties of lubricant base stocks from epoxidized karanja oil and its alkyl esters. *Ind. Eng. Chem. Res.* **2013**, *52*, 16598−16605.
(21) Sammaiah, A.; Padmaja, K. V.; Prasad, R. B. N. Synthesis and evaluation of novel acyl derivatives from jatropha oil as potential lubricant basestocks. *J. Agric. Food Chem.* **2014**, *62*, 4652−4660.
(22) Geethanjali, G.; Padmaja, K. V.; Sreedhar, B.; Prasad, R. B. N. Preparation of alkyl 11-anilino-10-hydroxy undecanoates and evaluation of their antioxidant activity. *Eur. J. Lipid Sci. Technol.* **2013**, *115*, 740−746.
(23) Rao, C. N. R.; Raghavan, V. R.; Kasturi, T. R. Contribution to the infrared spectra of organosulphur compounds. *Can. J. Chem.* **1964**, *42*, 36−42.
(24) Derzhinskii, A. R.; Kalugin, V. E.; Prilezhaeva, E. N. Syntheis and reaction of 2,3-epoxy(epthio)propyl alkyl sulphides, sulfoxides and sulphones (translation). *Izv. Akad. Nauk SSSR* **1984**, *6*, 1392−1395.
(25) Bell, J. P.; Don, T.-M.; Voong, S.; Fernandez, A.; Ku, W. Synthesis and properties of epoxy-episulfide resins. *Angew. Makromol.* **1996**, *240*, 67−81.
(26) Pereira-Caro, G.; Madrona, A.; Bravo, L.; Espartero, J. L.; Alcudia, F.; Cert, A.; Mateos, R. Antioxidant activity evaluation of alkyl hydroxytyrosyl ethers, a new class of hydroxytyrosol derivatives. *Food Chem.* **2009**, *115* (1), 86−91.
(27) Sorensen, A. D. M.; Lyneborg, K. S.; Villeneuve, P.; Jacobsen, C. Alkyl chain length impacts the antioxidative effect of lipophilized ferulic acid in fish oil enriched milk. *J. Funct. Foods* **2014**, DOI: 10.1016/j.jff.2014.04.008.
(28) Sharma, B. K.; Doll, K. M.; Erhan, S. Z. Ester hydroxyl derivatives of methyl oleate: Tribological, oxidation and low temperature properties. *Bioresour. Technol.* **2008**, *99*, 7333−7340.
(29) Sharma, B. K.; Adhvaryu, A.; Liu, Z.; Erhan, S. Z. Chemical modification of vegetable oils for lubricant applications. *J. Am. Oil Chem. Soc.* **2006**, *83*, 129−136.
(30) Tan, C. P.; Che Man, Y. B.; Selamat, J.; Yusof, M. S. A. Comparative studies of oxidative stability of edible oils by differential scanning calorimetry and oxidative stability index methods. *Food Chem.* **2002**, *76*, 385−389.
(31) Pardauil, J. J.; Souza, L. K.; Molfetta, F. A.; Zamian, J. R.; Rocha Filho, G. N.; da Costa, C. E. Determination of the oxidative stability by DSC of vegetable oils from the Amazonian area. *Bioresour. Technol.* **2011**, *102*, 5873−5877.
(32) Biresaw, G.; Laszio, J. A.; Evans, K. O.; Compton, D. L.; Bantchev, G. B. Synthesis and tribological investigation of lipoyl glycerides. *J. Agric. Food Chem.* **2014**, *62*, 2233−2243.
(33) Baek, S.Y.; Kim, Y.-W.; Chung, K.; Yoo, S.-H.; Kim, N. K.; Kim, Y.-J. Synthesis of succinic acid alkyl half-ester derivatives with improved lubricity characteristics. *Ind. Eng. Chem. Res.* **2012**, *51*, 3564−3568.
(34) Asadauskas, S. Z.; Biresaw, G.; McClure, T. G. Effects of chlorinated paraffin and ZDDP concentrations on boundary lubrication properties of mineral and soybean oils. *Tribol. Lett.* **2010**, *37* (2), 111−121.
(35) Zhou, M. L.; Li, F. F.; Zeng, X. J. Synthesis of two novel additives and study of their tribological properties in rapeseed oil. *China Petrol. Process. Petrochem. Technol.* **2007**, *3*, 29−33.
(36) Jianwei, Y.; Fenfang, L.; Yihui, H. Tribological performance of two potential environmentally friendly ash less vegetable oil additives. *China Petrol. Process. Petrochem. Technol.* **2010**, *12*, 43−48.

obstacle to improving the final amount of yields of cellulose hydrolysis.[13] Besides, previous studies showed that addition of BG during enzymatic hydrolysis of cellulose could promote the sugar yield effectively and reduce inhibition of cellobiose on CBH or EG.[13] Research also indicated that BG in hydrolysate having better glucose tolerance through directed mutation could also promote the yield of cellulose saccharification.[14]

A novel cellulytic strain, *Hypocrea orientalis*, has been isolated for enzymatic degradation of agricultural residues and production of bioethanol. Research found that the cellulase activity secreted by *H. orientalis* was obviously higher than that of *H. jecorina*, *T. koningii*, *P. decumbens*, and *A. niger*, and especially, *H. orientalis* secreted a relatively balanced cellulase system,[15] which showed good application of *H. orientalis* enzymes in the bioethanol industry. In recent work, BG of *H. orientalis* has been purified and the inhibition mechanism of glucose on BG was investigated. This study provided the basis for directed mutation of BG to improve the glucose tolerance of *H. orientalis* BG.

## MATERIALS AND METHODS

**Cassava Residues, Enzymes, and Reagents.** Cassava residues were generated in a local factory following starch production, and residual starch was stripped for the next process. The analysis of cassava residues was carried out according to the protocols of NREL.[16] *H. orientalis* strain was cultured in modified MS medium (1% cassava residues as carbon source).[7] Crude enzyme was prepared from the culture with centrifugation at 10000 rpm for 15 min at 4 °C. Homogeneous BG was isolated from the fermentation liquid sequentially through ammonium sulfate precipitation, DEAE chromatography, and Sephacryl S200 filtration. *p*-Nitrophenyl-*β*-D-glucopyranoside (pNPG) was from Sigma (St. Louis, MO, USA). Cellulase DF was purchased from Lizhudongfeng Biotechnology Co., Shanghai, China, and Cellulase R-10 was a product of Yakult in Japan. All other chemicals were local products of analytical grade.

**Enzymatic Activity and Hydrolysis of Cassava Residues.** Cassava residues were pretreated with NaOH for 30 min at 121 °C in an autoclave. After cooling, the residues was filtered and washed to neutral pH. Then the cassava residues were dried in an oven and chopped for hydrolysis. The hydrolysis reactions were run in 100 mL of 50 mM sodium acetate buffer (pH 5.0) containing 1.5% (w/v) residues and 0.1 mg/mL enzymes with incubation in a shaking water bath (160 rpm) for up to 24 h at the given temperature. Samples of hydrolysate were taken periodically and centrifuged (5000*g*, 5 min) for quantification of reducing sugars by DNS assay.[17] An Aminex HPX-87H column was used to determine the composition and quantity of the products with 5 mM $H_2SO_4$ as flow phase and pure glucose, cellobiose, and xylose as standards. Activities of CMCase, CBH, xylase and amylase were determined according to the method given in ref 15. One unit (U) of enzyme activity was defined as the amount of enzyme liberating 1 *μ*mol of glucose, xylose, *p*-nitrophenol, or maltose from the appropriate substrates per minute per milliliter of crude filtrate under assay conditions.

**Glucose Inhibition Assays.** *β*-Glucosidase activity was measured by adding 40 *μ*L of enzyme (0.03 *μ*g) into 960 *μ*L of substrate solution containing 0.16 mM pNPG and 50 mM NaAc buffer at pH 5.0. The mixture was incubated in a 60 °C water bath for 15 min, and then 2 mL of 0.5 M NaOH was added to stop the reaction; the adsorption at 405 nm of the reaction solution was measured by using a Beckman DU800 to determine the amount of liberated *p*-nitrophenolate using a standard curve. To determine the effect of D-glucose on BG, activity was measured in substrate solution containing different concentrations of glucose.

**Determination of Microscopic Inhibition Rate Constants.** The progress-of-substrate-reaction method described by Tsou[17] was used to study the inhibitory kinetics of BG by glucose. In this method, 40 *μ*L of enzyme was added to 1.0 mL of assay system 0.16 mM pNPG in the presence of different concentrations of glucose.

The substrate reaction progress curve was analyzed to obtain the reaction rate constants as detailed below. The results showed that the inhibition was a reversible reaction with fractional residual enzyme activity. This catalytic reaction can be written as where E, S, I, and P

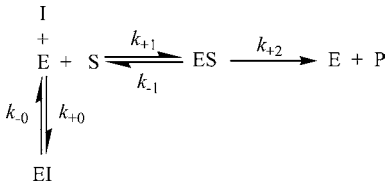


denote enzyme, substrate, inhibitor (glucose), and product, respectively. EI and ES are the respective compounds. $k_{+0}$ and $k_{-0}$ are the microscopic rate constants for the forward and reverse reactions of EI, respectively. As a rule, $[S] \gg [E_0]$ and $[I] \gg [E_0]$, and the product formation can be written as

$$[P]_t = \frac{vB}{(A[I] + B)} \times t + \frac{A[I]}{(A[I] + B)^2} - \frac{A[I]}{(A[I] + B)^2} \times e^{-(A[I]+B)t} \quad (1)$$

$$A = \frac{k_{+0} \times K_m}{K_m + [S]} \quad (2)$$

$$B = k_{-0} \quad (3)$$

where $[P]_t$ is the concentration of the product formed at time $t$, which is the reaction time; $A$ and $B$ are the apparent rate constants of inhibition; $[S]$ and $[I]$ are the concentrations of the substrate and inhibitor, respectively; $v$ is the initial rate of reaction in the absence of the inhibitor, where $v = (V_m \times [S])/(K_m + [S])$. When $t$ is sufficiently large, the curves become straight lines and the product concentration is written as $[P]_{calcd}$:

$$[P]_{calcd} = \frac{Bv}{A[I] + B} \times t + \frac{A[I]}{(A[I] + B)^2} \quad (4)$$

Combining eqs 1 and 4 yields

$$[P]_{calcd} - [P]_t = \frac{A[I]}{(A[I] + B)^2} \times e^{-(A[I]+B)t} \quad (5)$$

$$\ln([P]_{calcd} - [P]_t) = \text{constant} - (A[I] + B) \times t \quad (6)$$

where $[P]_{calcd}$ is the product concentration to be expected from the straight-line portions of the curves as calculated from eq 4 and $[P]_t$ is the product concentration actually observed at time $t$. Plots of $\ln([P]_{calcd} - [P]_t)$ versus $t$ give a series of straight lines at different concentrations of inhibitor ($[I]$) with slopes of $-(A[I] + B)$. A secondary plot of the slopes versus $[I]$ gives a straight line. The apparent forward and reverse rate constants, $A$ and $B$, can be obtained from the slope and intercept of this straight line. The value of $B$ directly gives the reverse rate constant $k_{-0}$.

From eq 2 and the Michaelis–Menten equation we can get

$$\frac{A}{v} = \frac{K_m \times k_{+0}}{V_m} \times \frac{1}{[S]} \quad (7)$$

A plot of $A/v$ versus $1/[S]$ gives a straight line with $(k_{+0} \times K_m/V_m)$ as the slope of the straight line; as $K_m$ and $V_m$ are obtained from measurement of the substrate reaction in the absence of glucose at different substrate concentrations, the rate constant $k_{+0}$ can be easily determined from the slope of the straight line.

## RESULTS AND DISCUSSION

**Enzymatic Hydrolysis of Cassava Residues.** The composition of cassava residue enzymes secreted by *H. orientalis* was previously determined to ensure what enzyme could be used for the hydrolysis (Tables 1 and 2). The optimum conditions for

**Table 1. Main Components of Cassava Residues**[a]

| NaOH for pretreatment | cellulose | hemicellulose | lignin | starch | ash | reducing sugars |
|---|---|---|---|---|---|---|
| 0% (nontreated) | 25.73 | 17.02 | 16.0 | 31.6 | 8.21 | 0.21 |
| 1% | 63.08 | 11.22 | 9.12 | —[b] | 3.08 | — |
| 4% | 68.08 | 10.95 | 9.03 | — | 3.70 | — |

[a]Grams per 100 g dry weight matter. Each value is average of three independent experiments. [b]Hard to detect.

**Table 2. Enzymatic Activity in *H. orientalis* Fermentation Liquid**[a]

| | activity (IU/mL) | | | | | |
|---|---|---|---|---|---|---|
| enzyme | CMCase | CBH | BG | Xylnase | α-amylase | protein |
| *H. orientalis* | 20.42 | 7.375 | 21.75 | 8530.55 | 2.17 | |
| cellulase DF | 37.5 | 1.4 | 3.15 | 4028.82 | nd[b] | 0.5 mg/mL |
| cellulase R-10 | 38.15 | 1.55 | 21.8 | 9253.15 | nd | |

[a]The values are average of the results of four independent tests. [b]Not detected.

saccharification yields of cassava residues were studied with 0.1 mg/mL enzymes and 1.5% matter. The results in Figure 1A show that, at pH 5.0, highest sugar yield (9.7 mg/mL) of enzymatic saccharification was obtained for 24 h of reaction.

The hydrolysis yields at different temperatures are presented in Figure 1B. As seen from the reaction curves, the highest yield of reducing sugar was obtained 10 mg/mL for 24 h of hydrolysis at 50 °C. Reaction kinetic study (data not shown) found that although enzymatic hydrolysis at 55 and 60 °C released sugars more quickly and more sugars were obtained at the initial stage, much less sugars were produced finally than at other temperatures due to thermo-inactivation of enzymes, which was in accordance with a previous study.[7] Effects of different concentrations of NaOH on sugar yields were determined. The results in Figure 1C indicate that alkali pretreatment can effectively and obviously improve yields of cellulase hydrolysis of cassava residues. Enzymatic hydrolysis of cassava residues pretreated with 0.5% (w/v) NaOH yielded 3-fold the amount of sugar of 0% NaOH pretreated residues (curve 3, from 2.5 to 7.5 mg/mL). However, there is a less significant increase in the amount of released sugar even alkaline up to 4%, showing the performances of NaOH above 0.5% were similar on removal of lignin of cassava residues.

Hydrolysis products were then separated and identified through Aminex HPX-87H (Figure 1D) chromatography. Major glucose (8.74 min) was found far more than xylose (9.36 min) and cellobiose (7.20 min), and the concentrations of the three sugars were 7.6, 0.75, and 0.34 mg/mL, respectively. Meanwhile, in a later phase of hydrolysis, a small amount of cellobiose emerged due to inhibition on β-glucosidase by accumulated glucose, with the yield of saccharification of cassava residues maintained but not increased.

**Hydrolysis of Cassava Residues by Different Enzymes.** Two resources of cellulases were used to hydrolyze cassava residues as compared with *H. orientalis* cellulase. Enzyme compositions of these three cellulases are presented in Table 2. It can be easily seen from the data that cellulase R-10 occupied the highest activity of each enzyme activity and that the BG activity of cellulase DF was lower much than those of the other two enzymes. The CMCase activity of *H. orientalis* was relatively small. When hydrolyzing cassava residues, CMCases of enzymes were all adjusted to 15 U/mL in the hydrolysis systems (pH 5.0, 50 °C). The yields of 24 h of hydrolysis catalyzed by *H. orientalis* enzyme and cellulase R-10 (Figure 2, curves 1 and 2) were close (9 mg/mL) and greater than that of cellulase DF (curve 5), which may be due to relatively small

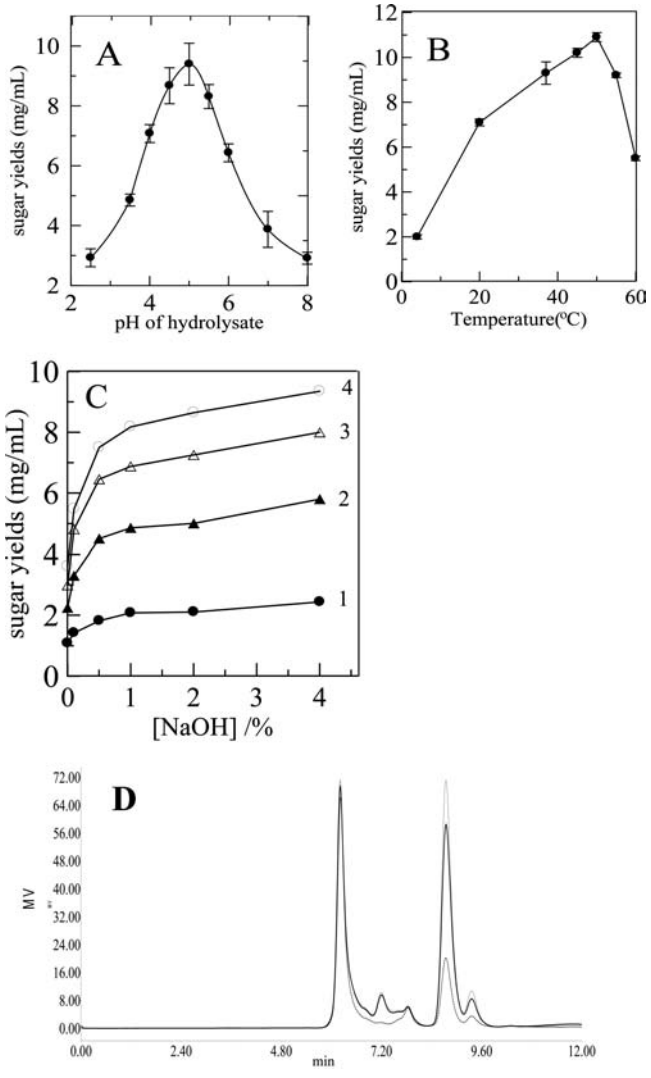


**Figure 1.** Enzymatic hydrolysis yield of pretreated cassava residues at different pH values (A) and temperatures (B) for 24 h of incubation at 50 °C with 0.1 mg/mL cellulase and 1.5% residues. (C) Enzymatic hydrolysis of cassava residues pretreated by different doses of NaOH. The hydrolysis times for curves 1−4 were 0.5, 2, 9, and 12 h, respectively. The values were means of duplicated experiments. (D) HPLC spectra of hydrolysate at three different hydrolysis times, 0.5 (dashed line), 9, and 12 h, respectively. The products were released from hydrolysis of 4% NaOH treated residues.


dx.doi.org/10.1021/jf5039663 | J. Agric. Food Chem. 2014, 62, 11512−11518

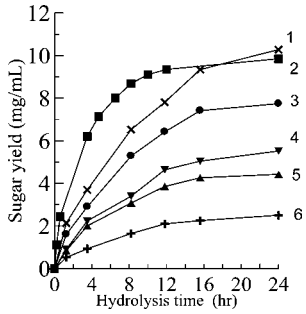


**Figure 2.** Enzymatic hydrolysis of cassava residues by different enzymes (50 °C, pH 5.0). The hydrolyzed residues were pretreated by 4% NaOH. Curves: 1, cellulase R-10 at 15 U/mL CMCase; 2, *H. orientalis* enzymes at 15 U/mL CMCase; 3, cellulase R-10 at 15 U/mL CMCase; 4, 2 U/mL CMCase *H. orientalis* enzymes with 7.5 U/mL cellulase R-10; 5, cellulase DF at 15 U/mL CMCase; 6, *H. orientalis* enzymes at 2 U/mL CMCase. The values are the average of three replicates.

activities of BG and xylase. Meanwhile, hydrolysis by *H. orientalis* enzyme reached the maximum yield faster than the other two enzymes, which could effectively and remarkably reduce the production costs.

To determine whether BG promotes the enzymatic hydrolysis, different enzyme blends were made to hydrolyze the residues. *H. orientalis* enzymes at 2 U/mL CMCase was respectively mixed with cellulase DF and cellulase R-10, both at 7.5 U/mL CMCase (total 9.5 U/mL CMCase with similar activity of xylase). Hydrolyses by the enzyme blends were run in the same conditions as above, respectively. The yields are shown in Figure 2 (curves 3 and 4) compared with respective enzymes. Results presented in the figure suggested that the sugar yields of the blends containing cellulase R-10 decreased significantly more than that of cellulase R-10 hydrolysis due to lower EG activity than that of cellulase R-10, whereas another enzyme blend containing *H. orientalis* enzymes and cellulase DF yielded a similar amount of sugars as that of cellulase DF, even though CMCase was relatively smaller. This result was in accordance with previous studies, which pointed out that adding BG could promote the yield of cellulose hydrolysis.[18,19]

**Hydrolysis of Various Residues by *H. orientalis* Enzymes.** Various resources of agricultural lignocelluloses producing sugars catalytically with *H. orientalis* cellulase (0.1 mg/mL enzymes loaded) were also studied. These cellulosic substrates were prepared from wheat grass, sugar cane bagasse, waste papers, peanut hulls, and stem dregs of swainsona salsula taubert (*Sphaerophysa salsula*, Chinese traditional medicine), respectively, which were all treated with 4% NaOH. Stems of swainsona salsula taubert were processed for extraction of flavonoids before this work. Hydrolysis yields of these materials are shown in Figure 3. The results showed that, without pretreatment, saccharification of cassava residues can produce more sugars than the other cellulose materials due to residual starch. With 4% NaOH pretreatment, sugar cane bagasse, wheat grass, and cassava residues produced similar amounts of sugars far greater than that of waste papers, peanut hulls, and stems of swainsona salsula taubert. Due to condensed lignin cortex, peanut hulls and stems of swainsona salsula taubert cannot release significant amounts of sugars by *H. orientalis* cellulase hydrolysis, whether 4% NaOH pretreated or not, and other effective treatment methods and enzymes were required for that saccharification.

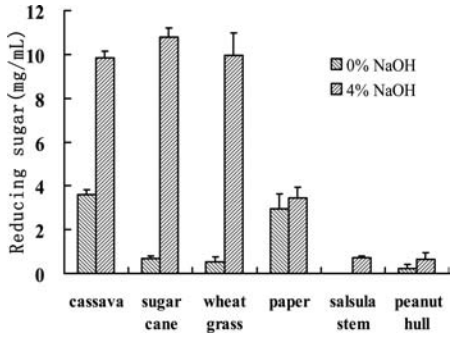


**Figure 3.** Enzymatic hydrolysis yields of pretreated wastes for 24 h of incubation at 50 °C and pH 5.0 with 0.1 mg/mL cellulase and 1.5% dry matter.

On the basis of the results above, with pretreatment, each gram of nonstarch cassava residues hydrolyzed by 0.1 mg/mL cellulase at 50 °C, pH 5.0, for 24 h can release the highest amount of 660 mg of reducing sugars, equal to that of bagasse and wheat grass. *H. orientalis* secreted enzymes were deficient to degrade peanut hulls and stems of swainsona salsula efficiently. The yield was similar to that of cellulase R-10.

**Glucose Gave Reversible and Competitive Inhibition on BG.** The relationship between the activity of *H. orientalis* BG and the concentrations of glucose is shown in Figure 4A.

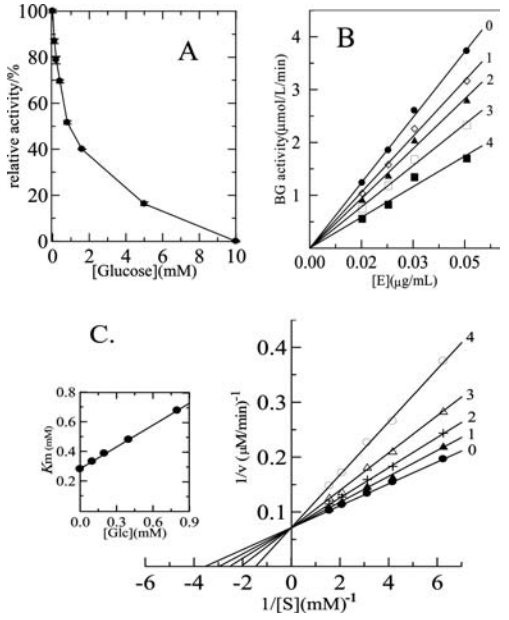


**Figure 4.** Inhibition of BG by glucose. Methods were described in the text. (A) Relative activity of BG at different concentrations of glucose. (B) Effects of BG concentrations on activity for the hydrolysis of pNPG with different concentrations of glucose. The concentrations of glucose for curves 0–4 were 0, 0.1, 0.2, 0.4, and 0.8 mM, respectively. (C) Lineweaver–Burk plots for the hydrolysis of pNPG catalyzed by BG in the presence of different concentrations of glucose. The glucose concentrations for lines 0–4 were 0, 0.1, 0.2, 0.4, and 0.8 mM, respectively. (Inset) Plot of $K_m$ versus glucose concentrations to determine the inhibition constant.

The effect of glucose on BG was dose-dependent inhibition, and the activity of BG was sharply reduced to 20% following the increase of glucose to 5 mM (0.9 mg/mL); the $IC_{50}$ value of glucose was estimated to be 0.87 ± 0.1 mM in the presence of 0.16 mM pNPG.


dx.doi.org/10.1021/jf5039663 | J. Agric. Food Chem. 2014, 62, 11512–11518

Plots of BG activity versus enzyme concentrations under various doses of glucose gave a family of straight lines all passing through the origin (Figure 4B), indicating that D-glucose was a reversible inhibitor of *H. orientalis* BG. Meanwhile, Lineweaver–Burk plots of $1/v$ versus $1/[S]$ under different concentrations of glucose gave a family of lines on a common intercept with slopes ascending along with the increase of glucose (Figure 4C), showing glucose can competitively inhibit BG activity in the progress of cellulose hydrolysis. The results indicated that adding enough enzymes or substrates can effectively reduce depression by glucose products during cellulose saccharification. From curve 0, values of $K_m$ and $V_m$ for pNPG hydrolysis in the absence of inhibitor were determined as 0.28 mM and 14.92 $\mu$M/min, respectively. The inhibition constant ($K_I$) of glucose was calculated to be 0.56 mM from the plot of $K_m$ versus concentrations of glucose as presented in the inset of Figure 4C, which was higher than BG from *P. purpurogenum*, *T. harzianum* C-4, *Daldinia eschscholzii* but lower than another six *Aspergillus* species.[20−25]

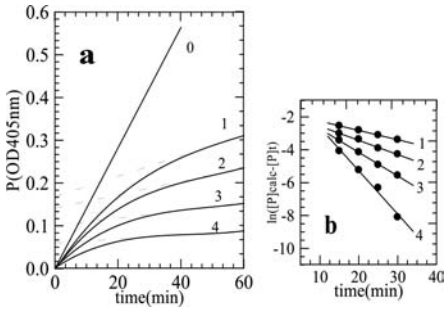


**Figure 5.** Courses of substrate reaction of BG in the presence of different concentrations of glucose. The substrate concentration was 0.16 mM in 0.1 M NaAc buffer (pH 5.0). (a) Substrate reaction course. The concentrations of glucose for curves 0−4 were 0, 0.1, 0.2, 0.4, and 0.8 mM, respectively. (b) Semilogrithmic plots of ln $([P]_{calcd} - [P]_t)$ against time. Data were taken from curves 0−4 in panel a.

**Determination of Microscopic Rate Constants of Glucose Inhibition on BG.** Reaction kinetics hydrolysis of pNPG by BG in the presence of different concentrations of D-glucose was measured as shown in Figure 5a. The results indicated that the reaction rate at each concentration of glucose decreased with increasing time until a straight line (identical with dash line) was approached. Plots of $\ln([P]_{calcd} - [P]_t)$ versus $t$ at different concentrations of glucose are shown in Figure 5b with slopes of $-(A[I] + B)$.

Time courses of the reaction at different concentrations of pNPG are shown in Figure 6a in the presence of 0.1 mM glucose. Plots of $\ln([P]_{calcd} - [P]_t)$ versus $t$ in Figure 6b gave a family of straight lines with slopes of $-(A[I] + B)$. The kinetic curves of substrate reaction at other concentrations of glucose can also be obtained with the same method.

With the presence of various substrate concentrations, plots of the values of $(A[I] + B)$ versus concentrations of glucose presented a series of straight lines with slopes of $A$, respectively, and had a common intercept on the ordinate (Figure 7A). The value of the apparent reverse rate constant $B$ was obtained from

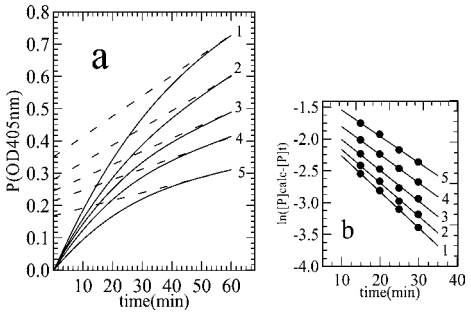


**Figure 6.** Courses of substrate reaction of BG in the presence of 0.1 mM glucose with different concentrations of pNPG. (A) Substrate reaction course. The concentrations of pNPG for curves 1−5 were 0.16, 0.24, 0.32, 0.48, and 0.64 mM, respectively. (B) Semilogrithmic plots of ln $([P]_{calcd} - [P]_t)$ against time. Data were taken from curves 1−5 in panel a.

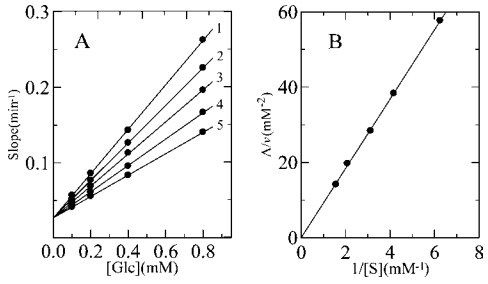


**Figure 7.** Determination of microscopic inhibition rate constants of BG by glucose. (A) Secondary plots of the slopes versus glucose concentrations for a series of fixed substrate concentrations. The concentrations pNPG for lines 1−5 were 0.16, 0.24, 0.32, 0.48, and 0.64 mM, respectively. (B) Plot of $A/v$ versus $1/[S]$. The $A$ value was calculated from the slopes of the straight lines in panel A.

the ordinate intercept, equal to the microscopic rate constant $k_{-0}$. Then, the plot of $A/v$ versus $1/[S]$ was obtained, a straight line that passed through the origin (Figure 7B) with the slope of $(K_m k_{+0}/V_m)$. The microscopic forward rate constant $k_{+0}$ was obtained according to eq 7. The results are summarized in Table 3.

**Relative BG Activities with Different Monosaccharides.** Effects of some monosaccharides (derivatives or isomers of glucose) on BG activity were studied as compared with glucose. Residual activities of BG at different concentrations of monosaccharides were assayed as described previously. It can be seen from the results (Table 4) that, within low concentrations of monosaccharides, BG was far more sensitive to D-glucose than to the other sugars. Meanwhile, the inhibitory effect of L-glucose, a chiral isomer of D-glucose, declined evidently with $IC_{50}$ to >5 mM. Moreover, mannose showed lower $IC_{50}$ than galactose, perhaps because the 2′-OH in the sugar molecule was more accessible to BG active residues than 3′-OH to block the catalytic site. Additionally, a 20% loss of BG activity caused by aminoglucose was detected at 200 mM, and no significant loss of BG activity was found in the presence of *N*-acetylglucose or fructose at a range below 200 mM.

Some of these sugars are components of many agricultural and food wastes,[12] which can be hydrolyzed catalytically

**Table 3. Inhibition Equilibrium Constants and Microscopic Rate Constants for BG by D-Glucose**

| $IC_{50}$ | $K_I$ | $k_{+0}$ | $k_{-0}$ |
|---|---|---|---|
| 0.87 ± 0.1 mM | 0.56 ± 0.02 mM | $4.88 \times 10^{-4}$ (mM· s)$^{-1}$ | $2.7 \times 10^{-4}$ s$^{-1}$ |


dx.doi.org/10.1021/jf5039663 | J. Agric. Food Chem. 2014, 62, 11512−11518

Table 4. Relative Activities of BG in the Presence of Different Concentrations of Monosaccharide

| | percentage of β-glucosidase activity | | | |
|---|---|---|---|---|
| | 1 mM | 5 mM | 50 mM | 200 mM |
| D-glucose | 48.0 ± 0.9 | 16.2 ± 0.7 | nd[a] | nd |
| L-glucose | 97.6 ± 2.8 | 86.1 ± 3.5 | 33.6 ± 1.3 | 8.5 ± 4.8 |
| D-mannose | 93.6 ± 3.1 | 87.1 ± 2.0 | 48.8 ± 3.0 | 18.6 ± 1.2 |
| D-galactose | 100.1 ± 3.4 | 96.8 ± 3.0 | 71.5 ± 1.7 | 42.2 ± 11.0 |
| D-aminoglucose | 99.0 ± 1.6 | 98.8 ± 5.6 | 88.4 ± 1.3 | 81.4 ± 3.5 |
| *N*-acetyl-D-glucose | 96.4 ± 2.8 | 95.7 ± 2.3 | 95.0 ± 6.3 | 95.9 ± 4.0 |
| D-fructose | 97.1 ± 5.1 | 99.0 ± 2.4 | 97.9 ± 6.7 | 94.3 ± 5.5 |

[a]nd, not determined.

accompanied with cellulosic materials for production of biofuels or other chemicals. This work provides theoretical support for that application. Furthermore, comparisons of effects on BG by these saccharides proved that the combination between the active site and chemicals required strict structural specificity, which guided molecular modification to improve sugar tolerance of cellulase.[14]

## AUTHOR INFORMATION

### Corresponding Author

*(Q.-X.C.) Phone/fax: +86-592-2185487. E-mail: chenqx@xmu.edu.cn.

### Funding

The present research was financially supported by the National Science Foundation for Fostering Talents in Basic Research of the National Natural Science Foundation of China (Grant J1310027/J0106) and a grant of the National Key Basic Research Program (NKBRP) (No. 2010CB732201).

### Notes

The authors declare no competing financial interest.

## ABBREVIATIONS USED

BG, β-glucosidase; CBH, cellobiohydrolase; DNS, 3,5-dinitrosalicylic; NaAc, sodium acetate; pNPG, *p*-nitrophenyl-β-D-glucopyranoside; $K_m$, Michaelis−Menten constant

## REFERENCES

(1) Tuck, C. O.; Pérez, E.; Horváth, I. T.; Sheldon, R. A.; Poliakoff, M. Valorization of biomass: deriving more value from waste. *Science* **2012**, *337*, 695−699.

(2) Himmel, M. E.; Ding, S. Y.; Johnson, D. K.; Adney, W. S.; Nimlos, M. R.; Brady, J. W.; Foust, T. D. Biomass recalcitrance engineering plants and enzymes for biofuels production. *Science* **2007**, *315*, 804−807.

(3) Hendriks, A. T. W. M.; Zeeman, G. Pretreatments to enhance the digestibility of lignocellulosic biomass. *Bioresour. Technol.* **2009**, *100*, 10−18.

(4) Binod, P.; Satyanagalakshmi, K.; Sindhu, R.; Janu, K. U.; Sukumaran, R. K.; Pandey, A. Short duration microwave assisted pretreatment enhances the enzymatic saccharification and fermentable sugar yield from sugarcane bagasse. *Renewable Energy* **2012**, *37*, 109−116.

(5) Yang, R.; Meng, D. M.; Hu, X. S.; Ni, Y. Y.; Li, Q. H. Saccharification of pumpkin residues by coculturing of *Trichoderma reesei* RUT-C30 and *Phanerochaete chrysosporium* burdsall with delayed inoculation timing. *J. Agric. Food Chem.* **2013**, *61*, 9192−9199.

(6) Wang, H.; Han, G.; Yu, X. Y.; Lv, X. B.; zhang, s. t. the influence of pretreatment methods on hydrolysis effect of cassava starch dregs. *J. Environ. Eng. Technol.* **2011**, *1* (6), 484−488.

(7) Tao, Y. M.; Xu, X. Q.; Ma, S. J.; Liang, G.; Wu, X. B.; Long, M. N.; Chen, Q. X. Cellulase hydrolysis of rice straw and inactivation of endoglucanase in urea solution. *J. Agric. Food Chem.* **2011**, *59*, 10971−10975.

(8) Kovacs, K.; Macrelli, S.; Szakacs, G.; Zacchi, G. Enzymatic hydrolysis of steam-pretreated lignocellulosic materials with *Trichoderma atroviride* enzymes produced in-house. *Biotechnol. Biofuels* **2009**, *2*, 14−24.

(9) Murphy, L.; Bohlin, C.; Baumann, M. J.; Søren, N. O.; Trine, H. S.; Lars, A.; Kim, B.; Peter, W. Product inhibition of five *Hypocrea jecorina* cellulases. *Enzyme Microb. Technol.* **2013**, *52*, 163−169.

(10) Hsieh, C. C.; Cannella, D.; Jørgensen, H.; Felby, C.; Thygesen, L. G. Cellulase inhibition by high concentrations of monosaccharides. *J. Agric. Food Chem.* **2014**, *62*, 3800−3805.

(11) Ma, S. J.; Leng, B.; Xu, X. Q.; Zhu, X. Z.; Shi, Y.; Tao, Y. M.; Chen, S. X.; Long, M. N.; Chen, Q. X. Purification and characterization of β-1,4-glucosidase from *Aspergillus glaucus*. *Afr. J. Biotechnol.* **2011**, *10* (84), 19607−19614.

(12) Tao, Y. M.; Zhu, X. Z.; Huang, J. H.; Ma, S. J.; Wu, X. B.; Long, M. N.; Chen, Q. X. Purification and properties of endoglucanase from a sugar cane bagasse hydrolyzing strain, *Aspergillus glaucus* XC9. *J. Agric. Food Chem.* **2010**, *58*, 6126−6130.

(13) Ma, L.; Zhang, J.; Zou, G.; Wang, C. S.; Zhou, Z. H. Improvement of cellulase activity in *Trichoderma reesei* by heterologous expression of a β-glucosidase gene from *Penicillium decumbens*. *Enzyme Microb. Technol.* **2011**, 366−371.

(14) Liu, J. J.; Zhang, X. C.; Fang, Z. M.; Fang, W.; Peng, H.; Xiao, Y. Z. The 184th residue of β-glucosidase Bgl1B plays an important role in glucose tolerance. *J. Biosci. Bioeng.* **2011**, *112* (5), 447−450.

(15) Long, C. N. *Study on Cellulose Degradation Enzymes and Gene Expression of Hypocrea orientalis EU7-22*. Ph.D. dissertation, Xiamen University, 2013.

(16) NREL. Chemical Analysis and Testing Laboratory Analytical Procedures, 1998.

(17) Miller, G. L. Use of the dinitrosalicylic acid reagent for the determination of reducing sugars. *Anal. Chem.* **1959**, *31*, 426−428.

(18) Tsou, C. L. Kinetics of substrate reaction during irreversible modification of enzyme activity. *Adv. Enzymol. Related Areas Mol. Biol.* **1988**, *61*, 381−436.

(19) Maeda, R. N.; Serpa, V. I.; Rocha, V. A. L.; Mesquita, R. A. A.; Santa Anna, L. M. M.; de Castro, A. M.; Driemeier, C. E.; Pereira, N., Jr.; Polikarpov, I. Enzymatic hydrolysis of pretreated sugar cane bagasse using *Penicillium funiculosum* and *Trichoderma harzianum* cellulases. *Process Biochem.* **2011**, 1196−1201.

(20) Paripok, P.; Kazuo, S.; Khanok, R. Improvement of lignocellulosic biomass in planta: a review of feedstocks, biomass recalcitrance, and strategic manipulation of ideal plants designed for ethanol production and processability. *Biomass Bioenrg.* **2013**, *58*, 390−405.

(21) Jeya, M.; Joo, A. R.; Lee, K. M.; Manish, K. T.; Lee, K. M.; Kim, S. H.; Lee, J. K. Characterization of β-glucosidase from a strain of *Penicillium purogenum* KJS506. *Appl. Microbiol. Biotechnol.* **2010**, *86*, 1473−1484.

(22) Decker, C. H.; Visser, J.; Schreier, P. β-Glucosidases from five black *Aspergillus* species: study of their physico-chemical and biocatalytic properties. *J. Agric. Food Chem.* **2000**, *48* (10), 4929−4936.

(23) Riou, C.; Salmon, J. M.; Vallier, M. J.; Günata, Z.; Barre, P. Purification, characterization, and substrate specificity of a novel highly glucose-tolerant β-glucosidase from *Aspergillus oryzae*. *Appl. Environ. Microbiol.* **1998**, *64* (10), 3607−3614.
(24) Soo, I. Y.; Choon, S. J.; Dae, K. C.; Hye, S. C. Purification and some properties of a β-glucosidase from *Trichoderma harzianum* type C-4. *Biosci., Biotechnol., Biochem.* **2001**, *65* (9), 2018−2032.
(25) Aphichart, K.; Amorn, P.; Polkit, S.; Jittra, P.; Anthony, J. S. W.; Colin, D. R.; Prakitsin, S. Purification and biochemical characterization of an extracellular β-glucosidase from the wood-decaying fungus *Daldinia eschscholzii* (Ehrenb.:Fr) Rehm. *Fed. Eur. Microbiol. Soc.* **2007**, *270*, 162−170.

M82.[15] The *S. pennellii* ILs were used to map several QTLs associated with characters related to tomato fruit quality.[17,18] By using these lines, in our laboratory two QTLs increasing fruit phenolics and AsA content were detected on tomato chromosomes 7 and 12.[19−21] In a subsequent study, these QTLs were pyramided in the genetic background of the cultivated line M82 using marker-assisted selection. The efficacy of pyramiding to improve tomato traits has been previously reported. For example, Gur et al.[22] developed genotypes carrying three independent yield-promoting genomic regions introduced from *S. pennellii* that resulted in a hybrid with 50% higher yields than leading commercial varieties in multiple environments and irrigation regimens. Moreover, introgressions originating from *S. pennellii* were introduced into lines of processing tomato, and the resulting hybrid, AB2, is presently a leading variety in California.[23] In our case, IL 7-3 and IL 12-4 were crossed, and four genotypes of the $F_3$ progenies were selected that carry both introgressions 7-3 and 12-4 at the homozygous condition (DHO).[24] Because the combined effect of these QTLs is unpredictable, here we evaluated the nutritional quality of the four genotypes obtained by QTL pyramiding. We analyzed the amount of phytochemicals associated with antioxidant activity in the cultivated line M82, in the two introgression lines IL 7-3 and IL 12-4 and in the DHO genotypes. In particular, the hydrophilic and lipophilic antioxidant activity and contents of AsA, total phenolics, flavonoids, phenolic acids, total carotenoids, lycopene, and $\beta$-carotene were investigated. In addition, to assess the nutraceutical potential of the DHO lines, we tested the activity of tomato fruit extracts on the proliferation of human normal and cancer cell lines.

## MATERIALS AND METHODS

**Chemicals and Reagents.** Ascorbic acid, Trolox, gallic acid, ferulic acid, quercetin, and kampferol were purchased from Sigma (St. Louis, MO, USA). All solvents used (water, methanol, chloroform) were obtained from Fluka (Swizerland), whereas HPLC grade formic acid was purchased from Aldrich Chemical Co. (Milwaukee, WI, USA). Folin−Ciocalteu's phenol was purchased by AppliChem (Darmstadt, Germany). $FeCl_3$, trichloroacetic acid (TCA), $Na_2CO_3$, $NaH_2PO_4$, $Na_2HPO_4$, 2,2′-dipyridil, $CH_3COOH$, 2,4,6-tripyridyl-*s*-triazine (TPTZ), 2,2′-azinobis(3-ethylbenzothiazoline-6-sulfonic acid) (ABTS), and $K_2S_2O_8$ were obtained from Sigma-Aldrich, $Na_2HPO_4$ and $H_3PO_4$ were obtained from J. T. Baker (Germany), and HCl was obtained from Riedel-deHaën (Germany). Deionized water was obtained from a Milli-Q water purification system (Millipore, Bedford, MA, USA). Chromatographic solvents were degassed for 20 min using a Branson 5200 (Branson Ultrasonic Corp., USA) ultrasonic bath.

**Plant Material and Growth Conditions.** Seeds from IL 12-4 (LA4102), IL 7-3 (LA4066), and their parental line M82 (LA3475) were kindly provided by the Tomato Genetics Resource Centre (TGRC) (http://tgrc.ucdavis.edu/).[25] Genotypes carrying introgressions IL 7-3 and IL 12-4 at the homozygous condition (DHO) were obtained using marker-assisted selection as described in Sacco et al.[24] During the year 2013, the double-homozygous plants of the $F_4$ progenies and their parents were grown according to a completely randomized design with three replicates (10 plants/replicate), in an experimental field located in Acerra (Naples, Italy). Samples of about 20 full mature red fruits per plot were collected.

Tomato fruits were chopped, ground in liquid nitrogen by a blender (FRI150, Fimar) to a fine powder, and kept at −80 °C until the analyses.

**Chemical Extractions.** For the biochemical analyses, each tomato fruit sample consisted of 20 pooled fruits per plot. The extraction of hydrophilic fraction was carried out according to the procedure reported by Choi et al.[26] with minor changes. Briefly, frozen powder (2 g) was weighed, placed into a 50 mL Falcon tube, and extracted with 25 mL of 80% methanol into an ultrasonic bath (Branson 5200 Ultrasonic Corp.) for 60 min at 30 °C. The mixture was centrifuged at 14000 rpm for 10 min at 4 °C, and the supernatant was stored at −20 °C until analysis of total phenolic compounds and hydrophilic antioxidant activity (HAA). The pellet was extracted with 10 mL of chloroform (100%) with the aid of a pestle and was centrifuged at 4000 rpm for 5 min at 4 °C according to the method reported by Wellburn[27] with some modifications. This procedure was repeated five consecutive times, and supernatants were collected and stored at −20 °C until analysis of carotenoids and lipophilic antioxidant activity (LAA).

**Carotenoid Determination.** The evaluation of total carotenoids was carried out according to the method reported by Wellburn,[27] whereas lycopene and $\beta$-carotene were determined according the method reported by Zouari et al.[28] with slight modifications. All biological replicates of samples were analyzed in triplicate. Results were expressed as milligrams per 100 g fresh weight (FW).

**Ascorbic Acid Determination.** AsA quantification was carried out according to the method reported by Stevens et al.[18] with slight modifications. Briefly, frozen powder (500 mg) was placed in a 2 mL eppendorf tube, and 300 $\mu$L of ice-cold 6% TCA was added. The mixture was vortexed for 10 s, incubated for 15 min on ice, and centrifuged at 14000 rpm for 20 min at 4 °C. Then, 20 $\mu$L of supernatant for each assay was transferred in a 1.5 mL eppendorf tube with 20 $\mu$L of 0.4 M phosphate buffer (pH 7.4) and 10 $\mu$L of double-distilled (dd) $H_2O$. Then, 80 $\mu$L of color reagent solution was prepared immediately before assay by mixing solution A (31% $H_3PO_4$, 4.6% (w/v) TCA, and 0.6% (w/v) $FeCl_3$) with solution B (4% 2,2′-dipyridil (w/v) made up in 70% ethanol) at a proportion of 2.75:1 v/v. The mixture was vortexed and incubated at 37 °C for 40 min prior to measurement at 525 nm by a NanoPhotometer (Implen) using 6% TCA as reference. Three separated biological replicates for each sample and three technical assays for each biological repetition were measured. The concentration was expressed in nanomoles of AsA according to the standard curve, designed over a range of 0−70 nmol; then the values were converted into milligrams per 100 g FW.

**Total Phenolic Compounds Determination.** Total polyphenolic amount was evaluated by using Folin−Ciocalteu's assay as reported by Singleton et al.[29] with some modifications. In an eppendorf tube (1.5 mL) 62.5 $\mu$L of methanolic extract, 62.5 $\mu$L of Folin−Ciocalteu's phenol reagent, and 250 $\mu$L of dd $H_2O$ were added and shaken. After 6 min, 625 $\mu$L of 7% $Na_2CO_3$ solution was added to the mixture. The solution was diluted with 500 $\mu$L of dd $H_2O$ and mixed. After incubation for 90 min at room temperature, the absorbance against prepared reagent blank was determined at 760 nm by a NanoPhotometer (Implen). All biological replicates of samples were analyzed in triplicate. Total phenolic content of tomato fruits was expressed as milligrams of gallic acid equivalents (GAE) per 100 g FW.

**Identification and Quantification of Individual Phenolic Compounds.** An aliquot (1 mL) of the methanolic extract was passed through a 0.45 $\mu$m Millipore nylon filter (Bedford, MA, USA) before HPLC analysis. Free phenolic acids and flavonoids were separated and quantified by using a HPLC (Spectra System SCM 1000) fitted with an UV−visible detector. Separation of compounds was carried out on a reversed phase C18 Prodigy column (Phenomenex, 250 × 4.6 mm; particle size = 5 $\mu$m), preceded by a guard column (Phenomenex, 4 × 3.0 mm) of the same stationary phase. A gradient of water acidified with 5% formic acid (A) and methanol (B) at a flow rate of 1 mL/min was applied with the following modes: A = 60% (0 min), 40% (3−18 min), 0% (23−28 min), and 60% (30 min) according to the method reported by Ferracane et al.[30] with minor modifications. To determine total flavonoids and total phenolic acids concentration, the sum of all peaks present in the chromatogram was considered at two characteristic wavelengths of 365 and 287 nm, respectively. Each sample was analyzed by HPLC in triplicate. The quantification was carried out using the calibration curves of quercetin, gallic acid and ferulic acid in the ranges of 1−100, 0.5−10, and 0.01−1 $\mu$g/mL, respectively. The amount of phenolic compounds was expressed as milligrams of

quercetin equivalents (QE) per kilogram FW for quercetin and total flavonoids, as milligrams of GAE per kilogram FW for gallic acid and total phenolic acids, and as milligrams of ferulic acid (FA) per kilogram FW for ferulic acid.

**Antioxidant Activity Determination.** HAA was evaluated in the water-soluble fraction using two different methods, the ferric reducing/antioxidant power (FRAP) method[31] and the 2,2′-azinobis-(3-ethylbenzothiazoline-6-sulfonic acid) (ABTS) method[32] with slight modifications.

The FRAP assay was carried out by adding in a vial (3 mL) 2.5 mL of acetate buffer, pH 3.6, 0.25 mL of TPTZ solution (10 mM) in 40 mM HCl, 0.25 mL of $FeCl_3 \cdot 6H_2O$ solution (12 mM), and 150 $\mu$L of methanolic extract. The mixture was incubated for 30 min in the dark, and then readings of the colored product (ferrous tripyridyltriazine complex) were taken at 593 nm using the spectrophotometer against a blank constituted by a mixture of reaction and 150 $\mu$L of extracting solution ($CH_3OH/H_2O$ 80:20 v/v). The standard curve was linear between 20 and 800 $\mu$M Trolox. Results were expressed as micromoles of Trolox equivalents (TE) per 100 g FW.

The ABTS assay was based on the reduction of the $ABTS^{\bullet+}$ radical action by the antioxidants present in the sample. A solution constituted by 7.4 mM $ABTS^{\bullet+}$ (5 mL) mixed with 140 mM $K_2S_2O_8$ (88 $\mu$L) was prepared and stabilized for 12 h at 4 °C in the dark. This mixture was then diluted by mixing $ABTS^{\bullet+}$ solution with ethanol (1:88) to obtain an absorbance of 0.70 ± 0.10 unit at 734 nm using a spectrophotometer. Methanolic extracts (100 $\mu$L) were allowed to react with 1 mL of diluted $ABTS^{\bullet+}$ solution for 2.5 min, and then the absorbance was taken at 734 nm using a spectrophotometer against a blank constituted by $ABTS^{\bullet+}$ solution added with 100 $\mu$L of ethanol. The standard curve was linear between 0 and 20 $\mu$M Trolox.

LAA determination was carried out according to the ABTS assay, using the extract in chloroform. All biological replicates of samples were analyzed in triplicate. Results were expressed as micromoles of TE per 100 g FW.

The percentage of the variations of quantitative parameters among genotypes was calculated by using the following formula: % increase and/or decrease = (value in genotype 1 − value in genotype 2)/value in genotype 2) × 100. Total antioxidant activity (TAA) was calculated by adding LAA to HAA obtained by using the ABTS test. HAA contribution to TAA was evaluated by dividing HAA value obtained by using the ABTS test by TAA.

**MTT Test Procedure.** Human renal cortical epithelial cells HRCE (Innoprot, Biscay, Spain) were cultured in basal medium, supplemented with 2% fetal bovine serum, epithelial cell growth supplement, and antibiotics, all from Innoprot. Human HeLa adenocarcinoma cells, human renal epithelial cells (Hek 293), and murine BALB/3T3 and SV-T2 fibroblasts (ATCC) were cultured in Dulbecco's modified Eagle's medium (Sigma-Aldrich), supplemented with 10% fetal bovine serum (HyClone, Logan, UT, USA), 2 mM L-glutamine, and antibiotics. Cells were grown in a 5% $CO_2$ humidified atmosphere at 37 °C. Cells were seeded in 96-well plates (100 $\mu$L/well) at a density of $5 \times 10^3$/well. Methanolic tomato extracts, obtained as reported above, were dried by rotovapor (R-210, Buchi), redissolved in dimethyl sulfoxide (DMSO) 5% in PBS, and then added to the cells 24 h after seeding for dose-dependent cytotoxicity assays. At the end of incubation, cell viability was assessed by the MTT assay. The MTT reagent, dissolved in DMEM in the absence of phenol red (Sigma-Aldrich), was added to the cells (100 $\mu$L/well) to a final concentration of 0.5 mg/mL. Following an incubation of 4 h at 37 °C, the culture medium was removed, and the resulting formazan salts were dissolved by adding isopropanol containing 0.1 N HCl (100 $\mu$L/well). Absorbance values of blue formazan were determined at 570 nm using an automatic plate reader (Microbeta Wallac 1420, PerkinElmer). The decrease in absorbance in the assay measures the extent of decrease in the number of viable cells following exposure to the test substances calculated by using the following formula: % inhibition of cells = $(A_{control} - A_{test\ substance})/A_{control} \times 100$. Three separate analyses were carried out with each extract. Control experiments were performed either by growing cells in the absence of the extract and by supplementing the cell cultures with identical volumes of extract buffer (5% DMSO in PBS). The method used avoids any possibility of a DMSO effect on the results.

**Statistical Analyses.** Quantitative results were expressed as the mean value ± SD for three replicates. Differences among genotypes for each evaluated parameter were determined by using SPSS (Statistical Package for Social Sciences) Package 6, version 15.0. Significance was determined by comparing mean values of DHOs to the common controls M82, IL 7-3, and IL 12-4 through a factorial analysis of variance (one-way ANOVA) with LSD post hoc test at a significance level of 0.05. Principal component analysis (PCA) was carried out using the same version of SPSS. For the MTT test all of the data are representative of at least three independent experiments (with comparable results). Statistical significance of the data was evaluated by *t* test analyses.

## RESULTS AND DISCUSSION

Tomato plants represent one of the major sources of antioxidants and other bioactive compounds that benefit nutrition and human health. It is well-known that carotenoids, phenolics, and AsA alone are not responsible for tomato functional effect, but they act synergistically.[12] In this study we report the characterization of novel tomato lines obtained by QTL pyramiding to combine different wild chromosomal regions and the evaluation of their phytochemical parameters in comparison with parental lines.

**Carotenoids.** In Table 1 the levels of total carotenoids, lycopene, and $\beta$-carotene in M82, the ILs, and DHO lines are reported. The cultivated line M82 showed a mean value of carotenoids of 11.10 ± 0.41 mg/100 g FW. The genotype IL 7-3 exhibited a significant ($p < 0.05$) increase (22.19%) of total carotenoids content compared to the cultivated line M82. On the contrary, IL 12-4 showed a significant decrease of total carotenoids content (35.6%) compared to M82. The DHO genotypes were characterized by an amount of carotenoids significantly lower than in M82, with a decrease ranging between 31.42 and 43.30% and comparable to the amount calculated in IL 12-4. In all of the genotypes lycopene constituted about 90−94% of total carotenoids, whereas $\beta$-carotene represented about 4−6% of total carotenoids. The reduction of carotenoids in the DHO lines and in IL 12-4 compared to the control M82 could be explained by taking into consideration the detection and fine-mapping of one major QTL (*lyc12.1*) for lycopene content in the chromosomal region 12-4.[33,34] In fact, wild alleles of the region 12-4 influenced negatively the levels of these metabolites in the tomato fruits of the DHO lines, even contrasting and overcoming the positive influence of the wild alleles located on the region 7-3 that may contribute increasing carotenoids levels. Therefore, we can

**Table 1. Lycopene, $\beta$-Carotene, and Total Carotenoids Contents in the Tomato Lines Analyzed[a]**

| genotype | lycopene (mg/100 g FW) | $\beta$-carotene (mg/100 g FW) | total carotenoids (mg/100 g FW) |
|---|---|---|---|
| M82 | 10.09 ± 0.38a | 0.67 ± 0.03a | 11.10 ± 0.41a |
| IL 12-4 | 6.66 ± 0.14b | 0.41 ± 0.01b | 7.15 ± 0.09b |
| IL 7-3 | 12.70 ± 0.20c | 0.58 ± 0.01c | 13.56 ± 0.22c |
| DHO1 | 6.15 ± 0.241b | 0.40 ± 0.02b | 6.78 ± 0.261b |
| DHO2 | 5.73 ± 0.64bd | 0.39 ± 0.05b | 6.40 ± 0.72bd |
| DHO3 | 5.75 ± 0.23bd | 0.33 ± 0.03bd | 6.29 ± 0.18bd |
| DHO4 | 6.85 ± 0.20b | 0.42 ± 0.01b | 7.61 ± 0.21b |

[a]Values are means ± SD ($n = 9$). Values with different letters are significantly different ($p < 0.05$).

speculate that a negative interaction exists between genes and/or transcription factors located in the *S. pennellii* regions 12-4 and 7-3. However, it is noteworthy that the amount of these metabolites calculated in the DHO lines and in IL 12-4 are comparable to those found in some cultivated tomato lines.[2,35−37]

**Ascorbic Acid.** The average AsA concentration in red ripe fruit of M82 was 14.27 ± 1.30 mg/100 g FW. Genotypes IL 12-4 and IL 7-3 showed significant increases (40 and 45%, respectively) compared to the cultivated genotype (Figure 1).

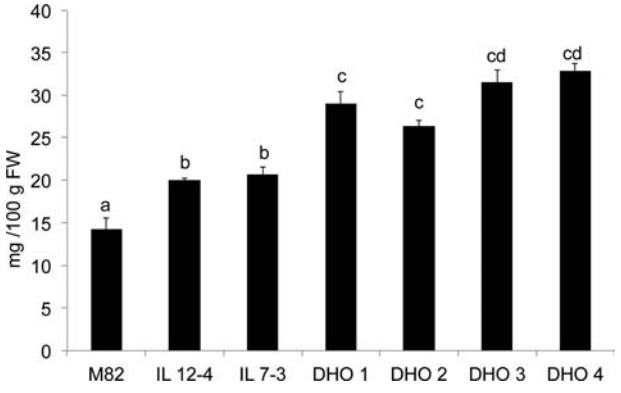


**Figure 1.** Ascorbic acid content (mg/100 g FW) in tomato lines analyzed. Values are means ± SD ($n$ = 9). Values with different letters are significantly different ($p$ < 0.05).

The amount of AsA calculated in M82 and in the IL lines is in agreement with the presence of QTLs for high AsA content previously identified in the 12-4 and 7-3 introgressed regions.[19,24] The mean value of ascorbic acid calculated in the DHO lines was between 28.99 and 32.84 mg/100 g FW. The DHO genotypes showed a significant increase of AsA content ranging between 84 and 130% compared to M82. Interestingly, the DHO genotypes also showed a significant mean increase of AsA content of 50% compared with IL 12-4 and of 45% compared to IL 7-3, indicating that in this case QTL pyramiding is effective in increasing AsA content. In addition, the DHO lines analyzed showed a higher AsA level compared to common commercial varieties,[2] for which a value of 20 mg/100 g FW was established as normal.[38] The high levels of AsA in DHOs may not only increase the nutritional value of these genotypes but might also have an effect on plant health, because AsA biosynthesis has been related to resistance to biotic and abiotic stresses.[39] Finally, the increase of AsA levels in the DHO lines compared to M82, but mostly compared to the two ILs, demonstrated that it is possible to have a positive interaction of the two wild chromosomal regions 7-3 and 12-4 on the level of this metabolite in tomato fruit.

**Phenolic Compounds.** The levels of total phenolic compounds were calculated in M82, ILs, and DHO lines. Results obtained from Folin−Ciocalteu's assay are reported in Figure 2. The cultivated line M82 showed a mean value of 18.12 ± 0.91 mg GAE/100 g FW. IL 12-4 did not exhibit a significant variation compared to M82, whereas IL 7-3 showed a significant increase (35.43%) compared to the cultivated genotype. The data obtained in the present study are in agreement with the levels reported for M82, IL 12-4, and IL 7-3 by Sacco et al.[24] Therefore, we could confirm the presence of a major QTL for fruit phenolic accumulation mapping to the introgressed region 3 of chromosome 7. DHO lines showed a

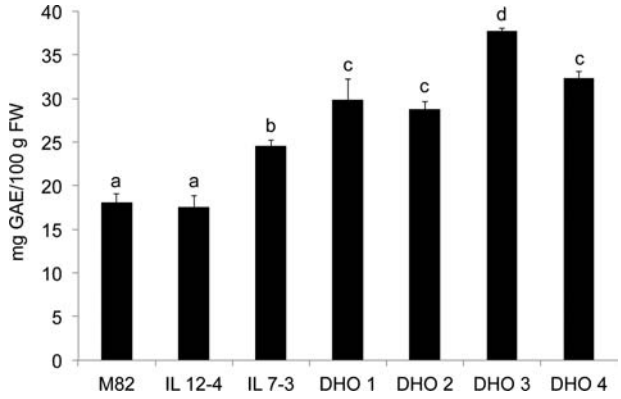


**Figure 2.** Total phenolics content (mg GAE/100 g FW) in tomato lines analyzed. Values are means ± SD ($n$ = 9). Values with different letters are significantly different ($p$ < 0.05).

significant increase of phenolics compared to the control M82 (ranging between 59.09 and 107.92%) and to IL 12-4 (ranging between 64.24 and 114.65%), but, interestingly, also compared to IL 7-3 (ranging between 17.46 and 53.52%). In the DHO lines the calculated amount of phenolic compounds ranged between 30 and 38 mg/GAE 100 g FW. These values are comparable with those observed by García-Valverde et al.[36] and by Martínez-Valverde et al.[40] in some tomato cultivated lines and higher than those reported by George et al.[35] and Hernández et al.[41]

Phenolic acids and flavonoids were also detected by HPLC (Table 2). Quercetin and gallic acid represent the majority of detected phenolics, whereas kampferol was not detected in any analyzed lines. These results are not in line with those reported by Slimestad et al.,[42] who observed that chlorogenic acid was the major phenolic acid and rutin the major flavonoid together with naringenin. This variability can be attributed mainly to the diverse genetic sources adopted in the different studies.[43] In particular, in our case quercetin was present in M82 at the mean level of 25.70 ± 4.26 mg QE/kg FW, and in IL lines it did not show significant variations compared to M82. By contrast, in DHOs a significant decrease ranging between 67.00 and 76.00% was found. Despite this decrease, values found for quercetin in the pyramided lines were higher than those reported by Vallverdú-Queralt et al.[44] in cultivated tomatoes. The same trend observed for quercetin in tested lines was observed for total flavonoids. The amount of total flavonoids in pyramided lines is comparable to that reported by Slimestad et al.[42] in different cultivars of tomato.

Total phenolic acids were significantly higher in IL 7-3 and DHO lines compared to M82 and IL 12-4. In particular, DHO genotypes showed an increase ranging between 94.11 and 154.16% compared to M82 and between 77.39 and 132.27% compared to IL 12-4. Interestingly, the DHO genotypes also showed a significant mean increase of total phenolic acid content up to 50.64% compared to IL 7-3. Frusciante et al.[2] established an optimum concentration of these compounds in tomato of 53.6 mg/kg FW. Therefore, the amount of total phenolic acid calculated in M82 in this study exceeded the recommended concentration of 53%, whereas in DHOs it exceeded this value of 197−288%.

There was also an increase in the level of gallic acid in the DHO genotypes compared to M82 and IL 12-4. These results are noteworthy because it has been demonstrated that gallic acid exerts a protective effect on diabetes due to its

Table 2. Flavonoids, Ferulic Acid, Gallic Acid, and Total Phenolic Acids Evaluated by HPLC[a]

| genotype | quercetin (mg QE/kg FW) | kampferol (mg QE/kg FW) | total flavonoids (mg QE/kg FW) | ferulic acid (mg FA/kg FW) | gallic acid (mg GAE/kg FW) | total phenolic acids (mg GAE/kg FW) |
|---|---|---|---|---|---|---|
| M82 | 25.70 ± 4.26a | nd | 27.53 ± 4.22a | 0.34 ± 0.05a | 78.48 ± 8.88a | 81.91 ± 9.86a |
| IL 12-4 | 23.82 ± 3.02a | nd | 26.52 ± 2.14a | 0.35 ± 0.03a | 86.02 ± 15.99a | 89.63 ± 15.48a |
| IL 7-3 | 21.57 ± 5.27a | nd | 28.00 ± 5.60a | 0.58 ± 0.05b | 129.99 ± 3.55b | 138.20 ± 4.51b |
| DHO1 | 8.13 ± 0.74b | nd | 12.87 ± 0.06b | 0.51 ± 0.09b | 147.58 ± 10.66b | 208.19 ± 18.79c |
| DHO2 | 8.43 ± 0.72b | nd | 12.81 ± 0.04b | 0.56 ± 0.15b | 98.58 ± 12.44a | 159.00 ± 3.76d |
| DHO3 | 6.19 ± 0.28b | nd | 9.73 ± 0.61b | 0.62 ± 0.07b | 131.25 ± 1.78b | 187.02 ± 15.58c |
| DHO4 | 6.55 ± 0.07b | nd | 11.29 ± 0.66b | 0.53 ± 0.01b | 147.58 ± 17.77b | 184.63 ± 19.63cd |

[a]Values are means ± SD ($n$ = 9). Values with different letters are significantly different ($p < 0.05$).

Table 3. Total Antioxidant Activity (TAA) and Its Lipophilic (LAA) and Hydrophilic (HAA) Fractions Evaluated by ABTS and FRAP Analyses[a]

| genotype | ABTS LAA (μmol TE/100 g FW) | ABTS HAA (μmol TE/100 g FW) | FRAP HAA (μmol TE/100 g FW) | TAA (μmol TE/100 g FW) |
|---|---|---|---|---|
| M82 | 104.79 ± 3.38a | 131.61 ± 13.34a | 115.36 ± 11.89a | 236.40 ± 16.72a |
| IL 12-4 | 83.27 ± 2.74b | 153.21 ± 5.17b | 154.52 ± 15.72b | 236.48 ± 7.91a |
| IL 7-3 | 112.05 ± 3.27a | 145.43 ± 3.10ab | 143.93 ± 4.57b | 257.48 ± 6.37a |
| DHO1 | 84.01 ± 3.88b | 183.86 ± 6.42c | 179.64 ± 2.63c | 267.87 ± 10.30a |
| DHO2 | 85.13 ± 5.80b | 253.98 ± 3.87d | 229.14 ± 3.18c | 339.11 ± 9.67b |
| DHO3 | 79.76 ± 4.76b | 246.07 ± 4.40d | 207.86 ± 4.02c | 325.83 ± 9.16b |
| DHO4 | 88.75 ± 0.50bc | 262.73 ± 3.38d | 289.71 ± 9.66d | 351.48 ± 3.88bc |

[a]Values are means ± SD ($n$ = 9). Values with different letters are significantly different ($p < 0.05$).

antihyperglycemic and antilipid peroxidative capacity as well as its strong antioxidant power.[45] In addition, a significant increase in the level of ferulic acid in the DHO lines compared to the cultivated line and IL 12-4 was detected. Also, the increase of ferulic acid in the DHO lines is significant from a nutritional point of view, because a positive effect derived from the combination of ferulic acid with AsA, in particular associated with the protection of the myocardium, has been demonstrated.[46]

Taken together, the data obtained from two independent assay procedures (Folin−Ciocalteau and phenolics estimation by HPLC-UV procedure) clearly indicated that the amount of phenolic compounds, in particular of phenolic acids, was increased in DHOs compared to ILs and M82, and above all compared to IL 7-3. This suggested that on the region 12-4 there are wild alleles that synergistically interact with those mapping to the 7-3 region, resulting in increased phenolic levels. On the contrary, the decrease of total flavonoid in the DHO lines must be due to negative interactions between the two wild regions. These findings highlight that detailed information regarding the interaction effects between detected QTLs and between QTLs and the recipient background genotype are necessary to design an efficient pyramiding strategy for increasing tomato nutritional quality.

**Antioxidant Activity.** Results regarding lipophilic (LAA), hydrophilic (HAA), and total antioxidant activity (TAA) of genotypes analyzed are reported in Table 3. In the cultivated M82 line, the LAA antioxidant activity showed a mean level of 104.79 ± 3.38 μmol TE/100 g FW. A significant 20% lower value of LAA was calculated in genotype IL 12-4 compared to the cultivated line, whereas in IL 7-3 the mean value of LAA (112.05 ± 3.27 μmol TE/100 g FW) was comparable to the value obtained in M82. In DHO lines, the detected values were not significantly different from those of IL 12-4 and showed a decrease compared to M82 ranging between 15.30 and 23.88%. Our LAA results confirmed the data obtained for carotenoids that constitute the major fraction of lipophilic compounds in tomato fruit. Nevertheless, the LAA decrease in the DHO lines and in IL 12-4 (estimated by ABTS) was lower than the decrease calculated for total carotenoids and lycopene. This is probably due to the presence of other lipophilic compounds such as tocopherol and lipophilic phenolics, as well as to the synergic effect of compounds contributing to LAA.[47]

The HAA determined by FRAP and ABTS tests in M82 showed values of 115.36 ± 11.89 and 131.61 ± 13.34 μmol TE/100 g FW, respectively. The parental lines IL 7-3 and IL 12-4 showed increased values of HAA compared to the cultivated line. Values calculated in DHO lines were significantly different from M82, with a mean increase of 96% by FRAP test and 80% by ABTS test. Compared to IL 12-4, DHO genotypes revealed significant mean increases of 46.63 and 54.46% according to FRAP and ABTS tests, respectively, and compared to IL 7-3 mean increases of 57.43 and 62.72% in the two assays. The mean contribution of HAA to TAA was estimated to be 55.67% in M82, 64.78% in IL 12-4, and 56.48% in IL 7-3, whereas in DHOs these percentages were between 68.63 and 75.52%. Overall, the TAA in DHOs revealed significant increased values in comparison to the cultivated M82 and IL lines, and this increase was attributed mostly to a higher contribution of HAA to TAA. Our data on HAA and TAA were comparable to those reported by Cano et al.,[48] and the contribution of HAA to TAA was comparable to that found by Kotíková et al[3] and Arnao et al.[49]

Comprehensively, our data demonstrated that there is a positive interaction between the two wild regions 7-3 and 12-4 that caused an increment of HAA. On the contrary, there is a negative influence of the wild alleles of the region 12-4 on LAA. Therefore, the improvement of the nutritional quality in DHO lines can be attributed mostly to the increment of the hydrophilic fraction that includes the majority of tomato phytochemicals, despite a general decrease of the lipophilic fraction.

Accordingly, by the PCA we observed that the separation of DHOs from M82 and from the two ILs is mainly due to the

hydrophilic fraction (Figure 3). Indeed, PC1 explained 71.92% of the variation in the data and was associated positively with

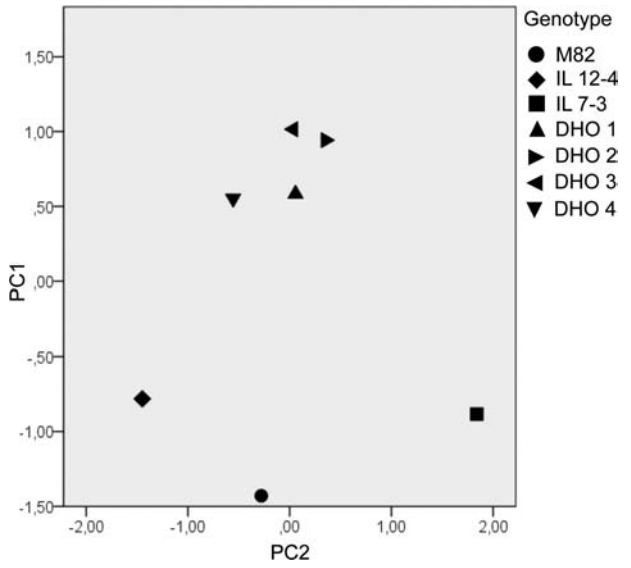


**Figure 3.** Principal component analysis (PCA) of metabolic profiles of analyzed genotypes.

AsA, phenolic acids, gallic acid, ferulic acid, total phenolics, total flavonoids, quercetin, hydrophilic ABTS, and FRAP (loading values > 0.60). PC2 explained 18.09% of the variation in the data and was associated positively with total carotenoids, lycopene, $\beta$-carotene, and lipophilic ABTS (loading values > 0.60). The PCA output shows an evident separation of both IL 12-4 and IL 7-3 from M82, mainly attributable to PC2 that included the lipophilic compounds and their contribution to the antioxidant activity. DHOs were well separated from the parental lines for both PC1 and PC2 and from M82 mainly for PC1, which represented the hydrophilic fraction of the analyzed metabolites and their relative antioxidant activity.

**Effects of Tomato Extracts on Cell Viability.** Finally, the biological activity of extracts from M82, IL 7-3, IL 12-4, and DHO has been tested in our study by using two normal cell lines (Figure 4): a primary human cell line derived from kidney (HRCE) and an immortalized murine fibroblast cell line (BALB/3T3). The viability of cells treated for 48 h with increasing amounts of tomato extracts was tested by the MTT reduction assay, as an indicator of metabolically active cells. In Figure 4 the results of dose−response experiments are shown. The values are the average of three independent experiments, each carried out with triplicate determinations. We observed that M82, IL 7-3, and IL 12-4 extracts had a cytotoxic effect on the HRCE cells and on the BALB/3T3 cells, which was very evident at the highest concentration tested. On the contrary, DHO extracts had no effect, independent of the concentration used on primary cells (HRCE cells), and small effects only at the highest concentration used (24 mg/mL) on immortalized normal cells (BALB/3T3 cells). The cytotoxic effect of M82, IL 7-3, and IL 12-4 extracts could be due to the presence in these genotypes of higher levels of compounds with reported antiproliferative activity such as flavonoids[50] compared with the lower levels observed in the DHO lines (Table 2). In fact, it has been demonstrated that exposure to high levels of flavonoids may potentially damage cells.[51] To test the anticarcinogenic potential of the tomato genotypes, we performed the same experiments using cancer cell lines of the same anatomical origin of normal cells (Figure 5). We examined the inhibition of the rapidly proliferating human cancer cell lines (HeLa cells), of BALB/3T3 murine fibroblasts transformed with SV40 virus, and of human renal cancer cell lines (Hek293). As shown in Figure 5, we observed a strong and selective cytotoxic effect of DHO extracts, particularly evident at the highest concentration used on all of the cancer cell lines tested. Generally, a lower cytotoxic effect was observed with the M82, IL 7-3, and IL 12-4 extracts. The effects of DHO extracts on cancer cells could be also dependent on the content of total phenolic acids[54] and on the presence of gallic acid, a compound known to have a selective cytotoxic effect on cancer cells.[55] The mechanism for the known selective effects of plant phenolics on cancer cell growth is still under debate and may also involve differences in gene expression between normal and tumor cell lines.[50] At low concentrations all of the tomato extracts caused an initial increase in HeLa and SV-T2 cell growth followed by inhibition of growth at higher concentration. This result was not observed on Hek293 cells. The proliferative effect here observed has been reported for several plant extracts used at low concentration on different cancer cells.[26,52,53] This could be due to the fact that cancer cells are actively proliferating; thus, the presence of nutrients in the plant extracts in combination with low levels and/or low

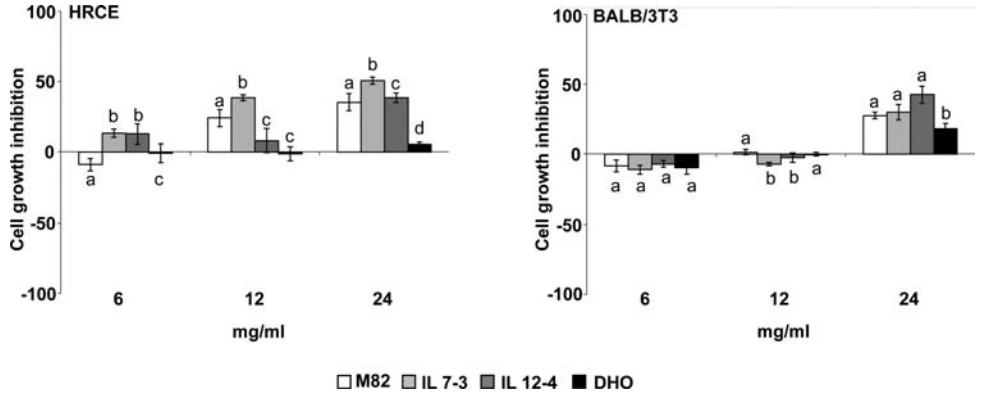


**Figure 4.** Dose−response curves obtained upon treatment of HRCE and BALB/3T3 cells with extracts from M82, IL 7-3, IL 12-4, or DHO after 48 h. Cell growth inhibition was assessed by the MTT assay and expressed as described under Materials and Methods. All values are given as means ± SD ($n \geq 3$). Within each treatment, values with different letters are significantly different ($p < 0.05$).

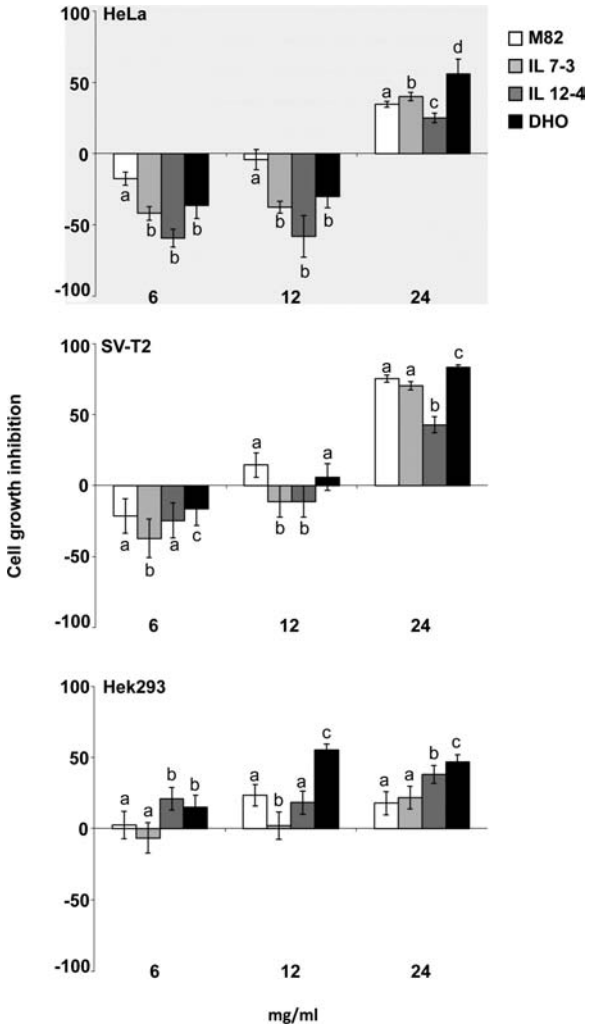


**Figure 5.** Dose–response curves obtained upon treatment of HeLa, SV-T2, and Hek 293 cells with extracts from M82, IL 7-3, IL 12-4, or DHO after 48 h. Cell growth inhibition was assessed by the MTT assay and expressed as described under Materials and Methods. All values are given as means ± SD ($n \geq 3$). Within each treatment values with different letters are significantly different ($p < 0.05$).

susceptibility to active compounds may have a positive effect on cell growth, as suggested by Choi et al.[26]

In conclusion, the combination of multiple QTLs, QTL pyramiding, offers a straightforward and useful way for improving target traits in crop plants.[56] Here we demonstrated that it is possible to incorporate favorable wild-species QTLs in the same genetic background to obtain genotypes with a reproducibly higher nutritional value. In particular, we have shown that QTL pyramiding resulted in genotypes with higher AsA and phenolics and increased the total antioxidant power. In addition, crude extracts from the pyramided genotypes showed antiproliferative activity only on human cancer cells, whereas they did not affect the growth of normal cells. On the contrary, extracts from the cultivated genotypes and the ILs did not show the same selective cytotoxic effect but inhibited proliferation of normal cells. The pyramided QTLs should now be transferred in cultivated genetic backgrounds different from M82 to verify that they might exert the same increase of the total antioxidant activity and the same selective cytotoxic effect on aggressive cancer cells. In particular, because compounds such as vitamin C (that are increased in DHO lines) are heat-labile, the pyramiding strategy here used to increase tomato nutritional value could be applied to varieties that are used for fresh consumption.

Consequently, these novel genotypes could be used as genetic material for breeding schemes aimed at generating new hybrids or improved varieties with higher nutritional levels. However, to use these DHO lines as breeding materials, it will be important to understand if introgressed wild regions determine taste alterations and/or allergenic effects. Finally, further studies aimed at dissecting the introgressed region into sublines, as well as in-depth analyses of candidate genes, will be necessary to elucidate the underlying mechanisms of the selected QTLs. These studies will help also to disrupt the linkage between the genes that promote AsA content and those that contribute to low carotenoid levels in region 4 of chromosome 12, thus facilitating the use of IL 12-4 as a source of favorable alleles for higher AsA.

## AUTHOR INFORMATION

### Corresponding Author

*(A.B.) E-mail: ambarone@unina.it. Phone: +39-081-2539491. Fax: +39-081-2539486.

### Author Contributions

‖M.M.R. and A.R. contributed equally to this work.

### Funding

We thank GenoPOM-pro Project (PON02_00395_3082360) for financial support of the activities reported in the present study and for its contribution to improve our scientific knowledge.

### Notes

The authors declare no competing financial interest.

## ABBREVIATIONS USED

ABTS, 2,2′-azinobis(3-ethylbenzothiazoline-6-sulfonic acid); AsA, ascorbic acid; CNCD, chronic noncommunicable diseases; CVD, cardiovascular diseases; dd, double distilled; DHO, double homozygote; FRAP, ferric reducing/antioxidant power; FW, fresh weight; GAE, gallic acid equivalents; HAA, hydrophilic antioxidant activity; IL, introgression line; LAA, lipophilic antioxidant activity; LDL, low-density lipoprotein; MTT, 3-(4,5-dimethylthiazol-2-yl)-2,5-diphenyltetrazolium bromide; PCA, principal component analysis; QE, quercetin equivalents; QTL, quantitative trait locus; ROS, reactive oxygen species; TAA, total antioxidant activity; TCA, trichloroacetic acid; TE, Trolox equivalents; TGRC, Tomato Genetics Resource Centre; TPTZ, 2,4,6-tripyridyl-*s*-triazine

## REFERENCES

(1) Canene-Adams, K.; Campbell, J. K.; Zaripheh, S.; Jeffery, E. H.; Erdman, J. W., Jr. The tomato as a functional food. *J. Nutr.* **2005**, *135*, 1226–1230.

(2) Frusciante, L.; Carli, P.; Ercolano, M. R.; Pernice, R.; Di Matteo, A.; Fogliano, V.; Pellegrini, N. Antioxidant nutritional quality of tomato. *Mol. Nutr. Food Res.* **2007**, *51*, 609–617.

(3) Kotíková, Z.; Lachman, J.; Hejtmánková, A.; Hejtmánková, K. Determination of antioxidant activity and antioxidant content in tomato varieties and evaluation of mutual interactions between antioxidants. *Food Sci. Technol.* **2011**, *44*, 1703–1710.

(4) Santangelo, C.; Varì, R.; Scazzocchio, B.; Di Benedetto, R.; Filasi, C.; Masella, R. Polyphenols, intracellular signalling and inflammation. *Ann. Ist. Super. Sanita* **2007**, *43*, 394–405.

(5) D'Introno, A.; Paradiso, A.; Scoditti, E.; D'Amico, L.; De Paolis, A.; Carluccio, M. A.; Nicoletti, I.; DeGara, L.; Santino, A.; Giovinazzo,

G. Antioxidant and anti-inflammatory properties of tomato fruits synthesizing different amounts of stilbenes. *Plant Biotechnol. J.* **2009**, *7*, 422−429.
(6) Kauss, T.; Moynet, D.; Rambert, J. Rutoside decreases human macrophage-derived inflammatory mediators and improves clinical signs in adjuvant-induced arthritis. *Arthritis Res. Ther.* **2008**, *10*, R19.
(7) González, R.; Ballester, I.; López-Posadas, R.; Suárez, M. D.; Zarzuelo, A.; Martínez-Augustin, O.; De Medina, F. S. Effects of flavonoids and other polyphenols on inflammation. *Crit. Rev. Food Sci. Nutr.* **2011**, *51*, 331−362.
(8) Raiola, A.; Rigano, M. M.; Calafiore, R.; Frusciante, L.; Barone, A. Enhancing the health-promoting effects of tomato fruit for biofortified food. *Mediators Inflamm.* **2014**, DOI: 10.1155/2014/139873.
(9) Moco, S.; Capanoglu, E.; Tikunov, Y.; Bino, R. J.; Boyacioglu, D.; Hall, R. D.; Vervoort, J.; De Vos, R. C. Tissue specialization at the metabolite level is perceived during the development of tomato fruit. *J. Exp. Bot.* **2007**, *58*, 4131−4146.
(10) Lodovici, M.; Guglielmi, F.; Meoni, M.; Dolara, P. Effect of natural phenolic acids on DNA oxidation in vitro. *Food Chem. Toxicol.* **2001**, *39*, 1205−1210.
(11) Naidu, K. A. Vitamin C in human health and disease is still a mystery? An overview. *Nutr. J.* **2003**, *21*, 7.
(12) Riso, P.; Visioli, F.; Erba, D.; Testolin, G.; Porrini, M. Lycopene and vitamin C concentrations increase in plasma and lymphocytes after tomato intake. Effects on cellular antioxidant protection. *Eur. J. Clin. Nutr.* **2004**, *58*, 1350−1358.
(13) Rao, A. V.; Rao, L. G. Carotenoids and human health. *Pharmacol. Res.* **2007**, *55*, 207−216.
(14) Frary, A.; Göl, D.; Keleş, D.; Ökmen, B.; Pınar, H.; Şığva, H. O.; Yemenicioğlu, A.; Doğanlar, S. Salt tolerance in *Solanum pennellii*: antioxidant response and related QTL. *BMC Plant Biol.* **2010**, *10*, 58.
(15) Eshed, Y.; Zamir, D. An introgression line population of *Lycopersicon pennellii* in the cultivated tomato enables the identification and fine mapping of yield-associated QTL. *Genetics* **1995**, *141*, 1147−1162.
(16) Gur, A.; Zamir, D. Unused natural variation can lift yield barriers in plant breeding. *PLoS Biol.* **2004**, *2*, No. e245.
(17) Rousseaux, M. C.; Jones, C. M.; Adams, D.; Chetelat, R.; Bennett, A.; Powell, A. QTL analysis of fruit antioxidants in tomato using *Lycopersicon pennellii* introgression lines. *Theor. Appl. Genet.* **2005**, *111*, 1396−1408.
(18) Stevens, R.; Buret, M.; Garchery, C.; Carretero, Y.; Causse, M. Technique for rapid small-scale analysis of vitamin C levels in fruit and application to a tomato mutant collection. *J. Agric. Food Chem.* **2006**, *54*, 6159−6165.
(19) Di Matteo, A.; Sacco, A.; Anacleria, M.; Pezzetti, M.; Delledonne, M.; Ferrarini, A.; Frusciante, L.; Barone, A. The ascorbic acid content of tomato fruits is associated with the expression of genes involved in pectin degradation. *BMC Plant Biol.* **2010**, *10*, 163.
(20) Di Matteo, A.; Sacco, A.; Ruggieri, V.; Trotta, N.; Nunziata, A.; Barone, A. Transcriptional network controlling antioxidants in tomato fruit. *J. Biotechnol.* **2010**, *150S*, 111−112.
(21) Di Matteo, A.; Ruggieri, V.; Sacco, A.; Rigano, M. M.; Carriero, F.; Bolger, A.; Fernie, A. R.; Frusciante, L.; Barone, A. Identification of candidate genes for phenolics accumulation in tomato fruit. *Plant Sci.* **2013**, *205*−*206*, 87−96.
(22) Gur, A.; Semel, Y.; Osorio, S.; Friedmann, M.; Seekh, S.; Ghareeb, B.; Mohammad, A.; Pleban, T.; Gera, G.; Fernie, A. R.; Zamir, D. Yield quantitative trait loci from wild tomato are predominately expressed by the shoot. *Theor. Appl. Genet.* **2011**, *122*, 405−420.
(23) http://www.ptab.org/ranking9.htm.
(24) Sacco, A.; Di Matteo, A.; Lombardi, N.; Trotta, N.; Punzo, B.; Mari, A.; Barone, A. Quantitative trait loci pyramiding for fruit quality traits in tomato. *Mol. Breed.* **2013**, *31*, 217−222.
(25) Tomato Genetics Resource Centre (TGRC), http://tgrc.ucdavis.edu/.
(26) Choi, S. H.; Kim, H. R.; Kim, H. J.; Lee, I. S.; Kozukue, N.; Levin, C. E.; Friedman, M. Free amino acid and phenolic contents and antioxidative and cancer cell-inhibiting activities of extracts of 11 greenhouse-grown tomato varieties and 13 tomato-based foods. *J. Agric. Food Chem.* **2011**, *59*, 12801−12814.
(27) Wellburn, A. R. The spectral determination of chlorophylls *a* and *b*, as well as total carotenoids, using various solvents with spectrophotometers of different resolution. *J. Plant Physiol.* **1994**, *144*, 307−313.
(28) Zouari, I.; Salvioli, A.; Chialva, M.; Novero, M.; Miozzi, L.; Tenore, G. C.; Bagnaresi, P.; Bonfante, P. From root to fruit: RNA-Seq analysis shows that arbuscular mycorrhizal simbiosi may affect tomato fruit metabolism. *BMC Genomics* **2014**, *15*, 1−19.
(29) Singleton, V. L.; Rossi, J. A. Colorimetry of total phenolics with phosphomolybdic phosphotungstic acid reagents. *Am. J. Enol. Vitic.* **1965**, *16*, 144−158.
(30) Ferracane, R.; Graziani, G.; Gallo, M.; Fogliano, V.; Ritieni, A. Metabolic profile of the bioactive compounds of burdock (*Arctium lappa*) seeds, roots and leaves. *J. Pharm. Biomed. Anal.* **2010**, *51*, 399−404.
(31) Benzie, I. F. F.; Strain, J. J. The ferric reducing ability of plasma (FRAP) as a measure of "antioxidant power": the FRAP assay. *Anal. Biochem.* **1996**, *239*, 70−76.
(32) Miller, J. N.; Rice-Evans, C. A. Factors influencing the antioxidant activity determined by the ABTS$^{\bullet+}$ radical cation assay. *Free Radical Res.* **1997**, *26*, 195−199.
(33) Tomato Functional Genomics database, 2010, http://solgenomics.net/ted/cgibin/TFGD/miame/experiment.cgi?ID=E037.
(34) Kinkade, M. P.; Foolad, M. R. Validation and fine mapping of lyc12.1, a QTL for increased tomato fruit lycopene content. *Theor. Appl. Genet.* **2013**, *126*, 2163−2175.
(35) George, B.; Kaur, C.; Khurdiya, D. S.; Kapoor, H. C. Antioxidant in tomato (*Lycopersicum esculentum*) as a function of genotype. *Food Chem.* **2004**, *84*, 45−51.
(36) García-Valverde, V.; Navarro-Gonzáles, I.; García-Alonso, J.; Periago, M. J. Antioxidant bioactive compounds in selected industrial processing and fresh consumption tomato cultivars. *Food Bioprocess. Technol.* **2013**, *6*, 391−402.
(37) Leonardi, C.; Ambrosino, P.; Esposito, F.; Fogliano, V. Antioxidative activity and carotenoid and tomatine contents in different typologies of fresh consumption tomatoes. *J. Agric. Food Chem.* **2000**, *48*, 4723−4727.
(38) Gould, W. A. Composition of tomatoes. In *Tomato Production, Processing & Technology*, 3rd ed.; Elsevier: Baltimore, MD, USA, 1992; pp 433−447.
(39) Gallie, D. R. The role of L-ascorbic acid recycling in responding to environmental stress and in promoting plant growth. *J. Exp. Bot.* **2013**, *64*, 433−443.
(40) Martínez-Valverde, I.; Periago, M. J.; Provan, G.; Chesson, A. Phenolic compounds, lycopene and antioxidant activity in commercial varieties of tomato (*Lycopersicum esculentum* Mill). *J. Sci. Food Agric.* **2002**, *82*, 323−330.
(41) Hernández, M.; Rodríguez, E.; Díaz, C. Free hydroxycinnamic acids, licopene and color parameters in tomato cultivars. *J. Agric. Food Chem.* **2007**, *55*, 8604−8615.
(42) Slimestad, R.; Verheul, M. Review of flavonoids and other phenolics from fruits of different tomato (*Lycopersicon esculentum* Mill.) cultivars. *J. Sci. Food Agric.* **2009**, *89*, 1255−1270.
(43) Rosales, M. A.; Cervilla, L. M.; Sánchez-Rodríguez, E.; Rubio-Wilhelmi, M. del M.; Blasco, B.; Ríos, J. J.; Soriano, T.; Castilla, N.; Romero, L.; Ruiz, J. M. The effect of environmental conditions on nutritional quality of cherry tomato fruits: evaluation of two experimental Mediterranean greenhouses. *J. Sci. Food Agric.* **2011**, *91*, 1014−1021.
(44) Vallverdú-Queralt, A.; Odriozola-Serrano, I.; Oms-Oliu, G.; Lamuela-Raventós, R. M.; Elez-Martínez, P.; Martín-Belloso, O. Changes in the polyphenol profile of tomato juices processed by pulsed electric fields. *J. Agric. Food Chem.* **2012**, *60*, 9667−9672.
(45) Punithavathi, V. R.; Prince, P. S. M.; Kumar, R.; Selvakumari, J. Antihyperglycaemic, antilipid peroxidative and antioxidant effects of

gallic acid on streptozotocin induced diabetic Wistar rats. *Eur. J. Pharmacol.* **2011**, *650*, 465−471.
(46) Yogeeta, S. K.; Hanumantra, R. B. R.; Gnanapragasam, A.; Senthilkumar, S.; Subhashini, R.; Devaki, T. Attenuation of abnormalities in the lipid metabolism during experimental myocardial infarction induced by isoproterenol in rats: beneficial effect of ferulic acid and ascorbic acid. *Basic Clin. Pharmacol. Toxicol.* **2006**, *98*, 467−472.
(47) Zanfini, A.; Corbini, G.; La Rosa, C.; Dreassi, E. Antioxidant activity of tomato lipophilic extracts and interactions between carotenoids and α-tocopherol in synthetic mixtures. *Food Sci. Technol.* **2010**, *43*, 67−72.
(48) Cano, A.; Acosta, M.; Arnao, M. B. Hydrophilic and lipophilic antioxidant activity changes during on-vine ripening of tomatoes (*Lycopersicon esculentum* Mill.). *Postharvest Biol. Technol.* **2003**, *28*, 59−65.
(49) Arnao, M. B.; Cano, A.; Acosta, M. The hydrophilic and lipophilic contribution to total antioxidant activity. *Food Chem.* **2001**, *73*, 239−244.
(50) Mazzucato, A.; Willems, D.; Bernini, R.; Picarella, M. E.; Santangelo, E.; Ruiu, F.; Tilesi, F.; Soressi, G. P. Novel phenotypes related to the breeding of purple-fruited tomatoes and effect of peel extracts on human cancer cell proliferation. *Plant Physiol. Biochem.* **2013**, *72*, 125−133.
(51) Skibola, C. F.; Smith, M. T. Potential health impacts of excessive flavonoid intake. *Free Radical Biol. Med.* **2000**, *29*, 375−383.
(52) Friedman, M.; Levin, C. E.; Lee, S.-U.; Kim, H.-J.; Lee, I.-S.; Byun, J.-O.; Kozukue, N. Tomatine-containing green tomato extracts inhibit growth of human breast, colon, liver, and stomach cancer cells. *J. Agric. Food Chem.* **2009**, *57*, 5727−5733.
(53) Weaver, J.; Briscoe, T.; Hou, M.; Goodman, C.; Kata, S.; Ross, H.; McDougall, G.; Stewart, D.; Riches, A. Strawberry polyphenols are equally cytotoxic to tumorigenic and normal human breast and prostate cell lines. *Int. J. Oncol.* **2009**, *34*, 777−786.
(54) Saunders, C. The anti-proliferative effect of different tomato varieties on the human colon-adenocarcinoma cells. *Biosci. Horizons* **2009**, *2*, 172−179.
(55) Russel, L. H., Jr.; Mazzio, E.; Badisa, R. B.; Zhu, Z.; Agharahimi, M.; Millington, D. J.; Goodman, C. B. Differential cytotoxicity of triphala and its phenolic constituent gallic acid on human prostate cancer LNCap and normal cells. *Anticancer Res.* **2011**, *31*, 3739−3746.
(56) Adachi, S.; Baptista, L. Z.; Sueyoshi, T.; Murata, K.; Yamamoto, T.; Ebitani, T.; Ookawa, T.; Hirasawa, T. Introgression of two chromosome regions for leaf photosynthesis from an indica rice into the genetic background of a japonica rice. *J. Exp. Bot.* **2014**, *65*, 2049−2056.

effect, in most experiments, the juice pH was modified using citrate buffer salts at a constant ionic strength. Given the possible role of double-layer interactions between particles on cloud stability, juice ionic strength could well be an important parameter in clarification rates.

Through research presented in this paper, we examine particle interactions as a function of pH, via static light scattering, turbidity, and $\zeta$ potential, and discuss the role of interparticle energy barriers in the observed cloud stability. We seek to elucidate cloud stability in low-acid carrot juice, which may have inherent properties different from those of juices previously studied that are naturally more acidic.

## MATERIALS AND METHODS

**Material Sourcing.** Refrigerated fresh carrot juice ("ready to drink"), commercially produced in Bakersfield, CA, was purchased from the local grocery store and used for all experiments. Juices prepared by us in the laboratory could not replicate the qualitative features and consistency of the particle size distributions of purchased fresh carrot juices, and thus, a study on commercial juice was preferred. According to the manufacturer, the juice was produced from finely ground fresh carrots that were separated into juice and pomace; the juice was then pasteurized, packed, stored, and distributed under refrigeration. There were no added ingredients, and the juice was not acidified. As indicated by the manufacturer, the average total solids of the commercial juice was 10−20% and the soluble solids was 5−6%. The weight fraction of all solids in carrot juice was estimated in our laboratory to be 0.09 g/g, by drying the juice in a 56 °C oven and weighing the residual. From this concentration, the amount of soluble solids in carrot juice was subtracted, to give a value of ∼0.04 g of insoluble solids/g of juice.[18] Turbidity of the juice was measured in our laboratory using ultraviolet (UV) absorption at 660 nm to be 14 $cm^{-1}$. The range of pH for carrots used by the manufacturer was reported to be 5.85−6.45, and the pH of the unbuffered juice was measured by us to be 6.2.

Citric acid monohydrate, sodium citrate, sodium chloride, and calcium chloride were obtained from Fisher Scientific (Fair Lawn, NJ).

**Acidification.** Citric acid and sodium citrate were added directly to commercial carrot juice to obtain seven samples of carrot juice with 0.1 M buffer concentrations and pH values spanning 3.5−6.1. Buffer salts were directly added to the carrot juice to ensure consistent ionic concentrations between the samples. All measurements were taken on the same day after 3 days of storage at 7 °C to ensure that particle flocculation was complete.

Certain juice samples were acidified by adding various small volumes of 2 M citric acid solution to commercial carrot juice, to achieve the desired pH value.

To explore the effect of neutralizing acidified juice back to its natural pH (6.2), 40 mL aliquots of juice were acidified with 2 M citric acid to pH 3.0 and left to sit for 1 day to allow for flocculation to occur. The juice was then neutralized back to pH 6.2 using 2 M NaOH.

**Relative Sediment Height.** Relative sediment height, also known as the sedimentation test, is a measure of the quantity of visible settling that occurs in the juice.[7,19] It is the height ($H_{sediment}$) of the cloud sediment divided by the total height ($H_{total}$) of the juice in a vial.

Roughly 5 mL of each juice sample was placed in a 7 mL glass vial with a screw cap and allowed to remain undisturbed, except for gentle transportation of the vials from the refrigerator to the laboratory bench for measurements. The height of the liquid in the vials was between 25 and 30 mm. A caliper was used to make height measurements in triplicate.

**Relative Turbidity.** Relative turbidity is a spectrophotometric method to determine cloud stability by comparing the turbidity in a juice sample before and after centrifugation.[3,5,7,12,20] For the carrot juices examined here, absorbance at 660 nm was used as the measure of juice turbidity. At this wavelength, absorbance is predominantly determined by the scattering as a result of the particles rather than specific chemical absorption.[21] Relative turbidities were determined by measuring the absorbance values for the homogeneously mixed whole juice and for the supernatants obtained after centrifugation (4200$g$ for 15 min at 20 °C). When absorbance values measured in standard 1 cm cuvettes were unacceptably high, shorter path length cuvettes (0.5 mm for whole juice and 5.0 mm for juice supernatants) were used. The absorbance of the whole commercial juice was determined to be 0.68, and the supernatant was 0.81. Turbidity ($\tau$) was calculated as the absorbance divided by the path length used for measurement. Relative turbidities (expressed as a percentage) were calculated as $\tau_{super}/\tau_{total} \times 100$, with $\tau_{super}$ obtained from the centrifuged supernatant layer and $\tau_{total}$ obtained from the uncentrifuged whole juice. Measurements were performed in triplicate.

**Particle Size Determination.** Static light scattering was used to measure the average particle size.[3−5,7,11,22] Measurements were performed using a Microtrac S3500 (Montgomeryville, PA). Results were obtained as the volume fraction of particles contained within a discrete size range (bin). The mean diameter was determined as a volume average:

$$D_{4,3} = \frac{\sum_i n_i d_i^4}{\sum_i n_i d_i^3} \quad (1)$$

where $D_{4,3}$ is the volume mean diameter, $n_i$ is the number of particles in bin $i$, and $d_i$ is their diameter. Carrot juice was inverted gently 10 times to ensure even distribution of particles and then added to the instrument sample port, which was operated at a flow rate of 15% of the maximum. Particles were assumed to be irregular in shape and absorbing, and a refractive index value for water of 1.333 was used. Three replicates were measured for each sample.

**$\zeta$ Potential.** Using a Malvern Zetasizer (Westborough, PA), the $\zeta$ potential ($\zeta$) of the cloud particles was determined by measuring the electrophoretic mobility ($\mu$) of the particles in the presence of an electric field. Carrot juice was diluted 1:40 with deionized water to ensure that it was in the appropriate concentration range for measurements, which in our experiments corresponded to a signal intensity of ∼100 kcps. The dielectric constant and viscosity of the continuous phase were set to 78.3 F/m and 0.8903 mPa s, respectively, at 25 °C. A minimum of 10 analysis runs were performed for each sample, the values for which were averaged together and analyzed via Smoluchowski's equation, $\zeta = \varepsilon\mu/\eta$, where $\varepsilon$ is the dielectric constant and $\eta$ is the viscosity of the continuous phase. This model requires the diffuse double layer to be thin compared to the particle radius. Three replicates were taken for each sample.

## RESULTS AND DISCUSSION

**Relative Sediment Height and Relative Turbidity.** Cloud stability decreased as juice pH was lowered by the use of citrate buffer. After 3 days of refrigerated storage, there was almost no precipitate in the buffered control juice (pH 6.1) nor in the juices at the two next highest pH values, whereas a separate sediment layer was seen in more acidified juices (Figure 1). The extent of the separation was quantified by

**Figure 1.** Cloud sedimentation in buffered commercial carrot juice after 3 days in refrigerated storage. pH 6.1 is the control buffered juice.

measuring the height of the sediment layer relative to the total juice height (Figure 2). This relative height increased with decreasing pH. These results were consistent with turbidity measurements of the supernatant before and after centrifugation (Figure 2). With a reduction in juice pH, the relative turbidity decreased monotonically, indicating that, most likely because of particle aggregation, particles sedimented more readily in lower pH samples upon centrifugation. The agreement between the results of relative sediment height and relative turbidity demonstrate that either method would be an appropriate way to measure the cloud instability in carrot juice. Results in Figure 1 also demonstrate that, as previously noted by Reiter et al.,[5] formation of a sediment in this experiment was not accompanied by the loss of visible turbidity in the supernatant, except to a small extent at the two lowest pH values.

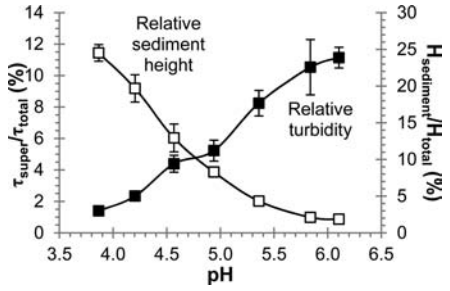


**Figure 2.** (■) Relative turbidity ($\tau_{super}/\tau_{total}$) and (□) relative sediment height ($H_{sediment}/H_{total}$) as a function of pH of commercial carrot juice with buffer salts added.

**Particle Size Distributions.** Particle size distributions were measured for the unbuffered juice at pH 6.2 (Figure 3a) as well as the samples with added buffers (panels b–h of Figure 3).

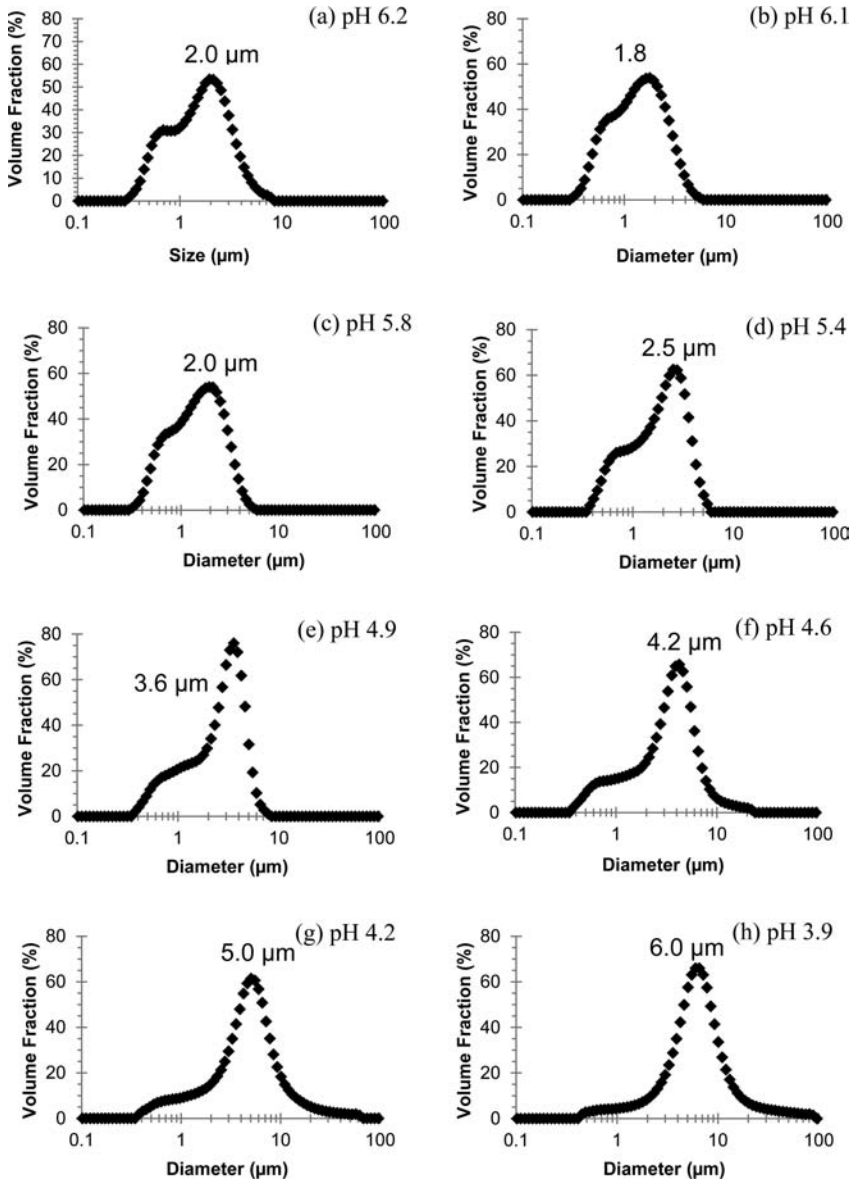


**Figure 3.** Particle size distribution graphs showing the volume fraction with the associated particle diameter (±0.04 μm) of (a) control unbuffered juice (pH 6.2) and (b–h) juices with added buffer salts at (b) pH 6.1, (c) pH 5.8, (d) pH 5.4, (e) pH 4.9, (f) pH 4.6, (g) pH 4.2, and (h) pH 3.9. The particle diameter at the maximum volume fraction is indicated above the main peak.

The distribution for the control buffered juice (Figure 3b, pH 6.1), shows evidence of two overlapping modes: one with particle sizes of a few micrometers and the other with sub-micrometer sizes. Particles of diameters less than 10 $\mu$m only were observed in the control juices, in contrast to typical juices analyzed by Reiter et al.,[5] which had particle sizes ranging from 0.1 to 700 $\mu$m. Thus, we did not observe a "coarse particle" fraction (defined as containing particles with a diameter of >10 $\mu$m),[5] and effects of acidification on fine particles (<10 $\mu$m) could be monitored directly (Figure 3). The average particle size ($D_{4,3}$) of the control juice (pH 6.1) was approximately 2 $\mu$m.

Juices with buffer at high pH levels, i.e., close to the natural juice pH, had particle distributions that were similar to the control (Figure 3c). As pH decreased, the main peak shifted toward larger particle sizes and increased in height. These particle distributions also exhibited a shoulder to the left of the main peak, and this mode decreased in height as the pH decreased (panels d–h of Figure 3). The rightward shift in the main peak with decreasing pH corresponded to only a moderate increase in the modal diameter (values marked in Figure 3), with this mode remaining below 10 $\mu$m for all pH conditions. Thus, it seems likely that, upon acidification, cloud particles of various sizes (sub-micrometer and micrometer) flocculated together to form clusters with just a few members, resulting in fewer sub-micrometer particles in the cloud and an accompanying growth in the size of the larger main mode. In addition, for pH values of ≤4.6, a new mode developed at larger particle sizes above 10 $\mu$m (panels f–h of Figure 3). The size of particles in this mode dramatically increased as the juice became more acidic. In contrast to particles in the main peak, it is clear that these largest particles are clusters with a large number of subparticles. These latter findings, in particular, are consistent with the work by Reiter et al.,[3] who observed that acidification of carrot juice to pH 4.4 increased the average diameter of the particles above 10 $\mu$m.

Overall, a monotonic increase in the average droplet size was observed with decreasing pH, as shown in Figure 4.

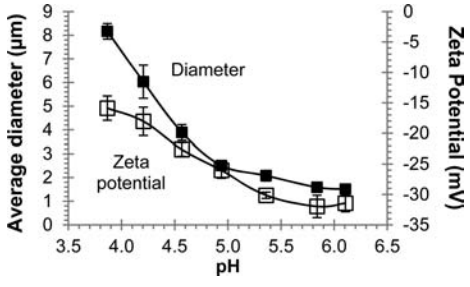


**Figure 4.** (■) Average particle size $D_{4,3}$ and (□) $\zeta$ potential of commercial carrot juice samples with added buffer.

Acidification caused particles to form aggregates that more rapidly sedimented and created an unstable cloud (Figures 1 and 2). The average particle size also increased in juices acidified by a method that was closer to industrial practice: by adding concentrated (2 M) citric acid in increasing amounts to the original juice. Measured results for the average diameter in the entire juice under these conditions are shown in Figure 5a.

Particle sizes in the supernatant and sediment of acidified (unbuffered) juices were also measured, with results in Figure 5a indicating that particles increased in size in both layers as the juices were acidified. During sedimentation of a monodisperse dispersion of particles, the vertical concentration profile exhibits three regions (Figure 5b): a stationary, concentrated region at the bottom of the container (the "sediment"), a region of intermediate concentration, which still falls toward the sediment layer, and above that, a particle-free region. In a polydisperse mixture, such as carrot juice cloud, these three distinct regions will occur simultaneously for different particle size fractions,[23] as shown schematically for a bidisperse suspension in Figure 5c. The "supernatant" region observable above the sediment layer in Figure 1 therefore comprises a mixture of different particle sizes, in sedimenting layers progressing toward the bottom, stationary layer. The influence of pH on the particle size in the supernatant is, thus, complex, because it results from opposing effects to the rate of particle settling and the size distribution remaining within the sedimenting supernatant regions. At high pH (pH ≥ 5.0), little sedimentation occurred over the 3 days of the experiment, and therefore, average sizes in the supernatant and sediment are the same as for the overall juice (Figure 5a). Under more acidic conditions, sedimentation partially separated the large and small particles, yielding smaller averages in the supernatant and larger averages in the sediment. However, because the sedimentation process was incomplete, the supernatant contained the still settling aggregates created at lower pH, and its average particle diameter is therefore larger than that measured at higher pH.

The process of particle separation described above depends upon not only the particle size but also the strength of the forces exerted on the particles. Thus, we expect differences in the extent of particle separation in juices sedimenting as a result of gravity (Figures 1 and 5a) and juices subjected to centrifugation. After centrifugation for 15 min at 4200*g*, control and acidified carrot juices studied by Reiter et al.[3] formed supernatants that displayed very similar particle size distributions. Large particles with diameters of > ~5 $\mu$m that were present in the intact juices were mainly absent from the supernatant in all cases, leading the authors to conclude that acidification causes only coarse particles to aggregate.[3] However, it is also possible that the centrifugation is effectively removing aggregates and other coarser particle fractions from all of the sample supernatants, regardless of the origins of those aggregates. In our results at lower pH values, we find that supernatants created by sedimentation of commercial carrot juice retained clear evidence of aggregates formed from fine particles.

**Aggregate Formation and Reversibility.** The effects of neutralizing acidified carrot juice back to its initial pH were also examined. Juice was acidified with 2 M citric acid to pH 3.0, causing the average particle size in the total juice to increase from 1.9 $\mu$m at the natural pH of carrot juice (6.2) to 13 $\mu$m at pH 3.0 (Figure 5). This aggregate growth led to almost complete clarification upon centrifugation, with a relative turbidity of 5.2% (data not shown). The juice at pH 3.0 was then neutralized back to pH 6.2 with the addition of 2 M NaOH. At 1 day after neutralization, the average particle size had decreased from 13 to 2.6 $\mu$m and the relative turbidity increased to 14%, although it did not recover fully to the initial value of 39%.

This partial recovery of cloud properties upon neutralization likely indicates that the aggregation of the particles at lower pH is reversible. These results are qualitatively similar to that seen in work performed on the more acidic apple and orange juices. In these systems, adjusting the juices to pH 7 retarded

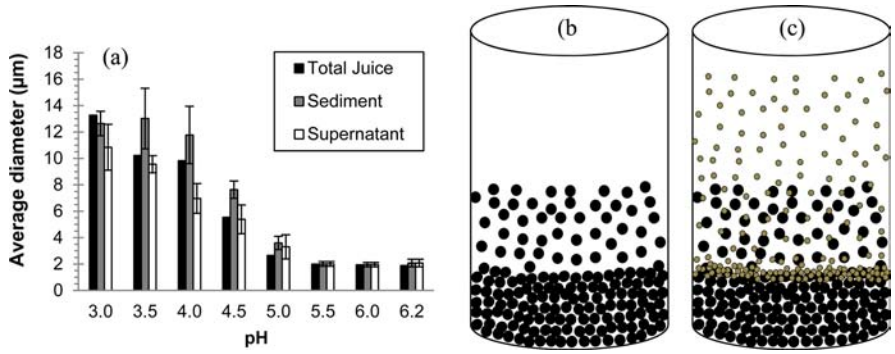


**Figure 5.** Effect of gravitational separation and pH on particle size: (a) $D_{4,3}$ measured in the entire juice (black bar), in the sediment (gray bar), and in the supernatant (white bar) in commercial juice acidified with 2 M citric acid and allowed to separate for 3 days, (b) particle layers in a monodisperse suspension during settling, and (c) particle layers in a bidisperse suspension during settling.

clarification and bringing the pH back down to the natural pH accelerated clarification.[24,25] Ellerbee and Wicker[11] also observed particle association and dissociation in orange juice aggregates at a fixed pH, which suggests formation of weak flocs. Likewise, carrot particles may flocculate at low pH, because of protonation and neutralization of the negatively charged pectin groups at the surface of the particles, which reduces repulsion sufficiently to allow for particles to be trapped together because of an attractive potential well, as discussed previously for orange juice.[24] When base is added and those groups are again deprotonated, the negative charges of the pectin become exposed again and the particles repel one another. This apparently reverses flocculation, decreasing the particle size. In this study, full recovery of the initial particle size may not have occurred because the attractive energy minimum between particles remained sufficiently large compared to thermal energy to allow for complete cluster separation. The protonation/deprotonation equilibrium of acid or base groups may also be altered within the cluster.

The growth in particle size with acidification can be seen more directly by viewing the particles under a light microscope at 20× magnification (Figure 6). A substantial increase in particle size between pH 4.9 and 4.6 was particularly visible. At pH values above 4.6, the aggregates appeared to consist of small rather symmetric clusters, whereas at the lower pH values, the clusters appeared to become more irregular and elongated. In addition, the dispersions at the lowest pH displayed some very large aggregates, approaching 100 $\mu$m in size, consistent with results in panels f–h of Figure 3.

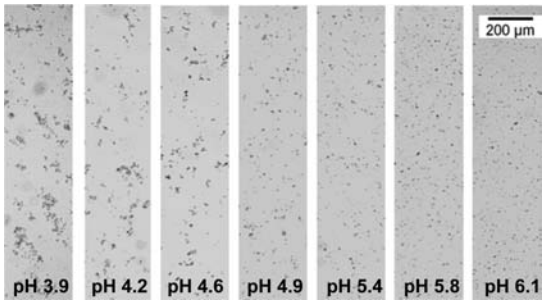


**Figure 6.** Optical micrographs with 20× magnification of carrot juice cloud particles at different pH values created by acidification of the juice.

**ζ Potential.** The $\zeta$ potential decreased in magnitude, from −31 to −15 mV, as pH decreased from 6.1 to 3.9. The average particle size increased over this same range (Figure 4). Below pH 4.6, the particle size increased and the magnitude of the potential decreased more steeply; this change corresponded to conditions where the large particle mode (diameter > 10 $\mu$m) appeared and grew on the size distribution graphs (Figure 3) and in the micrographs (Figure 6). From these results, a clear correlation between $\zeta$ potential and particle size increase is apparent.

Similar trends have been seen previously in apple and orange juices, which are naturally more acidic than carrot juice. Croak and Corredig[4] found that, when they adjusted the pH of orange juice over the range of pH 2.5–6.0, the most negative $\zeta$ potential existed when the pH was 6.0 and its magnitude decreased steeply until it nearly reached 0 mV at pH 2.5. Ellerbee and Wicker[11] also report a more negative $\zeta$ potential for pH 5.5 orange juice compared to that at the natural pH of 4.0. Larger average particle sizes and increased clarification were also observed at the lower pH condition. In apple juice, Benítez et al.[26] measured $\zeta$ potential and turbidity in diafiltered apple juice after allowing 1 h for sedimentation, comparing the control juice (pH 4.5) to those acidified with HCl to lower pH. Turbidity was the greatest, and thus, the cloud was most stable at the highest pH of 4.5, where the $\zeta$ potential was also most negative. The $\zeta$ potential for carrot juice at pH 4 was found to be only slightly more negative (−17 mV) than the value (−19 mV) published for the fruit juices; this difference may reflect the lower DM for carrot pectin.

For all three types of juice, decreasing the pH decreased the magnitude of the negative charge on the particle, and this change likely reduced the energy barrier between the particles. Thus, particle flocculation and cloud instability were enhanced at lower pH in these three types of juice. Interestingly, Mensah-Wilson et al.[7] demonstrated in a very different way the connection between the particle charge and cloud stability, by measuring the effects of adding pectin to pineapple juice and passion fruit nectar. The fruit particles were initially very weakly (positively) charged and would flocculate and separate but became negatively charged and stabilized upon the addition of pectin.

**Acidification and Ionic Strength Effects.** The practice of acidification by the addition of different amounts of strong acid to the juice modifies both the concentration and ionic strength of the juice, in addition to its pH. Modification of pH by the addition of 2 M citric acid required adding no more than 3% by volume of the concentrated acid, and thus, the dilution factor was insignificant. However, concentrations of the citric acid in

the final juice ranged up to 0.062 M at the lowest pH, and this would increase the juice ionic strength by up to ~0.04 M at pH values below 5.5.

These acidified juices can then be compared to those in which buffer salts were added directly to keep the ionic strength uniform between samples. The relative turbidity results from Figure 2, in which citric acid/sodium citrate buffers were used to alter pH, are replotted and compared in Figure 7 to carrot

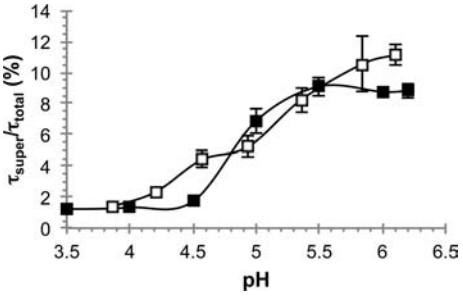


**Figure 7.** Relative turbidity ($\tau_{super}/\tau_{total}$) as a function of pH of commercial carrot juice with (■) 2 M citric acid solution or (□) buffer salts added. Buffer salts contributed 0.1 M to the ionic strength at all pH values.

juice to which 2 M citric acid was added to decrease pH. Juices acidified using citrate buffer salts (prepared at a constant ionic strength of 0.1 M) showed a smoother increase in turbidity over the entire pH range, while the turbidity data of the juice acidified with 2 M citric acid displayed a more sigmoidal shape. The latter juices were slightly less stable at high and low pH than the juices containing buffer salts. This result is somewhat surprising, because the higher ionic strength in the buffer salt-containing mixtures might be expected to promote flocculation by decreasing the Debye length and lowering the energy barrier between particles.[10,13]

To probe this effect further, the extent of clarification of juices was compared when sodium chloride versus calcium chloride was added in specific amounts to unbuffered commercial carrot juice at pH 6.2 (Figure 8). The juices

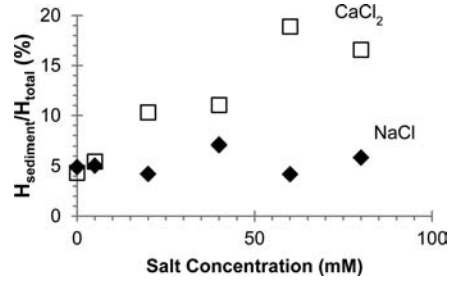


**Figure 8.** Relative sediment height ($H_{sediment}/H_{total}$) in commercial carrot juice (no acidification) after 3 days of storage at 4 °C, with added (□) $CaCl_2$ or (◆) NaCl.

were stored at 4 °C for 6 days, undisturbed, before relative sediment height was measured. The results in Figure 8 indicate that $CaCl_2$ significantly induced clarification, in contrast to NaCl, which had little effect on the cloud stability. Results with the sodium salt are consistent with those in Figure 7 and indicate that any effect of $Na^+$ on the particle diffuse double layer thicknesses does not seem to impact the particle stability.

Benítez et al.[10] explored the effect of the ionic strength on apple juice cloud stability, by first separating apple juice cloud particles from the juice serum and reconstituting them in aqueous solutions containing potassium chloride concentrations between $10^{-4}$ and $10^{-1}$ M. Turbidity and, hence, cloud stability were greatest at the lowest ionic strength, as expected.

A key difference between the results in Figure 8 and those by Benítez et al.[10] is that, in the latter study, the contributions of the native juice serum have been removed. To account for the surprisingly weak effect of ionic strength on our carrot juice cloud results, it is important to recognize that the native carrot juice serum will itself contain ions that contribute to the overall ionic strength. Data from the United States Department of Agriculture (USDA) National Nutrient Database[27] as well as measurements of electrolyte concentrations in other types of juices[28−32] suggest that native ionic strength values of the order of 20−100 mM[10] are likely. At such concentrations, the diffuse double layer is already less than 1−2 nm and further thinning upon addition of further ions may not have a large effect on modifying interparticle repulsion. In addition, with such small Debye lengths, electrostatic repulsion may occur over length scales comparable to short-range forces, such as steric interactions, giving the latter an important contributing role.[33] Benítez et al.[26] found that, even at very low pH values, where the $\zeta$ potential of isolated cloudy apple juice particles was close to zero, particles remained significantly stable because of a short-range repulsion. Ackerley and Wicker[24] also concluded that, at high pH values (pH 7), steric stabilization as a result of a hydrated pectin layer accompanies repulsive forces in preventing aggregation and clarification of orange juice. Thus, despite the high pH and high negative charge in the native carrot juice, such short-range interactions may be playing a significant role in carrot juice cloud stability, relative to the longer range double-layer interactions.

Results in Figure 8 also indicate an important contribution because of specific ion effects. Previous research has demonstrated that the presence of divalent cations increases fruit juice cloud instability, consistent with our results for carrot juice.[11,34−36] Calcium bridging of pectin is an important mechanism in the clarification of orange juice.[37] Such particle destabilization has been attributed to the formation of junction zones, in which divalent cations, such as calcium, induce pectin chain association.[34] Consequently, one explanation for the greater stability of the juices modified with buffer salts (Figure 7), despite their higher ionic strength, is that the higher concentration of sodium ions in the system competes with native calcium for binding to pectin. This would make calcium-induced flocculation less likely in these samples compared to juices acidified with citric acid.

**pH Threshold for Carrot Cloud Instability.** In summary, results from this study demonstrated that acidification of carrot juice caused clarification of the cloud because of particle flocculation. The growth in particle size was attributed to the particle $\zeta$ potential becoming less negative, which reduced the repulsion between particles and allowed them to approach one another and aggregate. Effects on $\zeta$ potential and particle clustering were observed over the entire pH of 3−6; however, the impact on cloud stability became more marked for pH values below 5. At these lower pH values, particle clusters between 10 and 100 $\mu$m developed as a significant portion of the size distribution. As the $\zeta$ potential increases more strongly below pH 5, these larger clusters may be promoted by a reduction in the energy barrier below a threshold value. However, the attractive interactions between particles in the cluster also appear quite weak, because the aggregation process

was at least partially reversible upon returning the juice to neutral pH.

However, salts had a complex effect on cloud stability. Small differences were only seen between juices acidified with buffer salts at a constant ionic strength versus those acidified by the addition of various amounts of concentrated citric acid; surprisingly, the juices at higher ionic strength were slightly more stable. The addition of monovalent sodium chloride to the juice had no clear influence on the stability, whereas the addition of divalent calcium chloride promoted clarification, likely because of its ability to bind to pectin and form bridges between different pectin molecules. Further work is needed to elucidate the types and concentrations of ions present in carrot juice, to understand how these ions influence interparticle interactions. Factors (such as chelators) that reduce the contribution of these ions in the juice as well as factors enhancing the negative charge of the particles could push the threshold pH for cloud stability lower and promote carrot juice stability in the presence of acidification.

## AUTHOR INFORMATION


### Corresponding Author

*Telephone: 530-752-5447. Fax: 530-752-4759. E-mail: srdungan@ucdavis.edu.

### Present Address

‡Alison K. Schultz: New Belgium Brewing, 500 Linden Street, Fort Collins, Colorado 80524, United States.



### Funding

The authors thank the National Science Foundation (NSF) Center for Advanced Processing and Packaging Studies for their funding of this research.


### Notes

The authors declare no competing financial interest.

## ABBREVIATIONS USED

DM, degree of methoxylation

## REFERENCES


(1) Castaldo, D.; Servillo, L.; Loiudice, R.; Balestrieri, C.; Laratta, B.; Quagliuolo, L.; Giovane, A. The detection of residual pectin methylesterase activity in pasteurized tomato juices. *Int. J. Food Sci. Technol.* **1996**, *31*, 313−318.

(2) Beveridge, T. Opalescent and cloudy fruit juices: Formation and particle stability. *Crit. Rev. Food Sci. Nutr.* **2002**, *42*, 317−337.

(3) Reiter, M.; Stuparić, M.; Neidhart, S.; Carle, R. The role of process technology in carrot juice cloud stability. *Lebensm.-Wiss. Technol.* **2003**, *36*, 165−172.

(4) Croak, S.; Corredig, M. The role of pectin in orange juice stabilization: Effect of pectin methylesterase and pectinase activity on the size of cloud particles. *Food Hydrocolloids* **2006**, *20*, 961−965.

(5) Reiter, M.; Neidhart, S.; Carle, R. Sedimentation behaviour and turbidity of carrot juices in relation to the characteristics of their cloud particles. *J. Sci. Food Agric.* **2003**, *83*, 745−751.

(6) Carle, R. Cloud stability of pulp-containing tropical fruit nectars. *Fruit Process.* **1998**, *8*, 266−272.

(7) Mensah-Wilson, M.; Reiter, M.; Bail, R.; Neidhart, S.; Carle, R. Cloud stabilizing potential of pectin on pulp-containing fruit beverages. *Fruit Process.* **2000**, *2*, 47−54.

(8) Sims, C. A.; Balaban, M. O.; Matthews, R. F. Optimization of carrot juice color and cloud stability. *J. Food Sci.* **1993**, *58*, 1129−1131.

(9) Yu, L. J.; Rupasinghe, H. P. V. Effect of acidification on quality and shelf-life of carrot juice. *Can. J. Plant Sci.* **2012**, *92*, 1113−1120.

(10) Benítez, E. I.; Lozano, J. E.; Genovese, D. B. Fractal dimension and mechanism of aggregation of apple juice particles. *Food Sci. Technol. Int.* **2010**, *16*, 179−186.

(11) Ellerbee, L.; Wicker, L. Calcium and pH influence on orange juice cloud stability. *J. Sci. Food Agric.* **2011**, *91*, 171−177.

(12) Mollov, P.; Mihalev, K.; Buleva, M.; Petkanchin, I. Cloud stability of apple juices in relation to their particle charge properties studied by electro-optics. *Food Res. Int.* **2006**, *39*, 519−524.

(13) Genovese, D. B.; Lozano, J. E. The effect of hydrocolloids on the stability and viscosity of cloudy apple juices. *Food Hydrocolloids* **2001**, *15*, 1−7.

(14) De Roeck, A.; Mols, J.; Duvetter, T.; Van Loey, A.; Hendrickx, M. Carrot texture degradation kinetics and pectin changes during thermal versus high-pressure/high-temperature processing: A comparative study. *Food Chem.* **2010**, *120*, 1104−1112.

(15) Ng, A.; Waldron, K. W. Effect of cooking and pre-cooking on cell-wall chemistry in relation to firmness of carrot tissues. *J. Sci. Food Agric.* **1997**, *73*, 503−512.

(16) Smout, C.; Sila, D. N.; Vu, T. S.; Van Loey, A. M. L.; Hendrickx, M. E. G. Effect of preheating and calcium pre-treatment on pectin structure and thermal texture degradation: A case study on carrots. *J. Food Eng.* **2005**, *67*, 419−425.

(17) Trejo Araya, X. I.; Hendrickx, M.; Verlinden, B. E.; Van Buggenhout, S.; Smale, N. J.; Stewart, C.; John Mawson, A. Understanding texture changes of high pressure processed fresh carrots: A microstructural and biochemical approach. *J. Food Eng.* **2007**, *80*, 873−884.

(18) Demir, N.; Bahceci, K. S.; Acar, J. The effect of processing method on the characteristics of carrot juice. *J. Food Qual.* **2007**, *30*, 813−822.

(19) Silva, V. M.; Sato, A. C. K.; Barbosa, G.; Dacanal, G.; Ciro-Velásquez, H. J.; Cunha, R. L. The effect of homogenisation on the stability of pineapple pulp. *Int. J. Food Sci. Technol.* **2010**, *45*, 2127−2133.

(20) Ibrahim, G. E.; Hassan, I. M.; Abd-Elrashid, A. M.; El-Massry, K. F.; Eh-Ghorab, A. H.; Manal, M. R.; Osman, F. Effect of clouding agents on the quality of apple juice during storage. *Food Hydrocolloids* **2011**, *25*, 91−97.

(21) Harrison, D.; Fisch, M. Turbidity measurement. In *Measurement, Instrumentation, and Sensors Handbook*, 2nd ed.; Webster, J. G., Eren, H., Eds.; CRC Press LLC: Boca Raton, FL, 2014; Chapter 51, pp 1−10, http://dx.doi.org/10.1201/b15664-57 (accessed May 1, 2014).

(22) Wicker, L.; Ackerley, J. L.; Corredig, M. Clarification of juice by thermolabile Valencia pectinmethylesterase is accelerated by cations. *J. Agric. Food Chem.* **2002**, *50*, 4091−4095.

(23) Bürger, R.; Concha, F.; Fjelde, K. K.; Karlsen, K. H. Numerical simulation of the settling of polydisperse suspensions of spheres. *Powder Technol.* **2000**, *113*, 30−54.

(24) Ackerley, J.; Wicker, L. Floc formation and changes in serum soluble cloud components of fresh Valencia orange juice. *J. Food Sci.* **2003**, *68*, 1169−1174.

(25) Yamasaki, M.; Kato, A.; Chu, S.-Y.; Arima, K. E. I. Pectic enzymes in the clarification of apple juice. II The mechanism of clarification. *Agric. Biol. Chem.* **1967**, *31*, 552−560.

(26) Benítez, E. I.; Genovese, D. B.; Lozano, J. E. Effect of pH and ionic strength on apple juice turbidity: Application of the extended DLVO theory. *Food Hydrocolloids* **2007**, *21*, 100−109.

(27) Holden, J. *National Nutrient Database for Standard Reference*; United States Department of Agriculture (USDA), Ed.; National Agricultural Library (NAL): Beltsville, MD, 2012.

(28) Eisele, T. A.; Drake, S. R. The partial compositional characteristics of apple juice from 175 apple varieties. *J. Food Compos. Anal.* **2005**, *18*, 213−221.

(29) Fung, Y. S.; Lau, K. M. Separation and determination of cations in beverage products by capillary zone electrophoresis. *J. Chromatogr.* **2006**, *1118*, 144−150.

(30) Genovese, D. B.; Lozano, J. E. Particle size determination of food suspensions: Application to cloudy apple juice. *J. Food Process Eng.* **2000**, *23*, 437−452.

(31) Tormen, L.; Torres, D. P.; Dittert, I. M.; Araújo, R. G. O.; Frescura, V. L. A.; Curtius, A. J. Rapid assessment of metal contamination in commercial fruit juices by inductively coupled mass spectrometry after a simple dilution. *J. Food Compos. Anal.* **2011**, *24*, 95−102.
(32) Vera, E.; Sandeaux, J.; Persin, F.; Pourcelly, G.; Dornier, M.; Piombo, G.; Ruales, J. Deacidification of clarified tropical fruit juices by electrodialysis. Part II. Characteristics of the deacidified juices. *J. Food Eng.* **2007**, *78*, 1439−1445.
(33) Genovese, D. B.; Lozano, J. E. Contribution of colloidal forces to the viscosity and stability of cloudy apple juice. *Food Hydrocolloids* **2006**, *20*, 767−773.
(34) Braccini, I.; Perez, S. Molecular basis of $Ca^{2+}$-induced gelation in alginates and pectins: The egg-box model revisited. *Biomacromolecules* **2001**, *2*, 1089−1096.
(35) Dronnet, V. M.; Renard, C. M. G. C.; Axelos, M. A. V.; Thibault, J. F. Characterisation and selectivity of divalent metal ions binding by citrus and sugar-beet pectins. *Carbohydr. Polym.* **1996**, *30*, 253−263.
(36) Whitaker, J. R. Pectic substances, pectic enzymes and haze formation in fruit juices. *Enzyme Microb. Technol.* **1984**, *6*, 341−349.
(37) Corredig, M.; Kerr, W.; Wicker, L. Particle size distribution of orange juice cloud after addition of sensitized pectin. *J. Agric. Food Chem.* **2001**, *49*, 2523−2526.

removed by decorticating sorghum cultivars prior to food use.[10] Soaking of sorghum grains decreases the content of phenolic compounds only moderately,[11] but the content and composition of phenolic compounds changes substantially during malting and spontaneous fermentation.[12] Hydrolysis of phenolic acid esters and flavonoid glycosides during sorghum fermentation with defined lactic starter cultures has been attributed to cereal enzymes.[4] Strain-specific esterase, glucosidase, phenolic acid decarboxylase, and phenolic acid reductase activities of lactobacilli contribute to the conversion of phenolic compounds in sorghum sourdoughs.[4,13]

Yeast metabolites that are produced during wine maturation, particularly pyruvate, acetoacetic acid, and acetaldehyde, have been shown to react with grape anthocyanins to form a multitude of pyranoanthocyanins.[14] Vinyl derivatives that are produced by enzymatic decarboxylation of hydroxycinnamic acids were also suggested to generate pyranoanthocyanidins.[15,16] Microbial metabolism of caffeic and coumaric acids in sorghum sourdoughs is known to yield vinylcatechol and vinylphenol, respectively;[4,13] however, the effect of these vinylaromatics on the fate of 3-deoxyanthocyanidins during sorghum fermentations has not been elucidated. It was, therefore, the aim of this study to determine the conversion of 3-deoxyanthocyanidins during fermentation of sorghum sourdoughs. Pure cultivar sorghum flour was fermented with defined strains of lactobacilli; 3-deoxyanthocyanidins and their derivatives formed during fermentation were identified with qualitative spectroscopic techniques including mass spectrometry and $^1$H nuclear magnetic resonance (NMR) spectroscopy.

## MATERIALS AND METHODS

**Chemicals and Reagents.** Apigeninidin and luteolinidin were purchased from Extrasynthése (Genay, France). High-performance liquid chromatography (HPLC)-grade acetonitrile, water, and formic acid (95%) were purchased from Fisher Scientific (Ottawa, ON, Canada). Deuterium oxide, methanol-$d_4$, and trifluoroacetic acid (TFA) were obtained from Sigma-Aldrich (Mississauga, ON, Canada). Solid-phase extraction (SPE) cartridges containing either 200 mg or 1 g of $C_{18}$ sorbent were obtained from Waters Corporation (Elstree, U.K.).

**Bacterial Strains and Culture Conditions.** *Lactobacillus plantarum* FUA 3171 and *Lactobacillus casei* FUA 3166 were isolated from ting, a fermented sorghum porridge.[9] Strains were grown on modified MRS (mMRS) agar for 24 h at 34 °C in modified atmosphere (1% $O_2$, 5% $CO_2$, 10% $H_2$, and balance $N_2$) and subcultured in mMRS broth for 24 h at 34 °C. The mMRS broth had the following composition per liter: 5.0 g of fructose, 5.0 g of glucose, 10.0 g of maltose, 10.0 g of tryptone, 5.0 g of beef extract, 5.0 g of yeast extract, 2.6 g of $H_2KPO_4$, 4.0 g of $HK_2PO_4$, 3.0 g of $NH_4Cl$, 0.5 g of L-cysteine HCl, 0.2 g of $MgSO_4$, 0.05 g of $MnSO_4$, 1.0 g of Tween 80, and 1.0 mL of vitamin mix (B12, B1, B2, B6, folic acid, and pantothenic acid). Solid media additionally contained 15 g·L$^{-1}$ agar.

**Fermentation of Sorghum Sourdough.** Pure cultivar *Sorghum bicolor* var. Town, a high-tannin red variety, was obtained from the Food Technology Research Centre, Kanye, Botswana. Grains were ground in an Ultra Centrifugal Mill ZM 200 (Retsch, Burlington, Canada) to a size of 0.5 mm, and the whole-grain flour was stored at −18 °C for less than 4 weeks until use. Starter cultures were prepared by harvesting cells from overnight cultures by centrifugation, washing with peptone saline solution (8.5 g·L$^{-1}$ sodium chloride and 1 g·L$^{-1}$ peptone), and resuspending the cells in an equal volume of sterile tap water. Sorghum sourdoughs were prepared by mixing 10 g of flour with 5 mL of each cell suspension of *L. plantarum* and *L. casei*, or by mixing with 10 mL of cell suspension of individual strains. Sourdoughs were fermented for 48 h at 34 °C. To account for modifications of 3-deoxyanthocyanidins in the absence of microbial activity, chemically acidified sorghum doughs were prepared with 10 g of ground sorghum and 10 mL of sterile tap water, acidified with 0.4 mL of 90% lactic acid and glacial acetic acid in a 4:1 ratio (v/v), and fermented for 48 h at 34 °C. The chemically acidified control had a pH of 3.8, comparable to the pH of sorghum sourdoughs. Fermentations were carried out in duplicate independent experiments. Before and after fermentation, samples were taken for the determination of cell counts and pH as described,[9] as well as for extraction of 3-deoxyanthocyanidins as described later.

**Table 1. Retention Times and Mass Spectra of 3-Deoxyanthocyanidins in Sorghum, Sorghum Sourdoughs, and Chemically Acidified Controls; Compounds That Were Observed Exclusively in Sorghum Sourdoughs but Were Absent in Unfermented Sorghum or Chemically Acidified Controls Are Shown in Bold Font**

| no. | identification | RT | $[M]^+$ ($m/z$) | $MS^2$ ($m/z$) |
|---|---|---|---|---|
| **1** | luteolinidin | 39.4 | 271 | 197, 187, 153, 141, 115 |
| **2** | apigeninidin | 46.2 | 255 | 227, 181, 171, 152, 121 |
| **3** | methoxyluteolinidin | 47.4 | 285 | 270, 253, 242, 165, 153 |
| **4** | methoxyapigeninidin | 52.1 | 269 | 254, 226, 197, 181, 121 |
| **5** | methoxyapigeninidin | 52.5 | 269 | 254, 226, 197, 181, 121 |
| **6** | **unknown** | 63.5 | 391 | 281 |
| **7** | dimer[a] | 66.8 | 525 | 385, 285, 255 |
| **8** | **unknown** | 68.7 | 375 | 281 |
| **9** | dimer | 69.5 | 525 | 435, 405, 281, 267 |
| **10** | **unknown** | 70.7 | 387 | 359, 255, 226, 202, 121 |
| **11** | dimer | 73.1 | 539 | 419, 399, 387, 285, 255 |
| **12** | dimer | 73.5 | 509 | 371, 198, 181, 153 |
| **13** | **unknown**[b] | 73.8 | 371 | 343, 239, 226, 202, 121 |
| **14** | **unknown** | 74.2 | 401 | 386, 358, 226, 202, 121 |
| **15** | **unknown** | 75.6 | 401 | 386, 358, 226, 202, 121 |
| **16** | dimer | 76.0 | 523 | 383, 163, 147, 145, 119 |
| **17** | dimer | 76.8 | 523 | 403, 383, 285, 269, 255 |
| **18** | dimer | 79.0 | 553 | 401, 281, 251 |
| **19** | dimer | 79.6 | 523 | 385, 216, 177, 145, 131 |
| **20** | **unknown** | 80.6 | 385 | 370, 342, 249, 165, 121 |
| **21** | apigeninidin−flavene dimer[c] | 84.7 | 509 | 384, 383, 255 |
| **22** | dimer | 86.1 | 537 | 509, 385, 383, 255 |

[a]Dimeric 3-deoxyanthocyanidin pigments. [b]Tentative identification as pyrano-3-deoxyanthocyanidin based on matching molecular mass.[24] [c]Apigeninidin−flavene dimer has previously been identified.[22]

**Extraction of 3-Deoxyanthocyanidins.** Ground sorghum (10 g), sorghum sourdoughs, or chemically acidified doughs were mixed with 50 mL of 70% (v/v) aqueous methanol for 1 h and then processed with high-intensity ultrasound for 20 min. After filtering, the residues were extracted again as described. Methanol was evaporated under vacuum at 40 °C (Rotavapor RE 21, Büchi, Flawil, Switzerland). Ethyl acetate (40 mL) was added, the organic phase was removed, and the liquid−liquid extraction was repeated. The ethyl acetate phases were combined and evaporated under vacuum at 30 °C. Solids were redissolved in 2 mL of methanol and filtered through a 0.22 μm filter prior to LC-DAD-MS (DAD, diode array detector) analysis. To concentrate 3-deoxyanthocyanidins, the methanol solution (1.5 mL) was diluted with water (9 mL) and loaded on a SPE C18 end-capped cartridge (1 g). The SPE cartridges were eluted with 30%, 45%, and 70% (v/v) aqueous

methanol. The fraction eluting with 70% aqueous methanol was collected and concentrated 10-fold prior to LC-DAD-MS analysis.

**Identification and Relative Quantitation of 3-Deoxyanthocyanidins by LC-MS/MS.** Analytes were separated using a Shimadzu UFLC system consisting of a degasser, binary pump, autosampler, thermostated column compartment, and SPD-M20A Prominence diode array detector (DAD). The LC was connected to a 4000 Q TRAP LC-MS/MS system (MDS SCIEX, Applied Biosystems, Streetville, ON, Canada). Phenolic compounds were separated on a Luna C18 HPLC column (5 $\mu$m, 250 × 4.6 mm, Phenomenex, Torrance, CA) and detected by diode array scanning from 190 to 800 nm; 3-deoxyanthocyanidins were monitored at 480 nm. Mobile phase A consisted of 1% (v/v) formic acid in water, and mobile phase B consisted of 1% (v/v) formic acid in water and acetonitrile (50:50, v/v) of HPLC grade (Fisher Scientific). Samples were eluted with the following gradient: 0−8 min, 10% B; 10−15 min, 10−20% B; 15−22 min, 20% B; 22−30 min, 20−30% B; 30−38 min, 30% B; 38−45 min, 30−40% B; 45−52 min, 40% B; 52−60 min, 40−50% B; 60−62 min, 50% B; 62−67 min, 50−60% B; 67−70 min, 60−65% B; 70−80 min, 65−65% B; 80−90 min, 65−68% B; 90−105 min, 68−100% B; 105−110 min, 100% B; 110−116 min, 100−10% B; 116−120 min, 10% B. The injection volume was 10 $\mu$L, and the flow rate was 0.8 mL·min$^{-1}$ at 35 °C.

Mass spectra were recorded in the positive-ion mode; the values of operating parameters were as follows: spray voltage, 5000 V in positive mode; source temperature, 600 °C; nebulizing gas (GS1), 55 psi; heating gas (GS2), 45 psi; and curtain gas, 15 psi. An information-dependent acquisition (IDA) method using enhanced MS, enhanced product ion, precursor ion scan modes, and MS$^3$ was used to tentatively identify 3-deoxyanthocyanidins. Both Q1 and Q3 were operated at unit mass resolution. The spectra were obtained over a range from $m/z$ 100 to 1000 in 0.8 s. The linear ion trap (LIT) fill time was set at 20 ms. The IDA threshold was set at 500 cps, above which enhanced product ion (EPI) spectra were collected from the three most intense peaks. The EPI scan rate was 4000 amu·s$^{-1}$. Collision-induced dissociation (CID) spectra were acquired using nitrogen as the collision gas under Rolling collision energy (CE) (CE = 0.008 × ($m/z$) + 37.75 for positive-ion mode). The data analysis was performed by Analyst 1.5 (Applied Biosystems).

**Isolation of Novel 3-Deoxyanthocyanidin Adducts from Sourdough.** Sterile tap water (3 L) was added to ground sorghum (3 kg), inoculated with 10 mL of a cell suspension of *L. plantarum*, and fermented for 48 h at 34 °C. After fermentation, doughs were extracted twice by mixing with 3 L of methanol for 1 h and processing with high-intensity ultrasound for 20 min. Extracts were combined and methanol was evaporated under vacuum at 40 °C. Ethyl acetate (3 L) was added to the water phase, and the liquid−liquid extraction was repeated as described. The ethyl acetate phase was combined and evaporated under vacuum at 30 °C. The solids were redissolved in 15 mL of methanol and filtered through a 0.45 $\mu$m nylon syringe filter (Fisher Scientific) prior to preliminary separation by preparative LC.

The resulting crude sample (3 mL) was passed through a PREP LC column (4 $\mu$m, 250 × 21.20 mm, Phenomenex) preequilibrated with 1% (v/v) formic acid in water and acetonitrile (60:40, v/v) of HPLC grade. The PREP LC column was eluted with the same solvent at a flow rate of 15 mL·min$^{-1}$. Fifty fractions (7.5 mL each) were collected. Fractions from 5 runs were combined; fractions containing deoxyanthocyanidins were identified on the basis of their color, and acetonitrile was removed by evaporation. SPE columns (1 g) were used to enrich each peak and to store pure compounds after separation on a Luna C18 RP-HPLC.[17] The separation on the analytical C18 column was repeated if necessary to obtain seven purified compounds. To reduce degradation the purified 3-deoxyanthocyanidin adducts were concentrated by SPE C18 end-capped cartridges (200 mg) for subsequent structure elucidation by $^1$H NMR, offline electrospray ionization−tandem mass spectrometry (ESI-MS/MS), and hydrogen/deuterium (H/D) exchange techniques for offline ESI-MS/MS.

**$^1$H NMR to Identify New 3-Deoxyanthocyanidins.** $^1$H NMR spectra were recorded on a Varian Inova 500 or 600 MHz spectrometer. For $^1$H NMR spectra, $\delta$ values were referenced to the solvent residual peak ($CHD_2OD$, 3.31 ppm). Samples were dissolved in a 1% TFA solution of $CD_3OD$ and analyzed immediately.

**Chemical Synthesis of Apigeninidin.** Apigeninidin was prepared from 2,4,6-triacetoxybenzaldehyde according to a previously published methodology[18,19] with the following modifications: 2,4,6-triacetoxybenzaldehyde (0.223 g) was cooled to 0 °C and a solution of hydrogen chloride in dioxane (4 M, 10.0 mL) and 4-hydroxyacetophenone (0.762 g, 7.00 equiv) was added. The solution was removed from ice and stirred for 1 h at room temperature, at which point dry methanol (7.5 mL) was added. After a further 30 min at room temperature, the solvents were removed under reduced pressure. Diethyl ether (25 mL) was then added to the dry residue to dissolve unreacted 4-hydroxyacetophenone, and the red insoluble fraction was collected by filtration (0.205 g). This solid proved to be a mixture of apigeninidin and aldehyde impurities. Attempts to purify apigeninidin by published methods[18,19] were unsuccessful. Instead, 110 mg of the crude apigeninidin chloride was divided into 25 mg segments, dissolved in 5 mL of 1:1 methanol/water, and purified via preparative HPLC on a Phenomenex Luna 5 $\mu$m C18(2) column with a gradient of 0.1% TFA in water (A) and 0.1% TFA in acetonitrile (B) as follows: 0 min, 5% B; 5 min, 5% B; 40 min, 24% B; 60 min, 40% B; 70 min, 64% B; 72 min, 95% B; followed by reequilibration to 5% B. Apigeninidin eluted as a single peak at 51.3 min, with strong absorbance at 254 and 480 nm. Fractions containing apigeninidin were pooled, partially concentrated under reduced pressure to remove acetonitrile, and stored wet on a Phenomenex Strata C18-E solid-phase extraction column (Phenomenex, U.S.A.) at 4 °C (1 mM HCl as the final wash). Elution with methanol provided pure apigeninidin triflate (0.0333 g, 21%). The NMR spectra and MS data were consistent with the structure and literature values.[20] Once it was purified via HPLC we found that concentration of apigeninidin chloride or triflate in the absence of C18 silica led to rapid degradation, as evidenced by a sharp decrease in methanol and water solubility. Storage in acidic methanol also led to degradation over time; apigeninidin and the apigeninidin adducts were thus stored on wet Phenomenex Strata C18-E columns at 4 °C.[17]

**Small-Scale Apigeninidin Adduct Synthesis.** To a solution of apigeninidin in methanol (0.50 mL at 1.0 mg/mL, 1.8 $\mu$mol) was added 1 mM hydrochloric acid (2 mL) and either a 10% solution of 4-vinylphenol in propylene glycol (5.10 $\mu$L, 3.25 equiv) or 4-coumaric acid (*p*-coumaric acid) (2.45 mg, 11.0 equiv). The solution was stirred for 24 h and then purified via HPLC on a Phenomenex Luna 5 $\mu$m C18(2) column as described above for the synthesis of apigeninidin. Samples were eluted at a flow of 1.0 mL min$^{-1}$. A third reaction lacking both 4-vinylphenol and 4-coumaric acid was used as a negative control, to account for the slow degradation of apigeninidin under these conditions.

**Large-Scale Synthesis of Apigeninidin Adducts.** To a solution of synthetic apigeninidin chloride (0.0323 g, 0.115 mmol) in 1 mM hydrogen chloride (30 mL, not degassed) was added a 10% solution of 4-vinylphenol in propylene glycol (0.430 mL, 3.25 equiv). After stirring in the dark for 24 h, the mixture was passed through a Phenomenex Strata C18-E column (MeOH elution) to remove excess water. This methanol/water mixture (1:1, 20 mL) was then purified via preparative HPLC on a Phenomenex Luna 5 $\mu$m C18(2) column as described above. Numerous new peaks with absorbances at 254 or 480 nm were detected. Those with strong absorbances at 480 nm were investigated further, and the structures of compounds **8** and **13** were determined via $^1$H NMR (Table 1).

**Offline ESI-MS/MS and Hydrogen/Deuterium Exchange Analysis of Novel Deoxyanthocyanidins.** Five $\mu$L of each purified compound was added into 1 mL of methanol/$H_2O$ (60:40, v/v) and directly injected into a Thermo LTQ-Orbitrap high-resolution mass spectrometer at a flow rate of 15 $\mu$L min$^{-1}$. The hydrogen/deuterium exchange (H/DX) reactions were initiated by diluting 5 $\mu$L of enriched solutions of each novel deoxyanthocyanidin into 1 mL of methanol-$d_4$/$D_2O$ (60:40, v/v). The MS experiments included full scan and MS/MS fragmentation in positive-ion mode to determine elemental compositions of ion formula and fragmentation pathways for the new 3-deoxyanthocyanidins and corresponding deuterated 3-deoxyanthocyanidins. Meanwhile, enhanced product ion (EPI) scan by AB Q-TRAP 4000 was also carried out to investigate the fragmentation pathways of

novel compounds via direct injection method, using a Harvard Apparatus syringe pump at a flow rate of 15 $\mu$L min$^{-1}$.

## RESULTS

**Conversion of 3-Deoxyanthocyanidins in Sorghum Sourdoughs.** Sorghum sourdoughs were fermented with a binary strain combination of ting isolates as previously described.[4] During fermentation of sorghum sourdoughs with *L. plantarum* and *L. casei*, the pH decreased from 6.1 to 3.7 and the cell count increased from $(5.8 \pm 0.6) \times 10^7$ to $(2.5 \pm 0.3) \times 10^8$ cfug$^{-1}$ after 48 h of fermentation. Cell counts of chemically acidified doughs remained below $10^5$ cfu g$^{-1}$ throughout fermentation. The separation of phenolic acids and flavonoids confirmed changes previously reported by Svensson et al.[4] by using the same strain combination but a different sorghum cultivar (data not shown). Separation of 3-deoxyanthocyanidins was achieved by LC-DAD-MS. Sourdough samples were additionally analyzed after concentration of 3-deoxyanthocyanidins by solid-phase microextraction and elution with 70% methanol. Retention times and mass spectra of 3-deoxyanthocyanidins detected in unfermented and fermented sorghum sourdoughs in positive-ion mode are listed in Table 1.

Compounds **1** and **2** were identified as luteolinidin and apigeninidin by comparison of retention times and mass spectra with external standards. Compounds **3**, **4**, and **5** were identified as methoxyluteolinidin and methoxyapigeninidins according to their molecular weights and fragmentation patterns.[21] Compounds **7**, **9**, **11**, **12**, **16**, **17**, **18**, **19**, **21**, and **22** were identified as various anthocyanidin dimers, according to their molecular weights.[22,23] The remaining compounds, **6**, **8**, **10**, **13**, **14**, **15**, and **20**, could not be identified with external standards or published mass spectra, although the molecular mass of compound **13** matched the mass of pyrano-3-apigeninidin 4-vinylphenol.[24] Deoxyanthocyanidin adducts were identified exclusively in sorghum sourdoughs. The relative quantitation of deoxyanthocyanidins in sorghum sourdoughs based on the peak height at 480 nm revealed that the pattern of deoxyanthocyanidins remained essentially unchanged in chemically acidified dough. During lactic fermentation, concentration of monomeric deoxyanthocyaninidins decreased and the relative abundance of adducts **6**, **8**, **10**, **13**, **14**, **15**, and **20** increased. To confirm that the formation of deoxyanthocyanidin adducts is dependent on microbial metabolism, sorghum sourdoughs were fermented with single strains of *L. plantarum* and *L. casei*. Adduct formation was detected in sorghum sourdoughs fermented with *L. plantarum* but not in sorghum sourdoughs fermented with *L. casei*. While both strains produce lactate as the main product of carbohydrate metabolism, only *L. plantarum* metabolizes phenolic acids. *L. plantarum* FUA3171 decarboxylates caffeic and coumaric acids to vinylphenols; ferulic acid is converted to dihydroferulic acid.[4] The formation of deoxyanthocyanidin derivatives thus corresponds to the formation of vinylcatechol and vinylphenol from caffeic and coumaric acids, respectively.

**Table 2. Elemental Composition of Novel 3-Deoxyanthocyanidins and the Deuterated 3-Deoxyanthocyanidins**

| | | *m/z* | | |
|---|---|---|---|---|
| no. | ion formula | theoretical | measured | error (ppm) |
| **6** | $C_{23}H_{19}O_6^+$ | 391.1176 | 391.1169 | 1.79 |
| **6-$d_5$**[a] | $C_{23}H_{14}D_5O_6^+$ | 396.1490 | 396.1487 | 0.76 |
| **8** | $C_{23}H_{19}O_5^+$ | 375.1227 | 375.1222 | 1.33 |
| **8-$d_4$** | $C_{23}H_{15}D_4O_5^+$ | 379.1478 | 379.1476 | 0.53 |
| **10** | $C_{23}H_{15}O_6^+$ | 387.0863 | 387.0858 | 1.29 |
| **10-$d_4$** | $C_{23}H_{11}D_4O_6^+$ | 391.1114 | 391.1118 | 1.02 |
| **13** | $C_{23}H_{15}O_5^+$ | 371.0914 | 371.0912 | 0.54 |
| **13-$d_3$** | $C_{23}H_{12}D_3O_5^+$ | 374.1102 | 374.1103 | 0.27 |
| **14** | $C_{24}H_{17}O_6^+$ | 401.1020 | 401.1013 | 1.75 |
| **14-$d_3$** | $C_{24}H_{14}D_3O_6^+$ | 404.1208 | 404.1205 | 0.74 |
| **15** | $C_{24}H_{17}O_6^+$ | 401.1020 | 401.1012 | 1.99 |
| **15-$d_3$** | $C_{24}H_{14}D_3O_6^+$ | 404.1208 | 404.1208 | 0.00 |
| **20** | $C_{24}H_{17}O_5^+$ | 385.1070 | 385.1065 | 1.30 |
| **20-$d_2$** | $C_{24}H_{15}D_2O_5^+$ | 387.1196 | 387.1198 | 0.52 |

[a]Deuterated compound **6**.

**Structure Elucidation of Novel Deoxyanthocyanidins.** Compounds **6**, **8**, **10**, **13**, **14**, **15**, and **20** were purified from sorghum sourdoughs. The elemental compositions of the 3-deoxyanthocyanidin derivatives and the corresponding deuterated compounds were determined by offline LTQ-Orbitrap mass spectrometry (Table 2).[25] Compounds **8** and **13** were purified in sufficient quantities to allow structure elucidation by $^1$H NMR (Table 3), although they proved unstable at room temperature and were not of sufficient concentration for heteronuclear single quantum coherence (HSQC), heteronuclear multiple-bond correlation (HMBC), or $^{13}$C analysis in the limited time window. While compound **8** displayed most of the peaks found in apigeninidin, the doublets at 6.66 and 6.95 ppm were absent. Instead a singlet was found at 7.01 ppm, suggesting substitution at C6.[20] Para-substituted phenols are excellent electrophiles, and both flavonoids and anthocyanins are known to undergo electrophilic aromatic substitution, although substitution is more common at C8 than at C6.[26] Peak assignments and the proposed structure of this vinylphenol/apigeninidin adduct are shown in Table 3.

The $^1$H spectra of compound **13** matched that of a symmetric pyrano-3-deoxyanthocyanidin that has been previously reported in sorghum extracts, although its biosynthesis was not determined.[24] The structure and peak assignments of compound **13** are also shown in Table 3. Under IUPAC naming conventions, compound **8** is 6-(1-(4-hydroxyphenyl)ethyl)-apigeninidin chloride and compound **13** is 8-hydroxy-2(4′-hydroxyphenyl)-5(4″-hydroxyphenyl)pyrano[4,3,2-*de*]1-benzopyrylium chloride.

Compounds **8** and **13**, as well as the other new deoxyanthocyanidins, were found only in sorghum sourdough fermented caffeic acid decarboxylase positive lactobacilli.[4] To confirm the role of vinyl derivatives of hydroxycinnamic acids as reactants in the formation of apigeninidin adducts, synthetic apigeninidin[18] was treated with 4-vinylphenol or 4-coumaric acid according to the procedure of Fulcrand et al.[27] While no reaction was observed between 4-coumaric acid and apigeninidin under these conditions, HPLC analysis of the 4-vinylphenol reaction revealed numerous new peaks with absorbance at 480 nm. The previously reported pyranoapigeninidin 4-vinylphenol[24] was a main component in a number of these peaks, often coeluting with compounds that had exact masses of 373.1067 and 375.1224. At least two different compounds with the latter mass were found, and $^1$H NMR analysis determined one was compound **8**, previously isolated during analysis of the fermentation samples (vide supra).

**MS Fragmentation Pathways of Deoxyanthocyanidin Adducts.** With the structure of compound **13** known and the structure of compound 8 tentatively assigned, we were able to identify the remaining unknown compounds (**6**, **10**, **14**, **15**, and

Table 3. $^1$H-NMR Spectral Data and Structures of Apigeninidin, Compound 8, and Compound 13[b]

| Carbon No.[a] | $\delta_H$ chemical shifts (Hz) Apigeninidin | Comp. 8 | Comp. 13 |
|---|---|---|---|
| 1 | – | – | – |
| 2 | – | – | – |
| 3 | 8.05 | 8.17 | 7.49 |
| 4 | 9.10 | 9.19 | – |
| 4a | – | – | – |
| 5 | – | – | – |
| 6 | 6.66 | – | 7.17 |
| 7 | – | – | – |
| 8 | 6.95 | 7.01 | 7.17 |
| 8a | – | – | – |
| 1′ | – | – | – |
| 2′ | 8.32 | 7.86 | 8.11 |
| 3′ | 7.08 | 7.01 | 7.04 |
| 4′ | – | – | – |
| 5′ | 7.08 | 7.01 | 7.04 |
| 6′ | 8.32 | 7.86 | 8.11 |
| 1″ | n.a. | – | – |
| 2″ | n.a. | 7.19 | 8.11 |
| 3″ | n.a. | 6.77 | 7.04 |
| 4″ | n.a. | – | – |
| 5″ | n.a. | 6.77 | 7.04 |
| 6″ | n.a. | 7.19 | 8.11 |
| 7″ | n.a. | 4.96 | – |
| 8″ | n.a. | 1.73 | 7.49 |

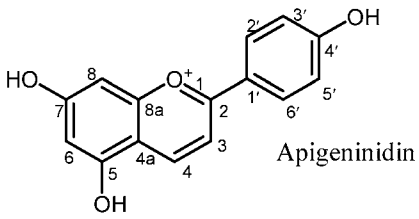


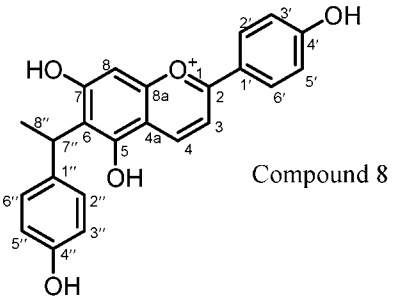


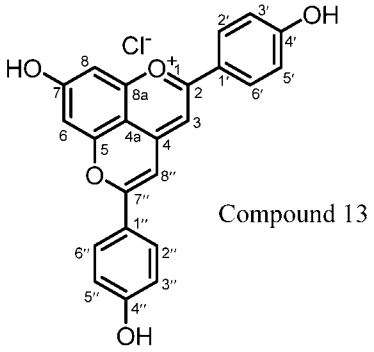


[a]Due to an imperfection in the cold probe used to collect several spectra, a deformation in signal is observed around high-intensity solvent peaks. This proved impossible to fully correct, although a minor baseline correction has been applied. [b]–, quarternary C atom; n.a., not applicable.

**20**) by comparing mass spectrometry fragmentation and isotope exchange patterns. In deuterated methanol/water, compound **8** gave a *m*/*z* of 379.1476, which corresponds to a molecular formula of $C_{23}H_{15}D_4O_5^+$ and the replacement of four protons with deuterium. Peaks at *m*/*z* 378.1413, *m*/*z* 377.1350, and *m*/*z* 376.1287 were also observed, suggesting ready back-exchange of the deuterated protons with water clusters during the ionization process.[28] This facile exchange suggests the presence of four hydroxyl groups, one more than apigeninidin. Supporting this conclusion was the fragmentation of compound **8** in protic media to a *m*/*z* of 281.0805, which corresponds to a molecular formula of $C_{17}H_{13}O_4^+$ and loss of phenol. This mass is ∼26 Da greater than that for apigeninidin, suggesting expulsion of phenol results in an alkene on the apigeninidin core (Figure 2a). One potential fragmentation pathway is transfer of a proton from a neighboring phenol via a six-membered ring transition state;[29] the other fragmentation pathway involves transfer of the hydrogen atom in the methyl group to the phenol group via a four-membered ring transition state.[30]

Similar to compound **8**, in deuterated media compound **6** displayed an increase in mass corresponding to proton-to-deuterium exchange. However, compound **6** gave a *m*/*z* of 396.1487, corresponding to a molecular formula of $C_{23}H_{14}D_5O_6^+$ (Table 2, Figure 2b). Fragmentation of compound **6** gave the same ions as in compound **8**, suggesting that the two share an apigeninidin core and that the difference in mass/deuterium substitution is a result of a different phenolic adducts. Compound **8** is formed from condensation of apigeninidin and 4-vinylphenol, the product of decarboxylation of coumaric acid. Both coumaric and caffeic acids are abundant in sorghum and both are decarboxylated by *L. plantarum* FUA3171, suggesting that compound **6** is the product of condensation between apigenindin and vinylcatechol.[4] The tentative structure of compound **6** is shown in Figure 3, and the fragmentation pathways of deuterated compound **6** are shown in Figure 2b.

Fragments generated with Q-TRAP 4000 were used to explain the structures of the symmetric pyrano-3-deoxyanthocyanidins, typified by compound **13**.[31] The conjugate $\pi$ system ordinarily provides a challenge for the structure elucidation of pyrano-3-deoxyanthocyanidins by MS/MS experimentation,[32] but by using pyranoapigeninidin 4-vinylphenol (compound **13**) as a reference, the structures of the remaining pyrano-3-deoxyanthocyanidins can be deduced. As in compounds **6** and **8**, comparison between mass spectra in deuterated and protic media was used to determine the number of phenolic hydrogens in compounds **10**, **14**, **15**, and **20** (Figure 3 and Table 4).


dx.doi.org/10.1021/jf503330b | J. Agric. Food Chem. 2014, 62, 11536−11546

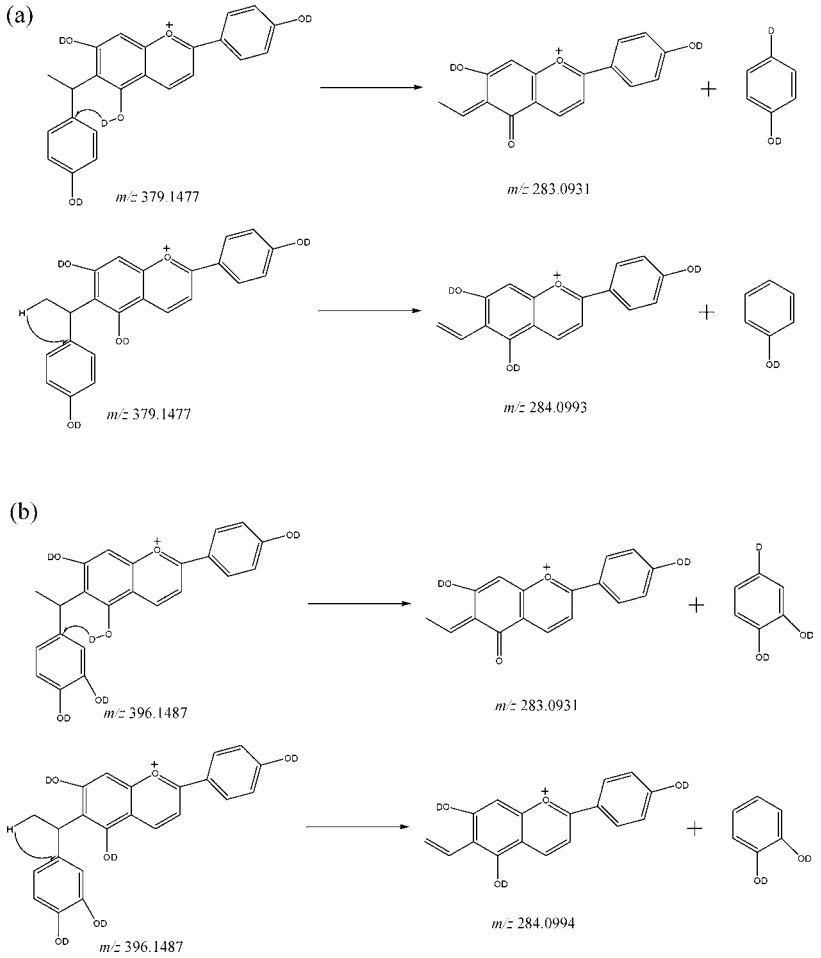


**Figure 2.** Fragmentation pathways of deuterated 3-deoxyanthocyanidin−vinylphenol adducts (compound **8**, panel a) and deuterated 3-deoxyanthocyanidin−vinylcatechol (compound **6**, panel b).

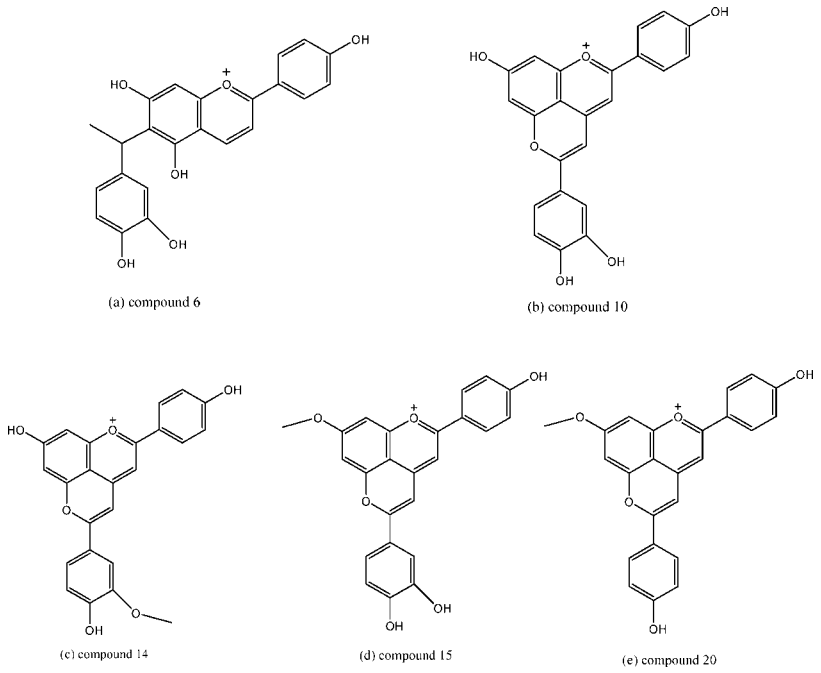


**Figure 3.** Proposed structures of compounds **6**, **10**, **14**, **15**, and **20**.

Figure 4 shows the proposed fragmentation pathways of deuterated pyranoapigeninidin 4-vinylphenol (compound **13**). Compound **13** does not contain nitrogen, and so even the deuterated fragments *m*/*z* 252, 228, and 204 in Figure 4 were


dx.doi.org/10.1021/jf503330b | J. Agric. Food Chem. 2014, 62, 11536−11546

**Table 4. Some Fragments from Compounds 13, 10, 14, 15, and 20 and Their Corresponding Deuterated Compounds; The Assignment of Product Ion Formula and Mass Difference from Deuterated Compounds**

| | *m/z* | | | | | | deuterated assignment | |
|---|---|---|---|---|---|---|---|---|
| no. | $[M]^+$ | $MS^2$ | mass difference | deuterated $[M]^+$ | $MS^2$ | mass difference | ion formula | mass difference |
| **13** | 371 | 371 | 0 | 374 | 374 | 0 | $C_{23}H_{12}D_3O_5^+$ | |
| | | 343 | 28 | | 346 | 28 | $C_{22}H_{12}D_3O_4^+$ | CO |
| | | 287 | 84 | | 289 | 85 | $C_{19}H_9D_2O_3^+$ | $C_4H_3DO_2$ |
| | | 250 | 121 | | 252 | 122 | $C_{16}H_8D_2O_3^{+\bullet}$ | $C_7H_4DO_2^\bullet$ |
| | | 239 | 132 | | 241 | 133 | $C_{15}H_9D_2O_3^+$ | $C_8H_3DO_2$ |
| | | 226 | 145 | | 228 | 146 | $C_{14}H_8D_2O_3^{+\bullet}$ | $C_9H_4DO_2^\bullet$ |
| | | 215 | 156 | | 217 | 157 | $C_{13}H_9D_2O_3^+$ | $C_{10}H_3DO_2$ |
| | | 202 | 169 | | 204 | 170 | $C_{12}H_8D_2O_3^{+\bullet}$ | $C_{11}H_4DO_2^\bullet$ |
| | | 165 | 206 | | 167 | 207 | $C_9H_7D_2O_3^+$ | $C_{14}H_5DO_2$ |
| | | 121 | 250 | | 122 | 252 | $C_7H_4DO_2^+$ | $C_{16}H_8D_2O_3$ |
| **10** | 387 | 387 | 0 | 391 | 391 | 0 | $C_{23}H_{11}D_4O_6^+$ | |
| | | 359 | 28 | | 363 | 28 | $C_{22}H_{11}D_4O_5^+$ | CO |
| | | 341 | 46 | | 343 | 48 | $C_{22}H_{11}D_2O_4^+$ | $CD_2O_2$ |
| | | 311 | 76 | | 313 | 78 | $C_{21}H_9D_2O_3^+$ | $C_2H_2D_2O_3$ |
| | | 255 | 132 | | 257 | 134 | $C_{15}H_9D_2O_4^+$ | $C_8H_2D_2O_2$ |
| | | 239 | 148 | | 240 | 151 | $C_{15}H_{10}DO_3^+$ | $C_8HD_3O_3$ |
| | | 226 | 161 | | 228 | 163 | $C_{14}H_8D_2O_3^{+\bullet}$ | $C_9H_3D_2O_3^\bullet$ |
| | | 202 | 185 | | 204 | 187 | $C_{12}H_8D_2O_3^{+\bullet}$ | $C_{11}H_3D_2O_3^\bullet$ |
| | | 165 | 222 | | 167 | 224 | $C_9H_7D_2O_3^+$ | $C_{14}H_4D_2O_3$ |
| | | 121 | 266 | | 122 | 269 | $C_7H_4DO_2^+$ | $C_{16}H_7D_3O_4$ |
| **14** | 401 | 401 | 0 | 404 | 404 | 0 | $C_{24}H_{14}D_3O_6^+$ | |
| | | 386 | 15 | | 389 | 15 | $C_{23}H_{11}D_3O_6^{+\bullet}$ | $CH_3^\bullet$ |
| | | 358 | 43 | | 361 | 43 | $C_{22}H_{11}D_3O_5^{+\bullet}$ | $C_2H_3O^\bullet$ |
| | | 329 | 72 | | 332 | 72 | $C_{21}H_{10}D_3O_4^+$ | $C_3H_4O_2$ |
| | | 303 | 98 | | 305 | 99 | $C_{19}H_9D_2O_4^+$ | $C_5H_5DO_2$ |
| | | 226 | 175 | | 228 | 176 | $C_{14}H_8D_2O_3^{+\bullet}$ | $C_{10}H_6DO_3^\bullet$ |
| | | 215 | 186 | | 217 | 187 | $C_{13}H_9D_2O_3^+$ | $C_{11}H_5DO_3$ |
| | | 202 | 199 | | 204 | 200 | $C_{12}H_8D_2O_3^{+\bullet}$ | $C_{12}H_6DO_3^\bullet$ |
| | | 165 | 236 | | 167 | 237 | $C_9H_7D_2O_3^+$ | $C_{15}H_7DO_3$ |
| | | 121 | 280 | | 122 | 282 | $C_7H_4DO_2^+$ | $C_{17}H_{10}D_2O_4$ |
| **15** | 401 | 401 | 0 | 404 | 404 | 0 | $C_{24}H_{14}D_3O_6^+$ | |
| | | 386 | 15 | | 389 | 15 | $C_{23}H_{11}D_3O_6^{+\bullet}$ | $CH_3^\bullet$ |
| | | 358 | 43 | | 361 | 43 | $C_{22}H_{11}D_3O_5^{+\bullet}$ | $C_2H_3O^\bullet$ |
| | | 341 | 60 | | 343 | 61 | $C_{22}H_{11}D_2O_4^+$ | $C_2H_3DO_2$ |
| | | 329 | 72 | | 332 | 72 | $C_{21}H_{10}D_3O_4^+$ | $C_3H_4O_2$ |
| | | 313 | 88 | | 315 | 89 | $C_{21}H_{11}D_2O_3^+$ | $C_3H_3DO_3$ |
| | | 255 | 146 | | 256 | 148 | $C_{15}H_{10}DO_4^+$ | $C_9H_4D_2O_2$ |
| | | 226 | 175 | | 227 | 177 | $C_{14}H_9DO_3^{+\bullet}$ | $C_{10}H_5D_2O_3^\bullet$ |
| | | 202 | 199 | | 204 | 200 | $C_{12}H_8D_2O_3^{+\bullet}$ | $C_{12}H_6DO_3^\bullet$ |
| | | 165 | 236 | | 166 | 238 | $C_9H_8DO_3^+$ | $C_{15}H_6D_2O_3$ |
| | | 121 | 280 | | 122 | 282 | $C_7H_4DO_2^+$ | $C_{17}H_{10}D_2O_4$ |
| **20** | 385 | 385 | 0 | 387 | 387 | 0 | $C_{24}H_{15}D_2O_5^+$ | |
| | | 370 | 15 | | 372 | 15 | $C_{23}H_{12}D_2O_5^{+\bullet}$ | $CH_3^\bullet$ |
| | | 342 | 43 | | 344 | 43 | $C_{22}H_{12}D_2O_4^{+\bullet}$ | $C_2H_3O^\bullet$ |
| | | 325 | 60 | | 326 | 61 | $C_{22}H_{12}DO_3^+$ | $C_2H_3DO_2$ |
| | | 313 | 72 | | 315 | 72 | $C_{21}H_{11}D_2O_3^+$ | $C_3H_4O_2$ |
| | | 297 | 88 | | 298 | 89 | $C_{21}H_{12}DO_2^+$ | $C_3H_3DO_3$ |
| | | 249 | 136 | | 250 | 137 | $C_{17}H_{12}DO_2^+$ | $C_7H_3DO_3$ |
| | | 239 | 146 | | 240 | 147 | $C_{15}H_{10}DO_3^+$ | $C_9H_5DO_2$ |
| | | 165 | 220 | | 166 | 221 | $C_9H_8DO_3^+$ | $C_{15}H_7DO_2$ |
| | | 121 | 264 | | 122 | 265 | $C_7H_4DO_2^+$ | $C_{17}H_{11}DO_3$ |

thus odd-electron radical cations.[31] The fragments of such homolytic cleavage of flavonoids should have stable aromatic structures;[33] the presence of two D atoms in the corresponding deuterated ions indicates the presence of two phenolic hydroxyl groups. Other fragments were even-electron cations.

In the low-mass region, the product ions of compounds **10**, **14**, **15**, and **20** are almost the same as those observed by fragmentation of pyranoapigeninidin 4-vinylphenol, including peaks at *m/z* 226, 202, 165, and 121. This suggests that all five compounds share a common pyrano-3-deoxyanthocyanidin core, with variation confined to the attached aromatic rings.


dx.doi.org/10.1021/jf503330b | J. Agric. Food Chem. 2014, 62, 11536−11546

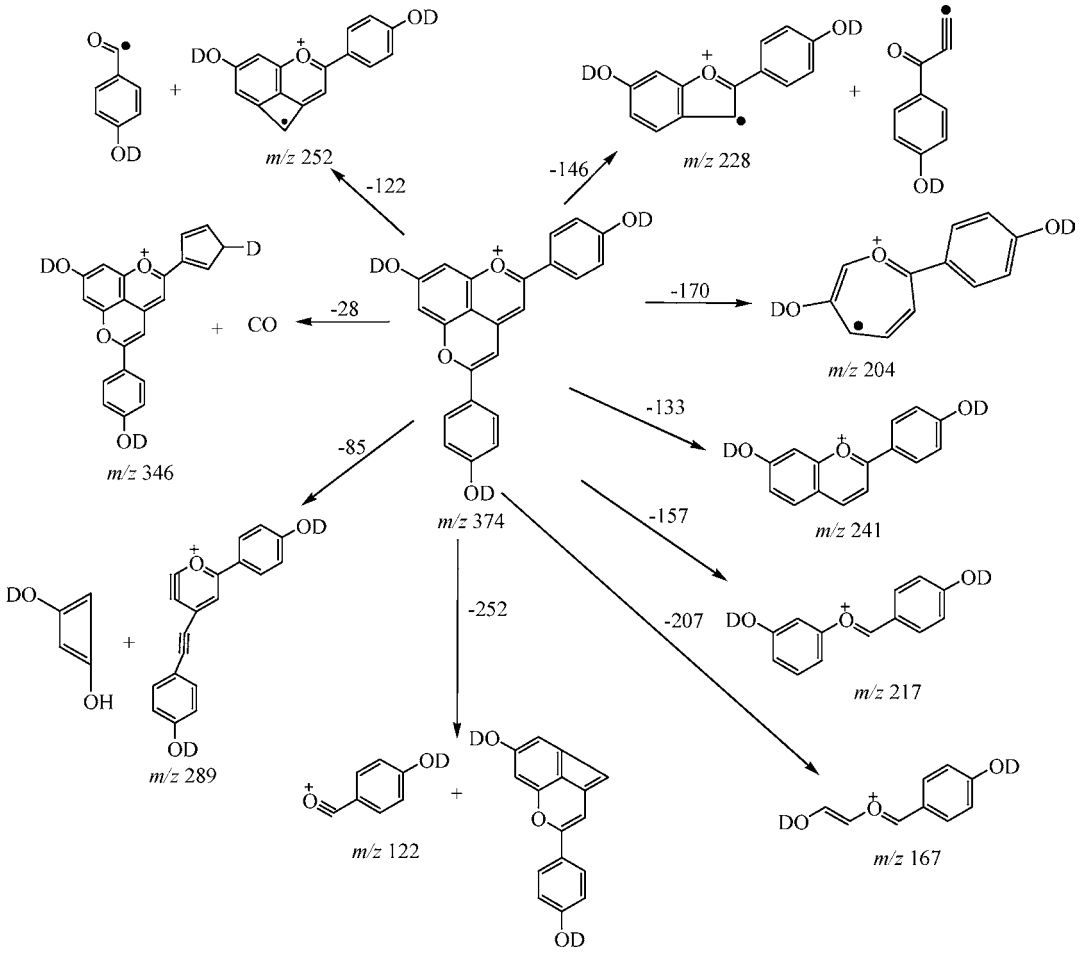


**Figure 4.** Proposed fragmentation pathways of deuterated compound **13**.

For compound **10**, the deuterated ion at *m*/*z* 343 was generated by the loss of $D_2O$ and CO, suggesting that compound **10** contains two adjacent phenolic hydroxyls (Figure 3b). Compounds **14**, **15**, and **20** all had peaks corresponding to the loss of $CH_3^{\bullet}$ and $COCH_3^{\bullet}$ radicals, which likely indicates the presence of OMe moieties.[34] Compounds **14** and **15** have the same molecular ion, suggesting that they are constitutional isomers. To determine the different connectivities, we ran multifragmentation experiments on an Orbitrap mass spectrometer. While both compounds gave precursor ions at *m*/*z* 358, significant differences in the $MS^4$ spectra were observed. Compound **14** largely yielded a single peak at *m*/*z* 329, corresponding to expulsion of COH•. In contrast, compound **15** appears to first lose H• to generate an ion at *m*/*z* 357 and then further degrade to a number of fragment ions.[33] The single peak in compound **14** indicates that loss of COH• is unusually facile, suggesting that there is a hydroxyl moiety adjacent to the OMe (Figure 5). As the core structure of the pyranoanthocyanidin was found in both compounds **14** and **15**, this suggests that one of the attached aromatic rings contains the pattern of interest. In contrast, compound **15** does not appear to be able to rapidly expel COH•, and thus the OMe group is not adjacent to a free hydroxyl. The two most likely structures for these compounds are shown in Figure 5. Compound **14** is formed analogous to pyranoapigeninidin 4-vinylphenol by condensation of apigeninidin and the decarboxylative product of caffeic acid, whereas compound **15** is likely a product of 7-methoxyapigeninidin and ferulic acid. Compound **20** can be identified analogously to compound **15** and is believed to be a product of 4-vinylphenol and 7-methoxyapigenidin (Figure 3e).

## DISCUSSION

Pyranoanthocyanidins are derivatives of anthocyanins that are generated during food processing. They have been previously identified in wine as well as juice from berries, blood orange, and black carrots.[14,35−37] This study tentatively identified four novel pyrano-3-deoxyanthocyanidins by MS/MS experimentation and comparison to a chemically synthesized reference compound, and it confirmed the presence of novel 3-deoxyanthocyanidin adducts with vinylphenol (Table 3 and Figure 3). Fragmentation pathways of pyranodeoxyanthocyanidins were elucidated by using the hydrogen/deuterium exchange technique in mass spectrometry.

A symmetric pyrano-3-deoxyanthocyanidin was previously identified in sorghum, but the pathways leading to its formation remained unknown.[24] Yeast metabolism contributes to the formation of pyranoanthocyanidins in wine maturation;[14,15] however, the formation of pyranoanthocyanidins in wine and unfermented juices was predominantly attributed to a reaction of hydroxycinnamic acids and anthocyanidins.[36−38] The use of defined decarboxylase-positive or -negative lactobacilli indicates that the formation of pyrano-3-deoxyanthocyanidins in fermented sorghum depends on bacterial decarboxylation of hydroxycinnamic acids. This hypothesis was confirmed by chemical synthesis of 3-deoxyanthocyanidin derivatives with

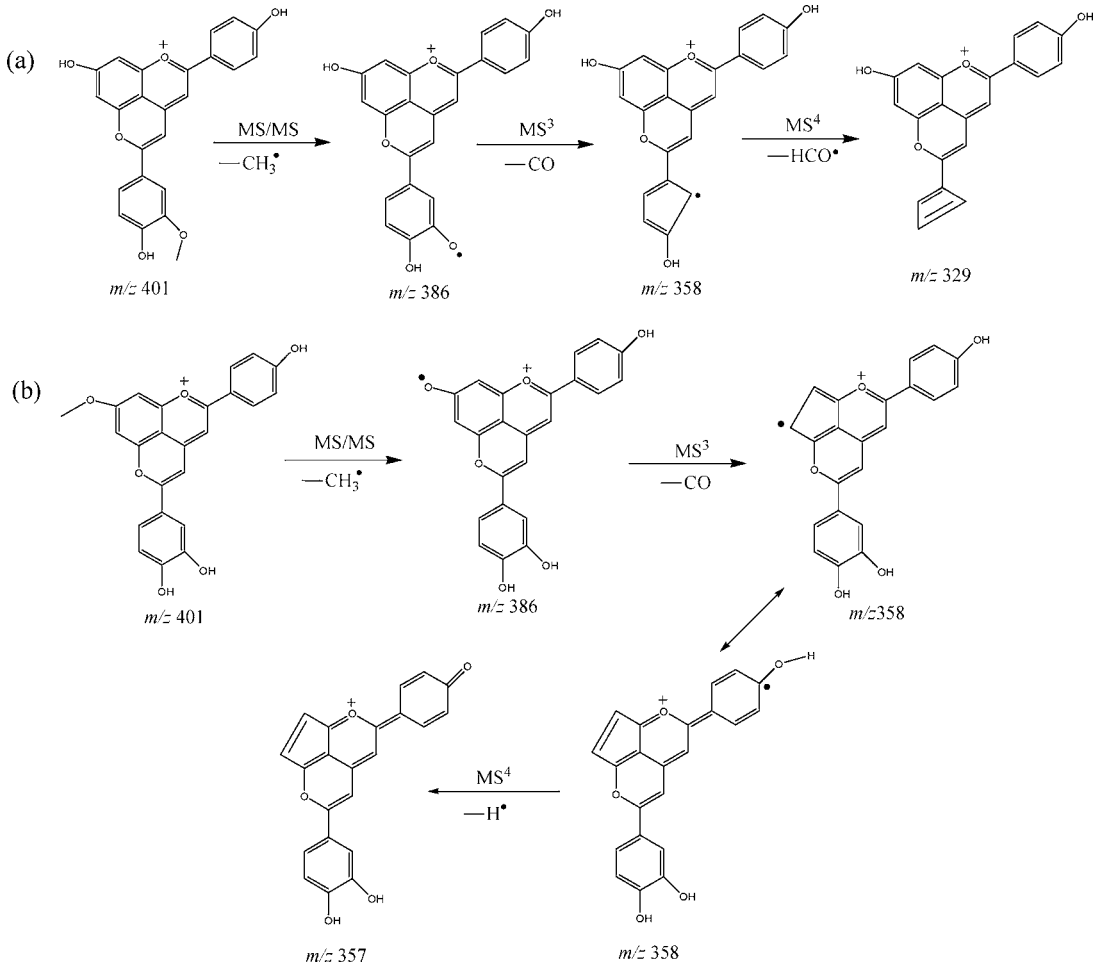


**Figure 5.** Fragmentation pathway of the isomer: (a) compound **14** and (b) compound **15**.

vinylphenol as a reactant; the use of 4-coumaric acid as reactant did not yield comparable adducts (Figure 6).

The novel pyrano-3-deoxyanthocyanidins found (Table 3 and Figure 3) are created via reaction of the most abundant 3-deoxyanthocyanidins in sorghum,[3,5] apigeninidin, and methoxyapigeninidin, with the decarboxylation products of the most abundant hydroxycinnamic acids, vinylphenol (coumaric acid), vinylcatechol (caffeic acid), and vinylguaiacol (ferulic acid) (Figure 6).[3,4,10] In contrast to previous reports,[24] pyrano-3-deoxyanthocyanidins were not identified in unfermented sorghum. We employed pure cultivar sorghum grains that were milled just prior to fermentation, thus minimizing the potential of chemical, microbial, or enzymatic conversions prior to extraction.

In addition to pyrano-3-deoxyanthocyanidins, we identified a second class of compounds, 3-deoxyanthocyanidin−vinylphenol adducts, which are also formed by reaction of 3-deoxyanthocyanidins with vinylphenols (Figure 6). Our study does not provide quantitative data on adduct formation; unfortunately, the compounds were isolated in minute quantity and were unstable in the liquid phase. Both derivatives are formed from the same reactants, 3-deoxyanthocyanidins and vinylphenols, suggesting that the formation of pyrano-3-deoxyanthocyanidins is favored at the conditions of sorghum sourdough fermentation. The identification of 3-deoxyanthocyanidin adducts linked at the C6 position may be attributable to a different reactivity of 3-deoxyanthocyanidins when compared to anthocyanidins or may simply relate to the higher concentration of reactants in sorghum sourdough when compared to wine or fruit juices. Of note, over several hours of storage in deuterated methanol we observed that the proton at C6 in apigeninidin was replaced with deuterium, via corresponding loss of signal at 6.66 ppm. The proton at C8 was unaffected under these conditions, suggesting that the C6 position is the more nucleophilic of the two.

The formation of pyranoanthocyanidins corresponds to color changes during aging of wine and may serve as an indicator of aging.[14,39] Pyranoanthocyanidins are also of interest as food colorants with increased stability, as well as because of their antioxidant properties.[39,40] The elucidation of microbial and chemical pathways leading to conversion of 3-deoxyanthocyanidins in sorghum fermentations is a major milestone toward an improved understanding of sorghum processing and fermentation on nutritional and sensory properties of the resulting cereal products. Results enable further studies to elucidate chemical and biological properties of novel pyrano-3-deoxyanthocyanidins and 3-deoxyanthocyanidin adducts and thus may aid to improve food quality, food security, and health benefits, particularly anticancer activities[7,21] of foods containing bioactive phenolic compounds.[8]

## ■ ASSOCIATED CONTENT

### Supporting Information

LC-DAD-MS data, solid-phase microextraction data, and fragmentation spectra. This material is available free of charge via the Internet at http://pubs.acs.org.

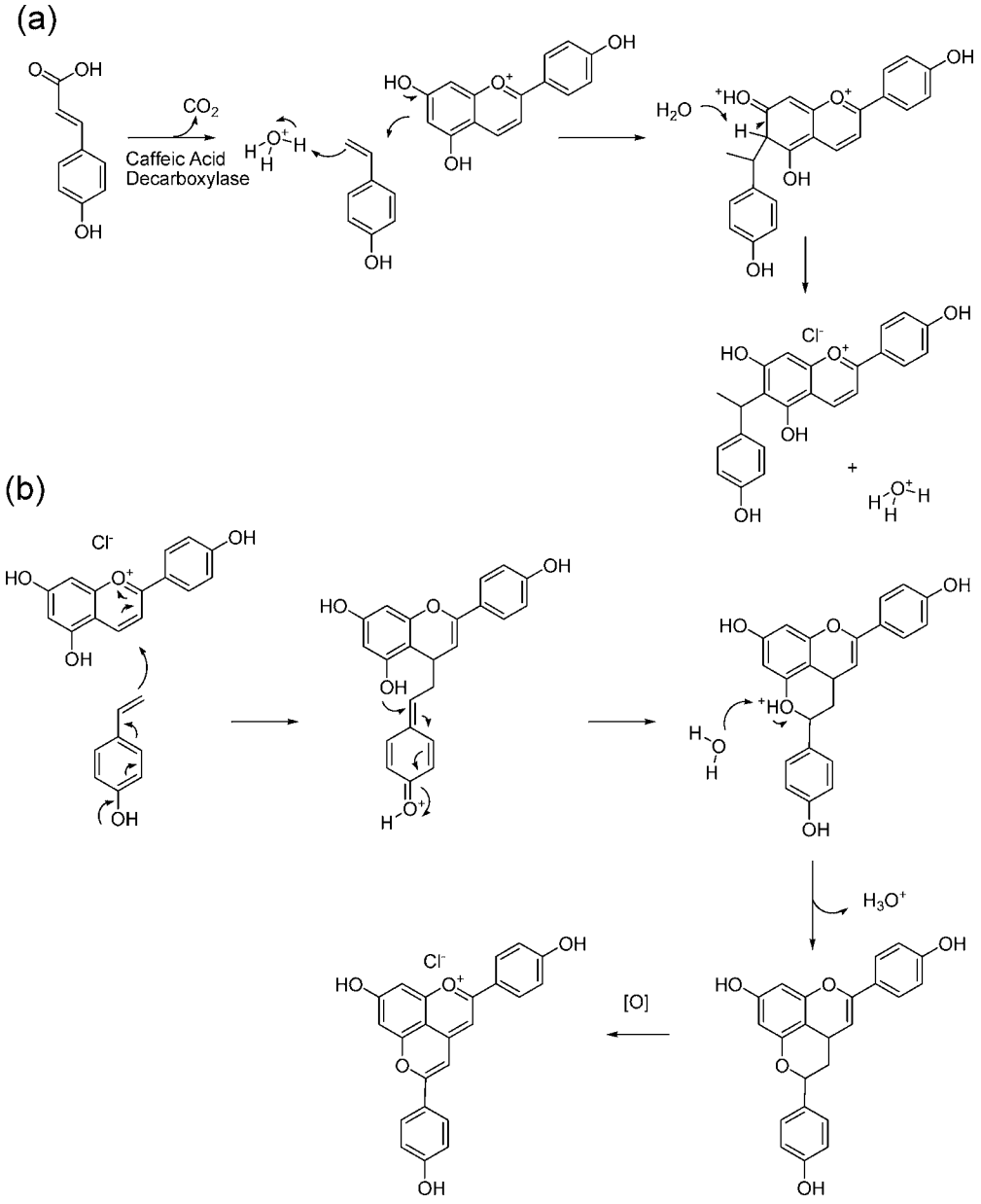


**Figure 6.** Proposed metabolic pathways of novel deoxyanthocyanidins: (a) pathway 1 leading to vinylphenol adducts and (b) pathway 2 leading to pyranoanthocyanidins.

## AUTHOR INFORMATION


### Corresponding Author

*University of Alberta, Department of Agricultural, Food and Nutritional Science, 4-10 Ag/For Centre, Edmonton, AB, T6G 2P5, Canada. E-mail: mgaenzle@ualberta.ca. Phone: + 1-780-492-0774. Fax: + 1-780-492-4265.



### Funding

The National Science and Engineering Council of Canada and the Canada Research Chairs Program are acknowledged for funding.


### Notes

The authors declare no competing financial interest.

## ACKNOWLEDGMENTS

We are grateful to Dr. Bonno Sekwati Monang for providing sorghum samples. Dr. Chengri Piao, Daewoong Pharmaceutical Co., Ltd., South Korea, is acknowledged for support with interpretation of mass spectra.

## REFERENCES


(1) FAO Faostat Gateway. Data retrieved from http://faostat3.fao.org/faostat-gateway/go/to/download/Q/QC/E on June 8, 2014.

(2) Dicko, M. H.; Hilhorst, R.; Gruppen, H.; Traore, A. S.; Laane, C.; van Berkel, W. J. H.; Voragen, A. G. J. Comparison of content in phenolic compounds, polyphenol oxidase, and peroxidase in grains of fifty sorghum varieties. *J. Agric. Food Chem.* **2002**, *50*, 3780−3788.

(3) Dykes, L.; Rooney, L. W. Sorghum and millet phenols and antioxidants. *J. Cereal Sci.* **2006**, *44*, 236−251.

(4) Svensson, L.; Sekwati Monang, B.; Lopez-Lutz, D.; Schieber, A.; Gänzle, M. Phenolic acids and flavonoids in nonfermented and fermented red sorghum (*Sorghum bicolor* (L.) Moench). *J. Agric. Food Chem.* **2010**, *58*, 9214−9220.

(5) Awika, J. M.; Rooney, L. W.; Waniska, R. D. Properties of 3-deoxyanthocyanins from sorghum. *J. Agric. Food Chem.* **2004**, *52*, 4388−4394.

(6) Ibraheem, F.; Gaffoor, I.; Chopra, S. Flavonoid phytoalexin-dependent resistance to anthracnose leaf blight requires a functional yellow seed in *Sorghum bicolor*. *Genetics* **2010**, *184*, 915−926.
(7) Shih, C. H.; Siu, S. O.; Ng, R.; Wong, E.; Chiu, L. C.; Chu, I. K.; Lo, C. Quantitative analysis of anticancer 3-deoxyanthocyanidins in infected sorghum seedlings. *J. Agric. Food Chem.* **2007**, *55*, 254−259.
(8) Nout, M. J. Rich nutrition from the poorest-cereal fermentations in Africa and Asia. *Food Microbiol.* **2009**, *26*, 685−692.
(9) Sekwati-Monang, B.; Gänzle, M. G. Microbiological and chemical characterisation of ting, a sorghum-based sourdough product from Botswana. *Int. J. Food Microbiol.* **2011**, *150*, 115−121.
(10) Awika, J. M.; McDonough, C. M.; Rooney, L. W. Decorticating sorghum to concentrate healthy phytochemicals. *J. Agric. Food Chem.* **2005**, *53*, 6230−6234.
(11) Afify, A.el-M.; El-Beltagi, H. S.; El-Salam, S. M.; Omran, A. A. Biochemical changes in phenols, flavonoids, tannins, vitamin E, $\beta$-carotene and antioxidant activity during soaking of three white sorghum varieties. *Asian Pac. J. Trop. Biomed.* **2012**, *2*, 203−209.
(12) Kayodé, A. P. P.; Mertz, C.; Guyot, J.-P.; Brat, P.; Mouquet-Rivier, C. Fate of phytochemicals during malting and fermentation of type III tannin sorghum and impact on product biofunctionality. *J. Agric. Food Chem.* **2013**, *61*, 1935−1942.
(13) Gänzle, M. G. Enzymatic and bacterial conversions during sourdough fermentation. *Food Microbiol.* **2014**, *37*, 2−10.
(14) de Freitas, V.; Mateus, N. Formation of pyranoanthocyanins in red wines: A new and diverse class of anthocyanin derivatives. *Anal. Bioanal. Chem.* **2011**, *401*, 1463−1473.
(15) Morata, A.; Benito, S.; Loira, I.; Palomero, F.; González, M. C.; Suárez-Lepe, J. A. Formation of pyranoanthocyanins by *Schizosaccharomyces pombe* during the fermentation of red must. *Int. J. Food Microbiol.* **2012**, *159*, 47−53.
(16) Morata, A.; González, C.; Suárez-Lepe, J..A. Formation of vinylphenolic pyranoanthocyanins by selected yeasts fermenting red grape musts supplemented with hydroxycinnamic acids. *Int. J. Food Microbiol.* **2007**, *116*, 144−152.
(17) Dao, L. T.; Takeoka, G. R.; Edwards, R. H.; Berrios, J. D. J. Improved method for the stabilization of anthocyanidins. *J. Agric. Food Chem.* **1998**, *46*, 3564−3569.
(18) Mas, T. A new and convenient one-step synthesis of the natural 3-deoxyanthocyanidins apigeninidin and luteolinidin chlorides from 2,4,6-triacetoxy-benzaldehyde. *Synthesis* **2003**, *12*, 1878−1880.
(19) Selenski, C.; Pettus, T. R. R. (±)-Diinsininone: Made nature's way. *Tetrahedron* **2006**, *62*, 5298−5307.
(20) Kouda-Bonafos, M.; Nacro, M.; Ancian, B. Total assignment of $^{1}$H and $^{13}$C NMR chemical shifts of a natural anthocyanidin, apigeninidin, using two-dimensional COLOC and HMBC techniques. *Magn. Reson. Chem.* **1996**, *34*, 389−392.
(21) Yang, L.; Browning, J. D.; Awika, J. M. Sorghum 3-deoxyanthocyanins possess strong phase II enzyme inducer activity and cancer cell growth inhibition properties. *J. Agric. Food Chem.* **2009**, *57*, 1797−1804.
(22) Geera, B.; Ojwang, L. O.; Awika, J. M. New highly stable dimeric 3-deoxyanthocyanidin pigments from *Sorghum bicolor* leaf sheath. *J. Food. Sci.* **2012**, *77*, C566−C572.
(23) González-Paramás, A. M.; Lopes da Silva, F.; Martín-López, P.; Macz-Pop, G.; González-Manzano, S.; Alcalde-Eon, C.; Pérez-Alonso, J. J.; Escribano-Bailón, M. T.; Rivas-Gonzalo, J. C.; Santos-Buelga, C. Flavanol-anthocyanin condensed pigments in plant extracts. *Food Chem.* **2006**, *94*, 428−436.
(24) Khalil, A.; Baltenweck-Guyot, R.; Ocampo-Torres, R.; Albrecht, P. A novel symmetrical pyrano-3-deoxyanthocyanidin from a *Sorghum* species. *Phytochem. Lett.* **2010**, *3*, 93−95.
(25) Sze, S. K.; Wang, W.; Meng, W.; Yuan, R.; Guo, T.; Zhu, Y.; Tam, J. P. Elucidating the structure of cyclotides by partial acid hydrolysis and LC-MS/MS Analysis. *Anal. Chem.* **2009**, *81*, 1079−1088.
(26) Atanasova, H.; Fulcrand, H.; Le Guernevé, C.; Cheynier, V.; Moutounet, M. Structure of a new dimeric acetaldehyde malvidin 3-glucoside condensation product. *Tetrahedron Lett.* **2002**, *43*, 6151−6153.
(27) Fulcrand, H.; Cameira dos Santos, P.-J.; Sarni-Manchado, P.; Cheynier, V.; Favre-Bonvin, J. Structure of new anthocyanin-derived wine pigments. *J. Chem. Soc., Perkin Trans.* **1996**, *1*, 735−739.
(28) Zhang, N.; Du, Y.; Cui, M.; Xing, J.; Liu, Z.; Liu, S. Probing the interaction of cisplatin with cytochrome *c* by electrospray ionization Fourier transform ion cyclotron resonance mass spectrometry. *Anal. Chem.* **2012**, *84*, 6206−6212.
(29) Winkler, J.; McLafferty, F. W. Stereochemical effects in the chemical ionization mass spectra of cyclic diols. *Tetrahedron* **1974**, *30*, 2971−2976.
(30) Sigsby, M. L.; Day, R. J.; Cooks, R. G. Fragmentation of even electron ions: Protonated amines and esters. *Org. Mass Spectrom.* **1979**, *14*, 556−561.
(31) de Hoffmann, E.; Stroobant, V. Appendix 5. In *Mass Spectrometry Principles and Applications*; De Hoffmann, E., Stroobant, V., Eds.; Wiley: Hoboken, NY, 2007; pp 457−466.
(32) Schildcrout, S. M.; Masnovi, J. Gaseous cation chemistry and chain-length effects in electron ionization and collision-induced dissociation mass spectra of symmetric 1,*n*-*bis*(9-anthracenyl)alkanes. *J. Mass Spectrom.* **2011**, *46*, 572−586.
(33) Hvattum, E.; Ekeberg, D. Study of the collision-induced radical cleavage of flavonoid glycosides using negative electrospray ionization tandem quadrupole mass spectrometry. *J. Mass Spectrom.* **2003**, *38*, 43−49.
(34) Lu, L.; Song, F.-R.; Tsao, R.; Jin, Y.-R.; Liu, Z.-Q.; Liu, S.-Y. Studies on the homolytic and heterolytic cleavage of kaempferol and kaempferide glycosides using electrospray ionization tandem mass spectrometry. *Rapid Commun. Mass Spectrom.* **2010**, *24*, 169−172.
(35) Hillebrand, S.; Schwarz, M.; Winterhalter, P. Characterization of anthocyanins and pyranoanthocyanins from blood orange [*Citrus sinensis* (L.) Osbeck] Juice. *J. Agric. Food Chem.* **2004**, *52*, 7331−7338.
(36) Schwarz, M.; Wray, V.; Winterhalter, P. Isolation and identification of novel pyranoanthocyanins from black carrot (*Daucus carota* L.) juice. *J. Agric. Food Chem.* **2004**, *52*, 5095−5101.
(37) Rein, M. J.; Ollilainen, V.; Vahermo, M.; Yli-Kauhaluoma, J.; Heinonen, M. Identification of novel pyranoanthocyanins in berry juices. *Eur. Food Res. Technol.* **2005**, *220*, 239−244.
(38) Schwarz, M.; Wabnitz, T. C.; Winterhalter, P. Pathway leading to the formation of anthocyanin−vinylphenol adducts and related pigments in red wines. *J. Agric. Food Chem.* **2003**, *51*, 3682−3687.
(39) He, F.; Liang, N. N.; Mu, L.; Pan, Q. H.; Wang, J.; Reeves, M. J.; Duan, C. Q. Anthocyanins and their variation in red wines. II. Anthocyanin derived pigments and their color evolution. *Molecules* **2012**, *17*, 1483−1519.
(40) Azevedo, J.; Oliveira, L., Cruz, L.; Teixeira, N.; Brás, N. F.; De Freitas, V.; Mateus, N. Antioxidant features of red wine pyranoanthocyanins: Experimental and theoretical approaches. *J. Agric. Food Chem.* **2014**, *62*, 7002−7009.

were extracted by shaking the leaf powder in a solution containing 50% (v/v) phenol, 0.45 M sucrose, 5 mM EDTA, 0.2% (v/v) 2-mercaptoethanol, and 50 mM Tris-HCl, pH 8.8 for 30 min at 4 °C. After centrifugation at 5000*g* at 4 °C for 10 min, the phenol phase was transferred to clean tube and proteins were precipitated by adding 5 volumes of ice-cold 0.1 M ammonium bicarbonate (ABC) in methanol followed by overnight incubation at −20 °C. After centrifugation at 5000*g* for 10 min at 4 °C, protein pellets were washed twice with ice-cold 0.1 M ammonium acetate in methanol, twice with ice-cold 80% acetone, and once in ice-cold 70% ethanol.

**Two-Dimensional (2D) Gel Electrophoresis and "In-Gel" Digestion.** Proteins were dissolved in rehydration sample buffer (8 M urea, 2 M thiourea, 2% (w/v) CHAPS, 2% (w/v) Triton X-100, 50 mM DTT, 0.5% ampholytes pH 3−10), and protein concentrations were determined according to Bradford.[23] Then, 50 μg of proteins were analyzed by 2-dimensional electrophoresis (2DE) using 7 cm immobilized pH gradient (IPG) strips with pH range 5−8, as described earlier.[24] Briefly, isoelectric focusing (IEF) was performed using a Protean IEF Cell (Bio-Rad) programmed for active rehydration for 12 h at 50 V followed by 150 V for 150 VH, 500 V for 500 VH, and 4000 V for 15000 VH. After IEF, the IPG strips were equilibrated in 6 M urea containing 30% (v/v) glycerol, 70 mM SDS, and 0.006% (w/v) bromphenol blue) for 15 min in equilibration solution with 1% (w/v) DTT, and then for an additional 15 min in equilibration solution containing 2.5% (w/v) iodoacetamide. Equilibrated IPG strips were placed on top of 10% SDS gels, and electrophoretic separation was performed at 10 mA per gel. Finally, triplicate gels were stained with colloidal Coomassie blue, the images digitalized (GS-800, Bio-Rad, Hercules, CA) at 300 dpi/16 bit grayscale and quantified using PDQuest 8.0 software (Figure 1 of the Supporting Information).

Protein spots present in at least two of the triplicate gels were excised, destained in wash solution [50% acetonitrile (ACN), 50 mM ABC], and dehydrated in 100% ACN. The dehydrated gel plugs were rehydrated in 50 mM ABC containing modified sequencing grade trypsin (Promega) and digested at 37 °C overnight. Tryptic peptides were extracted with 60% ACN containing 1% formic acid (FA). Solutions were reduced to dryness using a Concentrator plus (Eppendorf, Germany). The tryptic peptides were dissolved in 2% ACN containing 0.1% FA and stored at −80 °C until used.

**Protein Identification by Liquid Chromatography-Tandem Mass Spectrometry.** In total, 5 μL of tryptic peptides were separated using a nanoAcquity UPLC system (Waters). Samples were injected onto a Symmetry C18 trap column (20 mm length, 180 μm diameter, and 5 μm particle size). After 3 min of desalting/concentration with 3% ACN containing 0.1% FA at a flow rate 10 μL $min^{-1}$, peptides were separated on an analytical BEH130 C18 column (150 mm length, 75 μm diameter, and 1.7 μm particle size). For quick profiling, a 15 min gradient of 6−40% ACN containing 0.1% FA at a flow rate of 350 nl $min^{-1}$ was applied. The column outlet was connected to a precut noncoated PicoTip emitter (360 μm outer diameter, 20 μm inner diameter, 10 μm tip diameter; New Objective), mounted into the nanospray source of a Q-TOF Premier tandem mass spectrometer (Waters). The instrument was controlled by MassLynx software v. 4.1 (Waters). Basic settings were source temperature, 70 °C; nanospray voltage, 3.4 kV; nebulizer gas pressure, 0.4 bar; and collision gas flow, 0.48 mL $min^{-1}$. Data were acquired using the $MS^E$ method, which performed alternate scans at low and high collision energies. The quadrupole analyzer was operated in the radio frequency mode, allowing all ions to reach the TOF analyzer, so that in a single full-scan run, both precursor ions and accurate fragment masses were detected. In the MS channel, data were collected at a constant collision energy of 4 eV, while in tandem (MS/MS), channel fragments were recorded while the collision energy was ramped up from 20 to 35 eV. Spectra acquisition scan rate was 0.8 s, with a 0.05 s interscan delay; ions with 100−1900 m $z^{-1}$ were detected in both channels. The quadrupole mass profile settings allowed efficient deflection of masses of less than 400 in the low-energy mode, enabling filtering of contaminating ions.

**Analysis of the MS/MS Data.** Peak smoothing was performed, including background-subtraction, centroiding, and deisotoping. Noise filtering thresholds where set at intensity, 1200; low energy, 150; high energy, 20 counts. All data were lock-spray calibrated against Glu-Fibrinopeptide B, using data collected from the reference line during acquisition (500 fmol $\mu L^{-1}$ in 25% ACN with 0.1% FA, flow rate 350 nl $min^{-1}$, scans every 30 s). The lockmass-corrected data were deconvoluted to produce a single accurate monoisotopic mass for each peptide and associated fragment ions. Differently charged precursors were summed. The initial correlation of precursor and fragment ions was achieved by means of time alignment.

The MS/MS data were processed by the ProteinLynx Global Server (PLGS) v. 2.4 (Waters) against an in-house database consisting of sequences downloaded from UniProt during July 2013. In total, 742 Ginkgo species entries, 856836 Spermatophyta UniRef90 databank entries (taxonomy filter *Spermatophyta* and 90% sequence redundancy grouping), and 1573198 *Viridiplantae* entries were included. The databank was randomized to allow efficient correction for false-positive matches. The search parameters used were fixed modification, carbamidomethyl-Cys; variable modification, oxidized Met; one missed cleavage site; at least seven fragment ions per protein; and an automatic error tolerance value. Protein identifications were accepted after manual inspection of probabilistic PLGS assignment at the 95% confidence level. Additional parameters to accept protein identification required at least two peptides matched to the protein sequence, a minimum of three fragment ions per peptide, a 50 ppm tolerance of database-generated theoretical peptide ion masses, and a PLGS score greater than 50. The PLGS score is a statistical measure of accuracy of assignation and was calculated using a Monte Carlo algorithm. A higher score indicates a greater confidence in the assigned protein identity.

## RESULTS

Two-DE combined with MS/MS was used for analysis of the abundant gingko leaf proteins (Figure 1). Using this approach, we reliably quantified 190 abundant 2-DE spots (Table 1 of the Supporting Information), of which 157 were identified by MS/MS (Table 1). These data were used to establish the initial ginkgo leaf proteome reference map (Figure 2). As expected, the most abundant 2-DE spots were identified as ribulose-1,5-bisphosphate carboxylase/oxygenase (RuBisCO) subunits

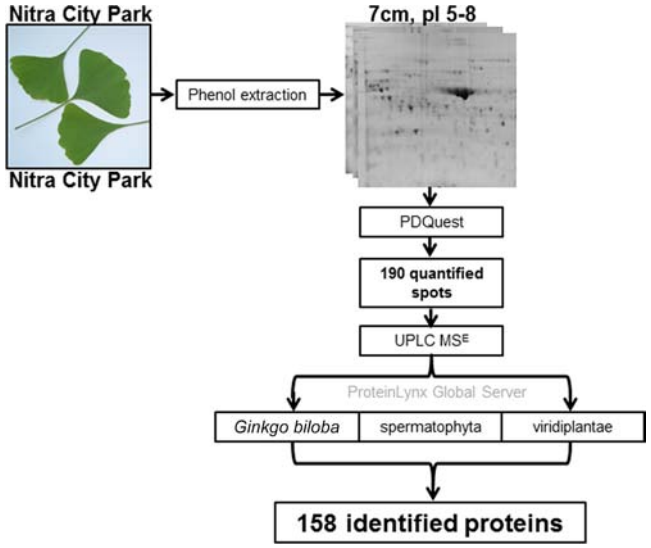


**Figure 1.** Experimental workflow. Proteins were isolated from ginkgo leaves using a phenol-based extraction method and separated by 2D electrophoresis. Protein spots were quantified using the PDQuest software. Excised spots were digested with trypsin, separated by nanoAcquity UPLC and analyzed by MS/MS in the $MS^E$ mode. Proteins were identified using ProteinLynx Global Server.

**Table 1. Proteins Located on the *Ginkgo biloba* L. Leaf Reference Map[a]**

| spot no. | UniProt | description | exp. MW/pI (kDa) | theoret. MW/pI (kDa) | PLGS score | pep | %*V* ± STDEV |
|---|---|---|---|---|---|---|---|
| | | | 01 Metabolism | | | | |
| | | | 01.01 Amino Acids | | | | |
| 3409 | H8YHW0 | adenosylmethionine synthetase | 45/6.24 | 16/6.04 | 143.12 | 2 | 0.28 ± 0.06 |
| 3401 | H8YHW0 | adenosylmethionine synthetase | 49/6.03 | 16/6.04 | 1575.12 | 3 | 0.10 ± 0.02 |
| 3406 | H8YHW0 | adenosylmethionine synthetase | 47/6.22 | 16/6.04 | 1147.95 | 6 | 0.10 ± 0.09 |
| 8401 | Q1M301 | alanine aminotransferase | 50/7.82 | 21/5.19 | 445.85 | 2 | 0.01 ± 0.00 |
| 7209 | A9NUJ0 | aspartate aminotransferase | 23/7.38 | 48/6.99 | 421.16 | 5 | 0.23 ± 0.11 |
| 4402 | M4CBV6 | glutamine synthetase | 40/6.42 | 39/7.91 | 325.49 | 2 | 0.28 ± 0.02 |
| 6307 | I1NWA3 | glycerate dehydrogenase | 40/7.1 | 44/6.37 | 499.95 | 6 | 0.03 ± 0.03 |
| 6704 | Q2YHN6 | methionine synthase | 105/7.1 | 18/5.83 | 461.24 | 6 | 0.16 ± 0.06 |
| 4703 | B0ZQ27 | phenylalanine ammonia lyase | 84/6.63 | 79/5.91 | 59.79 | 2 | 0.42 ± 0.28 |
| | | | 01.03 Nucleotides | | | | |
| 4303 | B9T0A9 | adenosine kinase putative | 37/6.5 | 38/4.99 | 221.05 | 3 | 0.06 ± 0.04 |
| | | | 01.05 Sugars and Polysaccharides | | | | |
| 2504 | B8LNV7 | glucose 1 phosphate adenylyltransferase | 55/5.8 | 58/5.94 | 230.2 | 9 | 0.10 ± 0.01 |
| 4201 | B9T2C3 | UDP glucosyltransferase putative | 29/6.3 | 54/5.68 | 68.26 | 2 | 0.07 ± 0.02 |
| | | | 01.06 Lipid and Sterol | | | | |
| 5701 | H9A985 | acetyl coenzyme A | 90/6.8 | 36/6.9 | 58.46 | 3 | 0.20 ± 0.08 |
| 7801 | H9A985 | acetyl coenzyme A | 110/7.5 | 36/6.9 | 134.48 | 3 | 0.13 ± 0.02 |
| | | | 02 Energy | | | | |
| | | | 02.01 Glycolysis | | | | |
| 4409 | I1KTX8 | phosphoglycerate kinase | 44/6.6 | 50/8.73 | 2168.39 | 12 | 0.46 ± 0.18 |
| 3413 | O24330 | phosphoglycerate kinase | 41/6.28 | 24/6.53 | 84.99 | 3 | 0.28 ± 0.08 |
| 4403 | I1KTX8 | phosphoglycerate kinase | 46/6.4 | 50/8.73 | 869.69 | 8 | 0.19 ± 0.08 |
| 5307 | M7ZR60 | phosphoglycerate kinase | 43/6.6 | 49/5.26 | 730.62 | 5 | 0.17 ± 0.11 |
| 7202 | A9NUC9 | fructose bisphosphate aldolase | 29/7.65 | 43/8.07 | 2368.93 | 10 | 1.14 ± 0.33 |
| 6303 | Q8LK59 | fructose bisphosphate aldolase | 35/7.08 | 34/9.53 | 267.41 | 4 | 0.18 ± 0.09 |
| 6316 | I3SDW4 | fructose bisphosphate aldolase | 30/6.9 | 43/8.2 | 135.71 | 3 | 0.09 ± 0.02 |
| 6310 | B9SJY9 | fructose bisphosphate aldolase | 28/7.32 | 43/8.58 | 228.15 | 4 | 0.07 ± 0.05 |
| 6403 | B9TQJ4 | glyceraldehyde 3 phosphate dehydrogenase | 41/7.12 | 21/5.64 | 866.6 | 3 | 0.35 ± 0.05 |
| 6407 | P12859 | glyceraldehyde 3 phosphate dehydrogenase B | 41/7.4 | 48/7.53 | 4794.78 | 19 | 0.43 ± 0.21 |
| 7302 | P09315 | glyceraldehyde-3-phosphate dehydrogenase A | 35/7.6 | 44/8.26 | 799.35 | 9 | 0.41 ± 0.06 |
| 2206 | A9NRN6 | triosephosphate isomerase | 19/5.63 | 27/4.82 | 1349.52 | 5 | 0.06 ± 0.04 |
| | | | 02.02 Gluconeogenesis | | | | |
| 6305 | G3BMW0 | Malate dehydrogenase | 32/7.1 | 35/9.22 | 2004.64 | 6 | 0.18 ± 0.02 |
| 5302 | O48906 | Malate dehydrogenase | 84/6.6 | 43/7.99 | 512.49 | 8 | 0.10 ± 0.01 |
| | | | 02.07 Pentose phosphate | | | | |
| 7102 | A9NP17 | ribulose-phosphate 3-epimerase | 15/7.5 | 31/7.93 | 594,00 | 4 | 0.09 ± 0.06 |
| 2303 | C4PAW8 | sedoheptulose 1 7 bisphosphatase | 39/5.7 | 42/5.89 | 257.02 | 10 | 0.41 ± 0.06 |
| 5703 | A5AS94 | transketolase | 91/6.9 | 74/6.37 | 220.84 | 4 | 0.22 ± 0.12 |
| 5702 | I1H1V5 | transketolase | 80/6.8 | 80/5.9 | 130.77 | 3 | 0.09 ± 0.00 |
| | | | 02.13 Respiration | | | | |
| 602 | I6N9D1 | ATP synthase subunit alpha | 54/5.05 | 56/4.83 | 635.21 | 10 | 0.34 ± 0.24 |
| 1605 | Q4FGJ3 | ATP synthase subunit alpha | 63/5.13 | 55/4.82 | 11218.78 | 24 | 0.72 ± 0.37 |
| 1611 | I6N9D1 | ATP synthase subunit alpha | 67/5.36 | 56/4.83 | 192.64 | 9 | 0.45 ± 0.12 |
| 2618 | H7CG64 | ATP synthase subunit alpha | 66/5.21 | 56/4.82 | 1317.53 | 17 | 0.38 ± 0.25 |
| 1609 | Q4FGJ3 | ATP synthase subunit alpha | 63/5.32 | 55/4.82 | 3390.77 | 19 | 0.32 ± 0.17 |
| 1507 | Q9MRI7 | ATP synthase subunit beta | 50/5.38 | 50/4.72 | 286.72 | 3 | 0.47 ± 0.26 |
| 1506 | H9A983 | ATP synthase subunit beta | 60/5.36 | 52/4.88 | 21867.13 | 57 | 2.53 ± 1.21 |
| 1607 | H9A983 | ATP synthase subunit beta | 58/5.23 | 52/4.88 | 19197.38 | 46 | 0.65 ± 0.15 |
| 2601 | Q9MRI7 | ATP synthase subunit beta | 60/5.48 | 50/4.72 | 4631.8 | 25 | 0.40 ± 0.14 |
| 2603 | Q9MRI7 | ATP synthase subunit beta | 62/5.6 | 50/4.72 | 399.81 | 6 | 0.07 ± 0.05 |
| | | | 02.30 Photosynthesis | | | | |
| 7203 | D8QZW2 | carbonic anhydrase | 18/7.73 | 22/7.12 | 366.27 | 2 | 0.29 ± 0.08 |
| 5201 | A9NNY0 | carbonic anhydrase | 23/6.75 | 30/6.42 | 135.46 | 2 | 0.17 ± 0.05 |
| 2304 | F8UAA7 | chloroplast rubisco activase | 39/5.93 | 48/6.01 | 1256.55 | 9 | 2.09 ± 1.26 |
| 7804 | G4XWZ6 | glycine decarboxylase complex subunit P | 110/7.58 | 30/6.86 | 282.38 | 5 | 0.26 ± 0.01 |
| 1204 | Q39768 | LHCB | 17/5.31 | 29/5.1 | 13220.84 | 8 | 0.27 ± 0.04 |
| 1110 | Q39768 | LHCB | 16/5.34 | 29/5.1 | 2232.48 | 3 | 0.27 ± 0.15 |
| 2211 | O49079 | oxygen evolving enhancer protein 1 | 26/5.78 | 35/6.24 | 1100.02 | 8 | 0.82 ± 0.12 |
| 3211 | O49079 | oxygen evolving enhancer protein 1 | 23/6.12 | 35/6.24 | 2461.32 | 11 | 0.22 ± 0.05 |

**Table 1. continued**

| spot no. | UniProt | description | exp. MW/pI (kDa) | theoret. MW/pI (kDa) | PLGS score | pep | %V ± STDEV |
|---|---|---|---|---|---|---|---|
| | | 02.30 Photosynthesis | | | | | |
| 3404 | B1PIE1 | RuBisCo oxygenase activase alpha 2 | 41/6.11 | 16/8.58 | 858.56 | 2 | 0.24 ± 0.06 |
| 2307 | B1PIE1 | RuBisCo oxygenase activase alpha 2 | 39/5.57 | 16/8.58 | 337.19 | 2 | 0.19 ± 0.10 |
| 8502 | I6N9F4 | RuBisCo large chain | 55/7.8 | 53/6.3 | 307.84 | 10 | 0.07 ± 0.08 |
| 5303 | I2AP09 | RuBisCo large chain | 41/6.8 | 53/5.97 | 417.05 | 8 | 0.12 ± 0.08 |
| 6601 | P48704 | RuBisCo large chain | 70/7.02 | 49/6.29 | 5734.4 | 4 | 0.10 ± 0.06 |
| 3501 | I2AP09 | RuBisCo large chain | 50/6.15 | 53/5.97 | 709.25 | 11 | 0.10 ± 0.05 |
| 5706 | P48704 | RuBisCo large chain | 83/6.74 | 49/6.29 | 219.14 | 6 | 0.08 ± 0.06 |
| 5912 | E7E875 | RuBisCo large chain | 250/6.9 | 20/6.94 | 1207.35 | 4 | 0.05 ± 0.03 |
| 3818 | P48704 | RuBisCo large chain | 102/6.25 | 49/6.29 | 139.9 | 4 | 0.03 ± 0.02 |
| 5502 | I6N9F4 | RuBisCo large chain | 55/6.8 | 53/6.3 | 6709.48 | 40 | 26.91 ± 2.63 |
| 6509 | I2AP09 | RuBisCo large chain | 55/6.9 | 53/5.97 | 12104.97 | 87 | 10.49 ± 2.79 |
| 4504 | I6N9F4 | RuBisCo large chain | 57/6.63 | 53/6.3 | 2349.38 | 28 | 7.80 ± 2.98 |
| 5501 | I6N9F4 | RuBisCo large chain | 58/6.7 | 53/6.3 | 5352.14 | 31 | 3.66 ± 3.72 |
| 4605 | I6N9F4 | RuBisCo large chain | 58/6.55 | 53/6.3 | 1590.2 | 12 | 1.02 ± 0.12 |
| 6814 | M8A2T1 | RuBisCo large chain | 180/6.83 | 46/5.71 | 240.85 | 6 | 0.29 ± 0.24 |
| 2616 | K9LMB1 | RuBisCo large chain | 66/5.21 | 53/5.98 | 70.41 | 3 | 0.24 ± 0.04 |
| 6501 | J7QBH1 | RuBisCo large chain | 57/7.07 | 22/5.4 | 12207.37 | 12 | 5.45 ± 3.69 |
| 6506 | E7E875 | RuBisCo large chain | 54/7.35 | 20/6.94 | 3631.08 | 6 | 0.43 ± 0.21 |
| 4602 | H8YV26 | RuBisCo large chain | 57/6.47 | 25/5.72 | 1666.18 | 10 | 0.41 ± 0.38 |
| 6508 | H8YV26 | RuBisCo large chain | 58/7.42 | 25/5.72 | 1357.03 | 3 | 0.27 ± 0.23 |
| 5907 | H8YV26 | RuBisCo large chain | 250/6.83 | 25/5.72 | 962.31 | 6 | 0.15 ± 0.06 |
| 7505 | O98722 | RuBisCo large subunit | 55/7.58 | 53/6.42 | 253.89 | 8 | 0.30 ± 0.07 |
| 604 | P21239 | RuBisCO large subunit binding protein | 67/5.05 | 58/4.64 | 134.75 | 3 | 0.34 ± 0.10 |
| 2403 | B1PIE1 | RuBisCo oxygenase activase alpha 2 | 42/5.56 | 16/8.58 | 606.05 | 2 | 0.29 ± 0.06 |
| 2402 | A9UHW7 | RuBisCo oxygenase activase small isoform | 45/5.56 | 48/8.18 | 458.21 | 9 | 0.08 ± 0.05 |
| | | 03 Cell Growth/Division | | | | | |
| 7803 | C0L3G8 | mother of FT and TFL1 like protein | 110/7.5 | 24/10.1 | 259.96 | 3 | 0.22 ± 0.02 |
| | | 04 Transcription | | | | | |
| 1108 | K9LNQ8 | DNA directed RNA polymerase | 13/5.2 | 78/9.66 | 77.05 | 2 | 0.14 ± 0.10 |
| 6706 | D4P3L6 | Ndly protein | 90/7.2 | 47/9.01 | 83.36 | 3 | 0.29 ± 0.11 |
| | | 04.1901 General TFs | | | | | |
| 2401 | Q20BK8 | class III homeodomain leucine zipper protein | 50/5.5 | 92/5.86 | 71.69 | 6 | 1.93 ± 0.99 |
| 6810 | A8HQJ4 | global transcription factor | 110/7.4 | 126/4.97 | 86.4 | 4 | 0.11 ± 0.01 |
| 6807 | K4CPZ3 | transcription factor KAN2 | 115/7.3 | 16/6.76 | 137.04 | 2 | 0.12 ± 0.04 |
| 807 | A1IKZ7 | transcription factor Tbx4 fragment | 133/5.0 | 17/9.37 | 74.11 | 2 | 0.14 ± 0.04 |
| | | 04.1904 Specific TFs | | | | | |
| 2404 | D7THU3 | agamous-like MADS-box protein AGL15-like | 48/5.7 | 21/9.5 | 185.27 | 5 | 0.13 ± 0.09 |
| | | 05 Protein Synthesis | | | | | |
| | | 05.01 Ribosomal Proteins | | | | | |
| 3804 | K9LMH5 | 50S ribosomal protein L14 | 103/6.1 | 14/9.39 | 199.07 | 5 | 0.11 ± 0.09 |
| | | 05.04 Translation Factors | | | | | |
| 8501 | H1ZY27 | putative elongation factor 1 alpha | 53/7.8 | 18/6.61 | 291.32 | 2 | 0.20 ± 0.11 |
| 6813 | Q1HPA9 | elongation factor 2 | 110/7.00 | 9/9.41 | 318.95 | 2 | 0.16 ± 0.05 |
| 6803 | O23755 | elongation factor 2 | 110/7.08 | 94/5.88 | 200.78 | 11 | 0.14 ± 0.05 |
| 7703 | P86349 | elongation factor G | 90/7.9 | 12/5.69 | 595.6 | 3 | 0.04 ± 0.01 |
| | | 06 Protein Destination and Storage | | | | | |
| | | 06.01 Folding and Stability | | | | | |
| 1702 | M0VTF2 | 70 kDa heat shock protein | 85/5.01 | 62/9.45 | 539.93 | 9 | 0.50 ± 0.15 |
| 2602 | A7Y7L7 | GloEL protein chaperonin 60 kDa | 67/5.5 | 18/10.53 | 1436.29 | 5 | 0.26 ± 0.11 |
| 3705 | M1B4C8 | heat shock cognate 70 kDa | 82/6.2 | 63/4.85 | 105.64 | 4 | 0.14 ± 0.05 |
| 1706 | P27322 | heat shock cognate 70 kDa protein 2 | 86/5.44 | 71/4.88 | 1701.94 | 13 | 0.34 ± 0.11 |
| 1705 | J3NEA8 | heat shock protein 70 | 86/5.4 | 71/7.9 | 1145.28 | 14 | 0.32 ± 0.25 |
| 3704 | D8RBE2 | heat shock protein 70 | 82/6.2 | 72/4.98 | 83.65 | 4 | 0.11 ± 0.03 |
| 2707 | A2XF47 | heat shock protein 70 | 87/6.0 | 45/4.93 | 111.68 | 5 | 0.08 ± 0.06 |
| | | 06.13 Proteolysis | | | | | |
| 3809 | P84565 | ATP dependent Clp protease | 103/6.3 | 8/4.17 | 696.96 | 3 | 0.19 ± 0.04 |
| 3807 | P84565 | ATP dependent Clp protease | 98/6.1 | 8/4.17 | 743.91 | 3 | 0.19 ± 0.05 |
| 3810 | P84565 | ATP dependent Clp protease | 97/6.3 | 8/4.17 | 1181.43 | 4 | 0.09 ± 0.06 |
| 3803 | P84565 | ATP dependent Clp protease | 104/6.1 | 8/4.17 | 274.81 | 2 | 0.09 ± 0.04 |
| 2706 | O82150 | ATP dependent zinc metalloprotease FTSH | 79/6.0 | 77/5.65 | 370.31 | 12 | 0.16 ± 0.03 |

**Table 1. continued**

| spot no. | UniProt | description | exp. MW/pI (kDa) | theoret. MW/pI (kDa) | PLGS score | pep | %V ± STDEV |
|---|---|---|---|---|---|---|---|
| | | 06.13 Proteolysis | | | | | |
| 4301 | I1LZJ2 | CAAX prenyl protease 2 | 36/6.4 | 38/8.54 | 96.2 | 2 | 0.26 ± 0.03 |
| 7807 | I1MXB2 | glycine dehydrogenase [decarboxylating] | 110/7.6 | 114/7.05 | 589.17 | 10 | 0.12 ± 0.13 |
| 8801 | O49954 | glycine dehydrogenase decarboxylating | 110/7.9 | 113/6.53 | 124.33 | 7 | 0.08 ± 0.05 |
| | | 06.20 Storage Proteins | | | | | |
| 6707 | Q8LPD3 | conlinin n 1 | 75/7.3 | 19/7.49 | 3504.32 | 2 | 0.03 ± 0.01 |
| 2405 | Q39772 | ginnacin | 42/5.8 | 51/8.0 | 95.72 | 3 | 0.69 ± 0.18 |
| 2406 | Q39772 | ginnacin | 46/5.8 | 51/8.0 | 65.8 | 7 | 0.50 ± 0.06 |
| 1202 | Q39772 | ginnacin | 25/5.1 | 51/8.0 | 93.6 | 4 | 0.40 ± 0.24 |
| 6302 | Q39772 | ginnacin | 32/7.1 | 51/8.0 | 93.06 | 4 | 0.35 ± 0.05 |
| 1214 | Q39772 | ginnacin | 18/5.0 | 51/8.0 | 134.23 | 5 | 0.35 ± 0.34 |
| 6309 | Q39772 | ginnacin | 37/7.2 | 51/8.0 | 95.07 | 4 | 0.24 ± 0.17 |
| 3701 | Q39772 | ginnacin | 73/6.1 | 51/8.0 | 92.51 | 5 | 0.10 ± 0.09 |
| 2506 | Q39772 | ginnacin | 50/5.9 | 51/8.0 | 70.87 | 6 | 0.16 ± 0.03 |
| 2407 | Q39772 | ginnacin | 47/5.9 | 51/8.0 | 75.19 | 4 | 0.15 ± 0.09 |
| 2502 | Q39772 | ginnacin | 49/5.7 | 51/8.0 | 63.87 | 4 | 0.15 ± 0.04 |
| 7601 | Q39772 | ginnacin | 57/7.5 | 51/8.0 | 50.7 | 3 | 0.12 ± 0.05 |
| 3706 | Q39772 | ginnacin | 74/6.24 | 51/8.0 | 66.55 | 5 | 0.16 ± 0.03 |
| 2802 | Q39772 | ginnacin | 103/6.0 | 51/8.0 | 88.29 | 4 | 0.04 ± 0.03 |
| 2708 | Q39772 | ginnacin | 77/6.0 | 51/8.0 | 88.29 | 4 | 0.01 ± 0.01 |
| 2704 | B7U6L4 | globulin 3 | 81/5.8 | 66/7.76 | 138.55 | 6 | 0.08 ± 0.03 |
| | | 10 Signal Transduction | | | | | |
| | | 1 Receptors | | | | | |
| 2715 | G7I4I2 | pheromone receptor like protein | 72/5.9 | 34/10.0 | 52.99 | 3 | 0.12 ± 0.02 |
| | | 11 Disease/Defense | | | | | |
| 2208 | Q6S9Z8 | ASR protein | 25/5.6 | 20/5.2 | 5891.91 | 8 | 0.70 ± 0.42 |
| 2204 | Q6S9Z8 | ASR protein | 25/5.5 | 20/5.2 | 3348.01 | 2 | 0.61 ± 0.07 |
| 2416 | Q6S9Z8 | ASR protein | 42/5.9 | 20/5.2 | 92.3 | 2 | 0.52 ± 0.52 |
| 2209 | Q6S9Z8 | ASR protein | 24/5.6 | 20/5.2 | 1910.87 | 3 | 0.41 ± 0.36 |
| 2302 | Q6S9Z8 | ASR protein | 33/5.5 | 20/5.2 | 97.93 | 2 | 0.11 ± 0.01 |
| | | 11.05 Stress (And Defense) Responses | | | | | |
| 5204 | B8YNY1 | ascorbate peroxidase | 18/6.8 | 27/5.8 | 3561.47 | 16 | 0.20 ± 0.03 |
| 6104 | B8YNY1 | ascorbate peroxidase | 17/6.8 | 27/5.8 | 2035.51 | 13 | 0.06 ± 0.05 |
| 3101 | B8YNX9 | superoxide dismutase | 14/6.2 | 27/6.9 | 260.77 | 4 | 0.28 ± 0.13 |
| 7105 | A6N9I6 | superoxide dismutase | 14/7.5 | 26/9.3 | 293.49 | 4 | 0.08 ± 0.09 |
| 5105 | B8YNX9 | superoxide dismutase | 14/6.4 | 27/6.9 | 1243.84 | 6 | 0.03 ± 0.02 |
| | | 11.06 Detoxification | | | | | |
| 4305 | Q01908 | ATP synthase gamma chain 1 | 36/6.5 | 41/8.1 | 354.9 | 2 | 0.24 ± 0.03 |
| 4309 | Q01908 | ATP synthase gamma chain 1 | 33/6.5 | 41/8.1 | 145.2 | 2 | 0.22 ± 0.10 |
| 4401 | A0MQ80 | monodehydroascorbate reductase | 47/6.3 | 47/5.2 | 248.68 | 5 | 0.06 ± 0.03 |
| 1113 | G7II43 | NAD P H quinone oxidoreductase | 15/5.1 | 30/9.4 | 74.35 | 2 | 0.30 ± 0.39 |
| 3305 | F6GY60 | peroxidase 12-like | 49/6.1 | 36/5.4 | 720.67 | 2 | 0.14 ± 0.02 |
| 1107 | H6VND7 | peroxiredoxin 2 | 13/5.1 | 30/7.1 | 1543.6 | 6 | 0.10 ± 0.08 |
| | | 12 Protein of Unknown Function (PUF) | | | | | |
| 8010 | M5XFL4 | chloro diff and palisade dev-related protein | 9/7.7 | 30/9.4 | 1213.14 | 2 | 0.05 ± 0.05 |
| 4103 | E4MXM1 | mRNA clone RTFL01 39 N23 | 17/6.6 | 50/5.7 | 154.17 | 2 | 0.13 ± 0.11 |
| 1201 | Q5QNF4 | Os01g0217100 protein | 23/5.1 | 19/10.2 | 422.25 | 2 | 0.35 ± 0.41 |
| 3403 | Q5QNF4 | Os01g0217100 protein | 43/6.0 | 19/10.2 | 607.16 | 2 | 0.27 ± 0.02 |
| 7301 | Q5QNF4 | Os01g0217100 protein | 42/7.6 | 19/10.2 | 693.39 | 4 | 0.06 ± 0.05 |
| 6804 | B9I1Z7 | predicted protein | 110/7.2 | 26/9.0 | 76.7 | 3 | 0.06 ± 0.04 |
| 2803 | A9PIA4 | predicted protein n | 110/6.0 | 24/7.5 | 445.74 | 2 | 0.11 ± 0.04 |
| 1501 | G7KFS4 | putative uncharacterized protein | 55/5.1 | 19/10.2 | 147.34 | 2 | 0.31 ± 0.24 |
| 5101 | M0TUE2 | uncharacterized protein | 14/6.7 | 44/6.4 | 84.73 | 2 | 0.19 ± 0.09 |
| 6702 | M4ECD1 | uncharacterized protein | 105/7.0 | 41/4.9 | 104.43 | 2 | 0.15 ± 0.05 |
| 915 | M0U8E4 | uncharacterized protein | 250/5.0 | 17/9.4 | 183.62 | 2 | 0.15 ± 0.06 |
| 6701 | M4EFH1 | uncharacterized protein | 85/7.0 | 15/5.0 | 347.02 | 2 | 0.11 ± 0.01 |
| 2605 | K3XJ71 | uncharacterized protein | 70/5.8 | 39/12.1 | 150.54 | 3 | 0.07 ± 0.01 |
| 3408 | M1CP73 | zinc finger CCCH domain-containing protein 11 | 40/6.2 | 48/6.8 | 131.11 | 4 | 0.21 ± 0.21 |

**Table 1. continued**

| spot no. | UniProt | description | exp. MW/pI (kDa) | theoret. MW/pI (kDa) | PLGS score | pep | %*V* ± STDEV |
|---|---|---|---|---|---|---|---|
| | | | 20 Secondary Metabolism | | | | |
| | | | 20.1 Phenylpropanoids/Phenolics | | | | |
| 1206 | K7YEU4 | caffeoyl CoA O methyltransferase | 21/5.4 | 29/5.5 | 537.88 | 4 | 0.19 ± 0.03 |
| 303 | G3EKI9 | cinnamoyl CoA reductase | 36/5.1 | 36/7.1 | 57.26 | 2 | 0.51 ± 0.15 |
| | | | 20.07 Flavonoids | | | | |
| 4306 | Q5XLY0 | anthocyanidin reductase | 36/6.6 | 37/5.5 | 1405.2 | 8 | 0.12 ± 0.03 |
| 6405 | Q6RIB2 | chalcone synthase | 41/7.3 | 43/6.3 | 174.41 | 6 | 0.28 ± 0.14 |
| 6204 | M1T9X3 | isoflavone reductase like protein | 28/7.4 | 33/6.2 | 445.65 | 5 | 0.20 ± 0.16 |
| | | | 20.99 Others | | | | |
| 5401 | I1NIQ0 | GDP-mannose 3,5-epimerase | 49/6.7 | 31/5.6 | 1077.03 | 10 | 0.12 ± 0.05 |
| 2210 | F6H9A9 | thiamine thiazole synthase 1 chloroplastic | 27/5.7 | 37/5.7 | 690.37 | 6 | 0.19 ± 0.01 |

[a]The table includes 2-DE spot number, UniProt accession number; description/name, observed MW (kDa)/p*I*, deduced MW (kDa)/p*I*, PLGS (Protein Lynx Global Server) score, number of peptides matched to protein sequence, and relative volume of 2-DE spot ± SD (%V ± STDEV) of biological triplicate analyses (Table 1 of the Supporting Information).

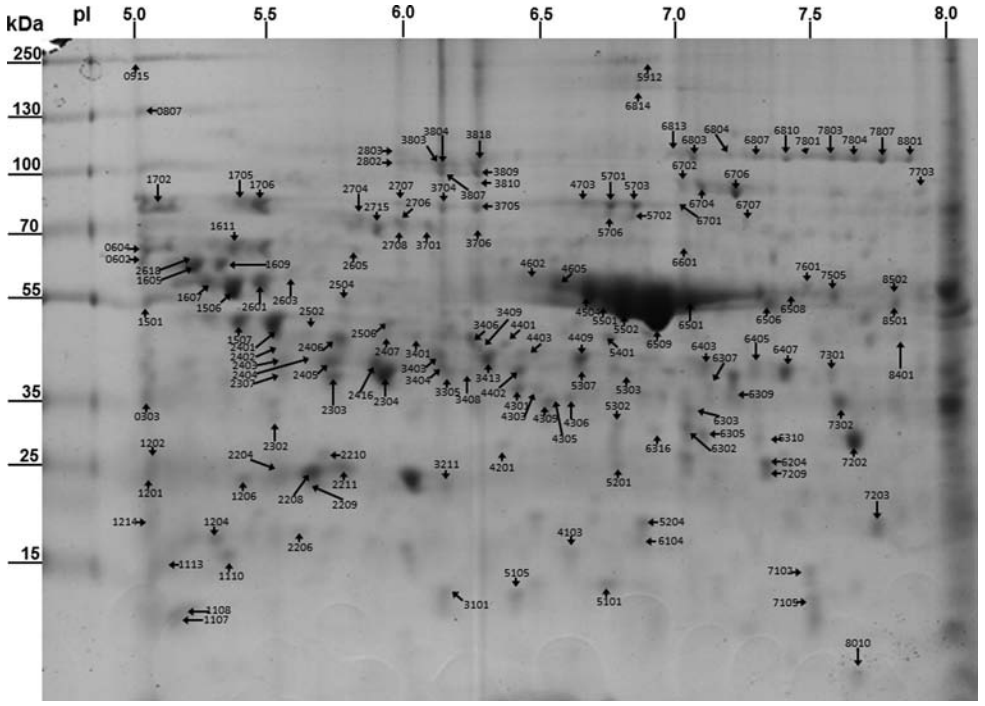


**Figure 2.** Map positions of 157 proteins extracted from *Ginkgo biloba* L. leaves. This quantitative reference map was established using 7 cm IPG strips (p*I* 5−8), PDQuest software (version 8.0), and Q-TOF Premier mass spectrometer.

(spots 5502, 6509, 4504, 6501, and 5501). The next most abundant proteins were ATP synthase (spot 1506), RuBisCO activase (spot 2304), and the class III homeodomain leucine-zipper protein C3HDZ3 (spot 2401) (Figure 2). The 2-DE spots with the lowest abundance values that contained an identifiable protein were spot 2708 (ginancin), followed by spot 8401 (alanine aminotransferase), spot 5105 (superoxide dismutase), and spot 6307 (protein similar to glycerate dehydrogenase/hyrdoxypyruvate reductase.

**Most of the Identified Ginkgo Leaf Proteins Were Assigned to the Energy Group.** Identified proteins presented on the reference map were assigned to one of 10 functional groups (Figure 3) according to Bevan et al.[25] Only one primary function was assigned per protein. Most of the identified proteins were associated with the energy group (61). Within this group, 24 2-DE spots were identified as subunits of RuBisCO. In total, 10 2-DE spots were identified as ATP synthase subunits (Table 1), 4 spots were identified as fructosebisphosphate aldolase, and another 4 as phosphoglycerate-kinase.

The second most populated category is proteins associated with destination/storage.[31] Within this group, 14 2-DE spots were identified as ginnacin, the 11S ginkgo seed storage protein.[26] Four 2-DE spots were identified as subunits of the ATP-dependent Clp protease (Table 1). A total of 16 proteins associated with disease/defense comprise the third largest functional group (Table 1). Five 2-DE spots contained proteins associated with abscisic acid stress and ripening (ASR).[27] The fourth largest functional group was proteins of unknown function (PUF).[15]

The relative volumes of all proteins within a particular functional class were summed in order to determine the most abundant functional group (Figure 2 of the Supporting Information. Proteins associated with energy contributed more than 70% to total protein abundance, followed by those associated with destination/storage, and disease/defense. The

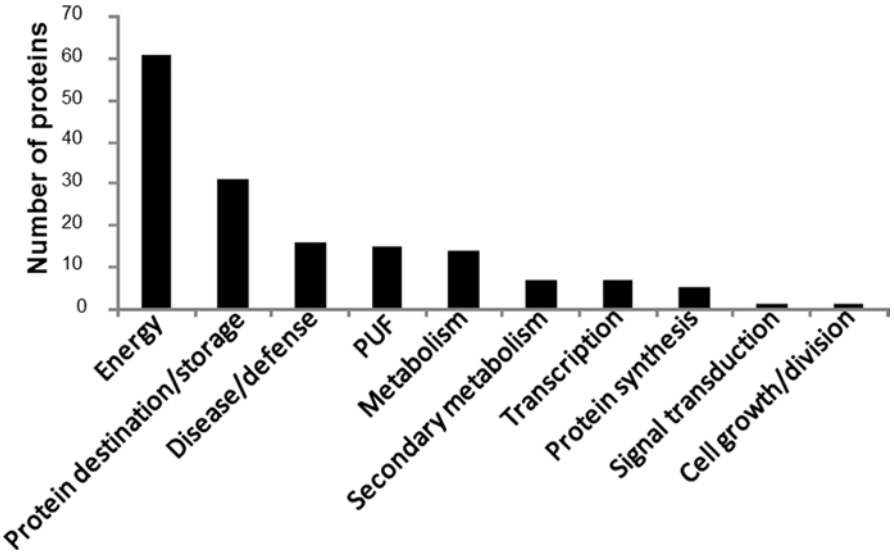


**Figure 3.** Functional classification of 157 proteins identified from *Ginkgo biloba* L. leaves, based upon the method of Bevan et al.[25]

fourth most abundant functional group was proteins associated with transcription, followed by PUF (Figure 2 of the Supporting Information).

**Abundant Protein of Unknown Function Is Similar to Nucleolar Protein 58 of the King Cobra.** We detected 14 proteins of unknown function (PUF). These proteins were subjected to BLASTP searches in order to reveal similarity with known proteins (Table 2 of the Supporting Information). The most abundant protein in this group was Os01g0217100 (spots 1201, 3403, and 7301) with UniProt accession number Q5QNF4 (Table 1). The NCBI Blast search revealed that the amino acid sequence of this unknown protein is 53% similar to the amino acid sequence of a purine permease from Foxtail millet (*Setaria italica*) (Table 2 of the Supporting Information). Unexpectedly, the second most abundant PUF was a putative uncharacterized protein (G7KFS4, spot 1501) that has the closest similarity (56%) to nucleolar protein 58 from the king cobra (*Ophiophagus hannah*) (Table 2 of the Supporting Information). Third most abundant PUF was the uncharacterized protein with UniProt accession M0TUE2 (Table 1). A BLAST search failed to reveal similarity to any known protein (Table 2 of the Supporting Information).

## DISCUSSION

The aim of this study was to use 2-DE based proteomics approach to establish a reference map of most abundant ginkgo leaf proteins. The application of a proteomics strategy for the characterization of medicinal plants is not new (e.g., studies of *Catharanthus roseus*,[28] *Pinellia ternata*,[29] *Podophyllum hexandrum*,[30] and Indian ginseng[31]). The previous analyses yielded meaningful results, such as in the case of *Gynura procumbens*, where the 92 characterized proteins from leaves included miraculin, a taste-masking agent with high commercial value.[32]

The majority of the proteins presented on the reference map (Figure 2) are involved with photosynthesis and energy metabolism. The abundance of many of these proteins in leaf proteomes has been noted previously (e.g., teak,[13] Indian ginseng,[31] *Gynura procumbens*,[32] barrel medic,[33] tomato,[34] holm oak,[18] and *Miscanthum sinensis*[35]). In the present study, we detected multiple spots containing subunits of RuBisCO (spots 5502, 6509, 4504, 6501, and 5501), the enzyme that catalyzes the first step of carbon fixation in the Calvin cycle, and the most abundant protein in the Ginkgo leaf proteome. Chloroplastidial ATP synthase, which generates ATP using a proton gradient, was represented by 10 2-DE spots on the reference map and was the second most abundant leaf protein (Figure 2). Half of the ATP synthase spots were identified as the $\alpha$-subunit and the other five as the $\beta$-subunit (Table 1).

Glycolytic enzymes are well-represented on the 2-DE reference map. Four spots were identified as fructose-bisphosphate aldolase (FBA), which catalyzes the aldol cleavage of fructose-1,6-bisphosphate to glyceraldehyde 3-phosphate and dihydroxyacetone-phosphate. Another three 2-DE spots (6407, 6403, and 7302) were identified as glyceraldehyde 3 phosphate dehydrogenase, which catalyzes the conversion of glyceraldehyde 3 phosphate to D-glycerate-1,3-bisphosphate. Two 2-DE spots (5302 and 6305) were identified as the Krebs cycle enzyme NAD-malate dehydrogenase.

Several stress-related proteins are present on the 2-DE map, including ascorbate peroxidase (APX, spots 5204 and 6104) and superoxide dismutase (SOD, spots 3101, 5105, and 7105). The APX reaction is part of the ascorbate-glutathione cycle for protection against oxidative stress. It uses two molecules of ascorbate to reduce $H_2O_2$ to water.[36] The SOD reaction is also involved with $H_2O_2$ detoxification.[37]

**Proteins Associated with Secondary Metabolism and Proteins of Unknown Function are Abundant in the Ginkgo Leaf Proteome.** Many of the spots on the reference map correspond to enzymes involved in secondary metabolism. Secondary metabolites are valuable targets for industrial applications.[38,39] It is known that Ginkgo leaves contain biologically active terpenes and a range of flavonoid glycosides.[40] More than 38 leaf flavonoids have been isolated so far.[41] Elaboration of the flavone core structure yields structurally related compounds with diverse functions.[42,43] In the present study, we detected 5 proteins associated with flavonoid metabolism: caffeoy-CoA O-methyltransferase (spot 1206), cinnamoyl-CoA reductase (spot 303), anthocyanidin reductase (spot 4306), an isoflavone reductase-like protein (spot 6204), and chalcone synthase (spot 6405). Chalcone synthase catalyzes the first committed step in flavonoid biosynthesis,[44] producing chalcone from which all other

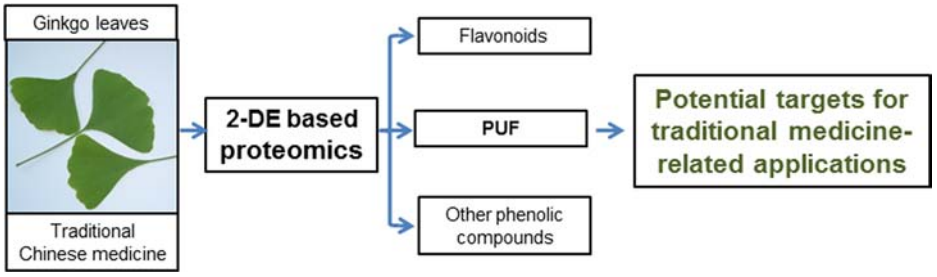


**Figure 4.** Quantitative analysis of proteins associated with synthesis of phenolic and flavonoids compounds with ethnobotanical applications. This approach was also applied to analysis of proteins of unknown function (PUF) that are potential targets for further analysis and with potential use in nontraditional medical applications.

flavonoids are derived. Anthocyanidin reductase (spot 4306) converts anthocyanidins to their corresponding 2,3-cis-flavan-3-ols and is responsible for formation of epicatechin and epigallocatechin in *Arabidopsis* and *Medicago*.[45] Flavonoids comprise a diverse group of polyphenolic compounds with neuroprotective properties in models of Alzheimer's disease, stroke, and Parkinson's disease.[46] Isoflavone reductase reduces achiral isoflavones to chiral isoflavanones in Ginkgo.[47] Cinnamoyl-CoA reductase (CCR) and caffeoyl-CoA O-methyltransferase (CCoAOMT) are enzymes active in phenylpropanoid biosynthesis. The CCR-catalyzed reaction is the first step of the lignin-specific branch of the phenylpropanoid pathway and is a key enzyme responsible for quality and quantity of lignin.[48−50]

Proteins with unknown function (PUF) are the fifth-most abundant functional group on an established map of ginkgo leaf proteome (Figure 2). Most abundant PUF was Os01g0217100 protein from rice (spot s1201, 3403, and 7301) with UniProt accession number Q5QNF4 (Table 1). Using the BLAST algorithm to search the NCBI databases revealed that the amino acid sequence of this protein is 77% similar to rice amino acid transporter-like protein (Table 2 of the Supporting Information). The nucleotide sequence for this protein was described during the sequencing of rice genome.[51]

The second-most abundant PUF was a putative uncharacterized protein (G7KFS4) that is for 56% similar to nucleolar protein 58 characterized from the blood of the king cobra (*Ophiophagus hannah*)[52] (Table 2 of the Supporting Information). Third-most abundant PUF protein was uncharacterized protein (spot 5101, M0TUE2). This protein showed similarity only to other unknown proteins (Table 2 of the Supporting Information). Additionally, this study quantified 10 other unknown proteins from ginkgo leaves (Table 1). It should be noted that unknown proteins constitute more than half of the proteins in plant genomes.[53] The characterization of unknown proteins is one of the greatest challenges of postgenomics biology and should lead to a broader understanding of metabolic processes. The ginkgo leaf PUF's constitute a pool of targets related to traditional medicine-related applications (Figure 4).

## CONCLUSIONS

A quantitative proteomics approach to analysis of the ginkgo leaf proteome led to detection of several proteins associated with secondary metabolism (Figure 4). Additionally, we also detected 14 proteins of unknown function that constitute pool of potential targets for ethnobotanical applications (Figure 4). Follow-up studies will be required to further characterize the ginkgo leaf PUF's and their potential contributions to the health benefits alluded to for centuries in traditional Chinese medicine.

## ASSOCIATED CONTENT

### Supporting Information

Supplemental Figure 1. Two-DE gels of the Ginkgo leaf proteome, presented in biological triplicate. Supplemental Figure 2. The summed relative volumes (%*V*) for all proteins assigned to each functional group. Supplemental Table 1. Relative volumes (%*V*) of all quantified 2-DE spots presented on 7 cm 2-DE gels of pH 5−8. Supplemental Table 2. The results of BLASTP queries of proteins of unknown functions (PUF) against NCBInr protein database, sorted by percent identity (max ident). The top three matches are shown. This material is available free of charge via the Internet at http://pubs.acs.org.

## AUTHOR INFORMATION

### Corresponding Author

*E-mail: hajduch@savba.sk. Tel: 421-37-6943346. Fax: 421-37-7336660.

### Funding

This research was partially funded by the European Community under project no. 26220220180: Building Research Centre "AgroBioTech" and by the Research & Development Operational Program funded by the ERDF, Centre of Excellence for White-Green Biotechnology (ITMS 26220120054).

### Notes

The authors declare no competing financial interest.

## REFERENCES

(1) Chen, L. Q.; Li, C. S.; Chaloner, W. G.; Beerling, D. J.; Sun, Q. G.; Collinson, M. E.; Mitchell, P. L. Assessing the potential for the stomatal characters of extant and fossil Ginkgo leaves to signal atmospheric CO2 change. *Am. J. Bot.* **2001**, *88*, 1309−1315.

(2) McKenna, D. J.; Jones, K.; Hughes, K. Efficacy, safety, and use of ginkgo biloba in clinical and preclinical applications. *Alternative Therapies in Health and Medicine* **2001**, *7*, 70.

(3) Tremouillaux-Guiller, J.; Rohr, T.; Rohr, R.; Huss, V. A. R. Discovery of an endophytic alga in Ginkgo biloba. *Am. J. Bot.* **2002**, *89*, 727−733.

(4) Major, R. T. The ginkgo, the most ancient living tree. The resistance of Ginkgo biloba L. to pests accounts in part for the longevity of this species. *Science (New York, N.Y.)* **1967**, *157*, 1270−1273.

(5) DeFeudis, F. V.; Drieu, K. Ginkgo biloba extract (EGb 761) and CNS functions: Basic studies and clinical applications. *Curr. Drug Targets* **2000**, *1*, 25−58.

(6) Glisson, J.; Crawford, R.; Street, S. The clinical applications of Ginkgo biloba, St. John's wort, saw palmetto, and soy. *Nurse Practitioner* **1999**, *24*, 35−6.
(7) Smith, J. V.; Luo, Y. Studies on molecular mechanisms of Ginkgo biloba extract. *Appl. Microbiol. Biotechnol.* **2004**, *64*, 465−472.
(8) Mazza, M.; Capuano, A.; Bria, P.; Mazza, S. Ginkgo biloba and donepezil: A comparison in the treatment of Alzheimer's dementia in a randomized placebo-controlled double-blind study. *European Journal of Neurology* **2006**, *13*, 981−985.
(9) Ude, C.; Schubert-Zsilavecz, M.; Wurglics, M. Ginkgo biloba extracts: A review of the pharmacokinetics of the active ingredients. *Clin. Pharmacokinet.* **2013**, *52*, 727−749.
(10) Sparreboom, A.; Cox, M. C.; Acharya, M. R.; Figg, W. D. Herbal remedies in the United States: Potential adverse interactions with anticancer agents. *J. Clin. Oncol.* **2004**, *22*, 2489−2503.
(11) Sagar, S. M.; Yance, D.; Wong, R. K. Natural health products that inhibit angiogenesis: A potential source for investigational new agents to treat cancer-Part 2. *Current Oncology (Toronto, Ont.)* **2006**, *13*, 99−107.
(12) Abril, N.; Gion, J.-M.; Kerner, R.; Mueller-Starck, G.; Navarro Cerrillo, R. M.; Plomion, C.; Renaut, J.; Valledor, L.; Jorrin-Novo, J. V. Proteomics research on forest trees, the most recalcitrant and orphan plant species. *Phytochemistry* **2011**, *72*, 1219−1242.
(13) Quiala, E.; Jesus Canal, M.; Rodriguez, R.; Yaguee, N.; Chavez, M.; Barbon, R.; Valledor, L. Proteomic profiling of Tectona grandis L. leaf. *Proteomics* **2012**, *12*, 1039−1044.
(14) Valledor, L.; Castillejo, M. A.; Lenz, C.; Rodriguez, R.; Canal, M. J.; Jorrin, J. Proteomic analysis of Pinus radiata needles: 2-DE map and protein identification by LC/MS/MS and substitution-tolerant database searching. *J. Proteome Res.* **2008**, *7*, 2616−2631.
(15) Valledor, L.; Jorrin, J. V.; Luis Rodriguez, J.; Lenz, C.; Meijon, M.; Rodriguez, R.; Jesus Canal, M. Combined proteomic and transcriptomic analysis identifies differentially expressed pathways associated to pinus radiata needle maturation. *J. Proteome Res.* **2010**, *9*, 3954−3979.
(16) Renaut, J.; Lutts, S.; Hoffmann, L.; Hausman, J. F. Responses of poplar to chilling temperatures: Proteomic and physiological aspects. *Plant Biol.* **2004**, *6*, 81−90.
(17) Yuan, K.; Zhang, B.; Zhang, Y.; Cheng, Q.; Wang, M.; Huang, M. Identification of differentially expressed proteins in poplar leaves induced by Marssonina brunnea f. sp Multigermtubi. *J. Genet. Genomics* **2008**, *35*, 49−60.
(18) Valero-Galvan, J.; Gonzalez-Fernandez, R.; Ma Navarro-Cerrillo, R.; Gil-Pelegrin, E.; Jorrin-Novo, J. V. Physiological and proteomic analyses of drought stress response in Holm Oak provenances. *J. Proteome Res.* **2013**, *12*, 5110−5123.
(19) Hu, W.-J.; Chen, J.; Liu, T.-W.; Wu, Q.; Wang, W.-H.; Liu, X.; Shen, Z.-J.; Simon, M.; Chen, J.; Wu, F.-H.; Pei, Z.-M.; Zheng, H.-L. Proteome and calcium-related gene expression in Pinus massoniana needles in response to acid rain under different calcium levels. *Plant and Soil* **2014**, *380*, 285−303.
(20) Yang, N.; Sun, Y.; Wang, Y.; Long, C.; Li, Y.; Li, Y. Proteomic analysis of the low mutation rate of diploid male gametes induced by colchicine in Ginkgo biloba L. *PLoS One* **2013**, 8.
(21) Wei, X.-D.; Shi, D.-W.; Chen, G.-X. Physiological, structural, and proteomic analysis of chloroplasts during natural senescence of Ginkgo leaves. *Plant Growth Regul.* **2013**, *69*, 191−201.
(22) Hajduch, M.; Ganapathy, A.; Stein, J. W.; Thelen, J. J. A systematic proteomic study of seed filling in soybean. Establishment of high-resolution two-dimensional reference maps, expression profiles, and an interactive proteome database. *Plant Physiol.* **2005**, *137*, 1397−1419.
(23) Bradford, M. M. A rapid and sensitive method for the quantitation of microgram quantities of protein utilizing the principle of protein-dye binding. *Anal. Biochem.* **1976**, *72*, 248−54.
(24) Takac, T.; Pechan, T.; Richter, H.; Mueller, J.; Eck, C.; Boehm, N.; Obert, B.; Ren, H.; Niehaus, K.; Samaj, J. Proteomics on brefeldin A-treated arabidopsis roots reveals profilin 2 as a new protein involved in the cross-talk between vesicular trafficking and the actin cytoskeleton. *J. Proteome Res.* **2011**, *10*, 488−501.
(25) Bevan, M.; Bancroft, I.; Bent, E.; Love, K.; Goodman, H.; Dean, C.; Bergkamp, R.; Dirkse, W.; Van Staveren, M.; Stiekema, W.; Drost, L.; Ridley, P.; Hudson, S. A.; Patel, K.; Murphy, G.; Piffanelli, P.; Wedler, H.; Wedler, E.; Wambutt, R.; Weitzenegger, T.; Pohl, T. M.; Terryn, N.; Gielen, J.; Villarroel, R.; De Clerck, R.; Van Montagu, M.; Lecharny, A.; Auborg, S.; Gy, I.; Kreis, M.; Lao, N.; Kavanagh, T.; Hempel, S.; Kotter, P.; Entian, K. D.; Rieger, M.; Schaeffer, M.; Funk, B.; Mueller-Auer, S.; Silvey, M.; James, R.; Montfort, A.; Pons, A.; Puigdomenech, P.; Douka, A.; Voukelatou, E.; Milioni, D.; Hatzopoulos, P.; Piravandi, E.; Obermaier, B.; Hilbert, H.; Dusterhoft, A.; Moores, T.; Jones, J. D. G.; Eneva, T.; Palme, K.; Benes, V.; Rechman, S.; Ansorge, W.; Cooke, R.; Berger, C.; Delseny, M.; Voet, M.; Volckaert, G.; Mewes, H. W.; Klosterman, S.; Schueller, C.; Chalwatzis, N. Project, E. U. A. G., Analysis of 1.9 Mb of contiguous sequence from chromosome 4 of Arabidopsis thaliana. *Nature* **1998**, *391*, 485−488.
(26) Arahira, M.; Fukazawa, C. Ginkgo 11s seed storage protein family messenger-RNA- unusual ASN-ASN linkage as posttranslational cleavage sitE. *Plant Mol. Biol.* **1994**, *25*, 597−605.
(27) Shen, G.; Pang, Y. Z.; Wu, W. S.; Deng, Z. X.; Liu, X. F.; Lin, J.; Zhao, L. X.; Sun, X. F.; Tang, K. X. Molecular cloning, characterization and expression of a novel Asr gene from Ginkgo biloba. *Plant Physiol. Biochem.* **2005**, *43*, 836−843.
(28) Jacobs, D. I.; Gaspari, M.; van der Greef, J.; van der Heijden, R.; Verpoorte, R. Proteome analysis of the medicinal plant Catharanthus roseus. *Planta* **2005**, *221*, 690−704.
(29) Wu, X.; Xiong, E.; An, S.; Gong, F.; Wang, W. Sequential extraction results in improved proteome profiling of medicinal plant Pinellia ternata tubers, which contain large amounts of high-abundance proteins. *PLoS One* **2012**, *7*.
(30) Dogra, V.; Ahuja, P. S.; Sreenivasulu, Y. Change in protein content during seed germination of a high altitude plant Podophyllum hexandrum Royle. *J. Proteomics* **2013**, *78*, 26−38.
(31) Dhar, R. S.; Gupta, S. B.; Singh, P. P.; Razdan, S.; Bhat, W. W.; Rana, S.; Lattoo, S. K.; Khan, S. Identification and characterization of protein composition in Withania somnifera-an Indian ginseng. *J. Plant Biochem. Biotechnol.* **2012**, *21*, 77−87.
(32) Hew, C.-S.; Gam, L.-H. Proteome analysis of abundant proteins extracted from the leaf of Gynura procumbens (Lour.) Merr. *Appl. Biochem. Biotechnol.* **2011**, *165*, 1577−1586.
(33) Watson, B. S.; Asirvatham, V. S.; Wang, L. J.; Sumner, L. W. Mapping the proteome of barrel medic (Medicago truncatula). *Plant Physiology* **2003**, *131*, 1104−1123.
(34) Guo, B.; He, W.; Wu, D.; Che, D.; Fan, P.; Xu, L.; Wei, Y. Proteomic Analysis of Tomato (Lycopersicum esculentum var. cerasifarm) Expressing the HBsAg Gene by 2-Dimensional Difference Gel Electrophoresis. *Plant Foods Hum. Nutr.* **2013**, *68*, 424−429.
(35) Sharmin, S. A.; Alam, I.; Rahman, M. A.; Kim, K.-H.; Kim, Y.-G.; Lee, B.-H. Mapping the leaf proteome of Miscanthus sinensis and its application to the identification of heat-responsive proteins. *Planta* **2013**, *238*, 459−474.
(36) Noctor, G.; Foyer, C. H. Ascorbate and glutathione: Keeping active oxygen under control. *Annu. Rev. Plant Physiol. Plant Mol. Biol.* **1998**, *49*, 249−279.
(37) Kosova, K.; Vitamvas, P.; Prasil, I. T.; Renaut, J. Plant proteome changes under abiotic stress: Contribution of proteomics studies to understanding plant stress response. *J. Proteomics* **2011**, *74*, 1301−1322.
(38) Jacobs, D. I.; van der Heijden, R.; Verpoorte, R. Proteomics in plant biotechnology and secondary metabolism research. *Phytochem. Anal.* **2000**, *11*, 277−287.
(39) Verpoorte, R.; Contin, A.; Memelink, J. Biotechnology for the production of plant secondary metabolites. *Phyto. Rev.* **2002**, *1*, 13−25.
(40) Vanbeek, T. A.; Scheeren, H. A.; Rantio, T.; Melger, W. C.; Lelyveld, G. P. Determination of ginkgolides and bilobalide in ginkgo-biloba leaves and phytopharmaceuticals. *J. Chromatogr.* **1991**, *543*, 375−387.

(41) van Beek, T. A.; Montoro, P. Chemical analysis and quality control of Ginkgo biloba leaves, extracts, and phytopharmaceuticals. *J. Chromatogr. A* **2009**, *1216*, 2002−2032.
(42) Winkel-Shirley, B. Flavonoid biosynthesis. A colorful model for genetics, biochemistry, cell biology, and biotechnology. *Plant Physiol.* **2001**, *126*, 485−493.
(43) Dixon, R. A.; Xie, D. Y.; Sharma, S. B. Proanthocyanidins: A final frontier in flavonoid research? *New Phytol.* **2005**, *165*, 9−28.
(44) Tohge, T.; Yonekura-Sakakibara, K.; Niida, R.; Watanabe-Takahashi, A.; Saito, K. Phytochemical genomics in Arabidopsis thaliana: A case study for functional identification of flavonoid biosynthesis genes. *Pure Appl. Chem.* **2007**, *79*, 811−823.
(45) Xie, D. Y.; Sharma, S. B.; Paiva, N. L.; Ferreira, D.; Dixon, R. A. Role of anthocyanidin reductase, encoded by BANYULS in plant flavonoid biosynthesis. *Science* **2003**, *299*, 396−399.
(46) Spencer, J. P. E. The interactions of flavonoids within neuronal signalling pathways. *Genes Nutr.* **2007**, *2*, 257−273.
(47) Hua, C.; Linling, L.; Feng, X.; Yan, W.; Honghui, Y.; Conghua, W.; Shaobing, W.; Zhiqin, L.; Juan, H.; Yuping, W.; Shuiyuan, C.; Fuliang, C. Expression patterns of an isoflavone reductase-like gene and its possible roles in secondary metabolism in Ginkgo biloba. *Plant Cell Rep.* **2013**, *32*, 637−50.
(48) Zhou, R.; Jackson, L.; Shadle, G.; Nakashima, J.; Temple, S.; Chen, F.; Dixon, R. A. Distinct cinnamoyl CoA reductases involved in parallel routes to lignin in Medicago truncatula. *Proc. Natl. Acad. Sci. U.S.A.* **2010**, *107*, 17803−17808.
(49) Zhong, R. Q.; Morrison, W. H.; Himmelsbach, D. S.; Poole, F. L.; Ye, Z. H. Essential role of caffeoyl coenzyme A O-methyltransferase in lignin biosynthesis in woody poplar plants. *Plant Physiol.* **2000**, *124*, 563−577.
(50) Martz, F.; Maury, S.; Pincon, G.; Legrand, M. cDNA cloning, substrate specificity and expression study of tobacco caffeoyl-CoA 3-O-methyltransferase, a lignin biosynthetic enzyme. *Plant Mol. Biol.* **1998**, *36*, 427−437.
(51) International Rice Genome Sequencing Project. The map-based sequence of the rice genome. *Nature* **2005**, *436*, 793−800.
(52) Vonk, F. J.; Casewell, N. R.; Henkel, C. V.; Heimberg, A. M.; Jansen, H. J.; McCleary, R. J. R.; Kerkkamp, H. M. E.; Vos, R. A.; Guerreiro, I.; Calvete, J. J.; Wuester, W.; Woods, A. E.; Logan, J. M.; Harrison, R. A.; Castoe, T. A.; de Koning, A. P. J.; Pollock, D. D.; Yandell, M.; Calderon, D.; Renjifo, C.; Currier, R. B.; Salgado, D.; Pla, D.; Sanz, L.; Hyder, A. S.; Ribeiro, J. M. C.; Arntzen, J. W.; van den Thillart, G. E. E. J. M.; Boetzer, M.; Pirovano, W.; Dirks, R. P.; Spaink, H. P.; Duboule, D.; McGlinn, E.; Kini, R. M.; Richardson, M. K. The king cobra genome reveals dynamic gene evolution and adaptation in the snake venom system. *Proc. Natl. Acad. Sci. U.S.A.* **2013**, *110*, 20651−20656.
(53) Hanson, A. D.; Pribat, A.; Waller, J. C.; de Crecy-Lagard, V. 'Unknown' proteins and 'orphan' enzymes: The missing half of the engineering parts list - and how to find it. *Biochem. J.* **2010**, *425*, 1−11.

addition, methods to improve the stability of SLN suspensions have been proposed, including (1) using a lipid source that prevents or retards the $\alpha$ to $\beta$ polymorphic transition, (2) adding sufficient emulsifier to completely cover the LNP surfaces in both the liquid and solid states, and (3) using an emulsifier that prevents particle aggregation by increasing the repulsion.

Despite the general use in foods, the permissible amount of emulsifier is often limited by regulations in many countries. Thus, it is not appropriate to use much emulsifier in the preparation of the LNP system for food applications. Meanwhile, sonication is commonly used to prepare emulsion systems, and the cavitation caused by sonication has various physical effects including dispersing molecules in liquids. In this paper, to prevent severe aggregation of LNPs, the effect of sonication during the cooling process was exploited rather than the addition of more emulsifier. For the LNP system, fully hydrogenated canola oil (FHCO) and liquid canola oil (LCO) were used as the solid and liquid lipids, respectively. We explored how the lipid oil (LCO) contents in the FHCO LNPs and the sonication time during the cooling process affected the stability of the dispersion system.

## MATERIALS AND METHODS

**Chemicals.** Lotte Samkang Co. Ltd. (Seoul, Korea) provided us with FHCO, which was composed of 79.5 wt % stearic acid, 8.8 wt % palmitic acid, 4.2 wt % oleic acid, 1.8 wt % lauric acid, 1.6 wt % arachidic acid, 1.4 wt % linoleic acid, 0.9 wt % myrisitc acid, and 1.8 wt % other ingredients. LCO was obtained from CJ Cheiljedang Co. (Seoul, Korea) and consisted of 58.3 wt % oleic acid, 20.0 wt % linoleic acid, 8.3 wt % linolenic acid, 4.4 wt % palmitic acid, 1.8 wt % stearic acid, 1.3 wt % erucic acid, 0.6 wt % arachidic acid, and 5.3 wt % other ingredients. Tween 20 (polyoxyethylene sorbitan monolaurate) was purchased from Sigma-Aldrich Co. (St. Louis, MO, USA). All other chemicals were of analytical reagent grade.

**Lipid Nanoparticle Preparation.** Oil-in-water emulsions were prepared by mixing 5 wt % lipid phase with 95 wt % aqueous phase (10 mM phosphate buffer, 1.67 wt % Tween 20, i.e., a third of the lipid phase weight, pH 7) at 85 °C. The lipid phase was prepared using blended bulk lipid consisting of FHCO and LCO. FHCO was liquefied by heating to 85 °C, and LCO was heated to 85 °C. A range of LCO-to-FHCO weight ratios was used to prepare the lipid phases (0, 10, 20, and 30 wt % of LCO). Coarse oil-in-water emulsions were prepared by homogenizing the oil and aqueous phases together using a high-speed blender (Ultra-Turrax T25D, Ika Werke GmbH & Co., Staufen, Germany) at 8000 rpm for 1 min and then at 11000 rpm for 1 min. The droplet size was further reduced by sonication (VCX 750, Sonics & Materials Inc., Newtown, CT, USA) for 4 min at an amplitude of 60% and a duty cycle of 1 s. To prevent lipid crystallization during emulsion preparation, all experiments were conducted at 95 °C, which was above the melting temperature of FHCO. After droplet size reduction, postsonication (4, 5, or 6 min) was applied to the emulsions as they cooled to 25 °C in a jacketed beaker, after which samples were maintained at room temperature (25 °C). The temperature changes in the emulsion samples during the process were monitored using a data logger (Agilent 34970A, Agilent Technologies Inc., Santa Clara, CA, USA).

**Microscopic Observation.** A drop of LNP sample was placed on a microscope slide and covered using a coverslip. The microstructure of the aggregated particles was observed using a conventional optical microscope (DCM130, Hangzhou HauXin IC Technology Inc., Hangzhou, China) equipped with a digital camera (DCM130E, BW Optics Co., Nanjing, China) and digital image processing software (ScopePhoto version 3.0, Hangzhou Scopetek Opto-Electric Co., Hangzhou, China).

The nanostructure of LNPs prepared using the postsonication process was observed using a transmission electron microscope (JEM1010, JEOL, Tokyo, Japan). First, LNP samples diluted with double-distilled water were placed on a film-coated copper grid and negatively stained with a 1% (w/v) aqueous solution of phosphotungstic acid for 30 s; ultimately, the overflow phosphotunstic acid on the sample was wiped off by filter paper before drying for 1 day at room temperature before observation.[27]

**Determination of Rheological Properties.** Storage modulus ($G'$) and phase angles ($\delta$) of the LNPs undergoing a sol-to-gel transition were measured using a Rheostress RS 100 (Haake Instruments, Karlsruhe, Germany) equipped with a cone and plate measurement system (diameter = 35 mm, cone angle = 1°) and a designated gap of 50 $\mu$m to avoid the effects of single particles. Initially, the shear stress that could cause the gelation of all fresh samples but not destoy the networks among gelled LNPs was determined by the rotational flow test. The stress level of 3 Pa was suitable to observe a time effect of shearing to gelation. Consequently, all time sweep tests were conducted under the controlled stress mode at a stress of 3 Pa and a frequency of 1 Hz.

**Differential Scanning Calorimetry (DSC) Measurement.** The polymorphism of the blended bulk lipids and lipid phases in the prepared suspensions was determined using a differential scanning calorimeter (Diamond DSC, PerkinElmer, Waltham, MA, USA). Each sample (20 ± 5 mg) was placed in a hermetic aluminum pan, which was sealed and equilibrated at room temperature overnight prior to the measurements. An empty pan was used as a reference. The DSC scan started at 25 °C, increased by 5 °C $min^{-1}$ to 95 °C, and then decreased by 5 °C $min^{-1}$ to 10 °C. The crystallinity index (CI) was calculated on the basis of heating thermograms to determine the degree of crystallinity of lipid nanoparticles using the equation[28]

$$\mathrm{CI}\ (\%) = \frac{\Delta H_{\mathrm{m\ LNP}}(\mathrm{J\ g^{-1}}) \times 100}{\Delta H_{\mathrm{m\ FHCO}}(\mathrm{J\ g^{-1}}) \times c_{\mathrm{L}}(\%)} \times 100$$

where $\Delta H_{\mathrm{m\ LNP}}$ is the melting enthalpy of LNPs, $\Delta H_{\mathrm{m\ FHCO}}$ is the melting enthalpy of bulk FHCO, and $c_{\mathrm{L}}$ is the concentration of the lipid phase (i.e., 5 wt %).

**Powder X-ray Diffraction (XRD) Analysis.** The XRD patterns for FHCO stored overnight at room temperature were collected using the X-ray diffractometer (Bruker model D8 advance, Karlsruhe, Germany) with Cu K$\alpha$ radiation at $\lambda$ = 1.54 Å (30 kV, 30 mA). Both results of small-angle X-ray scattering ($2\theta$ = 0−9.1°, 0.005°/s) and wide-angle X-ray scattering ($2\theta$ = 0−40°, 0.2°/s) were obtained with a general area detector diffraction system.

**Measurement of Lipid Nanoparticle Size.** The microstructural size of the LNP microstructure was measured using a laser diffraction analyzer (S3500, Microtrac Inc., Montgomeryville, PA, USA) to figure out the size distribution of aggregated LNPs in the fresh LNP system before (fresh sample) and after the gelation (gelled sample). Samples were stirred continuously throughout the measurements to ensure that they were homogeneous with the water flow option. The particle size was reported as the mean diameter in micrometers of the volume distribution, MV = $\sum V_i d_i / \sum V_i$ (where $V_i$ is the volume percent of particles of diameter $d_i$ in the population).

The gelled LNPs (4.5 mL) were diluted with 40.5 mL of double-distilled water (DDW) in a vial. For the separation of the layer containing the creamed (creaming layer) and noncreamed LNPs (aqueous layer), the vial containing diluted LNPs was tightly sealed with a screw cap and kept overnight at room temperature. The LNPs in the aqueous layer were collected by filtering with a glass microfiber filter with a 1 $\mu$m pore size (GF/B, Whatman Ltd., Fisons, Loughborough, UK) to figure out the size of noncreamed LNP, and their mean nanostructural diameter ($z$-average) was measured using a Zetasizer (Nano ZS, Malvern Instruments Ltd., Worcestershire, UK) using a helium−neon laser ($\lambda$ = 633 nm).

**Quantification of Stable Lipid Nanoparticles.** The diluted LNPs in the vials were passed through a glass microfiber filter with a 1 $\mu$m pore size (GF/B, Whatman Ltd.). The micrometer-sized and aggregated LNPs remaining on the filter were weighed after drying in an oven at 50 °C. The difference in filter weight before and after the

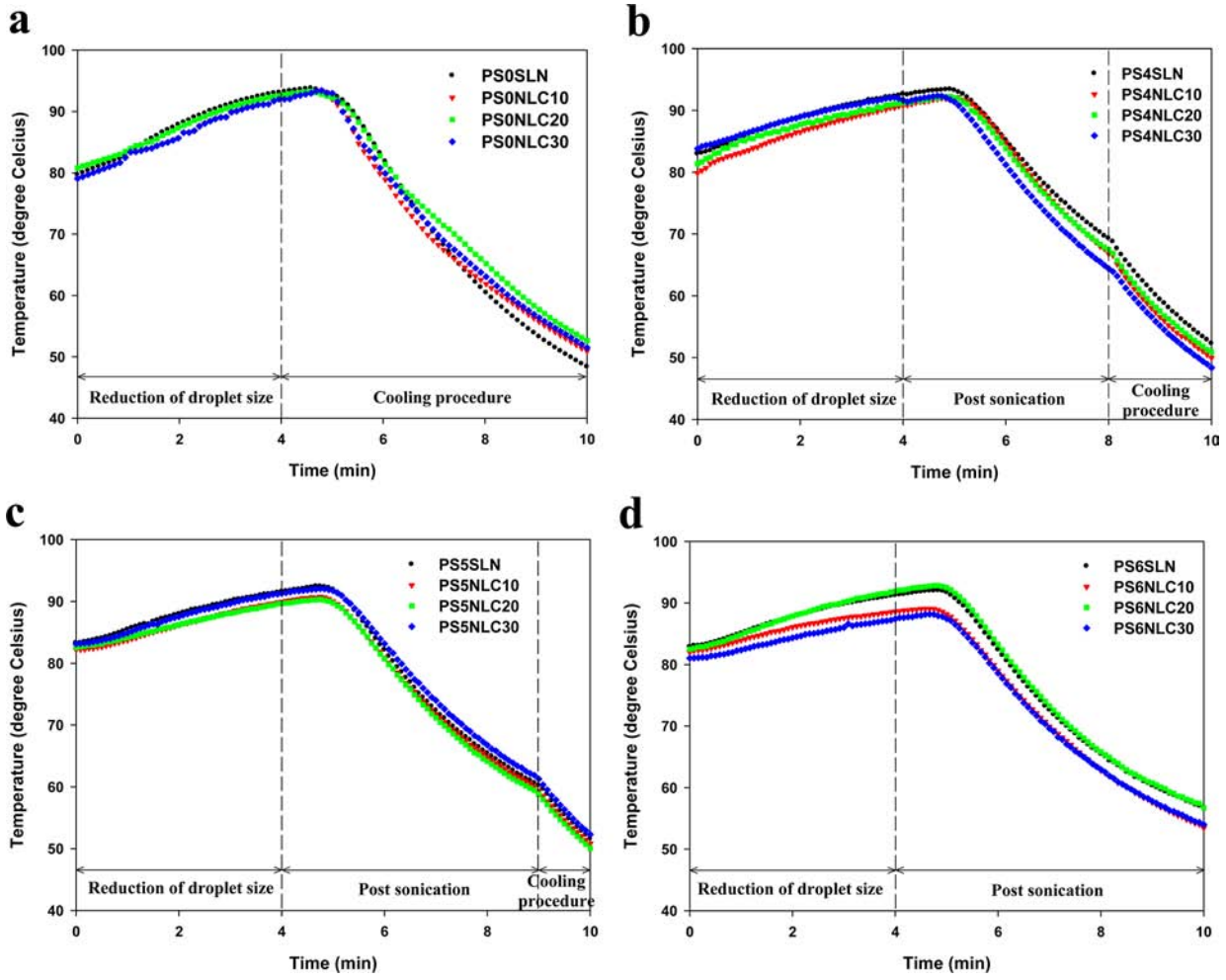


**Figure 1.** Temperature profiles during preparation of lipid nanoparticle suspensions by postsonication for (a) 0, (b) 4, (c) 5, and (d) 6 min, respectively. In the legend, the number following PS (0, 4, 5, and 6) represents the PS procedure time; SLN, NLC10, NLC20, and NLC30 indicate samples prepared using 0, 10, 20, and 30 wt %, respectively, liquid canola oil in the lipid phase.

procedure, which is the weight of the gelled or aggregated LNPs, was recorded.

**Determination of Tween 20 Surface Load.** From the TEM observations, the shape of LNPs was close to a sphere. Therefore, Tween 20 surface load ($\Gamma_s$) was calculated as $\Gamma_s = C_a D/6\Phi$, where $C_a$ is the concentration of the emulsifier adsorbed to the surface of lipid nanoparticles, $D$ is the mean diameter ($z$-average), and $\Phi$ is the lipid phase volume fraction (i.e., 0.05 lipid phase).[29] $C_a$ was determined by subtracting the concentration of Tween 20 suspended as single molecules or micelles from the initial concentration of total emulsifier in the water phase. A total of 2.5 mL of the previously diluted and filtered LNP dispersion was injected into the Sephadex G-25 column (GE Healthcare, Chalfont St Giles, UK) filled with DDW. Next, 1 mL of DDW was serially added, and then each fraction eluted from the column was collected in a microtube. Next, aliquots (1 mL) of the fractions in the fifth and sixth microtubes were selected as samples in which the Tween 20 molecules did not participate in emulsifying activity. Colorimetry for Tween 20 quantification has been reported previously.[30] Briefly, each sample (1 mL) was dried at 80 °C in an oven. The sample was then cooled, and 0.4 mL of ammonium cobaltothiocyanate (ACTC) solution and 0.8 mL of dichloromethane were added. The ACTC solution was fabricated using 3 g of cobalt nitrate hexahydrate and 18 g of ammonium thiocyanate in 100 mL of DDW. Samples were vortexed for 5 s and centrifuged at 10400 RCF for 10 min (Centrifuge Smart 15, Hanil Science Industrial Co., Ltd., Incheon, Korea). After centrifuging, the dichloromethane layer was transferred to a micro quartz cell, and the absorbance at 623.5 nm was determined using a spectrophotometer (Pharmaspec UV-1700, Shimadzu Corp., Kyoto, Japan). The amount of Tween 20 molecules in the LNP dispersion was calculated using standard curves ranging from 0.0167 to 0.0833 wt % for Tween 20 ($r^2$ = 0.9976).

**Statistical Analysis.** All results were analyzed using Tukey's significant difference test with IBM SPSS Statistics version 21.0 (IBM Co., Armonk, NY, USA). Data represent the averages of at least three independent experiments or measurements.

## RESULTS AND DISCUSSION

**Lipid Nanoparticle Preparation.** To differentiate our LNP preparation method from the general methods,[1,6,31] a new step, postsonication (PS), was added. After size reduction, sonication was performed for <6 min in a jacketed beaker maintained at 25 °C. Regardless of the PS time and the liquid oil content in the oil phase, all LNP solutions reached the melting temperature ($T_m$) and the crystallization temperature ($T_c$) of their lipids in approximately 4 and 6 min in the jacketed beaker at 25 °C, respectively (Figure 1). When the temperature of the LNP solution was lower than the $T_c$ of the blended oil, the sonication could partially coalesce the crystallized particles and the oil droplets as the source of turbulent flow rather than preventing the aggregation of LNPs.[21,22] Therefore, all PS should be performed at temperatures above the $T_c$ of the lipid phase, that is, 4−6 min.

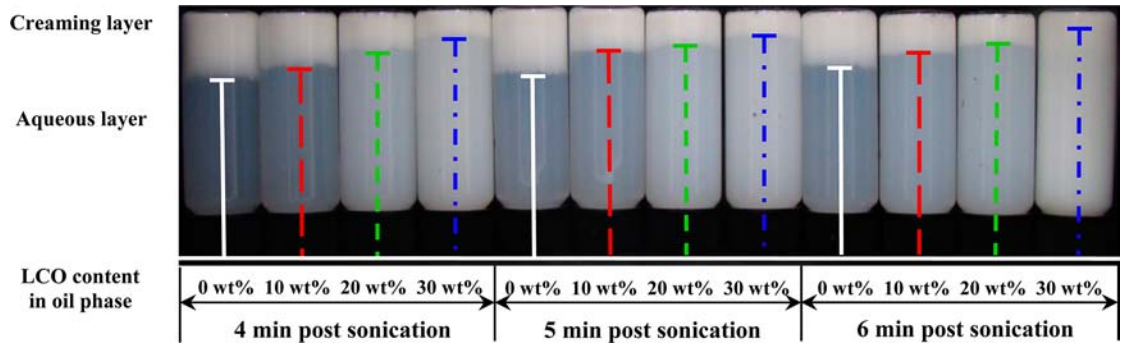


**Figure 2.** Creaming pattern of lipid nanoparticle dispersions diluted 10-fold.

All LNP samples prepared using the lipid containing the LCO concentration at 0−30 wt % would be solidified after the preparation. In other words, the LNP samples were not separately prepared as each of the solidified particles and the liquid droplets in a system, but fabricated as the solid state particles. However, in the LNP system prepared using the lipid containing 40 wt % LCO, both the solid state particles and the liquid state droplets were indirectly verified with DSC thermograms cooling from 95 to −65 °C and then heating from −65 to 95 °C (Figure S1 in Supporting Information). In both the cooling and heating graphs, LNP samples prepared using the lipid at 0−30 wt % LCO did not have the characteristic peaks, whereas distinguishing subzero peaks were observed in both LNP and an emulsion system prepared with 40 wt % LCO and 100 wt % LCO. Thus, the maximum LCO concentration for preparing the LNP system in the present study should be < 40 wt %.

**Visual Stability of Lipid Nanoparticles.** Collisions between some crystallized particles and some noncrystallized droplets could bring partial coalescence during cooling procedure for the LNP preparation,[21] which could force the solid particles together after the fabrication. Additionally, the hydrophobic patches exposed to aqueous solution interacted and aggregated to reduce the surface area exposed to aqueous solution.[32] As a result, the partially coalesced LNPs and the LNPs with surfactant-depleted patches on the surfaces naturally formed aggregates of a micrometer-level size. The creaming phenomenon of highly aggregated LNPs by the partial coalescence and the aggregation when the gelled LNP dispersion was diluted by a 10th part is observed in Figure 2. All samples were divided into two layers, that is, the creaming layer and the aqueous layer, and the length of the vertical line on the samples represents the thickness of the aqueous layer. These observations suggested that increases in the PS time and the LCO content of the oil phase enhance LNP stability.

Stokes' law for hindered settling could explain the creaming phenomenon of the dispersion system composed of LNPs.[33] Under the same composition, the effect of the particle size on the creaming rate predominates over the density difference. Therefore, the aggregated and gelled particles in micrometer size creamed readily, whereas the stable nanosize LNPs were well-dispersed in aqueous solution. Particle size measurement of the aqueous layer was conducted to verify this conjecture. All LNPs in the aqueous layer had mean particle size values (*z*-average) of 114.7−202.3 nm and a unimodal size distribution in the nanoscale range (Table S1 and Figure S1 in the Supporting Information). This supports our hypothesis that LNPs in the aqueous layer are nonaggregated particles.

**Morphological Characteristics of Lipid Nanoparticles and Gelation Phenomenon.** The freshly fabricated LNPs showed fluid properties. However, gelation of all LNP samples had occurred after the application of shear stress >3 Pa, and the fluid characteristics were lost (data not shown). This phenomenon is in agreement with a previous study.[19] Gelation of the LNPs can be accelerated by the interaction between hydrophobic patches on the LNPs, which were created by morphological changes, because the probability of particle collision is increased by shearing. Meanwhile, the partial coalescence among particles could not happen by shearing because the lipid matrix composing LNPs was solidified after the preparation.[21] Therefore, hydrophobic interactions could be an important factor for network formation with LNPs, resulting in their gelation.

Panels a−d of Figure 3 show microstructural morphologies of LNPs fabricated using LCO at diverse concentrations (0−30 wt %) using the PS step for 5 min after shearing and aggregating. LNP flocs at a micrometer-size were independently observed in all samples. The flocs consisted of LNPs, and comparatively small LNPs were suspended in the remaining space within the flocs. The LNPs comprising flocs might have hydrophobic patches or partially coalesced particles; that is, nonstable LNPs and the small LNPs suspended in the water phase might have been covered with Tween 20, that is, stable LNPs. Although it was assumed that LNPs composing flocs underwent morphological changes, shapes extremely deviated from a sphere were not observed among the LNPs in flocs.

After gelation by shearing, the aggregated LNP size changed significantly (Table 1). Before shearing, the LNPs generally showed a large decrease in mean particle diameter with increasing LCO content in the lipid phase. At the same LCO content in the lipid phase, intensive aggregation of the LNPs was observed as the PS time increased, with the exception of the 0 and 30 wt % LCO LNP. However, there was no trend in the change in LNP size following gelation. In addition, multiple peaks in the particle size distribution became unimodal after shearing, independent of the PS time and the LCO-to-FHCO weight ratio. For example, on aggregation in samples fabricated using PS for 5 min, whereas a single peak in a sample prepared using 0 wt % LCO contents simply shifted from 20.17 to 16.96 $\mu$m, multiple peaks in samples fabricated using 10, 20, and 30 wt % LCO contents (10% LCO, 1.50 and 14.27 $\mu$m; 20% LCO, 1.26 and 11.00 $\mu$m; 30% LCO, 1.16, 11.00, and 44.00 $\mu$m) formed unimodal peaks at 16.96, 16.96, 15.56, and 18.50 $\mu$m, respectively (Figure S2 in the Supporting Information). Surfactants on the surface of solidified LNPs could not re-emulsify the interface of LNP aggregates. Moreover, LNP

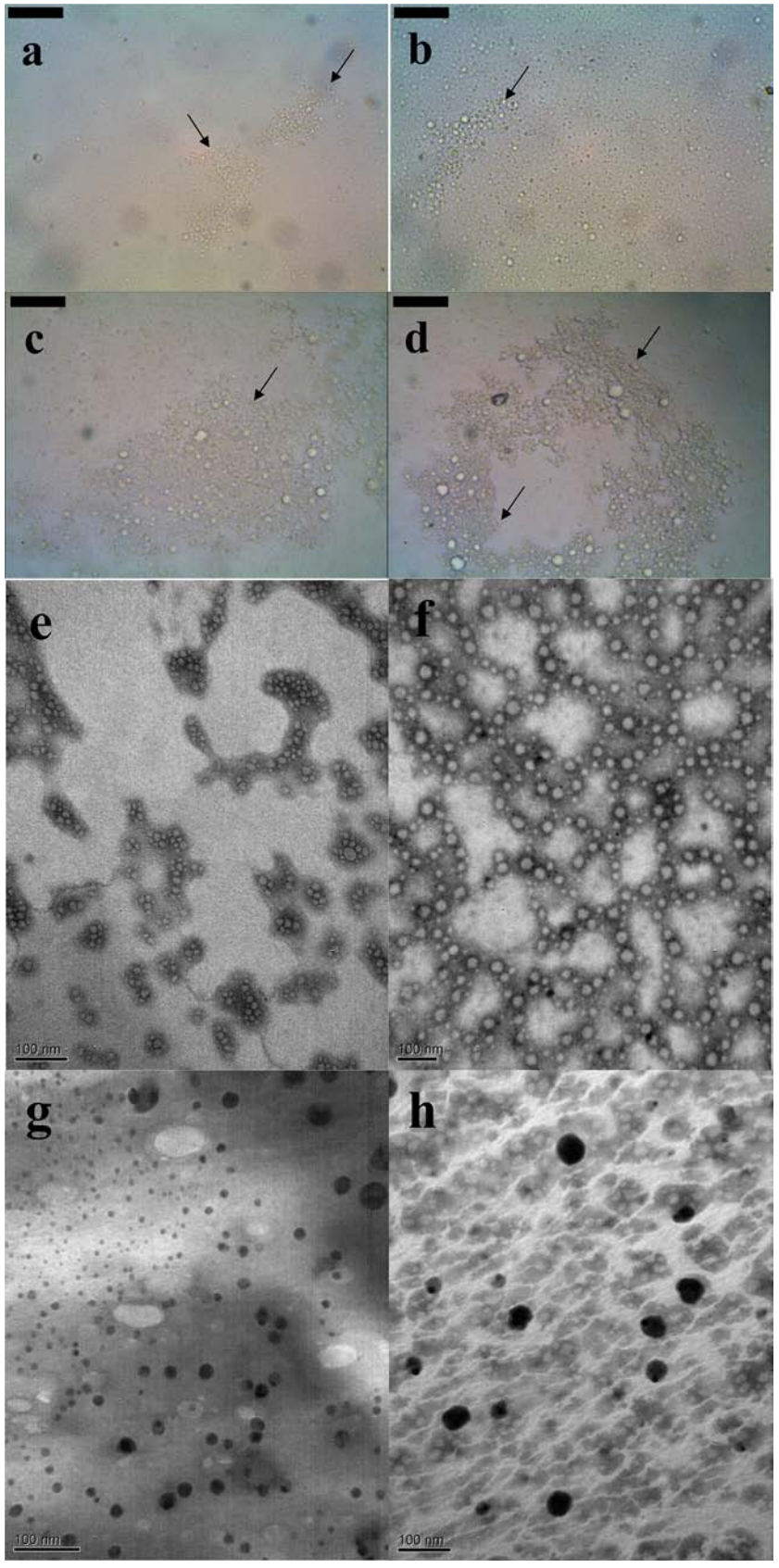


**Figure 3.** Microstructural images of lipid nanoparticles prepared by postsonication for 5 min after shearing and aggregating (optical microscopy): (a) SLN; (b) 10% NLC; (c) 20% NLC; (d) 30% NLC (arrows indicate flocs of aggregated lipid nanoparticles, and scale bars represent 20 $\mu$m). Nanostructural images of lipid nanoparticles prepared by postsonication for 5 min (TEM): (e) SLN; (f) 10% NLC; (g) 20% NLC; (h) 30% NLC.

**Table 1. Mean Diameters (MV) of Aggregated Lipid Nanoparticles before and after Gelling[a]**

| sample | | MV ($\mu$m) | |
|---|---|---|---|
| postsonication (min) | LCO content (wt %) | before shearing | after shearing |
| 0 | 0 | 6.27 ± 0.54 fg | 18.43 ± 1.26 def |
| | 10 | 5.86 ± 0.59 g | 15.39 ± 0.65 g |
| | 20 | 3.42 ± 0.41 i | 17.35 ± 0.57 efg |
| | 30 | 5.46 ± 0.08 gh | 26.00 ± 1.42 b |
| 4 | 0 | 20.10 ± 0.29 ab | 16.15 ± 0.17 fg |
| | 10 | 10.39 ± 0.71 d | 17.28 ± 0.59 efg |
| | 20 | 5.60 ± 0.39 g | 17.97 ± 0.33 cde |
| | 30 | 3.54 ± 0.34 hi | 20.74 ± 0.15 cd |
| 5 | 0 | 21.95 ± 0.21 a | 18.63 ± 0.87 def |
| | 10 | 15.13 ± 0.20 c | 19.14 ± 1.11 de |
| | 20 | 8.20 ± 1.27 ef | 17.62 ± 0.09 efg |
| | 30 | 4.80 ± 0.31 ghi | 23.59 ± 0.24 bc |
| 6 | 0 | 19.98 ± 0.59 ab | 18.20 ± 0.53 defg |
| | 10 | 18.25 ± 0.49 b | 16.46 ± 0.66 efg |
| | 20 | 8.75 ± 0.58 de | 22.42 ± 0.64 c |
| | 30 | 5.94 ± 1.59 g | 34.44 ± 2.80 a |

[a]Different letters a–i in a column are significantly different at $p < 0.05$.

aggregates could not be fully coalesced, which could be just rearranged in another size. Therefore, these results could indirectly support that the shearing in LNP systems could cause the aggregation and gelation of LNPs.

Panels e–h in Figure 3 show the nanostructural morphologies of LNPs prepared using various LCO contents (0–30 wt %) in the oil phase. The majority of each LNPs observed in the TEM images were nanoscaled, whereas micrometer-sized particles were rarely observed. In other words, either the LNPs making up the flocs or the LNPs suspended individually were composed of nanoscale LNPs. This observation suggested that although PS could not completely prevent floc formation, it facilitated maintenance of single particles at a nanoscale size. In addition, the shape of all LNPs in the microscopy was more similar to the sphere rather than the needle-shape referred to by several researchers.[16,19] This morphological shape similar to the sphere might come from the effects of the PS and the LCO content in the lipid matrix, which could cause the increase of surfactant coverage and improve the colloidal stability of the LNP system.

**Rheological Properties of Lipid Nanoparticles.** Changes in $G'$ and $\delta$ were monitored to determine the gelation time during the oscillatory dynamic measurement (Figure 4). Before a certain time, $G'$ remained close to zero and $\delta$ was maintained at a relatively high level (close to 90°), which indicated that the LNP suspension remained fluid. However, over time, the $G'$ of all LNP suspensions increased and their $\delta$

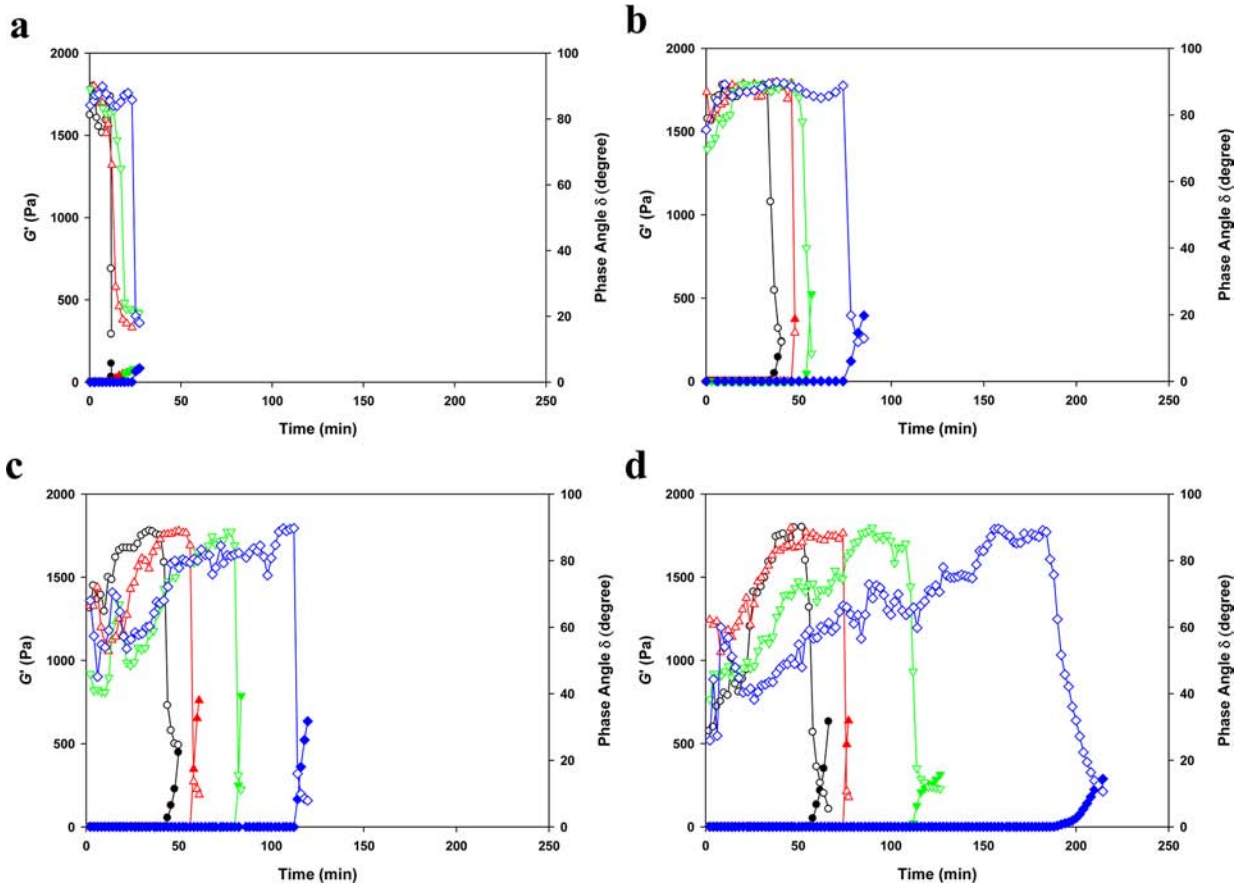


**Figure 4.** Storage modulus ($G'$) (left $Y$-axis) and phase angle ($\delta$) (right $Y$-axis) of lipid nanoparticle suspensions during the oscillation time sweep test: (a) SLN; (b) 10% NLC; (c) 20% NLC; (d) 30% NLC (solid circles, up triangles, down triangles, and diamonds are the $G'$ values of suspensions prepared by postsonication for 0, 4, 5, and 6 min, respectively; and open circles, up triangles, down triangles, and diamonds are the $\delta$ values of suspensions prepared by postsonication for 0, 4, 5, and 6 min, respectively).


dx.doi.org/10.1021/jf503489v | J. Agric. Food Chem. 2014, 62, 11557–11567

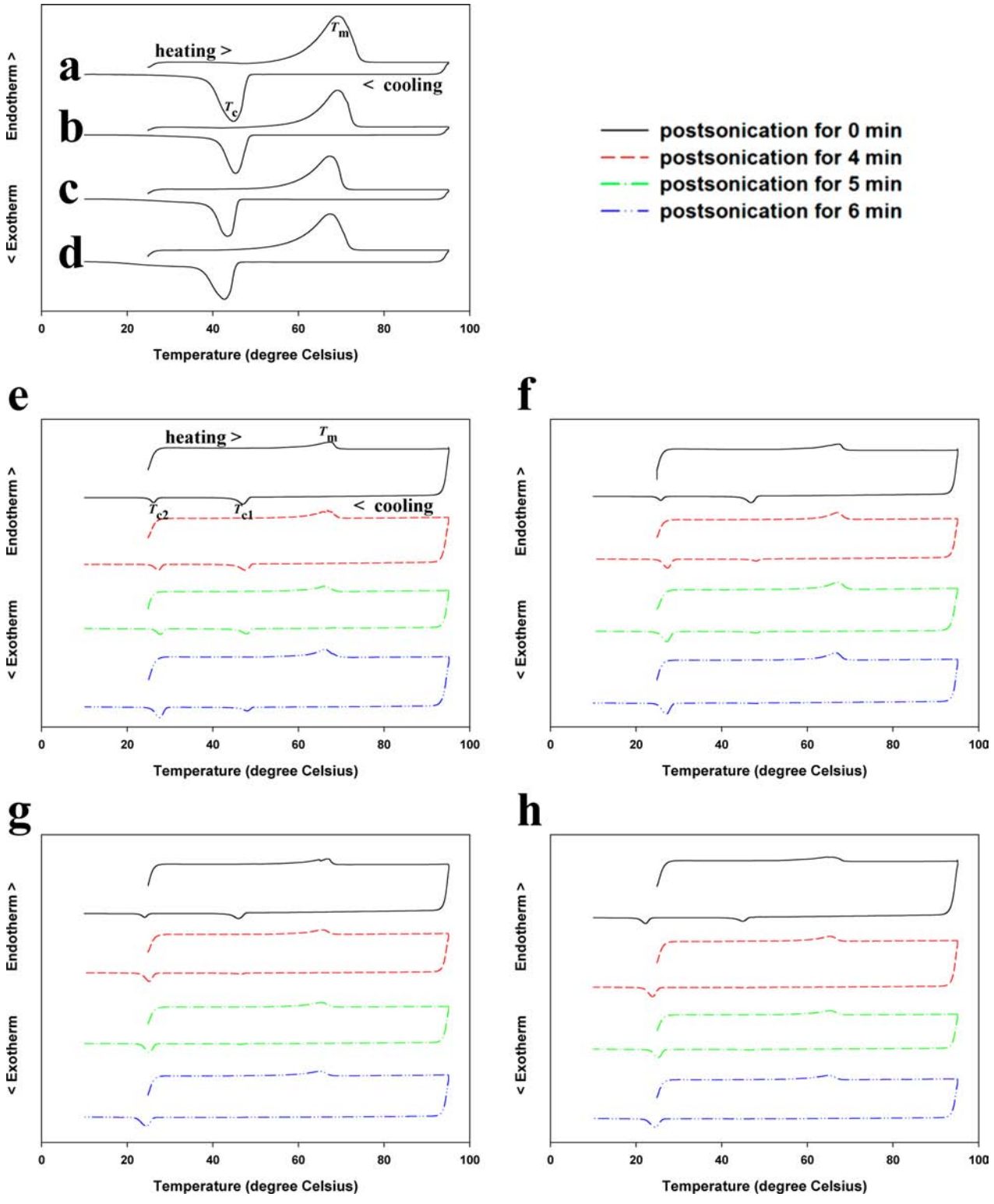


**Figure 5.** DSC thermograms of bulk FHCO lipids containing (a) 0, (b) 10, (c) 20, and (d) 30 wt % LCO; DSC thermograms of lipid nanoparticle suspensions: (e) SLN; (f) 10% NLC; (g) 20% NLC; (h) 30% NLC.

decreased, indicating that gelation occurred. With a higher LCO content in the oil phase and a longer PS time, gelation time was extended. Because the gelling phenomena of LNPs were derived from the building of networks with the LNPs and their flocs, a greater gelation time meant that the collision of LNPs and their flocs to create the gel network occurred less frequently at the same shear force. This may be indirect evidence that the LNPs prepared using a longer PS time and greater LCO contents in the oil phase contained more LNPs that did not play a role in gel network formation.

**Thermal Properties of Bulk Lipids and Lipid Nanoparticles.** The most abundant fatty acid in FHCO was stearic acid, which suggests that FHCO was composed of tristearin and other minor triacylglycerides. Therefore, the thermal


dx.doi.org/10.1021/jf503489v | J. Agric. Food Chem. 2014, 62, 11557−11567

**Table 2. Melting and Crystallization Temperatures and Enthalpy Values of Bulk Lipids and Lipid Nanoparticle Suspensions during Heating and Cooling on DSC[a]**

| | heating | | | cooling | | | | |
|---|---|---|---|---|---|---|---|---|
| sample | $T_m$ (°C) | $\Delta H_m$ (J g$^{-1}$) | CI (%) | $T_c$ (°C) | $T_{c1}$ (°C) | $T_{c2}$ (°C) | $\Delta H_c$ (J g$^{-1}$) | $\Delta H_{c2}/\Delta H_{c1}$ |
| bulk lipid | | | | | | | | |
| 0% LCO | 69.6 ± 0.4 y | 86.6 ± 1.8 x | | 44.8 ± 0.1 x | | | −61.5 ± 0.2 x | |
| 10% LCO | 69.1 ± 0.2 y | 86.5 ± 0.9 x | | 45.2 ± 0.1 w | | | −60.3 ± 0.3 y | |
| 20% LCO | 67.3 ± 0.3 z | 70.8 ± 2.0 y | | 43.4 ± 0.1 y | | | −52.7 ± 0.1 z | |
| 30% LCO | 67.3 ± 0.1 z | 66.0 ± 0.4 z | | 42.7 ± 0.1 z | | | −53.0 ± 0.1 z | |
| lipid phase | | | | | | | | |
| PS0SLN | 67.6 ± 0.2 ab | 4.3 ± 0.0 a | 98.2 ± 0.8 a | | 48.2 ± 0.2 a | 27.2 ± 0.1 a | | 0.4 ± 0.0 i |
| PS0NLC10 | 67.3 ± 0.0 ab | 4.0 ± 0.1 cd | 91.3 ± 1.7 cd | | 47.9 ± 0.1 a | 27.3 ± 0.1 a | | 0.4 ± 0.0 i |
| PS0NLC20 | 66.4 ± 0.4 bcd | 3.4 ± 0.1 f | 79.1 ± 2.6 f | | 46.3 ± 0.4 bc | 24.6 ± 0.2 b | | 0.4 ± 0.0 i |
| PS0NLC30 | 65.5 ± 0.3 de | 2.8 ± 0.0 hi | 64.9 ± 0.6 hi | | 45.3 ± 0.2 e | 23.3 ± 0.1 c | | 1.1 ± 0.1 i |
| PS4SLN | 67.7 ± 0.8 a | 4.2 ± 0.1 ab | 98.1 ± 1.2 ab | | 47.7 ± 0.4 a | 27.3 ± 0.1 a | | 0.8 ± 0.0 i |
| PS4NLC10 | 66.8 ± 0.1 ab | 3.8 ± 0.0 de | 87.9 ± 1.0 de | | 47.8 ± 0.2 a | 27.3 ± 0.3 a | | 4.5 ± 0.5 gh |
| PS4NLC20 | 65.0 ± 0.2 e | 3.1 ± 0.1 g | 72.0 ± 1.1 g | | 46.3 ± 0.4 bc | 24.5 ± 0.0 b | | 15.2 ± 0.7 f |
| PS4NLC30 | 64.7 ± 0.5 e | 2.7 ± 0.1 ij | 65.7 ± 1.1 ij | | 45.5 ± 0.1 de | 23.1 ± 0.0 c | | 32.9 ± 3.9 d |
| PS5SLN | 67.0 ± 0.7 ab | 4.2 ± 0.1 ab | 95.9 ± 2.2 ab | | 48.2 ± 0.2 a | 27.9 ± 0.3 a | | 1.0 ± 0.0 i |
| PS5NLC10 | 66.9 ± 0.2 ab | 3.8 ± 0.1 de | 87.0 ± 1.4 de | | 48.2 ± 0.5 a | 27.3 ± 0.1 a | | 8.7 ± 1.2 g |
| PS5NLC20 | 65.4 ± 0.2 de | 3.0 ± 0.0 gh | 68.2 ± 0.8 gh | | 46.3 ± 0.3 bcd | 24.7 ± 0.5 b | | 27.3 ± 2.4 e |
| PS5NLC30 | 65.2 ± 0.2 e | 2.6 ± 0.0 jk | 59.9 ± 0.8 jk | | 45.6 ± 0.3 cde | 23.3 ± 0.6 c | | 41.5 ± 4.7 c |
| PS6SLN | 67.3 ± 0.8 ab | 4.1 ± 0.1 bc | 93.7 ± 1.5 bc | | 47.9 ± 0.1 a | 27.8 ± 0.2 a | | 2.7 ± 0.1 i |
| PS6NLC10 | 66.7 ± 0.5 abc | 3.7 ± 0.1 e | 85.6 ± 1.2 e | | 48.0 ± 0.1 a | 27.3 ± 0.2 a | | 17.0 ± 1.1 f |
| PS6NLC20 | 65.4 ± 0.1 cde | 2.8 ± 0.0 hi | 65.0 ± 0.8 hi | | 46.5 ± 0.2 b | 25.0 ± 0.2 b | | 53.7 ± 0.7 b |
| PS6NLC30 | 65.1 ± 0.2 e | 2.5 ± 0.1 k | 57.5 ± 2.1 k | | 45.6 ± 0.2 cde | 23.5 ± 0.3 c | | 76.6 ± 0.7 a |

[a]Different letters w−z and a−k in a column within bulk lipid and lipid phase are significantly different at $p < 0.05$, respectively.

properties of FHCO were expected to be similar to those of tristearin.

In the present study, the DSC thermogram taken after overnight storage at 25 °C showed a single peak corresponding to the melting of $\beta$-polymorphic form crystals (Figure 5a). In other studies, multiple melting peaks of $\alpha$, $\beta'$, and $\beta$ forms were reported.[34] The reason for this discrepancy is transformation of $\alpha$-form into $\beta$-form crystals during overnight storage. The melting temperature ($T_m$) of the $\beta$-polymorphic forms of pure tristearin was 72.1 °C, and the $T_c$ of the $\alpha$-polymorphic form was 51 °C.[35] The $T_m$ (69.6 °C for $\beta$-polymorphic form) and $T_c$ (44.8 °C for $\alpha$-polymorphic form) of FHCO were similar to those of tristearin (Table 2). The specific XRD lines (0.46, 0.39, and 0.37 nm with WAXS and 4.49 nm with SAXS) for the $\beta$ form of FHCO in the current study were similar to the previous findings in the case of tristearin (Figure S4 in the Supporting Information).[35,36]

The thermogram patterns of FHCO blended with LCO in various weight ratios would be similar to the pattern of FHCO, which comprised a melting peak of the $\beta$ form and a crystallization peak of the $\alpha$ form (Figure 5b−d). However, the $T_m$ and $T_c$ of the $\beta$- and $\alpha$-polymorphic forms for each blended lipid differed from those for FHCO (Table 2).

During heating from 25 to 95 °C, the $\beta$-form $T_m$ (69.1 °C) of the lipid mixed with 90 wt % FHCO and 10 wt % LCO was similar to the $T_m$ (69.6 °C) of FHCO, whereas melting temperatures (both 67.3 °C) of the blended FHCOs with 20 and 30 wt % LCO were lower than the $T_m$ of the FHCO. Melting enthalpies ($\Delta H_m$) of bulk lipids decreased with increasing LCO contents, although enthalpies for the FHCO and the lipid mixed with 90 wt % FHCO and 10 wt % LCO were similar. In addition, all $\Delta H_m$ values for the lipids blended with LCO at each ratio (10−30 wt %) were greater than their own theoretical $\Delta H_m$ values. In other words, lipids mixed with FHCO and LCO formed more $\beta$-form crystals than all $\beta$ crystals of FHCO comprising the blended lipid matrix. This result suggested that triacylglycerol molecules in FHCO could be cocrystallized with molecules in LCO as the $\beta$-form crystals, which is in agreement with other research.[37,38]

With regard to melting of the lipid phase in the LNP system, in the lipid and LNP suspension prepared using the same LCO contents, the $T_m$ values of the lipid phase in the LNP suspension were generally ∼2.5 °C lower than those of the bulk lipid. However, the trend of the LNP, in which greater LCO contents decreased the $T_m$, was similar to those of bulk lipids. Moreover, $T_m$ values of the lipid phase were independent of PS times for preparation. The crystallinity indices (CI) decreased with increasing PS time and LCO contents. In other words, the additional sonication, PS, and the LCO in the lipid phase would inhibit lipid crystal formation.

The CI values of LNP suspensions were lower than those at the time for the crystallization of all FHCO molecules. For example, the lipid phase of the PS6NLC30 sample (Table 2) consisted of 70 wt % FHCO; nevertheless, the CI of the sample was 57.5%. This may be because LCO in the LNP interferes with formation of the perfect arrangement among FHCO $\beta$ crystals.[39] As a result, the decrease in crystal formation, which originated from increasing both the LCO content and PS time, improved the stability of the LNP system, which is discussed in the following section.

During cooling from 95 to 10 °C, the $\alpha$-form $T_c$ (44.8 °C) of the FHCO was lower than the $T_c$ (45.2 °C) of the lipid mixed with 90 wt % FHCO and 10 wt % LCO, and the $T_c$ values of the remainder, which were bulk lipids blended with 80 and 70 wt % FHCO and 20 and 30 wt % LCO, decreased with increasing LCO contents. The absolute values of the crystallization enthalpy ($\Delta H_c$) of bulk lipids from 0 to 20 wt % LCO contents decreased from 61.5 to 52.7 J g$^{-1}$, whereas the

absolute values of the $\Delta H_c$ of bulk lipids containing 20 and 30 wt % LCO were similar. In addition, on the basis of a comparison of experimental data and the theoretical values corresponding to the amount of FHCO, this result was in agreement with the melting enthalpies ($\Delta H_m$).

The $T_c$ of the $\alpha$-polymorphic form of emulsified tripalmitin at the nanoscale is lower than that of bulk tripalmitin.[25] This phenomenon was also observed in our study (Table 2). During the DSC scan, the LNPs melted during heating from 25 to 95 °C and then crystallized during cooling from 95 to 10 °C. The LNPs that did not participate in gelation formed individual liquid droplets at the nanoscale during heating, but either they partially coalesced during the LNP preparation or the highly gelled LNPs, which were attached to each other by hydrophobic interactions, underwent full coalescence and eventually formed large micrometer-scale liquid oil droplets. The DSC thermograms during cooling showed that LNP crystallization occurred at lower temperatures ($T_{c2}$) for the lipid droplets that were not coalesced compared to the coalesced ($T_{c1}$) LNPs. The $T_{c1}$ was similar to the $T_c$ of the bulk lipid (FHCO or blended FHCO/LCO), which is in agreement with previous studies.[15,25,40,41]

The ratios of the enthalpy values ($\Delta H_{c2}/\Delta H_{c1}$, $\Delta H_{c2}$, and $\Delta H_{c1}$ for $T_{c2}$ and $T_{c1}$, respectively) could be used to determine the quantity of LNPs that did not take part in the partial coalescence and the gelation. As $\Delta H_{c2}/\Delta H_{c1}$ increased, the quantity of particles not participating in the destabilization (the partial coalescence and the gelation) of LNPs increased. The increase in the LCO content in the oil phase increased $\Delta H_{c2}/\Delta H_{c1}$ (Table 2). Previous findings stated that a higher liquid oil content in the oil phase enhanced the stability of LNPs.[41,42] In this study, the increase in the LCO content of the oil phase improved the stability of the LNPs. In addition, the $\Delta H_{c2}/\Delta H_{c1}$ values increased with increasing PS time. This observation supported our hypothesis that additional sonication during the cooling step of LNP preparation improves the stability of LNPs.

**Proposed Mechanisms of the Increased Stability of Lipid Nanoparticles Due to Additional Sonication and Liquid Canola Oil in the Oil Phase.** Emulsifiers densely covering the surface of LNPs could prevent the FHCO from forming $\beta$-polymorphic crystals during cooling and storage.[15] As discussed above, the formation of $\beta$ crystals increases the likelihood of formation of hydrophobic patches on the surface of the particle. Thus, the increase in emulsifier density on the particle surface could prevent gelation and enhance the stability of LNPs. In the present study, the amount of Tween 20 per unit surface area of LNPs is shown in Table 3, which was based on the assumption that the shape of all LNPs was similar to a sphere. The Tween 20 surface load increased in proportion with increasing PS processing time or the LCO content in the oil phase. In particular, the surface load of the sample prepared using 6 min of PS and a 30 wt % LCO content was 10.29 mg $m^{-2}$. Despite the lower ratio (1/3) of the amount of Tween 20 to the lipid phase volume, this value was greater than that (8.1 mg $m^{-2}$) for SLN prepared using 10 wt % lipid and 10 wt % Tween 20 (1/1) reported by Nik et al.[34] Therefore, both the additional sonication process during cooling and the presence of liquid oil in the lipid matrix might result in effective emulsification of LNP by Tween 20 in contrast to that found by other researchers.

The nonaggregated stable LNPs were nanosized particles, but the aggregated nonstable particles were micrometer-sized. The stable particles could pass through the filter (pore size = 1 $\mu$m), whereas the aggregated particles remained on the filter. The contents of the nonaggregated LNPs are shown in Table 3. The amount of stable nanoparticles increased with increasing PS time and LCO content in the oil phase, which was similar to the tendency in the Tween 20 surface load. This result confirmed that a longer PS time and a greater LCO content in the oil phase are suitable conditions for preparing stable LNP systems.

**Table 3. Tween 20 Surface Load and the Quantity Values of Nonaggregated Lipid Nanoparticles[a]**

| sample | | | |
|---|---|---|---|
| postsonication (min) | LCO content (wt %) | Tween 20 surface load (mg $m^{-2}$) | content of nonaggregated particle (%) |
| 0 | 0 | 6.34 ± 0.03 h | 34.9 ± 0.2 i |
| | 10 | 6.39 ± 0.06 h | 34.6 ± 0.7 i |
| | 20 | 6.44 ± 0.01 h | 35.7 ± 0.9 hi |
| | 30 | 7.50 ± 0.04 ef | 49.1 ± 1.8 fg |
| 4 | 0 | 6.65 ± 0.14 gh | 39.5 ± 1.5 ghi |
| | 10 | 7.39 ± 0.08 f | 54.7 ± 5.7 ef |
| | 20 | 8.00 ± 0.03 d | 63.9 ± 3.9 de |
| | 30 | 9.57 ± 0.09 b | 76.7 ± 3.8 bc |
| 5 | 0 | 6.98 ± 0.10 g | 42.2 ± 2.6 ghi |
| | 10 | 7.77 ± 0.12 de | 61.4 ± 4.2 de |
| | 20 | 8.47 ± 0.10 c | 70.6 ± 5.8 bcd |
| | 30 | 9.77 ± 0.10 b | 80.6 ± 2.7 ab |
| 6 | 0 | 7.44 ± 0.05 ef | 47.1 ± 5.6 fgh |
| | 10 | 7.95 ± 0.14 d | 66.6 ± 3.3 cd |
| | 20 | 8.58 ± 0.09 c | 78.6 ± 5.5 b |
| | 30 | 10.29 ± 0.35 a | 90.1 ± 4.7 a |

[a]Different letters a–i in a column are significantly different at $p < 0.05$.

In the conventional method for LNP preparation (Figure 6a), the formation of Tween 20 micelles at high temperature could reduce the amount of Tween 20 molecules available to stabilize the interface between the oil and water phases[23,24] and induce the formation of coalesced micrometer-sized oil droplets. During the cooling procedure, these coalesced micrometer droplets at $T_{c1}$ could be crystallized and transformed to destabilized particles with hydrophobic patches, which may be partially coalesced with noncrystallized liquid droplets.[21] What was worse, nanoparticles with low Tween 20 surface load levels could be crystallized at $T_{c2}$ and transformed into unstable particles having hydrophobic patches,[25,26] which could be aggregates of nonstable particles. Consequently, flocs of these nonstable particles, which are the partially coalesced particles or the particles aggregated by hydrophobic patches, could float and be creamed.

In the present study, the positive effects on LNP stability of PS and liquid oil content could be explained by two mechanisms. First, the PS during the cooling procedure induces Tween 20 molecules to form micelles, which move and stabilize the LNP surface (Figure 6b). That is, Tween 20 molecules at higher temperature would be more stable in the form of micelles and less likely to adsorb at the interface of the LNP.[23,24] The PS could break the micelles and enhance the coating of the LNP by Tween 20. Therefore, the nanosized oil droplets processed with the PS, which are not coalesced, could crystallize at the $T_{c2}$ and disperse throughout the system.

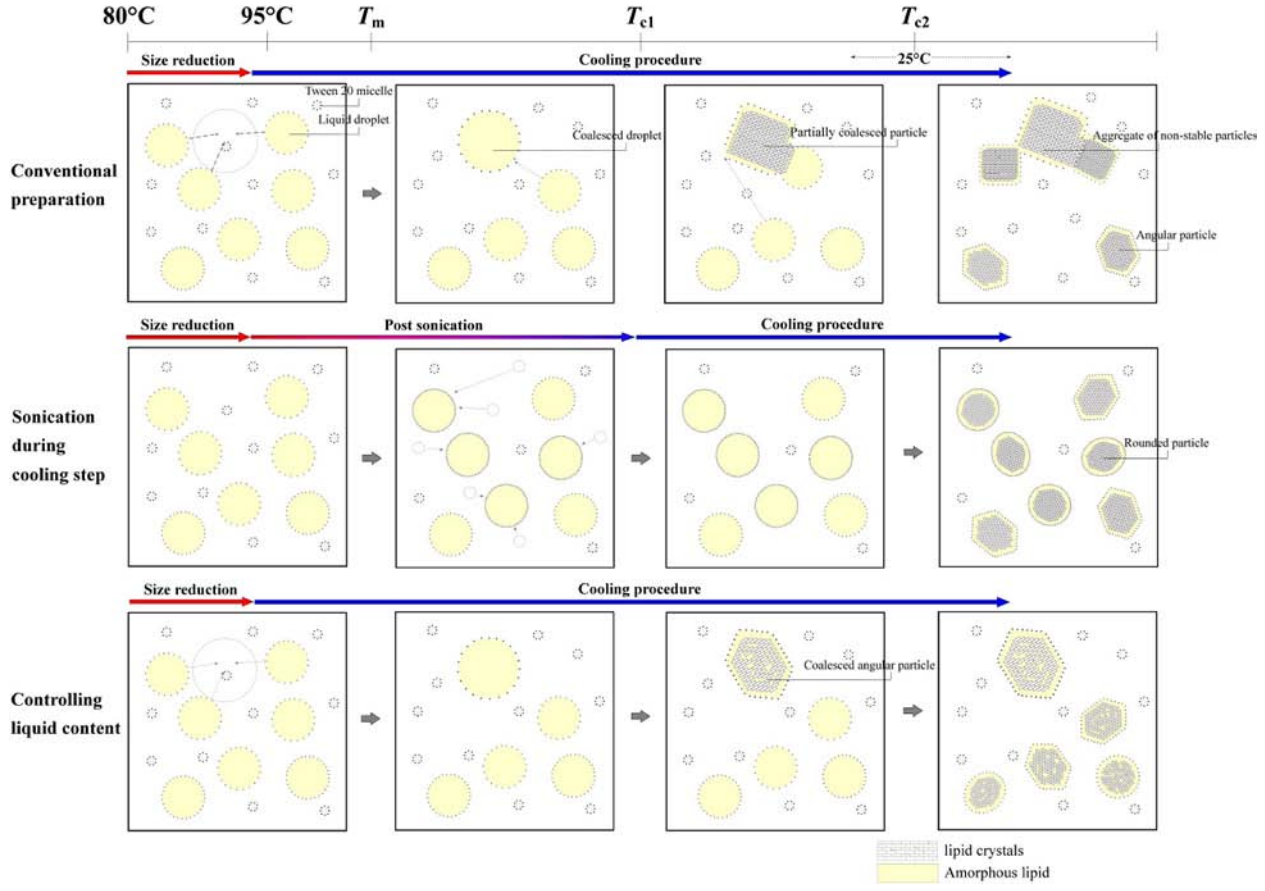


**Figure 6.** Schematic representation of the dispersion stability of lipid nanoparticles fabricated using the (a, top) conventional preparation, (b, middle) additional sonication (postsonication) during cooling, and (c, bottom) a solid lipid phase containing liquid canola oil.

Because the surfactant covering the lipid would compete with the lipid crystallization at the interface,[28,34] the PS process could decrease the CI of LNPs, as discussed in a previous section (Table 2). In other words, the better adsorption of surfactants at the interface, caused by the longer PS, could more effectively inhibit the crystallization of lipid matrices. Second, the liquid oil could interfere with crystallization of the oil phase and decrease the likelihood of morphological transition from a sphere to a rod shape (Figure 6c). Thus, the increase in liquid oil content in the oil phase could not only prevent the formation of hydrophobic patches but also reduce the surface area. This could contribute to the reduction of Tween 20 surface load (Table 3). Consequently, these synergetic effects that originated from the additional sonication during cooling and the presence of liquid oil in the oil phase increased the stability of the lipid nanoparticle system.

According to the characteristics of the blended lipid, FHCO and LCO are appropriate for use as carrier matrix lipids and for the application of LNPs in food systems. The PS step prevents the intensive aggregation and gelation of LNPs, which have been problems in LNP systems. These results confirmed our hypothesis that PS and the LCO content of a lipid matrix could improve LNP stability. Compared with the traditional methods for LNP preparation, the process introduced in this study could allow food companies to fabricate more stable LNPs. In conclusion, stable FHCO LNP systems as carrier systems of bioactive materials could be used for functional foods.

## ■ ASSOCIATED CONTENT

### Ⓢ Supporting Information

Table S1 and Figures S1−S4. This material is available free of charge via the Internet at http://pubs.acs.org.

## ■ AUTHOR INFORMATION

### Corresponding Author

*(Y.J.C.) Phone: +82 2 880 4851. Fax: +82 2 873 5095. E-mail: choiyj@snu.ac.kr.

### Author Contributions

‖C.B. and S.L. contributed equally to this work.

### Notes

The authors declare no competing financial interest.

## ■ REFERENCES

(1) Müller, R. H.; Mäder, K.; Gohla, S. H. Solid lipid nanoparticles (SLN) for controlled drug delivery − a review of the state of the art. *Eur. J. Pharm. Biopharm.* **2000**, *50*, 161−177.

(2) Müller, R. H.; Radtke, M.; Wissing, S. A. Nanostructured lipid matrices for improved microencapsulation of drugs. *Int. J. Pharm.* **2002**, *242*, 121−128.

(3) Müller, R. H. *Colloidal Carriers for Controlled Drug Delivery and Targeting: Modification, Characterization and in Vivo Distribution*; Taylor & Francis: Boca Raton, FL, USA, 1991.

(4) Wissing, S. A.; Kayser, O.; Müller, R. H. Solid lipid nanoparticles for parenteral drug delivery. *Adv. Drug Delivery Rev.* **2004**, *56*, 1257−1272.

(5) Hu, F. Q.; Jiang, S. P.; Du, Y. Z.; Yuan, H.; Ye, Y. Q.; Zeng, S. Preparation and characteristics of monostearin nanostructured lipid carriers. *Int. J. Pharm.* **2006**, *314*, 83−89.

(6) Mehnert, W.; Mäder, K. Solid lipid nanoparticles: production, characterization and applications. *Adv. Drug Delivery Rev.* **2001**, *47*, 165−196.
(7) Ricci, M.; Puglia, C.; Bonina, F.; Giovanni, C. D.; Giovagnoli, S.; Rossi, C. Evaluation of indomethacin percutaneous absorption from nanostructured lipid carriers (NLC): *in vitro* and *in vivo* studies. *J. Pharm. Sci.* **2005**, *94*, 1149−1159.
(8) Souto, E. B.; Müller, R. H. Investigation of the factors influencing the incorporation of clotrimazole in SLN and NLC prepared by hot high-pressure homogenization. *J. Microencapsul.* **2006**, *23*, 377−388.
(9) Hu, F. Q.; Jiang, S. P.; Du, Y. Z.; Yuan, H.; Ye, Y. Q.; Zeng, S. Preparation and characterization of stearic acid nanostructured lipid carriers by solvent diffusion method in an aqueous system. *Colloids Surf., B* **2005**, *45*, 167−173.
(10) Jenning, V.; Gohla, S. H. Encapsulation of retinoids in solid lipid nanoparticles (SLN). *J. Microencapsul.* **2001**, *18*, 149−158.
(11) Souto, E. B.; Wissing, S. A.; Barbosa, C. M.; Müller, R. H. Development of a controlled release formulation based on SLN and NLC for topical clotrimazole delivery. *Int. J. Pharm.* **2004**, *278*, 71−77.
(12) Souto, E. B.; Wissing, S. A.; Barbosa, C. M.; Müller, R. H. Evaluation of the physical stability of SLN and NLC before and after incorporation into hydrogel formulations. *Eur. J. Pharm. Biopharm.* **2004**, *58*, 83−90.
(13) Jores, K.; Mehnert, W.; Drechsler, M.; Bunjes, H.; Johann, C.; Mäder, K. Investigations on the structure of solid lipid nanoparticles (SLN) and oil-loaded solid lipid nanoparticles by photon correlation spectroscopy, field-flow fractionation and transmission electron microscopy. *J. Controlled Release* **2004**, *95*, 217−227.
(14) Castelli, F.; Puglia, C.; Sarpietro, M. G.; Rizza, L.; Bonina, F. Characterization of indomethacin-loaded lipid nanoparticles by differential scanning calorimetry. *Int. J. Pharm.* **2005**, *304*, 231−238.
(15) Helgason, T.; Awad, T. S.; Kristbergsson, K.; McClements, D. J.; Weiss, J. Effect of surfactant surface coverage on formation of solid lipid nanoparticles (SLN). *J. Colloid Interface Sci.* **2009**, *334*, 75−81.
(16) Bunjes, H.; Steiniger, F.; Richter, W. Visualizing the structure of triglyceride nanoparticles in different crystal modifications. *Langmuir* **2007**, *23*, 4005−4011.
(17) Hatziantoniou, S.; Deli, G.; Nikas, Y.; Demetzos, C.; Papaioannou, G. T. Scanning electron microscopy study on nano-emulsions and solid lipid nanoparticles containing high amounts of ceramides. *Micron* **2007**, *38*, 819−823.
(18) Jenning, V.; Schäfer-Korting, M.; Gohla, S. H. Vitamin A-loaded solid lipid nanoparticles for topical use: drug release properties. *J. Controlled Release* **2000**, *66*, 115−126.
(19) Westesen, K.; Siekmann, B. Investigation of the gel formation of phospholipid-stabilized solid lipid nanoparticles. *Int. J. Pharm.* **1997**, *151*, 35−45.
(20) Freitas, C.; Müller, R. H. Correlation between long-term stability of solid lipid nanoparticles (SLN) and crystallinity of the lipid phase. *Eur. J. Pharm. Biopharm.* **1999**, *47*, 125−132.
(21) Boode, K.; Walstra, P. Partial coalescence in oil-in-water emulsions. 1. Nature of the aggregation. *Colloids Surf., A* **1993**, *81*, 121−137.
(22) Vanapalli, S. A.; Coupland, J. N. Emulsions under shear − the formation and properties of partially coalesced lipid structures. *Food Hydrocolloids* **2001**, *15*, 507−512.
(23) Alexandridis, P.; Alan Hatton, T. Poly (ethylene oxide)-poly (propylene oxide)-poly (ethylene oxide) block copolymer surfactants in aqueous solutions and at interfaces: thermodynamics, structure, dynamics, and modeling. *Colloids Surf., A* **1995**, *96*, 1−46.
(24) Ruiz, C. C.; Molina-Bolívar, J.; Aguiar, J.; MacIsaac, G.; Moroze, S.; Palepu, R. Effect of ethylene glycol on the thermodynamic and micellar properties of Tween 20. *Colloid Polym. Sci.* **2003**, *281*, 531−541.
(25) Helgason, T.; Awad, T. S.; Kristbergsson, K.; McClements, D. J.; Weiss, J. Influence of polymorphic transformations on gelation of tripalmitin solid lipid nanoparticle suspensions. *J. Am. Oil Chem. Soc.* **2008**, *85*, 501−511.
(26) Trujillo, C. C.; Wright, A. J. Properties and stability of solid lipid particle dispersions based on canola stearin and Poloxamer 188. *J. Am. Oil Chem. Soc.* **2010**, *87*, 715−730.
(27) Jia, L.; Zhang, D.; Li, Z.; Duan, C.; Wang, Y.; Feng, F.; Wang, F.; Liu, Y.; Zhang, Q. Nanostructured lipid carriers for parenteral delivery of silybin: biodistribution and pharmacokinetic studies. *Colloids Surf., B* **2010**, *80*, 213−218.
(28) Schubert, M. A.; Müller-Goymann, C. C. Characterisation of surface-modified solid lipid nanoparticles (SLN): influence of lecithin and nonionic emulsifier. *Eur. J. Pharm. Biopharm.* **2005**, *61*, 77−86.
(29) McClements, D. J. Critical review of techniques and methodologies for characterization of emulsion stability. *Crit. Rev. Food Sci.* **2007**, *47*, 611−649.
(30) Khossravi, M.; Kao, Y. H.; Mrsny, R. J.; Sweeney, T. D. Analysis methods of polysorbate 20: a new method to assess the stability of polysorbate 20 and established methods that may overlook degraded polysorbate 20. *Pharm. Res.* **2002**, *19*, 634−639.
(31) Manjunath, K.; Venkateswarlu, V. Pharmacokinetics, tissue distribution and bioavailability of clozapine solid lipid nanoparticles after intravenous and intraduodenal administration. *J. Controlled Release* **2005**, *107*, 215−228.
(32) Silverstein, T. P. The real reason why oil and water don't mix. *J. Chem. Educ.* **1998**, *75*, 116.
(33) Reiffers-Magnani, C. K.; Cuq, J. L.; Watzke, H. J. Depletion flocculation and thermodynamic incompatibility in whey protein stabilised O/W emulsions. *Food Hydrocolloids* **2000**, *14*, 521−530.
(34) Nik, A. M.; Langmaid, S.; Wright, A. J. Nonionic surfactant and interfacial structure impact crystallinity and stability of $\beta$-carotene loaded lipid nanodispersions. *J. Agric. Food Chem.* **2012**, *60*, 4126−4135.
(35) Elisabettini, P.; Desmedt, A.; Durant, F. Polymorphism of stabilized and nonstabilized tristearin, pure and in the presence of food emulsifiers. *J. Am. Oil Chem. Soc.* **1996**, *73*, 187−192.
(36) Bunjes, H.; Westesen, K.; Koch, M. H. J. Crystallization tendency and polymorphic transitions in triglyceride nanoparticles. *Int. J. Pharm.* **1996**, *129*, 159−173.
(37) Danthine, S. Blending of hydrogenated low-erucic acid rapeseed oil, low-erucic acid rapeseed oil, and hydrogenated palm oil or palm oil in the preparation of shortenings. *J. Am. Oil Chem. Soc.* **2003**, *80*, 1069−1075.
(38) Himawan, C.; Starov, V. M.; Stapley, A. G. F. Thermodynamic and kinetic aspects of fat crystallization. *Adv. Colloid Interface Sci.* **2006**, *122*, 3−33.
(39) Teeranachaideekul, V.; Boonme, P.; Souto, E. B.; Müller, R. H.; Junyaprasert, V. B. Influence of oil content on physicochemical properties and skin distribution of Nile red-loaded NLC. *J. Controlled Release* **2008**, *128*, 134−141.
(40) Awad, T. S.; Helgason, T.; Kristbergsson, K.; Decker, E. A.; Weiss, J.; McClements, D. J. Effect of cooling and heating rates on polymorphic transformations and gelation of tripalmitin solid lipid nanoparticle (SLN) suspensions. *Food Biophys.* **2008**, *3*, 155−162.
(41) Qian, C.; Decker, E. A.; Xiao, H.; McClements, D. J. Solid lipid nanoparticles: effect of carrier oil and emulsifier type on phase behavior and physical stability. *J. Am. Oil Chem. Soc.* **2012**, *89*, 17−28.
(42) Yucel, U.; Elias, R. J.; Coupland, J. N. Effect of liquid oil on the distribution and reactivity of a hydrophobic solute in solid lipid nanoparticles. *J. Am. Oil Chem. Soc.* **2013**, *90*, 819−824.

by the LC−chip/TOF MS system,[13,14,20] but the reliability of such an approach for OS quantification is yet to be proven. In addition, all of the reports concerning OS profiling and/or quantification adopted a rather complex sample pretreatment procedure for protein elimination, thus affording limited sample throughput. Because OS are receiving increasing commercial attention for their role in enhancing human health, alternative LC−MS methods and simpler sample preparation protocols for the quantification of major OS species are needed.

Here, we report on the development and validation of a LC−MS method for the quantitative analysis of major OS in bovine milk based on the use of hydrophilic interaction liquid chromatography (HILIC) coupled to a linear ion trap (LTQ) Orbitrap mass spectrometer. We show that this method is sensitive, accurate, and able to quantify 13 major OS within a single run of 50 min with minimum sample pretreatment.

## MATERIALS AND METHODS

**Cows, Diets, and Milk Samples.** For method development, a full cream fresh milk (Farmdale) from the local market was used as a reference sample. For method application, milk samples from 32 individual Holstein-Friesian cows subjected to three different feeding treatments were analyzed. At the beginning of the experiment, the cows had body weights of 614 ± 57.6 kg, were 147 ± 18.2 days in milk (DIM), and were producing 25.2 ± 2.0 L of milk/day. All animal experimentation was conducted in accordance with the Australian Code of Practice for the Care and Use of Animals for Scientific Purposes.[23] Animal use was approved by the Animal Ethics Committee of the Department of Environment and Primary Industries, Victoria, Australia. The cows were fed one of three dietary treatments: (1) a control diet (CON), in which cows were individually offered daily, 6.0 kg of dry matter (DM) of crushed corn grain, 2.0 kg of DM of cold pressed canola meal, 0.2 kg of DM of minerals, and 14.0 kg of DM of alfalfa cubes; (2) an almond hull diet (ALH), in which cows were individually offered a diet similar to the CON diet, except that 4.0 kg of DM of almond hulls was substituted for 4.0 kg of DM of alfalfa cubes; and (3) a citrus diet (CIT), which was similar to the CON diet, but 3.0 kg of DM of citrus pulp (orange skins) was substituted for 3.0 kg of DM of alfalfa cubes. These diets were fed to the cows for 28 days, and samples of milk were collected on the last day of the experiment and kept at −80 °C before analysis.

**Chemicals.** OS standards [3′-sialyllactose (3′-SL), 6′-sialyllactose (6′-SL), 6′-sialyllactosamine (6′-SLN), stachyose, and verbascose] were purchased from Sigma. Molecular weight cutoff filters (10 kDa, Amicon) were obtained from Merck Millipore. Solvents were of analytical grade (for acetonitrile, Merck) or chromatographic purity (for water containing 0.1% formic acid and acetonitrile containing 0.1% formic acid, Fluka).

**Method for Removing Fat and Protein from Milk.** Full cream milk was centrifuged for 15 min (5000*g*), and the upper layer (fat) was removed. For protein elimination, three different methods were compared. Method 1 (chloroform extraction, standard method): to the defatted milk sample, 4 volumes of chloroform/MeOH (2:1, v/v) and 2 volumes of Milli-Q water were added.[13] The mixture was then centrifuged for 20 min (13000*g*) for complete phase separation. The upper layer, which contains the OS fraction, was carefully transferred to a new tube and dried by a SpeedVac concentrator (SPD2010, Thermo Scientific). The dried OS were reconstituted in water before LC−MS analysis. Method 2 (acetonitrile precipitation): acetonitrile was added to the defatted milk at a 1:1 ratio, and the mixture was placed in a fridge (4 °C) for 60 min to allow for protein precipitation.[24] After centrifugation (13000*g* for 20 min), the supernatant was analyzed directly by LC−MS. Method 3 (ultrafiltration): defatted milk was diluted by adding an equal volume of Milli-Q water and then filtered through a 10 kDa molecular weight cutoff filter in a microfuge (13000*g* for 30 min). Filtrate is expected to contain all OS and other low-molecular-weight compounds and was analyzed directly by LC−MS.

**OS Analysis by LC−MS.** Chromatographic separation of OS was achieved using a Luna HILIC column (250 × 4.6 mm, 5 μm, Phenomenex) on an Agilent 1290 Infinity HPLC system (Agilent, Walbronn, Germany), including a degasser, binary pump, temperature-controlled autosampler (maintained at 4 °C), and column compartment (maintained at 30 °C). The mobile phase was composed of water containing 0.1% formic acid (A) and acetonitrile containing 0.1% formic acid (B). The flow rate was 0.5 mL/min with a gradient elution of 5−50% A over 42 min and then increased to 1 mL/min for post-acquisition column washing and equilibration. The injection volume was 5 μL for both standards and milk samples. Analyte detection was by mass spectrometry LTQ Orbitrap Velos (Thermo Scientific, Waltham, MA) with a heated electrospray ionization (HESI) source. The heated capillary was maintained at 270 °C with a source heater temperature of 350 °C, and the sheath, auxiliary, and sweep gases were at 40, 15, and 8 units, respectively. The source voltage was set to 3.2 kV for negative mode.

The mass spectrometer was operated with full scan (*m*/*z* 120−2000) in negative Fourier transform (FT) mode (at a resolution of 60 000) for all OS analyses. Deprotonated molecular ions ($[M - H]^-$) were extracted from the full-scan chromatograms, and peak areas were integrated using Xcalibur software (Thermo Scientific). For structural confirmation of major OS identified on the basis of accurate mass information, tandem mass spectrometry (MS/MS) data were acquired in collision-induced dissociation (CID) mode using a normalized collision energy of 25 arbitrary units.

**Method Validation.** *Limit of Detection (LOD), Limit of Quantitation (LOQ), and Linear Range Determination.* Because of the fact that standards are not available for most milk OS, the LOD, LOQ, and linear range of the method were assessed for three representative acidic OS (3′-SL, 6′-SL, and 6′-SLN) and two neutral OS analogues (stachyose and verbascose). A series of 13 dilutions (ranging from 0.000 01 to 0.1 mg/mL) of the five OS standards were prepared in water and analyzed 3 times, and the LOD, LOQ, and linear range for each compound were determined as described previously.[25]

*Method Precision and Accuracy Assessment.* Three concentrations (one close to LOQ, one intermediate, and one close to the upper limit of the linear range) of the 5 OS standards were prepared in water and analyzed 5 times. Method precision was assessed by the variation [as judged by the relative standard deviation (RSD)] of the peak area between repeated injections of each standard dilution. Method accuracy was estimated by the ratio of the actual measured concentration to the nominal concentration prepared for each OS.

*Method Recovery.* A mix of four OS standards (6′-SL, 6′-SLN, stachyose, and verbascose) was spiked to the defatted reference milk sample at two different levels (0.1 or 1 μg each in 400 μL of milk) before ultrafiltration. The recovery of the standards was calculated using the following formula: recovery (%) = [(total mass in the spiked sample − mass in the non-spiked sample)/mass spiked] × 100.

**Method Application.** Having confirmed the precision, accuracy, and OS recovery using standards and the reference milk sample, we applied the method to relative and absolute quantification of the major OS in 32 milk samples. The results were analyzed for overall abundance of different OS, variation of OS content between samples, correlation between different OS species, and effect of feed on the milk OS profile.

## RESULTS

**Major OS Detected in the Reference Milk Sample.** Because the building blocks of cow milk OS are known to include glucose, galactose, *N*-acetylglucosamine, fucose, *N*-acetylneuraminic acid (NeuAc), and *N*-glycolylneuraminic acid (NeuGc),[3] an accurate mass of OS of different compositions can be calculated. This allowed us to detect a total of 18 OS in the non-enriched reference milk sample based on mass accuracy of less than 5 ppm. A total of 13 of them are

Table 1. Major OS Identified in the Reference Milk Sample[a]

| name (abbreviation) | composition | $m/z$ (exp) | $m/z$ (calcd) | retention time (min) |
|---|---|---|---|---|
| trisaccharides (Trisa) | 3 Hex | 503.1625 | 503.1612 | 29.00 |
| 3′-sialyllactose (3′-SL) | 2 Hex, 1 NeuAc | 632.2048 | 632.2038 | 35.86 |
| 6′-sialyllactose (6′-SL) | 2 Hex, 1 NeuAc | 632.2048 | 632.2038 | 35.19 |
| 6′-sialyl-*N*-acetyllactosamine (6′-SLN) | 1 Hex, 1 HexNAc, 1 NeuAc | 673.2314 | 673.2304 | 34.17 |
| disialyllactose (DSL) | 2 Hex, 2 NeuAc | 923.3011 | 923.2992 | 37.37 |
| *N*-acetylgalactosaminyllactose (GNL) | 2 Hex, 1 HexNAc | 544.1893 | 544.1878 | 27.80 |
| OS-A | 3 Hex, 1 NeuAc | 794.2585 | 794.2566 | 38.00 |
| OS-B | 4 Hex, 1 HexNAc | 868.2964 | 868.2934 | 33.37 |
| OS-C | 3 Hex, 1 HexNAc | 706.2417 | 706.2406 | 31.13 |
| OS-D | 3 Hex, 2 HexNAc | 909.3214 | 909.3200 | 32.91 |
| OS-E | 2 Hex, 1 NeuGc | 648.2002 | 648.1987 | 36.67 |
| OS-F | 2 Hex, 1 HexNAc, 1 NeuAc | 835.2836 | 835.2832 | 37.51 |
| OS-G | 4 Hex, 1 HexNAc, 1 NeuAc | 1159.3911 | 1159.3888 | 40.31 |

[a]exp and calcd, experimental and calculated $m/z$ values for deprotonated molecular ions (detected in negative mode); Hex, glucose or galactose; HexNAc, *N*-acetylglucosamine or *N*-acetylgalactosamine; NeuAc, *N*-acetylneuraminic acid (sialic acid); and NeuGc, *N*-glycolylneuraminic acid.

quantifiable and are thus considered as major OS (Table 1 and Figure 1).

It is worth noting that all 13 major OS are of lower degree of polymerization (DP) type and the dominant species (Trisa, OS-A, 3′-SL, 6′-SL, DSL, and GNL) contain three or four monosaccharide units. The composition of the major OS identified using accurate mass data was further confirmed by the standards (in the case of 3′-SL, 6′-SL, and 6′-SLN) and/or MS/MS data (see Figure S-1 of the Supporting Information). It is interesting to note that, of the pure hexose-based OS category, species containing more than three sugar units were not found in the sample nor were any fucose-containing OS species. Lactose, lactose phosphate, and *N*-acetyllactosamine were not considered as OS in this work.

**Comparison of Sample Pretreatment Methods.** Stachyose was used as an internal standard in our preliminary analysis, and comparable results were obtained with and without the internal standard. Therefore, no internal standards were used in subsequent experiments. The concentrations (as judged by peak areas) of the 13 major OS in the reference milk sample following different protein elimination procedures were measured in parallel. The experiment was designed in such a way that a same dilution factor was applicable to all three methods. The peak areas of the 13 OS generated with method 2 (acetonitrile precipitation) were highly correlated with those of method 1 (standard method), but the overall response was about 20% lower ($y = 0.7992x$; $R^2 = 0.9996$). This suggests that using acetonitrile to precipitate milk protein could lead to a significant underestimation of OS.

In contrast, the peak areas of the major OS measured using protein elimination method 3 (ultrafiltration) were not only highly correlated with those obtained with method 1 but also showed slightly higher overall ion abundance ($y = 1.0733x$; $R^2 = 0.9998$), implying a higher OS recovery using this new sample pretreatment method.

The ultrafiltration method (method 3) also displayed better measurement reproducibility than the standard method (method 1), with a RSD of the peak area of replicate extractions below 4% for 12 of the 13 major OS (Table 2). Consequently, the ultrafiltration was chosen as the protein elimination technique for further method validation.

**LOD, LOQ, and Linear Range of Representative OS.** This LC−MS method is highly sensitive for the detection of both acidic and neutral OS with a LOD for all species below 0.1 ng and a LOQ of 0.25 ng (Table 3). The linearity ranges from 0.25 to ≥100 ng ($R^2 > 0.99$).

**Precision and Accuracy of the Method.** This method also shows excellent reproducibility in the peak area for all representative OS and all injection levels. The peak area variation between repeated analyses of the five representative OS standards is below 9% for the low injection level (0.5 ng) and below 3% for intermediate (5 ng) and high (100 ng) injection levels (Table 4). The overall measurement accuracy of the method ranges from 91 to 104% for the three concentrations of OS standards (Table 4).

**Recovery of Spiked Standards.** The overall recovery of the four representative OS (stachyose, verbascose, 6′-SL, and 6′-SLN) spiked at two different levels (0.1 and 1 μg in 0.4 mL of defatted milk) is between 91 and 105% (Table 5). This suggests that no significant loss of the OS occurred during the ultrafiltration step nor was there a significant matrix effect on the detection of these compounds.

**Method Application.** The OS concentrations in 32 samples of milk were determined using the validated method. The major OS detected in these samples were the same as those found in the reference sample. The relative abundances (averaged from the 32 samples) of the 13 OS are shown in Table 6. Again, six OS (Trisa, OS-A, 3′-SL, 6′-SL, DSL, and GNL) were found in a larger amount, with 3′-SL and 6′-SL being the most dominant species, followed by Trisa, whereas OS-B, OS-C, OS-D, OS-E, OS-F, OS-G, and 6′-SLN were the lower abundance OS species in these samples.

Large variation was also observed between samples in the concentration of all major OS. For example, the 3′-SL content varied from 116 to 199 μg/mL across the 32 samples; the 6′-SL content varied from 6 to 32 μg/mL across the 32 samples; and the 6′-SLN content varied from 0.27 to 1.2 μg/mL across the 32 samples (Figure 2). The magnitude of variation appeared to be similar for milks from three different diets.

It is also interesting to note that the contents (as measured by peak areas) of some of the major OS are correlated with each other, with the most significant correlation ($R^2 > 0.6$) being found between the pairs 6′-SL/6′-SLN, OS-C/GNL, and OS-D/OS-G (Figure 3).

When the whole data matrix (13 OS contents of 32 samples) was subjected to PCA analysis, no clear separation was observed between the three feed groups, indicating that the intake of almond hulls or citrus pulp had little effect on the OS

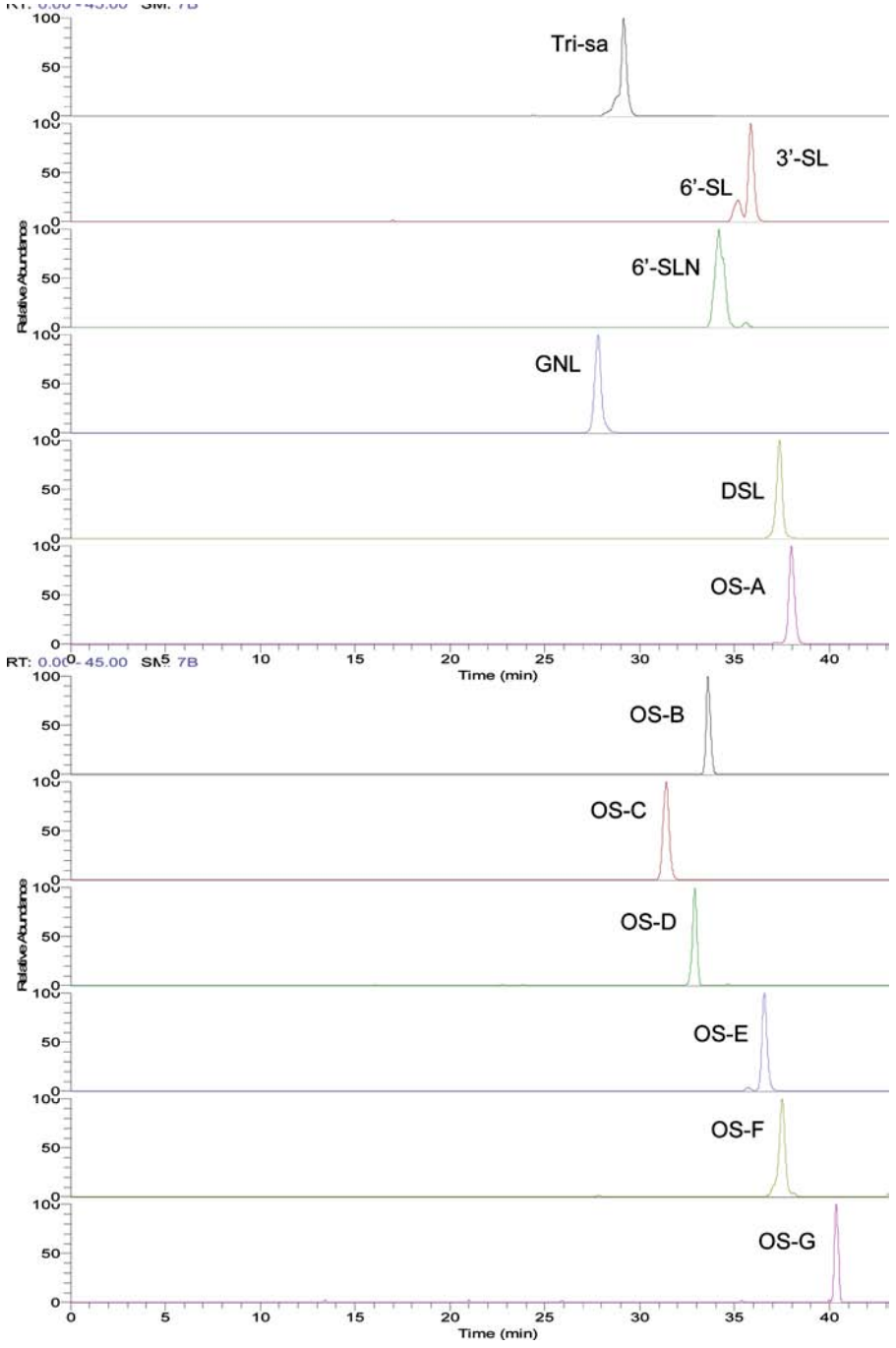


**Figure 1.** Extracted ion chromatogram of the 13 major OS detected in the reference milk sample. The deprotonated ion of each compound was extracted using a window of calculated accurate mass of $m/z$ ±0.005.

accumulation in milk (see Figure S-2 of the Supporting Information).

## DISCUSSION

The beneficial biological functions of OS are increasingly being recognized especially for neonates. It is generally accepted that the OS found in bovine milk are structurally similar to those in human milk.[5] Consequently, the use of bovine milk OS in infant formula and pharmaceutical and food industries is expected to intensify. Because OS in bovine milk are present as a mixture of a large number of linear and branched molecules with 3−10 monosaccharide units, measuring the total OS concentration in bovine milk is not as straightforward as determining the concentration of total fructo-oligosaccharide in plant tissue.[26] As a result, measuring the concentration of the major OS species is important to evaluate the potential beneficial value of OS in a milk sample.

Irrespective of analytical methods, absolute quantification of individual OS is currently possible only for a few major species, for which the standards are available.[16,18] Consequently, relative quantification (using ion intensity or peak area) is the only feasible way for estimating the content of most OS in milk. Indeed, ion intensity was used in a number of studies to estimate the relative content of OS in various milk samples,[13,14,20] but a robust and validated method for relative quantification of major OS is still lacking. Besides, all of the


dx.doi.org/10.1021/jf5037849 | J. Agric. Food Chem. 2014, 62, 11568−11574

**Table 2. Measurement Reproducibility of Methods 3 and 1**

| OS name | peak area RSD (%) ($n$ = 3) | |
|---|---|---|
| | method 3 | method 1 |
| Trisa | 1.68 | 4.50 |
| 3′-SL | 1.55 | 1.97 |
| 6′-SL | 2.25 | 1.00 |
| 6′-SLN | 2.80 | 1.09 |
| DSL | 0.47 | 3.50 |
| GNL | 0.77 | 6.49 |
| OS-A | 2.02 | 1.07 |
| OS-B | 3.13 | 4.02 |
| OS-C | 2.46 | 4.94 |
| OS-D | 8.18 | 7.81 |
| OS-E | 0.37 | 4.86 |
| OS-F | 2.45 | 7.16 |
| OS-G | 3.71 | 8.08 |

**Table 3. LOD, LOQ, and Linearity Range of Five Representative OS**

| OS | ion quantified | LOD (ng) | LOQ (ng) | linear range (ng) | $R^2$ |
|---|---|---|---|---|---|
| 3′-SL | $[M - H]^-$ | 0.05 | 0.25 | 0.25−500 | 0.9945 |
| 6′-SL | $[M - H]^-$ | 0.05 | 0.25 | 0.25−250 | 0.9970 |
| 6′-SLN | $[M - H]^-$ | 0.05 | 0.25 | 0.25−250 | 0.9974 |
| stachyose | $[M - H]^-$ | 0.05 | 0.25 | 0.25−100 | 0.9982 |
| verbascose | $[M - H]^-$ | 0.05 | 0.25 | 0.25−250 | 0.9937 |

previous analyses adopted a standard and complex protocol for protein elimination in milk samples, which consists of chloroform/methanol extraction, residual protein precipitation by ethanol, and OS fraction drying/reconstitution. Such a multi-step sample pretreatment procedure constitutes a bottleneck for measurement throughput. To simplify the sample preparation step, we have evaluated the performance of two new methods that are simpler than the standard method.

Acetonitrile precipitation appeared to be effective for protein elimination from milk, but this solvent also caused partial loss of OS in the supernatant, leading to a significant reduction in the OS yield. This may simply result from co-precipitation of OS in the presence of acetonitrile as reported by Ku et al. in the case of fructo-oligosaccharides.[27] In contrast, ultrafiltration is not only simple to perform but also afforded a higher OS yield with better reproducibility compared to the standard method. Consequently, we believe ultrafiltration has clear advantages over the standard method for protein elimination in milk samples prior to OS analysis.

Nano-LC−chip/TOF MS has been a technique of choice for OS profiling in milk and also for glycan profiling in human serum.[19,28,29] We have shown that HILIC separation coupled to an Orbitrap MS is also highly suitable for OS profiling, owing to its superior sensitivity and high mass accuracy capability.

**Table 5. Recovery (%) of Spiked Standards ($n$ = 3)**

| OS | spike I (0.1 μg) | | | spike II (1 μg) | | |
|---|---|---|---|---|---|---|
| | recovery (%) | SD (%) | RSD (%) | recovery (%) | SD (%) | RSD (%) |
| 6′-SL | 94.93 | 3.48 | 3.66 | 93.71 | 2.75 | 2.93 |
| 6′-SLN | 103.70 | 3.43 | 3.31 | 105.29 | 3.61 | 3.43 |
| stachyose | 95.28 | 2.34 | 2.45 | 94.23 | 4.23 | 4.49 |
| verbascose | 93.09 | 2.75 | 2.95 | 91.07 | 1.53 | 1.68 |

**Table 6. Relative Abundance (Peak Area) of the 13 Major OS ($n$ = 32)**

| OS name | mean ± SD |
|---|---|
| OS-A | 3716387 ± 1179608 |
| OS-B | 751707 ± 349185 |
| OS-C | 528108 ± 227577 |
| OS-D | 45560 ± 24728 |
| 6′-SL | 15374375 ± 6650642 |
| 3′-SL | 87002494 ± 12984817 |
| OS-E | 703177 ± 221299 |
| DSL | 2730046 ± 652066 |
| GNL | 3592667 ± 3376552 |
| Trisa | 9060101 ± 2021898 |
| 6′-SLN | 653564 ± 286207 |
| OS-F | 183795 ± 60414 |
| OS-G | 113112 ± 55621 |

Moreover, the Luna HILIC stationary phase that we used separated all major OS from lactose, thus avoiding the potential ion suppression effect of this most abundant sugar on the detection of other minor analogues. The minimal matrix effect observed in the recovery test may well have resulted from this. It is worth indicating that, except for 3′-SL and 6′-SL, no attempt was made to separate and quantify individual isomers of other major OS species. As a result, most major OS elute as a single peak, facilitating relative quantification.

Because of the limited availability of OS standards, we have used two galacto-oligosaccharides, stachyose (DP of 4) and verbascose (DP of 5), in the method validation to represent neutral OS. Given the similarity in molecular size and structure between these two compounds and the major neutral OS in milk, it is appropriate to assume that they have comparable ionization efficiency for MS detection. The fact that all of the tested OS standards had an on-column LOD of 0.05 ng suggests that, without any enrichment step, low-abundance OS (from 0.01 μg/mL) can be detected by this method. It should be pointed out that all OS species showed much higher response in negative ESI mode than in positive mode in our system and deprotonated molecular ions are dominant in all cases.

All OS detected in the reference sample have been identified previously in different studies.[9,14] Among the 13 major OS (of

**Table 4. Method Precision (% RSD; $n$ = 5) and Accuracy (% ± SD; $n$ = 5)**

| OS | 0.5 ng | | 5 ng | | 100 ng | |
|---|---|---|---|---|---|---|
| | precision (% RSD) | accuracy (% ± SD) | precision (% RSD) | accuracy (% ± SD) | precision (% RSD) | accuracy (% ± SD) |
| 3′-SL | 4.53 | 91.1 ± 4.1 | 1.76 | 95.5 ± 1.7 | 1.64 | 96.5 ± 1.6 |
| 6′-SL | 8.09 | 93.4 ± 7.6 | 2.49 | 99.5 ± 2.5 | 1.65 | 99.9 ± 1.6 |
| 6′-SLN | 2.78 | 96.9 ± 2.7 | 1.56 | 100.1 ± 1.6 | 1.02 | 102.2 ± 1.0 |
| stachyose | 3.71 | 93.5 ± 3.5 | 1.19 | 101.4 ± 1.2 | 2.82 | 103.6 ± 2.9 |
| verbascose | 7.65 | 97.8 ± 7.5 | 1.98 | 99.4 ± 2.0 | 1.38 | 99.5 ± 1.4 |


dx.doi.org/10.1021/jf5037849 | J. Agric. Food Chem. 2014, 62, 11568−11574

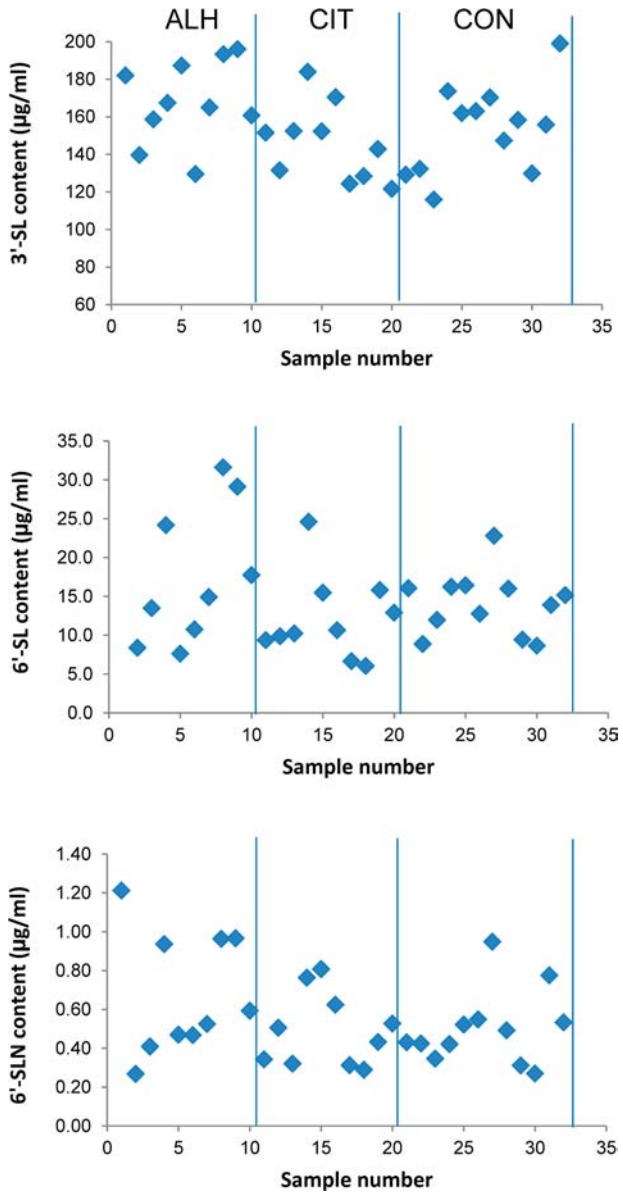


**Figure 2.** Variation in 3′-SL, 6′-SL, and 6′-SLN concentrations across the 32 samples (numbers 1−10, ALH; numbers 11−20, CIT; and numbers 21−32, CON.

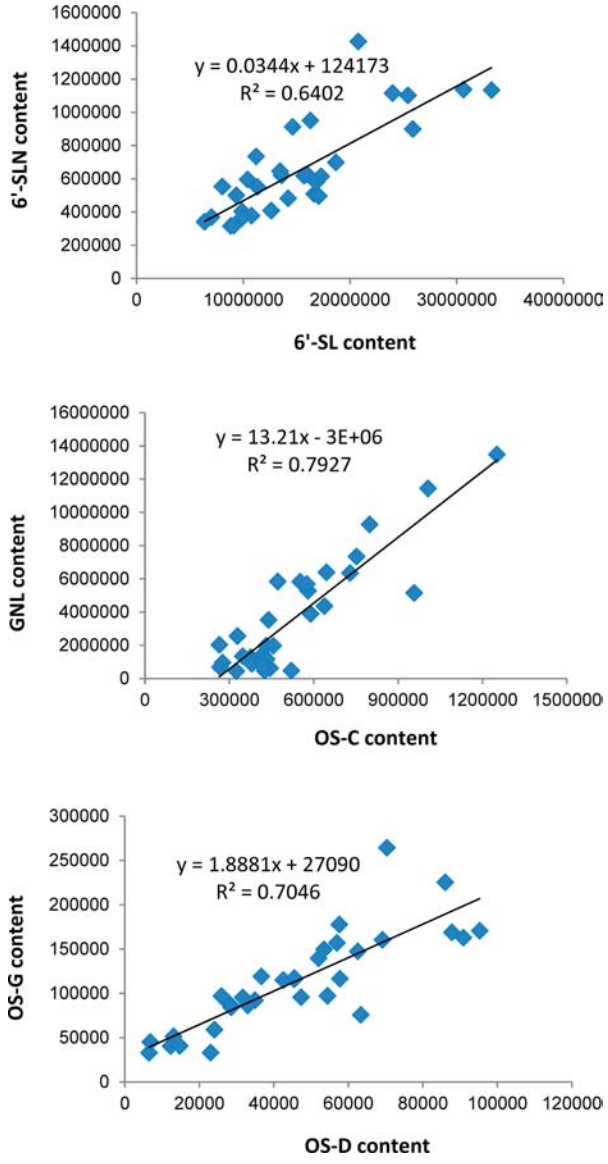


**Figure 3.** Significant correlations between the contents of some OS species ($n$ = 32).

which two are isomers) quantifiable, the structure of 12 have been reported previously.[9] Our observation of 3′-SL and 6′-SL being the most abundant OS across all samples has confirmed the results of other researchers.[12,16,18] The fact that 3′-SLN was not detected in any sample is also in agreement with the observation by Fong et al.[18] However, our finding of 6′-SLN being a low-abundance OS is significantly different to the results of Martin-Sosa et al.[15] and Tao et al.,[9] who found this same compound to be one of the most abundant OS. Such a discrepancy may be attributable to samples being derived from different cow breeds and/or lactation stages. An exhaustive search for more minor OS through sample enrichment was not the aim of this work.

Most of the previous work focused on the comprehensive identification of OS in human milk and animal milk and on the variation of the most abundant OS species, as influenced by various factors, e.g., lactation stages, mammal species, and bovine breeds. Our study has revealed the large variation of OS contents produced by individual cows of the same breed and under the same feeding regime. More samples over different seasons need to be tested to ascertain whether this is genetically based. Moreover, to increase the concentration of OS in cow milk requires a thorough understanding of OS metabolism in the mammary gland and in milk itself.[21] It has already been demonstrated that key genes for oligosaccharide synthesis undergo temporal changes in expression, and this expression differs between species.[30] In this regard, our finding regarding the correlation between some OS, which has not been reported previously to the best of our knowledge, is valuable for elucidating the biosynthesis pathways of OS. The correlation found between some OS species may be an indication of common biochemical steps used in their biosynthesis.

Our work also demonstrates the variability in the concentration of OS in milk from different cows in the same herd that is not associated with the feeding regime used in this study. This suggests that cows may be selected for their ability to produce larger quantities of certain OS that may be of value in human health products.


dx.doi.org/10.1021/jf5037849 | J. Agric. Food Chem. 2014, 62, 11568−11574

In conclusion, a novel LC−MS method has been developed, which, using a routine HILIC−LC and an Orbitrap mass analyzer, is able to provide relative quantification of 13 major OS in bovine milk with minimum sample preparation. The method is sensitive, accurate, and reproducible and can be used as an alternative to the widely used nano-LC−chip/TOF-based method. The applicability of this method to a large number of mature milk samples collected from cows after different feed treatments allowed us to confirm that almond hulls and citrus pulp when used as a feed supplement have no adverse effect on the accumulation of OS in milk.

## ■ ASSOCIATED CONTENT

### Ⓢ Supporting Information

MS/MS pattern of 13 OS (Figure S-1) and PCA plot of PC1 and PC2 showing unsupervised classification of 32 milk samples based on the content of 13 major OS (Figure S-2). This material is available free of charge via the Internet at http://pubs.acs.org.

## ■ AUTHOR INFORMATION

### Corresponding Author

*E-mail: simone.rochfort@depi.vic.gov.au.

### Notes

The authors declare no competing financial interest.

## ■ REFERENCES

(1) Stelwagen, K.; Carpenter, E.; Haigh, B.; Hodgkinson, A.; Wheeler, T. T. Immune components of bovine colostrum and milk. *J. Anim. Sci.* **2009**, *87*, 3−9.

(2) Bentley, P. A.; Shao, Y.; Misra, Y.; Morielli, A. D.; Zhao, F. Q. Characterization of bovine glucose transporter 1 kinetics and substrate specificities in *Xenopus* oocytes. *J. Dairy Sci.* **2012**, *95*, 1188−1197.

(3) Boehm, G.; Stahl, B. Oligosaccharides from milk. *J. Nutr.* **2007**, *137* (Supplement 2), 847S−849S.

(4) Gopal, P. K.; Gill, H. S. Oligosaccharides and glycoconjugates in bovine milk and colostrum. *Br. J. Nutr.* **2000**, *84* (Supplement 1), S69−S74.

(5) Zivkovic, A. M.; Barile, D. Bovine milk as a source of functional oligosaccharides for improving human health. *Adv. Nutr.* **2011**, *2*, 284−289.

(6) Ninonuevo, M. R.; Park, Y.; Yin, H.; Zhang, J.; Ward, R. E.; Clowers, B. H.; German, J. B.; Freeman, S. L.; Killeen, K.; Grimm, R.; Lebrilla, C. B. A strategy for annotating the human milkglycome. *J. Agric. Food Chem.* **2006**, *54*, 7471−7480.

(7) Wang, B. Sialic acid is an essential nutrient for brain development and cognition. *Annu. Rev. Nutr.* **2009**, *29*, 177−222.

(8) Tao, N.; Wu, S.; Kim, J.; An, H. J.; Hinde, K.; Power, M. L.; Gagneux, P.; German, J. B.; Lebrilla, C. B. Evolutionary glycomics: Characterization of milk oligosaccharides in primates. *J. Proteome Res.* **2011**, *10*, 1548−1557.

(9) Tao, N.; DePeters, E. J.; Freeman, S.; German, J. B.; Grimm, R.; Lebrilla, C. B. Bovine milk glycome. *J. Dairy Sci.* **2008**, *91*, 3768−3778.

(10) Urashima, T.; Taufik, E.; Fukuda, K.; Asakuma, S. Recent advances in studies on milk oligosaccharides of cows and other domestic farm animals. *Biosci., Biotechnol., Biochem.* **2013**, *77*, 455−466.

(11) Veh, R. W.; Michalski, J. C.; Corfield, A. P.; Sander-Wewer, M.; Gies, D.; Schauer, R. New chromatographic system for the rapid analysis and preparation of colostrum sialyloligosaccharides. *J. Chromatogr. A* **1981**, *212*, 312−322.

(12) MaJarrow, P.; van Amelsfort-Schoonbeek, J. Bovine sialyl oligosaccharides: Seasonal variations in their concentrations in milk, and a comparison of the colostrums of Jersey and Friesian cows. *Int. Dairy J.* **2004**, *14*, 571−579.

(13) Tao, N.; DePeters, E. J.; German, J. B.; Grimm, R.; Lebrilla, C. B. Variation in bovine milk oligosaccharides during early and middle lactation stages analysed by high-performance liquid chromatography−chip/mass spectrometry. *J. Dairy Sci.* **2009**, *92*, 2991−3001.

(14) Sundekilde, U. K.; Barile, D.; Meyrand, M.; Poulsen, N. A.; Larsen, L. B.; Lebrilla, C. B.; German, J. B.; Bertram, H. C. Natural variability in bovine milk oligosaccharides from Danish Jersey and Holstein-Friesian breeds. *J. Agric. Food Chem.* **2012**, *60*, 6188−6196.

(15) Martin-Sosa, S.; Martin, M. J.; Garcia-Pardo, L.; Hueso, P. Sialyloligosaccharides in human and bovine milk and in infant formulas: Variations with the progression of lactation. *J. Dairy Sci.* **2003**, *86*, 52−59.

(16) Nakamura, T.; Kawase, H.; Kimura, K.; Watanabe, Y.; Ohtani, M.; Arai, I.; Urashima, T. Concentrations of sialyloligosaccharides in bovine colostrum and milk during the prepartum and early lactation. *J. Dairy Sci.* **2003**, *86*, 1315−1320.

(17) Fong, B.; Ma, K.; McJarrow, P. Quantification of bovine milk oligosaccharides using liquid chromatography−selected reaction monitoring−mass spectrometry. *J. Agric. Food Chem.* **2011**, *59*, 9788−9795.

(18) Marino, K.; Lane, J. A.; Abrahams, J. L.; Struwe, W. B.; Harvey, D. J.; Marotta, M.; Hickey, R. M.; Rudd, P. M. Method for milk oligosaccharide profiling by 2-aminobenzamide labelling and hydrophilic interaction chromatography. *Glycobiology* **2011**, *21*, 1317−1330.

(19) Ninonuevo, M. R.; Lebrilla, C. B. Mass spectrometric method for analysis of oligosaccharides in human milk. *Nutr. Rev.* **2009**, *67* (Supplement 2), S216−S226.

(20) Barile, D.; Marotta, M.; Chu, C.; Mehra, R.; Grimm, R.; Lebrilla, C. B.; German, J. B. Neutral and acidic oligosaccharides in Holstein-Friesian colostrum during the first 3 days of lactation measured by high-performance liquid chromatography on a microfluidic chip and time-of-flight spectrometry. *J. Dairy Sci.* **2010**, *93*, 3940−3949.

(21) Wickramasinghe, S.; Hua, S.; Rincon, G.; Islas-Trejo, A.; German, J. B.; Lebrilla, C. B.; Medrano, J. F. Transcriptome profiling of bovine milk oligosaccharide metabolism genes using RNA-sequencing. *PLoS One* **2011**, *6* (4), No. e18895.

(22) Aldredge, D. L.; Geronimo, M. R.; Hua, S.; Nwosu, C. C.; Lebrilla, C. B.; Barile, D. Annotation and structural elucidation of bovine milk oligosaccharides and determination of novel fucosylated structures. *Glycobiology* **2013**, *23*, 664−676.

(23) National Health and Medical Research Council (NHMRC), Australian Government. *Australian Code of Practice for the Care and Use of Animals for Scientific Purposes*, 7th ed.; NHMRC, Australian Government: Canberra, Australian Capital Territory (ACT), Australia, 2004; http://www.nhmrc.gov.au/publications/synopses/ea16syn.htm.

(24) Coppa, G. V.; Pierani, P.; Zampini, L.; Carloni, I.; Carlucci, A.; Gabrielli, O. Oligosaccharides in human milk during different phases of lactation. *Acta Paediatr. Suppl.* **1999**, *430*, 89−94.

(25) Liu, Z.; Rochfort, S. A fast chromatography−mass spectrometry (LC−MS) method for quantification of major polar metabolites in plants. *J. Chromatogr. B: Anal. Technol. Biomed. Life Sci.* **2013**, *912*, 8−15.

(26) Liu, Z.; Mouradov, A.; Smith, K.; Spangenberg, G. An improved method for quantitative analysis of total fructans in plant tissues. *Anal. Biochem.* **2011**, *418*, 252−259.

(27) Ku, Y.; Jansen, O.; Oles, C. J.; Lazar, E. Z.; Rader, J. I. Precipitation of inulins and oligoglucoses by ethanol and other solvents. *Food Chem.* **2003**, *81*, 125−132.

(28) Hua, S.; An, H. J.; Ozcan, S.; Ro, G. S.; Soares, S.; DeVere-White, R.; Lebrilla, C. B. Comprehensive native glycan profiling with isomer separation and quantitation for the discovery of cancer biomarkers. *Analyst* **2011**, *136*, 3663−3671.

(29) Ninonuevo, M. R.; Park, Y.; Yin, H.; Zhang, J.; Ward, R. E.; Clowers, B. H.; German, J. B.; Freeman, S. L.; Killeen, K.; Grimm, R.; Lebrilla, C. B. A strategy for annotating the human milkglycome. *J. Agric. Food Chem.* **2006**, *54*, 7471−7480.

(30) Maksimovic, J.; Sharp, J. A.; Nicholas, K. R.; Cocks, B. G.; Savin, K. Conservation of the ST6Gal I gene and its expression in the mammary gland. *Glycobiology* **2011**, *21*, 467−481.

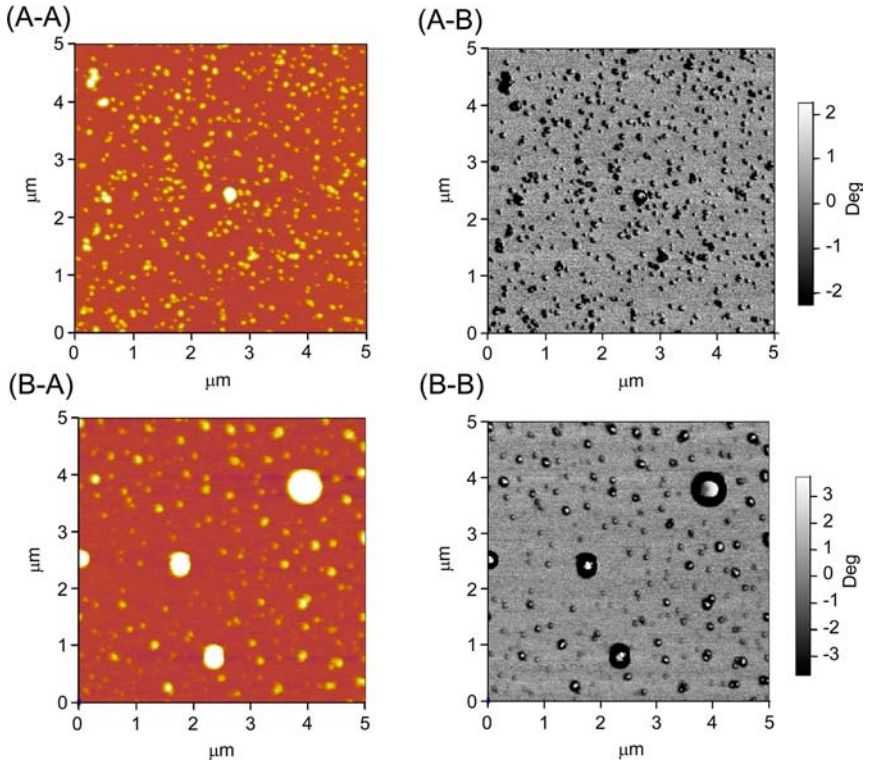


**Figure 1.** Atomic force microscopy images of fresh soybean O/W emulsions (10% w/w oil) prepared with 11.1 mg/mL Tween 20 + 20 mg/mL PPH using height retrace mode (A-A) and phase retrace mode (A-B) or with Tween 20 only using height retrace mode (B-A) and phase retrace mode (B-B) .

chased from Sigma-Aldrich Co. (St. Louis, MO, USA). All other chemicals were purchased from Sinopharm Chemical Reagent Co. (Shanghai, China), and they were of analytical grade unless otherwise specified. Deionized water was used for the preparation of all solutions.

**Preparation of Potato Protein Hydrolysate (PPH).** PPH was prepared through 1 h of hydrolysis of intact potato protein (40 mg/mL) in an aqueous solution at pH 8.0 and 50 °C using Alcalase.[3] The enzyme/protein substrate was at a weight ratio of 1:100. After hydrolysis, the broth was adjusted to pH 7.0 with 1 M NaOH and then heated at 80 °C for 15 min to inactivate the enzyme. The hydrolysate was freeze-dried, placed in sealed plastic bags, and stored at 4 °C. This PPH has been shown to be strongly antioxidative in an O/W emulsion due to its potent radical-scavenging capability.[3,14]

**Emulsion Preparation.** O/W emulsions were prepared from the mixture of 10% (w/w) soybean oil (Eastocean Oils and Grains Industries Co., Zhang Jiagang, Jiangsu, China) and 90% (w/w) 0.01 M phosphate buffer (pH 7.0) containing 11.1 mg/mL Tween 20 + 20 mg/mL PPH (treatment) or 11.1 mg/mL Tween 20 alone (control). In treatment emulsion, Tween 20 was used as coemulsifier because, unlike lecithin, Tween 80, or some other surfactants, it helps stabilize O/W emulsion droplets without affecting the oxidative stability.[13] Fine emulsions were produced by blending the mixture using a T18 Ultra-Turrax high-performance disperser (Ika-Werke Gmbh & Co., Staufen, Germany) at 21500 rpm for 2 min followed by passing through an ATS AH-basic high-pressure (32 MPa) valve homogenizer (ATS Engineering Inc., Brampton, Canada) twice.[13] The average particle size of the emulsions was determined by dynamic light scattering (DLS) (Mastersizer Nano-ZS, Malvern Instruments, Worcestershire, UK).

**Emulsion Microstructure.** Emulsion samples were diluted 10 times for the examination of the microstructure. For AFM, 2 μL of a diluted emulsion was dried on freshly cleaved mica. AFM images were obtained on Asylum MFP-3D-SA (Asylum Research, Santa Barbara, CA, USA) using the tapping mode and the phase mode. The surface of mica was scanned in air using OMCL-AC160TS cantilevers at a set point of 0.63 V, a 1 Hz scan rate, and a drive frequency of 336.3 kHz.

For CLSM, the procedure of Kerstens et al.[15] was followed. An aliquot of of 2 μL diluted emulsions was placed on a microscope slide, covered with a coverslip, and observed using a Carl Zeiss LSM 710 confocal system (Carl Zeiss MicroImaging GmbH, Göttingen, Germany) with an oil immersion 63× objective. Images were captured by a digital camera connected to the microscope. Photographs of the emulsions were analyzed using software ZEN 2008 Light Edition (Carl Zeiss MicroImaging GmbH) and recorded. The oil droplets in an emulsion were stained using Nile Red in such a way that 2.5 mL of emulsion was mixed with 25 μL of 0.1 mg/mL dye solution prepared with ethanol. On the other hand, peptides were stained with Nile Blue through mixing 2.5 mL of emulsion with 12.5 μL of the dye solution in a dye/protein ratio of 1:100. Nile Red and Nile Blue were excited at 488 and 639 nm, respectively. Emitted light was collected between 653 and 750 nm for Nile Red and between 503 and 613 nm for Nile Blue in two independent channels.

For cryo-TEM, 2 μL of a diluted emulsion was placed on a lacy carbon film supported by a copper grid and allowed to stabilize for 10 min. A filter paper was used to remove liquid for thin liquid films formation. The grid was then immersed in liquid nitrogen (−180 °C) for quenching. After 1 min, the specimen was mounted into the prechilled cryogenic sample holder (Gatan-626 Cryo-tansfer, Gatan, Inc., Tokyo, Japan), followed by being loaded to a JEOL JEM-2100 transmission electron microscope (JEOL Ltd., Tokyo, Japan) immediately. The acceleration voltage of 200 kV was used and the temperature of the holder was kept below the −170 °C during operation. The images of the specimen were captured using a digital camera connected to the microscope.

**Recovery of Interfacial Peptides.** PPH peptides present at the interfacial membrane were collected by means of centrifugation. Emulsion samples were placed in 50 mL tubes and centrifuged for 45 min at 50000*g* at 20 °C to separate into a cream layer and a serum layer. The cream layer was carefully removed using a syringe and dispersed in the same volume of 0.01 M phosphate buffer (pH 7.0). After centrifugation again under the same conditions as above to remove loosely bound peptides, the cream layer was collected and

extracted using chloroform/methanol mixture (2:1, v/v).[16] The methanol phase was dried, and the peptides were dissolved in water before analysis.

**Identification of Peptides at the Interface.** The peptide mixture obtained above was fractionated using Sephadex G15 gel filtration, and 50 fractions (2 min each) were collected. To obtain sufficient amounts of peptide samples, identical fractions from 10 separate gel filtration runs were combined and lyophilized. Each individual peptide fraction was tested for $ABTS^{\bullet+}$ scavenging activity at the protein concentration of 20 $\mu$g/mL; the fractions that exhibited strong radical scavenging aqctivity were subjected to solid phase extraction (SPE) to remove Tween 20 using a 3 mL Cleanert PCX SPE column (Agela Technologies Inc., Tianjin, China) preconditioned with 6 mL of methanol followed by 6 mL of deionized water. Peptide fractions loaded in the column were washed with 8 mL of deionized water and then 8 mL of a methanol/water solution (5:95, v/v) to remove Tween 20. Afterward, the samples were eluted with 3 mL of ammonia−water/methanol (5:95, v/v) and then dried by purging with nitrogen gas.

The purified peptide fractions were dissolved in 1 mL of water/acetonitrile (1:1, v/v). Ten microliters of the sample solutions was loaded and eluted in an Acquity UPLC BEH C18 column (2.1 × 120 mm) (Waters Corp., Milford, MA, USA). The mobile solvent (acetonitrile and formic acid for mobile phases A and B, respectively) flow rate was set at 0.3 mL/min, where a linear gradient (10−20% in 20 min for acetonitrile) was used. Eluted peptides were subjected to mass spectrometry sequencing using a Waters Synapt Mass Quadrupole TOF mass spectrometer (Waters Corp.) through an electrospray ionization source. Automated data acquisition using the information-dependent mode was performed using MassLynx software (Waters Corp.). The spectra were interpreted using the peptide sequencing module of the MassLynx software.

Properties of identified peptides were calculated using peptide property calculator from Innovagen (Innovagen AB, Lund, Sweden), which is also available at http://www.innovagen.se/peptide-design-tools.asp. The sequences identified were matched to the published sequences of potato proteins from the National Center for Biotechnology Information (NCBI) database.

**Evaluation of Radical Scavenging Activity.** The peptide fractions from the above gel filtration were diluted to 20 $\mu$g/mL and then subjected to the ABTS radical scavenging assay.[14] Briefly, samples (20 $\mu$L each) were reacted with 1980 $\mu$L of diluted $ABTS^{\bullet+}$, and the absorbance (734 nm) after 10 min was read. Radical scavenging activity was expressed as Trolox equivalent ($\mu$M) based on a standard curve generated with a series of concentrations of Trolox (0−3 mM).

**Statistical Analysis.** All experiments were repeated a minimum of three times ($n \geq 3$) in independent replication trials, each with duplicate or triplicate sample analyses. Data were subjected to one-way analysis of variance (ANOVA) using the Origin 7.5 statistics program (OriginLab Corp., Northampton, MA, USA). Differences ($P < 0.05$) between means were identified by Tukey's test.

## RESULTS AND DISCUSSION

**Emulsion Physical Stability.** The emulsions prepared either with Tween 20 alone or with Tween 20 + PPH had DLS-measured particle sizes of 215.3 and 218.1 nm, respectively. The value for the latter emulsion was larger than expected, which could have resulted from clustering of emulsion particles or peptide aggregates. Nevertheless, both the control and PPH treatment emulsions were very stable, showing no creaming even after 2 weeks of storage at 37 °C. During this period, the average particle size for both emulsions also did not show any significant change ($P > 0.05$).

**AFM.** The microscope images of emulsions prepared with Tween 20 with or without 20 mg/mL PPH are displayed in Figure 1. They represent height retrace and phase retrace obtained under the tapping mode. The emulsions prepared with combined Tween 20 and PPH (Figure 1A-A,A-B) consisted of numerous smaller and more uniformly distributed oil droplets when compared with those prepared with Tween 20 alone (Figure 1B-A,B-B). The particle numbers per measurement area (5 × 5 $\mu$m) for the two different emulsion systems were 365 and 137, respectively. This remarkable disparity was attributed to the surface activity of peptides present in PPH allowing more efficient dispersion of oil in the aqueous system.[13] In a typical O/W emulsion, the emulsifier concentration and type affect the particle size of emulsion droplets. Therefore, when PPH was combined with Tween 20, the peptides could impart additional emulsifying power by a sheer concentration effect. The imaging analysis result confirmed that the particle size measured by DLS in the PPH + Tween emulsion was likely an overestimate due to interactions between peptide-covered oil droplets and between peptides themselves. Because PPH alone was not capable of producing a stable emulsion (result not shown), there existed a cooperativity between Tween 20 and peptides.

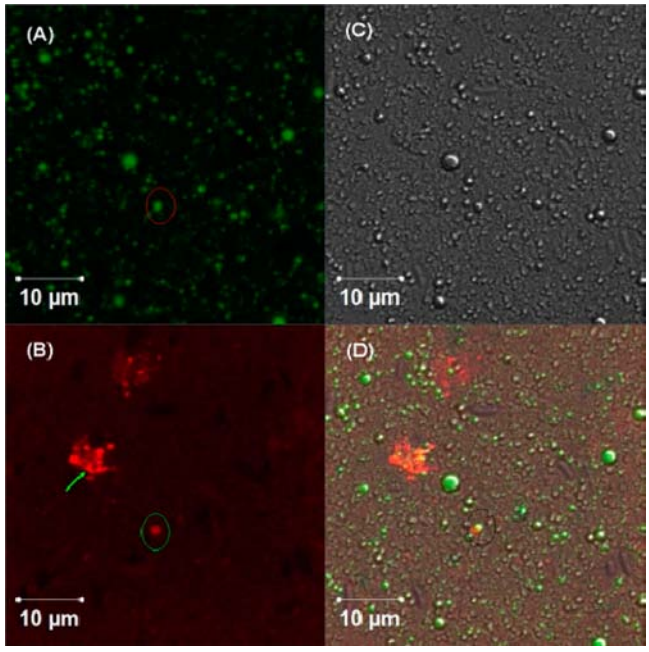


**Figure 2.** Confocal laser scanning micrographs of soybean O/W emulsions (10% w/w oil) prepared with 11.1 mg/mL Tween 20 + 20 mg/mL PPH: (A) image from Nile Red fluorescence (highlighting the oil phase); (B) image from Nile Blue/protein fluorescence; (C) phase contrast image without fluorescence; (D) overlay image combining fluorescence from both dyes. The arrow identifies a circular dark hole in the Nile Blue/protein image corresponding to a single large oil droplet. Scale bar represents 10 $\mu$m.

Phase angle shift, which is able to enhance the contrast of the AFM images, is a derivation of the tapping mode.[17,18] A phase image, taken by detecting the phase angle shift, is useful in distinguishing different chemical or physical features of the sample.[18−20] In phase images, dark and bright regions indicate different levels of hardness of the material.[20] It has been reported that interfacial characteristics and particle size affect not only the physical stability but also the chemical activity of emulsions.[21,22] An O/W emulsion could be regarded as a particle consisting of an oil core and a emulsifier shell. Because free oil inside an emulsion droplet is expected to have a higher fluidity than surface oil molecules with surfactants and the area-to-volume ratio is $3r^{-1}$ (where $r$ is radius), a large oil droplet would be softer than a small oil droplet. The poorly covered

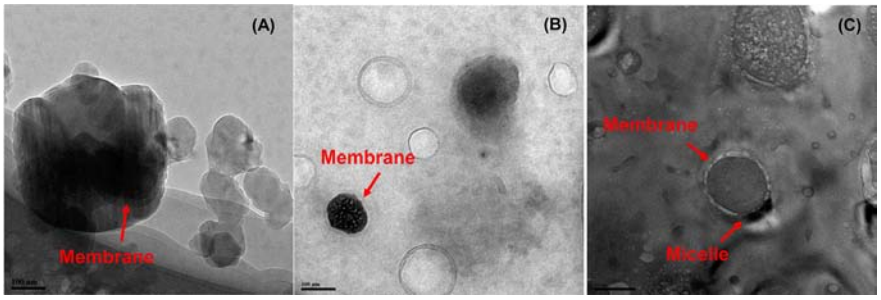


**Figure 3.** Cryo-TEM images of soybean O/W emulsions (10% w/w oil) prepared with (A) 11.1 mg/mL Tween 20, (B) 20 mg/mL PPH, and (C) 11.1 mg/mL Tween 20 + 20 mg/mL PPH. Bar = 100 nm.

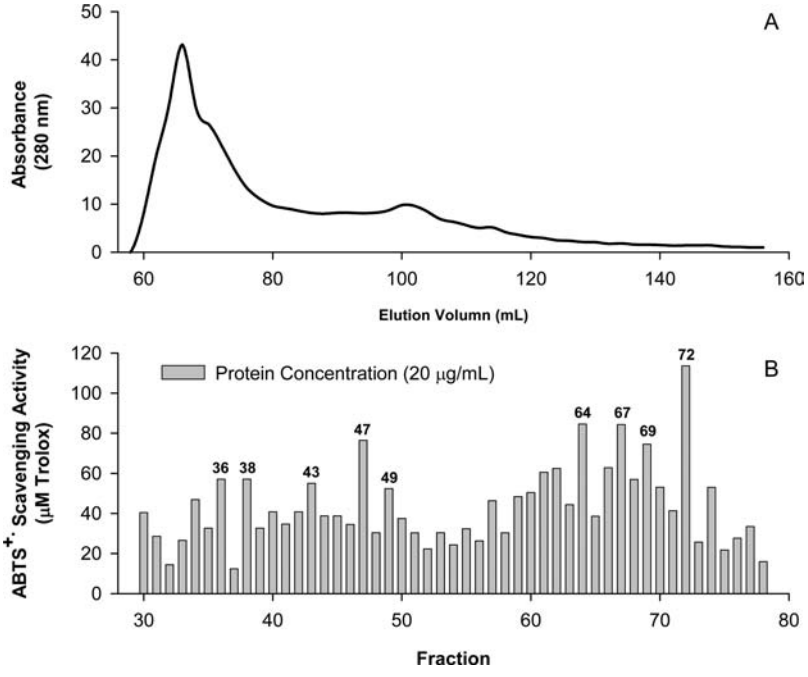


**Figure 4.** (A) Gel filtration spectra of PPH in the interface of soybean O/W emulsion prepared using 11.1 mg/mL Tween 20 + 20 mg/mL PPH; (B) $ABTS^{\bullet+}$ scavenging activity of gel filtration fractions from interfacial PPH. Every 2 mL of liquid was collected for one tube.

core region would be soft and appear bright, whereas the shell region would be hard and appear dark.

Indeed, in the Tween 20-stabilized oil emulsion, the emulsion droplets displayed a quite noticeable bright region in the surface center of the particles, indicating a soft matrix. In comparison, the emulsion prepared with combined PPH and Tween 20 exhibited a relatively dark region in the center of the oil droplets, indicating a harder or more intact membrane due to peptides. However, other parts of the surface of the emulsion droplets were not uniformly dark, suggesting that the distribution of PPH as a coemulsifier at the interface was not consistent. Moreover, the intensity of darkness appeared to be variable between oil droplets. If surface dilatational rheology measurements were carried out to determine the surface rheology, the results of AFM would be more convincing and mechanistic.

Inadequately covered (i.e., relatively exposed) surfaces of the emulsion droplets, notable for Tween 20 emulsions, would predispose the O/W emulsions to oxidative stress. When subjected to radicals and other oxidant species, the less well-protected oil particles would be prone to chemical degradation through oxidative chain reactions. Because peptides are emphateric ions, the less abundant presence of peptides at the interface would mean fewer charge repulsions against pro-oxidaitve metal and other oxidizing ionic species such as superoxide anion. Peptides located at the interface protect oil from oxidative stress through their radical scavenging activity and metal chelating actions. In addition, peptides dispersed in the aqueous phase are capable of enhancing the oxidative stability of emulsions by neutralizing radicals and sequestering pro-oxidaitve metal ions.[13,14,23]

**CLSM.** To substantiate that the physical location of peptides is an important factor for the inhibition of emulsion oxidation, CLSM images were presented to illustrate the distribution of peptides in different emulsion samples (Figure 2). Although CLSM was not able to display all particle sizes, we had found some typical particles to support out hypothesis. In these images, oil and peptides were labeled with fluorescent Nile Red and Nile Blue, respectively, enabling the delineation of peptide coating around the oil droplets. At the excitation wavelength of 639 nm, Nile Red-stained oil gave rise to a green color (Figure 2A), whereas at 488 nm, peptides stained with Nile Blue exhibited a red color (Figure 2B). The emulsion prepared with Tween 20 only showed numerous particles of varying sizes that emitted a green color. Because Tween 20 produces no fluorescence signals, these particles were oil droplets. On the

**Table 1. Peptides Identified by UPLC-Q-TOF-MS from Selected Fractions of PPH**

| fraction | peptide sequence | $M_w$ | prob % |
|---|---|---|---|
| 36 | ALEPRP | 681.4 | 95 |
| 38 | VTLLADKQ | 886.5 | 83 |
| | KPSQSLQ | 786.4 | 100 |
| | DLKSV | 560.3 | 74 |
| | RLCAK | 589.3 | 90 |
| 43 | LTEPGR | 671.4 | 75 |
| | NSVDLQ | 674.3 | 92 |
| 47 | KNGKAM | 647.3 | 87 |
| | LFVRAS | 691.4 | 74 |
| 49 | DF | 280.1 | 100 |
| 64 | PLAL | 412.3 | 100 |
| | RPALM | 586.3 | 97 |
| 67 | SFDL(I)K | 608.7 | 95 |
| 69 | TEVL | 460.2 | 99 |
| | GPVNLL | 611.4 | 99 |
| | SFY | 415.2 | 99 |
| | SFDL(I)K | 608.7 | 100 |
| 72 | PDE | 359.1 | 100 |
| | AQRVP | 569.3 | 100 |
| | ENYKT | 653.3 | 96 |
| | RTQ | 403.2 | 94 |

**Table 2. Properties of Peptides Identified by UPLC-Q-TOF-MS from Selected Fractions**

| fraction | peptide sequence | p*I* | hydrophilic residues/total number of residues (%) | average hydrophilicity | net charge at pH 7.0 |
|---|---|---|---|---|---|
| 36 | ALEPRP | 7.0 | 33 | 0.6 | 0 |
| 38 | VTLLADKQ | 10.1 | 38 | 0 | 1 |
| | KPSQSLQ | 14.0 | 71 | 0.3 | 2 |
| | DLKSV | 6.7 | 60 | 0.6 | 0 |
| | RLCAK | 10.1 | 40 | 0.5 | 2 |
| 43 | LTEPGR | 7.0 | 33 | 0.6 | 0 |
| | NSVDLQ | 6.7 | 67 | 0.1 | 0 |
| 47 | KNGKAM | 10.6 | 50 | 0.7 | 2 |
| | LFVRAS | 11.0 | 33 | −0.5 | 1 |
| 49 | DF | 3.1 | 50 | 0.3 | −1 |
| 64 | PLAL | 6.0 | 0 | 0 | −1 |
| | RPALM | 11 | 20 | −0.1 | 1 |
| 67 | SFDL(I)K | 6.7 | 60 | 0.4 | 0 |
| 69 | TEVL | 3.3 | 25 | −0.2 | −1 |
| | GPVNLL | 6.0 | 17 | −0.8 | 0 |
| | SFY | 5.9 | 33 | −1.5 | 0 |
| | SFDL(I)K | 6.7 | 60 | 0.4 | 0 |
| 72 | PDE | 3.0 | 67 | 2 | −2 |
| | AQRVP | 11.0 | 40 | 0.2 | 1 |
| | ENYKT | 6.9 | 60 | 0.7 | 0 |
| | RTQ | 14.0 | 67 | 0.9 | 2 |

other hand, when PPH was also present during the emulsion sample preparation, the product showed several conspicuous and many faint red droplets, indicting the presence of peptides surrounding the interface. In particular, a salient oil droplet and a remarkable cluster of red-colored particles are displayed (pointed by arrows), and these were peptide-coated particles (Figure 2B). Therefore, in these emulsions, Tween 20 and PPH coexisted at the interface for improved emulsion stability. Interestingly, apparently fewer oil droplets were visible in Nile Blue-stained samples (Figure 2B) than in Nile Red-stained samples (Figure 2A). This could be due to the lesser sensitivity of Nile Blue reacting with proteins than Nile Red reacting with oil.

Similar phenomena have been observed by Gallier et al.,[24] who used CLSM to analyze the membrane of milk fat globules. When some components absorbed in the membrane were replaced by other components with no fluorescence, their position in the membrane might turn to dark pores. The most prominent particle present in Figure 2A,B (arrow) was the same particle. When these two images were superimposed (Figure 2C), the color of the particle turned yellow, which was the overlay of green and red.[15] This was clear evidence that peptides in PPH were adsorbed at the interface as coemulsifiers. It was also shown in Figure 2B that some emulsion particles were surrounded by the aqueous environment consisting of peptides. This is in agreement with the result we reported previously with common transmission electron microscopy.[13]

On the basis of the results of AFM and CLSM, peptides from PPH were present at the interface, and they were distributed either through direct adsorption on the surface of oil droplets or by reinforcing the interface covered by Tween 20. Both scenarios are in agreement with the findings of Girardet et al.[25] that $\beta$-casein(f114−169) may cover the interface with Tween 20 or adsorb around the Tween 20 covering in the interface. Thus, the peptides partitioning in the interface filled in the space between individual Tween 20 molecules and prevented the exposure of oil to oxidants by means of physical obstacles in addition to chemical mechanisms. Peptides absorbed around Tween 20 might improve the interfacial charges and modify the electric double layers of the interface. This would lead to a stronger steric hindrance and enhanced electrostatic repulsions between oil droplets and oxidizing compounds as mentioned above to prevent oxidative chain reactions.

**Cyro-TEM.** Whereas CLSM yielded strong evidence that peptides in PPH were adsorbed at the interface of the soybean O/W emulsions, the structural details of the interfacial membrane were still missing. Hence, cyro-TEM, which operates in a nondestructive mode allowing emulsion samples to be examined in their intact state, was used to analyze the morphological characteristics of the interfacial membrane. The cyro-TEM images of the emulsion prepared with Tween 20 only exhibited no clear membrane (Figure 3A), whereas the emulsion prepared with PPH only showed a relatively uniform interfacial membrane-like structure (Figure 3B). On the other hand, the interface of the emulsion prepared using combined Tween 20 and PPH displayed a structurally heterogeneous membrane made up of several fragments with different lengths (Figure 3C). It appeared that the interface membrane was not composed of a single component; both Tween 20 and peptides were present. These two emulsifiers appeared to adsorb on the surface of the oil droplets alternatively but in an irregular pattern.

The dark segment in Figure 3C might be micelles of Tween 20 surrounding the surface of the emulsifier layer. A similar interfacial structure identified as a casein micelle sheath was found by other researchers who applied cyro-TEM to analyze the ultrastructure of dairy products.[26] It is possible that Tween 20 micelles, together with peptides from PPH, acted as physical barriers to prevent the penetration of peroxides and metal pro-oxidants, thereby inhibiting the oxidation of the oil.[12] Although the interfacial membrane of the emulsions prepared with combined Tween 20 and PPH appeared to be less tight than

Table 3. Identified Interfacial Peptides That Matched the Peptide Sequences of Potato Protein

| peptide sequence | matched protein[a] | sequence of matched protein[a] |
|---|---|---|
| DF | phosphoenolpyruvate carboxylase | f121 LKKKG**DF**GDE |
| | | f431 LL**DF**LRQVST |
| PLAL(I) | NAD(P)H-quinone oxidoreductase subunit 1 | f171 YEI**PLAL**CVL |
| | lipoxygenase 1 | f461 QDNGSLK**PLAI**ELSFPHPDG |
| ENYKT | ATP synthase subunit b | f121 L**ENYK**NE**T**IP |
| SFY | glucose-1-phosphate adenylyltransferase | f371 DF**SFY**DRSAP |
| TEVL(I) | pyruvate kinase, cytosolic isozyme | f461 AKATDSES**TEVI**LEAALKSA |
| GPVNLL | lipoxygenase 1 | f831 RS**GPVN**APYT**LL**FPTSEGGL |
| SFDL(I)K | patatin | f151 AIS**SFDIK**TN |
| PDE | isocitrate dehydrogenase | f80 **PDE**ARVKEFNL |
| AQRVP | ribulose-phosphate 3-epimerase | f121 LMIVEPD**QRVP**DFIKAGADI |

[a]From National Center for Biotechnology Information (NCBI).

the thin film in the emulsions prepared with Tween 20, the former clearly exhibited higher oxidation stability. This was not surprising because, in addition to the proposed physical effect, peptides can act as strong radical scavengers and reducing agents.[13,14] Emulsions stabilized by $\alpha$-lactalbumin and $\beta$-lactoglobulin, which exhibited similar thickness when absorbed in the emulsion interface, showed different oxidative stabilities for their different structures and properties in the interface.[27,28] It has been demonstrated that antioxidants partitioning at the O/W interface are more effective than antioxidants present in the aqueous phase in suppressing free radical.[29]

**Identification and Characterization of Interfacial Peptides.** As PPH distributed in the interface was still a mixture of peptides, it was fractionated using G15 gel filtration. Fractions 36, 38, 43, 47, 49, 64, 67, 69, and 72, which exhibited notably higher ($P < 0.05$) ABTS radical scavenging ability than most other fractions and represented a broad fraction distribution (Figure 4), were further analyzed. These selected fractions were subjected to UPLC-Q-TOF-MS for peptide separation and sequence identification. They were also characterized for physical properties to help explain their physical role in the mechanism of oxidation inhibition by PPH at the interfacial membrane. As displayed in Table 1, altogether 17 peptides were identified. The molecular weights ranged from 200 to 800 Da, corresponding to dipeptides to heptapeptides. The anchorage of peptides at the interface was thought to be independent of peptide length;[30] short peptides were able to participate at the interface and might fill the gap between monolayer Tween 20 molecules. Lysine, arginine, glutamic acid, aspartic acid, proline, and leucine were the most abundant amino acids in the peptides identified. The free amino group in lysine and arginine and free carboxyl group in glutamic acid and aspartic acid, which possess a pair of free electrons, were able to chelate pro-oxidative metal ions such as $Fe^{2+}$ and $Cu^{2+}$ through electrostatic coordination. The sequestration action would lead to less catalysis activity of metal ions and, hence, reduced lipid oxidation.

Proline and leucine, which were prone to oxidation, were contained in the peptides that exhibited high ABTS radical scavenging ability. It has been widely reported that many bioactive peptides are made up of two to nine amino acids. Proline, lysine, and arginine, along with most hydrophobic amino acids, were commonly present in antioxidative peptides.[31] This was not surprising because, during the course of neutralizing free radicals as antioxidants, these amino acid residues were sacrificed.[32] The hydrophobic amino acids that were identified in the peptides were leucine, methionine, phenylalanine, and tyrosine. These amino acids can effectively associate with hydrophobic group in lipids or Tween 20 through hydrophobic effect, shielding the oil droplets from oxidant attack.

Of the total amino acid constituents, the ratio of hydrophilic residues to total number of residues was 45% (Table 2). A similar ratio also applied to hydrophobic residues. The well-balanced hydrophilicity−hydrophobicity explained excellent partitioning of these identified peptides at the interface. Furthermore, the average hydrophilicity of the peptides displayed a small part of the peptides being negatively charged but a large part carrying positive charges. That could lead to different partitions of the peptides. In general, strongly hydrophobic peptides would effectively partition in the oil−water interface with Tween 20, whereasa strongly hydrophilic peptides would have the propensity to form a secondary layer surrounding the inner layer made up of hydrophobic peptides and Tween 20 by weak interactions. Most of the hydrophilic peptides exhibited a net positive charge. The ability of peptides to repel metal ions or other oxidizing ionic species from lipid in the microenvironment of the interface would improve the oxidative stability of emulsified lipid.[4,5]

The identified peptides extracted from the emulsion interface were matched with the known sequence of potato proteins available in the database (BLAST program in NCBI). A portion of several peptides matched the peptide sequences of potato protein either partially or totally (Table 3). Although most of the proteins are not the major proteins in potato, the peptide SFDIK matched the peptide sequence of patatin, which is the most abundant potato protein. However, the peptide SFDIK was not among the antioxidative peptides identified in our previous work.[14,23] This indicated that antioxidative peptides identified in our previous studies might be mostly located in the aqueous phase of the emulsions and act as an active blocking agent to prevent the passage of oxidants to the interface. It was clear that antioxidative peptides, including SFDIK, in the interfacial membrane functioned through both physical and chemical mechanisms.

In conclusion, the partition of peptides in the soybean O/W emulsion membrane was demonstrated using several biophysical methods. The results implied that peptides may be present in two different modes: (1) as an integral part of the interfacial membrane through partitioning and (2) forming a surrounding layer immediately adjacent to the inner interface layer through weak forces. The peptides comprising the interface were mostly small peptides made up of hydrophobic and hydrophilic amino acids, of which peptide SFDIK matched

the sequence of patatin. The antioxidant mechanism of peptides in the emulsion interface seemed to be both physical action including steric hindrance and possibly electrostatic effects and chemical action including radical scavenging capability. Further research should be carried out to measure the interfacial rheology in relation to the complex membrane structure so as to produce oxidation-resistant food emulsions.

## AUTHOR INFORMATION


### Corresponding Author

*(Y.L.X.) Phone: (859) 257-3822. Fax: (859) 257-5318. E-mail: ylxiong@uky.edu.



### Funding

The study was supported by the National Natural Science Foundation of China (Grant 31301422) and the Natural Science Foundation of Jiangsu Province (Grant BK20130494).

### Notes

The authors declare no competing financial interest.


## REFERENCES


(1) Zhang, L.; Li, J.; Zhou, K. Chelating and radical scavenging activities of soy protein hydrolysates prepared from microbial proteases and their effect on meat lipid peroxidation. *Bioresour. Technol.* **2010**, *101*, 2084−2089.

(2) Nieto, G.; Castillo, M.; Xiong, Y. L.; Álvarez, D.; Payne, F. A.; Garrido, M. D. Antioxidant and emulsifying properties of alcalase-hydrolyzed potato proteins in meat emulsions with different fat concentrations. *Meat Sci.* **2009**, *83*, 24−30.

(3) Wang, L. L.; Xiong, Y. L. Inhibition of lipid oxidation in cooked beef patties by hydrolyzed potato protein is related to its reducing and radical scavenging ability. *J. Agric. Food Chem.* **2005**, *53*, 9186−9192.

(4) Diaz, M.; Decker, E. A. Antioxidant mechanisms of caseinophosphopeptides and casein hydrolysates and their application in ground beef. *J. Agric. Food Chem.* **2004**, *52*, 8208−8213.

(5) McClements, D. J.; Decker, E. A.; Weiss, J. Emulsion-based delivery systems for lipophilic bioactive components. *J. Food Sci.* **2007**, *72*, R109−R124.

(6) Sanchez-Paz, V.; Pastoriza-Gallego, M. J.; Losada-Barreiro, S.; Bravo-Diaz, C.; Gunaseelan, K.; Romsted, L. S. Quantitative determination of $\alpha$-tocopherol distribution in a tributyrin/brij 30/water model food emulsion. *J. Colloid Interface Sci.* **2008**, *320*, 1−8.

(7) Huang, S. W.; Hopia, A.; Schwarz, K.; Frankel, E. N.; German, J. B. Antioxidant activity of alpha-tocopherol and trolox in different lipid substrates: bulk oils vs oil-in-water emulsions. *J. Agric. Food Chem.* **1996**, *44*, 444−452.

(8) Viljanen, K.; Kylli, P.; Hubbermann, E. M.; Schwarz, K.; Heinonen, M. Anthocyanin antioxidant activity and partition behavior in whey protein emulsion. *J. Agric. Food Chem.* **2005**, *53*, 2022−2027.

(9) Elias, R. J.; Bridgewater, J. D.; Vachet, R. W.; Waraho, T.; McClements, D. J.; Decker, E. A. Antioxidant mechanisms of enzymatic hydrolysates of $\beta$-lactoglobulin in food lipid dispersions. *J. Agric. Food Chem.* **2006**, *54*, 9565−9572.

(10) Diaz, M.; Dunn, C. M.; McClements, D. J.; Decker, E. A. Use of caseinophosphopeptides as natural antioxidants in oil-in-water emulsions. *J. Agric. Food Chem.* **2003**, *51*, 2365−2370.

(11) Elias, R. J.; Kellerby, S. S.; Decker, E. A. Antioxidant activity of proteins and peptides. *Crit. Rev. Food Sci. Nutr.* **2008**, *48*, 430−441.

(12) Nuchi, C. D.; Hernandez, P.; McClements, D. J.; Decker, E. A. Ability of lipid hydroperoxides to partition into surfactant micelles and alter lipid oxidation rates in emulsions. *J. Agric. Food Chem.* **2002**, *50*, 5445−5449.

(13) Cheng, Y.; Xiong, Y. L.; Chen, J. Antioxidant and emulsifying properties of potato protein hydrolysate in soybean oil-in-water emulsions. *Food Chem.* **2010**, *120*, 101−108.

(14) Cheng, Y.; Xiong, Y. L.; Chen, J. Fractionation, separation and identification of antioxidative peptides in potato protein hydrolysate that enhances oxidative stability of soybean emulsions. *J. Food Sci.* **2010**, *75*, C760−C765.

(15) Kerstens, S.; Murray, B. S.; Dickinson, E. Microstructure of $\beta$-lactoglobulin-stabilized emulsions containing non-ionic surfactant and excess free protein: influence of heating. *J. Colloid Interface Sci.* **2006**, *296*, 332−341.

(16) Dufour, E.; Dalgalarrondo, M.; Adam, L. Conformation of $\beta$-lactoglobulin at an oil/water interface as determined from proteolysis and spectroscopic methods. *J. Colloid Interface Sci.* **1998**, *207*, 264−272.

(17) Yang, H.; Wang, Y.; Lai, S.; An, H.; Li, Y.; Chen, F. Application of atomic force microscopy as a nanotechnology tool in food science. *J. Food Sci.* **2007**, *72*, R65−R75.

(18) Bar, G.; Thomann, Y.; Brandsch, R.; Cantow, H. J.; Whangbo, M. H. Factors affecting the height and phase images in tapping mode atomic force microscopy. Study of phase-separated polymer blends of poly(ethene-*co*-styrene) and poly(2,6-dimethyl-1,4-phenylene oxide). *Langmuir* **1997**, *13*, 3807−3812.

(19) Brandsch, R.; Bar, G.; Whangbo, M. H. On the factors affecting the contrast of height and phase images in tapping mode atomic force microscopy. *Langmuir* **1997**, *13*, 6349−6353.

(20) Parker, M.; Kirby, A.; Morris, V. In *situ* imaging of pea starch in seeds. *Food Biophys.* **2008**, *3*, 66−76.

(21) Degner, B. M.; Chung, C.; Schlegel, V.; Hutkins, R.; McClements, D. J. Factors influencing the freeze-thaw stability of emulsion-based foods. *Compr. Rev. Food Sci. Food Saf.* **2014**, *13*, 98−113.

(22) Berton-Carabin, C. C.; Ropers, M.-H.; Genot, C. Lipid oxidation in oil-in-water emulsions: involvement of the interfacial layer. *Compr. Rev. Food Sci. Food Saf.* **2014**, *13*, 945−977.

(23) Cheng, Y.; Chen, J.; Xiong, Y. L. Chromatographic separation and LC-MS/MS identification of active peptides in potato protein hydrolysate that inhibit lipid oxidation in soybean oil-in-water emulsions. *J. Agric. Food Chem.* **2010**, *58*, 8825−8832.

(24) Gallier, S.; Gragson, D.; Jimnez-Flores, R.; Everett, D. Using confocal laser scanning microscopy to probe the milk fat globule membrane and associated proteins. *J. Agric. Food Chem.* **2010**, *58*, 4250−4257.

(25) Girardet, J. M.; Humbert, G.; Creusot, N.; Chardot, V.; Campagna, S.; Courthaudon, J. L.; Gaillard, J. L. Dilational rheology of mixed $\beta$-casein/Tween 20 and $\beta$-casein (f114−169)/Tween 20 films at oil-water interface. *J. Colloid Interface Sci.* **2001**, *243*, 515−522.

(26) Zhang, Z.; Goff, H. D. Protein distribution at air interfaces in dairy foams and ice cream as affected by casein dissociation and emulsifiers. *Int. Dairy J.* **2004**, *14*, 647−657.

(27) Zhai, J.; Wooster, T. J.; Hoffmann, S. V.; Lee, T.-H.; Augustin, M. A.; Aguilar, M.-I. Structural rearrangement of $\beta$-lactoglobulin at different oil−water interfaces and its effect on emulsion stability. *Langmuir* **2011**, *27*, 9227−9236.

(28) Zhai, J.; Hoffmann, S. V.; Day, L.; Lee, T.-H.; Augustin, M. A.; Aguilar, M.-I.; Wooster, T. J. Conformational changes of $\alpha$-lactalbumin adsorbed at oil−water interfaces: interplay between protein structure and emulsion stability. *Langmuir* **2011**, *28*, 2357−2367.

(29) Bricarello, D. A.; Prada, M. J.; Nitin, N. Physical and chemical modifications of lipid structures to inhibit permeation of free radicals in a supported lipid membrane model. *Soft Matter* **2012**, *8*, 11144−11151.

(30) Rahali, V.; Chobert, J. M.; Haertlé, T.; Guéguen, J. Emulsification of chemical and enzymatic hydrolysates of $\beta$-lactoglobulin: characterization of the peptides adsorbed at the interface. *Food/Nahrung* **2000**, *44*, 89−95.

(31) Kitts, D. D.; Weiler, K. Bioactive proteins and peptides from food sources. Applications of bioprocesses used in isolation and recovery. *Curr. Pharm. Des.* **2003**, *9*, 1309−1323.

(32) Zhao, J.; Xiong, Y. L.; McNear, D. H. Changes in structural characteristics of antioxidative soy protein hydrolysates resulting from scavenging of hydroxyl radicals. *J. Food Sci.* **2013**, *78*, C152−C159.

degree of flavan-3-ol polymerization was found to have little effect on the kinetics of ACN loss and the color of pigments produced,[9,15] potentially indicating a minor role for tannin molecular mass in conferring a specific reactivity with ACN.

Yet, as highlighted above, skin tannin has a far higher mDP than seed tannin, and the relative reactivities of tannins of different sizes and compositions for ACN have not yet been studied. Whereas the detailed identification and quantification of low molecular mass ACN derivatives in model and commercial wines has been achieved using mass spectroscopy,[14,16,17] the pigmented tannin fraction is only partially resolved using LC-MS.[18] A review[11] has highlighted that research in this area is limited by a lack of information on the molecular mass distribution of grape flavanols and their reaction products in wine. In particular, there is limited information regarding grape tannins and their pigmented reaction products with ACN. A recent paper has indicated that the progression of red color incorporation to wine tannin is skewed in favor of smaller pigments in young wines, with a gradual conversion of larger, unpigmented tannin to smaller colored species during aging.[19] This highlights that the factors which drive partitioning of ACN to either complex with tannin or form low molecular mass pigments are currently unknown, leaving scope for aspects of earlier experiments[1,9,15] to be revisited.

It remains to be established how nonbleachable pigments, including polymeric pigments, form in the presence of tannins of very different structural characteristics. Using traditional techniques for colorimetric analysis of wines[20,21] in conjunction with newer methods to characterize wine pigmented polymers by solid-phase extraction (SPE),[22] phloroglucinolysis,[23] and gel permeation chromatography (GPC),[24] these knowledge gaps have been explored.

## MATERIALS AND METHODS

**Instrumentation.** An Agilent model 1100 HPLC (Agilent Technologies Australia Pty Ltd., Melbourne, Australia) was used with Chemstation software for chromatographic analyses.

**Grape Tannin Isolation.** Grapes were obtained from a 10-year-old commercial *V. vinifera* L. cv. Cabernet Sauvignon vineyard in the Langhorne Creek growing region of South Australia. Grapes were harvested corresponding with a commercial harvest point of ≅23 °Brix in the 2009 season. Skin and seed components were prepared from a 300-berry sample and were visually free of flesh material at the point of extraction. Tannin was extracted from frozen skins and seeds in 70% v/v acetone/water for 18 h and then purified from acetone extracts as described previously.[25] Extracts were concentrated under reduced pressure at 35 °C to remove acetone and then extracted with hexane to remove residual lipophilic material. The aqueous fraction was then recovered using a separatory funnel and made up to a final concentration of 60% v/v methanol containing 0.05% v/v trifluoroacetic acid (TFA) and applied (∼18.3 mL/min) to a 300 mm × 21 mm glass column (Michel-Miller, Vineland, NJ, USA) containing Sephadex LH20 chromatography resin (Amersham, Uppsala, Sweden) to a bed volume of 93 mL. Low molecular weight phenolics were eluted with 300 mL of 60% (v/v) HPLC grade methanol containing 0.05% v/v TFA. Tannin was then eluted with 250 mL of 70% v/v acetone containing 0.05% v/v TFA. The column was re-equilibrated with 60% v/v methanol containing 0.05% v/v TFA after each sample. The tannin fractions eluted were concentrated under reduced pressure at 35 °C to remove organic solvent and the aqueous fraction recovered (≅5 mL). The aqueous fraction was frozen at −80 °C and lyophilized to a dry powder. Dried tannin isolates were stored in the dark and under nitrogen at −20 °C prior to use.

**Grape Anthocyanin Isolation.** Shiraz grapes were sourced from the Coombe Vineyard, University of Adelaide, South Australia, at commercial ripeness (24 °Brix) in the 2011 season. Whole bunches were frozen at −20 °C until used. A 1 kg bunch sample was destemmed, allowed to thaw at room temperature, crushed, and partially homogenized using a blender. A 250 g sample of the coarse homogenate was extracted for 18 h with 2 L of 50% v/v MeOH, filtered, and concentrated under reduced pressure at 30 °C. The aqueous extract was loaded in 100 mL batches to a Toyopearl (660 mL bed volume) column equilibrated with 0.1% v/v aqueous TFA, and water-soluble nonadsorbent compounds were eluted in a further 2 L of 0.1% v/v TFA. The 3-*O*-monoglucoside ACN fraction was eluted with 1.5 L of 30% v/v MeOH containing 0.1% v/v aqueous TFA. The column was then washed with 2 L of 2:1 v/v acetone/water and re-equilibrated with 2 L of 0.1% v/v aqueous TFA. The eluate was concentrated under reduced pressure, frozen at −80 °C, and then lyophilized, yielding ≅200 mg of dry 3-*O*-monoglucoside ACNs, which were stored under nitrogen at −80 °C until used. Extract purity was verified by HPLC,[26] indicating the extract was free of acetylated or coumaroylated ACNs, other monomeric flavonoids, and polymeric material. It was found to have trace quantities of early eluting material at 280 nm, but this was below the detection limit for quantification. A calibration curve was established for the gravimetric concentration of the ACN isolate and the concentration estimated spectrophotometrically according to the method in ref 26 and is shown as Supporting Information (S1). This was to approximate the concentration of ACN addition (using the spectral method) to the concentration expected in grapes.

**Treatments.** Chemically defined medium (CDM) was based on the compositional specifications described by Schmidt et al.[27] All components used to prepare CDM were from Sigma-Aldrich, St. Louis, MO, USA. CDM was prepared in Milli-Q water as described by Contreras et al.[28] and contained (per L) glucose, 100 g; fructose, 100 g; citric acid, 0.2 g; malic acid, 3 g; potassium hydrogen tartrate, 2.5 g; $K_2HPO_4$, 1.1 g; $MgSO_4{\cdot}7H_2O$, 1.5 g; $CaCl_2{\cdot}2H_2O$, 0.4 g; $H_3BO_3$, 0.04 g; and proline, 0.84 g. To this solution were added stock solutions (described below) of nitrogen (20 mL), trace elements (1 mL), and vitamin (1 mL); the pH was adjusted to 3.5, and the mixture was sterile-filtered. The nitrogen stock solution contained the following (per L): 30% ammonium hydroxide solution, 27.7 g; alanine, 10.5 g; γ-amino butyrate, 7.2 g; arginine, 26.9 g; asparagine, 0.4 g; aspartate, 3.0 g; citrulline, 0.4 g; glutamate, 6.0 g; glutamine, 8.4 g; glycine, 0.4 g; histidine, 1.2 g; isoleucine, 1.2 g; leucine, 1.2 g; lysine, 0.4 g; methionine, 0.4 g; ornithine, 0.4 g; phenylalanine, 0.8 g; serine, 5.4 g; threonine, 6.0 g; tryptophan, 0.4 g; tyrosine, 0.4 g; valine, 2.1 g; and cysteine, 1.2 g. The trace elements stock solution contained (per L) $MnSO_4{\cdot}H_2O$, 3.5 g; $ZnCl_2$, 1.0 g; $FeSO_4{\cdot}7H_2O$, 6.0 g; $CuSO_4{\cdot}5H_2O$, 1.5 g; $KIO_3$, 0.01 g; $Co(NO_3)_2{\cdot}6H_2O$, 0.03 g; $Na_2MoO_4{\cdot}2H_2O$, 0.025 g; LiCl, 0.1 g; $NiSO_4{\cdot}6H_2O$, 0.05 g; and RbCl, 0.7 g. The vitamin stock solution contained (per L) thiamin HCl, 0.5 g; riboflavin, 0.2 g; pyridoxine HCl, 1.0 g; calcium D-pantothenate, 1.0 g; nicotinic acid, 1.0 g; *myo*-inositol, 10 g; biotin, 0.05 g; folic acid, 0.05 g; and 4-aminobenzoic acid, 0.05 g. Following sterile filtration, fatty acid and sterol (both 1 mL) stock solutions were added. The fatty acid stock solution contained (per L absolute ethanol) palmitic acids, 2.0 g; oleic acid, 1.0 g; linoleic acid, 3 g; and linolenic acid, 0.5 g. The sterol stock solution contained 1 g/L β-sitosterol in absolute ethanol.

Purified ACN, skin (Sk), and seed (Sd) tannin extracts were prepared as separate solutions either in sterile CDM or as a weakly acidified solution in 15% v/v ethanol containing 0.01% v/v TFA. Triplicate treatments were prepared with or without additions according to the experimental outline in Figure 1 to a final volume of 30 mL in 50 mL centrifuge tubes. Target final gravimetric ACN and tannin additions in 30 mL of CDM or 15% v/v acidified ethanol were to achieve concentrations of 1.15 and 1.5 g/L, respectively. For 15% v/v ethanol 0.01% v/v TFA treatments, additions were made at the same time, and tubes were sealed and mixed by shaking for 24 h prior to analysis. For ferments in CDM, ACN additions were made as a 5 mL aliquot in CDM prior to inoculation of yeast. Tannin addition was made as a 5 mL aliquot in CDM 24 h after inoculation to minimize the risk of yeast inhibition by excess tannin. The difference in the timing and type of additions was not found to affect fermentation kinetics.

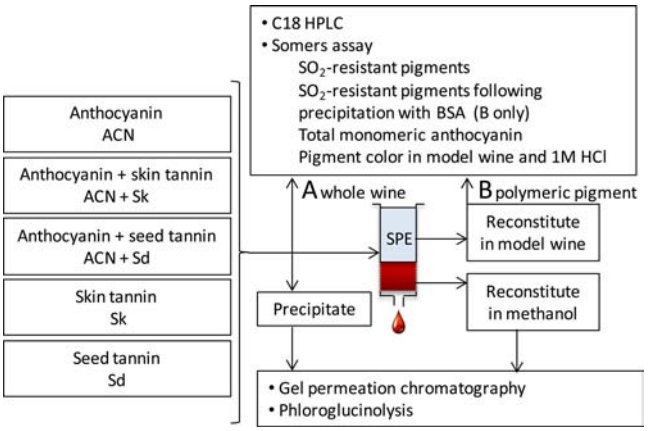


**Figure 1.** Diagrammatic representation of treatments, isolation of polymeric pigments, and general analysis performed.

For CDM ferments, the yeast added was *Saccharomyces cerevisiae* PDM (Maurivin, Sydney, Australia) at 200 ppm. After inoculation with yeast, tubes were sealed with a lid fitted with a gas release port. Ferments were carried out open to the atmosphere for 24 h at 22 °C in a temperature-controlled room and then sealed in plastic containers fitted with an airlock to continue fermentation. Glucose concentration was tracked during ferment using the Keto Diabur 5000 test strips (Roche Diagnostics, NSW, Australia), and following each sampling point, dry ice was added to the plastic ferment receptacles to minimize oxidation. When glucose fermented to dryness, a final aliquot was removed and tested for residual fructose and final ethanol concentrations by HPLC.[29] Fructose concentration was <0.5% w/v and ethanol was 10% v/v for all treatments, indicating complete fermentation. Although the target alcohol concentration of CDM ferments is lower than that of red wine, the approach was selected in favor of bottled wine or fresh grape juice to conduct the experiments under controlled conditions, in accordance with published experiments,[28] enabling comparison and replication in future studies. Model ferments did not undergo malolactic fermentation, were sealed under $CO_2$, and cold-settled at 4 °C. Completed ferments were centrifuged at 1730*g* for 5 min. Aliquots of wines and 15% v/v ethanol controls were sealed in glass vials with no ullage and placed in kegs that were fitted with a PreSens Pst6 oxygen sensor (Presens, Regensburg, Germany) and flushed with nitrogen. This system is described in detail in the Supporting Information (S2). A slight positive pressure of nitrogen was maintained and the oxygen concentration in the kegs maintained below 10 ppb. Samples were stored anaerobically for 6 months at 22 °C.

**Analysis of Tannin, Anthocyanin, and Pigments.** General analyses performed are summarized in Figure 1. Treatments at 0 and 6 months were centrifuged for 5 min at 16000*g*. Tannin concentration was analyzed in duplicate according to the published methyl cellulose precipitation assay.[26] ACN and pigment analysis was only done in treatments containing ACN, except for the Sk treatments. For Sk treatments with ACN addition, the Sk control was included as sample blank due to a minor contribution of color (but not monomeric ACN), which resulted from the tannin preparation step. Sample aliquots were analyzed by HPLC according to the method described by Mercurio et al.[26] ACNs, derived pigments, and polymeric pigments were quantified using their peak areas at 520 nm as malvidin-3-glucoside units based on a commercial standard (Polyphenols Laboratories, Norway). Vitisin A was identified according to its retention time and UV−visible spectrum (200−600 nm) in comparison with a synthesized standard[30] (Supporting Information S3). Vitisin B was not detected under the chromatographic conditions. The polymeric fraction, coeluting with tannin[26] as well as other nonpolymeric red pigments apparent by HPLC with absorbance maxima at 520−540 and 270 nm (Supporting Information S3), were quantified as malvidin-3-glucoside equivalents. After 6 months, polymeric pigments from triplicate experiments were purified from wine samples using SPE[22] with the modifications outlined in Kassara and Kennedy.[31] Duplicate extractions were done on 1 mL wine aliquots as preparation for different types of analysis. The first of the duplicate SPE extracts was reconstituted in 1 mL of model wine buffer containing 0.5% (w/v) tartaric acid and 12% (v/v) ethanol (pH 3.4). Color characteristics of unpurified treatments and SPE isolates were determined using a published protocol,[26] for which a brief description follows. All spectral analysis was performed in duplicate in a 370 μL 96-well UV plate, and 420 and 520 nm absorbances were measured using a SpectraMax M2Microplate Reader (Molecular Devices, Australia). Readings were corrected using an appropriate sample blank and a water constant correct function to approximate a 1 cm path length. For determination of total ACN, a 20 μL sample aliquot was added to 980 μL of 1 M HCl and mixed. Samples were left to stand in the dark for 1 h and a 300 μL aliquot analyzed. The 1 h period was modified from the original method stipulating 3 h, as we had demonstrated that maximal ionization of ACNs was achievable within this period (data not shown). A further 100 μL sample aliquot was added to 900 μL of model wine buffer and mixed, and a 300 μL aliquot was analyzed immediately. Buffer solution was also prepared containing 0.375% (w/v) sodium metabisulfite, and 900 μL was combined with a 100 μL sample aliquot, mixed, and left to stand in the dark for 1 h. Thereafter, a 300 μL aliquot was analyzed. Estimates of ACN were determined according to the calculations outlined in the published method.[26] The 520 nm analysis in the respective solutions were used to determine pigment color at pH 3.4 in 1 M HCl and in the presence of sodium metabisulfite ($SO_2$-resistant pigment). The 420 nm measure was not found to vary significantly during the limited aging period and was thereafter not included in the assessment of pigment color. Furthermore, the SPE isolate reconstituted in model wine was analyzed for protein precipitability of nonbleachable pigments using a published protocol.[32]

The second of the duplicate SPE extracts and a 1 mL aliquot of the treatments stored in 15% v/v ethanol were dried under a stream of nitrogen at 30 °C and reconstituted in 100 μL of methanol. Lyophilized powders of purified Sk and Sd tannins (pre-ferment) were reconsituted in methanol to a gravimetric concentration of 10 g/L and analyzed in duplicate, as described for the other samples. In wines, a small amount of precipitate was observed after 6 months of aging, which was not found for tannin solutions stored in 15% v/v acidified ethanol. The wine layer was carefully removed using a glass dropper to recover the precipitate. Wine precipitates were dried under a stream of nitrogen at 30 °C and reconstituted in methanol. Methanolic solutions of purified tannins, SPE isolates, dried (aged) ethanol solutions, and precipitates were analyzed by phloroglucinolysis and GPC using published protocols.[25,33] For phloroglucinolysis, (−)-epicatechin (Sigma-Aldrich, St. Louis, MO, USA) was the quantitative standard. To determine the proportion of wine tannin as precipitate, or retained in solution, the assumption was made that conversion yield differences would not differ significantly between the two fractions. Therefore, the proportion (%) of total wine tannin as precipitate was calculated directly from phloroglucinolysis product yields (on a mg/L wine volume basis). For GPC, separate calibration curves were established for skin and seed tannins using molecular mass standards reported previously.[33] This decision was based on our previous observation that seed and skin tannins differ in their hydrodynamic volume. In addition, oligomeric ACN-derived pigments and a standard of the chloride of malvidin-3-*O*-glucoside of molecular mass 528.9 g/mol (Polyphenols Laboratories, Norway) were analyzed by GPC, and nominal molecular mass values were assigned using the skin tannin calibration.

**Mass Spectrometric Analysis.** The SPE isolates of the 0- and 6-month-aged ACN wines and purified ACNs were mixed with the same portion of 0.25% v/v formic acid in 50% v/v methanol and then analyzed by direct infusion MS and MS/MS. The sample was infused to an electrospray (ESI) interface at a flow rate of 5 μL/min using a syringe pump (Harvard, Holliston, MA, USA). Mass spectrometric analysis was carried out using a 4000 QTrap mass spectrometer equipped with a Turbo ion source (AB Sciex, Mount Waverly, VIC, Australia). Data acquisition and processing were performed using

Table 1. General Compositional Analysis of Grape Skin and Seed Tannins and Their Combinations with Anthocyanin (ACN), Prepared in Acidified Aqueous Ethanol (15% EtOH) or Fermented and Stored Anaerobically for 6 Months[a]

| | seed tannin | | | skin tannin | | |
|---|---|---|---|---|---|---|
| treatment | %MC[b] | mDP[c] | %galloylation[d] | %MC[b] | mDP[c] | % prodelphinidin[e] |
| control | 76.0 | 5.2 | 22.3 | 64.7 | 25.6 | 58.2 |
| 15% EtOH | 78.7 ± 3.0 | 5.1 ± 0.1 | 21.3 ± 0.2 | 52.0* ± 0.4 | 26.5 ± 1.2 | 52.5* ± 0.2 |
| 15% EtOH + ACN | 76.5 ± 0.6 | 5.3 ± 0.0 | 22.0 ± 0.2 | 51.6* ± 0.6 | 23.6 ± 0.3 | 53.7* ± 0.9 |
| wine | 42.5* ± 2.6 | 5.5 ± 0.0 | 20.3* ± 0.1 | 25.4* ± 1.8 | 21.6 ± 0.8 | 54.8* ± 0.1 |
| wine + ACN | 34.9* ± 2.2 | 5.4 ± 0.1 | 20.7* ± 0.1 | 28.7* ± 1.6 | 26.0 ± 1.9 | 55.7* ± 0.3 |

[a]Data are the mean ± standard error. The control treatment was the respective purified seed or skin tannin powder at the point of addition to 15% v/v ethanol solution or model ferment. ACN, anthocyanin addition. Significant differences between ACN, seed tannin, or skin tannin additions in 15% v/v aqueous ethanol (15% EtOH) or wine after 6 months are compared with the respective skin and seed control preaddition using Dunnett's control test, where a significant difference is indicated by an asterisk. [b]Mass conversion is the recovery of tannin as its component subunits by phloroglucinolysis, as a proportion of the control, as the gravimetric mass. [c]Mean degree of polymerization. [d]Molar proportion of (−)-epicatechin-3-*O*-gallate expressed as the percentage galloylation. [e]Molar proportion of (−)-epigallocatechin expressed as the percentage prodelphinidin.

Analyst software 1.4.2 (AB Sciex). All ESI mass spectrometric data were obtained in positive ion mode. Nitrogen was used as curtain and nebulizer gases set at 10 and 12 (arbitrary units), respectively. The electrospray and declustering potentials were set at 5000 and 120 V, respectively. Mass spectra were obtained by linear ion trap mode. A full scan spectrum ranging from $m/z$ 300 to 2500 and a product ion spectrum from precursor ions of interest were consecutively accumulated until approximate ion intensity was obtained. For MS/MS, nitrogen was used as a collision gas setting at "high" and the collision energy was optimized in the range 30−60 eV as appropriate.

**Statistical Analysis.** Significant differences between treatments were determined by one-way analysis of variance (ANOVA). When ANOVA data were significant at $p < 0.05$ and follow-up statistics were required, differences between sample sets were analyzed by a post hoc Student's $t$ test. Dunnett's test was used for comparison of multiple treatments against a single pretreatment control. The JMP 5.0.1 statistical software package (SAS, Cary, NC, USA) was used for all statistical analysis.

## RESULTS AND DISCUSSION

**Tannin Concentration and Subunit Composition.** Tannin compositional information determined by phloroglucinolysis is shown in Table 1. According to the respective subunit yields by phloroglucinolysis, the Sd tannin extract prior to fermentation and aging had a higher conversion to component subunits on a w/w basis (% mass conversion) than the corresponding Sk tannin extract, at 76 and 65%, respectively (Table 1). It has been shown in various studies that seed and skin tannins differ in their conversion yields from phloroglucinolysis by ripeness stage and grape variety.[23,25,33,34] The composition of the Sd and Sk isolates pre-addition were clearly different, with Sd tannins having a far lower mDP as determined by phloroglucinolysis compared with Sk tannin. Sd tannins were distinguished by a high degree of galloylation (Table 1), which was low in Sk tannin at <2% (data not shown). Sk tannin contained a high molar proportion of trihydroxylated prodelphinidin as an extension unit (Table 1). It is important to note that the tannin preparation method using 70% v/v acetone extract tannins of a higher molecular mass than would be expected in wine. The tannins studied therefore provide a useful comparison of two extremes in tannin size distribution, molecular mass, and subunit composition, but cannot be said to be compositionally specific to wine. A marked decrease in tannin mass conversion was found following the 6 month aging of wines (Table 1). For the corresponding tannin combinations stored in acidified 15% v/v ethanol, mass conversion decreased ≅20% for Sk solutions after 6 months, but was unchanged in Sd solutions. The reduction in tannin mass conversion in aged ferment treatments was between 45 and 61%, and no trend was observed for Sd or Sk tannin preferentially or their respective combinations with ACN. Noting that the reduction in mass conversion could have been the result of tannin loss through precipitation, this was also quantified (Supporting Information S4). In wines, tannin precipitates were observed in all treatments, but were not found for stored acidified 15% v/v ethanol solutions. The absolute loss of wine tannin as precipitate was approximately 10% of the initial addition, with the exception of the Sd wine, for which tannin loss was only 4% (Supporting Information S4). Analysis of tannin before and after the 6 month aging period using the methyl cellulose precipitable tannin assay[26] confirmed these observations, showing that a reduction in tannin concentration did not occur during fermentation, but only during the aging of wine samples (data not shown).

Although the current results indicate that the reduction in wine tannin mass conversion with aging was the result of some tannin becoming insoluble, the decrease in percent conversion yield exceeded losses through precipitation. The decrease in mass conversion most likely reflects an altered tannin structure, with the incorporation of bonds resistant to acid-catalyzed depolymerization in the presence of phloroglucinol. This process is expected during wine aging[19,35,36] and has been suggested to be the result of multiple reactions, namely, acid-catalyzed depolymerization, condensation, rearrangement, and oxidation.[35] Specifically regarding the effect of oxidation reactions, a small reduction in the mass conversion of seed tannins (3.7%) has been reported following direct oxidation, with little change in tannin mDP.[37] The current study showed only small, nonsignificant changes in tannin mDP after 6 months (Table 1). However, the expected loss in tannin mass conversion resulting from oxidation (3.7−11.5%)[37] is far less than that observed during wine aging.[19,35,36] Although oxidation reactions cannot be definitively be excluded, it would be expected to contribute minimally to the observed changes and fails to account for the large difference in mass conversion between wines and 15% ethanol treatments.

An additional possibility that might reduce tannin mass conversion is depolymerization reactions under wine-like pH conditions.[38] At wine-like pH, decreased tannin mDP has been noted in model solutions of tannin and monomeric flavan-3-ols, consistent with the acid-catalyzed cleavage of interflavan bonds and subsequent incorporation of a flavan-3-ol. This process is supported by observed decreases in tannin mDP during the aging of real wine systems.[19,35,39] However, when monomeric

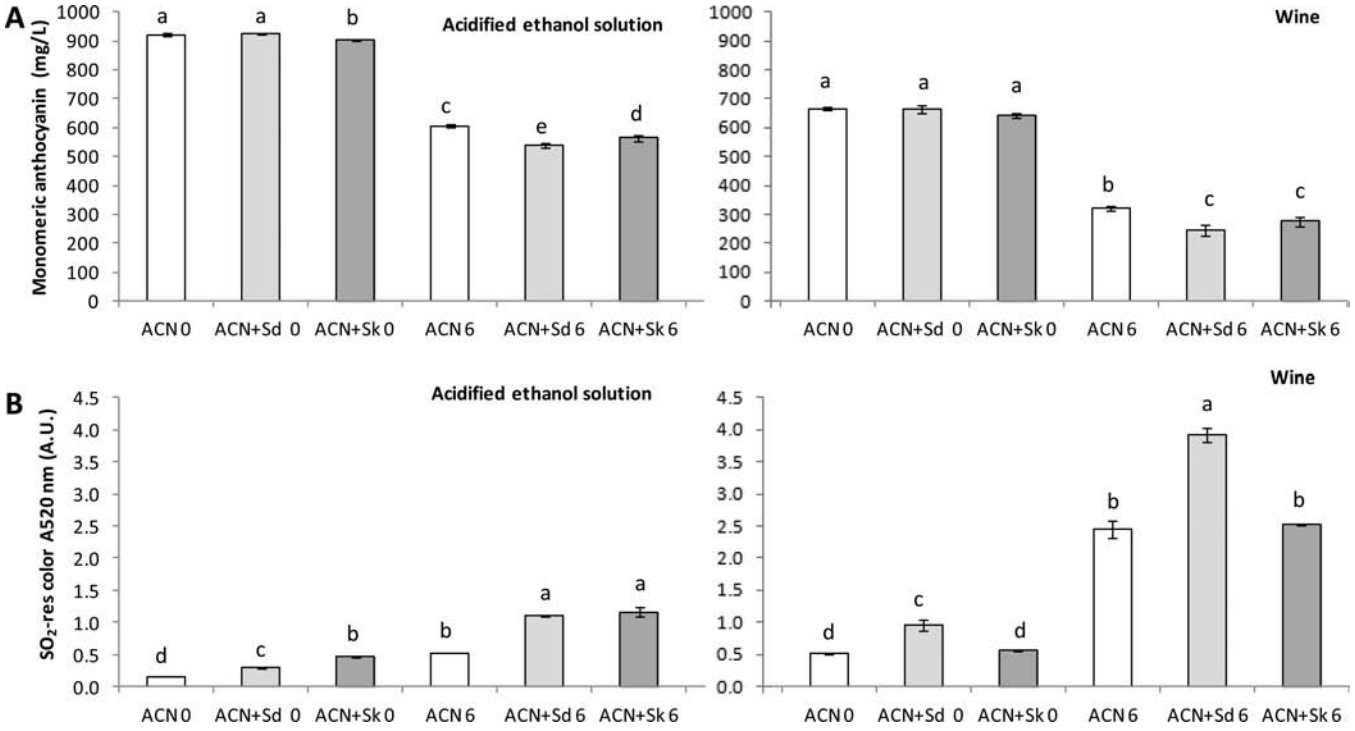


**Figure 2.** Changes in (A) monomeric anthocyanin and (B) nonbleachable pigments during the aging of anthocyanin (ACN, white bars) and its respective combinations with seed tannin (ACN+Sd, light gray bars) or skin tannin (ACN+Sk, dark gray bars) stored anaerobically for 6 months (initial analysis indicated as 0, after aging as 6) in 15% v/v acidified ethanol solution or as wine following fermentation. Significant differences between additions in their respective storage solutions are indicated by different letters, determined by one-way ANOVA, $P < 0.0001$, $n = 9$, followed by a post hoc Student's $t$ test.

flavan-3-ol is not present, such as in the current study, the loss of tannin subunits following acidic cleavage could lead to less significant changes in tannin mDP. This would appear to be supported by the current results. However, at wine-like pH[38] the condensation of ACN with tannin could occur in the absence of competing flavanols.[40] Evidence for this process exists up to the level of oligomers.[18,41,42] It would be expected that under mildly acidic conditions, that cleavage of the tannin polymer could yield smaller polymeric species with the addition of ACN, but would be expected to result in detectable changes in mDP subunit composition. On the contrary, in addition to the minimal effect on mDP, we also observed that the change in tannin subunit composition was minor, with Sd and Sk wines having only a marginally lower percent galloylation and percent prodelphinidin in comparison with the original tannin isolate (Table 1). Furthermore, no significant differences were observed in either tannin mass conversion or composition in the presence or absence of ACN. It is therefore likely that the aging reactions proceeded with tannin polymers in the nucleophilic form under the weakly acidic pH conditions.

On the basis of these observations, it appears that neither oxidation nor interflavan cleavage contributed significantly to the loss in mass conversion by phloroglucinolysis. Both of these mechanisms also fail to account for the marked differences in the responses of wine and 15% v/v ethanol preparations during aging. Although the CDM ferment approach has a lower target alcohol level than found in standard red wines, it enables the effect of a defined "wine matrix" in terms of yeast metabolites to be produced during fermentation. For the current results, we therefore propose that conditions produced during fermentation enhanced the formation of interflavan linkages leading to a reduction in tannin mass conversion, but there was limited evidence for cleavage of the tannin under the storage conditions.

**Anthocyanin, Pigment, and Color Properties.** ACN was found to decrease during the aging of both 15% v/v ethanol solutions and wines (Figure 2A). The estimate of ACN using the spectral method[26] approximates monomeric ACNs by subtracting the contribution of the $SO_2$-resistant fraction from total red color in ionized form[20] and is expected to correlate well with HPLC analysis.[26] In 15% v/v ethanol solutions ACN, measures of monomers using the spectral and HPLC methods were well-related, decreasing with age (Table 2). There were small increases in $SO_2$-resistant pigments in 15% v/v ethanol

**Table 2. Change in Anthocyanin (ACN) Concentration in 15% v/v Ethanol Containing 0.01% TFA before and after a 6 Month Aging Period[a]**

| | 0 months | 6 months |
|---|---|---|
| total ACN $A_{520\ nm}$[b] (mg/L) | 922.7a ± 5.1 | 605.8b ± 6.6 |
| total ACN HPLC[c] (mg/L) | 1160.9a ± 8.7 | 655.5b ± 4.7 |
| delphinidin-3-glucoside (mg/L) | 48.6a ± 1.3 | 27.4b ± 1.0 |
| cyanidin-3-glucoside (mg/L) | 10.6a ± 0.9 | 8.65b ± 0.9 |
| petunidin-3-glucoside (mg/L) | 119.3a ± 1.0 | 68.8b ± 1.3 |
| peonidin-3-glucoside (mg/L) | 147.2a ± 1.6 | 86.6b ± 1.3 |
| malvidin-3-glucoside (mg/L) | 838.3a ± 7.3 | 467.3b ± 3.5 |

[a]Data are the mean ± standard error. Significant differences at 0 and 6 months are indicated by different letters determined by one-way ANOVA, $P < 0.0001$. [b]Total wine anthocyanin determined spectrophotometrically in 1 M HCl, with estimated bisulfite-resistant absorbance at 520 nm subtracted. [c]Analysis of ACN and individual anthocyanins as their peak areas by HPLC, expressed as malvidin-3-glucoside units.

**Table 3. Change in Anthocyanin (ACN) Concentration and ACN-Derived Pigments in Wines Prepared from the Fermentation of ACN Alone or in Combination with Grape-Derived Seed (Sd) and Skin (Sk) Tannin, before and after a 6 Month Aging Period[a]**

| | 0 months | | | 6 months | | |
|---|---|---|---|---|---|---|
| | ACN | ACN+Sd | ACN+Sk | ACN | ACN+Sd | ACN+Sk |
| **Monomeric ACN** | | | | | | |
| total ACN $A_{520\ nm}$[b] (mg/L) | 666.9a ± 6.2 | 665.9a ± 5.9 | 641.8a ± 7.1 | 323.5b ± 7.7 | 246.0c ± 19.4 | 276.1c ± 14.5 |
| total ACN HPLC[c] (mg/L) | 601.8a ± 11.5 | 551.7b ± 13.9 | 579.8ab ± 5.8 | 184.7c ± 11.9 | 55.7e ± 12.3 | 117.9d ± 10.5 |
| delphinidin-3-glucoside (mg/L) | 19.01b ± 1.7 | 22.46a ± 1.1 | 22.1a ± 0.8 | 6.38c ± 0.9 | 5.45c ± 1.4 | 6.20c ± 0.9 |
| cyanidin-3-glucoside (mg/L) | 7.21a ± 0.7 | 5.98b ± 0.7 | 5.88b ± 0.8 | 1.61c ± 0.5 | nd[f] | nd |
| petunidin-3-glucoside (mg/L) | 61.13a ± 2.6 | 61.90a ± 2.2 | 62.57a ± 0.8 | 19.47b ± 1.6 | 7.51d ± 2.0 | 13.97c ± 1.8 |
| peonidin-3-glucoside (mg/L) | 17.88b ± 2.0 | 22.38a ± 0.7 | 22.84a ± 0.7 | 6.05c ± 1.0 | 2.81d ± 0.9 | 5.20c ± 0.9 |
| malvidin-3-glucoside (mg/L) | 499.7a ± 6.3 | 442.1c ± 11.5 | 469.6b ± 5.4 | 154.3d ± 10.2 | 42.3f ± 11.0 | 94.9e ± 8.3 |
| **ACN-Derived Pigments** | | | | | | |
| total ACN-derived pigments (mg/L)[d] | 30.08e ± 2.12 | 45.91d ± 3.25 | 35.16e ± 1.56 | 86.05b ± 7.85 | 94.48a ± 1.38 | 64.49c ± 1.19 |
| polymeric pigment (mg/L) | 2.01d ± 0.58 | 9.92c ± 1.21 | 6.51cd ± 0.69 | 41.78b ± 5.21 | 74.01a ± 2.50 | 38.39b ± 2.20 |
| nonpolymeric pigment color (mg/L) | 28.86c ± 1.67 | 36.78b ± 1.96 | 29.43c ± 1.61 | 45.07a ± 0.96 | 21.26d ± 2.77 | 26.89c ± 1.86 |
| vitisin A[e] (mg/L) | 6.03de ± 0.92 | 6.42cd ± 1.03 | 5.51e ± 0.88 | 11.83a ± 0.71 | 6.96cd ± 0.52 | 7.18bc ± 0.83 |

[a]Data are the mean ± standard error. Significant differences between ACN, Sd, or Sk additions in wine at 0 and 6 months are indicated by different letters determined by one-way ANOVA, $P < 0.001$ followed by Student's $t$ test. [b]Total wine anthocyanin determined spectrophotometrically in 1 M HCl, with estimated bisulfite-resistant absorbance at 520 nm subtracted. [c]Analysis of ACN and individual anthocyanins as their peak areas by HPLC, expressed as malvidin-3-glucoside units. [d]Sum of polymeric pigment and small derived pigments (including vitisin A) that did not coelute with the polymeric fraction determined as their peak areas by HPLC, quantified as malvidin-3-glucoside units. [e]Vitisin A identified according to elution time and spectra, quantified at 520 nm as malvidin-3-glucoside units. [f]nd, not detected.

solutions with aging (Figure 2B). However, apart from monomeric ACN, and a small increase in pigmentation within the tannin peak[26] during aging, no small (nonpolymeric) derived pigments were detected by HPLC (data not shown). Although potentially limited by the techniques used, this may indicate that the losses in monomeric ACN in aqueous ethanol were due to degradation or ACN−ACN condensation reactions[12] resulting in the colorless flavene ACN form. The reduction in monomeric ACN and the formation of $SO_2$-resistant pigments was higher in ethanol solutions containing tannin, confirming that some condensation of ACN and tannin may have occurred, maintaining the colored flavylium form of the ACN.[42] However, as alluded to in earlier studies,[8] it appears that this route of pigment formation is slow.

In contrast, the development of $SO_2$-resistant pigments in wine treatments was rapid, being similar to the aged 15% v/v ethanol treatments at the end of fermentation and then increasing markedly after 6 months of aging (Figure 2). The pattern of ACN loss and pigment formation in wine treatments differed markedly from that in 15% v/v ethanol solutions. In young wines, a reduction in monomeric ACN had already occurred during fermentation, with significant formation of $SO_2$-resistant pigments, including vitisin A and a number of derived pigments that were not identified, but quantified on the basis of their 520 nm absorbances (Table 3; Figure 2; Supporting Information S3). Hence, the initial concentration of monomeric ACN was lower in young wines than in ethanol solutions (Table 2). The correlation between measures of monomeric ACN using the spectral approach and HPLC were well-related in young wines, but were poorly related after aging (Table 3), likely indicating the high bleachability of a fraction of derived pigments by bisulfite.[20]

In wines, the reduction of monomeric ACN with aging was greatest in the treatment containing Sd tannin, followed by Sk tannin (Table 3). Consequently, the production of $SO_2$-resistant pigments was consistently greater in ACN+Sd wine, both at the end of fermentation and after 6 months of aging, whereas the ACN and ACN+Sk treatments were similar (Figure 2B). At the end of fermentation, only minor differences in the concentration of vitisin A and small derived pigments were observed between wine treatments (Table 3). After the aging period, vitisin A increased in ACN and ACN+Sk wines while remaining constant in the ACN+Sd treatment. Changes in total small derived pigments during aging differed between wine treatments, increasing in ACN wines, staying constant in the ACN+Sk wines, and decreasing in the ACN+Sd. This result suggests that in the case when tannin is present together with ACN in the wine matrix, the pool of derived pigments may undergo conversion to other forms during aging. Considering that the most remarkable aging-related increase in the color of the derived pigment fraction occurred within the polymeric pigment component (Table 3), this may reflect conversion of derived pigment intermediates to a polymeric form. The ACN +Sd wine had the highest concentration of polymeric pigment at 6 months, with ACN and ACN+Sk wines being equivalent. Changes within this fraction most closely reflected the changes observed in $SO_2$-resistant pigment formation.

From these results, it is evident that the Sd tannin favored the partitioning of ACN to form polymeric pigment by comparison with the Sk treatment. From the preliminary results, it would appear that the formation of polymeric pigments with Sk tannin was limited, such that the concentration of polymeric pigment did not differ from wines containing only ACN. Assessing the sum of total derived pigments (Table 3), the ACN+Sk wines produced the lowest total concentration, whereas the ACN+Sd and ACN treatments were similar. This may indicate that in the ACN+Sk treatment, a greater proportion of ACN was converted to a colorless form. The similarity in the total derived pigment concentrations formed in the ACN+Sd and ACN treatments is an important consideration. This potentially indicates that when conversion of ACN to the polymeric form was restricted due to the absence of tannin, the ongoing formation of small derived pigment forms was favored during aging.

Table 4. Spectrophotometric Analysis of Polymeric Pigments Isolated from 6-Month-Aged Wines Prepared from the Fermentation of Anthocyanin (ACN) Alone or in Combination with Grape-Derived Seed (Sd) and Skin (Sk) Tannin[a]

| | ACN | ACN+Sd | ACN+Sk |
|---|---|---|---|
| total color $A_{520\ nm}$[b] pH 3.4 (AU) | 6.45b ± 0.15 | 7.58a ± 0.22 | 6.65b ± 0.10 |
| total $SO_2$-res color $A_{520\ nm}$[c] (AU) | 2.45b ± 0.13 | 3.92a ± 0.10 | 2.52b ± 0.02 |
| polymeric $SO_2$-res color $A_{520\ nm}$[c] (AU) | 1.86b ± 0.06 | 3.18a ± 0.07 | 1.93b ± 0.07 |
| protein-precipitable polymeric $SO_2$-res color[d] (%) | 0.0c ± 0.02 | 32.39a ± 2.60 | 14.58b ± 3.71 |
| polymeric pigment color $A_{520\ nm}$ pH 3.4[b] (AU) | 4.45c ± 0.21 | 6.65a ± 0.06 | 5.30b ± 0.05 |
| polymeric pigment color $A_{520\ nm}$ 1 M HCl[e] (AU) | 6.84b ± 0.25 | 8.25a ± 0.37 | 7.00a ± 0.05 |

[a]Data are the mean ± standard error. $SO_2$-res, bisulfite-resistant pigments. Significant differences between ACN, Sd, or Sk additions in wine after 6 months are indicated by different letters determined by one-way ANOVA, $P < 0.05$, followed by Student's $t$ test. [b]Total wine color and polymeric pigment color following isolation by solid-phase extraction at 520 nm in model wine buffer. [c]Bisulfite-resistant absorbance of whole wine or polymeric pigments at 520 nm. [d]Proportion of bisulfite-resistant polymeric pigments precipitable by bovine serum albumin. [e]Absorbance of polymeric pigments at 520 nm in 1 M HCl.

To summarize the preliminary experiments, the main observation made was that following fermentation, the "matrix" conditions in wine facilitated a far greater production of bisulfite-resistant products than under acidified hydroalcoholic conditions. No further experimentation was performed on aged ethanol solutions. In aged wines, analysis was conducted to determine differences between the color and size distribution of the polymeric pigments formed.

**Color Characteristics of Wine Polymeric Pigments.** In 6-month-aged wine treatments, an SPE fractionation method that specifically selects for the polymeric fraction was used.[22] This method quantitatively recovered the fraction coincident with polymeric pigments identified by HPLC[22,26] and completely removed monomeric ACN and small derived pigments. Phloroglucinol analysis of the ACN treatment confirmed that proanthocyanidin cleavage products were not detected.

The contribution of the polymeric fraction to total pigment color was compared under wine-like conditions (pH 3.4), with and without the presence of bisulfite (Table 4). The results generated present minimum absorbance values, which exclude possible copigmentation effects that may have existed in the native wine matrix, becausse all samples were diluted in the modified Somers assay. The analysis confirmed the preliminary observations with HPLC described previously: that the ACN +Sd wines had the highest total polymeric color at wine pH and retained higher color in the presence of bisulfite of the wine treatments (Table 4). Total ionized color (in 1 M HCl) was also highest in the ACN+Sd polymeric pigment isolate, indicating that a greater quantity of ACN in the flavylium form was associated with this fraction. With regard to the previous observations with HPLC that the quantities of polymeric pigments formed in ACN and ACN+Sk were similar, this was found in terms of $SO_2$-resistant pigments, but it was found that the color of ACN+Sk polymeric pigments at pH 3.4 and in 1 M HCl was higher than for the ACN treatment. However, these differences were very small.

An important observation was that whereas significant differences between the wine treatments in terms of wine or polymeric pigment bleachability by bisulfite were found, absolute differences in total wine and polymeric pigment color were small by comparison. This indicates that the polymeric pigments formed in the presence of Sd tannins were less bleachable that those formed in the other treatments and points to differences in their structure. To qualify these observations, protein precipitation of polymeric pigments was performed with bovine serum albumin[32] (Table 4), and it was found that $SO_2$-resistant polymeric pigments from ACN+Sk wines were less effectively bound by protein than those isolated from ACN+Sd wines (Table 4). $SO_2$-resistant polymeric pigments formed from ACN were not precipitable by protein. This suggests differences in the extent of ACN incorporation by Sk and Sd tannins had occurred, but it is noteworthy that both model ferment treatments had proportionally low levels of protein-precipitable bisulfite-resistant pigments compared to real wines.[32] This result indicates that the omission of tannin (ACN wine) or reduced incorporation of ACN to tannin (ACN +Sk) potentially increases the formation of smaller (oligomeric) polymeric pigments, which were not precipitable by protein.

These results present a significant step forward in our understanding of the importance of polymeric pigments in conferring the color properties of wine. Recent work on the role of ACN pigment families in wine color properties has shown that the addition of pyranoanthocyanidins and flavanol–ACN condensation products to monomeric ACNs imparts quantitative increases in optical color, even at low concentration.[43] On the basis of the methodology used to fractionate wine pigments in that study,[43] it does not appear that oligomeric pigments were assessed. To add to these observations, the current results indicate that the polymeric ACN fraction makes an important contribution to wine optical properties, in addition to smaller ACN-derived pigments. In addition, the formation of small ACN-derived pigments appears to be favored in the absence of tannin.

**Assessment of Polymeric Pigment Size Distribution.** It is well-known that yeast-derived metabolites drive the formation of a diverse array of flavonoid linkages between flavan-3-ols, ACNs, and ACN-derived pigments in wine and are significantly correlated with increases in polymeric pigment with wine aging.[44−46] However, the current results indicate that differences in tannin structure may underpin the type of polymeric pigments formed. Sd tannins, which have a lower degree of polymerization and a higher degree of galloylation than Sk tannins (Table 2), appear to favor greater incorporation of ACN, yielding a higher concentration of polymeric pigments, which are resistant to $SO_2$ bleaching. Although limited incorporation of ACN by Sk tannin may point to a restriction imposed by tannin molecular mass, this could also reflect differences in the reactivity of flavan-3-ol subunits in pigment formation between Sk and Sd tannins. Our data therefore do not conclusively show an effect of tannin mDP as conferring reactivity for ACN and will require follow-up research.

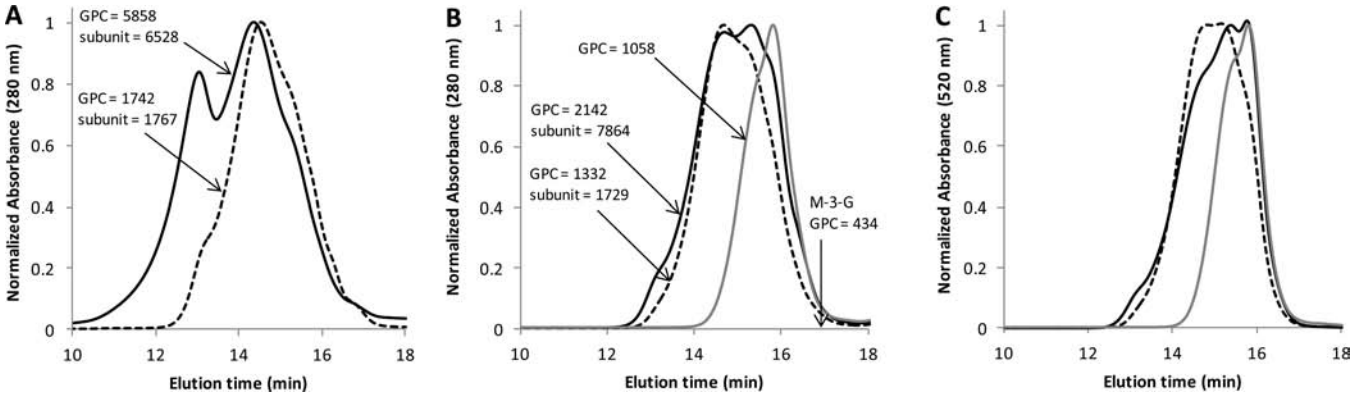


**Figure 3.** Elution profile of polymeric pigments in 6-month-aged wines containing skin (Sk, solid curve) and seed (Sd, broken curve) tannins, their respective combination with anthocyanin (ACN), or ACN only (gray curve) determined by gel permeation chromatography: (A) Sd and Sk wines produced without ACN, monitored at 280 nm; (B) Sd and Sk wines containing ACN in comparison with wine containing only ACN monitored at 280 nm; (C) Sd and Sk wines containing ACN in comparison with wine containing only ACN monitored at 520 nm. Annotations indicated as ↓ give the molecular mass average as g/mol by gel permeation chromatography (GPC), and when applicable a comparison with that determined by phloroglucinolysis (subunit) is given. The elution point of a malvidin-3-glucoside standard (M-3-G, 528.9 g/mol) is indicated as a reference.

To determine whether the differences in the type of polymeric pigments formed resulted in detectable changes in their molecular mass distribution (or hydrodynamic volume), GPC was performed on SPE isolates from 6-month-aged wines. The normalized chromatograms show size distribution differences on a comparable scale (Figure 3), but it was evident that the incorporation of ACN to polymeric pigments introduced large increases in 280 nm absorbance, which are included as Supporting Information (S5). Due to existing differences in conformational structure between seed and skin tannins, different molecular mass calibrations were used for the two tannin types. The presence of a significant proportion of early eluting, high molecular mass tannin in the Sk wine was evident (Figure 3A), which was absent in the Sd wine. The contribution of 520-nm-absorbing material from the Sk and Sd tannins themselves was negligible under the GPC conditions (data not shown). Molecular mass data obtained with GPC and phloroglucinolysis were similar in Sd and Sk wines without added ACN (Figure 3A). The molecular mass determined by GPC was also not significantly different between Sd and Sk wines and the corresponding tannin samples pre-ferment (data not shown).

When ACN was combined with Sd or Sk in wines, the apparent hydrodynamic volume of polymeric pigments determined by GPC was decreased significantly by comparison to Sd or Sk wines alone, and this was more significant for ACN +Sk (Figure 3B). An overlaid elution profile of the polymeric pigments isolated from wines containing only ACN showed that these eluted earlier than monomeric malvidin-3-*O*-glucoside (Figure 3B). Although the assigned molecular masses for ACNs are only nominal using the GPC (skin tannin) calibration, it was of interest to note that the predicted molecular mass for malvidin-3-*O*-glucoside of 434 g/mol (Figure 3B) was within the expected range for the compound and was higher than the lowest standard of calibration for monomeric epicatechin, 290.27 g/mol. The predicted molecular mass average of the ACN-derived wine pigments by GPC, assigned nominally as 1058 g/mol, therefore suggests an oligomeric form.

Material absorbing at 520 nm was evenly dispersed in ACN +Sd distribution (Figure 3C). In the case of ACN+Sk polymers, the 520 nm color was biased toward the lower molecular mass range. As a result, the overlaid elution profiles of ACN+Sk and ACN polymeric pigments were closely aligned within the lower molecular mass range. This possibly reflects a greater proportion of oligomeric pigments, not directly associated with tannin, in the ACN+Sk treatment. Because the 280 nm elution profile of ACN+Sk wine tannin showed a distinct loss of early eluting, high molecular mass material present in the Sk treatment (Figure 3A,B), which was not attributed to losses by precipitation (Supporting Information S4), this could indicate that the incorporation of ACN to high molecular mass Sk tannins rendered them more compact, thus eluting later by GPC.

In the absence of yeast-derived metabolites such as acetaldehyde and pyruvic acid, ACN and tannin can react directly with each other. Depending upon the intermediates of this reaction, the products may be rendered colorless. Oligomeric forms of ACNs can additionally polymerize with flavan-3-ols.[12,47] However, these processes all require acidic conditions, in particular, those processes that are facilitated by interflavan cleavage of the tannin polymer.[38] Under our experimental conditions, however, we hypothesized that hydrolysis was minimal due to limited changes in wine tannin composition (Table 1). Conversely, ethyl or vinyl linkages, formed in the presence of yeast metabolites, can facilitate reaction between ACN and tannin, as well as between tannin molecules.[48] Enhancement of ethyl linkages through manipulation of acetaldehyde concentration or wine aging has been related to increases in polymeric pigments.[44−46] Apart from this, intra- and intermolecular associations could occur within and between tannin molecules, respectively, leading to significant changes in tannin conformation (3-D structure).[37] Additional Π−Π stacking between aromatic rings of flavan-3-ols and bound ACN could also alter tannin conformation. It is noteworthy that tannin hydrodynamic volume determined by GPC was not affected when ACN was omitted from the ferment, which suggests ACN plays a significant role in conferring conformational changes to wine tannin during fermentation and aging (Table 1).

A reduction in hydrodynamic volume has also been observed for pigmented tannins with higher color incorporation, independent of wine tannin concentration and mDP.[19,49] Due to the use of dimethylformamide and lithium chloride in the

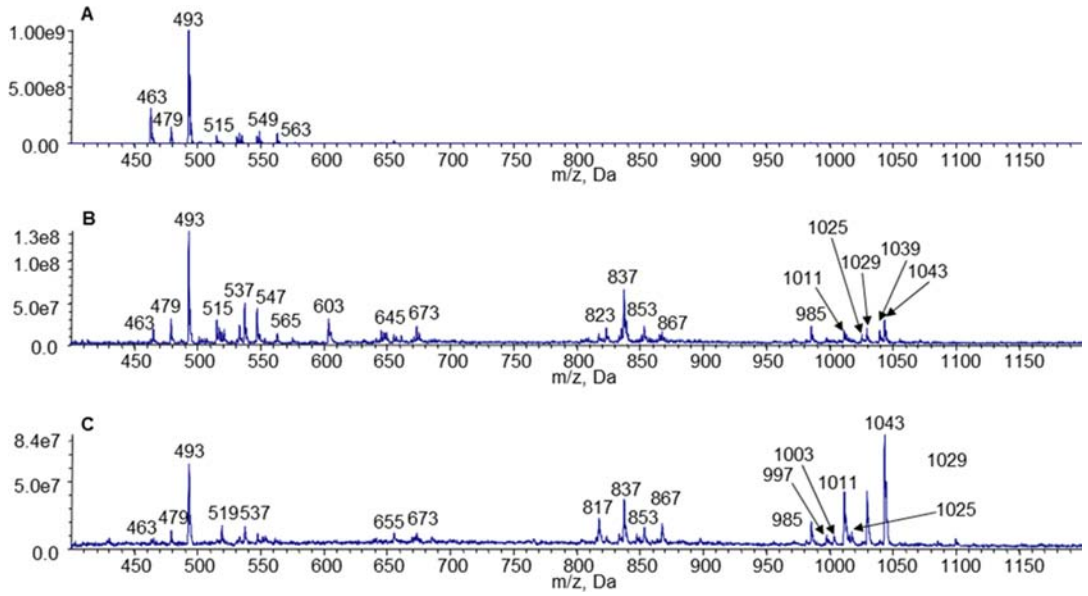


**Figure 4.** Mass spectra of (A) anthocyanin (ACN) solution, (B) 0-month-aged ACN wine, and (C) 6-month-aged ACN wine obtained by direct infusion MS.

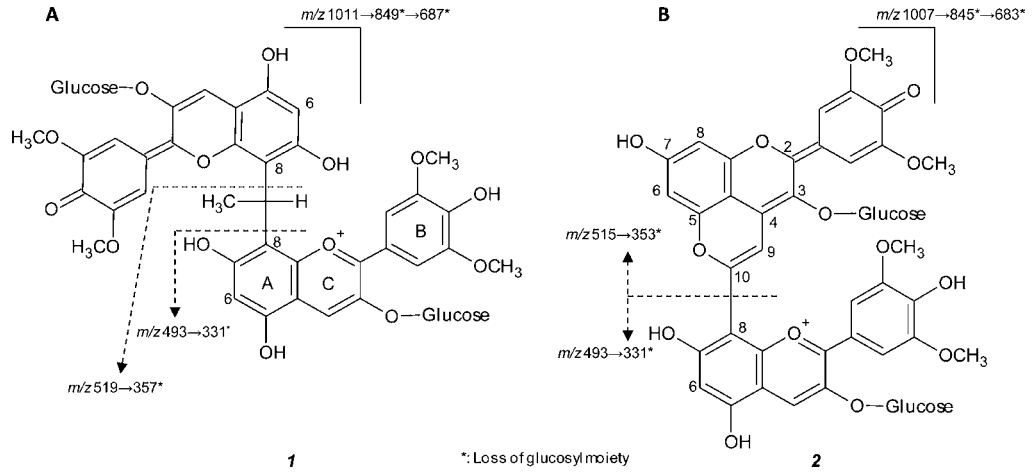


**Figure 5.** Possible structures of (A) ethyl-linked and (B) vinyl-linked malvidin-3-glucoside dimers.

GPC mobile phase, it is expected that interactions with the column itself are minimal. The reduction in the hydrodynamic volume of tannin/polymeric pigment isolates therefore reflects a possible dual effect of ACN on the mass distribution of wine polymeric pigments: first, a significant contribution of oligomeric pigments derived directly from ACNs; and second, a more compact tannin conformation following ACN incorporation, in particular for skin tannins.

From the current results, it is likely that a significant proportion of the pigment formed during the 6-month aging period was derived from reaction pathways other than direct condensation of ACN with tannin subunits, although this pathway is expected to contribute somewhat on the basis of the results of tannin and ACN combinations stored in acidified aqueous ethanol. What was unexpected was the formation of a significant quantity of polymeric pigments in wines containing only ACN, which contributed significantly to aging-related increases in total and bisulfite-resistant color. On the basis of the differences in the properties on polymeric pigments formed from Sk and Sd tannins, we can propose that tannin composition may limit the incorporation of ACN during fermentation and aging and could be due to differences in tannin molecular mass. Notably, the lack of ACN incorporation to tannin appears to facilitate the formation of small polymeric pigments, which are not precipitated by protein.

**Characterization of Anthocyanin-Derived Polymeric Pigments using Mass Spectrometry.** To confirm that the ACN wines formed pigments that were polymeric in nature, SPE isolates of the 0- and 6-month-aged ACN wines and ACN in aqueous ethanol solution were analyzed by direct infusion MS (Figure 4). Detailed fragment ion information on SPE isolates is provided as Supporting Information (S6). The ethanolic ACN solution gave a dominant ion at $m/z$ 493 corresponding to a mass of malvidin 3-glucoside (MvG), followed by $m/z$ 463 and 479 for the glucosides of peonidin (PnG) and petunidin (PtG), respectively (Figure 4A), which is an expected result. There were no obvious ion signals derived from ACN-related polymeric compounds.

On the other hand, the 0- and 6 month-aged ACN wines gave ions in a mass range greater than $m/z$ 1000 (Figure 4B,C), and the relative abundance ratio of these ions to the $m/z$ 493 (MvG) was markedly higher for 6-month-aged ACN wine than


dx.doi.org/10.1021/jf503922h | J. Agric. Food Chem. 2014, 62, 11582−11593

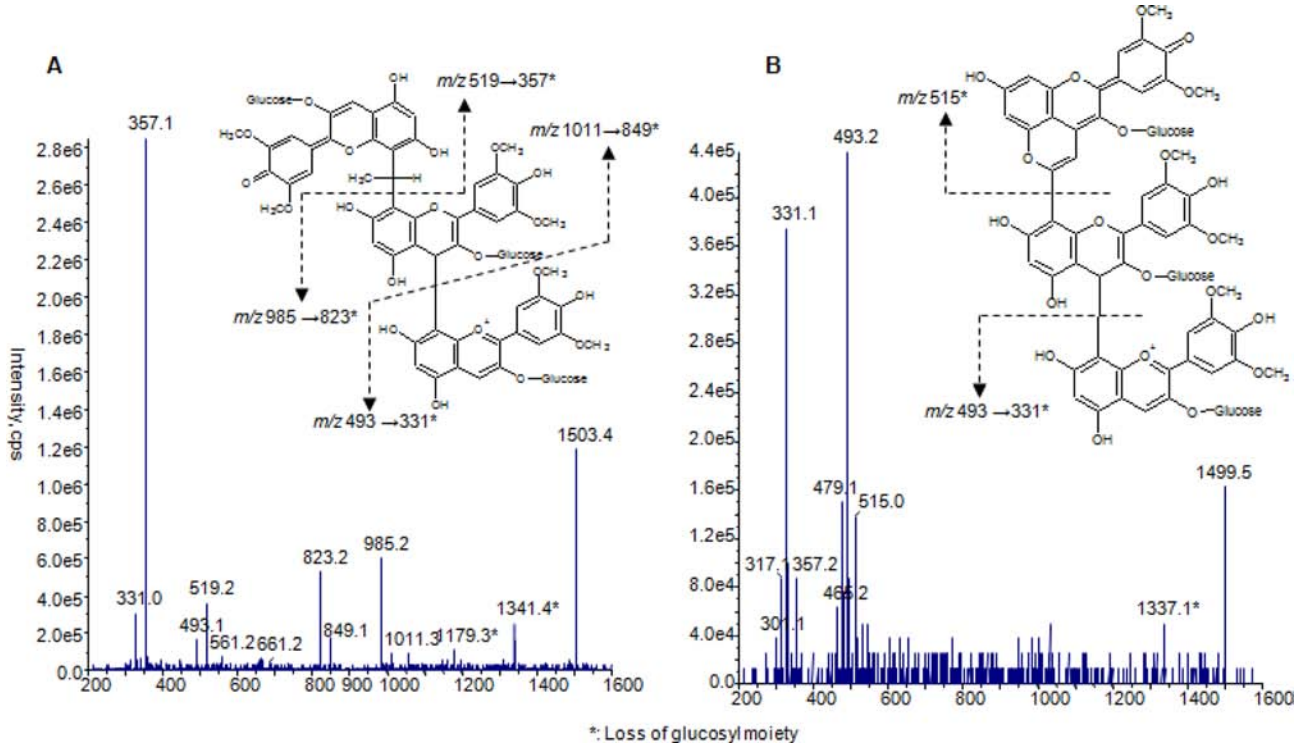


**Figure 6.** Product ion spectra and possible structures of (A) ethyl-linked and (B) vinyl-linked malvidin-3-glucoside trimers.

the young ACN wine. Direct infusion MS/MS analysis revealed that ions at *m/z* 1011, 1029, and 1043 were fragmented to common ions at *m/z* 849, 687, 519, 493, 357, and 331 (Supporting Information S7). In addition, both *m/z* 1029 and 1043 were fragmented to *m/z* 1011, indicating that these ions were likely hydrates (>18 Da) and methanol adducts (>32 Da). The ions at *m/z* 1011 and 1029 corresponded to masses of ethyl-linked MvG dimers containing one flavylium cation and either one quinoidal base (**1**) or hydrated form (Figure 5A). A doubly charged ion at *m/z* 506 was also detected by direct infusion MS analysis, demonstrating that the ethyl-linked MvG dimer with diflavylium cation was also present (data not shown). This result was consistent with the studies by Atanasova et al.[13] and Sun et al.,[50] who observed the formation of the same types of ethyl-linked MvG dimers in wine-like model solution containing MvG and acetaldehyde.

The fragment ions at *m/z* 519 (the loss of MvG in neutral quinoidal form), 357 (the losses of MvG and G), 493 (MvG), and 331 (Mv) (Supporting Information S8) were well-fitted with a possible fragmentation pattern of the proposed ethyl-linked MvG dimer. The ion at *m/z* 1043 (methanol adduct) was likely formed during the electrospray process due to the use of methanol as the solvent for LC-MS analysis. The ions at *m/z* 1025 and 1039 were fragmented into the same ion at *m/z* 1007, followed by giving the same fragment ions at *m/z* 845, 683, 515, 493, 353, and 331 as those derived from *m/z* 1007 (Supporting Information S8). Additional ions were observed at *m/z* 533 and 547 derived from *m/z* 1025 and 1039, respectively. The ion at *m/z* 1007 was assigned to be a vinyl-linked MvG dimer composed of pyranoMvG in quinoidal form and MvG in flavylium cation (**2**) (Figure 5B). The fragment ions appeared to be simply derived by the cleavage between the C10 position in the pyrano-MvG (*m/z* 515, probably vinyl carbocation) and C8 (or C6) position of MvG (*m/z* 493).

Pyranoanthocyanins have been reported to be highly stable and resistant to sulfur dioxide and water attack due to the substitution at the anthocyanin C4 position in ring C, resulting in no occurrence of hydration on these pigments.[51,52] Accordingly, the ion at *m/z* 1025 could be due to the adduction of a water molecule on the pyrano-MvG rather than the involvement of hydrated pyrano-MvG in dimerization. The adduction of a water or methanol molecule on the pyrano-MvG was also observed at fragment ions with *m/z* 533 or 547. In addition to the abundant ions derived from both dimers **1** and **2**, direct infusion MS analysis on the SPE isolates of the 0- and 6-month-aged ACN wines exhibited a large number of ions with low abundance in a mass range up to *m/z* 1600 (data not shown). The ions included *m/z* 997, 983, 981, and 967 and *m/z* 993, 979, 977, and 963 corresponding to masses of ethyl-linked and vinyl-linked dimers of MvG-PtG, MvG-DpG (delphinidin glucoside), MvG-PnG, and MvG-CyG (cyanidin glucoside), respectively.

Product ion spectra of these ions supported their identity by giving characteristic fragment ions derived from the cleavage of either the ethyl-linked or vinyl-linked ACN dimers (data not shown). Furthermore, a number of ions corresponding to masses of ethyl-linked and vinyl-linked ACN trimers were also observed (data not shown). For instance, the ions at *m/z* 1503 and 1499 were consistent with masses of ethyl-linked and vinyl-linked MvG trimers (Figure 6). Their product ions fitted well with their proposed structure.

The structural diversity of the ethyl- and vinyl-linked ACN oligomers can be extensive due to the variability in the composition and oxidation state of ACN units, linkage position and type, and molecular size. In addition, many structural isomers of the ACN oligomers can coexist, and the formation of adduct ions makes the structural elucidation of these pigments very difficult using the mass spectrometric techniques used here. In real wines, the possibility exists that ACN

condensation would occur with phenolics other than ACN itself, and these products have received greater attention in the literature to date. Due to the abundance of ACN in ferments and wines, the possibility exists that ACN-derived oligomers may be important intermediate products during wine aging and may in an ongoing manner form colored condensation products with polyphenols. Our work has demonstrated the existence of a broad range of ethyl- and vinyl-linked dimers and trimers in the 0- and 6-month-aged ACN wines, and to the best of our knowledge, the formation of vinyl-linked ACN oligomers is reported for the first time.

**General Implications of the Results.** This study has shown that the composition of grape tannin can significantly influence the formation of polymeric pigments in wine after reaction with ACN, notably their 520 nm absorbance properties and apparent hydrodynamic volume. A pertinent research direction will be to determine the long-term stability of polymeric pigments derived from tannins of different composition, in particular with respect to tannin size distribution and mDP. Whereas pigment reactions between ACN and Sd tannin were correlated with enhanced wine color stability, as inferred by lower pigment bleachability, the current study has shown that ACN alone can form significant quantities of polymeric pigments. Although these pigments are more bleachable by bisulfite than those formed with tannin, they contribute a strong 520 nm absorbance at wine pH. Using GPC and mass spectrometry, we have been able to demonstrate that pigments derived from ACN are oligomeric in nature. These may be important intermediates in the pathway for pigmented polymer formation in wine, which includes downstream condensation reactions with tannins and/or other polyphenols. The important contribution of these pigments to color at wine pH may have hitherto been overlooked due to their bleachability by bisulfite. The enhanced formation of non-bleachable pigments in wines as opposed to acidified ethanol solution suggests that reactions other than direct condensation or biphenyl linkages may drive their formation. Mass spectrometry confirmed that these are most likely to be ethyl or vinyl linkages.

## ■ ASSOCIATED CONTENT

### Supporting Information

S1−S8. This material is available free of charge via the Internet at http://pubs.acs.org.

## ■ AUTHOR INFORMATION

### Corresponding Author

*(K.B.) Phone: +61-8-83136190. Fax: +61-8-83136601. E-mail: keren.bindon@awri.com.au.

### Funding

The Australian Wine Research Institute, a member of the Wine Innovation Cluster in Adelaide, is supported by Australian grapegrowers and winemakers through their investment body, the Australian Grape and Wine Authority (AGWA), with matching funds from the Australian government.

### Notes

The authors declare no competing financial interest.

## ■ ACKNOWLEDGMENTS

We thank Pernod Ricard Australia (Orlando-Wyndham Vineyards) and the University of Adelaide for the donation of grape samples. We acknowledge Dr. Marlize Viviers for assistance in the anaerobic storage of wines. We also thank Dr. Toni Garcia Cordente for guidance in the preparation of chemically defined must. We are grateful to Dr. Eric Wilkes for proofreading the manuscript.

## ■ REFERENCES

(1) Singleton, V. L.; Trousdale, E. K. Anthocyanin-tannin interaction explaining differences in polymeric phenols between white and red wines. *Am. J. Enol. Vitic.* **1992**, *43*, 63−70.

(2) Canals, R.; Llaudy, M. C.; Valls, J.; Canals, J. M.; Zamora, F. Influence of ethanol concentration on the extraction of color and phenolic compounds from the skin and seeds of Tempranillo grapes at different stages of ripening. *J. Agric. Food Chem.* **2005**, *53*, 4019−4025.

(3) Carmen del Llaudy, M.; Canals, R.; Miquel Canals, J.; Zamora, F. Influence of ripening stage and maceration length on the contribution of grape skins, seeds and stems to phenolic composition and astringency in wine-simulated macerations. *Eur. Food Res. Technol.* **2008**, *226*, 337−344.

(4) Busse-Valverde, N.; Bautista-Ortin, A. B.; Gomez-Plaza, E.; Fernandez-Fernandez, J. I.; Gil-Munoz, R. Influence of skin maceration time on the proanthocyanidin content of red wines. *Eur. Food Res. Technol.* **2012**, *235*, 1117−1123.

(5) Cerpa-Calderon, F. K.; Kennedy, J. A. Berry integrity and extraction of skin and seed proanthocyanidins during red wine fermentation. *J. Agric. Food Chem.* **2008**, *56*, 9006−9014.

(6) Kennedy, J. A.; Hayasaka, Y.; Vidal, S.; Waters, E. J.; Jones, G. P. Composition of grape skin proanthocyanidins at different stages of berry development. *J. Agric. Food Chem.* **2001**, *49*, 5348−5355.

(7) Kennedy, J. A.; Matthews, M. A.; Waterhouse, A. L. Changes in grape seed polyphenols during fruit ripening. *Phytochemistry* **2000**, *55*, 77−85.

(8) Thorngate, J. H.; Singleton, V. L. Reactions of monomeric and polymeric flavan-3-ols with monomeric pigment in model wine solutions. *Am. J. Enol. Vitic.* **1994**, *45*, 349−352.

(9) Saucier, C.; Lopes, P.; Mirabel, M.; Guerra, C.; Glories, Y. Tannin-anthocyanin interactions: influence on wine color. In *Red Wine Color: Revealing the Mysteries*; Waterhouse, A. L., Kennedy, J. A., Eds.; ACS Symposium Series 886; American Chemical Society: Washington, DC, USA, 2004; pp 265−273.

(10) Cheynier, V.; Duenas-Paton, M.; Salas, E.; Maury, C.; Souquet, J. M.; Sarni-Manchado, P.; Fulcrand, H. Structure and properties of wine pigments and tannins. *Am. J. Enol. Vitic.* **2006**, *57*, 298−305.

(11) Fulcrand, H.; Duenas, M.; Salas, E.; Cheynier, V. Phenolic reactions during winemaking and aging. *Am. J. Enol. Vitic.* **2006**, *57*, 289−297.

(12) Vidal, S.; Meudec, E.; Cheynier, V.; Skouroumounis, G.; Hayasaka, Y. Mass spectrometric evidence for the existence of oligomeric anthocyanins in grape skins. *J. Agric. Food Chem.* **2004**, *52*, 7144−7151.

(13) Atanasova, V.; Fulcrand, H.; Le Guerneve, C.; Cheynier, W.; Moutounet, M. Structure of a new dimeric acetaldehyde malvidin 3-glucoside condensation product. *Tetrahedron Lett.* **2002**, *43*, 6151−6153.

(14) Pechamat, L.; Zeng, L. M.; Jourdes, M.; Ghidossi, R.; Teissedre, P. L. Occurrence and formation kinetics of pyranomalvidin-procyanidin dimer pigment in Merlot red wine: impact of acidity and oxygen concentrations. *J. Agric. Food Chem.* **2014**, *62*, 1701−1705.

(15) Timberlake, C. F.; Bridle, P. Interactions between anthocyanins, phenolic compounds and acetaldehyde and their significance in red wines. *Am. J. Enol. Vitic.* **1976**, *27*, 97−105.

(16) Blanco-Vega, D.; Lopez-Bellido, F. J.; Alia-Robledo, J. M.; Hermosin-Gutierrez, I. HPLC-DAD-ESI-MS/MS characterization of pyranoanthocyanins pigments formed in model wine. *J. Agric. Food Chem.* **2011**, *59*, 9523−9531.

(17) Blanco-Vega, D.; Gomez-Alonso, S.; Hermosin-Gutierrez, I. Identification, content and distribution of anthocyanins and low molecular weight anthocyanin-derived pigments in Spanish commercial red wines. *Food Chem.* **2014**, *158*, 449−458.

(18) Hayasaka, Y.; Kennedy, J. A. Mass spectrometric evidence for the formation of pigmented polymers in red wine. *Aust. J. Grape Wine Res.* **2003**, *9*, 210−220.
(19) Bindon, K. A.; McCarthy, M. G.; Smith, P. A. Development of wine colour and non-bleachable pigments during the fermentation and ageing of (*Vitis vinifera* L. cv.) Cabernet Sauvignon wines differing in anthocyanin and tannin concentration. *LWT−Food Sci. Technol.* **2014**, *59*, 923−932.
(20) Somers, C. T.; Evans, M. E. Spectral evaluation of young red wines: anthocyanin equilibria, total phenolics, free and molecular $SO_2$, "chemical age". *J. Sci. Food Agric.* **1977**, *28*, 279−287.
(21) Iland, P.; Bruer, N.; Edwards, G.; Weeks, S.; Wilkes, E. *Chemical Analysis of Grapes and Wine: Techniques and Concepts*; Patrick Iland Wine Promotions: Adelaide, Australia, 2004.
(22) Jeffery, D. W.; Mercurio, M. D.; Herderich, M. J.; Hayasaka, Y.; Smith, P. A. Rapid isolation of red wine polymeric polyphenols by solid-phase extraction. *J. Agric. Food Chem.* **2008**, *56*, 2571−2580.
(23) Kennedy, J. A.; Jones, G. P. Analysis of proanthocyanidin cleavage products following acid-catalysis in the presence of excess phloroglucinol. *J. Agric. Food Chem.* **2001**, *49*, 1740−1746.
(24) Kennedy, J. A.; Taylor, A. W. Analysis of proanthocyanidins by high-performance gel permeation chromatography. *J. Chromatogr., A* **2003**, *995*, 99−107.
(25) Bindon, K. A.; Kennedy, J. A. Ripening-induced changes in grape skin proanthocyanidins modify their interaction with cell walls. *J. Agric. Food Chem.* **2011**, *59*, 2696−2707.
(26) Mercurio, M. D.; Dambergs, R. G.; Herderich, M. J.; Smith, P. A. High throughput analysis of red wine and grape phenolics − adaptation and validation of methyl cellulose precipitable tannin assay and modified somers color assay to a rapid 96 well plate format. *J. Agric. Food Chem.* **2007**, *55*, 4651−4657.
(27) Schmidt, S. A.; Dillon, S.; Kolouchova, R.; Henschke, P. A.; Chambers, P. J. Impacts of variations in elemental nutrient concentration of Chardonnay musts on *Saccharomyces cerevisiae* fermentation kinetics and wine composition. *Appl. Microbiol. Biotechnol.* **2011**, *91*, 365−375.
(28) Contreras, A.; Hidalgo, C.; Henschke, P. A.; Chambers, P. J.; Curtin, C.; Varela, C. Evaluation of non-*Saccharomyces* yeasts for the reduction of alcohol content in wine. *Appl. Environ. Microbiol.* **2014**, *80*, 1670−1678.
(29) Varela, C.; Pizarro, F.; Agosin, E. Biomass content governs fermentation rate in nitrogen-deficient wine musts. *Appl. Environ. Microbiol.* **2004**, *70*, 3392−3400.
(30) Asenstorfer, R. E.; Markides, A. J.; Iland, P. G.; Jones, G. P. Formation of vitisin A during red wine fermentation and maturation. *Aust. J. Grape Wine Res.* **2003**, *9*, 40−46.
(31) Kassara, S.; Kennedy, J. A. Relationship between red wine grade and phenolics. 2. Tannin composition and size. *J. Agric. Food Chem.* **2011**, *59*, 8409−8412.
(32) Heredia, T. M.; Adams, D. O.; Fields, K. C.; Held, P. G.; Harbertson, J. F. Evaluation of a comprehensive red wine phenolics assay using a microplate reader. *Am. J. Enol. Vitic.* **2006**, *57*, 497−502.
(33) Bindon, K. A.; Smith, P. A.; Kennedy, J. A. Interaction between grape-derived proanthocyanidins and cell wall material. 1. Effect on proanthocyanidin composition and molecular mass. *J. Agric. Food Chem.* **2010**, *58*, 2520−2528.
(34) Bindon, K. A.; Smith, P. A.; Holt, H.; Kennedy, J. A. Interaction between grape-derived proanthocyanidins and cell wall material. 2. Implications for vinification. *J. Agric. Food Chem.* **2010**, *58*, 10736−10746.
(35) McRae, J. M.; Dambergs, R. G.; Kassara, S.; Parker, M.; Jeffery, D. W.; Herderich, M. J.; Smith, P. A. Phenolic compositions of 50 and 30 year sequences of Australian red wines: the impact of wine age. *J. Agric. Food Chem.* **2012**, *60*, 10093−10102.
(36) McRae, J. M.; Kassara, S.; Kennedy, J. A.; Waters, E. J.; Smith, P. A. Effect of wine pH and bottle closure on tannins. *J. Agric. Food Chem.* **2013**, *61*, 11618−11627.
(37) Poncet-Legrand, C.; Cabane, B.; Bautista-Ortin, A. B.; Carrillo, S.; Fulcrand, H.; Perez, J.; Vernhet, A. Tannin oxidation: intra- versus intermolecular reactions. *Biomacromolecules* **2010**, *11*, 2376−2386.
(38) Vidal, S.; Cartalade, D.; Souquet, J. M.; Fulcrand, H.; Cheynier, V. Changes in proanthocyanidin chain length in winelike model solutions. *J. Agric. Food Chem.* **2002**, *50*, 2261−2266.
(39) Chira, K.; Jourdes, M.; Teissedre, P. L. Cabernet Sauvignon red wine astringency quality control by tannin characterization and polymerization during storage. *Eur. Food Res. Technol.* **2012**, *234*, 253−261.
(40) Salas, E.; Fulcrand, H.; Meudec, E.; Cheynier, V. Reactions of anthocyanins and tannins in model solutions. *J. Agric. Food Chem.* **2003**, *51*, 7951−7961.
(41) Malien-Aubert, C.; Dangles, O.; Amiot, M. J. Influence of procyanidins on the color stability of oenin solutions. *J. Agric. Food Chem.* **2002**, *50*, 3299−3305.
(42) Salas, E.; Le Guerneve, C.; Fulcrand, H.; Poncet-Legrand, C.; Cheynier, W. Structure determination and colour properties of a new directly linked flavanol-anthocyanin dimer. *Tetrahedron Lett.* **2004**, *45*, 8725−8729.
(43) Garcia-Marino, M.; Escudero-Gilete, M. L.; Escribano-Bailon, M. T.; Gonzalez-Miret, M. L.; Rivas-Gonzalo, J. C.; Heredia, F. J. Colorimetric study of the interactions between different families of red wine pigments using transmittance and reflectance measurements. *Food Res. Int.* **2013**, *50*, 20−30.
(44) Drinkine, J.; Lopes, P.; Kennedy, J. A.; Teissedre, P. L.; Saucier, C. Analysis of ethylidene-bridged flavan-3-ols in wine. *J. Agric. Food Chem.* **2007**, *55*, 1109−1116.
(45) Drinkine, J.; Lopes, P.; Kennedy, J. A.; Teissedre, P. L.; Saucier, C. Ethylidene-bridged flavan-3-ols in red wine and correlation with wine age. *J. Agric. Food Chem.* **2007**, *55*, 6292−6299.
(46) Hayasaka, Y.; Birse, M.; Eglinton, J.; Herderich, M. The effect of *Saccharomyces cerevisiae* and *Saccharomyces bayanus* yeast on colour properties and pigment profiles of a Cabernet Sauvignon red wine. *Aust. J. Grape Wine Res.* **2007**, *13*, 176−185.
(47) Alcalde-Eon, C.; Escribano-Bailon, M. T.; Santos-Buelga, C.; Rivas-Gonzalo, J. C. Identification of dimeric anthocyanins and new oligomeric pigments in red wine by means of HPLC-DAD-ESI/MS*n*. *J. Mass Spectrom.* **2007**, *42*, 735−748.
(48) Cheynier, V.; Remy, S.; Fulcrand, H. *Mechanisms of Anthocyanin and Tannin Changes during Winemaking and Aging*, Proceedings of the ASEV 50th Anniversary Annual Meeting; Rantz, J. M., Ed.; American Society for Enology and Viticulture: Davis, CA, USA, 2000; pp 337−344.
(49) Bindon, K.; Varela, C.; Kennedy, J.; Holt, H.; Herderich, M. Relationships between harvest time and wine composition in *Vitis vinifera* L. cv. Cabernet Sauvignon 1. Grape and wine chemistry. *Food Chem.* **2013**, *138*, 1696−1705.
(50) Sun, B. S.; Santos, C. P. R.; Leandro, M. C.; De Freitas, V.; Spranger, M. I. High-performance liquid chromatography/electrospray ionization mass spectrometric characterization of new products formed by the reaction between flavanols and malvidin 3-glucoside in the presence of acetaldehyde. *Rapid Commun. Mass Spectrom.* **2007**, *21*, 2227−2236.
(51) Asenstorfer, R. E.; Lee, D. F.; Jones, G. P. Influence of structure on the ionisation constants of anthocyanin and anthocyanin-like wine pigments. *Anal. Chim. Acta* **2006**, *563*, 10−14.
(52) Cruz, L.; Petrov, V.; Teixeira, N.; Mateus, N.; Pina, F.; de Freitas, V. Establishment of the chemical equilibria of different types of pyranoanthocyanins in aqueous solutions: evidence for the formation of aggregation in pyranomalvidin-3-*O*-coumaroylglucoside-(+)-catechin. *J. Phys. Chem. B* **2010**, *114*, 13232−13240.

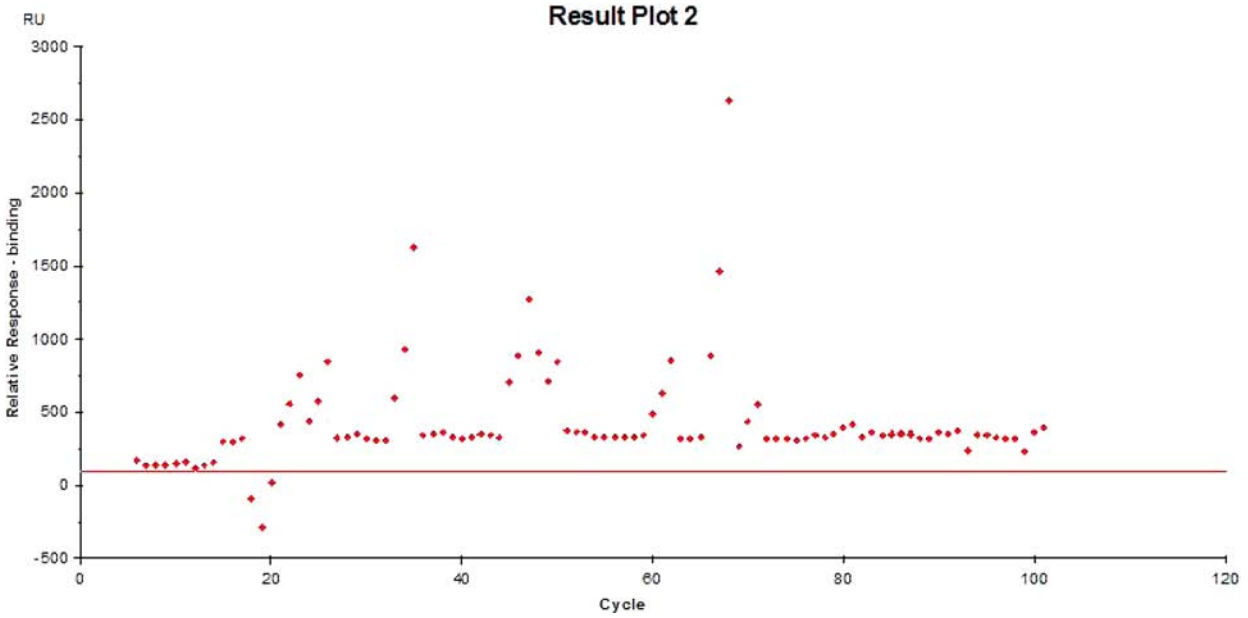


**Figure 1.** Binding sensogram of various compounds toward immobilized mushroom tyrosinase (2353 RU). Enzyme concentration was 50 $\mu$g mL$^{-1}$ in 0.1 M sodium acetate buffer, pH 4.5. Increasing concentrations for each compound (125, 250, and 500 $\mu$M) were injected simultaneously over the surface of immobilized enzyme and the total cycles ranging from 1 to 101 are as buffer (1−5), followed by L-DOPA, catechol, L-tyrosine, phloroglucinol, ABTS, *o*-toluidine, caffeic acid, gallic acid, guaiacol, syringaldehyde, pyrogallol, *p*-hydroxybenzoic acid, orcine, tannic acid, resorcinol, saffron, veratrol, vertryl alcohol, *o*-dianisidine hydroquinone, curcumin, glutathione, *o*-cresol, *p*-cresol, NaCl, sodium azide, ascorbic acid, kojic acid, thioglycolic acid, 2,6-dimethoxybenzoic acid, *m*-cresol, crocin, etc. (respective three cycles for each analyte). Flow rate was maintained constant throughout the binding (10 $\mu$L/min).

**Table 1. Interaction Kinetics of Mushroom Tyrosinase with Different Inhibitors Fit to a Two-State Model Using Biacore Evaluation Software**[a]

| inhibitor | $k_{a1}$(1/ms) | $k_{d1}$(1/s) | $K_{a2}$(1/s) | $K_{d2}$(1/s) | $K_D$ (M) |
|---|---|---|---|---|---|
| tannic acid | 397.4 ± 21 | 0.08624 ± 0.0033 | $8.708 \times 10^{-4} \pm 4.1 \times 10^{-5}$ | $0.001103 \pm 6.7 \times 10^{-5}$ | $1.213 \times 10^{-4} \pm 0.8$ |
| phloroglucinol | 4321 ± 41 | 0.3582 ± 0.019 | $5.208 \times 10^{-4} \pm 5.2 \times 10^{-4}$ | $0.003219 \pm 7.5 \times 10^{-5}$ | $7.136 \times 10^{-5} \pm 2$ |
| saffron | $2.774 \times 10^{4} \pm 3.2 \times 10^{3}$ | 0.9011 ± 0.089 | 0.003694 ± 0.0024 | 0.08329 ± 0.031 | $3.111 \times 10^{-5} \pm 0.3$ |
| catechol | $1.248 \times 10^{4} \pm 1.1 \times 10^{3}$ | 0.3185 ± 0.015 | $4.848 \times 10^{-4} \pm 2.6 \times 10^{-5}$ | $7.589\times 10^{-4} \pm 6.3 \times 10^{-5}$ | $1.557 \times 10^{-5} \pm 0.4$ |
| pyrogallol | 297.2 ± 7.5 | $0.02551 \pm 7.8 \times 10^{-4}$ | $0.005049 \pm 8.2 \times 10^{-5}$ | $5.176 \times 10^{-4} \pm 5.18 \times 10^{-5}$ | $7.981 \times 10^{-6} \pm 2$ |

[a]Standard error values were calculated from three measurements for each analyte by software itself.

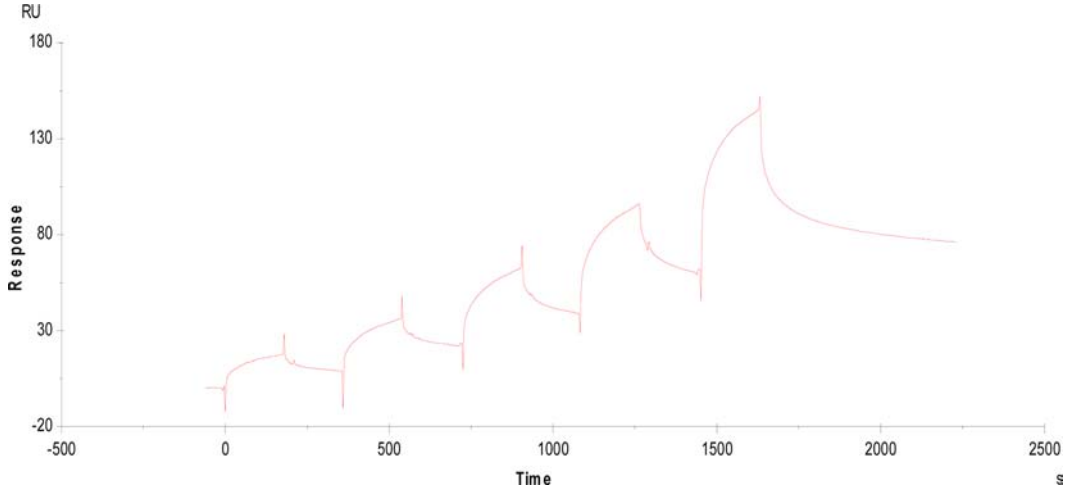


**Figure 2.** Binding sensogram for pyrogallol interaction with immobilized mushroom tyrosinase. Increasing concentrations of pyrogallol from 6.25, 12.5, 25, 50, to 100 $\mu$M were injected over the enzyme surface. Flow rate (30 $\mu$L/min) contact time and dissociation time were kept at 120 s. Regeneration was carried out with 10 mM glycine HCl, pH 2.5, for 30 s and at 30 $\mu$L/min. Data analysis was done with Biacore X100 evaluation software ver. 2.0.1, and data were fit to two states.

the surface of the flow cell was activated for 7 min using a 1:1 mixture of 100 mM EDC and 100 mM NHS (both dissolved in water), and subsequently tyrosinase was injected for 7 min; residual activated carboxymethyl groups on the surface were blocked by a 7 min injection of 1 M ethanolamine, pH 8.5. A total of 2353 RU of tyrosinase was immobilized. The activity of enzyme after immobilization was confirmed by plotting RI (RU) response against concentration of substrate (L-DOPA and L-tyrosine).

**Screening of Different Small Molecules.** For this study, one of the flow cells was blank immobilized (without protein) for use as a reference. Different analytes such as monohydroxy-, dihydroxy-, and trihydroxyphenols were screened against mushroom tyrosinase. Flow rate was maintained constant throughout the binding (10 $\mu$L/min) and kinetics experiment (30 $\mu$L/min); contact time and dissociation time were kept at 120 s. Regeneration was carried out with 10 mM glycine HCl, pH 2.5, for 30 s and at 30 $\mu$L/min. Kinetics was performed with various concentrations of compounds (12.5−200 $\mu$M) in a single-cycle kinetics[33,34] or multicycle kinetics mode. Data analysis was done with Biacore X100 evaluation software ver. 2.0.1, and data were fit to a 1:1 binding model or two-state fit.

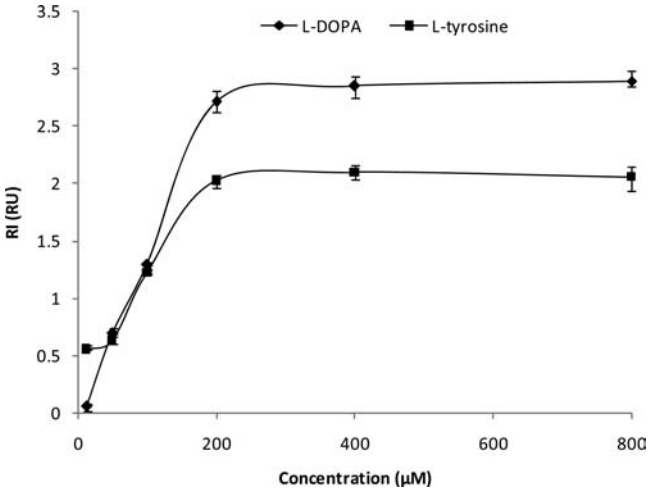


**Figure 3.** Activity of enzyme after immobilization was confirmed by plotting RI (RU) response against concentration of substrate for L-DOPA (◆) and L-tyrosine (■).

**Circular Dichroism (CD) Spectroscopy.** The CD spectra were recorded on a Jasco J-815 CD spectropolarimeter to give the content of regular secondary structure in mushroom tyrosinase. Protein solutions of 0.05 mg mL$^{-1}$ were prepared in the 0.1 mM PBS buffer at pH 6.8. Scans were performed at 20 °C using a 0.1 cm path length quartz cuvette with 8 s differential integration time at a scan rate of 50 nm min$^{-1}$. The protein solutions of 0.05 mg mL$^{-1}$ were incubated with and without pyrogallol, phloroglucinol, tannic acid, saffron, and catechol at a concentration of 200 $\mu$M for 15 min and were used to obtain the spectra. All spectra were collected in triplicate from 200 to 280 nm and a background corrected against buffer blank. The results were expressed as molar ellipticity (deg cm$^2$ dmol$^{-1}$) on the basis of a mean amino acid residue weight (MRW) of mushroom tyrosinase. The molar ellipticity was determined as $[\theta_{obs}] = (100 \times (MRW) \times \theta_{obs}/cl)$, where $\theta$ is the observed ellipticity in degrees at a given wavelength, $c$ is the protein concentration in mg/mL, and $l$ is the length of the light path in cm.[35]

## RESULT AND DISCUSSION

It has been recently discovered that various dermatological disorders such as age spots and freckles are caused by hyperpigmentation.[1] Hyperpigmentation in human skin and enzymatic browning in fruits are not desirable.[36] Thus, hyperpigmentation becomes a major problem in the food industry and one of the main causes of quality loss during postharvest handling and processing.[31] The regulation of melanin synthesis via the inhibition of tyrosinase is a current area of research in the context of preventing hyperpigmentation.[37] As a result, tyrosinase inhibitors have become increasingly important in the food, medical, and cosmetic industries.[38,39]

Various tyrosinase-based biosensors have been developed in the past few years.[22−26] Using these sensors, the detection of the large group of phenolic compounds as tyrosinase inhibitors was possible. However, low sensitivity is one of their major drawbacks.[40] In the present paper, the affinity and binding kinetics of various small molecules toward mushroom tyrosinase using SPR has been evaluated. In addition, this sensor has the ability to detect the number of different inhibitors of enzyme in a single run with high sensitivity and accuracy. Label-free interactions are more sensitive and less

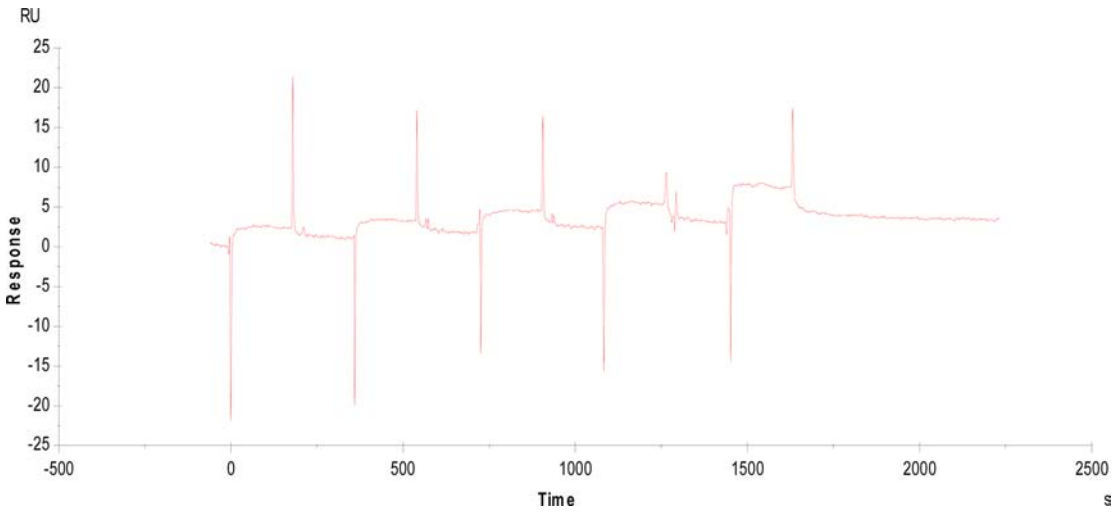


**Figure 4.** Binding sensogram for catechol interaction with immobilized mushroom tyrosinase. Increasing concentrations of catechol from 12.5, 25, 50, 100, to 200 $\mu$M were injected over the enzyme surface. Flow rate (30 $\mu$L/min) contact time and dissociation time were kept at 120 s. Regeneration was carried out with 10 mM glycine HCl, pH 2.5, for 30 s and at 30 $\mu$L/min. Data analysis was done with Biacore X100 evaluation software ver. 2.0.1, and data were fit to two states.

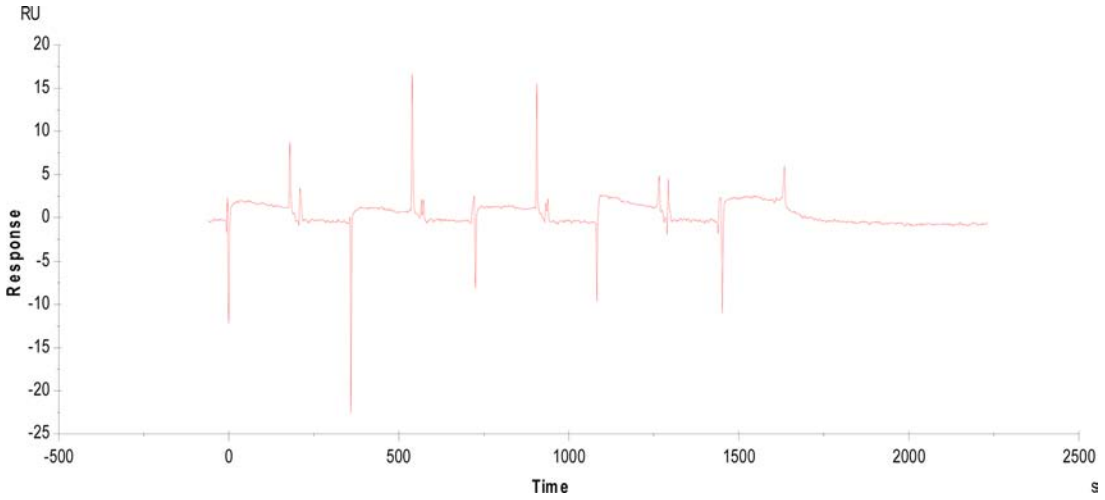


**Figure 5.** Binding sensogram for saffron interaction with immobilized mushroom tyrosinase. Increasing concentrations of saffron from 12.5, 25, 50, 100, to 200 $\mu$M were injected over the enzyme surface. Flow rate (30 $\mu$L/min) contact time and dissociation time were kept at 120 s. Regeneration was carried out with 10 mM glycine HCl, pH 2.5, for 30 s and at 30 $\mu$L/min. Data analysis was done with Biacore X100 evaluation software ver 2.0.1, and data were fit to two states. The resulting equilibrium dissociation constants are reported in Table 1.

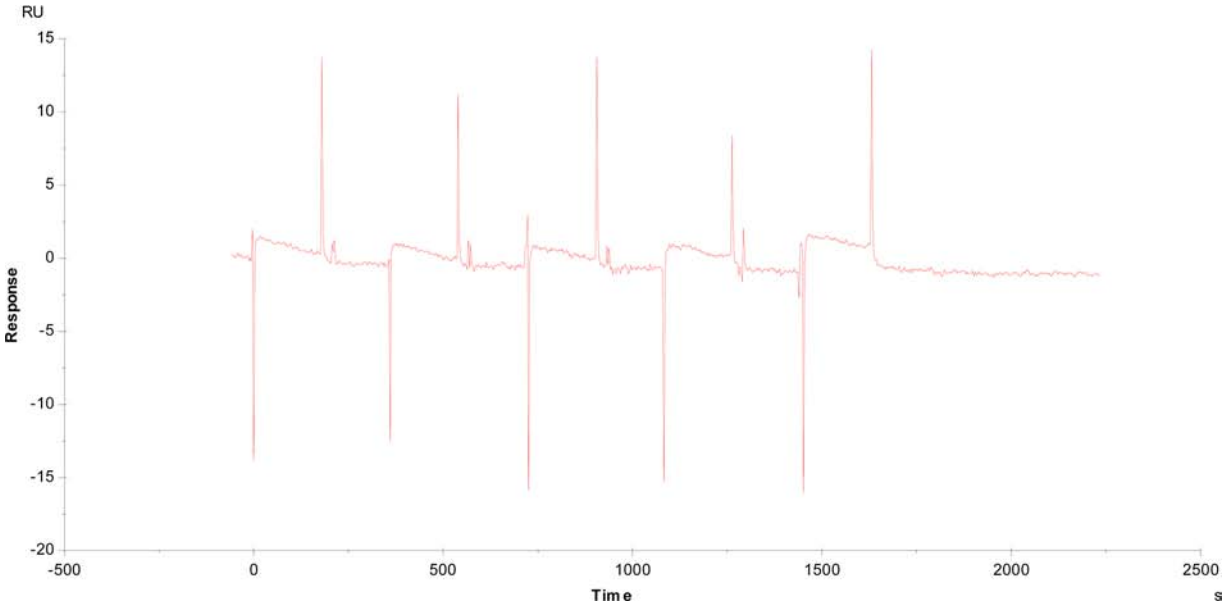


**Figure 6.** Binding sensogram for phloroglucinol interaction with immobilized mushroom tyrosinase. Increasing concentrations of phloroglucinol from 12.5, 25, 50, 100, to 200 $\mu$M were injected over the enzyme surface. Flow rate (30 $\mu$L/min) contact time and dissociation time were kept at 120 s. Regeneration was carried out with 10 mM glycine HCl, pH 2.5, for 30 s and at 30 $\mu$L/min. Data analysis was done with Biacore X100 evaluation software ver. 2.0.1, and data were fit to two states. The resulting equilibrium dissociation constants are reported in Table 1.

error prone compared with the conventional spectroscopic methods, which are based on color formation.

The screening results showed that the affinity toward mushroom tyrosinase varies from molecule to molecule, which is clearly observed from Figure 1. Many compounds showed high affinity for tyrosinase but possess low stability. Low-stability compounds were found to display a higher dissociation rate. On the basis of binding studies, various small molecules such as catechol, pyrogallol, saffron, tannic acid, and phloroglucinol were selected further for affinity and kinetic analysis against mushroom tyrosinase. This study shows that pyrogallol has a higher binding affinity for mushroom tyrosinase with a $K_D$ value of $7.981 \times 10^{-6}$ M. The data with different concentrations were fit to a two-state equation and are shown in Table 1. Pyrogallol has higher rates of association and dissociation and a higher equilibrium dissociation constant as evident from Figure 2. Pyrogallol is trihydroxyphenol: it perhaps binds more rapidly as compared to L-DOPA and L-tyrosine, which are dihydroxy- and monohydroxyphenols, respectively. Tyrosinase action on phenolic substrates follows the order trihydroxy > dihydroxy > monohydroxyphenol. The $K_D$ value for L-DOPA was reported by us before.[32] L-DOPA was also run between inhibitors during the kinetic runs to ascertain the activity of tyrosinase. The activity of enzyme after immobilization was proportional with increasing concentrations of L-DOPA and L-tyrosine (Figure 3), which confirmed the stability and reactivity of mushroom tyrosinase after immobilization. Pyrogallol was reported as a suicide inhibitor of tyrosinase and predicted to bind with high affinity.[41] The low affinity of catechol ($1.557 \times 10^{-5}$ M) (Figure 4) compared to

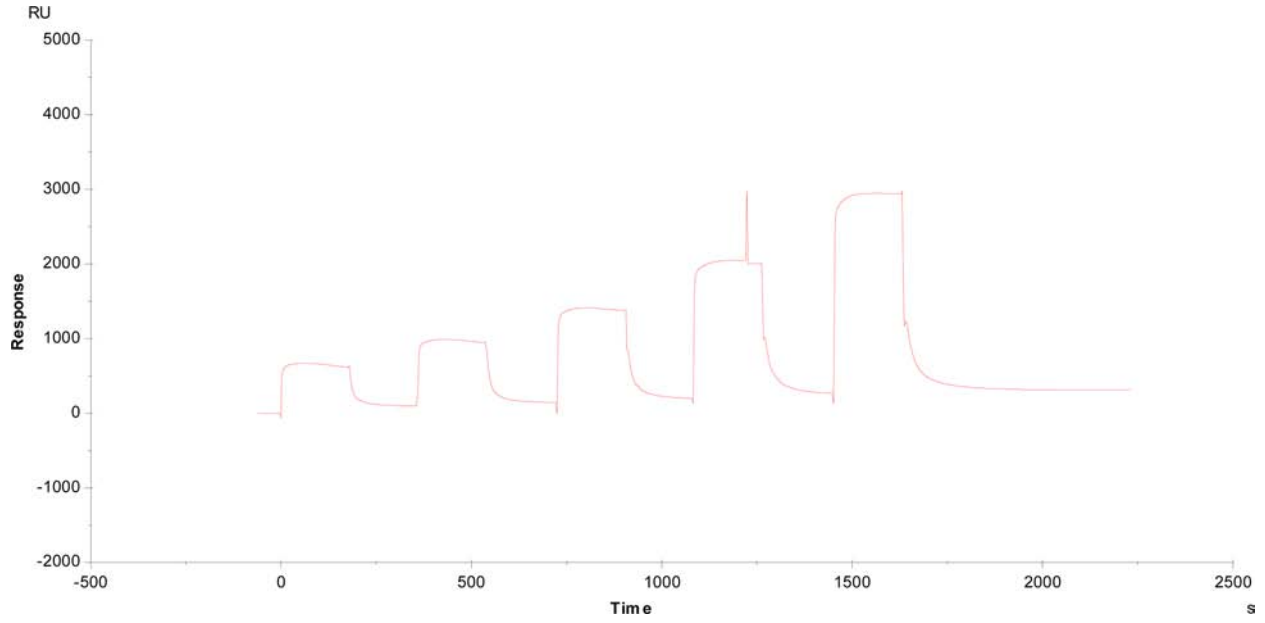


**Figure 7.** Binding sensogram for tannic acid interaction with immobilized mushroom tyrosinase. Increasing concentrations of tannic acid from 6.25, 12.5, 25, 50, to 100 $\mu$M were injected over the enzyme surface. Flow rate (30 $\mu$L/min) contact time and dissociation time were kept at 120 s. Regeneration was carried out with 10 mM glycine HCl, pH 2.5, for 30 s and at 30 $\mu$L/min. Data analysis was done with Biacore X100 evaluation software ver. 2.0.1, and data were fit to two states. The resulting equilibrium dissociation constants are reported in Table 1.

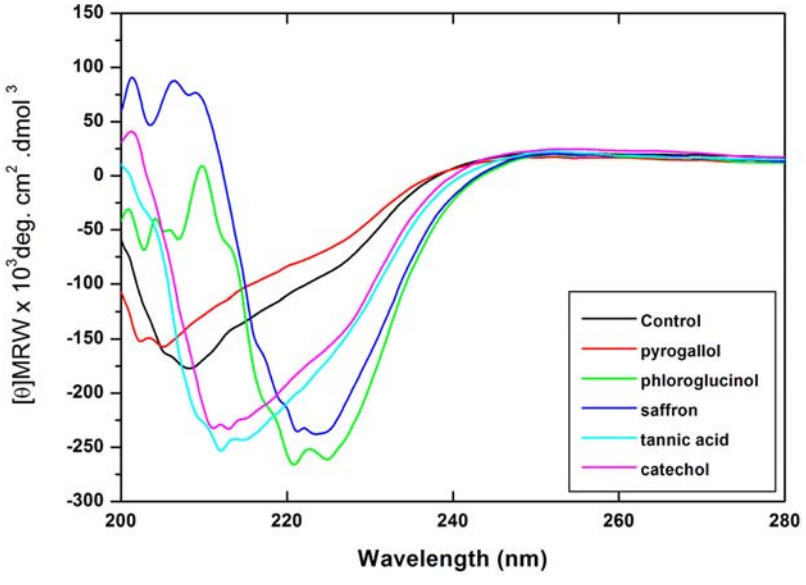


**Figure 8.** CD spectrum of mushroom tyrosinase without (black curve) and with pyrogallol (red curve), phloroglucinol (green curve), tannic acid (light blue curve), saffron (dark blue curve), and catechol (pink curve) at 200 $\mu$M concentration each.

pyrogallol may be because catechol follows "cresolase presentation", catechol being oxidized to form a product able to undergo deprotonation and reductive elimination, resulting in inactivation of the enzyme through the formation of copper at the active site. However, because the OH groups are equivalent, the probability of catalysis and inactivation increases in the cases of pyrogallol (trihydroxyphenol) and catechol (*o*-diphenol).[42] Catechol showed fast association and slow dissociation time as it is a substrate for tyrosinase (Table 1).

Saffron, phloroglucinol, and tannic acid have low binding affinities toward mushroom tyrosinase with $K_D$ values of $3.111 \times 10^{-5}$, $7.136 \times 10^{-5}$, and $1.213 \times 10^{-4}$ M, respectively (Table 1). Also, these three compounds showed slow association and fast dissociation in comparison with pyrogallol and catechol (Table 1). The binding kinetics for saffron (Figure 5), phloroglucinol (Figure 6), and tannic acid (Figure 7) with 1:1 fit clearly indicate almost similar association and dissociation rate constants, which perhaps suggests a similar mode of inhibition. The key component in saffron is crocin, reported as a potent inhibitor of tyrosinase.[32] Also, phloroglucinol ($IC_{50}$ > 300 $\mu$M) and tannic acid are reported as inhibitors of mushroom tyrosinase.[43,44] Inhibition of tannic acid is a reversible reaction.

The structural changes of the mushroom tyrosinase in the presence of inhibitors was studied by CD spectroscopy technique. As illustrated in Figure 8, there were significant

Table 2. Changes in Secondary Structure of MT in the Presence of Inhibitors

| | inhibitors | | | | | | | | | | | |
|---|---|---|---|---|---|---|---|---|---|---|---|---|
| | pyrogallol | | phloroglucinol | | tannic acid | | saffron | | catechol | |
| | 208 nm | 222 nm | 208 nm | 222 nm | 208 nm | 222 nm | 208 nm | 222 nm | 208 nm | 222 nm |
| % change | 21.97 ± 4.3 | 23.13 ± 4.16 | 78.03 ± 14.82 | 147 ± 29.4 | 60.41 ± 10.26 | 124.17 ± 24.83 | 9.63 ± 1.15 | 92.57 ± 16.6 | 73.87 ± 14.03 | 15.08 ± 2.41 |

differences in the secondary structure of the native enzyme and mushroom tyrosinase in the presence of inhibitors. CD studies also confirm the secondary structural changes analyzed using SPR. The percent changes in $\alpha$-helix in the presence of inhibitors are given in Table 2.

A number of tyrosinase inhibitors have earlier been reported to decrease hyperpigmentation resulting from the enzyme action. Most of these tyrosinase inhibitors were mono-, di-, and trihydroxylphenols, flavonoids, and peptides.[36,45] These reported activators and inhibitors are phenols and other common cosmetic ingredients well studied on mushroom tyrosinase.

The Biacore sensor has the ability to detect changes in protein conformation in addition to binding of inhibitors. Direct detection of low molecular weight analytes by SPR has been reported for binding of $Ca^{2+}$ ions to transglutaminase[46] and sulfonamide inhibitors to carbonic anhydrase.[47] The present study demonstrates for the first time direct detection of tyrosinase inhibitor binding using an SPR sensor. The study proves the ability of this sensor to screen the binding ability of different types of inhibitors toward mushroom tyrosinase at various concentrations and also to be used for the screening of new tyrosinase inhibitors. In addition, the sensor was relatively simple to make and did not require the use of antibodies to detect small-size inhibitors employed in the study. Once the enzyme is immobilized on the sensor surface, it will be useful for a long time through proper storage. Moreover, by immobilizing other enzymes or cell receptors of interest in the SPR sensor surface, their response on exposure to inhibitors and ligands can also be assessed, resulting in the development of novel and rapidly sensing biosensors. Other undesirable properties relate more to how the target and ligand interact. One such mechanism, recently described by McGovern et al.,[48,49] involves the formation of ligands into aggregates of 30−400 nm in diameter. These aggregates were proposed to inhibit either by absorption onto the surface of enzymes or by incorporating enzymes within them. Inhibitors acting in this manner were termed "promiscuous" inhibitors, as they appeared to inhibit a number of unrelated enzymes, although it is likely that there are other mechanisms by which compounds may inhibit numerous enzymes. McGovern et al.[48,49] identified and characterized a number of these promiscuous inhibitors by testing for properties that distinguished them from classical 1:1 reversible inhibitors.

In conclusion, pyrogallol, catechol, saffron, phloroglucinol, and tannic acid had anti-tyrosinase activity, but showed differences in their binding affinities for the tyrosinase. Therefore, this enzyme-based biosensor has the potential to be used in the detection and screening of new inhibitor drug candidates. Another advantage is that label-free interactions are more sensitive compared with the spectroscopic methods. Inhibitors may therefore have good potential as antibrowning agents to be applied in food industries as well as in cosmetics. The sensors can be used for high-throughput screening of potential pharmaceutical drug candidates.

## AUTHOR INFORMATION

### Corresponding Author

*(J.J.) Professor and Head, Department of Biotechnology, Shivaji University, Vidyanagar, Kolhapur 416004, India. E-mail: jpjbiochem@gmail.com. Phone: +91 231 2609365. Fax: +91 231 1691533.

### Funding

A BSR meritorious fellowship to S.P. from UGC, New Delhi, India, is gratefully acknowledged. J.J. thanks the Interdisciplinary Programme for Life Sciences sponsored by the Department of Biotechnology, government of India, under the DBT-IPLS program. All of the authors thank the Maharashtra state government for Golden Jubilee funding.

### Notes

The authors declare no competing financial interest.

## ■ ACKNOWLEDGMENTS

We are thankful to IIT − Mumbai for CD spectroscopy facility.

## ■ REFERENCES

(1) Yan, Q.; Cao, R.; Yi, W.; Chen, Z.; Wen, H.; Ma, L.; Song, H. Inhibitory effects of 5-benzylidene barbiturate derivatives on mushroom tyrosinase and their antibacterial activities. *Eur. J. Med. Chem.* **2009**, *44*, 4235−4243.

(2) Ando, H.; Kondoh, H.; Ichihashi, M.; Hearing, V. J. Approaches to identify inhibitors of melanin biosynthesis via quality control of tyrosinase. *J. Invest. Dermatol.* **2007**, *127*, 751−761.

(3) Mayer, A. M. Polyphenol oxidases in plants and fungi: going places? *Phytochemistry* **2006**, *67*, 2318−2331.

(4) Selinheimo, E.; NiEidhin, D.; Steffenson, C.; Nielson, J.; Lomascolo, A.; Halaouli, S.; Record, E.; O'Beirne, D.; Buchert, J.; Kruus, K. Comparison of the characteristics of fungal and plant tyrosinases. *J. Biotechnol.* **2007**, *130*, 471−480.

(5) Gandia-Herrero, F.; Escribano, J.; Garcia-Carmona, F. Betaxanthins as substrates for tyrosinase: an approach to the role of tyrosinase in the biosynthetic pathway of betalains. *Plant Physiol.* **2005**, *138*, 421−432.

(6) Yoruk, R.; Marshall, M. Physicochemical properties and function of plant polyphenol oxidase: a review. *J. Food Biochem.* **2003**, *27*, 361−422.

(7) Walker, J. R. L.; Ferrar, P. H. The control of enzymatic browning in foods. *Chem. Ind.* **1999**, *16*, 836−839.

(8) Kim, J.; Marshall, M. R.; Wei, C. Polyphenoloxidase. In *Sea Food Enzymes*; Haard, N. F., Simpson, B. K., Eds.; Dekker: New York, 2000; pp 271−315.

(9) Huang, X. H.; Chen, Q. X.; Wang, Q.; Song, K. K.; Wang, J.; Sha, L. Inhibition of the activity of mushroom tyrosinase by alkylbenzoic acids. *Food Chem.* **2006**, *94*, 1−6.

(10) Huang, X. H.; Chen, Q. X.; You, M. S.; Wang, Q.; Song, K. K.; Wang, J. Inhibitory effects of fluorobenzaldehydes on the activity of mushroom tyrosinase. *J. Enzyme Inhibition Med. Chem.* **2006**, *21*, 413−418.

(11) Wang, Q.; Shi, Y.; Song, K. K.; Guo, H. Y.; Qiu, L.; Chen, Q. X. Inhibitory effects of 4-halobenzoic acids on the diphenolase and monophenolase activity of mushroom tyrosinase. *Protein J.* **2004**, *23*, 303−308.

(12) Espin, J. C.; Wichers, H. J. Slow-binding inhibition of mushroom (*Agaricus bisporus*) tyrosinase isoforms by tropolone. *J. Agric. Food Chem.* **1999**, *47*, 2638−2644.

(13) Lee, Y. S.; Park, J. H.; Kim, M. H.; Seo, S. H.; Kim, H. J. Synthesis of tyrosinase inhibitory kojic acid derivative. *Arch. Pharm.* **2006**, *339*, 111−114.

(14) Jacobsohn, G. M.; Iskandar, R.; Jacobsohn, M. K. Activity of mushroom tyrosinase on catechol and on a catechol estrogen in an organic solvent. *Biochim. Biophys. Acta* **1993**, *1202*, 317−324.

(15) Fling, M.; Horowitz, N. H.; Heinemann, S. F. The isolation and properties of crystalline tyrosinase from *Neurospora*. *J. Biol. Chem.* **1963**, *238*, 2045−2053.

(16) Waite, J. H. Calculating extinction coefficients for enzymatically produced *o*-quinones. *Anal. Biochem.* **1976**, *75*, 211−218.

(17) Sussman, A. S. A comparison of the properties of two forms of tyrosinase from *Neurospora crassa*. *Arch. Biochem. Biophys.* **1961**, *95*, 407−415.

(18) Pfifferi, P. G.; Baldassari, L. A. Spectrophotometric method for the determination of the catecholase activity of tyrosinase by Besthorn's hydrazone. *Anal. Biochem.* **1973**, *52*, 325−335.

(19) Gauillard, F.; Richard-Forget, F.; Nicolas, J. New spectrophotometric assay for polyphenol oxidase activity. *Anal. Biochem.* **1993**, *215*, 59−65.

(20) Rezepecki, L. M.; Waite, J. H. A chromogenic assay for catecholoxidases based on the addition of L-proline to quinones. *Anal. Biochem.* **1989**, *179*, 375−381.

(21) Mayer, A. M.; Harel, E.; Ben-Shaul, R. Assay of catechol oxidsase − a critical comparison of methods. *Phytochemistry* **1966**, *5*, 783−789.

(22) Hu, X.; Leng, Z. Determination of cyanide using a tyrosinase amperometric biosensor with catechol as substrate. *Analyst* **1995**, *120*, 1555−1557.

(23) Besombes, J. L.; Cosnier, S.; Labbeâ, P.; Reverdy, G. A biosensor as warning device for the detection of cyanide, chlorophenols, atrazine and carbamate pesticides. *Anal. Chim. Acta* **1995**, *311*, 255−263.

(24) Macholan, L. Phenol-sensitive enzyme electrode with substrate cycling for quantification of certain inhibitory aromatic acids and thio compounds. *Collect. Czech. Chem. Commun.* **1990**, *55*, 2152−2160.

(25) Hasebe, Y.; Oshima, K.; Takise, O.; Uchiyama, S. Chemically amplified kojic acid responses of tyrosinase-based biosensor, based on inhibitory effect to substrate recycling driven by tyrosinase and L-ascorbic acid. *Talanta* **1995**, *42*, 2079−2085.

(26) Wang, J.; Nascimento, V. B.; Kane, S. A.; Rogers, K.; Smyth, M. R.; Angenes, L. Screen-printed tyrosinase-containing electrodes for the biosensing of enzyme inhibitors. *Talanta* **1996**, *43*, 1903−1907.

(27) Milkani, E.; Christopher, R.; Lambert, W.; Grant, M. G. Direct detection of acetylcholinesterase inhibitor binding with an enzyme-based surface plasmon resonance sensor. *Anal. Biochem.* **2011**, *408*, 212−219.

(28) Homola, J.; Yee, S. S.; Gauglitz, G. Surface plasmon resonance sensors: review. *Sens. Actuators, B* **1999**, *54*, 3−15.

(29) Germanas, J. P.; Wang, S.; Miner, A.; Hao, W.; Ready, J. M. Discovery of small-molecule inhibitors of tyrosinase. *Bioorg. Med. Chem. Lett.* **2007**, *17*, 6871−6875.

(30) Lee, H. Y.; Park, S. B. Surface modification for small-molecule microarrays and its application to the discovery of a tyrosinase inhibitor. *Mol. Biosyst.* **2011**, *7*, 304−310.

(31) Shi, Y.; Chen, Q.; Qin, W.; Song, K. K.; Qiu, L. Inhibitory effects of cinnamic acid and its derivatives on the diphenolase activity of mushroom (*Agaricus bisporus*) tyrosinase. *Food Chem.* **2005**, *92*, 707−712.

(32) Patil, S. A.; Sistla, S.; Jadhav, J. P. Evaluation of crocin and curcumin affinity on mushroom tyrosinase using surface plasmon resonance. *Biol. Macromol.* **2014**, *65*, 163−166.

(33) Karlsson, R.; Katsamba, P. S.; Nordin, H.; Pol, E.; Myszka, D. G. Analyzing a kinetic titration series using affinity biosensors. *Anal. Biochem.* **2006**, *349*, 136−147.

(34) William, P.; Carmelo, D. P. Simulated single-cycle kinetics improves the design of surface plasmon resonance assays. *Talanta* **2013**, *114*, 211−216.

(35) Yang, J. T.; Wu, C. S.; Martinez, H. M. Calculation of protein conformation from circular dichroism. *Methods Enzymol.* **1986**, *130*, 208−269.

(36) Kim, Y.; Uyama, H. Tyrosinase inhibitors from natural and synthetic sources: structure, inhibition mechanism and perspective for the future. *Cell. Mol. Life Sci.* **2005**, *62*, 1707−1723.

(37) Li, Z.; Huachen, L.; Yu, X.; Hu, Y.; Song, K.; Wangzhou, X.; Chen, Q. Inhibition kinetics of chlorobenzaldehyde thiosemicarbazones on mushroom tyrosinase. *J. Agric. Food Chem.* **2010**, *58*, 12537−12540.

(38) Fenoll, L.; Rodríguez-López, J.; García-Sevilla, F.; García-Ruiz, P.; Varón, R.; García-Cánovas, F. Analysis and interpretation of the action mechanism of mushroom tyrosinase on monophenols and diphenols generating highly unstable *o*-quinones. *Biochim. Biophys. Acta* **2001**, *1548*, 1−22.

(39) Han, P.; Chen, C.; Zhang, C.; Song, K.; Zhou, H.; Chen, Q. Inhibitory effects of 4-chlorosalicylic acid on mushroom tyrosinase and its antimicrobial activities. *Food Chem.* **2008**, *107*, 797−803.
(40) Streffer, K.; Kaatz, H.; Bauer, C. G.; Makower, A.; Schulmeister, T.; Scheller, F. W.; Peter, M. G.; Wollenberger, U. Application of a sensitive catechol detector for determination of tyrosinase inhibitors. *Anal. Chim. Acta* **1998**, *362*, 81−90.
(41) Munoz-Munoz, J. L.; Garcia-Molina, F.; Garcia-Ruiz, P. A.; Molina-Alarcon, M.; Tudela, J.; Garcia-Canovas, F.; Rodriguez-Lopez, J. N. Phenolic substrates and suicide inactivation of tyrosinase: kinetics and mechanism. *Biochem. J.* **2008**, *416*, 413−440.
(42) Munoz-Munoz, J. L.; Garcia-Molina, F.; Varon, R.; Garcia-Ruız, P. A.; Tudela, J.; Garcia-Canovas, F.; Rodrıguez-Lopez, J. N. Suicide inactivation of the diphenolase and monophenolase activities of tyrosinase. *IUBMB Life* **2010**, *62*, 539−547.
(43) Yoon, N. Y.; Eom, T. K.; Kim, M. M.; Kim, S. K. Inhibitory effect of phlorotannins isolated from *Ecklonia cava* on mushroom tyrosinase activity and melanin formation in mouse B16 f 10 melanoma cells. *J. Agric. Food Chem.* **2009**, *57*, 4124−4129.
(44) Xin, Q. L.; Hao, H.; Qingxi, C. The inhibitory effect on mushroom tyrosinase by tannic acid. *J. Xiaman Univ. Nat. Sci.* **2005**, *44*, 839−842.
(45) Song, Y. H. Why tyrosinase for treatment of melanoma. *Lancet* **1997**, *350*, 82−83.
(46) Gestwicki, J. E.; Hsieh, H. V.; Pitner, J. B. Using receptor conformational change to detect low molecular weight analytes by surface plasmon resonance. *Anal. Chem.* **2001**, *73*, 5732−5737.
(47) Myszka, D. G. Analysis of small-molecule interactions using Biacore S51 technology. *Anal. Biochem.* **2004**, *329*, 316−323.
(48) McGovern, S. L.; Caselli, E.; Grigorieff, N.; Shoichet, B. K. A common mechanism underlying promiscuous inhibitors from virtual and high-throughput screening. *J. Med. Chem.* **2002**, *45*, 1712−1722.
(49) McGovern, S. L.; Shoichet, B. K. Kinase inhibitors: not just for kinases anymore. *J. Med. Chem.* **2003**, *46*, 1478−1483.

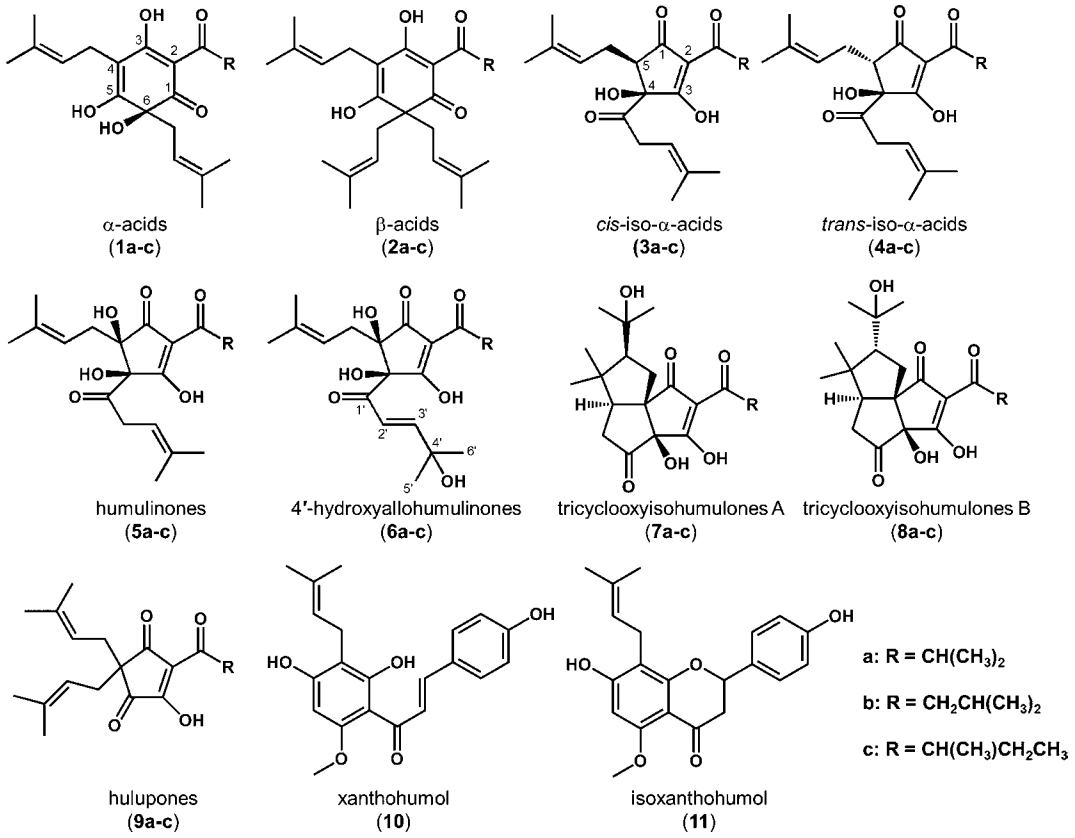


**Figure 1.** Structures of α-acids, cohumulone (**1a**), *n*-humulone (**1b**), and adhumulone (**1c**); β-acids, colupulone (**2a**), *n*-lupulone (**2b**), and adlupulone (**2c**); *cis*-iso-α-acids, *cis*-isocohumulone (**3a**), *cis*-iso-*n*-humulone (**3b**), and *cis*-isoadhumulone (**3c**); *trans*-iso-α-acids, *trans*-isocohumulone (**4a**), *trans*-iso-*n*-humulone (**4b**), and *trans*-isoadhumulone (**4c**); humulinones, cohumulinone (**5a**), *n*-humulinone (**5b**), and adhumulinone (**5c**); 4′-hydroxyallohumulinones, 4′-hydroxyallocohumulinone (**6a**), 4′-hydroxyallo-*n*-humulinone (**6b**), and 4′-hydroxyalloadhumulinone (**6c**); tricyclooxyisohumulones A, tricyclooxyisocohumulone A (**7a**), tricyclooxyiso-*n*-humulone A (**7b**), and tricyclooxyisoadhumulone A (**7c**); tricyclooxyisohumulones B, tricyclooxyisocohumulone B (**8a**), tricyclooxyiso-*n*-humulone B (**8b**), and tricyclooxyisoadhumulone B (**8c**); hulupones, cohulupone (**9a**), *n*-hulupone (**9b**), and adhulupone (**9c**); xanthohumol (**10**); and isoxanthohumol (**11**).

reported that the hard resin positively contributed to the foam stability of beer and produced a more pleasant bitter taste as opposed to the sharper bitterness of iso-α-acids. However, the hard-resin-enriched extracts used in the study were not subjected to rigorous chemical compositional analysis.[11] Thus, a suitable method to fully analyze the chemical composition of the hard resin was needed to properly examine its effect on the properties of beer. Furthermore, transformation of the hard-resin components during the wort boiling process, which is known to have a significant effect on beer taste, was not understood, except for the conversion of xanthohumol (**10**) into isoxanthohumol (**11**).[20] Knowledge of the transformation of hard-resin components during the wort boiling process is also essential to evaluate and optimize the effect of the hard resin on beer quality.

In our previous studies, we developed a high-performance liquid chromatography (HPLC) method suitable for investigation of the oxidation products in stored hops, which showed that α-acids are oxidized into humulinones (**5a**–**5c**), 4′-hydroxyallohumulinones (**6a**–**6c**), and tricyclooxyisohumulones A (**7a**–**7c**) and tricyclooxyisohumulones B (**8a**–**8c**) and that β-acids are oxidized into hulupones (**9a**–**9c**) (Figure 1).[21,22] These oxidation products are thought to be components in the soft or hard resins.

In this study, we analyzed the soft and hard resins derived from stored hops using our newly developed analytical method and clarified the existence of these oxidation compounds for the first time. We also investigated the transformation of the hard-resin components through wort boiling by using model boiling experiments and successively isolated and determined the structures of the transformation products. The concentration changes of these products and their precursors during the boiling process were also investigated.

## MATERIALS AND METHODS

**Chemicals and Materials.** The following chemicals were obtained commercially: ethylenediaminetetraacetic acid (EDTA), $H_3PO_4$, MeCN, EtOH, hexane, diethyl ether, and $CH_2Cl_2$ (Wako Pure Chemicals, Osaka, Japan) and xanthohumol and isoxanthohumol (Funakoshi, Tokyo, Japan). Deionized water for chromatography was purified by means of a Milli-Q Gradient A10 system (Millipore, Billerica, MA). Hop pellets, cultivar Hallertau Perle (HPE), were purchased from Hopsteiner (Mainburg, Germany).

**Preparation of Humulinones (5a–5c), Hulupones (9a–9c), Tricyclooxyiso-*n*-humulone A (7b), and Tricyclooxyiso-*n*-humulone B (8b).** Humulinones (**5a**–**5c**) and hulupones (**9a**–**9c**) were prepared according to a protocol reported previously.[21] Tricyclooxyiso-*n*-humulone A (**7b**) and tricyclooxyiso-*n*-humulone B (**8b**) were isolated from the autoxidation products of *n*-humulone.[22]

**Preparation of 4′-Hydroxyallohumulinones (6a–6c and 6c′) from Stored Hops.** Hop pellets (850 g) were stored at 60 °C for 120 h and extracted with $H_2O$ (8.5 L) at 50 °C for 1 h. The extract was filtered and then lyophilized to yield a brown powder (176 g). A portion of this powder (120 g) was dissolved in $H_2O$ (8.1 L) and

partitioned with $CH_2Cl_2$ (16.2 L) after adding 1 N HCl (810 mL) to the solution. The $CH_2Cl_2$ layer containing 4′-hydroxyallohumulinones was collected and dried over anhydrous $Na_2SO_4$ and concentrated to dryness *in vacuo* to give a yellowish brown oil (22 g). This oil was dissolved in EtOH and repeatedly subjected to preparative HPLC [column, 150 × 22 mm inner diameter, 5 μm, Alltima $C_{18}$ column (Systech, Tokyo, Japan); solvent, 100:1 (v/v) $H_2O/H_3PO_4$ (85%) (solvent A) and MeCN (solvent B), a linear gradient from 30 to 90% B in 0 → 40 min and 90% B for 40 → 45 min; flow rate, 18.8 mL/min; detector, 270 nm; and column temperature, room temperature] and divided into 11 fractions depending upon their elution times. Compounds **6a**, **6b**, and **6c**/**6c**′ were contained in fractions 3 ($t_R$, 8.6−9.5 min), 6 ($t_R$, 11.0−12.1 min), and 7 ($t_R$, 12.1−12.9 min), respectively. Compound **6a** in fraction 3 and compound **6b** in fraction 6 were further purified by repeatedly subjecting them to a second preparative HPLC step [column, 50 × 20 mm inner diameter, 5 μm, L-column 2 ODS (Chemicals Evaluation and Research Institute, Tokyo, Japan); solvent, 10 mM $NH_4HCO_3$ (solvent A) and MeCN (solvent B), isocratic elution at 20% B; flow rate, 9.5 mL/min; detector, 270 nm; and column temperature, 40 °C]. Compounds **6a** and **6b** were eluted at 3.8−4.7 and 5.5−7.5 min, respectively. Each eluate was immediately diluted 2 times with $H_2O$, adjusted to pH 2.0 with 1 N HCl, and partitioned with $CH_2Cl_2$ ($^1/_2$ volume of the diluted eluate, 2 times). The respective $CH_2Cl_2$ layer was dried over anhydrous $Na_2SO_4$ and concentrated to dryness to yield pure compounds **6a** (814 mg) and **6b** (1.2 g). Similarly, compounds **6c**/**6c**′ in fraction 7 were further purified by repeatedly subjecting them to a second preparative HPLC [column, 150 × 20 mm inner diameter, 5 μm, L-column 2 ODS (Chemicals Evaluation and Research Institute, Tokyo, Japan); solvent, 100 mM $NH_4HCO_3$ (solvent A) and MeCN (solvent B), isocratic elution at 20% B; flow rate, 18.8 mL/min; detector, 270 nm; and column temperature, room temperature]. Compounds **6c** and **6c**′ were eluted separately at 9.8−10.8 and 10.8−11.8 min, respectively. Pure compounds **6c** (40.3 mg) and **6c**′ (37.2 mg) were recovered from each eluate in the same way as that described for compounds **6a** and **6b**.

*4′-Hydroxyalloadhumulinone A (**6c**).* Pale yellow oil; $[\alpha]_D^{20}$, +4.01 (*c* 0.4, MeOH); $^1$H and $^{13}$C nuclear magnetic resonance (NMR) data, see Table 2; and high-resolution electrospray ionization mass spectrometry (HRESIMS) (negative), *m*/*z* 393.1916 $[M - H]^-$ (calcd for $C_{21}H_{29}O_7$, 393.1919).

*4′-Hydroxyalloadhumulinone B (**6c**′).* Pale yellow oil; $[\alpha]_D^{20}$, +12.1 (*c* 0.3, MeOH); $^1$H and $^{13}$C NMR data, see Table 2; and HRESIMS (negative), *m*/*z* 393.1914 $[M - H]^-$ (calcd for $C_{21}H_{29}O_7$, 393.1919).

**Preparation of Soft and Hard Resins.** Soft and hard resins from hops were prepared according to Analytica-EBC,[3] with some modification.

Hop pellets (100 g) were stored at 60 °C for 48 h, and a portion (10 g) was extracted with MeOH (100 mL) by stirring at room temperature for 1 h and then filtered. The filtrate was kept at 4 °C for 1 day, and a waxy precipitate that formed was removed by filtration. To a portion of the filtrate (20 mL), MeOH (10 mL), hexane (80 mL), and 1 N HCl (20 mL) were added, and the two-layer solution (hexane/acidic MeOH/$H_2O$) was partitioned in a separating funnel. The hexane layer, prepared by repeating the above partition 4 times (320 mL), was evaporated to dryness to give a yellowish brown oil (250 mg, soft resin).

The residual acidic MeOH/$H_2O$ layer was partitioned with diethyl ether (80 mL, 2 times). The diethyl ether layer (160 mL) was washed with saturated NaCl solution (160 mL), dried over anhydrous $Na_2SO_4$, and concentrated to dryness to give a brown solid (200 mg, hard resin).

**Boiling Test for the Hard Resin.** To 500 μL of 10 mM citrate buffer (pH 5.5) preheated to 100 °C was added a 25 μL solution of the hard resin in EtOH (5.0 mg/mL). The combined solution was kept at 100 °C and analyzed by HPLC at 30, 60, 90, and 120 min.

**Boiling Test of 4′-Hydroxyallohumulinones (6a−6c and 6c′).** To a 500 μL aliquot of 10 mM citrate buffer (pH 5.5) preheated to 100 °C was added a 25 μL solution of either 4′-hydroxyallocohumulinone (**6a**), 4′-hydroxyallo-*n*-humulinone (**6b**), 4′-hydroxyalloadhumulinone A (**6c**), or 4′-hydroxyalloadhumulinone B (**6c**′) (1.0 mg/mL in EtOH). Each combined solution was kept at 100 °C and analyzed by HPLC at 30, 60, 90, and 120 min.

**Isolation of the Transformation Products Produced by Boiling of 4′-Hydroxyallocohumulinone (6a) and 4′-Hydroxyallo-*n*-humulinone (6b).** 4′-Hydroxyallocohumulinone (**6a**) (200 mg) was dissolved in EtOH (50 mL), added to 10 mM citrate buffer (pH 5.5, 1 L) preheated to 100 °C, and maintained at this temperature for 90 min. After cooling to room temperature, the solution was acidified with 1 N HCl (100 mL) and partitioned with $CH_2Cl_2$ (250 mL, 3 times). The $CH_2Cl_2$ layer (750 mL) was washed with saturated NaCl solution (400 mL), dried over anhydrous $Na_2SO_4$, and concentrated to dryness to give a yellowish brown oil (150 mg).

The oil was dissolved in EtOH and repeatedly subjected to preparative HPLC [column, 150 × 10 mm inner diameter, 5 μm, Alltima $C_{18}$ column (Systech, Tokyo, Japan); solvent, 100:1 (v/v) $H_2O/H_3PO_4$ (85%) (solvent A) and MeCN (solvent B), a linear gradient from 30% B for 0 → 15 min, from 30 to 90% B in 15 → 18 min, and 90% B for 18 → 22 min; flow rate, 4.7 mL/min; detector, 270 nm; and column temperature, 40 °C]. In this preparative HPLC, 4′-hydroxyallo-*cis*-cohumulinone (**12a**) was eluted at 8.6−10.0 min and *cis*-oxycohumulinic acid (**13a**) was eluted at 10.0−10.6 min. Each eluate was diluted with $H_2O$ to lower the concentration of MeCN to less than 10% and extracted with $CH_2Cl_2$ ($^1/_4$ volume of the diluted eluate, 3 times). The $CH_2Cl_2$ layer was dried over anhydrous $Na_2SO_4$ and concentrated to dryness to yield compounds **12a** (33.4 mg) and **13a** (4.0 mg).

The transformation products (**12b** and **13b**) of 4′-hydroxyallo-*n*-humulinone (**6b**) were prepared and purified in almost the same way as described for compounds **12a** and **13a**. In summary, 4′-hydroxyallo-*n*-humulinone (**6b**) (200 mg) was boiled and partitioned between $CH_2Cl_2$ and acidic $H_2O$. The $CH_2Cl_2$ layer was concentrated to give an oil (167 mg). The oil was repeatedly subjected to preparative HPLC [column, flow rate, detector, and column temperature are identical to those used for the isolation of compounds **12a** and **13a**; solvent, 100:1, (v/v) $H_2O/H_3PO_4$ (85%) (solvent A) and MeCN (solvent B), a linear gradient from 30 to 48% B in 0 → 12 min, from 48 to 90% B in 12 → 18 min, and 90% B for 18 → 21 min]. In this preparative HPLC, 4′-hydroxyallo-*cis*-*n*-humulinone (**12b**) and *cis*-oxy-*n*-humulinic acid (**13b**) were eluted at 9.0−9.6 and 10.0−10.3 min, respectively. Pure compounds **12b** (41.3 mg) and **13b** (5.9 mg) were recovered from each eluate in the same way as described for compounds **12a** and **13a**.

*4′-Hydroxyallo-cis-cohumulinone (**12a**).* Pale yellow oil; $[\alpha]_D^{20}$, ±0 (*c* 0.7, MeOH); $^1$H and $^{13}$C NMR data, see Table 1; and HRESIMS (negative), *m*/*z* 379.1753 $[M - H]^-$ (calcd for $C_{20}H_{27}O_7$, 379.1762).

*4′-Hydroxyallo-cis-n-humulinone (**12b**).* Pale yellow oil; $[\alpha]_D^{20}$, ±0 (*c* 0.4, MeOH); $^1$H and $^{13}$C NMR data, see Table 1; and HRESIMS (negative), *m*/*z* 393.1911 $[M - H]^-$ (calcd for $C_{21}H_{29}O_7$, 393.1919).

*cis-Oxycohumulinic Acid (**13a**).* White, amorphous solid; $[\alpha]_D^{20}$, ±0 (*c* 0.1, MeOH); $^1$H and $^{13}$C NMR data, see Table 1; and HRESIMS (negative), *m*/*z* 267.1230 $[M - H]^-$ (calcd for $C_{14}H_{19}O_5$, 267.1238).

*cis-Oxy-n-humulinic Acid (**13b**).* Pale yellow oil; $[\alpha]_D^{20}$, ±0 (*c* 0.1, MeOH); $^1$H and $^{13}$C NMR data, see Table 1; and HRESIMS (negative), *m*/*z* 281.1390 $[M - H]^-$ (calcd for $C_{15}H_{21}O_5$, 281.1395).

**Preparation of *cis*-Oxy-*n*-humulinic Acid (13b) and *trans*-Oxy-*n*-humulinic Acid (14b) by Hydrolysis of *n*-Humulinone (5b).** Both *cis*- and *trans*-oxy-*n*-humulinic acids were prepared by alkaline hydrolysis of *n*-humulinone (**5b**) according to the previous report,[23] with some modification.

*n*-Humulinone was prepared according to a protocol reported previously.[21] To 2 M aqueous NaOH (300 mL) preheated at 100 °C, 30 mL of solution of *n*-humulinone in MeOH (10 mg/mL) was added and mixed well. The temperature was maintained at 100 °C for 10 min before cooling the solution to room temperature, acidifying with 6 N HCl (120 mL), and partitioning with $CH_2Cl_2$ (200 mL, 2 times). The $CH_2Cl_2$ layer was dried over anhydrous $Na_2SO_4$ and concentrated to dryness to give a yellow oil (270 mg). The oil was dissolved in EtOH and repeatedly subjected to preparative HPLC [column, 150 × 22 mm inner diameter, 5 μm, Alltima $C_{18}$ column (Systech, Tokyo, Japan);

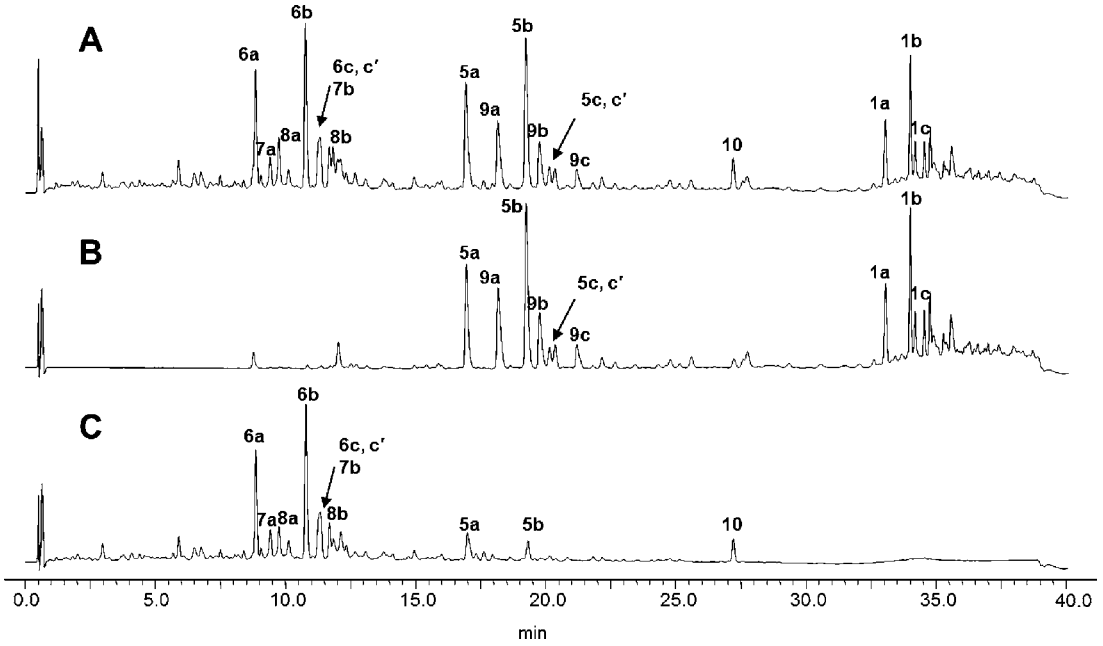


**Figure 2.** HPLC chromatograms of the (A) MeOH extract of hops stored at 60 °C for 48 h, (B) soft-resin fraction prepared from the MeOH extract, and (C) hard-resin fraction prepared from the MeOH extract. Structures of the compounds are given in Figures 1 and 6.

solvent, 100:1 (v/v) $H_2O/H_3PO_4$ (85%) (solvent A) and MeCN (solvent B), isocratic elution at 45% B; flow rate, 22.8 mL/min; detector, 270 nm; and column temperature, room temperature]. In this preparative HPLC, *cis*-oxy-*n*-humulinic acid (**13b**) and *trans*-oxy-*n*-humulinic acid (**14b**) were eluted at 5.1−5.5 and 6.7−7.2 min, respectively. Pure compounds **13b** (74.6 mg) and **14b** (94.6 mg) were recovered from each eluate in the same way as described for compounds **12a** and **13a**.

*trans-Oxy-n-humulinic Acid (**14b**).* White, amorphous solid; $[\alpha]_D^{20}$, ±0 (*c* 0.3, MeOH); $^1H$ and $^{13}C$ NMR data, see Table 1; and HRESIMS (negative), *m/z* 281.1389 $[M - H]^-$ (calcd for $C_{15}H_{21}O_5$, 281.1395).

**HPLC.** A Shimadzu Prominence UFLC system (Shimadzu, Kyoto, Japan) was used for all HPLC analyses. Data were processed with LCsolution software (Shimadzu, Kyoto, Japan).

HPLC analyses were performed to investigate the constituents in the soft and hard resins of hops and to analyze compositional changes in the hard-resin components in the boiling tests using the following conditions:[21,22] column, 100 × 2.1 mm inner diameter, 3 μm, Alltima $C_{18}$ column (Systech, Tokyo, Japan); solvent, 1000:0.2 (v/v) $H_2O/H_3PO_4$ (85%) containing EDTA (0.02%, w/v) (solvent A) and MeCN (solvent B), a linear gradient from 10 to 52% B in 0 → 26.7 min, 52% B for 26.7 → 30 min, from 52 to 75% B in 30 → 32.7 min, from 75 to 85% B in 32.7 → 36.7 min, and 85% B for 36.7 → 37.7 min; flow rate, 0.6 mL/min; detector, 270 nm; and column temperature, 40 °C. The injection volume was 3.0 μL. In the boiling tests, transformation products were quantified using isolated reference compounds. 4′-Hydroxyallo-*cis*-adhumulinone A (**12c**) and 4′-hydroxyallo-*cis*-adhumulinone B (**12c′**) were quantified using the calibration curve of 4′-hydroxyallo-*cis*-*n*-humulinone (**12b**), and *cis*-oxyadhumulinic acid A (**13c**) and *cis*-oxyadhumulinic acid B (**13c′**) were quantified using the calibration curve of *cis*-oxy-*n*-humulinic acid (**13b**).

To separate and check the purity of 4′-hydroxyalloadhumulinone A (**6c**) and 4′-hydroxyalloadhumulinone B (**6c′**) by HPLC (Figure 7), the following LC conditions were used: column, 100 × 2.1 mm inner diameter, 3 μm, L-column 2 ODS (Chemicals Evaluation and Research Institute, Tokyo, Japan); solvent, 5 mM $HCOONH_4$ (pH 8.5) (solvent A) and MeCN (solvent B), a linear gradient from 10 to 36% B in 0 → 39 min, from 36 to 80% B in 39 → 44 min, and 80% B for 44 → 52 min; flow rate, 0.25 mL/min; detector, 270 nm; and column temperature, 40 °C. The injection volume was 3.0 μL.

**HRESIMS.** HRESIMS of the purified compounds was measured using a Thermo Scientific LTQ Orbitrap mass spectrometer (Thermo Fisher Scientific, San Jose, CA). Before the samples were measured, accurate mass calibration was carried out using polytyrosine-1,3,6 as a mass standard (CS Bio Company, Menlo Park, CA).

**NMR.** $^1H$, $^{13}C$, and 2D NMR spectra were measured with a Bruker AVANCE400 spectrometer (Bruker BioSpin, Rheinstetten, Germany). Samples were dissolved in methanol-$d_4$. Chemical shifts were referenced to the solvent signals ($\delta_H/\delta_C$, 3.30/49.0). Data processing was performed using TopSpin-NMR software (version 3.0) (Bruker BioSpin). *J*-Resolved heteronuclear multiple-bond correlation (HMBC) experiments were conducted on a Varian INOVA-500 NMR spectrometer (Agilent, Santa Clara, CA) using the previously reported method.[24]

## RESULTS AND DISCUSSION

**Identification of the Components in the Soft and Hard Resins Derived from Stored Hops.** Recently, we reported the transformation of α-acids to humulinones (humulinones were further transformed to 4′-hydroxyallohumulinones) and to tricyclooxyisohumulones A and B because of oxidation.[21,22] During these studies, we also developed a HPLC method that is suitable for the analysis of α- and β-acid-derived oxidation compounds.[21,22] Using this HPLC method, we analyzed a MeOH extract of the stored hops and soft and hard resins prepared from the MeOH extract. The results are shown in Figure 2 (Figure 2A, MeOH extract of the stored hops; Figure 2B, soft resin; and Figure 2C, hard resin).

As shown in Figure 2B, the presence of humulinones (**5a**−**5c** and **5c′**) and hulupones (**9a**−**9c**) in addition to α-acids (**1a**−**1c**) in the soft resin can clearly be observed. This is the first study reporting the presence of humulinones (**5a**−**5c** and **5c′**) and hulupones (**9a**−**9c**) in soft resin.

The compounds contained in the soft resin were barely detectable in the hard resin (Figure 2C). Indeed, xanthohumol (**10**) and the hydrophilic α-acid-derived oxidation products, such as tricyclooxyisohumulones A (**7a** and **7b**) and tricyclooxyisohumulones B (**8a** and **8b**) and 4′-hydroxyallohumulinones (**6a**−**6c** and **6c′**), were found only in the hard-resin

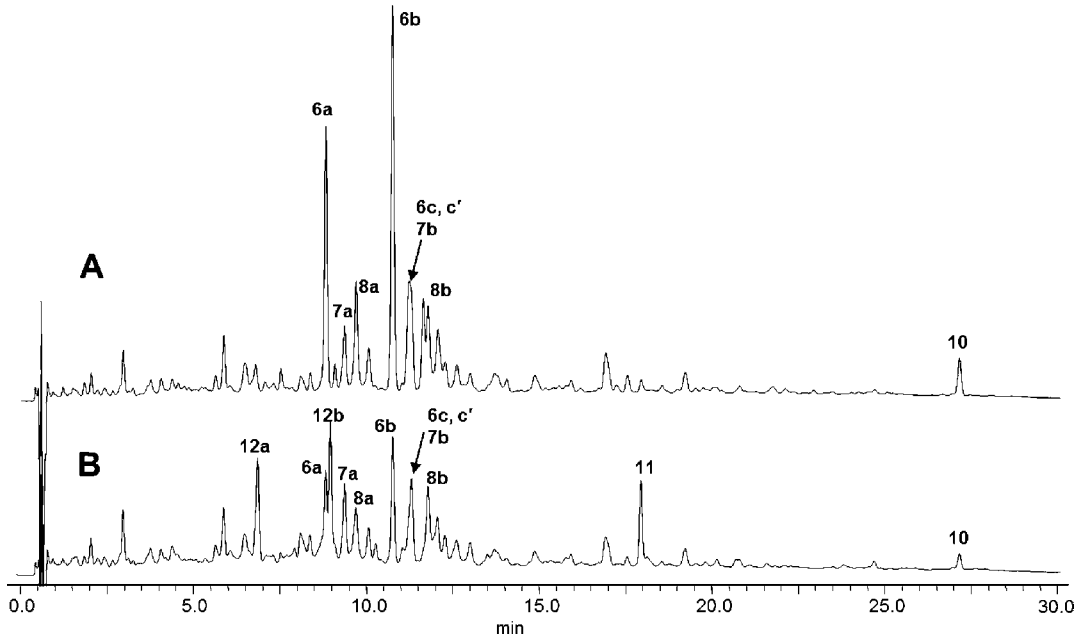


**Figure 3.** HPLC chromatograms of the hard resin (A) before and (B) after boiling in an aqueous buffer (pH 5.5) for 90 min. Structures of the compounds are given in Figures 1, 5, and 6.

extract. This is the first study to report the existence of these $\alpha$-acid-derived oxidation products in hard resin.

These findings also verify changes in the composition of the soft- and hard-resin constituents of hops caused by oxidation, because the concentration changes in $\alpha$- and $\beta$-acid-derived oxidation products in soft and hard resins detected in this study during oxidation of hops have been clarified in our previous studies.[21,22]

**Transformation of the Constituents of Hard Resin during the Wort Boiling Process.** There has been little reported data on the compositional changes in hard resin during the wort boiling process. Thus, we investigated the constituents in the hard resin after wort boiling. Changes in the chemical composition of hard-resin constituents were determined using a model boiling experiment conducted in an aqueous buffer (pH 5.5). HPLC analysis of the hard resin after 90 min of boiling (Figure 3B) clearly showed the transformation of xathohumol (**10**) into isoxanthohumol (**11**), which was reported previously.[20] In addition, the HPLC analysis also detected a decrease in the concentration of 4′-hydroxyallohumulinones [4′-hydroxyallocohumulinone (**6a**), 4′-hydroxyallo-*n*-humulinone (**6b**), and 4′-hydroxyalloadhumulinone (**6c**/**6c**′)] and the appearance of some new compounds (Figure 3B). These findings suggested, for the first time, further transformation of 4′-hydroxyallohumulinones in the hard resin during the wort boiling process.

**Isolation and Structural Elucidation of the Transformation Products of 4′-Hydroxyallocohumulinone (6a) and 4′-Hydroxyallo-*n*-humulinone (6b).** To verify the transformation of 4′-hydroxyallohumulinones into new compounds, isolated 4′-hydroxyallocohumulinone (**6a**) and 4′-hydroxyallo-*n*-humulinone (**6b**) were boiled in the same buffer. The HPLC analyses clearly showed the transformation of compound **6a** into compounds **12a** and **13a** (panels A1 and A2 of Figure 4) and compound **6b** into compounds **12b** and **13b** (panels B1 and B2 of Figure 4). We also boiled tricyclooxyiso-*n*-humulone A (**7b**) and tricyclooxyiso-*n*-humulone B (**8b**), but the compounds were stable (i.e., unchanged) under these conditions (data not shown).

To identify the transformation products of 4′-hydroxyallocohumulinone (**6a**) and 4′-hydroxyallo-*n*-humulinone (**6b**), each 200 mg sample of isolated compounds **6a** and **6b** was subjected to the boiling test. The compounds in the reaction products were purified using a two-phase solvent partition and preparative ODS HPLC, affording compounds **12a** (33.4 mg) and **13a** (4.0 mg) from compound **6a** and compounds **12b** (41.3 mg) and **13b** (5.9 mg) from compound **6b**.

Compound **12b** was obtained as a pale yellow oil. The HRESIMS data showed a $[M - H]^-$ ion at $m/z$ 393.1911 and, together with the $^{13}C$ NMR data, indicated a molecular formula of $C_{21}H_{30}O_7$, which is identical to that of compound **6b**. Analysis of the $^1H$ and $^{13}C$ NMR, $^1H-^1H$ correlation spectroscopy (COSY), heteronuclear multiple-quantum coherence (HMQC), and HMBC spectra of compound **12b** in methanol-$d_4$ established that compounds **12b** and **6b** possessed the same planar structure, whereas the $^{13}C$ NMR chemical shifts of C-5 and C-1″ were different between compounds **12b** [$\delta$ 85.1 (C-5) and 36.7 (C-1″)] and **6b** [$\delta$ 81.6 (C-5) and 31.3 (C-1″)][21] (Table 1). Furthermore, the nuclear Overhauser effect (NOE) observed between H-2′ and H-1″ in compound **6b**[21] was not observed in compound **12b**. From these results, compound **12b** was determined to be the C-5 epimer of compound **6b** and named 4′-hydroxyallo-*cis*-*n*-humulinone, which has not been previously reported (Figure 5).

Compound **13b** was obtained as a pale yellow oil. The HRESIMS data showed a $[M - H]^-$ ion at $m/z$ 281.1390 and, together with the $^{13}C$ NMR data, indicated a molecular formula of $C_{15}H_{22}O_5$ (**12b**$-C_6H_8O_2$). Analysis of the $^1H$ and $^{13}C$ NMR, $^1H-^1H$ COSY, HMQC, and HMBC spectra of compound **13b** in methanol-$d_4$ established that the *trans*-4-hydroxy-4-methyl-2-pentenosyl side chain attached at C-4 in compound **12b** was absent in compound **13b** (Table 1). Thus, the planar structure of compound **13b** was determined as oxy-*n*-humulinic acid (Figure 5). To determine relative configurations at C-4 and C-5 in compound **13b**, we prepared *cis*- and *trans*-oxy-*n*-humulinic

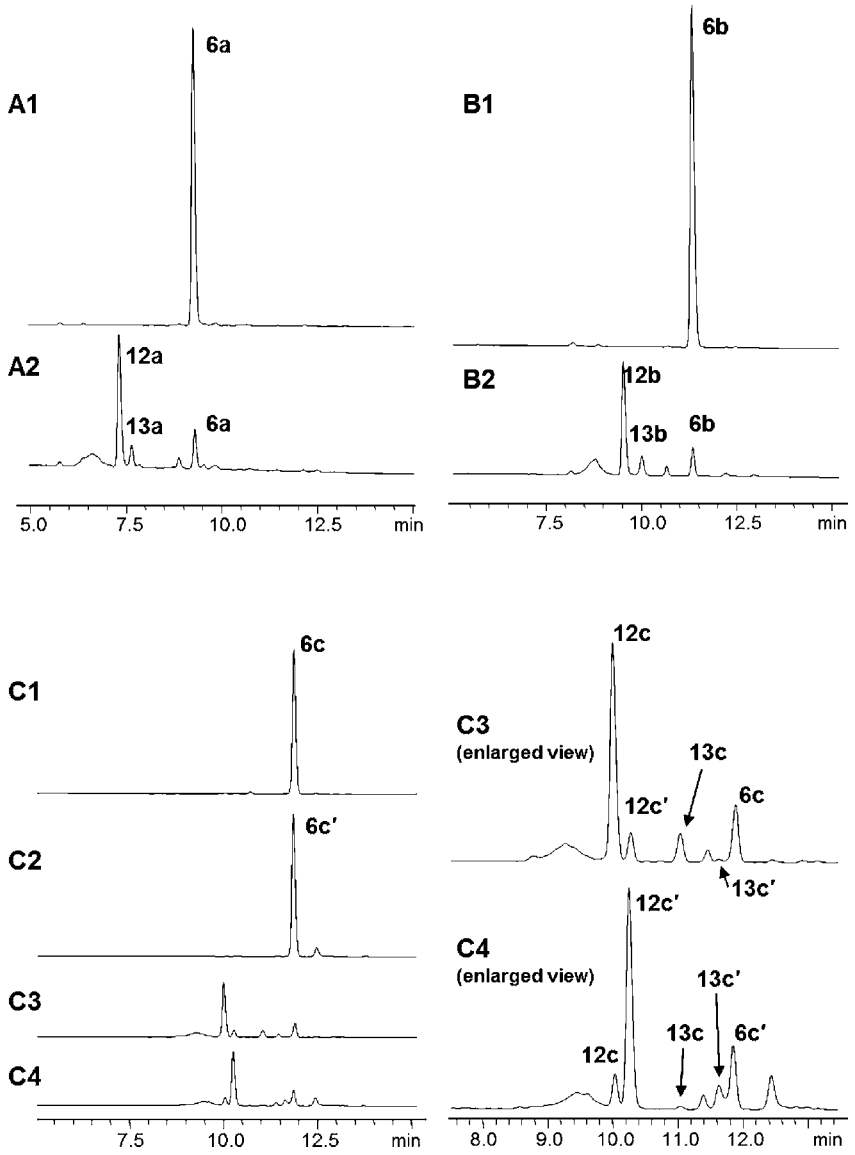


**Figure 4.** HPLC chromatograms of the isolated compounds before and after boiling in an aqueous buffer (pH 5.5) for 90 min. 4′-Hydroxyallocohumulinone (**6a**) (A1) before and (A2) after boiling, 4′-hydroxyallo-*n*-humulinone (**6b**) (B1) before and (B2) after boiling, and 4′-hydroxyalloadhumulinone A (**6c**) and 4′-hydroxyalloadhumulinone B (**6c′**) (C1 and C2, respectively) before and (C3 and C4, respectively) after boiling.

acids (epimers at C-5) by alkaline hydrolysis of *n*-humulinone (**5b**)[23] as a mixture and then isolated each isomer using preparative ODS HPLC. By $^{1}H$ and $^{13}C$ NMR analyses (Table 1), one of the two isomeric compounds was identified to be compound **13b**, and thus, the other (**14b**) was determined to be the C-5 epimer of compound **13b**. In the nuclear Overhauser effect spectroscopy (NOESY) experiments on compounds **13b** and **14b**, the NOE between H-4 and H-1″ (prenyl $CH_2$ attached at C-5) was clearly observed in compound **14b** but was barely detected in compound **13b** (see Figure S1 of the Supporting Information). Furthermore, *J*-resolved HMBC experiments[24] on compounds **13b** and **14b** showed that the absolute value of the two-bond $^{13}C-^{1}H$ coupling constant between H-4 and C-5 was greater in compound **13b** than in compound **14b** [$^{2}J$(C5, 4H) = 5.9 Hz in compound **13b**, and $^{2}J$(C5, 4H) $\leq$ 3.0 Hz in compound **14b**] (see Figure S2 of the Supporting Information), indicating a larger dihedral angle between H-4 and 5-OH in compound **14b** than compound **13b**.[25] These observations clearly indicated that H-4 and 5-OH were in the $\alpha$-orientation in compound **13b** and that H-4 and the prenyl group attached at C-5 were in the $\alpha$-orientation in compound **14b**. Thus, compound **13b** was determined as *cis*-oxy-*n*-humulinic acid, and compound **14b** was determined as *trans*-oxy-*n*-humulinic acid (Figure 5). Although the structures of compounds **13b** and **14b** were reported about 50 years ago,[23] we present their NMR data for the first time (Table 1).

Compound **12a** was obtained as a pale yellow oil. The HRESIMS data showed a $[M - H]^-$ ion at *m*/*z* 379.1753 and, together with the $^{13}C$ NMR data, indicated a molecular formula of $C_{20}H_{28}O_7$, which was the same as for compound **6a**. Analysis of the $^{1}H$ and $^{13}C$ NMR, $^{1}H-^{1}H$ COSY, HMQC, and HMBC spectra established that compound **12a** possessed an isobutyryl side chain at C-2 instead of an isovaleryl side chain in compound **12b** (Table 1). Thus, compound **12a** was identified


dx.doi.org/10.1021/jf504394h | J. Agric. Food Chem. 2014, 62, 11602−11612

Table 1. NMR Spectroscopic Data (400 MHz, Methanol-$d_4$) for Compounds 12a, 12b, 13a, 13b, and 14b[a]

| | 12a | | 12b | | 13a | | 13b | | 14b | |
|---|---|---|---|---|---|---|---|---|---|---|
| position | $\delta_C$, type | $\delta_H$, mult. ($J$ in Hz) | $\delta_C$, type | $\delta_H$, mult. ($J$ in Hz) | $\delta_C$, type | $\delta_H$, mult. ($J$ in Hz) | $\delta_C$, type | $\delta_H$, mult. ($J$ in Hz) | $\delta_C$, type | $\delta_H$, mult. ($J$ in Hz) |
| 1 | 200.9, C | | 201.6, C | | 199.6, C | | 200.2, C | | 200.5, C | |
| 2 | 113.3, C | | 114.1, C | | 111.6, C | | 112.6, C | | 112.8, C | |
| 3 | 195.4, C | | 196.0, C | | 197.8, C | | 198.3, C | | 199.8, C | |
| 4 | 92.0, C | | 92.3, C | | 80.6, CH | 4.35, s | 80.9, CH | 4.35, s | 74.2, CH | 4.14, s |
| 5 | 84.9, C | | 85.1, C | | 82.2, C | | 82.4, C | | 77.7, C | |
| 1′ | 198.2, C | | 198.3, C | | | | | | | |
| 2′ | 121.9, CH | 6.78, d (15.5) | 121.9, CH | 6.79, d (15.5) | | | | | | |
| 3′ | 155.9, CH | 6.92, d (15.5) | 156.0, CH | 6.92, d (15.5) | | | | | | |
| 4′ | 71.4, C | | 71.4, C | | | | | | | |
| 5′ | 29.1, $CH_3$ | 1.27, s | 29.1, $CH_3$ | 1.28, s | | | | | | |
| 6′ | 29.1, $CH_3$ | 1.29, s | 29.1, $CH_3$ | 1.29, s | | | | | | |
| 1″ | 36.79, $CH_2$ | 2.63, dd (13.9, 8.7) | 36.7, $CH_2$ | 2.62, dd (14.0, 8.5) | 34.8, $CH_2$ | 2.61, dd (13.5, 9.2) | 34.8, $CH_2$ | 2.60, dd (13.6, 9.1) | 34.6, $CH_2$ | 2.54, dd (14.0, 7.7) |
| | | 2.48, dd (13.9, 6.6) | | 2.45, dd (14.0, 6.7) | | 2.45, dd (13.5, 6.4) | | 2.43, dd (13.6, 6.4) | | 2.48, dd (14.0, 6.9) |
| 2″ | 119.1, CH | 5.10, m | 119.0, CH | 5.10, m | 119.3, CH | 5.03, m | 119.2, CH | 5.02, m | 118.3, CH | 5.03, m |
| 3″ | 136.6, C | | 136.6, C | | 136.5, C | | 136.4, C | | 137.6, C | |
| 4″ | 17.9, $CH_3$ | 1.52, s | 17.9, $CH_3$ | 1.53, s | 17.8, $CH_3$ | 1.52, s | 17.9, $CH_3$ | 1.52, s | 18.1, $CH_3$ | 1.65, s |
| 5″ | 26.2, $CH_3$ | 1.60, s | 26.2, $CH_3$ | 1.61, s | 26.1, $CH_3$ | 1.58, s | 26.1, $CH_3$ | 1.58, s | 26.1, $CH_3$ | 1.68, s |
| 1‴ | 203.5, C | | 197.8, C | | 205.2, C | | 199.9, C | | 201.9, C | |
| 2‴ | 36.75, CH | 3.50, sep (6.9) | 46.6, $CH_2$ | 2.74, dd (13.6, 7.2) | 37.3, CH | 3.49, sep (6.9) | 47.7, $CH_2$ | 2.77, dd (13.8, 7.0) | 48.4, $CH_2$ | 2.78, dd (14.5, 7.0) |
| | | | | 2.69, dd (13.6, 7.2) | | | | 2.64, dd (13.8, 7.1) | | 2.73, dd (14.5, 6.9) |
| 3‴ | 18.0, $CH_3$ | 1.10, d (6.9) | 27.6, CH | 2.11, m | 17.8, $CH_3$ | 1.09, d (6.9) | 27.1, CH | 2.11, m | 26.7, CH | 2.13, m |
| 4‴ | 18.6, $CH_3$ | 1.14, d (6.9) | 22.86, $CH_3$ | 0.95, d (6.7) | 18.7, $CH_3$ | 1.12, d (6.9) | 22.8, $CH_3$ | 0.94, d (6.2) | 22.8, $CH_3$ | 0.96, d (6.7) |
| 5‴ | | | 22.94, $CH_3$ | 0.97, d (6.7) | | | 22.9, $CH_3$ | 0.96, d (6.2) | 22.9, $CH_3$ | 0.96, d (6.7) |

[a]Arbitrary numbering according to structures **12a**, **12b**, **13a**, **13b**, and **14b** shown in Figure 5.



dx.doi.org/10.1021/jf504394h | J. Agric. Food Chem. 2014, 62, 11602−11612

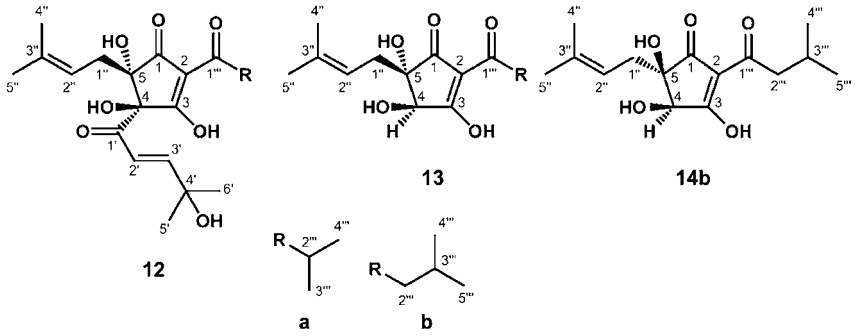


**Figure 5.** Chemical structures of 4′-hydroxyallo-*cis*-cohumulinone (**12a**), 4′-hydroxyallo-*cis*-*n*-humulinone (**12b**), *cis*-oxycohumulinic acid (**13a**), *cis*-oxy-*n*-humulinic acid (**13b**), and *trans*-oxy-*n*-humulinic acid (**14b**).

as 4′-hydroxyallo-*cis*-cohumulinone, which has not been previously reported (Figure 5).

Compound **13a** was obtained as a white, amorphous solid. The HRESIMS data showed a $[M - H]^-$ ion at *m*/*z* 267.1230 and, together with the $^{13}C$ NMR data, indicated a molecular formula of $C_{14}H_{20}O_5$ (**12a**−$C_6H_8O_2$). Analysis of the $^1H$ and $^{13}C$ NMR, $^1H$−$^1H$ COSY, HMQC, and HMBC spectra established that compound **13a** also possessed an isobutyryl side chain at C-2 instead of an isovaleryl side chain in compound **13b** (Table 1). Thus, compound **13a** was identified as *cis*-oxycohumulinic acid, which has not been previously reported (Figure 5).

Compounds **12a**, **12b**, **13a**, and **13b** were determined to be racemates because none of these compounds showed optical activity. Moreover, compounds **12a**, **12b**, **13a**, and **13b** were formed via a simple thermal reaction in aqueous solution from the precursors **6a** and **6b**, which do exist as racemates.[21]

**Analyses of the Transformation Products of 4′-Hydroxyalloadhumulinone (6c/6c′).** Adhumulinone, a precursor of 4′-hydroxyalloadhumulinone, is a mixture of two diastereomers (**5c** and **5c′**) (Figure 6).[21] Thus, 4′-hydroxyalloadhumulinone in hard resin is also a mixture of two diastereomers (**6c** and **6c′**) (Figure 6). Although ODS HPLC analysis using an acidic buffer could not separate the diastereomers (**6c** and **6c′**) (panels C1 and C2 of Figure 4), we successfully separated them through ODS HPLC analysis using a basic buffer (Figure 7). By employing a mobile phase containing the basic buffer, we isolated each diastereomer successively and named the former eluate in analytical HPLC ($t_R$, 16.6 min) as 4′-hydroxyalloadhumulinone A (**6c**) and the latter eluate ($t_R$, 17.5 min) as 4′-hydroxyalloadhumulinone B (**6c′**) (Figure 7). The $^1H$ and $^{13}C$ NMR data of compounds **6c** and **6c′** were almost identical (Table 2), and we could not analyze the respective stereochemistries of compounds **6c** and **6c′**.

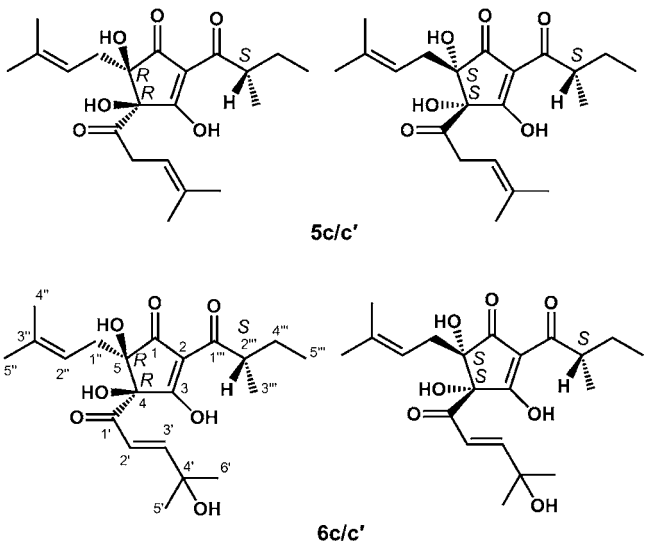


**Figure 6.** Chemical structures of adhumulinone diastereomers (**5c** and **5c′**) and 4′-hydroxyalloadhumulinones A and B (**6c** and **6c′**).

The yield of isolated compounds **6c** and **6c′** was too low to enable the separation of their transformation products in the boiling tests and perform structural determination by NMR analyses. Thus, we tentatively identified compound **12c** (main transformed product of compound **6c**) as 4′-hydroxyallo-*cis*-adhumulinone A and compound **13c** (minor transformed product of compound **6c**) as *cis*-oxyadhumulinic acid A, by comparison to the transformation products from 4′-hydroxyallocohumulinone (**6a**) and 4′-hydroxyallo-*n*-humulinone (**6b**) (Figure 4C3). Similarly, compounds **12c′** and **13c′** (transformed products of compound **6c′**) were tentatively identified as 4′-hydroxyallo-*cis*-adhumulinone B and *cis*-oxy-adhumulinic acid B, respectively (Figure 4C4).

The HPLC analysis of isolated compound **6c** demonstrated that it did not contain compound **6c′** (Figure 7B). Moreover, HPLC analysis of isolated compound **6c′** also showed that it did not contain compound **6c** (Figure 7C). However, the boiling test on compound **6c** afforded a small amount of compounds **12c′** and **13c′** in the HPLC analysis (Figure 4C3). A small quantity of compounds **12c** and **13c** was also obtained in the boiling test of compound **6c′** (Figure 4C4). These results suggested that the configuration at C-2‴ in compounds **6c**, **6c′**, **12c**, **12c′**, **13c**, and **13c′** may convert through proton exchange of H-2‴ during the boiling process. Figure 8 shows a plausible thermally induced epimerization of compound **12c** into the enantiomer of compound **12c′** and epimerization of compound **12c′** into the enantiomer of compound **12c**.

**Quantitative Analyses of 4′-Hydroxyallohumulinones and Their Transformation Products during the Boiling Process.** We aimed to quantitatively evaluate the changes in 4′-hydroxyallohumulinones and their transformation products during boiling. Thus, boiling solutions of compounds **6a**, **6b**, and **6c**/**6c′** were sampled at 30, 60, 90, and 120 min and analyzed by HPLC. Figure 9 shows the time-dependent decrease in 4′-hydroxyallohumulinones and compositional changes in the transformation products. The degree of conversion of 4′-hydroxyallo-*cis*-humulinones (**12a**, **12b**, and **12c**/**12c′**) increased until around 60 min and then slowly


dx.doi.org/10.1021/jf504394h | J. Agric. Food Chem. 2014, 62, 11602−11612

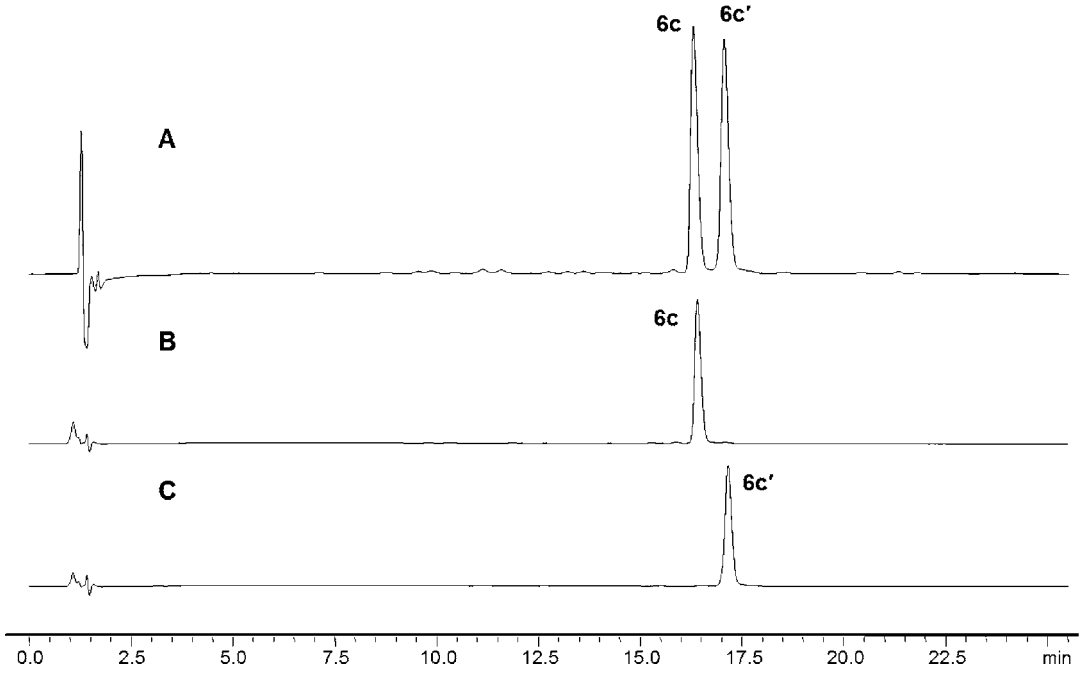


**Figure 7.** HPLC chromatograms of 4′-hydroxyalloadhumulinones A and B (**6c** and **6c′**, respectively) in the mobile phase using a basic aqueous buffer (A) before and (B and C) after their isolation.

**Table 2. NMR Spectroscopic Data (400 MHz, Methanol-$d_4$) for Compounds 6c and 6c′[a]**

| | 6c | | 6c′ | |
|---|---|---|---|---|
| position | $\delta_C$, type | $\delta_H$, mult. ($J$ in Hz) | $\delta_C$, type | $\delta_H$, mult. ($J$ in Hz) |
| 1 | 201.8, C | | 201.6, C | |
| 2 | 111.3, C | | 111.3, C | |
| 3 | 198.9, C | | 199.0, C | |
| 4 | 90.1, C | | 89.9, C | |
| 5 | 81.6, C | | 81.6, C | |
| 1′ | 200.0, C | | 200.0, C | |
| 2′ | 121.4, CH | 7.03, d (15.7) | 121.4, CH | 7.04, d (15.7) |
| 3′ | 155.8, CH | 6.87, d (15.7) | 155.8, CH | 6.87, d (15.7) |
| 4′ | 71.4, C | | 71.4, C | |
| 5′ | 29.3, $CH_3$ | 1.31, s | 29.3, $CH_3$ | 1.31, s |
| 6′ | 29.4, $CH_3$ | 1.31, s | 29.4, $CH_3$ | 1.31, s |
| 1″ | 31.0, $CH_2$ | 2.47, dd (14.8, 4.7) | 31.1, $CH_2$ | 2.47, dd (15.1, 5.5) |
| | | 2.42, dd (14.8, 8.9) | | 2.41, dd (15.1, 8.5) |
| 2″ | 118.9, CH | 5.30, m | 118.9, CH | 5.30, m |
| 3″ | 135.5, C | | 135.5, C | |
| 4″ | 18.1, $CH_3$ | 1.41, s | 18.1, $CH_3$ | 1.41, s |
| 5″ | 26.1, $CH_3$ | 1.62, s | 26.1, $CH_3$ | 1.62, s |
| 1‴ | 204.1, C | | 204.2, C | |
| 2‴ | 42.6, CH | 3.46, ddq (6.8, 6.8, 6.8) | 42.7, CH | 3.44, ddq (6.8, 6.8, 6.8) |
| 3‴ | 16.0, $CH_3$ | 1.13, d (6.8) | 15.9, $CH_3$ | 1.09, d (6.8) |
| 4‴ | 27.3, $CH_2$ | 1.64−1.74, m | 27.3, $CH_2$ | 1.70−1.80, m |
| | | 1.36−1.46, m | | 1.40−1.50, m |
| 5‴ | 11.9, $CH_3$ | 0.87, dd (7.4, 7.4) | 12.0, $CH_3$ | 0.92, dd (7.4, 7.4) |

[a]Arbitrary numbering according to structures **6c** and **6c′** shown in Figure 6.

decreased thereafter. In contrast, the amount of *cis*-oxyhumulinic acids (**13a**, **13b**, and **13c**/**13c′**) increased in inverse proportion to the decrease in the amount of 4′-hydroxyallo-*cis*-humulinones.

These results suggested that, during boiling, 4′-hydroxyallohumulinones (**6a**−**6c** and **6c′**) primarily isomerized into 4′-hydroxyallo-*cis*-humulinones (**12a**−**12c** and **12c′**), which then decomposed to *cis*-oxyhumulinic acids (**13a**−**13c** and **13c′**). The total amount of generated 4′-hydroxyallo-*cis*-humulinones and *cis*-oxyhumulinic acids accounted for 40−50% of the decomposed 4′-hydroxyallohumulinones. Our analysis indicates that, under these experimental conditions, about 10−15% of ad-congener substrates (**6c** and **6c′**) are epimerized through proton exchange at C-2‴ [calculated from the ratio of compounds **12c** and **12c′** generated from compound **6c** (Figure 9C) and compounds **12c′** and **12c** generated from


dx.doi.org/10.1021/jf504394h | J. Agric. Food Chem. 2014, 62, 11602−11612

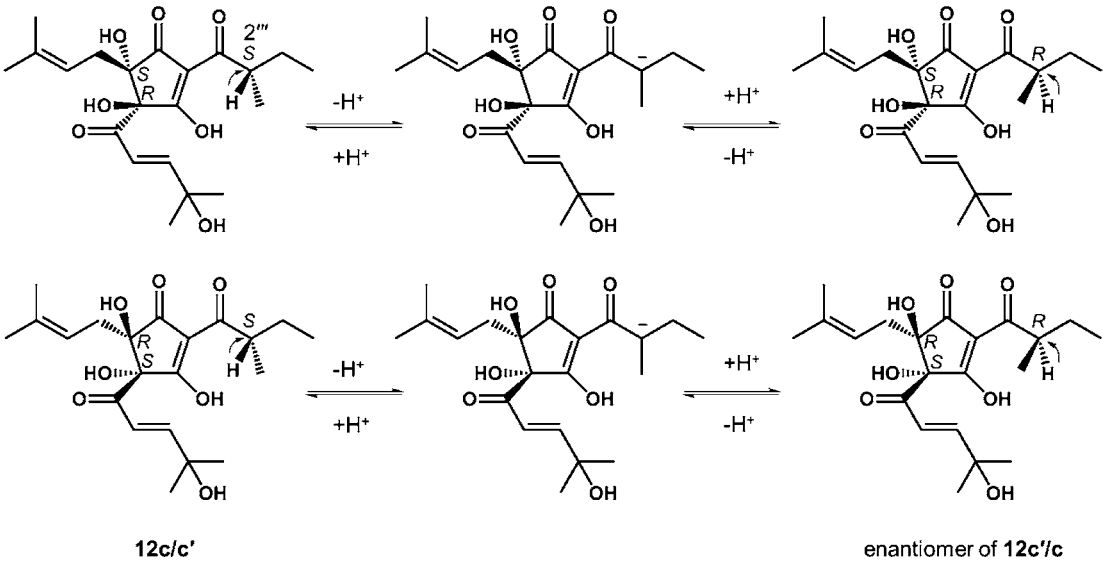


**Figure 8.** Proposed epimerization of 4′-hydroxyallo-*cis*-adhumulinones A and B (**12c** and **12c′**) through the proton exchange at C-2‴ as a result of boiling the sample.

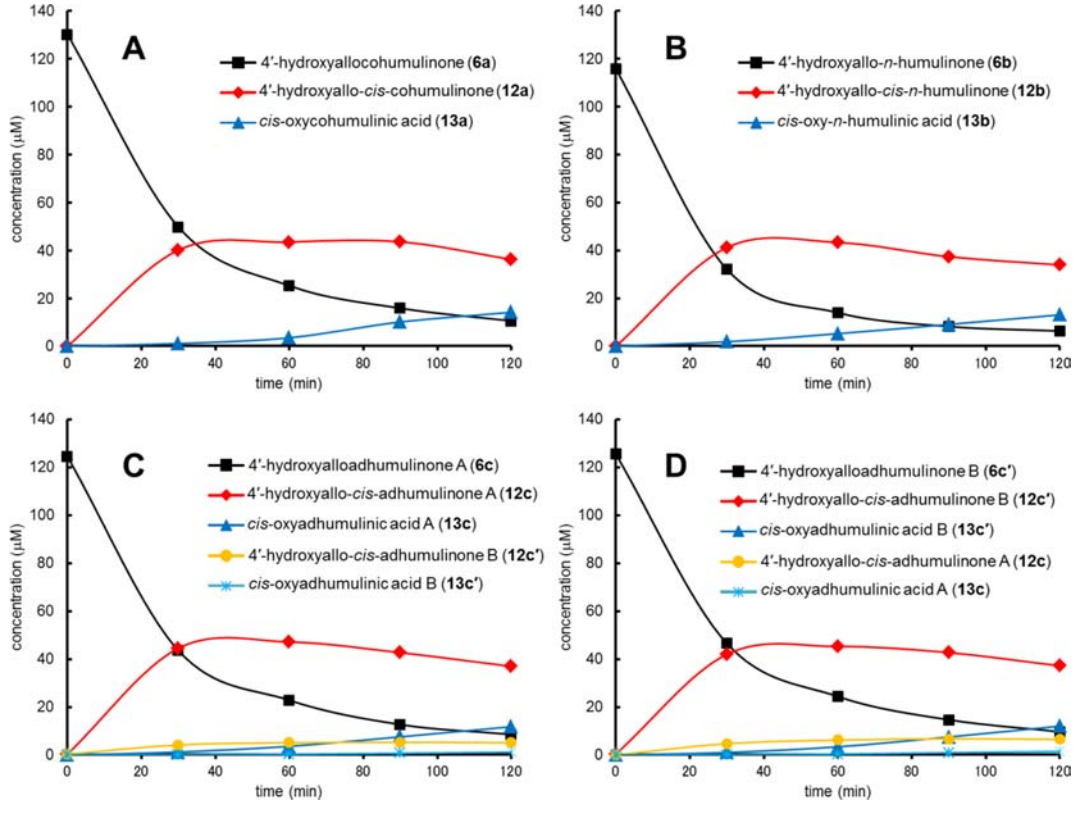


**Figure 9.** Concentration changes in (A) 4′-hydroxyallocohumulinone (**6a**), 4′-hydroxyallo-*cis*-cohumulinone (**12a**), and *cis*-oxycohumulinic acid (**13a**), in (B) 4′-hydroxyallo-*n*-humulinone (**6b**), 4′-hydroxyallo-*cis*-*n*-humulinone (**12b**), and *cis*-oxy-*n*-humulinic acid (**13b**), in (C) 4′-hydroxyalloadhumulinone A (**6c**), 4′-hydroxyallo-*cis*-adhumulinones A and B (**12c** and **12c′**), and *cis*-oxyadhumulinic acids A and B (**13c** and **13c′**), and in (D) 4′-hydroxyalloadhumulinone B (**6c′**), 4′-hydroxyallo-*cis*-adhumulinones A and B (**12c** and **12c′**), and *cis*-oxyadhumulinic acids A and B (**13c** and **13c′**) during boiling in an aqueous buffer (pH 5.5).

compound **6c′** (Figure 9D)]. This is the first study to report time-dependent changes of $\alpha$-acid-derived oxidation products in the hard resin during boiling. We believe these findings will be extremely valuable when evaluating effects of the hard resin generated through the oxidation of hops on beer properties.

In conclusion, we have clarified the main constituents, other than $\alpha$- and $\beta$-acids, of the soft and hard resins from stored hops. Furthermore, we investigated the compositional changes in the hard resin through wort boiling using model experiments and found that 4′-hydroxyallohumulinones (main constituents of the hard resin) were transformed to 4′-hydroxyallo-*cis*-humulinones and *cis*-oxyhumulinic acids. We believe our results will help to systematically evaluate the hard resin to optimize the effects of the hard resin on beer quality.


dx.doi.org/10.1021/jf504394h | *J. Agric. Food Chem.* 2014, 62, 11602−11612

## ■ ASSOCIATED CONTENT

### Supporting Information

NOESY spectra (Figure S1) and *J*-resolved HMBC spectra (Figure S2) of compounds **13b** and **14b**. This material is available free of charge via the Internet at http://pubs.acs.org.

## ■ AUTHOR INFORMATION


### Corresponding Author

*Telephone: +81-45-330-9007. Fax: +81-45-782-3657. E-mail: Yoshimasa_Taniguchi@kirin.co.jp.


### Notes

The authors declare no competing financial interest.

## ■ ACKNOWLEDGMENTS

The authors thank members of their research groups for valuable discussions, especially Mikio Katayama and Yasuji Kawachi.

## ■ REFERENCES


(1) European Brewery Convention (EBC). Current review. *J. Inst. Brew.* **1957**, *63*, 281−293.

(2) Krauss, G.; Cook, A. H.; Verzele, M. Recommendations concerning nomenclature of hop resin components. *J. Inst. Brew.* **1969**, *75*, 340−342.

(3) European Brewery Convention (EBC). Methods: 7.5 Bitter substances in hops and hop products: Lead conductance value and total resin, soft resin and hard resin. In *Analytica-EBC*; Fachverlag Hans Carl: Nürnberg, Germany, 2008.

(4) Palamand, S. R.; Aldenhoff, J. M. Bitter tasting compounds of beer. Chemistry and taste properties of some hop resin compounds. *J. Agric. Food Chem.* **1973**, *21*, 535−543.

(5) Urban, J.; Dahlberg, C. J.; Carroll, B. J.; Kaminsky, W. Absolute configuration of beer's bitter compounds. *Angew. Chem., Int. Ed.* **2013**, *52*, 1553−1555.

(6) Kowaka, M.; Kokubo, E. Composition of bitter substances of hops and characteristics of beer bitterness. *J. Am. Soc. Brew. Chem.* **1977**, *35*, 16−21.

(7) De Keukeleire, D. Fundamentals of beer and hop chemistry. *Quim. Nova* **2000**, *23*, 108−112.

(8) Bishop, L. R.; Whitear, A. L.; Inman, W. R. Scientific basis for beer foam formation and cling. *J. Inst. Brew.* **1974**, *80*, 68−80.

(9) Haseleu, G.; Intelmann, D.; Hofmann, T. Structure determination and sensory evaluation of novel bitter compounds formed from *β*-acids of hop (*Humulus lupulus* L.) upon wort boiling. *Food Chem.* **2009**, *116*, 71−81.

(10) Haseleu, G.; Intelmann, D.; Hofmann, T. Identification and RP-HPLC−ESI−MS/MS quantitation of bitter-tasting *β*-acid transformation products in beer. *J. Agric. Food Chem.* **2009**, *57*, 7480−7489.

(11) Almaguer, C.; Gastl, M.; Arendt, E. K.; Becker, T. Contributions of hop hard resins to beer quality. *BrewingSci.—Monatsschr. Brauwiss.* **2012**, *65*, 118−129.

(12) Burton, J. S.; Stevens, R. Evaluation of hops. XI. The hard resin and presence of hulupinic acid. *J. Inst. Brew.* **1965**, *71*, 51−56.

(13) Laws, D. R. J. Hops resins and beer flavor. V. The significance of oxidized hop resins in brewing. *J. Inst. Brew.* **1968**, *74*, 178−182.

(14) Ono, M.; Kakudo, Y.; Yamamoto, R.; Nagami, K.; Kumada, J. Simultaneous analysis of hop bittering components by high-performance liquid chromatography. II. Evaluation of hop deterioration. *J. Am. Soc. Brew. Chem.* **1987**, *45*, 61−69.

(15) Foster, R. T., II; Weber, K.; Jangaard, N. O. The effect of hop acids transformation on kettle utilization and finished beer flavor and aroma. *Tech. Q.—Master Brew. Assoc. Am.* **1981**, *18*, 109−115.

(16) Aitken, R. A.; Bruce, A.; Harris, J. O.; Seaton, J. C. The bitterness of hop-derived materials in beer. *J. Inst. Brew.* **1970**, *76*, 29−36.

(17) Whitear, A. L. Changes in resin composition and brewing behavior of hops during storage. *J. Inst. Brew.* **1966**, *72*, 177−183.

(18) Howard, G. A.; Martin, P. A. Bittering power of stored hops. *J. Inst. Brew.* **1964**, *70*, 424−439.

(19) Rigby, F. L. The practical significance of recent developments in the chemical analysis of hops. *Brew. Dig.* **1958**, 50−59.

(20) Stevens, J. F.; Taylor, A. W.; Clawson, J. E.; Deinzer, M. L. Fate of xanthohumol and related prenylflavonoids from hops to beer. *J. Agric. Food Chem.* **1999**, *47*, 2421−2428.

(21) Taniguchi, Y.; Matsukura, Y.; Ozaki, H.; Nishimura, K.; Shindo, K. Identification and quantification of the oxidation products derived from *α*-acids and *β*-acids during storage of hops (*Humulus lupulus* L.). *J. Agric. Food Chem.* **2013**, *61*, 3121−3130.

(22) Taniguchi, Y.; Taniguchi, H.; Matsukura, Y.; Kawachi, Y.; Shindo, K. Structural elucidation of humulone autoxidation products and analysis of their occurrence in stored hops. *J. Nat. Prod.* **2014**, *77*, 1252−1261.

(23) Dierckens, J.; Verzele, M. Oxidation products of humulone and their stereoisomerism. *J. Inst. Brew.* **1969**, *75*, 453−456.

(24) Furihata, K.; Seto, H. *J*-Resolved HMBC, a new NMR technique for measuring heteronuclear long-range coupling constants. *Tetrahedron Lett.* **1999**, *40*, 6271−6275.

(25) Morvai, M.; Nagy, T.; Kocsis, A.; Szabo, L. F.; Podanyi, B. Effect of oxygen substituents on two- and three-bond carbon−proton spin−spin coupling constants. *Magn. Reson. Chem.* **2000**, *38*, 343−359.

such natural materials as animals, plants, bacteria, and certain minerals".[3]

Biopesticides would be those things included in the definition of pesticide,[4] but with several modifications as noted above, in particular, "naturally occurring". Some people include synthetic pesticides derived from natural compounds as biopesticides. Third-generation pest control agents, reduced-risk pesticides, and biobased pesticides are other terms sometimes used interchangeably with biopesticides. Whatever the definition, the desirable qualities are

- Naturally occurring chemicals or their derivatives
- Reduced toxicity to nontarget organisms
- Reduced persistence in the environment
- Usable in organic agriculture
- Low mammalian toxicity
- Safe for farmworkers and nearby residents
- "Green" technology
- Nonrestricted use

Few products would fit all of these criteria. For example, no natural product-inspired or -derived synthetic compounds are approved for organic agriculture, nor would they be considered a biochemical biopesticide by the U.S. EPA.

## TRENDS

The market is growing, but still no biopesticides appear on the list of top 10 chemicals used in California. Some biopesticides are effective at low doses and would not be expected to appear on the list of pesticides used in largest quantities (Figure 1).[5] A

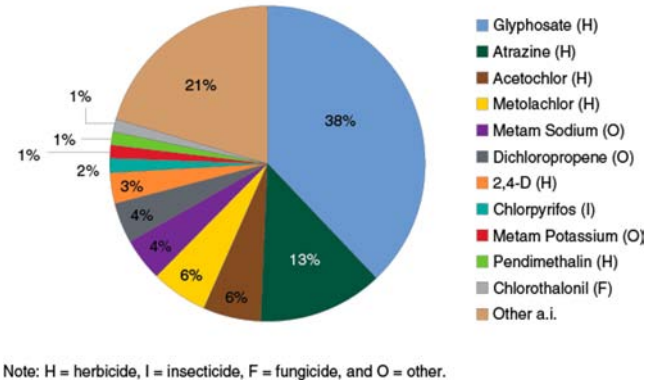


**Figure 1.** Most heavily used pesticides on 21 selected crops in the United States.[5]

reflection of the growing use of biopesticides may be found in trends in pesticide use, in California and worldwide, with compounds of nonconventional, bioderived structures such as spinosad and avermectins finding steadily increasing usage.

The trend both worldwide and in the United States is to reduce the amounts of pesticides since the peak in usage in the 1980s (Figure 2).[5] This trend reflects the phase-out of many high-dose chemicals such as toxaphene, DDT, and methyl bromide because of their environmental persistence and/or mammalian toxicity. More attention has been given to application methods that reduce drift and otherwise more precisely deliver the chemical to the target, thus reducing the amount of pesticide applied. The introduction of transgenic corn, soybeans, and cotton that are protected from insects by means of transgenes encoding *Bt* toxins (a PIP biopesticide) in the host plant has greatly decreased insecticide use in these crops. Integrated pest management tools, such as intercropping, cover crops, crop rotation, and use of hedgerows, have reduced pest populations without the use of external chemical application. The introduction of reduced risk pesticides such as spinosad that are effective at generally lower doses than conventional pesticides has furthered the reductions of amounts of pesticide applied.

Mechanical control, cover crops, solarization, and cultural methods can play a role in reducing the overall need for herbicides, as well as for other classes of pesticides. Agriculture is ripe for innovative approaches. Acquisitions and mergers may play into this as well as a society's desire for "green" technologies in helping with market development. In some cases the major retailers may favor organic or biopesticide approaches in products they market.

Smaller, specialty companies such as AgraQuest, Trécé, and Marrone Bio Innovations are leading the biopesticide technology as did Zoecon in the past, but larger companies such as Dow, DuPont, Monsanto, Syngenta, Merck, BASF, and Bayer are developing or marketing biopesticides along with the conventional chemicals that are their mainstays. The EPA has helped to catalyze the introduction of biopesticides by offering some regulatory relief for their registration. They include insect repellants and attractants, biochemical insecticides, fungicides, herbicides, nematicides, and others that were topics during this symposium. Figure 3 provides some examples of biochemical biopesticides approved by the EPA under their biopesticide program. The California Department of Pesticide Regulation (CDPR) does not offer a "fast track" for pesticide products involving biopesticides. However, if the biopesticide contains a new active ingredient, the applicant for registration can submit its application to CDPR concurrently with the application for federal registration with EPA. In addition, data requirements for biopesticides are reduced as compared to conventional chemicals, so the evaluation time period for a biopesticide may be shorter than for a conventional chemical.[6]

The trend toward reduced-risk pesticides, or toward little or no pesticide chemical at all, will likely continue and thus continue to lessen the load of xenobiotic chemicals in the environment. This said, it will be critical that practical levels of pest control be maintained, or even increased, so that agriculture can meet its challenge of providing more food within existing resources of land, water, and other resources to a world population expected to exceed 9 billion by 2050.

## NEEDS, OPPORTUNITIES, AND ALTERNATIVES

The case for new bioherbicides is particularly compelling in that the introduction of biochemical bioherbicides is lagging far behind those for pests other than weeds. Furthermore, there are strong needs for any new weed management technology because of the rapid evolution and spread of herbicide resistance.[7] Due to the widespread adoption of transgenic glyphosate-resistant (GR) crops, glyphosate has been over-used, resulting in evolution of extremely problematic GR weeds.[8,9] New herbicides with new modes of action are badly needed to combat GR weeds, as well as weeds with resistance to other herbicides, but no new herbicide mode of action has been introduced for well over 20 years.[10] Many natural phytotoxins that might be considered biochemical bioherbicides have novel modes of action that might fill this need.[11,12]

Weed management is the most costly pest management problem in organic agriculture.[13] In comparison to crop disease

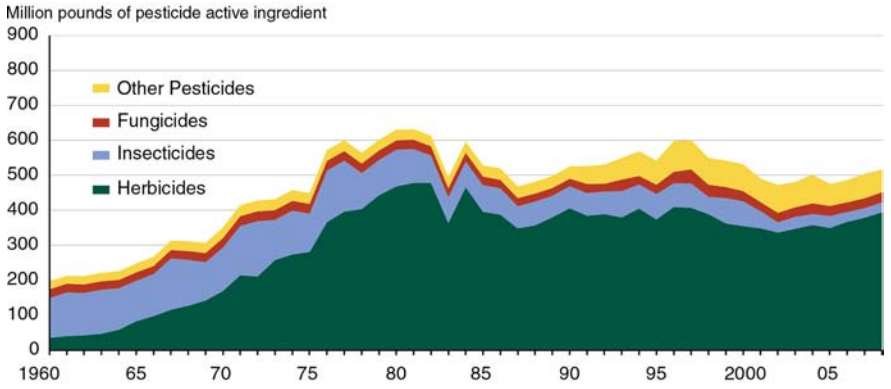


**Figure 2.** Pesticide use in U.S. agriculture, 21 selected crops, 1960–2008.[5]

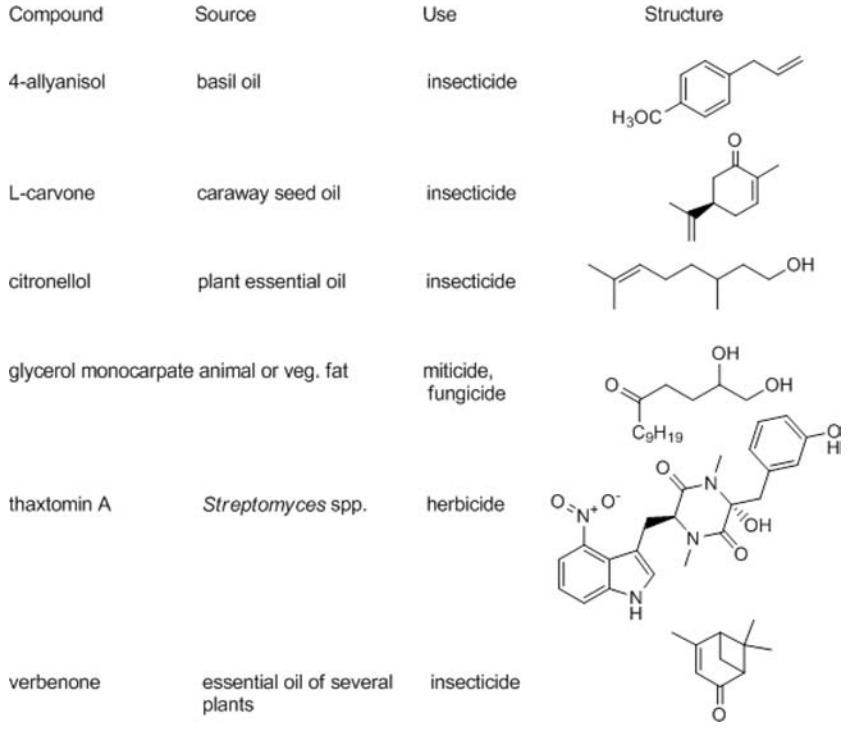


**Figure 3.** Examples of active ingredients for biochemical biopesticides registered by the U.S. EPA.

and insect management tools, organic farmers have relatively ineffective weed control products. Products such as corn gluten-based herbicides and vinegar require high dosage rates for control, and even then their performance is generally poor compared to that of synthetic herbicides. Furthermore, weed management with such tools is usually much more expensive than with conventional herbicides.[14] There are effective new bioherbicides in the pipeline (e.g., thaxtomin[15] from Marrone Bio Innovations), but some hurdles need to be surmounted before they are available for widespread use.

Similarly, new bionematicides for soil application and for use in stored products are critically needed. This is due to the mandated (Montreal Protocol) phase-out of methyl bromide and off-target movement and exposure issues with other fumigants such as methyl isothiocyanate (MITC) and chloropicrin.[16]

Semiochemicals, or sensing/communication chemicals, are another promising class of biopesticides that are far along in development including use in crop protection and related pest control needs. They include pheromones, allomones, kairomones, and other attractants and repellants for both monitoring and population control of pests. Some of the promising tools for orchard pest management come from the use of plant-biosynthesized pheromone mimics, such as the pheromone alternative found in pear leaves that can aid in control of the codling moth, a worldwide pest of apple, pear, walnut, almond, and other crops that is the reason for extensive pesticide-based control.[17] Controlling this damaging pest, and other boring insects that affect cotton seed and peanuts, is a critical element in controlling invasion of *Aspergillus* fungi, which can affect pome fruits, tree and ground nuts, and seeds, producing aflatoxins, a group of carcinogens, and other toxic mold metabolites. The use of semiochemicals to monitor insect pests in pistachio orchards was described by Beck et al.[18] in a presentation during the "Biopesticides: State of the Art and Future Opportunities" symposium.

Microbially produced biopesticides have been very successful in the past, with such products as bialaphos (bilanafos),

spinosyns, blasticidin, abamectins, validamycin, streptomycin, and milbemectin being sold as pesticides.[19] Semisynthetic modification of microbial products has also had some success in the generation of products such as emamectin from avermectin, lepimectin from milbemectin, and spinetoram from spinosyns. The impact of natural product-inspired pesticides (not biopesticides) has been tremendous, with such products as the strobilurin-based fungicides (e.g., azoxystrobin), and the synthetic version (glufosinate) of the natural herbicide phosphinothricin. Furthermore, there is an almost U.S. $1 billion market in live microbes as biocontrol agents, with or without natural product active ingredients. These include *Bacillus thuringiensis*, *Bacillus subtilis*, *Thichoderma* spp., and many others. New biopesticide products from microbes are being or may be introduced, such as the herbicides thaxatomin and mevalocidin. Microbial bioinsecticide products, such as formulations of *Chromobacterium subtsugae*, have been introduced into the marketplace. This product should be highly sustainable, in that it has a complex mode of action that causes repellency, oral toxicity, reduced egg hatch, and reduced fecundity.[20]

Pest management products from plants are also an important segment of the biopesticide market, including such products as pyrethrum and neem for insect control and many essential oil formulations for a range of pest management options. Isman[21] discussed botanical insecticides from a global perspective, noting that in 1980 <2% of all journal papers on insecticides dealt with botanicals, but the number exceeded 21% in 2011. There has been an explosive growth in reported studies of the insecticidal activity of plant essential oils, but this activity has not been reflected in increased commercialization of botanical insecticides, at least not in the major North American and European markets. Much of the interest in botanical insecticides has come from China and other Asian nations, Latin America, and Africa, perhaps a consequence of the potentially lower cost, local sourcing, and lower mammalian toxicity of many of these products relative to mainstream synthetics that have, regrettably, resulted in well-publicized human poisonings in earlier times.

Some of these plant products have inspired synthetic pesticides such as pyrethroids or could have inspired neonicotinoid and ryanodine receptor insecticides.[22−25] Although natural plant-derived triketones such as leptospermone show promise as bioherbicides, they provided the molecular scaffold for the synthetic triketone herbicides such as mesotrione.[26] Other phytochemicals are being used directly as biochemical biopesticides. These include an extract of the weed *Reynoutria* spp., which induces resistance to pathogens in crops,[27] and the compound sarmentine from *Piper longum*, which provides burndown-type weed management.[28]

Ashworth and coauthors[29] addressed MITC and other biofumigants using, for example, *Brassica* species incorporation in soil, which releases volatile isothiocyanate chemicals into the soil. They pointed out the disadvantages of the plant release scenario in soil, including relatively low release efficiency and rapid degradation and sorption within the soil, causing growers' reluctance to rely on biofumigants. On the other hand, bionematicides that do not operate by diffusion as vapors in the soil, such as ivermectins and ivermectin mixed with other chemicals, are showing promise in transitioning to a "fumigant-free" control strategy.[30]

RNAi is being rapidly developed for pest management.[31−37] RNAi may be ruled a biopesticide by the U.S. EPA because it leads to natural compounds that can be made to be highly selective with very little or no adverse environmental impact. Patents for different double-stranded RNA (dsRNA)-derived constructs to be used as insecticides, fungicides, nematicides, and herbicides have been filed by companies and public sector laboratories. Some of these products are at the trade name stage, and development is rapid.

## HIGHLIGHTS AND CHALLENGES

At the symposium it was stated that high levels of pest management (95% or better almost all of the time) that are expected with conventional pesticides may not be realistic for some biopesticides. Also, high levels of pest control with many biopesticides are more likely in integrated pest management systems that do not rely on a single technology for the control of a pest. In the long run, such an approach, although more complicated for the farmer, may be more sustainable because of the lower probability of evolved resistance to multiple technologies.

It is abundantly clear that research on semiochemicals for control of pests is advancing rapidly, especially the use of repellents and attractants. Attractants can be deployed several ways: (1) in traps for monitoring populations of pests (numbers and timing); (2) in attract-and-kill strategies that use baits laced with toxicants; or (3) in mating-disruption approaches, whereby an attractant pheromone is released in a large area to mask the gradients of pheromone emitted by female moths (for example), which would allow males to use the plume of pheromone to locate the female for mating, termed a "confusion" strategy. In addition, attractants can be utilized as part of a "push-pull" scenario, in which a repellent can push a pest species away from a specific habitat while an attractant pulls that species toward a different location, away from the host that needs protection from the pest.

One exciting highlight in the utilization of semiochemicals was the presentation of the novel delivery technology called specialized pheromone and lure application technology (SPLAT). Because nearly all attractants and repellents utilized in pest control are highly biodegradable (as well as chemically and physically degradable), their residence time in the environment is often less than optimal for the management of a pest. Progress on development of new slow-release technology has been gathering momentum recently, and the advances presented by Mafra-Neto et al.[38] are highly encouraging. The maximum value of highly specific pheromones, kairomones, or repellents will be realized only when a broadly applicable technology is developed for uses in multiple situations and becomes a somewhat standardized technology; the SPLAT slow-release methodology shows considerable promise toward that end.

Development of new classes of insecticides has often followed from identification of a natural pesticide's mechanism of toxic action. The current search for new target sites in insects, ticks, mites, and nematodes has focused on elucidation of receptors that are sensitive to natural ligands that may be encountered in a pest's habitat. Many secondary compounds in plants and microbes apparently have defensive functions, and we may be able to exploit that chemistry if we can determine the effects of those defensive compounds, for example, at specific receptors that are functionally important in the physiology of the pest species. Several classes are notable for being under-exploited in the management of pests: octopamine receptors, tyramine receptors, neuropeptide receptors, and

potassium channels are examples of target sites currently under investigation for expanded utility in pest management. Once mechanisms are understood, the natural ligands may be supplemented by the development of biorational derivatives and analogues and sometimes unrelated synthetic molecules. Among invertebrate groups of animals (insects, acarines, arachnids, nematodes, mollusks), their receptors vary in ways that can make a pesticide less broadly useful, but which may allow improved selectivity for controlling pests with minimal effects on nontarget species of many kinds. Creating selective toxicity differences for target/nontarget impacts is one of the inherent advantages to be gained from comprehension of how receptors function normally and how those processes can be disrupted biochemically or chemically. If a substantial series of closely related compounds are obtained (through bioprospecting or synthesis), quantitative structure−activity relationships can be developed, which often represent predictive information for us to find or design improved bioactive molecules.

The excitement offered in the 1970s with the publication of "third-generation pest control" by Carroll M. Williams[39] waned in the intervening years but is now on the upswing. Biopesticides are still only 3% of the global annual market for pesticides, but the market share is increasing, in part due to successful biopesticide products such as spinosad and avermectin. These products and others in the pipeline must offer efficacy against key pests, a useful spectrum of activity, robust performance, and a viable manufacturing and supply chain for continued success. The genes controlling the activity in some products, such as the Gram-positive Bt toxins, can be moved in such a way that control is delivered through the seed rather than through the air, water, or soil, an advantage for some biopesticides. However, Bt toxins are not efficacious against all pest species; for instance, hemipterans are less susceptible to Bt toxins.[40] Bonning and co-workers[41] discussed important advances in the modification of Bt toxins allowing them to be more effective pest control agents among less susceptible insects. This includes the addition of a short peptide sequence on a Bt cytolytic toxin (Cyt2A) showing efficacious effects against hemipteran pests (*Acyrthosiphon pisum* and *Myzus persicae*). This advance in biotechnology allows for a wider utilization of Bt toxins against a variety of pests.

It is evident that there is accelerated growth in biotechnology for pest control. The use of dsRNA has made rapid advances as a biotechnological tool for pest control. The RNAi pathway is a naturally evolved pathway, which creates a response against sequence-specific invading nucleic acids and is triggered by dsRNA. Successful use of RNAi machinery includes the identification of genes that have an essential physiological function, gene targets with high transcript levels and high protein turnover, and genes that have specific sequences that can be targeted. Siegfried[42] identified several areas of advancement of RNAi in pest management. Advancements include the use of baits for urban pest management,[43] nanoparticle stabilization for controlling the African malaria mosquito,[44] microbial formulation for spraying,[45] and plant expression for row crop agriculture.[46] This form of biopesticide offers new levels of target specificity for possible control of Varroa mites[47] or viruses[48] inside a bee hive without harm to the bees, a remarkable feat.

High-throughput discovery and microencapsulation (including in nanoparticle-based formulations) are technologies that can speed the development of biopesticides. Combinations of active chemicals are the rule in nature, perhaps because of synergies and/or reduced chances of evolved resistance. An organism may biosynthesize hundreds of related terpenes, for example, only some of which are active and then only in limited proportions. For example, there is good evidence of synergies in insect-active essential oil components, even involving compounds that are inactive when tested in isolation.[49] Whether mixtures will become more common in biopesticide products is an open question. Mixtures can increase the range of product properties, but they also raise regulatory questions for an approval process that values single, or just a few, active ingredients in a new pesticide product.

An example of the pitfalls to avoid with mixtures is provided by the second-generation insecticide toxaphene, for which a few of the more than 175 plus isomers and congeners of chlorinated camphene were responsible for most of the useful insecticidal activity. At least some of the compounds in this witch's brew were herbicidal, as toxaphene was also sold as a herbicide. The herbicidal components were never identified.[50] The bulk of the 175 related compounds contributed to widespread environmental contamination, and some possessed significant toxicity to nontarget organisms, including threatened or endangered wildlife.[51] It is important to understand the physical, chemical, and toxicological properties of each component of a mixture and its role in the utility of the mixture prepared for commercial use. This is often difficult for complex mixtures of naturally occurring or synthetic chemicals.

Goldblum, Warren, and Burlingame of Allylix discussed the future opportunities for novel pest control agents composed of terpenes, the most diverse class of biomolecules, or their derivatives.[52] Technology now exists for sustainable production of sesquiterpenes, a group of terpenes with many high-value applications including flavors and fragrances, cosmetic products, food ingredients, pharmaceuticals, and insecticides. Nootkatone, the flavor- and fragrance-defining chemical in grapefruit, is an effective acaricide and repellant. Terpene-based biopesticide products have the potential to compete with conventional pesticides on both efficacy and economic bases.

Because of the economic hurdles on the path from discovery to commercialization of new pesticides and new uses of existing pesticides, the IR-4 project was established in 1963 as a public sector program to facilitate registration of minor-use or specialty pesticides, including biopesticides. The biopesticide program of IR-4 was established in 1982 to assist in the registration of biochemical biopesticides such as plant extracts, pheromones, and minerals in addition to microbial and biotechnology projects.[53,54] Since its inception, IR-4 has provided over U.S, $6.7 million in grants for biopesticide R&D efforts.

Many of the symposium attendees echoed the need for additional sources of funds for research, development, education, and commercialization of biopesticides to advance this relatively new industry, much as public funds and incentives are being devoted to biofuels, bioenergy, and other aspects of the bioeconomy.

## ■ ASSOCIATED CONTENT

### Ⓢ Supporting Information

Table of the structures of compounds discussed. This material is available free of charge via the Internet at http://pubs.acs.org.

## AUTHOR INFORMATION


### Corresponding Author

*(J.N.S.) Phone: (530) 752-1141. Fax: (530) 752-3394. E-mail: jnseiber@ucdavis.edu.


### Notes

The authors declare no competing financial interest.

## REFERENCES


(1) Gross, A. D., Coats, J. R., Seiber, J. N., Duke, S. O., Eds. *Biopesticides: State of the Art and Future Opportunities*; ACS Symposium Series 1172; American Chemical Society: Washington, DC, USA, 2014.

(2) Cantrell, C. L.; Dayan, F. E.; Duke, S. O. Natural products as sources for new pesticides. *J. Nat. Prod.* **2012**, *75*, 1231−1242.

(3) U.S. Environmental Protection Agency (EPA). What are biopesticides? http://www.epa.gov/oppbppd1/biopesticides/whatarebiopesticides.htm (accessed July 2, 2014).

(4) Federal Insecticide, Fungicide, and Rodenticide Act (as amended through P.L. 110-246, effective May 22, 2008) Section 2.

(5) Fernandez-Cornejo, J.; Nehring, R.; Osteen, C.; Wechsler, S.; Martin, A.; Vialou, A. *Pesticide Use in U.S. Agriculture: 21 Selected Crops, 1960−2008*, EIB-124; U.S. Department of Agriculture, Economic Research Service: Washington, DC, USA, May 2014.

(6) Prichard, A., Pesticide Registration Branch, California Department of Pesticide Regulation, personal communication, July 14, 2014.

(7) Heap, I. Global perspective of herbicide-resistant weeds. *Pest Manage. Sci.* **2014**, *70*, 1306−1315.

(8) Duke, S. O.; Powles, S. B. Glyphosate-resistant crops and weeds: now and in the future. *AgBioForum* **2009**, *12*, 346−357.

(9) Duke, S. O. Comparing conventional and biotechnology-based pest management. *J. Agric. Food Chem.* **2011**, *59*, 5793−5798.

(10) Duke, S. O. Why have no new herbicide modes of action appeared in recent years? *Pest Manage. Sci.* **2012**, *68*, 505−512.

(11) Duke, S. O.; Dayan, F. E. Modes of action of microbially-produced phytotoxins. *Toxins* **2011**, *3*, 1038−1064.

(12) Dayan, F. E.; Owens, D. K.; Duke, S. O. Rationale for a natural products approach to herbicide discovery. *Pest Manage. Sci.* **2012**, *68*, 519−528.

(13) Bolda, M. P.; Tourte, L.; Klonsky, K. M.; De Moura, R. L. University of California Cooperative Extension Bulletin ST-CC-06-O, 2006.

(14) Young, S. L. Natural product herbicides for control of annual vegetation along roadsides. *Weed Technol.* **2004**, *18*, 580−587.

(15) Koivunen, M.; Marrone, P.; Boddy, L. Uses of thaxtomin and thaxtomin compositions as herbicides. U.S. Patent Appl. Publ. US20130217573, 2013.

(16) Ozone Secretariat. *The Montreal Protocol on Substances that Deplete the Ozone layer from United Nations Environment Programme*, 2000.

(17) Light, D. M.; Beck, J. J. Behavior of codling moth (Lepidoptera: Tortricidae) neonate larvae on surfaces treated with microencapsulated pear ester. *Environ. Entomol.* **2012**, *41*, 603−611.

(18) Beck, J. J.; Mahoney, N. E.; Higbee, B. S.; Gee, W. S.; Baig, N.; Griffith, C. M. Semiochemicals to monitor insect pests — future opportunities for an effective host plant volatile blend to attract navel orangeworm in pistachio orchards. In *Biopesticides: State of the Art and Future Opportunities*; Gross, A. D., Coats, J. R., Seiber, J. N., Duke, S. O., Eds.; ACS Symposium Series 1172; American Chemical Society: Washington, DC, USA, 2014; pp 191−210.

(19) Copping, L. G.; Duke, S. O. Natural products that have been used commercially as crop protection agents − a review. *Pest Manage. Sci.* **2007**, *63*, 524−554.

(20) Vasavada, A. Product stewardship: discovery and development of Grandevo to commercialization. In *Abstracts of Papers*, 248th National Meeting of the American Chemical Society, San Francisco, CA, Aug 10−14, 2014; American Chemical Society: Washington, DC, USA, 2013; IAC-38.

(21) Isman, M. B. Botanical insecticides: a global perspective. In *Biopesticides: State of the Art and Future Opportunities*; Gross, A. D., Coats, J. R., Seiber, J. N., Duke, S. O., Eds.; ACS Symposium Series 1172; American Chemical Society: Washington, DC, USA, 2014; pp 21−30.

(22) Katsuda, Y. Progress and future of pyrethroids. *Topics Curr. Chem.* **2012**, *314*, 1−30.

(23) Jeshke, P. Chemical structural features of commercialized neonicotinoids. In *Modern Crop Production Compounds*, 2nd ed.; Kraemer, W., Ed.; Wiley-VCH Verlag: Weinheim, Germany, 2012; Vol. 3, pp 1165−1169.

(24) Lahm, G. P.; Selby, T. P.; Stevenson, T. M.; Cordova, D.; Annan, I. B.; Andaloro, J. T. Pyrazolylpyridine activators of the insect ryanodine receptor. In *Bioactive Herterocyclic Compounds Classes*; Lambeth, C., Dinges, J., Eds.; Wiley-VCH Verlag: Weinheim, Germany, 2012; pp 251−263.

(25) Gerwick, B. C.; Sparks, T. C. Natural products for pest control: an analysis of their role, value and future. *Pest Manage. Sci.* **2014**, *70*, 1169−1185.

(26) Lee, D. L.; Prisbylla, M. P.; Cromartie, T. H.; Dagarin, D. P.; Howard, S. W.; Provan, W. M.; Ellis, M. K.; Fraser, T.; Mutter, L. C. The discovery and structural requirements of inhibitor of *p*-hydroxyphenylpyruvate dioxygenase. *Weed Sci.* **1997**, *45*, 601−609.

(27) Daayf, F.; Ongena, M.; Boulanger, R.; El Hadrami, I.; Belanger, R. I. Induction of phenolic compounds in two cultivars of cucumber by treatment of healthy and powdery mildew-infected plants with extracts of *Reynoutria sachalinensis*. *J. Chem. Ecol.* **2000**, *26*, 1579−1593.

(28) Huang, H.; Morgan, C. M.; Asolkar, R. N.; Koivunen, M. E.; Marrone, P. G. Phytotoxicity of sarmentine isolated from long pepper (*Piper longum*) fruit. *J. Agric. Food Chem.* **2010**, *58*, 9994−10000.

(29) Ashworth, D. J.; Yates, S. R.; Wang, D.; Luo, L. Natural and synthetic isothiocyanates for pest control in soil. In *Biopesticides: State of the Art and Future Opportunities*; Gross, A. D., Coats, J. R., Seiber, J. N., Duke, S. O., Eds.; ACS Symposium Series 1172; American Chemical Society: Washington, DC, USA, 2014; pp 159−177.

(30) Pesticide Action Network. Towards Fumigant-Free Fields, http://www.panna.org/blog/towards-fumigant-free-fields, April 10, 2013 (accessed Aug 28, 2014).

(31) Zhu, K. Y. RNA interference: a powerful tool in entomological research and a novel approach for insect pest management. *Insect Sci.* **2013**, *20*, 1−3.

(32) Katoch, R.; Thakur, N. Advances in RNA interference technology and is impact on nutritional improvement, disease and insect control in plants. *Appl. Biochem. Biotechnol.* **2013**, *169*, 1579−1605.

(33) Simon-Mateo, C.; Garcia, J. A. Antiviral strategies in plants based on RNA silencing. *Biochim. Biophys. Acta, Gene Regul. Mech.* **2011**, *1809*, 722−731.

(34) Bandaranayake, P. C. G.; Yoder, J. I. Trans-specific gene silencing of acetyl-CoA carboxylase in a root-parasitic plant. *Mol. Plant−Microbe Interact.* **2013**, *26*, 575−584.

(35) Huvenne, H.; Smagghe, G. Mechanisms of dsRNA uptake in insects and potential of RNAi for pest control: a review. *J. Insect Physiol.* **2010**, *56*, 227−235.

(36) Essigmann, B.; Paget, E.; Schmitt, F. RNA interference (RNAi) for functional genomics and as a tool for crop protection. In *Modern Methods in Crop Protection Research*; Jeschke, P., Ed.; Wiley-VCH: Weinheim, Germany, 2012; pp 131−160.

(37) Scott, J. G.; Michel, K.; Bartholomay, L. C.; Siegfried, B. D.; Hunter, W. B.; Smagghe, G.; Zhu, K. Y.; Douglas, A. E. Towards the elements of successful insect RNAi. *J. Insect Physiol.* **2013**, *59*, 1212−1221.

(38) Mafra-Neto, A.; Fettig, C. J.; Munson, A. S.; Rodriguez-Saona, C.; Holdcraft, R.; Faleiro, J. R.; El-Shafie, H.; Reinke, M.; Bernardi, C.; Villagran, K. M. Development of specialized pheromone and lure application technologies (SPLAT®) for management of coleopteran pests in agricultural and forest systems. In *Biopesticides: State of the Art and Future Opportunities*; Gross, A. D., Coats, J. R., Seiber, J. N., Duke,

S. O., Eds.; ACS Symposium Series 1172; American Chemical Society: Washington, DC, USA, 2014; pp 211−242.
(39) Williams, C. M. Third-generation pesticides. *Sci. Am.* **1967**, *217* (1), 13−17.
(40) Chougule, N. P.; Bonning, B. C. Toxins for transgenic resistance to hemipteran pests. *Toxins* **2012**, *4*, 405−429.
(41) Chougule, N. P.; Li, H.; Liu, S.; Linz, L. B.; Narva, K. E.; Meade, T.; Bonning, B. C. Retargeting of the *Bacillus thuringiensis* toxin Cyt2Aa against hemipteran insect pests. *Proc. Natl. Acad. Sci. U.S.A.* **2013**, *110*, 8465−8470.
(42) Vélez, A. M.; Siegfried, B. D. RNA interference in insect pest management: assessment of environmental risk. In *Biopesticides: State of the Art and Future Opportunities*; Gross, A. D., Coats, J. R., Seiber, J. N., Duke, S. O., Eds.; ACS Symposium Series 1172; American Chemical Society: Washington, DC, USA, 2014; pp 59−70.
(43) Zhou, X.; Wheeler, M. M.; Oi, F. M.; Scharf, M. E. RNA interference in the termite *Reticulitermes flavipes* through ingestion of double stranded RNA. *Insect Biochem. Mol. Biol.* **2008**, *38*, 805−815.
(44) Zhang, X.; Zhang, J.; Zhu, K. Y. Chitosan/double-stranded RNA nanoparticle-mediated RNA interference to silence chitin synthase genes through larval feeding in the African malaria mosquito (*Anopheles gambiae*). *Insect Mol. Biol.* **2010**, *19*, 683−693.
(45) Zhu, F.; Xu, J.; Palli, R.; Ferguson, J.; Palli, S. R. Ingested RNA interference for managing the populations of the Colorado potato beetle, *Leptinotarsa decemlineata*. *Pest Manage. Sci.* **2011**, *67*, 175−182.
(46) Price, D. R.; Gatehouse, J. A. RNAi-mediated crop protection against insects. *Trends Biotechnol.* **2008**, *26*, 393−400.
(47) Campbell, E. W.; Budge, G. E.; Bowman, A. S. Gene-knockdown in the honey bee mite *Varroa destructor* by non-invasive approach: studies on a glutathione *S*-transferase. *Parasites Vectors* **2010**, *3* (73), 10 DOI: 10.1186/1756-3305-3-73.
(48) Hunter, W.; Ells, J.; vanEngelsdorp, D.; Hayes, J.; Westervelt, D.; Glick, E.; Williams, M.; Sela, I.; Maori, E.; Pettis, J.; Cox-Foster, D.; Paldi, N. Large-scale field application of RNAi technology reducing Israeli acute disease in honey bees (*Apis mellifera*, Hymenoptera: Apidae). *PLoS Pathogens* **2010**, *6* (12), No. e1001160.
(49) Isman, M. B.; Miresmailli, S.; Machial, C. Commercial opportunities for pesticides based on plant essential oils in agriculture, industry and consumer products. *Phytochem. Rev.* **2011**, *10*, 197−204.
(50) Isenhour, D. J.; Todd, J. W.; Hauser, E. W. The impact of toxaphene applied as a post-emergence herbicide for control of sicklepod, *Cassia obtusifolia* L., on arthropods associated with soybean. *Crop Prot.* **1985**, *4*, 434−445.
(51) Angermann, J.; Fellers, G. M.; Matsumura, F. Polychlorinated biphenyls and toxaphene in pacific tree frog tadpoles (*Hyla regilla*) from the California Sierra Nevada, USA. *Environ. Toxicol. Chem.* **2002**, *21*, 2209−2215.
(52) Goldblum, S. D.; Warren, C. B.; Burlingame, R. P. Biopesticides: state of the art and future opportunities. In *Abstracts of Papers*, 246th National Meeting of the American Chemical Society, Indianapolis, IN, Sept 8−12, 2013; American Chemical Society: Washington, DC, USA, 2013; AGRO 227.
(53) IR-4 project. Year End Summary, 2013, http://issuu.com/snovack/docs/2013yes (accessed July 2, 2014).
(54) Braverman, M. P.; Kunkel, D. L.; Baron, J. J. Biopesticide registration successes of the IR-4 project and changes in regulatory requirements. In *Biopesticides: State of the Art and Future Opportunities*; Gross, A. D., Coats, J. R., Seiber, J. N., Duke, S. O., Eds.; ACS Symposium Series 1172; American Chemical Society: Washington, DC, USA, 2014; pp 259−265.

had previously been subjected to acidification by a technique involving ion-exchange resins.

**Table 1. 2-Bromo-4-methylphenol Levels in Wines[a]**

| concentration (ng/L) | harvest | concentration (ng/L) | harvest |
|---|---|---|---|
| | **(A) White Wines** | | |
| <LOD | 2011 | <LOQ | 2011 |
| <LOQ | 2011 | 260 | 2011 |
| <LOQ | 2011 | 272 | 2011 |
| <LOQ | 2011 | 28900 | 2011 |
| | **(B) Rosé Wines** | | |
| <LOQ | n.id | 47 | 2011 |
| <LOQ | 2012 | 49 | 2011 |
| <LOQ | 2012 | 49 | 2011 |
| <LOQ | 2012 | 50 | 2011 |
| <LOQ | 2012 | 52 | 2011 |
| <LOQ | 2012 | 60 | 2011 |
| <LOQ | 2011 | 72 | 2011 |
| <LOQ | 2011 | 73 | 2011 |
| <LOQ | 2011 | 79 | 2011 |
| <LOQ | 2011 | 136 | 2011 |
| <LOQ | 2011 | 152 | 2011 |
| <LOQ | 2011 | 184 | 2011 |
| <LOQ | 2011 | 234 | 2011 |
| <LOQ | 2011 | 278 | 2011 |
| <LOQ | 2011 | 342 | 2011 |
| <LOQ | 2011 | 434 | 2011 |
| <LOQ | 2011 | 522 | 2011 |
| <LOQ | 2011 | 653 | 2011 |
| <LOQ | 2011 | 813 | 2011 |
| 35 | 2011 | 6600 | 2011 |
| 41 | 2011 | 7556 | 2011 |
| | **(C) Red Wines** | | |
| <LOQ | n.id | 214 | 2010−2011 |
| <LOQ | 2010 | 313 | 2010 |
| <LOQ | 2011 | 542 | 2010 |
| <LOQ | 2011 | 699 | 2010 |
| <LOQ | 2011 | 787 | n.id |
| 63 | 2011 | 48000 | 2011 |
| 83 | 2009 | | |

[a]LOD, limit of detection; LOQ, limit of quantitation; n.id, no identification.

*High-Performance Liquid Chromatography (HPLC) Fraction Preparation.* Sample preparation was as optimized by Lytra et al.[7] A 500 mL wine sample was extracted with 80, 80, and 50 mL of dichloromethane, successively, for 10 min. The organic phases were collected, blended, dried over sodium sulfate, and concentrated using a Rotavapor (Laborota 4010 digital Rotary Evaporator, Heidolph, Germany) with a 20 °C bath temperature to obtain 1.25 mL of wine extract. Reversed-phase (RP) HPLC was performed on this raw extract using a Nova-Pak C18 column (300 × 3.9 mm i.d., 4 μm, 60 Å, Waters, Saint-Quentin, France) without a guard cartridge. The HPLC system consisted of an L-6200A pump (Merck-Hitachi, Germany). Chromatographic conditions were as optimized by Pineau et al.:[8] flow rate, 0.5 mL/min; injection volume, 250 μL wine extract; program gradient, phase A, water, phase B, ethanol; 0−2 min, 100% A, linearly programmed until 100% B at minute 50. The effluent was collected in 1 mL fractions. Twenty-five fractions with various aromas were obtained in dilute alcohol solution.

*HPLC Fraction Extraction.* Each fraction was diluted in distilled water to obtain 12% ethanol and then re-extracted by using the same method as for the wine, but with 4, 2, and 2 mL of dichloromethane (5 min stirring for each extraction). The organic phases were collected, dried over sodium sulfate, and concentrated under nitrogen flow to obtain 100 μL of extract.

**Gas Chromatography−Olfactometry (GC-O).** Olfactometry analyses were carried out by a panel of three judges during 40 min, using an HP-4890 gas chromatograph (Hewlett-Packard, Wilmington, DE, USA), equipped with a flame ionization detector (FID) and a sniffing port (ODO-I SGE, Ringwood, Australia), connected by a flow-splitter to the column exit. GC effluent was combined with humidified $N_2$ (Linde, France) at the bottom of the glass sniffing nose (SGE, Victoria, Australia) to avoid nasal dehydration. Two microliters of organic extract was injected in splitless mode (injector temperature, 250 °C). The column was a BP21 (SGE), 50 m × 0.32 mm i.d., film thickness = 0.25 μm. The oven was programmed at 40 °C for the first minute, and the temperature was increased at a rate of 4 °C/min to a final isotherm at 220 °C for 20 min. The carrier gas was hydrogen 5.0 (Linde) with a column head pressure of 15 psi.

**2-Bromo-4-methylphenol Identification.** Two microliter samples taken from the 100 μL of organic extract of fraction 19, corresponding to an initial volume of 3 L of wine, were injected in splitless−split mode (injector temperature, 250 °C; interface temperature, 280 °C; splitless time, 45 s; split flow, 50 mL/min) using an HP 7890 gas chromatograph (Hewlett-Packard) coupled to a mass spectrometer (HP 5975). The column was a BP21 (SGE), 50 m × 0.32 mm i.d., film thickness = 0.25 μm. The oven was programmed at 40 °C for the first minute and then heated at a rate of 4 °C/min to a final isotherm at 220 °C for 20 min. The carrier gas was helium N55 (Linde) with a column head pressure of 8 psi. The MSD was used in full-scan mode ($m/z$ 40−300, 3.09 scans/s). MS data were recorded and processed using Chemstation software equipped with NIST 2011 MS library (U.S. National Institute of Standards and Technology, Gaithersburg, MD, USA). The compound was then characterized by comparing its LRI and mass spectra with those of a standard.

**2-Bromo-4-methylphenol Quantitation.** *Solid Phase Microextraction (SPME).* Sample preparation was inspired by the protocol of OIV analysis of methods.[9] The fiber used was coated with polyacrylate stationary phases and an 85 μm film thickness. It was conditioned before use by insertion into the GC injector set at 280 °C during 1 h as recommended by the manufacturer. To a 20 mL headspace vial was added a 10 mL sample of either wine, spiked wine, or a blank solution of 12% (v/v) in water. To this were added 3 g of sodium chloride and 20 μL of a 5.6 mg/L solution of 2,4-dibromoanisole as internal standard, and then the vial was tightly sealed with a PTFE-lined cap. The solution was homogenized with a vortex shaker for 5 s and then loaded onto a Gerstel MPS2 autosampling device provided by R.I.C. (Saint Priest, France). The program consisted of whirling the vial at 500 rpm for 2 min at 60 °C, then inserting the fiber into the headspace for 50 min at 60 °C as the solution was swirled again, and then transferring the fiber to the injector for desorption at 250 °C for 5 min. Finally, the fiber was cleaned in a thermal desorption cleaner for 15 min at 200 °C.

*Gas Chromatography−Mass Spectrometry (GC-MS) Analysis.* The GC parameters were the same as those described in the identification method. The mass spectrometer was operated in electron ionization mode at 70 eV in selected-ion-monitoring (SIM) mode. The ions monitored were $m/z$ 107, 186, and 188 fragments from 20 to 37.2 min and $m/z$ 251, 264, 266 fragments from 37.2 min to the end of run with dwell time of 50 msec.

The limits of detection (LODs) (concentration for signal/noise = 3) and the limits of quantitation (LOQs) (concentration for signal/noise = 10) were calculated manually from the ratio of the peak heights to the average noise before and after each peak. These data are listed in Table 2.

For validation, repeatability assays were carried out on white, rosé, and red wines, which were not affected by the defect, spiked with **1** at 80, 60, and 100 ng/L, respectively. Recovery assays were carried out on white, rosé, and red wines, which were not affected by the defect, spiked with 50.5 ng/L.

**1** quantitation method parameters are shown in Table 2.

*Method Optimization.* Spiked white wine (Bordeaux, 2011) was use to optimize the method. Seven different fibers were tested to select

**Table 2. 2-Bromo-4-methylphenol Quantitation Method[a]**

| matrix | LOD (ng/L) | LOQ (ng/L) | linear range (ng/L) | $R^2$ | CV (%) | recovery (%) |
|---|---|---|---|---|---|---|
| white wine | 9 | 30 | 16–2736 | 0.9996 | 3.9 | 101.5 |
| rosé wine | 9 | 29 | 16–2736 | 0.9991 | 2.8 | 104.8 |
| red wine | 11 | 36 | 16–2736 | 0.9999 | 1.9 | 104.5 |

[a]LOD, limit of detection; LOQ, limit of quantitation; CV, coefficient of variation.

the best one for extracting 2-bromo-4-methylphenol. They were coated with various stationary phases and film thicknesses: 50/30 μm divinylbenzene/carboxen/polydimethylsiloxane (DVB/CAR/PDMS), 85 μm carboxen–polydimethylsiloxane (CAR-PDMS), 100 μm polydimethylsiloxane (PDMS-100), 65 μm polydimethylsiloxane–divinylbenzene (PDMS-DVB), 85 μm polyacrylate (PA), 70 μm carbowax–divinylbenzene (CW-DVB), and 60 μm polyethylene glycol (PEG) purchased from Supelco (Bellefonte, PA, USA). They were conditioned before use by insertion into the GC injector as recommended by the manufacturer. Adsorption time was set at 20 min at a temperature of 35 °C. Figure 1a shows that 85 μm polyacrylate (PA) fiber resulted in the highest signal-to-noise ratio for **1** and was thus selected as the best one for this analysis.

The effect of temperature was examined by sampling a spiked white wine at 30, 40, 50, 60, and 70 °C using the PA-85 fiber with a constant extraction time of 20 min. A temperature of 70 °C resulted in the highest absolute area for **1**, but 60 °C produced a better signal-to-noise ratio, as shown in Figure 1b. Consequently, 60 °C was selected as the adsorption temperature. A range of extraction times (20–70 min) were tested at 60 °C, using the PA-85 fiber to optimize the SPME sampling period. As shown in Figure 1c, adsorption onto the fiber increased with extraction time, reaching the best signal-to-noise ratio at 50 min.

To check the effect of ionic strength, the solution was supplemented with 0–4 g of sodium chloride and tested at 60 °C. The addition of 3 g resulted in the best signal-to-noise ratio for **1**, compared to 2 and 4 g (Figure 1d). All tests were duplicated.

**Sensory Studies.** *General Conditions.* Sensory analyses were performed according to the relevant ISO standards[10] and as described by Martin and de Revel.[11] Samples were evaluated in individual booths in a ventilated tasting room at controlled room temperature.

All samples were evaluated only orthonasally (all data were collected via olfaction alone).

*Materials.* Several matrices were used for sensory analyses: reverse osmosis water, a white wine (AOC Entre-deux-Mers, 2012), a rosé wine (AOC Buzet, 2012), and a red wine (Merlot Pays d'Oc). None of the wines contained **1** before it was added for sensory analysis (sensory and analytical controls).

Commercial **1** served as a base material. To make this compound soluble, a stock solution was prepared, containing an average of 1.1 g/L in ethanol.

*Panels.* Samples were selected (wine samples and HPLC fractions) for physicochemical analysis by a panel of three judges. Judges were selected on the basis of availability and interest. Participants (27–37) in the sensory panels were volunteers. All panelists were research laboratory staff at ISVV, Bordeaux University, with homogeneous sensory expertise. Detection threshold measurements in reverse osmosis water or in white wine as well as the qualitative effect of **1** addition in reverse osmosis water and in commercial wines naturally

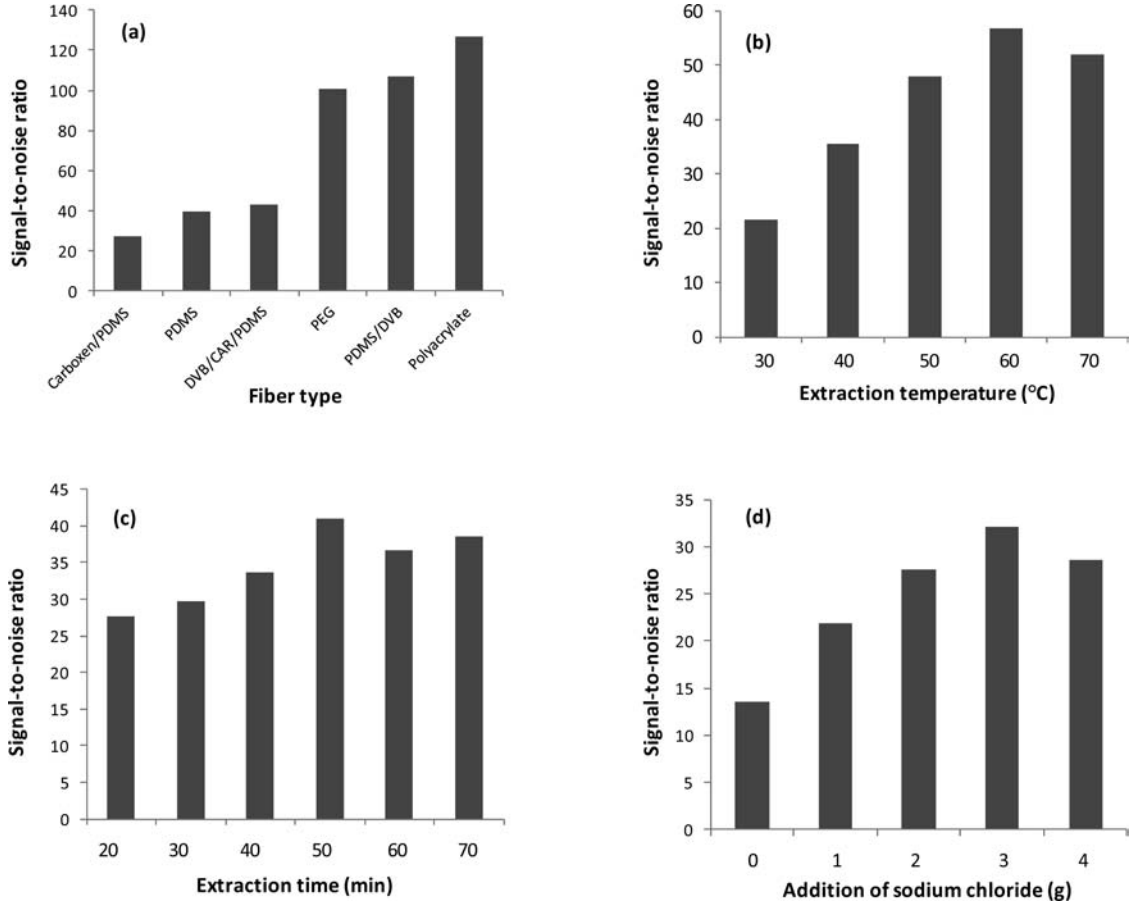


**Figure 1.** Signal-to-noise ratio in white wine depending on (a) fiber type, (b) extraction temperature, (c) extraction time, and (d) addition of sodium chloride.

affected by the defect were carried out by 37 assessors (panel 1), detection threshold in rosé wine by 27 assessors (panel 2), and detection threshold measurements in red wine by 35 assessors (panel 3). Ages ranged between 21 and 53 years, and the panels consisted of 54−68% females. The qualitative effect of **1** addition in red wine matrix was realized with a panel of 53 students (panel 4, 32 females and 21 males with an average age of 24) in enology in the first 6 months of their training.

**Quantitative Effect of 2-Bromo-4-methylphenol.** The detection thresholds were determined in water or in selected wines, with an ascending procedure (ten concentrations) and the three-alternative forced choice presentation method (AFC).[12]

For each concentration, the subject received a set of three covered ISO glasses coded with three-digit numbers.[13] Two of these glasses were blank samples (reverse osmosis water or selected wines) and one contained the **1** dilution (positive sample). For each concentration, the order of presentation was randomized.

For the whole series of dilution sets, each assessor was required to first sniff each glass in the prescribed order and then close the spiked sample in each set of three glasses.

The stimulating perithreshold concentration ranges to be used were determined on the basis of preliminary experiments (Table 3).

**Table 3. Concentration Ranges of 2-Bromo-4-methylphenol Used for Sensory Analysis**[a]

| matrix | concentration range used (ng/L) |
|---|---|
| reverse osmosis water | 0.2−109.4 |
| white wine | 0.5−273.6 |
| rosé wine | 2.1−1094.4 |
| red wine | 2.1−1094.4 |

[a]Concentration ranges were prepared in a geometric series (2-fold), and this table shows the extreme values of the ranges.

The individual detection threshold was estimated as the geometrical mean between the last concentration missed and the first concentration detected.[12]

**Qualitative Effect of 2-Bromo-4-methylphenol.** *Qualitative Effect of Adding 2-Bromo-4-methylphenol to Reverse Osmosis Water.* Each participant (panel 1) received a glass containing **1** solution at a supraliminal concentration (3283 ng/L), prepared in reverse osmosis water and presented in a covered ISO glass.[13] Participants were required to give the most precise olfactory description of the stimulus and answer the following question: "What terms would you use to characterize this sample?" No limit to the number of attributes was imposed on the subjects, and no specific instructions were given to participants concerning hedonic or subjective terms.

All of the descriptors for **1** evoked by the participant were recorded. The quotation frequency (QF) was calculated for each term, using the following formula: QF = NQ/$N$ (NQ = the number of participants who quoted the terms and $N$ = the number of terms quoted). Synonyms were included within an umbrella term or a higher level family.

*Qualitative Effect of Adding 2-Bromo-4-methylphenol to Red Wine.* This sensory task was conducted using red wine spiked with 22 ng/L **1**, antimode of the detection threshold distribution. Participants (panel 4) were required to give the most precise olfactory description of the wine presented. The QF was calculated for each term, using the following formula: QF = NQ/$N$ (NQ = the number of participants who quoted the terms and $N$ = the number of terms quoted).

*Qualitative Effect of 2-Bromo-4-methylphenol in Commercial Wines Naturally Affected by the Defect.* Six red and 7 rosé wines affected by the defect were presented to 37 assessors (panel 1), and they were asked if they perceived any off-odor. Participants who perceived an off-odor were then asked to describe the nuances in that sample by choosing a descriptor. For each sample, the subject rated the intensity of these descriptors on a 0−8 point structured scale, where 0 = no odor and 8 = high intensity.

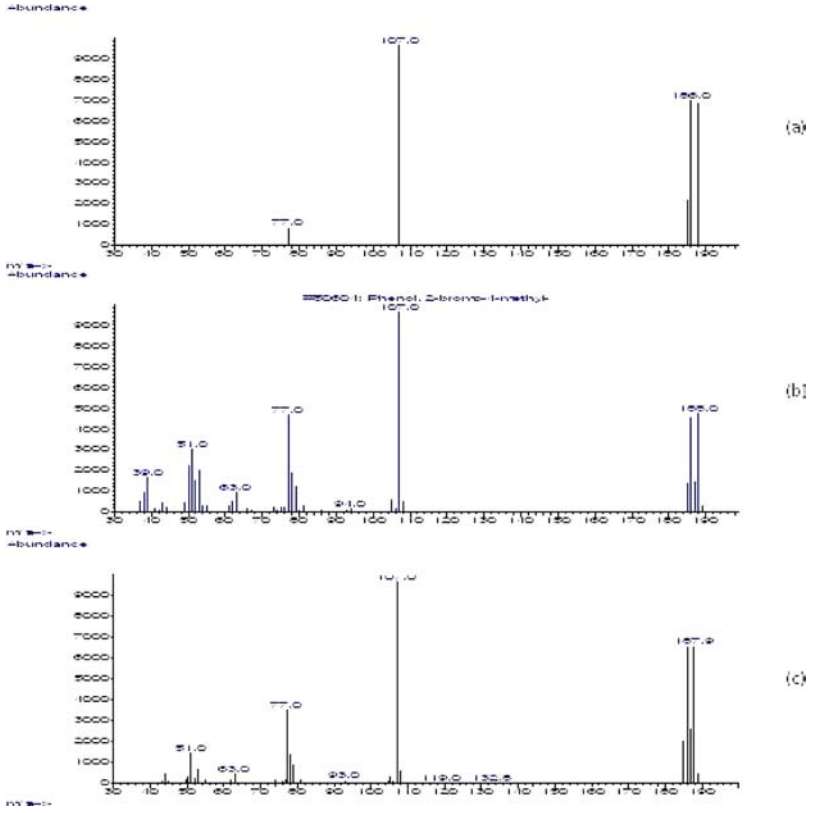


**Figure 2.** (a) Mass spectrum of a peak naturally present only in an affected wine. (b) Mass spectrum of 2-bromo-4-methylphenol from NIST 2011 Spectral Library (NIST Registry No. 50599; CAS Registry No. 006627-55-0). (c) Mass spectrum of 2-bromo-4-methylphenol reference compound.

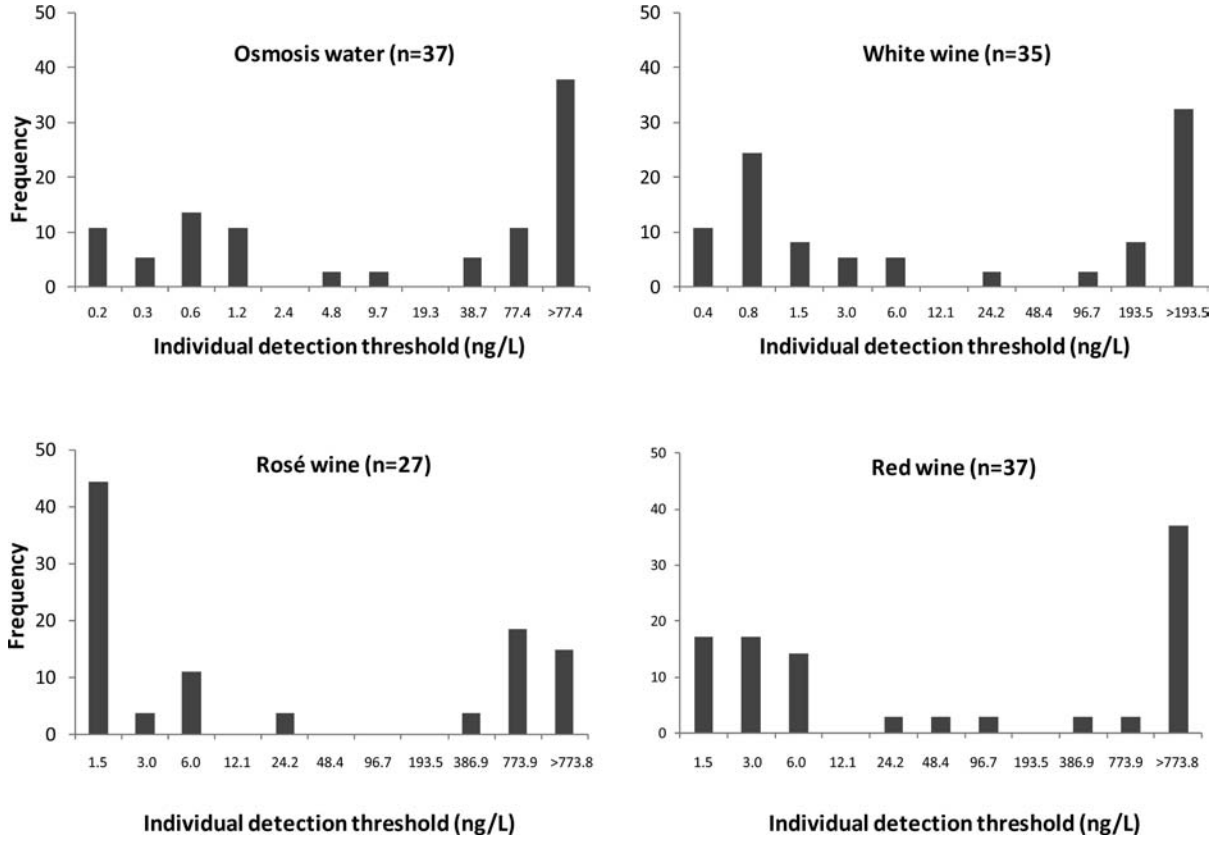


**Figure 3.** Individual detection threshold distribution for 2-bromo-4-methylphenol in different matrices. *n* = number of subjects tested.

## RESULTS AND DISCUSSION

**2-Bromo-4-methylphenol Identification.** Among 25 wine HPLC fractions, from 4 samples affected by this off-flavor, only fraction 19 was characterized by an iodine odor.

Its composition was analyzed using gas chromatography coupled to olfactometry (GC-O) and mass spectrometry (GC-MS). The olfactometry approach revealed that, in the wine fraction extract, only one iodine odor zone (OZ), with a linear retention index (LRI) of 2094, was perceived by the three members of the panel, who described it as "iodine" and "oysters".

GC-MS was used to identify the compound responsible for the iodine OZ. This OZ was first targeted by its LRI. GC-MS revealed that the spectrum of the OZ "iodine" compound, naturally present only in affected wines, exhibited the same peak, identical fragmentation, and comparable relative abundances to **1**, indexed in the NIST 2011 library. These results were confirmed by comparing the LRI and mass spectrum of the compound detected in wine with that of reference compound **1** (2095 on the BP21 column). The chromatograms and mass spectra obtained are presented in Figure 2. Finally, olfactometry (GC-O) confirmed that the odor quality of the pure compound matched that of the corresponding OZ eluted from the wine extract.

To our knowledge, this compound had never previously been identified in wine, so neither the concentrations present nor its aromatic impact had previously been described.

**2-Bromo-4-methylphenol Levels in Wines.** The **1** levels in the 8 white, 44 rosé, and 13 red wines assayed are shown in Table 1. The wines presented a wide range of levels, with maximum concentrations of 28900, 7556, and 48000 ng/L and minima of 260, 35, and 63 ng/L in white, rosé, and red wines, respectively. However, 4 white (Table 1A), 20 rosé (Table 1B), and 5 red wines (Table 1C) presented levels below the quantitation limit of this method. The average concentration was about 2754 ng/L in the wines studied where **1** was present at levels higher than the quantitation limit.

This study highlighted the occurrence of a new wine contaminant, 2-bromo-4-methylphenol, detected in wines acidified using ion-exchange resins. This compound was found at levels between 35 and 48000 ng/L, and this diversity suggests that levels may vary at different times during the resin treatment cycle. Regulations concerning cation-exchange resins are not necessarily in disagreement with our results. Indeed, only the maximum release of organic compounds is regulated (1 mg/kg when the first 40 volumes of liquid flow through the resin), and there is no specific limit value expressed for any individual compounds.[14] At this stage in our research, nevertheless, it is not possible to incriminate ion-exchange resins directly: the presence of **1** may also be linked to various processes accompanying the use of resins, such as regeneration conditions, washing, and flow rate, and further investigation is thus necessary.

**Quantitative Effect of 2-Bromo-4-methylphenol.** Figure 3 shows the distribution of individual detection thresholds for **1** in different matrices. In water, individual thresholds ranged from 0.15 to >77.4 ng/L, with a very wide distribution, suggesting the presence of two populations, sensitive and nonsensitive. Additional measurement revealed that some subjects were able to detect **1** in water at a concentration of 0.005 ng/L (2/37 subjects). Moreover, a few subjects (3/37 subjects) failed to detect **1** at a concentration of 2500 ng/L.

The range of dilution factors between the two extreme sensitivities revealed a panelist variability >5 × $10^5$.

Determination of anosmic frequencies for different compounds has been studied extensively,[15−17] but such a wide variation in sensitivity for a compound such as **1** had never been reported. These considerable variations in olfactory sensitivity to **1** affect the ability to detect this compound in wine. Individual thresholds ranged from 0.4 to >193.5 ng/L in white wine, from 0.5 to >774 ng/L in rosé wine, and from 0.5 to >774 ng/L in red wine. Moreover, the frequency distributions were apparently bimodal (continuous probability distribution with two different modes).[18] No gender or age effect was observed.

The pertinence of the olfactive detection threshold has been undermined by highlighting some remarkable perceptual interactions involving compounds at levels well below their individual detection thresholds in the experimental mixture.[19] In this study, the concept of an olfactive detection threshold may also be challenged, because **1** was perceived very differently depending on the subject and considering the detection threshold to be the "average" between those of sensitive and nonsensitive subjects would be meaningless.

**Qualitative Effect of Adding 2-Bromo-4-methylphenol to Reverse Osmosis Water.** After a session during which a glass containing a large subthreshold concentration of **1** was presented to the panel, 48 terms used by the subjects were counted: 25 different terms designating objects or families of objects were collected, and 2 hedonic descriptions (e.g., "unpleasant") were used. However, 8 of 37 subjects did not perceive any odor. In view of the wide range of sensitivities observed, only the results of the more sensitive group (16 subjects, representing 43% of the panel, whose individual detection thresholds in water were <19.3 ng/L) were considered (Figure 4). These more sensitive subjects used 19 different terms on varying levels. Therefore, synonyms were included within an umbrella term or a higher level family, as shown in Table 4.

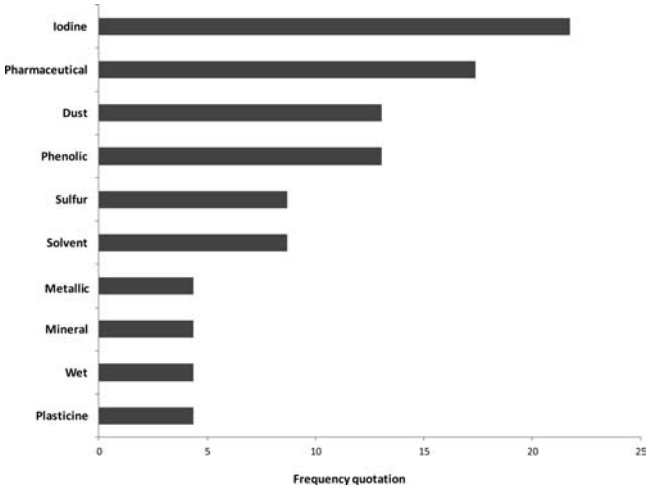


**Figure 4.** Quotation frequency, expressed in percentage, for each term cited by the 16 sensitive subjects (of 37) when 2-bromo-4-methylphenol was added to reverse osmosis water. Quotation frequency is the ratio of the number of participants who quoted the term to the number of terms collected.

**Table 4. Terms and Synonyms Cited by Sensitive Subjects Describing Reverse Osmosis Water Supplemented with 2-Bromo-4-methylphenol**

| terms | umbrella term |
|---|---|
| chlorine, bleach | chlorine |
| pharmaceutical, drug, laboratory, hospital | pharmaceutical |
| burnt rubber, tar, gouache, plastic | phenolic |
| fish, mud, iodine, oysters | iodine |
| solvent, glue | solvent |

The sum of the citations for umbrella terms and others was computed from the sensitive subjects' responses. The lexicon quoted by the participants is illustrated in Figure 4.

The characteristic odor descriptors for **1** had "iodine" or "pharmaceutical" connotations. This result is in agreement with those of Griffiths[4] and Strube et al.,[5] who indicated that halogenated compounds are generally characterized by musty, medicinal/chemical/iodine, or phenolic terms.

**Qualitative Effect of Adding 2-Bromo-4-methylphenol to Red Wine.** Fifteen of 53 subjects did not perceive any off-flavor in the wine spiked with **1** at 22 ng/L. Sixteen different terms were used by sensitive participants (38 subjects). **1** mainly imparted "iodine" notes to red wine, as described by sensitive panelists (Figure 5).

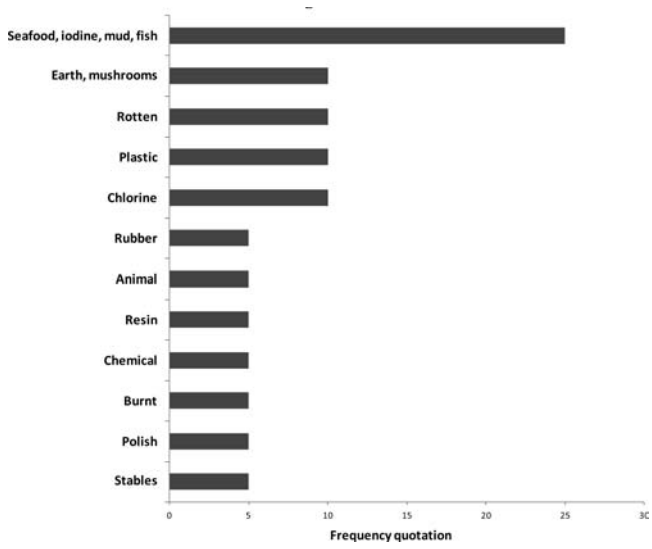


**Figure 5.** Quotation frequency, expressed in percentage, for each term cited by the 38 sensitive subjects (of 53) when 2-bromo-4-methylphenol was added to a red wine matrix. Quotation frequency is the ratio of the number of participants who quoted the term to the number of terms collected.

These results are in agreement with the individual detection thresholds: a 50/50 distribution of the population was found according to their sensitivity, thus explaining the wide variation in wine assessment. Olfactory perception of wine is dependent on mental construction;[20] however, when two sections of a population exhibit such wide variations in olfactory sensitivity, this is likely to have a significant impact on their evaluation of the product.

**Qualitative Impact of 2-Bromo-4-methylphenol on Commercial Wines Naturally Affected by the Defect.** The levels of **1** in commercial wines naturally affected by the defect were correlated with the sensory evaluation of each wine.

Panel 1 (37 subjects) strongly distinguished these wines according to their **1** levels. The average scores for defect intensity were significantly higher for wines containing the highest concentrations of **1**, thus confirming the sensory importance of this compound in wine quality perception (Figure 6). The terms used by sensitive subjects for rosé and red wines were retained: seafood, iodine, chemical, plastic, chlorine, moldy, mushroom, earth, rubber, burnt, pharmaceutical, mineral (chalk), and wet. As shown in Figure 7, the presence of **1** was not detected by a high proportion of subjects, irrespective of its concentration in the corresponding wine. This wide diversity of defect assessment was observed for both rosé and red wines (Figure 7). Figure 8 shows the distribution of perceived intensities of the defect attributed to the presence of **1** in rosé (concentration = 342.2 ng/L) and red (concentration = 787 ng/L) wines. These results demonstrate the wide diversity in perception among subjects: 46% of panelists perceived no defect when 19% gave a score of 7 (on the 8-point scale) to the commercial rosé wine naturally affected by the defect. Similarly, in the commercial red wine naturally affected by the defect, 30% of panelists perceived no defect when 16% gave a score of 7 (Figure 8).

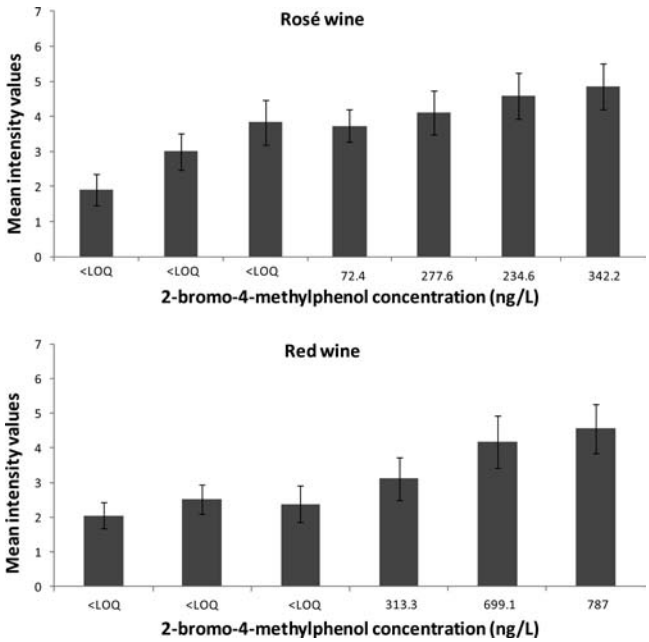


**Figure 6.** Mean aromatic defect intensities in wines with various concentrations of 2-bromo-4-methylphenol. Error bars indicate the 95% confidence interval on the mean intensity values.

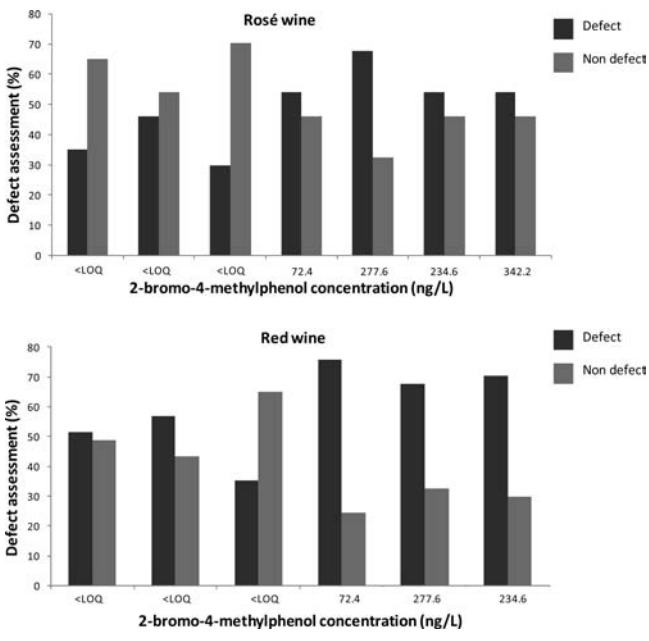


**Figure 7.** Percentage of subjects who detected a defect in commercial wines naturally containing 2-bromo-4-methylphenol.

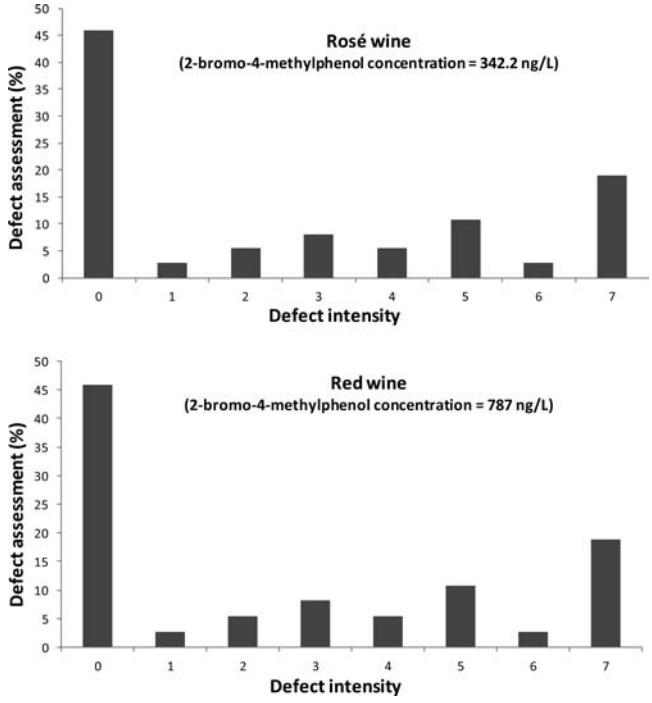


**Figure 8.** Distribution of perceived iodine defect intensity scores for rosé and red wines containing 342.2 and 787 ng/L 2-bromo-4-methylphenol, respectively.

Sensory studies concerning **1** gave very interesting results. This compound was perceptible at levels around 1 ng/L, which indicates its very powerful olfactive impact and highlights the major sensory consequences of its presence in the affected wines. **1** was identified as being responsible for a "chemical (phenolic)" taint in brine-salted Gouda cheese.[21] Several halogenated volatiles have been described as powerful odorants and identified as off-odors in mineral water, orange juice, salted Gouda cheese, cocoa powder, dried fruit, wine, fish sauce, and chicken.[5,22,23] For example, 2,4,6-trichloroanisole is responsible for "cork taint" in wine and the "Rio off-flavor" in coffee.[24] The odor detection threshold values for various halogenated volatiles in water generally range from milligrams per liter to the nanograms per liter.[5] Although these values depend on the matrix studied, some of these compounds had a major impact on odor. The odor detection threshold for the musty taint of 2,3,6-trichloroanisole was reported as $3 \times 10^{-10}$ mg/L in water.[5] In a recent study on the odor characteristics of ortho- and para-halogenated phenols and cresols, it was demonstrated that 2-halogenated-4-methylphenols had the lowest odor detection thresholds. Moreover, these compounds are almost fully characterized by medicinal, plaster-like descriptors.

The perception of **1** by the judges was very unusual, with a huge difference between the individual perception thresholds of sensitive and nonsensitive subjects, revealing a bimodal distribution. Similar phenomena were observed in all the test matrices. These results revealed the limitations of sensory analysis as a general tool for product quality control and assessment. For instance, according to individual sensitivity, an enologist may or may not be able to detect whether resin treatment has led to wine spoilage, with all of the consequences that may have. In the same way, a product's appreciation by consumers will be conditioned by their sensitivity, which will affect its economic value. Specific anosmia or hyperosmia for other organohalogenated compounds, such as 2,4,6-trichloroanisole, has also previously been reported.[25−27]

## AUTHOR INFORMATION


### Corresponding Author

*(J.-C.B.) Phone: +33 5 57 57 58 63. Fax: +33 5 57 57 58 13. E-mail: jean-christophe.barbe@agro-bordeaux.fr.


### Notes

The authors declare no competing financial interest.

## REFERENCES


(1) Commission Implementing Regulation (EU) No. 144/2013 of 19 February 2013. Amending Regulation (EC) No 606/2009 as regards certain oenological practices and the applicable restrictions and Regulation (EC) No. 436/2009 as regards the registering of these practices in the documents accompanying consignments of wine products and the wine sector registers to be kept.

(2) Escudier, J.-L.; Cauchy, B.; Lutin, F.; Moutounet, M. Acidification et stabilisation tartrique par méthodes soustractives. Comparaison de technologies d'échanges d'ions par résines et d'extraction d'ions par membranes. *Rev. Fr. Œnol.* **2012**, *254*, 324−332.

(3) Blaise, A.; Brun, S. Un phénomène enzymatique à l'origine du goût d'amande amère dans les vins. *C.R. Acad. Agric. Fr.* **1986**, *72*, 73−77.

(4) Griffiths, N. M. Sensory properties of the chloroanisoles. *Chem. Sens.* **1974**, *1*, 187−195.

(5) Strube, A.; Buettner, A.; Czerny, M. Influence of chemical structure on absolute odor thresholds and odor characteristics of ortho- and para-halogenated phenols and cresols. *Flavour Fragrance J.* **2012**, *27*, 304−312.

(6) Höfer, T. Tainting of seafood and marine pollution. *Water Res.* **1998**, *32*, 3505−3512.

(7) Lytra, G.; Tempere, S.; De Revel, G.; Barbe, J.-C. Distribution and organoleptic impact of ethyl 2-hydroxy-4-methylpentanoate enantiomers in wine. *J. Agric. Food Chem.* **2012**, *60*, 1503−1509.

(8) Pineau, B.; Barbe, J.-C.; Van Leeuwen, C.; Dubourdieu, D. Examples of perceptive interactions involved in specific "red- and blackberry" aromas in red wines. *J. Agric. Food Chem.* **2009**, *57*, 3702−3708.

(9) Organisation Internationale de la Vigne et du Vin. Recueil des méthodes internationales d'analyses. Dosage du 2,4,6-trichloroanisole relargable dans le vin par les bouchons de liège (Résolution OIV-Oeno 296-2009).

(10) Sensory Analysis − General guidance for the design of test rooms: ISO 8589. In *Analyse Sensorielle*; AFNOR: Paris, France, 2010.

(11) Martin, N.; De Revel, G. Sensory evaluation: scientific bases and oenological applications. *J. Int. Sci. Vigne Vin* **1999**, No. Special Issue, 81−93.

(12) Sensory Analysis − Methodology − General Guidance for Measuring Odor, Flavour and Test Detection Thresholds by a Three-Alternative Forced-Choice (3-AFC) Procedure: ISO 13301. In *Analyse Sensorielle*; AFNOR: Paris, France, 2002.

(13) Sensory Analysis − Apparatus − Wine-Tasting Glass: ISO 3591. In *Analyse Sensorielle*; AFNOR: Paris, France, 1977.

(14) Organisation Internationale de la Vigne et du Vin. *Codex Œnologique International*; OIV: Paris, France, 2013; 663 pp.

(15) Amoore, J. E. Specific anosmia and the concept of primary odors. *Chem. Senses* **1977**, *2*, 267−281.

(16) Baydar, A.; Petrzilka, M.; Schott, M. P. Olfactory thresholds for androstenone and galaxolide: sensitivity, insensitivity and specific anosmia. *Chem. Senses* **1993**, *18*, 661−668.

(17) Cain, W. S.; Schmidt, R. Sensory detection of glutaraldehyde in drinking water-emergence of sensitivity and specific anosmia. *Chem. Senses* **2002**, *27*, 425−433.

(18) Jarque, C. M.; Bera, A. K. A test for normality of observations and regression residuals. *Int. Stat. Rev.* **1987**, *55*, 163−172.

(19) Lytra, G.; Le Floch, A.; Tempere, S.; De Revel, G.; Barbe, J.-C. Study of sensory interactions among red wine fruity esters in a model solution. *J. Agric. Food Chem.* **2013**, *61*, 8504−8513.

(20) Brochet, F.; Dubourdieu, D. Wine descriptive language supports cognitive specific of chemical senses. *Brain Lang.* **2001**, *77*, 187−96.

(21) Mills, O. E.; Gregory, S. P.; Visser, F. R.; Broome, A. J. Chemical taint in rindless Gouda cheese. *J. Agric. Food Chem.* **1997**, *45*, 487−492.

(22) Curtis, R. F.; Land, D. G.; Griffiths, N. M.; Gee, M.; Robinson, D.; Peel, J. L. Chloroanisoles as a cause of musty taint in chicken and their microbiological formation from chlorophenols. *J. Sci. Food Agric.* **1974**, *25*, 811−828.

(23) Mottram, D. S. Chemical tainting of foods. *Int. J. Food Sci. Technol.* **1998**, *33*, 19−29.

(24) Spadone, J. C.; Takeoka, G.; Liardon, R. Analytical investigation, of Rio off-flavour in green coffee. *J. Agric. Food Chem.* **1990**, *38*, 226−230.

(25) Suprenant, A.; Butzke, C. E. Implications of odor threshold variations on sensory quality control of cork stoppers. *Am. J. Enol. Vitic.* **1997**, *48*, 269.

(26) Teixera, M. I. V.; Romao, M. V. S.; Bronze, M. 2,4,6-Trichloroanisole: a consumer panel evaluation. *Cienc. Tec. Vitivinic.* **2006**, *21*, 53−65.

(27) Tempere, S.; Cuzange, E.; Malak, J.; Bougeant, J. C.; De Revel, G.; Sicard, G. The training level of experts influences their ability to detect some wine key compounds. *Chemosens. Percept.* **2011**, *4*, 99−115.

polarities. The present extraction method, as well as the column and mobile phase used for the retention and isolation of HAAs or sugars, may not suitable for their simultaneous analysis in a single run. Meanwhile, due to the absence of a chromophore, the amino acids, sugar and creati(ni)ne often need to be derivatized with different derivatization reagents, which complicates detection.[22−24] To solve the extraction and retention problems, a suitable extraction solvent and a special column that promotes superior polar compound retention should be used. LC−MS/MS—a very sensitive technique for HAA determination at trace levels[25,26]—could eliminate the need for derivatization. Recently, this technique has been used as a tool to determine both amino acids and sugars in some published studies.[27,28]

In the present study, a robust method for the simultaneous quantification of two HAAs (PhIP and 4′-OH-PhIP) and their precursors (phenylalanine, tyrosine, creatine, creatinine, and glucose) in pork samples was established using ultra high-performance liquid chromatography coupled with triple quadrupole mass spectrometry (UHPLC−TQD−MS/MS). The appropriate extraction solvents and chromatographic columns for the simultaneous extraction and isolation of compounds with different polarities were compared and selected. The method was validated with regard to linearity, detection limitations, matrix effects, and recoveries. Finally, the new kinetic tools were applied to a kinetic study of HAAs and their precursors in fresh pork model systems with different heating time treatments.

## MATERIALS AND METHODS

**Reagents and Standard Solutions.** Optima LC/MS methanol, acetonitrile and HPLC-grade formic acids (99.9%) were obtained from Thermo Fisher Scientific (Waltham, MA). Distilled water was purified using a Milli-Q filtration system from Millipore Corp. (Bedford, MA). All of the reagents were filtered through a 0.22 $\mu$m nylon or cellulose filter before injecting them into the UHPLC−MS/MS system.

The SPE used Supelclean LC-18 columns were ordered from Supelco Corp. (St. Louis, MO). The Oasis MCX cartridges (60 mg, 3 mL) were obtained from Waters Corp. (Milford, MA) and the STYRE-SCREEN $SSH_2P$ columns were acquired from Sepax Technologies (Newark, NJ). The screw cap Tuf-Bond Teflon-fitted glass reaction vials (50 mL of capacity) were purchased from Pierce Company (Rockford, IL). All of the other chemicals used in this study were of analytical grade and purchased from Sinopharm Chemical Reagent Beijing Co. Ltd. (Beijing, China).

Creatine, creatinine, and two HAAs standards, PhIP and 4′−OH-PhIP (Figure 1), were purchased from Santa Cruz Biotechnology, Inc.

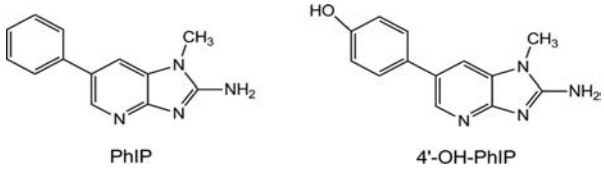


**Figure 1.** Structures of PhIP and 4′-OH-PhIP.

(Santa Cruz, CA). L-phenylalanine (Phe), L-tyrosine (Tyr) and D-glucose (Glc) were obtained from Sigma-Aldrich Company (St. Louis, MO). The standard stocking solutions of each compound (about 125 mg $L^{-1}$ for HAAs, about 1000 mg $L^{-1}$ for amino acids, creatine, creatinine, and glucose) were prepared and stored at −20 °C in the dark. The working standards of all of the above-mentioned chemicals were prepared by making the appropriate dilutions of stock solutions with a mixed solution of 0.1% formic acids and 50% methanol in water, and stored at 4 °C.

**Model System.** The dried fresh meat model system was established according to an earlier study, with some modification.[8] Pork was purchased at a local market and freeze-dried for 48 h. The lyophilized samples of raw pork (0.7 g) were mixed with diethylene glycol (3 mL) in the glass reaction vials and heated at 195 °C for 0−120 min using a thermostat-controlled oil-bath with electronically controlled temperature and temperature probe from RKC Instrument Inc. (Tokyo, Japan). The heating block was preheated for 2 h before sealing and inserting the vials. The temperature was checked every 30 s, and temperature fluctuations were within 2 °C. After heating, the vials were immediately cooled in an ice-bath to stop any further reaction. The model system experiments were performed in triplicate.

**Sample Preparation Procedures.** The content of the reaction vials was diluted and homogenized with 12 mL of 0.1 M hydrochloricacid (HCl) (four times for 15 s). Then the homogenate was extracted for 15 min using ultrasound. After the centrifugation of the mixture (11363 g for 20 min at 4 °C), the supernatant was collected. The extraction procedures were repeated twice, and then the extracting solutions were combined and the volume was fixed to 25 mL with the HCl solution. Ethanol was added to 10 mL of acidic solution with an end concentration of 80% to remove the protein.[29] The protein-free extract obtained was concentrated until it was dry in a rotary evaporator at 39 °C and then dissolved in 2 mL by solution of 0.1% formic acids and 50% methanol in water before being passed through a 0.22 $\mu$m filtration membrane. Alternatively, the SPE purification procedure with three cartridges (Supelclean LC-18, Oasis MCX, and STYRE-SCREEN $SSH_2P$) was implemented instead of the membrane filtration. For MCX cartridge, columns were first activated continuously with 6 mL of methanol, 6 mL of distilled water, and 6 mL of 0.1 M HCl solution, and were then rinsed sequentially with 6 mL of 0.1 M HCl solution and 6 mL of methanol after loading the sample. The retained analytes were finally eluted by a 6 mL mixture of methanol and ammonium hydroxide (25%) at a ratio of 95:5. For the LC-18 column, after conditioned with 6 mL of methanol and water, the columns were loaded the sample. First 1 mL of the sample solvents were discarded. And the subsequent sample solvents and the eluates from the 6 mL of the methanol were collected. With regard to the $SSH_2P$ cartridge, similar activate procedures as MCX were implemented. After loading the sample, the cartridges were then washed with water and 50% methanol in water. The target compounds were ultimately eluted with 6 mL of the methanol. All the elution obtained from the SPE procedure were then evaporated to dryness under a stream of nitrogen and then resuspended in 300 $\mu$L of the mixed solution (0.1% formic acids and 50% methanol in water). Finally, the filtrate or SPE elution was diluted to proper concentrations and transferred to an autosampler vial for UHPLC−MS/MS analysis.

**UHPLC−MS/MS Analysis.** The chromatographic analysis was performed on a Waters Acquity UPLC system equipped with a quaternary pump system, micro vacuum degasser, autosampler and column compartment setting the temperature at 35 °C. The separation was carried out on a Waters Atlantics $dC_{18}$ column (250 × 4.6 $mm^2$ i.d., 3.0 $\mu$m) (Milford, MA), which was selected from three other columns: Waters Acquity UPLC BEH $C_{18}$ (50 × 2.1 $mm^2$ i.d., 1.7 $\mu$m), Waters Acquity UPLC HSS $T_3$ (100 × 2.1 $mm^2$ i.d., 1.8 $\mu$m) and Waters XSELECT HSS $T_3$ (150 × 4.6 $mm^2$ i.d., 3.5 $\mu$m). The gradient elution was achieved with a binary mobile phase of methanol (A) and formic acid (0.1%, v/v) (B) at a flow rate of 0.5 mL $min^{-1}$. The gradient elution—0−10 min 5−100% A phase—was finally returned to its initial composition and equilibrated for 5 min before the next injection. Separation and stabilization were achieved in 15 min. The single injection volume was set at 1 $\mu$L.

The MS/MS detection was performed on a Waters Quattro Premier XE triple quadrupole mass spectrometer (TQD) (Milford, MA) using an electrospray ionization (ESI) source in positive mode. The data acquisition was carried out by MassLynxv 4.1 SCN 805 software from Waters. The capillary and extractor voltages were 3.5 kV and 3 V, respectively. Nitrogen (99.9% of purity) was used as the desolvation gas with the gas flow set to 800 L $h^{-1}$ at a temperature of 350 °C. The flow rate of the cone gas was set to 50 L $h^{-1}$ at a source temperature of 130 °C. Argon (99.9% of purity) was used as the collision gas at a flow

Table 1. Retention Time and MS/MS Parameters of the HAAs and Their Precursors

| compound | dwell time (secs) | cone voltage (V) | quantitation transition[a] | proposed assignation | conformation tranition[a] |
|---|---|---|---|---|---|
| PhIP | 0.037 | 54 | 225.03 > 210.01 (42) | $[M + H - \cdot CH_3]^+$ | |
| 4′-OH-PhIP | 0.037 | 54 | 241.03 > 225.76 (32) | $[M + H - \cdot CH_3]^+$ | |
| Phe | 0.037 | 22 | 165.98 > 119.68 (40) | $[M + H - COOH - H]^+$ | 165.98 > 102.80 (28) |
| Tyr | 0.037 | 24 | 181.98 > 122.73 (24) | $[M + H - COOH - NH_2 + 2H]^+$ | 181.98 > 90.81 (34) |
| creatine | 0.037 | 28 | 131.97 > 89.83 (16) | $[M + H - NH_2 - CN]^+$ | 131.97 > 43.77 (22) |
| creatinine | 0.037 | 34 | 114.03 > 44.02 (20) | $[M + H - NH_2 - CO - HCN]^+$ | 114.03 > 85.84 (16) |
| Glc | 0.037 | 14 | 382.90 > 202.73 (20) | $[2M + Na - M]^+$ | |

[a]Collision energy (V) is given in parentheses.

rate of 0.13 mL $min^{-1}$. The specific MS/MS parameters (compound transitions, collision energy, cone voltage, and dwell times) were optimized with 1 ng $\mu L^{-1}$ target compounds (Table 1).

**Validation.** The proposed method was validated in terms of linearity, recovery, limit of detection (LOD), limit of quantification (LOQ), and matrix effects. The calibration curve was established by plotting the peak area ratios of standards to the internal standard against seven analyte concentrations. The recoveries of the sample preparation were determined by analyzing blank samples spiked with two concentration mixed standards (low and high) and calculated as [(levels in spiked samples − levels in blank samples)/amount added] × 100.The precision of the overall method was studied by implementing intraday (repeatability) and interday (reproducibility) precision experiments. Intraday precision was investigated at a low spiked level in a recovery study with three replicates, whereas interday precision was evaluated at a high spiked level in a recovery study that was accomplished over three consecutive days. The matrix effects were evaluated using the slope comparison method.[30] The food sample extracts, which were spiked with diminishing concentrations of the standards, were used to establish standard addition calibration curves. Then, the slopes of these curves (A1, A2,···A*n*) were compared with the slopes obtained from the pure standards (B1, B2,···B*n*) at the same concentration levels, and the slope ratios $R_n$ were equal to A*n*/B*n*. The matrix effects could then be decided with $R_n$ as the ionization suppression effect (<1), ionization enhancement effect (>1) or without matrix effects (= 1).

## RESULTS AND DISCUSSION

**UHPLC−MS/MS Determination.** Given that the polarities of HAAs, sugars and creati(ni)ne are considerably different, the simultaneous detection of the HAAs and their precursors in a single run appears difficult. Therefore, the selection of a suitable chromatographic column is of great importance. Four columns, including Waters Acquity UPLC BEH $C_{18}$ column, Waters Acquity UPLC HSS $T_3$ column, Waters XSELECT HSS $T_3$ column, and Waters Atlantis $dC_{18}$ column were tested for obtaining well isolation and the suitable sensitivity of analytes (Figure 2). The BEH $C_{18}$ column, while widely used for the isolation of HAAs in previous studies,[26] was not suitable for the retention of Glc, creatine, creatinine, and Tyr, which are eluted before 1 min and could not have been isolated from their matrixes (Figure 2A). Both the UPLC HSS $T_3$ and Select HSS $T_3$ columns were developed by manufacturers to promote polar compound retention, and a charged surface hybrid (CSH) technique that controlled a small amount of charges on the surface of the fixed phase was applied to the latter column to further enhance the retention efficiency, according to the product description. The appropriate retentions of HAAs and amino acids were found when a UPLC HSS $T_3$ column was used, but for Glc, creatine, and creatinine, the retention remained poor (Figure 2B). Conversely, the Select HSS $T_3$ column provided proper retentions for all of the target compounds, but the poor symmetry for Glc and the bad separation between creatinine and Glc limit its application (Figure 2C). Using the same CSH technique, the Atlantics dC18 column is improved by the designer to pursue a simultaneous retaining and isolating of both the polar and nonpolar compounds with symmetrical peaks and proper retaining efficient. Compared with all of the above-mentioned columns, the use of the $dC_{18}$ column not only achieved favorable retention for all analytes, but also offered acceptable separation between creatinine and Glc. Therefore, this column was ultimately selected (Figure 2D). In order to improve the separation between Glc and create(ni)ne, different mobile phase and gradient conditions were tested. Due to the surface charge used in the packing to enhance the polar compound retention, no significant improvements were observed. However, without the baseline separation for all analytes, the quantifications are acceptable, since these compounds could be separated by their molecular ions in MRM mode, according to a statement from a previous study.[26] Therefore, a simple gradient condition was finally used to simultaneously detect the two HAAs and their precursors.

The ESI−MS/MS parameters were optimized by injecting 1 ng $\mu L^{-1}$ of the standard solution into the ESI source. Both the positive and negative ion modes were evaluated, and the results showed that all of the analytes were detectable in the positive mode. Amino acids could also be detected in the negative mode with relatively low sensitivity. Thus, the positive ion mode was ultimately preferred.

As for the ionization, saccharides were suggested to possess multiple ionization options. Previous studies have reported cesium positive ions $[M + Cs]^+$ or monosodiated cluster ions $[2M + Na]^+$ as the precursor ions of sugars.[27,31] Thus, the fragmentations of Glc were determined in this study. Supporting Information (SI) Figure S1 shows the fragmentation of Glc from monosodiated cluster ions $[2M + Na]^+$($m/z$ 383) to monosodiated adduct ions $[M + Na]^+$ ($m/z$ 203)—a transition that was ultimately chosen for the quantification of Glc in multiple reaction monitoring (MRM) mode. The ionization conditions for all seven targets are summarized in Table 1.

**Sample Extraction and Clean-Up.** To obtain the best extraction efficiency for PhIP, 4′-OH-PhIP, and their precursors, including Phe, Tyr, creatine, creatinine, and Glc, four solvents were tested with the same samples: water, 0.1% formic acids in water, 0.1 M HCl, and the solution of 0.1% formic acids and 50% methanol in water. The recoveries of all seven compounds after extraction are summarized in Table 2, which shows that all four solvents could successfully extract all of the target compounds with recoveries over 56.7%. Compared with the other three solvents, 0.1 M HCl could extract more PhIP and 4′-OH-PhIP, and was thus chosen.

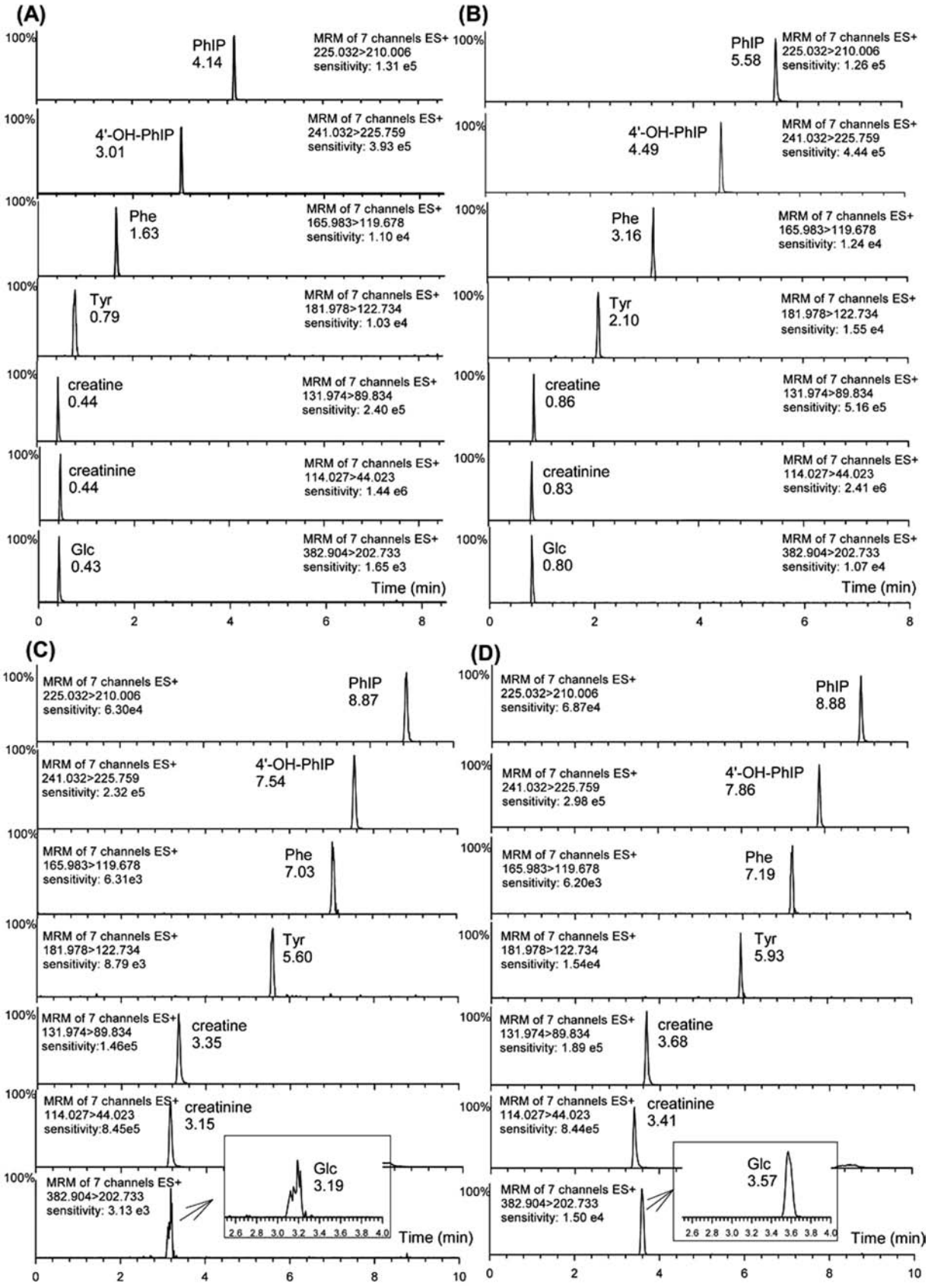


**Figure 2.** Comparison of separation effects for PhIP, 4′-OH-PhIP, and their precursors (Phe, Tyr, creatine, creatinine, and Glc) in same standard concentrations among four different candidate columns: (A) Waters Acquity UPLC BEH $C_{18}$ (50 × 2.1 $mm^2$ i.d., 1.7 $\mu$m), (B) Waters Acquity UPLC HSS $T_3$ (100 × 2.1 $mm^2$ i.d., 1.8 $\mu$m), (C) Waters XSELECT HSS $T_3$ (150 × 4.6 $mm^2$ i.d., 3.5 $\mu$m) and (D) Waters Atlantis $dC_{18}$ (150 × 4.6 $mm^2$ i.d., 3 $\mu$m). The $m/z$ of fragment and signal sensitivity values for each compounds channels were enclosed in these figures.


dx.doi.org/10.1021/jf503776e | J. Agric. Food Chem. 2014, 62, 11628−11636

**Table 2. Recoveries (Mean ± SD) of HAAs and Their Precursors by Extraction with Different Solvents**

| compound | water | 0.1% formic acid in water | 0.1 M HCl | 0.1% formic acid and 50% methanol in water |
|---|---|---|---|---|
| PhIP | 79.8 ± 16.2 | 73.4 ± 15.3 | 100.7 ± 7.3 | 72.0 ± 12.2 |
| 4′-OH-PhIP | 56.7 ± 6.9 | 57.9 ± 6.1 | 70.9 ± 12.3 | 57.5 ± 9.4 |
| Phe | 72.0 ± 7.8 | 71.6 ± 9.5 | 72.6 ± 9.8 | 71.0 ± 6.1 |
| Tyr | 98.8 ± 10.3 | 96.8 ± 14.5 | 105.7 ± 10.0 | 97.8 ± 12.3 |
| creatine | 98.6 ± 14.7 | 99.2 ± 8.8 | 99.7 ± 12.4 | 97.3 ± 9.8 |
| creatinine | 82.4 ± 8.7 | 80.5 ± 7.7 | 82.7 ± 16.8 | 79.7 ± 7.6 |
| Glc | 65.8 ± 9.6 | 61.4 ± 6.2 | 64.1 ± 11.4 | 63.7 ± 11.7 |

The SPE procedure used for purification was tested using three different SPE cartridges. The spiked solution obtained from the 0.1 M HCl extraction was used to evaluate the performance of every cartridge. The results are expressed by recovery rates and are summarized in Figure 3. As the figure shows, the HAAs were retained strongly on the MCX column (recoveries higher than 95%), agreeing with the previous study of MCX cartridge selected to purify the meat sample in HAAs analysis.[32] However, this column was found to be unsuitable for retaining the Glc. Appropriate spiked recoveries (>70%) for Glc were observed using both LC-18 and $SSH_2P$ columns, similar to the previous study which obtained appropriate recoveries of acrylamide and sugars using these two columns,[28] whereas the poor retaining efficiency for creatine and creatinine limited the application of these two types of columns. Therefore, the necessity of the SPE procedure should be considered for optimization purposes.

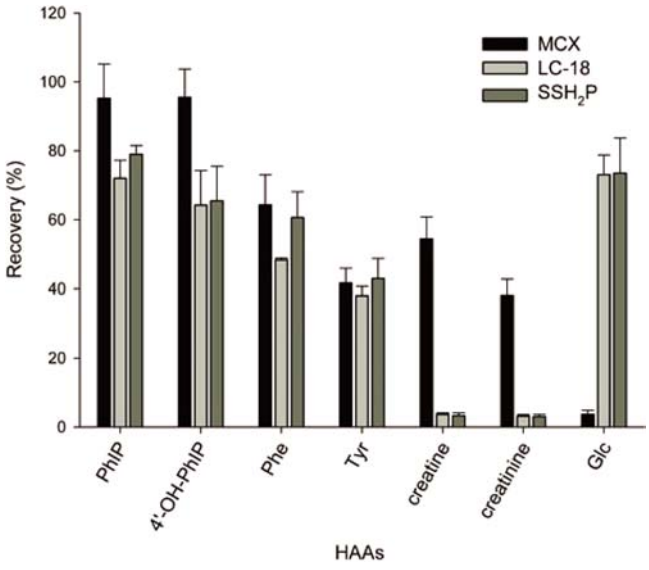


**Figure 3.** Recoveries of PhIP, 4′-OH-PhIP, and their precursors (Phe, Tyr, creatine, creatinine, and Glc) for SPE cleanup procedure using three different cartridges. The error bars were calculate from the three repeated tests ($n$ = 3).

The samples were then alternatively pretreated without SPE. After being spiked with the standards, the extraction solution was diluted and filtrated through a 0.22 $\mu$m membrane and then injected into the UHPLC−MS/MS. The chromatograms demonstrated that no impurities were found in any of the channels, except for Glc (Figure 4). Because the small interferential peak appearing in the Glc channel could be isolated to baseline from the Glc peak, this interference would not affect the quantification. Therefore, without the interference (including macro-interference, e.g., protein and fat), the pretreatment procedures could be simplified by omitting SPE cleanup. The simplified sample pretreatment used in the present study could contribute to the establishment of a rapid and robust quantification method for the simultaneous analysis of HAAs and their precursors, and thus may save analytical time in kinetic studies.

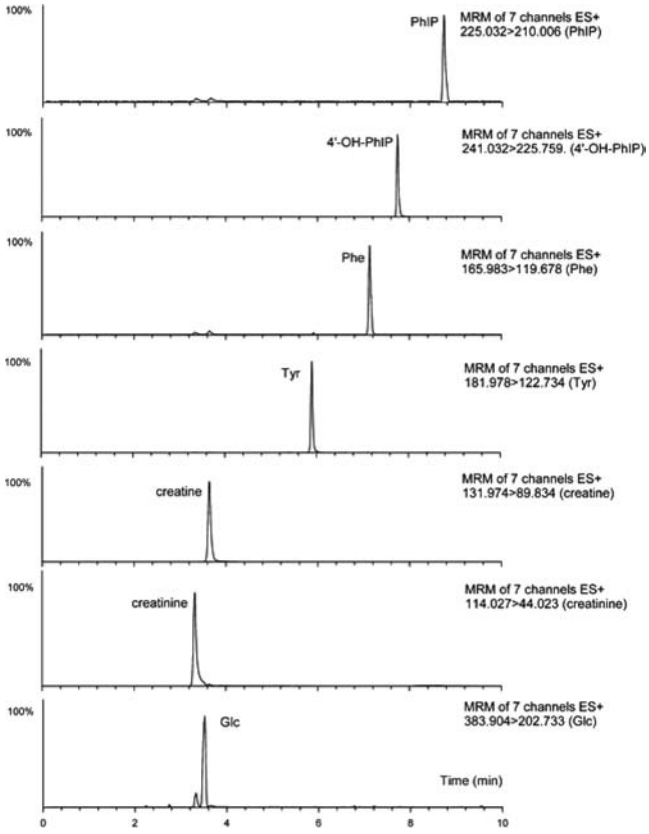


**Figure 4.** Representative UHPLC−MS/MS chromatograms of simultaneous determination of PhIP, 4′-OH-PhIP, and their precursors (Phe, Tyr, creatine, creatinine, and Glc) in a fresh pork model after heating and spiking with standards.

**Validation of the Proposed Method.** The characteristics of the proposed method were demonstrated by a validation procedure studying linearity, LOD, LOQ, recovery, precision, and matrix effects.

The linearity was evaluated by injecting different concentrations of standards and plotting the peak area versus the concentrations. As Table 3 shows, the detector response for individual compounds was linear over a broad concentration, with coefficients higher than 0.991. Glc was a fitted quadratic with a coefficient of 0.996 (SI Figure S2), which confirms an earlier study that reported the quadratic fitting of both Glc and sucrose.[27]

**Table 3. Validation Parameters of the Proposed Method**

| compound | linear range ($\mu$g L$^{-1}$) | coefficients ($r^2$) | LOD ($\mu$g L$^{-1}$) | LOQ ($\mu$g L$^{-1}$) | spiked level ($\mu$g g$^{-1}$) | mean recovery %[a] (RSD%) | matrix effects[b] (Rn ± SD) |
|---|---|---|---|---|---|---|---|
| PhIP | 1.15−147.50 | 0.995 | 0.14 | 0.58 | 0.2 | 106.8 (15.1) | 0.82 ± 0.07 |
| | | | | | 0.8 | 115.6 (15.4) | |
| 4′-OH-PhIP | 3.95−253.00 | 0.995 | 1.98 | 7.91 | 0.8 | 68.4 (14.3) | 0.78 ± 0.06 |
| | | | | | 3.0 | 72.7 (19.9) | |
| Phe | 8.44−1080.00 | 0.999 | 0.52 | 2.11 | 100.0 | 72.1 (9.9) | 0.89 ± 0.07 |
| | | | | | 400.0 | 89.7 (6.8) | |
| Tyr | 8.44−1080.00 | 0.999 | 4.22 | 16.88 | 150.0 | 102.0 (5.5) | 0.84 ± 0.11 |
| | | | | | 600.0 | 122.2 (19.4) | |
| creatine | 41.41−42400.00 | 0.998 | 5.18 | 20.70 | 3000.0 | 101.5 (13.5) | 0.73 ± 0.08 |
| | | | | | 6000.0 | 119.0 (3.6) | |
| creatinine | 115.23−7375.00 | 0.991 | 3.60 | 14.40 | 3000.0 | 80.1 (9.4) | 0.67 ± 0.05 |
| | | | | | 6000.0 | 100.8 (0.8) | |
| Glc | ----[c] | ----[c] | 325 | 650 | 20.0 | 64.3 (15.4) | 0.72 ± 0.07 |
| | | | | | 80.0 | 59.2 (13.2) | |

[a]Intraday and interday precisions are given in parentheses ($n$ = 3). [b]Matrix effects was expressed as the slope ratios ($R_n$) of standard spiked calibration curve to pure standard calibration curves at same analyte concentration. A value of >1.00 shows ionization enhancement, while <1.00 indicates ionization suppression ($n$ = 3). [c]Glc was fitted quadratic with calibration curves shown in SI Figure S2.

The LODs and LOQs, respectively defined as the amount of an analyte producing a signal-to-noise ratio of ≥3 and ≥10, were determined using standards (Table 3). The ranges were 0.14−325.00 $\mu$g L$^{-1}$ for LODs and 0.58−650.00 $\mu$g L$^{-1}$ for LOQs. Glc showed the highest detection limit of 325.00 $\mu$g L$^{-1}$, similar to a previous study,[33] which performed a new analytical setup to simultaneously analyze the precursors and products of the Maillard reaction using high-performance anion exchange chromatograph and obtained a LOQ of 1.00 $\mu$mol L$^{-1}$ for the Glc.

The standard spiking recoveries of the proposed method were evaluated using samples obtained from the fresh pork model system after heating. The results are also summarized in Table 3. The recoveries of compounds in the fresh pork model system ranged from 64.3% to106.4% at a low spiked level and 59.2% to122.2% at a high spiked level, demonstrating the accuracy of the proposed method compared with other published methods in terms of Glc or HAA recoveries.[28,32,34,35]

The precisions expressed as relative standard deviations (RSDs) were lower than 15.4% (19.9%) for intra(inter-)day studies, demonstrating the stability of the proposed method when large amounts of samples must be detected (Table 3).

The suppression or enhancement of ionization caused by coelute from the column was a common problem in LC−MS/MS when analyzing complex food samples, also known as matrix effects. In this study, the matrix effects for HAAs and their precursors were evaluated with the slope ratios ranging from 0.67 to 0.89, further verifying that the extracts obtained from the simple sample pretreatment used in the present work are relatively clean for UHPLC−MS/MS detection.

Summarizing all of the method validation results, the developed method proposed here can be regarded as a rapid and potent quantification method that could be successfully applied to the simultaneous analysis of PhIP, 4′-OH-PhIP, Phe, Tyr, creatine, creatinine, and Glc in a pork model system corresponding to the kinetic study, with simple and fast sample pretreatment procedures, appropriate recoveries and excellent method repeatability (Figure 5).

**Analysis of Model System Samples and Kinetic Evaluation.** As a specific application to the kinetic study, the proposed method was used to simultaneously detect HAAs and their precursors from lyophilized pork models with different heating times at 195 °C. The kinetic profiles of both the HAAs and their precursors were clearly depicted using the simultaneous method (Figure 4). Without heating (heating time, 0 min), the contents of the precursors were quantified as 34.3 $\mu$g g$^{-1}$ for Phe, 50.98 $\mu$g g$^{-1}$ for Tyr, 41054.26 $\mu$g g$^{-1}$ for creatine, 805.54 $\mu$g g$^{-1}$ for creatinine, and 1651 $\mu$g g$^{-1}$ for Glc using the current kinetic tool—similar to another study,[21] and further demonstrating the precision of our simultaneous method. The amino acid, creatine, and Glc contents sharply decreased within the initial 5 min, especially for creatine, indicating the violence of the reaction process. Then, as the reaction proceeded, the content variation became gentle. The elimination kinetics of creatine appeared to be faster than those of amino acids and Glc, which could be explained by creatine's simultaneous involvement in both creatinine and HAAs formations. The dehydration reaction from creatine to creatinine can be validated by a rapid increase in creatinine at the beginning, which gradually decreases in the subsequent reaction. A continuation of the HAAs formation is observed when the precursors are almost depleted by 20 min, indicating that there may be some other compound or multiple reactions involving in the formation process of HAAs. The kinetic profiles and levels of PhIP at different heating time is good in accordance with a previous study which used the similar lyophilized model,[8] further demonstrating the applicability of our simultaneous method. In the dry model used in this paper, water is removed to ensure the same chemical composition throughout all experiment. Compare with the actual pork model containing water, the PhIP level obtained in our lyophilized pork model are significant higher. For example, no PhIP are detected in wet pressed pork heated at 200 °C for 30 min in a previous study.[21] The author stated that water may play an important role in the PhIP formation, since a markedly higher PhIP level in the dry heated sample was observed. The effect of water or water activity in actual pork can be further demonstrated by the apparent decrease of the PhIP levels after adding the compounds that could enhance the water-holding capacity.[36]

The simultaneous quantitative method proposed in our work was successfully applied to the simultaneous detection of HAAs

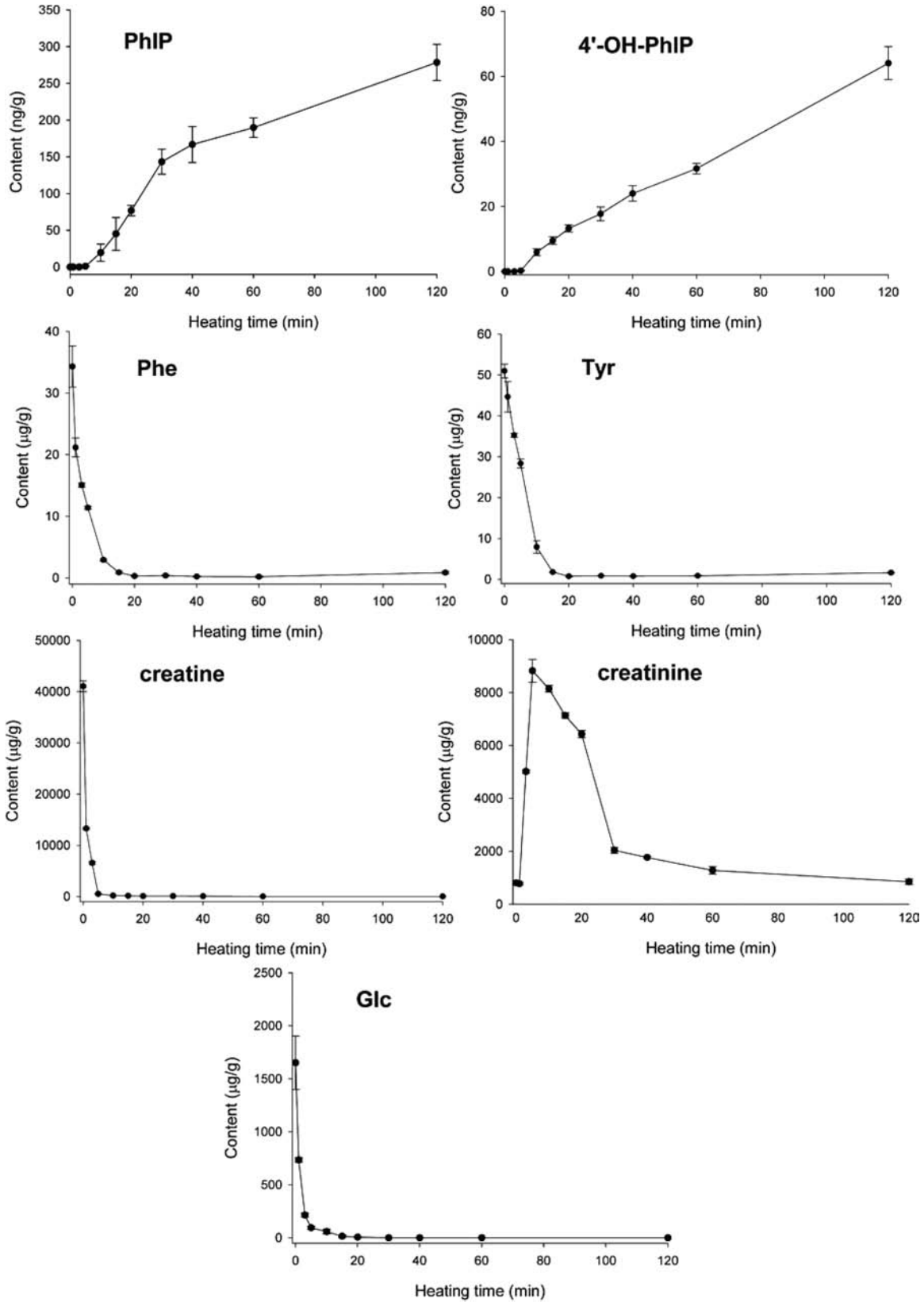


**Figure 5.** Content and kinetic profiles of PhIP, 4′-OH-PhIP, and their precursors (Phe, Tyr, creatine, creatinine, and Glc) in a fresh pork model with different heating time treatments. Each experiment was performed in triplicate repeats ($n$ = 3), and the standard deviation was calculated for the error bar of each point.

and their precursors during the kinetic evaluation. Compared with the separate analysis, the advantage of the proposed method is that it allows the simultaneous detection of all of the target compounds, which could reduce the analysis time and


dx.doi.org/10.1021/jf503776e | J. Agric. Food Chem. 2014, 62, 11628−11636

cost while eliminating the errors in the results obtained from the separate steps.

## ■ ASSOCIATED CONTENT

### Supporting Information

The fragmentation of Glc from monosodiated cluster ions $[2M + Na]^+$ ($m/z$ 383) to monosodiated adduct ions $[M + Na]^+$ ($m/z$ 203) was decided in this study (Figure S1). Glc was a fitted quadratic with a coefficient of 0.996 (Figure S2). This material is available free of charge via the Internet at http://pubs.acs.org.

## ■ AUTHOR INFORMATION

### Corresponding Author

*Phone: +86 139 6176 1357; fax: +86 510 85919065; e-mail: chenjie@jiangnan.edu.cn.

### Funding

The present work was supported by the 973 Program (2012 CB720801), the National Natural Science Foundation of China (NSFC, 31101287), the Research and Innovation Project for College Graduates of Jiangsu Province in China (CXZZ11_0490), and the Doctor Candidate Foundation of Jiangnan University (JUDCF 11020).

### Notes

The authors declare no competing financial interest.

## ■ REFERENCES

(1) Busquets, R.; Puignou, L.; Galceran, M. T.; Wakabayashi, K.; Skog, K. Liquid chromatography- tandem mass spectrometry analysis of 2-amino-1-methyl-6-(4-hydroxyphenyl)-imidazo 4,5-b-pyridine in cooked meats. *J. Agric. Food Chem.* **2007**, *55*, 9318−9324.

(2) Szterk, A. Chemical state of heterocyclic aromatic amines in grilled beef: Evaluation by in vitro digestion model and comparison of alkaline hydrolysis and organic solvent for extraction. *Food Chem. Toxicol.* **2013**, *62*, 653−660.

(3) Jinap, S.; Mohd-Mokhtar, M. S.; Farhadian, A.; Hasnol, N. D. S.; Jaafar, S. N.; Hajeb, P. Effects of varying degrees of doneness on the formation of heterocyclic aromatic amines in chicken and beef satay. *Meat Sci.* **2013**, *94*, 202−207.

(4) Costa, M.; Viegas, O.; Melo, A.; Petisca, C.; Pinho, O.; Ferreira, I. M. P. L. V. O. Heterocyclic aromatic amine formation in barbecued Sardines (*Sardina pilchardus*) and Atlantic Salmon (*Salmo salar*). *J. Agric. Food Chem.* **2009**, *57*, 3173−3179.

(5) Shioya, M.; Wakabayashi, K.; Sato, S.; Nagao, M.; Sugimura, T. Formation of a mutagen, 2-amino-1-methyl-6-phenylimidazo 4,5-b-pyridine (PhIP) in cooked beef, by heating a mixture containing creatinine, phenylalanine and glucose. *Mutat. Res.* **1987**, *191*, 133−8.

(6) Wakabayashi, K.; Kim, I. S.; Kurosaka, R.; Yamaizumi, Z.; Ushiyama, H.; Takahashi, M.; Koyota, S.; Tada, A.; Nukaya, H.; Goto, S. Identification of new mutagenic heterocyclic amines and quantification of known heterocyclic amines. *Princess Takamatsu Symposia* **1995**, *23*, 39−49.

(7) Szterk, A.; Waszkiewicz-Robak, B. Influence of selected quality factors of beef on the profile and the quantity of heterocyclic aromatic amines during processing at high temperature. *Meat Sci.* **2014**, *96*, 1177−1184.

(8) Messner, C.; Murkovic, M. Evaluation of a new model system for studying the formation of heterocyclic amines. *J. Chromatogr., B* **2004**, *802*, 19−26.

(9) Adamson, R. H.; Snyderwine, E. G.; Thorgeirsson, U. P.; Schut, H. A.; Turesky, R. J.; Thorgeirsson, S. S.; Takayama, S.; Sugimura, T. Metabolic processing and carcinogenicity of heterocyclic amines in nonhuman primates. *Princess Takamatsu Symposia* **1990**, *21*, 289−301.

(10) Ito, N.; Hasegawa, R.; Sano, M.; Tamano, S.; Esumi, H.; Takayama, S.; Sugimura, T. A new colon and mamary carcinogen in cooked food, 2-amino-1-methyl-6-phenyimidazo 4,5-b-pyridine (PhIP). *Carcinogenesis* **1991**, *12*, 1503−1506.

(11) Zhu, J. J.; Chang, P.; Bondy, M. L.; Sahin, A. A.; Singletary, S. E.; Takahashi, S.; Shirai, T.; Li, D. H. Detection of 2-amino-1-methyl-6-phenylimidazo 4,5-b-pyridine-DNA adducts in normal breast tissues and risk of breast cancer. *Cancer Epidemiol., Biomarkers Prev.* **2003**, *12*, 830−837.

(12) Zhu, J.; Rashid, A.; Cleary, K.; Abbruzzese, J. L.; Friess, H.; Takahashi, S.; Shirai, T.; Li, D. Detection of 2-amino-1-methyl-6-phenylimidazo 4,5-b-pyridine (PhIP)-DNA adducts in human pancreatic tissues. *Biomarkers* **2006**, *11*, 319−328.

(13) IARC. Some natural occurring substances: food items and constituents. Heterocyclic amines and mycotoxins. *IARC Monogr. Eval. Carcinog. Risks Hum.* **1993**, *56*, 163−242.

(14) Reistad, R.; Rossland, O. J.; Latva-Kala, K. J.; Rasmussen, T.; Vikse, R.; Becher, G.; Alexander, J. Heterocyclic aromatic amines in human urine following a fried meat meal. *Food Chem. Toxicol.* **1997**, *35*, 945−955.

(15) Kurosaka, R.; Wakabayashi, K.; Ushiyama, H.; Nukaya, H.; Arakawa, N.; Sugimura, T.; Nagao, M. Detection of 2-amino-1-methyl-6-(4-hydroxyphenyl)imidazo 4,5-b-pyridine in broiled beef. *Jpn. J. Cancer Res.* **1992**, *83*, 919−922.

(16) Sprague, M. A.; Colvin, M. E. A mixture-enthalpy fixed-grid model for temperature evolution and heterocyclic-amine formation in a frying beef patty. *Food Res. Int.* **2011**, *44*, 789−797.

(17) Kondjoyan, A.; Chevolleau, S.; Greve, E.; Gatellier, P.; Sante-Lhoutellier, V.; Bruel, S.; Touzet, C.; Portanguen, S.; Debrauwer, L. Modelling the formation of heterocyclic amines in slices of longissimus thoracis and semimembranosus beef muscles subjected to jets of hot air. *Food Chem.* **2010**, *123*, 659−668.

(18) Arvidsson, P.; van Boekel, M.; Skog, K.; Solyakov, A.; Jagerstad, M. Formation of heterocyclic amines in a meat juice model system. *J. Food Sci.* **1999**, *64*, 216−221.

(19) Olsson, V.; Solyakov, A.; Skog, K.; Lundstrom, K.; Jagerstad, M. Natural variations of precursors in pig meat affect the yield of heterocyclic amines—Effects of RN genotype, feeding regime, and sex. *J. Agric. Food Chem.* **2002**, *50*, 2962−2969.

(20) Puangsombat, K.; Gadgil, P.; Houser, T. A.; Hunt, M. C.; Smith, J. S. Heterocyclic amine content in commercial ready to eat meat products. *Meat Sci.* **2011**, *88*, 227−233.

(21) Borgen, E.; Solyakov, A.; Skog, K. Effects of precursor composition and water on the formation of heterocyclic amines in meat model systems. *Food Chem.* **2001**, *74*, 11−19.

(22) Smith-Palmer, T. Separation methods applicable to urinary creatine and creatinine. *J. Chromatogr., B* **2002**, *781*, 93−106.

(23) Castells, C. B.; Arias, V. C.; Castells, R. C. Precolumn derivatization of reducing carbohydrates with 4-(3-methyl-5-oxo-2-pyrazolin-1-*yl*) benzoic acid: Study of reaction, high-performance liquid chromatographic separation and quantitative performance of method. *Chromatographia* **2002**, *56*, 153−160.

(24) Gomez-Alonso, S.; Hermosin-Gutierrez, I.; Garcia-Romero, E. Simultaneous HPLC analysis of biogenic amines, amino acids, and ammonium ion as aminoenone derivatives in wine and beer samples. *J. Agric. Food Chem.* **2007**, *55*, 608−613.

(25) Chevolleau, S.; Touzet, C.; Jamin, E.; Tulliez, J.; Debramer, L. LC−APCI−MS/MS determination of heterocyclic aromatic amines formes during meat cooking. *Sci. Aliment.* **2007**, *27*, 381−396.

(26) Barcelo-Barrachina, E.; Moyano, E.; Galceran, M. T.; Lliberia, J. L.; Bago, B.; Cortes, M. A. Ultra-performance liquid chromatography-tandem mass spectrometry for the analysis of heterocyclic amines in food. *J. Chromatogr., A* **2006**, *1125*, 195−203.

(27) Nielsen, N. J.; Granby, K.; Hedegaard, R. V.; Skibsted, L. H. A liquid chromatography-tandem mass spectrometry method for simultaneous analysis of acrylamide and the precursors, asparagine and reducing sugars in bread. *Anal. Chim. Acta* **2006**, *557*, 211−220.

(28) Zhang, Y.; Ren, Y.; Jiao, J.; Li, D.; Zhang, Y. Ultra High-performance liquid chromatography-tandem mass spectrometry for the simultaneous analysis of asparagine, sugars, and acrylamide in Maillard reactions. *Anal. Chem.* **2011**, *83*, 3297−3304.

(29) Yoshikawa, H.; Hirano, A.; Arakawa, T.; Shiraki, K. Mechanistic insights into protein precipitation by alcohol. *Int. J. Biol. Macromol.* **2012**, *50*, 865−871.
(30) Jia, S.; Kang, Y. P.; Park, J. H.; Lee, J.; Kwon, S. W. Simultaneous determination of 23 amino acids and 7 biogenic amines in fermented food samples by liquid chromatography/quadrupole time-of-flight mass spectrometry. *J. Chromatogr., A* **2011**, *1218*, 9174−9182.
(31) Rogatsky, E.; Jayatillake, H.; Goswami, G.; Tomuta, V.; Stein, D. Sensitive LC MS quantitative analysis of carbohydrates by $Cs^+$ attachment. *J. Am. Soc. Mass Spectrom.* **2005**, *16*, 1805−1811.
(32) Szterk, A.; Roszko, M.; Malek, K.; Kurek, M.; Zbiec, M.; Waszkiewicz-Robak, B. Profiles and concentrations of heterocyclic aromatic amines formed in beef during various heat treatments depend on the time of ripening and muscle type. *Meat Sci.* **2012**, *92*, 587−595.
(33) Davidek, T.; Clety, N.; Devaud, S.; Robert, F.; Blank, I. Simultaneous quantitative analysis of Maillard reaction precursors and products by high-performance anion exchange chromatography. *J. Agric. Food Chem.* **2003**, *51*, 7259−7265.
(34) Lee, J.; Dong, A.; Jung, K.; Shin, H.-S. Influence of extra virgin olive oil on the formation of heterocyclic amines in roasted beef steak. *Food Sci. Biotechnol.* **2011**, *20*, 159−165.
(35) Toribio, F.; Busquets, R.; Puignou, L.; Galceran, M. T. Heterocyclic amines in griddled beef steak analysed using a single extract clean-up procedure. *Food Chem. Toxicol.* **2007**, *45*, 667−675.
(36) Persson, E.; Sjoholm, I.; Skog, K. Effect of high water-holding capacity on the formation of heterocyclic amines in fried beefburgers. *J. Agric. Food Chem.* **2003**, *51*, 4472−4477.

has not been studied yet. This study hypothesizes that VOO obtained from Picual olives of lower ripening index shows higher stability and lower thermal oxidation than VOO from higher ripening index counterparts when used in repeated frying operations of fresh potatoes. Thus, the aim of the present study was to evaluate the effect of olive ripeness on the thermal oxidation stability during frying of fresh potatoes of VOO obtained from Picual cultivars by quantifying (a) polar compounds, (b) thermal oxidation and hydrolytic compound profiles, (c) polar and nonpolar methyl esters, (d) fatty acid and tocopherol contents and profiles, (e) oxidative stability, and (f) the theoretical number of frying operations at which the three Picual VOOs must be discarded.

## MATERIALS AND METHODS

**Olive Harvesting, Ripening Index, and Oil Elaboration.** Olives of Picual variety were harvested during the 2011/2012 olive season in the Agricultural Experimental Station "La Chimenea", Instituto Madrileño de Investigación y Desarrollo Rural, Agrario y Alimentario (IMIDRA), located in the region of Madrid (Spain).

About 35 kg of olives was hand-picked in perfect sanitary conditions from olives trees at three ripening stages at three weekly intervals from November 19 to December 31. These three ripening stages were selected according to the normal harvesting period for the Picual olive variety. The olive ripening index was determined according to the method described by Uceda and Frias[26] based on the evaluation of the olive skin and pulp colors. Seven maturity states of the fruit (0, bright green skin; 1, green-yellowish skin; 2, green skin with reddish spots; 3, reddish-brown skin; 4, black skin with white flesh; 5, black skin with <50% purple flesh; 6, black skin with ≥50 and >100% purple flesh; and 7, black skin and purple flesh) were used.[22]

Olive oils were extracted using the Abencor system (MC2 Ingenierías y Sistemas, Sevilla, Spain). The oil was decanted, filtered, transferred into 500 mL amber glass bottles, and stored at 4 °C in darkness until analysis. Approximately 4.6 L of VOO was obtained in the first harvesting, 5.0 L in the second, and 6.1 L in the third.

**Fresh Potato Frying.** Domestic deep-fat fryers of 1.1 L stainless steel vessel equipped with a thermostat (SOLAC, Vitoria, Spain) were used for potato frying. A total of six fryers, two per VOO, were used. Spunta variety fresh potatoes (Valencia, Spain) were fried. The proportion of food to frying oil in the repeated frying was kept at 183 g to 1.1 L by replenishment with unused oil every five frying operations to maintain, insofar as possible, a constant food/oil ratio. Oil was heated to 180 °C for about 10 min. Potatoes were sliced to 2 mm thick using a mandolin slicer and introduced into the oil at 180 °C and fried for 8 min. Oil was allowed to cool until 30−35 °C between same-day fryings. The cooling time was approximately 4 h between frying operations. On the basis of previous studies,[27,28] a total of 40 frying operations at the rate of 4 fryings per day were performed with each VOO. The whole procedure was performed in duplicate by using two fryers for each oil. Thirty-five milliliters of oil from each of the two fryers was taken after 5, 10, 15, 20, 25, 30, 35, and 40 frying operations and kept frozen at −20 °C until analysis.

**Fatty Acid Profile.** Analysis of the fatty acid composition of oils was performed by GC after derivatization to fatty acid methyl esters (FAME) with 2 N KOH in methanol.[29] FAME were analyzed by GC using a chromatograph (Agilent Technologies 6850 series II network GC system) equipped with one capillary column Supelco 24111 of 60 m × 0.25 mm i.d. × 0.20 μm (Agilent Technologies). Samples were introduced into the column at 170 °C during 30 min; after this time, the temperature was increased at 5 °C/min to 200 °C and maintained for 12 min. The flow rate of He, used as carrier gas, was 0.6 mL/min. Injector and flame ionization detector temperatures were 230 and 250 °C, respectively.

The absolute amount of each individual FAME was calculated by multiplying the percentage of each FAME by the amount of nonoxidized fatty acid monomers (FAM) giving results equivalent to those obtained using internal standard.[30]

**Polar Compound Assessment.** Total PC contents in the unused oil and used frying oils were determined by gravimetric measurement using silica column chromatography.[23] One gram of sample was separated by column chromatography using 150 mL of hexane/diethyl ether (90:10, v/v) and 150 mL of diethyl ether to elute the nonpolar and polar fractions, respectively.

**Quantitation of Thermal Oxidation and Hydrolytic Compounds.** To obtain further information about changes due to thermal oxidation and hydrolysis during frying, high-performance size exclusion liquid chromatography (HPSEC) analysis of the PC fraction present in the unused and used frying oils was performed following a slight modification of the AOCS method.[23] Briefly, a sample concentration of the previously isolated PC (10−15 mg/mL tetrahydrofuran) was applied in a high-performance liquid chromatograph (HPLC) (Agilent 1100 series, Madrid, Spain) with a 20 μL sample loop. A refractive index detector (Agilent Technologies 1260 infinity, Madrid, Spain) and two 300 mm × 7.5 mm i.d. (5 μm particle size), 0.01 and 0.05 μm, PL gel columns (Agilent, Bellefonte, PA, USA), connected in series, were operated at 40 °C. HPLC grade tetrahydrofuran was used as the mobile phase with a flow of 1 mL/min. Polymers of triglycerides (PTG), dimers of triglycerides (DTG), oxidized triglycerides (OTG), diglycerides (DG), monoglycerides (MG), and free fatty acids (FFA) were quantified in the PC fraction. Hydrolytic compounds (HC) were calculated as the sum of DG, MG, and FFA, whereas thermally oxidized compounds (TC) were calculated as the sum of PTG, DTG, and OTG. Oligomers (OLIG) were calculated as the sum of DTG and PTG.

**Isolation and Quantitation of Altered and Unaltered Fatty Acid Methyl Esters.** Samples of the unused and used frying oils were saponified during 10 min with 0.5 N NaOH in methanol. Methylation was performed according to an AOAC method,[31] using 20% $BF_3$ in methanol, and required 15 min. After methylation, 1 g of sample was separated by column chromatography using 150 mL of hexane/diethyl ether (88:12, v/v) and 150 mL of diethyl ether to elute the nonpolar and polar fractions of methyl esters, respectively.[4,25] Thermal fatty acid dimers (thermal-FAD) and nonoxidized FAM were quantified in the nonpolar fraction, whereas fatty acid polymers (FAP), oxidized fatty acid dimers (oxFAD), and oxidized fatty acid monomers (oxFAM) were quantified in the polar fraction. Aliquot samples of both fractions (10−15 mg/mL tetrahydrofuran) were injected in a HPLC (Agilent 1100 series) with a 20 μL sample loop. The same equipment (refractive index detector and columns) and conditions (temperature and mobile phase flow) as for thermal oxidation and hydrolytic compound quantitations were used.

**Oxidative Stability.** Oxidative stability was analyzed in unused and used frying oils using the Rancimat equipment at 120 °C (Metrohm Ltd., Herisau, Swiss) with a continuous air flow of 20 L/h passing and 2.5 g oil samples. The inflection point of the curve was assigned as the induction time, measured in hours.[32,33]

**Determination of Total Polyphenolic Compounds.** Total phenolic compounds in unused and used frying oils were determined after methanol extraction and subsequent reaction with Folin−Ciocalteu reagent and measured in a Lambda 25 UV−vis spectrophotomer (PerkinElmer, Waltham, MA, USA) at a wavelength of 725 nm.[34]

**Determination of Tocopherols.** The determination of α- and γ-tocopherols present in unused and used frying oils was carried out by HPLC according to IUPAC methods.[35]

**Statistical Analyses.** All determinations were done in duplicate. The Pearson product−moment correlation test was used to find correlations between parameter data. Linear adjustments between the concentration of polar compounds, different thermal oxidation and hydrolytic compounds, various methyl esters compounds, and frying number were assessed. A stepwise multiple regression procedure was used to identify which of the following parameters, total phenolic content, tocopherol content, oleic, linoleic, and linolenic acids, explained better the extent of VOO thermal oxidation during frying. Regression collinearity diagnostics and regression case wise diagnostics were performed to prevent multicollinearity and influential cases. The SPSS 15.0 statistical packet was employed. Comparisons between linear adjustments for the different compounds in the three VOOs were checked by ANCOVA test using SAS 9.2 statistical package. Statistical significance was set at $p < 0.05$.

**Table 1. Changes (Grams per 100 g of Oil) in the Fatty Acid Profile after 40 Fryings of Fresh Potatoes with Virgin Olive Oils Obtained from Picual Olives of Different Ripeness Indices[a]**

| acid | VOO1-0 | VOO1-40 | VOO2-0 | VOO2-40 | VOO3-0 | VOO3-40 |
|---|---|---|---|---|---|---|
| myristic (14:0) | 0.01 ± 0.00 | 0.01 ± 0.00 | 0.01 ± 0.00 | 0.01 ± 0.00 | 0.01 ± 0.00 | 0.01 ± 0.00 |
| palmitic (16:0) | 12.81 ± 0.14 | 11.55 ± 0.02 | 10.69 ± 0.07 | 10.11 ± 0.03 | 10.88 ± 0.14 | 10.38 ± 0.20 |
| palmitelaidic (*t* 16:1 n-7) | 0.09 ± 0.00 | 0.09 ± 0.00 | 0.11 ± 0.00 | 0.11 ± 0.00 | 0.11 ± 0.00 | 0.11 ± 0.00 |
| palmitoleic (16:1 n-7) | 0.45 ± 0.01 | 0.98 ± 0.02 | 0.42 ± 0.01 | 0.86 ± 0.01 | 0.40 ± 0.00 | 0.39 ± 0.01 |
| margaric (17:0) | 0.20 ± 0.00 | 0.04 ± 0.00 | 0.18 ± 0.00 | 0.04 ± 0.00 | 0.19 ± 0.01 | 0.18 ± 0.00 |
| margaroleic (17:1 n-7) | 0.28 ± 0.00 | 0.08 ± 0.00 | 0.28 ± 0.00 | 0.07 ± 0.01 | 0.27 ± 0.00 | 0.26 ± 0.01 |
| stearic (18:0) | 3.20 ± 0.04 | 2.56 ± 0.04 | 3.21 ± 0.01 | 2.55 ± 0.07 | 3.51 ± 0.05 | 3.34 ± 0.08 |
| oleic (18:1 n-9) | 70.35 ± 0.68 | 71.60 ± 0.51 | 72.16 ± 0.44 | 70.66 ± 0.18 | 72.24 ± 0.84 | 69.60 ± 0.70 |
| *α*-linoleic (18:2 n-6) | 9.39 ± 0.11 | 2.26 ± 0.02 | 9.41 ± 0.04 | 2.68 ± 0.04 | 9.30 ± 0.11 | 2.55 ± 0.04 |
| arachidic (20:0) | 0.34 ± 0.00 | 0.45 ± 0.00 | 0.33 ± 0.00 | 0.43 ± 0.01 | 0.35 ± 0.01 | 0.34 ± 0.01 |
| *α*-linolenic (18:3 n-3) | 0.76 ± 0.02 | 0.37 ± 0.01 | 0.77 ± 0.01 | 0.43 ± 0.02 | 0.75 ± 0.01 | 0.50 ± 0.01 |
| gadoleic (20:1 n-9) | 0.26 ± 0.00 | 0.24 ± 0.00 | 0.29 ± 0.01 | 0.29 ± 0.02 | 0.29 ± 0.00 | 0.27 ± 0.01 |
| behenic (22:0) | 0.08 ± 0.00 | 0.13 ± 0.00 | 0.08 ± 0.00 | 0.13 ± 0.00 | 0.08 ± 0.00 | 0.09 ± 0.00 |
| lignoceric (24:0) | 0.03 ± 0.00 | 0.07 ± 0.00 | 0.03 ± 0.00 | 0.06 ± 0.00 | 0.03 ± 0.00 | 0.04 ± 0.00 |
| SFA | 17.07 ± 0.01 | 16.49 ± 0.15 | 14.95 ± 0.00 | 15.20 ± 0.05 | 15.42 ± 0.03 | 16.46 ± 0.15 |
| MUFA | 72.70 ± 0.03 | 80.08 ± 0.15 | 74.66 ± 0.02 | 81.28 ± 0.12 | 74.37 ± 0.03 | 80.08 ± 0.15 |
| PUFA | 10.33 ± 0.02 | 3.47 ± 0.01 | 10.39 ± 0.02 | 3.52 ± 0.07 | 10.21 ± 0.00 | 3.47 ± 0.01 |

[a]VOO1, VOO2, and VOO3 correspond to harvesting period; for more details see Material and Methods. Values (mg/100 mg oil) are the mean ± SD of two determinations. SFA, saturated fatty acids; MUFA, monounsaturated fatty acids; PUFA, polyunsaturated fatty acids. Sample and frying effects were not statistically tested as only duplicates of oil samples when unused (−0) and after 40 fryings (−40) were tested.

**Table 2. Changes (Grams per 100 g of Oil) of Polar Compounds and Thermal Oxidation Compounds during 40 Fryings of Fresh Potatoes with Virgin Olive Oils Obtained from Picual Olives of Different Ripeness Indices**

| frying no. | ripeness[a] | polar content | PTG | DTG | OTG | TC |
|---|---|---|---|---|---|---|
| 0 | VOO1 | 1.85 ± 0.08 | nd | 0.03 ± 0.00 | 0.37 ± 0.00 | 0.39 ± 0.00 |
| | VOO2 | 2.39 ± 0.00 | nd | 0.03 ± 0.00 | 0.49 ± 0.01 | 0.52 ± 0.00 |
| | VOO3 | 2.54 ± 0.19 | nd | 0.05 ± 0.02 | 0.61 ± 0.05 | 0.67 ± 0.08 |
| 5 | VOO1 | 3.03 ± 0.01 | 0.03 ± 0.01 | 0.42 ± 0.04 | 1.38 ± 0.01 | 1.83 ± 0.04 |
| | VOO2 | 3.86 ± 0.04 | 0.04 ± 0.00 | 0.70 ± 0.07 | 1.80 ± 0.09 | 2.54 ± 0.16 |
| | VOO3 | 4.78 ± 0.33 | 0.04 ± 0.01 | 0.72 ± 0.04 | 1.57 ± 0.11 | 2.34 ± 0.15 |
| 10 | VOO1 | 5.10 ± 0.14 | 0.10 ± 0.00 | 1.34 ± 0.03 | 1.86 ± 0.06 | 3.30 ± 0.09 |
| | VOO2 | 6.18 ± 0.25 | 0.14 ± 0.07 | 1.56 ± 0.65 | 2.80 ± 0.67 | 4.50 ± 1.39 |
| | VOO3 | 7.27 ± 0.04 | 0.25 ± 0.02 | 2.30 ± 0.02 | 2.88 ± 0.02 | 5.43 ± 0.02 |
| 15 | VOO1 | 7.18 ± 0.11 | 0.22 ± 0.01 | 2.16 ± 0.06 | 3.00 ± 0.07 | 5.38 ± 0.11 |
| | VOO2 | 9.94 ± 0.35 | 0.48 ± 0.11 | 3.22 ± 0.11 | 4.07 ± 0.26 | 7.78 ± 0.48 |
| | VOO3 | 9.83 ± 0.24 | 0.38 ± 0.08 | 3.03 ± 0.25 | 4.16 ± 0.01 | 7.57 ± 0.32 |
| 20 | VOO1 | 9.00 ± 0.04 | 0.45 ± 0.04 | 3.15 ± 0.07 | 3.58 ± 0.02 | 7.18 ± 0.05 |
| | VOO2 | 10.50 ± 0.37 | 0.53 ± 0.02 | 3.59 ± 0.13 | 4.15 ± 0.10 | 8.28 ± 0.21 |
| | VOO3 | 11.38 ± 0.30 | 0.63 ± 0.02 | 3.89 ± 0.08 | 4.73 ± 0.31 | 9.25 ± 0.41 |
| 25 | VOO1 | 10.34 ± 0.08 | 0.61 ± 0.02 | 3.60 ± 0.05 | 4.31 ± 0.07 | 8.53 ± 0.09 |
| | VOO2 | 12.23 ± 0.11 | 0.77 ± 0.07 | 4.06 ± 0.08 | 5.20 ± 0.08 | 10.04 ± 0.08 |
| | VOO3 | 13.93 ± 0.04 | 1.02 ± 0.07 | 5.04 ± 0.03 | 5.79 ± 0.06 | 11.84 ± 0.16 |
| 30 | VOO1 | 11.74 ± 0.08 | 0.72 ± 0.01 | 4.06 ± 0.02 | 5.09 ± 0.05 | 9.87 ± 0.08 |
| | VOO2 | 13.11 ± 0.13 | 0.91 ± 0.04 | 4.52 ± 0.02 | 5.36 ± 0.03 | 10.78 ± 0.09 |
| | VOO3 | 15.80 ± 0.20 | 1.35 ± 0.15 | 5.75 ± 0.10 | 6.48 ± 0.00 | 13.59 ± 0.25 |
| 35 | VOO1 | 12.99 ± 0.04 | 0.76 ± 0.25 | 4.73 ± 0.08 | 5.44 ± 0.15 | 10.92 ± 0.02 |
| | VOO2 | 14.46 ± 0.14 | 1.24 ± 0.17 | 5.09 ± 0.11 | 5.90 ± 0.13 | 12.23 ± 0.15 |
| | VOO3 | 17.56 ± 0.26 | 1.41 ± 0.16 | 6.19 ± 0.02 | 7.31 ± 0.04 | 14.91 ± 0.13 |
| 40 | VOO1 | 13.95 ± 0.10 | 1.17 ± 0.04 | 5.06 ± 0.11 | 5.78 ± 0.02 | 12.00 ± 0.17 |
| | VOO2 | 14.85 ± 0.21 | 1.22 ± 0.05 | 5.13 ± 0.03 | 6.13 ± 0.04 | 12.48 ± 0.12 |
| | VOO3 | 18.59 ± 0.27 | 1.96 ± 0.04 | 6.71 ± 0.13 | 7.58 ± 0.03 | 16.25 ± 0.20 |

[a]VOO1, VOO2, and VOO3 correspond to harvesting periods; for more details see text. Values are the mean ± SD of two determinations. PTG, triglyceride polymers; DTG, triglyceride dimers; OTG, oxidized triglycerides; TC, thermal oxidized compounds (PTG, DTG plus OTG); nd, nondetected.

Table 3. Changes (Grams per 100 g of Oil) in Hydrolytic Compounds and the Thermal Oxidized/Hydrolytic Compounds Ratio during 40 Fryings of Fresh Potatoes with Virgin Olive Oils Obtained from Picual Olives of Different Ripeness Indices

| frying no. | ripeness[a] | DG | MG | FFA | HC | TC/HC |
|---|---|---|---|---|---|---|
| 0 | VOO1 | 1.07 ± 0.06 | 0.01 ± 0.01 | 0.38 ± 0.04 | 1.46 ± 0.09 | 0.27 ± 0.02 |
| | VOO2 | 1.33 ± 0.00 | 0.06 ± 0.00 | 0.48 ± 0.01 | 1.87 ± 0.00 | 0.28 ± 0.00 |
| | VOO3 | 1.20 ± 0.05 | 0.09 ± 0.04 | 0.58 ± 0.02 | 1.87 ± 0.11 | 0.36 ± 0.02 |
| 5 | VOO1 | 1.36 ± 0.05 | 0.05 ± 0.08 | 0.62 ± 0.05 | 2.03 ± 0.08 | 0.91 ± 0.05 |
| | VOO2 | 1.47 ± 0.09 | nd | 0.76 ± 0.08 | 2.24 ± 0.17 | 1.14 ± 0.01 |
| | VOO3 | 1.75 ± 0.16 | nd | 0.72 ± 0.06 | 2.46 ± 0.10 | 0.95 ± 0.02 |
| 10 | VOO1 | 1.32 ± 0.04 | 0.07 ± 0.00 | 0.41 ± 0.00 | 1.80 ± 0.05 | 1.83 ± 0.00 |
| | VOO2 | 1.30 ± 0.76 | 0.09 ± 0.03 | 0.47 ± 0.34 | 1.86 ± 1.13 | 2.86 ± 1.20 |
| | VOO3 | 1.34 ± 0.05 | 0.10 ± 0.01 | 0.40 ± 0.01 | 1.84 ± 0.02 | 2.96 ± 0.02 |
| 15 | VOO1 | 1.31 ± 0.01 | 0.08 ± 0.00 | 0.40 ± 0.00 | 1.80 ± 0.01 | 2.99 ± 0.07 |
| | VOO2 | 1.57 ± 0.12 | 0.10 ± 0.01 | 0.48 ± 0.02 | 2.16 ± 0.13 | 3.62 ± 0.45 |
| | VOO3 | 1.62 ± 0.02 | 0.10 ± 0.04 | 0.54 ± 0.02 | 2.26 ± 0.08 | 3.36 ± 0.25 |
| 20 | VOO1 | 1.31 ± 0.05 | 0.09 ± 0.03 | 0.41 ± 0.03 | 1.82 ± 0.01 | 3.95 ± 0.04 |
| | VOO2 | 1.62 ± 0.13 | 0.07 ± 0.03 | 0.52 ± 0.01 | 2.22 ± 0.16 | 3.74 ± 0.18 |
| | VOO3 | 1.55 ± 0.08 | 0.08 ± 0.02 | 0.50 ± 0.01 | 2.13 ± 0.11 | 4.35 ± 0.42 |
| 25 | VOO1 | 1.30 ± 0.03 | 0.10 ± 0.02 | 0.41 ± 0.02 | 1.81 ± 0.01 | 4.72 ± 0.46 |
| | VOO2 | 1.58 ± 0.07 | 0.10 ± 0.02 | 0.52 ± 0.03 | 2.19 ± 0.02 | 4.59 ± 0.01 |
| | VOO3 | 1.56 ± 0.10 | 0.07 ± 0.01 | 0.46 ± 0.01 | 2.09 ± 0.12 | 5.68 ± 0.41 |
| 30 | VOO1 | 1.35 ± 0.01 | 0.08 ± 0.01 | 0.43 ± 0.01 | 1.87 ± 0.01 | 5.29 ± 0.02 |
| | VOO2 | 1.68 ± 0.02 | 0.09 ± 0.02 | 0.55 ± 0.01 | 2.32 ± 0.04 | 4.65 ± 0.05 |
| | VOO3 | 1.59 ± 0.10 | 0.12 ± 0.03 | 0.51 ± 0.02 | 2.21 ± 0.05 | 6.18 ± 0.24 |
| 35 | VOO1 | 1.46 ± 0.07 | 0.14 ± 0.01 | 0.47 ± 0.00 | 2.06 ± 0.06 | 5.30 ± 0.16 |
| | VOO2 | 1.61 ± 0.22 | 0.12 ± 0.01 | 0.50 ± 0.08 | 2.23 ± 0.30 | 5.55 ± 0.81 |
| | VOO3 | 1.93 ± 0.29 | 0.11 ± 0.02 | 0.61 ± 0.08 | 2.65 ± 0.40 | 5.70 ± 0.90 |
| 40 | VOO1 | 1.43 ± 0.00 | 0.11 ± 0.00 | 0.42 ± 0.07 | 1.95 ± 0.07 | 6.15 ± 0.30 |
| | VOO2 | 1.75 ± 0.05 | 0.14 ± 0.02 | 0.48 ± 0.01 | 2.37 ± 0.09 | 5.28 ± 0.15 |
| | VOO3 | 1.72 ± 0.07 | 0.12 ± 0.00 | 0.51 ± 0.01 | 2.37 ± 0.07 | 6.94 ± 0.13 |

[a]VOO1, VOO2, and VOO3 correspond to harvesting periods; for more details see text. Values are the mean ± SD of two determinations. DG, diglycerides; MG, monoglycerides; FFA, free fatty acids; HC, hydrolytic compounds (DG, MG plus FFA); TC, thermal oxidized compounds (PTG, DTG plus OTG); nd, nondetected.

## RESULTS AND DISCUSSION

**Unused Picual Virgin Olive Oil Characteristics.** Picual olives showed ripening indices of 4.9, 5.3, and 6.0 at the three ripening stages (VOO1, VOO2, and VOO3, respectively), which are normal values for this olive fruit variety.[22]

Initial fatty acid composition of the three VOOs obtained is shown in Table 1. VOO1 showed lower oleic acid and higher palmitic acid than the other two VOOs. Baccouri et al.[36] reported in virgin olive oils extracted from diverse fruits of selected oleasters that "at the beginning of fruit development, palmitic acid content was high, followed by an extreme decrease, then it remained unchanged until the end of fruit development" (sic), suggesting that very green olives are richer in this saturated fatty acid. Ontogenesis of the enzymes participating in the biosynthesis of oleic acid in olives seems to be important in determining the oil fatty acid profile and phenol content.[20] Stearoyl-acyl carrier protein (stearoyl-ACP) is obtained from acetyl-CoA by the action of an enzymatic complex called fatty acid synthase I and III (FAS III/I) followed by FAS II. Stearoyl-ACP is desaturated to oleoyl-ACP (C18:1-ACP) by the stearoyl-ACP Δ9-desaturase, which is highly active in the plastids.[20] As growth proceeds, desaturase transcripts accumulate at higher levels, and the high transcription rate remains up to 28 weeks after flowering. This transcription pattern observed during fruit development parallels well with the synthesis of oleic acid in olives.[37] Thus, Δ9-desaturase converting stearoyl in oleoyl moieties could be less active in less ripened olives.

Unused VOOs presented total PC levels ranging from 1.85 to 2.54 g per 100 g of oil (Table 2). These results suggest the good quality of the oils tested as the PC of fresh oils normally ranges between 0.4 and 6.4 g per 100 g of oil[38] and agree with previous findings of our group in olive oil[28] and extra VOO.[39] Similarly to other quality olive oils[28,39] DG were the major compounds in the polar fraction of the unused oils, whereas PTG and MG were rather low or not detected at all (Tables 2 and 3). Nevertheless, the VOO1 oil exhibited the lowest PC and OTG levels followed by the VOO2 oil. In addition, the TC/HC ratio also increased from VOO1 to VOO3 (Table 3).

As expected, unused VOOs showed low amounts of polar-ME, suggesting that the Picual monovarietal tested oils were

**Table 4. Changes (Grams per 100 g of Oil) of Polar Methyl Esters, Nonoxidized Fatty Acid Monomers, Fatty Acid Dimers (Oxidized and Thermal), Fatty Acid Polymers, and Oxidized Fatty Acid Monomers during 40 Fryings of Fresh Potatoes with Virgin Olive Oils Obtained from Picual Olives of Different Ripeness Indices**

| frying no. | ripeness[a] | polar-ME | thermal-FAD | nonoxidized FAM | FAP | oxFAD | oxFAM |
|---|---|---|---|---|---|---|---|
| 0 | VOO1 | 1.75 ± 0.99 | nd | 98.25 ± 0.99 | nd | 0.04 ± 0.02 | 1.71 ± 0.97 |
| | VOO2 | 2.03 ± 0.56 | nd | 97.98 ± 0.56 | nd | 0.05 ± 0.03 | 1.97 ± 0.53 |
| | VOO3 | 1.58 ± 0.62 | nd | 98.43 ± 1.18 | nd | 0.05 ± 0.03 | 1.52 ± 1.15 |
| 10 | VOO1 | 2.32 ± 0.01 | 3.22 ± 0.40 | 94.47 ± 0.42 | 0.15 ± 0.02 | 0.56 ± 0.04 | 1.61 ± 0.05 |
| | VOO2 | 2.68 ± 0.40 | 3.02 ± 0.16 | 94.30 ± 0.57 | 0.18 ± 0.05 | 0.57 ± 0.09 | 1.93 ± 0.27 |
| | VOO3 | 3.49 ± 0.22 | 2.93 ± 0.24 | 93.58 ± 0.02 | 0.17 ± 0.01 | 0.69 ± 0.10 | 2.63 ± 0.11 |
| 20 | VOO1 | 3.85 ± 0.36 | 3.66 ± 0.41 | 92.49 ± 0.77 | 0.28 ± 0.04 | 1.10 ± 0.09 | 2.46 ± 0.46 |
| | VOO2 | 4.48 ± 0.52 | 3.23 ± 0.28 | 92.29 ± 0.80 | 0.26 ± 0.00 | 1.07 ± 0.02 | 3.16 ± 0.54 |
| | VOO3 | 4.69 ± 1.27 | 3.57 ± 0.85 | 91.74 ± 0.12 | 0.27 ± 0.03 | 0.98 ± 0.11 | 3.44 ± 1.35 |
| 30 | VOO1 | 4.41 ± 0.04 | 4.14 ± 0.50 | 91.46 ± 0.55 | 0.34 ± 0.04 | 1.04 ± 0.00 | 3.03 ± 0.09 |
| | VOO2 | 5.96 ± 0.06 | 4.10 ± 0.54 | 89.94 ± 0.59 | 0.28 ± 0.04 | 1.47 ± 0.03 | 4.21 ± 0.04 |
| | VOO3 | 6.38 ± 0.01 | 4.53 ± 0.00 | 89.09 ± 0.01 | 0.32 ± 0.03 | 1.60 ± 0.05 | 4.46 ± 0.02 |
| 40 | VOO1 | 5.62 ± 0.22 | 3.94 ± 0.29 | 90.44 ± 0.51 | 0.46 ± 0.06 | 1.46 ± 0.05 | 3.69 ± 0.11 |
| | VOO2 | 6.31 ± 0.21 | 5.25 ± 0.12 | 88.44 ± 0.09 | 0.33 ± 0.06 | 1.58 ± 0.13 | 4.40 ± 0.02 |
| | VOO3 | 7.14 ± 0.73 | 4.79 ± 0.31 | 88.08 ± 1.04 | 0.41 ± 0.05 | 1.77 ± 0.07 | 4.95 ± 0.71 |

[a]VOO1, VOO2, and VOO3 correspond to harvesting periods; for more details see Materials and Methods. Values are the mean ± SD of two determinations. Polar-ME, polar methyl esters; thermal-FAD, thermal fatty acid dimers; nonoxidized FAM, nonoxidized fatty acid monomers; FAP, fatty acid polymers; oxFAD, oxidized fatty acid dimers; oxFAM, oxidized fatty acid monomers; nd, nondetected.

good-quality oils (Table 4). oxFAM where the main compounds followed by far from oxFAD as thermal-FAD and FAP were not detected in the polar-ME of the three unused VOOs tested. These results agree with those reported in previous studies.[40]

The determination of the oxidative stability of VOOs by the Rancimat test is a widely used method, as it is an easy, standardized, and well-controlled method. The oxidative stability, given by the Rancimat method, also decreases with olive fruit ripening, with values of 12.9, 7.6, and 4.0 h in VOO1, VOO2, and VOO3, respectively (Figure 1A). Total tocopherol content exhibited values of 236, 207, and 189 ppm in VOO1, VOO2, and VOO3, respectively (Figure 1B). $\alpha$-Tocopherol was the most abundant isoform of vitamin E in the three VOOs (about 92−93% of the total tocopherol content). Picual VOO1, VOO2, and VOO3 showed average total polyphenol contents of 394, 289, and 78 ppm, respectively (Figure 1C). Differences in the polyphenol content between VOOs were high, suggesting a dramatic effect of ripening in these antioxidant compounds.[20] Gómez-Rico et al.,[21] Baccouri et al.,[36] Beltrán et al.,[41] and Salvador et al.,[42] reported decreases in phenolic compounds and tocopherol content during olive ripening. Yousfi et al.[22] studied the effect of fruit ripening on the quality of the oil extracted and on the amount of phenolic compounds in the Arbequina and Picual varieties and observed that the oil quality was not affected by fruit ripening or by the increase in rainfall of the season. However, Yousfi et al.[22] reported that the changes in oil stability and phenolic compounds strongly differ depending on olive variety and ripeness of the olives from which oils were obtained.

**Oils Changes during Repeated Potato Frying.** *Changes in the Fatty Acid Composition.* As commented, VOO1 presented a higher amount of SFA. The differences in the fatty acid profile of the three tested VOOs have probably determined, at least partially, that VOO1 showed higher stability during frying (Table 1). It is well-known that oils rich in saturated fatty acids are highly thermostable.[1,43] Nonetheless, VOO1 also presents higher amounts of tocopherols and phenolic compounds, contributing to the higher thermal stability of VOO1.

After 40 frying operations, linoleic and linolenic acids markedly decreased (72−74 and 33.3−51.3%, respectively), whereas little difference was observed for oleic acid. These results are in line with general frying bibliography, reflecting that oleic acid decreases relevantly only when reduced linoleic acid content remains in the oil.[3,39,44] Results also confirm that the degradation rate of unsaturated fatty acids is higher than that of monounsaturated and saturated ones.

*Polar Content and Thermal Oxidation and Hydrolytic Changes during 40 Fryings.* As reported in previous studies with olive oils,[3,16,28,39,45] thermal oxidation compounds increased with the number of frying operations, whereas hydrolytic alteration products remained quite stable (Table 2). Casal et al.,[46] frying potatoes with commercial monovarietal extra VOO from the same cultivar region, a refined sunflower oil, and a refined oil and VOO blend, also observed PC increases. These authors reported that PC increased with the number of frying operations in all oils but that extra VOO showed the highest stability, whereas sunflower oil reached the 25% PC cutoff point at least 9 h before the other oils. However, in the present study, after 40 frying operations, the PC and OLIG contents (Table 2) were far from legal limits.[24] Table 2 also shows that after 40 frying operations, a large proportion of the polar fraction (~75%) was constituted by OTG and DTG and to a lesser degree by PTG. Changes in PC and thermal oxidation compounds but not those of most hydrolytic compounds were significantly fitted to linear adjustments (Table 5). These linear adjustments explain >92% ($r^2$ > 0.92) of the data variability of all the thermal oxidation compounds tested.

Previous studies by our group indicate that oil thermal oxidation changes fit linear adjustments when frying was

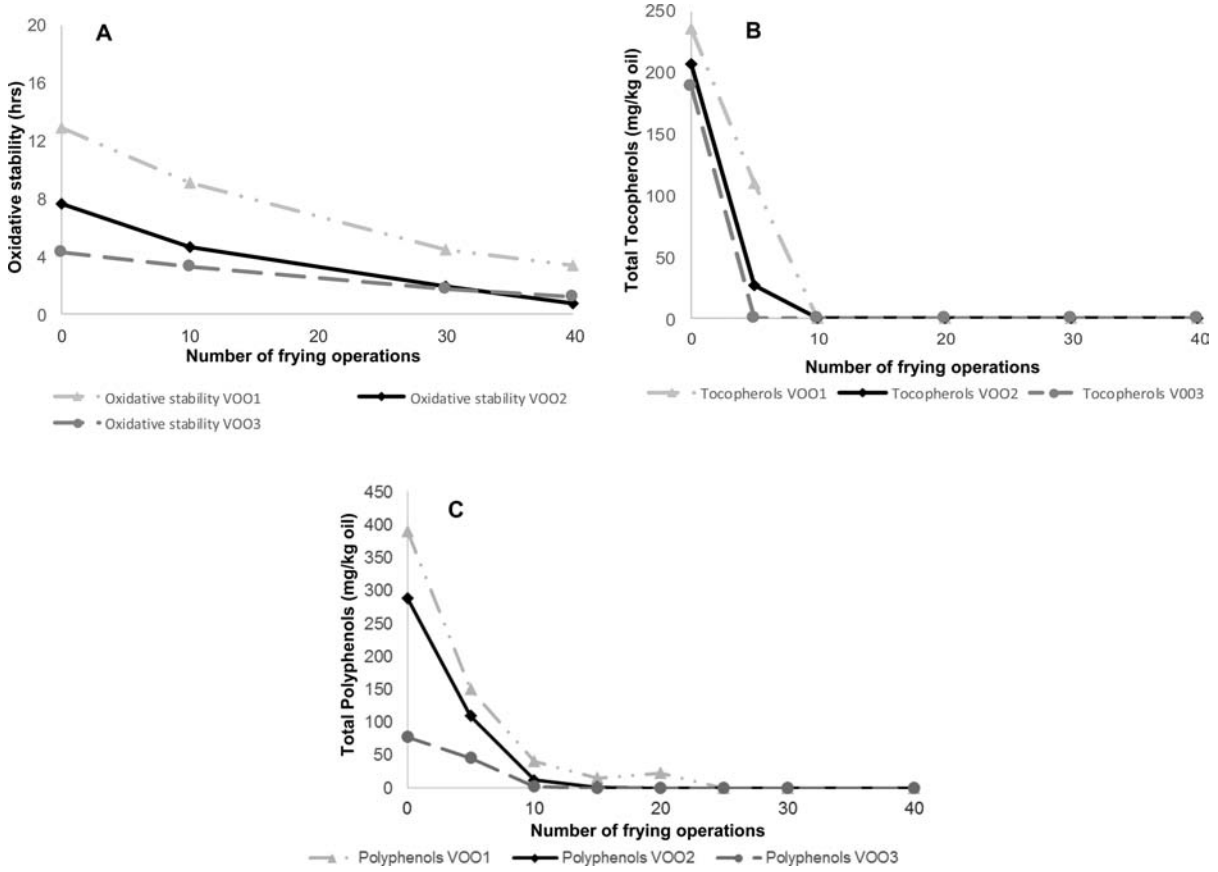


**Figure 1.** Changes in the oxidative stability, total tocopherols, and total polyphenols during 40 discontinuous fryings with virgin olive oils (VOO). (A) Oxidative stability changes (h) in the three Picual VOOs. VOO1, VOO2, and VOO3 correspond to virgin olive oils obtained from Picual olives at different ripening periods; for more details see text. Linear adjustment: $Y$ = intercept (with their values 95% CI) + slope (with their values 95% CI) × $X$, where $Y$ is the oxidative stability and $X$ the number of frying operations: (▲) VOO1, $Y$ = 11.571 (9.900; 13.242) − 0.236 (−0.309; −0.163) × $X$; $r^2$ = 0.839; ($p$ < 0.01); (♦) VOO2, $Y$ = 6.621 (5.567; 7.676) − 0.167 (−0.213; −0.121) × $X$; $r^2$ = 0.867; ($p$ < 0.01); (●) VOO3, $Y$ = 3.941 (3.484; 4.397) − 0.087 (−0.098; −0.058) × $X$; $r^2$ = 0.884; ($p$ < 0.01). Mean values of oxidative stability were significantly different for VOO1 versus VOO3 ($p$ = 0.01) and marginally significant for VOO2 versus VOO3 ($p$ = 0.054) although not significantly different for VOO1 versus VOO2 ($p$ = 0.099). (B) Total tocopherol changes (mg/kg oil) and (C) total polyphenol changes (mg/kg oil) in the three Picual VOOs. VOO1, VOO2, and VOO3 correspond to virgin olive oils obtained from Picual olives at different ripening periods; for more details see text. Nonlinear adjustments were found; thus, comparisons between oils were not performed.

performed with low or null oil turnover but to a power, logarithmic, or quadratic adjustment when frequent turnover was done.[47] The equations presented in Table 5 suggest that during frying of potatoes each frying operation induces increases of 0.307 and 0.317 g/100 g oil of PC and 0.161 and 0.172 mg/100 g oil OLIG in VOO1 and VOO2 oils, respectively, whereas these increases were of 0.412 and 0.222 g/100 g oil of PC and OLIG, respectively, in VOO3 oil. According to OLIG adjustments (Table 5), and in the case of keeping the same experimental frying conditions and trends, the VOO3 oils should be discarded at the 53rd frying, whereas the VOO1 oil should be discarded at the 73rd frying. The increased stability of the oils prepared from olive fruits of minor ripeness index seems to be related to their fatty acid profile and higher (4 and 5 times) polyphenol and higher (14 and 25%) tocopherol contents with respect to their VOO2 and VOO3 oil counterparts.

No linear relationships were found between the frying number and any hydrolytic compounds in any of the Picual VOO tested (data not shown).

*Changes in the Composition of FAME and Formation of Oxidative and Thermal Dimers and Polymers of FAME during 40 Fryings.* Evaluation of specific changes occurring in the fatty acyl chains of triglycerides, by far the most abundant compounds in oils, is an important tool to study in-depth oil degradation.[1] During frying, the formation of dimers (thermal-FAD and oxFAD) and polymers (oxFAD) derived of FAME increases the analysis complexity because of the presence of oxygenated (C−O−C) and nonoxygenated (C−C) bindings between triglyceride fatty acyl groups.[1] Following derivatization, results showed that thermal fatty acid monomers (thermal-FAM) and oxidized oxFAM significantly increased with the number of frying study (Table 4). These increases were fitted to linear adjustments (at least $p$ = 0.05) (Table 6). On the contrary, when the number of frying operations increased, nonoxidized FAM decreased (0.133−0.173 g/100 g oil per frying) (Table 6). After 40 frying operations, VOO3 oil showed less nonoxidized FAM and more oxFAM compared with the other two VOOs (Table 4). Linear adjustments for the different FAME related compounds tended to be higher, although in most cases nonsignificant, in VOO3 oil with respect to VOO1 and VOO2 counterparts. VOO1 showed lower polar-ME increase than VOO3 (0.098 vs 0.140 g/100 g oil increase each frying, $p$ = 0.029) (Table 6). Márquez-Ruiz et al.[25] observed a major increase in the altered fatty acid methyl esters content

**Table 5. Linear Adjustments between Polar Compounds, the Different Thermal Oxidation Compounds, and the Number of Fryings of Fresh Potatoes with Virgin Olive Oils Obtained from Picual Olives of Different Ripeness Indices**

| | ripeness[a] | $r^2$ | $\beta$ | intercept[b] | slope[b] | $P$[c] | VOO1 vs VOO2[d] | VOO1 vs VOO3[d] | VOO2 vs VOO3[d] |
|---|---|---|---|---|---|---|---|---|---|
| PC | VOO1 | 0.991 | 0.996 | 2.296 (1.938, 2.665) | 0.307 (0.292, 0.323) | <0.001 | ns | <0.001 | <0.001 |
| | VOO2 | 0.952 | 0.976 | 3.489 (2.595, 2.665) | 0.317 (0.279, 0.354) | <0.001 | | | |
| | VOO3 | 0.991 | 0.995 | 3.056 (2.558, 3.553) | 0.412 (0.391, 0.433) | <0.001 | | | |
| PTG | VOO1 | 0.927 | 0.963 | −0.114 (−0.214, −0.014) | 0.028 (0.240, 0.032) | <0.001 | ns | <0.001 | <0.001 |
| | VOO2 | 0.952 | 0.975 | −0.108 (−0.207, −0.009) | 0.350 (0.031, 0.039) | <0.001 | | | |
| | VOO3 | 0.955 | 0.977 | −0.204 (−0.339, −0.068) | 0.049 (0.044, 0.055) | <0.001 | | | |
| DTG | VOO1 | 0.983 | 0.991 | 0.063 (−0.157, 0.284) | 0.133 (0.124, 0.142) | <0.001 | ns | <0.001 | <0.001 |
| | VOO2 | 0.924 | 0.961 | 0.301 (−0.195, 0.798) | 0.137 (0.117, 0.158) | <0.001 | | | |
| | VOO3 | 0.980 | 0.990 | 0.280 (−0.035, 0.594) | 0.173 (0.160, 0.186) | <0.001 | | | |
| PTG + DTG (OLIG) | VOO1 | 0.989 | 0.995 | −0.050 (−0.261, 0.160) | 0.161 (0.153, 0.170) | <0.001 | ns | <0.001 | <0.001 |
| | VOO2 | 0.942 | 0.970 | 0.193 (−0.347, 0.734) | 0.172 (0.149, 0.195) | <0.001 | | | |
| | VOO3 | 0.989 | 0.994 | 0.076 (−0.220, 0.373) | 0.222 (0.210, 0.235) | <0.001 | | | |
| OTG | VOO1 | 0.982 | 0.991 | 0.651 (0.414, 0.888) | 0.139 (0.129, 0.149) | <0.001 | ns | <0.001 | <0.001 |
| | VOO2 | 0.931 | 0.965 | 1.135 (0.654, 1.616) | 0.140 (0.120, 0.160) | <0.001 | | | |
| | VOO3 | 0.980 | 0.990 | 0.975 (0.648, 1.303) | 0.180 (0.166, 0.193) | <0.001 | | | |
| TC | VOO1 | 0.990 | 0.995 | 0.601 (0.228, 0.973) | 0.300 (0.284, 0.316) | <0.001 | ns | <0.001 | <0.001 |
| | VOO2 | 0.942 | 0.971 | 1.328 (0.351, 2.305) | 0.312 (0.271, 0.353) | <0.001 | | | |
| | VOO3 | 0.988 | 0.994 | 1.051 (0.498, 1.605) | 0.402 (0.379, 0.425) | <0.001 | | | |

[a]VOO1, VOO2, and VOO3 correspond to different harvesting periods; for more details see text. [b]Values (95% CI). [c]$p$, lineal regression adjustment. [d]$p$, significant differences between lineal adjustments. PC, polar compounds; PTG, triglyceride polymers; DTG, triglyceride dimers; OLIG, triglyceride oligomers (PTG plus DTG); OTG, oxidized triglycerides; TC, thermal oxidized compounds (PTG, DTG plus OTG); ns, nonsignificant.

when the oils presented higher PC content in sunflower oil, high-oleic sunflower oil, and palm olein submitted to frying or thermal oxidation. Taking into account the correlation between PC and polar-ME found in the present study [polar-ME = PC × 0.345) + 0.855] it can be calculated that 25% PC corresponds to 9.5% polar-ME. Márquez-Ruiz et al.[25] and Sanchez-Muniz et al.[1] reported that PC values between 21 and 27% corresponded to 8−11% total altered fatty acid values. In the case of discarding oils at this 9.5% cutoff point, the VOO1 oil shelf life could be extended up to the 80th frying in contrast with VOO2 and VOO3 oils, which would be used for only 64 and 55 fryings, respectively. These results clearly indicate the highest stability of the oil obtained from olive fruits of low ripening index.

Pokorný and Dostálová[2] and Romero et al.[47,48] have suggested that slightly higher concentrations of these altered compounds are present in food than in the oil media. These results show the benefits of frying potatoes with the most stable oil as fewer alteration compounds are formed in the oil and absorbed by the food during frying.

*Changes in the Oxidative Stability and Tocopherol and Polyphenol Contents.* The oxidative stability of the three VOOs decreased with the number of frying operations. Andrikopoulos et al.[49] observed while obtaining chip potato that the increase in PC with the number of frying operations in VOO and a commercial vegetable oil was related to a decrease in the oxidative stability of both oils. After 40 fryings, VOO1 appears as the most stable (Figure 1A). However, with respect to its respective basal polyphenol content, VOO2 suffered the highest polyphenol losses followed by VOO1. The oxidative stability of the oils was significantly and negatively correlated ($p < 0.001$) with the contents of PC, OLIG, OTG, and TC and the TC/HC ratio and positively correlated (at least $p < 0.05$) with the TC/OLIG ratio (Table 7). Similarly, the oxidative stability was significantly and negatively correlated (at least $p < 0.01$) with polar-ME and oligomers of methyl esters (oligomers-ME) and positively correlated ($p < 0.001$) with nonpolar-ME (Table 7). The highest stability found for VOO1 with respect to VOO2 and VOO3 was closely related with the loss of tocopherols because approximately 50% of tocopherols remained after five frying operations in VOO1, and only 10% of basal levels remained in VOO2, whereas tocopherols were not detected in VOO3. Nevertheless, tocopherols were exhausted in all tested oils beyond the 10th frying operation (Figure 1B). Frying potatoes with olive oil, Chatzilazarou et al.[3] found a decrease of 41.2% after 10 h of frying, whereas Andrikopoulos et al.[49] described a retention of 50% of tocopherols after only three successive deep-fryings. Márquez-Ruiz et al.[40] suggested that oxidized triglyceride monomers and oligomers significantly increased only when oils were highly depleted in tocopherols.

In the three studied VOOs, the initial total polyphenol content decreased by >50% after six frying operations (Figure 1C). After 10 fryings, the polyphenol contents in VOO1 and VOO2 with respect to their respective basal values were 10 and 5%, respectively, whereas those compounds were not detected in VOO3. These amounts were further reduced as 3.5−5.5% of the initial polyphenol content was found in VOO1 between the 16th and 25th fryings, whereas those compounds were not detected in VOO2 and VOO3 (Figure 1C). Andrikopoulos et al.[49] reported that the major phenols found in virgin olive oils have abruptly diminished (by 50%) after five successive deep-fryings of potatoes. The higher polyphenol content of

**Table 6. Linear Adjustments between Polar Methyl Esters, Thermal Fatty Acid Dimers, Nonoxidized Fatty Acid Monomers, Fatty Acid Polymers, Oxidized Fatty Acid Dimers, and the Number of Fryings of Fresh Potatoes with Virgin Olive Oils Obtained from Picual Olives of Different Ripeness Indices**

| | ripeness[a] | $r^2$ | $\beta$ | intercept[b] | slope[b] | $P^c$ | VOO1 vs VOO2[d] | VOO1 vs VOO3[d] | VOO2 vs VOO3[d] |
|---|---|---|---|---|---|---|---|---|---|
| polar-ME | VOO1 | 0.926 | 0.962 | 1.622 (1.066, 2.178) | 0.098 (0.076, 0.121) | <0.001 | ns | 0.029 | ns |
| | VOO2 | 0.934 | 0.967 | 1.919 (1.291, 2.547) | 0.119 (0.097, 0.144) | <0.001 | | | |
| | VOO3 | 0.902 | 0.950 | 1.850 (0.928, 2.772) | 0.140 (0.102, 0.178) | <0.001 | | | |
| thermal-FAD | VOO1 | 0.647 | 0.804 | 1.229 (−0.071, 2.529) | 0.088 (0.035, 0.141) | 0.050 | ns | ns | ns |
| | VOO2 | 0.868 | 0.932 | 0.804 (−0.099, 1.707) | 0.116 (0.079, 0.153) | <0.001 | | | |
| | VOO3 | 0.824 | 0.908 | 0.926 (−0.106, 1.958) | 0.112 (0.070, 0.154) | <0.001 | | | |
| nonoxidized FAM | VOO1 | 0.983 | 0.991 | 0.063 (−0.157, 0.284) | 0.133 (0.124, 0.142) | <0.001 | ns | 0.067 | ns |
| | VOO2 | 0.924 | 0.961 | 0.301 (−0.195, 0.798) | 0.137 (0.117, 0.158) | <0.001 | | | |
| | VOO3 | 0.980 | 0.990 | 0.280 (−0.035, 0.594) | 0.173 (0.160, 0.186) | <0.001 | | | |
| FAP | VOO1 | 0.989 | 0.995 | −0.050 (−0.261, 0.160) | 0.161 (0.153, 0.170) | <0.001 | ns | ns | ns |
| | VOO2 | 0.942 | 0.970 | 0.193 (−0.347, 0.734) | 0.172 (0.149, 0.195) | <0.001 | | | |
| | VOO3 | 0.989 | 0.994 | 0.076 (−0.220, 0.373) | 0.222 (0.210, 0.235) | <0.001 | | | |
| oxFAD | VOO1 | 0.907 | 0.952 | 0.178 (−0.034, 0.390) | 0.033 (0.024, 0.042) | <0.001 | ns | 0.033 | ns |
| | VOO2 | 0.951 | 0.975 | 0.160 (−0.018, 0.338) | 0.039 (0.032, 0.047) | <0.001 | | | |
| | VOO3 | 0.965 | 0.982 | 0.145 (−0.020, 0.310) | 0.044 (0.037, 0.050) | <0.001 | | | |
| oxFAM | VOO1 | 0.982 | 0.991 | 0.651 (0.414, 0.888) | 0.139 (0.129, 0.149) | <0.001 | ns | 0.067 | ns |
| | VOO2 | 0.931 | 0.965 | 1.135 (0.654, 1.616) | 0.140 (0.120, 0.160) | <0.001 | | | |
| | VOO3 | 0.980 | 0.990 | 0.975 (0.648, 1.303) | 0.180 (0.166, 0.193) | <0.001 | | | |

[a]VOO1, VOO2, and VOO3 correspond to harvesting periods; for more details see text. [b]Values (95% CI). [c]$p$, lineal regression significance. [d]$p$, significant differences between lineal adjustments. Polar-ME, polar methyl esters; thermal-FAD, thermal fatty acid dimers; nonoxidized FAM, nonoxidized fatty acid monomers; FAP, fatty acid polymers; oxFAD, oxidized fatty acid dimers; oxFAM, oxidized fatty acid monomers; NS, nonsignificant.

**Table 7. Product−Moment Correlations between the Oxidative Stability Determined by the Rancimat Method and Different Thermal Oxidative and Hydrolytic Alteration Compounds Present in Virgin Olive Oils Obtained from Picual Olives of Different Ripeness Indices**

| ripeness[a] | PC | OLIG | OTG | TC | DG | MG | FFA | HC | TC/HC | TC/OLIG | polar-ME | non polar-ME | total OLIG-ME |
|---|---|---|---|---|---|---|---|---|---|---|---|---|---|
| VOO1 | −0.947 *** | −0.940 *** | −0.948 *** | −0.944 *** | −0.864 ** | −0.919 *** | −0.405 | −0.876 ** | −0.958 *** | 0.843 ** | −0.897 ** | 0.970 *** | −0.955 *** |
| VOO2 | −0.978 *** | −0.951 *** | −0.974 *** | −0.964 *** | −0.396 | −0.579 | 0.070 | −0.286 | −0.953 *** | 0.885 ** | −0.922 *** | 0.971 *** | −0.968 *** |
| VOO3 | −0.960 *** | −0.950 *** | −0.968 *** | −0.959 *** | −0.965 *** | −0.204 | 0.141 | −0.885 ** | −0.960 *** | 0.731 * | −0.894 ** | 0.917 *** | −0.933 *** |

[a]VOO1, VOO2, and VOO3 correspond to harvesting period; for more details see text. ∗, $p < 0.05$; ∗∗, $p < 0.01$; ∗∗∗, $p < 0.001$. PC, polar compounds; OLIG, triglyceride polymers plus of triglyceride dimers; OTG, oxidized triglycerides; TC, thermal oxidized compounds (PTG plus DTG plus OTG); DG, diglycerides; MG, monoglycerides; FFA, free fatty acids; HC, hydrolytic compounds (DG plus MG plus FFA); polar-ME, polar methyl esters (fatty acid polymers plus oxidized fatty acid dimers plus oxidized fatty acid monomers); nonpolar-ME, nonpolar methyl esters; total OLIG-ME, total oligomers of methyl esters (fatty acid polymers plus thermal fatty acid dimers plus oxidized fatty acid dimers).

VOO1 throughout repeated fryings is probably due to its initial higher value and to the partial turnover of oil performed after each five fryings to keep the food/oil ratio constant. None of the three VOOs showed polyphenol detectable amounts after the 25th frying.

To identify which parameters explained better the extent of VOO thermal oxidation during frying, the basal contents of total polyphenols, total tocopherols, and oleic, linoleic, and linolenic acids were correlated with the polar content change. Polyphenols ($r = -0.928$; $p = 0.008$) and tocopherols ($r = -0,870$; $p = 0.024$) were negatively and significantly correlated, whereas the other parameters did not show significant relationships. According to the stepwise multiple-regression procedure, a total polyphenol content of unused VOOs explains about 86% ($p = 0.008$) of data variability for the extent of oil thermal oxidation (as polar content change) during 40 fryings in our experimental conditions. Other parameters of the unused VOOs tested were excluded from the stepwise multiple-regression model. This confirms the hypothesis that olive oil phenols play an important antioxidant role during frying.[2,10,49]

In conclusion, Picual olive ripeness affects the VOO composition and stability. Although repeated fryings increased the concentration of all thermal oxidation compounds and decreased the oxidative stability in the three VOOs studied,

oil stability was higher and degradation lower during frying in the VOOs obtained from olives of lower ripeness index. As the potential toxicity of oils used in repeated fryings is ascribed to the amount and profile of alteration compounds, the repeated domestic potato frying with VOO obtained from low ripeness index olives should be recommended to obtain high-quality fried potatoes.

## AUTHOR INFORMATION


### Corresponding Author

*(F.J.S.-M.) Phone: 34-91-3941828. Fax: 34-91-3941810. E-mail: frasan@ucm.es.


### Author Contributions

F.J.S.-M. is the corresponding author and guarantor of the paper and contributed to the study design, data discussion, and writing of the paper. R.O.-D., C.M., and B.S. contributed to the data acquisition and analysis, whereas G.M.R. contributed to the oxidative stability analysis. A.P.-J. and S.B. contributed to the study design.


### Funding

The study was granted by the Spanish INIA RTA2010-00097 project. We thank the FPI INIA fellowship associated with the former project given to C.M.


### Notes

The authors declare no competing financial interest.

## ACKNOWLEDGMENTS


We thank Dr. J. Velasco from the Instituto de la Grasa of Sevilla for help with the tocopherol determination and Dra. F Holgado for help with the oxidative stability analysis.


## ABBREVIATIONS USED

DG, diglycerides; DTG, dimers of triglycerides; FAME, fatty acid methyl esters; FAP, fatty acid polymers; HC, hydrolytic compounds; HPSEC, high-performance size exclusion chromatography; MG, monoglycerides; nonoxidized FAM, nonoxidized fatty acid monomers; OLIG, oligomers; OTG, oxidized triglycerides; oxFAD, oxidized fatty acid dimers; oxFAM, oxidized fatty acid methyl esters; PC, polar compounds; polar-ME; polar methyl esters; PTG, polymers of triglycerides; TC, thermal oxidized compounds; thermal-FAM, thermal fatty acid methyl esters; thermal-FAD, thermal fatty acid dimers; VOO, virgin olive oil

## REFERENCES


(1) Sánchez-Muniz, F. J.; Bastida, S.; Márquez-Ruiz, G.; Dobarganes, C. Effects of heating and frying on oil and food fatty acids. In *Fatty Acids in Foods and Their Implications*, 3rd ed.; Chow, C. K., Ed.; Taylor and Francis Group: Boca Raton, FL, USA, 2008; pp 511−543.

(2) Pokorný, J.; Dostálová, J. Changes in nutrients, antinutritional factors, and contaminants at frying temperatures. In *Frying of Foods: Oxidation, Nutrient and Non-Nutrient Antioxidants, Biologically Active Compounds and High Temperatures*, 2nd ed.; Boskou, D., Elmadfa, I., Eds.; Taylor and Francis Group: Boca Raton, FL, USA, 2011; pp 71−104.

(3) Chatzilazarou, A.; Gortzi, O.; Lalas, S.; Zoidis, E.; Tsaknis, J. Physicochemical changes of olive oils and selected vegetable oils during frying. *J. Food Lipids* **2006**, *13*, 27−35.

(4) Dobarganes, C.; Márquez-Ruiz, G. Analysis of used frying oils. *Lipid Technol.* **2013**, *25*, 159−162.

(5) Sanchez-Muniz, F. J.; Lopez-Varela, S.; Garrido-Polonio, M. C.; Cuesta, C. Dietary effects on growth, liver peroxides, and serum and lipoprotein lipids in rats fed a thermoxidised and polymerised sunflower oil. *J. Sci. Food Agric.* **1998**, *76*, 364−372.

(6) Sánchez-Muniz, F. J.; Bastida, S.; González Muñoz, M. J. Column and high performance size exclusion chromatography application to the *in vivo* digestibility study of a thermoxidized and polymerized olive oil. *Lipids* **1999**, *34*, 1187−1192.

(7) Dobarganes, M. C.; Márquez-Ruiz, G. Formation and analysis of oxidized monomeric, dimeric and higher oligomeric triglycerides. In *Deep Frying: Chemistry Nutrition and Practical Applications*, 2nd ed.; Erickson, M. D., Ed.; AOCS: Champaign, IL, USA, 2007; pp 87−110.

(8) Olivero-David, R.; González-Muñoz, M. J.; Benedí, J.; Bastida, S.; Sánchez-Muniz, F. J. Thermally oxidized palm olein exposure increases triglyceride polymer levels in rat small intestine. *Eur. J. Lipid Sci. Technol.* **2010**, *112*, 970−976.

(9) Olivero-David, R.; Paduano, A.; Fogliano, V.; Vitaglione, P.; Bastida, S.; Gonzalez-Muñoz, M. J.; Benedí, J.; Sacchi, R.; Sanchez-Muniz, F. J. Effect of thermally oxidized oil and fasting status on the short-term digestibility of ketolinoleic acids and total oxidized fatty acids in rats. *J. Agric. Food Chem.* **2011**, *59*, 4684−4691.

(10) Boskou, D. Non-nutrient antioxidants and stability of frying oils. In *Frying of Foods: Oxidation, Nutrient and Non-Nutrient Antioxidants, Biologically Active Compounds and High Temperatures*, 2nd ed.; Boskou, D., Elmadfa, I., Eds.; Taylor and Francis Group: Boca Raton, FL, USA, 2011; pp 199−223.

(11) deMan, J. M. Chemical and physical properties of fatty acid. In *Fatty Acids in Foods and Their Health Implications*, 3rd ed.; Chow, C. K., Ed.; CRC Press: Boca Raton, FL, USA, 2008; pp 17−45.

(12) Bastida, S.; Sánchez-Muniz, F. J. Chapter 21. Frying, a cultural way of cooking in the Mediterranean diet. In *The Mediterranean Diet: A Comprehensive Approach*; Preedy, V. R., Watson, R., Eds.; Elsevier: Amsterdam, The Netherlands, 2015 (in press); pp 217−234, ISBN 978-0-12-407849-9.

(13) Covas, M. I.; Nyyssönen, K.; Poulsen, H. E.; Kaikkonen, J.; Zunft, H. J.; Kiesewetter, H.; Gaddi, A.; de la Torre, R.; Mursu, J.; Bäumler, H.; Nascetti, S.; Salonen, J. T.; Fitó, M.; Virtanen, J.; Marrugat, J. EUROLIVE Study Group. The effect of polyphenols in olive oil on heart disease risk factors: a randomized trial. *Ann. Int. Med.* **2006**, *145*, 333−341.

(14) Mensink, R. P.; Katan, M. B. Effect of dietary fatty acids on serum lipids and lipoproteins: a meta-analysis of 27 trials. *Arterioscler. Thromb.* **1992**, *12*, 911−919.

(15) Estruch, R.; Ros, E.; Salas-Salvadó, J.; Covas, M. I.; Corella, D.; Arós, F.; Gómez-Gracia, E.; Ruiz-Gutiérrez, V.; Fiol, M.; Lapetra, J.; Lamuela-Raventos, M. R.; Serra-Majem, L.; Pintó, X.; Basora, J.; Muñoz, M. A.; Sorlí, J. V.; Martínez, J. A.; Martínez-González, M. A. For the PREDIMED Study Investigators. Primary prevention of cardiovascular disease with a Mediterranean diet. *N. Engl. J. Med.* **2013**, *368*, 1279−1290.

(16) Romero, A.; Cuesta, C.; Sánchez-Muniz, F. J. Cyclic fatty acid monomers in high oleic sunflower oil and extra virgin olive oil used in repeated frying of fresh potatoes. *J. Am. Oil Chem. Soc.* **2003**, *80*, 437−442.

(17) Velasco, J.; Dobarganes, C. Oxidative stability of virgin olive oil. *Eur. J. Lipid Sci. Technol.* **2002**, *104*, 661−676.

(18) Servili, M.; Selvaggini, R.; Esposto, S.; Taticchi, A.; Montedoro, G.; Morozzi, G. Health and sensory properties of virgin olive oil hydrophilic phenols: agronomic and technological aspects of production that affect their occurrence in the oil. *J. Chromatogr., A* **2004**, *1054*, 113−127.

(19) Kiralan, M.; Bayrak, A.; Özkaya, M. T. Oxidation stability of virgin olive oils from some important cultivars in east Mediterranean area in Turkey. *J. Am. Oil Chem. Soc.* **2009**, *86*, 247−252.

(20) Conde, C.; Delrot, S.; Gerós, H. Physiological, biochemical and molecular changes occurring during olive development and ripening. *J. Plant. Physiol.* **2008**, *165*, 1545−1562.

(21) Gómez-Rico, A.; Fregapane, G.; Salvador, M. D. Effect of cultivar and ripening on minor components in Spanish olive fruit and their corresponding virgin olive oils. *Food Res. Int.* **2008**, *41*, 433−440.

(22) Yousfi, K.; Cert, R. M.; García, J. M. Changes in quality and phenolic compounds of virgin olive oils during objectively described fruit maturation. *Eur. Food Res. Technol.* **2006**, *223*, 117−124.
(23) Dobarganes, M. C.; Velasco, J.; Dieffenbacher, A. Determination of polar compounds, polymerized an oxidized triacyglycerols, and diacylglycerols in oils and fats. *Pure Appl. Chem.* **2000**, *72*, 1563−1575.
(24) DGF (German Society for Fat Research). Proceedings of the 3rd international symposium of deep-fat frying. Final recommendations. *Eur. J. Lipid Sci. Technol.* **2000**, *102*, 594.
(25) Márquez-Ruiz, G.; Tasioula-Margari, M.; Dobarganes, M. C. Quantitation and distribution of altered fatty acids in frying fats. *J. Am. Oil Chem. Soc.* **1995**, *72*, 1171−1176.
(26) Uceda, M.; Frias, L. Época de recolección. Evolución del contenido graso y de la composición y la calidad del aceite. In *Proceeding II Seminario Oleícola Internacional*; Córdoba, Spain, 1975.
(27) Arroyo, R.; Cuesta, C.; Garrido-Polonio, C.; López-Varela, S.; Sánchez-Muniz, F. J. High performance size exclusion chromatographic studies on polar components formed in sunflower oil used for frying. *J. Am. Oil Chem. Soc.* **1992**, *69*, 557−563.
(28) Bastida, S.; Sanchez-Muniz, F. J. Polar content vs. TAG oligomer content in the frying-life assessment of monounsaturated and polyunsaturated oils used in deep-frying. *J. Am. Oil Chem. Soc.* **2002**, *79*, 447−451.
(29) AENOR (Asociación Española de Normalización). *Norma UNE 55-011*; Catalogo de normas UNE: Madrid, Spain, 1991.
(30) Cuesta, C.; Sánchez-Muniz, F. J.; Hernández, I. Evaluation of nonpolar methyl esters by column and gas chromatography for the assessment of used frying olive oil. *J. Am. Oil Chem. Soc.* **1991**, *68*, 443−445.
(31) Association of Official Analytical Chemists. *Official Methods of Analysis of AOAC*, 16th ed.; Washington, DC, USA, 1995; part 969.63.
(32) Wagner, K. H.; Elmadfa, I. Effects of tocopherols and their mixtures on the oxidative stability of olive oil and linseed oil under heating. *Eur. J. Lipid Sci. Technol.* **2000**, *102*, 624−629.
(33) Koprivnjak, O.; Škevin, D.; Valic, S.; Majetic, V.; Petricevic, S.; Ljubenkov, I. The antioxidant capacity and oxidative stability of virgin olive oil enriched with phospholipids. *Food Chem.* **2008**, *111*, 121−126.
(34) Vázquez-Roncero, A.; Janer, C.; Janer, M. L. Determinación de polifenoles totales del aceite de oliva. *Grasas Aceites* **1975**, *24*, 350−355.
(35) IUPAC Regulation no. 2432. *Standard Methods for the Analysis of Oils, Fat and Derivatives*; Pergamon: Oxford, UK, 1992.
(36) Baccouri, B.; Zarrouk, W.; Krichene, D.; Nouairi, I.; Youssef, N. B.; Douja, D.; Zarrouk, M. Influence of fruit ripening and crop yield on chemical properties of virgin olive oil from seven selected oleasters (*Olea europaea* L.). *J. Agron.* **2007**, *6*, 338−396.
(37) Haralampidis, K.; Milioni, D.; Sánchez, J.; Baltrusch, M.; Heinz, E.; Hatzopoulos, P. Temporal and transient expression of stearoyl-ACP carrier protein desaturase gene during olive fruit development. *J. Exp. Bot.* **1998**, *49*, 1661−1669.
(38) Lumley, I. D. Polar compounds in heated oil. In *Frying of Food. Principles, Changes, New Approaches*; Varela, G., Bender, A. E., Morton, I. D., Eds.; Ellis Horwood: Chichester, UK, 1988; pp 166−173.
(39) Romero, A.; Cuesta, C.; Sánchez-Muniz, F. J. Quantitation and distribution of polar compounds in an extra virgin olive oil used in fryings with turnover of fresh oil. *Fat Sci. Technol.* **1995**, *97*, 403−407.
(40) Márquez-Ruiz, G.; Martín-Polvillo, M.; Dobarganes, M. C. Quantitation of oxidized triglyceride monomers and dimers as an useful measurement for early and advanced stages of oxidation. *Grasas Aceites* **1996**, *47*, 48−53.
(41) Beltrán, G. C.; Aguilera, C.; Del Rio, C.; Sánchez, S.; Martínez, L. Influence of fruit ripening process on the natural antioxidant content of Hojiblanca virgin olive oils. *Food Chem.* **2005**, *89*, 207−215.
(42) Salvador, M. D.; Aranda, F.; Fregapane, G. Influence of fruit ripening on 'Cornicabra' virgin olive oil quality. A study of four successive crop seasons. *Food Chem.* **2001**, *73*, 45−53.
(43) Wagner, K. H.; Elmadfa, I. Nutrient antioxidants and stability of frying oil (thocochromanols, $\beta$-carotene, philloquinone, ubiquinone 50, and arcorbyl palmitate. In *Frying of Foods: Oxidation, Nutrient and Non-Nutrient Antioxidants, Biologically Active Compounds and High Temperatures*, 2nd ed.; Boskou, D., Elmadfa, I., Eds.; Taylor and Francis Group: Boca Raton, FL, USA, 2011; pp 177−197.
(44) Romero, A.; Cuesta, C.; Sánchez-Muniz, F. J. Deep fat frying of frozen foods in sunflower oil. Fatty acid composition in fryer oil and frozen prefried potatoes. *J. Sci. Food Agric.* **2000**, *80*, 2135−2141.
(45) Velasco, J.; Marmesat, S.; Berdeaux, O.; Márquez Ruiz, G.; Dobarganes, C. Quantitation of short-chain glycerol-bound compounds in thermoxidized and used frying oils. A monitoring study during thermoxidation of olive and sunflower oils. *J. Agric. Food Chem.* **2005**, *53*, 4006−4011.
(46) Casal, S.; Malheiro, S.; Sendas, A.; Oliveira, B.; Pereira, J. A. Olive oil stability under deep-frying conditions. *Food Chem. Toxicol.* **2010**, *48*, 2972−2979.
(47) Cuesta, C.; Romero, A.; Sánchez-Muniz, F. J. Fatty acid changes in high oleic acid sunflower oil during successive deep-fat frying of frozen foods. *Food Sci. Tech. Int.* **2001**, *7*, 317−328.
(48) Romero, A.; Bastida, S.; Sánchez-Muniz, F. J. Cyclic fatty acids in sunflower oils during frying of frozen foods with oil replenishment. *Eur. J. Lipid Sci. Technol.* **2007**, *109*, 165−173.
(49) Andrikopoulos, N. K.; Kalogeropoulos, N.; Falirea, A.; Barbagianni, M. N. Performance of virgin olive oil and vegetable shortening during domestic deep-frying and pan-frying of potatoes. *Int. J. Food Sci. Technol.* **2002**, *37*, 177−190.

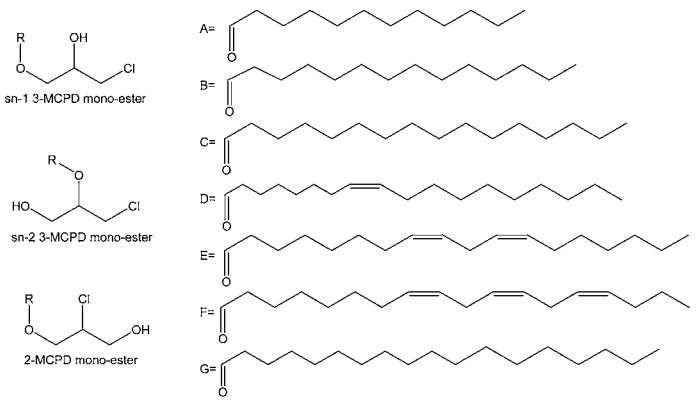


| MCPD mono-esters | | |
|---|---|---|
| **sn-1 3-MCPD mono-esters** | | |
| Name | Abbreviation | R |
| 1-Lauroyl-3-chloropropanediol | 1-La3 | A |
| 1-Myristoyl-3-chloropropanediol | 1-My3 | B |
| 1-Palmitoyl-3-chloropropanediol | 1-Pa3 | C |
| 1-Oleoyl-3-chloropropanediol | 1-Ol3 | D |
| 1-Linoleoyl-3-chloropropanediol | 1-Li3 | E |
| 1-Linolenoyl-3-chloropropanediol | 1-Ln3 | F |
| 1-Stearoyl-3-chloropropanediol | 1-St3 | G |
| **sn-2 3-MCPD mono-esters** | | |
| 2-Palmitoyl-3-chloropropanediol | 2-Pa3 | C |
| 2-Oleoyl-3-chloropropanediol | 2-Ol3 | D |
| **2-MCPD mono-esters** | | |
| 1-Palmitoyl-3-chloropropanediol | 1-Pa2 | C |
| 1-Oleoyl-3-chloropropanediol | 1-Ol2 | D |
| 1-Linoleoyl-3-chloropropanediol | 1-Li2 | E |

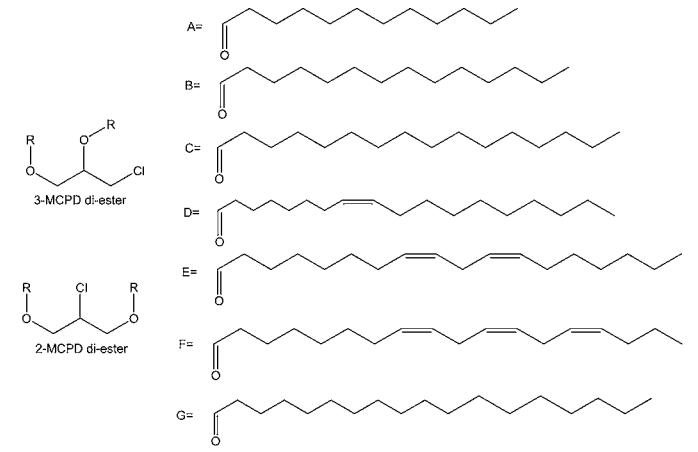


| MCPD di-esters | | | |
|---|---|---|---|
| Name | Abbreviation | R | R |
| Linoleoyl-linolenoyl-3-chloropropanediol | 3Li-Ln | E | F |
| Dilinoleoyl-3-chloropropanediol | 3Li-Li | E | E |
| Palmitoyl-linoleoyl-3-chloropropanediol | 3Pa-Li | C | E |
| Oleoyl-linoleoyl-3-chloropropanediol | 3Ol-Li | D | E |
| Dipalmitoyl-3-chloropropanediol | 3Pa-Pa | C | C |
| Palmitoyl-oleoyl-3-chloropropanediol | 3Pa-Ol | C | D |
| Dioleoyl-3-chloropropanediol | 3Ol-Ol | D | D |
| Stearoyl-linoleoyl-3-chloropropanediol | 3St-Li | G | E |
| Palmitoyl-stearoyl-3-chloropropanediol | 3Pa-St | C | G |
| Oleoyl-stearoyl-3-chloropropanediol | 3Ol-St | D | G |
| Distearoyl-3-chloropropanediol | 3St-St | G | G |
| 2-MCPD di-esters | | | |
| Linoleoyl-linolenoyl-2-chloropropanediol | 2Li-Ln | E | F |
| Dilinoleoyl-2-chloropropanediol | 2Li-Li | E | E |
| Palmitoyl-linoleoyl-2-chloropropanediol | 2Pa-Li | C | E |
| Oleoyl-linoleoyl-2-chloropropanediol | 2Ol-Li | D | E |
| Dipalmitoyl-2-chloropropanediol | 2Pa-Pa | C | C |
| Palmitoyl-oleoyl-2-chloropropanediol | 2Pa-Ol | C | D |
| Dioleoyl-2-chloropropanediol | 2Ol-Ol | D | D |
| Stearoyl-linoleoyl-2-chloropropanediol | 2St-Li | G | E |
| Palmitoyl-stearoyl-2-chloropropanediol | 2Pa-St | C | G |
| Oleoyl-stearoyl-2-chloropropanediol | 2Ol-St | D | G |
| Distearoyl-2-chloropropanediol | 2St-St | G | G |

**Figure 1.** Structures of analytes included in the method.

for 2-MCPD esters in edible oils. The scope of these methods has been expanded, as described herein, resulting in the first approach capable of determining exposure to intact 2-MCPD esters in edible oils. The method targets 14 2-MCPD esters (11 2-MCPD diester standards and 3 2-MCPD monoester standards) (see Figure 1) based on palimitic, linolenic, linoleic, oleic and stearic acid. Eleven standards were synthesized to target >90% of the 2-MCPD likely to be found in most commonly consumed edible oils. The method performance has been validated in soybean oil, olive oil, and palm oil matrices at spiked concentrations as low as 100 ng/g (ppb).

## MATERIALS AND METHODS

**Reagents and Materials.** Deuterated internal standards 1,2-dioleoyl-3-chloropropanediol-$d_5$ (3Ol-Old5) (CAS Registry No. 1246933-00-0), 1,2-dilinoleoyl-3-chloropropanediol-$d_5$ (3Li-Lid5), linoleoyl-linolenoyl-3-chloropropanediol-$d_5$ (3Li-Lnd5), palmitoyl-stearoyl-3-chloropropanediol-$d_5$ (3Pa-Std5), 1,2-distearoyl-3-chloropropanediol-$d_5$ (3St-Std5) (CAS Registry No. 1246818-85-8), 1-oleoyl-3-chloropropanediol-$d_5$ (1-Ol3-d5), and 1-palmitoyl-3-chloropropanediol-$d_5$ (1-Pa3-d5) were purchased from Toronto Research Chemicals (Toronto, ON, Canada). Standards 2-chloro-1,3-propanediol (2-MCPD) (CAS Registry No. 497-04-1), 1,3-distearoyl-2-chloropropandiol (2 St-St) (CAS Registry No. 26787-56-4), 1,3-dilinoleoyl-2-chloropropanediol (2Li-Li), 1-linoleoyl-3-linolenoyl-2-chloropropanediol (2Li-Ln), 1-palmitoyl-3-chloropropanediol (1-Pa3) (CAS Registry No. 30557-04-1), 1-linoleoyl-3-chloropropanediol (1-Li3) (CAS Registry No. 74875-98-2), 1-oleoyl-3-chloropropanediol (1-Ol3) (CAS Registry No. 10311-82-7), 2-oleoyl-3-chloropropanediol (2-Ol3) (CAS Registry No. 915297-48-2), 2-palmitoyl-3-chloropropanediol (2-Pa3) (CAS Registry No. 20618-92-2), linoleoyl-linolenoyl-3-chloropropanediol (3Li-Ln), dilinoleoyl-3-chloropropanediol (3Li-Li) (CAS Registry No. 74875-96-0), palmitoyl-linoleoyl-3-chloropropanediol (3Pa-Li) (CAS 1246833-87-3), oleoyl-linoleoyl-3-chloropropanediol (3Ol-Li) (CAS Registry No. 1336935-03-5), dipalmitoyl-3-chloropropanediol (3Pa-Pa) (CAS Registry No. 51930-97-3), palmitoyl-oleoyl-3-chloropropanediol (3Pa-Ol) (CAS Registry No. 1363153-60-9), dioleoyl-3-chloropropanediol (3Ol-Ol) (CAS Registry No. 69161-73-5), stearoyl-linoleoyl-3-chloropropanediol (3St-Li) (CAS Registry No. 1246833-46-4), palmitoyl-stearoyl-3-chloropropanediol (3Pa-St) (CAS Registry No. 1185060-41-6), oleoyl-stearoyl-3-chloropropanediol (3Ol-St) (CAS Registry No. 1336935-05-7), and distearoyl-3-chloropropanediol (3St-St) (CAS Registry No. 72468-92-9) were purchased from Toronto Research Chemicals. Standards for 2-MCPD esters 1-palmitoyl-2-chloropropanediol (1-Pa2) (CAS Registry No. 63326-63-6), 1-linoleoyl-2-chloropropanediol (1-Li2), 1-oleoyl-3-chloropropanediol (1-Ol2), palmitoyl-linoleoyl-2-chloropropanediol (2Pa-Li), oleoyl-linoleoyl-2-chloropropanediol (2Ol-Li), dipalmitoyl-2-chloropropanediol (2Pa-Pa) (CAS Registry No. 169471-41-4), palmitoyl-oleoyl-2-chloropropanediol (2Pa-Ol), dioleoyl-2-chloropropanediol (2Ol-Ol), stearoyl-linoleoyl-2-chloropropanediol (2St-Li), palmitoyl-stearoyl-2-chloropropanediol (2Pa-St), and oleoyl-stearoyl-2-chloropropanediol (2Ol-St) were synthesized according to the procedures described herein,

and their purity was confirmed by $^1$H NMR. *N,N′*-Dicyclohexylcarbodiimide (DCC) (CAS Registry No. 538-75-0), 4-(dimethylamino)-pyridine (DMAP) (CAS Registry No. 1122-58-3), carbon tetrachloride ($CCl_4$) (CAS Registry No. 56-23-5), and silica gel ($SiO_2$) (70−230 mesh, pore size = 40 Å) (CAS Registry No. 112926-00-8) were purchased from Sigma-Aldrich (St. Louis, MO, USA). Liquid chromatographic grade acetonitrile (ACN), isopropanol (IPA), methanol (MeOH), water ($H_2O$), *n*-hexane (hexane), ethyl acetate (EtOAc), methyl *tert*-butyl ether (MTBE), and diethyl ether ($Et_2O$) were from Burdick and Jackson. Formic acid and ammonium formate were of HPLC grade from Sigma-Aldrich. A Visiprep SPE manifold and Branson 2510 ultrasonic cleaner were purchased from Sigma-Aldrich. Silica SPE cartridges (500 mg Si, 3 mL and 1000 mg Si, 6 mL) and $C_{18}$ SPE cartridges (1000 mg $C_{18}$, 6 mL) were purchased from Supelco. Disposable 15 mL glass tubes were purchased from Thermo Fisher Scientific (Pittsburgh, PA, USA). A DB-3 Dri-Block Heater and Sample Concentrator were purchased from Bibby Scientific (Burlington, NJ, USA). Clear glass HPLC vials with preslit PTFE caps were purchased from National Scientific (Rockwood, TN, USA). Soybean oil and extra virgin olive oil were purchased from a local grocery store. Organic palm oil was purchased from Sigma-Aldrich.

**Synthesis of Analytical Standards.** The protocol is based on a published procedure for the synthesis of esters.[22]

*Synthesis of 2-MCPD Monoesters (1-Li2, 1-Ol2, 1-Pa2).* A solution of 2-chloro-1,3-propanediol (1 mmol) and the appropriate fatty acid (0.3 mmol) in $CCl_4$ (5 mL) was stirred at room temperature under nitrogen. A solution of DCC (1.1 mmol) and DMAP (0.3 mmol) in $CCl_4$ (3 mL) was added dropwise with stirring, and the resulting solution was stirred for 5 h. The solution was filtered, the solvent was removed in a rotary evaporator, and the material was purified by column chromatography ($SiO_2$, 20% ethyl acetate in hexane, 1-Li2 $R_f$ = 0.32; 1-Pa2 $R_f$ = 0.33; 1-Ol2 $R_f$ = 0.35). Identity and purity (95+%) were confirmed by LC-MS/MS and $^1$H NMR (400 MHz, $CDCl_3$) (1-Li2 LC-MS *m/z* 390.3 (M + $NH_4$): $^1$H NMR $\delta$ 0.9 (3H, t), 1.3 (14H, m), 1.6 (2H, m), 2.1 (4H, q), 2.4 (2H, t), 2.8 (2H, t), 3.8 (2H, m), 4.1 (1H, m), 4.3 (1H, m), 4.4 (1H, m), 5.3 (4H, m). 1-Pa2 (LC-MS *m/z* 366.2 (M + $NH_4$): $^1$H NMR $\delta$ 0.9 (3H, t), 1.3 (24H, m), 1.6 (2H, p), 2.2 (2H, t), 3.8 (2H, m), 4.1 (1H, m), 4.3 (1H, m), 4.4 (1H, m). 1-Ol2 (LC-MS *m/z* 392.3 (M + $NH_4$): $^1$H NMR $\delta$ 0.9 (3H, t), 1.3 (20H, m), 1.6 (2H, p), 2.0 (4H, m), 2.4 (2H, t), 3.8 (2H, d), 4.1 (1H, p), 4.3 (1H, m), 4.4 (1H, m), $\delta$ 5.3 ppm (2H, m).

*Synthesis of Symmetrical 2-MCPD Diesters (2Pa-Pa, 2Ol-Ol).* A solution of 2-chloro-1,3-propanediol (1 mmol) and the appropriate fatty acid (5 mmol) in $CCl_4$ (5 mL) was stirred at room temperature under nitrogen. A solution of DCC (5 mmol) and DMAP (0.3 mmol) in $CCl_4$ (3 mL) was added dropwise with stirring, and the resulting solution was stirred for 5 h. The solution was filtered, the solvent was removed in a rotary evaporator, and the material was purified by column chromatography ($SiO_2$, 7% ethyl acetate in hexane, 2Pa-Pa $R_f$ = 0.48; 2Ol-Ol $R_f$ = 0.46). Identity and purity (95+%) were confirmed by LC-MS/MS and $^1$H NMR (400 MHz, $CDCl_3$) 2Pa-Pa (LC-MS *m/z* 604.5 (M + $NH_4$): $^1$H NMR $\delta$ 0.9 (6H, t), 1.3 (48H, m), 1.6 (4H, p), 2.2 (4H, t), 4.2 (1H, m), 4.3 (4H, m). 2Ol-Ol (LC-MS *m/z* 656.5 (M + $NH_4$), $^1$H NMR $\delta$ 0.9 (6H, t), 1.3 (40H, m), 1.6 (4H, p), 2.0 (8H, m), 2.4 (4H, t), 4.1 (1H, p), 4.2 (4H, m), 5.3 (4H, m).

*Synthesis of Unsymmetrical 2-MCPD Diesters (2Pa-Li, 2Pa-Ol, 2Pa-St, 2Ol-St, 2Ol-Li, 2 St-Li).* A solution of the appropriate 2-MCPD monoester (0.7 mmol) and the appropriate fatty acid (3.5 mmol) in $CCl_4$ (5 mL) was stirred at room temperature under nitrogen. A solution of DCC (3.5 mmol) and DMAP (0.3 mmol) in $CCl_4$ (3 mL) was added dropwise with stirring, and the resulting solution was stirred for 5 h. The solution was filtered, the solvent was removed in a rotary evaporator, and the material was purified by column chromatography ($SiO_2$, 20% ethyl acetate in hexane, 2Pa-Li, 2Ol-Li, 2 St-Li, 2Ol-St $R_f$ = 0.46; 2Pa-Ol $R_f$ = 0.48; 2Pa-St $R_f$ = 0.50). Identity and purity (95+%) were confirmed by LC-MS/MS and $^1$H NMR (400 MHz, $CDCl_3$) 2Pa-Li (LC-MS *m/z* 628.5 (M + $NH_4$), $^1$H NMR: $\delta$ 0.9 (6H, m), 1.3 (38H, m), 1.6 (4H, m), 2.2 (4H, m), 2.4 (4H, t), 2.8 (2H, t), 4.2 (1H, m), 4.3 (4H, m), 5.3 (4H, m). 2 Pa-Ol (LC-MS *m/z* 630.5 (M + $NH_4$), $^1$H NMR: $\delta$ 0.9 (6H, t), 1.3 (44H, m), 1.6 (4H, p), 2.0 (4H, m), 2.4 (4H, t), 4.1 (1H, p), 4.2 (4H, m), 5.3 (2H, m). 2 Pa-St (LC-MS *m/z* 632.5 (M + $NH_4$), $^1$H NMR: $\delta$ 0.9 (6H, t), 1.3 (52H, m), 1.6 (4H, p), 2.2 (4H, t), 4.2 (1H, m), 4.3 (4H, m). 2Ol-St (LC-MS *m/z* 658.5 (M + $NH_4$), $^1$H NMR: $\delta$ 0.9 (6H, t), 1.3 (48H, m), 1.6 (4H, p), 2.0 (4H, m), 2.4 (4H, t), 4.1 (1H, p), 4.2 (4H, m), 5.3 (2H, m). 2Ol-Li (LC-MS *m/z* 654.5 (M + $NH_4$), $^1$H NMR: $\delta$ 0.9 (6H, m), 1.3 (34H, m), 1.6 (4H, m), 2.2 (8H, m), 2.4 (4H, t), 2.8 (2H, t), 4.2 (1H, m), 4.3 (4H, m), 5.3 (6H, m). 2 St-Li (LC-MS *m/z* 656.5 (M + $NH_4$), $^1$H NMR: $\delta$ 0.9 (6H, m), 1.3 (42H, m), 1.6 (4H, m), 2.2 (4H, m), 2.4 (4H, t), 2.8 (2H, t), 4.2 (1H, m), 4.3 (4H, m), 5.3 (4H, m).

**Standard Solutions.** Individual stock solutions of 500−1000 $\mu$g/mL (ppm) of each standard were prepared by weighing the appropriate amount of each reference standard (corrected for composition and purity) into separate tared 10 mL volumetric flasks (5 mL volumetric flasks for $d_5$ internal standards) and brought to volume with IPA. The spiking solution and the standard stock solution (containing 1-Ol, 1-Pa, 1-Li, 3Li-Ln, 3Li-Li, 3Pa-Li, 3Ol-Li, 3Pa-Ol, 3Ol-Ol, 3Pa-Pa, 3St-Li, 3Ol-St, 3Pa-St, 3St-St, 1-Ol2, 1-Pa2, 1-Li2, 2Li-Ln, 2Li-Li, 2Pa-Li, 2Ol-Li, 2Pa-Ol, 2Ol-Ol, 2Pa-Pa, 2St-Li, 2Ol-St, 2Pa-St, and 2St-St at 10 $\mu$g/mL (ppm)) were prepared by pipetting the appropriate volume of each individual stock solution into separate 25 mL volumetric flasks and brought to volume with IPA. The internal standard spiking solution and the internal standard stock solution (containing 1-Ol3-d5, 3Li-Ln-d5, 3Li-Li-d5, 3Ol-Ol-d5, 3Pa-St-d5, and 3St-St-d5 at 5 $\mu$g/mL (ppm)) were prepared by pipetting the appropriate volume of each individual stock solution into separate 10 mL volumetric flasks. One of the flasks was brought to volume with 20% EtOAc/MTBE, generating the internal standard spiking solution. The other flask was brought to volume with IPA, generating the internal standard stock solution. All individual stock solutions were stored at −20 °C and were stable for at least 1 year. The spiking and standard stock solutions were stored at 4 °C and were stable for at least 4 months.

**Sample Preparation.** The sample preparation used was optimized in previous work at the U.S. Food and Drug Administration.[20,21] A 1 g portion of oil was weighed in a tared 5 mL volumetric flask. A 250 $\mu$L aliquot of internal standard spiking solution and an appropriate volume of spiking solution were added to the flask, and the volume was brought to slightly below the 5 mL mark with 20% EtOAc/MTBE. The flasks were sonicated for 2 min to dissolve the entire sample, after which the solution was brought to the 5 mL mark to generate the sample solution.

For the analysis of 2-MCPD monoesters, a 1000 mg/6 mL $C_{18}$ SPE cartridge was preconditioned with 6 mL of ACN. A 200 $\mu$L portion of the sample solution was added to the cartridge; 14 mL of ACN was added and collected in a 15 mL glass tube. The resulting solution was dried at 70 °C under a stream of nitrogen. A 2 mL portion of 20% EtOAc/hexane was added to the glass tube containing the dried residue from the previous SPE cleanup, sonicated for 15 s, added to a 500 mg/3 mL Si cartridge (preconditioned with 3 mL of 20% EtOAc/hexane), and collected in a 15 mL glass tube. Another 2 mL portion of 20% EtOAc/hexane was added to the glass tube, vortex mixed for 15 s, and added to the Si SPE cartridge; this was repeated two more times, totaling 8 mL. A 1 mL portion of 20% EtOAC/hexane was added directly to the Si SPE cartridge, resulting in a total of 9 mL of elution solvent. The resulting solution was dried at 55 °C under a stream of nitrogen, reconstituted in 1 mL of IPA, vortex mixed for 30 s, and transferred to an HPLC vial for analysis.

For the analysis of 2-MCPD diesters, a 1000 mg/6 mL silica SPE cartridge was preconditioned with 5 mL of MeOH, 5.5 mL of dichloromethane, and two 6 mL portions (12 mL total) of 2% $Et_2O$/hexane. A 100 $\mu$L portion of the sample solution was added to a 15 mL glass tube and dried under a stream of nitrogen. A 2 mL portion of 2% $Et_2O$/hexane was added to the glass tube containing the dried residue from the previous step, sonicated for 15 s, added to the Si SPE cartridge, and collected in a new 15 mL glass tube. Another 2 mL portion of 2% $Et_2O$/hexane was added to the glass tube, vortex mixed for 15 s, and added to the Si SPE cartridge; this was repeated two more times, totaling 8 mL. A 5.5 mL portion of 2% $Et_2O$/hexane was added directly to the Si SPE cartridge, resulting in a total of 13.5 mL of

**Table 1. AB Sciex 5500 QTrap MS/MS Conditions for the 2-MCPD Monoesters and Isotopically Labeled Internal Standards (IS)**

| Q1 ($m/z$) | Q3 ($m/z$) | RT (min) | compound ID | IS | DP[a] | EP[a] | CE[a] | CXP[a] |
|---|---|---|---|---|---|---|---|---|
| 366.21 | 239.2 | 22.8 | 1Pa2.1 | 1Ol3.d5.1 | 65 | 10 | 16 | 12 |
| 368.21 | 239.2 | 22.8 | 1Pa2.2 | 1Ol3.d5.3 | 65 | 10 | 16 | 12 |
| 390.31 | 263.2 | 18.9 | 1Li2.1 | 1Ol3.d5.1 | 65 | 4 | 16 | 14 |
| 390.31 | 245.2 | 18.9 | 1Li2.2 | 1Ol3.d5.2 | 65 | 4 | 16 | 14 |
| 392.31 | 263.2 | 18.9 | 1Li2.3 | 1Ol3.d5.3 | 65 | 4 | 16 | 14 |
| 392.21 | 265.2 | 24.1 | 1Ol2.1 | 1Ol3.d5.1 | 75 | 14 | 20 | 14 |
| 392.21 | 247.2 | 24.1 | 1Ol2.2 | 1Ol3.d5.2 | 75 | 14 | 20 | 12 |
| 394.21 | 265.2 | 24.1 | 1Ol2.3 | 1Ol3.d5.3 | 75 | 14 | 20 | 14 |
| 397.2 | 265.2 | 23.1 | 1Ol3.d5.1 | | 75 | 14 | 20 | 14 |
| 397.2 | 247.2 | 23.1 | 1Ol3.d5.2 | | 75 | 14 | 20 | 12 |
| 399.2 | 265.2 | 23.1 | 1Ol3.d5.3 | | 75 | 14 | 20 | 14 |

[a]DP, declustering potential (V); EP, entrance potential (V); CE, collision energy (V); CXP, exit cell potential (V).

**Table 2. AB Sciex 5500 QTrap MS/MS Conditions for the 2-MCPD Diesters and Isotopically Labeled Internal Standards (IS)**

| Q1 ($m/z$) | Q3 ($m/z$) | RT (min) | compound ID | IS | DP[a] | EP[a] | CE[a] | CXP[a] |
|---|---|---|---|---|---|---|---|---|
| 655.5 | 261.2 | 22.7 | 3Li-Lnd5.1 | | 85 | 4 | 30 | 8 |
| 655.5 | 360.3 | 22.7 | 3Li-Lnd5.2 | | 85 | 4 | 30 | 8 |
| 650.51 | 261.2 | 23.6 | 2Li-Ln.1 | 3Li-Lnd5.1 | 85 | 4 | 30 | 8 |
| 650.51 | 355.3 | 23.6 | 2Li-Ln.2 | 3Li-Lnd5.2 | 85 | 4 | 28 | 8 |
| 657.5 | 360.2 | 25.0 | 3Li-Lid5.1 | | 85 | 4 | 30 | 8 |
| 657.5 | 263.2 | 25.0 | 3Li-Lid5.2 | | 85 | 4 | 27 | 16 |
| 652.51 | 355.2 | 26.0 | 2Li-Li.1 | 3Li-Lid5.1 | 85 | 4 | 30 | 8 |
| 652.51 | 263.2 | 26.0 | 2Li-Li.2 | 3Li-Lid5.2 | 85 | 4 | 27 | 14 |
| 628.51 | 331.2 | 28.2 | 2Pa-Li.1 | 3Ol-Old5.1 | 85 | 4 | 25 | 16 |
| 628.51 | 263.2 | 28.2 | 2Pa-Li.2 | 3Ol-Old5.3 | 85 | 4 | 25 | 12 |
| 654.51 | 357.3 | 28.5 | 2Ol-Li.1 | 3Ol-Old5.1 | 85 | 4 | 31 | 8 |
| 654.51 | 263.2 | 28.5 | 2Ol-Li.2 | 3Ol-Old5.3 | 85 | 4 | 28 | 8 |
| 604.51 | 331.2 | 30.4 | 2Pa-Pa.1 | 3Ol-Old5.1 | 85 | 4 | 25 | 8 |
| 606.51 | 333.2 | 30.4 | 2Pa-Pa.2 | 3Ol-Old5.2 | 85 | 4 | 25 | 8 |
| 630.51 | 265.2 | 30.6 | 2Pa-Ol.1 | 3Ol-Old5.3 | 85 | 4 | 27 | 8 |
| 630.51 | 331.2 | 30.6 | 2Pa-Ol.2 | 3Ol-Old5.1 | 85 | 4 | 27 | 8 |
| 630.51 | 357.3 | 30.6 | 2Pa-Ol.3 | 3Ol-Old5.1 | 85 | 4 | 27 | 8 |
| 661.5 | 362.3 | 29.9 | 3Ol-Old5.1 | | 85 | 4 | 28 | 8 |
| 663.5 | 364.2 | 29.9 | 3Ol-Old5.2 | | 85 | 4 | 28 | 8 |
| 661.5 | 265.2 | 29.9 | 3Ol-Old5.3 | | 85 | 4 | 27 | 8 |
| 656.5 | 357.3 | 30.8 | 2Ol-Ol.1 | 3Ol-Old5.1 | 85 | 4 | 28 | 8 |
| 656.5 | 265.2 | 30.8 | 2Ol-Ol.2 | 3Ol-Old5.2 | 85 | 4 | 20 | 7 |
| 658.5 | 359.2 | 30.8 | 2Ol-Ol.3 | 3Ol-Old5.3 | 85 | 4 | 28 | 8 |
| 656.51 | 263.2 | 31.5 | 2St-Li.1 | 3Ol-Old5.3 | 85 | 4 | 28 | 16 |
| 656.51 | 359.3 | 31.5 | 2St-Li.2 | 3Ol-Old5.1 | 85 | 4 | 28 | 8 |
| 637.5 | 364.3 | 32.5 | 3Pa-Std5.1 | | 85 | 10 | 21 | 16 |
| 637.5 | 336.2 | 32.5 | 3Pa-Std5.2 | | 85 | 10 | 21 | 16 |
| 632.51 | 331.2 | 33.4 | 2Pa-St.1 | 3Pa-Std5.1 | 85 | 10 | 21 | 16 |
| 632.51 | 359.2 | 33.4 | 2Pa-St.2 | 3Pa-Std5.2 | 85 | 10 | 21 | 16 |
| 658.51 | 357.2 | 33.5 | 2Ol-St.1 | 3Pa-Std5.1 | 85 | 4 | 23 | 7 |
| 658.5 | 359.3 | 33.5 | 2Ol-St.2 | 3Pa-Std5.2 | 85 | 4 | 26 | 8 |
| 658.5 | 265.2 | 33.5 | 2Ol-St.3 | 3Pa-Std5.1 | 85 | 4 | 23 | 7 |
| 665.6 | 364.3 | 35.1 | 3St-Std5.1 | | 85 | 4 | 26 | 8 |
| 667.6 | 366.3 | 35.1 | 3St-Std5.2 | | 85 | 4 | 28 | 8 |
| 660.6 | 359.3 | 36.0 | 2St-St.1 | 3St-Std5.1 | 85 | 4 | 28 | 8 |
| 662.6 | 361.3 | 36.0 | 2St-St.2 | 3St-Std5.2 | 85 | 4 | 28 | 8 |

[a]DP, declustering potential (V); EP, entrance potential (V); CE, collision energy (V); CXP, exit cell potential (V).

elution solvent. The solution was dried at 55 °C under a stream of nitrogen. A 2 mL portion of 40% EtOAc/ACN was added to the glass tube containing dried residue from the previous SPE cleanup, sonicated for 15 s, added to a 1000 mg/6 mL $C_{18}$ cartridge (preconditioned with 6 mL of 40% EtOAc/ACN), and collected in a new 15 mL glass tube. Another 2 mL portion of 40% EtOAc/ACN was added to the glass tube, vortex mixed for 15 s, and added to the Si SPE cartridge; this was repeated two more times, totaling 8 mL. A 1 mL portion of 40% EtOAc/ACN was added directly to the $C_{18}$ SPE cartridge, resulting in a total of 9 mL of elution solvent. The solution was dried at 70 °C under a stream of nitrogen, reconstituted in 0.500

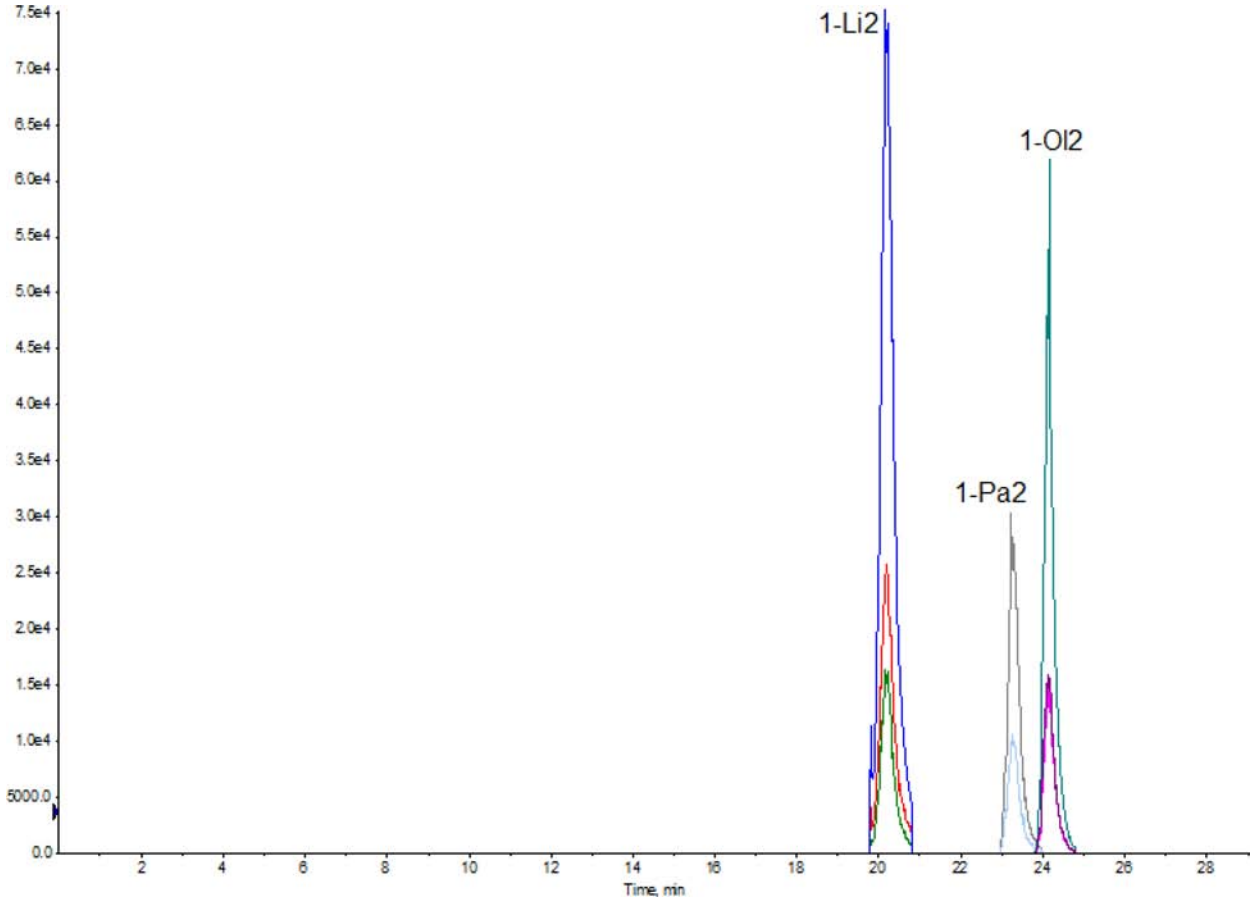


**Figure 2.** LC-MS/MS data for 2-MCPD monoesters.

mL of IPA, vortex mixed for 30 s, and added to an HPLC vial for analysis.

**LC-MS/MS Analysis.** A Prominence UFLC XR liquid chromatography system (Shimadzu, Columbia, MD, USA) with a Pursuit XRs $C_{18}$ column, 2.0 mm × 150 mm with 3.0 $\mu$m particles (Agilent, Santa Clara, CA, USA), was used for the HPLC separation of the 2-MCPD diesters. An initial flow rate of 200 $\mu$L/min of 100% mobile phase A (2 mM ammonium formate/0.05% formic acid in 92:8 MeOH/$H_2O$) was used for the first 2 min (min), stepping to 70% mobile phase A/30% mobile phase B (2 mM ammonium formate/0.05% formic acid in 98:2 IPA/$H_2O$) at 2.1 min, linearly ramped to 50% mobile phase A at 20 min, linearly ramped to 17% mobile phase A at 36 min, stepping to 0% mobile phase A and 250 $\mu$L/min at 36.25 min, holding at 0% mobile phase A until 42.5 min, returning to 100% mobile phase A with the increased flow rate of 250 $\mu$L/min at 42.75 min, holding these conditions until 48.75 min, and returning to initial flow rate of 200 $\mu$L/min at 49 min and stopping the controller. The integrated Valco valve was directed to waste at 0.0 min, to the mass spectrometer at 13.0 min, and to waste at 36.5 min. The injection volume was 5 $\mu$L.

Alternate chromatographic conditions to separate the 2-MCPD monoesters were developed using the same LC system and column described above. An initial flow rate of 200 $\mu$L/min of 100% mobile phase A (2 mM ammonium formate/0.05% formic acid in 75:25 MeOH/$H_2O$) was used for the first 2 min (min), followed by stepping to 70% mobile phase A/30% mobile phase B (2 mM ammonium formate/0.05% formic acid in 98:2 IPA/water) at 2.1 min, holding at 70% mobile phase A until 15 min, linearly ramping to 35% mobile phase A at 30.2 min, stepping to 0% mobile phase A and 250 $\mu$L/min at 30.5 min, holding at 0% mobile phase A until 40.5 min, returning to 100% mobile phase A at 40.75 min, holding at 100% mobile phase A at 250 $\mu$L/min until 46.75 min, returning to the initial flow rate of 200 $\mu$L/min at 47 min, and stopping the controller. The integrated Valco valve was directed to waste at 0.0 min, to the mass spectrometer at 9.0 min, and to waste at 30 min. The injection volume was 5 $\mu$L.

A 5500 QTRAP with an ESI source in positive ion mode with Analyst 1.5.2 software was used to control the LC and the MS (AB Sciex, Foster City, CA, USA). Source parameters such as gas flows, ion spray voltage, and source temperature were optimized for each analyte via T-infusion, combining a 20 $\mu$g/mL standard solution with LC mobile phase, as was collision energy (CE), declustering potential (DP), exit cell potential (CXP), and entrance potential (EP). Q1 and Q3 were set at unit resolution. For the analysis of 2-MCPD diesters, the curtain gas was set at 20 arbitrary units (au), the collisionally activated dissociation (CAD) gas was set at medium, the ion spray voltage was 5500 V, the source temperature was 500 °C, gas 1 pressure was set at 60 au, and gas 2 was 70 au. For the analysis of 2-MCPD monoesters, the curtain gas was set at 20 au, the CAD gas was set at medium, the ion spray voltage was 5500 V, the source temperature was 200 °C, gas 1 pressure was set at 50 au, and gas 2 was 80 au. The individual MS/MS transitions, approximate retention times (RT), internal standards, DP, EP, CE, and CXP for each analyte are shown in Tables 1 and 2 with the quantitation ions listed first, followed by one or two confirmatory ions for each analyte. The precursor ions for the 2-MCPD esters were increased by 0.01 $m/z$ to distinguish them from isomeric 3-MCPD diesters. This does not affect the data on a unit resolution mass spectrometer but is necessary to ensure the results can be processed separately.

Retention times for the target compounds were determined by analyzing a mixed standard under the conditions described above using standard MRM mode (not scheduled MRM). The MS/MS data for all validation samples were collected in scheduled MRM mode with unit resolution in Q1 and Q3, a 5 ms pause between mass ranges, an MRM detection window of 60 s, and a target scan time of 1 s.

**Quantitation.** To calculate recoveries for validation, a nine-point calibration curve with solutions at 1, 2, 5, 10, 25, 50, 125, 250, and 400

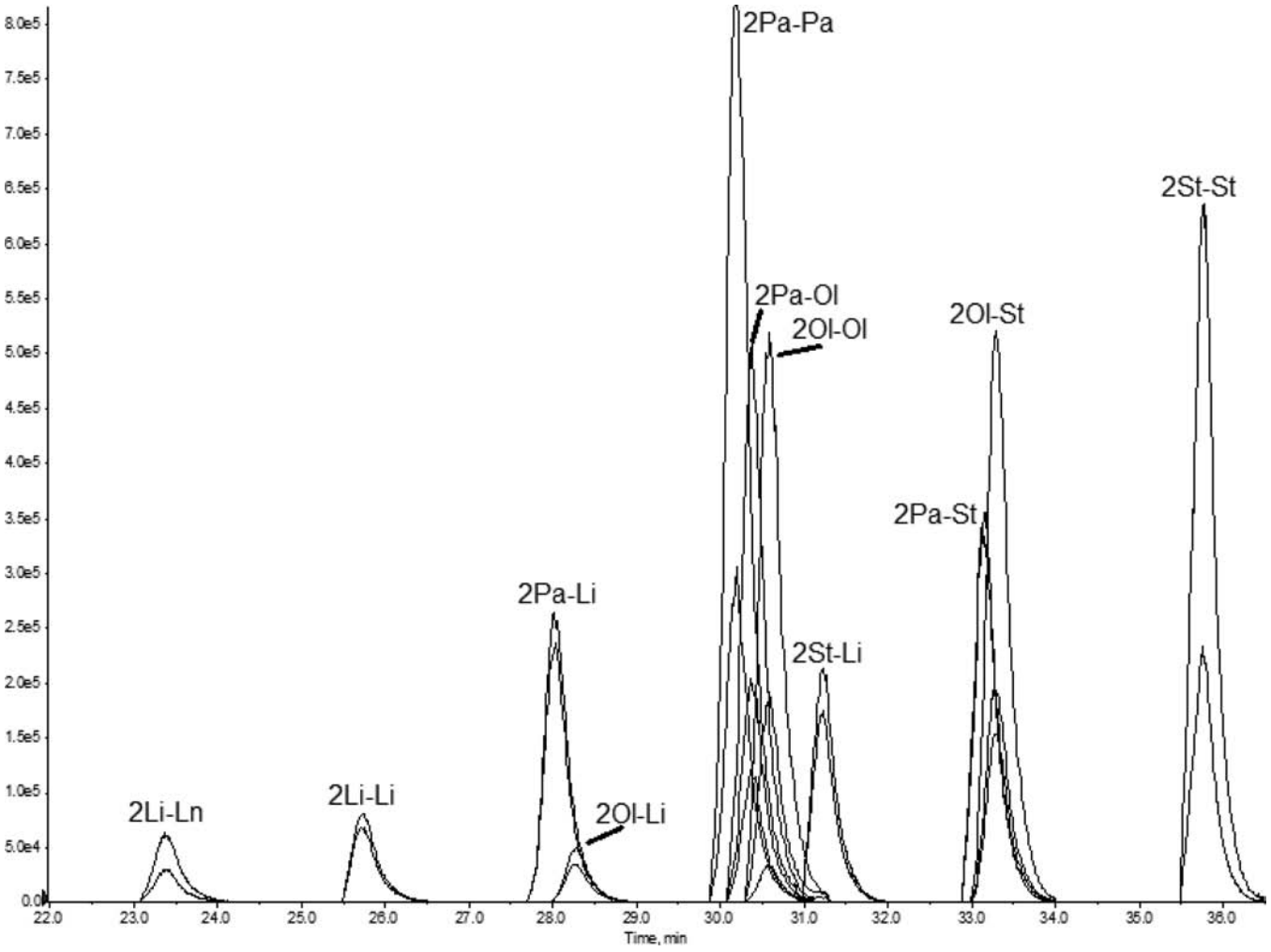


**Figure 3.** LC-MS/MS data for 2-MCPD diesters.

ng/mL (ppb) of each 2-MCPD ester standard (0.05−10.00 μg/g (ppm) on a sample basis), each with 50 ng/mL (ppb) of deuterated internal standard (1.25 μg/g (ppm) on a sample basis), was prepared in IPA and used for quantitation. The calibration curves were generated using the ratio of the MRM chromatographic peak area for each analyte to that of the corresponding internal standard. When appropriate internal standards were not available, analytes were quantified directly by their peak areas. A quadratic calibration curve with $1/X^2$ weighting provided the best fit for the 2-MCPD diesters; a linear fit with $1/X^2$ weighting was the best fit for the monoesters. The $1/X^2$ fit was used to ensure accurate low-end calibration, given the large dynamic range of the curve. All curves had $R^2$ values of ≥0.990.

## RESULTS AND DISCUSSION

**Selection of Standards.** The quality of the occurrence results produced by direct detection of intact 2-MCPD esters is related to the number of standards used in the analysis. Given that only a small number of 2-MCPD esters were commercially available, the standards required for collection of occurrence data in edible oils had to be synthesized. The seven most common fatty acids in edible oils (lauric acid, myristic acid, palmitic acid, linolenic acid, linoleic acid, oleic acid, and stearic acid) can theoretically lead to 28 2-MCPD diesters and 7 2-MCPD monoesters. However, relative 3-MCPD concentrations follow the fatty acid composition of the individual oils, with 2-MCPD ester concentrations likely to show the same trend. As a result, it is possible to target a large percentage of the MCPD esters with a much smaller group of analytical standards. On the basis of theoretical work from Nestlé[23] and later confirmed both by Nestlé's own experimental data[17] and our own occurrence results,[24] a group of nine 2-MCPD diester standards and three 2-MCPD monoester standards ensures >90% of the 2-MCPD will be detected in nearly all commonly consumed edible oils. As only 1 of these 12 standards was commercially available (2Li-Li), the additional fatty acid esters were synthesized to provide adequate detection capability for 2-MCPD in nearly all commonly consumed edible oils (see Figure 1). Representative LC-MS/MS chromatograms for the standards included in the method are shown in Figures 2 and 3. However, due to the absence of standards containing lauric acid and myristic acid, 2-MCPD esters in palm kernel oil and coconut oil will not be accurately accounted for in this method. Although efforts may be made in the future to synthesize additional standards and expand the validation, both oils contain relatively low concentrations of bound 3-MCPD (averages below 0.2 ppm (μg/g))[24] and would likely have low bound 2-MCPD concentrations, as well.

There were no commercially available isotopically labeled 2-MCPD ester standards at the time of analysis. Method development demonstrated that 1-Ol-d5 is a suitable internal standard for all three 2-MCPD monoesters. Average recoveries between 75 and 110% with relative standard deviation (RSD) values <15% demonstrate the success of this approach.

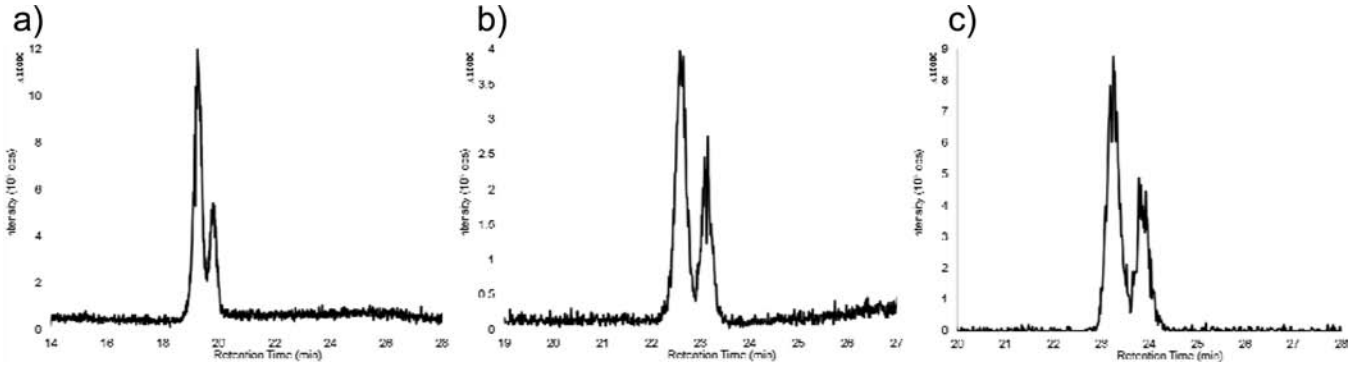


**Figure 4.** LC-MS/MS chromatograms showing the quantitation ion separation of sn-1 3-MCPD monoesters from isomeric 2-MCPD monoesters for (a) 1-Li3 and 1-Li2, (b) 1-Pa3 and 1-Pa2, and (c) 1-Ol3 and 1-Ol2. In all cases, the sn-1 3-MCPD monoester isomer elutes first.

**Method Development.** Standards for 11 of the analytes required for analysis of the most common oils were not commercially available. Because of this, research focused on the synthesis of these compounds, which have not been reported previously. The Steglich esterification was used for the synthesis of the esters[22] with $CCl_4$ as the reaction solvent. This approach leads to precipitation of the dicyclohexylurea reaction by-product, which can be difficult to separate from the desired final products. The reaction was run on a small scale due to the high cost of the 2-MCPD starting material.

The sample preparations for both the 2-MCPD monoesters and 2-MCPD diesters involve two solid-phase extractions. Following the silica cartridge solid-phase extraction, the subsequent $C_{18}$ cleanup for the 2-MCPD diesters does not measurably affect the recoveries of 2-MCPD esters in soybean, palm, or olive oil. The initial silica cleanup removes the majority of the triglycerides, as well as any free fatty acids and partial acylglycerols. The $C_{18}$ preparation is included to remove highly nonpolar material that could negatively affect long-term method and instrument performance. Removal of waxes and other nonpolar matrix components prior to analysis is potentially important in some oils, particularly sunflower oil, as well as in complex foods.

In the analysis of bound 3-MCPD in edible oils, monoesters generally account for a relatively small portion (<15%) of bound 3-MCPD in most oils.[23,24] No direct methods exist for the analysis of 2-MCPD monoesters, so it is unclear if they are actually present in processed oils. The monoesters of 2-MCPD can be separated from isomeric sn-1 3-MCPD monoesters (see Figure 4). However, attempts to chromatographically resolve 2-MCPD monoesters from sn-2 3-MCPD monoesters were not successful. Although they cannot be separated chromatographically, the two isomers have identical MS/MS responses, so it is possible to accurately quantify their combined concentration. However, given the differences in toxicology between 2-MCPD and 3-MCPD, they need to be separated for use in occurrence data. Alternate methods for their separation and individual quantitation are currently being explored. All 2-MCPD diesters were separated chromatographically from isomeric 3-MCPD diesters (see Figure 5).

Due to isomerism in 3-MCPD diesters containing two different fatty acids, the MS/MS fragment produced by the loss of $NH_4Cl$, although not the base peak, was used as the quantitation ion.[21] Unlike 3-MCPD diesters, 2-MCPD diesters with two different fatty acids exist as a single isomer, with the chlorine always occupying the sn-2 position. As a result, fragment ion selection for quantitation is not an issue and the cyclic acyloxonium ion base peak is suitable for quantitation of 2-MCPD diesters. Compared to 3-MCPD diesters, the diesters of 2-MCPD produce a higher relative response for the fatty acid acylium ion, and in several cases (2Li-Ln, 2Pa-Ol, 2St-Li) this ion was selected for quantitation.

**Method Performance.** The goal was to develop a validated method that is suitable for the analysis of a wide variety of edible oils. With this in mind, the method was validated using three different oil matrices to ensure robust performance. Extra virgin olive oil is unprocessed and consists mainly of unsaturated fatty acids, soybean oil is processed and contains primarily unsaturated fatty acids, and palm oil contains a relatively large portion of saturated fatty acids.

To confirm adequate recoveries for bound 2-MCPD in processed oils, each validation sample was spiked with an equivalent amount of the isomeric 3-MCPD ester standard. The presence of the isomeric 3-MCPD ester did not affect 2-MCPD ester isomer recoveries or reproducibilities, ensuring accurate results for the analysis of actual samples that are likely to contain both isomers. To generate validation data, four 1.0 ± 0.01 g portions of olive oil, soybean oil, and palm oil were prepared, in duplicate, and fortified with 0, 10, 100, and 800 $\mu$L of spiking solution, respectively. This produced one blank oil sample, as well as oils containing spiked MCPD ester concentrations of 0.1, 1.0, and 8.0 $\mu$g/g (ppm), respectively. Each fortified sample was spiked with 250 $\mu$L of internal standard spiking solution, generating oils containing 1.25 $\mu$g/g (ppm) of each internal standard. The method recoveries and relative standard deviations (RSD), incorporating labeled internal standards and averaged for three spiking concentrations in the three matrices, are depicted in Table 3. There were 2-MCPD monoesters in the organic palm oil sample blank (ranging from 58 to 263 ng/g (ppb)), along with 2-MCPD diesters in both the organic palm oil blank (ranging from 35 to 585 ng/g (ppb)) and the soybean oil blank (ranging from 31 to 103 ng/g (ppb)), which were subtracted before recoveries were calculated. Several of the analytes (2Pa-Pa, 2Pa-Ol, 2Ol-Li, 1-Li2, 1-Pa2, 1-Ol2) were present in the palm oil sample at higher concentrations than the low spikes, slightly affecting the reproducibility for these compounds.

Actual recoveries for the three 2-MCPD monoesters in olive oil, soybean oil, and palm oil, uncorrected by deuterated internal standards, ranged from 80 to 139% (RSD range, 24–55%), with the highest RSDs (>35%) seen in the 0.1 ppm spikes. As was the case with sn-2 3-MCPD monoester recoveries, 2-MCPD monoesters showed more variability than isomeric sn-1 3-MCPD monoesters. This was expected

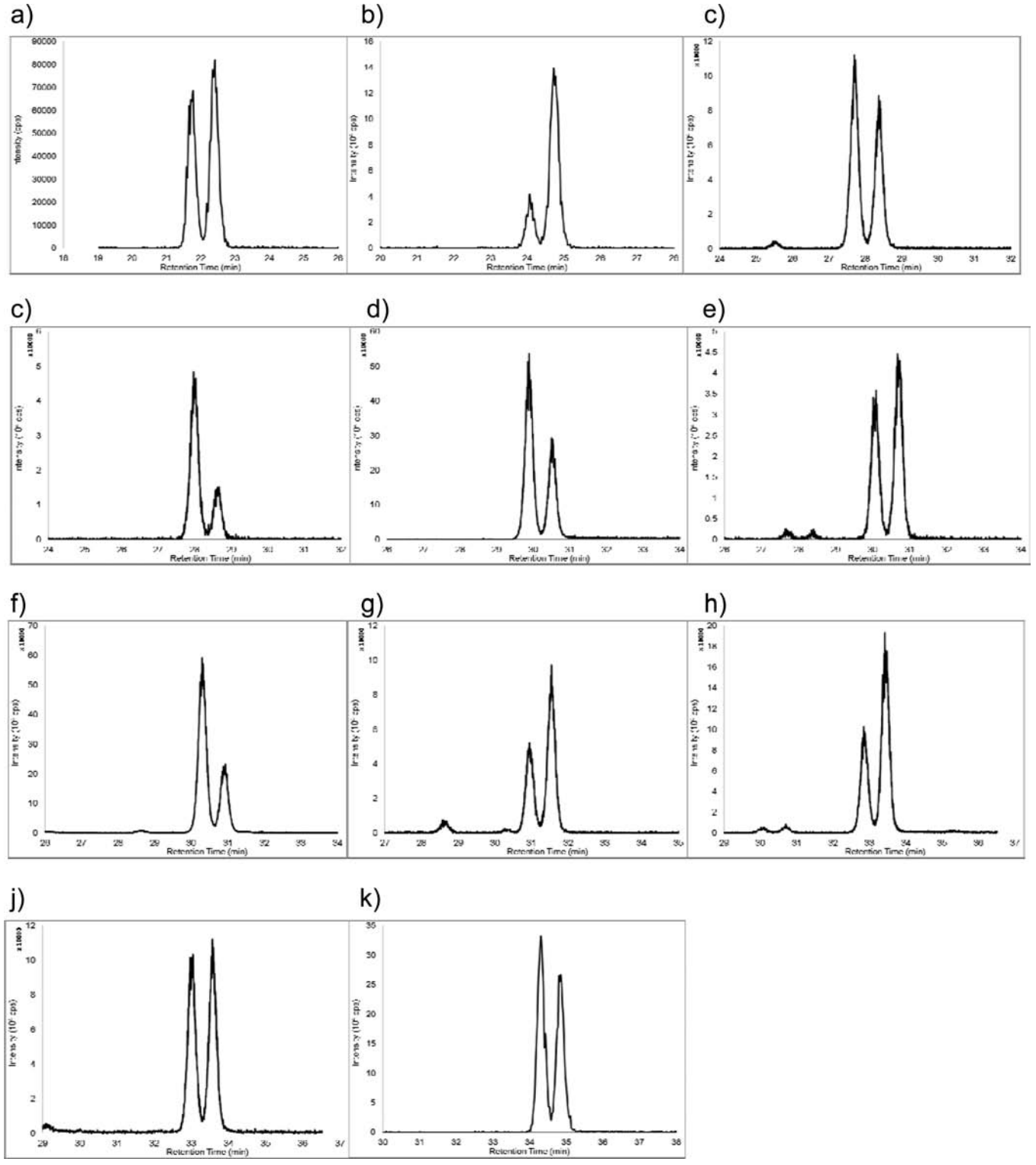


**Figure 5.** LC-MS/MS chromatograms showing the quantitation ion separation of 3-MCPD diesters from isomeric 2-MCPD diesters for (a) 3Li-Ln and 2Li-Ln, (b) 3Li-Li and 2Li-Li, (c) 3Pa-Li and 2Pa-Li, (d) 3Ol-Li and 2Ol-Li, (e) 3Pa-Pa and 2Pa-Pa, (f) 3Pa-Ol and 2Pa-Ol, (g) 3Ol-Ol and 2Ol-Ol, (h) 3St-Li and 2St-Li, (i) 3Pa-St and 2Pa-St, (j) 3Ol-St and 2Ol-St, and (k) 3St-St and 2St-St. In all cases, the 3-MCPD isomer elutes before the 2-MCPD isomer.

due to lower MS/MS responses for the 2-MCPD monoesters and close chromatographic proximity to the larger sn-1 monoester MS/MS peak (see Figure 4). Recoveries for 11 2-MCPD diesters in olive oil, soybean oil, and palm oil without the use of deuterated internal standards ranged from 61 to 104% (RSD range, 5−30%). However, after the incorporation of internal standards, the average recoveries and particularly the reproducibilities for all analytes in the method improved greatly.

The limit of detection (LOD) and limit of quantitation (LOQ) were defined as signal-to-noise (RMS noise) ratios of 3 and 10, respectively, and were determined experimentally by

**Table 3. Average Method Performance As Calculated by Use of an Eight-Point Calibration Curve with Deuterated Internal Standards for (a) 2-MCPD Monoesters and (b) 2-MCPD Diesters ($n$ = 6 at Each Concentration, Consisting of Duplicate Spikes in Olive Oil, Palm Oil, and Soybean Oil)**

| (a) 2-MCPD Monoesters | | | |
|---|---|---|---|
| | % recovery, % RSD | | |
| spike concn (ppm, μg/g) | 1-Li2 | 1-Pa2 | 1-Ol2 |
| 0.1 | 107.5, 11.7 | 84.0, 16.9 | 100.4, 11.3 |
| 1.0 | 84.7, 12.8 | 86.7, 10.4 | 92.2, 9.4 |
| 8.0 | 72.1, 11.2 | 82.9, 12.0 | 85.9, 4.2 |

| (b) 2-MCPD Diesters | | | | | | | | | | | |
|---|---|---|---|---|---|---|---|---|---|---|---|
| | % recovery, % RSD | | | | | | | | | | |
| spike concn (ppm, μg/g) | 2Li-Ln | 2Li-Li | 2Pa-Li | 2Ol-Li | 2Pa-Pa | 2Pa-Ol | 2Ol-Ol | 2St-Li | 2Pa-St | 2Ol-St | 2St-St |
| 0.1 | 86.2, 12.8 | 91.5, 3.1 | 93.7, 7.0 | 96.9, 9.0 | 98.5, 13.4 | 100.7, 13.2 | 91.6, 7.4 | 96.1, 10.1 | 93.2, 6.8 | 91.7, 3.1 | 91.9, 11.4 |
| 1.0 | 79.2, 13.3 | 86.0, 8.6 | 98.0, 10.2 | 91.6, 14.3 | 101.3, 7.4 | 85.7, 8.5 | 86.8, 8.6 | 91.5, 13.0 | 85.4, 8.8 | 86.1, 13.7 | 78.7, 8.7 |
| 8.0 | 81.7, 12.5 | 93.5, 11.4 | 101.7, 5.7 | 99.5, 8.6 | 106.3, 3.5 | 101.4, 10.2 | 98.2, 9.6 | 97.8, 6.1 | 96.1, 5.3 | 92.5, 6.3 | 93.9, 13.6 |

**Table 4. Method Limits of Detection (LOD) and Limits of Quantitation (LOQ) for (a) 2-MCPD Monoesters and (b) 2-MCPD Diesters Determined in Spiked Extra Virgin Olive Oil**

| (a) 2-MPCD Monoesters | | | |
|---|---|---|---|
| | 1-Li2 | 1-Pa2 | 1-Ol2 |
| LOD (ng/g, ppb) | 30 | 30 | 20 |
| LOQ (ng/g, ppb) | 90 | 90 | 60 |

| (b) 2-MPCD Diesters | | | | | | | | | | | |
|---|---|---|---|---|---|---|---|---|---|---|---|
| | 2Li-Ln | 2Li-Li | 2Pa-Li | 2Ol-Li | 2Pa-Pa | 2Pa-Ol | 2Ol-Ol | 2St-Li | 2Pa-St | 2Ol-St | 2St-St |
| LOD (ng/g, ppb) | 10 | 10 | 6 | 10 | 6 | 6 | 6 | 6 | 6 | 6 | 10 |
| LOQ (ng/g, ppb) | 30 | 30 | 20 | 30 | 20 | 20 | 20 | 20 | 20 | 20 | 30 |

analyzing spiked olive oil samples brought through the entire method; the results are shown in Table 4. Olive oil was chosen as the representative oil for limit determination because it consists predominantly of 18-carbon unsaturated fatty acids, as do most other commonly consumed edible oils, including soybean, canola, corn, sesame, sunflower, and peanut, and unlike those oils, unrefined olive oil is readily available commercially to provide a matrix free of incurred 2-MCPD esters. The three 2-MCPD monoesters have LOQs of ≤90 ppb, whereas the maximum LOQ detected among the 11 2-MCPD diesters was 30 ppb. Despite lower LC-MS responses for precursor ions, the LOQs for unsymmetrical 2-MCPD diesters are comparable to the limits in the 3-MCPD isomer. This is because all MS/MS transitions are suitable for accurate quantitation of 2-MCPD diesters.

**Applicability in Sample Analysis.** This is the first method that allows for quantitation of intact 2-MCPD esters in edible oils. It was validated using three different edible oil matrices to ensure reliable method performance and reproducibility. The lack of matrix-matched standards, combined with a straightforward two-step SPE cleanup, allows for rapid analysis of numerous samples in different matrices in a single analytical sequence. This is the first published approach that demonstrates chromatographic separation between sn-1 3-MCPD monoesters and 2-MCPD monoesters. These methods, which simultaneously quantify glycidyl esters and 3-MCPD esters,[20,21] can be used to determine the effectiveness of industrial processing mitigation approaches and in assessing the risk from these contaminants in edible oils.

## AUTHOR INFORMATION


### Corresponding Author

*(S.M.) Phone: (240) 402-1998. E-mail: shaun.macmahon@fda.hhs.gov. Fax: (301) 436-2634.


### Notes

The authors declare no competing financial interest.

## ACKNOWLEDGMENTS

We thank Dr. Gregory Noonan and Dr. Pierluigi Delmonte from the Center for Food Safety and Applied Nutrition for helpful discussions during the method development process. We acknowledge Dr. Mark Collison and Dr. Troy Haines from the Archer Daniels Midland Co. for kindly providing a full set of 3-MCPD diester standards at the outset of this research.

## REFERENCES


(1) Pudel, F.; Benecke, P.; Fehling, P.; Freudenstein, A.; Matthäus, B.; Schwaf, A. On the necessity of edible oil refining and possible sources of 3-MCPD and glycidyl esters. *Eur. J. Lipid Sci. Technol.* **2011**, *113*, 368−373.

(2) Hrncirik, K.; van Duijn, G. An initial study on the formation of 3-MCPD esters during oil refining. *Eur. J. Lipid Sci. Technol.* **2011**, *113*, 374−379.

(3) Matthäus, B.; Pudel, F.; Fehling, P.; Vosmann, K.l; Freudenstein, A. Strategies for the reduction of 3-MCPD esters and related compounds in vegetable oils. *Eur. J. Lipid Sci. Technol.* **2011**, *113*, 380−386.

(4) Ermacora, A.; Hrncirik, K. Influence of oil composition on the formation of fatty acid esters of 2-chloropropane-1,3-diol (2-MCPD) and 3-chloropropane-1,2-diol (3-MCPD) under conditions simulating oil refining. *Food Chem.* **2014**, *161*, 383−389.

(5) Schilter, B.; Scholz, G.; Seefelder, W. Fatty acid esters of chloropropanols and related compounds: toxicological aspects. *Eur. J. Lipid Sci. Technol.* **2011**, *113*, 309−313.
(6) Andres, S.; Appel, K. E.; Lampen, A. Toxicology, occurrence and risk characterisation of the chloropropanols in food: 2-monochloro-1,3-propanediol, 1,3-dichloro-2-propanol and 2,3-dichloro-1-propanol. *Food Chem. Toxicol.* **2013**, *58*, 467−478.
(7) Cho, W. S.; Han, B.S.; Nam, K. T.; Park, K.; Choi, M.; Kim, S. H.; Jeong, J.; Jang, D. D. Carcinogenicity study of 3-monochloropropane-1,2-diol in Sprague-Dawley rats. *Food Chem. Toxicol.* **2008**, *46*, 3172−3177.
(8) European Commission Health and Consumer Protection Directorate. Opinion of the scientific committee on food on 3-monochloro-propane-1,2-diol (3-MCPD), http://ec.europa.eu/food/fs/sc/scf/out91_en.pdf (accessed May 20, 2014).
(9) WHO Food Additives Series, no. 48, 2002, http://www.inchem.org/documents/jecfa/jecmono/v48je18.htm (accessed May 20, 2014).
(10) Weiβhaar, R. Determination of total 3-chloropropane-1,2-diol (3-MCPD) in edible oils by cleavage of MCPD esters with sodium methoxide. *Eur. J. Lipid Sci. Technol.* **2008**, *110*, 183−186.
(11) Haines, T. D.; Adlaf, K. J.; Pierceall, R. M.; Lee, I.; Venkitasubramanian, P.; Collison, M. Direct Ddetermination of MCPD fatty acid esters and glycidyl fatty acid esters in vegetable oils by LC-TOFMS. *J. Am. Oil Chem. Soc.* **2011**, *88*, 1−14.
(12) Kaze, N.; Sato, H.; Yamamoto, H.; Watanabe, Y. Bidirectional conversion between 3-monochloro-1,2-propanediol and glycidol in course of the procedure of DGF standard methods. *J. Am. Oil Chem. Soc.* **2011**, *88*, 1143−1151.
(13) Kuhlmann, J. Determination of bound 2,3-epoxy-1-propanol (glycidol) and bound monochloropropanediol (MCPD) in refined oils. *Eur. J. Lipid Sci. Technol.* **2011**, *113*, 335−344.
(14) Ermacora, A.; Hrncirik, K. A novel method for simultaneous monitoring of 2-MCPD, 3-MCPD and glycidyl esters in oils and fats. *J. Am. Oil Chem. Soc.* **2013**, *90*, 1−8.
(15) Hori, K.; Koriyama, N.; Omori, H.; Kuriyama, M.; Arishima, T.; Tsumura, K. Simultaneous determination of 3-MCPD fatty acid esters and glycidol fatty acid esters in edible oils using liquid chromatography time-of-flight mass spectrometry. *LWT−Food Sci. Technol.* **2012**, *48*, 204−208.
(16) Moravcova, E.; Vaclavik, L.; Lacina, O.; Hrbek, V.; Riddellova, K.; Hajslova, J. Novel approaches to analysis of 3-chloropropane-1,2-diol esters in vegetable oils. *Anal. Bioanal. Chem.* **2012**, *402*, 2871−2888.
(17) Dubois, M.; Tarres, A.; Goldmann, T.; Empl, A. M.; Donaubauer, A.; Seefelder, W. Comparison of indirect and direct quantification of esters of monochloropropanediol in vegetable oil. *J. Chromatogr., A* **2012**, *1236*, 189−201.
(18) Hori, K.; Matsubara, A.; Uchikata, T.; Tsumura, K.; Fukusaki, E.; Takeshi, B. High-throughput and sensitive analysis of 3-monochloropropane-1,2-diol fatty acid esters in edible oils by supercritical fluid chromatography/tandem mass spectrometry. *J. Chromatogr., A* **2012**, *1250*, 99−104.
(19) Yamazaki, K.; Ogiso, M.; Isagawa, S.; Urushiyama, T.; Ukena, T.; Kibune, N. A new, direct analytical method using LC-MS/MS for the fatty acid esters of 3-chloro-1,2-propanediol (3-MCPD) in edible oils. *Food Addit. Contam.* **2013**, *30*, 52−68.
(20) MacMahon, S.; Mazzola, E.; Begley, T. H.; Diachenko, G. W. Analysis of processing contaminants in edible oils. Part 1. A liquid chromatography-tandem mass spectrometry method for the direct detection of 3-monochloropropanediol monoesters and glycidyl esters. *J. Agric. Food Chem.* **2013**, *61*, 4737−4747.
(21) MacMahon, S.; Begley, T. H.; Diachenko, G. W. Analysis of processing contaminants in edible oils. Part 2. A liquid chromatography-tandem mass spectrometry method for the direct detection of 3-monochloropropanediol and 2-monochloropropanediol di-esters. *J. Agric. Food Chem.* **2013**, *61*, 4748−4757.
(22) Neises, B.; Steglich, W. Simple method for the esterification of carboxylic acids. *Angew. Chem. Int. Ed. Engl,* **1978**, *17*, 522−524.
(23) Dubois M. *Analysis of MCPD and glycidyl-esters in edible oils.* Presented at 102nd AOCS Annual Meeting & Expo, Cincinnati, OH, USA, 2001. http://www.aocs.org/files/resourcespdf/8_mdu_aocs.pdf (accessed May 19, 2014).
(24) MacMahon, S.; Begley, T. H.; Diachenko, G. W. Occurrence of 3-MCPD and glycidyl esters in edible oils in the United States. *Food Addit. Contam. A* **2013**, *30*, 2081−2092.

However, formulation-based drug delivery systems of silymarin in these studies are restricted to either in vitro dissolution studies or optimizing formulations. The major disadvantage of previous reports on the pharmacokinetics of silymarin is that the experimental animals are either restrained or under anesthesia. The stress associated with restraint and conventional blood sampling from conscious rodents affects their physiology, biochemistry, metabolism, and protein expression.[21,22]

In the present investigation, we designed liposome- and ethosome-encapsulated silymarin carriers to evaluate the differences between liposomes and ethosomes on pharmacokinetic profile and tissue distribution in free-moving rats.

Therefore, it is necessary to develop and validate an analysis method to investigate the pharmacokinetics and tissue distribution of liposome- and ethosome-encapsulated silymarin. Silibinin is the major active constituent of silymarin, which is the main target of analysis. A number of analytical methods for determining bioactive components of silymarin extracts in biological fluids and tissues have been reported, including liquid chromatography in combination with ultraviolet (LC-UV), mass spectrometry (MS), and tandem mass spectrometry (MS/MS) in human, dog (beagle and mongrel dog), rat, rabbit, and cat plasma or tissue.[17,18,23−28]

Among these analytical methods, HPLC has been most frequently used for pharmacokinetic studies of silibinin due to its simplicity, sensitivity, and selectivity. The objective of this study to develop and validate a sensitive and rapid LC-MS/MS method to quantify silymarin active compounds (silibinin in rat plasma and organ tissues, including liver, heart, spleen, lung, and kidney) after oral administration of silymarin loaded in liposomes and ethosomes. Furthermore, the pharmacokinetics and organ tissue distribution of silymarin in free form and formulations following oral administration were evaluated and compared.

## MATERIALS AND METHODS

**Chemicals and Reagents.** Cholesterol, heparin, naringin (internal standard, IS) and silymarin were obtained from Sigma−Aldrich Chemical Co. (St. Louis, MO). Hydrogenated soybean phosphatidylcholine (SPC, Phospholipon 80H) was supplied by American Lecithin Co. (Oxford, CT). Distearoylphosphatidylethanolamine−poly(ethylene glycol) with a mean molecular weight of 5000 (DSPE-PEG 5000) was purchased from Nippon Oil (Tokyo, Japan). Cellulose membrane (Cellu-Sep T2, with a molecular weight cutoff of 6000−8000) was obtained from Membrane Filtration Products (Seguin, TX). Acetonitrile, chloroform, ethyl acetate, and sodium chloride were purchased from Merck (Darmstadt, Germany). Milli-Q-grade water (Millipore, Bedford, MA) was used for preparation of solution and mobile phases.

**Preparation of Formulations.** The components of ethosome were similar to liposome, which contained soybean phosphatidylcholine [3.0% (w/v) of final product], cholesterol (0.5%), DSPE-PEG 5000 (0.5%), and triply deionized water with 20% ethanol (liposome only with triply deionized water that did not contain 20% ethanol). Formulations were prepared as follows: soybean phosphatidylcholine [3.0% (w/v) of final product], cholesterol (0.5%), and DSPE-PEG 5000 (0.5%) were dispersed in a chloroform/methanol (2:1) solution (5 mL). The organic solvent was evaporated in a rotary evaporator at 50 °C, and solvent traces were removed by retaining the lipid film under vacuum overnight. The films were hydrated with triply deionized water or triply deionized water with 20% ethanol containing silymarin by use of a probe-type sonicator (VCX600, Sonics and Materials, Newtown, CT) at 35 W for 30 min. The total volumes of the resulting products (liposome- and ethosome-encapsulated silymarin formulations, referred to as LSM and ESM, respectively) were set at 5 mL.

**Formulation Characteristics.** *Determination of Particle Size and ζ Potential.* The mean particle size and polydispersity index (PDI) of formulations were measured by dynamic light scattering (90 Plus, BIC, Holtsville, NY). The ζ potential of formulations was determined on a ζ potential analyzer (90 Plus, BIC, Holtsville, NY).

*Encapsulation of Silymarin in Liposomes and Ethosomes.* Entrapment capacity estimated the amount of LSM and ESM. These formulations were centrifuged at 48000*g* at 4 °C for 30 min in a Beckman Optima MAX ultracentrifuge (Beckman Coulter, Stanwood, WA) to separate the incorporated drug from the free form. The amount of silibinin in the formulation was analyzed by the HPLC-MS/MS system. Entrapment capacities of formulations were calculated as [(total amount of drug − amount of drug detected only in supernatant)/total amount of drug] × 100.[12]

*Morphological Observations by Transmission Electron Microscopy (TEM).* These vesicles were examined by TEM to characterize their microstructure. A drop of a formulation was applied to a 400-mesh carbon-film-covered copper grid to form a thin film specimen, which was stained with 1% phosphotungstic acid. After the stained samples were allowed to air-dry, TEM samples were obtained. Finally, the sample was then examined and photographed by a TEM (JEM-2000EXII, JEOL, Tokyo, Japan).

**Liquid Chromatography−Tandem Mass Spectrometry System and Analytical Method Validation.** *LC-MS/MS System.* An Agilent-1100 HPLC system (Agilent Technologies, Waldbronn, Germany) with an Applied Biosystems/MDS Sciex API 3000 tandem quadrupole mass spectrometer (Framingham, MA) equipped with quaternary pump, injector, vacuum degasser, and autosampler was used. The tandem quadrupole mass spectrometer equipped with electrospray ionization (ESI) turbo ion interface was used with the following parameters: turbo ion spray gas (GAS 2), 6 L/min; nebulizer gas (NEB), 10; curtain gas (CUR), 10; collisionally activated dissociation gas (CAD), 8; ion-spray voltage (IS), −4000 V; and turbo ionspray temperature (TIM), 500 °C. Nitrogen was used in all cases. Negative-ion mode with multiple reaction monitoring (MRM) was used for HPLC-MS/MS analysis. The following precursor → product ion transitions were used: $m/z$ 481.2 → 301.0 for silibinin [declustering potential (DP) −155 V, focusing potential (FP) −380 V, entrance potential (EP) −12 V, collision energy (CE) −22 V, collision cell exit potential (CXP) −12 V] and $m/z$ 579.3 → 271.6 for naringin as an internal standard (IS) (DP −86 V, FP −200 V, EP −11.5 V, CE −49 V, CXP −15 V). A reverse-phase C18 column (50 × 4.6 mm, particle size 5 μm, Phenomenex Luna) was used for HPLC separation. The mobile phase consisted of acetonitrile and 0.1% formic acid (67:33 v/v) at a flow rate of 0.3 mL/min. The sample injection volume was 10 μL.

*Analytical Method Validation.* The stock solution was silibinin and naringin (IS) in 100% acetonitrile (1 mg/mL). A set of standard solutions was prepared by appropriate dilution of the stock solution with mobile phase to make the calibration curve. These solutions were stored at −20 °C before use.

These solutions were further diluted to give a series of working standard solutions and samples for calibration in blank plasma and organ tissues (including liver, heart, spleen, lung, and kidney), prepared by spiking aliquots of the stock solutions into biosamples to obtain final concentrations in the range of 5−1000 ng/mL for plasma and 10−1000 ng/mL for organ tissues (including liver, heart, spleen, lung, and kidney). Samples were processed as described under Sample Preparation.

Pharmacokinetic studies and tissue distribution for bioanalytical assays were based on method validation practices according to FDA guidelines,[29] including tests of selectivity, sensitivity, linearity, precision, accuracy, recovery, and matrix effect.

Selectivity of analytes was determined by confirming the presence or absence of interference as well as the lot-to-lot variation regarding interference in blank plasma and organ tissues.

The limit of quantification (LOQ) is defined as the lowest concentration of the linear range, and the limit of detection (LOD) is

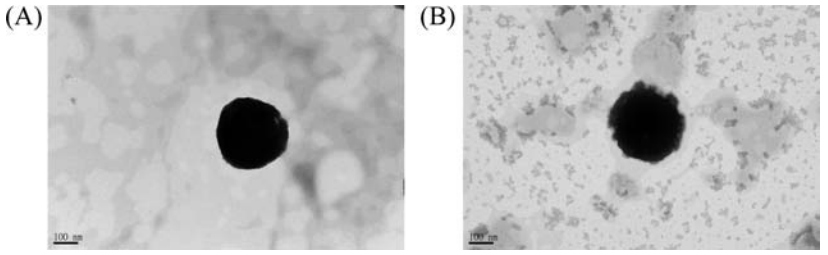


**Figure 1.** TEM micrographs of (A) liposome-encapsulated silymarin formulation (LSM) and (B) ethosome-encapsulated silymarin formulation (ESM). Original magnification 120000×, scale bars 100 nm.

defined as the concentration of analyte that gives a signal-to-noise ratio (S/N) of 3. Calibration curves were constructed by plotting the peak area ratio of silibinin and naringin (IS) versus concentration.

Quantitation of silibinin in plasma and organ samples (including liver, heart, spleen, lung, and kidney) was based on calibration curves, ranging from 5−1000 ng/mL for plasma samples and 10−1000 ng/mL for organ samples. These calibration curves were required to have a correlation coefficient ($r^2$) greater than 0.995.

Precision and accuracy of the analytical method for different biological matrices were assayed by testing the samples in five replicates on the same day (intraday) and on five successive days (interday). Accuracy (bias, as a percentage) was calculated from the nominal concentration ($C_{nom}$) and the mean value of observed concentration ($C_{obs}$) as follows:

$$\text{accuracy (bias)} = [(C_{nom} - C_{obs})/C_{nom}] \times 100$$

Precision (relative standard deviation, RSD, as a percentage) was calculated from the standard deviation and observed concentration as follows:

$$\text{precision (RSD)} = [\text{standard deviation (SD)}/C_{obs}] \times 100$$

Percentage bias (% bias) and percentage RSD (% RSD) for the lowest acceptable reproducibility concentration were defined as being within ±15% (±20% at the low limit of detection).

Matrix effect and recovery of silibinin in various biological samples were assessed at three different concentration levels (25, 250, and 1000 ng/mL). The naringin (IS) concentration was 250 ng/mL in rat plasma and organ tissues. Matrix effect (%) and recovery (%) were calculated by use of the following formulas:

$$\text{matrix effect} = \frac{\text{peak areas for standards spiked after extraction}}{\text{peak areas obtained in neat solution standards}} \times 100$$

$$\text{recovery} = \frac{\text{peak areas for standards spiked before extraction}}{\text{peak areas for standards spiked after extraction}} \times 100$$

**Animal Experiments: Freely Moving Rat Model.** Adult male Sprague-Dawley rats weighing 200 ± 30 g were obtained from the National Yang-Ming University Animal Center, Taipei, Taiwan. The animals were specifically pathogen-free and had free access to food (laboratory rodent diet 5001, PMI Nutrition International LLC, St. Louis, MO) and water. The rats were housed with a 12-h light and 12-h dark cycle. All experimental protocols involving animals were reviewed and approved by the Institutional Animal Care and Use Committee (IACUC number 1020613) of the National Yang-Ming University.

Experimental rats were initially anesthetized by pentobarbital (50 mg/kg, ip), and then polyethylene tubes were implanted in the right jugular and right femoral veins for iv administration. For the oral administration group, only the right jugular was catheterized for blood sampling. The catheter crossed the subcutaneous tissue and was fixed in the dorsal neck region. The patency tubing was maintained by flushing with heparinized normal saline [0.9% NaCl (w/v) solution containing 20 IU/mL heparin sodium salt]. After surgery, the rat was placed in an experimental cage and allowed to recover for 1 day. During the recovery period, the rat was kept warm under a light.

The oral administration group was given silymarin (free form) dissolved in triple-distilled deionized water and present in suspension; for iv administration, silymarin (free form) was completely dissolved in PEG 400 with 15% ethanol.

**Biodistribution.** Blood samples were collected by cardiac puncture at 30 min after silibinin administration (free drug and formulations) and then perfused with normal saline through the left ventricle. The organs (including liver, heart, spleen, lung, and kidney) were collected, weighed, and homogenized. Finally, the biological samples were stored at −20 °C for sample analysis.

**Sample Preparation.** *Plasma Samples.* The real plasma sample (45 μL) was mixed with 5 μL of naringin (IS) and vortexed for 30 s. Next, 1 mL of ethyl acetate was added and the mixture was vortexed for 5 min. The mixture was centrifuged at 16000*g* for 10 min at 4 °C. The supernatant (1 mL) was transferred to an Eppendorf vial and dried at 40 °C in a centrifugation evaporator. The dried sample was reconstituted in 100 μL of mobile phase (acetonitrile/0.1% formic acid = 67:33 v/v) and filtered through a 0.22 μm filter. Finally, the filtrate (10 μL) was applied to the HPLC-MS/MS system for analysis.

*Organ Samples.* After homogenization of the organs with 100% aqueous acetonitrile solution (1:3 w/v), the homogenate was centrifuged at 16000*g* for 10 min at 4 °C and the supernatant was collected and frozen at −20 °C until analysis. To determine silibinin concentration in the organs, sample preparation was similar to that described under Plasma Samples). Additionally, if the concentration of silibinin was over the limit of the linearity range (1000 ng/mL), these analytes were diluted with blank biological samples.

**Pharmacokinetics and Statistics.** All pharmacokinetic analysis was processed by WinNonlin standard edition, version 1.0 (Scientific Consulting Inc., Apex, NC). The Akaike information criterion (AIC) value was used to select the compartment model used for data analysis.

Pharmacokinetic parameters are explained as follows: the area under the concentration−time curve (AUC) is defined as the plot of concentration of drug in blood plasma against time. $t_{1/2,\alpha}$ and $t_{1/2,\beta}$ are the distribution half-life and elimination half-life, respectively. Peak plasma concentration of a drug after administration and time to reach this peak plasma concentration are $C_{max}$ and $T_{max}$, respectively. Clearance (CL), an indicator of drug elimination from the body, is calculated by CL = $D$ (dose)/AUC. Mean residence time (MRT) is the apparent average period drug molecules staying in the body. Bioavailability (%) = $100(AUC_{oral}/D_{oral})/(AUC_{iv}/D_{iv})$.

Pharmacokinetic results are represented as the mean ± standard error of measurement (SEM). Statistical significance was determined by using a one-way analysis of variance (ANOVA), followed by a Schieff post-test (SPSS version 10, SPSS, Chicago, IL) with $p < 0.05$ as the minimal level of significance.

## RESULTS AND DISCUSSION

**Physicochemical Characteristics of Formulations.** These formulations can be prepared successfully by a thin-film dispersion/homogenization method. The physicochemical characteristics of LSM and ESM were investigated by evaluating the formulations' appearance, vesicle size, ζ potential, and drug encapsulation percentage.

In this study, a formulation system containied SPC, DSPE-PEG 5000, and cholesterol, which functioned as the emulsifiers, located at the oil/water interface as a phospholipid membrane surrounding the quercetin-containing core.

TEM images of LSM and ESM are shown in Figure 1. These vesicles were both spherical, and their sizes and $\zeta$ potentials are shown in Table 1. Dynamic light scattering determinted the sizes of LSM and ESM were approximately 272 and 321 nm, respectively. The polydispersity index (PDI) is a measure of the width of the particle size distribution. The values of these formulations were smaller than 0.32, demonstrating highly homogeneous populations of particles for the formulations.[30] $\zeta$ potentials of the LSM and ESM were −27.14 and −36.32 mV, respectively.

**Table 1. Characterization of LSM and ESM by Vesicle Size, $\zeta$ Potential, PDI, and Drug Encapsulation**[a]

| | size (nm) | $\zeta$ potential (mV) | PDI | encapsulation (%) |
|---|---|---|---|---|
| LSM | 272.5 ± 5.11 | −27.14 ± 0.84 | 0.32 ± 0.02 | 60.36 ± 1.78 |
| ESM | 321.1 ± 22.4 | −36.32 ± 4.65 | 0.30 ± 0.01 | 69.13 ± 3.25 |

[a]PDI, polydispersity index; LSM, liposome-encapsulated silymarin formulation; ESM, ethosome-encapsulated silymarin formulation.

From a morphological point of view, the structure of ethosomes is very similar to that of liposomes; however, the results showed that ESM exhibited higher encapsulation efficiency (69.13% ± 3.25%) than LSM (60.36% ± 1.78%). This may be because ethosomes have ethanol, which provides better solubility for lipophilic drugs.[31]

**In Vitro Release.** To examine if silibinin could be readily released from silymarin solution (free form) and formulation groups, in vitro release tests were performed. As shown in Figure 2, release of silibinin from the silymarin solution (free form) was rapid at 24 h; the release kinetics of silibinin from LSM and ESM exhibited slower, more continuous release over 48 h. The drug release percentage of silibinin from the silymarin solution (free form) at the end of the experiment (48 h) showed enhancements of 2.33-fold compared to the formulation groups.

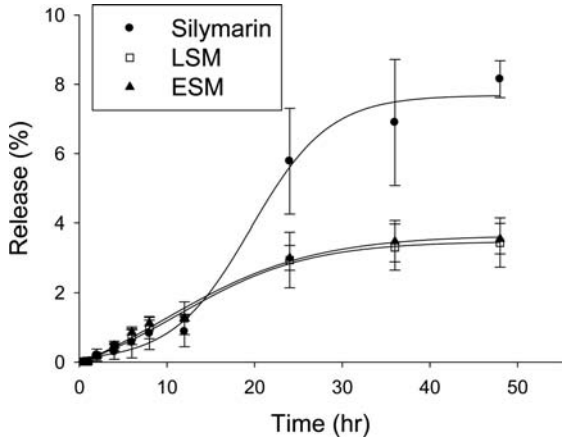


**Figure 2.** In vitro release-time profiles of silibinin from silymarin (free form), LSM, and ESM across a cellulose membrane added to the donor compartment of a Franz diffusion cell (mean ± SD, $n$ = 4).

The sustained release profiles of silymarin from LSM and ESM were consistent with the Higuchi diffusion equation ($r^2$ = 0.97).[32] There were no significant differences between LSM and ESM for in vitro release. LSM and ESM showed suppressed and sustained release of silymarin compared to the control groups.

**LC-MS/MS System and Method Validation.** To develop a sensitive and accurate LC-MS/MS method for the determination of silymarin's major active compound, silibinin, in rat plasma, liver, heart, spleen, lung, and kidney, the triple quadrupole mass spectrometer equipped with an electrospray ionization (ESI) source is currently one of the most useful tools available because of its high sensitivity and selectivity. Therefore, the process of analytical method development and validation could be divided into several parts, including optimization of MS and LC conditions, assessed matrix and recovery of sample preparation, selected calibration range, precision (RSD, %), and accuracy.

In the study, we used an MRM system for qualification analysis, which consisted of selecting the precursor ion (MS 1) and selecting a specific fragment of precursor ion (MS 2); therefore, the analysis method was specific and sensitive. Negative-ion electrospray ionization was used to optimize the HPLC-MS/MS analysis, and the MS/MS conditions of silibinin and naringin (IS) are shown in Table S1 in Supporting Information. The mass transit ion patterns $m/z$ 481.2 → 301.0 and $m/z$ 579.3 → 271.2 were selected to monitor silibinin and naringin (IS), respectively. Mass spectra and chemical structures of silibinin and naringin (IS) are shown in Figure 3.

In this method, the degree of interference was assessed by inspection of the MRM mode. Separation and quantification of silibinin in plasma and organ samples without other endogenous interfering peaks were performed in an optimal mobile phase containing acetonitrile with 0.1% formic acid (67:33 v/v) with a reverse-phase C18 column (50 × 4.6 mm, particle size 5 $\mu$m).

To assess pharmacokinetic and tissue distribution, a suitable assay system for the plasma and different tissue samples should be developed and optimized. In the process optimization, we have examined many methods for sample preparation, including protein precipitation and liquid−liquid extraction. However, we found that background interference appeared in the blank matrix extract after protein precipitation, whether the samples were treated with methanol or acetonitrile. However, background interference did not exist when the samples were treated by liquid−liquid extraction. The results showed that liquid−liquid extraction, using the liquid solvent ethyl acetate, provides the most effective extraction of silibinin from various biological samples.

Panels A−F in Figure S1 (Supporting Information) show the chromatograms of blank plasma, liver, heart, spleen, lung, and kidney, respectively. The chromatograms showed that no significant interfering peaks from the plasma and tissues after liquid−liquid extraction were found at the retention times or the ion channel of silibinin or naringin (IS). Panels G−L in Figure S1 (Supporting Information) shows chromatograms of the plasma and different organ samples containing naringin (IS) and silibinin collected from rats after iv administration of silymarin (100 mg/kg). Retention times of silibinin and naringin (IS) in the chromatograms were 1.4 and 1.9 min, respectively. The analysis time is shorter than previous analysis methods.[16,27]

Analyte matrix effect and recovery were used to assess suitability of the sample preparation method. The matrix effect and recovery percentages were determined at three different

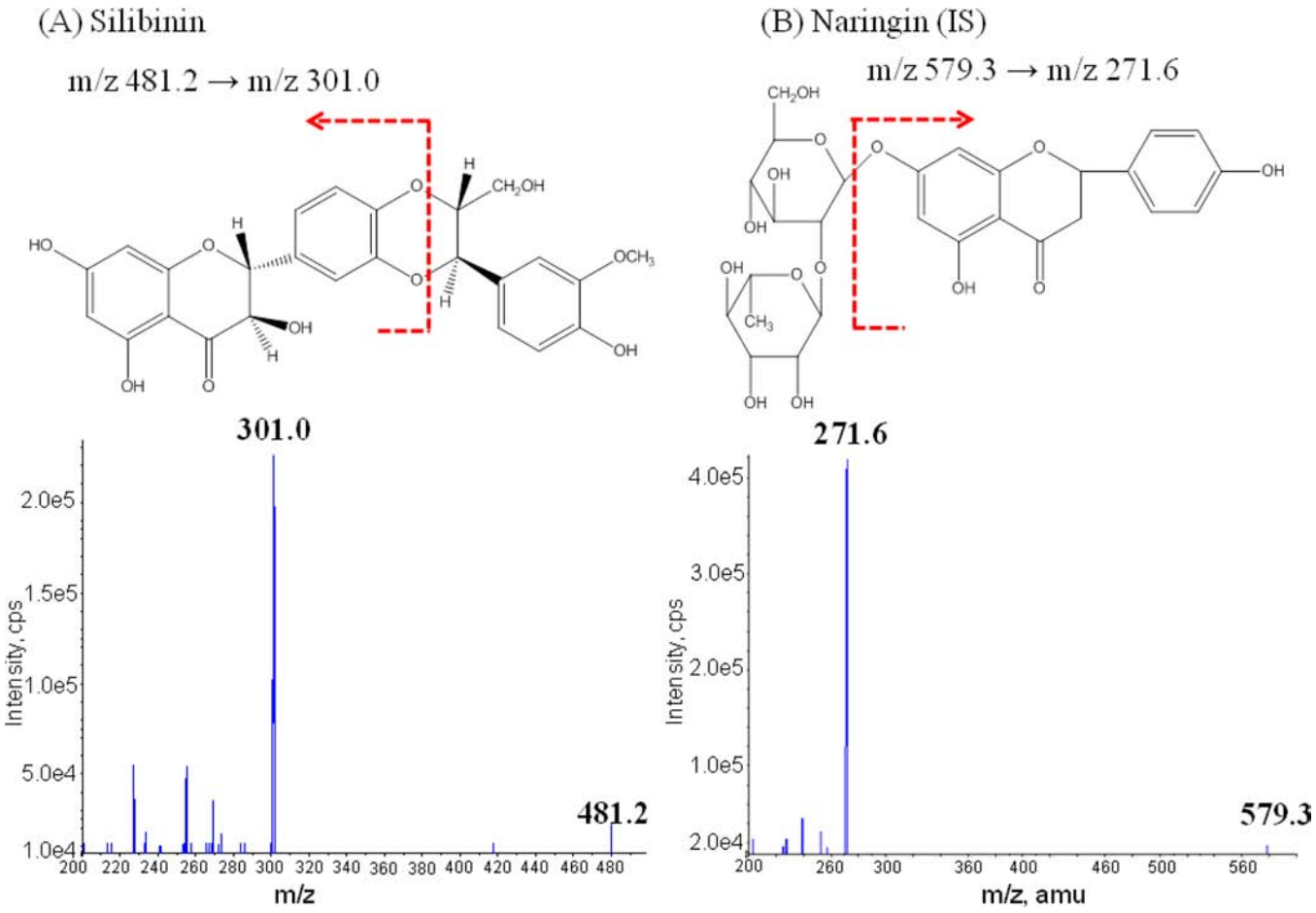


**Figure 3.** Representative product ion mass spectra and chemical structures of (A) silibinin and (B) naringin (IS).

concentrations (low, middle, and high concentrations) for all analytes. The data demonstrated that the mean matrix effect of silibinin in rat plasma and organ samples was 98.26% ± 3.93% and within the range 86.69−100.45%, respectively. No significant matrix effects of silibinin were observed in rat plasma and organ samples, which could be ignored in quantitative analysis (Table S2, Supporting Information). The extraction recovery of silibinin in rat plasma and organ samples was 86.64% ± 3.40% and within the range 88.40−95.57%, which were both considered acceptable (Table S2, Supporting Information).

Average matrix effects and recoveries of naringin (IS) in rat plasma and organ samples are shown in Table S2 (Supporting Information). Because the value of the matrix effect in the organ samples had only a small standard deviation, naringin could be used as a suitable internal standard for the analysis. To evaluate the analytical linearity of the developed method, the peak area ratio of silibinin to naringin (IS) versus concentration was used.

The data demonstrated that the linearity was related to concentration in the range 5−1000 ng/mL for plasma samples and 10−1000 ng/mL for biological samples. The results showed a good correlation coefficient ($r^2 \geq 0.995$) for silibinin over the concentration range from separately prepared analytical runs on different days. The inter- and intraday precision and accuracy values for plasma and organ samples are presented in Tables S3 and S4 (Supporting Information). Precision (RSD, %) and accuracy (bias, %) of plasma ranged from 0.77% to 17.62% and −6.23 to 12.78%, respectively; for organ samples, the percentages ranged from 0.48% to 15.26% and 15.41% to 10.64%, respectively. The LOQ of silibinin was 5 ng/mL in plasma samples and 10 ng/mL in organ sample.

These results showed that the analytical method was sensitive, repeatable, and reliable. The system could be applied to quantification of silibinin in pharmacokinetic studies and tissue distribution.

**Pharmacokinetics and Oral Bioavailability.** Pharmacokinetic and biodistribution assessment of nanoparticles is necessary. Many types of nanoparticles could improve drug distribution profiles, which usually influence drug delivery properties.[33] The morphological structure of ethosomes is similar to that of liposomes, but there have not been any studies about pharmacokinetic differences between them.

To assess the pharmacokinetics and bioavailability of silymarin (free form), LSM, and ESM, each was administered orally (100 mg/kg, po) and intravenously (10 mg/kg, iv) to rats. Rats have also been widely used to test drug efficacy and safety because they are mammals. Their systems could react to medicines, formulations, food products, or cosmetics in a similar manner as human systems; therefore, studying drug efficacy on rats is useful to test if a drug is considered safe enough for human consumption or exposure. Therefore, this animal model is suitable to investigate pharmacokinetics of silymarin loaded in liposomes and ethosomes.

The plasma drug concentration−time profile after intravenous and oral administration of silymarin, LSM, and ESM in


dx.doi.org/10.1021/jf504139g | J. Agric. Food Chem. 2014, 62, 11657−11665

rats is presented in Figures 4 and 5. As seen in Figure 4, there were no differences between silymarin (free form) and

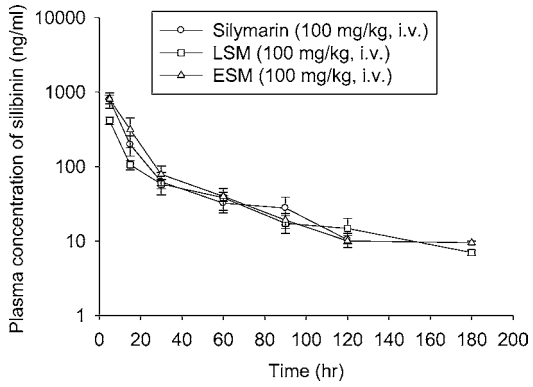


**Figure 4.** Concentration curve of silibinin in rat plasma after iv administration of silymarin (10 mg/kg, iv), LSM (10 mg/kg, iv), and ESM (10 mg/kg, iv); mean ± SEM, $n$ = 5.

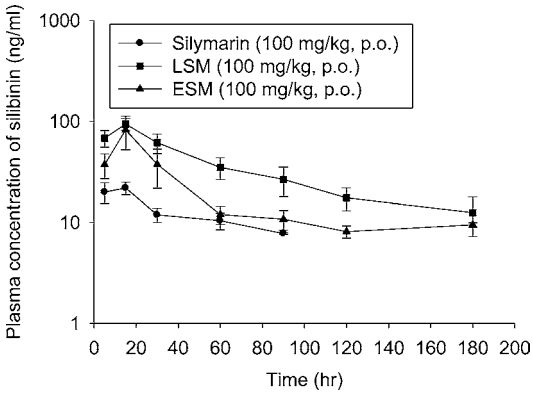


**Figure 5.** Concentration curve of silibinin in rat plasma after oral administration of silymarin (100 mg/kg, po), LSM (100 mg/kg, po), and ESM (100 mg/kg, po); mean ± SEM, $n$ = 5.

silymarin loaded in formulations. However, we found that silibinin could be detected in plasma up to 90 min after oral administration (100 mg/kg, po), while the time was prolonged to 120 min in the group administered LSM and ESM (Figure 5).

Pharmacokinetic parameters were calculated by use of the software program WinNonlin (version 1.1), and the results are summarized in Table 2. The pharmacokinetic models (one- versus two-compartment) were selected according to Akaike's information criterion (AIC),[34] which was calculated by WinNonlin. Smaller AIC values can be observed when the model is more suitable to fit the concentration−time curve.

In this study, the average AIC values from the one-compartment model after silymarin (10 mg/kg, iv), LSM (10 mg/kg, iv), and ESM (10 mg/kg, iv) administration were 56.97, 65.24, and 66.39, respectively. Additionally, the mean AIC values from the two-compartment model after silymarin (10 mg/kg, iv), LSM (10 mg/kg, iv), and ESM (10 mg/kg, iv) administration were 37.56, 52.99, and 57.47, respectively. From these results, the two-compartment model was more suitable than the one-compartment model for intravenous administration in rats (Figure 4 and Table 2).

The two-compartment pharmacokinetic model follows the equation $C_p = Ae^{-\alpha t} + Be^{-\beta t}$, which indicated that there are two different processes in the body, including a distribution phase and an elimination phase, presented as $Ae^{-\alpha t}$ and $Be^{-\beta t}$, respectively. The parameters of the equation, $A$ and $B$, are the concentration ($C$) intercepts for fast and slow disposition phases, respectively, and $\alpha$ and $\beta$ are the disposition rate constants for fast and slow disposition phases, respectively. Analysis of the data after silymarin (10 mg/kg, iv), LSM (10 mg/kg, iv), and ESM (10 mg/kg, iv) administration yielded the pharmacokinetic equations $C = 1.63e^{-0.20t} + 0.12e^{-0.03t}$, $C = 0.82e^{-0.23t} + 0.09e^{-0.03t}$, and $C = 1.49e^{-0.61t} + 0.06e^{-0.02t}$, respectively.

The data showed that the pharmacokinetic parameters for $t_{1/2,\beta}$ (43.1 ± 20.9, 32.54 ± 7.81, and 41.19 ± 6.69 min), CL (1.01 ± 0.34, 1.33 ± 0.16, and 0.78 ± 0.10 L·min$^{-1}$·kg$^{-1}$), and MRT (25.1 ± 9.9, 27.12 ± 5.93, and 23.23 ± 5.33 min) of silymarin, LSM, and ESM were not found to be significantly different between the three groups of each parameter.

Pharmacokinetic parameters for oral administration were calculated by noncompartmental analysis, also called model-independent analysis. The AUC values of silymarin (free form),

**Table 2. Pharmacokinetic Parameters of Silibinin in Rat Plasma**[a]

| | 10 mg/kg, iv | | | 100 mg/kg, po | | |
|---|---|---|---|---|---|---|
| PK parameter | silymarin | LSM | ESM | silymarin | LSM | ESM |
| AIC, one compartment | 57.0 ± 4.5 | 65.24 ± 3.60 | 66.39 ± 8.17 | | | |
| AIC, two compartment | 37.6 ± 7.2 | 52.99 ± 8.31 | 57.47 ± 11.52 | | | |
| $A$ ($\mu$g/mL) | 1.63 ± 0.64 | 0.82 ± 0.14 | 1.49 ± 0.34 | | | |
| $B$ ($\mu$g/mL) | 0.12 ± 0.05 | 0.09 ± 0.02 | 0.06 ± 0.03 | | | |
| $\alpha$ (1/min) | 0.20 ± 0.04 | 0.23 ± 0.04 | 0.61 ± 0.04 | | | |
| $\beta$ (1/min) | 0.03 ± 0.01 | 0.03 ± 0.01 | 0.02 ± 0.01 | | | |
| $t_{1/2,\alpha}$ (min) | 3.92 ± 0.70 | 3.54 ± 0.71 | 6.05 ± 3.14 | | | |
| $t_{1/2,\beta}$ (min) | 43.1 ± 20.9 | 32.54 ± 7.81 | 41.19 ± 6.69 | 80.2 ± 33.6 | 232 ± 108 | 48.1 ± 2.5 |
| $C_{max}$ ($\mu$g/mL) | 1.75 ± 0.69 | 0.92 ± 0.13 | 1.55 ± 0.34 | 0.02 ± 0.01 | 0.11 ± 0.01[b] | 0.08 ± 0.02[b] |
| $T_{max}$ (min) | | | | 10.0 ± 2.9 | 13.0 ± 2.0 | 20.0 ± 10.3 |
| CL (L·min$^{-1}$·kg$^{-1}$) | 1.01 ± 0.34 | 1.33 ± 0.16 | 0.78 ± 0.10 | 130 ± 87 | 9.54 ± 2.10[b] | 32.1 ± 12.2 |
| MRT (min) | 25.1 ± 9.9 | 27.12 ± 5.93 | 23.23 ± 5.33 | 119 ± 45 | 308 ± 153 | 70.2 ± 9.1 |
| AUC (min·$\mu$g·mL$^{-1}$) | 12.9 ± 3.5 | 7.99 ± 0.9 | 14.7 ± 3.2 | 2.04 ± 0.74 | 15.2 ± 6.5[b] | 4.48 ± 1.03 |
| bioavailability (%) | | | | 1.58 | 11.78 | 3.47 |

[a]Data are expressed as mean ± SEM, $n$ = 5. LSM, liposome-encapsulated silymarin formulation; ESM, ethosome-encapsulated silymarin formulation. [b]$P < 0.05$, significantly different from silymarin.

LSM, and ESM were found to be 2.04 ± 0.74, 15.17 ± 6.51, 4.48 ± 1.03 min·μg·mL$^{-1}$, respectively; the results showed that the AUC of LSM was significantly higher than that of silymarin.

$C_{max}$ is often assessed in an effort to show bioequivalence between a known and innovative drug product.[35] Values for LSM and ESM were both significantly higher ($p < 0.05$) than for silymarin, but differences between LSM and ESM were insignificant ($p > 0.05$). The AUC and $C_{max}$ of LSM after oral administration were 7.7- and 5.5-fold higher than for silymarin, respectively. These values for ESM were 2.19- and 4-fold higher than for silymarin, respectively.

The mean $T_{max}$ is the time to maximum concentration of a drug in plasma, which can be used as an indicator of the drug absorption rate. In our study, after oral administration, the $T_{max}$ values for silymarin (free form), LSM, and ESM were not significantly different (approximately 10 min), which was shorter than results reported by Parveen et al.[19] Anesthesia has an influence on the disposition of drugs in animals.[36] Therefore, this discrepancy may be because the previous study used blood samples collected from anesthesized animals, whereas our blood samples were collected from conscious rats.

Additionally, LSM was significantly improved as evidenced by 13.65-fold reduction in CL from silymarin. ESM clearance also decreased by 4.05-fold from silymarin, indicating that these formulations could increase the circulation time of silymarin in rats instead of rapid elimination. Previous in vitro study indicated that silymarin was metabolized by CYP2C8 in the liver.[9] Weingarten et al.[37] supported that liposome could protect the drugs from enzymatic metabolism via oral administration. Our data also observed that LSM and ESM could increase AUC and reduce CL of silibinin after oral administration.

Bioavailability is a term used to indicate the fractional extent to which a dose of drug reaches its site of action or a biological fluid from which the drug has access to its site of action. The formula for calculating bioavailability of a drug administered orally is given as bioavailability (%) = $100(AUC_{oral}/D_{oral})/(AUC_{iv}/D_{iv})$

According to the definition of pharmacokinetics, the bioavailability of iv administration is 100%. However, bioavailability of oral administration usually decreases due to incomplete absorption and first-pass metabolism. In this study, we used the $AUC_{iv}$ value of silymarin (free form) to calculate the bioavailabilities of silymarin (free form), LSM, and ESM. According to the experimental data, the oral bioavailability of silymarin (free form) was 100(2.04/100)/(12.9/10) = 1.58%, that of LSM was 100(15.2/100)/(12.9/10) = 11.78%, and that of ESM was 100(4.48/100)/(12.9/10) = 3.47%. The bioavailability of a substance in the body can be improved by increasing the absorption of the substance in the gastrointestinal tract or by reducing its metabolism in the body.[38]

As discussed above, the higher AUC and shorter CL for LSM and ESM caused their relative bioavailabilities to decrease by 7.45- and 2.2-fold compared to silymarin (free form), respectively. As a result, ethosomes have higher encapsulation efficiency than liposomes. In vitro release tests showed no differences between liposomes and ethosomes, but liposomes have better pharmacokinetic properties than ethosomes when liposomes are encapsulating silymarin.

**Biodistribution Study.** Biodistribution, which could be used to predict the possible mechanisms of action of nanoparticles, was demonstrated to be important for the application of nanoparticles.[39] According to the results from pharmacokinetic profiles, we observed that silibinin was around the intersection between the first and second compartment at 30 min after a single dose of silymarin was administered intravenously (10 mg/kg). Due to the possible high distribution of silibinin in various tissues at 30 min after intravenous administration, we selected this time point for assessing biodistribution of silymarin.

Concentrations of silibinin were determined in rat plasma and various tissues including liver, heart, spleen, lung, and kidney at 30 min after a single dose of silymarin and injectable formulation groups (LSM and ESM) were administered intravenously (10 mg/kg). Biodistribution study results are shown in Figure 6.

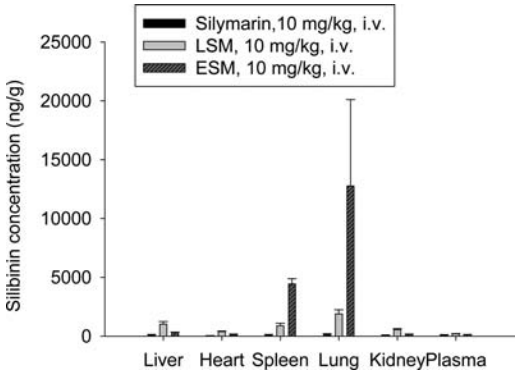


**Figure 6.** Silibinin concentration of rat liver, heart, spleen, lung, kidney, and plasma at 30 min following iv administration of silymarin (free form), LSM, and ESM at 10 mg/kg (mean ± SEM, $n = 6$).

It was shown that the concentrations of silymarin in various organs were lower than for the formulation groups. Distribution patterns of LSM and ESM were in the following order (from high to low): lung > liver > spleen > kidney> heart for LSM and lung > spleen > liver > kidney > heart for ESM. These formulation groups, when administered intravenously, are unable to leave general circulation and rapidly accumulate in mononuclear phagocyte systems (MPS), which are abundant in special tissues and organs such as liver, lung and spleen.[40,41] Therefore, the main organs of distribution in the formation groups were the spleen, lung, and liver instead of kidney.

From the perspective of treatment, silymarin has therapeutic efficacy for liver disease;[42,43] therefore, the level of silymarin accumulation in the liver should be considered. Relatively low levels of silibinin accumulate in the liver following administration of silymarin. The exposures of total silibinin levels in the liver following administration of LSM and ESM were approximately 9- and 3-fold higher than that for silymarin; these results are beneficial for therapy of liver disease. Additionally, according to the data of biodistribution, LSM and ESM appear at low accumulation in the kidney, which may reduce nephrotoxicity.

The tissue distribution patterns of LSM and ESM are similar, except the lung and spleen accumulation of ESM was higher than that of LSM. It is well-known that the biodistribution of vectors could be first affected by their particle size. The sizes of LSM and ESM were not significantly different. Therefore, if distribution differences between LSM and ESM occur, the size factor could be ignored. From a morphological point of view, ethosomes are very similar to liposomes; however, ethosomes

exhibit high encapsulation and soft structure, which may cause the high accumulation of ESM in some tissues.

To our knowledge, this is the first description of biodistribution of ethosomes. The results clarify the difference between ethosomes and liposomes in tissue distribution. ESM had high accumulation in the lung, suggesting that ethosomes have great potential as a lung-targeting drug carrier for the treatment of lung diseases.

In this study, the experiment was divided into four major areas, including development and establishment of analytical methods, formulation of design, pharmacokinetic property studies in awake rats, and biodistribution determination.

The LC-MS/MS method was developed and validated to assess pharmacokinetic profiles and biodistribution of silymarin-loaded liposomes and ethosomes in preclinical study phases. The analysis method is rapid, specific, sensitive, accurate, precise, and linear in the analytical range and has been successfully used in pharmacokinetic and biodistribution studies of silymarin in free-moving rats.

The pharmacokinetic results demonstrated liposome and ethosome could improve the bioavailability of silymarin and that liposomes perform better than ethosomes. Furthermore, LSM and ESM were taken up by the reticuloendothelial system (RES) with good targeting to the liver. Therefore, ethosomes have potential as a therapeutic for lung diseases. Although these results provide preliminary clinical feasibility, more detailed assessments should be required before clinical applications.

## ■ ASSOCIATED CONTENT

### Ⓢ Supporting Information

Four tables and one figure showing method validation results and typical HPLC-MS/MS chromatograms. This material is available free of charge via the Internet at http://pubs.acs.org.

## ■ AUTHOR INFORMATION

### Corresponding Author

*Fax (886-2) 2822 5044; tel (886-2) 2826 7115; e-mail thtsai@ym.edu.tw.

### Funding

This work was supported in part by research grants from the National Science Council Taiwan (NSC102-2113-M-010-001-MY3) and by TCH 103-02 and TCH 10301-62-021 from Taipei City Hospital, Taiwan.

### Notes

The authors declare no competing financial interest.

## ■ REFERENCES

(1) Mayer, K. E.; Myers, R. P.; Lee, S. S. Silymarin treatment of viral hepatitis: A systematic review. *J. Viral Hepatitis* **2005**, *12*, 559−567.

(2) Hackett, E. S.; Twedt, D. C.; Gustafson, D. L. Milk thistle and its derivative compounds: A review of opportunities for treatment of liver disease. *J. Vet. Intern. Med.* **2013**, *27*, 10−16.

(3) Singh, R. P.; Agarwal, R. Flavonoid antioxidant silymarin and skin cancer. *Antioxid. Redox Signaling* **2002**, *4*, 655−663.

(4) Pradhan, S. C.; Girish, C. Hepatoprotective herbal drug, silymarin from experimental pharmacology to clinical medicine. *Indian J. Med. Res.* **2006**, *124*, 491−504.

(5) Crocenzi, F. A.; Roma, M. G. Silymarin as a new hepatoprotective agent in experimental cholestasis: New possibilities for an ancient medication. *Curr. Med. Chem.* **2006**, *13*, 1055−1074.

(6) Vitaglione, P.; Morisco, F.; Caporaso, N.; Fogliano, V. Dietary antioxidant compounds and liver health. *Crit. Rev. Food Sci. Nutr.* **2004**, *44*, 575−586.

(7) Wallace, S.; Vaughn, K.; Stewart, B. W.; Viswanathan, T.; Clausen, E.; Nagarajan, S.; Carrier, D. J. Milk thistle extracts inhibit the oxidation of low-density lipoprotein (LDL) and subsequent scavenger receptor-dependent monocyte adhesion. *J. Agric. Food Chem.* **2008**, *56*, 3966−3972.

(8) Garg, R.; Gupta, G. D. Preparation and evaluation of gastroretentive floating tablets of silymarin. *Chem. Pharm. Bull.* **2009**, *57*, 545−549.

(9) Javed, S.; Kohli, K.; Ali, M. Reassessing bioavailability of silymarin. *Altern. Med. Rev.* **2011**, *16*, 239−249.

(10) Yuan, F.; Dellian, M.; Fukumura, D.; Leunig, M.; Berk, D. A.; Torchilin, V. P.; Jain, R. K. Vascular permeability in a human tumor xenograft: Molecular size dependence and cutoff size. *Cancer Res.* **1995**, *55*, 3752−3756.

(11) Cortesi, R.; Romagnoli, R.; Drechsler, M.; Menegatti, E.; Zaid, A. N.; Ravani, L.; Esposito, E. Liposomes- and ethosomes-associated distamycins: A comparative study. *J. Liposome Res.* **2010**, *20*, 277−285.

(12) Touitou, E.; Dayan, N.; Bergelson, L.; Godin, B.; Eliaz, M. Ethosomes, novel vesicular carriers for enhanced delivery: Characterization and skin penetration properties. *J. Controlled Release* **2000**, *65*, 403−418.

(13) Touitou, E.; Godin, B.; Dayan, N.; Weiss, C.; Piliponsky, A.; Levi-Schaffer, F. Intracellular delivery mediated by an ethosomal carrier. *Biomaterials* **2001**, *22*, 3053−3059.

(14) Li, C.; Deng, L.; Zhang, Y.; Su, T. T.; Jiang, Y.; Chen, Z. B. Silica-coated ethosome as a novel oral delivery system for enhanced oral bioavailability of curcumin. *Acta Pharm. Sin.* **2012**, *47*, 1541−1547.

(15) Abrol, S.; Trehan, A.; Katare, O. P. Formulation, characterization, and in vitro evaluation of silymarin-loaded lipid microspheres. *Drug Delivery* **2004**, *11*, 185−191.

(16) Yan-yu, X.; Yun-mei, S.; Zhi-peng, C.; Qi-neng, P. Preparation of silymarin proliposome: a new way to increase oral bioavailability of silymarin in beagle dogs. *Int. J. Pharm.* **2006**, *319*, 162−168.

(17) Li, X.; Yuan, Q.; Huang, Y.; Zhou, Y.; Liu, Y. Development of silymarin self-microemulsifying drug delivery system with enhanced oral bioavailability. *AAPS PharmSciTech* **2010**, *11*, 672−678.

(18) Jia, L.; Zhang, D.; Li, Z.; Duan, C.; Wang, Y.; Feng, F.; Wang, F.; Liu, Y.; Zhang, Q. Nanostructured lipid carriers for parenteral delivery of silybin: Biodistribution and pharmacokinetic studies. *Colloids Surf., B* **2010**, *80*, 213−218.

(19) Parveen, R.; Baboota, S.; Ali, J.; Ahuja, A.; Vasudev, S. S.; Ahmad, S. Oil based nanocarrier for improved oral delivery of silymarin: In vitro and in vivo studies. *Int. J. Pharm.* **2011**, *413*, 245−253.

(20) Lian, R.; Lu, Y.; Qi, J.; Tan, Y.; Niu, M.; Guan, P.; Hu, F.; Wu, W. Silymarin glyceryl monooleate/poloxamer 407 liquid crystalline matrices: Physical characterization and enhanced oral bioavailability. *AAPS PharmSciTech* **2011**, *12*, 1234−1240.

(21) Kissinger, P. T. The history of automatic blood sampling at BAS. *Curr. Sep.* **2002**, *19*, 113−115.

(22) Wu, Y. T.; Chen, Y. F.; Hsieh, Y. J.; Jaw, I.; Shiao, M. S.; Tsai, T. H. Bioavailability of salvianolic acid B in conscious and freely moving rats. *Int. J. Pharm.* **2006**, *326*, 25−31.

(23) Brinda, B. J.; Zhu, H. J.; Markowitz, J. S. A sensitive LC-MS/MS assay for the simultaneous analysis of the major active components of silymarin in human plasma. *J. Chromatogr. B: Anal. Technol. Biomed. Life Sci.* **2012**, *902*, 1−9.

(24) Malekinejad, H.; Rokhsartalab-Azar, S.; Hassani-Dizaj, S.; Alizadeh-Fanalou, S.; Rezabakhsh, A.; Amniattalab, A. Effects of silymarin on the pharmacokinetics of atorvastatin in diabetic rats. *Eur. J. Drug Metab. Pharmacokinet.* **2013**, *39*, 311−320.

(25) Voruganti, S.; Yamsani, S. K.; Yamsani, M. R. Effect of silibinin on the pharmacokinetics of nitrendipine in rabbits. *Eur. J. Drug Metab. Pharmacokinet.* **2013**, *39*, 277−281.

(26) Zhu, H. J.; Brinda, B. J.; Chavin, K. D.; Bernstein, H. J.; Patrick, K. S.; Markowitz, J. S. An assessment of pharmacokinetics and antioxidant activity of free silymarin flavonolignans in healthy

volunteers: A dose escalation study. *Drug Metab. Dispos.* **2013**, *41*, 1679−1685.
(27) Wen, Z.; Dumas, T. E.; Schrieber, S. J.; Hawke, R. L.; Fried, M. W.; Smith, P. C. Pharmacokinetics and metabolic profile of free, conjugated, and total silymarin flavonolignans in human plasma after oral administration of milk thistle extract. *Drug Metab. Dispos.* **2008**, *36*, 65−72.
(28) Webb, C. B.; McCord, K. W.; Twedt, D. C. Assessment of oxidative stress in leukocytes and granulocyte function following oral administration of a silibinin-phosphatidylcholine complex in cats. *Am. J. Vet. Res.* **2009**, *70*, 57−62.
(29) *Guidance for Industry, Bioanalytical Method Validation*. Center for Drug Evaluation and Research, U.S. Food and Drug Administration: Rockville, MD, May 2001.
(30) Martin, T. B.; Dodd, P. M.; Jayaraman, A. Polydispersity for tuning the potential of mean force between polymer grafted nanoparticles in a polymer matrix. *Phys. Rev. Lett.* **2013**, *110*, No. 018301.
(31) Tarun Parashar, S.; Sachan, R.; Singh, V.; Singh, G.; Tyagi, S.; Patel, C.; Gupta, A. Ethosome: A recent vesicle of transdermal drug delivery system. *Int. J. Res. Dev. Pharm. Life Sci.* **2013**, *2*, 285−292.
(32) Higuchi, T. Mechanism of sustained-action medication. Theoretical analysis of rate of release of solid drugs dispersed in solid matrices. *J. Pharm. Sci.* **1963**, *52*, 1145−1149.
(33) Farokhzad, O. C.; Langer, R. Nanomedicine: Developing smarter therapeutic and diagnostic modalities. *Adv. Drug Delivery Rev.* **2006**, *58*, 1456−9.
(34) Yamaoka, K.; Nakagawa, T.; Uno, T. Application of Akaike's information criterion (AIC) in the evaluation of linear pharmacokinetic equations. *J. Pharmacokinet. Biopharm.* **1978**, *6*, 165−175.
(35) Midha, K. K.; Rawson, M. J.; Hubbard, J. W. The bioequivalence of highly variable drugs and drug products. *Int. J. Clin. Pharmacol. Ther.* **2005**, *43*, 485−498.
(36) Feary, D. J.; Mama, K. R.; Wagner, A. E.; Thomasy, S. Influence of general anesthesia on pharmacokinetics of intravenous lidocaine infusion in horses. *Am. J. Vet. Res.* **2005**, *66*, 574−580.
(37) Weingarten, C.; Moufti, A.; Delattre, J.; Puisieux, F.; Ryman, B. E. Protection of insulin from enzymatic degradation by its association to liposomes. *Int. J. Pharm.* **1985**, *26*, 251−255.
(38) Fasinu, P.; Pillay, V.; Ndesendo, V. M.; du Toit, L. C.; Choonara, Y. E. Diverse approaches for the enhancement of oral drug bioavailability. *Biopharm. Drug Dispos.* **2011**, *32*, 185−209.
(39) Sa, L. T.; Albernaz Mde, S.; Patricio, B. F.; Falcao, M. V., Jr.; Coelho, B. F.; Bordim, A.; Almeida, J. C.; Santos-Oliveira, R. Biodistribution of nanoparticles: Initial considerations. *J. Pharm. Biomed. Anal.* **2012**, *70*, 602−604.
(40) Yang, S. C.; Lu, L. F.; Cai, Y.; Zhu, J. B.; Liang, B. W.; Yang, C. Z. Body distribution in mice of intravenously injected camptothecin solid lipid nanoparticles and targeting effect on brain. *J. Controlled Release* **1999**, *59*, 299−307.
(41) Bakker-Woudenberg, I. A. J. M. Delivery of antimicrobials to infected tissue macrophages. *Adv. Drug Delivery Rev.* **1995**, *17*, 5−20.
(42) Feher, J.; Lengyel, G. Silymarin in the prevention and treatment of liver diseases and primary liver cancer. *Curr. Pharm. Biotechnol.* **2012**, *13*, 210−217.
(43) Saller, R.; Meier, R.; Brignoli, R. The use of silymarin in the treatment of liver diseases. *Drugs* **2001**, *61*, 2035−2063.

propose a process to purify broccoli myrosinase and also a partial characterization of the enzyme.

## MATERIALS AND METHODS

**Plant Material.** Broccoli (*B. oleracea* cv. Avenger) heads (3 days from harvesting) were purchased at the local market (Santiago, Chile) through a single supplier. The vegetables were immediately subjected to protein extraction.

**Protein Extract.** Protein was extracted as previously described.[16] Briefly, samples were pulverized with liquid nitrogen in a mortar until obtaining a homogeneous pulp. After that, 1 mL of buffer was added to 0.25 g of powder. The buffers were 0.1 M acetate at pH 5.0 and 0.1 M phosphate buffer at pH 6.0 and 7.0. The mixture was vortexed and then centrifuged at 15000*g* for 20 min at 4 °C. The supernatant was recovered for analysis.

**Purification.** *Purification Process Design.* In a first stage, the crude broccoli extract was analyzed by sodium dodecyl sulfate−polyacrylamide gel electrophoresis (SDS−PAGE) to visualize the complexity of the sample from which myrosinase was to be purified.[17] The molecular mass of each band was estimated by comparison to full-range rainbow molecular weight markers (12 000−225 000 Da) (GE Healthcare, Uppsala, Sweden). With this information, we performed a database search to characterize the main proteins that must be separated in the purification process. In parallel, the physicochemical properties of Brassicaceae myrosinases were obtained from databases and literature. The database searches were carried out in UniProtKB (http://www.uniprot.org). Finally, considering the characterization of the broccoli protein extract and also the information about purification processes reported for myrosinases from different sources, the purification process was designed.

*Ammonium Sulfate Precipitation.* The protein extract was precipitated with ammonium sulfate at 55% saturation.[17] This saturation percentage was chosen on the basis of literature.[15] The mixture was agitated in a beaker for 10 min in an ice bath and then left at room temperature for 30 min. After that, the suspension was centrifuged at 7000*g* for 30 min, the precipitate was discarded because no activity was detected in it, and the supernatant was used in the subsequent purification steps.

*Dialysis.* The supernatant from ammonium sulfate precipitation (5 mL) was subjected to dialysis against 500 mL of 20 mM Tris−HCl buffer at pH 8.0 plus 0.15 mM NaCl in 0.2 μm dialysis bags [Spectra/Por molecular weight cut-off (MWCO) of 3500]. After 24 h of stirring at room temperature, the sample solution (10.5 mL) was recovered from the dialysis bag.

*Affinity Chromatography.* Chromatographic runs were performed in a BioLogic LP system equipped with a fraction collector and the LP Data View software (Bio-Rad, Hercules, CA). A 1 mL column was packed with concanavalin A resin (GE Healthcare, Uppsala, Sweden). The column was washed and equilibrated (5 column volumes) with 20 mM Tris−HCl at pH 8.0 plus 0.15 mM NaCl (buffer A). The protein extract (5 mL) was loaded into the column and subsequently washed with buffer A (5 column volumes). Elution of myrosinase was obtained with an increasing gradient of methyl-α-D-mannopyranoside (Sigma-Aldrich, Schnelldorf, Germany) formed by mixing buffer A with buffer A added with 0.5 M methyl-α-D-mannopyranoside (buffer B). The elution gradient was 3.33% B/min. The flow rate was constant and equal to 0.5 mL/min. The experiments were conducted at room temperature. All buffers were filtered through 0.22 μm Millipore filters. Absorbance at 280 nm was registered.

**Myrosinase Characterization.** *Native Molecular Mass.* The native molecular mass of broccoli myrosinase was determined by size-exclusion chromatography. A 0.7 × 30 cm Econo-Column (Bio-Rad, Hercules, CA) was packed with 11.5 mL of Sephacryl 200-HR (Sigma-Aldrich, Schnelldorf, Germany). The calibration curve was built using the Gel Filtration Marker Kit for protein molecular weights of 29 000−700 000 Da (Sigma-Aldrich, Schnelldorf, Germany). A total of 1 mL of the purified myrosinase fraction was loaded into the column and eluted with 50 mM Tris−HCl at pH 7.4 plus 0.15 M NaCl at 0.5 mL/min.

*Protein Identification.* Protein spots were excised directly from the SDS−PAGE gels and analyzed by matrix-assisted laser desorption ionization/time-of-flight (MALDI−TOF) at the Central Proteomics Facility of Sir William Dunn Pathology School at Oxford University. Samples were destained using a 25 mM ammonium bicarbonate in 50% acetonitrile/water (Mili-Q-grade) solution. Destained gel pieces were reduced with 10 mM dithiothreitol (DTT) and alkylated with 55 mM iodoacetamide. Reduced and alkylated gel pieces were washed 3 times with solution of 25 mM ammonium bicarbonate in 50% acetonitrile/water and dehydrated with 100% acetonitrile before adding 400 ng of Promega sequencing grade modified trypsin. Samples were left for 1 h at 4 °C to rehydrate. A 25 mM ammonium bicarbonate solution was added to cover the gel pieces, and the samples were incubated at 37 °C overnight. Digestion was stopped with 1 μL of acetic acid, and the supernatant was placed in new low binding microtubes. The gel pieces were covered with 50% acetonitrile/water with 2% formic acid solution and sonicated for 30 min to extract more peptides. The supernatant was added to new microtubes and dried down in a vacuum centrifuge. Samples were resuspended in 10 μL of 0.1% trifluoroacetic acid (TFA) and desalted using Millipore $C_{18}$ ZipTips. Samples were eluted in 3 μL of 0.1% TFA in 50% acetonitrile/water solution, and 0.5 μL of the eluent was spotted onto the MALDI plate and left to air-dry. Dried samples were overlaid with 0.5 μL of MALDI matrix α-cyano-4-hydroxycinnamic acid and left to air-dry. Then, dried samples were analyzed on AB Sciex 4800 MALDI ToF−ToF. The instrument was calibrated using 4700 calibration mixture, and after that, samples were analyzed using mass spectrometry (MS) reflector positive (for MS spectra) and MS/MS 1 kV positive (for MS/MS spectra) methods. The data were searched by GPS explorer software, using Mascot search engine, National Center for Biotechnology Information (NCBI) non-redundant (nr) green plant database (NCBInr 20131208; Sept 30, 2014).

*Effect of pH and Temperature.* The activity of myrosinase was determined at different pH (4.0, 5.0, 6.0, 7.0, and 8.0) and temperature (20, 40, 60, and 70 °C) conditions. We used 0.1 M acetate buffer to achieve pH 4.0 and 5.0 and 0.1 M phosphate buffer to achieve pH 6.0, 7.0, and 8.0. Activity assays were conducted using a thermostatic bath (Stuart, U.K.). All determinations were made in triplicate.

*Kinetic Characterization.* The kinetic behavior of broccoli myrosinase was studied using sinigrin (Sigma-Aldrich, Schnelldorf, Germany) as the substrate at different initial concentrations (0.035, 0.050, 0.075, 0.100, 0.125, and 0.250 mM) at pH 7.0 and 40 °C. The experimental data were adjusted to Michaelis−Menten kinetic models, and the respective parameters were estimated.

**Analytical Determinations.** *Protein Concentration.* The protein concentration was measured by the Bradford method using the Protein Quantification Kit-Rapid (Sigma-Aldrich, Schnelldorf, Germany). Absorbance at 595 nm was registered, and the protein concentration was estimated from a calibration curve made with bovine serum albumin (BSA) as the protein standard.

*Myrosinase Activity.* Enzyme activity was assessed spectrophotometrically through the method described in the literature.[18] A total of 1 mL of substrate buffer (33 mM sodium phosphate buffer at pH 7.4 containing 10 mM sinigrin, 3 mM MgCl, 0.55 mM ATP, 0.72 mM NADP, 3.5 units of hexokinase, and 1.75 units of glucose-6-phosphate dehydrogenase) was preincubated for a sufficient time (3−10 min) at 30 °C. Then, appropriate amounts of the enzyme were added. After mixing, the reaction was monitored at 346 nm. Myrosinase activity was calculated from the absorbance increasing rate, which was due to the formation of NADPH. A total of 1 unit of myrosinase activity was defined as the amount of enzyme that catalyzed the liberation of 1 μmol of glucose/min from sinigrin under the conditions described above. Results were expressed in units per milligram of protein. All chemicals were purchased from Sigma-Aldrich (Schnelldorf, Germany). All determinations were made in triplicate.

*SDS−PAGE.* SDS−PAGE was performed in a mini-chamber (Bio-Rad, Hercules, CA).[17] Each gel (12% acrylamide) had 10 wells, and in each well, 20 μL of protein solution was loaded (14 μg of protein of crude extract and dialysis fraction and 7 μg of the affinity chromatography fraction that contains the pure enzyme). The gels

were run at 120 V for 10 min and after that at 180 V until the advancing front reached the bottom of the gel. After that, the gels were soaked in a solution of 25% methanol and 7.5% acetic acid for 30 min, stained with Coomassie Brilliant Blue R-250 for 12 h (0.1% Coomassie Brilliant Blue R-250, 25% methanol, and 7.5% acetic acid), and destained in a solution of 25% methanol and 7.5% acetic acid. AccuRuler Prestained Protein Ladder (11 000−180 000 Da) (Lamda Biotech, Inc., Ballwin, MO) was used. The protein samples, except for the crude extract, were concentrated by acetone precipitation before SDS−PAGE.[19] Image acquisition was performed with an Image-Scanner II device (GE Healthcare, Uppsala, Sweden). All chemicals were analytical-grade and were purchased from Sigma-Aldrich (Schnelldorf, Germany).

## RESULTS AND DISCUSSION

**Purification.** The analysis of the proteins found in the crude broccoli extract yielded that there are approximately 21 main proteins, detected in the SDS−PAGE (shown in Figure 1), that must be eliminated in the purification process. The molecular weight of the monomers fluctuated between 93 and 19 kDa. According to the literature, among them, there are only two glycoproteins, $\beta$-galactosidase[10] and myrosinase,[2] which should be possible to separate through concanavalin A affinity chromatography. On the other hand, these two proteins differ considerably in their molecular weight. The molecular weight of most Brassicaceae myrosinases is about 62 kDa, while the molecular weight of $\beta$-galactosidase may vary between 52[21] and 130 kDa,[22] and it is usually 93 kDa in Brassicaceae.[20] Besides, myrosinase usually forms homodimers, whereas $\beta$-galactosidase may form dimers or tetramers.[23] As a consequence, a separation technique that exploits size differences would be adequate to purify broccoli myrosinase, such as ammonium sulfate precipitation. Hence, the purification process consisted of ammonium sulfate precipitation followed by concanavalin A affinity chromatography. An intermediate dialysis step was included to eliminate ammonium sulfate excess from the supernatant and also to perform a buffer change.

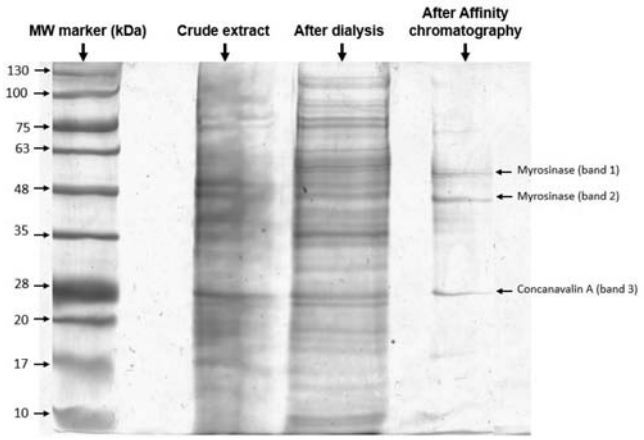


**Figure 1.** Image of SDS−PAGE that shows protein fractions along the purification process: lane 1, molecular weight ladder; lane 2, crude extract; lane 3, fraction after precipitation and dialysis; and lane 4, protein fraction after affinity chromatography.

Figure 1 shows SDS−PAGE that resolved the proteins present in the crude extract (second lane), the sample after ammonium sulfate precipitation and dialysis (third lane), and the active fraction obtained after concanavalin A affinity chromatography (fourth lane). The complexity of the crude protein extract is evident from Figure 1; besides, it is clear that the fraction composition changed after ammonium sulfate precipitation. In the chromatography fraction, three bands were detected, whose identity was elucidated through MS.

Table 1 shows the results from the MS analysis performed on the three bands detected in SDS−PAGE. Bands 1 and 2 were identified as myrosinase from *Brassica napus*, with an acceptable statistical significance (scores higher than 120 and e-values lower than $10 \times 10^{-5}$). These bands differ in their molecular size, in about 5 kDa. This difference can be attributed to different glycosylation states. Band 3 was identified as concanavalin A, which probably was released from the affinity resin.

Figure 2 shows the concanavalin A affinity chromatogram. Two peaks eluted during the elution gradient, the smallest peak at 74% buffer B and the second peak at 95% buffer B, which agrees with the activity curve. The smallest peak showed no myrosinase activity and probably corresponds to one of the myrosinase bands detected in SDS−PAGE. Then, it is likely that this peak corresponds to an inactive isoform of myrosinase.

The purification process proposed here was successful in purifying myrosinase from broccoli extract. Table 2 shows a summary of the purification process. The total myrosinase activity had only a small decrease (12.5%) with respect to the crude extract. Additionally, a high recovery was achieved, with a yield of 88%. Finally, purity increased 1328-fold. These values indicate that the process designed here is very efficient.

This process is simpler than other processes proposed to purify myrosinases from other sources. For example, a four-step process was proposed to purify myrosinase from daikon seedlings, consisting of anion-exchange chromatography, hydrophobic interaction chromatography, size-exclusion chromatography, and a final concanavalin A affinity chromatography.[13] The authors achieved a 49% recovery and a 230-fold purification. Another three-step process was also proposed, concanavalin A affinity chromatography, cation-exchange chromatography, and size-exclusion chromatography, for purifying crambe seed myrosinase.[3] The authors reported a 4% yield and a purification factor of 40-fold. Another three-step process to purify myrosinase from horseradish consisted of ammonium sulfate precipitation, Q-sepharose, and concanavalin A affinity chromatography,[15] resulting in a yield of 20% and a 34-fold purification. A two-step process was developed to separate myrosinase complexes from different Brassicaceae seeds, with a recovery between 18 and 48% and a maximum purification of 573-fold for *Sinapis alba* myrosinase.[2] Then, the process proposed in the present work gave the highest recovery and the highest purification factor compared to the data available in the literature.

**Myrosinase Characterization.** On the basis of the SDS−PAGE, myrosinase subunits have a molecular mass of 50−55 kDa. This value falls within the expected range of 10−110 kDa[1] but differs slightly from the value of 62 kDa reported for myrosinases from *Arabidopsis*, *Wasabia japonica*, *B. napus*, and *B. oleracea* var. Capitata. The number of subunits in the native structure of broccoli myrosinase was determined by size-exclusion chromatography (data not shown). The native molecular mass was equal to 157 kDa, and considering that each subunit weights 50−55 kDa, the native structure of broccoli myrosinase is composed of three subunits.

It is very frequent that myrosinases form complexes with other proteins. These complexes exhibit a high molecular weight (200−600 kDa) and show myrosinase activity.[2] In the

**Table 1. Identification of Protein Bands by MS**

| band | identity | score | e value | NCBInr access | matched peptide |
|---|---|---|---|---|---|
| 1 | myrosinase (*B. napus*) | 213 | $1.8 \times 10^{-9}$ | gil127733 | FSFAWSR |
| | | | | | GVNQGGLDYYHK |
| | | | | | DYADLCFK |
| | | | | | IGPVMITRWFLPFDESDPASIEAAER |
| | | | | | LTYDNSRGEFLGPLFVEDK |
| | | | | | GIYYVMDYFK |
| | | | | | YGDPLIYVTENGFSTPSSENREQAIADYKR |
| | | | | | EKGVNVR |
| | | | | | FGLSYVNW |
| | | | | | EDLDDR |
| 2 | myrosinase (*B. napus*) | 128 | $1.0 \times 10^{-5}$ | gil127733 | FSFAWSR |
| | | | | | GVNQGGLDYYHKLIDALLEK |
| | | | | | IGPVMITRWFLPFDESDPASIEAAER |
| | | | | | GRYPDIMR |
| | | | | | LTYDNSRGEFLGPLFVEDK |
| | | | | | GIYYVMDYFK--YGDPLIYVTENGFSTPSSENR |
| | | | | | EKGVNVR |
| 3 | concanavalin A (*Canavalia ensiformis*) | 1507 | $2.2 \times 10^{-5}$ | gil167013346 | XDTIVAVELD |
| | | | | | TYPNTDIGDP |
| | | | | | SYPHIGIDIK |
| | | | | | NMQNGKVGT |
| | | | | | HIIYNSVDKR |
| | | | | | VGLSASTGLY |
| | | | | | KETNTILSWS |
| | | | | | HETNALHFMF |
| | | | | | QFSKDQKDL |
| | | | | | ILQGDATTGTDGNLELTRVSSNGSPQGSSVGR |
| | | | | | SPDSHPADGIAFFISNIDSSIPSGSTGRLLGLFPDAX |

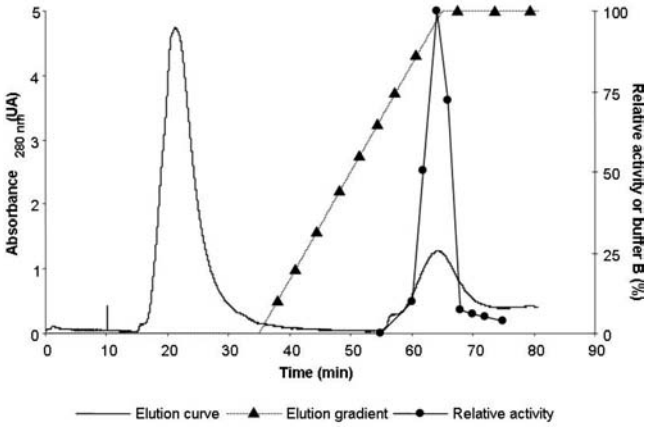


**Figure 2.** Chromatogram of the concanavalin A affinity step. The protein elution curve (flat line) is overlapped with the myrosinase activity curve (circles).

**Table 2. Purification of Myrosinase from Broccoli Extract**

| stage | total protein content (mg) | total activity (units) | specific activity (unit $mg^{-1}$) | yield (%) | purification factor (fold) |
|---|---|---|---|---|---|
| crude extract | 608.8 | 2.65 | 0.0044 | | |
| ammonium sulfate precipitation | 302.2 | 2.65 | 0.0088 | 100 | 2.0 |
| dialysis | 56.5 | 1.16 | 0.0205 | 44 | 4.6 |
| concanavalin A affinity chromatography | 0.4 | 2.32 | 5.8000 | 88 | 1318.2 |

case of broccoli, we can presume that such complexes were not formed. High-molecular-mass proteins or protein complexes are less soluble than small proteins; hence, if broccoli myrosinase forms complexes, they would have precipitated at 55% ammonium sulfate. However, the precipitate showed no myrosinase activity, but the supernatant did. Additionally, when forming complexes, myrosinase would still glycosylated, and therefore, the complexes should have been retained by the concanavalin A affinity column. However, this did not happen, because in SDS−PAGE, only myrosinase and concanavalin A (released from the affinity column) were detected after affinity chromatography. If there were complexes with other proteins, we should have detected different bands corresponding to the proteins bound to myrosinase.

Figure 3 shows myrosinase activity at different pH (Figure 3a) and temperature (Figure 3b) conditions. Myrosinase remained active at acidic pH and showed a decrease in its activity as pH increased, showing a significant loss of activity at pH above 5.0. Myrosinase was active in the temperature range from 20 to 70 °C, agreeing with the literature.[24,25] The optimum temperature at pH 6.0 was around 40 °C. The optimum pH would be below 4.0, differing from the optimum pH reported for other myrosinases. Crambe seed myrosinase has an optimum pH equal to 7.5,[3] and the optimum pH of horseradish myrosinase is 5.7,[15] both using sinigrin as the substrate.

Figure 4 shows myrosinase kinetics on sinigrin. Myrosinase exhibits substrate inhibition, because there is a maximum initial activity at 0.25 mM sinigrin, and at higher sinigrin concentrations, the initial reaction rate decreased drastically. This result agrees with another study[25] about the effect of

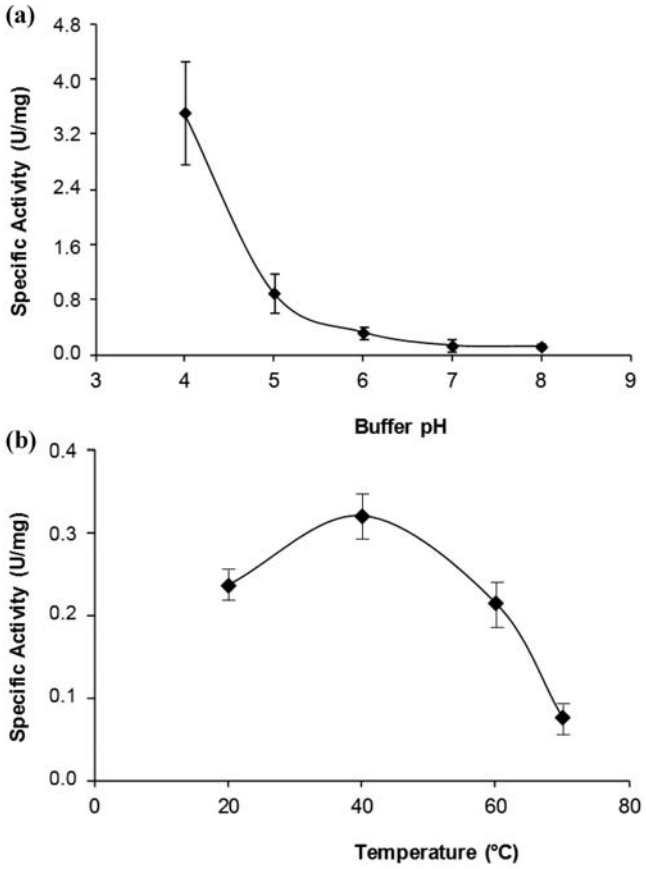


**Figure 3.** Myrosinase stability at different pH and temperature: (a) myrosinase stability between pH 4.0 and 8.0 at 40 °C and (b) myrosinase stability between 20 and 70 °C at pH 6.0.

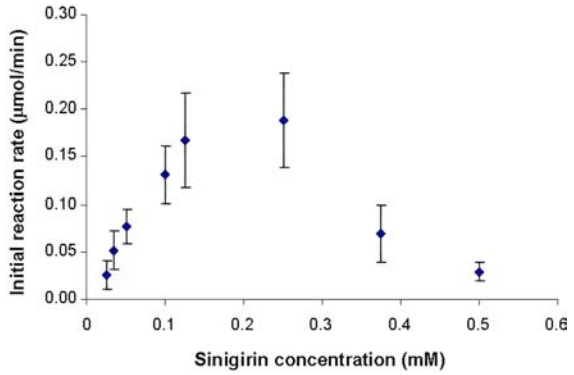


**Figure 4.** Initial reaction rate of myrosinase at different initial sinigrin concentrations.

broccoli blanching on sulforaphane synthesis. The authors suggest that a decrease in myrosinase activity at temperatures above 57 °C may be explained by substrate inhibition, owing to the higher release of glucosinolates from the vegetal matrix. The behavior of broccoli myrosinase differs from that exhibited by horseradish and *Raphanus sativus* myrosinases, which showed no substrate inhibition.[13,15]

The kinetic parameters $V_{mas}$, $K_m$, and $K_I$ were estimated from the Michaelis–Menten model with substrate inhibition (eq 1). Here, $V$ is the initial reaction rate, and $[S]$ is the substrate concentration. The maximum activity predicted by the model occurred at 0.18 mM sinigrin $[S_{max}]$. Myrosinase from *R. sativus* has a $K_m$ value of 2.06 $\mu$mol min$^{-1}$ mg$^{-1}$ and a $V_{max}$ equal to 23 $\mu$M,[13] whereas the kinetic parameters reported for horseradish myrosinase were 0.128 mM and 0.624 $\mu$mol min$^{-1}$, respectively.[15] Despite these authors not considering substrate inhibition, our values are of the same order of magnitude.

$$V = \frac{0.246[S]}{0.086 + [S] + \frac{[S]^2}{0.368}} \quad (1)$$

In summary, broccoli myrosinase was successfully purified by means of a rationally designed process that consists of ammonium sulfate precipitation, followed by concanavalin A affinity chromatography. The process resulted in an 88% recovery and a 1318-fold purification, the highest values reported for the purification of any myrosinase. The subunits of broccoli myrosinase have a molecular weight of 50–55 kDa, and the native structure is composed of three subunits. The maximum myrosinase activity was achieved at pH 4.0 and 40 °C. Broccoli myrosinase is subjected to substrate inhibition, with kinetic parameters that coincide in order of magnitude with those reported for other myrosinases.

## AUTHOR INFORMATION

### Corresponding Author

*Telephone: 56-2-27181833. Fax: 56-2-27181800. E-mail: andrea.mahn@usach.cl.

### Funding

This work was funded by Fondecyt Grant 1130384.

### Notes

The authors declare no competing financial interest.

## REFERENCES

(1) James, D. C.; Rossiter, J. T. Development and characteristics of myrosinase in *Brassica napus* during early seedling growth. *Physiol. Plant.* **1992**, *82*, 163–170.

(2) Bellostas, N.; Petersen, I. L.; Sørensen, J. C.; Sørensen, H. A fast and gentle method for the isolation of myrosinase complexes from brassicaceous seeds. *J. Biochem. Biophys. Methods* **2008**, *70*, 918–925.

(3) Bernardi, R.; Finiguerra, M. G.; Rossi, A. A.; Palmieri, S. Isolation and biochemical characterization of a basic myrosinase from ripe *Crambe abyssinica* seeds, highly specific for *epi*-progoitrin. *J. Agric. Food Chem.* **2003**, *51*, 2737–2744.

(4) Sivakumar, G.; Aliboni, A.; Bacchetta, L. HPLC screening of anticancer sulforaphane from important European *Brassica* species. *Food Chem.* **2007**, *104*, 1761–1764.

(5) Quazi, A.; Pal, J.; Maitah, M.; Fulciniti, M.; Pelluru, D.; Nanjappa, P.; Lee, S.; Batchu, R.; Prasad, M.; Bryant, C.; Rajput, S.; Gryaznov, S.; Beer, D.; Weaver, D.; Munshi, N.; Goyal, R.; Shammas, M. Anticancer activity of a broccoli derivative, sulforaphane, in Barrett adenocarcinoma: Potential use in chemoprevention and as adjuvant in chemotherapy. *Transl. Oncol.* **2010**, *3*, 389–399.

(6) Devi, J. R.; Thangam, E. B. Mechanisms of anticancer activity of sulforaphane from *Brassica oleracea* in HEp-2 human epithelial carcinoma cell line. *Asian Pac. J. Cancer Prev.* **2012**, *13*, 2095–2100.

(7) Vyas, A. R.; Singh, S. V. Functional relevance of D,L-sulforaphane-mediated induction of vimentin and plasminogen activator inhibitor-1 in human prostate cancer cells. *Eur. J. Nutr.* **2014**, *53*, 843–852.

(8) Fahey, J. W.; Wehage, S. L.; Holtzclaw, W. D.; Kensler, T. W.; Egner, P. A.; Shapiro, T. A.; Talalay, P. Protection of humans by plant glucosinolates: Efficiency of conversion of glucosinolates to isothiocyanates by the gastrointestinal microflora. *Cancer Prev. Res.* **2012**, *5*, 603–611.

(9) Ghawi, S. K.; Methven, L.; Niranjan, K. The potential to intensify sulforaphane formation in cooked broccoli (*Brassica oleracea* var.

*italica*) using mustard seeds (*Sinapis alba*). *Food Chem.* **2013**, *138*, 1734−1741.
(10) Yen, G.; Wei, Q. Myrosinase activity and total glucosinolate content of cruciferous vegetables, and some properties of cabbage myrosinase in Taiwan. *J. Sci. Food Agric.* **1993**, *61*, 471−475.
(11) Ludikhuyze, L.; Rodrigo, L.; Hendrickx, M. The activity of myrosinase from broccoli (*Brassica oleracea* L. cv. *italica*): Influence of intrinsic and extrinsic factors. *J. Food Prot.* **2000**, *63*, 400−403.
(12) Ludikhuyze, L.; Ooms, V.; Weemaes, C.; Hendrickx, M. Kinetic study of the irreversible thermal and pressure inactivation of myrosinase from broccoli (*Brassica oleracea* L. cv. *italica*). *J. Agric. Food Chem.* **1999**, *47*, 1794−1800.
(13) Shikita, M.; Fahey, J. W.; Golden, T. R.; Holtzclaw, W. D.; Talalay, P. An unusual case of "uncompetitive activation" by ascorbic acid: Purification and kinetic properties of a myrosinase from *Raphanus sativus* seedlings. *Biochem. J.* **1999**, *341*, 725−732.
(14) Van Eylen, D.; Indrawati; Hendrickx, M.; Van Loey, A. Temperature and pressure stability of mustard seed (*Sinapis alba* L.) myrosinase. *Food Chem.* **2006**, *97*, 263−271.
(15) Li, X.; Kushad, M. M. Purification and characterization of myrosinase from horseradish (*Armoracia rusticana*) roots. *Plant Physiol. Biochem.* **2005**, *43*, 503−511.
(16) Guo, R.; Yuan, G.; Wang, Q. Effect of sucrose and mannitol on the accumulation of health-promoting compounds and the activity of metabolic enzymes in broccoli sprouts. *Sci. Hortic.* **2011**, *128*, 159−165.
(17) Bollag, D. M.; Rozycki, M. D.; Edelstein, S. J. *Protein Methods*, 2nd ed.; Wiley-Liss, Inc.: New York, 1996.
(18) Rakariyatham, N.; Butr-Indr, B.; Niamsup, H.; Shank, L. Improvement of myrosinase activity of *Aspergillus* sp. NR4617 by chemical mutagenesis. *Electron. J. Biotechnol.* **2006**, *9*, 379−385.
(19) Sepulveda, I.; Barrientos, H.; Moenne, A.; Mahn, A. Changes in SMSeC, glucosinolates and sulforaphane levels, and in proteome profile in Broccoli (*Brassica oleracea* var. *italica*) fertilized with sodium selenate. *Molecules* **2013**, *18*, 5221−5234.
(20) Downs, G. R.; Almira, E. A $\beta$-galactosidase (GeneBank X84684) cDNA homolog from broccoli (*Brassica oleraccea* L.). *Plant Physiol.* **1995**, *108*, 1342.
(21) Alcantara, P. H. N.; Martima, L.; Silva, C. O.; Dietrich, S. M. C.; Buckeridge, M. S. Purification of a $\beta$-galactosidase from cotyledons of *Hymenaea courbaril* L. (Leguminosae). Enzyme properties and biological function. *Plant Physiol. Biochem.* **2006**, *44*, 619−627.
(22) Balasubramaniam, S.; Lee, H. C.; Lazan, H.; Othman, R.; Ali, Z. M. Purification and properties of a $\beta$-galactosidase from carambola fruit with significant activity towards cell wall polysaccharides. *Phytochemistry* **2005**, *66*, 153−163.
(23) Song, C.; Liu, G.; Xu, J.; Chi, Z. Purification and characterization of extracellular $\beta$-galactosidase from the psychrotolerant yeast *Guehomyces pullulans* 17-1 isolated from sea sediment in Antarctica. *Proc. Biochem.* **2010**, *45*, 954−960.
(24) Matusheski, N. V.; Juvik, J. A.; Jeffery, E. H. Heating decreases epithiospecifier protein activity and increases sulforaphane formation in broccoli. *Phytochemistry* **2004**, *65*, 1273−1281.
(25) Pérez, C.; Barrientos, H.; Roman, J.; Mahn, A. Optimization of a blanching step to maximize sulforaphane synthesis in broccoli florets. *Food Chem.* **2014**, *145*, 264−271.

using a DNA laddering assay, flow cytometric analysis, and Western blotting. To investigate the global influences within melanoma cells caused by GA induction, two-dimensional gel electrophoresis (2-DE) was used to monitor comprehensive protein expression comparatively from B16F10 melanoma cells with and without GA treatment. Using this method, quantitative analysis of protein expression profiling on a large scale can be achieved by intensity comparison of protein spots stained by silver or Coomassie blue on the gels of control and experimental samples. Differentially displayed proteins can be further hydrolyzed using in-gel digestion, and the protein identities can be identified using tandem mass spectrometry (MS/MS) and database matching. In this study, the regulated proteins from B16F10 melanoma cells under GA stimulation were uncovered, and their relative expressions were validated by Western blotting. The functions of the differentially displayed proteins were further correlated for exploring a more comprehensive mechanism underlying GA-mediated biological action.

## MATERIALS AND METHODS

**Materials.** Protease inhibitor cocktail, Dulbecco's modified Eagle medium (DMEM), and 3-(4,5-dimethylthiazol-2-yl)-2,5-diphenyltetrazolium bromide (MTT) were purchased from Sigma-Aldrich Corp. (St. Louis, MO, USA). Fetal bovine serum (FBS) was from Gibco (Carlsbad, CA, USA). Cell extraction buffer was obtained from BioSource International (Camarillo, CA, USA). The immobilized pH gradient (IPG) strips and sampling buffer were from GE Healthcare (Buckinghamshire, UK). Gallic acid (GA), iodoacetamide (IAA), dimethyl sulfoxide (DMSO), sodium dodecyl sulfate (SDS), trichloroacetic acid (TCA), propidium iodide (PI), RNase A, Triton X-100, cyclosporine A (CyA), and trifluoperazine (TFZ) (mitochondrial permeability transition inhibitors) were obtained from Sigma. Formic acid (FA), acetone, acetonitrile (ACN), ammonium bicarbonate (ABC), and 1,4-dithiothreitol (DTT) were obtained from J. T. Baker (Phillipsburg, NJ, USA). Trypsin used in in-gel digestion was purchased from Promega (Madison, WI, USA). Rabbit anti-mouse TCP1, PRDX-1, Rho-GDI, G-3-P DHase, SOD, aldolase, HSP 60, HSC 71, VDAC-1, ATPase, enolase, and glucokinase antibodies were purchased from ProteinTech Group (Chicago, IL, USA). Antibodies for apoptosis-related proteins such as cleaved caspase-8, cleaved caspase-9, cleaved caspase-3, PARP-1, Bad, AIF, Bax, cytochrome *c*, Mcl-1, Bcl-xL, and Bcl-2 were obtained from Cell Signaling Technology (Danvers, MA, USA). Rabbit anti-mouse $\beta$-actin antibodies (used to recognize $\beta$-actin as the internal control) were obtained from Sigma. Horseradish peroxidase conjugated IgG (goat anti-rabbit) was purchased from Millipore (Bellerica, MA, USA). Chemiluminescent HRP substrate and polyvinylidene difluoride (PVDF) membranes were obtained from Pierce (Rockford, IL, USA). The water used in this study was produced using a Milli-Q (Millipore) water purification system.

**Cell Culture.** The mouse melanoma cell line (B16F10) was obtained from the Food Industry Research and Development Institute (Hsinchu, Taiwan). The cells were cultured in 75 $cm^2$ flasks at approximately $1 \times 10^6$ cells/mL cell density with 90% MEM, 10% FBS, penicillin/streptomycin (100 $\mu$g/mL streptomycin and 100 U/mL penicillin), and 2 mM L-glutamine, and the cells were incubated at 37 °C in 100% humidity, 5% $CO_2$−95% air.

**Viability Assay.** B16F10 cells ($2 \times 10^5$ cells/well) were placed onto 12-well plates and incubated at 37 °C for 24 h prior to be treated with GA at different concentrations (0, 50, 100, 200, and 400 $\mu$M) for various time periods (0, 6, 12, and 24 h). Cell viabilities under different conditions were determined using the MTT assay. A control was carried out using DMSO (0.5%); 0.5% of DMSO did not show any significant impact on cell viability. After incubation, cells were photographed using contrast phase microscope for the observation of morphological changes of B16F10 cells with and without GA stimulation.

**Cell Migration Assay and Wound-Healing Assay.** To validate GA's cytotoxic effect, B16F10 melanoma cells were seeded onto polycarbonate (PC) membranes (8.0 $\mu$m, BD Biosciences, San Jose, CA, USA) in the culture inserts. Then these inserts were transferred into wells with DMEM containing 10% FBS. B16F10 cells with or without GA treatment were incubated for 24 h. After removal of cells on the upper site, migrated cells on the lower site were fixed by 100% methanol and stained using Giemsa (Merck, Darmstadt, Germany). The migrated cells were photographed and counted at 100× magnification under microscope. GA's cytotoxic effect was also examined using the wound-healing assay. B16F10 cells were seeded in 6-well plates to allow the cells to grow to conflux. A pipet tip was used to create an artificial scratch/wound in each well. Detached B16F10 cells were removed by washing with PBS. Images of control and treated samples at different concentrations (0, 100, 200, and 400 $\mu$M of GA) were acquired at 0, 6, 12, and 24 h after the treatments.

**Analysis of DNA Fragmentation by Agarose Gel Electrophoresis.** B16F10 cells ($2 \times 10^5$ cells/well) were incubated in a medium containing GA with various concentrations (0, 100, 200, and 400 $\mu$M) for 24 h. The cells were then washed using cold PBS buffer and kept in a lysis buffer containing 10 mM EDTA, 50 mM Tris-HCl (pH at pH 8.0), 0.5 g/L proteinase K, and 0.25% NP-40 at 50 °C for 2 h. The precipitated DNA was collected using ethanol at 25 °C. The resulting DNA pellets were washed with 70% ice-cold ethanol and then dissolved in TE buffer (0.6 g/mL RNase A and 1 mM EDTA in 10 mM Tris-HCl at pH 8.0), and the DNA mixture was further incubated at 37 °C for 1 h. The DNA separation was performed using horizontal electrophoresis at 200 V on a 1.5% agarose gel using tris/acetic acid/EDTA (TAE) as the running buffer. Finally, the DNA gel was stained with ethidium bromide (EtBr) and visualized under a 2 UV transilluminator (MacroVue UV-20 Hoefer).

**Analysis of Cell Cycle Distribution and Apoptosis.** B16F10 cells were treated with DMSO (0.5%) or with various concentrations (0, 100, 200, and 400 $\mu$M) of GA for 24 h. After treatment, the cells were collected and the reagents were removed by washing with PBS twice. Then the cells were fixed in 70% ethanol overnight. The phase distribution of cell DNA content was determined using PI (Sigma) staining. The cells were precipitated using centrifugation at 700 rpm for 5 min at 4 °C, and the resulting cell pellet was stained with 10 $\mu$g/mL of PI (in PBS buffer containing 10 $\mu$g/mL of RNase A) for 15 min at room temperature in the dark. The apoptotic cells induced by GA were observed using annexin V staining. B16F10 cells at a density of $1 \times 10^6$ cells per 100 mm Petri dish were treated with DMSO (0.5%) or GA at various concentrations (0, 100, 200, and 400 $\mu$M) for 24 h and subsequently labeled with 10 $\mu$g/mL of annexin V−FITC individually. The analysis of cell cycle distribution and apoptosis of GA-treated B16F10 cells were performed using FACScan flow cytometer (Becton-Dickinson, Mansfield, MA, USA) coupled with Cell-Quest software (Becton-Dickinson).

**Protein Extraction and Quantification.** B16F10 cells were treated with solvent vehicle (0.5% DMSO) or indicated concentrations of GA for 24 h, and then the cells were lysed using cell extraction buffer (BioSource International), and protease inhibitor cocktail (Sigma) was added to avoid protein degradation. The protein precipitation from supernatant was carried out using 10% TCA/acetone solution containing 20 mM DTT overnight (−20 °C). The protein pellet was collected, and the supernatant was discarded after centrifugation at 8000 rpm for 30 min at 4 °C. The resulting pellet was dissolved in a rehydration buffer that contained 6 M urea, 2 M thiourea, 0.5% CHAPS, 0.002% bromophenol blue, 20 mM DTT, and 0.5% IPG buffer. The quantification of protein content was performed using a 2-D Quant Kit (GE Healthcare). Here, the calibration curve was established using bovine serum albumin (BSA).

**Two-Dimensional Gel Electrophoresis.** Two-dimensional gel electrophoresis procedure was carried out according to a previous study.[19] The isoelectric focusing (IEF) was performed on GE Healthcare Ettan IPGphor 3 at 20 °C with a current limit of 30 A. Protein mixture was dissolved in a rehydration buffer and applied on

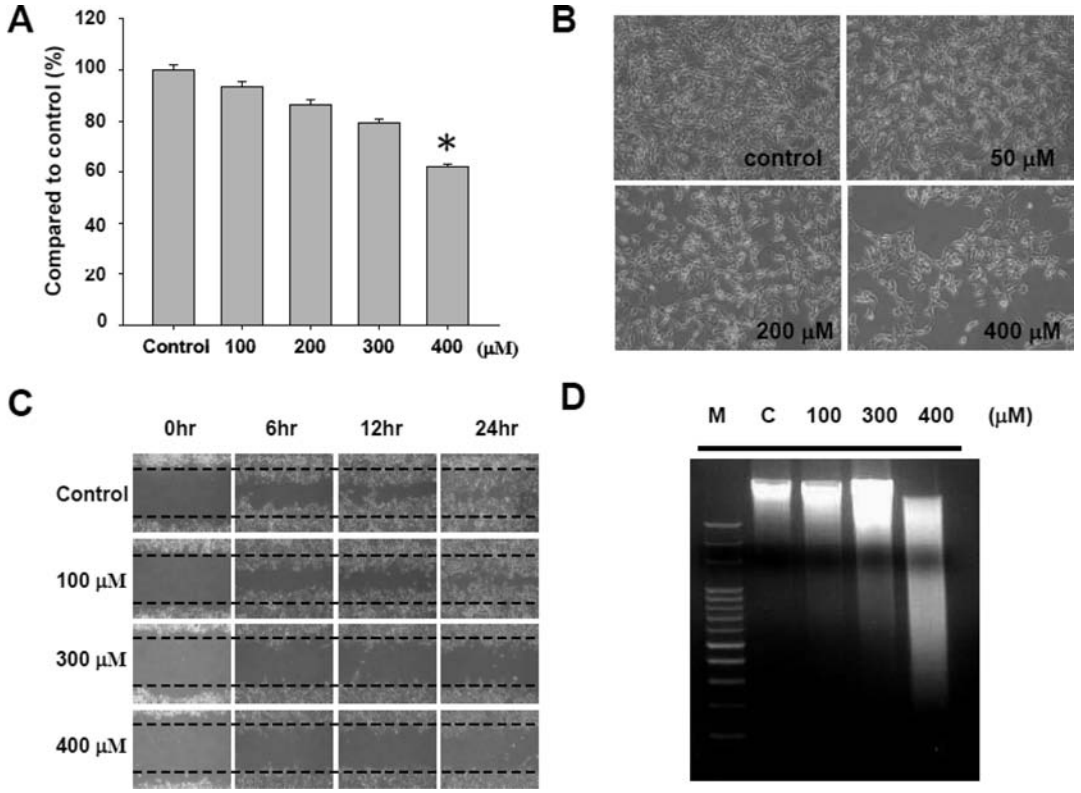


**Figure 1.** Evaluation of cytotoxicity and antimigratory effects of GA at different concentrations on B16F10 cells: (A) MTT assay for B16F10 cells treated with GA at 50−400 $\mu$M for 24 h (data are presented as the mean ± SEM from three independent experiments); (B) population and morphological changes of B16F10 cells treated with GA at different concentrations for 24 h; (C) wound-healing assay at different concentrations and time periods; (D) DNA laddering assay of B16F10 cells treated with GA at different concentrations (M, markers).

an IPG strip. An 11 cm IPG strip (p*I* 3−10) was rehydrated at 30 V for 12 h, and then proteins with different p*I* values were separated and focused using different stages of applied voltages according to the program 200 V (0−2 h), 500 V (2−4 h), 1000 V (4−6 h), 4000 V (6−7 h), 8000 V (7−11 h), until the total voltage (V) × hour (h) reached 39400. The equilibrated strip was placed on the top of a SDS-PAGE gel (12.5%), sealed with 0.5% agarose, and then the gel electrophoresis was performed under SE 600 Ruby (Hoefer, Holliston, MA, USA) at 150 V for 6.5 h. After that, the 2-DE gel was stained by silver, and the resulting silver-stained gel was scanned and analyzed using PDQuest image analysis software (Bio-Rad). 2-DE images were obtained from triplicates for each sample and normalized prior to statistical analysis. Protein spots (the same p*I* and $M_w$) in experimental and control samples showing more than 1.5-fold intensity difference were regarded as statistically significant.

**In-Gel Digestion.** A protein spot of interest was excised, cut into pieces, and immersed in 100 $\mu$L of 25 mM ammonium bicarbonate (ABC) (pH 8.5) containing 50 mM DTT at 37 °C for 1 h. After removal of supernatant, the gel pieces were resuspended in 100 $\mu$L of 100 mM iodoacetamide (IAA) in 25 mM ABC (pH 8.5) and then shaken for 30 min at room temperature in the dark. After removal of supernatant, the gel pieces were soaked in 100 $\mu$L of 50% acetonitrile in 25 mM ABC (pH 8.5) for 30 min, and then the buffer was completely removed by vacuum. The gel pieces were rehydrated and soaked in 100 $\mu$L of 25 mM ABC (pH 8.5) containing 0.1 $\mu$g of trypsin. The trypsin digestion was performed at 37 °C for 16 h. The reaction was quenched using 5 $\mu$L of 5% formic acid, and the resulting peptide mixture was obtained after removal of buffer.

**LC-MS/MS Analysis and Database Search.** The peptide mixture obtained from in-gel digestion was separated by a reversed phase C18 column (PepMap100 C18, 150 mm length, 2.1 mm i.d., 2.6 $\mu$m particle size) on a nano LC (Agilent 1200) system with a gradient from 5 to 70% acetonitrile containing 0.1% formic acid over 90 min at 300 nL/min. The separated peptides were online analyzed using an AB SCIEX QTRAP 5500 Q mass spectrometer (Applied Biosystems, Foster City CA, USA). The LC-MS/MS was performed under a positive survey scan in the range of $m/z$ 100−1000. The raw data were processed into WIFF format with Analyst 1.5.1. The database-assisted protein identification was carried out using Mascot search engine v2.3 (Matrix Science, UK) with the following search parameters: (1) protein database, Swiss-Prot; (2) taxonomy, *Mus musculus* (house mouse); (3) allowed trypsin missed cleavage, 1; (4) precursor and product ion mass tolerance, 2 Da/1 Da; (5) fixed modification, carbamidomethyl (C); (6) variable modifications, oxidation (M); (7) significance threshold, $p < 0.05$. Proteins with scores higher than the threshold were regarded as significant hits.

**Western Blotting Analysis.** GA-treated samples and controls were separated on SDS-PAGE gels, and the separated proteins on gels were transferred to PVDF membranes (Millipore) for 1.5 h at a fixed current of 400 mA under Transphor TE 62 (Hoefer). The membranes were then incubated with mouse antibodies of caspase-3/cleaved caspase-3, caspase-9/cleaved caspase-9, cleaved poly-ADP ribose polymerase (PARP), cytochrome *c*, AIF, Bcl-2, Bcl-xL, Mcl-1, Bax, p-Bad, Bad, TCP1, PRDX-1, Rho-GDI, G-3-P DHase, SOD, aldolase, HSP 60, HSC 71, VDAC-1, ATPase, $\alpha$-enolase, glucokinase, and $\beta$-actin at 4 °C for 2 h or overnight. The membranes were washed three times using PBST (10 mM $NaH_2PO_4$, 130 mM NaCl, 0.05% Tween 20), and then the primary antibodies were recognized and probed with the secondary antibodies (goat anti-rabbit) conjugated with horseradish peroxidase in blocking solution (1:5000) for 1 h. After removal of the excess secondary antibodies and blocking solution, the membranes were washed with PBST three times. The chemiluminescence on the blot was visualized through the redox reaction between horseradish peroxidase and substrate (ECL Western blotting reagent, Pierce).

**Statistical Analysis.** Experiments were done in triplicate or quaduplicate, and data of MTT assay, cell migration assay, and flow cytometric analysis were expressed as the mean ± SE. For the

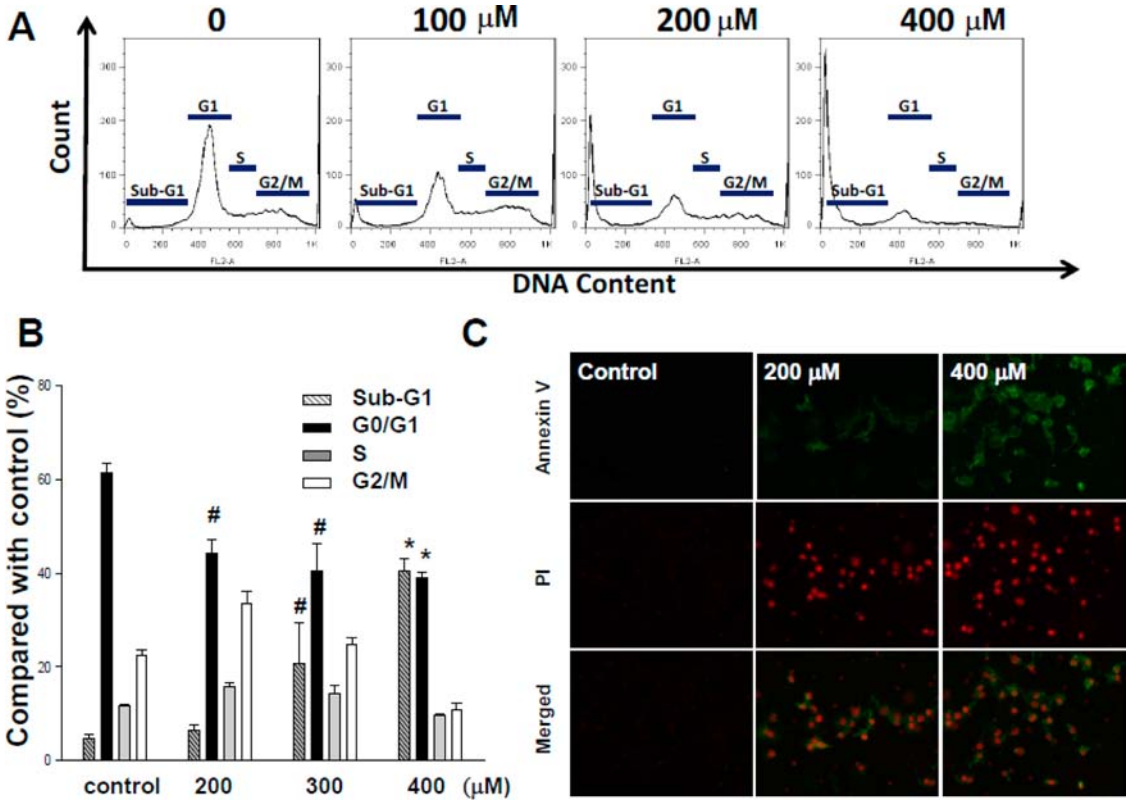


**Figure 2.** Cell cycle distribution and apoptosis: (A) flow cytometric measurement of cell cycle distribution of B16F10 cells treated with GA at different concentrations; (B) quantitative data obtained according to the DNA content measurement in panel A; (C) annexin V-FITC/PI analysis of B16F10 cells treated with GA at different concentrations.

determination of significant differences ($p \leq 0.05$) between experimental groups, one-way ANOVA followed by the Tukey–Kramer test, which was carried out on GraphPad InStat 3 (San Diego, CA, USA), was used in this study.

## RESULTS AND DISCUSSION

**Antitumor Effects of GA on B16F10 Cells.** B16F10 cells were treated with GA of various concentrations (0, 50, 100, 200, 400 $\mu$M) for 24 h. The MTT assay showed that significant cell death occurred (around 40%) when 400 $\mu$M GA was added (Figure 1A). The morphological change and reduced population of GA-treated cells observed by inverted light microscopy also displayed a similar trend (Figure 1B), which indicated that GA at a concentration of 400 $\mu$M can inhibit the proliferation of B16F10 cells. This result was similar to that reported by Locatelli et al.[15] The migratory capability of cells was measured by cell migration and wound-healing assay. After treatment with GA of various concentrations (50, 200, and 400 $\mu$M) in different time periods (6, 12, and 24 h), suppression of B16F10 cell migration was observed, and the migration suppression was also dose-dependent (Figure 1C and Supporting Information Figure S1). To study whether cell death was caused by apoptosis or not, the cells were treated with 0, 100, 200, and 400 $\mu$M GA for 24 h. After incubation, the cellular DNA was extracted and analyzed using agarose gel electrophoresis. As shown in Figure 1D, 400 $\mu$M GA induced the chromatin breakdown and the degraded DNA fragments resulting in ladder-like gel patterns, which indicated that cell death occurred via apoptosis instead of necrosis. According to a previous study, the cytotoxicities of GA and its derivatives toward other cell lines were mainly proposed to be involved in apoptosis-mediated cell death. Some phenomena such as mitochondrial dysfunction, intracellular $Ca^{2+}$ level increase, and DNA fragmentation were associated with this GA-induced apoptosis.[20,21] In fact, the effect of GA and its alkyl esters varies toward different tumor cell lines and results in cell-specific behavior. For example, the apoptotic DNA ladder fragmentation can be observed when mouse B cell lymphoma WEHI 231 cell line is stimulated by GA; however, in the case of GA-treated fibroblast L929 cells, some morphological changes such as cell shrinkage, chromatin condensation, and apoptotic body formation can be simultaneously observed, whereas the DNA fragmentation characteristic does not occur.[20] In this study, GA induced the breakdown of chromatin, resulting in apparent DNA fragmentation in B16F10 cells.

**GA-Induced Apoptosis of B16 Cells.** To investigate the effect of GA on cell cycle, B16F10 cells pretreated with GA at various concentrations (0, 100, 200, and 400 $\mu$M) were analyzed using annexin V–FITC and PI staining on flow cytometry (Becton-Dickinson). Apparently, B16F10 cells at sub-G1 phase were increased dose-dependently, which indicated that the accumulation of small DNA fragments was caused by apoptosis. The percentage of 400 $\mu$M GA-treated B16F10 cells at sub-G1 was enhanced to 41% while the control was only 6% (Figure 2A,B). The GA-induced apoptosis of B16F10 cells was further determined using the flow cytometer based-annexin V staining. Under fluorescent microscopy, the formation of apoptotic bodies indicated that GA concentrations of 200 and 400 $\mu$M dose-dependently increased the percentage of apoptotic cells (Figure 2C). These results all indicated that the cytotoxic effect of GA against B16F10 cells was due to its apparent apoptosis induction. According to the hypothesis

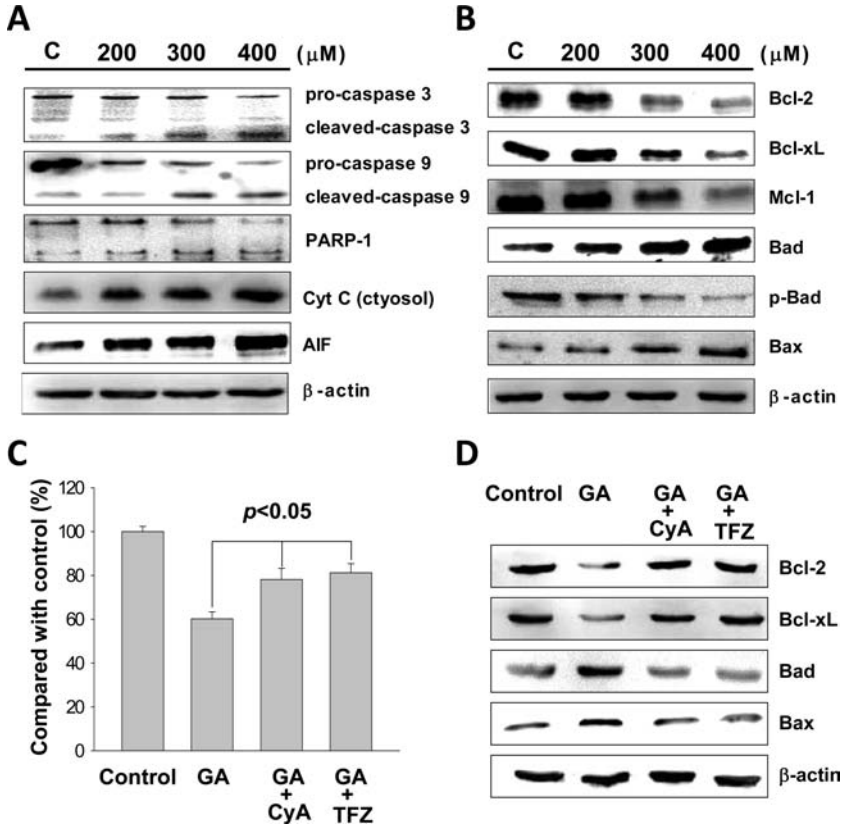


**Figure 3.** Expressions of apoptosis-related proteins in GA-treated B16F10 cells: (A) Western blotting analysis of caspase-3/cleaved caspase-3, caspase-9/cleaved caspase-9, cleaved-poly-ADP ribose polymerase (PARP), cytochrome *c* (cytosolic), and apoptosis-inducing factor (AIF) in B16F10 cells treated with GA at different concentrations; (B) Western blotting analysis of Bcl-2, Bcl-xL, induced myeloid leukemia cell differentiation protein (MCl-1), Bax, p-Bad, and Bad in B16F10 cells treated with GA at different concentrations; (C) cell viabilities (%, compared with the control) of GA (400 $\mu$M)-induced cell apoptosis with and without the mitochondrial permeability transition inhibitors cyclosporine A (CyA) or trifluoperazine (TFZ); (D) expression levels of Bcl2, Bcl-xl, Bax, and Bad proteins in the GA (400 $\mu$M)-induced B16F10 cells with and without mitochondrial permeability transition inhibitors. $\beta$-Actin was used as the internal control.

proposed by Serrano et al., GA can induce apoptosis not only because it can promote the generation of reactive oxygen species (ROS) but also as a consequence of its inhibitory activity toward protein tyrosine kinases (PTKs).[21] In the study of anticancer effects of GA on A549 human lung adenocarcinoma cells, Maurya et al. presented that GA treatment simultaneously decreased mitochondrial membrane potential and increased intracellular ROS, and the caspase activity measurement further showed the activation of caspase-3 but not caspase-8, indicating the involvement of intrinsic cell apoptosis.[10] Ou et al. presented that GA can induce G2/M phase cell cycle arrest in human bladder transitional carcinoma cells through regulating 14-3-3$\beta$ release from activation of Cdc25C and Chk2.[22] In normal human lymphocytes, however, GA shows anti-apoptotic ability via Bcl-2 independent mechanism.[23] Therefore, the detailed mechanism of apoptosis induction by GA in different tumor cells so far is not well-defined.

**Western Blot of Apoptosis Related Proteins.** To determine the mechanism for GA-induced apoptosis, we further analyzed the expression levels of several apoptotic markers including cytosolic cytochrome *c*, caspase-3, caspase-9, cleaved PARP, and apoptosis-inducing factor (AIF) from GA-treated B16F10 cells. Western blot showed dose-dependent down-regulations of pro-caspase-9 and pro-caspase-3. Expression of caspase-3 (17 kDa proteolytic fragments) was elevated when the concentration of GA increased to 200 $\mu$M or higher. Similarly, the increase of cleaved form of caspase-9 was also found at 37 kDa after GA treatment; the enhancement of cytosolic cytochrome *c* released from mitochondria, which activated caspase-dependent cell death, was simultaneously observed. Interestingly, the decrease of PARP-1 (116 kDa) was accompanied by dose-dependent increases of cleaved PARP-1 (89 kDa) and AIF after GA treatment (Figure 3A). This implied that the PARP-1 activation propagated to mitochondria, triggered the AIF translocation from mitochondria to the nucleus, and induced chromatin condensation and DNA fragmentation. The overexpression of AIF in the nucleus suggested that GA-induced apoptosis was also through a caspase-independent apoptosis. Unlike other cancer cell lines in which the GA-induced apoptosis was reported to be occurred solely via a caspase-dependent pathway, GA-induced apoptosis involved in B16F10 cells was simultaneously through caspase-dependent and -independent pathways, which is consistent with the phenomenon occurring in the other melanoma cell, A375.S2.[14] To further verify this conclusion, the expression levels of some mitochondrial cell death effectors such as pro-apoptotic B-cell lymphoma-2 (Bcl-2) family members Bax, Bak, and Bad were simultaneously evaluated with the increase of GA concentration. Meanwhile, the expression of anti-apoptotic Bcl-2, Bcl-xL, Mcl-1, and p-Bad was simultaneously suppressed (Figure 3B). The combined effects promoted the mitochondrial outer membrane permeablization and the release of cytochrome *c* from mitochondria into the cytosol and led to the

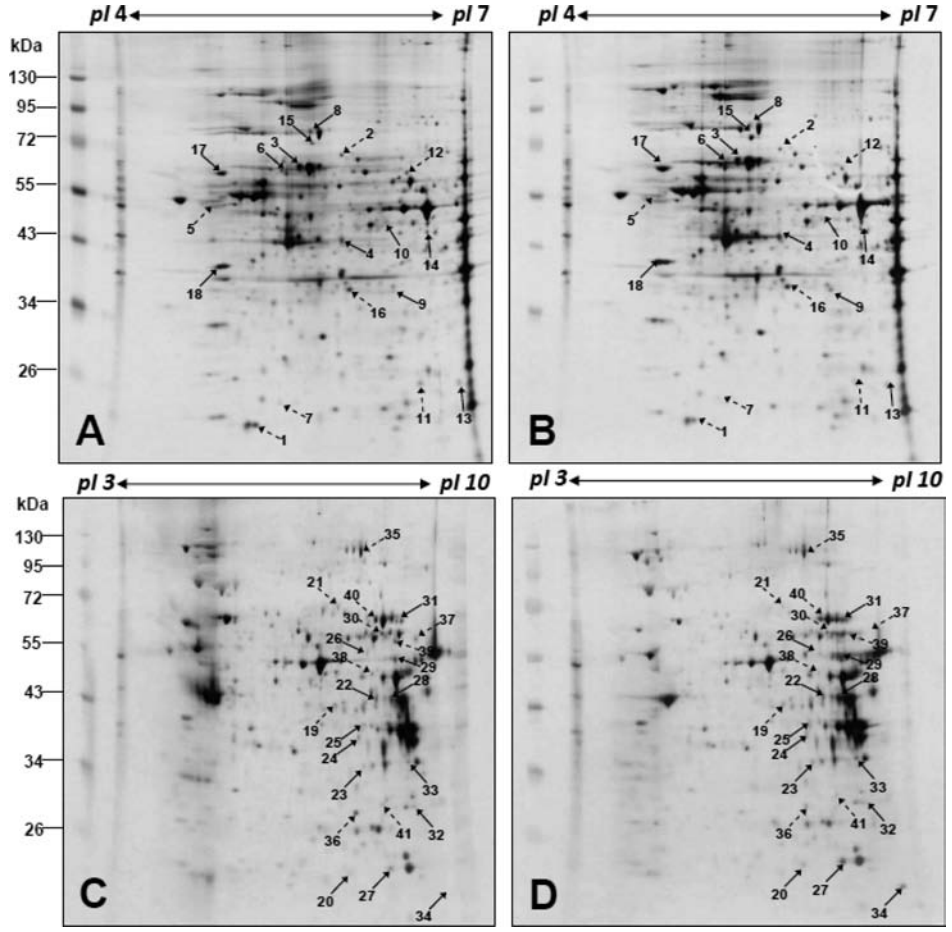


**Figure 4.** 2-DE maps of B16F10 cells treated with 400 $\mu$M GA and the control sample processed in different p*I* ranges: (A) control and (B) treated with 400 $\mu$M GA for 24 h in a range of p*I* 4−7; (C) control and (D) treated samples in p*I* 3−10. Protein spots marked on the maps were considered differentially expressed and identified by LC-MS/MS. The results are representative of three independent runs. Solid arrows denote up-regulated proteins, and dashed ones denote down-regulated proteins.

subsequent activation of caspase-3 and the executioner caspases. The data all indicated that GA induced B16F10 cell apoptosis via a mitochondrial intrinsic pathway. To further confirm that GA-induced cell apoptosis is through a mitochondria-related apoptotic pathway, B16F10 cells were pretreated with either cyclosporine A (CyA) or trifluoperazine (TFZ) (both are mitochondrial permeability transition inhibitors) prior to the GA treatment. The results showed that GA-induced cell apoptosis was significantly decreased when CyA or TFZ was added (Figure 3C). In addition, several mitochondrial-related apoptotic proteins, including Bcl2, Bcl-xl, Bax, and Bad proteins, were estimated by Western blotting, respectively. The expressions of Bcl2 and Bcl-xl were promoted when the cells were pretreated with CyA and TFZ. By contrast, the expression levels of Bax and Bad were decreased in the GA-treated cells when the cells were pretreated with CyA and TFZ (Figure 3D). Taken together, these results suggested that mitochondria dysfunction-mediated apoptotic pathway was involved in GA-induced cell apoptosis. To further uncover the pathway networks associated with this apoptosis, a comprehensive proteome study was used to globally analyze proteins regulated in GA-induced B16F10 cells.

**Proteomic Analysis of B16F10 Cells with GA Stimulation.** Protein spots from samples with and without 400 $\mu$M GA treatment were visualized by silver staining on 2-DE gels, as shown in Figure 4A,B with p*I* 4−7 and Figure 4C,D with p*I* 3−10. The quantitative analysis of protein spots in 2-DE maps between the GA-treated and the control samples was achieved using PDQuest image analysis software (Bio-Rad). Proteins with >1.5-fold spot intensity difference between the experimental and the control samples were defined as differentially expressed proteins. The differentially expressed proteins were hydrolyzed using in-gel trypsin digestion followed by LC-MS/MS analysis. The database-assisted protein identification was achieved using the MASCOT protein identification search engine. A total of 41 differentially expressed proteins were quantified and identified. Using a 1.5-fold intensity difference compared to control as threshold, 25 spots were overexpressed and 16 spots were underexpressed. The identified proteins with their MASCOT scores, identified peptide sequences, calculated $M_w$, p*I*, coverages, and folds of change in expression level (up-regulation or down-regulation) are shown in Table 1. Some up-regulated proteins such as 60 kDa heat shock protein (HSP60), heat shock cognate 71 kDa protein (HSC 71), nucleophosmin (NPM), peroxiredoxin-1 (PRDX-1), succinyl-CoA ligase (SCS-$\beta$G), poly(rC)-binding protein 1 (PCBP1), superoxide dismutase (SOD), voltage-dependent anion-selective channel protein 1 (VDAC-1), and voltage-dependent anion-selective channel protein 2 (VDAC-2) have been reported to be associated with apoptosis.[24−27] Among these up-regulated proteins, HSP60 acts as a chaperone protein to maintain proper folding and assembling of polypeptide chains in

**Table 1. Regulated Proteins Identified Using 2-DE-Based Comparative Proteomics**

| spot no. | protein name (short name) | accession no. | calcd $M_w$/p$I$ | peptides matched | sequence covered (%) | MASCOT score | regulation (-fold change)[a] |
|---|---|---|---|---|---|---|---|
| 1 | phosphatidylethanolamine-binding protein 1 (PEBP-1) | P70296 | 20.81/5.19 | 9 | 41 | 98 | −1.7 |
| 2 | T-complex protein 1 subunit epsilon (TCP-1) | P80316 | 59.58/5.72 | 10 | 14 | 142 | −2.1 |
| 3 | 60 kDa heat shock protein (HSP60) | P63038 | 60.9/5.91 | 74 | 60 | 1057 | +2.4 |
| 4 | succinyl-CoA ligase (SCS-$\beta$G) | Q9Z2I8 | 46.81/6.58 | 12 | 27 | 219 | +2.1 |
| 5 | vimentin | P20152 | 53.65/5.06 | 13 | 55 | 1888 | −1.9 |
| 6 | 60 kDa heat shock protein (HSP60) | P63038 | 60.9/5.91 | 4 | 5 | 77 | +2.5 |
| 7 | Rho GDP-dissociation inhibitor 1 (Rho-GDI) | Q99PT1 | 23.39/5.12 | 16 | 45 | 288 | −2.2 |
| 8 | heat shock cognate 71 kDa protein (HSC 71) | P63017 | 70.82/5.37 | 41 | 37 | 445 | +3.1 |
| 9 | inorganic pyrophosphatase 2 (PPase 2) | Q91VM9 | 38.09/6.51 | 4 | 15 | 51 | +2.4 |
| 10 | mannose-6-phosphate (perilipin-3) | Q9DBG5 | 47.2/5.45 | 36 | 21 | 358 | +2.3 |
| 11 | peroxiredoxin-6 (PRDX-6) | O08709 | 24.8/5.71 | 19 | 58 | 281 | −2.1 |
| 12 | glucose-6-phosphate 1-dehydrogenase (G6PD) | Q00612 | 59.0/6.07 | 33 | 38 | 502 | +2.2 |
| 13 | proteasome subunit $\alpha$ type 2 | P49722 | 25.9/8.39 | 4 | 16 | 81 | +2.1 |
| 14 | isovaleryl-CoA dehydrogenase (IVD) | Q9JHI5 | 46.2/8.53 | 17 | 30 | 250 | +2.6 |
| 15 | vacuolar ATP synthase catalytic subunit A | P50516 | 68.2/5.62 | 84 | 50 | 1041 | +2.9 |
| 16 | 60S acidic ribosmal protein P0 | P14869 | 34.1/5.91 | 42 | 42 | 483 | −2.8 |
| 17 | protein disulfide-isomerase precursor (PDI) | P09103 | 57.1/4.79 | 3 | 4 | 36 | −1.8 |
| 18 | nucleophosmin (NPM) | Q61937 | 32.54/4.62 | 5 | 12 | 55 | +2.1 |
| 19 | import inner membrane translocase subunit (Timm50) | Q9D880 | 39.75/8.26 | 13 | 19 | 228 | −2.2 |
| 20 | peroxiredoxin-1 (PRDX-1) | P35700 | 22.16/8.26 | 13 | 40 | 119 | +2.5 |
| 21 | phosphoenolpyruvate carboxykinase (PEPCK-M) | Q8BH04 | 70.48/6.92 | 19 | 25 | 265 | −2.7 |
| 22 | aspartate aminotransferase (transaminase A) | P05201 | 45.2/6.68 | 34 | 43 | 518 | +2.4 |
| 23 | voltage-dependent anion-selective channel protein 2 (VDAC-2) | Q60930 | 31.71/7.44 | 13 | 26 | 271 | +2.1 |
| 24 | poly(rC)-binding protein 1 (PCBP1) | P60335 | 37.47/6.66 | 27 | 31 | 624 | +2.2 |
| 25 | G-3-P dehydrogenase (GAPDH) | P16858 | 35.78/8.44 | 6 | 21 | 70 | +2.4 |
| 26 | $\alpha$-enolase (enolase) | P17182 | 47.1/6.37 | 10 | 21 | 101 | +2.9 |
| 27 | superoxide dismutase (SOD) | P09671 | 24.5/8.8 | 4 | 22 | 66 | +3.2 |
| 28 | fructose-bisphosphate aldolase (aldolase 1) | P05064 | 39.3/8.31 | 17 | 31 | 264 | +2.6 |
| 29 | fumarate hydratase (Fh1) | P97807 | 54.33/9.12 | 40 | 31 | 360 | +3.4 |
| 30 | ATP synthase subunit $\alpha$ (ATPase) | Q03265 | 59.71/9.22 | 48 | 45 | 737 | −2.8 |
| 31 | pyruvate kinase isozyme M2 (PKM) | P52480 | 57.85/7.18 | 11 | 17 | 99 | +2.8 |
| 32 | ChChd3Domain-containing protein (ChChd3) | Q9CRB9 | 26.31/8.56 | 6 | 21 | 117 | +1.7 |
| 33 | voltage-dependent anion-selective channel protein 1 (VDAC-1) | Q60932 | 32.33/8.55 | 41 | 59 | 470 | +2.4 |
| 34 | peptidyl-prolyl cis−trans isomerase B (cyclophilin B, CypB, PPlase B) | | 22.69/9.48 | 33 | 49 | 415 | +3.4 |
| 35 | elongation factor 2 (EF-2) | P58252 | 92.25/6.41 | 30 | 17 | 564 | −1.8 |
| 36 | phosphoglycerate mutase 1 (PGAM-1) | Q9DBJ1 | 28.81/6.67 | 14 | 35 | 164 | −2.4 |
| 37 | ATP synthase subunit $\alpha$ | Q03265 | 59.71/9.22 | 3 | 5 | 52 | −3.4 |
| 38 | 26S protease regulatory subunit 8 (mSUG1) | P62196 | 45.59/7.11 | 14 | 32 | 207 | −2.1 |
| 39 | serine hydroxymethyltransferase (SHMT) | P50431 | 52.55/6.47 | 5 | 4 | 106 | −2.4 |
| 40 | inosine-5′-monophosphate dehydrogenase 2 (IMPD 2) | P24547 | 55.78/6.84 | 32 | 35 | 720 | +1.7 |
| 41 | calcyclin-binding protein (CacyBP) | Q9CXW3 | 26.49/7.63 | 14 | 45 | 200 | −2.1 |

[a]Regulations (-fold changes) of differentially expression proteins are expressed at 24 h of treatment of gallic acid.

mitochondria, and overexpression of HSP60 is regarded as sustaining cellular survival under toxic or stressful conditions;[24] HSC 71 also acts as a chaperone involved in cell proliferation, differentiation, and tumorigenesis. Its increasing level in B16F10 cells after treatment with 400 $\mu$M GA suggested the association with the responses of either apoptosis or cell survival.[25] Similarly, the expressions of some down-regulated proteins such as T-complex protein 1 subunit $\varepsilon$ (TCP-1), vimentin, Rho GDP-dissociation inhibitor 1 (Rho-GDI), peroxiredoxin-6 (PRDX-6), elongation factor 2 (EF-2), and calcyclin-binding protein (CacyBP) are also consistent with those involved in apoptosis reported in the literature.[18,28−31]

The identities and relative expressions of some regulated proteins under GA treatment with various concentrations were further validated by Western blotting (Figure 5). HSP60, HSC 71, VDAC-1, SOD, and PRDX-1 were dose-dependently up-regulated, and their expression levels upon 400 $\mu$M GA treatment were consistent with those measured by 2-DE experiment. Meanwhile, TCP1, Rho-GDI, and ATPase were simultaneously down-regulated, which showed trends similar to those using a proteomics approach. In addition to these regulated proteins, which were regarded as being associated with apoptosis, interestingly, some proteins involved in glycolysis such as $\alpha$-enolase, aldolase, pyruvate kinase, and

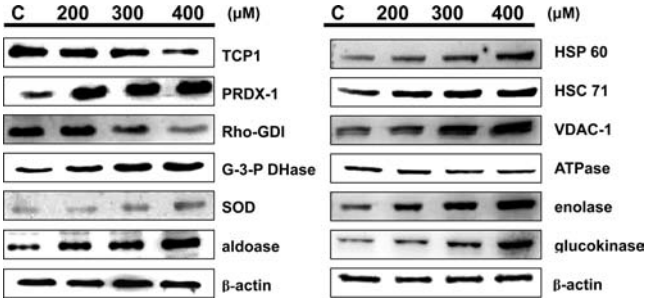


**Figure 5.** Validations of some regulated proteins identified from 2-DE experiment. Western blotting analysis of TCP1, PRDX-1, Rho-GDI, G-3-P DHase, SOD, aldolase, HSP 60, HSC 71, VDAC-1, ATPase, enolase, and glucokinase in B16F10 cells treated with increasing concentrations of GA. $\beta$-Actin was used as the internal control.

GAPDH were simultaneously up-regulated during the GA-induced apoptosis according to 2-DE experiment. The dose-dependent effects of GA on these glycolytic proteins were further confirmed by Western blotting, as shown in Figure 5. The result indicated that enolase, aldolase, pyruvate kinase, and GAPDH were up-regulated dose-dependently in GA-induced B16F10 cells, which implied that GA plays a dual role in both glycolysis and apoptosis. To further validate the activation of glycolysis, the expression of glucokinase, the key glycolysis enzyme, was also examined. The expression of glucokinase was up-regulated accordingly (Figure 5), which further provided evidence for this correlation. As we know, the oxidative phosphorylation of cancer cells is usually suppressed when they are under stressful condition, such as under GA stimulation. The energy supply of cancer cells shifts from oxidative phosphorylation to glycolysis, aiming to produce sufficient ATP, which is known as the Warburg effect.[32] The over-expression of glycolytic proteins in GA-treated B16F10 cells may be due to this effect. Typically, glycolysis and apoptosis are considered as major but independent pathways that are critical for cell survival. Through comparative proteomics, an association between GA-induced apoptosis and metabolic glycolysis in B16F10 melanoma cells was identified and correlated in this study. The interaction between GA-induced apoptosis and metabolic glycolysis may be also explained by the following two reasons: (1) Danial et al. combined the study of proteomics, genetics, and physiology to conclude that BAD and glucokinase reside in a mitochondrial complex that integrates glycolysis and apoptosis,[33] which suggests that GA triggered the intrinsic apoptosis accompanied by glycolysis; (2) GA induces intensive glycolysis and produces a highly reactive metabolite methylglyoxal (MG), which leads to B16F10 cell apoptosis via a mitochondrial intrinsic pathway.[34] However, these two reasons can not fully explain the co-occurrence of GA-induced apoptosis and metabolic glycolysis in B16F10 melanoma cells, so further exploration and validation experiments are required.

In this study, we comprehensively investigated the cytotoxicity on B16F10 melanoma cells caused by gallic acid with a concentration >200 $\mu$M using the MTT assay, wound-healing assay, and cell migration assay. The result of DNA laddering assay and flow cytometry assay further indicated that cell death occurred via apoptosis instead of necrosis. The overexpressions of cleaved forms of caspase-9, caspase-3, and PARP-1 and pro-apoptic Bax and Bad, accompanied by underexpressed anti-apoptotic Bcl-2 and Bcl-XL, indicated that GA induced B16F10 cell apoptosis via a mitochondrial pathway. 2-DE-based comparative proteomics showed that most regulated proteins were associated with apoptosis, consistent with the Western blot data. Notably, the proteomics data also revealed that most proteins involved in glycolysis were simultaneously up-regulated in this GA-induced cell apoptosis. The correlation between glycolysis and apoptosis was further confirmed by Western blot of glucokinase, $\alpha$-enolase, aldolase, and GAPDH.

## ■ ASSOCIATED CONTENT

### Ⓢ Supporting Information

Figure S1: Cell migration assay of GA. This material is available free of charge via the Internet at http://pubs.acs.org.

## ■ AUTHOR INFORMATION

### Corresponding Authors

*(J.-L.H.) E-mail: jlhsu@mail.npust.edu.tw.

*(Y.-J.W.) Mail: 23 Pingkung Road, Neipu Hsiang, Pingtung 91202, Taiwan. Phone: +886-8-7799821, ext 8613. Fax: +886-8-7797821. E-mail: wyr924@ms24.hinet.net or x00002180@meiho.edu.tw.

### Author Contributions

‖J.-L.H. and Y.-J.W. contributed equally to this work.

### Funding

This work was supported by Taiwan NSC grants (NSC 102-2313-B-276-001-MY3 for Dr. Yu-Jen Wu; NSC 102-2113-M-020-001-MY2 for Dr. Jue-Liang Hsu).

### Notes

The authors declare no competing financial interest.

## ■ ACKNOWLEDGMENTS

We gratefully acknowledge the MS technical assistance of Tzu-Chun Lin in the Food Science and Nutrition Department in Meiho University of Science and Technology and Dr. Ann Na Gong for English editing.

## ■ REFERENCES

(1) Yilmaz, Y.; Toledo, R. T. Major flavonoids in grape seeds and skins: antioxidant capacity of catechin, epicatechin, and gallic acid. *J. Agric. Food Chem.* **2004**, *52*, 255−260.

(2) Strlic, M.; Radovic, T.; Kolar, J.; Pihlar, B. Anti- and prooxidative properties of gallic acid in Fenton-type systems. *J. Agric. Food Chem.* **2002**, *50*, 6313−6317.

(3) Li, A.; Chen, J.; Zhu, W.; Jiang, T.; Zhang, X.; Gu, Q. Antibacterial activity of gallic acid from the flowers of *Rosa chinensis* Jacq. against fish pathogens. *Aquacult. Res.* **2007**, *38*, 1110−1112.

(4) Al-Adhroey, A. H.; Nor, Z. M.; Al-Mekhlafi, H. M.; Mahmud, R. Median lethal dose, antimalarial activity, phytochemical screening and radical scavenging of methanolic *Languas galanga* rhizome extract. *Molecules* **2010**, *15*, 8366−8376.

(5) Kroes, B. H.; van den Berg, A. J.; Quarles van Ufford, H. C.; van Dijk, H.; Labadie, R. P. Anti-inflammatory activity of gallic acid. *Planta Med.* **1992**, *58*, 499−504.

(6) Patel, S. S.; Goyal, R. K. Cardioprotective effects of gallic acid in diabetes-induced myocardial dysfunction in rats. *Pharmacognosy Res.* **2011**, *3*, 239−245.

(7) Kim, D. O.; Lee, K. W.; Lee, H. J.; Lee, C. Y. Vitamin C equivalent antioxidant capacity of phenolic phytochemicals. *J. Agric. Food Chem.* **2002**, *50*, 3713−3717.

(8) Hockenbery, D. M.; Oltval, Z. N.; Yin, X. M.; Milliam, C. L.; Korsmeyer, S. J. Bcl-2 functions in an antioxidant pathway to prevent apoptosis. *Cell* **1993**, *74*, 241−251.

(9) Sakaguchi, N.; Inoue, M.; Ogihara, Y. Reactive oxygen species and intracellular $Ca^{2+}$, common signals for apoptosis induced by gallic acid. *Biochem. Pharmacol.* **1998**, *55*, 1973−1981.
(10) Maurya, D. K.; Nandakumar, N.; Devasagayam, T. P. Anticancer property of gallic acid in A549, a human lung adenocarcinoma cell line, and possible mechanisms. *J. Clin. Biochem. Nutr.* **2011**, *28*, 85−90.
(11) Hsu, J. D.; Kao, S. H.; Ou, T. T.; Chen, Y. J.; Li, Y. Y.; Wang, C. J. Gallic acid induces G2/M phase arrest of breast cancer cell MCF-7 through stabilization of $p27^{Kip1}$ attributed to disruption of $p27^{Kip1}$/Skp2 complex. *J. Agric. Food Chem.* **2011**, *59*, 1996−2003.
(12) Kaur, M.; Singh, R. P.; Gu, M.; Agarwa, R.; Agarwal, C. Grape seed extract inhibits in vitro and in vivo growth of human colorectal carcinoma cells. *Clin. Cancer Res.* **2006**, *12*, 6194−6202.
(13) Yoshioka, K.; Kataoka, T.; Hayashi, T.; Hasegawa, M.; Ishi, Y.; Hibasami, H. Induction of apoptosis by gallic acid in human stomach cancer KATO III and colon adenocarcinoma COLO 205 cell lines. *Oncol. Rep.* **2000**, *7*, 1221−1223.
(14) Lo, C.; Lai, T. Y.; Yang, J. H.; Yang, J. S.; Ma, Y. S.; Weng, S. W.; Chen, Y. Y.; Lin, J. G.; Chung, J. G. Gallic acid induces apoptosis in A375.S2 human melanoma cells through caspase-dependent and -independent pathways. *Int. J. Oncol.* **2010**, *37*, 377−385.
(15) Locatelli, C.; Leal, P. C.; Yunes, R. A.; Nunes, R. J.; Creczynski-Pasa, T. B. Gallic acid ester derivatives induce apoptosis and cell adhesion inhibition in melanoma cells: the relationship between free radical generation, glutathione depletion and cell death. *Chem.−Biol. Interact.* **2009**, *181*, 175−184.
(16) Chatterjee, S. J.; Pandey, S. Chemo-resistant melanoma sensitized by tamoxifen to low dose curcumin treatment through induction of apoptosis and autophagy. *Cancer Biol. Ther.* **2011**, *11*, 216−228.
(17) Kim, Y. J. Antimelanogenic and antioxidant properties of gallic acid. *Biol. Pharm. Bull.* **2007**, *30*, 1052−1055.
(18) Monti, C.; Tosco, A.; De Marino, S.; Margarucci, L.; Riccio, R.; Casapullo, A. Differential in gel electrophoresis (DIGE) comparative proteomic analysis of macrophages cell cultures in response to perthamide C treatment. *Mar. Drugs* **2013**, *11*, 1288−1299.
(19) Li, H. H.; Su, J. H.; Chiu, C. C.; Lin, J. J.; Yang, Z. Y.; Hwang, W. I.; Chen, Y. K.; Lo, Y. H.; Wu, Y. J. Proteomic investigation of the sinulariolide-treated melanoma cells A375: effects on the cell apoptosis through mitochondrial-related pathway and activation of caspase cascade. *Mar. Drugs* **2013**, *11*, 2625−2642.
(20) Serrano, A.; Palacios, C.; Roy, G.; Cespón, C.; Villar, M. L.; Nocito, M.; González-Porqué, P. Derivatives of gallic acid induce apoptosis in tumoral cell lines and inhibit lymphocyte proliferation. *Arch. Biochem. Biophys.* **1998**, *350*, 49−54.
(21) Inoue, M.; Sakaguchi, N.; Isuzugawa, K.; Tani, H.; Ogihara, Y. Role of reactive oxygen species in gallic acid-induced apoptosis. *Biol. Pharm. Bull.* **2000**, *23*, 1153−1157.
(22) Ou, T. T.; Wang, C. J.; Lee, Y. S.; Wu, C. H.; Lee, H. J. Gallic acid induces G2/M phase cell cycle arrest via regulating 14-3-3$\beta$ release from Cdc25C and Chk2 activation in human bladder transitional carcinoma cells. *Mol. Nutr. Food Res.* **2010**, *54*, 1781−1790.
(23) Sohi, K. K.; Mittal, N.; Hundal, M. K.; Khanduja, K. L. Gallic acid, an antioxidant, exhibits antiapoptotic potential in normal human lymphocytes: a Bcl-2 independent mechanism. *J. Nutr. Sci. Vitaminol. (Tokyo)* **2003**, *49*, 221−227.
(24) Chandra, D.; Choy, G.; Tang, D. G. Cytosolic accumulation of HSP60 during apoptosis with or without apparent mitochondrial release: evidence that its pro-apoptotic or pro-survival functions involve differential interactions with caspase-3. *J. Biol. Chem.* **2007**, *282*, 31289−31301.
(25) Eleuterio, E.; Di Giuseppe, F.; Sulpizio, M.; di Giacomo, V.; Rapino, M.; Cataldi, A.; Di Ilio, C.; Angelucci, S. Proteome analysis of X-ray irradiated human erythroleukemia cells. *Biochim. Biophys. Acta* **2008**, *1784*, 611−620.
(26) Su, T. R.; Lin, J. J.; Chiu, C. C.; Chen, J. Y.; Su, J. H.; Cheng, Z. J.; Hwang, W. I.; Huang, H. H.; Wu, Y. J. Proteomic investigation of anti-tumor activities exerted by sinularin against A2058 melanoma cells. *Electrophoresis* **2012**, *33*, 1139−1152.
(27) Kumar, S. N.; Konorev, E. A.; Aggarwal, D.; Kalyanaraman, B. Analysis of proteome changes in doxorubicin-treated adult rat cardiomyocyte. *J. Proteomics* **2011**, *74*, 683−697.
(28) Zelivianski, S.; Liang, D.; Chen, M.; Mirkin, B. L.; Zhao, R. Y. Suppressive effect of elongation factor 2 on apoptosis induced by HIV-1 viral protein R. *Apoptosis* **2006**, *11*, 377−388.
(29) Lu, B.; Zhao, J.; Xu, L.; Xu, Y.; Wang, X.; Peng, J. Identification of molecular target proteins in berberine-treated cervix adenocarcinoma HeLa cells by proteomic and bioinformatic analyses. *Phytother. Res.* **2012**, *26*, 646−656.
(30) Rong, F.; Li, W.; Chen, K.; Li, D. M.; Duan, W. M.; Feng, Y. Z.; Li, F.; Zhou, X. W.; Fan, S. J.; Liu, Y.; Tao, M. Knockdown of RhoGDI$\alpha$ induces apoptosis and increases lung cancer cell chemosensitivity to paclitaxel. *Neoplasma* **2012**, *59*, 541−550.
(31) Jo, M.; Yun, H. M.; Park, K. R.; Park, M. H.; Lee, D. H.; Cho, S. H.; Yoo, H. S.; Lee, Y. M.; Jeong, H. S.; Kim, Y.; Jung, J. K.; Hwang, B. Y.; Lee, M. K.; Kim, N. D.; Han, S. B.; Hong, J. T. Anti-cancer effect of thiacremonone through down regulation of peroxiredoxin 6. *PLoS One* **2014**, *9*, No. e91508.
(32) Gasparre, G.; Porcelli, A. M.; Lenaz, G.; Romeo, G. Relevance of mitochondrial genetics and metabolism in cancer development. *Cold Spring Harbor Perspect. Biol.* **2013**, 5 DOI: 10.1101/cshperspect.a011411.
(33) Danial, N. N.; Gramm, C. F.; Scorrano, L.; Zhang, C. Y.; Krauss, S.; Ranger, A. M.; Datta, S. R.; Greenberg, M. E.; Licklider, L. J.; Lowell, B. B.; Gygi, S. P.; Korsmeyer, S. J. BAD and glucokinase reside in a mitochondrial complex that integrates glycolysis and apoptosis. *Nature* **2003**, *424*, 952−956.
(34) Okado, A.; Kawasaki, Y.; Hasuike, Y.; Takahashi, M.; Teshima, T.; Fujii, J.; Taniguchi, N. Induction of apoptotic cell death by methylglyoxal and 3-deoxyglucosone in macrophage-derived cell lines. *Biochem. Biophys. Res. Commun.* **1996**, *225*, 219−224.

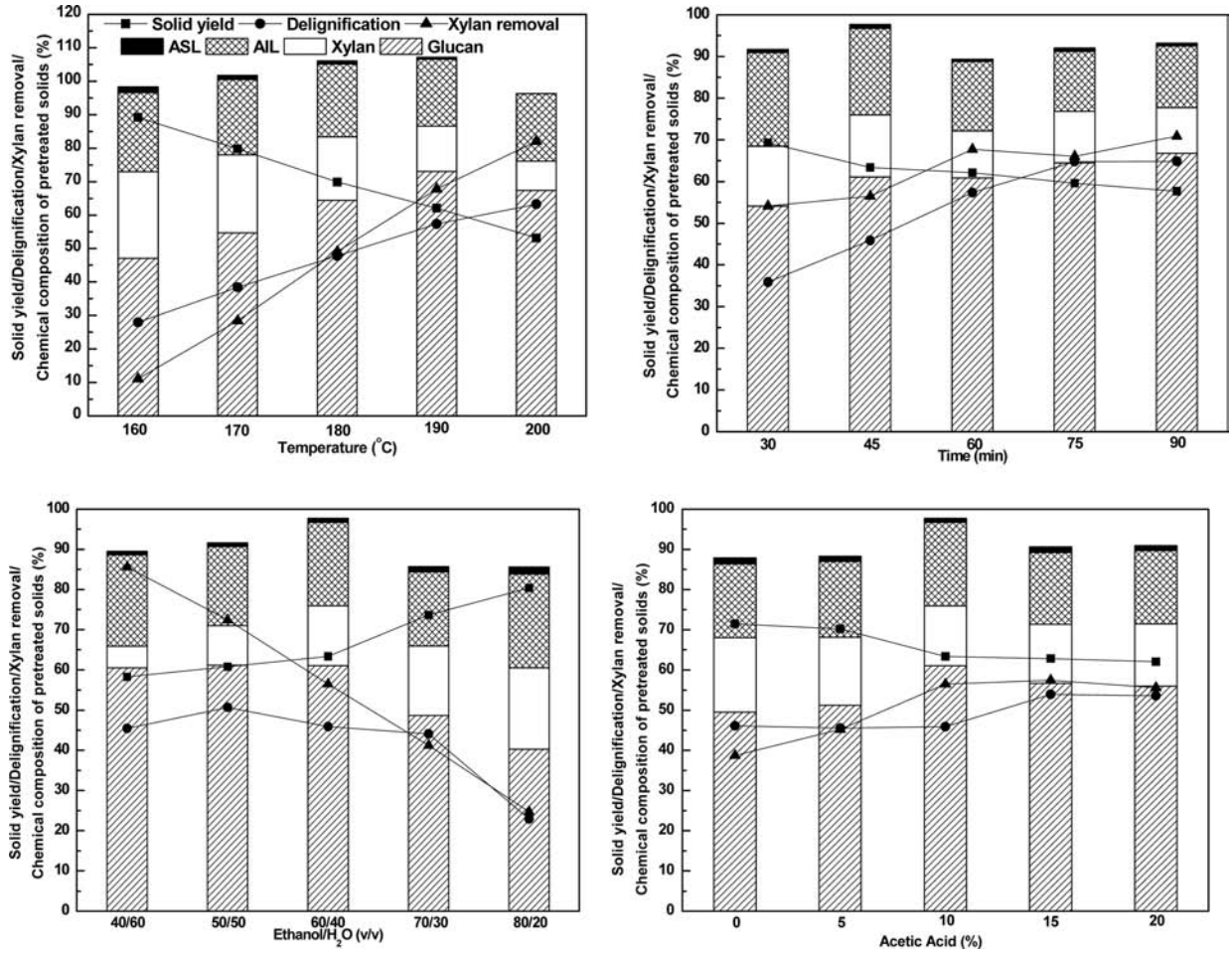


**Figure 1.** Effect of pretreatment conditions on the chemical composition of pretreated solids.

On the basis of the above viewpoint, sugar cane bagasse was subjected to acetic acid organosolv pretreatment for enzymatic saccharification. A parametric study focusing on the temperature, reaction time, ethanol concentration, and acid catalyst dose was performed to determine their influence on compositional changes of pretreated solids and the glucose and xylose yields during the pretreatment process and subsequent enzymatic hydrolysis. Moreover, the parametric effects on the total sugar yields were also investigated. Furthermore, we detected changes in the raw material and pretreated samples (pretreatment conditions of 190 °C, 45 min, 60:40 ethanol/water, and 5 wt % dosage of acetic acid) in crystallinity by X-ray diffraction (XRD) and in the surface structure by scanning electron microscopy (SEM) to provide a relation between delignification, xylan removal, and enzymatic hydrolysis.

## MATERIALS AND METHODS

**Materials.** Sugar cane bagasse obtained in Guangdong, China, was milled to a particle size of <1 mm using a refiner. Then, the milled raw material was air-dried for further use. The chemical composition of the milled sugar cane bagasse (on a dry weight basis) was 39.4 ± 0.7% glucan, 21.6 ± 0.3% xylan, 1.6 ± 0.2% arabinan, 0.4 ± 0.1% galactan, 24.3 ± 0.6% acid-insoluble lignin (AIL), 1.4 ± 0.2% acid-soluble lignin (ASL), and 4.5 ± 0.5% ash.

Ethanol and acetic acid were purchased from Sinopharm Chemical Reagent Co., Ltd. and China Sun Specialty Products Co., Ltd., respectively.

**Organosolv Pretreatment.** A total of 50 g (dry weight) of sugar cane bagasse was treated with aqueous ethanol (40:60−80:20 ethanol/water, v/v) at 1:8 solid/liquid ratio. The pretreatments were carried out in a 1 L high-pressure vessel (Parr Instrument Company, Moline, IL) equipped with a motor-driven electromagnetic stirrer (300 rpm). The reaction mixture were heated at 160−200 °C for 30−90 min in the presence of 0−10 wt % acetic acid based on the weight of raw material. It took 25−35 min to reach the prescribed temperature for the reactor. When the pretreatment was finished, the reactor was immediately cooled to room temperature by cooling water. The pretreated solution were separated by filtration and washed with ethanol/water (60 °C, 60:40, v/v). Then, the washes were combined, and 2 volumes of water were added to precipitate the ethanol organosolv lignin, which could be collected by centrifugation. The pretreated solids were stored in a refrigerator for further enzymatic hydrolysis. The concentration of sugars (glucose and xylose) and inhibitors [hydroxymethylfurfural (HMF) and furfural] in the prehydrolyzate and enzymatic hydrolysis process were analyzed by ion chromatography (IC) and high-pressure liquid chromatography (HPLC), respectively.

**Enzymatic Hydrolysis.** Pretreated sugar cane bagasse samples were immersed in 0.05 mol/L acetic acid sodium acetate buffer (pH 4.8) with 2% (w/w) dry matter and then incubated on a shaker at 150 rpm and 50 °C up to 60 h. The pretreated solids were subjected to enzymatic hydrolysis using the commercial cellulase mixture provided by Genencor (Shanghai, China), with a filter paper activity of 20 filter paper units (FPU)/mL. The cellulases were added at the loading of 20 FPU/g of dry substrate for all hydrolysis experiments. Two drops of acetic ether were added to avoid microorganisms. When the enzymatic hydrolysis reached the setting time, the samples were boiled for 10 min to quench the enzymatic reaction. Then, the enzymatic samples were centrifuged, the supernatants were retained for subsequent sugar analysis, and enzymatic residues were stored for further analysis.

**Table 1. Composition of the Prehydrolyzate after Ethanol-Based Organosolv Pretreatment of Sugar Cane Bagasse under Different Pretreatment Conditions**

| pretreatment condition | | | | composition of prehydrolyzate (g/100 g of raw material) | | | | | | inhibitor (g/L) | |
|---|---|---|---|---|---|---|---|---|---|---|---|
| temperature (°C) | time (min) | ethanol/$H_2O$ (v/v) | acetic acid (%) | glucose | glu-oligo | total glucose | xylose | xyl-oligo | total xylose | HMF | furfural |
| 160 | 60 | 60:40 | 5 | 0.04 | 0.10 | 0.14 | 0.06 | 2.51 | 2.57 | 0.00 | 0.00 |
| 170 | | | | 0.06 | 0.12 | 0.18 | 0.14 | 6.07 | 6.21 | 0.01 | 0.03 |
| 180 | | | | 0.09 | 0.08 | 0.17 | 0.29 | 10.31 | 10.60 | 0.02 | 0.18 |
| 190 | | | | 0.12 | 0.06 | 0.18 | 0.56 | 11.27 | 11.83 | 0.02 | 0.53 |
| 200 | | | | 0.09 | 0.19 | 0.28 | 0.72 | 4.89 | 5.61 | 0.03 | 0.71 |
| 190 | 30 | 60:40 | 5 | 0.05 | 0.17 | 0.22 | 0.28 | 10.43 | 10.71 | 0.01 | 0.23 |
| | 45 | | | 0.09 | 0.17 | 0.26 | 0.52 | 10.71 | 11.23 | 0.02 | 0.40 |
| | 60 | | | 0.12 | 0.06 | 0.18 | 0.56 | 11.27 | 11.83 | 0.02 | 0.53 |
| | 75 | | | 0.10 | 0.19 | 0.29 | 0.73 | 9.60 | 10.33 | 0.03 | 0.66 |
| | 90 | | | 0.08 | 0.20 | 0.28 | 0.83 | 7.59 | 8.42 | 0.03 | 0.76 |
| 190 | 45 | 40:60 | 5 | 0.09 | 0.31 | 0.40 | 1.87 | 6.86 | 8.73 | 0.02 | 0.48 |
| | | 50:50 | | 0.09 | 0.19 | 0.28 | 1.08 | 10.30 | 11.38 | 0.01 | 0.26 |
| | | 60:40 | | 0.09 | 0.17 | 0.26 | 0.52 | 10.71 | 11.23 | 0.02 | 0.40 |
| | | 70:30 | | 0.04 | 0.04 | 0.08 | 0.13 | 6.57 | 6.70 | 0.01 | 0.09 |
| | | 80:20 | | 0.02 | 0.05 | 0.07 | 0.05 | 2.92 | 2.97 | 0.00 | 0.07 |
| 190 | 45 | 60:40 | 0 | 0.06 | 0.07 | 0.13 | 0.25 | 7.13 | 7.38 | 0.02 | 0.24 |
| | | | 2.5 | 0.05 | 0.12 | 0.17 | 0.23 | 8.28 | 8.51 | 0.02 | 0.27 |
| | | | 5 | 0.09 | 0.17 | 0.26 | 0.52 | 10.71 | 11.23 | 0.02 | 0.40 |
| | | | 7.5 | 0.08 | 0.01 | 0.09 | 0.43 | 5.60 | 6.03 | 0.03 | 0.46 |
| | | | 10 | 0.07 | 0.08 | 0.15 | 0.36 | 7.31 | 7.67 | 0.02 | 0.35 |

**Analytical Techniques.** The chemical composition of sugar cane bagasse and pretreated solids were determined using the standard provided by the National Renewable Energy Laboratory (NREL) in Golden, CO.[21] Because some of the sugars obtained from organosolv pretreatment were oligosaccharides, an acid hydrolysis [4% (w/w) $H_2SO_4$, 121 °C, and 60 min] was performed to obtain monosaccharides for analysis.

All liquid products from the pretreatment process and enzymatic hydrolysis were diluted appropriately with the deionized water and then filtered using a 0.22 $\mu$m filter. The concentration of glucose and xylose were quantitatively analyzed at 30 °C by the IC system (Dionex ICS-3000) with a CarboPac PA20 column. The sugar derivatives (furfural and HMF) were determined using a HPLC system ($C_{18}$ column) at 30 °C based on a diode array detector (DAD). The mobile phase consisted of methanol/water (30:70, v/v) with a flow rate of 1.0 mL/min.[6]

**Crystallinity Measurements.** The crystallinity of native material and pretreated solid (190 °C, 45 min, 60:40 ethanol/$H_2O$, and 5 wt % acetic acid) was determined by XRD using a Bruker D8-ADVANCE (Germany) with Cu Ni radiation ($k$ = 0.154 18 nm). The scattering angle ($2\theta$) was from 5° to 60°. The crystalline index (CrI) was determined on the basis of the formula by Segal et al.[22] as follows:

$$\mathrm{CrI} = \frac{I_{002} - I_{\mathrm{am}}}{I_{002}} \times 100\%$$

in which $I_{002}$ is the scattered intensity at the main peak around 22.5° and $I_{\mathrm{am}}$ is the scattered intensity as a result of the amorphous portion evaluated as the minimum intensity between the main and secondary (the broad peak at 18.0°) peaks.

**SEM Analysis.** SEM of the two samples (raw material and solid pretreated at 190 °C, 45 min, 60:40 ethanol/$H_2O$, and 5 wt % acetic acid) was carried out with a ZEISS EVO18 (Germany) instrument at 10 kV. Each sample was sputter-coated with gold for 180 s prior to the observation. All observations were used at 2000× magnification.

## RESULTS AND DISCUSSION

**Chemical Composition of Sugar Cane Bagasse Pretreated by Different Ethanol Concentrations.** The effect of pretreatment parameters (temperature, reaction time, ethanol concentration, and acetic acid dose) on the solid recoveries and chemical composition of pretreated solids were discussed and presented in Figure 1. Ethanol and acetic acid in the pretreatment process were employed to remove hemicellulose and lignin; thus, the relative content of glucan (cellulose) in pretreated solids was higher than in raw material. Because of the different pretreatment conditions, the solid yields and chemical composition of pretreated biomass differed greatly.[23]

The solid yields decreased with the increment of the pretreatment temperature. When the pretreatment temperature increased from 160 to 200 °C, the solid yields decreased from 89.2 to 53.2%. However, within the same pretreatment parameters, the delignification and xylan removal increased from 27.9 and 11.1% to 63.3 and 82.0%, respectively. The increased delignification and xylan hydrolysis (generation of sugars and inhibitors) made a great contribution to the decreased solid yields. When the reaction time is taken as an example, extension of the reaction time (30−60 min) lead to a decrease of the solid yield (from 69.3 to 62.1%) but increment of the delignification (from 35.9 to 57.4%) and xylan removal (from 54.1 to 67.8%). However, when the reaction time was prolonged from 60 to 90 min, the increment of delignification and xylan removal were not significant. These results suggested that the reaction time seemed not to be a major process parameter for the organosolv pretreatment within a long reaction time (more than 60 min).[15]

As shown in Figure 1, the solid yields increased with the ethanol concentration because of the decreased delignification and xylan hydrolysis. The glucan content of the pretreated solid

**Table 2. Yields of Glucose and Xylose (g/100 g of Raw Material) from Both Ethanol-Based Organosolv Pretreatment and Enzymatic Hydrolysis**

| pretreatment condition | | | | enzyme hydrolyzate | | prehydrolyzate | | | | |
|---|---|---|---|---|---|---|---|---|---|---|
| temperature (°C) | time (min) | ethanol/$H_2O$ (v/v) | acetic acid (%) | glucose | xylose | glucose | xylose | total glucose | total xylose | total sugars |
| 160 | 60 | 60:40 | 5 | 12.87 | 6.30 | 0.14 | 2.57 | 13.01 | 8.87 | 21.88 |
| 170 | | | | 21.22 | 8.48 | 0.18 | 6.21 | 21.40 | 14.69 | 36.09 |
| 180 | | | | 29.84 | 7.74 | 0.17 | 10.60 | 30.01 | 18.34 | 48.35 |
| 190 | | | | 39.52 | 6.21 | 0.18 | 11.83 | 39.70 | 18.04 | 57.74 |
| 200 | | | | 32.98 | 4.13 | 0.28 | 5.61 | 33.26 | 9.74 | 43.00 |
| 190 | 30 | 60:40 | 5 | 32.90 | 7.12 | 0.22 | 10.71 | 33.12 | 17.83 | 50.95 |
| | 45 | | | 40.42 | 6.45 | 0.26 | 11.23 | 40.68 | 17.68 | 58.36 |
| | 60 | | | 39.52 | 6.21 | 0.18 | 11.83 | 39.70 | 18.04 | 57.74 |
| | 75 | | | 40.99 | 5.53 | 0.29 | 10.33 | 41.28 | 15.86 | 57.14 |
| | 90 | | | 39.90 | 5.17 | 0.28 | 8.42 | 40.18 | 13.59 | 53.77 |
| 190 | 45 | 40:60 | 5 | 38.92 | 2.44 | 0.40 | 8.73 | 39.32 | 11.17 | 50.49 |
| | | 50:50 | | 39.69 | 4.29 | 0.28 | 11.38 | 39.97 | 15.67 | 55.64 |
| | | 60:40 | | 40.42 | 6.45 | 0.26 | 11.23 | 40.68 | 17.68 | 58.36 |
| | | 70:30 | | 20.12 | 7.18 | 0.08 | 6.70 | 20.20 | 13.88 | 34.08 |
| | | 80:20 | | 14.46 | 6.92 | 0.07 | 2.97 | 14.53 | 9.89 | 24.42 |
| 190 | 45 | 60:40 | 0 | 28.25 | 6.80 | 0.13 | 7.38 | 28.38 | 14.18 | 42.56 |
| | | | 2.5 | 28.37 | 6.44 | 0.17 | 8.51 | 28.54 | 14.95 | 43.49 |
| | | | 5 | 40.42 | 6.45 | 0.26 | 11.23 | 40.68 | 17.68 | 58.36 |
| | | | 7.5 | 38.49 | 6.34 | 0.09 | 6.03 | 38.58 | 12.37 | 50.95 |
| | | | 10 | 38.30 | 6.56 | 0.15 | 7.67 | 38.45 | 14.23 | 52.68 |

decreased from 60.5% (40% ethanol) to 40.2% (80% ethanol). The increased ethanol concentration made a great contribution to the decreased xylan removal, which dropped from 85.6 to 24.7% . This phenomenon could be concluded that a higher concentration of ethanol inhibited xylan hydrolysis, which was in agreement with previous work.[24] As the ethanol concentration increased, more lignin could be soluble in the ethanol.[15] However, the delignification were decreased with the increased ethanol concentration (as shown in Figure 1). This observation suggested that the lower removal of xylan resulted in decreased delignification because of the linkages between lignin and hemicelluloses.

During the organosolv pretreatment process, the hemicellulose hydrolysis could be improved by the addition of the acid catalyst. As a consequence of increasing the acetic acid dose from 0 to 10 wt %, delignification and xylan hydrolysis increased and the solid yield decreased. For acid-soluble lignin (ASL), the composition of pretreated solids was lower than the raw material, suggesting that part of ASL was solubilized by ethanol and/or acetic acid.

**Organosolv Pretreatment.** The influence of reaction parameters on the composition of prehydrolyzate (including monomeric and oligomeric sugars of glucose and xylose) were examined and displayed in Table 1. Xylan was the principal component in hemicellulose, and its monomeric component (xylose) was the major carbohydrate in the prehydrolyzate, as shown in Table 1. When the pretreatment temperature is taken as an example, the xylose yield increased with the temperature, reaching 11.83 g (including 11.27 g of xylo-oligomers) based on 100 g of raw material at 190 °C, representing 48.1% xylose in the raw material. A further increase in the temperature reduced the xylose yield. This was probably due to the degradation of xylose to furfural with a serious pretreatment temperature.[25]

At the same reaction temperature, the reaction time shows a slight influence of the pretreatment at the process conditions tested. However, it may be an important parameter for the production of xylose. During different reaction times, the xylose yield was in the range of 8.42−11.83 g based on 100 g of raw material. When the reaction time reached 45 min, the xylose yield was 11.23 g/100 g of raw material. Although the xylose yield was a little lower than the prehydrolyzate pretreated at 60 min (11.83 g), within the reducing energy consumption during pretreatment, the reaction time of 45 min was regarded as the optimum. The xylose yield with different ethanol concentrations first increased from 8.73 g (40:60 ethanol/water) to 11.38 g (50:50 ethanol/water) and then decreased sharply to 2.97 g (80:20 ethanol/water). These results suggested that the ethanol concentration had significantly impacted the pretreatment and a higher ethanol concentration did not result in the large removal of xylan and high recovery of xylose.[26] The presence of ethanol in the reaction allowed for the performance of the delignification, which was confirmed in Figure 1. With the removal of lignin during the pretreatment, the subsequent enzymatic digestibility could be enhanced because of the removal of the physical barrier preventing enzyme access and nonproductive binding with enzyme,[27] which would be discussed in the following section. In addition, the removal of xylan also played an important role in enzymatic hydrolysis, as shown in the following discussion.

Hemicellulose hydrolysis during the organosolv pretreatment process could be enhanced by acid, thereby improving the subsequent enzymatic cellulose hydrolysis.[15] In this study, acetic acid was regarded as the catalyst and introduced in the pretreatment reaction. It is observed that the acetic acid concentration showed a strong influence on xylose production. As the acetic acid dosage increased from 0 to 10 wt %, the

xylose yield ranged from 6.03 to 11.23 g based on 100 g of raw material. The relative high concentration of acetic acid seemed to favor the production of xylose in the prehydrolyzate.[23] However, more acetic acid lead to the drastic degradation of xylose to furfural, as shown in Table 1.

From Table 1, it could be known that most of the xylose yield was obtained in the form of oligomers. This phenomenon could be concluded that the weak acid (acetic acid) during the pretreatment may enhance acid-catalyzed hydrolysis of hemicellulose to xylo-oligomes but was not strong enough to hydrolyze to xylose monomers. Because of the low content of glucan in hemicellulose and the crystallization structure of cellulose, the glucose yields obtained from organosolv pretreatment were limited. The maximal yield of glucose (0.40 g/100 g of raw material) was obtained at 190 °C, 45 min, 40:60 ethanol/water, and 5 wt % dosage of acetic acid, representing only 0.9% glucose in the raw material. Table 1 also depicted the formation of furfural and HMF during the pretreatment process. The quantities of furfural and HMF were estimated to be below 0.76 and 0.03 g/L, respectively. The very low concentration of furfural and HMF in prehydrolyzate attested to the limited degradation of pentose and hexose, respectively. These results suggested that organosolv pretreatment prevented the degradation of saccharides, which agreed with the former literature.[12]

**Enzymatic Hydrolysis.** Enzymatic hydrolysis of the organolsolv pretreated solid residues were performed using standard literature conditions.[6] The effects of pretreatment factors were analyzed on the basis of the sugar yields during enzymatic hydrolysis, and the results were displayed in Table 2. In comparison to the enzymatic hydrolysis of raw material without pretreatment (4.05 g of glucose and 1.42 g of xylose), the enzymatic hydrolysis of the organosolv pretreated solids showed higher sugar yields after a 60 h hydrolysis time. The result indicated that delignification and hemicellulose removal were beneficial to the subsequent enzymatic hydrolysis of the pretreated solids because lignin and hemicellulose in the raw material as physical barriers could prevent the accessibility of enzyme to cellulose.[19]

From Table 2, it could know that glucose, as the major carbohydrate in enzyme hydrolyzate, differed from each other because of the different pretreatment parameters. When the pretreatment temperature is taken as an example, when it increased from 160 to 190 °C, a rapid growth of the glucose yield could be observed (from 12.87 to 39.52 g/100 g of raw material). As the temperature continued to rise (200 °C), the glucose yield decreased sharply to 32.98 g/100 g of raw material. As the pretreatment time was prolonged from 30 to 45 min at 190 °C, with ethanol/water (60:40, v/v) and 5 wt % dosage of acetic acid, the glucose yield increased from 32.90 to 40.42 g/100 g of raw material. A maximal glucose yield (40.99 g based on 100 g of raw material) could be obtained at 75 min, representing 93.8% of glucose in raw material. For the ethanol concentration, when the ethanol/water ratio increased from 40:60 to 60:40 (v/v), the glucose yield increased gradually (from 38.92 to 40.42 g/100 g of raw material). As the ethanol/water ratio continued to grow, the glucose decreased sharply to 14.46 g based on 100 g of raw material, suggesting that an increase in the ethanol concentration at a certain extent reduced the enzymatic digestibility because of the reduced xylan hydrolysis (shown in Figure 1).[15] A rise in the glucose yield (from 28.25 to 40.42 g/100 g of raw material) upon an increase of the acetic acid dosage from 0 to 5 wt % could be obtained, which could be concluded that acetic acid contributed to the hydrolysis of hemicellulose and the linkages between hemicellulose and lignin breakdown. However, when the acetic acid dose increased to 10 wt %, the glucose yield dropped to 38.30 g based on 100 g of raw material. Moreover, a certain amount of xylose could also be obtained during enzymatic hydrolysis. This phenomenon could be concluded that organosolv pretreatment was beneficial to the recovery of xylose.

As an overview of the efficiency of the pretreatment and subsequent enzymatic hydrolysis, the total sugars recovered from both pretreatment (mainly xylose) and enzymatic hydrolysis (mainly glucose) were also summarized and presented in Table 2. The maximum xylose yield (including xylose monomer and xylo-oligomer) was obtained at 180 °C, 60 min, 60:40 ethanol/water ratio, and 5 wt % dosage of acetic acid, reaching 18.34 g/100 g of raw material, representing 74.6% xylose in the sugar cane bagasse, and 43.1% was obtained from the pretreatment process. The results indicated that amorphous hemicellulose could be easily degraded during pretreatment because of the acidity provided by acetic acid. The highest glucose yield (41.28 g/100 g of raw material) was obtained at 190 °C, 75 min, 60:40 ethanol/water ratio, and 5 wt % dosage of acetic acid, representing 94.4% of glucose in raw material. Among them, 93.8% was obtained during the enzymatic hydrolysis process. This phenomenon suggested that organosolv pretreatment could greatly enhance the efficiency of subsequent enzymatic hydrolysis. To take full use of lignocellulosic biomass, Table 2 also illustrated the combined sugar (xylose and glucose) yields. The largest total sugar yields occurred at 190 °C, 45 min, 60:40 ethanol/water ratio, and 5 wt % dosage of acetic acid, reaching 58.36 g/100 g of raw material (including 40.68 g of glucose and 17.68 g of xylose), representing 85.4% of total sugars in sugar cane bagasse. Although most sugars were obtained during pretreatment and enzymatic hydrolysis processes, there is still some carbohydrates (including 3.30 g of glucan and 9.46 g of xylan based on 100 g of raw material) in the enzymatic residue; how to use the enzymatic residue well is still to be explored.

**Delignification and Xylan Removal.** From Table 2, it could be seen that the enzymatic hydrolysis of pretreated sugar cane bagasse was enhanced greatly. During the ethanol-based organosolv pretreatment, a portion of lignin and hemicellulose was solubilized and the enzymatic hydrolysis of pretreated solids was enhanced greatly, suggesting that the enhanced glucose conversion may have correlation with delignification and xylan removal. TableCurve 3D was used to determine the best fit for glucan conversion, delignification, and xylan removal. A surface representation of these data points was presented in Figure 2, with $R^2 = 1$. As shown in Figure 2, the glucan conversion increased with the increment of delignification and xylan removal to a certain extent. As lignin and/or xylan were extensively removed, the glucan conversion decreased. One possible explanation was that the cellulose structure may be affected by ethanol/water or the extensive delignification and xylan removal.[20] Another explanation may be the degradation of carbohydrates, such as xylan, which formed on the cellulose surface and retarded enzymatic hydrolysis.[28]

**XRD Analysis.** The XRD spectra of untreated and pretreated sugar cane bagasse (190 °C, 45 min, 60:40 ethanol/$H_2O$, and 5 wt % acetic acid) were investigated and depicted in Figure 3. The untreated sugar cane bagasse had a

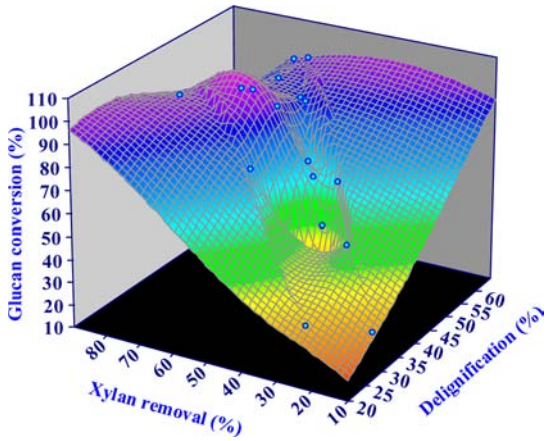


**Figure 2.** Glucan conversion as a function of delignification and xylan removal.

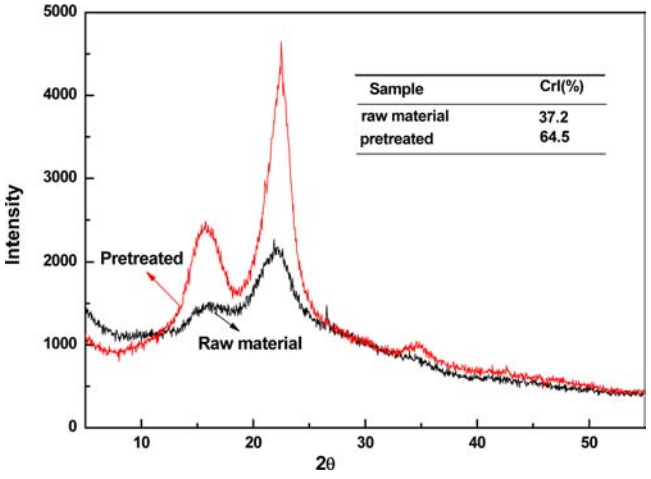


**Figure 3.** XRD patterns and CrI of native material and pretreated solid.

broader peak ($I_{002}$) with a crystallinity degree of 37.2%. The peak ($I_{002}$) became sharper after the pretreatment, and the CrI increased to 64.5%. This phenomenon could be concluded that a large proportion of amorphous lignin and hemicellulose were removed during the pretreatment process; thus, the relative content of crystalline cellulose increased, which was in accordance with previous research.[18,29] However, because of delignification and removal of hemicellulose during the pretreatment process, the intricate structure of native material was destroyed, became less rigid, and made the fibrils more accessible for enzyme. Then, the enzymatic hydrolysis of cellulose in pretreated solids was enhanced greatly, as shown in Figure 2.

**SEM Analysis.** To study the morphologic changes of sugar cane bagasse after ethanol-based organosolv pretreatment, SEM images were carried out. The surface microstructures of sugar cane bagasse before and after pretreatment (190 °C, 45 min, 60:40 ethanol/$H_2O$, and 5% acetic acid) at 2000× magnification are shown in Figure 4. From Figure 4A, it could be seen that the native material exhibited a relatively smooth and rigid surface structure. After ethanol-based organosolv pretreatment, as shown in Figure 4B, the structure became disordered and separated, together with some fragments and a considerable surface roughness, which was probably due to the dissolving of parts of hemicellulose and lignin or the linkages between carbohydrates and lignin breakdown.[30] Because of delignification and removal of hemicellulose, more cellulose fibers were exposed and the enzymatic hydrolysis digestibility could be enhanced (as shown in Table 2 and Figure 2), which is in great agreement with the difference structures apparent in these micrographs.

In conclusion, this study investigated the effect of different pretreatment parameters on the ethanol-based organosolv pretreatment and subsequent enzymatic hydrolysis of sugar cane bagasse. During the pretreatment process, 11.83 g of xylose based on 100 g of raw material could be obtained. After the removal of hemicellulose and lignin, the glucan composition of pretreated solids increased. The maximum glucose yield generated from enzymatic hydrolysis was 40.99 g based on 100 g of raw material, representing 93.8% of glucose in raw material. The highest total sugar yields occurred at 190 °C, 45 min, 60:40 ethanol/water, and 5% dosage of acetic acid, reaching 58.36 g (including 17.68 g of xylose and 40.68 g of glucose) based on 100 g of raw material, representing 85.4% of total sugars in sugar cane bagasse. The enhanced enzymatic hydrolysis was partly due to delignification, xylan removal,

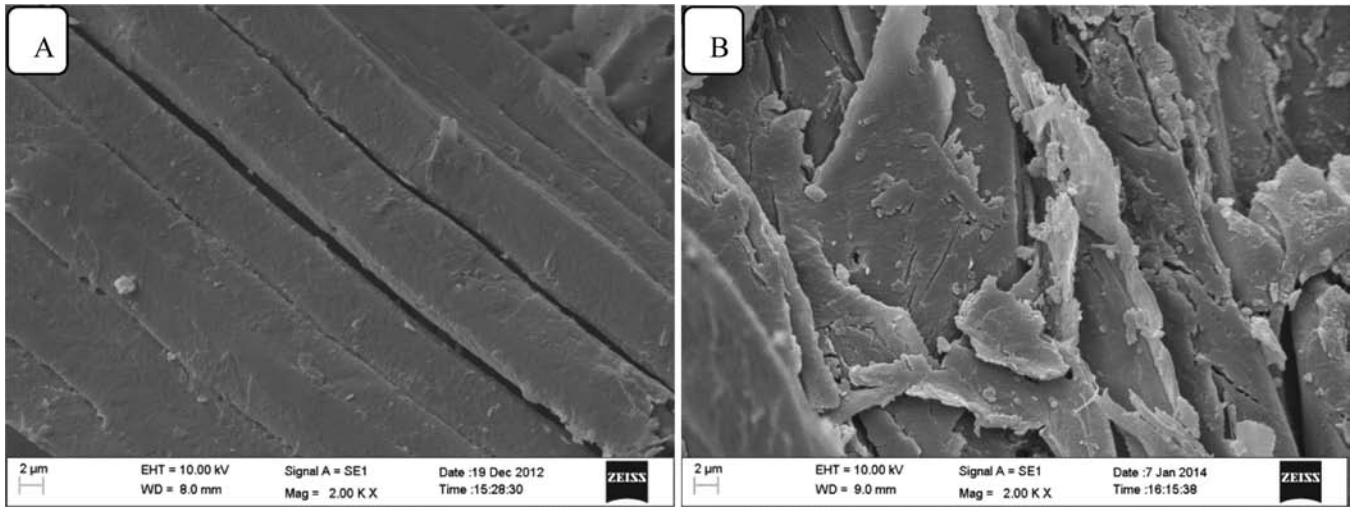


**Figure 4.** SEM images at 2000× magnification for native material and pretreated solid.


dx.doi.org/10.1021/jf503386b | J. Agric. Food Chem. 2014, 62, 11681−11687

change crystallinity, and exposure of cellulose. The results indicated that ethanol-based organosolv pretreatment with acetic acid can improve the efficiency of subsequent enzymatic hydrolysis; thus, it could be successfully applied to the conversion of sugar cane bagasse to sugars.

## AUTHOR INFORMATION


### Corresponding Author

*Telephone: +86-20-22236808. Fax: +86-20-87518783. E-mail: shubinwu@scut.edu.cn.



### Funding

This work was supported by the National High Technology Research and Development Program of China (2012AA101806), the National Key Basic Research Program of China (2013CB228101), the National Natural Science Foundation of China (31270635), and the Fundamental Research Funds for the Central Universities.


### Notes

The authors declare no competing financial interest.

## REFERENCES


(1) Cao, G. L.; Guo, W. Q.; Wang, A. J.; Zhao, L.; Xu, C. J.; Zhao, Q. L.; Ren, N. Q. Enhanced cellulosic hydrogen production from lime-treated cornstalk wastes using thermophilic anaerobic microflora. *Int. J. Hydrogen Energy* **2012**, *37*, 13161−13166.

(2) Brosse, N.; Sannigrahi, P.; Ragauskas, A. Pretreatment of *Miscanthus* × *giganteus* using the ethanol organosolv process for ethanol production. *Ind. Eng. Chem. Res.* **2009**, *48*, 8328−8334.

(3) Ruiz, H. A.; Rodriguez-Jasso, R. M.; Fernandes, B. D.; Vicente, A. A.; Teixeira, J. A. Hydrothermal processing, as an alternative for upgrading agriculture residues and marine biomass according to the biorefinery concept: A review. *Renewable Sustainable Energy Rev.* **2013**, *21*, 35−51.

(4) Yunus, R.; Salleh, S. F.; Abdullah, N.; Biak, D. R. A. Effect of ultrasonic pre-treatment on low temperature acid hydrolysis of oil palm empty fruit bunch. *Bioresour. Technol.* **2010**, *101*, 9792−9796.

(5) Moxley, G.; Zhu, Z.; Zhang, Y. H. P. Efficient sugar release by the cellulose solvent-based lignocellulose fractionation technology and enzymatic cellulose hydrolysis. *J. Agric. Food Chem.* **2008**, *56*, 7885−7890.

(6) Zhang, H. D.; Xu, S. H.; Wu, S. B. Enhancement of enzymatic saccharification of sugarcane bagasse by liquid hot water pretreatment. *Bioresour. Technol.* **2013**, *143*, 391−396.

(7) Krishnan, C.; Sousa, L. C.; Jin, M.; Chang, L.; Dale, B. E.; Balan, V. Alkali-based AFEX pretreatment for the conversion of sugarcane bagasse and cane leaf residues to ethanol. *Biotechnol. Bioeng.* **2010**, *107*, 441−450.

(8) Schwiderski, M.; Kruse, A.; Grandl, R.; Dockendorfa, D. Comparison of the influence of a Lewis acid $AlCl_3$ and a Brønsted acid HCl on the organosolv pulping of beech wood. *Green Chem.* **2014**, *16*, 1569−1578.

(9) Fu, D.; Maxxa, G.; Tamaki, Y. Lignin extraction from straw by ionic liquids and enzymatic hydrolysis of the cellulosic residues. *J. Agric. Food Chem.* **2010**, *58*, 2915−2922.

(10) Alvira, P.; Tomas-Pejo, E.; Ballesteros, M.; Negro, M. J. Pretreatment technologies for an efficient bioethanol production process based on enzymatic hydrolysis: A review. *Bioresour. Technol.* **2010**, *101*, 4851−4861.

(11) Himmel, M. E.; Ding, S. Y.; Johnson, D. K.; Adney, W. S.; Nimlos, M. R.; Brady, J. W.; Foust, T. D. Biomass recalcitrance: Engineering plants and enzymes for biofuels production. *Science* **2007**, *315*, 804−807.

(12) Teramoto, Y.; Lee, S. H.; Endo, T. Pretreatment of woody and herbaceous biomass for enzymatic saccharification using sulfuric acid-free ethanol cooking. *Bioresour. Technol.* **2008**, *99*, 8856−8863.

(13) Zhao, X.; Cheng, K.; Liu, D. Organosolv pretreatment of lignocellulosic biomass for enzymatic hydrolysis. *Appl. Microbiol. Biotechnol.* **2009**, *82*, 815−827.

(14) Shatalov, A. A.; Pereira, H. High-grade sulfur-free cellulose fibers by pre-hydrolysis and ethanol−alkali delignification of giant reed (*Arundo donax* L.) stems. *Ind. Crops Prod.* **2013**, *43*, 623−630.

(15) Wildschut, J.; Smit, A. T.; Reith, J. H.; Huijgen, W. J. J. Ethanol-based organosolv fractionation of wheat straw for the production of lignin and enzymatically digestible cellulose. *Bioresour. Technol.* **2013**, *135*, 58−66.

(16) Zhu, Z.; Sathitsuksanoh, N.; Vinzant, T.; Schell, D. J.; McMillan, J. D.; Zhang, Y. H. P. Comparative study of corn stover pretreated by dilute acid and cellulose solvent-based lignocellulose fractionation: Enzymatic hydrolysis, supramolecular structure, and substrate accessibility. *Biotechnol. Bioeng.* **2009**, *103*, 715−724.

(17) Chandra, R.; Bura, R.; Mabee, W.; Berlin, A.; Pan, X.; Saddler, J. Substrate pretreatment: The key to effective enzymatic hydrolysis of lignocellulosics. *Adv. Biochem. Eng. Biotechnol.* **2007**, *108*, 67−93.

(18) Kumar, S.; Kothari, U.; Kong, L.; Lee, Y. Y.; Gupta, R. B. Hydrothermal pretreatment of switchgrass and corn stover for production of ethanol and carbon microspheres. *Biomass Bioenergy* **2011**, *35*, 956−968.

(19) Kumar, R.; Wyman, C. E. Access of cellulase to cellulose and lignin for poplar solids produced by leading pretreatment technologies. *Biotechnol. Prog.* **2009**, *25*, 807−819.

(20) Rollin, J.; Zhu, Z.; Sathitsuksanoh, N.; Zhang, Y. H. P. Increasing cellulose accessibility is more important than removing lignin: A comparison of cellulose solvent-based lignocelluloses fractionation and soaking in aqueous ammonia. *Biotechnol. Bioeng.* **2011**, *108*, 22−30.

(21) Sluiter, A.; Hames, B.; Ruiz, R.; Scarlata, C.; Sluiter, J.; Templeton, D. *Determination of Sugars, Byproducts, and Degradation Products in Liquid Fraction Process Samples*; National Renewable Energy Laboratory (NREL): Golden, CO, 2006; NREL/TP-510-42623.

(22) Segal, L.; Creely, L.; Martin, A. E. An empirical method for estimating the degree of crystallinity of native cellulose using X-ray diffractormeter. *Text. Res. J.* **1959**, *29*, 786−794.

(23) Lim, W. S.; Lee, J. W. Influence of pretreatment condition on the fermentable sugar production and enzymatic hydrolysis of dilute acid-pretreated mixed softwood. *Bioresour. Technol.* **2013**, *140*, 306−311.

(24) Huijgen, W. J. J.; Reith, J. H.; Uil, D. H. Pretreatment and fractionation of wheat straw by an acetone-based organosolv process. *Ind. Eng. Chem. Res.* **2010**, *49*, 10132−10140.

(25) Lloyd, T. A.; Wyman, C. E. Combined sugar yields for dilute sulfuric acid pretreatment of corn stover followed by enzymatic hydrolysis of the remaining solids. *Bioresour. Technol.* **2005**, *96*, 1967−1977.

(26) Pan, X.; Xie, D.; Yu, R. W.; Lam, D.; Saddler, J. N. Pretreatment of lodgepole pine killed by mountain pine beetle using the ethanol organosolv process: Fractionation and process optimization. *Ind. Eng. Chem. Res.* **2007**, *46*, 2609−2617.

(27) Yuan, T. Q.; Wang, W.; Zhang, L. M.; Xu, F.; Sun, R. C. Reconstitution of cellulose and lignin after $[C_2mim][OAc]$ pretreatment and its relation to enzymatic hydrolysis. *Biotechnol. Bioeng.* **2013**, *110*, 729−736.

(28) Kumar, R.; Hu, F.; Sannigrahi, P.; Jung, S.; Ragauskas, A. J.; Wyman, C. E. Carbohydrate derived-pseudo-lignin can retard cellulose biological conversion. *Biotechnol. Bioeng.* **2013**, *110*, 737−753.

(29) Rezende, C. A.; de Lima, M. A.; Maziero, P.; deAzevedo, E. R.; Garcia, W.; Polikarpov, I. Chemical and morphological characterization of sugarcane bagasse submitted to a delignification process for enhanced enzymatic digestibility. *Biotechnol. Biofuels* **2011**, *11*, 54−72.

(30) Qiu, Z. H.; Aita, G. M.; Walker, M. S. Effect of ionic liquid pretreatment on the chemical composition, structure and enzymatic hydrolysis of energy cane bagasse. *Bioresour. Technol.* **2012**, *117*, 251−256.

isoflavone flour (Sinosoy40) was purchased from Jinmen Deai Biological Engineering Co., Ltd., China. All other chemicals and reagents were of analytical grade unless otherwise stated.

**Production of BglW5 by SSF.** *Gongronella* sp. W5 was cultured on potato dextrose agar (PDA) slants at 4 °C. The PDA medium contained 200.0 g potato extract liquid, 20.0 g glucose, 3.0 g $KH_2PO_4$, 1.5 g $MgSO_4{\cdot}7H_2O$, 0.02 g vitamin B1, and 15.0 g agar powder per liter.

To prepare the primary inoculum, an agar plug of 1 $cm^2$ containing actively growing mycelium of *Gongronella* sp. W5 was inoculated into 100 mL basal medium which contained (g/L) 10.0 g glucose, 0.3 g urea, 1.0 g peptone, 1.4 g $(NH_4)_2SO_4$, 2.0 g $KH_2PO_4$, 0.4 g $CaCl_2{\cdot}2H_2O$, 0.3 g $MgSO_4{\cdot}7H_2O$, 50.0 mg $FeSO_4{\cdot}7H_2O$, 16.0 mg $MnSO_4{\cdot}H_2O$, 14.0 mg $ZnSO_4{\cdot}7H_2O$, and 37.0 mg $CoCl_2{\cdot}6H_2O$. The culture was then incubated on a rotary shaker at 28 °C for 48 h.

After incubation, the mycelium was broken into pieces with a homogenizer. Then, 1 mL of the homogenate was inoculated into 4.0 g wheat bran, supplemented with the required volume of mineral salt buffer, which contained (g/L) 0.3 g urea, 0.75 g peptone, 1.4 g $(NH_4)_2SO_4$, 2.0 g $KH_2PO_4$, 0.4 g $CaCl_2{\cdot}2H_2O$, 0.5 g $MgSO_4{\cdot}7H_2O$, 5.0 mg $FeSO_4{\cdot}7H_2O$, 1.6 mg $MnSO_4{\cdot}H_2O$, 1.4 mg $ZnSO_4{\cdot}7H_2O$, and 3.7 mg $CoCl_2{\cdot}6H_2O$.

Fermentation was conducted for 21 days at 28 °C, with the substrate to moisture ratio of 1:1, 1:2, 1:3, and 1:4. At 24 h intervals, 40 mL of Tris-HCl buffer (50 mM, pH 8.5) was added to the fermented wheat bran, and the content was incubated at 25 °C and 200 rpm for 1 h with agitation. The culture suspension was squeezed through sterile absorbent gauze and centrifuged at 12 000 rpm and 4 °C for 30 min. Thus, the cell-free culture supernatant was obtained and assayed for $\beta$-glucosidase activity to study the time course of enzyme production. The enzyme activities were expressed as U/g solid.

**Enzyme Purification.** The cell-free culture broth supernatant was concentrated at 4 °C by ultrafiltration using Minitan Ultrafiltration System with a low-binding regenerated cellulose membrane (Millipore, Bedford, MA., U.S.A.). The supernatant was dialyzed against 20 mM Tris-HCl buffer (pH 7.5). The dialyzed enzyme solution was loaded onto a DEAE Sepharose FF column (10 × 200 mm, Amersham Pharmacia, Uppsala, Sweden) pre-equilibrated with 20 mM Tris-HCl buffer (pH 7.5). The column was washed with 0−0.3 M NaCl linear gradient at 0.8 mL/min. Then, the fractions with high specific activity were pooled and loaded onto a Superdex-75 column pre-equilibrated with 50 mM Tris-HCl buffer (pH 7.5) containing 0.2 M NaCl. The column was eluted with the same buffer at 1 mL/min. The active fractions were pooled and dialyzed against Tris-HCl buffer (50 mM, pH 7.5).

**Molecular Mass and pI Determination.** The apparent molecular mass of the denatured protein was estimated by sodium dodecyl sulfate polyacrylamide gel electrophoresis (SDS-PAGE) with 8% polyacrylamide gel. The molecular mass of the native protein was determined by dynamic light scattering system (Dynapro-99, ProteinSolution Corp.). The isoelectric point (pI) of the purified protein was determined by isoelectric focusing (IEF) in gels of 5% polyacrylamide, with 2% ampholine to obtain a pH range of 4 to 6, and 1 M $H_3PO_4$ and 1 M NaOH in anode and cathode, respectively. After IEF, the pH values were directly measured from the gel to obtain the pI calibration line. Proteins were stained with Coomassie brilliant blue R-250.

**Zymogram Analysis and Protein Deglycosylation.** For zymogram analysis, native-PAGE was separated on 8% polyacrylamide gel and the activity was measured by staining in 50 mM citrate-phosphate buffer (pH 4.5) with the use of 0.1% esculin hydrate (Bio Basic Inc., Canada) and 0.25% ferric ammonium citrate (Bio Basic Inc., Canada).

The enzymatic deglycosylation of BglW5 was performed by incubating the purified enzyme with endoglycosidase H (Endo H, New England BioLabs) following the manufacturer's instructions. After enzymatic treatment, the samples were analyzed by SDS-PAGE. Proteins were stained with Coomassie brilliant blue R-250.

**Enzyme Assays.** The protein concentration was assayed at $A_{595}$ based on the Bradford method with bovine serum albumin as the standard, following the manufacturer's instructions (Sangon Biotech, Co., Ltd., China). $\beta$-Glucosidase activity was assayed using *p*NPG as substrate. The reaction mixture contained 25 $\mu$L of appropriately diluted enzyme, 25 $\mu$L of 10 mM *p*NPG and 450 $\mu$L of 50 mM citrate-phosphate buffer (pH 4.5). After incubation at 70 °C for 10 min, the reaction was stopped by adding ice-cold 0.5 mL of 1 M $Na_2CO_3$, and the enzymatic activity was monitored at 405 nm for the amount of *p*-nitrophenol released. One unit of enzymatic activity (U) was defined as that the amount of enzyme that produced 1 $\mu$mol of *p*-nitrophenol per minute in the reaction mixture under the described assay conditions.

The alternative natural glycoside substrates used for the measurement of $\beta$-glucosidase activity were cellobiose, laminaribiose, sucrose, maltose, lactose, and trehalose. The assay mixture consisted of 25 $\mu$L of appropriately diluted enzyme and 475 $\mu$L of 50 mM citrate−$Na_2HPO_4$ buffer (pH 4.5) containing 5 mM of the specific glycoside substrate. The reaction mixtures were incubated at 70 °C for 30 min, and the amount of glucose released in each mixture was monitored using glucose oxidase/peroxidase reagent according to the manufacturer's instruction (Shanghai Rongsheng Biotech Co., Ltd., China).

**Effects of pH and Temperature on BglW5.** The optimum pH of the purified $\beta$-glucosidase activity was determined at varying pH values ranging from 3.0 to 7.0 by using 50 mM citrate−$Na_2HPO_4$ buffer supplemented with 10 mM *p*NPG or 5 mM cellobiose as substrate. The relative activity was determined. For pH stability assay, the enzyme was preincubated in 50 mM citrate−$Na_2HPO_4$ buffer (pH 3.0 to pH 7.0), or Tris-HCl (pH 7.0 to pH 8.5) buffer at 25 °C for 96 h. The residual activities at different pH levels were determined with 10 mM *p*NPG as substrate. The optimal temperature of BglW5 was measured using *p*NPG or cellobiose as substrate by incubating the reaction mixture for 10 min at varying temperatures ranging from 45 to 85 °C. The enzyme stabilities against temperature were established by incubating the enzyme in 50 mM citrate-phosphate buffer (pH 4.5) under 50 °C, 60 and 70 °C. The residual activities were estimated every hour using 10 mM *p*NPG as substrate.

**Effects of Metal Ions and Chemical Reagents on BglW5 Activity.** The effects of metal ions and chemicals on enzyme activity was measured using *p*NPG as substrate under standard enzyme assay conditions in the presence of $Ca^{2+}$, $Na^+$, $Co^{2+}$, $Mn^{2+}$, $Zn^{2+}$, $Cu^{2+}$, $Fe^{2+}$, $K^+$, $Mg^{2+}$, ethylene diamine tetraacetic acid (EDTA) and sodium dodecyl sulfate (SDS) at concentration of 5 mM and 10 mM, respectively. The relative activity, defined as the activity value relative to the activity of control (without any effector), was also determined using *p*NPG as substrate.

**Determination of Kinetic Parameters.** To determine the kinetic parameters ($K_m$, $V_{max}$, and $K_{cat}/K_m$), appropriate concentration of BglW5 was used under the optimal conditions. The reaction was performed by incubating 0.187 $\mu$g enzyme in 50 mM citrate−$Na_2HPO_4$ (pH 4.5) containing *p*NPG at five concentrations in the range 0.1−1.0 mM, at 70 °C for 10 min. For determination of the kinetic parameters toward cellobiose and laminaribiose, 1.87 $\mu$g purified enzyme was assayed with the substrate at concentrations ranging from 0.1 to 1.0 mM under optimal conditions.

Various concentrations of pure soy isoflavones, daidzin (from 0.1 to 1.0 mM), glycitin (from 0.05 to 1.0 mM), and genistin (from 0.05 to 1.0 mM) were used to determine the kinetic parameters. The reactions were performed in 50 mM citrate-phosphate buffer (pH 5.5) containing 0.4 $\mu$g enzyme at 50 °C for 5 min. The amount of isoflavone aglycones was determined by HPLC assay.

All of the $K_m$ and $V_{max}$ values were calculated by the Lineweaver−Burk equation. The catalytic constant, $K_{cat}$ is equal to $V_{max}$ divided by the total enzyme molar concentration calculated by using the molecular weight of the purified enzyme (105 kDa). The kinetic parameters are given as the mean ± standard deviation of the values calculated from three different experiments ($n$ = 3).

**Effects of Monosaccharides on Bglw5 Activity.** The effects of monosaccharides were evaluated by determining the activities of

BglW5 toward *p*NPG in the presence of glucose (0 mM to 100 mM), xylose (0 to 1.8 M), and fructose (0 to 3.5 M).

The kinetic parameters ($K_m$, $V_{max}$, and $K_{cat}/K_m$) for *p*NPG hydrolysis in the presence of different concentrations of xylose or fructose were estimated under optimal conditions.

**Preparation of Soy Isoflavones Flour Extract.** To evaluate the potential application of BglW5, the commercial soy isoflavone flour (Sinosoy40) was used as substrate for bioconversion. Soy isoflavone flour was produced from soybean cake and contained 10.08% daidzin, 26.85% genistin, 1.6% glycitin, and 3.88% of isoflavone aglycones according to the material data sheet of the manufacturer. According to the method of Rostagno et al., acetonitrile, ethanol, and methanol mixed with certain amount of water are the most used solvents to extract isoflavones.[20] In our study, 50% (v/v) ethanol was used to extract isoflavones from Sinosoy40. Briefly, 1 g of Sinosoy40 flour was dispersed in 5 mL of 50% (v/v) ethanol. The ethanol extract was incubated in an ultrasonic bath at 60 °C for 30 min and then centrifuged at 15 000 rpm for 5 min. The supernatant was stored at 4 °C for further assays.

**Enzymatic Hydrolysis of Soy Isoflavones Flour Extract.** For analysis of hydrolysis products, 0.5 mL reaction mixture was performed at 20 °C, 40 °C, and 60 °C in 50 mM citrate-phosphate buffer (pH 5.5), containing 0.045U β-glucosidase, and 100 μL soybean isoflavone flour extract (containing 1.08 mg daidzin and 0.93 mg genistin). The reaction was stopped by adding 4.5 mL of 50% (v/v) ethanol, and the mixture was centrifuged at 12 000 rpm for 20 min. The supernatant was filtered through a 0.22 μm filter for the quantification of isoflavones by HPLC analysis. Reactions with heat-inactivated (20 min in boiling water bath) enzyme were used as controls.

The productivity (mM/h) was defined as the increase in the concentration of isoflavone aglycones produced in 1 h.[21]

The hydrolysis rate was calculated using the following equation:[22]

$$\text{hydrolysis rate (\%)} = 100 \times (\text{isoflavone glycosides in control samples} - \text{isoflavone glycosides in hydrolyzed samples})/\text{isoflavone glycosides in control samples}$$

**HPLC Analysis of Isoflavones.** Isoflavones were assayed using an Agilent Eclipse Plus C18 column on an HPLC system (Agilent Corp., Palo Alto, CA) equipped with a UV detector set at 254 nm. The column was eluted with a gradient of solvent A (0.1% acetic acid in water) and solvent B (0.1% acetic acid in acetonitrile) at 25 °C. Following injection of 20 μL of the sample, solvent B was gradually increased from 5% to 100% over 60 min. The solvent flow rate was 0.5 mL/min. The peaks of daidzin, glycitin, and genistin, as well as their corresponding isoflavone aglycones, were identified by comparing their elution profile with those of the commercial standards (Sigma Chemical Co., U.S.A.).

## RESULTS AND DISCUSSION

**Production of β-Glucosidase BglW5.** The order of Mucorales consists of genera such as *Mucor*, *Rhizopus*, and *Rhizomucor*, from which some β-glucosidases with excellent features were isolated. Although belonging to the order of Mucorales, Cunninghamellaceae is distinguished from other families. No β-glucosidase-producing fungus has been isolated from this family. Thus, for the first time, β-glucosidase BglW5 was identified from the genus *Gongronella*, family Cunninghamellaceae. Under SSF condition, the maximum activity of 49.9 U/g solid was obtained on ninth day at 28 °C, with the substrate to moisture ratio of 1:2 (Figure S1 in the Supporting Information). Since *Gongronella* sp.W5 was isolated from the soil, its growth and enzyme expression in solid-state is comparable to the natural conditions of the fungus. Thus, under SSF, *Gongronella* sp.W5 is a good producer of β-glucosidase, similar to some known zygomycetous producers from the genera *Gilbertella*, *Mucor*, *Rhizomucor*, and *Rhizopus*, with the β-glucosidase yields of 6 U/g to 426 U/g wheat bran.[9]

Several studies showed that the filamentous fungi from *Gongronella* sp. were good producers of chitosanases.[17,18] Here we reported the isolation of a β-glucosidase from *Gongronella* sp. The chitinolytic and glucanolytic enzyme system may be involved in the metabolism of endogenous or exogenous fungal cell wall polysaccharides to provide the carbon and nitrogen source for fungi.[13] With regard to the distribution of the fungus in soil and its saprotrophic lifestyle, the ability to express glycoside hydrolases may be an adaptation of *Gongronella* sp. to its environment.

**β-Glucosidase Purification.** β-Glucosidase BglW5 was purified from the culture supernatant of *Gongronella* sp.W5 by ultrafiltration, ion exchange and gel filtration chromatography. As shown in Table 1, the enzyme was 5.5-fold purified to a specific activity of 59.0 U/mg with a yield of 2%.

**Table 1. Purification of β-Glucosidase BglW5 from *Gongronella* sp. W5**

| purification steps | total activity (U) | total protein (mg) | specific activity (U/mg) | yield (%) | purification (fold) |
|---|---|---|---|---|---|
| crude extract | 3498 | 321 | 10.8 | 100 | 1 |
| ultrafiltration | 2493 | 185 | 13.5 | 71 | 1.3 |
| DEAE sepharose FF | 600 | 40 | 15.0 | 17 | 1.4 |
| superdex-75 | 83 | 1.4 | 59.0 | 2 | 5.5 |

The purified enzyme exhibited one single band in SDS-PAGE and the apparent molecular weight was approximately 105 kDa (Figure 1A), which is located within the broad range of molecular weights of fungal β-glucosidases (35 kDa to 250 kDa).[22] By dynamic light scattering analysis, the particle size of native BglW5 was assumed to be 4.3 nm with particle dispersion index (PDI) of 13.5%. According to the particle size, the molecular mass of native BglW5 was estimated to be

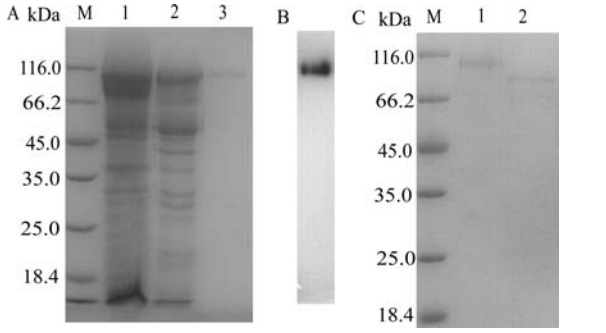


**Figure 1.** SDS-PAGE and native-PAGE analysis of β-glucosidase BglW5. (A) SDS-PAGE analysis of each purification step. M, Protein molecular weight marker (Thermo Fisher Scientific, Inc.); lane 1, crude extract; lane 2, purified BglW5 after DEAE sepharose; lane 3, purified BglW5 after Superdex-75. (B) Native-PAGE analysis of BglW5. BglW5 was stained using 0.1% esculin hydrate and 0.25% ferric ammonium citrate in 50 mM citrate−$Na_2HPO_4$ buffer (pH 4.5). (C) SDS-PAGE analysis of BglW5 hydrolyzed with endoglycosidase H (Endo H). Lane 1, BglW5 without Endo H treatment; lane 2, Endo H treated BglW5. The reduction in molecular mass indicates the presence of the N-glycosylation modification.

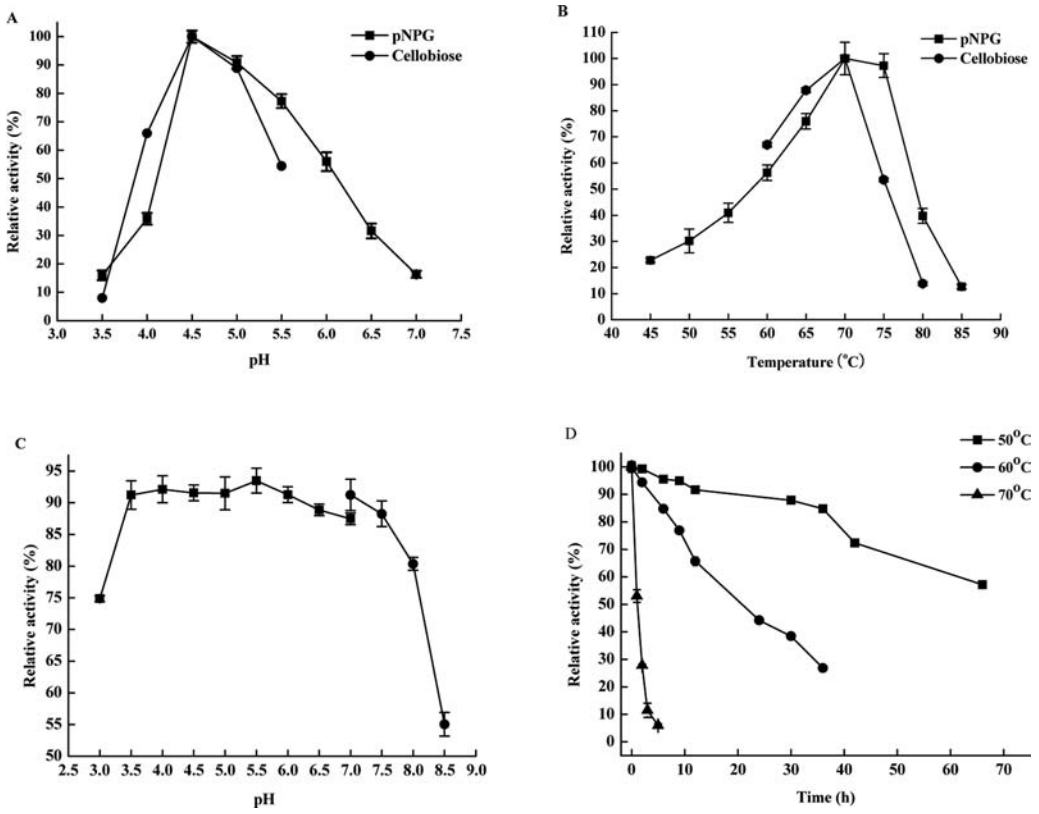


**Figure 2.** Effects of pH and temperature on the activity and stability of $\beta$-glucosidase BglW5. (A) Optimum pH of BglW5. The optimum pH was determined at varying pH levels ranging from 3.0 to 7.0 with *p*NPG or cellobiose as substrate. (B) Optimum temperature of BglW5. The optimal temperature of the enzyme was measured at various temperatures (45 to 85 °C) with *p*NPG or cellobiose as substrate. (C) Effect of pH on enzyme stability. The purified enzyme was preincubated in 50 mM citrate−$Na_2HPO_4$ buffer (pH 3.0−7.0) or Tris-HCl (pH 7.0−8.5) buffer at 25 °C for 96 h, and the remaining activities were measured using *p*NPG as substrate. (D) Effect of temperature on enzyme stability. The purified enzyme was incubated at 50 °C, 60 or 70 °C, and the remaining activity was determined using *p*NPG as substrate. All figures are the average of results from triplicate experiments.

100 kDa, indicating the presence of a monomeric protein. Consistent with this result, native-PAGE showed that the enzyme exhibited activity in the form of monomer (Figure 1B). After treated with Endo H, the molecular weight shifted to 89 kDa, which indicated that the molecular mass was increased about 16 kDa by N-glycosylation (Figure 1C). By IEF analysis, the pI value was estimated to be 4.6.

**Biochemical Properties of BglW5.** The biochemical properties of BglW5 were evaluated. BglW5 exhibited its highest activity at pH 4.5 and 70 °C with *p*NPG or cellobiose as substrates (Figure 2A and B). The enzyme was stable in the pH range from 3.0 to 8.5 at 25 °C for 96 h, maintaining more than 50% of its maximal activity (Figure 2C). Analysis of enzyme activity using *p*NPG as substrate demonstrated that Bglw5 maintained approximately 50% residual activity for 20 h at 60 °C. When incubated at 70 °C, the half-life of BglW5 was 1 h (Figure 2D). The high thermostability of BglW5 is comparable with the enzymes from some thermophilic fungi.[23] Since most applications of $\beta$-glucosidases require higher temperature (50 °C or above),[3,24] BglW5 should have high potential for use as catalysts in industrial bioconversion processes for its thermostability.

The effect of metal ions on BglW5 activity was investigated (Table 2). Significant inactivation was observed by adding $Cu^{2+}$ or $Fe^{2+}$. Interestingly, the activity of BglW5 was stimulated up to 126% in the presence of 10 mM $Mn^{2+}$. BglW5 retained more than 80% of its activity after addition of 10 mM $K^+$, $Zn^{2+}$, $Co^{2+}$, $Mg^{2+}$, $Ca^{2+}$, or $Na^+$, respectively. It is also noted that SDS completely inhibited the activity of BglW5, whereas EDTA only slightly decreased the enzyme activity, implicating that the enzyme is not a metalloprotein.

**Table 2. Effects of Metal Ions and Reagents on Activities of BglW5**[a]

| | relative activity (%) | |
|---|---|---|
| substances | 5 mM | 10 mM |
| $Mn^{2+}$ | 107.62 ± 1.83 | 125.87 ± 3.17 |
| $Na^+$ | 94.53 ± 0.17 | 94.28 ± 2.58 |
| $K^+$ | 93.76 ± 1.10 | 93.43 ± 0.67 |
| $Co^{2+}$ | 90.35 ± 0.51 | 89.62 ± 0.85 |
| $Mg^{2+}$ | 90.75 ± 1.03 | 89.38 ± 1.71 |
| $Zn^{2+}$ | 97.45 ± 1.89 | 89.09 ± 0.50 |
| $Ca^{2+}$ | 93.43 ± 1.72 | 87.92 ± 1.10 |
| $Cu^{2+}$ | 62.17 ± 2.92 | 0 |
| $Fe^{2+}$ | 0 | 0 |
| EDTA | 93.43 ± 0.65 | 85.78 ± 1.06 |
| SDS | 40.21 ± 0.26 | 0 |

[a]Data are expressed as the mean of three experiments ± standard deviation ($n$ = 3).

**Substrate Specificity of BglW5.** Among the saccharides tested, laminaribiose ($\beta$-1,3-linked glucose) and cellobiose ($\beta$-1,4-linked glucose) were the preferred substrates, with similar affinity ($K_m$) values of 1.66 ± 0.02 mM and 1.67 ± 0.03 mM,

respectively (Table 3). However, the higher $K_{cat}/K_m$ of laminaribiose indicated that BglW5 exhibited higher catalytic

**Table 3. Kinetic Parameters of BglW5 Towards Different Substrates**[a]

| substrates | $K_m$ (mM) | $K_{cat}$ ($s^{-1}$) | $K_{cat}/K_m$ ($s^{-1}$ $mmol^{-1}$ L) |
|---|---|---|---|
| *p*NPG | 0.39 ± 0.02 | 19.60 ± 0.98 | 50.26 ± 2.25 |
| cellobiose | 1.67 ± 0.03 | 17.38 ± 0.63 | 10.41 ± 0.20 |
| laminaribiose | 1.66 ± 0.02 | 60.61 ± 0.65 | 36.50 ± 1.66 |
| daidzin | 1.20 ± 0.04 | 328.13 ± 6.90 | 273.52 ± 4.51 |
| glycitin | 0.59 ± 0.02 | 122.50 ± 6.19 | 207.63 ± 10.49 |
| genistin | 1.30 ± 0.03 | 323.75 ± 12.37 | 249.04 ± 9.52 |

[a]The kinetic parameters were determined at the optimal pH and temperature, with the substrate concentrations ranging from 0.05 to 1.0 mM. Data are expressed as the mean of three experiments ± standard deviation ($n$ = 3).

efficiency toward the disaccharide with $\beta$ (1 → 3) linkage than $\beta$ (1 → 4) linkage. In general, $\beta$-glucosidases show stronger activity toward oligosaccharides with $\beta$ (1 → 4) linkages, but several $\beta$-glucosidases, such as the enzymes from *Aspergillus fumigatus*,[23] *Trichoderma koningii*,[23] and *Nasutitermes takasagoensis*,[25] exhibit relatively higher activity toward glucans with $\beta$ (1 → 3) linkages. Such enzymes may be involved not only in cellulose breakdown with cellobiase activity but also in other biological functions with $\beta$-1,3-glucanolytic activity. By using the Carbohydrate Active enzyme (CAZy) annotation analysis of the *Rhizopus oryzae* genome, several candidate protein-encoding ORFs of $\beta$-glucosidase related to exo-1,3-$\beta$-glucanases were identified, which indicated a potential role of $\beta$-glucosidases in the degradation of cell walls of ascomycetes and basidiomycetes, whose cell walls are riched in $\beta$-1,3-glucans.[13] The fact that BglW5 showed high activity toward the disaccharide with $\beta$ (1 → 3) linkage may be an indication that BglW5 is part of the glucanase complex, participating in the degradation of $\beta$-1,3 glucan in the environment to provide carbon and nitrogen source for the fungi.[13] Given that BglW5 exhibited both activities of laminaribiase and cellobiase, its importance in the hydrolysis of biomass is emphasized.[25] Furthermore, BglW5 showed no activity toward sucrose ($\alpha$-D-glucose-(1,2)-$\beta$-D-fructose), maltose ($\alpha$-1,4-linked glucose), and trehalose ($\alpha$-1,1-linked glucose).

Among the pure isoflavones tested, the most preferred substrate for BglW5 was glycitin, following the order glycitin > daidzin > genistin, similar to that of *Pyrococcus furiosus* $\beta$-glucosidase.[21] BglW5 showed the highest catalytic efficiency ($K_{cat}/K_m$) toward daidzin, indicating that daidzin was clearly the preferred substrate among the nonconjugated isoflavone glycosides.

**Effects of Monosaccharides on Enzyme Activity.** In the process of biological degradation of biomass, glucose yields are normally decreased in the presence of other monosaccharides, such as xylose, fructose, mannose, and galactose that are not end products of degradation.[26] Thus, the $\beta$-glucosidases activated by monosaccharides are a group of uncommon yet interesting enzymes,[27] which has the potential to remove a major bottleneck in the industrial application of $\beta$-glucosidases and to broaden their application range.[28] In the present study, BglW5 retained 65% of the maximum activity in the presence of glucose at a concentration up to 30 mM, which is close to the glucose concentration (~27 mM) retained in a simultaneous hydrolysis and fermentation process.[26] Interestingly, at a concentration of 0.5 M, both fructose and xylose significantly stimulated $\beta$-glucosidase activity with a maximal increase of approximately 2.2-fold and 1.6-fold, respectively (Figure 3). However, the activity of BglW5 was gradually inhibited as fructose and xylose concentration is further increased, with IC50 (the concentration of an inhibitor causing 50% activity reduction) of 1.8 M for xylose, and more than 3.5 M for fructose.

Although a few $\beta$-glucosidases with improved activity in the presence of xylose were identified from some thermophilic fungal sources,[29−31] no $\beta$-glucosidase has been reported to be stimulated by both xylose and fructose. To understand the effect of xylose and fructose on BglW5, the kinetic constants of BglW5 were determined in the presence of various concentrations of xylose and fructose (Table 4). The $K_m$ values of BglW5 toward *p*NPG gradually increased at stimulatory concentrations of xylose or fructose, indicating that monosaccharide compete with the substrate to bind to the catalytic site. Nonetheless, the catalytic activity of BglW5 was promoted. The uncommon properties of BglW5 activated by monosaccharides indicated that the monosaccharides may compete with the substrate for the catalytic site, meanwhile bind to some modulator binding site to induce conformational changes, and thus enhance the catalytic activity.[27] At higher monosaccharide

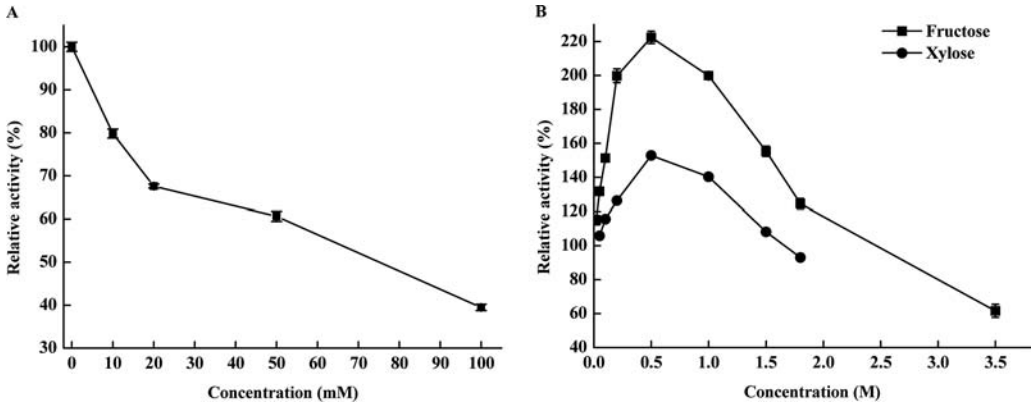


**Figure 3.** Effects of glucose (A), xylose, and fructose (B) on the enzyme activity. Influence of monosaccharide on enzyme activity was measured with *p*NPG as substrate in the presence of glucose, fructose or xylose at the concentrations indicated. All figures are the average of results from triplicate experiments.

**Table 4. Kinetic Parameters of BglW5 for Hydrolysis of *p*NPG in the Presence of Xylose or Fructose[a]**

| | monosaccharide (mol $L^{-1}$) | $K_m$ (mmol $L^{-1}$) | $V_{max}$ (U/mg) | $K_{cat}$ ($s^{-1}$) | $K_{cat}/K_m$ ($s^{-1}$ $mmol^{-1}$ L) |
|---|---|---|---|---|---|
| *p*NPG | 0 | 0.39 ± 0.02 | 11.76 ± 0.60 | 19.60 ± 0.98 | 50.26 ± 2.25 |
| fructose | 0.05 | 0.74 ± 0.01 | 20.59 ± 0.82 | 34.31 ± 1.36 | 46.37 ± 0.88 |
| | 0.50 | 1.87 ± 0.08 | 39.57 ± 1.13 | 59.42 ± 1.89 | 31.77 ± 0.34 |
| | 1.80 | 2.02 ± 0.13 | 34.58 ± 1.60 | 57.64 ± 2.27 | 28.50 ± 0.47 |
| | 3.50 | 2.70 ± 0.18 | 13.73 ± 0.76 | 22.88 ± 1.26 | 8.47 ± 0.08 |
| xylose | 0.05 | 2.22 ± 0.14 | 26.74 ± 1.51 | 44.56 ± 2.52 | 20.08 ± 0.14 |
| | 0.50 | 2.95 ± 0.15 | 56.15 ± 1.89 | 93.58 ± 3.51 | 31.80 ± 0.53 |
| | 1.00 | 3.76 ± 0.03 | 33.96 ± 0.38 | 56.6 ± 0.63 | 15.05 ± 0.05 |
| | 1.80 | 6.65 ± 0.20 | 26.47 ± 0.60 | 44.12 ± 1.15 | 6.63 ± 0.08 |

[a] $\beta$-Glucosidase activity was assayed using 0.187 $\mu$g protein at 70 °C in 50 mM citrate−$Na_2HPO_4$ buffer (pH 4.5), containing fructose or xylose at the concentrations indicated. Data are expressed as the mean of three experiments ± standard deviation ($n$ = 3).

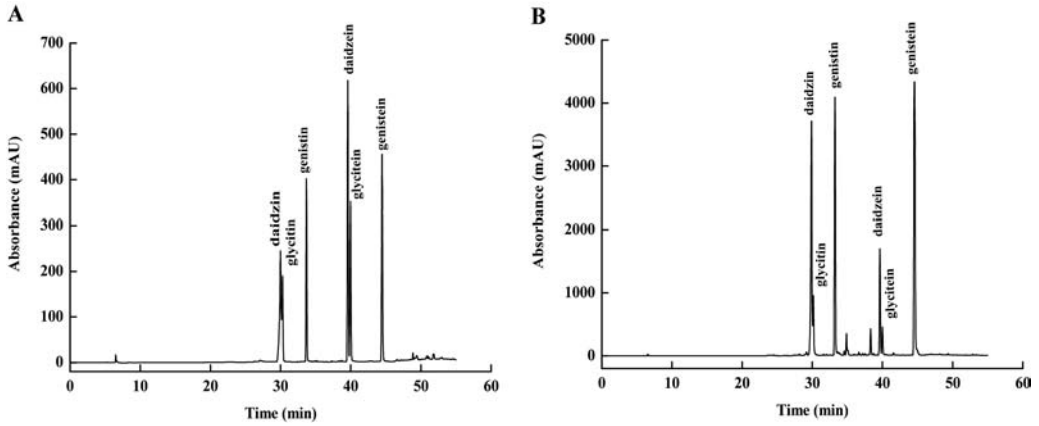


**Figure 4.** HPLC profiles for isoflavone standards and soy isoflavone flour extract. (A) HPLC profiles of daidzin, glycitin, genistin, daidzein, glycitein, and genistein. (B) HPLC profiles of soy isoflavone flour extract. One gram of sample was extracted by 5 mL of 50% (v/v) ethanol at 60 °C during 30 min on the ultrasonic bath.

concentrations, the competition for the catalytic site played a dominant role to decrease the apparent affinity of the enzyme to *p*NPG, which eventually inhibited the enzyme activity.

**Soy Isoflavone Flour Extraction.** Using ultrasound-assisted extraction, a total of 139.39 mg isoflavones was extracted from 1 g soy isoflavone flour, which consisted of 54.10 mg daidzin, 46.44 mg genistin, 13.46 mg glycitin, 15.30 mg daidzein, 2.70 mg glycitein, and 7.39 mg genistein (Figure 4). Daidzin and genistin were the predominant isoflavones in the extract, which occupied 72% of the total amount. Thus, enzymatic hydrolysis toward daidzin and genistin were evaluated in our study.

**Hydrolysis of Soy Isoflavone Flour Extract.** Enzymatic hydrolysis of $\beta$-glucosidases toward isoflavone glycosides is an important application with high commercial value,[3] which has been investigated by direct use of $\beta$-glucosidases from leguminous plants and microorganisms.[32−35] However, in industrial production of isoflavones, low solubility of isoflavones reduces the productivity of isoflavone aglycones.[36] To test the reactivity of BglW5 toward high concentration of isoflavones, the hydrolysis rate and the productivity were measured using isoflavone flour extract as substrate. As shown in Figure 5, BglW5 exhibited maximal hydrolytic activity for daidzin and genistin at 40 and 60 °C after 3 h treatment, with hydrolysis rate more than 96%. By comparison, the hydrolysis rate at 20 °C after 4 h was <50%. Due to its excellent thermostability, BglW5 exhibited effective hydrolysis of isoflavone glycosides at 60 °C within 3 h, with the hydrolysis rates of 96.2% and 96.7%, respectively. Temperature has been

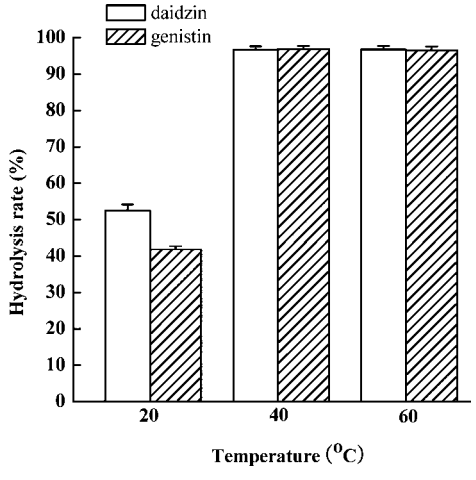


**Figure 5.** Hydrolysis rates of BglW5 toward daidzin and genistin in soy isoflavone flour extract. The reactions were performed in 50 mM citrate−$Na_2HPO_4$ buffer (pH 5.5) containing 0.045 U $\beta$-glucosidase, and isoflavone glucosides (5.20 mM daidzin and 4.30 mM genistin). All figures are the average of results from triplicate experiments.

reported to be a significant factor influencing the extraction of soy isoflavones.[20] Higher extraction efficiencies of isoflavone glycosides were obtained at relatively higher temperatures (e.g., 60∼80 °C).[20,37] Thus, BglW5 offers an advantage for the hydrolysis process of isoflavone glycosides at higher temperature, in which heat treatment of substrates is desirable.

Table 5. Conversion Efficiency of Isoflavone Glycosides to the Aglycone by β-Glucosidases

| substrate | source | daidzin (mM) | daidzein (mM) | genistin (mM) | genistein (mM) | productivity (mM/h) daidzein | productivity (mM/h) genistein | ref |
|---|---|---|---|---|---|---|---|---|
| daidzin | *Sulfolobus solfataricus* | 1.00 | 1.00 | NR | NR | 1.00 | NR | 34 |
| daidzin and genistin | unculturable microbes | 0.50[a] | NR | 0.50[a] | NR | 0.60 | 0.58 | 3 |
| soybean flour extract | *Pyrococcus furiosus* | 0.90 | NR | 1.00 | NR | 0.80 | 1.00 | 21 |
| soybean flour extract | *Aspergillus oryzae* | 2.50 | 1.83 | 1.20 | 0.54 | 0.61 | 0.11 | 35 |
| soy isoflavone flour extract | *Gongronella* sp.W5 | 5.00 | 4.50 | 4.10 | 3.70 | 1.50 | 1.23 | this study |

[a]mg/mL. NR, not reported.

As shown in Table 5, BglW5 converted 5.0 mM daidzin and 4.1 mM genistin to aglycones, with the productivities of 1.5 mM/h for daidzein and 1.23 mM/h for genistein, respectively. Although the experimental conditions and the components of isoflavone glycosides extracted were different, BglW5 exhibited higher productivities than *Aspergillus oryzae* β-glucosidase when using high concentration of isoflavones as substrate.[36] These results showed that BglW5 from *Gongronella* sp. can efficiently convert high concentrations of isoflavone glycosides into aglycones.

In summary, a novel β-glucosidase, BglW5 from *Gongronella* sp. was identified, purified, and characterized for the first time. The enzyme exhibited pH-stability and thermostability, and it displayed enhanced activity in the presence of fructose and xylose. Considering its high hydrolysis rate and high productivity on isoflavone glycosides, BglW5 is a promising candidate for enzymatic hydrolysis of soybean isoflavone glycosides.

## ■ ASSOCIATED CONTENT

### Supporting Information

Figure S1, BglW5 produced by *Gongronella* sp.W5 under solid state fermentation (SSF). This material is available free of charge via the Internet at http://pubs.acs.org.

## ■ AUTHOR INFORMATION


### Corresponding Authors

*Phone/fax: 86-551-63861861. E-mail: zemin_fang@163.com.
*Phone/fax: 86-551-63861861. E-mail: xiaoyazh@sina.com.



### Funding

This work was supported by grants from the National High Technology Research and Development Program of China (No. 2014AA093515); the National Natural Science Foundation of China (No. 31300062); the Key Scientific and Technological project of Anhui Province (1301032154); the Introduction Project of Academic and Technology Leaders in Anhui University (32030066); and the Innovative Research Team Program of 211 Project in Anhui University.


### Notes

The authors declare no competing financial interest.

## ■ REFERENCES


(1) Krisch, J.; Bencsik, O.; Papp, T.; Vágvölgyi, C.; Takó, M. Characterization of a β-glucosidase with transgalactosylation capacity from the zygomycete *Rhizomucor miehei*. *Bioresour. Technol.* **2012**, *114*, 555−560.

(2) Park, A. R.; Hong, J. H.; Kim, J. J.; Yoon, J. J. Biochemical characterization of an extracellular β-glucosidase from the fungus, *Penicillium italicum*, isolated from rotten citrus peel. *Mycobiology* **2012**, *40*, 173−180.

(3) Li, G.; Jiang, Y.; Fan, X. J.; Liu, Y. H. Molecular cloning and characterization of a novel β-glucosidase with high hydrolyzing ability for soybean isoflavone glycosides and glucose-tolerance from soil metagenomic library. *Bioresour. Technol.* **2012**, *123*, 15−22.

(4) Ketudat Cairns, J. R.; Esen, A. β-Glucosidases. *Cell. Mol. Life Sci.* **2010**, *67*, 3389−3405.

(5) Baldrian, P.; Valášková, V. Degradation of cellulose by basidiomycetous fungi. *FEMS Microbiol. Rev.* **2008**, *32*, 501−521.

(6) Gong, G.; Zheng, Z.; Liu, H.; Wang, L.; Diao, J.; Wang, P.; Zhao, G. Purification and characterization of a β-glucosidase from *Aspergillus niger* and its application in the hydrolysis of geniposide to genipin. *J. Microbiol. Biotechnol.* **2014**, *24*, 788−789.

(7) Dashtban, M.; Schraft, H.; Qin, W. Fungal bioconversion of lignocellulosic residues: opportunities & perspectives. *Int. J. Biol. Sci.* **2009**, *5*, 578−595.

(8) Takó, M.; Tóth, A.; Nagy, L.; Krisch, J.; Vágvölgyi, C.; Papp, T. A new β-glucosidase gene from the zygomycete fungus *Rhizomucor miehei*. *Antonie. Van. Leeuwenhoek.* **2010**, *97*, 1−10.

(9) Takó, M.; Farkas, E.; Lung, S.; Krisch, J.; Vágvölgyi, C.; Papp, T. Identification of acid- and thermotolerant extracellular β-glucosidase activities in zygomycetes fungi. *Acta. Biol. Hung.* **2010**, *61*, 101−110.

(10) Borgia, P. I.; Mehnert, D. W. Purification of a soluble and a wall-bound form of β-glucosidase from *Mucor racemosus*. *J. Bacteriol.* **1982**, *149*, 515−522.

(11) Karmakar, M.; Ray, R. R. A statistical approach for optimization of simultaneous production of β-glucosidase and endoglucanase by *Rhizopus oryzae* from solid-state fermentation of water hyacinth using central composite design. *Biotechnol. Res. Int.* **2011**, 574983 DOI: 10.4061/2011/574983.

(12) Tsuneo, W. Diversities of fungi. In *Pictorial Atlas of Soil and Seed Fungi: Morphologies of Cultured Fungi and Key to Species*, 2nd revised ed.; CRC Press Inc: Boca Raton, FL, 2002; pp 3−7.

(13) Battaglia, E.; Benoit, I.; van den Brink, J.; Wiebenga, A.; Coutinho, P. M.; Henrissat, B.; de Vries, R. P. Carbohydrate-active enzymes from the zygomycete fungus *Rhizopus oryzae*: A highly specialized approach to carbohydrate degradation depicted at genome level. *BMC Genomics* **2011**, *12*, 38 DOI: 10.1186/1471-2164-12-38.

(14) Espagne, E.; Lespinet, O.; Malagnac, F.; Da Silva, C.; Jaillon, O.; Porcel, B. M.; Couloux, A.; Aury, J. M.; Segurens, B.; Poulain, J.; et al. The genome sequence of the model ascomycete fungus *Podospora anserina*. *Genome Biol.* **2008**, *9*, R77.

(15) Martinez, D.; Challacombe, J.; Morgenstern, I.; Hibbett, D.; Schmoll, M.; Kubicek, C. P.; Ferreira, P.; Ruiz-Duenas, F. J.; Martinez, A. T.; Kersten, P.; et al. Genome, transcriptome, and secretome analysis of wood decay fungus *Postia placenta* supports unique mechanisms of lignocellulose conversion. *Proc. Natl. Acad. Sci. U.S.A.* **2009**, *106*, 1954−1959.

(16) Martin, F.; Aerts, A.; Ahren, D.; Brun, A.; Danchin, E. G.; Duchaussoy, F.; Gibon, J.; Kohler, A.; Lindquist, E.; Pereda, V.; et al. The genome of *Laccaria bicolor* provides insights into mycorrhizal symbiosis. *Nature* **2008**, *452*, 88−92.

(17) Wang, J.; Zhou, W.; Yuan, H.; Wang, Y. Characterization of a novel fungal chitosanase Csn2 from *Gongronella* sp. JG. *Carbohydr. Res.* **2008**, *343*, 2583−2588.

(18) Zhou, W.; Yuan, H.; Wang, J.; Yao, J. Production, purification and characterization of chitosanase produced by *Gongronella* sp. JG. *Lett. Appl. Microbiol.* **2008**, *46*, 49−54.
(19) Wei, F.; Hong, Y.; Liu, J.; Yuan, J.; Fang, W.; Peng, H.; Xiao, Y. *Gongronella* sp. induces overproduction of laccase in *Panus rudis*. *J. Basic Microbiol.* **2010**, *50*, 98−103.
(20) Rostagno, M. A.; Palma, M.; Barroso, C. G. Ultrasound-assisted extraction of soy isoflavones. *J. Chromatogr. A* **2003**, *1012*, 119−128.
(21) Yeom, S. J.; Kim, B. N.; Kim, Y. S.; Oh, D. K. Hydrolysis of isoflavone glycosides by a thermostable β-glucosidase from *Pyrococcus furiosus*. *J. Agric. Food Chem.* **2012**, *60*, 1535−1541.
(22) Song, X.; Xue, Y.; Wang, Q.; Wu, X. Comparison of three thermostable β-glucosidases for application in the hydrolysis of soybean isoflavone glycosides. *J. Agric. Food Chem.* **2011**, *59*, 1954−1961.
(23) Eyzaguirre, J.; Hidalgo, M.; Leschot, A. β-Glucosidases from filamentous fungi: Properties, structure, and applications. In *Handbook of Carbohydrate Engineering*; Yarema, K. J., Ed.; CRC Press Inc: Boca Raton, FL, 2005; pp 645−675.
(24) Li, D.; Li, X.; Dang, W.; Tran, P. L.; Park, S. H.; Oh, B. C.; Hong, W. S.; Lee, J. S.; Park, K. H. Characterization and application of an acidophilic and thermostable β-glucosidase from *Thermofilum pendens*. *J. Biosci. Bioeng.* **2013**, *115*, 490−496.
(25) Uchima, C. A.; Tokuda, G.; Watanabe, H.; Kitamoto, K.; Arioka, M. Heterologous expression in *Pichia pastoris* and characterization of an endogenous thermostable and high-glucose-tolerant β-glucosidase from the termite *Nasutitermes takasagoensis*. *Appl. Environ. Microbiol.* **2012**, *78*, 4288−4293.
(26) Hsieh, C. W.; Cannella, D.; Jørgensen, H.; Felby, C.; Thygesen, L. G. Cellulase inhibition by high concentrations of monosaccharides. *J. Agric. Food Chem.* **2014**, *62*, 3800−3805.
(27) Souza, F. H. M.; Inocentes, R. F.; Ward, R. J.; Jorge, J. A.; Furriel, R. P. M. Glucose and xylose stimulation of a β-glucosidase from the thermophilic fungus *Humicola insolens*: A kinetic and biophysical study. *J. Mol. Catal. B Enzym.* **2013**, *94*, 119−128.
(28) Xu, H.; Xiong, A. S.; Zhao, W.; Tian, Y. S.; Peng, R. H.; Chen, J. M.; Yao, Q. H. Characterization of a glucose-, xylose-, sucrose-, and D-galactose-stimulated β-glucosidase from the alkalophilic bacterium *Bacillus halodurans* C-125. *Curr. Microbiol.* **2011**, *62*, 833−839.
(29) Masui, D. C.; Zimbardi, A. L.; Souza, F. H.; Guimarães, L. H.; Furriel, R. P.; Jorge, J. A. Production of a xylose-stimulated β-glucosidase and a cellulase-free thermostable xylanase by the thermophilic fungus *Humicola brevis* var. *thermoidea* under solid state fermentation. *World J. Microbiol. Biotechnol.* **2012**, *28*, 2689−2701.
(30) Souza, F. H. M.; Nascimento, C. V.; Rosa, J. C.; Masui, D. C.; Leone, F. A.; Jorge, J. A.; Furriel, R. P. M. Purification and biochemical characterization of a mycelial glucose-and xylose-stimulated β-glucosidase from the thermophilic fungus *Humicola insolens*. *Proc. Biochem.* **2010**, *45*, 272−278.
(31) Zanoelo, F. F.; Polizeli, M. L.; Terenzi, H. F.; Jorge, J. A. β-Glucosidase activity from the thermophilic fungus *Scytalidium thermophilum* is stimulated by glucose and xylose. *FEMS Microbiol. Lett.* **2004**, *240*, 137−143.
(32) Kaya, M.; Ito, J.; Kotaka, A.; Matsumura, K.; Bando, H.; Sahara, H.; Ogino, C.; Shibasaki, S.; Kuroda, K.; Ueda, M.; Kondo, A.; Hata, Y. Isoflavone aglycones production from isoflavone glycosides by display of β-glucosidase from *Aspergillus oryzae* on yeast cell surface. *Appl. Microbiol. Biotechnol.* **2008**, *79*, 51−60.
(33) Yang, S.; Wang, L.; Yan, Q.; Jiang, Z.; Li, L. Hydrolysis of soybean isoflavone glycosides by a thermostable β-glucosidase from *Paecilomyces thermophila*. *Food Chem.* **2009**, *115*, 1247−1252.
(34) Kim, B. N.; Yeom, S. J.; Kim, Y. S.; Oh, D. K. Characterization of a β-glucosidase from *Sulfolobus solfataricus* for isoflavone glycosides. *Biotechnol. Lett.* **2012**, *34*, 125−129.
(35) Chuankhayan, P.; Rimlumduan, T.; Svasti, J.; Cairns, J. R. Hydrolysis of soybean isoflavonoid glycosides by *Dalbergia* β-glucosidases. *J. Agric. Food Chem.* **2007**, *55*, 2407−2412.
(36) Horii, K.; Adachi, T.; Matsuda, T.; Tanaka, T.; Sahara, H.; Shibasaki, S.; Ogino, C.; Hatad, Y.; Ueda, M.; Kondo, A. Improvement of isoflavone aglycones production using β-glucosidase secretory produced in recombinant *Aspergillus oryzae*. *J. Mol. Catal. B Enzym.* **2009**, *59*, 297−301.
(37) Xue, Y.; Yu, J.; Song, X. Hydrolysis of soy isoflavone glycosides by recombinant β-glucosidase from hyperthermophile *Thermotoga maritima*. *J. Ind. Microbiol. Biotechnol.* **2009**, *36*, 1401−1408.

At the molecular level, OSA substitution positions on anhydroglucosyl units varied for the modified starches by esterification reaction with different physical forms. For chemically modified granular starch, the OSA group was found to preferentially occur on the C-2 and C-3 hydroxyl groups of anhydroglucosyl units, and OSA group distribution was not uniform at the branch level of amylopectin.[23,25] However, OSA substitutions were grafted at C-2, C-3, and C-6 hydroxyl groups as well as the reducing ends of modified maltodextrin.[25]

Although the preparation and physicochemical properties of OSA modified starch have been studied extensively, little work has been reported on the substituted ester group position in OSA modified soluble starch. In this study, OSA starches with low and high degrees of substitution were prepared from sugary maize soluble starch. The substituted starches were hydrolyzed using amyloglucosidase followed by instrumental analysis. The OSA substituent distribution in modified soluble starch was deduced from the comprehensive analyses, which would be helpful in designing a modified starch with tailored functional properties.

## MATERIALS AND METHODS

**Materials.** Sugary-1 maize kernels were purchased from the Chinese Academy of Agricultural Sciences (Beijing, China). Octenylsuccinic anhydride (catalog no. 416487, 97%) and amyloglucosidase from *Rhizopus* sp. (catalog no. A9228, ≥40 units/mg solid) were purchased from Sigma-Aldrich Chemical Co. (St. Louis, MO, USA). All chemicals were of reagent grade and were obtained from Sinopharm Chemical Reagent Co., Ltd. (Shanghai, China).

**Methods.** *Isolating Soluble Starch from Sugary-1 Maize.* The sugary maize soluble starch (SMSS) was isolated from sugary maize in the laboratory following the methods described in a previous study.[5] The sugary-1 maize fresh kernels were dehulled, and endosperm was separated from germ and soaked in 5 times their weight of deionized water at 20 °C overnight. The softened grains were ground in a laboratory blender. The mixture was filtered through 100-mesh sieves and then centrifuged at 10000*g* for 10 min. The supernatant was collected, and the sediment was extracted twice with deionized water. The resulting decantate was heated in a boiling water bath for 30 min to denature the protein. After centrifugation, 1 volume of liquid was measured and 3 volumes of ethanol were added to precipitate the soluble starch. The precipitate was then collected and placed in a fume hood to remove the residual ethanol. The dried solid was ground to form a powder, which was then used for further studies within the next few months.

*Octenylsuccinic Anhydride Modification.* The isolated SMSS was esterification-modified with OSA according to the method of Miao et al.[16] The soluble starch (10 g, dry weight) was suspended in distilled water (30%, w/w) with agitation. OSA (3 or 10% based on the weight of soluble starch) was added to the starch dispersion, whereas the pH was maintained at 8.5 using 3% (w/v) NaOH. After the esterification at 35 °C for 8 h, the pH was adjusted to 6.5 using 2.5 M HCl. The reaction mixture was centrifuged (3000*g*) and washed three times with distilled water and three times with 70% ethanol. The collected material was oven-dried at 40 °C for 24 h and then ground to form a powder (100 mesh) for further analysis. The two types of OSA modified starch samples were named SMSS-OSA-3-0 and SMSS-OSA-10-0, respectively.

*Amyloglucosidase Hydrolysis.* The enzymatic preparation of starch derivatives was carried out by using the method of Huang at al.[10] with some modifications. The soluble starch or OSA starch (OSA-SMSS-3-0 and OSA-SMSS-10-0) dispersion in sodium acetate buffer (50 mM, pH 4.5) was prepared and then heated with agitation in a water bath at 95 °C for 60 min. The temperature of the starch sample was adjusted to 40 °C, and amyloglucosidase (50 U/g dry weight of soluble starch) was added to the each dispersion. Aliquots were withdrawn from each test reaction at 0.5, 1, 2, 3, 5, 10, 20, 30, 60, 120, 240, 360, 600, and 1440 min. The amount of glucose was determined using the Nelson−Somogyi method.[26] Each sample was analyzed in triplicate.

*Determination of the Degree of Substitution.* The DS was measured using the titration method as suggested by He et al.[14] The OSA starch or enzyme-treated OSA starch (0.5 g) was acidified by stirring for 30 min in 3 mL of HCl solution (2.5 M). Ten milliliters of 90% aqueous isopropanol (v/v) was added and stirred for an additional 10 min. The suspension was filtered, and the residue was washed with 90% aqueous isopropanol until no chloride ions were present, as determined by the addition 0.1 M $AgNO_3$; no chloride was present when a white haze of AgCl was no longer observed upon addition. The residue was redispersed in distilled water (30 mL) and heated in a boiling water bath for 30 min. The mixture was titrated with 0.1 M NaOH using phenolphthalein as the end-point indicator. The DS was calculated using the formula

$$\mathrm{DS} = \frac{0.162 \times (A \times M)/W}{1 - [0.210 \times (A \times M)/W]}$$

where $A$ is the titration volume of NaOH, $M$ is the molarity of NaOH, $W$ is the dry weight of sample, and 0.162 and 0.210 are the molecular weight of a glucose unit and an OSA group, respectively. Each sample was analyzed in triplicate.

*Zeta-Potential and Particle Size.* Zeta-potential and particle size analysis was conducted using a Zetasizer Nano ZS (Malvern Instruments Ltd., Malvern, UK) at room temperature. The sample powder (0.01%, w/v) was suspended in distilled water and heated in a boiling water bath for 20 min before measurement. The polystyrene latex nanoparticles were used as a model material; the refractive index and absorption of particle were 1.590 and 0.010, respectively, and data processing was performed using the Nanoapplication program.

*Molecular Weight Distribution Profiles.* The starch sample (10 mg) was added to 5 mL of deionized water and boiled for 15 min to completely dissolve. The dissolved samples were filtered through 5 $\mu$m cellulose acetate filters (Whatman, Maidstone, UK) and injected into a high-performance size exclusion column chromatography system with multiangle laser light scattering detector and a refractive index detector (HPSEC-MALLS-RI) (Wyatt Technology, Santa Barbara, CA, USA). Two series tandem columns (300 × 8 mm, Shodex OH-pak SB-806 and 804, Showa Denko K.K., Japan) with a OH-pak SB-G guard column, a DAWN HELEOS II laser photometer fitted with a He−Ne laser ($\lambda$ = 632.8 nm) with a K-5 flow cell, and a OPTILAB T-rEX Interferometric Refractometer were used. The flow rate was set at 0.5 mL/min with a mobile phase of distilled−deionized water (pH 6.8, 18.2 MΩ cm) containing 0.02% $NaN_3$. A d$n$/d$c$ value of 0.138 was used in the molecular weight calculation, and data processing was performed using ASTRA software (version 5.3.4.14, Wyatt Technology) as described by Miao et al.[5] Weight-average molecular weight ($M_w$, g/mol) and $z$-average radius of gyration ($R_z$, nm) were obtained using the second-order Berry method. The molecular density ($\rho$, g/mol·nm$^3$) was calculated as $M_w/R_z^3$. Each sample was analyzed in triplicate.

*Fourier Transform Infrared Spectroscopy.* The FT-IR spectrum was recorded on a Nicolet Nexus 470 FT-IR spectrometer (Thermo Electron Corp., Waltham, MA, USA) at room temperature. The starch powder was blended with KBr powder at a 1:100 ratio and pressed into tablets before measurement. A region from 400 to 4000 cm$^{-1}$ was used for scanning at 4 cm$^{-1}$ resolution with 32 scans.

*Nuclear Magnetic Resonance.* The $^1$H and $^{13}$C spectra were recorded at 70 °C using a 400 MHz AVANCE III NMR spectrometer (Bruker Co., Billerica, MA, USA) according to the procedure of Gidley.[27] The starch sample (60 mg) was exchanged with deuterium in three rounds of lyophilization with 99.99% deuterium oxide and then dissolved in 0.45 mL of 99.99% deuterium oxide. The parameters of sweep width, center band pulse frequency, npoints, nscans, and probe temperature were respectively set for 20 ppm, 6.175 ppm, 64 K, 64 scans, 333 K, and 240 ppm, 100 ppm, 64 K, 2048 scans, and 333 K for $^1$H and $^{13}$C NMR spectra. Using MestReNova software (version 8.0), chemical shifts ($\delta$) were expressed in parts per million and referenced

internally with acetone and 1,4-dioxane for $^{1}H$ and $^{13}C$ NMR spectra, respectively.

*Confocal Laser Scanning Microscopy (CLSM).* OSA starch sample (0.4 g) was added to 20 mL of deionized water. The pH of the starch dispersion was adjusted to 8.0, and 1% Methylene Blue ($MB^{+}$) solution was added. The mixture was incubated in a shaking water bath at 25 °C for 3 h, and the particles were washed with methanol to remove the excess dye. A TCS SP8 CLSM (Leica, Wetzlar, Germany) was used for the detection of the fluorescence signal from the dye-stained starch particles. The details of the Leica objective lens used were 63 ×plan apo/1.40 oil UV. A laser with a wavelength of 488 nm operating at 30% capacity was used to generate fluorescence. During the image acquisition, each line was scanned four times, and the average was calculated to reduce the noise.

## RESULTS AND DISCUSSION

**Amyloglucosidase Hydrolysis.** As shown in Figure 1, the glucose release from SMSS increased substantially to 182.4 mg/mL in the first 4 h and then incrementally increased to a value of 192.3 mg/mL at 24 h. For enzyme catalytic reaction, enzyme needs first to diffuse toward and bind the substrate and then cleave the glycosidic linkages. Amyloglucosidase is an exoacting enzyme that hydrolyzed both $\alpha$-1,4 and $\alpha$-1,6 glucosidic linkages from the nonreducing ends to yield glucose.[10] Thus, the rate of glucose release was governed by the dendrimer-like structure of soluble starch. On the basis of previous studies,[5−10] the SMSS nanoparticle is believed to have short linear chains densely distributed at the outer surface. At the initial stage of enzyme hydrolysis, effective binding occurred between amyloglucosidase molecules and nonreducing ends. Therefore, only the nonreducing ends at the outer surface of soluble starch were accessible to amyloglucosidase. As enzymatic hydrolysis proceeded, the linear chains were trimmed, resulting in exposure of the $\alpha$-1,6 linkages. According to Pazur and Ando,[28] an $\alpha$-1,4 linkage is hydrolyzed at about 30 times the rate for an $\alpha$-1,6 linkage, which suggested that the presence of $\alpha$-1,6 linkages substantially reduced the hydrolysis rate. Moreover, Butterworth et al.[29] reported that the amylolysis curve for starch with amylase in vitro followed a first-order kinetic equation.

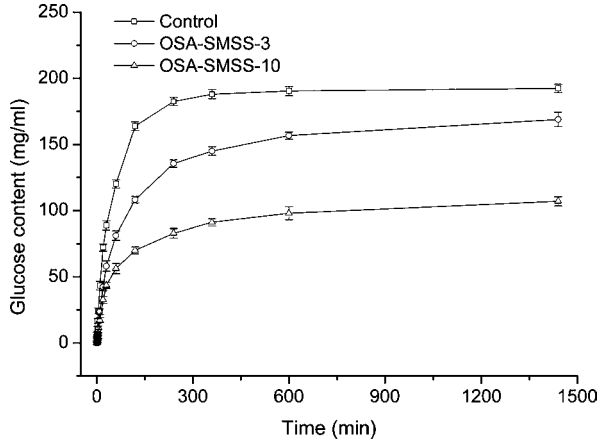


**Figure 1.** Hydrolysis of OSA modified soluble starch by amyloglucosidase over time. Each data point is the mean value of three measurements with error bar of standard deviation.

As depicted in Figure 1, the glucose release profiles between OSA modified starch (OSA-SMSS-3-0, DS 0.019, and OSA-SMSS-10-0, DS 0.0504) and native starch (SMSS) were basically similar; however, the glucose release from OSA modified starch was lower than that from native starch, which was due to OSA modification. According to a review by Sweedman et al.,[12] starch modified with OSA is either more slowly biodegraded or completely resistant to degradation. Viswanathan[30] found that when subjected to multiple enzymes ($\alpha$-amylase, amyloglucosidase, and pullulanase), even small amounts of OSA substitution might cause a considerable decrease in the extent of degradation, indicating that the action of enzyme was inhibited by OSA groups. He et al.[17] also revealed that starch modified by OSA acted like an uncompetitive inhibitor to amyloglucosidase in which the release of enzyme from substrate was delayed due to the physical hindrance or the hydrophobic microenvironment caused by the bulky group of OSA. The enzymatic hydrolysis reaction would stop when amyloglucosidase encounters the OSA groups, which was due to the substitution groups interfering with the binding processing between enzyme and the substrates. Hood and Mercier[31] reported that amyloglucosidase could hydrolyze every glucosidic bond of native starch in an exoenzyme pattern until it reached a modified residue, suggesting that the attachment of enzyme to the substrate was inhibited by the modifying groups on the inner or outer chains near the branch points. Our data revealed that the glucose units released by amyloglucosidase would contain no OSA substituents, whereas the hydrolysis residuals would contain all of the OSA groups. According to the soluble starch model of Huang and Yao,[10] the dispersed molecular density of external

**Table 1. Degree of Substitution, Zeta-Potential, Molecular Weight, Radius of Gyration, and Molecular Density of OSA Modified Soluble Starch after Amyloglucosidase Hydrolysis[a]**

| sample | DS ($\times 10^{-2}$) | zeta-potential (mV) | $M_w$ ($10^7$g/mol) | $R_z$ (nm) | $\rho^b$ (g/mol·nm$^3$) |
|---|---|---|---|---|---|
| OSA-SMSS-3-0 | 1.91 ± 0.08 | −11.1 ± 0.4 | 2.16 ± 0.01 | 32.9 ± 0.0 | 605 ± 3 |
| OSA-SMSS-3-10 | 1.98 ± 0.04 | −10.9 ± 1.2 | 1.74 ± 0.04 | 30.5 ± 0.5 | 612 ± 15 |
| OSA-SMSS-3-30 | 2.12 ± 0.01 | −11.7 ± 1.0 | 1.67 ± 0.02 | 32.8 ± 0.7 | 472 ± 8 |
| OSA-SMSS-3-60 | 2.32 ± 0.06 | −11.2 ± 0.7 | 1.35 ± 0.06 | 31.0 ± 0.2 | 451 ± 12 |
| OSA-SMSS-3-120 | 2.66 ± 0.03 | −10.6 ± 0.3 | 1.22 ± 0.15 | 30.1 ± 0.6 | 446 ± 10 |
| OSA-SMSS-10-0 | 5.04 ± 0.05 | −44.4 ± 0.2 | 2.23 ± 0.07 | 34.8 ± 0.2 | 530 ± 3 |
| OSA-SMSS-10-10 | 5.17 ± 0.00 | −43.7 ± 0.9 | 1.88 ± 0.06 | 32.3 ± 0.9 | 558 ± 21 |
| OSA-SMSS-10-30 | 5.34 ± 0.04 | −44.2 ± 0.6 | 1.79 ± 0.05 | 33.9 ± 0.5 | 461 ± 13 |
| OSA-SMSS-10-60 | 5.49 ± 0.06 | −43.5 ± 0.8 | 1.64 ± 0.02 | 33.2 ± 0.4 | 448 ± 6 |
| OSA-SMSS-10-120 | 5.71 ± 0.03 | −43.7 ± 0.5 | 1.60 ± 0.09 | 33.1 ± 0.1 | 440 ± 9 |

[a]Data expressed as mean ± SD ($n$ = 3). DS, degree of substitution; $M_w$, weight-average molecular weight; $R_z$, $z$-root-mean-square radius of gyration; $\rho$, molecular density. [b]$\rho$ was calculated as $M_w/R_z^3$.


dx.doi.org/10.1021/jf5035064 | J. Agric. Food Chem. 2014, 62, 11696−11705

region (1600 g/mol·nm$^3$) is higher than that of internal regions (950 g/mol·nm$^3$). It is likely that, during the esterification modification of starch, the chemical reagents penetrate more readily into the less dense areas. Therefore, the OSA-SMSS-3-0 (DS 0.019, low OSA modification) contained almost no OSA groups near the nonreducing ends at the outer surface, as opposed to OSA-SMSS-10-0 (DS 0.0504, high OSA modification). On the basis of the above results, five types of dual-modified starches (10 g of OSA starch subjected to amyloglucosidase hydrolysis for 10, 30, 60, or 120 min and then conducted with the same protocol as described SMSS extraction, named OSA-SMSS-3-10, OSA-SMSS-3-30, OSA-SMSS-3-60, and OSA-SMSS-3-120 or OSA-SMSS-10-10, OSA-SMSS-10-30, OSA-SMSS-10-60, and OSA-SMSS-10-120, respectively), were selected to study OSA group distribution in subsequent experiments.

**Degree of Substitution, Zeta-Potential, and Particle Size.** As shown in Table 1, the DS values of modified SMSS using 3 and 10% OSA were 0.0191 and 0.0504, respectively, indicating DS increased with the increased amount of OSA for esterification. In addition, the DS value of amyloglucosidase hydrolyzed OSA starch was increased as the enzyme reaction proceeded, which might be related with OSA substituted position on starch chains as suggested from glucose release profiles.

It is known that the zeta-potential is used to characterize the negative charge at the surface of OSA modified starch. Table 1 shows the zeta-potential of dual-modified starch (OSA modification followed by enzymatic hydrolysis). The zeta-potentials of OSA-SMSS-3-0 (DS 0.0191) and OSA-SMSS-10-0 (DS 0.0504) were −11.1 and −44.4 mV, respectively, which were consistent with previous studies.[12,16] The higher DS was related with a lower zeta-potential, revealing that there were more OSA groups in highly OSA modified starch (OSA-SMSS-10-0). After amyloglucosidase hydrolysis, the zeta-potential of OSA-SMSS (OSA-SMSS-3-0 or OSA-SMSS-10-0) remained at approximately the same value, which indicated that the hydrolysate of OSA starch would contain all of the OSA groups regardless of excessive hydrolysis.

As shown in Figure 2, the particle size distributions of SMSS-OSA have been observed to exhibit ranges from 25 to 400 nm. The average particle size of OSA starch was in the order OSA-SMSS-3-0 (84.9 nm) < OSA-SMSS-10-0 (93.1 nm), which confirmed the higher DS value (high level of OSA esterification) in OSA-SMSS-10-0 obtained using titration method. After amyloglucosidase hydrolysis, the average particle sizes of OSA-SMSS-3-120 and OSA-SMSS-10-120 were 68.0 and 78.3 nm, respectively, revealing that the size decreased as the time increased; however, OSA-SMSS-10 (high OSA modificaition) was more resistant to degradation than OSA-SMSS-3 (low OSA modificaition), which was consistent with the data from glucose release profiles (Figure 1).

**Molecular Weight, Radius of Gyration, and Molecular Density.** As shown by HPSEC-MALLS-RI in Table 1, weight-average molecular weight ($M_w$), $z$-average radius of gyration ($R_z$), and molecular density ($\rho$) of OSA-SMSS-3-0 and OSA-SMSS-10-0 are 2.16 × 10$^7$ g/mol, 32.9 nm, and 605 g/mol·nm$^3$ and 34.8 × 10$^7$ g/mol, 34.8 nm, and 530 g/mol·nm$^3$, respectively. $M_w$ of OSA-SMSS increased accompanied by a rise in substitution of OSA esterification, which was due to the starch chains grafting OSA groups. Similar observations have been reported by Miao et al.[16] and Scheffler et al.[19] During amyloglucosidase hydrolysis, the $M_w$ decreased and reached

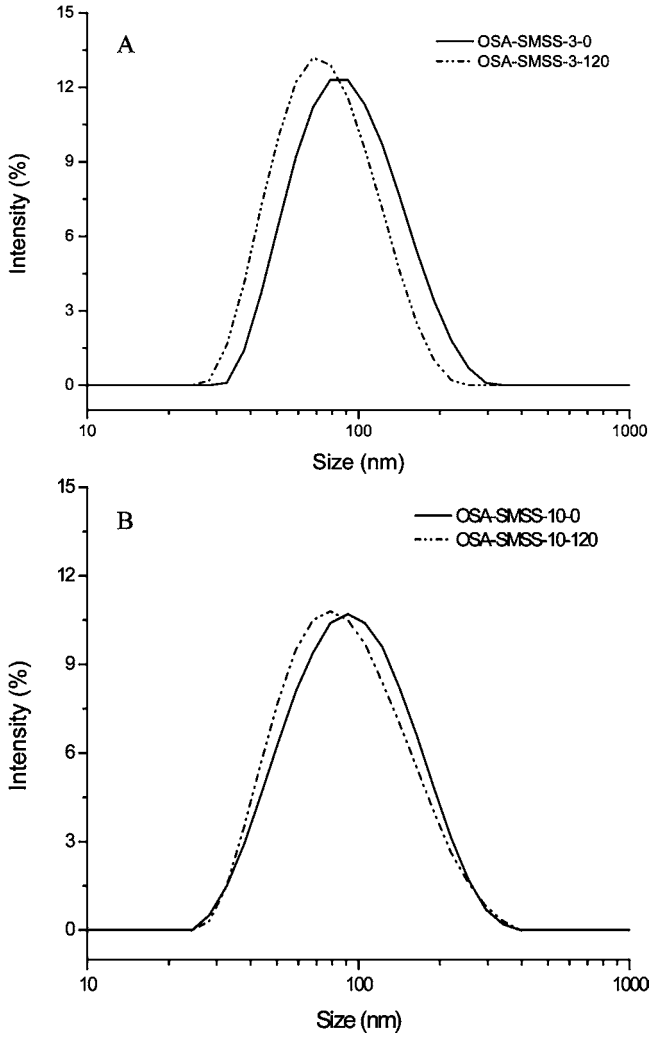


**Figure 2.** Particle size distribution profiles of OSA modified soluble starch after amyloglucosidase hydrolysis: (A) OSA-SMSS-3; (B) OSA-SMSS-10.

1.22 × 10$^7$ and 1.60 × 10$^7$ g/mol after 120 min for OSA-SMSS-3-0 and OSA-SMSS-10-0, respectively.

For OSA modification, the dendritic structure with higher integrity of soluble starch limited the stretching of external chains and restricted the expansion of the particles,[10,16] as evidenced by a slight increase of $R_z$ along with higher DS (Table 1). During the enzyme treatment, the value of $R_z$ for 10 min of hydrolysis dropped off significantly for OSA starch (both OSA-SMSS-3-0 and OSA-SMSS-10-0), indicating that amyloglucosidase hydrolysis primarily reduced the size of soluble starch nanoparticles. After 10 min of hydrolysis, the value of $R_z$ returned to a nearly constant value in each case that was slightly below the native OSA starch, which could be related to a subtle stretching of outer chains caused by an electrostatic repelling force among neighboring negatively charged OSA groups.[16] However, such stretching was limited from causing a substantial change of soluble starch particle size. Moreover, the whole pattern of $R_z$ change was similar to that of $M_w$: $R_z$ decreased much more slowly for 120 min of hydrolysis, reaching 30.1 and 32.9 nm, respectively, which is comparable with the results of particle size analysis (Figure 2).

The $\rho$ value of OSA-SMSS-3-0 was higher than of OSA-SMSS-10-0, which indicated that an increase of DS led to

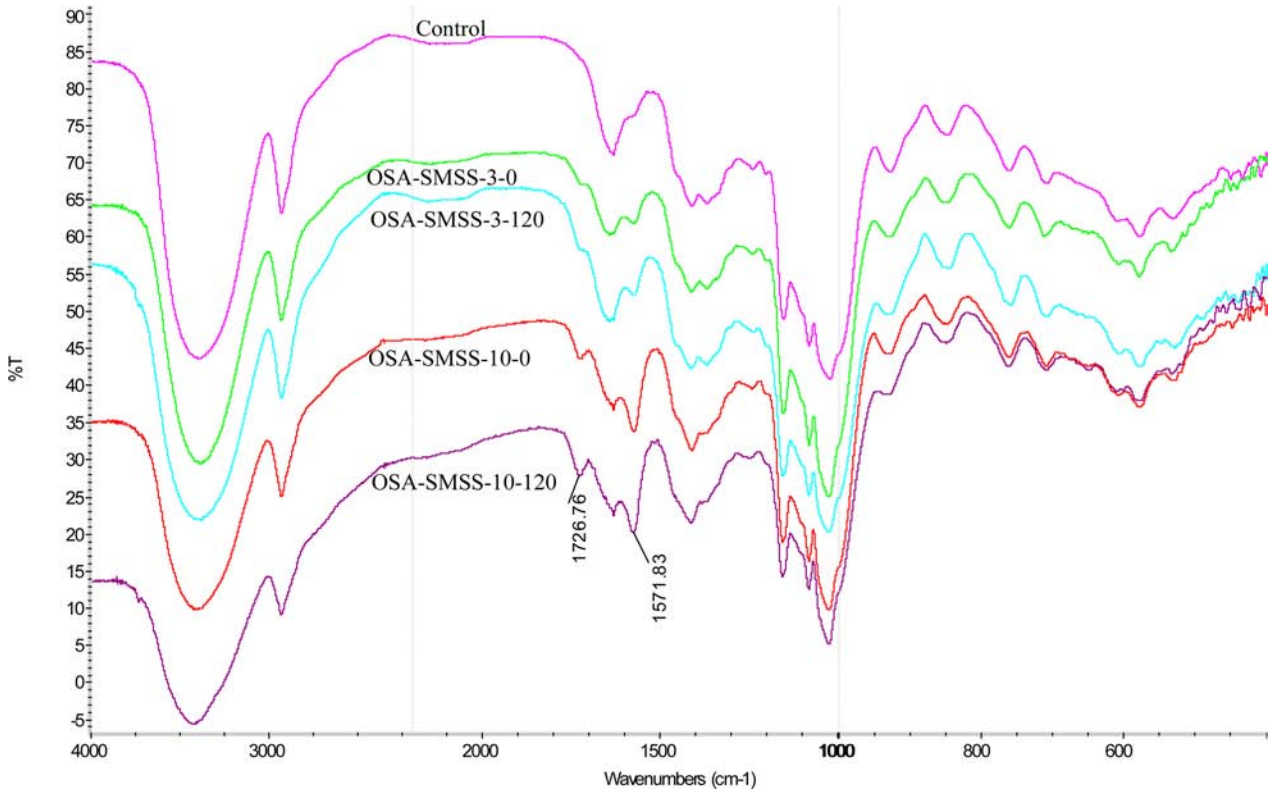


**Figure 3.** FT-IR spectra of OSA modified soluble starch after amyloglucosidase hydrolysis. The vertical lines represented the split of the *X*-axis at 2200 and 1000 $cm^{-1}$.

reduced $\rho$ value. According to some previous studies,[16,19] an increased DS led to reduced density (a low $\rho$ value), which would be caused by electrostatic repulsion among chains grafted with OSA groups. Besides, during amyloglucosidase hydrolysis, $\rho$ remained fairly constant (612 and 558 g/mol·$nm^3$) for the first 10 min and decreased to 446 and 440 g/mol·$nm^3$ after 120 min for OSA-SMSS-3-0 and OSA-SMSS-10-0, respectively. It should be revealed that the change in $M_w$ was due to OSA derivatization, whereas the changes of $R_z$ and $\rho$ were related to the rigid structure of OSA starch, subtle stretching of starch chains grafting OSA groups, and electrostatic repulsion.

**FT-IR Spectroscopy.** The FT-IR spectra of native and OSA starches with different DS (0.0191, 0.0266, 0.0504, 0.0571) are presented in Figure 3. For native starch (control), the FT-IR spectrum contained the following characteristic bands: $\nu$(O−H) 3400 $cm^{-1}$, $\nu$(C−H) 2930 $cm^{-1}$, $\delta$(HOH) 1640 $cm^{-1}$, $\delta$(O−H) 1420 $cm^{-1}$, $\delta$(C−H) 1370 $cm^{-1}$, a complex band $\nu$(C−O) and $\nu$(C−C) 1200−1000 $cm^{-1}$, and $\gamma$(C−H) 1000−700 $cm^{-1}$.[5,32,33] A broad peak appeared around 3400 $cm^{-1}$, indicating the presence of a hydroxyl group (O−H). The characteristic peaks at 2930 and 1640 $cm^{-1}$ were from the C−H stretching vibration and adsorbed water bending vibration, respectively. The spectra also showed C−H deformation at approximately 1410 and 1370 $cm^{-1}$. In the fingerprint region, three characteristic peaks appear between 1000 and 1200 $cm^{-1}$, which have been attributed to C−O bond stretching. The peak around 1020 $cm^{-1}$ also indicated the presence of the $\alpha$-1,6 linkage, the peak near 930 $cm^{-1}$ was assigned to the skeletal mode vibrations of $\alpha$-1,4 linkage, and the peak near 850 $cm^{-1}$ corresponded to C−H and $CH_2$ deformation.

For OSA starches (DS 0.0191, 0.0266, 0.0504, and 0.0571), the FT-IR spectra exhibited an essentially identical major peak, which was similar to that of native starch. By looking into the details, some minor changes are observed in Figure 3. Compared to native starch, two new absorption peaks at 1726.76 and 1571.83 $cm^{-1}$ were shown in OSA modified starch. The characteristic peak occurring at 1726.76 $cm^{-1}$ was C═O stretching vibration of the ester substituent, and the band at 1571.83 $cm^{-1}$ was attributed to an asymmetric stretch of vibration of the carboxyl group.[16,23] The intensity of absorption peaks at 1726.76 and 1571.83 $cm^{-1}$ increased with increasing DS of OSA starch, which was consistent with a previous study by Zhang and co-workers.[34]

**NMR Spectroscopy.** As shown by $^1$H NMR in Figure 4A, all characteristic peaks are assigned as suggested by Bai et al.[20,21,25] The signals at 4.5−5.4 ppm were from anomeric proton; for instance, the small peak at 4.96 ppm was the H-1 at $\alpha$-1,6 branching point, and H-1 at $\alpha$-1,4 internal linkage was characterized at 5.35 ppm. The signals for protons of H-2, H-3, H-4, and H-5 overlapped with each other at 3.19−4.09 ppm, and the peak at 4.37 ppm was assigned to water. The signal at 3.95 ppm was from the internal H-3, and the peak at 3.84 ppm was the overlapping of internal H-3 and H-5, whereas the signal at 3.63 ppm was assigned to the combination of internal H-2 and H-4. Compared to the native starch (control), OSA-SMSS had several additional peaks at 0.8−3.0 ppm and a shoulder at 5.56 ppm, which was from the OSA group. The intensities of signals also increased as DS increased. The peak at 0.8−1.0 ppm was from the methyl protons of the OSA substituent. The signals at 1.0−3.0 ppm were from the methylene and methine protons of the side chain of the OSA group. The signal at 5.56 ppm was from CH═CH of the OSA side chain. Moreover,

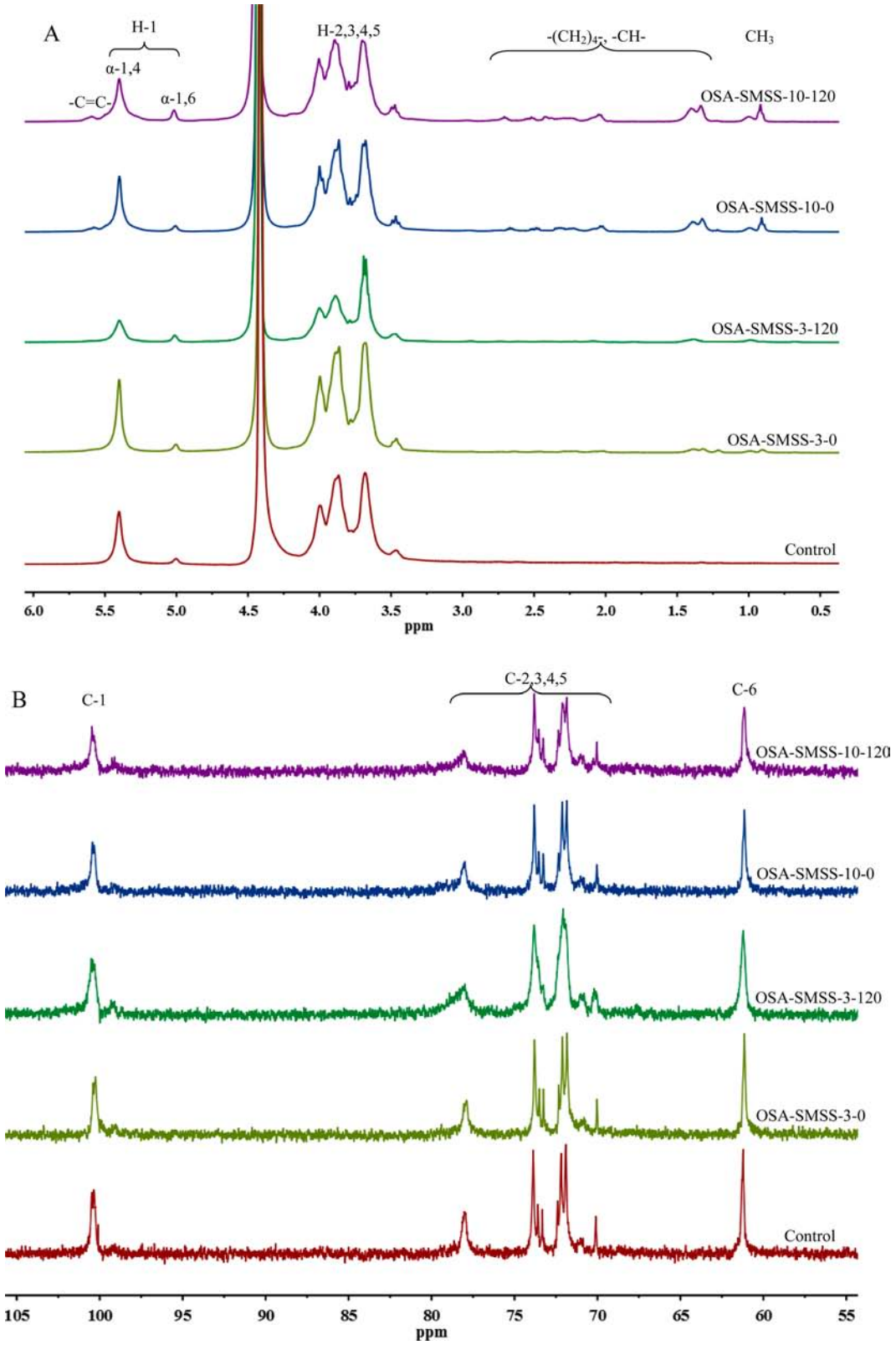


**Figure 4.** $^{1}H$ (A) and $^{13}C$ (B) NMR spectra of OSA modified soluble starch after amyloglucosidase hydrolysis.

peak broadening at 5.35 ppm was observed, which was presumed to be the substitution of OSA at the O-2 position of starch.[20,25]

The percentage of $\alpha$-1,4 and $\alpha$-1,6 linkages was determined using the area ratios of signals at 5.35 and 4.96 ppm. The results show that native SMSS has 6.9% $\alpha$-1,6 linkage, in accordance with several previous papers.[5−9] For OSA starches (DS 0.019, 0.0266, 0.0504, and 0.0571), the concentrations of $\alpha$-1,6 linkage were 13.4, 9.1, 11.7, and 8.2%, respectively. OSA-SMSS-3-0 had a lower ratio of $\alpha$-1,4 to $\alpha$-1,6 linkage than OSA-SMSS-3-10, which might be related to minor hydrolysis of glucosidic linkages at the surface during OSA esterification,[16] Also, the


dx.doi.org/10.1021/jf5035064 | J. Agric. Food Chem. 2014, 62, 11696−11705

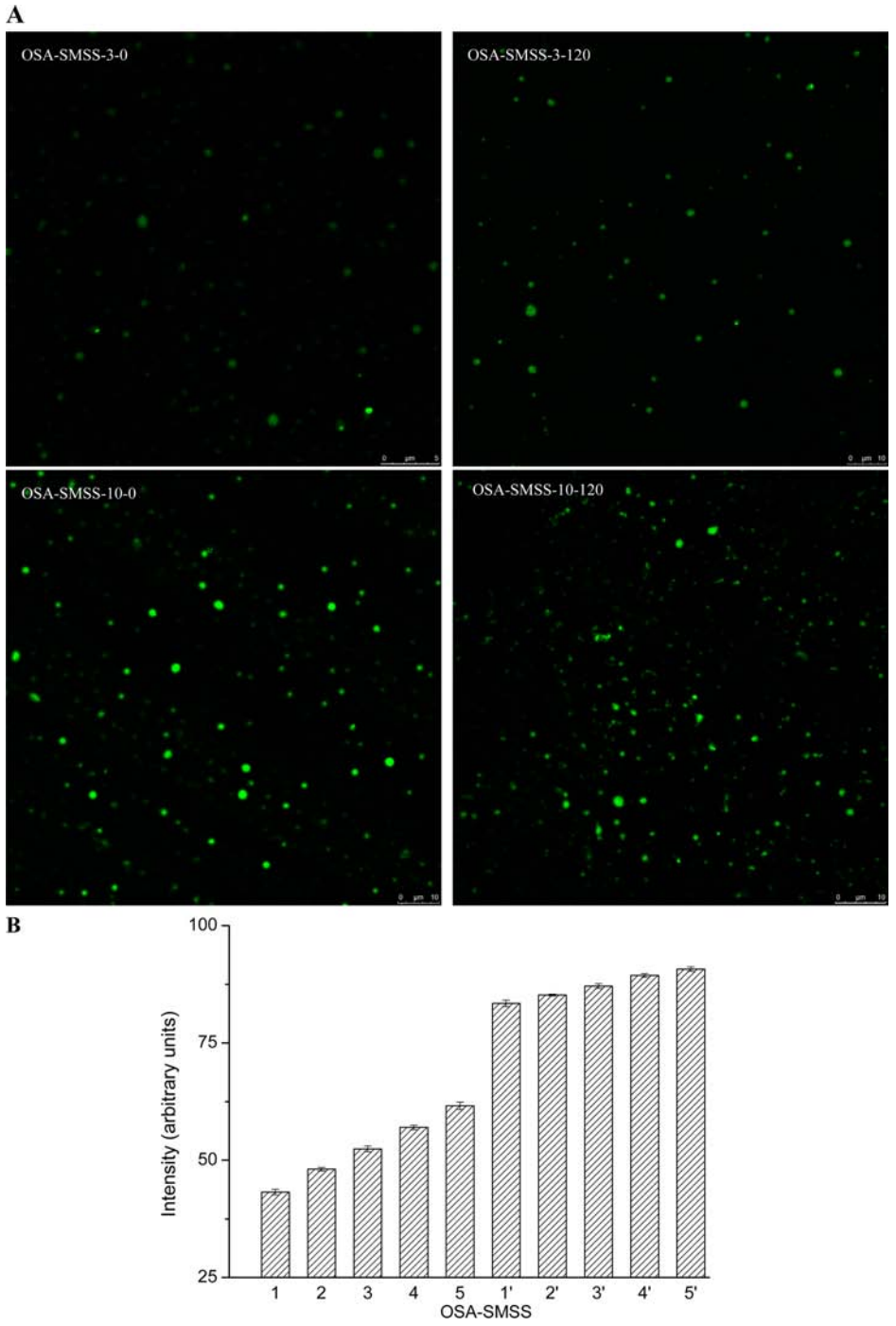


**Figure 5.** CLSM optical sections (A) and fluorescence intensity (B) of OSA modified soluble starch after amyloglucosidase hydrolysis. 1, 2, 3, 4, 5, 1′, 2′, 3′, 4′, 5′ are OSA-SMSS-3-0, OSA-SMSS-3-10, OSA-SMSS-3-30, OSA-SMSS-3-60, OSA-SMSS-3-120, OSA-SMSS-10-0, OSA-SMSS-10-10, OSA-SMSS-10-30, OSA-SMSS-10-60, and OSA-SMSS-10-120, respectively.

percentage of $\alpha$-1,4 linkage increased as DS increased, which was due to relative loss of glucose units resulting from enzyme hydrolysis. After 120 min of enzyme hydrolysis, $\alpha$-1,6 linkages (branching density) reduced 4.3 and 3.5% for OSA-SMSS-3-0 and OSA-SMSS-10-0, respectively, which was comparable with the above results.

As shown by $^{13}$C NMR in Figure 4B, the signal at around 100.47 ppm is from internal anomeric C-1, the multiplets at 70.0−80.0 ppm are from C-2, C-3, C-4, and C-5, and the peak at 61.22 was assigned to C-6. The resonances at 70.20 and 78.10 ppm are assigned to C-4 terminal and internal, whereas the other peaks at 73.80, 72.07, and 71.34 ppm, respectively, are assigned to C-3, C-2, and C-5 of internal $\alpha$-1,4-linked glucosyl units. Compared to SMSS, the C-1 signals of the internal glucosyl units of OSA-SMSS became broader, suggesting that the OS substitution occurred at O-2 and that the O-2 substituent affected the chemical shift of the neighboring C-1.[20] Moreover, additional resonances (shoulder peaks) of C-4 of internal glucosyl units were noted at approximately 78.10 ppm, suggesting that OS groups were substituted at the neighboring O-3 position in OSA-SMSS.[20] As the DS increased to 0.0571, there was no significant difference for the signal at

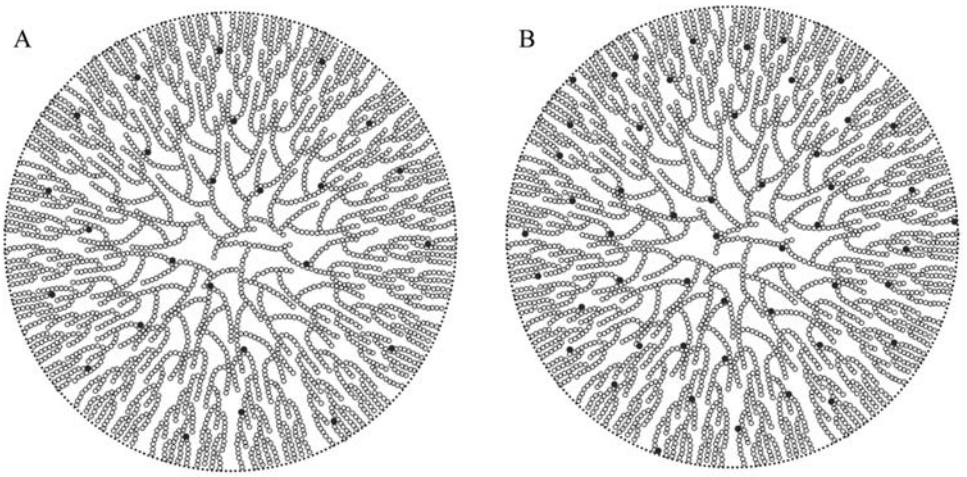


**Figure 6.** Proposed model structure of OSA modified soluble starch: (A) OSA-SMSS-3-0; (B) OSA-SMSS-10-0; (●) OSA group; (○) glucosyl unit.

61.22 ppm, revealing OH at C-6 was not connected with OSA groups.[25]

**CLSM Observation.** According to the transmission electron microscope image in previous studies,[5,6,10] SMSS had a spherical shape with diameters around 30−100 nm, which was comparable with our observations. As shown by CLSM after staining with $MB^+$ dye in Figure 5A, the OSA starches are shown as spherical particles with bright fluorescence. CLSM is used to visualize the internal structures of starch granules to avoid the complicated or invasive sample preparation, such as growth rings, equatorial grooves, channels, cavities, and the distribution of protein, lipid, amylose, or phosphate.[34,35] According to Jayaraj et al.,[36] $MB^+$ is one of the fluorescence dyes that highlight anionic substances, which has been used for specific labeling of $-COO^-$ of OSA substituents. Thus, the OSA group distribution in starch could be clearly revealed. It is observed that OSA groups appeared to be distributed throughout the OSA-SMSS nanoparticles, especially at internal regions of starch sphere. Moreover, OSA starch showed stronger fluorescence intensity as the DS increased (Figure 5B). The higher DS (0.0504, 0.0571) of OSA starch showed stronger fluorescence intensity, indicating that there were more negatively charged groups available to stain with $MB^+$. Zhang et al.[34] reported that OSA starch had only fairly uniform bright fluorescence on the granule surface, which was different from our observation. The cause of the difference might be related to substrate (starch) form during OSA esterification. SMSS is a water-soluble $\alpha$-glucan and well dispersed in the reaction solution, whereas granular starch is in a solid state during reaction. For the starch granule, most OSA droplets could react with the granular surface; only a few penetrate granule channels and arrive at the inner cavity, resulting in higher fluorescence of the granular surface in comparison to the interior under heterogeneous reaction conditions. For soluble starch, the OSA could penetrate the entire SMSS particles and evenly connect at the starch inner chain of internal regions with less density, resulting in a fluorescence sphere. These results reinforced the postulate that more OSA was substituted on the chains near the branch points at less dense areas. After enzyme treatment, there were no changes in the size of OSA starch, suggesting the OSA group was hardly connected at the surface for low OSA modification. Together with the particle size and NMR results, this would suggest fewer glucose units were removed from the OSA-SMSS-10 with higher DS and more $\alpha$-1,4 linkages, indicating that more OSA groups were substituted near the nonreducing end of the starch chains for high OSA modification. The above results revealed that even distribution of OSA groups in the center area of soluble starch particle has been directly observed under CLSM.

**Models of Substitution Distribution in OSA Starch.** The distribution of chemical groups in the granular starch has been revealed to react preferentially in the interior, amorphous domains of amylopectin molecules as well as on the surface,[23,24,34] which revealed that modification reagents penetrate less easily into the crystalline region during chemical derivatization of starch. It is known that the amorphous regions of starch are rich in $\alpha$-1,6 linkages.[31] Thus, the modifying substituents would be expected on the starch molecule near the branch points. Previous works on modified starches have confirmed that substitution reaction takes place preferably at the branched regions of amylopectin and that the linear regions of amylopectin are substituted more heterogeneously than the branched regions.[37−39] Biliaderis[40] reported that waxy maize starch favored a more uniform distribution of the substituent in the starch macromolecules, indicating substitution occurred near the branching points as well as at the nonreducing ends for hydroxypropyl distarch phosphate of waxy starch (DS 0.09). Shogren et al.[23] also found that 72% or less of the branches in an OSA waxy starch molecule (DS 0.11) contained at least one OSA group on the basis of the analysis of the debranched chains, which suggested that some branches were more accessible or reactive toward OSA than others. Recently, Bai et al.[41] investigated the position of OSA groups along the starch chains in the OSA waxy maize starch by enzyme hydrolysis followed by chromatographic analysis. They found that OSA substituents were located on the repeat units near the branching points of amylopectin at a low substitution value (DS 0.018), whereas a high substitution value (DS 0.092) occurred near both the branching points and the nonreducing ends.

In our study, we attempt to envisage the substituted OSA group location in soluble starch on the basis of the above data and the model structures present in Figure 6. The OSA group in modified starch with low DS (0.0191) was postulated to locate near branching points of soluble starch molecules, whereas the OSA starch with DS of 0.0504 had substitution

groups close to nonreducing ends together with near branches. OSA is insoluble in water, and the esterification is a heterogeneous reaction. In the initial stage of OSA esterification, OSA groups were grafted exclusively in the branch part at less dense internal areas of SMSS molecules. Those initial substituted ester groups might cause both electrostatic repelling force and steric hindrance for starch chain stretching, resulting in the outer surface or at least near that surface of SMSS (nonreducing end) being subjected to OSA substitution with increasing DS.

In summary, the substituted OSA group distribution and location in modified sugary maize soluble starch were elucidated by amyloglucosidase hydrolysis and followed by structural analysis of reaction residue. For low OSA modification (DS 0.0191), most substitutions were located near branching points of soluble starch molecules. For high OSA modification (DS 0.0504), substituted ester groups were located near branching points as well as at the nonreducing ends. Further work is underway to obtain the relationship between OSA group distribution and the functionalities and to design a tailor-made OSA starch for some niche applications with high-value-added products.

## ■ ASSOCIATED CONTENT

### Supporting Information

Molecular weight distribution of OSA-SMSS. This material is available free of charge via the Internet at http://pubs.acs.org.

## ■ AUTHOR INFORMATION


### Corresponding Author

*(M.M.) Phone: +86 (0)510 853 27859. Fax: +86 (0)510 859 19161. E-mail: miaoming@jiangnan.edu.cn.



### Funding

The research was financially supported by the National Natural Science Foundation of China (31000764, 31230057) and the Science and Technology Pillar Program of Jiangsu Province (BE2012613, BY2012049, BE2014703).


### Notes

The authors declare no competing financial interest.

## ■ REFERENCES


(1) Ball, S. G.; Morell, M. K. From bacterial glycogen to starch: understanding the biogenesis of the plant starch granule. *Annu. Rev. Plant Physiol.* **2003**, *54*, 207−233.

(2) Tetlow, I. J.; Morell, M. K.; Emes, M. J. Recent developments in understanding the regulation of starch metabolism in higher plants. *J. Exp. Bot.* **2004**, *55*, 2131−2145.

(3) BeMiller, J. N.; Whistler, R. L. *Starch: Chemistry and Technology*, 3rd ed.; Academic Press: New York, 2009.

(4) Boyer, C. D.; Liu, K.-C. Starch and water-soluble polysaccharides from sugary endosperm of sorghum. *Phytochemistry* **1983**, *22*, 2513−2515.

(5) Miao, M.; Li, R.; Jiang, B.; Cui, S. W.; Lu, K.; Zhang, T. Structure and digestibility of endosperm water-soluble α-glucans from different sugary maize mutants. *Food Chem.* **2014**, *143*, 156−162.

(6) Putaux, J.-L.; Buléon, A.; Borsali, R.; Chanzy, H. Ultrastructural aspects of phytoglycogen from cryo-transmission electron microscopy and quasi-elastic light scattering data. *Int. J. Biol. Macromol.* **1999**, *26*, 145−150.

(7) Yun, S.-H.; Matheson, N. K. Structures of the amylopectins of waxy, normal, amylose-extender, and wx ae genotypes and of the phytoglycogen of maize. *Carbohydr. Res.* **1993**, *243*, 307−321.

(8) Inouchi, N.; Glover, D. V.; Fuwa, H. Chain length distribution of amylopectins of several single mutants and the normal counterpart, and sugary-1 phytoglycogen in maize (*Zea mays* L.). *Starch* **1987**, *39*, 259−266.

(9) Wong, K.-S.; Kubo, A.; Jane, J.-l.; Harada, K.; Satoh, H.; Nakamura, Y. Structures and properties of amylopectin and phytoglycogen in the endosperm of sugary-1 mutants of rice. *J. Cereal Sci.* **2003**, *37*, 139−149.

(10) Huang, L.; Yao, Y. Particulate structure of phytoglycogen nanoparticles probed using amyloglucosidase. *Carbohydr. Polym.* **2011**, *83*, 1665−1671.

(11) Tharanathan, R. N. Starch − value addition by modification. *Crit. Rev. Food Sci.* **2005**, *45*, 371−384.

(12) Sweedman, M. C.; Tizzotti, M. J.; Schäfer, C.; Gilbert, R. G. Structure and physicochemical properties of octenyl succinic anhydride modified starches: a review. *Carbohydr. Polym.* **2013**, *92*, 905−920.

(13) Wolf, B. W.; Wolever, T. M. S.; Bolognesi, C.; Zinker, B. A.; Garleb, K. A.; Firkins, J. L. Glycemic response to a food starch esterified by 1-octenyl succinic anhydride in humans. *J. Agric. Food Chem.* **2001**, *49*, 2674−2678.

(14) He, G. Q.; Song, X. Y.; Ruan, H.; Chen, F. Octenyl succinic anhydride modified early indica rice starches differing in amylose content. *J. Agric. Food Chem.* **2006**, *54*, 2775−2779.

(15) Nilsson, L.; Bergenståhl, B. Emulsification and adsorption properties of hydrophobically modified potato and barley starch. *J. Agric. Food Chem.* **2007**, *55*, 1469−1474.

(16) Miao, M.; Li, R.; Jiang, B.; Cui, S. W.; Zhang, T.; Jin, Z. Structure and physicochemical properties of octenyl succinic esters of sugary maize soluble starch and waxy maize starch. *Food Chem.* **2014**, *151*, 154−160.

(17) He, J. H.; Liu, J.; Zhang, G. Y. Slowly digestible waxy maize starch prepared by octenyl succinic anhydride esterification and heat-moisture treatment: glycemic response and mechanism. *Biomacromolecules* **2008**, *9*, 175−184.

(18) Wang, X.; Li, X.; Chen, L.; Xie, F.; Yu, L.; Li, B. Preparation and characterisation of octenyl succinate starch as a delivery carrier for bioactive food components. *Food Chem.* **2011**, *126*, 1218−1225.

(19) Scheffler, S. L.; Wang, X.; Huang, L.; Gonzalez, F. S.-M.; Yao, Y. Phytoglycogen octenyl succinate, an amphiphilic carbohydrate nanoparticle, and ε-polylysine to improve lipid oxidative stability of emulsions. *J. Agric. Food Chem.* **2010**, *58*, 660−667.

(20) Bai, Y.; Shia, Y.-C.; Herrera, A.; Prakash, O. Study of octenyl succinic anhydride-modified waxy maize starch by nuclear magnetic resonance spectroscopy. *Carbohydr. Polym.* **2011**, *83*, 407−413.

(21) Bai, Y.; Shi, Y.-C.; Wetzel, D. L. Fourier transform infrared (FT-IR) microspectroscopic census of single starch granules for octenyl succinate ester modification. *J. Agric. Food Chem.* **2009**, *57*, 6443−6448.

(22) Wetzel, D. L.; Shi, Y.-C.; Schmidt, U. Confocal Raman and AFM imaging of individual granules of octenyl succinate modified and natural waxy maize starch. *Vib. Spectrosc.* **2010**, *53*, 173−177.

(23) Shogren, R. L.; Viswanathan, A.; Felker, F.; Gross, R. A. Distribution of octenyl succinate groups in octenyl succinic anhydride modified waxy maize starch. *Starch/Staerke* **2000**, *52*, 196−204.

(24) Huang, Q.; Fu, X.; He, X. W.; Luo, F. X.; Yu, S. J.; Li, L. The effect of enzymatic pretreatments on subsequent octenyl succinic anhydride modifications of cornstarch. *Food Hydrocolloids* **2010**, *24*, 60−65.

(25) Bai, Y.; Shi, Y.-C. Structure and preparation of octenyl succinic esters of granular starch, microporous starch and soluble maltodextrin. *Carbohydr. Polym.* **2011**, *83*, 520−527.

(26) Somogyi, M. Notes on sugar determination. *J. Biol. Chem.* **1952**, *195*, 19−23.

(27) Gidley, M. J. Quantification of the structural features of starch polysaccharides by N.M.R. spectroscopy. *Carbohydr. Res.* **1985**, *139*, 85−93.

(28) Pazur, J. H.; Ando, T. The hydrolysis of glucosyl oligosaccharides with α-D-(1,4) and α-D-(1,6) bonds by fungal amyloglucosidase. *J. Biol. Chem.* **1960**, *235*, 297−302.

(29) Butterworth, P. J.; Warren, F. J.; Grassby, T.; Patel, H.; Ellis, P. R. Analysis of starch amylolysis using plots for first-order kinetics. *Carbohydr. Polym.* **2012**, *87*, 2189−2197.
(30) Viswanathan, A. Effect of degree of substitution of octenyl succinate starch on enzymatic degradation. *J. Environ. Polym. Degrad.* **1999**, *7*, 185−190.
(31) Hood, L. F.; Mercier, C. Molecular structure of unmodified and chemically modified manioc starches. *Carbohydr. Res.* **1987**, *61*, 53−66.
(32) Kizil, R.; Irudayaraj, J.; Seetharaman, K. Characterization of irradiated starches by using FT-Raman and FTIR spectroscopy. *J. Agric. Food Chem.* **2002**, *50*, 3912−3918.
(33) Miao, M.; Ma, Y.; Jiang, B.; Huang, C.; Li, X.; Cui, S. W.; Zhang, T. Structural investigation of a neutral extracellular glucan from *Lactobacillus reuteri* SK24.003. *Carbohydr. Polym.* **2014**, *106*, 384−392.
(34) Zhang, B.; Huang, Q.; Luo, F.; Fu, X.; Jiang, H.; Jane, J.-L. Effects of octenylsuccinylation on the structure and properties of high-amylose maize starch. *Carbohydr. Polym.* **2011**, *84*, 1276−1281.
(35) Wang, C.; He, X.; Huang, Q.; Fu, X.; Luo, F.; Li, L. Distribution of octenylsuccinic substituents in modified A and B polymorph starch granules. *J. Agric. Food Chem.* **2013**, *61*, 12492−12498.
(36) Jayaraj, S. E.; Umadevi, M.; Ramakrishnan, V. Environmental effect on the laser-excited fluorescence spectra of methylene blue and methylene green dyes. *J. Inclusion Phenom. Macrocycl. Chem.* **2001**, *40*, 203−206.
(37) van der Brugt, Y. E. M.; Bergsma, J.; Bleeker, I. P.; Mijland, P. J. H. C.; van der Kerk-van Hoof, A.; Kamerling, J. P.; Vliegenthart, J. F. G. Distribution of methyl substituents over branched and linear regions in methylated starches. *Carbohydr. Res.* **1998**, *312*, 201−208.
(38) van der Brugt, Y. E. M.; Bergsma, J.; Bleeker, I. P.; Mijland, P. J. H. C.; van der Kerk-van Hoof, A.; Kamerling, J. P.; Vliegenthart, J. F. G. Distribution of methyl substituents in amylose and amylopectin from methylated potato starches. *Carbohydr. Res.* **2000**, *325*, 183−191.
(39) van der Brugt, Y. E. M.; Bergsma, J.; Bleeker, I. P.; Mijland, P. J. H. C.; van der Kerk-van Hoof, A.; Kamerling, J. P.; Vliegenthart, J. F. G. Substituent distribution in highly branched dextrins from methylated starches. *Carbohydr. Res.* **2000**, *327*, 423−429.
(40) Biliaderis, C. G. Physical characteristics, enzymic digestibility and structure of chemically modified smooth pea and waxy maize starches. *J. Agric. Food Chem.* **1982**, *30*, 925−930.
(41) Bai, Y.; Kaufman, R. C.; Wilson, J. D.; Shi, Y.-C. Position of modifying groups on starch chains of octenylsuccinic anhydride-modified waxy maize starch. *Food Chem.* **2014**, *153*, 193−199.

analysis indicated that there might be more than one copy of *SeFAD2* gene in the sesame genome.[15]

So far, *Sesame indicum* L. is the only large-scale cultivated species in the genus. For improvement of sesame in breeding programs by introgression of useful traits, e.g., resistance to diseases and pests, tolerance to abiotic and biotic stresses, etc., wild relative species of sesame need to be explored. The sesame germplasm collection in the U.S. is maintained by the USDA-ARS, PGRCU, in Griffin, Georgia. Fatty acid composition of the entire USDA collection (1232 accessions) has been evaluated, and significant variability was identified within the collection (Wang et al., unpublished results). From this screening, we selected seven accessions (including two wild species) with significant variation in fatty acid composition, and O/L ratio. These accessions were planted for sequencing the *FAD2* gene coding region and for chemical analysis of the harvested seeds. To our knowledge, we are not aware of any report on association of *FAD2* genotypes with fatty acid profiles in sesame. The objectives of this study were therefore to (1) confirm fatty acid composition and O/L ratio using newly harvested seeds, (2) identify nucleotide diversity in the *FAD2* gene coding region, and (3) identify nucleotide polymorphisms possibly contributing to alter the fatty acid profile and O/L ratio.

## MATERIALS AND METHODS

**Plant Materials and Seed Harvest.** Information on the seven selected sesame accessions is listed in Table 1. Among these, five were from the cultivated form (*S. indicum* L.) and two were from the wild form (*S. radiatum* Schum & Thonn.) based on the passport data (www.ars-grin.gov). One hundred seeds for each accession were acquired from the seed store of USDA-ARS-PGRCU, Griffin, Georgia. Twenty seeds from each accession were planted in large pots (Poly-Tainer-Can, No. 7s, Nursery Supplies Inc., Orange, CA) containing potting soil (Metromix-360, Griffin House and Nursery Inc., Griffin, GA) on April 30, 2012. Two weeks after germination, seedlings were thinned from 20 to 8. During plant growth, water and fertilizer for each pot were controlled. Seeds were harvested on multiple occasions from newly opened capsules. The capsules were collected into a paper bag and dried for 2 weeks at low humidity. After drying, the seeds were removed from the capsules and cleaned for seed morphology observation and chemical analysis.

**Table 1. Information on the Seven Selected Accessions from Seed Quality Analysis**

| PI no. | species | collection site | linoleic acid | O/L ratio |
|---|---|---|---|---|
| 188815 | *S. indicum* L. | Luzon, Philippines | 53.22 | 0.58 |
| 224663 | *S. indicum* L. | Libya | 45.78 | 0.86 |
| 278164 | *S. radiatum* Schum. & Thonn. | Angola | 47.35 | 0.78 |
| 367899 | *S. radiatum* Schum. & Thonn. | Tanzania | 61.79 | 0.34 |
| 490268 | *S. indicum* L. | India | 54.5 | 0.5 |
| 599435 | *S. indicum* L. | Texas, United States | 34.99 | 1.4 |
| 599442 | *S. indicum* L. | Texas, United States | 33.49 | 1.5 |

**Morphological Observation and Chemical Analysis.** Flowering time, leaf shape, plant stature, and seed morphology were observed, measured, and recorded. All samples were measured in triplicate and results averaged for each accession. Fatty acid methyl esters (FAMEs) were prepared from sesame seeds by alkaline transmethylation.[20] Fatty acid composition was determined on an Agilent 7890A GC equipped with a flame ionization detector (FID) following a previously described method.[21] A fatty acid methyl ester (FAME) standard mix was purchased from Sigma. The relative percentage of each fatty acid was calculated from the corresponding peak area. The O/L ratio was determined by % oleic acid/% linoleic acid. Data on fatty acids were recorded by replicates, accessions, and batches (old or new seeds). An analysis of variance was performed on the data, and means were separated using Tukey's multiple comparison procedure (SAS, 2008, Online Doc 9.2. Cary, NC: SAS Institute Inc.). Significant correlations between seed traits were determined using Pearson correlation coefficients.

**Amplification and Sequence of DNA Fragments in the *FAD2* Coding Region.** Genomic DNA was extracted from fresh leaf tissue using an E.Z.N.A. Plant DNA kit from Omega Bio-Tek (Doraville, GA). All DNA samples were dissolved and diluted in 0.1 × TE (1 mM Tris, 0.1 mM EDTA, pH 8.0) to a final concentration 10 ng/$\mu$L for use in PCR. For primer design, the sequence of the *FAD2* gene region was downloaded from GenBank (AY770501). Due to nucleotide divergence between cultivated and wild sesame, some specific primers were designed only for wild species (including some degenerate primers) (Table 2). In total, 33 sets of primers were designed and synthesized by Operon (Qiagen, Germantown, MD, USA, http://www.operon.com). Different PCR conditions were used based on the amplicon size and annealing temperature for DNA fragment amplification.

**Table 2. Primers Designed for Amplification of *FAD2* Coding Region in Cultivated and Wild Species**

| amplified fragment | forward and reverse primers (5′−3′) |
|---|---|
| cultivated 1 | btFAD-5F: TTTTTCGGGTGTTCGTTACC |
| | btFAD-5R: GCCACTGGTAATCGCTGAAT |
| cultivated 2 | btFAD-6F: GCTACCTAGCTTGGCCCATT |
| | btFAD-6R: AGAGCTCCCCTTAGCCAGTC |
| cultivated 3 | btFAD-7F: TGGGGTACCGTTACTCATTG |
| | btFAD-7R: AGAATCCGACCAGCACAGAC |
| wild 1 | SeWCodF1: TTGGGAGGTTTTGATTCAG |
| | SeWCodR1: GAGGCCAACCRAGAGTAAGA |
| wild 2 | SeWCodF2: CCTTGCTTGTGCCCTATTTC |
| | SeWCodR2: CACTAACARAGGAYGCATCTTA |

**Identification of Nucleotide Polymorphisms in the Coding Region and Amino Acid Substitution in the Polypeptides.** After trimming and editing each DNA sequence, gene coding sequences were aligned with a sesame reference sequence (AY770501) using Sequencher (ver. 4.10.1). Following sequence alignment, nucleotide polymorphisms were identified among accessions. From the deduced amino acid sequence, substitutions were identified in the polypeptides.

**Evaluation of Selected Accessions.** An integrated approach including morphological observation, chemical analysis, and DNA sequence analysis was used for evaluation of the selected accessions. A phylogenetic dendrogram was generated from nucleotide polymorphisms in the coding region using the Arlequin 3.01 program.[22] Subsequently, a cladogram was generated from the deduced amino acid sequences along with *Glycine* and *Arachis* sequences using the ClustalW2 (http://www.ebi.ac.uk/Tools/msa/clustalw2) program. The selected accessions clustered into different groups. Misnamed accessions were identified and reclassified.

## RESULTS AND DISCUSSION

**Variation on Plant and Seed Morphology.** There was significant variation in plant and seed morphology among the seven accessions. Variation in plant and seed morphology is shown in Figure 1. All seven accessions were planted on the same day, April 30, 2012. Four accessions flowered 7 weeks after planting, and PI 278164 flowered a week later. PI 490268 flowered in the middle of August, and PI 367899 eventually

**Figure 1.** Plant and seed morphology of the selected sesame accessions. The picture of seed morphology was taken using newly harvested seeds from the plants shown above. The scale bar represents one centimeter.

flowered, but did not produce seeds until the middle of November. This accession was originally collected from Tanzania (Table 1) and may be temperature sensitive (high temperature leading to unsuccessful pollination). PI 224663 produced purple petioles whereas PI 599442 produced curly leaves (Figure 1). By the latter developmental stages, PIs 188815, 367899, and 490268 were taller than 1.2 m with big branches on the main stems. Three accessions (PIs 188815, 367899, and 490268) produced dark, almost black seeds, and the other four accessions produced lighter colored seeds.

**Variation on Fatty Acid Composition.** Significant variation in the fatty acid composition was detected between stored (old) seeds and freshly harvested (new) seeds (Table 3). On average, the freshly harvested seeds contained a higher amount of palmitic acid (C16:0) than the stored seeds (9.22% vs 8.87%), whereas the stored seeds contained higher amounts of stearic (C18:0), arachidic (C20:0), gadoleic (C20:1), and lignoceric (24:0) acids than the freshly harvested seeds (5.73% vs 5.26%; 0.69% vs 0.66%; 0.19% vs 0.16%; and 0.10% vs 0.06%). This variability may be due to environmental conditions. No significant variability in the other five traits was detected between the old and new seeds (Table 3). Since the old seeds were collected from different locations and/or years, comparisons among accessions with the old seeds would not be biologically informative. Only data collected on the new seeds grown under the same conditions in 2012 were used for comparison between accessions, and the data on the old seeds were used simply as reference information.

There was significant variability in oleic acid (23.85% to 42.92%), linoleic acid (41.67% to 58.63%), and O/L ratio (0.41 to 1.03) (Table 3 and Figure S1 in the Supporting Information). Oleic acid had a significantly negative correlation with linoleic acid ($r = -0.99$ at $p < 0.0001$ level). For example, PI 367899 had the highest percentage of linoleic acid (58.63%) and the lowest percentage of oleic acid (23.85%). The ratio of oleic acid and linoleic acid (O/L) can reflect the seed quality and oil properties. Oils with higher oleic acid content generally have a longer shelf life and are healthier for consumption. Among these seven accessions, oil from PI 599442 may have the best quality based on this criterion, containing the lowest percentage of linoleic acid (41.67%) and the highest oleic acid (42.92%).

**Single Nucleotide Polymorphisms, Deduced Amino Acid Substitutions in the Coding Region, Polypeptides**

**Table 3. Fatty Acid Composition from Old and New Seeds[a]**

| | 188815[b] | 224663[b] | 278164[b] | 367899[b] | 490268[b] | 599435[b] | 599442[b] | mean | LSD[c] |
|---|---|---|---|---|---|---|---|---|---|
| C16:0 % | 9.225 | 8.66 | 9.27 | 8.975 | 8.875 | 8.545 | 8.505 | 8.865 b | 0.294 |
| | 9.88 | 8.82 | 9.7 | 8.26 | 10.01 | 8.86 | 9.03 | 9.223 a | |
| C16:1 % | 0.115 | 0.13 | 0.11 | 0.14 | 0.115 | 0.1 | 0.08 | 0.113 a | 0.072 |
| | 0.12 | 0.13 | 0.1 | 0.2 | 0 | 0.155 | 0.105 | 0.116 a | |
| C18:0 % | 5.08 | 4.71 | 4.955 | 5.51 | 7.215 | 6.23 | 6.4 | 5.729 a | 0.342 |
| | 4.905 | 4.875 | 4.66 | 6.57 | 5.99 | 4.795 | 5.005 | 5.257 b | |
| C18:1 % | 30.96 | 39.4 | 36.91 | 21.07 | 27.08 | 48.81 | 50.07 | 36.33 a | 3.661 |
| | 30.545 | 39.22 | 32.395 | 23.85 | 28.435 | 39.165 | 42.915 | 33.79 a | |
| C18:2 % | 53.22 | 45.78 | 47.35 | 61.79 | 54.5 | 34.99 | 33.49 | 47.30 a | 3.621 |
| | 53.155 | 45.695 | 51.605 | 58.625 | 53.375 | 45.695 | 41.67 | 49.97 a | |
| C18:3 % | 0.36 | 0.34 | 0.375 | 1.235 | 0.83 | 0.265 | 0.37 | 0.539 a | 0.103 |
| | 0.365 | 0.325 | 0.5 | 1.27 | 0.97 | 0.345 | 0.31 | 0.584 a | |
| C20:0 % | 0.625 | 0.56 | 0.605 | 0.795 | 0.92 | 0.655 | 0.67 | 0.690 a | 0.001 |
| | 0.61 | 0.545 | 0.605 | 0.835 | 0.87 | 0.575 | 0.56 | 0.657 b | |
| C20:1 % | 0.175 | 0.2 | 0.19 | 0.15 | 0.17 | 0.21 | 0.2 | 0.185 a | 0.008 |
| | 0.17 | 0.19 | 0.19 | 0.185 | 0 | 0.19 | 0.185 | 0.159 b | |
| C22:0 % | 0.155 | 0.14 | 0.15 | 0.22 | 0.22 | 0.12 | 0.125 | 0.161 a | 0.072 |
| | 0.145 | 0.125 | 0.165 | 0.22 | 0.35 | 0.135 | 0.135 | 0.182 a | |
| C24:0 % | 0.09 | 0.08 | 0.09 | 0.125 | 0.11 | 0.1 | 0.095 | 0.099 a | 0.008 |
| | 0.1 | 0.075 | 0.095 | 0 | 0 | 0.085 | 0.08 | 0.062 b | |
| O/L ratio | 0.58 | 0.86 | 0.78 | 0.34 | 0.5 | 1.4 | 1.5 | 0.851 a | 0.136 |
| | 0.575 | 0.858 | 0.629 | 0.407 | 0.533 | 0.857 | 1.03 | 0.698 b | |

[a]For each trait, the data in the upper and lower rows were from the old and new seeds, respectively. There is a significant difference if the letters (after values) are different in the same column. [b]PI no. [c]Least significant difference.

**of the *FAD2*, and Phylogenetic Relationship among Accessions.** The sequences in the coding region (1152 bp) of the *SeFAD2* were aligned (Figure S2 in the Supporting Information), and 61 single nucleotide polymorphisms (SNPs) were identified among the seven accessions. The deduced amino acid sequences (383 aa) of *SeFAD2* were aligned (Figure S3 in the Supporting Information), and 12 amino acid substitutions were identified. A phylogenetic dendrogram and cladogram were generated using nucleotide sequences and deduced amino acid sequences, respectively (Figures 2a and 2b). There were no DNA polymorphisms among four accessions (PI 224663, PI 278164, PI 599435, and PI 599442) which were identical to the sesame reference sequence (previously deposited *FAD2* coding sequence, AY770501). These four accessions may belong to the cultivated sesame type (*S. indicum* L., Cluster I). In comparison to these four accessions, PI 188815 had eight SNPs, but only one led to an amino acid substitution (T71A). This accession may still belong to the cultivated type but with significant divergence. Compared to the reference sequence, both PI 367899 and PI 490268 had 46 SNPs resulting in 6 and 8 amino acid substitutions, respectively. These two accessions were closely related and may belong to the wild sesame type (*S. radiatum* Schum. & Thonn., Cluster II). Most SNPs originated between the wild and cultivated sesame. There was an amino acid substitution at 317 from alanine (A) to threonine (T) between the wild and cultivated sesame which was located in the H Box 3 (in the active site of the fatty acid desaturase). This critical substitution may contribute to the altered fatty acid composition between wild and cultivated sesame.

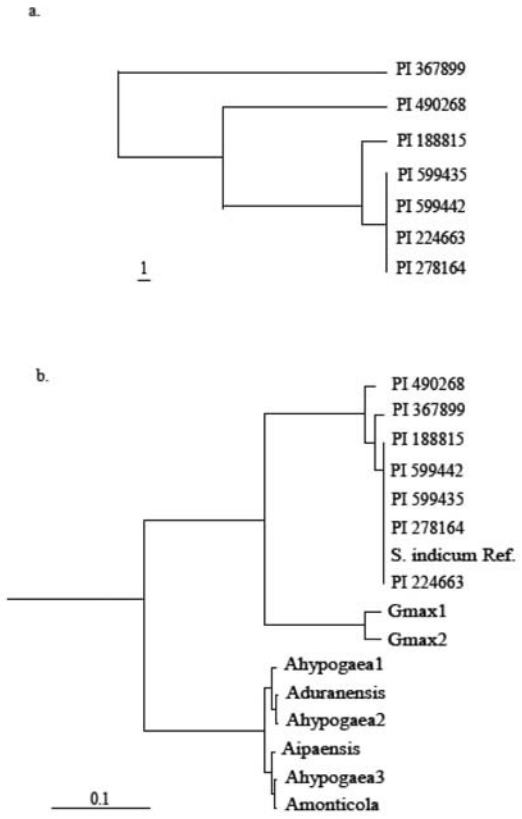


**Figure 2.** Dendrogram and cladogram from cluster analysis using nucleotide and amino acid sequence data, respectively. (a) Dendrogram was generated using nucleotide sequences from seven sesame accessions and (b) cladogram was generated from amino acid sequences from seven sesame accessions plus one sesame reference and two soybean (*Glycine*) and six peanut (*Arachis*) accessions: sesame reference, AAX11454.1; *G. max*1, BAD89862.1; *G. max*2, P48631; *A. hypogaea*1, AAY53559.1; *A. hypogaea*2, AAB84262.1; *A. hypogaea*3, AAK67829.1; *A. duranensis*, AAF82294.1; *A. ipaensis*, AAF82295.1; and *A. monticola*, AAX14399.1. Scale bar represents coefficient similarity.

In general, the results from the dendrogram and the cladogram were consistent; and they suggest that two accessions were misnamed in the GRIN database. PI 278164 does not belong to the wild species (*S. radiatum* Schum. & Thonn.) and should be classified as cultivated sesame (*S. indicum* L.). PI 490268 does not belong to the cultivated sesame and should be classified with the wild species. Our cladogram analysis also indicated that the sesame *FAD2* coding sequence had a higher similarity to the corresponding soybean sequences than to the *Arachis* sequences.

The results from morphological observation, chemical analysis, and *FAD2* gene coding sequence were consistent when freshly harvested seeds were analyzed. PI 278164 and PI 490268 were misnamed in the GRIN database. PI 278164 should be classified with the cultivated form (*S. indicum* L.) instead of the wild form (*S. radiatum* Schum & Thonn.), whereas PI 490268 should be classified as the wild form instead of the cultivated form. Ultimately, more research is still required to determine to which wild form PI 490268 belongs. The wild accessions PI 367899 and PI 490268 flowered and matured later, and they produced seeds with lower amounts of oleic acid (23.85% and 28.44%) but higher amounts of linoleic acid (58.63% and 53.38%) than the cultivated form. Our results demonstrate how an integrated approach including morphological observation, chemical analysis, and genetic analysis can be used to properly characterize and evaluate plant germplasm accessions.

High oleate cultivars have been developed in several major oilseed crops including soybean, canola, sunflower, and peanut;[23] but so far none in sesame. A high oleate sesame line (Ant-33 containing 41.4% oleic acid) was identified by screening 103 Turkey cultivated sesame landraces,[4] but this is much lower than the high oleate soybean containing over 80% oleic acid.[24] This high oleate soybean was developed by crossing two accessions (PI 603452 and PI 283327) which contained spontaneous mutations in *FAD2-1A* and *FAD2-1B*, respectively, and then by selection of the mutant alleles using marker-assisted selection (MAS) in breeding programs. Mutagenesis has been explored in sesame. Closed capsule and determinate growth habit mutants have been successfully identified using $\gamma$-irradiation, but there was limited enhancement of oleic acid only up to 46%.[25] If there are two copies of the *FAD2* gene in the sesame genome, the probability of simultaneously mutating both copies in one individual would be very low. Natural genetic variation in the level of oleic acid may exist in the sesame genome. More sesame germplasm accessions need to be screened for identification of new *FAD2* mutations. Newly identified accessions encompassing different mutant alleles of *FAD2* can be used as breeding materials for further developing high oleate sesame cultivars.

## ■ ASSOCIATED CONTENT

### Ⓢ Supporting Information

Figure S1, comparison of oleic acid (C18:1) and linoleic acid (C18:2) levels among seven accessions. Figure S2, DNA sequence alignment in the *FAD2* gene coding region among

accessions. Figure S3, amino acid sequence alignment for the *FAD2* among accessions. This material is available free of charge via the Internet at http://pubs.acs.org.

## AUTHOR INFORMATION


### Corresponding Authors

*(Z.C.) E-mail: zchen@uga.edu. Phone: 770-228-7331.
*(M.L.W.) E-mail: mingli.wang@ars.usda.gov. Phone: 770-229-3342.


### Notes

The authors declare no competing financial interest.

## ACKNOWLEDGMENTS

The authors would like to thank Drs. Paul Raymer and Charles Y. Chen for their useful comments and suggestions for improving the quality of this manuscript and Ken Manley for his help in planting sesame seeds.

## REFERENCES


(1) Nimmakayala, P.; Perumal, R.; Mulpuri, S.; Reddy, U. K. Sesame. In *Wild Crop Relatives: Genomic and Breeding Resources, Oilseeds*; Kole, C., Ed.; Springer-Verlag: Berlin Heidelberg, 2011; pp 261−273.

(2) Nayar, N. M.; Mehra, K. L. Sesame: its uses, botany, cytogenetics, and origin. *Econ. Bot.* **1970**, *24*, 20−31.

(3) Cheung, S. C. M.; Szeto, Y. T.; Benzie, I. F. F. (2007) Antioxidant protection of edible oils. *Plant Foods Hum. Nutr.* **2007**, *62*, 39−42.

(4) Uzun, B.; Arslan, Ç.; Furat, Ş. Variation in fatty acid composition, oil content and oil yield in germplasm collection of sesame (*Sesamum indicum* L.). *J. Am. Oil Chem. Soc.* **2008**, *85*, 1135−1142.

(5) Chen, P. R.; Chien, K. L.; Su, T. C.; Chang, C. J.; Liu, T. L.; Cheng, H.; Tsai, C. Dietary sesame reduces serum cholesterol and enhances antioxidant capacity in hypercholesterolemia. *Nutr. Res. (N.Y.)* **2005**, *25*, 559−567.

(6) Kapadia, G. J.; Azuine, M. A.; Tokuda, H.; Takasaki, M.; Mukainaka, T.; Konoshima, T.; Nishino, H. Chemopreventive effect of resveratrol, sesamol, sesame oil and sunflower oil in the epstein-barr virus early antigen activation assay and the mouse skin two-stage carcinogenesis. *Pharmacol. Res.* **2002**, *45*, 499−505.

(7) Yermanos, D. M. Sesame. In *Hybridization of crop plants*; Fehr, D. M., Hadley, H. H., Eds.; American Society of Agronomy and Crop Science Society: Madison, WI, 1980; pp 549−563.

(8) Morris, J. B. Characterization of sesame (*Sesamum indicum* L.) germplasm regenerated in Georgia, USA. *Genet. Resour. Crop Evol.* **2009**, *56*, 925−936.

(9) Morinaga, T.; Fukushima, E.; Kano, T.; Yamasaki, Y. Chromosome numbers of cultivated plants. II. *Bot. Mag.* **1929**, *43*, 589−594.

(10) Zhang, H.; Miao, H.; Wang, L.; Qu, L.; Liu, H.; Wang, Q.; Yue, M. Genome sequencing of the important oilseed crop *Sesamum indicum* L. *Genome Biol.* **2013**, *13*, 401.

(11) Cronquist, A. *An integrated system of classification of flowering plants*; Columbia University Press: New York, 1981; 1262 pp.

(12) Kim, M. J.; Kim, H.; Shin, J. S.; Chung, C. H.; Ohirogge, J. B.; Suh, M. C. Seed specific expression of sesame microsomal oleic acid desaturase is controlled by combinational properties between negative *cis*-regulatory elements in the *SeFAD2* promoter and enhancers in the 5′-UTR intron. *Mol. Genet. Genomics* **2006**, *276*, 351−368.

(13) Kim, M. J.; Kim, J. K.; Shin, J. S.; Suh, M. C. The SebHLH transcription factor mediates trans-activation of the Se*FAD2* gene promoter through binding to E- and G-box elements. *Plant Mol. Biol.* **2007**, *64*, 453−466.

(14) Kim, M. J.; Go, Y. S.; Lee, S. B.; Kim, Y. S.; Shin, J. S.; Min, M. K.; Hwang, I.; Suh, M. C. Seed-expressed casein kinase I acts as positive regulator of the SeFAD2 promoter via phosphorylation of the SebHLH transcription factor. *Plant Mol. Biol.* **2010**, *73*, 425−437.

(15) Jin, U. H.; Lee, J. W.; Chung, Y. S.; Lee, J. H.; Yi, Y. B.; Kim, Y. K.; Hyung, N. I.; Pyee, J. H.; Chung, C. H. Characterization and temporal expression of a ω-6 fatty acid desaturase cDNA from sesame (*Sesamum indicum* L.) seeds. *Plant Sci.* **2001**, *161*, 935−941.

(16) Okuley, J.; Lightner, J.; Feldmann, K.; Yadav, N.; Lark, E.; Browsw, J. *Arabidopsis FAD2* gene encodes the enzyme that is essential for polyunsaturated lipid synthesis. *Plant Cell* **1994**, *6*, 147−158.

(17) Heppard, E. P.; Kinney, A. J.; Stecca, K. L.; Miao, G. H. Developmental and growth temperature regulation of two different microsomal [omega]-6 desaturase genes in soybeans. *Plant Physiol.* **1996**, *110*, 311−319.

(18) Martínez-Rivas, J. M.; Sperling, P.; Lühs, W.; Heinz, E. Spatial and temporal regulation of three different microsomal oleate desaturase genes (*FAD2*) from normal type and high-oleic varieties of sunflower (*Helianthus annuus* L.). *Mol. Breed.* **2001**, *8*, 159−168.

(19) Liu, Q.; Singh, S. P.; Brubake, C. L.; Sharp, P. J.; Green, A. G.; Marshall, D. R. Molecular cloning and expression on a cDNA encoding a microsomal ω-6 fatty acid desaturase from cotton (*Gossypium hirsutum*). *Funct. Plant Biol.* **1999**, *26*, 101−106.

(20) Liu, K. Preparation of fatty acid methyl esters for gas chromatographic analysis of lipids in biological materials. *J. Am. Oil Chem. Soc.* **1994**, *71*, 1179−1187.

(21) Wang, M. L.; Chen, C. Y.; Tonnis, B.; Barkley, N. A.; Pinnow, D. L.; Pittman, R. N.; Davis, J.; Holbrook, C. C.; Stalker, H. T.; Pederson, G. A. Oil, fatty acid, flavonoid, and resveratrol content variability and *FAD2A* functional SNP genotypes in the U.S. peanut mini-core collection. *J. Agric. Food Chem.* **2013**, *61*, 2875−2882.

(22) Excoffier, L.; Laval, G.; Schneider, S. Arlequin ver. 3.0: An integrated software package for population genetics data analysis. *Evol. Bioinformatics Online* **2005**, *1*, 47−50.

(23) Barkley, N. A.; Wang, M. L. Oleic acid: Natural variation and potential enhancement in oilseed crops. In *Oleic acid: Dietary sources, functions and health benefits*; Silva, L. P., Ed.; Nova Scientific Publishers, Inc.: 2012; pp 59−72.

(24) Pham, A. T.; Lee, J. D.; Shannon, J. G.; Bilyeu, K. D. A novel *FAD2-1A* allele in a soybean plant introduction offers an alternate means to produce soybean seed oil with 85% oleic acid content. *Theor. Appl. Genet.* **2011**, *123*, 793−802.

(25) Arslan, Ç.; Uzun, B.; Ülger, S.; Çağirgan, M. İ. Determination of oil content and fatty acid composition of sesame mutants suitable for intensive management conditions. *J. Am. Oil Chem. Soc.* **2007**, *84*, 917−920.

be useful for various applications of high-amylose starches in the food and nonfood industries.

## MATERIALS AND METHODS

**Materials.** Native normal maize starch (S4126) (NS) and high-amylose maize starch (S4180) (HS) were purchased from Sigma-Aldrich.

**Separation of Large-, Medium-, and Small-Sized Fractions.** The native normal and high-amylose maize starches were separated into large-, medium-, and small-sized fractions using five methods (Supporting Information Figures S1−S5). The main procedure of the method is briefly explained below.

**Microsieving.** The starches were separated into different-sized fractions by microsieving according to the method of Kaur et al.[9] with some modifications (Supporting Information Figure S1). Starch suspension (0.2%, w/v) in distilled water was passed sequentially through 10 and 5 $\mu$m sieves. The granules retained on the 10 $\mu$m sieve were collected as the large-sized fraction. The filtrate that passed through the 10 $\mu$m sieve was screened further through the 5 $\mu$m sieve to obtain a filtrate containing the small-sized fraction. The starch retained on the 5 $\mu$m sieve was collected as the medium-sized fraction. The collected starch fractions were centrifuged and washed in distilled water and twice in anhydrous ethanol and then dried at 40 °C for 2 days, ground into powders in a mortar with pestle, and passed through a 100 mesh sieve.

**Extreme Sedimentation.** The starches were separated into different-sized fractions by extreme sedimentation according to the method of Ao and Jane[2] with some modifications (Supporting Information Figure S2). Starch suspension (0.2%, w/v; 150 mL) in distilled water was allowed to settle for 0.5 h in a graduated cylinder (250 mL). The supernatant was decanted to a glass beaker. The starch pellet was made up to 150 mL with distilled water and mixed and then was allowed to settle for 0.5 h to obtain the supernatant and starch precipitate again. The process was repeated 10 times. The starch precipitate was collected as the large-sized fraction. The suspensions were pooled and centrifuged at 5000*g* for 10 min. The resulting precipitate was suspended to 150 mL in the cylinder and allowed to settle for 1 h. The supernatant was decanted to another cylinder and made up to 150 mL with distilled water and was mixed and allowed to settle for 1 h to obtain the supernatant and starch precipitate again. The process was repeated 10 times. The starch in the supernatant was collected as the small-sized fraction. The starch precipitate during the separation of small-sized granules was pooled and collected as the medium-sized fraction. Finally, the starch fractions were washed and dried as described above for microsieving.

**Differential Sedimentation.** The starches were separated into different-sized fractions by differential sedimentation according to the method of Takeda et al.[26] with some modifications (Supporting Information Figure S3). Starch suspension (0.2%, w/v; 150 mL) in distilled water was allowed to settle in 250 mL cylinders for 0.5 and 2 h. The fractions of 0.5 h precipitate, 0.5−2 h precipitate, and 2 h supernatant were collected as large-, medium-, and small-sized granules, respectively. The fractionation was repeated 10 times on each fraction to be refined. Finally, the starch fractions were washed and dried as described above for microsieving.

**Differential Supernatant.** The starches were separated into different-sized fractions by differential supernatant according to the method of Dhital et al.[27] with some modifications (Supporting Information Figure S4). Starch suspension (0.2%, w/v) in distilled water was allowed to settle in a cylinder for 2 and 0.5 h. After the desired time, the top 10 cm of supernatant was pipetted to a beaker. The remaining suspension in the cylinder was then made up to the original volume with distilled water and mixed and then was allowed to settle for collecting supernatant. The pipetting supernatant was repeated 10 times. The starches in the supernatants of 2 and 0.5 h settlement were collected as small- and medium-sized fractions, respectively. The starch precipitate of 0.5 h settlement was collected as large-sized fraction. Finally, the starch fractions were washed and dried as described above for microsieving.

**Glycerol Centrifugation.** The starches were separated into different-sized fractions by glycerol centrifugation according to the method of Peng et al.[28] with some modifications (Supporting Information Figure S5). Starch suspension (2.5%, w/v; 40 mL) in 80% glycerol was centrifuged at 100*g* for 5 min. The supernatant was removed to a beaker. The pellet was suspended with 40 mL of 80% glycerol and centrifuged five times to obtain starch precipitate that constituted the large-sized fraction. The supernatants were pooled and centrifuged at 5000*g* for 10 min. The resulting starch pellet was suspended with 40 mL of 60% glycerol and centrifuged at 100*g* for 5 min. The supernatant was removed to a beaker. The pellet was suspended with 40 mL of 60% glycerol and centrifuged five times to obtain starch precipitate that constituted the medium-sized fraction. The supernatants were pooled and centrifuged at 5000*g* for 10 min. The resulting starch pellet comprised the small-sized fraction. Finally, the starch fractions were washed and dried as described above for microsieving.

**Morphology Observation.** The micromorphology of starch granules was viewed with an Olympus BX53 light microscope according to the method described by Cai et al.[22] For scanning electron microscope (SEM) observation, starch granules were suspended in anhydrous ethanol. Twenty microliters of the starch−ethanol suspension was applied to an aluminum stub using double-sided adhesive tape, and the starch was coated with gold using a sputter coater. Starch samples were observed and photographed using an environmental SEM (ESEM XL-30, Philips, The Netherlands).

**Granule Size Analysis.** Granule size analysis was carried out using a laser diffraction particle size analyzer (Mastersizer 2000, Malvern, UK). The starches were suspended in distilled water and stirred at 2000 rpm. The obscuration in all measurements was >10%. Particle size is defined in terms of the 10th percentile [$d(0.1)$], median [$d(0.5)$], 90th percentile [$d(0.9)$], surface-weighted mean [$D(3,2)$], and volume-weighted mean [$D(4,3)$].

**Apparent Amylose Content (AC) Determination.** Apparent AC was determined using an iodine colorimetric method as described by Man et al.[15]

**Molecular Weight Distribution Analysis.** Starch was deproteinized with protease and sodium bisulfite and debranched with isoamylase according to the methods of Tran et al.[29] and Li et al.[30] The molecular weight distribution of debranched starch was analyzed using a PL-GPC 220 high-temperature chromatograph (Agilent Technologies UK Limited, Shropshire, UK) with three columns (PL110-6100, 6300, 6525) and a differential refractive index detector according to the method of Cai et al.[31]

**Crystal Structure Analysis.** The crystal structure of starch was analyzed on an XRD (D8, Bruker, Germany) spectroscope. The XRD analysis and determination of the relative crystallinity were carried out following the method described by Man et al.[15] Before measurements, all of the specimens were stored in a moist chamber where a saturated solution of NaCl maintained a constant humidity (relative humidity = 75%) for 1 week.

**Short-Range Ordered Structure Analysis.** Short-range ordered structure of starch was analyzed on a Varian 7 000 FTIR spectrometer with a DTGS detector equipped with an ATR single-reflectance cell containing a germanium crystal (45° incidence angle) (PIKE Technologies, USA) as previously described by Man et al.[15] Original spectra were corrected by subtraction of the baseline in the region from 1200 to 800 $cm^{-1}$ before deconvolution was applied using Resolutions Pro. The assumed line shape was Lorentzian with a half-width of 19 $cm^{-1}$ and a resolution enhancement factor of 1.9. Intensity measurements at 1045, 1022, and 995 $cm^{-1}$ were performed on the deconvoluted spectra by recording the height of the absorbance bands from the baseline using Adobe Photoshop 7.0 image software.

**Solid-State $^{13}C$ CP/MAS NMR Analysis.** High-resolution solid-state $^{13}C$ CP/MAS NMR analysis of starch was carried out at $B_0$ = 9.4T on a Bruker AVANCE III 400 WB spectrometer as described previously by Cai et al.[31] Amorphous starch was prepared by gelatinizing native starch following the method of Atichokudomchai et al.[32] The spectrum of amorphous starch was matched to the intensity of native starch at 84 ppm and subtracted to produce the

ordered subspectrum. The quantitative analyses of single-helix, double-helix, and amorphous conformational features within starch were carried out according to the method described by Tan et al.[33]

**SAXS Analysis.** SAXS measurement of starch was performed according to the method of Yuryev et al.[34] with some modifications. Starch was dispersed in an excess of distilled water to form slurries. SAXS measurement was obtained using a Bruker NanoStar SAXS instrument equipped with Vantec 2000 detector and pinhole collimation for point focus geometry. The X-ray source was a copper rotating anode (0.1 mm filament) operating at 50 kV and 30 W, fitted with cross-coupled Göbel mirrors, resulting in Cu K$\alpha$ radiation wavelength of 1.5418 Å. The optics and sample chamber were under vacuum to minimize air scattering. During X-ray exposure, the starch slurries were kept in sealed cells to prevent dehydration. SAXS data sets were analyzed using DIFFRAC$^{plus}$ NanoFit software. Parameters of the SAXS spectrum were determined according to the simple graphical method.[34]

**Statistical Analysis.** The data reported in all tables are mean values and standard deviation. Analysis of variance (ANOVA) by Tukey's test ($p < 0.05$) was evaluated using the SPSS 16.0 Statistical Software Program.

## RESULTS AND DISCUSSION

**Morphology of Large-, Medium-, and Small-Sized Starch Fractions.** Figures S6 and S7 in the Supporting Information show the micromorphologies of native starches and their different-sized fractions. For native normal maize starch, most of the granules were polygonal with large size, and some granules were spherical with small size (Figure S6). For native high-amylose maize starch, some elongated starch granules were also observed except polygonal granules with large size and spherical granules with small size (Figure S7). It is very important to establish the size separation methods that give narrow granule size fractions for investigating the structural properties of different-sized starch granules. In this study, five procedures, including microsieving, extreme sedimentation, differential sedimentation, differential supernatant, and glycerol centrifugation separation, have been used to separate large-, middle-, and small-sized fractions from normal and high-amylose maize starches. Microsieving could not completely separate large-, medium-, and small-sized fractions. Some medium- and small-sized granules were retained in the large-sized fraction. Some large-sized granules passed through the screen and were present with medium- and small-sized granules in the filtrate (Figures S6 and S7). Some literature also reports that microsieving can not give a homogeneous size granule population.[28] Sedimentation in a water column separates different-sized granules on the basis of the difference in sedimentation rates. Different sedimentation procedures have been reported in refs 2, 26, and 27. In this study, extreme sedimentation, differential sedimentation, and differential supernatant separation methods were compared (Figures S6 and S7). The results showed that the extreme sedimentation and differential supernatant separation methods were better than differential sedimentation for giving homogeneous size granules. Because of the low density of water, the difference among sedimentation rates of different-sized granules in water is not large enough to separate the different-sized granules. In addition, it takes a very long time to obtain enough small-sized granules by extreme sedimentation and differential supernatant separation methods. Because glycerol solution has higher density than water, the difference among sedimentation rates of different-sized granules in glycerol is large enough to separate the different-sized granules. Thus, in the present study, the glycerol centrifugations through two glycerol solutions (80 and 60%, v/v) were used to purify large-, medium-, and small-sized granules from native normal and high-amylose maize starches. The granule morphology and sizes were significantly different in different-sized fractions separated by glycerol centrifugation (Figures S6 and S7).

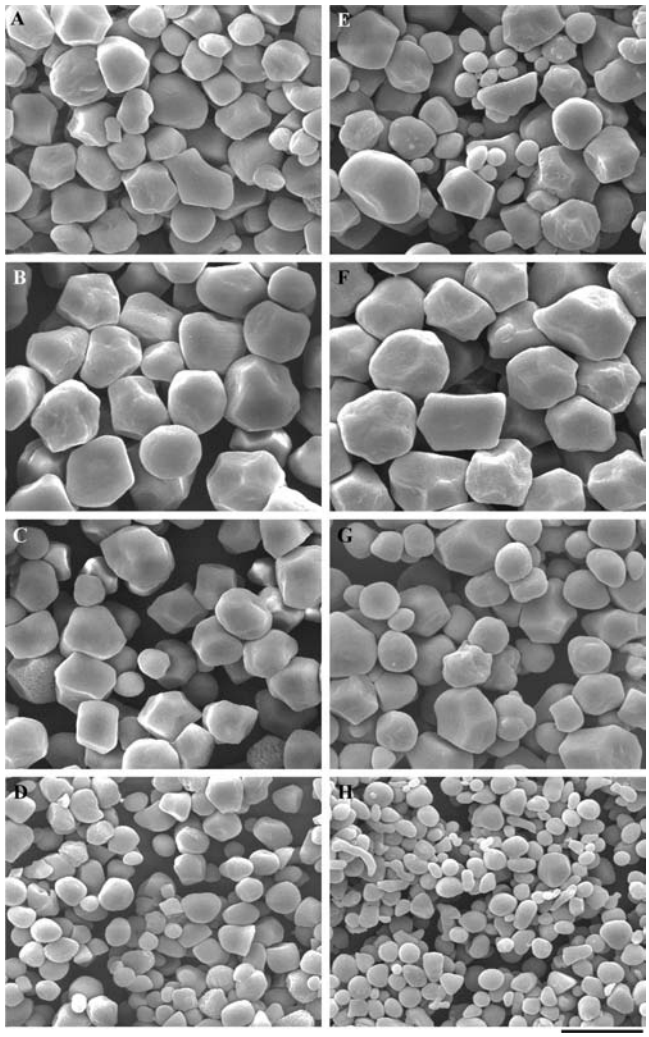


**Figure 1.** SEM photographs of native (A, E) and large- (B, F), medium- (C, G), and small-sized (D, H) fractions of normal (A–D) and high-amylose (E–H) maize starches separated by glycerol centrifugation method. Scale bar = 20 $\mu$m.

SEM was used to complement the light microscope images in an effort to reveal details about the granule surface that could not be distinguished by light microscope (Figure 1). The surfaces of the granules from native and large-, medium-, and small-sized fractions of normal and high-amylose maize starches were smooth. The native starches from normal and high-amylose maizes consisted of mixed populations of large, medium, and small granules. The large and medium granules were mainly polyhedral or irregular in shape, whereas the small granules were mainly spherical or ellipsoidal. In addition, some elongated granules were also observed in the small-sized fraction of high-amylose starch.

**Size of Large-, Medium-, and Small-Sized Starch Fractions.** The laser diffraction instrument for granule size measurement provides derived outputs of a volume distribution, standard mean diameters [$D(3,2)$ and $D(4,3)$], and distribution information [$d(0.1)$, $d(0.5)$, and $d(0.9)$]. The

**Table 1. Diameters of Native and Large-, Medium-, and Small-Sized Fractions of Normal and High-Amylose Maize Starches Separated by Glycerol Centrifugation Method[a]**

| | normal maize (μm) | | | | | high-amylose maize (μm) | | | | |
|---|---|---|---|---|---|---|---|---|---|---|
| fraction | $d(0.1)^b$ | $d(0.5)^b$ | $d(0.9)^b$ | $D(3,2)^c$ | $D(4,3)^c$ | $d(0.1)^b$ | $d(0.5)^b$ | $d(0.9)^b$ | $D(3,2)^c$ | $D(4,3)^c$ |
| native | 8.30 ± 0.01b | 13.86 ± 0.01c | 20.38 ± 0.02b | 7.49 ± 0.01a | 13.88 ± 0.01b | 6.60 ± 0.01b | 13.22 ± 0.01b | 22.53 ± 0.02c | 7.70 ± 0.00c | 13.83 ± 0.01b |
| large-sized | 12.54 ± 0.01d | 17.72 ± 0.01d | 25.11 ± 0.02d | 17.11 ± 0.01d | 18.38 ± 0.01d | 13.96 ± 0.00d | 19.75 ± 0.00d | 28.01 ± 0.01d | 19.07 ± 0.00d | 20.48 ± 0.00d |
| medium-sized | 9.12 ± 0.00c | 13.84 ± 0.00b | 20.99 ± 0.01c | 13.16 ± 0.00c | 14.54 ± 0.01c | 8.55 ± 0.01c | 14.36 ± 0.03c | 21.36 ± 0.08b | 7.64 ± 0.01b | 14.41 ± 0.04c |
| small-sized | 5.02 ± 0.00a | 8.40 ± 0.01a | 14.00 ± 0.03a | 7.79 ± 0.01b | 9.03 ± 0.01a | 4.26 ± 0.00a | 8.15 ± 0.01a | 13.70 ± 0.02a | 5.45 ± 0.00a | 8.52 ± 0.01a |

[a]Data are means ± standard deviations, $n = 3$. Values in the same column with different letters are significantly different ($P < 0.05$). [b]$d(0.1)$, $d(0.5)$, and $d(0.9)$ are the granule sizes at which 10, 50, and 90% of all the granules by volume are smaller, respectively. [c]$D(3,2)$ is the surface area-weighted mean diameter. $D(4,3)$ is the volume-weighted mean diameter.

**Table 2. Apparent Amylose Contents of Native and Large-, Medium-, and Small-Sized Fractions of Normal and High-Amylose Maize Starches[a]**

| | normal maize (%) | | | | | high-amylose maize (%) | | | | |
|---|---|---|---|---|---|---|---|---|---|---|
| fraction | $M_A{}^b$ | $M_B{}^b$ | $M_C{}^b$ | $M_D{}^b$ | $M_E{}^b$ | $M_A{}^b$ | $M_B{}^b$ | $M_C{}^b$ | $M_D{}^b$ | $M_E{}^b$ |
| native | 30.9 ± 0.4ab | 30.9 ± 0.4ab | 30.9 ± 0.4a | 30.9 ± 0.4bc | 30.9 ± 0.4b | 56.0 ± 0.4b | 56.0 ± 0.4c | 56.0 ± 0.4c | 56.0 ± 0.4c | 56.0 ± 0.4c |
| large-sized | 31.5 ± 0.4b | 32.4 ± 0.5c | 31.4 ± 0.7a | 31.7 ± 0.4c | 31.9 ± 0.4c | 45.5 ± 0.8a | 32.1 ± 0.9a | 31.6 ± 0.9a | 32.6 ± 0.9a | 33.2 ± 0.4a |
| medium-sized | 30.1 ± 0.6a | 31.4 ± 0.7bc | 31.0 ± 0.5a | 29.8 ± 0.7ab | 31.2 ± 0.3bc | 56.3 ± 1.0b | 46.5 ± 0.9b | 46.5 ± 0.8b | 48.9 ± 0.9b | 50.5 ± 0.9b |
| small-sized | 29.8 ± 0.4a | 29.8 ± 0.3a | 30.3 ± 0.8a | 29.3 ± 0.5a | 29.7 ± 0.4a | 65.5 ± 0.8c | 68.5 ± 0.8d | 58.1 ± 0.7d | 75.3 ± 1.0d | 74.1 ± 0.3d |

[a]Data are means ± standard deviations, $n = 3$. Values in the same column with different letters are significantly different ($P < 0.05$). [b]$M_A$, $M_B$, $M_C$, $M_D$, and $M_E$ indicate the separation methods of microsieving, extreme sedimentation, differential sedimentation, differential supernatant, and glycerol centrifugation, respectively.



dx.doi.org/10.1021/jf503865e | J. Agric. Food Chem. 2014, 62, 11711−11721

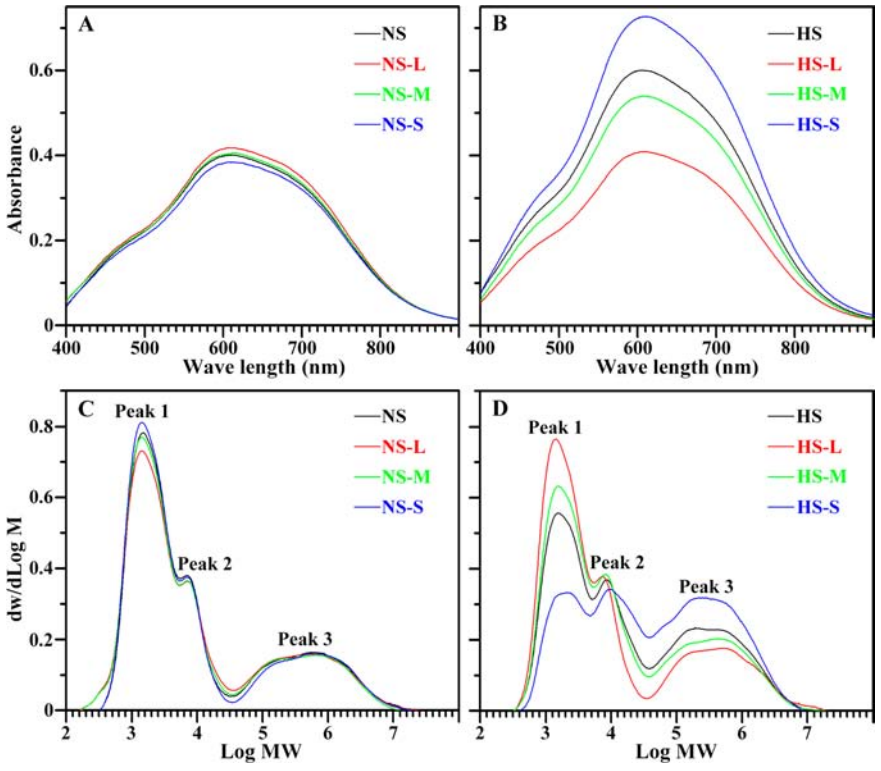


**Figure 2.** Absorbance spectra of starches in the $I_2$/KI solution (A, B) and GPC chromatograms of isoamylase-debranched starches (C, D) from normal (A, C) and high-amylose (B, D) maize starches separated by glycerol centrifugation method. NS, NS-L, NS-M, and NS-S: native and large-, medium-, and small-sized fractions of normal maize starch. HS, HS-L, HS-M, and HS-S: native and large-, medium-, and small-sized fractions of high-amylose maize starch.

volume distributions of different-sized fractions of normal and high-amylose maize starches are presented in Figure S8 in the Supporting Information. Native starches were unimodal distribution and could be separated into large-, medium-, and small-sized fractions. The granule size range of high-amylose maize starch was broader than that of normal maize starch, especially for native starch. An overlap between the fractions could be seen. The results of granule size measurements are listed in Table 1. The $d(0.5)$, $D(3,2)$, and $D(4,3)$ values of large-, medium-, and small-sized fractions were reduced from 17.72 to 13.84 and 8.40 $\mu$m, from 17.11 to 13.16 and 7.79 $\mu$m, and from 18.38 to 14.54 and 9.03 $\mu$m, respectively, for normal maize starch and from 19.75 to 14.36 and 8.15 $\mu$m, from 19.07 to 7.64 and 5.45 $\mu$m, and from 20.48 to 14.41 and 8.52 $\mu$m, respectively, for high-amylose maize starch.

**Apparent AC of Large-, Medium-, and Small-Sized Starch Fractions.** Apparent ACs of native and large-, medium-, and small-sized fractions of normal and high-amylose maize starches were determined using the iodine colorimetric method and are shown in Table 2. The results of five separation methods all showed that the apparent AC slightly decreased with decrease of granule size for normal maize starch, but markedly increased with decrease of granule size for high-amylose starch. For normal unimodal starch, the decrease in AC with decrease of granule size has been previously reported.[6,8−10] However, the significant increase of AC with decrease of granule size was not reported in previous studies. For high-amylose maize starch, it is noteworthy that the large-sized granules had only about 32% apparent AC and the small-sized granules had about 75% apparent AC for differential supernatant and glycerol centrifugation separation methods.

On the basis of the morphologies (Supporting Information Figures S6 and S7), ACs (Table 2), and purified efficiency of different-sized fractions separated by five methods, the separation effectiveness of glycerol centrifugation method was the best among five methods. In this study, structural properties of starches were investigated in the different-sized fractions separated by glycerol centrifugation method.

**Iodine Absorption Spectra of Large-, Medium-, and Small-Sized Starch Fractions.** The absorption spectra of iodine−starch complex are shown in Figure 2A,B. The absorption spectra were similar among native and large-, medium-, and small-sized starch fractions of normal maize (Figure 2A), but significantly different among native and large-, medium-, and small-sized starch fractions of high-amylose maize (Figure 2B). The maximum absorption wavelength was similar among different-sized fractions of normal and high-amylose maize starches. The iodine blue value slightly decreased with decrease of granule size for normal maize starch, but markedly increased with decrease of granule size for high-amylose starch (Table 3).

**Molecular Weight Distribution of Large-, Medium-, and Small-Sized Starch Fractions.** The molecular weight distributions of isoamylase-debranched starches as determined by GPC are shown in Figure 2C,D. A trimodal distribution of low, middle, and high molecular weight peaks, designated peak 1, peak 2, and peak 3, respectively, was observed. Peaks 1 and 2 consist of short (A and short B chains) and long (long B chains) branch-chains of amylopectin, respectively. The area ratio of peak 1 to peak 2 might be used as an index of the extent of branching of amylopectin; the higher the ratio, the higher the branching degree.[35] Peak 3 includes amylose.[36] The GPC

Table 3. Iodine Blue Values and GPC Parameters of Native and Large-, Medium-, and Small-Sized Fractions of Normal and High-Amylose Maize Starches Separated by Glycerol Centrifugation Method[a]

| fraction | iodine blue value[b] | | peak area of normal maize[c] (%) | | | peak area of high-amylose maize[c] (%) | | | peak 1/peak 2[c] | |
|---|---|---|---|---|---|---|---|---|---|---|
| | normal maize | high-amylose maize | peak 1 | peak 2 | peak 3 | peak 1 | peak 2 | peak 3 | normal maize | high-amylose maize |
| native | 0.355 ± 0.006b | 0.520 ± 0.002c | 56.6 ± 1.1a | 16.0 ± 0.6a | 27.5 ± 0.5a | 41.9 ± 1.4b | 22.6 ± 0.1b | 35.6 ± 1.3c | 3.5 ± 0.2a | 1.9 ± 0.1b |
| large-sized | 0.367 ± 0.009b | 0.367 ± 0.006a | 56.5 ± 0.3a | 15.8 ± 0.1a | 27.8 ± 0.4a | 56.4 ± 1.1d | 15.8 ± 1.6a | 27.9 ± 0.6a | 3.6 ± 0.0a | 3.6 ± 0.4c |
| medium-sized | 0.354 ± 0.006b | 0.476 ± 0.005b | 58.6 ± 0.8a | 16.3 ± 0.2a | 25.2 ± 1.1a | 47.9 ± 1.6c | 20.7 ± 1.2b | 31.5 ± 0.4b | 3.6 ± 0.0a | 2.3 ± 0.2b |
| small-sized | 0.334 ± 0.010a | 0.636 ± 0.006d | 58.4 ± 0.7a | 15.4 ± 0.1a | 26.3 ± 0.8a | 24.5 ± 0.2a | 26.5 ± 0.5c | 49.1 ± 0.7d | 3.8 ± 0.0a | 0.9 ± 0.0a |

[a]Data are means ± standard deviations, $n = 3$ for iodine blue values and =2 for GPC parameters. Values in the same column with different letters are significantly different ($P < 0.05$). [b]Iodine blue values are the absorbance at 680 nm of starch–iodine complex. [c]GPC parameters of isoamylase-debranched starches. The peak 1/peak 2 ratio is determined according to the area ratio of peak 1 and peak 2.

parameters are summarized in Table 3. The AC determined on the basis of iodine and starch affinity is described as apparent AC, which overestimates AC if there are branched molecules with long side chains that bind iodine.[37] The present results showed that the AC determined by GPC (Table 3) was significantly lower than the apparent AC obtained by iodine colorimetric method (Table 2), which was in agreement with the report of Shi et al.[37] and indicated that the intermediate chain and amylopectin long branch-chain could bind iodine to increase the value of apparent AC. The study of Dhital et al.[6] showed that the molecular weight distributions of fully branched normal maize starch fractions were almost similar, although their apparent ACs were different. In the present study, the small-sized fraction of normal starch also showed significantly lower apparent AC than the large-sized fraction, but the ACs and amylopectin branching degree determined by GPC had no significant difference among different-sized fractions of normal maize starch. The results agreed with the conclusion of Dhital et al.[6] that the lower apparent AC in the smaller normal starch granules was predominantly due to the higher amount of lipids in these granules that might have complexed with amylose and thereby reduced the amount of free amylose available to form a complex with iodine. For high-amylose starch, the AC determined by GPC was markedly lower than the apparent AC, the branching degree of high-amylose starch was also markedly lower than that of normal starch. These results indicated that high-amylose starch contained high levels of intermediate chain and amylopectin long branch-chain. The different-sized fractions of high-amylose starch had a significant increase in the amylopectin long branch-chain and AC and a marked decrease in the amylopectin short branch-chain and branching degree with the decrease of granule size, indicating that the different-sized fractions of high-amylose starch had significantly different molecular structures. However, it is noteworthy that the molecular structure of large-sized fraction of high-amylose starch was similar to that of normal starch.

**XRD Spectra of Large-, Medium-, and Small-Sized Starch Fractions.** Starches can be classified into A-, B-, and C-type crystallinity on the basis of their XRD spectra. C-type starch is a mixture of both A- and B-type polymorphs and can be further classified to $C_A$-type (closer to A-type), C-type, and $C_B$-type (closer to B-type) according to the proportion of A-type and B-type polymorphs.[38] The XRD patterns of native and large-, medium-, and small-sized fractions of normal maize starches are shown in Figure 3A. They all showed strong reflection at about 15° and 23° 2$\theta$, and an unresolved doublet at 17° and 18° 2$\theta$, which resembled the typical A-type XRD pattern of normal cereal starches,[38] indicating that the nature of individual crystallites is similar in all normal maize granules regardless of the granule size. This result was in agreement with previous papers.[2,6]

Native high-amylose maize starch showed strong reflection at about 15°, 17°, and 23° 2$\theta$, a small peak at about 5.6° 2$\theta$, and a shoulder peak at about 18° 2$\theta$ (Figure 3B). The peak at 5.6° 2$\theta$ was characteristic of B-type crystallinity, and the shoulder peak of 18° 2$\theta$ was indicative of the A-type polymorph, which suggested that the starch consisted of A- and B-type polymorphs, with the A-type polymorph being the main component. Therefore, native high-amylose maize starch was $C_A$-type crystallinity. For the large-sized fraction of high-amylose maize starch, the peak at 5.6° 2$\theta$ disappeared, the peaks at 17° and 18° 2$\theta$ became an unresolved doublet, and the

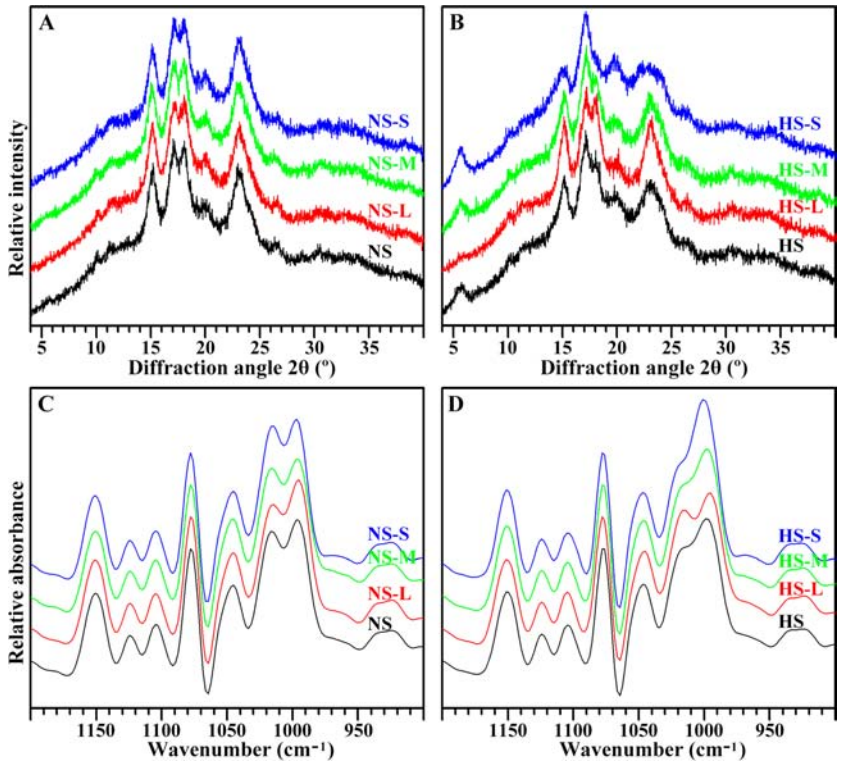


**Figure 3.** XRD spectra (A, B) and ATR-FTIR deconvoluted spectra (C, D) of native and large-, medium-, and small-sized fractions of normal (A, C) and high-amylose (B, D) maize starches separated by glycerol centrifugation method. NS, NS-L, NS-M, and NS-S: native and large-, medium-, and small-sized fractions of normal maize starch. HS, HS-L, HS-M, and HS-S: native and large-, medium-, and small-sized fractions of high-amylose maize starch.

**Table 4. Relative Crystallinities and IR Ratios of Native and Large-, Medium-, and Small-Sized Fractions of Normal and High-Amylose Maize Starches Separated by Glycerol Centrifugation Method[a]**

| | relative crystallinity (%) | | 1045/1022 ($cm^{-1}$) | | 1022/995 ($cm^{-1}$) | |
|---|---|---|---|---|---|---|
| fraction | normal maize | high-amylose maize | normal maize | high-amylose maize | normal maize | high-amylose maize |
| native | 22.31 ± 0.77a | 19.33 ± 0.63b | 0.60 ± 0.01b | 0.68 ± 0.00b | 0.91 ± 0.01b | 0.80 ± 0.01c |
| large-sized | 21.49 ± 0.96a | 22.26 ± 0.97c | 0.61 ± 0.01b | 0.65 ± 0.01a | 0.84 ± 0.01a | 0.88 ± 0.00d |
| medium-sized | 22.25 ± 0.71a | 19.61 ± 1.02b | 0.61 ± 0.01b | 0.67 ± 0.00b | 0.93 ± 0.01c | 0.76 ± 0.01b |
| small-sized | 21.42 ± 0.91a | 16.36 ± 0.97a | 0.53 ± 0.00a | 0.70 ± 0.01c | 0.95 ± 0.01d | 0.64 ± 0.01a |

[a]Data are means ± standard deviations, $n = 3$. Values in the same column with different letters are significantly different ($P < 0.05$).

peaks at 15° and 23° 2$\theta$ appeared to sharpen, indicating that the large-sized fraction of high-amylose maize starch was typical A-type crystallinity. The spectrum of the medium-sized fraction of high-amylose maize starch was very similar to that of native high-amylose maize and exhibited a $C_A$-type crystallinity. However, the shoulder peak at 18° 2$\theta$ disappeared and the peak at 23° 2$\theta$ became broad in the small-sized fraction of high-amylose maize starch, exhibiting a typical C-type crystallinity. Most high-amylose starches are B-type crystallinity,[12,14] but some C-type starches have also been reported in high-amylose cereal crops.[20,38] Cheetham and Tao[38] thought that the crystal type of maize starch could be varied from A- to B- via C-type when AC increased; the transition occurred at about 40% AC. In the present study, the AC of native high-amylose maize starch determined by GPC was about 35.6%. The result was in agreement with the report of Cheetham and Tao[38] that maize starch with about 40% AC had C-type crystallinity. C-type starch contains A- and B-type allomorphs. To date, the literature reports that A- and B-type allomorphs are distributed in the same granule. It is never reported that A- and B-type polymorphs are distributed in different granules; that is, C-type starches consist of A-type and B-type granules. In the present study, the results of C-type native starch and A-type large-sized starch from high-amylose maize indicated that C-type starches could contain some A-type granules.

Table 4 shows the relative crystallinities of starches, which were calculated from the XRD patterns. For normal maize starch, the crystallinities did not show significant difference among different-sized fractions. For high-amylose maize starch, the crystallinities significantly decreased with the decrease of granule size. This result was consistent with the findings of Cheetham and Tao[38] that relative crystallinity was negatively correlated with AC.

**ATR-FTIR Spectra of Large-, Medium-, and Small-Sized Starch Fractions.** The ATR-FTIR spectrum of starch is sensitive to the short-range ordered structure, defined as the double-helical order, as opposed to the long-range ordered structure related to the packing of double helices.[39] The variations in spectra among different starches can be interpreted in terms of the short-range ordered structure present in the

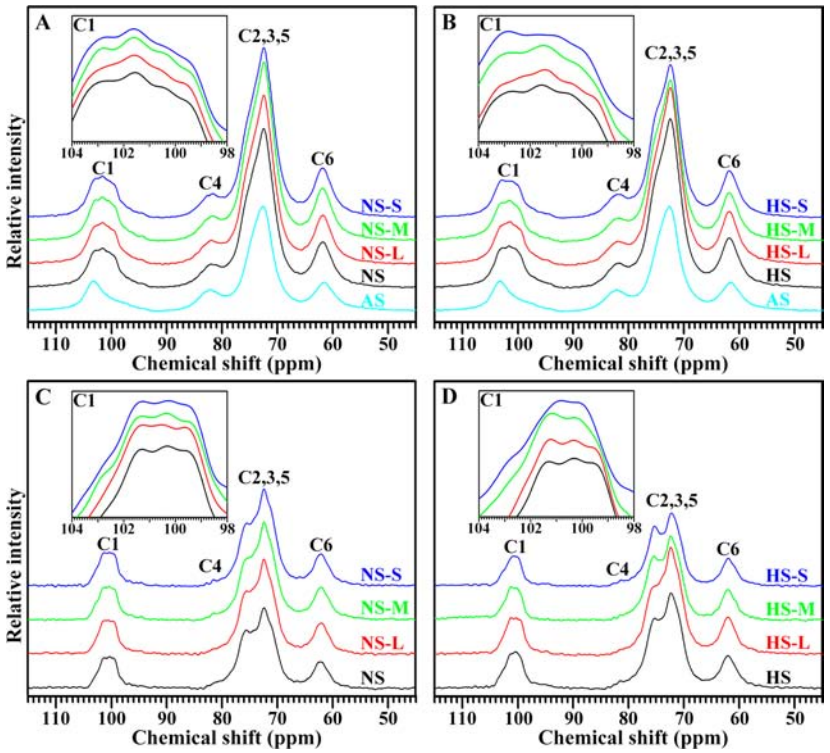


**Figure 4.** $^{13}C$ CP/MAS NMR original spectra (A, B) and ordered subspectra (C, D) of native and large-, medium-, and small-sized fractions of normal (A, C) and high-amylose (B, D) maize starches separated by glycerol centrifugation method. AS: amorphous starch. NS, NS-L, NS-M, and NS-S: native and large-, medium-, and small-sized fractions of normal maize starch. HS, HS-L, HS-M, and HS-S: native and large-, medium-, and small-sized fractions of high-amylose maize starch.

external region of starch granule. The intensity of absorbance at 1045, 1022, and 995 $cm^{-1}$ is sensitive to changes in starch conformation. The bands at 1045 and 1022 $cm^{-1}$ are associated with ordered/crystalline and amorphous regions in starch, respectively. The ratio of absorbance 1045/1022 $cm^{-1}$ is used to quantify the degree of order, and that of 1022/995 $cm^{-1}$ can be used as a measure of the proportion of amorphous to ordered carbohydrate structure in the starch.[39]

The ATR-FTIR spectra of native and large-, medium-, and small-sized fractions of normal and high-amylose maize starches in the 1200−900 $cm^{-1}$ region are shown in Figure 3C,D. The ratios for 1045/1022 and 1022/995 $cm^{-1}$ of starches from normal and high-amylose maizes are shown in Table 4. On the basis of both the spectra and calculated data, the ATR-FTIR characteristics of different-sized fractions of normal maize starch were similar, but high-amylose maize starch had significantly different ATR-FTIR characteristics among different-sized fractions. The ATR-FTIR characteristics of the large-sized fraction of high-amylose maize starch was much closer to those of different-sized fractions of normal maize starch. It is noteworthy that the ratio of 1022/995 $cm^{-1}$ significantly increased with the decrease of granule size for normal maize starch, but markedly decreased for high-amylose maize starch. These results indicated that the different-sized fractions of normal maize starch and large-sized granules of high-amylose maize starch had similar short-range ordered structure, whereas granule size significantly affected the short-range ordered structure of high-amylose maize starch.

**$^{13}C$ CP/MAS NMR Spectra of Large-, Medium-, and Small-Sized Starch Fractions.** The solid-state $^{13}C$ CP/MAS NMR patterns for starches are shown in Figure 4. The resonances at different parts per million were assigned according to data reported in the literature.[32,40] The C1 resonance, which gives information about both the crystalline nature as well as the noncrystalline (but rigid) chains, has been used to examine the structure of different types of starches. The multiplicity of C1 resonance corresponds to the packing type of the starch granule. A-type starch, which has three nonidentical sugar residues, shows a triplet at the C1 region, whereas B-type starch, which has two nonidentical sugar residues, shows a doublet.[32] In general, typical C-type starch has an inconspicuous triplet or doublet at the C1 region. However, $C_A$-type starch shows a triplet at the C1 region and $C_B$-type starch shows a doublet at the C1 region.[40]

The C1 resonances of native and large-, medium-, and small-sized fractions of normal maize starch occurred as triplets at about 99.5, 100.5, and 101.5 ppm (Figure 4A), those of native and large-sized fractions of high-amylose maize starch showed an inconspicuous triplet, and those of medium- and small-sized fractions of high-amylose maize starch showed an inconspicuous doublet (Figure 4B). Panels C and D of Figure 4 show the ordered subspectra of starches. In this analysis, the standard amorphous starch spectrum was subtracted from the test spectrum until there was no residual intensity at 84 ppm (a region of the spectrum with intensity due solely to amorphous conformations).[33] The ordered subspectra were similar to the original spectra, but they had clearer crystalline peaks of C1 resonances than those in the original spectra. The clear triplets were observed in the spectra of different-sized fractions of normal maize starch and native and large-sized fractions of high-amylose maize starch, and the clear doublet was observed in the spectra of medium- and small-sized fractions of high-amylose maize starch. These results, combined with the results from the XRD analysis, further confirmed that the different-

Table 5. Proportions of Single-Helix, Double-Helix, and Amorphous Conformations and SAXS Parameters of Native and Large-, Medium-, and Small-Sized Fractions of Normal and High-Amylose Maize Starches Separated by Glycerol Centrifugation Method[a]

| | normal maize | | | | | high-amylose maize | | | | |
|---|---|---|---|---|---|---|---|---|---|---|
| fraction | single helix[b] (%) | double helix[b] (%) | amorphous[b] (%) | $I_{max}$[c] (counts) | $D$[c] (nm) | single helix[b] (%) | double helix[b] (%) | amorphous[b] (%) | $I_{max}$[c] (counts) | $D$[c] (nm) |
| native | 6.2 ± 0.2a | 32.5 ± 0.5a | 61.2 ± 0.8a | 200.7 ± 0.0b | 10.0 ± 0.0a | 5.7 ± 0.5a | 30.8 ± 0.7b | 63.6 ± 0.9a | 171.3 ± 5.8b | 10.0 ± 0.0a |
| large-sized | 6.1 ± 0.2a | 31.7 ± 0.6a | 62.2 ± 0.9a | 215.0 ± 7.0c | 10.0 ± 0.0a | 6.8 ± 0.6a | 32.0 ± 0.9b | 61.2 ± 0.9a | 224.1 ± 0.3c | 10.0 ± 0.0a |
| medium-sized | 6.3 ± 1.0a | 33.7 ± 1.0a | 60.0 ± 1.1a | 205.8 ± 0.6bc | 10.0 ± 0.0a | 6.5 ± 0.2a | 30.2 ± 0.6b | 63.3 ± 0.7a | 181.2 ± 18.6b | 10.0 ± 0.0a |
| small-sized | 6.9 ± 0.3a | 32.9 ± 0.7a | 60.2 ± 0.9a | 187.9 ± 1.9a | 10.0 ± 0.0a | 7.2 ± 0.9a | 26.7 ± 1.0a | 66.2 ± 0.7b | 74.6 ± 1.4a | 10.0 ± 0.0a |

[a]Data are means ± standard deviations, $n = 3$ for the proportions of single-helix, double-helix, and amorphous conformations and = 2 for SAXS parameters. Values in the same column with different letters are significantly different ($P < 0.05$). [b]Relative proportions of single-helix, double-helix, and amorphous conformations are determined by $^{13}C$ CP/MAS NMR. [c]$I_{max}$, peak intensity; $D$, lamellar distance (Bragg spacing).

sized fractions of normal maize starch and the large-sized fraction of high-amylose maize starch were all A-type crystallinity, native and medium-sized fractions of high-amylose maize starch were $C_A$-type crystallinity, and the small-sized fraction was C-type crystallinity.

The ordered subspectra were peak-fitted. A combination (50/50) of Lorentzian and Gaussian profiles gave an acceptable fit (data not shown). The proportions of single-helix, double-helix, and amorphous components are listed in Table 5 and showed similarity among different-sized fractions of normal maize starch but some difference among different-sized fractions of high-amylose maize starch. The amylopectin side chains can form two types of helices in starch granule. Helices that are packed in the short-range order are defined as the double-helical order, and helices that are packed in long-range order are related to the packing of double helices forming crystallinity. The double helices in the short- and long-range distance can both be detected by $^{13}C$ CP/MAS NMR, but only the double helices in the long-range distance can be detected by XRD.[32] Therefore, the double-helix content of starch was generally higher than its relative crystallinity.

**SAXS Spectra of Large-, Medium-, and Small-Sized Starch Fractions.** A comparison of the SAXS patterns of the starches is shown in Figure 5. The well-resolved main scattering peak around scattering vector ($q_0$) of about 0.06 Å$^{-1}$ is thought to arise from the periodic arrangement of alternating crystalline and amorphous lamellae of amylopectin and corresponds to the lamellar repeat distance or Bragg spacing. The location of the peak depends on the size of lamella and may differ among starches from different plants, whereas the peak area or intensity depends mainly on the degree of order in semi-crystalline regions.[41] As shown in Figure 5, all starches were scaled to equal intensity at high $q$ ($q$ = 0.2 Å$^{-1}$) to account for variations in sample concentrations, according to the method of Sanderson et al.[42] The SAXS patterns were at the same relative scale and, therefore, were directly comparable. Native and large-, medium-, and small-sized fractions of normal and high-amylose maize starches all showed the most defined lamellar peak centered at 0.063 Å$^{-1}$, which corresponded to a lamellar repeat distance of 10.0 nm. However, the lamellar peak intensity showed significant difference among these starch fractions, especially for high-amylose maize starch (Table 5). The extremely low lamellar peak intensity of small-sized fraction of high-amylose starch likely indicated a severely disrupted or nonexistent lamellar structure compared to that of large- and medium-sized fractions. Yuryev et al.[34] reported that an increase in AC in wheat starches was accompanied by decreased peak scattering intensity, which resulted from accumulation of amylose tie-chains with increasing AC in the granules. The starch fractions from high-amylose maize showed significantly lower peak intensities with decrease of granule size, which might result from the elevated AC (Tables 2 and 3).

In conclusion, the structural properties of native and large-, medium-, and small-sized fractions of normal and high-amylose maize starches separated by glycerol centrifugation method were investigated to reveal whether structural properties differed among the different-sized fractions of the starches. The results showed that the granule sizes had no significant effect on structural properties of normal starch, but the different-sized fractions of high-amylose maize starch showed markedly different structural properties. The small-sized granules of high-amylose starch had significantly higher AC, amylopectin long branch-chain, and IR ratio of 1045/1022

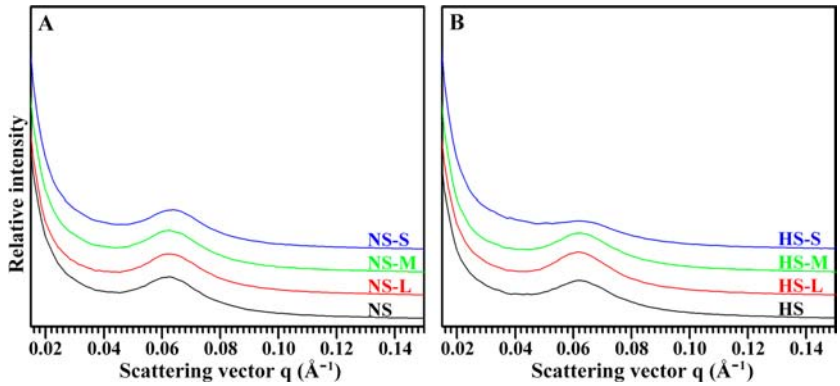


**Figure 5.** SAXS patterns of native and large-, medium-, and small-sized fractions of normal (A) and high-amylose (B) maize starches separated by glycerol centrifugation method. NS, NS-L, NS-M, and NS-S: native and large-, medium-, and small-sized fractions of normal maize starch. HS, HS-L, HS-M, and HS-S: native and large-, medium-, and small-sized fractions of high-amylose maize starch.

cm$^{-1}$, lower amylopectin short branch-chain and branching degree, relative crystallinity, IR ratio of 1022/995 cm$^{-1}$, and peak intensities of lamellar structure than the large-sized granules. The differences in crystal structure among the different-sized fractions indicated that C-type starch might contain A-type starch granules.

## ■ ASSOCIATED CONTENT

### Supporting Information

Schematic diagrams of the microsieving separation, the extreme sedimentation separation, the differential sedimentation separation, the differential supernatant separation, and the glycerol centrifugation separation of starch granules (Figures S1−S5); micrographs of different-sized fractions of normal and high-amylose maize starches separated by different methods (Figures S6 and S7); granule size distribution of native and large-, medium-, and small-sized fractions of normal and high-amylose maize starches separated by glycerol centrifugation method (Figure S8). This material is available free of charge via the Internet at http://pubs.acs.org.

## ■ AUTHOR INFORMATION

### Corresponding Author

*(C.W.) Mail: College of Bioscience and Biotechnology, Yangzhou University, Yangzhou 225009, China. Phone: +86 514 87997217. E-mail: cxwei@yzu.edu.cn.

### Funding

This study was financially supported by grants from the National Natural Science Foundation of China (31270221), the Talent Project of Yangzhou University, the Innovation Program for Graduates of Jiangsu Province (CXZZ13_0895), and the Priority Academic Program Development of Jiangsu Higher Education Institutions.

### Notes

The authors declare no competing financial interest.

## ■ ACKNOWLEDGMENTS

We are grateful to Prof. Robert G. Gilbert (Huazhong University of Science and Technology, China) and Prof. Chengjun Zhu (Wuhan Ausinorigin High Tech Co., Ltd., China) for kindly providing technical assistance in GPC analysis.

## ■ ABBREVIATIONS USED

AC, amylose content; ATR-FTIR, attenuated total reflectance Fourier transform infrared; $^{13}$C CP/MAS NMR, solid-state $^{13}$C cross-polarization magic-angle spinning nuclear magnetic resonance; GPC, gel permeation chromatography; SAXS, small-angle X-ray scattering; SEM, scanning electron microscope; XRD, X-ray powder diffraction

## ■ REFERENCES

(1) Tester, R. F.; Karkalas, J.; Qi, X. Starch structure and digestibility enzyme-substrate relationship. *World's Poult. Sci. J.* **2004**, *60*, 186−195.
(2) Ao, Z.; Jane, J. L. Characterization and modeling of the A- and B-granule starches of wheat, triticale, and barley. *Carbohydr. Polym.* **2007**, *67*, 46−55.
(3) Chiotelli, E.; Le Meste, M. Effect of small and large wheat starch granules on thermomechanical behavior of starch. *Cereal Chem.* **2002**, *79*, 286−293.
(4) Tang, H.; Ando, H.; Watanabe, K.; Takeda, Y.; Mitsunaga, T. Fine structures of amylose and amylopectin from large, medium, and small waxy barley starch granules. *Cereal Chem.* **2001**, *78*, 111−115.
(5) Vasanthan, T.; Bhatty, R. S. Physicochemical properties of small- and large-granule starches of waxy, regular, and high-amylose barleys. *Cereal Chem.* **1996**, *73*, 199−207.
(6) Dhital, S.; Shrestha, A. K.; Hasjim, J.; Gidley, M. J. Physicochemical and structural properties of maize and potato starches as a function of granule size. *J. Agric. Food Chem.* **2011**, *59*, 10151−10161.
(7) Noda, T.; Takigawa, S.; Matsuura-Endo, C.; Kim, S. J.; Hashimoto, N.; Yamauchi, H.; Hanashiro, I.; Takeda, Y. Physicochemical properties and amylopectin structures of large, small, and extremely small potato starch granules. *Carbohydr. Polym.* **2005**, *60*, 245−251.
(8) Utrilla-Coello, R. G.; Agama-Acevedo, E.; de la Rosa, A. P. B.; Rodríguez-Ambriz, S. L.; Bello-Pérez, L. A. Physicochemical and enzyme characterization of small and large starch granules isolated from two maize cultivars. *Cereal Chem.* **2010**, *87*, 50−56.
(9) Kaur, L.; Singh, J.; McCarthy, O. J.; Singh, H. Physico-chemical, rheological and structural properties of fractionated potato starches. *J. Food Eng.* **2007**, *82*, 383−394.
(10) Singh, N.; Kaur, L. Morphological, thermal, rheological and retrogradation properties of potato starch fractions varying in granule size. *J. Sci. Food Agric.* **2004**, *84*, 1241−1252.
(11) Bird, A. R.; Jackson, M.; King, R. A.; Davies, D. A.; Usher, S.; Topping, D. L. A novel high-amylose barley cultivar (*Hordeum vulgare* var. Himalaya 292) lowers plasma cholesterol and alters indices of large-bowel fermentation in pigs. *Br. J. Nutr.* **2004**, *92*, 607−615.
(12) Jiang, H. X.; Campbell, M.; Blanco, M.; Jane, J. L. Characterization of maize amylose-extender (*ae*) mutant starches: Part II. Structures and properties of starch residues remaining after

enzymatic hydrolysis at boiling-water temperature. *Carbohydr. Polym.* **2010**, *80*, 1−12.
(13) Kim, K. S.; Hwang, H. G.; Kang, H. J.; Hwang, I. K.; Lee, Y. T.; Choi, H. C. Ultrastructure of individual and compound starch granules in isolation preparation from a high-quality, low-amylose rice, Ilpumbyeo, and its mutant, G2, a high-dietary fiber, high-amylose rice. *J. Agric. Food Chem.* **2005**, *53*, 8745−8751.
(14) Li, L.; Jiang, H. X.; Campbell, M.; Blanco, M.; Jane, J. L. Characterization of maize amylose-extender (*ae*) mutant starches. Part I: relationship between resistant starch contents and molecular structures. *Carbohydr. Polym.* **2008**, *74*, 396−404.
(15) Man, J. M.; Yang, Y.; Zhang, C. Q.; Zhou, X. H.; Dong, Y.; Zhang, F. M.; Liu, Q. Q.; Wei, C. X. Structural changes of high-amylose rice starch residues following in vitro and in vivo digestion. *J. Agric. Food Chem.* **2012**, *60*, 9332−9341.
(16) Regina, A.; Bird, A.; Topping, D.; Bowden, S.; Freeman, J.; Barsby, T.; Kosar-Hashemi, B.; Li, Z. Y.; Rahman, S.; Morell, M. High-amylose wheat generated by RNA interference improves indices of large-bowel health in rats. *Proc. Natl. Acad. Sci. U.S.A.* **2006**, *103*, 3546−3551.
(17) Regina, A.; Kosar-Hashemi, B.; Ling, S.; Li, Z. Y.; Rahman, S.; Morell, M. Control of starch branching in barley defined through differential RNAi suppression of starch branching enzyme IIa and IIb. *J. Exp. Bot.* **2010**, *61*, 1469−1482.
(18) Slade, A. J.; McGuire, C.; Loeffler, D.; Mullenberg, J.; Skinner, W.; Fazio, G.; Holm, A.; Brandt, K. M.; Steine, M. N.; Goodstal, J. F.; Knauf, V. Development of high amylose wheat through TILLING. *BMC Plant Biol.* **2012**, *12*, 69.
(19) Wei, C. X.; Qin, F. L.; Zhu, L. J.; Zhou, W. D.; Chen, Y. F.; Wang, Y. P.; Gu, M. H.; Liu, Q. Q. Microstructure and ultrastructure of high-amylose rice resistant starch granules modified by antisense RNA inhibition of starch branching enzyme. *J. Agric. Food Chem.* **2010**, *58*, 1224−1232.
(20) Wei, C. X.; Xu, B.; Qin, F. L.; Yu, H. G.; Chen, C.; Meng, X. L.; Zhu, L. J.; Wang, Y. P.; Gu, M. H.; Liu, Q. Q. C-type starch from high-amylose rice resistant starch granules modified by antisense RNA inhibition of starch branching enzyme. *J. Agric. Food Chem.* **2010**, *58*, 7383−7388.
(21) Chen, P.; Yu, L.; Simon, G.; Petinakis, E.; Dean, K.; Chen, L. Morphologies and microstructures of corn starches with different amylose-amylopectin ratios studied by confocal laser scanning microscope. *J. Cereal Sci.* **2009**, *50*, 241−247.
(22) Cai, C. H.; Zhao, L. X.; Huang, J.; Chen, Y. F.; Wei, C. X. Morphology, structure and gelatinization properties of heterogeneous starch granules from high-amylose maize. *Carbohydr. Polym.* **2014**, *102*, 606−614.
(23) Dhital, S.; Shelat, K. J.; Shrestha, A. K.; Gidley, M. J. Heterogeneity in maize starch granule internal architecture deduced from diffusion of fluorescent dextran probes. *Carbohydr. Polym.* **2013**, *93*, 365−373.
(24) Liu, D.; Parker, M. L.; Wellner, N.; Kirby, A. R.; Cross, K.; Morris, V. J.; Cheng, F. Structural variability between starch granules in wild type and in *ae* high-amylose mutant maize kernels. *Carbohydr. Polym.* **2013**, *97*, 458−468.
(25) Wellner, N.; Georget, D. M. R.; Parker, M. L.; Morris, V. J. In situ Raman microscopy of starch granule structures in wild type and *ae* mutant maize kernels. *Starch* **2011**, *63*, 128−138.
(26) Takeda, Y.; Takeda, C.; Mizukami, H.; Hanashiro, I. Structures of large, medium and small starch granules of barley grain. *Carbohydr. Polym.* **1999**, *38*, 109−114.
(27) Dhital, S.; Shrestha, A. K.; Gidley, M. J. Relationship between granule size and *in vitro* digestibility of maize and potato starches. *Carbohydr. Polym.* **2010**, *82*, 480−488.
(28) Peng, M.; Gao, M.; Abdel-Aal, E. S. M.; Hucl, P.; Chibbar, R. N. Separation and characterization of A- and B-type starch granules in wheat endosperm. *Cereal Chem.* **1999**, *76*, 375−379.
(29) Tran, T. T. B.; Shelat, K. J.; Tang, D.; Li, E.; Gilbert, R. G.; Hasjim, J. Milling of rice grains. The degradation on three structural levels of starch in rice flour can be independently controlled during grinding. *J. Agric. Food Chem.* **2011**, *59*, 3964−3973.
(30) Li, E.; Hasjim, J.; Dhital, S.; Godwin, I. D.; Gilbert, R. G. Effect of a gibberellin-biosynthesis inhibitor treatment on the physicochemical properties of sorghum starch. *J. Cereal Sci.* **2011**, *53*, 328−334.
(31) Cai, J. W.; Cai, C. H.; Man, J. M.; Zhou, W. D.; Wei, C. X. Structural and functional properties of C-type starches. *Carbohydr. Polym.* **2014**, *101*, 289−300.
(32) Atichokudomchai, N.; Varavinit, S.; Chinachoti, P. A study of ordered structure in acid-modified tapioca starch by $^{13}C$ CP/MAS solid-state NMR. *Carbohydr. Polym.* **2004**, *58*, 383−389.
(33) Tan, I.; Flanagan, B. M.; Halley, P. J.; Whittaker, A. K.; Gidley, M. J. A method for estimating the nature and relative proportions of amorphous, single, and double-helical components in starch granules by $^{13}C$ CP/MAS NMR. *Biomacromolecules* **2007**, *8*, 885−891.
(34) Yuryev, V. P.; Krivandin, A. V.; Kiseleva, V. I.; Wasserman, L. A.; Genkina, N. K.; Fornal, J.; Blaszczak, W.; Schiraldi, A. Structural parameters of amylopectin clusters and semi-crystalline growth rings in wheat starches with different amylose content. *Carbohydr. Res.* **2004**, *339*, 2683−2691.
(35) Wang, Y. J.; White, P.; Pollak, L.; Jane, J. Characterization of starch structures of 17 maize endosperm mutant genotypes with Oh43 inbred line background. *Cereal Chem.* **1993**, *70*, 171−179.
(36) Song, Y.; Jane, J. Characterization of barley starches of waxy, normal, and high amylose varieties. *Carbohydr. Polym.* **2000**, *41*, 365−377.
(37) Shi, Y. C.; Capitani, T.; Trzasko, P.; Jeffcoat, R. Molecular structure of a low-amylopectin starch and other high-amylose maize starches. *J. Cereal Sci.* **1998**, *27*, 289−299.
(38) Cheetham, N. W. H.; Tao, L. Variation in crystalline type with amylose content in maize starch granules: an X-ray powder diffraction study. *Carbohydr. Polym.* **1998**, *36*, 277−284.
(39) Sevenou, O.; Hill, S. E.; Farhat, I. A.; Mitchell, J. R. Organisation of the external region of the starch granule as determined by infrared spectroscopy. *Int. J. Biol. Macromol.* **2002**, *31*, 79−85.
(40) Bogracheva, T. Y.; Wang, Y. L.; Hedley, C. L. The effect of water content on the ordered/disordered structures in starches. *Biopolymers* **2001**, *58*, 247−259.
(41) Blazek, J.; Gilbert, E. P. Application of small-angle X-ray and neutron scattering techniques to the characterisation of starch structure: a review. *Carbohydr. Polym.* **2011**, *85*, 281−293.
(42) Sanderson, J. S.; Daniels, R. D.; Donald, A. M.; Blennow, A.; Engelsen, S. B. Exploratory SAXS and HPAEC-PAD studies of starches from diverse plant genotypes. *Carbohydr. Polym.* **2006**, *64*, 433−443.

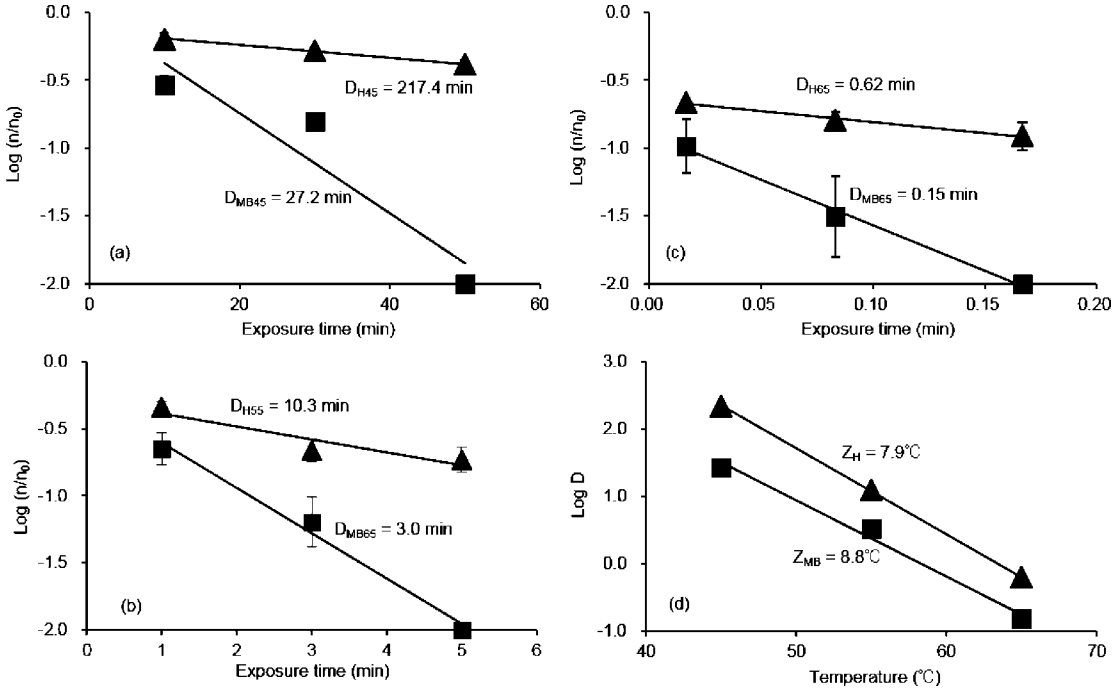


**Figure 1.** Effects of temperature on the heating coil during $\alpha$-glucosidase inactivation by the two-stage MB-$CO_2$ and heat treatments. The two-stage MB-$CO_2$ treatment was performed under the following conditions: the mixing vessel was set to 5 °C and 2 MPa, and the heating coil was set to 45, 55, 65, or 75 °C and 6 MPa. Data are presented as means with standard errors of the results from triplicate experiments.

**Two-Stage MB-$CO_2$ Apparatus and Procedure for Treating the UPS.** The experimental equipment for two-stage MB-$CO_2$ in the present study was used with the modification of the equipment in a previous report.[17] That is, two types of heating coils (5 mm diameter × 5100 mm length, volume 100 mL for 45 and 55 °C, or 4 mm diameter × 2000 mm length, volume 25 mL for 65 and 75 °C) were used.

The two-stage MB-$CO_2$ treatment was performed under the following conditions: temperature and pressure in the mixing vessel were 5 °C and 2 MPa, respectively; temperature, pressure, and exposure time in the heating coil were 45 °C for 10, 30, and 50 min, 55 °C for 1, 3, and 5 min, 65 °C for 1, 5, and 10 s, or 75 °C for 1 s, respectively, under a pressure of 6 MPa; temperature and pressure in the cooling coil were −15 °C and 6 MPa, respectively.

**Heat Treatment.** For comparison, heat treatments were performed only using the heating coil of two-stage MB-$CO_2$ equipment under the same conditions as two-stage MB-$CO_2$ treatment. In addition, to make heat-treated sake (HTS) for sensory evaluation and analysis of the components, a heat treatment was performed at 65 °C for 3 min, which was the same condition as the typical heat treatment of sake.

**Measurement of $\alpha$-Glucosidase Activity.** Residual $\alpha$-glucosidase activity in the sakes was measured using a glucoamylase and $\alpha$-glucosidase assay kit (Kikkoman Co., Noda, Japan). One unit of $\alpha$-glucosidase activity was defined as the amount required to produce 1 $\mu$mol of 4-nitrophenol in 1 min. The residual activity (RA) of $\alpha$-glucosidase was estimated using the following formula.

$$\text{RA}\,(\%) = (\alpha\text{-glucosidase activity after treatment} / \alpha\text{-glucosidase activity before treatment}) \times 100 \quad (1)$$

All experiments were performed in triplicate. Data are presented as means with standard error of the results from triplicate experiments.

**Kinetics Analysis on the Inactivation of $\alpha$-Glucosidase.** The inactivation kinetics of $\alpha$-glucosidase was analyzed using a conventional first-order model as in a previous report.[16]

$$\log(A_t/A_0) = (k/2.303)t \quad (2)$$

$$D = 2.303/k \quad (3)$$

where $A_t$ is the residual enzymatic activity at any time $t$, $A_0$ is the initial enzymatic activity, $k$ is the reaction rate constant ($\text{min}^{-1}$) in a given condition, and the decimal reduction time ($D$ value) is defined as the treatment time required for 90% inactivation of the initial activity at fixed temperature and pressure conditions. $D$ value is calculated using the following equation.[21]

$$\log(D_1/D_2) = (T_2 - T_1)/Z \quad (4)$$

where $Z$ is the temperature increase needed for a 90% reduction in the $D$, and $T_2$ and $T_1$ are the temperatures and pressures that correspond to $D_1$ and $D_2$. The $Z$ value is obtained from the negative slope of the regression line of log $D$ versus $T$.

**Sensory Evaluation.** Sensory evaluation of UPS, HTS, and the sakes treated by two-stage MB-$CO_2$ with a heating coil at 45 °C for 50 min (MB45), 55 °C for 5 min (MB55), 65 °C for 10 s (MB65), and 75 °C for 1 s (MB75) was performed by 10 panelists trained in sensory evaluation (age, 21−61 years; 5 men and 5 women). The panelists evaluated the total aroma and total taste of the sakes on a seven-point scale (3, very good; 2, good; 1, slightly good; 0, normal; −1, slightly bad; −2, bad; and −3, very bad). Data are presented as means with standard errors of the results from 10 panelists.

**Analysis of Organic Acids.** To analyze the organic acid content, 500 $\mu$L of sake filtered through a 0.45 $\mu$m filter was allowed to pass through a Sep-Pak C18 column (Waters Co., Ltd., Milford, MA) and eluted with 2 mL of 5% phosphoric acid solution. The eluate was used for the analysis of organic acids by high pressure liquid chromatography (HPLC, Shimadzu Co., Kyoto, Japan). Measuring conditions of the HPLC were as follows: column, ODS-3 (4.6 mm i.d. × 250 mm, GL Science Inc., Tokyo, Japan); mobile phase, 0.02 mol/L diammonium hydrogen phosphate: methanol at a ratio of 97:3 (pH 2.35); flow rate, 0.5 mL/min; detector, UV detector (SPD-20A, 210 nm); oven temperature, 25 °C. All experiments were performed in triplicate. Data are presented as means with standard errors of the results from triplicate experiments.

**Analysis of Glucose and Isomaltose.** Glucose and isomaltose contents were measured by HPLC (Jasco Co., Hachioji, Japan). Sake diluted 3-fold with distilled water was filtered through a 0.45 $\mu$m filter

and was used as sample. Running conditions for HPLC were as follows: column, Shodex Sugar SC1011 (8 mm i.d. × 300 mm, Showa Denko K. K., Tokyo, Japan); mobile phase, distilled water; flow rate, 1.0 mL/min; detector, RI detector (JASCO RI-930); oven temperature, 80 °C. All experiments were performed in triplicate. Data are presented as means with standard errors of the results from triplicate experiments.

**Analysis of Free Amino Acids.** Sake and 3% sulfosalicylic acid were mixed at a ratio of 1:1, refrigerated overnight, and then filtered through a 0.45 μm filter. Free amino acids in the filtrate were measured by an automated amino acid analyzer (JLC500-500/V2, JEOL Ltd., Akishima, Japan). All experiments were performed in triplicate. Data are presented as means with standard deviation of the results from triplicate experiments.

**Analysis of Volatile Compounds.** Volatile compounds in the sake were measured by gas chromatography mass spectrometry (GC–MS, 6890GC-5973MSD, Agilent Technologies, CA), which was connected to an Entech 7200 (7200 Preconcentrator, Entech Instruments Inc., CA) based on reports by Yoshizaki et al.[22,23] Afterward a 500 mL purpose-built capped glass pot containing 100 mL of sake (diluted to 1/3 with deionized water) and 100 μL of 0.1% methyl hexanoate (Wako Pure Chemical Industries Co. Ltd., Osaka, Japan) as internal standard was heated in a water bath for 15 min at 50 °C. Then, the volatile compounds in the headspace of the glass pots were automatically concentrated by the Entech 7200 and analyzed by GC–MS. Running conditions of GC–MS were as follows: A DB-WAX capillary column (0.25 mm i.d. × 30 m, thickness 0.25 μm; Agilent Technologies, Folsom, CA) was used. The oven temperature was held at 40 °C for 4 min, elevated to 240 °C at 8 °C/min, and then held for 2 min. Helium was used at 30 cm/s as a carrier gas. The interface temperature was 230 °C. Volatile compounds were identified using the NIST mass spectrum database and retention time of authentic compounds, and determined relatively using the internal standard. All experiments were performed in triplicate. Data are presented as means with standard deviation of the results from triplicate experiments.

**Statistical Analyses.** Significant differences were evaluated by the Tukey–Kramer test ($p < 0.01$).

## RESULTS AND DISCUSSION

**Inactivation of α-Glucosidase.** Inactivation of α-glucosidase by two-stage MB-$CO_2$ and heat treatments is shown in Figure 1. α-Glucosidase activity decreased with increasing temperature of the heating coil for both the two-stage MB-$CO_2$ and heat treatments. Complete inactivation of α-glucosidase by two-stage MB-$CO_2$ with a heating coil at 45, 55 and 65 °C was achieved at 50 min, 5 min, and 10 s, respectively. Both two-stage MB-$CO_2$ and heat treatments at 75 °C could completely inactivate α-glucosidase within 1 s of the shortest exposure time. So, the results at 75 °C could not be plotted (data not shown). *D* values for the inactivation of α-glucosidase by two-stage MB-$CO_2$ with a heating coil at 45, 55, and 65 °C were 27.2, 3.0, and 0.15 min, respectively, and the *D* values by the heat treatment were 217.4, 10.3, and 0.62 min, respectively. Therefore, inactivation of α-glucosidase by two-stage MB-$CO_2$ was more effective than that by heat. This result was identical to a previous report that inactivation efficiency of PPO by two-stage MB-$CO_2$ was significantly higher than that by heat.[16] Furthermore, heat resistance of α-glucosidase by two-stage MB-$CO_2$ became lower than that by heat, because *Z* values, which indicated heat resistance, for the two-stage MB-$CO_2$ and heat treatments were 7.9 and 8.8 °C, respectively (Figure 1d). This result was consistent with our report,[16] which showed how the heat resistance of PPO was decreased by two-stage MB-$CO_2$.

**Sensory Evaluation.** Sensory evaluation of UPS, HTS, and sakes in which α-glucosidase was completely inactivated by two-stage MB-$CO_2$ with a heating coil at 45 °C for 50 min (MB45), 55 °C for 5 min (MB55), 65 °C for 10 s (MB65), and 75 °C for 1 s (MB75) is shown in Figure 2. For the evaluation

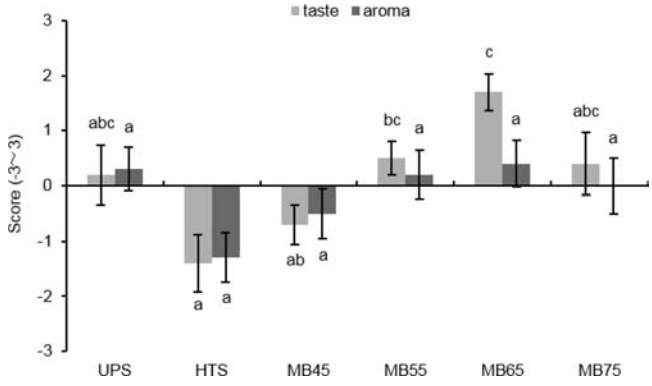


**Figure 2.** Sensory evaluation of unpasteurized, two-stage MB-$CO_2$-treated and heat-treated sakes. Two-stage MB-$CO_2$ treatment was performed under the following conditions: the mixing vessel was set to 5 °C and 2 MPa, and the heating coil was set to 45 °C for 50 min (MB45), 55 °C for 5 min (MB55), 65 °C for 10 s (MB65), or 75 °C for 1 s (MB75), under 6 MPa of pressure. Heat-treated sake (HTS) was produced at 65 °C for 3 min. Data are presented as means with standard errors of the results from triplicate experiments. Different letters indicate significant differences by the Tukey–Kramer method ($p < 0.01$).

of taste, the highest score was observed for MB65, followed in decreasing order by MB55, MB75, UPS, MB45, and HTS. Also, the evaluation of aroma followed the same pattern as those seen for taste, although no significant differences were recognized. Each sake was evaluated by the panelists as follows: strong bitterness and sweetness in UPS; strong bitterness and sourness, and weak sweetness in HTS; strong bitterness and spicy flavor in MB45; overall weakness in MB55; fresh sourness and moderate sweetness in MB65; and strong bitterness and sourness in MB75. Thus, to investigate the differences of taste and flavor in each sake determined by the sensory evaluation, free amino acids, organic acids, sugars, and volatile compounds in the sakes were measured.

**Free Amino Acids.** The main free amino acids in the UPS, HTS, MB45, MB55, MB65, and MB75 are shown in Table 1. The highest total amount of free amino acids in UPS was determined to be in the UPS, followed in decreasing order by HTS, MB75, MB45, MB65, and MB55. A significant amount of the free amino acids in UPS were likely due to decomposition of proteins and peptides by residual enzymes, while most of the free amino acids in MB75 and HTS were probably due to decomposition of proteins and peptides by excess heat. The present results on sensory evaluation and free amino acid contents are consistent with the results reported by Iwano et al. that sensory evaluation index of sake was negatively correlated with free amino acid contents.[24] Glutamic acid, arginine, alanine, and aspartic acid were also reported as taste components in sake.[25] No significant differences were recognized for glutamic acid, arginine, and alanine among all tested sakes, although aspartic acid, which causes sourness,[26,27] was significantly elevated in UPS, HTS, and MB75, thus contributing to the sourness of HTS and MB75 indicated by the sensory evaluation. Furthermore, amino acids that cause bitterness, such as phenylalanine, lysine, leucine, and valine,[28] were significantly higher in the UPS, HTS, and MB75. This

**Table 1. Amino Acids in Unpasteurized, Heat-Treated, and Two-Stage MB-$CO_2$-Treated Sakes**

| amino acids | UPS | HTS | MB45 | MB55 | MB65 | MB75 |
|---|---|---|---|---|---|---|
| P-Ser | 8.3 ± 0.6[a] a[b] | 8.6 ± 0.1 ab | 9.7 ± 0.6 a | 9.3 ± 0.7 ab | 9.8 ± 0.5 b | 8.6 ± 0.2 ab |
| urea | 296.0 ± 15.2 a | 294.8 ± 4.4 a | 277.8 ± 3.1 a | 268.1 ± 23.0 a | 277.0 ± 5.2 a | 284.3 ± 8.4 a |
| Asp | 18.4 ± 1.4 b | 19.8 ± 0.1 b | 15.1 ± 0.5 a | 14.9 ± 1.2 a | 15.4 ± 0.8 a | 18.4 ± 0.7 b |
| Thr | 230.6 ± 16.1 c | 200.6 ± 0.8 b | 159.6 ± 5.1 a | 156.3 ± 12.7 a | 159.0 ± 6.7 a | 188.4 ± 4.6 b |
| Ser | 464.7 ± 32.2 c | 410.7 ± 1.7 b | 348.4 ± 9.5 a | 342.5 ± 27.5 a | 349.6 ± 13.8 a | 389.1 ± 8.2 ab |
| Asn | 421.7 ± 27.8 b | 420.3 ± 1.3 b | 364.2 ± 11.2 a | 359.4 ± 29.2 a | 363.0 ± 16.4 a | 397.5 ± 10.7 ab |
| Glu | 1196.4 ± 79.4 a | 1201.6 ± 3.5 a | 1122.5 ± 35.8 a | 1099.2 ± 89.6 a | 1115.5 ± 47.3 a | 1144.0 ± 29.7 a |
| Gln | 415.5 ± 28.2 d | 347.5 ± 1.3 c | 288.5 ± 8.5 ab | 281.4 ± 22.6 a | 283.9 ± 12.7 ab | 327.2 ± 8.2 bc |
| AAA | 27.6 ± 2.0 a | 29.2 ± 0.2 a | 32.4 ± 1.2 a | 30.9 ± 2.8 a | 31.5 ± 0.8 a | 27.9 ± 1.4 a |
| Gly | 1118.7 ± 81.0 a | 1054.2 ± 3.2 a | 1072.5 ± 33.2 a | 1048.8 ± 85.5 a | 1065.8 ± 45.6 a | 1010.1 ± 26.5 a |
| Ala | 2019.3 ± 127.6 a | 2117.0 ± 63.6 a | 1935.1 ± 42.0 a | 1906.8 ± 148.6 a | 1963.3 ± 90.0 a | 1999.3 ± 56.7 a |
| Val | 551.3 ± 36.5 c | 529.9 ± 1.8 bc | 466.5 ± 14.4 ab | 457.1 ± 37.9 a | 468.9 ± 20.6 ab | 494.3 ± 8.0 abc |
| Cys | 37.6 ± 2.4 b | 24.7 ± 0.4 a | 23.5 ± 0.9 a | 22.3 ± 1.4 a | 22.7 ± 1.6 a | 23.7 ± 0.6 a |
| Met | 53.2 ± 3.2 c | 40.6 ± 0.3 b | 31.3 ± 0.7 a | 30.3 ± 2.3 a | 29.6 ± 1.3 a | 37.7 ± 1.1 b |
| Cysta | 28.1 ± 2.3 b | 27.5 ± 1.0 b | 23.1 ± 1.3 a | 22.2 ± 1.7 a | 22.7 ± 1.1 a | 25.4 ± 1.0 ab |
| Ile | 366.9 ± 23.9 b | 351.5 ± 1.3 b | 307.7 ± 9.1 a | 300.5 ± 24.0 a | 306.8 ± 12.9 a | 332.3 ± 7.5 ab |
| Leu | 722.0 ± 48.2 b | 693.1 ± 1.7 b | 590.8 ± 17.7 a | 578.2 ± 46.7 a | 590.1 ± 25.4 a | 653.3 ± 16.1 ab |
| Tyr | 428.4 ± 28.3 b | 404.9 ± 1.1 ab | 376.9 ± 11.2 ab | 369.0 ± 29.2 a | 375.3 ± 16.3 a | 385.0 ± 10.0 ab |
| Phe | 295.5 ± 19.5 b | 280.7 ± 1.1 b | 235.9 ± 7.1 a | 231.2 ± 19.0 a | 234.7 ± 10.2 a | 260.8 ± 13.7 ab |
| GABA | 164.8 ± 11.5 a | 168.9 ± 0.3 a | 184.1 ± 5.9 a | 179.9 ± 14.2 a | 184.3 ± 7.8 a | 163.1 ± 4.6 a |
| MEA | 1031.3 ± 69.9 a | 967.0 ± 4.0 a | 994.7 ± 38.0 a | 937.9 ± 69.6 a | 925.4 ± 45.2 a | 899.6 ± 25.9 a |
| Orn | 134.2 ± 8.9 b | 151.1 ± 0.0 c | 95.7 ± 2.8 a | 94.0 ± 7.4 a | 97.0 ± 3.5 a | 139.9 ± 3.2 bc |
| His | 203.1 ± 13.1 d | 183.6 ± 0.4 cd | 154.3 ± 5.1 ab | 147.3 ± 11.8 a | 147.9 ± 6.1 a | 172.2 ± 4.2 bc |
| Lys | 320.8 ± 20.2 c | 297.5 ± 1.3 bc | 216.6 ± 7.0 a | 211.4 ± 16.0 a | 213.1 ± 8.6 a | 276.9 ± 7.2 b |
| Arg | 1655.9 ± 109.1 a | 1599.1 ± 5.3 a | 1639.5 ± 51.0 a | 1590.8 ± 129.0 a | 1580.9 ± 65.3 a | 1533.7 ± 40.6 a |
| Pro | 959.2 ± 67.6 a | 884.5 ± 1.9 a | 918.3 ± 29.1 a | 897.7 ± 70.4 a | 901.4 ± 36.1 a | 848.3 ± 22.6 a |
| total | 13169.5 ± 889.6 a | 12708.7 ± 68.0 a | 11884.5 ± 351.0 a | 11587.2 ± 923.6 a | 11734.8 ± 1102.9 a | 12041.2 ± 142.7 a |

[a]Different letters indicate significant differences in each row. [b]Unit is μmol/mL.

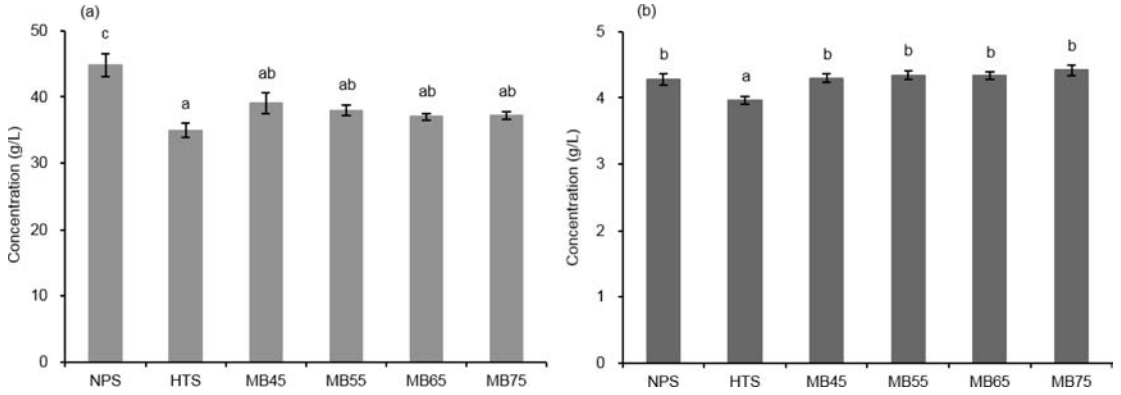


**Figure 3.** Glucose and isomaltose contents in unpasteurized, two-stage MB-$CO_2$-treated and heat-treated sakes. Measured sakes were the same as those used for the sensory evaluation. Data are presented as means with standard errors of the results from triplicate experiments. Different letters indicate significant differences by the Tukey–Kramer method ($p < 0.01$).

may be a cause of the bitterness of UPS, HTS, and MB75 indicated on sensory evaluation.

**Organic Acids.** Organic acids in UPS, HTS, MB45, MB55, MB65, and MB75 are shown in Figure 3. Organic acids in sake are metabolites that are produced by yeast during fermentation.[29] Lactic, succinic, malic, and citric acids contribute largely to the taste of sake.[30] In addition, Iwano et al. reported that succinic, citric, and malic acids had a strong correlation with the sensory evaluation of sake,[31] while pyroglutamic acid showed a weak correlation, and lactic, pyrvic, and acetic acids were not related. The amount of lactic acid, which is a bitter component in sake, was higher in HTS and all two-stage MB-$CO_2$-treated sakes than in UPS, and its levels were the greatest in MB65. Succinic acid, which is a taste component of sake, was significantly increased in MB65. Malic acid, which is a fresh sour component in sake, increased with increasing temperature of the heating coil in two-stage MB-$CO_2$ and was comparable in MB75, UPS, and HTS. Citric acid, which is a sour component in sake, in MB45 and MB55 was significantly lower than that in UPS, HTS, MB65, and MB75. Also, the acetic acid content in UPS, HTS, and MB75 was significantly lower than that in MB45, MB55, and MB65. However, the reason was still in the dark. So, further research is needed to determine the cause of the phenomenon. Acetic acid has been commonly controlled to low concentration, because sake containing acetic acid at high concentration has an acid smell.[32] The fumaric acid content,

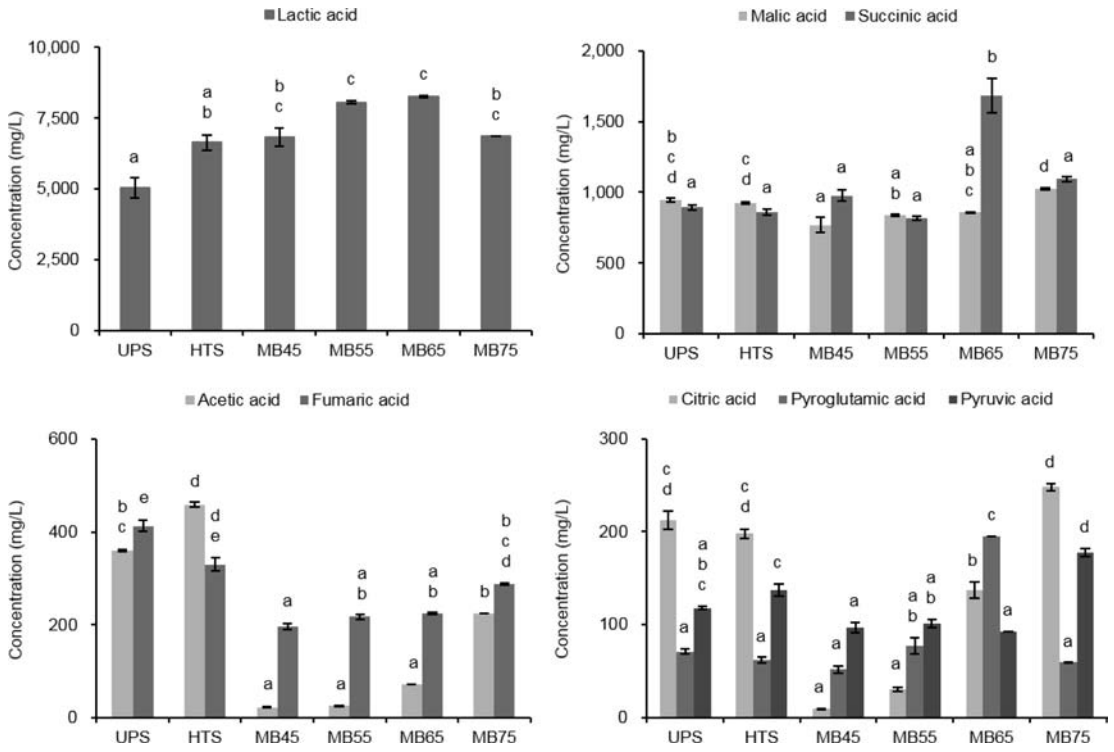


**Figure 4.** Organic acid contents in unpasteurized, two-stage MB-$CO_2$-treated, and heat-treated sakes. Measured sakes were the same as those used for the sensory evaluation. Data are presented as means with standard errors of the results from triplicate experiments. Different letters indicate significant differences by the Tukey–Kramer method ($p < 0.01$).

which is the light sour component in sake,[33] showed a similar pattern as that observed for the malic acid content. Pyroglutamic acid, which is weakly correlated with the sensory evaluation of sake[31] and contributes to umami of food,[34,35] was the highest in the MB65. Therefore, the result was suggested to influence the highest sensory evaluation index of MB65. Also, pyruvic acid, made during early stages of the TCA cycle along with acetic acid,[29,32] was significantly increased in HTS and MB75. It may be related to low sensory evaluation index of HTS and MB75, because pyruvic acid content in sake with high sensory evaluation index is apt to be low.[36] MB65, which was judged to be best by sensory evaluation, had the highest amount of succinic and lactic acids, and contained more malic and citric acids than MB45 and MB55. This suggested that balance of organic acids had a strong influence on the taste of sake. It was reported that malic and succinic acids in sake are decreased, and lactic and acetic acids are increased by heat treatment.[37] In this study, lactic, acetic, and pyruvic acids in HTS were higher than those in UPS and fumaric acid was lower.

**Glucose and Isomaltose.** Glucose and isomaltose in UPS, HTS, MB45, MB55, MB65, and MB75 are shown in Figure 4. The glucose content in HTS and all two-stage MB-$CO_2$-treated sakes was less than that in UPS. Particularly, the content in HTS was the lowest in all sakes. Also, isomaltose content did not differ significantly among UPS and all two-stage MB-$CO_2$-treated sakes, although it was significantly decreased in HTS. High glucose and isomaltose contents in UPS and low glucose and isomaltose contents in HTS contribute to the strong and weak sweetness indicated for UPS and HTS, respectively. The decrease in glucose and isomaltose contents in HTS was probably due to the Maillard reaction, which accelerated with heating time or temperature. However, it was considered that the glucose and isomaltose contents had an insignificant effect on the differences of the sensory evaluation among all the two-stage MB-$CO_2$-treated sakes, since there were no significant differences among these contents in all the two-stage MB-$CO_2$-treated sakes and no correlation between these contents and the sensory evaluation index was shown on the two-stage MB-$CO_2$-treated sake.

**Volatile Compounds.** Volatile compounds in UPS, HTS, MB45, MB55, MB65, and MB75 are shown in Table 2. Total amount of volatile compounds was highest in UPS, followed in decreasing order by MB65, MB55, MB75, MB45, and HTS. Ethyl acetate, 1-propanol, isoamyl acetate, isoamyl alcohol + 2-methyl-1-butanol, and ethyl hexanoate, which are the main compounds of orthonasal aroma in sake,[38] were significantly decreased in MB45, MB75, and HTS, while their levels in MB55 and MB65 were similar to those in UTS. These results are consistent with a previous study that showed that these compounds could be maintained over 80% by using a cooling coil.[17] The decrease of volatile compounds in MB75 and MB45 was considered to be due to high temperature and long exposure time, respectively. It was reported that the extraction efficiency of volatile compounds by supercritical $CO_2$ varies according to the type of compounds, and extraction temperature, pressure and time, respectively.[39−41] Also, changes of amino acids, organic acids, and sugar contents in the two-stage MB-$CO_2$-treated sake may influence flavor release, because volatile compounds were analyzed by concentrating headspace of sake in the study. It was noted that flavor release was changed by adding sucrose and starch into the solution.[42,43] Also, isovaleraldehyde, one of the off-flavors in sake,[44] was significantly decreased by both two-stage MB-$CO_2$ and heat treatments. These results were consistent with the reports by Chen et al., Gasperi et al., and Da Porto et al. that aldehydes in


dx.doi.org/10.1021/jf5038618 | J. Agric. Food Chem. 2014, 62, 11722−11729

**Table 2. Volatile Compounds in Unpasteurized, Heat-Treated, and Two-Stage MB-$CO_2$-Treated Sakes**

| KI[a] | compds[b] | UPS | HTS | MB45 | MB55 | MB65 | MB75 |
|---|---|---|---|---|---|---|---|
| 686 | acetaldehyde | 0.022 ± 0.002[c] b[d] | 0.013 ± 0.002 a | 0.021 ± 0.001 b | 0.021 ± 0.003 b | 0.021 ± 0.003 b | 0.020 ± 0.0001 ab |
| 809 | ethyl formate | 0.155 ± 0.036 b | 0.075 ± 0.020 a | 0.121 ± 0.005 ab | 0.138 ± 0.027 ab | 0.133 ± 0.022 ab | 0.128 ± 0.003 ab |
| 901 | ethyl acetate | 32.433 ± 2.268 c | 21.832 ± 0.844 a | 25.541 ± 0.278 ab | 27.716 ± 2.404 bc | 25.665 ± 2.064 ab | 25.493 ± 0.467 ab |
| 915 | 3-methylbutanal | 0.647 ± 0.032 c | 0.324 ± 0.009 a | 0.375 ± 0.004 ab | 0.411 ± 0.042 b | 0.394 ± 0.012 b | 0.383 ± 0.011 ab |
| 955 | ethyl propanoate | 1.243 ± 0.054 b | 0.877 ± 0.015 a | 0.910 ± 0.035 a | 1.033 ± 0.087 ab | 1.011 ± 0.095 a | 0.993 ± 0.032 a |
| 963 | ethyl 2-methylpropanoate | 0.128 ± 0.004 b | 0.070 ± 0.023 a | 0.128 ± 0.014 b | 0.120 ± 0.004 ab | 0.115 ± 0.020 ab | 0.116 ± 0.007 ab |
| 970 | *n*-propyl acetate | 0.461 ± 0.021 b | 0.341 ± 0.006 a | 0.400 ± 0.045 ab | 0.367 ± 0.021 a | 0.374 ± 0.017 ab | 0.391 ± 0.028 ab |
| 1009 | 2-methylpropyl acetate | 0.345 ± 0.013 c | 0.196 ± 0.005 a | 0.249 ± 0.009 ab | 0.276 ± 0.033 b | 0.298 ± 0.021 bc | 0.257 ± 0.016 ab |
| 1037 | ethyl butanoate | 2.970 ± 0.132 c | 1.723 ± 0.069 a | 2.080 ± 0.033 ab | 2.344 ± 0.265 b | 2.440 ± 0.177 b | 2.189 ± 0.087 ab |
| 1048 | 1-propanol | 2.522 ± 0.282 ab | 2.067 ± 0.423 a | 2.983 ± 0.057 b | 2.721 ± 0.160 ab | 2.609 ± 0.225 ab | 2.747 ± 0.257 ab |
| 1072 | ethyl 3-methyl-butanoate | 0.043 ± 0.001 c | 0.028 ± 0.002 a | 0.035 ± 0.001 b | 0.036 ± 0.003 b | 0.038 ± 0.002 bc | 0.035 ± 0.001 ab |
| 1076 | butyl acetate | 0.039 ± 0.000 a | 0.039 ± 0.002 a | 0.044 ± 0.004 a | 0.041 ± 0.005 a | 0.047 ± 0.003 a | 0.042 ± 0.006 a |
| 1086 | methyl 2-ethylbutanoate | 0.028 ± 0.004 a | 0.022 ± 0.003 a | 0.027 ± 0.004 a | 0.026 ± 0.001 a | 0.025 ± 0.001 a | 0.026 ± 0.004 a |
| 1097 | undecane | 0.017 ± 0.001 a | 0.017 ± 0.002 a | 0.020 ± 0.004 a | 0.016 ± 0.002 a | 0.016 ± 0.001 a | 0.016 ± 0.001 a |
| 1117 | 2-methyl-1-propanol | 5.690 ± 0.412 b | 4.763 ± 0.262 a | 4.941 ± 0.079 ab | 5.028 ± 0.168 ab | 5.029 ± 0.092 ab | 5.045 ± 0.173 ab |
| 1132 | isoamyl acetate | 8.466 ± 0.511 c | 5.300 ± 0.104 a | 5.962 ± 0.297 ab | 6.534 ± 0.670 ab | 7.148 ± 0.525 bc | 6.378 ± 0.436 ab |
| 1139 | ethyl pentanoate | 0.332 ± 0.012 b | 0.167 ± 0.054 a | 0.266 ± 0.016 ab | 0.298 ± 0.035 b | 0.295 ± 0.016 b | 0.273 ± 0.013 b |
| 1159 | 1-butanol | 0.273 ± 0.008 b | 0.228 ± 0.006 a | 0.280 ± 0.003 b | 0.276 ± 0.006 b | 0.277 ± 0.008 b | 0.259 ± 0.005 b |
| 1166 | ethyl 2-butanoate | 0.048 ± 0.006 b | 0.029 ± 0.001 a | 0.036 ± 0.005 ab | 0.042 ± 0.005 ab | 0.047 ± 0.002 b | 0.041 ± 0.006 ab |
| 1176 | pentyl acetate | 0.025 ± 0.002 a | 0.017 ± 0.001 a | 0.019 ± 0.005 a | 0.023 ± 0.003 a | 0.025 ± 0.002 a | 0.022 ± 0.001 a |
| 1235 | isoamyl alcohol + 2-methyl-1-butanol | 29.050 ± 1.438 c | 23.997 ± 0.606 a | 25.874 ± 0.432 ab | 26.729 ± 0.447 abc | 26.795 ± 0.860 bc | 25.959 ± 0.353 ab |
| 1248 | ethyl hexanoate | 17.628 ± 1.279 b | 12.411 ± 0.430 a | 12.829 ± 0.510 a | 13.995 ± 1.345 a | 15.183 ± 0.841 ab | 13.744 ± 0.980 a |
| 1303 | tridecane | 0.065 ± 0.017 a | 0.056 ± 0.023 a | 0.046 ± 0.010 a | 0.041 ± 0.012 a | 0.059 ± 0.010 a | 0.053 ± 0.018 a |
| 1323 | 4-methyl-1-pentanol | 0.049 ± 0.003 b | 0.037 ± 0.001 a | 0.044 ± 0.003 ab | 0.044 ± 0.004 ab | 0.048 ± 0.002 b | 0.044 ± 0.001 ab |
| 1328 | 2-heptanol | 0.042 ± 0.002 b | 0.033 ± 0.001 a | 0.037 ± 0.003 ab | 0.039 ± 0.003 ab | 0.042 ± 0.002 b | 0.038 ± 0.002 ab |
| 1335 | 3-methyl-1-pentanol | 0.044 ± 0.002 ab | 0.036 ± 0.001 a | 0.049 ± 0.004 b | 0.046 ± 0.003 b | 0.049 ± 0.003 b | 0.045 ± 0.003 ab |
| 1348 | ethyl 2-hydroxy-propanoate | 0.037 ± 0.004 a | 0.035 ± 0.001 a | 0.045 ± 0.007 a | 0.051 ± 0.014 a | 0.051 ± 0.012 a | 0.049 ± 0.008 a |
| 1361 | 1-hexanol | 0.032 ± 0.004 a | 0.022 ± 0.002 a | 0.031 ± 0.007 a | 0.029 ± 0.006 a | 0.032 ± 0.004 a | 0.026 ± 0.006 a |
| 1401 | tetradecane | 0.023 ± 0.007 a | 0.024 ± 0.005 a | 0.029 ± 0.002 a | 0.031 ± 0.005 a | 0.035 ± 0.005 a | 0.029 ± 0.001 a |
| 1424 | ethyl octanoate | 2.306 ± 0.293 b | 1.449 ± 0.055 a | 1.577 ± 0.125 a | 1.611 ± 0.183 a | 1.924 ± 0.227 ab | 1.609 ± 0.210 a |
| 1436 | 1-heptanol | 0.076 ± 0.002 a | 0.063 ± 0.003 a | 0.072 ± 0.003 a | 0.072 ± 0.013 a | 0.080 ± 0.008 a | 0.072 ± 0.004 a |
| 1442 | pentyl hexanoate | 0.032 ± 0.004 a | 0.027 ± 0.004 a | 0.034 ± 0.012 a | 0.035 ± 0.004 a | 0.033 ± 0.008 a | 0.027 ± 0.001 a |
| 1471 | benzaldehyde | 0.012 ± 0.002 a | 0.016 ± 0.003 a | 0.017 ± 0.001 a | 0.015 ± 0.002 a | 0.012 ± 0.003 a | 0.013 ± 0.003 a |
| 1633 | ethyl decanoate | 0.057 ± 0.006 a | 0.041 ± 0.002 a | 0.044 ± 0.006 a | 0.039 ± 0.001 a | 0.040 ± 0.004 a | 0.035 ± 0.005 a |
| 1830 | 2-phenylethyl acetate | 0.013 ± 0.002 a | 0.013 ± 0.001 a | 0.018 ± 0.002 a | 0.015 ± 0.002 a | 0.013 ± 0.003 a | 0.015 ± 0.001 a |
| 1858 | ethyl dodecanoate | 0.001 ± 0.000 a | 0.003 ± 0.000 ab | 0.005 ± 0.000 b | 0.005 ± 0.000 b | 0.004 ± 0.002 ab | 0.004 ± 0.000 b |
| 1997 | phenylethyl alcohol | 0.008 ± 0.000 a | 0.008 ± 0.001 a | 0.009 ± 0.001 a | 0.008 ± 0.002 a | 0.009 ± 0.001 a | 0.008 ± 0.001 a |
| | total | 105.347 ± 5.545 c | 76.398 ± 1.948 a | 85.185 ± 1.060 ab | 90.273 ± 5.423 b | 90.414 ± 0.835 b | 86.624 ± 2.279 ab |

[a]KI indicates Kovats Index on DW-WAX column. [b]Volatile compounds identify by GC−MS. [c]Unit is mg/L. [d]Different letters indicate significant differences.



dx.doi.org/10.1021/jf5038618 | J. Agric. Food Chem. 2014, 62, 11722−11729

hami melon and apple juices are significantly decreased by pasteurization by SC-$CO_2$. These factors may be related to the excellent results of MB65 in sensory evaluation.[9−11]

In this study, MB65 was revealed to be extremely good based on sensory evaluations. The reason is that level of free amino acids, which are negatively correlated with sensory evaluation, in MB65 was less than the levels in UPS, HTS, and MB75. Succinic and lactic acid levels were highest in MB65, and malic, citric, and acetic acids were higher than those in MB45 and MB55. However, further research is needed because it is not clear why free amino acid and organic acid contents in sake are changed by two-stage MB-$CO_2$.

## AUTHOR INFORMATION


### Corresponding Author

*Tel: +81-422-31-4151. Fax: +81-422-33-2094. E-mail: fkoba@nvlu.ac.jp.


### Notes

The authors declare no competing financial interest.

## ACKNOWLEDGMENTS

We thank Dr. Ai Egusa-Saiga of Faculty of Applied Life Science, Nippon Veterinary and Life Science University (Musashino, Tokyo, Japan), for technical assistance.

## REFERENCES


(1) Sato, S. In *Aging of Food*; Kohrin: Tokyo, Japan, 1984; pp 23−30 (in Japanese).

(2) Noshiro, K.; Momose, H. Hiochi bacteria. *J. Brew. Soc. Jpn.* **1970**, *65*, 88−91 (in Japanese).

(3) Yamamoto, N.; Saito, T. Pasteurization and storage condition of ginjoshu. *J. Brew. Soc. Jpn.* **1989**, *84*, 496−498 (in Japanese with English Abstract).

(4) Tanimoto, S.; Matsumoto, H.; Fujii, K.; Ohdoi, R.; Sakamoto, K.; Izuwa, S.; Yamane, Y.; Shimoda, M.; Osajima, Y. Thermal inactivation behavior of enzymes in fresh sake during pasteurization. *J. Brew. Soc. Japan.* **2004**, *99*, 208−214 (in Japanese with English Abstract).

(5) Damar, S.; Balaban, M. O. Review of dense phase $CO_2$ technology: microbial and enzyme inactivation, and effects on food quality. *J. Food Sci.* **2006**, *71*, R1−11.

(6) Garcia-Gonzalez, L.; Geeraerd, A. H.; Spilimbergo, S.; Elst, K.; Van Ginneken, L.; Debevere, J.; Van Impe, J. F.; Devlieghere, F. High pressure carbon dioxide inactivation of microorganism in foods: The past, the present and the future. *Int. J. Food Microbiol.* **2007**, *117*, 1−28.

(7) Spilimbergo, S.; Bertucco, A. Non-thermal bacteria inactivation with dense $CO_2$. *Biotechnol. Bioeng.* **2003**, *84*, 627−639.

(8) Kazazi, H.; Rezaei, K.; Ghotb-Sharif, S. J.; Emam-Djomeh, Z.; Yamini, Y. Supercritical fluid extraction of flavors and fragrances from *Hyssopus officinalis* L. cultivated in Iran. *Food Chem.* **2007**, *105*, 805−811.

(9) Chen, J.; Zhang, J.; Feng, Z.; Song, L.; Wu, J.; Hu, X. Influence of thermal and dense-phase carbon dioxide pasteurization on physicochemical properties and flavor compounds in Hami melon juice. *J. Agric. Food Chem.* **2009**, *57*, 5805−5808.

(10) Gasperi, F.; Aprea, E.; Biasioli, F.; Carlin, S.; Endrizzi, I.; Pirretti, G.; Spilimbergo, S. Effect of supercritical $CO_2$ and $N_2O$ pasterisation on the quality of fresh apple juice. *Food Chem.* **2009**, *115*, 129−136.

(11) Da Porto, C.; Decorti, D.; Tubaro, F. Effects of continuous dense-phase $CO_2$ system on antioxidant capacity and volatile compounds of apple juice. *Int. J. Food Sci. Technol.* **2010**, *45*, 1821−1827.

(12) Kobayashi, F.; Hayata, Y.; Ikeura, H.; Tamaki, M.; Muto, N.; Osajima, Y. Inactivation of *Escherichia coli* by $CO_2$ microbubbles at a lower pressure and near room temperature. *Trans. ASABE* **2009**, *52*, 1621−1626.

(13) Kobayashi, F.; Hayata, Y.; Ikeura, H.; Muto, N.; Osajima, Y. Inactivation of *Saccharomyces cerevisiae* by $CO_2$ microbubbles at a lower pressure and near ambient temperature. *Trans. ASABE* **2010**, *53*, 1217−1222.

(14) Kobayashi, F.; Sugawara, S.; Takatomi, T.; Ikeura, H.; Odake, S.; Tanimoto, S.; Hayata, Y. Inactivation of *Lactobacillus fructivorans* in physiological saline and unpasteurized sake using $CO_2$ microbubbles at ambient temperature and low pressure. *Int. J. Food Sci. Technol.* **2012**, *47*, 1151−1157.

(15) Kobayashi, F.; Ikeura, H.; Odake, S.; Tanimoto, S.; Hayata, Y. Inactivation of *Lactobacillus fructivorans* suspended in various buffer solutions by low-pressure $CO_2$ microbubbles. *LWT—Food Sci. Technol.* **2012b**, *48*, 330−333.

(16) Kobayashi, F.; Ikeura, H.; Odake, S.; Hayata, Y. Inactivation kinetics of polyphenol oxidase using a two-stage method with low pressurized carbon dioxide microbubbles. *J. Food Eng.* **2013a**, *114*, 215−220.

(17) Kobayashi, F.; Ikeura, H.; Odake, S.; Hayata, Y. Inactivation of enzymes and *Lactobacillus fructivorans* in unpasteurized sake by a two-stage method with low-pressure $CO_2$ microbubbles and quality of the treated sake. *Innovative Food Sci. Emerging Technol.* **2013b**, *18*, 108−114.

(18) Tanimoto, S.; Matsumoto, H.; Fujii, K.; Ohdoi, R.; Sakamoto, K.; Izuwa, S.; Yamane, Y.; Miyake, M.; Shimoda, M.; Osajima, Y. Inactivation of enzymes in fresh sake using a continuous flow system for high-pressure carbonation. *Biosci., Biotechnol., Biochem.* **2005**, *69*, 2094−2100.

(19) Hashizume, K.; Tokuda, K.; Kokubo, S.; Kawase, N.; Kurosu, T.; Shimizu, S.; Ueda, M.; Samuta, T.; Kuwabara, K.; Obata, T.; Tsugawa, M.; Ito, K.; Sugama, S.; Yoshizawa, K. Studies on brewing conditions affecting the qualities of sake. *J. Brew. Soc. Jpn.* **1982**, *77*, 670−675 (in Japanese).

(20) Tanimoto, S.; Matsumoto, H.; Fujii, K.; Ohdoi, R.; Sakamoto, K.; Izuwa, S.; Yamane, Y.; Shimoda, M.; Osajima, Y. Thermal inactivation behaviour of enzymes in fresh sake during pasteurization. *J. Brew. Soc. Jpn.* **2004**, *99*, 208−214 (in Japanese with English abstract).

(21) Zhang, Y.; Wang, Y.; Zhou, L.; Liao, X. A comparative study of inactivation of peach polyphenol oxidase and carrot polyphenol oxidase induced by high-pressure carbon dioxide. *Int. J. Food Sci. Technol.* **2010**, *45*, 2297−2305.

(22) Yoshizaki, Y.; Yamato, H.; Takamine, K.; Tamaki, H.; Ito, K.; Sameshima, Y. Analysis of volatile compounds in Shochu koji, Sake koji, and steamed rice by gas chromatography-mass spectrometry. *J. Inst. Brew.* **2010**, *116*, 49−55.

(23) Yoshizaki, Y.; Takamine, K.; Shimada, S.; Uchihori, K.; Okutsu, K.; Tamaki, H.; Ito, K.; Sameshima, Y. The formation of $\beta$-damascenone in sweet potato Shochu. *J. Inst. Brew.* **2011**, *117*, 217−223.

(24) Iwano, K.; Ito, T.; Nakazawa, N. Characteristics of amino acid compositions of ginjyo-shu, junmai-shu, honjyozo-shu, and futsu-shu. *J. Brew. Soc. Jpn.* **2004a**, *99*, 526−533 (in Japanese with English abstract).

(25) Iwano, K.; Takahashi, K.; Ito, T.; Nakazawa, N. Search for amino acids affecting the taste of Japanese sake. *J. Brew. Soc. Jpn.* **2004b**, *99*, 659−664 (in Japanese with English abstract).

(26) Yoshida, M.; Ninomiya, T.; Ikeda, S.; Yamaguchi, S.; Yoshikawa, T.; Ohara, M. Studies on the taste of amino acids. Part I. Detaermination of threshold values of various amino acids. *Agric. Biol. Chem.* **1966**, *40*, 295−299 (in Japanese with English abstract).

(27) Otsuka, H.; Take, T. Preparation of the sapid solution by mixture with various amino acids. *Eiyotosyokuryo* **1973**, *26*, 463−469 (in Japanese with English abstract).

(28) Fushiki, T. Koku and Japanese sake. *J. Brew. Soc. Jpn.* **2003**, *98*, 388−391 (in Japanese).

(29) The Brewing Society of Japan. In *Jouzoubutunoseibun*; The Brewing Society of Japan: Tokyo, Japan, 1999; pp 50−62 (in Japanese).

(30) Sato, S.; Oba, T.; Takahashi, K.; Kokubun, S.; Kobayashi, M.; Kobayashi, K. A study of taste of sake (The seventh report). *J. Brew. Soc. Jpn.* **1977**, *72*, 801−805 (in Japanese).
(31) Iwano, K.; Ito, T.; Nakazawa, N. Correlation analysis of a sensory evaluation and the chemical components of *Ginjyo-shu*. *J. Brew. Soc. Jpn* **2005**, *100*, 639−649 (in Japanese with English abstract).
(32) Asano, T.; Kurose, N. Mechanism of organic acids production by sake yeast. *J. Brew. Soc. Jpn.* **2000**, *95*, 227−234 (in Japanese).
(33) Kadokura, T.; Tanaka, K.; Takahashi, K.; Nakazato, A.; Takeda, M. Development of a sparkling sake containing yeast cells. *J. Brew. Soc. Jpn.* **1992**, *87*, 394−396 (in Japanese with English abstract).
(34) Watanabe, T. Seasoning. Japan Tobacco Inc.: 2007; Patent No. JP 4040823.
(35) Park, J. N.; Watanabe, T.; Endou, K.; Watanabe, K.; Abe, H. Taste-active components in a Vietnamese fish sauce. *Fish. Sci.* **2002**, *68*, 913−920.
(36) Suenaga, H.; Ichimatsu, T.; Oba, T. Analysis and evaluation technology of the sake, −Component analysis of Japanese sake-. *Bul. Fukuoka Ind. Technol. Center* **2009**, *19*, 54−57 (in Japanese).
(37) Ueda, R.; Hayashida, M.; Kitagawa, E. A Study of organic acids on sake brewing (I). *Hakko Kogaku Zasshi* **1960**, *38*, 337 (in Japanese).
(38) Ohta, T. In *The Annotation of the Official Analysis Methods of the National Tax Agency of Japan*, 4th ed.; The Brewing Society of Japan: Tokyo, Japan, 1993; pp 273 (in Japanese).
(39) Shimoda, M.; Ishikawa, H.; Kawano, T.; Osajima, Y. Extraction of volatile compounds from aqueous solution using micro bubble, gaseous, supercritical and liquid carbon dioxide. *J. Food Sci.* **1994**, *59*, 231−233.
(40) Pourmortazavi, S. M.; Sefidkon, F.; Hosseini, S. G. Supercritical carbon dioxide extraction of essential oils from *Perovskia atriplicifolia* Benth. *J. Agric. Food Chem.* **2003**, *51*, 5414−5419.
(41) Fornari, T.; Vicente, G.; Vázquez, E.; García-Risco, M. R.; Reglero, G. Isolation of essential oil from different plants and herbs by supercritical fluid extraction. *J. Chromatogr. A* **2012**, *1250*, 34−48.
(42) Friel, E. N.; Linforth, R. S. T.; Taylor, A. J. An empirical model to predict the headspace concentration of volatile compounds above solutions containing sucrose. *Food Chem.* **2000**, *71*, 309−317.
(43) Kant, A.; Linforth, R. S. T.; Taylor, A. J. Flavour retention and release from starch solutions. In *Flavour research at the dawn of the twenty-first century*; Lequéré, J. L., Ětiévant, P. X. S. Eds.; Intercept: 2003; pp103−106.
(44) Motoyoshi, T.; Nishimura, A.; Kondo, K.; Nakazawa, E.; Mishima, H.; Takemura, S. Changes of "Mureka" compounds in sake and the presumed pathway forming these compounds. *Hakko Kogaku* **1991**, *69*, 1−6 (in Japanese with English abstract).

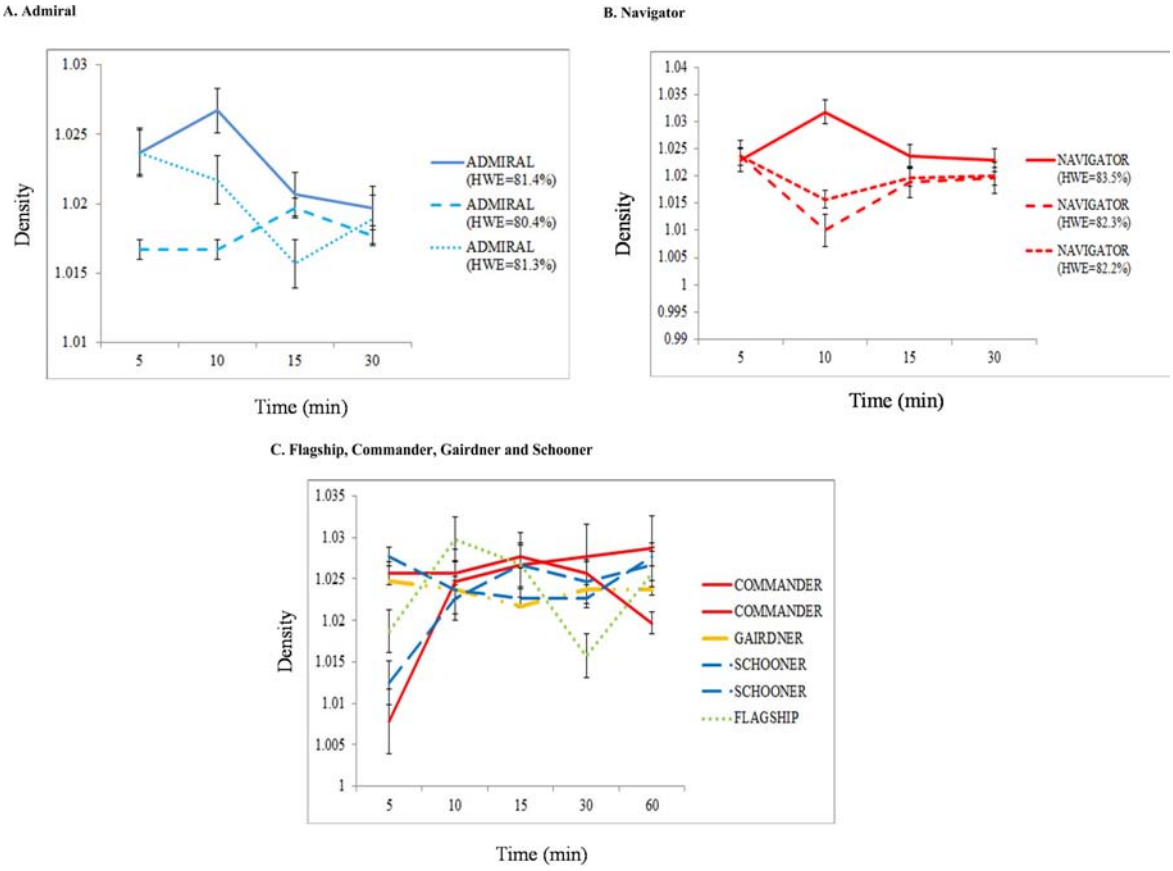


**Figure 1.** Patterns of hydrolysis in different malt varieties having different hot water extract values.

order to ensure the quality and consistency of raw materials and products, as well as allow screening of large quantities of samples.[14−18] Therefore, the combination of multivariate data analysis and IR spectroscopy will be of interest in order to develop high-throughput methods to monitor different steps during malt production or rapid screening of varieties during selection or trade.

The objectives of this study were (a) to compare the time course of hydrolysis of different malting barley varieties and (b) to evaluate the usefulness of mid-infrared (MIR) spectroscopy as high-throughput method to monitor malt hydrolysis.

## MATERIALS AND METHODS

Barley grain (*Hordeum vulgare* L) and corresponding malt samples were sourced from commercial varieties from the Barley Breeding Program (The University of Adelaide, Australia). The commercial barley malt varieties analyzed were Admiral ($n$ = 6), Commander ($n$ = 2), Flagship ($n$ = 2), Gairdner ($n$ = 2), Navigator ($n$ = 6) and Schooner ($n$ = 2), harvested in 2012 at one locality in South Australia (Charlick). Grain samples were malted using a Phoenix automatic micromalting system as reported previously.[19] Hot water extract (HWE) was analyzed using small scale versions of the Analytica-EBC Official methods (European Brewery Convention Analytica-EBC 1998, HWE method 4.5.1).[11,20]

Malt samples (1 ± 0.05 g) were placed in polypropylene tubes (in duplicate), and 10 mL of hot water (65 ± 5 °C) was added to each tube. The tubes were stirred allowing the water to have total contact with the sample and then placed in a water bath (65 ± 5 °C) with continuous agitation. Tubes were taken sequentially at 5, 10, 15, 30, 40, and 60 min and placed immediately in a container with ice to stop any further biochemical reaction. Samples were centrifuged at 2500$g$ for 20 min (Beckman, TJ6, USA). Total soluble solids (°Brix) were measured in the liquid (wort) using a digital portable refractometer (Hanna, HI 96801, Hanna Instruments, Inc. Rhode Island, USA) and converted to density.

The supernatant (wort) samples were scanned using a platinum diamond attenuated total reflectance (ATR) single reflection sampling module cell, mounted in a Bruker Alpha instrument (Bruker Optics GmbH, Ettlingen, Germany). Duplicates of each sample were scanned twice, and the average ATR-mid-infrared (MIR) spectrum of each sample was used for further analysis. The ATR-MIR spectra were recorded on OPUS software version 7.0 provided by Bruker Optics. The spectrum for each sample was obtained by taking the average of 24 scans (resolution of 4 $cm^{-1}$, between 4000 and 375 $cm^{-1}$) with a scanner speed of 7.5 kHz (background of 24 scans). Air was used as reference background spectra. The ATR diamond surface was cleaned with ethanol (95% v/v) before each sample was scanned. The absorption region between 2500 and 2000 $cm^{-1}$ due to carbon dioxide and the ATR diamond cell was discarded prior the calculation.[21,22]

The Unscrambler X software (v. 10.1, CAMO ASA, Norway) was used for preprocessing and chemometric analysis. Principal component analysis (PCA) was performed to determine any relevant and interpretable structure in the data, to detect outlier samples, and to visualize the changes in the MIR spectra related to the time course of the hydrolysis.[23,24] The ATR-MIR spectral data was preprocessed using Savitzky−Golay second derivative (40 smoothing points and second polynomial order) in order to remove and correct for baseline effects.[25] The second derivative is a measure of the change in the slope of the curve ignoring the offset and is very effective in removing both baseline offset and slope from a spectrum.[25]

Classification models were developed separately for each variety and time course of hydrolysis. Discrimination models were developed using partial least-squares discriminant analysis (PLS-DA) (The Unscrambler X, CAMO ASA, Norway).[23,24] Group membership of a new unknown sample was determined by its predicted value using PLS-DA.[23,24] PCA and PLS-DA models were developed by using full cross validation (leave one out) where the number of terms

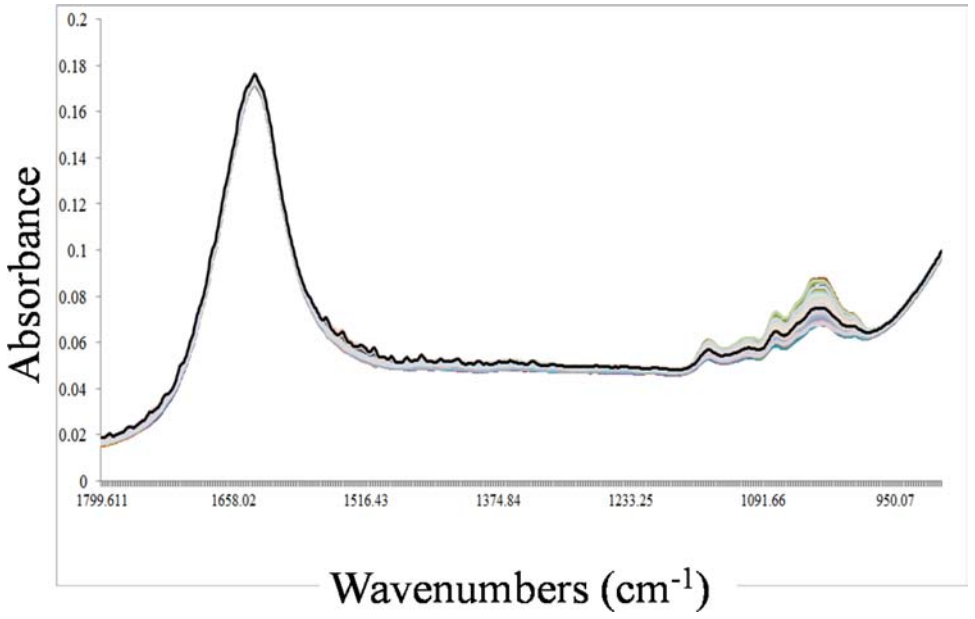


**Figure 2.** Attenuated total reflectance mid-infrared spectra of malt samples sourced from different time points during the malt hydrolysis.

(eigenvectors/loadings) were defined by the prediction residual error sum of squares (PRESS) function in order to avoid overfitting of the models (The Unscrambler, CAMO AS, v. 10.1, Oslo, Norway).

## RESULTS AND DISCUSSION

**Patterns of Hydrolysis: Reference Method.** Figure 1A–C shows the changes in density at different time points during the monitoring of the time course of starch hydrolysis in the different barley malt varieties analyzed. A nonlinear trend in the pattern of hydrolysis was observed between the different malt varieties. However, this pattern was not the same for all malt varieties analyzed. In malt varieties such as Admiral, Commander, and Flagship, an increase in density from 0 to 10 min was observed followed by a steady decrease in density after 15 min, after which time point density tends to increase until 60 min (end point). The opposite trend was observed for malting varieties such as Gairdner, Navigator, and Schooner. Moreover, malt samples from the same variety that have similar HWE (measured using the EBC method) tend to have the same pattern of hydrolysis (Figure 1A,B). At 10 min was observed either a peak or trough in the trend of hydrolysis.

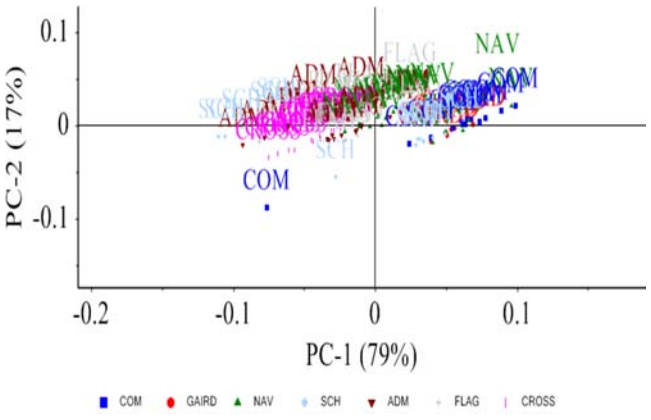


**Figure 3.** Principal component score plot (PC1 vs PC2) of all malt varieties analyzed using attenuated total reflectance mid-infrared spectroscopy.

These differences might be attributed to the different composition in sugars between the barley varieties analyzed. It is well-known that more than 90% of the solids present in wort are related to carbohydrates, where free sugars such as fructose, mannose, glucose, galactose, sucrose, and maltose are the most abundant. Nonstarch water-soluble sugars and cell wall components (e.g., hemicellulose) can also contribute to this.[3,26] Variations in the proportion of free and water-soluble sugars in different varieties of barley grain have been reported by other authors might also explain the observed patterns.[3,26]

It has been reported that HWE extracts from the malt are lower than those for the corresponding polysaccharides from the same grain, indicating that cleavage of some glycosidic bonds has occurred during malting.[3,26] However, all the reported studies on malt extract usually refer to the end point of HWE measured using the EBC method. The results of this study showed that the pattern or trend of starch hydrolysis might be more important than the end value. In particular, the amount of sucrose equivalent or the overall final density that is routinely used to calculate HWE might not explain the observed differences in HWE between barley varieties having high malt extract (HWE > 80%).

The results from this study also suggested that the pool of sugars in the wort tend to have high density such as fructose (1.69 g/cm$^3$) compared with glucose (1.54 g/cm$^3$). The observed differences in density might explain the increases in HWE between the malt varieties analyzed and are in agreement with early reports by other authors.[27−30] These authors reported that during kilning of the malt both glucose and sucrose increased, where the increase in sucrose is particularly well marked, indicating the important role that is played by kilning in altering the characteristics of the grain as well as the action of amylase that naturally becomes more important as malting progresses.[27−30] Some other sugars or oligosaccharides tend also to increase, among these fructosans being the most important.[30]

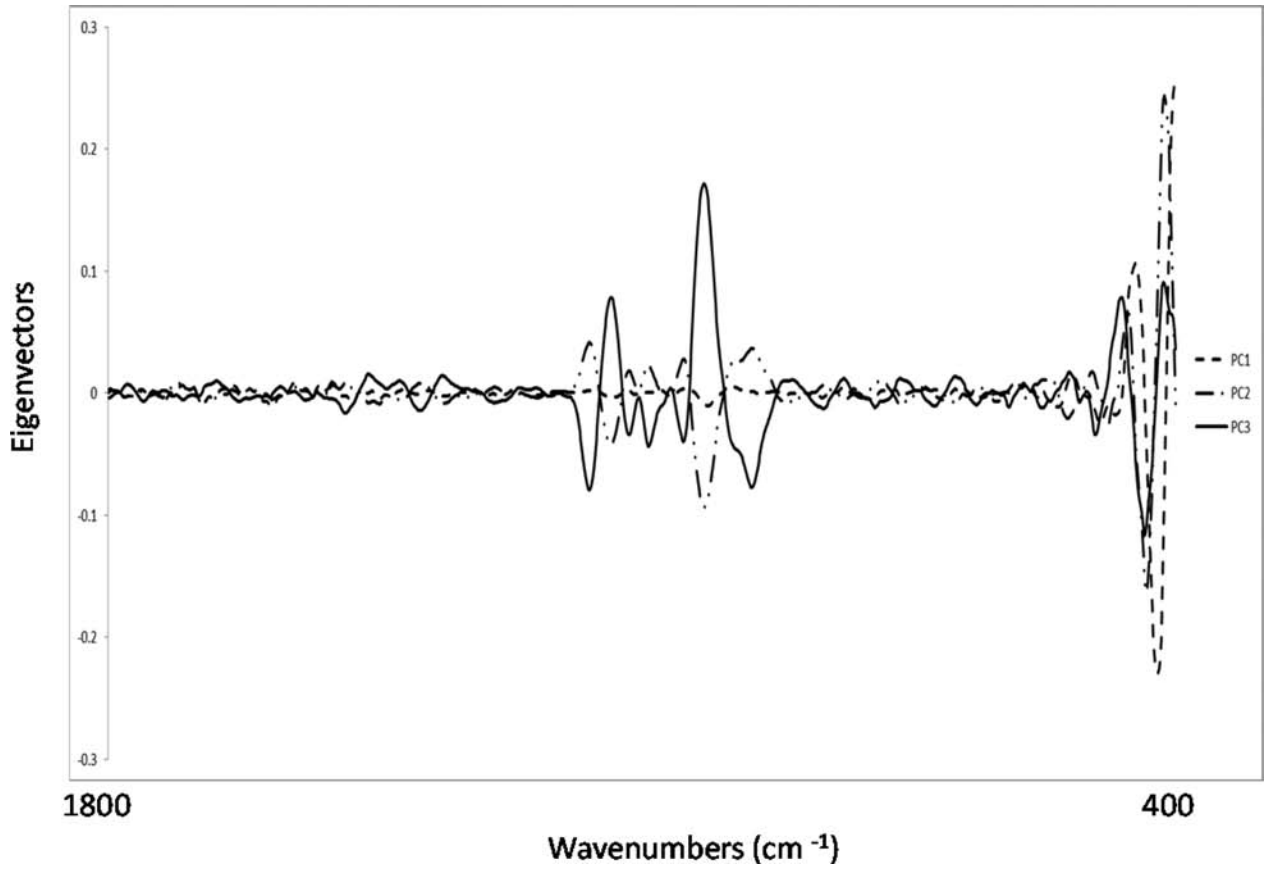


**Figure 4.** Eigenvectors derived from the first three principal component analyses of all malt varieties analyzed using attenuated total reflectance mid-infrared spectroscopy.

It is well-known that the major source of extract in malt wort is starch; however free sugars are also important, sucrose being one of the most abundant. Both mannose and galactose occur combined in malt, but neither is released during mashing. In wort samples, maltose, along with many other compounds, is produced during mashing by the partial hydrolysis of starch. There is some evidence that small amounts of fructans might also occur in malt.[3] These can be regarded as sucrose molecules to which one or more fructose residues have been attached. However, because the levels of fructose do not increase appreciably during mashing, it is likely that the fructans, which are very soluble, are not hydrolyzed, and so they remain with the nonfermentable carbohydrates.[3] Mashing constitutes the enzymatic hydrolysis of starch, resulting in the production of glucose, maltose, and glucose-based oligosaccharides.[31] However, there are other starch based carbohydrates in malted barley, which also contains sucrose.[31] In this context, the activity of the invertase enzyme facilitates the hydrolysis of sucrose to yield both glucose and fructose altering the density of the wort.[31] Therefore, the accumulation of fructose can be similar to the hydrolysis of sucrose, while the accumulation of glucose during mashing can be up to five times greater than the theoretical yield from utilized sucrose alone.[31] This large accumulation of glucose during mashing is most likely due to the combined activity of different enzymes such as invertases, glucoamylases, and $\alpha$-amylase.[31]

**Infrared Analysis: Spectra Interpretation.** In order to further interpret the patterns related to the time course of hydrolysis and the fate of sugars, the ATR-MIR spectra of the wort were recorded and evaluated. Figure 2 shows the ATR-MIR spectra in the fingerprint region of the wort samples analyzed. The spectra were dominated by intense peaks around 1030, 1070, 1160, and 1630 $cm^{-1}$ due to water, sugars, and nitrogen compounds. These peaks might be related to the CH−OH and alkyl frequencies for sugars mainly associated with glucose and fructose, between 1000 and 1200 $cm^{-1}$.[32−38] Most of the variation in the ATR-MIR spectra was observed between 1000 and 1200 $cm^{-1}$ (related to stretching modes of C−C and C−O groups), and it has been mainly related to differences in the release of sugars (measured as density) as a function of the time course of the hydrolysis as reported by other authors.[32−38]

Figure 3 shows the principal component score plot of the time course of hydrolysis using all the malting varieties analyzed using ATR-MIR. The first three principal components explain more than 90% of the variation in the ATR-MIR spectra (PC1 = 79%, PC2 = 17%, and PC3 = 2%). Differences in the patterns of the scores between the malt varieties and within the samples from the same variety as a consequence of the time course of hydrolysis were observed. Figure 4 shows the eigenvectors derived from the score plot of the first three principal components obtained from the analysis of wort samples using ATR-MIR spectra. The analysis of the first three eigenvectors indicated that the MIR regions related to sugars explain most of the observed differences between the malt samples. The highset eigenvectors were observed at 1130 and 1025 $cm^{-1}$ characteristic of sucrose and at 1032 $cm^{-1}$ characteristic of glucose.[32] Characteristic absorption bands of fructose are observed in the range between 1000 and 1100 $cm^{-1}$, while the region between 1056 and 1116 $cm^{-1}$ corresponds to the interference between

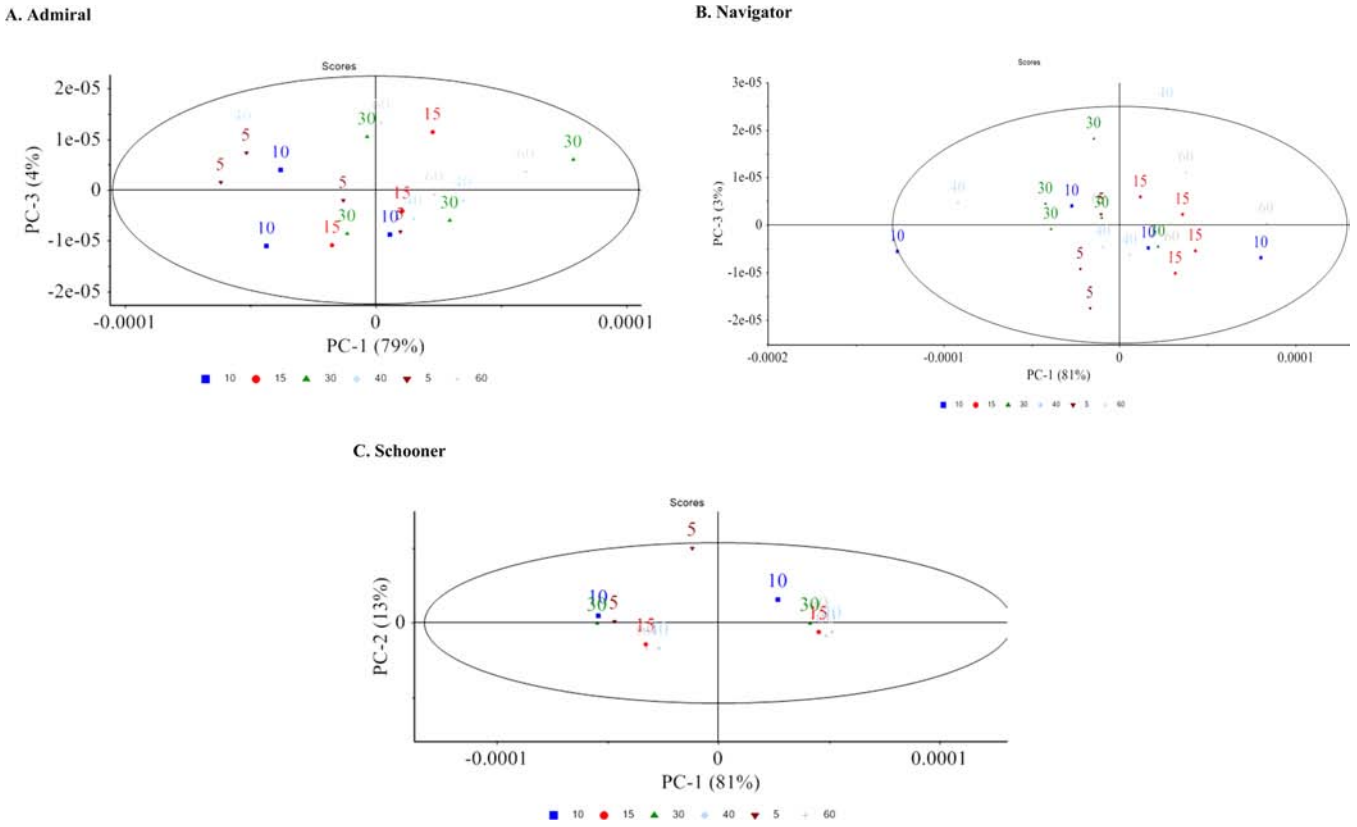


**Figure 5.** Principal component score plot (PC1 vs PC2) of Admiral, Navigator and Schooner malt samples analyzed using attenuated total reflectance mid-infrared spectroscopy labeled by the time course of hydrolysis.

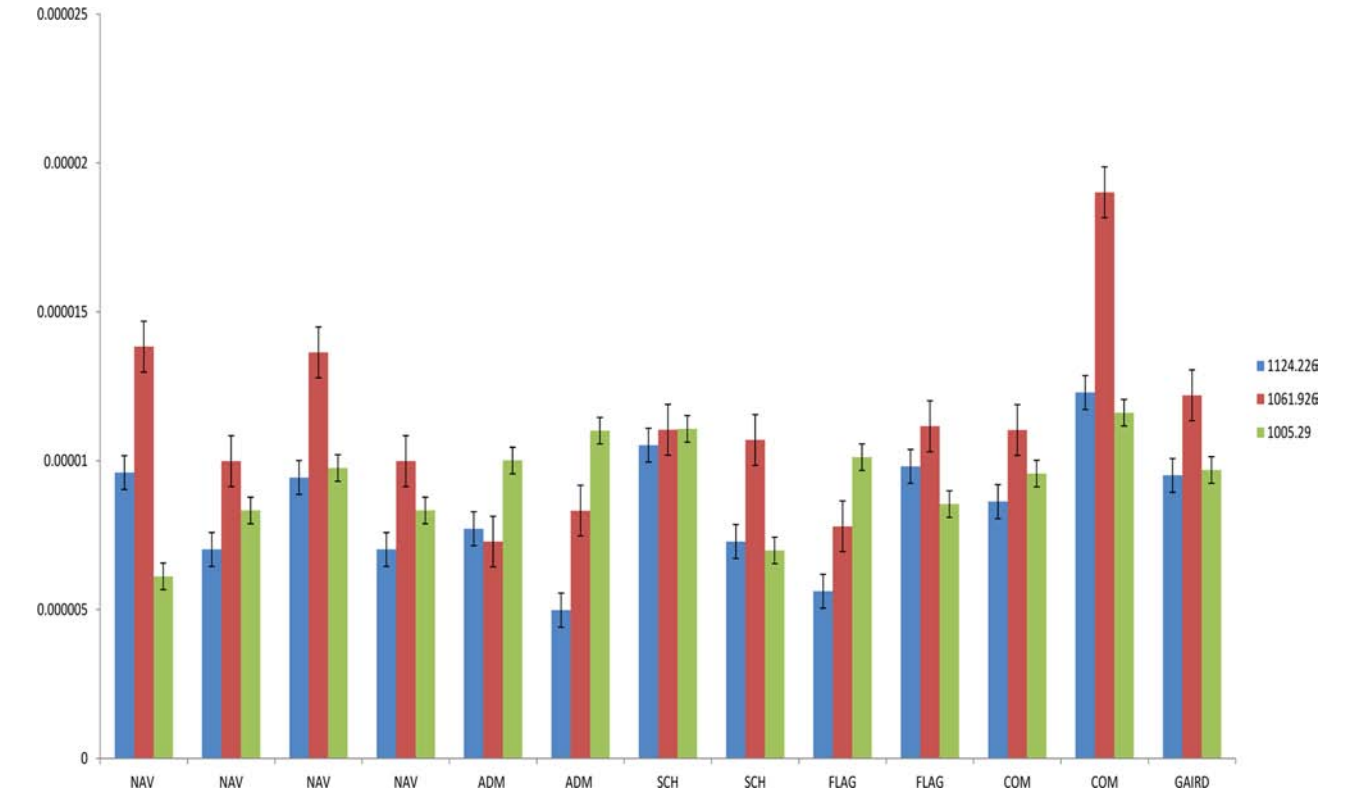


**Figure 6.** Absorbance values at specific frequencies from different barley malt varieties analyzed using attenuated total reflectance mid-infrared spectroscopy.


dx.doi.org/10.1021/jf504116j | J. Agric. Food Chem. 2014, 62, 11730−11736

glucose and fructose as reported by other authors.[32−38] Bands between 900 and 1100 $cm^{-1}$ are assigned to C−O and C−C stretching modes, while those between 1300 and 1100 $cm^{-1}$ are associated with the bending modes of O−C−H, C−C−H, and C−O−H. It has been reported by other authors that the spectra of aqueous solution of glucose show absorbance bands at 917 and 1034 $cm^{-1}$, those of fructose at 1062 and 1151 $cm^{-1}$, and those of sucrose at 926, 1005, 1048, and 1124 $cm^{-1}$,[32−38] while sucrose is characterized by a peak at 1005 $cm^{-1}$ owing to the presence of glycosidic links.[39,40] A major peak at 1034 and 1062 $cm^{-1}$ was observed for glucose and fructose, respectively, while three distinct peaks were obtained for sucrose with the major peak being centered at 1048 $cm^{-1}$. This shift in the frequencies of the major peaks can be explained by the difference in the chemical environment surrounding the atoms concerned with this vibrational band.[41]

**Principal Component Analysis of the Time Course of Hydrolysis in Different Varieties.** In an attempt to gain greater insight into the changes within the different malt varieties analyzed, PCA analysis was carried out for the single varieties separately (Figure 5). Changes in the direction of the scores derived from the MIR spectra were linear from 5 to 15 min, while a change in this trend was observed from 30 to 60 min. Similar changes were observed in the raw and transformed spectra (data not shown). Three main peaks were selected and compared between the varieties, and the relative frequencies for each variety are shown in Figure 6, around 1060 $cm^{-1}$ related to fructose and around 1160 $cm^{-1}$ with the combination of glucose and fructose as reported by other authors.[32−38] It has been observed that malt varieties that tend to yield high HWE present high frequencies in the wavenumber regions associated with high density sugars such as fructose (e.g., Navigator) while malt varieties that tend yield intermediate to high HWE have high frequencies in the region associated with glucose (e.g., Admiral, Flagship).

**Discriminant Analysis.** PLS-DA was used to classify malt samples according to their corresponding variety and time course of hydrolysis. The coefficient of determination ($R^2$) and the standard error of cross validation (SECV) obtained for the prediction of variety and time course of hydrolysis were 0.67 (SECV = 1.01) and 0.38 (SECV = 19.90), respectively. These results suggested that the time course and patterns of hydrolysis are affected by the variety and might be explained by the different composition in sugars as well as other chemical components of the grain.

In this study, the combination of spectroscopy and chemometrics as an analytical tool gave the advantage of rapid monitoring of the changes occurring during malt hydrolysis without the need for quantitative data. These results also suggested that the observed patterns in malt hydrolysis (reference data and PCA scores from the MIR spectra) and the information derived from the eigenvectors indicated that the observed differences in the patterns are mainly associated with variety and not with the time course of the hydrolysis. Although other biochemical components influence the final level of extract including husk thickness, grain size, protein, starch, nonstarch polysaccharides, and enzyme production, as well as the malting process and mashing conditions (pH, temperature, mash time, grist/particle size) only the patterns related to sugars were evaluated in this study.[7]

Compared with traditional laboratory methods, IR provides with new and better insight into complex problems by measuring a great number of chemical compounds at once. These methods are attractive due to their inherent features of versatility, flexibility, effectiveness, and richness of information. Further studies will be carried out in order to validate the proposed methodology with the addition of more samples derived from different harvests, localities and varieties.

## AUTHOR INFORMATION

### Corresponding Author

*E-mail: d.cozzolino@adelaide.edu.au.

### Funding

This project (UA00126) is supported by Australia's grain growers through their investment body, the Grain Research and Development Corporation (GRDC), with matching funds from the Australian government.

### Notes

The authors declare no competing financial interest.

## ACKNOWLEDGMENTS

The authors thank technical staff of the Barley Quality Laboratory and Barley Breeding Program, University of Adelaide.

## REFERENCES

(1) Meredith, W. S.; Anderson, J. A.; Hudson, L. E. Evaluation of malting barley. In *Barley and Malt. Biology, Biochemistry and Technology*; Cook, A. H., Eds.; Academic Press: New York, 1962; pp 207−270.

(2) Burger, W. C.; LaBerge, D. E. Malting and brewing quality. In *Barley*; Rasmusson, D. C., Eds.; American Society of Agronomy: Madison, WI, 1985; pp 367−401.

(3) Briggs, D. E.; Boulton, C. A.; Brookes, P. A.; Stevens, R. *Brewing science and practice*; Woodhead Publishing Limited: Abington Hall, Abington Cambridge, England, 2004.

(4) Fox, G. P. Chemical composition in barley grains and malt quality. In *Genetics and improvement of barley malt quality*; Zhang, G., Li, Ch.; Eds.; Zhejiang University Press: Hangzhou, China; 2009.

(5) Hayes, P.; Castro, A.; Marquez-Cedillo, L.; Corey, A.; Henson, C.; Jones, B. L.; Kling, J.; Mather, D.; Matus, I.; Rossi, C.; Sato, K. Genetic diversity inherited agronomic and malting quality traits. In *Diversity in Barley (Hordeum vulgare)*; Von Bothmer, R.; Von Hintum, T.; Knupffer, H.; Sato, K., Eds.; Elsevier: Amsterdam, 2003; pp 201−226.

(6) Hayes, P. M.; Jones, B. L. Malting quality from a QTL perspective, In Proceedings of the Eighth International Barley Genetics Symposium, Logue, S., Eds.; Adelaide University: Adelaide, Australia, 2000; pp 99−106.

(7) Fox, G. P.; Panozzo, J. F.; Li, C. D.; Lance, R. C. M. Molecular basis of barley quality. *Aust. J. Agric. Res.* **2003**, *54*, 1081−1101.

(8) Igartua, E.; Hayes, P. M.; Thomas, W. T. B.; Meyer, R.; Mather, D. E. Genetic control of quantitative grain and malt quality traits in barley. *J. Crop Prod.* **2002**, *5*, 131−164.

(9) Fox, G. P.; Henry, R. J. Rapid small scale method for the determination of malt extract. *J. Inst. Brew.* **1993**, *99*, 73−75.

(10) Morgan, A. G.; Gothard, P. G. A rapid test for identifying potential malting quality in the early generations of a barley breeding program. *J. Sci. Food Agric.* **1981**, *32*, 333−338.

(11) *European Brewery Convention. Analytica−EBC*. Verlag Hans Carl: Nürnberg, Germany, 1998.

(12) Ellis, R. P.; Swanston, J. S.; Bruce, F. M. A comparison of some rapid screening tests for malting quality. *J. Inst. Brew.* **1979**, *85*, 282−285.

(13) Edney, M. J.; MacLeod, A. L.; LaBerge, D. E. Evolution of a quality testing program for improving malting barley in Canada. *Can. J. Plant Sci.* **2014**, *94*, 535−544.

(14) Vandenberg, F. W. J.; Vanosenbruggen, W. A.; Smilde, A. K. Process analytical chemistry in the distillation industry using near-infrared spectroscopy. *Process Control Qual.* **1997**, *9*, 51−57.
(15) Hassell, D.Ch.; Bowman, E. Process analytical ahemistry for spectroscopists. *Appl. Spectros.* **1998**, *52*, 18A−29A.
(16) Wise, B. M.; Gallagher, N. B. The process chemometrics approach to process monitoring and fault detection. *J. Process Control* **1996**, *6*, 329−348.
(17) Cozzolino, D.; Parker, M.; Dambergs, R. G.; Herderich, M.; Gishen, M. Chemometrics and visible-near infrared spectroscopic monitoring of red wine fermentation in a pilot scale. *Biotechnol. Bioeng.* **2006**, *95*, 1101−1107.
(18) Karoui, R.; Downey, G.; Blecker, Ch. Mid-infrared spectroscopy coupled with chemometrics: A tool for the analysis of intact food systems and the exploration of their molecular structure-quality relationships - A Review. *Chem. Rev.* **2010**, *110*, 6144−6168.
(19) Roumeliotis, S.; Logue, S. J.; Jefferies, S. P.; Barr, A. R. In *Near Infrared Spectroscopy: Proceedings of the 9th International Conference*; Davies, A. M. C., Giangiacomo, R., Eds.; NIR Publications: Chichester, U.K., 2000; pp 673−678.
(20) Roumeliotis, S.; Tansing, P. *Season barley quality report*; The University of Adelaide: Waite Campus, 2003.
(21) Cozzolino, D.; Roumeliotis, S.; Eglinton, J. Feasibility study on the use of attenuated total reflectance infrared spectroscopy as high throughput screening tool to phenotype single barley seeds (*Hordeum vulgare L.*). *Biosys. Eng.* **2013**, *116*, 379−384.
(22) Cozzolino, D.; Roumeliotis, S.; Eglinton, J. An attenuated total reflectance mid infrared (ATR-MIR) spectroscopy study of gelatinization in barley. *Carbohydr. Polym.* **2014**, *108*, 266−271.
(23) Adams, M. J. *Chemometrics in analytical spectroscopy*; Barnett, N. W., Eds.; The Royal Society of Chemistry: Cambridge, UK, 1995; 216 pp.
(24) Brereton, R. G. Introduction to multivariate calibration in analytical chemistry. *Analyst* **2000**, *125*, 2125−2154.
(25) Savitzky, A.; Golay, M. J. E. Smoothing and differentiation of data by simplified least squares procedures. *Anal. Chem.* **1964**, *36*, 1627−1639.
(26) MacWilliam, I. C. Wort composition—A review. *J. Inst. Brew.* **1968**, *74*, 38−54.
(27) Harris, Ph.; MacWilliam, I. C. Changes in the carbohydrates op barley during malting. *J. Inst. Brew.* **1954**, *60*, 149−157.
(28) MacLeod, A. M.; Travis, D. C.; Wreay, D. G. Studies on the free sugars of the barley grain III. changes in sugar content during malting. *J. Inst. Brew.* **1953**, *59*, 154−165.
(29) Woolard, G. R.; Rathbone, E. B.; Novellie, L. Studies on the free sugars, water-soluble gums and hemicelluloses from barley grains and malts. *J. Sci. Food Agric.* **1977**, *28*, 469−476.
(30) Harris, G.; Barton-Wright, E.-C. Carbohydrate composition of wort and some aspects of the biochemistry of fermentation. *J. Inst. Brew.* **1954**, *57*, 264.
(31) Vriesekoop, F.; Rathband, A.; MacKinlay, J.; Bryce, J. H. The evolution of dextrins during the mashing and fermentation of all-malt whisky production. *J. Inst. Brew.* **2010**, *116*, 230−238.
(32) Kemsley, E. K.; Zhuo, L.; Hammouri, M. K.; Wilson, R. H. Quantitative analysis of sugar solutions using infrared spectroscopy. *Food Chem.* **1992**, *44*, 299−302.
(33) Li, W.; Dobraszczyk, B. J.; Dias, A.; Gil, A. M. Polymer conformation structure of wheat proteins and gluten subtractions revealed by ATR-FTIR. *Cereal Chem.* **2006**, *83*, 407−410.
(34) Van de Weert, M.; Haris, P. I.; Hennink, W. E.; Crommelin, D. J. Fourier transform infrared spectrometric analysis of protein conformation: Effect of sampling method and stress factors. *Anal. Biochem.* **2001**, *297*, 160−169.
(35) Warren, F. J.; Perston, B. B.; Royall, P. G.; Butterworth, P. J.; Ellis, P. R. Infrared spectroscopy with heated attenuated total internal reflectance enabling precise measurement of thermally induced transitions in complex biological polymers. *Anal. Chem.* **2013**, *85*, 3999−4006.
(36) Goodfellow, B. J.; Wilson, R. H. A Fourier transform IR study of the gelation of amylose and amylopectin. *Biopolymers* **1990**, *30*, 1183−1189.
(37) Van Soest, J. J. G.; Tournois, H.; De Wit, D.; Vliegenthart, J. J. G. Short-range structure in (partially) crystalline potato starch determined with attenuated total reflectance Fourier transform IR spectroscopy. *Carbohydr. Res.* **1995**, *279*, 201−214.
(38) Stuart, B. *Modern infrared spectroscopy*; Ando, D. J., Eds.; Analytical Chemistry by Open Learning Series; John Wiley and Sons: Chichester, U.K., 1996; 180 pp.
(39) Cadet, F.; Offmann, B. Extraction of characteristic bands of sugars by multidimensional analysis of their infrared spectra. *Spectrosc. Lett.* **1996**, *29*, 523−526.
(40) Cadet, F.; Robert, Ch.; Offmann, B. Simultaneous determination of sugars by multivariate analysis applied to mid-infrared spectra of biological samples. *Appl. Spectros.* **1997**, *51*, 369−375.
(41) Sivakesava, S.; Irudayaraj, J. Determination of sugars in aqueous mixtures using mid-infrared spectroscopy. *Appl. Eng. Agric.* **2000**, *16*, 543−550.

technique to pear, it is hypothesized that this method could be applied as pear is a $C_3$ plant and its $^{13}C/^{12}C$ ratio is very similar to that of apple.[14] This technique is limited by its detection limit of approximately 10−15% for $C_4$-based sweeteners (e.g., HFCS) and its inability to detect the addition of beet sugar- or inulin-derived syrups as these are produced from $C_3$ (Jerusalem artichoke and chicory) and Crassulacean acid metabolism (CAM) pathway plants (agave), respectively.[10,15−17] In addition, this technique requires the use of specialized and expensive equipment that limits its routine application.

Another method for the detection of fruit juice adulteration is by oligosaccharide profiling. This technique works by identifying oligosaccharides that are present in the adulterants but are not naturally occurring in the product in question.[18] One of the benefits of this method is that it is a targeted approach; that is, it can be used to not only determine whether a product has been adulterated but also identify which adulterant was used. The two most common techniques used for oligosaccharide profiling are high-performance anion exchange chromatography with pulsed amperometric detection (HPAE-PAD) and capillary gas chromatography with flame ionization detection (CGC-FID). Both HPAE-PAD and CGC-FID methods have been developed and successfully used to detect the debasing of foods rich in carbohydrates such as agave syrup, honey, and maple syrup, as well as in select fruit juices such as apple and grapefruit.[19−23]

To date, no literature reports on the application or development of analytical techniques to detect the debasing of pear juice with less expensive nutritive sweeteners exist. Therefore, the primary goal of this research was to develop an analytical method employing oligosaccharide profiling that would be able to detect the debasing of pear juice at low concentrations (5−10%) with a series of commercially available carbohydrate syrups including HFCS, hydrolyzed inulin syrup (HIS), and total invert sugar (TIS) in a single chromatographic analysis. In addition, a secondary research goal was to expand the developed analytical method to detect select juice-to-juice adulteration (i.e., pear to apple) and to detect juices produced using a total fruit liquefaction process.

## MATERIALS AND METHODS

**Samples.** Thirty-two pure commercial pear juice concentrates (~70 °Brix) representing three production years (2012−2014) and five world production regions (Argentina, Chile, China, New Zealand, United States) were analyzed in this study. Commercial nutritive sweeteners used in this study as debasing agents (i.e., adulterants) included HFCS (HFCS 55 and HFCS 90; CASCO, Canada), HIS (Raffinerie Tirlemontoise S.A., Belgium), and TIS (Lantic Sugar Ltd., Canada).

**Chemicals.** Arbutin, D-fructose, D-glucose, $\beta$-glucosidase (from almond), isomaltose, maltoheptaose, maltohexaose, maltopentaose, maltose, maltotetraose, maltotriose, sodium hydroxide (NaOH) solution (50% w/w), D-sorbitol, D-sucrose, and Sylon TP (TMSI + pyridine, 1:4) were purchased from Sigma-Aldrich Canada Ltd. (Oakville, ON, Canada). Sodium acetate (NaOAc) was obtained from Fisher Scientific (Ottawa, ON, Canada). The water used throughout this study was obtained from a Millipore Milli-Q water system (Millipore Corp., Milford, MA, USA).

**Major Carbohydrate and Polyol Analysis by High-Performance Liquid Chromatography with Refractive Index Detection (HPLC-RI).** Major carbohydrate and polyol analysis was carried out employing an Agilent 1100 series HPLC system with a refractive index detector controlled by ChemStation LC-3D software (Agilent Technologies Canada Inc., Mississauga, ON, Canada). Samples were initially diluted to 12.0 ± 0.1 °Brix (Auto Abbe refractometer; Leica Inc., Buffalo, NY, USA) before being further diluted 1:1 with water. Samples were syringe filtered (nylon, 0.2 $\mu$m pore size; 13 mm diameter; Chromatographic Specialties, Brockville, ON, Canada) prior to analysis. Carbohydrate separation was accomplished on a Capcell-Pak-$NH_2$ column (250 × 4 mm, 5 $\mu$m; Phenomenex, Torrance, CA, USA) in series with a guard column (4 × 3 mm) of the same stationary phase. The mobile phase consisted of acetonitrile/water (75:25, v/v) run isocratically at a flow rate of 1.0 mL/min. The injection volume was 5.0 $\mu$L, and the column and RI detector were maintained at 25 and 35 °C, respectively. Standard curves for fructose, glucose, sorbitol, and sucrose were prepared in water at concentrations ranging from 0.06 to 5.00 g/100.00 mL. Standard curves had $R^2$ values of ≥0.999. All samples and standards were analyzed in triplicate.

**Arbutin Analysis by High-Performance Liquid Chromatography with Photodiode Array Detection (HPLC-PDA).** Samples were initially diluted with water to 12.0 ± 0.1 °Brix before being further diluted 1:1. Arbutin (4-hydroxyphenyl-$\beta$-D-glucopyranoside) content in the pear juice samples was determined employing HPLC with photodiode array (PDA) detection (Agilent Technologies Canada Inc.). Samples were syringe filtered prior to analysis. Arbutin separation from other sample phenolics was carried out employing an ODS-3 (250 × 4.6 mm; 5 $\mu$m $C_{18}$, 100 Å) column (Phenomenex) in series with a guard column (4 × 3 mm) of the same stationary phase. A gradient program employing aqueous 10 mM formic acid (pH 3.5; mobile phase A) and 70% acetonitrile/30% solvent A (v/v; mobile phase B) was used for arbutin separation as follows: initial 100% A for 3.0 min, followed by a linear gradient to 4.0% B at 6.0 min, followed by a linear gradient to 7.0% B at 15.5 min, followed by column washing with 100% B for 10.0 min prior to re-equilibration with 100% A. The flow rate was 0.8 mL/min, and the injection volume was 20.0 $\mu$L. Arbutin detection was afforded by PDA at a wavelength of 280 nm. A standard curve for arbutin prepared in water at concentrations ranging from 5.0 to 110.0 $\mu$g/mL was employed for quantification. Standard curves had $R^2$ values of ≥0.999. All samples and standards were analyzed in triplicate.

**Pure and Intentionally Adulterated Pear Juice Oligosaccharide and Arbutin Analysis by Capillary Gas Chromatography with Flame Ionization Detection (CGC-FID).** Pure pear juice concentrates and debasing agents were individually prepared by dilution with water to 5.5 ± 0.1 °Brix. For pure pear juice samples a 150 $\mu$L aliquot of each sample was freeze-dried (Heto Lab Equipment, Allerod, Denmark) in a 12 × 32 mm glass vial (Chromatographic Specialties) for 1 h. To the resulting dried foam was added 500 $\mu$L of Sylon TP using a gastight glass syringe, and the vials were capped and heated in a block heater (Denville Scientific Inc., Metuchen, NJ, USA) at 70 °C for 1 h with shaking every 10−15 min. Selected pear juice samples were intentionally adulterated with equivalent soluble solid content solutions of HFCS 55 and HFCS 90, HIS, and TIS at levels of 15.0, 10.0, 5.0, and 2.0% (v/v) and prepared as outlined previously. Sample oligosaccharide analysis was carried out using an Agilent 6890 gas chromatograph equipped with an Agilent 6890 series injector autosampler (Agilent Technologies Canada Inc.). Samples were analyzed in the splitless mode using ultrapure hydrogen as the carrier gas at a constant flow rate of 1.5 mL/min. Ultrapure nitrogen was used as the makeup gas at a flow rate of 30.0 mL/min. The injection port temperature was maintained at 250 °C and the detector at 300 °C. Oligosaccharide separation was afforded using an Agilent J&W DB-5 (95% dimethyl−5% diphenyl polysiloxane; 30 m × 0.25 mm, 0.25 $\mu$m film thickness) open tubular fused-silica capillary column (Chromatographic Specialties). The injection volume was 3.0 $\mu$L. Data acquisition and processing were carried out using Agilent ChemStation rev. A.06.03 software (Agilent Technologies Canada Inc.). The following temperature profile was used for oligosaccharide and arbutin analysis: initial temperature of 210 °C for 10.0 min; raised at 0.55 °C/min from 210 to 235 °C; held at 235 °C for 5.0 min; raised at 30 °C/min from 235 to 295 °C; held at 295 °C for 12.0 min. The total run time was 74.45 min. The minimum qualitative detection limit for arbutin was determined as the concentration that would give a peak height equivalent to 3 times the signal-to-noise ratio (s/n).

Table 1. Mean, Range, and Standard Deviation Results for Fructose, Glucose, Sucrose, Sorbitol, and Arbutin Concentrations and Fructose/Glucose Ratios in 32 Commercial Pear Juice Samples ($n$ = 3)

| sample | country of origin | fructose (g/100 mL) | glucose (g/100 mL) | sucrose (g/100 mL) | sorbitol (g/100 mL) | F/G ratio[a] | arbutin ($\mu$g/mL) |
|---|---|---|---|---|---|---|---|
| 1 | Argentina | 5.48 | 1.78 | 0.64 | 2.56 | 3.1 | 68.6 |
| 2 | Argentina | 5.41 | 1.92 | 0.56 | 2.57 | 2.8 | 70.3 |
| 3 | Argentina | 6.04 | 1.83 | 0.33 | 2.34 | 3.3 | 69.0 |
| 4 | Argentina | 5.57 | 1.92 | 0.60 | 2.55 | 2.9 | 68.4 |
| 5 | Argentina | 5.69 | 1.92 | 0.58 | 2.59 | 3.0 | 67.0 |
| 6 | Argentina | 5.47 | 1.71 | 0.50 | 2.41 | 3.2 | 66.1 |
| 7 | Argentina | 5.52 | 1.93 | 0.54 | 2.72 | 2.9 | 67.5 |
| 8 | Argentina | 5.54 | 1.94 | 0.59 | 2.79 | 2.9 | 69.3 |
| 9 | Argentina | 5.44 | 1.83 | 0.66 | 2.58 | 3.0 | 73.3 |
| 10 | Argentina | 5.58 | 1.77 | 0.54 | 2.53 | 3.2 | 62.1 |
| 11 | Argentina | 5.61 | 1.96 | 0.52 | 2.70 | 2.9 | 64.7 |
| 12 | Chile | 5.85 | 2.03 | 0.23 | 2.62 | 2.9 | 72.3 |
| 13 | Chile | 5.71 | 1.98 | 0.21 | 2.59 | 2.9 | 77.5 |
| 14 | Chile | 5.79 | 2.04 | 0.20 | 2.53 | 2.8 | 77.0 |
| 15 | Chile | 5.98 | 1.97 | 0.19 | 2.58 | 3.0 | 73.3 |
| 16 | Chile | 5.84 | 2.03 | 0.77 | 2.38 | 2.9 | 83.1 |
| 17 | Chile | 5.97 | 1.99 | 0.24 | 2.52 | 3.0 | 74.5 |
| 18 | Chile | 5.72 | 1.99 | 0.26 | 2.60 | 2.9 | 75.0 |
| 19 | China | 5.26 | 2.32 | 0.62 | 2.98 | 2.3 | 128.7 |
| 20 | China | 5.97 | 2.50 | 0.74 | 1.73 | 2.4 | 286.9 |
| 21 | China | 4.88 | 2.35 | 0.80 | 3.25 | 2.1 | 114.0 |
| 22 | China | 4.97 | 2.28 | 0.37 | 3.19 | 2.2 | 223.7 |
| 23 | New Zealand | 6.32 | 1.29 | 1.45 | 1.99 | 4.9 | 69.9 |
| 24 | New Zealand | 6.19 | 1.08 | 1.35 | 2.72 | 5.7 | 64.9 |
| 25 | New Zealand | 6.86 | 1.03 | 1.10 | 2.60 | 6.7 | 58.8 |
| 26 | New Zealand | 6.48 | 1.37 | 0.47 | 2.41 | 4.7 | 134.0 |
| 27 | New Zealand | 6.44 | 1.22 | 0.50 | 2.37 | 5.3 | 128.8 |
| 28 | USA | 5.80 | 1.80 | 0.68 | 2.51 | 3.2 | 53.7 |
| 29 | USA | 5.80 | 1.79 | 0.63 | 2.50 | 3.2 | 50.6 |
| 30 | USA | 5.79 | 1.76 | 0.55 | 2.44 | 3.3 | 60.7 |
| 31 | USA | 5.94 | 1.90 | 0.51 | 2.50 | 3.1 | 64.8 |
| 32 | USA | 5.92 | 1.83 | 0.52 | 2.54 | 3.2 | 57.1 |
| mean | | 5.78 | 1.85 | 0.58 | 2.56 | 3.3 | 86.7 |
| SD | | 0.41 | 0.34 | 0.29 | 0.28 | 1.0 | 49.6 |
| range | | 4.88−6.86 | 1.03−2.50 | 0.19−1.45 | 1.73−3.25 | 2.1−6.7 | 50.6−286.9 |

[a]Fructose-to-glucose ratio.

**Pure and Intentionally Adulterated Pear Juice Oligosaccharide and Arbutin Analysis by High-Performance Anion Exchange Chromatography with Pulsed Amperometric Detection (HPAE-PAD).** Pure pear juice samples and debasing agents were individually prepared by dilution with water to 5.5 ± 0.1 °Brix followed by syringe filtration. Select pear juice samples were intentionally adulterated with equivalent soluble solid content HFCS 55 and HFCS 90, HIS, and TIS solutions at levels of 20.0, 10.0, and 5.0% (v/v). For pear juice intentionally adulterated with HIS, a further dilution (1:3) with water was required. Sample oligosaccharide analysis was carried out on a Dionex Bio LC 4000 gradient HPLC system (Dionex Corp., Sunnyvale, CA, USA) containing a 50.0 $\mu$L sample loop. Carbohydrate separation was performed using two Dionex CarboPac PA1 (Thermo Fisher Scientific) columns (4 × 250 mm) connected in series without a guard column. The flow rate was 0.7 mL/min, and the carbohydrates were detected using a gold electrode employing triple-pulsed amperometry at a sensitivity of 10 K. The electrode was maintained at the following potentials and durations: $E_1$ = 0.05 V, $t_1$ = 120 ms; $E_2$ = 0.80 V, $t_2$ = 120 ms; $E_3$ = −0.60 V, $t_3$ = 420 ms. The gradient mobile phase consisted of 160 mM NaOH (mobile phase A), 160 mM NaOH/1 M NaOAc (mobile phase B), and 1 M NaOH (mobile phase C) with the following linear gradient elution program: initial conditions of 96.0% A and 4.0% B for 15.0 min; gradient to 70.0% A and 30.0% B at 41.0 min; 100% B from 41.1 to 44.0 min; 100% C from 44.1 to 48.0 min. The system was re-equilibrated at the initial conditions for 12.0 min prior to the next injection. Data acquisition and analysis was carried using Chromatography Data Station software (Wei Ma Long Chromatographic Techniques Ltd., Nanning, China).

**Arbutin Identification by Capillary Gas Chromatography−Mass Spectrometry (CG-MS).** Gas chromatographic conditions were as described above for CGC-FID analysis, with the exception of the use of ultrapure helium as the carrier gas. Mass spectrometry was carried out on a VG Analytical 70SE mass analyzer (VG Instruments Canada Inc., St. Laurent, QC, Canada) operated in the electron impact (EI) mode at an ionization energy of 70.0 eV. The source temperature was set at 200.0 °C. Measurements were carried out in full scan mode with scanning from $m/z$ 50.0 to 650.0. A solvent delay of 10.0 min was used. Samples of arbutin and select pure pear juices were prepared as outlined previously for CGC-FID analysis.

**Arbutin Hydrolysis with $\beta$-Glucosidase.** Three pure pear juices representing low (<64.9 $\mu$g/mL; PJ 28), medium (65.0−79.9 $\mu$g/mL; PJ 15), and high (>80.0 $\mu$g/mL; PJ 27) concentrations of arbutin were selected for analysis. These juice concentrates were diluted to 5.5 ± 0.1 °Brix, and approximately 10 U/mL of $\beta$-glucosidase was added to each sample. The solutions were stirred at ambient temperature, and samples were taken after 16 and 24 h. The enzyme reaction was

Table 2. Mean, Range, and Standard Deviation Results for Fructose, Glucose, Sucrose, and Sorbitol Concentrations and Fructose/Glucose Ratios in the Four Commercial Nutritive Sweeteners[a] Used in This Study ($n$ = 3)

| | fructose (g/100 mL) | glucose (g/100 mL) | sucrose (g/100 mL) | sorbtiol (g/100 mL) | F/G ratio[b] |
|---|---|---|---|---|---|
| HFCS 55 | 7.62 | 4.07 | nd[c] | nd | 1.9 |
| HFCS 90 | 10.99 | 0.81 | nd | nd | 13.5 |
| HIS | 8.21 | 2.54 | nd | nd | 3.2 |
| TIS | 5.16 | 5.58 | 1.29 | nd | 0.9 |

[a]HFCS, high-fructose corn syrup; HIS, hydrolyzed inulin syrup; TIS, total invert sugar. [b]Fructose-to-glucose ratio. [c]Not detected, <0.02 g/100 mL.

Table 3. Calculated[a] Fructose, Glucose, Sucrose, and Sorbitol Concentrations and Fructose/Glucose Ratios of Select Pear Juices (9 and 14) with the Four Debasing Agents

| | fructose (g/100 mL) | glucose (g/100 mL) | sucrose (g/100 mL) | sorbitol (g/100 mL) | F/G ratio[b] |
|---|---|---|---|---|---|
| PJ[c] 9 | 5.44 | 1.83 | 0.66 | 2.58 | 3.0 |
| PJ 9 + 30% HIS | 6.27 | 2.05 | 0.46 | 1.81 | 3.1 |
| PJ 14 | 5.79 | 2.04 | 0.20 | 2.53 | 2.8 |
| PJ 14 + 10% TIS | 5.73 | 2.40 | 0.31 | 2.27 | 2.4 |
| PJ 14 + 10% HFCS 90 | 6.31 | 1.92 | 0.18 | 2.27 | 3.3 |
| PJ 14 + 15% TIS + 15% HFCS 90 | 6.48 | 2.39 | 0.33 | 1.77 | 2.7 |

[a]Calculated amounts based on the analytically determined concentrations at equivalent soluble solids. [b]Fructose-to-glucose ratio. [c]PJ, pear juice.

quenched by placing the samples in boiling water for 5 min. Samples were syringe filtered and analyzed by CGC-FID and HPAE-PAD as outlined previously. Samples of the same juices without enzyme addition were also analyzed as controls.

**Preparation of a Multiply Adulterated Pear Juice Sample with Cellobiose.** A commercial pear juice concentrate (PJ 7) was diluted with water to 5.5 ± 0.1 °Brix; HFCS 55, HIS, and TIS (at the same °Brix) were added at levels of 10.0, 3.0, and 10.0% (v/v), respectively, and cellobiose was added to yield a final concentration of 50.0 ppm. The sample was then freeze-dried, derivatized, and analyzed by CGC-FID as described previously.

## RESULTS AND DISCUSSION

**Major Carbohydrate and Sorbitol Analysis.** The major carbohydrates and polyol in pear juice have been reported to be fructose, glucose, sucrose, and sorbitol, respectively.[7,8] Together, these compounds comprise >95% of the total soluble solids found in pear juice. The major carbohydrate/polyol composition plays an important role in the nutritional and sensory attributes of fruit juices such as pear. In addition, their concentrations and ratios have been used to determine the authenticity of a variety of fruit juices.[20]

The concentrations of fructose, glucose, sucrose, and sorbitol in the 32 commercial pear juice samples used in this study were determined by normal phase HPLC-RI. The mean, range, standard deviation, and fructose/glucose (F/G) ratio results for each of these major pear juice components are reported in Table 1. Comparisons of these values for each of the major carbohydrates were within the literature-reported ranges (adjusted to 12.0 °Brix) of 4.59−8.89% (w/v) for fructose, 0.76−3.90% (w/v) for glucose, and 0.18−3.70% (w/v) for sucrose.[7,8,20,21] The maximum concentration of 3.25% (w/v) observed for sorbitol in this study was greater than that reported in the literature for this compound of 2.96% (w/v).[7]

The observed high content and the wide natural concentration ranges for each of these carbohydrates and sorbitol make pear juice susceptible to adulteration through debasing with commercial sweeteners of lower economic value. Four commercial sweeteners, HFCS 55, HFCS 90, HIS, and TIS, were chosen as potential debasing agents for pear juice on the basis of both their lower economic value and their natural carbohydrate content. The major carbohydrate concentrations and F/G results for each of the commercial sweeteners used as debasing agents in this study are shown in Table 2. On the basis of these values, it is clear that the debasing of commercial pear juices analyzed in this study with any of the analyzed commercial sweeteners on their own or in combination at appreciable (15−30%) levels would not significantly change the major carbohydrate and sorbitol profiles present in the adulterated juices and would also maintain the industry standard final °Brix value (Table 3). As examples, (a) the addition of 30% HIS to a pear juice with average major carbohydrate and sorbitol concentrations (PJ 9) and (b) the additions of 10% TIS, 10% HFCS 90, or 15% TIS + 15% HFCS 90 to PJ 14 would all result in calculated final glucose, fructose, sucrose, and sorbitol concentrations that would fall within the natural ranges (Tables 1 and 3) for these compounds as determined in this study. These results show that the limiting factor in the amount of debasing agent that can be added without resulting in a value below the published minimum is the sorbitol concentration of the starting juice as none of the commonly used commercial sweeteners contain this compound. Therefore, unscrupulous producers may be able to disguise even higher amounts of debasing by the addition of exogenous sorbitol.

It has been suggested that the fructose-to-glucose ratio is a better indicator of pear juice authenticity as it is more constant than absolute concentrations.[8] As such, a fructose-to-glucose ratio of >2.7 with a lower limit of 2.4 has been proposed as the indicator for pear juice authenticity.[7] In this study, 28 of the 32 commercial pear juices showed fructose-to-glucose ratios >2.7; the remaining 4 samples, which had F/G ratios ranging from 2.1 to 2.4, originated from China. Of the four commercial sweeteners analyzed in this study, two (HFCS 90 and HIS) had fructose-to-glucose ratios greater than the lower limit for authentic pear juice of 2.4. As such, pear juice debasing with either of these commercial sweeteners would maintain the major carbohydrate and sorbitol levels within the natural range and would also result in F/G ratios >2.7. The same results would be observed if blends of debasing agents were used such as HIS/TIS, where a 7:1 ratio of these specific samples would result in a calculated F/G ratio of at least 2.7.

It should also be noted that three of the four samples from China (PJ 19, PJ 21, and PJ22) had sorbitol concentrations at the upper end of the natural sorbitol range as determined by this study (Table 1). This indicates that greater amounts of debasing can occur in these samples without their sorbitol concentration dropping below the lower natural sorbitol level. As well, all four of the Chinese pear juices had F/G ratios at or below the lower limit for authentic samples (2.4) due to high glucose concentrations and/or lower than average fructose concentrations (Table 1). This indicates that care must be taken to avoid false positives when the F/G ratio is applied for pear juice authenticity analysis, especially to samples originating from China or to samples of unknown origin.

On the basis of the potential issues previously discussed and the data presented in Table 3, it is clear that the untargeted approach to pear juice adulteration detection based on major carbohydrate and sorbitol concentrations, ranges, and select ratios (i.e., F/G) is not a reliable means for pear juice authenticity analysis and that there is a significant need for a more targeted approach to detect the debasing of this juice with common commercial sweeteners.

A more targeted approach to detecting the adulteration of foods rich in carbohydrates is oligosaccharide fingerprinting.[19−23] This method is based on the formation of oligosaccharides in commercial sweeteners by acid reversion and/or transglycosylation reactions that are unique to each of the identified debasing agents. On this premise, the natural oligosaccharide profiles of the 32 pure commercial pear juice concentrates and the 4 identified debasing agents used in this study were determined by CGC-FID and HPAE-PAD.

**Pear Juice Adulteration with High Fructose Corn Syrup.** High-fructose syrups are produced from a number of different starting materials throughout the world, including a variety of starches isolated from rice, wheat, tapioca, and potato.[24] However, the most common substrate used for the production of high-fructose syrups is corn starch.[24] The commercial production of HFCS from starch normally involves both acid and enzymatic hydrolyses. Starch is first treated with acid (typically hydrochloric acid) to produce a reduced-viscosity syrup with low amounts of reducing sugars (low dextrose equivalent, DE). This syrup is then treated with $\alpha$-amylase (EC 3.2.1.1), glucoamylase (EC 3.2.1.3), and glucose isomerase (xylose isomerase; EC 5.3.1.18).[18] $\alpha$-Amylase and glucoamylase are added first to break down the remaining starch into free glucose molecules forming a monosaccharide-rich syrup. Some of the glucose in this syrup is then isomerized to fructose using glucose isomerase.[24,25] Theoretically, the highest concentration of fructose possible from a typical glucose stream is 47% at equilibrium. However, most processing plants settle for yields around 42% (HFCS 42) due to the amount of enzyme and reaction time needed to produce higher fructose concentrations.[24] To achieve higher concentrations of fructose in the final product, the HFCS 42 syrup is fractionated using a cation exchange resin to separate fructose from glucose and other carbohydrates.[24] The fructose and glucose fractions are then blended in the appropriate proportions to obtain a product with the desired fructose concentration (e.g., HFCS 55 or HFCS 90).

During the production of high-fructose corn syrup a number of oligosaccharides are formed including maltose and isomaltose along with a variety of higher molecular weight glucose polymers.[18] The concentration of these oligosaccharides can be significant. For example, HFCS 42 and HFCS 55 have been reported to contain 5 and 3% oligosaccharides, respectively.[24] This is due to the incomplete hydrolysis of starch, as well as the lack of a debranching enzyme (i.e., isoamylase/pullulanse), which can hydrolyze the $\alpha$-(1→6) glycosidic bonds in starch.[18,25] It is also possible that oligosaccharide formation can occur via the transglycosylation activity of the carbohydrases employed in HFCS production. One method to detect the adulteration of pear juice with HFCS is to look for the presence of these oligosaccharides, which can act as a chemical fingerprint facilitating the identification of this sweetener. A CGC-FID method has been previously developed and successfully used for the detection of HFCS in apple juice at low levels via the detection of isomaltose.[26] However, when the published protocol/temperature program was applied to pear juice, it was found that this method either gave a false positive for HFCS due to the presence of naturally occurring compounds in pure pear juice, which eluted at retention times similar to that of isomaltose, or indicated that isomaltose was a natural constituent of pear juice. To test these hypotheses, a new CGC-FID carbohydrate temperature program was developed that separated the interfering compound(s) that coeluted with $\beta$-isomaltose. This clearly showed that isomaltose was not a natural constituent of pear juice and established that the debasing of pear juice with HFCS could be detected by oligosaccharide fingerprinting employing the developed temperature gradient program. These results are illustrated in Figure 1, where chromatogram A shows the CGC-FID carbohydrate profile of pure pear juice (PJ 7) and chromatogram B shows the same juice intentionally adulterated with 5.0% (v:v) HFCS 55. The ∗ symbol in Figure 1 corresponds to an unknown compound(s) that coelutes with $\alpha$-isomaltose, and the arrow identifies $\beta$-isomaltose with retention times (RT) of 51.6 and 57.5 min, respectively. As supported by the lack of both $\alpha$- and $\beta$-isomaltose peaks, isomaltose was not found in any of the analyzed pure pear juice samples at a detection limit of 6.5 ppm; therefore, its presence in pear juice would be indicative of adulteration with HFCS or a glucose/maltose syrup. Maltose is also formed during the production of HFCS and is a potential fingerprint compound for adulteration detection. However, under the temperature program conditions employed in this study maltose eluted in a region of the chromatogram where pear juice is naturally rich in compounds that interfered with its detection. The detection limit for HFCS 90 in pear juice by CGC-FID was determined to be 2.0% (v/v) on the basis of $\beta$-isomaltose detector response and the 3 times the signal-to-noise ratio detection limit used throughout this study. The concentration of isomaltose in HFCS 55 is >1.5 times that found in HFCS 90,[23] resulting in a lower detection limit (1.0%) for this commercial sweetener. The third sweetener in this class, HFCS 42, was not analyzed in this study due to the fact that its fructose to glucose ratio of approximately 0.7 is considerably lower than that observed in this study for pure pear juices at ≥2.1 and the other commercial sweeteners used in this research. In addition, HFCS 42 has been shown to contain higher concentrations of oligosaccharides such as isomaltose than either HFCS 90 or HFCS 55[24,27] making its undeclared addition to pear juice even easier to detect by the developed CGC-FID method.

The detection of intentionally added HFCS to pear juice by HPAE-PAD posed a significant challenge due to the high monosaccharide content of these samples, which obscured not only the isomaltose peak (RT = 8.5 min) but also that of maltose (RT = 15.2 min). However, the excellent resolving

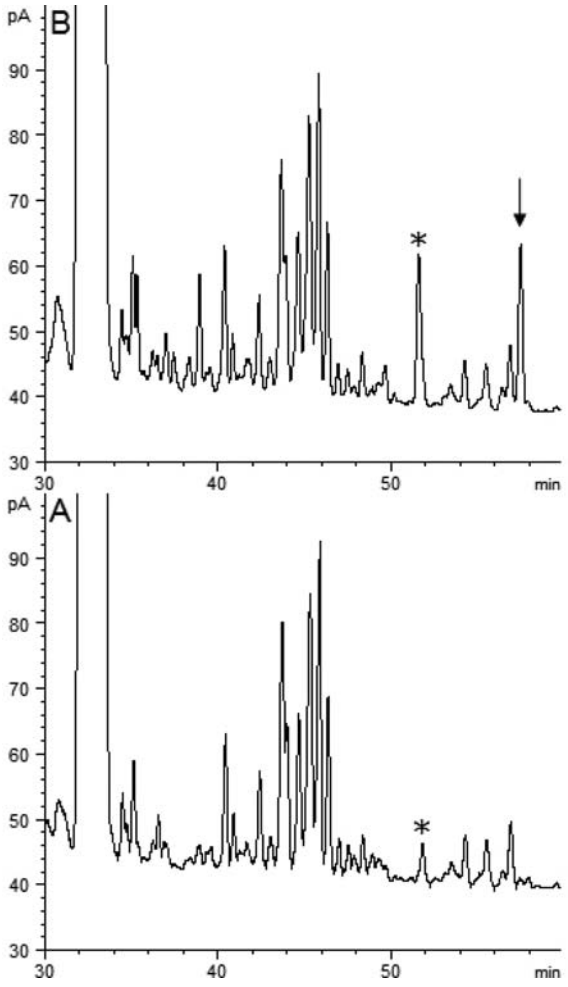


**Figure 1.** CGC-FID chromatograms from 30.0 to 60.0 min of (A) pure pear juice (PJ 7) and the same juice adulterated with (B) 5.0% (v/v) HFCS 55. The compound marked with ∗ corresponds to a naturally occurring oligosaccharide that coelutes with $\alpha$-isomaltose, and the arrow indicates $\beta$-isomaltose.

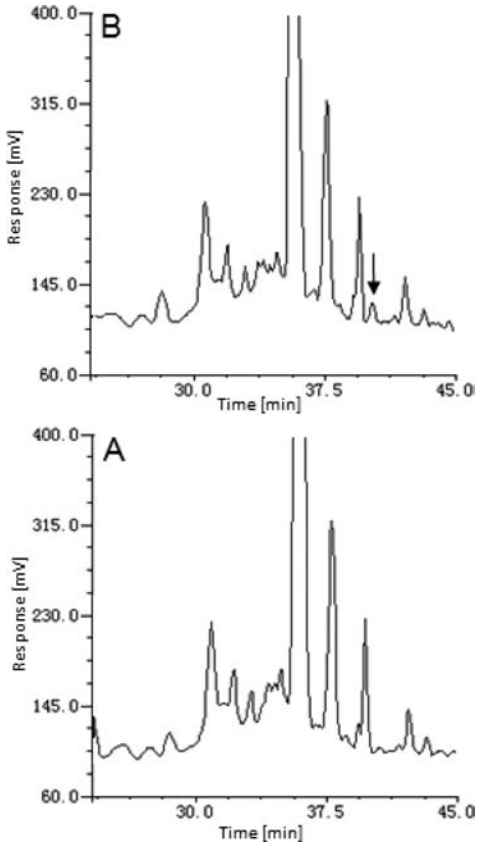


**Figure 2.** HPAE-PAD chromatograms from 22.0 to 45.0 min of (A) pure pear juice (PJ 23) at 5.5 °Brix and (B) the same pear juice intentionally adulterated with 10.0% (v/v) HFCS 55 at 5.5 °Brix. The fingerprint oligosaccharide tentatively identified as maltohexaose is indicated by an arrow.

power and low detection limits of high molecular weight glucose polymers by HPAE-PAD could readily detect the adulteration of pear juice with HFCS. These results are shown in Figure 2, where chromatogram A is of pure pear juice (PJ 23) and chromatogram B is the same pear juice intentionally adulterated with 10.0% (v/v) HFCS 55. We employed the peak eluting at approximately 40.2 min for adulteration detection on the basis of its relative intensity. This peak was tentatively identified as maltohexaose (DP 6) on the basis of retention time comparison to glucose polymer standards (DP 2−7; maltose to maltoheptaose) analyzed under the same conditions. Under the experimental conditions used in this study the detection limit for HFCS 55 by HPAE-PAD was determined to be 3.0% (v/v). Due to the fractionation and blending involved in the production of HFCS 90, the concentration of the DP6 marker is approximately 40−50% lower than in HFCS 55, resulting in a higher detection limit of 5.0% (v/v).

**Pear Juice Adulteration with Total Invert Sugar.** Invert sugar is produced from the treatment of beet or cane sucrose with either acid (typically hydrochloric acid) or invertase (EC 3.2.1.26), which hydrolyzes the glycosidic bond so as to yield equimolar amounts of glucose and fructose.[27] In industry, invert sugar is mainly produced using acid hydrolysis. Invert sugar can be produced to different degrees of inversion by controlling the time and temperature conditions used in its production.[28] Total invert sugar is produced when this reaction is allowed to proceed until only small amounts of sucrose remain (∼5−8%), resulting in a syrup containing a high concentrations of glucose and fructose in a 1:1 ratio.[25] During the production of invert sugar, oligosaccharides may be formed via a process known as reversion.[29] Three of these oligosaccharides have been previously identified as *O*-$\alpha$-D-glucopyranosyl-(1→3)-D-fructose, *O*-$\beta$-D-fructofuranosyl-(2→6)-D-glucose, and *O*-$\alpha$-D-glucopyranosyl-$\beta$-D-glucopyranoside.[28]

Total invert sugar was selected as a potential adulterant in pear juice due to its low level of sucrose as compared to medium invert sugar, which has a glucose to fructose to sucrose ratio of 1:1:2.[25] This means that the addition of medium invert sugar to pear juice should be detectable by a noticeable change in the glucose/fructose/sucrose ratios of the juice. The debasing of pear juice with TIS was readily detected employing the developed CGC-FID method and is illustrated in Figure 3, where chromatogram A shows the CGC-FID carbohydrate profile of pure pear juice (PJ 7) and chromatogram B shows the same juice intentionally adulterated with 10.0% (v/v) TIS. The fingerprint oligosaccharides for TIS detection have retention times of approximately 41.9 and 49.7 min, respectively. The peak eluting at 49.7 min was tentatively identified as IS2 (*O*-$\beta$-D-fructofuranosyl-(2→6)-D-glucose) on the basis of literature results,[3,28] whereas the peak at 41.9 min is currently unidentified. The detection limit for TIS addition to pear

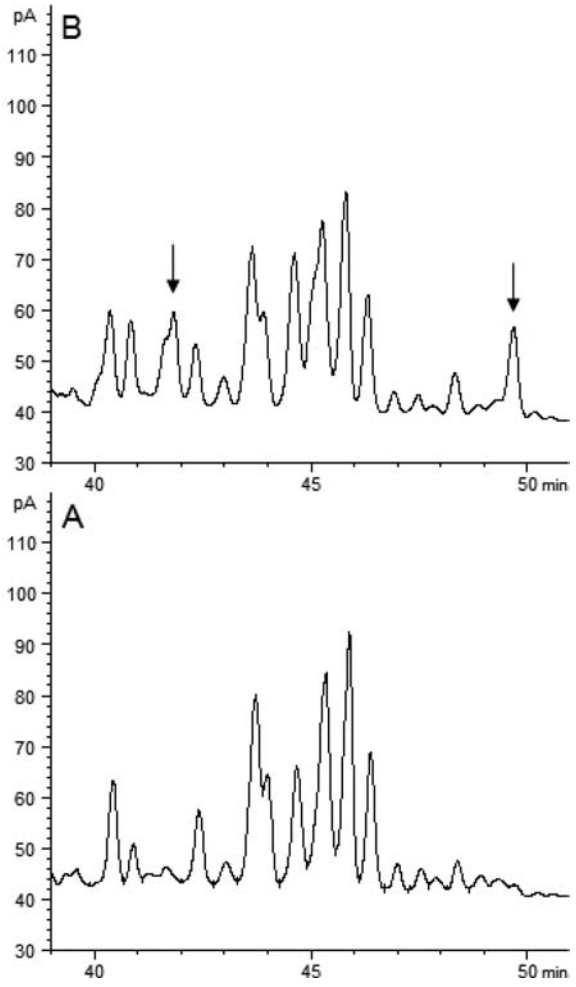


**Figure 3.** CGC-FID chromatograms from 39.0 to 51.0 min of (A) pure pear juice (PJ 7) and (B) the same pear juice intentionally adulterated with 10.0% (v/v) TIS. The fingerprint oligosaccharides tentatively identified as IS2 (*O*-$\beta$-D-fructofuranosyl-(2→6)-D-glucose) and an unknown compound are indicated by arrows.

juice by the developed CGC-FID method was found to be 3.0% (v/v).

Pear juice samples intentionally adulterated with TIS were also analyzed by the developed HPAE-PAD method. Unfortunately, the presence of naturally occurring oligosaccharides and the high concentration of monosaccharides in pure pear juice samples precluded the use of this technique to detect pear juice adulterated with TIS.

**Pear Juice Adulteration with Hydrolyzed Inulin Syrup.** Inulin is a naturally occurring polysaccharide found in plants and some bacterial and fungal species.[30] It is a mostly linear polysaccharide of varying chain length composed of fructose units glycosidically linked by $\beta$-(2→1)-D-fructosyl-fructose units terminated by D-glucose linked via an $\alpha$-(2→1) bond as in sucrose.[31,32] HIS is produced by the controlled enzymatic or acid (typically hydrochloric) hydrolysis of inulin. This results in the production of a syrup that is rich in fructose with minor amounts of glucose present.[33] It has been reported that the hydrolysis of inulin can result in the formation of a variety of different oligosaccharides, which consist either solely of fructose units (inulo-oligosaccharides) or of fructose units linked with a terminal glucose unit (fructo-oligosaccharides).[32]

CGC-FID oligosaccharide profiling of HIS shows the presence of two fingerprint oligosaccharides with retention times of approximately 21.5 and 34.9 min, respectively. When HIS is added to pear juice, the peak at 34.9 min was masked by the naturally occurring oligosaccharides; however, the peak at 21.5 min eluted in a region devoid of interfering compounds. These results are illustrated in Figure 4, where chromatogram A

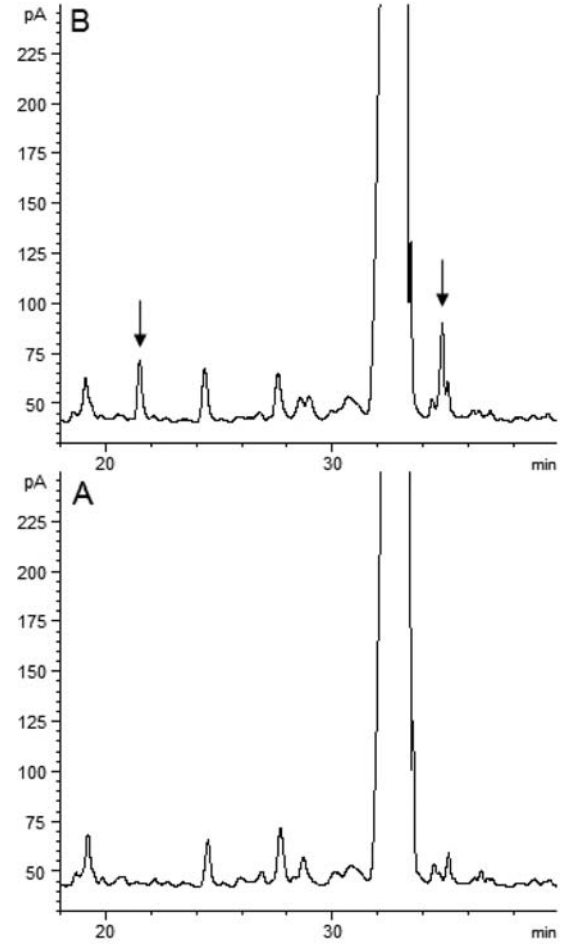


**Figure 4.** CGC-FID chromatograms from 18.0 to 40.0 min of (A) pure pear juice (PJ 7) and (B) the same pear juice intentionally adulterated with 2.0% (v/v) HIS. The fingerprint oligosaccharides tentatively identified as $\alpha$- and $\beta$-inulobiose are indicated by arrows.

shows the CGC-FID carbohydrate profile of pure pear juice (PJ 7) and chromatogram B shows the same juice intentionally adulterated with 2.0% (v/v) HIS. This fingerprint oligosaccharide for HIS is postulated to be a carbohydrate composed of two fructose moieties (i.e., disaccharide) based on inulin structure and hydrolysis and its elution time, which occurs in the typical range for disaccharides.[34] This oligosaccharide has been tentatively identified as inulobiose (*O*-$\beta$-D-fructofuranosyl-(2→1)-D-fructose), a disaccharide commonly reported to be formed during the hydrolysis of inulin, on the basis of both literature results and HPAE-PAD analysis of standards (unpublished results). Supporting evidence for this identification is based on the inulin source used in this study, which was chicory root, which has been reported to contain low amounts of branching (1−2%) when compared to other sources (e.g., bacterial; branching >15%).[33] The detection limit for HIS

addition to pear juice by the developed CGC-FID method was found to be 0.5% (v/v).

Pear juice samples intentionally adulterated with HIS were also analyzed by the developed HPAE-PAD method. A fingerprint oligosaccharide with a retention time of ∼17.5 min was readily identified when HIS was intentionally added to pure pear juice. The application of this method to a pure pear juice (PJ 23; chromatogram A) and the same pear juice intentionally adulterated with 5.0 and 10.0% (v/v) HIS (chromatograms B and C) is shown in Figure 5. The detection limit for HIS addition to pear juice by the developed HPAE-PAD method was found to be 2.0% (v/v).

**Detection of Juice-to-Juice Adulteration by Arbutin Analysis.** The developed chromatographic techniques were examined for their potential to detect types of adulteration besides debasing with less expensive commercial sweeteners. One common method of fruit juice adulteration is the addition of a juice of lesser value to one of higher value. This type of adulteration is referred to as juice-to-juice debasing. Due to the fact that apple and pear juices share similarities in properties such as major carbohydrate and polyol profiles, juice-to-juice adulteration between these two can be a significant problem as it is difficult to detect using traditional methods such as the matrix approach.[7] Arbutin (4-hydroxyphenyl-$\beta$-D-glucopyranoside) has been previously identified as a natural constituent of pear juice that is not found in apple juice.[7] It was found that arbutin could be detected by both of the developed chromatographic methods (i.e., CGC-FID and HPAE-PAD). The presence of arbutin was confirmed in all 32 pure pear juice concentrates by both CGC-FID and HPAE-PAD with retention times of 27.6 and 37.8 min, respectively.

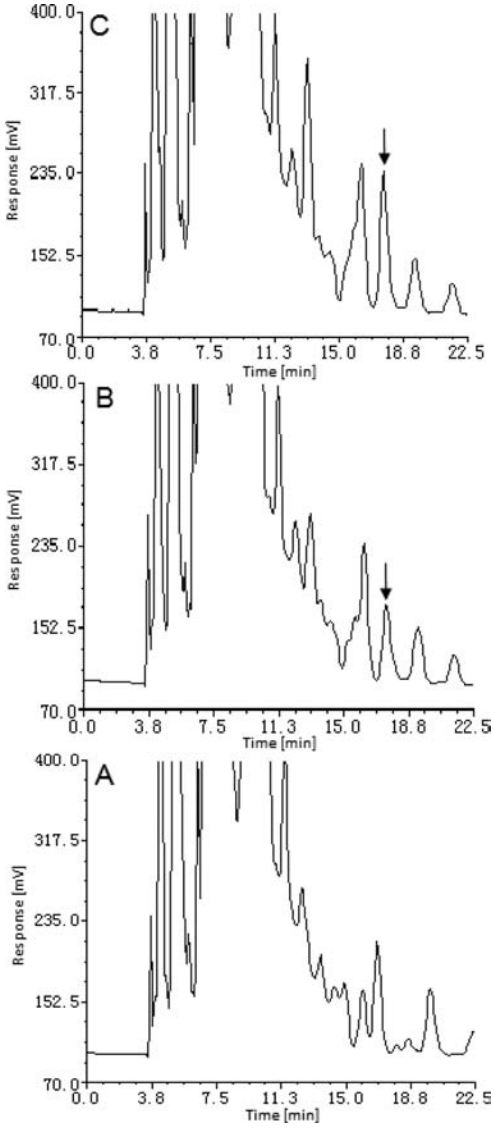


**Figure 5.** HPAE-PAD chromatograms from 0.0 to 22.5 min of (A) pure pear juice (PJ 23) and the same pear juice intentionally adulterated with (B) 5.0% and (C) 10.0% (v/v) HIS. The fingerprint oligosaccharide tentatively identified as inulobiose is indicated by an arrow.

GC-MS was carried out to confirm that the peak observed by CGC-FID corresponded to arbutin and not another compound with a similar retention time. The mass spectra of the silylated arbutin standard and the peak with the matching retention time in pear juice showed good agreement. The spectrum was also matched against those found in the National Institute of Standards and Technology (NIST) Mass Spectral Library as well as with literature data.[35,36] Figure 6 shows the mass spectra of silylated arbutin as found under these conditions. As can be seen, no fragments greater than a mass-to-charge ($m/z$) ratio of 450 were observed even though silylated arbutin has a molecular weight of 632 g/mol. This indicates that the molecular ion readily fragments under the conditions used in this study. Currently, there is only one literature report in which the identities of any of the observed fragments are suggested.[35] However, the authors do not give detailed structures of the proposed fragments and fail to identify a major fragment ($m/z$ 254). As well, the fragment at $m/z$ 217 is clearly misidentified as the proposed structure has an $m/z$ value of only 130. Therefore, more work in this area is needed. A number of the fragments were tentatively identified in this study and are shown in Figure 7.

Loss of the hydroquinone portion of arbutin as a neutral species results in the formation of the fragment at $m/z$ 450 with further fragmentation by loss of trimethylsilyl (TMS) groups and by ring cleavage. This type of behavior has been previously reported for TMS-derivatized glucose during analysis by CG-MS.[37] As well, a structure for the fragment observed at $m/z$ 254 has been suggested. The fragments at $m/z$ 147 (TMS-O-DMS) and $m/z$ 73 (TMS) have been previously identified and are characteristic of trimethylsilylated compounds.[35,37]

A second method was also applied to confirm the presence of arbutin in the pear juice samples. In this method $\beta$-glucosidase (EC 3.2.1.21) was added to select pear juice samples, which resulted in the hydrolysis of arbutin to free D-glucose and hydroquinone. As expected, this hydrolysis resulted in a disappearance of the arbutin peak as observed by both CGC-FID and HPAE-PAD. The use of $\beta$-glucosidase for arbutin identification is beneficial as it is simple to carry out and allows confirmation of the presence of arbutin by both CGC-FID and HPAE-PAD without the use of a mass spectrometer.

The concentration of arbutin in the pure samples was analyzed by HPLC-PDA to determine how effective this compound would be for adulteration detection. The average arbutin content of the 32 samples was found to be 86.7 ± 49.6 $\mu$g/mL with a range of 50.6−286.9 $\mu$g/mL (Table 1). The experimental average was found to be higher than the average arbutin content reported for a similar set of samples of 75.5 $\mu$g/mL (after adjustment to 12.0 °Brix).[7] This is likely due to the

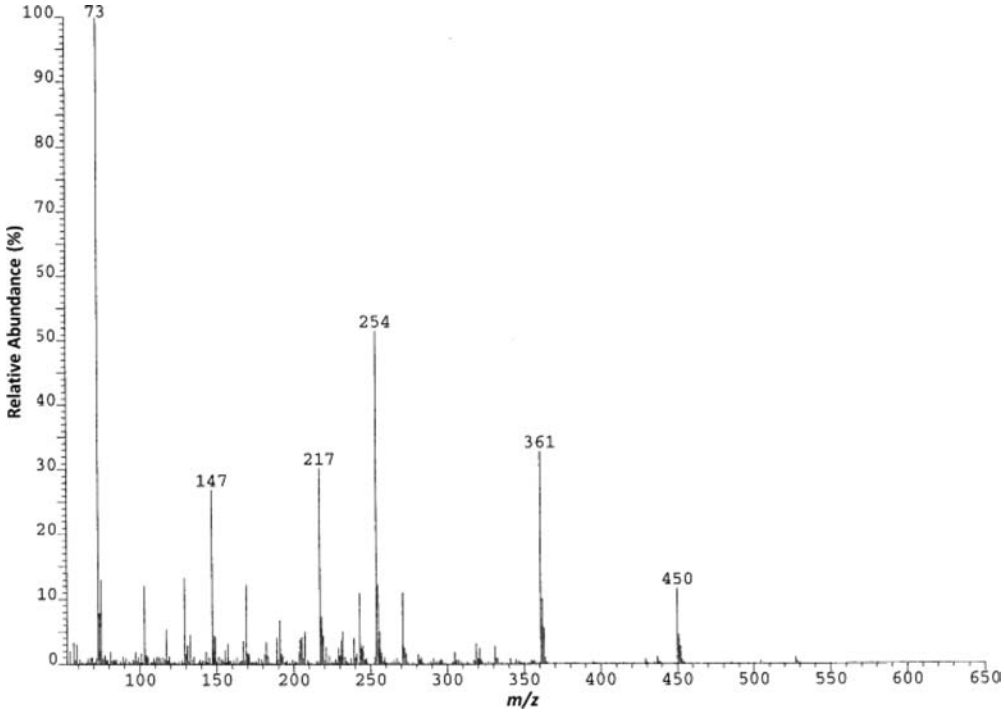


**Figure 6.** CG-MS spectra of silylated arbutin in pear juice.

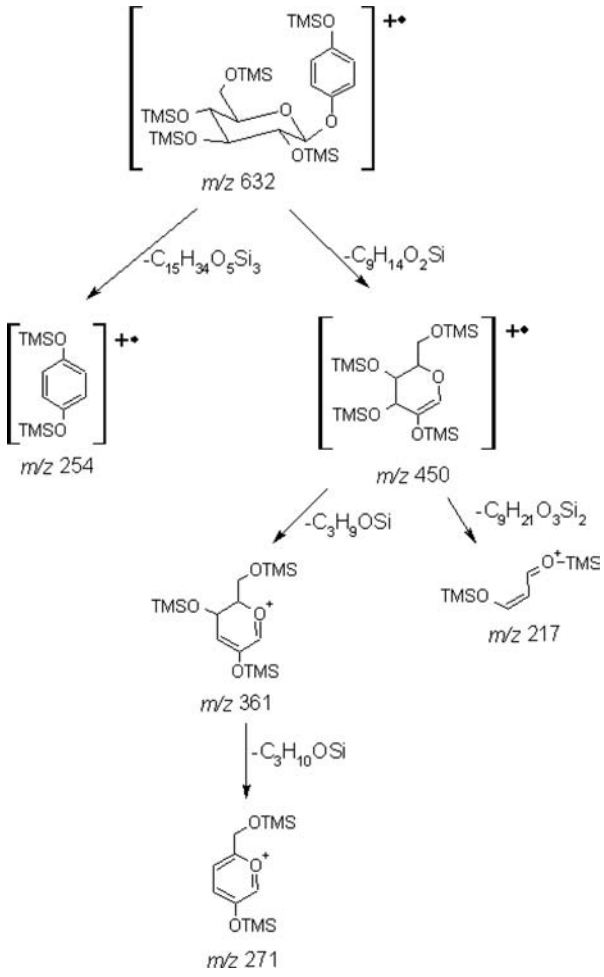


**Figure 7.** Proposed fragments of silylated arbutin under CG-MS condtions. TMS, $-Si(CH_3)_3$.

presence of six samples with arbutin contents >100.0 μg/mL in the present study. Of these six samples, four were obtained from China and two from New Zealand. The arbutin content in all of the remaining 26 pear juice samples was <85.0 μg/mL.

A literature range for pear arbutin content has been reported as 42.3−157.7 μg/mL, which is in agreement with the arbutin values obtained in this study with the exception of PJ 20 and PJ 22, which had concentrations of 223.7 and 286.9 μg/mL, respectively.[7] On the basis of the pear juice sample in this study with the lowest concentration of arbutin and a detection level of 3 times the signal-to-noise ratio, the addition of pear juice to apple juice can be detected at levels down to 3.0% (v/v). This detection limit would be even lower if a pear juice rich in arbutin was used to adulterate a sample. As well, it may be possible to lower this detection limit even further by the application of CG-MS for arbutin detection due to the increased sensitivity of this method.

Arbutin also shows the potential of acting as an indicator for pear juice authenticity. The absence of arbutin in a product claiming to contain pear would be a good indication that pear juice is not actually present in the product. As well, if a sample claiming to be a pure pear juice contains arbutin in concentrations considerably lower than those reported for authentic pear juice, it is likely that the sample is not pure and that further authenticity analysis needs to be undertaken.

**Detection of Total Liquefaction by Cellobiose Detection.** The production of pear and apple juice is aided by the use of enzymes, such as pectinases and amylases, which aid in cell wall breakdown, improving juice extraction and filtration.[38] Total liquefaction involves the addition of cellulases and excess pectinases to the fruit mash to achieve a more complete breakdown of the cell walls, resulting in an increase in the total soluble solids of the final juice.[39] This process is illegal in both North America and the European Union as there are no regulatory guidelines in place for cellulase use in fruit juice production and because little is known about the nutritional

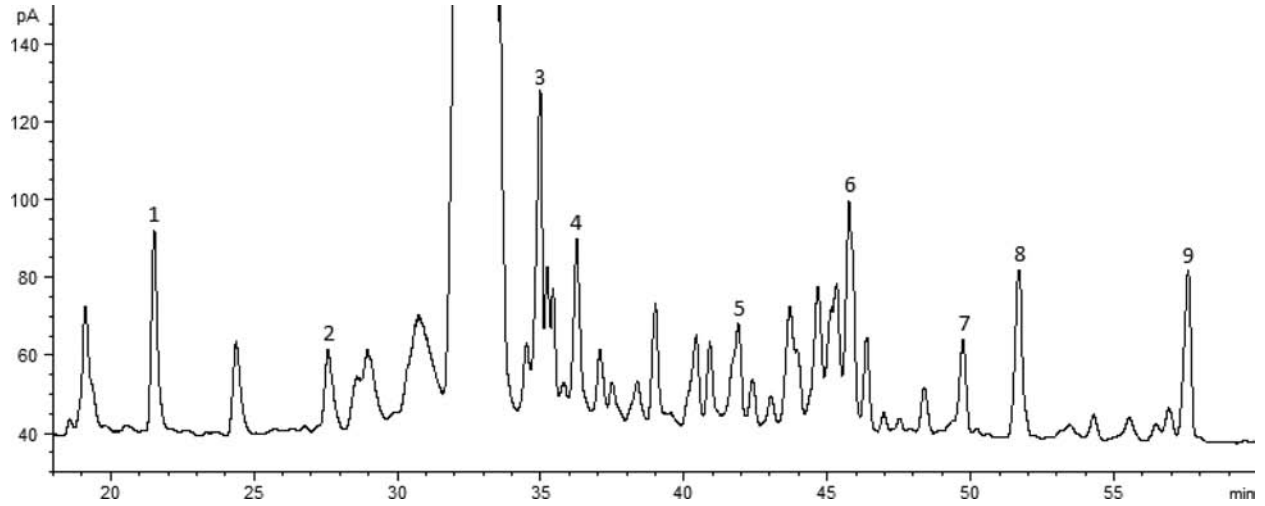


**Figure 8.** CGC-FID chromatogram of pear juice (PJ 7) to which HFCS 55, HIS, TIS, and cellobiose have been added. Identified peaks are as follows: 1, $\alpha$-inulobiose (HIS marker); 2, arbutin (pear marker); 3, $\beta$-inulobiose (HIS marker); 4, $\alpha$-cellobiose (liquefaction marker); 5, unidentified TIS marker; 6, $\beta$-cellobiose; 7, *O*-$\beta$-D-fructofuranosyl-(2→6)-D-glucose (TIS marker); 8, $\alpha$-isomaltose; 9, $\beta$-isomaltose (HFCS marker).

aspects of the liquefaction juice.[39,40] It should also be noted that total liquefaction leads to a lower quality juice with an increased propensity to browning and haze formation.[39] The undeclared substitution or blending of a premium juice with a juice of lower quality produced by liquefaction constitutes adulteration and would be considered illegal. Consequently, it is important to be able to distinguish between juices produced by these different methods.

Cellobiose, a disaccharide composed of two glucose units linked via a $\beta$-(1→4) glycosidic bond, is formed by the breakdown of cellulose found in the cell wall of fruits when cellulases are used for juice production. In one study, cellobiose was not found in apple juices produced using normal enzymatic treatments (premium juice), but was detected in three of four juices produced by total liquefaction at concentrations ranging from 16.6 to 55.4 ppm.[41] The presence of cellobiose, in combination with excess galacturonic acid, is considered to be indicative of pomace liquefaction by the fruit juice industry.[41] Currently, no official limits exist on the concentration of cellobiose in pear and apple juices.[41]

The developed CGC-FID method was shown to be able to effectively separate and detect cellobiose in pear juice. As it is a reducing carbohydrate, cellobiose has two chromatographic peaks at 36.2 and 45.8 min, corresponding to $\alpha$- and $\beta$-cellobiose, respectively. Whereas $\beta$-cellobiose overlaps with naturally occurring pear compounds, $\alpha$-cellobiose is free of such interferences. When analyzed by HPAE-PAD, the high monosaccharide content of pear juice obscured the cellobiose peak (RT = 10.4 min), precluding the use of this method for total liquefaction detection.

Cellobiose was not detected by CGC-FID in any of the 32 pure pear juice concentrates analyzed in this study at a detection limit of 8.0 ppm in the 12.0 °Brix juice by the developed analytical method, clearly indicating that these juices were not produced by total liquefaction.

In summary, these results show that the addition of less expensive nutritive sweeteners, namely, HFCS, HIS, and TIS, can be readily detected in pear juice by the application of the developed CGC-FID method at levels of 0.5−3.0% (v/v). In addition, HPAE-PAD profiling can also be used to confirm the presence of HFCS and HIS in pear juice. CGC-FID fingerprinting also affords the detection of pear to apple (and potentially apple to pear) juice debasing and process adulteration all within a single chromatographic analysis. Figure 8 shows the CGC-FID chromatogram of pear juice to which the studied pear juice adulterants (HFCS, HIS/ and TIS) and cellobiose have been added. The ability to detect each of these adulterants at low concentrations, arbutin (to confirm the presence or absence of pear), and cellobiose (indicator of liquefaction processing) in a single chromatographic run is beneficial as it is both a robust and accurate method and reduces sample preparation and analysis time. In addition, the use of the developed method not only allows an adulterated sample to be identified but also provides information on the adulterant used. It is envisaged that this method will result in a decrease in food fraud so as to maintain consumer confidence in the food industry.

## AUTHOR INFORMATION

### Corresponding Author

*(N.H.L.) Phone: (306) 966-5037. Fax: (306) 966-8898. E-mail: nicholas.low@usask.ca.

### Notes

The authors declare no competing financial interest.

## ABBREVIATIONS USED

CGC-FID, capillary gas chromatography with flame ionization detection; G/F ratio, glucose-to-fructose ratio; HFCS, high-fructose corn syrup; HIS, hydrolyzed inulin syrup; HPAE-PAD, high-performance anion exchange chromatography with pulsed amperometric detection; IS2, *O*-$\beta$-D-fructofuranosyl-(2→6)-D-glucose; TIS, total invert sugar

## REFERENCES

(1) Food and Agricultural Organization of the United Nations, FAOSTAT. http://faostat3.fao.org/faostat-gateway/go/to/home/E (accessed April 7, 2014).

(2) Fresh deciduous fruit (apples, grapes, and pears): world markets and trade. USDA, Foreign Agricultural Services, December 2012.

(3) Thavarajah, P. *Isolation, Structural Determination and Mechanism of Formation of Oligosaccharides in Total Invert Sugar; Phenolic Fingerprinting for Apple and Pear Juice Adulteration Detection*. Ph.D. thesis, University of Saskatchewan, Saskatoon, SK, Canada, 2004.

(4) Ginsberg's Foods. February 2014 Market Conditions Report. http://www.ginsbergs.com/resources/market-conditions/february-2014-market-conditions-report/ (accessed May 29, 2014).
(5) Tree Top Fruit Ingredients. Fruit Crop Update. http://foodingredients.treetop.com/crop-information/field-report (accessed May 29, 2014).
(6) Bates, R. P.; Morris, J. R.; Crandall, P. G. *Principles and Practices of Small- and Medium-Scale Fruit Juice Processing*; FAO Agricultural Services Bulletin; Rome, Italy, 2001.
(7) Thavarajah, P.; Low, N. H. Adulteration of apple with pear juice: emphasis on major carbohydrates, proline and arbutin. *J. Agric. Food Chem.* **2006**, *54*, 4861−4867.
(8) Wallrauch, S.; Faethe, W. Germany: RSK values − guidelines and tolerances for specified constituents in fruit juice. In *Adulteration of Fruit Juices Beverages*; Nagy, S., Attaway, J. A., Rhodes, M. E., Eds.; Dekker: New York, 1988; pp 405−470.
(9) Perez, A. L.; Smith, B. W.; Anderson, K. A. Stable isotope and trace element profiling combined with classification models to differentiate geographic growing origin for three fruits: effects of subregion and variety. *J. Agric. Food Chem.* **2006**, *54*, 4506−4516.
(10) Krueger, D. A. Applications of stable isotope ratio analysis to problems of fruit juice adulteration. In *Adulteration of Fruit Juices Beverages*; Nagy, S., Attaway, J. A., Rhodes, M. E., Eds.; Dekker: New York, 1988; pp 109−124.
(11) Reid, L. M.; O'Donnell, C. P.; Downey, G. Recent technological advances for the determination of food authenticity. *Trends Food Sci. Technol.* **2006**, *17*, 344−353.
(12) Doner, L. W. Application of natural variations in $^{13}C/^{12}C$ ratios to detect adulteration of orange, lemon, and apple juices. In *Adulteration of Fruit Juices Beverages*; Nagy, S., Attaway, J. A., Rhodes, M. E., Eds.; Dekker: New York, 1988; pp 125−138.
(13) Pupin, A. M.; Dennis, M. J.; Parker, I.; Kelly, S.; Bigwood, T.; Toledo, M. C. F. Use of isotopic analyses to determine the authenticity of Brazilian orange juice (*Citrus sinensis*). *J. Agric. Food Chem.* **1998**, *46*, 1369−1373.
(14) Krueger, D. A. Stable isotope analysis by mass spectrometry. In *Analytical Methods of Food Authentication*; Ashurst, P. R., Dennis, M. J., Eds.; Blackie Academic & Professional: London, UK, 1998; pp 14−29.
(15) Kelly, J. F. D.; Downey, G. Detection of sugar adulterants in apple juice using fourier transform infrared spectroscopy and chemometrics. *J. Agric. Food Chem.* **2005**, *53*, 3281−3286.
(16) Nobel, P. S.; Hartsock, T. L. Resistance analysis of nocturnal carbon dioxide by a Crassulacean acid metabolism succulent *Agave deserti*. *Plant Physiol.* **1978**, *61*, 510−514.
(17) Yan, K.; Chen, P.; Shao, H.; Zhao, S.; Zhang, L.; Zhang, L.; Xu, G.; Sun, J. Photosynthetic characterization of Jerusalem artichoke during leaf expansion. *Acta Physiol. Plant.* **2012**, *34*, 353−360.
(18) Low, N. Oligosaccharide analysis. In *Analytical Methods of Food Authentication*; Ashurst, P. R., Dennis, M. J., Eds.; Blackie Academic & Professional: London, UK, 1998; pp 97−136.
(19) Low, N. H.; McLaughlin, M.; Hofsommer, H.; Hammond, D. A. Capillary gas chromatography detection of invert sugar in heated, adulterated, and adulterated and heated apple juice concentrates employing the equilibrium method. *J. Agric. Food Chem.* **1999**, *47*, 4261−4266.
(20) Low, N. H.; Wudrich, G. G. Detection of inexpensive sweetener addition to grapefruit juice by HPLC-PAD. *J. Agric. Food Chem.* **1993**, *41*, 902−909.
(21) Morales, V.; Corzo, N.; Sanz, M. L. HPAEC-PAD oligosaccharide analysis to detect adulterations of honey with sugar syrups. *Food Chem.* **2008**, *107*, 922−928.
(22) Stuckel, J. G.; Low, N. H. Maple syrup authenticity analysis by anion-exchange liquid chromatography with pulsed amperometric detection. *J. Agric. Food Chem.* **1995**, *43*, 3046−3051.
(23) Willems, J. L.; Low, N. H. Major carbohydrate, polyol, and oligosaccharide profiles of agave syrup. Application of this data to authenticity analysis. *J. Agric. Food Chem.* **2012**, *60*, 8745−8754.
(24) Hanover, L. M.; White, J. S. Manufacturing, consumption, and applications of fructose. *Am. J. Clin. Nutr.* **1993**, *58*, 724S−732S.
(25) Low, N. H. Food authenticity analysis by high performance anion exchange chromatography with pulsed amperometric detection. *Semin. Food Anal.* **1997**, *2*, 55−70.
(26) Low, N. H.; McLaughlin, M. A.; Page, S. W. Identification of hydrolyzed inulin syrup and high-fructose corn syrup in apple juice by capillary gas chromatography. *J. AOAC Int.* **2001**, *84*, 486−492.
(27) White, J. S. Straight talk about high-fructose corn syrup: what it is and what it ain't. *Am. J. Clin. Nutr.* **2008**, *88*, 1716S−1721S.
(28) Thavarajah, P.; Low, N. H. Isolation and identification of select oligosaccharides from commercially produced total invert sugar with a proposed mechanism for their formation. *J. Agric. Food Chem.* **2006**, *54*, 2754−2760.
(29) Swallow, K. W.; Low, N. H. Isolation and identification of oligosaccharides in a commercial beet medium invert sugar. *J. Agric. Food Chem.* **1993**, *41*, 1587−1592.
(30) Franck, A. Technological functionality of inulin and oligofructose. *Br. J. Nutr.* **2002**, *87*, S287−S291.
(31) Borromei, C.; Cavazza, A.; Merusi, C.; Corrandini, C. Characterization and quantitation of short-chain fructooligosaccharides and inulooligosaccharides in fermented milks by high-performance anion-exchange chromatography with pulsed amperometric detection. *J. Sep. Sci.* **2009**, *32*, 3635−3642.
(32) Ronkart, S. N.; Blecker, C. S.; Fourmanoir, H.; Fougnies, C.; Deroanne, C.; Van Herck, J. C.; Paquot, M. Isolation and identification of inulooligosaccharides resulting from inulin hydrolysis. *Anal. Chim. Acta* **2007**, *606*, 81−87.
(33) Ricca, E.; Calabrò, V.; Curcio, S.; Iorio, G. The state of the art in the production of fructose from inulin enzymatic hydrolysis. *Crit. Rev. Biotechnol.* **2007**, *27*, 129−145.
(34) Low, N. H.; Sporns, P. Analysis and quantitation of minor di- and trisaccharides in honey, using capillary gas chromatography. *J. Food Sci.* **1988**, *53*, 558−561.
(35) Chisvert, A.; Sisternes, J.; Balaguer, Á.; Salvador, A. A gas chromatography-mass spectrometric method to determine skin-whitening agents in cosmetic products. *Talanta* **2010**, *81*, 530−536.
(36) Lamien-Meda, A.; Lukas, B.; Schmiderer, C.; Franz, C.; Novak, J. Validation of a quantitative assay of arbutin using gas chromatography in *Origanum majorana* and *Arctostaphylos uva-ursi* extracts. *Phytochem. Anal.* **2009**, *20*, 416−420.
(37) DeJongh, D. C.; Radford, T.; Hribar, J. D.; Hanessian, S.; Bieber, M.; Dawson, G.; Sweeley, C. C. Analysis of trimethylsilyl derivatives of carbohydrates by gas chromatography and mass spectrometry. *J. Am. Chem. Soc.* **1969**, *91*, 1728−1740.
(38) Kashyap, D. R.; Vohra, P. K.; Chopra, S.; Tewari, R. Applications of pectinases in the commercial sector: a review. *Bioresour. Technol.* **2001**, *77*, 215−277.
(39) Mehrländer, K.; Dietrich, H.; Sembries, S.; Dongowski, G.; Will, F. Structural characterization of oligosaccharides and polysaccharides from apple juices produced by enzymatic pomace liquefaction. *J. Agric. Food Chem.* **2002**, *50*, 1230−1236.
(40) Piatka, D.; Wilkowska, A.; Pogorzelski, E.; Ambroziak, W. Enzymatic liquefaction of apple pomace. *Food Chem. Biotechnol.* **2010**, *74*, 65−73.
(41) Will, F.; Bauckhage, K.; Dietrich, H. Apple pomace liquefaction with pectinases and cellulases: analytical data of the corresponding juices. *Eur. Food Res. Technol.* **2000**, *211*, 291−297.

transesterification and esterification reactions.[17] Moreover, Lewis acid has also been proven to be active for the esterification reaction.[18]

Thus far, numerous studies concerning the synthesis of phytosterol esters have been reported. However, the related research on the synthesis of ergosterol esters is still rare in the literature, except for a recent report concerning the synthesis of ergosteryl oleate,[10] in which the highest conversion (72.4%) was obtained using Lipozyme TL IM as the biocatalyst. The present study was aimed at the efficient synthesis of ergosterol ester by esterification using lauric acid as an acyl donor in the presence of a Lewis acid or an acid−surfactant-combined catalyst in a solvent-free system. The synthesized product was separated by silica gel column chromatography, and its chemical structure was characterized by Fourier transform infrared spectroscopy (FTIR), mass spectroscopy (MS), and nuclear magnetic resonance (NMR). The influence of different catalysts, catalyst dose, substrate molar ratio, reaction temperature, and reaction time was also considered. Furthermore, the solubility of ergosterol and its laurate in vegetable oil was studied and compared.

## MATERIALS AND METHODS

**Materials.** Ergosterol (purity of >95%) was provided by Sigma-Aldrich Co., Ltd. (Shanghai, China). Methanol and *n*-hexane used for high-performance liquid chromatography (HPLC) analysis were of spectral grade and provided from Tedia Company, Inc. (Shanghai, China). Petroleum ether (60−90 °C), ethyl acetate, formic acid, *n*-hexane, ethanol, hydrochloric acid (HCl), sodium dodecyl sulfate (SDS), stannous chloride ($SnCl_2$), cuprous chloride (CuCl), and other common reagents used were of analytical grade and purchased from Sinopharm Chemical Reagent Co., Ltd. (Shanghai, China). Silica gel (100−200 mesh) was obtained from Qingdao Haiyang Chemical Co., Ltd. (Qingdao, China).

**Preparation of the Catalyst.** In this study, SDS, SDS + HCl, $SnCl_2$, and CuCl were selected as the potential catalyst. Among these catalysts, SDS + HCl was prepared according to a previous report with minor modification.[11] Briefly, 0.3 g of SDS was weighed and put into a mortar in a fume hood, and 0.2 mL of HCl was added to the mortar. The mixture was ground for 10 min and stood for 20 min in a fume hood to remove the excess HCl by evaporation. The catalyst SDS + HCl was finally obtained. This catalyst was newly prepared every time prior to use. The other catalysts were directly used as catalyst for the esterification.

**Esterification Reaction.** The esterification reaction for ergosterol laurate synthesis was performed on a 20 mL special reaction tube. First, the reaction tube was placed and fixed in a digital oil bath heating device equipped with a magnetic stirring apparatus, and a magnetic stirrer was added. Then, the mixture of lauric acid (1.0−4.0 g) and catalyst (0.02−0.08 g) were added to the reaction tube and, subsequently, heated to the desired temperature under a constant nitrogen flow. A total of 2.0 g of ergosterol was added to the reaction system until lauric acid and catalyst melted completely, starting the reaction and lasting for some time (0.5−4.0 h). Over the time course of the reaction, a portion of the sample was periodically taken out for thin-layer chromatography (TLC) and HPLC analyses. At the end of the reaction, nitrogen flow was stopped until all samples were removed.

**TLC Analysis and Product Purification.** The sample (0.05 g) removed periodically from the reaction system was dissolved in 10 mL of *n*-hexane/ethanol (1:1, v/v) and then used for TLC analysis. A small quantity of sample solution (10 μL) was evenly pointed on a activated TLC plate. Development was then carried out using petroleum ether (60−90 °C)/ethyl acetate (9:1, v/v) as the developing agent, and the TLC plate was located by iodine vapor staining for 20 min. $R_f$ values of different substrates and products were as follows: 0.05−0.09 (lauric acid), 0.16−0.21 (ergosterol), and 0.85−0.91 (ergosterol laurate).

The sample (1.0 g) at the end of the reaction was dissolved in 20 mL of petroleum ether (60−90 °C)/ethyl acetate (9:1, v/v) and then applied to a silica gel column (12 × 1000 mm), eluted with petroleum ether (60−90 °C)/ethyl acetate (9:1, v/v) at the flow rate of 0.8 mL/min. The eluent was collected, and the purity of the product was preliminarily detected by TLC analysis and further analyzed by HPLC. The fractions only containing ergosterol laurate were collected by rotary evaporation under vacuum.

**FTIR Analysis.** The above purified ergosterol laurate was dried under vacuum and then characterized by FTIR analysis. FTIR measurement was performed on a FTIR spectrophotometer (Thermo Nicolet IS50 FT-IR, Waltham, MA) using an attenuated total reflectance method with the spectral scanning scope for 600−4000 $cm^{-1}$, number of scans of 32, and resolution of 4 $cm^{-1}$.

**MS Analysis.** The mass spectrum was obtained by liquid chromatography ion trap mass spectrometry (Thermo LXQ, Waltham, MA) with positive-ion atmospheric pressure chemical ionization (APCI) mode. The MS operating parameters were as follows: vaporizer temperature, 350 °C; sheath gas flow rate, 25 arb; auxiliary gas flow rate, 5 arb; discharge current, 4.0 μA; capillary temperature, 275 °C; capillary voltage, 30 V; tube lens, 120 V; and mass scan range, 100−800 amu.

**NMR Analysis.** The chemical structure of the purified product was further identified by NMR. In detail, $^1H$ and $^{13}C$ NMR and distortionless enhancement by polarization transfer 135 (DEPT 135) spectra of the product were recorded using $CDCl_3$ as the solvent with a Bruker NMR spectrometer (Avance II 400 MHz, Switzerland). The $^1H$ NMR spectrum was acquired using the following settings: temperature, 294.5 K; frequency, 400.13 MHz; acquisition time, 4 s; and number of scans, 16. $^{13}C$ NMR and DEPT 135 spectra were acquired using the same settings as follows: temperature, 295.2 K; frequency, 100.61 MHz; acquisition time, 1.4 s; and number of scans, 549.

**HPLC Analysis.** The reaction sample (0.05 g) periodically removed from the reaction tube was diluted in 20 mL of absolute ethyl alcohol/*n*-hexane (1:1, v/v). The sample (10 μL) was analyzed by Agilent 1100 HPLC using a symmetry-$C_{18}$ column (5 μm, 4.6 × 150 mm, Waters, Milford, MA) controlled at 35 °C. The sample was eluted with methanol/*n*-hexane (9:1, v/v) as the mobile phase at the flow rate of 1.0 mL/min. The eluate was monitored with a Schambeck ZAM 4000 evaporative light scattering detector (ELSD) at 60 °C and nitrogen as the carrier gas at a pressure of 0.5 bar. The purified ergosterol laurate and ergosterol were used as standards, and the corresponding calibration curves were prepared for quantitative analysis. The conversion and selectivity were defined as follows:

$$\text{conversion of ergosterol (\%)} = (\text{EB} - \text{EE})/\text{EB} \times 100$$

$$\text{selectivity of ergosterol laurate (\%)} = \text{ELE}/(\text{EB} - \text{EE}) \times 100$$

where EB is the molar amount of ergosterol at the beginning of the reaction, EE is the molar amount of ergosterol at the end of the reaction, and ELE is the molar amount of ergosterol laurate at the end of the reaction.

**Determination of the Oil Solubility of Ergosterol and Its Laurate.** The solubility of ergosterol and ergosterol laurate in vegetable oil was investigated as follows: 0.2 g of ergosterol or 0.5 g of ergosterol laurate was added to a 100 mL flask, successively. The flask was heated with a oil bath equipped with a magnetic stirring apparatus to 30 °C. Subsequently, the soybean oil was added dropwise until the sample was completely dissolved. Thereafter, the flask stood for 6 h with the help of magnetic stirring. The oil volume were promptly adjusted and recorded on the basis of the dissolution. The oil solubility can be calculated by the amount of sunflower oil to be added and expressed as grams per 100 mL at 30 °C.

## RESULTS AND DISCUSSION

**Product Analysis.** The product was quantified by HPLC. After the purification procedure, the purity of the product was also determined by HPLC. The purified product was characterized by FTIR, MS, and NMR analyses.

*HPLC Analysis.* The conversion of ergosterol to ergosterol laurate was determined by HPLC. ELSD was a kind of universal detector and selected for this study because of lauric acid without ultraviolet (UV) absorption. The peaks of ergosterol and lauric acid were characterized on the basis of their retention times with reference to standards. Lauric acid was first eluted with the retention time of 3.4 min, and then ergosterol was eluted with the retention time of 5.8 min. From the HPLC chromatogram of the reaction mixtures, a new peak at 22.4 min was observed and corresponded to the product ergosterol laurate. Apparently, the products can be clearly distinguished from the reaction substrates.

*FTIR Analysis.* The FTIR spectral data of lauric acid and the potential functional groups were displayed in Figure 1a.

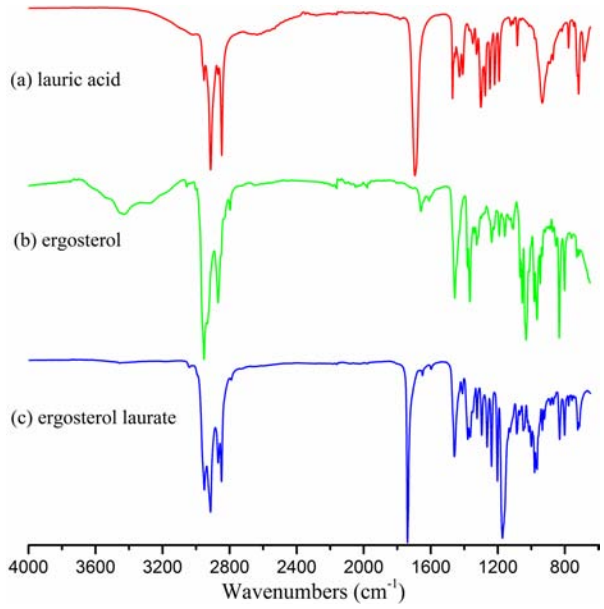


**Figure 1.** FTIR spectra of (a) lauric acid, (b) ergosterol, and (c) ergosterol laurate.

Obviously, the broad peak between 2450 and 3300 $cm^{-1}$ was the characteristic absorption signal of −OH in −COOH, and the strong peak at 1694 $cm^{-1}$ was the characteristic absorption signal of C═O in −COOH, suggesting the presence of a free carboxyl group. The peak at 2953 $cm^{-1}$ was the asymmetrical stretching vibration of C−H in the $CH_3$ group. The peaks at 2913 and 2847 $cm^{-1}$ were the asymmetrical and symmetrical stretching vibrations of C−H in the $CH_2$ group, respectively. The peak at 1471 $cm^{-1}$ was the bending vibration of C−H in the $CH_2$ group. The band at 718 $cm^{-1}$ indicated the presence of four or more $CH_2$ groups in the carbon chain.

The FTIR spectral data of ergosterol and the potential functional groups were displayed in Figure 1b. The broad and weak peak at 3430 $cm^{-1}$ corresponded to the stretching vibration of the hydroxyl group. The weak peak at 3056 $cm^{-1}$ was the signal of C−H in −C═C−H. The peaks at 2953 and 2869 $cm^{-1}$ were the asymmetrical and symmetrical stretching vibrations of C−H in the $CH_3$ group, respectively. The peak at 1366 $cm^{-1}$ was the bending vibration of C−H in the $CH_3$ group. The peaks at 2932 and 1456 $cm^{-1}$ were the asymmetrical and bending stretching vibrations of C−H in the $CH_2$ group, respectively. The medium peak at 1658 $cm^{-1}$ was the vibration signal of C═C. The strong peak at 1031 $cm^{-1}$ corresponded to the vibration of C−O.

The FTIR spectral data of the product and the potential functional groups were displayed in Figure 1c. The weak peak at 3040 $cm^{-1}$ was the signal of C−H in −C═C−H. The peaks at 2952 and 2869 $cm^{-1}$ were the asymmetrical and symmetrical stretching vibration of C−H in the $CH_3$ group, respectively. The peak at 1380 $cm^{-1}$ was the bending vibration of C−H in the $CH_3$ group. The peaks at 2915 and 1460 $cm^{-1}$ were the asymmetrical and bending stretching vibrations of C−H in the $CH_2$ group, respectively. The weak peak at 1651 $cm^{-1}$ was the vibration signal of C═C. The strong peaks at 1740 and 1173 $cm^{-1}$ were the characteristic absorption signals of C═O and C−O in the ester group, respectively. In comparison to the FTIR spectrum of lauric acid, the characteristic absorption signal of the carbonyl group in the product moved to a higher wavenumber, indicating that presence of the ester group. The band at 724 $cm^{-1}$ implied the presence of four or more $CH_2$ groups in the carbon chain.

The absorption signal of the free carboxyl group was observed in lauric acid but not in the product. The characteristic signal of the free hydroxyl group was observed in ergosterol. Nevertheless, the appearance of the ester group and the disappearance of the free hydroxyl group in the product suggesting that the new product may be ergosterol laurate.

**MS Analysis.** A direct sample infusion APCI−MS with positive-ion mode was used to identify the product. A major advantage of this approach was no need of separating the targeted compound from other compounds prior to analysis. The positive APCI−MS spectrum of the purified product was displayed in Figure 2. Theoretically, the relative molecular weight for ergosterol laurate was 578. In Figure 2, the protonated molecular ion $[M + H]^+$ at $m/z$ 579 was observed, indicating that the product was ergosterol laurate. Similarly, the molecular ion $[M + H]^+$ at $m/z$ 661 for oleyl ergosterol was observed in a previous report of the analysis of ergosterol esters isolated from the fruiting bodies of *Mycena chlorinella* using positive APCI−MS.[19] The base peak at $m/z$ 379 [M + H − lauric acid]$^+$ indicated the loss of lauric acid, providing strong evidence for the presence of ergosterol laurate. A similar result was also observed in a previous study, in which dehydrated molecular ions ($[M + H - H_2O]^+$) at $m/z$ 379 were found in ergosterol with strong intensity using positive APCI−MS.[20,21]

**NMR Analysis.** Following the purification procedure, the purified product showed only a single peak in the HPLC chromatograms, indicating that the purity of the product was very high (>98%). The microstructure of the product was further analyzed by $^1H$ and $^{13}C$ NMR and DEPT 135 spectroscopy (Figure 3). The $^1H$ and $^{13}C$ chemical shifts for the product were assigned by the interpretation of their $^1H$ and $^{13}C$ NMR and DEPT 135 spectra and further comparison to those of ergosterol in the literature.[21]

As displayed in Figure 3a, the $^1H$ NMR spectrum was complex, owing to the overlapping of the absorption signal of methylene and/or methylidyne between 1.2 and 2.1 ppm. The resonances below 1.1 ppm were mainly ascribable to methyl units, and those above 2.1 ppm were due to methylidyne units. The 3-H signal at 4.7 ppm in the product had a downfield shift of 1.0 ppm in comparison to that of ergosterol (3.7 ppm),[21]

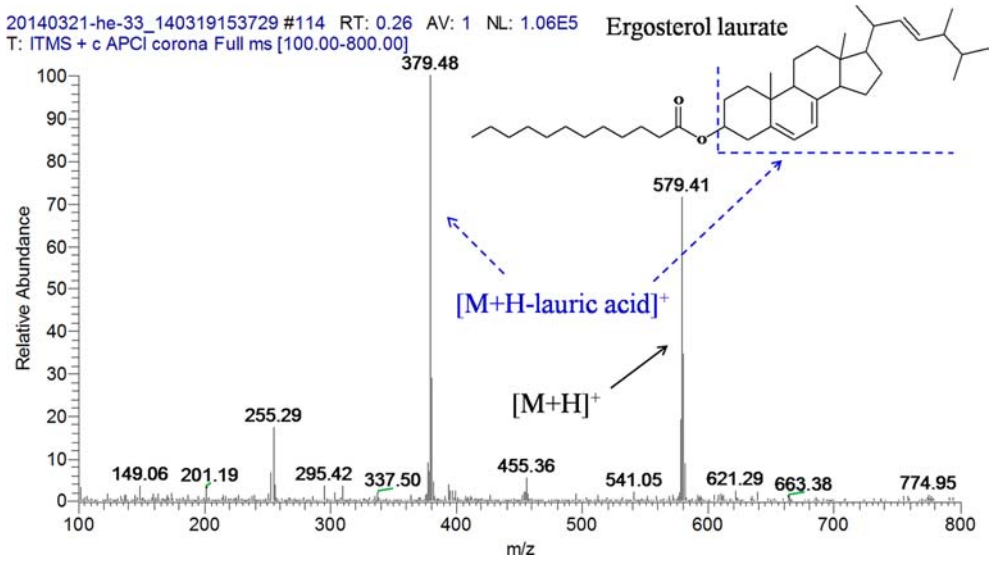


**Figure 2.** MS spectrum of ergosterol laurate.

indicating the presence of an ester bond in the ergosteryl moiety. The signals at 5.2 ppm were attributed to 22-H and 23-H. Furthermore, The resonances at 5.38 or 5.56 ppm were owing to 6-H or 7-H.

DEPT was a very useful method for determining the presence of primary, secondary, and tertiary carbon atoms. The DEPT experiment distinguished between CH, $CH_2$, and $CH_3$ groups by variation of the selection angle parameter. In DEPT 135, all $CH_2$ signals faced downward (negative), CH or $CH_3$ signals faced upward (positive), and quaternary carbon did not appear.

The $^{13}C$ NMR spectrum in Figure 3b illustrated the distribution of all carbon atoms in the product, while the DEPT 135 spectrum in Figure 3c only contained primary, secondary, and tertiary carbon atoms. Obviously, the peaks at 37.11, 37.11, 138.64, 141.47, and 173.33 ppm appearing in the $^{13}C$ NMR spectrum but disappearing in the DEPT 135 spectrum were ascribed to 10-, 13-, 5-, 8-, and 1′-quaternary carbon atoms, in agreement with proposed chemical structure for ergosterol laurate. In Figure 3c, the downward peaks between 21.0 and 39.1 ppm were mainly attributed to secondary carbon atoms. The resonances below 21.0 ppm were mainly ascribed to primary carbon atoms, and those above 39.1 ppm were mainly due to tertiary carbon atoms. By comparison, the number of primary, secondary, tertiary, and quaternary carbon atoms was in close agreement with the proposed chemical structure for ergosterol laurate. Furthermore, the 3-carbon atom signal at 72.5 ppm in the product exhibited a downfield shift of 2.0 ppm in comparison to that of ergosterol (70.5 ppm),[21] indicating the presence of an ester bond on the 3-carbon atom of the ergosteryl moiety. These NMR results together with FTIR and MS results proved that ergosterol laurate was successfully synthesized.

**Determination of Reaction Parameters.** For this esterification reaction, the main product was ergosterol laurate produced by direct esterfication of ergosterol with lauric acid, while there were also some unknown side products generated during the reaction. It has been reported that ergosterol was a rather unstable molecule and could be easily oxidized and photoxidized.[22] Meng et al. considered that the high temperature may be in favor of the dehydration of sterols to dienes.[15,23] In addition, ergosterol in mushrooms has also been found to be converted into vitamin $D_2$ by UV irradiation or sunlight exposure.[24] In this study, the side reaction was partially inhibited under constant nitrogen flow. Therefore, the conversion of ergosterol and the selectivity of the desired product (ergosterol laurate) were synchronously considered. The yield of the desired product (ergosterol laurate) was directly correlated to the selectivity. Under the same conversion, the higher the selectivity, the higher the yield of ergosterol laurate. On the contrary, the lower the selectivity, the higher the yield of side products.

*Selection of the Catalyst.* The effect of different catalysts on the conversion of ergosterol and the selectivity of ergosterol laurate was investigated, and the result is shown in Figure 4. These catalysts were used for the synthesis of ergosterol ester on the basis of the previous reports concerning the synthesis of phytostanyl esters.[11,15] Furthermore, CuCl was also selected to explore the catalytic efficiency for ergosterol ester synthesis because of its potential catalytic activity.[25]

As shown in Figure 4, the catalysts displayed different catalytic activities for the esterification of ergosterol with lauric acid. Among these catalysts, although $SnCl_2$ and CuCl showed excellent selectivity, lower conversion was observed when using $SnCl_2$ or CuCl as the catalyst. In a previous study, SDS + HCl has been found to be effective for the synthesis of phytostanyl esters in a solvent-free system.[11] In this study, the effect of SDS, HCl, or SDS + HCl on the conversion and selectivity was considered and compared for the synthesis of ergosterol ester. Almost no formation of the desired product occurred using HCl alone as the catalyst (data not shown), which was ascribed to be the rapid evaporation of hydrochloride at a high temperature. SDS had a comparable effect to SDS + HCl in the selectivity for this esterification, while the latter was better in the conversion. Therefore, SDS + HCl was used on the basis of the conversion and selectivity for the following experiments.

*Effect of the Reaction Temperature.* The influence of the reaction temperature on the conversion of ergosterol and the selectivity of ergosterol laurate was evaluated varying the reaction temperature from 80 to 120 °C. As shown in Figure 5, the conversion of ergosterol gradually improved as the temperature increased from 80 to 120 °C and then slightly

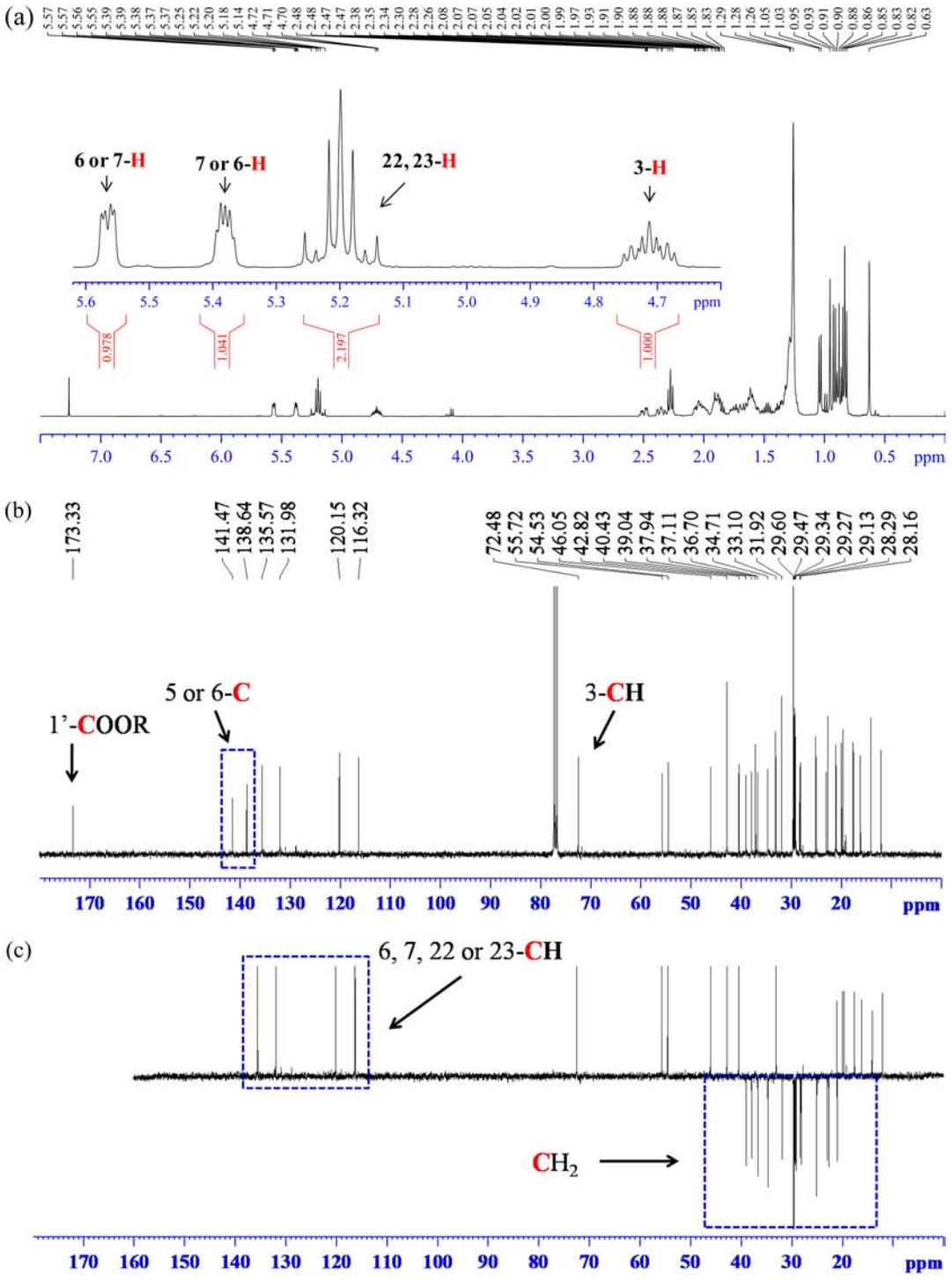


**Figure 3.** (a) $^{1}$H and (b) $^{13}$C NMR and (c) DEPT 135 spectra of ergosterol laurate.

decreased with a further increase of the reaction temperature from 120 to 140 °C. Moreover, the selectivity of ergosterol laurate varied slightly with the increase of the reaction temperature from 80 to 120 °C and then decreased when the temperature surpassed 120 °C. Although there was a high selectivity, the conversion of ergosterol was below 40% at 80 °C. The conversion was significantly improved at 140 °C, while the selectivity of ergosterol laurate was markedly decreased. In general, the esterification reaction would be enhanced as the substrates gradually melted and fully mixed with the gradual increase of the reaction temperature. Nevertheless, side reactions, such as oxidation, dehydration, and degradation, may also be accelerated as the reaction temperature increased, thus resulting in the lower selectivity.

*Effect of the Catalyst Dose.* The influence of the catalyst load on the conversion of ergosterol and the selectivity of ergosterol laurate was considered varying the amount of SDS + HCl from 1 to 5% (w/w), and the results were displayed in Figure 6. Although some ergosterol was consumed and the conversion below 8% was observed in the absence of SDS + HCl, almost no ergosterol laurate was formed at 120 °C (data not shown). As shown in Figure 6, the conversion of ergosterol

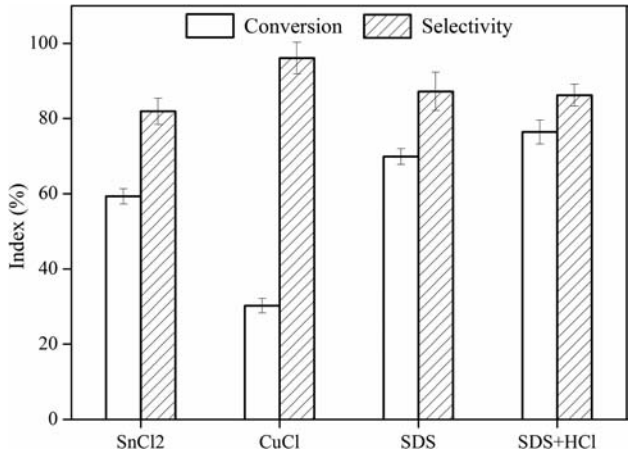


**Figure 4.** Effect of different catalysts on the conversion of ergosterol and the selectivity of ergosterol laurate (2:1 molar ratio of lauric acid/ergosterol, 100 °C, catalyst dose of 4%, and 2 h).

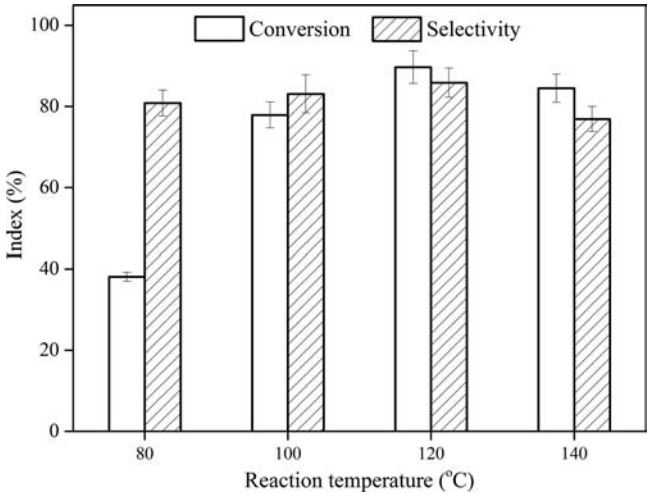


**Figure 5.** Effect of the reaction temperature on the conversion of ergosterol and the selectivity of ergosterol laurate (SDS + HCl as the catalyst, 2:1 molar ratio of lauric acid/ergosterol, catalyst dose of 4%, and 2 h).

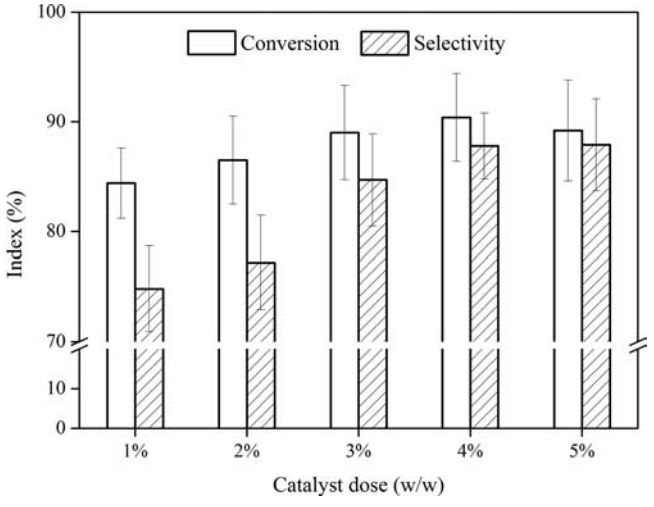


**Figure 6.** Effect of the catalyst dose on the conversion of ergosterol and the selectivity of ergosterol laurate (SDS + HCl as the catalyst, 2:1 molar ratio of lauric acid/ergosterol, 120 °C, and 2 h).

significantly promoted with the addition of 1% SDS + HCl and then gradually increased with a further increase of SDS + HCl and the highest conversion of ergosterol was achieved with 4% SDS + HCl. Meanwhile, the selectivity of ergosterol laurate also improved with the rise of SDS + HCl and then remained steady when the catalyst dose exceeded 4%. At a low catalyst dose, low conversion of ergosterol was still observed, while no ergosterol laurate was formed, which should be the occurrence of a side reaction under a high temperature. With the increase of the catalyst dose, the esterification of ergosterol with lauric acid was gradually activated and the conversion and selectivity also synchronously increased. However, the conversion and selectivity slightly varied with a further rise in the catalyst dose from 4 to 5%, indicating that 4% SDS + HCl was enough to make the substrate fully esterified.

*Effect of the Substrate Molar Ratio.* The influence of the molar ratio of lauric acid/ergosterol on the conversion of ergosterol and the selectivity of ergosterol laurate was evaluated using a molar ratio of lauric acid/ergosterol from 1:1 to 4:1 (Figure 7). In general, equimolar lauric acid and ergosterol

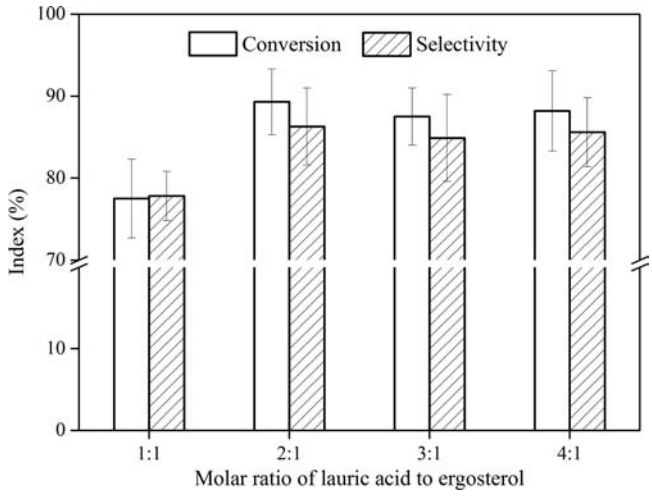


**Figure 7.** Effect of the molar ratio of lauric acid/ergosterol on the conversion of ergosterol and the selectivity of ergosterol laurate (SDS + HCl as the catalyst, 120 °C, catalyst dose of 4%, and 2 h).

should be ideal for direct esterification in view of the economic perspective and further purification. However, such a ratio was not favorable for the desirable product synthesis, and the conversion was below 80%. The conversion were improved with the rise of the molar ratio of lauric acid/ergosterol from 1:1 to 2:1, which was ascribed to a chemical equilibrium shift toward esterification. However, the conversion of ergosterol slightly varied with a further increase of lauric acid/ergosterol from 2:1 to 4:1, indicating that excessive lauric acid could not promote the conversion when the molar ratio exceeded 2:1. Low selectivity of ergosterol laurate was observed at a 1:1 molar ratio of lauric acid/ergosterol, and the selectivity was enhanced with the increase of the molar amount of lauric acid. For this reaction system, both the esterification reaction and side reaction were carried out at the same time, while the selectivity of ergosterol laurate was improved as the esterification shifted with the increase of the molar amount of lauric acid. Therefore, a 2:1 molar ratio of lauric acid/ergosterol was considered to be optimal.

*Effect of the Reaction Time.* The effect of the reaction time on the conversion of ergosterol and the selectivity of ergosterol

laurate was investigated under the above parameters, and the results are shown in Figure 8. In this experiment, all parameters

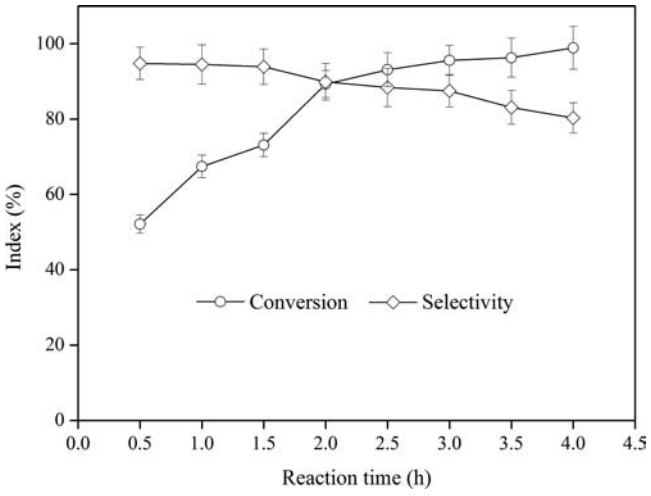


**Figure 8.** Effect of the reaction time on the conversion of ergosterol and the selectivity of ergosterol laurate (SDS + HCl as the catalyst, 2:1 molar ratio of lauric acid/ergosterol, catalyst dose of 4%, and 120 °C).

used have been selected by the above works. Obviously, the conversion of ergosterol rapidly increased with the extension of the reaction time, and the conversion reached 89% at 2 h. Furthermore, the highest selectivity was observed at 0.5 h and then slightly decreased with the rise of the reaction time. The conversion tended to gradually increase as the reaction time further extended from 2 to 4 h, indicating that the esterification of ergosterol with lauric acid had nearly reached equilibrium at 2 h. However, the selectivity of ergosterol laurate still decreased with a further increase of the reaction time from 2 to 4 h, suggesting that a small quantity of ergosterol and its laurate may be converted into side products. Therefore, the conversion and selectivity should be excellent when the esterification of ergosterol with lauric acid was performed for 2 h.

**Comparison of Solubility.** The solubility of ergosterol in vegetable oil was below 0.9 g/100 mL, while the solubility of ergosterol laurate could reach above 5.7 g/100 mL under the same conditions, indicating that the coupling of ergosterol and lauric acid by direct esterification can significantly improve the solubility of ergosterol in oil, thus greatly facilitating the incorporation into a variety of oil-based systems.

In recent years, ergosterol and its derivatives have attracted much attention for a variety of health benefits, while the latter showed excellent advantage in solubility. In the present study, ergosterol laurate was successfully and efficiently synthesized for the first time by direct esterification using SDS + HCl as the catalyst in a solvent-free system. Nevertheless, the side reaction should be prohibited further by exploring some moderate routes. Although the desired product (ergosterol laurate) was purified and characterized, its properties and application still need to be studied.

## AUTHOR INFORMATION

### Corresponding Authors

*Telephone/Fax: +86-511-88780201. E-mail: wshe2013@163.com.

*Telephone: +86-510-85913669. Fax: +86-510-85884496. E-mail: bfeng@jiangnan.edu.cn.

### Funding

This study was financially supported by the National Natural Science Foundation of China (31401664), the China Postdoctoral Science Foundation Funded Project (2014M560406), the Research Fund for the Doctoral Program of Higher Education of China (20130093110010), and the Research Fund for Advanced Talents of Jiangsu University (13JDG070).

### Notes

The authors declare no competing financial interest.

## REFERENCES

(1) Porep, J. U.; Walter, R.; Kortekamp, A.; Carle, R. Ergosterol as an objective indicator for grape rot and fungal biomass in grapes. *Food Control* **2014**, *37*, 77−84.

(2) Barreira, J. C. M.; Oliveira, M. B. P. P.; Ferreira, I. C. F. R. Development of a novel methodology for the analysis of ergosterol in mushrooms. *Food Anal. Methods* **2014**, *7*, 217−223.

(3) Villares, A.; García-Lafuente, A.; Guillamón, E.; Ramos, Á. Identification and quantification of ergosterol and phenolic compounds occurring in *Tuber* spp. truffles. *J. Food Compos. Anal.* **2012**, *26*, 177−182.

(4) Phillips, K. M.; Ruggio, D. M.; Horst, R. L.; Minor, B.; Simon, R. R.; Feeney, M. J.; Byrdwell, W. C.; Haytowitz, D. B. Vitamin D and sterol composition of 10 types of mushrooms from retail suppliers in the United States. *J. Agric. Food Chem.* **2011**, *59*, 7841−7853.

(5) Abe, F.; Hiraki, T. Mechanistic role of ergosterol in membrane rigidity and cycloheximide resistance in *Saccharomyces cerevisiae*. *Biochim. Biophys. Acta* **2009**, *1788*, 743−752.

(6) Kuo, C. F.; Hsieh, C. H.; Lin, W. Y. Proteomic response of LAP-activated RAW 264.7 macrophages to the anti-inflammatory property of fungal ergosterol. *Food Chem.* **2011**, *126* (1), 207−212.

(7) Hu, S. H.; Liang, Z. C.; Chia, Y. C.; Lien, J. L.; Chen, K. S.; Lee, M. Y.; Wang, J. C. Antihyperlipidemic and antioxidant effects of extracts from *Pleurotus citrinopileatus*. *J. Agric. Food Chem.* **2006**, *54* (6), 2103−2110.

(8) Schneider, I.; Kressel, G.; Meyer, A.; Krings, U.; Berger, R. G.; Hahn, A. Lipid lowering effects of oyster mushroom (*Pleurotus ostreatus*) in humans. *J. Funct. Foods* **2011**, *3*, 17−24.

(9) Shao, S. Q.; Hernandez, M.; Kramer, J. K. G.; Rinker, D. L.; Tsao, R. Ergosterol profiles, fatty acid composition, and antioxidant activities of button mushrooms as affected by tissue part and developmental stage. *J. Agric. Food Chem.* **2010**, *58*, 11616−11625.

(10) Chaibakhsh, N.; Basri, M.; Rahman, M. B. A.; Adnani, A.; Salleh, A. B. Lipase-catalyzed synthesis of ergosterol ester. *Biocatal. Agric. Biotechnol.* **2012**, *1*, 51−56.

(11) He, W. S.; Ma, Y.; Pan, X. X.; Li, J. J.; Wang, M. G.; Yang, Y. B.; Jia, C. S.; Zhang, X. M.; Feng, B. Efficient solvent-free synthesis of phytostanyl esters in the presence of acid-surfactant-combined catalyst. *J. Agric. Food Chem.* **2012**, *60*, 9763−9769.

(12) Tan, Z.; Le, K.; Moghadasian, M.; Shahidi, F. Enzymatic synthesis of phytosteryl docosahexaneates and evaluation of their anti-atherogenic effects in apo-E deficient mice. *Food Chem.* **2012**, *134*, 2097−2104.

(13) He, W.; Jia, C.; Ma, Y.; Yang, Y.; Zhang, X.; Feng, B.; Yue, L. Lipase-catalyzed synthesis of phytostanyl esters in non-aqueous media. *J. Mol. Catal. B: Enzym.* **2010**, *67*, 60−65.

(14) Pouilloux, Y.; Courtois, G.; Boisseau, M.; Piccirilli, A.; Barrault, J. Solid base catalysts for the synthesis of phytosterol esters. *Green Chem.* **2003**, *5*, 89−91.

(15) Zhou, Y.; Jia, C.; Li, R.; Zhang, X.; He, W.; Li, J.; Feng, B.; Xia, Q. An efficient and expeditious synthesis of phytostanyl esters in a solvent-free system. *Eur. J. Lipid Sci. Technol.* **2012**, *114*, 896−904.

(16) Meng, X.; Sun, P.; Pan, Q.; Shi, Z.; Yang, K.; He, R. Synthesis of plant sterol esters catalyzed by heteropoly acid in a solvent-free system. *Eur. J. Lipid Sci. Technol.* **2006**, *108*, 13−18.

(17) Ghesti, G. F.; de Macedo, J. L.; Parente, V. C. I.; Dias, J. A.; Dias, S. C. L. Synthesis, characterization and reactivity of Lewis acid/

surfactant cerium trisdodecylsulfate catalyst for transesterification and esterification reactions. *Appl. Catal., A* **2009**, *355*, 139−147.
(18) Jin, B.; Duan, P.; Xu, Y.; Wang, B.; Wang, F.; Zhang, L. Lewis acid-catalyzed in situ transesterification/esterification of microalgae in supercritical ethanol. *Bioresour. Technol.* **2014**, *162*, 341−349.
(19) Piovano, M.; Clericuzio, M.; Tabasso, S.; Chamy, M. C.; Garbarino, J. A.; Vidari, G.; Vita-finzi, P. Studies on chilean fungi III. Free and bound sterols from *Mycena chlorinella* (Basidiomycetes). *J. Chil. Chem. Soc.* **2005**, *50*, 389−390.
(20) Igarashi, F.; Hikiba, J.; Ogihara, M. H.; Nakaoka, T.; Suzuki, M.; Kataoka, H. A highly specific and sensitive quantification analysis of the sterols in silkworm larvae by high performance liquid chromatography−atmospheric pressure chemical ionization−tandem mass spectrometry. *Anal. Biochem.* **2011**, *419*, 123−132.
(21) Huang, L.; Cao, Y.; Xu, H.; Chen, G. Separation and purification of ergosterol and stigmasterol in *Anoectochilus roxburghii* (Wall.) Lindl. by high-speed counter-current chromatography. *J. Sep. Sci.* **2011**, *34*, 385−392.
(22) Villares, A.; Mateo-Vivaracho, L.; García-Lafuente, A.; Guillamón, E. Storage temperature and UV irradiation influence on the ergosterol content in edible mushrooms. *Food Chem.* **2014**, *147*, 252−256.
(23) Meng, X.; Pan, Q.; Yang, T. Synthesis of phytosteryl esters by using alumina-supported zinc oxide ($ZnO/Al_2O_3$) from esterification production of phytosterol with fatty acid. *J. Am. Oil Chem. Soc.* **2010**, *88*, 143−149.
(24) Jasinghe, V. J.; Perera, C. O. Distribution of ergosterol in different tissues of mushrooms and its effect on the conversion of ergosterol to vitamin $D_2$ by UV irradiation. *Food Chem.* **2005**, *92*, 541−546.
(25) Hajipour, A. R.; Nazemzadeh, S. H.; Mohammadsaleh, F. Choline chloride/CuCl as an effective homogeneous catalyst for palladium-free Sonogashira cross-coupling reactions. *Tetrahedron Lett.* **2014**, *55*, 654−656.

dioxide in fumigated tomatoes and cantaloupe. An additional objective was to investigate the effect of laboratory illumination on the formation of chloroxyanion byproducts such as chlorate and perchlorate during chlorine dioxide fumigation.

## MATERIALS AND METHODS

**Radiolabel.** Stock $Na^{36}ClO_2$, having a radiochemical purity of 90.5% and a specific activity of 14,000 dpm/$\mu$g was generated from $Na^{36}ClO_3$ as described by Hakk et al.[12] The 9.5% radiochemical impurity present in the stock $Na^{36}ClO_2$ solution was $Na^{36}Cl$ as determined by ion chromatography with radiochemical detection. Radioactive chlorine dioxide ($^{36}ClO_2$) was generated by the mineral acid catalyzed oxidation of $Na^{36}ClO_2$ (aq). For the tomato studies, 315 $\mu$L of stock $Na^{36}ClO_2$ was combined with 36 $\mu$L of sodium chlorite technical solution (318 mg/mL by iodometric titration; ICA TriNova), to a specific activity of 389 dpm/$\mu$g, and 49 $\mu$L of water in a Tyvek sachet (2.6 × 13 cm). Acidification of the chlorite solution with 1.8 M HCl (250 $\mu$L) initiated the release of $^{36}ClO_2$. The specific activity of the $^{36}ClO_2$ gas was 521 dpm/$\mu$g.

For the cantaloupe studies, sequential volumes of 4.925 mL of water; 1.390 mL of stock $Na^{36}ClO_2$, corrected for radiochemical purity; 0.628 mL of sodium chlorite technical solution; and 4.340 mL of 1.8 M HCl were added to a Tyvek sachet (19 × 5 cm, L × W) to initiate $^{36}ClO_2$ release. The specific activity of the $^{36}ClO_2$ gas was 134 dpm/$\mu$g.

**Tomato Studies.** *Tomato Fumigation.* Three separate $^{36}ClO_2$-fumigation experiments (trials A, B, and C) were conducted. In each experiment, approximately 100 g of tomato was exposed to approximately 5 mg of $^{36}ClO_2$ gas during a 2 h fumigation period. Fumigations occurred within a 5.5 L (11 × 22 × 23.5 cm; W × L × D) sealable glass tank (Figure 1). During experiments A and B, no effort was made to protect the fumigation tank from light, but for trial C the fumigation tank and lid were each protected from laboratory illumination by an aluminum foil wrap. Fumigation tanks were placed onto a magnetic stirring plate, and tomatoes were placed onto a slotted glass pedestal within each tank. A stir bar was also placed in the glass chamber and was allowed to rotate during fumigation to facilitate mixing of gases. Reactions were initiated, and the reaction chamber was sealed with a glass plate previously lined with vacuum grease. Glass lids were equipped with butyl-stoppered (20 mm; Kimble Chase; Vineland, NJ) entry and exit holes through which gases could be purged. Exposure periods were 2 h each. Experimental protocols varied slightly between experiments A, B, and C, and these variations are shown in Table 1.

**Recovery of Chamber Gas Radioactivity.** At the end of each fumigation experiment unreacted gas was either released into the fume hood (trial A) or trapped into 2 L of 0.1 N sodium thiosulfate after air was pumped (0.6 to 1.0 h) through the exposure chamber (trials B and C). To this end, entry and exit septa of the chamber lids were pierced with 11-gauge needles connected to Tygon tubing; gas pumped through the fumigation chambers was passed through coarse micro gas dispersion tubes (Chemglass Life Sciences, Vineland, NJ) housed within the thiosulfate.

*Recovery of Tomato Radioactivity.* Tomatoes were removed from the reaction vessel using tongs and placed into a 250 mL beaker containing about 200 mL of water. Tomatoes were rinsed for about 1 min, after which the tomato was removed and the rinsewater placed into a 250 mL volumetric flask; the beaker was rinsed, and the rinsewater was added to the volumetric flask. The volumetric flask was diluted to the mark and mixed, and radiochlorine in 1−2 mL aliquots was quantified by liquid scintillation counting (LSC).

*Recovery of Chamber Residual Radioactivity.* Stir bars and glass pedestals were placed in 250 mL beakers and rinsed with water, which was placed into volumetric flasks (0.5−1 L). Radioactive residues were recovered from the reaction chamber by rinsing sequentially with water. Rinses were transferred to the volumetric flask; the volumetric was diluted to the mark and mixed by inversion. Radioactivity in 1 to 2 mL aliquots was determined by LSC.

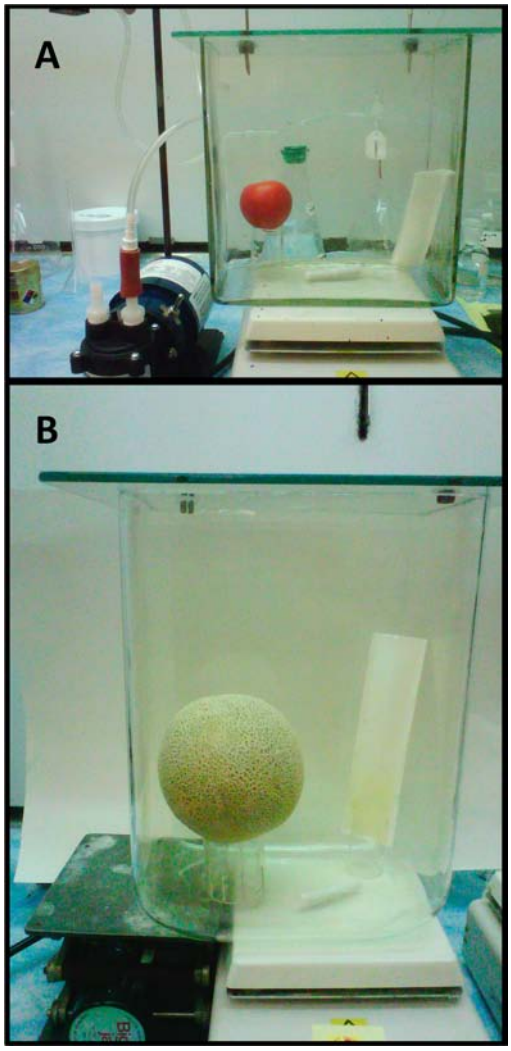


**Figure 1.** Experimental chambers for tomato (panel A) and cantaloupe (panel B) fumigations with $^{36}$Cl-chlorine dioxide. Panel A shows a tomato experiment at the initiation of the venting process. Panel B shows a cantaloupe experiment during fumigation; $^{36}$Cl-chlorine dioxide gas can be clearly seen as the greenish tint in the fumigation chamber. For each fumigation experiment, a slotted glass pedestal was used to support tomatoes or cantaloupe, a stir bar was used to provide gas circulation, and a Tyvek sachet contained the $^{36}ClO_2$ generating system. Glass lids were sealed with vacuum grease, and two butyl septa (embedded in the lids) served as portals through which air was pumped into sodium thiosulfate traps at the termination of the experiment. No effort was made to prevent laboratory illumination of either of the fumigations shown.

Radioactivity remaining within gas generation sachets was recovered after sequential rinsing with water and transfer of the rinse fractions into a 1 L volumetric as described for the tank rinse. Sachet radioactivity not removed by the water rinse was quantified after cutting each sachet into 1 cm strips and counting each strip directly in liquid scintillation fluid by LSC.

*Recovery of Tomato Radioactivity.* Rinsed tomatoes were weighed and homogenized whole (trial A), or the stem scar area was removed (trials B and C) and then the tomato was weighed and homogenized. The stem scar area was removed with a razor so that it contained minimal to no tomato skin or flesh. Aliquots (0.25 g) of puree were placed into glass LSC vials, digested overnight with 6 mL of Carbosorb E (PerkinElmer Life Sci.; Waltham, MA), and counted after the addition of 12 mL of Permaflour E (PerkinElmer Life Sci.; Waltham, MA) using LSC to obtain total radioactive residues (TRR). Stem scar

**Table 1. Experimental Differences between Tomato Fumigation Trials A, B, and C**

| | variable | | |
|---|---|---|---|
| trial | gas purge[a] | stem scar collection[b] | illumination[c] |
| A | no | no | yes |
| B | yes | yes | yes |
| C | yes | yes | no |

[a]Unreacted chlorine dioxide gas was either purged and trapped from the reaction vessel or vented into the fume hood. [b]The stem scar was either left on the tomato during postexposure processing or removed and processed separately. [c]The reaction chamber was unprotected from light for the 2 h reaction period, or it was covered with aluminum foil during the fumigation period and protected from illumination.

areas were added to a known amount of water and (or) crushed ice and were homogenized in a 25 mL stainless steel Waring blender cup. Radioactivity in scar puree was then quantified by LSC as described for tomato puree.

*Preparation of Tomato Serum and Pellet Fractions.* Aliquots of tomato puree were fractionated into liquid serum and solid pellet fractions by centrifugation at 30600*g* for 20 min. Aliquots (0.5 mL) of the serum fraction were counted directly in 15 mL of Ultima Gold LSC fluid; TRR in pellet aliquots (0.25 g) was quantified by LSC after overnight treatment in 6 mL of Carbosorb E followed by dilution in 12 mL of Permafluor LSC fluid.

*Speciation of Radioactive Residues in Tomato Rinse, in Serum Fractions, and in Tank Rinse Fractions.* The strategy for identification and quantification of radioactive metabolites was to fortify aliquots of tomato serum or water rinse samples with nonradioactive chlorite, chloride, and chlorate (21 to 23 $\mu$g; for use as chromatographic markers) and to inject the fortified aliquots onto the ion chromatograph. Each metabolite fraction was collected into a LSC vial as it eluted from the detector, and radioactivity in each fraction was determined by LSC. This strategy is essentially the same as described by Smith et al.[13] for the analysis of radioactive chlorate metabolites in beef tissues. Chlorite, chloride, and chlorate were separated using a Dionex AS11-HC (Thermo-Fisher) column; for perchlorate analysis, a Dionex AS16-HC column was used (see conditions below). Guard columns were not used. For trial C, quantification of perchlorate in the tomato rinse fraction was accomplished using ion chromatography with conductivity detection (described below); conductivity detection was more sensitive than radiochemical determination and could be used because the rinse fraction was free of interferences.

*Digestion of Tomato Pellets and Characterization of Radioactivity.* Radioactivity associated with the pellet fraction formed during the centrifugation of the tomato puree was released by digestion of pellet aliquots (1 g) in 1 M NaOH (50 °C for 72 h). Subsequent to digestion, slurries were recentrifuged at 50000*g* and the supernatant was assayed to determine recovery of radioactivity. Aliquots of digesta supernatant were treated with 0.3 M silver nitrate to precipitate silver $^{36}$Cl-chloride, as were aliquots of blank sodium hydroxide matrix, and sodium $^{36}$Cl-chloride and sodium $^{36}$Cl-chlorate fortified saline samples (controls). The amount of radioactivity remaining in supernatant aliquots was determined by LSC.

*LSC Techniques.* Background radiochlorine and limits of quantification were determined for individual matrices (i.e., tank rinse, tomato puree, tomato serum, tomato pellet, etc.) as described by Smith et al.[14] Individual aliquots of sample within a matrix set were counted for 10 to 20 min each. Radiochlorine was quantified using a Packard 1900 CA (Meriden, CT) liquid scintillation counter calibrated using a sealed radiochlorine standard (Analytics Inc., Atlanta, GA) prepared in Ultima Gold LSC fluid. Quench was corrected using the tSIE (transformed spectral index of the external standard; Packard) option. Net dpm of a sample was determined by subtracting the mean background dpm of a sample set from the gross dpm of a test sample.

*Ion Chromatography.* Chromatography was conducted using a Waters model 600 pump and controller having PEEK pump heads and tubing. For $^{36}$Cl-chlorite, $^{36}$Cl-chloride, and $^{36}$Cl-chlorate analyses, 10 mM NaOH was isocratically pumped at 1 mL/min through a Dionex AS11-HC, 4 × 250 mm, column. A conductivity detector (Dionex CD-25; 0.1 V, 100 mA, range, 3000) with external water suppression (Dionex ASRS 300; 4 mm) was used to monitor the elution of sample components. $^{36}$Cl-Perchlorate was separated using the same chromatograph equipped with a Dionex AS16-HC, 4 × 250 mm column with an isocratic mobile phase of 50 mM NaOH flowing at 1 mL/min. All samples were introduced through a Rheodyne 9725i Teflon injector equipped with a 1 mL injection loop. For each analysis, the detector signal was captured on paper using a Waters model 746 data module.

For some analyses of water rinses, perchlorate analysis was conducted using a Thermo-Fisher ICS-2100 ion chromatograph using the framework outlined in EPA method 314.0.[15] Briefly, sodium perchlorate standards (4, 10, 25, 100, 200, and 400 $\mu$g/L) were prepared in nanopure water. The limit of quantitation (LOQ) was equivalent to the lowest standard (4 $\mu$g/L) with the limit of detection (LOD) at 2 $\mu$g/L. Tomato rinse sample aliquots (1 mL) were injected onto the column, and perchlorate was separated from interferences on a Dionex AS16-HC column protected by an AG16-HC guard column (both 4 mm). An isocratic mobile phase of 50 mM KOH with a flow rate of 1.5 mL/min was generated using a Thermo-Fisher eluent generator. Perchlorate was measured using suppressed conductivity detection in-line with external water ASRS suppression (186 mA).

*Fate of Sodium $^{36}$Cl-Chlorite Injected into Tomatoes.* Fifty individual grape tomatoes (average wt 6.6 g) were each washed with water, blotted dry, weighed, and injected with 50 $\mu$L of sodium $Na^{36}ClO_2$ (862 $\mu$g; 90.5% radiochemical purity; 99 dpm/$\mu$g of sodium chlorite; radiochemical impurity was $Na^{36}Cl$). The injected tomatoes were collectively transferred into a Cuisinart blender and homogenized as described above for fumigated tomatoes. Likewise, total radioactive residues and the composition of residues in injected-tomato serum was determined as described for fumigated tomatoes.

**Cantaloupe Studies.** *Cantaloupe Fumigation.* Two experiments were conducted; for each trial, a single 18-count (851.6 g, trial A; 850.0 g, trial B) cantaloupe was supplied by SunFed Produce, Nogales, AZ; or Frontera Produce, Honduras. Test $^{36}ClO_2$ was generated in a Tyvek sachet as described for tomatoes. After acid addition, the glass exposure chamber (23.2 × 17.1 × 32.3 cm; L × W × D; 12.9 L) was sealed as rapidly as possible. The glass lid used for sealing the chamber was equipped with two 1 cm ports which were each sealed with 2 cm butyl septa. Cantaloupes were treated for 2 h with $^{36}ClO_2$ gas to meet a target exposure of 100 mg of $^{36}ClO_2$ per kg of cantaloupe (Figure 1). Mixing of gases within the exposure chamber was accomplished with magnetic stirring. No attempt to protect either cantaloupe experiment from laboratory light was made. Average light intensity in the laboratory that the experiments were conducted in is 900 ± 17 lx.

*Recovery of Chamber Radioactivity.* Chamber gases were collected as described for tomatoes except that a 1 N sodium thiosulfate trapping solution was used. Exposure chambers were purged for 1 (trial A) or 1.5 (trial B) h each. Radioactive residues were recovered from glass surfaces of the reaction chamber and Tyvek sachets as described for tomatoes.

*Recovery of Cantaloupe Radioactivity.* Cantaloupe were not rinsed after fumigation. Each cantaloupe was bisected with a single stroke of a stainless steel blade, and the seed bed was carefully removed and weighed. Edible cantaloupe flesh was separated from the rind with careful attention directed toward not contaminating the edible flesh with dry or liquid material from the inedible rind. The edible cantaloupe flesh was placed into a clean container and weighed; the rind portion was sliced into manageable pieces and weighed. Seed bed, edible flesh, and rind fractions were homogenized (Cuisinart CB-500) separately, and the resulting purees were analyzed for TRR content by LSC as described for the tomatoes.

*Preparation of Edible Flesh and Inedible Rind Serum and Pellet Fractions.* Aliquots (50 mL) of edible flesh or inedible rind puree were fractionated into liquid (serum) and solid (pellet) fractions by centrifugation at 30600*g* for 20 min. The serum and pellet fractions were separated, and quintuplicate aliquots (0.5 to 1.0 mL) of the sera fractions were counted directly in 15 mL of Ultima Gold

**Table 2. Distribution of Radioactivity after the Fumigation of Test Tomatoes with $^{36}ClO_2$ Gas**

| | trial A | | trial B | | trial C | |
|---|---|---|---|---|---|---|
| | wt (g) | act. (%) | wt (g) | act.[a] (%) | wt (g) | act. (%) |
| starting amounts[b] | | | | | | |
| tomato wt | 74.62 | | 97.54 | | 108.27 | |
| $Na^{36}ClO_2$ | | 90.5 | | 90.5 | | 90.5 |
| $Na^{36}Cl$ | | 9.5 | | 9.5 | | 9.5 |
| total | | 100.0 | | 100.0 | | 100.0 |
| tomato activity | | | | | | |
| tomato rinse | | 1.9 | | 2.2 | | 1.1 |
| puree | 74.62 | 10.0 | 96.77 | 7.5 | 108.03 | 7.8 |
| stem area puree | NA[c] | NA | 0.64 | 3.9 | 0.24 | 2.2 |
| tomato | | 11.9 | | 13.7 | | 11.0 |
| gas purge | | NM[d] | | 14.8 | | 18.0 |
| equipment rinse | | | | | | |
| tank rinse | | 12.5 | | 10.1 | | 0.6 |
| tank seal | | NM | | 0.5 | | 1.0 |
| lid seal | | NM | | 0.2 | | NM |
| equipment | | 12.5 | | 10.8 | | 1.6 |
| nonsachet activity[e] | | NC[f] | | 39.2 | | 31.4 |
| sachet activity | | | | | | |
| sachet rinse | | 42.3 | | 42.3 | | 47.8 |
| sachet | | 1.4 | | 1.9 | | 1.2 |
| sachet | | 43.7 | | 44.2 | | 49.0 |
| total recovery | 74.62 | *f* | 97.41 | 83.5 | 108.27 | 80.4 |

[a]Expressed as a percentage of the starting radioactivity. [b]Total starting radioactivity was 2.27 $\mu$Ci. [c]NA, the stem area was not removed in tomato trial A. [d]NM, not measured. [e]Nonsachet activity is the sum of total tomato activity, gas purge activity, and equipment rinse activity. [f]NC, not calculated because gas was not collected after the termination of the experiment.

(PerkinElmer; Waltham, MA) LSC fluid. Total radioactive residues in quintuplicate pellet aliquots (0.25 g for edible flesh, 0.05 g for inedible rind) were quantified by LSC after overnight treatment in 6 mL of Carbosorb E followed by dilution in 9 mL of Permafluor LSC fluid. Use of greater than 0.05 g of inedible rind pellet caused sample quench due to the intensity of color.

An untreated control cantaloupe was also fractioned into inedible rind, seed bed, and edible flesh fractions. In addition, control serum and pellet fractions were prepared from cantaloupe rind and edible flesh as described for treated melons. Sample aliquots from fractions of the control cantaloupe were used as blanks for determination of background radioactivity during the analysis of treated cantaloupe.

*Speciation of Radioactive Residues.* Radioactive residues in edible flesh, inedible rind sera, and tank rinse fractions were identified as described for tomatoes. Edible flesh serum from cantaloupe trial B, which contained TRR just above the detection limits, was thawed, and quintuplicate 1.25 mL aliquots of serum were fortified with 0.5 mL of 0.85% aqueous NaCl. Additional quintuplicate 1.25 mL aliquots of edible flesh serum were diluted with 0.5 mL of 0.3 M $AgNO_3$. Both sets of samples were centrifuged (15000*g* for 20 min), and 1.25 mL aliquots of each vial were transferred to glass LSC vials for determination of soluble radioactive residues in 15 mL of UltimaGold LSC fluid. For the saline treated serum, soluble radioactive residues would represent the TRR; for the $AgNO_3$ treated serum, the soluble residues would represent any residue present as $^{36}$Cl-chlorite, $^{36}$Cl-chlorate, and (or) $^{36}$Cl-perchlorate.

*Factors Impacting the Formation of Chloroxyanion Byproducts during $ClO_2$ Fumigation.* A 2 × 2 × 2 factorial experiment was designed to investigate the major variables that might impact chlorate and perchlorate formation from chlorine dioxide gas in glass reaction chambers. Main factors were reagent matrix (liquid or dry), chlorine dioxide gas concentration (1.6 or 7.8 mg per 0.95 L), and the presence or absence of light. The complete experiment was replicated on each of four consecutive days for a total "*n*" of four observations for each treatment combination. Reactions were conducted in clear glass quart jars (0.95 L) in the absence of vegetable matter. Jars containing treatments protected from light were entirely covered with aluminum foil, whereas jars containing treatments exposed to light were left uncovered. The levels of chlorine dioxide gas (1.6 and 7.8 mg; nominal concentrations of 600 and 3000 ppmv) were selected to bracket the mass of chlorine dioxide used in radiolabeled experiments (5.5 mg) with tomatoes.

Experiments were conducted in a laboratory illuminated by indirect sunlight, electronically ballasted F28T8 fluorescent laboratory lights (28 W), and F40T12 magnetically ballasted fluorescent laboratory hood lights. With the laboratory and hood lights illuminated, the light intensity was 900 ± 17 lx (mean ± std dev; 54 observations on 6 separate days). With laboratory and hood lights on, overcast or sunny days did not significantly influence in-hood light intensity ($P$ = 0.10).

Dry media chlorine dioxide generation employed FruitGard granules (ICA TriNova; Atlanta, GA). In the dry media experiments equal amounts of FruitGard chlorite impregnate and ICA dry acid activator impregnate were combined in Tyvek sachets or in glass beakers. The media were mixed by hand agitation to commence chlorine dioxide generation. Dry matrix reagents were sequentially and separately weighed (0.21 and 1.05 g of impregnate and activator, respectively, for the 1.6 and 7.8 mg $ClO_2$ treatments). Upon the addition of matrix part B, the contents of each sachet were mixed by hand agitation. Sachets were immediately placed in labeled, transparent 0.95 L canning jars and sealed with a canning jar lid and ring. The time at which each reaction was started was recorded.

Liquid reagents were added to Tyvek sachets in the sequence for 1.6 and 7.8 mg treatments respectively: nanopure water (96 or 529 $\mu$L) and technical grade sodium chlorite (10 or 52 $\mu$L; 318 mg/mL; ICA-TriNova; Atlanta, GA) followed by 1.8 M HCl (66 or 363 $\mu$L). After the addition of HCl, sachets were mixed by hand agitation and immediately placed into labeled, transparent 0.95 L canning jars and jars sealed. The start time was then recorded.

Reactions were allowed to proceed for 2 h, after which each container was unsealed and vented into the fume hood. Sachets were removed and each jar was rinsed sequentially by vigorously shaking four 50 mL aliquots of nanopure water within the sealed jars. Water rinses were transferred to labeled 250 mL volumetric flasks, the flasks were diluted to volume, and each flask was mixed by inverting a

minimum of 10 times. Aliquots of each sample were placed in labeled containers and were frozen until analysis by ion chromatography.

Perchlorate analyses were conducted using a Thermo-Fisher ICS-2100 ion chromatograph using the framework outlined in EPA method 314.0.[15] Sample aliquots (1 mL) were injected onto a Dionex AS16-HC column (4 × 250 mm) protected by an AG16-HC guard column (4 × 50 mm). An isocratic mobile phase of 50 mM KOH, produced using a Thermo-Fisher eluent generator, with a flow rate of 1.5 mL/min was used to elute perchlorate from the column. Perchlorate was measured using suppressed conductivity detection in-line with external water (ASRS 300) suppression (186 mA). Sodium perchlorate standards (4, 10, 25, 100, 200, and 400 μg/L), prepared in nanopure water, were injected in replicate 1 mL aliquots onto the ion chromatograph. Peak areas were regressed against perchlorate concentration using Chromeleon CHM-2 software (Thermo-Fisher). The LOQ was equivalent to the lowest standard (4 μg/L). The LOD of 0.001 μg/L was determined empirically by injecting replicate 1 mL aliquots of 0.5, 1, and 4 μg/L sodium perchlorate standards.

Chlorate analyses were also conducted using a Thermo-Fisher ICS-2100 ion chromatograph. Standards consisting of 5, 25, 100, 500, 1000, and 5000 μg/L of sodium chlorate were prepared in nanopure water. Chlorate was separated from interferences on a 4 × 250 mm Dionex AC19HC column protected by a 4 × 50 mm AS19HC guard column with an isocratic mobile phase of 20 mM KOH. Mobile phase was prepared using a Thermo Fisher eluent generator. Ions were detected using a DS6 conductivity detector with external water suppression (ASRS 300; 50 mA). Sodium chlorate standards were run at the beginning and end of each sample set. Blank samples were also concurrently run with each analysis. For the chlorate analysis, the LOQ was 5 μg/L; the LOD of 1 μg/L was determined empirically.

*Statistics.* SigmaPlot 12.0 (Systat Software, Inc.; San Jose, CA) was used to determine differences in treatment (dry or liquid reagent; chlorine dioxide concentration; or illuminated or dark fumigation) means for perchlorate and chlorate. Main effects of media and chlorine dioxide concentration on chlorate and perchlorate formation were determined using two-way analysis of variance (ANOVA) after passing tests of normality and equal variance. The effect of light was not included in the analyses because of the low to nondetectable levels of chlorate and perchlorate in samples protected from light. Chlorate residues were log-transformed prior to statistical analyses in order to meet the equal variance assumption. The Holm−Sidak method was used to determine differences in treatment means after the 2-way ANOVA *F* statistic indicated significant main effects. *F* statistics of less than 0.05 were considered to be significant.

## RESULTS AND DISCUSSION

**Fate of $^{36}$Cl-Chlorine Dioxide in a Tomato Fumigation System.** Table 2 shows the distribution of radioactivity in tomato fumigation systems after 2 h fumigations with $^{36}ClO_2$. Across trials approximately 12% of the system radioactivity was present on the tomato itself; 2 to 13% was rinsed from the fumigation tank and its associated parts (stir bar, glass pedestal); 15 to 19% was purged from the tank and trapped into sodium thiosulfate; and 44 to 49% was associated with the reaction sachet itself. Total recovery of radioactivity was 80 to 84%. Potential losses of radiochlorine include losses realized immediately after the acid activation of the reaction while the sachet was positioned in the reaction chamber and while sealing the chamber. Additional losses could have occurred during chamber evacuation by chlorine dioxide absorption or condensation on the Tygon tubing that transported gases from the reaction chamber to the thiosulfate trap or during the fumigation period by leakage from the tank. Of the total system radioactivity, approximately 55.9% was converted to $^{36}Cl$-$ClO_2$ (total starting radioactivity less activity remaining in the sachet); thus, of the total chlorine dioxide formed, approximately 22% was associated with the tomato itself.

Of note with regard to the gross disposition of the radioactivity was the apparently smaller amount of radioactivity that was rinsed from the tank wall, lid, pedestal, and stir rod in trial C (1.6%) compared to tank rinses of trials A and B (11 and 13%, respectively). Gases in trial C were protected from light, compared to trials A and B. Because the dark-phase radioactive experiment was not replicated, it would be unwise to make too many inferences from a single observation.

Tomato radioactive residues were the collective residues present in the tomato rinsewater, in the tomato puree, and in the stem scar region (for trials B and C). For trial A, 11.9% of the total starting activity was associated with the tomato after a 2 h exposure period, with 13.7 and 11.0% of the starting radioactivity associated with the tomatoes of trials B and C, respectively. While the surface area of the tomato was small relative to the surface area of the tank and its components, $^{36}ClO_2$ deposition was disproportionately associated with tomatoes. That is, approximately 56% of the total starting radioactivity was converted to $^{36}ClO_2$, with 20−25% of the $^{36}ClO_2$ radioactivity associated with the tomato. The disproportional deposition of radioactivity onto the tomato is not surprising given the water solubility of chlorine dioxide and the expected availability of reducing agents in a tomato matrix. The attraction of chlorine dioxide to the tomato itself also provides context for its efficacy at killing pathogens[16−18] and rot organisms[9,19] on vegetable surfaces.

Between 1.1 and 2.2% of the total system radioactivity was rinsed from the surface of tomatoes after the 2 h exposure. When expressed as the total activity present on the tomato, the rinse contained 10 (trial C) to 16% (trials A and B) of the tomato TRR. Data from trials B and C clearly show that the stem scar region of the tomato preferentially accumulated radioactive residues. For example, the stem scar from trial B contained 28.5% of the total activity associated with the tomato even though the scar region was only 0.64 g; for trial C, the scar area contained 20% of the total tomato activity, while comprising only 0.24 g of the total tomato mass. Given the low mass and the high concentration of TRR, one would expect that chlorine dioxide would have high efficacy at the moist, porous area of the fruit, those regions in which pathogens and rot organisms might have the highest probability of colonizing.

Figure 2 shows example chromatograms of sodium chlorite, sodium chloride, and sodium chlorate standards in water and a representative chromatogram of tomato rinsewater assayed for radiochlorine content by ion chromatography with subsequent trapping of radioactive fractions. Using the AS11-HC column chlorite, chloride, and chlorate were well resolved. The large peaks shown in Figure 2 are a reflection of the fact that each aliquot of tomato rinse chromatographed was fortified with unlabeled standards to assist in accurate trapping. Across trials, radioactive sodium chlorite was typically not present in rinse fractions; in contrast, the sodium chloride and chlorate fractions contained detectable radioactivity across trials. Total recovery of radioactivity was low (generally less than 70%) when sample aliquots were analyzed on the AS11-HC column so sample aliquots were also analyzed using an AS16-HC column which allowed perchlorate elution. Using the AS16-HC column, perchlorate was well resolved from chlorite, chloride, and chlorate, which coeluted (Figure 3).

Table 3 shows the composition of radioactive residues in tomato fractions of trials A, B, and C. Tomato rinse fractions did not contain detectable sodium chlorite in trials A and B, but did contain detectable (0.01 μg/g of tomato) $^{36}$Cl-chlorite in

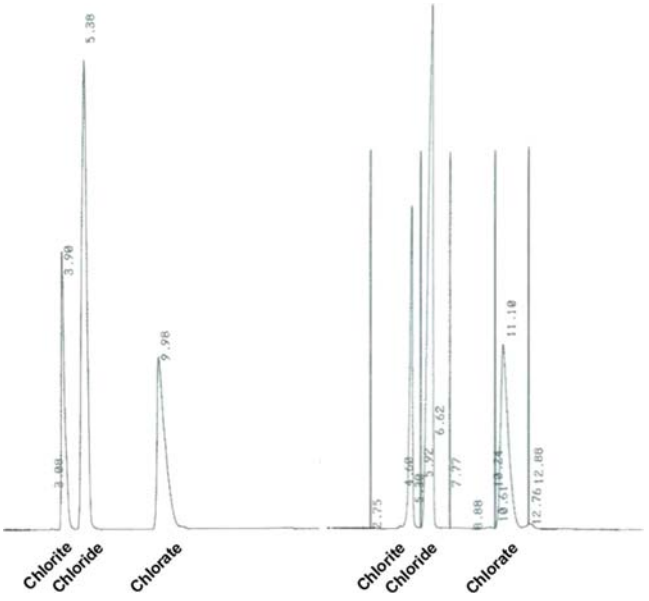


**Figure 2.** Ion chromatographic separation of unlabeled chlorite, chloride, and chlorate standards in water (10 $\mu$L; left panel), and an aliquot (1000 $\mu$L) of tomato rinse fortified with the standard mix (right panel). Vertical lines in the chromatogram of the tomato rinse fraction represent the regions collected directly into LSC vials for determining radioactive residues. Radioactivity was never present in the chlorite fraction of the tomato rinse, but it was significantly above background for the chloride and chlorate fractions in the tomato rinse aliquot. Differences in retention times of standards in the two injections are a function of the differing injection volumes at a constant flow rate (1 mL/min).

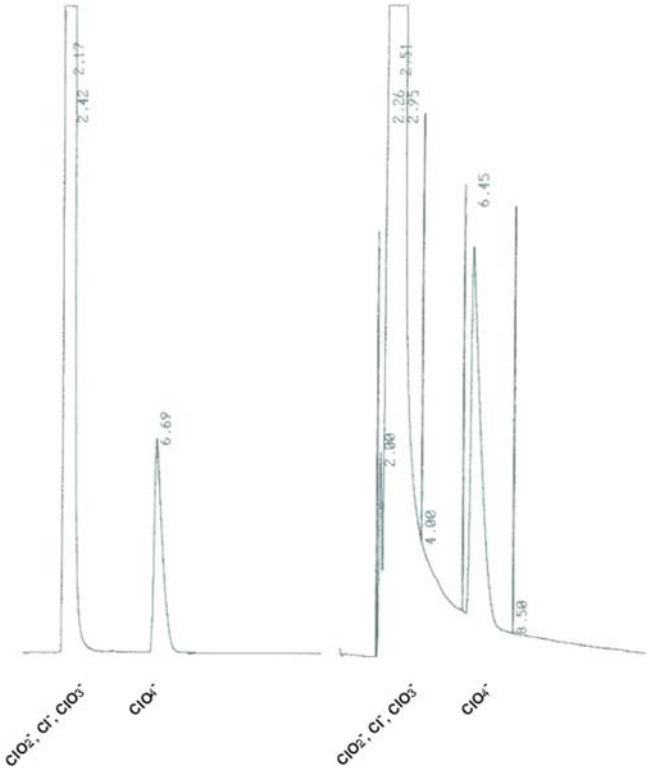


**Figure 3.** Ion chromatographic separation of unlabeled chlorite, chloride, chlorate, and perchlorate standards (left panel) and an aliquot of tomato serum containing incurred residue (right panel) and fortified with the standard mix. Radioactivity present as chlorite, chloride, and chlorate was not resolved on the AS16-HC column and was trapped together; perchlorate was trapped as a single peak, well resolved from chlorite, chloride, and chlorate. Vertical lines in the chromatogram of the tomato rinse fraction represent the regions collected directly into LSC vials for determining radioactive residues.

one of three sample aliquots measured from trial C. Sodium chlorate was the major residue rinsed from tomatoes of trials A and B (56.5 to 67.5% of total residue) but represented 10% of the total residue in trial C, which was run under dark conditions. Similarly, when reactions were run under laboratory illumination (trials A and B), $^{36}$Cl-perchlorate represented significant quantities of radioactivity in the tomato rinse (8.2 to 17.7% of rinse activity), but under conditions protected from light, no detectable $^{36}$Cl-perchlorate was present (trial C; LOQ of 4 ng/mL using ion chromatography). Radioactive chloride ion present on tomato surfaces was greatly influenced by illumination during the experiment, with trial A and B tomato rinses containing 14.8 to 35.2% chloride and trial C (dark) TRR being composed of 89.1% $^{36}$Cl-chloride. Thus, the major factor affecting the composition of residues rinsed from the surface of tomatoes was whether fumigations were exposed to laboratory light.

Of the total radioactive residues present in tomato puree, 53.9 $\pm$ 1.6 of the activity partitioned into the serum, while 46.1% partitioned into the pulp. Tomato serum, prepared from tomato puree, contained no detectable sodium chlorite (Table 3). Radioactive chloride ion represented 80 to 87% of the serum radioactivity in illuminated fumigations (trials A and B) and 93% of the serum radioactivity in the darkened fumigation (trial C). In illuminated fumigations, chlorate represented 13 to 19% of the serum activity, with the proportion dropping to 5% of the total activity for trial C serum (dark). Perchlorate was not consistently detected in sera of tomatoes, regardless of trial (LOQ 0.07 to 0.17 $\mu$g/g).

Stem scar radioactivity, measured in trials B and C, was composed primarily of sodium chloride (86 to 90% of total) and chlorate (9 to 13% of scar radiochlorine); perchlorate residues comprised about 1% of the total stem scar radiochlorine. It should be recalled, however, that the stem area of the tomato, while representing less than 1% of the tomato weight, contained 20 to 25% of the total radioactivity rinsed from, or deposited onto, the tomatoes.

Pellet radioactivity could not be measured directly via ion chromatography, so pellet aliquots were digested in NaOH and then reacted with an excess of silver nitrate to precipitate the $^{36}$Cl-chloride ion. It was assumed that radioactivity not precipitated by silver nitrate had the same chemical composition as stem scar. For trials A and B, 91 to 100% of the radioactivity released by NaOH digestion was precipitated by silver nitrate, indicating that the released radiochlorine was $^{36}$Cl-chloride ion. For trial C, 100% of the radioactivity was released by NaOH digestion, but only 97% of this radiochlorine was precipitated as $^{36}$Cl-chloride ion.

From a qualitative perspective, residues rinsed from the surface of the glass reaction chamber were similar to residues rinsed from tomato surfaces, with laboratory illumination being the major influence on the composition of residues. Oxidized products of chlorine dioxide present in tank rinsewater from trial A represented a major amount of residue (95.3% of tank rinse residue), but for trial C (dark) the major residue was chloride (78.1% of tank rinse activity) with only 13.9% of the radioactivity being present as chlorate or perchlorate. The presence of light greatly influences the propensity of radioactive

**Table 3. Composition of Radioactive Residues in Tomato Fractions and Tank Rinses of Tomato Trials A, B, and C**

| | | residue composition and concn[a] | | | | | | LOQ[b] |
|---|---|---|---|---|---|---|---|---|
| | | trial A | | trial B | | trial C | | trial A, B, C |
| fraction | residue[c] | | | | | | | |
| | | % | μg/g | % | μg/g | % | μg/g | μg/g |
| tomato rinse | $Na^{36}ClO_2$ | 0 | <0.01 | 0 | <0.01 | 0.8[d] | <0.01[d] | 0.01, 0.01, 0.01 |
| | $Na^{36}Cl$[e] | 35.2 | 0.22 | 14.8 | 0.11 | 89.1 | 0.32 | 0.01, 0.003, 0.01 |
| | $Na^{36}ClO_3$ | 56.5 | 0.65 | 67.5 | 0.92 | 10.1 | 0.7 | 0.01, 0.01, 0.005 |
| | $Na^{36}ClO_4$ | 8.2 | 0.11 | 17.7 | 0.28 | 0 | NDR[f] | 0.02, 0.02, 0.004[f] |
| serum | $Na^{36}ClO_2$ | 0 | <0.080 | 0 | <0.05 | 0 | <0.08 | 0.08, 0.05, 0.08 |
| | $Na^{36}Cl$[e] | 86.7 | 6.5 | 79.6 | 3.1 | 93.2 | 3.6 | 0.05, 0.03, 0.05 |
| | $Na^{36}ClO_3$ | 12.8 | 1.8 | 19.1 | 1.3 | 5.4 | 0.4 | 0.09, 0.06, 0.09 |
| | $Na^{36}ClO_4$ | 0.5[g] | <0.17[g] | 1.3[g] | <0.17[g] | 1.4[h] | 0.1[h] | 0.17, 0.17, 0.07 |
| stem scar | $Na^{36}ClO_2$ | | | 0 | <2.2 | 0.7 | 8.0 | [ ], 2.2, 6.1 |
| | $Na^{36}Cl$[e] | | | 86.2 | 444.1 | 89.5 | 685 | [ ], 1.4, 6.7 |
| | $Na^{36}ClO_3$ | | | 12.5 | 116.9 | 9.0 | 125 | [ ], 2.6, 4.3 |
| | $Na^{36}ClO_4$ | | | 1.1 | 11.9 | 0.8 | 12 | [ ], 5.4, 7.9 |
| pellet | $Na^{36}ClO_2$ | 0 | <0.43 | 0 | <0.65 | 0.2 | <0.86 | 0.43, 0.65, 0.86 |
| | $Na^{36}Cl$[e] | 100[i] | 6.0 | 91.0[j] | 12.8 | 97.3[k] | 25.9 | 0.28, 0.42, 0.56 |
| | $Na^{36}ClO_3$ | 0 | <0.51 | 8.3 | 2.1 | 2.3 | 1.13 | 0.51, 0.76, 1.02 |
| | $Na^{36}ClO_4$ | 0 | <0.58 | 0.7 | <0.88 | 0.2 | <1.17 | 0.58, 0.88, 1.17 |
| | | % | μg/mL | % | μg/mL | % | μg/mL | μg/g |
| tank rinse | $Na^{36}ClO_2$ | 0.4[h] | 0.01 | | | 8.0 | 0.01 | 0.01, [ ], 0.008 |
| | $Na^{36}Cl$[e] | 3.7 | 0.08 | | | 78.1 | 0.08 | 0.007, [ ], 0.005 |
| | $Na^{36}ClO_3$ | 82.5 | 3.14 | | | 7.2 | 0.01 | 0.012, [ ], 0.009 |
| | $Na^{36}ClO_4$ | 13.4 | 0.59 | 31.0 | 1.10 | 6.7 | 0.01 | 0.017, 0.031, 0.007 |

[a]Concentration in fraction; calculated by dividing the mass of residue by the fraction wt. (μg ÷ g = μg/g). [b]Limit of quantitation; based on the background radioactivity that was determined with each sample set and also based on the sample aliquot size used. [c]Based on the ion chromatographic separation of $^{36}$Cl-chlorite, $^{36}$Cl-chloride, $^{36}$Cl-chlorate, and $^{36}$Cl-perchlorate with determination of radioactivity in trapped fractions by liquid scintillation counting. [d]Radioactivity was detected and quantified in only 1 of 3 replicates. Thus, the calculated concentration is less than the limit of quantification. [e]Sodium chloride derived from $^{36}ClO_2$ gas; residues do not account for endogenous sodium chloride. [f]NDR, no detectable residue; perchlorate concentration in trial C rinsewater was also determined using ion chromatography having an LOQ of 4 ng/L. [g]Analyte was detected in one of three replicates, thus the calculated concentration is less than the LOQ. [h]Analyte was detected in two of three replicates. [i]98.6% of the pellet radioactivity was released by digestion in NaOH; of the released radioactivity, 100% was precipitated with silver nitrate. [j]97.3% of the pellet radioactivity was released by digestion in NaOH; of this, 91% was precipitated with silver nitrate (indicating chloride ions); it was assumed that the remaining 9% of the radioactivity was chlorate and perchlorate in the same proportion as in the stem scar. [k]100% of the pellet radioactivity was released by digestion in NaOH; of this, 97.3% was precipitated with silver nitrate (indicating chloride ions); it was assumed that the remaining 2.7% of the radioactivity was chlorate and perchlorate in the same proportion as in the stem scar.

residue to be deposited on the tank surface (Table 1), with light exposed chamber rinses containing 10.1 to 12.5% of the total starting activity; only 0.6% of the starting radioactivity in the chamber protected from light was deposited on the tank surface.

**Fate of Sodium $^{36}$Cl-Chlorite Injected into Tomatoes.** We hypothesized that instability of sodium chlorite in weak acids[20] would make it virtually impossible for chlorite residues to survive the acidity of tomatoes during processing. This hypothesis was tested by directly injecting sodium $^{36}$Cl-chlorite into tomatoes and subsequently following the chemical fate of the radiolabel. The exposure level selected (131 μg/g of tomato) was chosen to greatly exaggerate concentrations of chlorite in an anticipated commercial fumigation, even if 100% of a chlorine dioxide fumigation were to be converted to chlorite residue.

Radioactive residues injected into tomatoes distributed primarily to the serum fraction (87.3%) after centrifugation with only 13.7% of the activity distributing to the tomato solids. Radioactivity associated with chloride ion represented 98.3% the serum activity, with chlorate ion composing the complement. No chlorite ion was detected, indicating that 100% of the starting chlorite had been consumed. The qualitative (formation of chloride and chlorate) results are consistent with the aqueous degradation of sodium chlorite in the presence of organic acids.[21]

**Fate of $^{36}$Cl-Chlorine Dioxide in a Cantaloupe Fumigation System.** *Disposition of Radioactive Residues.* Table 4 shows the distribution of radioactivity expressed as total dpm in each fraction and as the percentages of the total starting radioactivity for cantaloupe trials A and B. Table 4 also shows the initial cantaloupe weights, the weights of the edible flesh, seed bed, and inedible rind fractions, and the total recovery of weight for each melon. The total recovery of radioactivity was comparable between cantaloupe trials A (89.4%) and B (88.3%). Unrecovered radioactivity (10.6 and 11.7% of the total for trials A and B, respectively) likely resulted from two factors. First, some $^{36}ClO_2$ was almost certainly lost to the atmosphere between sachet activation, positioning in the exposure tank, and sealing the tank. Additionally, $^{36}ClO_2$ may have been lost because of incomplete gas purging at the end of the treatment period or leakage during fumigation.

The total amount of released $^{36}ClO_2$ was calculated as the difference between the total starting activity and the radioactivity recovered in, and on, the reaction sachet. Therefore, about 63% of the starting activity was associated with the

**Table 4. Distribution of Radioactivity after the Fumigation of Cantaloupe with $^{36}ClO_2$ Gas**

| | trial A | | | | trial B | | | |
|---|---|---|---|---|---|---|---|---|
| | wt[a] | | act.[b] | | wt[a] | | act.[b] | |
| item | g | % | dpm | % | g | % | dpm | % |
| starting amt | | | | | | | | |
| melon | 851.6 | 100.0 | | | 850.0 | 100.0 | | |
| total act.[c] | | | 22,270,000 | 100.0 | | | 22,270,000 | 100.0 |
| $Na^{36}ClO_2$ | | | 20,150,000 | 90.5 | | | 20,150,000 | 90.5 |
| $Na^{36}Cl$ | | | 2,115,000 | 9.5 | | | 2,115,000 | 9.5 |
| residues from $^{36}ClO_2$ exposure[d] | | | | | | | | |
| edible flesh puree | 325.8 | 38.3 | <LOD | 0 | 294.9 | 34.7 | <LOD | 0.0 |
| seed bed puree | 62.4 | 7.3 | 3,532 | <0.1 | 49.3 | 5.8 | 4,669 | <.1 |
| rind puree | 458.5 | 53.8 | 7,225,000 | 32.5 | 500.9 | 58.9 | 8,331,000 | 37.4 |
| recovery, melon | 846.7 | 99.4 | 7,229,000 | 32.5 | 845.1 | 99.4 | 8,336,000 | 37.4 |
| chamber gas purge | | | 4,059,000 | 18.2 | | | 2,328,000 | 10.5 |
| chamber rinse | | | 382,000 | 1.7 | | | 636,900 | 2.9 |
| recovery, chamber | | | 4,441,000 | 19.9 | | | 2,965,000 | 13.3 |
| sachet activity (non $^{36}ClO_2$)[e] | | | | | | | | |
| rinse | | | 8,111,000 | 36.4 | | | 8,235,000 | 37.0 |
| bound | | | 124,000 | 0.6 | | | 132,000 | 0.6 |
| recovery, sachet | | | 8,235,000 | 37.0 | | | 8,367,000 | 37.6 |
| total recovery | 846.7 | 99.4 | 19,900,000 | 89.4 | 845.1 | 99.4 | 19,670,000 | 88.3 |
| unrecovered (gas phase)[f] | | | 2,361,000 | 10.6 | | | 2,598,000 | 11.7 |
| total gas phase[g] | | | 14,030,000 | 63.0 | | | 13,900,000 | 62.4 |

[a]Weight of melon and melon fractions. [b]Radioactive residues in indicated fraction, percentage of starting radioactivity. [c]Total amount of radiochlorine added to the Tyvek sachet; radiochemical purity of the sodium $^{36}Cl$-chlorite was 90.5% [d]Radioactive residues present on the melon fractions, in the chamber gas purge, and on the chamber walls, glass stand, and stir bar could only occur through the production of $^{36}ClO_2$ gas. [e]Sachet activity; residual radioactivity that did not exit the Tyvek sachet as chlorine dioxide gas. [f]Radioactivity not present in the melon residues, chamber gas purge or rinse, and sachet. [g]Sum of "recovery, melon", "recovery, chamber"; and "unrecovered (gas phase)" items.

**Table 5. Speciation of Radioactivity Present in Cantaloupe Edible Flesh, Inedible Rind Serum, and Tank Rinse Fractions of Cantaloupe Trials A and B**

| | | residue composition and concn[a] | | | | |
|---|---|---|---|---|---|---|
| | | trial A | | trial B | | LOQ[b] A, B |
| fraction | residue[c] | | | | | |
| | | % | μg/g | % | μg/g | μg/g |
| edible flesh | TRR[d] | 0.0 | NDR[e] | 0.0 | NDR | 0.4, 0.3[f] |
| rind serum | $Na^{36}ClO_2$ | 0.0 | <0.8 | 0.0 | <1.0 | 0.8, 1.0 |
| | $Na^{36}Cl$[g] | 86.3 | 74.4 | 87.0 | 69.6 | 0.5, 0.6 |
| | $Na^{36}ClO_3$ | 13.7 | 21.6 | 12.3 | 18.0 | 0.9, 1.2 |
| | $Na^{36}ClO_4$ | 0.0 | <0.3 | 0.7 | 1.2 | 0.3, 0.7 |
| | | % | μg/mL | % | μg/mL | μg/mL |
| tank rinse | $Na^{36}ClO_2$ | 0.0 | <0.1 | 0.0 | <0.1 | 0.11 |
| | $Na^{36}Cl$[g] | 11.3 | 0.3 | 6.2 | 0.3 | 0.07 |
| | $Na^{36}ClO_3$ | 55.5 | 2.5 | 79.7 | 6.0 | 0.13 |
| | $Na^{36}ClO_4$ | 33.3 | 1.7 | 14.1 | 1.2 | 0.03, 0.07 |

[a]Concentration in fraction; calculated by dividing the mass of residue by the fraction wt. (μg ÷ g = μg/g). [b]Limit of quantitation; based on the background radioactivity that was determined with each sample set and also based on the sample aliquot size used. [c]Based on the ion chromatographic separation of $^{36}Cl$-chlorite, $^{36}Cl$-chloride, $^{36}Cl$-chlorate, and $^{36}Cl$-perchlorate with determination of radioactivity in trapped fractions by liquid scintillation counting. [d]TRR, total radioactive residue. [e]NDR, no detectable residue. [f]LOQ for total radioactive residues assumes all residue is present as sodium chlorate equivalents. [g]Sodium chloride derived from $^{36}ClO_2$ gas; residues do not account for endogenous sodium chloride.

formation of $^{36}ClO_2$ gas in trials A and B. The specific activity of $^{36}ClO_2$ for each trial was 135 dpm/μg; therefore 104 and 103 mg of $^{36}ClO_2$ were produced in trials A and B, respectively. The cantaloupe weights used for trials A and B were 851.6 and 850.0 g, respectively, corresponding to $ClO_2$ exposures of 123 and 122 mg/kg of cantaloupe. Because *maximal* commercial exposures to chlorine dioxide are expected to be 100 mg of chlorine dioxide per kg of cantaloupe, data presented in this study represent residue levels commensurate with 120% over exposure relative to expected.

Cantaloupes retained 32.5 and 37.4% of the total radioactive charge in trials A and B (Table 4), respectively, representing 51.5 and 60.0% of the total $^{36}ClO_2$ produced from each reaction. Of the TRR present on the cantaloupe, greater than 99.97% of the cantaloupe radiochlorine was associated with the rind, regardless of trial (Table 4). Radioactive residues present

**Table 6. Production of Chlorine Dioxide Degradation Products in Rinses of Jars Treated with 1.6 or 7.8 mg of Chlorine Dioxide Using Dry or Liquid Reagent Matrices and in the Presence or Absence of Light[a]**

| | light | | | dark | |
|---|---|---|---|---|---|
| | μg/L | | | μg/L | |
| level of chlorine dioxide[b] | dry matrix | liquid matrix | *P* | dry matrix | liquid matrix |
| | | Perchlorate[c] | | | |
| low: 1.6 mg | 456 ± 233 | 438 ± 98 | 0.96 | NDR[d] | NDR |
| high: 7.8 mg | 4334 ± 838 | 880 ± 211 | <0.01 | NDR | NDR |
| *P* | <0.01 | 0.19 | | | |
| | | Chlorate[e] | | | |
| low: 1.6 mg | 998 ± 58 | 2,734 ± 289 | <0.01 | 11[f] | <LOQ[g] |
| high: 7.8 mg | 4,858 ± 693 | 17,497 ± 837 | <0.01 | NDR | 11 ± 2 |
| *P* | <0.01 | <0.01 | | | |

[a]Data are means ± standard deviations of four observations unless indicated by a footnote. NDR signifies no detectable residue. Statistical inferences of chlorate residues generated under lighted conditions were generated using log-transformed data (to meet the equal variance assumption). [b]Nominal concentrations of 600 and 3000 ppmv for the 1.6 and 7.8 mg reactions, respectively. [c]LOQ, 4 μg/L; LOD, 1 μg/L. Data are expressed on a sodium perchlorate equivalent basis. [d]Three of four replicates had no detectable residue; a single replicate had residues >LOD but less than the LOQ. [e]LOQ, 5 μg/L; LOD, 1 μg/L. Data are expressed on a sodium chlorate equivalent basis. [f]Single observation; remaining replicates had NDR. [g]All replicates had chlorate residues less than the LOQ, but greater than the LOD.

in the edible flesh portion of the cantaloupe were below the LOQ of the radiochemical assay (0.240 to 0.360 μg/g of sodium chlorite equivalents). Total radioactive residues present in seed beds represented 0.03% of the total radioactivity produced as $^{36}ClO_2$. Activity removed from the surfaces of the exposure tank, glass pedestal, and stir bar accounted for 1.7% of the total radioactivity in trial A and 2.9% in trial B. Gas purged from the exposure tank represented 18.2% of the initial activity for trial A and 10.5% for trial B. The sachet and its contents contained 37.0 and 37.6% of initial activity respectively for A and B.

Radioactive residues were not detected in edible cantaloupe flesh, indicating that chlorine dioxide gas does not penetrate the rind and acts at the cantaloupe surface. In the inedible rind fraction, radioactivity was nearly equally distributed between the rind serum (57.4 and 45.2% of rind radioactivity in trials A and B, respectively) and pellet fractions (42.6 and 54.8% of rind radioactivity in trials A and B, respectively) even though the serum fraction was the greatest by weight. Because the serum fractions represented 64 to 80% of the total rind fraction, relative concentrations of radioactivity were greater in the rind pellet fractions than in the rind serum fractions.

*Speciation of Radioactive Residues.* Table 5 summarizes residues of $^{36}$Cl-chlorite, $^{36}$Cl-chloride, $^{36}$Cl-chlorate, and $^{36}$Cl-perchlorate measured in fractions containing sufficient radioactive residues for speciation: rind serum and tank rinse fractions for both trials A and B. No sodium $^{36}$Cl-chlorite was detected in inedible rind serum or tank rinse, whereas sodium $^{36}$Cl-chloride was the predominant $^{36}ClO_2$-derived residue on cantaloupe rind comprising 86 to 87% of the rind radioactivity. The only other non-chloride residue on cantaloupe rind of trial A was sodium $^{36}$Cl-chlorate representing about 13% of the rind TRR with sodium $^{36}$Cl-perchlorate being nondetectable in rind serum of trial A, but representing 0.7% of the rind radioactivity in trial B (1.2 μg/g). In the tank rinse fraction, sodium $^{36}$Cl-chlorate and sodium $^{36}$Cl-perchlorate were the predominant radioactive residues, with sodium chlorate representing 56 to 80% of the total residue, and sodium perchlorate representing 14 to 33% of the total residue with sodium chloride a minor radioactive residue, representing 6 to 11% of the TRR. No effort to protect the cantaloupe exposures from light was made. Subsequent experiments with nonlabeled chlorine dioxide have demonstrated that chlorate and perchlorate formation during fumigation of cantaloupe can be essentially eliminated by protecting the reaction from light.

It is notable that the percentage compositions of radioactive residues on the cantaloupe rind and tank rinse fractions were not very similar. On the rind, sodium chloride was, by far, the major chlorine dioxide degradation product, representing between 86 and 87% of the radioactivity, with chlorate representing essentially the balance of activity. Such results are consistent with chlorine dioxide reductive processes and aqueous disproportionation reactions.[21,22] In contrast, glass surfaces contained mainly chlorate (55 to 80% of total glass rinse residue) and perchlorate (14 to 33% of total glass rinse residue), with lesser quantities of sodium chloride (6 to 11% of rinse radioactivity). The formation of mainly perchlorate and chlorate on glass surfaces is consistent with light catalyzed gas-phase reactions.[23,24] The formation of perchlorate from chlorine dioxide gas generated under a number of conditions is light dependent.[25,26]

As stated earlier, puree of edible flesh had no detectable residues in either trial A or B with LOD/Qs below 0.5 μg/g for sodium chlorite, sodium chlorate, and sodium perchlorate. Because it was reasoned that radioactive residues might concentrate in either the solid or liquid portions of the edible flesh, the puree was centrifuged to form liquid (serum) and pellet fractions. When serum was assayed, radioactive residues were detected in trial B cantaloupe edible flesh serum, but not in serum from trial A. Because a 1 g sample size was used to assay serum from trial B, a lower detection limit (<0.12 μg/g for each of sodium chlorite, sodium chlorate, and sodium perchlorate) was obtained. Precipitation of radioactive residues present in trial B serum with silver nitrate caused a 90% loss of activity from the serum, indicating that at least 90% of the edible flesh serum was sodium $^{36}$Cl-chloride. Assuming that the remaining 10% of the radioactive residue in edible flesh serum of trial B was either sodium $^{36}$Cl-chlorate or sodium $^{36}$Cl-perchlorate, then the concentration of radioactivity, expressed as sodium chlorate or sodium perchlorate equivalents, in serum would be 0.017 or 0.019 ng/g, respectively.

*Factors Impacting the Formation of Chlorate and Perchlorate Byproducts from Chlorine Dioxide Fumigation.* This experiment was conducted with a balanced factorial design

with level of chlorine dioxide, laboratory illumination, and reagent matrix (dry vs liquid) as main factors. Table 6 summarizes results of the experiment in which chlorate and perchlorate recovered in reaction jar rinsewater are expressed as $\mu$g/L of the sodium salt equivalents.

Data presented in Table 6 clearly demonstrate that light had a major impact on the formation of both perchlorate and chlorate from chlorine dioxide. Under dark conditions, insufficient perchlorate was formed to exceed the assay LOQ of 4 $\mu$g/L. Of the 16 samples excluded from light, perchlorate was formed in only two samples at levels that surpassed the assay LOD of 1 $\mu$g/L. In contrast, the reaction chambers exposed to light had mean perchlorate concentrations ranging from 438 to 4,334 $\mu$g/L, depending upon the amount of chlorine dioxide produced. In a similar manner, light catalyzed the formation of chlorate (means of 998 to 17,947 $\mu$g/L) on vessel walls; but under dark conditions, chlorate residues were either not detectable (LOD of 1 $\mu$g/L) or low, with a maximum concentration of 11 $\mu$g/L (Table 6). Statistical comparisons between means from dark and light exposed vessels were not possible because the darkened vessels contained insufficient chlorate and perchlorate for the calculation of treatment means (Table 6).

For the treatments exposed to light, however, significant ($P < 0.001$) main effects for both chlorine dioxide concentration and the reaction matrix were noted (Table 3). For perchlorate, a highly significant ($P < 0.001$) interaction between the target chlorine dioxide concentration and reaction matrix was observed, so no simple relationship existed. For chlorate, main effects of chlorine dioxide concentration ($P < 0.01$) and reaction matrix ($P = 0.02$) were significant, with the high chlorine dioxide concentration and liquid reaction matrix consistently producing greater quantities of chlorate than the low chlorine dioxide target concentration and the dry matrix.

The literature suggests that both light[23,24] and gas concentration[27] affect chlorine dioxide stability. Our data are also consistent with the notion that chlorine dioxide decomposition is catalyzed by light and (or) high gas concentrations. Spinks and Porter[23] reported the formation of perchlorate by gaseous chlorine dioxide decomposition, and the formation of perchlorate was dependent upon the presence of water vapor. Crawford and Dewitt[24] suggested that water vapor reacts with unstable chloroxy intermediates to form acid gases of chlorate and perchlorate. They also reported a wall to vessel volume relationship in the rate of reaction intermediate termination; presumably vessel walls act as terminal points for unstable radicals created during gas decomposition. Such data might explain the relatively high degree of deposition of $^{36}$Cl-chorate and $^{36}$Cl-perchlorate on vessel walls in which light exposure was not controlled, even with the presence of chlorine dioxide sinks (tomatoes or cantaloupe).

In the absence of light, but in the presence of water vapor, the terminal (i.e., stable) decomposition products of chlorine dioxide gas would be chlorate and chloride, consistent with the aqueous decomposition of chlorine dioxide.[22,28] Our data (Table 6), however, strongly suggest that, even in the presence of water vapor (i.e., liquid matrix), light must be present to catalyze the formation of chlorate (and also perchlorate). Thus, the mechanism for the formation of both perchlorate and chlorate is through the light catalyzed formation of unstable[25] intermediates such as chlorine perchlorate ($Cl_2O_4$).[26]

Collectively, the experiments reported herein clearly indicate the potential for chlorine dioxide fumigation of vegetables and melons from a residue chemistry perspective. Studies using radiolabel, for example, indicate that edible flesh of cantaloupe contains no chlorine dioxide related residue whatsoever. Additionally, for either tomato or cantaloupe, the major residue associated with vegetable matter is the chloride ion. Nevertheless, radiolabeled studies also show the potential for both chlorate and perchlorate formation during $ClO_2$ fumigation, especially if the fumigation is not protected from light. Further work is being conducted to determine fumigation conditions under which the formation of chlorate and perchlorate on vegetable matter may be minimized or prevented entirely. These studies will provide data supporting or refuting the concept that chlorine dioxide fumigation of produce can be accomplished without the formation of undesirable residual chloroxyanions.

## AUTHOR INFORMATION

### Corresponding Author

*Phone: 701-239-1238. E-mail: david.j.smith@ars.usda.gov.

### Funding

This study was collaboratively funded by ICA-TriNova (Agreement No. 58-5442-1-431) and the USDA ARS (Project No. 5442-32000-014).

### Notes

The authors declare no competing financial interest.

## ACKNOWLEDGMENTS

The use of trade, firm or corporation names in this publication is for the information and convenience of the reader. Such use does not constitute an official endorsement or approval by the United States Department of Agriculture or the Agricultural Research Service of any product or service to the exclusion of others that may be suitable. USDA is an equal opportunity employer.

## REFERENCES

(1) United Nations, Food and Agriculture Organization. *Global Food Losses and Food Waste: Extent, Causes and Prevention*; Rome, Italy, 2011. http://www.fao.org/docrep/014/mb060e/mb060e00.pdf. Accessed 3/19/2014.

(2) Code of Federal Regulations, 40§180.41. 2013.

(3) Laio, C.-H. Bacterial soft rot. In *Microbiology of Fruits and Vegetables*; Sapers, G. M., Gorny, J. R., Yousef, A. E., Eds.; CRC Taylor and Francis: Boca Raton, FL, USA, 2006; pp 117−134.

(4) Moss, M. O. Fungi, quality and safety issues in fresh fruits and vegetables. *J. Appl. Microbiol.* **2008**, *104*, 1239−1243.

(5) Gorny, J. Microbial contamination of fresh fruits and vegetables. In *Microbiology of Fruits and Vegetables*; Sapers, G. M., Gorny, J. R., Yousef, A. E., Eds.; CRC Taylor and Francis: Boca Raton, FL, USA, 2006; pp 3−32.

(6) US EPA. *Registration of pesticides containing chlorine dioxide*; 2009. http://www.epa.gov/pesticides/factsheets/chemicals/chlorinedioxidefactsheet.htm.

(7) Trinetta, V.; Vaidya, N.; Linton, R.; Morgan, M. Evaluation of chlorine dioxide gas residues on selected food produce. *J. Food Sci.* **2010**, *76*, T11−T15.

(8) Trinetta, V.; Linton, R. H.; Morgan, M. T. Use of chlorine dioxide gas for the postharvest control of *Alternaria alternate* and *Stemphylium vesicarium* on Roma tomatoes. *J. Sci. Food Agric.* **2013**, *93*, 3330−3333.

(9) Mahovic, M. J.; Tenney, J. D.; Bartz, J. A. Applications of chlorine dioxide gas for control of bacterial soft rot in tomatoes. *Plant Dis.* **2007**, *91*, 1316−1320.

(10) Sy, K. V.; Murray, M. B.; Harrison, D.; Beuchat, L. R. Evaluation of gaseous chlorine dioxide as a sanitizer for killing *Salmonella*, *E. coli*

O157:H7, *Listeria monocytogenes*, and yeasts and molds on fresh and fresh-cut produce. *J. Food Prot.* **2005**, *68*, 1176−1187.
(11) Sy, K. V.; McWatters, K. H.; Beuchat, L. R. Efficacy of gaseous chlorine dioxide as a sanitizer for killing *Salmonella*, yeasts, and molds on blueberries, strawberries, and raspberries. *J. Food Prot.* **2005**, *68*, 1165−1175.
(12) Hakk, H.; Smith, D. J.; Shappell, N. W. Tissue residues, metabolism, and excretion of radiolabeled sodium chlorate ($Na[^{36}Cl]ClO_3$) in rats. *J. Agric. Food Chem.* **2007**, *55*, 2034−2042.
(13) Smith, D. J.; Anderson, R. C.; Ellig, D. A.; Larsen, G. Tissue distribution, elimination, and metabolism of dietary sodium $[^{36}Cl]$-chlorate in beef cattle. *J. Agric. Food Chem.* **2005**, *53*, 4272−4280.
(14) Smith, D. J.; Stehly, G. S.; Turberg, M. T. Procedures and practices for conducting residue studies of animal health compounds in food animals. In *Handbook of Residue Analytical Methods for Agrochemicals*; Lee, P., Ed.; John Wiley & Sons, Ltd.: 2003; Vol. *1*, pp 248−299.
(15) US EPA. *Method 314.0 Determination of perchlorate in drinking water using ion chromatography. Revision 1.0*; 1999. http://www.epa.gov/ogwdw/methods/pdfs/methods/met314.pdf (accessed 8/01/2014).
(16) Han, Y.; Floros, J. D.; Linton, R. H.; Nielsen, S. S.; Nelson, P. E. Response surface modeling for the inactivation of *Escherichia coli* O157:H7 on green peppers (*Capsicum annuum* L.) by chlorine dioxide gas treatments. *J. Food Prot.* **2001**, *64*, 1128−1133.
(17) Han, Y.; Selby, L. T.; Schultze, K. K.; Nelson, P. E.; Linton, R. H. Decontamination of strawberries using batch and continuous chlorine dioxide gas treatments. *J. Food Prot.* **2004**, *67*, 2450−2455.
(18) Mahovic, M.; Bartz, J. A.; Schneider, K. R.; Tenney, J. D. Chlorine dioxide gas from an aqueous solution: Reduction of *Salmonella* in wounds on tomato fruit and movement to sinks in a treatment chamber. *J. Food Prot.* **2009**, *72*, 952−958.
(19) Wu, V. C. H.; Rioux, A. A simple instrument-free gaseous chlorine dioxide method for microbial decontamination of potatoes during storage. *Food Microbiol.* **2010**, *27*, 179−184.
(20) White, J. F.; Taylor, M. C.; Vincent, G. P. Chemistry of chlorites. *Ind. Eng. Chem.* **1942**, *34*, 782−792.
(21) Nabar, G. M.; Ramachandran, C. R.; Shenai, V. A. Studies in sodium chlorite: Part II-The mechanism of photodecomposition of sodium chlorite. *Ind. J. Technol.* **1964**, *2*, 11−14.
(22) Vel Leitner, N. K.; De Laat, J.; Dore, M. Photodecomposition of chlorine dioxide and chlorite by U.V.-irradiation—Part I. Photoproducts. *Water Res.* **1992**, *26*, 1655−1664.
(23) Spinks, J. W. T.; Porter, J. M. Photodecomposition of chlorine dioxide. *J. Am. Chem. Soc.* **1934**, *56*, 264−270.
(24) Crawford, R. A.; Dewitt, B. J. Decomposition rate studies in the gaseous chlorine dioxide-water system. *TAPPI* **1968**, *51*, 226−230.
(25) Schack, C. J.; Pilipovich, D. Chlorine perchlorate. *Inorg. Chem.* **1970**, *9*, 1387−1390.
(26) Schell-Sorokin, A. J.; Bethune, D. S.; Lankard, J. R.; Loy, M. M. T.; Sorokin, P. P. Chlorine perchlorate: A major photolysis product of chlorine dioxide. *J. Phys. Chem.* **1971**, *86*, 4653−4655.
(27) Brickhouse, M. D.; Lalain, T.; Bartram, P. W.; Hall, M.; Hess, Z.; Mantooth, B.; Reiff, L.; Zander, Z.; Stark, D.; Humphreys, P.; Ryan, S.; Martin, B. *Effects of vapor-based decontamination systems on selected building interior materials: Chlorine dioxide*; EPA/600/R-08/054; United States Environmental Protection Agency: 2008.
(28) Cosson, H.; Ernst, W. R. Photodecompostion of chlorine dioxide and sodium chlorite in aqueous solution by irradiation with ultraviolet light. *Ind. Eng. Chem. Res.* **1994**, *33*, 1468−1475.

**Table 1. Clinical Characteristics of Walnut-Allergic Subjects**

| location and subject ID | age | gender | walnut sIgE CAP (kU/L) | total IgE CAP (ku/L) | walnut SPT[a] | symptoms reported upon walnut ingestion |
|---|---|---|---|---|---|---|
| Madrid | | | | | | |
| 1 | 4 | F | 3.75 | 90 | + | anaphylaxis[b] (erythema, OAS,[c] pruritus, abdominal pain, diarrhea, dyspnea) |
| 2 | 10 | F | 1.95 | 314 | − | anaphylaxis (conjunctivitis, urticaria, bronchospasm) |
| 3 | 28 | M | 14.70 | 119 | + | anaphylaxis (eyelid angioedema, laryngeal edema, OAS, urticaria, dyspnea, blurred vision, cold sweating, malaise) |
| Manchester | | | | | | |
| 4 | 22 | M | 36.00 | 480 | nd[d] | anaphylaxis (OAS, urticaria, abdominal pain, vomiting) |
| 5 | 29 | F | 2.00 | 1200 | + | anaphylaxis (angioedema, urticaria, bronchospasm) |
| 6 | 16 | F | 21.00 | 140 | nd | anaphylaxis (lip and face angioedema, pharyngitis, urticaria, bronchospasm) |
| 7 | 21 | F | 2.30 | 470 | + | OAS |
| 8 | 21 | M | 0.50 | 170 | + | anaphylaxis (laryngeal edema, urticaria, dyspnea, wheezing, dizziness, light-headedness) |
| 9 | 18 | F | 27.10 | 130 | nd | anaphylaxis (lip and eyelid angioedema, face erythema, OAS, rhinitis, diarrhea, vomiting, dyspnea, wheezing, dizziness) |
| Barcelona | | | | | | |
| 10 | 28 | F | 1.91 | 82 | + | anaphylaxis (urticaria, abdominal pain, diarrhea, hypotension, loss of consciousness) |
| 11 | 23 | F | 12.10 | 218 | + | anaphylaxis (face urticaria, abdominal pain, vomiting) |

[a]Positive skin prick test (SPT); wheal diameter at least 3 mm greater than negative control. [b]Anaphylaxis, as defined by World Allergy Organization criteria.[38] [c]OAS, oral allergy symptoms. [d]nd, not done.

processing of preproproteins,[20] and the 7S globulin from certain plant species also undergoes N-glycosylation.[22] The 7S (Jug r 2) and 11S (Jug r 4) globulin allergens of walnut appear to follow similar patterns of posttranslational modification, but the specific processing mechanisms for this plant are poorly characterized, and the presence of N-linked glycans on Jug r 2 has yet to be demonstrated.[11,13]

Despite their early entrance into the study of plant proteins and their importance for food allergy, relatively few characterization studies have been conducted on walnut proteins, particularly regarding the natural form of the protein occurring in the nut. The objective of this study was to purify and characterize the natural 2S albumin allergen from English walnut. During the course of the study, however, an additional low molecular weight protein species was encountered with its own potential allergenic activity. Electrophoresis and mass spectrometry were employed to characterize these low molecular weight proteins, and their allergenic activity was assessed with a panel of walnut-allergic subjects' sera.

## MATERIALS AND METHODS

**Walnut-Allergic Subject Samples.** A panel of either serum or plasma was assembled from individuals with positive walnut-specific IgE (ImmunoCAP; Thermo Scientific, Uppsala, Sweden) and a convincing history of food allergy to walnut (Table 1). The patient panel was identified from clinic populations in either the United Kingdom (Manchester Respiratory and Allergy Biobank; ManRAB) or Spain (Hospital Clínico San Carlos, Madrid or Hospital Clínic, Barcelona). A pool of plasma from nine atopic, non-food-allergic subjects from Manchester was used as a negative control. Written informed consent was obtained from all patients, either specifically for this study (Madrid and Barcelona) or for future research studies following donation (ManRAB). Ethical approvals for the use of sera were obtained from the appropriate committees (National Research Ethics Service, Research Ethics Committee, 10/H1010/7, ManRAB; Comité Ético de Investigación Clínica and Comité de Investigación del Hospital Clínic, 2012/7805, Barcelona; Comité Ético de Investigación Clínica del Hospital Clínico San Carlos de Madrid, C.P.-C.I 12/365-E, Madrid).

**Materials and Walnut Preparation.** English walnuts (*J. regia* cv. Chandler) were purchased from Gold River Orchards (Oakdale, CA, USA) as raw light halves and pieces. The walnuts were ground (under liquid nitrogen, which was subsequently allowed to evaporate), and defatted walnut flour (DWNF) was produced by combining ground walnuts with hexane at a 1:5 (v/v) ratio and stirring for 1 h at room temperature. The lipid fraction was removed, the partially defatted flour was allowed to dry overnight, the dried flour was ground further, and the defatting process was repeated to produce the final DWNF (stored at −80 °C). Unless stated otherwise, all other chemical reagents were obtained from Sigma-Aldrich (Dorset, UK).

**Purification of Low Molecular Weight Walnut Proteins.** Extraction of protein from DWNF was performed with a high-salt buffer (25 mM Tris-HCl, pH 7.5, containing 1.5 M NaCl, 3 mM sodium azide). Following hydration of 3.5% (w/v) poly(vinylpolypyrrolidone) in the buffer, soluble proteins were extracted from DWNF at a 1:50 (w/v) ratio for 1 h at room temperature, with constant stirring and pH adjustment to 7.5 every 30 min. The extract was centrifuged (3600*g*, 30 min, 15 °C), and the supernatant was filtered (Whatman no. 1 filter paper and sequential 0.45 and 0.2 $\mu$m syringe filters). Total soluble protein concentrations of the DWNF extract and selected protein fractions were determined by microwell BCA assay.

The chromatographic portion of the purification consisted of ConA, gel filtration, and anion exchange stages. The high salt concentration in buffers (1.5 M NaCl) was retained for ConA and gel filtration chromatography to maintain protein solubility. The ConA chromatography was conducted with a Pharmacia XK 16 column (GE Healthcare Life Sciences, Little Chalfont, UK), packed with Concanavalin A Sepharose conjugate and connected to a BioCAD Sprint LC system (Applied Biosystems, Life Technologies, Paisley, UK). Following column equilibration and walnut extract loading, unbound (non-glycosylated) proteins were eluted (in the high-salt buffer used for extraction), followed by bound (glycosylated) proteins (in 25 mM Tris-HCl, pH 7.5, containing 0.4 M methyl $\alpha$-D-mannopyranoside, 1.5 M NaCl, and 3 mM sodium azide). The unbound, protein-containing fractions were pooled and concentrated 4-fold using a stirred-cell ultrafiltration apparatus (5 kDa nominal molecular weight limit (NMWL) membrane; Amicon, Millipore, Watford, UK). The concentrated, unbound fraction (UB pool) was subsequently used for gel filtration chromatography. The bound (glycosylated) fractions were not used further in this study, as they primarily contained higher molecular weight proteins (gel electrophoresis, data not shown).

Separation of UB pool proteins by gel filtration was conducted with a HiLoad 16/600 Superdex 200 column (GE Healthcare Life Sciences, calibrated with Bio-Rad (Hercules, CA, USA) Gel Filtration Standard

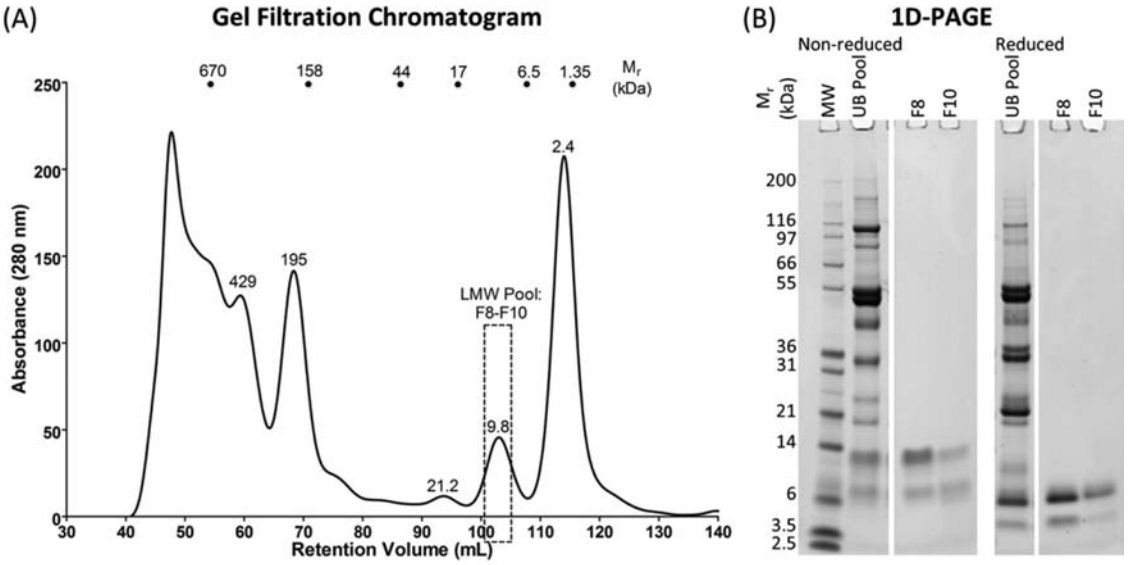


**Figure 1.** Gel filtration and 1D-PAGE analysis of nonglycosylated walnut proteins. (A) The gel filtration chromatogram has the calculated $M_r$ values labeled above each major peak and a dashed box indicating the fractions included in the LMW pool. Points along the top of the chromatogram indicate retention volumes of MW standards. (B) The 1D-PAGE image includes unbound material obtained from ConA chromatography (UB pool, 7.8 $\mu$g of protein loaded) and gel filtration fractions F8 and F10 (loaded in equal volumes) analyzed under nonreducing and reducing conditions. Molecular weight markers (MW) were also loaded (Mark12 unstained standards, Invitrogen; 5 $\mu$L loaded).

and Sigma-Aldrich aprotinin) connected to an ÄKTA FPLC system (Amersham Pharmacia Biotech, GE Healthcare Life Sciences). Following loading, proteins were eluted with the high-salt extraction buffer over 1.2 column volumes. Fractions F8−F10 (retention volume 100.5−105 mL) were combined in equal volumes to give a pooled low molecular weight fraction (LMW pool).

The LMW pooled fraction was dialyzed (3500 Da molecular weight cutoff membrane, against 20 mM Tris-HCl, pH 8.0) and concentrated by ultrafiltration (1 kDa NMWL membrane, Millipore). Anion exchange was conducted with a POROS HQ20 column (4.6 × 100 mm) connected to a BioCAD Sprint LC system. The column was equilibrated in 20 mM Tris-HCl, pH 8.0, running buffer [40% A (50 mM Tris-HCl), 60% B ($H_2O$)]. The LMW pooled fraction was loaded, the column was washed (2.0 column volumes of running buffer, 3.00 mL/min), and proteins were eluted [0−300 mM NaCl linear gradient; 40% A and 60% B to 40% A, 45% B, and 15% C (2.0 M NaCl); 3.00 mL/min]. Fractions were analyzed by gel electrophoresis and mass spectrometry.

**Gel Electrophoresis.** One-dimensional PAGE (1D-PAGE) was conducted with NuPAGE Novex 4−12% Bis-Tris precast gels. Samples were prepared per the manufacturer's instructions, under reducing (50 mM DTT) or nonreducing conditions. Equal volumes of purification fractions (following each chromatographic stage) were loaded, along with Mark12 Unstained Standards, and separated (MES SDS running buffer, 200 V, 35 min). Gels were fixed [50% (v/v) methanol, 10% (v/v) acetic acid; 2 h], stained (SimplyBlue Safe Stain, overnight), and destained (deonized water, 2 h). Gel images were acquired with a Bio-Rad GS-800 scanner. All 1D-PAGE reagents were obtained from Invitrogen (Life Technologies).

**Identification of Protein Bands by MS.** Protein bands were excised from 1D-PAGE gels for in-gel trypsin digestion. Briefly, gel plugs were destained, reduced (10 mM DTT, 30 min at 60 °C), and alkylated (100 mM iodoacetamide, 30 min at room temperature in the dark) and proteins digested with trypsin (Promega Trypsin Gold, Mass Spectrometry grade, 50 ng per plug, 3 h at 37 °C). The digestion was stopped (1% (v/v) formic acid) and peptides were eluted from the gel (50% (v/v) acetonitrile). The peptide solutions were dried in a vacuum centrifuge and resuspended in 0.1% (v/v) formic acid in water for LC-MS/MS analysis.

The tryptic digest samples were analyzed by LC-MS/MS (nanoACQUITY UPLC, Waters Corp., Milford, MA; LTQ Orbitrap XL, Thermo Scientific, Waltman, MA, USA). Peptides were trapped online to a Symmetry C18 trap column (5 $\mu$m, 180 $\mu$m × 20 mm; Waters Corp.), which was subsequently switched to an inline UPLC with a 75 mm × 250 $\mu$m i.d., 1.7 $\mu$m, BEH C18 analytical column (Waters Corp.). Peptides were separated with a gradient of 3−60% (v/v) acetonitrile in water with 0.1% (v/v) formic acid over 25 min at 250 nL $min^{-1}$. A nanospray source was used, and the mass spectrometer was operated in positive ion mode. Precursor ions were measured in the Orbitrap (60000 resolution over the mass range $m/z$ 300−2000). The Orbitrap was operated in data-dependent acquisition mode, and the top five precursor ions (2+ or 3+ charge states) were selected for collision-induced dissociation (CID) fragmentation (dynamic exclusion enabled). Product ions were analyzed in the ion trap (rapid scan rate and normal mass range).

Mascot generic format (mgf) files were generated (Proteome Discoverer software, Thermo Scientific) and searched against the UniProt database (downloaded March 3, 2011; Viridiplantae taxonomy; 592,152 sequences with filter) using a local Mascot server (version 2.2.06, Matrix Science, London, UK). The search parameters were as follows: one missed tryptic cleavage; carbamidomethyl (C) and oxidation (M) as fixed and variable modifications, respectively; peptide mass tolerance of 5 ppm; MS/MS tolerance of 0.6 Da; and Mascot peptide significance threshold of 0.05. The MS proteomics data have been deposited to the ProteomeXchange Consortium (http://proteomecentral.proteomexchange.org) via the PRIDE partner repository[23] (data set identifier PXD000634 and DOI 10.6019/PXD000634).

**Intact Mass Determination by MS.** MALDI-TOF MS was used to analyze the intact masses of the LMW proteins. The LMW pooled fraction (prior to dialysis, concentration, and anion exchange chromatography) was analyzed before and after reduction (DTT added to 5 mM, 10 min at 90 °C) and alkylation (iodoacetamide added to 10 mM, 20 min at room temperature in the dark). Samples were plated onto a polished stainless steel target with a DHB matrix [10 mg of 2,5-dihydroxybenzoic acid in 30% (v/v) acetonitrile, 70% (v/v) water with 0.1% (v/v) TFA] using the dried drop method (0.5 $\mu$L each of matrix and sample). Calibration standards (ProteoMass Peptide & Protein MALDI-MS Calibration Kit; Sigma-Aldrich) were prepared according to the manufacturer's instructions and plated in the same manner. Intact protein spectra were acquired using a Bruker Ultraflex II MALDI-TOF/TOF instrument (Coventry, UK). Positive

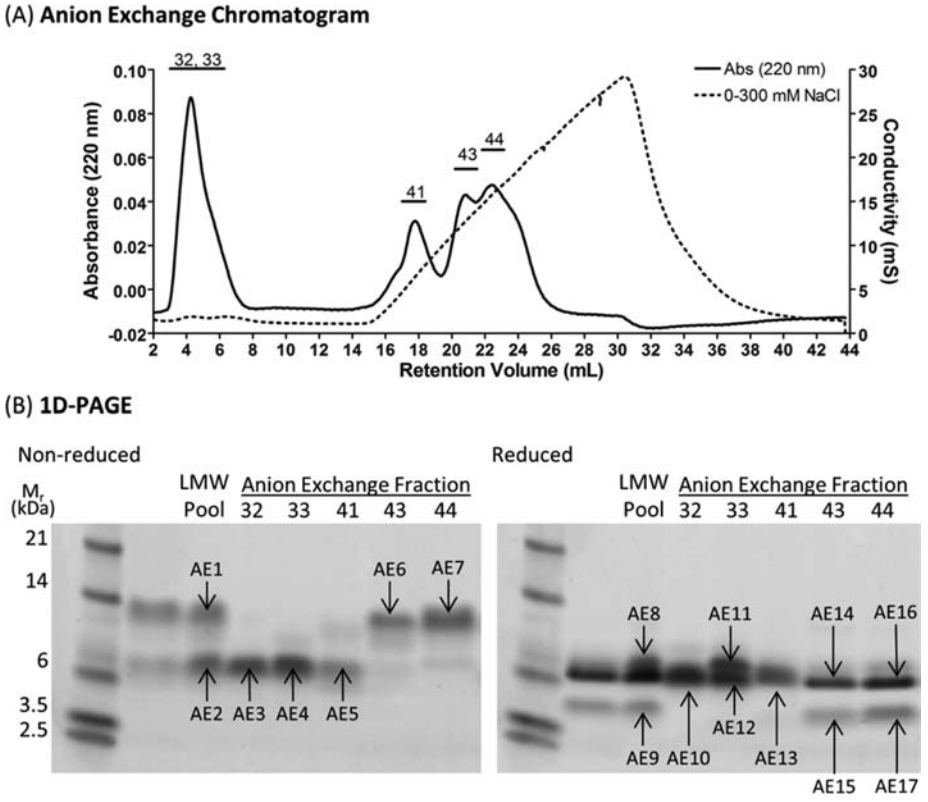


**Figure 2.** Anion exchange separation of LMW pool proteins and 1D-PAGE analysis of resultant fractions. (A) Anion exchange chromatogram shows separation of polypeptides in LMW pool obtained from gel filtration chromatography. (B) The 1D-PAGE of the low molecular weight (LMW) pool (1.8 μg protein) and equal volumes of the anion exchange fractions includes analysis under nonreducing and reducing conditions, with labels indicating bands selected for LC-MS/MS analysis.

ions were analyzed in linear mode, with 200 shots per sample used to produce a summed spectrum.

**IgE Immunoblotting.** Proteins in the LMW pooled fraction (1.0 μg per lane), along with SeeBlue Prestained Standards (Invitrogen), were separated by 1D-PAGE under nonreducing and reducing conditions (described above) and electroblotted onto a polyvinylidene fluoride membrane (0.2 μm, Immobiolon-P$^{SQ}$; Millipore) using a semidry transfer apparatus (Trans-Blot SD Semi-Dry Cell, Bio-Rad). Following protein transfer, membranes were blocked with 0.01 M PBST [0.002 M $NaH_2PO_4$, 0.008 M $Na_2HPO_4$, pH 7.4, containing 0.85% (w/v) NaCl and 0.05% (v/v) Tween 20] containing 5% (w/v) nonfat dry milk (NFDM) for 2 h at room temperature with gentle shaking. Individual serum/plasma samples were diluted 1:10 (v/v) in 0.01 M PBST containing 2.5% (w/v) NFDM. Diluted serum or plasma (0.05 mL/cm$^2$) was applied to the blocked membranes and incubated overnight at room temperature. Bound IgE was detected with a horseradish peroxidase-conjugated mouse anti-human IgE antibody (SouthernBiotech; Birmingham, AL, USA) and a chemiluminescent substrate (Pierce SuperSignal West Dura Extended Duration Substrate, Rockford, IL, USA). Images of chemiluminescence were acquired for 5 min with a CCD camera (FUJIFILM Luminescent Image Analyzer LAS-1000plus, Bedford, UK).

## RESULTS AND DISCUSSION

An extract of defatted walnut flour, prepared using a high-salt buffer, was subjected to ConA affinity chromatography to selectively remove N-glycosylated proteins. Although 2S albumins are classically extracted in water, the addition of salt was found to enhance their extraction from walnut (data not shown).The resulting fraction enriched in nonglycosylated proteins was further separated using gel filtration chromatography. A protein peak with a median relative molecular mass ($M_r$) of 9.8 kDa (LMW Pool, Figure 1A) was retained and analyzed by 1D-PAGE (Figure 1B). This analysis revealed the presence of two protein bands ($M_r$ 11.8 and 6.5 kDa), which after reduction showed a change in mobility, resolving as two bands ($M_r$ 6.0 and 4.2 kDa; Figure 1B).

The polypeptides in the LMW pool were further fractionated using anion exchange chromatography (Figure 2A). 1D-PAGE analysis of fractions from all protein-containing peaks revealed multiple protein band patterns (Figure 2B). The patterns observed with fractions 43 and 44 were analogous to the characteristic bands of other 2S albumins. Specifically, an intact protein of approximately 12 kDa under nonreducing conditions (AE6 and AE7) separated into large (6 kDa; AE14 and AE16) and small (4 kDa; AE15 and AE17) subunits upon reduction. The other fractions (32, 33, and 41) did not exhibit protein band patterns consistent with typical 2S albumin behavior. These fractions all delivered bands of 6−7 kDa on 1D-PAGE, under both nonreducing and reducing conditions (AE3, AE5, and AE10−13). The band patterns from the LMW pool demonstrated the coexistence of these two mobility patterns prior to anion exchange fractionation (AE1, AE2, AE8, and AE9).

In-gel trypsin digestion and LC-MS/MS analysis were used to identify the polypeptides observed with 1D-PAGE (Figure 2B; Table 2). A full listing of peptide spectrum matches is provided in Supporting Information Table S1. As expected, the polypeptides exhibiting typical 2S albumin mobility patterns in the LMW pooled fraction (AE1, AE8, AE9) and in fractions 43 and 44 (AE6, AE7, and AE14−17) were identified as English walnut 2S albumin (UniProt P93198; Figure 2; Table 2). This

**Table 2. LC-MS/MS Identifications of Anion Exchange 1D-PAGE Bands[a]**

| 1D-PAGE band | protein (UniProt accession) | Mascot protein score |
|---|---|---|
| AE1 | 2S albumin (P93198) | 366 |
| AE2 | 7S globulin; pecan (B3STU4/B3STU7) | 239 |
| AE3 | 7S globulin; pecan (B3STU4/B3STU7) | 151 |
| AE4 | 7S globulin; pecan (B3STU4/B3STU7) | 200 |
| AE5 | 7S globulin; walnut (Q9SEW4) | 224 |
| AE6 | 2S albumin (P93198) | 294 |
| AE7 | 2S albumin (P93198) | 349 |
| AE8 | 2S albumin (P93198) | 308 |
| AE9 | 2S albumin (P93198) | 177 |
| AE10 | 7S globulin; pecan (B3STU4/B3STU7) | 116 |
| AE11 | 7S globulin; pecan (B3STU4/B3STU7) | 206 |
| AE12 | 2S albumin (P93198) | 204 |
| AE13 | 7S globulin; pecan (B3STU4/B3STU7) | 226 |
| AE14 | 2S albumin (P93198) | 282 |
| AE15 | 2S albumin (P93198) | 213 |
| AE16 | 2S albumin (P93198) | 339 |
| AE17 | 2S albumin (P93198) | 186 |

[a]The top-ranked protein match (and UniProt accession number) for each band labeled in Figure 2B is given in the table, along with the corresponding Mascot protein score.

walnut 2S albumin was also identified as the top-ranking protein in band AE12, indicating the presence of the protein or a protein fragment in fraction 33.

The remaining low $M_r$ polypeptides in the second set of ion exchange fractions (32, 33, 42) were identified as the 7S seed storage globulin from pecan (*Carya illinoinensis*, B3STU4/B3STU7) and English walnut (Q9SEW4) (Figure 2; Table 2). This result is inconsistent with the experimentally determined $M_r$ of the mature 7S globulin from walnut (44−48 kDa by SDS-PAGE).[11] Inspection of the peptide spectrum matches from these bands showed that the peptide matches were located exclusively in the N-terminal regions of the pecan and walnut 7S globulin sequences (Figure 3A). However, all peptides were not identified in all 1D-PAGE bands (Figure 3B), indicating differences among the bands or in the compatibility of the various peptides with LC-MS/MS. The localization of peptides in the N-terminal region also explains the higher protein scores for the 7S globulin from pecan, as the walnut sequence currently in the public databases is incomplete in the N-terminal region. The walnut and pecan sequences are very similar throughout the portion of the walnut 7S sequence present in the database (92% identical), and therefore the peptide spectrum matches assigned exclusively to the pecan proteins can be assumed to be homology-based matches to walnut proteins and not indicative of the presence of pecan.

As is the case with many seed storage proteins, the 7S vicilin-like globulins are frequently synthesized as a pre-proprotein, which undergoes posttranslational proteolytic processing to produce the mature protein.[20] In some plant species (e.g., peanut, soy, pumpkin, cocoa, and cotton) evidence indicates that along with the proteolytic removal of the signal peptide, an additional hydrophilic portion of the proprotein N-terminal region is removed during the production of the 7S globulin.[24−31] On the basis of N-terminal sequencing data from the mature walnut 7S globulin (indicating an N-terminus at amino acid 173 of the full sequence), the walnut 7S globulin preproprotein processing appears to be similar to that observed in cocoa and cotton, where a large hydrophilic N-terminal region is removed.[11,24,26] Despite the well-documented presence of posttranslational processing of the 7S preproproteins in various plants, the fates of the hydrophilic N-terminal regions are often unknown, as studies have focused primarily on characterization of the mature 7S proteins.

The peptide matches obtained from the LC-MS/MS analysis spanned the entire length of the N-terminal regions of the pecan and walnut 7S proprotein sequences, but the corresponding theoretical masses (46.3 and 21.8 kDa, respectively) are much larger than the molecular masses estimated for the 1D-PAGE bands (5.8−6.7 kDa), implying that this region has undergone significant proteolysis in the seed. MALDI-TOF MS was undertaken on the LMW pooled fraction (under nonreduced and reduced/alkylated conditions) to characterize the molecular masses of the 7S globulin N-terminal fragments and the 2S albumin (Figure 4). Due to the unfractionated nature of the LMW pool, the resulting spectra were complex. On the basis of the LC-MS/MS identifications from 1D-PAGE, the 2S albumins are responsible for peaks near $m/z$ 12600 in the nonreduced sample and $m/z$ 8400 and 3000−4000 in the reduced/alkylated sample. The 7S globulin N-terminal peptides were responsible for the remaining peaks in the $m/z$ 5500−7500 region of both spectra.

Inspection of the $m/z$ range corresponding to the 7S globulin N-terminal peptides ($m/z$ 5500−7500) revealed a consistent pattern of peaks, which showed an $m/z$ shift of +232 Da between the nonreduced and reduced/alkylated samples (Figure 4, inset; Table 3). A shift of this mass is equivalent to the reduction of two disulfide bonds and alkylation of four cysteine residues (net mass change of +58 Da per cysteine residue). The N-terminal regions of the walnut and pecan 7S proproteins are rich in cysteine residues (containing 12 and 25 residues, respectively), which appear to be arranged in clusters of 4 (Figure 3C).

In addition to providing information about the 7S globulin N-terminal peptides, the MALDI-TOF spectra also revealed characteristics of the 2S albumin from walnut. The main peak corresponding to the intact (nonreduced) protein had a mass of 12617.2 Da (Figure 4). The predominant peaks for the small and large subunits were observed at $[M + H]^+$ 4640.1 and 8440.72 Da, respectively, which corresponds well with the predicted mass following reduction and alkylation of four cysteine bonds of the intact protein. Minor peaks were also observed in the regions associated with the intact 2S albumin ($m/z$ 12373.25) and its subunits ($m/z$ 8571.20, 8457.65, 4768.26, 4395.25, 4229.24, 4073.20, 4002.19, 3828.19, 3591.67, 3552.70, and 3435.28). Other tree nut 2S albumins, such as Brazil nut, have a documented level of heterogeneity, due to both sequence isoforms and posttranslational proteolytic processing.[32] In the case of the 2S albumin from English walnut, however, it is difficult to assign all MALDI-TOF or LC-MS/MS spectra as there is only one sequence isoform present in the protein databases.

The role of the English walnut 2S albumin as an allergen was established previously,[10] and it was given the allergen designation Jug r 1. The importance of the 7S N-terminal peptides as allergens in walnut is less well-understood. IgE immunoblotting of the LMW pooled fraction revealed that 3/

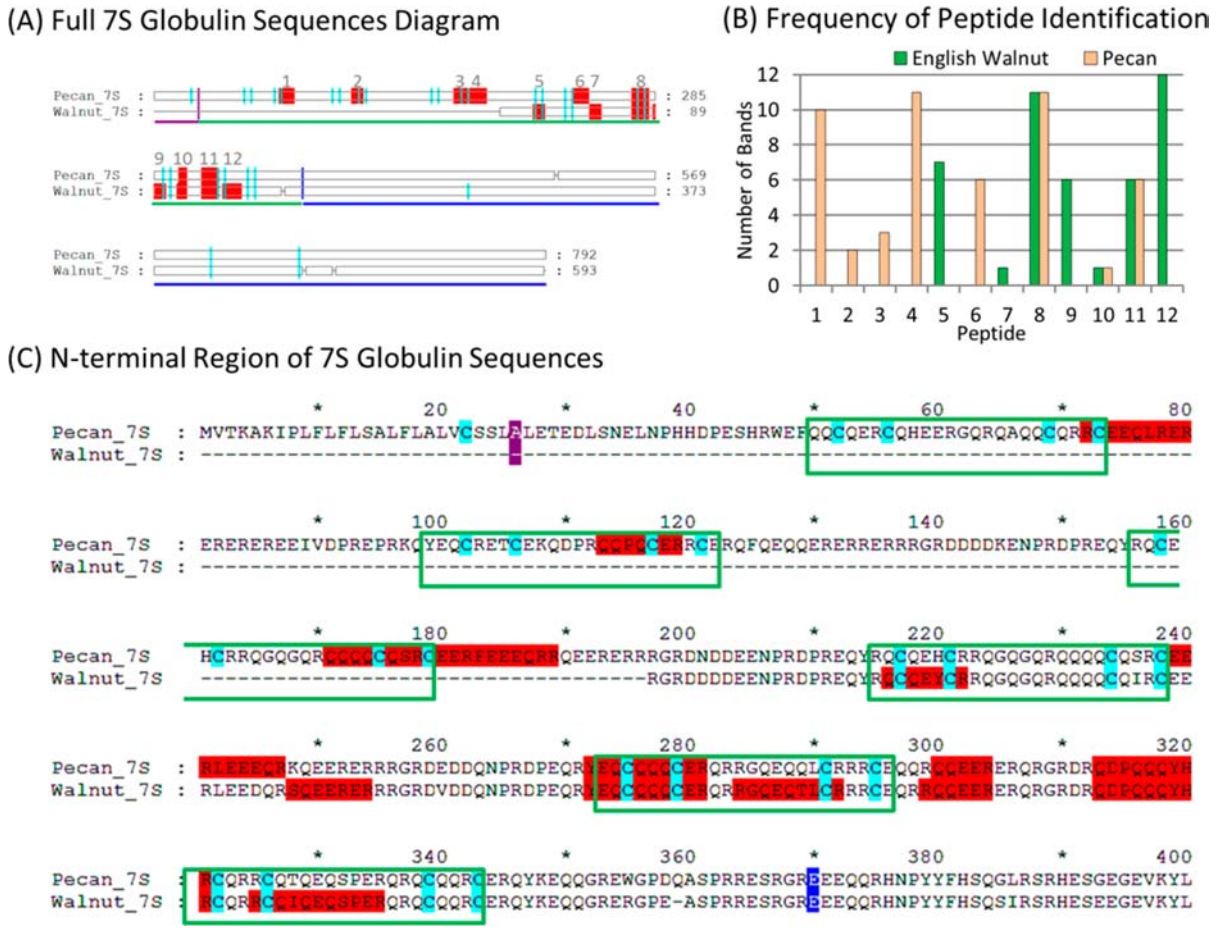


**Figure 3.** Peptide spectrum matches from anion exchange 1D-PAGE bands: (A) aligned, full-length English walnut and pecan 7S globlulin sequences (Q9SEW4 and B3STU4, respectively) are represented as white bars, labeled with red compiled sequence coverage, cyan cysteine residues, purple predicted signal peptide, green N-terminal region, and blue mature 7S globulin protein.[11] (B) The frequency of peptide occurrence is indicated as the number of 1D-PAGE bands in which each peptide (as numbered in panel A) was identified. (C) N-terminal regions of aligned English walnut and 7S globulin sequences are shown with red compiled peptide spectrum matches from all anion exchange LC-MS/MS analysis, purple predicted end of signal peptide, blue N-terminus of mature peptide,[11] and green conserved four-cysteine motifs (C-X-X-X-C-X$_{10-12}$-C-X-X-X-C) labeled.

11 (27%) sera from walnut-sensitized individuals demonstrated IgE binding to the 7S N-terminal peptides, whereas 5/11 (45%) showed IgE binding to the 2S albumin (Figure 5).

The proportion of sera reacting to the 2S albumin was less than the 75% reported by Teuber et al., but the differences could be due to a number of factors, including differences in patient geographical distribution.[10] Interestingly, in the current study, the IgE binding activity seems to be greatly decreased (to levels below the detection limit of the system utilized) when the proteins are analyzed under reducing conditions, which could indicate the presence of conformational epitopes. During the purification of nonspecific lipid transfer protein from English walnut, Pastorello et al. also isolated two peptides originating from the N-terminal region of the 7S vicilin-like globulin, which could be similar to the ones obtained in the present study based on N-terminal sequencing data.[12] In their study population, 10/46 (22%) patient sera showed IgE reactivity to at least one of the 7S globulin fragments, indicating similar levels of reactivity in the two populations.

The polypeptides from the N-terminal region of the English walnut 7S globulin proprotein described in this study are not an isolated occurrence. Similar cysteine-rich peptide fragments have been observed in macadamia nuts. Marcus et al. reported the presence of a series of antimicrobial peptides originating from the N-terminal region of the macadamia nut 7S globulin proprotein.[33] All of the peptides contained the following four-cysteine motif: C-X-X-X-C-X$_{10-12}$-C-X-X-X-C. Both the walnut and pecan 7S globulin sequences contain the same motif repeated three and six times, respectively, throughout the N-terminal region (Figure 3C), and this type of four-cysteine motif is consistent with the mass shifts observed in the MALDI-TOF spectra. The cumulative evidence in the current study indicates that the walnut 7S N-terminal fractions contain a heterogeneous mixture of peptides centered around these types of four-cysteine motifs. The presence of these motifs provides valuable information about the structure and possible biological function of these peptides.

In addition to their documented presence in some tree nut species, similar peptides have been described in other plant species.[34−36] The homologous peptide BWI-2b from buckwheat (*Fagopyrum esculentum*) functions as a trypsin inhibitor and exhibited IgE reactivity in 4/12 buckwheat-allergic subject sera.[34] In addition, the major buckwheat allergen, Fag e 3, also has homology with the 7S globulin proprotein N-terminal region.[35] Another homologous peptide from buckwheat, BWI-2c, was recently sequenced and described as having potent trypsin inhibition functionality and an $\alpha$-helical hairpin structure, stabilized by disulfide bonds of the four-cysteine

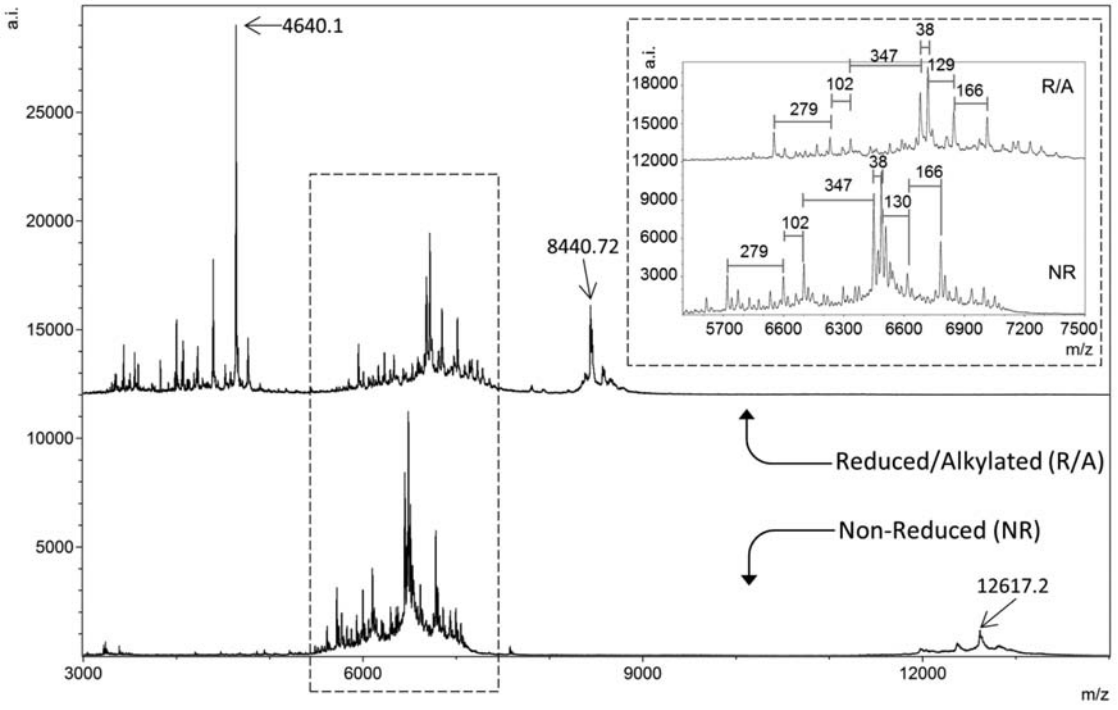


**Figure 4.** MALDI-TOF analysis of walnut LMW pool. Averaged spectra of the LMW gel filtration pool under nonreduced (NR) or reduced and alkylated (R/A) conditions are shown above, with average intensity (a.i.) displayed on the *y*-axis. Labels on inset spectra indicate conserved $m/z$ differences between peaks.

**Table 3. Mass Shifts of 7S Globulin N-Terminal Peptide MALDI-TOF Peaks Following Reduction and Alkylation**[a]

| NR mean $m/z$ | R/A mean $m/z$ | Δ $m/z$ (R/A-NR) |
|---|---|---|
| 5720.2395 | 5952.9377 | 232.6981 |
| 5999.1986 | 6231.6017 | 232.4032 |
| 6101.4799 | 6333.9527 | 232.4728 |
| 6448.7647 | 6681.1299 | 232.3652 |
| 6486.8504 | 6718.6630 | 231.8126 |
| 6616.5919 | 6848.1240 | 231.5321 |
| 6782.3607 | 7014.4832 | 232.1224 |

[a]Values shown indicate calculations of the $m/z$ shift of the conserved pattern of peaks illustrated in Figure 4 (inset), under nonreduced (NR) and reduced and alkylated (R/A) conditions.

motif.[36] Finally, cotton (*Gossypium hirsutum*) also has a 7S globulin gene encoding for a hydrophilic N-terminal region (containing three repetitions of the four-cysteine motif), and an isolated heterogeneous population of peptides from this region demonstrated antifungal properties.[37] The independent description of similar N-terminal peptides derived from 7S globulin proprotein sequences in seeds from several different plant species implies that this type of peptide is produced consistently in a variety of plants. Due to the lack of complete plant genomes and proteomes, however, it is difficult to assess the full range of affected plant species.

Purification and analysis of the LMW, nonglycosylated fraction of walnut revealed the presence of two main polypeptide species: the 2S albumin and a mixture of

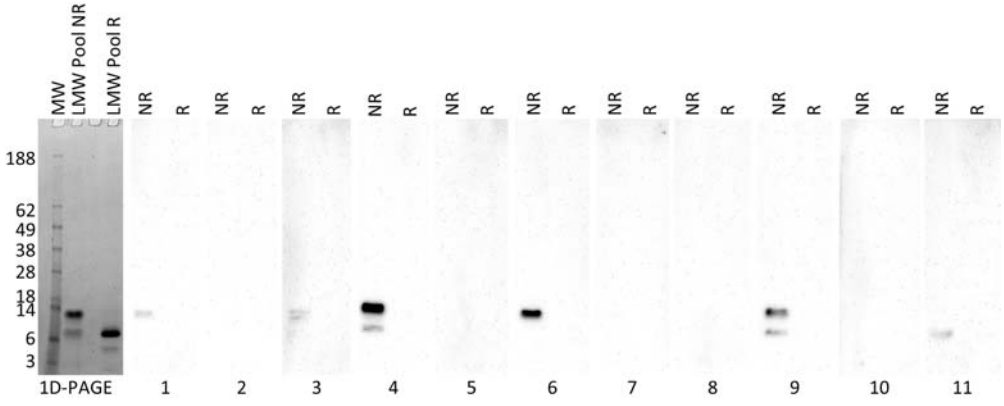


**Figure 5.** IgE reactivity to low molecular weight walnut proteins. Each IgE immunoblot includes the LMW pool (1.0 μg of protein) under nonreducing (NR) and reducing conditions (R), run in the same manner as on the 1D-PAGE gel replicate. Molecular weight markers (MW, SeeBlue prestained standards, 2 μL) were also run for each gel and blot. The numerical labels (1−11) below each immunoblot correspond to the individual serum samples from the walnut-allergic subjects described in Table 1.

polypeptides derived from the N-terminal region of the 7S seed storage globulin proprotein. N-terminal peptides derived from 7S globulin proprotein sequences and containing a conserved four-cysteine motif have been observed in a variety of plants, including walnuts, macadamia nuts, buckwheat, pumpkin, and cotton,[12,24,27,33−37] and gene sequences suggest they may be produced in a number of other plants such as cocoa.[26] In cotton and pumpkin, there is quite convincing evidence that multiple protein products with separate functionalities are produced from the single proprotein sequence typically designated a 7S globulin.[24,27,37] In cases when the peptides have been characterized, they seem to function primarily as a defense mechanism, with antimicrobial or trypsin inhibition activity.[33,34,36,37]

Additionally, these four-cysteine motif containing peptides can be potential allergens, as illustrated by the IgE reactivity observed in walnut- or buckwheat-allergic subjects using immunoblot, ELISA, or RAST analysis.[12,34,35] These data suggest that the N-terminal fragments could represent a subset of the 7S seed storage globulin allergens, which should be considered alongside other low molecular weight allergens such as 2S albumin and LTPs. However, as IgE reactivity alone is not fully indicative of biological activity, further in vivo or in vitro experiments (e.g., histamine release assays) should be conducted to confirm the clinical significance of the N-terminal peptides containing the four-cysteine motif. The implications for these peptides as potential allergens extend particularly to diagnostic and detection methods that aim to characterize allergens at the molecular level.

Component-resolved diagnosis using recombinant allergens, for example, could provide misleading or incomplete information if the N-terminal region of the 7S globulin proprotein is not analyzed separately from the mature protein, as these represent two independent allergenic components. In addition, the development of mass spectrometry-based methods for the detection of allergens in foods must properly assign peptide targets to particular proteins of interest and should recognize the independent nature of the 7S globulin proprotein N-terminal region. This study also shows that the 2S albumin from walnut exhibits a substantial amount of heterogeneity, which is not reflected in protein sequence databases. Without in-depth knowledge of protein isoforms and posttranslational processing, these types of heterogeneity make full characterization of native walnut proteins by mass spectrometry more challenging. As is the case with many plant foods, the genetic characterization of these species lags behind that of many animal and bacterial species. The continued expansion of genomic and proteomic data from plant foods is key to increasing our understanding of plant food allergens and will enhance our ability to use advanced techniques for characterization and quantitation of allergens in foods.

## ■ ASSOCIATED CONTENT

### Ⓢ Supporting Information

Table S1: Mascot Identification of Peptides and Proteins from LMW English Walnut Anion Exchange Bands. This material is available free of charge via the Internet at http://pubs.acs.org.

## ■ AUTHOR INFORMATION

### Corresponding Author

*(M.L.D.) E-mail: mdowns2@unl.edu. Phone: (402) 472-5423. Fax: (402) 472-4474.

### Funding

Research funding was provided by the Food Allergy Research & Resource Program at the University of Nebraska, a food industry-sponsored consortium of 80 food processing companies and their suppliers. This paper is independent research supported by the National Institute for Health Research Clinical Research Facility at University Hospital of South Manchester NHS Foundation Trust. The views expressed in this publication are those of the authors and not necessarily those of the NHS, the National Institute for Health Research, or the Department of Health.

### Notes

The authors declare no competing financial interest.

## ■ ACKNOWLEDGMENTS

We acknowledge the Manchester Respiratory and Allergy Biobank (funded by the UK National Institute for Health Research) and the North West Lung Centre Charity for supporting this project. In addition we thank the study participants for their contribution. We also thank Francis Mulholland (Institute of Food Research, Norwich, UK) for mass spectrometry technical support and Dr. Claire Eyers (Institute of Integrative Biology, University of Liverpool, UK) for helpful discussions.

## ■ ABBREVIATIONS USED

DWNF, defatted walnut flour; LMW, low molecular weight

## ■ REFERENCES

(1) Osborne, T. B.; Campbell, G. F. Conglutin and vitellin. *J. Am. Chem. Soc.* **1896**, *18*, 609−623.

(2) Osborne, T. B.; Harris, I. F. The globulin of the English walnut, the American black walnut and the butternut. *J. Am. Chem. Soc.* **1903**, *25*, 848−853.

(3) Sicherer, S. H.; Muñoz-Furlong, A.; Godbold, J. H.; Sampson, H. A. US prevalence of self-reported peanut, tree nut, and sesame allergy: 11-year follow-up. *J. Allergy Clin. Immunol.* **2010**, *125*, 1322−1326.

(4) Ben-Shoshan, M.; Harrington, D. W.; Soller, L.; Fragapane, J.; Joseph, L.; St. Pierre, Y.; Godefroy, S. B.; Elliot, S. J. A population-based study on peanut, tree nut, fish, shellfish, and sesame allergy prevalence in Canada. *J. Allergy Clin. Immunol.* **2010**, *125*, 1327−1335.

(5) Sicherer, S. H.; Furlong, T. J.; Muñoz-Furlong, A.; Burks, A. W.; Sampson, H. A. A voluntary registry for peanut and tree nut allergy: characteristics of the first 5149 registrants. *J. Allergy Clin. Immunol.* **2001**, *108*, 128−132.

(6) Sampson, H. A.; Mendelson, L.; Rosen, J. P. Fatal and near-fatal anaphylactic reactions to food in children and adolescents. *N. Engl. J. Med.* **1992**, *327*, 380−384.

(7) Pumphrey, R. S. H. Lessons for management of anaphylaxis from a study of fatal reactions. *Clin. Exp. Allergy* **2000**, *30*, 1144−1150.

(8) Bock, S. A.; Muñoz-Furlong, A.; Sampson, H. A. Fatalities due to anaphylactic reactions to foods. *J. Allergy Clin. Immunol.* **2001**, *107*, 191−193.

(9) Asero, R.; Antonicelli, L.; Arena, A.; Bommarito, L.; Caruso, B.; Colombo, G.; Crivellaro, M.; De Carli, M.; Della Torre, E.; Della Torre, F.; Heffler, E.; Lodi Rizzini, F.; Longo, R.; Manzotti, G.; Marcotulli, M.; Melchiorre, A.; Minale, P.; Morandi, P.; Moreni, B.; Moschella, A.; Murzilli, F.; Nebiolo, F.; Poppa, M.; Randazzo, S.; Rossi, G.; Senna, G. E. Causes of food-induced anaphylaxis in Italian adults: a multi-centre study. *Int. Arch. Allergy Immunol.* **2009**, *150*, 271−277.

(10) Teuber, S. S.; Dandekar, A. M.; Peterson, W. R.; Sellers, C. L. Cloning and sequencing of a gene encoding a 2S albumin seed storage protein precursor from English walnut (*Juglans regia*), a major food allergen. *J. Allergy Clin. Immunol.* **1998**, *101*, 807−814.

(11) Teuber, S. S.; Jarvis, K. C.; Dandekar, A. M.; Peterson, W. R.; Ansari, A. A. Identification and cloning of a complementary DNA encoding a vicilin-like proprotein, Jug r 2, from English walnut kernel (*Juglans regia*), a major food allergen. *J. Allergy Clin. Immunol.* **1999**, *104*, 1311−1320.
(12) Pastorello, E. A.; Farioli, L.; Pravettoni, V.; Robino, A. M.; Scibilia, J.; Fortunato, D.; Conti, A.; Borgonovo, L.; Bengtsson, A.; Ortolani, C. Lipid transfer protein and vicilin are important walnut allergens in patients not allergic to pollen. *J. Allergy Clin. Immunol.* **2004**, *114*, 908−914.
(13) Wallowitz, M.; Peterson, W. R.; Uratsu, S.; Comstock, S. S.; Dandekar, A. M.; Teuber, S. S. Jug r 4, a legumin group food allergen from walnut (*Juglans regia* Cv. Chandler). *J. Agric. Food Chem.* **2006**, *54*, 8369−8375.
(14) Breiteneder, H.; Radauer, C. A classification of plant food allergens. *J. Allergy Clin. Immunol.* **2004**, *113*, 821−830.
(15) Beyer, K.; Bardina, L.; Grishina, G.; Sampson, H. A. Identification of sesame seed allergens by 2-dimensional proteomics and Edman sequencing: seed storage proteins as common food allergens. *J. Allergy Clin. Immunol.* **2002**, *110*, 154−159.
(16) Kleber-Janke, T.; Crameri, R.; Appenzeller, U.; Schlaak, M.; Becker, W.-M. Selective cloning of peanut allergens, including profilin and 2S albumins, by phage display technology. *Int. Arch. Allergy Immunol.* **1999**, *119*, 265−274.
(17) Pastorello, E. A.; Farioli, L.; Pravettoni, V.; Ispano, M.; Conti, A.; Ansaloni, R.; Rotondo, F.; Incorvaia, C.; Bengtsson, A.; Rivolta, F.; Trambaioli, C.; Previdi, M.; Ortolani, C. Sensitization to the major allergen of Brazil nut is correlated with the clinical expression of allergy. *J. Allergy Clin. Immunol.* **1998**, *102*, 1021−1027.
(18) Pastorello, E. A.; Varin, E.; Farioli, L.; Pravettoni, V.; Ortolani, C.; Trambaioli, C.; Fortunato, D.; Giuffrida, M. G.; Rivolta, F.; Robino, A.; Calamari, A. M.; Lacava, L.; Conti, A. The major allergen of sesame seeds (*Sesamum indicum*) is a 2S albumin. *J. Chromatogr., B: Biomed. Sci. Appl.* **2001**, *756*, 85−93.
(19) Robotham, J. M.; Wang, F.; Seamon, V.; Teuber, S. S.; Sathe, S. K.; Sampson, H. A.; Beyer, K.; Seavy, M.; Roux, K. H. Ana o 3, an important cashew nut (*Anacardium occidentale* L.) allergen of the 2S albumin family. *J. Allergy Clin. Immunol.* **2005**, *115*, 1284−1290.
(20) Shewry, P. R.; Napier, J. A.; Tatham, A. S. Seed storage proteins: structures and biosynthesis. *Plant Cell* **1995**, *7*, 945−956.
(21) Sordet, C.; Culerrier, R.; Granier, C.; Rance, F.; Didier, A.; Barre, A.; Rouge, P. Expression of Jug r 1, the 2S albumin allergen from walnut (*Juglans regia*), as a correctly folded and functional recombinant protein. *Peptides* **2009**, *30*, 1213−1221.
(22) van Ree, R.; Cabanes-Macheteau, M.; Akkerdaas, J.; Milazzo, J.-P.; Loutelier-Bourhis, C.; Rayon, C.; Villalba, M.; Koppelman, S.; Aalberse, R.; Rodríguez, R.; Faye, L.; Lerouge, P. $\beta$(1,2)-Xylose and $\alpha$(1,3)-fucose residues have a strong contribution in IgE binding to plant glycoallergens. *J. Biol. Chem.* **2000**, *275*, 11451−11458.
(23) Vizcaíno, J. A.; Côté, R. G.; Csordas, A.; Dianes, J. A.; Fabregat, A.; Foster, J. M.; Griss, J.; Alpi, E.; Birim, M.; Contell, J.; O'Kelly, G.; Schoenegger, A.; Ovelleiro, D.; Pérez-Riverol, Y.; Reisinger, F.; Ríos, D.; Wang, R.; Hermjakob, H. The Proteomics Identifications (PRIDE) database and associated tools: status in 2013. *Nucleic Acids Res.* **2013**, *41*, D1063−D1069.
(24) Chlan, C.; Pyle, J. B.; Legocki, A. B.; Dure, L., III. Developmental biochemistry of cottonseed embryogenesis and germination XVIII cDNA and amino acid sequences of members of the storage protein families. *Plant Mol. Biol.* **1986**, *7*, 475−489.
(25) Doyle, J. J.; Schuler, M. A.; Godette, W. D.; Zenger, V.; Beachy, R. N.; Slightom, J. L. The glycosylated seed storage proteins of *Glycine max* and *Phaseolus vulgaris*. Structural homologies of genes and proteins. *J. Biol. Chem.* **1986**, *261*, 9228−9238.
(26) Spencer, M.; Hodge, R. Cloning and sequencing of a cDNA encoding the major storage proteins of *Theobroma cacao*. *Planta* **1992**, *186*, 567−576.
(27) Yamada, K.; Shimada, T.; Kondo, M.; Nishimura, M.; Hara-Nishimura, I. Multiple functional proteins are produced by cleaving Asn-Gln Bonds of a single precursor by vacuolar processing enzyme. *J. Biol. Chem.* **1999**, *274*, 2563−2570.
(28) Coates, J. B.; Medeiros, J. S.; Thanh, V. H.; Nielsen, N. C. Characterization of the subunits of $\beta$-conglycinin. *Arch. Biochem. Biophys.* **1985**, *243*, 184−194.
(29) de Jong, E. C.; van Zijverden, M.; Spanhaak, S.; Koppelman, S. J.; Pellegrom, H.; Penninks, A. H. Identification and partial characterization of multiple major allergens in peanut proteins. *Clin. Exp. Allergy* **1998**, *28*, 743−751.
(30) Wichers, H. J.; De Beijer, T.; Savelkoul, H. F. J.; van Amerongen, A. The major peanut allergen Ara h 1 and its cleaved-off N-terminal peptide; possible implications for peanut allergen detection. *J. Agric. Food Chem.* **2004**, *52*, 4903−4907.
(31) Marsh, J.; Rigby, N.; Wellner, K.; Reese, G.; Knulst, A.; Akkerdaas, J.; van Ree, R.; Radauer, C.; Lovegrove, A.; Sancho, A.; Mills, C.; Vieths, S.; Hoffmann-Sommergruber, K.; Shewry, P. R. Purification and characterisation of a panel of peanut allergens suitable for use in allergy diagnosis. *Mol. Nutr. Food Res.* **2008**, *52*, S272−S285.
(32) Moreno, F. J.; Jenkins, J. A.; Mellon, F. A.; Rigby, N. M.; Robertson, J. A.; Wellner, N.; Mills, E. N. C. Mass spectrometry and structural characterization of 2S albumin isoforms from Brazil nuts (*Bertholletia excelsa*). *Biochim. Biophys. Acta* **2004**, *1698*, 175−186.
(33) Marcus, J. P.; Green, J. L.; Goulter, K. C.; Manners, J. M. A family of antimicrobial peptides is produced by processing of a 7S globulin protein in *Macadamia integrifolia* kernels. *Plant J.* **1999**, *19*, 699−710.
(34) Park, S.-S.; Abe, K.; Kimura, M.; Urisu, A.; Yamasaki, N. Primary structure and allergenic activity of trypsin inhibitors from the seeds of buckwheat (*Fagopyrum esculentum* Moench). *FEBS Lett.* **1997**, *400*, 103−107.
(35) Choi, S.-Y.; Sohn, J.-H.; Lee, Y.-W.; Lee, E.-K.; Hong, C.-S.; Park, J.-W. Characterization of buckwheat 19-kD allergen and its application for diagnosing clinical reactivity. *Int. Arch. Allergy Immunol.* **2007**, *144*, 267−274.
(36) Oparin, P. B.; Mineev, K. S.; Dunaevsky, Y. E.; Arseniev, A. S.; Belozersky, M. A.; Grishin, E. V.; Egorov, T. A.; Vassilevski, A. A. Buckwheat trypsin inhibitor with helical hairpin structure belongs to a new family of plant defence peptides. *Biochem. J.* **2012**, *446*, 69−77.
(37) Chung, R. P. T.; Neumann, G. M.; Polya, G. M. Purification and characterization of basic proteins with in vitro antifungal activity from seeds of cotton, *Gossypium hirsutum*. *Plant Sci.* **1997**, *127*, 1−16.
(38) Simons, F. E. R.; Ardusso, L. R. F.; Bilò, M. B.; El-Gamal, Y. M.; Ledford, D. K.; Ring, J.; Sánchez-Borges, M.; Senna, G.; Sheikh, A.; Thong, B. Y. World Allergy Organization anaphylaxis guidelines: summary. *J. Allergy Clin. Immunol.* **2011**, *127*, 587−593.

**Table 1. Treatment Protocols**[a]

| | pot cultures | | | | field |
|---|---|---|---|---|---|
| products | sulcotrione | Mikado | grape marc | mixtures | Mikado |
| | | | **Spray** | | |
| liquid volumes | | | 1.12 mL | | 1 L |
| area (four leaves) | | | 1 $dm^2$ | | 1 ha |
| application rates | | | | | |
| A1 | 300 $\mu$g | 1 $\mu$L (300 $\mu$g sulcotrione) | 900 $\mu$g | 300 $\mu$g sulcotrione/900 $\mu$g grape marc/ $dm^2$ | 300 g sulcotrione/ha, i.e., 300 $\mu g/dm^2$ |
| A2 | 600 $\mu$g | 2 $\mu$L (600 $\mu$g sulcotrione) | 1800 $\mu$g | 600 $\mu$g sulcotrione/1800 $\mu$g grape marc /$dm^2$ | |
| A3 | 900 $\mu$g | 3 $\mu$L (900 $\mu$g sulcotrione) | 2700 $\mu$g | 900 $\mu$g sulcotrione/2700 $\mu$g grape marc/ $dm^2$ | |
| | | | **Infiltration** | | |
| liquid volumes | | | 50 $\mu$L | | 1 L |
| area | | | 1 $cm^2$ | | 1 ha |
| application rates | | | | | |
| C1 | 300 $\mu g$/1.12 mL, i.e., 13.4 $\mu g$/50 $\mu L/cm^2$ | 1 $\mu$L (300 $\mu$g sulcotrione)/1.12 mL, i.e., 13.4 $\mu$g sulcotrione/50 $\mu L/cm^2$ | 900 $\mu g$/1.12 mL, i.e., 40 $\mu g$/50 $\mu L/cm^{-2}$ | 13.4 $\mu$g sulcotrione/40 $\mu$g grape marc/ 50 $\mu L/cm^2$ | 300 g/ha, i.e., 3 $\mu g/cm^2$ |
| C2 | 27 $\mu g$/50 $\mu L/cm^2$ | 27 $\mu$g sulcotrione/50 $\mu L/cm^2$ | 80 $\mu g$/50 $\mu L/cm^{-2}$ | 27 $\mu$g sulcotrione/80 $\mu$g grape marc/ 50 $\mu L/cm^2$ | |
| C3 | 40 $\mu g$/50 $\mu L/cm^2$ | 40 $\mu$g sulcotrione/50 $\mu L/cm^2$ | 120 $\mu$g grape marc/ 50 $\mu L/cm^2$ | 40 $\mu$g sulcotrione/120 $\mu$g grape marc/ 50 $\mu L/cm^2$ | |

[a]*Leaf spray protocol:* plants with four leaves, covering 1 $dm^2$, were sprayed twice on each leaf. Volume of one spray was 0.14 mL. Therefore, treatments for 1 plant (1 $dm^2$) required 1.12 mL of solution, containing 300 $\mu$g of sulcotrione or 1 $\mu$L of Mikado and/or 900 $\mu$g grape marc for application rates called A1. Treatments A2 and A3 used 2 and 3 times A1 rates, respectively, for each product. For comparison, the application rate of sulcotrione used in fields is reported. *Leaf infiltration protocol:* usually, 50 $\mu$L of liquid (products in ultrapure water) was infiltrated until solutions spread across leaf area of 1 $cm^2$. C1 treatments used 268 $\mu$g/mL sulcotrione solution, either active ingredient or trademark Mikado, and 9 $\mu$g/mL grape marc, either alone or in mixtures. C2 and C3 treatments used 2 and 3 times C1 application rates, respectively, for each product. For comparison, the application rate of sulcotrione used in fields is reported.

commercial product Mikado. The aim of the work was to evaluate consequences of treatments by sulcotrione and trademark Mikado on plant cell physiology and the ability of grape marc to control plant response to determine if such treatments can modify pesticide effects on stress metabolism.

## MATERIALS AND METHODS

**Plant Material and Chemicals.** Sulcotrione, 2-(2-chloro-4-(methylsulfonyl) benzoyl)-1,3-cyclohexanedione ($M_m$ 328.77; dissociation constant, $pK_a$, 3.13; boiling point, 574.5 °C at 760 mmHg; Riedel de Haën, Pestanal, Saint-Quentin Fallavier, France), and commercial product as a concentrated suspension of sulcotrione at 300 g/L (liquid Mikado; Bayer CropScience) were used. Water was purified through a sterile Millipore Milli-Q system (Millipore $\alpha$Q; resistivity, 18 M·cm, DOC, <0.1 mg/L).

The experimental model of *V. faba* var. Aguadulce, is a cultivar with a high sensitivity to pollutants.[5,30] *V. faba* was also used to study responses of oxidative stress markers[31] and other antitoxic plant defenses, such as phytochelatins,[32] to environmental pollutants. Seeds of *V. faba* were surface sterilized with 10% sodium hypochloride, rinsed several times with distilled water, and placed on moistened paper at 25 °C for 4−5 days, allowing them to germinate, then put in pots filled with commercial substrate (40% black, 30% brown, and 30% blond peat moss, pH 6.1) and transfer to greenhouse (22 ± 5 °C; photoperiod, 16 h light/8 h dark). Grape marc (powder Acys; 60% polyphenols containing 25% anthocyanins) was a product from Grap'Sud (30360 Cruviers-Lascours).[21]

**Plant Treatments.** Herbicides, grape marc, and mixtures were applied as aqueous solutions on leaf tissue either as aerosol spray or by infiltration.

*Foliar Spray Treatments.* Spray treatment (1.12 mL per plant) on foliage was made onto the upper face of four leaves (two sprays per leaf). Plants were thus treated as in fields, that is, sulcotrione 300 g/ha or Mikado, 1 L/ha, a trademark that contains sulcotrione (300 g/L). Plants were thus treated using 0.3 mg/$dm^2$ (A1) sulcotrione active ingredient (ai) or sulcotrione in commercial product (i.e., 1 $\mu$L of Mikado). Treatments with grape marc contained 0.9 mg/$dm^2$ grape product for A1 treatments. The mixture of grape marc and sulcotrione then had a ratio 3:1 (w/w), respectively. To use similar ratios of sulcotrione and grape marc for treatments, the mixture made of grape marc and Mikado was 0.9 mg/1 $\mu$L (w/v), respectively. A2 and A3 application rates were 2 and 3 times the A1 rate, respectively, for every product. All products and mixtures were solubilized in 6 mL of sterile ultrapure water before being sprayed. Control leaf samples were sprayed with 1.12 mL of ultrapure water alone.

*Leaf Infiltrations.* These were carried out on leaf blades using plastic syringes. For infiltration treatments, 50 $\mu$L of solutions was usually infiltrated into a leaf area of 1 $cm^2$. Three replicates were performed on different plants. Table 1 describes experimental conditions compared to sulcotrione pesticide used in fields. For transcript analysis by leaf infiltrations, C1 treatments used sulcotrione active ingredient, Mikado (300 mg/mL), and grape marc (0.9 mg/mL), either alone or in mixtures. C2 and C3 treatments were used 2 and 3 times the C1 application rate for each product, respectively. Negative controls were obtained with sterile ultrapure water infiltrated leaves. Plant responses were observed after 2 or 4 days as indicated for treatments.

**Analysis of Membrane Lipoperoxides.** Fresh bean roots were ground in a buffer solution consisting of 0.5% thiobarbituric acid (TBA) and 20% trichloroacetic acid (TCA) (w/v = 1:10) with sterile Fontainebleau sand. The ground material was heated in a water bath at 95 °C for 30 min. During incubation, TBA and aldehyde compounds were bound. The reaction was stopped by immediate cooling in an ice bath. After centrifugation at 10000*g* for 10 min, the supernatant was recovered for a colorimetric assay of lipoperoxides. Their concentrations were determined according to the method of Heath and Packer.[33] The lipid peroxidation products that react with TBA mainly are malondialdehyde, MDA, and endoperoxides.[34] Absorbance of the TBA−MDA complex was measured by spectrophotometer at 532 nm

**Table 2. Primer Sequences for Gene Probes**

| target gene | primer sequences | product length (bp) | accession no. |
|---|---|---|---|
| actin | F: 5′-CAGCAGAGCGGGAAATTGTGAGGG-3′<br>R: 5′-AGGGCATCTGAATCTTTCAGCACCG-3′ | 147 | EU884301 |
| Apx | F: 5′-GGAAAGGCTATGGGGCTTAG-3′<br>R: 5′-TCAACAAGAGGGCGGAATAC-3′ | 230 | X62077.1 |
| ubiquitin | F: 5′-TCATCTTGTCCTCCGTCTCC-3′<br>R: 5′-AGCCAAAGTCCTTCCATCCT-3′ | 199 | AJ012552.1 |
| hsp 70.1 | F: 5′-TGTGCTTTGACATTGATGCCAACGG-3′<br>R: 5′-ATCCTCAGACTTGTACTTCTCAGCC-3′ | 136 | EU884304 |
| Cu-ZnSOD Cy | F: 5′-TGGACCACATTTCAATCCTAATGG-3′<br>R: 5′-CTTTCCCAAGATCATCAGGATCGG-3′ | 177 | EU884303 |
| Cu-ZnSOD CH | F: 5′-CTGGACCACATTTCAATCCTAATGG-3′<br>R: 5′-CTTTCCCAAGATCATCAGGATCGG-3′ | 207 | AB087845 |
| catalase | F: 5′-TGAACAGCTTGCATTTTGTCCTGCC-3′<br>R: 5′-ATTGTTGTGGTGAGACCACTTGGG-3′ | 132 | EU884302 |

and corrected by reading at 600 nm. MDA concentration was calculated using a molar extinction coefficient ($\varepsilon$ = 155 mm/cm).

**Cell Death Assays.** Cell death in leaf tissue was monitored by Evans Blue staining[35] as previously described.[21] Each assay was performed with 10 leaf disks (1 cm in diameter) punched out from each infiltrated area of the same leaf; triplicates were obtained from three different plants. Leaf disks were incubated for 30 min in 0.25% Evans Blue (Sigma, France) at room temperature on a shaker, extensively rinsed to remove excess dye, and ground in a tissue grind tube with 1 mL of 1% SDS solution. Treated leaf extracts were then centrifuged for 20 min at 20000*g*, and supernatants were diluted 8-fold with distilled water. Dye absorbencies were measured with a spectrophotometer at 600 nm and referred to the absorbance versus leaf disk weight, for either sprayed or infiltrated plants. Cell death was measured with plants treated by spray, either with different concentrations of products (A1−A3), pesticide, and grape marc for 4 days, or using the highest rates of products (A3) but for two periods, 2 and 4 days.

**RNA Isolation and Quantification.** Leaf tissues (200 mg) were ground in liquid nitrogen, and RNA extractions were performed using 1 mL of Trireagent solution (Euromedex, France) according to the manufacturer's instructions. Total RNA was cleaned up with 0.5 U DNase I solution (Euromedex, France), containing 20 U RNase inhibitor (Euromedex, France). RNA integrity was analyzed on 1% agarose gel by observation of rRNA spots. RNA concentrations were measured by absorbance at 260 nm. Reverse transcription was performed using total RNA and Euroscript Reverse Transcriptase (Eurogentec, France) according to the manufacturer's instructions. Quantitative assessment of mRNA levels was performed using an iCycler iQv3 (Bio-Rad). PCR reactions were prepared with qPCR kit Mastermix for SYBR green (Eurogentec, France) according to the manufacturer's protocol. The cDNA concentration used threshold cycle values (CT) between 15 and 30 cycles. Amplification specificity was checked by melting-curve analysis[22] and involved 42 cycles (melting, 95 °C; hybridization, 56 °C; elongation, 30 s for each step). PCR efficiencies were calculated for each gene according to Pfaffl.[36] Accumulations of gene transcripts were calculated using reference transcript and actin gene and set relative to control plants (water infiltration). Primer sequences of the studied gene are shown in Table 2.

**Statistical Analysis.** All experiments were done in triplicates. Bars represent the mean of three values ± standard error (SE). Student's test was used to compare the means for determination of significant differences between treated samples and control. The data are written as the mean ± SE. Values were determined to be significant when $p \leq 0.05$.

## RESULTS

**Cell Death Analyses.** Effects of treatments on plants exposed to the herbicide are illustrated in Figure 1. Sulcotrione or Mikado sprayed on leaves displayed a significant depletion of leaf surfaces (Figure 1A) and a higher MDA content in roots (Figure 1B) than control after 2 days of treatment. Treatment by grape marc alone did not show a significant effect. A significant increase was observed in MDA of plant treated by the mixtures sulcotrione or Mikado and grape marc. Such peroxidation could be a result of oxidative degradation of lipids due to a significant change in the cellular redox status in plants generated by herbicide as previously reported.[37] This observation indicated that herbicide spray led to plant membrane modification.

Sulcotrione pesticides, active ingredient and trademark (Mikado), induced higher cell death rate than observed in control leaves. Cell death was also enhanced with trademark product treatments (Figure 2A). Cell death was increased when grape marc was added either to sulcotrione (ai) or to commercial product (Figure 2A). Cell death was shown to be concentration-dependent (Figure 2A). It was triggered by grape marc or pesticides (sulcotrione or Mikado) treatments, but at high rates of pesticides. Mixtures then induced a great cell death, which seems to be related to an addition of product toxicity for sulcotrione but that still was enhanced with Mikado (Figure 2A).

Cell death evolutions were similar for plants treated either with grape marc or sulcotrione (Figure 2B). Addition of grape marc to sulcotrione enhanced cell death (Figure 2B). Mikado treatment displayed quicker cell death than grape marc treatment alone, but a mixture of both products still accelerated cell death, suggesting a synergy effect (Figure 2B).

**Gene Expressions.** Accumulations of intracellular ROS belong to cell death markers. Study of gene expression involved in oxidative burst metabolism clarified effects of plant treatments. Plants were treated by leaf infiltration with

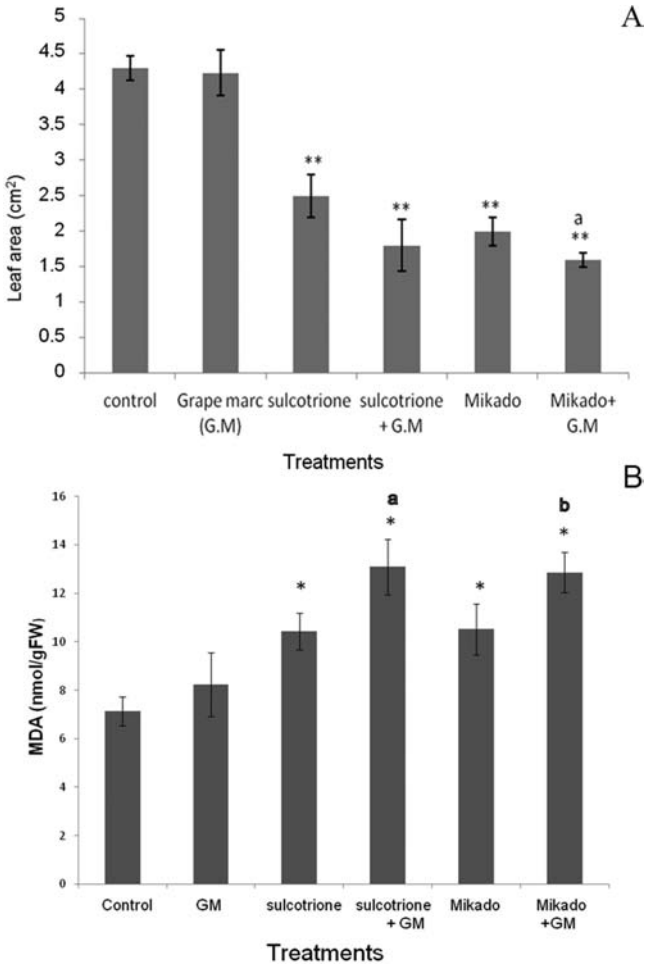


**Figure 1.** Physiological changes of plant, 2 days after treatments, by spray at application rate A3 for each product, as described in Table 1: (A) surfaces of treated *V. faba* leaves; (B) malondialdehyde content in *V. faba* roots. Control leaves were sprayed with ultrapure water. Each independent experiment was performed in triplicates. Bars represent mean values ± SE. Stars are significant differences between treatment samples and control, and a and b letters are significant differences between mixture treatments and corresponding herbicide alone ($p < 0.05$).

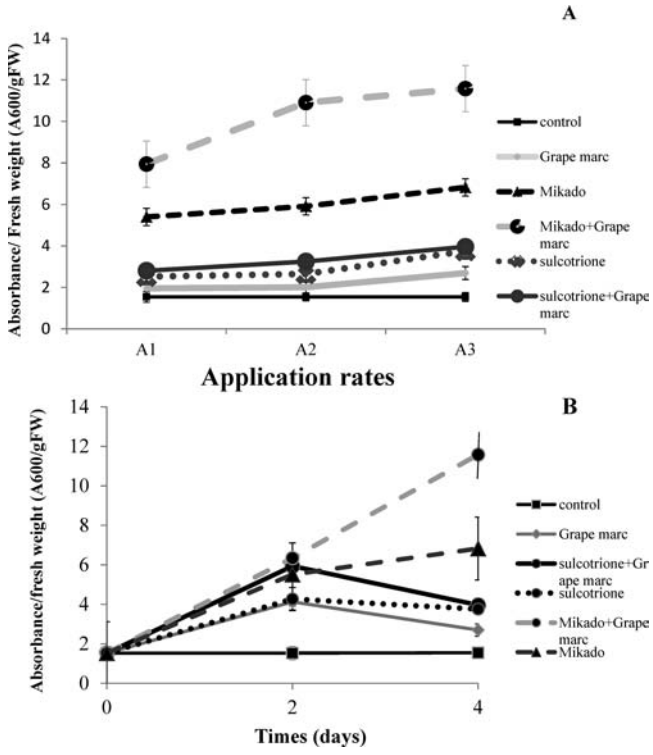


**Figure 2.** Cell death analysis. (A) Cell death induced after 4 days of treatments of *V. faba* leaves by spray. Treatments were done with sulcotrione, Mikado, grape marc, and a mixture of components, compared with *V. faba* control leaves. Application rates for plant treatment (A1) were 0.3 mg/dm$^2$ sulcotrione (ai) or in commercial product (i.e., 1 $\mu$L of Mikado). Grape marc was used at a rate 0.9 mg/dm$^2$ for A1. Mixture of grape marc and sulcotrione was used at a ratio 3:1 (w/w), respectively. Mixture made of grape marc and Mikado had a ratio 0.9:1 (w/v), respectively, to obtain a similar ratio for sulcotrione quantities. A2 and A3 were 2 and 3 times A1 rates for each product, respectively. Control samples were sprayed out with ultrapure water. Dye absorbance was measured at 600 nm. (B) Cell death induced by different spray treatment in leaves. Beans were treated by the highest product concentrations (A3). Absorbencies were measured after 2 and 4 days of treatments.

application rates called C1 for sulcotrione or Mikado (13.4 $\mu$g of active ingredient) and grape marc (40 $\mu$g per infiltration). Mixtures of grape marc and sulcotrione products were used at a ratio 3:1 (w/w), respectively. C2 and C3 are 2 and 3 times C1 rates, respectively, for sulcotrione products or grape marc quantities.

Sulcotrione treatments showed an increase of plastid copper−zinc superoxide dismutase (Cu/Zn-SOD CH) transcripts in leaves of *V. faba*, which was dose-dependent (Figure 3A). Other treatments, grape marc or Mikado (Figures 3A and 4A), displayed increases of transcripts for high concentrations. Addition of grape marc to herbicide enhanced sulcotrione effect (Figure 3A), but lowered induction by Mikado (Figure 4A).

Sulcotrione or Mikado treatments showed increases of cytosol copper−zinc superoxide dismutase (Cu/Zn-SOD CY) transcripts in leaves of *V. faba*, which displayed a dose−response relationship (Figures 3B and 4B). These treatments enhanced ascorbate peroxidase transcript accumulation in *V. faba* leaves mainly for the first rate C1, with a slight decrease for other application rates (Figures 3C and 4C). They also showed increases of catalase, ubiquitin, and hsp 70 transcript accumulations in leaves of *V. faba* that were dose-dependent (Figures 3 and 4D−F, respectively).

Grape marc treatments displayed an increase of cytosol copper−zinc superoxide dismutase (Cu/Zn-SOD CY) transcripts; addition of grape marc to herbicide enhanced effects of sulcotrione and Mikado for all rates (Figures 3B and 4B). In contrast, grape marc treatments displayed ascorbate peroxidase transcript increases that are dose-dependent (Figures 3C and 4C); addition of grape marc to herbicide did not markedly change effects of sulcotrione and Mikado (Figures 3C and 4C). Grape marc treatments displayed an increase of catalase transcript accumulation from the lowest rate C1 (Figures 3D and 4D); addition of grape marc to herbicide enhanced effects of sulcotrione and Mikado, at least for C1and C2 application rates; in contrast, the C3 rate lowered Mikado induction, whereas the effect of sulcotrione still was enhanced (Figures 3D and 4D). Addition of grape marc to herbicide also enhanced ubiquitin and hsp 70 transcript accumulations by sulcotrione and Mikado for every rate (Figures 3E,F and 4E,F, respectively).

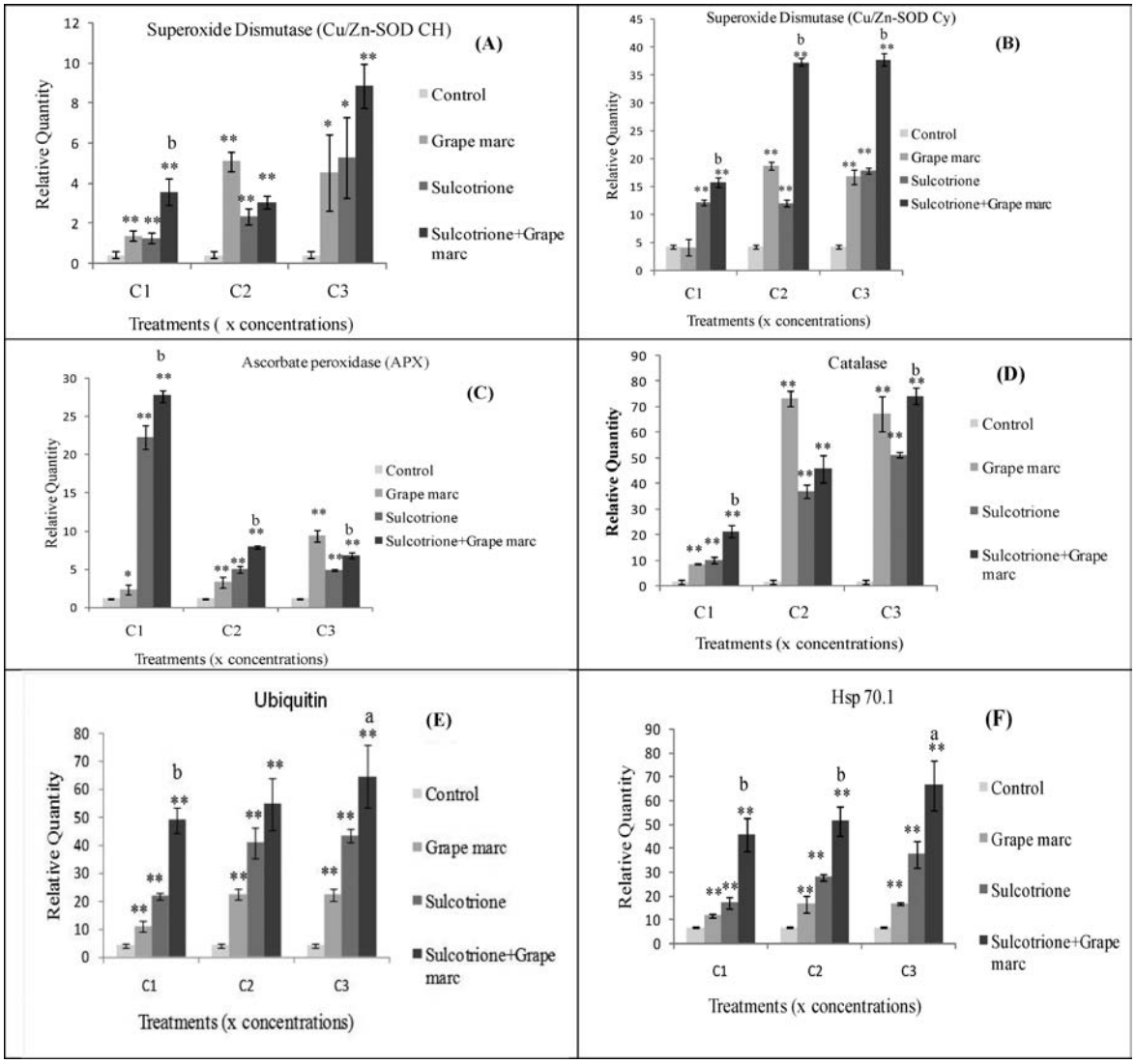


**Figure 3.** Transcript accumulation in *V. faba* leaves after infiltration treatments with sulcotrione, grape marc, and mixture of both components: (A) chloroplast copper−zinc superoxide (Cu/Zn-SOD CH) dismutase; (B) cytosolic copper−zinc superoxide dismutase (Cu/Zn-SOD CY); (C) ascorbate peroxidase (APX); (D) catalase; (E) ubiquitinl; (F) heat shock protein hsp 70.1. Values of treated leaves, with both sulcotrione or Mikado and grape marc, that have letters "a" or "b" are statistically different from values of treated leaves by sulcotrione or Mikado alone, at 5 or 1% significance level, respectively, according to Student's *t* test. Values with one or two stars are statistically different from control at 5 and 1% significance level, respectively. C2 and C3 treatments used 2 and 3 times, respectively, C1 rates for each product as described in Table 1.

## DISCUSSION

We have shown that herbicide can trigger oxidative stress resulting in disruption of cell metabolism, in experimental conditions that did not display leaf bleaching. Sulcotrione, as active ingredient or in a formulated product, Mikado, induced accumulation of MDA; it was suggested that pure sulcotrione or Mikado may induce cell membrane destruction, as was previously reported.[38] Lipid peroxidation has been suggested as one of the mechanisms involved in toxicity induced by pesticides.[39] Treatments of *V. faba* leaves with herbicides sulcotrione or Mikado displayed cell death increases that changed according to active ingredient concentrations and were enhanced using trademark Mikado. Grape marc also displayed slight bean cell death in a dose-dependent manner. Addition of grape marc either to sulcotrione or Mikado enhanced cell death, with higher increases using Mikado than with active ingredient alone. A potentiating effect between grape marc action and adjuvant elements of Mikado was then suggested.

Commercial product Mikado showed greater cell toxicity than active product sulcotrione. This was previously shown with mesotrione and Callisto or glyphosate and Roundup using growth inhibition criteria in several toxicity test organisms.[28,29] Mikado was shown to be toxic for *Pseudokirchneriella subcapitata* growth, whereas its toxicity was quite reduced for *Chlorella vulgaris*.[2] Pesticide action thus may strongly enhance ecotoxicological effects of other chemicals at high mixture concentrations, thereby showing potential synergy. Adjuvant added to herbicide formulations could enhance cell toxicity, as was potentially the case for methanol in Viper.[40] In contrast, it was previously shown that absorption of sulcotrione in maize was not significantly enhanced by adjuvant contained in commercial Mikado.[41] Moreover, most of the absorbed sulcotrione remained in the treated leaf and <14% was translocated to other organs; the presence of adjuvant in Mikado did not significantly modify the translocation of sulcotrione.[41]

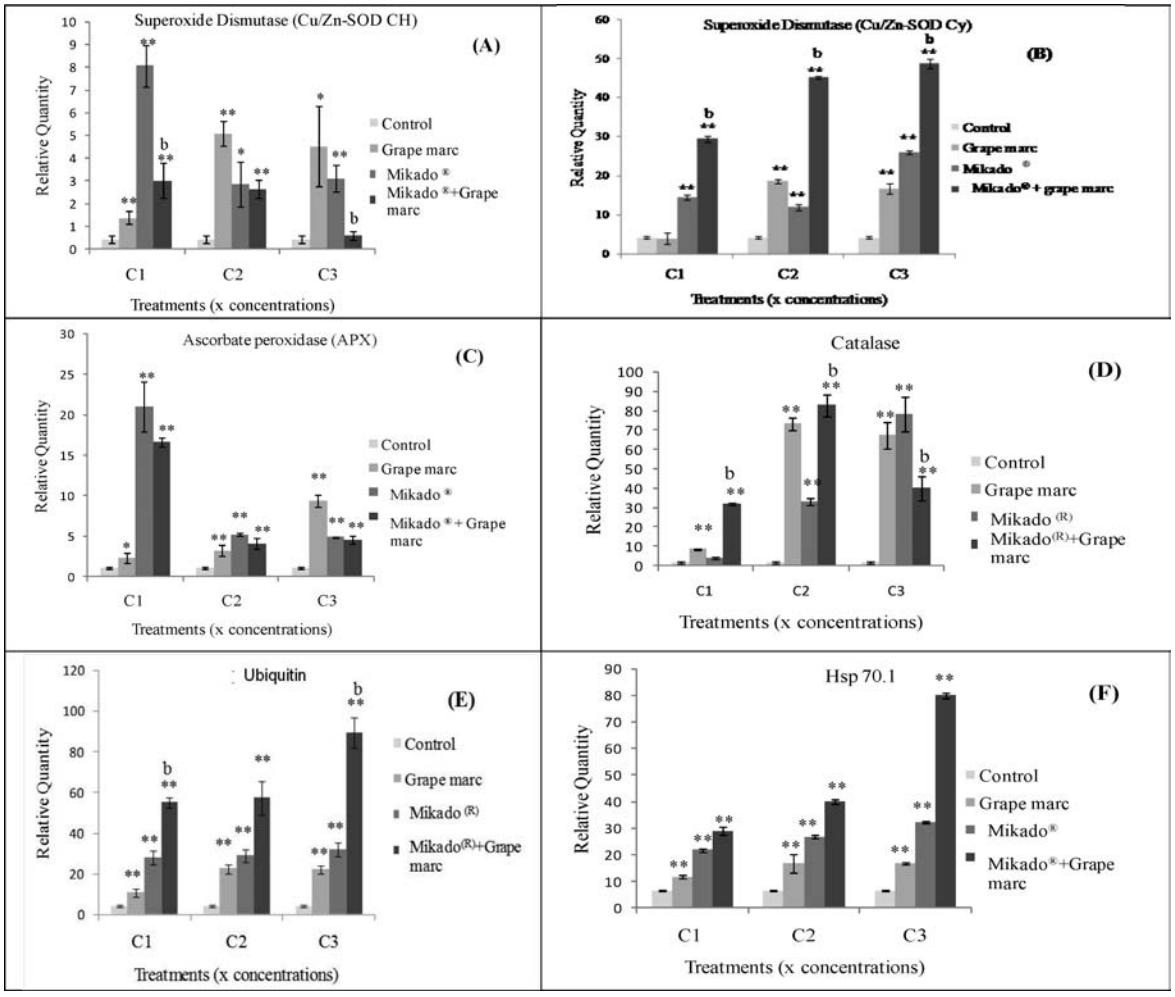


**Figure 4.** Transcript accumulation in *V. faba* leaves after infiltration treatments with Mikado, grape marc, and mixture of both components: (A) chloroplast copper−zinc superoxide (Cu/Zn-SOD CH) dismutase; (B) cytosolic copper−zinc superoxide dismutase (Cu/Zn-SOD CY); (C) ascorbate peroxidase (APX); (D) catalase; (E) ubiquitin; (F) heat shock protein hsp 70.1. Treatment values with letters "a" or "b" are statistically different from pesticide treatment at 5 or 1% significance level, respectively, and those with one or two stars are statistically different from control at 5 and 1% significance level, respectively, according to Student's *t* test. C2 and C3 treatments used 2 and 3 times, respectively, C1 rates for each product as described in Table 1.

Earlier, it was observed that formulation surprisingly increased the rate of sulcotrione phototransformation.[12] Synergistic joint effects on survival of daphnids for fungicide/insecticide and fungicide/herbicide mixtures[42] and for mixtures composed with only herbicides were found.[2,43] It was often explained that the effect of one chemical could be synergized by the presence of others, usually regulated by changes of detoxifying/biotransformation processes.[42] Recently, we have shown that sulcotrione and photoproducts increase chromosomal abnormality frequencies, but photodegraded sulcotrione cocktail has shown a greater toxicity than the parent molecule.[11]

Polyphenols can directly influence different points of apoptotic process and/or expression of regulatory proteins.[44] Mosse et al.[45] have shown that winery wastewater delayed germination and inhibited vegetative growth of several plants. We have studied and shown variations of oxidative stress in bean leaves exposed to pesticides and grape marc, measuring transcript accumulations of stress gene markers, such as superoxide dismutases, catalase, ascorbate peroxidase, ubiquitin, and hsp 70, as previously described.[46−50] Agati et al.[51] recently proposed a model in which chloroplast-located flavonoids scavenge generated ROS, thus avoiding programmed cell death. They suggested that flavonoids in conjunction with peroxidases and ascorbic acid constitute a secondary antioxidant system. In contrast, we showed that the addition of grape marc to herbicide products, sulcotrione or Mikado, had various effects according to herbicide composition (active ingredient alone or commercial product). Marker genes are differently expressed. Mixtures of grape marc and herbicide enhanced transcript accumulation for ubiquitin, hsp 70, and cytosolic SOD genes. Mixtures of grape marc and sulcotrione or Mikado gave different results at the highest rates for chloroplast SOD and catalase transcript accumulations. Grape marc mixtures markedly did not change effects of sulcotrione and Mikado for ascorbate peroxidase transcript accumulation. Depletion of catalase activity was previously reported in fishes exposed to endosulfan (ES) and was attributed to flux of superoxide radicals.[52,53]

Chromosome breakage, misrepaired DNA lesions, or chromosome unsegregation can be induced by oxidative stress[54,55] and could explain a genotoxic effect of sulcotrione previously described.[5] Other herbicide and pesticide chemicals such as insecticides may induce oxidative stress leading to

generation of free radicals and alterations in antioxidative or free radical scavenging enzyme systems.[56−59] It was indicated that enzymes associated with antioxidative defense mechanisms are altered under the influence of pesticides.[59] Moreover, oxidative stress and DNA damage have been proposed as mechanisms linking pesticide exposure to health effects such as cancer and neurological diseases.[60]

Proteins that are involved in cell stress metabolism, such as hsp 70 and ubiquitin, showed transcript increase following treatments by either sulcotrione or Mikado on *V. faba* leaves. Grape marc treatments alone displayed an increased accumulation of the same transcripts. In our conditions, mixtures of grape marc and herbicide enhanced effects of sulcotrione or Mikado for each concentration.

Earlier, it has been shown that intracellular ROS accumulation was attenuated by pretreatment with procyanidin B2.[61] In addition to antioxidative capacity, polyphenols may exert a protective effect by selective inhibition or stimulation of key protein into cell signaling cascades. Flavanols are also potent antioxidants in lipid systems, where they reduce oxidative modifications of membranes by restricting access of oxidants to the bilayer and propagation of lipid oxidation in hydrophobic membrane matrix.[62] In different experimental conditions, changes in catalase (CAT) and superoxide dismutase (SOD) gene expressions were observed after chronic consumption of wine phenolics by men.[63]

In conclusion, transcript accumulations of described genes were shown to be enhanced after treatments of leaves at three different product concentrations of sulcotrione or Mikado, grape marc, and mixtures. Genes that are involved in oxidative species induction (cytoplasmic and plastid SODs),[64] that encode antioxidative enzymes (catalase and ascorbate peroxidase, APX)[65] or which are involved in cellular defense (hsp 70 and ubiquitin)[66−69] were up-regulated after leaf treatments by pesticides and grape marc. Finally, cell death was increased after treatments but with high rates for pesticide cocktails supplemented with grape marc, especially for Mikado (Figure 5). Expression of these genes was also involved in the regulation of different cellular signalization pathways either triggering (SOD) or inhibiting various signal ways (Figure 5). Using suspension-cultured cells of tobacco, grape marc was shown to elicit early perception events and, then activating defense-related genes, ultimately leading to cell death.[70]Pesticide, sulcotrione or Mikado, and grape marc, alone, can induce target plant cell death. Signal transduction may involve ROS as shown in plant stressed conditions.[64,71] A mixture of pesticide and grape marc suggests a potentiating effect of grape marc by adjuvant elements of Mikado. Sulcotrione and mesotrione are herbicides related to a natural $\beta$-triketone, leptospermone from *Leptospermum scoparium*, that specifically inhibits the enzyme HPPD. Plant $\beta$-triketones also possess an array of biological activities such as antimicrobial activities and may protect plants from biotic stresses.[72] Leptospermone has shown toxicity against mite development, a nonherbicide target.[73]

Sulcotrione doses used for gene expression studies were similar for spray treatments or 3 to 4 times higher for infiltration treatments than the sulcotrione amount used in agriculture, as shown in Table 1. Herbicides and grape marc can trigger oxidative stress, resulting in disruption of cellular metabolism. We provide evidence that mixtures (herbicide and grape marc) induced specific gene expression for stress-associated proteins. Addition of grape marc to herbicide products, sulcotrione or Mikado, had different effects according to herbicide composition (active product or commercial product) and, meanwhile, genes are shown to be differently expressed. Therefore, adjuvant can modify the biological features of sulcotrione. Moreover, grape marc can enhance the biological effects of sulcotrione and Mikado but with different gene expression features.

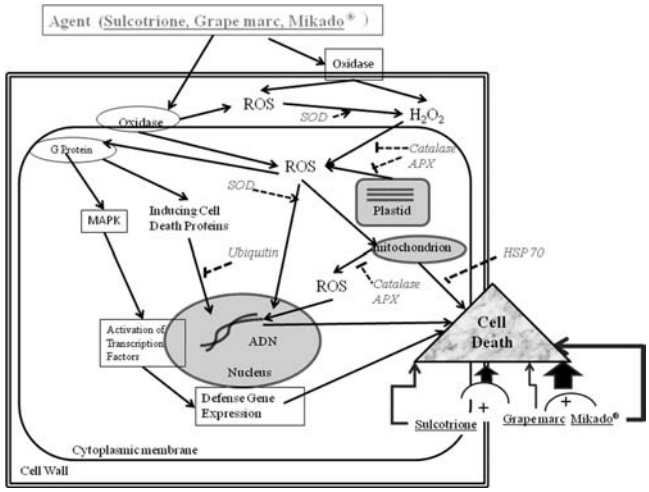


**Figure 5.** Putative interactions of products, such as herbicide (sulcotrione or Mikado) or grape marc, with cellular signalization pathways that can trigger cell defenses or death. Gene expressions are shown activating (arrow) or inhibiting (dash lines) signalization pathways. Gene markers are involved in accumulation of oxidative species (cytoplasmic and plastid superoxide dismutases, SOD, catalase, and ascorbate peroxidase, APX) or in cell defense (hsp 70 and ubiquitin). Cell death is shown to be increased after treatments using high application rates when pesticide cocktails with grape marc were used, especially associated with Mikado, as displayed by arrow thickness.

## AUTHOR INFORMATION

### Corresponding Author

*(G.L.) Phone: +33 473407908. Fax: +33 473407951. E-mail: gerard.ledoigt@univ-bpclermont.fr.

### Funding

This work was supported by grants from Europe (FEDER) and Région Auvergne Council.

### Notes

The authors declare no competing financial interest.

## ACKNOWLEDGMENTS

We thank Céline Sac and Dominique Marcon for their skillful assistance.

## REFERENCES

(1) Dayan, F. E.; Cantrell, C. L.; Duke, S. O. Natural products in crop protection. *Bioorg. Med. Chem.* **2009**, *17*, 4022−4034.

(2) Marques, C. R.; Goncalves, A. M. M.; Pereira, R.; Goncalves, F. Ecotoxicological effects of Mikado® and Viper® on algae and daphnids. *Environ. Toxicol.* **2012**, *27*, 685−699.

(3) Wiszniowski, J.; ter Halle, A.; Richard, C.; Hitmi, A.; Ledoigt, G. Photodegradation product of sulcotrione and the physiological response of maize (*Zea mays*) and white mustard (*Sinapis alba*). *Chemosphere* **2009**, *74*, 1224−1230.

(4) Chaabane, H.; Vulliet, E.; Joux, F.; Lantoine, F.; Conan, P.; Cooper, J. F.; Coste, C. M. Photodegradation of sulcotrione in various

aquatic environments and toxicity of its photoproducts for some marine micro-organisms. *Water Res.* **2007**, *41*, 1781−1789.
(5) Sta, C.; Ledoigt, G.; Ferjani, E.; Goupil, P. Exposure of *Vicia faba* to sulcotrione pesticide induced genotoxicity. *Pestic. Biochem. Physiol.* **2012**, *103*, 9−14.
(6) EFSA European Food Safety Authority: Conclusion on the peer review of sulcotrione . *EFSA Sci. Rep.* **2008**, *150*, 1−86.
(7) INERIS: Normes de Qualité Environnementale Sulcotrione − No. CAS 99105-77-8 08/11/2011, DRC-11-118981-11879A.
(8) Cherrier, R.; Boivin, A.; Perrin-Ganier, C.; Schiavon, M. Sulcotrione versus atrazine transport and degradation in soil columns. *Pest Manage. Sci.* **2005**, *61*, 899−904.
(9) Cherrier, R.; Perrin-Ganier, C.; Schiavon, M. Degradation of sulcotrione in a brown soil amended with various organic matters. *Agronomie* **2004**, *24*, 29−33.
(10) Chaabane, H.; Cooper, J. F.; Azouzi, L.; Coste, C. M. Influence of soil properties on the adsorption−desorption of sulcotrione and its hydrolysis metabolites on various soils. *J. Agric. Food Chem.* **2005**, *53*, 4091−4095.
(11) Goujon, E.; Sta, C.; Trivella, A.; Goupil, P.; Richard, C.; Ledoigt, G. Genotoxicity of sulcotrione pesticide and photoproducts on *Allium cepa* root meristem. *Pestic. Biochem. Physiol.* **2014**, *113*, 47−54.
(12) ter Halle, A.; Drncova, D.; Richard, C. Phototransformation of the herbicide sulcotrione on maize cuticular wax. *Environ. Sci. Technol.* **2006**, *40*, 2989−2995.
(13) ter Halle, A.; Wiszniowski, J.; Hitmi, A.; Ledoigt, G.; Bonnemoy, F.; Bonnet, J. L.; Bohatier, J.; Richard, C. Photolysis of the herbicide sulcotrione: formation of a major photoproduct and its toxicity evaluation. *Pest Manage. Sci.* **2009**, *65*, 14−18.
(14) Vulliet, E.; Emmelin, C.; Chovelon, J. M.; Chouteau, C.; Clement, B. Assessment of the toxicity of triasulfuron and its photoproducts using aquatic organisms. *Environ. Toxicol. Chem.* **2004**, *23*, 2837−2843.
(15) Bonnet, J. L.; Bonnemoy, F.; Dusser, M.; Bohatier, J. Assessment of the potential toxicity of herbicides and their degradation products to nontarget cells using two microorganisms, the bacteria *Vibrio fischeri* and the ciliate *Tetrahymena pyriformis*. *Environ. Toxicol.* **2007**, *22*, 78−91.
(16) Bonnet, J. L.; Bonnemoy, F.; Dusser, M.; Bohatier, J. Toxicity assessment of the herbicides sulcotrione and mesotrione toward two reference environmental microorganisms: *Tetrahymena pyriformis* and *Vibrio fischeri*. *Arch. Environ. Contam. Toxicol.* **2008**, *55*, 576−583.
(17) Jovic, M.; Manojlovic, D.; Stankovic, D.; Dojcinovic, B.; Obradovic, B.; Gasic, U.; Roglic, G. Degradation of triketone herbicides, mesotrione and sulcotrione, using advanced oxidation processes. *J. Hazard. Mater.* **2013**, *260*, 1092−1099.
(18) ter Halle, A.; Richard, C.; Ledoigt, G. Phytosanitary formulations containing plant extracts as photoprotectants for pesticides. Patent WO/2008/090476-PCT/IB2008/001007, 2008.
(19) Eyheraguibel, B.; Richard, C.; Ledoigt, G.; ter Halle, A. Photoprotection by plant extracts: a new ecological means to reduce pesticide photodegradation. *J. Agric. Food Chem.* **2010**, *58*, 9692−9696.
(20) Eyheraguibel, B.; Richard, C.; Ledoigt, G.; ter Halle, A. Inhibition of herbicide photodegradation by plant products. *J. Agric. Food Chem.* **2011**, *59*, 4868−4873.
(21) Goupil, P.; Benouaret, R.; Charrier, O.; ter Halle, A.; Richard, C.; Eyheraguibel, B.; Thiery, D.; Ledoigt, G. Grape marc extract acts as elicitor of plant defence responses. *Ecotoxicology* **2012**, *21*, 1541−1549.
(22) Benouaret, R.; Goujon, E.; Trivella, A.; Richard, C.; Ledoigt, G.; Joubert, J.-L.; Mery-Bernardon, A.; Goupil, P. Water extracts from winery by-products as tobacco defense inducers. *Ecotoxicology* **2014**, DOI: 10.1007/s10646-014-1298-3.
(23) Khanal, R. C.; Howard, L. R. Procyanidin content of grape seed and pomace, and total anthocyanin content of grape pomace as affected by extrusion processing. *J. Food Sci.* **2009**, *74*, H174−H182.
(24) Steyn, W. J.; Wand, S. J. E.; Holcroft, D. M.; Jacobs, G. Anthocyanins in vegetative tissues: a proposed unified function in photoprotection. *New Phytol.* **2002**, *155*, 349−361.
(25) Ross, J. A.; Kasum, C. M. Dietary flavonoids: bioavailability, metabolic effects and safety. *Annu. Rev. Nutr.* **2002**, *22*, 19−34.
(26) Souguir, D.; Ferjani, E.; Ledoigt, G.; Goupil, P. Exposure of *Vicia faba* and *Pisum sativum* to copper induced genotoxicity. *Protoplasma* **2008**, *233*, 203−207.
(27) Foltête, A. S.; Dhyèvre, A.; Férard, J. F.; Cotelle, S. Improvement of *Vicia*-micronucleus test for assessment of soil quality: a proposal for international standardization. *Chemosphere* **2011**, *85*, 1624−1629.
(28) Tsui, M. T.; Chu, L. M. Aquatic toxicity of glyphosate-based formulations: comparison between different organisms and the effects of environmental factors. *Chemosphere* **2003**, *52*, 1189−1197.
(29) Cedergreen, N.; Streibig, J. C. The toxicity of herbicides to non-target aquatic plants and algae: assessment of predictive factors and hazard. *Pest Manag. Sci.* **2005**, *61*, 1152−1160.
(30) Rahoui, S.; Chaoui, A.; El Ferjani, E. Differential sensitivity to cadmium in germinating seeds of three cultivars of faba bean (*Vicia faba* L.). *Acta Physiol. Plant.* **2008**, *30*, 451−456.
(31) Radetski, C. M.; Ferrari, B.; Cotelle, S.; Masfaraud, J.-F.; Ferard, J. F. Evaluation of the genotoxic, mutagenic and oxidant stress potentials of municipal solid waste incinerator bottom ash leachates. *Sci. Total Environ.* **2004**, *333*, 209−216.
(32) Béraud, E.; Cotelle, S.; Leroy, P.; Férard, J. F. Genotoxic effects and induction of phytochelatins in the presence of cadmium in *Vicia faba* roots. *Mutat. Res.* **2007**, *633*, 112−116 (Epub 2007 Jun 17).
(33) Heath, R. L.; Packer, L. Photoperoxidation in isolated chloroplasts. I. Kinetics and stoichiometry of fatty acid peroxidation. *Arch. Biochem. Biophys.* **1968**, *125*, 189−198.
(34) Buege, J. A.; Aust, S. D. Microsomal lipid peroxidation. *Methods Enzymol.* **1978**, *52*, 302−310.
(35) Baker, C. J.; Mock, N. M. An improved method for monitoring cell death in cell suspension and leaf disc assays using Evans Blue. *Plant Cell Tiss. Org.* **1994**, *39*, 7−12.
(36) Pfaffl, M. W. A new mathematical model for relative quantification 1 in real-time RT-PCR. *Nucleic Acids Res.* **2001**, *29*, No. e45.
(37) Schützendübel, A.; Schwanz, P.; Teichmann, T.; Gross, K.; Langenfeld-Heyser, R.; Goldbold, D. L.; Polle, A. Cadmium-induced changes in antioxidative systems, $H_2O_2$ content and differentiation in pine (*Pinus sylvestris*) roots. *Plant Physiol.* **2001**, *127*, 887−892.
(38) Abendroth, J. A.; Martin, A. R.; Roeth, F. W. Plant response to combinations of mesotrione and photosystem II inhibitors. *Weed Technol.* **2006**, *20*, 267−274.
(39) Kehrer, J. P. Free radicals as mediators of tissue injury and disease. *Crit. Rev. Toxicol.* **1993**, *23*, 21−48.
(40) Cabanne, F.; Gaudry, J. C. Effect of formulation agents on the joint action of aclonifen and bentazone. *Weed Control Congr. Proc.* **1996**, *1*−*4* (2ndInt.), 881−886.
(41) Doublet, J.; Mamy, M.; Barriuso, E. Delayed degradation in soil of foliar herbicides gluphosate and sulcotrione previously absorbed by plants: consequences on herbicide fate and risk assessment. *Chemosphere* **2009**, *77*, 582−589.
(42) Cedergreen, N.; Kamper, A.; Streibig, J. C. Is prochloraz a potent synergist across aquatic species? A study on bacteria, daphnia, algae and higher plants. *Aquat. Toxicol.* **2006**, *78*, 243−252.
(43) Banks, K. E.; Turner, P. K.; Wood, S. H.; Matthews, C. Increased toxicity to *Ceriodaphnia dubia* in mixtures of atrazine and diazinon at environmentally realistic concentrations. *Ecotoxicol. Environ. Saf.* **2005**, *60*, 28−36.
(44) D'Archivio, M.; Santangelo, C.; Scazzocchio, B.; Varì, R.; Filesi, C.; Masella, R.; Giovannini, C. Modulatory effects of polyphenols on apoptosis induction: relevance for cancer prevention. *Int. J. Mol. Sci.* **2008**, *9*, 213−228.
(45) Mosse, K. P. M.; Patti, A. F.; Christen, E. W.; Cavagnaro, T. R. Winery wastewater inhibits seed germination and vegetative growth of common crop species. *J. Hazard. Mater.* **2010**, *180*, 63−70.
(46) Song, Y.; Zhu, L. S.; Xie, H.; Wang, J.; Wang, J. H.; Liu, W.; Dong, X. L. Effects of atrazine on DNA damage and antioxidative enzymes in *Vicia faba*. *Environ. Toxicol. Chem.* **2009**, *28*, 1059−1062.

(47) Ahmad, R.; Kim, Y. H.; Kim, M. D.; Kwon, S. Y.; Cho, K.; Lee, H. S.; Kwak, S. S. Simultaneous expression of choline oxidase, superoxide dismutase and ascorbate peroxidase in potato plant chloroplasts provides synergistically enhanced protection against various abiotic stresses. *Physiol. Plant.* **2010**, *138*, 520−533.
(48) Romero, D. M.; Rios de Molina, M. C.; Juarez, A. B. Oxidative stress induced by a commercial glyphosate formulation in a tolerant strain of *Chlorella kessleri*. *Toxicol. Environ. Saf.* **2011**, *74*, 741−747.
(49) Cao, J.; Zhang, X.; Wang, Q.; Jia, L.; Zhang, Y.; Zhao, X. Influence of flavonoid extracts from celery on oxidative stress induced by dichlorvos in rats. *Hum. Exp. Toxicol.* **2012**, *31*, 617−625.
(50) Soydam, A. S.; Büyük, I.; Aras, S. Relationships among lipid peroxidation, SOD enzyme activity, and SOD gene expression profile in *Lycopersicon esculentum* L. exposed to cold stress. *Genet. Mol. Res.* **2013**, *12*, 3220−3229.
(51) Agati, G.; Brunetti, C.; Di Ferdinando, M.; Ferrini, F.; Pollastri, S.; Tattin, M. Functional roles of flavonoids in photoprotection: new evidence, lessons from the past. *Plant Physiol. Biochem.* **2013**, *72*, 35−45.
(52) Pandey, S.; Ahmad, I.; Parvez, S.; Bin-Hafeez, B.; Haque, R.; Raisuddin, S. Effect of endosulfan on antioxidants of freshwater fish *Channa punctatus* Bloch, 1. Protection against lipid peroxidation in liver by copper preexposure. *Arch. Environ. Contam. Toxicol.* **2001**, *41*, 345−352.
(53) Ballesteros, M. L.; Wunderlin, D. A.; Bistoni, M. A. Oxidative stress responses in different organs of *Jenynsia multidentata* exposed to endosulfan. *Ecotoxicol. Environ. Saf.* **2009**, *72*, 199−205.
(54) Pérez, D. J.; Lukaszewicz, G.; Menone, M. L.; Camadro, E. L. Sensitivity of *Bidens laevis* L. to mutagenic compounds. Use of chromosomal aberrations as biomarkers of genotoxicity. *Environ. Pollut.* **2011**, *159*, 281−286.
(55) Crupkin, A. C.; Carriquiriborde, P.; Mendieta, J.; Panzeri, A. M.; Ballesteros, M. L.; Miglioranza, K. S. B.; Menone, M. L. Oxidative stress and genotoxicity in the South American cichlid, *Australoheros facetus*, after short-term sublethal exposure to endosulfan. *Pestic. Biochem. Physiol.* **2013**, *105*, 102−110.
(56) Doulis, A. G.; Donahue, J. L.; Alscher, R. G. Differential responses to paraquat induced oxidative injury in a pea (*Pisum sativum*) protoplast system. *Physiol. Plant.* **1998**, *102*, 461−471.
(57) Štajner, D.; Popovic, M.; Štajner, M. Herbicide induced oxidative stress in lettuce, beans, pea seeds and leaves. *Biol. Plant.* **2004**, *47*, 575−579.
(58) Chagas, R. M.; Silveira, J. A. G.; Ribeiro, R. V.; Vitorello, V. A.; Carrer, H. Photochemical damage and comparative performance of superoxide dismutase and ascorbate peroxidase in sugarcane leaves exposed to paraquat-induced oxidative stress. *Pestic. Biochem. Physiol.* **2008**, *90*, 181−188.
(59) Duzguner, V.; Erdogan, S. Acute oxidant and inflammatory effects of imidacloprid on the mammalian central nervous system and liver in rats. *Pestic. Biochem. Physiol.* **2010**, *97*, 13−18.
(60) Duzguner, V.; Erdogan, S. Chronic exposure to imidacloprid induces inflammation and oxidative stress in the liver and central nervous system of rats. *Pestic. Biochem. Physiol.* **2012**, *104*, 58−64.
(61) Mazumdar, M.; Giri, S.; Giri, A. Role of quercetin on mitomycin C induced genotoxicity: analysis of micronucleus and chromosome aberrations *in vivo*. *Mutat. Res.* **2011**, *721*, 147−152.
(62) Verstraeten, S. V.; Keen, C. L.; Schmitz, H. H.; Fraga, C. G.; Oteiza, P. I. Flavan-3-ols and procyanidins protect liposomes against lipid oxidation and disruption of the bilayer structure. *Free Radical Biol. Med.* **2003**, *34*, 84−92.
(63) Fernandez-Pachon, M. S.; Berna, G.; Otaolaurruchi, E.; Troncoso, A. M.; Martin, F.; Garcia-Parrilla, M. C. Changes in antioxidant endogenous enzymes (activity and gene expression levels) after repeated red wine intake. *J. Agric. Food Chem.* **2009**, *57*, 6578−6583.
(64) Mahalingam, R.; Fedoroff, N. Stress response, cell death and signaling: the many faces of reactive oxygen species. *Physiol. Plant.* **2003**, *119*, 56−68.
(65) Mittler, R. Oxidative stress, antioxidants and stress tolerance. *TIPS, Trends Plant Sci.* **2002**, *7*, 405−410.
(66) Beere, H. M. Death versus survival: functional interaction between the apoptotic and stress-inducible heat shock protein pathways. *J. Clin. Invest.* **2005**, *115*, 2633−2639.
(67) Mace, P. D.; Shirley, S.; Day, C. L. Assembling the building blocks: structure and function of inhibitor of apoptosis proteins. *Cell Death Differentiat.* **2010**, *17*, 46−53.
(68) Liu, S.; Chen, Z. J. Expanding role of ubiquitination en NF-κB signaling. *Cell Res.* **2011**, *21*, 6−21.
(69) Fang, S.; Li, L.; Cui, B.; Men, S.; Shena, Y.; Yang, X. Structural insight into plant programmed cell death mediated by BAG proteins in *Arabidopsis thaliana*. *Acta Crystallogr.* **2013**, *D69*, 934−945.
(70) Benouaret, R.; Goujon, E.; Goupil, P. Grape marc extract causes early perception events, defence reactions and hypersensitive response in cultured tobacco cells. *Plant Physiol. Biochem.* **2014**, *77*, 84−89.
(71) Møller, I. M.; Jensen, P. E.; Hansson, A. Oxidative modifications to cellular components in plants. *Annu. Rev. Plant Biol.* **2007**, *58*, 459−481.
(72) Owens, D. K.; Dhammika Nanayakkara, N. P.; Dayan, F. E. *In planta* mechanism of action of Leptospermone: impact of its physico-chemical properties on uptake, translocation, and metabolism. *J. Chem. Ecol.* **2013**, *39*, 262−270.
(73) Jeong, E.-Y.; Kim, M.-G.; Lee, H.-S. Acaricidal activity of triketone analogues derived from *Leptospermum scoparium* oil against house-dust and stored-food mites. *Pest Manage. Sci.* **2009**, *65*, 327−331.

**Table 1. Chemical Structures, Postemergence Herbicidal Activities (Inhibition Rating of 0−100) of Compounds I, and Their Inhibitory Activities against *At*HPPD[a]**

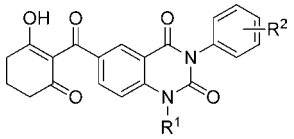

| compound | $R^1$ | $R^2$ | dose (g of ai/ha) | EC[b] | SF[b] | DS[b] | AR[b] | EP[b] | AJ[b] | $K_i$ (nM)[c] |
|---|---|---|---|---|---|---|---|---|---|---|
| **I-a** | $CH_3$ | 4-Cl | 150 | 90 | 100 | 90 | 90 | 85 | 90 | 21 ± 2 |
| | | | 75 | 70 | 60 | 60 | 60 | 50 | 50 | |
| | | | 37.5 | 50 | 50 | 50 | 60 | 0 | 0 | |
| **I-b** | $CH_3$ | 3-Cl | 150 | 80 | 100 | 70 | 100 | 80 | 80 | 27 ± 5 |
| | | | 75 | 50 | 20 | 40 | 70 | 30 | 20 | |
| | | | 37.5 | 40 | 0 | 0 | 60 | 30 | 20 | |
| **I-c** | $CH_3$ | 2-Cl | 150 | 100 | 100 | 100 | 80 | 80 | 85 | 23 ± 1 |
| | | | 75 | 90 | 90 | 90 | 75 | 40 | 70 | |
| | | | 37.5 | 60 | 60 | 40 | 60 | 30 | 60 | |
| **I-d** | $CH_3$ | 4-$CH_3$ | 150 | 75 | 75 | 75 | 100 | 75 | 75 | 42 ± 1 |
| **I-e** | $CH_3$ | 3-$CH_3$ | 150 | 70 | 100 | 75 | 100 | 95 | 70 | 39 ± 6 |
| **I-f** | $CH_3$ | 2-$CH_3$ | 150 | 100 | 100 | 100 | 100 | 100 | 100 | 32 ± 1 |
| | | | 75 | 100 | 100 | 95 | 100 | 87.5 | 100 | |
| | | | 37.5 | 95 | 90 | 85 | 97.5 | 82.5 | 97.5 | |
| **I-g** | H | 2-$CH_3$ | 150 | 0 | 10 | 0 | 0 | 0 | 15 | 627 ± 42 |
| **I-h** | $CH_2CH_3$ | 2-$CH_3$ | 150 | 100 | 100 | 100 | 100 | 100 | 100 | 5 ± 1 |
| | | | 75 | 100 | 100 | 97.5 | 100 | 100 | 100 | |
| | | | 37.5 | 100 | 97.5 | 60 | 90 | 95 | 100 | |
| **I-i** | $CH_2CH_2CH_3$ | 2-$CH_3$ | 150 | 87.5 | 90 | 60 | 95 | 97.5 | 100 | 15 ± 2 |
| | | | 75 | 80 | 87.5 | 50 | 80 | 87.5 | 100 | |
| | | | 37.5 | 70 | 65 | 30 | 50 | 70 | 87.5 | |
| **I-j** | $CH_2C{\equiv}CH$ | 2-$CH_3$ | 150 | 50 | 20 | 0 | 90 | 35 | 90 | 33 ± 1 |
| **I-k** | $CH_2CH_2CH_2CH_3$ | 2-$CH_3$ | 150 | 0 | 10 | 0 | 30 | 0 | 50 | 19 ± 1 |
| **I-l** | $CH_2CH(CH_3)_2$ | 2-$CH_3$ | 150 | 0 | 10 | 0 | 20 | 20 | 90 | 17 ± 2 |
| **I-m** | $CH_2C_6H_5$ | 2-$CH_3$ | 150 | 0 | 10 | 0 | 0 | 0 | 0 | 355 ± 9 |
| **I-n** | $CH_2$−2-F−$C_6H_4$ | 2-$CH_3$ | 150 | 50 | 50 | 30 | 0 | 90 | 0 | 139 ± 8 |
| **I-o** | $CH_2$−3-$OCH_3$−$C_6H_4$ | 2-$CH_3$ | 150 | 50 | 10 | 25 | 0 | 80 | 0 | 141 ± 55 |
| mesotrione | | | 150 | 85 | 20 | 95 | 100 | 100 | 100 | 13 ± 1 |
| | | | 75 | 75 | 0 | 60 | 100 | 100 | 100 | |
| | | | 37.5 | 30 | 0 | 30 | 100 | 100 | 100 | |

[a]For the method for the preparation of compounds **I**, see ref 15. [b]Abbreviations: EC, *Echinochloa crus-galli*; SF, *Setaria faberii*; DS, *Digitaria sanguinalis*; AR, *Amaranthus retroflexu*; EP, *Eclipta prostrata*; AJ, *Abutilon juncea*. [c]Inhibition constant of the enzymatic reaction.

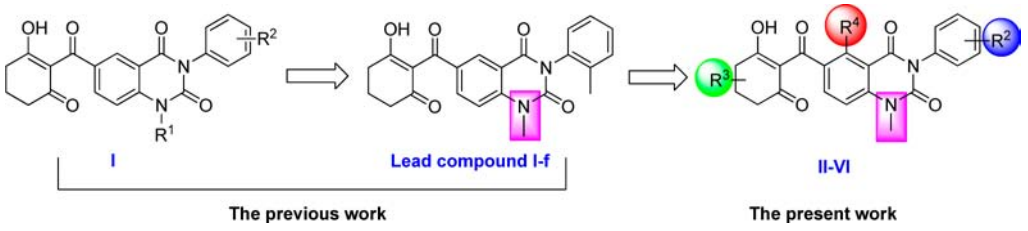


**Figure 1.** Design of title compounds (**II**−**VI**).

containing quinazoline-2,4-dione derivatives possessing a methyl group at the N-1 position of the quinazoline-2,4-dione ring (Figure 1). The biological test indicated that most newly synthesized compounds showed excellent herbicidal activity against broadleaf and monocotyledonous weeds at the dosages of 37.5−150 g of ai/ha. Notably, some compounds showed significantly improved crop selectivity compared to mesotrione. Herein, we have revealed the detailed synthesis, herbicidal activity, and structure−activity relationship (SAR) of compounds **II**−**VI** as potent herbicide candidates.

## MATERIALS AND METHODS

The experimental details and analytical data for all of the intermediates and compounds **II**−**VI** are shown in the Supporting Information.

**X-ray Diffraction.** Compound **IV-d** was recrystallized from a mixture of chloroform and *n*-hexane to afford a suitable single crystal. Light brown crystals of **IV-d** (0.12 × 0.10 × 0.10 mm) were mounted on a quartz fiber with protection oil. Cell dimensions and intensities were measured at 296 K on a Bruker SMART APEX DUO area detector diffractometer with graphite monochromated Mo K$\alpha$ radiation ($\lambda$ = 0.710 73 Å), with $\theta_{max}$ = 25.49, 16 744 measured reflections, and 4817 independent reflections ($R_{int}$ = 0.0253). The data sets were integrated and reduced using SAINT Plus Programme.[16]


dx.doi.org/10.1021/jf5048089 | J. Agric. Food Chem. 2014, 62, 11786−11796

**Table 2. Chemical Structures, Postemergent Herbicidal Activity (Inhibition Rating of 0−100) of Compounds II, and Their Inhibitory Activities against *At*HPPD**

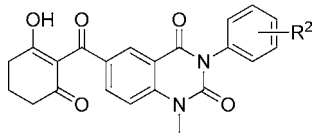


| compound | $R^2$ | dose (g of ai/ha) | EC[a] | SF[a] | DS[a] | AR[a] | EP[a] | AJ[a] | $K_i$ (nM) |
|---|---|---|---|---|---|---|---|---|---|
| **II-a** | H | 150 | 65 | 50 | 65 | 100 | 70 | 80 | 51 ± 9 |
| **II-b** | 2-F | 150 | 80 | 100 | 80 | 80 | 80 | 85 | 53 ± 3 |
| | | 75 | 70 | 40 | 60 | 75 | 50 | 50 | |
| | | 37.5 | 50 | 30 | 40 | 70 | 30 | 0 | |
| **II-c** | 3-F | 150 | 85 | 80 | 75 | 85 | 80 | 100 | 28 ± 4 |
| | | 75 | 60 | 40 | 60 | 80 | 50 | 30 | |
| | | 37.5 | 50 | 0 | 30 | 70 | 30 | 0 | |
| **II-d** | 4-F | 150 | 85 | 100 | 75 | 100 | 95 | 100 | 29 ± 1 |
| | | 75 | 70 | 20 | 60 | 70 | 60 | 40 | |
| | | 37.5 | 60 | 20 | 20 | 60 | 0 | 20 | |
| **II-e** | 2-Br | 150 | 87.5 | 90 | 70 | 100 | 82.5 | 100 | 27 ± 2 |
| | | 75 | 75 | 82.5 | 50 | 100 | 70 | 90 | |
| | | 37.5 | 45 | 75 | 20 | 100 | 60 | 65 | |
| **II-f** | 3-Br | 150 | 85 | 45 | 30 | 95 | 50 | 85 | 16 ± 1 |
| **II-g** | 4-Br | 150 | 85 | 85 | 70 | 100 | 100 | 100 | 17 ± 4 |
| | | 75 | 55 | 60 | 30 | 100 | 100 | 65 | |
| | | 37.5 | 30 | 45 | 0 | 100 | 95 | 50 | |
| **II-h** | 2-$OCH_3$ | 150 | 100 | 100 | 100 | 100 | 82.5 | 97.5 | 68 ± 5 |
| | | 75 | 100 | 100 | 100 | 100 | 75 | 90 | |
| | | 37.5 | 92.5 | 90 | 100 | 97.5 | 60 | 85 | |
| **II-i** | 3-$OCH_3$ | 150 | 92.5 | 25 | 60 | 95 | 67.5 | 100 | 17 ± 4 |
| **II-j** | 4-$OCH_3$ | 150 | 85 | 50 | 75 | 95 | 80 | 60 | 15 ± 3 |
| **II-k** | 2-$CF_3$ | 150 | 95 | 100 | 95 | 100 | 85 | 100 | 46 ± 5 |
| | | 75 | 90 | 95 | 90 | 95 | 80 | 97.5 | |
| | | 37.5 | 87.5 | 92.5 | 65 | 90 | 75 | 90 | |
| **II-l** | 3-$CF_3$ | 150 | 85 | 80 | 50 | 97.5 | 75 | 55 | 65 ± 1 |
| **II-m** | 4-$CF_3$ | 150 | 85 | 30 | 60 | 100 | 60 | 100 | 24 ± 2 |
| **II-n** | 2-$OCF_3$ | 150 | 85 | 80 | 85 | 97.5 | 85 | 95 | 47 ± 2 |
| | | 75 | 77.5 | 80 | 85 | 95 | 65 | 50 | |
| | | 37.5 | 70 | 50 | 75 | 90 | 50 | 30 | |
| **II-o** | 4-$OCF_3$ | 150 | 77.5 | 50 | 60 | 95 | 80 | 50 | 12 ± 1 |
| **II-p** | 4-$NO_2$ | 150 | 50 | 10 | 40 | 90 | 82.5 | 60 | 18 ± 4 |
| **II-q** | 2-$C_2H_5$ | 150 | 85 | 82.5 | 95 | 100 | 85 | 100 | 29 ± 1 |
| | | 75 | 87.5 | 90 | 85 | 95 | 0 | 90 | |
| | | 37.5 | 80 | 87.5 | 80 | 90 | 0 | 60 | |
| **II-r** | 2-iPr | 150 | 80 | 97.5 | 100 | 90 | 80 | 97.5 | 29 ± 3 |
| | | 75 | 82.5 | 87.5 | 92.5 | 95 | 60 | 80 | |
| | | 37.5 | 70 | 50 | 75 | 90 | 50 | 60 | |
| **II-s** | 2,6-di-iPr | 150 | 60 | 20 | 55 | 100 | 70 | 35 | 106 ± 3 |
| **II-t** | 2,6-di-Cl | 150 | 80 | 40 | 80 | 85 | 50 | 80 | 47 ± 2 |
| **II-u** | 2,6-di-$CH_3$ | 150 | 100 | 100 | 95 | 100 | 70 | 100 | 66 ± 5 |
| | | 75 | 92.5 | 100 | 85 | 100 | 65 | 100 | |
| | | 37.5 | 87.5 | 100 | 80 | 100 | 55 | 97.5 | |
| **II-v** | 2,4-di-Cl | 150 | 82.5 | 92.5 | 65 | 87.5 | 20 | 100 | 13 ± 3 |
| **II-w** | 2-$CH_3$-5-Cl | 150 | 85 | 60 | 80 | 90 | 82.5 | 85 | 53 ± 1 |
| | | 75 | 85 | 80 | 70 | 100 | 60 | 65 | |
| | | 37.5 | 70 | 55 | 30 | 100 | 50 | 30 | |
| **II-x** | 3,5-di-Cl | 150 | 80 | 80 | 70 | 90 | 60 | 100 | 17 ± 2 |
| mesotrione | | 150 | 85 | 20 | 95 | 100 | 100 | 100 | 13 ± 1 |
| | | 75 | 75 | 0 | 60 | 100 | 100 | 100 | |
| | | 37.5 | 30 | 0 | 30 | 100 | 100 | 100 | |

[a]Abbreviations: EC, *Echinochloa crus-galli*; SF, *Setaria faberii*; DS, *Digitaria sanguinalis*; AR, *Amaranthus retroflexu*; EP, *Eclipta prostrata*; AJ, *Abutilon juncea*.


dx.doi.org/10.1021/jf5048089 | *J. Agric. Food Chem.* 2014, 62, 11786−11796

**Table 3. Chemical Structures, Postemergent Herbicidal Activity (Inhibition Rating of 0−100) of Compounds III−V, and Their Inhibitory Activities against *At*HPPD**

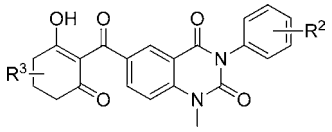


| compound | $R^2$ | $R^3$ | dose (g of ai/ha) | EC[a] | SF[a] | DS[a] | AR[a] | EP[a] | AJ[a] | $K_i$ (nM) |
|---|---|---|---|---|---|---|---|---|---|---|
| **III-a** | 4-Br | 5-$CH_3$ | 150 | 80 | 50 | 90 | 95 | 95 | 92.5 | 25 ± 1 |
| | | | 75 | 70 | 40 | 80 | 90 | 90 | 87.5 | |
| | | | 37.5 | 60 | 30 | 65 | 82.5 | 80 | 80 | |
| **III-b** | 2,4-di-Cl | 5-$CH_3$ | 150 | 100 | 100 | 100 | 100 | 95 | 100 | 15 ± 4 |
| | | | 75 | 100 | 95 | 95 | 95 | 92.5 | 100 | |
| | | | 37.5 | 95 | 90 | 92.5 | 90 | 85 | 100 | |
| **IV-a** | H | 5,5-di-$CH_3$ | 150 | 77.5 | 45 | 85 | 95 | 80 | 100 | 54 ± 5 |
| **IV-b** | 2-F | 5,5-di-$CH_3$ | 150 | 90 | 100 | 90 | 100 | 90 | 100 | 20 ± 3 |
| | | | 75 | 70 | 50 | 50 | 70 | 70 | 60 | |
| | | | 37.5 | 50 | 40 | 50 | 60 | 50 | 40 | |
| **IV-c** | 3-F | 5,5-di-$CH_3$ | 150 | 85 | 80 | 95 | 85 | 85 | 85 | 56 ± 5 |
| | | | 75 | 50 | 50 | 50 | 70 | 70 | 30 | |
| | | | 37.5 | 40 | 30 | 50 | 60 | 60 | 30 | |
| **IV-d** | 4-F | 5,5-di-$CH_3$ | 150 | 80 | 95 | 95 | 100 | 90 | 100 | 100 ± 9 |
| | | | 75 | 50 | 50 | 30 | 60 | 50 | 50 | |
| | | | 37.5 | 40 | 40 | 30 | 50 | 40 | 40 | |
| **IV-e** | 2-Br | 5,5-di-$CH_3$ | 150 | 75 | 35 | 95 | 95 | 82.5 | 100 | 245 ± 21 |
| **IV-f** | 3-Br | 5,5-di-$CH_3$ | 150 | 70 | 50 | 85 | 100 | 100 | 100 | 29 ± 3 |
| | | | 75 | 20 | 50 | 65 | 100 | 100 | 100 | |
| | | | 37.5 | 0 | 30 | 20 | 100 | 100 | 100 | |
| **IV-g** | 4-Br | 5,5-di-$CH_3$ | 150 | 60 | 30 | 92.5 | 100 | 87.5 | 100 | 24 ± 4 |
| **IV-h** | 2-$OCH_3$ | 5,5-di-$CH_3$ | 150 | 85 | 50 | 85 | 95 | 85 | 50 | 287 ± 21 |
| **IV-i** | 3-$OCH_3$ | 5,5-di-$CH_3$ | 150 | 60 | 60 | 55 | 80 | 75 | 55 | 103 ± 12 |
| **IV-j** | 4-$OCH_3$ | 5,5-di-$CH_3$ | 150 | 80 | 60 | 87.5 | 90 | 67.5 | 100 | 118 ± 19 |
| **IV-k** | 3-$CF_3$ | 5,5-di-$CH_3$ | 150 | 50 | 40 | 82.5 | 90 | 80 | 92.5 | 48 ± 1 |
| **IV-l** | 4-$CF_3$ | 5,5-di-$CH_3$ | 150 | 40 | 10 | 60 | 80 | 55 | 60 | 42 ± 9 |
| **IV-m** | 4-$OCF_3$ | 5,5-di-$CH_3$ | 150 | 65 | 50 | 90 | 95 | 80 | 100 | 24 ± 4 |
| **IV-n** | 4-$NO_2$ | 5,5-di-$CH_3$ | 150 | 0 | 80 | 25 | 80 | 80 | 100 | 58 ± 5 |
| **IV-o** | 2-$CH_2CH_3$ | 5,5-di-$CH_3$ | 150 | 80 | 75 | 60 | 100 | 70 | 100 | 23 ± 3 |
| **IV-p** | 2-iPr | 5,5-di-$CH_3$ | 150 | 55 | 50 | 50 | 100 | 90 | 97.5 | 249 ± 37 |
| **IV-q** | 2,6-di-Cl | 5,5-di-$CH_3$ | 150 | 92.5 | 95 | 87.5 | 95 | 97.5 | 95 | 180 ± 10 |
| | | | 75 | 97.5 | 85 | 85 | 82.5 | 80 | 90 | |
| | | | 37.5 | 90 | 80 | 70 | 70 | 70 | 80 | |
| **IV-r** | 2,6-di-$CH_3$ | 5,5-di-$CH_3$ | 150 | 85 | 80 | 50 | 100 | 87.5 | 100 | 262 ± 8 |
| | | | 75 | 87.5 | 87.5 | 82.5 | 80 | 60 | 85 | |
| | | | 37.5 | 75 | 82.5 | 75 | 75 | 50 | 80 | |
| **IV-s** | 2,4-di-Cl | 5,5-di-$CH_3$ | 150 | 25 | 30 | 20 | 30 | 50 | 100 | 362 ± 39 |
| **IV-t** | 2-$CH_3$-5-Cl | 5,5-di-$CH_3$ | 150 | 80 | 40 | 82.5 | 95 | 80 | 65 | 138 ± 11 |
| **IV-u** | 3,5-di-Cl | 5,5-di-$CH_3$ | 150 | 75 | 85 | 90 | 100 | 80 | 0 | 39 ± 3 |
| **V** | 2,6-di-Cl | 6,6-di-$CH_3$ | 150 | 95 | 45 | 60 | 97.5 | 80 | 100 | 49 ± 5 |
| mesotrione | | | 150 | 85 | 20 | 95 | 100 | 100 | 100 | 13 ± 1 |
| | | | 75 | 75 | 0 | 60 | 100 | 100 | 100 | |
| | | | 37.5 | 30 | 0 | 30 | 100 | 100 | 100 | |

[a]Abbreviations: EC, *Echinochloa crus-galli*; SF, *Setaria faberii*; DS, *Digitaria sanguinalis*; AR, *Amaranthus retroflexu*; EP, *Eclipta prostrata*; AJ, *Abutilon juncea*.

Data were corrected for Lorentz and polarization effects and absorption ($T_{max}$ = 0.9613, and $T_{min}$ = 0.9538). The structure was solved by a direct method using SHELXS97 and refined with SHELXL970.[17] Full-matrix least-squares refinement based on $F^2$ using the weight of $1/[\sigma^2(F_0^2) + (0.1322P)^2 + 0.6124P]$ gave final values of $R_1$ = 0.0628, $\omega R_2$ = 0.2008, and GOF($F$) = 1.116 for 403 variables, 403 parameters, and 4817 contributing reflections. Maximum shift/error = 0.002, and maximum/minimum residual electron density = 0.679/−0.506 e Å$^{-3}$. Hydrogen atoms were observed and placed at their ideal positions with a fixed value of their isotropic displacement parameter.

Crystallographic data for compound **IV-d** has been deposited with the Cambridge Crystallographic Data Centre as a supplementary publication with the deposition number 977355. These data can be obtained free of charge from http://www.ccdc.cam.ac.uk/.

**Herbicidal Activities.** The postemergent herbicidal activities of compounds **I−VI**, against *Echinochloa crus-galli* (EC), *Setaria faberii* (SF), *Digitaria sanguinalis* (DS), *Amaranthus retroflexus* (AR), *Eclipta*

**Table 4. Chemical Structures, Postemergent Herbicidal Activity (Inhibition Rating of 0−100) of Compounds III−V, and Their Inhibitory Activities against *At*HPPD**

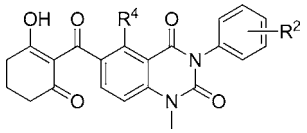


| | $R^2$ | $R^4$ | dose (g of ai/ha) | EC[a] | SF[a] | DS[a] | AR[a] | EP[a] | AJ[a] | $K_i$ (nM) |
|---|---|---|---|---|---|---|---|---|---|---|
| **VI-a** | 2-$CH_3$ | $CH_3$ | 150 | 100 | 100 | 100 | 100 | 100 | 100 | 16 ± 1 |
| | | | 75 | 100 | 100 | 100 | 100 | 100 | 100 | |
| | | | 37.5 | 100 | 100 | 100 | 100 | 100 | 97.5 | |
| **VI-b** | 2-$OCH_3$ | $CH_3$ | 150 | 100 | 100 | 100 | 100 | 100 | 100 | 28 ± 4 |
| | | | 75 | 100 | 100 | 100 | 100 | 100 | 100 | |
| | | | 37.5 | 97.5 | 92.5 | 100 | 95 | 95 | 97.5 | |
| **VI-c** | 2-$CF_3$ | $CH_3$ | 150 | 100 | 100 | 100 | 100 | 100 | 100 | 10 ± 1 |
| | | | 75 | 97.5 | 97.5 | 95 | 95 | 95 | 90 | |
| | | | 37.5 | 90 | 95 | 90 | 90 | 90 | 90 | |
| **VI-d** | 2,6-di-$CH_3$ | $CH_3$ | 150 | 100 | 100 | 100 | 100 | 100 | 100 | 9 ± 1 |
| | | | 75 | 100 | 100 | 100 | 100 | 95 | 100 | |
| | | | 37.5 | 95 | 95 | 100 | 95 | 87.5 | 97.5 | |
| mesotrione | | | 150 | 85 | 20 | 95 | 100 | 100 | 100 | 13 ± 1 |
| | | | 75 | 75 | 0 | 60 | 100 | 100 | 100 | |
| | | | 37.5 | 30 | 0 | 30 | 100 | 100 | 100 | |

[a]Abbreviations: EC, *Echinochloa crus-galli*; SF, *Setaria faberii*; DS, *Digitaria sanguinalis*; AR, *Amaranthus retroflexu*; EP, *Eclipta prostrata*; AJ, *Abutilon juncea*.

*prostrata* (EP), and *Abutilon juncea* (AJ) were evaluated according to the above-mentioned procedure;[18−20] the commercially available triketone herbicide mesotrione was selected as a positive control. All test compounds were formulated as 100 g/L emulsified concentrates using *N*,*N*-dimethylformamide (DMF) as the solvent and Tween-80 as the emulsification reagent. The concentrates were diluted with water to the required concentration and applied to pot-grown plants in a greenhouse. Clay soil was used with pH 6.5, 1.6% organic matter, 37.3% clay particles, and cation-exchange capacity (CEC) of 12.1 mol/kg. The rate of application (g of ai/ha) was calculated by the total amount of active ingredient in the formulation divided by the surface area of the pot. Plastic pots with a diameter of 9 cm were filled with soil to a depth of 8 cm. Approximately 20 seeds of selected weeds were sown in soil at the depth of 1−3 cm and grown at the temperature of 15−30 °C in a greenhouse. Atmospheric relative humidity was 50%. The diluted formulation solutions were applied as a postemergence treatment. Broadleaf weeds were treated at the 2-leaf stage, and monocotyledon weeds were treated at the 1-leaf stage. The postemergence application rate was 150 g of ai/ha. Untreated seedlings were used as the control group, and the solvent (DMF + Tween-80)-treated seedlings were used as the solvent control group. Herbicidal activity was evaluated visually after 15 days from post-treatment. The results of herbicidal activities are shown in Tables 1−4, with three replicates per treatment.

**Crop Selectivity.** The conventional rice, soybean, cotton, wheat, rape, and maize were planted separately in pots (diameter = 12 cm) containing selected soil and grown in a greenhouse at 20−25 °C.[21] After the (crop) plants had reached the 4-leaf stage, new herbicides were applied (spraying) at the dosage of 150 g of ai/ha. The visual injury and growth rate of the individual plants were observed at regular intervals. After 15 days, the final results of crop safety were determined (Table 5), using three replicates per treatment.

**Plasmid Construction, Protein Expression and Extraction, HPPD Purification, Activity Assays, and Kinetic Inhibition Studies.** *Arabidopsis thaliana* HPPD (*At*HPPD) was constructed by polymerase chain reaction (PCR) using cDNA of HPPD in pMD19-T Simple (Hangzhou BIOSCI Biotechnology Company) as the template. The primers, used here were 5′-CATGCCATGGGCCAC-CAAAACGCCGC-3′ (*Nco*I) and 5′-CGCGGATCCT-CAGTGGTGGTGGTGGTGGTGTCCCACTAACTGTTT-3′ (*Bam*HI). PCR conditions were 35 cycles at 94 °C for 30 s, 55 °C for 30 s, and 68 °C for 1.5 min. The amplion was introduced into the expression vector pET-15b and subsequently transformed into *Escherichia coli* BL21(DE3). The DNA sequences of the positive clones were confirmed by DNA sequencing with Shanghai SANGON Company.

**Table 5. Crop Selectivity (Injury Rating of 0−100) of Selected Compounds (Postemergence, 150 g of ai/ha)**

| compound | soybean | rape | cotton | maize | rice | wheat |
|---|---|---|---|---|---|---|
| **II-h** | 20 | 0 | 20 | 40 | 50 | 30 |
| **II-k** | 45 | 100 | 25 | 0 | 20 | 35 |
| **II-u** | 55 | 85 | 30 | 0 | 20 | 10 |
| **III-b** | 65 | 45 | 0 | 0 | 20 | 10 |
| **VI-a** | 100 | 100 | 100 | 15 | 100 | 90 |
| **VI-b** | 100 | 100 | 86 | 50 | 100 | 60 |
| **VI-c** | 90 | 100 | 90 | 30 | 100 | 100 |
| **VI-d** | 100 | 100 | 90 | 70 | 100 | 60 |
| mesotrione | 55 | 100 | 70 | 10 | 50 | 40 |

Recombinant *At*HPPD was overexpressed in *E. coli* BL21(DE3) cells with pET-15b-HPPD plasmid. Recombinant HGD from human was overexpressed in *E. coli* BL21(DE3) cells with pET-28a-HGD plasmid. The cells were grown at 37 °C in Luria−Bertani broth supplemented with 50 μg/mL kanamycin (pET-28a plasmid) or 100 μg/mL antimycin (pET-15b plasmid) according to the previous publication.[22] Expression of the *At*HPPD plasmid was incubated at 37 °C for 12 h. HGD was induced by 0.5 mM isopropyl-β-D-thiogalactopyranoside (IPTG) when bacterial growth reached $A_{600}$ of 0.6, and then the cells were incubated for another 40 h at 15 °C. After harvesting by centrifugation (5000*g* for 30 min), the pellet was resuspended in buffer [20 mM *N*-2-hydroxyethylpiperazine-*N*′-2-ethanesulfonic acid (HEPES) and 20 mM NaCl at pH 7.0] and washed twice, followed by sonication using a cell disruptor. A crude cell-free supernatant was obtained by centrifugation at 20000*g* for 30 min. The over-expression and the relative molecular weight of recombinant *At*HPPD were validated by both sodium dodecyl sulfate polyacrylamide gel electrophoresis (SDS-PAGE) stained with Coomassie Brilliant Blue-R250 and Simple Western analysis using Simon instrumentation (ProteinSimple, CA)

**Table 6. Binding Free Energies (kcal/mol) of Compounds II-k and VI-c**

| compound | $\Delta E_{ELE}$ | $\Delta E_{VDW}$ | $\Delta E_{GAS}$ | $\Delta G_{SOL}$ | $\Delta E_{MM}$ | $-T\Delta S$ | $\Delta G_{cal}{}^{a}$ | $\Delta G_{exp}{}^{b}$ |
|---|---|---|---|---|---|---|---|---|
| **II-k** | −128.75 (8.15) | −33.57 (3.46) | −162.31 (8.11) | 115.98 (7.74) | −46.33 (4.91) | 34.42 (2.65) | −11.91 | −10.93 |
| **VI-c** | −138.94 (7.44) | −31.98 (3.81) | −170.91 (6.57) | 124.09 (7.11) | −46.82 (5.31) | 37.72 (3.01) | −9.16 | −10.02 |

[a]The results were determined by the MM/PBSA calculations. [b]The experimental values of $\Delta G_{exp}$ were derived from the reported experimental $K_i$ values.

**Scheme 1. Synthetic Route for the Title Compounds II–V[a]**

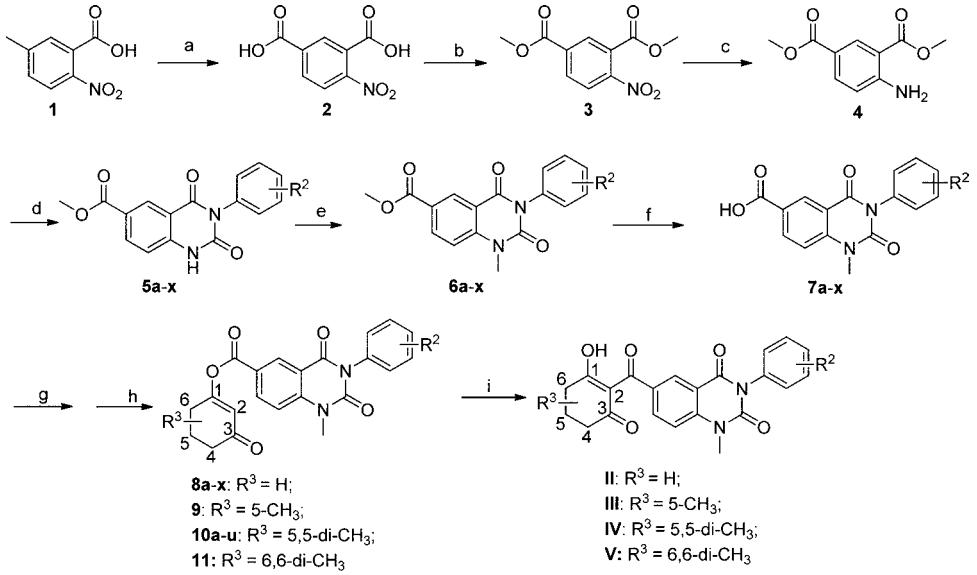


[a]Reagents and conditions: (a) KOH, $KMnO_4$, HCl; (b) $CH_3OH$, $H_2SO_4$, reflux; (c) $H_2$, 10% Pd/C; (d) (un)substituted phenyl isocyanates, pyridine, 100 °C; (e) $Cs_2CO_3$, $CH_3I$, DMF, rt; (f) HOAc, $H_2SO_4$, $H_2O$, 100 °C; (g) $SOCl_2$, THF, reflux; (h) substituted 1,3-cyclohexanediones, $Et_3N$, $CHCl_3$, 0 °C; (i) acetone cyanohydrin, $Et_3N$, $CH_2Cl_2$, rt.

*At*HPPD was purified in two chromatographic steps. The crude cell-free supernatant was loaded onto a nickel–nitrilotriacetic acid (Ni–NTA) column (Qiagen, Canada), equilibrated with 20 mM HEPES at pH 7.0. Then, HPPD was eluted with 20 mM HEPES at pH 7.0, 150 mM NaCl, and 250 mM imidazole. The fractions containing HPPD were concentrated, and the buffer was exchanged for 20 mM HEPES at pH 7.0 by ultrafiltration in Ultrafree filter devices (Millipore, MA). For further purification of the recombinant HPPD, anion-exchange chromatography was carried out on Q resin (Amersham-Pharmacia Biotech, Germany) in 20 mM HEPES at pH 7.0. Elution of the recombinant HPPD was carried out in a linear gradient from 0 to 250 mM NaCl. Again, the HPPD-containing fractions were collected, and the buffer was exchanged to 20 mM HEPES at pH 7.0 by ultrafiltration.

Our coupled enzyme assays for the *in vitro* activity and inhibition of HPPD were measured by a modification of methods previously reported in the literature.[23] Assays were performed in 96-well plates at 30 °C using an ultraviolet/visible plate reader to monitor the formation of maleylacetoacetate at 318 nm ($\varepsilon_{330}$ = 13 500 $M^{-1}$ $cm^{-1}$). The reaction mixture in a total assay volume of 200 $\mu$L contained appropriate amounts of HPPA, 100 $\mu$M $FeSO_4$, 2 mM sodium ascorbate, 20 mM HEPES buffer (pH 7.0), HPPD, and HGD. Before assays were conducted, all reaction components were pre-equilibrated at 30 °C for at least 10 min. The amount of HGD activity was predetermined to be in a large excess of the HPPD activity to ensure that the reaction was tightly coupled (the $K_m$ of HGD for HGA was 25 $\mu$M). Each experiment was repeated at least 3 times, and the values were averaged. HPPD inhibitors were dissolved in dimethyl sulfoxide (DMSO) for stock solution and diluted to various concentrations with reaction buffer just before use. The inhibition constant ($K_i$), the indication of the potency of an inhibitor, was obtained from the Dixon plot of plotting $1/v$ against the concentration of the inhibitor at certain concentrations of substrate. Bovine serum albumin is usually added up to 0.5% of the total reaction volume for coating of the target enzyme during the incubation. In our assay, no obvious effect from bovine serum albumin on the activity of the compounds has been found, which indicated that the new compounds selectively inhibited the target enzyme but did not interact with bovine serum albumin.

**Computational Methods.** The crystal structure of *At*HPPD was taken from the Protein Data Bank (PDB ID 1TFZ). Compounds were constructed and optimized using SYBYL 7.0 (Tripos, Inc.), and Gasteiger–Huckel charges were calculated for them. Docking calculations were performed on the two molecules using AutoDock4.0.[24] The protein and ligand structures were prepared with AutoDock Tools. A total of 256 runs were launched for each molecule. Each docked structure was scored by the built-in scoring function and clustered by 0.8 Å of root-mean-square deviation (RMSD) criterions. The best binding modes were determined by docking scores and also the comparison to available complex crystal structure of HPPD and commercial inhibitors (*Streptomyces avermitilis* HPPD complexed with inhibitor NTBC). Standard Amber ff99 force field parameters were assigned to protein, and general AMBER force field (gaff) was assigned to ligands. The partial atomic charges of ligands were calculated using the AM1-BCC method, and the system was solvated in an octahedral box of TIP3P water with the crystallographic water molecules kept. The edge of the box was at least 8 Å from the solute, and appropriate counterions were added to the system to preserve neutrality. In each step, energy minimization was first performed using the steepest descent algorithm for 1000 steps and then the conjugated gradient algorithm for another 2000 steps.

The MD simulation was performed under periodic boundary conditions using the Sander module of the AMBER9 program.[25] The stable MD trajectory was used to perform the binding free energy ($\Delta G_{bind}$) calculation using a modified MM/PBSA method (Table 6). A total of 100 snapshots were taken from the last 500 ps trajectory with an interval of 5 ps to analyze the binding energy, and at the same time,

**Scheme 2. Synthetic Route for the Title Compounds VI**[a]

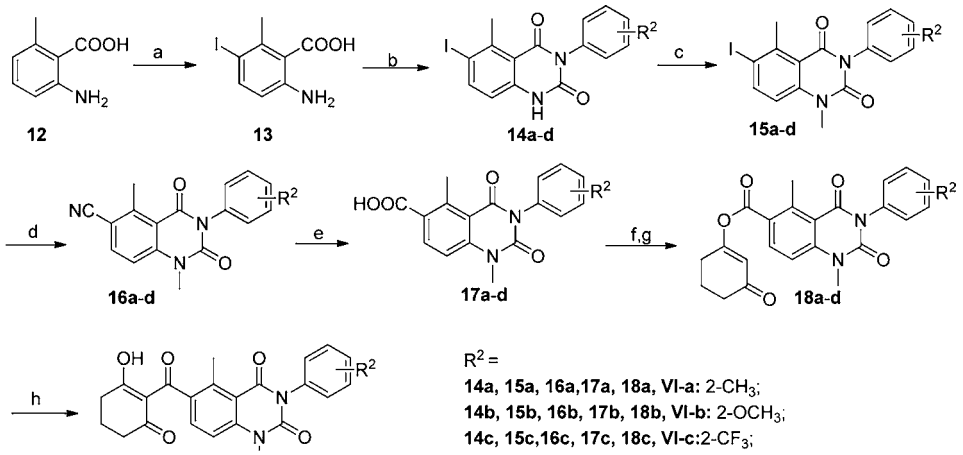


[a]Reagents and conditions: (a) ICl, $CH_3COOH$, rt; (b) substituted phenyl isocyanates, pyridine, 100 °C; (c) $Cs_2CO_3$, $CH_3I$, DMF, rt; (d) CuCN, DMF, reflux; (e) $H_2SO_4$, $CH_3COOH$, $H_2O$, 100 °C; (f) $SOCl_2$, THF, reflux; (g) 1,3-cyclohexanediones, $Et_3N$, $CHCl_3$, 0 °C; (h) acetone cyanohydrin, $Et_3N$, $CH_2Cl_2$, rt.

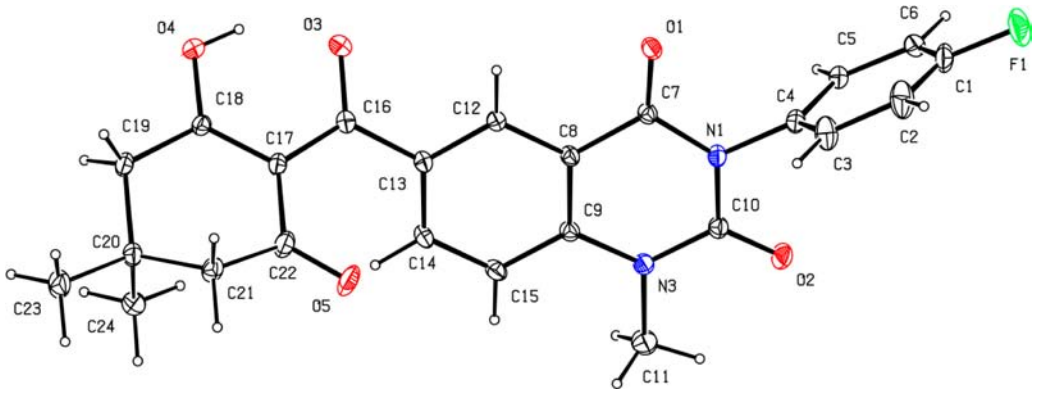


**Figure 2.** Crystal structure of compound **IV-d**.

the counterions and water molecules (water related to the crucial hydrogen bond was not included) were stripped.

## RESULTS AND DISCUSSION

**Chemistry.** Dependent upon the substituent at $R^4$, compounds **II**–**VI** were synthesized by two different synthetic routes. When the substituent at $R^4$ is H, the detailed synthetic routes of compounds **II**–**V** are outlined in Scheme 1. When $R^4$ is methyl, the detailed synthetic routes of title compounds **VI** are outlined in Scheme 2. As seen in Scheme 1, the target compounds **II**–**V** can be prepared in 10-step synthetic routes using 5-methyl-2-nitrobenzoic acid as the starting material. After oxidation, esterification, and reduction reactions, the key intermediate dimethyl 4-aminoisophthalate (**4**) was obtained in a yield of 83%. According to the reported methods,[26,27] the key intermediate **4** reacted with various (un)substituted phenyl isocyanates in pyridine to afford quinazoline-2,4-dione intermediates **5a**–**5x** in good yields. Then, the intermediates **5a**–**5x** reacted with $CH_3I$ to afford the corresponding intermediates **6a**–**6x** in yields of 81–99%. It was found that the intermediates **6a**–**6x** were very unstable in strong base solution, such as aqueous concentrated NaOH and KOH solution, because of the decomposition of the quinazoline-2,4-dione rings of **6a**–**6x** caused by base. However, to our delight, the quinazoline-2,4-dione rings of intermediates **6a**–**6x** were very stable in acid solution. Finally, using mixed acids (HOAc and $H_2SO_4$) as the hydrolysis reagents, the hydrolysis of intermediates **6a**–**6x** could smoothly proceed with yields of 78–98%. Subsequently, intermediates **7a**–**7y** reacted with $SOCl_2$ in tetrahydrofuran (THF) to obtain the corresponding acid chlorides that were very unstable. Thus, the acid chlorides were used directly in the next step without further isolation. After the reaction of the acid chlorides with substituted-1,3-cyclohexanediones, the key enol esters (**8a**–**8x**, **9a** and **9b**, **10a**–**10v**, and **11**) were generated. Finally, using acetone cyanohydrin as the Fries rearrangement catalyst, the target compounds **II**–**V** were obtained in yields of 64–94%.

Similarly, the title compounds **VI** can be prepared, in an 8-step synthetic route using 2-amino-6-methylbenzoic acid as the starting material, after an iodination reaction with ICl in acetic acid; the key intermediate 6-amino-3-iodo-2-methylbenzoic acid (**13**) was obtained in a yield of 73%. Intermediates **14a**–**14d** and **15a**–**15d** were obtained using the same methods as the preparation of intermediates **6a**–**6x**. Then, compounds **15a**–**15d** reacted with 2 equiv of CuCN in DMF, and the intermediates **16a**–**16d** were obtained in yields of 69–85%. Because the quinazoline-2,4-dione rings of intermediates **16a**–**16d** were also very sensitive to strong base, the reaction could not be proceeded in aqueous base solution. Using mixed acids ($H_2SO_4$ and HOAc) as the reactant, the hydrolysis of the cyano group in the intermediates **16a**–**16d** proceeded smoothly. Using the same method as the synthesis of previously enol


dx.doi.org/10.1021/jf5048089 | J. Agric. Food Chem. 2014, 62, 11786–11796

esters, the intermediates **18a−18d** could be prepared from intermediates **17a−17d** in yields of 62−80%. Subsequent Fries rearrangement reaction using acetone cyanohydrin as the catalyst afforded compounds **VI** in yields of 71−78%.

The structures of all of the synthetic triketone-containing compounds were confirmed by $^{1}H$ and $^{13}C$ nuclear magnetic resonance (NMR) and high-resolution mass spectrometry (HRMS) spectral data. In addition, the crystal structure of compound **IV-d** was further determined by X-ray diffraction analysis (Figure 2).

**Herbicidal Activity and SAR.** The postemergence herbicidal activities of all of the target compounds were evaluated against monocotyledon weeds (*E. crus-galli*, *S. faberii*, and *D. sanguinalis*) and broadleaf weeds (*A. retroflexus*, *E. prostrata*, and *A. juncea*) in the greenhouse environment. Mesotrione was used as the positive control, and the results are shown in Tables 1−4. As anticipated, the treated weeds developed unique bleaching symptoms, as typical HPPD herbicides. The herbicidal activity evaluation indicated that most of the synthetic compounds showed between "good" to "excellent" herbicidal activity against the test weeds. Among them, compounds **III-b** and **VI-a−VI-d** showed an even broader spectrum of weed control than mesotrione, because of their superior control efficacy against the monocotyledon weeds to mesotrione. To summarize systematically the SAR of triketone-containing quinazoline-2,4-diones, some of our previously synthesized compounds were also added to the results depicted in Table 1.[15]

Previously, we have found that compound **I-f** was worth considering for further optimization; therefore, a series of substituents with diversity were introduced at the N-1 position of the quinazoline-2,4-dione ring. As shown in Table 1, compound **I-h** with an ethyl group at $R^1$ displayed almost equipotent herbicidal activity as compound **I-f**. However, compound **I-i** with *n*-Pr at $R^1$ displayed reduced herbicidal activity compared to compound **I-h**. It seems that too small or sterically bulky substituents at $R^1$ are detrimental to the activity of target compounds; for example, compounds **I-g** ($R^1$ = H), **I-k** ($R^1$ = *n*-Bu), and **I-m** ($R^1$ = $CH_2C_6H_5$) are almost inactive against six tested weeds. A possible reason for the poor herbicidal activity of these compounds may be due to their uneasily access into the weeds or rapid degradation in the weeds. However, when we placed an electron-withdrawing (**I-n**, F) or electron-donating (**I-o**, $OCH_3$) group on the benzyl group of **I-m**, the herbicidal activity usually displayed enhanced effects (**I-n** and **I-o** > **I-m**). Therefore, the SAR at this position can be summarized as follows: $CH_3$ and $CH_2CH_3$ > *n*-Pr > $CH_2C{\equiv}CH$ > $CH_2$−2-F−$C_6H_4$, $CH_2$−3-$OCH_3$−$C_6H_4$, iBu, *n*-Bu, H, and $CH_2C_6H_5$.

On the basis of the above SAR results, we kept the methyl group at $R^1$ and synthesized a series of novel compounds with different $R^2$ substitutions to explore further their herbicidal activity (Scheme 1). A variety of substituents were introduced at $R^2$, including electron-withdrawing (F, Br, $OCF_3$, $CF_3$, and $NO_2$), electron-donating ($OCH_3$), sterically small (H), or bulky (2-iPr and 2.6-di-iPr) groups, to evaluate the substituent effect of the substituent at this position on herbicidal activity. As depicted in Tables 1 and 2, when a single group was introduced at $R^2$, in most cases, compounds with substituents at the *ortho* positions would have increased activity and broader spectrum weed control than those with equivalent substitutions on *para* and *meta* positions. For example, the above rule is applied to the chloro-substituted analogues (**I-c** > **I-a** and **I-b**), the methyl-substituted analogues (**I-f** > **I-e** and **I-d**), the methoxyl-substituted analogues (**II-h** > **II-i** and **II-j**), and the trifluoromethyl-substituted analogues (**II-k** > **II-m** and **II-l**). Notably, compounds with multiple substitutions on the phenyl ring showed a decreased herbicidal activity (**II-s−II-x**), even through some of them with substituents at the *ortho* positions. It was also found that compounds with *ortho* substitiutions of electron-donating groups (**I-f**, $CH_3$; **II-h**, $OCH_3$) displayed improved herbicidal activity compared to that of the compounds with electron-withdrawing groups (**I-c**, Cl; **II-b**, F; **II-e**, Br; **II-k**, $CF_3$; and **II-n**, $OCF_3$). The similar structure−activity trends could also be observed for the compounds with substituents at the *para* positions, although there may be a few exceptions.

The SAR results suggested that substituents in the *ortho* positions of compounds can usually improve their herbicidal activity. Inspired by this, we then synthesized compounds **II-q−II-s** with different sizes of substituents on *ortho* positions to examine the steric effects on herbicidal activity. As shown in Table 2, the steric factors had a significant impact on herbicidal activity. Compounds **II-q** ($R^2$ = 2-$C_2H_5$) and **II-r** ($R^2$ = 2-iPr) showed over 80% control in six deferent weed tests at the rate of 150 g of ai/ha. However, compound **II-s** ($R^2$ = 2,6-di-iPr) with more sterically bulky substituents in its *ortho* positions displayed decreased effects and was almost inactive toward *S. faberii* and *A. juncea*. A possible explanation for compound **II-s** with lower activity is that the large subsitutuents would prevent making bonds with plant HPPD.[28]

To examine the effect of $R^3$ substitution on herbicidal activity, we then synthesized another set of compounds (**III−V**). As in Table 3, compounds **III-a** and **III-b**, with a methyl on the 5 position of the 1,3-cyclohexanedione ring, displayed an increased herbicidal effect compared to their non-substituted analogues **II-g** and **II-v**, respectively. Furthermore, compound **III-b** exhibited over 85% control in six deferent weed tests, even at a rate as low as 37.5 g of ai/ha, demonstrating broader spectrum of weed control than mesotrione. However, when another methyl group was also introduced to the 5 position, the herbicidal activity (**IV-g** and **IV-s**) was impaired in most cases. Because of our curiosity, two methyl groups were introduced at 6 positions, with compound **V** displaying an improved herbicidal activity compared to its parent compound **II-t**. One possible reason for this phenomenon is that introducing two methyl groups on 6 posotions would block the metabolism of weeds *in vivo*.[7]

We found that most of the commercial HPPD herbicides have substituents in the *ortho* positions of their benzoyl groups.[7,8,10] It is assumed that placing a substitutent in the *ortho* position would be favorable for increasing their herbicidal activity. In addition, introducing a methyl group in the *ortho* position has been reported, to be able to enhance the herbicidal activity.[9,13] Owning to the structure feature of the triketone-containing quinazoline-2,4-dione motif, we intended to introduce a methyl group in the 5 position of the quinazoline-2,4-dione ring (*ortho* position). To understand whether placing a methyl group in the 5 position is beneficial for herbicidal activity or not, four representative compounds **I-f**, **II-h**, **II-k**, and **II-u** with a promising and broad spectrum of weed control were selected for further optimization. The synthetic methods for these methyl-substituted analogues (**VI-a−VI-d**) are outlined in Scheme 2, the herbicidal activity results are shown in Table 4. Surprisingly, compounds **VI-a−VI-d**, with a methyl group in the *ortho* positions, showed significantly

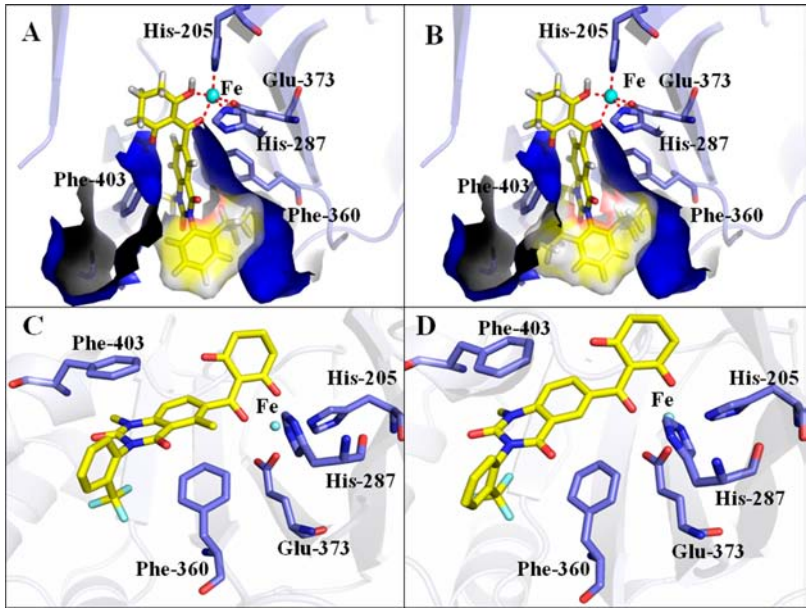


**Figure 3.** Simulated binding models of four representative compounds (A) **II-r**, (B) **II-s**, (C) **II-k**, and (D) **VI-c** in the active site of *At*HPPD, with panels A and B shown as translucent surfaces and panels C and D shown as directly binding models. Fe(II) is depicted as the aquamarine sphere; the structures of inhibitors are indicated in yellow sticks; and the key residues surrounding the active site are displayed in light blue.

improved herbicidal activity compared to their corresponding parent compounds **I-f**, **II-h**, **II-k**, and **II-u**, respectively. All four methyl-substituted analogues displayed strong inhibition (>85%) and broad spectrum for weed control, even at a dosage as low as 37.5 g of ai/ha. Especially, compound **VI-a** displayed almost 100% inhibition in both tests against monocotyledon and dicotyledon weeds, with its herbicidal potency against dicotyledon weeds (*A. retroflexus*, *E. prostrata*, and *A. juncea*) being almost equipotent to mesotrione and its potency against monocotyledon weeds (*E. crus-galli*, *S. faberii*, and *D. sanguinalis*) being superior to mesotrione.

**Crop Selectivity.** Crop selectivity is one of the vital concerns in pesticide discovery. Some representative compounds (**II-h**, **II-k**, **II-u**, **III-b**, and **VI-a**−**VI-d**) were chosen for crop selectivity evaluation. The results are listed in Table 5. It is very interesting that compound **III-b** was safe for three crops of cotton, maize, and wheat after postemergence application at a rate of 150 g of ai/ha, whereas mesotrione was not selective for cotton (70% injury) and wheat (40% injury) at the concentration of 150 g of ai/ha. This result indicated that there is a great potential for **III-b** to be used in cotton, maize, and wheat fields to control weeds. Furthermore, **II-u** was safe for maize and wheat, suggesting that **II-u** has potential to develop as a effective herbicide for controlling weeds in maize and wheat fields. In addition, **II-h** was safe for rape at the rate of 150 g of ai/ha, whereas mesotrione displayed 100% injury effect against it at the same conditions, indicating that **II-h** might has potential to develop as a new herbicide in a rape field. Moreover, **II-k** was safe for maize at the rate of 150 g of ai/ha, which indicated that **II-k** can be developed as a herbicide for maize field. Although compounds **VI-a**−**VI-d** displayed excellent herbicidal activity, they were not safe for the six selected crops. A possible explanation of compounds **VI-a**−**VI-d** to improve their herbicidal activity while decreasing crop selectivity is that the methyl group at $R^4$ would block metabolism of plants at this site.[13]

**HPPD Inhibition and SAR.** For further understanding, the structural basis for these compounds as HPPD inhibitors and the $K_i$ values of compounds **II**−**VI** against *At*HPPD are shown in Tables 2−4. Mesotrione was used as the positive control. Notably, most of newly synthesized herbicides displayed a strong *At*HPPD inhibitory activity, and some of them showed even better potency than mesotrione. Compound **VI-d** ($K_i$ = 9 nM) displayed the highest HPPD inhibitory activity, showing slightly more potency than mesotrione ($K_i$ = 13 nM). Furthermore, compounds **VI-c** ($K_i$ = 10 nM), **II-o** ($K_i$ = 12 nM), and **II-v** ($K_i$ = 13 nM) also showed excellent inhibitory activity, which are comparable to mesotrione.

On the basis of the *in vitro* activity of those compounds, some SARs can be drawn. As shown in Table 2, when the right side of the benzene ring is single-substituted, compounds with *para* substitutions generally have improved activity compared to those with the same substituents in *meta* and *ortho* positions. With regard to the multi-substituted analogues, the positions of substituents can also affect the HPPD inhibitory activity. Compounds with substituents at 2,4 and 3,5 positions would have enhanced activity compared to those at 2,6 positions (**II-v** and **II-x** > **II-t**). It seemed that the electronic factors did not significantly affect the activity; for example, compounds with either *para* substitutions of strongly electron-donating (**II-j**, $OCH_3$) groups or electron-withdrawing (**II-p**, $NO_2$) groups showed almost equal activity (**II-j** = **II-p**). In addition, the steric factors of substituents also have a significant impact on the inhibitory activity. Compounds with sterically bulky groups on the *ortho* position were found detrimental to activity (**II-r** > **II-s**). This was consistent with the herbicide inhibition activity. To understand the structural basis, we investigated the binding modes of the new compounds using compounds **II-r** and **II-s** as two representatives. As shown in panels A and B of Figure 3, the two compounds can form a bidentate association with the active site ferrous ion via its 5′ and 7′ oxygens and the quinazoline-2,4-dione ring can form $\pi-\pi$ stacking interaction with the conserved Phe360 and Phe403. In addition, the 2-isopropyl-substituted benzene ring on the quinazoline-2,4-dione moiety of compound **II-r** embedded deep into the hydrophobic cavity and occupied a major part of this pocket.


dx.doi.org/10.1021/jf5048089 | *J. Agric. Food Chem.* 2014, 62, 11786−11796

However, the 2,6-diisopropyl-substituted benzene ring of compound **II-s** occupied beyond the hydrophobic pocket, showing a strong steric repulsion effect.

It is worth mentioning that, when a methyl group was introduced to the 5 position of the quinazoline-2,4-dione ring, the inhibition of compounds **VI-a**−**VI-d** against *At*HPPD has improved significantly compared to their parent compounds **I-f**, **II-h**, **II-k**, and **II-u**, respectively (Table 4). To investigate why the methyl group at the $R^4$ position significantly improved the activity of the target compounds, compounds **II-k** and **VI-c** were chosen as the representative inhibitors for computational modeling. The energy component analysis showed that the difference mainly came from the electrostatic interaction, solvation, and entropy effects (Table 5). Compound **II-k** had an electrostatic interaction of −128.75 kcal/mol and a solvation penalty of 115.98 kcal/mol, which result in an enthalpy change of −46.33 kcal/mol. Compound **VI-c** had a lower electrostatic interaction of −138.94 kcal/mol and a higher solvation penalty of 124.09 kcal/mol, which result in a similar enthalpy change of −46.82 kcal/mol. However, a higher entropy penalty of **VI-c** (37.72 kcal/mol compared to 34.42 kcal/mol for **II-k**) resulted in a lower binding affinity (−9.16 kcal/mol compared to −11.91 kcal/mol for **II-k**), which demonstrated that the introduction of the methyl group at the 5 position of the quinazoline-2,4-dione ring can help reduce the entropy penalty and be advantageous for activity improvement.

In summary, a series of novel triketone-containing quinazoline-2,4-diones were designed and subsequently optimized on the basis of a systemic SAR study, leading to the discovery of several novel HPPD inhibitors with the excellent *in vitro* inhibitory potency and greenhouse herbicidal activity. Specifically, compounds **II-h**, **II-k**, **II-u**, **III-b**, and **VI-a**−**VI-d** were found with a potential of displaying a broader spectrum of weed control than mesotrione. More importantly, compound **III-b** was very safe for three crops of cotton, maize, and wheat at the rate of 150 g of ai/ha, showing great applicability in the field. Furthermore, at the dosage of 150 g of ai/ha, compound **II-h** was safe for rape, compound **II-k** was safe for maize, and compound **II-u** was safe for maize and wheat. The promising results suggested that the triketone-containing quinazoline-2,4-dione motif is well worth further optimization. Further structural optimizations and field trials of compounds **II-h**, **II-k**, **II-u**, and **III-b** are still ongoing.

## ■ ASSOCIATED CONTENT

### Ⓢ Supporting Information

Experimental details and analytical data for all of the intermediates and compounds **II**−**VI**. This material is available free of charge via the Internet at http://pubs.acs.org.

## ■ AUTHOR INFORMATION


### Corresponding Authors

*Telephone: +86-27-67867800. Fax: +86-27-67867141. E-mail: tomyang@mail.ccnu.edu.cn.

*Telephone: +86-27-67867800. Fax: +86-27-67867141. E-mail: gfyang@mail.ccnu.edu.cn.



### Funding

The authors are very grateful to the National Key Technologies Research and Development Program of China (2011BAE06B05) for the financial support for this work.


### Notes

The authors declare no competing financial interest.

## ■ REFERENCES


(1) Neidig, M. L.; Decker, A.; Choroba, O. W.; Huang, F. l.; Kavana, M.; Moran, G. R.; Spencer, J. B.; Solomon, E. I. Spectroscopic and electronic structure studies of aromatic electrophilic attack and hydrogen-atom abstraction by non-heme iron enzymes. *Proc. Natl. Acad. Sci. U. S. A.* **2006**, *103*, 12966−12973.

(2) He, P.; Moran, G. R. We two alone will sing: The two-substrate α-keto acid-dependent oxygenases. *Curr. Opin. Chem. Biol.* **2009**, *13*, 443−450.

(3) Purpero, V. M.; Moran, G. R. Catalytic, noncatalytic, and inhibitory phenomena: Kinetic analysis of (4-hydroxyphenyl)pyruvate dioxygenase from *Arabidopsis thaliana*. *Biochemistry* **2006**, *45*, 6044−6055.

(4) Wu, C. S.; Huang, J. L.; Sun, Y. S.; Yang, D. Y. Mode of action of 4-hydroxyphenylpyruvate dioxygenase inhibition by triketone-type inhibitors. *J. Med. Chem.* **2002**, *45*, 2222−2228.

(5) Yang, C.; Pflugrath, J. W.; Camper, D. L.; Foster, M. L.; Pernich, D. J.; Walsh, T. A. Structural basis for herbicidal inhibitor selectivity revealed by comparison of crystal structures of plant and mammalian 4-hydroxyphenylpyruvate dioxygenases. *Biochemistry* **2004**, *43*, 10414−10423.

(6) Borowski, T.; Bassan, A.; Siegbahn, P. E. 4-Hydroxyphenylpyruvate dioxygenase: A hybrid density functional study of the catalytic reaction mechanism. *Biochemistry* **2004**, *43*, 12331−12342.

(7) Beaudegnies, R.; Edmunds, A. J. F.; Fraser, T. E. M.; Hall, R. G.; Hawkes, T. R.; Mitchell, G.; Schaetzer, J.; Wendeborn, S.; Wibley, J. Herbicidal 4-hydroxyphenylpyruvate dioxygenase inhibitors—A review of the triketone chemistry story from a Syngenta perspective. *Bioorg. Med. Chem.* **2009**, *17*, 4134−4152.

(8) Ahrens, H.; Lange, G.; Müller, T.; Rosinger, C.; Willms, L.; van Almsick, A. 4-Hydroxyphenylpyruvate dioxygenase inhibitors in combination with safeners: Solutions for modern and sustainable agriculture. *Angew. Chem., Int. Ed.* **2013**, *52*, 9388−9398.

(9) Witschel, M. Design, synthesis and herbicidal activity of new iron chelating motifs for HPPD inhibitors. *Bioorg. Med. Chem.* **2009**, *17*, 4221−4229.

(10) Lee, D. L.; Prisbylla, M. P.; Cromartie, T. H.; Dagarin, D. P.; Howard, S. W.; Provan, W. M.; Ellis, M. K.; Fraser, T.; Mutter, L. C. The discovery and structural requirements of inhibitors of *p*-hydroxyphenylpyruvate dioxygenase. *Weed Sci.* **1997**, *45*, 601−609.

(11) Zhu, Y. Q.; Zou, X. M.; Hu, F. Z.; Yao, C. S.; Liu, B.; Yang, H. Z. Synthesis and herbicidal evaluation of novel 3-[(α-hydroxy-substituted)benzylidene]pyrrolidine-2,4-diones. *J. Agric. Food Chem.* **2005**, *53*, 9566−9570.

(12) Mitchell, G.; Bartlett, D. W.; Fraser, T. E.; Hawkes, T. R.; Holt, D. C.; Townson, J. K.; Wichert, R. A. Mesotrione: A new selective herbicide for use in maize. *Pest Manage. Sci.* **2001**, *57*, 120−128.

(13) Hamprecht, G.; Witschel, M.; Hawkes, T. R.; Edmunds, A. J. F.; Morris, J. A.; van Almsick, A. Herbicides with bleaching properties. In *Modern Crop Protection Compounds*, 2nd ed.; Krämer, W., Schirmer, U., Jeschke, P., Witschel, M., Eds.; Wiley-VCH: Weinheim, Germany, 2012; pp 197−276.

(14) Matringe, M.; Sailland, A.; Pelissier, B.; Rolland, A.; Zink, O. *p*-Hydroxyphenylpyruvate dioxygenase inhibitor-resistant plants. *Pest Manage. Sci.* **2005**, *61*, 269−276.

(15) Wang, D. W.; Lin, H. Y.; Cao, R. J.; Ming, Z. Z.; Chen, T.; Hao, G. F.; Yang, W. C.; Yang, G. F. Design, synthesis and herbicidal activity of novel quinazoline-2,4-diones as 4-hydroxyphenylpyruvate dioxygenase inhibitors. *Pest Manage. Sci.* **2014**, DOI: 10.1002/ps.3894.

(16) Bruker AXS. *SAINT and SMART*; Bruker AXS: Madison, WI, 2003.

(17) Sheldrick, G. M. *SHELXS97*; University of Gottingen: Gottingen, Germany, 1997.

(18) Luo, Y. P.; Jiang, L. L.; Wang, G. D.; Chen, Q.; Yang, G. F. Syntheses and herbicidal activities of novel triazolinone derivatives. *J. Agric. Food Chem.* **2008**, *56*, 2118−2124.

(19) Jiang, L. L.; Tan, Y.; Zhu, X. L.; Wang, Z. F.; Zuo, Y.; Chen, Q.; Xi, Z.; Yang, G. F. Design, synthesis, and 3D-QSAR analysis of novel

1,3,4-oxadiazol-2(3*H*)-ones as protoporphyrinogen oxidase inhibitors. *J. Agric. Food Chem.* **2010**, *58*, 2643−2651.
(20) Jiang, L. L.; Zuo, Y.; Wang, Z. F.; Tan, Y.; Wu, Q. Y.; Xi, Z.; Yang, G. F. Design and syntheses of novel *N*-(benzothiazol-5-yl)-4,5,6,7-tetrahydro-1*H*-isoindole-1,3(2*H*)-dione and *N*-(benzothiazol-5-yl)isoindoline-1,3-dione as potent protoporphyrinogen oxidase inhibitors. *J. Agric. Food Chem.* **2011**, *59*, 6172−6179.
(21) Zuo, Y.; Yang, S. G.; Luo, Y. P.; Tan, Y.; Hao, G. F.; Wu, Q. Y.; Xi, Z.; Yang, G. F. Design and synthesis of 1-(benzothiazol-5-yl)-1*H*-1,2,4-triazol-5-ones as protoporphyrinogen oxidase inhibitors. *Bioorg. Med. Chem.* **2013**, *21*, 3245−3255.
(22) Meazza, G.; Scheffler, B. E.; Tellez, M. R.; Rimando, A. M.; Romagni, J. G.; Duke, S. O.; Nanayakkara, D.; Khan, I. A.; Abourashed, E. A.; Dayan, F. E. The inhibitory activity of natural products on plant *p*-hydroxyphenylpyruvate dioxygenase. *Phytochemistry* **2002**, *60*, 281−288.
(23) Schmidt, S. R.; Müller, C. R.; Kress, W. Murine liver homogentisate 1,2-dioxygenase. Purification to homogeneity and novel biochemical properties. *Eur. J. Biochem.* **1995**, *228*, 425−430.
(24) Huey, R.; Morris, G. M.; Olson, A. J.; Goodsell, D. S. A semiempirical free energy force field with charge-based desolvation. *J. Comput. Chem.* **2007**, *28*, 1145−1152.
(25) Hao, G.-F.; Tan, Y.; Xu, W.-F.; Cao, R.-J.; Xi, Z.; Yang, G.-F. Understanding resistance mechanism of protoporphyrinogen oxidase-inhibiting herbicides: Insights from computational mutation scanning and site-directed mutagenesis. *J. Agric. Food Chem.* **2014**, *62*, 7209−7215.
(26) Charles, A.; Nicole, C. B.; Bernard, G.; Henri, J.; Fred, O. D.; Chester, P. W.; Ly, P.; Rose, K. C.; William, W. M. Quinazolines as mmp-13 inhibitors. WO Patent 2002064572 A1, 2002.
(27) Güngör, T.; Chen, Y.; Golla, R.; Ma, Z.; Corte, J. R.; Northrop, J. P.; Bin, B.; Dickson, J. K.; Stouch, T.; Zhou, R.; Johnson, S. E.; Seethala, R.; Feyen, J. H. Synthesis and characterization of 3-arylquinazolinone and 3-arylquinazolinethione derivatives as selective estrogen receptor beta modulators. *J. Med. Chem.* **2006**, *49*, 2440−2455.
(28) Lin, Y. L.; Wu, C. S.; Lin, S. W.; Huang, J. L.; Sun, Y. S.; Yang, D. Y. SAR studies of 3-cyclopropanecarbonyloxy-2-cyclohexen-1-one as inhibitors of 4-hydroxyphenylpyruvate dioxygenase. *Bioorg. Med. Chem.* **2002**, *10*, 685−690.

strategies prefer an aqueous purification process, where neither the glycosides are modified nor organic solvents are included in the purification.[9] Alternatively, some strategies focus on the isolation of specific constituents, such as rebaudioside A (Ra).[10] Moreover, enzymatic transglycosylation of stevioside and its congeners has been used by some manufacturers to improve the sweetness and reduce the undesirable bitter aftertaste of these compounds. Often, cyclodextrin glycosyltransferases (CGTases) have been used for this purpose. CGTases transfer glycosyl residues from donor substrates, such as cyclodextrins[11] or starch, to the $C_{13}$ and/or $C_{19}$ sugar residues of the natural compounds, yielding a complex mixture of transglycosylated products.[12,13]

Ultrahigh-performance liquid chromatography (UHPLC) is the method of choice for compositional analysis of steviol glycosides in extracts. Different kinds of detectors have been used for identification and quantification: UV,[14,15] pulsed amperometric detection[16] (PAD), charged aerosol detector (CAD),[17] and mass spectrometry (MS).[18,19]

The aim of this study was to determine the chemical composition of the major and minor steviol glycosides by ultrahigh performance liquid chromatography−electrospray ionization−mass spectrometry (UHPLC-ESI-MS) of four commercial *Stevia* products. In addition, the sensory properties of the latter were evaluated by a trained panel to assess the impact of the different manufacturing processes and resulting chemical composition on the sensory quality of the extracts.

## MATERIALS AND METHODS

**Chemicals and Materials.** Stevioside (Sv), rubososide (Ru), steviolbioside (Sb), rebaudioside A (Ra), rebaudioside B (Rb), rebaudioside C (Rc), rebaudioside D (Rd), rebaudioside F (Rf), and dulcoside A (DuA) were purchased from ChromaDex (Irvine, CA, USA); their purity was >97%. UHPLC-MS grade water and acetonitrile (ACN) were purchased from Biosolve BV (Valkenswaard, The Netherlands).

The following materials were used: sucrose (Merck, Darmstadt, Germany), commercial *Stevia* (Daily, Santiago, Chile), caffeine (Sigma-Aldrich, Germany), iron sulfate (Merck), D-sorbitol 98% (Sigma-Aldrich), sucralose (Sugafor, Santiago, Chile), glycyrrhizic acid ammonium salt from *Glycyrrhiza uralensis* root (Sigma-Aldrich), and unsalted rice cookies (Jumbo, Santiago, Chile).

***Stevia* Samples.** Purified *S. rebaudiana* extracts obtained by different process technologies, that is, membrane purification (MP), enzymatic modification (EM), and two samples from ethanol crystallization (EC1 and EC2), were provided by Prodalysa (Concón, Chile), AccoBio (Jiangsu, China), GLG Life Tech Corp. (Vancouver, Canada), and Cargill Truvia (Minneapolis, MN, USA), respectively.

**UHPLC-DAD-ESI-MS$^n$ Analysis.** Samples were analyzed in a Thermo Accela UHPLC system (Thermo Scientific, San Jose, CA, USA) equipped with a pump and autosampler using an Acquity UPLC HSS C18 column (Waters; 150 mm × 2.1 mm i.d.; particle size = 1.8 $\mu$m) at 20 °C. The eluents used were water/acetic acid (100:0.1, v/v) (eluent A) and ACN/acetic acid/dichloromethane (100:0.1:0.1, v/v/v) (eluent B). The elution program was as follows: 0−1 min, 25% B (v/v); 1−16 min, linear gradient of 25−50% B (v/v); 16−22 min, linear gradient of 50−100% B (v/v); 22−28 min, linear gradient of 100−25% B (v/v). The flow rate was 300 $\mu$L/min. MS$^n$ analysis was performed on a Thermo Scientific LTQ VELOS, using electrospray ionization (ESI) and detection in negative mode, with a source voltage of 3.5 kV and an ion transfer tube temperature of 350 °C. The instrument was tuned manually to optimize the ionization process and sensitivity using rebaudioside A. Control of the instrument and data processing were carried out using Xcalibur 2.07 (Thermo Scientific). Identification of compounds was based on the molecular mass of the parent ion and MS$^n$ spectral data. The most abundant ion of MS$^2$ was used for MS$^3$.

To visualize the minor compounds, the analyses were carried out with a divert valve (DV), by which the main peaks (Ra and Sv) could be removed from the chromatograms. The injection volumes were 1 and 5 $\mu$L for analysis without or with DV, respectively. Quantification of Ru, Sb, Rb, Rc, Rd, Rf, and DuA was conducted in SRM mode. Due to their coelution and overlapping fragments in MS$^2$, Ra and Sv were quantified in single ion monitoring (SIR) mode, as the rest of the minor compounds, using the corresponding $[M - H]^-$ ion.

**Calibration Curves.** The standard compounds were accurately weighed and dissolved in MeOH/$H_2O$ (50:50 v/v) to obtain stock solutions with a final concentration of ∼0.1 mg/mL. Dilutions were prepared in MeOH/$H_2O$ (50:50 v/v) in the range of 0.005−1 $\mu$g/mL for Ru, Sb, Rb, Rc, Rd, Rf, and DuA and in the range of 0.1−10 $\mu$g/mL for Sv and Ra. Three independent determinations were conducted for each concentration. Calibration curves were calculated by linear regression of double-logarithmic plots of the area of the selected ions versus the concentration of the respective steviol glycoside standard. These calibration curves were employed to calculate the amount of major and minor steviol glycosides present in the original samples. The obtained linearity coefficients were >0.998 (see Table S1 in the Supporting Information). For some steviol glycosides, no commercial standards were available. Thus, Rd was used for the quantification of minor steviol glycosides and transglycosylated products containing the Glc$\beta$1−2(Glc$\beta$1−3)Glc$\beta$1- chain; and Rc was used for the quantification of compounds containing the Rha$\alpha$1−2(Glc$\beta$1−3)Glc$\beta$1- chain.

**Sensory Analysis.** The sensory attributes 'sweetness', 'bitterness', 'licorice', and 'metallic' of the four commercial samples of *Stevia* (MP, EM, EC1 and EC2) were assessed by a trained panel that was previously recruited by the Centro de Aromas y Sabores following ISO norms.[20] All panelists ($n$ = 13) had previous experience in sensory analysis of other products. The panel received a specific training to assess the sensory properties of the *Stevia* extracts and employed a category-specific scale of 100 mm (product specific) for the sensory assessment.[21] Sensory data were acquired with the software Compusense Five release 5.4 (Guelph, Canada) and analyzed (ANOVA, means, SD) with Senstools (version 3.0.11, OP&P Product Research, Utrecht, The Netherlands).

**Selection and Training of the Panelists.** The selection procedure consisted of two phases. First, 33 female candidates 45 ± 5 years of age were asked to rank seven randomly presented sucrose solutions (2, 3, 5, 7, 9, 11, and 13% w/v sucrose) in order of increasing sweetness. In the second phase, the panelists had to position samples of sorbitol (86200 mg/L), sucralose (78.6 mg/L), and commercial *Stevia* (276 mg/L) within the correctly ordered sucrose solutions. These samples were designed to match the sweetness of a 5% w/v sucrose solution, as proposed elsewhere.[22,23] All of the sessions were performed in standardized sensory booths. Among the candidates, 13 panelists that performed correctly both tests were selected for further training.

The selected panelists completed five introductory training sessions of 2 h each during a 2 month period. First, they were introduced to the main sensory attributes describing sweeteners (sweetness, bitterness, licorice, and metallic taste). For this purpose, five solutions were shown to the panelists to familiarize them with the attributes: sucrose (sweetness), commercial *Stevia* (sweetness), caffeine (bitterness), glycyrrhizic acid ammonium salt (licorice), and iron sulfate (metallic taste).

In a second phase, a product-specific scale was developed to reflect the typical bitterness, licorice, metallic, and sweet tastes of the solutions that were assessed later by the panelists. The intensity range of each attribute was assessed on a scale from 0 to 100 mm. For each attribute, a reference stimulus was provided, which was anchored with an intensity in the middle of the scale at 50 mm. A series of 5% w/v sucrose solutions with increasing concentrations of tastants were presented to estimate the concentration of the reference stimulus, such as its perceived intensity, was similar to the intensity of each attribute present in the four *Stevia* samples. The reference stimuli for each

sensory attribute, with their respective concentrations, were as follows: caffeine for bitterness (0, 65, 110, 155, 210, and 250 mg/L), glycyrrhizic acid ammonium salt for licorice (100, 300, 500, 700, 900, and 1000 mg/L), and iron sulfate for metallic (0, 8, 10, 12, and 14 mg/L). The panelists had to position an aqueous 300 mg/L *Stevia* solution in each of the rankings of standards. For this purpose, the MP extract was randomly selected among the *Stevia* samples.

For determination of the concentration of the reference, the arithmetic mean of the positions selected for each attribute was calculated, and the resulting proportion was assigned to the respective concentration of the standard. The resulting concentrations of the reference stimuli in a 5% w/v sucrose solution anchored at 50 mm of the line scale were 114 mg/L of caffeine for bitterness, 280 mg/L of glycyrrhizic acid ammonium salt for licorice, and 11 mg/L of iron sulfate for metallic. Then, subjects were further trained employing these solutions as reference stimuli.

**Training of the Subjects of the Category Specific Scale.** The training of the panelists on the sensory space of the *Stevia* samples was carried out employing the Feedback Calibration Method (FCM) from Compusense Five software. FCM allows the training time of the panel to be reduced significantly by giving instant feedback on the attribute intensity after performing the assessment of a specific attribute.[24] An introductory session was used to present the 100 mm line scale. The training consisted of dedicated training sessions for each attribute. At least three training sessions were conducted for each attribute separately.

Training sessions in which all attributes were evaluated for one sample composed of mixtures of the reference stimuli were assessed with FCM. In at least six sessions, the levels below and above the anchor of each attribute were evaluated by the panelists. The following concentrations, in a 5% w/v sucrose solution, were evaluated in the training sessions: for bitterness, 75, 85, 95, 114, 150, and 200 mg/L caffeine; for licorice, 140, 210, 280, 420, 490, and 560 mg/L glycyrrhizic acid; for metallic, 8, 9, 11, 13, and 15 mg/L iron sulfate. The maximum concentration represented the highest intensity on the line scale (100 mm), and a blank represented the lowest intensity on the line scale (0 mm). Additionally, a mixture of these standards was prepared to train the panelists in the assessment of all the attributes simultaneously. In the final step of the training, the panel worked on sessions of consensus, where the panelists calibrated themselves with the mean values achieved by the group after evaluating the different *Stevia* samples. The training aimed to allow the panelists to differentiate small differences between the *Stevia* samples, as well as a correct use of the scale. The training sessions were carried out until the standard deviation from the mean of the intensity of each attribute (SD) assessed by the 13 subjects was <20 scale units.[21]

**Sensory Evaluation Procedure.** The four *Stevia* samples, chemically characterized by UHPLC ESI MS, were evaluated in aqueous solution by the trained panel. *Stevia* samples were dissolved in purified water at a concentration close to the sweetness of a 5% w/v sucrose solution, previously estimated by the panel leader and experienced professionals of the field. The following concentrations were used for the sensory evaluation of the *Stevia* samples by the trained subjects: 300 mg/L for MP, 700 mg/L for EM, 250 mg/L for EC1 and 220 mg/L for EC2. All samples were prepared freshly the day the sensory assessment was performed. The reference stimuli for each attribute in solutions of 5% w/v of sucrose were presented prior to the evaluation.

The trained panelists ($n$ = 13) performed a descriptive analysis[25] of the four *Stevia* samples in duplicate, evaluating the attributes sweetness, bitterness, licorice, and metallic. For mouth cleansing between samples, assessors had to use unsalted rice cookies and filtered water. The minimum resting time between samples was set at 3 min to minimize carry-over effects between samples.[4] Samples were presented in a volume of 20 mL in plastic cups with three-digit random numbers in a balanced manner. Panelists drank the sample, swirled it in the mouth for 7 s before swallowing, and then assessed the intensity of each attribute on the category scale presented in the screen of the computer.

**Statistical Data Analysis.** The means and standard deviations were calculated using the software Senstools. A repeated-measures ANOVA was used with samples as factor and judges to test for the significance of differences. A LSD post hoc comparison was performed. A significance level of $p < 0.05$ was chosen.

## RESULTS AND DISCUSSION

**Liquid Chromatography of *Stevia* Extracts Obtained by Different Manufacturing Processes.** Figure 2 illustrates

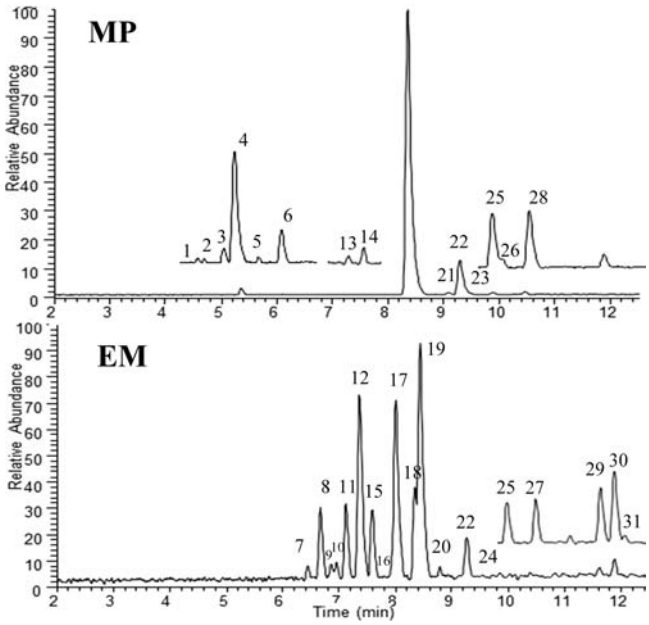


**Figure 2.** Chromatograms (MS-SIR) of *Stevia* extract from Chile (MP, membrane purified) and from China (EM, enzymatically modified). Zooms (100×) of regions with lower intensity signals have been added as insets.

the full MS chromatograms of the MP and EM samples, with a complete separation of 31 compounds, except rebaudioside A (**18**) and stevioside (**19**). The steviol glycosides Rd, Ra, Sv, Rf, Rc, DuA, Ru, Rb, and Sb (Table 1, peaks 4, 18, 19, 21, 22, 23, 28, 29, and 30, respectively) were identified on the basis of coelution with their authentic standards, as well as on their fragmentation pattern upon mass spectrometry. All steviol glycosides showed a consecutive loss of sugar moieties in $MS^2$ fragmentation of the $[M - H]^-$ parent ion (Table 1).

The MP extract is used here to illustrate a typical chromatogram of a purified *Stevia* extract. This chromatogram is similar to that of both EC extracts (not shown), with the main peak corresponding to the sum of Ra (**18**) and Sv (**19**). On the contrary, the chromatogram of the EM sample is very different, with several major peaks eluting earlier than Sv and Ra.

**Identification of Minor Natural Steviol Glycosides.** The various compounds were identified on the basis of the $m/z$ of their $[M - H]^-$ ions, their respective fragmentation patterns, and the literature. Compound **3** with $[M - H]^-$ of $m/z$ 1273 has one deoxyhexose and five hexose moieties attached. In $MS^2$, this parent ion yielded $m/z$ 803 (Table 1), indicating the loss of two hexoses and one deoxyhexose. As $MS^2$ of the commercial standards always showed cleavage of the ester-linked $O-R_1$ bond, prior to the ether-linked $O-R_2$ bond, the $R_1$ side chain might consist of one deoxyhexose and two hexoses moieties, whereas $R_2$ consists of three hexoses. Compound **3** was

**Table 1. Tandem Mass Spectra Data of the Steviol Glycosides Detected in *Stevia* Extracts from Different Suppliers[a]**

| no. | RT (min) | putative identification and commercial name* | RI | R2 | skeleton | MW | $MS^1$ ($m/z$) | $MS^2$ ($m/z$) | $MS^3$ ($m/z$) |
|---|---|---|---|---|---|---|---|---|---|
| 1 | 4.3 | I | hex- | $hex_3$- | 2 | 982 | **981** | **819** | **465**, 627, 657 |
| 2 | 5.1 | rebaudioside K (Rk) | $hex_2$- | deshex-$hex_2$- | 1 | 1112 | **1111** | 625, **787** | 479, **625**, 641 |
| 3 | 5.2 | rebaudioside N (Rn) | deshex-$hex_2$- | $hex_3$- | 1 | 1274 | **1273** | 641, **803** | **641** |
| 4 | 5.3 | *rebaudioside D (Rd) | Glc$\beta$1−2Glc$\beta$1- | Glc$\beta$1−2(Glc$\beta$1−3)Glc$\beta$1- | 1 | 1128 | **1127** | 641, **803** | **641** |
| 5 | 5.7 | rebaudioside J (Rj) | deshex-hex- | $hex_3$- | 1 | 1112 | **1111** | 641, **803** | **641** |
| 6 | 6.1 | rebaudioside M (Rm) | $hex_3$- | $hex_3$− | 1 | 1290 | **1289** | 641, **803**, 1127 | **641** |
| 7 | 6.4 | steviol-$(glucosyl)_6$ | Glc- hex- | Glc-Glc-$hex_2$- | 1 | 1290 | **1289** | **965** | 479, **641**, 803 |
| 8 | 6.7 | steviol-$(glucosyl)_5$ | Glc- | Glc-Glc-$hex_2$− | 1 | 1128 | **1127** | 641, 803, **965** | |
| 9 | 6.8 | steviol-$(glucosyl)_6$ | Glc-$hex_2$- | Glc-Glc-hex- | 1 | 1290 | **1289** | **803** | 479, **641** |
| 10 | 6.9 | steviol-$(glucosyl)_6$ | Glc-$hex_3$- | Glc-Glc- | 1 | 1290 | **1289** | **641**, 803, 965 | 317, **479** |
| 11 | 7.1 | steviol-$(glucosyl)_5$ | Glc- hex- | Glc-Glc-hex- | 1 | 1128 | **1127** | **803** | 479, 623, **641** |
| 12 | 7.3 | steviol-$(glucosyl)_4$ | Glc- | Glc-Glc-hex- | 1 | 966 | **965** | **803** | 479, **641** |
| 13 | 7.4 | rebaudioside H (Rh) | hex- | deshex-$hex_3$- | 1 | 1112 | 949, **1111** | 803, **949** | |
| 14 | 7.6 | II | hex- | $hex_3$- | 1 | 966 | 803, **965** | 641, 803, **845** | 655, **683**, 817 |
| 15 | 7.6 | steviol-$(glucosyl)_5$ | Glc-$hex_2$- | Glc-Glc- | 1 | 1128 | **1127** | **641** | 317, **479** |
| 16 | 8.0 | rebaudioside I | $hex_2$- | $hex_3$- | 1 | 1128 | **1127** | **803** | 479, **641** |
| 17 | 8.0 | steviol-$(glucosyl)_4$ | Glc- hex- | Glc-Glc- | 1 | 966 | **965** | **641** | 317, **479** |
| 18 | 8.4 | *rebaudioside A (Ra) | Glc$\beta$1- | Glc$\beta$1−2(Glc$\beta$1−3)Glc$\beta$1- | 1 | 966 | **965** | **803** | 317, 479, **641** |
| 19 | 8.4 | *stevioside (Sv) | Glc$\beta$1- | Glc$\beta$1−2Glc$\beta$1- | 1 | 804 | 642, **803** | **641** | **479** |
| 20 | 8.9 | steviol- $(glucosyl)_4$ - $(rhamnosyl)_1$ | Glc- hex- | Glc-Rha-Glc- | 1 | 1112 | **1111** | **787** | 479, **625** |
| 21 | 9.0 | *rebaudioside F (Rf) | Glc$\beta$1- | Xyl$\beta$1−2(Glc$\beta$1−3)Glc$\beta$1- | 1 | 936 | **935** | **773** | 479, 611, **641** |
| 22 | 9.2 | *rebaudioside C (Rc) | Glc$\beta$1- | Rha$\alpha$1−2(Glc$\beta$1−3)Glc$\beta$1- | 1 | 950 | **949** | **787** | 479, **625**, 641 |
| 23 | 9.4 | *dulcoside A (DuA) | Glc$\beta$1- | Rha$\alpha$1−2Glc$\beta$1- | 1 | 788 | 625, **787**, 949 | 479, **625**, 641 | **479** |
| 24 | 9.5 | steviol - $(glucosyl)_4$ | $hex_2$- | Glc-Glc- | 1 | 966 | **965** | 479, **641**, 803 | 317, **479** |
| 25 | 9.8 | rebaudioside G (Rg) | hex- | $hex_2$- | 1 | 804 | 641, **803** | **641** | **479** |
| 26 | 10.3 | III | hex- | deshex-$hex_2$- | 1 | 951 | **949** | **787** | **625**, 641 |
| 27 | 10.4 | steviol-$(glucosyl)_3$ | hex- | Glc−Glc- | 1 | 804 | 641, **803** | 479, **641**, 804 | **479** |
| 28 | 10.5 | *rubososide (Ru) | Glc$\beta$1- | Glc$\beta$1- | 1 | 642 | 480, **641**, 701 | **479** | **317** |
| 29 | 11.6 | *rebaudioside B (Rb) | H | Glc$\beta$1−2(Glc$\beta$1−3)Glc$\beta$1- | 1 | 804 | **803** | 479, **641** | **479** |
| 30 | 11.8 | *steviolbioside (Sb) | H | Glc$\beta$1−2Glc $\beta$1- | 1 | 642 | **641** | 317, **479**, 642 | **317** |
| 31 | 12.08 | dulcoside B (DuB) | H | deshex-$hex_2$- | 1 | 788 | 641, **787** | 479, **625**, 641 | **479** |

[a]Most abundant ions are shown in bold, in $MS^1$ it corresponds to $[M-H]^-$ ion), structures of previously described steviol glycosides confirmed with commercial standards (*) and the others represents the hypothetical distribution of sugar moieties in identified compounds without available commercial standards, see Figure 1. In enzymatic transglycosylation products, the additional glucosyl residues attached to the natural steviol glycoside are underlined. Glc, glucoside; Rha, rhamnoside; Xyl, xyloside; hex, hexoside; deohex, deoxyhexoside.

annotated as rebaudioside N (Rn). Compound **6** with $[M-H]^-$ of $m/z$ 1289 gave the fragment ion of $m/z$ 803 in $MS^2$ (Table 1), indicating the loss of three hexoses from $R_1$. Therefore, **6** was annotated as rebaudioside M (Rm), containing two trihexosyl side chains. Compound **25** with $[M-H]^-$ of $m/z$ 803 is an isomer of Sv, comprising three hexose moieties. The main fragment ion in $MS^2$ was $m/z$ 641 (Table 1), indicating the loss of one hexose, most likely $R_1$. A loss of 324 Da in $MS^3$ represents the dihexosyl moiety of $R_2$. Compound **25** is suggested to be rebaudioside G (Rg). Sv and Rg have the same fragmentation pattern, but they might differ in the type of glycosidic linkage or kind of hexose. Compounds **3**, **6**, and **25** have been previously described.[5] Compounds **1**, **14**, and **26** were annotated as I, II, and III, respectively, similar to steviol glycosides. Compound **I** was described before as compound 6,[27] **II** as compound 1[19] and **III** as compound 2.[26]

Compound **1** with $[M-H]^-$ of $m/z$ 981 had four hexose moieties attached to the kaurene skeleton with a mass of 332 Da (previously described by Ohtani et al.[28]). In $MS^2$, the parent ion yielded $m/z$ 819 (Figure 1), indicating the loss of one hexose, most likely ester-linked to $C_{19}$. The observed ion $m/z$ 465 in $MS^3$ would indicate the loss of two hexoses and $-CH_2OH$ from skeleton 2 (Figure 1). Therefore, peak 1 might be the same degradation product of rebaudioside A, previously described by Chaturvedula et al.[27] Compound **14**, with $[M-H]^-$ of $m/z$ 965, is an isomer of Ra. The $m/z$ 803, the second most abundant fragment ion in $MS^2$, points to the loss of one hexose at the $C_{19}$ and three hexoses moieties at $C_{13}$ (Table 1), similar to Ra, but with different interglycosidic bonds. Therefore, we suggest that **14** is the same as II, as previously reported.[19] Compound **26**, with $[M-H]^-$ of $m/z$ 949, has three hexoses and deoxyhexose moieties attached, confirmed with the observed loss of 146, 162, and 324 Da (Table 1). Compound **26** is the same compound previously reported by Chaturvedula and Prakash.[26]

**Identification of Transglycosylated Products.** The manufacturer of the EM product declared the use of enzymes in the production process. Stevioside and rebaudioside A are the most abundant compounds in *Stevia* leaves. However, a low bitterness threshold for stevioside has been reported recently,[4] which affects their sensory quality.[29] Enzymatic modification of the structure of this compound reduced, at least in part, its residual bitterness.[30] At industrial level, the enzymatic modification of stevioside is widely employed. On the contrary, industrial transglycosylation of rebaudioside A is not feasible.[30]

Therefore, and considering the resulting fragmentation patterns of the EM sample, the identified compounds in this sample probably correspond to transglycosylation products of Sv and Sb (or Ru). Their structural identification must be confirmed, however, by isolating these compounds by semipreparative HPLC and further NMR characterization. Similar fragmentation patterns of a group of these transglycosylated compounds have been reported for natural steviol glycosides obtained from *Stevia* leaves.[5] However, the concentrations of these natural compounds are lower than the concentrations obtained by transglycosylation.

Eleven peaks were proposed to be transglycosylated products in the EM sample. All of these compounds share the same principal structure (steviol), although they show differences in the number (mono-, tri-, tetra-, penta-, and hexasaccharides) and type of sugar moieties (glucose and/or rhamnose) at positions $C_{13}$ and $C_{19}$. We hypothesize that these compounds are transglycosylation products of Sv, Sb, and Rc, resulting from the action of CGTase, because of their earlier elution (higher polarity) and higher masses than the latter. Several authors[13,31] have described the modification of stevioside with CGTases in the presence of soluble starch or cyclodextrins, resulting in a mixture of products with extra mono, di, tri, or larger $\alpha$-glucosyl chains attached at the $C_{19}$- and/or $C_{13}$-glucosyl unit.[11,13,31] The proposed structures are indicated in Table 1.

Compounds **8**, **11**, and **15** eluted at 6.7, 7.1, and 7.6 min, respectively, with the same quasi molecular ion peaks $[M - H]^-$ at $m/z$ 1127 (Figure 3). The tandem mass spectrometric fragmentation patterns of these three compounds were different from each other (Table 1), suggesting that they were isomers with different numbers of glucosyl moieties attached to the $C_{19}$- or $C_{13}$-glucosyl unit of Sv. The molecular weight of Sv is 804 Da, so the above three isomers were assumed to be diglucosylated products, consisting of stevioside with two hexoses attached (stevioside-$(glucosyl)_2$).

Compound **8** had a deprotonated molecular ion at $m/z$ 1127; the fragmentation of this ion yielded a main ion at $m/z$ 965 in $MS^2$ (Table 1), indicating the loss of a hexose attached at $C_{19}$. Therefore, the two hexoses added by CGTase transglycosylation are attached to the $C_{13}$–O-glucosyl unit (Table 1). This structure was also proposed as rebaudioside L,[5] a compound naturally present in *Stevia* leaf, but not in such a high concentration as that found in the EM sample (Table 2). Compound **11**, with a $[M - H]^-$ of $m/z$ 1127, gave a fragment ion of $m/z$ 803 in the $MS^2$ (Table 1), indicating the loss of two hexoses attached at $C_{19}$- and another hexose attached at $C_{19}$-glucosyl (Table 1). Compound **15** showed a product ion at $m/z$ 641 in $MS^2$ (Table 1), indicating the loss of three hexoses attached at $C_{19}$ (Table 1). It is worth noting that compound **16** represents another isomer of $m/z$ 1127, with a fragmentation pattern similar to that of compound **11**. Compound **16**, found in the MP sample, was assumed to be rebaudioside I (Ri), a natural steviol glycoside. It is different from compound **11**, a transglycosylation product, and it has a different retention time in the EM sample (Table 1). Although both compounds have similar fragmentation patterns and the same distributions of sugar moieties (Table 1), they might be different compounds because one of them was found in MP (sample without enzymatic treatment) and the other in the transglycosylation product (EM). Other examples of isomers identified as natural and transglycosylated steviol glycosides that are present in different products are, for instance, compounds **17**, **18**, and **24** with $[M - H]^-$ of $m/z$ 965 and compounds **19**, **25**, and **27**

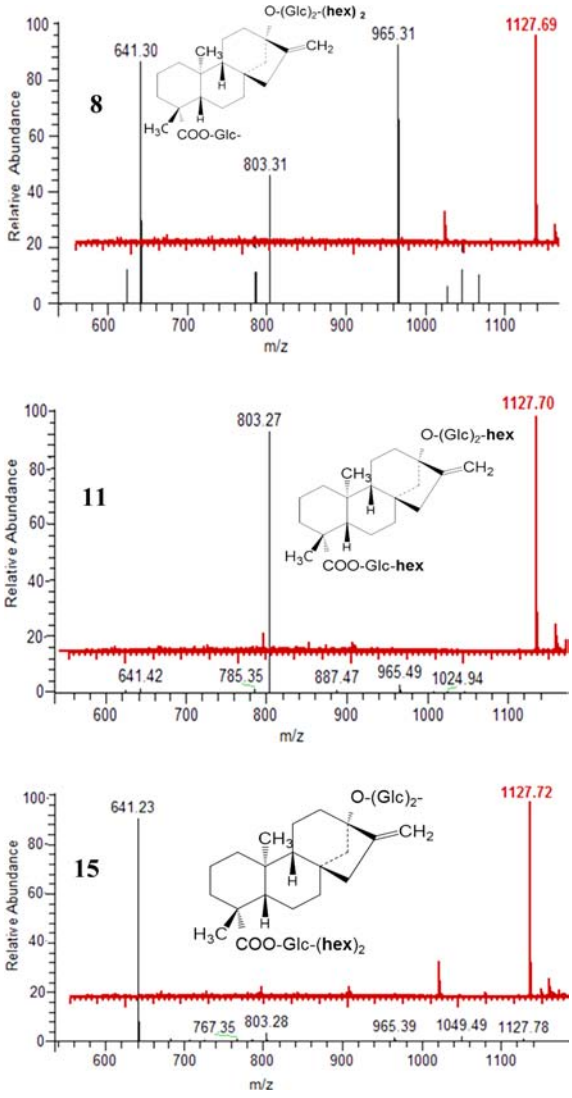


**Figure 3.** Tandem mass spectra ($MS^1$ (in red) and $MS^2$) of the transglycosylated compounds **8**, **11**, and **15**.

with $[M - H]^-$ of $m/z$ 803[5,32] (Table 1). These molecules were annotated in essentially the same way as those with $m/z$ 1127. Furthermore, the natural compounds **18** and **19** were confirmed with their respective commercial standard. The different type of interglycosidic linkage between natural and transglycosylated molecules leads to different elution behavior, on the basis of which these molecules could be distinguished. By this analysis, we demonstrated that the EM sample was obtained by transglycosylation. Of the 24 peaks present in EM, 11 are suggested to be transglycosylation products (Table 1).

**Quantitative Analysis of Steviol Glycosides.** In all commercial *Stevia* extracts, except EM, Ra was the most abundant compound, with a concentration >60 mg/100 mg of extract. Interestingly, MP contained a wide variety of minor steviol glycosides, up to 24 mg/100 mg (Table 2), resulting from the aqueous extraction and membrane purification processes employed for this sample. The slightly higher than 100% total sweetener content obtained for the three samples might result from inaccuracies of the quantification method.

**Descriptive Sensory Analysis of the Commercial *Stevia* Extracts.** The results of the sensory evaluation of MP, EM, EC1, and EC2 samples are presented in Table 3. The

**Table 2. Quantification of Major and Minor Steviol Glycosides (Milligrams per 100 mg of Extract) from the *Stevia* Extracts[a]**

| | | origin | | | | sensory properties[b] | | |
|---|---|---|---|---|---|---|---|---|
| no. | compound | MP | EM | EC1 | EC2 | sweet | bitter | refs |
| | major glycosides | | | | | | | |
| 18 | Ra | 67.2(±3.5) | 2.7(±0.03) | 84.4(±0.6) | 102.6 | 8.3 | 0.194 | 4, 33 |
| 19 | SV | 14.9(±0.4) | 6.3(±0.02) | 17.9(±0.3) | nd[c] | 11.2 | 112 | 4, 33 |
| | subtotal | 82.1 | 9.0 | 102.3 | 102.6 | | | |
| | minor glycosides | | | | | | | |
| 1 | I | 0.2(±0.01) | nd | 0.3(±0.01) | 0.2(±0.02) | nd | nd | 27 |
| 2 | Rk | 0.2(±0.006) | nd | nd | nd | nd | nd | 5 |
| 3 | Rn | 0.6(±0.04) | nd | nd | nd | nd | nd | 5 |
| 4 | Rd | 2.8(±0.16) | 0.2(±0.002) | 0.5(±0.001) | 0.1(±0.005) | 5.3 | 162 | 4, 33 |
| 5 | Rj | 0.3(±0.02) | nd | nd | nd | nd | nd | 5 |
| 6 | Rm | 1.6(±0.09) | 0.9(±0.05) | nd | nd | nd | nd | 5 |
| 13 | Rh | 0.4(±0.02) | nd | nd | nd | nd | nd | 5 |
| 14 | II | 0.7(±0.08) | nd | nd | nd | nd | nd | 19 |
| 16 | Ri | 0.05(±0.001) | 3.3(±0.05) | nd | nd | nd | nd | 5 |
| 21 | Rf | 1.2(±0.1) | 0.3(±0.03) | 0.1(±0.01) | 0.3(±0.004) | nd | nd | 33, 34 |
| 22 | Rc | 8.4(±0.7) | 1.3(±0.06) | 0.6(±0.04) | nd | 27.8 | 49 | 4, 33 |
| 23 | DuA | 1.3(±0.09) | 0.4(±0.01) | n.d | n.d | 32.9 | 49 | 4, 33 |
| 25 | Rg | 2.9(±0.1) | 1.7(±0.06) | nd | nd | nd | nd | 5 |
| 26 | III | 0.5(±0.01) | nd | nd | nd | nd | nd | 26 |
| 28 | Ru | 1.6(±0.1) | 0.3(±0.1) | nd | nd | 27.3 | 61 | 4, 33 |
| 29 | Rb | 0.4(±0.002) | 0.8(±0.001) | 0.8(±0.05) | 1.6(±0.1) | 18.1 | 137 | 4, 33 |
| 30 | Sb | nd | 0.9(±0.05) | 0.3(±0.002) | nd | 26.8 | 84 | 4, 33 |
| 31 | DuB | nd | 0.4(±0.04) | nd | nd | nd | nd | 5 |
| | **subtotal** | **23.2** | **10.5** | **2.6** | **2.2** | | | |
| | minor transglycosylated products | | | | | | | |
| 7 | steviol-$(glucosyl)_6$ | nd | 2.2(±0.03) | nd | nd | nd | nd | 35 |
| 8 | steviol-$(glucosyl)_5$ | nd | 5.2(±0.2) | nd | nd | nd | nd | 35 |
| 9 | steviol-$(glucosyl)_6$ | nd | 1.7(±0.2) | nd | nd | nd | nd | 35 |
| 10 | steviol-$(glucosyl)_6$ | nd | 2.0(±0.6) | nd | nd | nd | nd | 35 |
| 11 | steviol-$(glucosyl)_5$ | nd | 5.4(±0.2) | nd | nd | nd | nd | 35 |
| 12 | steviol-$(glucosyl)_4$ | nd | 10.2(±0.3) | nd | nd | nd | nd | 35 |
| 15 | steviol-$(glucosyl)_5$ | nd | 4.9(±0.08) | nd | nd | nd | nd | 35 |
| 17 | steviol-$(glucosyl)_4$ | nd | 11.2(±0.1) | nd | nd | nd | nd | 35 |
| 20 | steviol-$(glucosyl)_4$ - $(rhamnosyl)_1$ | nd | 0.9(±0.05) | nd | nd | nd | nd | 35 |
| 24 | steviol-$(glucosyl)_4$ | nd | 1.3(±0.08) | nd | nd | nd | nd | 35 |
| 27 | steviol-$(glucosyl)_3$ | nd | 1.7(±0.07) | nd | nd | nd | nd | 35 |
| | **subtotal** | **0.0** | **46.7** | **0.0** | **0.0** | | | |
| | **total** | **105.3** | **66.2** | **104.9** | **104.8** | | | |

[a]The standard deviation ($n$ = 3) is given in parentheses. [b]Taste threshold ($\mu$M). [c]nd, not detected.

**Table 3. Intensity of Sensory Attributes of *Stevia* Extracts Determined by a Trained Panel ($n$ = 13 in Duplicate)[a]**

| attribute | MP | EM | EC1 | EC2 |
|---|---|---|---|---|
| sweetness | 49.2 ± 7.3a | 49.5 ± 5.0a | 48.3 ± 5.2a | 48.0 ± 2.4a |
| bitterness | 59.1 ± 12.6c | 53.3 ± 11.1bc | 49.7 ± 15.2ab | 44.3 ± 16.4a |
| licorice | 68.3 ± 12.8c | 58.9 ± 12.3b | 51.2 ± 17.9ab | 48.6 ± 16.2a |
| metallic | 53.0 ± 12.0a | 49.1 ± 7.9a | 47.9 ± 8.1a | 45.3 ± 12.6a |

[a]A category specific line scale 0−100 mm was employed for the sensory evaluation. Means and standard deviations are shown (mean ± SD). The same letter indicates that means of intensity are not significantly different between samples at $p < 0.05$ confidence level.

means of intensity, together with the standard deviations, are reported. An ANOVA was performed on all attributes. The intensity of the attributes bitterness [$F(3,36) = 4.19$, $p = 0.01$] and licorice [$F(3,36) = 8.17$, $p = 0.00$] differed significantly between samples. On the contrary, the intensity of the attribute metallic did not differ significantly between samples [$F(3,36) = 2.39$, $p = 0.09$]. Sweetness was not significantly different between samples [$F(3,36) = 0.32$, $p = 0.814$]. All *Stevia* samples were perceived as iso-sweet and compared in sweetness with the reference stimulus (5% w/v sucrose solution anchored at 50 mm of the scale), matching the level of sweetness. The evaluation of the 5% w/v sucrose reference yielded 49.8 ± 0.3 in the attribute sweetness, 4.4 ± 7.7 in bitterness, 1.8 ± 2.9 in licorice, and 3.6 ± 8.9 in metallic.

In the case of MP, the presence of natural minor glycosides, and eventually the remaining impurities that were not

analytically identified in this study, might be responsible for the significantly higher licorice and bitterness intensities. It is worth mentioning that the MP sample has the highest concentration of rebaudioside D, a steviol glycoside containing the highest amount of $\beta$-glycosyl moieties, recently characterized by its high sweetness intensity and low bitterness intensity.[4] However, the amount of rebaudioside D was below its threshold concentration (Table 2) and, therefore, its contribution to the whole sweetness of the sample might be limited. The additive impact of the different constituents, however, should be considered in further research. MP sample also has the highest amount of rebaudioside C, but still below the threshold for bitterness; again, an additive effect among the different rebaudiosides could contribute to the higher perceived bitterness level and should be considered. EC1 and EC2 samples showed no significant differences for any of the attributes, demonstrating that the intensities of the off-flavor are equally intense when compared under iso-sweet conditions, despite their different contents in rebaudioside A and stevioside (Table 2). This difference in composition, however, has a cost impact that is worth considering for industrial applications. All samples do not significantly differ in metallic taste.

The impact of the fraction in the EM sample that remained compositionally unknown (ca. 35% w/w) on the sensory properties could not be assessed. On the other hand, in the EM sample, the concentration of Ra and Sv represents only 9% w/w of the total composition; instead, transglycosylated constituents (Table 2) accounting for almost 47% w/w are accountable for the remaining sweetness.[11]

In conclusion, this study shows that the MP sample contains a wide range of natural steviol glycosides. However, when compared at iso-sweet conditions, this *Stevia* product shows the strongest intensities of the off-taste attributes bitterness, licorice, and metallic compared to *Stevia* samples obtained by other processing techniques. Furthermore, extracts resulting from similar, solvent-extracted, purification processing but with different composition (EC1 and EC2) present similar sensory properties, although the extracts vary considerably in chemical composition. Finally, considering that *Stevia* leaves are particularly rich in Sv, a compound with high bitterness off-taste, our results show that the enzymatic modification occurring in the EM sample is an effective alternative to reduce off-tastes; the similar levels in all attributes of EM and EC1 support this conjecture.

The UHPLC-MS$^n$ method proposed here should allow identifying major and minor steviol glycosides in a single run and could be applied as a routine quality control method for natural and transglycosylated commercial extracts of *Stevia*.

## ■ ASSOCIATED CONTENT

### Supporting Information

Purity, fragment ions used to obtain calibration curves of all standards except Ra and Sv; slope and linearity coefficients obtained. This material is available free of charge via the Internet at http://pubs.acs.org.

## ■ AUTHOR INFORMATION

### Corresponding Author

*(E.A.) Phone: +56 2 2354 4253. Fax: +56 2 2354 5803. E-mail: agosin@ing.puc.cl.

### Funding

This research was funded by the Chilean Economic Development Agency, CORFO, through the project "Technological platform for formulating naturally sweetened healthy foods". This project is part of Wageningen UR Chile, the International Center of Excellence for Foods in Chile, Project 11 CEII-9568.

### Notes

The authors declare no competing financial interest.

## ■ ACKNOWLEDGMENTS

We acknowledge Romina Montealegre and Ricardo Rodríguez, from the Centro de Aromas y Sabores, DICTUC, for their excellent technical skills in managing the trained panel during the sensory evaluation sessions. We are particularly grateful to Javier Sainz, general manager of Prodalysa, Chile, for very fruitful discussions and permanent collaboration.

## ■ REFERENCES

(1) Brandle, J. E.; Starratt, A. N.; Gijzen, M. *Stevia rebaudiana*: its agricultural, biological, and chemical properties. *Can. J. Plant Sci.* **1998**, *78*, 527−536.

(2) Food and Drug Administration. Notification 252 Merisant GRAS Notification for Rebaudioside A.

(3) The European Comission. Commission Regulation (EU) No. 1131/2011 of 11 November 2011 Amending Annex II to Regulation (EC) No. 1333/2008 of the European Parliament and of the Council with Regard to Steviol Glycosides. *Off. J. Eur. Union* **2011** (Dec 11), 205−2011.

(4) Hellfritsch, C.; Brockhoff, A.; Stähler, F.; Meyerhof, W.; Hofmann, T. Human psychometric and taste receptor responses to steviol glycosides. *J. Agric. Food Chem.* **2012**, *60*, 6782−6793.

(5) Ohta, M.; Sasa, S.; Inoue, A.; Tamai, T.; Fujita, I.; Morita, K.; Matsuura, F. Characterization of novel steviol glycosides from leaves of *Stevia rebaudiana* Morita. *J. Appl. Glycosci.* **2010**, *57*, 199−209.

(6) Chaturvedula, V. S. P.; Prakash, I. Cucurbitane glycosides from *Siraitia grosvenorii*. *J. Carbohydr. Chem.* **2011**, *30*, 16−26.

(7) Chaturvedula, V. S. P.; Prakash, I. Structural characterization and hydrolysis studies of rebaudioside E, a minor sweet component of *Stevia rebaudiana*. *Eur. Chem. Bull.* **2013**, *2*, 298−302.

(8) Mizutani, K. T. O. Use of *Stevia rebaudiana* sweeteners in Japan. In *Stevia: the Genus Stevia*; Kinghorn, A. D., Ed.; Medicinal and Aromatic Plants − Industrial Profiles; Taylor & Francis: London, UK, 2002; pp 178−195.

(9) Joint FAO/WHO Expert Committee on Food Additives (JECFA). Steviol glycosides. *Compend. Food Addit. Specif.* **2004**, 47−50.

(10) Yang, M.; Hua, J.; Qin, L. *High-Purity Rebaudioside A and Method of Extracting Same*; Google Patents, 2011.

(11) Abelyan, V. A.; Balayan, A. M.; Ghochikyan, V. T.; Markosyan, A. A. Transglycosylation of stevioside by cyclodextrin glucanotransferases of various groups of microorganisms. *Appl. Biochem. Microbiol.* **2004**, *40*, 129−134.

(12) Li, S.; Li, W.; Xiao, Q.; Xia, Y. Transglycosylation of stevioside to improve the edulcorant quality by lower substitution using cornstarch hydrolyzate and CGTase. *Food Chem.* **2013**, *138*, 2064−2069.

(13) Ye, F.; Yang, R.; Hua, X.; Shen, Q.; Zhao, W.; Zhang, W. Modification of stevioside using transglucosylation activity of *Bacillus amyloliquefaciens* $\alpha$-amylase to reduce its bitter aftertaste. *LWT−Food Sci. Technol.* **2013**, *51*, 524−530.

(14) Geuns, J. M. C. European Stevia Association. Analysis of steviol glycosides. In *Stevia and Steviol Glycosides: Properties, Techniques, Uses, Exposure, Toxicology, Pharmacological Effects*; Euprint: Heverlee, Belgium, 2010; pp 11−17.

(15) Cacciola, F.; Delmonte, P.; Jaworska, K.; Dugo, P.; Mondello, L.; Rader, J. I. Employing ultra high pressure liquid chromatography as the second dimension in a comprehensive two-dimensional system for

analysis of *Stevia rebaudiana* extracts. *J. Chromatogr., A* **2011**, *1218*, 2012−2018.
(16) Jamaluddin Ahmed, M.; Smith, R. M. Determination of stevioside by high-performance liquid chromatography with pulsed amperometric detection. *J. Sep. Sci.* **2002**, *25*, 170−172.
(17) Clos, J. F.; DuBois, G. E.; Prakash, I. Photostability of rebaudioside A and stevioside in beverages. *J. Agric. Food Chem.* **2008**, *56*, 8507−8513.
(18) Zimmermann, B. F.; Woelwer-Rieck, U.; Papagiannopoulos, M. Separation of steviol glycosides by hydrophilic liquid interaction chromatography. *Food Anal. Methods* **2012**, *5*, 266−271.
(19) Chaturvedula, V. S. P.; Rhea, J.; Milanowski, D.; Mocek, U.; Prakash, I. Two minor diterpene glycosides from the leaves of *Stevia rebaudiana*. *Nat. Prod. Commun.* **2011**, *6*, 175−178.
(20) ISO 8586:2012. *Sensory Analysis — General Guidelines for the Selection, Training and Monitoring of Selected Assessors and Expert Sensory Assessors*, 2012.
(21) Kemp, S. E. *Sensory Evaluation: A Practical Handbook*; Wiley-Blackwell: Chichester, UK, 2009.
(22) DuBois, G. E.; Walters, D. E.; Schiffman, S. S.; Warwick, Z. S.; Booth, B. J.; Pecore, S. D.; Gibes, K.; Carr, B. T.; Brands, L. M. Concentration—response relationships of sweeteners: a systematic study. In *Sweeteners*; Walters, D. E., Orthoefer, F. T., DuBois, G. E., Eds.; American Chemical Society: Washington, DC, USA, 1991; Vol. 450, pp 261−276.
(23) Schiffman, S. S.; Sattely-Miller, E. A.; Bishay, I. E. Time to maximum sweetness intensity of binary and ternary blends of sweeteners. *Food Qual. Pref.* **2007**, *18*, 405−415.
(24) Findlay, C. J.; Castura, J. C.; Lesschaeve, I. Feedback calibration: a training method for descriptive panels. *Food Qual. Pref.* **2007**, *18*, 321−328.
(25) Meilgaard, M. *Sensory Evaluation Techniques*, 3rd ed.; CRC Press: Boca Raton, FL, USA, 1999.
(26) Chaturvedula, V. S. P.; Prakash, I. Structures of the novel diterpene glycosides from *Stevia rebaudiana*. *Carbohydr. Res.* **2011**, *346*, 1057−1060.
(27) Chaturvedula, V. S. P.; Clos, J. F.; Prakash, I. Fluorescent light exposure of rebaudioside A in mock beverages under International Conference on Harmonization (ICH) guidelines. *Int. J. Chem.* **2012**, *4*.
(28) Ohtani, K.; Aikawa, Y.; Kasai, R.; Chou, W.-H.; Yamasaki, K.; Tanaka, O. Minor diterpene glycosides from sweet leaves of *Rubus suavissimus*. *Phytochemistry* **1992**, *31*, 1553−1559.
(29) DuBois, G. E.; Stephenson, R. A. Diterpenoid sweeteners. Synthesis and sensory evaluation of stevioside analogs with improved organoleptic properties. *J. Med. Chem.* **1985**, *28*, 93−98.
(30) Kochikyan, V. T.; Markosyan, A. A.; Abelyan, L. A.; Balayan, A. M.; Abelyan, V. A. Combined enzymatic modification of stevioside and rebaudioside A. *Appl. Biochem. Microbiol.* **2006**, *42*, 31−37.
(31) Jaitak, V.; Kaul, V. K.; Bandna; Kumar, N.; Singh, B.; Savergave, L. S.; Jogdand, V. V.; Nene, S. Simple and efficient enzymatic transglycosylation of stevioside by $\beta$-cyclodextrin glucanotransferase from *Bacillus firmus*. *Biotechnol. Lett.* **2009**, *31*, 1415−1420.
(32) Zimmermann, B. F. Tandem mass spectrometric fragmentation patterns of known and new steviol glycosides with structure proposals: fragmentation patterns of steviol glycosides. *Rapid Commun. Mass Spectrom.* **2011**, *25*, 1575−1582.
(33) Joint FAO/WHO Expert Committee on Food Additives (JECFA). Steviol Glycosides. *Compend. Food Addit. Specif. 73th Meet. FAO JECFA Monogr.* **2010**, *10*, 17−22.
(34) Starratt, A. N.; Kirby, C. W.; Pocs, R.; Brandle, J. E.; Rebaudioside, F. A diterpene glycoside from *Stevia rebaudiana*. *Phytochemistry* **2002**, *59*, 367−370.
(35) Fukunaga, Y.; Miyata, T.; Nakayasu, N.; Mizutani, K.; Kasai, R.; Tanaka, O. Enzymic transglucosylation products of stevioside: separation and sweetness-evaluation. *Agric. Biol. Chem.* **1989**, *53*, 1603−1607.

and some sulfur containing compounds like dimethyl disulfide and dimethyl trisulfide.[17]

Different from previous literature reports on goat's milk, this study aimed to characterize not the entire volatile fraction of the milk or some specific odorants, but the most potent aroma compounds by use of GC/O and AEDA. In detail, the odor profile of raw milks from winter and summer season of different farms were compared with each other, also including a human sensory evaluation by means of aroma profile analysis (APA). Since the composition of milk fat is known to be an important contributor to milks' odor profiles, also the fatty acid composition of the raw goat milk was investigated. Furthermore, changes in goat milks' odor profiles as a result of heat-treatment were investigated. In a comparative approach, pasteurized, UHT-treated, and sterilized goat milk were studied by means of analytical and descriptive profiling.

## MATERIALS AND METHODS

**Chemicals.** *Fatty Acid Analysis.* The following chemicals with the stated purities were used (supplier in parentheses): ascorbic acid 95% p.a., 1-butanol 95%, formic acid 85%, sodium dihydrogen phosphate-dihydrate 95% p.a., tridecanoic acid 99% (Fluka, Steinheim, Germany), Celite 545, potassium hydroxide 98.5% p.a. (Sigma-Aldrich, St. Louis, MO), fatty acids calibration kit (Büchi, Essen, Germany).

*GC/O Analysis.* Dichloromethane p.a. was used as the organic solvent and extracting agent (Th. Geyer GmbH and Co. KG, Renningen, Germany). Anhydrous sodium sulfate was purchased from CHEMSOLUTE (Th. Geyer GmbH and Co. KG, Renningen, Germany). For unequivocal identification, the following reference compounds were used in stated purities: 4-hydroxy-3-methoxybenzaldehyde (vanillin) 99% (ABCR, Karlsruhe, Germany), 2-aminoacetophenone 98%, 1-benzopyran-2-one (coumarin) 99%, δ-decalactone 98%, γ-decalactone 98%, decanoic acid 98%, dimethyl trisulfide 98%, dodecanoic acid 98%, 4-ethyloctanoic acid 98%, 2-furaldehyde (furfural) 99%, hexanoic acid 99.5%, 3-hydroxy-4,5-dimethyl-2(5*H*)-furanone (sotolone) 97%, 3-hydroxy-2-methyl-4-pyrone (maltol) 99%, 2-methoxyphenol (guaiacol) 98%, 2 methylbutanoic acid 98%, 3-methylbutanoic acid 99%, 3-methylindole (skatol) 98%, 4-methyloctanoic acid 98%, 3-methylphenol (*m*-cresol) 99%, 3-methylthiopropanal (methional), (*E*,*E*)-nona-2,4-dienal 85%, (*E*,*Z*)-nona-2,6-dienal 95%, γ-nonalactone 98%, δ-nonalactone 98%, nonanoic acid 97%, (*E*)-non-2-enal 97%, octanal 99%, octanoic acid 98%, (*E*)-oct-2-enal 94%, oct-1-en-3-one 50%, phenylacetic acid 99%, phenylethan-2-ol 99%, γ-undecalactone 98% (Aldrich, Steinheim, Germany), 2-acetyl-1-pyrroline 90%, γ-(*Z*)-6-dodecenolactone, *trans*-4,5-epoxy-(*E*)-dec-2-enal 90% (aromaLAB AG, Freising, Germany), γ-octalactone (EGA Chemie, Steinheim, Germany), 1*H*-benzo[*b*]pyrrole (indole) 98.5%, butan-2,3-dione (diacetyl) 99%, butanoic acid 99.5%, (*E*,*E*)-deca-2,4-dienal 85%, dimethyl disulfide 98%, 4-hydroxy-2,5-dimethyl-3(2*H*)-furanone (furaneol) 99%, pentanoic acid 99% (Fluka, Steinheim, Germany), 3-ethylphenol 98% (Riedel-de-Haen, Seelze, Germany), δ-dodecalactone 98%, γ-dodecalactone 97%, 3-propylphenol 99%, (*E*)-undec-2-enal 90% (SAFC, Hamburg, Germany).

**Goat Milk.** Two types of raw milk (winter season, summer season) as well as three types of heat-treated goat milk (pasteurized, UHT-treated, sterilized) were analyzed in a comparative approach. In the case of raw milk, the milks were obtained from two different farms during two periods: winter season ("W", from 15 February to 21 March) and summer season ("S", from 19 July to 10 August). Farm 1 (W1, S1) had a flock size of 120 goats of the breed "Bunte Deutsche Edelziege"; farm 2 had a flock size of 85 goats of the same breed. According to the farmer's statements, both herds were fed on a mixture of home-grown pasture and grains (trefoil-grass, mixture of oat, barley, pea, triticale), given as straw/dried fodder and hay (conserved feed). Farm 2 additionally fed rapeseed meal, sugar beet slices, and carrots. At the beginning of the lactation period, both herds were additionally fed on concentrated feed, including rapeseed meal and sugar beet slices. Both farms fed their herds according to their good practice, and no specific feeding protocol was established in terms of this study to stay as close as possible to a conventional goat milk aroma and fatty acid composition.

Sterilized goat milk was produced by sterilizing raw milk at 121 °C and a pressure of 2 bar for 15 min in a laboratory autoclave (Fedegari Autoklavi Spa, Albuzzano, Italy). Pasteurized and UHT-treated goat milk were purchased from local supermarkets: Leeb Vital Bio-goat milk, pasteurized (Leeb Biomilch GmbH, Schlierbach, Austria), and Andechser Bio-goat milk, UHT-teated (Andechser Molkerei Scheitz GmbH, Andechs, Germany).

**Preparation of Milk Samples and Fatty Acid Analysis.** Sample preparation and gas chromatographic determination of the total fat content and fatty acid profiles were performed according to the DGF standard method C-III 19 (99).[18] By means of this DGF method, both free fatty acids and fatty acids bound in mono-, di-, and triglycerides, phospholipids, and sterols can be detected.

**Isolation of Volatile Organic Compounds (VOCs).** Solvent assisted flavor evaporation (SAFE)[19] was applied for the isolation of volatiles from fresh goat milk samples and heated goat milks. At room temperature (21 ± 1 °C), 25.0 ± 0.1 mL of goat milk was combined with freshly distilled dichloromethane at a ratio of 2:1 (milk/solvent). The mixture was stirred and distilled, and the organic phase of the distillate was separated, dried, and concentrated as it was reported before by Siefarth et al.[20]

**Characterization and Identification of Goat Milk Odorants.** *Characterization.* Concentrated distillates were characterized by applying them to a high resolution gas chromatography/olfactometry system (HRGC/O, type Trace GC Ultra, Thermo Fisher Scientific, Schwerte, Germany). Application was performed by use of the cold-on-column technique (at 40 °C) using the same GC capillaries and settings as described in an earlier study.[20] Two panelists screened the distillate for odor-active volatiles. Screening was performed by sniffing the effluent after gas chromatographic separation at the sniffing port and simultaneously describing the perceived odor impressions (GC/O). Additionally, AEDA was performed on all goat milk samples to screen for the most potent odorants. In detail, an FD series was sniffed via HRGC-O by diluting the concentrated distillates (FD factor $2^n$, concentrate, FD $2^0$ = FD 1) stepwise with dichloromethane (1:1, v/v). Two microliters of each dilution was analyzed on a DB-FFAP capillary.

*Identification.* Odorants were identified based on the following criteria: odor quality, RIs on two stationary phases, and mass spectra. Linear RIs of the compounds were calculated as described by Van Den Dool and Kratz.[21] Identification was performed using a two-dimensional gas chromatographic system (2D-HRGC-MS/O), of which the setup and GC conditions were described in an earlier study.[20] Mass spectra in the electron impact mode (MS/EI) or chemical ionization mode (MS/CI) were acquired ($m/z$ range 35−249 and 60−299, respectively). In the case of EI mode, mass spectra were generated at ionization energy of 70 eV; in CI mode, methanol was used as the reagent gas at a flow of 2.5 mL $min^{-1}$.

**Aroma Profile Analysis (APA).** Sensory analyses were performed in a sensory room at 21 ± 1 °C. Goat milk samples (20 mL) were filled into sensory glass beakers (140 mL, J. Weck GmbH u. Co. KG, Wehr, Germany) and closed with a lid. Trained panelists ($n$ = 11−16, male/female, age 23−45) with normal olfactory and gustatory function participated in the APA sessions. They exhibited no known illness at the time of examination. Prior to this study, the assessors were recruited in weekly training sessions for the recognition of about 200 selected odor-active compounds according to their odor qualities by means of an in-house developed flavor language. A preliminary sensory session was performed to evaluate and collect orthonasal (o) and retronasal (r) odor attributes of the different goat milks. Attributes that were detected by more than 50% of the panelists were selected for subsequent sensory evaluations. Panelists were asked to score the perceived intensities (o, r) of the selected attributes on a seven-point-scale from not perceivable (0) to weak (1), medium (2) and intensely perceivable (3), in increments of 0.5. The results for each odor attribute and goat milk sample were averaged and plotted in spider-web diagrams.

**Table 1. Main Fatty Acid Composition of Raw Goat Milk from Winter (W) and Summer (S) Seasons and Different Farms (1,2)[a]**

| | winter milk (W) (Φ total FA, 3.2 g/100 g) | | | summer milk (S) (Φ total FA, 2.4 g/100 g) | | | level of significance | | | | |
|---|---|---|---|---|---|---|---|---|---|---|---|
| | | | | | | | seasonal effects | | | farm-specific effects | |
| fatty acid | W1 | W2 | mean | S1 | S2 | mean | W1/S1 | W2/S2 | $W_{mean}/S_{mean}$ | W1/W2 | S1/S2 |
| $C_{4:0}$ butyric | 0.10 ± 0.01 (3.8%) | 0.15 ± 0.01 (3.8%) | 0.12 (3.8%) | 0.09 ± 0.01 (3.9%) | 0.09 ± 0.01 (3.7%) | 0.09 (3.8%) | *b* | *b* | *b* | *b* | *b* |
| $C_{6:0}$ caproic | 0.01 ± 0.00 (0.4%) | 0.01 ± 0.00 (0.3%) | 0.01 (0.3%) | 0.01 ± 0.00 (0.5%) | 0.01 ± 0.00 (0.4%) | 0.01 (0.4%) | *c* | *c* | *c* | *c* | *c* |
| $C_{8:0}$ caprylic | 0.08 ± 0.01 (3.3%) | 0.12 ± 0.01 (3.0%) | 0.10 (3.1%) | 0.07 ± 0.01 (3.1%) | 0.07 ± 0.00 (2.8%) | 0.07 (2.9%) | *b* | *b* | *b* | *b* | *b* |
| $C_{10:0}$ capric | 0.26 ± 0.02 (10.4%) | 0.34 ± 0.02 (9.0%) | 0.30 (9.6%) | 0.24 ± 0.01 (10.8%) | 0.24 ± 0.01 (9.7%) | 0.24 (10.2%) | *b* | *c* | *b* | *c* | *d* |
| $C_{12:0}$ lauric | 0.11 ± 0.01 (4.5%) | 0.16 ± 0.01 (4.1%) | 0.13 (4.2%) | 0.11 ± 0.01 (4.9%) | 0.11 ± 0.00 (4.4%) | 0.11 (4.6%) | *b* | *c* | *b* | *b* | *c* |
| $C_{14:0}$ myristic | 0.30 ± 0.02 (11.8%) | 0.39 ± 0.01 (10.3%) | 0.34 (10.9%) | 0.28 ± 0.01 (12.5%) | 0.31 ± 0.01 (12.2%) | 0.30 (12.3%) | *b* | *e* | *c* | *d* | *b* |
| $C_{16:0}$ palmitic | 0.60 ± 0.05 (23.9%) | 0.86 ± 0.04 (22.5%) | 0.73 (23.1%) | 0.60 ± 0.02 (27.4%) | 0.72 ± 0.01 (28.7%) | 0.66 (28.0%) | *c* | *e* | *c* | *b* | *c* |
| $C_{18:0}$ stearic | 0.22 ± 0.02 (8.8%) | 0.34 ± 0.02 (9.0%) | 0.28 (8.9%) | 0.16 ± 0.01 (7.0%) | 0.16 ± 0.00 (6.4%) | 0.16 (6.7%) | *c* | *e* | *c* | *b* | *c* |
| $C_{4:0-18:0}$ total SFA | 1.68 (67.2%) | 2.37 (62.4%) | 2.02 (63.9%) | 1.56 (70.9%) | 1.71 (68.4%) | 1.64 (69.0%) | | | | | |
| $C_{16:1}$ palmitoleic | 0.06 ± 0.01 (1.7%) | 0.09 ± 0.01 (2.7%) | 0.07 (2.2%) | 0.04 ± 0.01 (1.8%) | 0.05 ± 0.00 (2.1%) | 0.05 (2.0%) | *b* | *d* | *b* | *e* | *b* |
| $C_{18:1}$ oleic | 0.64 ± 0.05 (20.3%) | 1.09 ± 0.05 (34.4%) | 0.86 (27.6%) | 0.48 ± 0.01 (20.4%) | 0.61 ± 0.01 (26.1%) | 0.55 (23.1%) | *b* | *e* | *b* | *e* | *e* |
| $C_{16:1-18:1}$ total MUFA | 0.70 (28.0%) | 1.18 (31.1%) | 0.93 (29.8%) | 0.52 (23.6%) | 0.66 (26.4%) | 0.59 (25.1%) | | | | | |
| $C_{18:2}$ linoleic | 0.12 ± 0.01 (4.7%) | 0.20 ± 0.01 (5.1%) | 0.16 (5.0%) | 0.10 ± 0.01 (4.3%) | 0.12 ± 0.01 (4.6%) | 0.11 (4.5%) | *b* | *c* | *b* | *b* | *b* |
| $C_{18:3}$ linolenic | 0.03 ± 0.00 (1.2%) | 0.01 ± 0.00 (0.3%) | 0.02 (0.6%) | 0.02 ± 0.01 (1.0%) | 0.01 (0.4%) | 0.02 (0.7%) | *b* | *e* | *b* | *e* | *d* |
| $C_{18:2-18:3}$ total PUFA | 0.15 (6.0%) | 0.21 (5.5%) | 0.18 (5.6%) | 0.12 (5.5%) | 0.13 (5.2%) | 0.13 (5.2%) | | | | | |

[a]Mean values and relative amounts (percentage of total fatty acids) of individual fatty acids in milk (g/100 g of milk). SFA = saturated fatty acids; MUFA = monounsaturated fatty acids; PUFA = polyunsaturated fatty acids. [b]Not significant. [c]$p < 0.05$. [d]$p < 0.01$. [e]$p < 0.001$.



dx.doi.org/10.1021/jf5040724 | J. Agric. Food Chem. 2014, 62, 11805−11817

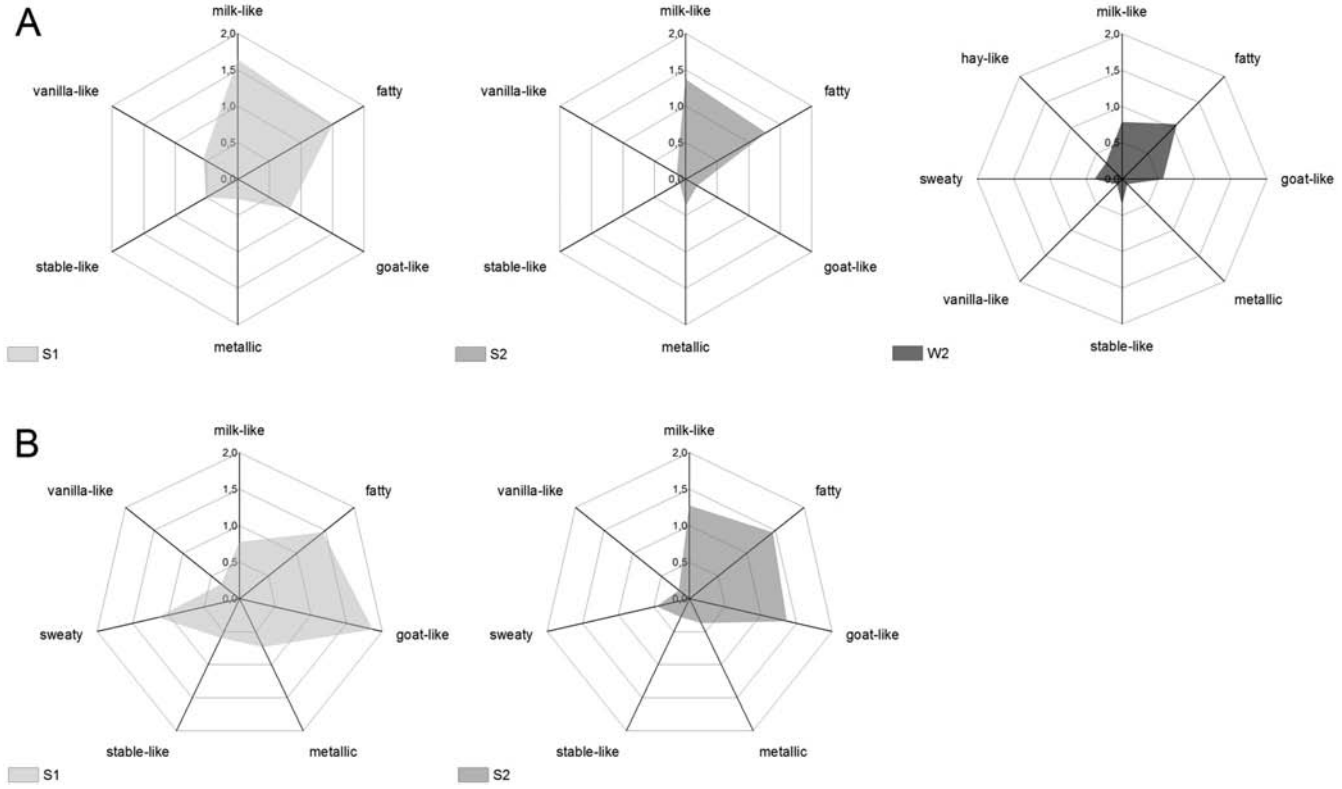


**Figure 1.** Orthonasal (A) and retronasal (B) odor profiles of goat milk: raw milk profiles from summer (S) and winter (W) season.

**Statistical Analysis.** For statistical analyses, Student's *t* test (Welch-test) or Mann–Whitney U-test was performed using OriginPro 9.1 (OriginLab Co., Northampton, MA). The level of statistical significance was set at 5%.

## RESULTS

**Fatty Acids Composition of Raw Milks.** The fatty acid composition of goat's milk was investigated in a comparative approach of winter versus summer milk and thus during different lactation stages (Table 1). Overall, the fatty acid percentage composition of summer and winter milk was quite similar to each other as the statistical comparison of $W_{mean}$ and $S_{mean}$ shows. Thus, average seasonal effects on fatty acid composition of goat's milk were found to be low. Significances were only detected in a few cases ($C_{6:0}$, $C_{14:0}$, $C_{16:0}$, $C_{18:0}$, $p < 0.05$).

Generally, winter milk contained a higher percentage of total MUFAs (monounsaturated fatty acids) while summer milk contained a higher percentage of total SFAs (saturated fatty acids). PUFA (polyunsaturated fatty acid) contents were quite similar between summer and winter milks. However, differences in fatty acid composition were more significant by direct comparison of (a) winter/summer milks from the same farm (W1/S1, W2/S2, seasonal effect) or (b) winter/summer milks from the same season but different farms/herds (W1/W2, S1/S2, farm-specific effect) (Table 1). In detail, most variations were detected in case of the fatty acids $C_{10:0}$, $C_{14:0}$, $C_{16:0}$, $C_{18:0}$, $C_{16:1}$, $C_{18:1}$, $C_{18:3}$, $p < 0.01$. Thus, farmer's seasonal changes in the goat's diet (types of pasture, grains) as well as farm-specific differences between two farms/herds of the same breed (e.g., due to feeding or animal-specific differences) showed an effect on percentage fatty acid composition.

**Sensory Characterization of the Raw Goat Milks by Means of APA.** Orthonasal (o) and retronasal (r) odor profiles of the raw goat milk samples were described by the following eight attributes: milk-like, fatty, goat-like, metallic, stable-like, vanilla-like, sweaty, and hay-like (Figure 1). Those attributes were detected by more than 50% of the trained panelists in one or more of the different raw milks.

Orthonasally, the strongest odor attributes were milk-like and fatty (weak to medium intense; mean values 1.3) followed by weak perception of the attribute *goat-like* (mean value 0.5). All other attributes were just slightly perceivable with mean values below 0.5.

Retronasally, goat-like and fatty were the strongest perceived odor attributes (medium intense; mean values 1.6 and 1.5). The attributes milk-like, sweaty, and metallic were evaluated with weak intensities (mean values 1.0, 0.8, and 0.6), and stable/vanilla-like odors were just slightly perceived (mean values <0.5).

When S1 and S2 (o, r), and thus milks from the same season but two different farms, were compared, odor profiles were evaluated for farm-specific effects. Orthonasally, the summer raw milks were ranked similar with respect to the attributes milk-like, fatty, and metallic (Figure 1). S1 was rated slightly more stable-like and vanilla-like and considerably more goat-like (>0.5 units). Retronasally, odor differences became more clear with respect to the attribute goat-like (mean intensities $_{S1,S2}$: 1.9 and 1.4), but also *sweaty* was perceived more intense in S1 (mean intensities $_{S1,S2}$: 1.1 and 0.5) and *milk-like* in S2 (mean intensities S1 and S2, 0.8 and 1.3). Metallic and stable-like were ranked slightly higher in S1. Thus, the raw milk odor profiles of one season were found to vary from one farm to another.

**Table 2. Characterization and Identification of Potent Odorants (FD ≥ 8) in Raw Goat Milk from Summer and Winter Season Using Gas Chromatography/Olfactometry (GC/O)**

| | | | RI on | | FD-factor[d] in raw goat milk | | | |
|---|---|---|---|---|---|---|---|---|
| | | | | | summer milk | | winter milk | |
| no. | odorant[a] | odor quality[c] | DB-FFAP | DB-5 | S1 | S2 | W1 | W2 |
| 1 | butan-2,3-dione (diacetyl) | buttery | 996−1004 | | 8 | <8 | 8 | <8 |
| 2 | dimethyl disulfide[b] | sweaty, fatty | 1138−1144 | 761−768 | *e* | *e* | *e* | 16 |
| 3 | oct-1-en-3-one | mushroom-like | 1294−1297 | 975−981 | 16 | 8 | 8 | 16 |
| 4 | (*E*)-oct-2-enal | green, fatty, plastic-like | 1414−1419 | 1060−1066 | 8 | *e* | <8 | 128 |
| 5 | (*Z*)-non-4-enal[b] | green, fatty | 1429−1433 | 1096−1099 | 16 | 8 | 8 | <8 |
| 6 | 3-methylthiopropanal (methional) | cooked potato-like | 1445−1449 | 908−909 | 8 | 16 | 16 | 16 |
| 7 | (*E*)-non-2-enal | fatty, green | 1512−1526 | 1156−1166 | 8 | 16 | 32 | <8 |
| 8 | (*E*,*Z*)-nona-2,6-dienal | fatty, cucumber-like | 1576−1580 | 1148−1151 | *e* | 8 | <8 | <8 |
| 9 | butanoic acid | cheesy, sweaty | 1614−1618 | 826−833 | 64 | 64 | 32 | 16 |
| 10/11 | 2-/3-methylbutanoic acid | sweaty, cheesy | 1652−1659 | 866−868 | 64 | 32 | 16 | 16 |
| 12 | (*E*,*E*)-nona-2,4-dienal | fatty, green | 1689−1691 | 1210−1215 | 16 | 16 | 16 | 16 |
| 13 | pentanoic acid[b] | sweaty, cheesy | 1715−1727 | 912−914 | 16 | <8 | <8 | <8 |
| 14 | (*E*,*E*)-deca-2,4-dienal | fatty, green | 1797−1799 | 1303−1314 | <8 | 8 | <8 | 8 |
| 15 | hexanoic acid | urine-like, pungent | 1829−1834 | 1020−1022 | 64 | 64 | 64 | 8 |
| 16 | phenylethan-2-ol[b] | flowery, fruity, sweet | 1885−1904 | 1103−1113 | <8 | *e* | 8 | 8 |
| 17 | γ-octalactone | coconut-like | 1904−1908 | 1251−1260 | *e* | <8 | 8 | 8 |
| 18 | *trans*-4,5-epoxy-(*E*)-dec-2-enal | metallic | 1983−1996 | 1371−1375 | 128 | 128 | 64 | 8 |
| 19 | γ-nonalactone | peach-like, woodruff-like | 2010−2017 | 1351−1360 | 64 | 32 | 32 | 32 |
| 20 | octanoic acid | medicinal, fatty, musty | 2037−2046 | 1262−1275 | 8 | 16 | 8 | 8 |
| 21 | δ-nonalactone | sweet, peach-like | 2063−2066 | 1333−1336 | 16 | 16 | 16 | 16 |
| 22 | 4-methyloctanoic acid (4-meC8) | musty, urine-, stable-like | 2074−2082 | 1228−1242 | 16 | 16 | 16 | 8 |
| 23 | unknown | fruity, soapy, sweet | 2097−2103 | | 256 | 32 | 8 | 8 |
| 24 | 3-methylphenol (*m*-cresol) | leather-like, medicinal | 2089−2099 | 1082−1091 | *e* | <8 | <8 | 8 |
| 25 | γ-decalactone | peach-like | 2130−2132 | 1459−1468 | 32 | 32 | 64 | 16 |
| 26 | nonanoic acid | fatty, fecal, goaty | 2147−2160 | 1271−1288 | 16 | 16 | 8 | 16 |
| 27 | 3-ethylphenol | fatty, leather-like, medicinal | 2151−2167 | 1166−1171 | <8 | 8 | <8 | 32 |
| 28 | δ-decalactone | coconut-like | 2178−2188 | 1487−1497 | 128 | 32 | <8 | 8 |
| 29 | 3-hydroxy-4,5-dimethyl-2(5*H*)-furanone (sotolone)[b] | spicy, maggi-like | 2189−2197 | 1079−1082 | *e* | 8 | <8 | *e* |
| 30 | 4-ethyloctanoic acid (4-etC8) | goaty, stable-like | 2190−2202 | 1318−1323 | 1024 | 512 | 256 | 1024 |
| 31 | 2-aminoacetophenon | flowery, peach-like, soapy | 2208−2214 | 1290−1295 | 32 | 32 | 32 | 16 |
| 32 | 3-propylphenol | musty, medicinal, leather-like | 2235−2244 | | 128 | 128 | 128 | 256 |
| 33 | γ-undecalactone | peach-like | 2247−2255 | 1564−1574 | <8 | 8 | 8 | 16 |
| 34 | decanoic acid | fatty, goaty, leather-like | 2253−2264 | 1368−1388 | 64 | 128 | 32 | 256 |
| 35 | unknown | fatty, pungent, plastic-like | 2331−2341 | | 128 | 32 | 64 | 256 |
| 36 | unknown | sweaty, goaty | 2345−2353 | | *e* | *e* | 8 | 128 |
| 37 | γ-dodecalactone | soapy, fatty, flowery | 2368−2381 | 1676−1682 | 32 | 64 | 64 | 32 |
| 38 | γ-(*Z*)-6-dodecenolactone | flowery | 2395−2405 | 1664−1674 | *e* | *e* | 8 | <8 |
| 39 | δ-dodecalactone | flowery, daisy-like | 2421−2430 | 1713−1718 | *e* | 32 | 32 | <8 |
| 40 | 1-benzopyran-2-one (coumarin) | cinnamon-like, sweet | 2437−2445 | 1433−1446 | 8 | <8 | <8 | 8 |
| 41 | 1*H*-benzo[*b*]pyrrole (indole) | fecal, goaty | 2440−2458 | 1306−1309 | 16 | <8 | 128 | 64 |
| 42 | unknown | flowery, soapy | 2456−2465 | | *e* | 8 | 8 | <8 |
| 43 | dodecanoic acid | soapy, goaty, fecal | 2468−2477 | 1566−1585 | 16 | 8 | *e* | 32 |
| 44 | 3-methylindole (skatol) | fecal, stable-like | 2478−2482 | 1379−1383 | 2048 | 2048 | 2048 | 512 |
| 45 | unknown | rubber-like, balloon-like | 2507−2512 | 1789−1791 | 256 | 32 | 64 | 256 |
| 46 | unknown | fruity, flowery, pleasant | 2530−2535 | 1785−1799 | 16 | 8 | 64 | 16 |
| 47 | phenylacetic acid | honey-like | 2543−2551 | 1246−1268 | 128 | 64 | 64 | 64 |
| 48 | 4-hydroxy-3-methoxybenzaldehyde (vanillin) | vanilla-like | 2549−2557 | 1392−1410 | 128 | 64 | 64 | 64 |
| 49 | unknown | spicy, meat-like | 2565−2567 | | *e* | 8 | <8 | 8 |
| 50 | unknown | canola-like, metallic, green | 2712−2716 | | 2048 | 1024 | 1024 | 32 |
| 51 | unknown | flowery | 2755−2759 | | <8 | <8 | 16 | 16 |
| 52 | unknown | spicy, urine-like | 2760−2764 | | <8 | <8 | 8 | <8 |
| 53 | unknown | flowery, soapy | 2832−2835 | | 64 | 16 | 16 | 16 |
| 54 | unknown | facial cream-like, oil paint-like | >2900 | 1471−1474 | 16 | 16 | 64 | 16 |

[a]The compound was identified by comparison with the respective reference substance on the basis of the following criteria: retention indices (RI) on two stationary phases given in the table (DB-FFAP, DB-5), mass spectra obtained by MS/EI or MS/CI, and odor qualities perceived at the sniffing


dx.doi.org/10.1021/jf5040724 | J. Agric. Food Chem. 2014, 62, 11805−11817

**Table 2. continued**

port(s). [b]MS signals were too weak for an unequivocal interpretation. The compound was identified based on the remaining criteria given in footnote *a*. [c]Odor quality as perceived at the sniffing port. [d]Only compounds that were detected with FD values >8 are displayed. [e]Not determined.

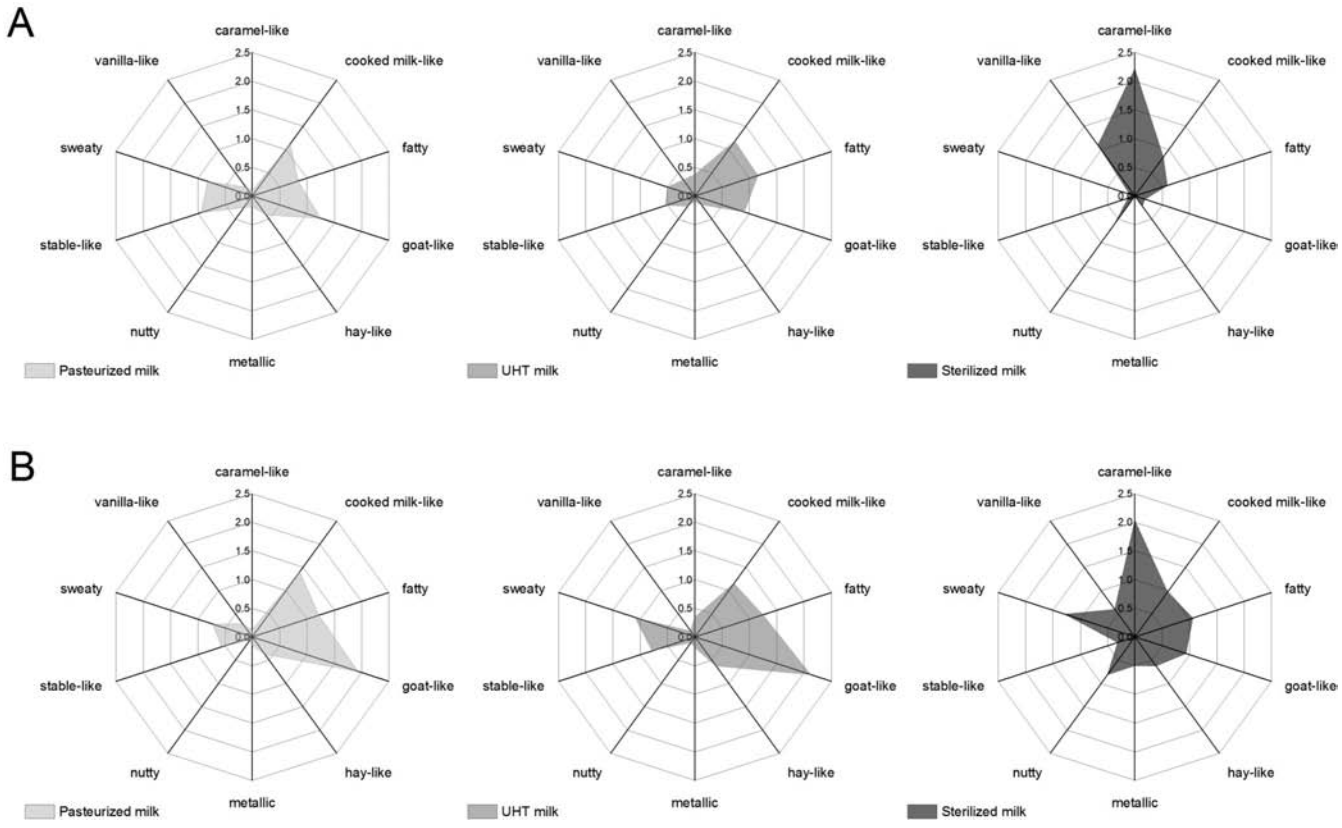


**Figure 2.** Orthonasal (A) and retronasal (B) odor profiles of goat milk: heated milk profiles after pasteurization, UHT-treatment, and sterilization.

Seasonal effects were detected by comparison of the odor profiles (o) of winter and summer raw milks of the same farm. Again, differences in the odor profiles became obvious (here W2, S2) (Figure 1): while S2 had higher rankings for the attribute milk-like (mean intensities S2 and W2, 1.4 and 0.8), W2 was rated more intense with respect to goat-like (mean intensities S2 and W2, 0.2 and 0.6). Metallic and fatty were evaluated slightly higher in S2 and stable-like slightly more intense in W2. The odor attributes sweaty (o) and hay-like (o) were only described for winter raw milk (here: W2), even if ratings were below 0.5.

Hence, besides farm-specific variations in odor profiles of goat milks from different farms (e.g., due to animal-specific or feeding differences), also seasonal variations were detected. These findings correspond with the observations made when studying the fatty acid composition (section Fatty Acids Composition of Raw Milks).

Overall, the only odor attributes ranked with weak to medium intensity ($1.0 < x < 2.0$) were milk-like (o, r), fatty (o, r), goat-like (r), and sweaty (r). No attribute was ranked with intensities above 2.0 (Figure 1), indicating that the overall odor intensity of the raw milks was low. In fact, it needs to be mentioned that the panelists reported that some of the raw milks, like S2, were orthonasally very close to the familiarized plain flavor of cow milk; this is also mirrored by the high ranking of milk-like and fatty odors.

**Characterization of Goat Milks' Odorant Composition.** Raw goat milks were characterized by GC/O, followed by AEDA to reveal the most potent odor-active compounds. Identification was performed by comparing their odor qualities, RIs, and mass spectra (MS-EI; MS-CI) with respective reference compounds.

A total of 54 odor-active volatile compounds were detected with FD factors between 8 and 2048 (Table 2). Especially fatty, sweaty/cheesy, goaty/musty, fecal/stable-like, leather-like/medicinal, and green odor attributes were often recorded descriptors of the odor characters of the volatiles. Additionally, peach-like, coconut-like, fruity, and flowery odor impressions occurred regularly as odor descriptions; these attributes were specifically related to higher FD factors.

A total of 37 compounds were identified unequivocally, as well as five compounds tentatively (without mass spectrum but based on their retention indices and olfactory properties). Compounds with very high intensities (FD $\geq$ 512) in all raw milks were identified as 4-etC8, 3-methylindole (skatol), and one unknown compound with a canola-like, metallic, and green odor character (RI 2715). Generally, a range of (branched-chain) saturated acids and lactones was identified, as well as alkenals and alkadienals (Table 2).

Interestingly, six compounds were associated with goat-like odor characteristics accompanied by the attributes stable-like, fecal, or leather-like. Identification revealed that besides 4-etC8, various saturated acids were among them, namely, nonanoic acid, decanoic acid, dodecanoic acid, and 1*H*-benzo[*b*]pyrrole (indole).

**Table 3. Characterization and Identification of Potent Odorants (FD ≥8) in Heated Goat Milk by Comparison of Pasteurized, UHT-Treated and Sterilized Goat Milk, Using Gas Chromatography/Olfactometry (GC/O)**

| | | | RI on | | FD-factor[d] in heated goat milk | | | |
|---|---|---|---|---|---|---|---|---|
| no. | odorant[a] | odor quality[c] | DB-FFAP | DB-5 | pasteurized | UHT-treated | sterilized | earlier identified in dairy products[e] |
| 1 | butan-2,3-dione (diacetyl) | buttery | 991−998 | | 8 | 32 | 256 | 1,4,5,9,10 |
| 2 | dimethyl disulfide[b] | sweaty, fatty | 1139−1145 | 759−761 | 256 | 128 | 32 | 7,10 |
| 55 | octanal | fatty, soapy | 1280−1289 | | <8 | nd | 8 | 1,3,4,6,7,10 |
| 3 | oct-1-en-3-one | mushroom-like | 1290−1299 | 979−983 | 16 | 16 | 8 | 1,4,5,7,8 |
| 56 | 2-acetyl-1-pyrroline | roasty, popcorn-like | 1330−1333 | 929−934 | <8 | <8 | 8 | 1,4,5,8,9 |
| 57 | dimethyl trisulfide | sweaty, cabbage-like | 1362−1371 | 994−1004 | <8 | 64 | 256 | 4,5,7,10 |
| 4 | (*E*)-oct-2-enal | green, fatty, plastic-like | 1414−1421 | 1060−1066 | 16 | 32 | 8 | 4,5 |
| 5 | (*Z*)-non-4-enal[b] | green, sweaty | 1429−1438 | 1082−1098 | <8 | 16 | 8 | 9 |
| 6 | 3-methylthiopropanal (methional) | cooked potato-like | 1445−1449 | 908−917 | 32 | 256 | 512 | 1,4,5,7,8,9 |
| 58 | 2-furaldehyde (furfural) | sweet, caramel-like | 1462−1468 | | *f* | 8 | <8 | 7,8,10 |
| 59 | (*Z*)-non-2-enal[b] | fatty, green | 1503−1508 | 1148−1151 | 16 | 8 | 8 | 5,9 |
| 7 | (*E*)-non-2-enal | fatty, green | 1514−1523 | 1156−1166 | 32 | 16 | 16 | 1,4,5,8,9 |
| 8 | (*E*,*Z*)-nona-2,6-dienal | fatty, cucumber-like | 1589−1594 | 1148−1153 | 8 | <8 | 8 | 1,4,5,8,9 |
| 9 | butanoic acid | cheesy, sweaty | 1604−1609 | 817−820 | 128 | 16 | 16 | 1,2,3,4,5,7,8,9 |
| 10/11 | 2-/3-methylbutanoic acid | sweaty, cheesy | 1647−1652 | 868−876 | 64 | 32 | 128 | 3,4,5/2,3,4,5,8 |
| 12 | (*E*,*E*)-nona-2,4-dienal | fatty, green | 1684−1691 | 1201−1207 | 64 | 8 | 8 | 1,4,5,8 |
| 13 | pentanoic acid[b] | sweaty, cheesy | 1713−1731 | 912−914 | 64 | 256 | 512 | 1,2,3,4,5,7 |
| 60 | (*E*)-undec-2-enal | coriander-like, fatty | 1733−1736 | 1336−1339 | 8 | 8 | *f* | 5 |
| 14 | (*E*,*E*)-deca-2,4-dienal | fatty, green | 1789−1796 | 1312−1323 | 32 | 32 | 16 | 1,4,5 |
| 15 | hexanoic acid | urine-like, pungent | 1822−1823 | 1022−1027 | 128 | 32 | 16 | 1,2,3,4,5,7,8,9 |
| 61 | 2-methoxyphenol (guaiacol) | spicy, ham-like | 1841−1844 | 1085−1090 | 32 | 16 | <8 | 4 |
| 16 | phenylethan-2-ol[b] | flowery, fruity, sweet | 1875−1885 | 1103−1113 | 8 | <8 | *f* | 2,3,4,5 |
| 17 | γ-octalactone | coconut-like | 1897−1804 | 1251−1260 | 8 | 8 | *f* | 1,4 |
| 62 | 3-hydroxy-2-methyl-4-pyrone (maltol) | caramel-like, creamy | 1943−1946 | 1111−1117 | 8 | 8 | 128 | 4,5 |
| 18 | *trans*-4,5-epoxy-(*E*)-dec-2-enal | metallic | 1983−1990 | 1371−1377 | 32 | 32 | 256 | 9 |
| 63 | unknown | cinnamon-like, coconut-like | 1990−2003 | | 8 | 8 | 8 | |
| 19 | γ-nonalactone | peach-like, woodruff-like | 2005−2008 | 1355−1364 | 16 | 16 | 16 | 4,9 |
| 64 | 4-hydroxy-2,5-dimethyl-3(2*H*)-furanone (furaneol) | caramel-like | 2009−2010 | 1070−1072 | *f* | *f* | 8192 | 4,5,8 |
| 20 | octanoic acid | medicinal, fatty, musty | 2031−2043 | 1258−1269 | 64 | 16 | 128 | 1,2,3,4,5,7,8,9 |
| 21 | δ-nonalactone | sweet, peach-like | 2057−2068 | 1333−1338 | 16 | 32 | 256 | 9 |
| 22 | 4-methyloctanoic acid (4-meC8) | musty, urine-, stable-like | 2063−2072 | 1228−1242 | 8 | 16 | 64 | 1,2,3,4 |
| 23 | unknown | fruity, soapy, sweet | 2093−2099 | | 16 | 16 | 8 | |
| 24 | 3-methylphenol (*m*-cresol) | leather-like, medicinal | 2089−2107 | 1079−1091 | 8 | 8 | 8 | 7,13 |
| 25 | γ-decalactone | peach-like | 2128−2133 | 1463−1472 | 128 | 128 | 512 | 1,4,8 |
| 26 | nonanoic acid | fatty, earthy, goaty | 2140−2152 | 1271−1288 | 64 | 32 | 8 | 1,2,3,4,5,7,8 |
| 27 | 3-ethylphenol | fatty, leather-like, medicinal | 2151−2164 | 1166−1171 | 16 | 16 | 8 | 13 |
| 28 | δ-decalactone | coconut-like | 2168−2174 | 1487−1497 | 256 | 512 | 2048 | 1,3,4,5,6,8,9 |
| 29 | 3-hydroxy-4,5-dimethyl-2(5*H*)-furanone (sotolone)[b] | spicy, maggi-like | 2178−2180 | 1081−1087 | 8 | 8 | 8 | 1,4,5,8 |
| 30 | 4-ethyloctanoic acid (4-etC8) | goaty, stable-like | 2175−2289 | 1320−1325 | 1024 | 2048 | 4096 | 1,2,3 |
| 31 | 2-aminoacetophenon | flowery, peach-like, soapy | 2203−2208 | 1294−1297 | 64 | 64 | 64 | 1,4,5 |
| 32 | 3-propylphenol | earthy, medicinal, leather-like | 2219−2230 | | 8 | 8 | 8 | 11 |
| 33 | γ-undecalactone | peach-like | 2237−2247 | 1566−1576 | 256 | 128 | 64 | 12 |
| 34 | decanoic acid | fatty, goaty, leather-like | 2245−2253 | 1368−1388 | 256 | 64 | 256 | 1,2,3,5,7,8,9 |
| 35 | unknown | fatty, creamy, plastic-like | 2310−2326 | | 64 | 64 | 32 | |
| 36 | unknown | sweaty, goaty | 2342−2353 | | 8 | 16 | <8 | |
| 37 | γ-dodecalactone | soapy, fatty, peach-like | 2361−2371 | 1682−1692 | 64 | 64 | 32 | 1,4,5,6,9 |
| 38 | γ-(*Z*)-6-dodecenolactone | flowery, pungent | 2382−2385 | 1662−1672 | 512 | 256 | 256 | 4,8,9 |


dx.doi.org/10.1021/jf5040724 | J. Agric. Food Chem. 2014, 62, 11805−11817

**Table 3. continued**

| no. | odorant[a] | odor quality[c] | RI on | | FD-factor[d] in heated goat milk | | | earlier identified in dairy products[e] |
|---|---|---|---|---|---|---|---|---|
| | | | DB-FFAP | DB-5 | pasteurized | UHT-treated | sterilized | |
| 39 | δ-dodecalactone | flowery, daisy-like | 2421−2430 | 1709−1713 | <8 | 16 | <8 | 1,3,4,6,9 |
| 40 | 1-benzopyran-2-one (coumarin) | cinnamon-like, sweet | 2429−2438 | 1433−1446 | 16 | 64 | 32 | *f* |
| 41 | 1*H*-benzo[*b*]pyrrole (indole) | fecal, goaty | 2431−2440 | 1308−1312 | 8 | 8 | 8 | 1,3,6,7 |
| 43 | dodecanoic acid | soapy, goaty, fecal | 2458−2470 | 1566−1586 | 64 | 32 | 32 | 2,5,7 |
| 44 | 3-methylindole (skatol) | fecal, stable-like | 2470−2478 | 1378−1382 | 512 | 512 | 1024 | 1,3,4,5,6,7,8 |
| 45 | unknown | rubber-like, balloon-like | 2500−2510 | 1790−1799 | 64 | 64 | 64 | |
| 46 | unknown | fruity, flowery, pleasant | 2521−2527 | 1797−1800 | 8 | 64 | 16 | |
| 47 | phenylacetic acid | honey-like | 2536−2547 | 1246−1268 | 4096 | 4096 | 8192 | 1,2,4,5,7,8 |
| 48 | 4-hydroxy-3-methoxybenzaldehyde (vanillin) | vanilla-like | 2547−2555 | 1392−1401 | 64 | 64 | 64 | 1,4,5,7,9 |
| 49 | unknown | spicy, meat-like | 2558−2565 | | 8 | <8 | <8 | |
| 50 | unknown | canola-like, metallic, green | 2705−2707 | | 256 | 256 | 128 | |
| 51 | unknown | flowery | 2759−2767 | | 8 | 8 | *f* | |
| 52 | unknown | spicy, urine-like | 2740−2749 | | 8 | 8 | *f* | |
| 53 | unknown | flowery, soapy | 2832−2840 | | 32 | 32 | 16 | |
| 65 | unknown | fecal, stable-like | >2900 | | <8 | 8 | *f* | |
| 54 | unknown | face-cream-like, oil-paint | >2900 | | 64 | 32 | 8 | |
| 66 | unknown | fruity, artificial cherry-like | >2900 | | 16 | 32 | 8 | |

[a]The compound was identified by comparison with the respective reference substance on the basis of the following criteria: retention index (RI) on two stationary phases given in the table (DB-FFAP, DB-5), mass spectra obtained by MS/EI or MS/CI, and odor quality as well as odor intensity perceived at the sniffing port. [b]MS signals were too weak for an unequivocal interpretation. The compound was identified based on the remaining criteria given in footnote *a*. [c]Odor quality as perceived at the sniffing port. [d]Only compounds that were detected with FD values >8 are displayed. [e]Earlier identified in 1,[3] 2[2] (goat cheese), 3[4−6] (goat milk), 4,[33] 5[51] (cow milk powder), 6,[4,5] 7,[17] 8,[16] 9,[15] 10[14] (heated cow milk), 11[47] (conjugates in cow milk), 12[52] (cow's milk cheese), 13[46] (ruminant milks). [f]Not determined.

AEDA revealed only slight differences with respect to seasonal (W1/S1, W2/S2) or farm-specific (W1/W2, S1/S2) effects (Table 2). For most odorants, the variation was no more than 1 FD factor.

**Sensory Characterization of Goat Milk after Different Heat Treatments.** Odor profiles (o, r) of the heated goat milk samples were described by the trained sensory panel, and 10 attributes were selected for APA: caramel-like, cooked milk-like, fatty, goat-like, hay-like, metallic, nutty, stable-like, sweaty, and vanilla-like (Figure 2). Generally, the odor profiles of pasteurized and UHT-treated milks were more similar to each other than sterilized milk, as the orthonasal and retronasal spider web diagrams demonstrate.

Highest ratings (mean values ≥2.0) were given to goat-like (r) in case of pasteurized/UHT-treated goat milk and caramel-like (o, r) in case of sterilized milk. With mean values ≥1.0, dominant attributes (o/r) of pasteurized and UHT-treated goat milk were also cooked milk-like, fatty, stable-like, and sweaty. Sterilized milk was additionally characterized by vanilla-like odors (o), as well as cooked milk-like, fatty, goat-like, and sweaty odors (r) with weak to medium intensities (mean values ≥1.0).

Overall, increasing rankings with thermal treatment were found for the attributes caramel-like, vanilla-like, and nutty, whereas for the following attributes intensity ratings decreased: cooked milk-like, goat-like, and stable-like (Figure 2). The odor impressions metallic and sweaty were orthonasally (slightly) stronger perceived in pasteurized milk and UHT samples, while retronasally they were stronger in sterilized milk.

**Heat-Induced Changes in Goat Milks' Odorant Composition.** Heated goat milks (pasteurized, UHT-treated and sterilized) were also characterized by GC/O and AEDA for the main odor-active volatiles. Overall, 66 compounds were detected with FD factors in the range of 8 and 2048 (Table 3). Besides fatty, sweaty/cheesy, goaty/musty, fecal/stable-like, leather-like/medicinal, and green odor attributes that were typical odor characters in raw milk (section Characterization of Goat Milks' Odorant Composition), also roasty, caramel-like, popcorn-like, cinnamon-like, and creamy odors were detected. Again, also peach-like, coconut-like, fruity, and flowery odor impressions were among those descriptors that were recorded with higher FD factors.

A total of 45 compounds were identified unequivocally, as well as 6 compounds tentatively (without mass spectrum but based on their retention indices and olfactory properties). Compounds with very high intensities (FD > 512) were identified as 3-methylthiopropanal (methional), pentanoic acid, 4-hydroxy-2,5-dimethyl-3(2*H*)-furanone (furaneol), γ-decalactone, δ-decalactone, 4-etC8, γ-(*Z*)-6-dodecenolactone, skatol, and phenylacetic acid. In all heated milks, 4-etC8, skatol, and phenylacetic acid were the most potent odor-active compounds. Furaneol was only detected in sterilized milk samples, but in a very high intensity (FD 8192) (Table 3). Among all flavor compounds that were only detected in the heated milk samples with FD ≥ 8, the following compounds could be identified: octanal, 2-acetyl-1-pyrroline, dimethyl trisulfide, 2-furaldehyde (furfural), (*Z*)-non-2-enal, (*E*)-undec-2-enal, 2-methoxyphenol (guaiacol), 3-hydroxy-2-methyl-4-pyrone (maltol), and furaneol.

Comparing the results of Table 3 with data on the main odorants in raw milk (Table 2), odor intensities were found to increase for a range of substances with heat treatment. While 14 odor-active volatiles with FD factors ≥128 were detected in raw milk samples, 22 compounds were detected with at least the same intensity in heated milk samples. Among the heated milk samples, sterilized goat milk showed highest odor intensities with 18 compounds of FD ≥ 128 (pasteurized and UHT, 11 and 12 compounds). Overall, the following compounds showed increasing FD factors with increasing thermal treatment: diacetyl, dimethyl trisulfide, methional, pentanoic acid, maltol, furaneol, δ-nonalactone, 4-meC8, γ-decalactone, δ-decalactone, 4-etC8, and phenylacetic acid (Table 3).

## DISCUSSION

**Fatty Acid Composition of Raw Milk.** Generally, the fatty acid composition of goat's milk shows a higher proportion of medium-chain fatty acids, like $C_{6:0}$ (caproic), $C_{8:0}$ (caprylic), and $C_{10:0}$ (capric), compared with cow's milk (8% vs up to 16% of total fatty acids).[22] In our study, fatty acid percentage composition was quite comparable to literature reports, with exception of $C_{6:0}$, which was detected in very low amounts (section Fatty Acids Composition of Raw Milks).[23,24] Alonso et al.[23] reported values for caprylic acid of 2.7% ± 0.1% by investigating milk from five different goat herds that were collected from November to May and 10.0% ± 0.3% for capric acid. Our results in Table 1 show the same characteristics (caprylic acid 3.1% ± 0.1%, capric acid 9.9% ± 0.3%) with just slight, not significant differences between summer and winter milk. According to Alonso et al.[23] and Park et al.,[25] the following five fatty acids (FA) make up the largest part (>75% of total FA) in goat milk: $C_{10:0}$, $C_{14:0}$, $C_{16:0}$, $C_{18:0}$, and $C_{18:1}$. This observation is in agreement with the results from Table 1, where those fatty acids account for 80.2% of total FA in the winter milk (3.1 g total FA/100 g goat milk) and 80.9% of total FA in the summer milk (2.4 g total FA/100 g goat milk).

A marker of authenticity for caprine milk and cheeses is the ratio of $C_{12:0}/C_{10:0}$. In literature, values from 0.46% ± 0.04% to 0.50% ± 0.04% were reported.[23,26] In accordance, a $C_{12:0}/C_{10:0}$ ratio of 0.44% ± 0.03% and 0.45% ± 0.03% was found in case of winter and summer milk, respectively. In the case of cow milk or sheep milk, this ratio is higher.[26]

Regarding seasonal effects, fatty acid analysis in section Fatty Acids Composition of Raw Milks revealed a very similar average percentage composition of summer and winter milk. Winter milk was found to contain a higher percentage of total MUFA while summer milk contained a higher percentage of total SFA. For milks in general, higher levels of SFA are reported during winter season while higher levels of PUFA are stated during summer season. Lock and Garnsworthy[27] described monthly changes of individual fatty acids in cow milk and reported high SFA levels from October to December and high PUFA levels from May to October with maximum values in October (SFA) and July (PUFA), respectively. In our study, PUFA contents were found to be quite similar between summer and winter milks; this observation might be explained by the fact that the diets of both herds were based on home-grown conserved forage all year round (cf. section Goat Milk). At the beginning of lactation, the goats were also fed on concentrate that included high values of rapeseed meal. The latter fact might be responsible for an increased percentage of MUFA in winter milks. Similar observations were reported by Butler et al.,[28] investigating SFA, MUFA, and PUFA composition of cow's milk fat of organic low-input production systems: high SFA levels in August, high MUFA levels in March, and no major differences in PUFA levels comparing March and August.

By direct comparison of winter/summer milks from the same farm (W1/S1, W2/S2; seasonal effect) and season (W1/W2, S1/S2;: farm-specific effect), differences in fatty acid composition were more significant ($C_{10:0}$, $C_{14:0}$, $C_{16:0}$, $C_{18:0}$, $C_{16:1}$, $C_{18:1}$, and $C_{18:3}$). However, the breed and general type of feeding was the same (breed "Bunte Deutsche Edelziege") or similar to each other (mainly conserved pasture and grains). Thus, the farmer's seasonal changes in their home-grown feed as well as individual differences of the animals or fed forage from one farm to the other (e.g., of rapeseed meal, sugar beet slices, and carrots) showed an effect on fatty acid composition. Similar findings on changes in percentage fatty acid composition due to seasonal changes in a goat herd feed were reported by Eknaes et al..[24] Bakke et al.[29] additionally reported differences in milk quality between individuals of the same breed, indicating that milk from different farms will show some variation, for example, in fatty acids profile.

**Characterization of Goat Milk Odor and Odorant Composition.** Descriptive profiling of raw goats' milk revealed milk-like, fatty, and goat-like odor attributes with weak to medium intensity (o, r), among some weak perception of metallic, stable-like, vanilla-like, sweaty, and hay-like odors (section Sensory Characterization of the Raw Goat Milks by Means of APA).

Characterization and identification of the odorant composition by HRGC/O, AEDA, and 2D-HRGC-MS/O (section Characterization of Goat Milks' Odorant Composition) pointed out >50 aroma compounds belonging to various substance classes (e.g., lactones, (branched-chain) saturated acids, alkenals, and alkadienals). Generally, a number of the identified compounds were described in literature before in the context of goat cheese, cow milk, or respective dairy products. However, only 16 of the 42 identified odorants were reported before in raw goat's milk since generally, literature lacks information on that topic (cf. Table 3). Furthermore, to the best of our knowledge, nine odorants were described for the very first time in a goat milk originating product: dimethyl disulfide, (*E*)-oct-2-enal, (*Z*)-non-4-enal, *trans*-4,5-epoxy-(*E*)-dec-2-enal, γ-nonalactone, δ-nonalactone, 3-propylphenol, γ-undecalactone, and γ-(*Z*)-6-dodecenolactone. Details are given in Table 3 and are further discussed in section Heat-Induced Changes in Goat Milk Odor and Odorant Composition.

Some of the raw milk odor-active substances were described with a goaty character, among them 4-etC8, as well as some saturated acids: nonanoic, decanoic, and dodecanoic acid. In literature, $C_{6:0}$ (caproic), $C_{8:0}$ (caprylic), and $C_{10:0}$ (capric) acids were described to be very dominant fatty acids in goat milk (cf. section Fatty Acid Composition of Raw Milk) and, additionally, defined to be partly responsible for the typical "goaty" odor of the milk.[1,2] In agreement with our results, Le Quere et al.[2] also described nonanoic acid and 4-etC8 as odor-active volatiles with a goat-like or goat cheese-like odor.

Generally, the characteristic goat-like or muttony flavor of goat milk (fat) is reported to depend on a wide range of monomethyl-branched and monoethyl-branched compounds, mainly with substitution on $C_4$.[30] Especially, 4-etC8 was found to be the main responsible odorant for the characteristic goat-like aroma in goat milk products, which is, other than 4-meC8, not present in cow's milk.[31−33] However, 4-meC8 lacks the typical goat-like odor note but has, according to literature, a

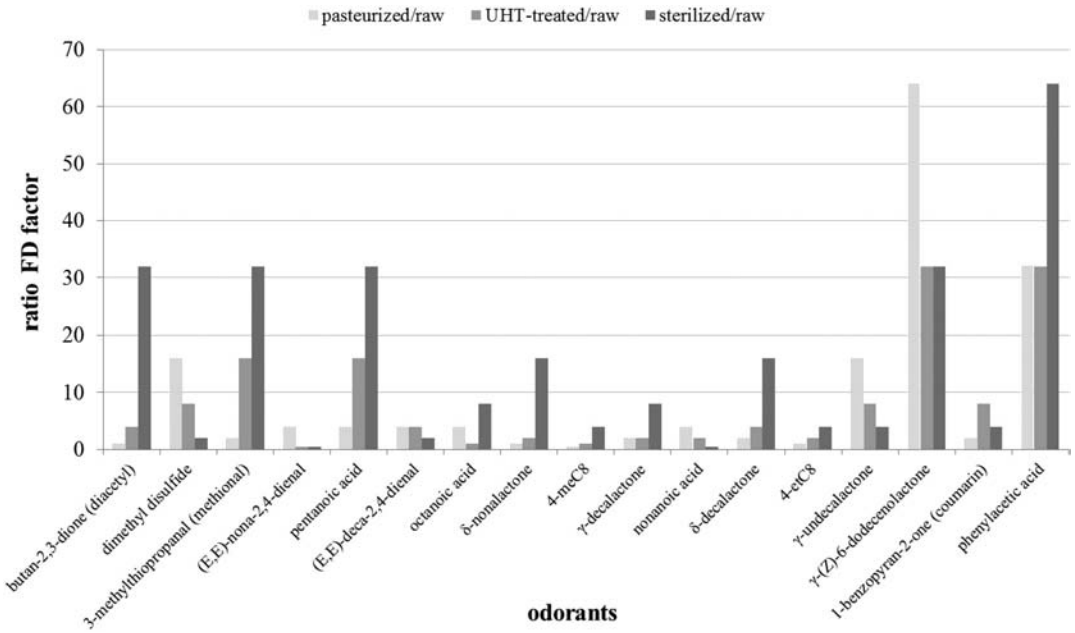


**Figure 3.** Ratio of flavor dilution (FD) factors: $FD_{heated\ milk}/FD_{raw\ milk}$ of selected odorants with $\Delta FD \geq 4$. Raw milk's highest detected FD factor was chosen for calculation. Compounds that were only detected in heated goat milks with FD values ≥8 (e.g., maltol, furaneol) are not displayed.

characteristic muttony smell, which we described as musty, urine-like, and stable-like.[34] In our study, 4-etC8 and skatol were found to be the most potent odorants in goats' raw milk, besides one unknown compound smelling canola-like, metallic, and green with RI 2715. With regard to these very intense odorants, no differences between the diverse types of raw milk were found (Table 2). Overall, only some slight seasonal or farm-specific alterations were observed, mostly within the range of ±1 FD factor.

However, in sensory sessions some differences in the odor profiles of the different raw milks were observed that were confirmed by fatty acid variations in the different raw milks. For example, winter milk was orthonasally found to smell slightly sweaty and hay-like, attributes that were not detectable or were only retronasally detected in summer milk. Indeed, dimethyl disulfide and an unknown compound with a sweaty, goat-like smell (no. 35) were detected in W2 milk in highest FD factors. However, some other compounds with sweaty odor impression were more strongly perceived in summer milks (butanoic acid, 2-/3-methylbutanoic acid, pentanoic acid). Specific hay-like odors were not detected in the course of GC/O screening. Nonetheless, some unsaturated aldehydes and acids were found with comparatively high FD factors in winter milks (e.g., (*E*)-oct-2-enal, (*E*)-non-2-enal), which were described in literature in the context of hay-like (off-) flavors.[35] The sensorial evaluation of summer milk S1 revealed sweaty, goat-like, stable-like, and metallic impressions to be more intense compared with S2. Indeed, a number of odor compounds were found with slightly higher FD factors in S1 (S1 and S2, 11 vs 6 compounds with ≥ FD 128) even if they could not be assigned specifically to one or more of the named attributes (Table 2). The intensities of single odorants in winter milks of different farms were even more similar to each other (W1 and W2, 5 vs 7 compounds with ≥ FD 128). Thus, APA revealed differences between the different raw milks, but FD values were primarily in the range of ±1 FD factor. Accordingly, future quantitative determinations would be required to objectify the differences obtained by our olfactory screening approach; these might then better visualize even minor quantitative variations between the milk samples. Such an observation of minor concentration differences but different substances or substance classes acting additively or synergistically and having a significant influence on the overall flavor of foods or beverages has already been reported in the context of other studies.[20,36,37] Especially odorants with very low odor thresholds, like alkenals, alkadienals, or branched-chain fatty acids, were described to greatly affect the overall flavor profile when concentration ratios slightly change.[20] Due to their comparable odor properties, such substances can also act as a whole in terms of aroma effects.

Overall, coupling of GC/O, AEDA, and 2D-HRGC-MS/O revealed a complete description of the slightly varying odorant composition of unheated goat milk that was obtained directly from two different farms during two seasons. Such detailed information on the odorant composition has, to the best of our knowledge, not been reported in literature before. A complete change of the odor profile between winter and summer milk, as reported by Fedele et al.,[11] was not confirmed by our study.

**Heat-Induced Changes in Goat Milk Odor and Odorant Composition.** Odor profiles of heated milks were also investigated in a comparative approach (pasteurized vs UHT-treated vs sterilized). Caramel-like, vanilla-like, and nutty attributes were found to increase as the heat treatment increased, whereas cooked milk-like, goat-like, and stable-like aroma notes were less perceivable. However, sterilized milks showed not only the highest FD factors in case of, for example, furaneol, maltol, or various lactones, but also of 4-etC8 (goat-like) and some stable-like compounds (4-meC8, skatol), as well as sweaty/sulfurous compounds (pentanoic acid, dimethyl trisulfide). Still, obviously a sensory dominance of the heating-related aroma notes results in the overall profile that might be related to additive or synergistic effects of the increased odorants such as maltol and furaneol, and the lactones; such phenomenon can be often observed in foods but would need to be further substantiated by quantification and aroma reconstitution experiments as done in other cases.[36,38]

In our study, furaneol was only detected in sterilized milk samples but with very high intensity (FD 8192), while 4-etC8, skatol, and phenylacetic acid were dominant odorants in all heated milks. 4-etC8 and skatol were also found among the most potent odor compounds in goats' raw milk. However, skatol was generally more intensely perceived in raw milk (~FD 2048) and 4-etC8 in UHT and sterilized milk (up to FD 4096). While skatol, as well as indol, are typically found in milk, especially from pasture-fed animals, presumably formed due to the degradation of tryptophan,[39,40] the formation of 4-etC8 is attributed to the activity of specific lipases and the specific composition of caprine milk fat.[32] Phenylacetic acid was detected in much lower intensities (FD ≤ 128) in raw milk. Its formation is assumed to derive from Strecker degradation of phenylalanine and oxidation processes.[40,41] A general overview of odorants with increased odor intensities in heated milk compared with raw goat milk is given in Figure 3.

Besides furaneol, some other compounds were only detected in heated goat milks (FD ≥ 8): octanal, 2-acetyl-1-pyrroline, dimethyl trisulfide, furfural, (*Z*)-non-2-enal, (*E*)-undec-2-enal, guaiacol, and maltol. Furaneol, as well as furfural and maltol are typically formed due to thermally induced decomposition of lactose (caramelization) or amino-carbonyl reactions in the course of the Maillard reaction.[42,43] Other thermally generated compounds identified in heated goat milk are vanillin, diacetyl, 2-acetyl-1-pyrroline, and 2-acetyl-2-thiazoline.[41] The latter substance was detected with FD < 8 in heated goat milk and thus was identified but not listed in Table 3. Other dominant odor compounds in the heated milk were methional, γ-decalactone, δ-decalactone, and γ-(*Z*)-6-dodecenolactone. Interestingly, goat milk lacks the amino acid cysteine compared with human and cow milk, which is balanced by a higher methionine content, presumably affecting flavor formation.[44] Indeed, methional is a typical product from Strecker degradation of methionine, as well as dimethyl disulfide or dimethyl trisulfide.[45] Lactones as well as saturated and unsaturated aldehydes are known from fatty acid oxidation, primarily as secondary oxidation products.[20] However, $C_{8:0}$, $C_{10:0}$, and $C_{12:0}$ δ-lactones were also reported in the context of a heat induced formation.[41] Besides δ-decalactone and δ-dodecalactone, we also identified δ-octalactone in heated goat milks, but in lower intensities than for the other substances shown in Table 3 (FD <8).

Moreover, 3-methylphenol (*m*-cresol) was detected in raw and heated goat's milk as well as 3-ethyphenol and 3-propylphenol, all showing leather-like, medicinal odor descriptions. Skjevdal[8] cited a Norwegian report on *o*- and *m*-cresols where both compounds were identified in whey cheese from goat's milk but not from cow's milk origin. According to Kilic and Lindsay,[46] the presence of 3-ethylphenols might contribute to the strong, animal-like flavor of goat milk. To the best of our knowledge, 3-propylphenol was not reported in goat milk products before. However, it was identified as a conjugated compound in cow's milk.[47] 1-Benzopyran-2-one (coumarin) was found in raw milks and with increasing FD values in heated goat milks (Figure 3). To our knowledge, this compound was not identified in goat milk or other ruminant milks before. However, the biosynthesis of coumarin in *Melilotus albus*, a legume used for forage, has been reported in previous studies, as well as the observation that the legume's sweet flavor is transferred into cow's milk.[48,49] Thus, a forage-based origin of coumarin can be assumed.

Apart from that, some odorants showed highest intensities in pasteurized milk samples but decreased with temperature and time of heat treatment: dimethyl disulfide, guaiacol, and γ-undecalactone (Figure 3). Those compounds were not detected or were detected with just low intensity, in the raw milk samples. Other odorants, like butanoic acid, (*E*,*E*)-nona-2,4-dienal, hexanoic acid, nonanoic acid, and an unknown compound with high FD factor (RI > 2900) were detected with high intensities in raw milk samples but decreased from pasteurized to UHT-treated and sterilized milk samples. Oxidations (e.g., fatty acid oxidation) and other thermally induced reactions might have been responsible for chemical rearrangements or degradation processes of those odorants. Thereby, it needs to be kept in mind that many odorants that are formed in the course of thermal and oxidative processes are labile themselves so that they can undergo further degradation if thermal or oxidative stress is continued.[50]

Overall, the main odorants in goat's milk were found to show high analogies to the most potent odorants reported in cow's UHT milk: a variety of lactones and acids, besides some sweet, sulfurous, and roasty compounds like methional (cooked potato-like), furaneol (caramel-like), 2-acetyl-1-pyrroline, 2-acetyl-2-thiazoline, furfural (roasty, popcorn-like), dimethyl disulfide, and dimethyl trisulfide (sweaty, cabbage-like).[15−17] However, since literature lacks information not only on raw goat milk odorants but also on detailed odorant investigations in heated goat milk, seven potent odorants were reported in our study for the first time in heated goat's milk (in addition to the large amount of odorants that were described in section Characterization of Goat Milks' Odorant Composition in raw goat's milk already, but were also reported in our study for the first time, these are dimethyl trisulfide, furfural, (*Z*)-non-2-enal, (*E*)-undec-2-enal, guaiacol, maltol, and furaneol.

Overall, the aim of this study was to characterize and identify the most potent odorants in goat's milk before and after heat treatment. More than 50 odor-active VOCs were described and up to 45 of them were unequivocally identified in the different milks. Of these substances, a total of 16 compounds are reported here for the first time for raw and heated goat's milk that were not described in any goat milk product before. Hence, comprehensive information on goat's milk aroma quality and aroma changes during the year and with thermal treatment is provided in this study, information that has not been as comprehensively reported before. Thus, our findings will close a gap in literature on important quality aspects of goat milk, which is increasingly consumed beside goat cheese worldwide, not least because new markets recently sprang up, like the use of goat milk in infant formulas.

## AUTHOR INFORMATION

### Corresponding Author

*Prof. Dr. Andrea Buettner. Tel: +49-8161-491-715. Fax: +49-8161-491-777. E-mail: andrea.buettner@ivv.fraunhofer.de.

### Funding

The research activities on the topic of the present study were funded by a Ph.D. scholarship of the Heinrich-Stockmeyer foundation (Bad Rothenfelde, Germany). The authors would like to thank the foundation for this support.

### Notes

The authors declare no competing financial interest.

## ABBREVIATIONS USED

AEDA, aroma extract dilution analysis; APA, aroma profile analysis; CI, chemical ionization; EI, electron impact; FA, fatty acid; FD, flavor dilution; FID, flame ionization detector; GC/O, gas chromatography/olfactometry; MUFA, monounsaturated fatty acid; o, orthonasal; PUFA, polyunsaturated fatty acid; r, retronasal; RI, retention index; S, summer milk; SAFE, solvent assisted flavor evaporation; SFA, saturated fatty acid; UHT, ultrahigh temperature; VOC, volatile organic compound; W, winter milk; 2D-HRGC-MS/O, two-dimensional high resolution gas chromatography−mass spectrometry/olfactometry; 4-etC8, 4-ethyloctanoic acid; 4-meC8, 4-methyloctanoic acid

## REFERENCES


(1) Silanikove, N.; Leitner, G.; Merin, U.; Prosser, C. G. Recent advances in exploiting goat's milk: Quality, safety and production aspects. *Small Ruminant Res.* **2010**, *89*, 110−124.

(2) Le Quere, J. L.; Pierre, A.; Riaublanc, A.; Demaizieres, D. Characterization of aroma compounds in the volatile fraction of soft goat cheese during ripening. *Lait* **1998**, *78*, 279−290.

(3) Whetstine, M. E. C.; Karagul-Yuceer, Y.; Avsar, Y. K.; Drake, M. A. Identification and quantification of character aroma components in fresh Chevre-style goat cheese. *J. Food Sci.* **2003**, *68*, 2441−2447.

(4) Moio, L.; Dekimpe, J.; Etievant, P.; Addeo, F. Neutral volatile compounds in the raw milks from different species. *J. Dairy Res.* **1993**, *60*, 199−213.

(5) Moio, L.; Langlois, D.; Etievant, P.; Addeo, F. Powerful odorants in bovine, ovine, caprine and water buffalo milk determined by means of gas chromatography-olfactometry. *J. Dairy Res.* **1993**, *60*, 215−222.

(6) Whetstine, M. E. C.; Drake, M. A. Flavor Characteristics of Goat Milk and Other Minor Species Milk Products. In *Handbook of Milk of Non-Bovine Mammals*; Park, Y. W., Haenlein, G. F. W., Eds.; Blackwell Publishing: Oxford, U.K., 2006; Vol. *1*, pp 107−120.

(7) Le Quere, J. L.; Septier, C.; Demaizieres, D.; Salles, C. Identification and sensory evaluation of the character impact compounds of goat cheese flavor. In *Flavor Science: Recent Developments*; Taylor, A. J., Mottram, D. S., Eds.; The Royal Society of Chemistry: Cambridge, U.K., 1996; pp 325−330.

(8) Skjevdal, T. Flavour of goat's milk: A review of studies on the sources of its variations. *Livest. Prod. Sci.* **1979**, *6*, 397−405.

(9) Ha, J. K.; Lindsay, R. C. Contributions of Cow, Sheep, and Goat Milks to Characterizing Branched-Chain Fatty Acid and Phenolic Flavors in Varietal Cheeses. *J. Dairy Sci.* **1991**, *74*, 3267−3274.

(10) Boelens, H.; Haring, H. G.; De Rijke, D. Threshold values of and human preferences for 4-ethyloctanoic and 3-methylbutanoic acids. *Perfum. Flavor.* **1983**, *8*, 71−74.

(11) Fedele, V.; Rubino, R.; Claps, S.; Sepe, L.; Morone, G. Seasonal evolution of volatile compounds content and aromatic profile in milk and cheese from grazing goat. *Small Ruminant Res.* **2005**, *59*, 273−279.

(12) Ormiston, E. E.; Herreid, E. O. Effect of Sterilization and Storage on Flavor of Goat Milk. *J. Dairy Sci.* **1965**, *48*, 501.

(13) Christensen, K. R.; Reineccius, G. A. Gas Chromatographic Analysis of Volatile Sulfur Compounds from Heated Milk Using Static Headspace Sampling. *J. Dairy Sci.* **1992**, *75*, 2098−2104.

(14) Zabbia, A.; Buys, E. M.; De Kock, H. L. Undesirable Sulphur and Carbonyl Flavor Compounds in UHT Milk: A Review. *Crit. Rev. Food Sci. Nutr.* **2011**, *52*, 21−30.

(15) Czerny, M.; Schieberle, P. Influence of the polyethylene packaging on the adsorption of odour-active compounds from UHT-milk. *Eur. Food Res. Technol.* **2007**, *225*, 215−223.

(16) Colahan-Sederstrom, P. M.; Peterson, D. G. Inhibition of Key Aroma Compound Generated during Ultrahigh-Temperature Processing of Bovine Milk via Epicatechin Addition. *J. Agric. Food Chem.* **2005**, *53*, 398−402.

(17) Iwatsuki, K.; Mizota, Y.; Kubota, T.; Nishimura, O.; Masuda, H.; Sotomiya, K.; Tomita, M. Evaluation of aroma of pasteurized and UHT processed milk by aroma extract dilution analysis. *J. Jpn. Soc. Food Sci. Technol.* **1999**, *46*, 587−597.

(18) DGF Standard Methods Section C − Fats C-III 19 (99), Bestimmung des Fettgehaltes nach Caviezel (R) (Schnellmethode). http://www.wiley-vch.de/vch/journals/2114/stand_meth/caviez.pdf (13.08.2014).

(19) Engel, W.; Bahr, W.; Schieberle, P. Solvent assisted flavour evaporation - a new and versatile technique for the careful and direct isolation of aroma compounds from complex food matrices. *Eur. Food Res. Technol.* **1999**, *209*, 237−241.

(20) Siefarth, C.; Serfert, Y.; Drusch, S.; Buettner, A. Comparative Evaluation of Diagnostic Tools for Oxidative Deterioration of Polyunsaturated Fatty Acid-Enriched Infant Formulas during Storage. *Foods* **2013**, *3*, 30−65.

(21) Van Den Dool, H.; Kratz, P. D. A generalization of the retention index system including linear temperature programmed gas-liquid partition chromatography. *J. Chromatogr.* **1963**, *11*, 463−471.

(22) Raynal-Ljutovac, K.; Lagriffoul, G.; Paccard, P.; Guillet, I.; Chilliard, Y. Composition of goat and sheep milk products: An update. *Small Ruminant Res.* **2008**, *79*, 57−72.

(23) Alonso, L.; Fontecha, J.; Lozada, L.; Fraga, M. J.; Juarez, M. Fatty acid composition of caprine milk: Major, branched-chain, and trans fatty acids. *J. Dairy Sci.* **1999**, *82*, 878−884.

(24) Eknaes, M.; Kolstad, K.; Volden, H.; Hove, K. Changes in body reserves and milk quality throughout lactation in dairy goats. *Small Ruminant Res.* **2006**, *63*, 1−11.

(25) Park, Y. W.; Juárez, M.; Ramos, M.; Haenlein, G. F. W. Physico-chemical characteristics of goat and sheep milk. *Small Ruminant Res.* **2007**, *68*, 88−113.

(26) Iverson, J. L.; Sheppard, A. J. Detection of Adulteration in Cow, Goat, and Sheep Cheeses Utilizing Gas-Liquid Chromatographic Fatty Acid Data. *J. Dairy Sci.* **1989**, *72*, 1707−1712.

(27) Lock, A. L.; Garnsworthy, P. C. Seasonal variation in milk conjugated linoleic acid and Δ9-desaturase activity in dairy cows. *Livest. Prod. Sci.* **2003**, *79*, 47−59.

(28) Butler, G.; Nielsen, J. H.; Slots, T.; Seal, C.; Eyre, M. D.; Sanderson, R.; Leifert, C. Fatty acid and fat-soluble antioxidant concentrations in milk from high- and low-input conventional and organic systems: seasonal variation. *J. Sci. Food Agric.* **2008**, *88*, 1431−1441.

(29) Bakke, H.; Steine, T.; Eggum, A. Flavor score and content of free fatty-acids in goat milk. *Acta Agric. Scand.* **1977**, *27*, 245−249.

(30) Ha, J. K.; Lindsay, R. Volatile Branched-chain Fatty Acids and Phenolic Compounds in Aged Italian Cheese Flavors. *J. Food Sci.* **1991**, *56*, 1241−1247.

(31) Sugiyama, T.; Sasada, H.; Masaki, J.; Yamashita, K. Unusual fatty acids with specific odor from mature male goat. *Agric. Biol. Chem.* **1981**, *45*, 2655−2658.

(32) Ha, J. K.; Lindsay, R. C. Release of volatile branched-chain and other fatty acids from ruminant milk fats by various lipases. *J. Dairy Sci.* **1993**, *76*, 677−690.

(33) Carunchia Whetstine, M. E.; Drake, M. The Flavor and Flavor Stability of Skim and Whole Milk Powders. In *Flavor of Dairy Products*; Cadwallader, K. R., Drake, M., McGorrin, R. J., Eds.; ACS Symposium Series; American Chemical Society: Washington, DC, 2007; Vol. *971*, pp 217−251.

(34) Wong, E.; Nixon, L. N.; Johnson, C. B. Volatile medium chain fatty acids and mutton flavor. *J. Agric. Food Chem.* **1975**, *23*, 495−498.

(35) Masanetz, C.; Grosch, W. Hay-like off-flavour of dry parsley. *Z. Lebensm.-Unters. Forsch.* **1998**, *206*, 114−120.

(36) Grosch, W. Evaluation of the key odorants of foods by dilution experiments, aroma models and omission. *Chem. Senses* **2001**, *26*, 533−545.

(37) Lorenz, S.; Buettner, A.; Ender, K.; Nürnberg, G.; Papstein, H.-J.; Schieberle, P.; Nürnberg, K. Influence of keeping system on the fatty acid composition in the longissimus muscle of bulls and odorants formed after pressure-cooking. *Eur. Food Res. Technol.* **2002**, *214*, 112−118.

(38) Hinterholzer, A.; Lemos, T.; Schieberle, P. Identification of the key odorants in raw French beans and changes during cooking. *Z. Lebensm.-Unters. Forsch. A* **1998**, *207*, 219−222.
(39) Bendall, J. G. Aroma Compounds of Fresh Milk from New Zealand Cows Fed Different Diets. *J. Agric. Food Chem.* **2001**, *49*, 4825−4832.
(40) Yvon, M.; Rijnen, L. Cheese flavour formation by amino acid catabolism. *Int. Dairy J.* **2001**, *11*, 185−201.
(41) Scanlan, R.; Lindsay, R.; Libbey, L.; Day, E. Heat-induced volatile compounds in milk. *J. Dairy Sci.* **1968**, *51*, 1001−1007.
(42) Kroh, L. W. Caramelisation in food and beverages. *Food Chem.* **1994**, *51*, 373−379.
(43) Newton, A. E.; Fairbanks, A. J.; Golding, M.; Andrewes, P.; Gerrard, J. A. The role of the Maillard reaction in the formation of flavour compounds in dairy products−not only a deleterious reaction but also a rich source of flavour compounds. *Food Funct.* **2012**, *3*, 1231−1241.
(44) Rutherfurd, S. M.; Moughan, P. J.; Lowry, D.; Prosser, C. G. Amino acid composition determined using multiple hydrolysis times for three goat milk formulations. *Int. J. Food Sci. Nutr.* **2008**, *59*, 679−690.
(45) Ballance, P. Production of volatile compounds related to the flavour of foods from the Strecker degradation of DL-methionine. *J. Sci. Food Agric.* **1961**, *12*, 532−536.
(46) Kilic, M.; Lindsay, R. C. Distribution of Conjugates of Alkylphenols in Milk from Different Ruminant Species. *J. Dairy Sci.* **2005**, *88*, 7−12.
(47) Brewington, C. R.; Parks, O. W.; Schwartz, D. P. Conjugated compounds in cow's milk. II. *J. Agric. Food Chem.* **1974**, *22*, 293−294.
(48) Stoker, J.; Bellis, D. The biosynthesis of coumarin in *Melilotus alba*. *J. Biol. Chem.* **1962**, *237*, 2303−2305.
(49) Honkanen, E.; Karvonen, P.; Virtanen, A. I. Studies on the transfer of some flavor compounds to milk. *Acta Chem. Scand.* **1964**, *18*, 612−618.
(50) Belitz, H.-D.; Grosch, W.; Schieberle, P. *Lehrbuch der Lebensmittelchemie*; Springer: Berlin, Heidelberg, 2008; Vol. *6*.
(51) Karagül-Yüceer, Y.; Cadwallader, K. R.; Drake, M. Volatile flavor components of stored nonfat dry milk. *J. Agric. Food Chem.* **2002**, *50*, 305−312.
(52) Van Leuven, I.; Van Caelenberg, T.; Dirinck, P. Aroma characterisation of Gouda-type cheeses. *Int. Dairy J.* **2008**, *18*, 790−800.

volatiles and chemical reactions responsible for the aroma changes after sunlight exposure.

## MATERIALS AND METHODS

**Standards and Reagents.** A standard series of $C_8$−$C_{20}$ and $C_{10}$−$C_{40}$ alkanes used for retention index (RI) determination were obtained from Sigma-Aldrich Co. Ltd. (St. Louis, MO, USA). Internal standards of ethyl 2-methylbutyrate and ethyl benzoate were also purchased from Sigma-Aldrich Co. Ltd. HPLC grade *n*-hexane was purchased from the Oceanpak Chemical Co. (Gothenburg, Sweden). Volatile standards, including α-pinene, sabinene, β-pinene, and D-limonene, etc. (listed in Table 2), were purchased from Sigma-Aldrich Co. Ltd., Alfa Aesar Co. Ltd. (Heysham, Lancashire, U.K.), Ormah Chemical Inc. Tic Co. (TIC, Hadimkoy, Istanbul), and Penta Manufacturing Co. (PMC, Livingston, NJ, USA). Other chemicals were obtained from Sinopharm Chemical Reagent Co. Ltd. (Shanghai, China).

**Preparation of the Essential Oils Exposed to Sunlight, Oxygen, and Heat.** GuanXi pummelo, a native pummelo species in southeastern China, was harvested by Fujian GuoNong Agricultural Development Co. (PingHe county, Fujian province, China) in October 2013. The fresh flavedo with oil sacs was mechanically pressed to squeeze the oil into a tube containing icy brine water. Then, the oil−water mixture was centrifuged at 13500*g* for 5 min to collect the oil, subsequently dehydrated with $Na_2SO_4$, and immediately stored at −20 °C in a freezer. To differentiate the effects of sunlight, heat, and oxygen on the aroma changes of the EO, the EO was pipetted into small glass tubes with screw caps and respectively treated by the following procedure.

(1) The fresh EO (sample 1) was stored at −20 °C until sensory evaluation and GC-MS analysis. This sample was used as a control for chemical comparison.

(2) For the sunlight-exposed EO under $N_2$ protection (sample 2) the EO was saturateded with pure nitrogen and then exposed under sunlight (i.e., sun) for 72 h at ambient temperature (30 °C) and stored at −20 °C until analysis. This sample was used to test the effect of sunlight (and/or UV) without oxygen on the volatile changes.

(3) To obtain the EO exposed to both sunlight and oxygen (sample 3), the EO was saturated with air and then exposed to sunlight for 72 h simultaneously with the second group. This sample was used to test the combined effect of sunlight and oxygen on the volatile changes.

(4) To obtain the oxygen-exposed EO in darkness (sample 4), the glass tube that contained the EO was filled with air and covered with an aluminum film to avoid exposure to sunlight for 72 h simultaneously with the second group. This sample was used to test the effect of oxygen without sunlight (or UV) on the volatile changes.

(5) Sample 5, the EO heated in darkness under $N_2$ protection, was obtained in a glass tube that contained the EO covered with an aluminum film and filled with nitrogen, followed by incubation at 40 °C in a water bath for 72 h. This sample was used to test the effect of temperature without sunlight and oxygen on the volatile changes.

**Sensory Evaluation of EO Samples after Different Treatments.** An aliquot of 100 μL of the pummelo EO was diluted with 900 μL of ethanol. Thereafter, 10 μL of the dilution was pipetted onto a fragrance test strip and then dried in the open air for 120 s, immediately followed by the sensory evaluation at room temperature under clean air conditions.

The sensory evaluation was conducted by 18 trained panelists, including 8 women and 7 men in a range of 20−30 years old, and another 3 trained panelists including 1 woman and 2 men aged in a range of 30−40 years old. The sensory evaluation adopted a 10-point scale according to the relevant references (refs 14, 19, and 20) and ISO 8589, in which 0 indicates an unperceived attribute intensity and 9 indicates a very strong attribute intensity. Before the sensory evaluation, the panelists were instructed to be familiar with the odor of standards and, as necessary, during the session. The panelists were asked to rate the EOs in a random order for sweet, minty, herbaceous, lemon, floral, and oily notes and gave a score within 0−9. Among these notes, herbaceous and lemon aromas contributed to the fresh odor; sweet and floral aromas contributed to the ripened odor (reduced freshness), whereas oily aroma was an off-flavor like machinery oil or resinous.[21] Mean values were calculated after corrections of effects of session and removal of outliers. An interval gap of 20 s was kept, which was sufficient between individual odor assessments.

**GC-MS Analysis of the Volatiles of Different EO Samples.** Each EO sample (1 μL) was diluted at two degrees. The 5000 times dilution was used for the analysis of the most abundant volatiles, that is, D-limonene and β-myrcene, whereas the 100 times dilution was used for the analysis of the volatiles other than D-limonene and β-myrcene by a gas chromatograph coupled with a mass spectrometer (GC-MS, Shimadzu, QP 2010 plus). Helium was used as the carrier gas, and the column flow rate was 3 mL/min. The injector temperature was set at 250 °C, and the split ratio was 1:5. The oven temperature for the Rtx-5MS column was initially programmed from 50 °C for 3 min, then increased to 220 °C at the rate of 5 °C/min, and held at this temperature for 3 min. The oven temperature for another column (i.e., Rtx-wax) was initially programmed from 30 °C for 3 min, then increased to 200 °C at the rate of 2 °C/min, and held at this temperature for 3 min. The temperatures of the ion source and the interface were set at 250 and 250 °C, respectively. The MS spectrum was operated in a positive electron ionization (EI) mode at 70 eV, and the MS spectra were recorded within a $m/z$ range from 29 to 500 amu.

Two columns, that is, an Rtx-5MS column (60 m × 0.32 mm × 0.25 μm, Restek Corp., Bellefonte, PA, USA) and an Rtx-wax column (60 m × 0.32 mm × 0.25 μm, Restek Corp.), were used to separate and identify the volatiles with a cross-check and comparison of the Kovats retention indices (RI). Most of the volatiles were identified by matching their MS spectra and RI values on both columns to those of standards. Some other volatiles that currently lack standards were temporarily identified by matching their MS spectra to those in the Mass Spectral Library (NIST08, NIST08s, FFNSC1.3) and their RI values to those from relevant references or the database book (Table 2). The volatile with a matching standard was quantified according to their respective calibration curves using the internal standard method. The concentrations of other volatiles were estimated using the calibration curve of the internal reference of ethyl benzoate.

**Analysis of the Odor of the Volatiles and Calculation of the Odor Activity Values.** Single standards, that is, α-pinene, sabinene, β-myrcene, D-limonene, *cis*- and *trans*-limonene oxides mixture (ratio = 1.6:1), *cis*- and *trans*-linalool oxides mixture (ratio = 1:1), neral and geranial mixture (ratio = 0.7:1), octanal, linalool, nonanal, decanal, carvone, geranyl acetate, nootkatone, and α-terpineol, were tested through sensory evaluation by three panelists. Each standard (0.5−50 μL) was properly diluted in propylene glycol and adjusted to a 10 mL volume, followed by sniffing their odors. Afterward, OAVs were calculated by dividing the concentrations of the aroma active compounds with their respective odor threshold values in water obtained from the corresponding literature.[20,22,23]

**Verifying the Contributions of Volatiles to the Changed Aroma.** The omission test was used to investigate the contributions of some aroma-impact volatiles to the change of the aroma profile. A formulated flavoring model sample (FMS) that represented the aroma of the fresh EO (FMS 0) was prepared with the following authentic standard chemicals (ASCs), including β-myrcene (220,000 μg/mL), octanal (500 μg/mL), D-limonene (500,000 μg/mL), linalool (2700 μg/mL), decanal (1000 μg/mL), neral and geranial mixture (17,000 μg/mL, ratio = 0.7:1), dodecanal (350 μg/mL), and nootkatone (1000 μg/mL), according to their concentrations in the fresh EO. Other series of artificial model samples were respectively composed by either adding or removing some volatiles from the model sample (FMS 0) according to the OAVs of the EOs that had been treated with sunlight exposure, oxygen exposure, and heat. In detail, (1) FMS 1 was composed by adding 3000 μg/mL of *cis*- and *trans*-linalool oxides mixture (ratio = 1:1), 10,000 μg/mL of *cis*- and *trans*-limonene oxides mixture (ratio = 1.6:1) into the model sample of the fresh EO (FMS 0) that had pre-excluded 13,000 μg/mL of neral and geranial mixture to simulate the aroma of the sunlight-exposed EO; (2) FMS 2 was formulated by adding 200 μg/mL of *cis*- and *trans*-linalool oxides mixture and 200 μg/mL of *cis*- and *trans*-limonene oxides mixture into

**Table 1. Sensory Evaluation and Average PCA Scores of the Essential Oils[a]**

| | sensory evaluation scores | | | | | | | PCA scores[b] | |
|---|---|---|---|---|---|---|---|---|---|
| EO sample | sweet | minty | herbaceous | lemon | floral | oily | aromatic profile | PC1 (58%) | PC2 (25%) |
| fresh | 1.6 b | 2.8 a | 7.4 a | 8.2 a | 1.8 b | 0.2 c | fresh pummelo | 1.19 | −0.41 |
| sunlight, $N_2$ | 1.5 b | 1.2 b | 1.6 c | 1.5 c | 1.1 b | 8.3 a | off-flavor, soapy | −0.19 | −0.36 |
| sunlight, $O_2$ | 1.4 b | 1.4 b | 1.5 c | 1.4 c | 1.5 b | 8.2 a | off-flavor, soapy | −1.07 | −0.26 |
| dark, $O_2$ | 1.8 b | 2.2 a | 7.6 a | 7.2 ab | 2.2 b | 1.5 b | freshness reduced | 0.79 | 0.03 |
| 40 °C, dark, $N_2$ | 2.5 a | 2.0 ab | 5.8 b | 6.7 b | 3.2 a | 1.0 b | freshness reduced, ripened | 0.30 | 1.11 |

[a]Different letters (a−d) in the same column indicate the data ahead have statistical differences ($p < 0.05$). In the column "EO samples", "sunlight, $N_2$" indicates the EO that was exposed under sunlight but was free from oxygen, "sunlight, $O_2$" indicates the EO exposed in both sunlight and oxygen, "dark $O_2$" indicates the EO that was exposed in oxygen but covered with an aluminum film under sunlight, "40 °C, dark, $N_2$" indicates the EO that underwent heating but was free from sunlight and oxygen. The panelists were trained to be familiar with the odors using the standard series. In short, the odors of limonene oxides and carvone were used to train panelists to score sweet and minty, respectively. A neral and geranial mixture was used as the herbaceous note, a nootkatone and D-limonene mixture was used as the lemon note, a geraniol and $\beta$-myrcene mixture was used as the floral note, and a linalool oxides and $\alpha$-terpineol mixture was used as the oily note. [b]PCA scores were the average scores of PC1 and PC2.

FMS 0, which was used to simulate the oxygen-exposed EO; (3) FMS 3 was prepared by adding 700 $\mu$g/mL of *cis*- and *trans*-limonene oxides mixture into FMS 0 to simulate the heated EO. Besides, other experiments to test the impacts of aroma constituents in EOs included (4) FMS 4 was composed by adding 3000 $\mu$g/mL of *cis*- and *trans*-linalool oxides mixture into FMS 0; (5) FMS 5 was composed by adding 400 $\mu$g/mL of $\alpha$-terpineol into FMS 0; (6) FMS 6 was prepared by removing 14,000 $\mu$g/mL of neral and geranial mixture from FMS 0; and (7) FMS 7 was modified by subtracting 400 $\mu$g/mL nootkatone from FMS 0. Then, the artificially reconstituted samples (FMS 0−7) were analyzed by the sensory evaluation, which was subsequently compared via principal component analysis (PCA).

**Comparison of the Effects of UV and Daylight Lamp Irradiation on the EOs.** The UV-exposed EOs with or without nitrogen gas protection were exposed under irradiation of two UV modulator tubes (FL20SE×2 sunlamps with peak emission at 305 nm; Toshiba Medical Supply, Tokyo, Japan) for 96 h at 30 °C. The electronic power was 40 W, and the distance between the light and the samples was 30 cm. Meanwhile, the same EOs with or without nitrogen gas protection were exposed under a daylight modulator tube (FL40T8DY, Toshiba Medical Supply) for 96 h at 30 °C. The electronic power was 40 W, and the distance between the light and samples was 30 cm. After the treatments, the EOs were subjected to the sensory evaluation and GC-MS analysis.

**Verifying the Chemical Reactions Induced by UV Irradiation.** The single standards, for example, D-limonene and $\beta$-myrcene, were saturated with nitrogen and exposed under irradiation of a UV modulator tube for 96 h at 30 °C, followed by GC-MS analysis to track the chemical changes using the Rtx-5MS column. The oven temperature was initially programmed from 50 °C for 3 min, then increased to 220 °C at the rate of 15 °C/min, and held at this temperature for 3 min.

**Statistical Analysis.** The data from sensory evaluation was analyzed by reliability and validity analysis using SPSS-IBM 19.0 software. The mean values were calculated after a correction for session, panelist effects, and removal of outliers (five of the data). PCA was conducted using the method of biplot visualization (SPSS-IBM 19.0 software), which was used to show relationships between the flavor attributes. The PCA was under varimax orthogonal rotation.

The significant statistical analyses were conducted according to previous methods[13,24] (SPSS-IBM 19.0 software, Microsoft Excel 2013). Cluster analysis was used to classify the volatiles and OAVs through the cosine correlation metric (SPSS-IBM 19.0 software).

## RESULT AND DISCUSSION

**Investigation of the Aroma Changes by Sensory Evaluation.** Sensory evaluation is a commonly used technique to evaluate the human perception of aroma attributes of many flavoring products. For example, it has been used to characterize the aromatic profiles of EOs.[17] By this method

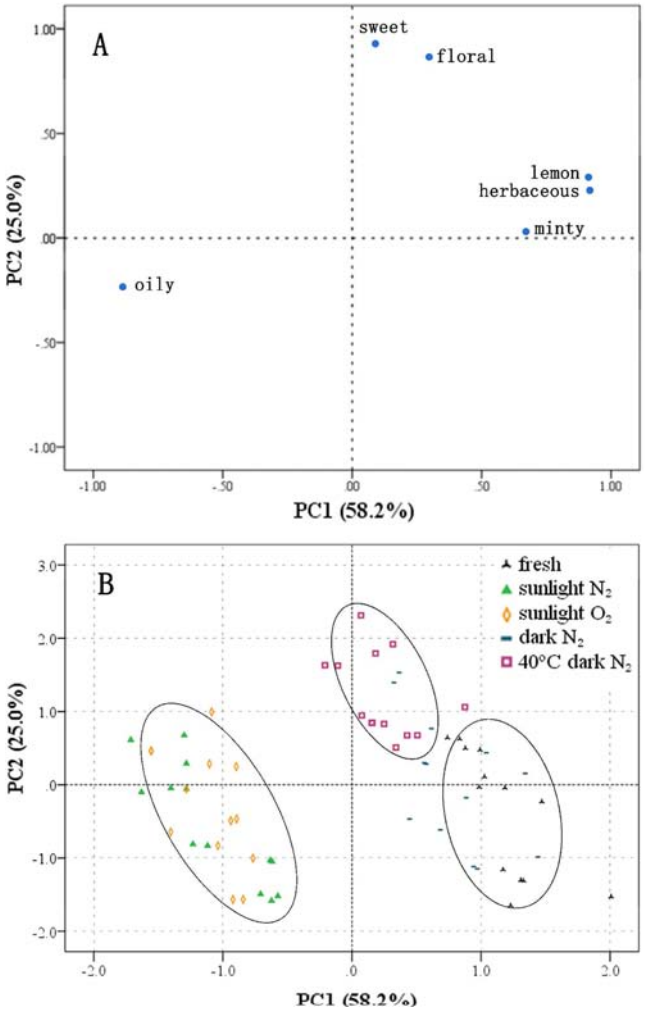


**Figure 1.** PCA scatter plot of the note of the EOs (A) and scatter diagram (B).

and/or in combination with other instrumental methods, the citrus EO was found to be able to maintain its natural aroma when stored at −20 °C.[16,17] In this study, the fresh pummelo EO (sample 1) showed a strong natural fresh flavor, whereas the sunlight-exposed EOs, no matter whether they were protected by $N_2$ (sample 2) or exposed under $O_2$ (sample 3), showed strong off-flavors and a soapy odor. By contrast, the oxygen-exposed EO in darkness (sample 4) possessed a

**Table 2. Volatile Calibration Equations and Identification of the Volatiles in the Essential Oils**

| | | Rtx-5 MS | | | Rtx-wax | | | | | | | | | |
|---|---|---|---|---|---|---|---|---|---|---|---|---|---|---|
| no. | volatile | RT[a] | RI[b] | RI[c] | RT | RI[d] | RI[e] | characteristic fragment | ref[f] | range (μg/mL) | curve[g] | $R^2$ | CF[h] | $R^i$ |
| 1 | α-pinene | 8.13 | 934 | 938 | 2.97 | 1027 | 1027 | 136, 93, 41 | Std R12 | 0.08−84.3 | $Y = 0.01262 + 0.01933x$ | 0.998 | 51.7 | 91 |
| 2 | sabinene | 9.19 | 974 | 979 | 5.46 | 1123 | 1119 | 136, 93, 41 | Std R12 | 0.07−66.0 | $Y = 0.00536 + 0.01260x$ | 1 | 79.4 | 89 |
| 3 | β-pinene | 9.31 | 977 | 982 | 4.9 | 1102 | 1108 | 136, 93, 41 | Std R12 | 0.09−85.3 | $Y = 0.01349 + 0.02320x$ | 0.998 | 43.1 | 95 |
| 4 | β-myrcene | 9.65 | 992 | 994 | 6.78 | 1158 | 1156 | 136, 93, 41 | Std R12 | 2.25−72.0 | $Y = -0.04046 + 0.02295x$ | 1 | 43.6 | 101 |
| 5 | octanal | 9.95 | 1004 | 1014 | 12.63 | 1286 | 1276 | 99, 44, 43 | Std R12 | 0.08−16.2 | $Y = 0.00231 + 0.00619x$ | 0.999 | 162 | 100 |
| 6 | α-phellandrene | 10.06 | 1005 | 1011 | 7.02 | 1164 | 1177 | 136, 93 | Std R12 | 0.08−16.1 | $Y = 0.00727 + 0.01762x$ | 0.998 | 56.8 | 103 |
| 7 | pseudolimonene | 10.22 | 1011 | 1004 | 7.35 | 1172 | 1184 | 136, 93 | R9 | | | | | |
| 8 | D-limonene | 10.73 | 1030 | 1038 | 7.95 | 1187 | 1196 | 99, 44, 43 | Std R12 | 2.55−81.5 | $Y = -0.03730 + 0.02466x$ | 0.998 | 40.6 | 102 |
| 9 | *cis*-β-ocimene | 11.27 | 1048 | 1055 | 10.54 | 1246 | 1239 | 136, 93, 41 | Std R12 | 0.07−73.8 | $Y = 0.00081 + 0.00544x$ | 1 | 107 | 94 |
| 10 | *cis*-linalool oxide | 12.05 | 1078 | 1078 | 21.38 | 1439 | 1440 | 59, 41 | Std R12 | 0.09−91.2 | $Y = -0.00020 + 0.00799x$ | 0.999 | 125 | 105 |
| 11 | *trans*-linalool oxide | 12.60 | 1090 | 1093 | 22.53 | 1458 | 1469 | 59, 41 | Std R12 | 0.09−91.2 | $Y = -0.00112 + 0.00790x$ | 1 | 130 | 94 |
| 12 | terpinolene | 12.65 | 1092 | 1090 | 12.18 | 1277 | 1269 | 150, 69, 41 | Std R12 | 0.07−68.8 | $Y = 0.00254 + 0.01056x$ | 0.999 | 94.7 | 89 |
| 13 | linalool | 12.79 | 1102 | 1107 | 28.26 | 1554 | 1557 | 136, 41 | Std R12 | 0.08−84.3 | $Y = -0.00167 + 0.00823x$ | 1 | 122 | 94 |
| 14 | perillene | 12.86 | 1104 | 1102 | 20.06 | 1417 | 1431 | 136, 93 | Std R8 | 0.07−46.3 | $Y = -0.00124 + 0.0134x$ | 0.998 | 71 | 99 |
| 15 | nonanal | 12.92 | 1105 | 1116 | 18.74 | 1394 | 1387 | 57, 44, 43 | Std R12 | 0.08−15.7 | $Y = 0.00209 + 0.00945x$ | 1 | 106 | 100 |
| 16 | α-pinene oxide | 13.27 | 1122 | 1115 | 16.31 | 1355 | 1365 | 137, 67, 41 | Std R9 | 0.04−16.5 | $Y = 0.00054 + 0.00859x$ | 0.998 | 119 | 96 |
| 17 | *cis*-limonene oxide | 13.86 | 1126 | 1134 | 21.36 | 1440 | 1451 | 152, 43 | Std R12 | 0.04−8.7 | $Y = -0.00187 + 0.00177x$ | 1 | 565 | 94 |
| 18 | *trans*-limonene oxide | 13.99 | 1141 | 1139 | 22.92 | 1465 | 1472 | 152, 43 | Std R12 | 0.05−9.3 | $Y = -0.00047 + 0.0028x$ | 1 | 354 | 98 |
| 19 | chrysanthemol | 14.34 | 1150 | 1163 | 34.67 | 1667 | 1684 | 123, 81, 41 | Std R34 | 0.08−16.9 | $Y = -0.00121 + 0.0072x$ | 0.996 | 141 | 103 |
| 20 | citronellal | 14.39 | 1155 | 1155 | 23.17 | 1469 | 1481 | 136, 41 | Std R8 | 0.09−17.7 | $Y = 0.00030 + 0.01038x$ | 0.999 | 96.3 | 119 |
| 21 | *trans*-verbenol | 15.03 | 1193 | 1206 | 35.91 | 1689 | 1688 | 93, 41 | Std R35 | 0.09−18.4 | $Y = 0.00271 + 0.00739x$ | 0.999 | 139 | 89 |
| 22 | α-terpineol | 15.60 | 1201 | 1206 | 35.64 | 1684 | 1680 | 109, 94, 41 | Std R12 | 0.09−18.2 | $Y = -0.00071 + 0.01520x$ | 1 | 65.8 | 102 |
| 23 | *trans*-carveol | 15.80 | 1205 | 1225 | 43.42 | 1826 | 1833 | 152, 106, 41 | Std R32 | 0.09−18.4 | $Y = -0.00449 + 0.00571x$ | 1 | 175 | 80 |
| 24 | decanal | 15.85 | 1207 | 1216 | 24.8 | 1496 | 1499 | 57, 43 | Std R12 | 0.08−80.5 | $Y = -0.00048 + 0.00376x$ | 1 | 266 | 105 |
| 25 | *cis*-carveol | 16.65 | 1223 | 1238 | 44.45 | 1849 | 1841 | 152, 106, 41 | Std R32 | 0.05−9.9 | $Y = 0.00003 + 0.00207x$ | 0.997 | 147 | 72 |
| 26 | neral | 16.91 | 1243 | 1251 | 35.31 | 1678 | 1683 | 150, 43, 41 | Std R12 | 0.04−40.1 | $Y = 0.00018 + 0.00674x$ | 0.998 | 148 | 100 |
| 27 | carvone | 17.06 | 1247 | 1251 | 37.48 | 1718 | 1731 | 150 82 58 | Std R32 | 0.10−19.0 | $Y = -0.00057 + 0.01600x$ | 1 | 62.5 | 99 |
| 28 | geranial | 17.73 | 1273 | 1281 | 36.52 | 1697 | 1686 | 150, 43, 41 | Std R12 | 0.09−86.3 | $Y = -0.00523 + 0.00961x$ | 1 | 104 | 99 |
| 29 | perilla alcohol | 18.01 | 1283 | 1299 | 48.95 | 1915 | 1892 | 134, 68, 41 | Std R36 | 0.07−32.1 | $Y = -0.00114 + 0.0101x$ | 1 | 99 | 102 |
| 30 | indole | 18.43 | 1296 | 1288 | 71.26 | 2433 | 2435 | 117, 58 | Std R12 | 0.12−120 | $Y = 0.00839 + 0.03136x$ | 0.999 | 11.9 | 87 |
| 31 | δ-elemene | 19.92 | 1341 | 1338 | 23.57 | 1475 | 1479 | 204, 93, 41 | R12 | | | | | |
| 32 | neryl acetate | 20.21 | 1366 | 1366 | 37.83 | 1724 | 1702 | 69, 43 | Std R12 | 0.09−17.3 | $Y = -0.01352 + 0.01450x$ | 1 | 69 | 100 |
| 33 | geranyl acetate | 20.71 | 1386 | 1385 | 40.32 | 1770 | 1762 | 106, 69, 41 | Std R12 | 0.09−17.5 | $Y = -0.01351 + 0.01794x$ | 1 | 55.7 | 102 |
| 34 | bourbonene | 20.99 | 1393 | 1382 | 24.08 | 1484 | 1501 | 204, 93, 41 | R14 | | | | | |
| 35 | β-elemene | 21.11 | 1396 | 1393 | 28.38 | 1556 | 1561 | 93, 41 | Std R12 | 0.09−88.5 | $Y = -0.00341 + 0.00812x$ | 0.998 | 122 | 88 |
| 36 | dodecanal | 21.38 | 1410 | 1418 | 37.41 | 1716 | 1718 | 71, 57 43 | Std R12 | 0.08−16.0 | $Y = -0.00457 + 0.00875x$ | 1 | 114 | 101 |
| 37 | β-cubebene | 21.52 | 1414 | 1435 | 27.89 | 1531 | 1539 | 204, 93, 41 | R12 | | | | | |
| 38 | *trans*-caryophyllene | 21.91 | 1425 | 1424 | 30.32 | 1589 | 1595 | 204, 93, 41 | Std R12 | 0.09−17.6 | $Y = -0.00108 + 0.00648x$ | 1 | 154 | 104 |
| 39 | perillyl acetate | 22.14 | 1423 | 1442 | 48.17 | 1895 | 1903 | 106, 79, 43 | R14 | | | | | |
| 40 | dodecenal | 22.40 | 1440 | 1466 | 45.32 | 1864 | 1856 | 204, 93, 43 | Std R33 | 0.08−15.8 | $Y = -0.00553 + 0.00617x$ | 1 | 161 | 88 |
| 41 | γ-elemene | 22.53 | 1443 | 1434 | 32.22 | 1605 | 1608 | 204, 93, 41 | Std R14 | 0.09−17.6 | $Y = -0.00572 + 0.00928x$ | 0.999 | 101 | 83 |
| 42 | α-humulene | 23.12 | 1459 | 1452 | 33.81 | 1650 | 1667 | 204, 93, 41 | Std R33 | 0.09−17.1 | $Y = -0.00241 + 0.01928x$ | 1 | 51.9 | 85 |



dx.doi.org/10.1021/jf5042946 | J. Agric. Food Chem. 2014, 62, 11818−11830

**Table 2. continued**

| | | Rtx-5 MS | | | Rtx-wax | | | | | | | | | |
|---|---|---|---|---|---|---|---|---|---|---|---|---|---|---|
| no. | volatile | RT[a] | RI[b] | RI[c] | RT | RI[d] | RI[e] | characteristic fragment | ref[f] | range ($\mu$g/mL) | curve[g] | $R^2$ | CF[h] | $R^i$ |
| 43 | germacrene D | 23.46 | 1487 | 1487 | 36.8 | 1705 | 1706 | 204, 93, 41 | R12 | | | | | |
| 44 | $\beta$-selinene | 23.85 | 1490 | 1493 | 36.02 | 1691 | 1695 | 204, 121, 93 | R32 | | | | | |
| 45 | elemol | 25.05 | 1535 | 1549 | 55.26 | 2067 | 2070 | 69, 41 | R12 | | | | | |
| 46 | *trans*-nerolidol | 25.25 | 1564 | 1567 | 52.88 | 2016 | 2025 | 69, 41 | Std R12 | 0.09−85.4 | $Y = -0.00758 + 0.00584x$ | 0.999 | 171 | 74 |
| 47 | germacrene B | 25.36 | 1567 | 1567 | 42.05 | 1801 | 1820 | 204, 93, 41 | R12 | | | | | |
| 48 | spathulenol | 27.83 | 1636 | 1589 | 57.63 | 2106 | 2119 | 119, 41 | R32 | | | | | |
| 49 | caryophyllene oxide | 27.99 | 1641 | 1595 | 51.12 | 1979 | 1960 | 93, 43, 41 | Std R32 | 0.10−64.2 | $Y = -0.00571 + 0.00646x$ | 1 | 156 | 82 |
| 50 | *cis*-farnesol | 28.85 | 1726 | 1714 | 68.99 | 2366 | 2371 | 222, 69, 41 | Std R8 | 0.09−85.4 | $Y = -0.02007 + 0.00706x$ | 0.998 | 142 | 76 |
| 51 | nootkatone | 30.95 | 1815 | 1824 | 75.1 | 2528 | 2532 | 218, 147, 43 | Std R12 | 0.10−98.0 | $Y = -0.00486 + 0.00369x$ | 0.997 | 271 | 80 |

[a]RT represents the retention time. [b]RI was obtained by GC-MS analysis using an Rtx-5MS column. [c]RI was reported in the literature or NIST Chemistry Web Book (http://webbook.nist.gov/chemistry), which was using a column similar to Rtx-5MS (the column stationary phase is 5% diphenyl and 95% dimethyl polysiloxane, equivalent to United States Pharmacopoeia G27). [d]RI was obtained by GC-MS analysis using an Rtx-wax column. [e]RI was reported in the literature or NIST Chemistry Web Book (http://webbook.nist.gov/chemistry) using a column similar to Rtx-wax (the column stationary phases is polyethylene glycol, equivalent to United States Pharmacopoeia G16). [f]Std indicates the identification has been confirmed by matching a standard; the number following R is the corresponding reference showing the RI values (R8 represents the reference of Njoroge et al. (2005); R9 is Lanphi et al. (2009); R12 is Liu et al. (2012); R14 is Cheong et al. (2012); R26 is Nguyen et al. (2009); R32 is Espina et al. (2011); R33 is Deterre et al. (2012); R34 is Alkateb et al. (2014); R35 is Lan et al. (2006); R36 is Cejudo et al. (2013). The authentic standard chemicals (ASCs) were obtained from Sigma-Aldrich Co. Ltd. (St. Louis, MO, USA); Alfa Aesar Co. Ltd. (Heysham, Lancashire, UK); Ormah Chemical Inc. Tic. Ltd. (TIC, Turkey); and Penta Manufacturing Co. Ltd. (PMC, Livingston, NJ, USA). [g]All of the equations of the calibration curves of ASCs were calculated in the SIM mode. $Y$ is the ratio of the peak area of the ASC to that of the internal standard (IS), and $x$ is the ratio of the concentration of the ASC to that of the IS. [h]CF represents correction factors using this formula: CF = (As/Ms)/(Ar/Mr). As represents the corresponding quantitative ion (SIM mode) area of the IS; Ar represents the corresponding quantitative ion (SIM mode) area of the ASC, Ms represents the concentration of IS, Mr represents the concentration of the ASC (QI of 2-methylbutyrate was 57, QI of ethyl benzoate was 105). [i]R is the Recovery rate, which is measured by adding the standards into either a fresh EO (if the volatile was detected in the fresh EO) or a sunlight-exposed EO (if the volatile was not detected in the fresh EO). The fresh EO and the sunlight-exposed EO show similar recoveries for all of the standards.



dx.doi.org/10.1021/jf504294g | J. Agric. Food Chem. 2014, 62, 11818−11830

**Table 3. Quantitation of the Volatiles in Each Essential Oil Sample**

| | | concentration[a] (μg/mL) | | | | | |
|---|---|---|---|---|---|---|---|
| no. | volatile | fresh | sunlight, $N_2$ | sunlight, $O_2$ | dark, $O_2$ | 40 °C, dark, $N_2$ | cluster |
| 1 | α-pinene | 2012 a | 1924 a | 1987 a | 1909 a | 1832 a | 3 |
| 2 | sabinene | 2556 a | 2821 a | 2901 a | 2580 a | 2356 a | 3 |
| 3 | β-pinene | 7698 a | 8571 a | 8648 a | 7610 a | 6624 a | 3 |
| 4 | β-myrcene | 220631 a | 209654 b | 208932 b | 218937 a | 221341 a | 3 |
| 5 | octanal | 656 a | 408 a | 636 a | 568 a | 494 a | 3 |
| 6 | α-phellandrene | 265 a | 261 a | 225 a | 248 a | 234 a | 3 |
| 7 | pseudolimonene | 0 b | 4340 a | 5904 a | 0 b | 0 b | 1 |
| 8 | D-limonene | 505803 a | 498996 a | 497689 a | 499062 a | 498789 a | 3 |
| 9 | *cis*-β-ocimene | 6816 a | 4448 b | 4173 b | 6962 a | 6450 a | 3 |
| 10 | *cis*-linalool oxide | 0 c | 534 a | 516 a | 97 b | 141 b | 1 |
| 11 | *trans*-linalool oxide | 0 c | 2585 a | 2633 a | 110 b | 120 b | 1 |
| 12 | terpinolene | 195 a | 0 b | 0 b | 131 a | 137 a | 2 |
| 13 | linalool | 2684 a | 2654 a | 2598 a | 2864 a | 2774 a | 3 |
| 14 | perillene | 0 b | 318 a | 241 a | 0 b | 0 b | 1 |
| 15 | nonanal | 116 a | 118 a | 102 a | 96 a | 90 a | 3 |
| 16 | α-pinene oxide | 0 c | 726 a | 698 a | 280 b | 204 b | 1 |
| 17 | *cis*-limonene oxide | 0 d | 5225 b | 9029 a | 191 c | 455 c | 1 |
| 18 | *trans*-limonene oxide | 0 d | 546 b | 3183 a | 61 c | 151 c | 1 |
| 19 | chrysanthemol | 68 b | 807 a | 556 a | 101 b | 115 b | 1 |
| 20 | citronellal | 0 c | 637 a | 265 ab | 70 b | 55 b | 1 |
| 21 | *trans*-verbenol | 0 b | 421 a | 391 a | 0 b | 0 b | 1 |
| 22 | α-terpineol | 583 b | 942 a | 919 a | 629 b | 618 b | 3 |
| 23 | *trans*-carveol | 0 b | 83 a | 91 a | 83 a | 74 a | 4 |
| 24 | decanal | 1629 a | 962 b | 1003 b | 1671 a | 1631 a | 3 |
| 25 | *cis*-carveol | 0 b | 112 a | 141 a | 101 a | 69 a | 3 |
| 26 | neral | 8100 a | 2564 b | 1522 b | 9537 a | 8991 a | 2 |
| 27 | carvone | 0 b | 607 a | 662 a | 0 b | 0 b | 1 |
| 28 | geranial | 9101 a | 843 b | 299 b | 7357 a | 8456 a | 2 |
| 29 | perilla alcohol | 0 b | 216 a | 230 a | 0 b | 0 b | 1 |
| 30 | indole | 186 a | 170 a | 248 a | 201 a | 218 a | 3 |
| 31 | δ-elemene | 2040 a | 109 b | 162 b | 1913 a | 1952 a | 2 |
| 32 | neryl acetate | 229 a | 168 b | 162 b | 221 a | 263 a | 3 |
| 33 | geranyl acetate | 512 a | 699 a | 663 a | 599 a | 628 a | 3 |
| 34 | bourbonene | 0 b | 3287 a | 2440 a | 0 b | 0 b | 1 |
| 35 | β-elemene | 100 b | 845 a | 840 a | 107 b | 106 b | 1 |
| 36 | dodecanal | 186 a | 160 a | 154 a | 205 a | 229 a | 3 |
| 37 | β-cubebene | 750 b | 1498 a | 1377 a | 799 b | 799 b | 3 |
| 38 | *trans*-caryophyllene | 856 b | 1335 a | 1257 a | 927 b | 920 b | 3 |
| 39 | perillyl acetate | 64 a | 89 a | 81 a | 74 a | 90 a | 3 |
| 40 | dodecenal | 350 a | 0 b | 0 b | 404 a | 455 a | 2 |
| 41 | γ-elemene | 0 b | 318 a | 191 a | 0 b | 0 b | 1 |
| 42 | α-humulene | 0 b | 237 a | 195 a | 0 b | 0 b | 1 |
| 43 | germacrene D | 8082 a | 1314 b | 1962 b | 7886 a | 7354 a | 2 |
| 44 | β-selinene | 785 a | 281 b | 289 b | 841 a | 863 a | 2 |
| 45 | elemol | 0 b | 0 b | 0 b | 0 b | 114 a | 5 |
| 46 | *trans*-nerolidol | 459 a | 521 a | 600 a | 600 a | 672 a | 3 |
| 47 | germacrene B | 400 a | 0 b | 0 b | 452 a | 517 a | 2 |
| 48 | spathulenol | 0 b | 186 a | 169 a | 0 b | 0 b | 1 |
| 49 | caryophyllene oxide | 0 b | 176 a | 169 a | 0 b | 0 b | 1 |
| 50 | *cis*-farnesol | 0 b | 312 a | 345 a | 282 a | 296 a | 4 |
| 51 | nootkatone | 964 a | 478 b | 479 b | 1137 a | 1165 a | 2 |
| | total (μg/mL) | 784876 | 764506 | 767957 | 779133 | 778842 | |

[a]0 means the concentration was <50 μg/mL or not detected. All of the identified chemicals were previously reported in citrus volatiles. Rows with different letters (a–d) indicate significant statistical differences ($p < 0.05$).

reduced fresh odor, whereas the heated EO (sample 5) displayed a reduced freshness and a ripened odor (Table 1). In more detail, the fresh EO (sample 1) had the highest scores for herbaceous and lemon notes, simultaneously with the lowest oily note; the sunlight-exposed EOs (samples 2 and 3) presented the strongest oily note and the weakest herbaceous

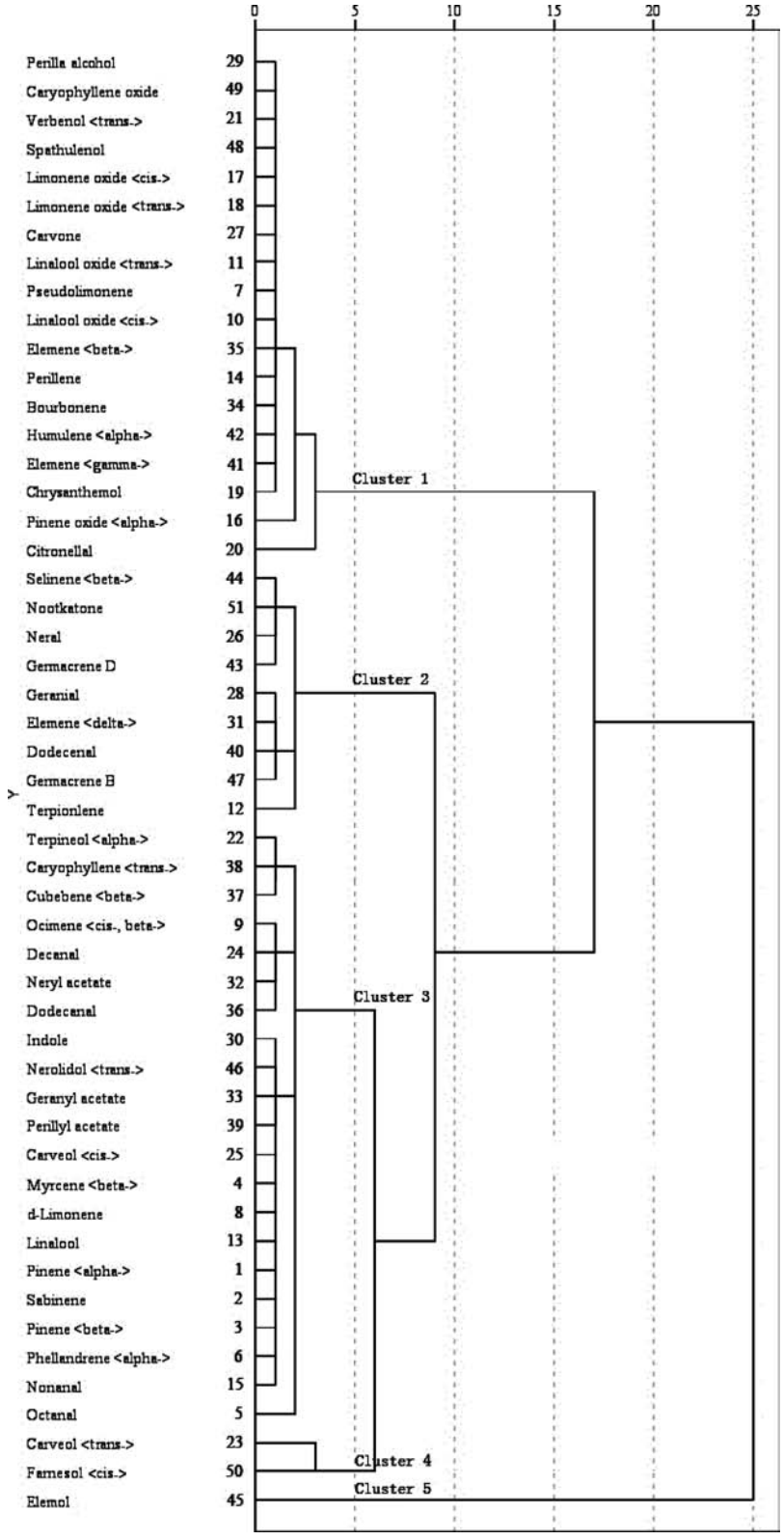


**Figure 2.** Cluster analysis of the volatiles based on their concentration changes after different treatments. The numbers (0−25) above the top line of the figure represent the relative distance using cosine correlation metric method. Cluster 1 represents the volatiles that were not detected or had very low concentrations in fresh EO but increased to a remarkable concentration in the sunlight-exposed EOs. Cluster 2 represents the volatiles that had decreased concentrations after the sunlight exposure. Cluster 3 represents the volatiles that had no significant changes in their concentrations after all of the treatments. Cluster 4 represents the volatiles that did not exist in the fresh EO but appeared in other EOs at low concentrations. Cluster 5 represents the volatiles existing only in heated EO.

**Table 4. Odor Activity Values and Characteristic Aromas of Essential Oil Samples**

| | | | | odor activity values | | | | | | |
|---|---|---|---|---|---|---|---|---|---|---|
| no. | volatile | odor characteristic | threshold[a] ($\mu$g/mL) | fresh | sunlight, $N_2$ | sunlight, $O_2$ | dark, $O_2$ | 40 °C, dark, $N_2$ | refs[b] | cluster |
| 1 | $\alpha$-pinene | harsh, pine-like | 0.18 | 1118 | 1069 | 1104 | 1061 | 1018 | 12, 26 | 4 |
| 2 | sabinene | woody, floral | 0.15 | 1704 | 1881 | 1934 | 1720 | 1571 | 33 | 4 |
| 3 | $\beta$-pinene | resinous, pine-like | 4.16 | 185 | 206 | 208 | 183 | 159 | 12, 26, 33 | 4 |
| 4 | $\beta$-myrcene | floral | 0.099 | 222860 | 211772 | 211042 | 221148 | 223577 | 12, 33 | 4 |
| 5 | octanal | spicy, fruity-peel | 0.003 | 21867 | 13600 | 21200 | 18933 | 16467 | 12, 29, 38 | 4 |
| 6 | $\alpha$-phellandrene | herbaceous, floral | 0.5 | 53 | 52 | 45 | 50 | 47 | 12, 33 | 4 |
| 7 | D-limonene | lemon, green | 1.2 | 42150 | 41583 | 41474 | 41589 | 41566 | 12, 29, 33 | 4 |
| 8 | *cis*-$\beta$-ocimene | pungent, burnt | 0.2 | 3408 | 2224 | 2087 | 3481 | 3225 | 12, 33 | 3 |
| 9 | *cis*-linalool oxide | oily, harsh | 0.1 | 0 | 534 | 516 | 97 | 141 | 12, 33 | 1 |
| 10 | *trans*-linalool oxide | oily, harsh | 0.1 | 0 | 2585 | 2633 | 110 | 120 | 12 | 1 |
| 11 | terpinolene | oily, resinous | 0.26 | 75 | 0 | 0 | 50 | 53 | 33 | 2 |
| 12 | linalool | sweet, floral, orange | 0.008 | 33550 | 33175 | 32475 | 35800 | 34675 | 12, 33, 38 | 4 |
| 13 | nonanal | floral, sweet, green | 0.001 | 11600 | 11800 | 10200 | 9600 | 9000 | 12, 29 | 4 |
| 14 | *cis*-limonene oxide | sweet, floral | 0.1 | 0 | 8225 | 9029 | 191 | 455 | 12, | 1 |
| 15 | *trans*-limonene oxide | sweet, floral | 0.19 | 0 | 1493 | 1675 | 32 | 79 | 26 | 1 |
| 16 | *a*-terpineol | oily, resinous | 0.3 | 194 | 314 | 306 | 210 | 206 | 30, 33 | 5 |
| 17 | decanal | floral, fruity | 0.002 | 81450 | 48100 | 50150 | 83550 | 81550 | 12, 30, 33 | 3 |
| 18 | neral | herbaceous, citrus | 0.3 | 2700 | 855 | 507 | 3179 | 2997 | 29, 30 | 2 |
| 19 | carvone | mint | 0.05 | 0 | 1214 | 1324 | 0 | 0 | 30, 33 | 1 |
| 20 | geranial | herbaceous, citrus | 0.04 | 22753 | 2108 | 748 | 18393 | 21140 | 29, 30 | 2 |
| 21 | geranyl acetate | green, sweet | 0.14 | 366 | 499 | 474 | 428 | 449 | 33 | 4 |
| 22 | dodecanal | oily, aldehyde | 0.002 | 9300 | 8000 | 7700 | 10250 | 11450 | 33 | 3 |
| 23 | germacrene D | oily, green, woody | 1.8 | 449 | 73 | 109 | 438 | 409 | 33 | 2 |
| 24 | nootkatone | pummelo like | 0.8 | 121 | 60 | 60 | 142 | 146 | 29, 38 | 3 |
| | total | | | 455903 | 391422 | 397000 | 450635 | 450500 | | |

[a]Thresholds in water were provided by Du et al. (2011), Guadagni (1963), and Ruth (1986). [b]Odor characteristics were evaluated by standards coupled with the corresponding references in the reference list: 12 is Liu et al. (2012); 26 is Nguyen et al. (2009); 29 is Chisholm et al. (2003); 30 is Perez et al. (2008); 33 is Deterre et al. (2012); and 38 is Lin et al. (2002).

and lemon notes; the oxygen-exposed EO (sample 4) gave light lemon and green notes; and the heated EO (sample 5) attained the highest score for its sweet and floral notes among all of the EOs (Table 1). These results were consistent with a previous study that the herbaceous and lemon aroma resulted in the fresh odor, the sweet and floral aroma was related to the ripened and reduced fresh odor, and the oily odor was a contributor to the off-flavor.[21]

The characteristic aromas were further identified, compared, and illustrated via PCA, which is commonly used to extract interpretable and statistically reliable information from data sets. As a result, two PCs that contributed >83% of the total variances of flavor contributors were extracted to express the main variables affecting the sensory characteristics, among which PC1 mainly represented the herbaceous, lemon, and oily notes, which accounted for 58.2% of the total variance among EO flavors, and PC2 mainly represented the sweet and floral notes, which accounted for 25.0% of total variance (Figure 1A).

The PCA scores showed that the heated EO (sample 5) possessed a higher PC2 score and a lower PC1 score than those of the fresh EO (sample 1) (Table 1; Figure 1B). This result was attributed to the thermal treatment that slightly increased the scores of sweet and floral notes while decreasing the scores of lemon and herbaceous notes (Table 1), which was consistent with previous studies that high temperature reduced the freshness odor of EOs.[14,25] The oxygen-exposed EO (sample 4) showed a slightly lower PC1 score than the fresh EO (Table 1; Figure 1B). This result could be attributed to the slight increase in the scores of sweet and oily notes and the decrease of lemon note (Table 1), which was consistent with a previous study that oxygen was an important factor affecting the aroma of an EO.[26] As shown in Figure 1, the sunlight-exposed EOs (samples 2 and 3) possessed very similar aromatic profiles, which obviously differentiated them from other EOs (Table 1; Figure 1B). This result was in agreement with the increase of the score of an oily note (from 0.2 to 8.3 and 8.2) and a decrease in the scores of the lemon (from 8.2 to 1.5 and 1.6) and decreased herbaceous notes (from 7.4 to 1.6 and 1.5). Both the sensory evaluation (Table 1) and PCA (Table 1; Figure 1) clearly indicated the flavor profiles of the sunlight-exposed EOs were dramatically different from those of the fresh EO, the oxygen-exposed EO, and the heated EO. In this context, sunlight is a key factor for the generation of an oily note and the decrease of herbaceous and lemon notes, whereas oxygen exposure and heating were the causes for the decline in fresh odor and increase in ripened odor.

**Investigation of the Volatile Changes by GC-MS Analysis.** It has been reported that many volatiles are subjected to degradation and oxidation during extraction and storage.[25,27] For instance, monoterpenes could transform to monoterpene alcohols and monoterpene oxide.[28,29] Previous studies have demonstrated that heat and oxygen were the major factors affecting the volatile compositions of citrus EOs.[17,26,30] However, the chemical basis of the sunlight-induced changes in aroma is still unclear. Although the effect of sunlight on milk flavors has been confirmed,[31] its effect on citrus EO has not

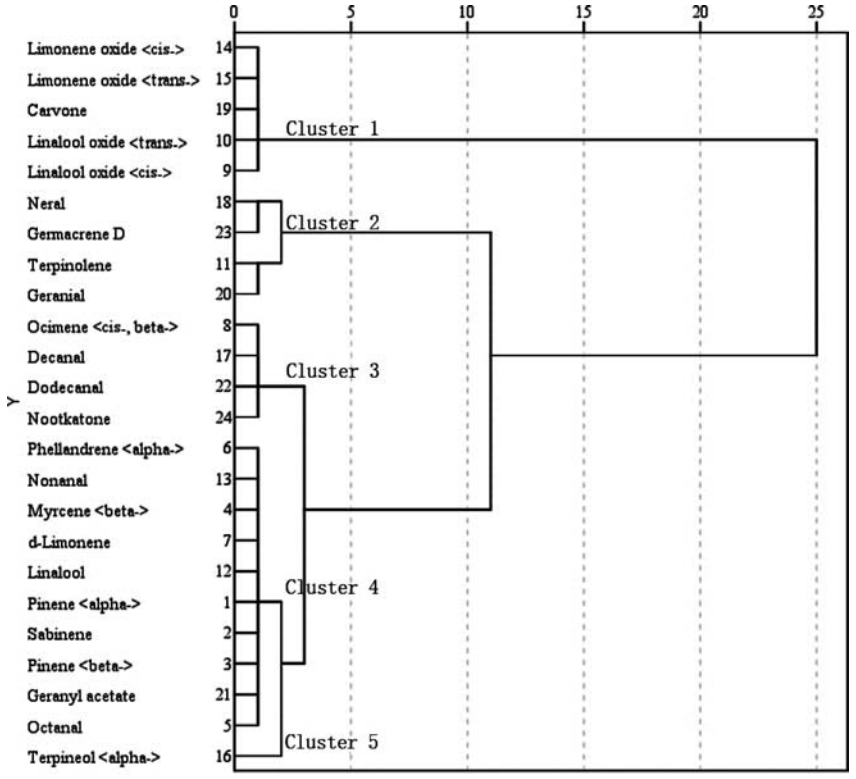


**Figure 3.** Cluster analysis of volatiles based on their changes in OAVs after different treatments. The numbers (0–25) above the top line of the figure represent the relative distance using cosine correlation metric method. Cluster 1 represents the volatiles that had 0 OAV in the fresh EO but increased to show remarkable OAVs in the sunlight-exposed and heated EOs. Clusters 2 and 3 represent the volatiles that had decreased OAVs in the sunlight-exposed EOs. Cluster 4 represents the volatiles that had no significant changes in their OAVs, and cluster 5 represents the volatiles that had increased OAVs in the sunlight-exposed EOs.

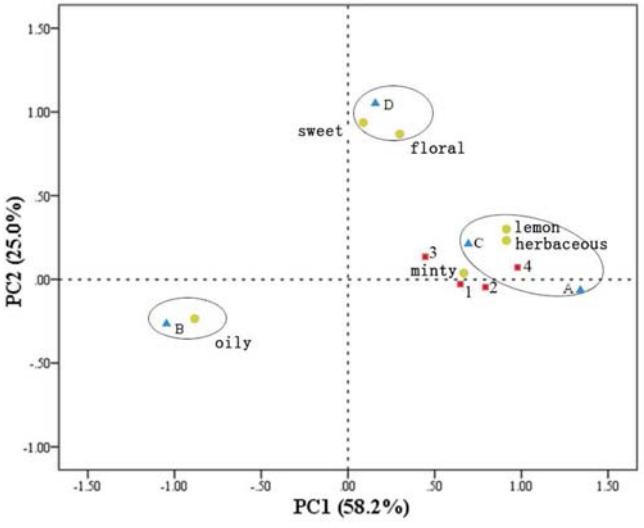


**Figure 4.** CA analysis of the aromas of the samples in the omission test. PC1 mainly represents the fresh odor, and PC2 mainly represents the ripened odor. "A" is the model sample of the fresh EO, "B" is the model sample of the sunlight-exposed EO, "C" is the model sample of the oxygen-exposed EO, and "D" is the model of the heated EO. "1" is the linalool oxides-added sample, "2" is $\alpha$-terpineol-added sample, "3" is neral and geranial mixture decreased sample, and "4" is nootkatone decreased sample.

been reported by other researchers. To explore the more accurate quantitative changes of the volatile constituents after sunlight exposure, oxygen exposure, and heating, the EO samples were subjected to GC-MS analysis.

A total of 51 compounds were detected in the EOs (Table 2), among which 41 volatiles were identifief on the basis of matching their MS and RI with those of standards (Table 2); another 10 volatiles were identified according to the comparison with the MS library and matching the RI with those from previous citrus fruit references.[8,9,12,14,26,32−36] Most of these volatiles have been found in other citrus fruits. Furthermore, the concentrations of the volatiles were quantified by using the calibration curves of the standards obtained in the selective ion monitoring (SIM) mode (Table 2), and the accuracy is shown using the recovery method (Table 2). Other volatiles were quantified through the calibration curve of the internal reference ethyl benzoate (Table 2). The result showed that all of the EOs had similar volatile components consisting of D-limonene and $\beta$-myrcene, germacrene D, geranial, neral, *cis*-$\beta$-ocimene, $\beta$-pinene, linalool, sabinene, and $\alpha$-pinene (Table 3), which are also the major constituents of other citrus EOs.[17]

The cluster analysis showed five clusters of volatiles according to their concentration changes after the treatments of sunlight exposure, oxygen exposure, or heating (Figure 2). Cluster 1 included perilla alcohol, caryophyllene oxide, *trans*-verbenol, spathulenol, *cis*-limonene oxide, *trans*-limonene oxide, carvone, *cis*-linalool oxide, *trans*-linalool oxide, pseudolimonene, $\beta$-elemene, perillene, bourbonene, $\alpha$-humulene, $\gamma$-elemene, chrysanthemol, $\alpha$-pinene oxide, and citronellal. These volatiles had much higher concentrations in the sunlight-exposed EOs (samples 2 and 3) than in other EOs ($p < 0.05$). Among these volatiles, pseudolimonene, perillene, perilla alcohol, *trans*-

**Table 5. Changes of the Major Volatiles and Their Odor Activity Values of the Fresh Essential Oil after UV and Daylight Irradiation**

| | concentration ($\mu$g/mL) | | | OAVs | | | |
|---|---|---|---|---|---|---|---|
| volatile | fresh | daylight, $N_2$ | UV, $N_2$ | fresh | daylight, $N_2$ | UV, $N_2$ | cluster[a] |
| $\beta$-pinene | 7698 | 7069 | 9009 | 185 | 170 | 217 | 1 |
| $\beta$-myrcene | 220631 | 218272 | 202181 | 222860 | 220477 | 204223 | 1 |
| octanal | 656 | 391 | 559 | 21867 | 13033 | 18633 | 1 |
| D-limonene | 505803 | 500185 | 490176 | 42150 | 41682 | 40848 | 1 |
| linalool | 2684 | 2883 | 2511 | 33550 | 36038 | 31388 | 1 |
| $\alpha$-terpineol | 583 | 635 | 899 | 194 | 212 | 300 | 1 |
| pseudolimonene | 0 | 0 | 3544 | | | | 2 |
| *trans*-linalool oxide | 0 | 66 | 1733 | 0 | 66 | 1733 | 2 |
| perillene | 0 | 0 | 199 | | | | 2 |
| *cis*-limonene oxide | 0 | 121 | 8971 | 0 | 121 | 8971 | 2 |
| *trans*-limonene oxide | 0 | 55 | 5522 | 0 | 29 | 2906 | 2 |
| citronellal | 0 | 58 | 332 | | | | 2 |
| perilla alcohol | 0 | 0 | 421 | | | | 2 |
| *trans*-verbenol | 0 | 0 | 327 | | | | 2 |
| carvone | 0 | 0 | 1378 | 0 | 0 | 2756 | 2 |
| citronellal hydrate | 0 | 0 | 115 | | | | 2 |
| bourbonene | 0 | 0 | 2211 | | | | 2 |
| $\beta$-elemene | 100 | 103 | 656 | | | | 2 |
| $\gamma$-elemene | 0 | 0 | 111 | | | | 2 |
| $\alpha$-humulene | 0 | 0 | 121 | | | | 2 |
| *cis*-$\beta$-ocimene | 6816 | 7020 | 1912 | 3408 | 3510 | 956 | 3 |
| terpinolene | 195 | 141 | 0 | 75 | 54 | 0 | 3 |
| decanal | 1629 | 1679 | 898 | 81450 | 83950 | 44900 | 3 |
| neral | 8100 | 8436 | 1311 | 2700 | 2812 | 437 | 3 |
| geranial | 9101 | 8809 | 267 | 22753 | 22023 | 668 | 3 |
| dodecenal | 350 | 442 | 0 | | | | 3 |
| germacrene D | 8082 | 7445 | 1131 | 449 | 414 | 63 | 3 |
| nootkatone | 964 | 1066 | 443 | 121 | 133 | 55 | 3 |
| *cis*-linalool oxide | 0 | 75 | 200 | 0 | 75 | 200 | 4 |
| $\alpha$-pinene oxide | 0 | 295 | 522 | | | | 4 |
| *trans*-carveol | 0 | 81 | 92 | | | | 4 |

[a]Cluster 1 represents the volatiles that had no significant changes in their concentrations, cluster 2 represents the volatiles that had increased concentrations and OAVs in the UV-exposed EO, cluster 3 represents the volatiles that had decreased concentrations and OAVs after UV exposure, cluster 4 represents the volatiles that had increased concentrations and OAVs in both the daylight-exposed and UV-exposed EOs.

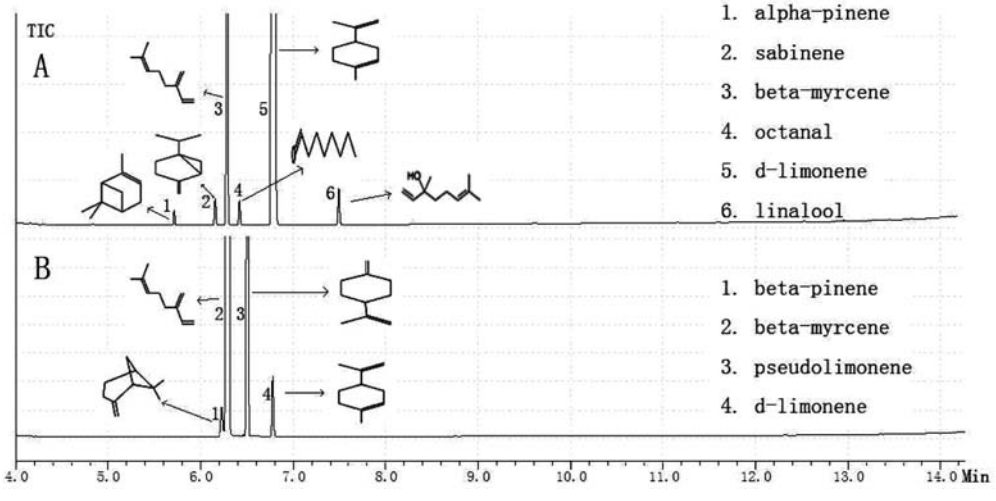


**Figure 5.** Transforming products of D-limonene (A) and $\beta$-myrcene (B) after UV exposure.

verbenol, carvone, bourbonene, $\gamma$-elemene, $\alpha$-humulene, spathulenol, and caryophyllene oxide were detected only in the sunlight-exposed EOs (samples 2 and 3). The volatiles in cluster 2, including $\beta$-selinene, nootkatone, neral, germacrene D, geranial, $\delta$-elemene, dodecenal, germacrene B, and terpinolene, showed significantly lower ($p < 0.05$) concen-


dx.doi.org/10.1021/jf504294g | J. Agric. Food Chem. 2014, 62, 11818−11830

trations after sunlight exposure (samples 2 and 3). Most volatiles in cluster 3 (i.e., α-terpineol, *trans*-caryophyllene, β-cubebene, *cis*-β-ocimene, decanal, neryl acetate, dodecanal, indole, *trans*-nerolidol, geranyl acetate, perillyl acetate, *cis*-carveol, β-myrcene, D-limonene, linalool, α-pinene, sabinene, β-pinene, α-phellandrene, nonanal, and octanal) had no significant statistical differences ($p < 0.05$) in their concentrations in all of the EOs. This result indicated that the volatiles in cluster 3 were relatively stable under the treatments by sunlight, oxygen, and heating, which was consistent with other studies showing most of these volatiles were relatively stable.[16,30] Cluster 4 had two compounds, including *trans*-carveol and *cis*-farnesol. These volatiles did not exist in the fresh EO but could be detected in the sunlight-exposed and heated EOs. Cluster 5 had only one volatile elemol that was generated in the heated EO, which might be transformed from elemene.[16] By comparing the volatile concentrations through cluster analysis, it was obvious that both oxygen and heating had significant influence on the volatile compositions, but sunlight was a more important factor responsible for the changes of volatile chemicals when exposed under sunlight and oxygen at room temperature. Moreover, the sunlight-exposed EOs (samples 2 and 3) presented volatiles (in clusters 1 and 2) entirely different from those of the oxygen-exposed and heated EOs, which indicated sunlight exposure could cause chemical changes different from those induced by oxygen exposure and heating.

**Investigation of the Volatiles Responsible for the Aroma Change by the Analysis of Odor Activity Values.** The aromas that had been reported to be the main aromatic volatiles in citrus fruits and exhibited remarkable changes in concentration after the above-mentioned treatments were analyzed by sensory evaluation,[12,26,30,33,37,38] which confirmed that *cis*- and *trans*-limonene oxides showed typical notes of sweet and floral notes; neral, geranial, and nootkatone had typical herbaceous and lemon notes, whereas α-terpineol, *cis*- and *trans*-linalool oxides displayed a strong oily note (Table 4). Furthermore, the OAVs of these volatiles in the EOs were estimated on the basis of their odor thresholds according to previous studies.[20,22,23] β-Myrcene, decanal, D-limonene, linalool, and octanal had OAVs in ranges of 211,042−223,577, 48,100−83,950, 41,453−42,150, 32,475−36,038, and 13,033−21,867 (Table 4), respectively. These chemicals contributed to the majority of the total OAVs of the EOs, which was consistent with previous studies that D-limonene, β-myrcene, linalool, octanal, citronellal, nonanal, linalool oxide, and nootkatone were the major contributors to the aroma of citrus oils.[12,17,33]

Studies have shown that an overall aromatic profile could be significantly changed by some changes of volatiles in small concentrations but with very low odor thresholds.[17,39] For instance, many oxygenated compounds have been recognized with high OAVs that may have significant impacts on overall flavors.[9,12] To explore the potent volatiles responsible for the aroma changes, the EOs were further compared by the OAVs of their inherent volatiles by cluster analysis, which showed the existence of five principal clusters according to the OAV changes (Table 4 and Figure 3). Cluster 1 represented the volatiles that did not exist in the fresh EO (sample 1) but had been generated with significantly high OAVs in the sunlight-exposed EOs (samples 2 and 3) and heated EOs (sample 5), which contributed to the oily and ripened notes. Clusters 2 and 3 represented the volatiles that presented herbaceous and lemon notes and had decreased OAVs in the sunlight-exposed EOs (samples 2 and 3). Cluster 4 represented the volatiles that had no significant changes in their OAVs among all of the EOs. Cluster 5 represented the volatiles that had increased OAVs of the sunlight-exposed EOs and contributed to the oily note.

In cluster 1, *cis*- and *trans*-limonene oxides that were reported having sweet and floral notes[29] had much higher OAVs in the heated (sample 5) and the sunlight-exposed EOs (samples 2 and 3) than in the fresh EO (sample 1), which was consistent with the reduced freshness of the heated and sunlight-exposed EOs (Table 1). Other volatiles in cluster 1, such as *cis*- and *trans*-linalool oxides that were reported to have the woody and linalool-like odor of *mangshanyegan*,[12] showed much higher OAVs in the sunlight-exposed EOs (samples 2 and 3) than their counterparts in other EOs, providing a reasonable explanation for the strong oily off-flavor of the sunlight-exposed EOs (Table 1). In cluster 2, neral and geranial, which had been reported having herbaceous and lemon notes of kumquat[14] and orange juice,[30] exhibited much lower OAVs in the sunlight-exposed EOs (samples 2 and 3), which was in agreement with the result from the sensory evaluation of the sunlight-exposed EO, which had a decrease in its lemon and herbaceous odor (Table 1). The volatiles (i.e., *cis*-β-ocimene, decanal, dodecanal, nootkatone) in cluster 3 had much lower OAVs in sunlight-exposed EOs. Among these volatiles, nootkatone was identified to possess a strong odor of fresh pummelo aroma and considered as the most important aroma of grapefruit oil.[40] The decreased OAVs of neral, geranial, and nootkatone seemed to provide a reasonable explanation for the less green notes of the sunlight-exposed EOs (samples 2 and 3). The volatiles in cluster 4, that is, α-pinene, sabinene, β-pinene, β-myrcene, D-limonene, linalool, α-phellandrene, nonanal, geranyl acetate, and octanal, showed constant OAVs in all of the EOs (Table 4; Figure 3), which indicated these compounds had little influence on the aroma changes of the EO. In cluster 5, α-terpineol, which was reported to have a strong oily off-flavor,[41] showed much higher OAVs in the sunlight-exposed EOs than that in other EOs, which gave the sunlight-exposed EOs (samples 2 and 3) a more oily note.

The comparison of the OAVs of the volatiles and the cluster analysis suggested that *cis*- and *trans*-linalool oxides, *cis*- and *trans*-limonene oxides, neral, geranial, nootkatone, and α-terpineol were the volatiles that had significantly affected the aroma changes of the sunlight-exposed EOs. Furthermore, *cis*- and *trans*-limonene oxides were also the volatiles responsible for the aroma changes of the heated EO.

**Verifying the Contributions of the Aroma-Impact Volatiles to the Aroma Changes by Omission Test.** The formulated sample model (i.e., FMS 0) possessed a typical fresh odor like the fresh EO. In comparison, FMS 1 possessed a typical oily off-flavor and reduced herbaceous and lemon notes like that in the sunlight-exposed EO; FMS 2 had a reduced freshness like that in the oxygen-exposed EO; FMS 3 showed a reduced freshness and sweet and floral notes like that in the heated EO. In addition, the linalool oxides-added sample (FMS 4) was found to have a slight oily off-flavor by sensory evaluation; the α-terpineol-increased sample (FMS 5) and the nootkatone-decreased sample (FMS 7) did not show obvious differences in comparison to the model sample of fresh EO (FMS 0); the neral and geranial mixture-excluded sample (FMS 6) released the reduced herbaceous and lemon notes (Figure 4). The above results from the reconstituted flavor models (from FMS 0 to 7) confirmed that increasing the contents of

*cis*- and *trans*-linalool oxides and *cis*- and *trans*-limonene oxides could result in the generation of the strong oily off-flavor, whereas increasing the concentrations of *cis*- and *trans*-limonene oxides gave strong sweet and floral notes, resulting in the suppression of the citrus freshness note. Lack of citral (i.e., neral and geranial) was considered to cause the decreased herbaceous and lemon notes. Surprisingly, nootkatone and $\alpha$-terpineol exhibited little effect on the flavor profiles of the formulated aroma models due to their negligible OAVs in comparison to those of the main OAV contributors such as linalool oxides and limonene oxides (Table 4). Nevertheless, all other results supported that the linalool oxides, limonene oxides, and citral (i.e., neral and geranial) were the main volatiles responsible for the aroma changes during sunlight exposure.

**Illustration of UV for the Sunlight-Induced Aroma Deterioration.** UV is the short wavelength light of sunlight; therefore, it has a higher energy than its counterparts in daylight beams. UV can cause the oxidation and degradation of some chemicals, resulting in the generation of free radicals.[25] Previous studies have shown that some volatiles, for example, terpinolene, germacrene D, neral, and geranial, were susceptible to degradation under UV irradiation.[15,26] For instance, Iwanami et al.[15] found the lemon EO had a dusty flavor after UV irradiation. To investigate whether the short-wavelength light is the cause for the sunlight-induced deterioration of the aromas, the pummelo EOs were exposed under a UV light and a daylight lamp, respectively, followed by monitoring of the changes of their aromatic profiles and volatile constituents. As a result, the UV-exposed EO exhibited a strong oily note and decreased lemon and herbaceous notes, whereas the EO exposed under the daylight lamp showed little change from its original aroma. Moreover, the UV-exposed EO had significant increases in the concentrations and OAVs of *cis*- and *trans*-linalool oxides and significant decreases in the contents and OAVs of neral, geranial, and nootkatone (Table 5). Besides, another parallel experiment using the single chemical standards, that is, $\beta$-myrcene and D-limonene, that account for the majority of the pummelo EO, was conducted to expose the chemicals under UV irradiation, respectively. It was found that D-limonene was turned into $\alpha$-pinene, sabinene, $\beta$-myrcene, octanal, and linalool, whereas $\beta$-myrcene was transformed to $\beta$-pinene, pseudolimonene, and D-limonene (Figure 5). These transformation trends were consistent with the concentration changes of these chemicals in the sunlight-exposed EOs (Table 3) and the UV-irradiated EO (Table 5). These results validated that the UV irradiation-initiated degradation and transformation was the main reason for the sunlight-induced deterioration of the EO.

In summary, sunlight exposure could cause remarkable aroma deterioration of pummelo EO. The sunlight-exposed EO had a strong oily and off-flavor odor and a reduced fresh aroma, which was significantly different from that of the oxygen-exposed and heated EOs. The strong oily and off-flavor notes were attributed to the generation of high concentrations of linalool oxides and limonene oxides. The reduced freshness was related to the decrease of neral and geranial. Moreover, the aroma deterioration of pummelo EO induced by sunlight was confirmed to be caused by the degradation and transformation of some aroma-impact volatiles, such as $\beta$-myrcene and D-limonene, initiated by the UV wavelength.

This information might be valuable for industries involved in the production and storage of aromatic products from citrus fruit.

## AUTHOR INFORMATION


### Corresponding Author

*(F.C.) Mail: Department of Food, Nutrition and Packaging Sciences, Clemson University, Clemson, South Carolina 29634, USA. Phone: (864) 656-5702. E-mail: fchen@clemson.edu.



### Funding

This research is financially supported by grants from the National Natural Science Foundation of China (31271914), the Science Foundation for Distinguished Young Scholars of Xiamen City (3502Z20126008), and the Foundation for Innovative Research Team of Jimei University (2010A006).

### Notes

The authors declare no competing financial interest.


## REFERENCES


(1) Fisher, K.; Phillips, C. Potential antimicrobial uses of essential oils in food: is citrus the answer? *Trends Food Sci. Technol.* **2008**, *19*, 156−164.

(2) Van, H. P.; Chi, P. T. L.; Phi, N. T. L. Comparison of antifungal activities of Vietnamese citrus essential oils. *Nat. Prod. Res.* **2013**, *27*, 506−508.

(3) Viuda-Martos, M.; Ruiz-Navajas, Y.; Fernández-López, J.; Pérez-Álvarez, J. Antifungal activity of lemon (*Citrus lemon* L.), mandarin (*Citrus reticulata* L.), grapefruit (*Citrus paradisi* L.) and orange (*Citrus sinensis* L.) essential oils. *Food Control* **2008**, *19*, 1130−1138.

(4) Razzaghi-Abyaneh, M.; Shams-Ghahfarokhi, M.; Rezaee, M.-B.; Jaimand, K.; Alinezhad, S.; Saberi, R.; Yoshinari, T. Chemical composition and antiaflatoxigenic activity of *Carum carvi* L., *Thymus vulgaris* and *Citrus aurantifolia* essential oils. *Food Control* **2009**, *20*, 1018−1024.

(5) Singh, P.; Shukla, R.; Prakash, B.; Kumar, A.; Singh, S.; Mishra, P. K.; Dubey, N. K. Chemical profile, antifungal, antiaflatoxigenic and antioxidant activity of *Citrus maxima* Burm. and *Citrus sinensis* (L.) *Osbeck* essential oils and their cyclic monoterpene, DL-limonene. *Food Chem. Toxicol.* **2010**, *48*, 1734−1740.

(6) Symrise TM annual report, 2009 (http://ar2009.symrise.com/).

(7) Steuer, B.; Schulz, H.; Läger, E. Classification and analysis of citrus oils by NIR spectroscopy. *Food Chem.* **2001**, *72*, 113−117.

(8) Njoroge, S. M.; Koaze, H.; Karanja, P. N.; Sawamura, M. Volatile constituents of redblush grapefruit (*Citrus paradisi*) and pummelo (*Citrus grandis*) peel essential oils from Kenya. *J. Agric. Food Chem.* **2005**, *53*, 9790−9794.

(9) Lanphi, N.; Shimamura, T.; Ukeda, H.; Sawamura, M. Chemical and aroma profiles of yuzu (*Citrus junos*) peel oils of different cultivars. *Food Chem.* **2009**, *115*, 1042−1047.

(10) Cheng, M. W.; Loke, X. Q.; Liu, S. Q.; Pramudya, K.; Curran, P.; Yu, B. Characterization of volatile compounds and aroma profiles of malaysian pomelo (*Citrus grandis* (L.) Osbeck) blossom and peel. *J. Essent. Oil Res.* **2011**, *23*, 34−44.

(11) Hosni, K.; Zahed, N.; Chrif, R.; Abid, I.; Medfei, W.; Kallel, M.; Brahim, N. B.; Sebei, H. Composition of peel essential oils from four selected Tunisian *Citrus* species: evidence for the genotypic influence. *Food Chem.* **2010**, *123*, 1098−1104.

(12) Liu, C. H.; Cheng, Y.; Zhang, H.; Deng, X.; Chen, F.; Xu, J. Volatile constituents of wild citrus Mangshanyegan (*Citrus nobilis* Lauriro) peel oil. *J. Agric. Food Chem.* **2012**, *60*, 2617−2628.

(13) Liu, C. H.; Jiang, D.; Cheng, Y.; Deng, X.; Chen, F.; Fang, L.; Ma, Z.; Xu, J. Chemotaxonomic study of Citrus, Poncirus and Fortunella genotypes based on peel oil volatile compounds − deciphering the genetic origin of Mangshanyegan (*Citrus nobilis* Lauriro). *PLoS One* **2013**, *8*, No. e58411.

(14) Cheong, M. W.; Chong, Z. S.; Liu, S. Q.; Zhou, W.; Curran, P.; Bin, Y. Characterisation of calamansi (*Citrus microcarpa*). Part I:

Volatiles, aromatic profiles and phenolic acids in the peel. *Food Chem.* **2012**, *134*, 686−695.
(15) Iwanami, Y.; Tateba, H.; Kodama, N.; Kishino, K. Changes of lemon flavor components in an aqueous solution during UV irradiation. *J. Agric. Food Chem.* **1997**, *45*, 463−466.
(16) Njoroge, S. M.; Ukeda, H.; Sawamura, M. Changes in the volatile composition of yuzu (*Citrus junos* Tanaka) cold-pressed oil during storage. *J. Agric. Food Chem.* **1996**, *44*, 550−556.
(17) Rouseff, R. L.; Ruiz Perez-Cacho, P.; Jabalpurwala, F. Historical review of citrus flavor research during the past 100 years. *J. Agric. Food Chem.* **2009**, *57*, 8115−8124.
(18) Buettner, A.; Mestres, M.; Fischer, A.; Guasch, J.; Schieberle, P. Evaluation of the most odour-active compounds in the peel oil of clementines (*Citrus reticulata* Blanco cv. Clementine). *Eur. Food Res. Technol.* **2003**, *216*, 11−14.
(19) Jelen, H. H.; Obuchowska, M.; Zawirska-Wojtasiak, R.; Wąsowicz, E. Headspace solid-phase microextraction use for the characterization of volatile compounds in vegetable oils of different sensory quality. *J. Agric. Food Chem.* **2000**, *48*, 2360−2367.
(20) Du, X.; Plotto, A.; Baldwin, E.; Rouseff, R. Evaluation of volatiles from two subtropical strawberry cultivars using GC-olfactometry, GC-MS odor activity values, and sensory analysis. *J. Agric. Food Chem.* **2011**, *59*, 12569−12577.
(21) Sawamura, M.; Onishi, Y.; Ikemoto, J.; Tu, N. T. M.; Phi, N. T. L. Characteristic odour components of bergamot (*Citrus bergamia* Risso) essential oil. *Flavour Fragrance J.* **2006**, *21*, 609−615.
(22) Guadagni, D. G.; Buttery, R. G.; Okano, S. Odour thresholds of some organic compounds associated with food flavours. *J. Sci. Food Agric.* **1963**, *14*, 761−765.
(23) Ruth, J. H. Odor thresholds and irritation levels of several chemical substances: a review. *Am. Ind. Hyg. Assoc. J.* **1986**, *47*, A-142−A-151.
(24) Burgard, D. R.; Kuznicki, J. T. *Chemometrics: Chemical and Sensory Data*; CRC Press: Boca Raton, FL, USA, 1990.
(25) Kashiwagi, T.; Lan Phi, N. T.; Sawamura, M. Compositional changes in Yuzu (*Citrus junos*) steam-distilled oil and effects of antioxidants on oil quality during storage. *Food Sci. Technol. Res.* **2010**, *16*, 51−58.
(26) Nguyen, H.; Campi, E. M.; Roy Jackson, W.; Patti, A. F. Effect of oxidative deterioration on flavour and aroma components of lemon oil. *Food Chem.* **2009**, *112*, 388−393.
(27) Ferhat, M. A.; Meklati, B. Y.; Chemat, F. Comparison of different isolation methods of essential oil from *Citrus* fruits: cold pressing, hydrodistillation and microwave 'dry' distillation. *Flavour Fragrance J.* **2007**, *22*, 494−504.
(28) Njoroge, S. M.; Ukeda, H.; Sawamura, M. Changes of the volatile profile and artifact formation in Daidai (*Citrus aurantium*) cold-pressed peel oil on storage. *J. Agric. Food Chem.* **2003**, *51*, 4029−4035.
(29) Chisholm, M. G.; Wilson, M. A.; Gaskey, G. M. Characterization of aroma volatiles in key lime essential oils (*Citrus aurantifolia* Swingle). *Flavour Fragrance J.* **2003**, *18*, 106−115.
(30) Perez, P. R.; Rouseff, R. Processing and storage effects on orange juice aroma: a review. *J. Agric. Food Chem.* **2008**, *56*, 9785−9796.
(31) Ramirez, E. Relation of the use of tygon plastic tubing to the lncidence of solar activated flavor in milk products. *Rev. CEIBA* **2013**, *10*, 57−62.
(32) Espina, L.; Somolinos, M.; Lorán, S.; Conchello, P.; García, D.; Pagán, R. Chemical composition of commercial citrus fruit essential oils and evaluation of their antimicrobial activity acting alone or in combined processes. *Food Control* **2011**, *22*, 896−902.
(33) Deterre, S.; Rega, B.; Delarue, J.; Decloux, M.; Lebrun, M.; Giampaoli, P. Identification of key aroma compounds from bitter orange (*Citrus aurantium* L.) products: essential oil and macerate-distillate extract. *Flavour Fragrance J.* **2012**, *27*, 77−88.
(34) Al-Kateb, H.; Mottram, D. S. The relationship between growth stages and aroma composition of lemon basil *Ocimum citriodorum* Vis. *Food Chem.* **2014**, *152*, 440−446.
(35) Lan Phi, N. T.; Minh Tu, N. T.; Nishiyama, C.; Sawamura, M. Characterisation of the odour volatiles in *Citrus aurantifolia* Persa lime oil from Vietnam. *Dev. Food Sci.* **2006**, *43*, 193−196.
(36) Cejudo, B. M. J.; Durán, E.; Castro, R.; Rodríguez-Dodero, M. C.; Natera, R.; García-Barroso, C. Study of the volatile composition and sensory characteristics of new Sherry vinegar-derived products by maceration with fruits. *LWT−Food Sci. Technol.* **2013**, *50*, 469−479.
(37) Chisholm, M. G.; Jell, J. A.; Cass, D. M. Characterization of the major odorants found in the peel oil of *Citrus reticulata* Blanco cv. Clementine using gas chromatography-olfactometry. *Flavour Fragrance J.* **2003**, *18*, 275−281.
(38) Lin, J.; Rouseff, R. L.; Barros, S.; Naim, M. Aroma composition changes in early season grapefruit juice produced from thermal concentration. *J. Agric. Food Chem.* **2002**, *50*, 813−819.
(39) Baldwin, E. A.; Bai, J.; Plotto, A.; Cameron, R.; Luzio, G.; Narciso, J.; Manthey, J.; Widmer, W.; Ford, B. L. Effect of extraction method on quality of orange juice: hand-squeezed, commercial-fresh squeezed and processed. *J. Sci. Food Agric.* **2012**, *92*, 2029−2042.
(40) Shaw, P. E.; Wilson, C. W. Importance of nootkatone to the aroma of grapefruit oil and the flavor of grapefruit juice. *J. Agric. Food Chem.* **1981**, *29*, 677−679.
(41) Ruiz, P.; Mahattanatawee, K.; Smoot, J. M.; Rouseff, R. Identification of sulfur volatiles in canned orange juices lacking orange flavor. *J. Agric. Food Chem.* **2007**, *55*, 5761−5767.

MCs in aquatic environments may be transferred to farmland through agricultural irrigation using toxin-contaminated water and fertilization using harvested toxic cyanobacterial paste.[14] In order to reduce the water contamination, thousands of tons of cyanobacterial blooms have been mechanically salvaged from the eutrophicated water in the past decade in China. Some cyanobacterial blooms from this collection were discharged as organic fertilizers directly onto the farmlands near the waters. Following transfer of the cyanobacterial blooms and the toxin-contaminated water to farmlands, a considerable quantity of toxins is released to farmlands. High levels of MCs, ranging from 2.1 to 6.6 ng/g and 1.4 to 21.3 ng/g, were detected in the cropland soil near Taihu Lake and Dianchi Lake in China, respectively.[15,16]

Previous studies have shown that the morphological characteristics and the productivity of crop plants were affected when exposed to microcystins.[17,18] Furthermore, the exposure of edible crops to microcystins would cause human health risks, as terrestrial crops can take up and accumulate these compounds in the roots, stems, and leaves.[19−21] MCs accumulation in crops (such as vegetables) irrigated with toxin-contaminated water or fertilized with toxic cyanobacterial blooms could introduce MCs to the human food chain and consequently pose a hazard health risk to humans. Recent studies have reported that the consumption of vegetables (for example, salad lettuce) is another important exposure route of MCs to humans, in addition to aquatic products and drinking water exposure.[20,22,23]

The increasing awareness of the human health hazard and occurrence of cyanobacterial toxins in plants highlights the need for highly sensitive and selective analytical methods to examine MCs in plants. The methods commonly used to examine MCs can be categorized as those used for screening and quantitation. The former consisted of enzyme-linked immunosorbent assays (ELISA) and protein phosphatase inhibition assays (PPIA), which detect MCs in samples with high sensitivity. However, they cannot discriminate among MC analogues. The latter methods utilized high performance liquid chromatography (HPLC) combined with ultraviolet (UV) or mass spectrometric detection. Compared to ELISA and PPIA, the recently developed reverse-phase HPLC method can separate toxins and identify each microcystin variant. HPLC with a UV detector has been used for the identification and quantitation of microcystins through the characteristic UV spectra absorption of conjugated Adda diene, trypotophan, or tyrosine at 238, 223, or 232 nm, respectively.[24] However, identifying the target MCs based on chromatographic retention time alone is prone to false positives due to the complicated sample matrices and the similar UV spectra among MCs, which can also interfere with quantitation. Furthermore, the sensitivity of HPLC-DAD is not sufficient to detect trace amounts of MCs in plants.

HPLC coupled with mass spectrometry is an effective and powerful technology to detect the trace organic toxins in complex matrices, as it can provide the necessary sensitivity and selectivity. The feasibility of HPLC−MS/MS used to identify and quantitate trace amounts of microcystins in water and aquatic products, such as fish, shrimps, clams, and crabs, has been described in previous reports.[25−28] However, to our knowledge, simultaneous assays of trace amounts of microcystin variants in vegetable matrices using HPLC−MS/MS have not been reported. In previous studies, the detection of MCs in vegetables was performed using ELISA or HPLC-UV methods, which analyzed total MCs and did not distinguish among MC variants.[17,18]

This study was performed to establish a reliable, sensitive, and convenient method for the determination of MC variants in vegetables. The microcystins selected in our study were the toxins detected most frequently in previous environmental analyses, which included MC-LR, MC-RR, and MC-YR.

Overall, a sensitive and selective method was established for the simultaneous analysis of microcystin variants in various vegetable matrices using solid-phase extraction and HPLC-MS/MS in positive-ionization mode. This method comprised sample treatment procedures and methodologies, was validated with accuracy, precision, and matrix effect, and was applied to assay the MCs in real vegetables with acceptable results.

## MATERIALS AND METHODS

**Reagents.** The microcystin standards were bought from Taiwan Algal Science (Taoyuan, Taiwan) and Enzo Biochem (NewYork, NY), respectively, with purities >95%. Single and mixture microcystin standard stock solutions were prepared in methanol and stored in a refrigerator. Matrix-matched standard solutions were generated by adding serially diluted standard mixture to the microcystin-free (blank) vegetables (lettuce, water spinach, cabbage, choi sum, carrot, turnip, potato, pumpkin, cucumber, and eggplant). The microcystin-free vegetables detected without the target micocystins were purchased from an organic vegetable production base, which was irrigated with clean water and fertilized without the paste of cyanobacterial bloom. All the standard solutions were stored in a refrigerator and used within 3 months.

HPLC-grade acetonitrile and methanol were purchased from Fisher Co. (Fair Lawn, NJ). The solid-phase extraction (SPE) system with 24-port vacuum manifolds was bought from Sigma-Aldrich (St. Louis, MO). The Sep-pak $C_{18}$ cartridges and Oasis HLB were obtained from Waters Corporation (Milford, MA). The cartridge was pretreated with 3 mL of methanol and 6 mL of ultrapure water sequentially before sample extraction. Trifluoroacetic acid (TFA) (≥99%) was purchased from Aladdin Reagent Company (Shanghai, China). All other reagents were analytical grade. Ultrapure water used throughout the entire analytical process was obtained from a Unique-R20 system (Research Scientific Instruments Corporation, Xiamen, China).

**Instrument and Apparatus.** The Applied Biosystems API 4000Q-Trap triple-quadrupole mass spectrometer (Applied Biosystems, FosterCity, Canada) equipped with an electrospray ionization (ESI) source was used in this study. The liquid chromatography system was an Agilent 1100 system equipped with a G1379A degasser, G1311A binary pump, G1313A autosampler and G1316A column oven (Agilent Technologies, Palo Alto, CA). HPLC separation was performed using a 150 mm × 2.1 mm i.d., 5 $\mu$m, Eclipse Plus $C_{18}$ column (Agilent Technologies, PaloAlto, CA).

**Recommended Procedure.** The tested vegetable samples (lettuce, water spinach, cabbage, choi sum, carrot, turnip, potato, pumpkin, cucumber and eggplant), with moisture content of 80.9−95.4%, were collected and immediately transported to the laboratory under the cool conditions, then the fresh vegetables were lyophilized and ground to powder (0.45 mm). Two g (accurate to 0.01 g) of the lyophilized powder of vegetable sample was extracted using 10 mL of acidified methanol aqueous solution (methanol/water/TFA, 80/19.9/0.1 or 80/19/1, v/v/v) by 20 min of vortexing

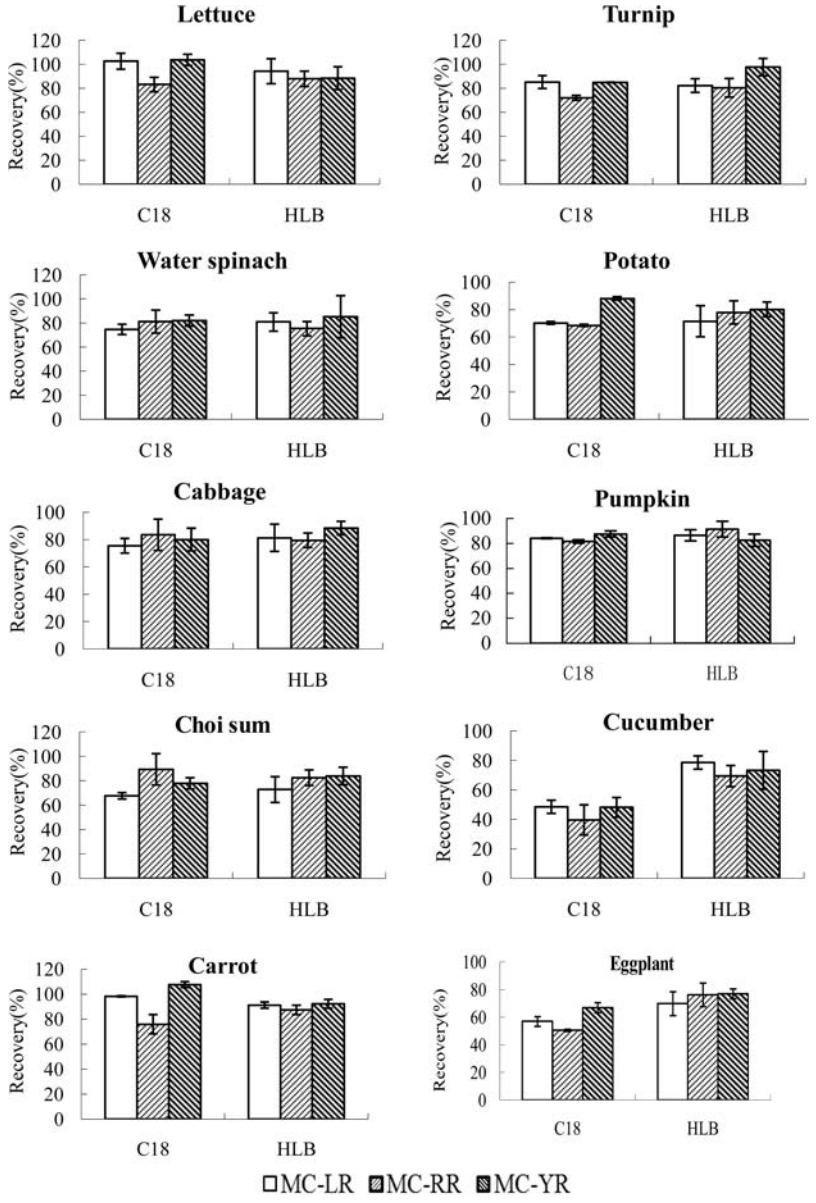


**Figure 2.** Effect of sorbents ($C_{18}$ and HLB) on the recovery of microcystins in different vegetables ($n$ = 5).

extraction and 10 min of ultrasonic extraction, followed by centrifugation at 10000 rpm and 10 °C for 10 min. The supernatant was collected and the vegetable residue was extracted again with 10 mL of acidified aqueous methanol. The supernatants were combined and concentrated to ~2 mL using a rotary evaporator below 40 °C under reduced pressure. The obtained extract was introduced into the $C_{18}$ (HLB cartridge was used for cucumber and eggplant sample) cartridge (500 mg/6 mL) for solid-phase extraction cleanup. The effluent was collected and reintroduced into a $C_{18}$ (or HLB) cartridge for re-extraction. Then the cartridge was rinsed with 5 mL of ultrapure water and vacuum-dried. It was then eluted with 5 mL of acidified aqueous methanol (methanol/water/TFA, 80/19.9/0.1, v/v/v) and the resulting eluate was filtered through a 0.22 $\mu$m filter and concentrated to 1 mL using a nitrogen stream for LC-MS/MS detection. Quantitation was performed using matrix-matched standard calibrations.

Microcystin-free vegetables were used as blanks for validation experiments and matrix-matched standard calibrations. Fortification of the vegetable samples for recovery studies was carried out by delivering 0.4 mL of mixed microcystin standard solutions at 0.1, 1, and 5 $\mu$g/mL in methanol to 2 g of lyophilized vegetable samples to obtain 20, 200, and 1000 $\mu$g/kg dw fortification levels (roughly equivalent to 1, 10, and 50 $\mu$g/kg fresh weight fortification levels, respectively). The fortified samples were left for 12 h at room temperature prior to the sample extraction procedure.

**Chromatographic and Mass Spectrometric Conditions.** *HPLC Operating Conditions.* The mobile phase consisted of acetonitrile (solvent A) and water containing 0.2% (v/v) formic acid (solvent B), the flow rate was 0.3 mL/min. The optimal gradient program started with 20% acetonitrile at the time of injection and increased linearly to 80% acetonitrile over 2 min, which was kept for 4.5 min, and then brought back to 20% acetonitrile over 0.1 min and held for 9.4 min until the next injection. The column oven temperature was maintained at 35 °C. The sample injection volume was 5 $\mu$L. All the three microcystins were eluted within 6.0 min.


dx.doi.org/10.1021/jf5033075 | J. Agric. Food Chem. 2014, 62, 11831−11839

*MS Operating Conditions.* The ESI source in positive multiple-reaction-monitoring (MRM) mode was used for the identification and quantitation of the three microcystin variants. The monitoring parameters were optimized as follows: ion source spray voltage (IS), 5500 V; atomization temperature (TEM), 450 °C; atomization gas pressure (GAS1), 55 psi (nitrogen); heated auxiliary gas (GAS2), 50 psi (nitrogen); air curtain gas pressure (CUR), 25 psi (nitrogen); collision flow ratio (CAD), high.

**Data Analysis.** Microcystin concentrations from LC-MS/MS analysis were determined using Analyst software(version 1.4, Applied Biosystems). The data were exported to Microsoft Excel 2003 (Microsoft Co., Redmond, WA, USA) to calculate the average and to perform statistical (ANOVA) analysis.

## RESULTS AND DISCUSSION

**Optimization of Sample Pretreatment.** Ten vegetables—lettuce, water spinach, cabbage, choi sum, carrot, turnip, potato, pumpkin, cucumber, and eggplant—were selected for the study to represent tropical and subtropical vegetables commonly consumed in China. Ten vegetables were chosen to examine the matrix effects of each vegetable on the determination of MCs in vegetables because the matrix components in the samples can affect the analyte signals. It is believed that the same species of vegetables should have similar matrix effects. Thus, lettuce, water spinach, cabbage, and choi sum could represent green leafy vegetables with high content of chlorophyll.[29] Carrot, turnip, and potato were the representatives of root vegetables, while pumpkin, cucumber, and eggplant represent fruit vegetables.

Microcystin variants in vegetable samples were usually present at trace or even ultratrace amounts, and the vegetable matrix effect may interfere with the HPLC separation and reduce the sensitivity of the mass spectrometry detector; therefore, analyte enrichment and sample cleanup were required prior to HPLC-MS/MS analysis. During the sample treatment process, lyophilization was used to dehydrate the vegetables and concentrate microcystins, with less loss of analyte under vacuum and cool conditions. Furthermore, the volumes of reagents used for sample extraction decreased by 80% compared to the fresh vegetable samples, which could also reduce the time required for the extract to pass through the cartridge.

Previous studies suggested that an acidified aqueous methanol solvent was suitable for the extraction of both hydrophilic and hydrophobic microcystins.[30] Therefore, the extraction efficiencies of solvents at several methanol−water ratios (60%, 80%, and 100% methanol) and acidities (1%, 0.1%, and 0.01% TFA, v/v) were evaluated.

Extraction with 80% methanol provided recoveries higher than 67.6% in all vegetable samples for the three target MCs, while extraction with 60% and 100% methanol yielded low recoveries of 42.6% and 45.3% for MC-LR, 48.1% and 48.8% for MC-RR, and 44.4% and 45.5% for MC-YR in the vegetable samples, respectively. In most of the selected vegetable matrices, the highest extraction efficiencies for the three microcystins were obtained by addition of 0.1% TFA (v/v) in aqueous methanol (19.9/80, v/v) solution, while the highest extraction efficiencies of MC-LR in potato and choi sum, of MC-RR in cucumber and pumpkin, and of MC-YR in water spinach and cabbage were obtained by addition of 1% TFA (v/v) in aqueous methanol.

In the sample cleanup and preconcentration step, two commonly used sorbents, Oasis Sep-Pak $C_{18}$ and HLB cartridges, which could simultaneously retain nonpolar to moderately polar toxins from complicated matrices,[31] were tested in various vegetable matrices to optimize extraction and concentration efficiency. As shown in Figure 2, both recovery and RSD were satisfied when Sep-Pak $C_{18}$ or Oasis HLB was used in lettuce, water spinach, cabbage, choi sum, carrot, turnip, potato, and pumpkin samples. However, the $C_{18}$ cartridge was selected as a sorbent for the above-mentioned eight species of vegetable because it was relatively cheap compared with the HLB cartridge. Nevertheless, microcystin recoveries were very poor (less than 60%) when the $C_{18}$ cartridge was used for cucumber and eggplant samples, suggesting that interfering impurities in the matrices were not completely eliminated. Otherwise, when HLB was used in these matrices, both recoveries (>70%) and RSD were acceptable in terms of removing pigments from cucumber and eggplant (Figure 2). Therefore, $C_{18}$ (500 mg/6 mL) was used to clean up lettuce, water spinach, cabbage, choi sum, carrot, turnip, potato, and pumpkin samples, while HLB (500 mg/6 mL) was chosen to purify cucumber and eggplant in the study.

In the elution step, the retained microcystins should be completely eluted using as little volume of eluent as possible. Microcystins are relatively polar molecules with hydrophobic regions, such as the Adda residue or hydrophobic substituents of amino acids. Some investigations found that the efficiency of eluting solvents depended on various factors, such as the water content of the sample and eluent polarity.[32,33] Thus, various aqueous/methanol ratios from 10% to 100% methanol were tested for elution of the adsorbed microcystins from the cartridges. When the solutions (5 mL) contained less than 50% methanol, they could not remove the target microcystins. The pure methanol resulted in more efficient elution of MC-LR and MC-YR, but the yield of MC-RR, a strong polar, was not sufficient. However, the desired elution yields of the three microcystin variants were obtained when using 80% methanol. Therefore, 5 mL of 80% methanol aqueous solution was optimal to elute the tested microcystin variants from the cartridges.

**Liquid Chromatography.** The reverse-phase HPLC system with a $C_{18}$ stationary phase and an acetonitrile in the water mobile phase is a typical method of separating microcystin variants.[34] Two Agilent Eclipse Plus $C_{18}$ columns, both 150 mm × 2.1 mm i.d., but with different particle sizes of 5 and 3.5 $\mu$m were compared for separation of the target microcystins. A better reproducibility and sensitivity of the three target microcystins was observed when separated with the 5 $\mu$m particle size column compared to the 3.5 $\mu$m particle size column. Thus, the Agilent Eclipse Plus $C_{18}$ column with 5 $\mu$m particle size was selected.

The mobile phase, which consists of acetonitrile gradients in the presence of organic acid, such as formic acid, is capable of separating microcystin variants with greater chromatographic efficiency than the neutral mobile phase because the acid could improve the protonation of carboxylic acid groups in the toxins and decrease the interactions between basic groups of the microcystin molecule and the silanol groups coated on the particle surface in the column.[35] The effects of the formic acid addition ratio in the mobile phase on the MCs defect sensitivity were evaluated. It can be found that a mobile phase containing 0.2% formic acid provided the highest sensitivity. Under this

condition, the liquid chromatography elution order was MC-RR, MC-YR, and MC-LR.

**Mass Spectrometry.** Individual standard solutions of each microcystin were infused into the ESI source to create an ion transition under the positive-ionization mode. In the full-scan mass spectrum, the protonated molecules ($[M + H]^+$) of $m/z$ 996.1 and 1046 were produced by MC-LR and MC-YR, respectively, and the double-charged protonated molecular ion $[M + 2H]^{2+}$ of $m/z$ 520 was produced by MC-RR, which contains two basic Arg residues in the molecule. The protonated molecule was selected as a precursor ion and was subjected to fragmentation. The fragment ions of $m/z$ 135 and 213 were the major product ions for the three target microcystins and used as the quantitative and qualitative ions, respectively. The product ion mass spectra of MC-LR, MC-RR, and MC-YR are shown n Figure 3. The fragment ion of $m/z$ 135 was identified as the $[\text{phenyl-CH}_2\text{–CH(OCH}_3)]^+$ ion formed by cleavage of the Adda residue between C-8 and C-9, and $m/z$ 213 was $[\text{Glu-Mdha+H}]^+$ formed by the cleavage of the $\alpha$-linked glutamic acid (D-Glu) and *N*-methyldehydroalanine (Mdha) residue.[36] Two major ion pairs for each analyte and the optimal MS/MS parameters for each ion pair are described in Table 1.

**Method Validation.** *Matrix Effects.* The matrix effect (ME), which impacts the quantitation greatly, depends on various factors, including the instrument, the type and amount of matrix, the treatment procedure, and the properties of the analyte.[37,38] The matrix effect in vegetable matrices was studied by comparing the slopes of the calibration curves of standards in methanol and sample matrices. The following expression was used to quantitate signal suppression or enhancement for each microcystin:

$$ME = 100 \times \left(\frac{slope_m}{slope_s} - 1\right)\%$$

The $\text{slope}_m$ and $\text{slope}_s$ represent the slopes of the matrix-matched and solvent-only (matrix-free) calibration curves, respectively. The matrix effect was considered mild when it ranged from −20% to −10% or from +10% to +20%, medium when it ranged from −50% to −20% or from +20% to +50%, and strong when it was below −50% or above +50%. If it ranged from −10% to +10%, the effect could be ignored. These results reveal the suppressive effects of vegetable components on the tested microcystins in the range of −63% to −2%. The matrix effects of three tested microcystins in lettuce (−13 to −5%) and carrot (−10 to −2%) could almost be ignored, but those in water spinach, choi sum, turnip, cucumber, and eggplant matrices showed medium suppression (−50 to −20%). A strong signal-suppressive effect was detected in potato and pumpkin for MC-RR and in cabbage and pumpkin for MC-YR. Generally, matrix effects originated from insufficient elimination of sample endogenous materials such as pigments and fatty acids. The coexistence of the impurities would affect the ionization efficiency and weaken the response of the analytes. Therefore, in order to get more accurate results, the matrix-matched calibration curves should be used for quantitation due to the existence of matrix effects.

*Linearity and Limit of Quantitation (LOQ).* The linearity and LOQ were obtained using the peak areas of the product ions acquired from the MS/MS mode. The matrix-matched calibration curves were constructed using least-squares linear regression analysis of the matrices (lettuce, water spinach, cabbage, choi sum, carrot, turnip, potato, pumpkin, cucumber, and eggplant) spiked with MC-LR, MC-RR, and MC-YR at 5–2500 ng/mL. The correlation coefficients ($R^2$) were higher than 0.9876 in all cases, and the limit of detection (LOD) was below 7.5 μg/kg, while the LOQ was 1.6–10.0 μg/kg (dw), 6.3–25.0 μg/kg (dw), and 5.6–25.0 μg/kg (dw) for MC-LR, MC-RR, and MC-YR in different vegetable matrices, respectively. Regarding specificity, no responses were detected in the

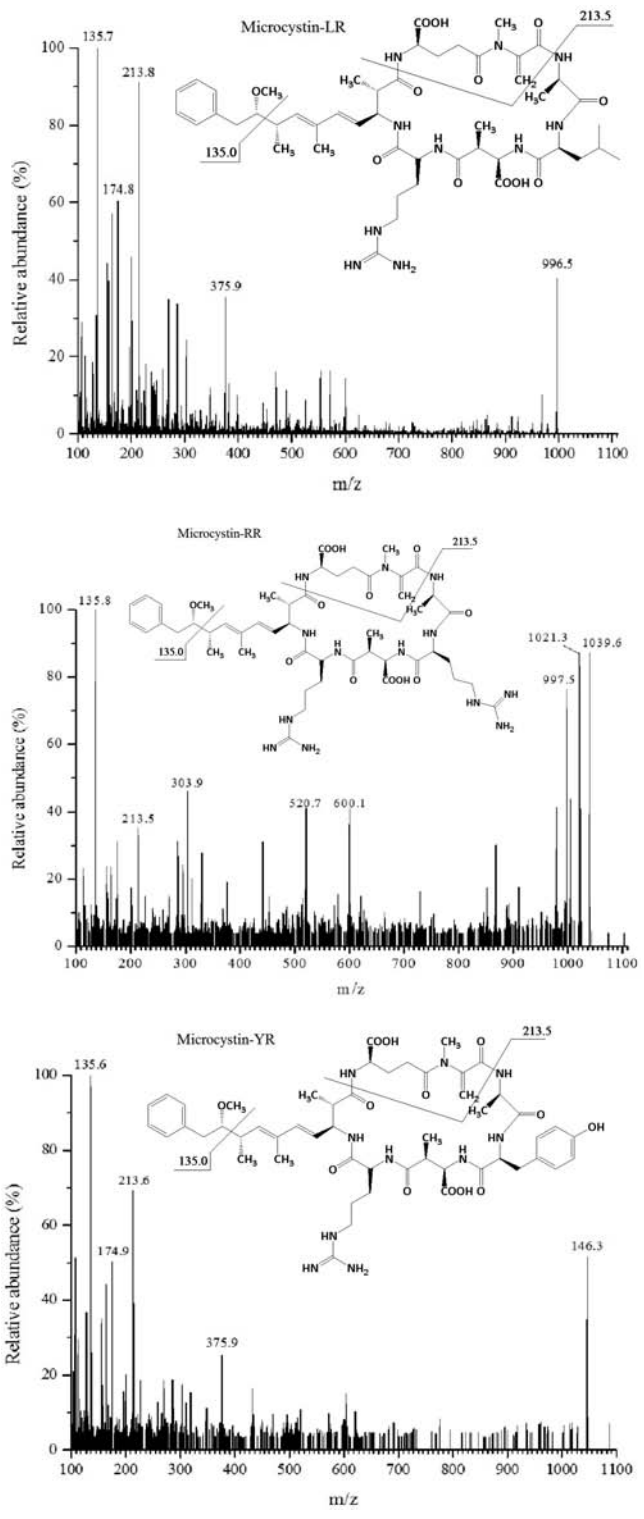


**Figure 3.** MS/MS spectra of the three target microcystins.


dx.doi.org/10.1021/jf5033075 | J. Agric. Food Chem. 2014, 62, 11831–11839

**Table 1. Mass Spectrometry Characteristics of the Target Microcystins as Determined Using LC-MS/MS**

| Compound | Mol wt | Retention time (min) | Precursor ion | Product ion | DP[a] | CE[b] |
|---|---|---|---|---|---|---|
| Microcystin-LR | 995.2 | 5.5 | 996.1 $[M + 1]^+$ | 135[c]/ 213[d] | 96/91 | 100/85 |
| Microcystin-RR | 1038.2 | 5.2 | 520 $[M + 2]^{2+}$ | 135/213 | 90/90 | 56/56 |
| Microcystin-YR | 1045.2 | 5.4 | 1046 $[M + 1]^+$ | 135/213 | 150/150 | 100/90 |

[a]DP, decluster potential. [b]CE, collision energy voltages. [c]Quantitative ion. [d]Qualitative ion.

**Table 2. Recoveries and RSD for the Target Microcystins from Different Matrices at Three Fortified Levels**

| | | MC-LR | | | MC-RR | | | MC-YR | | |
|---|---|---|---|---|---|---|---|---|---|---|
| Matrix | Fortification level ($\mu$g/kg dw) | Recovery (%) | RSD[a] (%) | RSD[b] (%) | Recovery (%) | RSD[a] (%) | RSD[b] (%) | Recovery (%) | RSD[a] (%) | RSD[b] (%) |
| Lettuce | 20 | 61.3 | 9.1 | 9.8 | 83.9 | 11.5 | 12.1 | 116.1 | 6.4 | 6.9 |
| | 200 | 102.6 | 6.6 | 8.7 | 83.2 | 6.1 | 8.2 | 103.8 | 4.7 | 5.3 |
| | 1000 | 95.2 | 4.7 | 7.3 | 92.5 | 4.8 | 5.9 | 93.3 | 5.0 | 5.8 |
| Water spinach | 20 | 85.5 | 5.8 | 4.2 | 62.1 | 16.4 | 13.8 | 91.2 | 0.8 | 4.9 |
| | 200 | 74.7 | 4.3 | 6.9 | 81.2 | 9.6 | 9.7 | 82.0 | 4.7 | 8.5 |
| | 1000 | 77.6 | 7.2 | 6.8 | 65.6 | 3.5 | 10.1 | 81.8 | 8.8 | 8.5 |
| Cabbage | 20 | 78.4 | 3.4 | 5.5 | 117.3 | 4.3 | 6.7 | 97.0 | 16.7 | 12.3 |
| | 200 | 65.4 | 5.3 | 9.4 | 83.5 | 11.5 | 9.9 | 79.9 | 8.3 | 13.5 |
| | 1000 | 82.2 | 6.8 | 10.2 | 70.4 | 6.9 | 7.9 | 82.5 | 7.8 | 9.1 |
| Choi sum | 20 | 102.5 | 0.6 | 6.7 | 79.4 | 7.9 | 8.5 | 84.0 | 17.9 | 11.6 |
| | 200 | 67.6 | 2.6 | 3.8 | 89.3 | 12.8 | 10.5 | 67.8 | 4.6 | 18.3 |
| | 1000 | 68.3 | 2.1 | 11.2 | 70.0 | 9.1 | 11.4 | 68.0 | 2.9 | 10.9 |
| Carrot | 20 | 107.9 | 8.5 | 4.4 | 85.9 | 11.2 | 10.9 | 100.3 | 7.4 | 11.3 |
| | 200 | 98.3 | 0.5 | 3.9 | 76.0 | 7.7 | 9.8 | 107.6 | 2.3 | 5.6 |
| | 1000 | 89.3 | 4.0 | 5.0 | 92.7 | 11.4 | 8.9 | 111.4 | 4.0 | 6.3 |
| Turnip | 20 | 81.7 | 4.7 | 5.1 | 72.2 | 6.8 | 9.9 | 86.7 | 5.4 | 9.2 |
| | 200 | 85.2 | 5.4 | 3.8 | 72.1 | 2.0 | 6.9 | 84.9 | 0.2 | 2.1 |
| | 1000 | 72.9 | 2.6 | 8.1 | 71.5 | 3.5 | 7.2 | 81.5 | 0.7 | 1.6 |
| Potato | 20 | 70.2 | 5.3 | 2.4 | 68.9 | 4.5 | 6.4 | 95.3 | 7.3 | 5.6 |
| | 200 | 70.2 | 11.0 | 9.5 | 68.4 | 0.8 | 2.1 | 88.1 | 1.2 | 4.1 |
| | 1000 | 74.1 | 4.3 | 5.8 | 79.6 | 2.9 | 2.9 | 78.2 | 1.6 | 7.5 |
| Pumpkin | 20 | 93.7 | 9.8 | 9.2 | 77.8 | 9.3 | 10.4 | 92.9 | 4.9 | 6.5 |
| | 200 | 84.0 | 0.4 | 4.3 | 81.5 | 1.4 | 3.6 | 87.5 | 2.4 | 3.2 |
| | 1000 | 91.7 | 3.1 | 11.6 | 87.3 | 5.4 | 6.9 | 90.7 | 2.9 | 4.6 |
| Cucumber | 20 | 74.1 | 4.3 | 8.9 | 79.6 | 2.9 | 5.4 | 78.2 | 1.6 | 2.4 |
| | 200 | 78.5 | 4.5 | 9.4 | 69.4 | 1.2 | 7.1 | 73.2 | 12.8 | 14.3 |
| | 1000 | 76.1 | 4.4 | 6.6 | 79.3 | 4.0 | 4.2 | 78.2 | 6.6 | 5.9 |
| Eggplant | 20 | 75.0 | 9.4 | 8.4 | 81.9 | 8.7 | 8.8 | 83.9 | 7.3 | 9.4 |
| | 200 | 69.9 | 8.6 | 8.2 | 76.3 | 8.5 | 9.4 | 77.0 | 3.6 | 5.4 |
| | 1000 | 68.1 | 0.7 | 6.7 | 87.5 | 7.0 | 9.1 | 70.6 | 0.8 | 6.9 |

[a]Intraday precision ($n$ = 5). [b]Interday precision ($n$ = 15).

procedure blank or vegetable sample blank, suggesting the high specificity of MS-MS detection.

*Accuracy and Precision.* The recovery analysis was performed to evaluate the performance of the proposed method by analyzing 10 species of vegetable samples spiked with 20, 200, or 1000 $\mu$g/kg of MC-LR, MC-RR, and MC-YR. The precision of the method was expressed using the intraday and interday relative standard deviation (RSD). The intraday RSD was measured by comparing the standard deviation of the recovery rates of the spiked samples analyzed in the same day. The intraday RSD was determined by analyzing the spiked samples for three distinct days. Table 2 showed the detailed recovery and repeatability data for the microcystins in various vegetable matrices. The recoveries of the microcystins were in the range of 61.3−117.3% ($n$ = 5), and the RSD of the intraday ($n$ = 5) and interday ($n$ = 15) ranged from 0.2−17.9% and 1.6−18.3%, respectively. The MRM chromatograms of the blank and the positive lettuce sample are shown in Figure 4, and this indicates that the proposed method can maintain blanks below a critical threshold.

**Method Application.** To demonstrate its functionality, the proposed method was applied to determine the field vegetable samples collected from the farmlands irrigated with Dianchi Lake water. Dianchi Lake is China's sixth largest fresh water lake, fed by several rivers and located at 1700 m above sea level in Yungui Plateau in southwest China. This lake is used to irrigate millions of hectares of grains and vegetables in a lush agricultural region in Yunnan Province, and it was formerly one of China's most important freshwater fisheries. With the rapid economic development over the past 30 years, the lake has been subjected to serious eutrophication, which has caused frequent outbreaks of cyanobacteria blooms during years.[39−41]

A total of 28 vegetable samples (8 lettuce samples, 3 water spinach samples, 12 cabbage samples and 5 choi sum samples) with moisture content ranging from 91.4% (water spinach) to 95.4% (lettuce) were collected in the winter of 2013 from

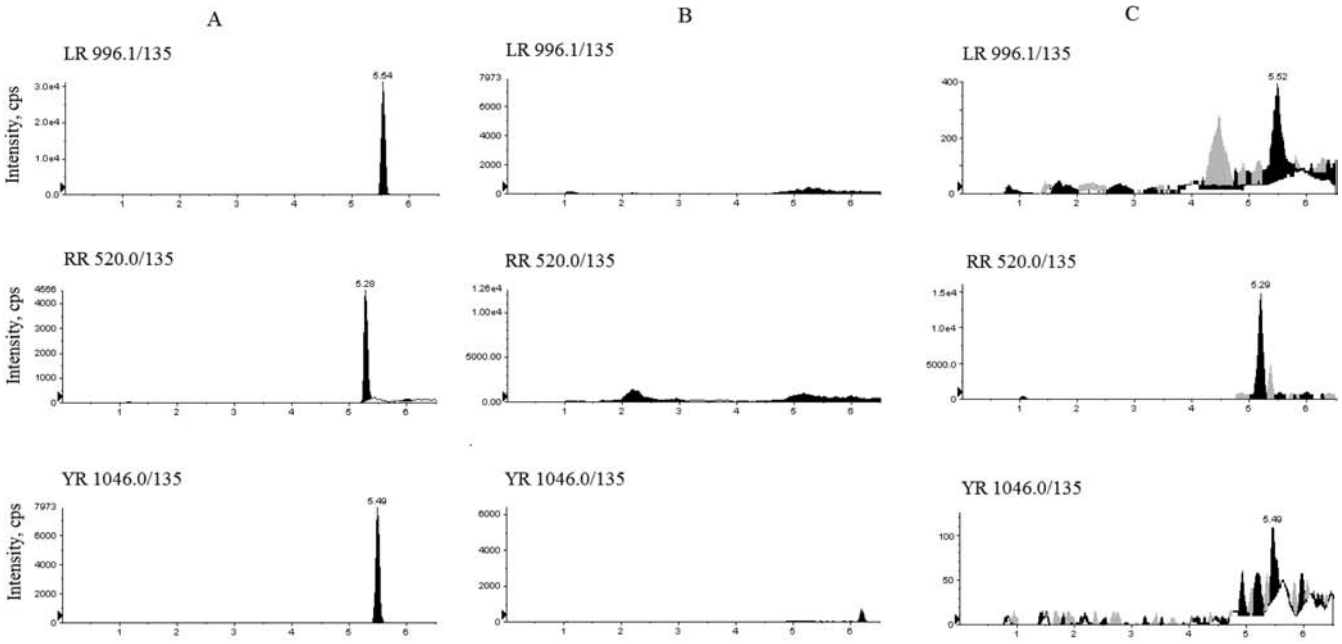


**Figure 4.** MRM chromatograms of (A) standard solution; (B) lettuce matrix; and (C) positive lettuce sample by HPLC-MS/MS.

**Table 3. Concentrations of the Three Microcystin Variants in Vegetables**

| MC | Vegetable | Moisture content (%) | Sample no. | Positive sample no. | Range (dw[a]/fw[b]) (μg/kg) | Average (dw) ± SD (μg/kg) |
|---|---|---|---|---|---|---|
| MC-LR | Lettuce | 95.4 | 8 | 0 | ND[c]/ND | |
| | Water spinach | 91.4 | 3 | 1 | 23.7/2.0 | |
| | Cabbage | 94.9 | 12 | 0 | ND/ND | |
| | Choi sum | 92.7 | 5 | 0 | ND/ND | |
| MC-RR | Lettuce | 95.4 | 8 | 8 | 46.1−2352.2/2.1−108.2 | 973.7 ± 849.4 |
| | Water spinach | 91.4 | 3 | 3 | 36.4−765.2/3.1−65.8 | 298.8 ± 330.6 |
| | Cabbage | 94.9 | 12 | 10 | 53.1−394.1/2.7−20.1 | 138.6 ± 54.4 |
| | Choi sum | 92.7 | 5 | 4 | 86.2−553.3/6.3−40.4 | 196.4 ± 189.0 |
| MC-YR | Lettuce | 95.4 | 8 | 1 | 22.8/1.0 | |
| | Water spinach | 91.4 | 3 | 0 | ND/ND | |
| | Cabbage | 94.9 | 12 | 0 | ND/ND | |
| | Choi sum | 92.7 | 5 | 0 | ND/ND | |
| ∑MCs | Lettuce | 95.4 | 8 | 8 | ND-2352.2/ND-108.2 | |
| | Water spinach | 91.4 | 3 | 3 | ND-788.9/ND-67.8 | |
| | Cabbage | 94.9 | 12 | 11 | ND-394.1/ND-20.1 | |
| | Choi sum | 92.7 | 5 | 4 | ND-553.3/ND-40.4 | |

[a]dry weight. [b]fresh weight. [c]not detected.

farmlands along the lake shore, which were irrigated with the lake water. Three quality controls (QCs) at 20, 200, and 1000 μg/kg were included for each vegetable sample in the analysis sequence.

The concentrations of MCs in the analyzed samples are listed in Table 3. The detected frequencies of the target microcystins were 3.6%, 89.3%, and 7.1% for MC-LR, MC-RR, and MC-YR, respectively, in the Dianchi Lake vegetable samples. The most frequently detected microcystin in the vegetable samples was MC-RR, which was consistent with the results reported previously in Dianchi Lake water.[22] All the tested vegetable samples, with the exception of two cabbage samples and a choi sum sample, contained MC-RR at 36.4−2352.2 μg/kg (dw). The vegetable samples with high MC-RR concentrations, exceeding 1000 μg/kg, were cultivated in a greenhouse. One water spinach sample and one lettuce sample contained MC-LR and MC-YR with 23.7 and 22.8 μg/kg, respectively. Similar concentrations were found in various vegetables cultivated around Taihu Lake (the third largest freshwater lake in China) using an ELISA screening method (∑MCs concentration: 30−360 μg/kg).[14]

In summary, a sensitive, selective, and reliable method based on HPLC-MS/MS was developed through stepwise optimization for the individual analysis of three microcystins in common vegetables. This method requires less than 6 min to perform each sample analysis. Using a simple solid-phase extraction procedure consuming only 2 g of lyophilized vegetable samples for cleanup and analyte enrichment, the method can be used to simultaneously determine trace microcystin variants (MC-LR, MC-RR, and MC-YR) in various vegetables at μg/kg levels. The optimized method was applied to analysis of vegetables collected from farmlands irrigated with cyanobacterial bloom water. The results indicated that vegetables were contaminated with microcystins, of which MC-RR exhibited the highest concentration, 2352.2 μg/kg. More research is clearly needed to

evaluate the human health risk exposed to microcystins via edible terrestrial plants such as vegetables in the future.

## ■ ASSOCIATED CONTENT

### Supporting Information

Table S1. Effects of formic acid on the microcystin detection sensitivity of MS. Table S2. Linear range, calibration curves, limits of detection (LOD), and limits of quantitation (LOQ) of microcystins in various vegetables (to be continued). Figure S1. Effect of water/methanol ratio on extraction efficiency of microcystins in different vegetables ($n$ = 5). Figure S2. Effect of acidity on extraction efficiency of microcystins in different vegetables ($n$ = 5). This material is available free of charge via the Internet at http://pubs.acs.org.

## ■ AUTHOR INFORMATION

### Corresponding Author

*Tel: +86 020 85220564. Fax: +86 020 85226615. E-mail: tchmo@jnu.edu.cn.

### Funding

This work was supported by the National Natural Science Foundation of China (41301337, 41173101), Natural Science Foundation of Guangdong Province (2011020003196), the project of Science and Technology of Dongguan City (201210815000399), and the High-Level Talents Program of Guangdong Higher Education Institutions, granted to C.-H.M., Jinan University, and by a Scientific Research Innovation Project for Graduates without Requiring Entrance Examinations, granted to T.-F.S.

### Notes

The authors declare no competing financial interest.

## ■ REFERENCES

(1) Rinehart, K. L.; Harada, K.; Namikoshi, M.; Chen, C.; Harvis, C. A.; Munro, M. H. G.; Blunt, J. W.; Mulligan, P. E.; Beasley, V. R.; Dahlem, A. M.; Carmichael, W. W. Nodularin, microcystin, and the configuration of Adda. *J. Am. Chem. Soc.* **1988**, *110*, 8557−8558.

(2) Sandra, P.; Diana, S. A. Recent advances in the sample preparation, liquid chromatography tandem mass spectrometric analysis and environmental fate of microcystins in water. *TrAC Trends in Anal. Chem.* **2005**, *24*, 658−670.

(3) Falconer, I. R. Is there a human health hazard from microcystins in the drinking water supply. *Acta Hydroch. Hydrob.* **2005**, *33*, 65−71.

(4) Carmichael, W. W. Health effects of toxin-producing cyanobacteria: "the CyanoHABs. *Hum. Ecol. Risk Assess.* **2001**, *7*, 1393−1407.

(5) Sivonen, K.; et al. Cyanobacterial toxins. In *Toxic Cyanobacteria in Water: A Guide to Their Public Health Consequences, Monitoring and Management*; Chorus, I., Bartram, J., Eds.; E & FN Spon: London, 1999; Chapter 3, p 26.

(6) Yu, S. Z. Drinking water and primary liver cancer. In *Primary Liver Cancer*; Tang, Z. Y., Wu, M. C., Xia, S. S., Eds.; China Academic Publications: Beijing, China, 1989; p 495.

(7) Yu, S. Z. Primary prevention of hepatocellular carcinoma. *J. Gastroen. Hepatol.* **1995**, *10*, 674−682.

(8) Xu, C.; Chen, J. A.; Huang, Y. J.; Qiu, Z. Q.; Luo, J. H.; Zeng, H.; Zhao, Q.; Cao, J.; Shu, W. Q. Identification of microcystins contamination in surface water samples from the Three Gorges Reservoir, China. *Environ. Monit. Assess.* **2011**, *180*, 77−86.

(9) Song, L. R.; Chen, W.; Peng, L.; Wan, N.; Gan, N. Q.; Zhang, X. M. Distribution and bioaccumulation of microcystins in water columns: A systematic investigation into the environmental fate and the risks associated with microcystins in Meiliang Bay, Lake Taihu. *Water Res.* **2007**, *41*, 2853−2864.

(10) Li, S.; Xie, P.; Xu, J.; Zhang, X.; Qin, J.; Zheng, L.; Liang, G. Factors shaping the pattern of seasonal variations of microcystins in Lake Xingyun, a subtropical plateau lake in China. *Bull. Environ. Contam. Toxicol.* **2007**, *78* (3−4), 226−230.

(11) Zhang, X.; Xie, P.; Hao, L.; Guo, N. C.; Gong, Y. G.; Hu, X. L.; Chen, J.; Liang, G. D. Effects of the phytoplanktivorous silver carp (*Hypophthalmichthys molitrixon*) on plankton and the hepatotoxic microcystins in an enclosure experiment in a eutrophic lake, Lake Shichahai in Beijing. *Aquaculture* **2006**, *257*, 173−186.

(12) Wang, J.; Pang, X. L.; Ge, F.; Ma, Z. Y. An ultra-performance liquid chromatography-tandem mass spectrometry method for determination of microcystins occurrence in surface water in Zhejiang Province, China. *Toxicon* **2007**, *49*, 1120−1128.

(13) Meriluoto, J. A. O.; Spoof, L. E. M. Cyanotoxins: sampling, sample processing and toxin uptake. *Adv. Exp. Med. Biol.* **2008**, *619*, 483−499.

(14) Chen, W.; Song, L. R.; Gan, N. Q.; Li, L. Sorption, degradation and mobility of microcystins in Chinese agriculture soils: risk assessment for groundwater protection. *Environ. Pollut.* **2006**, *144*, 752−758.

(15) Chen, W.; Jia, Y. L.; Li, E. H.; Zhao, S.; Zhou, Q. C.; Liu, L. M.; Song, L. R. Soil-Based treatments of mechanically collected cyanobacterial blooms from Lake Taihu: efficiencies and potential risks. *Environ. Sci. Technol.* **2012**, *46*, 13370−13376.

(16) Li, Y. W.; Huang, X. P.; Wu, X. L.; Xiang, L.; Zhan, X. J.; Li, Z. J.; Wen, H. F.; Zhong, F. L.; Mo, C. H.; Hong, A. H. Simultaneous extraction and determination of three Microcystins from soil using solid phase extraction and liquid chromatography-tandem mass spectrometry. *Chin. J. Anal. Chem.* **2013**, *41*, 88−92.

(17) McElhiney, J.; Lawton, L. A.; Leifert, C. Investigations into the inhibitory effects of microcystins on plant growth, and the toxicity of plant tissues following exposure. *Toxicon* **2001**, *39*, 1411−1420.

(18) Chen, J.; Han, F. X. X.; Wang, F.; Zhang, H. Q.; Shi, Z. Q. Accumulation and phytotoxicity of microcystin-LR in rice (*Oryza sativa*). *Ecotoxicol. Environ. Saf.* **2012**, *76*, 193−199.

(19) Codd, G. A.; Bell, S. G.; Kaya, K.; Ward, C. J.; Beattie, K. A.; Metcalf, J. S. Cyanobacterial toxins, exposure routes and human health. *Eur. J. Phycol.* **1999**, *34*, 405−415.

(20) Codd, G. A.; Metcalf, J. S.; Beattie, K. A. Retention of Microcystis aeruginosa and microcystin by salad lettuce (*Lactuca sativa*) after spray irrigation with water containing cyanobacteria. *Toxicon* **1999**, *37*, 1181−1185.

(21) Crush, J. R.; Briggs, L. R.; Sprosen, J. M.; Nichols, S. N. Effect of irrigation with lake water containing microcystins on microcystin content and growth of ryegrass, clover, rape, and lettuce. *Environ. Toxicol.* **2008**, *23*, 246−252.

(22) Peng, L.; Liu, Y. M.; Chen, W.; Liu, L. M.; Kent, M.; Song, L. R. Health risks associated with consumption of microcystin-contaminated fish and shellfish in three Chinese lakes: Significance for freshwater aquacultures. *Ecotoxicol. Environ. Saf.* **2010**, *73*, 1804−1811.

(23) Zhang, D.; Xie, P.; Liu, Y.; Chen, J.; Wen, Z. Spatial and temporal variations of microcystins in hepatopancreas of a freshwater snail from Lake Taihu. *Ecotoxicol. Environ. Saf.* **2009**, *72*, 466−472.

(24) Chorus, I.; et al. Laboratory analysis of cyanotoxins. In *Toxic Cyanobacteria in Water: A Guide to Their Public Health Consequences, Monitoring and Management*; Chorus, I., Bartram, J., Eds.; E & FN Spon: London, 1999; Chapter 13, pp 384−400.

(25) Ruiz, M. J.; Cameán, A. M.; Moreno, I. M.; Picó, Y. Determination of microcystins in biological samples by matrix solid-phase dispersion and liquid chromatography−mass spectrometry. *J. Chromatogr., A* **2005**, *1073*, 257−262.

(26) Lawrence, J. F.; Menard, C. Determination of microcystins in blue-green algae, fish and water using liquid chromatography with ultraviolet detection after sample clean-up employing immunoaffinity chromatography. *J. Chromatogr., A* **2001**, *922*, 111−117.

(27) McElhiney, J.; Lawton, L. A. Detection of the cyanobacterial hepatotoxins microcystins. *Toxicol. Appl. Pharmacol.* **2005**, *203*, 219−230.

(28) Edwards, C.; Lawton, L. A.; Coyle, S. M.; Ross, P. Laboratory-scale purification of microcystins using flash chromatography and reversed-phase high-performance liquid chromatography. *J. Chromatogr., A* **1996**, *734*, 163−173.
(29) Aranzazu, P.; Carmen, H.; Juan, V.; Sancho, F. Development of a fast analytical method for the individual determination of pyrethrins residues in fruits and vegetables by liquid chromatography−tandem mass spectrometry. *J. Chromatogr., A* **2013**, *1307*, 126−134.
(30) Barco, M.; Lawton, L. A.; Rivera, J.; Caixach, J. Optimization of intracellular microcystin extraction for their subsequent analysis by high-performance liquid chromatography. *J. Chromatogr., A* **2005**, *1074*, 23−30.
(31) Liu, X. G.; Xu, J.; Dong, F. S.; Li, Y. B.; Song, W. C.; Zheng, Y. Q. Residue analysis of four diacylhydrazine insecticides in fruits and vegetables by quick, easy, cheap, effective, rugged, and safe (QuEChERS) method using ultra-performance liquid chromatography coupled to tandem mass spectrometry. *Anal. Bioanal. Chem.* **2011**, *401*, 1051−1058.
(32) Lawton, L. A.; Edwards, C.; Codd, G. A. Extraction and high-performance liquid chromatographic method for the determination of microcystins in raw and treated waters. *Analyst* **1994**, *119*, 1525−1530.
(33) Fastner, J.; Flieger, I.; Neumann, U. Optimized extraction of microcystins from field samples—A comparison of different solvents and procedures. *Wat. Res.* **1998**, *32*, 3177−3181.
(34) Biochemical Samples: Proteins, Nucleic Acids, Carbohydrates, and Related Compounds. In *Practical HPLC Method Development*; Snyder, L. R., Kirkland, J. J., Glajch, J. L., Eds.; John Wiley & Sons, Inc: New York, 1997; Chapter 11, p 497.
(35) Meriluoto, J. Chromatography of microcystins. *Anal. Chim. Acta* **1997**, *352*, 277−298.
(36) Yuan, M.; Namikoshi, M.; Otsuki, A.; Rinehart, K. L.; Sivonen, K.; Watanabe, M. F. Low-energy collisionally activated decomposition and structural characterization of cyclic heptapeptide microcystins by electrospray ionization mass spectrometry. *J. Mass Spectrom.* **1999**, *34*, 33−43.
(37) Mol, H. G. J.; van Dam, R. C. J.; Steijger, O. M. Determination of polar organophosphorus pesticides in vegetables and fruits using liquid chromatography with tandem mass spectrometry: selection of extraction solvent. *J. Chromatogr., A* **2003**, *1015*, 119−127.
(38) Kebarle, P.; Tang, L. From ions in solution to ions in the gas phase—the mechanism of electrospray mass spectrometry. *Anal. Chem.* **1993**, *65*, 972−986.
(39) Wu, Y. L.; Li, L.; Gan, N. Q.; Zheng, L. L.; Ma, H. Y.; Shan, K.; Liu, J.; Xiao, B. D.; Song, L. R. Seasonal dynamics of water bloom-forming Microcystis morphospecies and the associated extracellular microcystin concentrations in large, shallow, eutrophic Dianchi Lake. *J. Environ. Sci.* **2014**, *26*, 1921−1926.
(40) Pan, X. J.; Chang, F. Y.; Shen, Y. W.; Liu, Y. D.; Li, D. H.; Li, G. B. The correlation between the variation of microcystin content and environment factors in Dianchi Lake. *J. Lake Sci.* **2006**, *18*, 572−578 (in Chinese with English abstract).
(41) Liu, Y. M.; Chen, W.; Li, D. H.; Shen, Y. W.; Li, G. B.; Liu, Y. D. First report of aphantoxins in China—waterblooms of toxigenic *Aphanizomenon flos-aquae* in Lake Dianchi. *Ecotoxicol. Environ. Saf.* **2006**, *65*, 84−92.

recently become an emerging method for protein quantification.[18−20] If the power of the speciation and quantification of mass spectrometry technology can be used for the analysis of mammalian gelatins, it will definitely be of great interest to the food industry.

Currently, most of the quantitative proteomics approaches by mass spectrometry use the isotopic labels as the reference for either relative or absolute quantification.[21] The incorporation of stable isotopes into peptides results in a fixed mass shift with no effect on the chemical properties of the peptides (i.e., peptide LC elution time or ionization efficiency). Therefore, the relative abundances of the labeled peptides from different samples can be accurately quantified using LC-MS.[22−24] Isotopes can be introduced by many methods including metabolic labeling,[25,26] chemical labeling through derivatization,[27,28] and enzymatic labeling.[29,30] Among these methods, as a powerful labeling strategy for quantitative proteomics application, enzymatic $^{18}O$ labeling shows many advantages including high labeling specificity, relatively lower price, and compatibility with almost any source of protein.[31,32] Serine proteases such as trypsin, chymotrypsin, Lys-C, and Glu-C can catalyze C-terminal carboxyl group oxygen exchange for $^{18}O$ labeling; nevertheless, different enzymes target various amino acid C-termini.[24,33] It was reported that trypsin, Glu-C, or Lys-C could incorporate two $^{18}O$ atoms into the C-terminus of the resulting peptide, whereas chymotrypsin and Asp-N introduced only one $^{18}O$ atom.[34,35] Trypsin-catalyzed $^{18}O$ labeling is particularly popular because it is simple, cost-effective, and able to specifically label all peptides that end with Arg or Lys residue on the peptide C-terminus.[24] Combined with mass spectrometry, trypsin-catalyzed $^{18}O$ labeling has been used to quantify many proteins in the biochemistry and medicine fields including human plasma proteins[36] and plasma membrane proteins.[37]

The purpose of this study was to establish a method by combining trypsin-catalyzed $^{18}O$ labeling and high-resolution mass spectrometry to quantify the bovine or porcine gelatins. At the first step, we identified characteristic marker peptides for the gelatins with or without $^{18}O$ labeling. High-energy C-trap dissociation (HCD) was selected to determine the sequence and identify the modification owing to its capability to detect the low mass fragments, which are often not detectable due to the low mass cutoff in ion trap collision-induced dissociation (CID). We then mixed the gelatin peptides with different ratios of $^{16}O$−$^{18}O$ to check whether the method was suitable to quantify the gelatins. Our results clearly demonstrated that trypsin-catalyzed $^{18}O$ labeling combined with mass spectrometric analysis was an accurate approach for the quantification of bovine and porcine gelatins.

## MATERIALS AND METHODS

**Materials.** Bovine gelatin (G9382), porcine gelatin (G2500), and Lys-C were purchased from Sigma Chemical Co. (St. Louis, MO, USA). $H_2{}^{18}O$ (97%) was obtained from Cambridge Isotope Laboratories, Inc. (Andover, MA, USA). Water ($H_2{}^{16}O$) was purified with a Milli-Q apparatus (Millipore, Schwalbach, Germany). Trypsin was purchased from Promega Corp. (Madison, WI, USA). All other reagents used were of analytical grade.

**Sample Digestion.** The bovine or porcine gelatin was dissolved in the digestion buffer composed of 20 mM, pH 8.0, Tris-HCl, 50 mM NaCl, and 50 mM $CaCl_2$. One hundred microliters of the gelatin solution (1 mg/mL) was mixed with 100 μL of the digestion solution in a 500 μL centrifuge tube. ProteaseMax Surfactant (Promega Corp.) was added into the mixed solution at the concentration of 0.01% (w/v). Fifteen microliters of 100 mM DTT was added to the tube, and the whole sample was incubated at 95 °C for 5 min and then cooled in an ice bath. Thirty microliters of the alkylation buffer (100 mM iodoacetamide) was added to the tube and incubated in the dark at room temperature for 20 min. Twenty microliters of 0.05 μg/μL Lys-C was added to hydrolyze the gelatin sample at 37 °C for 4 h. Twenty micorliters of 0.1 μg/μL trypsin was added to further hydrolyze the gelatin at 37 °C overnight.

**$^{18}O$-Labeling for Sample.** Fifty microliters of 0.1 μg/μL trypsin was added to the tube and mixed uniformly. The solution was split into two aliquots and freeze-dried. Eighty microliters of acetonitrile was added to every aliquot, and then the sample was dried by vacuum centrifugation at room temperature. Ten microliters of acetonitrile and 40 μL of $H_2{}^{18}O$ were added to one aliquot, whereas 10 μL of acetonitrile and 40 μL of $H_2{}^{16}O$ were added to another aliquot. The samples were incubated at 30 °C for overnight. After labeling, trypsin was inactivated by cysteine alkylation to minimize the back-exchange of $^{18}O$ to $^{16}O$. The inactivation of trypsin was done according to the protocol reported by Staes et al.[38] with slight modifications. Ten microliters of 50 mM tris(2-carboxyethyl)phosphine (TCEP) was dried in a centrifugation tube, and 15 μL of 100 mM iodoacetamide was dried in another tube in the dark. The labeled sample was transferred to the tube containing TCEP and incubated at 37 °C for 1 h. The solution was then transferred to the tube containing iodoacetamide and incubated at 37 °C for 90 min in the dark. The $^{16}O$ labeling sample was also prepared by the trypsin inactivation step. After the above steps, the samples were stored at −80 °C for further use.

**Liquid Chromatography and Mass Spectrometry Analysis.** A Shimadzu HPLC (Shimadzu, Kyoto, Japan), with two LC-10AD pumps, was used to generate a gradient with a 50 μL/min flow rate. Solvent A was 5% acetonitrile in $H_2O$ and 0.1% formic acid (FA), whereas solvent B consisted of 95% acetonitrile in $H_2O$ and 0.1% FA. For analysis of proteolytic peptides, 3 μg of digested gelatin sample was injected onto a 2.0 mm i.d. × 100 mm C18 column (Phenomenex Inc., Torrance, CA, USA). After desalting for 5 min with 2% B, the peptides were eluted at 50 μL/min with a 2−20% gradient for 40 min and 20−95% gradient for 2 min. The effluent was infused into a LTQ-Orbitrap Velos mass spectrometer (Thermo Fisher Scientific, Waltham, MA, USA) for MS/MS analysis to identify the characteristic peptides of the gelatins. The signals detected in the precursor ion scanning were further submitted to a HCD fragmentation to detect those fragment ions including low $m/z$ range. The normalized collision energy was set to 35% for HCD. Dynamic exclusion was enabled with exclusion duration of 90 s.

**Database Search.** Thermo proteome discoverer (ver. 1.4.0.288) was used to generate the mgf file from mass spectrometric data, and then Mascot Daemon (ver. 2.4.0, Matrix Science, Boston, MA, USA) was used to perform the searches against the in-house database including bovine and porcine collagen sequences, which were acquired from the uniprot database and a published patent.[39] Carbamidomethyl (C) was set as a fixed modification, and oxidations on P and K were set as variable modifications. Additional search settings included a maximum of five missed cleavages, peptide tolerance of ±25 ppm, and MS/MS tolerance of ±0.5 Da. The peptides with a Mascot ion score >40 were considered to be positive identification or extensive similarity ($p < 0.05$).[40] The targeted peptides are those characteristic peptides unique to either bovine or porcine gelatin.[16]

**$^{18}O/^{16}O$ Ratio Calculation.** The ratio of the abundance of the $^{18}O$-labeled peptide to the $^{16}O$-labeled peptide can be calculated from the heights of the monoisotopic peaks. Corrected for $^{13}C$ contributions and single $^{18}O$ incorporation, the calculated formula is

$$\frac{^{18}O}{^{16}O} = \frac{I_4 - \frac{M_4}{M_0}I_0 - \frac{M_2}{M_0}\left(I_2 - \frac{M_2}{M_0}I_0\right) + I_2 - \frac{M_2}{M_0}I_0}{I_0} \quad (1)$$

where $I_0$, $I_2$, and $I_4$ represent the observed relative intensities of the monoisotopic peak for the peptides without $^{18}O$ label, the peak with masses 2 Da higher, and the peak with 4 Da higher masses, respectively. $M_0$, $M_2$, and $M_4$ represent the theoretical relative intensities of the monoisotopic peak for the peptides, the peak with masses 2 Da higher, and the peak with 4 Da higher masses, respectively. In this work, the

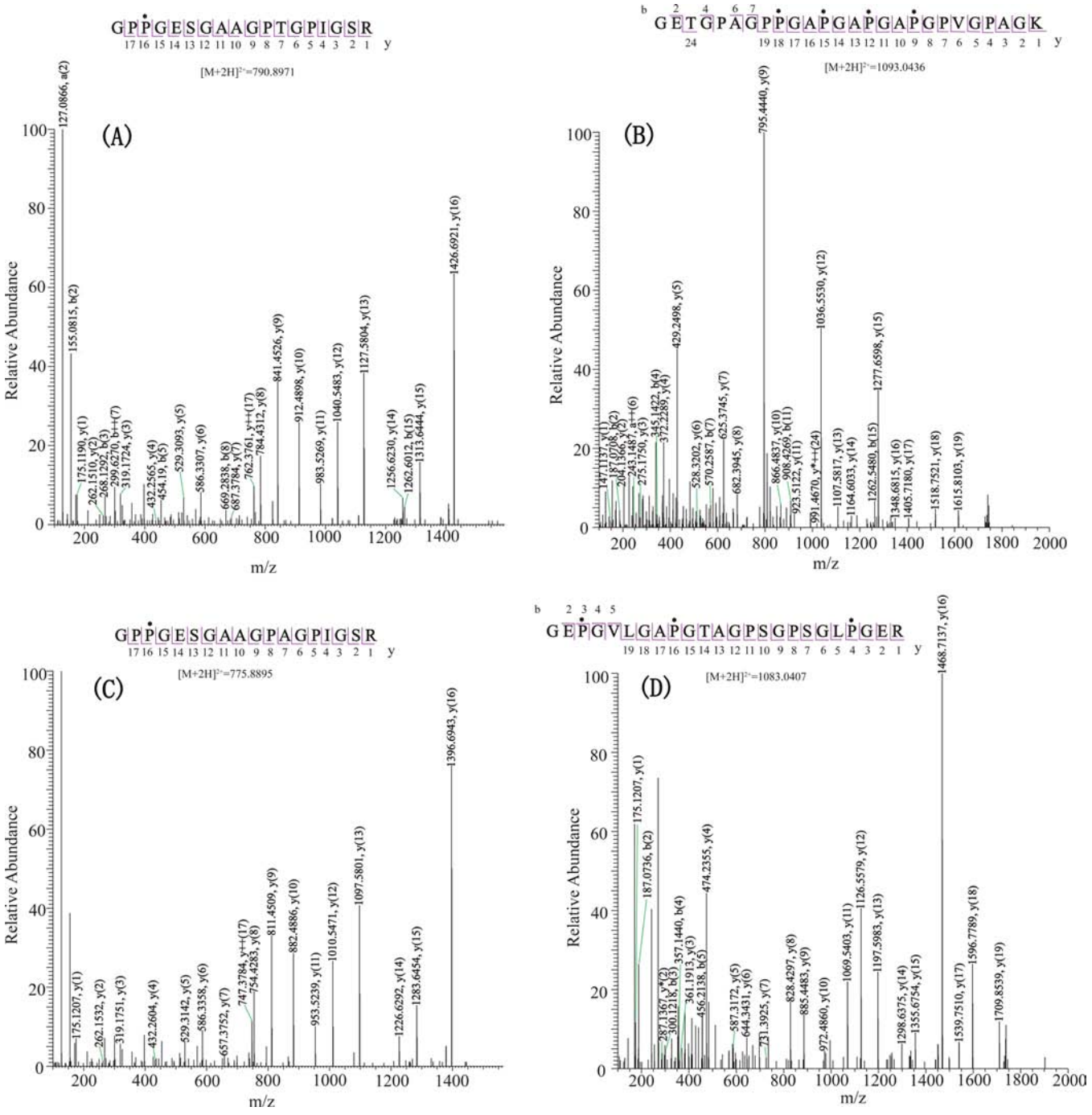


**Figure 1.** Sequence identification and hydroxylation determination by tandem mass spectrometry for marker peptides: (A) peptide from bovine gelatin at $m/z$ 790.8971$^{2+}$; (B) peptide from bovine gelatin at $m/z$ 1093.0436$^{2+}$; (C) peptide from porcine gelatin at $m/z$ 775.8895$^{2+}$; (D) peptide from porcine gelatin at $m/z$ 1083.0407$^{2+}$. The sequence of each peptide is shown on top of the peptide. The hydroxylated prolines are indicated by the asterisk. The b and y ions are indicated by the numbers and lines.

values of $M_4/M_0$ and $M_2/M_0$ are replaced by $2 \times 10^{-12}M_r^{3.2684}$ and $3 \times 10^{-7}M_r^{1.9241}$ ($M_r$ is the molecular weight of the peptide) according to the procedure of Johnson and Muddiman.[41] For bovine and porcine gelatins, 10 characteristic peaks were chosen to obtain the average $^{18}O/^{16}O$ ratio for minimum error.

## RESULTS AND DISCUSSION

**Gelatin Modification Identification.** Collagen contains a range of post-translational modifications that are essential for triple-helix assembly and stability, intermolecular cross-linking, and strength of fibrils and tissue function.[42] For instance, collagen includes abundant hydroxyproline (Hyp) resulting from the post-translational hydroxylation of some proline residues.[43] From the partial hydrolysis of the collagen, the gelatin also has a number of Hyp residues. Therefore, prior to the quantification of bovine or porcine gelatins, it is necessary to identify the modification sites by accurate mass and tandem mass spectrometry.

With the optimized hydrolysis of the gelatin followed by high-performance liquid chromatography−LTQ/Orbitrap high-resolution mass spectrometry, we accurately identified many modified sites of bovine and porcine gelatins. Figure 1 shows

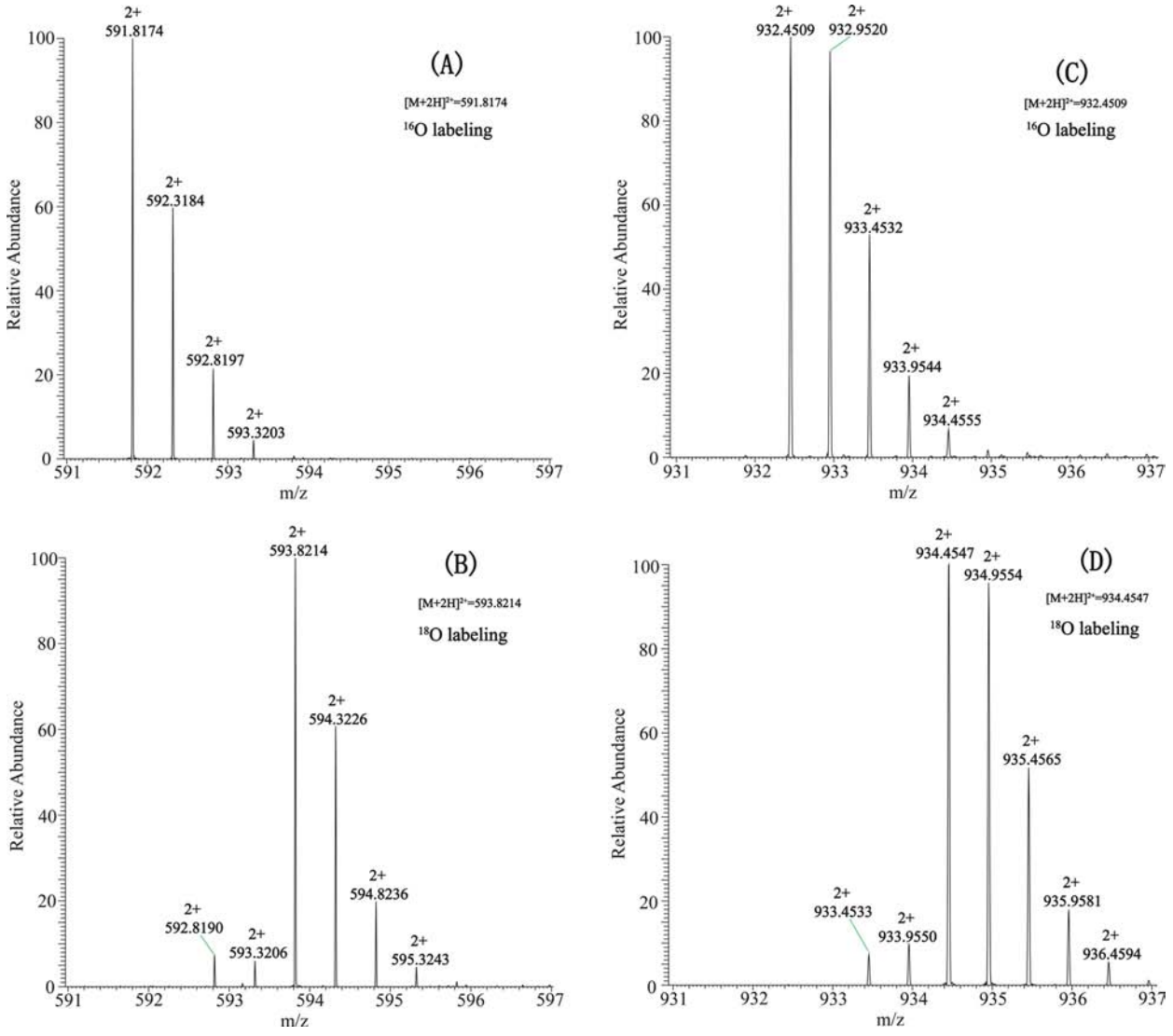


**Figure 2.** Comparison of the mass spectra of bovine gelatin peptides after $^{16}O$ and $^{18}O$ labeling: (A, B) peptide $^{465}$EGPVGL*PGIDGR$^{476}$ after $^{16}O$ and $^{18}O$ labeling, respectively; (C, D) peptide $^{451}$GEPG*PTGIQGP*PGPAGEEGK$^{470}$ after $^{16}O$ and $^{18}O$ labeling, respectively.

the determination of hydroxylated proline sites for four peptides from the bovine or porcine gelatin. From Figure 1A, the mass of the peptide (1579.7796) with $m/z$ 790.8971$^{2+}$ matched well with that of the Pro oxidation form (1579.7591) with the sequence $^{592}$GP*PGESGAAGPTGPIGSR$^{609}$ (the asterisk indicates that Pro594 was hydroxylated) from the $\alpha_2$ chain of the bovine gelatin. Moreover, the HCD MS/MS of the peptide generated a series of b and y ions (y1−y17 in Figure 1A), unambiguously confirming the sequence of the peptide. The location of the hydroxylation (Pro594) was obtained by the mass difference between the y15 and y16 ions, which is the corresponding mass of Hyp. From Figure 1B, Pro1047, Pro1050, Pro1053, and Pro1056 were identified as the hydroxylated proline sites in the sequence of $^{1039}$GETGPAGP*PGA*PGA*PGA*PGPVGPAGK$^{1064}$ with $m/z$ of 1093.0436$^{2+}$ from the $\alpha_1$ chain of the bovine gelatin. The series of b and y ions ensured the positive identification of the peptide sequence (b2, b4, b6, b7, y1−y19, and y24) and Hyp location (y8, y9, y11, y12, y14, y15, y17, and y18). Similarly, on the basis of the y15 and y16 ions in Figure 1C, Pro594 was identified to be the Hyp in the peptide $^{592}$GP*PGESGAAGPAGPIGSR$^{609}$ with $m/z$ 775.8895$^{2+}$ from the $\alpha_2$ chain of the porcine gelatin. On the basis of the b2, b3, y15, y16, y3, and y4 ions in Figure 1D, Pro624, Pro630, and Pro642 were identified to be three hydroxylated proline sites in the peptide with the sequence of $^{622}$GE*PGVLGA*PGTAGPSGPSGL*PGER$^{645}$ with $m/z$ 1083.0407$^{2+}$ from the $\alpha_2$ chain of the porcine gelatin.

**$^{18}$O-Labeling Identification.** To use the $^{18}O$ labeling to quantify the bovine or porcine gelatin, it is important to ensure all of the characteristic peptides from the targeted gelatin are labeled at their maximum. Figure 2 shows the mass spectra of two characteristic $^{16}O$ labeling peptides from bovine gelatin and their corresponding peptides labeled by $^{18}O$, respectively. During the $^{18}O$ labeling processing for the gelatin peptides, two $^{18}O$ atoms are exchanged by trypsin into the $\alpha$-carboxyl group of peptides C-terminally ending with a lysine or arginine residue because tryptic peptides interact with trypsin by forming covalent intermediates with repeated binding/hydrolyses cycles in the $H_2{}^{18}O$.[44] As a result, the $m/z$ of the peptides will increase by 4 Da when the $^{18}O$ labeling is complete. As shown in Figure 2A, the monoisotopic peak at $m/z$ of 591.8174$^{2+}$ was found from $^{16}O$ labeling peptides after bovine gelatin digestion. The MS and MS/MS confirmed that this peptide was from $\alpha_2$ chain of the bovine gelatin with the sequence of $^{465}$EGPVGL*PGIDGR$^{476}$. Among the two proline


dx.doi.org/10.1021/jf503876a | J. Agric. Food Chem. 2014, 62, 11840−11853

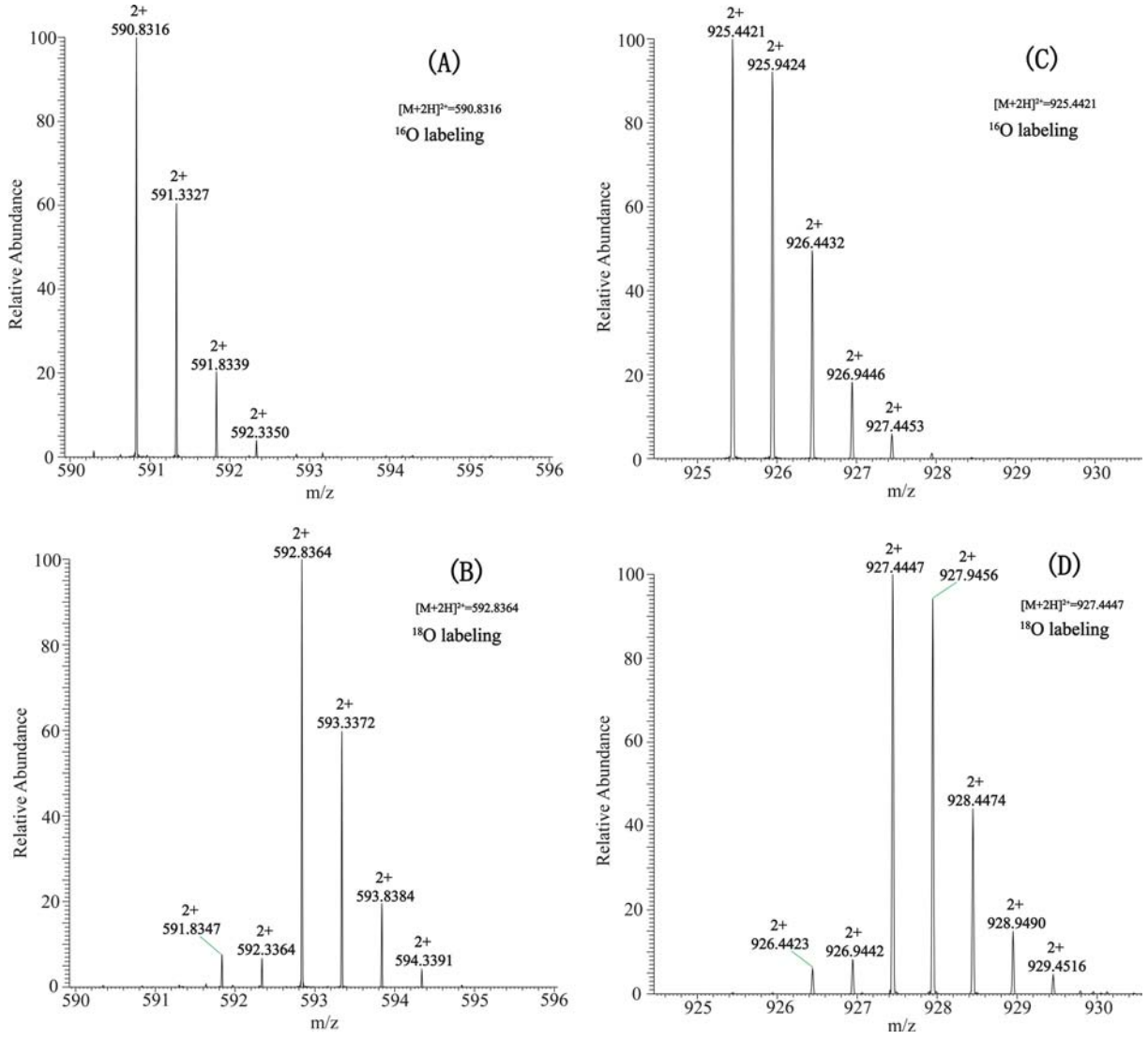


**Figure 3.** Comparison of the mass spectra of porcine gelatin peptides after $^{16}O$ and $^{18}O$ labeling: (A, B) peptide $^{1068}$TGQPGAVGPAGIR$^{1080}$ after $^{16}O$ and $^{18}O$ labeling, respectively; (C, D) peptide $^{451}$GEPG*PTGVQGP*PGPAGEEGK$^{470}$ after $^{16}O$ and $^{18}O$ labeling, respectively.

residues contained in this sequence, only proline 471 was oxidized. After $^{18}O$ labeling, the monoisotopic peak of this peptide shifted to $m/z$ of 593.8214$^{2+}$ (Figure 2B). The mass shift of 4.0080 Da was well matched to the theoretical shift of 4.0085 Da for $^{18}O$ labeling with only 0.4 ppm difference. Figure 2C shows another example of the mass shift of a bovine peptide after $^{16}O$ labeling. The peak with $m/z$ 932.4509$^{2+}$ represents the peptide $^{451}$GEPG*PTGIQGP*PGPAGEEGK$^{470}$ with two oxidized proline. As shown in Figure 2D, the $^{18}O$ labeling resulted in the disappearance of this peak and the appearance of a new peak at $m/z$ 934.4547$^{2+}$. Again, the mass shift of 4.0076 Da was well matched to the theoretical shift of 4.0085 Da for $^{18}O$ labeling. Similarly, $^{18}O$ labeling for porcine samples is given in Figure 3. The peaks with $m/z$ 590.8316$^{2+}$ and 925.4421$^{2+}$ found in the $^{16}O$ labeling porcine gelatin sample represent the peptides $^{1068}$TGQPGAVGPAGIR$^{1080}$ and $^{451}$GEPG*PTGVQGP*P GPAGEEGK$^{470}$, respectively. The $^{18}O$ labeling shifted these two peptides to the expected $m/z$ of 592.8364$^{2+}$ and 927.4447$^{2+}$, with mass changes of 4.0096 and 4.0052 Da, respectively. The exact mass shift of 4 Da by $^{18}O$ labeling indicates that two $^{18}O$ atoms have been incorporated into these peptides. Table 3 lists 10 characteristic peptides for both bovine and porcine gelatin samples. All of these peptides reached their optimal $^{18}O$ labeling as indicated by complete $^{16}O$ to $^{18}O$ exchange (disappearance of $^{16}O$ in concert with the appearance of $^{18}O$ peptide).

It should be noted, however, because the labeling reagent ($H_2{}^{18}O$) is not 100% pure, there will be a small fraction of $^{16}O$ incorporated into one or two C-terminal carboxyl groups of the $^{18}O$-labeling peptides.[24] In this work, the purity of $H_2{}^{18}O$ was 97%, resulting in the peaks with one $^{16}O$ atom being detected with very low intensities in the $^{18}O$-labeled peptides (Figures 2 and 3). In addition, the $^{18}O$ back-exchange can readily happen and affect the accuracy of this quantitative method. In this work, TCEP reduction followed by cysteine alkylation was performed to disrupt the three-dimensional structure of trypsin and thus minimize the $^{18}O$ back-exchange.[43] As shown in Figures 2 and 3, the minimal $^{16}O$ incorporation indicated the samples were well labeled by $H_2{}^{18}O$.

To ensure the 4 Da shifted peptides resulted from the $^{18}O$ labeling, we further verified these peptides by tandem mass spectrometry. Figure 4 shows the MS/MS spectra of the peptides carrying $^{18}O$ or $^{16}O$ labels from the digested bovine or porcine gelatin. The accurate mass of the peptide as well as the complete sequencing by HCD with consecutive y ions (y1−y11,

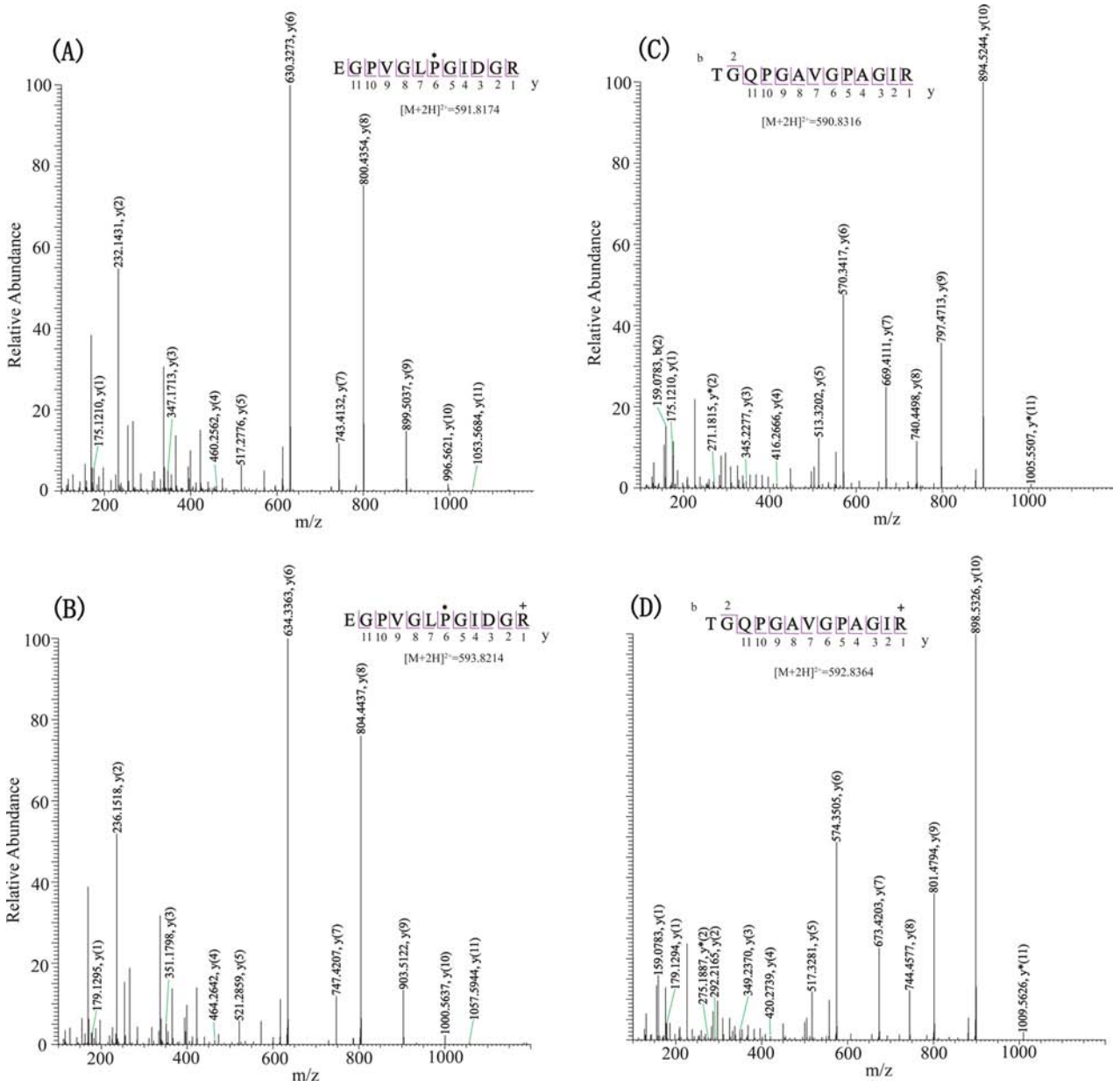


**Figure 4.** Sequence identification and localization of $^{18}O$ labeling by comparing MS/MS spectra of marker peptides labeled by $^{16}O$ and $^{18}O$: (A) peptide from bovine gelatin with $^{16}O$ labeling at $m/z$ 591.8174$^{2+}$; (B) peptide from bovine gelatin with $^{18}O$ labeling at $m/z$ 593.8214$^{2+}$; (C) peptide from porcine gelatin with $^{16}O$ labeling at $m/z$ 590.8316$^{2+}$; (D) peptide from porcine gelatin with $^{18}O$ labeling at $m/z$ 592.8364$^{2+}$. The sequence of each peptide is shown on top of the peptide. The $^{18}O$-labeled arginine is marked by the plus sign. The identified hydroxylated prolines are marked by the asterisk. The b and y ions are indicated by the numbers and lines.

unambiguously confirmed the sequence of the peptide and proline oxidation at positive of 471 ($^{465}$EGPVGL*PGIDGR$^{476}$). The mass of the $^{18}O$-labeled peptide at $m/z$ 593.8214$^{2+}$ matched well with that of the Pro oxidation and $^{18}O$ labeling (1185.6127). Two $^{18}O$ atoms were confirmed to attach to the terminal residue, Arg476, as suggested by the 4 Da mass increase of y1 ions. This is further confirmed by all y ions exhibiting a mass increase of 4 Da. The mass spectrometric results determined that the sequence was $^{465}$EGPVGL*PGIDG$^{+}$R$^{476}$ ($^{18}O$ labeling is indicated by the plus sign) from the $\alpha_2$ chain of the bovine gelatin. Similarly, accurate mass and tandem mass spectrometry of the peak with $m/z$ 590.8316$^{2+}$ determined the sequence of this peptide was $^{1068}$TGQPGAVGPAGIR$^{1080}$ in the $\alpha_2$ chain of the porcine gelatin, without any modification. After $^{18}O$ labeling, the peak moved to $m/z$ 592.8364$^{2+}$ with a mass increase of 4 Da, and this mass increase was found to be in the C-terminal amino acid residue of Arg1080.

Isotopic peaks annotated A, A+2, and A+4 are typically used in $^{18}O/^{16}O$ quantification.[41] A is the monoisotopic peak, representing the light sample. The A+2 peak is a composite of signals arising from (1) single $^{18}O$ labeled sample and (2) the third peak of the naturally occurring isotopes (e.g., $^{13}C$, $^{34}S$) of the light sample. The A+4 peak is also a composite containing three variables: (1) double $^{18}O$ labeled sample, (2) the third peak of the naturally occurring isotopes of the single $^{18}O$ labeled sample, and (3) the fifth peak of the naturally occurring isotopes of the light sample. Because of these three variables in A+4 peak, eq 1 is necessary to eliminate the interference from these isotopic


dx.doi.org/10.1021/jf503876a | J. Agric. Food Chem. 2014, 62, 11840−11853

**Table 1. Marker Peptides for Bovine Gelatin Identification and Quantification**

| unique peptides from bovine gelatin[a] | $m/z$ | $M_r$ obsd | $M_r$ theor | $M_r$ error (ppm) |
|---|---|---|---|---|
| $\alpha$1: $^{451}$GEPG*PTGIQGP*PGPAGEEGK$^{470}$ | 932.4509$^{2+}$ | 1862.8872 | 1862.8647 | 12.1 |
| $\alpha$1: $^{1039}$GETGPAGP*PGA*PGAPGAPGPVGPAGK$^{1064}$ | 1077.0491$^{2+}$ | 2152.0836 | 2152.0549 | 13.3 |
| $\alpha$1: $^{1039}$GETGPAGP*PGA*PGA*PGAPGPVGPAGK$^{1064}$ | 1085.0461$^{2+}$ | 2168.0777 | 2168.0498 | 12.9 |
| $\alpha$1: $^{1039}$GETGPAGP*PGA*PGA*PGA*PGPVGPAGK$^{1064}$ | 1093.0436$^{2+}$ | 2184.0726 | 2184.0448 | 12.7 |
| $\alpha$1: $^{1069}$GETGPAGPAGPIGPVGAR$^{1086}$ | 780.9210$^{2+}$ | 1559.8275 | 1559.8056 | 14.0 |
| $\alpha$2: $^{328}$GI*PGPVGAAGATGAR$^{342}$ | 634.3497$^{2+}$ | 1266.6849 | 1266.6681 | 13.3 |
| $\alpha$2: $^{382}$GSTGEIGPAGP*PGPPGLR$^{399}$ | 816.9313$^{2+}$ | 1631.8481 | 1631.8268 | 13.1 |
| $\alpha$2: $^{382}$GSTGEIGPAGP*PGP*PGLR$^{399}$ | 824.9285$^{2+}$ | 1647.8425 | 1647.8217 | 12.6 |
| $\alpha$2: $^{465}$EGPVGL*PGIDGR$^{476}$ | 591.8174$^{2+}$ | 1181.6202 | 1181.6041 | 13.6 |
| $\alpha$2: $^{574}$GI*PGEFGL*PGPAGAR$^{588}$ | 714.3776$^{2+}$ | 1426.7406 | 1426.7205 | 14.1 |
| $\alpha$2: $^{574}$GI*PGEFGL*PG*PAGAR$^{588}$ | 722.3748$^{2+}$ | 1442.7350 | 1442.7154 | 13.6 |
| $\alpha$2: $^{592}$GP*PGESGAAGPTGPIGSR$^{609}$ | 790.8971$^{2+}$ | 1579.7796 | 1579.7591 | 13.0 |
| $\alpha$2: $^{622}$GE*PGVVGA*PGTAGPSGPSGLPGER$^{645}$ | 1068.0354$^{2+}$ | 2134.0562 | 2134.0291 | 12.7 |
| $\alpha$2: $^{622}$GE*PGVVGA*PGTAGPSGPSGL*PGER$^{645}$ | 1076.0321$^{2+}$ | 2150.0496 | 2150.0240 | 11.9 |
| $\alpha$2: $^{795}$TG*P*PGPSGISGPPGP*PG*PAGK$^{815}$ | 923.4631$^{2+}$ | 1844.9117 | 1844.8905 | 11.5 |
| $\alpha$2: $^{831}$SGETGASGP*PGFVGEK$^{846}$ | 746.8590$^{2+}$ | 1491.7034 | 1491.6842 | 12.9 |
| $\alpha$2: $^{949}$GY*PGNAGPVGAAGA*PGPQGPVGPVGK$^{974}$ | 1131.0834$^{2+}$ | 2260.1522 | 2260.1237 | 12.6 |
| $\alpha$2: $^{1068}$IGQPGAVGPAGIR$^{1080}$ | 596.8522$^{2+}$ | 1191.6898 | 1191.6724 | 14.6 |
| $\alpha$1: $^{315}$PGAPGPAGAR$^{324}$ | 425.7301$^{2+b}$ | —[c] | — | — |
| $\alpha$1: $^{508}$GPAGERGAPGPAGPK$^{522}$ | 659.8468$^{2+}$ | — | — | — |
| $\alpha$1: $^{784}$GEAGPSGPAGPTGAR$^{798}$ | 641.3127$^{2+}$ | — | — | — |
| $\alpha$1: $^{921}$PGEVGPPGPPGPAGEK$^{936}$ | 721.8673$^{2+}$ | — | — | — |
| $\alpha$1: $^{937}$GAPGADGPAGAPGTPGPQGIAGQR$^{960}$ | 1029.0116$^{2+}$ | — | — | — |
| $\alpha$1: $^{987}$QGPSGASGER$^{996}$ | 473.2229$^{2+}$ | — | — | — |
| $\alpha$1: $^{1029}$DGSPGAK$^{1035}$ | 316.1559$^{2+}$ | — | — | — |
| $\alpha$1:$^{1144}$GPPGSAGSPGK$^{1154}$ | 456.2327$^{2+}$ | — | — | — |
| $\alpha$2: $^{235}$GSDGSVGPVGPAGPIGSAGPPGFPGAPGPK$^{264}$ | 1271.1403$^{2+}$ | — | — | — |
| $\alpha$2: $^{283}$GEVGLPGLSGPVGPPGNPGANGLPGAK$^{309}$ | 1183.6268$^{2+}$ | — | — | — |
| $\alpha$2: $^{310}$GAAGLPGVAGAPGLPGPR$^{327}$ | 757.9255$^{2+}$ | — | — | — |
| $\alpha$2: $^{361}$GEPGAVGQPGPPGPSGEEGK$^{380}$ | 902.4290$^{2+}$ | — | — | — |
| $\alpha$2: $^{414}$AGVMGPAGSR$^{423}$ | 451.7293$^{2+}$ | — | — | — |
| $\alpha$2: $^{424}$GATGPAGVR$^{432}$ | 393.2169$^{2+}$ | — | — | — |
| $\alpha$2: $^{451}$GFPGSPGNIGPAGK$^{464}$ | 628.3251$^{2+}$ | — | — | — |
| $\alpha$2: $^{499}$GPSGDPGK$^{506}$ | 357.6745$^{2+}$ | — | — | — |
| $\alpha$2: $^{520}$GAPGPDGNNGAQGPPGLQGVQGGK$^{543}$ | 1065.5198$^{2+}$ | — | — | — |
| $\alpha$2: $^{544}$GEQGPAGPPGFQGLPGPAGTAGEAGK$^{569}$ | 1153.0640$^{2+}$ | — | — | — |
| $\alpha$2: $^{664}$GDIGSPGR$^{671}$ | 379.6932$^{2+}$ | — | — | — |
| $\alpha$2: $^{676}$GAPGAIGAPGPAGANGDR$^{693}$ | 753.3764$^{2+}$ | — | — | — |
| $\alpha$2: $^{748}$GENGPVGPTGPVGAAGPSGPNGPPGPAGSR$^{777}$ | 1283.1257$^{2+}$ | — | — | — |
| $\alpha$2: $^{907}$GPPGNVGNPGVNGAPGEAGR$^{926}$ | 887.4350$^{2+}$ | — | — | — |
| $\alpha$2: $^{927}$DGNPGNDGPPGR$^{938}$ | 576.7551$^{2+}$ | — | — | — |
| $\alpha$2: $^{939}$DGQPGHK$^{945}$ | 369.6801$^{2+}$ | — | — | — |
| $\alpha$2: $^{979}$GEPGPAGAVGPAGAVGPR$^{996}$ | 758.8970$^{2+}$ | — | — | — |
| $\alpha$2: $^{1024}$GHNGLQGLPGLAGHHGDQGAPGAVGPAGPR$^{1053}$ | 1376.6924$^{2+}$ | — | — | — |

[a]The marker peptides and their sequence numbers, based on the sequence alignment results, were obtained from Zhang et al. *P indicates the hydroxylated proline. The modification site, $m/z$ value, and match condition are only shown in the detected unique peptides in this work. [b]$m/z$ within the same row as "—" denotes the theoretical monoisotopic peak in charge state of 2+ without any modification. [c]—, theoretical unique peptides that were not detected in this work.

contributions. Theoretically, peptides being doubly, triply, or quadruply charged can all be used for the quantitative purpose. However, because triply and quadruply charged ions are usually longer peptides, the isotopic interference from light sample via its naturally occurring A+4 isotopic peak will be much higher than that of shorter peptides that are doubly charged. For example, for the peptide $^{1068}$TGQPGAVGPAGIR$^{1080}$ with $m/z$ 590.8316$^{2+}$, the contribution from the light sample via its naturally occurring A+4 isotopic peak is only 1.12%, whereas it is drastically increased to 19.31% for the longer peptide $^{544}$GEQG*PAGPPGFQGLPG*PAGTAGEVGK*PGER$^{573}$ with $m/z$ 940.8010$^{3+}$. Therefore, to minimize this effect, we chose doubly charged shorter peptides for the following quantitative analysis.

The sequence homologies for $\alpha_1$ and $\alpha_2$ chains from bovine and porcine gelatins were 95.9 and 95.3%, respectively. A little less than 5% of the sequence divergence between two types of gelatin can generate many characteristic tryptic peptides.[16] Tables 1 and 2 list the theoretical characteristic peptides for bovine and porcine gelatins. In this work, with the combined digestion by Lys-C and trypsin and high-performance liquid

**Table 2. Marker Peptides for Porcine Gelatin Identification and Quantification**

| unique peptides from porcine gelatin[a] | $m/z$ | $M_r$ obsd | $M_r$ theor | $M_r$ error (ppm) |
|---|---|---|---|---|
| $\alpha$1:[451]GEPG*PTGVQGP*PGPAGEEGK[470] | 925.4421$^{2+}$ | 1848.8696 | 1848.8490 | 11.1 |
| $\alpha$1:[937]GS*PGADGPAGA*PGT*PGPQGIAGQR[960] | 1061.0131$^{2+}$ | 2120.0116 | 2119.9883 | 11.0 |
| $\alpha$1:[1039]GESGPAGP*PGA*PGA*PGAPGPVGPAGK[1064] | 1078.0370$^{2+}$ | 2154.0594 | 2154.0342 | 11.7 |
| $\alpha$1:[1036]GDRGESGPAGPPGA*PGA*PGAPGPVGPAGK[1064] | 1234.1156$^{2+}$ | 2466.2166 | 2466.1888 | 11.3 |
| $\alpha$2:[235]GNDGSVGPVGPAGPIGSAGP*PGF*PGAPGP*K[264] | 1308.6522$^{2+}$ | 2615.2899 | 2615.2617 | 10.8 |
| $\alpha$2:[235]GEVGL*PGVSGPVGP*PGNPGANGLPGA*K[309] | 1200.6263$^{2+}$ | 2399.2380 | 2399.2081 | 12.5 |
| $\alpha$2:[382]GPNGEVGSAGP*PGP*PGLR[399] | 824.4170$^{2+}$ | 1646.8194 | 1646.8013 | 11.0 |
| $\alpha$2:[451]GF*PGSPGNVGPAGK[464] | 629.3225$^{2+}$ | 1256.6305 | 1256.6150 | 12.3 |
| $\alpha$2:[451]EGPAGL*PGIDGRPGPIGPAGAR[486] | 1014.5465$^{2+}$ | 2027.0784 | 2027.0548 | 11.7 |
| $\alpha$2:[544]GEQGPAGP*PGFQGL*PGPAGTAGEVGK[569] | 1183.0894$^{2+}$ | 2364.1642 | 2364.1346 | 12.5 |
| $\alpha$2:[544]GEQG*PAGPPGFQGLPG*PAGTAGEVGK*PGER[573] | 1410.6967$^{2+}$ | 2819.3788 | 2819.3475 | 11.1 |
| $\alpha$2:[592]GP*PGESGAAGPAGPIGSR[609] | 775.8895$^{2+}$ | 1549.7644 | 1549.7485 | 10.3 |
| $\alpha$2:[622]GE*PGVLGA*PGTAGPSGPSGL*PGER[645] | 1083.0407$^{2+}$ | 2164.0669 | 2164.0397 | 12.6 |
| $\alpha$2:[748]GENGPVGPTGPVGAAGPAGPNGP*PGPAGSR[777] | 1283.1388$^{2+}$ | 2564.2630 | 2564.2368 | 10.2 |
| $\alpha$2:[795]IG*P*PGPSGISGPPGP*PG*PAGK[815] | 929.4823$^{2+}$ | 1856.9500 | 1856.9269 | 12.4 |
| $\alpha$2:[831]TGETGASGP*PGFAGEK[846] | 739.8483$^{2+}$ | 1477.6820 | 1477.6685 | 9.1 |
| $\alpha$2:[949]GY*PGNPGPAGAAGA*PGPQGAVGPAGK[974] | 1103.0501$^{2+}$ | 2204.0855 | 2204.0611 | 11.1 |
| $\alpha$2:[1068]TGQPGAVGPAGIR[1080] | 590.8316$^{2+}$ | 1179.6486 | 1179.6360 | 10.7 |
| $\alpha$1:[315]PGPPGPAGAR[324] | 438.7380$^{2+b}$ | —[c] | — | — |
| $\alpha$1:[508]GPAGERGSPGPAGPK[522] | 667.8442$^{2+}$ | — | — | — |
| $\alpha$1:[784]GETGPSGPAGPTGAR[798] | 656.3180$^{2+}$ | — | — | — |
| $\alpha$1:[921]PGEAGPPGPPGPAGEK[936] | 707.8517$^{2+}$ | — | — | — |
| $\alpha$1:[987]QGPSGPSGER[996] | 486.2307$^{2+}$ | — | — | — |
| $\alpha$1:[1029]DGAPGPK[1035] | 321.1663$^{2+}$ | — | — | — |
| $\alpha$1:[1069]GETGPAGPAGPVGPVGAR[1086] | 773.9023$^{2+}$ | — | — | — |
| $\alpha$1:[1144]GPPGSAGAPGK[1154] | 448.2352$^{2+}$ | — | — | — |
| $\alpha$2:[310]GAAGLLGVAGAPGLPGPR[327] | 765.9412$^{2+}$ | — | — | — |
| $\alpha$2:[328]GIPGPAGAAGATGAR[342] | 612.3282$^{2+}$ | — | — | — |
| $\alpha$2:[361]GEPGAAGPQGPPGPSGEEGK[380] | 888.4134$^{2+}$ | — | — | — |
| $\alpha$2:[414]AGVMGPPGSR[423] | 464.7371$^{2+}$ | — | — | — |
| $\alpha$2:[424]GPTGPAGVR[432] | 406.2247$^{2+}$ | — | — | — |
| $\alpha$2:[499]GPTGDPGK[506] | 364.6823$^{2+}$ | — | — | — |
| $\alpha$2:[520]GAPGPDGNNGAQGPPGPQGVQGGK[543] | 1057.5041$^{2+}$ | — | — | — |
| $\alpha$2:[574]GIPGEFGLPGPAGPR[588] | 711.3804$^{2+}$ | — | — | — |
| $\alpha$2:[664]GDVGSPGR[671] | 372.6854$^{2+}$ | — | — | — |
| $\alpha$2:[676]GAPGAVGAPGPAGANGDR[693] | 746.3686$^{2+}$ | — | — | — |
| $\alpha$2:[907]GPPGAVGNPGVNGAPGEAGR[926] | 865.9321$^{2+}$ | — | — | — |
| $\alpha$2:[927]DGNPGSDGPPGR[938] | 563.2496$^{2+}$ | — | — | — |
| $\alpha$2:[939]DGQAGHK[945] | 356.6723$^{2+}$ | — | — | — |
| $\alpha$2:[979]GEPGPAGSVGPAGAVGPR[996] | 766.8944$^{2+}$ | — | — | — |
| $\alpha$2:[1024]GHNGLQGLPGLAGHHGDQGAPGPVGPAGPR[1053] | 1389.7002$^{2+}$ | — | — | — |

[a]The marker peptides and their sequence numbers based on the sequence alignment results were obtained from Zhang et al. *P and *K indicate the hydroxylated proline and lysine, respectively. The modification site, $m/z$ value and match condition were only shown in the detected unique peptides in this work. [b]The $m/z$ within the same row as "—" denotes the theoretical monoisotopic peak in charge state of 2+ without any modification. [c]—, theoretical unique peptides that were not detected in this work.

chromatography-LTQ/Orbitrap high-resolution mass spectrometry, the sequence coverages for $\alpha_1$ and $\alpha_2$ chains from bovine gelatin were 62 and 70%, respectively. The sequence coverages for $\alpha_1$ and $\alpha_2$ chains from porcine gelatin were 64 and 73%, respectively. In total, we detected 18 distinctive peptides from bovine gelatin (591.8174$^{2+}$, 596.8522$^{2+}$, 634.3497$^{2+}$, 714.3776$^{2+}$, 722.3748$^{2+}$, 746.8590$^{2+}$, 780.9210$^{2+}$, 790.8971$^{2+}$, 816.9313$^{2+}$, 824.9285$^{2+}$, 923.4631$^{2+}$, 932.4509$^{2+}$, 1068.0354$^{2+}$, 1076.0321$^{2+}$, 1077.0491$^{2+}$, 1085.0461$^{2+}$, 1093.0436$^{2+}$, and 1131.0834$^{2+}$) and 18 peptides from the porcine gelatin (590.8316$^{2+}$, 629.3225$^{2+}$, 739.8483$^{2+}$, 775.8895$^{2+}$, 824.4170$^{2+}$, 925.4421$^{2+}$, 929.4823$^{2+}$, 1014.5465$^{2+}$, 1061.0131$^{2+}$, 1078.0370$^{2+}$, 1083.0407$^{2+}$, 1103.0501$^{2+}$, 1183.0894$^{2+}$, 1200.6263$^{2+}$, 1234.1156$^{2+}$, 1283.1388$^{2+}$, 1308.6522$^{2+}$, and 1410.6967$^{2+}$), respectively. As shown in Tables 1 and 2, all detected peaks of the characteristic peptides from bovine and porcine gelatins matched well with the theoretical values below 15 ppm. Moreover, the $^{18}$O labeling forms of all above unique peptides were also positively confirmed with less than 15 ppm using accurate mass and tandem mass spectrometry. From the above unique peaks, we selected the 10 strongest peaks for further quantification of the bovine or porcine gelatin. The corresponding sequences of the 10 peptides are shown in Table 3.

**$^{18}$O/$^{16}$O Ratio Determination.** To validate the $^{18}$O labeling method for quantification of gelatins, we prepared gelatin digests with four different mixing ratios of $^{18}$O and $^{16}$O, those being 20:1,

**Table 3. Relative $^{18}O/^{16}O$ Ratio Quantification of the Marker Peptides for Bovine and Porcine Gelatins**

| selected characteristic sequence[a] | monoisotopic peak at 2+ charge state | $M_r$ obsd | $M_r$ theor | error (ppm) | average ratio of $^{18}O$ to $^{16}O$ 20:1 | 5:1 | 1:1 | 1:5 |
|---|---|---|---|---|---|---|---|---|
| **Bovine Gelatin** | | | | | | | | |
| $^{465}$EGPVGL*PGIDGR$^{476}$ | 591.8174 | 1181.6202 | 1181.6041 | 13.6 | 20.41 ± 0.84 | 4.93 ± 0.07 | 1.00 ± 0.02 | 0.19 ± 0.02 |
| $^{1068}$IGQPGAVGPAGIR$^{1080}$ | 596.8522 | 1191.6898 | 1191.6724 | 14.6 | | | | |
| $^{328}$GI*PGPVGAAGATGAR$^{342}$ | 634.3497 | 1266.6849 | 1266.6681 | 13.3 | | | | |
| $^{574}$GI*PGEFGL*PGPAGAR$^{588}$ | 714.3776 | 1426.7406 | 1426.7205 | 14.1 | | | | |
| $^{1069}$GETGPAGPAGPIGPVGAR$^{1086}$ | 780.9210 | 1559.8275 | 1559.8056 | 14.0 | | | | |
| $^{592}$GP*PGESGAAGPTGPIGSR$^{609}$ | 790.8971 | 1579.7796 | 1579.7591 | 13.0 | | | | |
| $^{795}$TG*P*PGPSGISGPPGP*PG*PAGK$^{815}$ | 923.4631 | 1844.9117 | 1844.8905 | 11.5 | | | | |
| $^{451}$GEPG*PTGIQGP*PGPAGEEGK$^{470}$ | 932.4509 | 1862.8873 | 1862.8647 | 12.1 | | | | |
| $^{622}$GE*PGVVGA*PGTAGPSGPSGL*PGER$^{645}$ | 1076.0321 | 2150.0496 | 2150.0240 | 11.9 | | | | |
| $^{1039}$GETGPAGP*PGA*PGA*PGA*PGPVGPAGK$^{1064}$ | 1093.0436 | 2184.0726 | 2184.0448 | 12.7 | | | | |
| **Porcine Gelatin** | | | | | | | | |
| $^{1068}$TGQPGAVGPAGIR$^{1080}$ | 590.8316 | 1179.6486 | 1179.6360 | 10.7 | 20.59 ± 0.56 | 4.97 ± 0.11 | 0.99 ± 0.04 | 0.20 ± 0.02 |
| $^{831}$TGETGASGP*PGFAGEK$^{846}$ | 739.8483 | 1477.6820 | 1477.6685 | 9.1 | | | | |
| $^{592}$GP*PGESGAAGPAGPIGSR$^{609}$ | 775.8895 | 1549.7644 | 1549.7485 | 10.3 | | | | |
| $^{382}$GPNGEVGSAGP*PGP*PGLR$^{399}$ | 824.4170 | 1646.8194 | 1646.8013 | 11.0 | | | | |
| $^{451}$GEPG*PTGVQGP*PGPAGEEGK$^{470}$ | 925.4421 | 1848.8696 | 1848.8490 | 11.1 | | | | |
| $^{795}$IG*P*PGPSGISGPPGP*PG*PAGK$^{815}$ | 929.4823 | 1856.9500 | 1856.9269 | 12.4 | | | | |
| $^{1039}$GESGPAGP*PGA*PGA*PGAPGPVGPAGK$^{1064}$ | 1078.0370 | 2154.0594 | 2154.0342 | 11.7 | | | | |
| $^{622}$GE*PGVLGA*PGTAGPSGPSGL*PGER$^{645}$ | 1083.0407 | 2164.0669 | 2164.0397 | 12.6 | | | | |
| $^{949}$GY*PGNPGPAGAAGA*PGPQGAVGPAGK$^{974}$ | 1103.0501 | 2204.0855 | 2204.0611 | 11.1 | | | | |
| $^{748}$GENGPVGPTGPVGAAGPAGPNGP*PGPAGSR$^{777}$ | 1283.1388 | 2564.2630 | 2564.2368 | 10.2 | | | | |

[a] *P indicates the hydroxylated proline.



dx.doi.org/10.1021/jf503876a | J. Agric. Food Chem. 2014, 62, 11840−11853

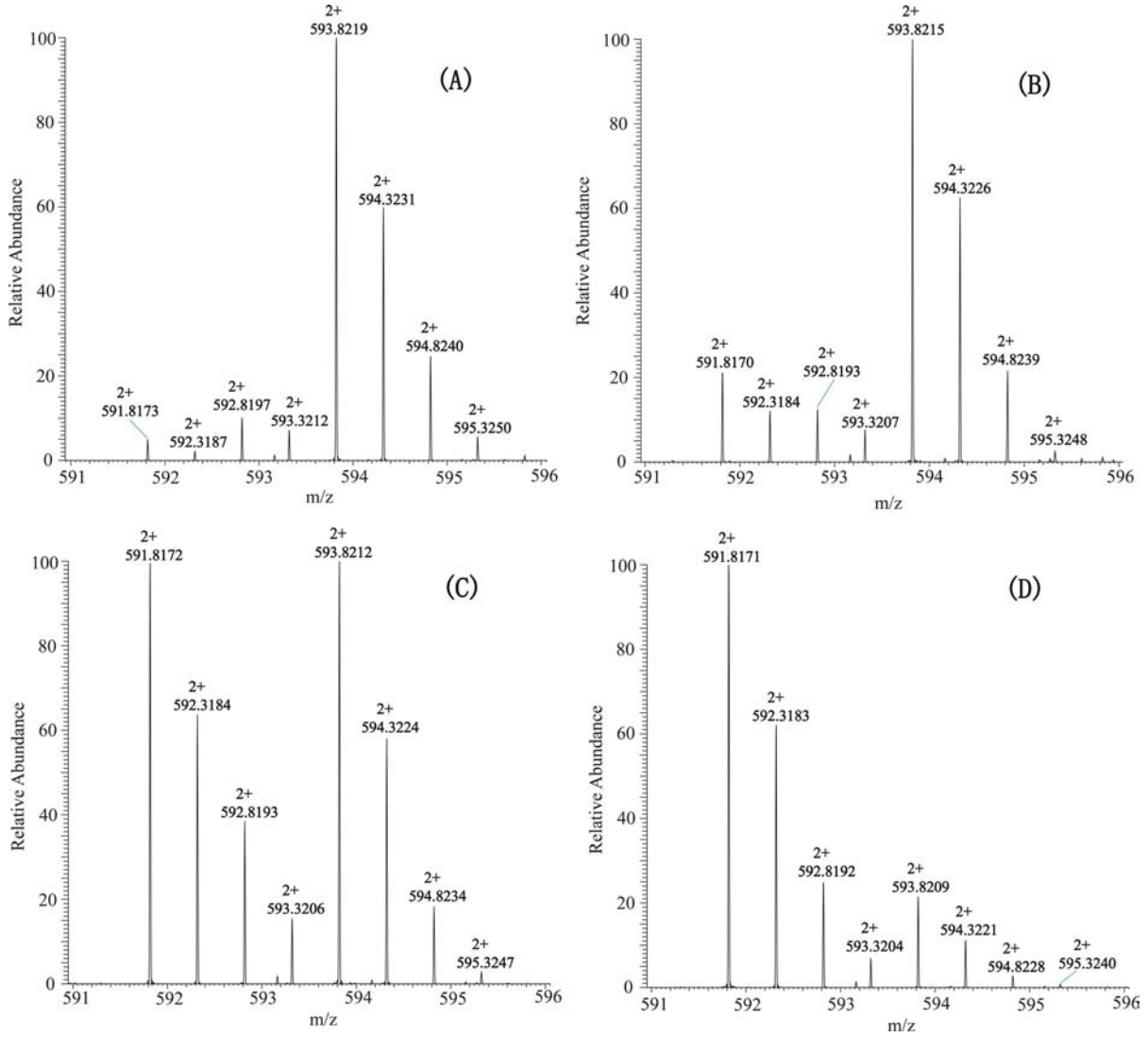


**Figure 5.** Mass spectra of the peptide $^{465}$EGPVGL*PGIDGR$^{476}$ from bovine gelatin with various $^{18}O/^{16}O$ mixing ratios: (A) 20:1; (B) 5:1; (C) 1:1; (D) 1:5.

5:1, 1:1, and 1:5, respectively. The deviation of the measured values from the mixing values for the characteristic peaks will allow us to evaluate the accuracy of this method. For each type of gelatin, 10 characteristic peptides with strongest signal were used for quantification by averaging the measured $^{18}O/^{16}O$ ratios. For example, Figure 5 shows the mass spectra at various mixing ratios of the $^{16}O$ labeling peptide at $m/z$ 591.8174$^{2+}$ and corresponding $^{18}O$-labeled peptide at $m/z$ 593.8219$^{2+}$ from bovine gelatin sample. The S/N ratios of these two peaks were high, and the $^{18}O/^{16}O$ ratios of these two peaks were visually very close to the mixing ratios. Similarly, for the porcine gelatin sample as shown in Figure 6, the mass spectra of the peptide with $m/z$ 590.8316$^{2+}$ exhibited relative intensities very close to their mixing ratios.

Table 3 lists the sequences and mixing ratios of 10 characteristic peptides from bovine and porcine gelatins, respectively. The samples with mixing $^{18}O/^{16}O$ ratios of 20:1, 5:1, 1:1, and 1:5 from the bovine gelatin were measured to be 20.41 ± 0.84, 4.93 ± 0.07, 1.00 ± 0.02, and 0.19 ± 0.02, respectively. For porcine gelatin, the ratios of the peptides for $^{18}O/^{16}O$ mixing ratio at 20:1, 5:1, 1:1, and 1:5 were measured to be 20.59 ± 0.56, 4.97 ± 0.11, 0.99 ± 0.04, and 0.20 ± 0.02, respectively. The experimental values were very close to the mixing value with small standard deviation, suggesting this mass spectrometry-based method is very accurate.

**Specificity of the Quantitative Method.** $^{16}O$- and $^{18}O$-labeled peaks for all characteristic peptides from bovine and porcine gelatins were unambiguously identified by accurate mass and tandem mass spectrometry. As demonstrated in Figures 5 and 6, all characteristic peptides showed the coelution of the $^{16}O$- and $^{18}O$-labeled forms. The retention time for each unique peptide in the chromatography remained consistent in the samples with various mixing ratios of $^{18}O$ to $^{16}O$ (data not shown). Moreover, 10 characteristic peptides for each type of gelatin all showed easily recognizable peaks without strong impurity peak interference in the mass spectra. The $^{16}O$- and $^{18}O$-labeled peaks could be clearly distinguished in LTQ/Orbitrap high-resolution mass spectrometry. All of these indicate that the specificity of this method for gelatin quantification is excellent.

**Sensitivity of the Quantitative Method.** In this work, a HPLC equipped with a microcolumn was used for the separation of the digested mixture of gelatin. When 3 μg/mL digested gelatin mixture was loaded, the signal-to-noise level for all characteristic peptides of bovine or porcine gelatin was much


dx.doi.org/10.1021/jf503876a | J. Agric. Food Chem. 2014, 62, 11840−11853

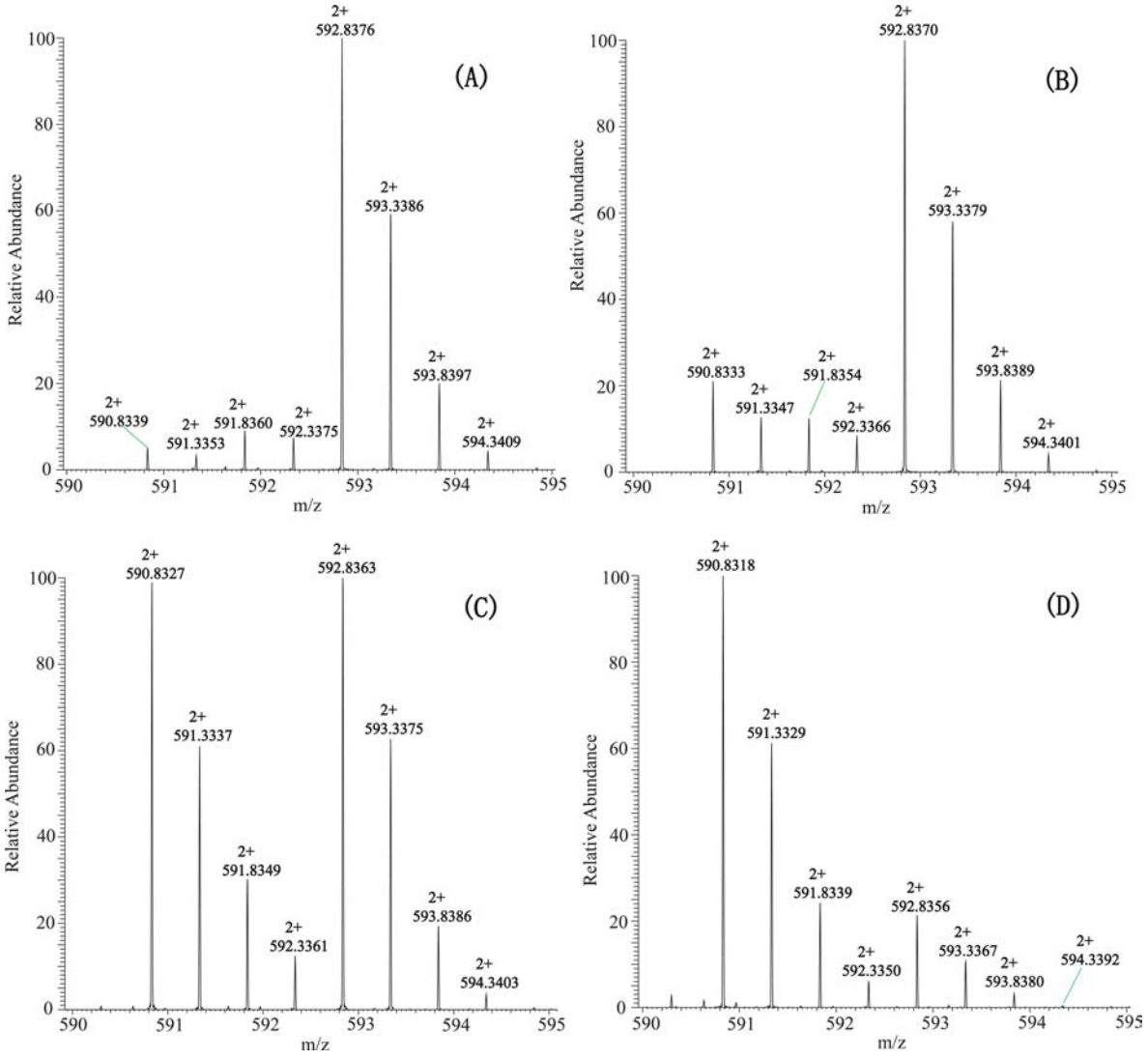


**Figure 6.** Mass spectra of the peptide $^{1068}$TGQPGAVGPAGIR$^{1080}$ from porcine gelatin with various $^{18}O/^{16}O$ mixing ratios: (A) 20:1; (B) 5:1; (C) 1:1; (D) 1:5.

larger than 10, providing a reliable identification and quantification for $^{16}O$- and $^{18}O$-labeled peptides. In a separate experiment, we were able to detect the characteristic peptides of bovine gelatin at a concentration of 0.11 $\mu$g/mL when a UPLC equipped with a nanocolumn (the nanoACQUITY UPLC system) was utilized (Supporting Information Supplemental Figure 1).

**Dynamic Range of the Quantitative Method.** To access the dynamic range of relative quantification, we plotted the $^{18}O/^{16}O$ ratios of peak height ($y$) against the concentration ratios of all 10 peptides. For example, Figure 7A shows two of the plots represented by bovine peptide $^{592}$GP*PGESGAAGPTG-PIGSR$^{609}$ with $m/z$ 790.8971$^{2+}$ and porcine peptide $^{451}$GEPG*PTGVQGP*PGPAGEEGK$^{470}$ with $m/z$ 925.4421$^{2+}$, respectively. Both peptides exhibited a linear response in relative $^{18}O/^{16}O$ concentration ratios from 0.2 to 20 with correlation coefficients ($R^2$) of 0.9995 and 0.9993, respectively. To evaluate the overall dynamic range for the gelatin quantification, $^{18}O/^{16}O$ ratios of all 10 peptides were averaged and plotted against concentration ratios of these peptides (Figure 7B). The results indicated the quantification method by $^{18}O$ labeling and high-resolution mass spectrometry had the excellent linear relationship in relative $^{18}O/^{16}O$ concentration ratios from 0.2 to 20 with $R^2$ of 0.9997 and 0.9995 for bovine gelatin and porcine gelatin, respectively. The dynamic range of relative quantification based on $^{18}O/^{16}O$ labeling can be defined as the ranges of $^{18}O/^{16}O$ concentration ratios that show linear response on isotopic peak area/height ratios.[45] Fenselau and Yao[46] summarized previous work on the quantification method by $^{18}O$ labeling and mass spectrometry and concluded that the dynamic range was limited to about 1:20, which is consistent with our results. It should be noted that the typical quantification method by $^{18}O$ labeling and mass spectrometry employs direct comparison of the peak area or height of the $^{18}O$-labeled and unlabeled peptide pair. A recent quantification method developed by Kim et al.[45] suggests that selected reaction monitoring (SRM) could potentially improve the dynamic range of this type of quantification method.

**Reproducibility of the Quantitative Method.** The reproducibility of the method was evaluated by analyzing the relative standard deviation (RSD) from triplicate. As shown in Table 4, the peptides with $m/z$ values of 790.8971$^{2+}$ and 925.4421$^{2+}$ were used to represent the characteristic peaks from the bovine and porcine gelatins, respectively. The average values of three replicates were very close to the real mixing $^{18}O/^{16}O$

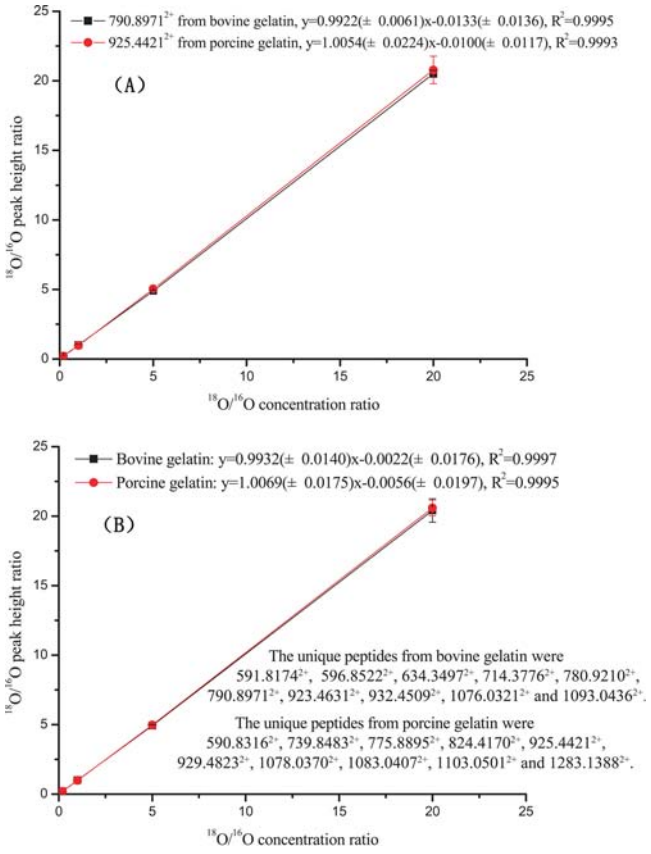


**Figure 7.** Calibration curves of bovine and porcine gelatins: (A) calibration curves of the peptides with $m/z$ 790.8971$^{2+}$ ($^{592}$GP*PGESGAAGPTGPIGSR$^{609}$) and 925.4421$^{2+}$ ($^{451}$GEPG*PTGVQGP*PGPAGEEGK$^{470}$) from bovine and porcine gelatins, respectively; (B) calibration curves by averaging 10 characteristic peptides from bovine and porcine gelatins, respectively.

ratios of 20:1, 5:1, 1:1, and 1:5. All RSD values of below 7.11% were obtained for the peptides from both bovine and porcine gelatins, indicating excellent reproducibility of the gelatin quantification method by $^{18}$O labeling and high-resolution mass spectrometry. The reproducibility is visualized in Supplemental Figure 2, represented by the mass spectra of the peptide 925.4421$^{2+}$ from porcine gelatin at the mixing ratios of 20:1, 5;1, 1:1, and 1:5. At all $^{18}O/^{16}O$ ratios, the mass spectra from three replicates showed peak height ratios close to their mixing ratios.

Gelatin quantification by oxygen-18 labeling utilizes isotopically labeled peptides as internal standards. The $^{18}O/^{16}O$ peptide pairs share the same elution time and ionization efficiency. The interference of the matrix, if there is any, will be equally executed on both $^{18}$O and $^{16}$O peptides. Therefore, the reproducibility of the quantification results should be minimally affected by matrix for the real gelatin sample. To evaluate the reproducibility of this quantification method for the real sample, we performed wide selected ion monitoring (SIM) experiments on gelatin films prepared by mixing bovine and porcine gelatins with glycerol and sorbitol. Five SIM scans with a wide mass window of 200 Da covering the mass range from 500 to 1500 Da were acquired with high resolution and mass accuracy by LTQ-Orbitrap. This method allows us to perform protein/peptide quantification and evaluate whether there are any changes when matrix is present. As shown in Supplemental Figure 3, the extracted ion peak area for the bovine peptide $^{592}$GP*PGESGAAGPTGPIGSR$^{609}$ with $m/z$ 790.8971$^{2+}$ was consistent for three replicates with an RSD value of 7.94%, indicating excellent reproducibility for the samples in the matrix. Similarly, the extracted ion peak area for the peptide from porcine gelatin with $m/z$ 925.4421$^{2+}$ showed excellent reproducibility with an RSD value of 3.81%.

Our results proved that the trypsin-catalyzed $^{18}$O labeling can serve as an excellent internal standard. When combined with high-resolution mass spectrometry, it can be a highly accurate and sensitive method for quantification of the bovine or porcine gelatin. It is important to note that high-resolution mass spectrometry is crucial for this type of analysis. After $^{18}$O labeling, the peptide pair labeled by $^{18}$O and $^{16}$O differ only by 4 Da (4.0085 Da for high resolution) in mass. Under electrospray ionization (ESI), peptides are typically detected as multiple charged ions including doubly, triply, or quadruply charged ions. The differences between the peptide pair are thus only 2, 1.33, and 1 Da in $m/z$, respectively, for these charges. Use of high-resolution mass spectrometers is always considered to be necessary for such close mass difference as it can be difficult with low-resolution mass spectrometers such as ion traps to differentiate the peak pair. An LTQ Orbitrap Velos mass spectrometer can routinely provide mass resolution of 100,000, which can sufficiently separate the peptide pair even at higher charge state. In addition, because proline hydroxylation commonly occurs on bovine or porcine collagen, it is always suggested to use a high-resolution mass spectrometer, which can offer a much easier determination of the sequence modified by hydroxylation.[47] For example, a pair of marker peptides from bovine and porcine gelatins contains very similar sequences of $^{520}$GAGPDGNNGAQGPPGLQGVQGGK$^{542}$ and $^{520}$GAGPDGNNGAQGPPGPQG VQGGK$^{542}$, respectively. If Pro$^{535}$ is hydroxylated, the two sequences will be essentially the same for low-resolution mass spectrometers as the mass difference between Leu and Hyp (0.036 Da) is too small to be differentiated. However, this mass difference can be accurately distinguished when high resolution is applied. In this case, a resolution of 56000 or a mass accuracy of 17 ppm will be able to make a distinction between these two peptides. The LTQ Orbitrap mass spectrometer used in this work constantly provides resolution and mass accuracy better than 60000 and 15 ppm, respectively, and therefore is suitable for this type of analysis.

**Table 4. Reproducibility of the Method**

| | | | average ratio of $^{18}$O to $^{16}$O | | | | | | | |
|---|---|---|---|---|---|---|---|---|---|---|
| gelatin source | selected characteristic sequence[a] | $m/z$ | 20:1 | RSD[b] (%) | 5:1 | RSD (%) | 1:1 | RSD (%) | 1:5 | RSD (%) |
| bovine skin | $^{592}$GP*PGESGAAGPTGPIGSR$^{609}$ | 790.8971$^{2+}$ | 20.50 | 1.20 | 4.91 | 0.62 | 1.00 | 5.40 | 0.19 | 7.11 |
| porcine skin | $^{451}$GEPG*PTGVQGP*PGPAGEEGK$^{470}$ | 925.4421$^{2+}$ | 20.78 | 4.76 | 5.03 | 3.03 | 0.97 | 3.08 | 0.19 | 5.25 |

[a]*P indicates the hydroxylated proline. [b]RSD (%) represents relative standard deviation. The RSD value was obtained by data analysis from three replicates.

Using trypsin-catalyzed $^{18}O$ labeling coupled with high-resolution mass spectrometry, we are able to accurately determine the ratios of the marker peptides ranging from 20:1 to 1:5 ($^{18}O$ vs $^{16}O$). The peptide pair with an $^{18}O/^{16}O$ mixing ratio of 1:20 was also tested; the computed ratio of $^{18}O/^{16}O$ mixture from eq 1 deviated a lot from the mixing ratio. As the contribution of the naturally occurring A+4 isotopic peak from $^{16}O$-labeled peptide and naturally occurring A+2 from single-$^{18}O$-labeled peptide are required to be taken out, any variation of the signal will deposit error in the computation. At an $^{18}O/^{16}O$ mixing ratio of 1:20, $^{18}O$-labeled peptide is only 5%, which is similar or even smaller than the naturally occurring A+4 isotopic peak from $^{16}O$-labeled peptide. When subjected to calculation by eq 1, the resulting error will be intolerant to the signal variation. In contrast, when the mixing ratio is higher than 1:5, the results are mostly accepted because at 20% relative intensity, the signal variation is more forgivable. Among all of the results of various ratios for $^{18}O/^{16}O$ mixtures, the 1:1 mixing ratio showed the most veracity with $1.00 \pm 0.02$ and $0.99 \pm 0.04$ for the bovine and porcine gelatin quantification, respectively. Therefore, the most accurate measurement can be obtained by mixing the equivalent of $^{18}O$- and $^{16}O$-labeled samples.

It is anticipated that this quantification method can be applied to any other type of gelatin under the conditions that the gelatin can be purified and measured accurately so $^{18}O$-labeled internal standard can be prepared. Because this method compares the relative intensities of the marker peptides, matrix effects should not be a problem as long as these marker peptides can be detected by mass spectrometry. The divergent sequence can generate unique marker peptides for each type of gelatin, and this quantification can be extended to mixtures of gelatins. Under this circumstance, an $^{18}O$-labeled internal standard for each gelatin is required. As a simple and accurate way, trypsin-catalyzed $^{18}O$ labeling is also a promising method to quantify other proteins in the food industry.

## ■ ASSOCIATED CONTENT

### Ⓢ Supporting Information

Supplemental Figures 1-3. This material is available free of charge via the Internet at http://pubs.acs.org.

## ■ AUTHOR INFORMATION


### Corresponding Authors

*(H.X.) Phone.: (718) 430-3469. Fax: (718) 430-8939. E-mail: hui.xiao@einstein.yu.edu.

*(Z.-C.T.) E-mail: tuzc_mail@aliyun.com.



### Funding

This study was supported by the National High Technology Research and Development Program of China (863 Program) (No. 2011AA100803), the earmarked fund for Jiangxi Agriculture Research System, the Research Fund for the Doctoral Program of Higher Education (20123604110001), Jiangxi Province Science and Technology Support Program (20122BBF60060), and Project of Education Department of Jiangxi Province (GJJ12018).


### Notes

The authors declare no competing financial interest.

## ■ ABBREVIATIONS USED

HPLC, high-performance liquid chromatography; HCD, high-energy C-trap dissociation; BSE, bovine spongiform encephalopathy; FMD, foot-and-mouth disease; PCR, polymerase chain reaction; ELISA, enzyme-linked immunosorbent assay; Hyp, hydroxyproline; ESI, electrospray ionization

## ■ REFERENCES


(1) Karim, A.; Bhat, R. Fish gelatin: properties, challenges, and prospects as an alternative to mammalian gelatins. *Food Hydrocolloids* **2009**, *23*, 563−576.

(2) Gómez-Guillén, M.; Pérez-Mateos, M.; Gómez-Estaca, J.; López-Caballero, E.; Giménez, B.; Montero, P. Fish gelatin: a renewable material for developing active biodegradable films. *Trends Food Sci. Technol.* **2009**, *20*, 3−16.

(3) Karim, A.; Bhat, R. Gelatin alternatives for the food industry: recent developments, challenges and prospects. *Trends Food Sci. Technol.* **2008**, *19*, 644−656.

(4) Nur Hanani, Z.; Roos, Y.; Kerry, J. P. Use of beef, pork and fish gelatin sources in the manufacture of films and assessment of their composition and mechanical properties. *Food Hydrocolloids* **2012**, *29*, 144−151.

(5) Fernandez-Dıaz, M.; Montero, P.; Gómez-Guillén, M. Effect of freezing fish skins on molecular and rheological properties of extracted gelatin. *Food Hydrocolloids* **2003**, *17*, 281−286.

(6) Tabarestani, H. S.; Maghsoudlou, Y.; Motamedzadegan, A.; Sadeghi Mahoonak, A. Optimization of physico-chemical properties of gelatin extracted from fish skin of rainbow trout (*Onchorhynchus mykiss*). *Bioresour. Technol.* **2010**, *101*, 6207−6214.

(7) Morrison, N.; Clark, R.; Chen, Y.; Talashek, T.; Sworn, G. Gelatin alternatives for the food industry. In *Physical Chemistry and Industrial Application of Gellan Gum*; Springer: Berlin, Germany, 1999; pp 127−131.

(8) Kaewruang, P.; Benjakul, S.; Prodpran, T. Characteristics and gelling property of phosphorylated gelatin from the skin of unicorn leatherjacket. *Food Chem.* **2014**, *146*, 591−596.

(9) Wasswa, J.; Tang, J.; Gu, X. Utilization of fish processing by-products in the gelatin industry. *Food Rev. Int.* **2007**, *23*, 159−174.

(10) O'Mahony, P. Finding horse meat in beef products − a global problem. *QJM* **2013**, *106*, 595−597.

(11) Nemati, M.; Oveisi, M.; Abdollahi, H.; Sabzevari, O. Differentiation of bovine and porcine gelatins using principal component analysis. *J. Pharm. Biomed. Anal.* **2004**, *34*, 485−492.

(12) Hidaka, S.; Liu, S. Effects of gelatins on calcium phosphate precipitation: a possible application for distinguishing bovine bone gelatin from porcine skin gelatin. *J. Food Compos. Anal.* **2003**, *16*, 477−483.

(13) Venien, A.; Levieux, D. Differentiation of bovine from porcine gelatines using polyclonal anti-peptide antibodies in indirect and competitive indirect ELISA. *J. Pharm. Biomed. Anal.* **2005**, *39*, 418−424.

(14) Tasara, T.; Schumacher, S.; Stephan, R. Conventional and real-time PCR−based approaches for molecular detection and quantitation of bovine species material in edible gelatin. *J. Food Prot.* **2005**, *68*, 2420−2426.

(15) Hashim, D.; Man, Y.; Norakasha, R.; Shuhaimi, M.; Salmah, Y.; Syahariza, Z. Potential use of Fourier transform infrared spectroscopy for differentiation of bovine and porcine gelatins. *Food Chem.* **2010**, *118*, 856−860.

(16) Zhang, G.; Liu, T.; Wang, Q.; Chen, L.; Lei, J.; Luo, J.; Ma, G.; Su, Z. Mass spectrometric detection of marker peptides in tryptic digests of gelatin: a new method to differentiate between bovine and porcine gelatin. *Food Hydrocolloids* **2009**, *23*, 2001−2007.

(17) Yilmaz, M. T.; Kesmen, Z.; Baykal, B.; Sagdic, O.; Kulen, O.; Kacar, O.; Yetim, H.; Baykal, A. T. A novel method to differentiate bovine and porcine gelatins in food products: nanoUPLC-ESI-Q-TOF-MS$^E$ based data independent acquisition technique to detect marker peptides in gelatin. *Food Chem.* **2013**, *141*, 2450−2458.

(18) Zhang, H.; Li, X.-J.; Martin, D. B.; Aebersold, R. Identification and quantification of N-linked glycoproteins using hydrazide chemistry, stable isotope labeling and mass spectrometry. *Nat. Biotechnol.* **2003**, *21*, 660−666.

(19) Bantscheff, M.; Schirle, M.; Sweetman, G.; Rick, J.; Kuster, B. Quantitative mass spectrometry in proteomics: a critical review. *Anal. Bioanal. Chem.* **2007**, *389*, 1017−1031.
(20) de Godoy, L. M.; Olsen, J. V.; Cox, J.; Nielsen, M. L.; Hubner, N. C.; Fröhlich, F.; Walther, T. C.; Mann, M. Comprehensive mass-spectrometry-based proteome quantification of haploid versus diploid yeast. *Nature* **2008**, *455*, 1251−1254.
(21) Sechi, S. *Quantitative Proteomics by Mass Spectrometry*; Springer: Berlin, Germany, 2007; Vol. 359.
(22) Goshe, M. B.; Smith, R. D. Stable isotope-coded proteomic mass spectrometry. *Curr. Opin. Biotechnol.* **2003**, *14*, 101−109.
(23) Qian, W.-J.; Camp, D. G., II; Smith, R. D. High-throughput proteomics using Fourier transform ion cyclotron resonance mass spectrometry. *Expert Rev. Proteomics* **2004**, *1*, 87−95.
(24) Qian, W.-J.; Petritis, B. O.; Nicora, C. D.; Smith, R. D. Trypsin-catalyzed oxygen-18 labeling for quantitative proteomics. In *Gel-Free Proteomics*; Springer: Berlin, Germany, 2011; pp 43−54.
(25) Gouw, J. W.; Tops, B. B.; Krijgsveld, J. Metabolic labeling of model organisms using heavy nitrogen ($^{15}$N). In *Gel-Free Proteomics*; Springer: Berlin, Germany, 2011; pp 29−42.
(26) Gouw, J. W.; Krijgsveld, J.; Heck, A. J. Quantitative proteomics by metabolic labeling of model organisms. *Mol. Cell. Proteomics* **2010**, *9*, 11−24.
(27) Ross, P. L.; Huang, Y. N.; Marchese, J. N.; Williamson, B.; Parker, K.; Hattan, S.; Khainovski, N.; Pillai, S.; Dey, S.; Daniels, S. Multiplexed protein quantitation in Saccharomyces cerevisiae using amine-reactive isobaric tagging reagents. *Mol. Cell. Proteomics* **2004**, *3*, 1154−1169.
(28) Tao, W. A.; Wollscheid, B.; O'Brien, R.; Eng, J. K.; Li, X.-J.; Bodenmiller, B.; Watts, J. D.; Hood, L.; Aebersold, R. Quantitative phosphoproteome analysis using a dendrimer conjugation chemistry and tandem mass spectrometry. *Nat. Methods* **2005**, *2*, 591−598.
(29) Reynolds, K. J.; Yao, X.; Fenselau, C. Proteolytic $^{18}$O labeling for comparative proteomics: evaluation of endoprotease Glu-C as the catalytic agent. *J. Proteome Res.* **2002**, *1*, 27−33.
(30) Qin, W.; Song, Z.; Fan, C.; Zhang, W.; Cai, Y.; Zhang, Y.; Qian, X. Trypsin immobilization on hairy polymer chains hybrid magnetic nanoparticles for ultra fast, highly efficient proteome digestion, facile $^{18}$O labeling and absolute protein quantification. *Anal. Chem.* **2012**, *84*, 3138−3144.
(31) Shetty, V.; Nickens, Z.; Shah, P.; Sinnathamby, G.; Semmes, O. J.; Philip, R. Investigation of sialylation aberration in N-linked glycopeptides by lectin and tandem labeling (LTL) quantitative proteomics. *Anal. Chem.* **2010**, *82*, 9201−9210.
(32) Ueda, K.; Takami, S.; Saichi, N.; Daigo, Y.; Ishikawa, N.; Kohno, N.; Katsumata, M.; Yamane, A.; Ota, M.; Sato, T.-A. Development of serum glycoproteomic profiling technique; simultaneous identification of glycosylation sites and site-specific quantification of glycan structure changes. *Mol. Cell. Proteomics* **2010**, *9*, 1819−1828.
(33) Fenselau, C.; Yao, X. $^{18}O_2$-labeling in quantitative proteomic strategies: a status report. *J. Proteome Res.* **2009**, *8*, 2140−2143.
(34) Schnölzer, M.; Jedrzejewski, P.; Lehmann, W. D. Protease-catalyzed incorporation of $^{18}$O into peptide fragments and its application for protein sequencing by electrospray and matrix-assisted laser desorption/ionization mass spectrometry. *Electrophoresis* **1996**, *17*, 945−953.
(35) Yao, X.; Freas, A.; Ramirez, J.; Demirev, P. A.; Fenselau, C. Proteolytic $^{18}$O labeling for comparative proteomics: model studies with two serotypes of adenovirus. *Anal. Chem.* **2001**, *73*, 2836−2842.
(36) Qian, W.-J.; Monroe, M. E.; Liu, T.; Jacobs, J. M.; Anderson, G. A.; Shen, Y.; Moore, R. J.; Anderson, D. J.; Zhang, R.; Calvano, S. E. Quantitative proteome analysis of human plasma following in vivo lipopolysaccharide administration using $^{16}$O/$^{18}$O labeling and the accurate mass and time tag approach. *Mol. Cell. Proteomics* **2005**, *4*, 700−709.
(37) Nelson, C. J.; Hegeman, A. D.; Harms, A. C.; Sussman, M. R. A quantitative analysis of *Arabidopsis* plasma membrane using trypsin-catalyzed $^{18}$O labeling. *Mol. Cell. Proteomics* **2006**, *5*, 1382−1395.
(38) Staes, A.; Demol, H.; Van Damme, J.; Martens, L.; Vandekerckhove, J.; Gevaert, K. Global differential non-gel proteomics by quantitative and stable labeling of tryptic peptides with oxygen-18. *J. Proteome Res.* **2004**, *3*, 786−791.
(39) Bell, M.; Neff, T.; Polarek, J.; Seeley, T. Animal collagen and gelatins. World Patent PCT/034647, 2001.
(40) Zhang, Q.; Tu, Z.; Wang, H.; Huang, X.; Shi, Y.; Sha, X.; Xiao, H. Improved glycation after ultrasonic pretreatment revealed by high-performance liquid chromatography−linear ion trap/orbitrap high-resolution mass spectrometry. *J. Agric. Food Chem.* **2014**, *62*, 2522−2530.
(41) Johnson, K. L.; Muddiman, D. C. A method for calculating $^{16}$O/$^{18}$O peptide ion ratios for the relative quantification of proteomes. *J. Am. Soc. Mass Spectrom.* **2004**, *15*, 437−445.
(42) Fernandes, R. J.; Farnand, A. W.; Traeger, G. R.; Weis, M. A.; Eyre, D. R. A role for prolyl 3-hydroxylase 2 in post-translational modification of fibril-forming collagens. *J. Biol. Chem.* **2011**, *286*, 30662−30669.
(43) Song, E.; Mechref, Y. LC−MS/MS identification of the O-glycosylation and hydroxylation of amino acid residues of collagen $\alpha$-1 (II) chain from bovine cartilage. *J. Proteome Res.* **2013**, *12*, 3599−3609.
(44) Heller, M.; Mattou, H.; Menzel, C.; Yao, X. Trypsin catalyzed $^{16}$O-to-$^{18}$O exchange for comparative proteomics: tandem mass spectrometry comparison using MALDI-TOF, ESI-QTOF, and ESI-ion trap mass spectrometers. *J. Am. Soc. Mass Spectrom.* **2003**, *14*, 704−718.
(45) Kim, J.-S.; Fillmore, T. L.; Liu, T.; Robinson, E.; Hossain, M.; Champion, B. L.; Moore, R. J.; Camp, D. G.; Smith, R. D.; Qian, W.-J. $^{18}$O-labeled proteome reference as global internal standards for targeted quantification by selected reaction monitoring-mass spectrometry. *Mol. Cell. Proteomics* **2011**, *10*, DOI: 10.1074/mcp.M110.007302.
(46) Fenselau, C.; Yao, X. Proteolytic labeling with $^{18}$O for comparative proteomics studies. In *Quantitative Proteomics by Mass Spectrometry*; Springer: Berlin, Germany, 2007; pp 135−142.
(47) Steen, H.; Mann, M. Analysis of bromotryptophan and hydroxyproline modifications by high-resolution, high-accuracy precursor ion scanning utilizing fragment ions with mass-deficient mass tags. *Anal. Chem.* **2002**, *74*, 6230−6236.

conducted using high-performance liquid chromatography (HPLC), carried out with a Sunniest-C18 column (150 × 4.6 mm, 5 μm; ChromaNik, Osaka, Japan). Analytes were dissolved in a methanol ($CH_3OH$) gradient solvent system (5 min hold at 15%, 5−50 min, linear gradient of 15−40%, and 50−160 min, linear gradient of 40−80%) in 0.1% trifluoroacetic acid in water. The flow rate was 1.0 mL/min, and analytes were detected at 275 nm. All analyses by HPLC were carried out at the Institute for Bee Products & Health Science, Yamada Bee Company, Inc.

**Shaving and Depilation of Mice.** Female C57BL/6N mice were purchased from Japan SLC (Shizuoka, Japan) and were maintained under conventional conditions at 22−25 °C. At 8 weeks of age, when the back skin was at the telogen stage, mice were anesthetized by intraperitoneal administration of sodium pentobarbital and were then shaved or depilated.

For the gentle anagen induction experiments, the back skin of mice ($n$ = 10), under anesthesia, was shaved with an electric shaver, and ethanol-extracted propolis, diluted 10-fold in 99.5% ethanol, was topically applied to the shaved skin at 100 μL/d for 3 weeks. Control mice ($n$ = 10) were similarly shaved, and 99.5% ethanol was used in place of diluted propolis. The treated skin regions of all 20 mice were excised and fixed in 4% formaldehyde in phosphate buffered saline (PBS).

For the forced anagen induction experiments, the back hair of anesthetized mice was shortened with an electric shaver, and then club hairs were removed from the back skin using depilatory wax. Eight days after depilation, 10% ethanol-extracted propolis was topically applied to the dorsal skin at 100 μL/d for 3 d ($n$ = 6). Control mice ($n$ = 5) were depilated and then treated with ethanol only. The treated skin regions were excised and fixed in 4% formaldehyde in PBS.

All experimental procedures in this study were approved by the Animal Resource Committee of Hokkaido University (approval number: #09-0125) and were conducted in accordance with Hokkaido University guidelines for the care and use of laboratory animals.

**Identification of Anagen Induction in Shaved Mice.** In shaved mice, the hair cycle progresses from the caudal end toward the cranial end of the back skin, and melanin granules are produced in the hair bulb during middle and late anagen.[16,27] Therefore, we visually identified middle anagen induction based on the degree of melanization of the caudal regions of the back skin in shaved mice.

**Antibodies.** The following antibodies were used as primary antibodies for immunofluorescence staining: mouse antibodies against pan-keratin (Sigma-Aldrich, St. Louis, MO, U.S.A.), cytokeratin 10 (CK10; Progen, Heidelberg, Germany), cytokeratin 14 (CK14; Sigma-Aldrich), cytokeratin 15 (CK15; Thermo Scientific, Fremont, CA, U.S.A.), and 5-bromo-2′-deoxyuridine (BrdU; BioLegend, San Diego, CA, U.S.A.). Similarly, rabbit antibodies against perilipin (Cell Signaling Technology, Danvers, MA, U.S.A.), laminin (LSL, Tokyo, Japan), and zonula occludens-1 (ZO-1; Life Technologies, Gaithersburg, MD, U.S.A.), a rat antibody against Ki-67 (DakoCytomation, Glostrup, Denmark), and a goat antibody against versican (R&D Systems, Minneapolis, MN, U.S.A.) were also used as primary antibodies.

The following antibodies were purchased from Cell Signaling Technology and were used as secondary antibodies: Alexa Fluor 488-conjugated goat anti-rabbit, Alexa Fluor 488-conjugated and Alexa Fluor 546-conjugated goat anti-mouse, Alexa Fluor 488-conjugated donkey anti-mouse, Alexa Fluor 546-conjugated donkey anti-goat, and Alexa Fluor 488-conjugated and Alexa Fluor 546-conjugated goat anti-rat antibodies.

**Immunofluorescence Staining.** After fixation (as described above), surgically excised regions of skin were embedded in paraffin and sliced into 5 μm sections. The sections were deparaffinized and rehydrated. After they were heated in a microwave oven in antigen retrieval buffer consisting of 10 mM Tris-HCl (pH 9.0) and 0.5 mM ethylene glycol tetraacetic acid (Sigma-Aldrich), the sections were incubated in blocking solution (5% bovine serum albumin in PBS) to preclude nonspecific interactions. The sections were then incubated overnight at 4 °C in various primary antibodies diluted in blocking solution. After the sections were washed with PBS containing 0.05% Tween 20, they were exposed to secondary antibodies diluted in blocking solution for 1 h at room temperature. Controls for autofluorescence and the unspecific binding of the secondary antibody were treated in the same manner, but without primary antibodies. Images of the stained sections were obtained using a confocal laser-scanning microscope (TCS SP5; Leica, Mannheim, Germany).

**Measurement of Matrix Cell Migration Distance.** In middle and late anagen, hair matrix keratinocytes actively proliferate and then migrate toward the upper part of the HFs, leading to hair shaft elongation.[19] Therefore, to evaluate hair growth activity, proliferating matrix keratinocytes were labeled by intraperitoneal injection of BrdU into mice (1 mg/mouse in 100 μL of PBS, Sigma-Aldrich). Mice were sacrificed 24 h after injection, and skin samples were excised and fixed (as described above). The migration distance between the bottom of the hair bulb and the furthermost BrdU-positive cells in the hair shaft was measured in 19 sagittally sectioned HFs from 6 propolis-treated and 5 vehicle-treated (control) mice.

**Skin Organ Culture.** Organ culture was performed using depilated, middle anagen stage back skin to investigate the influence of propolis on the proliferation of hair matrix keratinocytes. The back skin was harvested from mice 5 d after depilation and washed with RPMI-1640 medium containing penicillin and streptomycin. Each skin sample was placed on a cell culture insert with a pore size of 0.2 μm and was then cultured for 3 d in RPMI-1640 containing 10 μg/mL insulin, 10 ng/mL hydrocortisone, and either a low concentration (0.005%) of propolis ($n$ = 6), a high concentration (0.05%) of propolis ($n$ = 6), or ethanol as vehicle ($n$ = 6). After 3 d in culture, skin samples were fixed in 4% formaldehyde in PBS, and paraffin sections were prepared.

To measure the proliferation rate of hair matrix keratinocytes, paraffin sections were assayed by immunofluorescence with anti-Ki-67 antibodies and stained with 4′,6-diamidino-2-phenylindole (DAPI). The Ki-67-positive cells were counted, and the percentages of proliferating cells were calculated by dividing this count by the total number of DAPI-stained matrix cells.

**Keratinocyte Isolation and Culture.** Keratinocytes were isolated from the back skin of neonatal C57BL/6N mice 1 d after birth, as follows. Excised regions of back skin were immersed in 0.1% collagenase type III (Worthington Biochemical, Freehold, NJ, U.S.A.), and the epidermis and dermis were separated with fine forceps. Keratinocytes in the separated epidermis were collected by washing with keratinocyte growth medium (CELLnTEC Advanced Cell Systems, Bern, Switzerland), and the cell suspension was passed through a 40 μm cell strainer (BD Biosciences, San Jose, CA, U.S.A.). The cell suspension was then centrifuged at 500$g$ for 5 min, and the epidermal keratinocytes obtained were seeded in 96-well plates at $1 \times 10^3$ cells/well and cultured for 1 d. The medium was then replaced with new medium that lacked growth factors but contained either propolis or vehicle (ethanol). After 2 d of culture, the proliferation activity of these keratinocytes was evaluated using a WST-8 Cell Counting Kit (Dojindo, Osaka, Japan).

**Statistical Analysis.** Statistical analysis was performed using the Analyze-It add-in (Analyze-it Software, Ltd., Leeds, United Kingdom) for Microsoft Excel (Microsoft Corporation, Redmond, WA, U.S.A.). In the case of in vitro experiments, differences between propolis and vehicle groups were analyzed using the unpaired Student's $t$-test. Differences were considered significant at a $p$-value of <0.05 and very significant at a $p$-value of <0.005. These $p$-values are indicated herein by * and **, respectively.

## RESULTS

To confirm the concentrations of specific propolis components, the propolis ethanol extract was analyzed by HPLC (Table 1). The propolis extract contained physiologically active substances responsible for keratinocyte differentiation and reepithelialization, such as caffeic acid and chlorogenic acid.[12,15] Likewise, artepillin C, baccharin, $p$-coumaric acid, drupanin, and kaempferide, which suppress tumor cell growth,[28−30] were abundant in the propolis extract. Propolis also contained a small

**Table 1. Concentrations of Specific Components of Ethanol-Extracted Propolis**

| compd | concn (% w/v) |
|---|---|
| artepillin C | 8.1 ± 0.110 |
| baccharin | 1.5 ± 0.026 |
| caffeic acid | 0.13 ± 0.001 |
| chlorogenic acid | 0.074 ± 0.001 |
| *p*-coumaric acid | 1.2 ± 0.019 |
| drupanin | 1.7 ± 0.027 |
| kaempferide | 1.4 ± 0.024 |
| kaempferol | 0.13 ± 0.001 |

quantity of kaempferol, which promotes apoptosis in human bladder and ovarian cancer cells.[9,10]

**Propolis Facilitates Normal Hair Growth in the Shaved-Mouse Model.** The influence of the propolis extract on hair growth was investigated using two types of in vivo mouse models. In the shaved-mouse model (also known as the gentle anagen induction model), the middle anagen stage was identified by the degree of melanization of the caudal back skin. In those mice that were treated with topical application of propolis, it was induced around 10 d after the mice were shaved, versus around 18 d after shaving in the mice that were treated with topical application of ethanol (vehicle) (Figure 1A). There was a significant difference in the timing of induction of middle anagen between propolis-treated and vehicle-treated mice (Figure 1B). Additionally, 21 d after treatment, 33.3% (5 out of 15) of the propolis-treated mice, compared with only 14.3% (2 out of 14) of the vehicle-treated mice, had hair covering over half of the back skin area.

The histology of the HFs induced into late anagen by propolis treatment was compared with that of the late-anagen HFs in vehicle-treated skin. Hematoxylin and eosin (H&E) staining did not reveal any detectable morphological differences between HFs in propolis-treated and vehicle-treated mice (Figure 2A). The pan-keratin-positive ORS structures were invaginated normally into the perilipin-positive subcutaneous fat layer in both propolis-treated and vehicle-treated skin (Figure 2B). Likewise, in both propolis-treated and vehicle-treated HFs, most of the hair matrix keratinocytes in the hair bulb were Ki-67 positive (Figure 2C). Versican, a dermal papilla-specific proteoglycan,[31] was observed by immunofluorescence in both propolis-treated and vehicle-treated skin, and no obvious differences in versican expression were noted between the two (Figure 2D). CK15 is an intermediate filament protein that is expressed in stem cells in the bulge region and in precursor cells in the ORS and in the epidermal basal layer.[32] In the propolis-treated skin, CK15-positive cells were distributed in the bulge and in the ORS, as well as in the basal layer in the epidermis, similarly to those in vehicle-treated skin (Figure 2E).

**Propolis Facilitates Hair Shaft Elongation in the Depilated-Mouse Model.** The effects of propolis on hair growth in the forced anagen induction model were investigated using depilated mice. Depilation synchronized the hair cycles, such that there were no temporal differences between individuals or spatial differences between caudal and cranial regions of the back skin, regardless of whether the mice were treated with propolis or with vehicle (Figure 3A). HFs were observed to be in late anagen in mice that were depilated and then, 8 d later, treated with either propolis or vehicle for 3 d. Most of the matrix keratinocytes in the hair bulb were Ki-67 positive, and there were no detectable differences between propolis-treated and vehicle-treated HFs (Figure 3B). In contrast, cells that had been labeled with BrdU in the hair matrix 24 h prior were found to have migrated more distally along the hair shaft in the propolis-treated HFs than in the vehicle-treated HFs (Figure 3B). Thus, the migration distance of BrdU-labeled cells significantly increased with propolis treatment (Figure 3C).

**Propolis Facilitates Keratinocyte Proliferation in Vivo and in Vitro.** The effects of propolis on the epidermis were also examined. H&E staining showed the stratified squamous structure of the epidermis in both propolis-treated and vehicle-treated skin, 3 d after initiation of treatment and 11 d after depilation (Figure 4A). Propolis-treated epidermis was somewhat thickened compared with vehicle-treated epidermis. Ki-67-positive cells were detected in the basal layer of the epidermis in both propolis-treated and vehicle-treated skin (Figure 4B); however, the ratio of Ki-67-positive cells to total

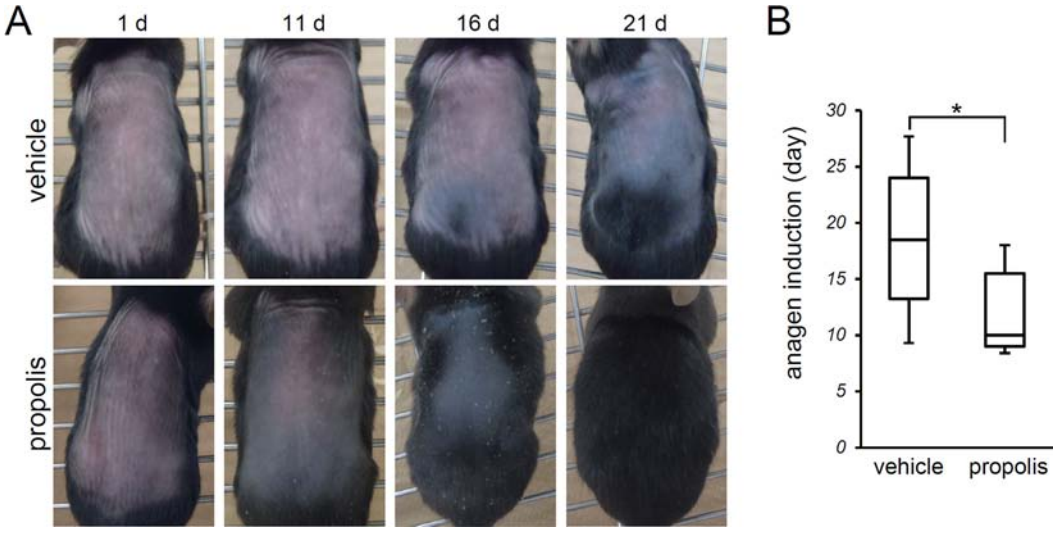


**Figure 1.** Stimulatory effect of propolis on anagen induction in the shaved-mouse model. (A) Representative images of mice treated with topical applications of propolis or vehicle to shaved back skin. (B) Box plots displaying the day of anagen induction, identified based on the degree of melanization of the caudal region of the back skin. *$p < 0.05$.

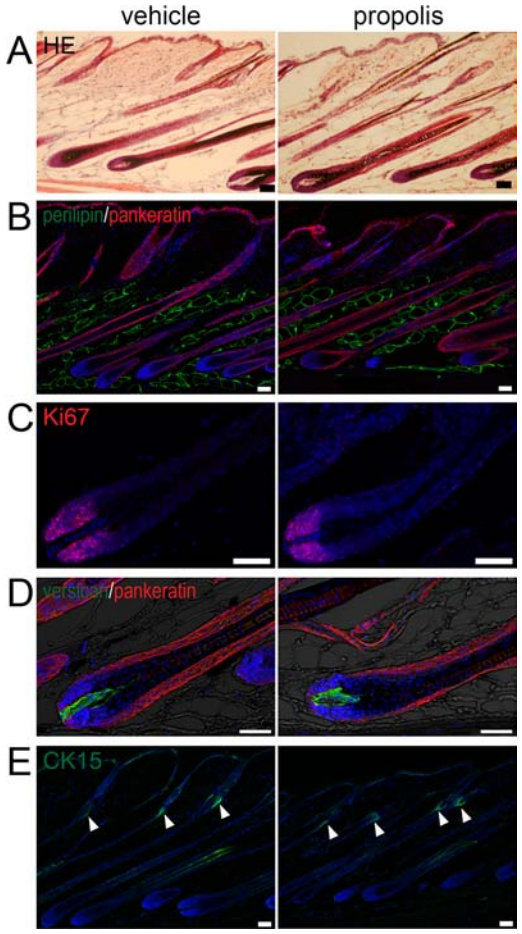


**Figure 2.** Histological assessment of hair follicles induced into anagen stage by propolis in the shaved-mouse model. Images show (A) hematoxylin and eosin (H&E) staining and (B–E) immunofluorescence detection of pan-keratin (red; B, D), perilipin (green; B), Ki-67 (red; C), versican (green; D), and CK15 (green; E) in mouse back skin treated with propolis (left) or vehicle (right) at late anagen stage. Arrowheads indicate the hair stem cells in the bulge region. Nuclei were stained with 4′,6-diamidino-2-phenylindole (DAPI; blue). Bars = 50 $\mu$m.

epidermal cells significantly increased in propolis-treated epidermis (Figure 4C). CK14 and CK10 are specific markers of undifferentiated keratinocytes in the basal layer and of differentiated keratinocytes in the suprabasal layer, respectively.[33] In propolis-treated skin, CK14-positive and CK10-positive keratinocytes lined the basal and suprabasal layers of the epidermis, respectively, similarly to those in vehicle-treated skin (Figure 4D). A continuous basal membrane was observed as a laminin-positive line beneath the basal layer in propolis-treated skin, similar to that observed in the vehicle-treated skin. ZO-1 is a membrane-associated component of both the tight junctions and adherens junctions found at sites of cell–cell contact.[34] In both propolis-treated and vehicle-treated skin, ZO-1 was localized between keratinocytes, except in the fully keratinized cornified layer, as expected in normal skin.

The influence of propolis on the proliferation of hair matrix keratinocytes was examined by organotypic culture of depilated back skin. Some of the matrix keratinocytes in the hair bulb were Ki-67 positive under both vehicle and propolis treatments (Figure 5A). Approximately 45%–48% of matrix keratinocytes were Ki-67 positive in vehicle-treated skin and in skin treated with 0.005% propolis (Figure 5B). However, after treatment with 0.05% propolis, the number of Ki-67-positive hair matrix keratinocytes significantly increased, compared with vehicle treatment.

The influence of propolis on the proliferation of epidermal keratinocytes was examined by culturing isolated epidermal keratinocytes. Isolated keratinocytes exhibited a cobblestone-like shape (Figure 6A), which is the typical shape of epidermal keratinocytes. The proliferation activity of these cells significantly increased when they were treated with 0.05% propolis, compared with vehicle treatment, although lower concentrations of propolis did not influence proliferation (Figure 6B).

## DISCUSSION

During anagen, the hair shaft is produced by active proliferation of hair matrix keratinocytes in the hair bulb. Active proliferation and differentiation of hair epithelial cells is also required to develop hair follicle structures during the telogen–anagen transition. In this study, propolis facilitated anagen induction and activated the proliferation of matrix keratinocytes and the growth of the hair shaft. Propolis is a traditional medicine used for accelerating skin regeneration in wounds, and its components have various stimulatory and regulatory roles in epithelial cell proliferation and differentiation.[14,21,22,35] In particular, chlorogenic acid and caffeic acid facilitate keratinocyte proliferation and differentiation, respectively.[12,15] The Brazilian propolis ethanol extract used in this study contained both chlorogenic acid (0.7 mg/mL) and caffeic acid (1.3 mg/mL). Therefore, it is possible that propolis stimulated hair growth in shaved and depilated mice via the effects of its components on hair keratinocyte proliferation and differentiation.

We confirmed that propolis could influence the morphologically normal development of HFs. HFs stimulated by propolis treatment were normally invaginated into the subcutaneous fat layer and formed well-developed hair bulb structures with hair matrix cells that could actively proliferate. Hair stem cells in the bulge region and progenitor cells in the epidermal basal layer exhibited similar distribution patterns in propolis-treated skin and vehicle-treated skin. The size and shape of hair shafts were not noticeably different in vehicle-treated versus propolis-treated HFs. Versican, which is a marker protein for functional dermal papilla cells,[36] was also distributed normally in propolis-treated HFs. These results indicate that propolis facilitates normal hair growth.

The influence of propolis on the epidermis was also assessed. The normal multilayer structure of the epidermis consists of a CK14-positive basal layer, a CK10-positive suprabasal layer, and a denucleated squamous cell layer.[33] A similar multilayer structure was observed in the epidermis of propolis-treated mice, and tight cell–cell contacts and a continuous basal membrane were observed by ZO-1 and laminin immunofluorescence, respectively, with no detectable differences between vehicle-treated and propolis-treated skin. In contrast, the number of Ki-67-positive proliferating keratinocytes increased in the epidermis with the topical application of propolis. The stimulatory effects of propolis on epidermal keratinocytes were confirmed in assays utilizing cultured isolated keratinocytes. Thus, propolis appears to stimulate the proliferation of epidermal keratinocytes, which stratify into the normal multilayer structure of the epidermis. These results are

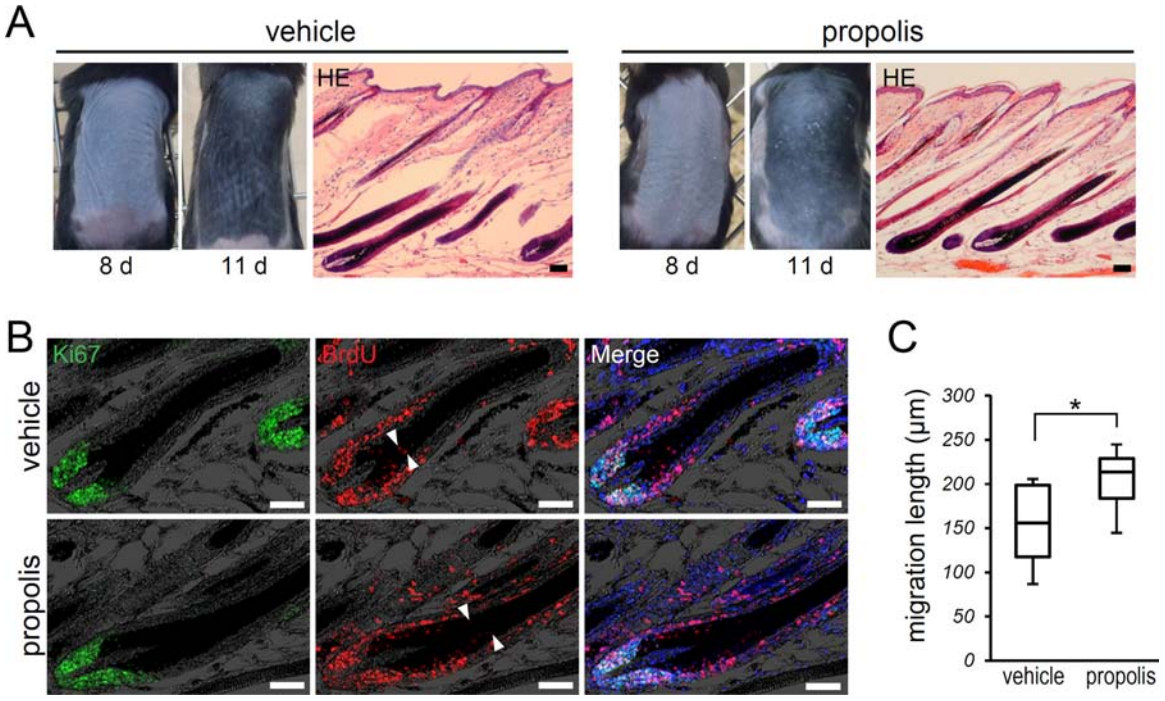


**Figure 3.** Representative images of mice after topical applications of propolis or vehicle to the depilated back skin. (A) Melanization of the back skin and elongation of hair shafts occurred after 8 and 11 d in mice, respectively, following depilation. H&E staining of the back skin 11 d after depilation revealed that hair follicles were at anagen stage following 3 d of propolis or vehicle treatment. (B) Images show immunofluorescence detection of Ki-67 (green) and 5-bromo-2′-deoxyuridine (BrdU; red); rightmost pictures are merged images. Nuclei were stained with DAPI (blue). Over 24 h, BrdU-positive cells migrated out of the hair matrix region and along the hair shaft (arrowheads). (C) Propolis increased the extent of migration, as indicated by a graph of distances traveled by BrdU-labeled cells from the bottom of the hair matrix region. Bars = 50 $\mu$m. *$p$ < 0.05.

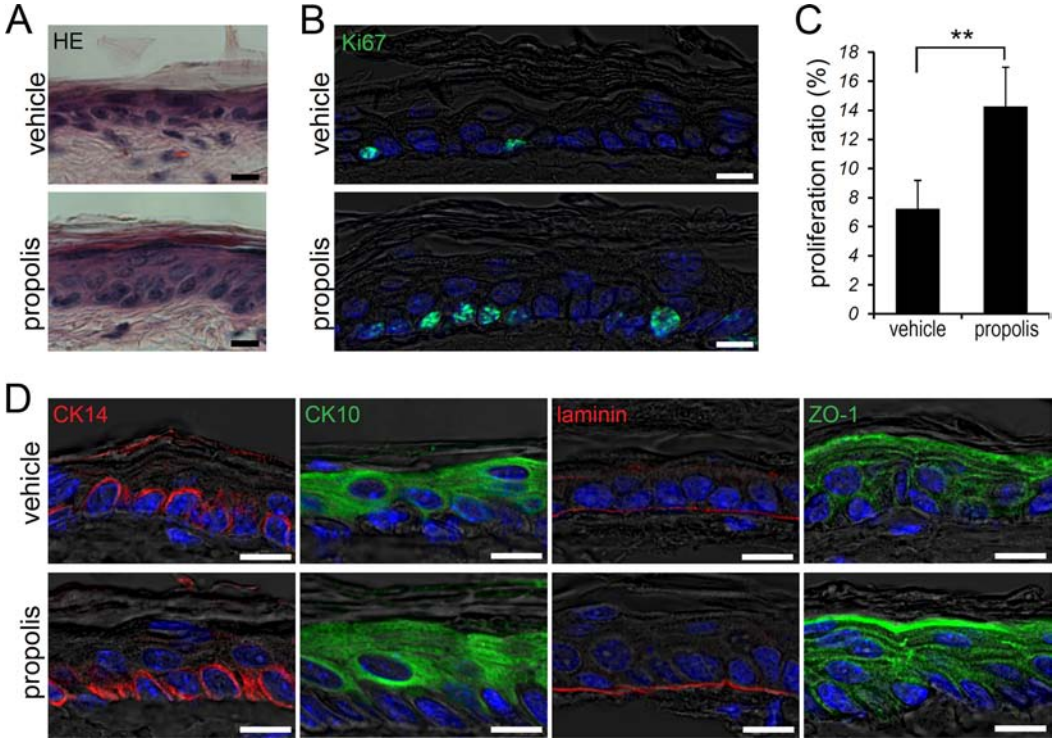


**Figure 4.** Images show (A) H&E staining and (B, D) immunofluorescence detection of Ki-67 (green; B), CK14 (red; D), CK10 (green; D), laminin (red; D), and ZO-1 (green; D) in the skin of mice after topical application of propolis (top half) or vehicle (bottom half) to depilated back skin. Nuclei were stained with DAPI (blue). Bars = 10 $\mu$m. (C) Propolis increased keratinocyte proliferation, as indicated by a graph of the ratio of Ki-67-positive, proliferating cells to total epidermal cells. **$p$ < 0.005.

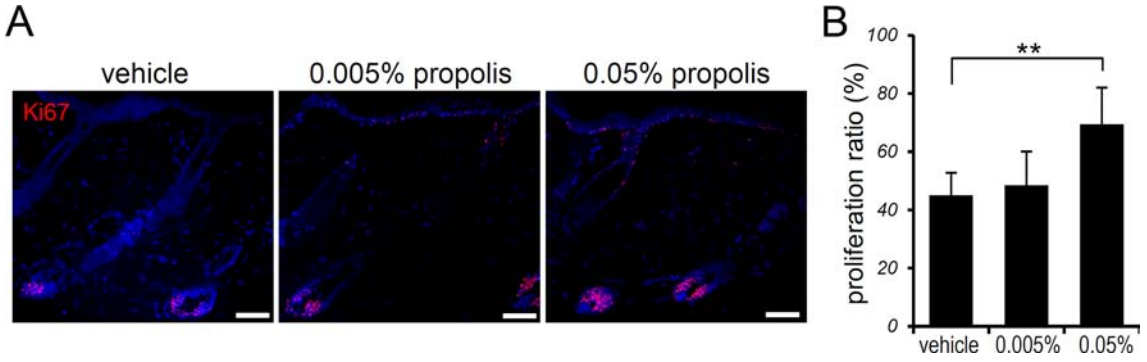


**Figure 5.** (A) Representative images of Ki-67 immunofluorescence in organ skin cultures treated with vehicle, 0.005% propolis, or 0.05% propolis. Nuclei were stained with DAPI (blue). Bar = 50 $\mu$m. (B) The higher concentration of propolis increased proliferation, as indicated by a graph of the ratio of Ki-67-positive matrix cells to total matrix cells. $^{**}p < 0.005$.

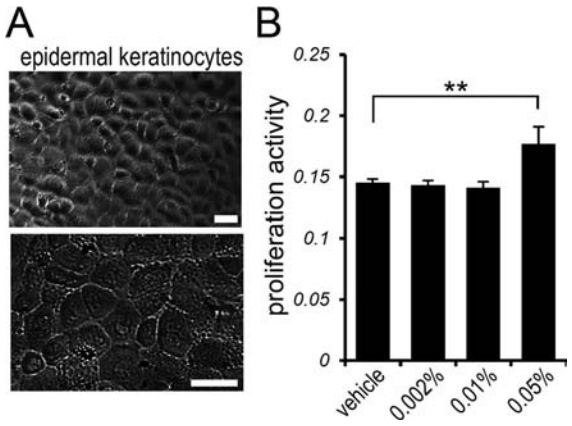


**Figure 6.** (A) The upper and lower panels are a representative phase-contrast image of epidermal keratinocytes cultured for 4 d and a magnified image of the same, respectively. Bars = 10 $\mu$m. (B) A graph of keratinocyte proliferation activity, as assessed by a WST-8 assay, displays an increase in proliferation induced at the highest concentration of propolis tested. $^{**}p < 0.005$.

supported by previously published research that investigated the relationships between propolis and epithelial cells.[14,21,22,35]

Several substances, such as finasteride and minoxidil, have been reported to facilitate hair growth via distinct pathways. Finasteride blocks the hair loss that occurs in androgenetic alopecia by inhibiting steroid 5$\alpha$-reductase, which catalyzes the conversion of testosterone into dihydrotestosterone.[37] Minoxidil extends anagen by activating $\beta$-catenin signaling and the opening of ATP-sensitive potassium channels in dermal papilla cells.[38,39] Conversely, neither finasteride nor minoxidil stimulates keratinocyte proliferation, although minoxidil does slow the senescence of keratinocytes.[40] Thus, propolis utilizes a different pathway from finasteride and minoxidil in promoting hair growth. Therefore, propolis and either minoxidil or finasteride, if applied in combination, would be expected to promote hair growth synergistically.

In this study, we demonstrated the effects of propolis on hair growth through its effects on keratinocyte proliferation. However, the components in propolis that are responsible for the induction of keratinocyte proliferation remain unclear; it is also not known whether propolis has multiple components that contribute to hair growth. Propolis contains several components, such as coumaric acid, artepillin C, and CAPE. Artepillin C acts as a ligand for peroxisome proliferator-activated receptor gamma (PPAR$\gamma$) and enhances adipocyte differentiation, while also inhibiting the macrophage inflammatory response.[41,42] CAPE is a specific inhibitor of nuclear factor kappa B (NF-$\kappa$B) and demonstrates anti-inflammatory and antioxidant effects in several kinds of cells through inhibition of NF-$\kappa$B signaling.[43−46] *p*-Coumaric acid inhibits human tyrosinase activity and melanin synthesis in human epidermal melanocytes.[47,48] PPAR$\gamma$, NF-$\kappa$B, and tyrosinase all take part in biological processes related to hair growth.[49−51] Further investigation is required to elucidate which of these or other components of propolis stimulate hair growth and to determine how to best apply propolis, or its active components, in a clinical setting.

## AUTHOR INFORMATION

### Corresponding Author

*Laboratory of Dairy Food Science, Research Faculty of Agriculture, Hokkaido University, North 9, West 9, Sapporo 060-8589, Japan. Tel: +81-11-706-3642. Fax: +81-11-706-2540. E-mail: kkobaya@anim.agr.hokudai.ac.jp.

### Funding

This work was supported by a Yamada Research Grant from Yamada Bee Company, Inc., and a Grant-in-Aid for Young Scientists (24780281) from the Japan Society for the Promotion of Science.

### Notes

The authors declare no competing financial interest.

## ACKNOWLEDGMENTS

We are grateful to the Yamada Bee Company, Inc., for providing propolis ethanol extracts and for the supporting HPLC analysis.

## ABBREVIATIONS USED

CAPE, caffeic acid phenethyl ester; CK, cytokeratin; HF, hair follicle; HPLC, high-performance liquid chromatography; NF-$\kappa$B, nuclear factor $\kappa$B; ORS, outer root sheath; PPAR, peroxisome proliferator-activated receptor; ZO-1, zonula occludens-1

## REFERENCES

(1) Bankova, V. Chemical diversity of propolis and the problem of standardization. *J. Ethnopharmacol.* **2005**, *100*, 114−117.

(2) Falcao, S. I.; Vale, N.; Cos, P.; Gomes, P.; Freire, C.; Maes, L.; Vilas-Boas, M. In vitro evaluation of Portuguese propolis and floral sources for antiprotozoal, antibacterial and antifungal activity. *Phytother. Res.* **2014**, *28*, 437−443.

(3) Kujumgiev, A.; Tsvetkova, I.; Serkedjieva, Y.; Bankova, V.; Christov, R.; Popov, S. Antibacterial, antifungal and antiviral activity of propolis of different geographic origin. *J. Ethnopharmacol.* **1999**, *64*, 235−240.
(4) Sforcin, J. M.; Bankova, V. Propolis: is there a potential for the development of new drugs? *J. Ethnopharmacol.* **2011**, *133*, 253−260.
(5) Wagh, V. D. Propolis: a wonder bees product and its pharmacological potentials. *Adv. Pharmacol. Sci.* **2013**, *2013*, 308249.
(6) Ruifeng, G.; Yunhe, F.; Zhengkai, W.; Ershun, Z.; Yimeng, L.; Minjun, Y.; Xiaojing, S.; Zhengtao, Y.; Naisheng, Z. Chlorogenic acid attenuates lipopolysaccharide-induced mice mastitis by suppressing TLR4-mediated NF-kappaB signaling pathway. *Eur. J. Pharmacol.* **2014**, *729*, 54−58.
(7) Al-Musayeib, N.; Perveen, S.; Fatima, I.; Nasir, M.; Hussain, A. Antioxidant, anti-glycation and anti-inflammatory activities of phenolic constituents from Cordia sinensis. *Molecules* **2011**, *16*, 10214−10226.
(8) Zhang, M.; Zhou, J.; Wang, L.; Li, B.; Guo, J.; Guan, X.; Han, Q.; Zhang, H. Caffeic acid reduces cutaneous tumor necrosis factor alpha (TNF-alpha), IL-6 and IL-1beta levels and ameliorates skin edema in acute and chronic model of cutaneous inflammation in mice. *Biol. Pharm. Bull.* **2014**, *37*, 347−354.
(9) Xie, F.; Su, M.; Qiu, W.; Zhang, M.; Guo, Z.; Su, B.; Liu, J.; Li, X.; Zhou, L. Kaempferol promotes apoptosis in human bladder cancer cells by inducing the tumor suppressor, PTEN. *Int. J. Mol. Sci.* **2013**, *14*, 21215−21226.
(10) Luo, H.; Rankin, G. O.; Li, Z.; Depriest, L.; Chen, Y. C. Kaempferol induces apoptosis in ovarian cancer cells through activating p53 in the intrinsic pathway. *Food Chem.* **2011**, *128*, 513−519.
(11) Mishima, S.; Ono, Y.; Araki, Y.; Akao, Y.; Nozawa, Y. Two related cinnamic Acid derivatives from Brazilian honey bee propolis, baccharin and drupanin, induce growth inhibition in allografted sarcoma S-180 in mice. *Biol. Pharm. Bull.* **2005**, *28*, 1025−1030.
(12) Kim, B.; Kim, J. E.; Kim, H. S. Caffeic acid induces keratinocyte differentiation by activation of PPAR-alpha. *J. Pharm. Pharmacol.* **2014**, *66*, 84−92.
(13) dos Santos, J. S.; Monte-Alto-Costa, A. Caffeic acid phenethyl ester improves burn healing in rats through anti-inflammatory and antioxidant effects. *J. Burn Care Res.* **2013**, *34*, 682−688.
(14) Serarslan, G.; Altug, E.; Kontas, T.; Atik, E.; Avci, G. Caffeic acid phenethyl ester accelerates cutaneous wound healing in a rat model and decreases oxidative stress. *Clin. Exp. Dermatol.* **2007**, *32*, 709−715.
(15) Chen, W. C.; Liou, S. S.; Tzeng, T. F.; Lee, S. L.; Liu, I. M. Effect of topical application of chlorogenic acid on excision wound healing in rats. *Planta Med.* **2013**, *79*, 616−621.
(16) Muller-Rover, S.; Handjiski, B.; van der Veen, C.; Eichmuller, S.; Foitzik, K.; McKay, I. A.; Stenn, K. S.; Paus, R. A comprehensive guide for the accurate classification of murine hair follicles in distinct hair cycle stages. *J. Invest. Dermatol.* **2001**, *117*, 3−15.
(17) Paus, R. Principles of hair cycle control. *J. Dermatol.* **1998**, *25*, 793−802.
(18) Hsu, Y. C.; Pasolli, H. A.; Fuchs, E. Dynamics between stem cells, niche, and progeny in the hair follicle. *Cell* **2011**, *144*, 92−105.
(19) Schneider, M. R.; Schmidt-Ullrich, R.; Paus, R. The hair follicle as a dynamic miniorgan. *Curr. Biol.* **2009**, *19*, R132−142.
(20) Botchkarev, V. A.; Paus, R. Molecular biology of hair morphogenesis: development and cycling. *J. Exp. Zool., Part B* **2003**, *298*, 164−180.
(21) Sehn, E.; Hernandes, L.; Franco, S. L.; Goncalves, C. C.; Baesso, M. L. Dynamics of reepithelialisation and penetration rate of a bee propolis formulation during cutaneous wounds healing. *Anal. Chim. Acta* **2009**, *635*, 115−120.
(22) McLennan, S. V.; Bonner, J.; Milne, S.; Lo, L.; Charlton, A.; Kurup, S.; Jia, J.; Yue, D. K.; Twigg, S. M. The anti-inflammatory agent Propolis improves wound healing in a rodent model of experimental diabetes. *Wound Repair Regener.* **2008**, *16*, 706−713.
(23) Martin, L. F.; Rocha, E. M.; Garcia, S. B.; Paula, J. S. Topical Brazilian propolis improves corneal wound healing and inflammation in rats following alkali burns. *BMC Complementary Altern. Med.* **2013**, *13*, 337.
(24) Abdulrhman, M.; El Barbary, N. S.; Ahmed Amin, D.; Saeid Ebrahim, R. Honey and a mixture of honey, beeswax, and olive oil-propolis extract in treatment of chemotherapy-induced oral mucositis: a randomized controlled pilot study. *Pediatr. Hematol. Oncol* **2012**, *29*, 285−292.
(25) Ogawa, H.; Hattori, M. Regulation mechanisms of hair growth. *Curr. Probl. Dermatol.* **1983**, *11*, 159−170.
(26) Ishimatsu-Tsuji, Y.; Moro, O.; Kishimoto, J. Expression profiling and cellular localization of genes associated with the hair cycle induced by wax depilation. *J. Invest. Dermatol.* **2005**, *125*, 410−420.
(27) Yamamoto, K.; Yamauchi, M. Characterization of dermal type I collagen of C3H mouse at different stages of the hair cycle. *Br. J. Dermatol.* **1999**, *141*, 667−675.
(28) Akao, Y.; Maruyama, H.; Matsumoto, K.; Ohguchi, K.; Nishizawa, K.; Sakamoto, T.; Araki, Y.; Mishima, S.; Nozawa, Y. Cell growth inhibitory effect of cinnamic acid derivatives from propolis on human tumor cell lines. *Biol. Pharm. Bull.* **2003**, *26*, 1057−1059.
(29) Janicke, B.; Onning, G.; Oredsson, S. M. Differential effects of ferulic acid and p-coumaric acid on S phase distribution and length of S phase in the human colonic cell line Caco-2. *J. Agric. Food Chem.* **2005**, *53*, 6658−6665.
(30) Martineti, V.; Tognarini, I.; Azzari, C.; Carbonell Sala, S.; Clematis, F.; Dolci, M.; Lanzotti, V.; Tonelli, F.; Brandi, M. L.; Curir, P. Inhibition of in vitro growth and arrest in the G0/G1 phase of HCT8 line human colon cancer cells by kaempferide triglycoside from Dianthus caryophyllus. *Phytother. Res.* **2010**, *24*, 1302−1308.
(31) du Cros, D. L.; LeBaron, R. G.; Couchman, J. R. Association of versican with dermal matrices and its potential role in hair follicle development and cycling. *J. Invest. Dermatol.* **1995**, *105*, 426−431.
(32) Morris, R. J.; Liu, Y.; Marles, L.; Yang, Z.; Trempus, C.; Li, S.; Lin, J. S.; Sawicki, J. A.; Cotsarelis, G. Capturing and profiling adult hair follicle stem cells. *Nat. Biotechnol.* **2004**, *22*, 411−417.
(33) Broekaert, D.; Leigh, I. M.; Lane, E. B.; Van Muijen, G. N.; Ramaekers, F. C.; De Bersaques, J.; Coucke, P. An immunohistochemical and histochemical study of cytokeratin, involucrin and transglutaminase in seborrhoeic keratosis. *Arch. Dermatol. Res.* **1993**, *285*, 482−490.
(34) Hartsock, A.; Nelson, W. J. Adherens and tight junctions: structure, function and connections to the actin cytoskeleton. *Biochim. Biophys. Acta* **2008**, *1778*, 660−669.
(35) de Groot, A. C. Propolis: a review of properties, applications, chemical composition, contact allergy, and other adverse effects. *Dermatitis* **2013**, *24*, 263−282.
(36) Feng, M.; Yang, G.; Wu, J. Versican targeting by RNA interference suppresses aggregative growth of dermal papilla cells. *Clin. Exp. Dermatol.* **2011**, *36*, 77−84.
(37) Wright, A. S.; Thomas, L. N.; Douglas, R. C.; Lazier, C. B.; Rittmaster, R. S. Relative potency of testosterone and dihydrotestosterone in preventing atrophy and apoptosis in the prostate of the castrated rat. *J. Clin. Invest.* **1996**, *98*, 2558−2563.
(38) Kwack, M. H.; Kang, B. M.; Kim, M. K.; Kim, J. C.; Sung, Y. K. Minoxidil activates beta-catenin pathway in human dermal papilla cells: a possible explanation for its anagen prolongation effect. *J. Dermatol. Sci.* **2011**, *62*, 154−159.
(39) Shorter, K.; Farjo, N. P.; Picksley, S. M.; Randall, V. A. Human hair follicles contain two forms of ATP-sensitive potassium channels, only one of which is sensitive to minoxidil. *FASEB J.* **2008**, *22*, 1725−1736.
(40) Baden, H. P.; Kubilus, J. Effect of minoxidil on cultured keratinocytes. *J. Invest. Dermatol.* **1983**, *81*, 558−560.
(41) Choi, S. S.; Cha, B. Y.; Iida, K.; Lee, Y. S.; Yonezawa, T.; Teruya, T.; Nagai, K.; Woo, J. T.; Artepillin, C. as a PPARgamma ligand, enhances adipocyte differentiation and glucose uptake in 3T3-L1 cells. *Biochem. Pharmacol.* **2011**, *81*, 925−933.
(42) Szliszka, E.; Mertas, A.; Czuba, Z. P.; Krol, W. Inhibition of Inflammatory Response by Artepillin C in Activated RAW264.7

Macrophages. *Evidence-Based Complementary Altern. Med.* **2013**, *2013*, 735176.
(43) Yasui, N.; Nishiyama, E.; Juman, S.; Negishi, H.; Miki, T.; Yamori, Y.; Ikeda, K. Caffeic acid phenethyl ester suppresses oxidative stress in 3T3-L1 adipocytes. *J. Asian Nat. Prod. Res.* **2013**, *15*, 1189−1196.
(44) Bezerra, R. M.; Veiga, L. F.; Caetano, A. C.; Rosalen, P. L.; Amaral, M. E.; Palanch, A. C.; de Alencar, S. M. Caffeic acid phenethyl ester reduces the activation of the nuclear factor kappaB pathway by high-fat diet-induced obesity in mice. *Metabolism* **2012**, *61*, 1606−1614.
(45) Zhao, W. X.; Wang, L.; Yang, J. L.; Li, L. Z.; Xu, W. M.; Li, T. Caffeic acid phenethyl ester attenuates pro-inflammatory and fibrogenic phenotypes of LPS-stimulated hepatic stellate cells through the inhibition of NF-kappaB signaling. *Int. J. Mol. Med.* **2014**, *33*, 687−694.
(46) Natarajan, K.; Singh, S.; Burke, T. R., Jr.; Grunberger, D.; Aggarwal, B. B. Caffeic acid phenethyl ester is a potent and specific inhibitor of activation of nuclear transcription factor NF-kappa B. *Proc. Natl. Acad. Sci. U.S.A.* **1996**, *93*, 9090−9095.
(47) Song, K.; An, S. M.; Kim, M.; Koh, J. S.; Boo, Y. C. Comparison of the antimelanogenic effects of p-coumaric acid and its methyl ester and their skin permeabilities. *J. Dermatol. Sci.* **2011**, *63*, 17−22.
(48) An, S. M.; Koh, J. S.; Boo, Y. C. p-coumaric acid not only inhibits human tyrosinase activity in vitro but also melanogenesis in cells exposed to UVB. *Phytother. Res.* **2010**, *24*, 1175−1180.
(49) Billoni, N.; Buan, B.; Gautier, B.; Collin, C.; Gaillard, O.; Mahe, Y. F.; Bernard, B. A. Expression of peroxisome proliferator activated receptors (PPARs) in human hair follicles and PPAR alpha involvement in hair growth. *Acta Derm.-Venereol.* **2000**, *80*, 329−334.
(50) Kloepper, J. E.; Ernst, N.; Krieger, K.; Bodo, E.; Biro, T.; Haslam, I. S.; Schmidt-Ullrich, R.; Paus, R. NF-kappaB Activity is Required for Anagen Maintenance in Human Hair Follicles in vitro. *J. Invest. Dermatol.* **2014**, *134*, 2036−2038.
(51) Slominski, A.; Paus, R. Melanogenesis is coupled to murine anagen: toward new concepts for the role of melanocytes and the regulation of melanogenesis in hair growth. *J. Invest. Dermatol.* **1993**, *101*, 90S−97S.

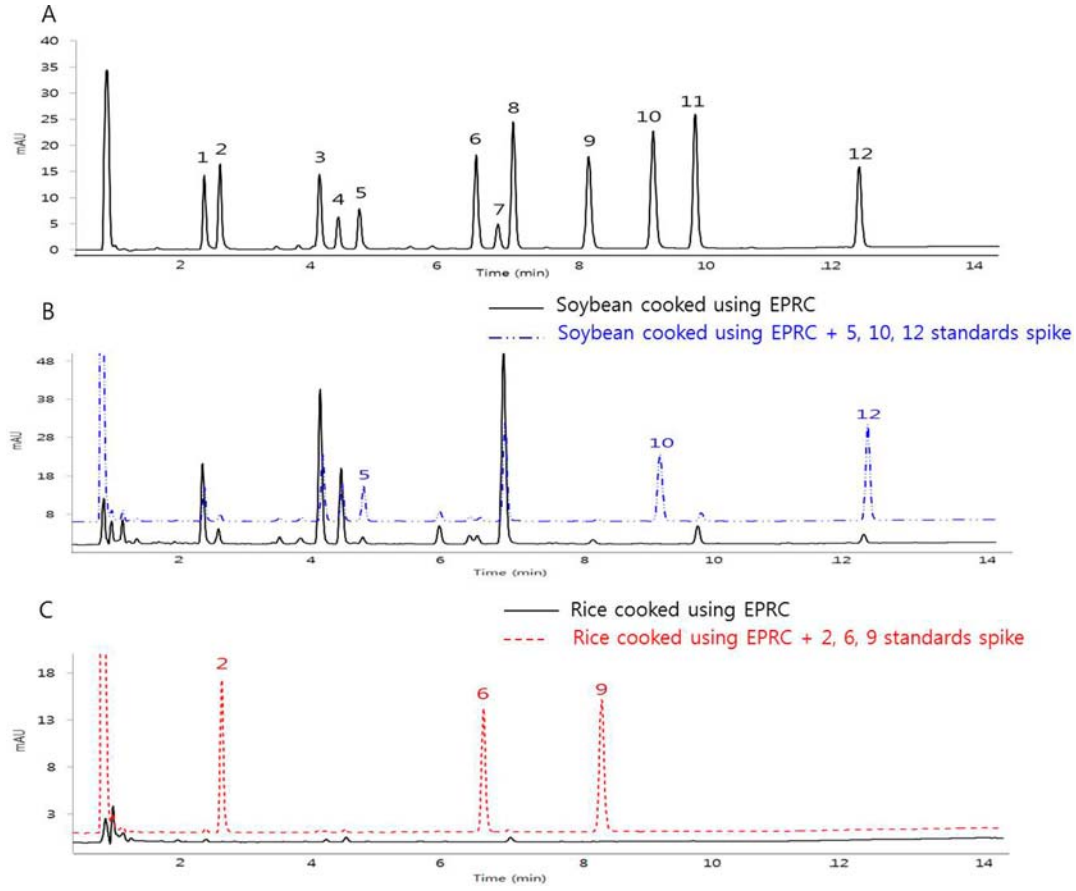


**Figure 1.** (A) Representative UPLC chromatograms of 12 isoflavone STDs and the isoflavones in cooked soybeans and rice. (B) Comparison of chromatograms of the soybeans cooked using an EPRC (black solid line) and the same soybean aliquot spiked with isoflavone STDs 5, 10, and 12 (blue dotted line). (C) Comparison of chromatograms of the rice cooked using the EPRC (black solid line) and the same rice aliquot spiked with isoflavone STDs 2, 6, and 9 (red dotted line). Isoflavone STDs: 1, Din; 2, Glin; 3, Gin; 4, MD; 5, MGl; 6, AD; 7, MG; 8, AGl; 9, Dein; 10, Glein; 11, AG; and 12, Gein.

of soybeans and soy foods.[8,15,21−24] However, to the best of our knowledge, few studies have examined the effects of a combination cooking method involving heat and pressure treatment on isoflavone composition and content of soybean−rice mixtures cooked using rice cookers. Therefore, the present study investigated the effects of heat and pressure processing on the composition and content of 12 isoflavones in soybeans during soybean−rice mixture cooking using an ERC and an EPRC. The present study also examined the transfer of these 12 isoflavones between soybeans and rice after ERC and EPRC cooking of a soybean−rice mixture. The results of the present study describe the effects of cooking on the composition and content of isoflavones in soybeans and provide basic information for the development of functional foods using soybeans in the food industry.

## MATERIALS AND METHODS

**Chemicals.** All solvents used for isoflavone extraction and analysis were of high-performance liquid chromatography grade. All solvents and reagents were obtained from Fischer Scientific Korea, Ltd. (Seoul, Korea), Merck (Darmstadt, Germany), J.T.Baker (Phillipsburg, NJ), or Daejung Chemical & Materials Co., Ltd. (Gyeonggi-Do, Korea). A total of 12 isoflavone standards (STDs) were purchased from Wako Pure Chemical Industries, Ltd. (Osaka, Japan).

**Rice and Soybean Materials.** The soybean cultivar "Chung-ja" (black-coated soybean seed) was cultivated, harvested, and obtained from the Rural Development Administration in 2012. In general, "Chung-ja" is classified as the type of soybean cooked with rice in Korea.[25] The rice cultivar "Choochung" was purchased from a local market in Seoul, Korea, to be cooked with the soybeans. This rice grain had a moisture content of approximately 14% and was stored at room temperature until it was cooked with the soybeans.

**Soybean−Rice Mixture Cooking.** Two rice cookers were used in the present study: an ERC (LJ-MG0402) and an EPRC (LJP-SA063E), both from Lihom (Seoul, Korea). During the soybean−rice mixture cooking, the ERC was operated at a cooking temperature of ∼100 °C and a cooking pressure of ∼14.7 psi, whereas the EPRC was operated at a cooking temperature of 120−130 °C and a cooking pressure of 25−30 psi. For soybean−rice mixture cooking, 40 and 300 g of soybeans and rice, respectively, were weighed and combined. Tap water (400 mL) was added, and the soybeans and rice were soaked together in water for 30 min at room temperature. Thereafter, the soybeans and rice were cooked using the ERC and EPRC ($n$ = 3). Then, the soybeans and rice were separated and lyophilized at −45 °C for 3 days and pulverized for isoflavone analysis.

**Isoflavone Extraction.** Isoflavones from the soybean and rice samples were extracted using acidic extraction.[7] Pulverized samples (2 g each; $n$ = 3) were added to 10 mL of acetonitrile and 2 mL of 0.1 N hydrochloric acid and then extracted for 2 h at room temperature on a shaker at 200 rpm (Green-Sseriker, Vision Scientific Co., Ltd., Gyeonggi-Do, Korea). The crude extract was filtered through No. 42 Whatman filter paper (125 mm diameter, Maidstone, U.K.), and the filtrate was evaporated at a temperature lower than 32 °C with a vacuum evaporator (EYELA, SB-1200, Tokyo Rikakikai Co., Ltd., Gyeonggi-Do, Korea). The dried samples were reconstituted with

Table 1. Calibration Curve, Concentration Range, Linearity, LOD, and LOQ of 12 Isoflavone STDs

| group | STD[a] | concentration range[b] ($\mu$g mL$^{-1}$) | linearity ($r^2$) | slope ($S$) | SD of $y$ intercept | LOD[c] ($\mu$g mL$^{-1}$) | LOQ[c] ($\mu$g mL$^{-1}$) |
|---|---|---|---|---|---|---|---|
| aglucon | Dein | 0.5−2.5 | 1 | 7.37 | 0.06 | 0.02 | 0.08 |
| | Gein | 0.5−2.5 | 1 | 12.14 | 0.05 | 0.01 | 0.04 |
| | Glein | 0.5−2.5 | 1 | 9.19 | 0.02 | 0.01 | 0.02 |
| glucoside | Din | 0.5−25 | 0.999 | 8.15 | 0.41 | 0.16 | 0.52 |
| | Gin | 0.5−25 | 1 | 9.55 | 0.51 | 0.16 | 0.53 |
| | Glin | 0.5−5 | 1 | 7.63 | 0.07 | 0.03 | 0.09 |
| acetyl glucoside | AD | 0.5−5 | 0.999 | 5.58 | 0.43 | 0.23 | 0.78 |
| | AG | 0.5−10 | 0.999 | 10.11 | 0.44 | 0.13 | 0.44 |
| | AGl | 0.5−5 | 0.999 | 8.21 | 0.23 | 0.08 | 0.28 |
| malonyl glucoside | MD | 0.5−25 | 0.999 | 4.78 | 0.04 | 0.02 | 0.07 |
| | MG | 0.5−75 | 0.999 | 4.40 | 0.07 | 0.05 | 0.15 |
| | MGl | 0.5−5 | 1 | 2.70 | 0.01 | 0.01 | 0.04 |

[a]Dein, daidzein; Gein, genistein; Glein, glycitein; Din, daidzin; Gin, genistin; Glin, glycitin; AD, acetyldaidzin; AG, acetylgenistin; AGl, acetylglycitin; MD, malonyldaidzin; MG, malonylgenistin; and MGl, malonylglycitin. [b]The calibration curve was composed of 4−8 different concentrations for each standard solution. [c]The LOD and LOQ were calculated as follows: LOD = 3SD/$S$ and LOQ = 10SD/$S$, where SD is the standard deviation of the $y$ intercept in the calibration curve and $S$ is the slope of each calibration curve.[26]

10 mL of 80% methanol and then filtered through a 0.2 $\mu$m nylon membrane syringe filter (Sun Sri, Rockwood, TN).

**Isoflavone Analysis with Ultraperformance Liquid Chromatography (UPLC).** Isoflavones were analyzed with an Agilent UPLC system coupled with a diode array detector (1290 infinity binary pump, Agilent, Seoul, Korea). A reverse-phase column (Agilent Zorbax Eclipse $C_{18}$, 100 × 2.1 mm internal diameter, 1.8 $\mu$m) was used to separate the 12 isoflavones. The ultraviolet and reference wavelengths were set at 254 and 360 nm, respectively. The mobile phase consisted of 0.1% glacial acetic acid in water (solvent A) and 0.1% glacial acetic acid in acetonitrile (solvent B). The gradient conditions of the mobile phases were slightly modified as previously described[7] and optimized for isoflavone analysis using UPLC as follows: initial, 85% A/15% B; 10 min, 75% A/25% B; 13 min, 65% A/35% B; 16 min, 65% A/35% B; and 20 min, 85% A/15% B. The stop time was set at 20 min, and the post time (equilibrium time) was set at 5 min. The injection volume was 1 $\mu$L, and the flow rate was 0.5 mL min$^{-1}$. The isoflavones were identified by comparing the retention times of the authentic STDs and the peaks in the sample aliquots. Furthermore, each isoflavone STD was added to the sample aliquots (sample aliquot + isoflavone STD) to confirm the correct peak assignment in the sample aliquots; we could then properly assign the isoflavone peaks in the samples (Figure 1). The limit of detection (LOD) and limit of quantification (LOQ) were calculated using the calibration curve as follows: LOD = 3SD/$S$ and LOQ = 10SD/$S$, where SD is the standard deviation of the $y$ intercept of the calibration curve, and $S$ is the slope of the calibration curve.[26] The LOD and LOQ of the 12 isoflavones were 0.01−0.23 and 0.02−0.78 $\mu$g mL$^{-1}$, respectively (Table 1).

**Statistical Analysis.** Statistical analysis was performed using the general linear model procedure of the SAS software (SAS Institute, Inc., Cary, NC). The results were analyzed using a variance analysis. Additionally, Fisher's least significant difference test at the 0.05 probability level ($LSD_{0.05}$) was used to determine differences among the means of the samples.

## RESULTS

**Composition and Content of Isoflavones in Soybeans and Rice before Cooking.** The composition and content of the 12 isoflavones in soybeans and rice before cooking are shown in Table 2. The total isoflavone content in the soybeans was 562.9 ± 21.2 $\mu$g g$^{-1}$. Among the four isoflavone groups, malonylglucosides (sum of malonyldaidzin, malonylgenistin, and malonylglycitin) were the most abundant (83.5 ± 3.1%) in the soybeans before cooking. Glucosides (12.8 ± 0.5%), acetylglucosides (2.8 ± 0.1%), and aglucon (0.9 ± 0.1%) were the next most abundant isoflavone groups, and the differences in abundance were statistically significant ($p < 0.05$). The total daidzein (sum of daidzein, daidzin, acetyldaidzin, and malonyldaidzin), total genistein, and total glycitein in the soybeans before cooking were 69.4 ± 3.1, 220.9 ± 7.8, and 12.1 ± 0.6 $\mu$g g$^{-1}$ (aglucon equivalents), respectively ($p < 0.05$; Table 3). Among the 12 isoflavones, malonylgenistin was the major isoflavone type (359.1 ± 12.6 $\mu$g g$^{-1}$), accounting for approximately 64% of the total isoflavone content in the soybeans before cooking. Acetylglycitin and glycitein were not detected or found in only trace levels (indicating levels below the limit of detection, <LOD). In addition, isoflavones were not found in the rice before cooking (Table 2 and Figure 2).

**Changes in Isoflavone Composition and Content in the Soybean−Rice Mixture after ERC Cooking.** In comparison to that before cooking, the total isoflavone content in soybeans cooked using the ERC decreased by approximately 10% (before cooking, 562.9 $\mu$g g$^{-1}$; after cooking, 504.4 ± 2.9 $\mu$g g$^{-1}$). Malonylglucosides and glucosides constituted approximately 68 and 26%, respectively, of the total isoflavone content in the soybeans cooked using the ERC. In comparison to that before cooking, the malonylglucoside content in the soybeans decreased by ∼16% and the glucoside content increased by ∼13% after ERC cooking. Therefore, some of the malonylglucosides in the soybeans were converted to the glucosides during ERC cooking (Table 2). In comparison to the isoflavones (total daidzein, total genistein, and total glycitein) in the soybeans before cooking, the total genistein and total glycitein in the soybeans cooked using the ERC decreased by ∼11 and ∼7%, respectively ($p < 0.05$). The total daidzein content increased by ∼3% in the ERC-cooked soybeans; however, the difference was not statistically significant (see Table 3). Among the 12 isoflavones, malonylgenistin was the major isoflavone (52.3 ± 0.3%) in the soybeans cooked using the ERC and glycitin and acetylglycitin were detected at trace levels (<LOD) or not detected. Furthermore, the genistin content increased by approximately 82% (before cooking, 42.6 $\mu$g g$^{-1}$; after cooking, 77.4 $\mu$g g$^{-1}$) in the soybeans after ERC cooking (Table 2).

After soybean−rice mixture cooking using the ERC, the total isoflavone content in the rice was 14.0 ± 0.1 $\mu$g g$^{-1}$ (dry basis of ERC-cooked rice), which equaled approximately 85 $\mu$g g$^{-1}$ (dry basis of ERC-cooked soybeans), approximately 15% of the total isoflavones in the soybeans before cooking. Malonylglucosides were the major isoflavones (∼90%) in the rice cooked

**Table 2. Composition and Contents of 12 Isoflavones in Soybeans and Rice before and after Soybean−Rice Cooking Using ERC and EPRC ($\mu$g g$^{-1}$, Dry Basis)[a]**

| | aglucon | | | | glucoside | | | | acetylglucoside | | | | malonylglucoside | | | | |
|---|---|---|---|---|---|---|---|---|---|---|---|---|---|---|---|---|---|
| sample | Dein | Gein | Glein | Ta | Din | Gin | Glin | Tg | AD | AG | AGl | Tac | MD | MG | MGl | Tm | total |
| soybean before cooking[b] | 2.8 ± 0.1 b | 2.3 ± 0.3 b | <LOD | 5.1 ± 0.4 b | 22.3 ± 0.9 c | 42.6 ± 1.5 c | 7.2 ± 0.4 c | 72.1 ± 2.7 a | 7.2 ± 0.3 c | 8.5 ± 0.2 c | ND | 15.7 ± 0.5 c | 96.8 ± 4.4 a | 359.1 ± 12.6 a | 14.1 ± 0.7 a | 470.0 ± 17.6 a | 562.9 ± 21.2 a |
| soybean cooked using ERC[b] | 3.8 ± 0.03 a | 4.0 ± 0.2 a | <LOD | 7.7 ± 0.1 a | 43.8 ± 0.5 b | 77.4 ± 0.6 b | 9.1 ± 0.5 b | 130.3 ± 1.2 b | 10.7 ± 0.1 b | 13.1 ± 0.1 b | ND | 23.8 ± 0.2 b | 68.8 ± 1.5 b | 263.6 ± 1.7 b | 10.3 ± 0.5 b | 342.6 ± 2.3 b | 504.4 ± 2.9 b |
| soybean cooked using EPRC[b] | 2.7 ± 0.3 b | 2.4 ± 0.1 b | <LOD | 5.2 ± 0.4 b | 65.8 ± 1.8 a | 120.2 ± 2.9 a | 11.4 ± 0.4 a | 197.3 ± 5.0 b | 25.2 ± 0.6 a | 31.8 ± 0.9 a | ND | 57.1 ± 1.4 a | 47.5 ± 1.2 c | 187.8 ± 5.7 c | 8.6 ± 0.2 c | 243.9 ± 6.9 c | 503.5 ± 13.5 b |
| CV (%) | 5.3 | 7.0 | | 5.3 | 2.7 | 2.4 | 4.6 | 2.7 | 2.7 | 3.0 | | 2.6 | 3.9 | 3.0 | 4.9 | 3.2 | 2.8 |
| $LSD_{0.05}$ | 0.2 | 0.3 | | 0.4 | 1.5 | 2.3 | 0.5 | 6.7 | 0.5 | 0.7 | | 1.0 | 3.4 | 9.9 | 0.7 | 13.5 | 18.0 |
| rice before cooking[c] | ND | ND | ND | | ND | ND | ND | | ND | ND | ND | | ND | ND | ND | | |
| rice cooked using ERC[c] | ND | ND | ND | | 0.5 ± 0.02 b | 0.7 ± 0.03 b | 0.2 ± 0.01 a | 1.5 ± 0.04 b | <LOD | <LOD | ND | | 3.5 ± 0.04 a | 5.6 ± 0.06 a | 3.3 ± 0.01 a | 12.5 ± 0.1 a | 14.0 ± 0.1 a |
| rice cooked using EPRC[c] | ND | ND | ND | | 0.7 ± 0.06 a | 0.7 ± 0.03 b | 0.3 ± 0.01 a | 1.5 ± 0.04 b | <LOD | <LOD | ND | | 2.8 ± 0.09 b | 4.7 ± 0.06 b | 3.3 ± 0.04 b | 10.8 ± 0.2 b | 12.7 ± 0.3 b |
| CV (%) | | | | | 8.1 | 5.7 | 7.0 | 1.8 | | | | | 2.2 | 1.1 | 0.9 | 1.2 | 2.8 |
| $LSD_{0.05}$ | | | | | 0.06 | 0.06 | 0.02 | 0.07 | | | | | 0.09 | 0.08 | 0.04 | 0.2 | 18.0 |

[a]Dein, daidzein; Gein, genistein; Glein, glycitein; Din, daidzin; Gin, genistin; Glin, glycitin; AD, acetyldaidzin; AG, acetylgenistin; AGl, acetylglycitin; MD, malonyldaidzin; MG, malonylgenistin; MGl, malonylglycitin; Ta, total content of aglucon; Tg, total content of glucosides; Tac, total content of acetylglucosides; Tm, total content of malonylglucosides; and ND, not detected. [b]Isoflavone contents were expressed as micrograms per 1 g of lyophilized/pulverized soybean ($\mu$g g$^{-1}$, on a dry basis of the soybean). [c]Isoflavone contents were expressed as micrograms per 1 g of lyophilized/pulverized rice ($\mu$g g$^{-1}$, on a dry basis of the rice).



dx.doi.org/10.1021/jf5033944 | J. Agric. Food Chem. 2014, 62, 11862−11868

Table 3. Change of Total Daidzein, Total Genistein, and Total Glycitein Contents in Soybeans and Rice before and after Soybean−Rice Cooking Using ERC and EPRC

| sample | aglucon equivalents[a] ($\mu$g g$^{-1}$) | | |
|---|---|---|---|
| | total daidzein | total genistein | total glycitein |
| soybean before cooking[b] | 69.4 ± 3.1 b | 220.9 ± 7.8 a | 12.1 ± 0.6 a |
| soybean cooked using ERC[b] | 71.2 ± 1.0 b | 197.1 ± 1.04 b | 11.3 ± 0.6 b |
| soybean cooked using EPRC[b] | 81.0 ± 2.2 a | 193.5 ± 5.2 b | 11.9 ± 0.3 ab |
| CV (%) | 3.0 | 2.7 | 4.6 |
| $LSD_{0.05}$ | 2.8 | 6.7 | 0.7 |
| rice before cooking[c] | ND[d] | ND | ND |
| rice cooked using ERC[c] | 2.1 ± 0.02 a | 3.4 ± 0.04 a | 1.9 ± 0.01 a |
| rice cooked using EPRC[c] | 1.8 ± 0.08 b | 3.0 ± 0.7 b | 1.9 ± 0.03 a |
| CV (%) | 3.1 | 1.8 | 1.3 |
| $LSD_{0.05}$ | 0.08 | 0.07 | 0.03 |

[a]Aglucon equivalents were calculated as follows: total daidzein = [daidzein + (0.611 × daidzin) + (0.555 × acetyldaidzin) + (0.506 × malonyldaidzin)], total genistein = [genistein + (0.625 × genistin) (0.570 × acetylgenistin) + (0.521 × malonylgenistin)], total glycitein = [glycitein + (0.637 × glycitin) + (0.582 × acetylglycitin) + (0.534 × malonylglycitin)]. The constant used for aglucon equivalent calculation was from a normalization of the molecular weight of individual algulcon and glucoside isoflavones. [b]Isoflavone contents were expressed as micrograms per 1 g of lyophilized/pulverized soybean (aglucon equivalents, $\mu$g g$^{-1}$, on a dry basis of the soybean). [c]Isoflavone contents were expressed as micrograms per 1 g of lyophilized/pulverized rice (aglucon equivalents, $\mu$g g$^{-1}$, on a dry basis of the rice). [d]ND = not detected.

using the ERC. Furthermore, aglucons and acetylglucosides were not found or found below LOD in rice cooked using the ERC (Table 2 and Figure 2).

**Changes in Isoflavone Composition and Content in the Soybean−Rice Mixture after EPRC Cooking.** In comparison to that before cooking, the total isoflavone content in the EPRC-cooked soybeans decreased by ∼10%. Malonylglucosides and glucosides comprised approximately 48 and 40%, respectively, of the total isoflavones in the soybeans cooked using the EPRC (Table 2). In particular, the genistin (before cooking, 42.6 $\mu$g g$^{-1}$; after cooking, 120.2 $\mu$g g$^{-1}$) and daidzin (before cooking, 22.3 $\mu$g g$^{-1}$; after cooking, 65.8 $\mu$g g$^{-1}$) contents in the EPRC-cooked soybeans increased ∼3-fold compared to those in the soybeans before cooking because of the conversion of malonylglucosides to glucosides (Table 2 and Figure 2). Furthermore, in comparison to that before cooking, the acetylglucoside content in the soybeans cooked using the EPRC increased by >3-fold (Table 2). In comparison to that before cooking, the total genistein and total glycitein contents in the EPRC-cooked soybeans decreased by 2−12%, whereas the total daidzein content increased by ∼17% in the soybeans cooked using the EPRC ($p < 0.05$; Table 3). Malonylgenistin and genistin comprised 37 and 24%, respectively, of the total isoflavone content in the soybeans cooked using the EPRC and were the most abundant isoflavones. Acetylglycitin and glycitein were also found at trace levels (<LOD) or not detected in soybeans cooked using the EPRC (Table 2).

After soybean−rice cooking using the EPRC, the total isoflavone content in the rice was 12.7 ± 0.3 $\mu$g g$^{-1}$ (dry basis of EPRC-cooked rice), which equaled approximately 78 $\mu$g g$^{-1}$ (dry basis of EPRC-cooked soybean), approximately 14% of the total isoflavones in the soybeans before cooking. Among the isoflavones in the rice cooked using the EPRC, 85% were malonylglucosides; aglucons and acetylglucosides were found at trace levels (<LOD; Table 2) or not detected.

## DISCUSSION

In many countries, soybeans are usually consumed as soy curd, soy paste, soy sauces, soy milk, soy bread, and other soy products. Among the various functional substances in soybeans and soy foods, isoflavones in particular have attracted attention as nutraceutical compounds, owing to constituents, such as phytoestrogens, which have health benefits.[27,28] To increase the nutritive value of rice, particularly essential amino acid content,[5] the practice of cereal−legume complementation is widely followed in Korea. Both ERCs and EPRCs are generally used for soybean−rice mixture cooking. The difference in these cooking methods is that EPRCs use a relatively higher pressure than ERCs. Therefore, the soybean−rice mixture cooking time is usually accelerated when cooking with EPRCs, resulting in a greater degree of gelatination because of the higher boiling point of water, which can be attributed to the higher pressure during cooking.[29,30]

The composition and content of isoflavones in soybeans and soy foods are influenced by various processing conditions, such as soaking, heating, acid hydrolysis, deforming, and pressure treatment.[7,20,31,32] During soybean and soy food processing, isoflavones are usually generated by converting malonylglucosides to acetylglucosides, glucosides, and aglucon through chemical reactions, such as decarboxylation or ester hydrolysis.[33,34] Previous studies have shown that heat treatment affects the conversion of malonylglucosides to acetylglucosides and glucosides,[35] whereas microbial fermentation affects the conversion of glucoside isoflavones to aglucon.[7] In particular, the conversion of malonylglucosides to other types of isoflavones is most likely and rapid during heating.[35] Furthermore, in comparison to dry heat treatment, moist heat treatment converts a higher number of malonylglucosides to glucosides but only limited amounts of malonylglucosides to acetylglucosides.[17,36,37] The order of isoflavone stability under heat treatment conditions (above 160 °C) is daidzin > genistin > glycitin.[33]

In the present study, the total isoflavone content in the cooked soybeans and rice relative to that in the soybeans before cooking was ∼90 and 14−15%, respectively, after both ERC and EPRC cooking, which indicates that most isoflavones in soybeans were preserved during soybean−rice mixture cooking. However, the composition of isoflavones in soybeans cooked using the ERC and EPRC was significantly different from that in soybeans before cooking ($p < 0.05$). Furthermore, the malonylglucoside content in soybeans cooked using the EPRC showed an additional ∼20% decrease relative to that in soybeans cooked using the ERC, whereas the glucoside content in soybeans cooked using the EPRC showed a further increase of ∼15% relative to that in soybeans cooked using the ERC (Table 2 and Figure 2). In the present study, malonylgenistin was highly susceptible to isoflavone conversion under the cooking conditions. These results were partially similar to those of a prior study showing that the malonylglucoside content is significantly decreased relative to glucoside and aglucon contents in yellow and black soybeans under boiling and steaming processing conditions.[21] The reduced conversion of malonylglucoside to aglucon in the present study may have resulted from differences in cooking conditions (e.g., cooking temperature and cooking period). Furthermore, the other previous study[33] showed that the aglucon content also increases during heating

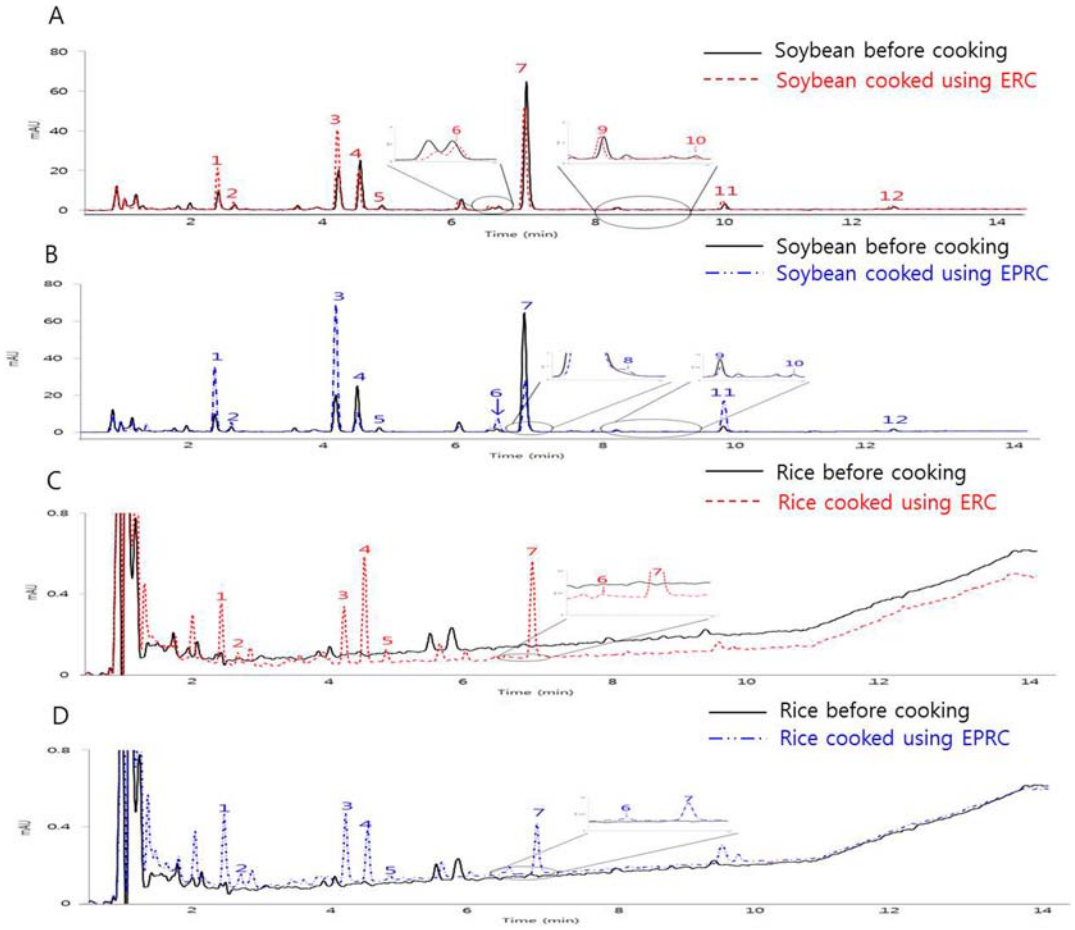


**Figure 2.** Representative UPLC chromatograms of isoflavones in soybeans and rice cooked using an ERC and an EPRC. (A) Comparison of the soybeans before and after soybean−rice mixture cooking using the ERC. (B) Comparison of the soybeans before and after soybean−rice mixture cooking using the EPRC. (C) Comparison of the rice before and after soybean−rice mixture cooking using the ERC. (D) Comparison of the rice before and after soybean−rice mixture cooking using the EPRC. Isoflavone STDs: 1, Din; 2, Glin; 3, Gin; 4, MD; 5, MGl; 6, AD; 7, MG; 8, AGl; 9, Dein; 10, Glein; 11, AG; and 12, Gein.

at temperatures above 135 °C. In the present study, soybeans prepared using the EPRC were cooked under conditions with a higher boiling point of water (120−130 °C) compared to that used to cook soybeans with the ERC; however, the aglucon content in the soybeans did not change significantly during the soybean−rice mixture cooking (Table 2). The combination of adiabatic heating and pressure treatment has been shown to affect isoflavone conversion in soy milk significantly, especially the conversion of malonylglucosides to glucosides. The aglucon content in soy milk also remains constant under adiabatic heating and pressure treatments.[20] These results may explain why isoflavone conversion, especially that of malonylglucosides, in soybeans cooked using the EPRC was decreased to a greater extent than that in soybeans cooked using the ERC in the present study.

Isoflavone composition is generally changed by various processes, but the total isoflavone content does not change if sample mass loss does not occur.[7] In the present study, no mass loss occurred during soybean−rice mixture cooking using the ERC or the EPRC, and 14−15% of the total isoflavone content in the soybeans before cooking was transferred to the rice through ERC and EPRC cooking. However, soybean−rice mixture cooking using the EPRC slightly increased the total daidzein content of the cooked soybeans but decreased the total genistein and glycitein contents. The increase in total daidzein in EPRC-cooked soybeans was caused by the greater increase of acetyldaidzin and daidzin in the EPRC-cooked soybeans compared to those in the soybeans before cooking. However, although no sample loss occurred during the soybean−rice cooking, it remains unclear why the total daidzein content in the EPRC-cooked soybeans was slightly higher than that in the soybeans before cooking.

In conclusion, the composition of isoflavones in soybeans was significantly changed by heat treatment, pressure treatment, or both during soybean−rice cooking. In particular, the combination of heat and pressure treatments had a greater effect on isoflavone composition compared to the effect of heat treatment alone ($p < 0.05$) but did not affect the total isoflavone content. In comparison to that in the soybeans before cooking, a total isoflavone content of 90% was found in the soybeans cooked using the ERC and EPRC; the rest of the isoflavones were transferred to the rice during soybean−rice mixture cooking. Malonylglucosides, especially malonylgenistin, were the isoflavone types most susceptible to conversion, and they were normally converted to glucosides rather than acetylglucosides or aglucons during ERC and EPRC cooking of the soybean−rice mixture. The results of the present study describe the alteration of isoflavone composition and content in a soybean−rice mixture after ERC and EPRC cooking and may provide insight into the use of functional substances, such as isoflavones, in soybeans or soy foods.

## AUTHOR INFORMATION


### Corresponding Author

*Telephone: 82-02-2049-6163. Fax: 82-02-450-3726. E-mail: kshkim@konkuk.ac.kr.



### Funding

This paper was supported by Konkuk University in 2014.


### Notes

The authors declare no competing financial interest.

## ACKNOWLEDGMENTS

The authors thank the reviewers for their perceptive and helpful comments.

## REFERENCES


(1) United States Department of Agriculture (USDA). *Production, Supply and Distribution (PSD) Online*; http://apps.fas.usda.gov/psdonline/psdhome.aspx.

(2) Shimamoto, K. The molecular biology of rice. *Science* **1995**, *270*, 1772−1773.

(3) Wu, J. G.; Shi, C.; Zhang, X. Estimating the amino acid composition in milled rice by near-infrared reflectance spectroscopy. *Field Crops Res.* **2002**, *75*, 1−7.

(4) Chavan, J. K.; Duggal, S. K. Studies on the essential amino acid composition, protein fractions and biological value (BV) of some new varieties of rice. *J. Sci. Food Agric.* **1978**, *29*, 225−229.

(5) Kannan, S.; Nielsen, S. S.; Mason, A. C. Protein digestibility-corrected amino acid scores for bean and bean−rice infant weaning food products. *J. Agric. Food Chem.* **2001**, *49*, 5070−5074.

(6) Tikkanen, M. J.; Adlercreutz, H. Dietary soy-derived isoflavone phytoestrogens: Could they have a role in coronary heart disease prevention? *Biochem. Pharmacol.* **2000**, *60*, 1−5.

(7) Wang, H.-J.; Murphy, P. A. Mass balance study of isoflavones during soybean processing. *J. Agric. Food Chem.* **1996**, *44*, 2377−2383.

(8) Huang, R.-Y.; Chou, C.-C. Heating affects the content and distribution profile of isoflavones in steamed black soybeans and black soybean Koji. *J. Agric. Food Chem.* **2008**, *56*, 8484−8489.

(9) Vincent, A.; Fitzpatrick, L. A. Soy isoflavones: Are they useful in menopause? *Mayo Clin. Proc.* **2000**, *75*, 1174−1184.

(10) Setchell, K. D. Phytoestrogens: The biochemistry, physiology, and implications for human health of soy isoflavones. *Am. J. Clin. Nutr.* **1998**, *68*, 1333S−1346S.

(11) Messina, M. J.; Persky, V.; Setchell, K. D. R.; Barnes, S. Soy intake and cancer risk: A review of the *in vitro* and *in vivo* data. *Nutr. Cancer* **1994**, *21*, 113−131.

(12) Andrade, J. E.; Ju, Y. H.; Baker, C.; Doerge, D. R.; Helferich, W. G. Long-term exposure to dietary sources of genistein induces estrogen-independence in the human breast cancer (MCF-7) xenograft model. *Mol. Nutr. Food Res.* **2014**, DOI: 10.1002/mnfr.201300780.

(13) Riedl, K. M.; Lee, J. H.; Renita, M.; St Martin, S. K.; Schwartz, S. J.; Vodovotz, Y. Isoflavone profiles, phenol content, and antioxidant activity of soybean seeds as influenced by cultivar and growing location in Ohio. *J. Sci. Food Agric.* **2007**, *87*, 1197−1206.

(14) Chung, I.-M.; Seo, S.-H.; Park, I.; Ahn, J.-K.; Kim, E.-H.; Kim, M.-Y.; Kim, S.-H. Changes in isoflavone composition of soya seeds, soya curd and soya paste at different processing conditions. *J. Food. Nutr. Res.* **2012**, *51*, 40−51.

(15) Coward, L.; Smith, M.; Kirk, M.; Barnes, S. Chemical modification of isoflavones in soyfoods during cooking and processing. *Am. J. Clin. Nutr.* **1998**, *68*, 1486S−1491S.

(16) Kim, J. J.; Kim, S. H.; Hahn, S. J.; Chung, I. M. Changing soybean isoflavone composition and concentrations under two different storage conditions over three years. *Food Res. Int.* **2005**, *38*, 435−444.

(17) Coward, L.; Barnes, N. C.; Setchell, K. D. R.; Barnes, S. Genistein, daidzein, and their $\beta$-glycoside conjugates: Antitumor isoflavones in soybean foods from American and Asian diets. *J. Agric. Food Chem.* **1993**, *41*, 1961−1967.

(18) Knorr, D.; Heinz, V.; Buckow, R. High pressure application for food biopolymers. *Biochim. Biophys. Acta* **2006**, *1764*, 619−631.

(19) Xu, B.; Chang, S. K. C. Reduction of antiproliferative capacities, cell-based antioxidant capacities and phytochemical contents of common beans and soybeans upon thermal processing. *Food Chem.* **2011**, *129*, 974−981.

(20) Jung, S.; Murphy, P. A.; Sala, I. Isoflavone profiles of soymilk as affected by high-pressure treatments of soymilk and soybeans. *Food Chem.* **2008**, *111*, 592−598.

(21) Xu, B.; Chang, S. K. C. Total phenolics, phenolic acids, isoflavones, and anthocyanins and antioxidant properties of yellow and black soybeans as affected by thermal processing. *J. Agric. Food Chem.* **2008**, *56*, 7165−7175.

(22) Lee, S. W.; Lee, J. H. Effects of oven-drying, roasting, and explosive puffing process on isoflavone distributions in soybeans. *Food Chem.* **2009**, *112*, 316−320.

(23) Chun, J.; Kim, J. S.; Kim, J. H. Enrichment of isoflavone aglycones in soymilk by fermentation with single and mixed cultures of *Streptococcus infantarius* 12 and *Weissella* sp. 4. *Food Chem.* **2008**, *109*, 278−284.

(24) Xiao, C. W.; Wood, C. M.; Robertson, P.; Gilani, G. S. Protease inhibitor activities and isoflavone content in commercial soymilks and soy-based infant formulas sold in Ottawa, Canada. *J. Food Compos. Anal.* **2012**, *25*, 130−136.

(25) Chung, I.-M.; Seo, S.-H.; Ahn, J.-K.; Kim, S.-H. Effect of processing, fermentation, and aging treatment to content and profile of phenolic compounds in soybean seed, soy curd and soy paste. *Food Chem.* **2011**, *127*, 960−967.

(26) Shrivastava, A.; Gupta, B. B. Methods for the determination of limit of detection and limit of quantitation of the analytical methods. *Chron. Young Sci.* **2011**, *2*, 21−24.

(27) Kawakami, Y.; Tsurugasaki, W.; Yoshida, Y.; Igarashi, Y.; Nakamura, S.; Osada, K. Regulative actions of dietary soy isoflavone on biological antioxidative system and lipid metabolism in rats. *J. Agric. Food Chem.* **2004**, *52*, 1764−1768.

(28) Arjmandi, B. H.; Alekel, L.; Hollis, B. W.; Amin, D.; Stacewicz-Sapuntzakis, M.; Guo, P.; Kukreja, S. C. Dietary soybean protein prevents bone loss in an ovariectomized rat model of osteoporosis. *J. Nutr.* **1996**, *126*, 161−167.

(29) Park, S. J.; Lee, H. K. The patent history of rice cooker. *J. Korean Intell. Pat. Soc.* **2008**, *13*, 55−60.

(30) Kim, H. Y.; Kim, K. O. Sensory characteristics of rice cooked with pressure cookers and electric cookers. *Korean J. Food Sci. Technol.* **1986**, *18*, 319−324.

(31) Shimoni, E. Stability and shelf life of bioactive compounds during food processing and storage: Soy isoflavones. *J. Food Sci.* **2004**, *69*, R160−R165.

(32) Barnes, S.; Kirk, M.; Coward, L. Isoflavones and their conjugation soy foods: extraction conditions and analysis by HPLC−mass spectrometry. *J. Agric. Food Chem.* **1994**, *42*, 2466−2474.

(33) Xu, Z.; Wu, Q.; Godber, J. S. Stabilities of daidzin, glycitin, genistin, and generation of derivatives during heating. *J. Agric. Food Chem.* **2002**, *50*, 7402−7406.

(34) Rostagno, M. A.; Villares, A.; Guillamón, E.; García-Lafuente, A.; Martínez, J. A. Sample preparation for the analysis of isoflavones from soybeans and soy foods. *J. Chromatogr. A* **2009**, *1216*, 2−29.

(35) Chien, J. T.; Hsieh, H. C.; Kao, T. H.; Chen, B. H. Kinetic model for studying the conversion and degradation of isoflavones during heating. *Food Chem.* **2005**, *91*, 425−434.

(36) Mathias, K.; Ismail, B.; Corvalan, C. M.; Hayes, K. D. Heat and pH effects on the conjugated forms of genistin and daidzin isoflavones. *J. Agric. Food Chem.* **2006**, *54*, 7495−7502.

(37) Grün, I. U.; Adhikari, K.; Li, C.; Li, Y.; Lin, B.; Zhang, J.; Fernando, L. N. Changes in the profile of genistein, daidzein, and their conjugates during thermal processing of tofu. *J. Agric. Food Chem.* **2001**, *49*, 2839−2843.

analytical techniques.[13] van Platerink et al.[14] developed a sensitive method to detect peptides in human plasma samples with detection limits from 0.01 to 0.001 ng/mL. Although the research on the absorption of antihypertensive peptides has revealed that certain short peptides, di- and tripeptides such as VY and IPP, can reach bloodstream undegraded after oral administration, either in fasted or fed states, very low absorption extents were reported.[15−17] To the best of our knowledge, kinetic studies with longer peptides than tripeptides from dietary sources have not been reported.

Because the information regarding the kinetic profile is needed to establish a scientific basis for efficacy in the use of any food supplement, the objective of this study was to investigate the oral bioavailability and the kinetic behavior of the antihypertensive peptide HLPLP after its administration to rats, determining HLPLP plasma concentrations using a sensitive and specific analytical method. In addition, this technique allowed us to monitor the plasma concentrations of two derived peptide fragments, LPLP [β-casein fragment f(135−138)] and HLPL [β-casein fragment f(134−137)].

## MATERIALS AND METHODS

**Chemicals.** The peptides HLPLP, β-casein f(134−138), HLPL, β-casein f(134−137), HLP, β-casein f(134−136), LPLP, β-casein f(135−138), LPL, β-casein f(135−137), PLP, and β-casein f(136−138) were used in this study. These peptides were prepared in-house following the solid-phase synthesis method with fluorenyl-methoxy-carbonyl (FMOC), using a 431A peptide synthesizer (Applied Biosystems Inc. Überlingen, Germany). Their purities, verified by reversed phase high performance liquid chromatography−ultraviolet−mass spectrometry (RP-HPLC-UV-MS) as previously described,[18] were 98.0%, 97.68%, 96.20%, 93.43%, and 99.36%, respectively. Peptide PLP, with a purity of 92.94%, was purchased from SynPeptide CO, LDT (Shanghai, China). All other chemicals were of the highest quality grade and obtained from commercial sources.

**Animals and Experimental Design.** The study was undertaken in accordance with the ethics requirements and authorized by the official ethical committee of University Complutense of Madrid. Adult male Wistar rats (Charles River Inc., Margate, Kent, UK) each weighing 220−230 g at 9 weeks of age were used. The animals were individually housed in polycarbonate cages with sawdust bedding and maintained in environmentally controlled rooms (22 ± 2 °C and 50 ± 10% relative humidity) with a 12 h light/dark cycle (light from 08.00 to 20.00 h). Food (A04 rodent diet, Panlab SL, Barcelona, Spain) and water were available ad libitum. The rats were divided into two groups, one group of 60 animals (group 1) received the synthetic peptide HLPLP intravenously and the other group of 84 animals (group 2) orally. Group 2 rats were deprived of food for 12 h before the single oral administration of 40 mg/kg body weight, but they had ad libitum access to water. The peptide was dissolved in distilled water (10 mg/mL) and was administered by oral gavage in a volume of 1 mL peptide solution/rat of 250 g of body weight. Group 1 rats were given a single iv injection of 4 mg/kg body weight into the lateral tail vein (in this case a peptide solution of 4 mg/mL was prepared, and 0.25 mL peptide solution/rat of 250 g of body weight was injected). The iv 4 mg/kg and oral 40 mg/kg doses of peptide HLPLP were selected on the basis of preliminary experiments where both doses and routes of administration did not show any adverse effects, abnormal clinical signs, behavioral changes, body weight changes, or change in food and water consumption in the animals treated (data not shown). The oral HLPLP dose was higher than the iv dose due to the low absolute oral bioavailability described for other food-derived peptides in pigs, approximately 0.1%.[17] The administered oral dose is higher than that reported to cause a significant decrease in the systolic blood pressure in spontaneously hypertensive rats (SHR).[10] Five additional animals were used as control to collect blank blood samples and to prepare calibration curves from plasma control fortified with the synthetic peptides HLPLP, LPLP, and HLPL.

Animals in groups 1 and 2 were killed by cervical dislocation (six animals at each time) and then exsanguination at 0, 1.5, 2, 3, 5, 8, 10, 15, 20, and 30 min after iv and at 0, 3, 5, 10, 15, 20, 30, 40, 45, 50, 55, 60, 65, and 70 min after oral administration of peptide HLPLP, respectively. Time points were selected based on preliminary experiments, and the limit of quantification (LOQ) of the analytical method was taken into account. Blood samples (1 mL) were withdrawn from the jugular vein and collected in heparinized tubes. Plasma was separated by centrifugation and stored frozen at −80 °C until analyzed. Blood samples at times greater than 70 or 30 min after oral or iv HLPLP doses, respectively, were not collected, because preliminary experiments (data not shown) showed that at these times no levels of the synthetic peptides HLPLP, LPLP, and HLPL were detected.

**Analysis of Plasma Samples.** *Plasma Sample Preparation.* Plasma samples from rats were prepared by adding 40 μL of an aqueous solution of 10% of trifluoroacetic acid (TFA) to 1 mL of plasma and homogenized in a vortex, and the mixture was heated at 99 °C for 2 min to precipitate proteins, as previously described.[14] Then the samples were centrifuged (MiniSpin, Eppendorf, Hamburg, Germany) at 8500*g* for 30 min. The supernatant was purified using mixed mode cation exchange cartridges (Bond Elut Plexa PCX, 60 mg, 1 mL, Agilent, Santa Clara, CA). Cartridges were preconditioned with 1500 μL of methanol and 2500 μL of Milli-Q water (Millipore, Bedford, MA). The plasma sample, previously mixed (1:3 v/v) with an aqueous solution containing 2% orthophosphoric acid, was loaded. The cleaning step consisted of the addition of 1500 μL of 2% formic acid in Milli-Q water and 2500 μL of a mixture composed of 50% methanol and 50% acetonitrile (v/v). The elution step was carried out by adding 1 mL of ammonia at 5% (35% purity) in methanol:acetonitrile (50:50, v/v). The elution volume was afterward totally dried by vacuum centrifugation (SpeedVac SC 200 Savant, Irving, TX). For the injection, the dried samples were reconstituted with 50 μL of 0.1% formic acid.

To prepare the standard curves, the synthetic peptides HLPLP, LPLP, and HLPL were diluted in Milli-Q water to final concentrations that ranged from 0.08 to 300 ng/mL, corresponding to 0.13 to 521 nmol/L, 0.18 to 682.9 nmol/L, and 0.17 to 625.9 nmol/L, respectively, in rat control plasma. Immediately after addition of the peptide solution to the plasma, they were treated as described previously for the preparation of plasma samples from rat assays. The calibration curves were injected on the same day as the rat samples.

*Peptide Analysis by UPLC-Q-TOF.* The analyses of samples were performed on an Acquity ultrahigh performance liquid chromatography (UPLC) instrument from Waters (Milford, MA), coupled to a Microtof-QII (Bruker Daltonik, Bremen, Germany). The LC-MS system was controlled by HyStar 3.2 software (Bruker). The column employed for the analyses was an Acquity UPLC BEH 130 $C_{18}$ of 2.1 mm × 100 mm (Waters), with a particle size of 1.7 μm. The analyses were run at 30 °C, the flow rate was 0.2 mL/min, and the injection volume was 25 μL. A linear gradient was set from 0 to 45% of solvent B (acetonitrile/formic acid 0.1%) and 55% of solvent A (water/formic acid 0.1%) in 16 min. The nebulizer pressure was set at 3 bar, the temperature of the source at 180 °C, and the capillary voltage at 4.5 kV. MS full-scan acquisitions were first performed during UPLC runs, using a 50−1200 mass-to-charge ratio ($m/z$) range. The method developed was pseudoselected reaction monitoring (SRM) in which the parent ion with $m/z$ 576.343 was selected for fragmentation. The peptide HLPLP was identified by its retention time and also by its fragmentation profile. The identification of the possible derived peptide fragments, i.e., LPLP and HLPL, HLP, LPL, and PLP, was performed using the retention time and the extraction of the characteristic molecular ions $m/z$ 439.284, 479.290, 366.206, 342.231, and 326.200, respectively. The Q-TOF analyzer was calibrated on a daily basis in MS mode, using the $m/z$ ratios of adduct ions arising from sodium formate as reference.

**Data Analysis.** The mean plasma concentration versus time after iv and oral administration was sequentially fitted to one-, two-, and

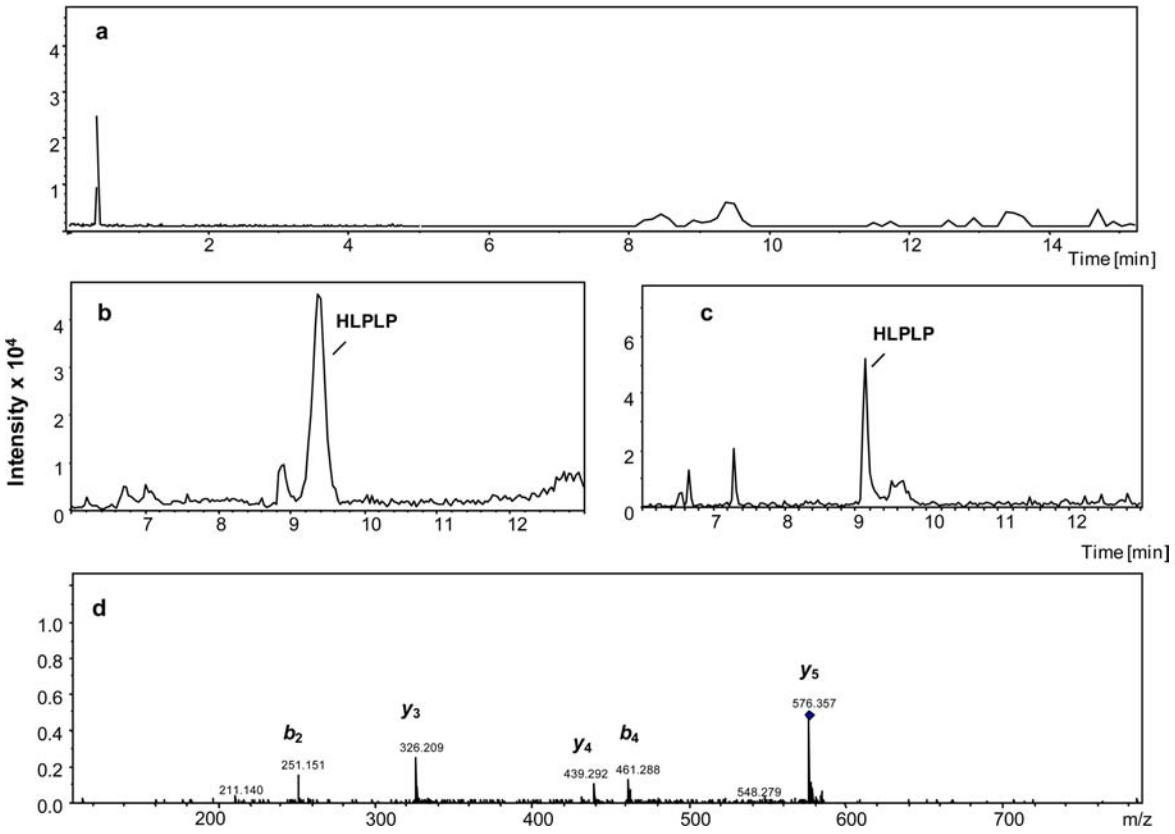


**Figure 1.** (a) Extracted ion chromatogram (EIC) of HLPLP ($m/z$ 576.343; $t_R$ 9.4), LPLP ($m/z$ 439.284; $t_R$ 10.5), and HLPL ($m/z$ 479.290; $t_R$ 8.4) in blank plasma. EIC of the peptide HLPLP ($m/z$: 576.343; $t_R$ 9.4 min) (b) at 15 after oral administration and (c) at 20 min after intravenous administration. (d) Fragmentation pattern of HLPLP at 15 min after oral administration.

multiple-compartment models, using the computer program WinNonlin (Version 6.3; Pharsight Corporation, Mountain View, CA). The model was determined for best fit on the basis of a smaller value for the Akaike's Information Criterion (AIC).[19] The two-compartment model was the best fit for the two animal groups. This model was used to establish pharmacokinetic characteristics. Mean plasma concentration curves of peptide HLPLP after a single iv and oral administration and those of the peptides LPLP and HLPL (metabolites in plasma) after a single iv administration of HLPLP were fitted to the following exponential equations:

$$C = A_1 \times e^{-\alpha t} + A_2 \times e^{-\beta t} \text{ (iv)}$$

$$C = A_1 \times e^{-\alpha t} + A_2 \times e^{-\beta t} - A_3 \times e^{-K_a t} \text{ (oral)}$$

where $C$ is the plasma concentration of the compound, $A_1$, $A_2$, and $A_3$ are mathematical coefficients (i.e., $A_1$ and $A_2$ are the plasma concentrations extrapolated to time zero of the first and second elimination phases of the compound and $A_3$ for the absorption phase), $\alpha$ is the hybrid rate constant for the distribution phase, $\beta$ is the hybrid rate constant for the elimination terminal phase (i.e., $\alpha$ and $\beta$ are the slopes of the first and second elimination phases of the compound disposition), and $t$ is the time. Absorption half-life ($T_{1/2a}$), half-life of $\alpha$ phase ($T_{1/2\alpha}$), the half-life of $\beta$ phase ($T_{1/2\beta}$), distribution rate constants for transfer of the compound from the central to the peripheral compartment ($K_{12}$) and from the peripheral to the central compartment ($K_{21}$), and the elimination rate constant ($K_{10}$) were calculated using standard equations as described.[20,21] After iv and oral administration, the area under the concentration−time curves (AUC) was calculated as follows:

$$\text{AUC} = (A_1/\alpha) + (A_2/\beta)$$

or

$$\text{AUC} = (A_1/\alpha) + (A_2/\beta) - (A_3/K_a)$$

where bioavailability ($F$) is $(\text{dose}_{iv} \times \text{AUC}_{oral})/(\text{dose}_{oral} \times \text{AUC}_{iv})$.

Total plasma clearance (CL) was calculated, using the following formula:

$$\text{CL} = [\text{dose (mg/kg)}]/\text{AUC}$$

or

$$\text{CL} = [\text{dose (mg/kg)}](F)/\text{AUC}$$

Mean residence time (MRT) (only for HLPLP iv administration) was calculated as follows:

$$\text{MRT} = [(A_1/\alpha^2) + (A_2/\beta^2) \times (1/\text{AUC})]$$

Volume of distribution in the central compartment ($V_1$) (only for HLPLP iv administration) was determined as follows:

$$V_1 = [\text{dose (mg/kg)}]/A_1 + A_2$$

Apparent volume of distribution in the second compartment ($V_2$) (only for HLPLP iv administration) was determined as follows:

$$V_2 = (V_1) \times (K_{12}/K_{21})$$

Volume of distribution at steady state ($V_{ss}$) (only for HLPLP iv administration) was determined as follows:

$$V_{ss} = \text{MRT} \times \text{CL}$$

Maximum drug plasma concentration ($C_{max}$) after oral administration and the time at which $C_{max}$ was achieved ($T_{max}$) was determined directly from the concentration versus time curve.


dx.doi.org/10.1021/jf5035256 | J. Agric. Food Chem. 2014, 62, 11869−11875

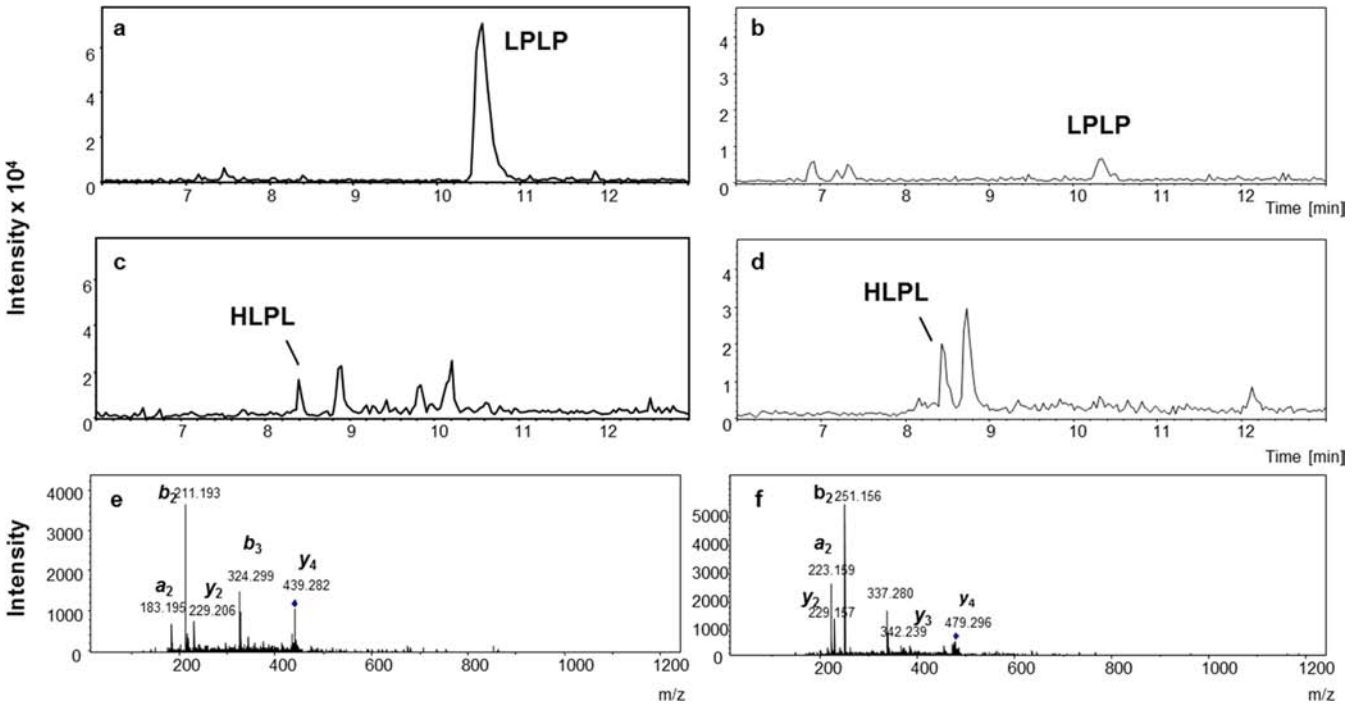


**Figure 2.** (a) Extracted ion chromatogram (EIC) of LPLP ($t_R$ 10.5 min) at 2 min after intravenous administration and (b) at 40 min after oral administration of the peptide HLPLP; (c) EIC of HLPL ($t_R$ 8.4 min) at 2 min after intravenous administration and (d) at 60 min after oral administration of HLPLP; fragmentation pattern of (e) LPLP and (f) HLPL.

## RESULTS

**Quantitative Determination of Peptides by UPLC-Q-TOF.** In preliminary experiments, the quantification of the HLPLP peptide was attempted with a sample preparation protocol consisting of the addition of 10% TFA to 1 mL of plasma followed by heating at 99 °C for 2 min to precipitate the proteins and further centrifugation. However, this protocol did not allow determining plasma peptide concentrations below 12.5 ng/mL. Therefore, peptide purification and concentration was investigated by using different solid-phase extraction (SPE) cartridges, such as reversed phase $C_{18}$ cartridges, mixed-mode cation, anion, and weak cation exchangers, and several solvent mixtures for the elution step. The best recovery values were obtained with a cation exchanger with mixed sorbent characteristics suitable for polar and nonpolar bases. The elution solvent selected was ammonia at 5% (35% purity) in methanol:acetonitrile (50:50, v/v).

The calibration curves provided linear results for HLPLP concentration values from 0.13 to 521 nmol/L in plasma ($R^2$ = 0.99). Figure 1a shows the extracted ion chromatogram of a blank plasma sample indicating the masses of the pentapeptide HLPLP and both tetrapeptides, HLPL and LPLP, where no interferences with endogenous compounds are expected. The extracted ion chromatogram of the pentapeptide after oral and iv administration and its fragmentation pattern are shown in Figure 1b, 1c, and 1d, respectively. One of the most intense fragment ions was observed at $m/z$ 326.207, corresponding to $y$-type ion $y_3$. Other major fragment ions were detected at $m/z$ 251.149 and 461.290, corresponding to $b$-type ions $b_2$ and $b_4$, respectively. These fragments ($y_3$, $b_2$, and $b_4$) resulted from the cleavage at N-terminal proline, which often generates highly intense $b$- and $y$-type fragment ions.[22] The recovery was calculated as the ratio between the concentration determined in a blank plasma sample spiked with HLPLP and further subjected to SPE purification and the concentration determined in a spiked sample after SPE purification. This was performed in triplicate using two concentrations of the peptide. The recovery values ranged from 96.9% to 98.7%. The reproducibility was estimated by the analyses of five spiked plasma extracts purified by SPE on three different days separated by 10 days, and repeatability by performing these determinations in consecutive analyses. Relative standard deviations (RSD) of the peak areas were 6% and 5% for reproducibility and repeatability, respectively. These values reflect the high performance achieved in the present study in terms of accuracy and precision. The limit of detection (LOD) was estimated to be 0.03 nmol/L, equivalent to 0.02 ng/mL, and was calculated as the concentration of peptide that gave a signal equal to 3 times the standard deviation of the blank. The LOQ was estimated at 0.17 nmol/L, equivalent to 0.10 ng/mL, by using 10 times the standard deviation of blank signal. With respect to the peptides LPLP and HLPL, the calibration curves provided linear results from 0.18 to 682.9 nmol/L ($R^2$ = 0.98) and 0.17 to 625.9 nmol/L ($R^2$ = 0.99), respectively. The LOD values for LPLP and HLPL were estimated at 1.13 ng/mL (0.50 nmol/L) and 0.11 ng/mL (0.22 nmol/L), respectively. The LOQ values for these peptides resulted in 1.67 ng/mL (3.71 nmol/L) and 0.36 ng/mL (0.75 nmol/L), respectively.

**Pharmacokinetics of Peptide HLPLP and Its Biotransformed Peptides LPLP and HLPL.** In the plasma samples collected at time 0, i.e., before HLPLP iv and oral administration, peptides HLPLP, HLPL, and LPLP were not detected. The two peptide fragments ($m/z$ 479.290, 439.284) corresponding to HLPL and LPLP respectively, were found in plasma from 1.5 min until 30 min after iv administration of HLPLP. However, after oral administration, peptide fragments were detected between 5 and 60 min although they could not be quantified at all time points. Figure 2 shows the extracted

ion chromatogram of the derived peptides, LPLP and HLPL, at different times after oral and iv administration, and their corresponding fragmentation patterns.

Mean plasma concentrations of peptide HLPLP and its biotransformed peptides LPLP and HLPL after single HLPLP iv administration and mean plasma concentrations of peptide HLPLP after single oral administration are shown in Figure 3.

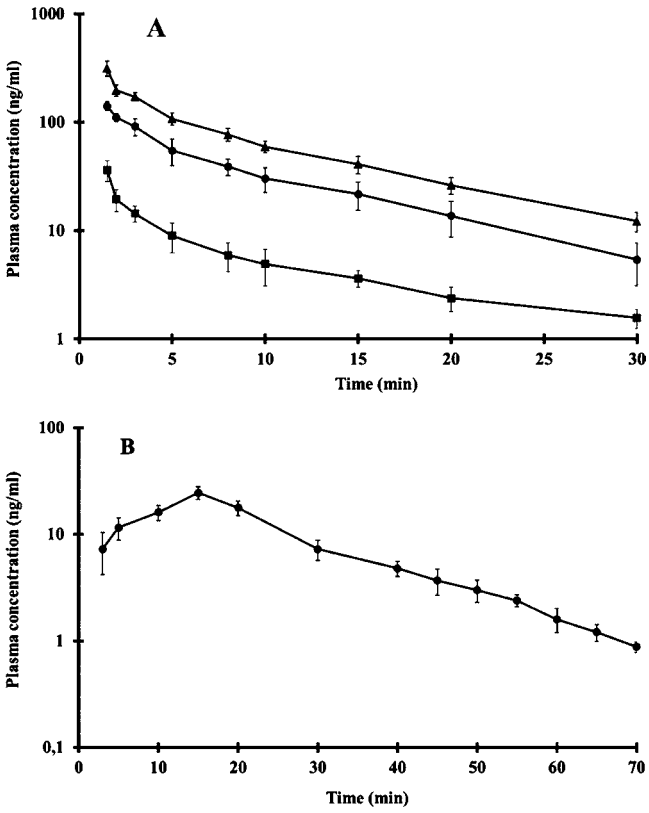


**Figure 3.** (A) Mean plasma concentrations of the peptides HLPLP (●), LPLP (▲), and HLPL (■) after single HLPLP intravenous dose of 4 mg/kg of body weight. (B) Mean plasma concentrations of the peptide HLPLP (●) after single oral dose of 40 mg/kg of body weight. Data represent mean ± SD values for six rats (i.e., six rats/time) (one-way ANOVA). Symbols without bars indicate that SD is within the symbols.

**Table 1. Kinetic Parameters for Peptide HLPLP and Its Biotransformed Peptides LPLP and HLPL after a Single HLPLP iv Dose of 4 mg/kg Body Weight in Rats**

| parameters[a] | HLPLP | LPLP | HLPL |
|---|---|---|---|
| $A_1$ (ng/mL) | 189 | 537 | 91.8 |
| $A_2$ (ng/mL) | 75.7 | 141 | 9.60 |
| $\alpha$ (1/min) | 0.64 | 0.77 | 0.90 |
| $\beta$ (1/min) | 0.09 | 0.08 | 0.06 |
| $T_{1/2\alpha}$ (min) | 1.08 | 0.90 | 0.77 |
| $T_{1/2\beta}$ (min) | 7.95 | 8.38 | 10.9 |
| $V_1$ (L/kg) | 15.1 | – | – |
| $V_2$ (L/kg) | 15.7 | – | – |
| $V_{ss}$ (L/kg) | 30.8 | – | – |
| $K_{12}$ (1/min) | 0.25 | 0.35 | 0.42 |
| $K_{21}$ (1/min) | 0.24 | 0.23 | 0.14 |
| $K_{10}$ (1/min) | 0.23 | 0.28 | 0.40 |
| AUC ($\mu$g min/L) | 1163 | 2404 | 253 |
| MRT (min) | 8.95 | 8.97 | 9.87 |
| CL (L/min/kg) | 3.41 | – | – |

[a]Kinetic parameters were calculated from the mean plasma concentration−time curves.

**Table 2. Kinetic Parameters for Peptide HLPLP after Oral Administration in Rats**

| parameters[a] | oral dose (40 mg/kg body weight) |
|---|---|
| $B_1$ (ng/mL) | 242 |
| $B_2$ (ng/mL) | 56.9 |
| $B_3$ (ng/mL) | 299 |
| $\alpha$ (1/min) | 0.29 |
| $\beta$ (1/min) | 0.06 |
| $K_a$ (1/min) | 0.25 |
| $T_{1/2\alpha}$ (min) | 2.38 |
| $T_{1/2\beta}$ (min) | 11.7 |
| $T_{1/2a}$ (min) | 2.79 |
| AUC ($\mu$g min/L) | 603 |
| $F$ (%) | 5.18 |
| CL (L/min/kg) | 3.41 |
| $C_{max}$ (ng/mL) | 20.1 |
| $T_{max}$ (min) | 11.8 |

[a]Kinetic parameters were calculated from the mean plasma concentration−time curve.

Analysis of plasma concentration-versus-time curves indicated a biphasic decrease after iv and oral administration. Good fit of the observed data for a two-compartment open model was obtained. The values of the kinetic parameters of HLPLP and its derived peptides LPLP and HLPL after iv administration of HLPLP are presented in Table 1. Values of the relevant kinetic variables that described absorption and disposition kinetics of HLPLP after oral administration are presented in Table 2.

## ■ DISCUSSION

The limited information available on the absorption of antihypertensive peptides derived from food proteins makes it difficult to interpret the functional properties of these bioactive peptides and to make an efficacy assessment as a new food supplement. These topics are commonly under debate for most functional ingredients.

Efficacy and safety assessment of many substances are normally extrapolated from animal data to humans. Laboratory animals, particularly rodents, are widely used for these evaluations. When several factors such as differences in species sensitivity are considered, kinetic variables are of major importance and should be taken into account in extrapolation of laboratory data to humans, because changes in various kinetic parameters are either easily determined experimentally or can be predicted with a reasonable accuracy. It is apparent that the principles of pharmacokinetics are indispensable in the overall assessment of human health risk.

Kinetic characteristics combined with dynamic patterns should be considered in the efficacy evaluation of peptide HLPLP. Preclinical pharmacokinetic information in experimental animals, such as the rat, is essential in designing further pharmacokinetic studies in humans which should be applied to the safe and effective use of this bioactive peptide.[23]

To the best of our knowledge, the present paper is the first report of plasma disposition of HLPLP peptide in rats using a selective analytical method to evaluate its pharmacokinetic profile. The LC-MS determination of the peptide was carefully optimized by selecting the parameters and analysis mode

providing the highest signal-to-noise ratio. The validation parameters used show that the method is reliable and sensitive and allow an adequate characterization of the disposition of peptide HLPLP in rat plasma. In addition, this analytical method also allowed the identification and the quantification of two derived fragments, LPLP and HLPL, from the hydrolysis of HLPLP by the action of plasma peptidases. However, the presence of shorter fragments derived from the action of plasma peptidases on HLPLP cannot be excluded. The inherent limitations of the mass spectrometry techniques to identify small peptides and the complexity of the matrix may have impaired detection of shorter fragments.

This study reports the kinetics of the peptide HLPLP after a single iv (4 mg/kg body weight) and oral (40 mg/kg body weight) administration in rats. Plasma disposition of HLPLP after iv and oral administration in rats as well as the appearance of the peptide fragments, LPLP and HLPL, after iv administration of HLPLP were best described by use of a two-compartment open model. Disappearance of the peptide from plasma was characterized by an initial rapid distribution phase followed by a rapid elimination phase. van der Pijl et al.[17] reported in pigs that elimination from plasma of the proline-rich tripeptides IPP, VPP, and LPP followed a two-compartment decay process only for 18 of the 30 observations. Therefore, it was concluded that the pharmacokinetic behavior of these peptides in pigs can be described with both one- and two-compartment models, although values for AIC for fitted peptide plasma concentrations after iv administration were lower using a two-compartment model.[17]

In the present study, after iv administration of HLPLP at 4 mg/kg, the distribution phase was rapid ($T_{1/2\alpha}$ = 1.08 min) and with a high value of $V_{ss}$ (30.79 L/kg) which suggests that the peptide HLPLP is distributed into extravascular tissues. The elimination half-life ($T_{1/2\beta}$) calculated after iv administration was 7.95 min, much longer than that reported in pigs for peptides IPP, LPP or VPP (range $T_{1/2el}$ = 2.5−3.1 min)[17] The $T_{1/2\beta}$ of peptide HLPLP increased from 7.95 min after iv to 11.7 min after oral administration. This may indicate that the plasma disposition of HLPLP after oral administration could be conditioned by the absorption process.

Peptide HLPLP was extensively biotransformed to peptides LPLP and HLPL in rats and, after iv administration, represented 206% and 21.8% of the HLPLP plasma concentrations, respectively, as calculated by the ratio between the AUC for LPLP or HLPL and AUC for HLPLP. This suggests that these biotransformed peptides might contribute to the physiological activity of the peptide. In this respect, further experiments aiming at the evaluation of the activity of these derived peptides are already in progress.

When orally administered, HLPLP was rapidly absorbed through the gastrointestinal tract in rats, as reflected in a $T_{1/2a}$ of 2.79 min. This $T_{1/2a}$ is comparable to that previously obtained in pigs for the tripeptides IPP, LPP, and VPP, where after a single oral dose of 4 mg/kg body weight, the absorption half-life ranged from 2.0 to 4.6 min.[17] The absorption rate of the peptide HLPLP was low with a $C_{max}$ of 20.1 ng/mL at 11.8 min ($T_{max}$) after an oral dose of 40 mg/kg body weight. However, it has to be highlighted that, as shown after iv administration, HLPLP is rapidly hydrolyzed by plasma peptidases into smaller fragments but were not considered in the calculation of absorption rate. In addition, it is hypothesized that other smaller fragments, tri- and dipeptides, might be released by the action of the peptidases, and due to the rapid degradation of the peptide, the effective absorption is underestimated. Nevertheless, the oral bioavailability found for HLPLP (5.18%) in rats was higher than that estimated for peptides IPP, LPP, and VPP in pigs, for which approximately 0.059−0.077% of the dose was absorbed.[17] Probably, the low bioavailability of HLPLP observed in the present study could be due to first-pass effect (metabolism in gastrointestinal tract or liver before reaching systemic circulation).[24,25] However, the absolute bioavailability of 5.18% after oral administration of the peptide HLPLP, which is not high for a small organic molecule, is valuable data for a peptide, given that they are subjected to extensive metabolism by peptidases before, during, and after the absorption process. The bioavailability of a chemical compound is a prime consideration in formulation approaches, especially when attempting to increase bioavailability through physico-chemical and technical manipulations in regard to the dosage form. Further studies in this concern should be conducted.

In summary, the present study indicates that when orally given, peptide HLPLP is absorbed and distributed throughout the body by the bloodstream. The kinetic characteristics of peptide HLPLP identified in this study warrant further research on possible new ways of supplementation in food to increase its absorption and time of exposure. The present pharmacokinetic information in rats can play an important role designing future kinetic studies in humans for assessing HLPLP dose−response relationship. In addition, this work reports an accurate analytical method for the determination of HLPLP, which also allowed the identification and quantification of some derived peptide fragments. Although the pentapeptide reaches the bloodstream, its rapid degradation in plasma affects the estimation of the kinetic parameters. This study raises, as well, the question about the final active form of dietary compounds, and specifically of dietary peptides, in the organism.

## AUTHOR INFORMATION

### Corresponding Author

*E-mail: anadon@vet.ucm.es. Phone: +34-91-394.38.34. Fax: +34-91-394.38.40.

### Funding

This work was supported by projects Consolider-Ingenio FUN-C-Food CSD 2007-063, FP7-SME-2012-315349 (FOFIND), and AGL2011-24643 from Ministerio de Economía y Competitividad, projects P2009/AGR-1469 and (ALIBIRD-CM) S2013/ABI-2728 from Comunidad de Madrid, and project 920204 UCM-BSCH from Universidad Complutense de Madrid.

### Notes

The authors declare no competing financial interest.

## ACKNOWLEDGMENTS

The authors are participants in the FA1005 COST Action INFOGEST on food digestion. L. Sanchez-Rivera acknowledges CSIC for a JAE Program fellowship.

## REFERENCES

(1) Fitzgerald, R. J.; Murray, B. A. Bioactive peptides and lactic fermentations. *Int. J. Dairy Technol.* **2006**, *59*, 118−125.

(2) Korhonen, H.; Pihlanto, A. Bioactive peptides: Production and functionality. *Int. Dairy J.* **2006**, *16*, 945−960.

(3) Martínez-Maqueda, D.; Miralles, B.; Recio, I.; Hernández-Ledesma, B. Antihypertensive peptides from food proteins: a review. *Food Funct.* **2012**, *3*, 350−361.

(4) García-Tejedor, A.; Sánchez-Rivera, L.; Castelló-Ruiz, M.; Recio, I.; Salom, J.; Manzanares, P. Novel antihypertensive lactoferrin-derived peptides produced by *Kluyveromyces marxianus*: Gastrointestinal stability profile and *in vivo* angiotensin I-converting enzyme (ACE) inhibition. *J. Agric. Food Chem.* **2014**, *62*, 1609−1616.
(5) Muguerza, B.; Ramos, M.; Sánchez, E.; Manso, M. A.; Miguel, M.; Aleixandre, A.; Delgado, M. A.; Recio, I. Antihypertensive activity of milk fermented by *Enterococcus faecalis* strains isolated from raw milk. *Int. Dairy J.* **2006**, *16*, 61−69.
(6) Miguel, M.; Muguerza, B.; Sánchez, E.; Delgado, M. A.; Recio, I.; Ramos, M.; Aleixandre, M. A. Changes in arterial blood pressure in hypertensive rats caused by long-term intake of milk fermented by *Enterococcus faecalis* CECT 5728. *Br. J. Nutr.* **2005**, *94*, 36−43.
(7) Miguel, M.; Recio, I.; Ramos, M.; Delgado, M. A.; Aleixandre, M. A. Antihypertensive effect of peptides obtained from *Enterococcus faecalis*-fermented milk in rats. *J. Dairy Sci.* **2006**, *89*, 3352−3359.
(8) Quirós, A.; Contreras, M. d. M.; Ramos, M.; Amigo, L.; Recio, I. Stability to gastrointestinal enzymes and structure-activity relationship of [beta]-casein-peptides with antihypertensive properties. *Peptides* **2009**, *30*, 1848−1853.
(9) Quirós, A.; Dávalos, A.; Lasunción, M. A.; Ramos, M.; Recio, I. Bioavailability of the antihypertensive peptide LHLPLP: Trans-epithelial flux of HLPLP. *Int. Dairy J.* **2008**, *18*, 279−286.
(10) Miguel, M.; Gómez-Ruiz, J. Á.; Recio, I.; Aleixandre, A. Changes in arterial blood pressure after single oral administration of milk-casein-derived peptides in spontaneously hypertensive rats. *Mol. Nutr. Food Res.* **2010**, *54*, 1422−1427.
(11) Quirós, A.; Hernández-Ledesma, B.; Ramos, M.; Martín-Álvarez, P. J.; Recio, I. Production of antihypertensive peptide HLPLP by enzymatic hydrolysis: Optimization by response surface methodology. *J. Dairy Sci.* **2012**, *95*, 4280−4285.
(12) Franz, C. M. A.; Huch, M.; Abriouel, H.; Holzapfel, W.; Gálvez, A. Enterococci as probiotics and their implications in food safety. *Int. J. Food Microbiol.* **2011**, *151*, 125−140.
(13) Foltz, M.; van der Pijl, P. C.; Duchateau, G. S. M. J. E. Current in vitro testing of bioactive peptides is not valuable. *J. Nutr.* **2010**, *140*, 117−118.
(14) van Platerink, C. J.; Janssen, H.-G. M.; Horsten, R.; Haverkamp, J. Quantification of ACE inhibiting peptides in human plasma using high performance liquid chromatography-mass spectrometry. *J. Chromatogr. B* **2006**, *830*, 151−157.
(15) Matsui, T.; Tamaya, K.; Seki, E.; Osajima, K.; Matsumoto, K.; Kawasaki, T. Val-Tyr as a natural antihypertensive dipeptide can be absorbed into the human circulatory blood system. *Clin. Exp. Pharmacol. Physiol.* **2002**, *29*, 204−208.
(16) Foltz, M.; Meynen, E. E.; Bianco, V.; van Platerink, C.; Koning, T. M. M. G.; Kloek, J. Angiotensin converting enzyme inhibitory peptides from a lactotripeptide-enriched milk beverage are absorbed intact into the circulation. *J. Nutr.* **2007**, *137*, 953−958.
(17) van der Pijl, P.; Kies, A. K.; Ten Have, G. A. M.; Duchateau, G. S. M. J. E.; Deutz, E. P. Pharmacokinetics of proline-rich tripeptides in the pig. *Peptides* **2008**, *29*, 2196−2202.
(18) Gomez-Ruiz, J. A.; Ramos, M.; Recio, I. Angiotensin-converting enzyme-inhibitory peptides in Manchego cheeses manufactured with different starter cultures. *Int. Dairy J.* **2002**, *12*, 697−706.
(19) Yamaoka, K.; Nakagawa, T.; Uno, T. Application of Akaike's Information Criterion (AIC) in the evaluation of linear pharmacokinetic equations. *J. Pharmacokinet. Biopharm.* **1978**, *6*, 165−175.
(20) Wagner, J. G. *Fundamentals of Clinical Pharmacokinetics*; Drug Intelligence Publications: Hamilton, IL, 1975.
(21) Wagner, J. G. Linear pharmacokinetic equations allowing direct calculation of many needed pharmacokinetic parameters from the coefficients and exponents of poly-exponential equations which have been titled to the data. *J. Pharmacokinet. Biopharm.* **1975**, *4*, 443−467.
(22) Papayannopoulos, I. A. The interpretation of collision-induced dissociation tandem mass spectra of peptides. *Mass Spectrom. Rev.* **1995**, *14*, 49−73.
(23) EMEA (European Medicines Agency). *CPMP/ICH/286/95 Guideline. Non-Clinical Safety Studies for the Conduct of Human Clinical Trials and Marketing Authorization for Pharmaceuticals*; EMEA: London, 2008.
(24) Li, Z.; Jiand, H.; Xu, C.; Gu, L. A review. Using nanoparticles to enhance absorption and bioavailability of phenolic phytochemicals. *Food Hydrocolloids* **2014**, *43*, 153−164.
(25) Gao, S.; Hu, M. Bioavailability challenges associated with development of anti-cancer phenolic. *Mini-Rev. Med. Chem.* **2014**, *10*, 550−567.

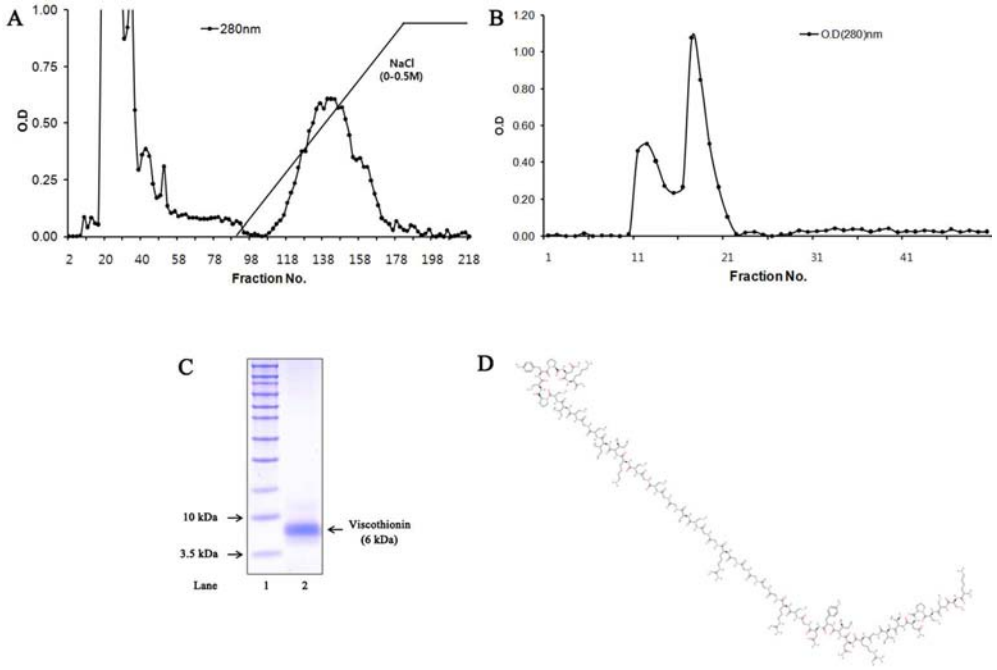


**Figure 1.** Isolation of viscothionin from Korean mistletoe: (A) activity-guided chromatography fractionation of viscothionin from Korean mistletoe using a CM Sepharose FF cation exchange column; (B) chromatographic isolation of viscothionin from the CM Sepharose−NaCl elution fraction using a Sephadex G-50 gel filtration column; (C) SDS-PAGE pattern of purified viscothionin obtained from mistletoe extracts (lanes: 1, molecular weight marker; 2, purified viscothionin (9 kDa cutoff)).

activity and, if so, what the underlying mechanisms of this activity are.

Thus, in the present study, we extracted and identified viscothionin from Korean mistletoe and investigated its effects on AMPK-mediated lipid metabolism as it relates to NAFLD using in vitro and in vivo models.

## MATERIALS AND METHODS

**Preparation of Korean Mistletoe.** Korean mistletoe, growing on oak trees, was collected in February 2013 in the Kangwon province of South Korea. Mistletoe plants were washed twice with distilled water before removal of the excess water by drying in the shade for 2 days, after which the plants were freeze-dried. Mistletoe leaves and branches were ground in a homogenizer (Hanil, Seoul, South Korea) and strained through a sieve with a mesh size of 500 $\mu$m. The resultant mistletoe powder was stored at −80 °C until use.

**Isolation of Viscothionin from Korean Mistletoe.** Isolation of viscothionin from mistletoe was performed as described previously with slight modification.[18] Briefly, 50 g of powdered mistletoe was mixed with 750 mL of 2% acetic acid and stirred overnight at 4 °C. The homogenate was centrifuged at 6000 rpm for 30 min, and the resulting supernatant was lyophilized. The dried matter was then dialyzed using membrane tubing (molecular weight cutoff 3.5 kDa) against 25 mM sodium acetate buffer (pH 4.8) at 4 °C. The dialysate was loaded on a CM Sepharose Fast Flow cation exchange column (20 × 4.6 cm) and washed with the same acetate buffer. Retained compounds were then eluted with a NaCl gradient (0−0.5 M), and 15 mL fractions were collected using a DC-1200 fraction collector (Eyela, Sunnyvale, CA, USA). The eluted fractions were monitored by determining their absorbance at 280 nm (Figure 1A), and the appropriate fractions were pooled for eventual lyophilization. Specifically, the pooled fractions were first dialyzed against distilled water using the same membrane tubing as described above. Next, the NaCl-free dialysate was relyophilized, dissolved in 1.5 mL of distilled water, and passed through a Sephadex G-50 gel filtration column (70 × 1.4 cm). Among the collected fractions, the fractions in the second peak, which showed cytotoxic activity (Figure 1B), were pooled and concentrated by centrifugation using a centrifugal filtration unit with a molecular weight cutoff of 9 kDa (Thermo Scientific, Rockford, IL, USA). The preparation of isolated viscothionin resulted in a single polypeptide band, approximately 6 kDa in size, as determined by SDS-PAGE analysis (Figure 1C).

**Polyacrylamide Gel Electrophoresis and Immunoblotting.** Polyacrylamide gel electrophoresis of isolated viscothionin was carried out using precast 12% NuPAGE Bis-Tris gels (Invitrogen, San Diego, CA, USA) at 100 V for 1 h in NuPAGE 2-(*N*-morpholino)-ethanesulfonic acid (MES) sodium dodecyl sulfate running buffer (Invitrogen) according to the manufacturer's instructions. A SeeBlue Plus2 prestained standard protein marker (Invitrogen) was used to determine the apparent molecular masses of the extracted and concentrated mistletoe proteins. Gels were stained with Coomassie Brilliant Blue R-250 for visualization.

**Chemicals.** DMSO, oleic acid (OA), and compound C were purchased from Sigma (St. Louis, MO, USA). Primary antibodies for AMPK, phosphorylated AMPK (pAMPK), ACC, phosphorylated ACC (pACC), and $\beta$-actin were purchased from Cell Signaling (Beverly, MA, USA). Secondary antibodies (horseradish peroxidase-conjugated anti-rabbit, anti-goat, and anti-mouse IgG antibodies) were obtained from Millipore (Temecula, CA, USA). Cell culture medium and other in vitro ingredients were purchased from Hyclone (Logan, UT, USA).

**Cell Culture.** HepG2 cells (American Type Culture Collection, Manassas, VA, USA) were cultured at 37 °C under a humidified atmosphere supplemented with 5% $CO_2$. Cells were routinely subcultured twice per week and maintained in Dulbecco's modified Eagle's medium (DMEM) supplemented with 10% fetal bovine serum (FBS), 100 U/mL penicillin, 100 $\mu$g/mL streptomycin, and 5.5 mM D-glucose. Upon reaching 70% confluence, medium on HUVEC cells was replaced with serum-free DMEM overnight, and cells were used as described previously.[19]

**Cell Viability Assay.** Cell survival was determined using a 3-(4,5-dimethylthiazoldimethylthiazol-2-yl)-2,5-diphenyltetrazolium bromide (MTT) assay kit from Sigma. HepG2 cells were seeded in 48-well plates at a density of $2.0 \times 10^4$ cells per well, incubated for 48 h, and treated with various concentrations (0.5−10 $\mu$M) of viscothionin for

24 h. After the incubation period, 20 μL of the kit solution was added to each well. Plates were then incubated for 3 h at 37 °C in 5% $CO_2$. The resultant formazan crystals were subsequently dissolved in MTT solubilization solution, and the absorbance of each well at 540 nm was determined using a PowerWave2 multiplate reader spectrophotometer (Bio-Tek Instruments, Winooski, VT, USA).

**Lipid Accumulation Analysis.** Lipid accumulation was analyzed using an Oil Red O staining kit according to the manufacturer's suggested protocol (Lifeline Cell Technology, Carlsbad, CA, USA). Oil Red O-stained cells were imaged with an Observer A1 microscope (Carl Zeiss, Jena, Germany) at 100× magnification. After image acquisition, accumulated intracellular Oil Red O dye was eluted with isopropanol and quantified by determining its optical absorbance at 540 nm using a PowerWave2 multiplate reader spectrophotometer (Bio-Tek Instruments).

**Animals and in Vivo Experimental Design.** Forty male C57BL/6J mice, approximately 6 weeks of age, were purchased from Dae-han Biolink (Daejeon, South Korea). All mice were verified to be free of murine viruses, bacteria, and parasites and were maintained in microisolator cages under pathogen-free conditions on a 12 h light/dark schedule for 1 week. Mice were randomly divided into two groups and fed either a normal diet ($n$ = 8) or a high-fat diet (HFD, $n$ = 32) containing 45% of its calories from fat. HFD mice were fed for 8 weeks to induce obesity. After 8 weeks, mice receiving the normal diet were orally administered 0.1 mL of saline daily, whereas HFD-fed mice were randomly divided into four subgroups. Each subgroup was orally administered either 0.1 mL of saline ($n$ = 8), 1 mg/kg viscothionin in 0.1 mL of saline ($n$ = 8), 10 mg/kg viscothionin in 0.1 mL of saline ($n$ = 8), or 10 mg/kg simvastatin in 0.1 mL of saline daily for 4 weeks. Treatments were maintained while the mice were fed a HFD from weeks 0 to 4. All mice had free access to food and water. Body weight for each mouse was measured 1 and 4 weeks after beginning the treatments. At the end of the experimental period, food was withheld for 12 h and the mice were anesthetized with ether. Subsequently, cardiac punctures were performed, and the mice were perfused with cold physiological saline. The livers were then harvested, weighed, photographed, and processed. Livers were processed for histology, real-time RT-PCR, immunoblotting, and other analyses; samples were stored at −80 °C until needed for analysis. All animals were cared for in accordance with the Chonbuk National University institutional guidelines for the care and use of experimental animals.

**Histopathology.** Trimmed liver tissues were fixed in 10% normal buffered formalin for 24 h. All of the fixed samples were embedded in paraffin and cut into 4−5 μm sections. The resulting sections were deparaffinized with xylene, rehydrated with a graded alcohol series, and stained with hematoxylin and eosin (H&E). Tissue histopathology was then evaluated using a conventional light microscope (magnification 200×; Carl Zeiss). H&E-stained sample sections were imaged, and the areas of the stained regions, in pixels, were quantified using the Image Pro analysis program.

**Measurement of Intracellular Triglyceride Contents.** Intracellular triglyceride contents were measured using a commercial triglyceride assay kit (BioAssay Systems, Hayward, CA, USA) according to the manufacturer's instructions. Briefly, HepG2 cells were pretreated with viscothionin at various concentrations (0, 1, or 5 μM) for 1 h before treatment with 10 mM OA in conditioned medium for 48 h. Additionally, cells were pretreated either with or without compound C (20 μM) or viscothionin (5 μM) for 1 h and then treated with OA for 48 h. After treatment, cells were washed twice with phosphate-buffered saline (PBS) prior to the addition of 75 μL of homogenizing solution (154 mM KCl, 1 mM EDTA, 50 mM Tris, pH 7.4) to lyse the cells. The resultant cell lysate was centrifuged at 3000$g$ for 5 min at 4 °C to remove cellular lipids. The supernatants were then assayed for triglyceride and protein contents. Triglyceride contents were normalized to protein concentrations, which were determined from a standard BSA curve. Results were expressed as milligrams of triglyceride per milligram of cellular protein. To evaluate the triglyceride contents in liver tissues, the tissues were homogenized in 1 mL of PBS, and the protein concentrations of the resultant lysates were determined. Homogenates were extracted with 5 mL of a chloroform/methanol mixture, vortexed vigorously, allowed to separate into two phases, and centrifuged at 2500 rpm for 15 min at 4 °C. The total hepatic triglyceride concentrations were normalized to the respective protein concentrations and are presented as milligrams of lipid per gram of tissue protein.

**Immunoblotting.** Total proteins from HepG2 cell lysates and liver tissue lysates were subjected to sodium dodecyl sulfate−polyacrylamide gel electrophoresis using 12−15% gels. Proteins were then electrophoretically transferred to polyvinylidene difluoride membranes (Bio-Rad Laboratories, Hercules, CA, USA). Membranes were blocked in 5% skim milk in PBS and then incubated with primary antibodies, which were diluted 1:500 in 1% skim milk in PBS overnight at 4 °C. Membranes were then incubated with peroxidase-conjugated goat anti-rabbit IgG antibodies (1:5000; Millipore, Bedford, MA, USA) for 1 h. Immunoreactive bands were visualized with SuperSignal West Dura Extended Duration Substrate (Thermo Scientific, San Jose, CA, USA) and analyzed using a chemiImager analyzer system (Alpha Innotech, San Leandro, CA, USA).

**RNA Preparation and Real-Time RT-PCR.** Total RNA was isolated from cells and precipitated with Ribo EX (Geneall, Daejeon, South Korea) according to the manufacturer's instructions. mRNA was reverse transcribed to cDNA using a Maxime RT PreMix kit (Intron, Seongnam, South Korea) according to the manufacturer's instructions. For real-time RT-PCR, cDNA was amplified using a Mastercycler Gradient 5331 thermal cycler (Eppendorf, Germany). Real-time PCR runs were monitored by measuring the fluorescence signal after each cycle with an ABI Step One Plus Sequence Detection System (Applied Biosystems, Singapore). Specific primers for each gene were designed using Primer Express software (Applied Biosystems). The following sense and antisense primers were used for real-time RT-PCR quantification in HepG2 cells (forward and reverse): 5′-GGAGCCATGGATTGCACTTT-3′ and 5′-TCAAATAGGCCAGGGAAGTCA-3′ for SREBP-1; 5′-CGTCCTCTTCCCCGCCACT-3′ and 5′-GCACCACATCCTCAAACACCACA-3′ for FAS; and 5′-TCTCCTCTGACTTCAACAGCGAC-3′ and 5′-CCCTGTTGCTGTAGCCAAATTC-3′ for glyceraldehyde-3-phosphate dehydrogenase (GAPDH), which was used as a housekeeping gene. The following sense and antisense primers were used in real-time RT-PCR for quantification in liver tissue (forward and reverse): 5′-GCAGCCACCATCTAGCCTG-3′ and 5′-CAGCAGTGAGTCTGCCTTGAT-3′ for SREBP-1; 5′-CCTGGATAGCATTCCGAACCT-3′ and 5′-AGCACATCTCGAAGGCTACACA-3′ for FAS; and 5′-GCATGGCCTTCCGTGTTC-3′ and 5′-GATGTCATCATACTTGGCAGGTTT-3′ for GAPDH, which was used as a housekeeping gene. All experiments were performed at least three times.

**Statistical Analysis.** Results are presented as the mean ± standard error. Data were analyzed using Student's $t$ test (for two groups), one-way ANOVA, and Tukey's test (for more than two groups). $P$ values <0.05 were considered statistically significant. All analyses were performed using the Statistical Package for Social Sciences, version 13.0, for Windows (SPSS, Inc., Chicago, IL, USA).

## RESULTS

**Cell Viability in HepG2 Cells Treated with Viscothionin.** Figure 1D shows the structure of viscothionin. Before proceeding with the main experiment, we evaluated the effect of viscothionin on HepG2 cell viability using an MTT assay. We found that viscothionin was not significantly cytotoxic at concentrations <10 μM (Figure 2). Thus, viscothionin concentrations ≤5 μM, which were found to be nontoxic in HepG2 cells, were used in subsequent experiments.

**Viscothionin Increases Phosphorylation of the AMPK/ACC Signaling Pathway.** AMPK plays a critical role in the regulation of lipogenesis in the liver. To examine whether AMPK is activated by viscothionin, the phosphorylation status of AMPK was analyzed by immunoblotting cellular extracts after various treatments. As shown in Figure 3A, viscothionin treatment increased the levels of phosphorylated AMPK and

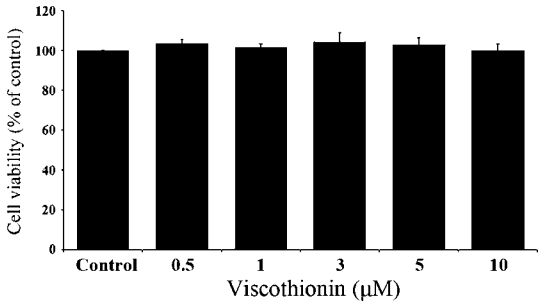


**Figure 2.** Viability of HepG2 cells treated with viscothionin. HepG2 cells were treated with various concentrations of viscothionin (0.5−10 $\mu$M) for 24 h and analyzed by MTT assay.

ACC compared with untreated controls. Importantly, this effect was dose-dependent, although 10 $\mu$M viscothionin did not stimulate AMPK or ACC phosphorylation to the same extent as 5 $\mu$M viscothionin. We hypothesized that this apparent discrepancy could be explained by different kinetics of phosphorylation associated with the two doses. Specifically, we confirmed that phosphorylation occurs more rapidly and transiently with high doses of viscothionin compared with low doses of viscothionin (data not shown), which likely explains the apparent inconsistency of the dose-dependent results. A number of previous studies have established that OA-treated HepG2 cells are an appropriate in vitro model of NAFLD.[20−22] On the basis of these studies, we used OA (10 mM) to induce lipid accumulation in HepG2 cells. As shown in Figure 3B, the levels of phosphorylated AMPK and ACC were decreased by treatment with 10 mM OA, whereas treatment with viscothionin counteracted the OA-induced reduction of phosphorylated AMPK and ACC in a dose-dependent manner. These results indicated that viscothionin was able to activate the AMPK signaling pathway. To determine whether viscothionin acts via AMPK, HepG2 cells were pretreated for 1 h with compound C, a selective AMPK inhibitor. The levels of phosphorylated AMPK and ACC in cells treated with compound C alone were significantly decreased compared with those in control cells. As predicted, pretreatment with compound C counteracted the viscothionin-induced increase in levels of phosphorylated AMPK and ACC in the OA-treated group (Figure 3C). Taken together, these results suggest that viscothionin counteracts the effect of OA on HepG2 cells by activating AMPK.

**Viscothionin Attenuates OA-Induced Lipid Accumulation in HepG2 Cells via Activation of the AMPK Signaling Pathway.** To verify the inhibitory effect of viscothionin on OA-induced lipid accumulation, HepG2 cells were treated with the indicated concentrations of viscothionin in the presence of OA for 48 h. As shown in Figure 4A, lipid accumulation was visualized with Oil Red O, which stains lipid droplets red in HepG2 cells. Quantification of intracellular lipids revealed that viscothionin treatment significantly attenuated OA-induced lipid accumulation in a dose-dependent manner. Moreover, treatment with compound C significantly reduced the effect of viscothionin in OA-treated cells. Consistent with previous results, cellular triglyceride levels (Figure 4B) and the expression of lipogenic genes such as SREBP-1 (Figure 4C) and FAS (Figure 4D) were reduced in viscothionin-treated HepG2 cells compared with OA-treated HepG2 cells. Moreover, compound C reduced the effects of viscothionin on cellular triglyceride concentration as well as on the expression of SREBP-1 and FAS in OA-treated HepG2 cells. These results are consistent with those presented in Figure 4A and suggest that viscothionin antagonizes OA-induced hepatic lipid accumulation via activation of the AMPK signaling pathway.

**Viscothionin Treatment Improves Some Symptoms of NAFLD.** To validate our in vitro results in vivo, we utilized the HFD-induced obese mouse model of NAFLD. Initial histopathological examinations indicated that viscothionin was not cytotoxic to any of the organs examined, including the liver, kidney, and spleen in normal mice (data not shown). As shown

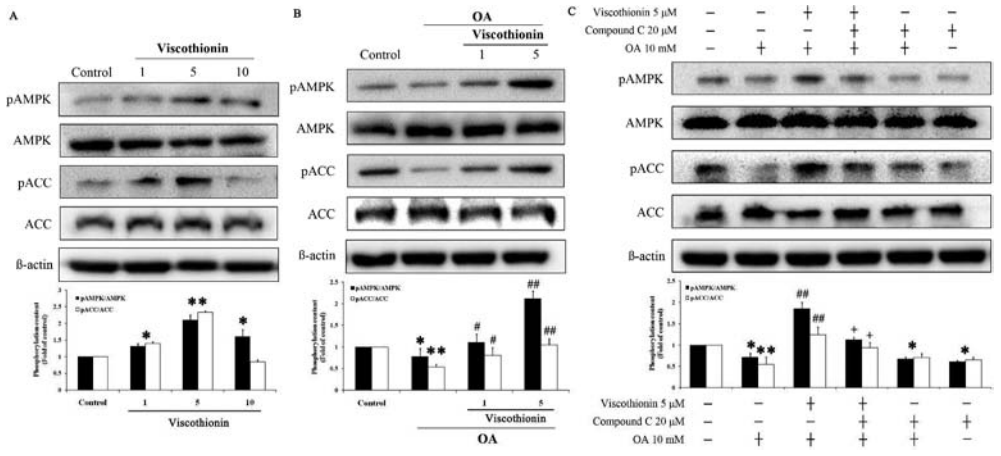


**Figure 3.** Effects of viscothionin on the levels of phosphorylated AMPK and ACC in HepG2 cells. Immunoblotting analysis was used to determine the levels of phosphorylated AMPK and ACC. (A) HepG2 cells were treated with viscothionin (1, 5, or 10 $\mu$M) for 1 h. (B) HepG2 cells were pretreated with the indicated concentrations of viscothionin (1 or 5 $\mu$M) for 1 h and then incubated with 10 mM OA for 1 h. (C) HepG2 cells were treated with compound C (20 $\mu$M) for 1 h and then incubated with or without 5 $\mu$M viscothionin for an additional 1 h. Cells were then incubated with OA for 1 h. The intensities of the control bands were set to 100%, and the relative intensities of all other bands were calculated. Protein levels were normalized to the levels of total AMPK or ACC as appropriate. Immunoblots were analyzed by densitometry; data are presented as relative intensity units. Data are presented as the mean ± SEM ($n$ = 3). (*) $p < 0.05$ compared with the control; (**) $p < 0.01$ compared with the control; (#) $p < 0.05$ compared with the OA-alone group; (##) $p < 0.01$ compared with the OA-alone group; (+) $p < 0.05$ compared with the viscothionin + OA group.

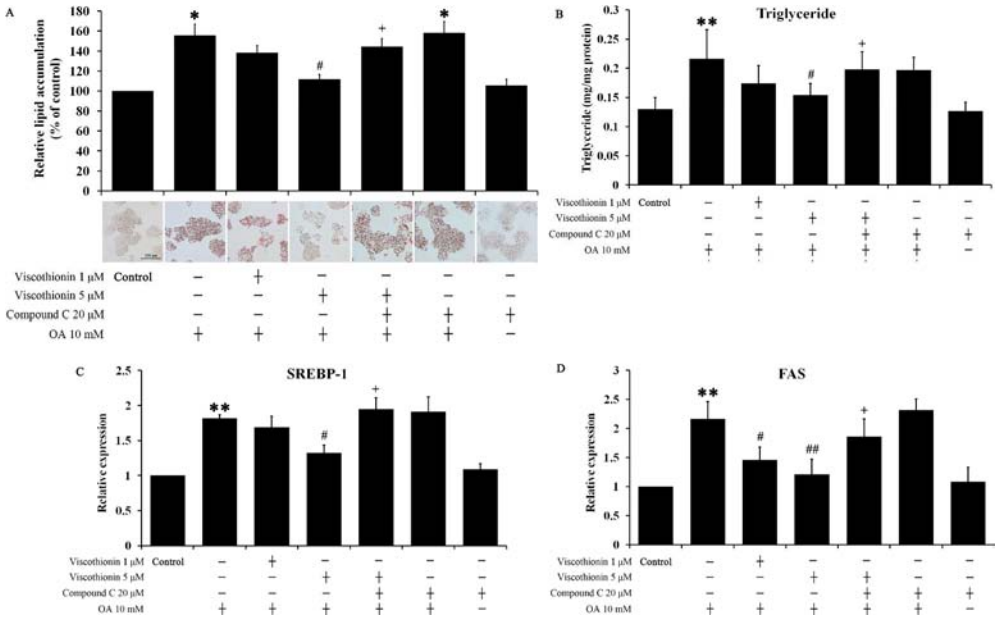


**Figure 4.** Viscothionin-mediated effects on AMPK activation, lipid accumulation, and expression of lipogenic genes in OA-treated HepG2 cells. HepG2 cells were treated with the AMPK inhibitor compound C (20 $\mu$M) for 1 h. Cells were then incubated with or without 5 $\mu$M viscothionin for an additional 1 h followed by OA for 24 h. (A) Intracellular lipid droplets in HepG2 cells were stained with Oil Red O and observed at 200× magnification. Lipid droplets were quantified by measuring the resultant absorbance at 540 nm. (B) Intracellular triglyceride contents were measured. The expression levels of the lipogenic genes SREBP-1 (C) and FAS (D) were examined by real-time RT-PCR. Data are presented as the mean ± SEM ($n$ = 3). (*) $p < 0.05$ compared with the control; (**) $p < 0.01$ compared with the controlL (#) $p < 0.05$ compared with the OA-alone group; (##) $p < 0.01$ compared with the OA-alone group; (+) $p < 0.05$ compared with the 5 $\mu$M viscothionin + OA group.

in Figure 5A,B, significant differences in the average body and liver weights of the experimental groups were observed at the end of the study. To investigate the effects of viscothionin in the liver, HFD-induced obese mice (1 week of treatment) were used at 14 weeks. Specifically, these mice were administered either viscothionin or simvastatin orally until reaching 17 weeks (4 weeks of treatment). Viscothionin treatment decreased the average body weight (10 mg/kg, 28.5 ± 1.1) and liver weight (10 mg/kg, 2.62 ± 0.22) in HFD-induced obese mice compared with the saline control group. These measurements were similar to those of mice treated with 10 mg/kg simvastatin, a commercially available antiobesity agent. Moreover, notable morphological changes were observed in the gross appearances of the livers from each experimental group. Compared with those of the control group, livers from the saline-only group were significantly enlarged and had a pale appearance. These apparent abnormalities of the liver, reminiscent of those found in NAFLD, were improved in a dose-dependent manner by viscothionin (Figure 5C). Accordingly, histological evaluation with H&E staining revealed significant differences among the groups (Figure 5C). Specifically, liver sections in the saline-only group exhibited typical ballooning signs of degeneration, whereas these histological changes in the liver, which were digitized from section images, were almost completely prevented by treatment with viscothionin in a dose-dependent manner. These results suggested that viscothionin improved the pathogenesis of NAFLD in HFD-induced obese mice. Additionally, several factors involved in lipid metabolism were analyzed in hepatic tissue. The levels of triglycerides in the livers of the saline-only group were significantly elevated compared to those in the normal control group (Figure 5D). Furthermore, viscothionin treatment (10 mg/kg) led to a marked decrease in the levels of liver triglycerides (about 0.5-fold) compared with the saline-only group. The liver mRNA expression of several factors involved in lipid metabolism, namely SREBP-1 and FAS, were also examined (Figure 5E,F). The expression levels of SREBP-1 and FAS in the saline-only group were increased 6.8- and 17.3-fold, respectively, compared with those of the normal control group. On the other hand, viscothionin treatment (10 mg/kg) resulted in 0.6- and 0.87-fold lower levels of SREBP-1 and FAS, respectively, compared with the saline-only group. Taken together, these results indicated that viscothionin exerts effects similar to those of simvastatin, a known antiobesity agent, against HFD-induced NAFLD.

**Viscothionin-Mediated Effects on AMPK Activation in NAFLD.** To extend our in vitro results and confirm whether the hypolipidemic effects of viscothionin were mediated by AMPK, we examined the levels of phosphorylated AMPK in liver tissues. Viscothionin treatment increased the levels of ACC and AMPK phosphorylation in a dose-dependent manner in the livers of the experimental groups compared with the livers in the saline-only group (Figure 6). These data suggested that viscothionin also exerts hypolipidemic effects against NAFLD via AMPK activation in vivo. Additionally, we confirmed that viscothionin and simvastatin exert similar effects on AMPK phosphorylation. Thus, we concluded that viscothionin exerts effects against NAFLD similar to those of simvastatin.

## DISCUSSION

NAFLD is globally recognized as a hepatic sign of lipid metabolic syndrome and is rising as one of the most general causes of chronic liver disease.[23] NAFLD stimulates progression of various liver diseases such as simple hepatic steatosis to steatohepatitis, advanced fibrosis, and cirrhosis.[24] Although the pathogenic mechanisms by which steatosis advances to early and advanced stages of NAFLD have not yet been clearly identified, the "two-hit" hypothesis[25] is now generally accepted.

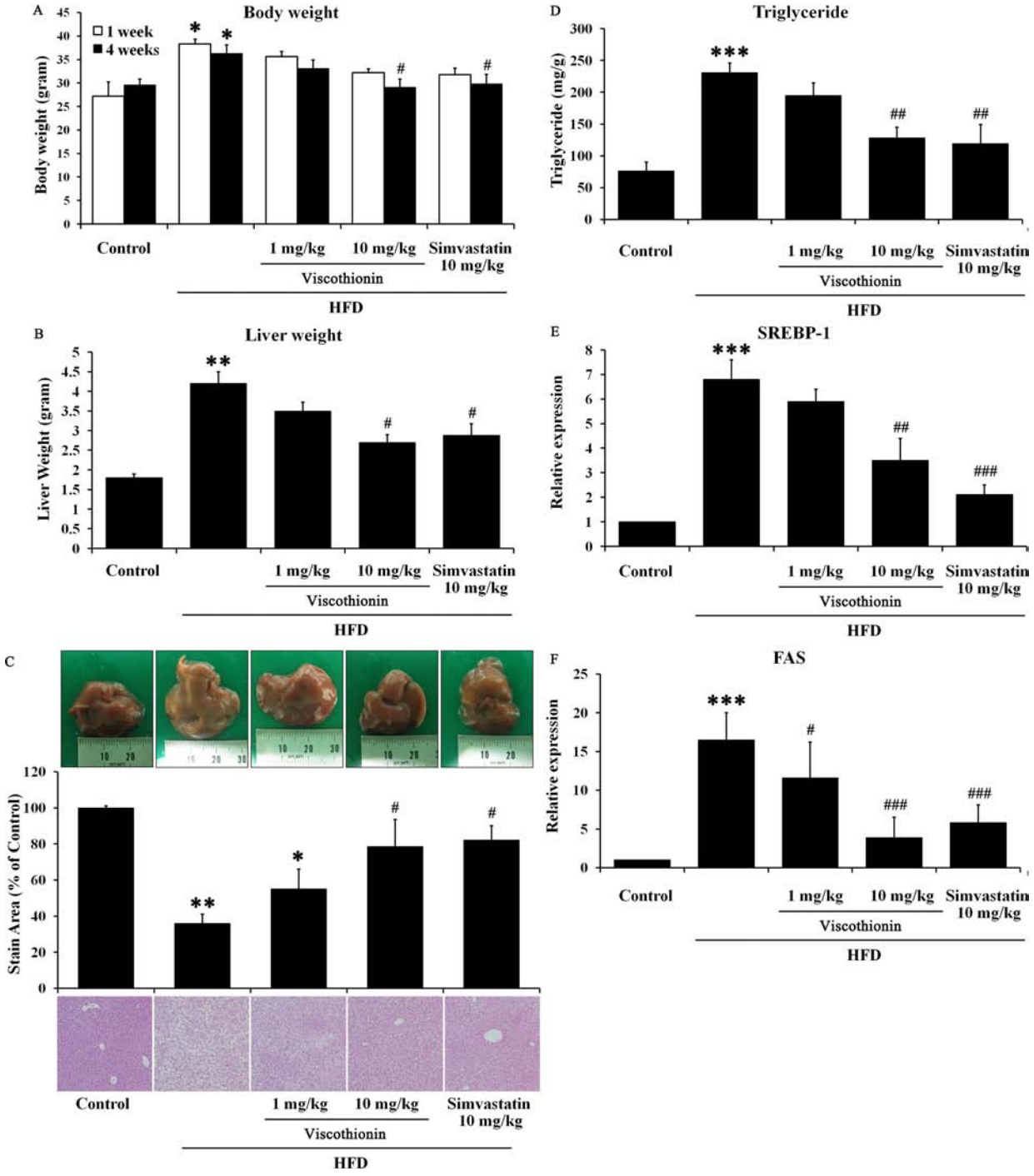


**Figure 5.** Effects of viscothionin on a mouse model of NAFLD. (A) Body weights were determined at 14 weeks (1 week of treatment) and 17 weeks (4 weeks of treatment). (B) Liver weights for all experimental mice were determined at 17 weeks. Panel C shows gross appearances and histological analyses of liver sections from each experimental group. Liver sections were obtained at 17 weeks. H&E staining (magnification 200×) was quantified by determining the stained area, in pixels, in each image using the Image Pro analysis program. (D) Hepatic concentrations of triglycerides were measured in all experimental groups. The expression levels of SREBP-1 (E) and FAS (F) in livers were determined by real-time RT-PCR. Data are presented as the mean ± SEM ($n$ = 8). (*) $p < 0.05$ compared with the control; (**) $p < 0.01$ compared with the control; (***) $p < 0.001$ compared with the control; (#) $p < 0.05$ compared with the saline-only group; (##) $p < 0.01$ compared with the saline-only group; (###) $p < 0.001$ compared with the saline-only group.

Hepatic lipid accumulation, which was thought to be an initial developmental factor, represents the "first-hit" in this progression and can therefore be an early indication of NAFLD. Thus, reducing hepatic lipid accumulation is thought to be an important strategy for preventing and treating NAFLD.

In the present study, we examined whether viscothionin, a compound isolated from Korean mistletoe, could improve NAFLD in both in vitro and in vivo models. Moreover, we explored the possible mechanisms of action of viscothionin, in particular the role of AMPK. Mistletoe is a semiparasitic plant that grows on many different kinds of deciduous trees all over


dx.doi.org/10.1021/jf503535s | J. Agric. Food Chem. 2014, 62, 11876−11883

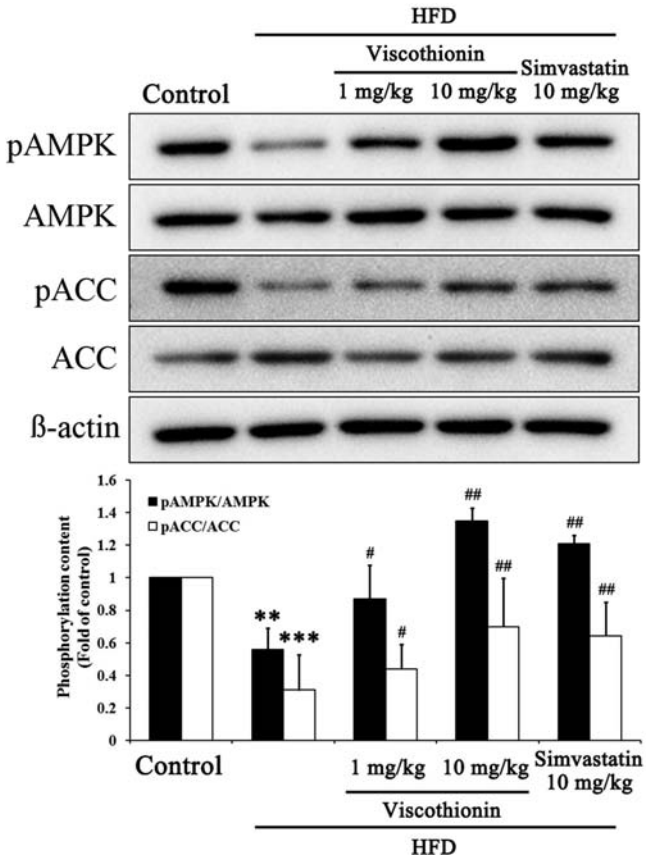


**Figure 6.** Effects of viscothionin on AMPK activation in an animal model of NAFLD. Levels of pAMPK, AMPK, pACC, ACC, and $\beta$-actin in liver lysates were determined by immunoblot analysis. The intensities of the control bands were set to 100%, and the relative intensities of all other bands were calculated. Protein levels were normalized to that of total AMPK or ACC as appropriate. Immunoblots were analyzed by densitometry. Data are presented as relative intensity units as the mean ± SEM ($n$ = 8). (**) $p < 0.01$ compared with the control; (***) $p < 0.001$ compared with the control; (#) $p < 0.05$ compared with the saline-only group; (##) $p < 0.01$ compared with the saline-only group.

the world. Importantly, mistletoe has been investigated as an alternative treatment for many diseases including cancer, hypertension, cardiac vascular disease, epilepsy, arthritis, menopausal symptoms, and rheumatism.[13−16] Likewise, several recent studies have demonstrated that Korean mistletoe has potential anticancer[16] and antiobesity effects.[17] On the basis of these findings, we purified potential candidate molecules from Korean mistletoe and confirmed that viscothionin is the active component involved in lipid metabolism. Moreover, we investigated the effect of viscothionin on the liver, which is the organ most vulnerable to excessive lipid accumulation.

AMPK is a heterotrimeric protein consisting of one catalytic subunit ($\alpha$) and two noncatalytic subunits ($\beta$ and $\gamma$). Phosphorylation of AMPK on threonine 172 (Thr172) of the $\alpha$-subunit changes the cellular energy ratio and leads to AMPK activation. The activity of ACC, an enzyme that converts acetyl-CoA into malonyl-CoA and thus provides substrates for fatty acid synthesis,[27] can be regulated by AMPK-mediated phosphorylation,[26] and phosphorylation of ACC potently reduces lipogenesis, because the carboxylase activity of ACC is suppressed.[26] These studies suggest that AMPK signaling pathways are potential targets for the treatment of metabolic disorders such as insulin resistance and NAFLD.[27] Thus, we examined the relationship between AMPK activation and viscothionin. As expected, viscothionin increased the levels of phosphorylated AMPK and ACC in a dose-dependent manner (Figure 3A). Viscothionin also increased the levels of phosphorylated AMPK and ACC, even in the presence of OA, which normally reduces the levels of phosphorylated AMPK and ACC (Figure 3B). Moreover, compound C, a known inhibitor of AMPK, significantly reduced the effects of viscothionin on the phosphorylation of AMPK and ACC (Figure 3C). These results indicated that viscothionin acts via the AMPK signaling pathway. We also confirmed the presence of lipid accumulation in our model of NAFLD. As shown in Figure 4, OA-induced lipid accumulation was attenuated by 5 $\mu$M viscothionin. Additionally, we also observed reduced SREBP-1 gene expression and down-regulation of its target adipogenic gene, FAS, in viscothionin-treated HepG2 cells (Figure 4C,D). SREBP-1 is an important transcription factor that stimulates several adipogenic enzymes related in liver fatty acid synthesis[28] and also regulates the expression of ACC. AMPK activation has been shown to directly inhibit ACC activity and to also indirectly inhibit FAS expression via suppression of SREBP-1.[29] Consistent with our immunoblotting data, compound C significantly attenuated the effects of viscothionin on SREBP-1 and FAS gene expression in OA-treated HepG2 cells. Together, these findings indicated that viscothionin exerts its lipid-reducing effects via the AMPK signaling pathway.

We confirmed the effects of viscothionin in an in vivo model of NAFLD. As expected, viscothionin treatment resulted in notably improved liver histology in mice with obesity-induced NAFLD. Moreover, the average body weight of the viscothionin-treated group (10 mg/kg) was lower than that of the saline-treated group (Figure 5A). Weight, gross abnormalities, and ballooning degeneration in the liver are considered to be early indicators of NAFLD.[23] Consistent with these observations and our results to this point, we found that viscothionin treatment resulted in reduced liver weight, improvements in gross abnormalities, and reduced ballooning degeneration of the liver in mice with NAFLD compared with mice with NAFLD treated with saline alone (Figure 5B,C). As expected, viscothionin treatment also reduced the level of hepatic triglycerides (Figure 5D), high levels of which are a marker of lipid metabolism in NAFLD.[30] Promotion of triglyceride synthesis has been proposed to excessively provoke other deleterious reactions such as lipid peroxidation.[31] Moreover, the expression levels of SREBP-1 and FAS in the liver were also reduced in the viscothionin-treated group. Viscothionin also significantly increased the levels of phosphorylated AMPK and ACC compared with the saline-only group in a dose-dependent manner, which was consistent with our in vitro data. On the basis of these results, we concluded that viscothionin exerts its anti-NAFLD actions via activation of AMPK.

In conclusion, this study demonstrated that viscothionin isolated from Korean mistletoe decreases hepatic lipid accumulation. The beneficial effect of viscothionin was shown to involve AMPK-mediated regulation of fatty acid metabolism and was confirmed in both in vitro and in vivo models of NAFLD. Thus, viscothionin appears to exert notable hepatic protective and therapeutic properties against NAFLD, and we obtained insight into the underlying molecular mechanisms regarding the effects of viscothionin. Taken together, our

findings indicate that viscothionin is a novel potential therapeutic agent for the treatment of NAFLD.

## AUTHOR INFORMATION


### Corresponding Author

*(J.K.) Mail: Department of Laboratory Animal Medicine, College of Veterinary Medicine, Chonbuk National University, 664-14, Duckjin-Dong, Jeonju, Jeonbuk 561-156, Republic of Korea. Phone: +82-63-270-3884. Fax: +82-63-270-3780. E-mail: jkwon@chonbuk.ac.kr.

### Author Contributions

‖S.K. and D.L. contributed equally to this study.



### Funding

This work was supported by a grant from the National Research Foundation of Korea, funded by the Korean government (NRF-2013R1A1A2065158). This work was also supported by the Nuclear Research & Development Program of the Korea Science and Engineering Foundation, through a grant funded by the government of the Republic of Korea.


### Notes

The authors declare no competing financial interest.

## ABBREVIATIONS USED

OA, oleic acid; SREBP-1, sterol regulatory element binding protein-1; FAS, fatty acid synthase; AMPK, 5′-adenosine monophosphate-activated protein kinase; ACC, acetyl-CoA carboxylase; HFD, high-fat diet

## REFERENCES


(1) Matteoni, C. A.; Younossi, Z. M.; Gramlich, T.; Boparai, N.; Liu, Y. C.; McCullough, A. J. Nonalcoholic fatty liver disease: a spectrum of clinical and pathological severity. *Gastroenterology* **1999**, *116*, 1413−1419.

(2) Madan, K.; Bhardwaj, P.; Thareja, S.; Gupta, S. D.; Saraya, A. Oxidant stress and antioxidant status among patients with non-alcoholic fatty liver disease (NAFLD). *J. Clin. Gastroenterol.* **2006**, *40*, 930−935.

(3) Browning, J. D.; Horton, J. D. Molecular mediators of hepatic steatosis and liver injury. *J. Clin. Invest.* **2004**, *114*, 147−152.

(4) Targher, G.; Bertolini, L.; Rodella, S.; Tessari, R.; Zenari, L.; Lippi, G.; Arcaro, G. Nonalcoholic fatty liver disease is independently associated with an increased incidence of cardiovascular events in type 2 diabetic patients. *Diabetes Care* **2007**, *30*, 2119−2121.

(5) Charlton, M. Nonalcoholic fatty liver disease: a review of current understanding and future impact. *Clin. Gastroenterol. Hepatol.* **2004**, *2*, 1048−1058.

(6) Steinberg, G. R.; Kemp, B. E. AMPK in health and disease. *Physiol. Rev.* **2009**, *89*, 1025−1078.

(7) Musso, G.; Gambino, R.; Cassader, M. Emerging molecular targets for the treatment of nonalcoholic fatty liver disease. *Annu. Rev. Med.* **2010**, *61*, 375−392.

(8) Chirala, S. S.; Jayakumar, A.; Gu, Z.-W.; Wakil, S. J. Human fatty acid synthase: role of interdomain in the formation of catalytically active synthase dimer. *Proc. Natl. Acad. Sci. U.S.A.* **2001**, *98*, 3104−3108.

(9) Smith, S. The animal fatty acid synthase: one gene, one polypeptide, seven enzymes. *FASEB J.* **1994**, *8*, 1248−1259.

(10) Bennett, M. K.; Lopez, J. M.; Sanchez, H. B.; Osborne, T. F. Sterol regulation of fatty acid synthase promoter coordinate feedback regulation of two major lipid pathways. *J. Biol. Chem.* **1995**, *270*, 25578−25583.

(11) Kim, J. B.; Spiegelman, B. M. ADD1/SREBP1 promotes adipocyte differentiation and gene expression linked to fatty acid metabolism. *Genes Dev.* **1996**, *10*, 1096−1107.

(12) Eberle, D.; Hegarty, B.; Bossard, P.; Ferré, P.; Foufelle, F. SREBP transcription factors: master regulators of lipid homeostasis. *Biochimie* **2004**, *86*, 839−848.

(13) Kienle, G. S.; Kiene, H. Review article: Influence of *Viscum album* L (European mistletoe) extracts on quality of life in cancer patients: a systematic review of controlled clinical studies. *Integr. Cancer Ther.* **2010**, *9*, 142−157.

(14) Ostermann, T.; Bussing, A. Retrolective studies on the survival of cancer patients treated with mistletoe extracts: a meta-analysis. *Explore (N.Y.)* **2012**, *8*, 277−281.

(15) Pearl, P. L.; Drillings, I. M.; Conry, J. A. Herbs in epilepsy: evidence for efficacy, toxicity, and interactions. *Semin. Pediatr. Neurol.* **2011**, *18*, 203−208.

(16) Khil, L.-Y.; Kim, W.; Lyu, S.; Park, W. B.; Yoon, J.-W.; Jun, H.-S. Mechanisms involved in Korean mistletoe lectin-induced apoptosis of cancer cells. *World J. Gastroenterol.* **2007**, *13*, 2811.

(17) Jung, H.-Y.; Kim, Y.-H.; Kim, I.-B.; Jeong, J.; Lee, J.-H.; Do, M.-S.; Jung, S.-P.; Kim, K.; Kim, J.-B. The Korean mistletoe (*Viscum album coloratum*) extract has an anti-obesity effect and protects against hepatic steatosis in mice with high-fat diet-induced obesity. *Evidence-Based Complement. Altern. Med.* **2013**, No. 168207, DOI: 10.1155/2013/168207.

(18) Park, J. H.; Hyun, C. K.; Shin, H. K. Cytotoxic effects of the components in heat-treated mistletoe (*Viscum album*). *Cancer Lett.* **1999**, *139*, 207−213.

(19) Zang, M.; Zuccollo, A.; Hou, X.; Nagata, D.; Walsh, K.; Herscovitz, H.; Brecher, P.; Ruderman, N. B.; Cohen, R. A. AMP-activated protein kinase is required for the lipid-lowering effect of metformin in insulin-resistant human HepG2 cells. *J. Biol. Chem.* **2004**, *279*, 47898−47905.

(20) Chang, J. J.; Hsu, M. J.; Huang, H. P.; Chung, D. J.; Chang, Y. C.; Wang, C. J. Mulberry anthocyanins inhibit oleic acid induced lipid accumulation by reduction of lipogenesis and promotion of hepatic lipid clearance. *J. Agric. Food Chem.* **2013**, *61*, 6069−6076.

(21) Liao, C. C.; Ou, T. T.; Huang, H. P.; Wang, C. J. The inhibition of oleic acid induced hepatic lipogenesis and the promotion of lipolysis by caffeic acid via up-regulation of AMP-activated kinase. *J. Sci. Food Agric.* **2014**, *94*, 1154−1162.

(22) Zhang, T.; Yamamoto, N.; Ashida, H. Chalcones suppress fatty acid-induced lipid accumulation through a LKB1/AMPK signaling pathway in HepG2 cells. *Food Funct.* **2014**, *5*, 1134−1141.

(23) Hjelkrem, M. C.; Torres, D. M.; Harrison, S. A. Nonalcoholic fatty liver disease. *Minerva Med.* **2008**, *99*, 583−593.

(24) Angulo, P. Nonalcoholic fatty liver disease. *Rev. Gastroenterol. Mex.* **2005**, *70* (Suppl. 3), 52−56.

(25) Day, C. P. Pathogenesis of steatohepatitis. *Best Pract. Res. Clin. Gastroenterol.* **2002**, *16*, 663−678.

(26) Park, S. H.; Gammon, S. R.; Knippers, J. D.; Paulsen, S. R.; Rubink, D. S.; Winder, W. W. Phosphorylation-activity relationships of AMPK and acetyl-CoA carboxylase in muscle. *J. Appl. Physiol.* **2002**, *92*, 2475−2482.

(27) Viollet, B.; Foretz, M.; Guigas, B.; Horman, S.; Dentin, R.; Bertrand, L.; Hue, L.; Andreelli, F. Activation of AMP-activated protein kinase in the liver: a new strategy for the management of metabolic hepatic disorders. *J. Physiol.* **2006**, *574*, 41−53.

(28) Brown, M. S.; Goldstein, J. L. The SREBP pathway: regulation of cholesterol metabolism by proteolysis of a membrane-bound transcription factor. *Cell* **1997**, *89*, 331−340.

(29) Hardie, D. G. AMP-activated/SNF1 protein kinases: conserved guardians of cellular energy. *Nat. Rev. Mol. Cell Biol.* **2007**, *8*, 774−785.

(30) Yamabe, N.; Noh, J. S.; Park, C. H.; Kang, K. S.; Shibahara, N.; Tanaka, T.; Yokozawa, T. Evaluation of loganin, iridoid glycoside from Corni Fructus, on hepatic and renal glucolipotoxicity and inflammation in type 2 diabetic db/db mice. *Eur. J. Pharmacol.* **2010**, *648*, 179−187.

(31) Wymann, M. P.; Schneiter, R. Lipid signalling in disease. *Nat. Rev. Mol. Cell Biol.* **2008**, *9*, 162−176.

Table 1. Sequences of the Primers Used for PCR[a]

| gene | forward (5′−3′) | reverse (5′−3′) |
|---|---|---|
| LDL receptor | CAGCTCTGTGTGAACCTGGA | TTCTTCAGGTTCGGGATCAG |
| CYP7A1 | CACCATTCCTGCAACCTTTT | GTACCGGCAGGTCATTCAGT |
| GLUT-4 | GACATTTGGCGGAGCCTAAC | TAACTCCAGCAGGGTGACACAG |
| PPAR-$\alpha$ | GGTCATACTCGCAGGAAA | AGCAAATTATAGCAGCCAC |
| PPAR-$\gamma$ | TCAGGGCTGCCAGTTTCG | GCTTTTGGCATACTCTGTGATCTC |
| $\beta$-actin | TGTTGTCCCTGTATGCCTCT | TAATGTCACGCACGATTTCC |

[a]LDL receptor, low-density lipoprotein receptor; CYP7A1, cholesterol 7$\alpha$-hydroxylase; GLUT-4, glucose transporter-4; PPAR-$\alpha$, peroxisome proliferator-activated receptor-$\alpha$; and PPAR-$\gamma$, peroxisome proliferator-activated receptor-$\gamma$.

[certificate number SCXK (Su) 2011-0003, Changzhou, China]. All animals were housed under the conditions of 23 ± 1 °C and 12/12 h of light/dark cycle with *ad libitum* food and water for 1 week before commencement of the animal experiment. All animals used in this study were cared for in accordance with the Guidelines for the Care and Use of Laboratory Animals published by the U.S. National Institutes of Health (NIH Publication 85-23, 1996), and all experimental procedures were approved by the Nanchang University Medical College Animal Care Review Committee.

**Experimental Design.** After acclimation, 10 rats were fed a standard normal chow diet and the others were fed with a high-fat diet. The high-fat diet consists of 66.5% (w/w) normal chow diet, 10% lard, 20% sucrose, 2.5% cholesterol, and 1% sodium cholate.[14] After 8 weeks of dietary manipulation, rats fed a high-fat diet were fasted for 12 h and injected with STZ (Sigma Chemical Co., St. Louis, MO) at the dose of 30 mg/kg of body weight into the tail vein to induce type 2 diabetes. Rats fed on a standard normal chow diet received an equivalent volume of vehicle. Hyperglycemia was confirmed by the levels of fasting blood glucose (FBG) higher than 11.1 mmol/L at day 7 after STZ injection.

A total of 40 type 2 diabetic rats were randomly divided into four groups ($n$ = 10 in each group) as follows: untreated diabetes mellitus (DM), DM treated with $10^9$ CFU/mL *L. plantarum* NCU116 (NCU), DM treated with fermented carrot juice with *L. plantarum* NCU116 (FCJ, $10^9$ CFU/mL), and DM treated with non-fermented carrot juice (NFCJ). A total of 10 rats fed on a standard normal chow diet served as a non-diabetes mellitus group (NDM) and received the same volume of saline. All treatments were conducted with 10 mL/kg of body weight by oral administration once daily over a 5 week period.

**Measurement of Metabolites in Carrot Juices.** $\beta$-Carotene,[17] short-chain fatty acid (SCFA),[18] and other organic acids (citric acid, malic acid, and lactic acid)[19] in the carrot juices were measured as described in previous reports. Amino acids in the juices were determined by an amino acid analyzer (L-8900, Hitachi, Japan).

**Measurements of Blood Glucose, Lipids, and Hormones.** At the end of the 5 week experimental period, blood glucose levels in the rats were determined following food deprivation for 12 h by Accu-Chek Performa (Roche Diagnostics, Mannheim, Germany). Then, the rats were humanly anesthetized with chloral hydrate via peritoneal injection. Blood samples were obtained by cardiac puncture and centrifuged at 1000*g* for 10 min, and the serum was recovered for further analyses. Samples of liver, pancreas, kidney, skeletal muscle, and feces in colon were quickly removed and stored at −80 °C until use. Levels of serum lipids, including total cholesterol (TC), high-density lipoprotein cholesterol (HDL-C), low-density lipoprotein cholesterol (LDL-C), and triacylglycerols (TG), as well as hormones, including serum insulin, leptin, and glucagon, were measured by a radioimmunoassay method, as described previously.[13] Contents of glucagon-like peptide (GLP)-1 and peptide tyrosine-tyrosine (PYY) were determined by enzyme-linked immunosorbent assay (ELISA) kits (Xinyu Biotech Co., Shanghai, China).

**Determination of Serum Oxidative Stress and Kidney Function.** Activities of superoxide dismutase (SOD), glutathione peroxidase (GSH-Px), and catalase (CAT) and levels of malondialdehyde (MDA), total antioxidant capacity (T-AOC), uric acid, creatinine, and urea nitrogen were determined using commercial kits (Jiancheng Bioengineering, Nanjing, China) according to the instructions of the manufacturer.

**Determination of SCFA in Colonic Feces.** SCFA of colonic feces were measured as described in a previous report.[18]

**Histopathological Examination.** The pancreas and kidney samples were collected from the animals under anaesthetized conditions, and a portion of the samples was fixed in 10% buffered formalin, dehydrated through graded alcohol, and embedded in paraffin wax. Sections with 5 $\mu$m thickness were mounted on slides. The samples were stained with hematoxylin and eosin after deparaffinization. The stained slides were mounted in neutral balsam and covered with coverslips. Histopathological changes were observed with a Nikon Ti series inverted microscope equipped with bright-field high-quality objectives. Images were acquired by a digital camera (Nikon Digital Sight DS-Fi1c) and image acquisition software.

**Reverse Transcription Quantitative Polymerase Chain Reaction (RT-qPCR) Analyses of Gene Expression.** Total RNA was extracted from the liver and skeletal muscle, and cDNA was obtained by reverse transcription using the RevertAid First Strand cDNA Synthesis Kit (Thermo Scientific, Vilnius, Lithuania) according to the instructions of the manufacturer. The PCR reactions were performed by a 7900HT fast real-time PCR system (Applied Biosystems, Foster City, CA) using SYBR Premix Ex Taq (Takara, Kusatsu, Japan). Data analysis was carried out using the $2^{-\Delta\Delta C_T}$ method. The housekeeping gene, $\beta$-actin, was used for normalization. The sequences of the primers (Invitrogen China, Ltd., Beijing, China) used for RT-qPCR are shown in Table 1.

**Statistical Analysis.** Results were expressed as the mean ± standard error of mean (SEM), and the data were analyzed by SPSS 17.0 software (SPSS, Inc., Chicago, IL). One-way analysis of variance (ANOVA) with Duncan's multiple range test was used to compare the differences among various groups. A value of $p < 0.05$ was considered to be statistically significant.

## RESULTS

**Metabolite Composition in Carrot Juices.** The metabolite concentrations in NFCJ and FCJ are shown in Table 2. In

Table 2. Metabolite Composition in Carrot Juices[a]

| parameter | NFCJ | FCJ |
|---|---|---|
| acetic acid (mmol/L) | 8.99 ± 0.41 | 18.58 ± 0.66 |
| propionic acid (mmol/L) | 0.31 ± 0.02 | 0.47 ± 0.03 |
| butyric acid (mmol/L) | ND | 0.25 ± 0.02 |
| SCFA (mmol/L) | 9.30 ± 0.42 | 19.29 ± 0.67 |
| citric acid (mmol/L) | 1.28 ± 0.02 | 1.46 ± 0.01 |
| malic acid (mmol/L) | 26.11 ± 0.08 | 12.54 ± 0.06 |
| lactic acid (mmol/L) | 3.59 ± 0.05 | 68.88 ± 0.06 |
| $\beta$-carotene ($\mu$mol/L) | 89.22 ± 1.30 | 79.72 ± 0.74 |
| amino acids (mmol/L) | 84.94 ± 5.14 | 107.31 ± 9.03 |

[a]FCJ, fermented carrot juice with *L. plantarum* NCU116; NFCJ, non-fermented carrot juice; and ND, not detected. SCFA = acetic acid + propionic acid + butyric acid. Data are expressed as the mean ± SEM ($n$ = 6).

Table 3. Effect of NCU and FCJ Treatments on Levels of Blood Glucose, Hormones, and Serum Lipids in Diabetic Rats[a]

| parameter | NDM | DM | NCU | FCJ | NFCJ |
|---|---|---|---|---|---|
| FBG (mmol/L) | 4.55 ± 0.19 a | 26.60 ± 0.84 d | 19.37 ± 0.73 b | 17.19 ± 0.98 b | 23.34 ± 0.83 c |
| insulin (μIU/mL) | 20.64 ± 1.06 a | 65.04 ± 4.13 c | 39.22 ± 3.49 b | 44.54 ± 7.88 b | 59.77 ± 2.44 c |
| glucagon (pg/mL) | 88.26 ± 4.78 a | 158.77 ± 10.17 c | 130.29 ± 9.10 b | 107.50 ± 6.54 a | 169.57 ± 4.74 c |
| leptin (ng/mL) | 4.92 ± 0.71 a | 7.33 ± 0.68 b | 5.52 ± 0.46 ab | 4.97 ± 0.30 a | 6.48 ± 0.74 ab |
| GLP-1 (pmol/L) | 3.42 ± 0.23 c | 1.51 ± 0.09 a | 2.49 ± 0.11 b | 2.81 ± 0.15 b | 1.76 ± 0.06 a |
| PYY (pg/mL) | 97.61 ± 3.05 d | 41.86 ± 4.21 a | 64.02 ± 3.67 b | 78.53 ± 2.31 c | 44.98 ± 3.37 a |
| TC (mmol/L) | 1.89 ± 0.10 a | 8.08 ± 0.51 c | 5.24 ± 0.63 b | 6.37 ± 0.65 b | 6.75 ± 0.36 bc |
| TG (mmol/L) | 1.10 ± 0.10 a | 9.86 ± 0.56 c | 7.31 ± 0.81 b | 7.47 ± 0.37 b | 8.60 ± 0.56 bc |
| HDL-C (mmol/L) | 1.00 ± 0.04 b | 0.74 ± 0.03 a | 0.85 ± 0.07 a | 0.81 ± 0.05 a | 0.80 ± 0.02 a |
| LDL-C (mmol/L) | 0.39 ± 0.09 a | 2.86 ± 0.32 d | 1.07 ± 0.20 ab | 1.54 ± 0.19 bc | 2.04 ± 0.34 c |

[a]NDM, non-diabetes mellitus + saline; DM, diabetes mellitus + saline; NCU, DM + $10^9$ CFU/mL *L. plantarum* NCU116; FCJ, DM + fermented carrot juice with *L. plantarum* NCU116; and NFCJ, DM + non-fermented carrot juice. Data are expressed as the mean ± SEM ($n$ = 10). Values within a row with different letters are significantly different ($p < 0.05$).

Table 4. Effect of NCU and FCJ Treatment on Oxidative Stress and Kidney Function in Diabetic Rats[a]

| parameter | NDM | DM | NCU | FCJ | NFCJ |
|---|---|---|---|---|---|
| SOD (units/mL) | 219.53 ± 4.76 c | 156.94 ± 6.03 a | 191.29 ± 6.20 b | 200.35 ± 8.95 b | 166.43 ± 3.61 a |
| GSH-Px (units/mL) | 402.73 ± 16.18 b | 289.28 ± 34.29 a | 353.65 ± 4.22 b | 361.72 ± 9.71 b | 293.52 ± 10.86 a |
| MDA (nmol/mL) | 3.59 ± 0.19 a | 5.36 ± 0.41 ab | 3.73 ± 0.14 a | 3.70 ± 0.17 a | 5.74 ± 1.21 b |
| T-AOC (units/mL) | 14.77 ± 0.80 c | 6.67 ± 0.56 a | 11.62 ± 0.63 b | 13.35 ± 0.66 bc | 8.23 ± 0.83 a |
| CAT (units/mL) | 198.59 ± 12.36 c | 98.65 ± 7.13 a | 120.18 ± 9.67 ab | 150.32 ± 18.96 b | 107.48 ± 7.00 a |
| urea nitrogen (mmol/L) | 2.79 ± 0.36 a | 13.30 ± 1.87 c | 9.25 ± 0.24 b | 6.84 ± 0.67 b | 7.82 ± 0.86 b |
| creatinine (mmol/L) | 0.16 ± 0.01 a | 0.98 ± 0.05 c | 0.58 ± 0.06 b | 0.44 ± 0.08 b | 0.42 ± 0.04 b |
| uric acid (mmol/L) | 0.26 ± 0.04 a | 0.56 ± 0.08 b | 0.48 ± 0.10 ab | 0.43 ± 0.12 ab | 0.51 ± 0.08 ab |

[a]NDM, non-diabetes mellitus + saline; DM, diabetes mellitus + saline; NCU, DM + $10^9$ CFU/mL *L. plantarum* NCU116; FCJ, DM + fermented carrot juice with *L. plantarum* NCU116; and NFCJ, DM + non-fermented carrot juice. Data are expressed as the mean ± SEM ($n$ = 10). Values within a row with different letters are significantly different ($p < 0.05$).

comparison to the NFCJ, with the fermentation of *L. plantarum* NCU116, FCJ showed more concentrations of acetic acid, propionic acid, total SCFA (=acetic acid + propionic acid + butyric acid), citric acid, lactic acid, and amino acids. In addition, the butyric acid in NFCJ was not detected, but the FCJ contained about 0.25 mmol/L of the acid. However, the concentrations of malic acid and β-carotene in FCJ decreased in comparison to that of NFCJ.

**Blood Glucose.** As expected, the level of fasting blood glucose (FGB) in the DM group (26.72 mmol/L) was markedly higher than that in the NDM group (4.55 mmol/L). Interestingly, the FGB levels in NCU and FCJ groups (19.37 and 17.19 mmol/L, respectively) were significantly lower than that of the DM group ($p < 0.05$). The animals that received NFCJ (23.34 mmol/L) also showed a significant decrease in the blood glucose level compared to the DM group.

**Hormones.** The levels of serum insulin, glucagon, and leptin in the DM group were significantly higher than those in the NDM group ($p < 0.05$). Supplementation of NCU and FCJ reduced their levels close to the NDM group, especially glucagon and leptin levels in the FCJ group. The levels of the three hormones in the NFCJ group were not significantly different from the DM group. Meanwhile, levels of GLP-1 and PYY in the DM group were abatement compared to the NDM group, and the levels of these two parameters in NCU and FCJ groups were obviously increased ($p < 0.05$; Table 3).

**Serum Lipids.** As shown in Table 3, TC, TG, and LDL-C levels in DM group were all notably increased in comparison to the NDM group. Interestingly, the levels of these three parameters in NCU and FCJ groups declined significantly ($p < 0.05$). The HDL-C contents in the four diabetic groups were all significantly lower than that in the NDM group (1.00 mmol/L), but there were no significant differences between the four groups (0.74−0.85 mmol/L; Table 3).

**Oxidative Stress.** As shown in Table 4, the activities of SOD (156.94 units/mL), GSH-Px (289.28 units/mL), and CAT (98.65 units/mL) and level of T-AOC (6.67 unit/mL) in the DM group were significantly lower than those in the NDM group ($p < 0.05$). The treatment of FCJ significantly increased the levels of these parameters (200.35, 361.72, 150.32, and 13.35 units/mL, respectively). MDA contents in NCU and FCJ groups decreased to lower levels compared to that in the NFCJ group.

**Kidney Function.** A high-fat diet and STZ-induced diabetes were found to raise the levels of urea nitrogen, creatinine, and uric acid. Interestingly, the treatment of NCU and FCJ led to a significant reduction in the levels of these parameters. These results suggested that supplementation of NCU and FCJ improved kidney function in diabetes (Table 4).

**SCFA Composition in Feces.** As shown in Figure 1, the DM group contained significantly lower concentrations of acetic acid (120.54 μmol/g), propionic acid (49.15 μmol/g), butyric acid (16.44 μmol/g), and total SCFA (186.13 μmol/g) in feces compared to the NDM group ($p < 0.05$). These acids in feces of the NCU-, FCJ-, and NFCJ-treated groups were higher than those in the DM group, especially the NCU and FCJ groups ($p < 0.05$).

**Histopathology of the Pancreas and Kidney.** Histological analysis of the pancreas showed that pancreatic cells of the NDM group had normal proportions of islets of Langerhans. Acinar cells, which stained strongly, were arranged in lobules with prominent nuclei and surrounding healthy islet

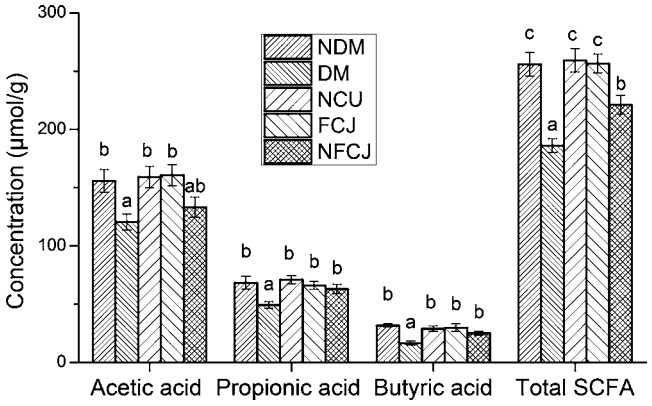


**Figure 1.** Changes in SCFA in feces of five groups of rats: non-diabetes mellitus (NDM), untreated diabetes mellitus (DM), DM plus *L. plantarum* NCU116 (NCU), DM plus fermented carrot juice with *L. plantarum* NCU116 (FCJ), and DM plus non-fermented carrot juice (NFCJ). Data are expressed as the mean ± SEM ($n$ = 10). Values with different letters are significantly different ($p$ < 0.05).

cells. A marked decrease in pancreatic $\beta$-cell size and number of Langerhans was found in the DM group compared to that in the NDM group, and the DM group also showed degeneration and atrophy of the islets. DM rats treated with NCU and FCJ showed an improvement of cell damage, as shown by partial restoration of islet cells, increase in the number of islets, and decrease in $\beta$-cell necrosis and vacuolization, respectively (Figure 2A).

Similarly, in comparison to the NDM group, diabetic rats exhibited a prominent feature of glomerular injury, with evidence of both diffuse and nodular glomerulosclerosis. In addition, tubulointerstitial pathology was present in these diabetic rats. This pathological appearance was reversed by NCU and its fermented carrot juice treatments. This reduction was greater with FCJ than with NCU. However, the NFCJ group had no notable change compared to the DM group (Figure 2B).

**mRNA Expression of Lipid and Glucose Metabolism.** As shown in Figure 3, diabetes downregulated the expression of LDL receptor, GLUT4, and PPAR-$\alpha$, and the supplementation of *L. plantarum* NCU116 increased the expression of these

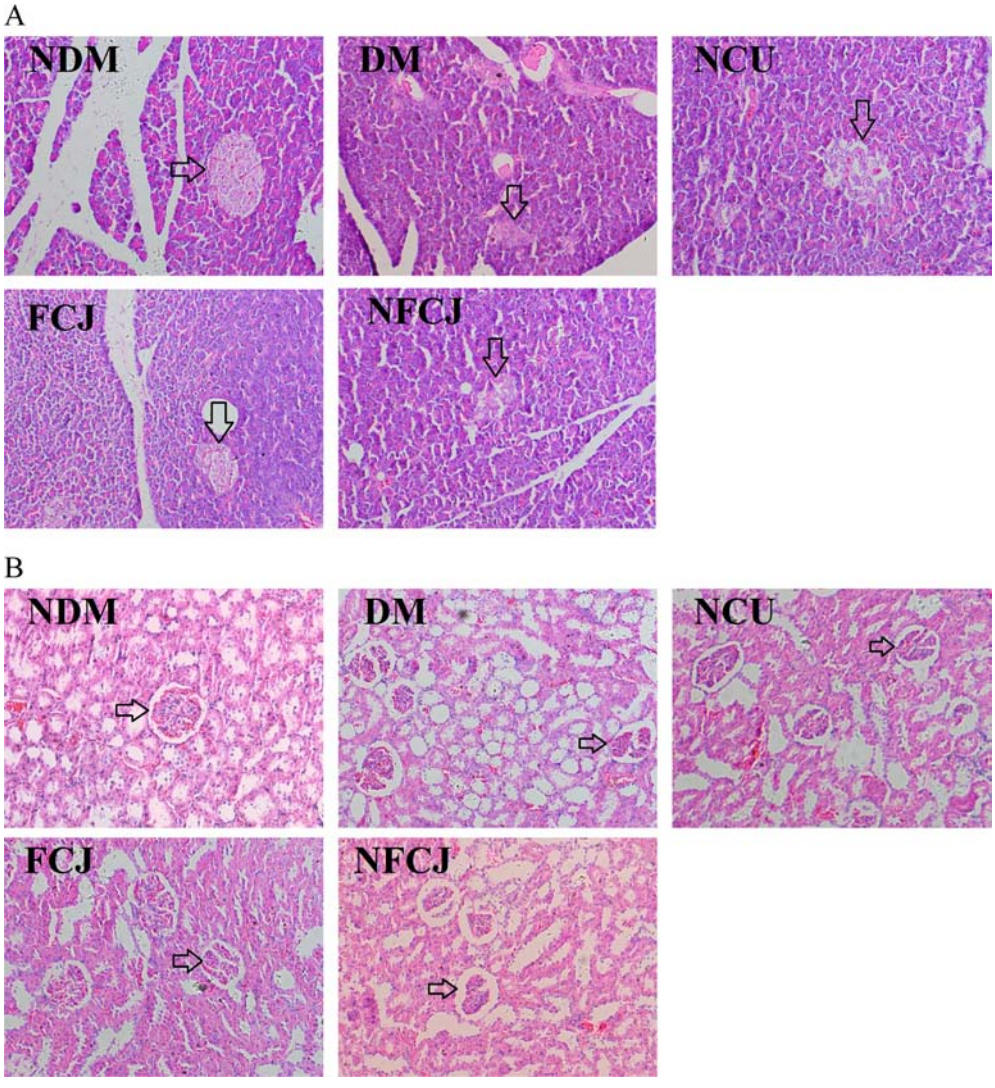


**Figure 2.** Effect of NCU and FCJ treatments on histology (100×) of the pancreas and kidney in five groups of rats: non-diabetes mellitus (NDM), untreated diabetes mellitus (DM), DM plus *L. plantarum* NCU116 (NCU), DM plus fermented carrot juice with *L. plantarum* NCU116 (FCJ), and DM plus non-fermented carrot juice (NFCJ). A, pancreas; B, kidney, with hematoxylin and eosin staining.

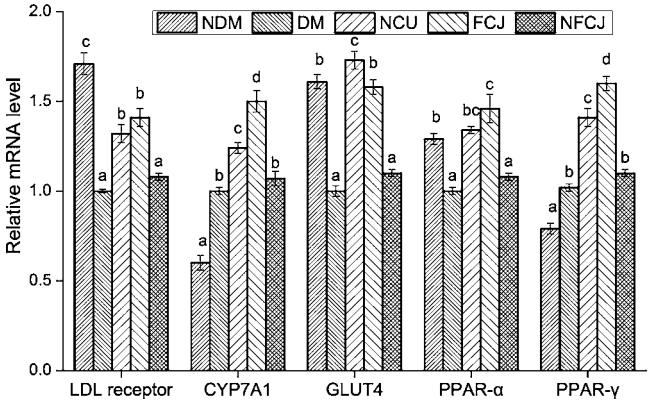


**Figure 3.** Effect of NCU and FCJ treatments on mRNA levels of low-density lipoprotein (LDL) receptor, cholesterol 7$\alpha$-hydroxylase (CYP7A1), glucose transporter-4 (GLUT-4), peroxisome proliferator-activated receptor-$\alpha$ (PPAR-$\alpha$), and peroxisome proliferator-activated receptor-$\gamma$ (PPAR-$\gamma$) in five groups of rats: non-diabetes mellitus (NDM), untreated diabetes mellitus (DM), DM plus *L. plantarum* NCU116 (NCU), DM plus fermented carrot juice with *L. plantarum* NCU116 (FCJ), and DM plus non-fermented carrot juice (NFCJ). The graph represents the mRNA levels relative to $\beta$-actin. Data are expressed as the mean ± SEM ($n$ = 10). Values with different letters are significantly different ($p < 0.05$).

genes after the 5 week experimental period. Simultaneously, the expression of CYP7A1 and PPAR-$\gamma$ in diabetic rats was raised, and higher expression levels of these two genes were found in the NCU and FCJ groups.

## DISCUSSION

T2DM, which has a higher incidence (90−95%) than T1DM, previously referred to as non-insulin-dependent diabetes or adult onset diabetes, encompasses individuals who have insulin resistance and usually have relative (rather than absolute) insulin deficiency.[2] A high-fat diet and low-dose STZ used in the study resulted in destruction of pancreatic $\beta$-cells, an increased blood glucose level (hyperglycemia), and induced oxidative stress. The T2DM experimental rat model mimics closely metabolic characteristics of human T2DM.[20]

The T2DM model used in this study apparently showed the basic phenotypes of hyperglycemia and insulin resistance (Table 3). Evidence from our study clearly demonstrated that supplementation of NCU and FCJ significantly attenuated hyperglycemia and insulin resistance.

Organic acids, the main products of probiotic fermentation, contribute toward an appropriate colonic pH and protect against pathological changes in the colonic mucosa.[21] In this study, it must be noted that the concentrations of SCFA in fermented carrot juice (FCJ) supplemented with *L. plantarum* NCU116 were significantly increased compared to those of non-fermented carrot juice (NFCJ). Interestingly, the butyric acid was not detected in non-fermented carrot juice (NFCJ), which means *L. plantarum* NCU116 could ferment the dietary fiber in the carrot juice to produce certain kinds of SCFA, such as butyric acid. Thus, in this study, we focused on the function of SCFA to the diabetic rats.

Because *L. plantarum* NCU116 had the property of promotion of SCFA production *in vitro*, we determined the SCFA concentrations *in vivo* of rat colonic feces. Studies showed that 90−95% of the SCFA present in the colon is constituted by acetic acid, propionic acid, and butyric acid. Ingestion of a high-fat diet reduced the SCFA concentration, and fermentable dietary fibers increased SCFA in the colon.[22,23] In these high-fat diet (fed) and low-dose STZ-induced diabetic rats, the fecal SCFA was obviously decreased in comparison to that of the NDM group. The NCU and FCJ groups showed a higher levels of SCFA than the DM and NFCJ groups (Figure 1). SCFA has several physiological properties that might suppress diabetes by different pathways; SCFA is probably a key component in the growth of lactobacilli and bifidobacteria and in lowering intestinal pH, all of which are expected to have beneficial effects on diabetes.[24] The main beneficial activities of SCFA were identified in the decrease of levels of glucose in serum, insulin resistance, inflammation, and increase in protective PYY and GLP-1 secretion.[22]

Propionate has been shown to decrease glucose production in rat hepatocytes.[25] In this experiment, the results suggested that the consumption of *L. plantarum* NCU116 and carrot juice led to an increase of propionic acid for preventing hyperglycemia, but a more pronounced effect was found when carrot juice was fermented with *L. plantarum* NCU116. The hypoglycemic effect of the FCJ observed in this study could be related to the synergistic effects of both $\beta$-carotene in carrot, gut microbiota, and the production of SCFA.[26] In addition, hormones, such as insulin, glucagon, and leptin, play an important role in diabetes. Previous studies have suggested that leptin secretion is affected by insulin and that rats with metabolic syndrome exhibit high plasma levels of leptin.[27] It has been reported that supplementation of *L. plantarum* NCU116 significantly decreased the oral glucose tolerance and insulin resistance in hyperlipidaemic rats, indicating that the probiotic fermented carrot juice could regulate the production of insulin and glucagon by pancreatic cells.[13] These results suggested that the decrease in insulin, glucagon, and leptin levels may have resulted from the improvement of insulin sensitivity by the oral supplementation of *L. plantarum* NCU116. Changes in the microbiota and, consequently, in SCFA composition have been hypothesized to be associated with the development of insulin resistance and diabetes.[22] Alterations to the composition and metabolic capacity of gut microbiota in metabolic syndrome influence metabolic processes in peripheral organs, the release of hormones from the gut (such as GLP-1 and PYY; Table 3), and the synthesis, storage, or metabolism of lipids in the adipose tissue, liver, and muscle.[28] Studies performed in G-protein-coupled receptor 41 (GPR41)-deficient mice suggested that the activation of GPR41 by SCFA is responsible for the release of the gut hormones PYY. The peptide has been shown to decrease the intestinal transit time, which indicates that it promotes the absorption of nutrients, mostly glucose.[29] It has been reported that propionic and butyric acids were shown to reduce low-grade inflammation and induce hormone release. In addition, SCFA have been linked to increased GLP-1 secretion in both animal and human models. GLP-1 is an incretin hormone that participates in glucose homeostasis, mainly by lowering the plasma glucose concentration and preserving pancreatic $\beta$-cell function.[22] The gastrointestinal hormones have antidiabetic effects primarily by stimulating glucose-dependent insulin release and promoting glucose homeostasis.[7,30]

Dyslipidemia is the common character in T2DM and is the primary cause of cardiovascular diseases in patients with diabetes.[6] In the STZ-induced diabetic rat model, it has been shown that TC, TG, and LDL-C levels increased and the HDL-C level decreased and that the supplementation with soymilk

fermented with *Lactobacillus rhamnosus* CRL981 could ameliorate lipid profiles compared to the unfermented soymilk.[16] It is well-known that high levels of serum TC and LDL-C can increase the risk of cardiovascular events. Decreasing TC and LDL-C levels in serum is effective for reducing the risk of atherosclerosis. A previous study showed that *L. plantarum* NCU116 significantly decreased the levels of serum TC, TG, and LDL-C and increased the HDL-C level in a hyperlipidaemic rat model.[13] Butyrate-producing intestinal bacteria seem to play an important role in blood glucose regulation and lipid metabolism, as shown by fecal transplantation studies.[22] In the present study, the administration of FCJ showed the best ability of regulating TC, TG, and LDL-C compared to the other treatments, and it might relate to the increase of butyric acid production in the colonic content by the gut microbiota (Table 3).

Oxidative stress is considered to play an important role in the pathogenesis of type 2 diabetes. The increased risk of dyslipidemia and hyperglycemia damage the antioxidant system of tissues.[31] Diabetes is associated with the increase of oxidative stress, which is essentially an imbalance of free radicals and antioxidant defenses.[32] Oxidative stress can impair the living cell membrane, and this may be the reason for the injury to the islets of Langerhans and glomeruli of kidney. It has been shown that STZ-induced diabetes in rats caused an abnormal decrease of SOD, GSH-Px, and CAT activities and T-AOC level, resulting in the accumulation of reactive oxygen species (ROS), such as hydrogen peroxide and superoxide radicals.[33] MDA, as an end product and marker of the lipid peroxidation process, is toxic to DNA and protein. In this study, the administration of NCU and FCJ caused as a significant increase in activities of SOD, GSH-Px, and CAT and level of T-AOC. This may be due to the biologically active $\beta$-carotene present in the fermented carrot juice with *L. plantarum* NCU116 bioconversion, because non-fermented carrot juice did not show the same level of increase (Table 4).

Hyperglycemia and dyslipidemia in diabetes are related to the increased production of free radicals. Consequently, oxidative damages and pancreas and kidney injuries leading to failure and dysfunctions were observed. Interestingly, after NCU and FCJ supplementation, reduction of pancreas and kidney injuries was found in the histopathology study (Figure 2). NCU and FCJ could enhance pancreatic activity in regenerating $\beta$-cells by reducing $\beta$-cell necrosis and vacuolization.[34] To our knowledge, rare studies have shown the effect of fermented carrot juice administration on histology, except for a few studies showing the effect of $\beta$-carotene supplementation on the incidence of type 2 diabetes.[35]

A long period of hyperglycemia can induce damage to blood vessels that can affect the functionality of some organs, such as the pancreas, liver, and kidney. Consequently, oxidative damages and kidney tissue damage leading to failure and dysfunctions were observed. The disability of the kidney in the diabetic rats to filter properly leads to the accumulation of waste and toxic substances, such as uric acid, creatinine, and urea nitrogen in the blood.[36] STZ-induced diabetic rats showed an increase of uric acid, creatinine, and urea nitrogen, and the supplementation with soymilk fermented with *L. rhamnosus* CRL981 did not have any effect in diabetic rats.[16] Morphologically, the findings of this study revealed the efficiency of NCU and FCJ in protecting the kidney of diabetic rats, which was evidenced by the lower rates observed for kidney dysfunction indices (Table 4 and Figure 2).

The gut microbiota not only affect the metabolic syndrome by SCFA production but also influence the expression of host genes and control fatty acid absorption, oxidation, and storage.[29] A previous study showed that oral administration of *L. plantarum* NCU116 could regulate LDL receptor and CYP7A1 to alleviate the high-fat diet induced hyperlipidaemic symptom in rats. The increased expression of these genes in liver may be the mechanism by which *L. plantarum* NCU116 reduces TC and LDL-C in serum.[13] In this study, mRNA expression levels of LDL receptor and CYP7A1 in NCU and FCJ groups were significantly increased, which may result in the decrease of the serum LDL-C level. GLUT-4 is the insulin-regulated glucose transporter found primarily in adipose tissues and skeletal muscle, which is responsible for insulin-stimulated glucose transport into the cell. Conditional depletion of GLUT4 in certain organs caused a roughly equivalent incidence of diabetes in animals.[37] We found that GLUT4 mRNA expression was increased in the skeletal muscle of NCU and FCJ groups compared to the untreated DM group. With more than 80% insulin-stimulated glucose disposal in the skeletal muscle, the increased GLUT4 mRNA expression by supplementation of NCU and FCJ could enhance glucose uptake in diabetic rats.[38] It has been known that PPARs play a key role in inflammation and glucose homeostasis. PPAR-$\alpha$ may relate to the improvement insulin sensitivity, and PPAR-$\gamma$ is a therapeutic drug target for metabolic syndrome.[39,40] Our results suggested that NCU and FCJ could regulate glucose homeostasis and insulin sensitivity in the diabetic rats via regulating the expression of these genes (Figure 3). The possible mechanism involved in antidiabetic effects of *L. plantarum* NCU116 and its fermented carrot juice on a high-fat diet (fed) and low-dose STZ-induced type 2 diabetic rat model is provided in Figure 4.

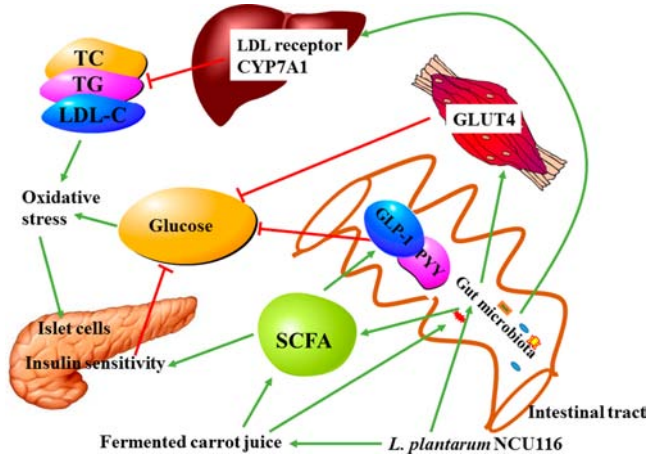


**Figure 4.** Possible mechanism involved in antidiabetic effects of *L. plantarum* NCU116 and its fermented carrot juice on a high-fat diet (fed) and low-dose STZ-induced type 2 diabetic rat model. Red arrows represent inhibition, and green arrows represent promotion.

In conclusion, this study demonstrated that the antidiabetic effect of NCU and FCJ on a high-fat diet (fed) and low-dose STZ-induced type 2 diabetic rat model. *L. plantarum* NCU116 was found to increase SCFA in the fermented carrot juice (FCJ); meanwhile, NCU and FCJ increased SCFA in the colonic feces of diabetic rats. The results have shown that NCU and FCJ had the potential abilities to regulate levels of blood glucose and its related hormones (insulin, glucagon, GLP-1,

and PYY) and ameliorated diabetes induced damage of the pancreas and kidney. In addition, NCU and FCJ also decreased serum lipids and oxidative stress and regulated the expression levels of lipid and glucose metabolism. The possible mechanism of the paper was that NCU and FCJ changed the gut microbiota and, consequently, SCFA composition, which were associated with the development of diabetes. Thus, these results indicated that *L. plantarum* NCU116 and the probiotic fermented carrot juice have potential for the treatment of diabetes.

## ■ ASSOCIATED CONTENT

### Supporting Information

Amino acids in carrot juices (Supplementary Table) and final body weight, food intake, and water consumption in the last week (Supplementary Figure). This material is available free of charge via the Internet at http://pubs.acs.org.

## ■ AUTHOR INFORMATION


### Corresponding Authors

*Telephone: +86-791-88304452. Fax: +86-791-88304452. E-mail: spnie@ncu.edu.cn.

*Telephone: +86-791-83969009. Fax: +86-791-83969009. E-mail: myxie@ncu.edu.cn.

### Author Contributions

†Chuan Li and Qiao Ding contributed equally to this work.



### Funding

The authors are grateful for financial support from the National High Technology Research and Development Key Program of China (863 Key Program, 2011AA100904) and the Program for New Century Excellent Talents in University (NCET-12-0749).


### Notes

The authors declare no competing financial interest.

## ■ REFERENCES


(1) Ristagno, G.; Fumagalli, F.; Porretta-Serapiglia, C.; Orrù, A.; Cassina, C.; Pesaresi, M.; Masson, S.; Villanova, L.; Merendino, A.; Villanova, A. Hydroxytyrosol attenuates peripheral neuropathy in streptozotocin-induced diabetes in rats. *J. Agric. Food Chem.* **2012**, *60*, 5859−5865.

(2) Association, A. D. Diagnosis and classification of diabetes mellitus. *Diabetes Care* **2013**, *36*, S67−S74.

(3) Karlsson, F. H.; Tremaroli, V.; Nookaew, I.; Bergström, G.; Behre, C. J.; Fagerberg, B.; Nielsen, J.; Bäckhed, F. Gut metagenome in European women with normal, impaired and diabetic glucose control. *Nature* **2013**, *498*, 99−103.

(4) Qin, J.; Li, Y.; Cai, Z.; Li, S.; Zhu, J.; Zhang, F.; Liang, S.; Zhang, W.; Guan, Y.; Shen, D. A metagenome-wide association study of gut microbiota in type 2 diabetes. *Nature* **2012**, *490*, 55−60.

(5) Krentz, A. J.; Bailey, C. J. Oral antidiabetic agents. *Drugs* **2005**, *65*, 385−411.

(6) Chen, P.; Zhang, Q.; Dang, H.; Liu, X.; Tian, F.; Zhao, J.; Chen, Y.; Zhang, H.; Chen, W. Antidiabetic effect of *Lactobacillus casei* CCFM0412 in high-fat-fed, streptozotocin-induced type 2 diabetic mice. *Nutrition* **2014**, *30*, 1061−1068.

(7) Devaraj, S.; Hemarajata, P.; Versalovic, J. The human gut microbiome and body metabolism: Implications for obesity and diabetes. *Clin. Chem.* **2013**, *59*, 617−628.

(8) Kootte, R.; Vrieze, A.; Holleman, F.; Dallinga-Thie, G.; Zoetendal, E.; De Vos, W.; Groen, A.; Hoekstra, J.; Stroes, E.; Nieuwdorp, M. The therapeutic potential of manipulating gut microbiota in obesity and type 2 diabetes mellitus. *Diabetes, Obes. Metab.* **2012**, *14*, 112−120.

(9) Wallace, T. C.; Guarner, F.; Madsen, K.; Cabana, M. D.; Gibson, G.; Hentges, E.; Sanders, M. E. Human gut microbiota and its relationship to health and disease. *Nutr. Rev.* **2011**, *69*, 392−403.

(10) Rupa, P.; Mine, Y. Recent advances in the role of probiotics in human inflammation and gut health. *J. Agric. Food Chem.* **2012**, *60*, 8249−8256.

(11) Lye, H.-S.; Kuan, C.-Y.; Ewe, J.-A.; Fung, W.-Y.; Liong, M.-T. The improvement of hypertension by probiotics: Effects on cholesterol, diabetes, renin, and phytoestrogens. *Int. J. Mol. Sci.* **2009**, *10*, 3755−3775.

(12) Xiong, T.; Song, S.; Huang, X.; Feng, C.; Liu, G.; Huang, J.; Xie, M. Screening and identification of functional *Lactobacillus* specific for vegetable fermentation. *J. Food Sci.* **2013**, *78*, 84−89.

(13) Li, C.; Nie, S.-P.; Ding, Q.; Zhu, K.-X.; Wang, Z.-J.; Xiong, T.; Gong, J.; Xie, M.-Y. Cholesterol-lowering effect of *Lactobacillus plantarum* NCU116 in a hyperlipidaemic rat model. *J. Funct. Foods* **2014**, *8*, 340−347.

(14) Li, C.; Nie, S.; Zhu, K.-X.; Ding, Q.; Li, C.; Xiong, T.; Xie, M.-Y. *Lactobacillus plantarum* NCU116 improves liver function, oxidative stress and lipid metabolism in high fat diet induced non-alcoholic fatty liver disease rats. *Food Funct.* **2014**, *5*, 3216−3223.

(15) Demir, N.; Bahçeci, K. S.; Acar, J. The effects of different initial *Lactobacillus plantarum* concentrations on some properties of fermented carrot juice. *J. Food Process. Preserv.* **2006**, *30*, 352−363.

(16) Marazza, J. A.; LeBlanc, J. G.; de Giori, G. S.; Garro, M. S. Soymilk fermented with *Lactobacillus rhamnosus* CRL981 ameliorates hyperglycemia, lipid profiles and increases antioxidant enzyme activities in diabetic mice. *J. Funct. Foods* **2013**, *5*, 1848−1853.

(17) Barba, A.; Hurtado, M. C.; Mata, M.; Ruiz, V. F.; Tejada, M. Application of a UV−vis detection−HPLC method for a rapid determination of lycopene and $\beta$-carotene in vegetables. *Food Chem.* **2006**, *95*, 328−336.

(18) Hu, J. L.; Nie, S. P.; Min, F. F.; Xie, M. Y. Polysaccharide from seeds of *Plantago asiatica* L. increases short-chain fatty acid production and fecal moisture along with lowering pH in mouse colon. *J. Agric. Food Chem.* **2012**, *60*, 11525−11532.

(19) Kun, S.; Rezessy-Szabó, J. M.; Nguyen, Q. D.; Hoschke, Á. Changes of microbial population and some components in carrot juice during fermentation with selected *Bifidobacterium* strains. *Process Biochem.* **2008**, *43*, 816−821.

(20) Srinivasan, K.; Viswanad, B.; Asrat, L.; Kaul, C.; Ramarao, P. Combination of high-fat diet-fed and low-dose streptozotocin-treated rat: A model for type 2 diabetes and pharmacological screening. *Pharmacol. Res.* **2005**, *52*, 313−320.

(21) Parvez, S.; Malik, K.; Ah Kang, S.; Kim, H. Y. Probiotics and their fermented food products are beneficial for health. *J. Appl. Microbiol.* **2006**, *100*, 1171−1185.

(22) Puddu, A.; Sanguineti, R.; Montecucco, F.; Viviani, G. L. Evidence for the gut microbiota short-chain fatty acids as key pathophysiological molecules improving diabetes. *Mediators Inflammation* **2014**, *2014*, 1−9.

(23) Jakobsdottir, G.; Xu, J.; Molin, G.; Ahrné, S.; Nyman, M. High-fat diet reduces the formation of butyrate, but increases succinate, inflammation, liver fat and cholesterol in rats, while dietary fibre counteracts these effects. *PLoS One* **2013**, *8*, No. e80476.

(24) Mehal, W. Z. The Gordian Knot of dysbiosis, obesity and NAFLD. *Nat. Rev. Gastroenterol. Hepatol.* **2013**, *10*, 637−644.

(25) Cameron-Smith, D.; Collier, G.; O'Dea, K. Effect of propionate on in vivo carbohydrate metabolism in streptozocin-induced diabetic rats. *Metabolism* **1994**, *43*, 728−734.

(26) Nicolle, C.; Gueux, E.; Jaffrelo, L.; Rock, E.; Mazur, A.; Amouroux, P.; Rémésy, C. Lyophilized carrot ingestion lowers lipemia and beneficially affects cholesterol metabolism in cholesterol-fed C57BL/6J mice. *Eur. J. Nutr.* **2004**, *43*, 237−245.

(27) Lee, M. J.; Fried, S. K. Multilevel regulation of leptin storage, turnover, and secretion by feeding and insulin in rat adipose tissue. *J. Lipid Res.* **2006**, *47*, 1984−1993.

(28) Tremaroli, V.; Bäckhed, F. Functional interactions between the gut microbiota and host metabolism. *Nature* **2012**, *489*, 242−249.

(29) Delzenne, N. M.; Neyrinck, A. M.; Bäckhed, F.; Cani, P. D. Targeting gut microbiota in obesity: Effects of prebiotics and probiotics. *Nat. Rev. Endocrinol.* **2011**, *7*, 639−646.
(30) Nachnani, J.; Bulchandani, D.; Nookala, A.; Herndon, B.; Molteni, A.; Pandya, P.; Taylor, R.; Quinn, T.; Weide, L.; Alba, L. Biochemical and histological effects of exendin-4 (exenatide) on the rat pancreas. *Diabetologia* **2010**, *53*, 153−159.
(31) Yadav, H.; Jain, S.; Sinha, P. Antidiabetic effect of probiotic dahi containing *Lactobacillus acidophilus* and *Lactobacillus casei* in high fructose fed rats. *Nutrition* **2007**, *23*, 62−68.
(32) Betteridge, D. J. What is oxidative stress? *Metabolism* **2000**, *49*, 3−8.
(33) Lee, J.-S. Effects of soy protein and genistein on blood glucose, antioxidant enzyme activities, and lipid profile in streptozotocin-induced diabetic rats. *Life Sci.* **2006**, *79*, 1578−1584.
(34) Posuwan, J.; Prangthip, P.; Leardkamolkarn, V.; Yamborisut, U.; Surasiang, R.; Charoensiri, R.; Kongkachuichai, R. Long-term supplementation of high pigmented rice bran oil (*Oryza sativa* L.) on amelioration of oxidative stress and histological changes in streptozotocin-induced diabetic rats fed a high fat diet; Riceberry bran oil. *Food Chem.* **2013**, *138*, 501−508.
(35) Kataja-Tuomola, M.; Sundell, J.; Männistö, S.; Virtanen, M.; Kontto, J.; Albanes, D.; Virtamo, J. Effect of $\alpha$-tocopherol and $\beta$-carotene supplementation on the incidence of type 2 diabetes. *Diabetologia* **2008**, *51*, 47−53.
(36) Bejar, W.; Hamden, K.; Ben Salah, R.; Chouayekh, H. *Lactobacillus plantarum* TN627 significantly reduces complications of alloxan-induced diabetes in rats. *Anaerobe* **2013**, *24*, 4−11.
(37) Huang, S.; Czech, M. P. The GLUT4 glucose transporter. *Cell Metab.* **2007**, *5*, 237−252.
(38) Kim, S.-W.; Park, K.-Y.; Kim, B.; Kim, E.; Hyun, C.-K. *Lactobacillus rhamnosus* GG improves insulin sensitivity and reduces adiposity in high-fat diet-fed mice through enhancement of adiponectin production. *Biochem. Biophys. Res. Commun.* **2013**, *431*, 258−263.
(39) Soares, F. L. P.; de Oliveira Matoso, R.; Teixeira, L. G.; Menezes, Z.; Pereira, S. S.; Alves, A. C.; Batista, N. V.; de Faria, A. M. C.; Cara, D. C.; Ferreira, A. V. M Gluten-free diet reduces adiposity, inflammation and insulin resistance associated with the induction of PPAR-$\alpha$ and PPAR-$\gamma$ expression. *J. Nutr. Biochem.* **2013**, *24*, 1105−1111.
(40) Mohamed, S. Functional foods against metabolic syndrome (obesity, diabetes, hypertension and dyslipidemia) and cardiovasular disease. *Trends Food Sci. Technol.* **2014**, *35*, 114−128.

Table 1. Carotenoid and Theoretical Retinol Feed Concentrations (nmol/g feed)[A] Prepared for Laying Hens using a Combination of Different maize Genotypes and Fortificants

| | treatment[B] | | | |
|---|---|---|---|---|
| carotenoid | orange | tangerine | yellow | white |
| lutein | 6.2 ± 0.32[b] | 4.40 ± 0.48[b] | 24.8 ± 5.83[a] | 4.0 ± 0.89[b] |
| zeaxanthin | 3.42 ± 0.57[a] | 0.72 ± 0.09[c] | 2.14 ± 0.73[b] | 0.68 ± 0.27[c] |
| β-cryptoxanthin | 5.64 ± 0.39[a] | 4.85 ± 0.75[a] | 0.79 ± 0.03[b] | 0.13 ± 0.06[c] |
| α-carotene | 0.24 ± 0.11[a] | 0.13 ± 0.03[bc] | 0.20 ± 0.05[ab] | 0.06 ± 0.03[c] |
| 9-*cis*-β-carotene | 0.93 ± 0.13[a] | 0.20 ± 0.07[b] | 0.23 ± 0.02[b] | 0.10 ± 0.01[c] |
| all-*trans*-β-carotene | 3.37 ± 0.20[a] | 0.87 ± 0.29[b] | 0.60 ± 0.03[c] | 0.27 ± 0.03[d] |
| 13-*cis*-β-carotene | 1.03 ± 0.30[a] | 0.22 ± 0.07[b] | 0.33 ± 0.04[b] | 0.15 ± 0.06[b] |
| theoretical retinol | 16.3 ± 1.36[a] | 8.69 ± 1.71[b] | 3.24 ± 0.26[c] | 1.07 ± 0.33[c] |

[A]Concentrations are mean ± SD; $n$ = 27 for white maize; $n$ = 21 for other treatment feeds. All carotenoid and theoretical retinol differed by treatment using one-way ANOVA (All $P < 0.0001$). Lowercase superscript letters in a row designate differences between feeds (tested with LSMEANS at $P < 0.05$). [B]Treatment groups are designated by color regarding maize and/or fortification. Orange = high β-cryptoxanthin biofortified maize, tangerine = white maize + tangerine-peel fortificant, yellow = yellow maize + lutein fortificant, white = white maize only.

The source of β-cryptoxanthin may impact the bioavailability of β-cryptoxanthin in hens for egg yolk deposition. The objective of this study was to comprehensively compare the source of β-cryptoxanthin in hens' feed, that is, orange maize or tangerine peel, and the impact on egg yolk color, skin color, carotenoid concentrations, and VA status of the laying hens compared with the industry-recommended lutein standard.

## MATERIALS AND METHODS

**Maize, Feed Preparation, and Analysis.** Four different maize feeds were prepared. The high β-cryptoxanthin (orange) maize genotype was conventionally bred and obtained from the International Maize and Wheat Improvement Center/HarvestPlus maize provitamin A biofortification project and was grown in Mexico at Agua Fria, Puebla (20°32′N, 97°28′ W; 110 m above sea level). Ears were harvested and dried, and grain was stored at −20 °C before shipping to University of Wisconsin-Madison. The kernels were stored at −24 °C for the duration of the study. Kernels were ground to a fine powder before hen feed preparation using a C&N Hammermill No. 8 (Christy-Norris Ltd., Ipswich, U.K.). Feed composition was identical to Liu et al. with the only source of VA through the orange and yellow maize[25] or tangerine peel. Tangerine peel was freeze-dried for 48 h, finely ground, and stored at −80 °C until preparation of the tangerine-fortified white maize feed. The white maize was sourced locally (DeLong Co., Inc., Clinton, WI) and approximately 40 g ground freeze-dried tangerine peel was added per 1 kg feed, which was based on the β-cryptoxanthin concentration of the orange maize feed (5.64 ± 0.39 nmol/g feed). Concentrations were based on saponified β-cryptoxanthin because 75 to 94% of β-cryptoxanthin is esterified in tangerine peel,[27] but only 1−5% of xanthophylls are esterified in maize.[28,29] Lutein ORO GLO-20 (graciously donated by Kemin Industries, Inc., Des Moines, IA) was added to the yellow maize (DeLong Co., Inc., Clinton, WI) at 0.05%, according to industry recommendations.[30]

Feeds were mixed and analyzed weekly, and stored at −20 °C to prevent carotenoid degradation. Carotenoid composition of maize and feeds (Table 1) was determined using an adapted saponification method.[10,29] This ensured that the carotenyl esters present in the tangerine peel were hydrolyzed to the free form,[31] which was subsequently quantified in the tissues. After preheating 0.6 g maize feed suspended in 6 mL ethanol at 85 °C for 5 min, saponification was done with addition of 500 μL 80:20 potassium hydroxide/water (w/v) for 10 additional min. Water (3 mL) was added to aid phase separation during hexane extraction (3 × 3 mL hexane). The hexane extracts were dried, reconstituted in 500 μL 50:50 methanol/dichloroethane, and 50 μL aliquots were analyzed by HPLC using a YMC C30 column (4.6 × 250 mm).[4] A 40 min multistep, binary gradient [A: 92:8 methanol/water (10 mM ammonium acetate); B: methyl tertiary butyl ether] was run at 2 mL/min (Supporting Information Table S1). Extraction efficiencies ranged from 90 ± 7 to 95 ± 3% for the different maize feeds.

**Hens.** All animal procedures were approved by the College of Agricultural and Life Sciences Animal Care and Use Committee, University of Wisconsin-Madison. Single Comb White Leghorns ($n$ = 32), 28 wk into their laying cycle, were individually housed in metal battery cages under a 16-h light/8-h dark cycle. The hens were checked daily to ensure adequate supply of ad libitum feed and water and to monitor health status. Hens were given approximately 110 g feed/d, but total feed intake was not measured. Hens were killed by $CO_2$ fixation on intervention d 50. Hens were weighed before blood, liver, and breast skin were harvested.

**Experimental Design.** Laying hens were fed a white-maize feed for a 10-d depletion period. For the next 40 d, hens were divided into 4 treatments based on maize genotype and fortificant ($n$ = 8/treatment): high β-cryptoxanthin biofortified orange maize (orange), tangerine-fortified white maize (tangerine), lutein-fortified yellow maize (yellow), and white maize only (white) as a negative control. Eggs were collected every day and subjected to colorization every other day. Upon breaking the shell, yolks were separated from the whites and color was analyzed using a portable Konica Minolta colorimeter (Chroma Meter CR-300, Konica Minolta Sensing Americas, Inc., Ramsey, NJ) using the complementary color model. Color space (often referred to as L*a*b*) was used for assessment of changes in yolk color over the course of the study ($n$ = 6−8/treatment and collection time). The L-scale represents lightness, with a value of 0−100 (L = 0 indicates darkest, L = 100 lightest). The a-scale represents redness on a scale from −60 (green), to +60 (red). The b-scale represents yellowness on a scale from −60 (blue) to +60 (yellow). After color analysis, yolks were transferred into black conical tubes and stored at −80 °C.

**Analysis of Egg Yolk.** Egg yolk samples from every 4 d were prepared for carotenoid and retinol equivalent composition analysis using an adaptation from a previously published method.[22] Yolk (0.3 g) was mixed with 1 mL deionized water using a vortex, followed by 3 mL ethanol (0.1% butylated hydroxytoluene as antioxidant). Potassium hydroxide/water (500 μL, 50:50, w/v) was added and the mixture was saponified for 30 min at 60 °C. One mL cold deionized water was added to quench the reaction and 200 μL C-23-*apo*-carotenol was added as internal standard. The mixture was extracted with 4 mL 9:1 hexane/ethyl acetate (v/v) and then twice more with 3 mL. The organic layers were pooled, dried under nitrogen, and reconstituted in 200 μL 75:25 methanol/dichloroethane (v/v); 4 μL was injected onto a Waters Ultra Performance Liquid Chromatograph (UPLC) equipped with an ACQUITY HSS C18 1.8 μm, 2.1 × 150 mm column at 35 °C (Milford, MA). Solvent A was 90:10 water/isopropanol (10 mM ammonium acetate) and solvent B was 80:20 acetonitrile/isopropanol at 0.45 mL/min with a total runtime of 25 min. The gradient started with 30% solvent A and 70% solvent B switching to 5% A and 95% B from 0 to 10 min, with a change to 1% A

and 99% B at 12 min and holding until reverse conditions from 21.5 to 25 min. Retention times are noted in Supporting Information Table S1.

All-*trans*-$\beta$-carotene (537 g/mol; Sigma-Aldrich, St. Louis, MO), $\beta$-cryptoxanthin (553 g/mol; CaroteNature, GmbH, Lupsingen, Switzerland), lutein (569 g/mol; GNC, Inc., Pittsburgh, PA), and zeaxanthin (569 g/mol; GNC, Inc., Pittsburgh, PA) were quantified using HPLC-purified standards. Provitamin A equivalents were the sum of $\beta$-cryptoxanthin, $\alpha$-carotene, and twice the $\beta$-carotene due to the theoretical yield of retinol from the chemical structures.

**Analysis of Chicken Livers, Serum, and Skin.** Livers were prepared and analyzed for carotenoids, retinol, and retinyl esters using an adaptation of published methods.[32] Serum was prepared and analyzed for carotenoids and retinol and retinyl esters using previously published methods.[10] Retinol and retinyl esters were quantified at 325 nm and carotenoids were quantified at 450 nm. Chicken skin was colorized with the colorimeter.[25] Skin (1 g) was ground with 4−5 g sodium sulfate, 150 $\mu$L $\beta$-*apo*-8′-carotenal was added as internal standard, and the mixture was extracted with 25 mL dichloromethane. A 5 mL aliquot was dried under nitrogen, suspended in 750 $\mu$L ethanol (0.1% butylated hydroxytoluene), and saponified with 300 $\mu$L potassium hydroxide/water (50:50, w/v) for 15 min at 45 °C. After saponification, 1 mL deionized water was added to quench the reaction and the mixture was extracted 3 times with 2 mL hexanes. Organic layers were pooled and dried under nitrogen, reconstituted in 150 $\mu$L methanol/dichloroethane (50:50, v/v); 75 $\mu$L was injected onto a Waters Resolve $C_{30}$ 5 $\mu$m, 3.9 × 300 mm reversed-phase column (Waters, Milford, MA) equipped with a guard column. The HPLC system consisted of a 1525 binary pump, a 717 autosampler, and a 996 photodiode array detector (Waters). Solvents and run-time were similar to published methods[32] (Supporting Information Table S1).

**Statistical Analysis.** Values are means ± SD. Data were analyzed using Statistical Analysis System software (SAS version 9.2, SAS Institute, Cary, NC). A repeated measures two-way ANOVA with mixed effects was used with PROC MIXED for egg color analysis and carotenoid and retinol concentrations of saponified egg yolk. The overall differences in color were evaluated using eq 1:[33]

$$\Delta E = \sqrt{(\Delta L)^2 + (\Delta a)^2 + (\Delta b)^2} \quad (1)$$

The influence of treatment on liver VA stores and serum retinol concentrations were evaluated using one-way ANOVA for the hens. LSMEANS was used to determine differences between treatments. Main treatment effects for feed type and time, and the interaction of treatment by time were considered significant at $P \leq 0.05$.

## RESULTS

**Carotenoid Concentration of Feeds.** By design, orange and tangerine feeds did not differ in total $\beta$-cryptoxanthin concentration determined after saponification, although they presumably did differ in percentage of free versus esterified $\beta$-cryptoxanthin. The theoretical value of provitamin A equivalents were different due to the endogenous $\beta$-carotene in the orange maize (Table 1). Much lower amounts of provitamin A equivalents were present in the yellow and white maize feeds (Table 1). The yellow feed had four times more lutein than the orange feed. Zeaxanthin was similar in orange and yellow feeds, and it was more than four times higher than that of the tangerine and white feeds.

**Egg and Hen Weight.** Egg weights (53.4 ± 2.80 g) among treatment groups across all time periods did not differ (Supporting Information Figure S1). However, egg weight increased over time as the hens aged ($P < 0.0001$). A paired $t$ test comparing eggs at d 10 (end of washout period) and d 50 (end of treatment phase) found a significant increase in egg weight (5.07 ± 3.31 g) from hens in all treatment groups ($P < 0.0001$). A treatment by time interaction occurred ($P = 0.02$) where egg weight increase in the tangerine group (3.1 ± 3.3 g) was less than the other treatment groups (5.2 ± 3.2 g). Egg production differed among treatment groups ($P < 0.01$), but was almost 1 egg/d. Egg percent production (eggs/d on treatment × 100) were 93.0 ± 5.3%, 90.8 ± 7.2%, 97.2 ± 2.4%, and 99.0 ± 3.6% for hens fed the orange, tangerine, yellow, and white treatments, respectively, where yellow and white groups produced more eggs than orange and tangerine groups. One hen in the white group was euthanized early due to a prolapsed follicle. Hen weight at kill (1.40 ± 0.11 kg) did not differ among treatment groups.

**Color Assessment of Egg Yolk.** The L-scales for the yolks were different among treatments, time, and an interaction existed ($P < 0.0001$ for all; Supporting Information Figure S2). Although the L-scale remained relatively flat over time, yolks from all hens were significantly lighter on d 10 at the end of the washout period with VA-depleted white maize than d 0 at the beginning of the study ($P < 0.0001$). Similar to the L-scale, the a-scale responded to treatment, time, and an interaction existed ($P < 0.0001$) (Supporting Information Figure S3). The yolks from orange and yellow groups had similar a-scale values throughout the treatment phase of the study and were significantly higher than the tangerine and white groups' yolks ($P < 0.0001$). Similar to the other scales, the b-scale differed by treatment, time, and an interaction between the two existed ($P < 0.0001$; Supporting Information Figure S4). After the initial washout period, the b-scale remained relatively flat. Total color differences (Table 2) were significant by treatment group ($P = 0.006$), as well as overall between treatment groups ($P < 0.011$). The orange and yellow groups' yolks had similar values as did the tangerine and white groups' yolks.

**Egg Yolk Carotenoid and Retinol Concentrations.** Carotenoid concentrations in yolks from the orange group, but not other treatment groups, increased until d 24 and then stabilized ($P < 0.0001$) (Table 3). $\beta$-Cryptoxanthin concentrations were significantly different among treatment groups, increased with time, and a treatment by time interaction occurred (all $P < 0.0001$). $\beta$-Cryptoxanthin concentration was highest in yolks from chickens fed orange maize, followed by tangerine, yellow, and white groups. $\beta$-Cryptoxanthin increased following the wash-out period in the orange, tangerine, and yellow treatments, but little change occurred in the white control (Table 3). In eggs from hens fed orange maize, $\beta$-cryptoxanthin concentration increased >2 times between d 16 and 24 and plateaued throughout the remainder of the study. As expected, lutein concentration was significantly higher in eggs from chickens fed yellow maize than that of any other group, but also increased with time across all groups and a treatment by time interaction occurred (all $P < 0.0001$). Yolks from the yellow group were the only yolks to reach lutein concentrations similar to the beginning of the washout period. Zeaxanthin was significantly higher in yolks from the orange group throughout the treatment period but decreased with time across all groups and a treatment by time interaction occurred (all $P < 0.0001$). Thus, after the washout period, yolk lutein was high from yellow maize but generally abundant from all feeds, while yolk zeaxanthin was particularly high from orange and yellow feeds. Yolk $\beta$-cryptoxanthin had moderate increases according to feed but remained less than lutein or zeaxanthin concentrations. Treatment alone did not impact yolk retinol concentration, but time had a significant effect, and an interaction between treatment and time occurred (both $P <$

**Table 2. Color Scale Readings (L*a*b*) on Select Days and Total Color Difference of Egg Yolks Assessed by $\Delta E$. Hens were fed Orange, Tangerine-fortified White, Lutein-fortified Yellow, or Unfortified White Maize for 40 d**

| color scale measurements[A,B] | | Day 10 | Day 50 |
|---|---|---|---|
| orange[C] | L | 60.2 ± 2.63 | 58.3 ± 0.94 |
| | a | −3.27 ± 0.56 | 2.79 ± 0.72 |
| | b | 38.4 ± 3.43 | 44.6 ± 2.46 |
| tangerine | L | 61.1 ± 2.00 | 61.9 ± 2.40 |
| | a | −3.50 ± 0.36 | −2.80 ± 0.64 |
| | b | 37.5 ± 1.57 | 38.1 ± 2.70 |
| yellow | L | 61.3 ± 1.07 | 57.8 ± 1.73 |
| | a | −3.09 ± 0.55 | 1.96 ± 0.61 |
| | b | 38.5 ± 2.70 | 46.1 ± 1.40 |
| white | L | 62.7 ± 1.16 | 61.2 ± 2.50 |
| | a | −3.43 ± 0.57 | −4.03 ± 0.43 |
| | b | 39.1 ± 5.26 | 36.7 ± 1.47 |

| within treatment group[B,D] | $\Delta E$[E] |
|---|---|
| orange | 9.46 ± 2.36[a] |
| tangerine | 4.15 ± 2.38[b] |
| yellow | 8.59 ± 2.72[a] |
| White | 4.72 ± 5.16[b] |

| between treatment group means[F] | $\Delta E$[E] |
|---|---|
| orange vs tangerine | 10.3 |
| orange vs yellow | 1.36 |
| orange vs white | 10.8 |
| tangerine vs yellow | 9.74 |
| tangerine vs white | 1.62 |
| yellow vs white | 10.2 |

[A]All L*a*b* scale measurements can be found in Supporting Information Figures S2−4. [B]Values are means ± SD; $n$ = 8/treatment group. [C]Treatment groups: orange = high $\beta$-cryptoxanthin maize, tangerine = white maize + tangerine peel fortificant, yellow = yellow maize + lutein fortificant, white = white maize only. [D]The treatment effect within a group is significant ($P$ = 0.006); means with lowercase superscript letters are significantly different using LSMEANS at $P$ < 0.05. [E]$\Delta E$ is a measure of change in L-, a-, and b-scales from the beginning (d 10) to end (d 50) of the experimental feeding period (see eq 1). [F]Means of each group on d 50 of the experiment were compared between groups for $\Delta E$; $P \leq 0.011$.

0.0001). Egg yolk retinol concentrations were lower on d 50 than d 0 (Table 4).

**Chicken Liver and Serum Retinol and Carotenoid Concentrations.** Hen liver weights (37.0 ± 6.4 g) did not differ among treatment groups. Liver VA concentration and total liver VA reserves, which includes both retinol and retinyl esters, were significantly different among treatment groups (Figure 1A, B; $P$ < 0.0001, $P$ = 0.0004, respectively), and total retinol decreased in the order of orange ≥ tangerine = yellow = white groups. Treatment also affected liver carotenoid concentrations (Figure 2A). $\beta$-Cryptoxanthin, zeaxanthin, and $\beta$-carotene concentrations of free carotenoids and total carotenoid liver reserves were highest in chickens from the orange group (Figure 2A, B, all $P$ < 0.0001). Lutein concentration and total liver lutein reserves were highest in the yellow group. However, zeaxanthin was consistently the most abundant carotenoid in liver, except for in the tangerine group where $\beta$-cryptoxanthin was similar to zeaxanthin (Figures 2A, B). $\alpha$-Carotene was not detected in the chicken liver.

Hen serum retinol concentrations differed among treatment groups ($P$ < 0.0001) and were highest in the tangerine group (Figure 1C). Serum retinol concentrations did not follow the same pattern as the retinol concentrations in the liver. All hens had serum retinol concentrations ≥1.0 $\mu$mol/L. Hen serum $\beta$-cryptoxanthin and zeaxanthin concentrations were highest in the orange group ($P$ < 0.0001). Serum lutein was highest in the yellow group ($P$ < 0.0001) (Figure 2C). While serum lutein, zeaxanthin, and $\beta$-cryptoxanthin concentrations reflected those in the liver, $\beta$-carotene was not detectable in any group. In contrast, liver $\beta$-carotene concentrations were detectable and highest in the orange group compared with other groups.

**Chicken Skin Colorization and Carotenoids.** No differences were observed among the skin from any of the feeding groups for the L-, a-, and b-color scales. Lutein and zeaxanthin were highest in the yellow group's skin, but no significant differences existed (Table 5, $P$ = 0.09, $P$ = 0.38, respectively). Skin $\beta$-cryptoxanthin concentration was low compared with lutein and zeaxanthin but was significantly higher in the orange group than other groups (Table 5, $P$ = 0.002).

## DISCUSSION

This study evaluated the impact of $\beta$-cryptoxanthin from biofortified orange maize or tangerine peel powder on egg yolk color and VA status of laying hens fed for 40 d. The orange feed resulted in deeper orange yolk, which was visible to the naked eye, significantly higher concentrations of $\beta$-cryptoxanthin (∼2 times higher) and zeaxanthin (∼4 times higher), and differentiated color from the tangerine group on all color scales, even though both feeds contained similar concentrations of $\beta$-cryptoxanthin. Eggs from hens that were fed orange maize became significantly darker on the L-scale, redder on the a-scale, and more yellow on the b-scale. Total color difference was small between white and tangerine and between orange and yellow, which was expected because they were similar on each color-scale measurement.

Hens consuming the orange maize had the highest liver VA stores, which were 1.5 times higher than the tangerine group and 2.6 times higher than the yellow group. Tangerine peel was chosen as a fortificant because it is considered a waste product in juice production and therefore could be repurposed in chicken feed manufacturing. Considering the difference in theoretical retinol equivalents between the orange maize and tangerine peel feeds, it is likely that the $\beta$-cryptoxanthin from the tangerine peel was serving as a major source of VA for the hen itself, because other provitamin A carotenoids were absent in the tangerine peel feed. Follow-up studies should equalize maize feeds for provitamin A equivalents to determine if $\beta$-cryptoxanthin is less bioavailable from the tangerine peel matrix compared with orange maize, and to investigate different levels of tangerine fortificant to maximize the $\beta$-cryptoxanthin response in the egg yolk in addition to meeting the hen's VA needs. In addition, the degree of fatty acid esterification of the $\beta$-cryptoxanthin in the tangerine peel should be determined to investigate whether this has any effect on bioavailability in the chicken.[31]

In addition to this study, two prior studies fed biofortified maize feeds to laying hens that resulted in enhanced $\beta$-cryptoxanthin of the yolks.[25,26] The $\beta$-cryptoxanthin concentration in egg yolks from this study, on d 28, were twice that (8.66 ± 0.53 nmol/g) of a previous study (4.20 nmol/g), yet similar $\beta$-cryptoxanthin concentrations were fed (4.71 nmol/g and 5.64 nmol/g, respectively).[25] Furthermore, a recent study in which biofortified $\beta$-cryptoxanthin maize was fed to laying hens for 140 d with a concentration of 9.8 nmol/g, found a

**Table 3. Carotenoid Concentrations in Egg Yolk (nmol/g) from Hens Fed a Variety of Feeds with Orange, Tangerine-fortified White, Lutein-fortified Yellow, or Unfortified White Maize[A]**

| | | treatment | | | |
|---|---|---|---|---|---|
| carotenoid | day | orange | tangerine | yellow | white |
| β-cryptoxanthin[B] | 0 | 1.98 ± 0.23 | 1.77 ± 0.14 | 1.87 ± 0.33 | 1.99 ± 0.21 |
| | 8 | 1.25 ± 0.13 | 1.41 ± 0.18 | 1.41 ± 0.17 | 1.22 ± 0.11 |
| | 16 | 3.49 ± 1.91 | 3.22 ± 0.41 | 2.44 ± 0.29 | 1.14 ± 0.28 |
| | 24 | 10.4 ± 0.60 | 3.71 ± 0.86 | 2.52 ± 0.32 | 1.35 ± 0.13 |
| | 32 | 6.98 ± 0.55 | 3.75 ± 0.78 | 2.11 ± 0.29 | 1.35 ± 0.84 |
| | 40 | 7.98 ± 1.14 | 3.88 ± 0.69 | 2.07 ± 0.28 | 1.11 ± 0.10 |
| | 50 | 8.82 ± 1.00 | 3.74 ± 0.53 | 1.93 ± 0.29 | 1.55 ± 0.79 |
| lutein[B] | 0 | 22.5 ± 4.29 | 22.2 ± 2.38 | 25.5 ± 6.13 | 23.0 ± 4.30 |
| | 8 | 7.23 ± 1.25 | 7.43 ± 1.12 | 8.08 ± 1.84 | 6.29 ± 0.99 |
| | 16 | 10.4 ± 1.05 | 6.0 ± 0.39 | 14.6 ± 4.32 | 5.30 ± 1.38 |
| | 24 | 11.7 ± 1.13 | 4.15 ± 0.58 | 31.8 ± 4.82 | 5.85 ± 0.86 |
| | 32 | 8.54 ± 1.24 | 6.05 ± 0.88 | 43.4 ± 6.88 | 6.40 ± 2.35 |
| | 40 | 8.95 ± 2.43 | 6.50 ± 1.40 | 38.4 ± 6.76 | 5.45 ± 0.35 |
| | 50 | 10.3 ± 1.55 | 5.09 ± 0.87 | 27.3 ± 2.95 | 5.86 ± 0.87 |
| zeaxanthin[B] | 0 | 16.3 ± 3.56 | 18.0 ± 3.86 | 17.7 ± 4.08 | 16.6 ± 3.25 |
| | 8 | 6.16 ± 0.89 | 6.49 ± 0.98 | 6.85 ± 1.42 | 6.50 ± 1.07 |
| | 16 | 24.3 ± 3.69 | 5.13 ± 0.34 | 8.40 ± 2.26 | 4.69 ± 1.28 |
| | 24 | 29.6 ± 2.91 | 3.33 ± 0.46 | 14.3 ± 2.07 | 5.00 ± 0.78 |
| | 32 | 19.1 ± 2.82 | 5.21 ± 0.82 | 20.0 ± 3.76 | 3.67 ± 0.63 |
| | 40 | 19.4 ± 3.18 | 5.03 ± 1.06 | 16.0 ± 3.43 | 3.49 ± 0.39 |
| | 50 | 23.1 ± 3.73 | 3.77 ± 0.81 | 16.1 ± 1.80 | 4.48 ± 0.75 |
| β-carotene[B] | 0 | ND | ND | ND | ND |
| | 8 | 0.06 ± 0.04 | ND | ND | ND |
| | 16 | 0.02 ± 0.008 | ND | ND | ND |
| | 24 | 0.16 ± 0.08 | ND | ND | ND |
| | 32 | 0.10 ± 0.02 | ND | ND | ND |
| | 40 | 0.22 ± 0.21 | ND | ND | ND |
| | 50 | 0.15 ± 0.10 | ND | ND | ND |

[A]Eggs were collected every other day and analyzed every 4 d; data shown are every 8 d. ND, not detected. Values are means ± SD; $n$ = 8/treatment group. [B]Indicates a significant treatment, time, and treatment by time interaction using two-way ANOVA (all $P < 0.0001$).

**Table 4. Egg Yolk Retinol[A] Concentrations (nmol/g) from Hens Fed Feeds with Different Mixtures of Maize and Fortificants[B]**

| day[C] ($n$ = 32) | all hens[C] | orange | tangerine | yellow | white |
|---|---|---|---|---|---|
| 0 | 19.2 ± 4.01$^{a}$ | 18.7 ± 3.03 | 19.0 ± 2.31 | 21.3 ± 6.44 | 18.1 ± 2.7 |
| 4 | 16.6 ± 3.53$^{ab}$ | 15.4 ± 1.58 | 17.0 ± 2.30 | 15.7 ± 6.35 | 17.9 ± 2.1 |
| 8 | 15.7 ± 3.56$^{bcd}$ | 14.2 ± 1.31 | 17.5 ± 1.97 | 16.7 ± 3.01 | 14.0 ± 5.47 |
| 12 | 16.3 ± 3.10$^{bc}$ | 14.2 ± 1.38 | 16.2 ± 3.25 | 17.0 ± 2.82 | 17.3 ± 4.16 |
| 16 | 11.7 ± 3.79$^{e}$ | 8.55 ± 0.84 | 14.3 ± 1.17 | 8.70 ± 3.04 | 14.3 ± 3.60 |
| 20 | 14.3 ± 4.18$^{bcde}$ | 17.1 ± 1.09 | 15.1 ± 1.14 | 15.3 ± 1.29 | 8.60 ± 1.13 |
| 24 | 15.4 ± 2.50$^{bcd}$ | 15.6 ± 1.08 | 16.0 ± 3.26 | 14.2 ± 2.96 | 16.2 ± 2.40 |
| 28 | 14.9 ± 2.76$^{bcd}$ | 15.2 ± 1.2 | 15.1 ± 1.14 | 14.7 ± 2.02 | 14.7 ± 5.30 |
| 32 | 13.7 ± 2.19$^{cde}$ | 13.6 ± 2.65 | 13.4 ± 1.99 | 13.9 ± 2.12 | 13.2 ± 2.42 |
| 36 | 13.8 ± 2.01$^{bcde}$ | 13.6 ± 1.96 | 13.3 ± 0.90 | 14.4 ± 2.65 | 13.9 ± 3.09 |
| 40 | 15.3 ± 2.42$^{bcd}$ | 15.4 ± 3.30 | 14.6 ± 1.00 | 16.2 ± 2.77 | 14.7 ± 1.76 |
| 44 | 14.0 ± 2.03$^{bcde}$ | 15.7 ± 1.14 | 14.3 ± 1.91 | 12.9 ± 2.06 | 13.0 ± 1.71 |
| 48 | 13.3 ± 4.11$^{de}$ | 13.7 ± 3.78 | 8.41 ± 1.92 | 13.9 ± 1.56 | 17.1 ± 5.31 |
| 50 | 14.9 ± 3.51$^{bcd}$ | 16.8 ± 3.79 | 15.2 ± 2.18 | 15.6 ± 3.26 | 11.7 ± 2.33 |

[A]Retinol is defined as free retinol and retinyl esters hydrolyzed during saponification in egg yolk. [B]Values are mean ± SD; $n$ = 6−8/time and feed group. [C]Using two-way ANOVA, time and an interaction between treatment and time were significant (both $P < 0.0001$); feed alone was not significant. Using LSMEANS, unlike lowercase superscript letters represent significant differences by time ($P < 0.05$).

mean egg yolk β-cryptoxanthin concentration of 10.1 nmol/g after freeze-drying.[26] Raw egg yolk is approximately 50% water;[34] therefore, the prior two study values are similar. Interaction between zeaxanthin and β-cryptoxanthin for uptake into the egg yolk may contribute to these discrepancies. However, yolk concentration of β-cryptoxanthin did mirror theoretical provitamin A intake in this study. β-Carotene in the orange maize likely met the VA requirements of the hens, which allowed for more β-cryptoxanthin to be deposited into the egg yolk than utilized for VA needs.

Unlike the prior studies, this study also evaluated the VA statuses of the hens, which were impacted by the level of β-

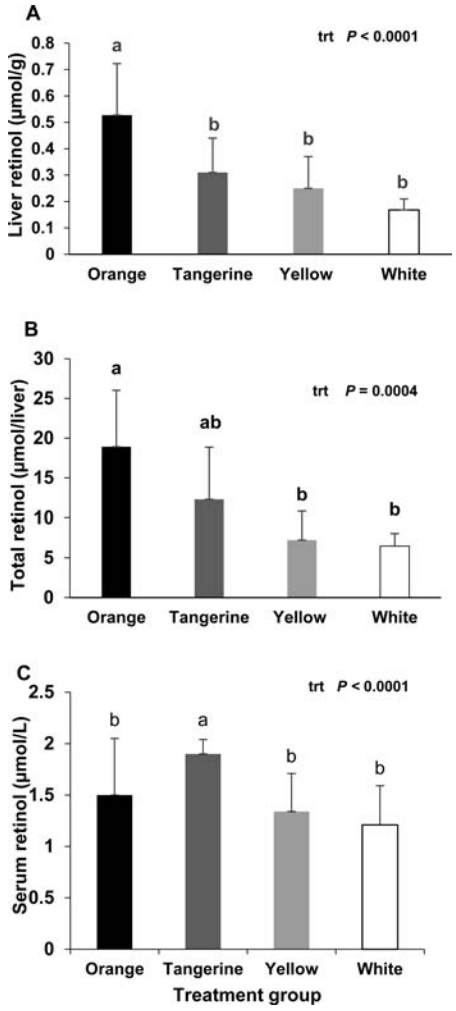


**Figure 1.** Liver VA concentrations and reserves, which includes retinol and retinyl esters, in hens ($n$ = 7 white maize, $n$ = 8 all other treatment groups) fed either orange, tangerine-fortified white, lutein-fortified yellow, or white maize feeds. Means were analyzed using PROC MIXED and LSMEANS was used to make comparisons between groups. Bars with unlike lowercase letters are different at $P < 0.05$. (A) Liver VA concentrations were significantly different among treatment groups ($P < 0.0001$). (B) Total liver VA reserves were significantly different among treatment groups ($P = 0.0004$). (C) Serum retinol concentrations were higher in the tangerine-fortified white maize group and did not reflect the relationship of liver VA concentrations.

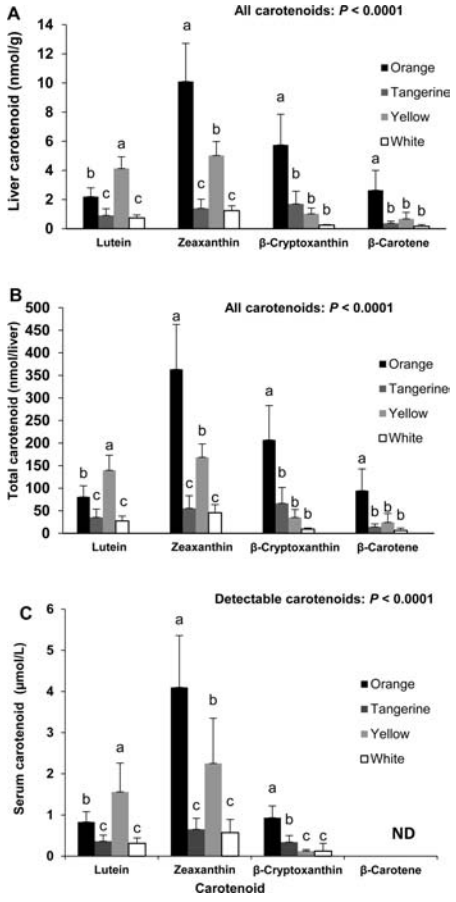


**Figure 2.** Liver and serum carotenoid concentrations and reserves in hens ($n$ = 7 white maize, $n$ = 8 all other treatment groups) fed either orange, tangerine-fortified white, lutein-fortified yellow, or white maize feeds. Means were analyzed using PROC MIXED and LSMEANS was used to make comparisons between groups. Bars with unlike lowercase letters are different at $P < 0.05$. (A) Liver carotenoid concentrations were significantly different among treatment groups for lutein, zeaxanthin, $\beta$-cryptoxanthin, and $\beta$-carotene. (B) Total liver carotenoid reserves differed among treatment groups for lutein, zeaxanthin, $\beta$-cryptoxanthin, and $\beta$-carotene. (C) Serum carotenoid concentrations were significantly different among treatment groups for lutein, zeaxanthin, and $\beta$-cryptoxanthin. ND, not detected.

cryptoxanthin and other provitamin A carotenoids. Currently, there is no carotenoid requirement for poultry, although dietary carotenoids contribute to plumage, beak, skin, and egg yolk color.[15] Consequences of VA deficiency in laying hens are decreased egg production and yolk VA concentration, and lesions in the upper respiratory tract (esophagus) and ovarian follicle.[35] The National Research Council's VA requirement for mature Leghorn laying hens is 300 IU VA/d (90 $\mu$g/d).[36] According to international standards and theoretical VA concentrations in the feeds, all hens except those on the white maize feed met 300 IU/day. Assuming they ate ~100 g feed/day, hens fed orange maize theoretically consumed 1555 IU/d, the tangerine group consumed 828 IU/d, the yellow group consumed 309 IU/d, and the white group consumed 102 IU/d. Although they were theoretically consuming one-third the VA requirement, hens fed the white maize had adequate liver reserves [0.17 $\mu$mol/g liver compared with 0.1 $\mu$mol/g liver[37]] after 50 d treatment. Retinol concentration in the eggs was not impacted by the level of provitamin A equivalents in the feed during this short-term study, which indicates highly regulated deposition of VA into the yolk. Hens fed orange maize had higher liver VA concentrations and total reserves than other groups. Using biofortified orange maize or tangerine fortificant could eliminate the need for addition of preformed retinyl palmitate to feed. According to serum retinol and liver VA concentrations, hens on all treatments were VA-adequate meeting the cutoffs of 0.7 $\mu$mol retinol/L serum and 0.1 $\mu$mol VA/g liver, respectively.

The orange feed was higher in $\beta$-carotene than other groups. Hens are efficient at cleaving $\beta$-carotene to retinol, most likely contributing to the increased VA concentration and reserves in hen liver; however, liver $\beta$-carotene concentrations were significantly higher in hens fed orange maize, indicating that some absorption of intact $\beta$-carotene did occur in this study. Hens fed the orange maize also had higher liver $\beta$-cryptoxanthin concentrations than other groups, reflective of $\beta$-cryptoxanthin concentrations in the feed. Lutein and


dx.doi.org/10.1021/jf5037195 | J. Agric. Food Chem. 2014, 62, 11892−11900

Table 5. Hen Skin Xanthophyll Concentrations (nmol/g) from Hens Fed Different Maize Feeds for 40 d[A]

| | maize feed | | | | |
|---|---|---|---|---|---|
| | orange | tangerine peel-fortified white | lutein-fortified yellow | white | *P* value |
| lutein | 0.38 ± 0.16 | 0.39 ± 0.22 | 0.53 ± 0.18 | 0.28 ± 0.14 | 0.09 |
| zeaxanthin | 0.40 ± 0.24 | 0.31 ± 0.24 | 0.84 ± 1.46 | 0.19 ± 0.11 | 0.38 |
| β-cryptoxanthin | 0.07 ± 0.04[a] | 0.03 ± 0.02[b] | 0.03 ± 0.01[b] | 0.01 ± 0.005[b] | 0.002 |

[A]Values are means ± SD; $n = 7$ white maize, $n = 8$ all other treatment groups. One-way ANOVA was used to determine differences among treatment groups for each carotenoid. Using LSMEANS, different lowercase superscript letters in a row designate differences ($P < 0.05$).

zeaxanthin accumulation in liver reflected feed intake, similar to results found when feeding high lutein and zeaxanthin feeds to Leghorn chicks.[38] Lutein concentration was highest in the yellow group's livers. Zeaxanthin was highest in the orange group and greater than the β-cryptoxanthin concentration. Furthermore, the ratio of liver β-cryptoxanthin to lutein (2.6) was higher than the ratio in the orange feed (0.9), which may indicate a bias against accumulation of lutein in the chicken liver. Differences among animal models in carotenoid metabolism are interesting. A common model used for provitamin A carotenoid metabolism is Mongolian gerbils, but they have the limitation of only absorbing and storing very small amounts of lutein and zeaxanthin.[39,40] Chickens appear to be a better model for studying xanthophyll carotenoid bioavailability. Similar to gerbils, serum concentrations of β-carotene were not detectable, which may be because chickens have higher HDL than LDL.[41] β-Carotene is predominantly carried by LDL, whereas lutein and zeaxanthin are carried by HDL.[42]

Chicken skin color is strongly associated with dietary concentration of carotenoids,[43] but there were no color differences among treatment groups in this study using L*a*b* scales. β-Cryptoxanthin was present in small amounts in chicken skin and was significantly higher in chickens fed orange maize. Even though the lutein concentration in the yellow group was extremely high, lutein concentrations did not differ in the skin. However, the hens used in this study were young and early in their laying cycle. Hens in peak egg production withdraw xanthophyll carotenoids from skin and deposit them in egg yolk. Increased deposition of xanthophyll carotenoids into skin is probably best studied in non-egg-laying chickens.

In order to be effective, biofortified foods must be accepted by targeted populations. Consumers have documented egg yolk preferences. Consumers in Germany, Belgium, Netherlands, and Spain prefer an orange-colored yolk, whereas those in Ireland and Sweden prefer a lighter yolk.[43] Dietary sources of β-cryptoxanthin are few and most humans obtain it from orange citrus fruits. Although β-cryptoxanthin concentration varies by fruit source, a mean value for orange juice is ∼200 μg/100 mL.[44] Thus, two biofortifed egg yolks (e.g., 30 g yolk with 5 μg β-cryptoxanthin/g) could provide about 75% of that amount or provide more than a medium fresh orange, which contains ∼60 mL juice.

The consumption of white staple foods by both humans and livestock in developing countries provides no VA. Many countries prefer nutrient-poor white maize to meet their daily calorie needs.[45] The introduction of provitamin A biofortified crops, such as orange maize, has the potential to raise xanthophyll intakes in humans and animals.[4,10−14] Due to the xanthophyll profile of maize, it should be especially targeted, because it is the primary ingredient in many livestock feeds, such as chickens, swine, and cattle. By substituting biofortified orange maize, which has enhanced β-cryptoxanthin, lutein, and zeaxanthin, for white or yellow maize in chicken feed, the need for VA or lutein-fortified feeds could be diverted lowering the cost for hen husbandry and improving the nutritional profile of eggs for human consumption.

The introduction of biofortified maize as a human food and an animal feed in developed and developing countries could have economic and health considerations for all. Eggs are a target for provitamin A carotenoid biofortification through feeding orange maize to laying hens, which could further eggs' status as a functional food with enhanced nutrition.[46] Furthermore, lutein and zeaxanthin, which are also enhanced in many genotypes of biofortified maize, may contribute to decreased risk of macular degeneration.[47] Thus, future studies should determine the impact of the complete carotenoid profile of the biofortified egg on human health.

## ■ ASSOCIATED CONTENT

### Supporting Information

Table S1 and Figures S1−4. This material is available free of charge via the Internet at http://pubs.acs.org.

## ■ AUTHOR INFORMATION

### Corresponding Author

*Phone: 608-265-0792. E-mail: sherry@nutrisci.wisc.edu.

### Author Contributions

E.K.H. conducted research, analyzed samples, analyzed data, and wrote the first draft of the manuscript. J.P.T. and V.V. were responsible for the day-to-day care of the hens, colorized the eggs, and analyzed samples. M.C. was responsible for animal care training and oversight of hen husbandry. N.P.-R. and S.A.T. designed the research. S.A.T. provided input for the statistical analysis and revised the manuscript. All authors read and approved the final manuscript.

### Funding

This research was supported by MASAGRO (Modernizacion Sustentable de la Agricultura), a program of SAGARPA-Mexico in collaboration with the International Center of Wheat and Maize Improvement and USDA Hatch WIS01528 and WIS01804.

### Notes

**Disclosure** Part of this work was presented at the Experimental Biology Meeting in 2014, San Diego, CA.

The authors declare no competing financial interest.

## ■ ACKNOWLEDGMENTS

The authors thank James Claus, University of Wisconsin-Madison, for guidance and use of the colorimeter. The authors thank Michael Grahn, Chris Davis, and Shellen Goltz for assisting with sample analysis and guidance during this study. The authors also thank Chris Davis for assisting us with the preparation of Supporting Information Table S1.

## REFERENCES


(1) Arscott, S. A. Food sources of carotenoids. In *Carotenoids and Human Health*; Tanumihardjo, S. A., Ed.; Springer Science and Business Media: New York, 2013; pp 21−28.

(2) Liu, C.; Bronson, R. T.; Russell, R. M.; Wang, W. D. β-Cryptoxanthin supplementation prevents cigarette smoke-induced lung inflammation, oxidative damage, and squamous metaplasia in ferrets. *Am. Assoc. Cancer Res.* **2011**, *4*, 1255−1266.

(3) Institute of Medicine. *Dietary Reference Intakes for Vitamin A, Vitamin K, Arsenic, Boron, Chromium, Copper, Iodine, Iron, Manganese, Molybdenum, Nickel, Silicon, Vanadium, and Zinc*; National Academy Press: Washington, DC, 2001; pp 65−126.

(4) Davis, C.; Jing, H.; Howe, J. A.; Rocheford, T.; Tanumihardjo, S. A. β-Cryptoxanthin from supplements or carotenoid-enhanced maize maintains liver vitamin A in Mongolian gerbils (*Meriones unguiculatus*) better than or equal to β-carotene supplements. *Br. J. Nutr.* **2008**, *100*, 786−793.

(5) Dhuique-Mayer, C.; Borel, P.; Reboul, E.; Caporiccio, B.; Besancon, P.; Amiot, M. J. β-Cryptoxanthin from citrus juices: Assessment of bioaccessibility using an in vitro/Caco-2 cell culture model. *Br. J. Nutr.* **2007**, *97*, 883−890.

(6) Burri, B. J.; Chang, J. S. T.; Neidlinger, T. R. β-Cryptoxanthin and α-carotene rich foods have greater apparent bioavailability than β-carotene-rich foods in Western diets. *Br. J. Nutr.* **2011**, *105*, 212−219.

(7) Fu, H.; Xie, B.; Fan, G.; Ma, S.; Zhu, X.; Pan, S. Effect of esterification with fatty acid of β-cryptoxanthin on its thermal stability and antioxidant activity by chemiluminescence method. *J. Food Chem.* **2010**, *122*, 602−609.

(8) Ciccone, M. M.; Cortese, F.; Gesualdo, M.; Carbonara, S.; Zito, A.; Ricci, G.; De Pascalis, F.; Scicchitano, P.; Riccioni, G. Dietary intake of carotenoids and their antioxidant and anti-inflammatory effects in cardiovascular care. *Mediators Inflamm.* **2013**, No. 782137.

(9) Yamaguchi, M. Role of carotenoid β-cryptoxanthin in bone homeostasis. *J. Biomed. Sci.* **2012**, *19*, 36 DOI: 10.1186/1423-0127-19-36.

(10) Howe, J. A.; Tanumihardjo, S. A. Carotenoid-biofortified maize maintains adequate vitamin A status in Mongolian gerbils. *J. Nutr.* **2006**, *136*, 2562−2567.

(11) Li, S.; Nugroho, A.; Rocheford, T.; White, W. S. Vitamin A equivalence of the β-carotene in β-carotene-biofortified maize porridge consumed by women. *Am. J. Clin. Nutr.* **2010**, *92*, 1105−1112.

(12) Muzhingi, T.; Gadaga, T. H.; Siwela, A. H.; Grusak, M. A.; Russell, R. M.; Tang, G. Yellow maize with high β-carotene is an effective source of vitamin A in healthy Zimbabwean men. *Am. J. Clin. Nutr.* **2011**, *94*, 510−519.

(13) Gannon, B.; Kaliwile, C.; Arscott, S. A.; Schmaelzle, S.; Masi, C.; Chileshe, J.; Kalungwana, N.; Mosonda, M.; Pixley, K.; Masi, C.; Tanumihardjo, S. A. Biofortified orange maize is as efficacious as a vitamin A supplement in Zambian children even in the presence of high liver reserves of vitamin A: A community-based, randomized placebo-controlled trial. *Am. J. Clin. Nutr.* **2014**, No. 10.3945/ajcn.114.087379.

(14) Heying, E. K.; Grahn, M.; Pixley, K. V.; Rocheford, T.; Tanumihardjo, S. A. High-provitamin A carotenoid (orange) maize increases hepatic vitamin A reserves of offspring in a vitamin A-depleted sow-piglet model during lactation. *J. Nutr.* **2013**, *143*, 1141−1146.

(15) Goodwin, T. W. Avian carotenoids. In *Carotenoids, Their Comparative Biochemistry*; Chemical Publishing Co.: New York, 1954; pp 259−268.

(16) Hencken, H. Chemical and physiological behavior of feed carotenoids and their effects on pigmentation. *Poult. Sci.* **1992**, *71*, 711−717.

(17) Castaneda, M. P.; Hirschler, E. M.; Sams, A. R. Skin pigmentation evaluation in broilers fed natural and synthetic pigments. *Poult. Sci.* **2005**, *84*, 143−147.

(18) Perez-Vendrell, J.; Hernández, M.; Llauradó, L.; Schierle, J.; Brufau, J. Influence of source and ratio of xanthophyll pigments on broiler chicken pigmentation and performance. *Poult. Sci.* **2001**, *80*, 320−326.

(19) Martinez, P. M.; Cortes, C. A.; Avila, G. E. Evaluation of three pigment levels of marigold petals (*Tagetes erecta*) on skin pigmentation of broiler chicken. *Tec. Pecu. Mex.* **2004**, *42*, 105−111.

(20) Schaeffer, J. L.; Tyczkowski, J. K.; Parkhurst, C. R.; Hamilton, P. B. Carotenoid composition of serum and egg yolks of hens fed diets varying in carotenoid composition. *Poult. Sci.* **1988**, *67*, 608−614.

(21) Mangels, A. R.; Holden, J. M.; Beecher, G. R.; Forman, M. R.; Lanza, E. Carotenoid contents of fruits and vegetables: An evaluation of analytic data. *J. Am. Diet. Assoc.* **1993**, *93*, 284−296.

(22) Handelman, G. J.; Nightingale, Z. D.; Lichtenstein, A. H.; Schaefer, E. J.; Blumberg, J. B. Lutein and zeaxanthin concentrations in plasma after dietary supplementation with egg yolk. *Am. J. Clin. Nutr.* **1999**, *70*, 247−251.

(23) Poor, C. L.; Miller, S. D.; Fahey, G. C.; Easter, R. A.; Erdman, J. W., Jr. Animal models for carotenoid utilization studies: Evaluation of the chick and the pig. *Nutr. Rep. Int.* **1987**, *36*, 229−234.

(24) Surai, P. F.; Noble, R. C.; Speake, B. K. Tissue-specific differences in antioxidant distribution and susceptibility to lipid peroxidation during development of the chick embryo. *Biochim. Biophys. Acta* **1996**, *1304*, 1−10.

(25) Liu, Y. Q.; Davis, C. R.; Schmaelzle, S. T.; Rocheford, T.; Cook, M. E.; Tanumihardjo, S. A. β-Cryptoxanthin biofortified maize (*Zea mays*) increases β-cryptoxanthin concentration and enhances the color of chicken egg yolk. *Poult. Sci.* **2012**, *91*, 432−438.

(26) Burt, A. J.; Caston, L.; Leeson, S.; Shelp, B. J.; Lee, E. A. Development and utilization of high carotenoid maize germplasm: Proof of concept. *Crop Sci.* **2013**, *53*, 554−563.

(27) Breithaupt, D. E.; Bamedi, A. Carotenoid esters in vegetables and fruits: A screening with emphasis on β-cryptoxanthin esters. *J. Agric. Food Chem.* **2001**, *49*, 2064−2070.

(28) Blessin, C. W. Carotenoids of corn and sorghum. *Cereal Chem.* **1962**, *39*, 236−242.

(29) Howe, J. A.; Tanumihardjo, S. A. Evaluation of analytical methods for carotenoid extraction from biofortified maize (*Zea mays* sp.). *J. Agric. Food Chem.* **2006**, *54*, 7992−7997.

(30) Kemin Industries. *Utilization of Dry Kem GLO Brand and Dry ORO GLO Brand for Pigmentation of Egg Yolks As Quantitated through Fan Score Comparison and Reflectance Colorimeter Readings*; Kemin Industries: Des Moines, IA, 2000.

(31) Pérez-Gálvez, A.; Mínguez-Mosquera, M. I. Esterification of xanthophylls and its effect on chemical behavior and bioavailability of carotenoids in the human. *Nutr. Res. (N.Y.)* **2005**, *25*, 631−640.

(32) Tanumihardjo, S. A.; Howe, J. A. Twice the amount of α-carotene isolated from carrots is as effective as β-carotene in maintaining the vitamin A status of Mongolian gerbils. *J. Nutr.* **2005**, *135*, 2622−2626.

(33) *Interpretation of Color Data*; Technical service report No. 79; PolyOne Corp.: Avon Lake, OH, 2005.

(34) U.S. Department of Agriculture, Agricultural Research Service. 2013. USDA National Nutrient Database for Standard Reference, Release 26. Nutrient Data Laboratory Home Page: http://www.ars.usda.gov/ba/bhnrc/ndl (accessed in June 2014).

(35) Bermudez, A. J.; Swayne, D. E.; Squires, M. W.; Radin, M. J. Effects of vitamin A deficiency on the reproductive system of mature White Leghorn hens. *Avian Dis.* **1993**, *37*, 274−283.

(36) National Research Council. *Nutrient Requirements of Laboratory Animals*, 4th ed.; National Academy Press: Washington, DC, 1995.

(37) Tanumihardjo, S. A. Vitamin A: Biomarkers of nutrition for development. *Am. J. Clin. Nutr.* **2011**, *94*, S658−S665.

(38) Wang, Y.; Illingworth, D. R.; Connor, S. L.; Duell, P. B.; Connor, W. E. Competitive inhibition of carotenoid transport and tissue concentrations by high dose supplements of lutein, zeaxanthin, and β-carotene. *Eur. J. Nutr.* **2010**, *49*, 327−336.

(39) Molldrem, K.; Tanumihardjo, S. A. Lutein supplements are not bioavailable in the Mongolian gerbil while consuming a diet with or without cranberries. *Int. J. Vitam. Nutr. Res.* **2004**, *74*, 153−160.

(40) Escaron, A. L.; Tanumihardjo, S. A. Absorption and transit of lutein and β-carotene supplements in the Mongolian gerbil (*Meriones unguiculatus*). *Int. J. Vitam. Nutr. Res.* **2006**, *76*, 315−323.
(41) Arshad, M. S.; Anjum, F. M.; Khan, M. I.; Shahid, M. Wheat germ oil and α-lipoic acid predominantly improve the lipid profile of broiler meat. *J. Agric. Food Chem.* **2013**, *61*, 11158−11165.
(42) Clevidence, B. A.; Bieri, J. G. Association of carotenoids with human plasma lipoproteins. *Methods Enzymol.* **1993**, *214*, 33−46.
(43) Tarique, T. M.; Yang, S.; Mohsina, Z.; Qiu, J.; Zhao, Y.; Gang, C.; Ailiang, C. Role of carotenoids in poultry industry in China: A review. *J. Nat. Sci. Res.* **2013**, *3*, 111−121.
(44) Stinco, C. M.; Fernández-Vázquez, R.; Escudero-Gilete, M. L.; Heredia, F. J.; Meléndez-Martínez, A. J.; Vicario, I. M. Effect of orange juice's processing on the color, particle size, and bioaccessibility of carotenoids. *J. Agric. Food Chem.* **2012**, *60*, 1447−55.
(45) Nuss, E. T.; Tanumihardjo, S. A. Maize: A paramount staple crop in the context of global nutrition. *Compr. Rev. Food Sci. Food Saf.* **2010**, *9*, 417−436.
(46) Applegate, E. Introduction: Nutritional and functional roles of eggs in the diet. *J. Am. Coll. Nutr.* **2000**, *19*, 495S−498S.
(47) Vishwanathan, R.; Johnson, E. J. Lutein and zeaxanthin and eye disease. In *Carotenoids and Human Health*; Tanumihardjo, S. A., Ed.; Springer Science and Business Media: New York, 2013; pp 215−235.

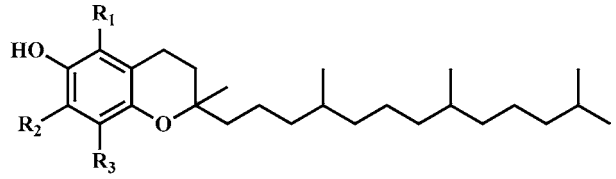


Toc

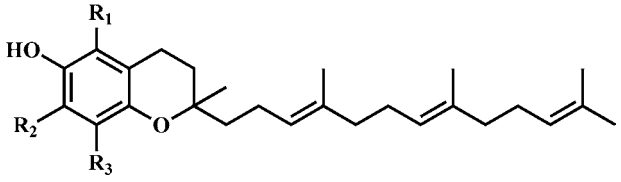


Toc-3

| | $R_1$ | $R_2$ | $R_3$ |
|---|---|---|---|
| α | $CH_3$ | $CH_3$ | $CH_3$ |
| β | $CH_3$ | H | $CH_3$ |
| γ | H | $CH_3$ | $CH_3$ |
| δ | H | H | $CH_3$ |

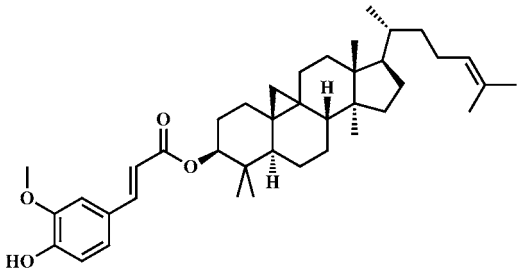


γ - Oryzanol (Cycloartenyl ferulate)

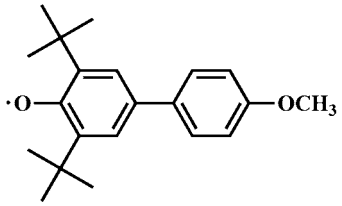


ArO•

**Figure 1.** Molecular structures of α-, β-, γ-, and δ-tocopherols (Tocs) and α-, β-, γ-, and δ-tocotrienols (Toc-3s), γ-oryzanol, and aroxyl radical (ArO•).

brans prepared from many kinds of rice were found to contain different concentrations of α-, β-, γ-, δ-Tocs and -Toc-3s. However, to the best of our knowledge, a detailed kinetic study of the free radical scavenging activity of rice brans has not been carried out.

In the present study, measurements of the rate constants ($k_s^{Extract}$ ($f$) and $k_s^{Extract}$ ($t_{1/2}$)) and the relative ARAC values were performed for seven kinds of rice bran extracts 1−7 (Table 1), which were prepared from Japanese and Korean rice varieties, in ethanol, to evaluate the free radical scavenging activity of rice brans, and to demonstrate that the ARAC method is applicable to not only pure α-, β-, γ-, δ-TocHs, but also general food extracts. Measurement of the rate constants ($k_s^{\gamma\text{-Ory}}$ ($f$) and $k_s^{\gamma\text{-Ory}}$ ($t_{1/2}$)) for γ-Ory was also performed, as rice brans generally include high concentrations of γ-Ory.[14,18,19,22]

In addition, the concentrations (in mg/100 g) of α-, β-, γ-, δ-Tocs and -Toc-3s included in extracts 1−7 were determined using HPLC-MS/MS.[24] The concentration of γ-Ory was determined from the UV−vis absorption spectra of rice bran extracts 1−7.[14] Furthermore, comparison of the $k_s^{Extract}$ ($f$) values observed for the above extracts 1−7 with the sum of the product $\{\sum k_s^{AOH\text{-}i}$ ($f$) [AOH-$i$]/$10^5\}$ of the $k_s^{AOH\text{-}i}$ ($f$) values obtained for each AOH-$i$ and the concentration ([AOH-$i$]/$10^5$) of AOH-i included in the extracts was performed, in order to ascertain the validity of the ARAC assay method developed.[17]

## MATERIALS AND METHODS

**Materials.** α-, β-, γ-, δ-Tocs, and -Toc-3s were kindly supplied by Eisai Co. Ltd. (Tokyo, Japan). γ-Ory extracted from rice germ is commercially available (Wako Chemicals, Japan). The ArO• radical was prepared by following the method of Rieker et al.[25]

**Preparation of Rice Bran Extracts 1−7.** Seven kinds of crude rice bran samples 1−7 (Nipponbare (1), Wataribune (2), Koshihikari (3), Oiran (4), Moritawase (5), γ-rich Koshihikari (6), Milyang-23 (7); Table 1) were prepared from domestic Japanese (or Korean) dehulled rice using a Toyo-Tester grain-polishing machine (Toyo Rice Corporation, Tokyo, Japan).[15] γ-Rich Koshihikari (extract 6), which includes high concentrations of γ-Toc and -Toc-3 (Table 2), is a mutant of Koshihikari (extract 3). The weight of each sample was approximately 10% of the dehulled rice.

Measurements of the amounts of Tocs and Toc-3s and total γ-oryzanol in the rice bran were performed by Chen and Bergman[14] and Sookwong et al.,[15] using 2-propanol as an extraction solvent. In the present work, 2-propanol was similarly used to prepare the seven rice bran extracts 1−7.

Specifically, freshly prepared rice bran powder (40.2 g) of Nipponbare (1) was ground in a mortar using a pestle and subsequently freeze-dried for 6 h. To 38.3 g of dried powder, 150 mL of 2-propanol was added, and extraction was performed for 10 min at 20 °C using a magnetic stirrer. The extraction was repeated 3 times. Approximately 400 mL of the extracted 2-propanol solution was evaporated using a rotary evaporator. The resultant oil was then dried for 2 h using a vacuum pump to eliminate the remaining 2-propanol and water. Finally, 7.75 g of rice bran extract 1 was obtained. Repeating the extraction by 2-propanol from dried powder resulted in a notable decrease in the weight of the extract, so that the final quantity of the extract obtained by the third extraction was only 8% of that of the first extraction.

Rice bran extracts 2−7 were prepared similarly from ∼40 g of rice brans 2−7. An approximately 5% weight loss was observed by freeze-drying rice brans 2−7 for 6 h. The weight ratios of rice bran extracts 1−7 to freeze-dried rice bran powders 1−7 were 0.200, 0.243, 0.191, 0.123, 0.196, 0.178, and 0.189, respectively, all of which were similar to each other with the exception of Oiran (4). Taken together, these results suggest that the method of preparation of rice bran extracts 1−7 via 2-propanol extraction is reasonable.

Measurements of the ArO•-radical scavenging rates ($k_s^{Extract}$($f$) and $k_s^{Extract}$($t_{1/2}$)) and the concentrations of 4 Tocs and 4 Toc-3s included in extracts 1−7 were performed using the extracts prepared as described above.

**HPLC-MS/MS Measurement of the Concentrations of α-, β-, γ-, δ-Tocopherols and -Tocotrienols Included in Rice Bran Extracts 1−7.** Concentrations of α-, β-, γ-, δ-Tocs and -Toc-3s included in rice bran extracts 1−7 were determined by using a HPLC-MS/MS technique.

Approximately 10 mg of rice bran extracts whose weight was correctly measured was dissolved in 3.00 mL of $n$-hexane. This solution (50.0 μL) was further diluted with $n$-hexane to yield a final volume of 250 μL. Next, a portion (20.0 μL) of the prepared solution was subjected to


dx.doi.org/10.1021/jf503996z | J. Agric. Food Chem. 2014, 62, 11901−11909

**Table 1. $k_s^{Extract}$ ($f$) and $k_s^{Extract}$ ($t_{1/2}$) Values and Relative ARAC ($f$) and ARAC ($t_{1/2}$) Values**

| rice bran extract | $k_s^{Extract}$ ($f$) (L g$^{-1}$ s$^{-1}$) | ARAC ($f$) value | $k_s^{Extract}$ ($t_{1/2}$) (L g$^{-1}$ s$^{-1}$) | ARAC ($t_{1/2}$) value |
|---|---|---|---|---|
| Nipponbare (1) | $1.26 \times 10^{-2}$ | $1.06 \times 10^{-3}$ | $1.19 \times 10^{-2}$ | $1.01 \times 10^{-3}$ |
| Wataribune (2) | $1.08 \times 10^{-2}$ | $9.08 \times 10^{-4}$ | $1.10 \times 10^{-2}$ | $9.32 \times 10^{-4}$ |
| Koshihikari (3) | $1.07 \times 10^{-2}$ | $8.99 \times 10^{-4}$ | $1.08 \times 10^{-2}$ | $9.15 \times 10^{-4}$ |
| Oiran (4) | $9.30 \times 10^{-3}$ | $7.82 \times 10^{-4}$ | $9.74 \times 10^{-3}$ | $8.25 \times 10^{-4}$ |
| Moritawase (5) | $9.30 \times 10^{-3}$ | $7.82 \times 10^{-4}$ | $9.07 \times 10^{-3}$ | $7.69 \times 10^{-4}$ |
| $\gamma$-rich Koshihikari (6) | $8.70 \times 10^{-3}$ | $7.31 \times 10^{-4}$ | $8.53 \times 10^{-3}$ | $7.23 \times 10^{-4}$ |
| Milyang-23 (7) | $8.29 \times 10^{-3}$ | $6.96 \times 10^{-4}$ | $8.45 \times 10^{-3}$ | $7.16 \times 10^{-4}$ |
| $\gamma$-oryzanol | $2.64 \times 10^{-2}$ | $2.22 \times 10^{-3}$ | $2.67 \times 10^{-2}$ | $2.26 \times 10^{-3}$ |
| $\alpha$-Toc | 11.9 | 1.00 | 11.8 | 1.00 |

**Table 2. Contents of 8 Vitamin E Homologues (4 Tocs and Toc-3s) and $\gamma$-Oryzanol Included in Rice Bran Extracts 1−7**

| rice bran extract | $\alpha$-Toc (mg/100 g)[a] | $\beta$-Toc (mg/100 g) | $\gamma$-Toc (mg/100 g) | $\delta$-Toc (mg/100 g) | $\alpha$-Toc-3 (mg/100 g) | $\beta$-Toc-3 (mg/100 g) | $\gamma$-Toc-3 (mg/100 g) | $\delta$-Toc-3 (mg/100 g) | Total Tocs and Toc-3s (mg/100 g) | $\gamma$-Ory (mg/100 g) |
|---|---|---|---|---|---|---|---|---|---|---|
| Nipponbare (1) | 50.4 ± 4.2[b] | 2.0 ± 0.1 | 5.0 ± 0.5 | 0.4 ± 0.1 | 34.5 ± 4.5 | 0.3 ± 0.1 | 40.8 ± 2.4 | 2.9 ± 0.2 | 136.3 | 1560 |
| Wataribune (2) | 43.8 ± 5.3 | 3.1 ± 0.3 | 13.1 ± 0.6 | 2.0 ± 0.3 | 20.8 ± 0.5 | 0.3 ± 0.1 | 47.5 ± 2.4 | 5.2 ± 0.3 | 135.8 | 1400 |
| Koshihikari (3) | 37.4 ± 3.3 | 1.7 ± 0.2 | 6.8 ± 0.6 | 0.6 ± 0.1 | 22.1 ± 0.8 | 0.2 ± 0.1 | 47.2 ± 2.5 | 2.7 ± 0.1 | 118.7 | 1420 |
| Oiran (4) | 60.4 ± 1.0 | 3.3 ± 0.3 | 2.6 ± 0.1 | 0.7 ± 0.1 | 20.3 ± 0.4 | 0.3 ± 0.1 | 23.4 ± 0.8 | 1.4 ± 0.1 | 112.3 | 1400 |
| Moritawase (5) | 33.5 ± 1.6 | 2.7 ± 0.2 | 3.0 ± 0.3 | 0.7 ± 0.3 | 24.3 ± 2.4 | 0.6 ± 0.1 | 46.1 ± 5.5 | 4.9 ± 0.1 | 115.9 | 1970 |
| $\gamma$-rich Koshihikari (6) | 9.6 ± 0.1 | 0.2 ± 0.1 | 43.4 ± 2.0 | 3.0 ± 0.4 | 3.3 ± 0.2 | 0.0 ± 0.0 | 84.8 ± 6.3 | 3.4 ± 0.5 | 147.6 | 1610 |
| Milyang-23 (7) | 11.2 ± 0.1 | 0.8 ± 0.1 | 24.1 ± 1.8 | 1.8 ± 0.3 | 8.4 ± 1.0 | 0.0 ± 0.0 | 99.4 ± 8.5 | 5.7 ± 0.4 | 151.5 | 1530 |

[a]mg/100 g shows the contents (mg) of 4 Tocs and 4 Toc-3s and $\gamma$-Ory included in 100 g of rice bran extracts 1−7. [b]Values are expressed as mean ± SD ($n$ = 3).

HPLC-MS/MS measurement.[15,24] Separation was performed at 40 °C using a silica column (ZORBAX Rx-SIL, 4.6 × 250 mm; Agilent, Palo Alto, CA). A mixture of hexane/1,4-dioxane/2-propanol (100:4:0.5) was used as the mobile phase at a flow rate of 1.0 mL/min. Tocs and Toc-3s were detected in atmospheric pressure chemical ionization mode (APCI). MS/MS parameters were optimized with Tocs and Toc-3s standards in APCI mode (positive). Tocs and Toc-3s were detected using multiple reaction monitoring (MRM) as follows: $\alpha$-Toc, $m/z$ 431.3 > $m/z$ 165.1; $\beta$-Toc, $m/z$ 417.3 > $m/z$ 151.3; $\gamma$-Toc, $m/z$ 417.3 > $m/z$ 151.0; $\delta$-Toc, $m/z$ 403.3 > $m/z$137.0; $\alpha$-Toc-3, $m/z$ 425.3 > $m/z$ 165.1; $\beta$-Toc-3, $m/z$ 411.3 > $m/z$ 151.1; $\gamma$-Toc-3, $m/z$ 411.3 > $m/z$ 151.2; $\delta$-Toc-3, $m/z$ 397.2 > $m/z$ 137.0. Typical MRM chromatograms of standard vitamin E homologues (A) and a rice bran extract (B) are shown in Figure S1A and B, respectively (Supporting Information). Tocs and Toc-3s concentrations in the rice bran extracts were calculated using calibration curves of standard Tocs and Toc-3s. The concentration was determined three times for each sample, and the average values are summarized in Table 2.

**UV−Vis Absorption Measurement of the Concentration of $\gamma$-Oryzanol Included in Rice Bran Extracts 1−7.** As reported previously,[14,19] $\gamma$-Ory extracted from rice germ oil contains 10 kinds of phytosterols. However, measurement of the concentration of each phytosterol included in rice bran extracts 1−7 was not performed in the present work, because the ArO•-scavenging rate of $\gamma$-Ory is two to 3 orders of magnitude smaller than those of $\alpha$-, $\beta$-, $\gamma$-, and $\delta$-Tocs and -Toc-3s, as will be discussed later. In the present work, the total concentration of $\gamma$-Ory included in rice bran extracts 1−7 was determined in ethanol from the UV−vis absorption spectrum, following the method performed by Chen and Bergman.[14] The values obtained are listed in Table 2, together with those for $\alpha$-, $\beta$-, $\gamma$-, and $\delta$-Toc and -Toc-3.

**Measurements.** Measurement of the second-order rate constants ($k_s^{AOH}(f)$ and $k_s^{AOH}(t_{1/2})$) and ARAC values for the reaction of ArO• with AOH (reaction 1) was performed using a Unisoku single-mixing stopped-flow spectrophotometer (Model RSP-1000), by mixing equal volumes of ethanol solutions of ArO• and AOH under nitrogen atmosphere.[17,26−28] The reaction was monitored with either single wavelength detection (Figure 2B) or a photodiode array detector (Figure 2A) attached to the stopped-flow spectrophotometer. All measurements were performed at 25.0 ± 0.5 °C. Experimental errors in the rate constants ($k_s^{AOH}(f)$ and $k_s^{AOH}(t_{1/2})$) were estimated to be about 7% in ethanol solution. Details of the measurements were described previously.[17,26−28]

## RESULTS AND DISCUSSION

**Rates of the Aroxyl-Radical-Scavenging ($k_s$) of Rice Bran Extracts 1−7 and $\gamma$-Oryzanol in Ethanol Solution.** UV−vis absorption spectra of rice bran extracts 1−7 and $\gamma$-Ory were measured in ethanol. The spectra observed for Koshihikari (3) and $\gamma$-Ory are shown in Figure 3A and B, respectively. The spectrum of Koshihikari (3) shows an absorption maximum ($\lambda_{max}$) at 328 nm and a shoulder ($\lambda_{shoulder}$) at ∼300 nm. Similar spectra were observed for extracts 1, 2, and 4−7. The absorption at 328 nm is attributable to $\gamma$-Ory ($\lambda_{max}$ = 328 nm ($\varepsilon_{max}$ = 35.6 L g$^{-1}$cm$^{-1}$) and $\lambda_{shoulder}$ ∼ 300 nm).[14,19] Weak broad absorption in the region between 380−500 nm (Figure 3A) is due to several carotenoids included in rice brans, as previously reported.[19] $\alpha$-, $\beta$-, $\gamma$-, $\delta$-Tocs and -Toc-3s show absorption maxima, $\lambda_{max}$, between 292−298 nm in ethanol, as previously reported.[29] The absorption bands of these Tocs and Toc-3s are thought to overlap with that of $\gamma$-Ory, because the $\varepsilon_{max}$ values (7.24−9.00 L g$^{-1}$cm$^{-1}$) of Tocs and Toc-3s are several times smaller than that of $\gamma$-Ory ($\varepsilon_{max}$ = 35.6 L g$^{-1}$cm$^{-1}$), and the concentrations of Tocs and Toc-3s are lower than that of $\gamma$-Ory (Table 2), as will be discussed later.[29]

The rate constant ($k_s^{Extract}$) for the reaction of the ArO• radical with rice bran extracts 1−7 was determined in ethanol at 25.0 °C (reaction 1). By reacting Oiran 4 with ArO• radical, the absorbance at 376 and 580 nm of the ArO• decreases, and the absorbance at 428 nm of Toc• and Toc-3• radicals, which will be mainly due to $\alpha$-Tocs• and $\alpha$-Toc-3•, increases, as shown in Figure 2A.[27,28] The decay rate ($k_{obsd}(f)$) of the ArO• radical was measured by following the decrease in absorbance at 580 nm (Figure 2B), because the absorption at 376 nm overlaps with that of Oiran 4 (specifically that of $\gamma$-Ory, as described above[19]). The pseudo-first-order rate constants ($k_{obsd}(f)$) at 580 nm were


dx.doi.org/10.1021/jf503996z | J. Agric. Food Chem. 2014, 62, 11901−11909

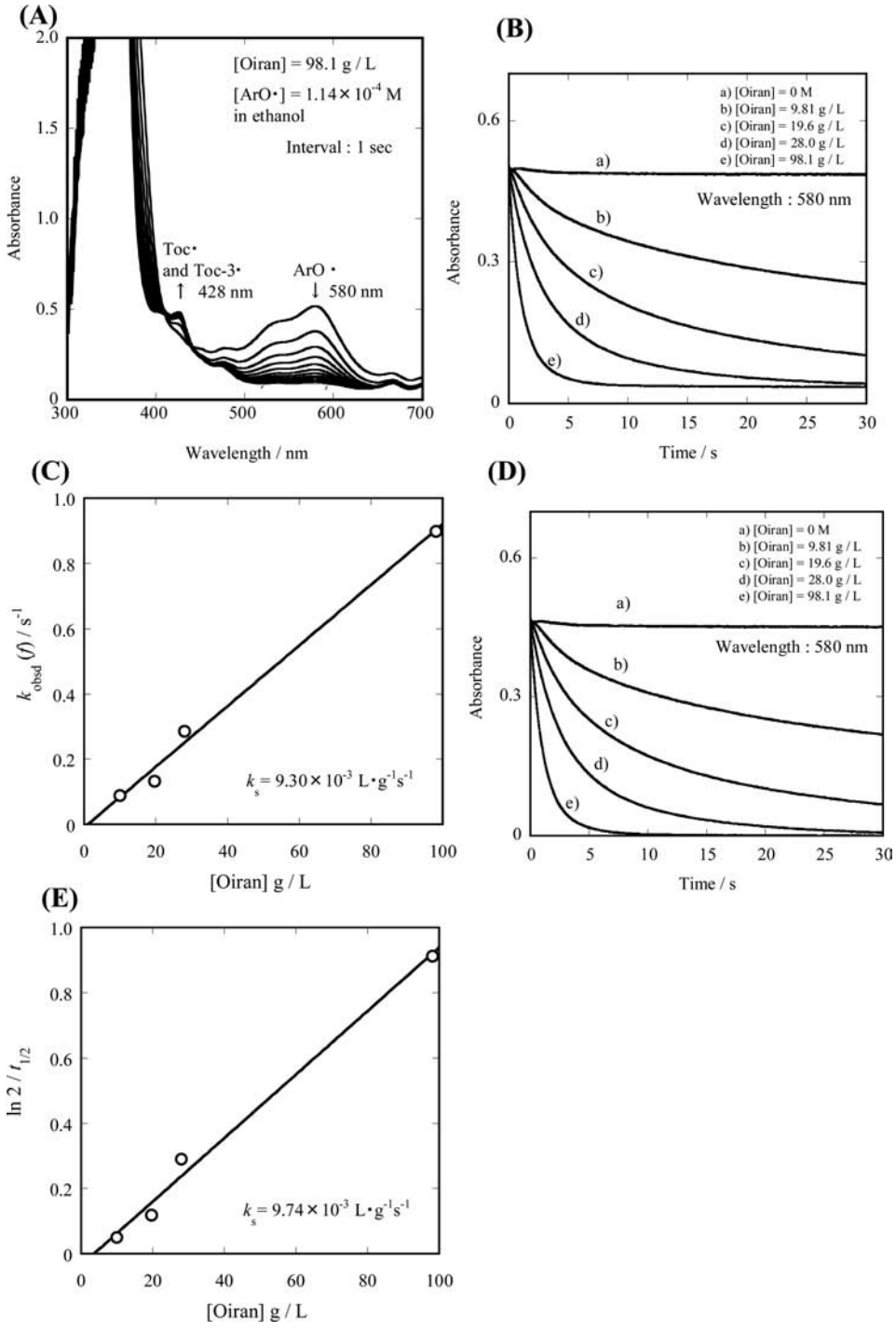


**Figure 2.** (A) Change in electronic absorption spectra of ArO• and Toc• (and Toc-3•) radicals during the reaction of ArO• with Oiran (4) in ethanol solution at 25.0 °C. The initial concentrations are [ArO•] = $1.14 \times 10^{-4}$ M and [Oiran] = 98.1 g/L. The spectra were recorded at 1 s intervals. The arrow indicates a decrease (ArO•) and increase (Toc• and Toc-3•) in absorbance with time. (B) Time dependences of the absorbance of the ArO• radical (at 580 nm) in solution containing five different concentrations of extract 4 at 25.0 °C. (C) Pseudo-first-order rate constant ($k_{obsd}$ ($f$)) versus [Oiran] plot. (D) Baseline correction. (E) ln $2/t_{1/2}$ versus [Oiran] plot.

linearly dependent on the concentration of the extract ([Extract]), and thus the rate equation is expressed as

$$-\mathrm{d}[\mathrm{ArO}\bullet]/\mathrm{d}t = k_{obsd}(f)\,[\mathrm{ArO}\bullet] = k_s^{\mathrm{Extract}}(f)\,[\mathrm{Extract}]\,[\mathrm{ArO}\bullet] \quad (2)$$

where $k_s$ ($f$) is the second-order rate constant for the oxidation of the extract by the ArO• radical. The rate constants ($k_s(f)$) were obtained by plotting $k_{obsd}(f)$ against [Extract], as shown in Figure 2C. Units of g/L were used for the concentrations of rice bran extracts 1−7. The $k_s(f)$ value obtained for Oiran (4) is $9.30 \times 10^{-3}$ L $g^{-1}s^{-1}$ (Table 1).

Equation 3 is easily obtained by substituting the relation for the first-order reaction ($k_{obsd}(f) = \ln 2/t_{1/2}$) into eq 2:

$$\ln 2/t_{1/2} = k_s^{\mathrm{Extract}}(t_{1/2})\,[\mathrm{Extract}] \quad (3)$$


dx.doi.org/10.1021/jf503996z | J. Agric. Food Chem. 2014, 62, 11901−11909

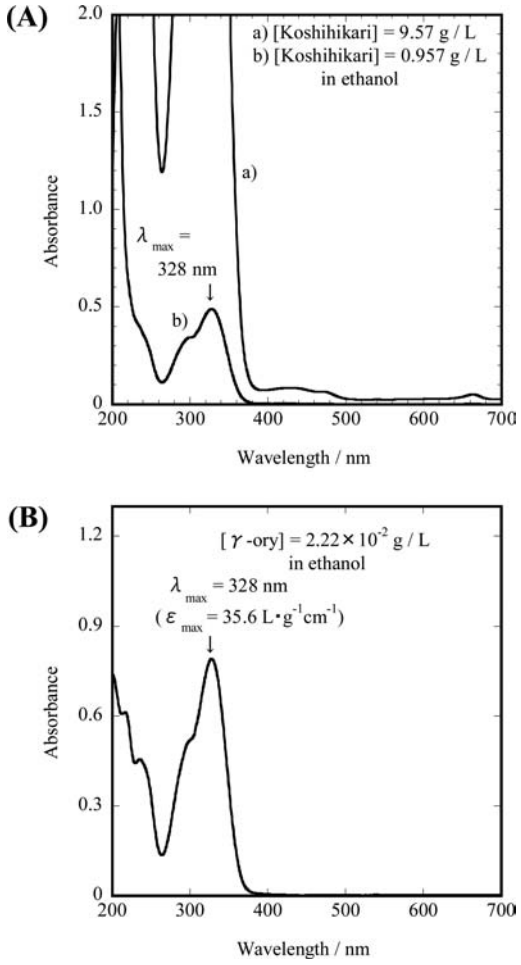


**Figure 3.** UV−vis absorption spectra of (A) Koshihikari (extract 3) and (B) γ-oryzanol in ethanol.

where $t_{1/2}$ is the half-life of ArO● in the presence of extract. To obtain the correct $t_{1/2}$ value in eq 3, baseline correction was performed for the decay curve of ArO● in Figure 2B. The results obtained are shown in Figure 2D. Equation 3 indicates that the $k_s^{Extract}$ ($t_{1/2}$) value can be obtained from a plot of ln $2/t_{1/2}$ versus [Extract]. An example for Oiran (4) is shown in Figure 2E. The value of $k_s^{Oiran}(t_{1/2})$ (= $9.74 \times 10^{-3}$ L $g^{-1}s^{-1}$) obtained for Oiran (4) was in good agreement with that of $k_s^{Oiran}(f)$ (= $9.30 \times 10^{-3}$ L $g^{-1}s^{-1}$), as listed in Table 1.

Similar measurements were performed for the reaction of ArO● with extracts 1−3, 5−7, and γ-Ory in ethanol solution. The result obtained for γ-Ory is shown in Figure 4. The $k_s^{Extract}(f)$ and $k_s^{Extract}(t_{1/2})$ values obtained for extracts 1−7 are summarized in Table 1, together with those of γ-Ory and α-Toc. Both $k_s^{Extract}(f)$ and $k_s^{Extract}(t_{1/2})$ increase in the following order:

$$\text{Milyang-23 (7)} \leq \gamma\text{-rich Koshihikari (6)} < \text{Moritawase (5)} \sim \text{Oiran (4)} < \text{Wataribune (3)} \sim \text{Koshihikari (2)} < \text{Nipponbare (1)} < \gamma\text{-oryzanol} < \alpha\text{-Toc} \quad (4)$$

Nipponbare (1) exhibits a $k_s^{Extract}(f)$ value 1.5 times larger than that of Milyang-23 (7). The $k_s^{\gamma\text{-Ory}}(f)$ value of γ-Ory is 2.1 times larger than that of Nipponbare (1). However, the value is 450 times smaller than that of α-Toc. The $k_s^{Extract}(f)$ values obtained for extracts 1−7 are shown as a bar graph in Figure 5A.

**Development of an Aroxyl Radical Absorption Capacity (ARAC) Assay Method for Food Extracts.** As

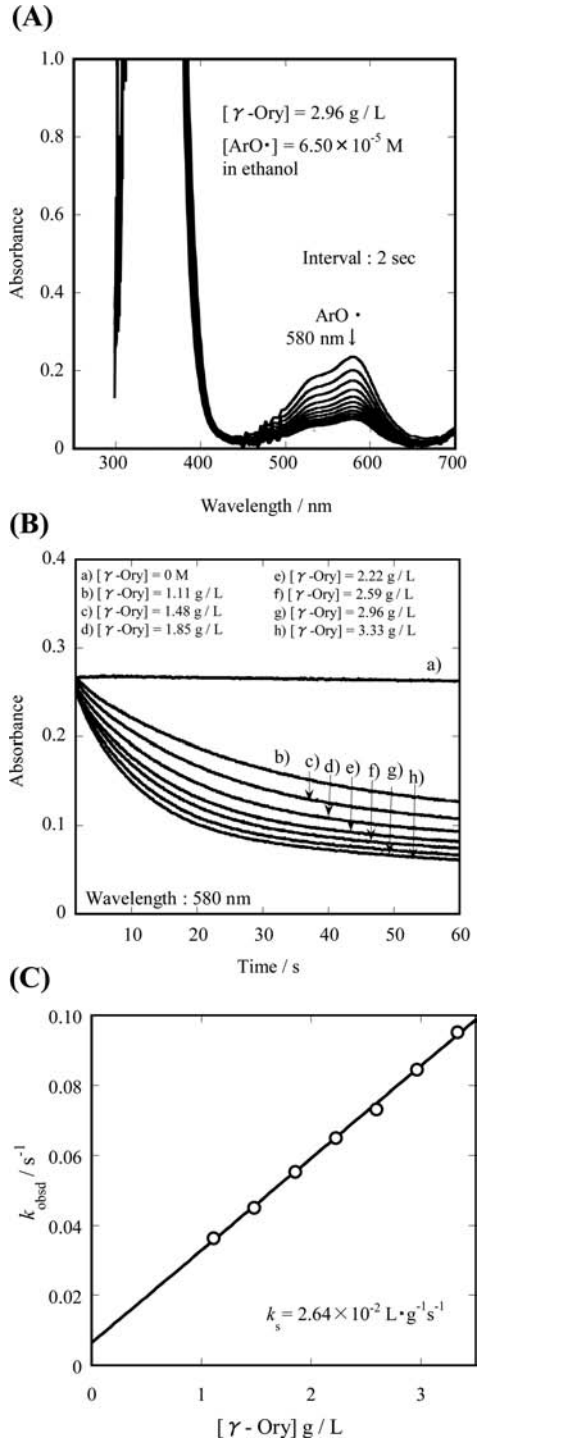


**Figure 4.** (A) Change in electronic absorption spectrum of the ArO● radical during the reaction of ArO● with γ-Ory in ethanol at 25.0 °C. [ArO●] = $6.50 \times 10^{-5}$ M and [γ-Ory] = 2.96 g/L. (B) Time dependences of the absorbance of the ArO● radical (at 580 nm) in ethanol containing eight different concentrations of γ-Ory at 25.0 °C. (C) Pseudo-first-order rate constant ($k_{obsd}(f)$) versus [γ-Ory] plot.

proposed previously,[17] relative ARAC ($f$) and ARAC ($t_{1/2}$) values for AOH were defined according to eqs 5 and 6:

$$\text{relative ARAC } (f) \text{ value (based on molar concentration unit (M = mol/L))} = k_s^{AOH}(f)\ (M^{-1}\,s^{-1}) / k_s^{\alpha\text{-Toc}}(f)\ (M^{-1}\,s^{-1}) \quad (5)$$


dx.doi.org/10.1021/jf503996z | J. Agric. Food Chem. 2014, 62, 11901−11909

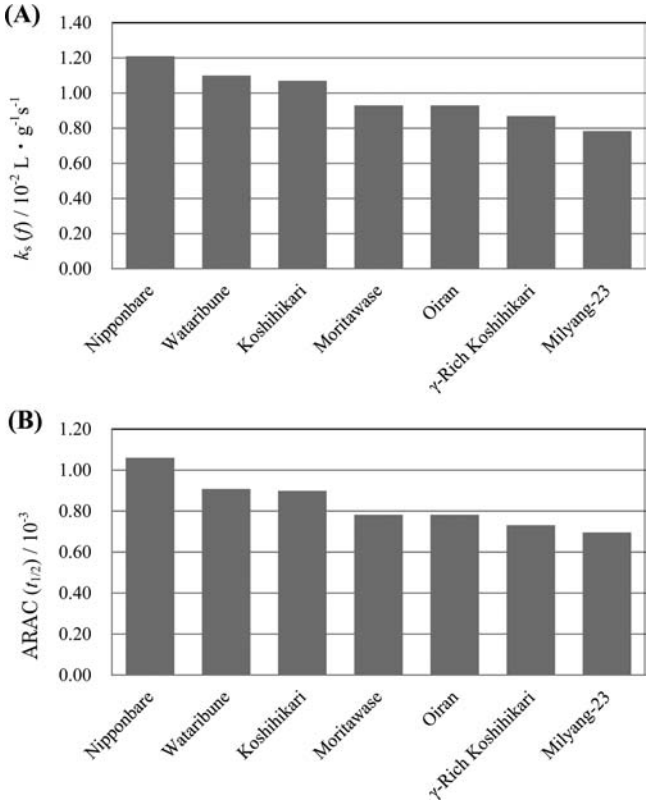


**Figure 5.** Comparison of (A) the $k_s(f)$ values and (B) the relative ARAC ($t_{1/2}$) values for seven kinds of rice bran extracts 1−7 in ethanol.

$$\text{relative ARAC } (t_{1/2}) \text{ value} = k_s^{\text{AOH}}(t_{1/2})\ (\text{M}^{-1}\,\text{s}^{-1}) / k_s^{\alpha\text{-Toc}}(t_{1/2})\ (\text{M}^{-1}\,\text{s}^{-1}) = (t_{1/2}{}^{\alpha\text{-Toc}}/t_{1/2}{}^{\text{AOH}}) \times ([\alpha\text{-Toc}]/[\text{AOH}]) \quad (6)$$

Equation 5 indicates that the ARAC ($f$) value corresponds to the ratio ($k_s^{\text{AOH}}(f)/k_s^{\alpha\text{-Toc}}(f)$) of the scavenging rate of ArO• ($k_s^{\text{AOH}}(f)$) by AOH to that ($k_s^{\alpha\text{-Toc}}(f)$) by $\alpha$-Toc. $\alpha$-Toc was used as a standard compound of ARAC assay.

By substituting the relation eq 3 into the second line of eq 6, we can obtain the third line of eq 6. According to eq 6, ARAC ($t_{1/2}$) value may be determined by the measurement of the half-life of the ArO• radical ($t_{1/2}{}^{\text{AOH}}$) and the concentration of AOH ([AOH]) without analysis of the decay rate of ArO•.

In the ARAC assay method, $\alpha$-Toc was used as a standard compound for the following reasons: (i) $\alpha$-Toc is a representative phenolic antioxidant, (ii) $\alpha$-Toc shows the same order of $k_s$ value as those for the other phenolic antioxidants (such as tocopherol homologues (4 Tocs and 4 Toc-3s), catechins, and ubiquinol-10),[17,26−28,30] (iii) $\alpha$-Toc and the above phenolic antioxidants often coexist in general foods[31−33] and biological systems (such as plasma[34] and mitochondria[35]), and function as free radical scavengers at a similar reaction field. Furthermore, $\alpha$-Toc was used as a standard compound in the singlet oxygen absorption capacity (SOAC) assay method, which was recently developed to evaluate the singlet oxygen quenching activity of many natural AOHs and food extracts.[36−38]

Units of g/L were used for the concentrations of rice bran extracts 1−7, while units of L $g^{-1}$ $s^{-1}$ were used for $k_s^{\text{Extract}}(f)$ and $k_s^{\text{Extract}}(t_{1/2})$ values. The ARAC values for extracts 1−7 were also calculated using g/L as the unit of concentration for AOH in eqs 5 and 6. The relative ARAC ($f$) (and ARAC ($t_{1/2}$)) values obtained for extracts 1−7 are shown as a bar graph in Figure 5B.

As summarized in Table 1, the $k_s^{\text{Extract}}(f)$ and $k_s^{\text{Extract}}(t_{1/2})$ values and the relative ARAC ($f$) and ARAC ($t_{1/2}$) values obtained for rice bran extracts 1−7 and $\gamma$-Ory are in good agreement with each other, suggesting that the ARAC assay method developed is applicable to the estimation of the free radical scavenging activity of food extracts. Measurement of ARAC values for many kinds of food extracts, including vegetable and fruit extracts and edible oils, will be necessary to verify the applicability of the ARAC assay method to food extracts, as performed for the SOAC assay method.[29,36−38]

**Contents of Eight Vitamin E Homologues and $\gamma$-Oryzanol in Rice Bran Extracts 1−7.** To compare the $k_s^{\text{Extract}}(f)$ value observed for rice bran extracts 1−7 with the value of $k_s^{\text{Extract}}(f)$ calculated using the rate constants ($k_s^{\text{AOH-i}}(f)$) and the concentrations ([AOH-i]) of each AOH included in extracts 1−7, measurements of the concentrations of 4 Tocs and 4 Toc-3s and $\gamma$-Ory were performed.

The concentrations (in mg/100 g) of 4 Tocs and 4 Toc-3s included in extracts 1−7 were measured using HPLC-MS/MS, as described in Materials and Methods. The results obtained are listed in Table 2. The concentrations of $\alpha$-, $\beta$-, $\gamma$-, $\delta$-Tocs, and -Toc-3s obtained for extracts 1−7 are in reasonable agreement with previously reported values.[15] High concentrations of Toc-3s are included in rice bran extracts 1−7, as listed in Table 2. Nipponbare (1) and Oiran (4) contain high total concentrations of $\alpha$-Toc and $\alpha$-Toc-3. Specifically, high concentrations of $\gamma$-Toc and $\gamma$-Toc-3 were included in $\gamma$-rich Koshihikari (6) and Milyang-23 (7).

On the other hand, the total concentration of $\gamma$-Ory included in extracts 1−7 was determined from the UV−vis absorption spectrum. As reported previously,[14,19] $\gamma$-Ory extracted from rice germ oil contains 10 kinds of phytosterols. Three of these, namely, cycloartenyl ferulate, 24-methylenecycloartanyl ferulate, and campesteryl ferulate, were major components of $\gamma$-Ory. In the present work, commercially available $\gamma$-Ory extracted from rice germ oil was used as a standard. The $\varepsilon_{\text{max}}$ value (35.6 L $g^{-1}cm^{-1}$) of $\gamma$-Ory at 328 nm in ethanol was determined from the UV−vis absorption spectrum of $\gamma$-Ory (see Figure 3B). Using this $\varepsilon_{\text{max}}$ value, the concentration (in mg/100 g) of $\gamma$-Ory included in extracts 1−7 was tentatively estimated. The values obtained are listed in Table 2, together with those for $\alpha$-, $\beta$-, $\gamma$-, and $\delta$-Toc, and -Toc-3. The concentration of $\gamma$-Ory in extracts 1−7 were similar (between 1400−1970 mg/100 g), and about 1 order of magnitude larger than those of total Tocs and Toc-3s (112−152 mg/100 g), as listed in Table 2.

**Comparison of Observed and Calculated ArO•-Scavenging Activities for Rice Bran Extracts 1−7.** It is well-known that various AOHs coexist not only in foods and plants, but also in human tissues. The $k_s^{\text{Extract}}(f)$ (L $g^{-1}s^{-1}$) values for rice bran extracts 1−7 were determined from a plot of $k_{\text{obsd}}(f)$ versus [Extract (g/L)] using eq 7.

$$k_{\text{obsd}}(f) = k_s^{\text{Extract}}(f)\ [\text{Extract}] \quad (7)$$

$$k_{\text{obsd}}(f) = \{\Sigma k_s^{\text{AOH-}i}(f)[\text{AOH-}i]/10^5\}\ [\text{Extract}] \quad (8)$$

As listed in Table 2, 4 Tocs and 4 Toc-3s and $\gamma$-Ory (abbreviated as AOH-i) are included in extracts 1−7. Polyphenols are also included in rice bran.[21,23] However, the concentrations of these polyphenols are not reported. Furthermore, carotenoids are included in rice bran extracts, as shown in Figure 3A.[21] However, as the free radical scavenging activity of

Table 3. Comparison between Observed and Calculated ArO• Scavenging Rates ($k_s^{Koshihikari}$ (Obsd.) and $\Sigma k_s^{AOH\text{-}i}(f) \times ([AOH\text{-}i]/10^5)$ (Calcd.)) for Koshihikari (3) in Ethanol Solution

| antioxidant | $k_s^{AOH\text{-}i}(f)$ ($M^{-1}$ $s^{-1}$) | Mw | $k_s^{AOH\text{-}i}(f)$ (L $g^{-1}$ $s^{-1}$) | [AOH-$i$] (mg/100 g) | $k_s^{AOH\text{-}i}(f) \times ([AOH\text{-}i]/10^5)$ (L $g^{-1}$ $s^{-1}$) |
|---|---|---|---|---|---|
| $\alpha$-Toc | $5.12 \times 10^3$ | 430.71 | 11.9 | 37.4 | $4.45 \times 10^{-3}$ |
| $\alpha$-Toc-3 | $4.97 \times 10^3$ | 424.66 | 11.7 | 22.1 | $2.58 \times 10^{-3}$ |
| $\beta$-Toc | $2.77 \times 10^3$ | 416.69 | 6.65 | 1.7 | $0.115 \times 10^{-3}$ |
| $\beta$-Toc-3 | $3.11 \times 10^3$ | 410.64 | 7.57 | 0.2 | $0.0126 \times 10^{-3}$ |
| $\gamma$-Toc | $2.82 \times 10^3$ | 416.69 | 6.77 | 6.8 | $0.460 \times 10^{-3}$ |
| $\gamma$-Toc-3 | $2.76 \times 10^3$ | 410.64 | 6.72 | 47.2 | $3.17 \times 10^{-3}$ |
| $\delta$-Toc | $1.02 \times 10^3$ | 402.67 | 2.53 | 0.6 | $0.0152 \times 10^{-3}$ |
| $\delta$-Toc-3 | $1.09 \times 10^3$ | 396.62 | 2.75 | 2.7 | $0.0743 \times 10^{-3}$ |
| $\gamma$-Oryzanol | | | $2.64 \times 10^{-2}$ | 1420 | $0.375 \times 10^{-3}$ |
| $\Sigma k_s^{AOH\text{-}i}(f) \times ([AOH\text{-}i]/10^5)$ (Calcd.) | | | | | $11.3 \times 10^{-3}$ |
| $k_s^{Extract}(f)$ (Obsd.) | | | | | $10.7 \times 10^{-3}$ |

Table 4. Comparison between Observed and Calculated ArO•-Scavenging Rates ($k_s^{Extract}(f)$ (Obsd.) and $k_s^{Extract}(f)$ (Calcd.)) for Rice Bran Extracts 1−7 in Ethanol, Ratio of the Rate Constants ($k_s^{Extract}(f)$ (Obsd.)/$k_s^{Extract}(f)$ (Calcd.)), and Contribution of $\gamma$-Oryzanol ($k_s^{\gamma\text{-}Ory}(f)$ (Calcd.))

| rice bran extract | $k_s^{Extract}(f)$ (Obsd.) (L $g^{-1}$ $s^{-1}$) | $k_s^{Extract}(f)$ (Calcd) (L $g^{-1}$ $s^{-1}$) | $k_s^{Extract}(f)$ (Obsd.)/$k_s^{Extract}(f)$ (Calcd) | $k_s^{\gamma\text{-}Ory}(f)$ (Calcd) (contribution of $\gamma$-Ory) |
|---|---|---|---|---|
| Nipponbare (1) | $1.26 \times 10^{-2}$ | $1.38 \times 10^{-2}$ | 0.913 | $4.12 \times 10^{-4}$ |
| Wataribune (2) | $1.08 \times 10^{-2}$ | $1.25 \times 10^{-2}$ | 0.864 | $3.70 \times 10^{-4}$ |
| Koshihikari (3) | $1.07 \times 10^{-2}$ | $1.13 \times 10^{-2}$ | 0.947 | $3.75 \times 10^{-4}$ |
| Oiran (4) | $9.30 \times 10^{-3}$ | $1.20 \times 10^{-2}$ | 0.775 | $3.70 \times 10^{-4}$ |
| Moritawase (5) | $9.30 \times 10^{-3}$ | $1.10 \times 10^{-2}$ | 0.845 | $5.20 \times 10^{-4}$ |
| $\gamma$-rich Koshihikari (6) | $8.70 \times 10^{-3}$ | $1.08 \times 10^{-2}$ | 0.806 | $4.25 \times 10^{-4}$ |
| Milyang-23 (7) | $8.29 \times 10^{-3}$ | $1.13 \times 10^{-2}$ | 0.734 | $4.04 \times 10^{-4}$ |

carotenoids is generally low, the contribution of carotenoids to the ArO•-scavenging rate is thought to be small and negligible.

Recently, measurements of the ArO•-scavenging rate constants ($k_s^{AOH}(f)$) of AOHs ($\alpha$-, $\beta$-, $\gamma$-, $\delta$-Tocs and -Toc-3s) were performed in ethanol solution.[30] $k_s^{AOH}(f)$ values of $\alpha$-, $\beta$-, $\gamma$-, $\delta$-Toc-3s were in good agreement with those of the corresponding $\alpha$-, $\beta$-, $\gamma$-, $\delta$-Tocs. The $k_s^{AOH}(f)$ values reported are listed in Table 3. The $k_s^{AOH}(f)$ value for $\gamma$-Ory was measured in the present work.

Consequently, the $k_s^{Extract}(f)$ values for extracts 1−7 were calculated using eq 8, that is, $\{\Sigma k_s^{AOH\text{-}i}(f)\,[AOH\text{-}i]/10^5\}$, where the $k_s^{AOH\text{-}i}(f)$ (L $g^{-1}s^{-1}$) values are the rate constants for 4 Tocs, 4 Toc-3s, and $\gamma$-Ory in ethanol (see Tables 3 and 4). [AOH-$i$] is the concentration (in mg/100 g) of Tocs, Toc-3s, and $\gamma$-Ory included in extracts 1−7 (see Table 2). As an example, the result of the detailed analysis performed for Koshihikari (3) is listed in Table 3. Good agreement between the observed $k_s^{Koshihikari}(f)$ value (= $1.07 \times 10^{-2}$ L $g^{-1}s^{-1}$) and calculated $\{\Sigma k_s^{AOH\text{-}i}(f)\,[AOH\text{-}i]/10^5\}$ value (= $1.13 \times 10^{-2}$ L $g^{-1}s^{-1}$) observed for Koshihikari (3). The contribution of $\gamma$-Ory to the total $k_s^{Koshihikari}(f)$ value is small and about 3.3% of the total rate. A similar result was obtained for Nipponbare (1) (see Table 4). These results indicate that the total ArO•-scavenging activity of Nipponbare (1) and Koshihikari (3) may be explained by only considering the contribution of 8 kinds of vitamin E homologues and $\gamma$-Ory included in Nipponbare (1) and Koshihikari (3). The contribution of the other AOHs is negligible. Furthermore, this result suggests that the interactions between 8 vitamin E homologues and among vitamin E homologues and many molecules included in rice bran extracts are weak and negligible in solution.

On the other hand, as listed in Table 4, $k_s^{Extract}(f)$ (Obsd.) values for extracts 2 and 4−7 are 14−27% smaller than the corresponding ($k_s^{Extract}(f)$ (Calcd.)) values calculated using only the concentrations of 4 Tocs, 4 Toc-3s, and $\gamma$-Ory. We may expect that the $k_s^{Extract}(f)$ (Obsd.) values for extracts 1−7 are similar to or larger than those ($k_s^{Extract}(f)$ (Calcd.)) calculated, because the other AOHs, such as polyphenols included in extracts 1−7, may also contribute to the $k_s^{Extract}(f)$ (Obsd.) values.[26]

In a previous study, measurements of the ArO•-scavenging rate constants ($k_s^{AOH}(f)$) of AOHs ($\alpha$-Toc, ubiquinol-10 ($UQ_{10}H_2$) and sodium ascorbate ($Na^+AsH^-$)) were performed in 2-propanol/water (5/1, v/v) solution.[28] $k_s^{AOH}(f)$ values were measured not only for each AOH but also for the mixtures of two AOHs ((i) $\alpha$-Toc and $UQ_{10}H_2$ and (ii) $\alpha$-Toc and $Na^+AsH^-$). A notable synergistic effect, namely, that the $k_s^{AOH}(f)$ values increase 1.6, 2.5, and 6.8 times for $\alpha$-Toc, $UQ_{10}H_2$, and $Na^+AsH^-$, respectively, was observed for the solutions containing two kinds of AOHs.

Furthermore, measurements of the ArO•-scavenging rate constants ($k_s^{AOH}(f)$) of AOHs ($\alpha$-, $\beta$-, $\gamma$-, $\delta$-Tocs) were recently performed in ethanol solution, not only for each AOH but also for the mixtures of two AOHs ((i) $\alpha$-Toc and $\beta$-Toc, (ii) $\alpha$-Toc and $\gamma$-Toc, and (iii) $\alpha$-Toc and $\delta$-Toc).[30] A considerable synergistic effect, namely, that the $k_s^{AOH}(f)$ value increases 12%, was observed for the solutions containing $\alpha$-Toc and $\gamma$-Toc. On the other hand, a canceling effect, namely that the $k_s^{AOH}(f)$ value decreases by (i) 7% and (ii) 24%, respectively, was observed for the solutions containing (i) $\alpha$-Toc and $\beta$-Toc and (ii) $\alpha$-Toc and $\delta$-Toc. Similar results were observed for the mixtures of $\alpha$-, $\beta$-, $\gamma$-, $\delta$-Toc-3s.[30]

In rice bran extracts 1−3 and 5, the concentrations of total $\alpha$-Toc and $\alpha$-Toc-3 and of total $\gamma$-Toc and $\gamma$-Toc-3 were higher than those of total $\beta$-Toc and $\beta$-Toc-3 (and total $\delta$-Toc and $\delta$-Toc-3), while the concentrations of total $\alpha$-Toc and $\alpha$-Toc-3

were similar to those of total γ-Toc and γ-Toc-3 (Table 2). Consequently, we may expect a synergistic effect (that is, an increase of the $k_s^{Extract}(f)$ values) for rice bran extracts 1−3 and 5. However, the $k_s^{Extract}(f)$ values observed for extracts 1−3 and 5 were similar to or smaller than the corresponding calculated values. High concentrations of proteins, lipids, and carbohydrates are included in rice bran extracts. The interactions between these compounds and Tocs (and Toc-3s) molecules may affect the ArO•-radical scavenging activity of AOHs. However, the reason is not clear at present. A detailed study will be necessary to clarify the reason why the values of the ratio ($k_s^{Extract}(f)$ (Obsd.)/$k_s^{Extract}(f)$ (Calcd.)) obtained for extracts 1−7 are ≤1 (Table 4).

In recent years, various methods to assess the free radical scavenging activity of natural antioxidants and vegetable and fruit extracts have been proposed.[16] The oxygen radical absorbance capacity (ORAC) assay method is one of the most frequently used methods.[39−42] The ORAC values for extracts of nearly 300 vegetables and fruits have been measured and are listed on the US Department of Agriculture (USDA) Web site (http://www.ars.usda.gov/SP2UserFiles/Place/12354500/Data/ORAC/ORAC07.pdf). However, to our regret, in 2012 the USDA's Nutrient Data Laboratory (NDL) removed the USDA ORAC Database for Selected Foods from the NDL Web site because of mounting evidence that the values indicating antioxidant capacity have no relevance to the effects of specific bioactive compounds, including polyphenols, on human health.[43] Accordingly, several alternative methods have been proposed to assess antioxidant capacity against free radicals.[16,44]

In a previous work, a new assay method that can quantify the aroxyl radical absorption capacity (ARAC) of phenolic AOHs, including α-, β-, γ-, δ-Tocs and five tocopherol derivatives, was proposed.[17] However, the examples of food extracts investigated were limited to a palm oil extract. In the present work, relative ARAC ($f$) and ARAC ($t_{1/2}$) values were measured for seven rice bran extracts 1−7, which include eight kinds of vitamin E homologues (4 Tocs and 4 Toc-3s) and γ-Ory. Results suggest that the ARAC assay method may be applicable not only to general natural AOHs but also to food extracts that include many kinds of AOHs.

## ■ ASSOCIATED CONTENT

### Supporting Information

Figure showing typical MRM chromatograms of standard vitamin E homologues (A) and a rice bran extract (B). This material is available free of charge via the Internet at http://pubs.acs.org.

## ■ AUTHOR INFORMATION

### Corresponding Author

*Tel: 81-89-927-9588. Fax: 81-89-927-9590. E-mail: mukai-k@dpc.ehime-u.ac.jp.

### Notes

The authors declare no competing financial interest.

## ■ ACKNOWLEDGMENTS

We are very grateful to Prof. Shin-ichi Nagaoka of Ehime University for his kind support. We also are very grateful to Prof. Hisako Sato and to Eri Ishikawa of Ehime University for their kind help in the preparation of rice bran extracts.

## ■ REFERENCES

(1) Niki, E. Antioxidant action of tocotrienols . *Tocotrienols: Vitamin E Beyond Tocopherols*, 2nd ed.; Tan, B., Watson, R., Preedy, V., Eds.; CRC/AOCS Press: Boca Raton, FL, 2012; Chapter 17, pp 233−240; and references cited therein.

(2) Parker, R. A.; Pearce, B. C.; Clark, R. W.; Gordon, D. A.; Wright, J. J. K. Tocotrienols regulate cholesterol production in mammalian cells by post-transcriptional suppression of 3-hydroxy-3-methylglutaryl-coenzyme A reductase. *J. Biol. Chem.* **1993**, *268*, 11230−11238.

(3) Black, T. M.; Wang, P.; Maeda, N.; Coleman, R. A. Palm tocotrienols protect ApoE ± mice from diet-induced atheroma formation. *J. Nutr.* **2000**, *130*, 2420−2426.

(4) Qureshi, A. A.; Sami, S. A.; Salser, W. A.; Khan, F. A. Dose-dependent suppression of serum cholesterol by tocotrienol-rich fraction ($TRF_{25}$) of rice bran in hypercholesterolemic humans. *Atherosclerosis* **2002**, *161*, 199−207.

(5) Sakai, M.; Okabe, M.; Tachibana, H.; Yamada, K. Apoptosis induction by γ-tocotrienol in human hepatoma Hep3B cells. *J. Nutr. Biochem.* **2006**, *17*, 672−676.

(6) Eitsuka, T.; Nakagawa, K.; Miyazawa, T. Down-regulation of telomerase activity in DLD-1 human colorectal adenocarcinoma cells by tocotrienol. *Biochem. Biophys. Res. Commun.* **2006**, *348*, 170−175.

(7) Nesaretnam, K.; Meganathan, P. Tocotrienols: inflammation and cancer. *Ann. N.Y. Acad. Sci.* **2011**, *1229*, 18−22.

(8) Shibata, A.; Nakagawa, K.; Kawakami, Y.; Tsuzuki, T.; Miyazawa, T. Suppression of γ-tocotrienol on UVB induced inflammation in HaCaT keratinocytes and HR-1 hairless mice via inflammatory mediators multiple signaling. *J. Agric. Food Chem.* **2010**, *58*, 7013−7020.

(9) Nakagawa, K.; Shibata, A.; Yamashita, S.; Tsuzuki, T.; Kariya, J.; Oikawa, S.; Miyazawa, T. In vivo angiogenesis is suppressed by unsaturated vitamin E, tocotrienol. *J. Nutr.* **2007**, *137*, 1938−1943.

(10) Shibata, A.; Nakagawa, K.; Sookwong, P.; Tsuduki, T.; Tomita, S.; Shirakawa, H.; Komai, M.; Miyazawa, T. Tocotrienol inhibits secretion of angiogenic factors from human colorectal adenocarcinoma cells by suppressing hypoxia-inducible factor-1α. *J. Nutr.* **2008**, *138*, 2136−2142.

(11) Khanna, S.; Roy, S.; Slivka, A.; Craft, T. K. S.; Chaki, S.; Rink, C.; Notestine, M. A.; DeVries, A. C.; Parinandi, N. L.; Sen, C. K. Neuroprotective properties of the natural vitamin E α-tocotrienol. *Stroke* **2005**, *36*, 2258−2264.

(12) Sookwong, P.; Nakagawa, K.; Yamaguchi, Y.; Miyazawa, T.; Kato, S.; Kimura, F.; Miyazawa, T. Tocotrienol distribution in foods: Estimation of daily tocotrienol intake of Japanese population. *J. Agric. Food Chem.* **2010**, *58*, 3350−3355.

(13) Sambanthamurthi, R.; Sundram, K.; Tan, Y.-A. Chemistry and biochemistry of palm oil. *Prog. Lipid Res.* **2000**, *39*, 507−558.

(14) Chen, M. H.; Bergman, C. J. A rapid procedure for analyzing rice bran tocopherol, tocotrienol, and γ-oryzanol contents. *J. Food Compos. Anal.* **2005**, *18*, 319−331.

(15) Sookwong, P.; Nakagawa, K.; Murata, K.; Kojima, Y.; Miyazawa, T. Quantitation of tocotrienol and tocopherol in various rice brans. *J. Agric. Food Chem.* **2007**, *55*, 461−466.

(16) Niki, E. Assessment of antioxidant capacity in vitro and in vivo. *Free Radical Biol. Med.* **2010**, *49*, 503−515 (review article) and references cited therein..

(17) Nagaoka, S.; Nagai, K.; Fujii, Y.; Ouchi, A.; Mukai, K. Development of a new free radical absorption capacity assay method for antioxidants: Aroxyl radical absorption capacity (ARAC). *J. Agric. Food Chem.* **2013**, *61*, 10054−10062.

(18) Xu, Z.; Godber, J. S. Purification and identification of components of γ-oryzanol in rice bran oil. *J. Agric. Food Chem.* **1999**, *47*, 2724−2728.

(19) Stöggl, W.; Huck, C.; Wongyai, S.; Scherz, H.; Bonn, G. Simultaneous determination of carotenoids, tocopherols, and γ-oryzanol in crude rice bran oil by liquid chromatography coupled to diode array and mass spectrometric detection employing silica C30 stationary phases. *J. Sep. Sci.* **2005**, *28*, 1712−1718.

(20) Abdul-Hamid, A.; Sulaiman, R. R. R.; Osman, A.; Saari, N. Preliminary study of the chemical composition of rice milling fractions stabilized by microwave heating. *J. Food Comp. Anal.* **2007**, *20*, 627−637.

(21) Nakornriab, M.; Sriseadka, T.; Wongpornchai, S. Quantification of carotenoid and flavonoid components in brans of some Thai black rice cultivars using supercritical fluid extraction and high-performance liquid chromatography−mass spectrometry. *J. Food Lipids* **2008**, *15*, 488−503.
(22) Oka, T.; Fujimoto, M.; Nagasaka, R.; Ushio, H. H.; Hori, M.; Ozaki, H. Cycloartenyl ferulate, a component of rice bran oil-derived γ-oryzanol, attenuates mast cell degranulation. *Phytomedicine* **2010**, *17*, 152−156.
(23) Ajitha, M. J.; Mohanlal, S.; Suresh, C. H.; Jayalekshmy, A. DPPH radical scavenging activity of tricin and its conjugates isolated from "Njavara" rice bran: A density functional theory study. *J. Agric. Food Chem.* **2012**, *60*, 3693−3699.
(24) Gregor, C. B.; Nakagawa, K.; Abe, T.; Kimura, F.; Miyazawa, T. Tocotrienol modulates crucial lipid metabolism-related genes in differentiated 3T3-L1 preadipocytes. *Food Funct.* **2014**, *5*, 2221−2227.
(25) Rieker, A.; Scheffler, K. Die beteiligung von phenylresten an der aroxylmesomerie. *Liebigs Ann. Chem.* **1965**, *689*, 78−92.
(26) Mitani, S.; Ouchi, A.; Watanabe, E.; Kanesaki, Y.; Nagaoka, S.; Mukai, K. Stopped-flow kinetic study of the aroxyl radical-scavenging action of catechins and vitamin C in ethanol and micellar solutions. *J. Agric. Food Chem.* **2008**, *56*, 4406−4417.
(27) Mukai, K.; Ouchi, A.; Mitarai, A.; Ohara, K.; Matsuoka, C. Formation and decay dynamics of vitamin E radical in the antioxidasnt reaction of vitamin E. *Bull. Chem. Soc. Jpn.* **2009**, *82*, 494−503.
(28) Mukai, K.; Ouchi, A.; Nakaya, S.; Nagaoka, S. Aroxyl-radical-scavenging rate increases remarkably under the coexistence of α-tocopherol and ubiquinol-10 (or vitamin C): Finding of synergistic effect on the reaction rate. *J. Phys. Chem. B* **2013**, *117*, 8378−8391.
(29) Mukai, K.; Ishikawa, E.; Ouchi, A.; Nagaoka, S.; Suzuki, T.; Izumisawa, K.; Koike, T. Kinetic study of the quenching reaction of singlet oxygen by α-, β-, γ-, δ-tocotrienols and palm oil and soybean extracts in solution. *Biosci. Biotechnol. Biochem.* **2014**, in press.
(30) Ouchi, A.; Nagaoka, S.; Suzuki, T.; Izumisawa, K.; Koike, T.; Mukai, K. Finding of synergistic and cancel effects on the aroxyl radical-scavenging rate and suppression of prooxidant effect under the coexistence of α-tocopherol and β-, γ-, and δ-tocopherols (or -tocotrienols). *J. Agric. Food Chem.* **2014**, *62*, 8101−8113.
(31) Hewavitharana, A. K.; van Brakel, A. S.; Harnett, M. Simultaneous liquid chromatographic determination of vitamins A, E, and β-carotene in common diary foods. *Int. Dairy J.* **1996**, *6*, 613−624.
(32) Kurilich, A. C.; Tsau, G. J.; Brown, A.; Howard, L.; Klein, B. P.; Jeffery, E. H.; Kushad, M.; Wallig, M. A.; Juvik, J. A. Carotene, tocopherol, and ascorbate contents in subspecies of *Brassica oleracea*. *J. Agric. Food Chem.* **1999**, *47*, 1576−1581.
(33) Burns, J.; Fraser, P. D.; Bramley, P. M. Identification and quantification of carotenoids, tocopherols, and chlorophylls in commonly consumed fruits and vegetables. *Phytochemistry* **2003**, *62*, 939−947.
(34) Colome, C.; Artuch, R.; Vilaseca, M.-A.; Sierra, C.; Brandi, N.; Lambruschini, N.; Cambra, F. J.; Campistol, J. Lipophilic antioxidants in patients with phenylketonuria. *Am. J. Clin. Nutr.* **2003**, *77*, 185−188.
(35) Lass, A.; Foster, M. J.; Sohal, R. S. Effects of coenzyme $Q_{10}$ and α-tocopherol administration on their tissue levels in the mouse elevation of mitochondrial α-tocopherol by coenzyme $Q_{10}$. *Free Radical Biol. Med.* **1999**, *26*, 1375−1383.
(36) Ouchi, A.; Aizawa, K.; Iwasaki, Y.; Inakuma, T.; Terao, J.; Nagaoka, S.; Mukai, K. Kinetic study of the quenching reaction of singlet oxygen by carotenoids and food extracts in solution. Development of a singlet oxygen absorption capacity (SOAC) assay method. *J. Agric. Food Chem.* **2010**, *58*, 9967−9978.
(37) Aizawa, K.; Iwasaki, Y.; Ouchi, A.; Inakuma, T.; Nagaoka, S.; Terao, J.; Mukai, K. Development of singlet oxygen absorption capacity (SOAC) assay method. 2. Measurements of the SOAC values for carotenoids and food extracts. *J. Agric. Food Chem.* **2011**, *59*, 3717−3729.
(38) Mukai, K.; Ouchi, A.; Takahashi, S.; Aizawa, K.; Inakuma, T.; Terao, J.; Nagaoka, S. Development of singlet oxygen absorption capacity (SOAC) assay method. 3. Measurements of the SOAC values for phenolic antioxidants. *J. Agric. Food Chem.* **2012**, *60*, 7905−7916.
(39) Cao, G.; Alessio, H. M.; Cutler, R. G. Oxygen-radical absorbance capacity assay for antioxidants. *Free Radical Biol. Med.* **1993**, *14*, 303−311.
(40) Wang, H.; Cao, G.; Prior, R. L. Total antioxidant capacity of fruits. *J. Agric. Food Chem.* **1996**, *44*, 701−705.
(41) Ou, B.; Hampsch-Woodill, M.; Prior, R. L. Development and validation of an improved oxygen radical absorbance capacity assay using fluorescein as the fluorescent probe. *J. Agric. Food Chem.* **2001**, *49*, 4619−4626.
(42) Huang, D.; Ou, B.; Hampsch-Woodill, M.; Flanagan, J. A.; Deemer, E. K. Development and validation of oxygen radical absorbance capacity assay for lipophilic antioxidants using randomly methylated β-cyclodextrin as the solubility enhancer. *J. Agric. Food Chem.* **2002**, *50*, 1815−1821.
(43) U.S. Department of Agriculture, Agricultural Research Service. *Oxygen Radical Absorbance Capacity (ORAC) of Selected Foods, Release 2 (2010)*. http://www.ars.usda.gov/services/docs.htm?docid=15866 (accessed June 2013).
(44) Takashima, M.; Horie, M.; Shichiri, M.; Hagihara, Y.; Yoshida, Y.; Niki, E. Assessment of antioxidant capacity for scavenging free radicals in vitro: A rational basis and practical application. *Free Radical Biol. Med.* **2012**, *52*, 1242−1252 and references cited therein..

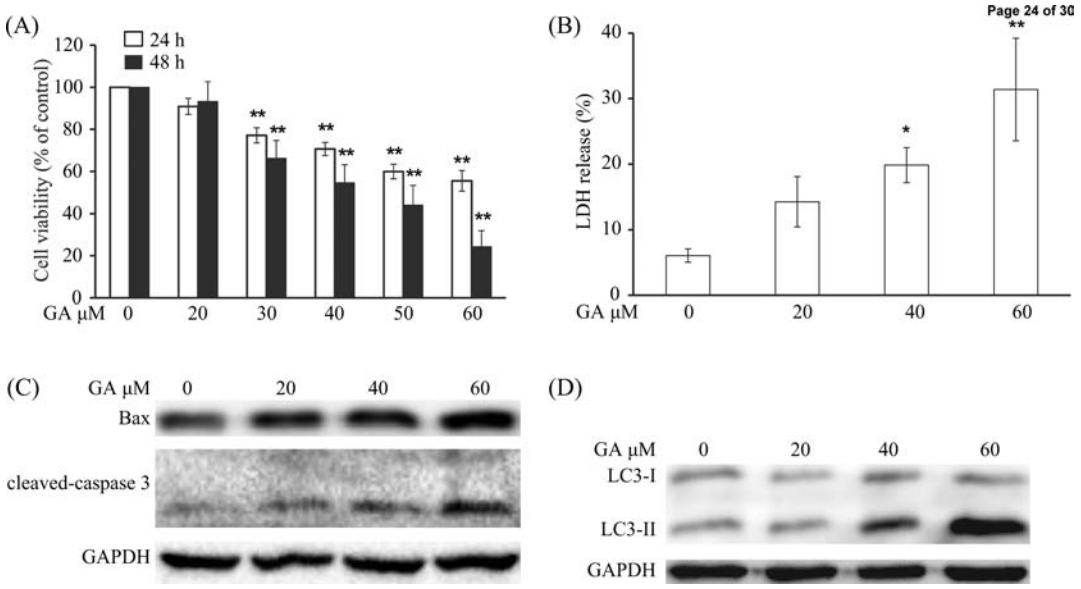


**Figure 1.** GA reduced the cell viability, enhanced LDH release, and increased the expression of Bax, cleaved caspase-3, and LC3-II in HCC cells. (A) Cells were treated with indicated concentrations of GA for 24 or 48 h. The cell viability was evaluated by MTT assay. (*) $P < 0.05$ and (**) $P < 0.01$, compared with 0 $\mu$M GA treatment. (B) Cells were treated with 0, 20, 40, and 60 $\mu$M GA for 24 h, and the LDH assay was performed according to the manufacturer. (*) $P < 0.05$ and (**) $P < 0.01$, compared with 0 $\mu$M GA treatment. (C, D) HepG2 cells were treated with indicated dosages of GA for 24 h. Cell extracts were analyzed for the expression levels of Bax, cleaved caspase-3, and LC3 by Western blot analysis.

dysfunctional cellular components through the actions of lysosomes.[18,19] In the initiation of tumors, autophagy inhibits tumor formation by degradation of damaged organelles or proteins.[20] However, after tumor formation, the tumors can utilize the autophagy as a survival mechanism to ensure growth advantage of cancer cells in a hypoxia, starvation, and acid environment.[21] Herein, we confirmed that GA induced autophagy in HCC cells by activation of extracellular regulated protein kinases (ERK), and inhibition of autophagy or ERK activation, GA-induced proliferative inhibition, and apoptosis were enhanced. Our study suggested that the GA triggered autophagic effect may attenuate the anticancer efficiency of GA or chemotherapeutic drugs loaded with GA-modified TDDS and requires further evaluation.

## MATERIALS AND METHODS

**Reagents.** GA was obtained from National Institutes for Food and Drug Control (Shenzhen, Guangdong, China). Monodansylcadaverine (MDC), chloroquine (CQ), bafilomycin A1 (BAF), and dimethyl sulfoxide (DMSO) were obtained from Sigma (St. Louis, MO, USA). PD98059 and U0126 were purchased from Beyotime Biotechnology Corp. (Shanghai, China). A Cytotoxicity Detection Kit (lactate dehydrogenase, LDH) was obtained from Roche Diagnostics (Mannheim, Germany). 3-(4,5-Dimethyl-2-thiazolyl)-2,5-diphenyltetrazolium bromide (MTT) was purchased from Molecular Probes (Eugene, OR, USA). Dulbecco's modified Eagle's medium (DMEM) medium, fetal bovine serum (FBS), antibiotics (100 U/mL penicillin and 100 mg/mL streptomycin), and phosphate-buffered saline (PBS) were purchased from Gibco (Carlsbad, CA, USA). Primary antibodies, that is, microtubule-associated protein light-chain 3 (LC3), ERK, p-ERK (Thr202/Tyr204), Bax, cleaved caspase-3, cleaved caspase-9, and GAPDH, and the secondary antibodies were purchased from Cell Signaling Technology Inc. (Beverly, MA, USA).

**Cell Culture.** Hepatocellular carcinoma HepG2 and Hep3B cells were obtained from the American Type Culture Collection (ATCC, Rockville, MD, USA) and cultured in a DMEM supplemented with 10% (v/v) FBS and 1% (v/v) antibiotics (100 U/mL penicillin, 100 $\mu$g/mL streptomycin). Cells were cultured in a 5% $CO_2$ incubator at 37 °C. Exponentially growing cells were used in the experiments.

**MTT Assay.** Cell viability was examined by the MTT assay. Exponentially growing HepG2 cells were seeded onto 96-well plates. Upon reaching approximately 70−80%, cells were incubated with a series of concentrations of the test compounds. Then, cell viability was determined by incubating the cells in a medium containing 1 mg/mL MTT for 4 h before 100 $\mu$L of DMSO was added to solubilize the formazan. The absorbance at 570 nm was measured with a microplate reader (PerkinElmer, 1420 Multilabel Counter Victor3, Wellesley, MA, USA).

**LDH Assay.** HepG2 cells were cultured to 70−80% concentration on 96-well plates and then treated with the indicated concentrations of GA for 24 h. The cellular toxicity was studied by detection of the LDH released into the incubation medium by the cytotoxicity detection kit according to the manufacturer's instructions.

**MDC Staining.** The autofluorescent agent MDC (excitation, 360 nm; emission, 535 nm) was utilized to evaluate the abundance of acidic vesicular organelles (AVOs) in the cells because it can accumulate in AVOs and exhibit fluoresced bright green dots.[22] For qualitative analysis, cells were seeded onto 96-well plates, treated with indicated concentrations of GA for 24 h and stained with 50 $\mu$M MDC in PBS for 30 min. Cells were washed with PBS three times and immediately analyzed using In Cell Analyzer 2000 imaging system (GE Healthcare, Uppsala, Sweden). For qualitative analysis, cells were seeded onto 24-well plates and treated with a series of concentrations of the test compounds. Then, cells were stained with 50 $\mu$M MDC in PBS for 30 min. After washed with PBS three times, the mean fluorescence intensities of the cells were determined with a flow cytometer (Becton Dickinson FACS CantoTM, BD Biosciences, San Jose, USA).

**Transmission Electron Microscopy (TEM) Assay.** After treatment or not with 40 $\mu$M GA for 24 h, the cells were harvested and washed with PBS and then fixed in ice-cold 2.5% glutaraldehyde for 1 h. After being washed with PBS three times for 15 min, cells were postfixed in 1% $OsO_4$ for 1 h and stained with 2% uranyl acetate for 30 min at room temperature. Then cells were dehydrated through a graded series of ethanol (50, 70, and 90%) for 15 min each, ethanol (100%) for 20 min, and 100% acetone for 20 min, respectively, and embedded in Epon812. Ultrathin sections (120 nm) were obtained before staining with 2% uranyl acetate for 20 min and lead citrate for 5 min and then examined using a TECNAI 10 transmission electron

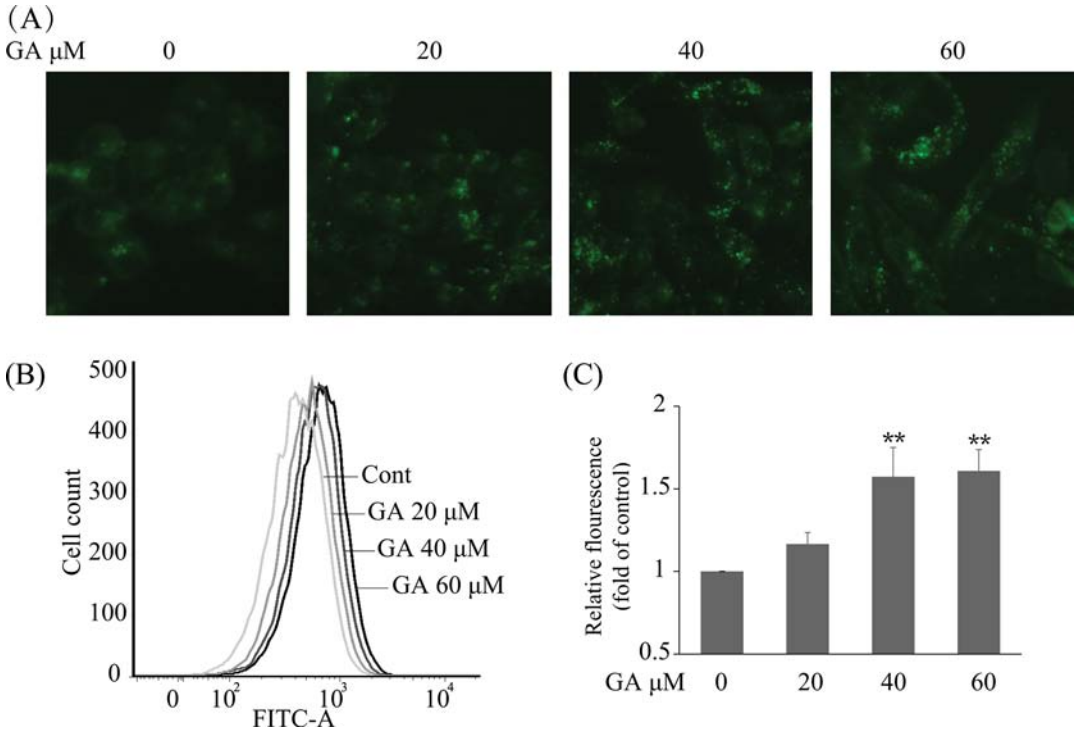


**Figure 2.** GA -triggered autophagy in HepG2 cells by MDC staining. (A) HepG2 cells were treated with GA at indicated concentrations for 24 h. The cells were collected, washed with PBS, and incubated with 50 $\mu$M MDC probe for 30 min. AVOs (bright green dots) in HepG2 cells were imaged with a fluorescent microscope. (B) The treated cells were stained with 50 $\mu$M MDC probe for 30 min, collected, washed, and resuspended. The intracellular fluorescence was quantified using flow cytometry. (C) Statistical result of three independent tests of (B). Data represent the mean ± SD, and one-way ANOVA was performed to evaluate the significance of different treatment. (∗) $P < 0.05$ and (∗∗) $P < 0.01$, compared with 0 $\mu$M GA treatment.

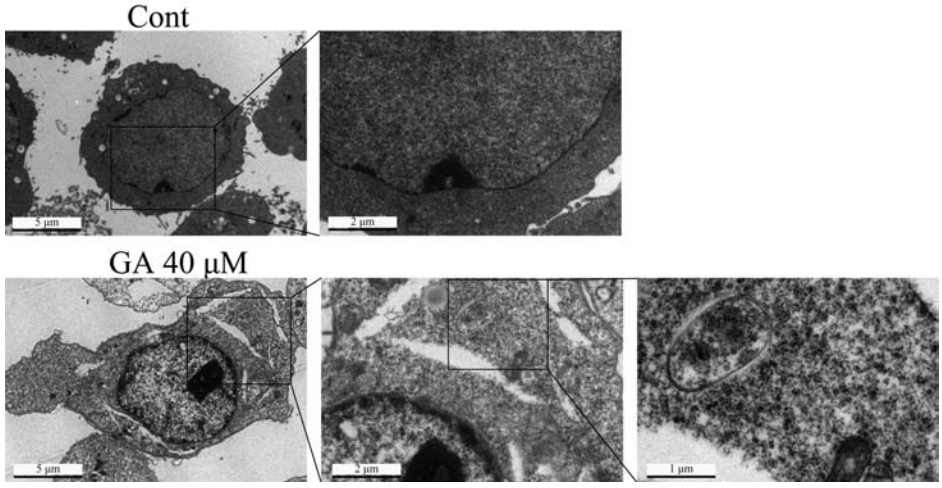


**Figure 3.** GA-triggered autophagy in HepG2 cells by TEM observation. HepG2 cells were treated with 40 $\mu$M GA or vehicle control for 24 h. Cells were collected, fixed, and observed under a TEM.

microscope (Phillips, Eindhoven, The Netherlands) at high voltage of 80 kV.

**Western Blot Analysis.** Proteins were extracted with a radioimmunoprecipitation lysis buffer containing 1% phenylmethanesulfonyl fluoride and 1% protease inhibitor cocktail for 25 min. The protein concentrations were measured with a BCA Protein Assay Kit (Pierce, Rockford, IL, USA). Equal amounts of proteins were separated using sodium dodecyl sulfate–polyacrylamide gel electrophoresis and transferred to a polyvinylidene fluoride membrane, which was blocked in 5% nonfat dried milk for 1 h. The membranes were probed with specific primary antibodies against LC3, p-ERK (Thr202/Tyr204), ERK, Bax, cleaved caspase-3, cleaved caspase-9, and GAPDH followed by incubation with the corresponding secondary antibodies. The specific protein bands were detected with an ECL advanced Western blot analysis detection kit (BD Biosciences, Bedford, MA, USA).

**Statistical Analysis.** The mean ± standard deviation (SD) was determined for each group. Statistical analysis was performed with one-way analysis of variance (ANOVA) and Tukey's test. Differences were considered statistically significant for (∗) $P < 0.05$ and (∗∗) $P < 0.01$.

## RESULTS

**GA Reduced the Cell Viability, Enhanced LDH Release, and Increased the Expression of Bax, Cleaved Caspase-3, and LC3-II in HCC Cells.** First, the MTT assay was used to evaluate the cell viability. As shown in Figure 1A, the cell viability of HepG2 cells was concentration- and time-dependently reduced after GA treatment. After treatment with 40 $\mu$M GA for 24 and 48 h, 71 and 55% HepG2 cells survived, respectively. We also found that GA increased LDH release into the medium in a concentration-dependent manner (Figure 1B), indicating that necrosis has occurred.[23] The apoptosis-related proteins, such as Bax and cleaved caspase-3, were also obviously enhanced after GA treatment (Figure 1C), which was similar to a previous study.[11] Besides, the expression of LC3-II, which correlates with the number of autophagosomes,[24] was concentration-dependently up-regulated after GA treatment (Figure 1D).

**GA Triggered Autophagy in HCC Cells.** To further confirm GA-triggered autophagy in HepG2 cells, multiple approaches were used. As AVOs are a hallmark of autophagy,[25] we initially evaluated the generation of AVOs by autofluorescent agent MDC, which accumulates in AVOs and fluoresces bright green dots.[22,26] The formation of AVOs in HepG2 cells was enhanced after treatment with various concentrations of GA for 24 h as evidenced by obvious green dot formation, whereas the control cells exhibited faint fluorescence only (Figure 2A). The GA-mediated AVO accumulation was also quantified using flow cytometry; GA concentration-dependently increased fluorescence intensity in HepG2 cells after 24 h of treatment. The 40 $\mu$M GA-treated cells exhibited an approximately 1.57-fold increase in fluorescence intensity compared with that of the control group (Figure 2B,C), which was consistent with morphological observations, suggesting that GA truly induces AVO production in HepG2 cells. Another traditional and classical method for autophagy observation is transmission electron microscopy (TEM) analysis.[27] Herein, the TEM experiment was performed to confirm the formation of AVOs after GA treatment in HepG2 cells. As shown in Figure 3, more AVOs were developed in the GA-treated group than in the control group. To further study GA-induced autophagic flux in HepG2 cells, two autophagy inhibitors, that is, chloroquine (CQ) and bafilomycin A1 (BAF), which cause accumulation of LC3-II protein by blocking the fusion between autophagosome and lysosome or suppressing the acidification of the lysosome,[27] were used. After pretreatment with CQ (10 $\mu$M) or BAF (100 nM), the GA-induced up-regulation of LC3-II was more prominent than in nontreated cells (Figure 4B), indicating that GA induces autophagic flux in HepG2 cells. GA-triggered autophagy was also confirmed in HCC Hep3B cells as evidenced by GA concentration-dependently increased expression of LC3-II (Supporting Information Supplemental Figure 1). Taken together, these data collectively indicate that GA triggers autophagy in HCC cells.

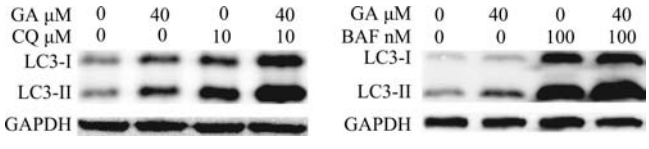


**Figure 4.** GA-triggered autophagic flux in HepG2 cells by Western blot analysis. HepG2 cells were incubated in 40 $\mu$M GA for 24 h with or without pretreatment of CQ (10 $\mu$M, 1 h) or BAF (100 nM, 1 h). Cell extracts were analyzed for LC3 expression levels using Western blot analysis.

**GA-Triggered Protective Autophagy in HCC Cells.** Natural compound-induced autophagy may be either pro-survival or pro-death in cancer therapy.[28,29] Herein, to clarify the effect of GA-induced autophagy in HCC cells, we evaluated the GA-mediated cell survival and apoptosis in cells pretreated with the autophagy inhibitors CQ (10 $\mu$M, 1 h) or BAF (100 nM, 1 h). MTT results indicated that survival rates of GA-treated HepG2 cells were decreased from 69.79 to 46.09 or 22.13% via pretreatment with CQ or BAF, respectively (Figure 5A). Western blot analysis indicated that pretreatment with CQ or BAF obviously enhanced the protein levels of cleaved caspase-3 and cleaved caspase-9 in HepG2 cells (Figure 5B). Besides, the cell viability of Hep3B cells was decreased from 63.47% (GA only) to 52.85% (GA + CQ) or 53.47% (GA + BAF), respectively (Supplemental Figure 2). Taken together, these data suggest that GA triggers a protective autophagy in HCC cells.

**GA-Triggered Autophagy by Activation of ERK in HepG2 Cells.** To further determine the molecular mechanism of GA-triggered autophagy induction in HepG2 cells, we evaluated the activation status of ERK signaling, a critical pathway of autophagy induction.[30,31] Phosphorylated ERK (p-ERK) and total ERK were assayed after cells had been treated with different concentrations of GA. As shown in Figure 6A, expression of p-ERK was concentration-dependently increased after treatment with GA for 24 h, indicating that GA activated ERK in HepG2 cells. In addition, we examined whether the activated ERK was critical for GA-triggered autophagy. Cells were pretreated with the MEK inhibitor (U0126 or PD98059), the p-ERK, as well as the GA-induced expression of LC3-II was decreased (Figure 6B,C). Furthermore, the GA-induced AVO formation was also decreased after pretreatment with PD98059 (Figure 6D).

**Inhibition of ERK Enhanced GA-Induced Cell Death and Apoptosis.** We further studied the effects of the ERK pathway in GA-induced cell death and apoptosis. As shown in Figure 7A, the cell viability of HepG2 was 69.79% after treatment with GA alone, whereas it decreased to 54.78% after combined treatment with PD98059 and GA. Furthermore, the expression of cleaved caspase-3 was more obvious in the PD98059 + GA group compared with the GA alone group (Figure 7B).

## DISCUSSION

Targeted drug treatment is a novel promising strategy for HCC, which specifically delivers chemotherapeutic drugs to HCC and results in increased local concentrations and reduced side effects.[32] GA is an excellent ligand for HCC-targeting due to the abundant binding sites on the cellular membrane of liver cells.[14] Besides, GA exhibits potential anti-HCC effects by inhibition of proliferation and induction of apoptosis and cell cycle arrest.[11] Herein, we demonstrated that GA induced cell viability reduction, LDH release, and up-regulation of Bax and cleaved caspase-3, indicating that necrosis and apoptosis may contribute to GA-induced cell death. We also found, for the first time, that GA triggered the autophagic response in HCC cells as evidenced by obvious up-regulation of AVO formation by MDC staining and TEM detection, and by elevation of LC3-II protein expression by Western blot analysis and that

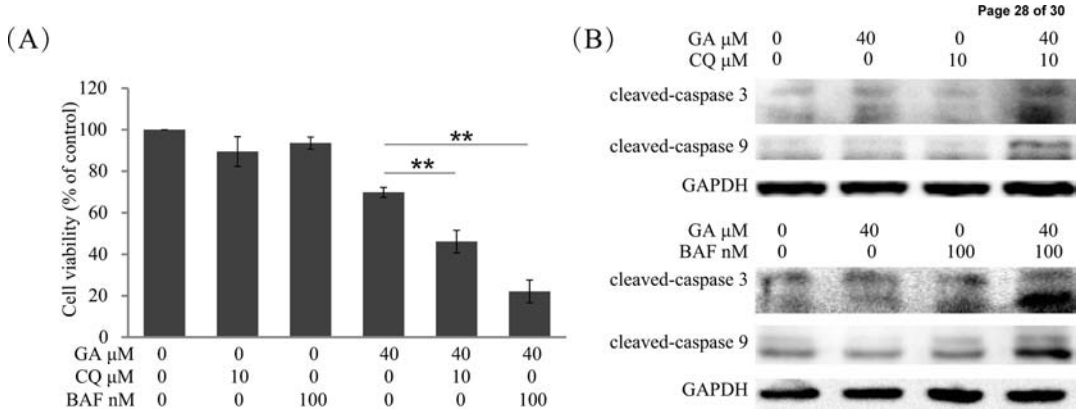


**Figure 5.** Inhibition of autophagy enhanced GA-induced cell death and apoptosis in HepG2 cells. (A) HepG2 cells were treated with indicated concentrations of GA for 24 h with or without pretreatment of CQ (10 $\mu$M, 1 h) or BAF (100 nM, 1 h). Cell viability was evaluated by MTT assay. (*) $P < 0.05$ and (**) $P < 0.01$. (B) HepG2 cells were treated with 40 $\mu$M GA for 24 h with or without pretreatment of CQ (10 $\mu$M, 1 h) or BAF (100 nM, 1 h). Cell extracts were analyzed for the levels of cleaved caspase-3 and cleaved caspase-9 by Western blot analysis.

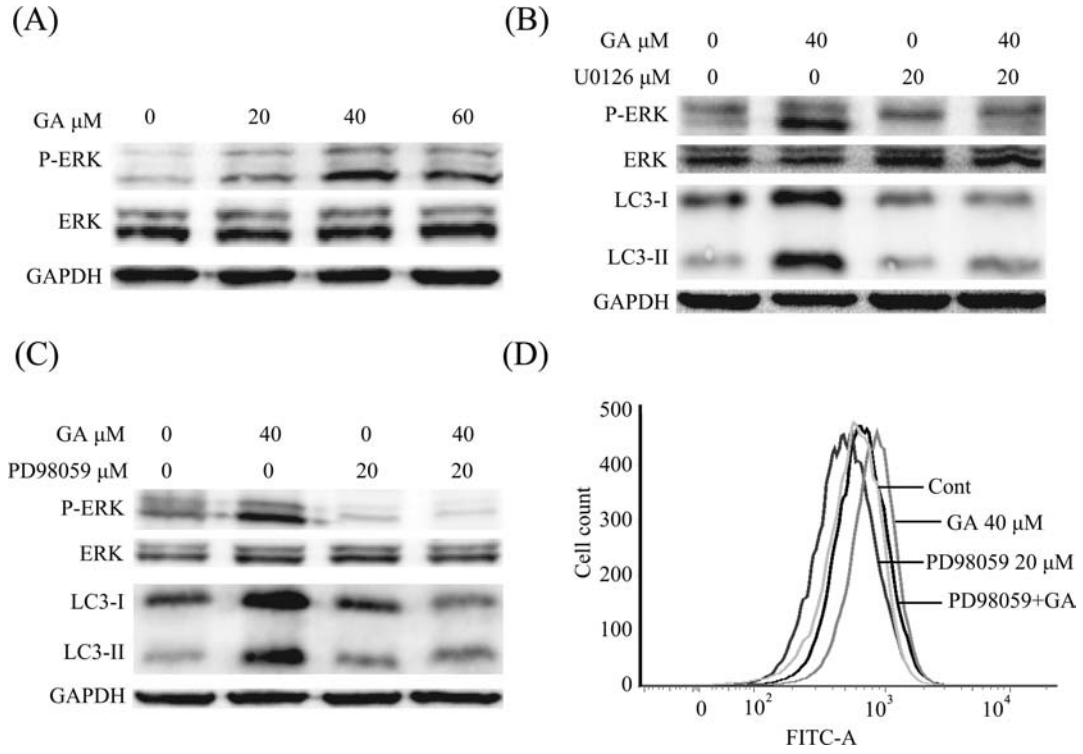


**Figure 6.** GA-triggered autophagy in HepG2 cells by activation of ERK pathway. (A) HepG2 cells were incubated with the indicated concentrations of GA for 24 h. Cell extracts were analyzed for phosphorylated ERK (Thr202/Tyr204), total ERK, and LC3 expression by Western blot analysis. (B, C) HepG2 cells were incubated with 40 $\mu$M GA for 24 h with or without pretreatment of U0126 (20 $\mu$M, 1 h) or PD98059 (20 $\mu$M, 1 h). Cell extracts were analyzed for phosphorylated ERK (Thr202/Tyr204), total ERK, and LC3-II expression by Western blot analysis. (D) Treated cells were stained with 50 $\mu$M MDC probe for 30 min, collected, washed, and resuspended. The intracellular fluorescence was quantified using flow cytometry.

cotreatment of GA and CQ or BAF caused an up-regulation of LC3-II protein expression.

The effects of autophagy, pro-survival or pro-death, are controversial in cancer.[33] In the progress of cancer cells, autophagy can be activated by hypoxia, starvation, and acid environment and act as a survival mechanism to protect cancer cells from those adverse environments.[21] However, excessive autophagy may result in cancer cell death.[34] The functions of autophagy induced by diverse compounds are also distinguishing.[35] For example, resveratrol and quercetin can induce a pro-survival autophagy in esophageal squamous carcinoma cells and gastric cancer cells, respectively,[28,36] whereas silibinin induces a pro-death autophagy in fibrosarcoma cells.[29] In the present study, we have demonstrated that GA triggered a protective autophagy in HCC HepG2 and Hep3B cells, as evidenced by the enhanced proliferative inhibition and/or apoptosis after blocking autophagy, which may be a mechanism for attenuating its anticancer effects or GA-modified TDDS loaded chemotherapeutic drugs. Besides, it has been reported that some nanoparticles can also induce protective autophagy in cancer cells.[37] These may partially explain why the GA-modified liposome nanoparticles loaded with docetaxel (0.7 $\mu$g/mL

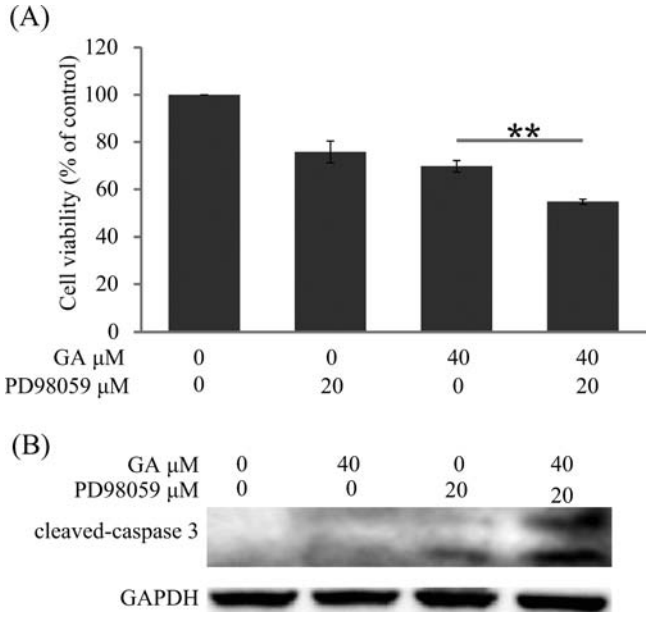


**Figure 7.** Inhibition of ERK enhanced GA-induced cell death and apoptosis. (A) HepG2 cells were treated with 40 $\mu$M GA for 24 h with or without pretreatment of PD98059 (20 $\mu$M, 1 h). The cell viability was evaluated by MTT assay. (*) $P < 0.05$ and (**) $P < 0.01$. (B) HepG2 cells were incubated with 40 $\mu$M GA for 24 h with or without pretreatment of PD98059 (20 $\mu$M, 1 h). Cell extracts were analyzed for cleaved caspase-3 expression by Western blot analysis.

docetaxel) presented fewer antiproliferative effects compared with docetaxel alone[17] and why GA-modified sulfated chitosan nanoparticles loaded with doxorubicin (0.0039, 0.0156, and 0.0625 $\mu$g/mL of doxorubicin) showed fewer antiproliferative effects compared with doxorubicin alone in HepG2 cells.[38] Thus, the autophagic effects might be a mechanism attenuating anticancer effects. In terms of cancer treatment by GA-modified TDDS, combination of an autophagy inhibitor might be a valuable strategy for TDDS-based HCC therapy.

Recently, accumulating studies have indicated the activation of ERK results in autophagic induction.[39] The present study showed that ERK was activated after GA treatment. ERK activity was remarkably inhibited by pretreatment with MEK inhibitor (U0126 or PD98059), and the autophagic protein marker LC3-II and the formation of AVOs were decreased accordingly, indicating that GA, at least partially, induced autophagy in HepG2 cells by activation of ERK. It is notable that inhibition of ERK activity by U0126 or PD98059 and the GA-induced protein expression of LC3-II and AVO formation were still slightly observed, compared with control group (Figure 6B−D), indicating other pathways might also participate in GA-induced autophagy, for example, the Akt/mammalian target of rapamycin pathway, which is one of the most important regulatory pathways for autophagy.[40] Moreover, as the Raf-MEK-ERK pathway (Raf activates MEK, which then activates ERK) is a classical signaling in cells,[39] how GA activates ERK warrants further study.

In summary, GA triggered a protective autophagy in HCC cells via activation of ERK, which might attenuate the anticancer effects of GA or GA-modified nanoparticle-loaded chemotherapeutics. The combined treatment with autophagy inhibitor and GA-modified nanoparticle-loaded anticancer drugs might be a promising strategy for HCC therapy.

## ■ ASSOCIATED CONTENT

### Supporting Information

Supplemental Figure 1. GA-triggered autophagy in Hep3B cells. Hep3B cells were treated with indicated concentrations of GA for 24 h. Cell extracts were analyzed for the expression of LC3 using Western blot analysis. Supplemental Figure 2. Inhibition of autophagy-enhanced GA-induced cytotoxicity in Hep3B cells. Hep3B cells were treated with indicated concentrations of GA for 24 h with or without pretreatment of CQ (10 $\mu$M, 1 h) or BAF (100 nM, 1 h). The cell viability was evaluated by MTT assay. (*) $P < 0.05$ and (**) $P < 0.01$. This material is available free of charge via the Internet at http://pubs.acs.org.

## ■ AUTHOR INFORMATION

### Corresponding Author

*(J.-J.L.) Mail: State Key Laboratory of Quality Research in Chinese Medicine, Institute of Chinese Medical Sciences, University of Macau, Avenida da Universidade, Taipa, Macao, China. Phone: 853-88224674. Fax: 853-28841358. E-mail: jinjianlu@umac.mo or jinjian.lu@163.com.

### Funding

This work was supported by the Macao Science and Technology Development Fund (074/2012/A3 and 070/2013/A) and the Research Fund of the University of Macau (MRG013/WYT/2013/ICMS, MRG008/LJJ2014/ICMS, and CPG2014-00012-ICMS). Y.-G.T. is supported by the National Cancer Institute of the National Institutes of Health under Award R00CA138914 and by the National Natural Science Foundation under Grant 81372216.

### Notes

The authors declare no competing financial interest.

## ■ ACKNOWLEDGMENTS

We thank Dr. Xue-Nong Zhang for his kindly help in doing the experiments and the Core Facilities (Imaging Facility), School of Medicine, Zhejiang University, for our TEM assay.

## ■ ABBREVIATIONS USED

ANOVA, analysis of variance; AVOs, acidic vesicular organelles; BAF, bafilomycin A1; CQ, chloroquine; DMEM, Dulbecco's modified Eagle's medium; DMSO, dimethyl sulfoxide; ERK, extracellular regulated protein kinases; FBS, fetal bovine serum; GA, glycyrrhetinic acid; HCC, hepatocellular carcinoma; LC3, microtubule-associated protein light-chain 3; LDH, lactate dehydrogenase; MDC, monodansylcadaverine; MTT, 3-(4,5-dimethyl-2-thiazolyl)-2,5-diphenyltetrazolium bromide; PBS, phosphate-buffered saline; p-ERK, phosphorylated of ERK; SD, standard deviation; TDDS, targeted drug delivery system; TEM, transmission electron microscopy

## ■ REFERENCES

(1) Parkin, D. M.; Bray, F.; Ferlay, J.; Pisani, P. Estimating the world cancer burden: Globocan 2000. *Int. J. Cancer* **2001**, *94*, 153−156.

(2) Chen, W. Q.; Zheng, R. S.; Zhang, S. W. Liver cancer incidence and mortality in China, 2009. *Chin. J. Cancer* **2013**, *32*, 162−169.

(3) Siegel, R.; Naishadham, D.; Jemal, A. Cancer statistics for Hispanics/Latinos, 2012. *CA Cancer J. Clin.* **2012**, *62*, 283−298.

(4) Zhang, Y.-W.; Shi, J.; Li, Y.-J.; Wei, L. Cardiomyocyte death in doxorubicin-induced cardiotoxicity. *Arch. Immunol. Ther. Exp.* **2009**, *57*, 435−445.

(5) Llovet, J. M.; Ricci, S.; Mazzaferro, V.; Hilgard, P.; Gane, E.; Blanc, J. F.; de Oliveira, A. C.; Santoro, A.; Raoul, J. L.; Forner, A.; Schwartz, M.; Porta, C.; Zeuzem, S.; Bolondi, L.; Greten, T. F.; Galle,

P. R.; Seitz, J. F.; Borbath, I.; Haussinger, D.; Giannaris, T.; Shan, M.; Moscovici, M.; Voliotis, D.; Bruix, J. Sorafenib in advanced hepatocellular carcinoma. *N. Engl. J. Med.* **2008**, *359*, 378−390.
(6) Han, J. H.; Oh, Y. K.; Kim, D. S.; Kim, C. K. Enhanced hepatocyte uptake and liver targeting of methotrexate using galactosylated albumin as a carrier. *Int. J. Pharm.* **1999**, *188*, 39−47.
(7) Zhang, C.; Wang, W.; Liu, T.; Wu, Y.; Guo, H.; Wang, P.; Tian, Q.; Wang, Y.; Yuan, Z. Doxorubicin-loaded glycyrrhetinic acid-modified alginate nanoparticles for liver tumor chemotherapy. *Biomaterials* **2012**, *33*, 2187−2196.
(8) Shibata, S. A drug over the millennia: pharmacognosy, chemistry, and pharmacology of licorice. *Yakugaku Zasshi* **2000**, *120*, 849−862.
(9) Kao, T.-C.; Wu, C.-H.; Yen, G.-C. Bioactivity and potential health benefits of licorice. *J. Agric. Food Chem.* **2014**, *62*, 542−553.
(10) Yo, Y.-T.; Shieh, G.-S.; Hsu, K.-F.; Wu, C.-L.; Shiau, A.-L. Licorice and licochalcone-A induce autophagy in LNCaP prostate cancer cells by suppression of Bcl-2 expression and the mTOR pathway. *J. Agric. Food Chem.* **2009**, *57*, 8266−8273.
(11) Satomi, Y.; Nishino, H.; Shibata, S. Glycyrrhetinic acid and related compounds induce G1 arrest and apoptosis in human hepatocellular carcinoma HepG2. *Anticancer Res.* **2005**, *25*, 4043−4047.
(12) Huiling, L.; Zhang, Z.; Qinian, W.; Huang, M.; Huang, W.; Zhang, D.; Fengyi, Y. 18$\beta$-glycyrrhetinic acid-induced apoptosis and relation with intracellular $Ca^{2+}$ release in human breast carcinoma cells. *Chin.−Germ. J. Clin. Oncol.* **2004**, *3*, 137−140.
(13) Csuk, R.; Schwarz, S.; Siewert, B.; Kluge, R.; Ströhl, D. Synthesis and antitumor activity of ring A modified glycyrrhetinic acid derivatives. *Eur. J. Med. Chem.* **2011**, *46*, 5356−5369.
(14) Negishi, M.; Irie, A.; Nagata, N.; Ichikawa, A. Specific binding of glycyrrhetinic acid to the rat liver membrane. *Biochim. Biophys. Acta−Biomembranes* **1991**, *1066*, 77−82.
(15) Cheng, M.; Gao, X.; Wang, Y.; Chen, H.; He, B.; Xu, H.; Li, Y.; Han, J.; Zhang, Z. Synthesis of glycyrrhetinic acid-modified chitosan 5-fluorouracil nanoparticles and its inhibition of liver cancer characteristics in vitro and in vivo. *Mar. Drugs* **2013**, *11*, 3517−3536.
(16) Cheng, M.; Gao, X.; Wang, Y.; Chen, H.; He, B.; Li, Y.; Han, J.; Zhang, Z. Synthesis of liver-targeting dual-ligand modified GCGA/5-FU nanoparticles and their characteristics in vitro and in vivo. *Int. J. Nanomed.* **2013**, *8*, 4265.
(17) Li, J.; Xu, H.; Ke, X.; Tian, J. The anti-tumor performance of docetaxel liposomes surface-modified with glycyrrhetinic acid. *J. Drug Targ.* **2012**, *20*, 467−473.
(18) Jiang, P.; Mizushima, N. Autophagy and human diseases. *Cell Res.* **2014**, *24*, 69−79.
(19) Yang, Z.; Klionsky, D. J. Eaten alive: a history of macroautophagy. *Nat. Cell Biol.* **2010**, *12*, 814−822.
(20) Mathew, R.; White, E. Why sick cells produce tumors: the protective role of autophagy. *Autophagy* **2007**, *3*, 502−505.
(21) White, E. Deconvoluting the context-dependent role for autophagy in cancer. *Nat. Rev. Cancer* **2012**, *12*, 401−410.
(22) Mizushima, N. Methods for monitoring autophagy. *Int. J. Biochem. Cell B* **2004**, *36*, 2491−2502.
(23) Chan, F. K.; Moriwaki, K.; De Rosa, M. J. Detection of necrosis by release of lactate dehydrogenase activity. *Methods Mol. Biol.* **2013**, *979*, 65−70.
(24) Rubinsztein, D. C.; Gestwicki, J. E.; Murphy, L. O.; Klionsky, D. J. Potential therapeutic applications of autophagy. *Nat. Rev. Drug Discovery* **2007**, *6*, 304−312.
(25) Mizushima, N.; Yamamoto, A.; Matsui, M.; Yoshimori, T.; Ohsumi, Y. In vivo analysis of autophagy in response to nutrient starvation using transgenic mice expressing a fluorescent autophagosome marker. *Mol. Biol. Cell* **2004**, *15*, 1101−1111.
(26) Paglin, S.; Hollister, T.; Delohery, T.; Hackett, N.; McMahill, M.; Sphicas, E.; Domingo, D.; Yahalom, J. A novel response of cancer cells to radiation involves autophagy and formation of acidic vesicles. *Cancer Res.* **2001**, *61*, 439−444.
(27) Mizushima, N.; Yoshimori, T.; Levine, B. Methods in mammalian autophagy research. *Cell* **2010**, *140*, 313−326.
(28) Wang, K.; Liu, R.; Li, J.; Mao, J.; Lei, Y.; Wu, J.; Zeng, J.; Zhang, T.; Wu, H.; Chen, L. Quercetin induces protective autophagy in gastric cancer cells: involvement of Akt-mTOR- and hypoxia-induced factor 1$\alpha$-mediated signaling. *Autophagy* **2011**, *7*, 966−978.
(29) Duan, W.; Jin, X.; Li, Q.; Tashiro, S.-i.; Onodera, S.; Ikejima, T. Silibinin induced autophagic and apoptotic cell death in HT1080 cells through a reactive oxygen species pathway. *J. Pharmacol. Sci.* **2010**, *113*, 48−56.
(30) Ogier-Denis, E.; Pattingre, S.; El Benna, J.; Codogno, P. Erk1/2-dependent phosphorylation of G$\alpha$-interacting protein stimulates its GTPase accelerating activity and autophagy in human colon cancer cells. *J. Biol. Chem.* **2000**, *275*, 39090−39095.
(31) Pattingre, S.; Bauvy, C.; Codogno, P. Amino acids interfere with the ERK1/2-dependent control of macroautophagy by controlling the activation of Raf-1 in human colon cancer HT-29 cells. *J. Biol. Chem.* **2003**, *278*, 16667−16674.
(32) Villanueva, A.; Llovet, J. M. Targeted therapies for hepatocellular carcinoma. *Gastroenterology* **2011**, *140*, 1410−1426.
(33) Mathew, R.; Karantza-Wadsworth, V.; White, E. Role of autophagy in cancer. *Nat. Rev. Cancer* **2007**, *7*, 961−967.
(34) Pardo, R.; Lo Ré, A.; Archange, C.; Ropolo, A.; Papademetrio, D. L.; Gonzalez, C. D.; Alvarez, E. M.; Iovanna, J. L.; Vaccaro, M. I. Gemcitabine induces the VMP1-mediated autophagy pathway to promote apoptotic death in human pancreatic cancer cells. *Pancreatology* **2010**, *10*, 19−26.
(35) Ding, Q.; Bao, J.; Zhao, W.; Hu, Y.; Lu, J.; Chen, X. Natural autophagy regulators in cancer therapy: a review. *Phytochem. Rev.* **2014**, 1−18.
(36) Tang, Q.; Li, G.; Wei, X.; Zhang, J.; Chiu, J. F.; Hasenmayer, D.; Zhang, D.; Zhang, H. Resveratrol-induced apoptosis is enhanced by inhibition of autophagy in esophageal squamous cell carcinoma. *Cancer Lett.* **2013**, *336*, 325−337.
(37) Zhang, X.; Dong, Y.; Zeng, X.; Liang, X.; Li, X.; Tao, W.; Chen, H.; Jiang, Y.; Mei, L.; Feng, S.-S. The effect of autophagy inhibitors on drug delivery using biodegradable polymer nanoparticles in cancer treatment. *Biomaterials* **2014**, *35*, 1932−1943.
(38) Tian, Q.; Wang, X.-H.; Wang, W.; Zhang, C.-N.; Wang, P.; Yuan, Z. Self-assembly and liver targeting of sulfated chitosan nanoparticles functionalized with glycyrrhetinic acid. *Nanomed.−Nanotechnol.* **2012**, *8*, 870−879.
(39) Roberts, P.; Der, C. Targeting the Raf-MEK-ERK mitogen-activated protein kinase cascade for the treatment of cancer. *Oncogene* **2007**, *26*, 3291−3310.
(40) Yu, L.; McPhee, C. K.; Zheng, L.; Mardones, G. A.; Rong, Y.; Peng, J.; Mi, N.; Zhao, Y.; Liu, Z.; Wan, F. Termination of autophagy and reformation of lysosomes regulated by mTOR. *Nature* **2010**, *465*, 942−946.

Seven strains of *Paecilomyces gunnii* were selected for rescreening (Figure 1). The strains were cultured with the same medium and

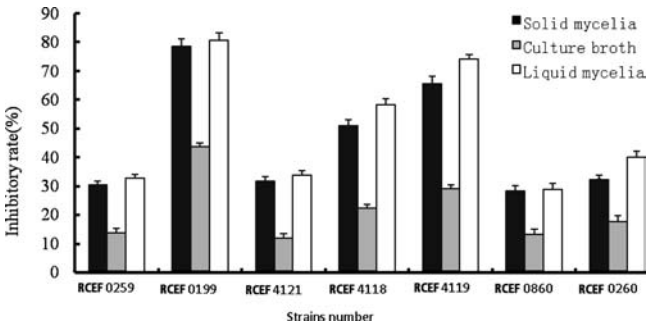


**Figure 1.** Inhibition rates of mycelia extracts and fermentation broth extracts from different strains against diphenolase of tyrosinase.

condition as that of the 50 fungal isolates or cultured in liquid medium (40 g/L glucose, 10 g/L yeast extract, and 10 g/L peptone) under shaking at 130 rpm and 25 °C for 10 days. The mycelia of the liquid cultures were separated from fermentation media. All of the mycelia were freeze-dried and then pulverized to save for use. The fermentation broths were condensed to $^1/_4$ of their original volume under reduced pressure and then freeze-dried.

The freeze-dried samples were sonicated in methanol by a solid/liquid ratio of 1 g/30 mL at 25 °C for 30 min and then statically extracted at 4 °C for 6 h. After centrifugation, the supernatants of the extracts were concentrated under reduced pressure and lyophilized to give the crude methanol extracts.

**Tyrosinase Inhibition Assay.** Extracts and isolated compounds (initial concentration of 5.0 mg/mL) were first dissolved in dimethyl sulfoxide (DMSO) and then diluted to different concentrations using DMSO. L-DOPA and tyrosinase were dissolved in 50 mmol/L phosphate buffer (pH 6.8). A total of 150 μL of substrate solution (1.0 mmol/L) and 10 μL of sample solution were added to 96 well microtiter plates and incubated at 30 °C for 5 min, and then 40 μL of tyrosinase solution (100 μg/mL) was quickly added and immediately mixed. After thorough mixing by vortex, initial absorbance at 475 nm was measured.

The enzyme activity was obtained by calculation of the slope of the time line through tracking and measuring the optical density ($OD_{475}$) at a wavelength of 475 nm. The molar extinction coefficient of the product at 475 nm was calculated as 3700 mol $L^{-1}$ $cm^{-1}$, and the relative inhibition rate was calculated as follows:

$$\text{relative inhibition rate } (\%) = (1 - \Delta A_m/\Delta A_c) \times 100\%$$

where $\Delta A_m$ is the enzyme activity of the sample and $\Delta A_c$ is the enzyme activity of the control (sample was replaced by an equal volume of solvent). Triplicate experiments were performed, and half inhibition concentration ($IC_{50}$) of the extract on tyrosinase was determined for each compound. The inhibition type was assayed by the Lineweaver−Burk plot, and the inhibition constant was determined by the second plot of the apparent $K_m/V_m$ or $1/V_m$ versus the concentration of the inhibitor.

**HPLC−PAD−HRMS Analysis.** A total of 10 μL of methanol solution of the sample (1.0 mg/mL) was injected into the analytical column. The flow rate was 0.8 mL/min. The column was eluted with a water/methanol (both contain 0.05% formic ammonium) gradient from 90:10 to 55:45 for 10 min, from 55:45 to 40:60 for a further 15 min, from 40:60 to 0:100 (%) for another 5 min, and pure methanol for the final 15 min. The eluates were monitored with a PAD at full length scan from 200 to 600 nm and a HRMS detector under negative and positive modes. Drying gas of the ESI ion source was 12 L/min at 325 °C. The nebulizer pressure was 35 psig. The capillary voltage was 3500 V for negative mode and 4000 V for positive mode. The fragmentor voltage was 175 V for negative mode and 215 V for positive mode. The scan range was 50−1200 amu.

**HPLC−MS−Bioactivity Combined Analysis.** A total of 10 μL of methanol solution of the sample (3.0 mg/mL) was injected into the analytical column and eluted with the above conditions. A total of 20% of the eluates was monitored with the MS detector through a distribution valve. The other 80% of the eluates was automatically collected every 5 min. The injection was repeated 9 times. Every three collections of the same time were combined as one sample and condensed to dry with the centrifugal concentrator. The dried eluates were dissolved with 15 μL of DMSO, and 10 μL of the solutions were transferred to 96 well microtiter plates for tyrosinase inhibitory activity detection.

**Selection of the Two-Phase Solvent System for HSCCC.** The two-phase solvent system was selected according to the partition coefficient ($K$) of each target component. The concentration of the target component in the upper phase ($C_A$) and lower phase ($C_B$) was analyzed by HPLC−MS. $K = C_A/C_B$.

According to the fact that the target components are methanol-soluble and possibly have moderate polarity, we selected a two-phase solvent system (*n*-hexane/ethyl acetate/methanol/water), which was suitable for the separation of compounds with medium polarity.[13] To obtain a better separation effect by HSCCC, a partition coefficient ($K$) between 0.5 and 2 is highly needed and the retention rate of the stationary phase has to be kept more than 50%.[14] On the basis of the selected basic solvent system and HSCCC separation pretests, we created a series of solvent systems (Table 1), and system 5 with 72% retention rate of the stationary phase was selected as the optimal solvent system for target compound preperation.

**HSCCC Separation.** The sample solution was prepared by dissolving the crude sample in a solvent mixture consisting of equal volumes of both upper and lower phases (4 mL for each phase). In each separation, the coiled column of HSCCC was first entirely filled with the upper phase as the stationary phase at a flow rate of 9.99 mL/min. Then, the lower phase (mobile phase) was pumped into the column at a flow rate of 2.0 mL/min, while the apparatus was run at a speed of 850 rpm. After the mobile phase front emerged and hydrodynamic equilibrium was established in the column, the sample solution (8 mL) containing 100 mg of crude extract was injected. All through the experiment, the separation temperature was controlled at 25 °C. The effluent of the column was monitored at 254 nm and automatically collected in a 10 mL test tube per 2 min.

**Structural Identification and Statistical Analysis.** The structural identification of each HSCCC peak fraction was carried out by the analysis of HPLC−PAD−ESI−HRMS, $^1$H and $^{13}$C NMR data, and two-dimensional (2D) NMR. Student's paired $t$ test for comparison of means was performed with the obtained data.

**Table 1. Distribution Coefficient ($K$) of the Target Compounds in Different Solvent Systems**

| | | $K$ | | |
|---|---|---|---|---|
| | *n*-hexane/ethyl acetate/ methanol/acetic acid/water | compound **1** | compound **2** | compound **3** |
| 1 | 5:5:5:0:5 | 0.45 | 0.18 | 0.14 |
| 2 | 2:5:2:0:5 | 7.35 | 2.25 | 1.80 |
| 3 | 2.5:5:2.5:0:5 | 1.55 | 0.90 | 0.68 |
| 4 | 2.5:5:2.5:0.15:5 | 5.32 | 1.45 | 0.91 |
| 5 | 3.5:5:3.5:0.15:5 | 1.56 | 0.86 | 0.53 |

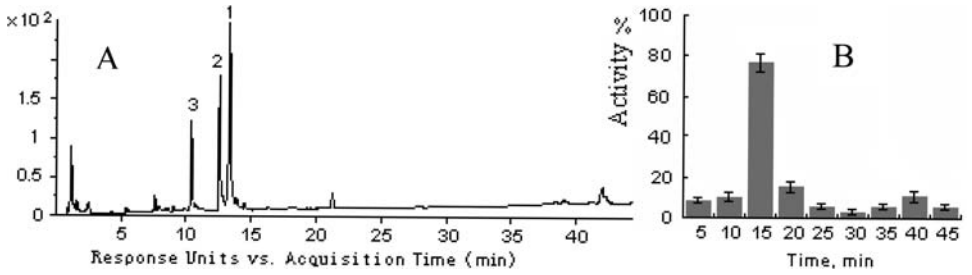


**Figure 2.** (A) HPLC chromatograms of the methanol extract from liquid mycelia of *P. gunnii*. (B) Inhibition rate of HPLC fractions on diphenolase activity.

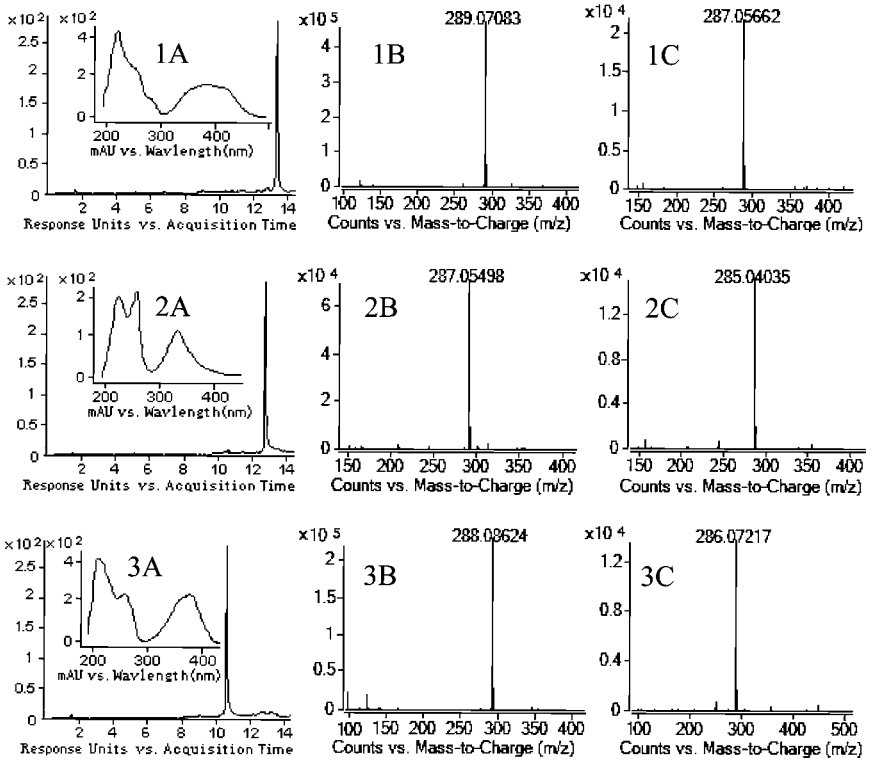


**Figure 3.** HPLC−PAD−HRMS analysis of compounds **1**−**3**: (A) HPLC and full wavelength scan spectrum (PAD), (B) HRMS of the compounds in positive mode, and (C) HRMS of the compounds in negative mode.

## RESULTS AND DISCUSSION

**Preliminary Screening of Tyrosinase Inhibitory Activity of Fungal Extracts.** Screening was conducted on the methanol extracts of solid-cultured mycelia of the selected 50 strains by testing their inhibition rates against tyrosinase diphenolase in Table S1 of the Supporting Information. An obvious difference was found in the tyrosinase inhibition activity among different species and strains of the same species. Among the measured strains, *P. gunnii* showed relative higher inhibitory activity; therefore, further rescreening experiment was carried out on multiple strains of *P. gunnii*.

**Rescreening of Seven Strains of *P. gunnii*.** To better understand the tyrosinase inhibitory activities of the active strains of *P. gunnii*, the methanol extracts of the solid-cultured mycelia, liquid-cultured mycelia, and broth were tested (Figure 1 and Table S2 of the Supporting Information). The inhibitory activities of the liquid-cultured mycelia were significantly ($p < 0.05$) higher than that of the others, and the differences between mycelia and broth were very significant ($p < 0.01$; see Table S2 of the Supporting Information), indicating that the active ingredients mainly exist in the mycelia. Of all of the tested samples, the methanol extract of the liquid-cultured mycelia of the strain RCEF0199 showed the highest activity; therefore, it was selected for further bioassays and follow-up searching for the active compounds.

**$IC_{50}$ of the Extract on Tyrosinase.** With L-DOPA as a substrate, inhibitory rates of different concentrations of the methanol extract of the strain RCEF0199 on tyrosinase were measured. The amount of product formation is proportional to the reaction time, and the response slope of the line is the enzyme activity. The effect curve was obtained through plotting the concentrations versus enzyme activities. The results showed that the enzyme activity decreased with an increased concentration of the extract, and the $IC_{50}$ of the extract on tyrosinase was calculated as 48 $\mu$g/mL (see Figure S1A of the Supporting Information).

**Tyrosinase Inhibitory Mechanism of the Extract.** The inhibition mechanism on the enzyme by the methanol extract for oxidation of L-DOPA was investigated. In the experiment, the concentration of the substrate L-DOPA was constant while changing the concentration of the extract and the enzyme. The

Table 2. $^{1}H$ and $^{13}C$ NMR Spectral Data ($\delta$ in ppm) of Compounds 1−3 in DMSO-$d_6$[a]

| | $^{1}H$ NMR | | | $^{13}C$ NMR | | |
|---|---|---|---|---|---|---|
| position | 1 | 2 | 3 | 1 | 2 | 3 |
| 1 | | | | 172.3 | 169.2 | 174.3 |
| 2 | 6.51 s | 6.53 s | 6.41 s | 97.4 | 97.4 | 96.3 |
| 3 | | | | 166.8 | 166.8 | 166.6 |
| 3a | | | | 111.6 | 111.5 | 110.7 |
| 3b | | | | 127.8 | 130.6 | 129.6 |
| 4 | | | | 144.9 | 145.1 | 144.8 |
| 5 | 6.82 s | 6.83 s | 6.67 s | 117.3 | 117.3 | 117.2 |
| 6 | | | | 162.2 | 171.2 | 165.0 |
| 6a | | | | 105.4 | 105.7 | 106.5 |
| 7 | | | | 172.0 | 162.7 | 169.9 |
| 8 | | | | 131.7 | 196.6 | 131.0 |
| 9 | | | | 166.8 | 166.8 | 174.0 |
| 9a | | | | 103.3 | 100.0 | 102.3 |
| $OCH_3$ | 4.00 s | 4.01 s | 3.96 s | 56.7 | 56.7 | 56.4 |
| $CH_3$ | 2.74 s | 2.76 s | 2.75 s | 25.8 | 25.8 | 25.8 |
| OH | | 12.85 s, 13.53 s | | | | |
| $NH_2$ | | | 8.95 br s | | | |

[a]s, singlet; br s, broad signal.

results are shown in Figure S1B of the Supporting Information. A group of straight lines through the origin was obtained for the extract, and the slop of the line decreased with the increased concentration of the sample, which indicated that the inhibitory effect of the extract on tyrosinase was a reversible process. Therefore, the extract was a reversible inhibitor of tyrosinase.

**Competitive Inhibitory Type of the Extract on Tyrosinase.** The effects on the enzyme activity of different concentrations of the extract were measured by changing the concentration of the substrate (L-DOPA) while maintaining the amount of the enzyme. Using the Lineweaver−Burk double-reciprocal plot method, a set of straight lines intersecting the $y$ linear axis was obtained, as shown in Figure S1C of the Supporting Information, indicating that the methanol extract was a competitive inhibitor on the tyrosinase. The Michaelis constant ($K_m$) increased with the ascended concentration of the extract. The affinity of the enzyme with the substrate was reduced with the increase of the concentration of the extract. The extract impeded the binding of the enzyme and substrate and led to a lower catalytic activity. The Michaelis constant ($K_m$) was calculated as 1.02 mM without adding extract in the reaction system. The maximum reaction velocity ($V_{max}$) was 186.44 units/min based on the linear slope and $K_m$ values. The equilibrium constant ($K_I$) for the extract binding to the free enzyme was obtained from the secondary plot of the line slope versus the concentration of the extract (see Figure S1D of the Supporting Information). The value of $K_I$ was 555.56 $\mu$g/mL.

**Bioactive Fractions of the Extract.** Combined analysis of HPLC−MS and tyrosinase inhibitory activities shows that the HPLC fraction collected from 10 to 15 min has the strongest bioactivity (Figure 2B). The HPLC chromatogram shows that the main bioactive fraction contains three components, where the purities of the target compounds **1**, **2**, and **3** were 23.9, 6.6, and 15.7%, respectively, based on the HPLC peak area percentage (Figure 2A). The three compounds will be used as targets for HSCCC separation.

**HSCCC Preparation for the Target Compounds.** The target components were isolated by the optimal solvent system as compounds **3**, **2**, and **1** with retention times at 70, 110, and 210 min, respectively (see Figure S2 of the Supporting Information). The collected fractions were analyzed by HPLC, and fractions with the same component were combined. After solvent evaporation under vacuum at 50 °C, compound **1** (20.4 mg), compound **2** (5.2 mg), and compound **3** (12.5 mg) were obtained with the purities of 96.8, 95.8, and 95.0%, respectively, based on HPLC analysis (panels 1A−3A of Figure 3).

**Structural Identification.** Full wavelength scan of active ingredient absorption spectra are shown in panels 1A−3A of Figure 3. Identification of peak fractions was performed with ESI−HRMS (panels 1B−3C of Figure 3), $^{1}H$ and $^{13}C$ NMR, and 2D NMR (see Figure S3 of the Supporting Information). The $^{1}H$ and $^{13}C$ NMR data are given in Table 2.

Compound **1**, peak 1 in Figure 2A, is a yellow powder. The ultraviolet (UV) spectrum (panel 1A of Figure 3) shows the existence of a long conjugated system. UV (MeOH) $\lambda_{max}$ (log $\varepsilon$): 218 (5.0), 256 (sh, 2.6), and 380 (2.0). ESI−HRMS ($m/z$) showed the pseudo-molecular peak at 289.07083 (M + H, calcd. 289.07066) in positive mode and 287.05662 (M − H, calcd. 287.05611) in negative mode (panels 1B and 1C of Figure 3). Thus, its molecular formula was calculated as $C_{15}H_{12}O_6$, which suggested that it has a carbon skeleton with 10 degrees of unsaturation. The $^{1}H$ and $^{13}C$ NMR (Table 2) spectra of compound **1** indicated the presence of one naphthalene ring system, which has 10 aromatic carbons, including 1 methine carbon ($\delta_H$ 6.82, $\delta_C$ 117.23) and 9 quaternary carbons ($\delta_C$ 111.6, 144.9, 162.2, 105.4, 170.0, 131.07, 173.0, and 103.3), as well as 1 methoxy group ($\delta_H$ 4.00, $\delta_C$ 56.7), 1 methyl group ($\delta_H$ 2.74, $\delta_C$ 25.8), and 1 conjugated carbonyl system ($\delta_{CO}$ 172.3, $\delta_C$ 97.3 and 166.8). The above NMR and HRMS data suggested that it has a very high degree of unsaturation, consistent with a tricyclic phenalenone framework. A literature search showed that it is very similar to the known phenalenone compound myeloconone A2 (Figure 4), which was found from the lichen *Myeloconis erumpens*,[15] except that compound **1** has a hydroxyl group instead of a methoxyl group at position C-8.

Further evidence for the structure of compound **1** was provided by heteronuclear multiple-bond correlation (HMBC) long-range C−H connectivities, as illustrated in Figure 4. The

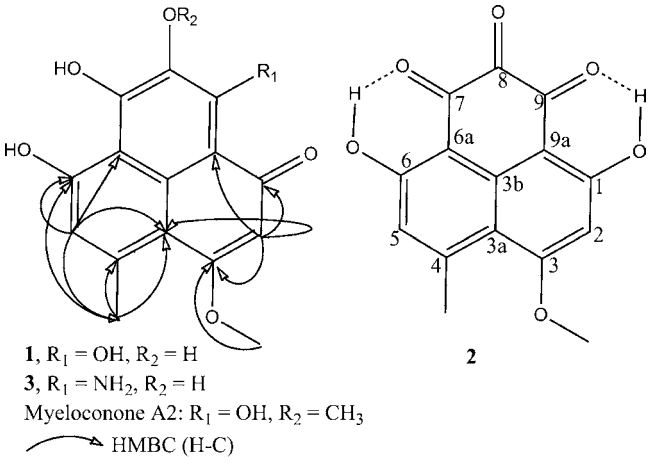


**Figure 4.** Chemical structures of phenanelones from methanol extracts of liquid-cultivated mycelia of *P. gunnii* and HMBC correlations (arrows with arrowhead) around the protons in the structure: H-5, $CH_3$, H-2, and $OCH_3$ of compound **1**.

aromatic proton singlet at $\delta_H$ 6.82 (H-5) yielded three strong C−H long-range correlations, assigned as $^3J_{CH}$ couplings, to quaternary carbon atoms at $\delta_C$ 111.6 (C-3a) and 105.4 (C-6a) and the methyl carbon atom at $\delta_C$ 25.8. In addition, a weak connectivity to an oxysubstituted carbon atom ($\delta$ 162.9) was assigned as a $^2J_{CH}$ correlation to C-6. Similarly, three strong correlations involving the methyl protons at $\delta_H$ 2.74 can be found at $\delta_C$ 111.6 (C-3a), 117.3 (C-5), and 144.9 (C-4), and a weak correlation at $\delta_C$ 166.8 (C-3) also existed. The strong correlations involving $\delta_H$ 6.51 (H-2) are at $\delta_C$ 103.3 (C-9a), 111.6 (C-3a), 166.8 (C-3), and 172.3 (C-1), with a weak correlation at $\delta_C$ 144.9 (C-4). The strong correlation involving the methoxy group $\delta_H$ 4.00 ($OCH_3$-3) is at $\delta_C$ 166.8 (C-3), which confirmed that the methoxy group is at position C-3. Besides, a weak correlation of $OCH_3$-3/C-2 ($\delta_C$ 97.4) was also found. Thus, the $^1$H and $^{13}$C NMR spectra of compound **1** were consistent with a highly oxygenated phenalenone and very similar to those of the known phenalenone myeloconone A2. Finally, in combination with the above HRMS and NMR information, compound **1** can be deduced as 6,7,8,9-tetrahydroxy-3-methoxy-4-methyl-1*H*-phenalen-1-one and named as paecilomycone A (Figure 4).[15,16]

Compound **2**, peak 2 in Figure 2A, is an orange powder. The UV spectrum (panel 2A of Figure 3) shows the existence of a long conjugated system. UV (MeOH) $\lambda_{max}$ (log $\varepsilon$): 220 (2.6), 255 (2.7), and 332 (1.5). ESI−HRMS ($m/z$) showed the pseudo-molecular peak at 287.05498 (M + H, calcd. 287.05501) in positive mode and 285.04035 (M − H, calcd. 285.04046) in negative mode (panels 2B and 2C of Figure 3). Thus, its molecular formula was calculated as $C_{15}H_{10}O_6$. The $^1$H NMR spectra of compound **2** showed similarity to those of compound **1** (Table 2). However, its molecular formula has one more oxygen atom while short of two hydrogen atoms, which suggests 1 more degree of unsaturaton in the structure. Thus, it should be a more oxygenated phenalenone-type compound compared to compound **1**. In the $^1$H NMR experiment, two lower field single peaks were found at $\delta_H$ 12.85 and 13.53, which are two typically strongly hydrogen-bonded hydroxyl groups ascribed to the positions OH-1 and OH-6 (Figure 4). In comparison of the above-mentioned HRMS and NMR data to those of compound **1**, its structure was decided as 4,9-dihydroxy-6-methoxy-7-methyl-1*H*-phenalene-1,2,3-trione, as shown in Figure 4, and named as paecilomycone B.

Compound **3**, peak 3 in Figure 2A, is an olive powder. The UV spectrum (panel 3A of Figure 3) shows the existence of a long conjugated system. UV (MeOH) $\lambda_{max}$ (log $\varepsilon$): 208 (2.2), 260 (sh, 1.3), and 380 (1.3). ESI−HRMS ($m/z$) showed the pseudo-molecular peak at 288.08624 (M + H, calcd. 288.08665) in positive mode and 286.07217 (M − H, calcd. 286.07210) in negative mode (panels 3B and 3C of Figure 3). Thus, its molecular formula was decided as $C_{15}H_{13}NO_5$. The $^1$H and $^{13}$C NMR (Table 2) spectra of compound **3** indicated the presence of one naphthalene ring system, which has 10 aromatic carbons, including 1 methine carbon ($\delta_H$ 6.67, $\delta_C$ 117.2) and 9 quaternary carbons ($\delta_C$ 110.7, 144.8, 165.0, 106.5, 169.9, 131.0, 174.0, and 102.3), as well as 1 methoxy group ($\delta_H$ 3.96, $\delta_C$ 56.4), 1 methyl group ($\delta_H$ 2.75, $\delta_C$ 25.8), and 1 conjugated carbonyl system ($\delta_{CO}$ 174.3, $\delta_C$ 96.3 and 166.6). The above NMR data are very similar to those of compound **1**. In comparison of its HRMS and NMR data to those of compound **1**, one $NH_2$ group ($\delta_H$ 8.95, br s, 2H) substituted one OH group in the structure of compound **3**, which was assigned to $NH_2$-9 because the $NH_2$ group is hydrogen-bonded with the carbonyl group of C-1, which led to the lower field signal ($\delta_H$ 8.95). In combination with the above HRMS and NMR information, compound **1** can be deduced as 9-amino-6,7,8-trihydroxy-3-methoxy-4-methyl-1*H*-phenalen-1-one and named as paecilomycone C (Figure 4).[15,16] For further confirmation of the presence of a $NH_2$ group in the deduced structure, compound **3** was tried with the ninhydrin reaction and showed a positive purple reaction in the TLC plate (see Figure S6 of the Supporting Information).[17]

**Inhibition Capacity of Paecilomycones A−C on Tyrosinase.** According to the above assay method, initial solutions of paecilomycones were diltuted to 3−9 fold and the inhibitory rates at each dilution were measured. $IC_{50}$ of the three new phenalenones paecilomycones A−C were 0.11, 0.17, and 0.14 mM, respectively (Table 3), which are almost as strong as that of kojic acid (0.10 mM) and stronger than that of arbutin (0.20 mM). Both kojic acid and arbutin are well-known tyrosinase inhibitors, which are usually used as the positive control of the tyrosinase inhibitor and commercially used in whitening cosmetics and food to prevent browning.[18]

**Table 3. $IC_{50}$ of Compounds 1−3 on Tyrosinase**

| compound | $IC_{50}$ (mM) ± SD |
|---|---|
| paecilomycone A (**1**) | 0.11 ± 0.010 |
| paecilomycone B (**2**) | 0.17 ± 0.009 |
| paecilomycone C (**3**) | 0.14 ± 0.004 |
| kojic acid | 0.10 ± 0.003 |
| arbutin | 0.20 ± 0.005 |

The three new phenalenones are the main tyrosinase inhibitors in the methanol extract of *P. gunnii*. The competitive inhibitory mechanism of the extract means that the three new compounds combine with tyrosinase in a manner that competes for the same binding site on the enzyme as the substrate L-DOPA or L-tyrosine. The three phenalenones are natural polyphenols with several phenolic hydroxyl groups in their structure. The tyrosinase inhibition test showed that the number of hydroxyl groups plays an important role in its activity: paecilomycone A has four hydroxyl groups with the highest activity ($IC_{50}$ = 0.11 mM); paecilomycone B has one

hydroxyl group with the lowest activity ($IC_{50}$ = 0.17 mM); and paecilomycone C has three hydroxyl groups with mid-activity ($IC_{50}$ = 0.14 mM) (Figure 4).

Phenalenone originated from very restricted natural resources, including Fungi Imperfecti.[19] *P. gunnii* is one species of Fungi Imperfecti, which suggested that its presence of related phenalenones is reasonable and it should share a similar biosynthetic pathway to produce the phenalenones through folding of a linear $C_{14}$-polyketide.[19] Phenalenones were reported to have antibacterial, antitumor, anti-HIV activity through inhibition of HIV-1 integrase, and antiprotozoal activities.[19−21] Recently, two phenalenone compounds were found to exhibit considerable effects against the malaria parasite, one of which maintained the same level of activity in a chloroquine-resistant strain, which is the first report of the antimalarial activity of this type of scaffold compound.[22] The structure of the newly isolated compound paecilomycone A is very similar to the anti-HIV target funalenone (anti-HIV, $IC_{50}$ = 1.7 $\mu$M),[20] while there is a $NH_2$ group at C-9 of paecilomycone C instead of the normal OH group, which could be a hint that the two new compounds could be potential effective anti-HIV compounds and highly valuable for continuing studies.

Entomogenous fungi are a treasury for searching for bioactive compounds, and many interesting results have been found from them.[23−30] However, few tyrosinase inhibitors were reported from these species. This study revealed that tyrosinase inhibitors truly existed in the secondary metabolites of entomopathogenic fungi. Tyrosinase is one of the main enzymes involved in immunity and defense response of insects;[9−11,31] therefore, tyrosinase inhibitors from metabolites of entomopathogenic fungi, such as paecilomycones A−C, must play an important role in virulence of the fungus and can possibly be used as virulence factors for high-virulent strain screening and used in novel pesticide production. Most of the currently used pesticides kill insects by targeting their nervous system and have a neurotoxic effect in mammals as well;[9,32] however, tyrosinase inhibitors targeting the immune and defensive systems of insects may have wider application prospects. Additionaly, similar to some popularly used tyrosinases in the food industry and cosmetics, paecilomycones A−C also have the possibility to be used in these areas.

## ■ ASSOCIATED CONTENT

### Supporting Information

Inhibiton of the methanol extracts of the strain RCEF0199 on tyrosinase diphenolase (Figure S1), preparative HSCCC separation of the crude sample from *P. gunnii* using two-step elution with solvent systems (Figure S2), $^1H$ and $^{13}C$ NMR and HMBC of compound **1** (Figure S3), $^1H$ and $^{13}C$ NMR of compound **2** (Figure S4), $^1H$ and $^{13}C$ NMR of compound **3** (Figure S5), ninhydrin reaction with the three compounds shown only in compound **3** reacted positively with a purple color (Figure 6), inhibition rates of mycelia extracts from different strains against diphenolase of tyrosinase (Table S1), and paired *t* tests on inhibibition rates of mycelia extracts and fermentation broth extracts (Table S2). This material is available free of charge via the Internet at http://pubs.acs.org.

## ■ AUTHOR INFORMATION


### Corresponding Authors

*Telephone/Fax: +86-551-5786887. E-mail: hufenglin@hotmail.com.

*Telephone: +86-551- 65786401. Fax: +86-551-65786765. E-mail: baoguanhu@ahau.edu.cn.

### Author Contributions

†Ruili Lu and Xiaoxiao Liu contributed equally to this work.



### Funding

This work was financially supported by the China National Science Foundation (30871676), the Foundation of the Ministry of Science and Technology of Anhui Province (1408085MC46 and KJ2012A107), the Anhui Agricultural University Talents Foundation (YJ2011-06), and the Anhui Outstanding Youth Science Foundation (1108085J04).


### Notes

The authors declare no competing financial interest.

## ■ REFERENCES


(1) Parvez, S.; Kang, M.; Chung, H. S.; Bae, H. Naturally occurring tyrosinase inhibitors: Mechanism and applications in skin health, cosmetics and agriculture industries. *Phytother. Res.* **2007**, *21*, 805−816.

(2) Chang, T. S. An updated review of tyrosinase inhibitors. *Int. J. Mol. Sci.* **2009**, *10*, 2440−2475.

(3) Chang, T. M. Tyrosinase and tyrosinase inhibitors. *J. Biocatal. Biotransform.* **2012**, *1*, 1−2.

(4) Kumar, C. M.; Sathisha, U. V.; Dharmesh, S.; Rao, A. G.; Singh, S. A. Interaction of sesamol (3,4-methylenedioxyphenol) with tyrosinase and its effect on melanin synthesis. *Biochimie* **2011**, *93*, 562−569.

(5) Demirkiran, O.; Sabudak, T.; Ozturk, M.; Topcu, G. Antioxidant and tyrosinase inhibitory activities of flavonoids from *Trifolium nigrescens* subsp. petrisavi. *J. Agric. Food Chem.* **2013**, *61*, 12598−12603.

(6) Lin, Y. F.; Hu, Y. H.; Lin, H. T.; Liu, X.; Chen, Y. H.; Zhang, S.; Chen, Q. X. Inhibitory effects of propyl gallate on tyrosinase and its application in controlling pericarp browning of harvested longan fruits. *J. Agric. Food Chem.* **2013**, *61*, 2889−2895.

(7) Espin, J.; Wichers, H. Effect of captopril on mushroom tyrosinase activity in vitro. *Biochim. Biophys. Acta* **2001**, *1544*, 289−300.

(8) Jimbow, K.; Luo, D.; Chen, H.; Hara, H.; Lee, M. H. Coordinated messenger-RNA and protein expression of human lamp-1 in induction of melanogenesis after UV-B exposure and contransfection of human tyrosinase and TRP-1 CDNAs. *Pigm. Cell Res.* **1994**, *7*, 311−319.

(9) Guerrero, A.; Rosell, G. Biorational approaches for insect control by enzymatic inhibition. *Curr. Med. Chem.* **2005**, *12*, 461−469.

(10) Ortiz-Urquiza, A.; Keyhani, N. O. Action on the surface: Entomopathogenic fungi versus the insect cuticle. *Insects* **2013**, *4*, 357−374.

(11) Hussein, K. A.; Abdel-Rahman, M. A. A.; Abdel-Mallek, A. Y.; El-Maraghy, S. S.; Joo, J. H. Pathogenicity of *Beauveria bassiana* and *Metarhizium anisopliae* against *Galleria mellonella*. *Phytoparasitica* **2012**, *40*, 117−126.

(12) Kramer, K. J.; Hopkins, T. L. Tyrosine metabolism for insect cuticle tanning. *Arch. Insect Biochem. Physiol.* **1987**, *4*, 279−301.

(13) Ito, Y. Golden rules and pitfalls in selecting optimum conditions for high-speed count-current chromatography. *J. Chromatogr. A* **2005**, *1065*, 145−168.

(14) Black, B.; Sun, C.; Zhao, Y. Y.; Gänzle, M. G.; Curtis, J. M. Antifungal lipids produced by lactobacilli and their structural identification by normal phase LC/atmospheric pressure photoionization−MS/MS. *J. Agric. Food Chem.* **2013**, *22*, 5338−5346.

(15) Ernst-Russell, M. A.; Chai, C. L. L.; Elix, J.; McCarthyC, P. M. Myeloconone A2, a new phenalenone from the lichen *Myeloconis erumpens*. *Aust. J. Chem.* **2000**, *53*, 1011−1013.

(16) Hölscher, D.; Schneider, B. Phenalenones from *Strelitzia reginae*. *J. Nat. Prod.* **2000**, *63*, 1027−1028.

(17) Harding, V. J.; Warneford, F. H. S. The ninhydrin reaction with amino acids and ammonium salts. *J. Biol. Chem.* **1916**, *25*, 319−335.

(18) Kim, Y. J.; Uyama, H. Tyrosinase inhibitors from natural and synthetic sources: Structure, inhibition mechanism and perspective for the future. *Cell. Mol. Life Sci.* **2005**, *62*, 1707−1723.
(19) Cooke, R. G.; Edwards, J. M. Naturally occurring phenalenones and related compounds. *Fortschr. Chem. Org. Naturst.* **1981**, *40*, 153−190.
(20) Shiomi, K.; Matsui, R.; Isozaki, M.; Chiba, H.; Sugai, T.; Yamaguchi, Y.; Masuma, R.; Tomoda, H.; Chiba, T.; Yan, H.; Kitamura, Y.; Sugiura, W.; Omura, S.; Tanaka, H. Fungal phenalenones inhibit HIV-1 integrase. *J. Antibiot.* **2005**, *5*, 65−68.
(21) Rosquete, L. I.; Cabrera-Serra, M. G.; Piñero, J. E.; Martín-Rodríguez, P.; Fernández-Pérez, L.; Luis, J. G.; McNaughton-Smith, G.; Abad-Grillo, T. Synthesis and in vitro antiprotozoal evaluation of substituted phenalenone analogues. *Bioorg. Med. Chem.* **2010**, *18*, 4530−4534.
(22) Gutiérrez, D.; Flores, N.; Abad-Grillo, T.; McNaughton-Smith, G. Evaluation of substituted phenalenone analogues as antiplasmodial agents. *Exp. Parasitol.* **2013**, *135*, 456−458.
(23) Molnar, I.; Gibson, D. M.; Krasnoff, S. B. Secondary metabolites from entomopathogenic Hypocrealean fungi. *Nat. Prod. Rep.* **2010**, *27*, 1241−1275.
(24) Isaka, M.; Srisanoh, U.; Sappan, M.; Supothina, S.; Boonpratuang, T.; Sterostreins, F.-O. Illudalanes and norilludalanes from cultures of the basidiomycete *Stereum ostrea* BCC 22955. *Phytochemistry* **2012**, *79*, 116−120.
(25) Hu, F. L.; He, Y. Q.; Huang, B.; Li, Z. Z. Secondary metabolites in a soybean fermentation broth of *Paecilomyces militaris*. *Food Chem.* **2009**, *116*, 198−201.
(26) Schimidt, K.; Riese, U.; Li, Z. Z.; Hamburger, M. Noval tetramic acids and pyridone alkaloids, militarinones B, C and D, from the insect pathogenic fungus *Paecilomyces militaris*. *J. Nat. Prod.* **2003**, *66*, 378−383.
(27) Cheng, Y. X.; Li, Z. Z.; Hamburger, M. Farinosones A−C, neurotrophic alkaloidal metabolites from the entomopathogenous deuteromycete *Paecilomyces farinosus*. *J. Nat. Prod.* **2004**, *67*, 1854−1858.
(28) Lu, R. L.; Bao, G. H.; Hu, F. L.; Huang, B.; Li, C. R.; Li, Z. Z. Comparison of cytotoxic extracts from fruiting bodies, infected insects and cultured mycelia of *Cordyceps formosana*. *Food Chem.* **2014**, *145*, 1066−1071.
(29) Lu, R. L.; Luo, F. F.; Hu, F. L.; Huang, B.; Li, C. R.; Bao, G. H. Identification and production of a novel natural pigment, cordycepoid A, from *Cordyceps bifusispora*. *Appl. Microbiol. Biotechnol.* **2013**, *97*, 6241−6249.
(30) Luo, F.; Lu, R.; Zhou, H.; Hu, F.; Bao, G.; Huang, B.; Li, Z. Metabolic effect of an exogenous gene on transgenic *Beauveria bassiana* using liquid chromatography−mass spectrometry-based metabolomics. *J. Agric. Food Chem.* **2013**, *61*, 7008−7017.
(31) Valadez-Lira, J. A.; Alcocer-Gonzalez, J. M.; Damas, G.; Nunez-Mejia, G.; Oppert, B.; Rodriguez-Padilla, C.; Tamez-Guerra, P. Comparative evaluation of phenoloxidase activity in different larval stages of four lepidopteran pests after exposure to *Bacillus thuringiensis*. *J. Insect Sci.* **2012**, *12*, 801−811.
(32) Costa, L. G.; Giordano, G.; Guizzetti, M.; Vitalone, A. Neurotoxicity of pesticides: A brief review. *Front. Biosci.* **2008**, *13*, 1240−1249.

**Table 1. Structures of the Tested Alkylpyrazines**

| no. | structure | name | MF[a] | MW[b] | purity |
|---|---|---|---|---|---|
| 1 | 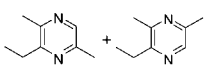 | 2-Ethyl -3,6-dimethylpyrazine, 2-Ethyl -3,5-dimethylpyrazine | $C_8H_{12}N_2$ | 136 | 95% |
| 2 | | 2-Methylpyrazine | $C_5H_6N_2$ | 94 | 99% |
| 3 | | 2,3-Dimethylpyrazine | $C_6H_8N_2$ | 108 | 99% |
| 4 | | 2,5-Dimethylpyrazine | $C_6H_8N_2$ | 108 | 99% |
| 5 | | 2,6-Dimethylpyrazine | $C_6H_8N_2$ | 108 | 98% |
| 6 | | Ethylpyrazine | $C_6H_8N_2$ | 108 | 98% |
| 7 | | 2,3,5-Trimethylpyrazine | $C_7H_{10}N_2$ | 122 | 99% |
| 8 | | 2-Ethyl-3-methylpyrazine | $C_7H_{10}N_2$ | 122 | 99% |
| 9 | | 2,3-Diethylpyrazine | $C_8H_{12}N_2$ | 136 | 98% |
| 10 | | 2-Methyl-3-propylpyrazine | $C_8H_{12}N_2$ | 136 | 97% |
| 11 | | 2,3,5,6-Tetramethylpyrazine | $C_8H_{12}N_2$ | 136 | 98% |
| 12 | | 2,3-Diethyl-5-methylpyrazine | $C_9H_{14}N_2$ | 150 | 99% |
| 13 | | 2-Isobutyl-3-methylpyrazine | $C_9H_{14}N_2$ | 150 | 98% |
| 14 | 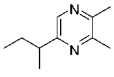 | 5-*sec*-Butyl-2,3-dimethylpyrazine | $C_{10}H_{16}N_2$ | 164 | 99% |

[a]MF = molecular formula. [b]MW = molecular weight.

is the most efficient tool for controlling fire ant colonies in large areas, even in phorid fly released areas. In the last several decades, numerous attempts have been made to develop efficient baits. A toxicant (the active ingredient usually less than 1.0%), an attractant, such as soybean oil, and an inert carrier, such as corn cob grits, were used to formulate bait for fire ant control.[16,17] A recently developed fire ant bait consisting of dried distillers grains with solubles as a carrier was found to be water-resistant and compatible with a number of pyrethroid insecticides.[18] Communication in social insects is based primarily on the use of pheromones, and many of these pheromones have attractive properties. The highly evolved fire ant uses a complex of pheromones, such as trail pheromone, alarm pheromone, and queen-produced recognition pheromone, for colony communications.[9] The incorporation of these ant pheromones with attractive properties could enhance the attractiveness and harvest of bait because the efficacy of bait largely depends upon ant foraging activity.[19] For instance, alarm pheromonal components from leaf-cutting ants (*Atta* spp.) have previously been proven to substantially increase the attractiveness and harvest of the bait.[20,21] The potential of alarm pheromones in fire ant control is that they elevate workers to a heightened state of alertness and movement, resulting in quicker location of a bait particle than otherwise possible.[22]

Previous studies have shown that pheromone homologues and analogues could elicit biological activity in insects comparable to the natural compounds[23−26] and may have a high potentiality as alternative material in integrated pest management strategies.[27] Thus, the present study aimed to examine both electroantennogram (EAG) and behavioral responses of *S. invicta* workers to the commercially available 2-ethyl-3,6(5)-dimethyl pyrazine (mixture of the 3,5- and 3,6-dimethyl isomers, herein referred to as pheromone isomers) and related alkylpyrazine analogues. Because an alarm response is a rapid reaction and, therefore, requires compounds of low molecular weight (between 100 and 200 with 5−10 carbons) with high volatility, we selected 13 alkylpyrazine analogues

whose molecular weights range from 94 to 164. For both EAG and behavioral bioassays, a series of dilutions were made to test both EAG and behavioral dose−responses of fire ant workers from various colonies to pheromone isomers and the selected analogues. The pyrazine analogues that proved to be very active in both EAG and behavioral bioassays would potentially be used as bait enhancers for the control of the fire ants in the invaded regions.

## MATERIALS AND METHODS

**Insects.** Eight mature colonies of *S. invicta* were collected on the campus of South China Agricultural University (Guangzhou, Guangdong, China). All colonies were considered polygyne because of the presence of multiple queens during collection. Colonies were reared with soil under laboratory conditions and provided daily with purified water, 10% honey solution, and larvae of *Tenebrio molitor* L. Tests were carried out within 1 month of ant collection.

**Reagents and Test Chemicals.** Acetonitrile ($CH_3CN$) was of high-performance liquid chromatography (HPLC) grade and was used without further purification. Water was purified with a model 7155 Barnstead Nanopure system (Thermo Scientific, Marietta, OH) and subsequently filtered through a 0.45 $\mu$m membrane. The alarm pheromone component, 2-ethyl-3,6-dimethylpyrazine (**1a**), was commercially available as a mixture with the 2-ethyl-3,5-dimethylpyrazine (**1b**) isomer (Sigma-Aldrich, St. Louis, MO). The mixture consisted of about 45% of compound **1a** and 55% of compound **1b** [gas chromatography (GC) analysis]. A total of 13 structurally related alkylpyrazine analogues were purchased from Sigma-Aldrich or Acros Organics (Geel, Belgium). The chemical structures of these compounds are shown in Table 1. Each compound was diluted with HPLC-grade *n*-hexane to make a 100 $\mu g/\mu L$ solution. Further serial 10-time dilutions were made to give solutions with different concentrations ranging from 0.01 ng/$\mu$L to 10 $\mu g/\mu L$ for EAG and behavioral tests. The solutions were kept in a freezer at −20 °C until use.

**HPLC Analysis.** HPLC separation of compound **1** was performed on an Agilent HP 1260 instrument (Agilent Technologies, Palo Alto, CA), using a stainless-steel, 250 × 4.6 mm inner diameter, 5 $\mu$m, HC C-18 column (Agilent Technologies, Middelburg, Netherlands). A solution of compound **1** at 10 $\mu g/\mu L$ was prepared with $CH_3CN$ for both analytical separation and semi-preparation. All chromatographic experiments were performed in the isocratic mode. $CH_3CN$/water was selected as the mobile phase, followed by a previously reported liquid chromatography−mass spectrometry (LC−MS) analysis.[28] Various percentages (20−50%) of $CH_3CN$ were tested to optimize the separation efficiency of the mobile phase. The flow rate was 0.2 mL/min, and the detection wavelength was ultraviolet (UV) 278 nm. The injection volume was 1 $\mu$L in analytical separations. On the basis of nuclear magnetic resonance (NMR) spectroscopic data obtained by LC−NMR, 2-ethyl-3,5-dimethylpyrazine (**1b**) was found to be eluted first, followed by 2-ethyl-3,6-dimethylpyrazine (**1a**).[28] In semi-preparative separation, a 5 $\mu$L sample loop was used. Each peak fraction was manually collected according to the elution profile. After 2 weeks of semi-preparative separation, the collected fractions were combined (**1a**, 150 mL; **1b**, 180 mL) and subjected to sequential liquid−liquid partitions to remove $CH_3CN$ and water. The pooled fractions were first partitioned with hexane (50 mL × 3), and then the resultant hexane layer was acidified with 20 mL of 0.1 N HCl. After removal of the hexane layer, the acid layer was neutralized to pH 10 with 15 mL of 0.2 N NaOH and subsequently partitioned with hexane (20 mL × 3). The resultant hexane layers were combined and dried over anhydrous $Na_2SO_4$. The hexane extract was finally concentrated to 2 mL under a mild stream of nitrogen and subjected to HPLC quantitation.

To quantitate pyrazine **1a** or **1b** in the hexane extract, 2,3-diethylpyrazine (**9**) was used as an external standard. A stock solution of standard compound **9** (10 $\mu g/\mu L$) was prepared and then diluted to a series of concentrations ranging from 0.25 to 8 $\mu g/\mu L$. All dilutions were transferred to the HPLC autosampler, and 1 $\mu$L of each dilution was used for HPLC analysis under the same conditions as above at a flow rate of 1 mL/min. A standard curve was calculated by linear regression analysis. The concentration of pyrazine in the 2 mL hexane extract was calculated against the standard curve. The hexane extracts of compounds **1a** and **1b** were thereafter diluted to 1 $\mu g/\mu L$ for EAG study and to 10 ng/$\mu$L for behavioral study. A mixture of an equal volume of both compound **1a** and **1b** solutions at the same concentration was bioassayed to determine the synergistic effect.

**EAG Experiment.** The EAG sensitivity of *S. invicta* workers was determined by conventional EAG methods.[29,30] Briefly, the reference glass electrode was connected to the neck of an isolated head of a major worker, and the recording electrode was connected to the antennal tip. The analogue signal was detected through a PRG-3 probe, amplified with a data acquisition controller IDAC-2, and analyzed with software EAG 2000 (all from Syntech, Kirchzarten, Germany). A 10 $\mu$L aliquot of each test compound (in hexane) was applied to a piece of filter paper (4 × 40 mm, Whatman no. 1). After solvent evaporation, the odor-impregnated filter paper strip was placed in a glass Pasteur pipet. Fresh stimulus pipets were prepared before each set of experiments. Hexane was used as the solvent control. Stimuli were delivered as 0.2 s puffs at a humidified flow rate of 1000 mL/min generated by an air stimulus controller CS-55 (Syntech, Kirchzarten, Germany).

A test series of the pyrazines of the same dose (0.1, 1, 10, 100, or 1000 $\mu$g) was applied to a single antennal preparation, and the presentation order of these compounds was randomized. A blank stimulus (solvent control) was presented before and after the 14 test compounds. EAG recordings were obtained from eight antennal preparations for each dose. For analyses, EAG response to the solvent control (average of two recordings per antennal preparation, less than 0.20 mV) was deducted from the EAG amplitudes elicited by the test compounds. The corrected EAG data were analyzed for each dose using one-way analysis of variance (ANOVA) to establish significant differences among the treatments (test compounds). Means across all 14 compounds for certain doses were compared by the Tukey−Kramer honestly significant difference (HSD) comparison test ($p < 0.05$).[31]

**Behavioral Bioassay.** Behavioral bioassays were conducted as described by Vander Meer et al.,[9] with slight modification. At least 2 h prior to a bioassay, 0.1 g of workers (approximately 100−150) from each colony were added to a plastic cup (9 cm tall × 14 cm inner diameter) with the inside wall coated with Fluon to prevent escape. A 1 $cm^3$ sugar-agar block (10% sugar water + 1% agar after boiling and chilling) was placed on the bottom of the cup to allow feeding. Water was provided by filling a 1.5 mL microcentrifuge tube with distilled water and threading a cotton string through a hole in the cap of the tube. A filter paper strip (1 × 3 cm) folded into a triangle was put in an empty space in the bottom of the cup. The experiment was not started until the worker ants had settled into a quiescent group. A total of 10 $\mu$L of sample solution was loaded onto the filter paper strip with a micropipet in a gentle movement that would not generate a response. The alarm response of ant workers was observed and recorded. The response to a test compound was evaluated on the number of workers that were running out of the quiescent group during the recording time. After each test, the filter paper strip was replaced with a new strip for the next test. All ant bioassay units (i.e., cups) were tested with the control (10 $\mu$L of hexane), and all of the samples were at the same dose. Bioassay units were evaluated in sequence, but the samples presented to the ants were randomized. In this way, workers of a test unit that were alarmed had enough time (more than 30 min) to recover prior to the next test. Ants from a colony were considered as one replicate. A test series of the alkylpyrazines of the same dose (0.1, 1, 10, 100, or 1000 ng) was replicated 8 times. Bioassay data were determined to be normally distributed and then analyzed using one-way ANOVA, followed by the Tukey−Kramer HSD comparison test ($p < 0.05$), to establish significant differences among the treatments.[31]

For correlation analysis, behavioral response to the solvent control was deducted from that elicited by the test compounds. It appears that all compounds elicited dose-dependent responses in both EAG experiment and behavioral bioassay. A pilot analysis indicated that the

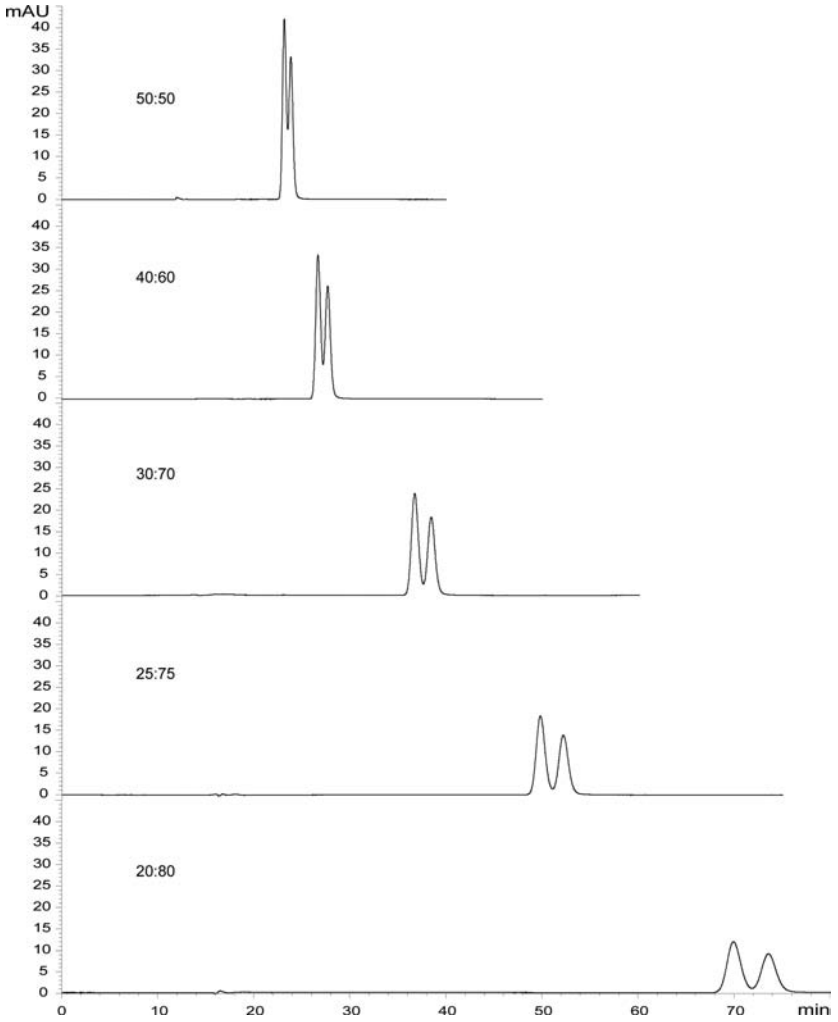


**Figure 1.** Separation of fire ant alarm pheromone isomers in $CH_3CN$/water mobile phases of various compositions (as indicated in the figure) on an Agilent HC C-18 column.

EAG data at five doses correspond well to the behavioral data from the low to high doses. Therefore, the correlation between the corrected EAG data and the corrected behavior data was analyzed using the PROC CORR procedure of SAS statistical software.[31]

**Bait Attraction Bioassay.** Three alkylpyrazines with relatively high activity in both EAG and behavior bioassays were selected for further food bait tests. The potential for using these alarm pheromone compounds to enhance the attractiveness of food bait was examined for *S. invicta* workers. A total of 0.5 g of ant workers was transferred into a plastic basin (55 cm diameter at the bottom) with the inside wall coated with Fluon to prevent escape. A moisturized cotton wad in a Petri dish cover ($d$ = 6 cm) for provision of water was placed at the center of the basin. Holes were made at the side wall of the Petri dish cover for ant movement. Ants were attracted to the water source and left for a 2 h period of acclimatization to settle into a quiescent group. During this period, three aluminum foil disks (5 cm diameter) were mounted on the bottom of the basin. Foil disks were positioned 20 cm away from the center of the basin and at an equal distance from each other. On the foil disk was then placed a filter paper disk (4 cm diameter). Prior to the start of evaluation, a block of ham sausage (0.1 g) used as food bait was placed onto the filter paper disk. A total of 10 $\mu$L of hexane was loaded onto both filter paper disk and food block with a micropipet in a gentle movement. For the other two food blocks, 10 $\mu$L of sample solution was loaded onto either the filter paper disk or the food block. The number of ants on a filter paper disk was counted at 2, 5, 15, 30, and 45 min after impregnation of the sample solution (or hexane control) onto a filter paper disk or food block. After each test, ants were discarded and the basin was cleaned with soap water and air-dried for the next test. Each sample solution was repeated 8 times. Two doses (10 and 100 ng) of each compound were tested. Mean numbers of ants for the same compound−dose combination on different filter paper disks were compared using the Tukey−Kramer HSD comparison test ($p < 0.05$).[31]

## RESULTS AND DISCUSSION

As expected, separation of 2-ethyl-3,6-dimethylpyrazine (**1a**) and 2-ethyl-3,5-dimethylpyrazine (**1b**) in the commercial product was accomplished on a reverse-phase C-18 column using $CH_3CN$/water mobile phase. Figure 1 illustrates elution profiles of compound **1** at a flow rate of 0.2 mL/min with variable ratios of $CH_3CN$/water mobile phase. The injection results in two chromatographic peaks, which correspond to the two regio-isomers. The percentage of $CH_3CN$ in the mobile phase had a significant influence on separation efficiency. The separation efficiency increases with the decrease of the $CH_3CN$/water ratio. However, when the $CH_3CN$/water ratio decreases, chromatographic retention time increases significantly. At a ratio of 20:80 (v/v), the two regio-isomers, compounds **1a** and **1b**, are nearly baseline-separated. Because general preparative separations are time-consuming and tedious, we used a ratio of 25:75 (v/v) for scaling-up the preparation of pure isomers at the semi-preparative level. The

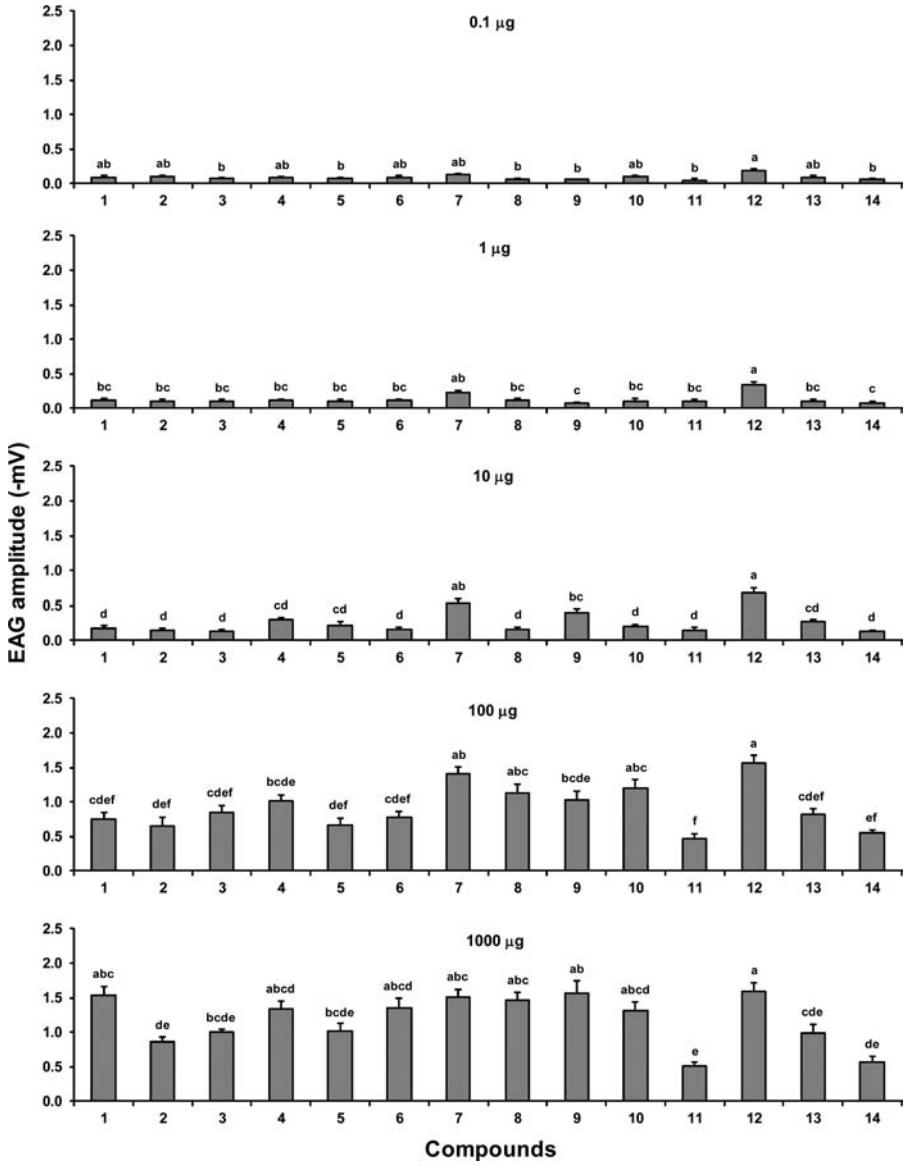


**Figure 2.** EAG response [−mV ± standard error (SE)] of *S. invicta* workers to 14 alkylpyrazines. Means for the same dose having no letter in common are significantly different ($p < 0.05$; Tukey HSD test).

two peaks derived from preparative compounds **1b** and **1a**, respectively, were observed at 49.6 and 51.7 min at 278 nm. The external standard method was used to obtain the regression equation, $A = 608.6090C + 2.7015$, where $A$ is the peak area and $C$ is the concentration of the standard compound ($\mu g/\mu L$). The standard compound showed excellent linearity ($r^2 = 0.999\,98$; $p < 0.001$) in selected concentration ranges. With the obtained calibration curve, the concentrations of 2 mL preparative compound **1a** and **1b** solutions were determined to be 2.14 and 3.02 $\mu g/\mu L$, respectively.

All tested compounds elicited dose-dependent responses from the antennae of *S. invicta* workers (Figure 2). Significant differences were recorded in the EAG response of ant workers to the various compounds at all tested doses. Statistical analyses (ANOVA) of the corrected EAG data revealed that both the chemical structures and doses of alkylpyrazines influenced electrophysiological responses. Antennal responses to pheromone isomers (**1**) varied between 0.09 and 1.53 mV across all doses. In comparison to compound **1**, EAG responses to 7 compounds of 13 tested analogues were similar or relatively higher at both the lowest and highest doses. At moderate doses (1, 10, and 100 $\mu g$), responses to compounds **7** and **12** were significantly higher than that to compound **1**, except for response to compound **7** at a dose of 1 $\mu g$. Among the 14 tested alkylpyrazines, compound **12** elicited the highest responses at every dose tested.

All alkylpyrazines elicited apparent alarm behavioral responses of *S. invicta* workers. When exposed to odors of pyrazine analogues, workers were observed to leave the quiescent group rapidly toward the source of odors. The alarm bioassay results for all tested compounds are shown in Figure 3. Among the 14 tested alkylpyrazines, three compounds, **1**, **7**, and **12**, elicited significant alarm responses at every dose tested. Furthermore, the responses to these three compounds increased in a dose-dependent manner. In contrast, the remaining 10 compounds failed to elicit significant behavioral response at low doses. In comparison to compound **1**, behavioral responses to the two active alkylpyrazines, compounds **7** and **12**, were not significantly different at all tested doses, except that the response to compound **12** was

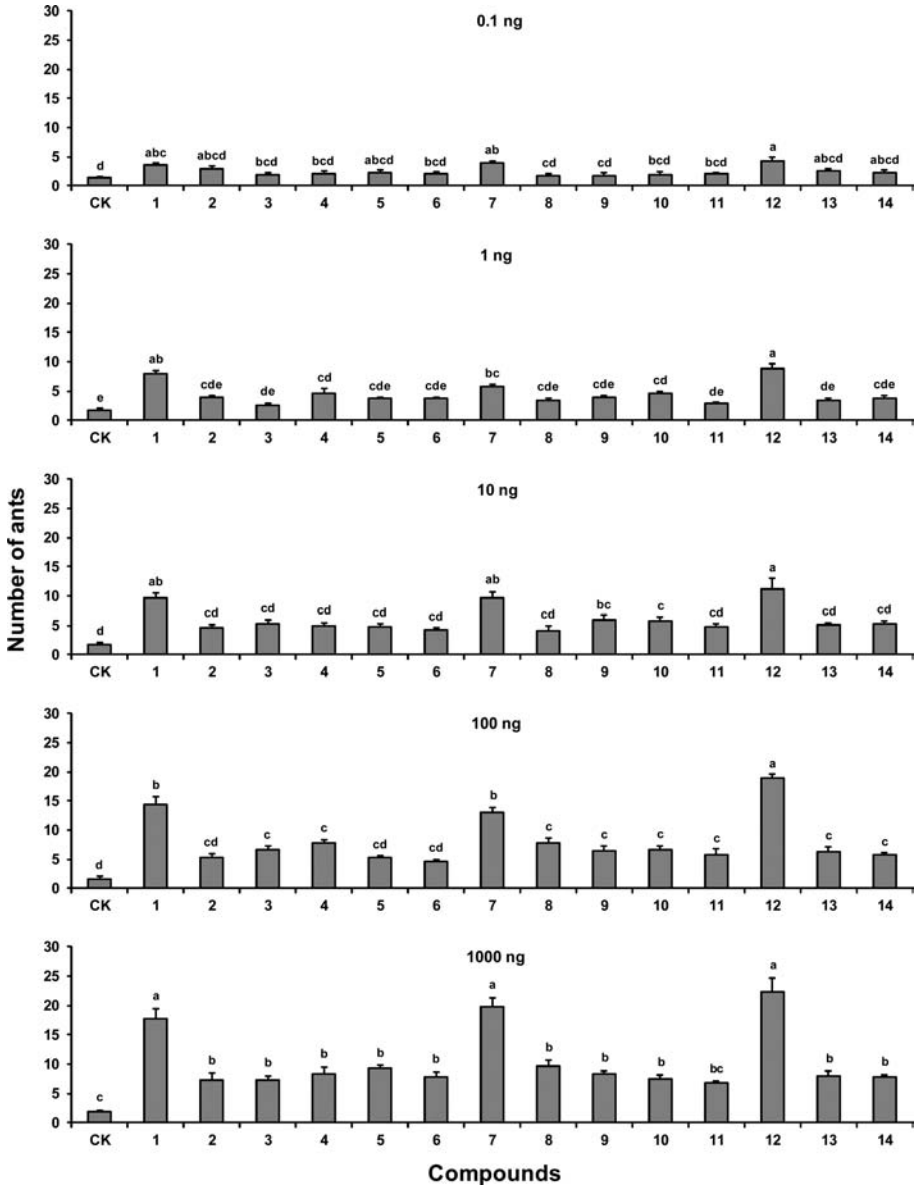


**Figure 3.** Alarm response of *S. invicta* workers to 14 alkylpyrazines. Means for the same dose having no letter in common are significantly different ($p < 0.05$; Tukey HSD test).

significantly higher than that to compound **1** at a dose of 100 ng. Generally, the alarm responses induced by the remaining 10 alkylpyrazine analogues were significantly less than that induced by compound **1** at all doses but the lowest dose (0.1 ng).

A good correlation between the EAG and behavioral responses was obtained for all 14 alkylpyrazines ($y = 6.3857x + 1.3999$; $r^2 = 0.5963$; $p < 0.0001$). This suggests that these alkylpyrazine analogues target the same olfactory neurons on the antennae of fire ant workers.

When pure isomers were tested at a dose of 10 $\mu$g, compound **1a** elicited significantly greater EAG response than compound **1b** (Table 2). A mixture of both isomers (1:1) at the same dose elicited intermediate EAG response, suggesting that there exists an addition effect between the two isomers. Furthermore, the EAG response to compound **1a** in the second EAG experiment was comparable to responses to compounds **7** and **12** in the first EAG experiment. The data from the behavioral bioassay with pure isomers of compound **1** at a dose of 100 ng showed that the number of workers responding to odors was significantly more than the number of workers responding to hexane (Table 3). Compound **1a** elicited a significantly higher alarm response than compound **1b**, and the activity of the mixture of both isomers (1:1) was similar to that of compound **1b**.

**Table 2. EAG Response of *S. invicta* Workers to Alarm Pheromone Isomers[a]**

| compound | EAG (−mV ± SE) |
|---|---|
| **1a** | 0.62 ± 0.043 a |
| **1b** | 0.43 ± 0.034 b |
| **1a** + **1b** | 0.54 ± 0.054 ab |

[a]Dose = 10 $\mu$g. Means followed by different letters are significantly different ($p < 0.05$; Tukey HSD test).

The results of the EAG and behavioral experiments demonstrated the responses of fire ant workers to the commercially available mixture of 2-ethyl-3,6(5)-dimethyl pyrazine and its individual components and support a previous


dx.doi.org/10.1021/jf505191s | J. Agric. Food Chem. 2014, 62, 11924−11932

**Table 3. Behavioral Response of *S. invicta* Workers to Alarm Pheromone Isomers[a]**

| compound | no. of ants (± SE) |
|---|---|
| CK | 3.2 ± 0.25 c |
| **1a** | 19.5 ± 0.42 a |
| **1b** | 16.4 ± 0.32 b |
| **1a** + **1b** | 16.7 ± 0.53 b |

[a]Dose = 100 ng. Means followed by different letters are significantly different ($p < 0.05$; Tukey HSD test).

identification of fire ant alarm pheromone component, 2-ethyl-3,6-dimethyl pyrazine (**1a**).[9] Compound **1a** was found to be significantly more active than 2-ethyl-3,5-dimethyl pyrazine (**1b**) in both EAG and behavior bioassays. This is in agreement with previous reports demonstrating that compound **1b** was less active than compound **1a** in the alarm response experiment with fire ant workers and in the trail following experiment with the Mediterranean ant *Pheidole pullidulu*.[9,32] Interestingly, 2,3-diethyl-5-methylpyrazine (**12**) elicited significantly higher EAG responses compared to pheromone isomers **1** for doses of 1, 10, and 100 μg. In the EAG experiment, we puffed 100 μg of compound **1** to serve as a standard before the tests of all samples. This stimulation may have significant influence on the EAG responsiveness of the isolated head preparation to the same compound **1**, especially at low doses, in the following tests. EAG responsiveness of the isolated head preparation to the same stimulus has proven to decrease rapidly, falling below 50% of initial EAG responses after 20 min.[33] It seems likely that compound **1** elicits the same level of EAG response of fresh antennal preparation that has not been tested to standard (100 μg of compound **1**) as the two active pyrazine analogues **7** and **12**. This interpretation is supported by the fact that EAG response to compound **1a** is similar to EAG responses to compounds **7** and **12** at a dose of 10 μg. At a dose of 100 ng, the alarm response to compound **12** was significantly greater than that to compounds **1** and **7** but was similar to the alarm response to compound **1a**, indicating that compound **12** is equally active as the fire ant alarm pheromone component (**1a**). Di- and trialkyl-substituted pyrazines are known components of alarm/trail pheromones of ant species, including *Linepithema humilis* (Mayr), *Eutetramorium mocquerysi* Emery, and *Wasmannia auropunctata* (Roger).[34−36] It is possible that compound **12** is an unidentified component of the alarm pheromone of *S. invicta* or the observed response to compound

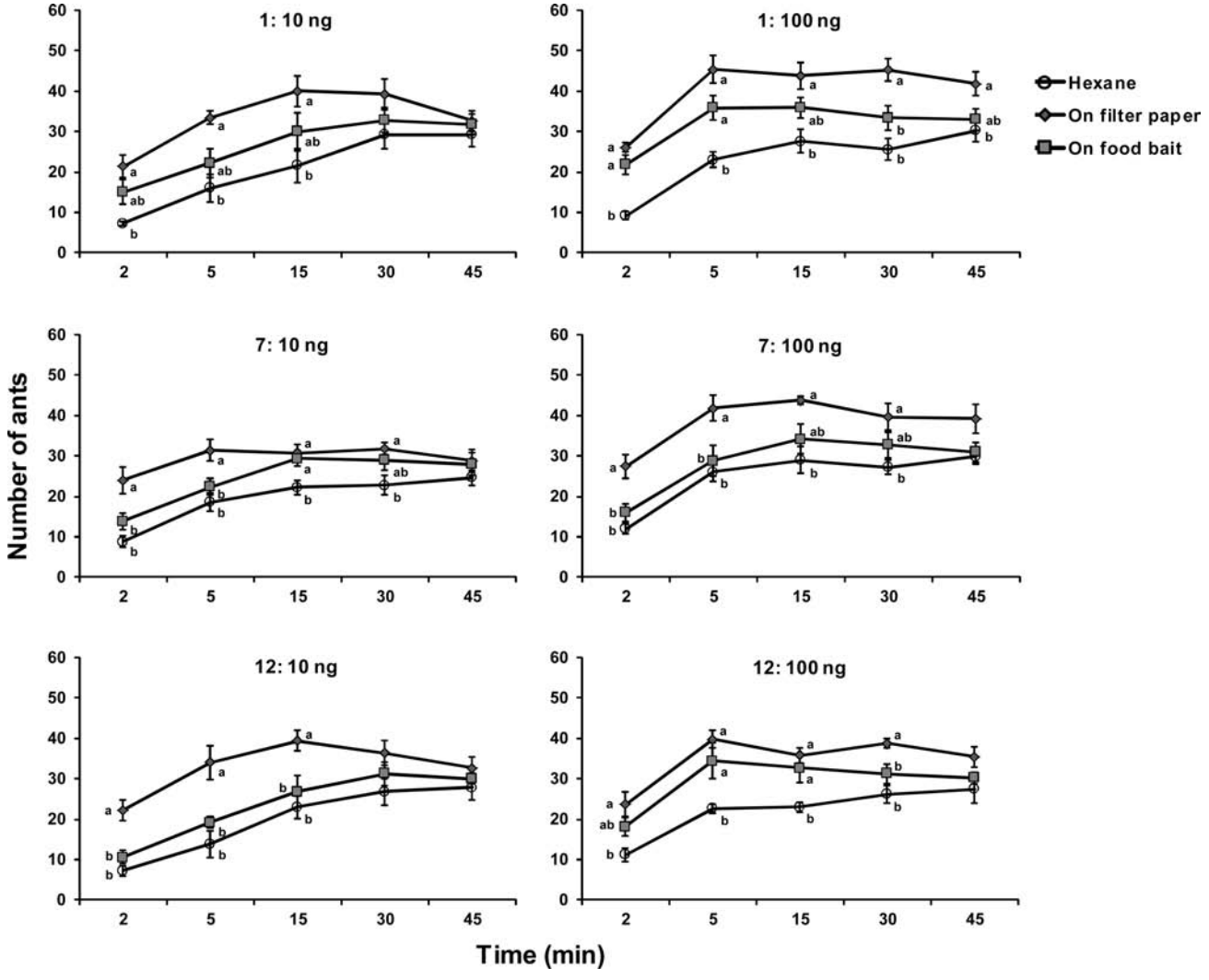


**Figure 4.** Responses of *S. invicta* workers in bait attraction bioassay to the three most active alkylpyrazines at two doses (10 and 100 ng). Means for the same time period having no letter in common are significantly different ($p < 0.05$; Tukey HSD test).

**12** may simply be due to their structural similarity to the alarm pheromone component **1a**.

For methyl-substituted pyrazines, only trimethyl-substituted pyrazine was EAG- and behaviorally active. In contrast, mono-, di-, and tetramethyl-substituted pyrazines turned out to be behaviorally much less active or even inactive, regardless of the position of the methyl substituents. In general, disubstituted pyrazines, for instance, 2-ethyl-3-methylpyrazine (**8**), 2,3-diethylpyrazine (**9**), 2-methyl-3-propylpyrazine (**10**), 2-isobutyl-3-methylpyrazine (**13**), attracted significantly more workers than hexane control but elicited significantly lower response than pheromone isomers **1**. The 6 substitution on the pyrazine ring of 2-ethylpyrazine appears to be important because 3-methyl- and 3-ethyl-2-ethylpyrazines (**8** and **9**) were much less behaviorally active than compound **1**. Thus, the number of substituents (methyl and ethyl) and the position of substituents in alkylpyrazines exerted a strong influence on the behavioral response. Substitution with propyl, isobutyl, or *sec*-butyl groups would result in a significant decrease of response. In contrast to the behavioral data, a relatively smaller influence of the chemical structure on the responsiveness was detected by the electrophysiological experiments with the EAG technique. All compounds tested, including the behaviorally inactive compounds, elicited dose-dependent physiological responses from the antennae of ant workers.

Three alkylpyrazines, **1**, **7**, and **12**, with both significant EAG and behavior responses were selected for bait discovery bioassays. Immediately after loading samples, ant workers were observed to run toward the odor sources, showing an alarm response. At the beginning of the test, workers ran around the food bait without feeding, then climbed up, and bit the bait intensely. After a few seconds, the workers turned back to their "nest" to recruit nestmates. About 4 min later, a large number of workers ran onto the food bait and started feeding. Workers near the sample-treated food bait appeared more agitated than those in the hexane control and fed on the food bait in a more aggressive manner. The number of workers around food bait increased rapidly over time (Figure 4), and reached the highest level in 45 min for the hexane control and in 15 min for both alkylpyrazine treatments. In general, the sample loaded onto filter paper disk attracted significantly more workers than the sample loaded on food bait and hexane control in 2 and 5 min periods, possibly because of the quick evaporation of the test compound on filter paper disk. In most cases, the number of workers in treatment of the sample loaded onto food bait were not significantly greater than that in the hexane control in a 15 min period. At the end of observation, generally no significant difference was observed in the number of workers among the three treatments of a pyrazine compound and among the six compound × dose combinations ($p > 0.05$). These results suggest that the three selected alkylpyrazines could significantly enhance bait attractiveness to *S. invicta* workers.

Eusocial insects are generally attracted to emission sources of alarm pheromones and exhibit a collective response to these chemical releasers. Alarm pheromones can also frequently function as recruitment stimuli that recruit large numbers of aggressive individuals to a pheromonal point source with incredible rapidity.[37,38] In this study, we observed this characteristic behavior in fire ants. Because excited ant workers would move rapidly to emission sources of alarm pheromones, we used the number of workers on the food bait to evaluate the activity of the three selected alkylpyrazines, **1**, **7**, and **12**, for food bait tests. These samples stimulated the same behaviors when incorporated in food baits. The sample loaded onto filter paper disk attracted more workers than loaded onto bait directly in the first 5 min period presumably because of faster recruitment of the sample evaporated in the air from the filter paper disk. Relatively more workers were attracted to bait incorporated with sample in the first 5 min period than to bait incorporated with hexane, but the difference was statistically significant only for compounds **1** and **12** at the high dose. The attraction to food bait by the sample-treated filter paper disk has potential applications. Alkylpyrazines can be used to improve harvest of toxic bait as proven by the alarm pheromone of leaf-cutting ants (*Atta* spp.), 4-methyl-3-heptanone, to significantly increase the attractiveness of enhanced bait sachets and the discovery of nearby unenhanced sachets in the field.[20] Future work will test the influence of alkylpyrazines on bait transportation and substantial control of the imported fire ants.

## ■ ASSOCIATED CONTENT

### Ⓢ Supporting Information

HPLC chromatographs of commercial mixture **1** and isolated isomers (Figure S1) and correlation between the EAG and behavioral responses (Figure S2). This material is available free of charge via the Internet at http://pubs.acs.org.

## ■ AUTHOR INFORMATION

### Corresponding Author

*Telephone/Fax: +86-10-64807780. E-mail: chenli@ioz.ac.cn.

### Funding

This research was supported by the National Basic Research Program of China (Grant 2012CB114105) and the National Natural Science Foundation of China (Grant 30970402).

### Notes

The authors declare no competing financial interest.

## ■ REFERENCES

(1) Hölldobler, B.; Wilson, E. O. *The Ants*; The Belknap Press and Harvard University Press: Cambridge, MA, 1990.

(2) Parry, K.; Morgan, E. D. Pheromones of ants: A review. *Physiol. Entomol.* **1979**, *4*, 161−189.

(3) Wilson, E. O.; Regnier, F. E., Jr. The evolution of the alarm defense system in the formicine ants. *Am. Nat.* **1971**, *105*, 279−289.

(4) Vander Meer, R. K.; Alonso, L. E. Pheromone directed behavior in ants. In *Pheromone Communication in Social Insects*; Vander Meer, R. K., Breed, M. D., Espelie, K. E., Winston, M. L., Eds.; Westview Press: Boulder, CO, 1998; pp 159−192.

(5) Brown, W. L. J.; Eisner, T.; Whittaker, R. H. Allomones and kairomones: Transspecific chemical messengers. *Bioscience* **1970**, *20*, 21−22.

(6) Wilson, E. O. Chemical communication among workers of the fire ant *Solenopsis saevissima* (Fr. Smith) 1. The organization of mass-foraging. *Anim. Behav.* **1962**, *10*, 134−147.

(7) Wilson, E. O. Chemical communication among workers of the fire ant *Solenopsis saevissima* (Fr. Smith) 2. An information analysis of the odour trail. *Anim. Behav.* **1962**, *10*, 148−158.

(8) Wilson, E. O. Chemical communication among workers of the fire ant *Solenopsis saevissima* (Fr. Smith) 3. The experimental induction of social responses. *Anim. Behav.* **1962**, *10*, 159−164.

(9) Vander Meer, R. K.; Preston, C.; Choi, M.-Y. Isolation of a pyrazine alarm pheromone component from the fire ant, *Solenopsis invicta*. *J. Chem. Ecol.* **2010**, *36*, 163−170.

(10) Vinson, S. B. Invasion of the red imported fire ant (Hymenoptera: Formicidae): Spread, biology, and impact. *Am. Entomol.* **1997**, *43*, 23−39.

(11) Wojcik, D. P.; Allen, C. R.; Brennan, R. J.; Forys, E. A.; Jouvenaz, D. P.; Lutz, R. S. Red imported fire ants: impact on biodiversity. *Am. Entomol.* **2001**, *47*, 24−50.
(12) Ascunce, M. S.; Yang, C.-C.; Oakey, J.; Calcaterra, L.; Wu, W.-J.; Shih, C.-J.; Goudet, J.; Ross, K. G.; Shoemaker, D. Global invasion history of the fire ant *Solenopsis invicta*. *Science* **2011**, *331*, 1066−1068.
(13) Morrison, L. W.; Porter, S. D.; Daniels, E.; Korzukhin, M. D. Potential global range expansion of the invasive fire ant, *Solenopsis invicta*. *Biol. Invasions* **2004**, *6*, 183−191.
(14) Morrison, L. W. Long-term impacts of an arthropod-community invasion by the imported fire ant, *Solenopsis invicta*. *Ecology* **2002**, *83*, 2337−2345.
(15) Callcott, A.-M. A.; Porter, S. D.; Weeks, R. D., Jr.; Graham, L. C. F.; Johnson, S. J.; Gilbert, L. E. Fire ant decapitating fly cooperative release programs (1994−2008): Two *Pseudacteon* species, *P. tricuspis* and *P. curvatus*, rapidly expand across imported fire ant populations in the southeastern United States. *J. Insect Sci.* **2011**, *11*, 1−25.
(16) Kafle, L.; Wu, W. J.; Vander Meer, R. K.; Huang, Y. Y.; Shih, C. J. Microencapsulated bait: Does it work with red imported fire ant, *Solenopsis invicta* Buren (Hymenoptera: Formicidae)? *Sociobiology* **2009**, *53*, 729−737.
(17) Williams, D. F.; Collins, H. L.; Oi, D. H. The red imported fire ant (Hymenoptera: Formicidae): An historical perspective of treatment programs and the development of chemical baits for control. *Am. Entomol.* **2001**, *46*, 146−159.
(18) Kafle, L.; Wu, W.-J.; Shih, C.-J. A new fire ant (Hymenoptera: Formicidae) bait base carrier for moist conditions. *Pest Manage. Sci.* **2010**, *66*, 1082−1088.
(19) Vogt, J. T.; Smith, W. A.; Grantham, R. A.; Wright, R. E. Effects of temperature and season on foraging activity of red imported fire ants (Hymenoptera: Formicidae) in Oklahoma. *Environ. Entomol.* **2003**, *32*, 447−451.
(20) Hughes, W. O. H.; Howse, P. E.; Vilela, E. F.; Knapp, J. J.; Goulson, D. Field evaluation of potential of alarm pheromone compounds to enhance baits for control of grass-cutting ants (Hymenoptera: Formicidae). *J. Econ. Entomol.* **2002**, *95*, 537−543.
(21) Hughes, W. O. H.; Goulson, D. The use of alarm pheromones to enhance bait harvest by grass-cutting ants. *Bull. Entomol. Res.* **2002**, *92*, 213−218.
(22) Vander Meer, R. K. Potential role of pheromones in fire ant control. In *Pest Management in the Subtropics: Integrated Pest Management—A Florida Perspective*; Rosen, D., Capinera, J., Bennett, F., Eds.; Intercept Press: Andover, U.K., 1996; pp 223−232.
(23) Kapitsky, S. V.; Zhukvoskaya, M. I. New analogs of sex pheromones of American cockroach (*Periplaneta americana* L.): Behavioral and electroantennographic study. *Pheromones* **1999**, *6*, 3−14.
(24) Solari, P.; Crnjar, R.; Frongia, A.; Sollai, G.; Secci, F.; Spiga, M.; Masala, C.; Liscia, A. Oxaspiropentane derivatives as effective sex pheromone analogs in the gypsy moth: Electrophysiological and behavioral evidence. *Chem. Senses* **2007**, *32*, 755−763.
(25) Bowers, W. S.; Nishino, C.; Montgomery, M. E.; Nault, L. R. Structure-activity relationships of analogs of the aphid alarm pheromone, (*E*)-*β*-farnesene. *J. Insect Physiol.* **1977**, *23*, 697−701.
(26) Briggs, G. G.; Cayley, G. R.; Dawson, G. W.; Griffiths, D. C.; Macaulay, E. D. M.; Pickett, J. A.; Pile, M. M.; Wadhams, L. J.; Woodcock, C. M. Some fluorine-containing pheromone analogues. *Pestic. Sci.* **1986**, *17*, 441−448.
(27) Renou, M.; Guerrero, A. Insect parapheromones in olfaction research and semiochemical-based pest control strategies. *Annu. Rev. Entomol.* **2000**, *45*, 605−630.
(28) Sugimoto, N.; Yomota, C.; Furusho, N.; Sato, K.; Yamazaki, T.; Tanamoto, K. Application of liquid chromatography−nuclear magnetic resonance spectroscopy for the identification of ethyldimethylpyrazine, a food flavouring agent. *Food Addit. Contam.* **2006**, *23*, 1253−1259.
(29) Chen, L.; Fadamiro, H. Y. Behavioral and electroantennogram responses of phorid fly *Pseudacteon tricuspis* (Diptera: Phoridae) to red imported fire ant *Solenopsis invicta* odor and trail pheromone. *J. Insect Behav.* **2007**, *20*, 267−287.
(30) Chen, L.; Sharma, K. R.; Fadamiro, H. Y. Fire ant venom alkaloids act as key attractants for the parasitic phorid fly, *Pseudacteon tricuspis* (Diptera: Phoridae). *Naturwissenschaften* **2009**, *96*, 1421−1429.
(31) SAS Institute. *SAS User Guide*; SAS Institute: Cary, NC, 2004.
(32) Ali, M. F.; Morgan, E. D.; Detrain, C.; Attygalle, A. B. Identification of a component of the trail pheromone of the ant *Pheidole pallidula* (Hymenoptera: Formicidae). *Physiol. Entomol.* **1988**, *13*, 257−265.
(33) Park, K. C.; Zhu, J.; Harris, J.; Ochieng, S. A.; Baker, T. C. Electroantennogram responses of a parasitic wasp, *Microplitis croceipes*, to host-related volatile and anthropogenic compounds. *Physiol. Entomol.* **2001**, *26*, 69−77.
(34) Cavill, G.; Houghton, E. Some pyrazine derivatives from the Argentine ant, *Iridomyrmex humilis*. *Aust. J. Chem.* **1974**, *27*, 879−889.
(35) Tentschert, J.; Bestmann, H. J.; Hölldobler, B.; Heinze, J. 2,3-Dimethyl-5-(2-methylpropyl)pyrazine, a trail pheromone component of *Eutetramorium mocquerysi* Emery (1899) (Hymenoptera: Formicidae). *Naturwissenschaften* **2000**, *87*, 377−380.
(36) Showalter, D.; Troyer, E.; Aklu, M.; Jang, E.; Siderhurst, M. Alkylpyrazines: Alarm pheromone components of the little fire ant, *Wasmannia auropunctata* (Roger) (Hymenoptera, Formicidae). *Insectes Soc.* **2010**, *57*, 223−232.
(37) Maschwitz, U. W. Alarm substances and alarm behaviour in social Hymenoptera. *Nature* **1964**, *204*, 324−327.
(38) Blum, M. S. Alarm pheromones. *Annu. Rev. Entomol.* **1969**, *14*, 57−80.

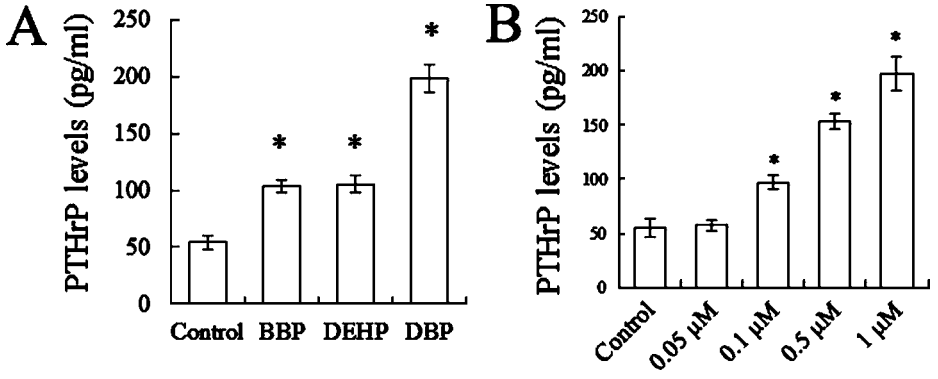


**Figure 1.** Phthalate esters increased PTHrP expression in breast cancer. (A) The effects of BBP, DBP, and DEHP on PTHrP levels in MDA-MB-231 cells. (B) DBP increased PTHrP expression in a dose-dependent manner. MDA-MB-231 cells treated with butylbenzyl phthalate (BBP), di-2-ethylhexyl phthalate (DEHP), and dibutyl phthalate (DBP) at the same concentration of 1 $\mu$M or various concentrations of DBP for 6 h. After washing and a 24-h culture, the condition media of phthalate esters-treated MDA-MB-231 cells (BBP-, DEHP-, and DBP-MDA-MB-231-CM) were harvested, and the PTHrP expression levels in these conditioned media were then assessed. The expression of PTHrP was assessed by ELISA. Each value is the mean ± SD of three independent experiments. * indicates significant difference between the control and test groups ($p < 0.05$).

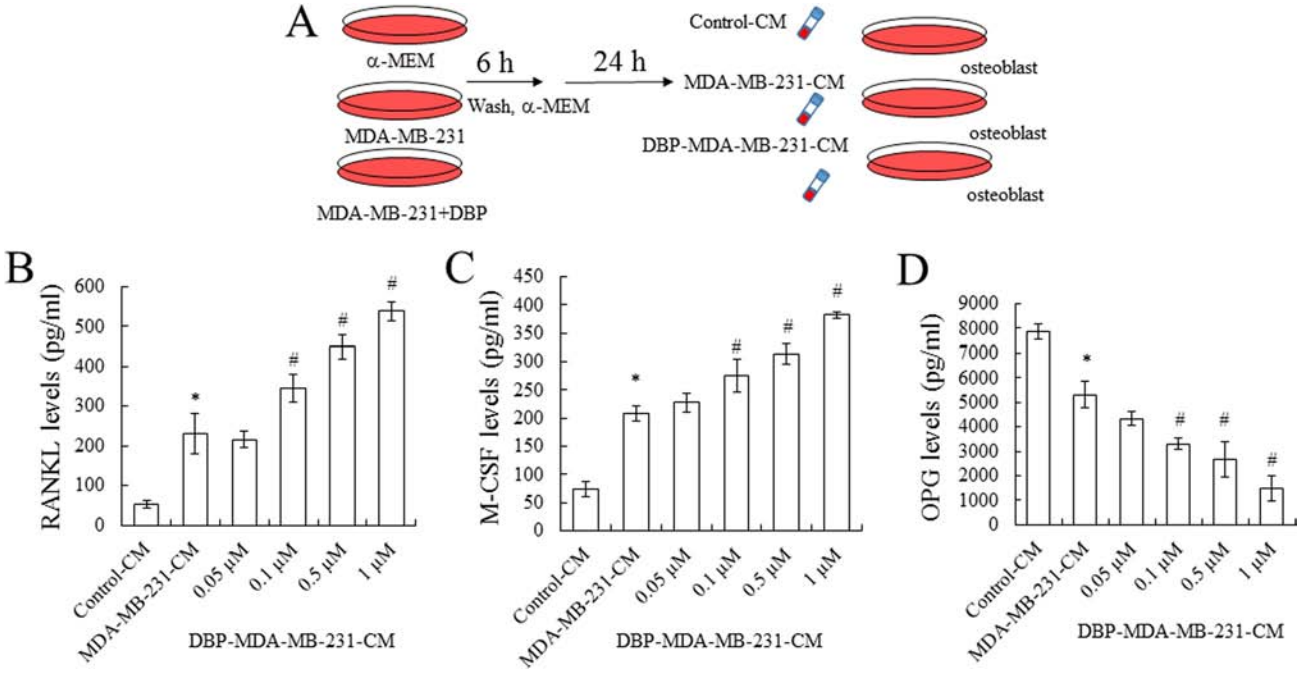


**Figure 2.** DBP reinforced the stimulatory effect of breast cancer in osteoblasts. (A) Flowchart showing production of control-MDA-MB-231-CM and DBP-MDA-MB-231-CM. DBP enhanced the stimulatory effect of MDA-MB-231 cells on the expression of (B) RANKL and (C) M-CSF in osteoblasts. (D) DBP potentiated the inhibitory effect of breast cancer on OPG expression in osteoblasts. MDA-MB-231 cells treated with or without DBP (0.05−1 $\mu$M) at for 6 h. After washing and a 24 h culture, the condition medium of nontreated or DBP-treated MDA-MB-231 cells (MDA-MB-231-CM and DBP-MB-231-CM) were harvested and stored at −80 °C. Osteoblasts were treated with various CMs for 24 h. The levels of M-CSF, RANKL or OPG in the supernatants of osteoblasts were assessed by ELISA. Each value is the mean ± SD of three independent experiments. * indicates significant difference with control-CM treatment, # indicates significant difference with MDA-MB-231-CM treatment, $p < 0.05$.

IL-8 were assessed and quantified using the DuoSet ELISA (enzyme-linked immuno-sorbent assay) (R&D Systems). Parathyroid hormone-related protein (PTHrP) levels were also determined by an ELISA kit (Abnova Corporation, Taipei, Taiwan).

**Analysis of Cell Viability.** MDA-MB-231 cells ($1 \times 10^5$ /well), osteoblasts ($0.5 \times 10^5$ /well), or CD14+monocytes ($1 \times 10^6$ /well) were seeded in a 96 well plate. Cells were treated with phthalates or various condition media for 24 h (BBP, DEHP, and DBP for MDA-MB-231 cells; control-MDA-MB-231-CM and DBP-MDA-MB-231-CM for osteoblasts and CD14 monocytes). The cell viability of MDA-MB-231 or CD14+ monoctytes was assessed using Premixed WST-1 Cell Proliferation Reagent (Clontech Laboratories Inc., Mountain View, CA, U.S.A.).

**Isolation of CD14$^+$ Monocytes and Differentiation of Osteoclasts.** Monocytes were purified from peripheral blood mononuclear cells (PBMCs) obtained from healthy consenting donors. Mononuclear cells were isolated from blood by Ficoll-Hypaque gradient (GE Healthcare Bio-Sciences, Little Chalfont, U.K.). CD14$^+$ monocytes were purified using CD14$^+$ monoclonal antibody-conjugated magnetic beads (MACS MicroBeads, Miltenyi Biotec), according to the manufacturer's protocol. Osteoclasts were generated by culturing CD14$^+$ monocytes in culture medium containing control 20% vehicle control-CM or DBP-MDA-MB-231-CM presented in 100 ng/mL M-CSF and 50 ng/mL RANKL (R&D Systems, Minneapolis, MN) for 14−21 days. The medium was replaced with fresh medium containing M-CSF and RANKL every 5 days. Osteoclast formation was measured by quan-


dx.doi.org/10.1021/jf5042905 | J. Agric. Food Chem. 2014, 62, 11933−11940

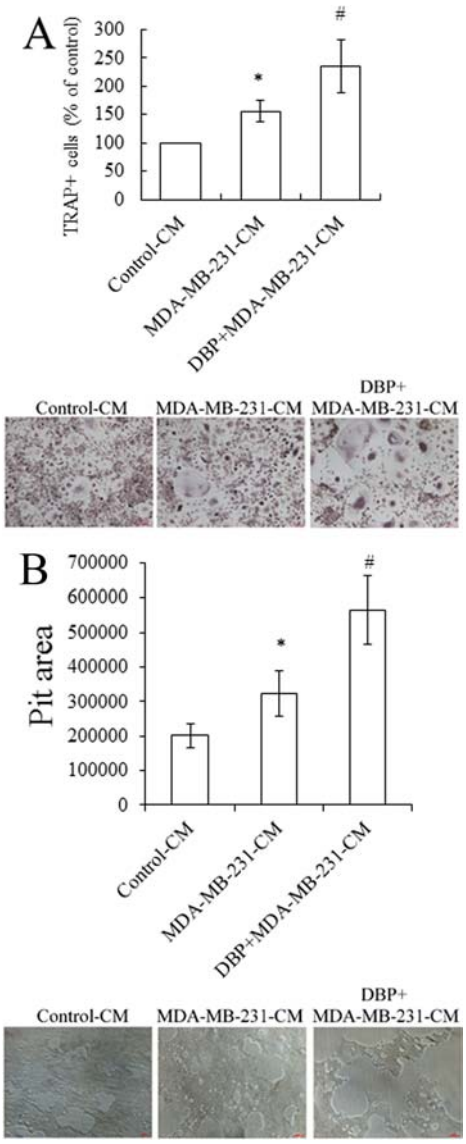


**Figure 3.** DBP reinforced the stimulatory effect of breast cancer in osteoclastogenesis and bone resorption. (A) DBP increased the effect of MDA-MB-231 cell on osteoclast differentiation and (B) their bone resorption activities. Osteoclastogenesis was determined by TRAP staining (osteoclast/nuclei > 3, TRAP positive). CD14+ monocytes were treated with MDA-MB-231-CM and DBP-MB-231-CM (20%) and cultured with M-CSF and RANKL for 14−21 days. Media were replaced every 5 days. Osteoclasts were stained by TRAP. Multinucleated (3+ nuclei) TRAP-positive cells are defined as osteoclasts. The pit area was determined by AlphaEase FC Software. Each value is the mean ± SD of three independent experiments. * indicates significant difference with control-CM treatment, # indicates significant difference with MDA-MB-231-CM treatment, $p < 0.05$.

tifying cells positively stained by TRAP (Sigma-Aldrich, St. Louis, MO, U.S.A.). Osteoclasts were deemed TRAP-positive by light microscopy that revealed staining of multinuclear (>3 nuclei) cells. The TRAP-positive cells and the number of nuclei per TRAP-positive cell in each well were counted. Osteoclasts' bone resorption activity was assessed by a 48-well plate bone resorption assay (Cosmo Bio Co., Ltd., Tokyo, Japan), under the same culture conditions as described above.

The Institutional Review Board (IRB) of Kaohsiung Medical University Hospital approved the study protocol and all of the participants provided written informed consent in accordance with the Declaration of Helsinki (IRB No.: KMUH-IRB-990174 and KMUH-IRB-20120362).

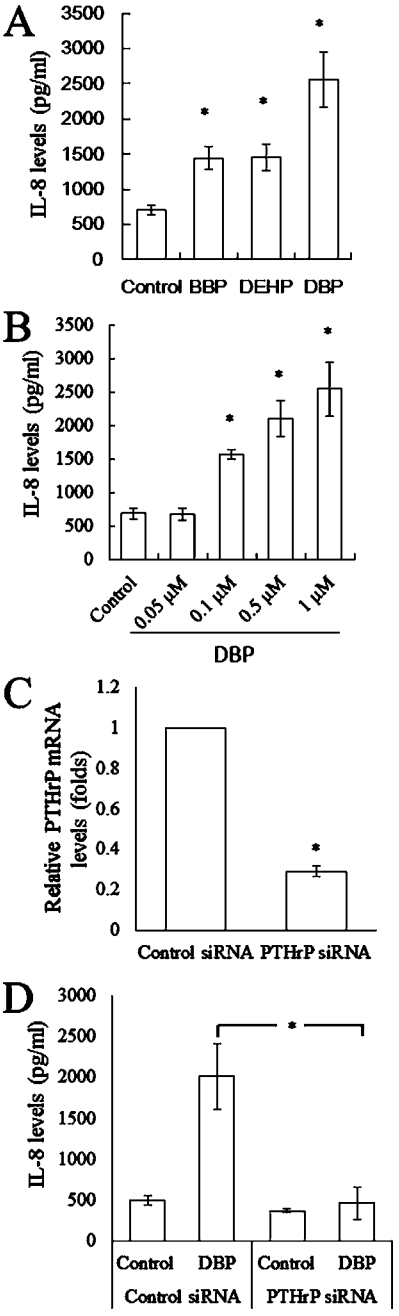


**Figure 4.** Phthalate esters increased the expression of IL-8 by increasing PTHrP in breast cancer. (A) The effect of BBP, DBP and DEHP on IL-8 levels in MDA-MB-231. (B) DBP increased IL-8 expression in a dose-dependent manner. (C) The efficiency of PTHrP siRNA transfection. (D) Inhibition of PTHrP decreased the up-regulation of IL-8 by DBP in MDA-MB-231 cells. MDA-MB-231 cells were transfected with either control siRNA or PTHrP siRNA (10 nM). After 24 h post-transfection, the knockdown efficacy was determined by qRT-PCR. MDA-MB-231 or siRNA transfected MDA-MB-231 cells treated with BBP, DBP or DEHP (1 $\mu$M) or various concentrations of DBP for 24 h. The PTHrP expression levels in these conditioned media were determined by ELISA. Each value is the mean ± SD of three independent experiments. *$p < 0.05$, or significant difference between the control and test groups.

**Real-Time Polymerase Chain Reaction (qRT-PCR).** The TRIzol reagent (Invitrogen, Carlsbad, CA, U.S.A.) was used for RNA isolation, while cDNA was prepared using an oligo-(dT) primer and reverse transcriptase (Takara, Shiga, Japan) following standard protocols. The

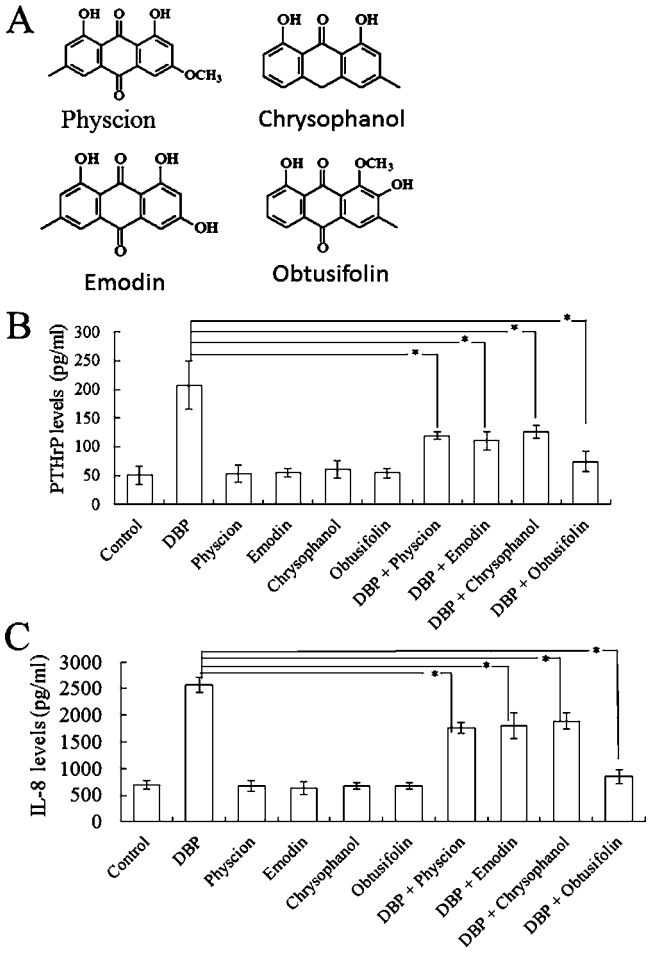


**Figure 5.** Active constituents of *Cassia tora* seeds decreased the effect of DBP on PTHrP and IL-8 expression. (A) Chemical structures of physcion, emodin, chrysophanol, and obtusifolin. The active components of *Cassia tora* L. seeds decreased the up-regulation of DBP on (B) PTHrP and (C) IL-8. MDA-MB-231 cells were pretreated with physcion, emodin, chrysophanol, and obtusifolin for 1 h, then incubated with DBP (1 $\mu$M) for another 6 h for PTHrP, or 24 h for IL-8 analysis. After washing and a 24 h culture, the culture media were collected and PTHrP levels were assessed using ELISA kit. Each value is the mean ± SD of three independent experiments. *$p$ < 0.05, or significant difference between the control and test groups.

qRT-PCR was performed using SYBR Green on the ABI 7500 Real-Time PCR System (Applied Biosystems, Foster City, CA, U.S.A.). Each PCR reaction mixture contained 200 nM of each primer, 10 $\mu$L of 2× SYBR Green PCR Master Mix (Applied Biosystems), and 5 $\mu$L of cDNA and RNase-free water for a total volume of 20 $\mu$L. The qRT-PCR was conducted with a denaturation step at 95 °C for 10 min, then for 40 cycles at 95 °C for 15 s, and 60 °C for 1 min. All PCRs were performed in triplicate and normalized to internal control glyceraldehyde-3-phosphate dehydrogenase (GAPDH) mRNA. The relative expression level was presented using the $2^{-\Delta\Delta CT}$ method.

**PTHrP Knockdown.** MDA-MB-231 cells were transfected with 20 nM nontarget or PTHrP siRNAs pool (Dharmacon, Lafayette, CO, U.S.A.) by DharmFECT 4 reagents, according to the manufacturer's instructions. After 24 h transfection, the medium was changed to whole medium and the cells treated with DBP. PTHrP changes were measured by qRT-PCR.

**Statistical Analysis.** Data were expressed as means ± standard errors. Statistical comparisons of the results were made using analysis of variance (ANOVA). Significant differences ($p$ < 0.05) between the means of the test groups were analyzed by Student's $t$ test.

## RESULTS

**Phthalate Esters Induced PTHrP Secretion in Human Breast Adenocarcinoma Cells.** To investigate the biological significance of the phthalate esters on PTHrP regulation in breast cancer cells, MDA-MB-231 cells were treated with butylbenzyl phthalate (BBP), di-2-ethylhexyl phthalate (DEHP), and dibutyl phthalate (DBP) at the same concentration of 1 $\mu$M for 6 h. After washing and culturing for 24 h, the condition medium of phthalate esters-treated MDA-MB-231 cells (BBP-, DEHP-, and DBP-MDA-MB-231-CM) were harvested, and the PTHrP expression levels of these conditioned media were then assessed. BBP, DEHP, and DBP increased the production of PTHrP in MDA-MB-231 cancer cells (Figure 1A). The effect of DBP on the induction of PTHrP expression was greater than that of BBP or DEHP. Because DBP had the strongest effect in increasing PTHrP secretion of MDA-MB-231, DBP was selected as the model to investigate the mechanism of phthalate esters in breast cancer bone metastasis. Consequently, treatment with different concentrations of DBP revealed that DBP increased the production of PTHrP in MDA-MB-231 cells in a dose-dependent manner after 6 h of stimulation followed by a 24 h culture (Figure 1B). To eliminate the possibility of PTHrP enhancement due to altered cell viability, we assessed the effect of phthalate esters on cell viability of MDA-MB-231 cells. The data shows that phthalate esters did not affect the viability of MDA-MB-231cells, suggesting that phthalate esters increased the expression of PHTrP (data not shown).

**Conditioned Medium of DBP-treated MDA-MB-231 Increased M-CSF and RANKL Expression, and Decreased OPG Expression in Osteoblasts.** PTHrP regulation enhanced osteoclastogenesis by changing the ratio of osteoclastogenesis activator (RANKL and M-CSF)/inhibitor (osteoprotegrin (OPG)) produced by osteoblasts.[23,24] To determine the effects of DBP on breast cancer in the secretion of RANKL, M-CSF, and OPG in osteoblasts, MDA-MB-231 cells were treated with 0.1% DMSO or DBP for 6 h. After removing DBP by washing, the cells were cultured with fresh medium before the medium was collected (defined as control-MDA-MB-231-CM and DBP-MDA-MB-231-CM). The CMs were added to human osteoblasts to assess the effect of DBP on breast cancer-osteoblast interaction (Figure 2A). Control-MDA-MB-231-CM increased M-CSF and RANKL expressions in osteoblasts, and this stimulatory effect was further enhanced when MDA-MB-231 cells were pretreated with DBP (Figure 2B and C). In contrast, MDA-MB-231 decreased the expression of OPG in osteoblasts (Figure 2D). To eliminate the likelihood of M-CSF, RANKL, and OPG changes resulting from different cell counts, we assessed the effect of control-MDA-MB-231-CM and DBP-MDA-MB-231-CM on the cell viability of osteoblasts. The data shows that neither control-MDA-MB-231-CM nor DBP-MDA-MB-231-CM affected the cell viability of osteoblasts, suggesting that DBP-MDA-MB-231-CM enhanced the M-CSF/RANKL and decreased OPG expression on osteoblasts (data not shown). This effect of breast cancer on osteoblasts worsened when breast cancer cells were exposed to DBP.

**Phthalate Esters Increased Breast Cancer Cell-Mediated Osteoclastogenesis and Bone Resorption.** The effect of DBP on breast-cancer-mediated osteoclastogenesis was assessed. MDA-MB-231-CM increased osteoclastogenesis, and this effect was reinforced when MDA-MB-231 cells were pretreated with DBP (Figure 3A). Similarly, MDA-MB-231-CM enhanced osteoclast bone resorption activity, and this

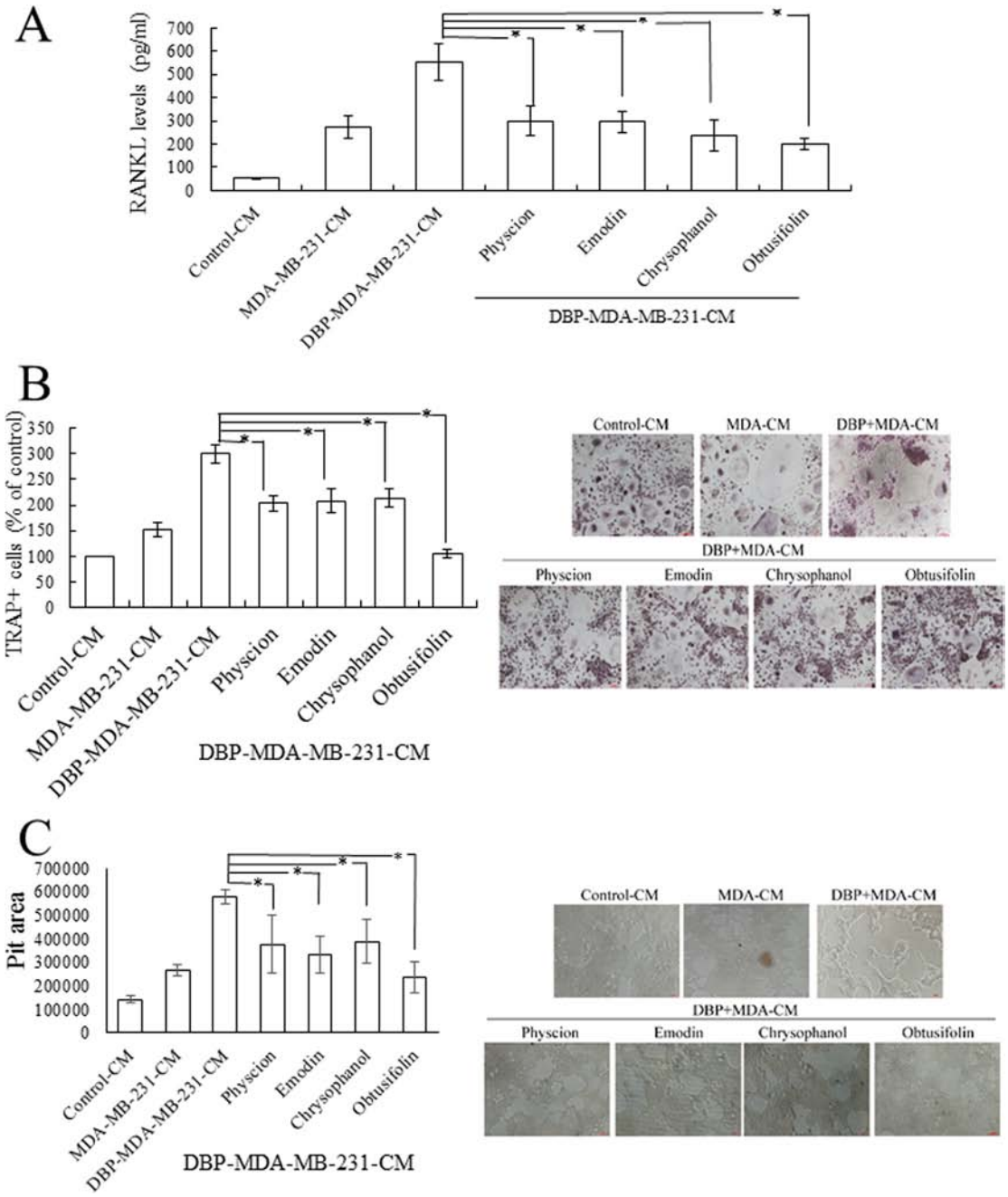


**Figure 6.** Active constituents of *Cassia tora* L. seeds decreased the effects of DBP on breast cancer bone metastasis events. *Cassia tora* L. seeds' compounds decreased the synergetic effects of DBP on (A) the RANKL expression of osteoblasts, (B) osteoclastogenesis, and (C) bone resorption. RANKL levels were measured by ELISA kit. For part A, MDA-MB-231 cells were pretreated with physcion, emodin, chrysophanol, and obtusifolin for 1 h, then incubated with DBP (1 $\mu$M) for another 6 h. After washing and a 24 h culture, the culture media were collected, then added to osteoblasts for a 24 h culture, The levels of RANKL in the supernatants of osteoblasts was assessed by ELISA. For parts B and C, MDA-MB-231 cells were pretreated with physcion, emodin, chrysophanol, and obtusifolin for 1 h, then incubated with DBP (1 $\mu$M) for another 6 h. After washing and a 24 h culture, the culture medium (20%) was collected, then added to CD14+ monocytes presenting in M-CSF and RANKL for a 14−21 days. The osteoclastogenesis and bone resorption was conducted as described above. Each value is the mean ± SD of three independent experiments. *$p$ < 0.05, or significant difference between the control and test groups.

stimulatory effect of breast cancer was further intensified by DBP pretreatment (Figure 3B). However, the cell viability of monocytes was not affected by MDA-MB-231-CM or DBP-MDA-MB-231-CM (data not shown).

**PTHrP/IL-8 Autocrine Loop Was Involved in the Stimulation of DBP on Breast-Cancer-Mediated Osteoclastogenesis.** Since PTHrP has been reported to increase cancer cell expression of IL-8,[25] this study assessed whether phthalate esters increased the inductive effect of MDA-MB-231 on osteoclastogenesis by targeting the PTHrP/IL-8 loop. The level of IL-8 was higher in BBP-, DEHP-, and DBP-treated MDA-MB-231 than in the control group (Figure 4A). In inducing PTHrP expression, the effect of DBP on IL-8 secretion was greater than that of BBP or DEHP in MDA-MB-231. DBP increased IL-8 expression in MDA-MB-231 in a dose-dependent manner (Figure 4B). To confirm the role of PTHrP on the

up-regulation of IL-8 induced by DBP, MDA-MB-231 cells were transfected with PTHrP siRNA. Transfection of MDA-MB-231 cells with PTHrP siRNA decreased PTHrP mRNA expression in MDA-MB-213 cells by 74.5% (Figure 4C). Silencing prevented the up-regulation of DBP on the expression of IL-8 in MDA-MB-231 cells (Figure 4D).

**Obtusifolin Suppressed Phthalate Esters-Mediated Bone Resorption.** This study assessed the effects of physcion, emodin, chrysophanol, and obtusifolin on DBP-induced breast cancer bone metastasis (Figure 5A). DBP induced PTHrP and IL-8 secretion in human breast adenocarcinoma cells, whereas physcion, emodin, chrysophanol, and obtusifolin treatment decreased PTHrP and IL-8 secretion (Figure 5B and C). Of these compounds, obtusifolin completely reversed PTHrP and IL-8 secretion of breast cancer cells upon exposure to DBP. Similarly, the CM of DBP-treated MDA-MB-231 mediated RANKL up-regulation in osteoblasts. Osteoclastogenesis and bone resorption were totally abrogated by obtusifolin treatment, whereas they were only partially reversed by treatment with physcion, emodin, or chrysophanol alone (Figure 6).

## DISCUSSION

Bone metastasis is a disturbing development in patient care because cancer's spread to the bone increases morbidity and mortality rates.[6,26,27] Previous studies indicate that exposure to phthalate esters is associated with increased risk of breast cancer.[11−14] Furthermore, Hsieh et al. have indicated that phthalate esters increase the proliferation and invasiveness of breast cancer cells.[15,16] This study is the first to demonstrate that phthalate increases the stimulatory effect of breast cancer on osteoclastogenesis and osteoclast bone resorption activity directly via PTHrP/IL8 and by interfering in the osteoblast-osteoclast interaction.

Parathyroid hormone-related protein (PTHrP), a potent activator of osteoclastic bone resorption, is an important pathologic factor for hypercalcemia among cancer patients.[28−30] PTHrP stimulates osteoclastogenesis by increasing receptor activator of NF-κB ligand (RANKL) expression and by reducing osteoprotegerin (OPG) expression in osteoblasts. However, it does not act directly on osteoclast precursors.[31,32] RANKL binds with the RANK receptor in osteoclast precursors and induces the formation of mature osteoclasts in the presence of macrophage colony stimulating factor (M-CSF).[33,34] Since OPG is a soluble decoy receptor for RANKL, with the ability to decrease osteoclastogenesis,[35] a relative increase of RANKL/OPG ratio by cancer-derived PTHrP results in osteoclastic bone resorption.[36] This study shows that phthalate esters, BBP, DEHP, and DBP, cause an up-regulation of PTHrP in breast cancer. Consistent with PTHrP enhancement, DBP reinforces the interference of breast cancer on osteoblasts, including increased M-CSF and RANKL, and decreased OPG. These results suggest that phthalate esters may worsen bone metastasis in breast cancer.

Many studies report that breast cancer expresses high levels of IL-8, which enhances both osteoclastogenesis and bone resorption.[37−39] PTHrP has been reported to increase osteoclastogenesis by increasing the expression of osteoclast stimulatory factors such as IL-8.[36] The present study reveals that phthalate esters increase IL-8 expression in breast cancer cells. Inhibition of PTHrP by siRNA transfection prevents phthalate-mediated up-regulation on IL-8 secretion, suggesting that PTHrP is the major mediator involved in the stimulatory effect of phthalate esters on IL-8 production. Moreover, DBP enhances the stimulatory effect of breast cancer on osteoclastogenesis and their bone resorption activity. Thus, the regulation of IL-8 expression by phthalate esters through PTHrP is a key point that contributes to phthalate esters-induced osteoclastogenesis and bone resorption.

Current treatments for bone metastases have limited efficacy and are merely palliative. Side effects such as renal toxicity and osteo-necrosis of the jaw are considered clinically significant, potentially painful, and debilitating enough to decrease the quality of life of breast cancer patients.[40] Since eliminating all phthalate exposure may be impossible because phthalate esters are widely used in modern life, it is therefore important that strategies be developed for the prevention of bone metastasis in breast cancer. The data here shows that the components of Jue-ming-zi, including physcion, emodin, chrysophanol, and obtusifolin, exhibit effects that decrease PTHrP expression in MDA-MB-231 cells. These agents also simultaneously decrease IL-8 expression, resulting in the inhibition of MDA-MB-231-mediated osteoclastogenesis and bone resorption.

Moreover, these agents also decrease the stimulatory effect of breast cancer on the expression of RANKL in osteoblasts. Among these active constituents of seeds from *Cassia tora* L., obtusifolin has the most significant effect on the prevention of breast cancer-mediated osteolytic events, suggesting that Jue-ming-zi or obtusifolin may be potential agents to prevent the exacerbating of breast cancer related bone metastasis by phthalate esters.

In conclusion, the present study is the first to investigate the interaction of breast cancer cells, osteoblasts, and osteoclasts after exposure to phthalate esters. These esters, BBP-, DEHP-, and DBP, cause human breast cancer cell line MDA-MB-231 to secrete PTHrP and IL-8, which mediate RANKL up-regulation and OPG down-regulation in osteoblasts, thereby inducing osteoclastogenesis and bone resorption. This is the first investigation that provides evidence that obtusifolin, a major bioactive compound present in the seeds of *Cassia tora* L., has great potential in preventing phthalate esters-associated breast cancer bone metastasis. This is also the first investigation to provide evidence that the seeds of *Cassia tora* L. have great potential as a novel antibreast cancer bone metastasis agent.

## AUTHOR INFORMATION

### Corresponding Author

*Phone: +886-7-312-1101 ext. 2512 #33. Fax: +886-7-321-0701. E-mail: kuopolin@seed.net.tw.

### Funding

This study was supported by grants from the National Science Council of Taiwan (NSC 102-2628-B-037-002-MY3; NSC 102-2632-B-037-001-MY3; and NSC 102-2314-B-037-035-MY3), the Kaohsiung Medical University "Aim for the Top 500 Universities Grant," grant No. KMU-DT103008, the Kaohsiung Medical University "Aim for the Top Universities Grant", grant No. KMU-TP103A15, and the Excellence for Cancer Research Center Grant, the Ministry of Health and Welfare, Executive Yuan, Taipei, Taiwan (MOHW 103-TD-B-111-05).

### Notes

The authors declare no competing financial interest.

## ACKNOWLEDGMENTS

The authors thank the Center for Resources, Research, and Development of Kaohsiung Medical University for its support with the instrumentation.

## REFERENCES


(1) Hess, K. R.; Varadhachary, G. R.; Taylor, S. H.; Wei, W.; Raber, M. N.; Lenzi, R.; Abbruzzese, J. L. Metastatic patterns in adenocarcinoma. *Cancer* **2006**, *106*, 1624−1633.

(2) Chappard, D.; Bouvard, B.; Baslé, M. F.; Legrand, E.; Audran, M. Bone metastasis: Histological changes and pathophysiological mechanisms in osteolytic or osteosclerotic localizations. A review. *Morphologie* **2011**, *95*, 65−75.

(3) Goldstein, R. H.; Reagan, M. R.; Anderson, K.; Kaplan, D. L.; Rosenblatt, M. Human bone marrow-derived MSCs can home to orthotopic breast cancer tumors and promote bone metastasis. *Cancer Res.* **2010**, *70*, 10044−10050.

(4) Onishi, T.; Hayashi, N.; Theriault, R. L.; Hortobagyi, G. N.; Ueno, N. T. Future directions of bone-targeted therapy for metastatic breast cancer. *Nat. Rev. Clin. Oncol.* **2010**, *7*, 641−651.

(5) Coleman, R. E.; Lipton, A.; Roodman, G. D.; Guise, T. A.; Boyce, B. F.; Brufsky, A. M.; Clézardin, P.; Croucher, P. I.; Gralow, J. R.; Hadji, P.; Holen, I.; Mundy, G. R.; Smith, M. R.; Suva, L. J. Metastasis and bone loss: Advancing treatment and prevention. *Cancer Treat. Rev.* **2010**, *36*, 615−620.

(6) Zheng, L.; Zhu, K.; Jiao, H.; Zhao, Z.; Zhang, L.; Liu, M.; Deng, W.; Chen, D.; Yao, Z.; Xiao, G. PTHrP expression in human MDA-MB-231 breast cancer cells is critical for tumor growth and survival and osteoblast inhibition. *Int. J. Biol. Sci.* **2013**, *9*, 830−41.

(7) Yoneda, T.; Tanaka, S.; Hata, K. Role of RANKL/RANK in primary and secondary breast cancer. *World J. Orthop.* **2013**, *4*, 178−185.

(8) Theriault, R. L.; Theriault, R. L. Biology of bone metastases. *Cancer Control* **2012**, *19*, 92−101.

(9) Martino-Andrade, A. J.; Chahoud, I. Reproductive toxicity of phthalate esters. *Mol. Nutr. Food Res.* **2010**, *54*, 148−157.

(10) Ge, R. S.; Chen, G. R.; Tanrikut, C.; Hardy, M. P. Phthalate ester toxicity in Leydig cells: Developmental timing and dosage considerations. *Reprod. Toxicol.* **2007**, *23*, 366−373.

(11) López-Carrillo, L.; Hernández-Ramírez, R. U.; Calafat, A. M.; Torres-Sánchez, L.; Galván-Portillo, M.; Needham, L. L.; Ruiz-Ramos, R.; Cebrián, M. E. Exposure to phthalates and breast cancer risk in northern Mexico. *Environ. Health Perspect.* **2010**, *118*, 539−544.

(12) Aschengrau, A.; Coogan, P. F.; Quinn, M.; Cashins, L. J. Occupational exposure to estrogenic chemicals and the occurrence of breast cancer: An exploratory analysis. *Am. J. Ind. Med.* **1998**, *34*, 6−14.

(13) Carran, M.; Shaw, I. C. New Zealand Malayan war veterans' exposure to dibutylphthalate is associated with an increased incidence of cryptorchidism, hypospadias, and breast cancer in their children. *N Z. Med. J.* **2012**, *125*, 52−63.

(14) Sprague, B. L.; Trentham-Dietz, A.; Hedman, C. J.; Wang, J.; Hemming, J. D.; Hampton, J. M.; Buist, D. S.; Aiello Bowles, E. J.; Sisney, G. S.; Burnside, E. S. Circulating serum xenoestrogens and mammographic breast density. *Breast Cancer Res.* **2013**, *15*, R45.

(15) Hsieh, T. H.; Tsai, C. F.; Hsu, C. Y.; Kuo, P. L.; His, E.; Suen, J. L.; Hung, C. H.; Lee, J. N.; Chai, C. Y.; Wang, S. C.; Tsai, E. M. *n*-Butyl benzyl phthalate promotes breast cancer progression by inducing expression of lymphoid enhancer factor 1. *PLoS One* **2012**, *7*, e42750.

(16) Hsieh, T. H.; Tsai, C. F.; Hsu, C. Y.; Kuo, P. L.; Lee, J. N.; Chai, C. Y.; Wang, S. C.; Tsai, E. M. Phthalates induce proliferation and invasiveness of estrogen receptor-negative breast cancer through the AhR/HDAC6/c-Myc signaling pathway. *FASEB J.* **2012**, *26*, 778−787.

(17) Chen, F. P.; Chien, M. H. Lower concentrations of phthalates induce proliferation in human breast cancer cells. *Climacteric* **2014**, *17*, 377−384.

(18) Yen, G. C.; Chung, D. Y. Antioxidant effects of extracts from *Cassia tora* L. prepared under different degrees of roasting on the oxidative damage to biomolecules. *J. Agric. Food Chem.* **1999**, *47*, 1326−1332.

(19) Zhao, X.; Wang, Q.; Qian, Y.; Pang, L. *Cassia tora* L. (Jue-ming-zi) has anticancer activity in TCA8113 cells in vitro and exerts anti-metastatic effects in vivo. *Oncol. Lett.* **2013**, *5*, 1036−1042.

(20) Chen, S.; Li, G.; Zhu, K.; Sun, P.; Wang, R.; Zhao, X. Antitumor activities of Juemingzi (*Cassia tora* L.) on Balb/c sarcoma 180-injected mice. *Oncol Lett.* **2014**, *7*, 250−254.

(21) Park, Y. B.; Kim, S. B. Isolation and identification of antitumor promoters from the seeds of *Cassia tora*. *J. Microbiol. Biotechnol.* **2011**, *21*, 1043−1048.

(22) Jang, D. S.; Lee, G. Y.; Kim, Y. S.; Lee, Y. M.; Kim, C. S.; Yoo, J. L.; Kim, J. S. Anthraquinones from the seeds of *Cassia tora* with inhibitory activity on protein glycation and aldose reductase. *Biol. Pharm. Bull.* **2007**, *30*, 2207−2210.

(23) Casimiro, S.; Mohammad, K. S.; Pires, R.; Tato-Costa, J.; Alho, I.; Teixeira, R.; Carvalho, A.; Ribeiro, S.; Lipton, A.; Guise, T. A.; Costa, L. RANKL/RANK/MMP-1 molecular triad contributes to the metastatic phenotype of breast and prostate cancer cells in vitro. *PLoS One* **2013**, *8*, e63153.

(24) Krishnan, V.; Vogler, E. A.; Sosnoski, D. M.; Mastro, A. M. In vitro mimics of bone remodeling and the vicious cycle of cancer in bone. *J. Cell Physiol.* **2014**, *229*, 453−62.

(25) Manenti, G.; Peissel, B.; Gariboldi, M.; Falvella, F. S.; Zaffaroni, D.; Allaria, B.; Pazzaglia, S.; Rebessi, S.; Covelli, V.; Saran, A.; Dragani, T. A. A cancer modifier role for parathyroid hormone-related protein. *Oncogene* **2000**, *19*, 5324−5328.

(26) van der Pol, C. B.; Schweitzer, M. E.; Di Primio, G.; Sampaio, M. L.; Kielar, A.; Clemons, M.; Jaberi, A. Breast cancer and bone metastases: The association of axial skeleton MRI findings with skeletal-related events and survival. *Breast Cancer Res. Treat.* **2014**, *146*, 583−589.

(27) Hsu, Y. L.; Hou, M. F.; Kuo, P. L.; Huang, Y. F.; Tsai, E. M. Breast tumor-associated osteoblast-derived CXCL5 increases cancer progression by ERK/MSK1/Elk-1/snail signaling pathway. *Oncogene* **2013**, *32*, 4436−4447.

(28) Hiraki, A.; Ueoka, H.; Bessho, A.; Segawa, Y.; Takigawa, N.; Kiura, K.; Eguchi, K.; Yoneda, T.; Tanimoto, M.; Harada, M. Parathyroid hormone-related protein measured at the time of first visit is an indicator of bone metastases and survival in lung carcinoma patients with hypercalcemia. *Cancer* **2002**, *95*, 1706−1713.

(29) Grill, V.; Ho, P.; Body, J. J.; Johanson, N.; Lee, S. C.; Kukreja, S. C.; Moseley, J. M.; Martin, T. J. Parathyroid hormone-related protein: Elevated levels in both humoral hypercalcemia of malignancy and hypercalcemia complicating metastatic breast cancer. *J. Clin. Endocrinol. Metab.* **1991**, *73*, 1309−1315.

(30) Shen, X.; Falzon, M. PTH-related protein upregulates integrin $\alpha 6\beta 4$ expression and activates Akt in breast cancer cells. *Exp. Cell Res.* **2006**, *312*, 3822−3834.

(31) Kitazawa, S.; Kitazawa, R. RANK ligand is a prerequisite for cancer-associated osteolytic lesions. *J. Pathol.* **2002**, *198*, 228−236.

(32) Thomas, R. J.; Guise, T. A.; Yin, J. J.; Elliott, J.; Horwood, N. J.; Martin, T. J.; Gillespie, M. T. Breast cancer cells interact with osteoblasts to support osteoclast formation. *Endocrinology* **1999**, *140*, 4451−8.

(33) Yasuda, H.; Shima, N.; Nakagawa, N.; Yamaguchi, K.; Kinosaki, M.; Goto, M.; Mochizuki, S. I.; Tsuda, E.; Morinaga, T.; Udagawa, N.; Takahashi, N.; Suda, T.; Higashio, K. A novel molecular mechanism modulating osteoclast differentiation and function. *Bone* **1999**, *25*, 109−113.

(34) Jansen, I. D.; Vermeer, J. A.; Bloemen, V.; Stap, J.; Everts, V. Osteoclast fusion and fission. *Calcif. Tissue Int.* **2012**, *90*, 515−522.

(35) Lacey, D. L.; Timms, E.; Tan, H. L.; Kelley, M. J.; Dunstan, C. R.; Burgess, T.; Elliott, R.; Colombero, A.; Elliott, G.; Scully, S.; Hsu, H.; Sullivan, J.; Hawkins, N.; Davy, E.; Capparelli, C.; Eli, A.; Qian, Y. X.; Kaufman, S.; Sarosi, I.; Shalhoub, V.; Senaldi, G.; Guo, J.; Delaney, J.; Boyle, W. J. Osteoprotegerin ligand is a cytokine that regulates osteoclast differentiation and activation. *Cell* **1998**, *93*, 165−176.

(36) Kuo, P. L.; Liao, S. H.; Hung, J. Y.; Huang, M. S.; Hsu, Y. L. MicroRNA-33a functions as a bone metastasis suppressor in lung cancer by targeting parathyroid hormone related protein. *Biochim. Biophys. Acta* **2013**, *1830*, 3756−3766.

(37) Kamalakar, A.; Bendre, M. S.; Washam, C. L.; Fowler, T. W.; Carver, A.; Dilley, J. D.; Bracey, J. W.; Akel, N. S.; Margulies, A. G.;

Skinner, R. A.; Swain, F. L.; Hogue, W. R.; Montgomery, C. O.; Lahiji, P.; Maher, J. J.; Leitzel, K. E.; Ali, S. M.; Lipton, A.; Nicholas, R. W.; Gaddy, D.; Suva, L. J. Circulating interleukin-8 levels explain breast cancer osteolysis in mice and humans. *Bone* **2014**, *61*, 176−185.

(38) Singh, B.; Berry, J. A.; Vincent, L. E.; Lucci, A. Involvement of IL-8 in COX-2-mediated bone metastases from breast cancer. *J. Surg. Res.* **2006**, *134*, 44−51.

(39) Bendre, M. S.; Margulies, A. G.; Walser, B.; Akel, N. S.; Bhattacharrya, S.; Skinner, R. A.; Swain, F.; Ramani, V.; Mohammad, K. S.; Wessner, L. L.; Martinez, A.; Guise, T. A.; Chirgwin, J. M.; Gaddy, D.; Suva, L. J. Tumor-derived interleukin-8 stimulates osteolysis independent of the receptor activator of nuclear factor-κB ligand pathway. *Cancer Res.* **2005**, *65*, 11001−11009.

(40) Jacobs, C.; Simos, D.; Addison, C.; Ibrahim, M.; Clemons, M. Pharmacotherapy of bone metastases in breast cancer patients—An update. *Expert. Opin. Pharmacother.* **2014**, *15*, 1109−1118.

MALDI matrix 2,5-dihydroxybenzoic acid (DHB), peptide calibration standard II, and protein calibration standard II were from Bruker (Billerica, MA). $C_4$ ziptips were from EMD Millipore (Darmstadt, Germany). Other reagents, including HPLC grade acetonitrile (ACN), trifluoroacetic acid (TFA), and ammonium bicarbonate (AMBIC) were from Fisher Scientific (Waltham, MA). Water was purified on a Milli-Q Advantage A10 system (EMD Millipore). Dithiothreitol was from Acros Organics (New Jersey) and iodoacetamide was from BioRad (Hercules, CA). For gene cloning, an RNeasy Plant Mini Kit (Qiagen, Venlo, Limburg), a SMARTer RACE cDNA Amplification kit, and an Advantage 2 PCR kit from Clontech (Mountain View, CA), a pGEM-T vector (Promega), and *Escherichia coli* strain JM109 were used.

**Molecular Mass Measurement.** Purified WPTP was dissolved in 0.1% TFA, mixed 1:1 with a MALDI matrix solution (20 g/L DHB in 50% ACN, 0.1% TFA), spotted onto a polished steel target plate (Bruker), and allowed to air-dry. The molecular mass was measured with an Ultraflex III MALDI-TOF/TOF mass spectrometer (Bruker) in linear positive mode. In 200 shot increments, 1500 laser shots were accumulated. The matrix suppression cutoff, using gating, was at 9500 $m/z$. Pulsed ion extraction (PIE) delay was set to 150 ns. Instrument voltages were at 25 kV (ion source 1 [IS1]), 23.1 kV (IS2), and 6.5 kV (lens). The WPTP molecular mass value was calibrated using the protein mix II calibration standard (Bruker). Spectrum processing, consisting of peak detection (centroid algorithm, peak width 1000 $m/z$) and smoothing (Savitzky−Golay algorithm, 1 cycle at 20 $m/z$), was performed in Flex Analysis 3.4 (Bruker).

**Top-Down Sequencing.** Top-down sequencing (TDS) of native WPTP was performed after solid-phase reduction of its disulfide bonds. BSA was used as the control and the molecular mass calibrator. For solid-phase disulfide bond reduction, a $C_4$ ziptip was wetted with 50% ACN in 250 mM AMBIC solution several times. The protein sample (25 pmol in 15 $\mu$L of 100 mM AMBIC) was loaded on the tip equilibrated with 100 mM AMBIC by slowly repipetting at least 10 times. Then, 50 mM dithiothreitol (200 $\mu$L) was introduced to the tip by aspirating and dispensing the solution for 2 min at 60 °C. The ziptip was then incubated in that solution for 30 min at 60 °C. The tip was washed three times with 0.1% TFA. The protein was eluted with 5 $\mu$L of a MALDI matrix solution (40 g/L DHB in 70% ACN, 0.1% TFA), and 0.25 $\mu$L was spotted directly on the target plate and allowed to air-dry.

TDS spectra were acquired with an Ultraflex III MALDI-TOF/TOF mass spectrometer in reflector positive mode. In 200 shot increments, 19 000 laser shots were accumulated. The matrix suppression cutoff, using deflection, was at 900 $m/z$. PIE delay was set to 40 ns. Instrument voltages were at 25 kV (IS1), 21.4 kV (IS2), 9.7 kV (lens), 26.3 kV (reflector 1), and 13.8 kV (reflector 2). Spectrum processing, consisting of peak detection (SNAP algorithm, peak width 0.75 $m/z$), baseline subtraction (TopHat algorithm), and smoothing (Savitzky−Golay algorithm, 5 cycles at 1.5 $m/z$), as well as peak annotation was carried out in Flex Analysis 3.4. Peaks were assigned with a mass tolerance of 300 ppm. Interpretation of the ions comprising the near C-terminus was aided by the characteristic $m/z$ difference of 15 ($\Delta$ $m/z$) between y- and z+2-ion series. Additional annotation was performed with BioTools (Bruker) and Sequence Editor (Bruker).

**Bottom-Up Sequencing.** WPTP (10 $\mu$g, 1 $\mu$g/$\mu$L in 25 mM AMBIC) was reduced with 50 mM dithiothreitol (20 $\mu$L) for 30 min at 60 °C, alkylated with 100 mM iodoacetamide (25 $\mu$L) for 45 min at room temperature in the dark. The alkylation reaction was quenched by addition of 1 $\mu$L of 143 mM dithiothreitol. Reduced and alkylated WPTP was diluted with water and then digested in solution with 0.5 $\mu$g of trypsin (50 $\mu$L) at 37 °C for 12 h. Peptides were dried via SpeedVac and resuspended in 5% ACN in 0.1% TFA. The peptide solution was mixed 1:1 with a MALDI matrix solution (20 g/L DHB in 50% ACN, 0.1% TFA) and then spotted on a target plate.

Mass spectra of the peptides were acquired with an Ultraflex III MALDI-TOF/TOF mass spectrometer in reflector positive mode. In 200 shot increments, 600 shots were accumulated. The matrix suppression cutoff, using deflection, was at 850 $m/z$. PIE delay was set to 0 ns. Instrument voltages were at 25 kV (IS1), 21.45 kV (IS2), 9.5 kV (lens), 26.3 kV (reflector 1), and 13.8 kV (reflector 2). External calibration was performed using peptide mix II calibration standard (Bruker). Spectrum processing, consisting of peak detection (SNAP algorithm, peak width 0.75 $m/z$) and smoothing (Savitzky−Golay algorithm, 1 cycle at 0.2 $m/z$), was performed in Flex Analysis 3.4.

Several peaks in the mass spectrum were selected for fragmentation in LIFT mode.[17] Several thousand laser shots were accumulated in 200 shot increments. PIE delay was set to 0 ns. Instrument voltages were at 8 kV (IS1), 7.2 kV (IS2), 3.6 kV (lens), 29.5 kV (reflector 1), and 13.85 kV (reflector 2). Spectrum processing, consisting of peak detection (SNAP algorithm, peak width 0.75 $m/z$) and smoothing (Savitzky−Golay algorithm, 4 cycles at 0.15 $m/z$) as well as peak annotation, was carried out in Flex Analysis 3.4. Additional annotation was performed with BioTools and Sequence Editor with a mass tolerance of 0.3 $m/z$ for peptides and 1 $m/z$ for glycopeptides. Fragmentation spectra were interpreted and used for primer design in the gene cloning experiment.

**Cloning and Sequencing of the cDNA.** Total RNA was isolated from 0.1 g of *T. fortunei* leaves using an RNeasy Plant Mini Kit (Qiagen). The first-strand cDNA was synthesized from the isolated RNA using a SMARTer RACE cDNA Amplification kit (Clontech). The WPTP gene was cloned in two steps. In the first step, the forward degenerate primers (5′-GAYCTNCARATHGGNTT-3′ and 5′-GAYTTRCAR-ATHGGNTT-3′) targeted the previously determined amino acid sequence of the N-terminus of WPTP (DLQGIFY).[15] The reverse primer, UPM, was provided with the same kit. PCR amplification was performed using an Advantage 2 PCR kit (Clontech). The PCR protocol consisted of an initial denaturation step at 94 °C (2 min), which was followed by 5 cycles of denaturation at 94 °C (30 s), annealing at 60 °C (30 s), and extension at 68 °C (1 min); then 5 cycles of denaturation at 94 °C (30 s), annealing at 55 °C (30 s), and extension at 68 °C (1 min); then followed by 25 cycles of denaturation at 94 °C (30 s), annealing at 50 °C (30 s), and extension at 68 °C (1 min); and then a final extension for 3 min at 68 °C. The resulting 1200 bp product was used as a template in the second step. The forward primer (5′-ATGCAYTTYCAYGAYTGYTT-3′) was designed from the amino acid sequence MHFHDCF, obtained by tandem mass spectrometry analysis of WPTP tryptic peptides in this study. The PCR protocol was the same as above except that the annealing temperatures were 65 °C, 62 °C, and 60 °C, respectively. The PCR product was cloned into a pGEM-T vector and transformed into *E. coli* strain JM109. Positive transformants were screened by PCR. Plasmids were extracted from positive clones and confirmed by sequencing. For 5′-RACE, the reverse primer, 5′-GGACCTGGTAGGTGATGTTGCCG-3′, was designed from the DNA sequence obtained in the previous step. The forward primer, UPM, was from the same kit. The PCR protocol was the same as above except that the annealing temperatures were 65 °C, 62 °C, and 58 °C, respectively. The PCR product was cloned, transformed, screened, and sequenced as before. The complete cDNA sequence of WPTP was obtained by combining the 5′- and 3′-cDNA sequences which were overlapping with each other. Analysis of the data was conducted with the software Mega5.[18] These data can be accessed at NCBI accession: KM504969.

## RESULTS AND DISCUSSION

**Determination of the Molecular Mass of WPTP.** The MALDI-TOF mass spectrum of WPTP indicated the presence of a single glycoprotein with considerable heterogeneity (Figure 1A). An expanded view of the +2 charged peak revealed that it was composed of many partially resolved peaks, probably corresponding to WPTP glycoforms, i.e., differentially glycosylated WPTP (Figure 1B). A similar view of the +1 charged peak also showed multiple, partially resolved peaks.

The obtained data allowed for calculation of the MW of WPTP which ranged from 41 to 45 kDa (Figure 1C). These values are a little lower than the value previously reported for WPTP (50 kDa), which was measured using SDS-PAGE.[15] Due to decreased binding of SDS to glycans relative to the polypeptide backbone, the migration of a glycoprotein during SDS-PAGE is altered relative to what is expected for a similarly sized nonglycosylated protein.[19] Therefore, the previous measurement

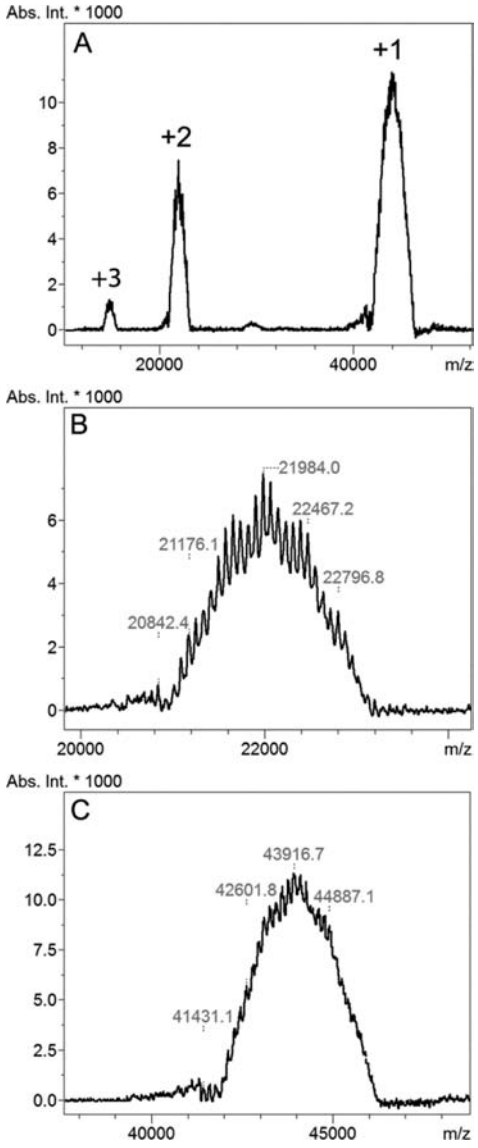


**Figure 1.** MALDI-TOF MS of WPTP to determine the molecular mass: (A) +1, +2, and +3 charged peaks and an expanded view of the (B) +2 charged and (C) +1 charged peak.

was likely an overestimation. Similarly, the first report of RPTP's MW, as measured by SDS-PAGE, was 51 kDa[20] and the MW as measured by mass spectrometry was 44 596 Da.[14]

**Top-Down Sequencing.** It is well-known that drawbacks of MALDI-TDS are the requirement of a high purity of analyte, low sensitivity, and lack of fragmentation in the presence of disulfide bonds.[21] The isolated WPTP used in this study was high purity.[15] WPTP was immobilized onto a C4 ziptip by hydrophobic interactions, and its disulfide bonds were then reduced. This provided a quick and effective way to reduce WPTP's disulfide bonds, remove contaminating salts, and concentrate the reduced protein in one simple step.

MALDI-TDS results in ladder fragmentation of the intact protein, leaving glycans attached to the modified Asn residues.[22] Partial amino acid sequence near the N-terminus of WPTP was gained through interpretation of the c-ion series in the MALDI-TDS spectrum (Figure 2A, MHFHD). The y- and $z$+2-ions were interpreted as a continuous 30-amino acid residue sequence (Figure 2A, DN*LTAWVAKFAQAIVKMGQIQVLTGTQ-GEI). A protein BLAST search of the NCBInr database (blast.ncbi.nlm.nih.gov) predicted that this sequence originated from a protein in the peroxidase superfamily. The top hit was RPTP (PDB: 3HDL; $E$ value: $6 \times 10^{-16}$). The y ions at $m/z$ 5290.1 and 6575.7 (N*) (and the corresponding $z$+2-ions) had a mass difference corresponding to a glycosylated Asn, Asn-$GlcNAc_2Man_3FucXyl$ (exact $\Delta$ $m/z$ 1284.5 and accurate $\Delta$ $m/z$ 1285.6). This glycan is the predominant glycan found on HRP,[23] soybean peroxidase (SBP),[24] RPTP,[14] and other plant peroxidases. A scheme of the glycan is depicted in Figure 2B according to the conventions of the Consortium for Functional Glycomics. All assigned peaks had a mass error within 200 ppm and the root-mean-square error (RMSError) was 65.32 ppm.

**Bottom-Up Sequencing.** Additional amino acid sequence information was gained through a more traditional "bottom-up" approach. For this, WPTP was digested with trypsin, and the resulting tryptic peptides were subjected to MALDI-TOF MS (Figure 3A). Tandem mass spectrometry was performed to obtain the amino acid sequence of the tryptic peptides of WPTP (Figure 3B–F). Among these, fragments of the parent ion at $m/z$ 1264.6 could be unambiguously interpreted as $M^{[ox]}$HFHDCFVR (Figure 3D). Furthermore, this sequence overlapped with an amino acid sequence ladder from the MALDI-TDS experiment. Thus, this amino acid sequence was used for primer design for cDNA cloning and sequencing of WPTP.

Fragments of the parent ion at $m/z$ 2890.3 displayed a characteristic spectrum of a glycopeptide (Figure 3F). Man and GlcNAc oxonium ions were observed at $m/z$ 162.7 and 203.7, respectively. We also observed cross-ring fragmentation of the innermost GlcNAc ($^{0,2}$X). Additionally, the glycan moiety fragmented into a series of y-ions corresponding to mass shifts indicative of the glycan $GlcNAc_2Man_3XylFuc$ (Figure 2C).

**cDNA Sequencing.** The gene for WPTP was cloned and sequenced from mRNA isolated from the leaves of *T. fortunei*. The gene consisted of 5′- and 3′- untranslated regions, which included a poly-A tail, and 1032 bp encoding a polypeptide of 344 amino acids (Figure 4). There was an N-terminal signal peptide upstream of the previously sequenced N-terminus of mature WPTP, which targets class III peroxidases to the secretory pathway.[25] Some peroxidases additionally bear a C-terminal signal peptide for vacuolar targeting.[25] Insights into in vivo processing of the C-terminus of WPTP were obtained by combining information from the MALDI-TDS spectrum of intact WPTP and its cDNA sequence. In a MALDI-TDS spectrum, the ion with the lowest $m/z$ value in each ion series corresponds to the mass of the N-terminus (for c-ions) or the C-terminus (for y- and z-type ions). Therefore, the y 11-ion corresponded to the mass of RTN*CSVVNSAS (Figure 2A; exact $m/z$ 2307.9 and accurate $m/z$ 2307.8), where the mass shift for $Asn^{298}$ (N*) in the WPTP sequence corresponded to $GlcNAc_2Man_3FucXyl$. Thus, the vacuolar targeting signal for WPTP was LGDIVMASGHLTEVATS (Figure 4, gray italics).

Using the same logic for the N-terminus, the c 38-ion at $m/z$ 6098.4 (Figure 2A) corresponded to the sequence DLQIG-FYN#QSCPSAESLVQQAVAAAFAN*NSGIAPGLIR (Figure 4), where the mass difference of 2178.3 relative to the expected peptide mass (3920.1 Da) could be accounted for by adding a glycan to $Asn^{8}$ (N#) and one to $Asn^{28}$ with the potential sequences $GlcNAc_2Man_2FucXyl$ ($\Delta$ $m/z$ 1008.4) and $GlcNAc_2Man_3FucXyl$ ($\Delta$ $m/z$ 1170.4), giving an overall mass error of 65.6 ppm (exact $m/z$ 6098.7 and accurate $m/z$ 6098.4).

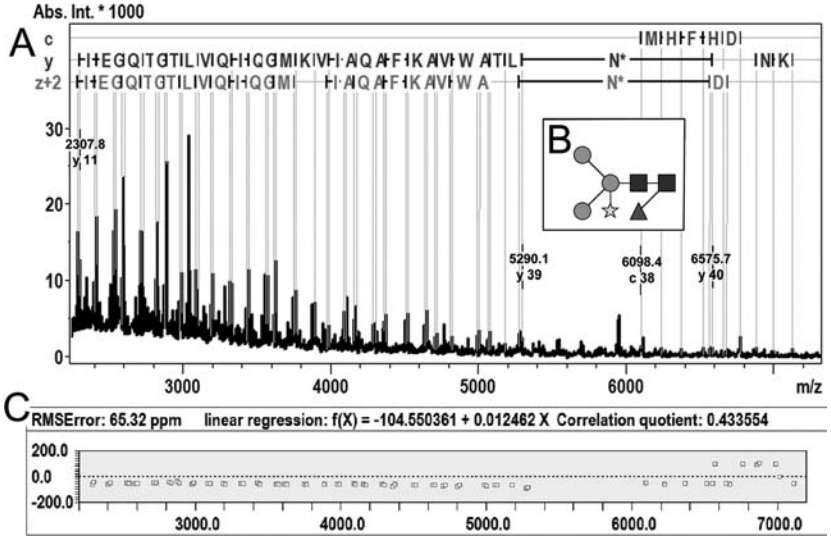


**Figure 2.** MALDI-top-down sequencing of WPTP to determine the amino acid sequence near the protein termini. The amino acid sequence was interpreted from c-, y-, and z+2-ion series. (A) Δ $m/z$ between y 39 at $m/z$ 5290.1 and y 40 at 6575.7 corresponded to Asn modified with the glycan $GlcNAc_2Man_3XylFuc$ (N*). (B) A cartoon structure of the glycan $GlcNAc_2Man_3XylFuc$. (C) A plot showing the mass error (ppm) for each matched ion. (■) *N*-Acetylglucosamine (GlcNAc); (●) mannose (Man); (▲) fucose (Fuc); (★) xylose (Xyl).

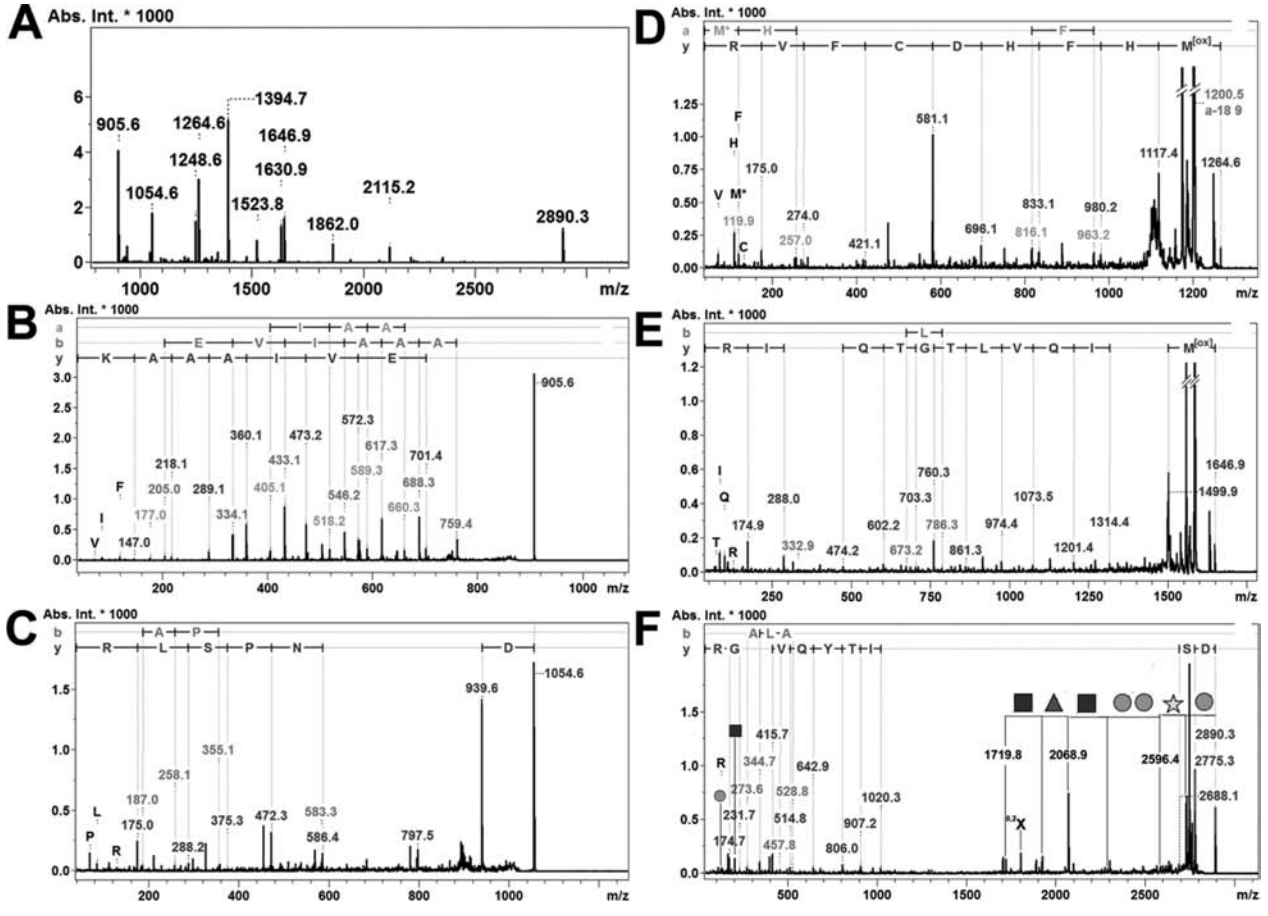


**Figure 3.** MALDI-TOF/TOF MS/MS of WPTP tryptic peptides for primer design: (A) mass spectrum WPTP tryptic peptides and fragmentation spectra of the parent ion at $m/z$ (B) 905.6, (C) 1054.6, (D) 1264.6, (E) 1646.9, and (F) 2980.3. ($M^{[ox]}$) oxidized methionine; (■) *N*-acetylglucosamine (GlcNAc); (●) mannose (Man); (▲) fucose (Fuc); (☆) xylose (Xyl).

**Structure Overview.** Mature WPTP was composed of a single polypeptide, 306 amino acid residues in length, with an average mass of 32 172 Da. The cDNA sequence showed that there were 13 potential glycosylation sites, identified by the sequence Asn-Xxx-Ser/Thr, where Xxx is any amino acid except Pro. The MW, as measured by MALDI-TOF MS (Figure 1), ranged from 41−45 kDa. Considering this and the polypeptide mass, WPTP has 21−29% glycans. This level of complexity made


dx.doi.org/10.1021/jf504511h | J. Agric. Food Chem. 2014, 62, 11941−11948

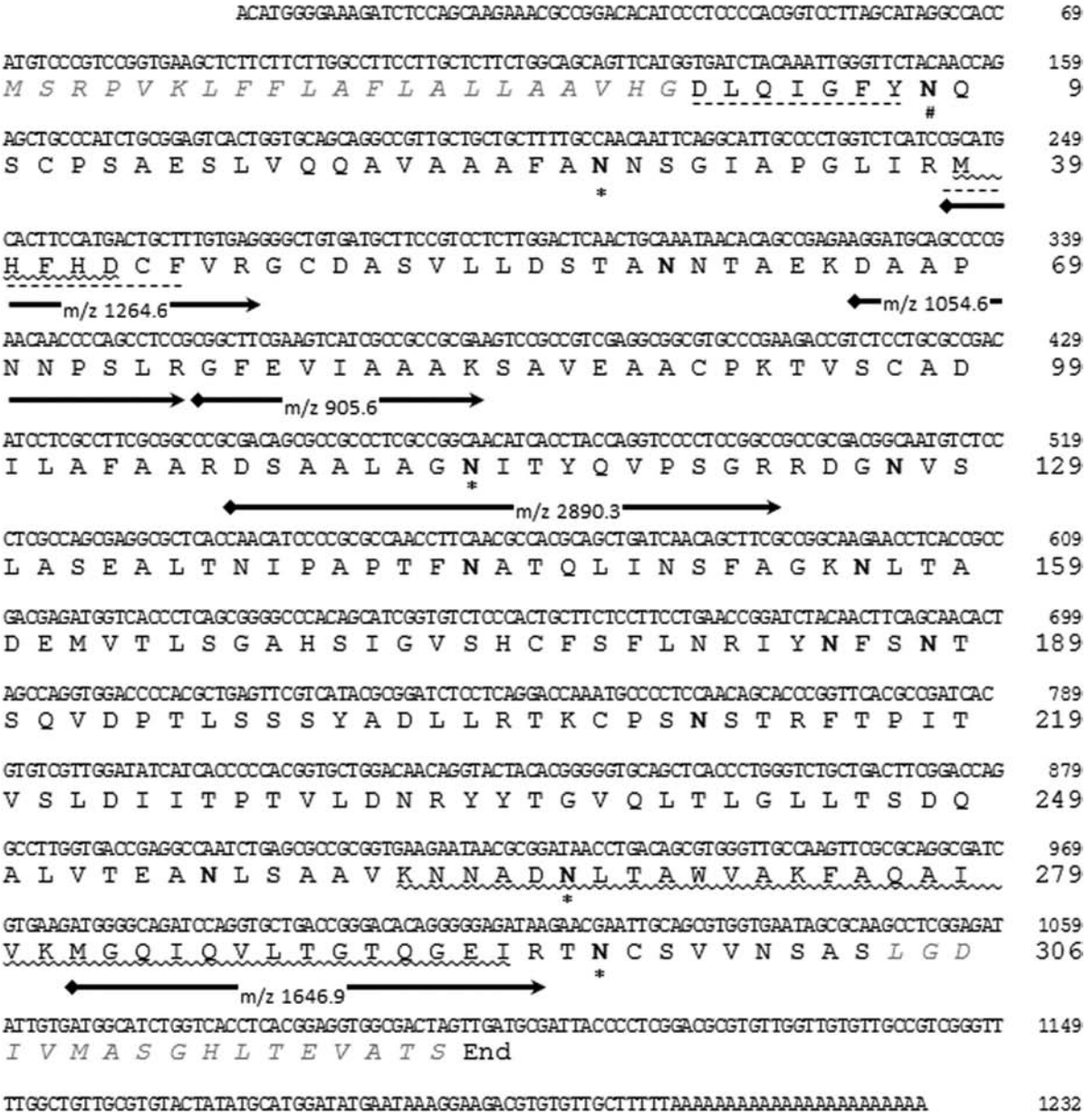


**Figure 4.** cDNA sequencing of WPTP to determine the complete amino acid sequence. Nucleotide and amino acid residue numbers are on the right. (gray italicized) N- and C-terminal signal peptides; amino acid sequence (----) used for primer design, (zig-zag) covered by MALDI-TDS, and (→) determined by MALDI-TOF/TOF MS/MS; (**N**) potential glycosylation site; (#) $GlcNAc_2Man_2FucXyl$; (*) $GlcNAc_2Man_3FucXyl$.

it difficult to assign a specific glycoform structure to each peak in that spectrum. Positions 8, 28, 114, 267, and 298 were glycosylated. A more detailed study of WPTP's glycosylation profile is underway.

Class III peroxidases share a common 3D structure despite a low sequence identity.[2,16,26] For example, RPTP and HRP were only 36% identical, but their C$\alpha$ backbone structures were closely related, having an overall root mean squared deviation of 1.07 Å.[14] A structurally guided alignment revealed that WPTP and RPTP were 88% identical in primary structure and likely were very similar in secondary and tertiary structures (Figure 5).

Structural integrity of plant peroxidases is maintained largely by an extensive hydrogen bonding network that extends above and below the heme-containing active site to distal and proximal $Ca^{2+}$.[32] Additionally, four invariant disulfide bridges tie the protein together. These eight cysteine residues were present in WPTP (Figure 5, c). Importantly, the disulfide bridge between $Cys^{44}$ and $Cys^{49}$ stabilizes the BC loop, which comprises the majority of the distal $Ca^{2+}$ binding residues (Figure 5, +). Distal $Ca^{2+}$ was critical for maintaining the proper tertiary structure of the active site.[33] The disulfide bridge between $Cys^{176}$ and $Cys^{208}$ stabilizes the region between helices F and H, which is important for substrate binding and contains residues necessary for binding proximal $Ca^{2+}$. The additional 4.5 $Ca^{2+}$ found in the WPTP structure were difficult to account for because only one other peroxidase, anionic peanut peroxidase,[34] had elevated $Ca^{2+}$ content and its 3D structure was still not available.

**Features of Potential Importance to Substrate Specificity.** The new WPTP structure information presented in this study allowed for exploration of features of potential importance in palm tree peroxidases. One striking functional difference is substrate reactivity differences between WPTP, RPTP, and HRP (Table 1). Ferulic acid was the better substrate for RPTP and HRP.[20] Moreover, the difference in reactivity

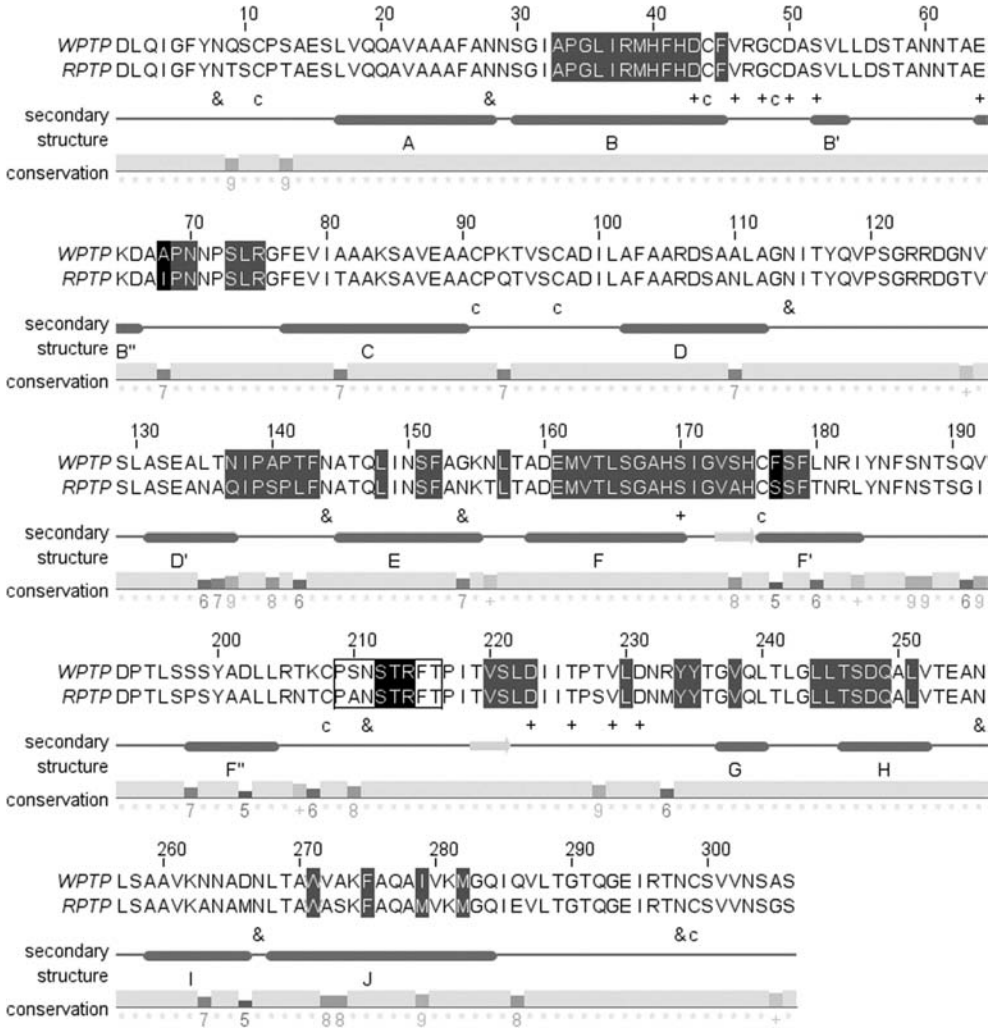


**Figure 5.** Alignment of WPTP and RPTP (PDB: 3HDL) according to the method of Armougom et al.[27] to determine features related to substrate specificity. Determination of (highlighted in gray) residues less than 12 Å from heme iron and (highlighted in black) less than 4.6 Å from MES with Swiss-PdbViewer 4.1.0[28] and (box) residues with significant structural deviation between RPTP and HRP (PDB: 1ATJ) with a protein structure alignment tool.[29] (&) Occupied glycosylation site;[14] (c) cysteine; (+) $Ca^{2+}$ binding. Secondary structure: (dark gray) helices; (light gray) sheets. Helices labeled according to Watanabe et al.[14] and conservation according to Livingston and Barton.[30] The figure was drawn in JalView.[31]

**Table 1. Substrate Reactivity As Measured by $k_{app}$ ($M^{-1}$ $s^{-1}$)**

| | WPTP[a] | RPTP[b] | HRP[b] |
|---|---|---|---|
| ferulic acid | $3.0 \times 10^6$ | $6.3 \times 10^7$ | $1.3 \times 10^7$ |
| ABTS[c] | $6.0 \times 10^7$ | $5.0 \times 10^7$ | $4.0 \times 10^6$ |

[a]The data for WPTP are from ref 15. [b]The data for RPTP and HRP are from ref 20. [c]2,2′-Azinobis(3-ethylbenzothiazoline-6-sulfonic acid).

between ferulic acid and ABTS was not too different for those two peroxidases, i.e., there was a 1.26-fold difference for RPTP and 3.25-fold difference for HRP.[20] The better substrate for WPTP was ABTS, and ferulic acid had 20-fold lower reactivity.[15] Investigation of the 3D structure of RPTP, using Swiss-PdbViewer 4.1.0,[28] revealed amino acid residues and features of known and putative importance to substrate binding (Table 2).

Amino acids involved in substrate binding should be within 12 Å of the heme iron, as indicated by NMR studies of HRP–substrate complexes.[38] There were 64 residues within this distance in RPTP (Figure 5, highlighted in gray) and 5 of those differed between WPTP and RPTP. Of those 5, the lowest conservation was at position 142. Interactions between residue 142 and conserved Phe[143] resulted in topological features thought to affect interactions with substrates.[2,39] Residue 142 was hydrophobic in HRP, RPTP, and WPTP, except that it was large in HRP (Phe) and RPTP (Leu) but small in WPTP (Thr). This difference could be a major factor causing the large deficit in WPTP's reactivity toward ferulic acid. The absence of a 3D structure complex between peroxidase and ABTS prevented speculation about features responsible WPTP's superior catalysis of that large substrate.

The RPTP crystal structure contained a potential inhibitor, an MES molecule.[14] Residues within van der Waals radius (4.6 Å) of MES may affect substrate reactivity. Nine residues (Ile[68], Ser[140], Pro[141], Leu[142], Ser[177], Ser[178], Ser[212], Thr[213], and Arg[214]) were within that region. Five of the nine residues did not overlap with the residues that were 12 Å from the heme iron (Figure 5, highlighted in black). The position with the lowest conservation between between RPTP and WPTP was at position 177 and WPTP was at position 177. In WPTP, it was large, hydrophobic, and aromatic Phe, whereas in RPTP, it was small and polar Ser. Moreover, this MES binding site was in the most structurally divergent region between HRP and RPTP (Figure 5, box). In

**Table 2. Residues of Known and Potential Importance for Protein−Substrate Interactions**

| position[a] | WPTP | RPTP | predicted effect | evidence |
|---|---|---|---|---|
| Distance within 12 Å of Heme Iron | | | | |
| 38 | R | R | critical | two H-bonds to ferulic acid (FA) (HRP);[35] $Arg^{38}$ to Leu 10−100 times slower substrate oxidation (HRP)[36] |
| 69 | P | P | minor | putative hydrophobic interaction between FA and anionic *Arabidopsis thaliana* peroxidase (ATP A2)[37] |
| 138 | I | I | minor | putative hydrophobic interaction with FA (ATP A2)[37] |
| 139 | P | P | major | H-bond to active site $H_2O$ which is H-bonded to FA (HRP)[35] |
| 140 | A | S | minor | Ala: tiny[b] and hydrophobic vs Ser: small[c] and polar; hydrophobic interaction with FA (HRP: $Ala^{140}$);[35] H-bond to MES[d] (RPTP)[14] |
| 142 | T | L | major | Thr: small[c] and hydrophobic vs Leu: large, hydrophobic, and aliphatic; hydrophobic interaction with FA (HRP)[35] |
| Distance within 4.6 Å of MES[d] | | | | |
| 68 | A | I | minor | Ile: large, hydrophobic, and aliphatic vs Ala: tiny[b] and hydrophobic; hydrophobic interaction with FA (HRP: $Gly^{68}$)[35] |
| 177 | F | S | major | Phe: large, hydrophobic, and aromatic vs Ser: small[c] and polar |
| 212−214 | STR | STR | major | structurally distinct region (HRP vs RPTP) and H-bond with MES[d] (RPTP: $Arg^{214}$)[14] |

[a]Position in the amino acid sequence (Figure 5). [b]Less than 35 $Å^3$. [c]Less than 60 $Å^3$. [d]2-(*N*-Morpholino)ethanesulfonic acid.

HRP, this loop region was pointing away from the active site, whereas in RPTP, it was pointing toward it. This difference in topology brought $Arg^{214}$ into hydrogen bonding distance with MES.[14] Further investigation into this distinct region is warranted.

## AUTHOR INFORMATION


### Corresponding Author

*Telephone: 808-956-2011; fax 808-956-3542; e-mail: qingl@hawaii.edu.



### Funding

M.R.B. was a NIFA Pre-Doctoral Fellowship recipient. This project was supported in part by the Agriculture and Food Research Initiative Competitive Grant 2012-67011-19671 from the USDA National Institute of Food and Agriculture, NIH RCMI Grant 8G12MD007601, and the Korean RDA Grant 2008131.


### Notes

The authors declare no competing financial interest.

## ACKNOWLEDGMENTS


The authors thank Mr. Sam Fu for consultation about the method for solid-phase reduction of disulfide bonds.


## ABBREVIATIONS USED

ABTS, 2,2′-azinobis(3-ethylbenzothiazoline-6-sulfonic acid); ACN, acetonitrile; AMBIC, ammonium bicarbonate; ATP A2, anionic *Arabidopsis thaliana* peroxidase 2; DHB, 2,5-dihydroxybenzoic acid; FA, ferulic acid; HRP, horseradish peroxidase; IS, ion source; MES, 2-(*N*-morpholino)ethanesulfonic acid; PDB, protein databank; PIE, pulsed ion extraction; PNP, peanut peroxidase; TDS, top-down sequencing; TFA, trifluoroacetic acid; WPTP, windmill palm tree peroxidase

## REFERENCES


(1) Zipor, G.; Oren-Shamir, M. Do vacuolar peroxidases act as plant caretakers? *Plant Sci.* **2013**, *199*, 41−47.

(2) Veitch, N. C. Structural determinants of plant peroxidase function. *Phytochem. Rev.* **2004**, *3*, 3−18.

(3) Gaspar, S.; Popescu, I. C.; Gazaryan, I. G.; Gerardo Bautista, A.; Sakharov, I. Yu.; Mattiasson, B.; Csöregi, E. Biosensors based on novel plant peroxidases: a comparative study. *Electrochim. Acta* **2000**, *46*, 255−264.

(4) Chen, S.; Yuan, R.; Chai, Y.; Hu, F. Electrochemical sensing of hydrogen peroxide using metal nanoparticles: A review. *Microchim. Acta* **2013**, *180*, 15−32.

(5) Farré, M.; Kantiani, L.; Barceló, D. Advances in immunochemical technologies for analysis of organic pollutants in the environment. *TrAC, Trends Anal. Chem.* **2007**, *26*, 1100−1112.

(6) Litescu, S. C.; Eremia, S.; Radu, G. L. Biosensors for the determination of phenolic metabolites. In *Bio-Farms for Nutraceuticals*; Giardi, M. T.; Rea, G.; Berra, B., Eds.; Springer: New York, 2010; pp 234−240.

(7) Zhang, H.; Lu, Y.; Ushio, H.; Shiomi, K. Development of sandwich ELISA for detection and quantification of invertebrate major allergen tropomyosin by a monoclonal antibody. *Food Chem.* **2014**, *150*, 151−157.

(8) Zhao, H.; Nan, T.; Tan, G.; Gao, W.; Cao, Z.; Sun, S.; Li, Z.; Li, Q. X.; Wang, B. Development of two highly sensitive immunoassays for detection of copper ions and a suite of relevant immunochemicals. *Anal. Chim. Acta* **2011**, *702*, 102−108.

(9) Sakharov, I. Yu. Palm tree peroxidases. *Biochemistry (Moscow)* **2004**, *69*, 823−829.

(10) Alpeeva, I. S.; Niculescu-Nistor, M.; Leon, J. C.; Csöregi, E.; Sakharov, I. Yu. Palm tree peroxidase-based biosensor with unique characteristics for hydrogen peroxide monitoring. *Biosens. Bioelectron.* **2005**, *21*, 742−748.

(11) Sakharov, I. Yu.; Vorobiev, A. C.; Leon, J. J. C. Synthesis of polyelectrolyte complexes of polyaniline and sulfonated polystyrene by palm tree peroxidase. *Enzyme Microb. Technol.* **2003**, *33*, 661−667.

(12) Caramyshev, A. V.; Evtushenko, E. G.; Ivanov, V. F.; Barceló, A. R.; Roig, M. G.; Shnyrov, V. L.; van Huystee, R. B.; Kurochkin, I. N.; Vorobiev, A. K.; Sakharov, I. Yu. Synthesis of conducting polyelectrolyte complexes of polyaniline and poly(2-acrylamido-3-methyl-1-propanesulfonic acid) catalyzed by pH-stable palm tree peroxidase. *Biomacromolecules* **2005**, *6*, 1360−1366.

(13) Caramyshev, A. V.; Lobachov, V. M.; Selivanov, D. V.; Sheval, E. V.; Vorobiev, A. K.; Katasova, O. N.; Polyakov, V. Y.; Makarov, A. A.; Sakharov, I. Yu. Micellar peroxidase-catalyzed synthesis of chiral polyaniline. *Biomacromolecules* **2007**, *8*, 2549−2555.

(14) Watanabe, L.; de Moura, P. R.; Bleicher, L.; Nascimento, A. S.; Zamorano, L. S.; Calvete, J. J.; Sanz, L.; Pérez, A.; Bursakov, S.; Roig, M. G. Crystal structure and statistical coupling analysis of highly glycosylated peroxidase from royal palm tree (*Roystonea regia*). *J. Struct. Biol.* **2010**, *169*, 226−242.

(15) Caramyshev, A. V.; Firsova, Y. N.; Slastya, E. A.; Tagaev, A. A.; Potapenko, N. V.; Lobakova, E. S.; Pletjushkina, O. Y.; Sakharov, I. Yu. Purification and characterization of windmill palm tree (*Trachycarpus fortunei*) peroxidase. *J. Agric. Food Chem.* **2006**, *54*, 9888−9894.

(16) Gajhede, M.; Schuller, D. J.; Henriksen, A.; Smith, A. T.; Poulos, T. L. Crystal structure of horseradish peroxidase C at 2.15 Å resolution. *Nat. Struct. Biol.* **1997**, *4*, 1032−1048.

(17) Suckau, D.; Resemann, A.; Schuerenberg, M.; Hufnagel, P.; Franzen, J.; Holle, A. A novel MALDI LIFT-TOF/TOF mass spectrometer for proteomics. *Anal. Bioanal. Chem.* **2003**, *376*, 952−965.

(18) Tamura, K.; Peterson, D.; Peterson, N.; Stecher, G.; Nei, M.; Kumar, S. MEGA5: Molecular evolutionary genetics analysis using maximum likelihood, evolutionary distance, and maximum parsimony methods. *Mol. Biol. Evol.* **2011**, *28*, 2731−2739.
(19) Segrest, J. P.; Jackson, R. L.; Andrews, E. P.; Marchesi, V. T. Human erythrocyte membrane glycoprotein: A re-evaluation of the molecular weight as determined by SDS polyacrylamide gel electrophoresis. *Biochem. Biophys. Res. Commun.* **1971**, *44*, 390−395.
(20) Sakharov, I. Yu.; Vesga B, M. K.; Galaev, I. Yu.; Sakharova, I. V.; Pletjushkina, O. Y. Peroxidase from leaves of royal palm tree *Roystonea regia*: Purification and some properties. *Plant Sci.* **2001**, *161*, 853−860.
(21) Resemann, A.; Wunderlich, D.; Rothbauer, U.; Warscheid, B.; Leonhardt, H.; Fuchser, J.; Kuhlmann, K.; Suckau, D. Top-down *de novo* protein sequencing of a 13.6 kDa camelid single heavy chain antibody by matrix-assisted laser desorption ionization-time-of-flight/time-of-flight mass spectrometry. *Anal. Chem.* **2010**, *82*, 3283−3292.
(22) Hanisch, F.-G. Top-down sequencing of *O*-glycoproteins by in-source decay matrix-assisted laser desorption ionization mass spectrometry for glycosylation site analysis. *Anal. Chem.* **2011**, *83*, 4829−4837.
(23) Yang, B. Y.; Gray, J. S.; Montgomery, R. The glycans of horseradish peroxidase. *Carbohydr. Res.* **1996**, *287*, 203−212.
(24) Gray, J. S. S.; Montgomery, R. Asymmetric glycosylation of soybean seed coat peroxidase. *Carbohydr. Res.* **2006**, *341*, 198−209.
(25) Welinder, K. G.; Justesen, A. F.; Kjaersgård, I. V. H.; Jensen, R. B.; Rasmussen, S. K.; Jespersen, H. M.; Duroux, L. Structural diversity and transcription of class III peroxidases from *Arabidopsis thaliana*: 73 peroxidases from *Arabidopsis*. *Eur. J. Biochem.* **2002**, *269*, 6063−6081.
(26) Schuller, D. J.; Ban, N.; van Huystee, R. B.; McPherson, A.; Poulos, T. L. The crystal structure of peanut peroxidase. *Structure* **1996**, *4*, 311−321.
(27) Armougom, F.; Moretti, S.; Poirot, O.; Audic, S.; Dumas, P.; Schaeli, B.; Keduas, V.; Notredame, C. Expresso: automatic incorporation of structural information in multiple sequence alignments using 3D-Coffee. *Nucleic Acids Res.* **2006**, *34*, W604−W608.
(28) Arnold, K.; Bordoli, L.; Kopp, J.; Schwede, T. The SWISS-MODEL workspace: A web-based environment for protein structure homology modelling. *Bioinformatics* **2006**, *22*, 195−201.
(29) Shindyalov, I. N.; Bourne, P. E. Protein structure alignment by incremental combinatorial extension (CE) of the optimal path. *Protein Eng.* **1998**, *11*, 739−747.
(30) Livingstone, C. D.; Barton, G. J. Protein sequence alignments: a strategy for the hierarchical analysis of residue conservation. *CABIOS, Comput. Appl. Biosci.* **1993**, *9*, 745−756.
(31) Waterhouse, A. M.; Procter, J. B.; Martin, D. M. A.; Clamp, M.; Barton, G. J. Jalview Version 2–a multiple sequence alignment editor and analysis workbench. *Bioinformatics* **2009**, *25*, 1189−1191.
(32) Smulevich, G.; Feis, A.; Howes, B. D. Fifteen Years of Raman Spectroscopy of Engineered Heme Containing Peroxidases: What Have We Learned? *Acc. Chem. Res.* **2005**, *38*, 433−440.
(33) Szigeti, K.; Smeller, L.; Osváth, S.; Majer, Z.; Fidy, J. The structure of horseradish peroxidase C characterized as a molten globule state after $Ca^{2+}$ depletion. *Biochim. Biophys. Acta, Proteins Proteomics* **2008**, *1784*, 1965−1974.
(34) Hu, C.; Lee, D.; Chibbar, R. N.; Huystee, R. B. $Ca^{2+}$ and peroxidase derived from cultured peanut cells. *Physiol. Plant.* **1987**, *70*, 99−102.
(35) Henriksen, A.; Smith, A. T.; Gajhede, M. The structures of the horseradish peroxidase c-ferulic acid complex and the ternary complex with cyanide suggest how peroxidases oxidize small phenolic substrates. *J. Biol. Chem.* **1999**, *274*, 35005−35011.
(36) Rodriguez-Lopez, J. N.; Smith, A. T.; Thorneley, R. N. F. Role of arginine 38 in horseradish peroxidase: A critical residue for substrate binding and catalysis. *J. Biol. Chem.* **1996**, *271*, 4023−4030.
(37) Nielsen, K. L.; Indiani, C.; Henriksen, A.; Feis, A.; Becucci, M.; Gajhede, M.; Smulevich, G.; Welinder, K. G. Differential activity and structure of highly similar peroxidases. Spectroscopic, crystallographic, and enzymatic analyses of lignifying *Arabidopsis thaliana* peroxidase A2 and horseradish peroxidase A2. *Biochemistry* **2001**, *40*, 11013−11021.
(38) Veitch, N. C. Aromatic donor molecule binding sites of haem peroxidases. *Biochem. Soc. Trans.* **1995**, *23*, 232−240.
(39) Henriksen, A.; Mirza, O.; Indiani, C.; Teilum, K.; Smulevich, G.; Welinder, K. G.; Gajhede, M. Structure of soybean seed coat peroxidase: A plant peroxidase with unusual stability and haem-apoprotein interactions. *Protein Sci.* **2001**, *10*, 108−115.

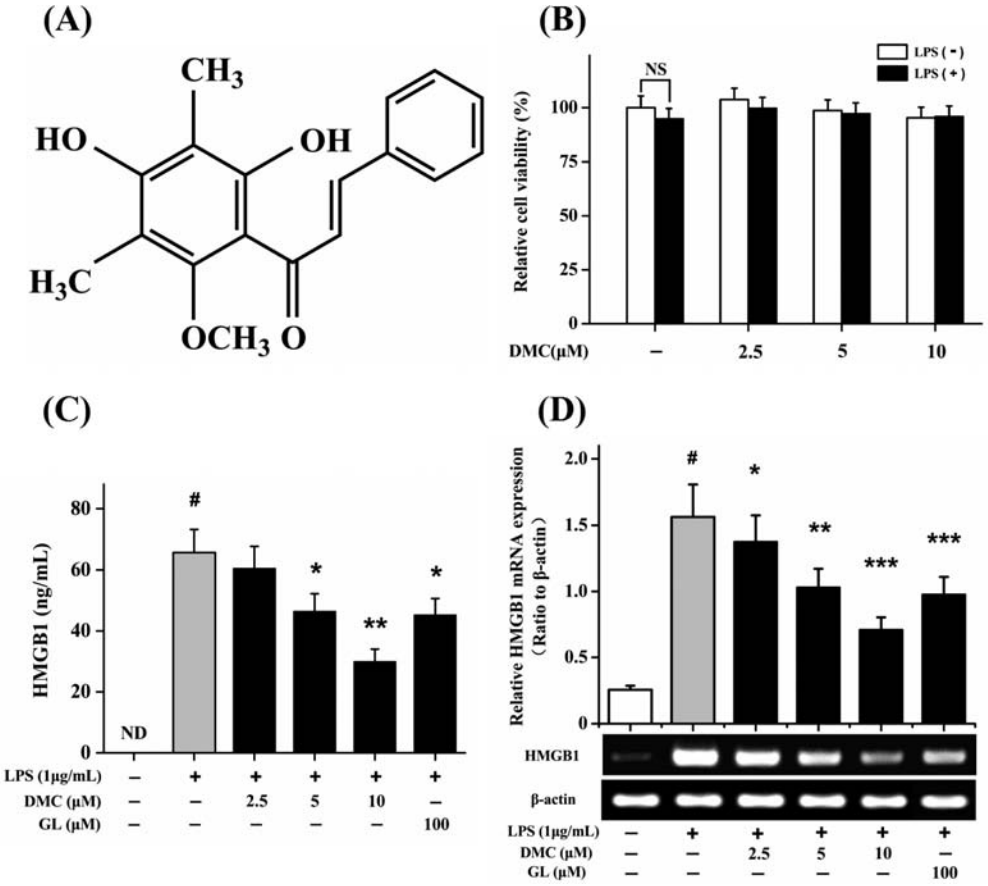


**Figure 1.** 2′,4′-Dihydroxy-6′-methoxy-3′,5′-dimethylchalcone (DMC) inhibits high-mobility group box 1 (HMGB1) secretion and transcription in lipopolysaccharide (LPS)-stimulated Kupffer cells. Kupffer cells were pretreated with or without the indicated concentrations of DMC or glycyrrhizin (GL) (100 $\mu$M) for 2 h before LPS (1 $\mu$g/mL) treatment for 24 h. Panel A shows the chemical structure of DMC. (B) CCK-8 assay data showed the concentrations of DMC in Kupffer cells. The data are expressed as percentage of surviving cells. (C) DMC dose-dependently decreased the LPS-stimulated HMGB1 secretion from Kupffer cells. Levels of HMGB1 were measured by ELISA. (D) RT-PCR was used to evaluate mRNA levels of HMGB1. $\beta$-Actin was used as a loading control. The bar graph showing semiquantitative densitometric analysis summarizes the fold change of HMGB1 expression in each group. Each value represents the mean ± SD of triplicate experiments. (#) $P < 0.001$ as compared with control group; (*) $P < 0.05$, (**) $P < 0.01$, and (***) $P < 0.001$ as compared with LPS-stimulated group only; NS, nonsignificant; ND, not detectable.

C (PKC), phospho-PKC, phospho-PKC$\alpha$, phospho-PKC$\beta$I, phospho-PKC$\beta$II, phospho-PKC$\gamma$, phosphoserine, $\beta$-actin, and histone H3.1 were obtained from Cell Signaling Technology (Danvers, MA, USA). Mouse anti-HMGB1 monoclonal antibody (mAb) and fluorescein-5-isothiocyanate (FITC) labeled anti-mouse immunoglobulin G (IgG) were purchased from Invitrogen (Carlsbad, CA, USA). Cell Counting Kit 8 (CCK-8) assay kit was purchased from Jiancheng Institute (NJ, China). HMGB1, tumor necrosis factor-alpha (TNF-$\alpha$), interleukin-1 beta (IL-1$\beta$), and interleukin-6 (IL-6) were respectively determined by using a double-antibody sandwich enzyme-linked immunosorbent assay (ELISA) kit from Jiancheng Institute. Alkaline phosphatase (AP) labeled anti-mouse IgG was purchased from Cell Signaling Technology.

**Primary Cell Isolation and Culture.** Kupffer cells were isolated from rat as described.[43] First, fresh cells were cultured in Roswell Park Memorial Institute 1640 (RPMI-1640) containing 2 mM glutamine, heat-inactivated fetal bovine serum (FBS, 10%), streptomycin, and penicillin. They were maintained in an incubator at 37 °C with an atmosphere of humidified 5% $CO_2$. Second, after 15 min of culture, nonadherent cells were removed and adherent cells were collected. Finally, Kupffer cell purity was >90% as evaluated by CD68 staining. The ability of phagocytosis with Kupffer cells was also examined.

**Cell Viability Assay and Stimulation.** The viability of the Kupffer cells was determined by the CCK-8 Counting Kit following the manufacturer's instructions. The cells were plated onto 96- and 6-well culture dishes. Cells cultured for 12 h were washed and replaced with fresh medium (RPMI-1640 medium containing 0.25% heat-inactivated FBS) with DMC (2.5, 5, and 10 $\mu$M) for 2 h before LPS (1 $\mu$g/mL) treatment for 24 h. Cell-free supernatants, protein, and RNA extracts were stored at −80 °C. Cells cultured in media alone acted as a negative control. Pretreatment with GL (100 $\mu$M) acted as the positive control in all tests.

**Measurement of Cytokines.** The cytokines including HMGB1, TNF-$\alpha$, IL-1$\beta$, and IL-6 were respectively evaluated by ELISA kits according to the manufacturer's instructions. NO assay was measured by Griess reagent.[44]

**Semiquantitative Reverse Transcription Polymerase Chain Reaction (RT-PCR).** Cell's total RNA extraction and cDNA synthesis were examined following the manufacturer's instructions (RT-PCR kit, Roche, Germany). The RT-PCR primer sequences for analysis of HMGB1, IL-6, IL-1$\beta$, inducible nitric oxide synthase (iNOS), TNF-$\alpha$, and $\beta$-actin expression were as follows: HMGB1, 5′-ATGGGCAAAGGAGATCCTAA-3′ and 5′-CTCTGTAGGCAGGAATATCC-3′; IL-6, 5′-GGATACCACCCACAACAGAC-3′ and 5′-TTGCCGAGTAGACCTCATAG-3′; IL-1$\beta$, 5′-TCATTGTGGCTGTGGAGAAG-3′ and 5′-CTATGTCCCGACCATTGCTG-3′; iNOS, 5′-GCATCCCAAGTACGAGTGGT-3′ and 5′-GAAGGCGTAGCTGAACAAGG-3′; TNF-$\alpha$, 5′-GTAGCCCACGTCGTAGCAAA-3′ and 5′-CCCTTCTCCAGCTGGAAGAC-3′; $\beta$-actin, 5′-TGCTGTCCCTGTATGCCTCT-3′ and 5′-TGATGTCACGCACGATTTCC-3′. The PCR products were resolved by electrophoresis and analyzed by staining ethidium bromide with ultraviolet light illumination. The band

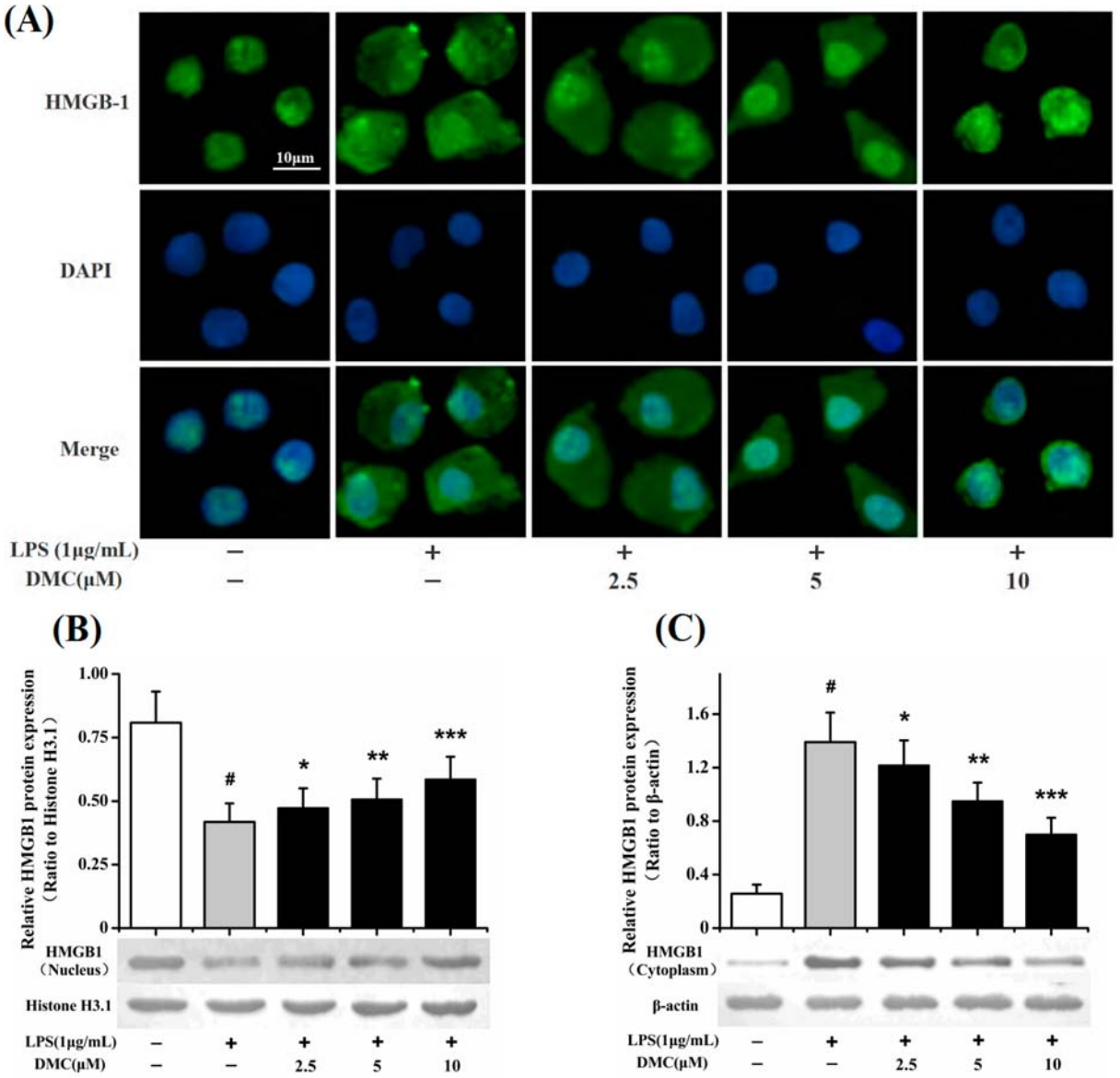


**Figure 2.** Inhibitory effect of DMC on nucleocytoplasmic translocation of HMGB1. Kupffer cells were pretreated with or without the indicated concentrations of DMC for 2 h before LPS (1 $\mu$g/mL) treatment for 24 h. HMGB1 nucleocytoplasmic translocation assay was measured by laser scanning confocal microscopy. Cell fractionation was evaluated by Western blotting. (A) HMGB1 was mostly distributed in the nuclear region of unstimulated group (first column). HMGB1 was localized in both nuclear and cytoplasmic regions of LPS-stimulated Kupffer cells (second column). The indicated concentrations of DMC treatment greatly inhibited LPS elicited intracellular HMGB1 movement (third to fifth columns). Nucleus (blue, DAPI staining), HMGB1 (green). Bar = 10 $\mu$m. The cytoplasmic and nuclear protein was extracted separately, and the level of HMGB1 was detected by Western blotting. (B) Nuclear HMGB1 protein, normalized by histone H3.1 protein. (C) Cytoplasmic HMGB1 protein, normalized by $\beta$-Actin protein. The bar graph showing semiquantitative densitometric analysis summarizes the fold change of HMGB1 expression in each group. Each value represents the mean ± SD of triplicate experiments. (#) $P < 0.001$ as compared with control group; (*) $P < 0.05$, (**) $P < 0.01$, and (***) $P < 0.001$ as compared with LPS-stimulated group only.

intensities were measured with a densitometer, and the results were normalized with $\beta$-actin.

**Immunofluorescence.** Kupffer cells were cultured in monolayers on glass coverslips. Cells were pretreated with the indicated concentrations of DMC for 2 h before LPS (1 $\mu$g/mL) treatment. The samples were fixed for 30 min with 4% formaldehyde. Cells were permeabilized for 15 min with 0.3% Triton X-100 and then blocked for 1 h with 2% bovine serum albumin. The samples were probed with anti-HMGB1. FITC-labeled IgG was used as secondary antibody. Finally, samples were stained for 15 min with DAPI. Fluorescence were analyzed by laser scanning confocal microscopy (Olympus Inc., Center Valley, PA, USA).

**Western Blot Analysis.** The samples were lysed with lysis buffer on ice for 30 min. For collection of nuclear and cytosolic proteins, protein extracts were respectively enriched according to the manufacturer's instructions (Cytoplasmic and Nuclear Extraction Kit, Roche, Germany). Protein samples were quantified by using an Enhanced BCA Protein Assay Kit (Beyotime, Jiangsu, China). The proteins were separated by SDS-PAGE and electroblotted to PVDF membranes (Millipore, Bedford, MA). Membranes were blocked with 5% nonfat milk and probed with primary antibodies (diluted at 1:1000) for HMGB1, PI3K, p-PI3K, PDK1, p-PDK1, p-PKC, p-PKC$\alpha$, p-PKC$\beta$I, p-PKC$\beta$II, p-PKC$\gamma$, $\beta$-actin, and histone H3.1 at 4 °C overnight. After three washings with PBS (0.1% Tween 20), the membranes were incubated with AP-labeled secondary antibody. Finally, membranes were stained for 10 min with BCIP/NBT. The relative band intensity was analyzed by a software Quantity


dx.doi.org/10.1021/jf504527r | J. Agric. Food Chem. 2014, 62, 11949−11956

One v4.62 (Bio-Rad, Inc., Berkeley, CA, USA) to quantify the protein levels.

**Co-immunoprecipitation.** Kupffer cells were pretreated with the indicated concentrations of DMC for 2 h before LPS treatment for 60 min. The nuclear extracts were harvested as described above. Nuclear extract (500 $\mu$g) was incubated with antiphosphoserine and anti-PKC onto protein G-Sepharose beads at 4 °C overnight. After three washings with lysis buffer and PBS, the precipitated complexes were solubilized by boiling in SDS buffer. Western blotting was performed using anti-HMGB1 antibody.

**Molecular Docking Calculations.** The crystal structures of the HMGB1 (entry 2GZK[45]) and the B box (entry 1hmf[46]) were from the RCSB Protein Data Bank. The three-dimensional structure of DMC was downloaded from the National Centre for Biotechnology Information PubChem. The interaction between B box and DMC was evaluated by AutoDock 4.2 (Scripps Research Institute, La Jolla, CA, USA). The interaction analysis was carried out by using Pymol 0.99 (DeLano Scientific LLC, Portland, OR, USA) and Ligplus v1.4.5 (EMBL-EBI, Cambridge, UK).

**Statistical Analysis.** Data were performed by using one-way ANOVA followed by Duncan's test. The results were expressed as the mean ± SD. Statistical difference of $P < 0.05$ was considered significant.

## RESULTS

**DMC Inhibits HMGB1 Secretion from Activated Liver Macrophage.** In our previous study, we have demonstrated that DMC had a potential hepatoprotective effect through preventing acute liver injury in mice.[20] In this work, to exclude cells' necrotic release of HMGB1, cytotoxic concentrations of DMC with LPS were evaluated by CCK-8 assay. As shown in Figure 1B, the indicated concentrations of DMC did not show cytotoxic effect, demonstrating that the release of HMGB1 was mostly from the active pathway. As shown in Figure 1C, LPS alone significantly ($P < 0.001$) stimulated HMGB1 release. DMC could dose-dependently reduce LPS-stimulated HMGB1 release. Pretreatment with DMC (5 $\mu$M) could be comparable to positive control group treated with GL (100 $\mu$M). The maximum inhibition was achieved at the DMC concentration of 10 $\mu$M ($P < 0.01$). In addition, treatment with DMC significantly ($P < 0.05$) inhibited the expression of HMGB1 mRNA (Figure 1D), the results were consistent with the changes of HMGB1 levels in the supernatant. These results demonstrated that the potential hepatoprotective effect of DMC might be related to the inhibition of HMGB1 release.

**DMC Inhibits LPS-Stimulated HMGB1 Release through Blocking Its Nucleocytoplasmic Translocation.** During normal conditions, HMGB1 was mainly distributed in the nuclear. LPS could visibly trigger the nucleocytoplasmic translocation of HMGB1 (Figure 2A). DMC could markedly inhibit HMGB1 nucleocytoplasmic translocation. Pretreatment of DMC (10 $\mu$M) almost completely blocked HMGB1 cytoplasmic translocation. To further investigate the above observations, cytoplasmic and nuclear fractions were respectively isolated and immunoblotted with mAb specific for HMGB1. The results of Western blot assay showed the ratio of nuclear (Figure 2B) to cytoplasm (Figure 2C) for HMGB1 protein expression levels. Pretreatment with DMC could not only significantly ($P < 0.05$) accumulate HMGB1 in cell nuclei but also markedly ($P < 0.05$) decrease HMGB1 in the cytoplasm. These data indicated that DMC could suppress HMGB1 nucleocytoplasmic translocation.

**DMC Modulates LPS-Elevated PI3K-PDK1-PKC$\alpha$ Signaling.** As shown in Figure 3A, LPS stimulation evoked obvious phosphorylation of PI3K ($P < 0.001$). Pretreatment

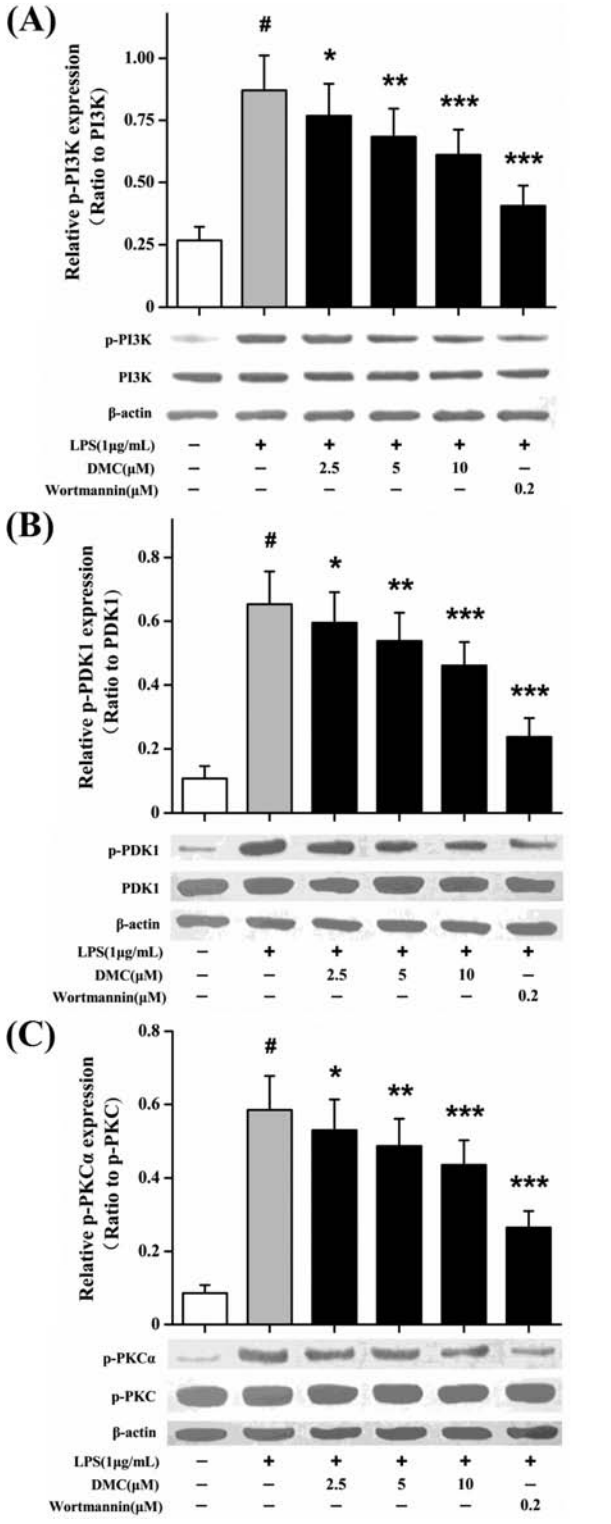


**Figure 3.** Effects of DMC on activation of the PI3K-PDK1-PKC$\alpha$ pathway in LPS-stimulated Kupffer cells. Kupffer cells were pretreated with or without the indicated concentrations of DMC for 2 h before LPS (1 $\mu$g/mL) treatment for 60 min. Phospho-PI3K (A), PDK1 (B), and PKC$\alpha$ (C) levels were measured by Western blotting. PI3K inhibitor wortmannin was used as a control. The bar graph showing semiquantitative densitometric analysis summarizes the fold change of total PI3K, PDK1, and p-PKC expression in each group. Each value represents the mean ± SD of triplicate experiments. (#) $P < 0.001$ as compared with control group; (*) $P < 0.05$, (**) $P < 0.01$, and (***) $P < 0.001$ as compared with the LPS-stimulated group only.

with DMC decreased dose-dependently the LPS-stimulated PI3K phosphorylation. Maximum inhibition was achieved at the DMC concentration of 10 $\mu$M ($P < 0.001$). To further explore the effect of DMC on PI3K-related pathway, we investigated the influence of DMC on PDK1 phosphorylation. Consistently, PDK1 phosphorylation was significantly ($P < 0.05$) inhibited by DMC in LPS-stimulated cells in a dose-dependent manner, and maximum inhibition was achieved at the DMC concentration of 10 $\mu$M ($P < 0.001$) (Figure 3B). It was interesting to note that DMC could dose-dependently reduce the LPS-stimulated phosphorylation of PKC$\alpha$ ($P < 0.001$) (Figure 3C), but not of p-PKC$\beta$I, p-PKC$\beta$II, and p-PKC$\gamma$ (data not shown). These results demonstrated that DMC could modulate the PI3K-PDK1-PKC$\alpha$ signaling pathway, and PKC$\alpha$ played a role in this pathway but had no apparent effect on all conventional PKC (cPKCs: $\alpha$, $\beta$, and $\gamma$).

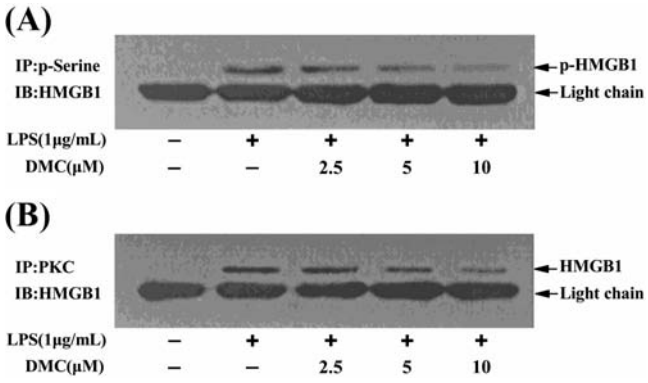


**Figure 4.** Inhibition of HMGB1 phosphorylation by DMC. Kupffer cells were pretreated with or without the indicated concentrations of DMC for 2 h before LPS (1 $\mu$g/mL) treatment for 60 min. The nuclear extracts were harvested. (A) HMGB1 phosphorylation was measured in LPS-stimulated Kupffer cells through immunoprecipitation-linked immunoblotting. Nuclear extracts were immunoprecipitated with antiphosphoserine antibody and then immunoblotted with anti-HMGB1 antibody. (B) The interaction between HMGB1 and PKC was measured in LPS-stimulated Kupffer cells through immunoprecipitation-linked immunoblotting. Nuclear extracts were immunoprecipitated with anti-PKC antibody, then immunoblotted with anti-HMGB1 antibody.

**DMC Blocks HMGB1 Nucleocytoplasmic Translocation through Suppressing HMGB1 Phosphorylation.** Several papers have suggested that HMGB1 phosphorylation and acetylation play a critical role in its nucleocytoplasmic translocation. During LPS stimulation, HMGB1 phosphorylation and acetylation localize to serine and lysine residues, respectively.[47] Therefore, we further investigated how DMC inhibited HMGB1 secretion. As shown in Figure 4A, various concentrations of DMC treatment markedly suppressed the phosphorylation of HMGB1, but not the acetylation (data not shown). Pretreatment of DMC (10 $\mu$M) almost completely blocked HMGB1 phosphorylation. Furthermore, DMC (10 $\mu$M) markedly inhibited the interaction between PKC and HMGB1 (Figure 4B). These results suggested that DMC directly suppressed HMGB1 phosphorylation through hampering the interaction between PKC and HMGB1.

**Modeling of DMC Interaction with B Box of HMGB1.** The detailed interaction between DMC and HMGB1 was analyzed by molecular modeling tools. Interestingly, the molecular modeling results revealed that the binding site was only localized to the B box of HMGB1. Specifically, this binding site localized to the L-shape fold (Figure 5A), which exhibited van der Waals with the hydrophobic side chains of Ala88, Pro89, Pro92, Pro93, Ala95, Phe96, and Phe97 (Figure 5B). Furthermore, DMC formed four hydrogen bonds with Lys90,

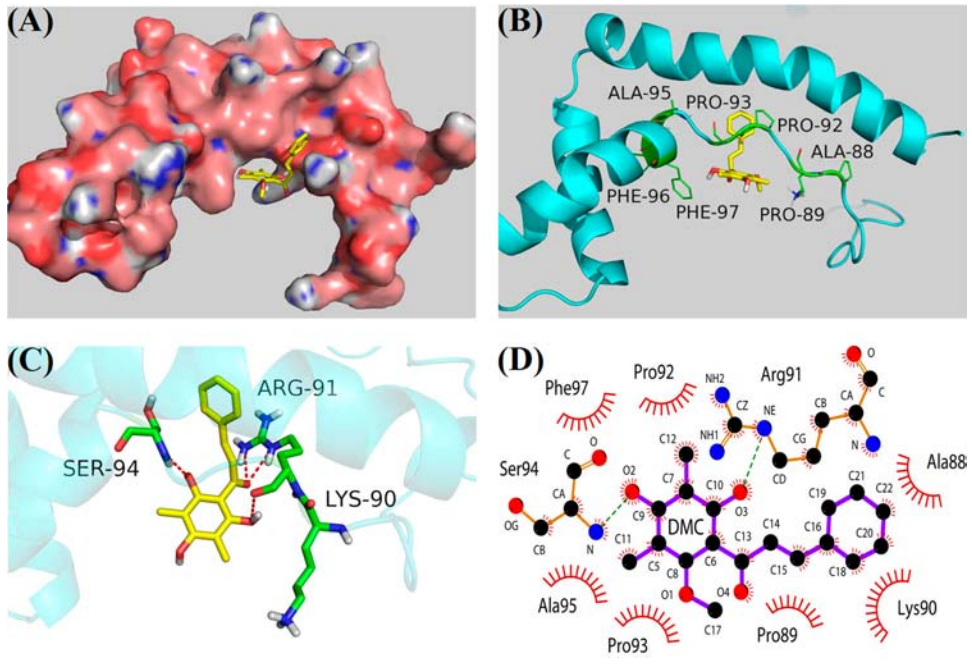


**Figure 5.** Predicted binding modes of DMC in the active site of the B box. (A) DMC was accommodated at the L-shape fold. (B) DMC exhibited favorable van der Waals with the hydrophobic side chains of Ala88, Pro89, Pro92, Pro93, Ala95, Phe96, and Phe97 (green). (C) DMC formed hydrogen bonds with Lys90, Arg91, and Ser94, respectively. The hydrogen bonds are depicted using a red dashed line. Panel D shows the hydrophobic interactions and hydrogen bonds for DMC binding with B box. The residues and DMC involved in hydrophobic interactions are highlighted using spoked arcs and spokes, respectively. The hydrogen bonds are depicted using a green dashed line.


dx.doi.org/10.1021/jf504527r | J. Agric. Food Chem. 2014, 62, 11949−11956

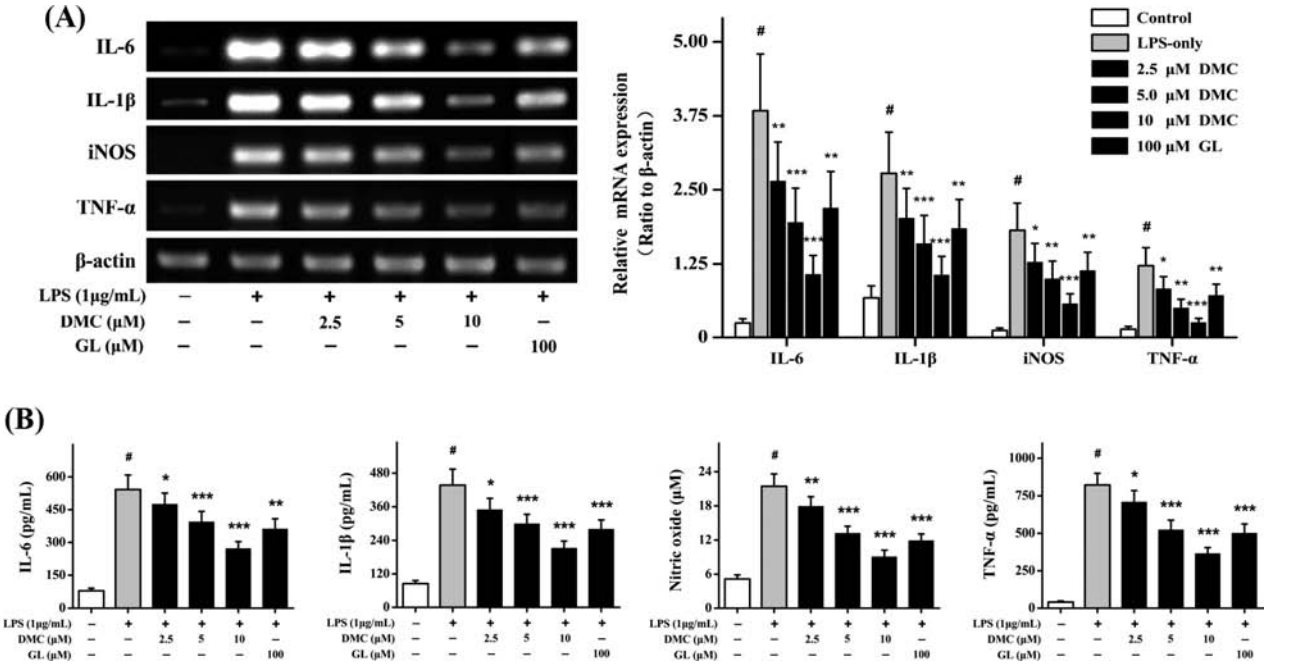


**Figure 6.** Effects of DMC on the expression of HMGB1-dependent inflammatory cytokines in LPS-stimulated Kupffer cells. (A) Representative blots show the effects of DMC with or without LPS treatment on mRNA expression levels of pro-inflammatory IL-6, IL-1$\beta$, iNOS, and TNF-$\alpha$. Similar treatment with GL (100 $\mu$M) was taken as positive control. $\beta$-Actin was used as a loading control. The bar graph showing semiquantitative densitometric analysis summarizes the fold changed of IL-6, IL-1$\beta$, iNOS, and TNF-$\alpha$ expression in each group. (B) DMC dose-dependently decreased the LPS-stimulated IL-6, IL-1$\beta$, NO, and TNF-$\alpha$ release from Kupffer cells. Levels of IL-6, IL-1$\beta$, and TNF-$\alpha$ were measured by ELISA. NO assay was measured by Griess reagent. Each value represents the mean ± SD of triplicate experiments. (#) $P < 0.001$ as compared with control group; (*) $P < 0.05$, (**) $P < 0.01$, and (***) $P < 0.001$ as compared with the LPS-stimulated group only.

Arg91, and Ser94, respectively (Figure 5C). The binding cavity was mainly formed by hydrophobic residues Ala88, Pro89, Lys90, Pro92, Pro93, Ala95, and Phe97 (Figure 5D). From the molecular modeling study, it could be speculated that DMC possessed the direct binding force to the B box of HMGB1.

**DMC Inhibits HMGB1-Dependent Inflammatory Molecule Expression.** The expression of mRNA was measured by RT-PCR. As shown in Figure 6A, LPS stimulation significantly ($P < 0.001$) up-regulated the mRNA expression of iNOS, IL-6, TNF-$\alpha$, and IL-1$\beta$ compared with the negative control group. Various concentrations of DMC treatment significantly ($P < 0.05$) reduced their expression in a dose-dependent manner. Pretreatment with DMC (5 $\mu$M) was found to be comparable to the positive group treated with GL (100 $\mu$M). Maximum inhibition was achieved at the DMC concentration of 10 $\mu$M ($P < 0.001$). Furthermore, DMC significantly decreased the levels of NO, IL-6, TNF-$\alpha$, and IL-1$\beta$ (Figure 6B), and the trends were consistent with the changes of mRNA expression. These data demonstrated that DMC could suppress HMGB1-dependent inflammatory molecule expression.

## DISCUSSION

In our previous study, we have demonstrated that DMC had a potential hepatoprotective effect through preventing acute liver injury in mice and the amelioration of inflammatory cells infiltration in the liver.[20] However, the anti-inflammatory activity of DMC and the underlying molecular mechanisms were still unclear. Thus, we further explored the direct correlation between HMGB1 and DMC and found that DMC suppressed both HMGB1 secretion and its pro-inflammatory activity.

The development of hepatic diseases is usually accompanied by inflammation. Upon inflammatory stimuli, HMGB1 would be rapidly and actively released by Kupffer cells (the resident macrophages of the liver) in response to pro-inflammatory cytokines.[11−14] During hepatic inflammation, activated HMGB1 promoted nucleocytoplasmic translocation. DMC could suppress both HMGB1 molecule expression and its nucleocytoplasmic translocation, suggesting that DMC might act as an inhibitor of HMGB1 secretion.

The underlying molecular mechanisms of how DMC down-regulated the expression of HMGB1 are still unknown. Some papers have suggested that secretion of HMGB1 was associated with the PI3K-PDK1-cPKC signal pathway.[48,49] The results showed that the phosphorylation of PI3K and PDK1 was significantly blocked by DMC. Interestingly, DMC dose-dependently blocked the phosphorylation of PKC$\alpha$, but not of p-PKC$\beta$I, p-PKC$\beta$II, and p-PKC$\gamma$ (data not shown). Therefore, it is possible that DMC could modulate the PI3K-PDK1-PKC$\alpha$ signaling pathway.

It has been reported that the important phosphorylation binding sites on HMGB1 localize to serine residues. In addition, PKC has been reported to be involved in HMGB1 phosphorylation.[47−49] DMC could directly suppress HMGB1 phosphorylation through hampering the interaction between PKC and HMGB1. Furthermore, some researchers have reported that the first 20 amino acid residues of B box are considered a potential pro-inflammatory agent.[15,16] According to molecular modeling results, it is possible that DMC has direct binding force to the B box of HMGB1. The direct binding between DMC and HMGB1 might map to a 10 residue fragment of the full-length protein (HMGB1 residues 88−97), reflecting the important role in blocking HMGB1 pro-inflammatory

activity. It is suggested that DMC could serve as a promising HMGB1 inhibitor.

HMGB1 not only is regarded as an inflammatory mediator but also mediates gene transcription.[11,12] Emerging evidence had suggested that HMGB1 might be an inflammatory inducer or booster in the progression of inflammation.[13,14] The late mediators (such as HMGB1) may promote the expression of early pro-inflammatory cytokines including iNOS, IL-6, TNF-$\alpha$, IL-1$\beta$, and so on.[50] DMC could decrease the production of NO, IL-6, TNF-$\alpha$, and IL-1$\beta$. Therefore, DMC exerts preventive effects on hepatitis through decreasing the production of pro-inflammatory factors.

In conclusion, the present study demonstrates that DMC is a promising HMGB1 inhibitor that exhibits a duplicate role in inhibiting both HMGB1 secretion and its pro-inflammatory activity, mostly related to (1) DMC markedly inhibiting the nucleocytoplasmic translocation and secretion of HMGB1, (2) DMC modulating the PI3K-PDK1-PKC$\alpha$ signaling pathway, (3) DMC hampering the interaction between PKC and HMGB1, (4) DMC possessing direct binding force to the B box of HMGB1, and (5) DMC suppressing HMGB1-dependent inflammatory molecule expression.

## AUTHOR INFORMATION


### Corresponding Authors

*(Y.-H.L.) Mail: State Key Laboratory of Bioreactor Engineering, East China University of Science and Technology, Box 283, 130 Meilong Road, Shanghai 200237, P. R. China. E-mail: luyanhua@ecust.edu.cn. Phone/fax: +86 21 64251185.

*(J.Q.) E-mail: Qianjie116@mail.tongji.edu.cn.



### Funding

This work was supported by the Fundamental Research Funds for the Central Universities (WF1113010) and partially supported by the National High Technology Research and Development Program of China (2013AA092901) and the National Special Fund for State Key Laboratory of Bioreactor Engineering (2060204).


### Notes

The authors declare no competing financial interest.

## ABBREVIATIONS USED

HMGB1, high-mobility group box 1 protein; DMC, 2′,4′-dihydroxy-6′-methoxy-3′,5′-dimethylchalcone; LPS, lipopolysaccharide; PDK1, phosphoinositide-dependent kinase 1; PI3K, phosphatidylinositol 3-kinase; PKC, protein kinase C; IL-6, interleukin 6; TNF-$\alpha$, tumor necrosis factor-alpha; IL-1$\beta$, interleukin 1 beta; iNOS, inducible nitric oxide synthase; GL, glycyrrhizin

## REFERENCES


(1) Herkel, J.; Schuchmann, M.; Tiegs, G.; Lohse, A. W. Immune-mediated liver injury. *J. Hepatol.* **2005**, *42*, 920−923.

(2) Adams, D. H.; Ju, C.; Ramaiah, S. K.; Uetrecht, J.; Jaeschke, H. Mechanisms of immune-mediated liver injury. *Toxicol. Sci.* **2010**, *115*, 307−321.

(3) Yang, J. Y.; Li, Y.; Wang, F.; Wu, C. F. Hepatoprotective effects of apple polyphenols on $CCl_4$-induced acute liver damage in mice. *J. Agric. Food Chem.* **2010**, *58*, 6525−6531.

(4) Muriel, P.; Rivera-Espinoza, Y. Beneficial drugs for liver diseases. *J. Appl. Toxicol.* **2008**, *28*, 93−103.

(5) Czura, C. J.; Yang, H.; Amella, C. A.; Tracey, K. J. HMGB1 in the immunology of sepsis (not septic shock) and arthritis. *Adv. Immunol.* **2004**, *84*, 181−200.

(6) Yang, H.; Wang, H. C.; Czura, C. J.; Tracey, K. J. The cytokine activity of HMGB1. *J. Leukocyte Biol.* **2005**, *78*, 1−8.

(7) Zhou, R. R.; Liu, H. B.; Peng, J. P.; Huang, Y.; Li, N.; Xiao, M. F.; Wang, H. C.; Fan, X. G. High mobility group box chromosomal protein 1 in acute-on-chronic liver failure patients and mice with ConA-induced acute liver injury. *Exp. Mol. Pathol.* **2012**, *93*, 213−219.

(8) Watanabe, T.; Kubota, S.; Nagaya, M.; Ozaki, S.; Nagafuchi, H.; Akashi, K.; Taira, Y.; Tsukikawa, S.; Oowada, S.; Nakano, S. The role of HMGB-1 on the development of necrosis during hepatic ischemia and hepatic ischemia/reperfusion injury in mice. *J. Surg. Res.* **2005**, *124*, 59−66.

(9) Gong, Q.; Zhang, H.; Li, J. H.; Duan, L. H.; Zhong, S.; et al. High-mobility group box 1 exacerbates concanavalin A-induced hepatic injury in mice. *J. Mol. Med.* **2010**, *88*, 1289−1298.

(10) Seki, E.; Minicis, S. D.; Osterreicher, C. H.; Kluwe, J.; Osawa, Y.; Brenner, D. A.; Schwabe, R. F. TLR4 enhances TGF-$\beta$ signaling and hepatic fibrosis. *Nat. Med.* **2007**, *13*, 1324−1332.

(11) Gong, G.; Xiang, L.; Yuan, L. B.; Hu, L.; Wu, W.; Cai, L.; Yin, L.; Dong, H. Protective effect of glycyrrhizin, a direct HMGB1 inhibitor, on focal cerebral ischemia/reperfusion-induced inflammation, oxidative stress, and apoptosis in rats. *PLoS One* **2014**, *9*, 89450−89460.

(12) Oozawa, S.; Mori, S.; Kanke, T.; Takahashi, H.; Liu, K. Y.; Tomono, Y.; Asanuma, M.; Miyazaki, I.; Nishibori, M.; Sano, S. Effects of HMGB1 on ischemia-reperfusion injury in the rat heart. *Circ. J.* **2008**, *72*, 1178−1184.

(13) Lakhan, S. E.; Kirchgessner, A.; Hofer, M. Inflammatory mechanisms in ischemic stroke: therapeutic approaches. *J. Transl. Med.* **2009**, *7*, 97−108.

(14) Lotze, M. T.; Tracey, K. J. High-mobility group box 1 protein (HMGB1): nuclear weapon in the immune arsenal. *Nat. Rev. Immunol.* **2005**, *5*, 331−342.

(15) Li, J.; Kokkola, R.; Tabibzadeh, S.; Yang, R.; Ochani, M.; Qiang, X.; Harris, H. E.; Czura, C. J.; Wang, H. C.; Ulloa, L.; Wang, H.; Warren, H. S.; Moldawer, L. L.; Fink, M. P.; Andersson, U.; Tracey, K. J.; Yang, H. Structure basis for the proinflammatory cytokine activity of high mobility group box 1. *Mol. Med.* **2003**, *9*, 37−45.

(16) Du, D.; Yan, J.; Ren, J. H.; Lv, H. N.; Li, Y.; Xu, S.; Wang, Y. D.; Ma, S. G.; Qu, J.; Tang, W. B.; Hu, Z. W.; Yu, S. S. Synthesis, biological evaluation, and molecular modeling of glycyrrhizin derivatives as potent high-mobility group box-1 inhibitors with anti-heart-failure activity in vivo. *J. Med. Chem.* **2013**, *56*, 97−108.

(17) Dung, N. T.; Kim, J. M.; Kang, S. C. Chemical composition, antimicrobial and antioxidant activities of the essential oil and the ethanol extract of *Cleistocalyx operculatus* (Roxb.) Merr and Perry buds. *Food Chem. Toxicol.* **2008**, *46*, 3632−3639.

(18) Mai, T. T.; Yamaguchi, K.; Yamanaka, M.; Lam, N. T.; Otsuka, Y.; Chuyen, N. V. Protective and anticataract effects of the aqueous extract of *Cleistocalyx operculatus* flower buds on $\beta$-cells of streptozotocin-diabetic rats. *J. Agric. Food Chem.* **2010**, *58*, 4162−4168.

(19) Ye, C. L.; Lu, Y. H.; Wei, D. Z. Flavonoids from *Cleistocalyx operculatus*. *Phytochemistry* **2004**, *65*, 445−447.

(20) Yu, W. G.; Qian, J.; Lu, Y. H. Hepatoprotective effects of 2′,4′-dihydroxy-6′-methoxy-3′,5′-dimethylchalcone on $CCl_4$-induced acute liver injury in mice. *J. Agric. Food Chem.* **2011**, *59*, 12821−12829.

(21) Dung, N. T.; Bajpai, V. K.; Yoon, J. I.; Kang, S. C. Anti-inflammatory effects of essential oil isolated from the buds of *Cleistocalyx operculatus* (Roxb.) Merr and Perry. *Food Chem. Toxicol.* **2009**, *47*, 449−453.

(22) Kim, Y. J.; Ko, H.; Park, J. S.; Han, I. H.; Amor, E. C.; Lee, J. W.; Yang, H. O. Dimethyl cardamonin inhibits lipopolysaccharide-induced inflammatory factors through blocking NF-$\kappa$B p65 activation. *Int. Immunopharmacol.* **2010**, *10*, 1127−1134.

(23) Dao, T. T.; Tung, B. T.; Nguyen, P. H.; Thuong, P. T.; Yoo, S. S.; Kim, E. H.; Kim, S. K.; Oh, W. K. C-Methylated flavonoids from *Cleistocalyx operculatus* and their inhibitory effects on novel influenza A (H1N1) neuraminidase. *J. Nat. Prod.* **2010**, *73*, 1636−1642.

(24) Ko, H.; Kim, Y. J.; Amor, E. C.; Lee, J. W.; Kim, H. C.; Kim, H. J.; Yang, H. O. Induction of autophagy by dimethyl cardamonin is

associated with proliferative arrest in human colorectal carcinoma HCT116 and LOVO cells. *J. Cell Biochem.* **2011**, *112*, 2471−2479.
(25) Li, D. D.; Wu, X. Q.; Tang, J.; Wei, X. Y.; Zhu, X. F. ON-III inhibits erbB-2 tyrosine kinase receptor signal pathway and triggers apoptosis through induction of Bim in breast cancer cells. *Cancer Biol. Ther.* **2009**, *8*, 739−743.
(26) Ye, C. L.; Liu, J. W.; Wei, D. Z.; Lu, Y. H.; Qian, F. In vitro anti-tumor activity of 2′,4′-dihydroxy-6′-methoxy-3′,5′-dimethylchalcone against six established human cancer cell lines. *Pharmacol. Res.* **2004**, *50*, 505−510.
(27) Ye, C. L.; Liu, J. W.; Wei, D. Z.; Lu, Y. H.; Qian, F. In vivo antitumor activity by 2′,4′-dihydroxy-6′-methoxy-3′,5′-dimethylchalcone in a solid human carcinoma xenograft model. *Cancer Chemother. Pharmacol.* **2005**, *55*, 447−452.
(28) Ye, C. L.; Liu, Y.; Wei, D. Z. Antioxidant and anticancer activity of 3′-formyl-4′,6′-dihydroxy-2′-methoxy-5′-methylchalcone and (2*S*)-8-formyl-5-hydroxy-7-methoxy-6-methylflavanone. *J. Pharm. Pharmacol.* **2007**, *59*, 553−559.
(29) Ye, C. L.; Qian, F.; Wei, D. Z.; Lu, Y. H.; Liu, J. W. Induction of apoptosis in K562 human leukemia cells by 2′,4′-dihydroxy-6′-methoxy-3′,5′-dimethyl chalcone. *Leukemia Res.* **2005**, *29*, 887−892.
(30) Zhu, X. F.; Xie, B. F.; Zhou, J. M.; Feng, G. K.; Liu, Z. C.; Wei, X. Y.; Zhang, F. X.; Liu, M. F.; Zeng, Y. X. Blockade of vascular endothelial growth factor receptor signal pathway and antitumor activity of ON-III (2′,4′-dihydroxy-6′-methoxy-3′,5′-dimethylchalcone), a component from Chinese herbal medicine. *Mol. Pharmacol.* **2005**, *67*, 1444−1450.
(31) Su, M. Y.; Huang, H. Y.; Li, L.; Lu, Y. H. Protective effects of 2′,4′-dihydroxy-6′-methoxy-3′,5′-dimethylchalcone to PC12 cells against cytotoxicity induced by hydrogen peroxide. *J. Agric. Food Chem.* **2011**, *59*, 521−527.
(32) Min, B. S.; Thu, C. V.; Dat, N. T.; Dang, N. H.; Jang, H. S.; Hung, T. M. Antioxidative flavonoids from *Cleistocalyx operculatus* buds. *Chem. Pharm. Bull.* **2008**, *56*, 1725−1728.
(33) Martinez, A.; Conde, E.; Moure, A.; Dominguez, H.; Estevez, R. J. Protective effect against oxygen reactive species and skin fibroblast stimulation of *Couroupita guianensis* leaf extracts. *Nat. Prod. Res.* **2012**, *26*, 314−322.
(34) Salem, M. M.; Werbovetz, K. A. Antiprotozoal compounds from *Psorothamnus polydenius*. *J. Nat. Prod.* **2005**, *68*, 108−111.
(35) Amor, E. C.; Villasenor, I. M.; Ghayur, M. N.; Gilani, A. H.; Choudhary, M. I. Spasmolytic flavonoids from *Syzygium samarangense* (Blume) Merr. & L.M. Perry. *Z. Naturforsch. C* **2005**, *60*, 67−71.
(36) Ghayur, M. N.; Gilani, A. H.; Khan, A.; Amor, E. C.; Villasenor, I. M.; Choudhary, M. I. Presence of calcium antagonist activity explains the use of *Syzygium samarangense* in diarrhoea. *Phytother. Res.* **2006**, *20*, 49−52.
(37) Hu, Y. C.; Luo, Y. D.; Li, L.; Joshi, M. K.; Lu, Y. H. In vitro investigation of 2′,4′-dihydroxy-6′-methoxy-3′,5′-dimethylchalcone for glycemic control. *J. Agric. Food Chem.* **2012**, *60*, 10683−10688.
(38) Hu, Y. C.; Hao, D. M.; Zhou, L. X.; Zhang, Z.; Huang, N.; Hoptroff, M.; Lu, Y. H. 2′,4′-Dihydroxy-6′-methoxy-3′,5′-dimethylchalcone protects the impaired insulin secretion induced by glucotoxicity in pancreatic $\beta$-cells. *J. Agric. Food Chem.* **2014**, *62*, 1602−1608.
(39) Hu, Y. C.; Zhang, Z.; Shi, W. G.; Mi, T. Y.; Zhou, L. X.; Huang, N.; Hoptroff, M.; Lu, Y. H. 2′,4′-Dihydroxy-6′-methoxy-3′,5′-dimethylchalcone promoted glucose uptake and imposed a paradoxical effect on adipocyte differentiation in 3T3-L1 cells. *J. Agric. Food Chem.* **2014**, *62*, 1898−1904.
(40) Qian, F.; Ye, C. L.; Wei, D. Z.; Lu, Y. H.; Yang, S. L. In vitro and in vivo reversal of cancer cell multidrug resistance by 2′,4′-dihydroxy-6′-methoxy-3′,5′-dimethyl chalcone. *J. Chemother.* **2005**, *17*, 309−314.
(41) Huang, H. Y.; Niu, J. L.; Lu, Y. H. Multidrug resistance reversal effect of DMC derived from buds of *Cleistocalyx operculatus* in human hepatocellular tumor xenograft model. *J. Sci. Food Agric.* **2012**, *92*, 135−140.
(42) Huang, H. Y.; Niu, J. L.; Zhao, L. M.; Lu, Y. H. Reversal effect of 2′,4′-dihydroxy-6′-methoxy-3′,5′-dimethylchalcone on multi-drug resistance in resistant human hepatocellular carcinoma cell line BEL-7402/5-FU. *Phytomedicine* **2011**, *18*, 1086−1092.
(43) Hsieh, W. T.; Tsai, C. T.; Wu, J. B.; Hsiao, H. B.; Yang, L. C.; Lin, W. C. Kinsenoside, a high yielding constituent from *Anoectochilus formosanus*, inhibits carbon tetrachloride induced Kupffer cells mediated liver damage. *J. Ethnopharmacol.* **2011**, *135*, 440−449.
(44) Huang, C. C.; Tung, Y. T.; Cheng, K. C.; Wu, J. H. Phytocompounds from *Vitis kelungensis* stem prevent carbon tetrachloride-induced acute liver injury in mice. *Food Chem.* **2011**, *125*, 726−731.
(45) Stott, K.; Tang, G. S. F.; Lee, K. B.; Thomas, J. O. Structure of a complex of tandem HMG boxes and DNA. *J. Mol. Biol.* **2006**, *360*, 90−104.
(46) Weir, H. M.; Kraulis, P. J.; Hill, C. S.; Raine, A. R.; Laue, E. D.; Thomas, J. O. Structure of the HMG box motif in the B-domain of HMG1. *EMBO J.* **1993**, *12*, 1311−1319.
(47) Oh, Y. J.; Youn, J. H.; Ji, Y.; Lee, S. E.; Lim, K. J.; Choi, J. E.; Shin, J. S. HMGB1 is phosphorylated by classical protein kinase C and is secreted by a calcium- dependent mechanism. *J. Immunol.* **2009**, *182*, 5800−5809.
(48) Youn, J. H.; Shin, J. S. Nucleocytoplasmic shuttling of HMGB1 is regulated by phosphorylation that redirects it toward secretion. *J. Immunol.* **2006**, *177*, 7889−7897.
(49) Zhang, X. H.; Wheeler, D.; Tang, Y.; Guo, L. P.; Shapiro, R. A.; Ribar, T. J.; Means, A. R.; Billiar, T. R.; Angus, D. C.; Rosengart, M. R. Calcium/calmodulin- dependent protein kinase (CaMK) IV mediates nucleocytoplasmic shuttling and release of HMGB1 during lipopolysaccharide stimulation of macrophages. *J. Immunol.* **2008**, *181*, 5015−5023.
(50) Andersson, B. U.; Wang, H.; Palmblad, K.; Aveberger, A. C.; Bloom, O.; Helena, E. H.; Janson, A.; Kokkola, R.; Zhang, M.; Yang, H.; Tracey, K. J. High mobility group 1 protein (HMG-1) stimulates proinflammatory cytokine synthesis in human monocytes. *J. Exp. Med.* **2000**, *192*, 565−570.

extracts enriched in phenolic antioxidants have also been broadly examined. It was reported, for instance, that *Curcuma longa* extract, besides acting as antioxidant, significantly increased anti-inflammatory cytokine IL-4 production and reduced A$\beta$ and tau levels in A$\beta$-overexpressing mice.[13] *Ginkgo biloba* extracts showed significant neuroprotective effects in murine models and improved cognitive function in AD patients.[14] Aqueous garlic extracts showed antiamyloidogenic properties inhibiting A$\beta$ fibril formation and also defibrillating A$\beta$ preformed fibrils.[15] In recent times, we have demonstrated the ability of a phenol-rich extracts from *Laurus nobilis* leaves to promote a dose-dependent regression of the formation of A$\beta$ oligomers in neuronal SH-SY5Y and SK-N-BE(2)C cell lines, pretreated in the previous 24 h with the A$\beta$(25−35) neurotoxic fragment, expounding a promising neuroprotective effect.[16]

In this context, the neuroprotective capability of an alcoholic extract from *Pistacia lentiscus* leaves (P*l*-M) was of interest. *Pistacia lentiscus* L., commonly known as mastic tree or lentisk, is an aromatic bush indigenous to Italy and other Mediterranean and Middle East countries. The plant, belonging to the Anacardiaceae family, is a dioecious species with red flowers and fruits, whose resin (Chios mastic gum), rich in terpene molecules, found extensive use in folk medicine for their antibacterial, antiasthmatic, hepatoprotective, sedative, anti-inflammatory, and antitumor activities.[17] *Pistacia lentiscus* essential oil was showed to exert beneficial effect in cerebral hyperfusion/reperfusion for preventing early neuroinflammatory events. The chemical composition of alcoholic *Pistacia lentiscus* leaf extracts was also investigated.[18,19] In particular, a comprehensive characterization of a methanol extract from *P. lentiscus* leaves, collected in Algeria, was recently reported:[20] As geographical and climatic conditions have remarkable influence in the plant phenol production, the LC-ESI-MS/MS analysis of a polyphenol leaf extract (P*l*-M) from *P. lentiscus* plants collected in Southern Italy was carried out. To this purpose, leaves were previously deprived of their apolar constituents through maceration in $CHCl_3$. In order to hypothesize the setting up of an antioxidant preparation with important effects in counteracting invalidating neurodegenerations as Alzheimer's disease, P*l*-M antioxidant and antiamyloidogenic effectiveness was evaluated.

## MATERIALS AND METHODS

**Reagents and Chemicals.** All of the solvents and reagents used for assessing antioxidant screening were purchased from Sigma-Aldrich Chemie (Buchs, Switzerland) except ABTS [2,2′-azinobis(3-ethylbenzothiazolin-6-sulfonic acid)], which was from Roche Diagnostics (Roche Diagnostics, Mannheim, Germany). Cell culture media and reagents for cytotoxicity testing were purchased from Invitrogen (Paisley, U.K.), MTT [3-(4,5-dimethyl-2-thiazolyl)-2,5-diphenyl-2H-tetrazolium bromide], SRB (sulforhodamine B), INT [(2-(4-iodophenyl)-3-(4-nitrophenyl)-5-phenyl-2H-tetrazolium chloride)], A$\beta$ 25−35 fragment, phenazine methosulfate, and lactic acid were from Sigma-Aldrich Chemie.

**Plant Collection and Fractionation.** Leaves from *Pistacia lentiscus* L. collected in May 2011 in Caserta (Italy) were identified by Dr. Assunta Esposito of the Second University of Naples. A voucher specimen has been deposited at the Herbarium of the Department of Environmental, Biological, and Pharmaceutical Sciences and Technologies of the Second University of Naples. These were dried in a thermo-ventilated oven at 40 °C for 7 days, powdered in a mill and extracted by sonication (Dr. Hielscher UP 200S) for 1 h, using $CHCl_3$ as extracting solvent. Then, the samples were centrifuged at 2044*g* for 10 min in a Beckman GS-15R centrifuge (Beckman Coulter, Milano, Italy) fitted with rotor S4180. The deterpenated and dried plant material underwent four sonication cycles (each sonication cycle was 40 min) using MeOH as extracting solvent. The supernatant was dried under vacuum to yield a crude extract (24.4 g, P*l*-M).

**RP-HPLC-ESI-MS/MS Analyses.** The chromatographic analyses were carried out using an HPLC Agilent 1200 system (Agilent Technologies Inc., Palo Alto, CA, U.S.A.), provided of binary pump, *microvacuum* degasser, and autosampler. The chromatographic separation was carried using the reverse phase column (Luna $C_{18}$, 5.0 $\mu$m, 250 × 4.6 mm id, Phenomenex) and as a mobile phase a mixture of A ($H_2O/CH_3COOH$, 975:25) and B (MeOH). The following gradient was applied: a linear gradient from 5% to 40% of B in 10 min, a linear gradient from 40% to 51% of B in 20 min, a linear gradient from 51% to 68% of B in 4 min, a linear gradient from 68% to 95% of B in 3 min, a linear gradient from 95% to 100% of B in 4 min, an isocratic elution for 5 min at 100% of B and a last linear gradient from 100% to 5% of B in 5 min. The flow was set at 0.4 mL/min. The P*l*-M injection volume (1.0 mg/mL) was of 10 $\mu$L. The LC system was coupled to the mass spectrometer API QTRAP 2000 (Applied Biosystem). The ESI mass spectra were recorded in negative mode. The HPLC eluates *full scan* MS mass spectra were acquired in the mass range 50−1000 *m*/*z* in *electrospray* mode with negative ions $[M-H]^-$. In order to obtain more structural information, MS/MS experiments (mass range: 20-value *m*/*z* of the parental ion) were performed.

**Assessment of the Antiradical Capacity.** Three methods were used to assess the ability of the extract of being *chain breaker*, which means free radicals' inactivating. MeOH extract, previously dissolved in DMSO as stock solutions of 125.0 mg/mL, was evaluated at different concentration levels (DMSO final concentration was equal to 0.1% (v/v)). Tests were carried out performing three replicate measurements for three samples ($n$ = 3) of the extract (in total, 3 × 3 measurements). Recorded activities were compared to a blank. Results are the mean ± SD values. Student *t*-test was applied in order to determine statistical significance (significance level was set at $P < 0.05$).[21,22]

**Determination of 2,2-Diphenyl-1-picrylhydrazyl (DPPH) Radical Scavenging Capacity.** In order to estimate the DPPH$^\bullet$ (2,2-diphenyl-1-picrylhydrazyl) scavenging capability, *P. lentiscus* leaf extract (2.5, 5.0, 10.0, 25.0, 50.0, and 100.0 $\mu$g/mL, final concentration levels) was dissolved in a DPPH$^\bullet$ methanol solution ($9.4 \times 10^{-5}$ M; 1.0 mL) at room temperature. After 10 min, when the reaction has gone to completion, the absorption at 515 nm was measured by a Shimadzu UV-1700 spectrophotometer in reference to a blank. The results were expressed in terms of the percentage decrease of the initial DPPH$^\bullet$ radical absorption by the test samples.

**Determination of ABTS$^{\bullet+}$ Scavenging Capacity.** The determination of ABTS$^{\bullet+}$ ([2,2′-azinobis(3-ethylbenzothiazolin-6-sulfonic acid)] radical cation) solution scavenging capacity was estimated as previously reported. ABTS radical cation was generated by reacting ABTS (7.0 mM) and $K_2S_2O_8$ (2.45 mM). The mixture was allowed to stand in the dark at room temperature for 12h. Thus, the ABTS$^{\bullet+}$ solution was diluted with PBS (pH 7.4) in order to reach an absorbance of 0.70 at 734 nm. P*l*-M extract (2.5, 5.0, 10.0, 25.0, 50.0, and 100.0 $\mu$g/mL, final concentration levels) was dissolved in 1.0 mL of diluted ABTS$^{\bullet+}$ solution. After 6 min of incubation, the absorption at 734 nm was measured by a Shimadzu UV-1700 spectrophotometer in reference to a blank. The results were expressed in terms of the percentage decrease of the initial ABTS$^{\bullet+}$ absorption by the test samples.

**Determination of Oxygen Radical Absorbance Capacity (ORAC).** The ORAC assay was performed as follows: P*l*-M extract (20 $\mu$L; 1.0, 2.5, and 5.0 $\mu$g/mL, final concentration levels) and fluorescein (FL, 120.0 $\mu$L; 70 nM, final concentration) were preincubated for 15 min at 37 °C in 75 mM phosphate buffer (pH 7.4). Then 2,2′-azobis(2-amidinopropane)-dihydrochloride (AAPH) solution (60.0 $\mu$L; 12 mM, final concentration) was rapidly added. In parallel with the test samples, a blank (FL + AAPH) and solutions of the reference antioxidant Trolox (1−8 $\mu$M, final concentration levels) were properly prepared in PBS. The fluorescence decay ($\lambda_{ex}$ = 485 nm, $\lambda_{em}$ = 525 nm) was recorded every minute for 120 min using a Tecan

**Table 1. Main Constituents of the Alcoholic Extract from *Pistacia lentiscus* L. Leaves Detected by LC-ESI-MS/MS in Negative Ionization Mode**

| peak no. | compd. assignment | $t_R$ [min] | MW [Da] | $[M-H]^-$ | MS/MS fragment ions [$m/z$] |
|---|---|---|---|---|---|
| 1 | shikimic acid | 11.40 | 174 | 173 | 155, 137, 111, 93 |
| 2 | quinic acid | 12.17 | 192 | 191 | 173, 151, 127, 111, 93, 85 |
| 3 | galloylhexose I | 13.30 | 332 | 331 | 271, 169, 125 |
| 4 | galloylhexose II | 13.78 | 332 | 331 | 271, 169 |
| 5 | galloylhexose III | 14.40 | 332 | 331 | 271, 211, 193, 169 |
| 6 | prodelphinidin B-4 | 14.65 | 610 | 609 | 441, 423, 305 |
| 7 | galloylhexose IV | 15.15 | 332 | 331 | 271, 223, 211, 169 |
| 8 | galloylhexose V | 15.58 | 332 | 331 | 313, 271, 241, 211, 169, 161 |
| 9 | gentisic acid hexoside | 16.29 | 316 | 315 | 255, 225, 195, 153 |
| 10 | (epi)gallocatechin | 17.50 | 306 | 305 | 261, 179, 137, 125 |
| 11 | (epi)catechin Gallate | 18.50 | 442 | 441 | 331, 169 |
| 12 | 1-*O*-galloyl-quinic acid | 19.36 | 344 | 343 | 325, 191, 169 |
| 13 | 3-*O*-galloyl-quinic acid | 19.50 | 344 | 343 | 191, 169 |
| 14 | 5-*O*-galloyl-quinic acid | 19.64 | 344 | 343 | 191, 169 |
| 15 | (epi)catechin | 20.20 | 290 | 289 | 245, 203, 179 |
| 16 | 4-*O*-galloyl-quinic acid | 20.85 | 344 | 343 | 191, 169 |
| 17 | *p*-coumaroyl hexose | 21.46 | 326 | 325 | 265, 231, 187, 163, 145, 137, 119 |
| 18 | gallocatechin gallate | 21.53 | 458 | 457 | 375, 331, 305, 287, 217, 179, 169, 161, 125 |
| 19 | ampelopsin *O*-hexoside | 21.90 | 482 | 481 | 463, 355, 319, 283, 193 |
| 20 | digalloyl quinic acid I | 23.31 | 496 | 495 | 435, 413, 343, 191, 169 |
| 21 | digalloyl quinic acid II | 23.50 | 496 | 495 | 343, 191, 169 |
| 22 | digalloyl quinic acid III | 24.81 | 496 | 495 | 343, 325, 191, 169 |
| 23 | digalloyl quinic acid IV | 24.95 | 496 | 495 | 343, 191, 169, 113 |
| 24 | trigalloyl quinic acid | 27.00 | 648 | 647 | 495, 343 |
| 25 | glabrol | 27.95 | 392 | 391 | 331, 309, 161 |
| 26 | taxifolin *O*-hexoside | 28.17 | 466 | 465 | 405, 303 |
| 27 | methyl digallate | 29.62 | 336 | 335 | 275, 253, 183 |
| 28 | myricetin *O*-rutinose | 31.95 | 626 | 625 | 479, 316 |
| 29 | myricetin *O*-hexoside I | 32.02 | 480 | 479 | 419, 316, 299 |
| 30 | myricetin *O*-hexoside II | 32.16 | 480 | 479 | 316, 299 |
| 31 | eriodictyol *O*-hexoside | 34.71 | 450 | 449 | 389, 367, 287, 217, 151 |
| 32 | myricetin *O*-deoxyhexoside | 35.49 | 464 | 463 | 381, 316, 299, 217, 179 |
| 33 | kaempferol (or Luteolin) *O*-hexoside | 35.56 | 448 | 447 | 387, 285,227, 193, 170 |
| 34 | rutin | 37.55 | 610 | 609 | 301 |
| 35 | quercetin *O*-hexoside I | 37.92 | 464 | 463 | 381, 301, 300, 217 |
| 36 | gentisic acid pentoside | 38.63 | 286 | 285 | 225, 203, 153, 108 |
| 37 | quercetin *O*-hexoside II | 40.29 | 464 | 463 | 316, 301, 300, 217 |
| 38 | myricetin *O*-galloyl-deoxyhexoside I | 40.77 | 616 | 615 | 316 |
| 39 | myricetin *O*-galloyl-deoxyhexoside II | 40.84 | 616 | 615 | 463, 317 |
| 40 | quercetin *O*-galloyl-pentoside I | 41.35 | 586 | 585 | 525, 301 |
| 41 | quercetin *O*-galloyl-pentoside II | 41.50 | 586 | 585 | 525, 301, 179 |
| 42 | myricetin *O*-galloyl-deoxyhexoside III | 41.82 | 616 | 615 | 463, 317 |
| 43 | quercetin *O*-deoxyhexoside | 42.10 | 448 | 447 | 365, 301, 300, 283, 201, 179, 151 |
| 44 | quercetin *O*-galloyl-deoxyhexoside | 43.93 | 600 | 599 | 539, 447, 301 |
| 45 | kaempferol (or luteolin) *O*-hexoside | 44.07 | 448 | 447 | 415, 365, 285, 201 |
| 46 | kaempferol (or luteolin) *O*-deoxyhexoside | 44.82 | 432 | 431 | 371, 285, 284 |

SpectraFluor fluorescence and absorbance reader. Antioxidant curves (fluorescence vs time) were normalized to the curve of the blank. From the normalized curves, the area under the fluorescence decay curve (AUC) was calculated. Linear regression equations between net AUC ($AUC_{antioxidant}-AUC_{blank}$) and antioxidant concentration were calculated for all the samples. The antioxidant activity (ORAC value) was calculated by using the Trolox calibration curve. The ORAC values were expressed as Trolox equivalents ($\mu$M).

**Cytotoxicity Assessment.** Cytotoxicity assays that use different parameters associated with cell death and proliferation were performed. P*l*-M extract was prepared as a stock solutions of 125.0 mg/mL in DMSO and further diluted in cell culture medium to appropriate final dose levels (DMSO final concentration was equal to 0.1% (v/v)). Tests were carried out performing 12 replicate ($n$ = 12) measurements for three samples of each extract (in total: 12 × 3 measurements). Recorded activities were compared to an untreated blank arranged in parallel to the samples. Results are the mean ± SD values. Student $t$-test was applied in order to verify statistical significance (significance level was set at $P < 0.05$).[21,22]

**Cell Cultures.** Rat C6 glioma cell line and human SH-SY5Y neuroblastoma cells were purchased from ATCC (American Type Culture Collection); SK-N-BE(2)-C human bone marrow neuroblastoma cells were purchased from ICLC (Interlab Cell Line Collection) at Istituto Nazionale per la Ricerca sul Cancro, Genoa (Italy). Rat C6 and SH-SY5Y cell lines were grown in DMEM high glucose medium while SK-N-BE(2)-C cell line in RPMI 1640. All the culture media were supplemented with 10% fetal bovine serum, 50.0 U/mL penicillin, and 100.0 $\mu$g/mL streptomycin. The cells were cultured at 37 °C in a humidified atmosphere containing 5% $CO_2$. The cell count, for each assay, was carried out using Countess Automated Cell Counter (Invitrogen).

**MTT Cell Viability Test.** The MTT is a colorimetric assay which values the activity of the mitochondrial dehydrogenase to reduce the tetrazolium ring of 3-(4,5-dimethyl-2-thiazolyl)-2,5-diphenyl-2H-tetrazolium bromide (MTT), yellow colored, generating a chromogenic compound, which is formazan. C6, SH-SY5Y, and SK-N-BE(2)-C cell lines were seeded in 96-multiwell plates at a density of $1.0 \times 10^4$ cells/well. After 24 h of incubation, cells were treated with P*l*-M at five dose levels (2.5, 10.0, 25.0, 50.0, and 100.0 $\mu$g/mL). At 24, 48, and 72 h of incubation, cells were treated with 150 $\mu$L of MTT (0.50 mg/mL), dissolved in the culture medium, for 1 h at 37 °C in a 5% $CO_2$ humidified atmosphere. The MTT solution was then removed and 100 $\mu$L of DMSO were added to dissolve the formazan originated. Finally, the absorbance at 570 nm of each well was determined using a Tecan Spectra Fluor fluorescence and absorbance reader. The results were expressed as percentage of mitochondrial redox activity of the cells treated with the extracts compared to the untreated control.

**SRB Cell Viability Test.** C6, SH-SY5Y, and SK-N-BE(2)-C cell lines were seeded in 96-multiwell plates at a density of $1.0 \times 10^4$ cells/well. After 24 h of incubation, cells were treated with P*l*-M at five dose

levels (2.5, 10.0, 25.0, 50.0, and 100.0 μg/mL). At 24, 48, and 72 h of incubation, cells were fixed with ice-cold TCA (10% w/v, 40 μL) for 1 h at 4 °C. The plates were washed five times in distilled water and allowed to dry. Then, 50 μL of sulforhodamine B (SBR, 0.4% w/v in 1% aqueous *acetic acid*) solution was added to each well of the dried 96-well plates and incubated at room temperature for 30 min. In order to remove unbound dye, the plates were quickly washed with 1% aqueous acetic acid and dried subsequently. The bound SRB was solubilized by adding 100 μL of 10 mM unbuffered Tris Base (pH 10.5) to each well and shaking for 5 min on a shaker platform. Finally, the absorbance at 570 nm of each well was measured using a Tecan SpectraFluor fluorescence and absorbance reader.

**Lactate Dehydrogenase (LDH) Leakage Assay.** The lactate dehydrogenase (LDH) leakage assay is a colorimetric assay for the quantification of cell death and cell lysis based on the measurement of LDH released into the supernatant from the cytosol of damaged cells. The oxidation reaction (LDH oxidizes lactate to pyruvate and converts $NAD^+$ to NADH) catalyzed by this enzyme produces NADH that is reacted in vitro with a tatrazolium salt 2-(4-iodophenyl)-3-(4-nitrophenyl)-5-phenyltetrazolium chloride (INT), yellow colored to generate a formazan salt purple/red colored; this coloration can be measured using a spectrophotometer. C6, SH-SY5Y, and SK-N-BE(2)-C cell lines were seeded in 24-multiwell plates at a density of $4.0 \times 10^4$ cells/well. Twenty-four hours after seeding, the cells were treated P*l*-M extract (100.0 μg/mL). After the exposure times of 24 h, 48 h, and 72 h, the supernatant (100 μL) was treated with 100 μL of the reaction mixture (0.7 mM INT; 54.0 mM lactic acid; 0.3 mM phenazine methosulfate; 0.8 mM $NAD^+$ in 0.2 M Tris-HCl pH 8.0) in a 96-wells plate. The reaction was carried out for 45 min in the dark under gentle stirring at 37 °C and stopped by addition of 1 M HCl (50 μL). The absorbance was red at 492 nm by a Tecan SpectraFluor fluorescence and absorbance reader. Data obtained were expressed in reference to a blank prepared using a Triton X-100 (1%) solution. The increase in the amount of formazan detected in culture supernatant reflects the membrane integrity and directly correlates to the increase in the number of lysed cells. Hence, cell vitality is inversely proportional to the LDH released.

**Determination of Cytoprotective Effect in Oxidized Cell Systems.** SK-N-BE(2)-C cell line was seeded in 96-multiwell plates at a density of $1.0 \times 10^4$ cells/well. After 24 h of incubation, cells were cotreated with P*l*-M extract (25.0, 50.0, and 100.0 μg/mL, final concentration levels) and $H_2O_2$ (400 μM) or A$\beta$(25−35) peptide domain (100 μM) for 24 h. After the treatment period, cell viability inhibition (CV) was assessed by MTT assay.[16]

## RESULTS AND DISCUSSION

The diverse array of bioactive nutrients present in plant natural products plays a pivotal role in prevention and cure of various neurodegenerative diseases, such as Alzheimer's disease (AD). Accumulated evidence suggests that naturally occurring phytocompounds, such as polyphenolic antioxidants may potentially hinder neurodegeneration, and improve memory and cognitive function.[23]

In order to investigate the neuroprotective potential of Mediterranean medicinal plants, *Pistacia lentiscus* was of interest. Leaf plant drug was analyzed for its antioxidant and cytoprotective effectiveness, whereas its chemical composition was characterized by means of a LC-MS/MS approach.

**LC-MS/MS Metabolic Profiling of the Alcoholic Extract from *Pistacia lentiscus* L. Leaves.** LC-ESI-MS/MS techniques allowed us to obtain qualitative information about the biochemical constitution of P*l*-M extract. Forty-six main secondary metabolites were tentatively identified by means of LC-MS/MS data (Table 1). Among them ten compounds (**6**, **11**, **17**−**19**, **27**, **31**, **36**, **40**, **41**) were tentatively characterized for the first time in *Pistacia lentiscus* leaves.

Compound **1** was identified on the basis of its mass spectrum, as shikimic acid.[24] A $[M\text{-}H]^-$ pseudomolecular ion at $m/z$ 173 and the corresponding dimeric deprotonated ion $[2M\text{-}H]^-$ a $m/z$ 347 were detectable. The selection of the $[M\text{-}H]^-$ precursor ion and the subsequent dissociation ($MS^2$ experiment) generated a fragment ion at $m/z$ 155, due to the loss of a water molecule, probably including the hydroxyl function at C-5. A second fragment ion at $m/z$ 111 was putatively attributed to the ion $[M\text{-}H\text{-}CO_2\text{-}H_2O]^-$.

Compound **2** was characterized as quinic acid on the basis of its fragmentation pattern. In fact, the collision activated decomposition of the deprotonated molecule at $m/z$ 191, beside the ion at $m/z$ 173 (- $H_2O$), led to the formation of the fragment ion at $m/z$ 127, corresponding to the loss of CO and of two water molecules.[25] Metabolites **12**−**14** and **16** are quinic acid derivatives, and in particular they were identified as galloyl-quinic acid isomers, showing a deprotonated pseudomolecular ion at $m/z$ 343, which in turn generated product ions at $m/z$ 191 and 169, following the neutral loss of a quinic acid residue and a gallic acid moiety, respectively. The discrimination between the four isomers was performed on the basis of their relative retention times and according to the data previously reported.[26] The P*l*-M extract also contained four peaks characterized by a pseudomolecular deprotonated ion at $m/z$ 495 (compounds **20**-**23**). The fragmentation of the $[M\text{−}H]^-$ ion at $m/z$ 495 provided the fragments at $m/z$ 343 ($[M\text{-}H\text{-}152]^-$) and $m/z$ 191 ($[M\text{-}H\text{-}304]^-$) corresponding to the loss of one and two galloyl moieties, respectively. The fragment at $m/z$ 169 was attributed to gallic acid anion. On the basis of these experimental evidence they were identified as isomers of digalloyl quinic acid, recently identified in *P. lentiscus* leaves.[20]

Metabolites **3**−**5**, **7**, **8** exibited the same pseudomolecolar deprotonated ion at $m/z$ 331. On the basis of the data arising from $MS^2$ experiments, compared with those present in literature,[27] the compounds were tentatively identified as hexoside isomers of gallic acid. In fact, the collision activated decomposition of the precursor ions at $m/z$ 331 led to the formation of product ions consistent with this hypothesis, namely the fragment ions at $m/z$ 271 ($[M\text{-}H\text{-}60]^-$), 241 ($[M\text{-}H\text{-}90]^-$), and 211 ($[M\text{-}H\text{-}120]^-$), due to the cross-ring fragmentation of the hexose moiety. Furthermore, the product ion at $m/z$ 169 ($[M\text{-}H\text{-}C_6H_{10}O_5]^-$) could be due to the neutral loss of the hexose residue, and could consequently be ascribed to the deprotonated gallic acid, which in turn lost a 44 Da moiety (likely $CO_2$) to give the ion at $m/z$ 125.

Compound **6** exhibited a pseudomolecular deprotonated ion at $m/z$ 609. The $MS^2$ spectrum showed characteristic fragment ions that allowed us to identify the molecule as the proanthocyanidin prodelphinidin B-4, a dimer of gallocatechin and epigallocathechin.[28] In fact, beside the ion at $m/z$ 305, due to the loss of one monomer ($[M\text{-}H\text{-}304]^-$), the ions at $m/z$ 441 and 423 could be formed following a retro Diels−Alder fragmentation mechanism involving the C ring (cleavage of O1−C2 and C3−C4 bonds) and subsequent water loss.

Metabolite **9**, characterized by a $[M\text{-}H]^-$ pseudomolecular ion at $m/z$ 315, was tentatively identified as gentisic acid hexoside.[20] The product ions deriving from MS/MS experiments were detected at $m/z$ 255, 225, 195, corresponding to cross-ring cleavage of the sugar moiety (−60, −90, and −120 Da, respectively), and at $m/z$ 153, attributable to the deprotonated gentisic acid. The deprotonated compound **36** differed from **9** for 30 mass units, having a $[M\text{-}H]^-$ pseudomolecular ion at $m/z$ 285. Its fragmentation pattern

showed product ions at $m/z$ 225, 203, 153 and 108, consistent with the presence of a pentose instead of hexose. For this reason, it was putatively identified as gentisic acid pentoside.

Compound **15** was characterized by a deprotonated pseudomolecular ion at $m/z$ 289, attributable at least in principle to catechin or epicatechin. The relative intensity of the characteristic fragment ions detected in the fragmentation pattern of this molecule (ions at $m/z$ 245, 203, 179), even if compared with literature,[29] was insufficient to discriminate between the two epimers.

Similarly the metabolite **10** was putatively identified as the flavonol (epi)gallocatechin. Indeed, the mass spectrum showed the peak of the $[M\text{-}H]^-$ ion at $m/z$ 305 and characteristic fragments at $m/z$ 261, 219, 179, and 125. The presence of the fragment at $m/z$ 125 was identifiable in the intact flavonoid A ring.[30] The metabolite **11**, on the basis of data provided by mass spectrometry experiments, was putatively identified as (epi)catechin gallate. The fragmentation of the $[M\text{-}H]^-$ ion at $m/z$ 441 generated two major fragments at $m/z$ 331 and 169. The formation of the former fragment could be due to the loss of the only catechol B ring and introduction of a new unsaturation between carbons C2−C3 of the C ring. The fragment at $m/z$ 169 consisted of gallic acid anion.

The $[M-H]^-$ ion for the metabolite **18** at $m/z$ 457 yielded main fragment ions at $m/z$ 331, 305, and 169. The product ion at $m/z$ 331 was due to the neutral loss of intact B-ring, whereas the ion at $m/z$ 305 consisted of deprotonated epigallocatechin or gallocatechin, formed by the loss of the galloyl moiety (−152 Da). Finally, the ion at $m/z$ 169 corresponded to the gallic acid anion.[31] The abundance of this latter, respect to that at $m/z$ 305, allowed us to unequivocally identify this compound as gallocatechin gallate.[29]

Compound **17** was identified as *p*-coumaroylhexose on the basis of its $MS^2$ spectrum compared with literature.[32] In fact, the deprotonated molecular ion at $m/z$ 325, once fragmented, yielded product ions at $m/z$ 163, likely corresponding to deprotonated *p*-coumaric acid formed after the loss of the hexose residue as 162 Da, and $m/z$ 145 and 119 due to the subsequent loss of a water molecule and $CO_2$, respectively.

The compound **24**, with the $[M\text{-}H]^-$ pseudomolecular ion at $m/z$ 647, was identified as trigalloylquinic acid (e.g., pistafolin A).[33] The fragments at $m/z$ 343 and 495 were reported as successive losses of two molecules of gallic acid.

The fragmentation pattern of the metabolite **25** was in agreement with the presence of glabrol, a molecule that reduces the absorption of cholesterol and modulates the expression of genes involved in lipid metabolism and recently was found in *P. lentiscus* leaves.[20] The pseudomolecular ion at $m/z$ 391 gave rise to the fragments at $m/z$ 331 and 161. The latter, corresponding to a residue of 2-(3-methylbut-2-enyl)phenol, could be formed after the loss of a benzo-$\gamma$-pyrane core that brought an isoprenic chain in C-8.

Metabolite **27** showed a deprotonated pseudomolecular ion at $m/z$ 335 and a characteristic fragment ion at $m/z$ 183, which allowed us to identify it as methyl digallate on the basis of literature data.[27]

It has previously reported that the Anacardiaceae family is characterized by the occurrence of both gallic acid and myricetin derivatives.[34] Our data confirmed these evidence. In fact, beside the gallic acid derivatives discussed above, the alcoholic extract of *P. lentiscus* under study also contained myricetin glycosides (compounds **28**−**30**, **32**). In particular, metabolite **28** was identified as the flavonol myricetin *O*-rutinoside ($[M-H]^-$ at $m/z$ 625). The presence of fragments at $m/z$ 479 and 316 in $MS^2$ spectrum was attributable to the loss of a deoxyhexose moiety $[M-H-146]^-$ and to the aglycone radical myricetin, respectively. The formation of this latter was probably due to the homolytic cleavage of the glycosidic bond. Compounds **29** and **30** were tentatively identified as myricetin *O*-hexoside isomers ($[M-H]^-$ at $m/z$ 479). Also in this case, the formation of the aglycone radical $[Aglicone-H]^{-\bullet}$ was observed. The metabolite **32** was putatively identified as myricetin *O*-deoxyhexoside. In fact, the homolytic cleavage of the $[M-H]^-$ ion at $m/z$ 463 generated the aglycone radical and a glycanic radical (−147 Da) of deoxyhexose nature. Other three myricetin derivatives (**38**, **39**, **42**) were found to be present in P*l*-M extract, characterized by the presence of a galloyl moiety as evidenced by neutral losses of 152 Da, beside a deoxyhexoside residue. They were tentatively identified as myricetin *O*-galloyl-deoxyhexoside isomers.

On the basis of their fragmentation pattern metabolites **34**, **35**, **37**, **43** were identified as quercetin glycosides, which differed for the sugar residue (rutinose, hexose, deoxyhexose). The product ions at 301 and 300 likely corresponded to deprotonated quercetin and quercetin radical, respectively. The two hexoside isomers (**35** and **37**) differed mainly for the relative abundance of these ions, whose ratio suggested the glycosylation position at the C-3 for compound **37**, and C-7 or C-4′ for compound **35**.[35,36] Compounds **40** and **41** were putatively identified as quercetin *O*-galloylpentoside isomers. In fact, following the collision induced dissociation of the deprotonated molecules at $m/z$ 585, the ions at $m/z$ 301 were generated, likely due to the loss of a pentose sugar and a galloyl moiety (132 + 152 Da). Metabolite **44** was characterized as quercitrin gallate, according to MS/MS evidence. In fact, it showed a molecular deprotonated ion at $m/z$ 599, which yielded fragment ions at $m/z$ 447, due to the loss of the galloyl moiety, and $m/z$ 301, likely the deprotonated quercetin arising from the further loss of a deoxyhexoside residue. This compound was recently reported as a component of *P. lentiscus* leaves.[20]

Compounds **19** and **26** were putatively ascribed to glycosylated dihydroflavonols. In particular the $MS^2$ spectrum of metabolite **19**, sharing a $[M\text{-}H]^-$ pseudomolecular ion at $m/z$ 481, showed the product ion at $m/z$ 319 after the loss of a hexose residue (162 Da), likely corresponding to dihydromyricen (ampelopsin), whereas deprotonated compound **26** at $m/z$ 465, once fragmented, gave rise to the ion at $m/z$ 303, likely dihydroquercetin (taxifolin). According to these experimental data, compounds **19** and **26** were tentatively characterized as ampelopsin *O*-hexoside and taxifolin *O*-hexoside, respectively.

Metabolite **31** was putatively identified as a hexoside of the flavanone eriodictyol ($[M-H]^-$ a $m/z$ 449). The fragment ion at $m/z$ 287 ($[M\text{-}H\text{-}C_6H_{10}O_5]^-$) suggested the presence of the flavonone for loss of a six carbon atoms glycidic moiety.[37]

Compounds **33** and **45** were tentatively identified as hexosides of the flavonoid kaempferol and/or luteolin. In fact, they showed the same $[M\text{-}H]^-$ molecular ion at $m/z$ 447, and the same product ion at $m/z$ 285, formed after the loss of a hexose residue (−162 Da). Unfortunately mass spectrometric data did not allow us to discriminate between the two aglycone isomers. For the same reason metabolite **46** was putatively identified as kaempferol-3-*O*-deoxyhexoside or luteolin-3-*O*-deoxyhexoside. The $MS^2$ spectrum of the deprotonated molecular ion at $m/z$ 431 provided a base peak at $m/z$ 285,

which allowed us to hypothesize the presence of kaempferol/luteolin as aglycone, and a deoxyhexosyl glyconic moiety (−146 Da).

**Antioxidant and Cytoprotective Capabilities of Pl-M Extract.** The antiradical properties of Pl-M extract were evaluated through three methods, useful to define the capability of the investigated plant complex to act as a source of secondary antioxidants (*chain breaker*), which are chemical species able to inactivate dangerous free radicals transferring them an hydrogen atom and/or a single electron (Figure 1).

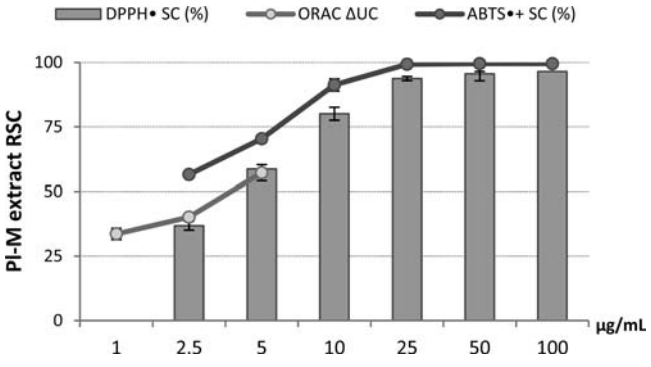


**Figure 1.** Radical scavenging capacity (RSC, %) of *P. lentiscus* investigated extract toward DPPH radical, $ABTS^{+}$ radical, and $ROO^{\bullet}$ radicals. These latter are reported as the mean of ΔAUC values from ORAC assay. Values, reported as percentage vs a blank, are the mean ± SD of measurements carried out on 3 samples ($n$ = 3) analyzed three times.

The extract showed an efficacious reducing power the target radical species $ABTS^{\bullet+}$ and $DPPH^{\bullet}$. In fact, 0.6 µg/mL Pl-M dose level was able to reduce $ABTS^{\bullet+}$ by 50%, whereas a dose equal to 2.9 µg/mL was required to scavenge the same percentage of DPPH radical. The scavenging effectiveness appeared to be strongly dependent on the dose tested. In particular, it was observed that the complete conversion of the radical cation ABTS in its reduced form was realized when the probe was exposed to an extract dose equal to 25.0 µg/mL. The massive antiradical activity was confirmed by ORAC data. The high sensitivity of the ORAC method required, in order to obtain useful information, the use of extract doses lower than those adopted in the colorimetric tests (1.0, 2.5, and 5.0 µg/mL). The values of ΔAUC (area under the curve) shown in Figure 1 and ORAC values, reported as equivalents of Trolox, a water-soluble analogue of vitamin E commonly used as a standard positive, highlighted the antiradical effectiveness of the extract capable to exercise at a dose of 1.0 µg/mL an activity comparable to that exerted by 3.1 µg/mL of Trolox.

The evaluation of the cytotoxic effects of the extract through MTT and SRB assays that it exerted only an mild cell viability inhibition (Figure 2A, B). In particular, it was observed that the extract influenced in a time dependent manner the proliferation of murine cell line, whereas both the human neuroblastoma cell lines showed a similar cytotoxic behavior at all the three exposure times. SK-N-BE(2)-C cell line appeared to be less sensitive to the addition of toxic. In fact, an inhibition of cell viability of approximately 10% was detected when SK-N-BE(2)-C cells were treated with the extract highest tested dose (100 µg/mL). Data obtained emphasize that Pl-M complex did not adversely influence the growth and proliferation of tested cell lines opening a favorable scenario for an its likely therapeutic application.

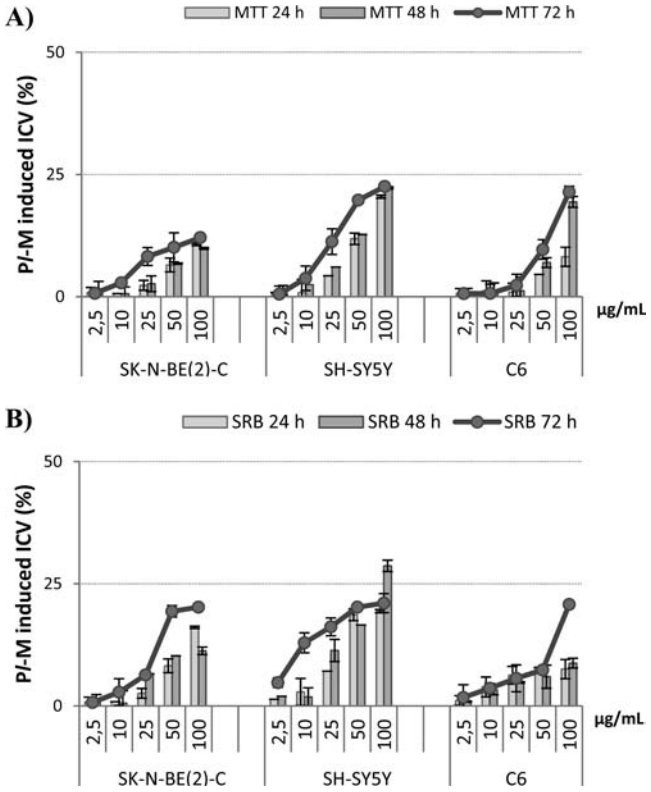


**Figure 2.** Pl-M cell viability inhibition (CVI, %) toward SK-N-BE(2)-C, SH-SY5Y, and C6 cell lines at 24, 48, and 72 h exposure times by means of (A) MTT test results, (B) SRB test results. Values, reported as percentage vs an untreated control, are the mean ± SD of measurements carried out on 3 samples ($n$ = 3) analyzed 12 times.

In order to further explore the Pl-M toxic effects, lactate dehydrogenase (LDH) release was also investigated. The test (Figure 3) was performed toward the three cell lines using the single dose of 100.0 µg/mL. Detected data allowed us to state that the extract did not affect LDH release.

The evaluation of the plant extract effect on $H_2O_2$-induced oxidative stress in SK-N-BE(2)-C cells was tested. Co-treatment with 25.0, and 50.0 µg/mL Pl-M extract showed viability values slightly lower than those elicited by $H_2O_2$-treated group (Figure 4A). Only the cells treated with Pl-M

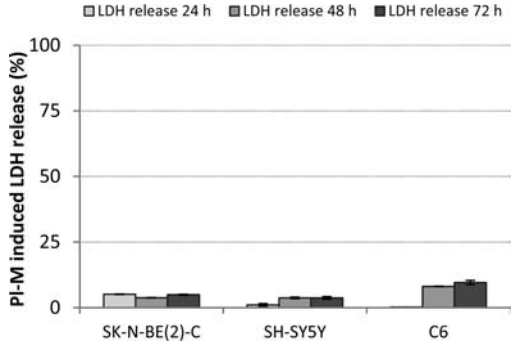


**Figure 3.** Pl-M induced LDH release (±SD) vs SK-N-BE(2)-C, SH-SY5Y, and C6 cell lines. The evaluation of LDH release was carried out treating cells with 100.0 µg/mL extract dose at 24, 48, and 72 h exposure times. Values, reported as percentage vs an untreated control, are the mean ± SD of measurements carried out on 3 samples ($n$ = 3) analyzed 12 times.

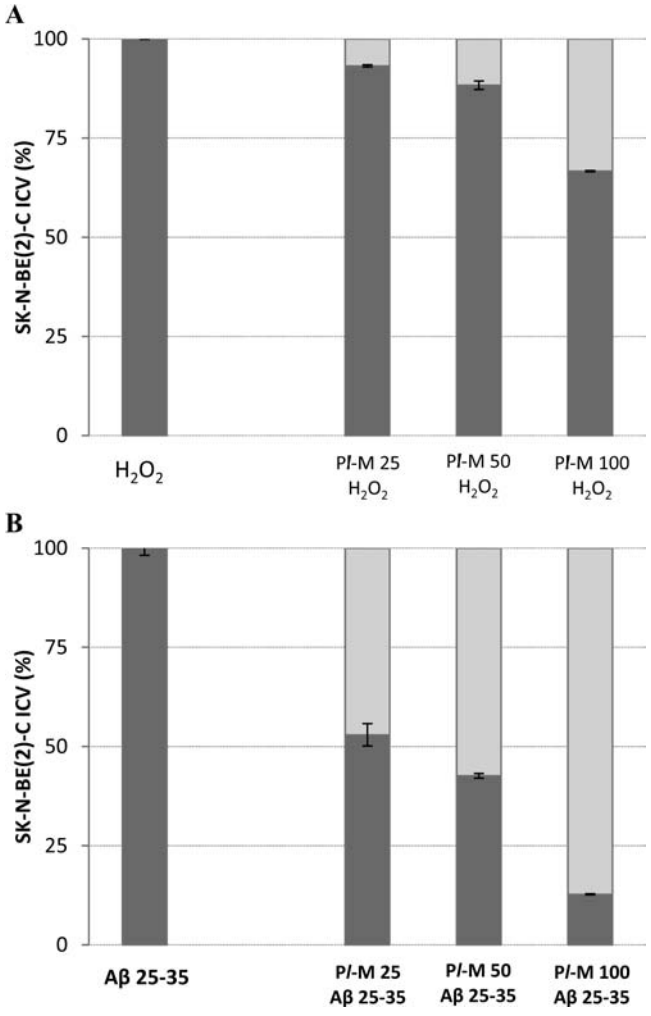


**Figure 4.** Cell viability inhibition (CVI, %) toward SK-N-BE(2)-C cell line cotreated with P*l*-M extract and (A) $H_2O_2$ (400 $\mu$M) or (B) A$\beta$(25−35) fragment (100 $\mu$M) at 24 h exposure time by means of MTT test results. Values, reported as percentage vs. an untreated control, are the mean ± SD of measurements carried out on 3 samples ($n$ = 3) analyzed 12 times.

100.0 $\mu$g/mL dose level presented a high and significant value of cell viability compared to $H_2O_2$-treated group. In order to determine the possible beneficial effect of the extract against the phenomena of oxidative stress induced by amyloid plaques in Alzheimer's dementia, its antioxidant capacity in a system utilizing the functional domain of the $\beta$-amyloid peptide, A$\beta$(25−35), as oxidizing agent, was tested. As the cellular reduction of MTT represents a specific indicator of the initial events underlying the mechanism of $\beta$-amyloid peptide toxicity,[38,39] MTT test was first carried out exposing the three cell lines at increasing concentrations of A$\beta$(25−35) fragment (12.5, 25.0, 50.0, and 100.0 $\mu$M). A$\beta$(25−35) fragment was found to induce cytotoxicity in SK-N-BE-(2)-C cell line. The results of the MTT test carried out after exposure of SK-N-BE-(2)-C cell line to A$\beta$ 25−35 increasing concentrations (12.5, 25.0, 50.0, and 100.0 $\mu$M) allowed us to identify the domain concentration to which it induced the highest cell viability inhibition. The effects of cotreatment of the cell line for 24 h with A$\beta$ 25−35 100.0 $\mu$M and increasing extract dose levels (25.0, 50.0, and 100.0 $\mu$g/mL) were assessed through MTT test (Figure 4B). P*l*-M extract was able to reduce by nearly 50%, the A$\beta$ 25−35-induced toxicity at the lowest dose level tested. A marked neuroprotective effect was observed when P*l*-M 100.0 $\mu$g/mL dose level was screened. In fact, the results underlined the high antioxidant capacity of this P*l*-M dose level able to counteract almost completely the cytotoxic action of the oxidant.

There is ample scientific and empirical evidence supporting the use of plant-derived antioxidants for the control of neurodegenerative disorders. Antioxidants may have neuroprotective (preventing apoptosis) and neuroregenerative roles, by reducing or reversing cellular damage and by slowing progression of neuronal cell loss.

Dementia pathologies such as Alzheimer's disease (AD) are reaching epidemic proportions, yet they are not successfully managed by effective symptomatic treatments.[40] Since two of the currently licensed drugs for AD are based on natural products (galantamine and rivastigmine), different plants are now being investigated as a potential source of new therapy for AD.[41,42] Furthermore, different studies have revealed that natural polyphenols can reduce A$\beta$ neurotoxicity[43,44] possibly via an antioxidative mechanism and inhibition of A$\beta$ oligomerization.[45] The A$\beta$ lowering properties of these substance could be mainly mediated via their effect on NF-$\kappa$B signaling which in turn could affect the regulation of BACE-1 expression.

A significant inverse association between phenolics intake and dementia risk, was found.[46] In neuronal cell cultures, it was observed that EGCG was able to regulate the proteolytic processing of APP (amyloid precursor protein) and to reduce A$\beta$ generation.[47] The molecular mechanism involved in the neuroprotection effect of EGCG could also due to its ability to decrease the expression of pro-apoptotic genes.[48] Upon their antioxidant properties, phenol compounds as chlorogenic acid, gallic acid, and quinic acid, together with various flavonoids, were reported to be potential inhibitors of acetylcholinesterase. Thus, the use of these substances could be used to counteract the AD deficiency in acetylcholine production.[49] Furthermore, previous bioavailability studies allow us to encourage the use of *Pistacia lentiscus* leaf alcoholic extract as an alternative source for the preparation of functional food enriched in flavan-3-ols and galloyl esters. Indeed, although absorption, distribution, metabolism, and excretion (ADME) studies highlighted that polyphenols bioavailability varies widely from one compound to another, as it is influenced by their chemical structure and molecular weight,[50] positive data are available on molecules identified in Pl-M extract. An acute feeding study, through HPLC-$MS^3$ analysis of plasma and urine samples of healthy human subjects fed with green tea products, showed that (−)-epigallocatechin-3-*O*-gallate and (−)-epicatechin-3-*O*-gallate appeared unmetabolized in plasma.[51] The passage of ECG and EGCG through the wall of the small intestine into the circulatory system without metabolism could be a consequence of the presence of the 3-*O*-galloyl moiety interfering with phase II metabolism. Gallic acid per se is readily absorbed with a reported urinary excretion of 37% of intake, and so, the gallate ester might exhibit improved absorption.[52] The absence of detectable amounts of EGCG in urine was hypothesized to be due to the kidney inability to remove it from the bloodstream.[53] Preclinical studies speculated that EGCG may be removed from the bloodstream in the liver and returned to the small intestine in the bile.[54] The level of EGCG found in the major organs was found to be ∼1/10 that found in the serum. Most interestingly, this includes the brain, suggesting that EGCG passes through

the blood-brain barrier.[55] In this latter context, little and controversial information deals with the interaction of polyphenols or their circulating metabolites with the blood brain barrier (BBB). The layer of brain endothelial cells is sealed by complex tight junctions that possess few pinocytotic vesicles but express a number of specific uptake and efflux transport systems and metabolic enzymes. Together, these properties enable the BBB to restrict the passage of most small polar molecules and macromolecules from the cerebrovascular circulation to the brain, to exert tight control over trans-endothelial molecular traffic and to contribute to regulation of brain extracellular fluid composition. Youdim and co-workers[56] investigated the potential BBB permeability of flavonoids and their physiologically relevant metabolites using the ECV304/C6 coculture BBB model. Aglycones, due to their lipophilicity, were found to cross BBB by passive transcellular diffusion. Moreover, some evidence suggested that polyphenol constituents from *Pistacia lentiscus* leaves could be able to cross BBB. Epigallocatechin gallate (EGCG), for instance, was reported to enter the brain after a gastric administration of [$^3$H]EGCG,[57] whereas gallic acid was found to pass through BBB and protect or improve neuronal function in critical brain regions involving cognition after cerebral damage by ischemia.[58] $^{14}$C-labeled grape polyphenols was also demonstrated to reach the brain following oral administration.[59] Importantly, in in vitro and in situ models of the blood brain barrier, it was demonstrated that quercetin was able to enter different regions of the brain as a substrate of P-glicoproteins, a BBB efflux transporter.[60] Studies have indicated that the accumulation of flavonoids in the brain is not dependent on the brain region. Vauzour and co-workers,[61] reviewing the neuroprotective potential of flavonoids, stated that these molecules traverse BBB and are able to localize in the brain, suggesting that they are candidates for direct neuroprotective and neuromodulatory actions. Indeed, although the uptake and distribution of dietary polyphenols within the brain are well documented, the question of the dose reaching the target tissues remains uncertain. Data from studies using exsanguinated and perfused animals or applying the recently published mathematical correction model suggest that polyphenols usually localize in the brain at levels below 1 nmol/g tissue.[62]

In conclusion, a host of products from plant species and derivatives have neuroprotectant effects in vitro and in vivo. Reported data are in accordance with the preparation of a polyphenol-rich alcoholic extract of *Pistacia lentiscus* (Pl-M) with strong antiradical and antioxidant activity. The extract, which was highly cytocompatible in neuronal and glial tested cell lines, at concentrations up to 100 $\mu$g/mL, showed protective effect against hydrogen peroxide-induced oxidative stress and marked antiamyloidogenic activity in neuronal cells. The positive and promising effects, probably the result of an appropriate mixture of ingredients, allow us to hypothesize that the enrichment of a food matrix with polyphenol bioactives from a broadly available and renewable source, as *Pistacia lentiscus* leaves, could represent a valuable method to counteract Alzheimer's disease onset.

In the present study, LC-MS analyses were performed to unravel the chemical complexity of this potential botanical dietary supplements, which represents, likely green tea and wine, an active and rich source of gallic acid esters and glycosides. The massive presence of some of these compounds, e.g. galloyl and digalloyl quinic acids, poorly available in human diet, addresses Pl-M extract bioavailability and preclinical studies, able to define its active doses and to assess *Pistacia lentiscus* polyphenol extract safety and efficacy as nutraceutical in an AD mouse model and aged mice.

## AUTHOR INFORMATION


### Corresponding Author

*E-mail: severina.pacifico@unina2.it. Phone: +39 0823 274572. Fax: +39 0823 274571.


### Notes

The authors declare no competing financial interest.

## REFERENCES


(1) De Flora, S.; Quaglia, A.; Bennicelli, C.; Vercelli, M. The epidemiological revolution of the 20th century. *FASEB J.* **2005**, *19*, 892−897.

(2) Alzheimer's Disease International. *World Alzheimer Report 2013*; Prince, M. J., Jackson, J., Eds.; Alzheimer's Disease International: London, 2013.

(3) Alzheimer's Disease International. *World Alzheimer Report 2012*; Prince, M. J., Jackson, J., Eds.; Alzheimer's Disease International: London, 2012.

(4) Ramesh, B. N.; Rao, T. S.; Prakasam, A.; Sambamurti, K.; Rao, K. S. Neuronutrition and Alzheimer's disease. *J. Alzheimers Dis.* **2010**, *19*, 1123−1139.

(5) Mattson, M. P. Pathways towards and away from Alzheimer's disease. *Nature* **2004**, *430*, 631−639.

(6) Cai, Z.; Zhao, B.; Ratka, A. Oxidative stress and $\beta$-amyloid protein in Alzheimer's disease. *Neuromol. Med.* **2011**, *13*, 223−250.

(7) Tamagno, E.; Guglielmotto, M.; Monteleone, D.; Tabaton, M. Amyloid-$\beta$ production: Major link between oxidative stress and BACE1. *Neurotox. Res.* **2012**, *22*, 208−219.

(8) Ono, K.; Hasegawa, K.; Naiki, H.; Yamada, M. Curcumin has potent anti-amyloidogenic effects for Alzheimer's $\beta$-amyloid fibrils in vitro. *J. Neurosci. Res.* **2004**, *75*, 742−750.

(9) Marambaud, P.; Zhao, H.; Davies, P. Resveratrol promotes clearance of Alzheimer's disease amyloid-$\beta$ peptides. *J. Biol. Chem.* **2005**, *280*, 37377−37382.

(10) Rezai-Zadeh, K.; Arendash, G. W.; Hou, H.; Fernandez, F.; Jensen, M.; Runfeldt, M.; Shytle, R. D.; Tan, J. Green tea epigallocatechin-3-gallate (EGCG) reduces $\beta$-amyloid mediated cognitive impairment and modulates tau pathology in Alzheimer transgenic mice. *Brain Res.* **2008**, *1214*, 177−187.

(11) Singh, M.; Arseneault, M.; Sanderson, T.; Murthy, V.; Ramassamy, C. Challenges for research on polyphenols from foods in Alzheimer's disease: Bioavailability, metabolism, and cellular and molecular mechanisms. *J. Agric. Food Chem.* **2008**, *56*, 4855−4873.

(12) Abuznait, A. H.; Qosa, H.; Busnena, B. A.; El Sayed, K. A.; Kaddoumi, A. Olive-oil-derived oleocanthal enhances $\beta$-amyloid clearance as a potential neuroprotective mechanism against Alzheimer's Disease: In vitro and in vivo studies. *ACS Chem. Neurosci.* **2013**, *4*, 973−982.

(13) Shytle, R. D.; Tan, J.; Bickford, P. C.; Rezai-Zadeh, K.; Hou, L.; Zeng, J.; Sanberg, P. R.; Sanberg, C. D.; Alberte, R. S.; Fink, R. C.; Roschek, B., Jr. Optimized turmeric extract reduces $\beta$-amyloid and phosphorylated Tau protein burden in Alzheimer's transgenic mice. *Curr. Alzheimer Res.* **2012**, *9*, 500−506.

(14) Shi, C.; Liu, J.; Wu, F.; Yew, D. T. *Ginkgo biloba* extract in Alzheimer's disease: From action mechanisms to medical practice. *Int. J. Mol. Sci.* **2010**, *11*, 107−123.

(15) Gupta, V. B.; Indi, S. S.; Rao, K. S. Garlic extract exhibits antiamyloidogenic activity on amyloid-$\beta$ fibrillogenesis: Relevance to Alzheimer's disease. *Phytother. Res.* **2009**, *23*, 111−115.

(16) Pacifico, S.; Gallicchio, M.; Lorenz, P.; Duckstein, S. M.; Potenza, N.; Galasso, S.; Marciano, S.; Fiorentino, A.; Stintzing, F. C.; Monaco, P. Neuroprotective potential of *Laurus nobilis* antioxidant polyphenol-enriched leaf extracts. *Chem. Res. Toxicol.* **2014**, *27*, 611−626.

(17) Nahida; Ansari, S. H.; Siddiqui, A. N. *Pistacia lentiscus*: A review on phytochemistry and pharmacological properties. *Int. J. Pharm. Pharm. Sci.* **2012**, *4* (suppl. 4), 16−20.
(18) Romani, A.; Pinelli, P.; Galardi, C.; Mulinacci, N.; Tattini, M. Identification and quantification of galloyl derivatives, flavonoid glycosides, and anthocyanins in leaves of *Pistacia lentiscus* L. *Phytochem. Anal.* **2002**, *13*, 79−86.
(19) Vaya, J.; Mahmood, S. Flavonoid content in leaf extracts of the fig (*Ficus carica* L.), carob (*Ceratonia siliqua* L.), and pistachio (*Pistacia lentiscus* L.). *Biofactors* **2006**, *28*, 169−175.
(20) Rodrìguez-Perez, C.; Quirantes-Pinè, R.; Amessis-Ouchemoukh, N.; Khodir, M.; Segura-Carretero, A.; Fernàndez-Gutierrez, A. A metabolite profiling approach allows the identification of new compounds from *Pistacia lentiscus* leaves. J. *Pharm. Biomed. Anal.* **2013**, *77*, 167−174.
(21) Pacifico, S.; Gallicchio, M.; Fiorentino, A.; Fischer, A.; Meyer, U.; Stintzing, F. C. Antioxidant properties and cytotoxic effects on human cancer cell lines of aqueous fermented and lipophilic quince (*Cydonia oblonga* Mill.) preparations. *Food Chem. Toxicol.* **2012**, *50*, 4130−4135.
(22) Pacifico, S.; Gallicchio, M.; Lorenz, P.; Potenza, N.; Galasso, S.; Marciano, S.; Fiorentino, A.; Stintzing, F. C.; Monaco, P. Apolar *Laurus nobilis* leaf extracts induce cytotoxicity and apoptosis towards three nervous system cell lines. *Food Chem. Toxicol.* **2013**, *62*, 628−637.
(23) Essa, M. M.; Vijayan, R. K.; Castellano-Gonzalez, G.; Memon, M. A.; Braidy, N.; Guillemin, G. J. Neuroprotective effect of natural products against Alzheimer's disease. *Neurochem. Res.* **2012**, *37*, 1829−1842.
(24) Flores, P.; Hellin, P.; Fenoll, J. Determination of organic acid in fruits and vegetables by liquid chromatography with tandem-mass spectroscopy. *Food Chem.* **2012**, *132*, 1049−1054.
(25) Pacifico, S.; Di Maro, A.; Petriccione, M.; Galasso, S.; Piccolella, S.; Di Giuseppe, A. M. A.; Scortichini, M.; Monaco, P. Chemical composition, nutritional value and antioxidant properties of autochthonous *Prunus avium* cultivars from Campania Region. *Food Res. Int.* **2014**, *64*, 188−199.
(26) Clifford, M. N.; Stoupi, S.; Kuhnert, N. Profiling and characterization by LC-MS$^n$ of the galloylquinic acids of green tea, tara tannin, and tannic acid. *J. Agric. Food Chem.* **2007**, *55*, 2797−2807.
(27) Abu-Reidah, I. M.; Ali-Shtayeh, M. S.; Jamous, R. M.; Arráez-Román, D.; Segura-Carretero, A. HPLC-DAD-ESI-MS/MS screening of bioactive components from *Rhus coriaria* L. (Sumac) fruits. *Food Chem.* **2015**, *166*, 179−191.
(28) Dou, J.; Lee, V. S. Y.; Tzen, J. T. C.; Lee, M.-R. Identification and comparison of phenolic compounds in the preparation of oolong tea manufactured by semifermentation and drying processes. *J. Agric. Food Chem.* **2007**, *55*, 7462−7468.
(29) Jaiswal, R.; Jayasinghe, L.; Kuhnerta, N. Identification and characterization of proanthocyanidins of 16 members of the *Rhododendron* genus (*Ericaceae*) by tandem LC−MS. *J. Mass. Spectrom.* **2012**, *47*, 502−515.
(30) Miketova, P.; Schram, K. H.; Whitney, J.; Li, M.; Huang, R.; Kerns, E.; Valcic, S.; Timmermann, B. N.; Rourick, R.; Klohr, S. Tandem mass spectrometry studies of green tea catechins. Identification of three minor components in the polyphenolic extract of green tea. *J. Mass Spectrom.* **2000**, *35*, 860−869.
(31) Mizooku, Y.; Yoshikawa, M.; Tsuneyoshi, T.; Arakawa, R. Analysis of oxidized epigallocatechin gallate by liquid chromatography/mass spectrometry. *Rapid Commun. Mass Spectrom.* **2003**, *17*, 1915−1918.
(32) Vanholme, R.; Storme, V.; Vanholme, B.; Sundin, L.; Christensen, J. H.; Goeminne, G.; Halpin, C.; Rohde, A.; Morreel, K.; Boerjan, W. A systems biology view of responses to lignin biosynthesis perturbations in Arabidopsis. *Plant Cell.* **2012**, *24*, 3506−3529.
(33) Hou, A. J.; Peng, L. J.; Liu, Y. Z.; Lin, Z. W.; Sun, H. D. Two new gallotannins from *Pistacia weinmannifolia*. *Chin. Chem. Lett.* **2000**, *11*, 53−56.
(34) Romani, A.; Pinelli, P.; Galardi, C.; Mulinacci, N.; Tattini, M. Identification and quantification of galloyl derivatives, flavonoid glycosides, and anthocyanins in leaves of *Pistacia lentiscus* L. *Phytochem. Anal.* **2002**, *13*, 79−86.
(35) Cuyckens, F.; Claeys, M. Determination of the glycosylation site in flavonoid mono-*O*-glycosides by collision-induced dissociation of electrospray-generated deprotonated and sodiated molecules. *J. Mass Spectrom.* **2005**, *40*, 364−372.
(36) March, R. E.; Lewars, E. G.; Stadey, C. J.; Miao, X.-S.; Zhao, X.; Metcalfe, C. D. A comparison of flavonoid glycosides by electrospray tandem mass spectrometry. *Int. J. Mass Spectrom.* **2006**, *248*, 61−85.
(37) Guimarães, R.; Barros, L.; Duenãs, M.; Carvalho, A. M.; Queiroz, M. J. R. P.; Santos-Buelga, C.; Ferreira, I. C. F. R. Characterization of phenolic compounds in wild fruits from Northeastern Portugal. *Food Chem.* **2013**, *141*, 3721−3730.
(38) Shearman, M. S.; Hawtin, S. R.; Tailor, V. J. The intracellular component of cellular 3-(4,5-dimethylthiazol-2-yl)-2,5-diphenyltetrazolium bromide (MTT) reduction is specifically inhibited by $\beta$-amyloid peptides. *J. Neurochem.* **1995**, *65*, 218−227.
(39) Liu, Y.; Schubert, D. Cytotoxic amyloid peptides inhibit cellular 3-(4,5-dimethylthiazol-2-yl)-2,5-diphenyltetrazolium bromide (MTT) reduction by enhancing MTT formazan exocytosis. *J. Neurochem.* **1997**, *69*, 2285−2293.
(40) Howes, M. J.; Perry, E. The role of phytochemicals in the treatment and prevention of dementia. *Drugs Aging* **2011**, *28*, 439−468.
(41) Williams, P.; Sorribas, A.; Howes, M. J. R. Natural products as a source of Alzheimer's drug leads. *Nat. Prod. Rep.* **2011**, *28*, 48−77.
(42) Howes, M. J.; Houghton, P. J. Ethnobotanical treatment strategies against Alzheimer's disease. *Curr. Alzheimer Res.* **2012**, *9*, 67−85.
(43) Bastianetto, S.; Yao, Z. X.; Papadopoulos, V.; Quirion, R. Neuroprotective effects of green and black teas and their catechin gallate esters against $\beta$-amyloid-induced toxicity. *Eur. J. Neurosci.* **2006**, *23*, 55−64.
(44) Kim, J. K.; Choi, S. J.; Cho, H. Y.; Hwang, H. J.; Kim, Y. J.; Lim, S. T.; Kim, C. J.; Kim, H. K.; Peterson, S.; Shin, D. H. Protective effects of kaempferol (3,4′,5,7-tetrahydroxyflavone) against amyloid $\beta$ peptide (A$\beta$)-induced neurotoxicity in ICR mice. *Biosci. Biotechnol. Biochem.* **2010**, *74*, 397−401.
(45) Ono, K.; Yoshiike, Y.; Takashima, A.; Hasegawa, K.; Naiki, H.; Yamada, M. Potent anti-amyloidogenic and fibril-destabilizing effects of polyphenols *in vitro*: Implications for the prevention and therapeutics of Alzheimer's disease. *J. Neurochem.* **2003**, *87*, 172−181.
(46) Commenges, D.; Scotet, V.; Renaud, S.; Jacqumin-Gadda, H.; Barberger-Gateau, P.; Dartigues, J. F. Intake of flavonoids and risk of dementia. *Eur. J. Epidemiol.* **2000**, *16*, 357−363.
(47) Ramassamy, C. Emerging role of polyphenolic compounds in the treatment of neurodegenerative diseases: A review of their intracellular targets. *Eur. J. Pharmacol.* **2008**, *545*, 51−64.
(48) Levites, Y.; Amit, T.; Youdim, M.; Mandel, S. Involvement of protein kinase C activation and cell survival/cell cycle genes in green tea polyphenol (−)-epigallocatechin 3-gallate neuroprotective action. *J. Biol. Chem.* **2002**, *277*, 30574−30580.
(49) Orhan, I.; Kartal, M.; Tosun, F.; Sener, B. Screening of various phenolic acids and flavonoid derivatives for their anticholinesterase potential. *Z. Naturforsch C* **2007**, *62*, 829−832.
(50) Singh, M.; Arseneault, M.; Sanderson, T.; Murthy, V.; Ramassamy, C. Challenges for research on polyphenols from foods in Alzheimer's disease: Bioavailability, metabolism, and cellular and molecular mechanisms. *J. Agric. Food Chem.* **2008**, *56*, 4855−4873.
(51) Del Rio, D.; Rodrigues-Mateos, A.; Spencer, J. P.; Tognolini, M.; Borges, G.; Grozier, A. Dietary (poly)phenolics in human health: Structures, bioavailability, and evidence of protective effects against chronic diseases. *Antioxid. Redox. Signal.* **2013**, *18*, 1818−1892.
(52) Shahrzad, S.; Bitsch, I. Determination of gallic acid and its metabolites in human plasma and urine by high-performance liquid chromatography. *J. Chromatogr. B* **1998**, *705*, 87−95.

(53) Lee, M. J.; Maliakal, P.; Chen, L.; Meng, X.; Bondoc, F. Y.; Prabhu, S.; Lambert, G.; Mohr, S.; Yang, C. S. Pharmacokinetics of tea catechins after ingestion of green tea and (−)-epigallocatechin-3-gallate by humans: Formation of different metabolites and individual variability. *Cancer Epidemiol Biomarkers Prev.* **2002**, *11*, 1025−1032.
(54) Kohri, T.; Nanjo, F.; Suziki, M.; Seto, R.; Matsumoto, N.; Yamakawa, M.; Hojo, H.; Hara, Y.; Desai, D.; Amin, S.; Conaway, C. C.; Chung, F. L. Synthesis of (−)-[4-$^{3}$H]epigallocatechin gallate and its metabolic fate in rats after intravenous administration. *J. Agric. Food Chem.* **2001**, *49*, 1042−1048.
(55) Smith, T. J. Green tea polyphenols in drug discovery—A success or failure? *Expert. Opin. Drug Discovery* **2011**, *6*, 589−595.
(56) Youdim, K. A.; Dobbie, S. M.; Kuhnle, G.; Proteggente, A. R.; Abbott, J. N.; Rice-Evans, C. Interaction between flavonoids and the blood−brain barrier: In vitro studies. *J. Neurochem.* **2003**, *85*, 180−192.
(57) Suganuma, M.; Okabe, S.; Oniyama, M.; Tada, Y.; Ito, H.; Fujiki, H. Wide distribution of [$^{3}$H](−)-epigallocatechin gallate, a cancer preventive tea polyphenol, in mouse tissue. *Carcinogenesis* **1998**, *19*, 1771−1776.
(58) Farbood, Y.; Sarkaki, A.; Hashemi, S.; Mansouri, M. T.; Dianat, M. The effects of gallic acid on pain and memory following transient global ischemia/reperfusion in Wistar rats. *Avicenna J. Phytomed.* **2013**, *3*, 329−340.
(59) Janle, E. M.; Lila, M. A.; Grannan, M.; Wood, L.; Higgins, A.; Yousef, G. G.; Rogers, R. B.; Kim, H.; Jackson, G. S.; Ho, L.; Weaver, C. M. Pharmacokinetics and tissue distribution of $^{14}$C-labeled grape polyphenols in the periphery and the central nervous system following oral administration. *J. Med. Food.* **2010**, *13*, 926−933.
(60) Youdim, K. A.; Qaiser, M. Z.; Begley, D. J.; Rice-Evance, C. A.; Abbott, N. J. Flavonoid permeability across an in situ model of blood−brain barrier. *Free Radic. Biol. Med.* **2004**, *36*, 592−604.
(61) Vauzour, D.; Vafeiadou, K.; Rodrigues-Mateos, A.; Rendeiro, C.; Spencer, J. P. E. The neuroprotective potential of flavonoids: A multiplicity of effects. *Genes Nutr.* **2008**, *3*, 115−126.
(62) Schaffer, S.; Halliwell, B. Do polyphenols enter the brain and does it matter? Some theoretical and practical considerations. *Genes Nutr.* **2012**, *7*, 99−109.

including the limit of polyphenol bioconversion and absorption as compared to in vivo studies which are less stable in human gut due to environmental conditions and diversity of microbes.[19] To our knowledge, there is no information regarding the nature or biological properties of naturally occurring phenolic lipids that could result from natural lipid−phenolic interactions in olive oil. The specific objectives of this research were the following: (i) to investigate the occurrence of natural lipid−phenolic interactions in virgin olive oil via evaluation of the total content of free and lipid-bound phenolic compounds and identification of individual lipid phenolic compounds in virgin olive oil; and (ii) test the biological properties of free and bound phenolic compounds in terms of antioxidant activity, α-amylase and ACE inhibitory activities, and antitumorigenic activity.

## MATERIALS AND METHODS

**Plant Materials.** Nepali olive sample was obtained from Rahoub Valley (Irbid, Jordan). Samples were harvested in the winter of 2010 at proper harvesting stages according to the International Olive Oil Council method (IOOC).[20] Olives were subjected to milling at commercial industrial two-phase olive oil (Irbid, Jordan) to obtain the virgin olive oil. Olive oil samples were filled in plastic containers of 10 L. The virgin olive oil was graded into upper and lower layers of 10 L containers after storage of three months to remove sediments and then stored at −18 °C prior to analysis.

**Phenolic Compounds Extraction.** *Free Phenolic Compounds Extraction.* Free phenolic compounds were extracted according to the method described by Alu'datt et al.[21] with modifications. A 15 mL sample of two layers from virgin olive oil was extracted with 25 mL of methanol at 30 °C for 1 h in a shaking water bath. The supernatant oil samples were filtered using Whatman 3 filter paper, and the resulting extract was designated as free phenolic extract at 30 °C (FP-30 °C). The supernatant that remained after methanol extraction at 30 °C was subjected to methanol extraction with 25 mL at 60 °C for 1 h in a shaking water bath. After filtration with Whatman 3 filter paper, the extract was designated as free phenolic extract at 60 °C (FP-60 °C). The FP-30 °C and FP-60 °C extracts were stored at −18 °C for further analysis.

*Bound Phenolic Compounds Extraction.* Bound phenolic compounds were extracted according to the method described by Alu'datt et al.[21] with modifications. The residue remaining after extraction of free phenolic compounds at 30 and 60 °C as described above was hydrolyzed with dilute alkaline solution (25 mL, pH 12.0, 0.1 M NaOH) for 24 h at 30 °C in a shaking water bath, and then the alkaline solution was freeze-dried (LFD-5508 freeze-dryer, Korea). The liberated bound phenolic compounds from alkaline hydrolysis were subjected to methanol extraction (25 mL) at 30 °C for 1 h. The supernatant was filtered using filter papers (Whatman 3), and the resulting extract was designated as bound phenolic at 30 °C (BP-30 °C). Following extraction with 25 mL of methanol at 60 °C for 1 h, the extract that was generated was designated as bound phenolic at 60 °C (BP-60 °C). All extracts were stored at −18 °C for further analysis.

*Total Phenolic Compounds Content.* Determination of the total phenol content in each phenolic extract was conducted by using the Folin−Ciocalteu method as previously described by Hoff and Singleton.[22] Standard curves of gallic acid were prepared using a stock solution of 5 mg/mL. A 100 μL portion of the extract containing phenolic compounds was added to 8.4 mL of distilled water. A 0.5 mL portion of the Folin−Ciocalteu solution was added and mixed well in the test tube after 4 min, which was followed by addition of 1.0 mL of 5% sodium carbonate and vortex-mixed for several seconds. The absorbance was measured 1 h later at 725 nm using UV−vis spectrophotometry (UV 1800, Biotech Engineering Management Co., Ltd., U.K.). The total phenolic content was expressed as mg/L gallic acid equivalents (mg GAE/L).

*Determination of Antioxidant Activity.* Antioxidant activity of phenolic extract was determined according to the method of Alu'datt et al.[21] with modifications. A 5 mg portion of β-carotene was dissolved in 50 mL of chloroform. The β-carotene/linoleic acid stock solution was prepared by mixing 3 mL of β-carotene solution with 50 μL of linoleic acid and 400 mg of Tween 20. The chloroform was evaporated under nitrogen gas followed by addition of 100 mL distilled water, and the resulting emulsion was shaken for 2 min. A 100 μL portion of the bound phenolic methanolic extract (BP-30 °C or BP-60 °C) was mixed with 3 mL of the emulsion. The absorbance was measured at time 0 and after incubation for 1 h at 50 °C at 470 nm. A 100 μL portion of solvent was used in the blank control sample. The percent antioxidant activity (AA%) was calculated as amount of β-carotene bleaching in sample to control according to the following equation:

$$AA\% = 100*((DRc - DRs)/DRc)$$

Here, AA% is the percent antioxidant activity. DRc is the degradation rate of the blank control sample [DRc = (ln(A/B)/60)]. DRs is the degradation rate of the sample DRs = (ln(A/B)/60). A is the absorbance at t = 0, and B is the absorbance at t = 60 min.

*Measurement Inhibitory activity for α-Amylase Enzyme.* The activity of α-amylase was evaluated according to the method described by McCue et al.[23] with modifications. Porcine pancreatic α-amylase (10080, Sigma Chemical Co.) was prepared by mixing 0.030 g of the enzyme in 100 mL of distilled water. A potato starch solution of 0.5% (w/v) was prepared by dissolving 0.125 g of starch in 25 mL of phosphate buffer (pH 6.9; 65 °C/20 min). A colorimetric reagent was prepared by mixing well 19.8 g of sodium hydroxide with 10.6 g of 3,5-dinitrosalicyclic acid solution (DNS) in 1.416 L of distilled water and then adding this to a mixture of 3.06 g of sodium potassium tartarate, 7.6 g of phenol, and 8.3 g of sodium metabisulfite, and mixing by shaking for 15 min. A 100 μL portion of phenolic extract (BP-30 °C or BP-60 °C), 500 μL of phosphate buffer (pH 7.0), and 500 μL of α-amylase solution were incubated at 25 °C for 10 min. The control sample consisted of 100 μL of solvent. After the preincubation, 500 μL of potato starch solution was added, and the mixture was incubated in a 25 °C water bath for 10 min. The reaction stopped by adding 1 mL of DNS. The mixture was then incubated in a boiling water bath for 5 min and then cooled to room temperature. The total volume of reaction mixture was diluted to 10 mL by adding distilled water. To determine the amount of liberated maltose the absorbance was measured at 540 nm via a spectrophotometer (Spectrophotometer-UV 1800, Biotech Engineering Management Co., Ltd., U.K.). The percent α-amylase inhibition was expressed as amount of liberated maltose in sample to control and calculated according to the followin equation:

$$\alpha\text{-amylase inhibition } \% = 100[(Ac - As)/Ac]$$

Here, Ac is the absorbance of the control sample at 540 nm, and As is sample absorbance.

*Determination Inhibitory Activity of Angiotensin 1-Converting Enzyme (ACE).* ACE inhibition was measured according to the method described by Cushman and Cheung[24] with modifications. A 0.3% (w/v) solution of hippuryl-L-histidyl-L-leucine (HHL) solution was dissolved in 50 mM 4-(2-hydroxyethyl)-1-piperazineethanesulfonic acid (HEPES) HCl buffer with 300 mM sodium chloride (pH 8.3 at 37 °C). The ACE enzyme solution was prepared by mixing of 0.33 U in 1 mL of distilled water. An aliquot of 200 μL of HHL was mixed with 100 μL of either the BP-30 °C or BP-60 °C phenolic extract. An aliquot of 50 μL of ACE solution was added, and the mixture was incubated at 37 °C for 15 min. The reaction was stopped by adding 0.25 mL of HCl, and then 2 mL of ethyl acetate was added to extract the liberated hippuric acid. A 1 mL portion of the ethyl acetate layer was separated by centrifugation (3000 rpm/3 min) and evaporated by using boiling water bath for 15 min, and then 3 mL of distilled water was added. The amount of liberated hippuric acid was quantified by measuring the absorbance at 228 nm (UV 1800, Biotech Engineering Management Co., Ltd., U.K.). A blank was prepared by adding of 200 μL of HHL and 50 μL of ACE in 100 μL of distilled water. The amount of hippuric acid liberated in the control samples was defined as 100% ACE activity. The ACE inhibition was expressed as the amount of liberated hippuric acid in the sample to the control and calculated using the following equation:

$$\text{ACE inhibition \%} = [(A228\ \text{blank} - A228\ \text{sample})/A228\ \text{blank})100]$$

Here, $A$ is the absorbance.

**Measurement of Anti-Tumorigenic Activity Using Human Colorectal Cancer Cells.** *Cell Culture.* Two different human colorectal cancer cells (CRC1 and CRC5) were supplied by Dr. Rick Throm, University of Newcastle, Australia. The cell lines were cultured as monolayer and attached in Dulbecco's modified essential medium (DMEM) supplemented with 10% fetal calf serum (FCS) (Lonza, Verviers, Belgium), 1% penicillin-streptomycin (5000 U penicillin/mL and 5000 U streptomycin/mL) (Lonza, Verviers, Belgium), and amphotericin B (250 μg/mL) (Lonza, Verviers, Belgium). Cells were incubated in a humidified atmosphere containing 5% $CO_2$, at 37 °C in $CO_2$ incubator (Shell Lab).

*Cell Viability Assay.* The four types of phenolic extracts derived from the virgin olive oil layer characterized by having the highest phenolic content were chosen for studying the antitumorigenic effects of phenolics in olive oil. The cytotoxic effect of different concentrations of phenolic extracts (10−200 μL) was determined by using 3-(4,5-dimethylthiazo-l-2-yl)-2,5-diphenyltetrazolium bromide (MTT) assay according to the method described by Wu et al.[25] Cells were seeded at 5000 cells/well onto flat-bottomed 96-well culture plates, and allowed to grow for 24 h before treatment. Cells were incubated with five different concentrations of phenolic extracts (0, 10, 50, 100, and 200 μL; 0.0, 1.4, 7.1, 14.2, and 28.4 μg for FP-30 °C; 0.0, 0.7, 3.5, 7.0, and 14.0 μg for FP-60 °C; 0.0, 0.6, 3.0, 6.0, and 12.0 μg for BP-30 °C; and 0.0, 0.68, 3.4, 6.8, and 13.6 μg for BP-60 °C). After 48 h of incubation, cells were incubated with 10 μL of MTT for 4 h from Vybrant MTT assay cell proliferation assay kit (Molecular Probes, Eugene, OR) according to manufacturer's instruction. After MTT incubation, the supernatant was aspirated, and the insoluble formozan product was dissolved with dimethyl sulfoxide (80 μL DMSO). Cell proliferation was measured by measuring absorbance using a microplate reader (model 3550, Bio-Rad Laboratories, CA) at 540 nm.

*Identification and Quantification of Individual Phenolic Compounds by Using Liquid Chromatography-Electrospray Ionization Tandem Mass Spectrometry (LC/ESI-MS/MS).* A 10 mL portion of free and bound phenolic extracts that were characterized with the highest phenolic content was evaporated under a stream of nitrogen and then dissolved in 1 mL of methanol and stored at −18 °C until further analysis. Standard curves were prepared by using a stock standard solution prepared by dissolving 5 mg of each phenolic standard in 50 mL of methanol. Virgin olive extracts were analyzed by LC-MS/MS according to the method described by Obied et al.[26] The analysis of phenolic compounds was carried out using Agilent 1100 chromatography system (Agilent 1100, Agilent Technologies, Wilmington, DE) equipped with a diode array UV detector. The samples were injected into a Thermo $C_{18}$ reversed phase column (pore size 5 μm, 250 mm × 4.6 mm i.d., Thermo Fisher Scientific, San Jose, CA).

The analysis was carried out by a gradient solvent system using aqueous formic acid (1%) as solvent A, and methanol/acetonitrile/formic acid mixture (89.5/9.5/1 v/v/v) as solvent B. A seven-step linear gradient elution for total run time of 65 min was carried out using the solvent gradient as follows: 0−10 min 90−70% solvent A and 10−30% solvent B, 10−15 min isocratic, 15−25 min 60% solvent A and 40% solvent B, 25−40 min 50% solvent A and 50% solvent B, 40−50 min to 100% solvent B, 50−55 min 90% solvent A and 10% solvent B and 55−65 min isocratic. An injection volume of 15 μL at constant flow of 0.75 mL/min was used for each analysis. The entire flow from the HPLC was directed into the tandem mass spectrometer. Triple-quadrupole mass spectrometer (API 3200; MDS Sciex, Concord, ON, Canada) was used. The mass spectral data was acquired on negative ion mode, capillary voltage 4000 V, ion source atmospheric pressure chemical ionization (APCI), a cone voltage 70 V, collision energy 10 eV, drying temperature 350 °C, drying gas $N_2$ with 4.0 L/min flow rate, nebulizer gas helium with 40 psi flow rate, software used for data processing was Analyst software version 3.5.1. Diode array UV detector was used to scan between 200 and 400 nm to evaluate contents of individual phenolic compounds. A maximum absorbance of 280 nm was selected to determine the contents of individual phenolic compounds. The eluted compounds of samples and standards were detected at 280 nm. Mixture of external standards (*p*-hydroxybenzoic acid, gallic acid, caffeic acid, ferulic acid, vanillic acid, tyrosol, hydroxytyrosol, *p*-coumaric acid, syringic acid, apigenin, hesperidin, luteolin, quercetin, rutin, sinapic acid, and oleuropein) was used to quantify the contents of individual phenolic compounds.

*Analysis of the Fatty Acids by Gas Chromatography (GC).* Fatty acid analysis was carried out according to the method described by Ereifej et al.[27] with modifications. Fatty acid profiles of virgin olive oil before and after removal of free and bound phenolic compounds were analyzed by GC-MS (Varian 450-GC/Varian 320-MS). Fatty acid methyl esters of virgin olive were prepared as follows: 0.1 g of olive oil was dissolved in 2 mL of heptane and mixed with a 0.2 mL solution of 2 M methanolic potassium hydroxide and then shaken vigorously for 30 s. The upper layer of the solution containing fatty acid methyl esters was separated, and 15 μL was injected in a split/split injector. An Agilent HP-INNOwax column (30 m × 0.25 mm i.d., 0.25 μm film thickness) was employed. The oven temperature program was as follows: column temperature was programmed from 50 °C (kept for 4 min) to 200 °C at 25 °C/min, 2 min at 200 °C, from 200 to 240 °C at 4 °C/min, 18 min at 240 °C. A constant helium carrier gas flow rate of 0.8 mL/min was used. A standard of fatty acid methyl esters was used to identify the content of fatty acids and was expressed as percent of total content of fatty acids.

*HPLC Separation of Acylglycerols.* Acylglycerols for virgin olive oil before and after removal of free and bound phenolic compounds were analyzed by HPLC. Olive oil samples were dissolved in tetrahydrofuran (THF). HPLC separation was carried out by Agilent 1100 series instrument (Wilmington, DE) equipped with UV−vis diode-array detection operated at 215 nm using a Zorbax SB-$C_{18}$ reverse phase column (pore size 5 μm, 250 mm × 4.6 mm i.d., Restek Co., Bellefonte, PA) operated at 60 °C. Elution was carried out at flow rate of 0.8 mL/min, with an injection sample volume of 10 μL. The elution of the injected sample was carried out by a gradient solvent system using distilled water as solvent A, and acetonitrile/methyl tetra-butyl ether mixture (9:1, v/v) as solvent B. Linear gradient started from 87% solvent B, and increased to 100% solvent B over 25 min. The initial conditions were then re-established over 4 min. The fractionation of individual peaks obtained from HPLC analysis of glycerols for virgin olive oil before and after removal of free and bound phenolic compounds involved elution from the column and collection of the fractions that were pooled and freeze-dried (LFD-5508 freeze-dryer, Korea). A 4 mL portion of distilled water were added to each fraction, which was divided into two parts and then freeze-dried. The first part was extracted with methanol, while the second part was hydrolyzed with dilute alkaline solution (2 mL, pH 12.0, 0.1 M NaOH) for 24 h at 30 °C water bath followed by freeze-drying and then extracted with methanol. All fractionated samples were stored at −18 °C for further analysis.

*Statistical Analysis.* Statistical analysis was performed by applying the General Linear Model (GLM) of the SAS software package (Version 9.1 SAS 2002 Institute Inc., NC). The least significant difference (LSD) multiple-range test was used for means separation using an $\alpha$ level of 0.05.

## RESULTS AND DISCUSSION

**Free and Bound Phenolic Distribution.** Table 1 shows the content of extracted free and bound phenolic compounds from the lower layer A and upper layer B. The total phenolic content of olive oil from the combined fractions was 567.83 mg/L for layer A and 506.64 mg/L for layer B. The total content of extracted free phenolics in virgin olive oil ranged from 330.8 to 353.53 mg/L while the total content of extracted bound phenolics ranged from 175.84 to 214.3 mg/L. The above results are comparable with the upper range phenolic concentrations noted in previous studies, which found that the total content of phenolic compounds in virgin olive oil ranged

**Table 1. Total Phenolic Content (mg/L), Antioxidant Activity (%), and Inhibitory Activities (%) of α-Amylase and ACE of Free (FP) and Bound (BP) Phenolic Compounds at 30 and 60 °C from Lower (A) and Upper (B) Layers of Extra Virgin Olive Oil[a]**

| layer of oil | FP-30 °C content (mg/L) | FP-60 °C content (mg/L) | BP-30 °C content (mg/L) | BP-60 °C content (mg/L) | SE |
|---|---|---|---|---|---|
| A | 237.37a A | 116.16b A | 100.74c A | 113.56b A | 2.72 |
| B | 232.32a A | 98.48b A | 86.09c B | 89.75bc B | 3.11 |
| SE | 2.52 | 3.99 | 1.83 | 2.90 | |
| layer of oil | antioxidant activity for FP-30 °C (%) | antioxidant activity for FP-60 °C (%) | antioxidant activity for BP-30 °C (%) | antioxidant activity for BP-60 °C (%) | SE |
| A | 58.1a A | 44.1b A | 45.3b A | 6.7c A | 0.46 |
| B | 55.0a A | 39.3c B | 45.1b A | 5.7d A | 0.43 |
| SE | 0.54 | 0.60 | 0.30 | 0.24 | |
| layer of oil | α-amylase inhibitory activity of FP-30 °C (%) | α-amylase inhibitory activity FP-60 °C (%) | α-amylase inhibitory activity BP-30 °C (%) | α-amylase inhibitory activity BP-60 °C (%) | SE |
| A | 33.41b A | 27.99c A | 37.67a A | 30.15c A | 0.71 |
| B | 27.70b B | 21.49c B | 33.20a B | 27.27b A | 0.94 |
| SE | 0.89 | 1.03 | 0.41 | 0.87 | |
| layer of oil | ACE inhibitory activity of FP-30 °C (%) | ACE inhibitory activity FP-60 °C (%) | ACE inhibitory activity BP-30 °C (%) | ACE inhibitory activity BP-60 °C (%) | SE |
| A | 33.12b A | 17.51d A | 37.57a A | 28.51c A | 0.36 |
| B | 24.89b B | 11.60c B | 29.39a B | 24.32b A | 1.08 |
| SE | 0.26 | 0.98 | 0.35 | 1.41 | |

[a]Means are averages of two replicates. Row values with the same small letters and column values with the same capital letters were not significantly different ($p < 0.05$). SE: standard error.

from 0.04 to 900 mg/kg.[28,29] The variations in phenolic content are likely related to varieties of cultivar, extraction method, storage, and package conditions.[8] In terms of individual fractions, the highest content of phenolic compounds in layers A and B was observed in the FP-30 °C extract with values of 237.37 and 232.2 mg/L, respectively. The lowest phenolic values were observed in the BP-30 °C extract with values of 100.74 and 86.09 mg/L for layers A and B, respectively. The above findings are in agreement with Alu'datt et al.[21] who found that the majority of free phenolics were extracted from olive cake in first step cycle.

Figure 1 illustrates the percent content of phenolic compounds of the FP-30 °C, FP-60 °C, BP-30 °C, and BP-60 °C extracts. The highest percent phenolic content was observed for the FP-30 °C extract, which had 41.80% and 45.86% for layers A and B, respectively. On the other hand, total phenolics in the FP-60 °C extract represented only 20.64% and 19.44%, respectively. These latter results were consistent with the finding of Alu'datt et al.[21] who found that a majority of phenolic compounds were extracted in the first three cycles of extraction from olive cake. The percent extraction of free phenolic compounds by heat treatment at 60 °C was lower than the percent phenolics obtained from the extraction carried out at 30 °C (Figure 1). The percent phenolic content of BP-30 °C in layers A and B was 17.74% and 16.99%, respectively. Similarly, the percent content of BP-60 °C in layers A and B was 20.00% and 17.71%, respectively. These results are in agreement with values obtained by Alu'datt et al.[21] who found that the percent content of bound phenolic

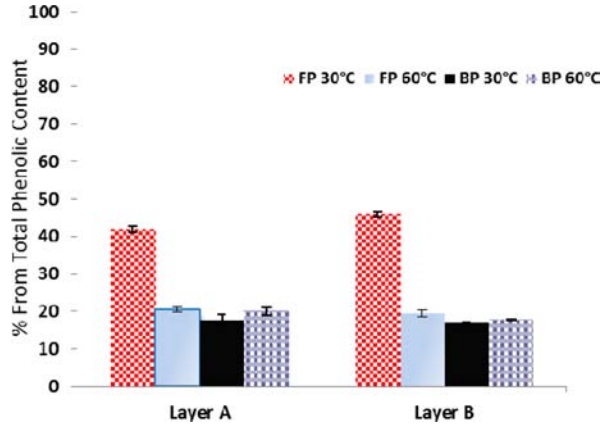


**Figure 1.** Distribution of free and bound phenolic compounds (percent of total phenolic content) at 30 and 60 °C.

compounds in olive cake ranged between 10% and 25%. In contrast, Alu'datt et al.[17] have reported that the percent content of bound phenolic compounds from olive meal represented less than 10% of total phenolic content. These results suggest that the phenolic compounds are present in free and bound forms in virgin olive oil.

**Antioxidant Activity of Free and Bound Phenolics Extracts.** Table 1 demonstrates the antioxidant activity of free and bound phenolic extracts of virgin olive oil. The antioxidant activities were the highest (55.0−58.1%) in layers B and A of FP-30 °C. The antioxidant activity of BP-30 °C in layer B was higher (45.1) as compared to antioxidant activities with layer B from FP-60 °C (39.3). The lowest antioxidant activities were found in BP-60 °C for both layers B and A with values in the range 5.7−6.7%. The above results indicate that the antioxidant activities of extracted free or bound phenolic compounds extracted at 30 °C are higher than those observed with the phenolics extracted at 60 °C. These latter results are inconsistent with previous findings showing a negative relationship between temperature of extraction and antioxidant activity.[30] The above ranges of antioxidant activities are similar to the 13.2−40.2% antioxidant activities reported by Gorinstein et al.[31] in Spanish olive oils. Conversely, Baiano et al.[16] found that the antioxidant activities of Italian virgin olive oils ranged between 70.67% and 87.83%. A weak positive linear correlation (0.571) was observed between total phenolic content and antioxidant activity (Table 2) which is in agreement with previous work showing that phenolic content was positively correlated with the antioxidant activity of olive oil.[16]

**Inhibitory Activity of α-Amylase of Free and Bound Phenolics Extracts.** Table 1 shows the α-amylase inhibitory activity of free and bound phenolic extracts from virgin olive oil. The maximum inhibitory activities of α-amylase were observed for layers A and B with the BP-30 °C extract with a range of values between 33.20% and 37.67%. The lowest inhibitory activities of α-amylase for the two layers were seen with the FP-60 °C extract with a range of values of 21.49−27.99%. The bound phenolic extracts of virgin olive oil generally had a better α-amylase inhibitory activity than the free phenolic extracts. Also, the free or bound phenolic extracts at 30 °C had higher inhibitory activity of α-amylase than free or bound phenolic extracts at 60 °C. Variations in inhibitory activities of α-amylase by the phenolic extracts may be due to differences in type, quantity, and polarity of phenolic compounds in extracts. These results are in agreement with the findings by Loizzo et al.[32] who

Table 2. Correlation Coefficients ($r$) between Phenolic Content, $\alpha$-Amylase Inhibitory Activity, Anticancer Activity (CRC1 and CRC5), Antioxidant Activity, and ACE Inhibitory Activity of Phenolic Extracts from Virgin Olive Oil

| | antioxidant activity | ACE inhibitory activity | $\alpha$-amylase inhibitory activity | anticancer (CRC1) | anticancer (CRC5) |
|---|---|---|---|---|---|
| content | 0.571 | 0.209 | 0.080 | 0.206 | −0.830 |
| antioxidant activity | | 0.117 | 0.241 | 0.115 | −0.495 |
| ace inhibitory activity | | | 0.943 | −0.911 | −0.720 |
| $\alpha$-amylase inhibitory activity | | | | −0.882 | −0.585 |

reported that the phenolic extracts of virgin olive oil inhibit $\alpha$-amylase activity. Several studies have reported the affinity of phenolic compounds to inhibit amylases and ACE enzymes.[30]

**Inhibitory Activity of Angiotensin 1-Converting Enzyme (ACE) of Free and Bound Phenolic Extracts.** Table 1 shows the inhibitory activities of free and bound phenolic extracts from olive oil on ACE enzyme inhibition. All free and bound phenolic extracts of olive oil had relatively good ACE inhibitory activity against enzyme apart from the free phenolic extract at 60 °C. Shahidi and Naczk[30] have reported that the ACE inhibitory activity of phenolic compounds depends upon the polarity and solubility of phenolic compounds. The highest inhibitory activity of ACE was observed with the bound phenolic extract in layer A at 30 °C with value of 37.57% whereas the lowest inhibitory activity (17.51%) was found in the free phenolic extract at 60 °C. Similarly, the highest ACE inhibitory activity in layer B was observed in bound phenolic extract at 30 °C with value of 29.39%, and the lowest inhibitory activity was found in free phenolic extract at 60 °C with value of 11.60%. Similar ACE inhibitory activities of phenolic extracts of extra virgin have been previously reported by Loizzo et al.[32] On the other hand, a high correlation was observed between ACE inhibitory activity and $\alpha$-amylase inhibitory activity (0.943).

**Proliferation Inhibition Activity of Free and Bound Phenolic Extracts.** The antiproliferative activity of extracted free and bound phenolic compounds from virgin olive oil against colorectal cancer cells is shown in Table 3. For the colorectal cancer cell line CRC 1, the lowest IC50 value was found with bound phenolic extract at 60 °C, which was significantly ($p < 0.05$) lower than both free phenolic extracts. For the CRC 5 colorectal cancer cell line, the lowest value of IC50 was found with the free phenolic extract at 60 °C that was significantly ($p < 0.05$) different from the IC50 of the free phenolic extract at 30 °C. The above results suggest that both free and bound phenolics can exert antiproliferative effects against CRC1 and CRC5 cells. These findings are consistent with previous observations that oleuropein and hydroxytyrosol can have antiproliferative effects against colon cancer cell lines (HT-29 and SW620).[33,34] Likewise, Fini et al.[35] have reported that extracted phenolics from virgin olive oil inhibited proliferation of RKO and HCT116 colorectal cancer cells lines. Results showed that the temperature does not have an effect on the anticancer properties.

Table 3. IC50 Values ($\mu$L/mL) of MTT Cytotoxicity Assay against Colorectal Cancer Cell Lines of Free Phenolic Compounds (FP) at 30 and 60 °C and Bound (BP) Phenolic Compounds at 30 and 60 °C from Virgin Olive Oil[a]

| | IC 50 ($\mu$L/mL) | | |
|---|---|---|---|
| type of extract | CRC1 | CRC5 | SE |
| FP-30 °C | 93.05a A | 140.37a A | 16.3 |
| FP-60 °C | 96.55a A | 86.52b A | 4.99 |
| BP-30 °C | 84.22ab A | 109.47ab A | 7.38 |
| BP-60 °C | 57.06b A | 100.61ab A | 8.96 |
| SE | 7.13 | 12.74 | |

[a]Means are average of two replicates. Column values with the same small letters and row values with same capital letters were not significantly different ($p < 0.05$). SE: standard error.

In contrast, CRC1 anticancer activity showed a strong negative correlation with ACE inhibitory and $\alpha$-amylase inhibitory activities with values of −0.911 and −0.882, respectively. The CRC5 anticancer activity had a weak negative correlation with antioxidant (−0.495) and $\alpha$-amylase inhibitory (−0.585) activities. The CRC5 antitumorigenic activity had a strong negative correlation with phenolic content (−0.830) and ACE inhibitory activity (−0.720).

**LC-MS/MS Analysis of Individual Free and Bound Phenolic Compounds.** Table 4 shows the phenolic profile identified by LC-MS/MS in the free and bound phenolic extracts of virgin olive oil. The LC-MS/MS profile of FP-30 °C extract showed the presence of gallic acid, *p*-hydroxybenzoic acid, vanillic acid, tyrosol, hydroxytyrosol, hesperidin, and quercetin that were not present in FP-60 °C extract. The major predominant individual phenolic compounds in FP-30 °C extract were luteolin, apigenin, and hydroxytyrosol with values of 49.02%, 32.33%, and 8.02% of total phenolic content, respectively, whereas the major predominant individual phenolic compounds in FP-60 °C extract were apigenin, luteolin, and sinapic acid with values of 45.84%, 25.04%, and 23.65% of total phenolic content, respectively. The above results are consistent with previous findings that gallic, *p*-hydroxybenzoic, vanillic, *p*-coumaric, and sinapic acids are the major phenolic acids found in virgin olive oil.[12] Reboredo-Rodríguez et al.[36] reported that the contents of apigenin, vanillic acid, and *p*-coumaric in extra virgin olive oil were present in minor amounts. Regueiro et al.[37] reported that the liquid chromatography-linear trap quadrupole (LC-LTQ-Orbitrap) analysis had an extensive identification of the phenolic compounds in walnuts. The LC-MS/MS profile of BP-30 °C was similar to the profile of BP-60 °C except for the presence of hesperidin in BP-30 °C extract and *p*-coumaric acid in BP-60 °C extract. The major predominant individual phenolic compounds in BP-30 °C extract were apigenin, luteolin, and quercetin with values of 44.39%, 25.04%, and 10.32% of total phenolic content, respectively, whereas the major predominant individual phenolic compounds in BP-60 °C extract were apigenin, luteolin, and rutin with values of 34.00%, 33.86%, and 25.18% of total phenolic content, respectively. The above results thus indicate the presence of flavonoids (apigenin, luteolin, and rutin) in detectable amounts as both free and bound phenolic compounds, which agrees with previous work showing that apigenin and lutolein are the major flavonoids compounds identified in virgin olive oil.[15] The presence of hesperidin, rutin, and quercetin in olives has been previously reported by Alu'datt et al.[17] On the other hand, Tuck and

Table 4. Percent of Total Phenolic Content of Free Phenolic Compounds (FP) at 30 and 60 °C and Bound (BP) Phenolic Compounds at 30 and 60 °C from Extra Virgin Olive Oil Identified using (LC/MS/MS)[a]

| type of phenolic compds | retention time (min) | FP-30 °C extract (%) | FP-60 °C extract (%) | BP-30 °C extract (%) | BP-60 °C extract (%) |
|---|---|---|---|---|---|
| gallic acid | 4.44 | 0.97efg | ND | ND | ND |
| hydroxytyrosol | 8.1 | 8.02c | ND | ND | ND |
| tyrosol | 12.2 | 1.53def | ND | ND | ND |
| *p*-hydroxybenzoic acid | 12.6 | 1.46ef | ND | ND | ND |
| vanillic acid | 15.1 | 2.58d | ND | ND | ND |
| *p*-coumaric acid | 19.2 | ND | ND | ND | 4.19c |
| sinapic acid | 21.4 | 0.91efg | 23.65b | ND | ND |
| rutin | 27.4 | 1.77de | 3.07c | 9.15c | 25.18b |
| hesperidin | 27.5 | 0.23g | ND | 1.72d | ND |
| oleuropein | 32.9 | 0.51fg | 2.4c | 4.00d | 1.39d |
| quercetin | 37.4 | 0.69efg | ND | 10.32c | 1.38d |
| luteolin | 39.2 | 49.02a | 25.04b | 30.43b | 33.86a |
| apigenin | 43.8 | 32.33b | 45.84a | 44.39a | 34.00a |
| SE | | 0.36 | 0.62 | 0.83 | 0.44 |

[a]Mean value of two replicates. Percentage of total phenolic content based on peak areas. Column values with the same letters were not significantly different ($p < 0.05$). SE: standard error. ND: not detected.

Hayball[11] reported that the major phenolic compounds in virgin olive oil are oleuropein, hydroxytyrosol, and tyrosol. The variation in profile of phenolic compounds for olive oil may be due to many factors including degree of olive maturity,[13] and filtration of virgin olive oil during extraction and processing.[14] Storage appears to be a major factor as tyrosol and hydroxytyrosol were found at low concentrations after storage of olive oil for more than six months.[16] Reboredo-Rodríguez et al.[38] reported that the contents of individual phenolic compounds were 19.3−66.8 mg/kg for hydroxytyrosol and tyrosol, 3.3−8.4 mg/kg for apigenin and luteolin, 2.9−5.8 mg/kg for pinoresinol, and trace contents for vanillic acid and *p*-coumaric acid.

**Effect of Removal of Free and Bound Phenolics on Fatty Acids Content.** Table 5 shows the fatty acid composition (g/100 g olive oil) for virgin olive oil before and after removal of free and bound phenolic compounds. The major predominant fatty acids in virgin olive oil in either the presence or absence of phenolic compounds were oleic acid (83.026−83.859%), palmitic acid (7.502−8.008%), and linoleic acid (5.837−6.190%) whereas myristic, palmitoleic, arachidic, eicosenoic, and behenic acids were found in minor amounts. Olive oil after removal of free and bound phenolic compounds showed a significant decrease in oleic acid (C18:1) content while concentrations of palmitoleic, stearic, linoleic, and linolenic acids were increased. The decrease in oleic acid content after removal of free and bound phenolics is likely due to conjugation of oleic acid with phenolic compounds in mono- and diacylglycerols. The alkaline hydrolysis may have released the conjugated complex of oleic acid with phenolic compounds into the extracts. The increased levels of palmitoleic, stearic, linoleic, and linolenic acids may be the result of the breakage of bound phenolic compounds with free fatty acids by alkaline hydrolysis leading to the release of free fatty acids following the methanolic extraction of phenolics. The above findings are suggestive that phenolic compounds can be bound to either oleic acid in mono- and diacyglycerols or to palmitoleic, stearic, linoleic, and linolenic acids as free fatty acids.

Table 5. Fatty Acid Composition (g/100 g Virgin Olive Oil) of Virgin Olive Oil, Virgin Olive Oil after Removal of Free Phenolic Compounds, Virgin Olive Oil after Removal of Free and Bound Phenolics[a]

| fatty acid | formula | olive oil (g/100 g) | olive oil after removal of free phenolics (g/100 g) | olive oil after removal of free and bound phenolics (g/100 g) | SE |
|---|---|---|---|---|---|
| myristic | C14:0 | 0.008a | 0.006a | 0.006a | 0.001 |
| palmitic | C16:0 | 7.502a | 7.876a | 8.008a | 0.138 |
| palmitoleic | C16:1 | 0.053b | 0.235a | 0.230a | 0.005 |
| stearic | C18:0 | 1.402b | 1.382b | 1.686a | 0.050 |
| oleic | C18:1 | 83.859a | 83.717a | 83.026b | 0.093 |
| linoleic | C18:2 | 6.053b | 5.837c | 6.190a | 0.028 |
| linolenic | C18:3 | 0.257b | 0.245b | 0.292a | 0.005 |
| arachidic | C20:0 | 0.191a | 0.189a | 0.197a | 0.005 |
| eicosenoic | C20:1 | 0.111a | 0.109a | 0.111a | 0.003 |
| behenicacid | C22:0 | 0.053a | 0.051a | 0.056a | 0.001 |
| squalene | C24:6 | 0.514a | 0.356a | 0.201a | 0.097 |

[a]Means are average of two replicates. Row values with the same letters were not significantly different ($p < 0.05$). SE: standard error.

**Effect of Removal of Free and Bound Phenolic Compounds on RP-HPLC Analysis of Acylglycerols.** The RP-HPLC chromatogram of virgin olive acylglycerols before removal of phenolic compounds showed the presence of four major fractions (F1, F2, F3, and F4) (Figure 2a). The chromatogram for olive oil before removal of phenolic compounds was similar to the profile of olive oil after removal of free phenolic compounds except the presence of F1, which was subdivided to three major peaks F1a, F1b, and F1c (Figure 2b). This latter result suggests that the removal of phenolic compounds in F1 may have affected the polarity of acylglycerols. The RP-HPLC chromatogram for olive oil after removal of free and bound phenolic compounds was similar to the chromatogram for olive oil before removal of those phenolics except that fraction F4 was subdivided into three major peaks after hydrolysis, which suggests that alkaline hydrolysis may have led to partial hydrolysis of acylglycerols in fraction F4. Reboredo-Rodríguez et al.[38] and Reboredo-Rodríguez et al.[39] reported that the predominant fatty acids in olive oil were oleic and linoleic acid.

**LC-MS/MS Analysis of Extracted Phenolic Compounds from Fractionated Acylglycerols via RP-HPLC.** Table 6 shows the percent content of free and bound phenolic

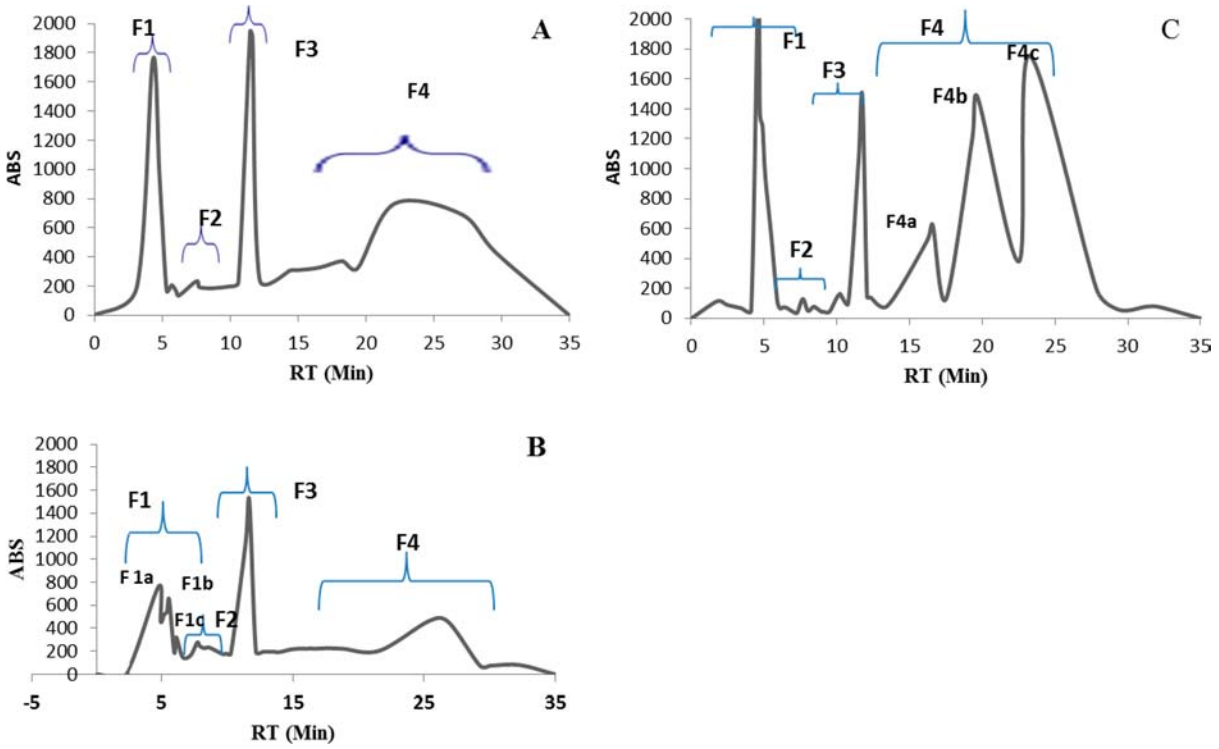


**Figure 2.** RP-HPLC separation for acylgycerols before and after removal of free and bound phenolic compounds from virgin olive oil: (A) olive oil before removal of phenolic compounds, (B) olive oil after removal of free phenolic compounds, (C) olive oil after removal of free and bound phenolic compounds.

**Table 6. Percent of Total Phenolic Content of Individual Phenolic Compounds of Free (before Hydrolysis) and Bound (after Hydrolysis) Phenolic Compounds by LC-MS/MS of RP-HPLC Fractionated Acylglycerols from Olive Oil before and after Removal of Free and Bound Phenolic Compounds[a]**

| | fraction 1 | | fraction 2 | | fraction 3 | | fraction 4 | |
|---|---|---|---|---|---|---|---|---|
| individual phenolic compd | free | free and bound | free | free and bound | free | free and bound | free | free and bound |
| Olive Oil before Removal of Phenolic Compounds, Percent of Total Phenolic Content | | | | | | | | |
| *p*-hydroxybenzoic acid | 80.05 | 47.07 | ND | ND | ND | ND | ND | ND |
| tyrosol | 19.95 | 52.93 | ND | ND | ND | ND | ND | ND |
| Olive Oil after Removal of Free Phenolic Compounds, Percent of Total Phenolic Content | | | | | | | | |
| *p*-hydroxybenzoic acid | ND | 45.63 | ND | ND | ND | ND | ND | ND |
| tyrosol | ND | 54.37 | ND | ND | ND | ND | ND | ND |
| Olive Oil after Removal of Free and Bound Phenolic Compounds, Percent of Total Phenolic Content | | | | | | | | |
| *p*-hydroxybenzoic acid | ND | ND | ND | ND | ND | ND | ND | ND |
| tyrosol | ND | ND | ND | ND | ND | ND | ND | ND |

[a]Percent of total phenolic content. ND: not detected.

compounds in RP-HPLC fractionated acylglycerols from olive oil before and after removal of the phenolic compounds. The presence of *p*-hydroxybenzoic acid and tyrosol was detected in both the free and acylglycerol-bound form. After removal of the free phenolic compounds, fraction number 1 showed the presence of *p*-hydroxybenzoic acid and tyrosol in the bound form, which were not detected before alkaline hydrolysis. After removal of free and bound phenolic compounds, *p*-hydroxybenzoic acid and tyrosol were not detected. This suggests that *p*-hydroxybenzoic acid and tyrosol were bound to the glycerol fraction. Phenolic compounds were not detected in the other RP-HPLC fractionated glycerols from olive oil either before or after removal of free and bound phenolic compounds. The above study is the first to demonstrate natural lipid and phenolic interactions in virgin olive oil although Alu'datt et al.[40] have previously suggested the presence of lipid−protein−phenolic interaction in oilseeds such as soybean and flaxseed. It appears that phenolic−lipid interaction in virgin olive oil can occur via two pathways that include either interaction of tyrosol with palmitoleic, stearic, linoleic, or linolenic acids in the free form or via interaction of *p*-hydroxybenzoic acid and oleic acid in conjugated form that is located in mono- and diacylglycerols.

Free and bound phenolic extracts from virgin olive oil showed antioxidant action, $\alpha$-amylase, and ACE inhibitory activities as well as antiproliferative effects in two colorectal cancer cell lines. Free phenolic extracts at 30 °C had superior antioxidant activities as compared to bound phenolic extracts whereas bound phenolic extracts at 30 °C had greater $\alpha$-amylase and ACE inhibitory activities than the free phenolic extracts. The major predominant phenolic compounds in free and bound phenolic extracts from virgin olive oil were apigenin, luteolin, and rutin. The presence of natural lipid−phenolic

interactions was indicated via the presence of *p*-hydroxybenzoic acid and tyrosol in the acylglycerol fractions of virgin olive oil. The biological effects demonstrated with the lipid-bound phenolics in the present work require in vivo verification since there is extensive biotransformation of polyphenols by gut microbiota to secondary metabolites. The present findings, however, present the possibility that naturally occurring lipid bound phenolics might affect the bioaccessibility and bioavailability of the phenolic compounds. The present study indicates natural phenolic lipid interactions are present in virgin olive oil that may generate biologically active natural phenolic lipids for use in pharmaceutical and nutraceutical applications.

## AUTHOR INFORMATION

### Corresponding Author

*E-mail: Muhammad.aludatt@mail.mcgill.ca, malodat@just.edu.jo, mhudatt@uqu.edu.sa. Phone: +962776579511. Fax: +9627201078.

### Funding

Authors acknowledge Jordan University of Science and Technology (JUST) for financial support.

### Notes

The authors declare no competing financial interest.

## REFERENCES

(1) Scalbert, A.; Manach, C.; Morand, C.; Remesy, C.; Jimenez, L. Dietary polyphenols and the prevention of diseases. *Crit. Rev. Food Sci. Nutr.* **2005**, *45*, 287−306.

(2) Figueroa-Espinoza, M. C.; Villeneuve, P. Phenolic acids enzymatic lipophilization. *J. Agric. Food Chem.* **2005**, *53*, 2779−2787.

(3) Sabally, K.; Karboune, S.; St-Louis, R.; Kermasha, S. Lipase-catalyzed synthesis of phenolic lipids from fish liver oil and dihydrocaffeic acid. *Biocatal. Biotransform.* **2007**, *25*, 211−218.

(4) Lue, B. M.; Karboune, S.; Yebaoh, F. K.; Kermasha, S. Lipase-catalyzed esterification of cinnamic acid and oleyl alcohol in organic solvent media. *J. Chem. Technol. Biotechnol.* **2005**, *80*, 462−468.

(5) Guyot, B.; Bosquette, B.; Pina, M.; Graille, J. Esterification of phenolic acids from green coffee with an immobilized lipase from Candida antarctica in solvent-free medium. *Biotechnol. Lett.* **1997**, *19*, 529−532.

(6) Trox, J.; Vadivel, V.; Vetter, W.; Stuetz, W.; Scherbaum, V.; Gola, U.; Nohr, D.; Biesalski, H. K. Bioactive compounds in cashew nut (*Anacardium occidentale* L.) kernels: Effect of different shelling methods. *J. Agric. Food Chem.* **2010**, *58*, 5341−5346.

(7) Khalil, M. L. Biological activity of bee propolis in health and disease. *Asian Pac. J. Cancer Prev.* **2006**, *7*, 22−31.

(8) Boskou, D.; Tsimidou, M.; Blekas, G. Polar phenolic compounds. In *Olive Oil: Chemistry and Technology II*; Boskou, D., Ed.; AOCS Press: Champaign, IL, 2006; pp 73−90.

(9) International Olive Council (IOC). COI/T.15/NC No 3/Rev. 6. Trade standard applying to olive oils and olive pomace oils. Madrid, 2011.

(10) Hashempour, A.; Ghazvini, R. F.; Bakhshi, D.; Sanam, S. A. Fatty acids composition and pigments changing of virgin olive oil (*Olea europea* L.) in five cultivars grown in Iran. *Aust. J. Crop Sci.* **2010**, *4*, 258−260.

(11) Tuck, K. L.; Hayball, P. J. Major phenolic compounds in olive oil: metabolism and health effects. *J. Nutr. Biochem.* **2002**, *13*, 636−644.

(12) Carrasco Pancorbo, A.; Cruces-Blanco, C.; Segura-Carretero, A.; Fernandez Gutierrez, A. Sensitive determination of phenolic acids in extra-virgin olive oil by capillary zone electrophoresis. *J. Agric. Food Chem.* **2004**, *52*, 6687−6693.

(13) Artajo, L. S.; Romero, M. P.; Motilva, M. J. Transfer of phenolic compounds during olive oil extraction in relation of ripening stage of the fruit. *J. Sci. Food Agric.* **2006**, *86*, 518−527.

(14) Gómez -Caravaca, A. M.; Cerretani, L.; Bendini, A.; Segura-Carretero, A.; Fernandez-Gutierrez, A.; Lercker, G. Effect of filtration systems on the phenolic content in virgin olive oil by HPLC-DAD-MSD. *Am. J. Food Technol.* **2007**, *2*, 671−678.

(15) Suárez, M.; Macià, A.; Romero, M. P.; Motilva, M. J. Improved liquid chromatography tandem mass spectrometry method for the determination of phenolic compounds in virgin olive oil. *J. Chromatogr. A* **2008**, *1214*, 90−99.

(16) Baiano, A.; Gambacorta, G.; Terracone, C.; Previtali, M. A.; Lamacchia, C.; La Notte, E. Changes in phenolic content and antioxidant activity of Italian extra-virgin olive oils during storage. *J. Food Sci.* **2009**, *74*, 177−183.

(17) Alu'datt, M. H.; Rababah, T.; Ereifej, K.; Alli, I. Distribution, antioxidant and characterisation of phenolic compounds in soybeans, flaxseed and olives. *Food Chem.* **2013**, *139*, 93−99.

(18) Fortes, C.; Forastiere, F.; Farchi, S.; Mallone, S.; Trequattrinni, T.; Anatra, F.; Schmid, G.; Perucci, C. A. The protective effect of the Mediterranean diet on lung cancer. *Nutr. Cancer* **2003**, *46*, 30−37.

(19) van Duynhoven, J. V.; Vaughan, E.; Jacobs, D.; Kemperman, R.; Velzen, E. V.; Gross, G.; Roger, L. C.; Possemiers, S.; Smilde, A. K.; Dore, J.; Westerhuis, J. A.; Wiele, T. V. D. Metabolic fate of polyphenols in the human superorganism. *Proc. Natl. Acad. Sci. U.S.A.* **2011**, *108*, 4531−4538.

(20) International Olive Oil Council (IOOC). *Olive Oil Quality Omprovement, Technical Handbook*; Madrid, Spain, 1984; pp 25−45.

(21) Alu'datt, M.; Alli, I.; Ereifej, K.; Alhamad, M.; Al-Tawaha, A.; Rababeh, T. Optimisation, characterisation and quantification of phenolic compounds in olive cake. *Food Chem.* **2010**, *123*, 117−122.

(22) Hoff, J. E.; Singleton, K. I. A method for determination of tannins in foods by means of immobilized protein. *J. Food Sci.* **1977**, *42*, 1566−1569.

(23) McCue, P.; Kwon, Y. I.; Shetty, K. Anti-amylase, anti-glucosidase and anti-angiotensin I-converting enzyme potential of selected foods. *Food Biotechnol.* **2005**, *29*, 278−294.

(24) Cushman, D. W.; Cheung, H. S. Spectrometric assay and properties of the angiotensin-converting-I-enzyme of rabbit lung. *Biochem. Pharmacol.* **1971**, *20*, 1637−1648.

(25) Wu, J. J.; Zhang, X. D.; Gillespie, S.; Hersey, P. Selection for TRAIL resistance results in melanoma cells with high proliferative potential. *FEBS Lett.* **2005**, *579*, 1940−1944.

(26) Obied, H.; Bedgood, D. R., Jr.; Prenzler, P.; Robards, K. Chemical screening of olive biophenol extracts by hyphenated liquid chromatography. *Anal. Chim. Acta* **2007**, *603*, 176−189.

(27) Ereifej, K.; Alu'datt, M. H.; Alkahalidy, H. A.; Alli, I.; Rababah, T. Comparison and characterization of fat and protein composition for camel milk from eight Jordanian locations. *Food Chem.* **2011**, *127*, 282−289.

(28) Baldioli, M.; Servili, M.; Perretti, G.; Montedoro, G. F. Antioxidant activity of tocopherols and phenolic compounds of virgin olive oil. *J. Am. Oil Chem. Soc.* **1996**, *73* (11), 1589−1593.

(29) Tripoli, E.; Giammanco, M.; Tabacchi, G.; Di Majo, D.; Giammanco, S.; LaGuardia, M. The phenolic compounds of olive oil: Structure, biological activity and beneficial effects on human health. *Nutr. Res. Rev.* **2005**, *18*, 98−112.

(30) Shahidi, F.; Naczk, M. *Phenolics in Food and Nutraceuticals*; CRC Press: Boca Raton, FL, 2004; pp 1−558.

(31) Gorinstein, S.; Martin-Belloso, O.; Katrich, E.; Lojek, A.; Cíz, M.; Gligelmo-Miguel, N.; Haruenkit, R.; Park, Y. S.; Jung, S. T.; Trakhtenberg, S. Comparison of the contents of the main biochemical compounds and the antioxidant activity of some Spanish olive oils as determined by four different radical scavenging tests. *J. Nutr. Biochem.* **2003**, *14*, 154−159.

(32) Loizzo, M. R.; Di Lecce, G.; Boselli, E.; Menichini, F.; Frega, N. G. Inhibitory activity of phenolic compounds from extra virgin olive oils on the enzymes involved in diabetes, obesity and hypertension. *J. Food Biochem.* **2011**, *35*, 381−399.

(33) Notarnicola, M.; Pisanti, S.; Tutino, V.; Bocale, D.; Rotelli, M. T.; Gentile, A.; Memeo, V.; Bifulco, M.; Perri, E.; Caruso, M. G. Effects of olive oil polyphenols on fatty acid synthase gene expression

and activity in human colorectal cancer cells. *Gene Nutr.* **2011**, *6*, 63−69.
(34) Fabiani, R.; De Bartolomeo, A.; Rosignoli, P.; Servili, M.; Montedoro, G. F.; Morozzi, G. Cancer chemoprevention by hydroxytyrosol isolated from virgin olive oil through G1 cell cycle arrest and apoptosis. *Eur. J. Cancer Prev.* **2002**, *11*, 351−358.
(35) Fini, L.; Hotchkiss, E.; Fogliano, V.; Graziani, G.; Romano, M.; De Vol, E. B.; Qin, H.; Selgrad, M.; Boland, C. R.; Ricciardiello, L. Chemo preventive properties of pinoresinol-rich olive oil involve a selective activation of the ATM-p53 cascade in colon cancer cell lines. *Carcinogenesis* **2008**, *29*, 139−146.
(36) Reboredo-Rodríguez, P.; Rey-Salgueiro, L.; Regueiro, J.; González-Barreiro, C.; Cancho-Grande, B.; Simal-Gándara, J. Ultrasound-assisted emulsification−microextraction for the determination of phenolic compounds in olive oils. *Food Chem.* **2014**, *150*, 128−136.
(37) Regueiro, J.; Sánchez-González, C.; Vallverdú-Queralt, A.; Simal-Gándara, J.; Lamuela-Raventós, R.; Izquierdo-Pulido, M. Comprehensive identification of walnut polyphenols by liquid chromatography coupled to linear ion trap−Orbitrap mass spectrometry. *Food Chem.* **2014**, *152*, 340−348.
(38) Reboredo-Rodríguez, P.; González-Barreiro, C.; Cancho-Grande, B.; Simal-Gándara, J. Quality of extra virgin olive oils produced in an emerging olive growing area in north-western Spain. *Food Chem.* **2014**, *164*, 418−426.
(39) Reboredo-Rodríguez, P.; González-Barreiro, C.; Cancho-Grande, B.; Simal-Gándara, J. Improvements in the malaxation process to enhance the aroma quality of extra virgin olive oils. *Food Chem.* **2014**, *158*, 534−545.
(40) Alu'datt, M. H.; Rababah, T.; Ereifej, K.; Brewer, S.; Alli, I. Phenolic−protein interactions in oilseed protein isolates. *Food Res. Int.* **2013**, *52*, 178−184.

carried out at 25 ± 2 °C and a relative humidity of 70 ± 10%. The photoperiod inside the rearing room was set to 16/8 h light/dark.

**Collection of Volatiles.** The three replicates of each experimental case were simultaneously collected by SPME using three Supelco SPME holders equipped with polydimethylsiloxane/divinylbenzene fibers (PDMS/DVB; 100 μm film thickness; Supelco Inc., Bellefonte, PA, USA). SPME fibers were conditioned before volatile sampling in a GC injector at 250 °C for 10 min with a He flow rate of 20 mL/min.

Each set of 10 olives was placed inside 50 mL round-bottom flasks with a screw-top connecting adapter. Sampling was static, and each SPME needle was inserted through the septum; then, the fibers were exposed to each sample headspace for 20 h at 25 ± 1 °C. After this period, fibers were removed and inserted into the GC injection port to desorb volatiles.

**Chromatographic and Spectroscopic Analysis.** SPME fibers were thermally desorbed into the GC injection port for 1 min. The injector temperature was set at 250 °C, and it was operated in splitless mode. The extracted volatiles were analyzed by gas chromatography coupled with mass spectrometry (GC-MS) using a Clarus 600 GC-MS from PerkinElmer Inc. (Wellesley, MA, USA), equipped with a ZB-5MS fused silica capillary column (30 m × 0.25 mm i.d. × 0.25 μm; Phenomenex Inc., Torrance, CA, USA). The oven was held at 40 °C for 2 min and then programmed at 5 °C/min to 180 °C and, when reached, raised to 280 °C at 10 °C/min and maintained at 280 °C for 1 min. Helium was used as the carrier gas with a flow of 1 mL/min. The detection was performed in EI mode (ionization energy, 70 eV; source temperature, 180 °C). The spectrum acquisition was performed in scanning mode (mass range $m/z$ 35−500). Chromatograms and spectra were recorded by means of GC-MS Turbomass software version 5.4 (PerkinElmer Inc.). Compounds were identified by comparing their retention indices and mass spectra with those of pure standards and high probability matches (>80%) according to the NIST MS Search routine (NIST Mass Spectral Search Program for the NIST\EPA\NIH mass Spectral Library, version 2.0, build 4/2005).

To confirm the presence of α-copaene and unequivocally identify each isomer, additional olive samples and both α-copaene enantiomer standards were analyzed by chiral GC-FID with a Clarus 500 GC (PerkinElmer Inc.), equipped with an InertCap CHIRAMIX capillary column (30 m × 0.25 mm i.d. × 0.25 μm; GL Sciences Inc.) supplied by Teknokroma Analítica SA (Barcelona, Spain). In this case, the oven was held at 60 °C for 1 min, then programmed at 1 °C/min to 180 °C, and maintained at this temperature for 10 min.

**Chemicals.** All reagents and solvents (reagent grade) were purchased from Sigma-Aldrich (Madrid, Spain) and employed without additional purification unless stated. (+)-α-Copaene (>95% purity by GC) and (−)-α-copaene (>97% purity by GC) were isolated from angelica seed oil (Sigma-Aldrich) or copaiba balsam oil (Sigma-Aldrich) respectively, according to the procedure described by Jacobson et al.[10]

**Oviposition Preference Bioassay.** Twenty mated 8−10-day-old *B. oleae* females were introduced in 30 × 25 × 25 cm PMMA cages and held there for 24 h for acclimation before olive fruits were offered for oviposition test. The flies had free access to food and water at any time.

Green olive fruits used in the experiments were freshly collected from *O. europaea* cv. Serrana and had an equivalent ripening grade (green colored and firm flesh) and size (19−21 mm length). The fruits were gently wiped with a cellulose towel and carefully examined for punctures after 24 h from the collection to ensure that they were uninfested before the assay. A set of 10 olive fruits was placed in a polystyrene 100 × 15 mm Petri dish plate; then, 50 μL of the test solution was dropwise added to each fruit, allowing the solvent to evaporate for 3 min. The test solutions consisted of 1 mg/mL enantiopure α-copaene standard solutions in pentane. Control olive fruits were treated with 50 μL of pentane each.

All treated pairs of olive sets consisting of one α-copaene-added set and one control set were simultaneously offered to the mated females by introducing them inside the assay cage for 240 min. Then, the plates were taken from the cage and allowed to stand for 24 h before examination and recording the number of punctures present in the fruits of each set.

Each experiment was repeated six times in different cages with flies that were not previously used for other bioassays. In each replicate of the assay, the relative position of test substances and control was randomized.

**Statistical Analysis.** Oviposition preference was evaluated by analysis of the ratio of damaged fruits on each set of olives from the offered pair. Ratio of attacked olives (RAO) was calculated by dividing the number of punctured fruits by the total number of fruits for each set. All of the calculated values were transformed to arcsine square root values to normalize the error distribution prior to the analysis of variance (ANOVA). The means were compared and separated by the Tukey−Kramer HSD test at $P = 0.05$. All statistical analyses were conducted using SPSS Statistics version 19 from IBM Corp. (Armonk, NY, USA).

## RESULTS AND DISCUSSION

The first approach for the present study was undertaken by means of a regression analysis between infestation degree and the relative areas of GC-MS peaks obtained from SPME sampling of a set of eight olive cultivars taken from the collection of varieties maintained at CIRGO (Universidad de Córdoba, ceiA3). The sesquiterpene fraction represented ca. 1% of the olive volatile profile for the analyzed samples, but a strong direct correlation was found only between the relative ratio of α-copaene (ranging from approximately 0.015 to 0.15% of the total chromatograms, KI 1381 in a ZB-5MS column) in the volatile fraction of the different samples and their respective percentage of infested olive fruits (Figure 1).

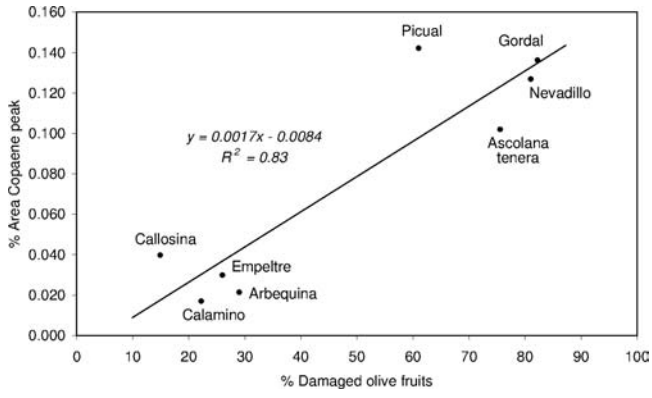


**Figure 1.** Scatter plot of data from different olive varieties according to the percentage of infested fruits and relative α-copaene amount in their volatile profiles. A regression model of these data was obtained by means of least-squares method and provided the depicted line.

This preliminary result encouraged us to carry out a two-year study to determine the changes in the relative amount of α-copaene released from uninfested fruit for a single variety (cv. Serrana) according to their phenological stage as they developed in the tree. This variety is included in the Regulation of Protected Designation of Origin (POD) for Valencian Olive Oil, and it is one of the most cultivated on the east coast of Spain, the latter being the main reason for our selection of this cultivar as it allowed us total availability to collect fresh samples when required.[11] These SPME-GC-MS analyses indicated that α-copaene is not detected until pit hardening is evident (Figure 2); then, the amount of this sesquiterpene rapidly increases to a maximum while the green fruit grows. The subsequent fast decrease of the α-copaene amount is related to fruit ripening,

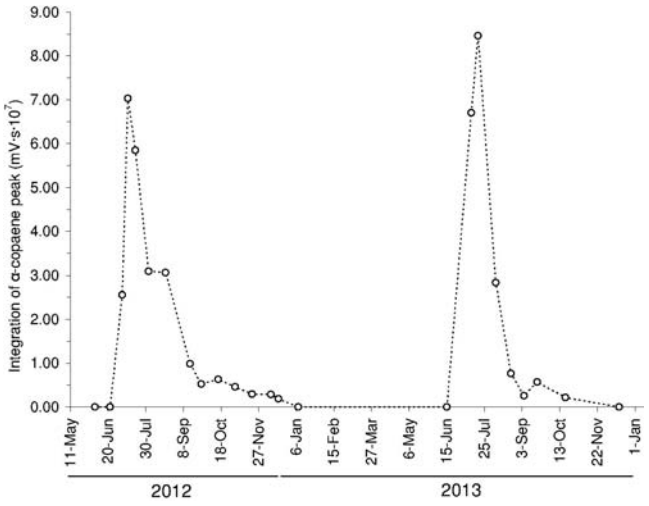


**Figure 2.** Variation of the relative amount of $\alpha$-copaene in the volatile fraction of *Olea europaea* L. cv. Serrana fruits collected at different dates during two years.

and this compound is no longer detected as fruit starts to soften and become darker (Figure 2). These results are in agreement with the decrease of $\alpha$-copaene content in olive oils obtained from fruits at different ripening states found by Vichi et al.[12] On the other hand, it is known that, within a variety, unripe green olives are preferred to ripe red or purple olives, reinforcing the hypothesis that $\alpha$-copaene could play an important role in fruit susceptibility to *B. oleae* attack.[7,13]

Males of many tephritid species are strongly attracted to the odors of particular synthetic or natural compounds.[14] Specifically, angelica seed and root oils from *Angelica archangelica* L. were found to be attractants for the Mediterranean fruit fly (*Ceratitis capitata* Wiedemann).[15] The potent activity of these oils was further attributed to the compound (+)-$\alpha$-copaene, the levorotatory isomer being much less attractive.[10,16] Although $\alpha$-copaene had been widely described as an olive oil volatile, no analysis of its enantiomeric identity has been addressed to date. Given the importance of the compound stereochemistry for the biological activity, the isomeric identity of this compound was assessed in the present study for both Serrana and Picual variety samples, showing a similar ratio of 70:30 for dextro and levo isomers, respectively, by means of chiral GC-FID analysis (according to retention indices of the respective enantiopure standards in a InertCap CHIRAMIX column, KI 1374 and KI 1382 for (+)- and (−)-$\alpha$-copaene, respectively). Although $\alpha$-copaene had been widely described as an olive oil volatile, to our knowledge, no analysis of its enantiomeric identity has been addressed to date.[17−19] In the present study, the isomeric identity of this compound was assessed for both Serrana and Picual variety samples, showing a similar ratio of 70:30 for dextro and levo isomers, respectively, by means of chiral GC-FID analysis according to retention times of the respective enantiopure standards.

To establish the activity of the isomers, an oviposition preference test was carried out for each enantiomer of $\alpha$-copaene from enantiopure standards that were isolated from essential oils and for the racemic mixture prepared from them. The results from these experiments revealed that the addition of (+)-$\alpha$-copaene to olive fruits increases significantly the ratio of attacked olives (Figure 3). On the other hand, the addition of the same amount of (−)-$\alpha$-copaene to olive fruits produced

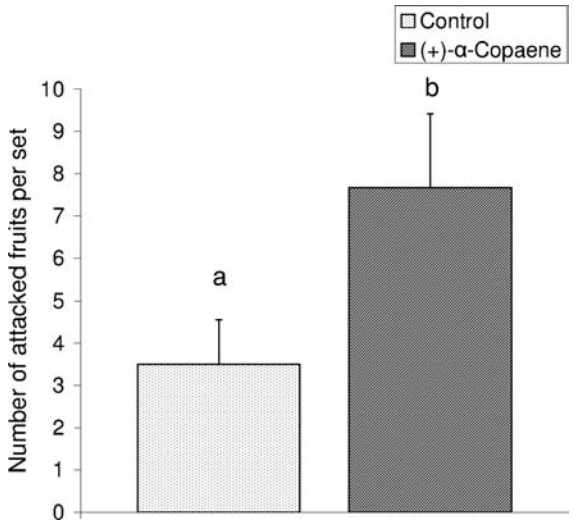


**Figure 3.** Mean (± SD, $N = 6$) number of attacked olive fruits per set in oviposition preference competitive bioassay between olives with added (+)-$\alpha$-copaene and control fruits. Results of ANOVA test performed over arcsine-square root transformed values of RAO: $F_{1,10} = 42.26$, $P < 0.001$. Bars with the same letters are not significantly different by means of Tukey−Kramer HSD test at $P = 0.05$.

no significant differences in this parameter when compared to control (Figure 4). Finally, no synergistic or detrimental effects of the levorotatory isomer on the activity of (+)-$\alpha$-copaene were observed when a racemic mixture was assessed (Figure 5).

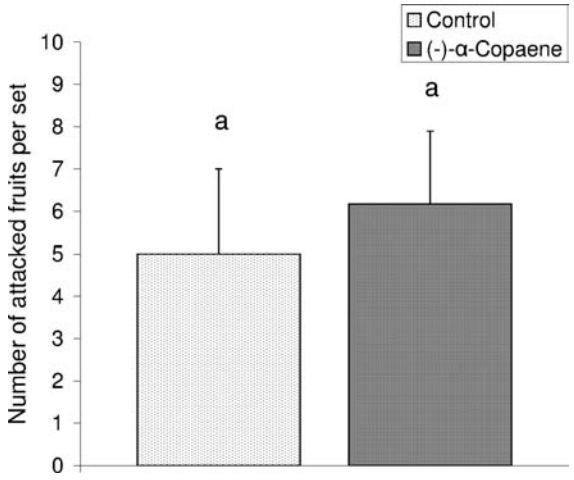


**Figure 4.** Mean (± SD, $N = 6$) number of attacked olive fruits per set in oviposition preference competitive bioassay between olives with added (−)-$\alpha$-copaene and control fruits. Results of ANOVA test performed over arcsine-square root transformed values of RAO: $F_{1,10} = 4.07$, $P = 0.08$. Bars with the same letters are not significantly different by means of Tukey−Kramer HSD test at $P = 0.05$.

The results of the present work showed that (+)-$\alpha$-copaene is clearly contributing to an increase in the susceptibility of olive fruits to attack by *B. oleae* females. Nevertheless, as suggested in previous studies carried out by other authors, it is likely that a combination of several factors is affecting the ovipositional preference for this insect−plant system.[20,21] This is the first study on the effect of the olive-occurring volatile compound $\alpha$-copaene on the behavior of *B. oleae*, contributing to a better understanding of the chemical ecology between this

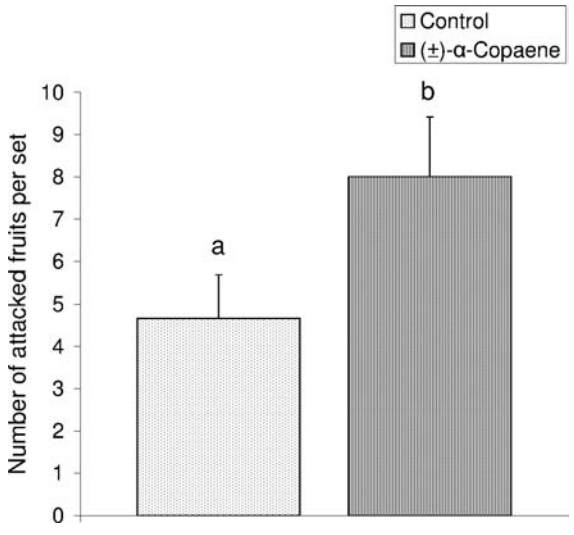


**Figure 5.** Mean (± SD, $N = 6$) number of attacked olive fruits per set in oviposition preference competitive bioassay between olives with added (±)-α-copaene and control fruits. Results of ANOVA test performed over arcsine-square root transformed values of RAO: $F_{1,10} = 91.62$, $P < 0.001$. Bars with the same letters are not significantly different by means of Tukey–Kramer HSD test at $P = 0.05$.

pest and its host, which may result in the development of new control strategies.

## AUTHOR INFORMATION

### Corresponding Author

*(I.A.) Phone: +34-674437680. E-mail: ignacio.alfonso@uv.es.

### Notes

The authors declare no competing financial interest.

## ACKNOWLEDGMENTS

We acknowledge Enrique Quesada-Moraga and Centro Internacional de Recursos Genéticos del Olivo (CIRGO) for providing fruit damage values and cultivar samples. We thank Vicente Navarro-Llopis and the rest of the CEQA staff for their technical support. Vincenzo Girolami deserves our special thanks for his permission to use the olive fruit fly picture as part of our TOC graphic.

## REFERENCES

(1) Daane, K. M.; Johnson, M. W. Olive fruit fly: managing an ancient pest in modern times. *Annu. Rev. Entomol.* **2010**, *55*, 151–169.

(2) Gómez-Caravaca, A. M.; Cerretani, L.; Bendini, A.; Segura-Carretero, A.; Fernández-Gutiérrez, A.; Del Carlo, M.; Compagnone, C.; Cicheli, A. Effects of fly attack (*Bactrocera oleae*) on the phenolic profile and selected chemical parameters of olive oil. *J. Agric. Food Chem.* **2008**, *56*, 4577–4583.

(3) Vossen, P. M. *Organic Olive Production Manual*; University of California, UCARN Publications: Oakland, CA, USA, 2007; 105 pp.

(4) Margaritopoulos, J. T.; Skavdis, G.; Kalogiannis, N.; Nikou, D.; Morou, E.; Skouras, P. J.; Tsitsipis, J. A.; Vontas, J. Efficacy of the pyrethroid α-cypermethrin against *Bactrocera oleae* populations from Greece, and improved diagnostic for an iAChE mutation. *Pest Manage. Sci.* **2008**, *64*, 900–908.

(5) International Atomic Energy Agency (IAEA). Development of improved attractants and their integration into fruit fly SIT managements program. In *Proceedings of a Final Research Coordination Meeting*, Vienna, Austria, May 5–7, 2005; IAEA-TECDOC-1574; International Atomic Energy Agency, IAEA Books, Vienna, Austria, 2007; 230 pp.

(6) Foster, S. P.; Harris, M. O. Behaviourial manipulation methods for insect pest-management. *Annu. Rev. Entomol.* **1997**, *42*, 123–146.

(7) Kombargi, W. S.; Michelakis, S. E.; Petrakis, C. A. Effect of olive surface waxes on oviposition by *Bactrocera oleae* (Diptera:Tephritidae). *J. Econ. Entomol.* **1998**, *91*, 993–998.

(8) Iannotta, N.; Scalercio, S. Susceptibility of cultivars to biotic stresses. In *Olive Germplasm – The Olive Cultivation, Table Olive and Olive Oil Industry in Italy*; Muzzalupo, I., Ed.; INTECH Publications: Rijeka, Croatia, 2012; 384 pp.

(9) Gomes da Silva, M. D. R.; Costa Freitas, A. M.; Cabrita, M. J. B.; García, R. Olive oil composition: volatile compounds. In *Olive Oil – Constituents, Quality, Health Properties and Bioconversions*; Muzzalupo, I., Ed.; INTECH Publications: Rijeka, Croatia, 2012; 522 pp.

(10) Jacobson, M.; Uebel, E. C.; Lusby, W. R.; Waters, R. M. Optical isomers of α-copaene derived from several plant sources. *J. Agric. Food Chem.* **1987**, *35*, 798–800.

(11) López-Cortés, I.; Salazar-García, D. C.; Velázquez-Martí, B.; Salazar, D. M. Chemical characterization of traditional varietal olive oils in East of Spain. *Food Res. Int.* **2013**, *54*, 1934–1940.

(12) Vichi, S.; Lazzez, A.; Kamoun, N. G.; López-Tamames, A.; Buxaderas, S. Evolution of sesquiterpene hydrocarbons in virgin olive oil during fruit ripening. *J. Agric. Food Chem.* **2010**, *58*, 6972–6976.

(13) Neuenschwander, P.; Michelakis, S.; Holloway, P.; Berchtold, W. Factors affecting the susceptibility of fruits of different olive varieties to attack by *Dacus oleae* (Gmel.) (Dipt., Tephritidae). *Z. Ang. Entomol.* **1985**, *100*, 174–188.

(14) Jang, E. B.; Light, D. M. Olfactory semiochemicals of tephritids. In *Fruit Fly Pests: A World Assessment of Their Biology and Management*; McPheron, B. E., Steck, G. J., Eds.; St. Lucie Press: Delray Beach, FL, USA, 1996; pp 73–90.

(15) Steiner, L. F.; Miyashita, D. H.; Christenson, L. D. Angelica oils as Mediterranean fruit fly lures. *J. Econ. Entomol* **1957**, *50*, 505–509.

(16) Flath, R. A.; Cunningham, R. T.; Mon, T. R.; John, J. O. Additional male Mediterranean fruitfly (*Ceratitis capitata* Wied.) attractants from angelica seed oil (*Angelica archangelica* L.). *J. Chem. Ecol.* **1994**, *20*, 1969–1984.

(17) Kesen, S.; Kelebek, H.; Selli, S. Characterization of the key aroma compounds in Turkish olive oils from different geographic origins by application of aroma extract dilution analysis (AEDA). *J. Agric. Food Chem.* **2014**, *62*, 391–401.

(18) Zunin, P.; Boggia, R.; Salvadeo, P.; Evangelisti, F. Geographical traceability of West Liguria extravirgin olive oils by the analysis of volatile terpenoid hydrocarbons. *J. Chromatogr., A* **2005**, *1089*, 243–249.

(19) Bortolomeatzi, R.; Berno, P.; Pizzale, L.; Conte, L. S. Sesquiterpene, alkene, and alkane hydrocarbons in virgin olive oils of different varieties and geographical origins. *J. Agric. Food Chem.* **2001**, *49*, 3278–3283.

(20) Gonçalves, M. F.; Malheiro, R.; Casal, S.; Torres, L.; Pereira, J. A. Influence of fruit traits on oviposition preference of the olive fly, *Bactrocera oleae* (Rossi) (Diptera, Tephritidae), on three Portuguese olive varieties (Cobrançosa, Madural and Verdeal Transmontana). *Sci. Hortic.* **2012**, *145*, 127–135.

(21) Burrack, H. J.; Zalom, F. G. Olive fruit fly (Diptera, Tephritidae) ovipositional preference and larval performance in several commercially important olive varieties in California. *J. Econ. Entomol.* **2008**, *101*, 750–758.

Further, to develop high viscous base stocks, the unsaturation in branched mono- and polyol esters was modified to the acylated derivatives. The base stocks with the above modifications are novel and are reported for the first time.

## MATERIALS AND METHODS

**Materials.** Sal fat was procured from M/s. Paras Vanaspathi, Raipur, India. Hydrogen peroxide, formic acid, sulfuric acid, acetic acid, 4 N hydrobromic acid, iodine monochloride (ICl), potassium hydroxide, hydrochloric acid, *n*-butanol, pyridine, chloroform, acetic anhydride, 2-ethylhexanol (2-EtH), NPG, TMP, *p*-tolunesulfonic acid (p-TSA), 4-(dimethylamino)pyridine (DMAP), xylene, aluminum oxide active basic, sodium hydroxide (NaOH), methanol, urea, and sodium sulfate were procured from M/s SD. Fine chemicals Pvt. Ltd., (Mumbai, India). Propionic, butyric, and hexanoic anhydrides were procured from Sigma-Aldrich (St. Louis, MO, U.S.A.). Hexane, methanol, and ethyl acetate were purchased from Industrial Solvents and Chemicals Pvt. Ltd. (Mumbai, India). All the solvents and reagents were of analytical grade and used directly without purification.

**Methods.** *Spectral Analysis.* Infrared (IR) spectra were obtained on a 1600 FT-IR PerkinElmer Spectrometer (Norwalk, CT) with a liquid film between NaCl cells. Proton nuclear magnetic resonance ($^1$H NMR) spectra were recorded in $CDCl_3$ on Avance 300 MHz spectrometer. Chemical shifts relative to TMS as internal standard are given as $\delta$ values in ppm. Carbon nuclear magnetic resonance ($^{13}$C NMR) spectra were recorded in $CDCl_3$ on a Varian (75 MHz) spectrometer.

*Thermogravimetric Analysis (TGA).* TGA studies were carried out in nonisothermal mode in a Mettler Toledo TGA instrument to get the decomposition pattern of the base stocks. About 5 mg of the sample was taken in an aluminum crucible and heated slowly up to 600 °C at a rate of 10 °C/min under nitrogen atmosphere. The TGA degradation onset temperature was obtained by extrapolating the horizontal baseline and intercept of this line with tangent to the downward portion of the weight curve was taken as onset temperature.

*Physico-Chemical Analyses.* The lubricant properties namely, acid value, hydroxyl value, density, specific gravity, kinematic viscosity, viscosity index, pour point, flash point, copper corrosion, TGA degradation onset temperature, oxidative stability, weld load, and wear of the lubricant base stocks were also determined using standard AOCS and ASTM methods. All the analyses were carried out in duplicates and the results are the average of the two values.

**Procedure for Enrichment of Unsaturation in Sal Fatty Acids.** Sal fatty acid methyl esters (SFAME) 100 g were taken in methanol (1000 mL, 1:10 w/v ratio of SFAME) and urea (200 g, 1:2 w/w ratio of SFAME) was added. The contents were stirred mechanically under reflux until urea was completely dissolved. The contents were cooled to room temperature and stored at 0−5 °C for 12 h. The material was then filtered to remove urea complex and concentrated. The filtrate was extracted with hexane, washed with diluted HCl to remove traces of urea followed by water until it was acid free.[22] The hexane extract was concentrated on rotary evaporator to obtain oleic acid rich SFAME (51 g, 51% yield). The fatty acid composition of enriched SFAME (72.6%, by GC) is shown in Table 1.

The enriched sal fame was hydrolyzed to get oleic acid rich sal fatty acids (ORSFA). ORSFA was further reacted with branched monoalcohol (2-ethylhexanol) and polyols (NPG, TMP) in the presence of a p-TSA and xylene medium at 135−140 °C to obtain corresponding oleic acid rich branched mono and polyol esters (ORS2-EtHE, ORSNPGE, ORSTMPE).[17]

**Table 1. Fatty Acid Composition (wt %) of Oleic Acid Rich Sal Fat**

| | fatty acid composition (wt %) | | | | |
|---|---|---|---|---|---|
| sample name | 16:0 | 18:0 | 18:1 | 18:2 | 20:0 |
| oleic acid rich sal FAME | 9.5 | 15.8 | 67.7 | 4.9 | 2.1 |

**Hydroxylation of Oleic Acid Rich Sal 2-Ethylhexyl Esters.** In a typical experiment, ORS2-EtHE (300 g, 0.764 mol), formic acid (85%) (43.35 mL, 1.14 mol), and concentrated sulfuric acid (3.37 mL, 2% weight of formic acid and hydrogen peroxide) were stirred under mechanical stirring at 5−10 °C. Hydrogen peroxide solution, 30% concentration (234.23 mL, 2.29 mol), which was pre-equilibrated at the same temperature was added slowly to the contents through addition funnel for a period of 2 h. This precaution was taken to prevent over heating of the system due to the exothermic nature of epoxidation. After addition of the $H_2O_2$ the temperature was slowly raised to 60 °C. After 3 h, the temperature of the reaction was raised to 90 °C and stirred for 24 h. The course of the reaction was monitored by withdrawing aliquots of the reaction mixture at various time intervals and analyzed for oxirane value. After complete conversion, the reaction mixture was cooled, extracted with ethyl acetate, and washed with water until it was acid free. The final product was analyzed for acid value, oxirane value, iodine value, and hydroxyl value. The structure of hydroxylated ORS2-EtHE was characterized by IR, $^1$H NMR, and $^{13}$C NMR.

A similar procedure was followed for the preparation of hydroxy ORSNPGE (HydORSNPGE) and hydroxy ORSTMPE (HydORSTMPE) taking ORSNPGE (0.477 mol), formic acid (46.1 mL, 1.19 mol), sulfuric acid (3.5 mL), and hydrogen peroxide solution, 30% concentration (2.38 mol); ORSTMPE (0.325 mol), formic acid (37.78 mL, 0.97 mol), sulfuric acid (3.26 mL), and hydrogen peroxide solution, 30% concentration (2.28 mol) respectively. The hydroxylated polyol esters were analyzed for acid, oxirane, iodine, and hydroxyl values. The structures of the compounds were characterized by IR, $^1$H NMR, and $^{13}$C NMR.

**HydORS2-EtHE.** IR (neat, cm$^{-1}$): 3448 (—OH), 2925 (C—H), 1736 (—C═O), 1168 (C—(C═O)—O); $^1$H NMR ($CDCl_3$, $\delta$ ppm): 0.89 (t, C$\underline{H}_3$—CH$_2$—), 1.19−1.41 (m, (—C$\underline{H}_2$—)$_n$), 1.46−1.51 (m, —CH(OH)—C$\underline{H}_2$—), 1.54−1.72 (m, —CH$_2$—C$\underline{H}_2$—CH$_2$—C═O), 2.31 (t, —CO—C$\underline{H}_2$—CH$_2$—), 3.36−3.45 (m, —C$\underline{H}$—OH), 3.98 (d, —CH—C$\underline{H}_2$—O—CO—CH$_2$—); $^{13}$C NMR ($CDCl_3$, $\delta$ ppm): 10.96, 14.02, 14.08, 22.64, 22.95, 23.76, 24.94, 25.03, 25.56, 25.64, 28.89−29.67, 30.38, 31.89, 34.36, 34.43, 38.70, 66.63, 74.49, 174.09.

**HydORSNPGE.** IR (neat, cm$^{-1}$): 3460 (—OH), 2928 (C—H), 1740 (—C═O), 1162 (C—(C═O)—O); $^1$H NMR ($CDCl_3$, $\delta$ ppm): 0.88 (t, C$\underline{H}_3$-CH$_2$—), 0.96 (s, C$\underline{H}_3$—C—C$\underline{H}_3$), 1.14−1.39 (m, (—C$\underline{H}_2$—)$_n$), 1.40−1.53 (m, —CH(OH)—C$\underline{H}_2$—), 1.54−1.7 (m, —CH$_2$—C$\underline{H}_2$—CH$_2$—C═O), 2.31 (t, —CO-—C$\underline{H}_2$—CH$_2$—), 3.36−3.45 (m, —C$\underline{H}$—OH), 3.87 (s, —C—C$\underline{H}_2$—O—CO—CH$_2$—); $^{13}$C NMR ($CDCl_3$, $\delta$ ppm): 14.08, 21.7, 22.63, 23.83, 24.93, 25.51, 25.63, 28.98−29.88, 31.83, 33.54, 34.21, 34.56, 68.95, 74.39, 74.45, 173.77.

**HydORSTMPE.** IR (neat, cm$^{-1}$): 3461 (—OH), 2924 (C—H), 1742 (—C═O), 1160 (C—(C═O)—O). $^1$H NMR ($CDCl_3$, $\delta$ ppm): 0.88 (t, C$\underline{H}_3$—CH$_2$—), 1.21−1.38 (m, (—C$\underline{H}_2$—)$_n$), 1.44−1.53 (m, —CH(OH)—C$\underline{H}_2$—, —C—C$\underline{H}_2$—CH$_3$), 1.54−1.67 (m, —CH$_2$—C$\underline{H}_2$—CH$_2$—C═O), 2.30 (t, —CO—C$\underline{H}_2$—CH$_2$—), 3.36−3.43 (m, —C$\underline{H}$—OH), 4.01 (s, —C—C$\underline{H}_2$—O—CO—CH$_2$—); $^{13}$C NMR ($CDCl_3$, $\delta$ ppm): 7.30, 14.08, 22.6, 22.9, 23.8, 24.87, 25.65, 28.9−29.6, 31.83, 33.54, 34.12, 40.5, 42.7, 63.62, 74.4, 173.5.

**Propionylation of HydORS2-EtHE.** HydORS2-EtHE (300 g, 0.716 mol), propionic anhydride (2.148 mol), DMAP (0.3 g, 0.1% DMAP based on weight of HydORS2-EtHE), and xylene (150 mL) were taken in a three-necked round-bottom flask and stirred at 135−140 °C for 8 h. The progress of the reaction was monitored by TLC using hexane/ethyl acetate (80:20 v/v) and IR. The crude product was distilled at 140 °C and 5 mm Hg to remove excess propionic anhydride and xylene. The residue was extracted into ethyl acetate, washed with water, passed over anhydrous sodium sulfate, and concentrated using a rotary evaporator and dried under reduced pressure to obtain acylated product. The product was further purified to remove traces of propionic acid by passage through a basic alumina column to obtain propionylated ORS2-EtHE (PrORS2-EtHE) with an acid value of <0.2. The product was analyzed for hydroxyl value. The

structure of the product was confirmed by IR, $^1$H NMR, and $^{13}$C NMR spectral studies.

Similar procedure was followed for the butanoylation and hexanoylation of HydORS2-EtHE (HydORS2-EtHE) and alkanoylation of HydORSNPGE and HydORSTMPE, by taking HydORSNPGE (300 g, 0.439 mol) and alkanoic anhydride (2.198 mol); HydORSTMPE (300 g, 0.439 mol) and alkanoic anhydride (2.097 mol), respectively. The products were analyzed for acid and hydroxyl values. The structures of all the alkanoylated esters were confirmed by IR, $^1$H NMR, and $^{13}$C NMR spectral studies.

**Propionylated Esters of Oleic Acid Rich Sal 2-Ethylhexyl Esters (PrORS2-EtHE).** IR (neat, cm$^{-1}$): 2928 (C—H), 1739 (—C═O), 1182 (C—(C═O)—O); $^1$H NMR ($CDCl_3$, $\delta$ ppm): 0.85–0.92 (m, C$\underline{H}_3$—CH$_2$—), 1.15 (t, C$\underline{H}_3$—CH$_2$–C═O), 1.20–1.39 (m, (—C$\underline{H}_2$—)$_n$), 1.47–1.53 (m, —C$\underline{H}_2$—CH—CO), 1.53–1.65 (—C$\underline{H}_2$—CH$_2$—C═O), 2.26–2.40 (m, —CH$_2$—C$\underline{H}_2$—C═O), 3.94–4.02 (m, —CH—C$\underline{H}_2$—O—CO—), 4.98–5.03 (m, O═C—O—C$\underline{H}$—); $^{13}$C NMR ($CDCl_3$, $\delta$ ppm): 9.25, 10.94, 13.99, 22.63, 22.93, 23.71, 24.90, 25.05, 27.61, 28.86–29.65, 30.34, 30.66, 31.77, 31.86, 34.33, 34.39, 38.66, 66.56, 73.57, 173.97, 174.09.

**Butanoylated Esters of Oleic Acid Rich Sal 2-Ethylhexyl Esters (BuORS2-EtHE).** IR (neat, cm$^{-1}$): 2929 (C—H), 1736 (—C═O), 1178 (C—(C═O)—O);$^1$H NMR ($CDCl_3$, $\delta$ ppm): 0.86–0.91 (m, C$\underline{H}_3$—CH$_2$—), 0.95 (t, C$\underline{H}_3$—(CH$_2$)$_2$—C═O), 1.19–1.39 (m, (—C$\underline{H}_2$—)$_n$), 1.47–1.53 (m, —C$\underline{H}_2$—CH—CO), 1.53–1.71 (—C$\underline{H}_2$—CH$_2$—C═O), 2.26–2.33 (m, —CH$_2$—C$\underline{H}_2$—C═O), 3.94–4.02 (m, —CH—C$\underline{H}_2$—O—CO—), 4.98–5.03 (m, O═C—O—C$\underline{H}$—); $^{13}$C NMR ($CDCl_3$, $\delta$ ppm): 10.96, 13.66, 14.00, 18.52, 22.61, 22.94, 23.76, 24.94, 25.03, 25.08, 28.89–29.66, 30.38, 30.73, 31.79, 31.89, 34.35, 34.42, 36.25, 38.71, 66.60, 73.48, 173.15, 174.00.

**Hexanoylated Esters of Oleic Acid Rich Sal 2-Ethylhexyl Esters (HeORS2-EtHE).** IR (neat, cm$^{-1}$): 2927 (C—H), 1735 (—C═O), 1171 (C—(C═O)—O); $^1$H NMR ($CDCl_3$, $\delta$ ppm): 0.85–0.92 (m, C$\underline{H}_3$—CH$_2$—), 1.20–1.39 (m, (—C$\underline{H}_2$—)$_n$), 1.46–1.52 (m, —C$\underline{H}_2$—CH—CO), 1.53–1.67 (—C$\underline{H}_2$—CH$_2$—C═O), 2.26–2.34 (m, —CH$_2$—C$\underline{H}_2$—C═O), 3.94–4.01 (m, —CH—C$\underline{H}_2$—O—CO—), 4.98–5.03 (m, O═C—O—C$\underline{H}$—); $^{13}$C NMR ($CDCl_3$, $\delta$ ppm): 10.94, 13.85, 13.99, 22.28, 22.63, 22.92, 23.71, 24.70, 24.90, 24.99, 25.07, 28.86–29.65, 30.34, 30.72, 31.27, 31.77, 31.86, 34.30, 38.66, 66.56, 73.43, 173.33, 173.97.

**Propionylated Esters of Oleic Acid Rich Sal NPG Esters (PrORSNPGE).** IR (neat, cm$^{-1}$): 2927 (C—H), 1740 (—C═O), 1177 (C—(C═O)—O); $^1$H NMR ($CDCl_3$, $\delta$ ppm): 0.88 (t, C$\underline{H}_3$—CH$_2$—), 0.96 (s, C$\underline{H}_3$—C—C$\underline{H}_3$), 1.15 (t, C$\underline{H}_3$—CH$_2$—C═O), 1.2–1.35 (m, (—C$\underline{H}_2$—)$_n$), 1.44–1.53 (m, —C$\underline{H}_2$—CH—CO), 1.54–1.67 (m, —C$\underline{H}_2$—CH$_2$—C═O), 2.27–2.40 (m, —CH$_2$—C$\underline{H}_2$—C═O), 3.88 (s, —C—C$\underline{H}_2$—O—CO—CH$_2$—), 4.98–5.03 (m, O═C—O—C$\underline{H}$—); $^{13}$C NMR ($CDCl_3$, $\delta$ ppm): 9.28, 14.08, 21.7, 22.63, 23.74, 24.85, 24.93, 25.05, 27.61, 29.03–29.88, 30.66, 31.77, 31.83, 32.9, 34.18, 34.56, 68.95, 73.61, 173.65, 173.97.

**Butanoylated Esters of Oleic Acid Rich Sal NPG Esters (BuORSNPGE).** IR (neat, cm$^{-1}$): 2926 (C–H), 1736 (—C═O), 1175 (C—(C═O)—O); $^1$H NMR ($CDCl_3$, $\delta$ ppm): 0.88 (t, C$\underline{H}_3$—CH$_2$—), 0.91–1.01 (m, C$\underline{H}_3$—C—C$\underline{H}_3$, C$\underline{H}_3$—(CH$_2$)$_2$—C═O), 1.19–1.36 (m, (—C$\underline{H}_2$—)$_n$), 1.45–1.54 (m, —C$\underline{H}_2$—CH—CO), 1.55–1.73 (m, —C$\underline{H}_2$—CH$_2$—C═O), 2.3 (t, —CH$_2$—C$\underline{H}_2$—C═O), 3.87 (s, —C—C$\underline{H}_2$—O—CO—CH$_2$—), 4.97–5.05 (m, O═C—O—C$\underline{H}$—); $^{13}$C NMR ($CDCl_3$, $\delta$ ppm): 7.3, 13.87, 14.07, 22.3, 22.6, 22.86, 24.73, 24.87, 25.1, 28.99–29.64, 30.72, 31.27, 31.77, 34.09, 34.30, 40.5, 63.56, 73.42, 173.32.

**Hexanoylated Esters of Oleic Acid Rich Sal NPG Esters (HeORSNPGE).** IR (neat, cm$^{-1}$): 2927 (C—H), 1740 (—C═O), 1170 (C—(C═O)—O); $^1$H NMR ($CDCl_3$, $\delta$ ppm): 0.86–0.91 (m, C$\underline{H}_3$—CH$_2$—, —CO—(CH$_2$)$_4$—C$\underline{H}_3$), 0.96 (s, C$\underline{H}_3$—C—C$\underline{H}_3$), 1.20–1.36 (m, (—C$\underline{H}_2$—)$_n$), 1.46–1.53 (m, —C$\underline{H}_2$—CH—CO), 1.54–1.66 (m, —C$\underline{H}_2$—CH$_2$—C═O), 2.26–2.35 (m, —CH$_2$—C$\underline{H}_2$—C═O), 3.87 (s, —C—C$\underline{H}_2$—O—CO—CH$_2$—), 4.97–5.03 (m, O═C—O—C$\underline{H}$—); $^{13}$C NMR ($CDCl_3$, $\delta$ ppm): 13.88, 14.08, 21.72, 22.3, 22.65, 23.75, 24.73, 24.96, 25.1, 26.04, 26.14, 29.06–29.9, 30.74, 31.3, 31.78, 31.89, 32.93, 34.2, 34.27, 34.33, 34.46, 34.61, 38.53, 42.8, 68.96, 73.46, 73.72, 173.32, 173.61, 173.71.

**Propionylated Esters of Oleic Acid Rich Sal TMP Esters (PrORSTMPE).** IR (neat, cm$^{-1}$): 2926 (C—H), 1741 (—C═O), 1180 (C—(C═O)—O); $^1$H NMR ($CDCl_3$, $\delta$ ppm): 0.88 (t, C$\underline{H}_3$—CH$_2$—), 1.15 (t, C$\underline{H}_3$—CH$_2$—C═O), 1.2–1.36 (m, (—C$\underline{H}_2$—)$_n$), 1.42–1.54 (m, —C$\underline{H}_2$—CH—CO), 1.55–1.66 (—C$\underline{H}_2$—CH$_2$—C═O), 2.24–2.42 (m, —CH$_2$—C$\underline{H}_2$—C═O), 4.0 (s, —C—C$\underline{H}_2$—O—CO—CH$_2$—), 4.96–5.05 (m, O═C—O—C$\underline{H}$—); $^{13}$C NMR ($CDCl_3$, $\delta$ ppm): 7.3, 9.25, 14.05, 22.63, 22.86, 23.74, 24.84. 25.05, 27.6, 28.88–29.64, 30.66, 31.83, 34.12, 40.49, 63.56, 73.61, 173.38, 173.97.

**Butanoylated Esters of Oleic Acid Rich Sal TMP Esters (BuORSTMPE).** IR (neat, cm$^{-1}$): 2926 (C—H), 1740 (—C═O), 1177 (C—(C═O)—O); $^1$H NMR ($CDCl_3$, $\delta$ ppm): 0.88 (t, C$\underline{H}_3$—CH$_2$—), 0.95 (t, —CO—(CH$_2$)$_2$—C$\underline{H}_3$), 1.2–1.34 (m, (—C$\underline{H}_2$—)$_n$), 1.44–1.53 (m, —C$\underline{H}_2$—H—CO), 1.53–1.71 (—C$\underline{H}_2$—CH$_2$—C═O), 2.25–2.34 (m, —CH$_2$—C$\underline{H}_2$—C═O), 2.38 (t, —CH$_2$—C$\underline{H}_2$—C═O), 4.01 (s, —C—C$\underline{H}_2$—O—CO—CH$_2$—), 4.97–5.03 (m, O═C—O—C$\underline{H}$—); $^{13}$C NMR ($CDCl_3$, $\delta$ ppm): 7.3, 13.64, 14.05, 18.5, 22.63, 22.89, 23.739, 24.87, 25.07, 29.20, 29.64, 30.72, 31.83, 34.12, 36.22, 40.50, 63.57, 73.46, 173.13, 173.42.

**Hexanoylated Esters of Oleic Acid Rich Sal TMP Esters (HeORSTMPE).** IR (neat, cm$^{-1}$): 2927 (C—H), 1740 (—C═O), 1168 (C—(C═O)—O); $^1$H NMR ($CDCl_3$, $\delta$ ppm): 0.83–0.95 (m, C$\underline{H}_3$—CH$_2$—, —CO—(CH$_2$)$_4$—C$\underline{H}_3$), 1.21–1.37 (m, (—C$\underline{H}_2$—)$_n$), 1.43–1.53 (m, —C$\underline{H}_2$—CH—CO), 1.55–1.69 (m, —C$\underline{H}_2$—CH$_2$—C═O), 2.24–2.41 (m, —CH$_2$—C$\underline{H}_2$—C═O), 4.01 (s, —C—C$\underline{H}_2$—O—CO—CH$_2$—), 4.95–5.06 (m, O═C—O—C$\underline{H}$—); $^{13}$C NMR ($CDCl_3$, $\delta$ ppm): 7.3, 13.87, 14.08, 22.28, 22.6, 22.86, 24.78, 25.1, 29.03–29.67, 30.72, 31.27, 31.82, 34.24, 40.49, 63.56, 73.43, 173.33.

## RESULTS AND DISCUSSION

Sal fat (containing 56.5% saturated fatty acids) based polyol esters synthesized in our earlier study[17] showed viscosities ranging between ISO viscosity grades 10 to 68 suitable for high temperature applications. However, the base stocks were found to exhibit high pour points.[17] With this background, an attempt was made to further chemically modify sal fat to generate high viscosity base stocks which are in more demand for high temperature industrial applications such as gear oil applications (involving BS 150 lubricant base stocks), forging lubricants and metal working fluids. As these base-stocks require very high viscosities and low pour points, sal fatty acids were chemically modified employing a four step process. Initially, oleic acid rich sal fatty acid esters were prepared employing urea complexation method and then hydrolyzed to get oleic acid rich sal fatty acids. These fatty acids were esterified with branched mono- and polyols such as 2-EtH, NPG, and TMP to prepare esters in 95.5 to 93% yields.

The branched mono- and polyol esters were hydroxylated using one pot synthesis of epoxidation followed by hydroxylation using Prilezhaev dihydroxylation method.[23] The hydroxylated products were analyzed for oxirane value, hydroxyl value, and iodine value and characterized using spectral techniques. The products with low oxirane < 0.1, iodine ≤ 1.5, and high hydroxyl values of 168–119, indicated complete hydroxylation of branched mono- and polyol esters. The presence of prominent —OH stretching band (~3450) as observed in IR spectra along with disappearance of ═C—H and epoxy stretching bands supported the complete hydroxylation. The presence of a multiplet at ~1.40–1.53 ppm related to —CH(OH)—C$\underline{H}_2$— and multiplet at ~3.36–3.45 ppm related to —C$\underline{H}$—OH in $^1$H NMR and also characteristic

**Scheme 1. Synthesis of Acylated Neopentyl Glycol Esters of Oleic Acid Rich Sal Fatty Acids**

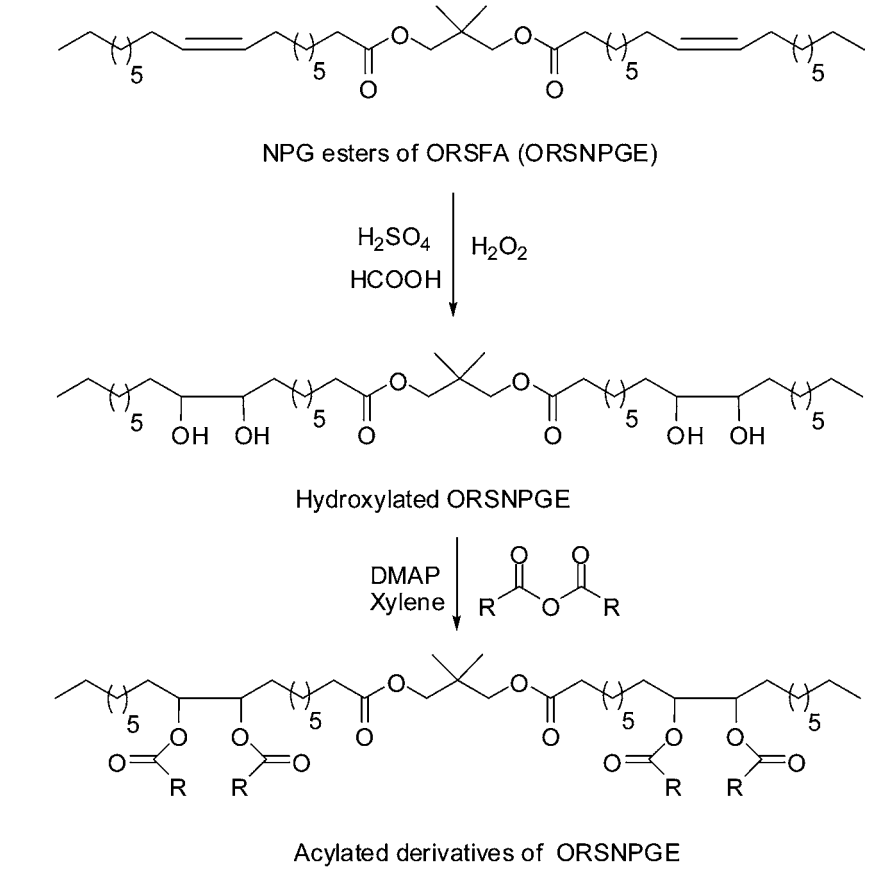


peaks at ~74.5 ppm related to $C_9$ and $C_{10}$ hydroxyl carbons in $^{13}C$ NMR further confirmed complete hydroxylation.

Further, the hydroxylated branched mono- and polyol esters were acylated by using propionic anhydride, butyric anhydride, and hexanoic anhydrides in the presence of DMAP and xylene medium at 135−140 °C, as branching helps in reducing the pour points and improving oxidation stability.[24] The progress of the reaction was monitored by TLC using hexane/ethyl acetate (80:20 v/v) and IR spectra. The lower hydroxyl value (≤3.1) indicated the completion of acylation. A total of nine products were prepared and thoroughly characterized using spectral data (IR, $^1H$ NMR, and $^{13}C$ NMR). The scheme involved in the preparation of the above esters is shown by taking NPG esters of ORSFA acylation as a representative in Scheme 1.

In IR spectra, the noticeable disappearance of −O−H stretching band in the region of (~3450) $cm^{-1}$ and appearance of prominent intensity of carbonyl functionality at ~1740 $cm^{-1}$ were also observed; this is due to increasing the ester functionality in the products confirming complete acylation.

In $^1H$ NMR spectra, the presence of triplet at 1.15 ppm related to methyl protons of the propanoyl side chain, multiplet at 4.98−5.03 ppm related to acylated $C_9$ and $C_{10}$ protons and also increase in area of peak at 2.2−2.4 ppm, related to methylene protons $\alpha$ to the corbonyl group of the acyl side chain, indicated the complete propanoylation of branched mono- and polyol esters. In butanoylation the presence of new peak, triplet at 0.95 ppm related to methyl protons of the butanoyl side chain and multiplet at 4.98−5.03 ppm related to acylated $C_9$ and $C_{10}$ protons and also increase in area of peak at around 2.2−2.3 ppm, related to methylene protons $\alpha$ to the corbonyl group of the acyl side chain, confirmed the butanoylation of branched mono- and polyol esters. The presence of multiplets at around 0.83−0.95 ppm, 4.98−5.03 ppm related to acylated $C_9$ and $C_{10}$ protons and also increasing the area of peak at 2.26−2.4 ppm due to methylene protons $\alpha$ to the carbonyl group of the acyl side chain confirmed the complete hexanoylation of branched mono- and polyol esters. The dissappearance of multiplet at 3.36−3.45 ppm related to −C<u>H</u>−OH further supported the acylation.

In $^{13}C$ NMR spectra, the peaks at around 9.25 ppm related to propanoyl side chain methyl carbon, 73.6 ppm of $C_9$ and $C_{10}$ carbons of propanoylated esters and 173.97 ppm confirmed the propanoylation. The peaks at around 13.7 ppm related to butanoyl side chain methyl carbon, $C_9$ and $C_{10}$ carbons of butanoylated esters 73.4 and 173.4 ppm indicates the butanoylation. The presence of peaks at 13.88 ppm related to hexanoyl side chain methyl carbon, 73.4 ppm of $C_9$ and $C_{10}$ carbons of hexanoylated esters and 173.4 ppm confirmed the hexanoylation of branched mono- and polyol esters.

All the nine base-stocks were characterized for lubricant properties such as density, specific gravity, kinematic viscosity, viscosity index, pour point, flash point, thermogravimetric analysis (TGA), rotating pressurized vessel oxidation test


dx.doi.org/10.1021/jf504700m | J. Agric. Food Chem. 2014, 62, 11980−11987

**Table 2. Physico-Chemical and Lubricant Properties of Propionylated Oleic Acid Rich Sal 2-Ethylhexyl Esters (PrORS2-EtHE), Butanoylated Oleic Rich Sal 2-Ethylhexyl Esters (BuORS2-EtHE), and Hexanoylated HeORS2-EtHE Oleic Rich Sal 2-Ethylhexyl Esters**

| test | | method | PrORS2-EtHE | BuORS2-EtHE | HeORS2-EtHE |
|---|---|---|---|---|---|
| total acid number | | AOCS Te 2a-64 | 0.28 | 0.33 | 0.35 |
| hydroxyl value | | AOCS Cd 13-60 | 1.2 | 2.3 | 1.8 |
| density at 15 °C (g/cm$^3$) | | ASTM D 4052 | 0.91412 | 0.91369 | 0.90012 |
| specific gravity at 15 °C | | ASTM D 4052 | 0.91494 | 0.91451 | 0.90093 |
| kinematic viscosity (cSt) | 40 °C | ASTM D 445 | 23.44 | 22.65 | 20.94 |
| | 100 °C | | 4.91 | 4.89 | 4.71 |
| viscosity index (VI) | | ASTM D 2270 | 137 | 144 | 150 |
| pour point (°C) | | ASTM D 97 | −3 | −3 | −6 |
| flash point (°C) | | ASTM D 93 | 238 | 244 | 252 |
| TGA onset temp. (°C) | | | 254 | 266 | 272 |
| copper corrosion | | ASTM D 130 | 1a | 1a | 1a |
| oxidative stability (min) (RPVOT) | | ASTM D 2272 | 18 | 20 | 16 |
| weld load (kg) | | IP 239 | 130 | 130 | 140 |
| wear (mm) | | ASTM D 4172 | 0.63 | 0.65 | 0.73 |

**Table 3. Physico-Chemical and Lubricant Properties of Propionylated Oleic Acid Rich Sal Neopentyl Glycol Esters (PrORSNPGE), Butanoylated Oleic Acid Rich Sal Neopentyl Glycol Esters (BuORSNPGE), and Hexanoylated Oleic Acid Rich Sal Neopentyl Glycol Esters (HeORSNPGE)**

| test | | method | PrORSNPGE | BuORSNPGE | HeORSNPGE |
|---|---|---|---|---|---|
| total acid number | | AOCS Te 2a-64 | 0.21 | 0.35 | 0.33 |
| hydroxyl value | | AOCS Cd 13-60 | 1.1 | 2.3 | 2.9 |
| density at 15 °C (g/cm$^3$) | | ASTM D 4052 | 0.95401 | 0.95101 | 0.94584 |
| specific gravity at 15 °C | | ASTM D 4052 | 0.95487 | 0.95687 | 0.94669 |
| kinematic viscosity (cSt) | 40 °C | ASTM D 445 | 318.84 | 301.73 | 268.81 |
| | 100 °C | | 32.45 | 31.94 | 30.09 |
| viscosity index (VI) | | ASTM D 2270 | 142 | 146 | 150 |
| pour point (°C) | | ASTM D 97 | 3 | 0 | −3 |
| flash point (°C) | | ASTM D 93 | 300 | 314 | 329 |
| TGA onset temp. (°C) | | | 347 | 349 | 357 |
| copper corrosion | | ASTM D 130 | 1a | 1a | 1a |
| oxidative stability (min) (RPVOT) | | ASTM D 2272 | 20 | 20 | 18 |
| weld load (kg) | | IP 239 | 165 | 170 | 180 |
| wear (mm) | | ASTM D 4172 | 0.78 | 0.73 | 0.69 |

**Table 4. Physico-Chemical and Lubricant Properties of Propionylated Oleic Acid Rich Sal Trimethylolpropane esters (PrORSTMPE), Butanoylated Oleic Acid Rich Sal Trimethylolpropane (BuORSTMPE), and Hexanoylated Oleic Acid Rich Sal Trimethylolpropane HeORSTMPE**

| test | | method | PrORSTMPE | BuORSTMPE | HeORSTMPE |
|---|---|---|---|---|---|
| total acid number | | AOCS Te 2a-64 | 0.15 | 0.31 | 0.29 |
| hydroxyl value | | AOCS Cd 13−60 | 1.5 | 2.5 | 3.1 |
| density at 15 °C (g/cm$^3$) | | ASTM D 4052 | 0.97181 | 0.96826 | 0.96065 |
| specific gravity at 15 °C | | ASTM D 4052 | 0.97268 | 0.96913 | 0.96151 |
| kinematic viscosity (cSt) | 40 °C | ASTM D 445 | 471.93 | 463.33 | 427.35 |
| | 100 °C | | 41.73 | 42.49 | 43.82 |
| viscosity index (VI) | | ASTM D 2270 | 138 | 143 | 157 |
| pour point (°C) | | ASTM D 97 | 9 | 6 | 3 |
| flash point (°C) | | ASTM D 93 | 333 | 351 | 375 |
| TGA onset temp. (°C) | | | 376 | 382 | 385 |
| copper corrosion | | ASTM D 130 | 1a | 1a | 1a |
| oxidative stability (min) (RPVOT) | | ASTM D 2272 | 20 | 16 | 15 |
| weld load (kg) | | IP 239 | 180 | 185 | 190 |
| wear (mm) | | ASTM D 4172 | 0.78 | 0.72 | 0.69 |

(RPVOT), weld load, and wear (Tables 2, 3 and 4) using standard test methods.

**Kinematic Viscosity.** Viscosity of lubricant is the resistance to flow and is directly related to the film formation. It was observed that in case of acylated TMP esters of oleic acid rich sal fatty acids the viscosities ranged between 427 to 468 cSt at 40 °C which could be due to larger number of acyl groups.[18] A lubricant oil with high viscosity flows very slowly and is good to

form stable film between two moving surfaces.[25] The base-stocks in this viscosity range lie within the viscosity of BS 150 mineral oil and those required for high temperature applications such as forging lubricants and metal working fluids. With the shift in polyol from TMP to NPG, the viscosities of the corresponding acylated NPG esters (268.81 to 318.84 cSt) showed a decrease by about 150−200 units. This could be due to the smaller number of acyl groups and difference in molecular size compared to TMP esters. Similar observations were found in case of rubber based polyol esters.[16] These viscosities are related to ISO VG 320 and well suited for the industrial applications such as SAE gear oil No. 80W-140, bearing lubricants and positive displacement blowers, forging lubricants and metal working fluids. On further acylation of 2-ethylhexyl esters, the viscosities drastically fell by several folds ranging from 20.94 to 23.44 cSt, related to ISO VG 22 viscosity grade base stocks. These low viscosity grade base stocks are in more demand today in several industrial applications.[9]

Among the nine acylated TMP, NPG, and 2-EtH esters, the viscosities and densities were found to decrease as the alkyl chain increased from propyl to butyl, butyl to hexanoylated polyol esters. The degree of attenuation in viscosity of acylated lubricant basestocks was observed with increased substituent group chain length. This could be the effect of branching in the chain, which tends to introduce sphericity in the molecule, causing attenuation in the viscosity.[8] Similar observations were found in viscosities of acylated derivatives of milkweed oil,[8] branched polysaccharides,[26] branched synthetic polymers[27,28] and oligomerized estolides of oleic acid.[29]

**Viscosity Index (VI).** VI describes the change of viscosity with change in temperature. A high VI indicates there is little change over a wide temperature range. The acylated polyol esters exhibited high viscosity indices ranging from 138 to 157 in acylated TMP esters, 142−150 in acylated NPG esters and 137−150 in the acylated 2-ethylhexyl esters indicating their multirange applications.[15,30] Even though the VI increased with the molecular weight of the acyl group, it slightly decreased with branching. A similar trend was reported by Yao et al.[31] for ricinoleic acid−based acylated products. The VI values of the reported acylated derivatives are comparable to those of synthetic oils and superior to those of mineral oils.[8,9,32,33] Based on viscosity index, sal oleic acid rich acylated polyol esters belong to group II and group III, category of base fluids as per API classification. The viscosity indices are also well within the specifications required for BS 150 mineral oil base stocks, forging, and metal working fluid applications.

**Pour Point.** Pour point indicates the low temperature fluidity of lubricants. Vegetable oils have a tendency to form macrocrystalline structures at low temperature through uniform stacking of the "bend" triacylglycerol backbone. Such macro-crystals restrict the easy flow of the system due to loss of kinetic energy of individual molecules during self-stacking. The property can be improved by increasing the unsaturation and modification at the unsaturation and also at −COOH. Presence of a polyol and branched mono alcohol attached to the fatty acid does not allow the molecules to come closer due to steric interactions, preventing easy stacking of the individual molecules resulting in better fluidity of the total mixture. Among the nine base stocks, acylated TMP esters of oleic acid rich sal fatty acids exhibited high pour points (3 to 9 °C) compared to the corresponding acylated NPG (−3 to 3 °C) and acylated 2-EtH esters of oleic acid rich sal fatty acids (−3 to −6 °C). It was observed that the pour points of the base stocks under study are much lower compared to corresponding sal fatty acid based branched mono and polyol esters.[17] This could be due to effective disruption of molecular packing in the former with high degree of branching due to acylated groups compared to the later. The pour points of TMP esters are higher compared to that of BS 150 mineral oil base stocks, which can be further reduced by using appropriate pour point depressants and diluents.[14] The pour point decreased with branching as seen in the corresponding acylated 2-ethylhexyl esters of oleic acid rich sal fatty acids (−6 to −3 °C). Similar observation was reported for acylated jatropha alkyl esters[9] and acylated soy bean oil derivatives.[13] The base stocks with low pour points are useful for machine tool and hydraulic systems applications.[34]

**Flash Point.** Flash point is useful in determining a biolubricant volatility, fire resistance, and transportation and storage temperature requirements. The flash point should be high to allow the safe operation and minimum volatilization at the maximum operating temperature. The flash point values of all the 9 acylated branched mono- and polyol esters as observed in the range 238−375 °C are useful for multirange applications. Among all the acylated derivatives acylated TMP esters exhibited high flash points (333−375 °C) followed by acylated NPG esters (300−329 °C) and acylated 2-EtH esters (238−252 °C). The high flash point of the acylated TMP esters is due to the high molecular weight and side chain branching. The flash point specification for hydraulic oils as per IS: 3098 is 150 °C. All the acylated derivatives with flash point of ≥165 °C lie well within the range of hydraulic oils.[35] The lubricant base stocks with high flash point ≥300 °C are suitable for the applications that are in more demand, such as gear oil lubricants and aviation jet engine lubricants.[36]

**TGA.** The thermal stability of a fluid is its ability to resist decomposition on exposure to high temperatures. It establishes the ultimate high-temperature limit for a tribological system fluid that will ensure continual unimpaired service. The most significant change in fluid properties caused by thermal decomposition of organic molecules is an increase in vapor pressure caused by the shearing of molecules into smaller, more volatile fragments. Ester functionality is more prone to thermolysis and removal of $\beta$-hydrogen in the triglyceride by reacting with a polyol and branched alcohols improves the thermal stability.[37]

Among the nine base stocks prepared, the acylated TMP esters exhibited very high thermal stabilities as observed by their TGA onset temperatures, 376−385 followed by NPG esters, 347−357. The stability of the branched mono esters was found to decrease drastically due to disturbance in crystalline packing.[37] However, the values were found higher compared to the undecenoic acid−based polyol esters and other vegetable oil based polyol esters.[15,39] The high thermal stabilities of the acylated TMP and NPG esters are suitable as substitutes to BS 150 mineral oil base stocks and for high temperature applications such as forging and metal working fluid applications.

**Rotating Pressurized Vessel Oxidation Test (RPVOT).** Oxidation stability is another important property which determines the degree of resistance of the lubricant to oxidation. In general, the ester group is oxidatively stable and increases the stability of the adjacent carbon atoms.[38,39] Removal of the $\beta$-hydrogen in the triglyceride by reacting with a polyol and branched alcohols improves the oxidation stability. In general, TMP esters are more stable compared to

NPG and branched esters.[37] However, in the present study, it was observed an increase in unsaturation by urea adduct complexation, followed by reaction with polyols and branched alcohols, which on further acylation increased the oxidation stabilities of all the base stocks. The oxidation stabilities of all the base stocks were higher or comparable to other vegetable oil-based synthetic esters.[9,15,16,33] All the nine base stocks with good oxidation stabilities can be well exploited as mineral oil base stock substitutes in a variety of lubricant formulations.

**Extreme Pressure Test (Weld Load).** Weld load is another important property of lubricant base stocks, which determines the load-carrying capacity of the lubricants. The weld load capacity of the acylated ORSTMP esters is found to be more (180−190 kg), followed by acylated ORSNPG esters (155−170 kg) and acylated ORS2-EtHE (130−140 kg). All the 9 acylated base stocks were is found to possess high load carrying capacity compared to other reported polyols.[16,17]

**Wear.** This property indicates the antiwear properties of the lubricant between two sliding surfaces preventing the surfaces from the dimensional loss of one solid, with or without any actual decoupling and loss of material. In case of polyol esters, the effect of nature of the polyol involved has hardly any effect on the property.[40] Similar observation was seen in the TMP and NPG acylated products understudy. However, all the acylated polyol and branched mono-esters exhibited good antiwear properties suitable for high pressure and high temperature applications such as the forging and metal working fluid applications.

In conclusion, Sal fat was chemically modified to develop acylated branched mono and polyol esters of oleic acid rich sal fatty acids with a wide range of properties matching with BS 150 mineral oil base stocks in case of TMP acylated products, forging and metal working fluid applications in case of NPG acylated products. The modification resulted in low viscous 2-EtH acylated products suitable for metal working and hydraulic fluid applications. The thermal and oxidative stabilities of the base stocks have been improved with the above modification and found comparable to synthetic esters. Overall, all the base stocks with stringent properties are promising candidates to replace most of the mineral oil base stocks in a variety of industrial applications either as such or after formulations.

## AUTHOR INFORMATION


### Corresponding Author

*Tel.: +91-40-27193179. Fax: +91-40-27193370. E-mail: karuna@iict.res.in.


### Notes

The authors declare no competing financial interest.

## REFERENCES


(1) Prerna, C. S.; Chhibber, V. K. Chemical modification in karanja oil for biolubricant industrial applications. *J. Drug Delivery Ther.* **2013**, 3 (3), 117−122.

(2) Adhvaryu, A.; Liu, Z.; Erhan, S. Z. Synthesis of novel alkoxylated triacylglycerols and their lubricant base oil properties. *Ind. Crops Prod.* **2005**, *21*, 113−119.

(3) Erhan, S. Z.; Asadauskas, S. Lubricant basestocks from vegetable oils. *Ind. Crops Prod.* **2000**, *11* (2−3), 277−282.

(4) Gapinski, R. E.; Joseph, I. E.; Layzell, B. D. A vegetable oil based tractor lubricant. SAE Technical Paper 941758, 1994, DOI: 10.4271/941758.

(5) Bunemann, T. F.; Steverink-de Zoete, M. C.; Van Aken, R. P. Synthetische ester—Wie kann mann die lebensdauer von biologisch schnell abbaueren hydraulikfleussigkeiten verlängern. In *Proceedings in International Colloquium Tribology, 2000-Plus, Ostfildern TAE*, 2000; pp 15−25.

(6) Knothe, G.; Dunn, R. O.; Shockley, M. W.; Bagby, M. O. Synthesis and characterization of some long-chain diesters with branched or bulky moieties. *J. Am. Chem. Soc.* **2000**, *77*, 865−871.

(7) Knothe, G. Characterization of esters of fatty acids and dicarboxylic acids with guerbet alcohols. *J. Am. Chem. Soc.* **2001**, *78*, 537−540.

(8) Harry-O'kuru, R. E.; Biresaw, G.; Cermak, S. C.; Gordon, S. H.; Vermillion, K. Investigation of some characteristics of polyhydroxy milkweed triglycerides and their acylated derivatives in relation to lubricity. *J. Agric. Food Chem.* **2011**, *59*, 4725−4735.

(9) Sammaiah, A.; Padmaja, K. V.; Prasad, R. B. N. Synthesis and evaluation of novel acyl derivatives from jatropha oil as potential lubricant basestocks. *J. Agric. Food Chem.* **2014**, *62*, 4652−4660.

(10) Abdelmalik, A. A. Chemically modified palm kernel oil ester: A possible sustainable alternative insulating fluid. *Sus. Mater. Technol.* **2014**, DOI: 10.1016/j.susmat.2014.06.001.

(11) Daniel, L.; Aridyanti, A. R.; Schuur, B.; Manurung, R.; Broekhuis, A. A.; Heeres, H. J. Synthesis and properties of highly branched *Jatropha curcas* L. oil derivatives. *Eur. J. Lipid Sci. Technol.* **2011**, *113*, 18−30.

(12) Sujay, U. M.; Priya, R. K.; Ravindra, D. K.; Pramod, P. M. Synthesis and characterization of chemically modified epoxidized mustard oil for biolubricant properties. *Inter. J. Appl. Eng. Res.* **2013**, *8* (17), 2023−2030.

(13) Erhan, S. Z.; Sharma, B. K.; Liu, Z.; Adhvaryu, A. Lubricant base stock potential of chemically modified vegetable oils. *J. Agric. Food Chem.* **2008**, *56*, 8919−8925.

(14) Hwang, H.-S.; Erhan, S. Z. Modification of epoxidized soybean oil for lubricant formulations with improved oxidative stability and low pour point. *J. Am. Oil Chem. Soc.* **2001**, *78*, 1179−1184.

(15) Padmaja, K. V.; Rao, B. V. S. K.; Reddy, R. K.; Bhaskar, P. S.; Singh, A. K.; Prasad, R. B. N. 10-Undecenoic acid-based polyol esters as potential lubricant base stocks. *Ind. Crops Prod.* **2012**, *35*, 237−240.

(16) Kamalakar, K.; Amit, K. R.; Prasad, R. B. N.; Karuna, M. S. L. Rubber seed oil-based biolubricant base stocks: A potential source for hydraulic oils. *Ind. Crops Prod.* **2013**, *51*, 249−257.

(17) Kamalakar, K.; Mohini, Y.; Rao, B. V. S. K.; Karuna, M. S. L.; Prasad, R. B. N. Sal fatty acid-based biolubricant base-stocks: A potential source for high temperature applications. *J. Lipid Sci. Technol.* **2013**, *45* (3), 79−85.

(18) Gryglewicz, S.; Piechocki, W.; Gryglewicz, G. Preparation of polyol esters based on vegetable and animal fats. *Bioresour. Technol.* **2003**, *87*, 35−39.

(19) Chang, T.-S.; Masood, H.; Yunus, R.; Rashid, U.; Choong, T. S. Y.; Biak, D. R. A. Activity of calcium methoxide catalyst for synthesis of high oleic palm oil based trimethylolpropane triester as lubricant base stock. *Ind. Eng. Chem. Res.* **2012**, *51*, 5438−5442.

(20) Edwards, D. M. Non-timber forest products from Nepal: Aspect of the trade in medicinal and aromatic plants. Forest Research and Survey Center: Kathmandu, 1996; p 134.

(21) Narayanmurti, D.; Das, N. A preliminary note on adhesives, building boards and moulding powders from tree's bark. *Indian For.* **1951**, *77*, 706−708.

(22) Christie, W. W. Isolation of individual fatty acids for structural analysis. In *Gas Chromatography of Lipids—A Practical Guide*; The Oily Press Ltd: Bridgwater, Somerset, 1989; Chapter 6, Section B, pp 76−77.

(23) Gurbanov, M. S.; Mamedov, B. A. Epoxidation of flax oil with hydrogen peroxide in a conjugate system in the presence of acetic acid and chlorinated cation exchanger KU-2x8 as catalyst. *Russ. J. Appl. Chem.* **2009**, *82*, 1483.

(24) Moser, B. R.; Erhan, S. Z. Synthesis and evaluation of a series of α-hydroxy ethers derived from isopropyl oleate. *J. Am. Oil Chem. Soc.* **2006**, *83*, 959−963.

(25) Salimon, J.; Salih, N.; Yousif, E. Synthesis characterization and physicochemical properies of oleic acid ether derivatives as bio-lubricant basestocks. *J. Oleo Sci.* **2011**, *60* (12), 613−618.

(26) Whistler, R. L.; BeMiller, J. N. Factors influencing gum costs and application. In *Industrial Gums, Polysaccharides and Their Derivatives*; Whistler, R. L., Ed.; Academic Press: New York, 1959; pp 1−13.
(27) Jonsson, U. J. Lubrication of rolling element bearings with HFC polyester mixtures. *Wear* **1999**, *232*, 185−191.
(28) Wood-Adams, P. The effect of long chain branches on the shear flow behavior of polyethylene. *J. Rheol.* **2001**, *45*, 203−210.
(29) Harry-O'kuru, R. E.; Isbell, T. A.; Weisleder, D. Synthesis of estolide esters from cis-9-octadecenoic acid estolides. *J. Am. Oil Chem. Soc.* **2001**, *78*, 219−222.
(30) Schneider, M. P. Plant-oil-based lubricants and hydraulic fluids. *J. Sci. Food Agric.* **2006**, *86*, 1769−1780.
(31) Yao, L.; Hammond, E. G.; Wang, T.; Bhuyan, S.; Sundararajan, S. Synthesis and physical properties of potential biolubricants based on ricinoleic acid. *J. Am. Oil Chem. Soc.* **2010**, *87*, 937−945.
(32) Rudnick, L. R. Polyalphaolefins. In *Synthetics, Mineral Oils and Bio-Based Lubricants*; Rudnick, L. R., Ed.; CRC Press, Taylor & Francis Group: Boca Raton, FL, 2006; pp 1−33.
(33) Mckeon, T. A.; Sharma, B. K.; Lin, J. T.; Erhan, S. Z.; Alander, J.; Gunstone, F. D. Non-food uses of oils and fats. In *The Lipid Hand Book*; Gunstone, F. D., Harwood, J. L., Dijkstra, A. L., Eds.; CRC Press: New York, 2007; pp 615−620.
(34) Booser, E. R. Lubrication and lubricants. In *Kirk−Othmer Encyclopedia of Chemical Technology*, 4th ed.; Grant, M. H., Ed.; Wiley-Interscience: Chichester, U.K., 1992; Vol. *15*, pp 463−517.
(35) Paeglis, T.; Karabeško, P.; Mieriņa, I.; Seržane, R.; Strēle, M.; Tupureina, V.; Jure, M. Compositions of hydraulic fluids based on rapeseed oil and its derivatives. In *8th International Scientific Conference: Engineering for Rural Development*, Jelgava, May 28−29, 2009; pp 171−175.
(36) Salimon, J.; Salih, N. Modification of epoxidized ricinoleic acid for biolubricant base oil with improved flash and pour points. *Asian J. Chem.* **2010**, *22*, 5468−5476.
(37) Stephen, B.; Randles, S. J. Esters. In *Synthetics, Mineral Oils and Bio-Based Lubricants*, 2nd ed.; Rudnick, L. R., Ed.; CRC Press, Taylor & Francis Group: Boca Raton, FL, 2013; pp 52−76.
(38) Schlosberg, R. H.; Chu, J. W.; Knudsen, G. A.; Suciu, E. N.; Aldrich, H. S. High stability ester for synthetic lubricant applications. *Lubr. Eng.* **2001**, *57* (2), 21−26.
(39) Sniegoski, p. J. Selectivity of the oxidation attack on a model ester lubricant. *ASLE Trans.* **1976**, *20* (4), 282−286.
(40) Havet, L.; Blouet, J.; Velloire, F. R.; Brasseur, E.; Slomka, D. Tribological characteristics of some environmentally friendly lubricants. *Wear* **2001**, *248*, 140−146.

Table 1. Nucleotide Sequences of Primers Used for PCR Amplification in the Present Study

| sequence number | name of the primer | sequence (5′−3′) |
|---|---|---|
| 1 | TomA-f | 5′-GGTACCGCATGCATATGCCTCGAGAACTTTGC-3′ |
| 2 | TomA-r | 5′-CTCGAGGATATCAGATCTCTCCACCAGCATTGATTAGG-3′ |
| 3 | TomC-f | 5′-CACCAGATCTGGATCCTAGAAAATGAGCACCACAAG-3′ |
| 4 | TomC-r | 5′-GTCGCTCGAGGTCGACCTAACGACTTCTCCGAGATC-3′ |
| 5 | TomD-f | 5′-AGATCTGATATCCTCGAGGACAAGCAATAGCAGGAGTG-3′ |
| 6 | TomD-r | 5′-GATCCTCTAGATAAGTGTGCCAACATCAGAC-3′ |
| 7 | NPTII f | 5′-GTCACTGAAGCGGGAAGGG-3′ |
| 8 | NPTII r | 5′-GGCGATACCGTAAAGCAC-3′ |
| 9 | TomA-qf | 5′-GAGGCGTGGGATAGGA-3′ |
| 10 | TomA-qr | 5′-GGATACGGGTAGTCAGCA-3′ |
| 11 | TomB-qf | 5′-TGCTACAATGACTTGGGTGAA-3′ |
| 12 | TomB-qr | 5′-CCTGTCCTGCCTCTACG-3′ |
| 13 | TomC-qf | 5′-ATGATCTCGGAGAAGTCG-3′ |
| 14 | TomC-qr | 5′-GTAGGGCGGAGTAAACG-3′ |
| 15 | TomD-qf | 5′-GACAAGCAATAGCAGGAGTG-3′ |
| 16 | TomD-qr | 5′-TAAGTGTGCCAACATCAGAC-3′ |
| 17 | TomE-qf | 5′-ATCTCAGTATCCGTATCCTCG-3′ |
| 18 | TomE-qr | 5′-TGTCCAAATCGCTCGTC-3′ |
| 19 | leEF-1-f | 5′-GGAACTTGAGAAGGAGCCTAAG-3′ |
| 20 | leEF-1-r | 5′-CAACACCAACAGCAACAGTCT-3′ |

volatiles do not have an important defensive function against this bacterial pathogen.[16] The overexpression of *TomloxD* gene in transgenic tomato plants resulted in a marked increase in the LOX activity and jasmonic acid (JA) accumulation, which indicted that TomloxD may use ALA as a substrate to produce (13*S*)-hydroperoxyoctadecatrienoic acid (13-HPOT), and 13-HPOT was further metabolized to synthesize JA.[15] In comparison to non-transformed tomato plants, the transgenic plants overexpressing TomloxD were more tolerant to *Cladosporium fulvum* and high-temperature stress.[15] The overexpression of TomLoxD also leads to elevated wound-induced JA biosynthesis and increased expression of wound-responsive genes, thereby enhanced resistance to insect herbivory attack and necrotrophic pathogen infection.[17] Therefore, TomloxD is involved in endogenous JA synthesis and tolerance to biotic and abiotic stress.[16,17]

Both ALA and LA in tomato are EFAs for humans. To improve the nutrition value of the tomato fruits, increasing the content of ALA or LA is advantageous. We produced some transgenic tomato plants silencing five LOX family genes. Transgenic tomato plants with greatly reduced TomloxA, TomloxB, TomloxC, TomloxD, and TomloxE were identified by quantitative real-time polymerase chain reaction (PCR) and LOX activity assays. Significant improvement in the contents of ALA or LA in tomato fruit was achieved.

## MATERIALS AND METHODS

**Experimental Materials and Growth Conditions.** All experiments were performed using a near-isogenic line of diploid tomato (*Solanum lycopersicum* cv. Ailsa Craig) plants. The inbred tomato was cultivated in soil. After 20 days of growth, seedlings were collected, frozen in liquid nitrogen, and used to extract RNA.

**Cloning of the Fragments of *TomloxA*, *TomloxC*, and *TomloxD* Genes.** Total RNA was isolated from the seedlings using the Trizol reagent (Gibco-BRL, Grand Island, NY). Reverse transcription (RT) was conducted with 500 ng of total RNA using the SuperScript III RNase H Reverse Transcriptase kit (Invitrogen, Carlsbad, CA) and 10 mM anchored olig(dT)$_{18}$ primer according to the instructions of the manufacturer.

On the basis of the TomloxA, TomloxC, and TomloxD cDNA sequences (GenBank accession numbers U09026, U37839, and U37840, respectively), the primers TomA-f, TomA-r, TomC-f, TomC-r, TomD-f, and TomD-r were designed. The appropriate restriction sites were added at the 5′ end of primers (Table 1). The fragments of *TomloxA*, *TomloxC*, and *TomloxD* genes were amplified from cDNA by PCR using PrimeSTAR HS DNA Polymerase (Takara, Dalian, China) with primers TomA-f and TomA-r, TomC-f and TomC-r, and TomD-f and TomD-r, respectively. The PCR products were cloned into pMD18-T vector (Invitrogen, Carlsbad, CA) and sequenced to obtain vectors TomloxA-T, TomloxC-T, and TomloxD-T, respectively.

**Construction of RNA Interference (RNAi) Vector TomloxACDi-pBIN19 and Plant Transformation.** RNAi expression vector TomloxACDi-pBIN19 was constructed as follows: (1) *TomloxC* gene fragment from the plasmid TomloxC-T (cut by *Bam*HI and *Sal*I) was cloned into the plasmid TomloxA-T in the sense orientation at *Bgl*II and *Sal*I restriction sites of the plasmid TomloxA-T and obtained TomloxAC-T vector. (2) *TomloxD* gene fragment from the plasmid TomloxD-T (digested with *Xho* I and *Sal*I) was cloned into the plasmid TomloxAC-T in the sense orientation at *Sal*I restriction sites of the plasmid TomloxAC-T and obtained TomloxACD-T vector. (3) ACD fragment from the plasmid TomloxACD-T (cut by *Bam*HI and *Sal*I) was linked into the pDHG 5.2 plasmid at *Bam*HI and *Sal*I restriction sites in the antisense orientation and obtained plasmid pDHG5.2-rTomloxACD. (4) The ACD fragment from the plasmid TomloxACD-T (digested by *Kpn*I and *Bam*HI) was linked into the plasmid pDHG5.2-rTomloxACD at *Kpn*I and *Bam*HI restriction sites in the sense orientation and was called pDHG5.2-fTomloxACD-rTomloxACD vector. (5) The double-stranded (ds) RNA expression unit from the plasmid pDHG5.2-fTomloxACD-rTomloxACD vector, including the cauliflower mosaic virus (CaMV) 35S promoter, *TomloxACD* fragment in sense orientation, *GFP* gene fragment, *TomloxACD* fragment in antisense orientation, and 35S terminator, was subcloned into the plant binary vector pBIN 19 (Takara, Dalian, China) with *Eco*RI to yield RNAi vector TomloxACDi-pBIN19 for Tomlox family genes silencing (Figure 1). The construct was confirmed by PCR, restriction digest analysis, and sequencing of the *TomloxACD* fragment.

The binary vector TomloxACDi-pBIN19 was used to transform tomato cotyledon explants. After the construct was transferred into *Agrobacterium tumefaciens* LBA4404 by the freeze−thaw method,[18] transformation was carried out according to the *Agrobacterium*-

**Figure 1.** Construct of RNAi vector TomloxACDi-pBIN19 for Tomlox family gene silencing. The fragments of *TomloxA*, *TomloxC*, and *TomloxD* genes in the sense and antisense orientations were linked with a GFP gene fragment and as a transcriptional unit for hairpin RNA expression, which was controlled by the CaMV 35S promoter and terminated by the 35S terminator.

mediated co-cultivation method.[19] Transgenic plants that rooted on kanamycin were transferred to compost and grown.[11]

**Confirmation and Phenotype Analysis of Positive Transgenic Plants.** The genomic DNA of transgenic and wild-type plants was isolated using Plant Genomic DNA Extraction kit (VOK-Bio, Beijing, China) according to the instructions of the manufacturer and used as templates. The forward primer *NPTII f* and reverse primer *NPTII r* were designed according to the *NPTII* gene sequence (Table 1). The positive transgenic plants were validated by PCR analysis. The phenotype of transgenic tomato plants was investigated.

**Real-Time RT-PCR Analysis of Transgenic Tomato Plants.** Total RNA was isolated from the leaf tissues of transgenic and wild-type tomato plants using Trizol reagent and subsequently treated with DNase I. The RNAs were reverse-transcribed as described above. The specific primers of real-time RT-PCR analysis are listed in Table 1. The real-time RT-PCR analysis of *TomloxA*, *TomloxB*, *TomloxC*, *TomloxD*, and *TomloxE* genes was carried out using the quantitative SYBR Green PCR kit (Tianwei, China) as described by He et al.[20] Real-time RT-PCR was performed using the CFX96 real-time system (C1000 thermal cycler, Bio-Rad, Hercules, CA). The gene expression was normalized to the *LeEF-1* gene from the tomato plant.[21]

**LOX Activity Assays.** LOX activity from leaf tissues was determined spectrophotometrically. The extraction of tomato LOXs and LOX activity assay were performed using the methods as described by Hu et al.[12] Proteins were measured by the Bradford method.[22] A total of 1 unit of activity was defined as the quantity of enzyme catalyzing an increase in absorbance of 0.01 at 234 nm/min under assay conditions.

**Quantification of Endogenous ALA and LA in Tomato Fruits.** Frozen samples of ripe fruits (8−10 days after breaker stage) were homogenized with a polytron apparatus, and 5 g of the homogenate was digested with 10 mL of HCl for 1 h at 70−80 °C. The mixture was cooled and extracted twice, each time being shaken for 2 min with 10 mL of ethanol, 10 mL of aether, and 25 mL of petroleum ether, followed by 10−20 min of quiescence. The supernatant liquid was transferred to another beaker and evaporated under reduced pressure. After saponification with 1 mL of 2 M NaOH−methanol for 15−20 min at 65 °C, the sample was methyl-esterified with 1 mL of 2 M HCl−methanol for 5 min at 65 °C. The resultant fatty acid methyl esters were recovered by adding 2 mL of saturated NaCl solution and 1 mL of hexane, vortexing, and centrifugation at 1000 rpm for 5 min to give the upper hexane layer.

Fatty acid analysis was performed by the application of 100 μL aliquots to a gas chromatograph (LC-2010, Shimadzu, Japan) equipped with a TC-70 capillary column (30 cm × 0.25 mm, GL Sciences, Japan) under a temperature program of 180−220 °C at a rate of 4 °C/min. ALA and LA were calculated on the basis of the area of each peak, and the amount was obtained by comparison to the ALA and LA standards, respectively.

**Statistical Analysis.** All experiments were repeated 3 times for two biological replicates. The data are means of six independent experiments ± standard deviation (SD). Student's *t* test was used for statistical analysis to compare the data. A *p* value of <0.05 was considered to indicate a statistically significant difference.

## RESULTS

**Generation, Confirmation, and Phenotype Analysis of Transgenic Plants.** To silence LOX family genes, RNAi expression vector TomloxACDi-pBIN19 was constructed. The plasmid TomloxACDi-pBIN19 was introduced to *A. tumefaciens* LBA4404 and transformed into *S. lycopersicum* cv. Ailsa Craig plants by the *Agrobacterium*-mediated co-cultivation method. The transgenic plants were selected with kanamycin. The regenerated seedlings were acclimated for 2 weeks in zippy pot soil in a greenhouse, then transferred to soil, and cultured under field conditions. The transgenic lines were obtained and further verified by PCR. Because the *NPTII* gene is closely adjacent to the target gene in the plasmid TomloxACDi-pBIN19 and not present in the wild-type tomato genome, the positive transgenic plants should have a specific 493 bp amplified product, which did not appear in wild-type tomato plants (Figure 2). The transgenic tomato lines were used for further analysis.

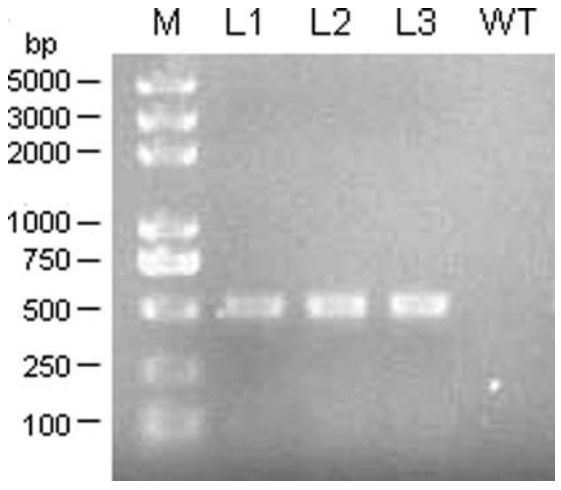


**Figure 2.** PCR analysis of transgenic tomato plants. M, DNA marker; L1, L2, and L3, independent transgenic lines; WT, wild-type tomato.

To examine the effect of silencing LOX family genes, the growth, development, and phenotype of the positive transgenic plants were analyzed. In comparison to wild-type tomato, the plant architectures, flowers, and fruits of transgenic tomato appeared normal. There was no detectable phenotypic difference between transgenic plants and wild-type tomato plants.

**Silence of LOX Family Genes in Transgenic Plants.** Real-time RT-PCR was used to investigate the expression of LOX family genes in transgenic tomato plants. The results showed that the expression of *TomloxA*, *TomloxB*, and *TomloxE* in transgenic tomato plants was drastically repressed. The expression of their transcript in transgenic lines 1, 2, and 3 was only approximately 0.05−5.79% of the wild-type tomato plants. The expression of *TomloxC* and *TomloxD* in transgenic plants was also seriously suppressed. There was no *TomloxC* expression in transgenic line 1, and the expression level of the *TomloxC* mRNA in transgenic lines 2 and 3 was 17.56 and 32.56% of the wild-type plants, respectively. The expression level of *TomloxD* mRNA in transgenic lines 1, 2, and 3 was only 2.45, 0.35, and 9.53% of the wild-type tomato, respectively (Figure 3).

**Repression of LOX Family Genes Decreased LOX Activity.** LOX activity of crude extracts from the transgenic and wild-type tomato plants was detected. The transgenic tomato always had lower LOX activities than the wild-type tomato (Figure 4). Among three transgenic lines, the LOX

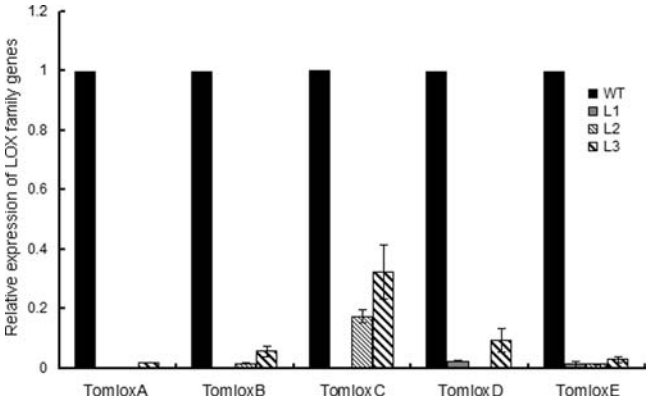


**Figure 3.** Expression of LOX family genes analyzed by real-time RT-PCR. WT, wild-type tomato; L1, L2, and L3, independent transgenic lines.

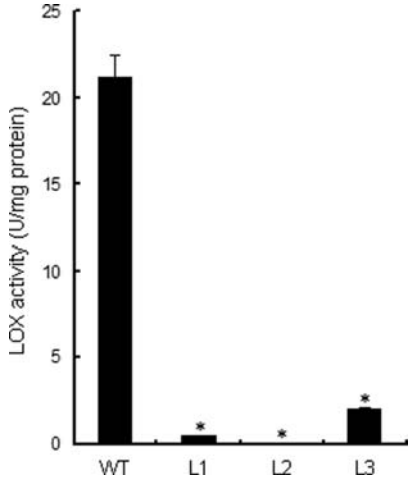


**Figure 4.** LOX activity in transgene tomato. WT, wild-type tomato; L1, L2, and L3, independent transgenic lines. (*) $p < 0.05$ versus wild-type tomato.

activities of lines 1, 2, and 3 were only 2.46, 0.35, and 9.53% of the wild-type plants, respectively (Figure 4). The result suggested that the repression of LOX family genes reduced LOX activity.

**Fruits of Transgenic Tomato Had Higher Endogenous ALA and LA.** Gas chromatographic analysis was used to determine the contents of endogenous ALA and LA in tomato fruits. The results showed that the contents of the endogenous ALA and LA in tomato fruits varied in the different transgenic lines. In comparison to the wild-type tomato, the transgenic tomato had higher accumulations of the endogenous ALA and LA in their fruits, which were 1.65−3.99 and 2.91−4.98 times that of the wild-type plants, respectively.

The highest levels of the endogenous ALA and LA were in the fruits of line 2, which contained 388.42 μg of ALA and 443.36 μg of LA per gram of tomato fruit (Table 2). The findings suggested the repression of LOX family genes resulted in a striking increase in the levels of endogenous ALA and LA in tomato fruits.

## DISCUSSION

The major objectives of genetic engineering of crops aim at improving tolerance toward various biotic and abiotic stresses, increasing output and enhancing nutritional value. Biotechnology techniques involving plant tissue culture and recombinant DNA technologies are powerful tools that can complement conventional breeding. In the case of tomato, genetic transformation via *Agrobacterium* is certainly an important tool to modify tomato growth,[23] nutritional quality,[24] facilitate genetic improvement against several diseases caused by phytopathogenic fungi, bacteria, and viruses,[25,26] and enhance resistance to abiotic stresses, such as high salinity, metal ions, hyperosmotic, heat, chilling stress, and ultraviolet radiation.[24,27,28]

**Table 2. Contents of ALA and LA in Tomato Fruits[a]**

| plant line | ALA (μg/g of fruit) | LA (μg/g of fruit) |
|---|---|---|
| wild type | 97.28 ± 27.89 | 88.99 ± 24.08 |
| line 1 | 160.70 ± 17.77 | 266.20 ± 55.86 |
| line 2 | 388.42 ± 63.22 | 443.36 ± 31.08 |
| line 3 | 223.99 ± 47.69 | 258.90 ± 47.89 |

[a]The data are means of six independent experiments ± SD.

In our present study, we constructed an RNAi expression vector using *TomloxC* fragment, *TomloxD* fragment, and partial *TomloxA* sequence that is highly identical with *TomloxB* and *TomloxE* to silence LOX family genes in tomato plants and investigated the expression levels of LOX family genes, LOX activity, and the contents of ALA and LA. In comparison to wild-type tomato, the expression of the LOX family genes *TomloxA*, *TomloxB*, *TomloxC*, *TomloxD*, and *TomloxE* was drastically repressed in transgenic tomato lines and the total LOX activity in transgenic tomato was lower. The contents of endogenous ALA and LA in transgenic tomato fruits were higher than that in the wild-type tomato fruits. LOXs can catalyze the dioxygenation of ALA and LA. In the transgenic lines, silencing LOX family genes resulted in the reduction of LOX activities, which led to a marked decrease in using ALA and LA substrates. Therefore, ALA and LA accumulated and transferred to fruit, and ALA and LA contents in fruit increase. The total LOX activities varied depending upon the transgenic lines and were relatively well-correlated with ALA and LA contents. Among three transgenic lines, line 2 had the lowest LOX activity and the highest contents of endogenous ALA and LA in their fruits, whereas lines 1 and 3 had higher LOX activity and less endogenous ALA and LA compared to line 2. The findings suggested that the lower the LOX activity, the higher the contents of endogenous ALA and LA (Figure 4 and Table 2).

The antisense suppression of TomloxA, TomloxB, and TomloxE in tomato fruits caused no significant changes in the contents of $C_6$ flavor volatile aldehydes and alcohols in tomato fruits compared to wild-type controls.[11,13] Taking into account that the majority of the hydroperoxides (HPOs) formed by LOX activity in tomato are the 9 isomers and that TomloxA, TomloxB, and TomloxE have high expression levels in wild-type tomato fruits, it is most likely that the majority of the HPOs formed by TomloxA, TomloxB, and TomloxE in tomato are the 9-HPOs.[11,29−32] Our previous work showed that TomloxC is a chloroplast-targeted lipoxygenase isoform that can use both ALA and LA as substrates and produce 13-hydroperoxy products, which appear to be specifically used as the precursors of volatile $C_6$ short-chain flavor compounds and metabolized further by the action of the 13-HPLs to give rise to hexanal, hexenal, and the corresponding alcohols.[11] The TomloxD protein also has a chloroplast target signal. Our previous investigation suggested that TomloxD can produce

13-HPOs, which is metabolized further to synthesize JA.[15] Therefore, it is the silencing of LOX family genes in tomato plants that leads to reduction of the LOX activity, in turn, causing the enhanced accumulation of ALA and LA in transgenic tomato fruits.

LOXs have been associated with some processes in a number of developmental stages and environmental stresses.[33,34] LOXs and the products of the LOX pathway were involved in a series of biological events, which include seed germination, tuber development, sex determination, nodule development, fruit ripening, plant senescence, and cell death.[11,34−40] Another important role of plant LOXs is an involvement in defense responses to wounding, heat, microbial pathogens, nematode infection, insect attack, and herbivore attack.[15,38,41−44] Therefore, inhibiting LOX activity is closely associated with plant development and defense mechanisms. Although there was no detectable phenotypic difference between transgenic and wild-type tomato plants, the suppression of *TomloxC* and *TomloxD* lead to the decrease of aroma volatile and JA in transgenic plants. JA regulates plant developmental plasticity and is the key regulators of plant defense mechanisms against pathogens, insects, and adaptation to abiotic stress.[45] Therefore, the transgenic tomatoes could potentially be a developmental defect and more venerable to biotic and abiotic stress factors, which are the potential ecological disadvantages of these transgenic plants. To overcome disadvantages of the transgenic tomato plants, further research is to construct a RNAi vector of LOX family genes using a fruit-specific promoter and transform wild-type tomato to obtain transgenic tomato plants, in which LOX family genes will be silenced only in tomato fruits.

In summary, the expressions of TomloxA, TomloxB, TomloxC, TomloxD, and TomloxE are greatly reduced by genetic transformation of RNAi constructs, which leads to the decrease of LOX activity and the increase of the contents of ALA and LA in transgenic tomato fruits. The research has the potential in engineering cropping plants that improve nutritional quality.

## AUTHOR INFORMATION


### Corresponding Author

*Telephone: +86-23-65112674. Fax: +86-23-65102507. E-mail: chenguoping@cqu.edu.cn.



### Funding

This work was supported by the National Natural Science Foundation of China (31100089 and 31171968) and the Natural Science Foundation of Chongqing of China (CSTC 2010BB5239).


### Notes

The authors declare no competing financial interest.

## ABBREVIATIONS USED

AA, arachidonic acid; ALA, $\alpha$-linolenic acid; CaMV, cauliflower mosaic virus; DHA, docosahexaenoic acid; DGLA, dihomo-$\gamma$-linolenic acid; EFA, essential fatty acid; EPA, eicosapentaenoic acid; HPL, hydroperoxide lyase; HPO, hydroperoxide; 13-HPOT, (13*S*)-hydroperoxyoctadecatrienoic acid; JA, jasmonic acid; LA, linoleic acid; LOX, lipoxygenase; PUFA, polyunsaturated fatty acid

## REFERENCES


(1) Chang, C. Y.; Ke, D. S.; Chen, J. Y. Essential fatty acids and human brain. *Acta Neurol. Taiwan* **2009**, *18*, 231−241.

(2) Higdon, J. Essential fatty acids (omega-3 and omega-6). *An Evidence-Based Approach to Dietary Phytochemicals*; Thieme Medical Publishers: New York, 2007; pp 78−99.

(3) Das, U. N. Essential Fatty acids—A review. *Curr. Pharm. Biotechnol.* **2006**, *7*, 467−482.

(4) Rege, S. A.; Momin, S. A.; Bhowmick, D. N.; Pratap, A. A. Stabilization of emulsion and butter like products containing essential fatty acids using kalonji seeds extract and curcuminoids. *J. Oleo Sci.* **2012**, *61*, 11−16.

(5) Brash, A. R. Lipoxygenases: Occurrence, functions, catalysis, and acquisition of substrate. *J. Biol. Chem.* **1999**, *274*, 23679−23682.

(6) Kühn, H.; Rŏmisch, I.; Belkner, J. The role of lipoxygenase-isoforms in atherogenesis. *Mol. Nutr. Food Res.* **2005**, *49*, 1014−1029.

(7) Liavonchanka, A.; Feussner, I. Lipoxygenases: Occurrence, functions and catalysis. *J. Plant Physiol.* **2006**, *163*, 348−357.

(8) Lang, I.; Feussner, I. Oxylipin formation in *Nostoc punctiforme* (PCC73102). *Phytochemistry* **2007**, *68*, 1120−1127.

(9) Loiseau, J.; Vu, B. L.; Macherel, M. H.; Le Deunff, Y. Seed lipoxygenases: Occurrence and functions. *Seed Sci. Res.* **2001**, *11*, 199−211.

(10) Feussner, I.; Wasternack, C. Lipoxygenase pathway. *Annu. Rev. Plant Biol.* **2002**, *53*, 275−297.

(11) Chen, G.; Hackett, R.; Walker, D.; Taylor, A.; Lin, Z.; Grierson, D. Identification of a specific isoform of tomato lipoxygenase (TomloxC) involved in the generation of fatty acid-derived flavor compounds. *Plant Physiol.* **2004**, *136*, 2641−2651.

(12) Hu, T.; Qy, X.; Hu, Z.; Chen, G.; Chen, Z. Expression, molecular characterization and detection of lipoxygenase activity of *tomloxD* from tomato. *Afr. J. Biotechnol.* **2011**, *10*, 490−498.

(13) Griffiths, A.; Prestage, S.; Linforth, R.; Zhang, J.; Taylor, A.; Grierson, D. Fruit-specific lipoxygenase suppression in antisense-transgenic tomatoes. *Postharvest Biol. Technol.* **1999**, *17*, 163−173.

(14) Heitz, T.; Bergey, D. R.; Ryan, C. A. A gene encoding a chloroplast-targeted lipoxygenase in tomato leaves is transiently induced by wounding, systemin, and methyl jasmonate. *Plant Physiol.* **1997**, *114*, 1085−1093.

(15) Hu, T.; Zeng, H.; Hu, Z.; Qv, X.; Chen, G. Overexpression of the tomato 13-lipoxygenase gene *TomloxD* increases generation of endogenous jasmonic acid and resistance to *Cladosporium fulvum* and high temperature. *Plant Mol. Biol. Rep.* **2013**, *31*, 1141−1149.

(16) Shen, J.; Tieman, D.; Jones, J. B.; Taylor, M. G.; Schmelz, E.; Huffaker, A.; Bies, D.; Chen, K.; Klee, H. J. A 13-lipoxygenase, TomloxC, is essential for synthesis of $C_5$ flavour volatiles in tomato. *J. Exp. Bot.* **2014**, *65*, 419−428.

(17) Yan, L.; Zhai, Q.; Wei, J.; Li, S.; Wang, B.; Huang, T.; Du, M.; Sun, J.; Kang, L.; Li, C. B.; Li, C. Role of tomato lipoxygenase D in wound-induced jasmonate biosynthesis and plant immunity to insect herbivores. *PLoS Genet.* **2013**, *9*, No. e1003964.

(18) Höfgen, R.; Willmitzer, L. Storage of competent cells for *Agrobacterium* transformation. *Nucleic Acids Res.* **1988**, *16*, 9877.

(19) Bird, C. R.; Smith, C. J. S.; Ray, J. A.; Moureau, P.; Bevan, M. W.; Bird, A. S.; Hughes, S.; Morris, P. C.; Grierson, D.; Schuch, W. The tomato polygalacturonase gene and ripening-specific expression in transgenic plants. *Plant Mol. Biol.* **1988**, *11*, 651−662.

(20) He, S.; Tan, L.; Hu, Z.; Chen, G.; Wang, G.; Hu, T. Molecular characterization and functional analysis by heterologous expression in *E. coli* under diverse abiotic stresses for OsLEA5, the atypical hydrophobic LEA protein from *Oryza sativa* L. *Mol. Genet. Genomics* **2012**, *287*, 39−54.

(21) Løvdal, T.; Lillo, C. Reference gene selection for quantitative real-time PCR normalization in tomato subjected to nitrogen, cold, and light stress. *Anal. Biochem.* **2009**, *387*, 238−242.

(22) Bradford, N. M. A rapid and sensitive method for the quantitation of microgram quantities of protein utilizing the principle of protein−dye binding. *Anal. Biochem.* **1976**, *72*, 248−254.

(23) Villagarcia, H.; Morin, A. C.; Shpak, E. D.; Khodakovskaya, M. V. Modification of tomato growth by expression of truncated ERECTA protein from *Arabidopsis thaliana*. *J. Exp. Bot.* **2012**, *63*, 6493−6504.

(24) Kamthan, A.; Kamthan, M.; Azam, M.; Chakraborty, N.; Chakraborty, S.; Datta, A. Expression of a fungal sterol desaturase improves tomato drought tolerance, pathogen resistance and nutritional quality. *Sci. Rep.* **2012**, *2*, 951.
(25) Horvath, D. M.; Stall, R. E.; Jones, J. B.; Pauly, M. H.; Vallad, G. E.; Dahlbeck, D.; Staskawicz, B. J.; Scott, J. W. Transgenic resistance confers effective field level control of bacterial spot disease in tomato. *PLoS One* **2012**, *7*, No. e42036.
(26) Kesanakurti, D.; Kolattukudy, P. E.; Kirti, P. B. Fruit-specific overexpression of wound-induced tap1 under E8 promoter in tomato confers resistance to fungal pathogens at ripening stage. *Physiol. Plant* **2012**, *146*, 136−148.
(27) Duan, M.; Feng, H. L.; Wang, L. Y.; Li, D.; Meng, Q. W. Overexpression of thylakoidal ascorbate peroxidase shows enhanced resistance to chilling stress in tomato. *J. Plant Physiol.* **2012**, *169*, 867−877.
(28) Liu, J.; Tang, X.; Gao, L.; Gao, Y.; Li, Y.; Huang, S.; Sun, X.; Miao, M.; Zeng, H.; Tian, X.; Niu, X.; Zheng, L.; Giovannoni, J.; Xiao, F.; Liu, Y. A role of tomato UV-damaged DNA binding protein 1 (DDB1) in organ size control via an epigenetic manner. *PLoS One* **2012**, *7*, No. e42621.
(29) Hatanaka, A. The biogeneration of green odour by green leaves. *Phytochemistry* **1993**, *34*, 1201−1218.
(30) Royo, J.; Vancanneyt, G.; Pérez, A. G.; Sanz, C.; Störmann, K.; Rosahl, S.; Sánchez-Serrano, J. J. Characterization of three potato lipoxygenases with distinct enzymatic activities and different organ-specific and wound-regulated expression patterns. *J. Biol. Chem.* **1996**, *271*, 21012−21019.
(31) Galliard, T.; Matthew, J. A. Lipoxygenase-mediated cleavage of the fatty acids to carbonyl fragments in tomato fruits. *Phytochemistry* **1977**, *16*, 339−343.
(32) Smith, J. J.; Linforth, R.; Tucker, G. A. Soluble lipoxygenase isoforms from tomato fruit. *Phytochemistry* **1997**, *45*, 453−458.
(33) Siedow, J. N. Plant lipoxygenase—Structure and function. *Annu. Rev. Plant Physiol. Mol. Biol.* **1991**, *42*, 145−188.
(34) Kolomiets, M. V.; Hannapel, D. J.; Chen, H.; Tymeson, M.; Gladon, R. J. Lipoxygenase is involved in the control of potato tuber development. *Plant Cell* **2001**, *13*, 613−626.
(35) Hayashi, S.; Gresshoff, P. M.; Kinkema, M. Molecular analysis of lipoxygenases associated with nodule development in soybean. *Mol. Plant-Microbe Interact.* **2008**, *21*, 843−853.
(36) Acosta, I. F.; Laparra, H.; Romero, S. P.; Schmelz, E.; Hamberg, M.; Mottinger, J. P.; Moreno, M. A.; Dellaporta, S. L. tasselseed1 is a lipoxygenase affecting jasmonic acid signaling in sex determination of maize. *Science* **2009**, *323*, 262−265.
(37) Palmieri-Thiers, C.; Canaan, S.; Brunini, V.; Lorenzi, V.; Tomi, F.; Desseyn, J. L.; Garscha, U.; Oliw, E. H.; Berti, L.; Maury, J. A lipoxygenase with dual positional specificity is expressed in olives (*Olea europaea* L.) during ripening. *Biochim. Biophys. Acta* **2009**, *1791*, 339−346.
(38) Hwang, I. S.; Hwang, B. K. The pepper 9-lipoxygenase gene CaLOX1 functions in defense and cell death responses to microbial pathogens. *Plant Physiol.* **2010**, *152*, 948−967.
(39) Liu, S.; Han, B. Differential expression pattern of an acidic 9/13-lipoxygenase in flower opening and senescence and in leaf response to phloem feeders in the tea plant. *BMC Plant Biol.* **2010**, *10*, 228−242.
(40) Rudolph, M.; Schlereth, A.; Körner, M.; Feussner, K.; Berndt, E.; Melzer, M.; Hornung, E.; Feussner, I. The lipoxygenase-dependent oxygenation of lipid body membranes is promoted by a patatin-type phospholipase in cucumber cotyledons. *J. Exp. Bot.* **2011**, *62*, 749−760.
(41) Veronico, P.; Giannino, D.; Melillo, M. T.; Leone, A.; Reyes, A.; Kennedy, M. W.; Bleve-Zacheo, T. A novel lipoxygenase in pea roots. Its function in wounding and biotic stress. *Plant Physiol.* **2006**, *141*, 1045−1055.
(42) Wang, R.; Shen, W.; Liu, L.; Jiang, L.; Liu, Y.; Su, N.; Wan, J. A novel lipoxygenase gene from developing rice seeds confers dual position specificity and responds to wounding and insect attack. *Plant Mol. Biol.* **2008**, *66*, 401−414.
(43) Zhou, G.; Qi, J.; Ren, N.; Cheng, J.; Erb, M.; Mao, B.; Lou, Y. Silencing OsHI-LOX makes rice more susceptible to chewing herbivores, but enhances resistance to a phloem feeder. *Plant J.* **2009**, *60*, 638−648.
(44) Vicente, J.; Cascón, T.; Vicedo, B.; García-Agustín, P.; Hamberg, M.; Castresana, C. Role of 9-lipoxygenase and α-dioxygenase oxylipin pathways as modulators of local and systemic defense. *Mol. Plant* **2012**, *5*, 914−928.
(45) Howe, G. A.; Schilmiller, A. L. Oxylipin metabolism in response to stress. *Curr. Opin. Plant Biol.* **2002**, *5*, 230−236.

We have previously developed a construct-specific method for detection and quantitation of Embrapa 5.1 GM common bean, named OLA assay.[14,15] However, it is necessary to develop an event-specific assay in order to distinguish authorized and unauthorized GM events containing the same inserted DNA. OLA assay was unable to differentiate between Embrapa 2.3 and Embrapa 5.1 events. The present work reports the development of an event-specific method for detection and quantitation of Embrapa 5.1 GM common bean. In the present work, we designed a primer pair and a hydrolysis probe targeting a junction sequence between the common bean genomic DNA and the inserted DNA of Embrapa 5.1 GM common bean. This event-specific DNA assay, named FGM assay, was the first assay successfully developed for specific real-time PCR quantitation of Embrapa 5.1 event.

## MATERIALS AND METHODS

**Plant Material.** Two Embrapa 5.1 GM common bean lines, namely GM Pérola and GM Pontal, derived from the cultivars Pérola and Pontal, respectively, were used as positive controls. Non-GM Pérola, non-GM Pontal, 44 different *Phaseolus vulgaris* L. non-GM varieties, cowpea (*Vigna unguiculata* L.), lima bean (*Phaseolus lunatus*), and sword bean (*Canavalia gladiata*) were used as negative controls. The GM common bean Embrapa 2.3, a noncommercial event that contains the same construct of Embrapa 5.1, was used as the main negative control. Seeds of these samples were provided by Embrapa Arroz e Feijão (Santo Antônio de Goiás, GO, Brazil). Non-GM soybean and pea grains were purchased from local markets in Florianópolis, SC, Brazil. Certified reference materials (CRM) from RR soybean (5%, BF410), MON810 (5%, BF413f), Bt11 (4.89%, BF412f) and Bt176 (5%, BF411f) were purchased from IRMM (Institute for Reference Material and Measurements, Geel, Belgium).

Leaf material was obtained as follows: Two seeds of each sample were placed on moistened germination paper and germinated in a growth chamber at 25 °C without light for 2 days. Afterward, seeds were transferred to seedling pots containing soil and cultivated in a controlled environment growth chamber, adjusted to 12 h photoperiod, photosynthetic active radiation of 150 $\mu mol \cdot m^{-2} \cdot s^{-1}$, at 25 °C, watered daily. After 11 days, leaves were collected and stored at −80 °C. Powder seed material was obtained as follows: Embrapa 5.1 GM common bean seeds were cryo-ground in an analytical mill (IKA model A11 basic), followed by manual crushing with mortar and pestle in the presence of liquid nitrogen.

**DNA Extraction.** Genomic DNA was extracted from frozen leaf material by two protocols: cetyltrimethylammonium bromide (CTAB) and DNeasy plant minikit (Qiagen).[16] Genomic DNA was extracted from seed material by use of DNeasy plant minikit (Qiagen). DNA was extracted at least twice for each sample. DNA concentration was estimated from measurements at 260 and 280 nm on a Thermo Scientific NanoDrop 2000 spectrophotometer (Wilmington, DE).

**Primers and Probe Design.** Primers and probe were designed on the basis of the Embrapa 5.1 GM common bean DNA sequence that was provided by EMBRAPA (Figure S1, Supporting Information). Primer Express 3.0 software (Applied Biosystems) was used for designing the primers and the probe in the border junction sequence of common bean DNA and inserted DNA (Table 1).

**Table 1. Primers and FGM Probe Sequences Designed for Event-Specific qPCR of Embrapa 5.1 GM Common Bean[a]**

| oligonucleotide | sequence 5′−3′ |
|---|---|
| BeanF primer | CTGATTCAATCGACGCCTTACTT |
| VectorR primer | CGCGGTATTATCCCGTATTGAC |
| FGM probe | VIC-TTAATAAATAAGTGGATCTCTTGCC-MGB |

[a]Amplicon size is 77 bp.

**Chemicals.** DNA extraction performed with DNeasy plant minikit used all reagents provided by Qiagen (Valencia, CA): buffer AP1, RNase A, buffer P3, QIAshredder spin column, buffer AW1, DNeasy mini spin column, buffer AW2, and buffer AE. Ethanol, chloroform, and sodium chloride were purchased from Synth (São Paulo, Brazil); 2-propanol was purchased from Vetec (Rio de Janeiro, Brazil), proteinase K was from Promega (Madison, WI), and CTAB was from USB (Cleveland, OH). qPCR reagents (2× SYBR Green master mix and 2× TaqMan universal PCR master mix) were purchased from Applied Biosystems (Foster City, CA). The primer pair, named BeanF/VectorR, was synthesized by IDT (Coralville, IA) and the TaqMan probe, named FGM, was synthesized by Life Technologies (Foster City, CA).

**Real-Time PCR Conditions.** Quantitative real-time polymerase chain reaction (qPCR) was performed in ABI PRISM 7500 detection system (Applied Biosystems, Foster City, CA). The amplification reactions were carried out in a final volume of 25 $\mu$L containing 12.5 $\mu$L of 2× SYBR Green master mix or 2× TaqMan universal PCR master mix, primer pair, probe, water, and 50 ng of template DNA. All reactions were carried out in duplicate under the following cycling conditions: 2 min at 50 °C; 10 min at 95 °C; 40 cycles of 15 s at 94 °C and 1 min at 60 °C. All real-time PCR runs were evaluated separately by using the automatic software settings for each run. Tested and optimized primer pair and probe concentrations are presented in Table 2.

**Table 2. Primers and FGM Probe Concentrations Used for Event-Specific qPCR of Embrapa 5.1 GM Common Bean**

| | SYBR Green | TaqMan |
|---|---|---|
| Tested Concentrations (nmol/L) | | |
| BeanF/VectorR primers | 100, 200, 300, 400, 500 | 300 |
| FGM probe | | 150, 250 |
| Optimized Concentrations (nmol/L) | | |
| BeanF/VectorR primers | 300 | 300 |
| FGM probe | | 250 |

**Specificity of Primer Pair and Probe.** The specificity of SYBR Green assay was assessed by use of DNA extracted from soybean, pea, non-GM common beans Pérola and Pontal, GM common bean Embrapa 2.3, and two GM common beans Embrapa 5.1 (GM Pérola and GM Pontal). Primer specificity was evaluated under the PCR conditions described in the previous section.

In order to evaluate the specificity of FGM assay, negative samples were tested, including 46 *P. vulgaris* varieties (including non-GM Pérola and Pontal), one *P. lunatus*, one *V. unguiculata*, one *C. gladiata*, and Embrapa 2.3 GM. Primers and probe concentrations were respectively 300 and 250 nM.

**Construction of Standard Curves.** Genomic DNA isolated from leaves of Embrapa 5.1 GM common bean was used for serial dilution in water, to final concentrations from $10^5$ to $10^0$ DNA copies, or in DNA solution of non-GM common bean, to final concentrations of $10^2$ and $10^1$ DNA copies. The number of genome copies was calculated from the equation $m = n(660)(1/6.023 \times 10^{23})$, incorporating the 1C value of 637 Mbp for *P. vulgaris* L., the molecular weight of DNA (660 Da/bp), and Avogadro's constant. Therefore, the estimated number of genome copies in standard curves ranged from $10^5$ to $10^0$ copies of haploid genome, corresponding to mass quantities of 69.8 to $(6.98 \times 10^{-4})$ ng of DNA that were used as template in PCR. Amplification efficiency values were calculated from the equation $E = (10^{-1/S} - 1) \times 100$, where $E$ is the efficiency (percent) and $s$ is the slope obtained from the standard curve.

**qPCR Assay Repeatability.** Repeatability of the TaqMan FGM assay for DNA samples extracted with DNeasy plant minikit was evaluated by two approaches. In the first approach, DNA samples extracted from Embrapa 5.1 GM Pérola and Embrapa 5.1 GM Pontal were analyzed in three PCR runs, on different days, in duplicate. The second approach was performed with three DNA extracts from

Embrapa 5.1 GM Pérola. The PCR runs were performed in 4 days, by use of the three DNA extracts, in duplicate.

Repeatability of the TaqMan assay for samples extracted with CTAB was performed with one DNA sample extracted from Embrapa 5.1 GM Pérola and one DNA sample extracted from Embrapa 5.1 GM Pontal in four qPCR runs, in duplicate.

## RESULTS

**qPCR Parameters for SYBR Green Assay.** In order to test the specificity of the primers, SYBR Green assays were performed at four primer concentrations: 400, 300, 200, and 100 nM with negative and positive control samples. Low variation in Cq values of positive samples (GM Pérola and GM Pontal) was observed for primer concentrations of 400, 300, and 200 nM (Table S1, Supporting Information). For primer concentration of 100 nM, quantitation cycle (Cq) values of the positive samples were higher than Cq values at other primer concentrations.

Regarding the negative controls (pea, GM and non-GM soybean, GM maize, non-GM Pérola, non-GM Pontal, and Embrapa 2.3), amplification signals with late Cq were verified for GM and non-GM soybean, GM maize, and non-GM common bean Pontal samples at primer concentration of 400 nM and for non-GM common bean Pérola, GM and non-GM soybean, and GM maize at primer concentration of 200 nM. For 300 nM primer concentration, no amplification signals were observed for the large majority of negative controls. In this case, only five positive signals were observed out of 25 with late Cq (Cq > 34.9) (Table S1, Supporting Information).

Standard curves were obtained at five primer concentrations (500, 400, 300, 200, and 100 nM) with DNA samples extracted with DNeasy plant minikit from Embrapa 5.1 GM Pérola and GM Pontal. Efficiency values ranged from 95% to 110% for GM Pérola and from 94% to 112% for GM Pontal (Table 3). Primer concentrations of 300 and 200 nM showed suitable efficiency values, and they were selected to obtain standard curves for GM Pérola and GM Pontal samples extracted by the CTAB method. For GM Pérola the amplification efficiency values were 107% and 104%, respectively, and for GM Pontal the efficiencies were 104% and 110%, respectively (Table 3). For primer concentrations of 200 and 300 nM, amplification efficiency values presented standard deviation of 4.55 and 2.52, respectively, for the samples extracted with both DNA extraction methods. Given the amplification efficiency values and the results obtained in the specificity tests, the primer concentration of 300 nM was selected to be used in further experiments.

**Table 3. qPCR Efficiency Values and $R^2$ of SYBR Green Assay[a]**

| | Embrapa 5.1 Pérola | | Embrapa 5.1 Pontal | |
|---|---|---|---|---|
| [primer] (nmol/L) | efficiency (%) | $R^2$ | efficiency (%) | $R^2$ |
| DNA from DNeasy Plant Minikit | | | | |
| 500 | 95 | 0.987 | 103 | 0.999 |
| 400 | 106 | 1.000 | 94 | 0.998 |
| 300 | 110 | 0.997 | 110 | 1.000 |
| 200 | 104 | 0.999 | 100 | 1.000 |
| 100 | 106 | 0.993 | 112 | 0.988 |
| DNA from CTAB Method | | | | |
| 300 | 107 | 1.000 | 104 | 0.993 |
| 200 | 104 | 0.999 | 110 | 0.991 |

[a]Template DNA came from Embrapa 5.1 GM Pérola and Embrapa 5.1 GM Pontal common bean varieties, extracted by DNeasy plant minikit or CTAB method..

**qPCR Parameters for TaqMan Assay of Leaf DNA.** Standard curves were obtained for 250 and 150 nM FGM probe concentrations, 300 nM BeanF/VectorR primer pair, and GM Pérola and GM Pontal samples extracted from leaf material with DNeasy plant minikit. Curves for 250 nM FGM probe showed efficiency values close to 100%, and this concentration was selected to be used in further experiments (Figure 1).

The specificity of FGM probe was assessed under optimized conditions of primers and probe concentrations. For *P. vulgaris* varieties, only 35 out of 158 reactions (22%) presented a positive signal. For Embrapa 2.3 GM event, only six out of 26 reactions (23%) present a positive signal (Table 4). All positive results presented a late Cq, higher than 37.

**Repeatability of TaqMan Assay.** The repeatability assay was performed in four PCR runs with three GM Pérola DNA extracts (Table 5). Each DNA extract resulted in a standard curve obtained from a 10-fold serial dilution. The efficiency values ranged from 85% to 101%. A mean standard curve was generated by use of all data obtained from this experiment ($n$ = 24). The mean efficiency value was 95% and the correlation coefficient was 0.998 (Figure 2).

Repeatability of the TaqMan assay was also assessed for one DNA extract of Embrapa 5.1 GM Pérola and one DNA extract of Embrapa 5.1 GM Pontal, in 3 days. Efficiency values ranged from 90% to 103% for GM Pérola and from 94% to 98% for GM Pontal (Figure S2, Supporting Information).

DNA samples extracted by the CTAB method were also used to verify the repeatability of the TaqMan assay. Efficiency values for GM Pérola and GM Pontal were 89% and 86%, respectively. Both curves presented a correlation coefficient of 0.97 (Figure 3).

**Limit of Detection of qPCR Assay.** The limit of detection (LOD) for FGM assay was determined through the repeatability test: four qPCR runs for three DNA extracts (A, B, and C), in duplicate. The limit of detection also was assessed with DNA from Embrapa 5.1 diluted with non-GM common bean DNA and compared with results obtained in the construct-specific OLA assay (Table 6).

Embrapa 5.1 DNA extracted with DNeasy plant minikit and diluted in water was detected in 24 out of 24 reactions (100%) to $10^1$ DNA copy number. Positive reactions were observed in 14 out of 24 (58%) for $10^0$ DNA copy number. For samples extracted with CTAB, Embrapa 5.1 DNA diluted in water was detected in 16 out of 16 reactions (100%) for $10^2$ DNA copy number. A positive signal was observed in 12 out of 16 reactions (75%) for $10^1$ DNA copy number.

Embrapa 5.1 DNA diluted in non-GM common bean was detected in all 12 reactions (100%) evaluated up to the dilution of $10^2$ for FGM assay and in 11 out of 12 reactions (92%) for OLA assay. OLA assay showed positive signal in 21 out 24 reactions (87.5%) for $10^1$ DNA copies while FGM probe showed 22 out of 24 reactions (92%) for $10^1$ DNA copies (Table 6).

**qPCR Parameters for TaqMan Assay of Seed DNA.** Standard curves were also obtained for four DNA extracts from bean material. DNA was extracted from powder seeds by use of DNeasy plant minikit. Standard curve with 250 nM FGM probe and 300 nM primers showed mean efficiency value of 100% (Figure 4).

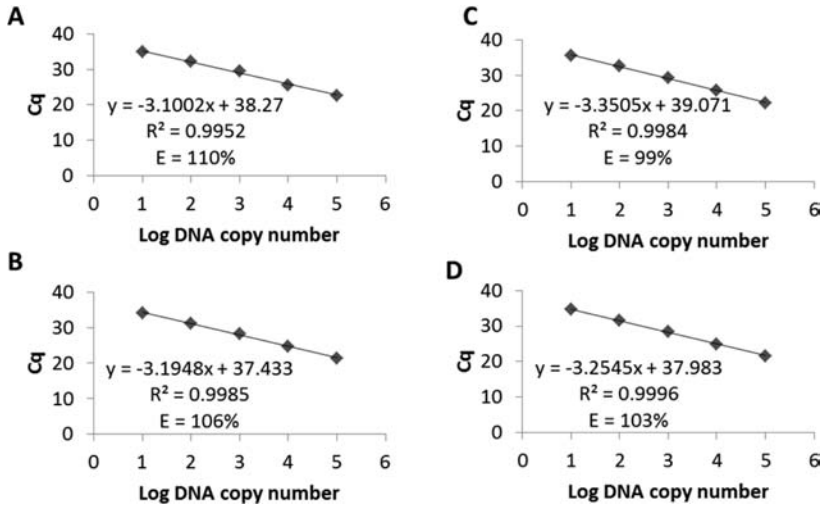


**Figure 1.** TaqMan FGM assay stardard curves for two FGM probe concentrations (250 and 150 nM) and template DNA extracted by use of DNeasy plant minikit from leaves of two GM common beans. (A) Embrapa 5.1 GM Pérola DNA and 150 nM FGM probe ($n$ = 4); (B) Embrapa 5.1 GM Pérola DNA and 250 nM FGM probe ($n$ = 4); (C) Embrapa 5.1 GM Pontal DNA and 150 nM FGM probe ($n$ = 2); (D) Embrapa 5.1 GM Pontal DNA and 250 nM FGM probe ($n$ = 2). Assays were performed with 300 nM BeanF/VectorR primer pair.

**Table 4. Specificity Test for TaqMan FGM Assay with Optimized Primers and Probe Concentrations**

| DNA sample[a] | positive/total | mean Cq | SD |
|---|---|---|---|
| Embrapa 5.1 GM Pérola | 4/4 | 21.20 | 0.21 |
| Embrapa 5.1 GM Pontal | 4/4 | 21.81 | 0.20 |
| *P. vulgaris* | 28/134 | 37.28 | 0.79 |
| non-GM Pérola | 4/12 | 38.47 | 0.63 |
| non-GM Pontal | 3/12 | 38.73 | 0.63 |
| *C. gradiata* | 0/2 | | |
| *P. lunatus* | 0/2 | | |
| *V. unguiculata* | 1/4 | 38.44 | |
| Embrapa 2.3 common bean | 6/26 | 38.05 | 0.89 |

[a]DNA was extracted by use of DNeasy plant minikit.

**Table 5. qPCR Parameters of TaqMan FGM Assay Standard Curves Based on Four PCR Runs and Three DNA Extracts**

| DNA sample[a] | efficiency (%) | slope | $R^2$ |
|---|---|---|---|
| | PCR Run 1 | | |
| A | 91 | −3.546 | 0.998 |
| B | 94 | −3.477 | 0.999 |
| C | 85 | −3.738 | 0.999 |
| | PCR Run 2 | | |
| A | 90 | −3.582 | 1.000 |
| B | 94 | −3.470 | 1.000 |
| C | 99 | −3.353 | 0.999 |
| | PCR Run 3 | | |
| A | 99 | −3.352 | 0.999 |
| B | 101 | −3.305 | 0.991 |
| C | 91 | −3.563 | 0.996 |
| | PCR Run 4 | | |
| A | 97 | −3.387 | 0.998 |
| B | 98 | −3.367 | 0.996 |
| C | 96 | −3.427 | 0.998 |
| mean | 95 | −3.464 | 0.998 |
| SD | 5.0 | 0.14 | 0.00 |

[a]DNA from Embrapa 5.1 GM Pérola was extracted from leaves by use of DNeasy plant minikit.

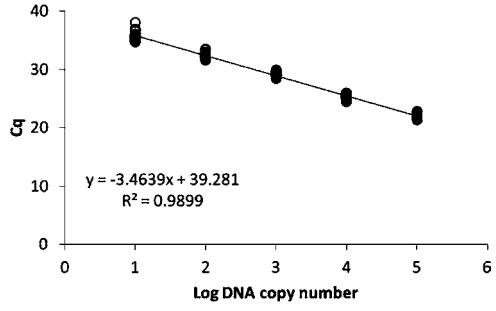


**Figure 2.** TaqMan FGM assay stardard curves performed in four qPCR runs on different days with three DNA extracts from leaves of Embrapa 5.1 GM Pérola in duplicate ($n$ = 24). Samples were extracted by use of DNeasy plant minikit.

**Comparison between OLA and FGM Assays.** In order to compare the efficiency values of FGM and OLA assays, serial dilutions were prepared for DNA from Embrapa 5.1 GM Pérola, Embrapa 5.1 GM Pontal, and Embrapa 2.3 GM event samples and tested for both assays. The results showed that for OLA assay the efficiency values ranged from 90% to 97%, while for FGM assay the efficiency values were 95% and 113% (Table 7). As expected, the FGM assay did not present positive amplification signals for DNA extracted from Embrapa 2.3 common bean event.

## DISCUSSION

Event-specific methods present the highest specificity in order to differentiate GMO events.[17] Two GM common bean events obtained with the same construct (Embrapa 2.3 and Embrapa 5.1) showed high resistance to bean golden mosaic virus,[2,18] but only Embrapa 5.1 GM common bean event was submitted for approval and approved for commercialization in Brazil.

In order to develop an event-specific assay for Embrapa 5.1, common bean DNA was extracted from leaf tissue to be used as certified reference material. Seed powder for GMO analysis presented some limitations, such as limited quantitation range, inconvenient preparation procedures, and difficulty in obtaining homogeneous candidate samples.[19] Furthermore, the genetic

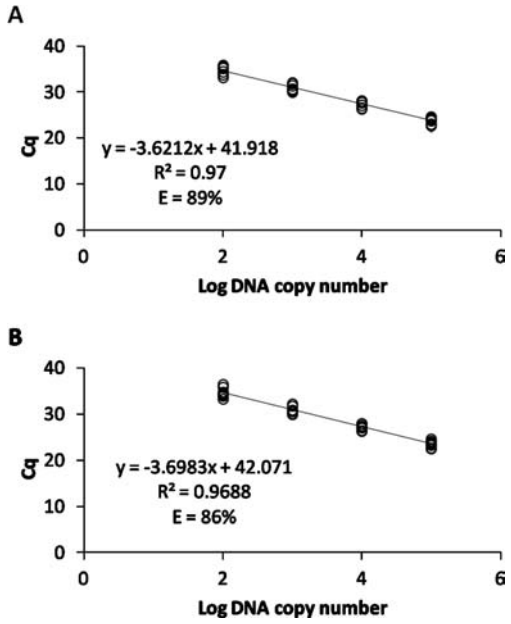


**Figure 3.** TaqMan FGM assay stardard curves performed in four qPCR runs on different days. Curves were generated for two DNA extracts from leaves: (A) Embrapa 5.1 GM Pérola ($n$ = 8) and (B) Embrapa 5.1 GM Pontal ($n$ = 8). Samples were extracted by the CTAB method.

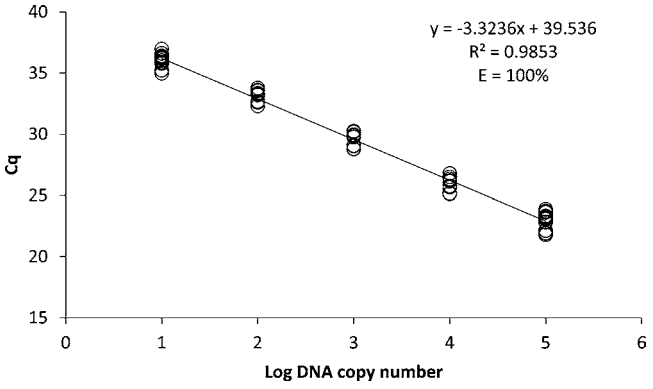


**Figure 4.** TaqMan FGM assay stardard curves performed in two qPCR runs on different days with four DNA extracts from seeds of Embrapa 5.1 GM Pérola in duplicate ($n$ = 12). Samples were extracted by use of DNeasy plant minikit.

purity of a powder produced from GM seeds is difficult to check.[9]

The specificity of the developed primers was assessed by SYBR Green assay. The results showed that Cq values were similar for Embrapa 5.1 DNA samples at 200, 300, and 400 nM primers. However, the 300 nM concentration detected the target with no cross-reaction with non-GM common bean. Efficiency values obtained in the SYBR Green assay, with five primer concentrations and samples extracted with DNeasy plant minikit or CTAB method, are in accordance with the European Network of Genetically Modified Organism Laboratory (ENGL).[20] According to this guideline, the efficiency values of standard curves must range from 90% to 110%, and the correlation coefficient ($R^2$) must be higher than 0.98. One efficiency value was out of this range (112%) and all correlation coefficients were higher than 0.98.

**Table 7. Comparison of Amplification Efficiency Values and $R^2$ for Two GM Events, Embrapa 2.3 and Embrapa 5.1[a]**

| | OLA assay | | FGM assay | |
|---|---|---|---|---|
| DNA sample | efficiency (%) | $R^2$ | efficiency (%) | $R^2$ |
| Embrapa 2.3 common bean | 95[b] | 1.000 | | |
| Embrapa 5.1 Pérola | 90[b] | 0.980 | 113[c] | 0.998 |
| Embrapa 5.1 Pontal | 97[c] | 0.924 | 95[c] | 0.993 |

[a]qPCR was performed in TaqMan OLA (construct-specific) assay and FGM (event-specific assay for Embrapa 5.1). [b]Limit of detection at $10^0$. [c]Limit of detection at $10^1$.

Because of its high specificity, a TaqMan probe was developed. FGM probe uses the minor-groove-binding (MGB) technology that allows the design of shorter probes with higher melting temperatures[21] and with high specificity of the hybridization.[22] When FGM probe was tested with nontarget samples, positive signals in 42 out of 192 samples (22%) were observed. The samples that showed a positive signal presented a late Cq (Cq > 37) for 50 ng of DNA, equivalent to $10^{4.85}$ DNA copies. The Cq value of positive samples (GM Pérola and GM Pontal) with the same DNA quantity (50 ng) is approximately 21. The observed ΔCq of 16

**Table 6. Cq Values Generated by qPCR TaqMan OLA (Construct-Specific) and FGM (Event-Specific) Assays for Mixed DNA Samples**

| samples | GM Pérola + Pérola[a] | GM Pérola + Pontal[a] | GM Pontal + Pérola[a] | GM Pontal + Pontal[a] |
|---|---|---|---|---|
| | | OLA Assay, $10^2$ DNA Copy Number | | |
| Cq ± SD | 31.91 ± 0.16 | 31.78 ± 0.10 | 31.78 ± 0.10 | 33.98 ± 2.17 |
| positive/total | 3/3 | 3/3 | 3/3 | 2/3 |
| | | OLA Assay, $10^1$ DNA Copy Number | | |
| Cq ± SD | 34.90 ± 1.28 | 34.64 ± 0.73 | 35.38 ± 0.74 | 35.66 ± 0.92 |
| positive/total | 5/6 | 6/6 | 5/6 | 5/6 |
| | | FGM Assay, $10^2$ DNA Copy Number | | |
| Cq ± SD | 32.12 ± 0.19 | 32.47 ± 0.39 | 33.02 ± 0.16 | 32.61 ± 0.37 |
| positive/total | 3/3 | 3/3 | 3/3 | 3/3 |
| | | FGM Assay, $10^1$ DNA Copy Number | | |
| Cq ± SD | 35.55 ± 0.73 | 35.04 ± 0.84 | 36.07 ± 0.8 | 36.57 ± 1.59 |
| positive/total | 5/6 | 5/6 | 6/6 | 6/6 |

[a]Template DNA was mixed DNA: Embrapa 5.1 GM Pérola ($10^2$ or $10^1$ DNA copies) in the presence of background DNA of non-GM common bean (Pérola and Pontal) varieties (10 ng or 14 327 copies)

is sufficient to propose that these amplifications of few negative samples were unspecific.

Standard curves for quantitation of Embrapa 5.1 GM common bean by the FGM probe were prepared from serial dilutions of GM Pérola and GM Pontal leaf material. For GM Pérola, 14 out 15 (93%) efficiency values were between 90% and 110%, in accordance with ENGL. For GM Pontal, the efficiency values were between 94% and 98%. All curves presented $R^2$ higher than 0.99. A mean standard curve was generated by the repeatability assay, using DNA samples of GM Pérola, presenting an efficiency of 95% and an $R^2$ of 0.99. Dinon et al.[14] reported an efficiency of 89% for the standard curve generated with OLA probe. By comparison of these results, FGM probe seems to be more suitable for detection and quantitation of Embrapa 5.1 GM common bean, as the efficiency of the assay was closer to 100% and mainly for being event-specific.

The LOD is defined as the lowest amount of DNA that can be reliably detected. According to ENGL,[20] qPCR methods should detect the presence of the analyte at least 95% of the time. For FGM assay, the LOD was 10 DNA copies based on the haploid genome of common bean for DNA extracted with DNeasy plant minikit diluted in water. The Cq value of 10 DNA copies (corresponding to 6.98 pg) is approximately 35.66. For Embrapa 5.1 DNA extracted by the CTAB method, FGM assay showed a LOD of 100 DNA copies. Wang et al.[10] reported a LOD of 100 copies for an event-specific qPCR assay of GM rice Kefeng-8. For a qPCR assay of GM rice Kefeng-6, Guertler et al.[11] reported a LOD of 5 copies. We observed that amplification occurred later for DNA samples extracted by the CTAB method since the Cq of these samples was approximately 24 for $10^5$ DNA copies, while the samples extracted with DNeasy plant mini kit presented a Cq of 22. The DNA extraction method can influence the quantitation because of its effectiveness in removing substances that can interfere in the PCR.[23] In order to verify applicability of the FGM assay for seed samples, standard curves for DNA extracted from powder seeds were obtained and efficiency value of 100% was obtained. DNA extraction methods applied to one matrix may not be suitable for other matrices. In this case, DNA extraction method (DNeasy plant minikit) was suitable for both leaf and seed materials.

When Embrapa 5.1 DNA was diluted in non-GM common bean DNA solution, the LOD of FGM assay was $10^2$ DNA copies, with a mean Cq of 32.5. Positive reactions were still observed in 22 out of 24 reactions (92%) for $10^1$ DNA copy numbers, with a mean Cq of 35.8, showing that amplification was not highly influenced by the presence of a background DNA. Andersen et al.[21] reported that the presence of large amounts of background DNA did not promote a severe effect in the results of DNA amplification. When OLA assay (construct-specific) and FGM assay for DNA samples diluted in non-GM common bean were compared, the methods presented the same LOD and the Cq values were very similar.

FGM and OLA assays were compared for serial dilutions of Embrapa 5.1 GM Pérola, Embrapa 5.1 GM Pontal, and Embrapa 2.3 GM event. For OLA probe the efficiency values were 90%, 97%, and 95%, respectively. For FGM probe the efficiency value for GM Pérola was 113% and for GM Pontal was 95%. DNA from Embrapa 2.3 was not detected in any of the points of the standard curves. Therefore, the FGM probe was suitable to differentiate authorized from nonauthorized GM common bean events.

Recent reports have been published about development of GM event-specific qPCR assays for several new GMOs. Guertler et al.[11] developed an assay for detection of Kefeng-6 GM rice. Event-specific assays were developed for specific detection of a GM herbicide-tolerant soybean, A2704-12 event,[24] of GM Chinese cabbage[25] and GM flax.[12] Other authors also reported the development of event-specific assays.[12,13,26−28]

The method developed in the present work is reliable for detection and quantitation of Embrapa 5.1 GM common bean. Even when it is considered that some negative samples presented a positive signal, the Cq values were higher than the Cq value of the LOD, considered to be 100 DNA copies in the presence of background DNA. Both qPCR chemistries used in this work are suitable for quantitation of GM common bean Embrapa 5.1. A new endogenous reference gene assay, named LEC assay, was developed for quantitation of common bean DNA in food.[29] The FGM assay developed here, together with the LEC assay, can be useful for surveys of compliance with GMO-labeling legislation by regulatory authorities in Brazil and in other countries.[30] Moreover, this new event-specific assay is an important tool in GMO analysis because it allows specific quantitation of an authorized GM event.

## ■ ASSOCIATED CONTENT

### Supporting Information

One table showing specificity test of SYBR Green assay and two figures showing border junction sequence of Embrapa 5.1 and TaqMan FGM assay standard curves. This material is available free of charge via the Internet at http://pubs.acs.org.

## ■ AUTHOR INFORMATION

### Corresponding Author

*Phone +554837215382; fax +554837219943; e-mail ana.arisi@ufsc.br.

### Funding

The work was financially supported by CNPq Grants 471401/2012-9 and 470683/2012-0. D.T. is the recipient of a CNPq Master fellowship; G.L.V., a CAPES Ph.D. fellowship; F.C.A.B., a CAPES PNPD postdoctoral fellowship; and A.C.M.A., a CNPq PQ-2 fellowship.

### Notes

The authors declare no competing financial interest.

## ■ ACKNOWLEDGMENTS

We express our gratitude to Francisco J. L. Aragão for providing the border junction DNA sequence of GM common bean Embrapa 5.1.

## ■ ABBREVIATIONS

BGMV, bean golden mosaic virus; Cq, quantitation cycle; CTAB, cetyltrimethylammonium bromide; Embrapa, Brazilian Agricultural Research Corporation; ENGL, European Network of GMO Laboratories; FGM, event-specific quantitative polymerase chain reaction assay for Embrapa 5.1 detection; GMO, genetically modified organism; GM, genetically modified; LOD, limit of detection; MGB, minor-groove binding; OLA, construct-specific quantitative polymerase chain reaction assay for Embrapa 5.1 and Embrapa 2.3 detection; PCR, polymerase chain reaction; qPCR, quantitative polymerase chain reaction; $R^2$, correlation coefficient

## REFERENCES


(1) Bonfim, K.; Faria, J. C.; Nogueira, E. O. P. L.; Mendes, E. A.; Aragao, F. J. L. RNAi-mediated resistance to Bean golden mosaic virus in genetically engineered common bean (*Phaseolus vulgaris*). *Mol. Plant-Microbe Interact.* **2007**, *20*, 717−726.

(2) Aragao, F. J. L.; Faria, J. C. First transgenic geminivirus-resistant plant in the field. *Nat. Biotechnol.* **2009**, *27*, 1086−1088.

(3) Faria, J. C.; Valdisser, P. A. M. R.; Nogueira, E. O. P. L.; Aragão, F. J. L. RNAi-based bean golden mosaic virus-resistant common bean (Embrapa 5.1) shows simple inheritance for both transgene and disease resistance. *Plant Breed.* **2014**, *133*, 649−653.

(4) Aragao, F. J. L.; Nogueira, E. O. P. L.; Tinoco, M. L. P.; Faria, J. C. Molecular characterization of the first commercial transgenic common bean immune to the bean golden mosaic virus. *J. Biotechnol.* **2013**, *166*, 42−50.

(5) Brazil, Decree 4.680 of 24 April 2003, regulates the information access concerning foods and ingredients containing or produced from genetically modified organisms. DOU, Official Journal of Brazil, Brasília, Brazil, 2003; http://www.anvisa.gov.br/e-legis/.

(6) European Commission.. EC Regulation 1830/2003 of 22 September 2003, concerning the traceability and labelling of genetically modified organisms and the traceability of food and feed products produced from genetically modified organisms. *Off. J. Eur. Commun.* **2003**, *L268*, 24−28.

(7) European Commission.. EC Regulation 619/2011 of 24 June 2011, laying down the methods of sampling and analysis for the official control of feed as regards presence of genetically modified material for which an authorization procedure is pending or the authorization of which has expired. *Off. J. Eur. Commun.* **2011**, *L166*, 9−15.

(8) Scholtens, I.; Laurensse, E.; Molenaar, B.; Zaaijer, S.; Gaballo, H.; Boleij, P.; Bak, A.; Kok, E. Practical experiences with an extended screening strategy for genetically modified organisms (GMOs) in real-life samples. *J. Agric. Food Chem.* **2013**, *61*, 9097−9109.

(9) Caprioara-Buda, M.; Meyer, W.; Jeynov, B.; Corbisier, P.; Trapmann, S.; Emons, H. Evaluation of plasmid and genomic DNA calibrants used for the quantification of genetically modified organisms. *Anal. Bioanal. Chem.* **2012**, *404*, 29−42.

(10) Wang, W.-x.; Zhu, T.-h.; Lai, F.-x.; Fu, Q. Event-specific qualitative and quantitative detection of transgenic rice Kefeng-8 by characterization of the transgene flanking sequence. *Eur. Food Res. Technol.* **2012**, *234*, 477−484.

(11) Guertler, P.; Huber, I.; Pecoraro, S.; Busch, U. Development of an event-specific detection method for genetically modified rice Kefeng 6 by quantitative real-time PCR. *J. Verbraucherschutz Lebensmittelsicherh.* **2012**, *7*, 63−70.

(12) Vanella, R.; Weston, A.; Brodmann, P.; Kuebler, E. Development of an event-specific assay for the qualitative and quantitative detection of the genetically modified flax CDC Triffid (FP967). *Food Control* **2014**, *41*, 128−133.

(13) Wu, Y.; Yang, L.; Cao, Y.; Song, G.; Shen, P.; Zhang, D.; Wu, G. Collaborative validation of an event-specific quantitative real-time PCR method for genetically modified rice event TT51-1 detection. *J. Agr. Food Chem.* **2013**, *61*, 5953−5960.

(14) Dinon, A. Z.; Brod, F. C. A.; Mello, C. S.; Oliveira, E. M. M.; Faria, J. C.; Arisi, A. C. M. Primers and probes development for specific PCR detection of genetically modified common bean (*Phaseolus vulgaris*) Embrapa 5.1. *J. Agric. Food Chem.* **2012**, *60*, 4672−4677.

(15) Brod, F. C. A.; Dinon, A. Z.; Kolling, D. J.; Faria, J. C.; Arisi, A. C. M. Development of plasmid DNA reference material for the quantification of genetically modified common bean Embrapa 5.1. *J. Agric. Food Chem.* **2013**, *61*, 4921−4926.

(16) Dinon, A. Z.; Prins, T. W.; van Dijk, J. P.; Arisi, A. C. M.; Scholtens, I. M. J.; Kok, E. J. Development and validation of real-time PCR screening methods for detection of cry1A.105 and cry2Ab2 genes in genetically modified organisms. *Anal. Bioanal. Chem.* **2011**, *400*, 1433−1442.

(17) Holst-Jensen, A.; Ronning, S. B.; Lovseth, A.; Berdal, K. G. PCR technology for screening and quantification of genetically modified organisms (GMOs). *Anal. Bioanal. Chem.* **2003**, *375*, 985−993.

(18) Aragao, F.; Faria, J. First transgenic geminivirus-resistant plant in the field: The development of a RNAi-based agriculture technology. *In Vitro Cell. Dev. Biol. Anim.* **2010**, *46*, S5.

(19) Meng, Y. A.; Liu, X.; Wang, S.; Zhang, D. B.; Yang, L. T. Applicability of plasmid calibrant pTC1507 in quantification of TC1507 maize: An interlaboratory study. *J. Agric. Food Chem.* **2012**, *60*, 23−28.

(20) ENGL, European Network of Genetically Modified Organism Laboratories. Definition of minimum performance requirements for analytical methods of GMO testing, 13 October 2008; http://gmo-crl.jrc.ec.europa.eu/doc/Min_Perf_Requirements_Analytical_methods.pdf.

(21) Andersen, C. B.; Holst-Jensen, A.; Berdal, K. G.; Thorstensen, T.; Tengs, T. Equal performance of TaqMan, MGB, molecular beacon, and SYBR green-based detection assays in detection and quantification of Roundup-ready soybean. *J. Agric. Food Chem.* **2006**, *54*, 9658−9663.

(22) Kutyavin, I. V.; Afonina, I. A.; Mills, A.; Gorn, V. V.; Lukhtanov, E. A.; Belousov, E. S.; Singer, M. J.; Walburger, D. K.; Lokhov, S. G.; Gall, A. A.; Dempcy, R.; Reed, M. W.; Meyer, R. B.; Hedgpeth, J. 3′-minor groove binder-DNA probes increase sequence specificity at PCR extension temperatures. *Nucleic Acids Res.* **2000**, *28*, 655−661.

(23) Cankar, K.; Stebih, D.; Dreo, T.; Zel, J.; Gruden, K. Critical points of DNA quantification by real-time PCR: Effects of DNA extraction method and sample matrix on quantification of genetically modified organisms. *BMC Biotechnol.* **2006**, *6*, 37.

(24) Ma, H.; Li, H.; Li, J.; Wang, X. F.; Wei, P. C.; Li, L.; Yang, J. B. High-throughput, low-cost, and event-specific polymerase chain reaction detection of herbicide tolerance in genetically modified soybean A2704-12. *GMR, Genet. Mol. Res.* **2014**, *13*, 696−703.

(25) Shin, K.-S.; Lim, M.-H.; Woo, H.-J.; Lim, S.-H.; Ahn, H.-I.; Lee, J.-H.; Cho, H.-S.; Kweon, S.-J.; Suh, S.-C. Event-specific qualitative and quantitative polymerase chain reaction methods for detection of insect-resistant genetically modified Chinese cabbage based on the 3′-junction of the insertion site. *J. Kor. Soc. Appl. Biol. Chem.* **2012**, *55*, 367−375.

(26) Xu, W. T.; Zhang, N.; Luo, Y. B.; Zhai, Z. F.; Shang, Y.; Yan, X. H.; Zheng, J. J.; Huang, K. L. Establishment and evaluation of event-specific qualitative and quantitative PCR method for genetically modified soybean DP-356043-5. *Eur. Food Res. Technol.* **2011**, *233*, 685−695.

(27) Zhang, N.; Xu, W.; Bai, W.; Zhai, Z.; Luo, Y.; Yan, X.; He, J.; Huang, K. Event-specific qualitative and quantitative PCR detection of LY038 maize in mixed samples. *Food Control* **2011**, *22*, 1287−1295.

(28) Zhang, M.; Huo, N.; Liu, Y.; Qiu, Y.; Ao, J.; Luan, F.; Li, Q.; Gao, X. Event-specific detection of genetically modified wheat B73−6-1 based on the 3′-flanking sequence. *Eur. Food Res. Technol.* **2012**, *235*, 1149−1159.

(29) Venturelli, G. L.; Brod, F. C.; Rossi, G. B.; Zimmermann, N. F.; Oliveira, J. P.; Faria, J. C.; Arisi, A. C. A Specific endogenous reference for genetically modified common bean (*Phaseolus vulgaris* L.) DNA quantification by real-time PCR targeting lectin gene. *Mol. Biotechnol.* **2014**, *56*, 1060−1068.

(30) Branquinho, M. R.; Ferreira, R. T. B.; Cardarelli-Leite, P. Survey of compliance with labeling legislation in food containing GMOs in Brazil. *J. Food Compos. Anal.* **2010**, *23*, 220−225.

2-picrylhydrazyl (DPPH•) and to distinguish the kinetic behavior of different antioxidants, quantifying the type of antioxidants and determining the molar ratio of antioxidant to DPPH•. Oszmianski et al.[13] also proved that EPR spectroscopy appeared to be a much better method than UV−visible spectrophotometry, the first methodology reflecting more accurately the content in procyanidins. Moreover, EPR detection is not affected either by the turbidity of samples or by the presence of colored samples, thus avoiding the necessity for corrections for background absorbance.[13]

With the present work we aimed at studying more in depth the behavior of hydrophilic extracts from lettuce related to a different phenolic composition. In fact, from preliminary analyses, the hydrophilic extract showed to be more interesting than the lipophilic one having an antioxidant capacity many fold higher (data not shown). To better discriminate the antioxidant capacity of phenolics, we focused our study on differently colored lettuces [green (G); green/red (G/R); and red (R)] with the aim of identifying the antioxidant kinetic behavior of the different antioxidant-rich cultivars.[15] The three cultivars of lettuce have been characterized for the profile and concentrations of phenols, including conjugated forms, which until now have been less studied.[8] Even if several authors have tried to correlate the antioxidant capacity of food with a specific antioxidant compound,[11,16] this is the first approach in lettuce that aimed at correlating the kinetic behavior of hydrophilic extracts from different pigmented cultivars with their relative antioxidant composition. This study could contribute to fully characterize plant antioxidants, adding useful information about the different importance of each hydrophilic antioxidant in the human diet.

## MATERIALS AND METHODS

**Chemicals and Reagents.** All solvents were of highest purity and were purchased from Sigma-Aldrich (Milan, Italy). Water was of Milli-Q grade. All solvents and water were accurately degassed before use in the analyses. The standards luteolin-7-*O*-glucoside, rutin, apigenin-7-*O*-glucoside, quercetin, quercitrin, luteolin, kaempferol, quercetin-3-*O*-glucuronide, cyanidin, and cyanidin-3-*O*-glucoside were purchased from Extrasynthèse (Genay, France). The standards gallic, protocatechuic, *p*-hydroxybenzoic, chlorogenic, vanillic, caffeic, syringic, *p*-coumaric, ferulic, and chicoric acids as well as free stable DPPH• and 2,2′-azinobis(3-ethylbenzothiazoline-6-sulfonic acid) (ABTS) were purchased from Sigma (Milan, Italy).

**Plant Material and Growing Conditions.** Seeds of three commercially available cultivars of lettuce, a green-leaf cultivar (Blonde of Paris Batavia, G), a green/red-leaf cultivar (Marvel of Four Seasons, G/R), and a red-leaf cultivar (Oak Leaf, R) (Clemente Viven, Vitoria-Gasteiz, Spain) were planted in plastic pots (13 cm side × 15 cm high) containing a mixture of perlite/vermiculite (3:1, v/v). Seven days after sowing (DAS), the most uniformly sized lettuce plants were selected, leaving one plant per pot. Seedlings were grown in a controlled growth chamber maintained at 24/20 °C (day/night) with a relative humidity of 60/80% (day/night); seedlings were watered with Hoagland's solution[17] every 2 days. Photosynthetic active radiation was 400 μmol photons $m^{-2}$ $s^{-1}$ with a photoperiod of 14 h. To minimize the effects of intrachamber environmental gradients, plants were randomly repositioned within the chamber each week. At the end of the experiment (46 DAS) the antioxidant capacity and the concentration of the different antioxidant compounds were measured in the fully expanded external leaves chosen at random.

**Sample Extracts.** Fresh leaves (0.5 g) were pulverized with liquid nitrogen by a tissue homogenizator (MM301, Fisher Bioblock Scientific, France). Extraction was performed in the dark with 70% methanol containing 1% HCl using a mortar. Homogenization was completed with sonication for 30 min. After centrifugation at 4 °C at 12100*g* for 15 min, supernatants were filtered by Sartorius (Goettingen, Germany) filters (Minisart 0.45 μm) to remove any suspended material.

**Quantification of Antioxidant Capacity by EPR Analysis.** The antioxidant capacity was measured using DPPH• quenching. DPPH• is a commercially available free radical compound that is soluble and stable in ethanol. All operations were performed in the dark to avoid photochemical effects on DPPH• as well as on leaf extracts. EPR spectra were recorded with a Varian E112 (X-band) spectrometer equipped as previously reported[2] at the conditions specified in Sgherri et al.[14] Computer-based simulations of EPR spectra were performed using the Winsim program.[18] All data analyses were performed using the CurveExpert software (version 1.34). The incubation mixture contained DPPH• at a final concentration of 400 μM in ethanol. This concentration was chosen by preliminary experiments because it was much in excess to the initial concentration of antioxidants in the sample, thus allowing all of the antioxidants to react with the radical.[12] In these conditions the reactions with DPPH• were completed after several hours. To determine the decay of the radical before measuring antioxidant capacity, decay kinetics of DPPH• without the extract were recorded. The amplitude of the central line of DPPH• spectra was taken for registration of kinetics, which started soon after the addition of the sample to the radical solution. In this way, the scan time was 1 min, and many experimental points could be monitored. Both rate constant and number of DPPH• molecules reduced by extracts in the tube were obtained by fitting of the kinetic curves. Antioxidant capacity was the result of the number of DPPH• molecules reduced by 1 g of plant material and of the EPR decay rate constants ($M^{-1}$ $s^{-1}$).

The following equation, 1, which is a special form of the pseudo-first-order kinetic model previously applied to the determination of antioxidant capacity of lipid extracts of basil[14] as well as of oil fractions,[12] was employed in the analyses of the experimental kinetic data:

$$A = A_S \exp(-k_S' t) + A_I \exp(-k_I' t) + A_F \exp(-k_F' t) + A_R \quad (1)$$

$A$ is DPPH• molar concentration at time $t$, $A_S$, $A_I$, and $A_F$ are the initial DPPH• molar concentrations that can be reduced by the slow, intermediate, and fast fractions, respectively, and $A_R$ is the remaining DPPH• concentration in the medium because of the antioxidant depletion.

$k_S$, $k_I$, and $k_F$ represent the rate constants of the slow, intermediate, and fast fractions, respectively, and were calculated as follows:

$$k_S = k_S'/[\mathrm{DPPH}]_{t0}$$

$$k_I = k_I'/[\mathrm{DPPH}]_{t0} \text{ and}$$

$$k_F = k_F'/[\mathrm{DPPH}]_{t0}$$

Equation 1 is the solution of more than one differential equation of second order assuming that the initial molar concentration of DPPH• ($[\mathrm{DPPH}]_{t0}$) is greater than the molar concentration of antioxidants in the reactions.[12]

**Quantification of Antioxidant Capacity by Spectrophotometric Analysis.** The radical cation 2,2′-azinobis(3-ethylbenzothiazoline-6-sulfonic acid) ($ABTS^{•+}$) was generated as described by Pellegrini et al.[19] The radical solution was diluted in ethanol to obtain an absorbance at 734 nm of 0.7 ± 0.05. After addition of the extract, the decrease in absorbance was monitored and compared to that of the trolox standard. Antioxidant capacity was expressed in terms of trolox equivalent antioxidant capacity (TEAC) per gram dry weight (DW) of plant material.

**Determination of Total Phenols.** Determination of total phenolic compounds was performed on methanolic extracts following the method reported by Nguyen and Niemeyer[20] based on the reaction between phenols with Folin−Ciocalteu reagent. Calculations were performed using a calibration curve prepared with gallic acid as standard.

**Determination of Total Anthocyanins.** Approximately 0.01 g of lettuce fresh weight was homogenized in liquid nitrogen and extracted

with 3 M HCl/$H_2O$/MeOH (1:3:16 v/v/v) using a tissue homogenizer. The extracts were centrifuged at 16100*g* for 5 min, and anthocyanin levels were estimated (as cyanidin-3-glycoside equivalents) using a molar extinction coefficient of 33000 $M^{-1}$ $cm^{-1}$.[21] Absorbance of anthocyanins at 524 nm was corrected by subtracting the interference due to pheophytin as $A_{524} - 0.24A_{653}$.[22]

**Analysis of Flavonoids.** Qualitative and quantitative analyses were performed by RP-HPLC. Twenty microliters of extract was injected into a Waters model 515 HPLC system fitted with a 4.6 mm × 250 mm Prodigy ODS column (Phenomenex, Bologna, Italy). Detection was at 360 nm, using a Waters 2487 dual $\lambda$ UV−visible detector. Mobile phase A contained water acidified with formic acid (pH 2.7), and mobile phase B contained methanol. A linear gradient of 10−90% mobile phase B was run for 26 min at 1 mL $min^{-1}$. The identity of the free flavonoids was confirmed by cochromatography with authentic standards. Quantification was performed using standard curves in the range of 10−500 ng of a standard mixture containing luteolin-7-*O*-glucoside, rutin, apigenin-7-*O*-glucoside, quercitrin, quercetin-3-glucuronide, quercetin, luteolin, and kaempferol. Chromatogram analysis was performed by the software Millennium 32 (Waters). Hydrolyzable flavonoids were detected after hydrolysis of methanolic extracts at 85 °C for 30 min with 4 N HCl containing 0.1% (w/v) ascorbic acid.

Detection of cyanidin and cyanidin-3-*O*-glucoside was performed in the dark similarly to that of flavonoids with the exception of absorbance, which was changed to 520 nm. The quantification of anthocyanins was obtained after cochromatography with cyanidin and cyanidin-3-*O*-glucoside in the range 0.1−0.5 $\mu$g.

**Analysis of Phenolic Acids.** Qualitative and quantitative analyses were performed by RP-HPLC as previously reported in Sgherri et al.[23] The identity of the free phenolic acids was confirmed by cochromatography with authentic standards, and quantification was performed using a standard curve in the range 0.1−0.5 $\mu$g of standard mixtures containing gallic, protocatechuic, *p*-hydroxybenzoic, chlorogenic, vanillic, caffeic, syringic, *p*-coumaric, ferulic, and chicoric acids. Chromatogram analysis was performed as previously reported for flavonoid determination.

Detection of conjugated phenolic acid was performed after alkaline hydrolysis of methanolic extracts. Samples were added of 4 N NaOH (1:1, v/v) containing 1% ascorbic acid and 10 mM ethylenediaminetetraacetic acid (EDTA) to prevent the degradation of phenolic acids during alkaline hydrolysis. After incubation for 1 h in the dark under a continuous flux of nitrogen, samples were acidified using 12 N HCl to achieve a pH value of about 2. The resulting mixtures were extracted three times with 1 mL of ethyl acetate. The organic phases were collected after centrifugation at 3000*g* for 5 min and evaporated to dryness at 35 °C in a rotary evaporator. Immediately before analysis, the residue was redissolved in 50% (v/v) acetonitrile and then passed through a Sartorius (Goettingen, Germany) filter (Minisart 0.45 $\mu$m) to remove any suspended material.

**Statistical Analysis.** The results are the means from three replicates of three independent experiments ($n$ = 9). All data are reported as mean values ± SE. The significance of differences among mean values was determined by one-way ANOVA. Comparisons among means were performed using Duncan's multiple-range test. Means in tables and figures accompanied by different letters are significantly different at $p \leq 0.05$. When necessary, an arc sin or angular transformation was applied before statistical analysis was performed.

## RESULTS

The EPR spectrum of DPPH•, previously reported by Sgherri et al.,[2,14] is characterized by five lines that are narrow enough, compared to the spectrum acquisition time, to be used for registration of kinetics with many points close. DPPH• shows a well-resolved quintet EPR spectrum with $a_{N1}$ = 0.927 mT and $a_{N2}$ = 0.846 mT at $g$ = 2.0036, and its unimolecular decay constant was 2.06 × $10^{-6}$ $s^{-1}$.[14,24] The model of scavenging stable DPPH• is a widely used method to evaluate antioxidant capacity, and the radical reactions involved during its scavenging by an antioxidant are well detailed in Espín et al.[12] Decay kinetics of DPPH• following the addition of the hydrophilic extracts from lettuce leaves (G, G/R, and R) are shown in Figure 1. The decay kinetics of DPPH• in the presence of the hydrophilic extract were due to the contribution of two or three pseudo-first-order kinetics, depending on the cultivar: two for G and R and three for G/R. This is related to the presence of different antioxidants or groups of antioxidants that differ in their velocity to scavenge the radical with the rate constants ($k$) to be considered as a measure of the speed of DPPH• disappearance.[12] G cultivar was characterized by an intermediate and a slow rate constant and R by a fast and an intermediate rate constant, whereas G/R was characterized by a fast, an intermediate, and a slow rate constant (Table 1). These $k$ values, which characterize the decay kinetics of DPPH•, are indicative of the presence of antioxidants in the hydrophilic extract distinguishable for a fast, intermediate, and slow action. For this reason, we can calculate (by EPR kinetics) a fast, an intermediate, and a slow antioxidant capacity of the hydrophilic extract. Each antioxidant capacity, detected by EPR, is expressed as the ability to reduce DPPH• molecules by 1 g of lettuce leaves (Table 1). Substantial increases in the fast antioxidant capacity of the hydrophilic extract were observed in G/R compared to G (not detectable) and in R compared to G/R. A significant increase in the slow antioxidant capacity of the hydrophilic extract was also observed in G/R compared to G, whereas R lettuce did not show any slow antioxidant capacity. Although G and G/R showed similar intermediate antioxidant capacities, in R lettuce intermediate antioxidant capacity was about 5 times higher than in G and G/R (Table 1).

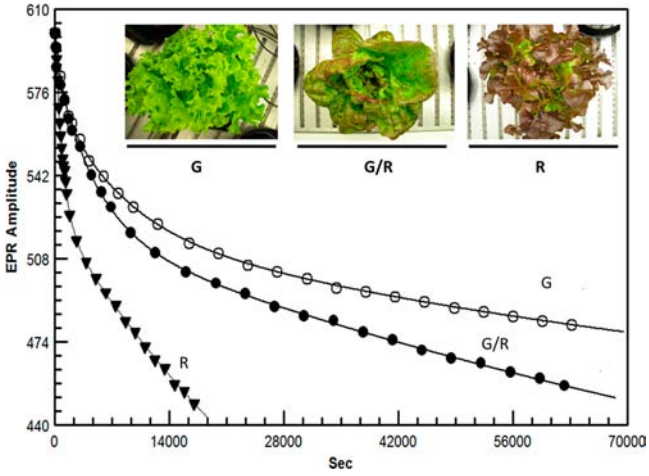


**Figure 1.** EPR decay kinetics of 400 $\mu$M 1,1-diphenyl-2-picrylhydrazyl (DPPH•) after the addition of hydrophilic extracts from green (G), green/red (G/R), and red (R) lettuces.

Data obtained by the discoloration of $ABTS^{\bullet+}$ (Figure 2A) confirmed what is reported in Table 1, namely, that antioxidant capacity of hydrophilic extracts increased with the increase in red pigmentation. In particular, the enhancement in antioxidant capacity was about 120% in G/R and 400% in R, compared to G lettuce. The enrichment in total phenols (Figure 2B) and total anthocyanins (Figure 2C) followed a similar trend. In fact, compared to G lettuce, the contents of total phenols and total anthocyanins increased by 3- and 5-fold in G/R and by 4- and 12-fold in R, respectively.

**Table 1. Decay Rate Constants and Number of Antioxidants Obtained from EPR Decay Kinetics of DPPH after the Addition of Hydrophilic Extract from Green (G), Green/Red (G/R), and Red (R) Lettuces[a]**

| | decay rate constant ($M^{-1}$ $s^{-1}$) | | | no. of antioxidants (no. DPPH• reduced × $10^{19}$/g) | | |
|---|---|---|---|---|---|---|
| | $k_F$ | $k_I$ | $k_S$ | FRA | IRA | SRA |
| G | nd | 0.51 ± 0.04 | 0.017 ± 0.003 | nd | 2.34 ± 0.07 | 3.85 ± 0.09 |
| G/R | 2.75 ± 0.09 | 0.32 ± 0.03 | 0.023 ± 0.005 | 1.43 ± 0.08 | 2.71 ± 0.05 | 4.62 ± 0.05 |
| R | 2.55 ± 0.06 | 0.41 ± 0.02 | nd | 3.70 ± 0.07 | 14.58 ± 0.09 | nd |

[a] $k_F$, fast rate constant; $k_I$, intermediate rate constant; $k_S$, slow rate constant; nd, not detectable. FRA, fast-rate antioxidants; IRA, intermediate-rate antioxidants; SRA, slow-rate antioxidants.

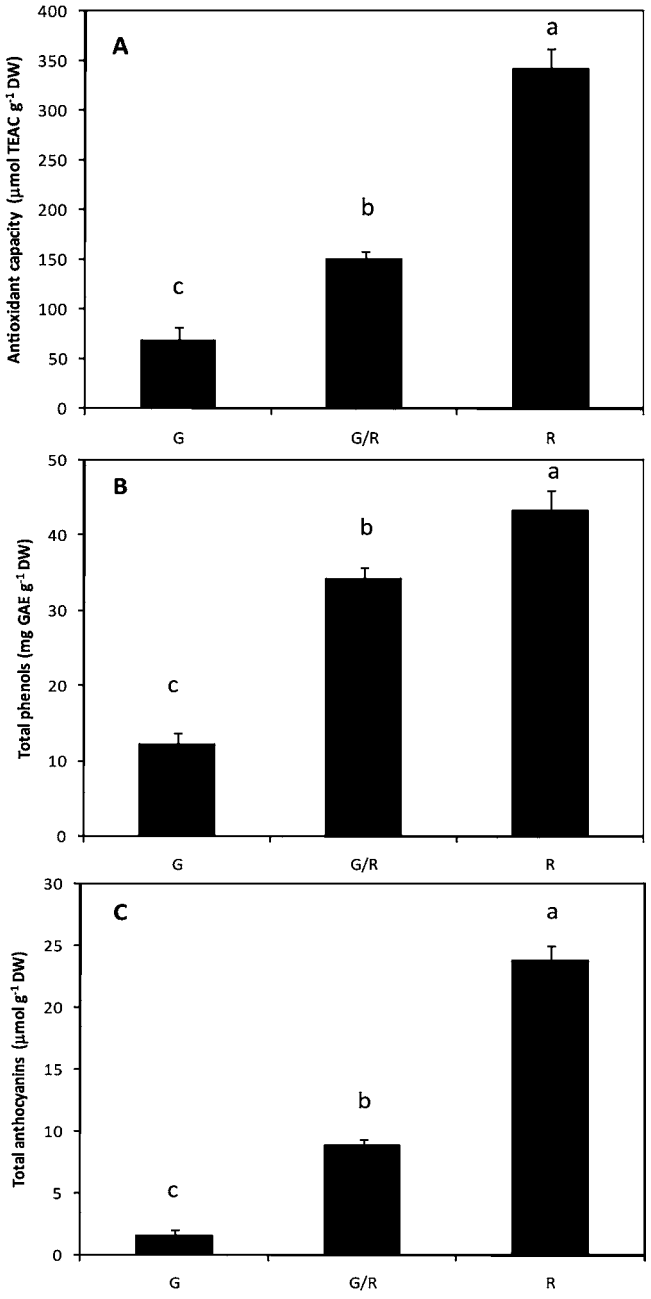


**Figure 2.** Antioxidant capacity determined by discoloration of 2,2′-azinobis(3-ethylbenzothiazoline-6-sulfonic acid) (A), total phenols (B), and total anthocyanins in leaves of green (G), green/red (G/R), and red cultivars (R) of lettuce. All data are reported as mean values ± SE. Means accompanied by different letters are significantly different at $p < 0.05$. TEAC, trolox equivalent antioxidant capacity; GAE, gallic acid equivalent.

Among phenols, Tables 2 and 3 showed that both flavonoids (in free and conjugated form) and phenolic acids (in free and conjugated form) were significantly affected by cultivar type, increasing their total amounts as a function of red pigmentation. In G the main free flavonoids were represented by quercetin and kaempferol, in G/R by kaempferol and quercetin-3-*O*-glucuronide, whereas in R by quercetin, quercetin-3-*O*-glucuronide, and luteolin-7-*O*-glucoside (Table 2). In each lettuce cultivar the most abundant conjugated flavonoid was quercetin, with an average contribution between 56 and 80%. Other hydrolyzable flavonoids identified in lettuce were luteolin and kaempferol (Table 2). In comparison with G, the G/R cultivar showed about double values of total free and hydrolyzable flavonoids. With regard to free flavonoids, this was due to a general increase in all flavonoids, with the exception of quercetin, which remained constant. The increase in the total amount of conjugated flavonoids was instead ascribable to a 2-fold increment of quercetin and kaempferol. R lettuce showed values 15- and 5-fold higher than G lettuce for total free and hydrolyzable flavonoids, respectively. In the R cultivar, each flavonoid took part in the increase in free flavonoids, whereas, similarly to what happened for G/R, only quercetin and kaempferol were responsible for the increase in hydrolyzable flavonoids, luteolin remaining almost constant (Table 2).

For all cultivars the composition in free phenolic acids was characterized by the prevalence of chlorogenic acid, contributing for 63−73% to the total (Table 3). Noteworthy was also the presence of ferulic and chicoric acids. After alkaline hydrolysis, the most representative phenolic acid became caffeic acid, contributing 70−80% to the total amounts of conjugated phenolic acids (Table 3). In comparison with G, higher contents in free phenolic acids showed by G/R and R were mainly related to the increases in chlorogenic, *p*-coumaric, and chicoric acids, whereas those of conjugated phenolic acids were prevalently ascribable to gallic, caffeic, *p*-coumaric, and chicoric acids (Table 3).

With regard to anthocyanins, we detected both cyanidin and cyanidin-3-*O*-glucoside, with cyanidin being prevalent (Figure 3). In G none of these compounds was observed, whereas in R lettuce values for cyanidin and cyanidin-3-*O*-glucoside were 22- and 12-fold higher than in G/R, respectively.

## DISCUSSION

Although in our previous studies DPPH• was employed to analyze the antioxidant behavior of lipid extracts,[2,14,24] the use of DPPH• in an ethanol mixture makes it suitable also for the determination of the antioxidant power of hydrophilic extracts (Figure 1; Table 1). Moreover, because without extract DPPH• shows a decay constant many times lower than that of Fremy's salt,[24] it is more suitable for monitoring long-lasting decay kinetics.

**Table 2. Changes in the Composition (Percent of the Total) and in the Total Amount (Micrograms per Gram Dry Weight) of Free and Conjugated Flavonoids in Different Cultivars of Lettuce[a]**

| | G cultivar | | G/R cultivar | | R cultivar | |
|---|---|---|---|---|---|---|
| | free | conjugated | free | conjugated | free | conjugated |
| luteolin-7-*O*-glucoside | 5.77 ± 0.42b | | 15.30 ± 1.45a | | 17.56 ± 0.37a | |
| rutin | 2.30 ± 0.33c | | 14.31 ± 1.26a | | 6.87 ± 0.29b | |
| apigenin-7-*O*-glucoside | 10.97 ± 0.98a | | 6.96 ± 0.54b | | 2.22 ± 0.17c | |
| quercitrin | 5.77 ± 0.05 | | tr | | tr | |
| quercetin | 32.40 ± 3.84b | 55.85 ± 0.79c | 11.52 ± 1.58c | 67.10 ± 1.98b | 43.82 ± 0.79a | 79.74 ± 1.14a |
| luteolin | 9.85 ± 0.33a | 17.39 ± 0.51a | 5.77 ± 0.12b | 10.39 ± 0.32b | 1.05 ± 0.03c | 4.69 ± 0.14c |
| kaempferol | 30.66 ± 1.55a | 26.76 ± 0.59a | 24.26 ± 1.33b | 22.51 ± 0.42b | 4.36 ± 0.28c | 15.56 ± 0.17c |
| quercetin-3-*O*-glucuronide | 2.30 ± 0.23b | | 21.87 ± 1.65a | | 24.13 ± 0.72a | |
| total | 21.33 ± 0.98c | 147.66 ± 1.29c | 58.75 ± 1.54b | 271.96 ± 4.58b | 319.10 ± 5.15a | 706.14 ± 7.34a |

[a]All data are reported as mean values ± SE. For each compound, in free or conjugated form, means accompanied by different letters are significantly different at $p \leq 0.05$ among cultivars. G, green; G/R, green/red; R, red.

**Table 3. Changes in the Composition (Percent of the Total) and in the Total Amount (Micrograms per Gram Dry Weight) of Free and Conjugated Phenolic Acids in Different Cultivars of Lettuce[a]**

| | G cultivar | | G/R cultivar | | R cultivar | |
|---|---|---|---|---|---|---|
| | free | conjugated | free | conjugated | free | conjugated |
| gallic acid | | 7.19 ± 0.31b | | 16.54 ± 0.53a | | 3.03 ± 0.14c |
| protocatechuic acid | | 3.15 ± 0.22b | | 0.77 ± 0.03c | | 4.01 ± 0.35a |
| chlorogenic acid | 73.78 ± 3.50a | 3.68 ± 0.26b | 68.80 ± 3.68a | 1.89 ± 0.12c | 63.34 ± 0.93b | 6.99 ± 0.54a |
| caffeic acid | | 76.59 ± 2.05b | | 71.04 ± 1.89b | | 81.08 ± 2.57a |
| *p*-coumaric acid | tr | 3.98 ± 0.25b | 2.85 ± 0.67b | 5.52 ± 0.25a | 10.97 ± 0.42a | 2.38 ± 0.12c |
| ferulic acid | 15.55 ± 0.12a | 3.88 ± 0.27a | 9.51 ± 0.11b | 2.66 ± 0.18b | 5.96 ± 0.34c | 1.38 ± 0.11c |
| chicoric acid | 10.67 ± 0.98b | 1.52 ± 0.11a | 18.84 ± 1.65a | 1.58 ± 0.11a | 19.73 ± 0.12a | 1.13 ± 0.13a |
| total | 111.10 ± 4.95c | 759.51 ± 17.98c | 135.16 ± 7.95b | 1141.82 ± 19.58b | 1166.18 ± 11.87a | 2980.61 ± 20.86a |

[a]All data are reported as mean values ± SE. For each compound, in free or conjugated form, means accompanied by different letters are significantly different at $p \leq 0.05$ among cultivars. G, green; G/R, green/red; R, red.

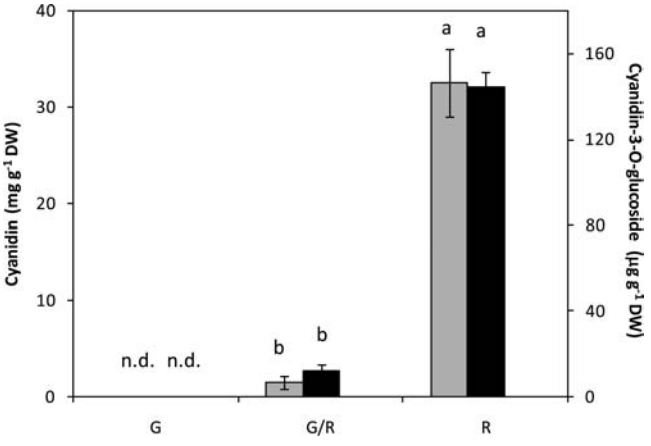


**Figure 3.** Contents of cyanidin (mg $g^{-1}$ DW, left axis; grey) and cyanidin 3-*O*-glucoside ($\mu$g $g^{-1}$ DW, right axis; black) in leaves of green (G), green/red (G/R), and red cultivars (R) of lettuce. All data are reported as mean values ± SE. Means accompanied by different letters are significantly different at $p < 0.05$.

The idea that a different pigmentation of plants is related to a different antioxidant capacity of their extracts is not new,[9,10,15] but the possibility to monitor and simulate EPR decay kinetics of DPPH•, as previously done for lipophilic extracts,[14] may add information about the kinetic behavior of the different antioxidants present in lettuce. Applying this methodology[14] to hydrophilic extracts, we could distinguish among slow-, intermediate-, and fast-rate antioxidants (Figure 1; Table 1). For the moment, we cannot attribute the kinetic behavior to a specific antioxidant, but only state that G/R contains antioxidants belonging to both G and R lettuce (SRA, IRA, FRA) and that G possesses the slowest antioxidants, whereas R the fastest ones (Table 1). The next step will be the identification of a specific kinetic behavior for each hydrophilic antioxidant (mostly representative for lettuce composition) by the study of the decay kinetics of authentic standards, which is currently underway in our laboratory and which was, in part, already performed for lipophilic antioxidants.[24]

Our results suggest that the different decay rates (Table 1) were related to the presence or absence of some antioxidants (Tables 2 and 3; Figure 3). Noteworthy is the relationship between the presence of cyanidin and cyanidin-3-*O*-glucoside and the fastest antioxidant behavior of R and R/G compared to G, which does not contain those antioxidants. Thus, as red pigmentation increased (see inset of Figure 1), the hydrophilic antioxidant capacity was higher (Figure 2A). This result from EPR analysis was further confirmed by spectrophotometric determinations (Figures 1 and 2; Table 1).

In the red lettuces (R and G/R) the higher antioxidant capacity, compared to G, could be also related to the presence of higher amounts of phenols (Figure 2B; Tables 2 and 3). In fact, the lettuce cultivars analyzed showed a positive correlation between the presence of phenols and the antioxidant potential (Figures 1−3; Tables 1−3). However, it is known that not all phenols have an antioxidant capacity,[25] making difficult the

understanding of the relative contribution of the different antioxidant compounds to the higher antioxidant capacity of R lettuce.

Because phenols represent the most important hydrophilic antioxidants in lettuce,[10,26] they are likely the most responsible for its antioxidant capacity. Chlorogenic and chicoric acids being the most representative free phenolic acids for all cultivars (Table 3), it was expected that after basic hydrolysis caffeic acid prevailed in all samples, reaching about 70−80% of the total (Table 3). In fact, chlorogenic acid is the ester of caffeic and quinic acid, whereas chicoric acid results from the esterification of caffeic with tartaric acid. The fact that other authors[10,11] found different values of phenolic acids in lettuce might be attributed to the different growing conditions, as environment affects significantly the phenolic composition.[10] Another source of variation might be represented by the extraction method and, in particular, by the solvent used in the extraction.[27]

Among the variety of phenolic compounds, phenolic acids have attracted considerable interest in the past few years due to their many potential health benefits.[7] The antioxidant nature of phenolic acids and their esters is related to the number of hydroxylations and methoxylations on their aromatic rings.[25] The increase, among others, in chlorogenic acid from G to R could account for the enhancement in antioxidant capacity because Zlotek et al.[11] found that the DPPH$^{\bullet}$ scavenging ability of lettuce was significantly and positively correlated with the presence of chlorogenic acid.

In lettuce the most commonly found flavones and flavonols, having dihydroxylations in the 3′- and 4′-positions of the B ring, were represented by quercetin, quercetin-3-*O*-glucuronide, rutin, luteolin, and luteolin-7-*O*-glucoside (Table 2). Less commonly present were instead those with the lone B-ring hydroxyl group in the 4′-position, that is, kaempferol and apigenin-7-*O*-glucoside (Table 2). It is known that aglycones such as quercetin, luteolin, and kaempferol are more potent antioxidants than their corresponding glycosides.[28] Furthermore, according to Rice-Evans et al.[5] the antioxidant capacity of flavonoids is related to the number and positions of hydroxyl groups, and Soobrattee et al.[4] found that quercetin (3,5,7,3′,4′-OH) has a higher TEAC value than luteolin (5,7,3′,4′-OH) and kaempferol (3,5,7,4′-OH). Thus, also the increase in flavonoids as well as in their glycoside forms (Table 2) could account for the enhancement in the antioxidant capacity of R lettuce compared to G and G/R.

From the results of the present study and the finding of Zlotek et al.[11] that the DPPH$^{\bullet}$ scavenging ability of lettuce is significantly and positively correlated with the presence of quercetin, we could hypothesize that this flavonoid might be one of the antioxidants responsible for the intermediate-decay activity. In fact, G/R and G contained similar concentrations of quercetin, showing the same levels of intermediate-rate antioxidants (Table 1), whereas in R, where quercetin approached a value 20-fold higher (Table 2), the concentration of intermediate-rate antioxidants was much higher (Table 1).

In the R cultivar cyanidin mostly contributed to the amount of total phenols, different from its glucosidic form cyanidin-3-*O*-glucoside (Figures 2 and 3). Anthocyanins are particularly important food bioactive compounds having a double interest: one technological (sensorial characteristics of food products) and the other one related to their health properties.[29] Because glycosylation of anthocyanidins in the 3-position diminishes the antioxidant capacity of its aglycone,[25] cyanidin should contribute mainly to the antioxidant capacity recorded in R lettuce (Figure 1; Table 1).

About 70% (in R) and 90% (in G and G/R) of the phenolic acids detected in lettuce were in the bound form (Table 3). The same pattern was detected for flavonoids (Table 2). Reasons for conjugation of phenolic compounds are related to their potential toxicity and their sequestration in the plant vacuoles.[30] Because it was previously demonstrated that the antioxidant capacity of a free phenolic acid mixture was higher than that of a mixture of bound phenolics,[31] we can assume that the higher antioxidant capacity of R lettuce, compared to G and G/R, could be also related to the decreased presence of the conjugated forms on the total (Tables 2 and 3). However, these results are in contrast with those reported for some barley varieties by Maillard and Berset,[32] who attributed a higher antioxidant capacity to bound phenolic acids. Moreover, it has been demonstrated that also flavonol glycosides can be absorbed as intact molecules.[33] Thus, it is advisible to give attention to the identification and quantification of both free and conjugated forms.

In conclusion, as long as lettuce had higher red pigmentation, the hydrophilic antioxidant capacity increased together with the contents in free and conjugated phenolic acids, free and conjugated flavonoids, and anthocyanins. The study of EPR decay kinetics allowed the identification of slow-, intermediate-, and fast-rate antioxidants in the three different lettuce cultivars. At present, we cannot attribute a kinetic behavior to a specific antioxidant, but we can suggest that the flavonoid quercetin accounted for the majority of the intermediate-rate antioxidants, whereas anthocyanins accounted for the majority of the fast-rate antioxidants.

## AUTHOR INFORMATION

### Corresponding Author

*(U.P.L.) Phone: +34 94 601 3374. Fax: +34 94 601 35 00. E-mail: usue.perez@ehu.es.

### Funding

This research was financially supported by the University of Pisa (Fondi di Ateneo) and by the following grants: UFI11/24, EHUA14/19 and GRUPO Gobierno Vasco-IT577-13.

### Notes

The authors declare no competing financial interest.

## ABBREVIATIONS USED

ABTS, 2,2′-azinobis(3-ethylbenzothiazoline-6-sulfonic acid); DAS, days after sowing; DPPH$^{\bullet}$, 1,1-diphenyl-2-picrylhydrazyl; EPR, electron paramagnetic resonance; G, green; G/R, green/red; GAE, gallic acid equivalent; R, red; TEAC, trolox equivalent antioxidant capacity

## REFERENCES

(1) Hooper, L.; Cassidy, A. A review of the health care potential of bioactive compounds. *J. Sci. Food Agric.* **2006**, *86*, 1805−1813.

(2) Sgherri, C.; Cecconami, S.; Pinzino, C.; Navari-Izzo, F.; Izzo, R. Levels of antioxidants and nutraceuticals in basil grown in hydroponics and soil. *Food Chem.* **2010**, *123*, 416−422.

(3) Choi, E. H.; Chang, H.-J.; Cho, J. Y.; Chun, H. S. Cytoprotective effect of anthocyanins against doxorubicin-induced toxicity in H9c2 cardiomyocytes in relation to their antioxidant activities. *Food Chem. Toxicol.* **2007**, *45*, 1873−1881.

(4) Soobrattee, M. A.; Neergheen, V. S.; Luximon-Ramma, A.; Aruoma, O. I.; Bahorum, T. Phenolics as potential antioxidant

therapeutic agents: mechanism and actions. *Mutat. Res.* **2005**, *579*, 200−213.
(5) Rice-Evans, C.; Miller, N. J.; Paganga, G. Antioxidant properties of phenolic compounds. *Trends Plant Sci.* **1997**, *2*, 152−159.
(6) Hollman, P. C. H.; Arts, I. C. W. Flavonols, flavones and flavanols-nature, occurrence and dietary burden. *J. Sci. Food Agric.* **2000**, *80*, 1081−1093.
(7) Mattila, P.; Hellström, J. Phenolic acids in potatoes, vegetables, and some of their products. *J. Food Compos. Anal.* **2007**, *20*, 152−160.
(8) Baslam, M.; Morales, F.; Garmendia, I.; Goicoechea, N. Nutritional quality of outer and inner leaves of green and red pigmented lettuces (*Lactuca sativa* L.) consumed as salads. *Sci. Hortic.* **2013**, *151*, 103−111.
(9) Llorach, R.; Martínez-Sánchez, A.; Tomás-Barberán, F. A.; Gil, M. I.; Ferreres, F. Characterisation of polyphenols and antioxidant properties of five lettuce varieties and escarole. *Food Chem.* **2008**, *108*, 1028−1038.
(10) Nicolle, C.; Carnat, A.; Fraisse, D.; Lamaison, J.; Rock, E.; Michel, H.; Amouroux, P.; Rémésy, C. Characterisation and variation of antioxidant micronutrients in lettuce (*Lactuca sativa* folium). *J. Sci. Food Agric.* **2004**, *84*, 2061−2069.
(11) Zlotek, U.; Swieca, M.; Jakubczyk, A. Effect of abiotic elicitation on main health-promoting compounds, antioxidant activity and commercial quality of butter lettuce (*Lactuca sativa* L.). *Food Chem.* **2014**, *148*, 253−260.
(12) Espín, J. C.; Soler-Rivas, C.; Wichers, H. J. Characterization of the total free radical scavenger capacity of vegetable oils and oil fractions using 2,2-diphenyl-1-picrylhydrazyl radical. *J. Agric. Food Chem.* **2000**, *48*, 648−656.
(13) Oszmianski, J.; Wolniak, M.; Wojdylo, A.; Wawer, I. Comparative study of polyphenolic content and antiradical activity of cloudy and clear apple juices. *J. Sci. Food Agric.* **2007**, *87*, 573−579.
(14) Sgherri, C.; Pinzino, C.; Navari-Izzo, F.; Izzo, R. Contribution of major lipophilic antioxidants to the antioxidant activity of basil extracts: an EPR study. *J. Sci. Food Agric.* **2011**, *91*, 1128−1134.
(15) Pérez-López, U.; Miranda-Apodaca, J.; Muñoz-Rueda, A.; Mena-Petite, A. Lettuce production and antioxidant capacity are differentially modified by salt stress and light intensity under ambient and elevated $CO_2$. *J. Plant Physiol.* **2013**, *170*, 1517−1525.
(16) Sun, B.; Yan, H.; Zhang, F.; Wang, Q. Effects of plant hormones on main health-promoting compounds and antioxidant activity of Chinese kale. *Food Res. Int.* **2012**, *48*, 359−366.
(17) Arnon, D. I.; Hoagland, D. R. Crop production in artificial solutions and in soils with special reference to factors influencing yields and absorption of inorganic nutrients. *Soil Sci.* **1940**, *50*, 462−85.
(18) Duling, D. R. Simulation of multiple isotropic spin trap EPR spectra. *J. Magn. Reson.* **1994**, *104B*, 105−110.
(19) Pellegrini, N.; Re, R.; Yang, M.; Rice-Evans, C. Screening of dietary carotenoids and carotenoid-rich fruit extracts for antioxidant activities applying 2,2′-azinobis (3-ethylenebenzothiazoline-6-sulfonic acid) radical cation decolorization assay. *Methods Enzymol.* **1999**, *299*, 379−389.
(20) Nguyen, P. M.; Niemeyer, E. D. Effect of nitrogen fertilization on the phenolic composition and antioxidant properties of basil (*Ocimum basilicum* L.). *J. Agric. Food Chem.* **2008**, *56*, 8685−8691.
(21) Gould, K. S.; Markhams, K. R.; Smith, R. H.; Goris, J. J. Functional role of anthocyanins in the leaves of *Quintinia serrata* A. Cunn. *J. Exp. Bot.* **2000**, *51*, 225−232.
(22) Murray, J. R.; Hackett, W. P. Dihydroflavonol reductase activity in relation to differential anthocyanin accumulation in juvenile and mature phase *Hedera helix* L. *Plant Physiol.* **1991**, *97*, 343−351.
(23) Sgherri, C.; Ranieri, A.; Quartacci, M. F. Antioxidative responses in *Vitis vinifera* infected by grapevine fanleaf virus. *J. Plant Physiol.* **2013**, *170*, 121−128.
(24) Sgherri, C.; Pinzino, C.; Navari-Izzo, F.; Izzo, R.; Quartacci, M. F. Antioxidant potential in lipophilic and hydrophilic extracts from medicinal herbs (*Salvia officinalis* and *Echinacea angustifolia*). A comparison between assays based on electron paramagnetic resonance and spectrophotometry. *Am. J. Agric. Biol. Sci.* **2012**, *7*, 417−424.
(25) Rice-Evans, C.; Miller, N. J.; Paganga, G. Structure-antioxidant activity relationships of flavonoids and phenolic acids. *Free Radical Biol. Med.* **1996**, *20*, 933−956.
(26) Llorach, R.; Tomás-Barberán, F. A.; Ferreres, F. Lettuce and chicory byproducts as a source of antioxidant extracts. *J. Agric. Food Chem.* **2004**, *52*, 5109−5116.
(27) Su, D.; Zhang, R.; Hou, F.; Zhang, M.; Guo, J.; Huang, F.; Deng, Y.; Wei, Z. Comparison of the free and bound phenolic profiles and cellular antioxidant activities of litchi pulp extracts from different solvents. *BMC Complement. Altern. Med.* **2014**, *14*, 1−10.
(28) Heim, K. E.; Tagliaferro, A. R.; Bobilya, D. J. Flavonoid antioxidants: chemistry, metabolism and structure-activity relationships. *J. Nutr. Biochem.* **2002**, *13*, 572−584.
(29) de Pascual-Teresa, S.; Sánchez-Ballesta, M. T. Anthocyanins: from plant to health. *Phytochem. Rev.* **2008**, *7*, 281−299.
(30) Harborne, J. B. Recent advances in and functional significance of phenolic conjugation in plants. *Recent Adv. Phytochem.* **1979**, *12*, 457−474.
(31) Subba Rao, M. V. S. S. T.; Muralikrishna, G. Evaluation of the antioxidant properties of free and bound phenolic acids from native and malted finger millet (Ragi, *Eleusine coracana* Indaf-15). *J. Agric. Food Chem.* **2002**, *50*, 889−892.
(32) Maillard, M. N.; Berset, C. Evolution of antioxidant activity during kilning: role of insoluble bound phenolic acids of barley and malt. *J. Agric. Food Chem.* **1995**, *43*, 1789−1793.
(33) Hollman, P. C. H.; van Trijp, J. M. P.; Buysman, M. N. C. P.; van der Gaag, M. S.; Mengelers, M. J. B.; de Vries, J. H. M.; Katan, M. B. Relative bioavailability of the antioxidant quercetin from various food in mans. *FEBS Lett.* **1997**, *418*, 152−156.

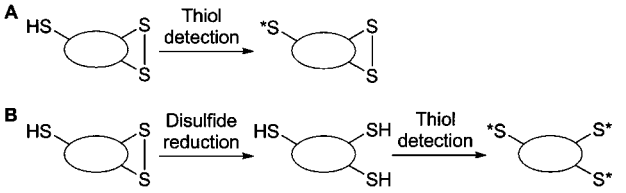


**Figure 1.** Approach for detection of (A) free thiols and (B) total thiols. Thiols destined for detection are denoted S* (modified with permission from ref 15. Copyright 2009 Elsevier).

maximum absorbance at 412 nm in the pH range from 6 to 9.5.[14,15] An alternative to DTNB is 4,4′-dithiodipyridine (4-DPS), which reacts in a similar way with thiol groups, forming 4-thiopyridone (4-TP) that absorbs at 324 nm. The small size of this detection reagent makes it easier to reach poorly accessible thiols within the protein core. 4-TP also has a higher extinction coefficient than NTB, suggesting that 4-DPS is a more sensitive thiol detection agent than DTNB.[16] Furthermore, 4-TP is stable in lower pH ranges (pH 3−7), making thiol detection possible at low pH as in common reversed-phase high-performance liquid chromatography (HPLC) conditions.[17] Ruan et al.[18] found 4-DPS to be less affected by pH and denaturants compared to DTNB and, thus, found 4-DPS more suitable and reliable for thiol detection in soy protein. The measurement of disulfide bonds is based on the reduction of disulfides, followed by detection of the newly reduced thiols (Figure 1B). The amount of disulfides can then be calculated by subtracting the amount of free thiols from total thiols. To reduce disulfide bonds during SDS−PAGE, dithiothreitol (DTT) is often used. This reagent is less suitable for disulfide quantification because of its slow reaction rate and the cross-reactivity with thiol detection agents.[15,17] Liu et al.[19] have quantified disulfide bonds in myofibrillar proteins based on a method described by Damodaran.[20] In this procedure, disulfides are cleaved by adding an excess of sodium sulfite. However, oxidative sulfitolysis of disulfide bonds is slow and rarely quantitative in the absence of catalysts.[15,21] An alternative reducing agent is sodium borohydride (BH), a highly reactive and strong reductant, whose main advantage is that its excess can be removed by acidification.[15,22]

The aim of the present study was to investigate the extent of reversible and irreversible thiol oxidation in ground beef during storage. A sensitive and reliable method for the quantification of protein disulfides in meat was established on the basis of disulfide reduction with sodium borohydride and thiol detection with 4-DPS. The method was subsequently used for quantification of reversible and irreversible thiol oxidation in ground beef during storage in high-oxygen modified atmosphere packaging (HiOx MAP) and compared to SDS−PAGE-based methodology.

## MATERIALS AND METHODS

**Chemicals.** All chemicals were of analytical grade or the highest available purity. Citric acid was purchased from Carl Roth GmbH (Karlsruhe, Germany). Disodium hydrogen phosphate was purchased from Panreac Química, S.A.U. (Castellar del Vallès, Barcelona, Spain). Trisodium citrate dihydrate, sodium dodecyl sulfate (SDS), hydrochloric acid, tris(hydroxymethyl)-aminomethane (Tris), 1-octanol, sodium hydroxide, and bovine serum albumin (BSA) were obtained from Merck (Darmstadt, Germany). Guanidine hydrochloride (GuHCl), L-cysteine, and sodium borohydride were purchased from Sigma-Aldrich Co. (St. Louis, MO). 4-DPS and oxidized glutathione (GSSG) were obtained from Acros Organics (Geel, Belgium). NuPAGE Novex 3−8% Tris−acetate gels, lithium dodecyl sulfate (LDS) sample buffer, SDS Tris−acetate running buffer, and Molecular Probes SYPRO Ruby Protein Gel Stain were purchased from Invitrogen (Carlsbad, CA). Precision Plus Protein Standard All Blue was obtained from Bio-Rad Laboratories, Inc. (Hercules, CA). DTT was purchased from Applichem GmbH (Darmstad, Germany). Water was prepared using a Millipore Mill-Q purification system (Millipore Corp., Bedford, MA).

**Sampling of HiOx MAP Ground Meat.** Two independent storage trials (trials 1 and 2) were performed for sampling of HiOx MAP ground beef. For trial 1, ground beef stored in HiOx MAP was obtained from a local Danish supermarket. The meat had been packed under modified atmosphere (high oxygen) the day before and consisted of nine packages of 400 g each. Three packages (replicates A, B, and C) were opened, and the meat was vacuum-packed in portions of 50 g and stored at −80 °C until analysis (day 0). The remaining six packages were stored in darkness at 4 °C until day 4 or 9, at which point another three replicates (A, B, and C) were collected, vacuum-packed, and frozen to −80 °C.

For trial 2, similar sampling was performed for freshly ground beef obtained from a local Belgian butcher, ground 3 days after slaughter of the animal. The meat was packed under modified atmosphere (70% $O_2$ and 30% $CO_2$) into 15 packages of 450 g each and stored at 4 °C until sampling day. On days 0, 3, 6, 9, and 12, three packages (replicates A, B, and C) were opened, vacuum-packed in portions of 75 g, and stored at −80 °C until analysis.

**Influence of pH and Denaturant on the Molar Extinction Coefficients of 4-TP.** A total of 24 buffers were prepared, by varying the buffering capacity, the pH value, and the presence of a denaturant. Six buffers with a low buffering capacity were prepared by mixing 0.1 M citric acid and 0.2 M $Na_2HPO_4$ to pH values of 2.5, 3.5, 4.5, 5.5, 6.5, and 7.5. Likewise, six high-capacity buffers were prepared by mixing 1 M citric acid and 1 M trisodium citrate dihydrate to the aforementioned pH values. SDS buffers were prepared by adding 5% (w/v) SDS to the low-capacity buffers. The same was performed for guanidine hydrochloride by adding 6 M GuHCl to the high-capacity buffers. Concentrations of L-cysteine ranging from 2.5 to 500 μM were prepared in all buffers. Thiol detection with 4-DPS was performed on the basis of the study by Riener et al.,[16] by diluting 500 μL of L-cysteine solution with 2 mL of the corresponding buffer and adding 500 μL of 4-DPS solution (4 mM 4-DPS in 12 mM HCl). The absorbances were measured at 324 nm against water before the addition of 4-DPS ($A_{pre}$) and after exactly 30 min of reaction with 4-DPS in the dark at room temperature ($A_{post}$). The absorbance corresponding to the thiol concentration was calculated by subtracting $A_{pre}$ and $A_{blank}$ (2.5 mL of buffer + 500 μL of 4-DPS solution) from $A_{post}$. Molar extinction coefficients ($\varepsilon$) were calculated from the slope of the standard curves according to the Lambert−Beer law ($A$ is the absorbance, and $l$ is the path length).

$$A = \varepsilon l c \quad (1)$$

**Optimization of Disulfide Reduction.** The efficiency of the disulfide reduction was tested by the reduction of known concentrations (25−200 μM) of commercially available GSSG. The expectation was to find thiol concentrations in the form of reduced glutathione (GSH) double the aforementioned molarities (50−400 μM). GSSG was dissolved in 6 M GuHCl in 100 μM Tris buffer (pH 8.0), because this was the buffer system that was chosen to solubilize the meat proteins. The method was developed on the basis of disulfide reduction according to Hansen et al.[17] The reduction was performed by adding 100 μL of 30% (w/v) alkaline borohydride to 3 mL of sample. After incubation at 50 °C, the excess of borohydride was removed with 6 M hydrochloride (final concentration of 1.8 M) at room temperature. Different conditions and parameters were tested by varying the solvent for sodium borohydride (1, 2, and 4 M NaOH), the incubation time for the reduction with borohydride (15, 30, 60, and 150 min), and the hydrolysis time of the residual borohydride (2, 10, 20, 30, 40, 45, 60, 90, 150, 165, and 180 min).

**Quantification of Free and Total Thiols in MAP Ground Beef Using 4-DPS.** The vacuum-packed meat was thawed in water at room

temperature for 30 min before homogenizing 1.0 g of meat in 25 mL of 6 M GuHCl in 100 mM Tris buffer (pH 8.0) using an Ultra Turrax. The homogenates were centrifuged (for 20 min at 5311*g* and 4 °C), and supernatants were filtered (qualitative filter paper, particle retention of 11 μm). Samples were kept on ice at all times. The protein concentration of the filtrates was determined spectrophotometrically at 280 nm using a five-point standard curve prepared from BSA. Disulfide reduction was performed according to the optimized procedure, as described in the previous section. Hence, an aliquot of 3 mL of filtrate was subjected to disulfide reduction by adding 50 μL of 1-octanol (as an anti-foaming agent) and 100 μL of freshly prepared 30% (w/v) sodium borohydride in 1 M NaOH. After incubation at 50 °C for 30 min, an aliquot of 1.35 mL of 6 M HCl was added, followed by stirring for 10 min.

Free and total thiols were determined with 4-DPS in the non-reduced and reduced filtrates, respectively. An aliquot of 500 μL of filtrate was mixed with 2 mL of 6 M GuHCl in 1 M citric acid buffer (pH 4.5) and 500 μL of 4-DPS solution (4 mM 4-DPS in 12 mM HCl). The absorbance was measured at 324 nm against 6 M GuHCl in 1 M citric acid buffer (pH 4.5) before the addition of 4-DPS ($A_{pre}$) and after exactly 30 min of reaction with 4-DPS in the dark at room temperature ($A_{post}$). A mixture of 2.5 mL of 6 M GuHCl in 1 M citric acid buffer (pH 4.5) and 500 μL of 4-DPS solution was prepared as a blank sample ($A_{blank}$). The absorbance corresponding to the thiol concentration was calculated by subtracting $A_{pre}$ and $A_{blank}$ from $A_{post}$. The thiol concentration was calculated on the basis of a five-point standard curve ranging from 2.5 to 500 μM L-cysteine in 6 M GuHCl in 1 M citric acid buffer (pH 4.5). The thiol content was expressed as nanomoles of thiol per milligram of protein. Because treatment of disulfide bonds with sodium borohydride yields two thiol groups,[23] the disulfide content was calculated as half of the difference between total and free thiols.

**SDS–PAGE Analysis.** The meat from trial 1 was subjected to SDS–PAGE analysis. The meat was thawed at room temperature for 30 min before an aliquot of 1.0 g of meat was homogenized in 25 mL of 5% (w/v) SDS dissolved in 100 mM Tris buffer at pH 8.0 using an Ultra Turrax. The homogenates were placed in a water bath at 80 °C for 30 min, followed by centrifugation for 20 min at 950*g*. The supernatant was filtered (particle retention of 5–13 μm), and the protein concentration was determined spectrophotometrically at 280 nm using a standard curve prepared from BSA. The homogenates were analyzed by gel electrophoresis using NuPAGE Novex 3–8% Tris–acetate gels according to the instructions of the manufacturer (Invitrogen, Carlsbad, CA). Reduced samples were prepared by mixing 1.6 μL of diluted sample (2.0 mg of protein/mL) and 14.4 μL of loading solution, which was prepared from 60 μL of LDS sample buffer, 24 μL of 1.0 M DTT, and 132 μL of Milli-Q water. The non-reduced samples were prepared by mixing 1.6 μL of diluted sample (2.0 mg of protein/mL) and 14.4 μL of loading solution, which was prepared from 60 μL of LDS sample buffer and 156 μL of Milli-Q water. Aliquots of 10 μL of reduced or non-reduced samples as well as 3 μL of Precision Plus Protein Standard All Blue marker were loaded to the wells of the gels. Electrophoresis was run for 90 min at 150 V in cassettes containing ice-cold SDS Tris–acetate running buffer. After electrophoresis, the gels were fixed overnight in fixation solution (50% ethanol and 7% acetic acid) at room temperature on a rocking table. Following staining overnight by the fluorescence SYPRO Ruby Protein Gel Stain, the gels were photographed by a charge-coupled device (CCD) camera (Raytest, Camilla II, Straubenhardt, Germany). The protein concentration of the bands were estimated by the pixel intensity as determined by the freeware GelAnalyzer by Dr. Istvan Lazar, www.gelanalyzer.com. Band intensities were quantified from the volume of the pixel intensity when analyzing the gels with GelAnalyzer. To correct for total protein content of each sample, the pixel intensities of cross-linked myosin heavy chain (CL-MHC) and myosin heavy chain (MHC) were divided by the total pixel volume of all bands in each lane of the gel to obtain the relative intensity of CL-MHC and MHC for each sample. The degree of cross-linking was calculated on the basis of gels containing both reduced and non-reduced samples and was considered equal to the ratio of the relative intensity of CL-MHC in the non-reduced samples to the relative intensity of MHC in the reduced samples at day 0 ($CL\text{-}MHC_{non\text{-}red}/MHC_{red,\ day\ 0}$, %).

**Statistical Analysis.** Statistical analysis was performed using SAS 9.3 package (SAS Institute, Inc., Cary, NC). Recovery percentages were analyzed using a linear model with the concentration as fixed effect. Free and total thiols were analyzed using a linear model with the storage time (days), treatment (with or without reduction), and their interaction as fixed effects. Disulfides and degrees of cross-linking were analyzed using a linear model with the storage time as fixed effect. The correlation between the 4-DPS assay and SDS–PAGE was assessed using Pearson correlation. Effects were considered significant at $p < 0.05$.

## RESULTS AND DISCUSSION

**Influence of pH and Denaturant on the Molar Extinction Coefficients of 4-TP.** To determine the optimal pH for thiol detection with 4-DPS, two types of buffer solutions with a low and high buffering capacity were prepared that ranged from pH 2.5 to 7.5. It is strictly necessary to include protein denaturants in the buffer during analysis of thiols in meat to prevent precipitation of some of the cross-linked protein. In the absence of protein denaturants, such precipitants would not be included in the assay, resulting in erroneous quantifications. The effect of denaturants was therefore tested by adding 5% SDS and 6 M GuHCl to the low- and high-capacity buffers, respectively. Molar extinction coefficients were calculated from the slope of a L-cysteine standard curve, which was subjected to the 4-DPS assay at all pH and denaturant conditions.

According to Riener et al.,[16] the molar extinction coefficient of 4-TP is 21 400 $M^{-1}$ $cm^{-1}$ at pH 7.0. As shown in Figure 2,

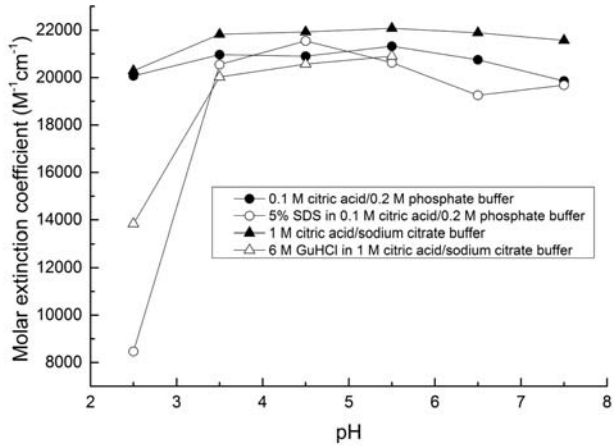


**Figure 2.** Molar extinction coefficients of 4-DPS as a function of pH.

the molar extinction coefficients in all low- and high-capacity buffers without denaturants stay close to this value. However, adding denaturants to the buffers clearly narrows the pH range in which the molar extinction coefficients are stable. This is in agreement with the findings by Hansen and Winther,[15] who found that the presence of denaturants decreased the alkylation rate of NTB by *N*-ethylmaleimide. The lowest 4-TP absorptions were measured at pH 2.5 with buffers added 5% SDS and 6 M GuHCl ($\varepsilon$ = 8500 and 13 800 $M^{-1}$ $cm^{-1}$, respectively). The amount of GuHCl was not soluble at pH 6.5 and 7.5; thus, Figure 2 shows no results for these conditions.

Overall, optimal molar extinction coefficients were found in buffers containing denaturants ranging from pH 3.5 to 5.5. Two

factors were considered to select the optimal working buffer. First, the pH value in the samples was very low after acidification in the reduction step. Therefore, a high-capacity buffer was needed to ensure correct pH adjustment. Second, a strong denaturant is crucial to ensure good solubility of meat proteins. We therefore chose to use 6 M GuHCl in 1 M citric acid buffer at pH 4.5 as a working buffer for determining the free and total thiols in meat using 4-DPS.

**Optimization of Disulfide Reduction.** It was necessary to optimize the disulfide reduction in the buffer systems chosen for the meat samples, and this was established by determination of recovery percentages for the reduction of GSSG based on incubation at 50 °C with alkaline borohydride, followed by removal of residual borohydride by acidification. The reduction procedure was tested by combining different sodium hydroxide concentrations with varying times of incubation and hydrolysis, as described above. For each combination, a known concentration of GSSG in 6 M GuHCl in 100 mM Tris buffer (pH 8.0) and a blank (6 M GuHCl in 100 mM Tris buffer at pH 8.0) were subjected to the reduction assay. Twice as much GSH as GSSG in molar concentrations was expected; thus, the recovery percentages were calculated according to eq 2.

$$\text{recovery percentage (\%)} = \frac{\text{thiols quantified}}{\text{thiols expected}} \times 100 \quad (2)$$

It is well-known that sodium borohydride rapidly decomposes at neutral or acidic pH.[24] Therefore, solutions of 30% (w/v) borohydride in 1, 2, and 4 M NaOH were freshly prepared for the reduction of GSSG. After mixing 3 mL of sample with 100 μL of BH dissolved in 1, 2, and 4 M NaOH, the pH was approximately 8.6, 11.0, and 12.0, respectively. Although Patsoukis and Georgiou[25] highlighted that a high alkaline environment (pH 12.0 rather than pH 8.0) is needed for optimal disulfide reduction by borohydride, we found similar recovery percentages with the 1 M NaOH treatment as with 2 and 4 M NaOH (data not shown). The lack of correlation between our results and those reported by Patsoukis and Georgiou[25] may be due to the use of different buffers and derivatization agents.

After the addition of BH, the mixtures were incubated at 50 °C as recommended by Patsoukis and Georgiou.[25] The optimal incubation time for effective reduction depends upon the concentration and reactivity of BH and the accessibility of the protein disulfides. Incubation must take long enough to let BH reach and reduce all disulfides. Prolonged incubation, however, might promote reoxidation of the newly formed thiols.[22] Furthermore, $NaBH_4$ can decompose over time, even at alkaline pH.[22,26] For the current method development, oxidized glutathione was incubated with BH during 15, 30, 60, and 150 min and optimal recovery percentages were found with 30 min of incubation (data not shown).

Subsequent to incubation, the residual BH was removed by acidification with 6 M HCl, bringing the final concentration of HCl in the mixture to 1.8 M. Acidification of $NaBH_4$ completely discharges the reactive hydride, yielding hydrogen gas ($H_2$)[15,27] and causing the protein solution to foam. This foaming was avoided by adding a small amount of 1-octanol.[15] During the method optimization, the acidified solutions were left to stir on a magnetic stirrer at room temperature for various time periods, ranging from 2 min to 3 h. The best recovery percentages were found when stirring for 10 min after the addition of HCl and subsequently readjusting the pH with 6 M GuHCl in 1 M citric acid buffer (pH 4.5) for the 4-DPS assay (data not shown). Although the low pH of the BH−HCl mixture is likely to protect the reduced thiols from reoxidation,[15] oxygen inclusion because of prolonged and vigorous stirring may induce further oxidation after the reducing agent has been deactivated.[22]

The method for disulfide reduction was adjusted on the basis of all of the above-mentioned considerations. Optimal recovery percentages in the range from 25 to 200 μM GSSG were obtained when carrying out the reduction as follows: 50 μL of 1-octanol and 100 μL of freshly prepared 30% (w/v) sodium borohydride in 1 M NaOH were added to 3 mL of sample. The mixture was incubated at 50 °C for 30 min with occasional stirring. After incubation, the excess of borohydride was removed by adding 1.35 mL of 6 M HCl, followed by stirring for 10 min. This procedure was applied for the reduction of various concentrations of GSSG. The quantified thiols and recovery percentages are presented in Table 1.

**Table 1. Recovery of GSH after Reduction of GSSG in 6 M GuHCl and 100 mM Tris Buffer (pH 8.0), with 30% (w/v) Sodium Borohydride in 1 M NaOH at 50 °C for 30 min, Followed by Acidification with 6 M HCl (Final Concentration of 1.8 M) and Stirring for 10 min[a]**

| GSSG (μM) | thiols expected (μM) | thiols quantified (μM) | recovery (%) |
|---|---|---|---|
| 0 (blank) | 0 | 3.8 ± 1.6 | |
| 25 | 50 | 42.9 ± 3.6 | 85.8 ± 7.1 |
| 50 | 100 | 82.7 ± 4.7 | 82.7 ± 4.7 |
| 75 | 150 | 129.1 ± 2.6 | 86.1 ± 1.7 |
| 100 | 200 | 175.3 ± 1.2 | 87.7 ± 0.6 |
| 125 | 250 | 211.5 ± 8.6 | 84.6 ± 3.4 |
| 150 | 300 | 262.7 ± 5.6 | 87.6 ± 1.9 |
| 175 | 350 | 304.7 ± 6.5 | 87.1 ± 1.9 |
| 200 | 400 | 350.1 ± 8.1 | 87.5 ± 2.0 |

[a]Recovery percentages are expressed as the ratio quantified to expected thiols (described in eq 2).

No significant differences between recovery percentages were found among the GSSG concentrations ($p = 0.642$), indicating that the reduction procedure is precise for concentrations ranging from 25 to 200 μM disulfides and resulted in an approximate recovery of 86%. According to AOAC International, the expected recovery is from 80−90 to 107−110% in the concentration range of the quantified thiols used in the present study; therefore, the observed accuracy is acceptable.[28]

**Quantification of Disulfides in MAP Ground Beef with 4-DPS.** MAP ground beef obtained from trials 1 and 2 were subjected to thiol and disulfide quantification by the 4-DPS assay at various storage times. Caution should be made when comparing the meat from trials 1 and 2 for several reasons: (1) the batches of meat were not obtained from the same animal; (2) ground beef often comes from different muscles; thus, any observed difference in thiol or disulfide concentrations between the two trials could be ascribed to differences in the types of muscles used in each batch of meat; and (3) there are differences in time between slaughter and packaging and the exact gas composition (unknown for trial 1).

The significant decrease in free thiols in the meat from trial 1 as well as trial 2 (Tables 2 and 3, respectively) shows that thiol oxidation (ca. 30 and 33% loss of thiols, respectively) took place during storage, which is in agreement with previous studies.[3,29] After reduction of the proteins from the beef

**Table 2. Thiol and Disulfide Quantification with 4-DPS in Ground Beef from Trial 1, Stored under High-Oxygen Atmosphere at 4 °C for up to 9 Days[a]**

| storage time | free thiols (nmol/mg of protein) | total thiols (nmol/mg of protein) | disulfides (nmol/mg of protein) |
|---|---|---|---|
| day 0 | 37.6 ± 0.5 a | 51.7 ± 0.8 a | 7.0 ± 0.6 a |
| day 4 | 30.0 ± 1.1 b | 49.2 ± 1.5 a | 9.6 ± 1.1 b |
| day 9 | 26.5 ± 1.7 c | 49.4 ± 1.4 a | 11.5 ± 1.4 c |

[a]Results are shown as the mean ± standard deviation (SD) of three independent replicates. Different letters (a–c) within a column denote statistical differences among storage times ($p < 0.05$).

**Table 3. Thiol and Disulfide Quantification with 4-DPS in Ground Beef from Trial 2, Stored under High-Oxygen Atmosphere at 4 °C during 12 Days[a]**

| storage time | free thiols (nmol/mg of protein) | total thiols (nmol/mg of protein) | disulfides (nmol/mg of protein) |
|---|---|---|---|
| day 0 | 58.3 ± 1.6 a | 61.8 ± 0.2 a | 1.8 ± 0.9 a |
| day 3 | 44.4 ± 1.2 b | 55.1 ± 1.2 b | 5.3 ± 1.1 b |
| day 6 | 42.4 ± 0.8 bc | 54.4 ± 1.6 b | 6.0 ± 1.1 b |
| day 9 | 40.4 ± 2.4 bc | 53.1 ± 2.2 b | 6.4 ± 2.1 b |
| day 12 | 39.2 ± 0.8 c | 52.1 ± 1.6 b | 6.4 ± 1.0 b |

[a]Results are shown as the mean ± SD of three independent replicates. Different letters (a–c) within a column denote statistical differences among storage times ($p < 0.05$).

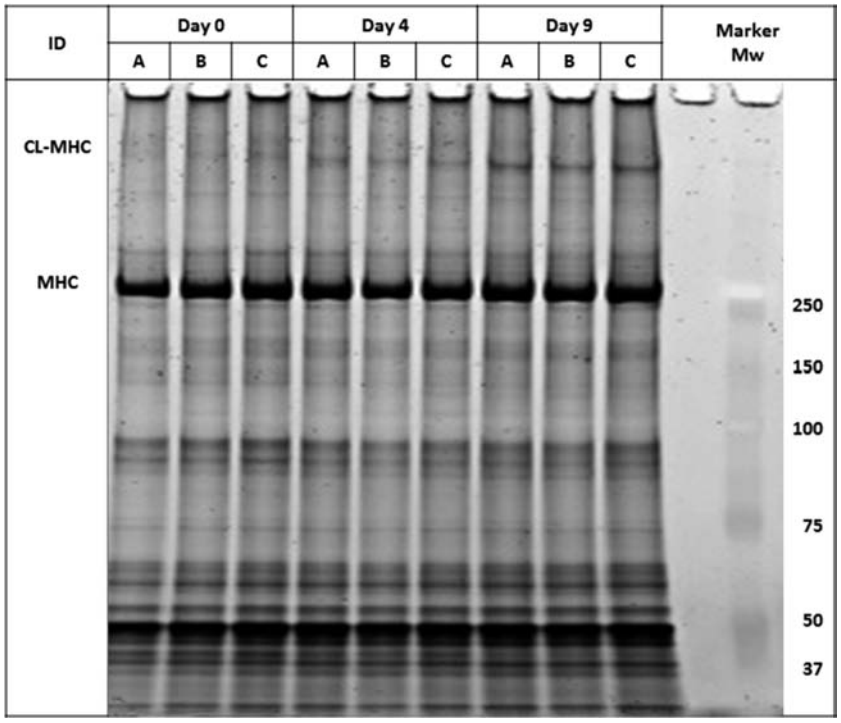


**Figure 3.** SDS–PAGE gel of non-reduced ground beef from trial 1 stored under high-oxygen atmosphere at 4 °C for 9 days. The gel shows all samples in triplicate (A–C). CL-MHC, cross-linked myosin heavy chain; MHC, myosin heavy chain.

samples from trial 1 with borohydride, the amount of total thiols was significantly higher than the amount of free thiols at all sampling days, indicating the formation of disulfides. No significant changes in total thiol levels were found during the 9 days of storage (Table 2). This suggests that all thiols lost during 9 days of storage could be fully reduced by borohydride and were, hence, lost because of reversible thiol oxidation (most likely disulfide formation).

When subjecting the beef from trial 2 to borohydride reduction, no significant difference was found between the free and total thiol level on day 0, indicating that the initial level of oxidation in this meat was minimal. After 3 days of storage, the concentration of free thiols was significantly lower than at day 0 (Table 3) ($p < 0.001$), confirming thiol oxidation during storage. Reduction of the beef proteins resulted in a significantly higher concentration of total thiols than free thiols at day 3 ($p < 0.001$), proving the formation of disulfides. However, the concentration of total thiols significantly decreased from day 0 to day 3 ($p < 0.001$), showing that irreversible thiol oxidation had taken place concomitantly to the disulfide formation. Although the amount of total thiols stayed constant between days 3 and 12, there was a significant decrease of free thiols between days 3 and 12, indicating that predominantly protein disulfides were formed in this storage period. With subtraction of the free thiol concentration on day 0 with the free thiol concentration on day 12, a loss in free

thiols of 19 nmol/mg of protein was obtained. Similarly, the loss in total thiols over 12 days of storage was only 10 nmol/mg of protein, which means that, over the full duration of storage, about half of the thiols was lost because of irreversible oxidation and the other half was lost because of reversible oxidation. The consequence of thiol oxidation in meat has previously been ascribed mainly to disulfide formation;[3,29] however, thiol oxidation is very complex, and numerous oxidation products may be formed, such as sulfenic acid, sulfinic acid, sulfonic acid, and thiosulfinates.[10] The present study shows that other thiol oxidation products than disulfides may be formed in meat during storage. While the formation of sulfonic acid is irreversible, sulfenic acid is extremely reactive and may react further to create compounds, such as disulfides or sulfonic acid. Because of the efficient reducing capacity of BH, it is likely that sulfenic acids are also reduced to thiols by this reducing agent; thus, it is unknown whether a part of the quantified total thiols is in fact derived from the reduction of sulfenic acid, thus overestimating the amount of disulfides. However, the approach based on BH and 4-DPS has previously been used for the quantification of the thiol−disulfide redox status in cells without considering a potential sulfenic acid formation.[30] The formation of sulfenic acids in living cells has been shown to be rather widespread in some cases,[31] but it has never been determined in meat samples during storage.

**Comparison between SDS−PAGE and 4-DPS for the Quantification of Disulfides in MAP Ground Beef.** The quantification of thiols and disulfides in the ground beef from trial 1 with 4-DPS was compared to the conventional cross-linking analysis by SDS−PAGE. MHC has previously been found to be the meat protein that is most susceptible to oxidation, and SDS−PAGE analysis has been widely used to study disulfide cross-link formation in meat and meat products.[3,8,13,29] The non-reduced samples showed an increase of the CL-MHC band intensity on the SDS gel as the storage time increased (Figure 3), whereas no CL-MHC was seen in the reduced samples (data not shown).

The degrees of disulfide formation in the ground beef according to the 4-DPS assay and SDS−PAGE are compared in Table 4. With both methods, a significant increase of disulfides was found in the ground beef during 9 days of storage under high-oxygen atmosphere ($p < 0.001$ and $p = 0.005$ for 4-DPS and SDS−PAGE, respectively). A Pearson correlation of 0.913 was found between the two methods, but the concentration of disulfides found by the 4-DPS assay was considerably higher than that by SDS−PAGE. This can be explained by the fact that two proteins may be cross-linked by several disulfide bridges; consequently, cleaving these disulfide bridges leads to more than two newly formed thiol groups. From the three-dimensional protein structure of MHC, it can be seen that several cysteine residues are transversely positioned in the tail of MHC; thus, it is likely that several intermolecular disulfides are formed between two MHC molecules. Furthermore, thiols may be lost to disulfide formation intramolecularly in MHC, without causing a cross-link between two proteins, that is, without generating the CL-MHC band that appears in the SDS−PAGE gel. Additionally, it is worth noting that severely CL-MHC polymers are probably too large to enter the SDS gel,[12] leading to an underestimation of CL-MHC. This is a problem that is actually one of the many drawbacks with the gel electrophoresis methods. Finally, even though MHC has been found to be the meat protein that is most prone to thiol oxidation,[32] disulfide formation in other meat proteins may also contribute to the values obtained with the 4-DPS assay, and as mentioned above, the potential presence of sulfenic acid may contribute to an overestimation of disulfides by the 4-DPS assay. In conclusion, SDS−PAGE analysis provides information about intermolecular disulfide formation in MHC for moderately oxidized samples, while the 4-DPS assay provides a more accurate and quantitative assessment of protein thiols and intra- and intermolecular disulfides and, thus, offers a good tool to investigate the thiol−disulfide reactions in meat and potentially also in meat products.

In the present study, we have shown that both reversible and irreversible thiol oxidation takes place in meat during storage. Disulfide formation is often the consequence of thiol oxidation, as observed by a thiol loss, but our results clearly show that disulfide formation in meat during storage is not the only consequence of thiol oxidation. This is an important observation in relation to the further development of strategies to avoid or repair thiol oxidation.

**Table 4. Degrees of Cross-Linking in Ground Beef Obtained from Trial 1 during 9 Days of Storage under High-Oxygen Atmosphere at 4 °C, Measured with 4-DPS and SDS−PAGE[a]**

| | 4-DPS assay | SDS−PAGE |
|---|---|---|
| storage time | disulfides/total thiols$_{day\ 0}$ (%) | CL-MHC$_{non\text{-}red}$/MHC$_{red,\ day\ 0}$ (%) |
| day 0 | 13.6 ± 0.4 a | 3.1 ± 1.6 a |
| day 4 | 18.6 ± 0.9 b | 6.9 ± 1.0 b |
| day 9 | 22.2 ± 0.3 c | 8.5 ± 1.2 b |

[a]Degrees of cross-linking are expressed as the level of cross-linking (disulfides and CL-MHC for 4-DPS and SDS−PAGE, respectively) divided by the reference level of reduced protein on day 0 (total thiols and MHC$_{red}$ for 4-DPS and SDS−PAGE, respectively). Results are shown as the mean ± SD of three independent replicates. CL-MHC, cross-linked myosin heavy chain; MHC, myosin heavy chain. Different letters (a−c) within a column denote statistical differences among storage times ($p < 0.05$).

## AUTHOR INFORMATION


### Corresponding Author

*Telephone: +45-35333547. Fax: +45-35333344. E-mail: mnl@food.ku.dk.


### Notes

The authors declare no competing financial interest.

## ACKNOWLEDGMENTS


The authors thank the Institute for Agricultural and Fisheries Research (ILVO) for granting the project entitled "Protein Oxidation in Meat Products: Effects of Natural Bioactive Compounds from Side Flows on Quality and Health Aspects". The authors also thank the Danish Council for Independent Research|Technology and Production within the Danish Agency for Science, Technology and Innovation for granting the project entitled "Antioxidant Mechanisms of Natural Phenolic Compounds against Protein Cross-Link Formation in Meat and Meat Systems" (11-117033).


## ABBREVIATIONS USED

4-DPS, 4,4′-dithiodipyridine; 4-TP, 4-thiopyridone; BH, sodium borohydride; BSA, bovine serum albumine; CL-MHC, cross-linked myosin heavy chain; DTNB, 5,5′-dithiobis-

(2-nitrobenzoic acid); DTT, dithiothreitol; GuHCl, guanidine hydrochloride; GSH, reduced glutathione; GSSG, oxidized glutathione; HiOx, high-oxygen; LDS, lithium dodecyl sulfate; MAP, modified atmosphere packaging; MHC, myosin heavy chain; NTB, 2-nitro-5-thiobenzoate; RSH, thiol; RSSR, disulfide; SDS, sodium dodecyl sulfate; SDS−PAGE, sodium dodecyl sulfate−polyacrylamide gel electrophoresis; Tris, tris(hydroxymethyl)-aminomethane

## REFERENCES


(1) Estévez, M. Protein carbonyls in meat systems: A review. *Meat Sci.* **2011**, *89*, 259−279.

(2) Lund, M. N.; Heinonen, M.; Baron, C. P.; Estévez, M. Protein oxidation in muscle foods: A review. *Mol. Nutr. Food Res.* **2011**, *55*, 83−95.

(3) Lund, M. N.; Lametsch, R.; Hviid, M. S.; Jensen, O. N.; Skibsted, L. H. High-oxygen packaging atmosphere influences protein oxidation and tenderness of porcine *longissimus dorsi* during chill storage. *Meat Sci.* **2007**, *77*, 295−303.

(4) Zakrys-Waliwander, P. I.; O'Sullivan, M.; O'Neill, E.; Kerry, J. The effects of high oxygen modified atmosphere packaging on protein oxidation of bovine *M. longissimus dorsi* muscle during chilled storage. *Food Chem.* **2012**, *131*, 527−532.

(5) Kim, Y. H.; Huff-Lonergan, E.; Sebranek, J. G.; Lonergan, S. M. High-oxygen modified atmosphere packaging system induces lipid and myoglobin oxidation and protein polymerization. *Meat Sci.* **2010**, *85*, 759−767.

(6) Jongberg, S.; Wen, J.; Tørngren, M. A.; Lund, M. N. Effect of high-oxygen atmosphere packaging on oxidative stability and sensory quality of two chicken muscles during chill storage. *Food Packag. Shelf Life* **2014**, *1*, 38−48.

(7) Rowe, L. J.; Maddock, K. R.; Lonergan, S. M.; Huff-Lonergan, E. Oxidative environments decrease tenderization of beef steaks through inactivation of $\mu$-calpain. *J. Anim. Sci.* **2004**, *82*, 3254−3266.

(8) Morzel, M.; Gatellier, P.; Sayd, T.; Renerre, M.; Laville, E. Chemical oxidation decreases proteolytic susceptibility of skeletal muscle myofibrillar proteins. *Meat Sci.* **2006**, *73*, 536−543.

(9) Santé-Lhoutellier, V.; Aubry, L.; Gatellier, P. Effect of oxidation on in vitro digestibility of skeletal muscle myofibrillar proteins. *J. Agric. Food Chem.* **2007**, *55*, 5343−5348.

(10) Nagy, P.; Winterbourn, C. C. Redox chemistry of biological thiols. In *Advances in Molecular Toxicology*, 4th ed.; Fishbein, J. C., Ed.; Elsevier B.V.: London, U.K., 2010; pp 183−222.

(11) Li, Y.; Kong, B.; Xia, X.; Liu, Q.; Li, P. Inhibition of frozen storage-induced oxidation and structural changes in myofibril of common carp (*Cyprinus carpio*) surimi by cryoprotectant and hydrolysed whey protein addition. *Int. J. Food Sci. Technol.* **2013**, *48*, 1916−1923.

(12) Jongberg, S.; Lund, M. N.; Waterhouse, A. L.; Skibsted, L. H. 4-Methylcatechol inhibits protein oxidation in meat but not disulfide formation. *J. Agric. Food Chem.* **2011**, *59*, 10329−10335.

(13) Decker, E. A.; Xiong, Y. L.; Calvert, J. T.; Crum, A. D.; Blanchard, S. P. Chemical, physical, and functional properties of oxidized turkey white muscle myofibrillar proteins. *J. Agric. Food Chem.* **1993**, *41*, 186−189.

(14) Estévez, M.; Morcuende, D.; Ventanas, S. Determination of oxidation. In *Handbook of Processed Meats and Poultry Analysis*; Nollet, L. M. L., Toldrá, F., Eds.; CRC Press: Boca Raton, FL, 2008; pp 141−162.

(15) Hansen, R. E.; Winther, J. R. An introduction to methods for analyzing thiols and disulfides: Reactions, reagents, and practical considerations. *Anal. Biochem.* **2009**, *394*, 147−158.

(16) Riener, C. K.; Kada, G.; Gruber, H. J. Quick measurement of protein sulfhydryls with Ellman's reagent and with 4,4′-dithiodipyridine. *Anal. Bioanal. Chem.* **2002**, *373*, 266−276.

(17) Hansen, R. E.; Ostergaard, H.; Norgaard, P.; Winther, J. R. Quantification of protein thiols and dithiols in the picomolar range using sodium borohydride and 4,4′-dithiodipyridine. *Anal. Biochem.* **2007**, *363*, 77−82.

(18) Ruan, Q.; Chen, Y.; Kong, X.; Hua, Y. Comparative studies on sulfhydryl determination of soy protein using two aromatic disulfide reagents and two fluorescent reagents. *J. Agric. Food Chem.* **2013**, *61*, 2661−2668.

(19) Liu, G.; Xiong, Y. L.; Butterfield, D. A. Chemical, physical, and gel-forming properties of oxidized myofibrils and whey- and soy-protein isolates. *J. Food Sci.* **2000**, *65*, 811−818.

(20) Damodaran, S. Estimation of disulfide bonds using 2-nitro-5-thiosulfobenzoic acid—Limitations. *Anal. Biochem.* **1985**, *145*, 200−204.

(21) Kella, N. K. D.; Kinsella, J. E. A method for the controlled cleavage of disulfide bonds in proteins in the absence of denaturants. *J. Biochem. Biophys. Methods* **1985**, *11*, 251−263.

(22) Gailit, J. Restoring free sulfhydryl groups in synthetic peptides. *Anal. Biochem.* **1993**, *214*, 334−335.

(23) Brown, W. D. Reduction of protein disulfide bonds by sodium borohydride. *Biochim. Biophys. Acta* **1960**, *44*, 365−367.

(24) Banfi, L.; Narisano, E.; Riva, R.; Stiasni, N.; Hiersemann, M. Sodium borohydride. In *Encyclopedia of Reagents for Organic Synthesis*; John Wiley and Sons, Ltd.: New York, 2001.

(25) Patsoukis, N.; Georgiou, C. D. Fluorometric determination of thiol redox state. *Anal. Bioanal. Chem.* **2005**, *383*, 923−929.

(26) Minkina, V. G.; Shabunya, S. I.; Kalinin, V. I.; Martynenko, V. V.; Smirnova, A. L. Stability of alkaline aqueous solutions of sodium borohydride. *Int. J. Hydrogen Energy* **2012**, *37*, 3313−3318.

(27) Winther, J. R.; Thorpe, C. Quantification of thiols and disulfides. *Biochim. Biophys. Acta, Gen. Subj.* **2014**, *1840*, 838−846.

(28) AOAC International. International guidelines for standard method performance requirements. In *Official Methods of Analysis*, 19th ed.; AOAC International: Rockville, MD, 2012.

(29) Jongberg, S.; Skov, S. H.; Tørngren, M. A.; Skibsted, L. H.; Lund, M. N. Effect of white grape extract and modified atmosphere packaging on lipid and protein oxidation in chill stored beef patties. *Food Chem.* **2011**, *128*, 276−283.

(30) Hansen, R. E.; Roth, D.; Winther, J. R. Quantifying the global cellular thiol−disulfide status. *Proc. Natl. Acad. Sci. U. S. A.* **2009**, *106*, 422−427.

(31) Saurin, A. T.; Neubert, H.; Brennan, J. P.; Eaton, P. Widespread sulfenic acid formation in tissues in response to hydrogen peroxide. *Proc. Natl. Acad. Sci. U. S. A.* **2004**, *101*, 17982−17987.

(32) Stagsted, J.; Bendixen, E.; Andersen, H. J. Identification of specific oxidatively modified proteins in chicken muscles using a combined immunologic and proteomic approach. *J. Agric. Food Chem.* **2004**, *52*, 3967−3974.

collected, and only green leaf was collected in other time points. Leaf samples of lingonberry (*V. vitis-idaea* L.) were collected in the forest of the Paattinen area, Turku, Finland (latitude, 60° 36′ 15″ N; longitude, 22° 22′ 33″ E) at intervals of approximately 10 days from the end of June to mid-September 2013. Both locations consisted of a moraine-type soil. The location in Paattinen was facing east/southeast, and the location in Kohmo was flat. Information on the weather conditions in the Turku area during the growth period can be found in Supplemenatary Table 1 in the Supporting Information. At each time point, samples were picked from five different blocks within the same area. After this, the samples were pooled together into a representative sample and mixed well before being frozen at −18 °C until analysis.

**Reference Compounds and Reagents.** Hyperoside (quercetin-3-*O*-galactoside), isoquercitrin (quercetin-3-*O*-glucoside), kaempferol-3-*O*-glucoside, rutin (quercetin-3-*O*-rutinoside), cyanidin-3-*O*-glucoside chloride, cyanidin-3-*O*-galactoside chloride, and cyanidin-3-*O*-arabinoside chloride were purchased from Extrasynthese (Genay, France). Quercetin-3-*O*-glucuronide, kaempferol-3-*O*-glucuronide, quercetin-3-*O*-rhamnoside, epicatechin, catechin, and chlorogenic acid (5-*O*-caffeoylquinic acid) were purchased from Sigma-Aldrich Co. (St. Louis, MO, USA), methanol (HPLC grade) and formic acid from J. T. Baker (Deventer, The Netherlands), and acetone (HPLC grade) and acetonitrile (HPLC grade) from VWR International Oy (Espoo, Finland).

Deuterium oxide ($D_2O$) was from VWR Internatinal BVBA (Leuven, Belgium). Acetone-$d_6$ and 3-(trimethylsilyl) propionic-2,2,3,3-$d_4$ acid sodium salt (TSP) were from Sigma-Aldrich Co.

**Sample Preparation for HPLC Analysis of Phenolic Compounds.** A sample of 10 g of frozen bilberry leaves or lingonberry leaves was milled to a fine powder with the aid of liquid nitrogen. About 1.5 g of leaf powder was extracted with 20 mL of 70% aqueous acetone in an ultrasonicator bath for 15 min, followed by centrifugation (4420*g*) for 5 min. The supernatant was collected. After centrifugation, the residue was extracted twice, and the supernatants of three extractions were combined and evaporated until dry with a vacuum rotary evaporator at 35 °C. The extract was redissolved in 5 mL of methanol and filtered through a 0.45 μm filter before analysis. Two parallel extracts were prepared for each leaf sample, and the extracts were analyzed twice.

**Sample Preparation for GC-FID Analysis of Fatty Acids.** Total lipids in the bilberry and lingonberry leaves were extracted using a modified method of Folch et al.[20] A sample of 100 mg of leaf powder (prepared in the same way as above) was taken, and 0.40 mg of triheptadecanoin (1,2,3-triheptadecanoylglycerol) dissolved in chloroform were added as an internal standard. The mixture was extracted with 5 mL of chloroform/methanol (2;1, v/v) in a sonicator bath for 30 min. The extract was washed with 1 mL of 0.88% KCl and centrifuged. The organic phase was transferred to a tube with a screw cap. After that, the solvent was evaporated under $N_2$ flow. The methylation of the total fatty acids was carried out by adding of 1 mL of 10% $BF_3$ in methanol to the extracts and incubating at 80 °C for 60 min. After that, 1 mL of water was added to the solution, and fatty acid methyl esters (FAMEs) were extracted with 1 mL of hexane. Two parallel samples were prepared for each time point, and each sample was analyzed twice.

**Measurement of Dry Mass.** The dry mass was determined gravimetrically by heating the samples in an oven at 105 °C until they reached a constant weight.

**Sample Preparation for NMR Analysis.** The leaf samples were lyophilized and ground, and 50 mg of leaf powder was extracted with 800 μL of solvent consisting of deuterated acetone/$D_2O$/TSP (95:5:0.05, v/v/w). The extraction lasted for 1 h in a shaker, followed by centrifugation for 5 min (1650*g*). The supernatant was collected and was either analyzed immediately or stored at −80 °C until analysis.

**Qualitative Analysis with HPLC-DAD-ESI-MS/MS.** HPLC-DAD-ESI-MS/MS analysis was performed using a Waters Acquity Ultra Performance LC system in combination with a Waters 2996 DAD and a Waters Quattro Premier mass spectrometer (Waters Corp., Milford, MA, USA) equipped with an electrospray interface. A Phenomenex Aeris peptide XB-C18 (3.6 μm, 150 × 4.60 mm, Torrance, CA, USA) column was used, and the temperature of the column oven was 25 °C. A binary solvent system was employed consisting of formic acid/water (0.1:99.9, v/v) as solvent A and formic acid/acetonitrile (0.1:99.9, v/v) as solvent B. The gradient program was as follows: 0 min with 15% solvent B, 0−15 min with 15−20% B, 15−20 min with 20−25% B, 20−25 min with 25% B, 25−30 min with 25−60% B, 30−35 min with 60−15% B, and 35−40 min with 15% B. The flow rate of the mobile phase was 0.5 mL/min, and the injection volume was 5 μL. UV chromatograms were recorded at four different wavelengths (280 nm for all phenolic compounds, 320 nm for phenolic acids, 360 nm for flavonol glycosides, and 520 nm for anthocyanins) with a DAD.

The mass spectrometer was operated in both positive and negative modes. The capillary voltage was set to 3.5 kV, the cone voltage to 22 V, and the extractor voltage to 3 V. The source temperature was 150 °C and the desolvation temperature, 300 °C. Mass spectra were obtained by scanning ions between $m/z$ 100 and 1000. For tandem MS, the collision energy was set at 25 eV. The HPLC-ESI-MS system was operated using MassLynx 4.1 software.

Phenolic compounds were identified by comparing the retention times, UV spectra, and mass spectra of the analytes with those of the reference compounds and on the basis of previous reports of these compounds in the literature. Both the methanol solution of reference compounds and the sample spiked with reference compounds were analyzed to confirm the retention times.

**LC-DAD-ESI-TOF-MS Analysis.** The exact masses of the identified compounds were achieved using a micrOTOF-Q mass spectrometer (Bruker Daltonics, Bremen, Germany) connected to an Agilent HPLC 1200 series (Agilent Technologies, Waldbronn, Germany) via an ESI interface. The chromatographic conditions were the same as described above. The HPLC system was controlled by Hystar software (Bruker BioSpin, Rheinstetten, Germany). The eluent flow was split before introduction into the ion source. The mass spectrometer was operated in both positive and negative ion modes. The capillary voltage was set to 4000 V (negative ion mode) or 4500 V (positive ion mode) and the end plate offset to −500 V. Nebulizer gas ($N_2$) pressure was 1.6 bar. The flow rate of the drying gas ($N_2$) was 12.0 L/min and the drying gas temperature, 200 °C. Mass spectra were obtained by scanning ions between $m/z$ 100 and 2000. The internal mass spectrum calibration was achieved with 5 mM sodium formate injected at the end of each LC-MS experiment, and the calibration was performed using HPC mode. The spectrometer was controlled by Compass micrOTOF control software, and the data were processed by Compass DataAnalysis software (both Bruker Daltonics, Bremen, Germany).

**Quantitative HPLC-DAD Analysis.** The HPLC-DAD system used for quantitative analysis consisted of a DGU-20A5 vacuum degasser, two LC-30AD pumps, an SIL 30AC automatic injector, a CTO-20AC column oven, an SPD-M20A VP photodiode array detector (DAD), and a CBM-20A system controller (Shimadzu, Kyoto, Japan). The system was operated using Labsolution Workstation software (Shimadzu). For the analysis of flavonol glycosides and phenolic acids, the HPLC columns, gradient program, temperature of the column oven, flow rate and injection volume were the same as described for the HPLC-DAD-ESI-MS/MS analysis. The peaks were recorded at 360 nm. For the analysis of anthocyanins in the extracts of red bilberry leaves, a binary solvent system was used consisting of formic acid/water (5:95, v/v) as solvent A and acetonitrile as solvent B, and the gradient program was as follows: 0−15 min with 10% solvent B, 15−25 min with 10−20% B, 25−30 min with 20% B, 30−35 min with 20−25% B, 35−40 min with 25−60% B, 40−45 min with 60−10% B, and 45−50 min with 10% B. The peaks were recorded at 520 nm.

Quantitative analysis of flavonol glycosides, phenolic acids, and anthocyanins in the extracts was carried out using an external standard method. The calibration curves were constructed by HPLC-DAD analysis of standard solutions of hyperoside, isoquercitrin, kaempferol-3-*O*-glucoside, quercetin-3-*O*-glucuronide, kaempferol-3-*O*-glucuronide, rutin, chlorogenic acid (5-*O*-caffeoyl quinic acid), cyanidin-3-*O*-glucoside chloride, cyanidin-3-*O*-galactoside chloride, and cyanidin-3-*O*-arabinoside in the concentration range of 0.01−0.15 mg/mL. The standard solutions of anthocyanins were prepared by dissolving the standards in methanol/HCl (99:1). The other standards were dissolved in pure methanol. The calibration curve of every compound was constructed using five different concentrations and by plotting the peak

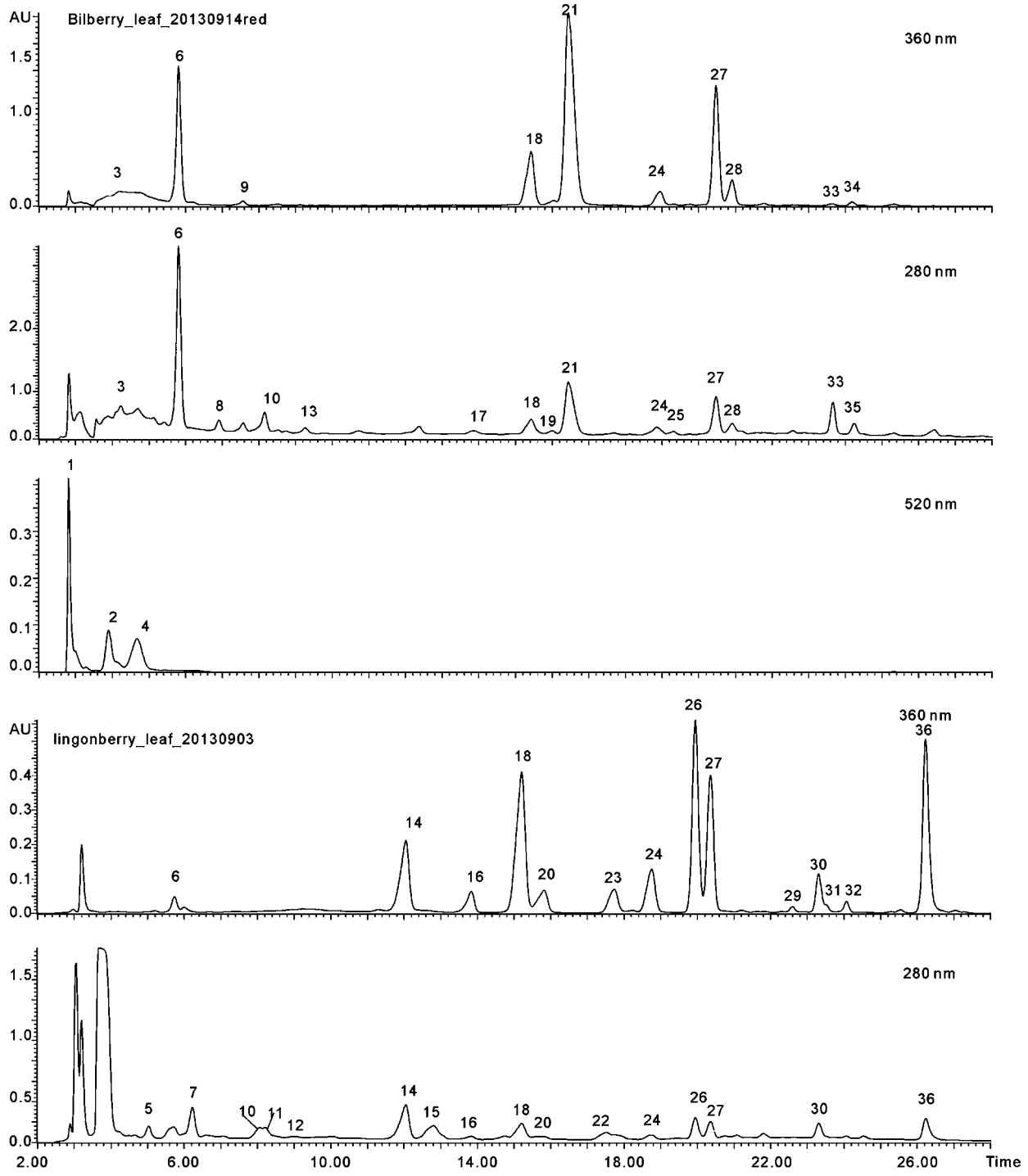


**Figure 1.** HPLC-UV chromatograms of extracts of bilberry leaves (red leaves picked on September 13, 2013) at 360, 280, and 520 nm and of lingonberry leaves (picked on September 3, 2013) at 360 and 280 nm. The numbering and identification of peaks are according to Table 1.

areas against the concentrations. The quantification of quercetin-pentosides and quercetin-3-*O*-(4″-3-hydroxy-3-methylglutaryl)-rhamnoside was carried out using the calibration curve of hyperoside, and the quantification of caffeoyl-hexose-hydroxyphenol and caffeoylquinic acid isomers was performed using the calibration curves of chlorogenic acid (5-*O*-caffeoylquinic acid).

**GC-FID Analysis.** The methyl esters of fatty acids were analyzed using a Shimadzu GC-2010 equipped with an AOC-20i autoinjector and a flame ionization detector. The column used was a DB-23 (60 m × 0.25 mm i.d × 0.25 $\mu$m $d_f$, Agilent Technologies, J. W. Scientific, Santa Clara, CA, USA). A sample of 0.5 $\mu$L was injected into a split/splitless injector (in splitless model). The flow rate of the carrier gas helium was 1.35 mL/min. The temperature of the injector was 270 °C and that of the detector, 280 °C. The column temperature was programmed as 1 min at 130 °C, raised to 170 °C at a rate of 4.5 °C/min, then raised to 220 °C at a rate of 10 °C/min, held at 220 °C for 14.5 min, raised to the final temperature of 230 °C at a rate of 60 °C/min, and held at 230 °C for 3 min.

The fatty acids were identified by comparing the retention times with those of the FAME mix standards Supelco 37 (Supelco, St. Louis, MO, USA) and 68D (Nu-Check-Prep, Elysian, MN, USA).

**NMR Data Acquisition.** NMR analyses were performed on a Bruker Avance 500 spectrometer operated at 500.13 MHz and equipped with a BBI-5 mm-Zgrad-ATM probe.

**Table 1. Phenolics Determined by HPLC-DAD and HPLC-ESI-MS in the Aqueous Acetone Extracts from Leaves of Bilberry and Lingonberry**

| compound[a] | $t_R$[b] (min) | $\lambda_{max}$ (nm) | $[M+H]^+$ ($m/z$) | other ions (positive) | $[M-H]^-$ ($m/z$) | other ions (negative) | $[M-H]^-$[c] ($m/z$) | identification[d] | source |
|---|---|---|---|---|---|---|---|---|---|
| **1** | 2.78 | 218, 518 | 449 | 287 | | | | cyanidin-3-*O*-galactoside* | red bilberry leaves |
| **2** | 3.85 | 210, 517 | 449 | 287 | | | | cyanidin-3-*O*-glucoside* | red bilberry leaves |
| **3** | 4.2 | 287, 329 | 355 | 163 | 353 | 191 | 353.0887 | caffeoylquinic acid I | bilberry leaves |
| **4** | 4.62 | 214, 517 | 419 | 287 | | | | cyanidin-3-*O*-arabinoside* | red bilberry leaves |
| **5** | 5.71 | 211, 279 | 579 | 291, 289, 867 | 577 | | 577.1344 | B-type procyanidin dimer I | bilberry leaves |
| **6** | 5.73 | 287,327 | 355 | 163 | 353 | 191 | 353.0898 | chlorogenic acid (5-*O*-caffeoylquinic acid)* | bilberry/lingonberry leaves |
| **7** | 6.3 | 225, 280 | 291 | | 289 | | 289.0719 | catechin* | bilberry/lingonberry leaves |
| **8** | 6.9 | 219, 280 | 579 | 291, 867 | 577 | 289 | 577.1364 | B-type procyanidin dimer II | bilberry/lingonberry leaves |
| **9** | 7.47 | 282, 329 | 355 | 163 | 353 | 191 | 353.0893 | caffeoylquinic acid II | bilberry leaves |
| **10** | 8.15 | 225, 280 | 291 | 581 | 289 | | 289.0707 | epicatechin* | bilberry/lingonberry leaves |
| **11** | 8.52 | 219, 280 | 865 | 291, 579 | 863 | 289 | 863.1814 | type A/B procyanidin trimer | bilberry/lingonberry leaves |
| **12** | 9.03 | 211, 279 | 865 | 291, 579, 887 | 863 | | 863.1840 | type A/B procyanidin trimer | lingonberry leaves |
| **13** | 9.27 | 211, 279 | 867 | 579, 889 | 865 | | 865.1985 | B-type procyanidin trimer | bilberry leaves |
| **14** | 12.05 | 288, 329 | 435 | 163, 325, 457 | 433 | 161, 323 | 433.1164 | 2-*O*-caffeoylarbutin** | lingonberry leaves |
| **15** | 12.82 | 211, 279 | 577 | | 575 | | 575.1221 | A-type procyanidin dimer I | lingonberry leaves |
| **16** | 13.83 | 263, 355 | 611 | 303, 465, 633 | 609 | 301 | 609.1497 | rutin* | lingonberry leaves |
| **17** | 13.87 | 280 | 741 | 579 | 739 | 577 | 739.1660 | B-type procyanidin dimer derivative | bilberry leaves |
| **18** | 15.42 | 263, 355 | 465 | 303, 487, 929 | 463 | 301 | 463.0874 | hyperoside* | bilberry/lingonberry leaves |
| **19** | 15.6 | 210, 282 | 579 | 867 | 577 | 289 | 577.1363 | B-type procyanidin dimer III | bilberry leaves |
| **20** | 15.82 | 263, 355 | 465 | 303, 487 | 463 | 301 | 463.0895 | quercetin-3-*O*-glucoside | lingonberry leaves |
| **21** | 16.45 | 257, 355 | 479 | 303, 501, 957 | 477 | 301 | 477.0677 | quercetin-3-*O*-glucuronide | bilberry leaves |
| **22** | 17.5 | 210, 279 | 577 | 599 | 575 | 289 | 575.1224 | A-type procyanidin dimer II | lingonberry leaves |
| **23** | 17.73 | 263, 355 | 435 | 303, 457 | 433 | 301 | 433.0779 | quercetin-pentoside I (quercetin-3-*O*-xyloside) | lingonberry leaves |
| **24** | 18.95 | 261, 356 | 435 | 303 | 433 | 301 | 433.0754 | quercetin-pentoside II (quercetin-3-*O*-arabinoside) | bilberry/lingonberry leaves |
| **25** | 19.3 | 210, 318 | 429 | 163, 267, 451 | 427 | 146 | 427.1598 | caffeoyl-hexoside derivative | bilberry leaves |
| **26** | 19.95 | 263, 355 | 435 | 303, 457 | 433 | 301 | 433.0787 | quercetin-pentoside III (quercetin-3-*O*-arabinofuranoside) | lingonberry leaves |
| **27** | 20.47 | 256, 349 | 449 | 303, 887 | 447 | 301 | 447.0918 | quercetin-3-*O*-rhamnoside* | bilberry/lingonberry leaves |
| **28** | 20.92 | 267, 347 | 463 | 287 | 461 | 285 | 461.0717 | kaemperol-3-*O*-glucuronide* | bilberry leaves |
| **29** | 22.60 | 260, 356 | 507 | 303, 529 | 505 | 301 | 505.1006 | quercetin-acetylglucoside | lingonberry leaves |
| **30** | 23.3 | 258, 354 | 579 | 303 | 577 | 301 | 577.1221 | quercetin derivatives | lingonberry leaves |
| **31** | 23.32 | 261, 357 | 477 | 367, 477, 499 | 475 | 161, 365, 475 | 475.1275 | 2-*O*-caffeoyl-6-*O*-acetylarbutin** | lingonberry leaves |
| **32** | 23.5 | 263, 355 | 419 | 287, 419 | 417 | 285 | 417.0831 | kaempferol pentoside | lingonberry leaves |
| **33** | 23.67 | 210, 312 | 413 | 146, 251, 425, 825 | 411 | | 411.1679 | *p*-coumaroyl-hexoside derivative I** | bilberry leaves |
| **34** | 24.2 | 261, 356 | 433 | 287 | 431 | 285 | 431.0985 | kaempferol-rhamnoside | bilberry/lingonberry leaves |
| **35** | 24.23 | 210, 312 | 413 | 146, 251, 425, 825 | 411 | | 411.1675 | *p*-coumaroyl- hexoside derivative II** | bilberry leaves |
| **36** | 26.23 | 263, 355 | 593 | 303, 615 | 591 | 301 | 591.1401 | quercetin-HMG[e]-rhamnoside | lingonberry leaves |
| **37** | 3.8 | | | | | | | arbutin** | lingonberry leaves |

[a]Compound numbers are according to peak labels in Figure 1. [b]Retention time according to HPLC-DAD chromatograms. [c]High-resolution mass spectra were obtained using LC-DAD-ESI-TOF-MS. [d]Compounds with * were identified with reference compounds, with **, with NMR; the others were identified on the basis of UV and mass spectra. [e]HMG, 3-hydroxy-3-methylglutaryl.

*1D $^1$H NMR.* $^1$H NMR spectra were acquired for all samples with 180 scans at 25 °C using an 1D pulse sequence with water suppression by presaturation (Bruker's pulse program zgpr) with a relaxation delay of 5 s. Free induction decays (FIDs) were collected with 64K data points, an acquisition time of 3.28 s, and a spectral width of 10000.0 Hz. Fourier transformation was applied to the FID.

*2D NMR.* Standard 2D NMR experiments DQF-COSY (cosygpmfqf), TOCSY (mlevgpph) with a mixing time of 300 ms, $CH_2$-edited HSQC (hsqcedetgpsisp.2), and HMBC (hmbcgplpndqf) with couplings of 5.0 and 10.0 Hz were performed for selected lingonberry leaf and bilberry leaf samples.

*Data Preprocessing.* All of the $^1$H NMR spectra were manually calibrated and corrected for phase and baseline using TopSpin 3.2 NMR

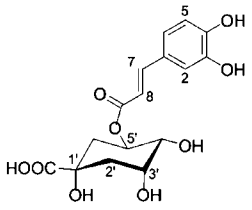

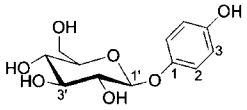

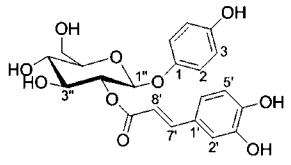

***trans*-5-*O*-caffeoyl quinic acid**

| Position | $\delta_H$ (ppm) | $J_H$ (Hz) | Type | $\delta C$ (ppm) | COSY (δH) | HMBC (δH) |
|---|---|---|---|---|---|---|
| 7 | 7.55 | 15.9 | d | 147.7 | 6.28 (8) | 7.16 (2); 7.00 (6) |
| 2 | 7.16 | 2.0 | d | 116.5 | 7.00 (6) | 7.55 (7); 7.00 (6) |
| 6 | 7.00 | 2.0; 8.3 | dd | 124.1 | | 7.55 (7); 7.16 (2) |
| 5 | 6.86 | 8.2 | d | 117.9 | 7.00 (6) | |
| 8 | 6.28 | 15.9 | d | 117.0 | 7.55 (7) | |
| 1 | | | | 129.2 | | 6.86 (5); 6.28 (8) |
| 9 | | | | 169.6 | | 7.55 (7); 6.28 (8) |
| 5' | 5.35 | | m | 73.1 | 3.72 (4'); 2.20 (2'a); 1.97 (2'b) | |
| 3' | 4.20 | 3.0 | q* | 73.0 | 3.72 (4'); 2.1 (6'a&b) | |
| 4' | 3.72 | | m | 72.4 | 5.35 (3'); 4.20 (5') | |
| 2'a&b, 6'a&b | 1.93–2.27 | | | 36.9–39.5 | | |

**beta-*p*-arbutin**

| Position | $\delta_H$ (ppm) | $J_H$ (Hz) | Type | $\delta_C$ (ppm) | COSY (δH) | HMBC (δH) |
|---|---|---|---|---|---|---|
| 2 & 6 | 6.93 | 9.0 | d | 120.6 | 6.72 (5,6) | 6.93 (2⇔6) |
| 3 & 5 | 6.72 | 9.0 | d | 117.9 | 6.93 (2,3) | 6.72 (3⇔5) |
| 1 | | | | 153.8 | | 4.74 (1'), 6.72 (3,5), 6.93 (2,6) |
| 4 | | | | 155.5 | | 6.72 (3,5); 6.93 (2,6) |
| 1' | 4.76 | 7.7 | d | 104.7 | 3.42 (2') | 3.42 (5') |
| 6'a | 3.86 | 2.0; 12.1 | dd | 64.1 | 3.66 (6'b) | 3.42 (5') |
| 6'b | 3.69 | 5.1; 12.1 | dd | 64.1 | 3.84 (6'a) | 3.42 (5') |
| 3' | 3.48 | | m | 79.2 | 3.42 (2', 4') | 3.42 (2') |
| 5' | 3.42 | | m | 79.2 | | 4.74 (1'), 3.86 (6'a), 3.69 (6'b) |
| 4' | 3.42 | | m | 72.7 | 3.47 (3') | 3.86 (6'a); 3.48 (3') |
| 2' | 3.41 | | m | 76.1 | 4.74 (1'); 3.47 (3') | 4.76 (1'); 3.42 (4') |

**2-*O*-caffeoyl-beta-*p*-arbutin**

| Position | $\delta_H$ (ppm) | $J_H$ (Hz) | Type | $\delta_C$ (ppm) | COSY (δH) | HMBC (δH) |
|---|---|---|---|---|---|---|
| 2 & 6 | 6.85 | 9.0 | d | 120.6 | 6.72 (3,5) | 6.85 (2⇔6) |
| 3 & 5 | 6.72 | 9.0 | d | 117.9 | 6.93 (2,6) | 6.72 (3⇔5) |
| 1 | | | | 153.1 | | 5.00 (1"), 6.72 (3,5), 6.93 (2,6) |
| 7' | 7.59 | 15.9 | d | 148.0 | 6.14 (8') | 7.16 (2'); 7.00 (6') |
| 2' | 7.16 | 2.0 | d | 116.8 | | |
| 6' | 7 | 2.1; 8.1 | dd | 124.1 | 6.86 (5') | |
| 5' | 6.86 | 1.8; 6.9 | dd | 117.5 | 7.00 (6') | |
| 8' | 6.32 | 15.9 | d | 116.9 | 7.59 (7') | |
| 9' | | | | 168.7 | | 7.59 (7'); 6.3 (8'), 5.05 (2") |
| 1' | | | | 129.0 | | 6.86 (5'); 6.32 (8') |
| 2" | 5.06 | 8.1; 9.5 | dd | 76.2 | 4.98 (1"); 3.75 (3") | |
| 1" | 4.98 | 8.1 | d | 103.1 | 5.06 (2") | |
| 3" | 3.75 | | m | 77.3 | 5.06 (2") | |
| 6"a | 3.95 | | m | 65.7 | 3.6 (6"b) | |
| 6"b | 3.6 | | m | 65.7 | 3.95 (6"a) | |
| 4", 5" | 3.5–3.54 | | m | 72.9–73.1 | 3.6 (6"b) | |

**Figure 2.** Chemical structures of chorogenic acid (5-*O*-caffeoylquinic acid), arbutin, and 2-*O*-caffeoylarbutin and their chemical shifts in crude bilberry/lingonberry leaf extracts in aqueous acetone-$d_6$.

software. Chemical shifts were referenced (internally) to TSP ($\delta$ 0.0). Preprocessed $^1$H NMR spectra were integrated to consecutive 0.005 ppm wide buckets using Amix software. Spectra of eight sampling points of bilberry leaves and six sampling points of lingonberry leaves were used for metabolomic comparison. The spectra of the rest of the samples (one sampling point of bilberry leaf and three sampling points of lingonberry leaves) were not included due to shifting of the signals caused by the residue of acetone used for washing the NMR tubes. The spectrum of red bilberry leaf was also excluded due to its highly exceptional profile.

**Analysis of Pearson Correlation Coefficient and Hierarchial Clustering.** Pearson correlation (Pearson product moment correlation) was applied in Excel to the spectral integrals generated by Amix to find correlations between the changes in concentrations of different metabolites. Specific integrals were chosen in turn as reference signals. R software (v. 3.0.1) with plotrix library was used to create graphical presentations of correlations between metabolites.[21,22]

The same integrated spectral areas were used to create a hierarchial clustering analysis visualized by dendrogram tree using SIMCA-P+ software package (version 12.0, Umetrics AB, Umeå, Sweden).

## RESULTS AND DISCUSSION

**Identification of Phenolics and Fatty Acids in Leaves of Bilberry and Lingonberry by Chromatographic Methods and NMR.** Figure 1 presents exemplary HPLC-DAD chromatograms of extracts of bilberry and lingonberry leaves. Thirty-seven phenolic compounds were identified/tentatively identified from the extracts (Table 1). Twenty-one phenolic compounds were detected from the extracts of the red bilberry leaves, 18 phenolics from the green bilberry leaves, and 25 phenolics from lingonberry leaves. 2D NMR analyses were used to support the identification based on HPLC and MS analyses.

Some of the compounds listed in Table 1 have been reported previously.[13,23,24] Quercetin-acetylglucoside (compound **29**), B-type procyanidin dimer-hexoside (compound **17**), 2-*O*-caffeoyl-6-*O*-acetylarbutin (compound **31**), caffeoyl-glucoside derivative (compound **25**), and *p*-coumaroyl-glucoside derivatives (compound **33** and **35**) are identified for the first time.

*Anthocyanins.* Compounds **1**, **2**, and **4** had UV spectra typical for anthocyanins with absorption maxima around 520 nm. By comparing their retention times and mass spectra with those of reference compounds, these compounds were identified as cyanidin-3-*O*-galactoside, cyanidin-3-*O*-glucoside, and cyanidin-3-*O*-arabinoside, respectively. These anthocyanins were found in the extracts of red bilberry leaves, but not in those of green leaves.

*Phenolic Acids and Arbutin Derivatives.* Derivatives of phenolic acids were identified on the basis of their UV spectra with typical absorption maxima around 280 and 320 nm.

Compound **6** was identified as chlorogenic acid (5-*O*-caffeoylquinic acid) by comparing its UV and mass spectra as well as retention time with those of the reference compound, and the identification was confirmed by the NMR data. The position of the caffeoyl group was concluded on the basis of the coupling constants of H3 and H5, where the first one showed only small couplings (equatorial) and the latter also large ones (axial) based on the total width of the signals. Thus, the correct structure could be identified even though exact values of coupling constants cannot be detected because of other overlapping signals from other compounds. Compounds **3** and **9** had very similar UV and mass spectra with compound **6**. The ion at $m/z$ 163 in the mass spectra in the positive mode derived from the caffeoyl unit and the ion at $m/z$ 191 in the negative mode from quinic acid. The $[M + H]^+$ at $m/z$ 355 indicated that they were isomers of chlorogenic acid. Chemical shifts and couplings of 5-*O*-caffeoylquinic acid obtained by NMR are presented in Figure 2.

The most dominant compound in lingonberry crude extract was identified as $\beta$-*p*-arbutin on the basis of the 2D NMR spectra

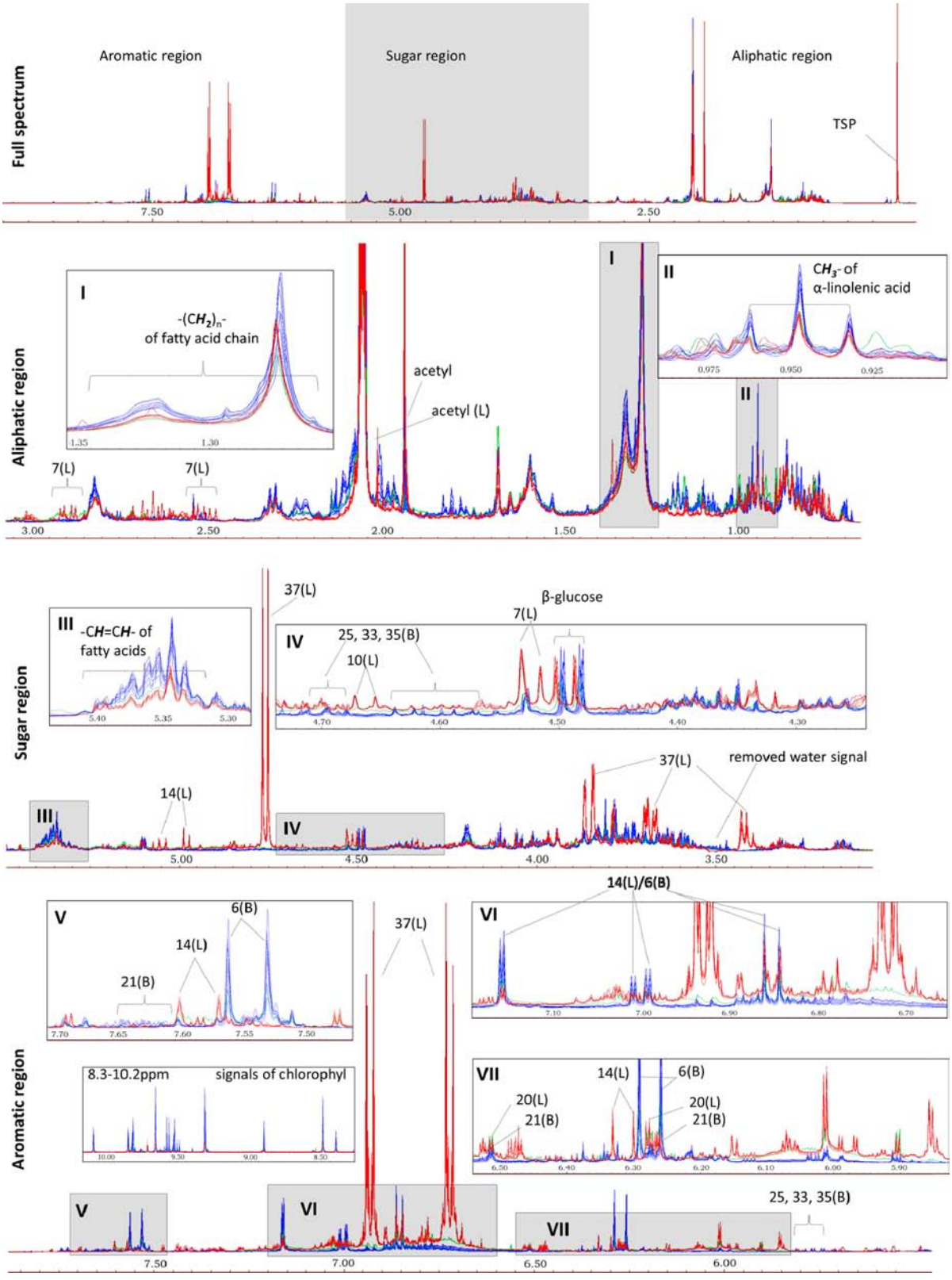


**Figure 3.** [1]H NMR spectra of crude extracts of green bilberry (blue), red bilberry (green), and lingonberry (red) leaves collected during the growing season. Spectra of lingonberry leaves are almost uniformly overlapping with each other, whereas more variation in spectral fingerprints can be found between bilberry leaves of different collection points. (L) refers to the compounds detected from lingonberry leaf samples, and (B) refers to bilberry leaves. Some of the compounds can be found in both plants (no letter attached). Compounds presented in the figure: chlorogenic acid (**6**), catechin (**7**), epicatechin (**10**), 2-*O*-caffeoyl arbutin (**14**), quercetin-3-*O*-glucoside (**20**), quercetin-3-*O*-glucuronide (**21**), *p*-coumaroyl and caffeoyl-glucoside derivatives (**25**, **33**, **35**), and *β*-*p*-arbutin (**37**).


dx.doi.org/10.1021/jf503521m | *J. Agric. Food Chem.* 2014, 62, 12015−12026

(Figure 2). The resonances originated from this compound were easily perceived due to their exceptionally high intensities. Two doublets ($J$ = 8.9 Hz) at the aromatic region ($\delta$ 6.72 of H2, H6; and $\delta$ 6.93 of H3, H5) indicated the presence of para-substituted aromatic ring structure. HMBC correlations from H2 and H6 to carbon at $\delta$ 155.3 indicated the presence of a hydroxyl group attached to the 4-carbon, and HMBC correlations from H3, H5, and H1′ to carbon at $\delta$ 153.8 linked the phenol group to a sugar moiety. Resonances from the sugar moiety are disrupted by the removal of the solvent signal at $\delta$ 3.50. However, by the selective 1D TOCSY experiment it was possible to specify all of the protons belonging to the same spin system as the anomeric doublet signal at $\delta$ 4.76 (Figure 2). The arbutin had maximum absorption at about 280 nm in the UV spectrum. However, the peak of arbutin in the HPLC chromatograms under 280 nm overlapped with the peaks of other compounds forming the huge peak from 3.5 to 4.1 min (Figure 1). This made it impossible to extract clear UV and mass spectra.

Compound **14** was a prevalent phenolic acid in the extracts of lingonberry. The ions at $m/z$ 435 and 457 represented $[M + H]^+$ and $[M + Na]^+$ ($[M + 23]^+$), respectively. The ion at $m/z$ 163 in the mass spectrum in the positive mode indicated the existence of a caffeoyl unit. The mass spectrum was identical to that of caffeoyl-hexose-hydroxyphenol previously reported.[23] 2-*O*-Caffeoylarbutin was reported to be the most abundant caffeoyl-hexose-hydroxyphenol isomer in lingonberry leaves.[23] In our 2D NMR analyses, correlations over the glycosidic bonds between the 1″-position of $\beta$-glucose and hydroxyphenol as well as the 2″-position of glucose and the caffeoyl vinyl group were detected, supporting the previous identification (Figure 2).

Compound **31** was identified as 2-*O*-caffeoyl-6-*O*-acetylarbutin on the basis of the UV and mass spectra and literature. An acetyl moiety was also detected in the $^1$H NMR spectra of lingonberry leaf extracts. Via HMBC a very weak coupling from the 6″ proton of a glucose moiety of the caffeoyl arbutin to carbonyl carbon of acetyl could be detected, supporting the identification (Supplementary Figure 1). However, the integration of the acetyl moiety revealed the concentration to be only one-sixth of the corresponding anomeric glucose doublet ($\delta$ 4.98), indicating that most of the caffeoyl arbutin remains without acetylation (compound **14**). Similar types of compounds with a hydroxyphenyl moiety have previously been identified from *Vaccinium dunalianum*, which is an evergreen perennial shrub distributed in China, Myanmar, and Vietnam.[25] Tea made from the leaves of this plant has been traditionally used as folk medicine to treat articular rheumatism, similarly to lingonberry leaves. Arbutin has been postulated to play an important role in the bioactivity of leaves in these two plants.[14,25] However, a potent mutagenic activity of hydroquinone and its analogues such as arbutin has also been reported.[26] The deleterious properties of the analogues are probably due to the cleavage of hydroquinone via deglycolysation.[26] On the contrary, in the study of Takebayashi et al., hydroquinone as well as arbutin showed strong antioxidant activity assessed by several methods,[27] yet the hydroquinone in higher concentrations exhibited cytotoxicity when the protective effects against oxidative stress in fibroblasts were studied in vitro, whereas arbutin retained its protective properties.

Compound **25** was detected in the extracts of bilberry leaves and identified as a caffeoyl derivative. Ions at $m/z$ 163 in the mass spectrum derived from the caffeoyl unit. The difference of 162 amu between the $[M + H]^+$ at $m/z$ 429 and a fragment at $m/z$ 267 indicated a hexose unit esterified to the caffeoyl. The mass spectrum also showed an unknown fragment (114 amu) likely linked to the caffeoyl unit. Compounds **33** and **35** were isomers with similar structures with compound **25**, but the caffeoyl unit being replaced by *p*-coumaroyl. A closer inspection of 2D NMR spectra established a cis orientation of a vinyl group in these hydroxycinnamic acid derivatives and a $\beta$-glucose to be the potential hexose unit based on the variation of the proton signals between different samples. In the 2D COSY experiment the signal of H2 protons of this sugar resonated at $\delta$ 4.67−4.89, which refers to a linkage of electronegative group to the 2-carbon. The cis conformation is supported by Kort et al., who demonstrated a shortening of the coupling constant from 15.9 Hz (trans) to 12.8 Hz (cis) as a result of photoisomerization in *p*-coumaric acid (Figure 3).[28]

*Flavanols and Procyanidins.* Flavanols and procyanidins commonly have clear absorption maxima at around 230 and 280 nm. Compounds **7** and **10** were identified as catechin and epicatechin, respectively, on the basis of their UV and mass spectra as well as confirmation with reference compounds. Signals of the C-ring of catechin and epicatechin were also detected by NMR measurements (Figure 3). Signals of A and B rings overlapped with others signals on the aromatic region, but HMBC couplings could be detected for catechin (Supplementary Figure 2).

Compounds **5**, **8**, **11**−**13**, **15**, **17**, **19**, and **22** were identified as procyanidins on the basis of their UV spectra. Compounds **5**, **8**, and **19** showed mass spectra typical for B-type procyanidin dimers.[29,30] In negative mode, the mass spectra of compounds **15** and **22** had $[M - H]^-$ ions at $m/z$ 575 and fragment ions at $m/z$ 289. These two compounds were identified as A-type procyanidins because the $m/z$ values of the $[M - H]^-$ ions were lower than those of the corresponding B-type procyanidin dimers by 2 amu. Compound **13** had $[M + H]^+$ at $m/z$ 867 and $[M + Na]^+$ at $m/z$ 889 in the mass spectrum and are assigned as a B-type procyanidin trimer. Compounds **11** and **12** had $[M + H]^+$ at $m/z$ 865 and were identified as A/B-type procyanidin trimers. The $m/z$ value of the $[M + H]^+$ ion of compound **17** was 162 amu higher than those of B-type procyanidin dimers, suggesting the presence of a hexose or a caffeoyl group linked to the procyanidin dimer.[30] The exact mass ($m/z$ 739.1660 for $[M - H]^-$) obtained using high-resolution mass spectrometry suggested it is a caffeoyl procyanidin dimer.

*Flavonol Glycosides.* Flavonol glycosides were among the major phenolics in the extracts from bilberry leaves and lingonberry leaves. All of the flavonol glycosides detected in bilberry and lingonberry leaves had quercetin or kaempferol as the aglycons. Compounds **16**, **18**, **20**, **21**, and **27** were identified as rutin (quercetin-3-*O*-rutinoside), hyperoside (quercetin-3-*O*-galactoside), isoquercitrin (quercetin-3-*O*-glucoside), quercetin-3-*O*-glucuronide, and quercetin-3-*O*-rhamnoside, respectively, with the aid of reference compounds. On the basis of the mass spectra, compounds **23**, **24**, and **26** were identified as quercetin-pentosides, and by comparing the order of the elution with references, these compounds were likely quercetin-3-*O*-xyloside, quercetin-3-*O*-arabinoside, and quercetin-3-*O*-arabinofuranoside, respectively.[13,23] Compound **29** was indentified as quercetin-acetylglucoside on the basis of the mass spectrum. The ions at $m/z$ 303 in the mass spectra indicated that compound **30** was a derivative of quercetin, and compound **36** was quercetin-3-*O*-(4″-3-hydroxy-3-methylglutaryl)-rhamnoside.[13,23]

Compound **28** was confirmed as kaempferol-3-*O*-glucuronide with reference compound. Compounds **32** and **34** were

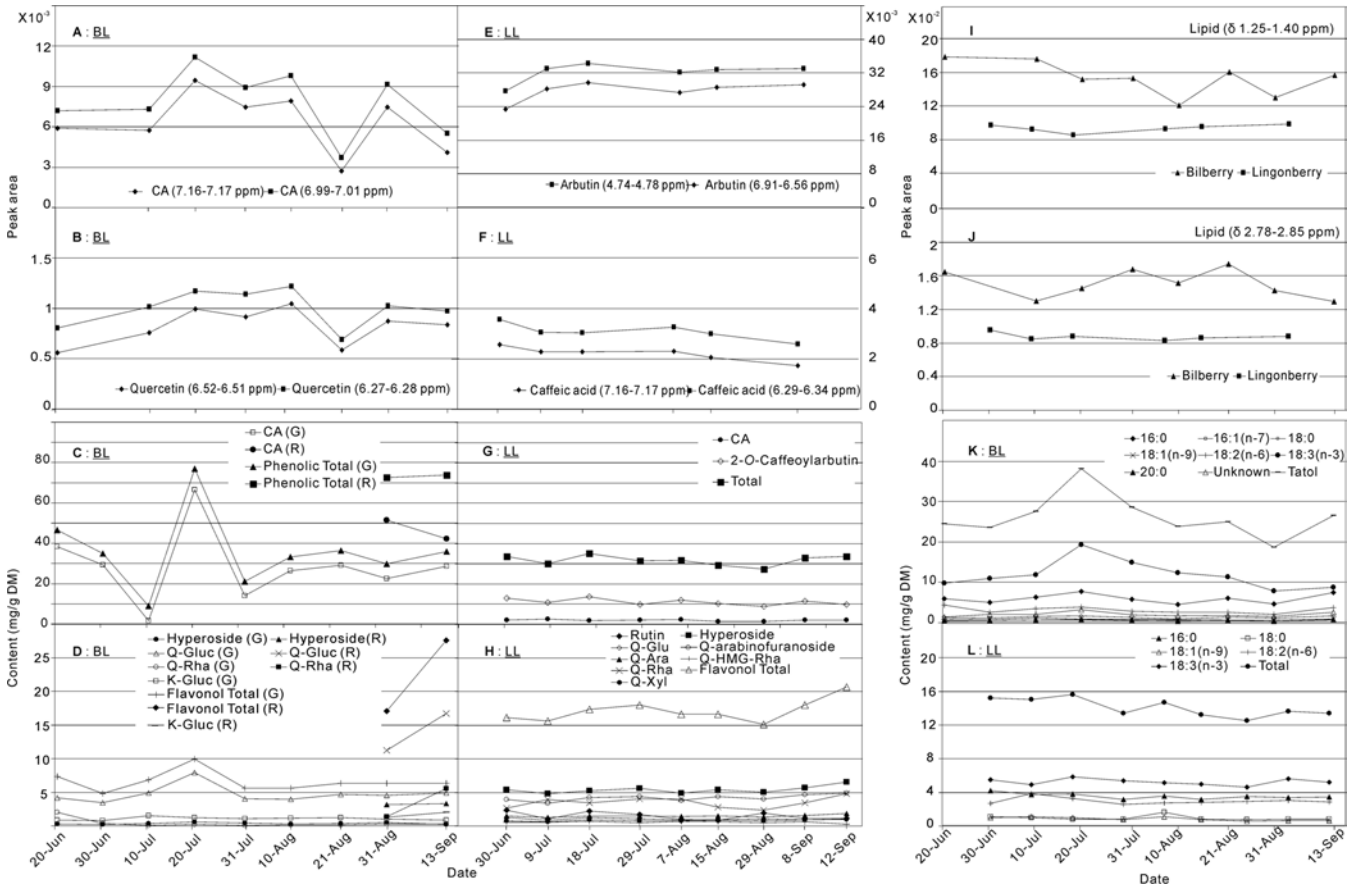


**Figure 4.** Changes in the content of phenolic compounds in bilberry leaves (A–D) and lingonberry leaves (E–H) and the content of lipids in bilberry and lingonberry leaves (I–L) during the growing season in 2013. Panels A, B, E, F, I, and J are based on the results of NMR analyses; panels C, D, G, and H are based on the results of HPLC-DAD analyses; panels K and L are based on the results of GC-FID analyses. BL, bilberry leaves; LL, lingonberry leaves; CA, chlorogenic acid; Q, quercetin; K, kaempferol; Gluc, glucuronide; Glu, glucoside; Rha, rhamnoside; Xyl, xyloside; Ara, arabinoside; HMG, 3-hydroxy-3-methylglutaryl; G, green leaves; R, red leaves.

identified as kaempferol-pentoside and kaempferol-rhamnoside, respectively.

*Fatty Acids.* $\alpha$-Linolenic acid (18:3n-3), palmitic acid (16:0), stearic acid (18:0), oleic acid (18:1n-9), linoleic acid (18:2n-6), and arachidic acid (20:0) were the major fatty acids in both lingonberry and bilberry leaves. Also, some minor fatty acids were found. An unknown fatty acid peak with retention time of 15.1 min was detected in the chromatograms of only bilberry leaves, but not in those of lingonberry leaves (Supplementary Figure 3).

**Metabolomic Changes during the Growing Season.** An untargeted approach was exploited to reveal the overall similarities and differences between bilberry and lingonberry samples and to investigate the changes occurring during the growing season. Targeted approaches were applied for more accurate quantification of specific metabolites.

*Untargeted Metabolomics.* The untargeted metabolomic analysis of metabolite fingerprints obtained by $^1$H NMR revealed differing compositional profiles of the crude extracts of bilberry and lingonberry leaves (Figure 3). The most notable differences occurred in the major phenolic compounds and lipids. In general, the aromatic region of the spectra of lingonberry leaf encompassed more intensive signals than the corresponding spectra of bilberry leaf. However, the fingerprints of red bilberry leaf extracts deviated from green bilberry leaves, especially by the broad signals in the aromatic region, as found in the lingonberry leaves. The intensities of several signals in bilberry spectra varied considerably among the collection points, whereas the signals of lingonberry extracts remained at relatively constant level regardless of the time of collection (see insets I–VII in Figure 3). These differences between different types of leaves were also indicated by statistical analysis (Supplymentary Figure 4). In dendrograms based on hierarchical clustering analysis of the samples analyzed by untargeted $^1$H NMR, two clearly separated groups were created, dividing the samples of lingonberry and bilberry into different branches. In addition, the red leaf of bilberry creates its own branch, being more similar to green bilberry leaves than lingonberry leaves. It is also indicated on the basis of the hierarchical clustering analysis that the differences in the metabolite composition between bilberry leaves are more notable than those between the lingonberry leaves at different collection times (Supplymentary Figure 4).

The major phenolic compounds as well as a few minor compounds could be addressed from the $^1$H NMR fingerprints obtained by untargeted approach (Figure 3). In the bilberry leaf extracts, chlorogenic acid (5-*O*-caffeoylquinic acid) was the most abundant phenolic compound in all of the collection points, whereas it remained as a minor one in the lingonberry leaf extracts. Arbutin or its derivates were not detected in the extracts from bilberry leaves, but they were the most prevalent compounds in all the lingonberry leaf extracts.

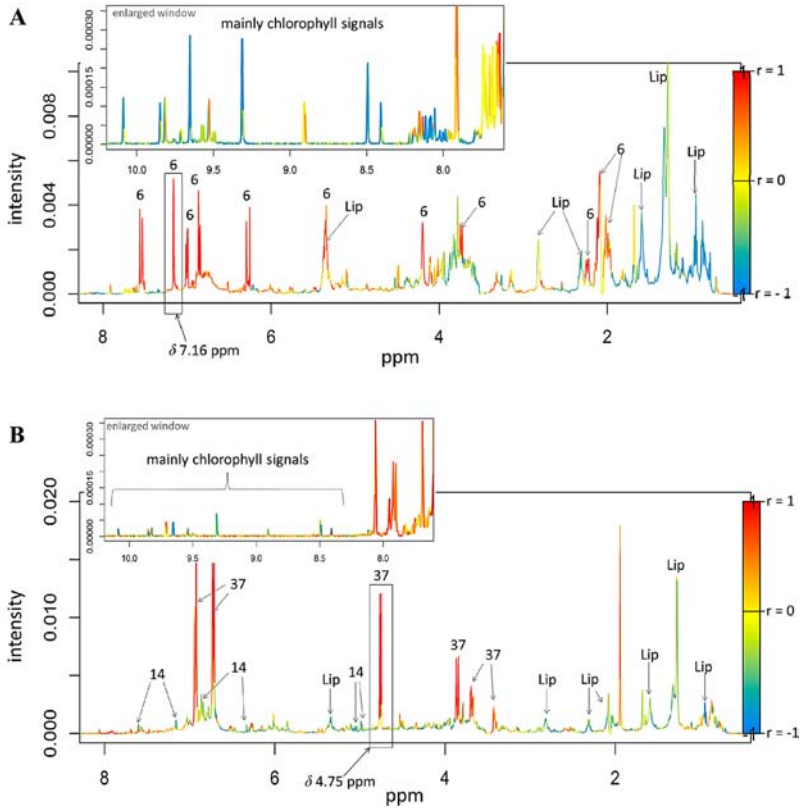


**Figure 5.** $^1$H NMR spectrum of leaf crude extract is colored according to Pearson correlation coefficients: (A) correlation between the changes of other bilberry leaf metabolites with chlorogenic acid signal at $\delta$ 7.16 during the growing season; (B) correlation between the changes of other lingonberry leaf metabolites with arbutin signal at $\delta$ 4.75 during the growing season. Correlation coefficients ($r$) of 0.5−1.0 (red) and 0.3−0.5 (orange) indicate strong and moderate positive correlations, respectively, and −0.5−1.0 (blue) and −0.3−0.5 (green) indicate strong and moderate negative correlations, respectively, between the metabolites. Compounds allocated in the figure: chlorogenic acid (**6**), 2-*O*-caffeoyl arbutin (**14**), *β*-*p*-arbutin (**37**), and lipid signals (Lip).

On the basis of $^1$H NMR spectra, the overall lipid content appeared to be higher in the crude extracts of bilberry leaves (Figure 3, insets I−III). Also, the changes in lipid content during the growth period were apparent in the bilberry samples, whereas lingonberry leaves showed less variation. Furthermore, the content of n-3 fatty acids was found to be slightly higher in bilberry leaves than in lingonberry leaves on the basis of the integrals of methyl groups of n-3 fatty acids ($\delta$ 0.95).

*Changes in Lipids Profiles of Bilberry and Lingonberry Leaves.* The integrated lipid areas of $^1$H NMR spectra resulted in different changing patterns in the lipids of leaf samples during the season, especially in the case of bilberry leaf extracts (Figure 4I,J, targeted NMR). The integrals of the signal $\delta$ 2.78−2.85, consisting of the resonances of =CH—C$\underline{H}_2$—CH= protons, showed a different changing trend from those of the integrals of $\delta$ 1.25−1.40 [−(C$\underline{H}_2$)$_n$−] and $\delta$ 2.29−2.36 (−OCO—C$\underline{H}_2$−), and the latter two showed a similar trend with each other (Figure 4I,J). This may reflect the compositional changes in the fatty acid profile.

Targeted analysis by GC-FID supported the results from untargeted analysis (Figure 4K,L). However, $^1$H NMR measures the amount of protons in the fatty acid chain, whereas peak integral in GC chromatogram indicates the number on fatty acid molecules, which might explain some of the differences between these two methods. By choosing very specific proton types, such as $\alpha$- or $\beta$-protons ($\delta$ 2.29...2.36 and 1.54...1.63, respectively) from the carbonyl group, for integration, the number of protons should linearly correlate with the number on fatty acid molecules.

Analyses by GC showed generally higher content and wider deviation of fatty acids in bilberry extracts than in lingonberry extracts. The content of fatty acids in extracts of bilberry leaves ranged from 19 to 38 mg/g DM (dry mass) during the growing season (Figure 4K). The highest contents were found in the samples picked on July 20 (Figure 4K). $\alpha$-Linolenic acid was the most abundant fatty acid, accounting for almost half of the total in all of the samples (Figure 4K). No major difference was noted in the content of fatty acids between the green leaves and red leaves picked on the same day.

The levels of fatty acids in lingonberry leaves were 13−16 mg/g DM during the season (Figure 4L). $\alpha$-Linolenic acid was the most abundant fatty acid in extracts of all the samples except the one collected on August 7. The contents of palmitic acid and linoleic acid were found similarly quite close (Figure 4L).

*Changes in Phenolic Profile in Bilberry and Lingonberry Leaves.* The changing trends constructed using selected signals of phenolic compounds based on NMR integrals are shown in Figure 4A,B. Changing trends of 10 major phenolic compounds (chlorogenic acid and its two isomers, hyperoside, quercetin-3-*O*-glucuronide, quercetin-rhamnoside, kaemperol-3-*O*-glucouronide, cyanidin-3-*O*-galatoside, cyanidin-3-*O*-glucosdie, and cyanidin-3-*O*-arabinoside) in the extracts from leaves studied by the HPLC-DAD method are shown in Figure 4C,D. Targeted analyses by HPLC-DAD showed results largely consistent with the findings obtained by NMR approach.

The total phenolics in green bilberry leaves ranged from 9 to 77 mg/g DM. The contents in red bilberry leaves were 73 mg/g

DM on August 31 and 74 mg/g DM on September 13, respectively. Chlorogenic acid accounted for a vast majority of the total content of phenolic compounds in bilberry leaves (Figure 4C).

The content of chlorogenic acid varied dramatically during the whole growing season from 2 to 66 mg/g DM in bilberry leaves (Figure 4C). The highest levels were found in the red leaves (51 and 42 mg/g) and the green leaf samples picked on July 20 (66 mg/g DM). The red leaves contained a higher amount of chlorogenic acid than the green ones picked on the same day. With minor deviations in the samples picked on July 10 and August 21, the changing pattern during the growth period shown by NMR spectral integrals was similar to the trend acquired by targeted HPLC method (Figure 4A,C).

Flavonol glycosides were the second most abundant group of phenolic compounds in the bilberry leaves. The total content ranged from 5 to 10 mg/g DM in green leaves and from 17 to 28 mg/g DM in red leaves (Figure 4D). Quercetin-3-*O*-glucuronide was the major flavonol glycoside in all of the samples. In the green leaves, the content of flavonol glycoside increased from the end of June and reached its highest level in the middle of July and then decreased. The changing pattern in phenolic profile obtained by HPLC and NMR results were analogous in the case of total flavonol content and quercetin-3-*O*-glucuronide (Figure 4B,D). The contents of flavonol glycosides in the red leaves were notably higher than the levels found in the green leaves.

Anthocyanins were found only in the extracts of the red bilberry at a level close to 3 mg/g DM.

The correlation between flavonoid biosynthesis in bilberry leaves and solar radiation has been investigated before. An increasing expression of the genes related to the biosynthesis of flavonoids has been detected in leaves growing under high radiation.[31] Red leaves are often found in bilberry shrubs in sunny locations. This might explain why the red bilberry leaves contained higher amounts of phenolics than the green leaves.

In the extracts of lingonberry leaf, 10 phenolic compounds, including chlorogenic acid (5-*O*-caffeoylquinic acid), 2-*O*-caffeoylarbutin, rutin, hyperoside, quercetin-3-*O*-glucoside, 3 isomers of quercetin-pentoside, quercetin-3-*O*-rhamnoside, and quercetin-3-*O*-(4″-3-hydroxy-3-methylglutaryl)-rhamnoside, were quantified using HPLC-DAD. During the growing season, the levels of contents of total phenolics and individual compounds did not vary remarkably in lingonberry leaves (Figure 4G,H).

2-*O*-Caffeoylarbutin was the most abundant polyphenol in all of the lingonberry samples quantified by HPLC-DAD, and its content ranged from 9 to 14 mg/g DM (Figure 4G).

On the basis of $^1$H NMR, arbutin was the most abundant phenolic compound in lingonberry leaf. It was not quantified with HPLC-DAD because of overlapping peaks of other compounds. On the basis of integrated areas in $^1$H NMR spectra, the content of arbutin was roughly 6−10-fold higher than the level of 2-*O*-caffeoylarbutin. The contents of two metabolites profiles correlated negatively in the samples collected at different time points (Figure 5).

Hyperoside, quercetin-3-*O*-arabinoside, and quercetin-3-*O*-rhamnoside were the major flavonol glycosides (5−7 mg/g DM) in the extract from lingonberry leaves, whereas quercetin-3-*O*-glucuronide (3−17 mg/g DM) was the major flavonol glycoside in bilberry leaves (Figure 4H). The total contents of flavonol glycosides in the extracts of lingonberry leaves (15−20 mg/g DM) were higher than those of green bilberry leaves (5−10 mg/g DM) but lower than the level found in the red bilberry leaves (17−28 mg/g DM).

In plants, the biosynthesis of phenolic compounds are influenced by a matrix of potentially overlapping regulatory signals, including developmental signals, such as during lignification of new growth or the production of anthocyanins during fruit and flower development, and environmental signals for protection against abiotic and biotic stresses.[32] Temperature, radiation, and other weather conditiond will also affect the accumulation of phenolic compounds in the plant tissues.[32] The weather information for the Turku region during the study period is presented in Supplementaty Table 1. During the period from early June to late July, the average temperature and hours of sunshine were higher than the periods before and after, which may have contributed to the variation in the content of phenolic compounds. A common phenomenon seems to be that the leaves contain less phenolics during the development period of berry/fruit than the other time, as in the cases of leaves of black currant and hawthorn.[33,34] The content of phenolic compounds in bilberry leaves followed this pattern very well. The ripening time of lingonberry (after mid August) occurs much later than that of the bilberry (early to mid July). This could explain the relatively stable content of the phenolics found in our study.

*Correlation between the Trends in Compositional Changes.* By comparing the integrals acquired by $^1$H NMR and spectral bucketing, some correlations were found between the metabolomic changes occurring between the collection points. In the fingerprints of bilberry leaf extracts, a negative correlation was found between the signals of chlorogenic acid and lipids (Figure 5A). A strong negative correlation was found between the signals in the aliphatic region and those of chlorogenic acid. The protons resonating on the aliphatic region close to 1 ppm commonly originate from methyl groups of fatty acid but also from short-chain hydroxyl fatty acid or amino acids. Moreover, in bilberry leaf fingerprints a strong negative correlation was revealed between the signals of chlorogenic acid and signals originating from chlorophyll structure.

On the basis of the $^1$H NMR fingerprints of lingonberry leaves a moderate negative correlation occurred between the changes of arbutin and lipids, and a strong negative correlation was observed between arbutin and caffeoylarbutin (Figure 5B).

In higher plants, acetyl-CoA carboxylase (ACCase) and fatty acid synthase (FAS) are the key enzymes for the biosynthesis of fatty acids. The cytosolic homomeric ACCase generates a malonyl-CoA pool for elongation of fatty acids and biosynthesis of secondary metabolites such as flavonoids and other phenolic compounds.[35] Therefore, there is competition for carbon sources between the biosynthesis of lipids and phenolic compounds. This competition may explain the negative correlation between the contents of these two groups of metabolites. For example, inhibition of lipid metabolism enhanced the accumulation of anthocyanins in rape (*Brassica napus* L.) leaves.[36]

Bilberry and lingonberry leaves collected during the growing season were studied by both targeted and untargeted approaches. Although bilberry and lingonberry belong to the same genus, *Vaccinium*, the compositional profiles of phenolic compounds and lipids in the leaves of the two species were very different. The contents of different metabolites varied remarkably in bilberry leaves, whereas in lingonberry leaves the metabolites maintained quite constant levels during the growing season. The different methods were complementary and could support each other in characterization of metabolomic profiles of the leaves during the growth season. The chromatographic−mass spectrometric

methods can give accurate detailed information on specific group of compounds, whereas NMR analysis gave a broader view of the overall profiles. The consistency between the key results obtained by targeted and nontargeted analyses suggests nontargeted NMR metabolomic analysis is an efficient tool for fast screening of various leaf materials.

Both lingonberry leaf and bilberry leaf are potential raw materials of health food and food ingredients. Phenolic compounds are the major bioactive components in these materials. Our results suggest that the collection time of bilberry should be carefully selected to achieve the highest concentration of phenolic compounds in the leaves. The content of phenolic compounds in lingonberry leaf seems to be rather constant during the season. It is important to note that samples collected from several years should be analyzed to reach a general conclusion on the optimal collection time for the leaves.

## ■ ASSOCIATED CONTENT

### Supporting Information

Supplementary Table 1 and Supplementary Figures 1−4. This material is available free of charge via the Internet at http://pubs.acs.org.

## ■ AUTHOR INFORMATION

### Corresponding Author

*(J.-P.S.) Phone: +358 2 333 6875. Fax: +358 2 231 7666. E-mail: jusuom@utu.fi.

### Funding

The study was funded by TEKES, the Finnish Funding Agency for Innovation (Project 2128/31/2012, TEKES Decision 40055/13), the Magnus Ehrnrooth Foundation, and food companies in Finland and Germany.

### Notes

The authors declare no competing financial interest.

## ■ ACKNOWLEDGMENTS

We sincerely thank Dr. Jaana Liimatainen (Food Chemistry and Food Development, Department of Biochemistry, University of Turku) for her assistance in high-resolution mass spectrometry.

## ■ REFERENCES

(1) Kivimäki, A. S.; Ehlers, P. I.; Turpeinen, A. M.; Vapaatalo, H.; Korpela, R. Lingonberry juice improves endothelium-dependent vasodilatation of mesenteric arteries in spontaneously hypertensive rats in a long-term intervention. *J. Funct. Foods* **2011**, *3*, 267−274.

(2) Kivimäki, A. S.; Ehlers, P. I.; Siltari, A.; Turpeinen, A. M.; Vapaatalo, H.; Korpela, R. Lingonberry, cranberry and blackcurrant juices affect mRNA expressions of inflammatory and atherothrombotic markers of SHR in a long-term treatment. *J. Funct. Foods* **2012**, *4*, 496−503.

(3) Aly, E. M.; Ali, M. A. Effects of bilberry on deoxyribonucleic Acid damage and oxidant-antioxidant balance in the lens, induced by ultraviolet radiation. *Malays. J. Med. Sci.* **2014**, *21*, 11−18.

(4) Bornsek, S. M.; Ziberna, L.; Polak, T.; Vanzo, A.; Ulrih, N. P.; Abram, V.; Tramer, F.; Passamonti, S. Bilberry and blueberry anthocyanins act as powerful intracellular antioxidants in mammalian cells. *Food Chem.* **2012**, *134*, 1878−1884.

(5) Davarmanesh, M.; Miri, R.; Haghnegahdar, S.; Tadbir, A. A.; Tanideh, N.; Saghiri, M. A.; Garcia-Godoy, F.; Asatourian, A. Protective effect of bilberry extract as a pretreatment on induced oral mucositis in hamsters. *Oral Surg., Oral Med., Oral Pathol. Oral Radiol.* **2013**, *116*, 702−708.

(6) Hara, S.; Morita, R.; Ogawa, T.; Segawa, R.; Takimoto, N.; Suzuki, K.; Hamadate, N.; Hayashi, S. M.; Odachi, A.; Ogiwara, I.; Shibusawa, S.; Yoshida, T.; Shibutani, M. Tumor suppression effects of bilberry extracts and enzymatically modified isoquercitrin in early preneoplastic liver cell lesions induced by piperonyl butoxide promotion in a two-stage rat hepatocarcinogenesis model. *Exp. Toxicol. Pathol.* **2014**, *66*, 225−234.

(7) Jakesevic, M.; Xu, J.; Aaby, K.; Jeppsson, B.; Ahrne, S.; Molin, G. Effects of bilberry (*Vaccinium myrtillus*) in combination with lactic acid bacteria on intestinal oxidative stress induced by ischemia-reperfusion in mouse. *J. Agric. Food Chem.* **2013**, *61*, 3468−3478.

(8) Kapusuz, Z.; Ozkiris, M.; Kala, M.; Saydam, L. Protective role of bilberry extract against Cisplatin induced ototoxicity in rats. *Indian J. Otolaryngol. Head Neck. Surg.* **2013**, *65*, 339−344.

(9) Luo, H.; Lv, X. D.; Wang, G. E.; Li, Y. F.; Kurihara, H.; He, R. R. Anti-inflammatory effects of anthocyanins-rich extract from bilberry (*Vaccinium myrtillus* L.) on croton oil-induced ear edema and *Propionibacterium acnes* plus LPS-induced liver damage in mice. *Int. J. Food Sci. Nutr.* **2014**, *65*, 594−601.

(10) Kivimäki, A. S.; Siltari, A.; Ehlers, P. I.; Korpela, R.; Vapaatalo, H. Lingonberry juice lowers blood pressure of spontaneously hypertensive rats (SHR). *J. Funct. Foods* **2013**, *5*, 1432−1440.

(11) Larmo, P. S.; Kangas, A. J.; Soininen, P.; Lehtonen, H. M.; Suomela, J. P.; Yang, B.; Viikari, J.; Ala-Korpela, M.; Kallio, H. P. Effects of sea buckthorn and bilberry on serum metabolites differ according to baseline metabolic profiles in overweight women: a randomized crossover trial. *Am. J. Clin. Nutr.* **2013**, *98*, 941−951.

(12) Cignarella, A.; Nastasi, M.; Cavalli, E.; Puglisi, L. Novel lipid-lowering properties of *Vaccinium myrtillus* L. leaves, a traditional antidiabetic treatment, in several models of rat dyslipidaemia: a comparison with ciprofibrate. *Thromb. Res.* **1996**, *84*, 311−322.

(13) Ieri, F.; Martini, S.; Innocenti, M.; Mulinacci, N. Phenolic distribution in liquid preparations of *Vaccinium myrtillus* L. and *Vaccinium vitis idaea* L. *Phytochem. Anal.* **2013**, *24*, 467−475.

(14) Wang, X.; Sun, H.; Fan, Y.; Li, L.; Makino, T.; Kano, Y. Analysis and bioactive evaluation of the compounds absorbed into blood after oral administration of the extracts of *Vaccinium vitis-idaea* in rat. *Biol. Pharm. Bull.* **2005**, *28*, 1106−1108.

(15) Vyas, P.; Kalidindi, S.; Chibrikova, L.; Igamberdiev, A. U.; Weber, J. T. Chemical analysis and effect of blueberry and lingonberry fruits and leaves against glutamate-mediated excitotoxicity. *J. Agric. Food Chem.* **2013**, *61*, 7769−7776.

(16) Moyer, R. A.; Hummer, K. E.; Finn, C. E.; Frei, B.; Wrolstad, R. E. Anthocyanins, phenolics, and antioxidant capacity in diverse small fruits: vaccinium, rubus, and ribes. *J. Agric. Food Chem.* **2002**, *50*, 519−525.

(17) Taruscio, T. G.; Barney, D. L.; Exon, J. Content and profile of flavanoid and phenolic acid compounds in conjunction with the antioxidant capacity for a variety of northwest *Vaccinium* berries. *J. Agric. Food Chem.* **2004**, *52*, 3169−3176.

(18) Brooks, J. S.; Feeny, P. Seasonal variation in *Daucus carota* leaf-surface and leaf-tissue chemical profiles. *Biochem. Syst. Ecol.* **2004**, *32*, 769−782.

(19) Scognamiglio, M.; D'Abrosca, B.; Fiumano, V.; Golino, M.; Esposito, A.; Fiorentino, A. Seasonal phytochemical changes in *Phillyrea angustifolia* L.: metabolomic analysis and phytotoxicity assessment. *Phytochem. Lett.* **2014**, *8*, 163−170.

(20) Folch, J.; Lees, M.; Sloane Stanley, G. H. A simple method for the isolation and purification of total lipides from animal tissues. *J. Biol. Chem.* **1957**, *226*, 497−509.

(21) R Core Team R: a language and environment for statistical computing, 2013; http://www.R-project.org/.

(22) Lemon, J. Plotrix: a package in the red light district of R. *R-News* **2006**, *6*, 8−12.

(23) Hokkanen, J.; Mattila, S.; Jaakola, L.; Pirttila, A. M.; Tolonen, A. Identification of phenolic compounds from lingonberry (*Vaccinium vitis-idaea* L.), bilberry (*Vaccinium myrtillus* L.) and hybrid bilberry (*Vaccinium* × *intermedium* Ruthe L.) leaves. *J. Agric. Food Chem.* **2009**, *57*, 9437−9447.

(24) Riihinen, K.; Jaakola, L.; Kärenlampi, S.; Hohtola, A. Organ-specific distribution of phenolic compounds in bilberry (*Vaccinium myrtillus*) and 'Northblue' blueberry (*Vaccinium corymbosum* × *V. angustifolium*). *Food Chem.* **2008**, *110*, 156−160.

(25) Zhao, P.; Tanaka, T.; Hirabayashi, K.; Zhang, Y. J.; Yang, C. R.; Kouno, I. Caffeoyl arbutin and related compounds from the buds of *Vaccinium dunalianum*. *Phytochemistry* **2008**, *69*, 3087−3094.
(26) Blaut, M.; Braune, A.; Wunderlich, S.; Sauer, P.; Schneider, H.; Glatt, H. Mutagenicity of arbutin in mammalian cells after activation by human intestinal bacteria. *Food Chem. Toxicol.* **2006**, *44*, 1940−1947.
(27) Takebayashi, J.; Ishii, R.; Chen, J.; Matsumoto, T.; Ishimi, Y.; Tai, A. Reassessment of antioxidant activity of arbutin: multifaceted evaluation using five antioxidant assay systems. *Free Radical Res.* **2010**, *44*, 473−478.
(28) Kort, R.; Vonk, H.; Xu, X.; Hoff, W. D.; Crielaard, W.; Hellingwerf, K. J. Evidence for trans-cis isomerization of the *p*-coumaric acid chromophore as the photochemical basis of the photocycle of photoactive yellow protein. *FEBS Lett.* **1996**, *382*, 73−78.
(29) Gu, L.; Kelm, M. A.; Hammerstone, J. F.; Zhang, Z.; Beecher, G.; Holden, J.; Haytowitz, D.; Prior, R. L. Liquid chromatographic/electrospray ionization mass spectrometric studies of proanthocyanidins in foods. *J. Mass Spectrom.* **2003**, *38*, 1272−1280.
(30) Liu, P.; Yang, B.; Kallio, H. Characterization of phenolic compounds in Chinese hawthorn (*Crataegus pinnatifida* Bge. var. major) fruit by high performance liquid chromatography−electrospray ionization mass spectrometry. *Food Chem.* **2010**, *121*, 1188−1197.
(31) Jaakola, L.; Maatta-Riihinen, K.; Karenlampi, S.; Hohtola, A. Activation of flavonoid biosynthesis by solar radiation in bilberry (*Vaccinium myrtillus* L) leaves. *Planta* **2004**, *218*, 721−728.
(32) Cheynier, V.; Comte, G.; Davies, K. M.; Lattanzio, V.; Martens, S. Plant phenolics: recent advances on their biosynthesis, genetics, and ecophysiology. *Plant Physiol. Biochem.* **2013**, *72*, 1−20.
(33) Liu, P.; Kallio, H.; Yang, B. Flavonol glycosides and other phenolic compounds in buds and leaves of different varieties of black currant (*Ribes nigrum* L.) and changes during growing season. *Food Chem.* **2014**, *160*, 180−189.
(34) Liu, P.; Kallio, H.; Yang, B. Phenolic compounds in hawthorn (*Crataegus grayana*) fruits and leaves and changes during fruit ripening. *J. Agric. Food Chem.* **2011**, *59*, 11141−11149.
(35) Sasaki, Y.; Nagano, Y. Plant acetyl-CoA carboxylase: structure, biosynthesis, regulation, and gene manipulation for plant breeding. *Biosci., Biotechnol., Biochem.* **2004**, *68*, 1175−1184.
(36) Belkebir, A.; Benhassaine-Kesri, G. Sethoxydim treatment inhibits lipid metabolism and enhances the accumulation of anthocyanins in rape (*Brassica napus* L.) leaves. *Pestic. Biochem. Physiol.* **2013**, *107*, 120−126.

carried out 15, 30, and 45 days after planting. Each pot was fertilized with a solution containing calcium nitrate (1.12 g), magnesium sulfate (0.50 g), potassium nitrate (0.36 g), monobasic potassium phosphate (0.30 g), iron chelate (0.07 g), and manganese sulfate (0.01 g). After 45 days, the plants were randomly subjected to different levels of water stress: 65, 35, 24, and 12% SM, by suppressing irrigation for a period of 7, 16, 21, and 26 days, respectively. For the same amount of time as for each treatment, a control was carried out (irrigation every 3 days, at 85% SM). Treatments and controls included 6 replicates, producing a total of 48 experimental units (pots).

Plant response to drought stress was determined by the increase in shoot length ($n$ = 12) as well as longitudinal growth and leaf expansion ($n$ = 24), which were evaluated by measuring the length of the leaf from the base to the apex (longitudinal growth) and at the broadest part (transverse growth). All of these parameters were measured at day 45 and after 7, 16, 21, and 26 days without water added.

**Harvest and Infusion Preparation.** Immediately after each drought treatment, after 7, 16, 21, and 26 days without water added, midlife leaves were collected from each experimental unit, dried at 45 °C for 24 h using a convection oven (Fisher Scientific, 650D, Waltham, MA), and milled in an herb grinder (Krups GX4100, Mexico) to a particle size of 0.7−1.0 mm. Infusions were prepared by adding 1 g of ground material to 100 mL of freshly boiled distilled water; the mixture was allowed to stand for 10 min and was then filtered using a 0.5 mm pore size filter. These conditions simulate the recommended preparation of commercial infusions.

**Total Phenolic and Flavonoid Contents.** The total phenolic compound content of the peppermint infusions was determined according to the Folin−Ciocalteu colorimetric method.[8] Briefly, 40 μL of the infusion diluted in 480 μL of water was mixture with 450 μL of a 1 M Folin−Ciocalteu reagent and 1250 μL of a sodium carbonate solution (5%, w/v). The tubes were left at room temperature for 120 min, and the absorbances were measured at 765 nm. Results are expressed as milligrams of gallic acid (GA) equivalents per milliliter of infusion (mg of GAE/mL).

The flavonoid content was determined according to the method described by Liu et al.[9] Briefly, 0.25 mL of each infusion were diluted with 1.25 mL of water and mixed with 75 μL of 5% $NaNO_2$. After 6 min, 150 μL of a 10% $AlCl_3{\cdot}6H_2O$ solution and 500 μL of 1 M NaOH were added, and the reaction was adjusted to 2.5 mL with distilled water. The absorbances were measured at 510 nm, and the results are expressed as milligrams of (+)-catechin equivalents per milliliter of infusion (mg of CAE/mL).

**Identification and Quantification of Phenolic Compounds.** For the identification of phenolic compounds by high-performance liquid chromatography with photodiode array detection and mass-spectrometric detection (HPLC/DAD−MSD) analysis, the extract was lyophilized and suspended in methanol at a concentration of 10 mg/mL. Separation and identification was carried out using an Agilent 1200 HPLC−DAD system connected to a SL quadrupole mass spectrometer Agilent 1100 equipped with an electrospray interface. The samples were injected into a reversed-phase column [Zorbax octadecylsilane (ODS-$C_{18}$), 15 × 4.6 mm] operated at room temperature. A total of 10 μL of sample was injected, and the compounds were eluted at 1 mL/min using a linear gradient system consisting of two solvents: (A) 2:98 (v/v) acetic acid/water and (B) (2:30:68, v/v/v) acetic acid/acetonitrile/water. The ratios of mobile phases were 90% A and 10% B at $t$ = 0 min and 0% A and 100% B at $t$ = 30 min. The absorbance was set at $\lambda_{max}$ of 260, 280, and 320 nm. The mass spectrometer was operated in the negative ion mode, under the following conditions: capillary voltage, 4000 V; nebulizer pressure, 40 psi; drying gas flow rate, 10 L/min; gas temperature, 300 °C; skimmer voltage, 50 V; octapolerf, 150 V; and fragmentor voltage, 130 V. Liquid chromatography−mass spectrometry (LC−MS) accurate mass spectra were recorded across the range of $m/z$ 50−1000. Quantification was carried out using phenolic acid and flavonoid standards (caffeic, coumaric, sinapic, and rosmarinic acids, eriocitrin, naringenin, rutin, vanillin, luteolin, quercetin, and hesperidin).

**Identification of Low-Molecular-Weight Metabolites.** A sample solution (10 mg/mL) was prepared in methanol with lyophilized infusions, which was concentrated with a nitrogen gas stream. Then, 50 μL of derivatizing agent, *N*,*O*-bis(trimethylsilyl)-trifluoroacetamide (BSTFA) + 1% trimethylchlorosilane (TMCS), was added and stirred for 2 min at room temperature. Finally, 1 μL was injected into an Agilent GC series 7890A (Wilmington, DE) coupled to an Agilent single quadrupole MS detector (Agilent 5975C), with electron energy set at 70 eV and mass range at $m/z$ 50−700. A HP-5MS capillary column (30 m × 0.25 mm inner diameter × 0.25 μm) was used. The injector temperature was set at 250 °C in splitless mode. The initial oven temperature was 100 °C, held for 1 min, and raised to 220 °C at 6 °C $min^{-1}$, which was held for 1.23 min, then raised to 290 °C at 10 °C $min^{-1}$, then raised to 310 °C at 40 °C/min, and held for 7.5 min. The flow rate of the carrier gas (helium) was maintained at 1 mL $min^{-1}$. Gas chromatography−mass spectrometry (GC−MS) control and data processing were performed using Chem-Station (Agilent Technologies) software.

**Free Radical Scavenging Assays.** The capacity of peppermint infusions to bleaching diphenylpicrylhydrazyl (DPPH) radical was determinate by the method described by Brand-Williams et al.[10] Aliquots of peppermint infusions were made to a total volume of 1 mL using methanol. A freshly prepared DPPH solution (98 μg/mL) was added, stirred, and left to stand at room temperature for 30 min in the dark. The inhibition capacity was determined by the decrease in absorbance at 517 nm.

The 2,2′-azinobis(3-ethyl-benzthiazoline-6-sulfonic acid) (ABTS) radical scavenning assay was carried out as described by Re et al.[11] $ABTS^{\bullet+}$ was obtained by reacting 7 mM ABTS stock solution with 2.45 mM potassium persulfate, and the mixture was left to stand in the dark at room temperature for 12−16 h before use. The $ABTS^{\bullet+}$ solution was diluted with 5 mM phosphate-buffered saline (pH 7.4) to an absorbance at 730 nm of 0.70. After the addition of 10 μL of aliquots of sample to 1 mL of diluted $ABTS^{\bullet+}$ solution, the absorbance was measured at 7 min.

Furthermore, nitric oxide radical scavenging capacity was measured as described by Marcocci and Parker,[12] with some modifications. Sodium nitroprusside (SNP, 5 mM) in phosphate-buffered saline was added to the sample at different concentrations to make up a volume of 3 mL and incubated at room temperature (27 °C) for 90 min. This incubated solution (1.5 mL) was added to 1.5 mL of Greiss reagent. The inhibition of nitrite formation was determined by the decrease in absorbance at 546 nm.

All of these results were expressed as the half-maximal inhibitory concentration ($IC_{50}$) and compared to a (+)-catechin standard.

***In Vitro* Digestive Enzyme Inhibition Assays.** The α-amylase activity was determined according to the methodology proposed by Kandra et al.[13] Thus, 50 μL of the peppermint infusions and 50 μL of α-amylase from *Bacillus subtilis* (50 units/mg) were pre-incubated for 20 min in a water bath at 37 °C. The substrate was starch (1%) prepared in phosphate buffer at pH 7.0 with 38 mmol/L NaCl. After the addition of 100 μL of the substrate, the mixture was incubated for 2 h. The product (glucose) was quantified by the glucose oxidase−peroxidase method with a commercial kit (Spinreact) and measured at 540 nm.

For determination of α-glucosidase inhibition, we used the method described by Apostolidis et al.,[14] with some modifications, using 5 mmol/L *p*-nitrophenyl-α-D-glucopyranoside as the substrate in a 0.1 mol/L citrate−phosphate buffer at pH 7. In the assay, 50 μL of the infusion and 100 μL of enzyme (10 units/mg) were incubated in a water bath at 37 °C for 30 min after the addition of 50 μL of the substrate. The reaction was interrupted adding 1.000 μL of 0.05 mol/L NaOH, and the product was read in a spectrophotometer at 410 nm.

Pancreatic lipase inhibition was measured according to the method described by McDougall et al.[15] The mixture of 100 μL of porcine pancreatic lipase, 50 μL of the infusion, and 50 μL of 4 mmol/L *p*-nitrophenyl laurate in 0.05 mmol/L Tris−HCl buffer at pH 8.0 containing 0.5% Triton X-100 was incubated for 30 min. The reaction was stopped, transferring the tubes to an ice bath and adding 1.000 μL of 0.05 mmol/L Tris−HCl buffer at pH 8.0. *p*-Nitrophenol, a product of the lipase action on *p*-nitrophenyl palmitate, was read in a spectrophotometer at 410 nm.

**Table 1. Changes in Fresh and Dry Weight of Leaves and Growth of Shoots and Leaves of Peppermint (*M. piperita*) Grown at Different Levels of SM[a]**

| | leaf growth (cm) | | | | |
|---|---|---|---|---|---|
| soil water content | leaf width | leaf length | shoot growth (cm) | fresh weight (mg leaf$^{-1}$) | dry weight (mg leaf$^{-1}$) |
| control | 2.8 ± 0.1 | 6.3 ± 0.2 | 7.1 ± 0.1 | 135.5 ± 8.1 | 39.8 ± 2.0 |
| 65% | 2.7 ± 0.1 a | 6.5 ± 0.3 a | 6.9 ± 0.3 a | 122.8 ± 6.3 b | 38.2 ± 1.8 b |
| control | 2.6 ± 0.2 | 6.4 ± 0.2 | 7.4 ± 0.3 | 147.2 ± 7.2 | 43.2 ± 2.1 |
| 35% | 2.1 ± 0.1 b[b] | 5.7 ± 0.4 b[b] | 6.4 ± 0.4 b[b] | 133.5 ± 5.6 b[b] | 41.2 ± 1.7 b |
| control | 2.7 ± 0.0 | 6.6 ± 0.3 | 7.8 ± 0.5 | 164.8 ± 7.2 | 48.5 ± 2.3 |
| 24% | 2.3 ± 0.1 b[b] | 5.5 ± 0.3 b[b] | 6.6 ± 0.3 b[b] | 126.9 ± 6.3 b[b] | 45.2 ± 1.6 a[b] |
| control | 2.8 ± 0.1 | 6.8 ± 0.4 | 7.6 ± 0.4 | 171.0 ± 8.2 | 50.3 ± 2.3 |
| 12% | 2.2 ± 0.0 b[b] | 5.7 ± 0.3 b[b] | 6.5 ± 0.3 b[b] | 138.3 ± 6.1 a[b] | 46.9 ± 1.7 a[b] |

[a]Results are the average of three independent determinations ± SE. Different letters indicate significant statistical differences between drought treatments ($p < 0.05$; Tukey's test). [b]Significant statistical differences between controls (plant growth of 85% SM over the same number of days of the respective treatment) and their respective treatment ($p < 0.05$; Dunnett's test).

The results of these determinations were expressed as a percentage of inhibition exhibited by a concentration of 10 mg/mL peppermint infusion.

**Statistical Analysis.** All results were expressed as the mean ± standard error (SE). Data were analyzed by one-way analysis of variation (ANOVA), and differences among treatments were determined by a comparison of means using Tukey's test or Dunnett's test when was compared to a control. The level of statistical significance was considered at $p < 0.05$. Pearson correlation was performed to verify the association between measurements ($p < 0.01$).

## RESULTS AND DISCUSSION

**Evaluation of Growth Parameters.** Table 1 shows the effect of drought stress on the growth parameters of the plants. The plants grown at 35, 24, and 12% SM decreased in leaf width (20, 15, and 21%), leaf length (11, 16, and 17%), and shoot length (14, 15, and 14%) compared to the control plants, while the 65% SM treatment did not produce significant effects on growth parameters compared to the control. A similar trend was observed in the fresh weight of leaves (11, 23, and 20% for 35, 24, and 12% SM, respectively). However, the dry weight was less affected by drought treatments, resulting in decreases of approximately 5, 7, and 7% for 35, 24, and 12% SM, as compared to their respective controls. These effects were similar to those reported by Moeini et al.,[16] who observed 2-, 6-, and 4-fold decreases in plant height, leaf area, and fresh yield, respectively, in basil (*Ocimum basilicum*) plants cultivated under constant water stress (at 60% of field capacity) for 6 weeks.

The reduced growth of the aerial part of the plant is widely described as a consequence of water stress and depends upon the severity and duration of the stress period. The decrease in growth is mainly due to a loss of cell turgor (a physical process). Under normal conditions, water enters the cells because of a difference in potential, which is more negative inside, the cell swells, and the plasma membrane exerts turgor pressure against the cell wall. In drought conditions, the water potential is lower outside than inside the cell; therefore, the water tends to leave the cell, and this also causes the closure of stomata. In these situations, turgor pressure disappears and the plasma membrane detaches from the cell wall in some sections. The main consequence of this loss of turgor is the absence of cell growth and a reduction in plant biomass production.[17,18] This may explain the decrease of fresh and dry weight observed in drought treatments. However, it is important to mention that the dry weight of leaves was not significantly affected in the treated plants, which may be of industrial importance, because peppermint infusions are prepared from dry material.

**Quantification of Total and Individual Phenolic Compounds.** The total polyphenol and flavonoid contents as well as the phenolic profile of infusions of peppermint leaves cultivated under water stress are shown in Figure 1 and Table 2, respectively. Infusions prepared from peppermint grown at 35, 24, and 12% SM showed an increase of 32, 60, and 12% in total

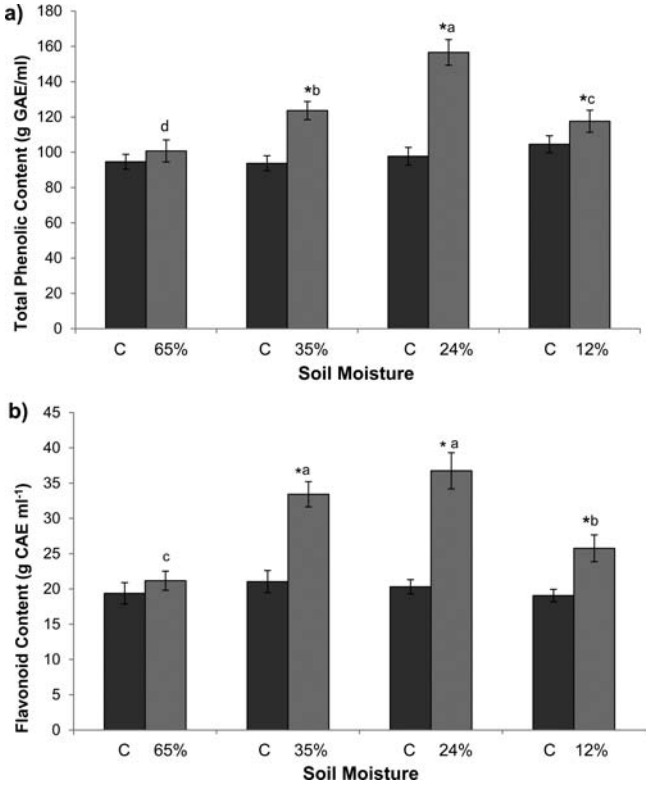


**Figure 1.** (a) Total phenolic and (b) flavonoid contents in infusions prepared from peppermint (*M. piperita*) leaves grown at different levels of SM. Results are expressed as milligrams of (a) gallic acid or (b) catechin equivalents per milliliter of peppermint infusion and are the average of three independent determinations ± SE. (*) Significant statistical differences between controls (black bars, plant growth at 85% SM over the same number of days as the respective treatment in gray bars) and treatments ($p < 0.05$; Dunnett's test). Different letters indicate significant statistical differences between treatments ($p < 0.05$; Tukey's test).

**Table 2. Chromatographic Profile of Phenolic Compounds Identified in Infusions Prepared from Peppermint (*M. piperita*) Leaves Grown at Different Levels of SM[a]**

| peak | compound | ion ($m/z$) | RT (min) | control | 65% | 35% | 24% | 12% |
|---|---|---|---|---|---|---|---|---|
| 1 | caffeic acid | 179 | 12.7 | 0.2 ± 0.0 c | 0.3 ± 0.0 b | 0.8 ± 0.0 a | 0.9 ± 0.0 a | 0.3 ± 0.0 b |
| 2 | coumaric acid | 146 | 16.6 | LDL[b] | LDL | 2.9 ± 0.0 a | 1.21 ± 0.0 b | 0.8 ± 0.0 c |
| 1 | luteolin | 285 | 17.3 | LDL | LDL | 1.5 ± 0.0 a | 1.6 ± 0.0 a | LDL |
| 2 | eriocitrin | 597 | 19.4 | 0.7 ± 0.0 d | 3.7 ± 0.1 c | 7.5 ± 0.2 a | 4.2 ± 0.1 c | 6.0 ± 0.2 b |
| 3 | rutin | 609 | 20.0 | 15.2 ± 0.6 c | 31.5 ± 0.8 b | 50.8 ± 0.4 a | 49.5 ± 0.2 a | 26.3 ± 0.3 b |
| 3 | sinapic acid | 207 | 21.6 | 0.1 ± 0.0 b | 0.1 ± 0.0 b | 2.2 ± 0.0 a | 2.5 ± 0.0 a | 2.3 ± 0.0 a |
| 4 | rosmarinic acid | 359 | 22.5 | 51.6 ± 2.3 b | 51.3 ± 1.5 b | 78.1 ± 3.2 a | 55.3 ± 1.8 b | 45.5 ± 3.1 c |
| 6 | hesperedin | 609 | 23.1 | 35.7 ± 2.1 d | 38.1 ± 3.5 c | 34.9 ± 1.8 d | 67.9 ± 4.5 a | 45.8 ± 2.6 b |
| 11 | quercetin | 301 | 28.4 | LDL | 0.4 ± 0.0 c | 0.8 ± 0.0 b | 1.2 ± 0.0 a | 0.5 ± 0.0 c |
| 13 | naringenin | 271 | 31.4 | LDL | LDL | 0.8 ± 0.0 a | 0.2 ± 0.0 b | LDL |
| 14 | vanillin | 285 | 33.4 | LDL | LDL | 0.2 ± 0.0 b | 0.4 ± 0.0 a | LDL |

[a]Results are expressed as ng $\mu L^{-1}$ of peppermint infusion and are the average of three independent determinations ± SE. Different letters indicate significant statistical differences for each compound ($p < 0.05$; Tukey's test). [b]LDL = lower than the detection limit.

**Table 3. Low-Molecular-Weight Metabolites of Infusions Prepared from Peppermint (*M. piperita*) Leaves Grown at Different Levels of SM[a]**

| | | | area (%) | | | | | |
|---|---|---|---|---|---|---|---|---|
| nature of compound | proposed compound | RT (min) | control | 65% | 35% | 24% | 12% | important ions in peaks ($m/z$) |
| amino acid | L-alanine | 4.1 | 0.73 | 0.51 | LDL[b] | LDL | LDL | 218, 190, 172, 116, 94 |
| | L-leucine | 6.8 | 1.47 | 0.15 | LDL | LDL | LDL | 260, 232, 203, 176, 158, 133, 103 |
| | isoleucine | 7.2 | 2.54 | 0.70 | 0.46 | LDL | 1.09 | 260, 218, 158, 149 |
| | L-proline | 7.3 | 7.35 | 7.14 | 6.68 | 8.23 | 9.20 | 244, 216, 170, 142, 119, 100 |
| | L-serine | 8.5 | 1.49 | LDL | LDL | LDL | LDL | 306, 278, 260, 222, 204, 174 |
| | threonine | 9.0 | 0.90 | LDL | LDL | LDL | LDL | 320, 291, 248, 218, 117 |
| | 4-aminobutiric acid | 11.7 | 0.82 | LDL | LDL | LDL | LDL | 304, 246, 216, 174 |
| | 5-oxo-L-proline | 11.6 | 10.79 | LDL | LDL | LDL | LDL | 258, 230, 174, 156, 133 |
| | glutamine | 13.4 | 0.02 | 0.05 | 0.04 | 0.02 | 0.03 | 363, 348, 320, 246, 218, 198, 174 |
| | phenylalanine | 13.5 | 0.11 | LDL | LDL | LDL | LDL | 294, 266, 218, 192, 174, 100 |
| | L-asparagine | 14.4 | 0.01 | LDL | LDL | LDL | LDL | 351, 333, 258, 188, 169, 116 |
| | L-tyrosine | 19.0 | 0.04 | LDL | LDL | LDL | LDL | 382, 354, 280, 218, 179 |
| | tryptophan | 23.8 | 0.03 | LDL | LDL | LDL | LDL | 357, 325, 291, 251, 202, 147 |
| carbohydrate | arabinose | 18.7 | 1.83 | 2.85 | 2.96 | 8.20 | 2.44 | 333, 305, 219, 204, 187, 147, 129 |
| | D-glucose | 20.0 | 0.03 | 8.26 | 27.10 | 21.17 | 20.04 | 435, 393, 345, 305, 231, 204 |
| organic acid | lactic acid | 3.6 | 1.87 | 15.67 | 19.54 | 9.15 | 22.97 | 219, 191, 147, 117 |
| | glycolic acid | 3.8 | 1.15 | 6.07 | 2.45 | 1.86 | 8.78 | 205, 177, 121 |
| | malonic acid | 5.6 | 0.71 | 0.99 | 0.18 | 0.13 | 0.57 | 233, 204, 117, 99 |
| | succinic acid | 7.5 | 9.34 | 5.51 | 6.41 | 1.81 | 3.39 | 247, 218, 190, 172 |
| | 2,3-hidroxipropionic acid | 7.9 | 1.34 | 4.22 | 3.64 | 2.19 | 9.74 | 322, 292, 265, 217, 189, 129, 103 |
| | fumaric acid | 8.1 | 0.75 | 0.61 | 0.53 | LDL | 1.51 | 245, 217, 191, 171, 115 |
| | malic acid | 11.0 | 16.26 | 2.20 | 1.27 | 0.85 | 1.76 | 355, 307, 265, 233, 189, 171, 129 |
| | threonic acid | 12.2 | 0.30 | 0.45 | LDL | LDL | LDL | 409, 379, 319, 292, 263, 245, 177, 117 |
| | lauric acid | 13.8 | 0.02 | 4.01 | LDL | 0.88 | LDL | 257, 229, 201, 171, 145 |
| | tartaric acid | 14.0 | 0.01 | 2.02 | 0.83 | 0.54 | 2.12 | 423, 395, 367, 333, 292, 219 |
| | citric acid | 17.2 | LDL | LDL | 1.83 | 2.78 | 9.27 | 465, 375, 305, 273, 217, 183, 129 |
| | myristic acid | 17.3 | 0.02 | LDL | 1.21 | LDL | 1.53 | 303, 285, 257, 201, 171, 145 |
| | pantothenic acid | 19.9 | 0.01 | LDL | LDL | LDL | LDL | 420, 363, 330, 291, 247, 219 |
| fatty acid | palmitic acid | 20.5 | 0.15 | 16.19 | 8.62 | 4.50 | 8.87 | 331, 313, 269, 171, 145, 117, 97 |
| | linoleic acid | 23.3 | 0.02 | LDL | LDL | LDL | LDL | 337, 309, 262, 220, 199 |
| | oleic acid | 23.4 | LDL | 5.43 | 3.21 | 1.99 | 5.35 | 339, 264, 222, 185, 145, 117 |
| | stearic acid | 24.0 | 2.69 | 4.37 | 3.14 | 1.04 | LDL | 341, 315, 297, 257, 227, 201 |
| | α-linolenic acid | 23.5 | 0.08 | LDL | LDL | LDL | LDL | 335, 291, 260, 213 |
| alcohol | glycerol | 6.9 | 18.01 | 17.88 | 5.55 | 13.08 | 15.02 | 293, 263, 205, 177, 125, 103 |
| | tyrosol | 12.4 | 0.25 | 1.89 | 0.56 | 0.41 | 1.99 | 282, 267, 193, 179 |

[a]Results are expressed as a percentage of the total area. [b]LDL = lower than the detection limit.

phenolic content and 71, 80, and 31% in total flavonoid content, respectively. However, the 65% SM treatment produced no significant effect on total phenolic and flavonoid contents. An increase of 10 and 71% in total phenolic content after 4 and 8 days of water stress in different tea (*Camellia sinensis*) cultivars has been reported, as compared to control

plants, along with a decrease of about 75% in these compounds when the stress period was prolonged for 12 days.[19]

Plants exposed to drought present increased levels of abscicic acid (ABA) in leaves, shoots, and roots, which induces several responses in the plant, including the accelerated production of ROS in chloroplasts, mitochondria, and peroxisomes, which stimulates antioxidant enzyme activity and the synthesis of phenolic compounds. This mechanism is used in plants as an adaptation strategy to overcome oxidative stress.[7]

The phenolic profile of the different controls used for each treatment was determined, and no significant differences were found; hence, only the control corresponding to the 24% SM treatment is shown in Table 2 and in the following results.

The main phenolic compounds identified in the peppermint infusions were phenolic acids and flavonoids. Most of these compounds were increased in infusions obtained from stressed plants, and this effect was greater in the 35 and 24% SM treatments. Among the compounds that were increased by drought treatment were rosmarinic acid (1.5-fold at 35% SM) and hesperidin (2-fold at 24% SM), which are the most abundant in this plant and have been related to the beneficial health effects of peppermint infusions.[1] Furthermore, coumaric acid, luteolin, quercetin, naringenin, and vanillin were found in infusions of stressed leaves but not in controls. In a previous study, we treated peppermint plants with different concentrations of elicitors [salicylic acid (SA) or hydrogen peroxide] and found similar results, increasing the hesperidin and rosmarinic acid in leaves, among other phenolic compounds, and we also found some compounds, such as naringinin, in SA-treated plants but not in controls; these compounds are different in comparison to those found in this study, which suggests that different types of abiotic stress induce different pathways involved in phenolic compound synthesis.[20]

**Identification of Low-Molecular-Weight Compounds.** Table 3 shows the identification of low-molecular-weight polar compounds, such as amino acids, carbohydrates, organic acids, fatty acids, and alcohols, obtained by GC−MSD analysis. Drought stress led to important changes in the metabolite profile of infusions compared to the control. For instance, most of the amino acids identified in the control, such as Ser, Thr, Phe, and Asn, among others, were not detected in infusions prepared from stressed plants. Similar results were previously reported in tobacco (*Nicotiana tabacum* L.) leaves after 4 days of water deprivation, where decreases of approximately 40−70% were observed in the concentrations of some amino acids, such as Asp, Glu, Ser, and Gly, as well as a decrease in $NO_3^-$. The low level of transpiration and turgor pressure because of water deficit leads to a decrease in root absorption of $NO_3^-$ and transport of $NO_3^-$ to the leaves, decreasing amino acid synthesis. This effect could explain the changes in the amino acid profile found in peppermint infusions made from stressed leaves, because some amino acids were not detected in plants grown under severe drought stress conditions.[21]

However, in several studies, the opposite effect has been shown for some amino acids, such as proline. Ghorbanli et al.[22] found that severe drought stress ($^1/_3$ field capacity) on tomato cultivars growing under greenhouse conditions for 9 weeks resulted in a 6-fold increase of the amount of proline in the leaves. It has been shown that increased proline in drought-stressed plants may be an adaptation to stress conditions, because this amino acid has a scavenger function and acts as a supply of osmolytes and energy for the growth and survival of cells, thereby helping the plant to tolerate water stress.[23] In this study, we found this amino acid in all water stress treatments; however, it is necessary to perform a quantitative study of proline to demonstrate the aforementioned effect.

Despite the fact that amino acids are not the main bioactive compound in peppermint infusions and that these beverages are not consumed for nutritional purposes, these results showed that drought stress affected amino acid biosynthesis in the leaves. Carbohydrates, such as arabinose and D-glucose, were identified in the peppermint infusions; however, these compounds were found in all infusions evaluated, both control and treated. In addition, a similar trend was found for the majority of organic and fatty acids, in which no differences were found between the profiles of control and stressed plants. However, some of these compounds, such as citric and oleic acids, were only identified in infusions made from stressed plants. These compounds are primary metabolites and can be found in large amounts in all plants; in a manner similar to that of phenolic compounds, some organic and fatty acids may also play a protective role against various oxidative diseases because of their antioxidant properties,[24] as is the case of citric acid because it has the ability to act as a singlet oxygen quencher and scavenger of $OH^\bullet$ radicals.[25] Moreover, these compounds are key components of some mechanisms used by plants for the management of nutrient deficiencies, plant−microbe interactions, and water stress, operating at the root−soil interface.[26]

Pantothenic, linoleic, and $\alpha$-linolenic acids were found only in infusions made from control plants, suggesting that drought conditions decrease the amount of these compounds in leaves. Gigon et al.[27] reported approximately 3-fold decreases of the total lipid content in *Arabidopsis thaliana* subjected to drought for 14 days. Similar results were found by Benhassaine-Kesri et al.,[28] who reported decreases in linoleic and linolenic acid contents in rape leaves (*Brassica napus*) growing under water stress conditions for 6 days. Several plant species respond to environmental stresses by altering their membrane lipid composition.[27] Indeed, membranes are primary targets of degradative processes induced by drought stress, and it has been shown that, under water stress, a decrease in the membrane lipid content is correlated with an inhibition of lipid biosynthesis and a stimulation of lipolytic and peroxidative activities, decreasing the lipid content of plant. However, the response may be different depending upon the class of lipid studied.[27−29]

**Evaluation of Antioxidant Capacity.** Antioxidant capacity is related to the presence of compounds with the ability to counteract the formation of free radicals by different mechanisms.[30] Table 4 shows the antioxidant capacity of peppermint infusions as determined by DPPH, ABTS, and

**Table 4. Capacity of Infusions Prepared from Peppermint (*M. piperita*) Leaves Grown at Different Levels of SM, for Inhibition of $ABTS^+$, $DPPH^\bullet$, and $NO^\bullet$ Radicals[a]**

| treatment | $IC_{50}$ $DPPH^\bullet$ | $IC_{50}$ $ABTS^+$ | $IC_{50}$ $NO^\bullet$ |
|---|---|---|---|
| control | 61.2 ± 1.4 a | 16.5 ± 0.4 a | 48.5 ± 0.9 a |
| 65% | 58.2 ± 1.2 a | 14.2 ± 0.3 b | 52.3 ± 1.2 a |
| 35% | 24.5 ± 1.5 d | 10.9 ± 0.5 c | 35.3 ± 0.8 b |
| 24% | 32.2 ± 1.2 c | 12.3 ± 0.3 bc | 32.8 ± 1.6 c |
| 12% | 53.4 ± 1.3 b | 15.2 ± 0.3 a | 51.2 ± 1.8 a |

[a]Results are expressed as $\mu$g/mL and reflect averages of triplicate assays ± SE. Different letters indicate significant statistical differences for each treatment ($p < 0.05$; Tukey's test).

nitric oxide scavenging assays, expressed as $IC_{50}$ values. ABTS and DPPH are the main assays used for the evaluation of the ability of compounds to donate electrons or hydrogen atoms, respectively.[30] We found that infusions made from control and stressed peppermint leaves reached a maximum inhibition percentage of approximately 92 and 94% for DDPH and ABTS, respectively (data not shown). However, the infusions obtained from peppermint subjected to water stress exhibited an important decrease in $IC_{50}$ values, as compared to the control in both assays. SM of 35 and 24% had the greatest antioxidant activity, because $IC_{50}$ values were reduced by 33 and 25% for ABTS and 60 and 47% for DPPH, respectively, as compared to the control infusion. These effects could be attributed to the increase of some phenolic compounds, such as coumaric acid, luteolin, rutin, rosmarinic acid, naringenin, and caffeic acid, in drought-stressed plants, because we found high correlation coefficients between these compound concentrations and the DPPH ($r$ = 0.67−0.98) and ABTS ($r$ = 0.80−0.98) scavenging capacities.

On the other hand, we measure the ability of infusions to compete with oxygen to scavenge nitric oxide, which was generated from SNP. Results showed that infusions from all treatments exhibited a maximum inhibition of approximately 82%, while (+)-catechin reached a maximum of 91% (data not shown). Infusions obtained from stressed peppermint showed decreased $IC_{50}$ values by approximately 31 and 37% for the 24 and 35% SM treatments, respectively, as compared to the control. Furthermore, we found a high correlation coefficient between the sinapic acid concentration and NO scavenging activity ($r$ = 0.98). These results suggest that all infusions are likely to have a nitric oxide scavenging activity, which was monitored indirectly by the nitrite production. Nitrite is the final product of the reaction of nitric oxide with oxygen through reactive intermediates, such as $NO_2$ and $N_2O_3$. Therefore, the inhibitory effect of peppermint infusions on nitrite production could be attributed to not only their NO scavenging activity but also their reaction with other nitrogen oxides.[12,31]

**Inhibition of Digestive Enzymes.** It has been demonstrated that peppermint infusions reduce the blood concentration of glucose and triglycerides; therefore, the evaluation of *in vitro* digestive enzyme inhibition represents a preliminary approach to the biological potential of peppermint infusions. Pancreatic α-amylase hydrolyzes starch to oligosaccharides, which are then hydrolyzed to glucose by intestinal α-glucosidase. Pancreatic lipase hydrolyzes triglycerides to free fatty acids and is responsible for the hydrolysis of 50−70% of total dietary fats.[32,33] Therefore, the inhibition of these digestive enzymes could reduce glucose and lipid absorption. It has been reported that some polyphenols may inhibit digestive enzymes involved in the breakdown of lipids and starches, leading to positive effects on obesity and blood glucose control.[15,32] Therefore, we evaluated the capacity of the infusions for inhibition of α-amylase, α-glucosidase, and pancreatic lipase activity.

Table 5 shows that infusions obtained with 35, 24, and 12% SM presented 4-, 24-, and 14-fold increases in α-amylase inhibition, as compared to the control; however, the maximum percentage of inhibition achieved was only 12% (with the 24% SM treatment), suggesting that peppermint infusions are not highly able to inhibit this enzyme. This inhibition was obtained with the concentration used to prepare this kind of beverage (10 mg/mL); however, the peppermint infusions presented a dose-dependent inhibitory capacity, and the maximum α-amylase inhibition (45%) was achieved with 60−80 mg/mL (data not shown). McCue and Shetty[34] reported that pure rosmarinic acid exhibits an inhibitory activity over pancreatic α-amylase in a concentration-dependent manner, and these authors suggested that phenolic synergies in plant extracts may contribute to additional amylase inhibitory activity. Nevertheless, this is not in agreement with our results because we found a low correlation coefficient between the rosmarinic acid concentration and inhibition values to this enzyme ($r$ = 0.19). However, high correlation coefficients were found between hesperidin ($r$ = 0.95), quercetin ($r$ = 0.77), and sinapic acid ($r$ = 0.76) and the amylase inhibition. On the other hand, peppermint infusions (10 mg/mL) inhibited about 7−8% of the activity of α-glucosidase, finding the highest correlation with vainillin and luteolin ($r$ = 0.86 and 0.82, respectively); however, no significant changes were found in infusions made from stressed leaves, as compared to the control. The maximum inhibitory capacity (24%) was reached at 50−65 mg/mL (data not shown). It has been reported that some phenolic compounds, such as quercetin, rutin, and chlorogenic acid, present in *Gynuramedica* leaf extracts have the capacity to inhibit α-glucosidase activity *in vitro*; however, we found low correlation coefficients between inhibition of this enzyme and rutin and quercetin concentrations ($r$ = 0.54 and 0.60, respectively), which suggest that these inhibitions could be related to synergic effects between different compounds in plants.[35]

**Table 5. Inhibition of Digestive Enzyme Activity by Infusions Prepared from Peppermint (*M. piperita*) Leaves (10 mg $mL^{-1}$) Grown at Different Levels of SM[a]**

| treatment | α-amylase | α-glucosidase | lipase |
|---|---|---|---|
| control | 0.5 ± 0.1 d | 7.6 ± 1.0 a | 45.6 ± 4.2 b |
| 65% | 0.7 ± 0.0 d | 8.1 ± 1.1 a | 49.0 ± 3.6 ab |
| 35% | 2.1 ± 0.1 c | 7.5 ± 0.6 a | 48.7 ± 4.1 b |
| 24% | 12.5 ± 0.1 a | 7.2 ± 0.5 a | 53.5 ± 4.9 a |
| 12% | 7.1 ± 0.1 b | 7.9 ± 1.2 a | 55.1 ± 6.5 a |

[a]Results are expressed as a percentage of enzyme inhibition and reflect averages of triplicate assays ± SE. Different letters indicate significant statistical differences for each treatment ($p$ < 0.05; Tukey's test).

Control infusions inhibited approximately 45% of the pancreatic lipase activity, while infusions made from plants stressed with 24 and 12% SM showed inhibitions of 53.5 and 55.1%, respectively. However, the 65 and 35% SM treatments produced no significant changes, as compared to the control. It has been previously reported that hesperidin has the ability to inhibit pancreatic lipase activity *in vitro*, and this effect is associated with its chemical structure, specifically with the 7 position of rutinose on the C ring of the flavonoid structure.[36] Furthermore, the highest correlation coefficient between phenolic compounds and lipase inhibition capacity was found for hesperidin ($r$ = 0.68).

The results of this study suggest that water deficit has an important effect on the synthesis of phenolic compounds in the peppermint plant, which is reflected in an increased *in vitro* antioxidant capacity and inhibition of digestive enzyme activity of the resulting infusions. However, drought stress negatively affected metabolites, such as amino acids and unsaturated fatty acids; therefore, further research is required to determine the biological significance of this effect in the peppermint plant and infusions.

## AUTHOR INFORMATION


### Corresponding Author

*Telephone: +52-442-1921300, ext. 5576. Fax: +52-442-1921304. E-mail: rrcamachomx@yahoo.com.mx.


### Notes

The authors declare no competing financial interest.

## REFERENCES


(1) McKay, D. L.; Blumberg, J. B. A review of the bioactivity and potential health benefits of peppermint tea (*Mentha piperita* L.). *Phytother. Res.* **2006**, *20*, 619−633.

(2) Mushtaq, N.; Schmatz, R.; Pereira, L.; Ahmad, M.; Stefanello, N.; Vieira, J. M.; Abdalla, F.; Rodrigues, M.; Baldissarelli, J.; Pelinson, L.; Dalenogare, D.; Reichert, K.; Dutra, E.; Mulinacci, N.; Innocenti, M.; Bellumori, M.; Morsch, V. M.; Schetinger, M. R. Rosmarinic acid prevents lipid peroxidation and increase in acetylcholinesterase activity in brain of streptozotocin-induced diabetic rats. *Cell Biochem. Funct.* **2013**, *32*, 287−293.

(3) Bentli, R.; Ciftci, O.; Cetin, A.; Unlu, M.; Basak, N.; Cay, M. Oral administration of hesperidin, a citrus flavonone, in rats counteracts the oxidative stress, the inflammatory cytokine production, and the hepatotoxicity induced by the ingestion of 2,3,7,8-tetrachlorodibenzo-*p*-dioxin (TCDD). *Eur. Cytokine Network* **2013**, *24*, 91−96.

(4) Barbalho, S.; Vazquez, S.; Machado, F.; Oshiiwa, M.; Abreu, M.; Tomazela, P.; Goulart, T. Investigation of the effects of peppermint (*Mentha piperita*) on the biochemical and anthropometric profile of university students. *Cienc. Tecnol. Aliment. (Campinas, Braz.)* **2011**, *31*, 584−588.

(5) Mani, R.; Badal, D.; Badal, P.; Khare, A.; Shrivastava, J.; Kumar, V. Pharmacological action of *Mentha piperita* on lipid profile in fructose-fed rats. *Iran. J. Pharm. Res.* **2011**, *10*, 843−848.

(6) Zingaretti, S. M.; Inácio, M. C.; de Matos Pereira, L.; Paz, T. A.; de Castro França, S. Water stress and agriculture. In *Responses of Organisms to Water Stress*, 1st ed.; Akinci, S., Ed.; InTech: Rijeka, Croatia, 2013; Chapter 7, pp 152−179.

(7) Cruz, M. Drought stress and reactive oxygen species. *Plant Signaling Behav.* **2008**, *3*, 156−165.

(8) Singleton, V. L.; Rossi, J. A. Colorimetry of total phenolics with phosphomolybdic and phosphotungstic acid reagents. *Am. J. Enol. Vitic.* **1965**, *16*, 144−153.

(9) Liu, M.; Li, X. Q.; Weber, C.; Lee, C. Y.; Brown, J.; Liu, R. H. Antioxidant and antiproliferative activities of raspberries. *J. Agric. Food Chem.* **2002**, *50*, 2926−2930.

(10) Brand-Williams, W.; Cuvelier, M.; Berset, C. Use of free radical method to evaluate antioxidant activity. *Lebensm.-Wiss. Technol.* **1995**, *28*, 25−30.

(11) Re, R.; Pellegrini, N.; Proteggente, A.; Pannala, A.; Yang, M.; Rice-Evans, C. Antioxidant activity applying an improved ABTS radical cation decolorization assay. *Free Radical Biol. Med.* **1999**, *26*, 1231−1237.

(12) Marcocci, T. K.; Parker, L. Antioxidant action of *Ginkgo biloba* extract EGB 761. *Methods Enzymol.* **1994**, *234*, 462−475.

(13) Kandra, L.; Zajacz, A.; Remenyik, J.; Gyemant, G. Kinetic investigation of a new inhibitor for human salivary α-amylase. *Biochem. Biophys. Res. Commun.* **2005**, *334*, 824−828.

(14) Apostolidis, E.; Kwon, Y.; Shetty, K. Inhibitory potential of herb, fruit, and fungal-enriched cheese against key enzymes linked to type 2 diabetes and hypertension. *Innovative Food Sci. Emerging Technol.* **2007**, *8*, 46−54.

(15) McDougall, G.; Kulkarni, N.; Stewart, D. Berry polyphenols inhibit pancreatic lipase activity *in vitro*. *Food Chem.* **2009**, *115*, 193−199.

(16) Moeini, H.; Heidari, A.; Dizaji, A. Effect of water stress on some morphological and biochemical characteristics of purple basil (*Ocimum basilicum*). *J. Biol. Sci.* **2006**, *6*, 763−767.

(17) Blum, A. *Plant Breeding for Water-Limited Environments*; Springer: New York, 2011.

(18) Yordanov, I.; Velikova, V.; Tsonev, T. Plant responses to drought and stress tolerance. *Bulg. J. Plant Physiol.* **2003**, 187−206.

(19) Chakraborty, U.; Chakaborty, B. Response of tea plants to water stress. *Biol. Plant.* **2002**, *45*, 557−562.

(20) Figueroa-Perez, M. G.; Rocha-Guzmán, N. E.; Mercado-Silva, E.; Loarca-Piña, G.; Reynoso-Camacho, R. Effect of chemical elicitors on peppermint (*Mentha piperita*) plants and their impact on the metabolite profile and antioxidant capacity of resulting infusions. *Food Chem.* **2014**, *156*, 273−278.

(21) Ferrario-Mery, S.; Valadier, M. H.; Foyer, C. H. Overexpression of nitrate reductase in tobacco delays drought-induced decreases in nitrate reductase activity and mRNA. *Plant Physiol.* **1998**, *117*, 293−302.

(22) Ghorbanli, M.; Gafarabad, M.; Amirkian, T.; Allahverdi, B. Investigation of proline, total protein, chlorophyll, ascobate and dehydroascorbate under drought stress in Akria and Mobil tomato cultivars. *Iran. J. Plant Physiol.* **2011**, *3*, 651−658.

(23) Sankar, B.; Jaleel, C. A.; Manivannan, P.; Kishorekumar, A.; Somasundaram, R.; Panneerselvam, R. Effect of paclobutrazol on water stress amelioration through antioxidants and free radical scavenging enzymes in *Arachis hypogaea* L. *Colloids Surf., B* **2007**, *60*, 229−235.

(24) Oliveira, A.; Pereira, J.; Andradec, P.; Valentãoc, P.; Seabrac, R.; Silva, B. Organic acids composition of *Cydonia oblonga* Miller leaf. *Food Chem.* **2008**, *111*, 393−399.

(25) Polumbryk, M.; Ivanov, S.; Polumbryk, O. Antioxidants in food systems. Mechanism of action. *Ukr. J. Food Sci.* **2013**, *1*, 15−40.

(26) Lopez-Bucio, J.; Nieto-Jacobo, F.; Ramírez-Rodriguez, V.; Herrera-Estrella, L. Organic acid metabolism in plants: From adaptive physiology to transgenic varieties for cultivation in extreme soils. *Plant Sci.* **2000**, *160*, 1−13.

(27) Gigon, A.; Matos, A. R.; Laffray, D.; Zuily-Fodil, Y. Effect of drought stress on lipid metabolism in the leaves of *Arabidopsis thaliana* (ecotype Columbia). *Ann. Bot.* **2004**, *94*, 345−351.

(28) Benhassaine-Kesri, G.; Aid, F.; Demandre, C.; Kader, J. C.; Mazliak, P. Drought stress affects chloroplast lipid metabolism in rape (*Brassica napus*) leaves. *Physiol. Plant.* **2002**, *115*, 221−227.

(29) Harwood, J. L. Recent advances in biosynthesis of plant fatty acids. *Biophys. Acta* **1996**, *1301*, 7−56.

(30) Prior, R. L.; Wu, X.; Schaich, K. Standardized methods for the determination of antioxidant capacity and phenolics in foods and dietary supplements. *J. Agric. Food Chem.* **2005**, *53*, 4290−4302.

(31) Stamler, J. S.; Singel, D. J.; Loscalzo, J. Biochemistry of nitric oxide and its redox-activated forms. *Science* **1992**, *258*, 1898−1902.

(32) McDougall, G.; Shpiro, F.; Dobson, P.; Smith, P.; Blake, A.; Stewart, D. Different polyphenolic components of soft fruits inhibit α-amylase and α-glucosidase. *J. Agric. Food Chem.* **2005**, *53*, 2760−2766.

(33) Shi, Y.; Burn, P. Lipid metabolic enzymes: Emerging drug targets for the treatment of obesity. *Nat. Rev. Drug Discovery* **2004**, *3*, 695−710.

(34) McCue, P.; Shetty, K. Inhibitory effects of rosmarinic acid extracts on porcine pancreatic amylase *in vitro*. *Asia Pac. J. Clin. Nutr.* **2004**, *13*, 101−106.

(35) Chao, T.; Qunxing, W.; Chunhua, L.; Sai, C.; Qianyuan, L.; Peng, Li Yeast α-glucosidase inhibitory phenolic compounds isolated from *Gynura medica* leaf. *Int. J. Mol. Sci.* **2013**, *14*, 2551−2558.

(36) Kawaguchi, K.; Mizuno, T.; Aida, K.; Uchino, K. Hesperedin as an inhibitor of lipases from porcine pancreas and *Pseudomonas*. *Biosci., Biotechnol., Biochem.* **1997**, *61*, 102−104.

α-amylase resistant, water-soluble oligosaccharides from maltodextrins (partially hydrolyzed starches). These enzymes cleave off the nonreducing glucose moiety and then reattach the glucose moiety to an α-glucan chain via an (α1 → 6)-, (α1 → 2)- or (α1 → 3)-glycosidic linkage, predominantly resulting in chain elongation, though branches are also formed.

A new development in this field are 4,6-α-glucanotransferase enzymes, which have been shown to convert (1 → 4)-α-D-gluco-oligosaccharides into linear α-glucans with consecutive (α1 → 6)-glycosidic bonds build onto (1 → 4)-α-D-gluco-oligosaccharides.[23−25] These enzymes cleave off the nonreducing glucose moiety of a (1 → 4)-α-D-gluco-oligosaccharide and attach this glucose moiety to the nonreducing end of another (α1 → 4)-glucan chain via an (α1 → 6) linkage without forming branches. This catalytic cycle is repeated several times, yielding α-glucans with consecutive (α1 → 6) linkages.

Here, we report the production of a novel type of dietary fiber from starch using the 4,6-α-glucanotransferase enzyme GTFB of *Lactobacillus reuteri* 121.

## MATERIALS AND METHODS

**GTFB Expression and Purification.** GTFB was produced in *Escherichia coli* BL21(DE3) carrying the plasmids pRSF-GTFB and pBAD22-GroELS. Plasmid vector pRSF-GTFB was constructed by cloning the *gtfB* gene of pET15b-GTFB[23] into the *Nco*I/*Eco*RV sites of pRSFduet (Novagen/EMD Chemicals Inc., Darmstadt, Germany). The encoded GTFB protein carries a C-terminal $(His)_6$-tag. *E. coli* was cultured at 30 °C in Luria Broth medium supplemented with ampicillin (100 mg $L^{-1}$) and kanamycin (25 mg $L^{-1}$). Expression of GTFB and GroELS was induced at an $OD_{600}$ of 0.4−0.5 by the addition of isopropyl β-D-1-thiogalactopyranoside (0.5 mM) and L-arabinose (0.02% w/v), respectively, and the incubation was continued for 8 h. Coexpression with the GroELS chaperones increases the yield of GTFB (data not shown). Cells were harvested by centrifugation, washed with buffer A (20 mM Tris/HCl pH 8.0, 250 mM NaCl, 1 mM $CaCl_2$) and stored at −20 °C. Following resuspension in buffer A supplemented with Triton X100 (0.25% v/v) and β-mercaptoethanol (5 mM), the cells were broken by sonication and the supernatant was obtained by centrifugation (10,000*g*; for 30 min). GTFB was purified by His-tag affinity column chromatography using buffer A and eluted with imidazole (200 mM). Purity was checked on sodium dodecyl sulfate-polyacrylamide gel electrophoresis (GTFB is ∼170 kDa) and the protein concentration was measured with Bradford reagent (Bio-Rad, Hercules, CA) and bovine serum albumin as standard.

**Starches, Maltodextrins, and Other Carbohydrates.** The native starches, maltodextrins and amylose V were provided by AVEBE (Veendam, The Netherlands) (Table 1). Maltoheptaose, glycogen type IX (bovine liver), glycogen type VIII (Crepidula), dextran with an average molecular weight of 6,000, and cellulose were from Sigma-Aldrich (St. Louis, MO). Vivinal GOS (galacto-oligosaccharides) was from Friesland-Campina Domo (Beilen, The Netherlands) and FOS Orafti P95 (fructo-oligosaccharides) was from BENEO-Orafti (Oreye, Belgium). Debranched Eliane 100 (waxy potato), Eliane MD6 and Etenia 457 (4-α-glucanotransferase-treated potato starch), also provided by AVEBE, were made using the debranching enzyme Promozyme D2 Pullulanase (Novozymes, Bagsvaerd, Denmark). Briefly, 10% (w/w) starch/maltodextrin was incubated with 5 mg of pullulanase per g of starch/maltodextrin at pH 4.7 and 60 °C for 1 day. Isoamylase (*Pseudomonas* sp.; Megazyme, Wicklow, Ireland) debranched Etenia 457 and glycogen type IX were made by dissolving 0.5 g in 20 mL of sodium acetate buffer (25 mM, pH 4.0) supplemented with 0.02% (w/v) sodium azide. Fifty units of isoamylase were added and the mixture was incubated at 37 °C for 68 h. The reactions were terminated by heating to 90 °C for 5 min.

**Table 1. Evaluation of Various Starches and Maltodextrins As Substrates in IMMP Synthesis[a]**

| substrate | amylose content (apparent) | average DP[f] | % (α1→6) in IMMP | % (α1→6) in IMMP using debranched substrate |
|---|---|---|---|---|
| | | maltodextrins | | |
| Etenia 457[b] | n/a[e] | n/a[e] | 33 | 83[j]/66[k] |
| Paselli SA2[b] | n/a[e] | 50 | 32 | |
| Paselli MD6[b] | n/a[e] | 20 | 34 | |
| Paselli MD10[b] | n/a[e] | 12 | 33 | |
| Avebe MD20[b] | n/a[e] | 6 | 25 | |
| Avebe SPG30[c] | n/a[e] | 4 | 24 | |
| Eliane MD6[d] | n/a[e] | 20 | 24 | 63[k] |
| maltoheptaose | n/a[e] | 7 | 38 | |
| | | starches | | |
| arrow root | 20.8[f] | n/a[e] | 24 | |
| barley | 25.5[g] | n/a[e] | 21 | |
| corn | 29.4[g] | n/a[e] | 21 | |
| corn, waxy | 0[g] | n/a[e] | 7 | |
| corn, hylon V | 52.0[g] | n/a[e] | 50 | |
| corn, hylon VII | 68.0[g] | n/a[e] | 61 | |
| mung bean | 37.9[g] | n/a[e] | 34 | |
| pea, yellow | 30.9 | n/a[e] | 35 | |
| pea, wrinkled | 52.8 | n/a[e] | 71 | |
| potato | 36.0[g] | n/a[e] | 28 | 92[k,l] |
| potato, waxy | 0 | n/a[e] | 14 | 63[k]/83[j,l] |
| amylose V of potato | 100 | n/a[e] | 91 | |
| rice, round grain | 25.0[g] | n/a[e] | 13 | |
| rice, waxy | 0[g] | n/a[e] | 7 | |
| sorghum | 23.7[h] | n/a[e] | 22 | |
| tapioca | 23.5[g] | n/a[e] | 20 | |
| wheat | 28.8[g] | n/a[e] | 22 | |

[a]The substrates were incubated with *Lactobacillus reuteri* 121 GTFB enzyme, and the percentages of (α1 → 6)-glycosidic linkages in the obtained products were determined by $^1$H NMR spectroscopy. [b]Maltodextrins manufactured from potato starch. [c]Maltodextrins manufactured from corn starch. [d]Maltodextrins manufactured from waxy potato starch. [e]n/a, not applicable. [f]Values as reported in ref 40. [g]Values as reported in ref 41. [h]Values as reported in ref 42. [i]Degree of polymerization. [j]Isoamylase debranched. [k]Pullulanase debranched. [l]The debranching and GTFB reactions were carried out simultaneously.

**Substrate Evaluation.** A series of starches and maltodextrins were incubated with GTFB at a concentration of 0.5% (w/v) in sodium acetate buffer (10 mM, pH 5.0) supplemented with $CaCl_2$ (1 mM) and sodium azide (0.02% w/v) at 37 °C. Native starches were pregelatinized by autoclaving (15 min, 120 °C), amylose V was dissolved in sodium hydroxide (1 M) and neutralized by hydrochloric acid, and maltodextrins were solubilized by heating to 90 °C in buffer. Incubations of the α-glucan solutions, cooled to 37 °C, were started by the addition of 0.5 mg of GTFB per gram of substrate. The progress of the reactions was followed by analyzing samples at different time intervals ($^1$H NMR analysis). The GTFB

reactions were stopped by heating the samples to 95 °C for 10 min. All reactions were performed at least in duplicate.

**IMMP Production on Gram Scale.** Seven different isomalto/malto-polysaccharide (IMMP) products were produced on multigram scale from the potato starch maltodextrins Paselli MD6, MD10, and SA2, from the waxy potato starch maltodextrin Eliane MD6 (2×), potato starch, and waxy potato starch. Production with the latter two was performed in the presence of a debranching enzyme. The substrate concentrations ranged from 2.5 to 5% (w/w). The other reaction parameters were as above.

**Simultaneous Starch Debranching and GTFB Conversion.** Starch debranching during GTFB conversion was performed by adding isoamylase (5 units per g of starch) or pullulanase (5 mg per g of starch) to the GTFB incubation mixtures under the above-described GTFB reaction conditions.

**α-Amylase Treatment of GTFB Products.** GTFB products (25 mg) were dissolved in 625 μL sodium acetate buffer (34 mM) and incubated with porcine pancreas type I-A α-amylase (Sigma Aldrich) at pH 7 and 37 °C for 24 h.

**Isolation of Individual α-Glucan Structures.** Ten milligrams of the reaction mixture product derived of Paselli MD10 by GTFB treatment, and 10 mg of the same product incubated with excess pig pancreatic α-amylase, were fractionated by size-exclusion chromatography on a Bio-Gel P-2 column (100 × 0.9 cm) (Bio-Rad) using ammonium bicarbonate (10 mM) as eluent at a rate of ∼10 mL $h^{-1}$. Selected fractions were lyophilized, dissolved in water, and further fractionated by high-pH anion-exchange chromatography (HPAEC) on a Carbo-Pac PA-1 column (250 × 9 mm) (Thermo Scientific Dionex, Amsterdam, The Netherlands), assembled in a Dionex DX500 workstation equipped with an ED40 pulsed amperometric detector, using a linear gradient of 30 to 600 mM sodium acetate in 100 mM sodium hydroxide (4 mL $min^{-1}$); see text for specific elution programs. Eluting fractions were collected manually and neutralized directly with 4 M acetic acid. The fractions were desalted using 150 mg CarboGraph SPE columns (Grace, Breda, The Netherlands) and analyzed by matrix-assisted laser-desorption ionization time-of-flight mass spectrometry (MALDI-TOF-MS) and nuclear magnetic resonance (NMR) spectroscopy.

**NMR Spectroscopy.** One-dimensional NMR spectra were recorded on a Varian Inova 500 spectrometer (NMR Center, University of Groningen) and one- and two-dimensional NMR spectra on a Bruker DRX-500 spectrometer (NMR Spectroscopy, Bijvoet Center, Utrecht University) at probe temperatures of 300 K. Prior to analysis, samples were exchanged twice in $D_2O$ (99.9 atom % D, Cambridge Isotope Laboratories, Inc., Andover, MA) with intermediate lyophilization, and then dissolved in 0.6 mL of $D_2O$. Suppression of the HOD signal was achieved by applying a WEFT (Bruker) or WET1D (Varian) pulse sequence for one-dimensional experiments and by a presaturation of 1 s during the relaxation delay in two-dimensional experiments. The two-dimensional TOCSY (total correlation spectroscopy) spectra were recorded using an MLEV-17 mixing sequence with spin-lock times of 20−200 ms. The two-dimensional ROESY (rotating frame Overhauser enhancement spectroscopy) spectra were recorded using standard Bruker XWINNMR software with a mixing time of 200 ms. The carrier frequency was set at the downfield edge of the spectrum to minimize TOCSY transfer during spin-locking. Natural abundance two-dimensional $^1H-^{13}C$ HSQC (heteronuclear single quantum coherence) experiments ($^1H$ frequency 500.0821 MHz, $^{13}C$ frequency 125.7552 MHz) were recorded without decoupling during acquisition of the $^1H$ FID. Resolution enhancement of the spectra was performed by a Lorentzian-to-Gaussian transformation for one-dimensional spectra or by multiplication with a squared-bell function phase shifted by $\pi/(2.3)$ for two-dimensional spectra, and when necessary, a fifth order polynomial baseline correction was performed. Chemical shifts ($\delta$) are expressed in ppm by reference to internal acetone ($\delta$ 2.225 for $^1H$ and $\delta$ 31.08 for $^{13}C$). Carbohydrate structures were determined using the previously developed $^1H$ NMR structural-reporter-group concept of α-D-glucans.[25,26]

**MALDI-TOF-MS.** MALDI-TOF-MS experiments were performed on an Axima mass spectrometer (Shimadzu Kratos Inc., Manchester, UK) equipped with a nitrogen laser (337 nm, 3 ns pulse width). Positive-ion mode spectra were recorded using the reflector mode at a resolution of 5000 fwhm and delayed extraction (450 ns). The accelerating voltage was 19 kV with a grid voltage of 75.2%; the mirror voltage ratio was 1.12, and the acquisition mass range was 200−7000 Da. Samples (1 μL) were mixed in 1:1 ratio with a solution of 10 mg $mL^{-1}$ 2,5-dihydroxybenzoic acid in 1:1 acetonitrile/$H_2O$.

**Dietary Fiber.** Dietary fiber measurements were performed according to an all-in-one measurement,[27] with slight modifications, which is based on the Englyst,[16] McClearly[28] and AOAC 2001.03 procedures. One gram of sample in 5 mL water was homogenized for 5 min (150 rpm). Subsequently, 10 mL of 7.5 g $L^{-1}$ pepsin (P7000, Sigma-Aldrich) in 0.05 M HCl, supplemented with 0.25% saturated benzoic acid, was added, and samples were incubated for 30 min at 37 °C (150 rpm). After raising the pH to 6.0 with 0.7 mL of 0.75 M NaOH and 4 mL of 0.4 M sodium maleate buffer (pH 6.0), 20 mL of 0.4 M sodium maleate buffer (pH 6.0), supplemented with 4 mM $CaCl_2$, 0.02% sodium azide, 0.27% (w/v) pancreatic α-amylase (P7545, Sigma-Aldrich) and 0.18% (v/v) amyloglucosidase (3.26 U $mL^{-1}$; Megazyme), was added. The samples were incubated at 37 °C (150 rpm) for 16 h. After incubation, the pH was adjusted to pH 4.3 with 2 M acetic acid. High-molecular-weight dietary fiber (HMWDF) was precipitated with 180 mL of preheated 95% ethanol of 60 °C. After 16 h at room temperature, the samples were sieved through a tarred and dried crucible containing 1 g of Celite filter, and washed twice with 15 mL of 76% ethanol, once with 95% ethanol, and once with acetone. The samples were dried overnight at 103 °C and weighed, resulting in the weight of the "residue". This fraction was subsequently used to determine ash content by heating at 550 °C for 5 h or protein content using Kjeldahl analysis. The amount of low-molecular-weight dietary fiber (LMWDF) was determined according to the AOAC 2001.03 procedure. In short, the filtrate containing the LMWDF was evaporated to near dryness, mixed with 10 mL of aqueous ethylene glycol (10.2 mg $mL^{-1}$) and water was added up to 50 mL. This sample was loaded on a column containing 25 g of Amberlite IRA-67 (anion-exchange resin) and 25 g of Amberlite 200 ($H^+$ form). After elution of the column with 250 mL of water at a flow rate of 0.8 mL per min, the collected eluate was evaporated to near dryness, and the sample was analyzed quantitatively using high-performance liquid chromatography (TSK-GEL G2500PWXL; Tosoh Corp, Tokyo, Japan). The total dietary fiber fraction (TDF) of a sample is the residue weight, minus protein and ash fraction, plus the LMWDF fraction, which was subsequently expressed as a w/w percentage of the original sample. Control samples were

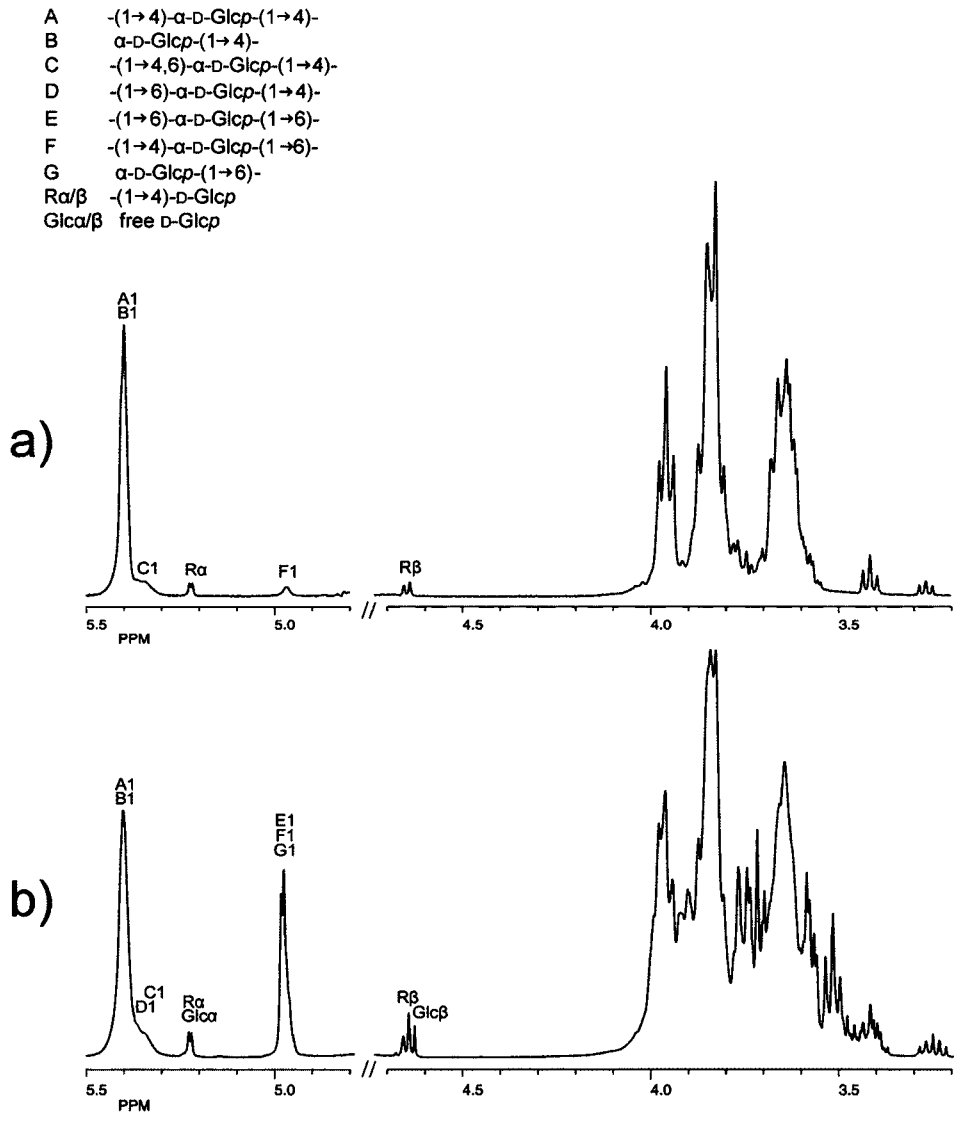


**Figure 1.** $^{1}$H NMR spectra ($D_2O$, 300 K) of (a) the Paselli MD10 maltodextrin substrate (average DP = 12) and (b) the IMMP product derived of Paselli MD10 maltodextrin upon GTFB treatment.

analyzed to compensate for any contribution of reagents and or enzymes used in the procedure.

**Enzymatic Digestion Using Brush Border Enzymes.** Fifty milligrams of rat intestinal acetone powder (Sigma-Aldrich), containing the rat brush border enzymes, was dissolved in 1.5 mL of 0.9% NaCl. Following sonication on ice and centrifugation (10,000*g*; 30 min), the supernatant was used as brush border preparation in the digestion assays. Serial dilutions of various oligosaccharides were prepared in sodium maleate (100 mM; pH 6.0). Incubations were performed in sealed 96-well plates containing 30 $\mu$L oligosaccharide solution and 20 $\mu$L of enzyme mixture at 37 °C. Progress of the digestion was followed in time by taking samples, heat inactivation (10 min; 100 °C), and measuring the amount of glucose released with a glucose assay kit (GAGO-20, Sigma-Aldrich).

**In Vitro Fecal Fermentation.** Culture media for in vitro fecal fermentations were prepared according to Kabel et al.,[29] with minor modifications. Solutions S1 and S3 were adapted to maintain a stable pH during the fermentation. Fermentation substrates were dissolved in S1 (1.05 g $L^{-1}$ $KH_2PO_4$, 1.05 g $L^{-1}$ $K_2HPO_4$ and 4.7 g $L^{-1}$ $Na_2CO_3$) and the pH was adjusted to 6.8. S2 is 6.7 g $L^{-1}$ bacto yeast nitrogen base (Difco, Detroit, MI) dissolved in water. S3 is a 40% (v/v) solution of 0.2 g $L^{-1}$ $MgSO_4$, 0.2 g $L^{-1}$ $CaCl_2$, 1 g $L^{-1}$ $K_2HPO_4$, 1 g $L^{-1}$ $KH_2PO_4$, and 2 g $L^{-1}$ NaCl, supplemented with 5% (w/v) casein enzymatic hydrolysate (N-Z Amine A, Sigma-Aldrich) and 0.5% (w/v) sodium thioglycolate. The pH of S2 and S3 were adjusted to 6−7 with 1 M NaOH. The three solutions S1, S2, and S3 were combined in a ratio of (v/v) 17:1:2 in serum flasks, which were filled at 50% and closed by a butyl rubber stopper. Filter-sterilized S2 was added only after the flasks had been autoclaved (15 min, 121 °C).

Anaerobic conditions were created by exchanging the air with nitrogen. Fecal samples were obtained from a healthy human volunteer in sterile plastic cups and were processed shortly after defecation to avoid aerobic conditions. Samples were processed as described by Kabel et al.[29]

A 10% (w/v) fecal slurry was prepared by adding ∼10 g of each fecal sample to 90 mL of inoculation solution, composed of 1 g $L^{-1}$ Bacto Peptone, 8 g $L^{-1}$ NaCl, and 0.5 g $L^{-1}$ L-cysteine-HCl at pH 6.9. The fecal slurry was mixed, and after an

equilibration time of 30 min, the slurry was diluted to 0.5% (w/v) with phosphate buffered saline solution (pH 6.8), of which 10 mL was added anaerobically to 40 mL culture media in serum flasks using a syringe adapted with a needle. The flasks were incubated at 37 °C. Samples were removed between 0 and 72 h for optical density measurements at 600 nm.

**Short Chain Fatty Acids.** Short chain fatty acids (SCFA) were measured by HPLC using an organic acids column (Column IOA-1000; Alltech) equipped with a refractive index detector. The column was hold at 60 °C and run with 5 mM sulfuric acid at a flow rate of 0.5 mL $min^{-1}$. Fermentation samples taken after 0, 3, 6, 14, 48, and 72 h were analyzed.

## RESULTS AND DISCUSSION

**Maltodextrins Are Substrates for the GTFB Enzyme.** Recently, we reported the synthesis of isomalto/malto-oligosaccharides from short (DP4-DP7) (1 → 4)-α-D-gluco-oligosaccharides using GTFB and two homologous enzymes.[23−25] Here we call the products isomalto/malto-**poly**saccharides (IMMPs), because this better reflects the molecular sizes of the molecules obtained with the larger substrate molecules used in this study. So, IMMPs are α-glucans with one or more (α1 → 4)-linked glucose monomers at its reducing end and one or more glucose units linked via (α1 → 6)-glycosidic bonds at its nonreducing end. They are synthesized via the stepwise addition of single glucose moieties, via (α1 → 6)-glycosidic bonds, onto the nonreducing end of an α-glucan chain.[25] Since α-amylases cannot hydrolyze (α1 → 6) linkages, IMMPs, or more precisely the IMMP fragments rich in (α1 → 6) linkages will not be digested in the upper part of the gastrointestinal tract, and may also escape digestion in the small intestine and then enter the large intestine, where they will be fermented. IMMPs can therefore be regarded as a novel type of dietary fiber and as such they are potentially valuable food ingredients. However, for IMMPs to be of commercial interest it is crucial to produce them from affordable and readily available materials, instead of the expensive monodisperse DP4 to DP7 (1 → 4)-α-D-gluco-oligosaccharides used in the original reports.[23−25] Therefore, it was explored whether GTFB can convert maltodextrins, that is, partially hydrolyzed starches, into IMMPs. Reaction progress was monitored by taking samples over time, followed by enzyme inactivation and subsequent $^1$H NMR analysis. The strong increase observed in the percentage of (α1 → 6)-glycosidic bonds (Table 1) demonstrates that maltodextrins are excellent substrates for GTFB. As a typical example, the $^1$H NMR spectrum of the IMMP product derived from Paselli MD10 maltodextrin (average DP = 12) with GTFB is presented in Figure 1. Figure 1a shows clearly the spectrum of a maltodextrin. The H-1 signal at δ 5.40 reflects high amounts of -(1 → 4)-α-D-Glc*p*-(1 → 4)- internal fragments (residue **A**) combined with α-D-Glc*p*-(1 → 4)-terminal units (residue **B**). The low percentage of branching is indicated by the broad H-1 resonance at δ ∼5.35, derived from -(1 → 4,6)-α-D-Glc*p*-(1 → 4)- branching fragments (residue **C**), combined with the low-intensity H-1 signal at δ 4.97 for -(1 → 4)-α-D-Glc*p*-(1 → 6)- internal fragments (residue **F**). Furthermore, the low-molecular mass of the maltodextrin is evident from the visible H-1α and H-1β signals at δ 5.223 and δ 4.650, respectively, of the -(1 → 4)-D-Glc*p* reducing end unit (residue **R**). Going to the spectrum in Figure 1b, recorded after GTFB treatment, besides the H-1 signals of the residues **A**, **B**, **C**, **F**, **Rα**, and **Rβ**, some new signals are detected. Especially, the H-1 signal at δ 4.97 (residue **F**) has strongly increased, now also belonging to -(1 → 6)-α-D-Glc*p*-(1 → 6)- internal fragments (residue **E**) combined with α-D-Glc*p*-(1 → 6)-terminal units (residue **G**). Furthermore, the broad signal at δ ∼5.35 (residue **C**) has somewhat increased, due to the presence of minor amounts of -(1 → 6)-α-D-Glc*p*-(1 → 4)- internal fragments (residue **D**). The signals present at δ 4.637 (α-D-Glc*p* H-1) and δ 5.223 (β-D-Glc*p* H-1) indicate the formation of a small amount of free glucose (**Glc**). The latter demonstrates that GTFB has a low hydrolytic activity on maltodextrin, as also observed with monodisperse DP4−7 maltooligosaccharide substrates.[25] Note that the products generated of the lowest average DP maltodextrins (i.e., average DP < 5) possessed somewhat less (α1 → 6) linkages (Table 1). This indicates that short chain oligosaccharides are relatively poor glucose donors, which is in agreement with our previous study showing that (1 → 4)-α-D-gluco-oligosaccharides shorter than maltotetraose are very slow glucose donor substrates of the enzyme.[23] Important to note here is that the IMMPs are more soluble in water than the substrates used, as based on visual observation. In conclusion, it can be stated that GTFB effectively converts maltodextrins into water-soluble IMMPs.

**High Amylose Starches Are Preferred Substrates of GTFB.** In the above section, it was shown that maltodextrins are good starting materials for modification with the GTFB enzyme. This raised the question whether starches themselves might be good starting materials. Because starches are not readily soluble in water, making the starch inaccessible to enzymatic modification, the starches were first gelatinized (i.e., solubilized). This was done at a low concentration of 5 g $L^{-1}$ to slow down the process of retrogradation, that is, aligning of (α1 → 4)-glucan chains in a solution enabling hydrogen bond formation which results in a kind of crystalline structure, which basically makes the (α1 → 4)-glucan chains inaccessible for enzymatic modification; note that the process of retrogradation is used to make type 3 resistant starch. $^1$H NMR analysis of the reaction products revealed that GTFB also utilizes native (gelatinized) starches as substrate (Table 1). Importantly, the percentage of (α1 → 6)-glycosidic linkages in the IMMP products obtained is strongly dependent on the type of starch. There are two important factors. First, the amylose content of the starch is positively correlated with the percentage of (α1 → 6)-glycosidic bonds in the IMMP product produced (Figure 2A). Second, the degree of branching (i.e., (α1 → 4,6)-glycosidic bonds) of the starch is negatively correlated with the percentage of (α1 → 6) linkages in the IMMP product (Figure 2B). Indeed, the highly branched α-glucan glycogen, with 7−10% branching, is not a substrate of GTFB, as incubation with GTFB did not significantly increase the percentage of (α1 → 6) linkages (data not shown). The negative correlation with the degree of branching is explained by the exoacting nature of GTFB which forces the enzyme to stop when it reaches a branch point in the glucose donor substrate. Thus, the fraction of glucose moieties available for transfer by GTFB will be lower in more branched substrates. Linear (1 → 4)-α-D-poly/oligosaccharides thus are the best substrates for producing IMMPs with a high percentage of (α1 → 6)-glycosidic bonds. Indeed, the virtually linear substrate amylose V delivered an IMMP product with 91% of (α1 → 6) linkages (Table 1, see Supporting Information Figure S1 for the $^1$H NMR spectrum). This high percentage of (α1 → 6) linkages reached with amylose V demonstrates that once the first elongation step occurs the product becomes a better acceptor substrate. Otherwise all available α-glucan chains would be rapidly

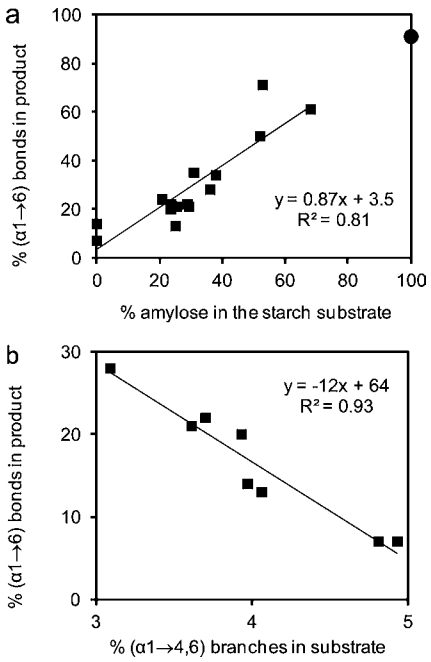


**Figure 2.** Preference of the GTFB enzyme for high amylose starches in the synthesis of IMMPs. (a) Plot of the percentage of ($\alpha$1 → 6) linkages in the IMMP products versus the percentage of apparent amylose in 16 starch substrates (see Table 1). The IMMP derived of amylose V is also indicated (filled circle), but is excluded from the linear regression. (b) Plot of the percentage of ($\alpha$1 → 6) linkages in the IMMP products versus the degree of ($\alpha$1 → 4,6) branching of eight starch substrates (see Table S1 of the Supporting Information).

capped with an ($\alpha$1 → 6)-linked glucose unit, which cannot be cleaved by GTFB at a measurable rate, which would effectively prohibit the further synthesis of IMMPs as there are no longer glucose donor substrates available. Note here that Amylose V is a slightly degraded amylose, as a result of the extraction procedure used to isolate it from regular potato starch. There are thus some shorter ($\alpha$1 → 4)-glucan chains that may serve as initial acceptor substrates. Starting with relative short acceptor substrates, instead of longer ($\alpha$1 → 4)-glucan chains, also ensures that less of the potential glucose donor substrates become inaccessible as donor substrate for GTFB due to the formation of the first ($\alpha$1 → 6) linkage at the nonreducing end of a long ($\alpha$1 → 4)-glucan chain. Overall, it is clear that native (gelatinized) starches are good substrates of GTFB and that high amylose starches can be converted into IMMPs with up to 70% ($\alpha$1 → 6) linkages (Table 1).

**Debranched Starches Are Efficient Substrates of GTFB.** Because high amylose starches are the preferred substrates of GTFB, it may be rationalized that debranched starches will deliver IMMPs with a higher percentage of ($\alpha$1 → 6) linkages compared to their native starches. However, this required confirmation as debranched amylopectin is composed of relatively low DP $\alpha$-glucan chains compared to native amylose chains. The experiment indeed demonstrated that all debranched $\alpha$-glucans evaluated are substrates of GTFB, producing IMMP products with over 60% of ($\alpha$1 → 6) linkages (Table 1). Even glycogen, which itself is not converted into IMMP by GTFB, becomes a substrate upon debranching. Since glycogens have about 7−10% branching, these results as such demonstrate that relative short chains with an average DP of around 10 are long enough to be converted into IMMPs with over 60% of ($\alpha$1 → 6) linkages. The higher percentage of ($\alpha$1 → 6) linkages obtained with isoamylase-debranched Etenia (4-$\alpha$-glucanotransferase-treated potato starch) compared to pullulanase-debranched Etenia, is in agreement with the typical incomplete hydrolysis of branches obtained with pullulanase.

In an industrial setting, it would be advantageous to perform the debranching and GTFB reactions simultaneously in a single reactor. Such one pot reactions are, in addition, also expected to slow down the retrogradation of the linear ($\alpha$1 → 4)-glucan chains resulting from debranching, as the in situ formed ($\alpha$1 → 4)-glucans can be directly utilized by GTFB. Since both GTFB and debranching enzymes (isoamylase as well as pullulanase) require slightly acidic conditions the tandem reaction is expected to work well. As proof of concept experiment, potato starch and waxy potato starch were converted into IMMP with GTFB under standard reaction conditions in the presence of pullulanase or isoamylase, respectively. This yielded products with 92 and 83% ($\alpha$1 → 6)-glycosidic bonds, which is much higher than without the debranching enzyme treatment (Table 1). Thus, incubations with debranching enzyme plus GTFB yield IMMPs with a high percentage of ($\alpha$1 → 6) linkages from starches with a regular amylose content or even waxy starches and glycogen.

**Molecular Structures of the IMMP Products.** To further explore the structural characteristics of the IMMP products, the IMMP generated of maltodextrin Paselli MD10 (average DP = 12) (Figure 1) was separated using Bio-Gel P-2 size-exclusion chromatography, yielding six fractions, denoted **F1**−**F6** (data not shown). MALDI-TOF-MS analysis showed that fraction **F1** contained polymeric material of DP > 30, **F2** mainly DP13−30, **F3** mainly DP10-DP17, **F4** mainly DP8-DP11, **F5** mainly DP5-DP7 and **F6** mainly DP3-DP5. Subsequent $^1$H NMR analysis, comparing the peak areas of the ($\alpha$1 → 4)- and ($\alpha$1 → 6)-related H-1 signals, demonstrated that the fractions consisting of DP8-DP30 $\alpha$-glucans (**F2**−**F3**−**F4**) have slightly more ($\alpha$1 → 6) than ($\alpha$1 → 4) linkages, whereas the shorter (**F5**−**F6**) and larger (**F1**) molecules have more ($\alpha$1 → 4) than ($\alpha$1 → 6) linkages (Figure 3). The fractions **F3** and **F6** were further

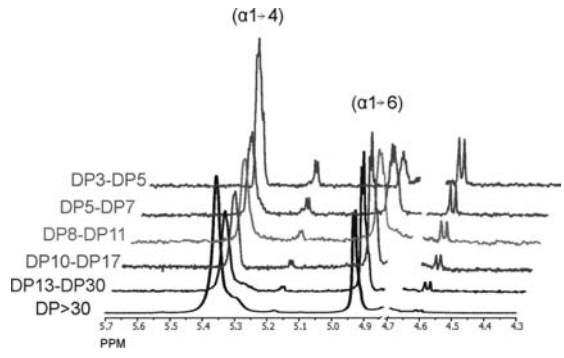


**Figure 3.** Anomeric regions of the $^1$H NMR spectra of Bio-Gel P-2 fractions **F1**−**F6**, varying in DP ranges, of the IMMP product derived of Paselli MD10 maltodextrin. The IMMP fractions in the DP8-DP30 range contain a higher percentage of ($\alpha$1 → 6) linkages, compared with the ($\alpha$1 → 4) linkages present.

fractionated by HPAEC on CarboPac PA-1 (Figure 4A/B) to yield fractions containing compounds of a single DP according to MALDI-TOF-MS analysis, that is, for **F3** compounds 1−7 and for **F6** compounds 8−10. The structures of the 10 oligosaccharides were elucidated by one- and two-dimensional NMR spectroscopy, making use of published $^1$H NMR data of a series of GTFB products prepared from short malto-

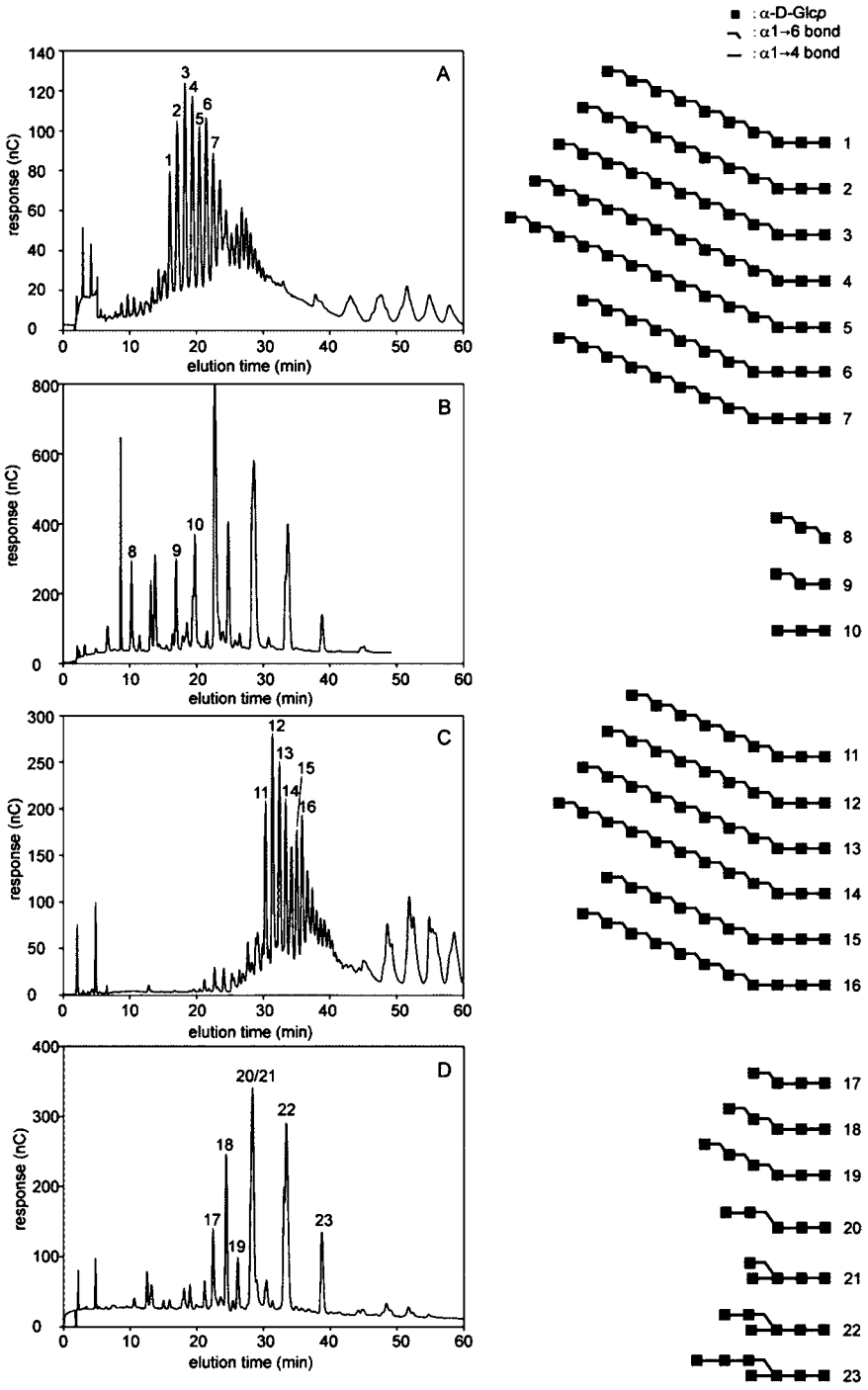


**Figure 4.** HPAEC separations on CarboPac PA-1 of Bio-Gel P-2 fractions, prepared from the IMMP product derived of Paselli MD10 maltodextrin before (A and B) and after (C and D) α-amylase treatment, together with 23 assigned α-glucan structures. (A) Profile of fraction **F3** (elution gradient 15−40% of 600 mM sodium acetate in 100 mM sodium hydroxide in 60 min); (B) Profile of fraction **F6** (elution gradient 5−28.5% in 40 min); (C) Profile of fraction **F′5** (5−50% in 78 min); and (D) Profile of fraction **F′7** (5−40% in 60 min).

oligosaccharides.[25,30] The identified α-glucan structures are depicted in Figure 4A/B, showing for **F3** long isomalto-elongations of maltotriose and maltotetraose and for **F6** maltotriose, panose, and isomaltotriose.

The IMMP product derived of Paselli MD10 was also treated with α-amylase, followed by fractionation on Bio-Gel P-2, yielding nine fractions, denoted **F′1**−**F′9** (data not shown). The α-amylase treatment resulted in a large amount of maltose (**F′9**), but also about 30% oligosaccharides and small polysaccharides. The fraction with the highest molecular masses (**F′1**, DP 17−35; MALDI-TOF-MS analysis) is composed of linear α-glucans (i.e., without branches) and has about 90% (α1 → 6) linkages ($^1$H NMR analysis). This demonstrates that GTFB is able to synthesize product mixtures that contain linear α-glucans with a DP up to 35. Possibly even larger α-glucans are present, but these are much harder to detect with MALDI-TOF-MS. Fractions **F′5** (DP9-DP16) and **F′7** (DP4-DP7) were further fractionated by HPAEC (Figure 4C/D), and the major peaks were isolated to yield for **F′5** compounds 11−16 and for **F′7** compounds 17−23. The


dx.doi.org/10.1021/jf503970a | J. Agric. Food Chem. 2014, 62, 12034−12044

structures of the 13 oligosaccharides were elucidated by one- and two-dimensional NMR spectroscopy, following the same approach as described for **F3** and **F6**, and are depicted in Figure 4C/D. Examples of the 1D $^1$H NMR spectra of isolated compounds (i.e., compounds 11, 15, 16, 20/21, 22, and 23 of Figure 4C/D) are shown in the Supporting Information (Supporting Information Figure S2 and S3). The 1D/2D NMR (HSQC, TOCSY, ROESY) spectra of the branched compound 22 (Figure 4D) is depicted and worked out in the Supporting Information (Figure S4). In total three branched molecules were identified, that is, compounds 21, 22, and 23 in the $\alpha$-amylase-treated IMMP, and these are all typical $\alpha$-amylase degradation products of starch.

Overall, the $\alpha$-glucan structures identified in the IMMP product mixtures, derived of Paselli MD10, convincingly demonstrate that GTFB builds linear ($\alpha$1 → 6)-glucan chains onto the nonreducing end of ($\alpha$1 → 4)-chains when acting on starches and maltodextrins, in analogy to the compounds synthesized from short-chain monodisperse (1 → 4)-$\alpha$-D-gluco-oligosaccharides.[23,25]

**IMMPs are Different from Dextran.** The simple fact that IMMPs have two or more glucose moieties linked via an ($\alpha$1 → 4) linkage at its reducing end makes IMMPs a different kind of $\alpha$-glucan than dextran. However, there are additional differences. Dextrans are much larger polymers, which are synthesized from sucrose by dextransucrase enzymes forming fructose as byproduct.[31,32] GTFB, in contrast, synthesizes IMMPs via disproportionation reactions resulting in a polydisperse mixture of small poly- and oligosaccharide molecules. The size of the dextran molecules can, however, be tuned by either the addition of acceptor molecules during synthesis or by partial acid hydrolysis or dextranase enzymes.[33,34] Even though the size of dextran molecules can be matched to that of IMMPs, dextrans also contain branches which are absent in the IMMPs generated by GTFB. Also dextran dextrinase enzymes act on maltodextrins and produce oligosaccharides rich in ($\alpha$1 → 6)-glycosidic bonds. However, dextran dextrinase products possess branches, involving all three $\alpha$-glycosidic linkage types possible: ($\alpha$1 → 2), ($\alpha$1 → 3), and ($\alpha$1 → 4).[21,35,36] Currently available isomalto-oligosaccharides are produced with transglucosidases (i.e., $\alpha$-glucosidases), however, these compounds are much smaller (DPs in the range of 3 to 6) than the IMMPs made by GTFB. These isomalto-oligosaccharides are so small because the transglucosidase enzymes used (i.e., $\alpha$-glucosidases) are glycoside hydrolases that are relative effective in catalyzing disproportionation reactions at the high substrate concentrations employed in production processes. Thus, the IMMPs described in this paper are a novel class of $\alpha$-glucan structures that can only be obtained with GTFB-like enzymes.

**IMMPs Have a High Dietary Fiber Content.** To evaluate the dietary fiber quality of the IMMPs, they were subjected to a dietary fiber analysis. As the procedure used requires larger amounts of carbohydrate, seven IMMP products derived of Paselli MD10, Paselli MD6, Paselli SA2, Eliane MD6, waxy potato starch, and potato starch were produced at ten gram scale, with the percentage of ($\alpha$1 → 6)-glycosidic bonds ranging from 32 to 92% (Figure 5A). The dietary fiber analysis mimics the passage through the human upper gastrointestinal tract and small intestine, by incubating the IMMPs with representative digestive enzymes, that is, $\alpha$-amylase and amyloglucosidase. As expected this treatment degraded maltodextrins completely, whereas the IMMPs were found to

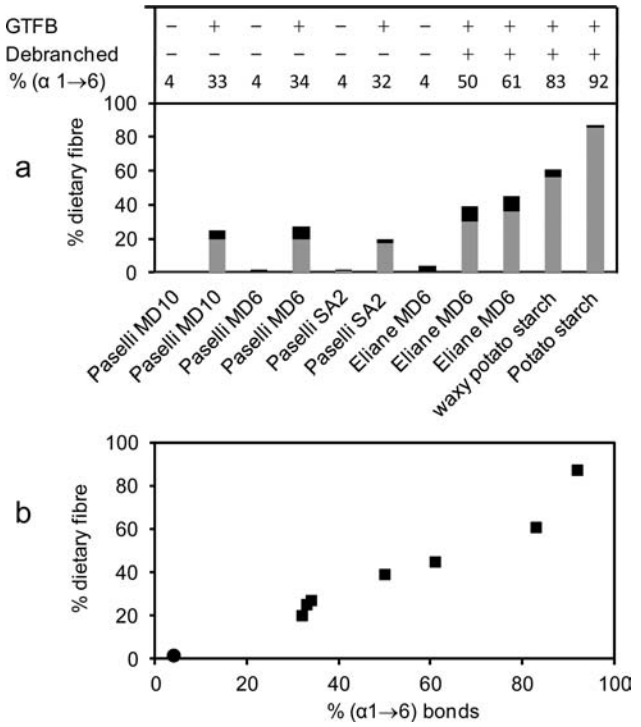


**Figure 5.** Dietary fiber content of seven IMMP products. (a) The percentages of total dietary fibers (height of bar), the high-molecular-weight dietary fiber (HMWDF, gray), and the low-molecular-weight dietary fiber (LMWDF, black) of the IMMP products derived of the indicated substrates. Note that the two Eliane MD6 samples are of incubations that were terminated before completion of the reaction. The numbers and the plus/minus symbols on top indicate the enzymes used in the conversion and the percentage of ($\alpha$1 → 6) linkages in the obtained IMMP product. (b) Increase of the percentage of total dietary fiber with the percentage of ($\alpha$1 → 6)-glycosidic bonds in the IMMP products (black squares). The unmodified maltodextrin Paselli MD6 (filled circle) is included as negative control. The exact numbers are reported in the Supporting Information (Table S2).

have a high dietary fiber fraction, reaching up to 87% (Figure 5A). The dietary fiber material of IMMP is largely composed of high-molecular-weight dietary fiber (HMWDF), which is defined as the fraction that precipitates with 72% ethanol, and a small amount of low-molecular-weight dietary fiber (LMWDF), which is the fraction that is soluble in 72% ethanol and has a DP ≥ 3. The HMWDF fractions obtained of the IMMPs derived of Paselli MD6, MD10 and SA2 maltodextrins were analyzed by $^1$H NMR spectroscopy, revealing that the HMWDF fractions contain about 90% ($\alpha$1 → 6) and 10% ($\alpha$1 → 4) linkages (data not shown). Thus, the dietary fiber analysis protocol specifically degrades the ($\alpha$1 → 4) linkages in the IMMPs products, which is as expected because of the $\alpha$-amylase used in the procedure. The dietary fiber analysis in addition demonstrated that the total dietary fiber fraction increased with the percentage of ($\alpha$1 → 6)-glycosidic bonds (Figure 5B).

Because the above dietary fiber method employs an amyloglucosidase enzyme, which has similar, but not identical, activities than the maltase-glucoamylase and sucrose-isomaltase enzymes of the brush border, two of the IMMP products, with 50 and 92% ($\alpha$1 → 6) linkages (Figure 5A), were also incubated with a rat intestine extract in an effort to closer resemble the digestive power of the small intestinal part of the gastrointestinal tract. The consideration here is that maltase-

glucoamylase and sucrose-isomaltase, which are known to hydrolyze ($\alpha$1 → 6) linkages in the $\alpha$-amylase degradation products of starch, may have a different effectivity toward ($\alpha$1 → 6) linkages in the IMMP products compared to amyloglucosidase. The brush border experiment with Eliane MD6 as example, revealed that as expected, this maltodextrin is rapidly converted into glucose. The 92% ($\alpha$1 → 6) IMMP (derived of potato starch by the combined action of GTFB and pullulanase, Figure 5A) is, in contrast, only very slowly degraded by the rat intestine extract, at the same rate as dextran (Figure 6). After 3 h the maltodextrin is completely converted to glucose, whereas only 9% of the glucose was released of the 92% ($\alpha$1 → 6) IMMP (Figure 6). The 50% ($\alpha$1 → 6) IMMP (derived of Eliane MD6 maltodextrin by the combined action of GTFB and isoamylase, Figure 5A) represents an interesting case. Initially it is degraded like maltodextrin with a rapid release of glucose, after which the further conversion to glucose is slow like that of the 92% ($\alpha$1 → 6) IMMP and dextran. Overall the brush border experiment indicates that the IMMP segments rich in ($\alpha$1 → 6) linkages will largely pass the human small intestine, acting as a soluble dietary fiber, and enter the large intestine were they can serve as carbon and energy source for the large intestine microbiota.

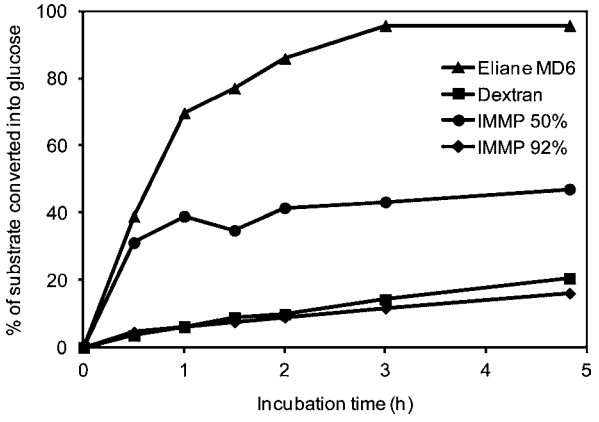


**Figure 6.** Formation of glucose from Eliane MD6 maltodextrin (average DP = 20), dextran (average DP = 37), IMMP derived of Eliane MD6 by the combined action of GTFB and isoamylase debranching enzyme [average DP = 15; 50% ($\alpha$1 → 6) linkages; see Figure 5A] and IMMP derived of potato starch by the combined action of GTFB and pullulanase debranching enzyme [average DP = 50; 92% ($\alpha$1 → 6) linkages; see Figure 5A].

**IMMP Degradation by the Large Intestine Microbiota.** It remained to be studied whether this novel type of dietary fiber is fermented in the large intestine. The human gut microbiota possesses an enormous diversity of carbohydrate degrading enzymes,[37] and short isomalto-oligosaccharides (≪DP10) have been shown to be fermented by the human fecal microbiota in vitro.[38] IMMPs will be partly digested before reaching the large intestine, depending on the percentage of ($\alpha$1 → 6) linkages. The passage through the upper gastrointestinal tract and the small intestine was therefore simulated by subjecting the IMMPs, and the dextran control, first to the dietary fiber analysis method. The HMWDF obtained in this procedure was then used as carbon source in anaerobic fermentations, that were inoculated with a thousand fold diluted fecal sample of one healthy adult human. The IMMP dietary fibers were readily fermented as visualized by a strong increase in the optical density at 600 nm (Figure 7),

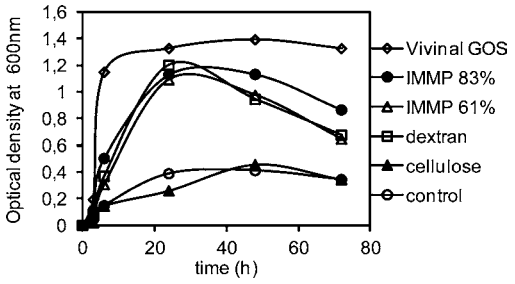


**Figure 7.** Fermentation of IMMP derived of Eliane MD6 by the combined action of GTFB and isoamylase debranching enzyme [61% ($\alpha$1 → 6) linkages; see Figure 5A], IMMP derived of waxy potato starch [83% ($\alpha$1 → 6) linkages; see Figure 5A], Vivinal GOS, dextran, cellulose and no added carbon source (control) by human fecal microbiota. See Materials and Methods for fermentation conditions. The IMMPs and dextran were first subjected to the dietary fiber analysis method, and that 1 g $L^{-1}$ of the obtained HMWDF was added as carbon source, because this is the part of the material that will reach the large intestine. Fermentations were inoculated with a 1,000-fold diluted fecal sample of one healthy adult human, and the optical density was followed in time.

compared to negative control samples with cellulose or without added carbon source. Note that this does not necessarily proof that IMMPs are fermented by the intestinal microbiota of all humans, because individuals significantly differ in their capacity to ferment dietary fibers. The small increase in optical density of these two negative control samples can be explained by the presence of some remaining but still fermentable carbon source in the diluted fecal sample. The faster increase in optical density with the commercially available prebiotic Vivinal GOS (galacto-oligosaccharides), which was included as positive control, is at least partly explained by the presence of glucose in this material. This glucose could not be removed by the dietary fiber method pretreatment, as performed with the IMMPs, simply because no HMWDF fraction is obtained, as the GOS does not precipitate in the dietary fiber analysis method used.

The fermentation experiment with IMMP as added carbon source showed an increased formation of the short fatty acids acetate and propionate compared to the control without added carbon source, after 6, 14, and 48 h. After 48 h, about 150 mg $L^{-1}$ acetate and 80 mg $mL^{-1}$ propionate is formed additional relative to the control. However, because this result is based on a fecal sample of one person only, it is not necessarily true for other individuals as well. Nevertheless, this preliminary result prompts us to further explore IMMPs, which is currently studied in more detail. The key question is whether short chain fatty acids are produced by all individuals of a large group, as these compounds are generally believed to have a positive impact on health.[15,39]

**Conclusions.** In this Article, we report the characterization of IMMP, representing a novel type of soluble dietary fiber, obtained by enzymatic modification of starch and starch-derived maltodextrins using the 4,6-$\alpha$-glucanotransferase GTFB of *Lactobacillus reuteri* 121. This enzyme is unique because it synthesizes completely linear chains of ($\alpha$1 → 6)-glucans onto the nonreducing ends of starch and starch-derived maltodextrin fragments. In the first catalytic cycle an ($\alpha$1 → 4)-glucan chain serves as acceptor substrate. The product displays a non-reducing end glucose moiety linked via an ($\alpha$1 → 6)-glycosidic bond, which apparently represents a better acceptor substrate that is further elongated. This explains the synthesis of products with a high percentage of ($\alpha$1 → 6)-glycosidic linkages.

The percentage of ($\alpha$1 → 6) linkages in the IMMP product can be controlled from 0 to 92% by substrate selection, in- or excluding debranching enzymes, and reaction time or GTFB enzyme concentration. With GTFB only, the highest percentages of ($\alpha$1 → 6) linkages are obtained when utilizing substrates rich in amylose and with a low degree of branching. But basically any starch compound can serve as good substrate, simply by using a debranching enzyme prior or during the incubation of starch with the GTFB enzyme.

Dietary fiber analysis methods, serving as in vitro models for the upper gastrointestinal tract and the small intestine, revealed that the dietary fiber content of the IMMPs is proportional to the fraction of ($\alpha$1 → 6) linkages in IMMP. The dietary fiber material remaining after this procedure, i.e. the material that will enter the large intestine, was used as carbon source by the large intestine microbiota. However, because the microbiota was of one person only it cannot yet been concluded that IMMPs are fermented by the intestinal microbiota of other individuals.

Thus, IMMPs represent a novel type of dietary fiber, and may constitute a new type of prebiotic.[43] Additional research is required to obtain solid evidence for the latter. Focus is on the identification of the groups of bacteria that ferment the IMMP dietary fibers. We still need to show that the IMMP dietary fibers reach the large intestine and promote the growth of beneficial microorganisms by in vivo studies in human subjects.

To conclude, this Article reports on a novel type of soluble dietary fiber, IMMP, which is produced by enzymatic modification of starch and is fermented by the microbiota of the large intestine.

## ■ ASSOCIATED CONTENT

### Supporting Information

Degree of branching of eight starches, dietary fiber content of IMMPs derived of indicated substrates, 1D $^1$H NMR spectra of (a) amylose V and (b) the IMMP product mixture derived of amylose V upon incubation with GTFB, 1D $^1$H NMR spectra of linear compounds 11 (a), 15 (b), and 16 (c) from Figure 4 of the main text, 1D $^1$H NMR spectra of branched compounds 21 (a), 22 (b), and 23 (c) from Figure 4 of the main text, and 1D/2D $^1$H NMR spectra of compound 22 from Figure 4 of main text. This material is available free of charge via the Internet at http://pubs.acs.org.

## ■ AUTHOR INFORMATION


### Corresponding Author

*Tel: 31-50-3632150. Fax: 31-50-3632154. E-mail: L. Dijkhuizen@rug.nl.

### Present Address

△M.J.E.C.v.d.M.: Aquatic Biotechnology and Bioproduct Engineering, Institute for Technology and Management, University of Groningen, Groningen, The Netherlands.



### Funding

This project is part-financed by the European Union, European Regional Development Fund and The Ministry of Economic Affairs, Agriculture and Innovation, Peaks in the Delta, the Municipality of Groningen, the Provinces of Groningen, Fryslân and Drenthe, as well as the Dutch Carbohydrate Competence Center (CCC WP2c).


### Notes

The authors declare no competing financial interest.

## ■ ABBREVIATIONS USED

DP, degree of polymerization; GOS, galacto-oligosaccharides; HMWDF, high-molecular-weight dietary fiber; HPAEC, high-pH anion-exchange chromatography; HSQC, heteronuclear single quantum coherence; IMMP, isomalto/malto-polysaccharide; LMWDF, low-molecular-weight dietary fiber; MALDI-TOF-MS, matrix-assisted laser-desorption ionization time-of-flight mass spectrometry; NMR, nuclear magnetic resonance; ROESY, rotating frame Overhauser enhancement spectroscopy; SDS, slowly digestible starch; TDF, total dietary fiber; TOCSY, total correlation spectroscopy

## ■ REFERENCES


(1) Buchholz, K.; Seibel, J. Industrial carbohydrate biotransformations. *Carbohydr. Res.* **2008**, *343*, 1966−1979.

(2) BeMiller, J.; Whistler, R. *Starch: Chemistry and Technology*; Elsevier, Academic Press: Amsterdam, 2009.

(3) Kaur, B.; Ariffin, F.; Bhat, R.; Karim, A. A. Progress in starch modification in the last decade. *Food Hydrocolloids* **2012**, *26*, 398−404.

(4) Van der Maarel, M. J. E. C.; Leemhuis, H. Starch modification with microbial alpha-glucanotransferase enzymes. *Carbohydr. Polym.* **2013**, *93*, 116−121.

(5) Kajiura, H.; Takata, H.; Kuriki, T.; Kitamura, S. Structure and solution properties of enzymatically synthesized glycogen. *Carbohydr. Res.* **2010**, *345*, 817−824.

(6) Palomo, M.; Pijning, T.; Booiman, T.; Dobruchowska, J. M.; van der Vlist, J.; Kralj, S.; Planas, A.; Loos, K.; Kamerling, J. P.; Dijkstra, B. W.; van der Maarel, M. J. E. C.; Dijkhuizen, L.; Leemhuis, H. *Thermus thermophilus* glycoside hydrolase family 57 branching enzyme: crystal structure, mechanism of action, and products formed. *J. Biol. Chem.* **2011**, *286*, 3520−3530.

(7) Lee, C.-K.; Le, Q.-T.; Kim, Y.-H.; Shim, J.-H.; Lee, S.-J.; Park, J.-H.; Lee, K.-P.; Song, S.-H.; Auh, J. H.; Lee, S.-J.; Park, K.-H. Enzymatic synthesis and properties of highly branched rice starch amylose and amylopectin cluster. *J. Agric. Food Chem.* **2008**, *56*, 126−131.

(8) Leemhuis, H.; Kelly, R. M.; Dijkhuizen, L. Engineering of cyclodextrin glucanotransferases and the impact for biotechnological applications. *Appl. Microbiol. Biotechnol.* **2010**, *85*, 823−835.

(9) Hansen, M. R.; Blennow, A.; Pedersen, S.; Nørgaard, L.; Engelsen, S. B. Gel texture and chain structure of amylomaltase-modified starches compared to gelatin. *Food Hydrocolloids* **2008**, *22*, 1551−1566.

(10) Alting, A. C.; van de Velde, F.; Kanning, M. W.; Burgering, M.; Mulleners, L.; Sein, A.; Buwalda, P. Improved creaminess of low-fat yoghurt: The impact of amylomaltase-treated starch domains. *Food Hydrocolloids* **2009**, *23*, 980−987.

(11) Janeček, S.; Svensson, B.; MacGregor, E. A. $\alpha$-Amylase: An enzyme specificity found in various families of glycoside hydrolases. *Cell. Mol. Life Sci.* **2014**, *71*, 1149−1170.

(12) Ludwig, D. S. The glycemic index: Physiological mechanisms relating to obesity, diabetes, and cardiovascular disease. *J. Am. Med. Assoc.* **2002**, *287*, 2414−2423.

(13) Lattimer, J. M.; Haub, M. D. Effects of dietary fiber and its components on metabolic health. *Nutrients* **2010**, *2*, 1266−1289.

(14) Howarth, N. C.; Saltzman, E.; Roberts, S. B. Dietary fiber and weight regulation. *Nutr. Rev.* **2001**, *59*, 129−139.

(15) Rastall, R. A. Functional oligosaccharides: Application and manufacture. *Annu. Rev. Food Sci. Technol.* **2010**, *1*, 305−339.

(16) Englyst, K. N.; Englyst, H. N.; Hudson, G. J.; Cole, T. J.; Cummings, J. H. Rapidly available glucose in foods: an in vitro measurement that reflects the glycemic response. *Am. J. Clin. Nutr.* **1999**, *69*, 448−454.

(17) Ao, Z.; Simsek, S.; Zhang, G.; Venkatachalam, M.; Reuhs, B. L.; Hamaker, B. R. Starch with a slow digestion property produced by altering its chain length, branch density, and crystalline structure. *J. Agric. Food Chem.* **2007**, *55*, 4540−4547.

(18) Lee, B.-H.; Yan, L.; Phillips, R. J.; Reuhs, B. L.; Jones, K.; Rose, D. R.; Nichols, B. L.; Quezada-Calvillo, R.; Yoo, S.-H.; Hamaker, B. R. Enzyme-synthesized highly branched maltodextrins have slow glucose generation at the mucosal α-glucosidase level and are slowly digestible in vivo. *PLoS One* **2013**, *8*, e59745.
(19) Tsusaki, K.; Watanabe, H.; Yamamoto, T.; Nishimoto, T.; Chaen, H.; Fukuda, S. Purification and characterization of highly branched α-glucan-producing enzymes from *Paenibacillus* sp. PP710. *Biosci. Biotechnol. Biochem.* **2012**, *76*, 721−731.
(20) Ota, M.; Okamoto, T.; Wakabayashi, H. Action of transglucosidase from *Aspergillus niger* on maltoheptaose and [U-$^{13}$C]-maltose. *Carbohydr. Res.* **2009**, *344*, 460−465.
(21) Wang, S.; Mao, X.; Wang, H.; Lin, J.; Li, F.; Wei, D. Characterization of a novel dextran produced by *Gluconobacter oxydans* DSM 2003. *Appl. Microbiol. Biotechnol.* **2011**, *91*, 287−294.
(22) Hehre, E. J. The biological synthesis of dextran from dextrins. *J. Biol. Chem.* **1951**, *192*, 161−174.
(23) Kralj, S.; Grijpstra, P.; van Leeuwen, S. S.; Leemhuis, H.; Dobruchowska, J. M.; van der Kaaij, R. M.; Malik, A.; Oetari, A.; Kamerling, J. P.; Dijkhuizen, L. 4,6-α-Glucanotransferase, A novel enzyme that structurally and functionally provides an evolutionary link between glycoside hydrolase enzyme families 13 and 70. *Appl. Environ. Microbiol.* **2011**, *77*, 8154−8163.
(24) Leemhuis, H.; Dijkman, W. P.; Dobruchowska, J. M.; Pijning, T.; Grijpstra, P.; Kralj, S.; Kamerling, J. P.; Dijkhuizen, L. 4,6-α-Glucanotransferase activity occurs more widespread in *Lactobacillus* strains and constitutes a separate GH70 subfamily. *Appl. Microbiol. Biotechnol.* **2013**, *97*, 181−193.
(25) Dobruchowska, J. M.; Gerwig, G. J.; Kralj, S.; Grijpstra, P.; Leemhuis, H.; Dijkhuizen, L.; Kamerling, J. P. Structural characterization of linear isomalto-/malto-oligomer products synthesized by the novel GTFB 4,6-α-glucanotransferase enzyme from *Lactobacillus reuteri* 121. *Glycobiology* **2012**, *22*, 517−528.
(26) Van Leeuwen, S. S.; Leeflang, B. R.; Gerwig, G. J.; Kamerling, J. P. Development of a $^{1}$H NMR structural-reporter-group concept for the primary structural characterisation of α-D-glucans. *Carbohydr. Res.* **2008**, *343*, 1114−1119.
(27) Van der Kaaij, R. M.; Sanders, P.; Drost, W. C.; Nagtegaal, R. M. A.; van Wandelen, M. T. R.; Burgering, M. J. M.; van der Kamp, J.-W. All-in-one measurement of dietary fibre, including resistant starch, in bread. *Qual. Assur. Saf. Crops Foods* **2009**, *1*, 256−260.
(28) McCleary, B. V. An integrated procedure for the measurement of total dietary fibre (including resistant starch), non-digestible oligosaccharides and available carbohydrates. *Anal. Bioanal. Chem.* **2007**, *389*, 291−308.
(29) Kabel, M. A.; Kortenoeven, L.; Schols, H. A.; Voragen, A. G. J. In vitro fermentability of differently substituted xylo-oligosaccharides. *J. Agric. Food Chem.* **2002**, *50*, 6205−6210.
(30) Dobruchowska, J. M.; Meng, X.; Leemhuis, H.; Gerwig, G. J.; Dijkhuizen, L.; Kamerling, J. P. Gluco-oligomers initially formed by the reuteransucrase enzyme of *Lactobacillus reuteri* 121 incubated with sucrose and malto-oligosaccharides. *Glycobiology* **2013**, *23*, 1084−1096.
(31) Leemhuis, H.; Pijning, T.; Dobruchowska, J. M.; van Leeuwen, S. S.; Kralj, S.; Dijkstra, B. W.; Dijkhuizen, L. Glucansucrases: Three-dimensional structures, reactions, mechanism, α-glucan analysis and their implications in biotechnology and food applications. *J. Biotechnol.* **2013**, *163*, 250−272.
(32) Moulis, C.; Joucla, G.; Harrison, D.; Fabre, E.; Potocki-Veronese, G.; Monsan, P.; Remaud-Simeon, M. Understanding the polymerization mechanism of glycoside-hydrolase family 70 glucansucrases. *J. Biol. Chem.* **2006**, *281*, 31254−31267.
(33) Goulas, A. K.; Cooper, J. M.; Grandison, A. S.; Rastall, R. A. Synthesis of isomaltooligosaccharides and oligodextrans in a recycle membrane bioreactor by the combined use of dextransucrase and dextranase. *Biotechnol. Bioeng.* **2004**, *88*, 778−787.
(34) Naessens, M.; Cerdobbel, A.; Soetaert, W.; Vandamme, E. J. *Leuconostoc* dextransucrase and dextran: production, properties and applications. *J. Chem. Technol. Biotechnol.* **2005**, *80*, 845−860.
(35) Sims, I. M.; Thomson, A.; Hubl, U.; Larsen, N. G.; Furneaux, R. H. Characterisation of polysaccharides synthesised by *Gluconobacter oxydans* NCIMB 4943. *Carbohydr. Polym.* **2001**, *45*, 285−292.
(36) Yamamoto, K.; Yoshikawa, K.; Okada, S. Structure of dextran synthesized by dextrin dextranase from *Acetobacter capsulatus* ATCC 11894. *Biosci. Biotechnol. Biochem.* **1993**, *57*, 1450−1453.
(37) El Kaoutari, A.; Armougom, F.; Gordon, J. I.; Raoult, D.; Henrissat, B. The abundance and variety of carbohydrate-active enzymes in the human gut microbiota. *Nat. Rev. Microbiol.* **2013**, *11*, 497−504.
(38) Sarbini, S. R.; Kolida, S.; Gibson, G. R.; Rastall, R. A. *In vitro* fermentation of commercial α-gluco-oligosaccharide by faecal microbiota from lean and obese human subjects. *Br. J. Nutr.* **2013**, *109*, 1980−1989.
(39) Kumar, V.; Sinha, A. K.; Makkar, H. P. S.; de Boeck, G.; Becker, K. Dietary roles of non-starch polysaccharides in human nutrition: A review. *Crit. Rev. Food Sci. Nutr.* **2012**, *52*, 899−935.
(40) Peroni, F. H. G.; Rocha, T. S.; Franco, C. M. L. Some structural and physicochemical characteristics of tuber and root starches. *Food Sci. Technol. Int.* **2006**, *12*, 505−513.
(41) Jane, J.; Chen, Y. Y.; Lee, L. F.; McPherson, A. E.; Wong, K. S.; Radosavljevic, M.; Kasemsuwan, T. Effects of amylopectin branch chain length and amylose content on the gelatinization and pasting properties of starch. *Cereal Chem.* **1999**, *76*, 629−637.
(42) Sang, Y.; Bean, S.; Seib, P. A.; Pedersen, J.; Shi, Y.-C. Structure and functional properties of sorghum starches differing in amylose content. *J. Agric. Food Chem.* **2008**, *56*, 6680−6685.
(43) Dijkhuizen, L.; van der Maarel, M. J. E. C.; Kamerling, J. P.; Leemhuis, R. J.; Kralj, S.; Dobruchowska, J. M. Gluco-oligosaccharides comprising (alpha→4) and (alpha1→6) glycosidic bonds, use thereof, and methods for providing them. Int. Patent WO 2010/128859 A2, 2010.

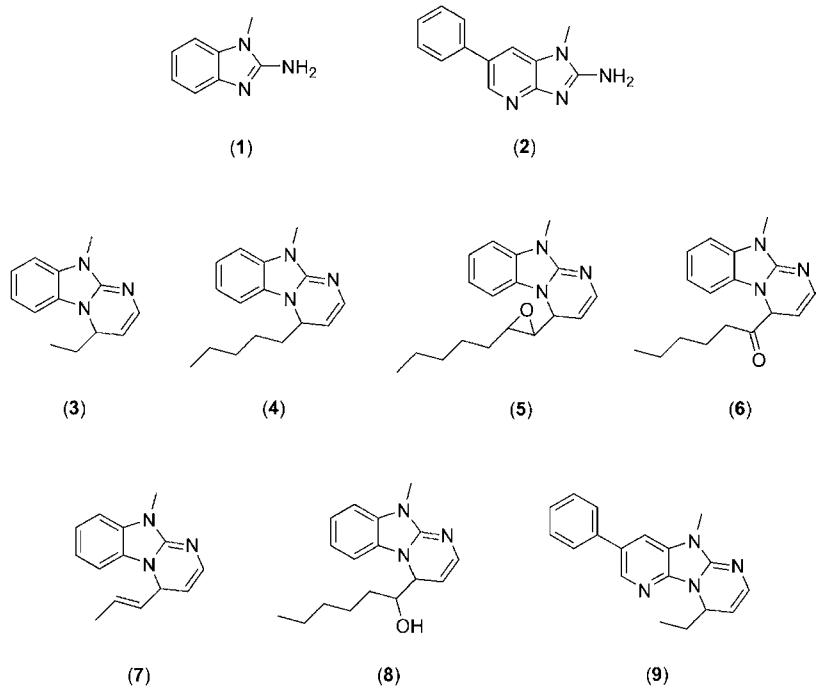


**Figure 1.** Chemical structures of the 2-aminoimidazoles (**1** and **2**) employed in this study and the adducts formed in their reactions with lipid-derived carbonyl compounds.

an Agilent 5973 MSD (mass selective detector, quadrupole type). Liquid chromatography−tandem mass spectrometry (LC−MS/MS) analyses were conducted by using an Agilent liquid chromatography system (1200 Series) consisting of a binary pump (G1312A), a degasser (G1379B), and an autosampler (G1329A), connected to a triple-quadrupole API 2000 mass spectrometer (Applied Biosystems) using an electrospray ionization interface in positive ionization mode ($ESI^+$). High-resolution mass spectra (HRMA) were recorded with a micrOTOF-QII mass spectrometer from Bruker equipped with an electrospray ionization source in positive ionization mode ($ESI^+$). $^1H$ and $^{13}C$ NMR spectra at 300 and 75.4 MHz, respectively, were recorded with a Bruker AC-300P instrument with tetramethylsilane as an internal standard.

Different reactive carbonyls derived from both $\omega$−6 and $\omega$−3 fatty acids were employed in these studies. Alkenals (2-octenal and 2-pentenal) and alkadienals (2,4-decadienal, 2,4-heptadienal, and 2,4-hexadienal) were purchased from Aldrich (Milwaukee, WI). Epoxyalkenals (4,5-epoxy-2-decenal and 4,5-epoxy-2-heptenal) were prepared by epoxidation of alkadienals (2,4-decadienal and 2,4-heptadienal, respectively) with 3-chloroperoxybenzoic acid.[14,15] Oxoalkenals (4-oxo-2-nonenal and 4-oxo-2-hexenal) were synthesized from 2-alkylfurans (2-pentylfuran and 2-ethylfuran, respectively) with *N*-bromosuccinimide.[16,17] 4-Hydroxy-2-nonenal was prepared according to the procedure of Gardner et al.[18]

PhIP was purchased from Toronto Research Chemicals (North York, ON). All other chemicals were purchased from Aldrich, Sigma (St. Louis, MO), Fluka (Buchs, Switzerland), or Merck (Darmstadt, Germany) and were analytical grade.

**Reaction of AMBI with Lipid-Derived Reactive Carbonyls.** A solution of AMBI (5 $\mu$mol in 100 $\mu$L of methanol), the reactive carbonyl (20 $\mu$mol in 170 $\mu$L of methanol), and 230 $\mu$L of 100 mM sodium phosphate buffer (pH 7.4) was heated for 15 h in closed test tubes at 37 °C. At the end of the heating period, samples were cooled and the formed adducts were studied by GC−MS.

In addition to the heating at 37 °C, other samples were also heated for 15 h at 100 °C in sodium citrate buffer (pH 5.0). The obtained results were similar, but reaction yields changed. The most stable adducts were produced with 2-alkenals, and these adducts were formed to a higher extent at high temperatures. When the reactive carbonyls had more functions than the aldehyde group and the carbon−carbon double bond, the produced adduct was more unstable. These adducts were better observed when heating was conducted at 37 °C.

To fully characterize the produced adducts, 2-pentenal was selected as the reactive carbonyl because the corresponding adduct was produced to a higher extent and was fairly stable. Thus, a mixture of AMBI and 2-pentenal heated at 100 °C overnight was fractionated by column chromatography using a diethyl ether/ethanol mixture (1:2) as the eluent. The formed adduct was identified as 2,10-dihydro-2-ethyl-10-methylpyrimido[1,2-*a*]benzimidazole (**3**) by one- and two-dimensional (2D) nuclear magnetic resonance (NMR) spectroscopy and high-resolution mass spectrometry (HRMS). Chemical structures of this and other adducts identified in this study are shown in Figure 1. $^1H$ NMR (300 MHz, $CDCl_3$): $\delta$ 0.88 (t, 3H, $J$ = 7.5 Hz, $C\underline{H}_3CH_2$), 1.25 (m, 2H, $CH_3C\underline{H}_2$), 3.46 (s, 3H, $NC\underline{H}_3$), 4.72 (dd, 1H, $J$ = 3.8 Hz, $J$ = 7.3 Hz, H3), 5.20 (m, 1H, H4), 6.60 (dd, 1H, $J$ = 1.2 Hz, $J$ = 7.3 Hz, H2), 7.05 (m, 4H, H6, H7, H8, H9). $^{13}C$ NMR (75.4 MHz, $CDCl_3$): $\delta$ 7.72 ($\underline{C}H_3CH_2$), 27.40 ($N\underline{C}H_3$), 29.70 ($CH_3\underline{C}H_2$), 54.43 (C4), 99.17 (C3), 106.87 and 107.79 (C6 and C9), 120.88 and 121.63 (C7 and C8), 129.66 and 131.91 (C5a and C9a), 135.88 (C2), 150.52 (C10a). HRMS: $m/z$ 427.259892 ($[2M + H]^+$, error of 1 ppm) and 214.133661 ($[2M + 2H]^{2+}$, error of 1 ppm).

**Study of AMBI/Reactive Carbonyl Adducts by GC−MS.** The formation of adducts between AMBI and lipid-derived reactive carbonyls was studied by GC−MS. Compounds were separated using a fused-silica HP5-MS capillary column (30 m × 0.25 m inside diameter; coating thickness, 0.25 $\mu$m) and injecting 1 $\mu$L of sample in the chromatograph in pulsed splitless mode. Working conditions were as follows: carrier gas, helium (1 mL/min at a constant flow); injector, 250 °C; oven temperature-programmed from 40 °C (1 min) to 240 °C at a rate of 5 °C/min and then to 300 °C at a rate of 10 °C/min; transfer line to MSD, 280 °C; ionization EI, 70 eV; ion source temperature, 230 °C; and mass range, 28−550 amu.

**Reaction of PhIP with 2-Pentenal.** A solution of PhIP (1 $\mu$mol in 150 $\mu$L of methanol), the reactive carbonyl (4 $\mu$mol), and 350 $\mu$L of 300 mM sodium citrate buffer (pH 5.0) was heated overnight in closed test tubes at 100 °C. At the end of the heating period, samples were cooled (5 min at room temperature and 10 min at −20 °C), and the formed adduct was studied by HRMS. HRMS: $m/z$ 581.309905 ($[2M + H]^+$, error of 6 ppm) and 291.159583 ($[2M + 2H]^{2+}$, error of 1 ppm).

**Study of PhIP Disappearance in the Presence of Lipid-Derived Reactive Carbonyls.** A solution of PhIP (1 nmol) and the reactive carbonyl (0−40 μmol) in 500 μL of 0.3 M buffer was heated in closed test tubes for the indicated time (0−1, 6, or 24 h) and temperature (60−200 °C). The buffers employed for controlling the reaction pH were sodium citrate buffer (pH 2.15−6), sodium phosphate buffer (pH 6−8), and sodium borate buffer (pH 8−10).

At the end of the heating period, samples were cooled (5 min at room temperature and 10 min at −20 °C) and analyzed to assess PhIP disappearance.

To study PhIP disappearance, 100 μL of the cooled reaction mixtures was diluted with 50 μL of an internal standard solution (1.29 mg of caffeine in 5 mL of a 30:70 mixture of 0.2% formic acid in acetonitrile and 4 mM ammonium acetate), and 850 μL of a 30:70 mixture of 0.2% formic acid in acetonitrile and 4 mM ammonium acetate, and PhIP was determined by LC−MS/MS.

Samples were separated on a Zorbax Eclipse XDB-C18 (150 mm × 4.6 mm, 5 μm) column from Agilent. As the eluent, a 30:70 mixture of 0.2% formic acid in acetonitrile and 4 mM ammonium acetate was used. The mobile phase was delivered at a rate of 0.5 mL/min in isocratic mode. Mass spectrometric detection was performed by using multiple-reaction monitoring (MRM). The nebulizer gas (synthetic air), the curtain gas (nitrogen), and the heater gas (synthetic air) were set at 45, 25, and 50 (arbitrary units), respectively. The collision gas (nitrogen) was set at 5 (arbitrary units). The heater gas temperature was set at 500 °C and the electrospray capillary voltage at 5.5 kV. The fragment ions in MRM mode were produced by collision-activated dissociation of selected precursor ions in the collision cell of the triple quadrupole, and the selected products were analyzed with the second analyzer of the instrument. Three transitions were acquired for the identification of both PhIP and the IS.

To establish the appropriate MRM conditions for the individual compounds, the mass spectrometric conditions were optimized using infusion with a syringe pump to select the most suitable ion transitions for the target analytes. Precursor and product ions used for confirmation purposes and operating conditions were described previously.[17] The $m/z$ 225.0 → $m/z$ 210.1 and $m/z$ 195.2 → $m/z$ 138.0 transitions for PhIP and caffeine, respectively, were used for quantitation purposes in this study.

Quantitation of PhIP was conducted by preparing five standard curves of this compound in 400 μL of 0.3 M sodium phosphate buffer (pH 8.0) and following the whole procedure described above. For each curve, seven different concentration levels of PhIP (0−2 nmol) were used. The PhIP content was directly proportional to the PhIP:IS area ratio ($r > 0.997$; $p < 0.0001$). The limit of detection (LOD), defined as the lowest sample concentration that could be detected with a signal-to-noise ratio (S/N) of >3,[19] was 0.005 nmol. The limit of quantitation (LOQ), defined as the lowest concentration that could be quantified with a precision of <15%, was 0.01 nmol.

**Statistical Analysis.** All data given are means ± the standard deviation of at least three independent experiments. Statistical comparisons among different groups were made using analysis of variance. When significant $F$ values were obtained, group differences were evaluated by the Tukey test.[20] Statistical comparisons were conducted using Origin version 7.0 (OriginLab Corp., Northampton, MA). The significance level is $p < 0.05$ unless otherwise indicated.

## RESULTS AND DISCUSSION

**Reaction between AMBI and 2-Pentenal.** 2-Pentenal reacted with AMBI producing an adduct that could be isolated and characterized by $^1$H and $^{13}$C NMR, and HRMS. Its $^1$H NMR spectrum was quite simple, and the original chain of 2-pentenal could be easily identified in the spectrum of the adduct by using 2D techniques. Thus, the carbonyl carbon of 2-pentenal was converted into an olefinic carbon in the adduct, and a shift of the carbon−carbon double bond of 2-pentenal was produced. In addition, the formed compound had the methyl group and the four aromatic protons of the original AMBI. The $^{13}$C NMR spectrum showed the positions of the 13 carbons of the adduct. According to these spectra, the adduct was identified as 2,10-dihydro-2-ethyl-10-methylpyrimido[1,2-*a*]benzimidazole (**3**). The structure for this compound is shown in Figure 1. Additional confirmation of the structure was obtained by HRMS. Curiously, compound **3** did not produce the usual $[M + H]^+$ ion, but ions $[2M + H]^+$ and $[2M + 2H]^{2+}$, the second one being the main ion. Compound **3** was fluorescent with excitation and emission maxima at 343 and 458 nm, respectively (Figure S1A of the Supporting Information).

**Reaction between AMBI and Other Lipid-Derived Reactive Carbonyls.** The reaction between AMBI and 2-pentenal described above was general for the different lipid-derived reactive carbonyls assayed, which involved alkenals, alkadienals, oxoalkenals, epoxyalkenals, and hydroxynonenal. All reactions developed fluorescence, and the obtained maxima were similar for all adducts, therefore suggesting a similar structure for all of them. Some the obtained fluorescence spectra are shown in Figure S1A of the Supporting Information.

This similarity among fluorescence spectra of the different adducts was also observed when adducts were studied by GC−MS. Figure S2 of the Supporting Information shows some of the obtained spectra. As one can see, the mass spectrum of adduct **3** produced between AMBI and 2-pentenal showed the molecular ion ($m/z$ 213) and a base ion at $m/z$ 184 that resulted from the loss of the ethyl chain (Figure S2A of the Supporting Information). A similar spectrum was obtained for the adduct **4** produced between AMBI and 2-octenal (Figure S2B of the Supporting Information). Thus, the molecular ion ($m/z$ 255) and the base ion at $m/z$ 184, resulting from the loss of the pentyl chain, were easily observed.

The reaction between AMBI and epoxyalkenals also produced adducts having analogous mass spectra. Thus, the spectrum obtained for adduct **5** resulting from the reaction between AMBI and 4,5-epoxy-2-octenal is shown in Figure S2C of the Supporting Information. This spectrum had the molecular ion at $m/z$ 297 and the base ion at $m/z$ 184 produced by the loss of the chain. An other important ion appeared at $m/z$ 281. This ion was produced by the loss of oxygen, which is in agreement with the presence of the epoxide ring.

The reaction between AMBI and oxoalkenals also produced adducts having similar mass spectra. Figure S2D of the Supporting Information shows the spectrum of adduct **6** produced between AMBI and 4-oxo-2-nonenal. This spectrum was also analogous to the other spectra, and the molecular ion at $m/z$ 283 and the base ion at $m/z$ 184 were the main ions in the spectrum.

The adducts between AMBI and 2,4-alkadienals were produced to an extent much lower than that of the previous adducts. Nevertheless, adduct **7** was produced between AMBI and 2,4-hexadienal. It also exhibited the characteristic molecular ion at $m/z$ 225 and the base ion at $m/z$ 184 (Figure S2E of the Supporting Information).

Finally, an adduct between AMBI and 4-hydroxy-2-nonenal was also produced, and its spectrum is shown in Figure S2F of the Supporting Information. It also exhibited the molecular ion at $m/z$ 285 and a fractionation pattern compatible with the dehydration of the adduct (Figure S2F of the Supporting Information). However, the base ion appeared at $m/z$ 186 and not at $m/z$ 184. For this reason, it is only tentatively assigned as adduct **8**. To obtain an additional confirmation of the structure

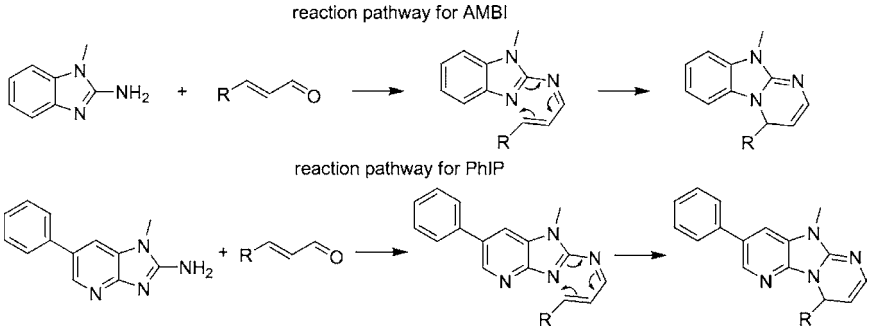


**Figure 2.** Proposed pathways for the formation of adducts between 2-amino-1-methylbenzimidazole (AMBI) or 2-amino-1-methyl-6-phenylimidazo[4,5-*b*]pyridine (PhIP) and lipid-derived reactive carbonyls.

**Table 1. Effect of Lipid-Derived Reactive Carbonyls on the Disappearance of PhIP as a Function of Heating Time and Temperature**[a]

| | 60 °C | | 100 °C | | 150 °C | | 200 °C |
|---|---|---|---|---|---|---|---|
| reactive carbonyl | 6 h | 24 h | 6 h | 24 h | 6 h | 24 h | 6 h |
| none | 1.98 ± 0.08 | 1.94 ± 0.05 | 1.99 ± 0.20 | 2.03 ± 0.11 | 2.02 ± 0.18 | 1.99 ± 0.33 | 1.13 ± 0.14 |
| 2-pentenal | 1.86 ± 0.26 | 1.02 ± 0.12[d] | 0.96 ± 0.02[d] | 0.26 ± 0.08[d] | 0.48 ± 0.08[d] | 0.10 ± 0.02[d] | 0.38 ± 0.08[c] |
| 2-octenal | 1.58 ± 0.06[c] | 1.28 ± 0.16[c] | 1.14 ± 0.12[c] | 0.44 ± 0.02[d] | 0.56 ± 0.06[d] | 0.28 ± 0.06[d] | 0.70 ± 0.12[b] |
| 2,4-heptadienal | 1.90 ± 0.12 | 1.84 ± 0.22 | 1.78 ± 0.28 | 1.60 ± 0.26 | 1.00 ± 0.18[c] | 0.40 ± 0.20[c] | 0.96 ± 0.10 |
| 2,4-decadienal | 1.98 ± 0.06 | 1.66 ± 0.14[b] | 1.88 ± 0.14 | 1.40 ± 0.20[c] | 1.14 ± 0.24[c] | 0.38 ± 0.08[c] | 0.84 ± 0.12 |
| 4,5-epoxy-2-heptenal | 2.04 ± 0.22 | 1.70 ± 0.28 | 1.22 ± 0.42[b] | 0.48 ± 0.06[d] | 0.96 ± 0.24[c] | 0.68 ± 0.16[c] | 0.38 ± 0.26[b] |
| 4,5-epoxy-2-decenal | 1.30 ± 0.04[d] | 0.66 ± 0.02[d] | 0.66 ± 0.06[d] | 0.24 ± 0.02[d] | 0.59 ± 0.06[d] | 0.22 ± 0.02[d] | 0.34 ± 0.12[c] |
| 4-oxo-2-hexenal | 1.72 ± 0.26 | 1.62 ± 0.14[b] | 1.66 ± 0.36 | 1.46 ± 0.12[c] | 1.05 ± 0.14[c] | 0.66 ± 0.16[c] | 0.66 ± 0.06[c] |
| 4-oxo-2-nonenal | 1.00 ± 0.06[d] | 0.54 ± 0.02[d] | 0.60 ± 0.04[d] | 0.34 ± 0.12[d] | 0.38 ± 0.10[d] | 0.32 ± 0.06[d] | 0.32 ± 0.08[d] |
| 4-hydroxy-2-nonenal | 1.86 ± 0.16 | 0.70 ± 0.14[d] | 1.00 ± 0.06[c] | 0.88 ± 0.18[d] | 0.80 ± 0.06[d] | 0.66 ± 0.08[c] | 0.74 ± 0.10[b] |

[a]Mixtures of PhIP (1 nmol) and the lipid (40 μmol) in 500 μL of sodium citrate buffer (pH 5) were heated for 6 or 24 h at the indicated temperatures. Values, in nanomoles of PhIP per milliliter of solution, are means ± the standard deviation of at least three different experiments. [b]For the significance of the differences between means, $p < 0.05$ compared to its control. [c]For the significance of the differences between means, $p < 0.01$ compared to its control. [d]For the significance of the differences between means, $p < 0.001$ compared to its control.

of adduct **8**, its HRMS spectrum was obtained. The $[M + H]^+$ ion appeared at $m/z$ 286.191389, which was close to the expected value (error of 5 ppm).

**Formation of the Adduct between PhIP and Lipid-Derived Reactive Carbonyls.** To confirm that the reaction between AMBI and lipid-derived reactive carbonyls was general for 2-aminoimidazoles, the reaction between the heterocyclic aromatic amine PhIP and 2-pentenal was studied by HRMS. This reaction produced a fluorescent adduct **9** that exhibited ions analogous to AMBI−2-pentenal adduct **3**. Thus, ions $[2M + 2H]^{2+}$ (error of 1 ppm) and $[2M + H]^+$ (error of 6 ppm) were observed.

Fluorescence provided a further confirmation that analogous adducts were also produced in the different reactions between lipid-derived reactive carbonyls and either AMBI or PhIP. As observed in Figure S1B of the Supporting Information, all adducts exhibited a similar fluorescence, and this fluorescence was also similar to that exhibited by AMBI−carbonyl adducts.

**Reaction Pathway for Formation of the Adduct between either AMBI or PhIP and Lipid-Derived Reactive Carbonyls.** The reaction between lipid-derived carbonyl compounds and either AMBI or PhIP is likely to take place as indicated in Figure 2. The primary amino group of the 2-aminoimidazole would react with the carbonyl compound producing the corresponding imine, and a later electronic rearrangement of this imine would produce the reaction product. This cyclization reaction, which does not have to be necessarily concerted (arrows are drawn only to indicate a hypothetical flow of electrons), would be favored because of the formation of a stable heterocyclic structure. This mechanism is valid for all α,β-unsaturated aldehydes, although reaction yields are expected to be different depending on the aldehyde structure. Thus, if the β-carbon belongs to a delocalized electronic system, such as in alkadienals, the reaction should be expected to proceed more difficulty, which was experimentally observed (see below). On the contrary, the reaction should be favored if the β-carbon is activated for the reaction, such as in oxoalkenals. In addition, the stability of the adduct will depend on the presence of functional groups in the side chain of the formed adduct. Thus, the adducts produced with alkenals would be the most stable, as observed.

**PhIP Disappearance in the Presence of Lipid-Derived Reactive Carbonyls.** A consequence of PhIP−carbonyl reactions is the disappearance of PhIP. This may be important as an alternative pathway to decrease the amount of heterocyclic aromatic amines in food products. For that reason, the disappearance of PhIP in the presence of lipid-derived reactive carbonyls was studied.

When PhIP was heated alone, PhIP was stable at most of the assayed temperatures (Table 1). Only when it was heated at 200 °C, did PhIP disappear as a function of heating time. Thus, 43% of PhIP disappeared after 6 h at 200 °C, and this level of disappearance was >80% after 24 h at 200 °C. However, the stability observed for PhIP at temperatures below 200 °C disappeared when PhIP was heated in the presence of lipid-derived reactive carbonyls. Furthermore, the ability of lipid-

derived carbonyls to destroy PhIP depended on the type of carbonyl involved and also on the reaction time and temperature (Table 1). Thus, 4-oxo-2-nonenal and 4,5-epoxy-2-decenal turned out to be the most efficient PhIP scavengers. In the presence of 4-oxo-2-nonenal, 49% of PhIP disappeared after 6 h at 60 °C. A similar treatment produced the disappearance of 34% of PhIP in the presence of 4,5-epoxy-2-decenal. On the other hand, alkadienals turned out to be the least reactive carbonyls for this reaction, and a disappearance of 50% of PhIP in the presence of these compounds was observed only after heating at 150 °C for 6 h.

For oxoalkenals and epoxyalkenals, carbonyls derived from $\omega-6$ fatty acids were usually more reactive than the corresponding reactive carbonyls derived from $\omega-3$ fatty acids. Thus, 4,5-epoxy-2-decenal was more reactive than 4,5-epoxy-2-heptenal, and 4-oxo-2-nonenal was more reactive than 4-oxo-2-hexenal. On the other hand, this difference was not so clear for alkenals and alkadienals, which exhibited mostly similar reactivities regardless of the chain length.

In a manner independent of the carbonyl compound involved, PhIP losses increased, in general, with reaction time and temperature. All carbonyl compounds exhibited significantly ($p < 0.05$) decreased PhIP content after being heated for 6 h at 150 °C, and most of them exhibited significantly ($p < 0.05$) decreased PhIP content after being heated for 24 h at 100 °C.

Because the larger PhIP losses were observed in the presence of 4-oxo-2-nonenal, this compound was employed as the lipid-derived reactive carbonyl to study the best reaction conditions that favored PhIP degradation.

**Effect of Reaction Conditions on PhIP Disappearance in the Presence of 4-Oxo-2-nonenal.** PhIP disappearance depended on the reaction conditions, including the pH, the concentration of the lipid-derived reactive carbonyls, the time, and the temperature. Figure 3 shows the effect of pH on the disappearance of PhIP. PhIP disappearance was mostly produced at pH 4–5 using citrate buffer, although PhIP also disappeared to a large extent at pH 3 and 6, when using the same buffer. The PhIP disappearance rate was much lower at pH <3 or >6. In addition, the PhIP disappearance rate was also lower when using sodium phosphate buffer than when using sodium citrate buffer. The study of other reaction conditions to determine PhIP disappearance was conducted at pH 5.

PhIP disappearance also depended on the amount of 4-oxo-2-nonenal added (Figure 4). In fact, the PhIP disappearance rate increased linearly ($r = 0.97$; $p = 0.0001$) within the range of 0–6 $\mu$mol of 4-oxo-2-nonenal and continued to increase at higher concentrations of the carbonyl compound but to a lesser extent.

The PhIP disappearance rate increased linearly ($r > 0.965$; $p < 0.0018$) as a function of time between 60 and 120 °C (Figure 5). In addition, the PhIP disappearance rate increased when the temperature increased. Reaction rates at the different assayed temperatures were calculated by using the equation

$$\text{PhIP disapperance} = kt$$

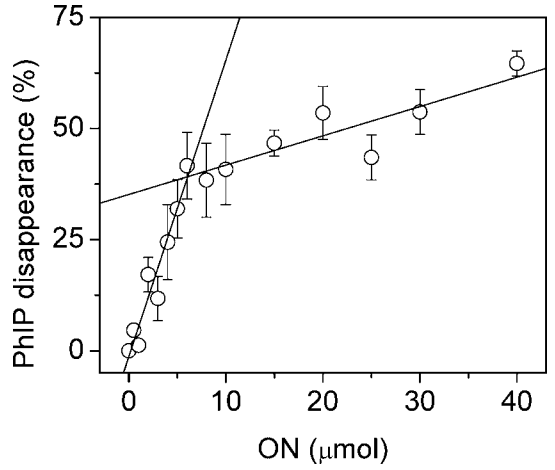


**Figure 4.** Effect of 4-oxo-2-nonenal (ON) concentration on the disappearance of PhIP. Mixtures containing PhIP (1 nmol) and 4-oxo-2-nonenal in 500 $\mu$L of 0.3 M sodium citrate buffer (pH 5) were heated at 100 °C for 24 h.

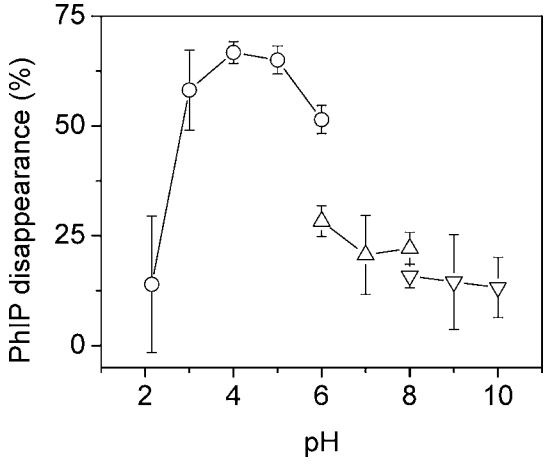


**Figure 3.** Effect of pH on the disappearance of PhIP in the presence of 4-oxo-2-nonenal. Mixtures containing PhIP (1 nmol) and 4-oxo-2-nonenal (40 $\mu$mol) in 500 $\mu$L of 0.3 M buffer were heated at 100 °C for 24 h. The employed buffers were sodium citrate for pH 2.15–6 (○), sodium phosphate for pH 6–8 (△), and sodium borate for pH 8–10 (▽).

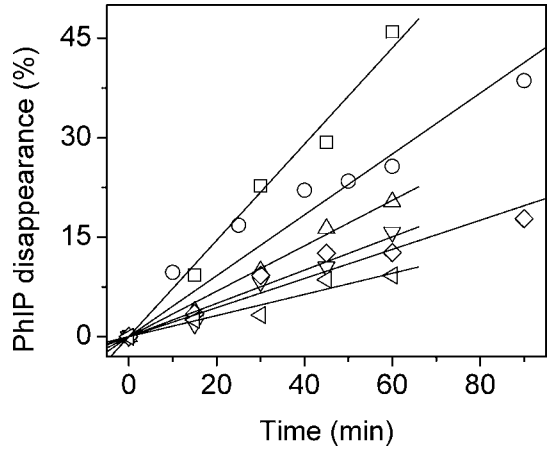


**Figure 5.** Effect of time and temperature on the disappearance of PhIP. Mixtures containing PhIP (1 nmol) and 4-oxo-2-nonenal (40 $\mu$mol) in 500 $\mu$L of 0.3 M sodium citrate buffer (pH 5) were heated at the indicated times and temperatures. The assayed temperatures were 60 (left-pointing triangles), 70 (◇), 80 (▽), 90 (△), 100 (○), and 120 °C (□).

where $k$ is the rate constant and $t$ is the reaction time. These rate constants were used in an Arrhenius plot for the calculation of the activation energy ($E_a$) of PhIP disappearance in the presence of 4-oxo-2-nonenal (Figure S3 of the Supporting Information). The determined $E_a$ was 27.4 kJ/mol.

These results show that 2-aminoimidazoles are able to react with reactive carbonyls, but at the same time, they disappear as a consequence of the produced reactions. Therefore, these reactions might be employed as a strategy for the removal of heterocyclic aromatic amines having this chemical structure, which include all aminoimidazoazarenes.[10]

The formation of the adducts between PhIP and the lipid-derived reactive carbonyl compounds, and therefore the disappearance of PhIP, is produced much more easily than the formation of PhIP in the presence of carbonyl compounds because the $E_a$ of the formation of the cyclic compound (27.4 kJ/mol) is much lower than that obtained for PhIP formation in the reaction among creatinine, phenylalanine, and 4-oxo-2-nonenal (80.9 kJ/mol).[21] Therefore, the results obtained in this study support the previous results of Randel et al.[9] that found losses of PhIP when this last compound was heated in the presence of frying fats. In addition, they also provide an explanation for the reduction of the mutagenic potential observed in parallel to PhIP disappearance.[9] Thus, the formed adduct has lost the primary amino group of the original PhIP, which seems to be the responsible for its metabolic activation.[22]

The results obtained in this study and previous studies[17,21] provide two opposite roles for lipid-derived reactive carbonyls in PhIP formation and disappearance. On one hand, reactive carbonyls promote the conversion of phenylalanine into phenylacetaldehyde, which is needed for PhIP formation.[23] On the other, they are able to react with PhIP after it is produced. Therefore, lipid-derived reactive carbonyls will play one role or another depending on whether PhIP is present. Thus, lipid oxidation in the presence of phenylalanine and creati(ni)ne will contribute to PhIP formation. However, once PhIP is present, lipid oxidation will destroy PhIP over favoring its formation (at least at low temperatures) because the $E_a$ of PhIP destruction in the presence of lipid-derived reactive carbonyls is much lower than the $E_a$ of PhIP formation in the presence of the same carbonyl compounds.[21] For that reason, significant increases in the level of PhIP formation were only observed when phenylalanine and creatinine were heated in the presence of small amounts of the lipid carbonyl compound.[21]

The results obtained in this study and previous studies show the complexity of the reactions involving carbonyl compounds in food because they can react with many food components and consequences for food will be different depending on the reaction that is finally produced to a larger extent. Therefore, identification of the different components that scavenge carbonyl compounds and the study of the competitive ability of carbonyl scavengers are essential for fully understanding many of the changes produced as a consequence of food processing.

## ■ ASSOCIATED CONTENT

### Supporting Information

Figures S1−S3. This material is available free of charge via the Internet at http://pubs.acs.org.

## ■ AUTHOR INFORMATION


### Corresponding Author

*Instituto de la Grasa, CSIC, Avenida Padre García Tejero 4, 41012 Seville, Spain. Phone: +34 954 611 550. Fax: +34 954 616 790. E-mail: rzamora@ig.csic.es.



### Funding

This study was supported in part by the European Union (FEDER funds) and the Plan Nacional de I + D of the Ministerio de Economía y Competitividad of Spain (Project AGL2012-35627).


### Notes

The authors declare no competing financial interest.

## ■ ACKNOWLEDGMENTS

We are indebted to José L. Navarro for technical assistance and José J. Ríos for the HRMS data.

## ■ ABBREVIATIONS USED

AMBI, 2-amino-1-methylbenzimidazole; PhIP, 2-amino-1-methyl-6-phenylimidazo[4,5-*b*]pyridine

## ■ REFERENCES


(1) Davidek, T.; Festring, D.; Dufosse, T.; Novotny, O.; Blank, I. Study to elucidate formation pathways of selected roast-smelling odorants upon extrusion cooking. *J. Agric. Food Chem.* **2013**, *61*, 10215−10219.

(2) Adams, A.; Kitryte, V.; Venskutonis, R.; De Kimpe, N. Model studies on the pattern of volatiles generated in mixtures of amino acids, lipid-oxidation-derived aldehydes, and glucose. *J. Agric. Food Chem.* **2011**, *59*, 1449−1456.

(3) Hidalgo, F. J.; Zamora, R. Amino acid degradations produced by lipid oxidation products. *Crit. Rev. Food Sci. Nutr.* **2014**, DOI: 10.1080/10408398.2012.761173.

(4) Muttucumaru, N.; Powers, S. J.; Elmore, J. S.; Mottram, D. S.; Halford, N. G. Effects of nitrogen and sulfur fertilization on free amino acids, sugars, and acrylamide-forming potential in potato. *J. Agric. Food Chem.* **2013**, *61*, 6734−6742.

(5) Zamora, R.; Hidalgo, F. J. Contribution of lipid oxidation products to acrylamide formation in model systems. *J. Agric. Food Chem.* **2008**, *56*, 6075−6080.

(6) Villaverde, A.; Estevez, M. Carbonylation of myofibrillar proteins through the Maillard pathway: Effect of reducing sugars and reaction temperature. *J. Agric. Food Chem.* **2013**, *61*, 3140−3147.

(7) Moskowitz, M. R.; Bin, Q.; Elias, R. J.; Peterson, D. G. Influence of endogenous ferulic acid in whole wheat flour on bread crust aroma. *J. Agric. Food Chem.* **2012**, *60*, 11245−11252.

(8) Hidalgo, F. J.; Zamora, R. 2-Alkenal-scavenging ability of m-diphenols. *Food Chem.* **2014**, *160*, 118−126.

(9) Randel, G.; Balzer, M.; Grupe, S.; Drusch, S.; Kaina, B.; Platt, K.-L.; Schwarz, K. Degradation of heterocyclic aromatic amines in oil under storage and frying conditions and reduction of their mutagenic potential. *Food Chem. Toxicol.* **2007**, *45*, 2245−2253.

(10) Sanz Alaejos, M.; Afonso, A. M. Factors that affect the content of heterocyclic aromatic amines in foods. *Compr. Rev. Food Sci. Food Saf.* **2010**, *10*, 52−108.

(11) Engst, R.; Schnaak, W. Determination of residues of the fungicide benzimidazole carbamic acid methyl-ester and its metabolites 2-aminobenzimidazole and benzimidazole. *Nahrung* **1979**, *23*, 701−706.

(12) Shaikh, B.; Rummel, N.; Reimschuessel, R. Determination of albendazole and its major metabolites in the muscle tissues of Atlantic salmon, tilapia, and rainbow trout by high performance liquid chromatography with fluorimetric detection. *J. Agric. Food Chem.* **2003**, *51*, 3254−3259.

(13) Zula, A.; Kikelj, D.; Ilas, J. 2-Aminoimidazoles in Medicinal Chemistry. *Mini-Rev. Med. Chem.* **2013**, *13*, 1921−1943.

(14) Hidalgo, F. J.; Zamora, R. Modification of bovine serum albumin structure following reaction with 4,5(*E*)-epoxy-2(*E*)-heptenal. *Chem. Res. Toxicol.* **2000**, *13*, 501−508.
(15) Zamora, R.; Navarro, J. L.; Gallardo, E.; Hidalgo, F. J. Chemical conversion of α-amino acids into α-keto acids by 4,5-epoxy-2-decenal. *J. Agric. Food Chem.* **2006**, *54*, 2398−2404.
(16) Shimozu, Y.; Shibata, T.; Ojika, M.; Uchida, K. Identification of advanced reaction products originating from the initial 4-oxo-2-nonenal-cysteine Michael adducts. *Chem. Res. Toxicol.* **2009**, *22*, 957−964.
(17) Zamora, R.; Alcon, E.; Hidalgo, F. J. Effect of lipid oxidation products on the formation of 2-amino-1-methyl-6-phenylimidazo[4,5-*b*]pyridine (PhIP) in model systems. *Food Chem.* **2012**, *135*, 2569−2574.
(18) Gardner, H. W.; Bartelt, R. J.; Weisleder, D. A facile synthesis of 4-hydroxy-2(*E*)-nonenal. *Lipids* **1992**, *27*, 686−689.
(19) Hidalgo, F. J.; Alaiz, M.; Zamora, R. Determination of peptides and proteins in fats and oils. *Anal. Chem.* **2001**, *73*, 698−702.
(20) Snedecor, G. W.; Cochran, W. G. *Statistical Methods*, 7th ed.; Iowa State University Press: Ames, IA, 1980.
(21) Zamora, R.; Alcon, E.; Hidalgo, F. J. Comparative formation of 2-amino-1-methyl-6-phenylimidazo[4,5-*b*]pyridine (PhIP) in creatinine/phenylalanine and creatinine/phenylalanine/4-oxo-2-nonenal reaction mixtures. *Food Chem.* **2013**, *138*, 180−185.
(22) Cheung, C.; Ma, X.; Krausz, K. W.; Kimura, S.; Feigenbaum, L.; Dalton, T. P.; Nebert, D. W.; Idle, J. R.; Gonzalez, F. J. Differential metabolism of 2-amino-1-methyl-6-phenylimidazo[4,5-*b*]pyridine (PhIP) in mice humanized for *CYP1A1* and *CYP1A2*. *Chem. Res. Toxicol.* **2005**, *18*, 1471−1478.
(23) Zamora, R.; Alcon, E.; Hidalgo, F. J. Strecker-type degradation of phenylalanine initiated by 4-oxo-2-alkenals in comparison to that initiated by 2,4-alkadienals, 4,5-epoxy-2-alkenals, or 4-hydroxy-2-nonenal. *J. Agric. Food Chem.* **2013**, *61*, 10231−10237.

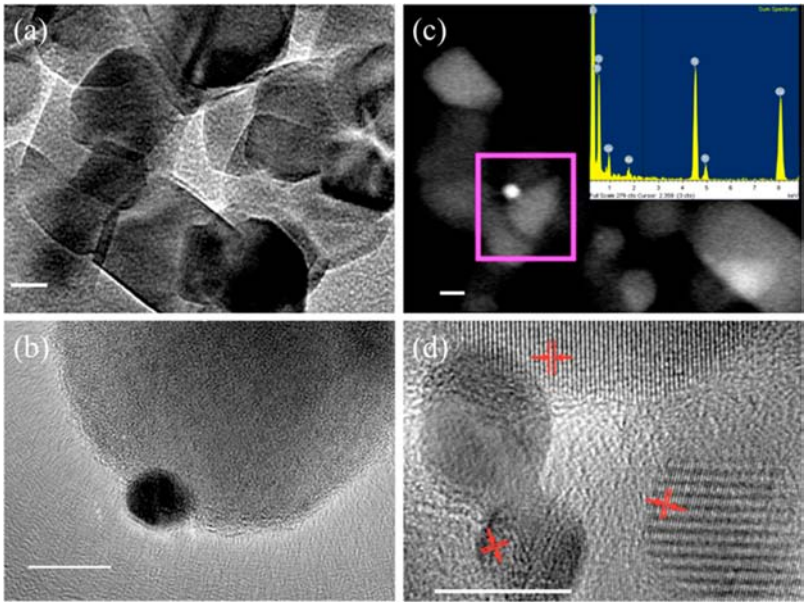


**Figure 1.** TEM images of (a) $TiO_2$ NPs and (b) Au/$TiO_2$ hybrid nanostructures; (c) dark field STEM of Au/$TiO_2$ hybrid nanostructures, inset shows EDS analysis; and (d) HRTEM of Au/$TiO_2$ (Au:$TiO_2$ ratio = 1:100 by weight) hybrid nanostructures formation after photodeposition. All scale bars are 10 nm.

## MATERIALS AND METHODS

**Materials.** The sample of FD&C Yellow No. 5 (Y5) used in this study originated from a batch submitted to the FDA for certification. The purified main component of FD&C Yellow No. 5 (MY5) was separated by countercurrent chromatography from a portion of Y5 and was generously provided by Dr. Adrian Weisz of the FDA.[23] Methanol (Fisher Scientific, Fair Lawn, NJ, USA), ammonium acetate ($NH_4OAc$, Fisher), and water were of chromatography grade. The mixed-phase titanium dioxide Deggussa Aeroxide P25 (75% anatase and 25% rutile phase; surface area, 50 ± 15 $m^2/g$) was purchased from Degussa Corporation (Parsippany, NJ). The spin-trap, 5-tert-butoxycarbonyl 5-methyl-1-pyrroline *N*-oxide (BMPO), was purchased from Applied Bioanalytical Laboratories (Sarasota, FL). The 2,2,6,6-tetramethyl-4-piperidone (TEMP) was purchased from Wako Pure Chemical Industry, Ltd. Japan; and 2,2,6,6-tetramethylpiperidine-1-oxyl (TEMPO) was purchased from Alexis, Enzo Life Sciences, Inc. (Farmingdale, NY). The $^{15}N$-labeled 4-oxo-2,2,6,6-tetramethyl-piperidine-d16−1-oxyl ($^{15}N$-PDT) was purchased from Cambridge Isotope Laboratories (Andover, MA). Superoxide dismutase (SOD) and standard buffer solutions were purchased from Sigma Chemical Co. (St. Louis, MO). Before use, each buffer stock solution (pH 3.9 HAc-NaAc, pH 5.0 PBS, pH 7.4 PBS, all at 0.1 M) was treated with Chelex100 molecular biology-grade resin from Bio-Rad Laboratories (Hercules, CA) to remove trace metal ions. Distilled deionized water (18.2 MΩ cm) from a Milli-Q water purification system was used in all experiments.

**Preparation of Au/$TiO_2$ Hybrid Nanostructures.** Au/$TiO_2$ hybrid nanostructures were prepared according to a previously reported photoreduction method with modifications.[24,25] To obtain a 1.00 wt % Au/$TiO_2$ sample, 10 mL of 2.0 mg/mL $TiO_2$ suspension in methanol (50% by volume) was mixed with 0.1 mL of an aqueous solution of $HAuCl_4$ (2 mg/mL Au) in a 50 mL quartz Erlenmeyer flask and sealed. The above mixture was sonicated for 5 min and then irradiated for 30 min under simulated sunlight with magnetic stirring in an ice water bath. The light source was an Oriel Xenon Arc Lamp Solar Simulator. A clearly evident color change from white to greyish pink was observed, which indicated the formation of Au/$TiO_2$ hybrid nanostructures. After centrifugation, UV spectral analysis of the supernatant after each photodeposition revealed that the Au had been almost completely (>99%) deposited as Au on the $TiO_2$ particles. The precipitate was collected, washed three times with double distilled water, and then dried at 45 °C overnight in oven and used for further experiments.

**Characterization of $TiO_2$ NPs and Au/$TiO_2$ Nanostructures.** UV−vis absorption spectra were obtained using a Varian Cary 300 spectrophotometer. Transmission electron microscopy (TEM) and high resolution TEM (HRTEM) images were captured on a JEM 2100 FEG (JEOL) transmission electron microscope (accelerating voltage of 200 kV) located at the NanoCenter, University of Maryland, College Park, MD. Energy-dispersive X-ray spectroscopy analysis (EDS) was conducted using the same microscope. The samples for TEM analysis were prepared by adding drops of the redispersed colloidal solutions onto standard holey carbon-coated copper grids, which were then air-dried at room temperature.

**Dye Degradation.** For examining the degradation of Y5, 10 mL of an aqueous solution containing 25 mg/L MY5 or Y5 and selected concentrations of $TiO_2$ or Au/$TiO_2$ NPs was continuously stirred in the dark for 30 min to establish an adsorption−desorption equilibrium between the NPs and dyes. The $TiO_2$ and Au/$TiO_2$ NPs were dispersed as suspensions for all experiments. Each suspension was transferred to a 50 mL quartz Erlenmeyer flask, sealed, and irradiated using a light source to deliver simulated sunlight. The light resource consisted of a Universal Arc Lamp Power Supply (69920 Universal Supply, Newport, Irvine, CA) and an Oriel Xenon Arc Lamp (880 W) solar simulator. During irradiation, the suspension was continuously stirred and kept in ice water bath. The degradation process was monitored using a Varian Cary 300 spectrophotometer. Before UV−vis analysis, the reaction mixture was centrifuged to remove the $TiO_2$ or Au/$TiO_2$ particles. The photocatalytic degradation of MY5 was observed to follow pseudo-first-order kinetics. When the dye concentration was in the millimolar range, the apparent first-order rate constant, $k_{app}$, was determined from the slope of ln ($C/C_0$) versus irradiation time according to the following relation:

$$-\ln \frac{C}{C_0} = k_{app} t \quad (1)$$

where $t$ is the irradiation time, $C_0$ is the initial concentration of dye, and $C$ is the concentration of dye (mg/L) at time $t$.[26] The concentration was determined by spectrophotometry. The UV−vis spectrum of MY5 consists of two characteristic peaks at 425 and 258 nm. The $\lambda_{max}$ value of the dye (425 nm) was chosen for quantitative degradation studies.

**Electron Spin Resonance.** ESR spin-trap spectroscopy is a powerful tool for evaluating the capability of NPs to generate reactive oxygen species and free radicals.[27] It was employed to detect the generation of ROS and occurrence of electron transfer during irradiation of samples with simulated sunlight. The spin-trap, BMPO, was used to detect the generation of superoxide radicals ($O_2^{-\bullet}$) or hydroxyl radicals (•OH). TEMP was used to investigate the generation of singlet oxygen ($^1O_2$). TEMPO, a stable radical that exhibits an ESR signal with three identical peaks, was used as spin probe to study the electrons generated in the $TiO_2$ aqueous suspension. Oxygen consumption during dye degradation photocatalyzed by $TiO_2$ NPs was monitored by ESR oximetry. A water-soluble spin label, $^{15}$N-PDT, was used to detect the oxygen content in sample solutions. The shape of the $^{15}$N-PDT ESR spectrum is dependent on the amount of $O_2$ that interacts with it, where higher peak-to-peak amplitude ($A$) and narrower peak-to-peak line width ($W$) are found when the levels of $O_2$ in solution are reduced.[28] The $O_2$ concentration was calculated by a calibration standard curve described by

$$[O_2] = 419.72 \times W - 44.12 \quad (2)$$

where $[O_2]$ is the concentration in solution ($\mu$M). The consumption of oxygen was expressed as $[O_{2\text{-time}}]/[O_{2\text{-initial}}]$.

Fifty microliter aliquots of control or sample solutions were put in glass capillary tubes with internal diameters of 1 mm and sealed using Critoseal capillary tube sealant, then placed into the microwave cavity of a Bruker EMX ESR Spectrometer (Billerica, MA) to obtain ESR spectra. All ESR measurements were carried out in situ using the following settings for detection of the spin adducts: 10 mW microwave power for detection of spin adducts using spin-traps and 1 mW microwave power for ESR oximetry using $^{15}$N-PDT, 100 G scan range, and 1 G field modulation. A Schoeffel xenon arc (450 W) solar simulator was used to irradiate samples during ESR measurements. ESR spectra were collected during irradiation at different time intervals. All measurements were performed in replicate at ambient temperature. Control groups, either without catalysts or without irradiation, were also recorded for comparison. The final concentration of each component is described in each figure caption. All experiments were repeated three times. Data are expressed as mean ± standard deviation.

## RESULTS AND DISCUSSION

**Characterization of $TiO_2$ NPs and Au/$TiO_2$ Hybrid Nanostructures.** The morphology of $TiO_2$ NPs and Au/$TiO_2$ hybrid nanostructures was characterized by TEM. Figure 1, panel a shows the original $TiO_2$ P25 agglomerates with the size range of 22−48 nm. Figure 1, panel b shows the Au NPs (dark dots) located on the surface of the individual $TiO_2$ NPs. The size of the photodeposited Au NPs was estimated to be 4−10 nm. After Au was doped onto $TiO_2$ surface, the surface characteristics and size of the $TiO_2$ NPs remained unchanged. EDS analysis was performed to further confirm the formation of Au/$TiO_2$ nanostructure. The EDS spectrum in Figure 1, panel c shows a strong signal for Ti and a weak signal for Au. The mass ratio of Au/$TiO_2$ for the selected area was estimated to be approximately 5% based on this spectrum. Elemental copper and carbon were also detected by EDS, which was associated with the supporting carbon-coated copper grids. The HRTEM image (Figure 1d) taken from the interfacial region of Au and $TiO_2$ shows the lattice image with a lattice spacing of 0.353 nm that corresponds to the {001} facets of anatase phase. Lattice fringes with interplanar distance of 0.202 nm were observed on the dark dots in Figure 1, panel d, which is similar to the planar distance for Au {200} ($d$ = 0.204 nm).

**Degradation of FD&C Yellow No. 5.** *Effect of Initial $TiO_2$ Concentration.* The degradation of Y5 and MY5 in the presence of nano-$TiO_2$ was carried out under simulated sunlight. Figure 2, panel a illustrates the effect of the initial

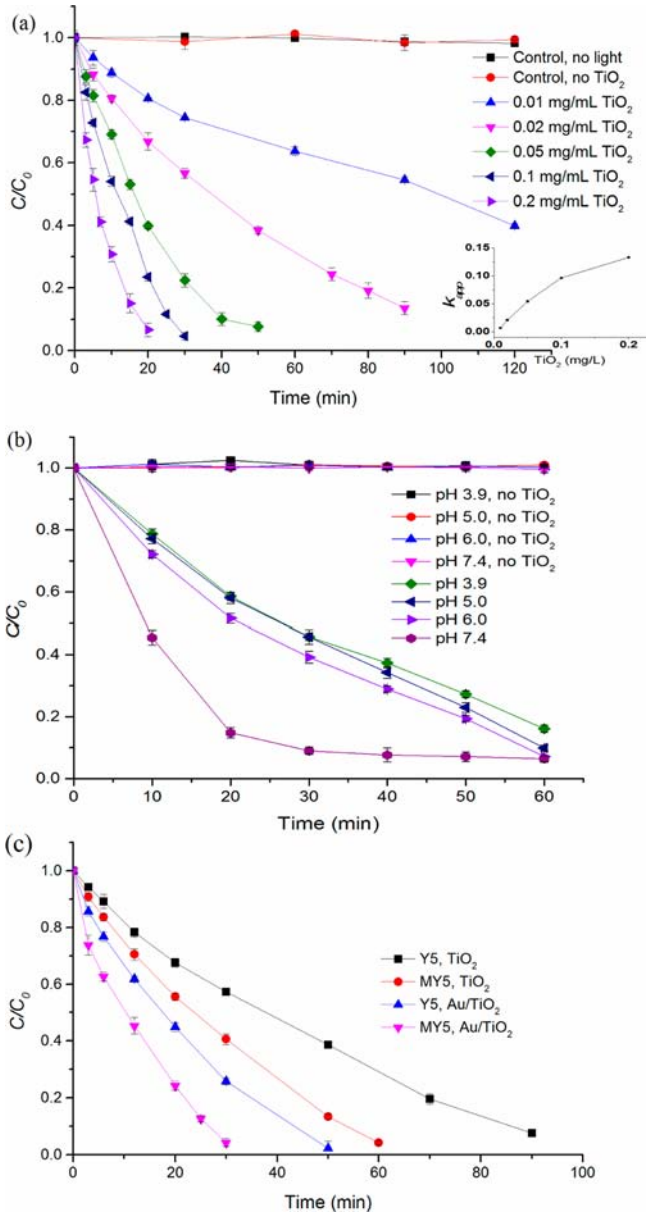


**Figure 2.** Decomposition of purified MY5 under simulated sunlight. $Y$-axis ($C/C_0$) shows the concentration of remaining dye at irradiation time divided by the initial dye concentration. Reactions were carried out in (a) water solutions of MY5 and 0 (control), 0.01, 0.02, 0.05, 0.1, and 0.2 mg/mL $TiO_2$ NPs irradiated by simulated sunlight for different time intervals or without sunlight exposure (control); (b) 10 mM PBS buffer (pH 5.0, 6.0, and 7.4) or 10 mM acetic acid buffer (pH 3.9) solutions containing MY5 and 0.1 mg/mL $TiO_2$ NPs; (c) water solutions of MY5 or batch-certified Y5 containing 0.1 mg/mL $TiO_2$ NPs or Au/$TiO_2$ hybrid nanostructures. The initial dye concentration in all samples was fixed at 25 mg/mL.

$TiO_2$ NPs concentration on degradation kinetics. The initial concentration of MY5 was fixed at 25 mg/L, while the concentration of $TiO_2$ NPs was adjusted to 0.01, 0.02, 0.05, 0.1, and 0.2 mg/mL. Figure 2, panel a demonstrates that MY5 remains unchanged after 120 min for the control groups, either without $TiO_2$ NPs but exposed to simulated sunlight or added with $TiO_2$ NPs but without exposure to simulated sunlight. Dos


dx.doi.org/10.1021/jf5045052 | J. Agric. Food Chem. 2014, 62, 12052−12060

Santos et al. reported a significant reduction of tartrazine in aqueous solution with 15 min of UV irradiation.[21] The difference between this study and our results may be attributed to the different light sources and intensities used. Figure 2, panel a shows that an increase in the concentration of $TiO_2$ resulted in a higher rate of degradation for MY5. At $TiO_2$ NP concentration of 0.1 mg/mL, the dye was not spectrophotometrically detectable after 30 min of exposure to simulated sunlight. The inset of Figure 1, panel a shows the calculated reaction constant, $k_{app}$, at different concentrations of $TiO_2$. The highest rate constant ($k_{app}$ = 0.133 $min^{-1}$) was observed at 0.2 mg/mL $TiO_2$ NPs.

*Effect of pH.* The pH value of the reaction mixture plays multiple roles in the dye degradation process by affecting the ionization state of the $TiO_2$ surface and hydroxyl radical generation in the solution[26] as well as the structure of tartrazine.[23] In this study, we investigated pH values of 3.9, 5.0, 6.0, and 7.4 to mimic the pH range of particular food products. Figure 2, panel b shows that under slightly alkaline conditions (pH = 7.4), the degradation rate was significantly promoted ($k_{app}$ = 0.084 $min^{-1}$), whereas the rate constant $k_{app}$ was calculated to be 0.028, 0.035, and 0.039 $min^{-1}$ for pH values 3.9, 5.0, and 6.0, respectively. The effect of pH value plays multiple roles in dye decomposition, including influences on •OH generation and adsorption as well as the adsorption of dye. Higher pH value could provide higher concentration of hydroxyl ions to react with valence band holes ($h^+$) to form •OH.[29] However, under acidic conditions (pH < 6.8), the $TiO_2$ surface is positively charged, whereas it is negatively charged for pH > 6.8.[30] When $TiO_2$ is negatively charged, Coulombic repulsion takes place, which repels the hydroxyl ion and oxygen molecule from adsorbing on its surface and thus decreases the availability of hydroxyl and superoxide radical for dye degradation.[31] On the other hand, in acidic media, a strong adsorption of the dye onto the $TiO_2$ particle has been observed, which results from the significantly high electrostatic attraction force between the positively-charged $TiO_2$ and the anionic dye molecule, which causes an increase in adsorption and accelerates the degradation process.[32,33] Therefore, with regard to the influence of pH on azo dye degradation, some reported a bell-shaped figure in which the dye degradation reaches its maximum around neutral pH.[34,35] For Y5 (tartrazine) decomposition triggered by $TiO_2$, the rate constant $k_{app}$ was found to increase with pH in the pH range of 2.2−11.[36]

*Effect of Dye Composition.* Y5 is batch certified by the FDA to ensure compliance with specifications in the Code of Federal Regulations (CFR).[23] Among the specifications is a limit of 1% for each of two polysulfonated subsidiary colors: the tetrasodium salt of 4-((4,5-disulfo(1,1-biphenyl)-2-yl) hydrazono)-4,5-dihydro-5-oxo-1-(4-sulfophenyl)-1H-pyrazole-3-carboxylic acid and the trisodium salt of 4,4′-(4,5-dihydro-5-oxo-4-((4-sulfophenyl)hydrazono)-1H-pyrazol-1,3-diyl)bis-(benzenesulfonic acid), which have been assigned the abbreviations Pk5 and Pk7, respectively.[23] To our best knowledge, most of the Y5 samples in previously published studies were obtained from commercially available tartrazine samples that contain around 85% MY5. It is noteworthy that the purity and composition of those samples may lead to different results. Therefore, we studied a certified batch of dye (Y5, ∼86% purity) used for coloring foods, drugs, and cosmetics as well as its purified main component (MY5, ∼99% purity). Under the same treatment conditions, the FDA-certified dye showed a lower degradation rate compared to the purified main component according to data obtained by spectrophotometric analysis. This result points to a higher stability of the batch-certified Y5 compared to MY5, which may be attributable to the more complex mixture of dye components in Y5.

*Effect of Deposition of Au onto $TiO_2$ Surface.* Noble metals have been widely used to enhance the photoactivity of $TiO_2$. Au NPs deposited on $TiO_2$ act as electron traps and enhance the electron−hole separation and the subsequent transfer of the trapped electron to the adsorbed $O_2$ that acts as an electron acceptor. Therefore, to investigate the relationship between dye degradation and electron/hole pair as well as ROS generation, we synthesized Au/$TiO_2$ hybrid nanostructure by depositing Au onto the surface of $TiO_2$. Figure 2, panel c shows that, for both MY5 and Y5, Au/$TiO_2$ exhibited enhanced photoactivity and accelerated color degradation, again with a higher degradation rate for MY5.

**$TiO_2$-Generated Electrons and ROS.** *Detection of Electron Reactivity during Photoexcitation of $TiO_2$ NPs.* ESR was employed to investigate the generation of ROS and occurrence of electron transfer during photoexcitation of $TiO_2$ in aqueous suspension. The reactive electrons generated in 0.1 mg/mL $TiO_2$ NPs were detected using a stable spin probe, TEMPO. TEMPO is a stable radical that has been widely used as a spin label in ESR spectroscopy, and it exhibits a triplet ESR spectrum, whereas its reduced form, hydroxyl amine (TEMPOH), is ESR silent.[37] As shown Figure 3, panel a, the

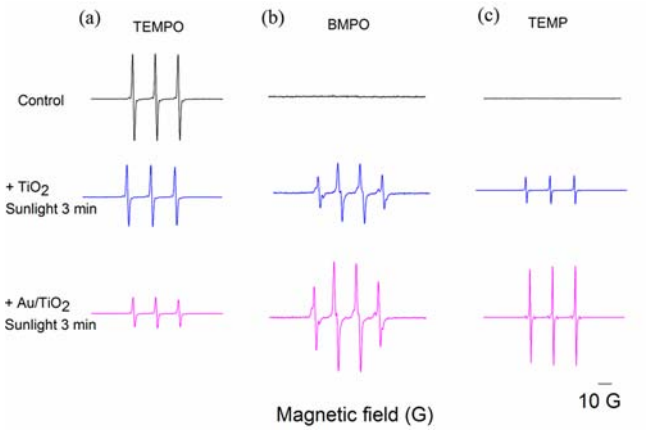


**Figure 3.** Detection of photogenerated electrons and ROS in solutions containing 0.1 mg/mL $TiO_2$ NPs or Au/$TiO_2$ hybrid nanostructures. ESR spectra obtained from samples mixed with different spin probes: (a) 0.02 mM TEMPO; (b) 25 mM BMPO; and (c) 2 mM TEMP. First row of each column presents both of the control groups, which contained the spin probe either without $TiO_2$ NPs or without simulated sunlight irradiation. All the spectra were recorded after 3 min of irradiation with simulated sunlight.

triplet-peak ESR signal of TEMPO remained unchanged for both control groups, either without $TiO_2$ NPs but exposed to simulated sunlight or added with $TiO_2$ $NP_S$ but without exposure to simulated sunlight. When $TiO_2$ NPs were added (0.1 mg/mL) and simulated sunlight irradiation was applied for 3 min, the TEMPO signal intensity was reduced. Further flattening of ESR spectrum was observed for samples containing the same amount of Au/$TiO_2$ NPs, which indicates a higher fraction of TEMPO being reduced to TEMPOH. Since our results indicated that TEMPO does not react with other species in the solution, such as hydroxyl radical or superoxide

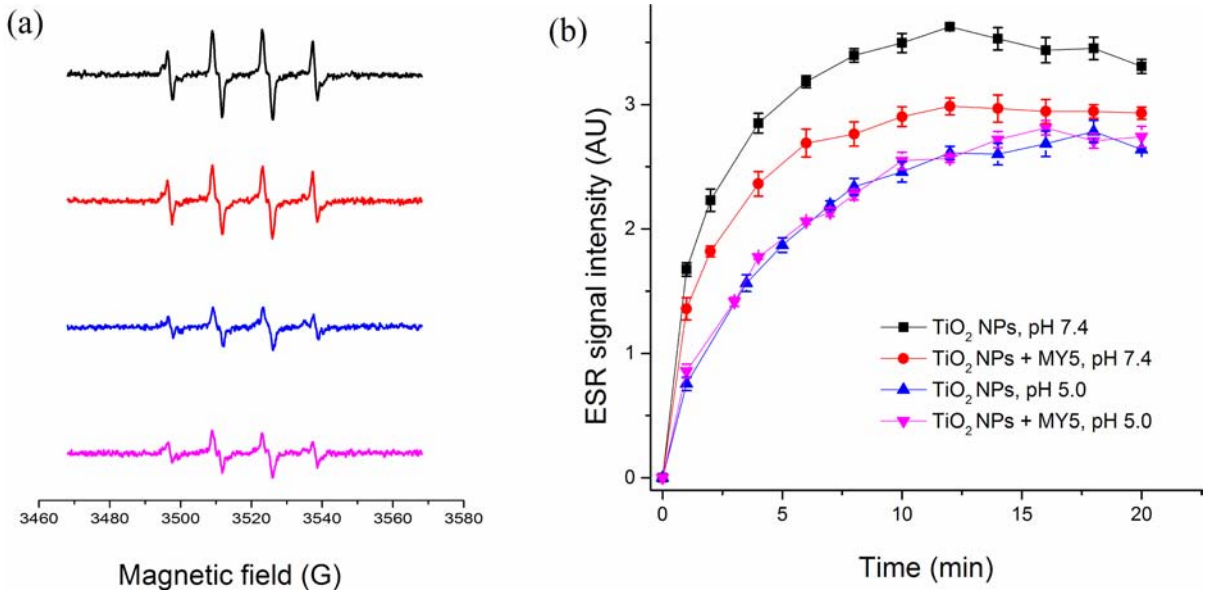


**Figure 4.** ESR detection of •OH during decomposition of dye upon simulated sunlight irradiance: (a) ESR spectra recorded after 1 min of irradiation by simulated sunlight; and (b) time-dependent ESR signal intensity obtained by measuring the peak-to-peak height of the second line of the ESR spectrum of BMPO/•OH. Reactions were conducted in 10 mM pH 5.0 or 7.4 PBS buffer solutions containing 25 mM BMPO spin-trap. All sample solutions contained 0.1 mg/mL $TiO_2$ NPs with (or without) 25 mg/mL MY5.

radical generated by $H_2O_2$ (Figure S1, Supporting Information), the reduction of TEMPO necessarily resulted from the electrons generated during photoexcitation of $TiO_2$ NPs.

*Generation of Hydroxyl and Superoxide Radicals.* The generation of hydroxyl radical by photoexcited $TiO_2$ NPs in aqueous suspension was confirmed using the spin-trap BMPO. Being ESR silent itself, BMPO can trap hydroxyl radical or superoxide radical and become ESR detectable. The spin-adduct BMPO/•OH exhibits a 1:2:2:1 ratio in peak ESR signal intensity, with hyperfine coupling constant $a_N$ = 13.5 G, $a_{H\beta}$ = 15.3 G, and $a_{H\gamma}$ = 0.62 G, while the spin-adduct of BMPO and superoxide radical (BMPO/O2$^{-\bullet}$) has a typical four-line ESR spectrum with hyperfine splitting structure ($a_N$ = 13.4 G, $a_{H\beta}$ = 12.1 G).[38] Figure 3, panel b shows an ESR spectrum identical to the BMPO/•OH spin-adduct signal for $TiO_2$ exposed to simulated sunlight. A similar ESR pattern with higher intensity was observed for Au/$TiO_2$ NPs under the same experimental conditions. Previous studies have reported difficulties when using BMPO as a spin-trap for a system containing both •OH and $O_2^{-\bullet}$ because of possible overlap of BMPO/•OH and BMPO/$O_2^{-\bullet}$ signal.[14] For irradiated $TiO_2$ solutions, the formation of •OH has been widely recognized, while several studies have reported observation of $O_2^{-\bullet}$ detected by ESR spectroscopy.[39] To determine whether superoxide radical is involved in this process, superoxide dismutase (SOD) was employed to scavenge superoxide radicals in order to eliminate any BMPO/$O_2^{-\bullet}$ signal (Figure S2, Supporting Information). With the addition of SOD (0.2 U/ml) to the above $TiO_2$ NP suspension, the 1:2:2:1 peak ESR signal remained the same pattern that is identical to BMPO/•OH spin-adduct. However, the intensity of the above signal was reduced to half. The reduction of this ESR signal suggests that that superoxide radical is involved in ROS generation in photoexcited $TiO_2$ NP suspensions.

*Generation of Singlet Oxygen.* In addition to hydroxyl and superoxide radicals, singlet oxygen is another important ROS that has been implicated in the degradation of dye mixtures.[40] We used the spin probe TEMP to study singlet oxygen ($^1O_2$) generation during irradiation of $TiO_2$ NPs. TEMP is ESR silent. When it reacts with singlet oxygen, the reaction product, a nitroxide radical, 2, 2, 6, 6-tetramethylpiperidine-*N*-oxyl (TEMPONE), is formed and shows a 1:1:1 peak ESR spectrum.[41] No ESR signal was observed for both control groups containing the spin probe TEMP, either without $TiO_2$ NPs but exposed to simulated sunlight or added with $TiO_2$ NP$_S$ but without exposure to simulated sunlight (Figure 3c). ESR spectra with three lines with equal intensities ($a_N$ = 16.0 G), typical of nitroxide radicals, were found for irradiated suspensions containing TEMP and $TiO_2$ (Figure 3c). The hyperfine splitting constant and *g* factor of the observed signal were identical to those of commercial TEMPONE, which indicates the generation of singlet oxygen during irradiation. A similar spectrum with higher intensity was observed for Au/$TiO_2$. Previous studies found evidence that singlet oxygen was formed through the following pathway:[42]

$$O_2^{-\bullet} + h^+_{vb} \rightarrow {}^1O_2 \quad (3)$$

To test this theory, SOD (0.2 U/mL) was added to the above mixture. This resulted in a reduction of this triplet ESR signal (Figure S2, Supporting Information). TEMPO signal significantly reduced upon the addition of SOD. Again, because of the fact that SOD is a specific enzyme that catalyzes the dismutation of superoxide ($O_2^{-\bullet}$), this result confirms that during photoexcitation of $TiO_2$ NP aqueous suspension, superoxide radicals play a role in the formation of singlet oxygen.

**Interaction between ROS and FD&C Yellow No. 5.** *Hydroxyl Radical Consumption.* A time and pH dependence study was carried out to further investigate the role of hydroxyl radical in the decomposition of Y5 (Figure 4). Figure 4, panel a shows the ESR spectra of the BMPO/$^{\bullet}$OH spin-adduct recorded for photoexcited $TiO_2$ NP suspensions with or without MY5 at pH 5.0 or 7.4 after 1 min of simulated sunlight irradiation. The time-dependent ESR signal intensity shown in

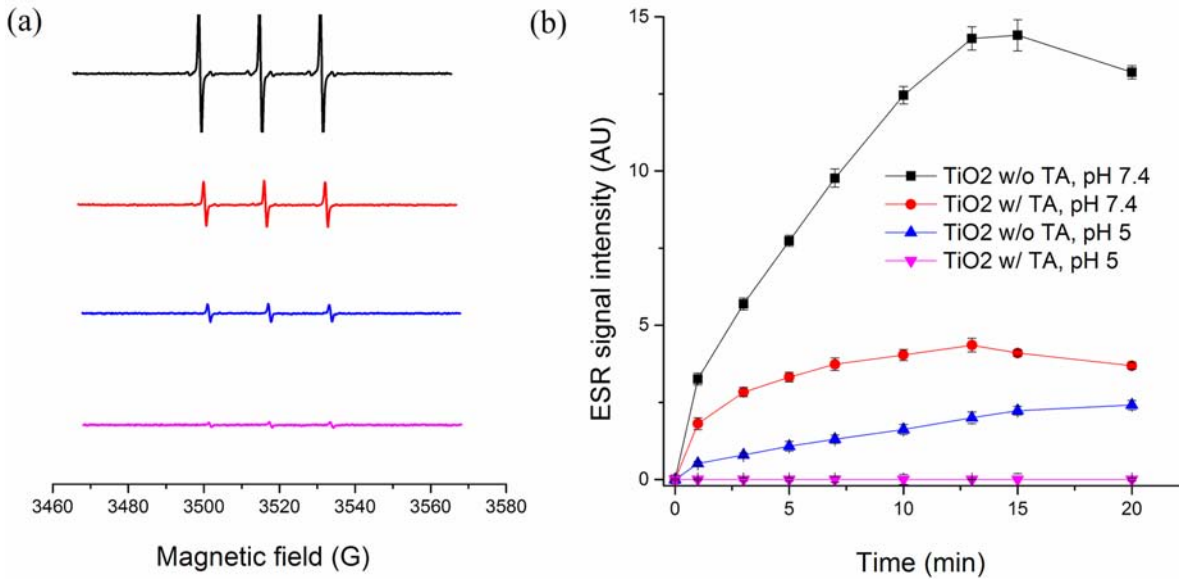


**Figure 5.** ESR detection of $^1O_2$ during decomposition of dye upon simulated sunlight irradiance: (a) ESR spectra recorded after 10 min of irradiation by simulated sunlight; (b) time-dependent ESR signal intensity obtained by measuring the peak-to-peak height of the first line of the ESR spectrum of TEMP/$^1O_2$ adduct. Reactions were conducted in 10 mM pH 5.0 or 7.4 PBS buffer solutions containing 5 mM TEMP spin probe. All sample solutions contained 0.1 mg/mL $TiO_2$ NPs with (or without) 25 mg/mL MY5.

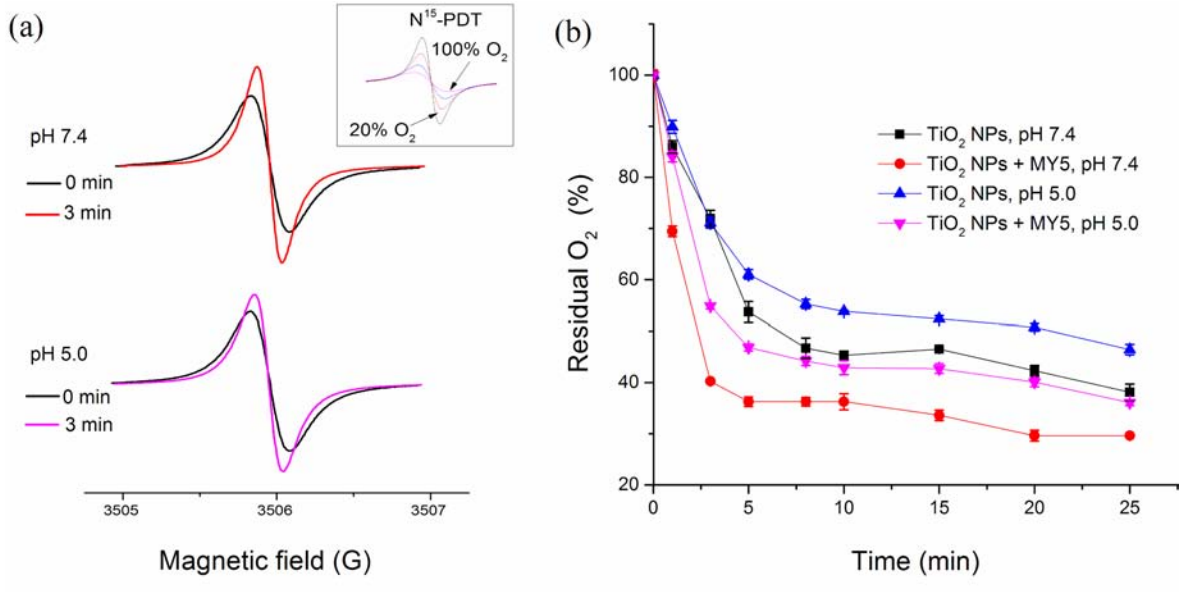


**Figure 6.** $O_2$ consumption detection using ESR oximetry during decomposition of dye upon simulated sunlight irradiation: (a) ESR spectra of spin-probe $^{15}$N-PDT in sample solutions containing 0.1 mg/mL $TiO_2$ and 25 mg/mL MY5 recorded before (0 min) or after 3 min of irradiation by simulated sunlight; and (b) $O_2$ consumption kinetics. $O_2$ concentration was calculated based on the peak-to-peak line width of spin-probe $^{15}$N-PDT using a calibrated standard curve described in the Material and Methods section. Reactions were conducted in 10 mM pH 5.0 or 7.4 PBS buffer solutions containing 0.2 mM $^{15}$N-PDT spin-probe. All sample solutions contained 0.1 mg/mL $TiO_2$ NPs with (or without) 25 mg/mL MY5.

Figure 4, panel b was obtained by measuring the peak-to-peak height of the second line of the ESR spectra. For suspensions containing only $TiO_2$ NPs, the signal intensities of BMPO/•OH adduct tested at pH 5.0 were significantly lower than those of samples tested at pH 7.4. This is most likely due to the lower availability of hydroxide ions in acidic media. It has been stated that in alkaline solution, •OH generation is promoted due to oxidation of more hydroxide ions available on $TiO_2$ surface.[26] At pH 7.4, $TiO_2$ solutions with MY5 show significantly lowered ESR intensity compared to $TiO_2$ NPs only, which indicates that under the simulated sunlight, hydroxyl radicals generated on photoexcited $TiO_2$ NPs were consumed by the azo dye MY5, which results in decomposition. Interestingly, at pH 5.0, the addition of MY5 did not result in a significant change in ESR intensity for •OH spin-adduct, which implies that little or no •OH was used for dye degradation. The results from this ESR time- and pH-dependent study agree with our previous observations shown in Figure 2, panel b, where a lower reaction rate constant was found for acidic solution.

*Singlet Oxygen Consumption.* Figure 5 shows the time dependence of ESR signal for the formation of TEMPONE from TEMP due to the generation of $^1O_2$. Figure 5, panel a exhibits the ESR spectra of TEMPONE observed after 10 min irradiation of $TiO_2$ NP suspensions with or without MY5 at pH 5.0 or 7.4. The time dependence of the ESR signal intensity (Figure 5b) was obtained by measuring the peak-to-peak height of the first line of this ESR spectrum. ESR intensity detected at pH 7.4 was significantly higher compared to that at pH 5. This observation agrees with a previous study by Daimon et al. in which the generation of $^1O_2$ was suppressed when pH < 5 and reaches its maximum between pH 6−11.[15] The decrease in $^1O_2$ at pH 5 compared to pH 7.4 is attributable to the suppression of $O_2^{-\bullet}$ at the $TiO_2$ surface by taking consideration that the $^1O_2$ originated from the oxidation of $O_2^{-\bullet}$ by the valence band holes $h^+$ (eq 1). Unlike hydroxyl radical, the consumption of $^1O_2$ by the azo dye MY5 was found for both acidic and alkaline conditions. At pH 5, the ESR signal for $^1O_2$ was largely reduced when MY5 was added into the reaction mixture; thus, we did not observe any ESR signal for $^1O_2$. However, when BMPO is used in the above solution, a six-peak ESR signal was recorded by ESR spectroscopy (data not shown), which indicates the formation of carbon center radical[28] that was associated the oxidation of dye MY5. The decrease in $^1O_2$ may take place by two mechanisms: one is by direct reaction with the Y5 dye anion, and the other is due to the decrease of available $O_2^{-\bullet}$ that has been consumed by dye oxidation.

*Oxygen Consumption.* It has been well established that the $O_2^{-\bullet}$ in aqueous solutions containing $TiO_2$ NPs results from the reduction of oxygen by conduction band electrons ($e^-_{cb}$):

$$O_2 + e^-_{cb} \rightarrow O_2^{-\bullet} \quad (4)$$

Although $O_2^{-\bullet}$ was indirectly detected by adding SOD to the suspension containing both $TiO_2$ NPs and BMPO spin-trap as discussed above, it was unclear how $O_2^{-\bullet}$ was involved in the decomposition process of MY5. Since difficulties arise when $O_2^{-\bullet}$ is detected by ESR due to the overlap of BMPO/$O_2^{-\bullet}$ and BMPO/•OH spin adducts, a time- and pH-dependent study was conducted for $O_2$ consumption using ESR oximetry. The inset in Figure 6, panel a depicts the ESR spectrum of a commonly used water-soluble spin-label $^{15}$N-PDT. Figure 6, panel a shows that after 3 min of light irradiation, higher peak intensity with broader line width was observed for the sample containing $TiO_2$ and food color, which is associated with the reduction of oxygen in the solution. Figure 6, panel b demonstrates that for suspensions only containing $TiO_2$ NPs, higher $O_2$ consumption was observed at pH 7.4 compared to that at pH 5. The addition of the dye MY5 led to a further decrease in $O_2$ level in both acidic (pH 5) and alkaline (pH 7.4) media, and the degree of this further consumption appeared to be similar for both pHs. On the basis of the observation that upon sunlight irradiation, $O_2$ did not directly react with the azo dye without $TiO_2$ or that the reaction was too slow to be observed and thus negligible (control groups in Figure 2a,b), the main reason for oxygen consumption is very likely to be the reduction of $O_2$ by $e^-$ (eq 4). Therefore, by determination of oxygen consumption, we observed the involvement of $O_2^{-\bullet}$ in the decomposition process. Our findings suggest it is very possible that pH primarily affects the initial rate of $O_2^{-\bullet}$ generation rather than the interaction between the azo dye and $O_2^{-\bullet}$.

Nanosized $TiO_2$ particles may be found in a broad range of consumer products. In conclusion, our results confirmed that when exposed to simulated sunlight, $TiO_2$ NPs at low concentration can trigger decomposition of the azo dye Y5, which is widely used in food, drug, and cosmetic products. By using ESR spin trapping, the only technique that directly monitors the existence of free radicals and identifies them,[43] we demonstrated that dye degradation proceeds via reaction with ROS generated on the surface of photoexcited $TiO_2$, and a higher degradation rate was associated with increased ROS generation. At pH 7.4, a significant reduction in both hydroxyl radical and singlet oxygen was observed after the dye was added into the suspension, while singlet oxygen became the main reactive species at pH 5.0. Our study characterized the decomposition mechanism and directly monitored the involvement of ROS that may occur in food, drugs, cosmetics, and other consumer products that contain both $TiO_2$ and Y5 as ingredients. The findings in this study may provide important insights for the design of new applications or evaluation of the safety of nano-$TiO_2$ in these products. Our results demonstrate that the interaction between nanomaterials and other ingredients should be investigated in addition to studies on the nanomaterials as independent components. Our results were obtained in a simplified chemical system. Further studies are needed to determine the effects of complex food matrices on factors such as aggregation, ROS quenching, and light transmission, which might moderate the photocatalytic activity of $TiO_2$.

## ■ ASSOCIATED CONTENT

### Ⓢ Supporting Information

Effect of hydroxyl radical on BMPO and TEMPO spin probes. Effect of SOD on ESR signal generated from $TiO_2$ NP solutions exposed to simulated sunlight. This material is available free of charge via the Internet at http://pubs.acs.org.

## ■ AUTHOR INFORMATION

### Corresponding Author

*E-mail: junjie.yin@fda.hhs.gov. Phone: 240-402-1991. Fax: 201-436-2624.

### Funding

This work was supported by a regulatory science grant under the FDA Nanotechnology CORES Program and by the Office of Cosmetics and Colors, CFSAN/FDA. W.H. appreciates the support from the National Natural Science Foundation of China (Grant No. 21303153) and the Program for Science and Technology Innovation Talents in Universities of Henan Province (Grant No. 14HASTIT008).

### Notes

The authors declare no competing financial interest.

## ■ ACKNOWLEDGMENTS

The authors thank Dr. Adrian Weisz (CFSAN/FDA) for his valuable help and comments. We acknowledge the support of the Maryland NanoCenter and its NispLab. This article is not an official U.S. FDA guidance or policy statement. No official support or endorsement by the U.S. FDA is intended or should be inferred.

## ■ ABBREVIATIONS USED

Y5, FD&C Yellow No. 5; MY5, purified main component of FD&C Yellow No. 5; NPs, nanoparticles; ESR, electron spin resonance; ROS, reactive oxygen species; $H_2O_2$, hydrogen peroxide; •OH, hydroxyl radical; $O_2^{\bullet-}$, superoxide radical; $^1O_2$,

singlet oxygen; BMPO, 5-tert-butoxycarbonyl 5-methyl-1-pyrroline *N*-oxide; TEMP, 2,2,6,6-tetramethyl-4-piperidone; TEMPO, 2,2,6,6 -tetramethylpiperidine-1-oxyl; $^{15}$N-PDT, 4-oxo-2,2,6,6-tetramethylpiperidine-d$_{16}$-1-oxyl; SOD, superoxide dismutase

## REFERENCES


(1) Carlotti, M. E.; Ugazio, E.; Gastaldi, L.; Sapino, S.; Vione, D.; Fenoglio, I.; Fubini, B. Specific effects of single antioxidants in the lipid peroxidation caused by nanotitania used in sunscreen lotions. *J. Photochem. Photobiol., B* **2009**, *96* (2), 130−135.

(2) Hamal, D. B.; Haggstrom, J. A.; Marchin, G. L.; Ikenberry, M. A.; Hohn, K.; Klabunde, K. J. A multifunctional biocide/sporocide and photocatalyst based on titanium dioxide ($TiO_2$) codoped with silver, carbon, and sulfur. *Langmuir* **2010**, *26* (4), 2805−2810.

(3) Ochiai, T.; Tago, S.; Nakano, R.; Nakata, K.; Murakami, T.; Fujishima, A.; Ikekita, M.; Morito, Y.; Hara, M.; Nojima, Y.; Masuko, K.; Suzuki, T.; Niitsu, Y.; Kobayashi, G.; Kurano, M.; Serizawa, I.; Horio, K. Development of a hybrid environmental purification unit by using of excimer VUV lamps with $TiO_2$-coated titanium mesh filter. *Chem. Eng. J.* **2013**, *218*, 327−332.

(4) Gomez, M.; Arancibia, V.; Rojas, C.; Nagles, E. Adsorptive stripping voltammetric determination of tartrazine and sunset yellow in gelatins and soft drink powder in the presence of cetylpyridinium bromide. *Int. J. Electrochem. Sci.* **2012**, *7* (8), 7493−7502.

(5) *Code of Federal Regulations, Title 21, Section 73.575*; U.S. Food and Drug Administration: Washington, DC, 2014.

(6) *Japan's Specifications and Standards for Food Additives*, 7th ed.; Ministry of Health and Welfare: Tokyo, Japan, 2000.

(7) EU European Parliament and Council Directive, 94/36/EC of 30 June 1994 on Colours for Use in Foodstuffs. *Off. J. Eur. Communities* **1994**, *L237*, 13−29.

(8) Chewing gum and bubble gum. In *The Prevention of Food Adulteration Act and Rules, 1955, Appendix B, Section A.25.02.01, Directorate General of Health Services*; Ministry of Health: New Delhi, India, 2004.

(9) Powdered concentrate mixes for fruit beverage drinks. In *The Prevention of Food Adulteration Act and Rules, 1955, Appendix C, Table 3, Directorate General of Health Services*; Ministry of Health: New Delhi, India, 2004.

(10) Yang, Y.; Doudrick, K.; Bi, X.; Hristovski, K.; Herckes, P.; Westerhoff, P.; Kaegi, R. Characterization of food-grade titanium dioxide: The presence of nanosized particles. *Environ. Sci. Technol.* **2014**, *48* (11), 6391−400.

(11) Weir, A.; Westerhoff, P.; Fabricius, L.; Hristovski, K.; Von, G. N. Titanium dioxide nanoparticles in food and personal care products. *Environ. Sci. Technol.* **2012**, *46* (4), 2242−50.

(12) Chen, X. X.; Cheng, B.; Yang, Y. X.; Cao, A.; Liu, J. H.; Du, L. J.; Liu, Y.; Zhao, Y.; Wang, H. Characterization and preliminary toxicity assay of nano-titanium dioxide additive in sugar-coated chewing gum. *Small* **2013**, *9*, 9−10.

(13) Mao, S. S.; Chen, X. Selected nanotechnologies for renewable energy applications. *Int. J. Energy Res.* **2007**, *31* (6−7), 619−636.

(14) Yin, J. J.; Liu, J.; Ehrenshaft, M.; Roberts, J. E.; Fu, P. P.; Mason, R. P.; Zhao, B. Phototoxicity of nano-titanium dioxides in HaCaT keratinocytes—Generation of reactive oxygen species and cell damage. *Toxicol. Appl. Pharmacol.* **2012**, *263* (1), 81−88.

(15) Daimon, T.; Hirakawa, T.; Kitazawa, M.; Suetake, J.; Nosaka, Y. Formation of singlet molecular oxygen associated with the formation of superoxide radicals in aqueous suspensions of $TiO_2$ photocatalysts. *Appl. Catal., A* **2008**, *340* (2), 169−175.

(16) Yu, K. P.; Huang, Y. T.; Yang, S. C. The antifungal efficacy of nanometals supported $TiO_2$ and ozone on the resistant *Aspergillus niger* spore. *J. Hazard Mater.* **2013**, *261*, 155−162.

(17) Wu, P.; Xie, R.; Imlay, K.; Shang, J. K. Visible-light-induced bactericidal activity of titanium dioxide codoped with nitrogen and silver. *Environ. Sci. Technol.* **2010**, *44* (18), 6992−6997.

(18) Mills, A. Oxygen indicators and intelligent inks for packaging food. *Chem. Soc. Rev.* **2005**, *34* (12), 1003−1011.

(19) Wamer, W. G.; Yin, J.-J.; Wei, R. R. Oxidative damage to nucleic acids photosensitized by titanium dioxide. *Free Radical Biol. Med.* **1997**, *23* (6), 851−858.

(20) Liu, S.; Xu, L.; Zhang, T.; Ren, G.; Yang, Z. Oxidative stress and apoptosis induced by nanosized titanium dioxide in PC12 cells. *Toxicology* **2012**, *267*, 1−3.

(21) Dos Santos, T. C.; Zocolo, G. J.; Zanoni, M. V. B.; Morales, D. A.; Umbuzeiro, G. D. A. Assessment of the breakdown products of solar/UV-induced photolytic degradation of food dye tartrazine. *Food Chem. Toxicol.* **2014**, *68*, 307−315.

(22) Oancea, P.; Meltzer, V. Photo-Fenton process for the degradation of tartrazine (E102) in aqueous medium. *J. Taiwan Inst. Chem. Eng.* **2013**, *44*, 990−994.

(23) Weisz, A.; Ridge, C. D.; Roque, J. A.; Mazzola, E. P.; Ito, Y. Preparative separation of two subsidiary colors of FD&C Yellow No. 5 (tartrazine) using spiral high-speed counter-current chromatography. *J. Chromatogr., A* **2014**, *1343*, 91−100.

(24) He, W.; Kim, H.-K.; Wamer, W. G.; Melka, D.; Callahan, J. H.; Yin, J.-J. Photogenerated reactive oxygen species and charge carriers in ZnO/Au hybrid nanostructures are correlated with enhanced photocatalytic and antibacterial activity. *J. Am. Chem. Soc.* **2014**, *136* (2), 750−757.

(25) Tanaka, A.; Ogino, A.; Iwaki, M.; Hashimoto, K.; Ohnuma, A.; Amano, F.; Ohtani, B.; Kominami, H. Gold−titanium(IV) oxide plasmonic photocatalysts prepared by a colloid-photodeposition method: Correlation between physical properties and photocatalytic activities. *Langmuir* **2012**, *28* (36), 13105−13111.

(26) Konstantinou, I. K.; Albanis, T. A. $TiO_2$-assisted photocatalytic degradation of azo dyes in aqueous solution: Kinetic and mechanistic investigations—A review. *Appl. Catal., B* **2004**, *49* (1), 1−14.

(27) He, W.; Liu, Y.; Wamer, W. G.; Yin, J. J. Electron spin resonance spectroscopy for the study of nanomaterial-mediated generation of reactive oxygen species. *J. Food Drug Anal.* **2014**, *22* (1), 49−63.

(28) Yin, J. J.; Zhao, B.; Xia, Q.; Fu, P. P. *Electron Spin Resonance Spectroscopy for Studying the Generation and Scavenging of Reactive Oxygen Species by Nanomaterials in Nanopharmaceutics: The Potential Application of Nanomaterials*; World Scientific Pub. Co.: Singapore, 2012; pp 375−400.

(29) Zhang, Y.; Wong, J. W.; Liu, P.; Yuan, M. Heterogeneous photocatalytic degradation of phenanthrene in surfactant solution containing $TiO_2$ particles. *J. Hazard Mater.* **2011**, *191* (1−3), 136−143.

(30) Poulios, I.; Tsachpinis, I. Photodegradation of the textile dye Reactive Black 5 in the presence of semiconducting oxides. *J. Chem. Technol. Biotechnol.* **1999**, *74* (4), 349−357.

(31) Choudhury, B.; Borah, B.; Choudhury, A. Extending photocatalytic activity of $TiO_2$ nanoparticles to visible region of illumination by doping of cerium. *Photochem. Photobiol.* **2012**, *88* (2), 257−264.

(32) Banerjee, S.; Chattopadhyaya, M. C. Adsorption characteristics for the removal of a toxic dye, tartrazine, from aqueous solutions by a low-cost agricultural by-product. *Arabian J. Chem.* **2013**, DOI: 10.1016/j.arabjc.2013.06.005.

(33) Rauf, M. A.; Meetani, M. A.; Hisaindee, S. An overview on the photocatalytic degradation of azo dyes in the presence of $TiO_2$ doped with selective transition metals. *Desalination* **2011**, *276* (1−3), 13−27.

(34) Meetani, M. A.; Rauf, M. A.; Hisaindee, S.; Khaleel, A.; Al Zamly, A.; Ahmad, A. Mechanistic studies of photoinduced degradation of Orange G using LC/MS. *RSC Adv.* **2011**, *1* (3), 490−497.

(35) Soutsas, K.; Karayannis, V.; Poulios, I.; Riga, A.; Ntampegliotis, K.; Spiliotis, X.; Papapolymerou, G. Decolorization and degradation of reactive azo dyes via heterogeneous photocatalytic processes. *Desalination* **2010**, *250* (1), 345−350.

(36) Gupta, V. K.; Jain, R.; Nayak, A.; Agarwal, S.; Shrivastava, M. Removal of the hazardous dye—Tartrazine by photodegradation on titanium dioxide surface. *Mater. Sci. Eng., C* **2011**, *31* (5), 1062−1067.

(37) Lavi, R.; Sinyakov, M.; Samuni, A.; Shatz, S.; Friedmann, H.; Shainberg, A.; Breitbart, H.; Lubart, R. ESR detection of $^1O_2$ reveals enhanced redox activity in illuminated cell cultures. *Free Radical Res.* **2004**, *38* (9), 893−902.
(38) Zhao, H.; Joseph, J.; Zhang, H.; Karoui, H.; Kalyanaraman, B. Synthesis and biochemical applications of a solid cyclic nitrone spin trap: A relatively superior trap for detecting superoxide anions and glutathiyl radicals. *Free Radical Biol. Med.* **2001**, *31* (5), 599−606.
(39) Li, M.; Yin, J. J.; Wamer, W. G.; Lo, Y. M. Mechanistic characterization of titanium dioxide nanoparticle-induced toxicity using electron spin resonance. *J. Food Drug Anal.* **2014**, *22* (1), 76−85.
(40) Rembold, M.; Kramer, H. Singlet oxygen as an intermediate in the catalytic fading of dye mixtures. *J. Soc. Dyers Colour.* **1978**, *94* (1), 12−17.
(41) Lion, Y.; Delmelle, M.; Van, V. A. New method of detecting singlet oxygen production. *Nature* **1976**, *263* (5576), 442−443.
(42) Daimon, T.; Nosaka, Y. Formation and behavior of singlet molecular oxygen in $TiO_2$ photocatalysis studied by detection of near-infrared phosphorescence. *J. Phys. Chem. C* **2007**, *111* (11), 4420−4424.
(43) Fu, P. P.; Xia, Q.; Hwang, H. M.; Ray, P. C.; Yu, H. Mechanisms of nanotoxicity: Generation of reactive oxygen species. *J. Food Drug Anal.* **2014**, *22* (1), 64−75.

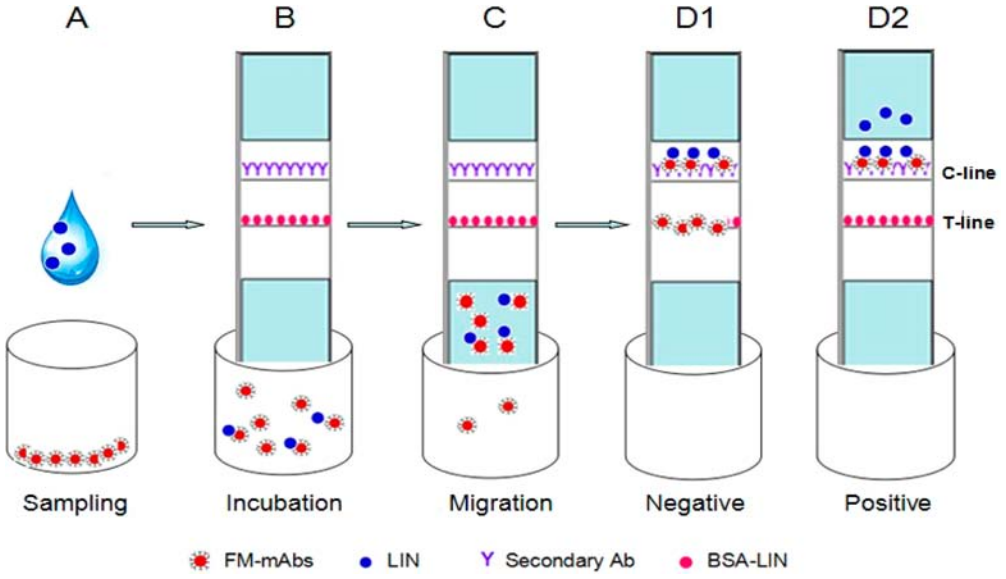


**Figure 1.** Experimental scheme includes sampling (A), incubation (B), migration (C), negative result (D1), and positive result (D2).

clinical diagnosis, bioanalysis, and environmental monitoring.[21−25]

According to our best knowledge, only two publications have been reported for the detection of LIN residues based on immunoassays.[10,11] Compared with these two time-consuming and laborious methods, we adopted FMIA for the detection of LIN based on anti-LIN monoclonal antibody (mAb) for successfully assaying the residues of LIN in milk, honey, beef, and swine urine samples.

## MATERIALS AND METHODS

**Reagents and Materials.** FluoSpheres carboxylate-modified microspheres, 200 nm, red fluorescent (580/605), 2% solids, were obtained from Invitrogen (Carlsbad, CA, USA). Bovine serum albumin (BSA), goat anti-mouse immunoglobulin G (IgG), lincomycin hydrochloride (>98%), 1-ethyl-3-(3-dimethylaminopropyl)-carbodiimide (EDC), and *N*-hydroxysuccinimide (NHS) were purchased from Sigma-Aldrich (St. Louis, MO, USA). 2-(4-Morpholino)ethanesulfonic acid (MES) and polyvinylpyrrolidone (PVP) were purchased from Aladdin Chemistry Co., Ltd. (Shanghai, China). Dextran 4000 and polyethylene glycol (PEG) were purchased from Wako Pure Chemical Industries, Ltd. (Osaka, Japan). A Milli-Q water purification system and nitrocellulose (NC) membrane were provided by Millipore Corp. (Bedford, MA, USA). The whole blood separation membrane (GF-2) and the absorbance pad (H5076) were supplied by Shanghai Jieyi Biotechnology Co., Ltd. (Shanghai, China). Purified anti-LIN monoclonal antibody (mAb) and an ELISA kit for the detection of LIN were purchased from Beijing WDWK Biotechnology Co., Ltd., and stored at 4 °C before use.

**Apparatus.** The ESE-Quant LFR fluorescence reader was supplied by QIAGEN (Dusseldorf, Germany). The NanoDrop ND-1000 spectrophotometer was obtained from Gene Co., Ltd. (Hong Kong, China). A multifunctional microplate reader SpectraMax M5 was purchased from Molecular Devices Co., Ltd. (Sunnyvale, CA, USA). The ZX1000 dispensing platform and the CM4000 Guillotine Cutting Module for the preparation of FMIA strips were provided by Bio Dot Inc. (Irvine, CA, USA). The UV spectrometer was provided by Qiangyun Co., Ltd. (Shanghai, China).

**Preparation of Capture Antigens.** The capture antigens were prepared by conjugating LIN to BSA using the sodium periodate ($NaIO_4$) reduction method as previously described.[11] More details can be found in the Supporting Information (Synthesis of BSA−LIN).

**Preparation of FMIA Strips.** The strip of FMIA consists of three parts: sample pad, NC membrane, and absorbent pad. The sample pad was made of whole blood separation membrane, pretreated with 0.02 M phosphate buffer (pH 6.2) containing 0.04% KCl, 0.2% PVP, and 2% Tween-20 and dried at 37 °C for 2 days. Then, 0.075 mg/mL BSA−LIN (0.7 μL/cm) and 0.9 mg/mL goat anti-mouse IgG (0.7 μL/cm) dissolved in 0.02 M coating buffer (pH 9.4) were sprayed onto the NC membrane as test line (T-line) and control line (C-line), respectively, as shown in Figure 1. Later, the NC membrane was dried at 37 °C for 2 h. Subsequently, different pads were laminated onto the baking part, sample pad, and absorbent pad with an overlap on NC membrane of about 2 mm to promote sample flow. Finally, the whole pad was cut into 3.5 mm wide strips and kept dry at room temperature.

**Conjugation of Fluorescent Microspheres and mAbs.** Thirty microliters of 2% fluorescent microspheres was suspended in 1 mL of 0.05 M MES (pH 6.5) in the dark. To activate the carboxylic groups on the surface of microspheres, 24 μL of 100 mg/mL immediately dissolved EDC solution and 32 μL of a 100 mg/mL NHS solution were dissolved in FM solution for 15 min at room temperature. Subsequently, 10 μL of 0.16 mg/mL mAbs in 0.01 M PBS (pH 7.4) was added for 2 h. One hundred microliters of 0.1 M glycine was added and incubated for another 15 min to terminate the reaction, and then the mixture was centrifuged at 8000 rpm for 10 min at 4 °C. The precipitate was resuspended in 200 μL of 0.05 M PBS (pH 7.4) containing 1% BSA, 2% PEG, and 1% Dextran 4000. Finally, the suspension was dispersed by supersonic vibration for 5 min and stored at 4 °C in the dark before use.

**Procedures of FMIA.** The principle of FMIA is based on the competitive binding of LIN and LIN−BSA conjugate to the anti-LIN mAbs labeled with fluorescent microspheres (FM−mAbs), as shown in Figure 1 (all steps were performed in the dark). Briefly, 2 μL of FM−mAb conjugates were added into one well of the 96-microtiter plate, and then 120 μL of the sample was added and fully mixed for 3 min (Figure 1A). Later the strip was vertically inserted into the corresponding microwell (Figure 1B), standing for another 15 min (Figure 1C). In the blank sample, the free FM−mAbs bound to the BSA−LIN conjugates at the T-line. Meanwhile, the free FM−mAbs were subsequently caught by the specific secondary anti-mouse antibodies at the C-line. All of these together indicated the samples were LIN negative (Figure 1D1). Contrarily, analyte in the sample would bind to FM−mAbs, leading to fewer fluorescent signals at the T-line, suggesting the sample was positive for LIN residues (Figure 1D2). Additionally, the results can be quantitated by an ESE Quant lateral flow reader to provide rich-information answers.

**Standard Curves and Specificity.** On the basis of the optimized conditions mentioned above, the standard curve of LIN was

established for FMIA. A 20 μg/mL LIN standard solution was disposed in dosages of 1, 2, 3, 4, 5, and 6 ng/mL in PBST. Calculations were performed on OrginPro 8.5 software (Origin, Northampton, MA, USA). A four-parameter logistic equation was used to calculate the obtained data.

$$Y = (A - B)/[1 + (X/C)^D] + B$$

$A$ = response value at high asymptote, $B$ = response value at low asymptote, $C$ = concentration corresponding to $IC_{50}$, $D$ = slope, and $X$ = calibration concentration. The $IC_{50}$, dynamic range, and limit of detection (LOD) served as quantitative criteria to evaluate the performance of FMIA. These parameters represent the calibration concentrations obtained at inhibition rates of 50%, between 20 and 80%, and at 90%, respectively.

Antibiotics with structures similar to LIN were studied for the cross-reactivity (CR) to determine the specificity of the FM−mAb conjugates. The corresponding CRs of each antibiotic in respective tests were quantitated from each standard curve on the basis of the following formula:

$$CR\ (\%) = 100 \times (IC_{50}\ \text{of LIN}/IC_{50}\ \text{of related compounds})$$

**Sample Preparations.** Matrix effect, an undesired unspecific obstruction of sample on antigen−antibody, mostly leads to decreased response values.

In this study, we tried three methods for the sample pretreatments: the trichloroacetic acid method (TCA), the dilution method, and the zinc sulfate method (ZSF). For the TCA method,[26] 200 μL of 3% TCA was added into 1 mL of spiked milk and then centrifuged at 8000 rpm for 8 min at room temperature; subsequently, 10 μL of 0.1 M NaOH was added to the supernatant to adjust the pH to 7.0. With regard to the dilution method, different extracting solutions were directly added to samples with series of dilutions. The ZSF method started by the addition of 60 μL of 1.04 M $ZnSO_4$ into 1 mL of spiked milk. After full mixture, the supernatant was obtained by centrifugation at 8000 rpm for 8 min. We also tried TCA and another two extracting solutions (water and 0.01 M PBST) to dilute the honey samples to different multiple factors (4-, 8-, 12-, 16-, and 20-fold). Similarly, we tried four extracting solutions (0.04 M PB, 0.04 M PB plus 0.1% Tween-20, water, and 0.01 M PBST) to deal with the beef samples. One gram of homogenized beef was dissolved into 8 mL of extracting solutions and centrifuged at 4000 rpm for 10 min. The supernatant was extracted for further use. Swine urine was directly diluted in four extracting solutions: 0.04 M PB, 0.04 M PB with 0.1% Tween-20, water, and 0.01 M PBST.

**Recovery Test.** LIN-free skimmed milk, honey, beef, and swine urine confirmed by liquid chromatography−electrospray ionization tandem mass spectrometry (LC-MS/MS) were obtained from the National Reference Laboratory for Veterinary Drug Residues (Beijing, China). The samples were spiked with different volumes of the 20 μg/mL LIN standard solution and treated as described for the sample preparations.

For the recovery test, LIN at final concentration levels of 1, 3, and 5 ng/mL was spiked into the samples. Then the samples were treated according to the methods mentioned above four times before fluorescent reading. Finally, the recoveries were calculated through the correspondence percentages of the fluorescence intensity between spiked and found LIN in the samples.

**Preparation of CGIA.** The principle of CGIA is similar to that of FMIA; they differ from each other by the biomarkers and the methods used to prepare biomarker and antibody conjugates. Unlike the covalent coupling method used for the preparation FM−mAb conjugates, the positively charged antibodies bind to the negatively charged surface of the gold nanoparticles on the basis of electronic interaction.[27] The preparation of CGIA strips has been previously described, as shown in the Supporting Information.[28]

## RESULTS AND DISCUSSION

**Optimization of FMIA.** The characteristics of different diameters (100 and 200 nm) and coloration (red, yellow, and blue) of FMs were first studied. Different sizes had discrepancy of brightness of coloration and sensitivity. Microspheres of 100 nm size showed lighter color and lower sensitivity than did those of 200 nm size. Figure S1 in the Supporting Information shows the coloration of FM−mAbs in the resuspended solution and the strips of negative samples under the UV light at 365 nm for three different FMs. Obviously, the blue light approximates white due to the UV light appearing purple close to blue, and the yellow has a high background value so that it is not easily distinguished. The red fluorescent is bright enough to distinguish. Thus, we chose the red 200 nm FMs to label anti-LIN mAbs. Then, red FMs (580/605) were 100-fold diluted in water and scanned from 300 to 700 nm. The excitation and emission peaks of FMs and FM−mAb conjugates were at 580 and 605 nm, respectively. In the present work, the carboxylic groups on the surface of microspheres were used to bind to the amino groups of the anti-LIN mAbs. Naturally, carboxyl can react with amino groups without the need of additional activator; however, the coupling efficiency was unsatisfactory. Hence, EDC was chosen to be an activator to accelerate the reaction. We have compared the single-step reaction (EDC only) with the two-step reaction (EDC and NHS) and found that the two-step reaction was more stable and showed higher response than the single-step reaction. Also, the dosage of EDC affected activation efficiency; we tried different dosages of EDC (as shown in Table S1 in the

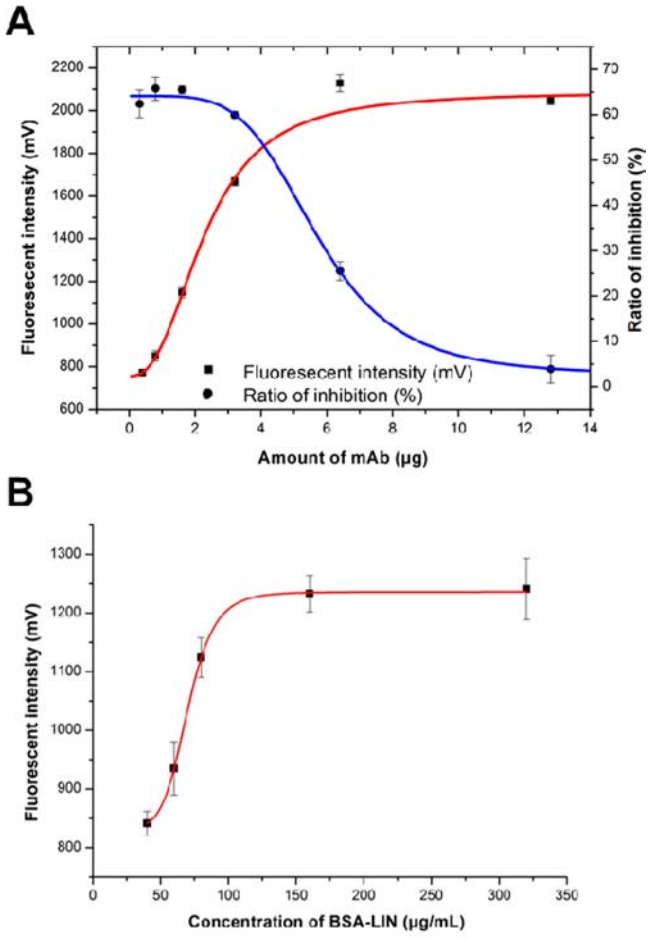


**Figure 2.** (A) Effects of the amount of mAb on the fluorescence intensity and inhibition ratio (at 3 ng/mL LIN). (B) Effect of the concentration of BSA−LIN on the fluorescence intensity.

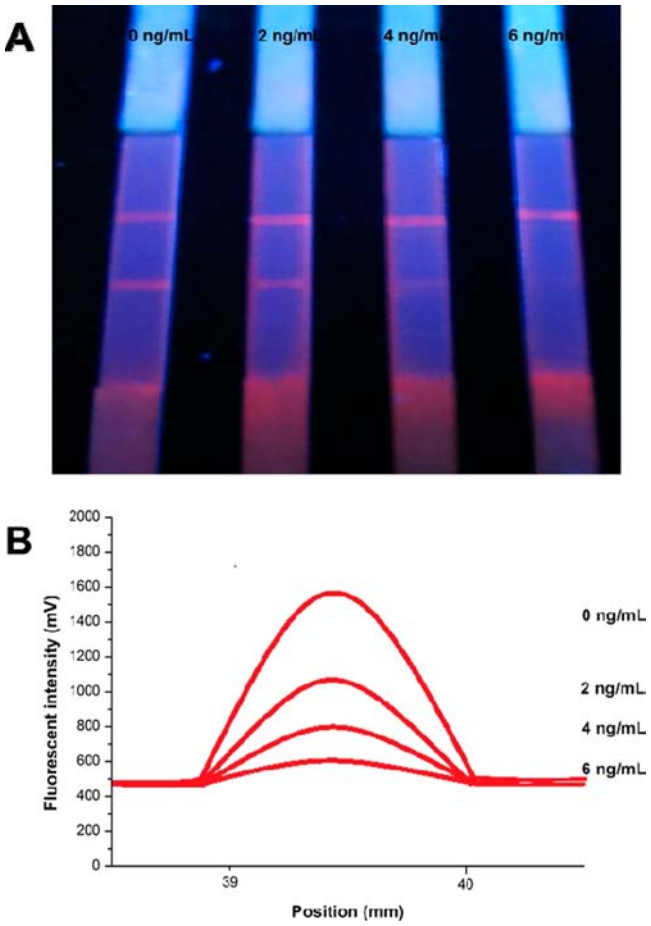


**Figure 3.** Detection of LIN in PBST by the naked eye (A) and fluorescence reader (B), under UV light with excitation wavelength at 365 nm.

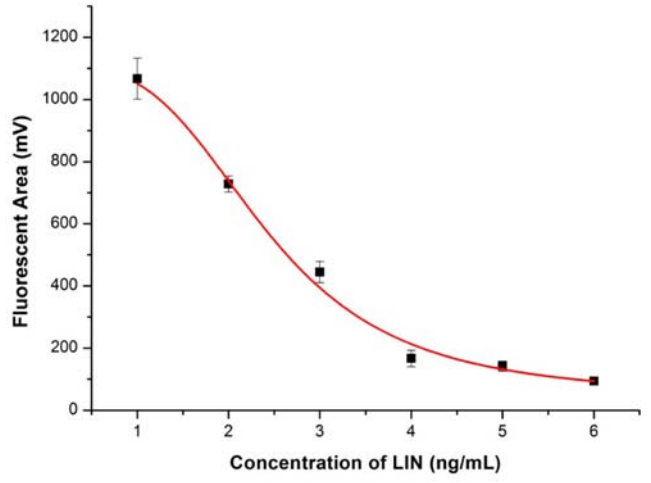


**Figure 4.** Standard curve of LIN in PBST by FMIA.

Supporting Information) to obtain good coloration and stability based on the naked eye and a fluorescence reader. With more EDC, a deeper color was found at the T-line. Meanwhile, the excess activator EDC led to obvious residue on the NC membrane. From Table S1 in the Supporting Information, the ratio of EDC to NHS at 2.4/3.2 showed the highest fluorescent intensity with satisfactory coloration of the T-line.

**Table 1. Recoveries of LIN from Various Biological Matrices Spiked at Different Concentration Levels by FMIA ($n$ = 4)**

| matrix | spiked (ng/mL) | tested (ng/mL) | recovery (%) | variation coefficient (%) |
|---|---|---|---|---|
| milk | 1 | 0.86 ± 0.07 | 86.21 | 8.14 |
| | 3 | 3.34 ± 0.35 | 111.30 | 10.48 |
| | 5 | 4.61 ± 0.80 | 92.27 | 17.35 |
| honey | 1 | 0.78 ± 0.04 | 77.63 | 5.13 |
| | 3 | 2.24 ± 0.16 | 74.74 | 7.14 |
| | 5 | 4.66 ± 0.29 | 93.28 | 6.22 |
| beef | 1 | 0.79 ± 0.09 | 78.50 | 11.39 |
| | 3 | 3.44 ± 0.19 | 114.50 | 5.52 |
| | 5 | 6.03 ± 1.31 | 120.50 | 21.76 |
| urine | 1 | 0.81 ± 0.09 | 80.98 | 11.11 |
| | 3 | 2.22 ± 0.22 | 73.92 | 9.91 |
| | 5 | 5.28 ± 0.18 | 105.50 | 3.41 |

FM−mAbs as the competitive binding targets between LIN of interest and the BSA−LIN conjugates play an important role in the stability and sensitivity of FMIA. The florescent intensity increased in a mAb-dependent manner and reached saturation point at 4 $\mu$g. In contrast, the trend of the inhibition ratio with LIN at 3 ng/mL sharply fell with increased concentration of mAb (Figure 2A). We found insufficient antibody led to the slight presence of the T-line, whereas excess antibody deposited flocks in the coupling process, and the FM−mAbs obviously aggregated on the bottom of the strips during testing for the sample. In addition, the T-line and C-line must be bright enough to distinguish the negative and positive samples. Taken together, 1.6 $\mu$g of mAbs was chosen to functionalize the surface of FMs. Moreover, the dosage of the BSA−LIN conjugates on the NC membrane to bind free FM−mAbs was subsequently optimized. The fluorescent intensity increased sharply in a BSA−LIN-dependent manner and became stable at 100 $\mu$g/mL. Finally, the last point in the linear range of fluorescence intensity (75 $\mu$g/mL) was chosen to achieve better coloration of FMIA (Figure 2B).

**Analytical Performance of the FMIA.** According to the principle described above, the performance of the T-line can represent the concentrations of LIN. As shown in Figure 3A, the coloration of the T-line obviously weakened as the concentration of LIN increased. The T-line disappeared with LIN at 6 ng/mL; thus, 6 ng/mL was the cutoff of this method. The semiquantitation of the corresponding strips is shown in Figure 3B by fluorescent reader. Figure 4 shows the competitive inhibition standard curves for LIN in PBST by FMIA. The dynamic range was from 1.35 to 3.57 ng/mL, with $R^2$ = 0.9825. The LOD and $IC_{50}$ were 0.69 and 2.20 ng/mL, respectively, and the cross-reactivity tests showed there was low cross-reactivity with clindamycin (4.4%) and negligible cross-reactivity (<0.1%) with streptomycin, roxithromycin, kanamycin, kitasamycin, and gentamicin. Therefore, this method showed high specificity to LIN. Furthermore, FMIA was challenged with authentic sample tests, as shown in Table 1. The recoveries ranged from 73.92 to 120.50%, with coefficients of variation under 21.76% in milk, honey, beef, and swine urine samples.

**Comparison of FMIA with CGIA and ELISA.** Compared with CGIA and ELISA methods, FMIA is a novel semi-


dx.doi.org/10.1021/jf5029416 | J. Agric. Food Chem. 2014, 62, 12061−12066

Table 2. Comparison of FMIA with CGIA and ELISA for the Detection in Milk, Honey, Beef, and Swine Urine Samples

| | CGIA | FMIA | ELISA |
|---|---|---|---|
| biomarker | colloidal gold | fluorescent microspheres | enzymes |
| type | qualitative | semiquantitative | quantitative |
| dilution factor | milk (1:1), honey (1:8), beef (1:8), swine urine (1:1) | milk (1:4), honey (1:8), beef (1:8), swine urine (1:8) | milk (1:2), beef (1:3) |
| method LOD (ng/mL) | void number | 0.69 | 1.00 |
| sample LOD/cutoff ($\mu$g/kg) | milk (10), honey (80), beef (80), swine urine (10) | milk (24), honey (48), beef (48), swine urine (48) | milk (50), beef (75) |
| time (min) | 5 | 15[a] and 30[b] | 120 |
| detection range | void number | 1.35−3.57 | 1.00−12.62 |
| $IC_{50}$ (ng/mL) | void number | 2.20 | 2.46 |

[a]Detected by fluorescence reader. [b]Detected by the naked eye under UV light.

quantitative immunoassay. Table 2 presents the main parameters among CGIA, ELISA, and FMIA. On the basis of covalent coupling between mAbs and FMs, FMIA was more stable and consumed fewer mAbs than CGIA. Meanwhile, the sensitivity of FMIA (6 ng/mL) was higher than that of CGIA (10 ng/mL). In addition, the $IC_{50}$ of FMIA was 2.20 ng/mL, lower than that of ELISA, 2.46 ng/mL (Figure S3), with advantages such as easy operation and time savings. Similar to previous papers,[27,29] the FMIA developed in the present work showed satisfactory results compared with the commonly used ELISA and CGIA.

**Sample Analysis.** Similar to the untreated milk samples, the sticky honey sample cannot move on the FMIA strips based on capillarity. Furthermore, the beef and urine samples always have complex matrix effects. To report a positive or negative result of the tested sample, the strip needs a clear background under UV light. In the present work, TCA and ZSF methods showed low response values, which cannot indicate the results. On the contrary, dilution can not only decrease the matrix effects of samples but also enhance the fluorescence response with the additional agents, such as polyvinylpyrrolidone (PVP) and Tween-20. Dilution and extraction of the samples by different solutions play important roles in the sample pretreatment. The best diluting schemes were as follows: milk was diluted 4-fold into 0.01 M PBS (pH 7.4) with 0.5% PVP; honey was diluted 8-fold into 0.01 M PBST; 1 g of homogenized beef was added into 8 mL of 0.04 M PB (pH 7.4) with 0.1% Tween-20, to extract the supernatant for further detection; swine urine was diluted 8-fold with double-distilled water (Table 2). Finally, the cutoff values were 24 ng/mL for raw milk and 48 $\mu$g/mL for honey, urine, and beef.

In conclusion, FMIA was a simple, effective, and semiquantitative method for the detection of LIN residues. A minimum of 0.69 ng/mL LIN was tested in 20 min. FMIA was used to assay the residues of LIN in four different matrices (i.e., milk, honey, beef, and swine urine). Thus, FMs can be widely used to couple antibodies for the detection of various resides of antibiotic or other chemicals in foodstuffs, providing an alternative method for immunoassay.

## ■ ASSOCIATED CONTENT

### Supporting Information

Synthesis of BSA−LIN and preparation of CGIA strips, Figures S1−S3 and Tables S1 and S2. This material is available free of charge via the Internet at http://pubs.acs.org.

## ■ AUTHOR INFORMATION

### Corresponding Author

*(S.D.) E-mail: dingsy@cau.edu.cn. Phone: +86-10-62732802. Fax: +86-10-62731032.

### Funding

This work was supported by the Special Fund for Agro-scientific Research in the Public Interest (201203069-2) and the Fund of Modern Agriculture Industry System Innovation in Beijing City Team.

### Notes

The authors declare no competing financial interest.

## ■ ABBREVIATIONS USED

BSA, bovine serum albumin; $IC_{50}$, half inhibitory concentration; ELISA, enzyme-linked immunosorbent assay; mAb, monoclonal antibody; PBS, phosphate-buffered saline; PBST, PBS containing 0.1% (v/v) Tween-20; NHS, *N*-hydroxysuccinimide; MES, 2-(4-morpholino)ethanesulfonic acid; PVP, polyvinylpyrrolidone; PEG, polyethylene glycol; $NaIO_4$, sodium periodate

## ■ REFERENCES

(1) Netting, R. M. *Smallholders, Householders: Farm Families and the Ecology of Intensive, Sustainable Agriculture*; Stanford University Press: Stanford, CA, USA, 1993; pp 265−270.

(2) Daughton, C. G.; Ternes, T. A. Pharmaceuticals and personal care products in the environment: agents of subtle change? *Environ. Health Perspect.* **1999**, *107*, 907−938.

(3) Boxall, A. B. A.; Fogg, L. A.; Blackwell, P. A.; Kay, P.; Pemberton, E. J.; Croxford, A. Veterinary medicines in the environment. *Rev. Environ. Contam. Toxicol.* **2004**, *180*, 81−91.

(4) Macleod, A. J.; Ross, H. B.; Ozere, R. L.; Digout, G.; van Rooyen, C. E. Lincomycin: a new antibiotic active against staphylococci and other Gram-positive cocci. *Can. Med. Assoc. J.* **1964**, *91*, 1056−1060.

(5) Spizek, J.; Rezanka, T. Lincomycin, clindamycin and their applications. *Appl. Microbiol. Biotechnol.* **2004**, *64*, 455−464.

(6) Gerasimova, S. S.; Berezina, E. K. Cytomorphological study of lincomycin toxicity. *Antibiotiki (Moscow)* **1977**, *22*, 539−544.

(7) Teuber, M. Veterinary use and antibiotic resistance. *Curr. Opin. Microbiol.* **2001**, *4*, 493−499.

(8) Enrica, C.; Anna, C.; Annamaria, F.; Edoardo, F.; Novella, P. Effect of lincomycin treatment on intestinal microflora composition and its bile-acid-metabolizing activity. *Curr. Microbiol.* **1985**, *12*, 1−4.

(9) Chiu, M. H.; Yang, H. H.; Liu, C. H.; Zen, J. M. Determination of lincomycin in urine and some foodstuffs by flow injection analysis coupled with liquid chromatography and electrochemical detection with a preanodized screen-printed carbon electrode. *J. Chromatogr., B* **2009**, *887*, 991−994.

(10) Wang, Y. Q.; Wang, R. M.; Wang, J. Q.; Yang, H.; Song, J.; Wang, Y. Z.; Deng, A. P. A sensitive and specific enzyme-linked immunosorbent assay for the detection of lincomycin in food samples. *J. Sci. Food Agric.* **2010**, *90*, 2083−2089.

(11) Burkin, M. A.; Galvidis, I. A. Development of a competitive indirect ELISA for the determination of lincomycin in milk, eggs, and honey. *J. Agric. Food Chem.* **2010**, *58*, 9893−9898.

(12) Zhou, J.; Xu, F.; Wu, C.; Liu, W. L.; Ding, S. Y. Study on two patterns comparison of gold immunochromatography test strip for

rapid detection of lincomycin. *China Anim. Husband. Vet. Med.* **2014**, *41*, 159−163 (in Chinese).
(13) Jiang, W. X.; Zhang, H. Y.; Li, X. M.; Liu, X. X.; Zhang, S. X.; Shi, W. M.; Shen, J. Z.; Wang, Z. H. Monoclonal antibody production and the development of an indirect competitive enzyme-linked immunosorbent assay for screening spiramycin in milk. *J. Agric. Food Chem.* **2013**, *61*, 10925−10931.
(14) Chilaka, C. A.; de Kock, S.; Dutton, M. F. Comparative profiling of different analytical methods for fumonisin detection in maize. *J. Microbiol.* **2012**, *2*, 833−849.
(15) Taranova, N. A.; Byzova, N. A.; Zaiko, V. V.; Starovoitova, T. A.; Vengerov, Y. Y.; Zherdev, A. V.; Dzantiev, B. B. Integration of lateral flow and microarray technologies for multiplex immunoassay: application to the determination of drugs of abuse. *Microchim. Acta* **2013**, *180*, 1165−1172.
(16) Baptista, P. V.; Doria, G.; Quaresma, P.; Cavadas, M.; Neves, C. S.; Gomes, I.; Eaton, P.; Pereira, E.; Franco, R. Nanoparticles in molecular diagnostics. *Prog. Mol. Biol. Transl. Sci.* **2011**, *104*, 427−488.
(17) Zhu, K.; Li, J. C.; Wang, Z. H.; Jiang, H. Y.; Beier, R. C.; Xu, F.; Shen, J. Z.; Ding, S. Y. Simultaneous detection of multiple chemical residues in milk using broad-specificity antibodies in a hybrid immunosorbent assay. *Biosens. Bioelectron.* **2011**, *26*, 2716−2719.
(18) Hu, Y. H.; Wang, C. C.; Bai, B.; Li, M. T.; Wang, R. H.; Li, Y. B. Detection of *Staphylococcus aureus* using quantum dots as fluorescence labels. *J. Agric. Biol. Eng.* **2014**, *7*, 77−83.
(19) Zhang, F.; Zou, M. Q.; Chen, Y.; Li, J. F.; Wang, Y. F.; Qi, X. H.; Xue, Q. Lanthanide-labeled immunochromatographic strips for the rapid detection of *Pantoea stewartii* subsp. *stewartii*. *Biosens. Bioelectron.* **2014**, *51*, 29−35.
(20) Langenhorst, R. J.; Lawson, S.; Kittawornrat, A.; Zimmerman, J. J.; Sun, Z.; Li, Y.; Christopher, H. J.; Nelson, E. A.; Fang, Y. Development of a fluorescent microsphere immunoassay for detection of antibodies against porcine reproductive and respiratory syndrome virus using oral fluid samples as an alternative to serum-based assays. *Clin. Vaccine Immunol.* **2012**, *19*, 180−189.
(21) Wang, Z. H.; Li, H.; Li, C. L.; Yu, Q.; Shen, J. Z.; Saeger, S. D. Development and application of a quantitative fluorescence-based immunochromatographic assay for fumonisin B1 in maize. *J. Agric. Food Chem.* **2014**, *62*, 6294−6298.
(22) Jerry, W. P.; Thomas, B. M.; Ryan, W. G.; Carl Schroder, M.; Mark, E. A.; Christine, M. L.; Stephen, W. H.; Harry, R. H. A multiplexed fluorescent microsphere immunoassay for antibodies to pneumococcal capsular polysaccharides. *J. Clin. Pathol.* **2002**, *117*, 589−596.
(23) Thomas, B. M.; Brian, M. P.; Jerry, W. P.; Troy, D. J.; Christine, M. L.; Harry, R. H. Determination of cytokine responses using a multiplexed fluorescent microsphere immunoassay. *J. Clin. Pathol.* **2002**, *118*, 346−353.
(24) Wang, L. B.; Chen, W.; Ma, W. W.; Liu, L.; Ma, W.; Zhao, Y.; Zhu, Y. Y.; Xu, L. G.; Kuang, H.; Xu, C. L. Fluorescent strip sensor for rapid determination of toxins. *Chem. Commun.* **2011**, *47*, 1574−1576.
(25) Czeh, A.; Mandy, F.; Feher-Toth, S.; Torok, L.; Mike, Z.; Koszegi, B.; Lustyik, G. A flow cytometry based competitive fluorescent microsphere immunoassay (CFIA) system for detecting up to six mycotoxins. *J. Immunol. Methods* **2012**, *384*, 71−80.
(26) Chen, Y. Q.; Chen, Q.; He, L. D.; Shang, B. R.; Zhang, L. Y. Enzyme immunoassay and liquid chromatography-fluorescence detection for amikacin in raw milk. *Food Chem.* **2012**, *135*, 380−385.
(27) Xie, Q. Y.; Wu, Y. H.; Xiong, Q. R.; Xu, H. Y.; Xiong, Y. H.; Liu, K.; Jin, Y.; Lai, W. H. Advantages of fluorescent microspheres compared with colloidal gold as a label in immunochromatographic lateral flow assays. *Biosens. Bioelectron.* **2014**, *54*, 262−265.
(28) Li, X. M.; Luo, P. J.; Tang, S. H.; Beier, R. C.; Wu, X. P.; Yang, L. L.; Li, Y. W.; Xiao, X. L. Development of an immunochromatographic strip test for rapid detection of melamine in raw milk, milk products and animal feed. *J. Agric. Food Chem.* **2011**, *59*, 6064−6070.
(29) Biagini, R. E.; Sammons, D. L.; Smith, J. P.; MacKenzie, B. A.; Striley, C. A.; Semenova, V.; Steward-Clark, E.; Stamey, K.; Freeman, A. E.; Quinn, C. P.; Snawder, J. E. Comparison of a multiplexed fluorescent covalent microsphere immunoassay and an enzyme-linked immunosorbent assay for measurement of human immunoglobulin G antibodies to anthrax toxins. *Clin. Diagn. Lab. Immunol.* **2004**, *11*, 50−55.

nucleotides 15−20.[15,16] Because the RNAi mechanism effectively parses sequence mismatches and ambiguities, it has been shown through in vitro studies conducted with transfected small RNAs that small RNAs can cause gene suppression of unintended gene targets.[17] This outcome, commonly referred to as the "off-target" effect, has led to increased scrutiny regarding the specificity of RNAi-based drugs and also been proposed as a putative concern for food crops that are engineered to produce small RNAs. However, this "off-target" effect has been characterized using in vitro systems and is orders of magnitude less potent than "on-target" suppression.[9,11] Such suppression also requires special sequence contexts, thermodynamic criteria, target accessibility, and other conditions.[18,19]

To investigate the level of significance of regularly consumed small RNAs that share sequence homology with human genes, the small RNA profiles of fresh market fruits and vegetables were examined. These were locally purchased tomatoes, watermelons, zucchinis, and onions that were selected because their appearance suggested they were likely to be infected with viral disease(s). Using a next-generation high-throughput sequencing method, between 1.6 and 3.6 million small RNA sequences were obtained from each sample. Although most of the small RNAs found in these vegetables were likely derived from endogenous genome, up to 9.5% were identified as sequences originating from viruses. Many of these small RNAs were found to share sequence similarity with human genes. Small RNA profiles such as these resemble those of plants genetically modified to express fragments of virus sequences for the purposes of conferring virus resistance.[14] The analysis of the small RNAs presented here provides insights into the plant−virus interaction and also evidence of a history of safe consumption for dietary small RNAs. By extension, this research supports the safety of biotechnology-derived crops employing RNA-based gene suppression when consumed by humans or animals.

## MATERIALS AND METHODS

**Plant Materials.** Vegetables suspected of virus diseases based on physical characteristics were selectively purchased at local farmers' markets or supermarkets in the region of Yolo county, California, USA. The tomato fruits displayed lesions with a chlorotic concentric ring pattern typical of those caused by *tomato spotted wilt virus* (TSWV, family Bunyaviridae, genus *Tospovirus*). The onion bulbs with attached green leaves exhibited elongated lesions typical of those caused by the *iris yellow spot virus* (INSV, family Bunyaviridae, genus *Tospovirus*). The squash fruits had mosaic symptoms consistent with those caused by viruses such as the *watermelon mosaic virus* (WMV), *zucchini yellow mosaic virus* (ZYMV), or *papaya ring spot virus* (PRSV) (all viruses in the family Potyviridae, genus *Potyvirus*). The melon fruit was chosen on the basis of mottling symptoms that might be caused by a number of different potyviruses.

**Plant RNA Isolation and Small RNA Sequencing.** Symptomatic portions of the fruits/bulbs were harvested and ground in liquid nitrogen. Total RNA was extracted using TRIzol (Invitrogen, Carlsbad, CA, USA) following the manufacturer's recommended protocol. RNA was quantified by Nanodrop (Thermo scientific, Wilmington, DE, USA), and its integrity was verified by gel electrophoresis. Small RNA library construction and sequencing were performed with Illumina technology (Illumina Inc., San Diego, CA, USA) as described previously.[20] Raw reads (4−6 million) were generated from each library. After the 5′ and 3′ adaptors were identified and removed from the raw reads, reads with sequence length from 18 to 26 nt were parsed out for further analysis (Figure 1). The sequences of these raw reads can be found in NCBI under BioProject accession PRJNA265505.

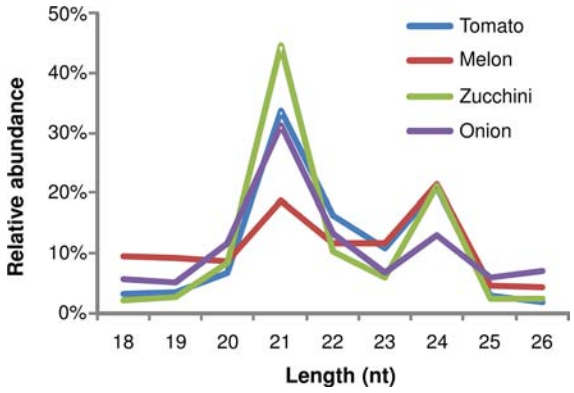


**Figure 1.** Relative abundance of small RNA size classes. The relative abundance of small RNA with lengths ranging from 18 to 26 nt is shown in the graph. All of the samples had the typical plant small RNA size distribution with peaks at 21 and 24 nt. With the exception of the melon sample, the 21 nt class was more abundant than the 24 nt class.

**Small RNA Sequence Analysis.** The parsed small RNAs were mapped to plant virus sequences downloaded from www.dpvweb.net on March 2, 2012. Small RNA matching was performed using "SHRiMP" v2.[21] Only perfectly mapped small RNAs were counted. RNAi plays an important antiviral role in plants. Upon virus infection, small RNAs are generated with the help of host plant Dicer-like protein from viral dsRNAs either as viral replicative intermediates or resulting from host RNA-dependent RNA polymerases on viral templates. The viral siRNAs are from both strands of the dsRNA and predominantly 21 and 22 nt in length. To remove noise from the virus mapping results, such as nonvirus sequence contamination, we applied three filters: (1) A virus is said to have infested the plant if only its sequence has at least 10 perfectly matched and sequence distinct small RNAs; (2) 21 and 22 nt small RNAs account for at least 60% of the small RNAs that mapped to a virus sequence; and (3) the abundance of small RNAs mapping to either strand of a virus sequences reflects a minimum of 5% of overall mapped small RNA abundance to the virus sequence. Virus-mapped small RNAs were then compared to the human reference RNA set downloaded from genome.ucsc.edu on February 7, 2012. For this analysis, up to 2 mismatches in 21 nt small RNAs and 3 mismatches in 22 nt small RNAs were allowed. Similarly, all small RNAs not mapped to virus sequences ("non-virus-mapped"), which were presumably derived from endogenous plant sequences, were also compared to the human reference RNA set. To match this subset of plant small RNAs against human reference genes, human miRNAs, rRNAs, small nucleolar RNAs, and small nuclear RNAs were excluded from the reference RNA set, and up to two mismatches were allowed for each match. Detailed lists of the virus-mapped small RNAs and small RNAs homologous to human genes can be found in the Supporting Information.

## RESULTS

**Deep Sequencing of Vegetable Small RNA Populations.** RNA extracted from tomato (fruit), melon (fruit), zucchini (fruit), and onion (bulb and stem) was sequenced using Illumina technology. Small RNA sequences ranging in length from 18 to 26 nt were parsed out for subsequent analyses (Figure 1 and Table 1). The peaks shown here are typical of plant small RNA distribution, showing major peaks at 21 and 24 nt, consistent with plant dicer-like protein (DCL) cleavage products.[22] The 21 nt class was more predominant than the 24 nt for all samples but melon. The total number of

**Table 1. Total Numbers of Small RNA Reads Obtained from Each Sample Library and the Numbers of Reads That Mapped to the Virus Sequences[a]**

| | | | | parsed reads (18−26 nt) | | virus-mapped reads | |
|---|---|---|---|---|---|---|---|
| sample ID | species | tissue | raw reads | total reads | unique reads | total reads | unique reads |
| tomato | *Solanum lycopersicum* | tomato RNA (fruit) | 5315393 | 3609317 | 1209206 | 196069 | 23929 |
| melon | *Cucumis melo* | melon RNA (fruit) | 4825754 | 1636524 | 536672 | 185 | 175 |
| zucchini | *Cucurbita pepo* | zucchini RNA (fruit) | 5184745 | 3344051 | 838271 | 191085 | 22949 |
| onion | *Allium cepa* | onion RNA (bulb + stem) | 6038349 | 3145549 | 915603 | 301913 | 33144 |

[a]Only parsed (18−26 nt) reads were used in the mapping.

reads varied from 1,636,524 to 3,609,317, with unique reads well represented in all of the libraries (Table 1).

**Size Class Distribution of Virus-Mapped Small RNAs.** Several filters were applied to map the parsed plant-derived small RNA sequences to the virus genome collections obtained from www.dpvweb.net (see Small RNA Sequence Analysis under Materials and Methods). The 21−22 nt size class siRNAs are significantly more abundant than the 24 nt in all four samples (Figure 2), consistent with the size of small RNA

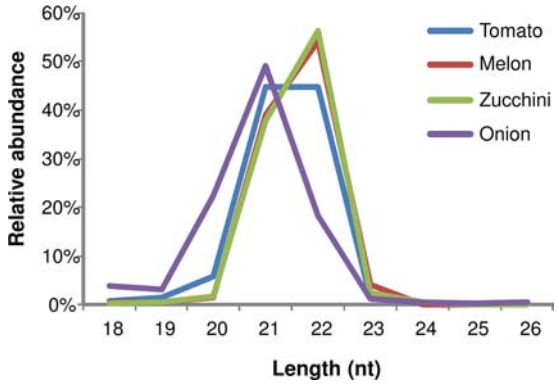


**Figure 2.** Relative abundance of small RNA size classes from small RNAs mapped to the virus sequence database. For all samples, most of the virus-mapped reads belong to the 21 and 22 nt size classes. These small RNAs, usually associated with post-transcriptional gene silencing, are likely generated upon viral infection.

products of post-transcriptional gene silencing usually associated with viral infection. However, the number of reads of the virus-mapped melon small RNA population is >100-fold less than in the other vegetable libraries (Table 1).

**Validation of Virus-Mapped Matches.** The genomic sequences of the top two virus matches (Table 2) generated from mapping the siRNA libraries to the virus sequence collection (except for the melon library where only one matching virus was identified) were plotted against the sequences of their respective small RNA matches to illustrate their distribution (Figure 3). In addition to applying the filters described earlier, the presence of small RNAs across the entire length of the putative virus hit serves as a validation criterion suggesting the legitimate presence of the virus in the sample (Figure 3A−D,F). In the case of the melon sample, although the number of small RNA matches is smaller in number (possibly reflecting low virus titer in the tissue) the virus hit seems to be authentic. Conversely, a sparsely distributed match pattern (Figure 3E,G) is an indication that the matching small RNAs likely originated from sources other than the matched virus. Due to sequence similarities between viruses, some small RNAs match to one virus and also cross-match to another: for

**Table 2. Top Two Virus Matches and the Numbers of Small RNA Reads Matched in Each Sample Library[a]**

| | | | mapped reads | |
|---|---|---|---|---|
| sample | virus species matched | GenBank accession | total reads | unique reads |
| tomato | *tomato spotted wilt virus* (TSWV), segment S | HQ402595 | 100079 | 6211 |
| | *potato virus Y* (PVY) | HQ912865 | 12076 | 4040 |
| melon | *watermelon mosaic virus* (WMV) | FJ623474 | 128 | 122 |
| zucchini | *watermelon mosaic virus* (WMV) | EU660583 | 146333 | 17542 |
| | *soybean mosaic virus* (SMV) | D00507 | 3607 | 419 |
| onion | *iris yellow spot virus* (INSV), segment L | FJ623474 | 108325 | 15979 |
| | *tomato yellow fruit ring virus* (TYFRV), partial L gene | AJ493271 | 802 | 91 |

[a]The melon sample had only one virus match. For viruses that have more than one genome segment, only one segment is shown in the table, although all other segments had similar significant matches.

example, in the zucchini sample, most of the small RNAs mapped to *soybean mosaic virus*, SMV (Figure 3E) were also mapped to WMV (Figure 3D) and in the onion sample, all of the small RNAs mapped to *tomato yellow fruit ring virus*, TYFRV (Figure 3G), also mapped to INSV (Figure 3F).

In the case of the *tomato spotted wilt virus*, segment S matched in the tomato sample (Figure 3A), and the small RNA reads in both the sense and antisense orientations come predominantly from the regions corresponding to the non-structural and nucleocapsid protein coding sequences, and noticeably less from the intergenic region that is not actively transcribed. For PVY (Figure 3B), WMV (Figure 3D), and INSV segment L (Figure 3F), all regions are evenly represented (note the change of scale), consistent with the generation of a single transcript over the genomic segment. The relative abundance of these virus-derived small RNAs across the virus genome and their sequence signatures could also reveal the biochemical properties of plant small RNA processing. For example, using virus-derived small RNA sequences from TSWV infected tomato and *Nicotiana benthamiana*, details of small RNA differential processing were examined previously.[23] Our small RNA sequencing results that include three additional viruses could be applied to such studies in the future.

**Characterization of Tomato Library Reads.** The tomato small RNA library was further investigated and mapped to the Monsanto in-house assembled tomato reference genome. Only sequences with perfect matches to the tomato and/or viral genomes are included in the analysis, and these matches

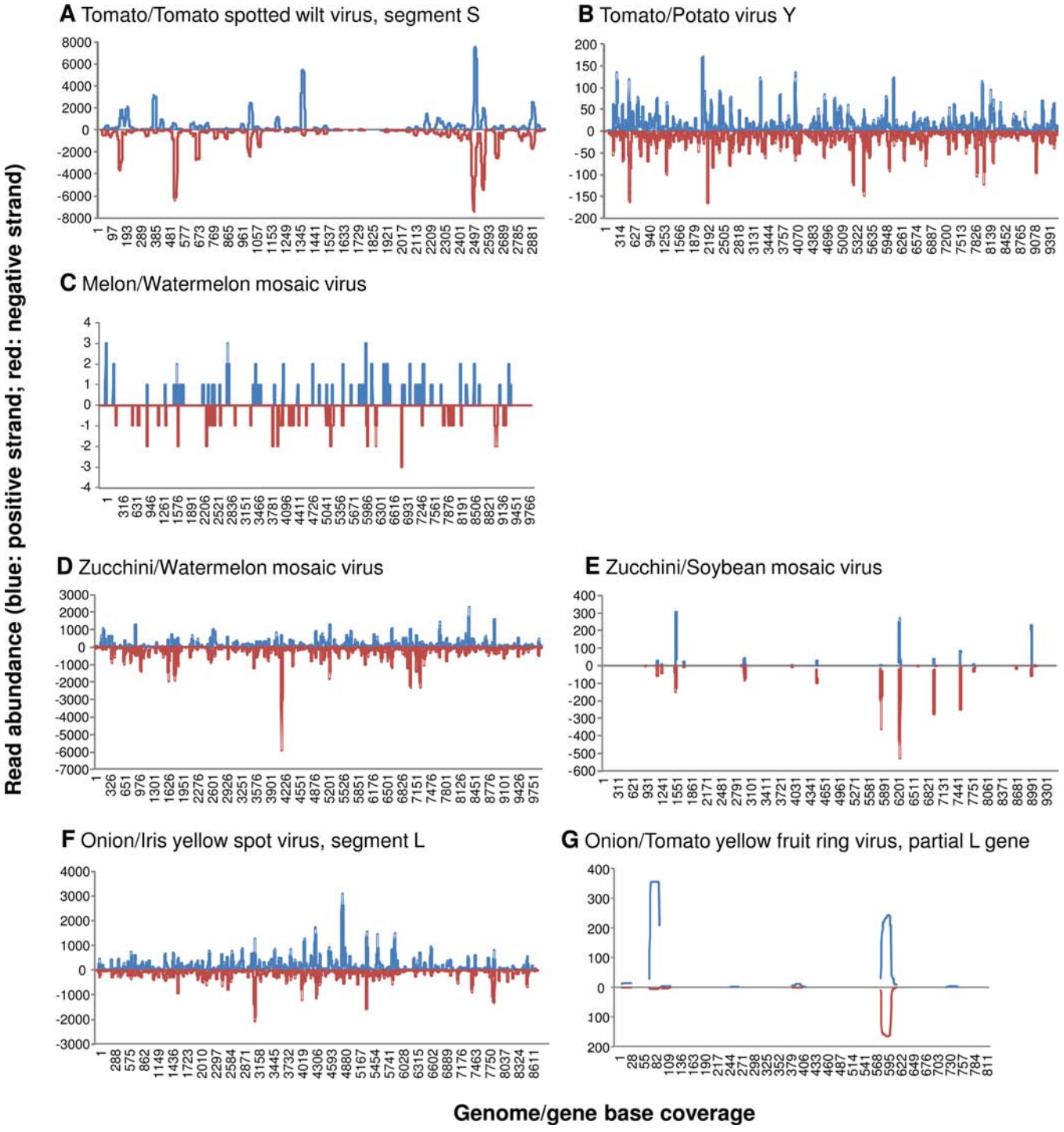


**Figure 3.** Validation of virus-mapped small RNA reads to their respective matching viral sequences. The top two virus matches for each sample were plotted against small RNAs mapped to them. Except for E and G, the small RNAs are mapped across the entire virus sequences. Therefore, there is a high probability that such a virus is present in the samples. On the contrary, only sparse matches were found on E and G, which suggests that these mapped small RNAs were derived from different sources.

**Table 3. Number of Total and Unique Small RNA Reads in Each Category in the Tomato Sample**

| | all reads | | tomato genome-mapped reads | | virus-mapped reads | | overlap reads | |
|---|---|---|---|---|---|---|---|---|
| sample | total reads | unique reads | total reads | unique reads | total reads | unique reads | total reads | unique reads |
| tomato | 3609317 | 120206 | 2596723 | 824996 | 196069 | 23929 | 2374 | 676 |

accounted for 78% of all reads (Table 3). The remaining, nonmatching reads could be mostly sequencing errors and some representing single-nucleotide polymorphisms (SNPs) because the sample is sourced from a tomato variety different


dx.doi.org/10.1021/jf503756v | J. Agric. Food Chem. 2014, 62, 12067−12074

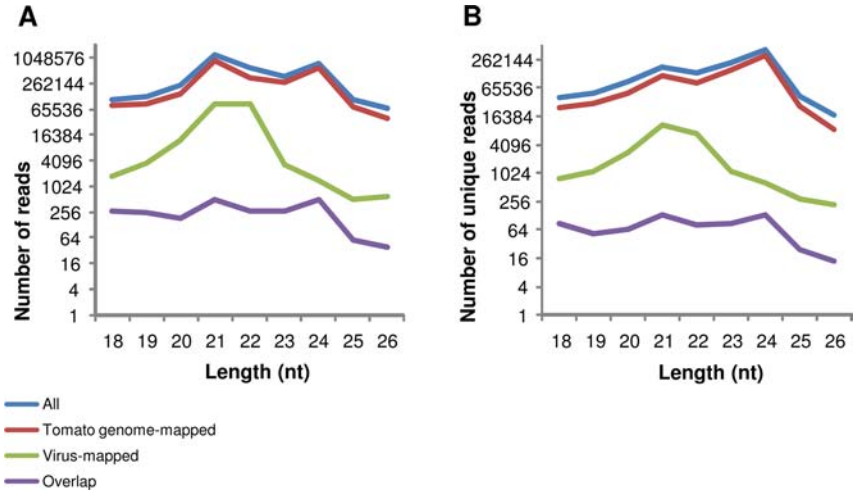


**Figure 4.** Categories of reads and unique reads in small RNA size classes from the tomato sample: the total number of reads (A) and the unique number of reads (B) of tomato small RNAs that matched perfectly to the in-house assembled reference tomato genome (red line), virus genome database (green line), or both (purple line). Together they account for 78% (Table 3) of all reads (blue line).

from the reference sequence. As previously observed, the abundance of 21−22 nt classes appears to have been enhanced by the virus-derived small RNAs (Figure 4A). The 24 nt class small RNAs, mostly derived from the endogenous tomato genome, are both abundant and rich in unique sequences (Figure 4). This is probably due to their roles in genome-wide transcriptional regulation and chromatin modification.[22]

**Comparison of Vegetable Small RNAs to the Human Transcriptome.** To evaluate if small RNAs derived from food have sequence similarity to human genes, we compared our libraries of small RNA sequences to small RNAs using a database of human reference RNAs. A recent study suggested that ingestion of a rice-derived miRNA matching a human gene over its open reading frame could cause transcript suppression in humans,[24] claims that have been strongly challenged in the peer-reviewed literature by several independent research groups collectively.[25−27] Nevertheless, similar matching criteria were used in this evaluation.

We divided the small RNAs in each library into virus-mapped and non-virus-mapped reads, representing exogenous and endogenous sources for the sequences, respectively. To simplify this bioinfomatic evaluation, the positions of the mismatches, which sometimes can have various degrees of impact in target gene suppression efficacy,[15,16] were not given special considerations. The results in Table 4 summarize that, when allowing up to 2 mismatches in the 21 nt size class and 3 mismatches in 22 size class, many human genes are homologous to virally derived small RNAs. Totals of 1580, 43, 884, and 1399 human genes have at least one subregion sharing sequence similarity to virus-mapped small RNAs in the tomato, melon, zucchini, and onion small RNA libraries, respectively (Supporting Information Tables S1−S4). Except for the melon library, where fewer virus-mapped small RNAs were found, virus-derived small RNAs that match to human gene transcripts appear abundant. For example, in the tomato library, 21816 reads or 11.1% of the virus-mapped reads are highly homologous to 1580 human genes (Table 4). In some instances, thousands of virus-derived small RNAs can match a single human gene. The top three human genes matched by the most virus-mapped small RNAs in the tomato, zucchini, and onion are listed in Table 5. However, there is no human gene match shared by the virus-derived small RNAs in all four libraries.

**Table 4. Virus-Mapped Small RNA Reads Sharing Sequence Homology to Human Reference RNA Set[a]**

| sample | no. of human RNAs matched | no. of unique reads | total reads | % of total virus-mapped reads sharing homology with human genes |
|---|---|---|---|---|
| tomato | 1580 | 1786 | 21816 | 11.1 |
| melon | 43 | 22 | 22 | 11.9 |
| zucchini | 884 | 1558 | 16634 | 8.7 |
| onion | 1399 | 1936 | 18005 | 6.0 |

[a]The virus-mapped reads, 21- and 22-nt size classes, in each sample (Figure 2) were matched against the human reference RNA set downloaded from genome.ucsc.edu (Feb 7, 2012), allowing up to two or three mismatches for each 21- and 22-nt small RNA read, respectively.

Beyond the virus-derived small RNAs, the remaining small RNAs in these fruit or vegetable small RNA libraries are probably derived from endogenous plant sequences. These small RNAs can also share sequence homology to human genes. To eliminate trivial and low-complexity matches, the miRNAs, rRNAs, small nucleolar RNAs, and small nuclear RNAs in the human reference RNA set that could be matched from the corresponding fruit or vegetable rRNA sequences were excluded from the sequence search. Up to two mismatches were allowed for each small RNA, and the results are shown in Table 6. These results imply that up to 10.9% of the total small RNAs in regularly consumed vegetables share a high degree of sequence similarity with human genes. Furthermore, 2774 human gene matches are shared by all four libraries (Supporting Information Tables S5−S8). This suggests that some human genes can have frequent matches by small RNAs derived from different fruits and vegetables. Although most of these matched sequences are few in numbers, numbers of endogenous small RNA with high copy numbers appear to have significant sequence similarity with human genes. For example, miRNA159a, which is abundant in all four libraries, can be mapped to a human gene encoding polycystic kidney and hepatic disease 1, PKHD1 protein (Tables S5−S8).

Table 5. Examples of Human RNAs Matching the Sequence of Virus-Mapped Small RNA Reads[a]

| sample | human RNA matched | GenBank ID | region matched | no. of unique reads | total reads |
|---|---|---|---|---|---|
| tomato | multiple EGF-like-domains 8 (MEGF8), mRNA | NM_001410 | 10253−10274 | 20 | 3451 |
| | family with sequence similarity 190, member A (FAM190A), transcript variant 1, mRNA | NM_001145065 | 5152−5170 | 1 | 2419 |
| | rho-associated, coiled-coil containing protein kinase 2 (ROCK2), mRNA | NM_004850 | 4525−4545, 997−1017 | 6 | 2337 |
| zucchini | WD repeat domain 3 (WDR3), mRNA | NM_006784 | 3424−3444 | 6 | 1019 |
| | regulator of G-protein signaling 7 (RGS7), mRNA | NM_002924 | 1273−1295 | 14 | 904 |
| | proline-rich transmembrane protein 2 (PRRT2), transcript variant 1, mRNA | NM_145239 | 1444−1464 | 4 | 462 |
| onion | triosephosphate isomerase 1 pseudogene 3 (TPI1P3), noncoding RNA | NR_027338 | 639−659 | 6 | 1043 |
| | olfactory receptor, family 6, subfamily P, member 1 (OR6P1), mRNA | NM_001160325 | 635−654 | 10 | 941 |
| | DYX1C1-CCPG1 readthrough (nonprotein coding) (DYX1C1-CCPG1), noncoding RNA | NR_037923 | 2962−2983, 3037−3056 | 11 | 689 |

[a]Except for the melon sample, where only a few matches were found, the top three human RNA matches in each sample are listed. The majority of the reads matched a single subregion of the transcript as shown using the base number referenced in GenBank.

Table 6. Non-Virus-Mapped Small RNA Reads Sharing Sequence Homology to Human Reference RNA Set[a]

| sample | no. of human RNAs matched | no. of unique reads | total reads | % of total non-virus-mapped reads sharing homology with human genes |
|---|---|---|---|---|
| tomato | 13683 | 33189 | 337610 | 9.4 |
| melon | 8664 | 14961 | 157019 | 9.6 |
| zucchini | 8286 | 14633 | 144654 | 4.3 |
| onion | 13851 | 34193 | 342541 | 10.9 |

[a]The virus-mapped small RNA reads were removed from each small RNA library. The rest of the small RNA reads, presumably derived from endogenous sequences, were matched against the human reference RNA set downloaded from genome.ucsc.edu. The miRNAs, ribosomal RNAs, small nucleolar RNAs, and small nuclear RNAs were excluded from the human reference RNA set and allowed up to two mismatches for each plant small RNA. The number of human genes matched as well as the numbers of unique and total small RNA reads whose sequences matched these human genes are shown.

## DISCUSSION

A typical plant small RNA size distribution is characterized by abundant 21 and 24 nt size classes; the 24 nt class is commonly present at an abundance similar to, or more than, that of the 21 nt size class.[22] The 24 nt class small RNA is responsible for transcriptional regulation and chromatin modification,[28] whereas the 21 nt class small RNA is mostly involved in post-transcriptional[29] and antiviral defense.[30,31] Except for the melon sample, the small RNA size profiles of all other fruit and vegetable samples displayed a higher abundance of 21 nt sized small RNAs (Figure 1). This is likely due to the presence of viruses in these tissues that induced an antiviral RNA silencing response, resulting in the accumulation of 21 nt small RNAs. Indeed, significant amounts of total small RNA populations are found to have originated from viral sequences, which partially contributed to the greater abundance of the 21 nt class seen in tomato, zucchini, and onion samples (Figure 2). However, directly comparing the small RNA populations between known infected and uninfected plants would be necessary to confirm these results.

Previously, we have shown that it is possible to reassemble significant portions of TSWV genome from overlapping small RNA sequences obtained by small RNA sequencing of tomato infected with the virus.[20] Here we report that several viruses can be easily and precisely detected in fresh market vegetables using small RNA sequencing. Furthermore, except for the WMV in the melon sample where the virus accumulation was likely to be low, the contigs assembled from the small RNA sequences from other samples embody large portions of the virus genomes. For example, as much as 89% of TSWV, 84% of PVY, 76% of WMV, and 96% of INSV total genomic sequences are covered by the small RNAs in their respective samples (data not shown). Therefore, it is possible to use small RNA sequencing to assemble the genome of a novel virus, especially when the endogenous small RNAs of host plant can be identified and excluded. With gradual reduction in cost since its invention, small RNA sequencing has the potential to be used as a one-step diagnostic and discovery tool for plant viruses in the future.

Because RNA-mediated gene suppression in plants and animals operated through fundamentally similar mechanisms and synthetic dsRNA or siRNA/miRNA are known to work in plant or animal cells in vitro in a sequence-specific manner, some have cautioned the use of this RNA-based gene suppression in plant biotechnology. Recently, a study claiming that a miRNA, miR168a, from rice can target a mouse gene for suppression through oral ingestion has intensified the debate.[24] The experimental design and assumptions of this study have been disputed.[11,27,32] This phenomenon of significant miRNA uptake in mice, nonhuman primates, and humans has not been reproduced by others[25−27] and the reported physiological impacts by Zhang and colleagues were not reproduced in a properly controlled feeding study with higher miR168a exposures.[27] In addition, these observations are inconsistent with the weight of the evidence for the safety of ingested nucleic acids, as evidenced by biological barriers to their uptake and/or activity in higher organisms, their extensive history of safe consumption, and the delivery challenges faced by pharmaceutical companies developing oligonucleotide-based therapeutics.[11,33] The human diet is made up of largely eukaryotic sources that contain an abundance of small RNAs. Therefore, it is not surprising that such small RNAs were found, intact, in food through small RNA sequencing.[24−27,34] Studies have also demonstrated that some endogenous long dsRNAs in crop plants share sequence complementarity of at least 21 nucleotides with human genes.[33,34]

In the current study, we have sequenced the small RNAs in fruits and vegetables readily available for purchase and likely to be ingested by consumers in an unprocessed or raw state. Sequences highly homologous to human genes were abundant in these fruits and vegetables, and we found that small RNAs originating within the plant and from infecting viruses can have matches to human genes. However, the consumption of fresh fruits and vegetables like these is not associated with an obvious heath risk; indeed, the opposite is true.[35,36]

It is logical to assume that small RNAs produced by transgenes are fundamentally no different from endogenously derived plant small RNAs. The data presented here provide additional support for the assumption that small RNAs derived from transgenic sources have no more impact on human health than the multitudes of endogenous plant small RNAs present in foods regularly consumed every day. This opinion is shared by the independent statutory agency Food Standards Australia New Zealand (FSANZ), who have noted that "there is no scientific basis for suggesting that small dsRNAs present in some GM foods have different properties or pose a greater risk than those already naturally abundant in conventional foods".[37] Coupled with the long history of safe consumption of these dietary small RNAs, the results described here provide further evidence to suggest that RNA-based gene suppression in biotech crops is unlikely to present a direct safety hazard to humans or animals.

## ■ ASSOCIATED CONTENT

### Supporting Information

Table S1, virus-mapped small RNA reads in the tomato sample that share sequence homology to human reference RNA set; Table S2, virus-mapped small RNA reads in the melon sample that share sequence homology to human reference RNA set; Table S3, virus-mapped small RNA reads in the zucchini sample that share sequence homology to human reference RNA set; Table S4, virus-mapped small RNA reads in the onion sample that share sequence homology to human reference RNA set; Table S5, non-virus-mapped small RNA reads in the tomato sample that share sequence homology to human reference RNA set; Table S6, non-virus-mapped small RNA reads in the melon sample that share sequence homology to human reference RNA set; Table S7, non-virus-mapped small RNA reads in the zucchini sample that share sequence homology to human reference RNA set; Table S8, non-virus-mapped small RNA reads in the onion sample that share sequence homology to human reference RNA set. This material is available free of charge via the Internet at http://pubs.acs.org.

## ■ AUTHOR INFORMATION

### Corresponding Author

*(S.H.) Fax: (530) 792-2005. E-mail: shihshieh.huang@monsanto.com.

### Author Contributions

‖A.F. and Y.Z. contributed equally to this work.

### Notes

The authors declare the following competing financial interest(s): All the authors are the employees of Monsanto.

## ■ ACKNOWLEDGMENTS

We thank Daniel Ader, Mingya Huang, and Mitchell Sudkamp for constructing the small RNA libraries and performing the small RNA sequencing and Jay Petrick for his valuable comments on the manuscript. We also thank Sofia Castiglioni for her contribution to the artwork in the Table of Contents graphic.

## ■ ABBREVIATIONS USED

TSWV, tomato spotted wilt virus; PVY, potato virus Y; WMV, watermelon mosaic virus; SMV, soybean mosaic virus; INSV, Iiris yellow spot virus; TYFRV, tomato yellow fruit ring virus; ZYMV, zucchini yellow mosaic virus; PRSV, papaya ring spot virus

## ■ REFERENCES

(1) Hannon, G. J. RNA interference. *Nature* **2002**, *418*, 244−251.
(2) Baulcombe, D. RNA silencing in plants. *Nature* **2004**, *431*, 356−33.
(3) Mello, C. C.; Conte, D., Jr. Revealing the world of RNA interference. *Nature* **2004**, *431*, 338−342.
(4) Kim, V. N. Small RNAs: classification, biogenesis, and function. *Mol. Cells* **2005**, *19*, 1−15.
(5) Brodersen, P.; Voinnet, O. The diversity of RNA silencing pathways in plants. *Trends Genet* **2006**, *22*, 268−280.
(6) Mallory, A. C.; Vaucheret, H. Functions of microRNAs and related small RNAs in plants. *Nat. Genetics* **2006**, *38* (Suppl), S31−S36.
(7) Siomi, H.; Siomi, M. C. On the road to reading the RNA-interference code. *Nature* **2009**, *457*, 396−404.
(8) Tiemann, K.; Rossi, J. J. RNAi-based therapeutics-current status, challenges and prospects. *EMBO Mol. Med.* **2009**, *1*, 142−151.
(9) Vaishnaw, A. K.; Gollob, J.; Gamba-Vitalo, C.; Hutabarat, R.; Sah, D.; Meyers, R.; de Fougerolles, T.; Maraganore, J. A status report on RNAi therapeutics. *Silence* **2010**, *1*, 14.
(10) O'Neill, M. J.; Bourre, L.; Melgar, S.; O'Driscoll, C. M. Intestinal delivery of non-viral gene therapeutics: physiological barriers and preclinical models. *Drug Discovery Today* **2011**, *16*, 203−218.
(11) Petrick, J. S.; Brower-Toland, B.; Jackson, A. L.; Kier, L. D. Safety assessment of food and feed from biotechnology-derived crops employing RNA-mediated gene regulation to achieve desired traits: a scientific review. *Regul. Toxicol. Pharmacol.* **2013**, *66*, 167−176.
(12) Sanders, R. A.; Hiatt, W. Tomato transgene structure and silencing. *Nat. Biotechnol.* **2005**, *23*, 287−289.
(13) Krieger, E. K.; Allen, E.; Gilbertson, L. A.; Roberts, J. K.; Hiatt, W.; Sanders, R. A. The Flavr Savr Tomato, an early example of RNAi technology. *HortScience* **2008**, *43*, 962−964.
(14) Frizzi, A.; Huang, S. Tapping RNA silencing pathways for plant biotechnology. *Plant Biotechnol. J.* **2010**, *8*, 655−677.
(15) Parizotto, E. A.; Dunoyer, P.; Rahm, N.; Himber, C.; Voinnet, O. In vivo investigation of the transcription, processing, endonucleolytic activity, and functional relevance of the spatial distribution of a plant miRNA. *Genes Dev.* **2004**, *18*, 2237−2242.
(16) Debernardi, J. M.; Rodriguez, R. E.; Mecchia, M. A.; Palatnik, J. F. Functional specialization of the plant miR396 regulatory network through distinct microRNA-target interactions. *PLoS Genet.* **2012**, *8*, No. e1002419.
(17) Jackson, A. L.; Burchard, J.; Schelter, J.; Chau, B. N.; Cleary, M.; Lim, L.; Linsley, P. S. Widespread siRNA "off-target" transcript silencing mediated by seed region sequence complementarity. *RNA* **2006**, *12*, 1179−1187.
(18) Liu, L.; Li, Q. Z.; Lin, H.; Zuo, Y. C. The effect of regions flanking target site on siRNA potency. *Genomics* **2013**, *102*, 215−222.
(19) Naito, Y.; Jun Yoshimura, J.; Morishita, S.; Ui-Tei, K. siDirect 2.0: updated software for designing functional siRNA with reduced seed-dependent off-target effect. *BMC Bioinf.* **2009**, *10*, 392.
(20) Hagen, C.; Frizzi, A.; Kao, J.; Jia, L.; Huang, M.; Zhang, Y.; Huang, S. Using small RNA sequences to diagnose, sequence, and investigate the infectivity characteristics of vegetable-infecting viruses. *Arch. Virol.* **2011**, *156*, 1209−1216.

(21) Rumble, S. M.; Lacroute, P.; Dalca, A. V.; Fiume, M.; Sidow, A.; Brudno, M. SHRiMP: accurate mapping of short color-space reads. *PLoS Comput. Biol.* **2009**, *5*, No. e1000386.
(22) Nobuta, K.; Lu, C.; Shrivastava, R.; Pillay, M.; De Paoli, E.; Accerbi, M.; Arteaga-Vazquez, M.; Sidorenko, L.; Jeong, D.-H.; Yen, Y.; Green, P. J.; Chandler, V. L.; Meyers, B. C. Distinct size distribution of endogeneous siRNAs in maize: evidence from deep sequencing in the mop1-1 mutant. *Proc. Natl. Acad. Sci. U.S.A.* **2008**, *105*, 14958−14963.
(23) Mitter, N.; Koundal, V.; Williams, S.; Pappu, H. Differential expression of tomato spotted wilt virus-derived viral small RNAs in infected commercial and experimental host plants. *PLoS One* **2013**, *8*, No. e76276.
(24) Zhang, L.; Hou, D.; Chen, X.; Li, D.; Zhu, L.; Zhang, Y.; Li, J.; Bian, Z.; Liang, X.; Cai, X.; Yin, Y.; Wang, C.; Zhang, T.; Zhu, D.; Zhang, D.; Xu, J.; Chen, Q.; Ba, Y.; Liu, J.; Wang, Q.; Chen, J.; Wang, J.; Wang, M.; Zhang, Q.; Zhang, J.; Zen, K.; Zhang, C.-Y. Exogenous plant MIR168a specifically targets mammalian LDLRAP1: evidence of cross-kingdom regulation by microRNA. *Cell Res.* **2011**, *22*, 107−126.
(25) Snow, J. W.; Hale, A.; Isaacs, S. K.; Baggish, A. L.; Chan, S. Y. Ineffective delivery of diet-derived microRNAs to recipient animal organisms. *RNA Biol.* **2013**, *10*, 1−10.
(26) Witwer, K. W.; McAlexander, M. A.; Queen, S. E.; Adams, R. J. Real-time quantitative PCR and droplet digital PCR for plant miRNAs in mammalian blood provide little evidence for general uptake of dietary miRNAs. *RNA Biol.* **2013**, *10*, 1−7.
(27) Dickinson, B.; Zhang, Y. J.; Petrick, J. S.; Heck, G.; Ivashuta, S.; Marshall, W. S. Lack of detectable oral bioavailability of plant microRNAs after feeding in mice. *Nat. Biotechnol.* **2013**, *31*, 965−967.
(28) Matzke, M. A.; Birchler, J. A. RNAi-mediated pathways in the nucleus. *Nat. Rev. Genet.* **2005**, *6*, 24−35.
(29) Vaucheret, H. Post-transcriptional small RNA pathways in plants: mechanisms and regulations. *Genes Dev.* **2006**, *20*, 759−771.
(30) Voinnet, O. Induction and suppression of RNA silencing: insights from viral infections. *Nat. Rev. Genet.* **2005**, *6*, 206−220.
(31) Wang, M. B.; Metzlaff, M. RNA silencing and antiviral defense in plants. *Curr. Opin. Plant Biol.* **2005**, *8*, 216−222.
(32) Zhang, Y.; Wiggins, B. E.; Lawrence, C.; Petrick, J.; Ivashuta, S.; Heck, G. Analysis of plant-derived miRNAs in animal small RNA datasets. *BMC Genomics* **2012**, *13*, 381.
(33) Jensen, P. D.; Zhang, Y.; Wiggins, B. E.; Petrick, J. S.; Zhu, J.; Kerstetter, R. A.; Heck, G. R.; Ivashuta, S. I. Computational sequence analysis of predicted long dsRNA transcriptomes of major crops reveals sequence complementarity with human genes. *GM Crops Food: Biotechnol. Agric. Food Chain* **2013**, *4*, 1−8.
(34) Ivashuta, S. I.; Petrick, J. S.; Heisel, S. E.; Zhang, Y.; Guo, L.; Reynolds, T. L.; Rice, J. F.; Allen, E.; Roberts, J. K. Endogenous small RNAs in grain: semi-quantification and sequence homology to human and animal genes. *Food Chem. Toxicol.* **2009**, *47*, 353−360.
(35) Bazzano, L. A. The high cost of not consuming fruits and vegetables. *J. Am. Diet. Assoc.* **2006**, *106*, 1364−1368.
(36) Steffen, L. M. Eat your fruit and vegetables. *Lancet* **2006**, *367*, 278−279.
(37) Food Standards Australia Zealand (FSANZ). *Response to Heinemann et al. on the regulation of GM crops and foods developed using gene silencing*; May 2013 (http://www.foodstandards.gov.au/consumer/gmfood/Pages/Response-to-Heinemann-et-al-on-the-regulation-of-GM-crops-and-foods-developed-using-gene-silencing.aspx).

Peach purée at different pH values was divided into 30 mL glass tubes and heated in a water bath at 90 °C for 10 min. The flasks were then cooled to room temperature in ice for 10 min. Tubes were stored in the dark for 90 days at room (ca. 23 °C) and refrigerated (4 °C) temperatures. The headspace gas was equivalent to the mixture existent in the atmospheric air (78 kPa $N_2$ + 21 kPa $O_2$ + 0.03 kPa $CO_2$). Sampling of individual flasks was carried out at 0, 7, 14, 30, 60, and 90 days of storage. This procedure was performed in triplicate.

**Microbiological Analysis.** Total mesophylls were assessed, in duplicate, using plate count agar (PCA, Biokar Diagnostics, Solabia, France) and a spread plate technique. Samples were incubated at 30 °C for 24 h.

Total yeasts and molds were assessed, in duplicate, using potato dextrose agar (PDA, Biokar Diagnostics, Solabia, France) and a spread plate technique. Samples were incubated at 30 °C for 48 h.

In both cases, colonies were enumerated and total viable cells (cfu/g) were determined.

**Color Measurement.** A Petri dish (inner diameter of 50 mm) with a whole in the lid was filled with the purée and placed directly over the Konica-Minolta CR-400 chromameter (Osaka, Japan) equipped with a $D_{65}$ illuminant and 2°. The instrument was calibrated using white ($Y$, 93.9; $x$, 0.3159; $y$, 0.3322) reference tiles. Two measurements from triplicates were performed, and results were averaged. The $L^*$, $a^*$, and $b^*$ CIE color system was used to evaluate the color.

The saturation index ($C^*$; eq 1) and hue angle ($H$; eq 2) were calculated using measured $L^*$, $a^*$, and $b^*$ values as follows and used to describe the color change compared to the control sample:

$$C^* = \sqrt{(a^*)^2 + (b^*)^2} \quad (1)$$

$$H = \tan^{-1}\left(\frac{b^*}{a^*}\right) \quad (2)$$

**Extract Preparation.** Hydrophilic extractions were performed by homogenizing 5 g of peach purée in 50 mL of 80% methanol in water at room temperature. Homogenization (IKA Ultraturrax T18, Wilmington, NC) was performed at 24 000 rpm for 30 s. The slurry was then centrifuged at 4000$g$ and 4 °C for 10 min; the supernatant was filtered through a 0.45 $\mu$m cellulose acetate filter (Orange Scientific, Braine-l'Alleud, Belgium); and the filtrate was used for the assessment of total activities. A 10 mL aliquot of the extract was evaporated to dryness in a RVC 2-18 speed-vacuum evaporator (Christ, Osterode am Harz, Germany) at 30 °C, and the residue was dissolved in 3 mL of methanol. The extract was then analyzed by high-performance liquid chromatography with photodiode array detection (HPLC−DAD) for phenolic compound identification and quantification over time.

Carotenoids were extracted as described by Wright and Kader,[9] where 5 g of peach purée was suspended in 10 mL of cold ethanol and homogenized at 24 000 rpm for 3 min using an IKA T18 Ultraturrax (Wilmington, NC). Hexane (8 mL) was added to the homogenate, and the resulting mixture was homogenized for an additional 2 min before the centrifugation for 10 min at 4000$g$. The hexane layer containing the carotenoids was transferred to a polypropylene tube. A solution of saturated sodium chloride (5 mL) and an additional 8 mL of hexane was added to the purée slurry, and the resulting mixture was homogenized for 1 min. The mixture was centrifuged as described above, and the hexane layer was collected. Both hexane layers were collected in the same polypropylene tube and used for saponification. Saponification was made as described by Kimura et al.,[10] where the resultant hexane fractions were mixed with 10% methanolic KOH and left under agitation overnight at 300 rpm. The mixture then was washed with 10% NaCl, and after three washes with deionized water, the sample was collected and used for spectrophotometric and HPLC−DAD analyses. The saponification procedure was carried out to remove chlorophylls and unwanted lipids and hydrolyzing carotenoid esters.[11]

**Analysis of Total Antioxidant Activity, Total Phenolics, and Total Carotenoids.** The total antioxidant activity was determined by 2,20-azinobis(3-thylbenzothiazoline-6-sulfonic acid) diammonium salt (ABTS) radical scavenging activity as described by Giao et al.[12] Briefly, the $ABTS^+$ radical cation was produced from the reaction of 7 mM ABTS and 2.45 mM potassium persulfate after incubation at room temperature in the dark for 16 h. The $ABTS^+$ solution was diluted with water to an absorbance of 0.70 ± 0.02 at 734 nm. The ascorbic acid concentrations used to give 20−80% inhibition of the blank absorbance for linearity purposes were between 0.02 and 0.50 g/L. The $ABTS^+$ solution was read after 10 $\mu$L of sample extract reacts for 6 min. The antioxidant capacity of the sample was calculated and expressed as milligrams of ascorbic acid equivalent per gram of peach purée.

The total phenolic content was determined spectrophotometrically with an ultraviolet (UV) mini 1240 spectrophotometer (Shimadzu, Tokyo, Japan) by the Folin−Ciocalteu method.[13] Briefly, 50 $\mu$L of methanolic extract, 50 $\mu$L of Folin−Ciocalteau reagent, 1 mL of $Na_2CO_3$ (75 g/L), and 1.4 mL of ultrapure water were mixed. The mixture was vortexed, and the tubes were left for 60 min in the dark at room temperature. The absorbance of the sample was read at 750 nm using gallic acid (0.06−0.5 g/L) as a standard. Results were expressed as milligrams of gallic acid equivalent per gram of peach purée.

Carotenoids were quantified after saponification by measuring the sample absorbance at 454 nm. $\beta$-Carotene was used to prepare the calibration curve in the range of 0.063−4.0 g/L.

**HPLC−DAD Analysis.** Qualitative and quantitative profiles of phenolic compounds and carotenoids present in the extracts were determined by HPLC−DAD (Waters Series 600, Milford, MA). Separation was performed in a reverse-phase Symmetry $C_{18}$ column (250 × 4.6 mm inner diameter, 5 mm particle size, and 125 Å pore size) with a guard column (Symmetry $C_{18}$).

Solvents used in chromatographic separation of phenolic compounds were solvent A, methanol, water, and formic acid (92.5:5:2.5, v/v/v), and solvent B, methanol and water (94:6, v/v). The linear gradient elution starts at 0−10% solvent B in 10 min at 0.5 mL/min, 10−30% in 40 min at 0.65 mL/min, 30−50% in 20 min at 0.75 mL/min, and 50−0% in 10 min at 1 mL/min. The injection volume was 20 $\mu$L.

Carotenoids were eluted using acetonitrile, methanol, dichloromethane, hexane, and ammonium acetate (55:22:11.5:11.5:0.02, v/v/v/v/w) under isocratic conditions at 1.0 mL/min flow rate for 20 min at 25 °C with an injection volume of 40 $\mu$L.

Detection was achieved by a diode array detector (Waters, MA) at wavelengths ranging from 200 to 600 nm in 2 nm intervals, and absorbance was measured at 320 and 454 nm.

The pure standards used were chlorogenic acid, neochlorogenic acid, and $\beta$-carotene (Sigma-Aldrich, Sintra, Portugal) and zeaxanthin and $\beta$-cryptoxanthin (Extrasynthése, Lyon, France), and results were expressed as micrograms per gram of fresh biomass.

**Statistical Analysis.** The changes in antioxidant activity and the contents of total and individual polyphenols and carotenoids were described during storage, where $Y$ represents the ratio between the concentration at time $t$ and the initial concentration at time 0 and $t$ is the storage time (days).

Statistical analysis was performed using GraphPad Prism, version 5.00, for Windows. Normality of data distribution was tested by the Kolmogorov−Smirnov method.

Statistically significant values of the means of groups were made by two-way analysis of variance with Bonferroni post-hoc test for the different pH conditions along time for both storage temperatures. The statistical analyses performed were considered significant when $p < 0.05$.

The case-wise principal component analysis (PCA) scores for the first three principal components were uploaded into the SPSS software package (version 17). PCA was conducted to the data set after normalization (the mean of the values for each variable is subtracted from each variable value, and the result is divided by the standard deviation of the values for each variable). Factor analysis was performed to reduce and explain the variability of the data. The Varimax method was used to produce orthogonal transformations to the reduced factors to better identify the high and low correlations.

## RESULTS AND DISCUSSION

**PCA.** A PCA model containing three principal components (PC1, PC2, and PC3) were calculated, which accounted for 75% of the total variation of the data set (Figure 1).

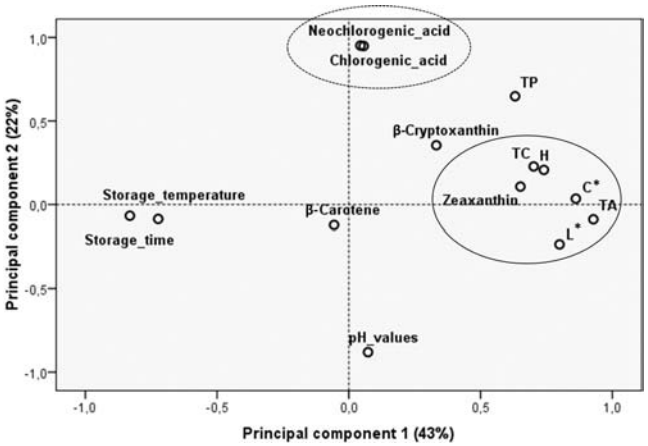


**Figure 1.** PCA of data from peach purée pasteurized and stored for 90 days at 4 and 23 °C for pH 2.5, 3.0, 3.5, 4.0, and 4.5. Total antioxidant activity, total phenolic content, and total carotenoid content are represented as TA, TP, and TC.

The most important component (PC1) explained 43% of the total variance. PC1 is related to purée overall quality, where the increase in storage time and temperature promoted a decrease of total antioxidant activity, total phenolic content, total carotenoid content, zeaxanthin and $\beta$-crytptoxanthin concentration, and color ($C^*$, $H$, and $L^*$). PC2 explained 22% of the total variance and mainly correlates pH variation with neochlorogenic and chlorogenic acids.

Finally, PC3 explained 10% of the variance, and this variation was mostly described by $\beta$-carotene. Variables that appear close together in this plot correlated positively, as seen in Figure 1; there is a close relationship between storage time and temperature, zeaxanthin, $C^*$, and total antioxidant activity.

Negative correlations were observed for storage time and temperature, $C^*$, $H$, $L^*$, total antioxidant activity, total carotenoids, and zeaxanthin.

The content of zeaxanthin was highly correlated with $H^*$ (Figure 1), which is consistent with the fact that an intense yellow color should be indicative of a higher zexanthin content. These results indicated that carotenoids as well as peach purée color were not strongly affected by pH variation, contrary to storage temperature and time, which were the main factors affecting these compounds.

A strong and negative correlation was also observed between pH and individual polyphenols, such as chlorogenic and neochlorogenic acids. Thus, the lower the pH, the greater the chlorogenic and neochlorogenic acid contents.

$\beta$-Carotene was found to be loaded on PC3, and the variables pH, storage time, and temperature seem to not affect the $\beta$-carotene content (Figure 1).

**Effect of pH Changes in Total Antioxidant Activity and Total Phenolic and Total Carotenoid Contents.** The pH value variations (2.5−4.5) on peach purée had no significant effect on antioxidant activity ($p > 0.05$; Figure 2). On the other hand, storage time showed a significant ($p < 0.05$) effect on antioxidant activity decrease, because longer storage periods were associated with lower antioxidant retention. The storage temperature was also a significant ($p < 0.05$) parameter, where, at 4 °C, antioxidant activity decreased 40% and, at 23 °C, antioxidant activity decreased 50% after 90 days (panels A and B of Figure 2).

The total phenolic content presented no significant variations in the range of pH values tested in samples for 90 days of storage at 4 and 23 °C. The total phenolic content decreased between 18 and 30% for 4 °C and between 29 and 40% for 23 °C after 90 days of storage (panels C and D of Figure 2). When açai juice was fortified with ascorbic acid and stored at 4 and 20 °C for 30 and 193 days, a maximum loss of soluble phenolics ranged from 8 to 13%. Authors related losses of total soluble phenolics during storage with polyphenolic oxidation and polymerization reactions that serve to reduce the number of free hydroxyl groups measured by the Folin−Ciocalteu assay.[14] The total phenolic content also decreased in orange juice stored at 18, 28, and 38 °C for 4 months by 7, 11, and 20%, respectively, also reflecting the decrease in antioxidant capacity of those juices.[15]

Total carotenoids were significantly ($p < 0.05$) affected by pH variation. At 4 °C, pH values of 3.0 and 3.5 presented the highest retention in total carotenoids, by decreasing 27 and 29%, respectively. The pH values of 4.0 and 4.5 presented both a similar decrease of ca. 56% (panels E and F of Figure 2). Similarly, at 23 °C and pH 3.0 and 3.5, there was a 40% decrease that was significantly ($p < 0.05$) lower than at pH 4.5 (68%). The percentage of total carotenoid losses was similar for the two storage temperatures, indicating no effect on the total carotenoid content. The present work demonstrates that the pH value of 4.0 and 4.5 induced a higher decrease rate for both storage temperatures and the pH values of 3.0 and 3.5 presented a better condition for a high stability of the carotenoids.

It may be hypothesized that, under acidic conditions, after thermal treatment, carotenoids may be entrapped or encapsulated within aggregates from the cellular components formed after cell wall depolymerization. This can protect the carotenoids from degradation reactions promoted by oxygen.[11] A significant loss of galacturonic acid after long acid hydrolysis times was found to be accompanied by changes in the size and branching of the single polymers and further breakdown of the complexes.[16] Palmero et al.[17] observed a decrease in carotenoid bioaccessibility upon heating carrots because of induced separation of intact cells that encapsulate carotenoids. On the one hand, cell wall components might be physically blocking carotenoid release.[17]

**Effect of pH Changes in Peach Polyphenols and Carotenoids.** In the literature, scarce information is available on the changes in individual phenolic and carotenoid constituents of pasteurized peach during storage at different pH conditions.

The individual phenolic compounds identified were neochlorogenic and chlorogenic acids, and they were stable throughout the storage period. At 4 °C, neochlorogenic acid decreased ($p < 0.001$) 34% after 90 days of storage for the higher pH values (4.0 and 4.5) (Figure 3A). With the increase of the storage temperature to 23 °C, pH variation did not affect the neochlorogenic acid concentration (Figure 3B).

The chlorogenic acid concentration decreased ($p < 0.001$) 32 and 39% for pH 4.0 and 4.5, respectively, for peach purée stored at 4 °C. The lower pH values (2.5, 3.0, and 3.5) presented decreases between 6 and 11% (Figure 3C).


dx.doi.org/10.1021/jf503913t | J. Agric. Food Chem. 2014, 62, 12075−12081

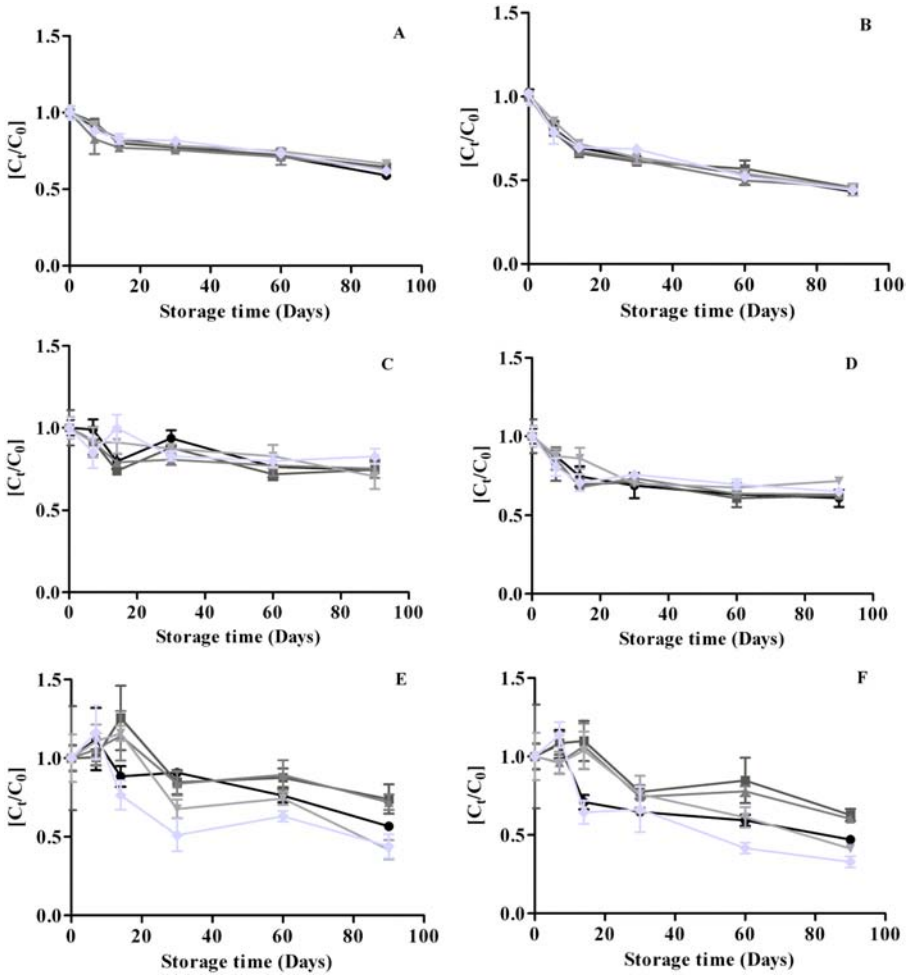


**Figure 2.** Evolution of (A and B) total antioxidant activity, (C and D) total phenolics, and (E and F) total carotenoids measured as the mean ± standard deviation ($n$ = 3) in pasteurized peach purée stored at 4 and 23 °C for 90 days, respectively. The different pH values are represented as (●) 2.5, (■) 3.0, (▲) 3.5, (▼) 4.0, and (◆) 4.5.

Storage at 23 °C led to a decrease of the chlorogenic acid concentration to ($p$ < 0.001) 37% on pH 4.5. The remaining pH values tested (2.5, 3.0, 3.5, and 4.0) presented a decrease of 14% (Figure 3D).

Previous studies revealed that chlorogenic acid was stable when added to apple juice at pH 3 and 4.5 and stored under refrigeration for up to 2 weeks. The susceptibility of phenolic compounds to pH strongly depends upon the structure of the phenol. Chlorogenic and neochlorogenic acids are compounds with OH groups, and their multi-ring aromatic structures are more complex than the mono-ring phenolic compounds. Their ionized and resonance forms are more resistant to acidic degradation than are the monocyclic polyphenolic compounds.[6] van der Sluis et al.[18] predicted by mathematical modeling that chlorogenic acid declined roughly by 40% in apple juice stored for 200 days at 20 °C in the absence of oxygen.

The individual carotenoids identified in peach purée extracts were zeaxanthin, β-cryptoxanthin, and β-carotene. The zeaxanthin concentration decreased ($p$ < 0.01) 11% for pH 3.0 by 90 days of storage at 4 °C. The remaining pH values, 2.5, 3.5, 4.0, and 4.5, decreased 67, 41, 60, and 68%, respectively (Figure 4A). At 23 °C, the zeaxanthin concentration decreased between 56 and 75%, without significant changes between pH conditions (Figure 4B).

The β-cryptoxanthin concentration decreased between 30 and 50% for purées stored under refrigeration, but pH variation did not affect its concentration. Storage under 23 °C caused the β-cryptoxanthin concentration to decrease 36% for pH 3.5, while pH 2.5, 3.0, 4.0, and 4.5 induced a higher significant decrease of 55, 46, 44, and 55%, respectively (panels C and D of Figure 4).

The concentration of β-carotene decreased ($p$ < 0.05) 47 and 52% for pH 2.5 and 4.5, respectively. The intermediate pH conditions resulted in a 24% decrease (Figure 4E) when purée was stored at 4 °C. Chen et al.[19] and Schieber and Carle[20] described that a high concentration of acids resulted in isomerization of β-carotene. At 23 °C, β-carotene decreased 39% at pH 2.5 and 4.5, while at pH 3.0, 3.5, and 4.0, it decreased between 24 and 26% (Figure 4F).

Carotenoids with carbonyl groups (astaxanthin and canthaxanthin) have slower rates of degradation than β-carotene and zeaxanthin, indicating preferential non-degradative protonation of the carbonyl groups.[4,21,22] However, other authors also demonstrated that low pH has a minor effect on β-carotene isomerization.[19,23] Nevertheless, other approaches report that carotenoids can undergo reactions of *cis*−*trans* isomerization containing double bonds through the formation of an intermediate carbocation when exposed to acidic conditions.[24,25] Protonation of carotenoids with a double bond


dx.doi.org/10.1021/jf503913t | J. Agric. Food Chem. 2014, 62, 12075−12081

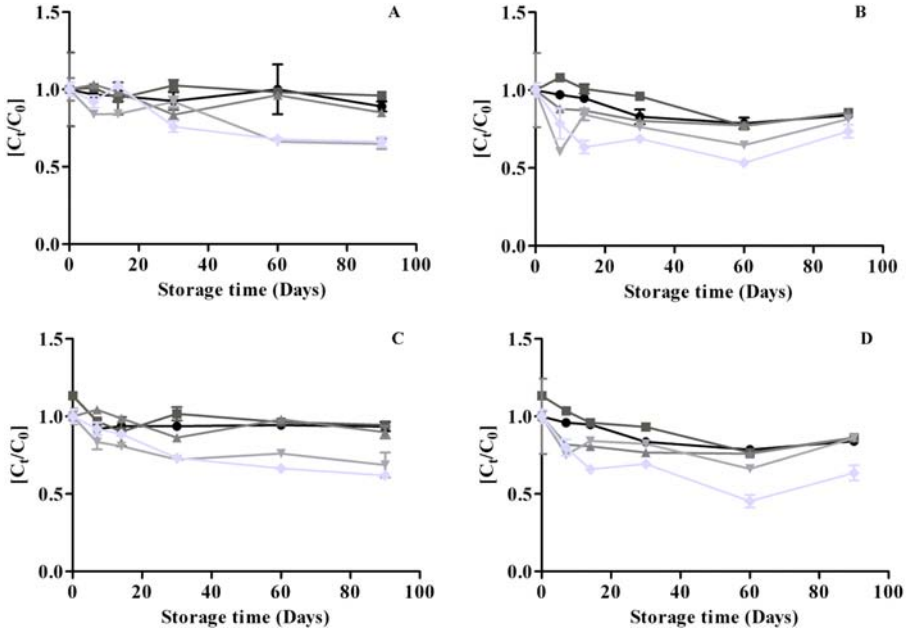


**Figure 3.** Concentration of individual phenolic compounds measured in pasteurized peach purée stored at 4 and 23 °C for 90 days for (A and B) neochlorogenic acid and (C and D) chlorogenic acid measured as the mean ± standard deviation ($n$ = 3), respectively. The different pH values are represented as (●) 2.5, (■) 3.0, (▲) 3.5, (▼) 4.0, and (◆) 4.5.

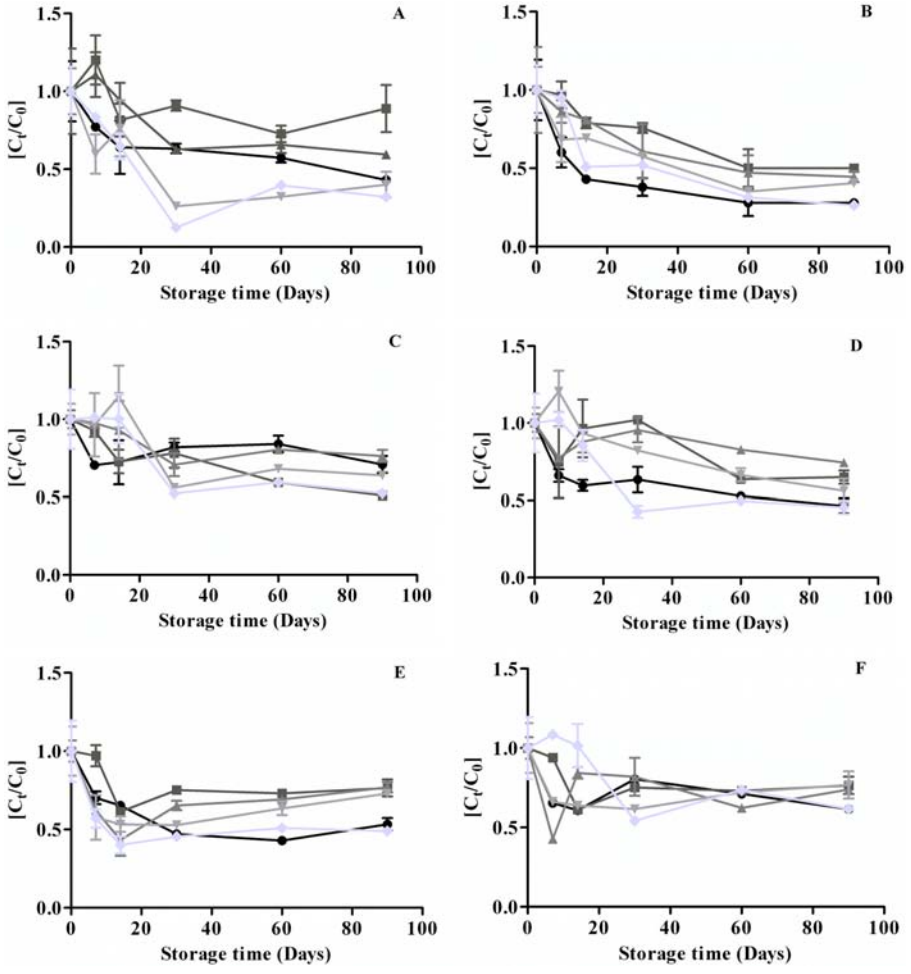


**Figure 4.** Concentration of individual carotenoids measured in pasteurized peach purée stored at 4 and 23 °C for 90 days for (A and B) zeaxanthin, (C and D) $\beta$-cryptoxanthin, and (E and F) $\beta$-carotene measured as the mean ± standard deviation ($n$ = 3), respectively. The different pH values are represented as (●) 2.5, (■) 3.0, (▲) 3.5, (▼) 4.0, and (◆) 4.5.


dx.doi.org/10.1021/jf503913t | J. Agric. Food Chem. 2014, 62, 12075−12081

Table 1. Changes in Color Values ($L^*$, $C$, and $H$) of Pasteurized Peach Purée Stored for 90 Days at 4 and 23 °C under Five Different pH Values (2.5, 3.0, 3.5, 4.0, and 4.5)[a]

| | | $L^*$ | | $C^*$ | | $H$ | |
|---|---|---|---|---|---|---|---|
| storage time (days) | | 0 | 90 | 0 | 90 | 0 | 90 |
| 4 °C | 2.5 | 42.78 ± 0.17 c | 38.20 ± 0.49 c | 32.70 ± 0.17 c | 26.11 ± 0.35 a | 84.28 ± 0.12 b | 85.42 ± 1.31 a |
| | 3.0 | 43.07 ± 0.28 c | 40.88 ± 0.38 b | 36.74 ± 0.13 b | 25.63 ± 0.75 a | 84.42 ± 0.10 b | 80.82 ± 0.05 ab |
| | 3.5 | 41.10 ± 0.78 d | 42.14 ± 0.11 ab | 36.10 ± 0.10 b | 27.23 ± 1.26 a | 85.43 ± 0.15 b | 80.51 ± 0.28 b |
| | 4.0 | 44.67 ± 0.20 b | 41.84 ± 0.21 ab | 37.87 ± 0.30 a | 24.76 ± 0.69 b | 86.63 ± 0.01 a | 81.14 ± 1.08 b |
| | 4.5 | 46.33 ± 0.07 a | 42.51 ± 0.44 a | 38.12 ± 0.10 a | 22.37 ± 3.32 b | 86.74 ± 2.10 a | 76.84 ± 0.58 b |
| 23 °C | 2.5 | 42.78 ± 0.17 bc | 38.69 ± 2.88 a | 32.70 ± 0.17 b | 30.68 ± 0.43 a | 84.28 ± 0.12 b | 81.28 ± 0.50 b |
| | 3.0 | 43.07 ± 0.28 bc | 38.89 ± 0.56 a | 36.74 ± 0.13 a | 31.00 ± 0.24 a | 84.42 ± 0.10 ab | 82.12 ± 0.01 a |
| | 3.5 | 41.10 ± 0.78 c | 39.15 ± 0.33 a | 36.16 ± 0.10 a | 33.57 ± 0.80 a | 85.43 ± 0.15 ab | 84.30 ± 0.23 a |
| | 4.0 | 44.67 ± 0.20 ba | 39.5 ± 0.21 a | 37.87 ± 0.30 a | 29.97 ± 0.30 ab | 86.63 ± 0.01 a | 83.38 ± 0.30 a |
| | 4.5 | 46.33 ± 0.07 a | 40.50 ± 2.67 a | 38.12 ± 0.10 a | 28.93 ± 1.07 b | 86.74 ± 2.10 a | 81.13 ± 0.21 b |

[a]Different letters in the same line indicate significant differences ($p < 0.05$).

carbon would result in hybridization and the formation of a single bond, leading to free rotation about the new single bond, forming *cis* isomers.[4] Some reports described carotenoids, such as β-carotene, canthaxanthin, and 8′-apo-caroten-8′-al, once dissolved in acetonitrile, benzene, and dichloromethane exposed to strong acid [trifluoroacetic acid (TFA)], revealing *cis* isomerization formed by protonation of carotenoids, and the reaction products are probably carotenoid esters.[4]

However, peach purée antioxidant activity and total phenolics were not affected by pH variation during 90 days of storage. Contrarily, carotenoids revealed a higher degradation for the higher pH values tested of 4.0 and 4.5. The pH values of 3.0 and 3.5, the most similar to the peach pH (3.6), were the optimum conditions for zeaxanthin, β-cryptoxanthin, and β-carotene retention. Chlorogenic and neochlorogenic acids presented a higher content for the lower pH (2.5).

**Color Measurements.** The highest $b^*$ values ($p < 0.05$) were obtained for pH 3.5, and the lowest $b^*$ value ($p < 0.05$) was obtained for pH 4.0 and 4.5; contrarily, the higher $a^*$ value was obtained for pH 4.5 (data not shown). The yellow color decrease had impact on saturation index ($C^*$) values, where the higher decrease was observed for pH 4.0 and 4.5 for both storage temperatures. The hue angle ($H$) values decreased highly for pH 4.0 and 4.5 but at a lower rate (Table 1).

The lowest ($p < 0.05$) lightness ($L^*$) values were obtained for pH 2.5 at 4 °C (Table 1), while for 23 °C, $L^*$ presented no significant differences between the different pH values (Table 1).

Over the 90 day storage period, $L^*$ and $b^*$ parameters decreased, while $a^*$ increased for all pH values. This means that, with the increase of the storage time, the color variation involves a shift from the yellow to red hues among the pH values tested. The decrease in lightness and, consequently, increase in darkening can be indicative of some precipitation along storage. The peach purée treated at 80 °C loses its yellowness and becomes redder, resulting from non-enzymatic browning (Maillard) reactions.[26,27]

This study allowed for the conclusion that pH between 3.0 and 3.5 lead to higher carotenoid content and higher color stability, with time and temperature of storage being more preponderant for peach purée overall quality.

## AUTHOR INFORMATION


### Corresponding Author

*Telephone: +351-225580097. E-mail: mpintado@porto.ucp.pt.



### Funding

The work was financially supported by Agência de Inovação, Portugal, and Quadro de Referência Estratégico Nacional (QREN, Portugal) through project Frutamais: Preservation of Functional Nutritional and Organoleptic Characteristic of Fruits and Derived Food (QREN-ADI 3436). This work was supported by the National Funds from Fundação para a Ciência e a Tecnologia (FCT) through Project PEst-OE/EQB/LA0016/2013 and the Ph.D. Grant SFRH/BD/75041/2010 to Ana Oliveira.


### Notes

The authors declare no competing financial interest.

## REFERENCES


(1) Bengoechea, M. L.; Sancho, A. I.; Bartolomé, B.; Estrella, I.; Gómez-Cordovés, C.; Hernández, M. T. Phenolic composition of industrially manufactured purées and concentrates from peach and apple fruits. *J. Agric. Food Chem.* **1997**, *45*, 4071−4075.

(2) Barrett, D. M.; Lloyd, B. Advanced preservation methods and nutrient retention in fruits and vegetables. *J. Sci. Food Agric.* **2012**, *92*, 7−22.

(3) Guerrero-Beltrán, J. A.; Barbosa-Cánovas, G. V.; Swanson, B. G. High hydrostatic pressure processing of peach puree with and without antibrowning agents. *J. Food Process. Preserv.* **2004**, *28*, 69−85.

(4) Konovalov, V.; Kispert, L. AM1, INDO/S and optical studies of carbocations of carotenoid molecules. Acid induced isomerization. *J. Chem. Soc., Perkin Trans. 2* **1999**, 901−910.

(5) Torskangerpoll, K.; Andersen, Ø. M. Colour stability of anthocyanins in aqueous solutions at various pH values. *Food Chem.* **2005**, *89*, 427−440.

(6) Friedman, M.; Jürgens, H. S. Effect of pH on the stability of plant phenolic compounds. *J. Agric. Food Chem.* **2000**, *48*, 2101−2110.

(7) Cabrita, L.; Fossen, T.; Andersen, Ø. M. Colour and stability of the six common anthocyanidin 3-glucosides in aqueous solutions. *Food Chem.* **2000**, *68*, 101−107.

(8) Davies, A. J.; Mazza, G. Copigmentation of simple and acylated anthocyanins with colorless phenolic compounds. *J. Agric. Food Chem.* **1993**, *41*, 716−720.

(9) Wright, K. P.; Kader, A. A. Effect of controlled-atmosphere storage on the quality and carotenoid content of sliced persimmons and peaches. *Postharvest Biol. Technol.* **1997**, *10*, 89−97.

(10) Kimura, M.; Rodriguez-Amaya, D. B.; Godoy, H. T. Assessment of the saponification step in the quantitative determination of carotenoids and provitamins A. *Food Chem.* **1990**, *35*, 187−195.

(11) Rodriguez-Amaya, D. B. *Carotenoids and Food Preparation: The Retention of Provitamin A Carotenoids in Prepared, Processed and Stored Foods*; John Snow Incorporated/OMNI Project: Arlington, VA, 1997.

(12) Giao, M. S.; Gonzalez-Sanjose, M. L.; Rivero-Perez, M. D.; Pereira, C. I.; Pintado, M. E.; Malcata, F. X. Infusions of Portuguese

medicinal plants: Dependence of final antioxidant capacity and phenol content on extraction features. *J. Sci. Food Agric.* **2007**, *87*, 2638−2647.
(13) Singleton, V.; Rossi, J. A. Colorimetry of total phenolics with phosphomolybdic−phosphotungstic acid reagents. *Am. J. Enol. Vitic.* **1965**, *16*, 144−158.
(14) Pacheco-palencia, L. A.; Hawken, P.; Talcott, S. T. Phytochemical, antioxidant and pigment stability of açai (*Euterpe oleracea* Mart.) as affected by clarification, ascorbic acid fortification and storage. *Food Res. Int.* **2007**, *40*, 620−628.
(15) Klimczak, I.; Małecka, M.; Szlachta, M.; Gliszczyńska-Świgło, A. Effect of storage on the content of polyphenols, vitamin C and the antioxidant activity of orange juices. *J. Food Compos. Anal.* **2007**, *20*, 313−322.
(16) Round, A. N.; Rigby, N. M.; MacDougall, A. J.; Morris, V. J. A new view of pectin structure revealed by acid hydrolysis and atomic force microscopy. *Carbohydr. Res.* **2010**, *345*, 487−497.
(17) Palmero, P.; Lemmens, L.; Hendrickx, M.; Van Loey, A. Role of carotenoid type on the effect of thermal processing on bioaccessibility. *Food Chem.* **2014**, *157*, 275−282.
(18) van der Sluis, A. A.; Dekker, M.; van Boekel, M. A. Activity and concentration of polyphenolic antioxidants in apple juice. 3. Stability during storage. *J. Agric. Food Chem.* **2005**, *53*, 1073−1080.
(19) Chen, B. H.; Peng, H. Y.; Chen, H. E. Changes of carotenoids, colour, and vitamin A contents during processing of carrot juice. *J. Agric. Food Chem.* **1995**, *43*, 1912−1918.
(20) Schieber, A.; Carle, R. Occurrence of carotenoid *cis*-isomers in food: Technological, analytical, and nutritional implications. *Trends Food Sci. Technol.* **2005**, *16*, 416−422.
(21) Mortensen, A.; Skibsted, L. H. Kinetics and mechanism of the primary steps of degradation of carotenoids by acid in homogeneous solution. *J. Agric. Food Chem.* **2000**, *48*, 279−286.
(22) Farhangi, M.; Guy Valadon, L. R. Effect of acidified processing and storage on carotenoids (provitamin A) and vitamin C in mung bean sprouts. *J. Food Sci.* **1981**, *46*, 1464−1466.
(23) Schwartz, S. J.; Patroni-Killam, M. Detection of *cis*−*trans* carotene isomers by two-dimensional thin-layer and high-performance liquid chromatography. *J. Agric. Food Chem.* **1985**, *33*, 1160−1163.
(24) Mortensen, A.; Skibsted, L. H.; Sampson, J.; Rice-Evans, C.; Everett, S. A. Comparative mechanisms and rates of free radical scavenging by carotenoid antioxidants. *FEBS Lett.* **1997**, *418*, 91−97.
(25) Qian, C.; Decker, E. A.; Xiao, H.; McClements, D. J. Physical and chemical stability of $\beta$-carotene-enriched nanoemulsions: Influence of pH, ionic strength, temperature, and emulsifier type. *Food Chem.* **2012**, *132*, 1221−1229.
(26) Ávila, I. M. L. B.; Silva, C. L. M. Modelling kinetics of thermal degradation of colour in peach puree. *J. Food Eng.* **1999**, *39*, 161−166.
(27) Garza, S.; Ibarz, A.; Pagan, J.; Giner, J. Non-enzymatic browning in peach puree during heating. *Food Res. Int.* **1999**, *32*, 335−343.

proposed, including milled wood lignin (MWL) and cellulolytic enzyme lignin (CEL),[15] they are not suitable for pummelo fruits due to low yield and contamination.[11,16,17] The organic solvent extraction method is an effective lignin extraction technique that produces less contaminant, does not alter lignin structure,[18−21] and is useful for isolating lignins from pummelo fruits.

Multiple studies assessing lignin have mainly focused on its application in bioenergy[22,23] and pulping;[17,24] however, the effect of lignin on pummelo fruit quality has been rarely studied. Here, we compare the composition and structure linkages of lignin between granulated juice sacs and three other tissues, in three severely granulated cultivars of pummelo. Our findings provide useful information about the main lignin synthesis pathway and specific lignin deposition in juice sacs, which is important for the further investigation of the relationship between lignin metabolism and juice sac granulation. To our knowledge, this is the first report evaluating the composition and structure of specific lignins accumulated in juice sacs of pummelo fruits.

## MATERIALS AND METHODS

**Plant Materials.** Plant materials used in this study included the granulated juice sacs, segment membranes, stems, and leaves. Granulated juice sacs were obtained from three cultivars, 'Hongroumiyou', 'Guanximiyou', and 'Sanhongmiyou', abbreviated HR, GX, and SH, respectively (Figure 1). Segment membranes, stems, and leaves were all from cultivar HR. The main leaf veins were removed before lignin extraction.

**Lignin Isolation.** Soluble substances in samples were washed out according to the modified method of Müse et al.[25] A total of 50 g (segment membranes, stems, and leaves) or 100 g (granulated juice sacs) of plant material was homogenized in 150 mL of homogenization buffer (50 mM Tris-HCl, 5 mL/L Triton X-100, 1 M NaCl; pH 8.3) using a juice extractor. After transfer to an 80 mL Beckman tube with screw cap, the homogenate was thoroughly vortexed and centrifuged (8000*g*, 10 min). The sediments were washed twice with the homogenization buffer, twice with 80% acetone, and twice with pure acetone. The washing procedure was repeated once for stem samples, twice for those from segment membranes and leaves, and three times for granulated juice sac specimens. The sediments from each tissue were combined and lyophilized. After lyophilization, the sediment samples were extracted with toluene/ethanol (2:1, v/v) for >7 h with a Soxhlet extractor and dried. Crude lignin was extracted and purified according to the method of Wu et al.,[19] with the following modifications. Sediment samples (8 g), 4 g/L nitric acid (16 mL), and a mixture of formic acid/acetic acid/$H_2O$ at the ratio of 11:5:4 were placed into a 250 mL three-necked flask. The solid to liquid material ratio was 1:20. After extraction of the crude lignin for 3 h at 110 °C, the liquid part was dried using a rotary evaporator. The sediments were washed with double-distilled water several times and dried by desiccation. The crude lignin was purified according to the method of Wu et al.[19]

**Preliminary Characterization of Lignin by UV.** Lignin was preliminarily characterized by UV−vis spectroscopy after solubilization in dioxane/$H_2O$ (9:1, v/v) according to the method described by Wu et al.[19] with minor modifications. The scanning spectrum was from 200 to 400 nm.

**HSQC NMR Sample Preparation.** Lignin acetylation was performed according to previous studies,[13,26] with minor changes. Purified lignin (20 mg) or segment membrane lignin (8 mg) was dissolved in 2 mL of pyridine/acetic anhydride (1:1, v/v) at room temperature in the dark for 72 h. After the sample had been transferred into an 80 mL Beckman tube, 30 mL of ethyl ether was added and the mixture centrifuged (15000*g*, 7 min). The sediments were washed with ethyl ether until disappearance of the pyridine odor. The sediments were then dissolved in dimethyl-$d_6$ sulfoxide (DMSO-$d_6$, containing 0.03% TMS) and used for HSQC NMR analysis.

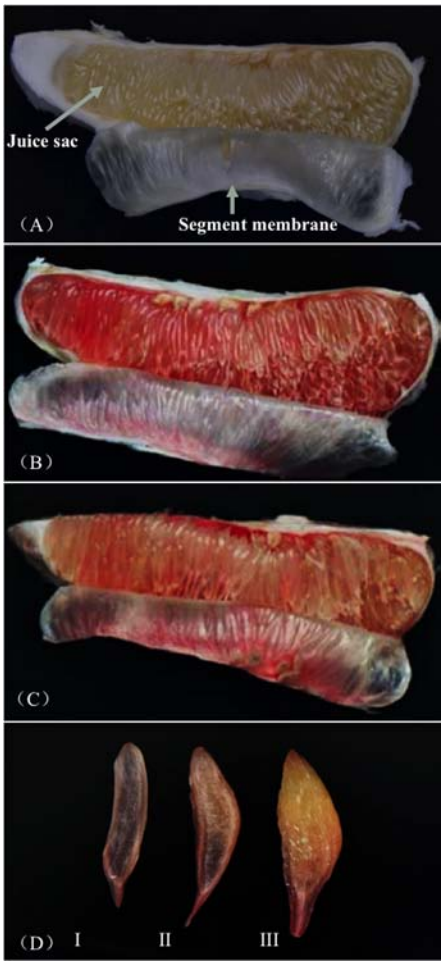


**Figure 1.** Cultivars and juice sacs of pummelo used in this study: (A) GX segment with white juice sacs and segment membranes; (B) HR segment with red juice sacs and segment membranes; (C) SH segment with red juice sacs and segment membranes; (D) comparison of normal juice sacs (I) with the different degrees of juice sac granulation (II and III) in cultivar HR. The granulation was more severe in III than in II.

**HSQC NMR Procedures.** All NMR experiments were conducted on a Bruker AVANCE III 500 instrument equipped with a *z*-gradient BBO probe at a temperature of 298 K. The Larmor frequencies of $^1H$ and $^{13}C$ were 500.0 and 125.7 MHz, respectively. The spectral widths in HSQC experiments were 5000 and 20833 Hz for the $^1H$ and $^{13}C$ dimensions, respectively. The number of complex points collected was 1024 for the $^1H$ dimension; the acquisition time was 0.1 s with a recycle delay of 2 s. The number of transients was 24 (except for the sample of segment membranes for which 96 transients were accumulated to achieve a reasonable signal-to-noise ratio), and 256 time increments were recorded in the $^{13}C$ dimension. The experiments were optimized for the $^1J_{CH}$ of 145 Hz. Prior to Fourier transformation, the data matrices were zero filled to 1024 points in the $^{13}C$ dimension. A squared cosine-bell apodization function was applied in both dimensions. The central solvent (DMSO-$d_6$) peak was used as an internal chemical shift reference point ($\delta_C/\delta_H$ 40.1/2.50).

Semiquantitative analysis of different linkages and basic compositions of lignins was carried out according to previous reports.[15,27] In the aliphatic oxygenated region, the relative abundances of interunit linkages were estimated from $C_\alpha-H_\alpha$ cross-signals. In the aromatic region, $C_2-H_2$ cross-signals from **G′** units were also incorporated into **G** units in the calculation. $C_{2,6}-H_{2,6}$ cross-signals from **S** units and

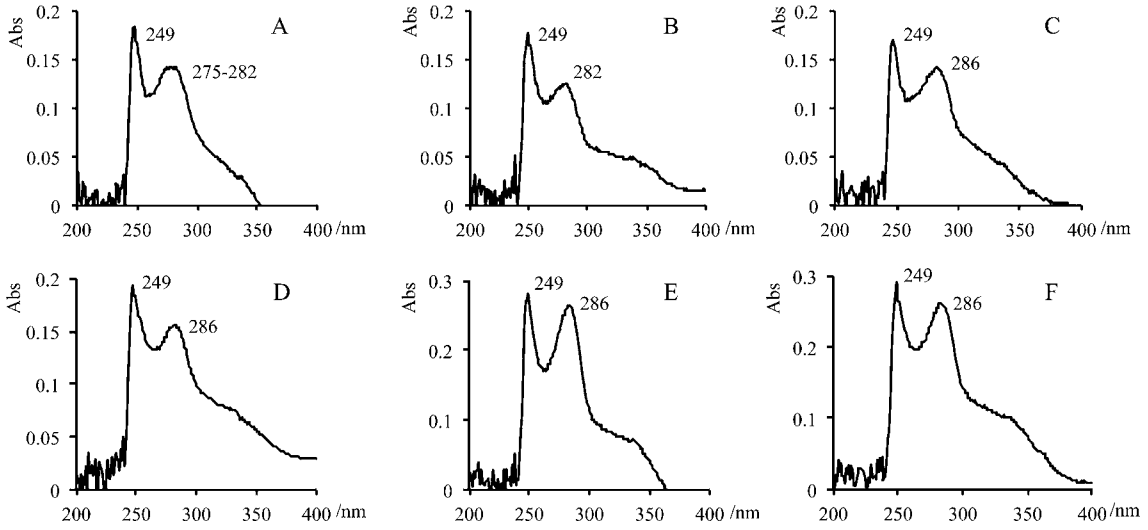


**Figure 2.** UV spectra of lignins isolated from different tissues: (A) lignin from HR leaves; (B) lignin from HR stems; (C) lignin from HR segment membranes; (D) lignin from HR granulated juice sacs; (E) lignin from GX granulated juice sacs; (F) lignin from SH granulated juice sacs.

doubles of $C_2$–$H_2$ cross-signals from **G** and **G′** units were used to estimate the **G**/**S** ratio.

## RESULTS

**Lignin Extraction and Characterization.** Because the lignin contents of the four tissues studied were very low compared with those of woody plants, and no previous work was available, we established a method appropriate to analyze the lignin content and purity of each sample. The organic solvent extraction method was good enough for us to obtain relatively pure lignin suitable for NMR analysis.

The preliminary characteristics of lignins from different tissues are shown in Figure 2. Lignins of all tested tissues displayed a wide absorption peak at 240–300 nm and a characteristic absorption peak at 249 nm. In addition, stem lignin showed a characteristic absorption at 282 nm, whereas that from segment membranes and granulated juice sacs in all three cultivars had an adsorption peak at 286 nm. The lignin from leaves did not have a characteristic peak, but adsorbed between 275 and 282 nm. Because lignins have a specific absorption at 200–300 nm,[28] we concluded that lignin might be present in our samples. These samples were then used for subsequent NMR analysis.

**HSQC NMR Analysis of Isolated Lignin.** The lignin samples from leaves, stems, and segment membranes in HR, and from granulated juice sacs in HR, GX, and SH were analyzed by HSQC NMR. Before measurement, the lignin samples were acetylated to ensure complete solubility in the NMR solvent[29] and acquisition of unique and well-resolved cross-signals.[15] Because the lignin content of segment membranes was low, only 8 mg was used for analysis, but the results were not affected.

The HSQC spectra revealing the key information regarding lignin structures are shown in Figures 3 and 4. Lignin contours in the HSQC spectra were assigned by comparison with data from previous studies.[15,26,30−33] The assignments and relative abundances of main lignin $^{13}C$–$^{1}H$ cross-signals are listed in Tables 1 and 2. The main lignin substructures identified in HSQC spectra are presented in Figure 5.

**Analysis of Lignin Interunit Linkages.** In the side-chain region of HSQC spectra, the main lignin interunit linkages *β*-O-4′, *β*-*β*′, and *β*-5′ were distinctly observed. All spectra showed prominent signals corresponding to the *β*-O-4′ substructures. The $C_\alpha$–$H_\alpha$ cross-signals in *β*-O-4′ substructures (**A** and **A′**) were observed at $\delta_C/\delta_H$ 73.81/5.88 (for *erythro*) and 74.05/5.96 ppm (for *threo*), whereas the $C_\beta$–$H_\beta$ cross-signals were observed at $\delta_C/\delta_H$ 78.96/4.86 and 80.64/4.57 for substructures linked to G and S units, respectively. The $C_\gamma$–$H_\gamma$ cross-signals of substructure **A** were seen at $\delta_C/\delta_H$ 62.37/3.96–4.29, whereas the *γ*-acylated *β*-ether units **A′** were identified at $\delta_C/\delta_H$ 63.60/3.90–4.26, partially overlapping with other signals. Strong signals from *β*-*β*′ substructures (**B**) were observed only in the spectrum of lignin samples from stems, with their $C_\alpha$–$H_\alpha$, $C_\beta$–$H_\beta$, and the two $C_\gamma$–$H_\gamma$ cross-signals at $\delta_C/\delta_H$ 85.35/4.71, 54.19/3.07, and 71.77/3.86 and 4.21, respectively. Phenylcoumaran (*β*-5′) substructures (**C**) were found in lignins of all samples except for leaves; their $C_\alpha$–$H_\alpha$ and $C_\beta$–$H_\beta$ cross-signals were observed at $\delta_C/\delta_H$ 87.29/5.53 and 49.80/3.78, respectively, and the $C_\gamma$–$H_\gamma$ correlation signal overlapped with other signals around $\delta_C/\delta_H$ 64.63/4.38.

The abundance of these three linkages varied among the tested tissues. Leaf lignin only had *β*-O-4′ substructures, whereas stem lignin contained all three linkages with a predominance of *β*-O-4′ units (**A** and **A′**, 76.48% of total side chains) followed by *β*-*β*′ substructures (**B**, 14.88%) and lower amounts of phenylcoumaran (*β*-5′) substructures (**C**, 8.64%). In the lignin of fruits (segment membranes and granulated juice sacs), *β*-O-4′ substructures (**A** and **A′**) were predominant with abundances between 78.76 and 87.65% and certain amounts of *β*-5′ substructures (**B**, 12.35–21.24%) were also observed; however, *β*-*β*′ substructures (**C**) were not detected.

**Analysis of Lignin Units.** The main lignin $^{13}C$–$^{1}H$ cross-signals in the aromatic region of HSQC spectra correspond to the aromatic rings of various lignin units.[11] According to our results, the three main lignin units from the monolignol metabolic pathway were clearly observed. Syringyl (**S**) units showed a prominent signal for $C_{2,6}$–$H_{2,6}$ correlation at $\delta_C/\delta_H$ 103.92/6.68, whereas guaiacyl (**G**) units displayed different cross-signals for $C_2$–$H_2$, $C_5$–$H_5$, and $C_6$–$H_6$ at $\delta_C/\delta_H$ 111.83/6.98, 117.13/7.01, and 120.06/6.93, respectively. In addition, signals corresponding to $C_2$–$H_2$ and $C_6$–$H_6$ cross-signals of $C_\alpha$-oxidized G units (**G′**) at $\delta_C/\delta_H$ 112.11/7.16 and 123.10/


dx.doi.org/10.1021/jf5041349 | J. Agric. Food Chem. 2014, 62, 12082−12089

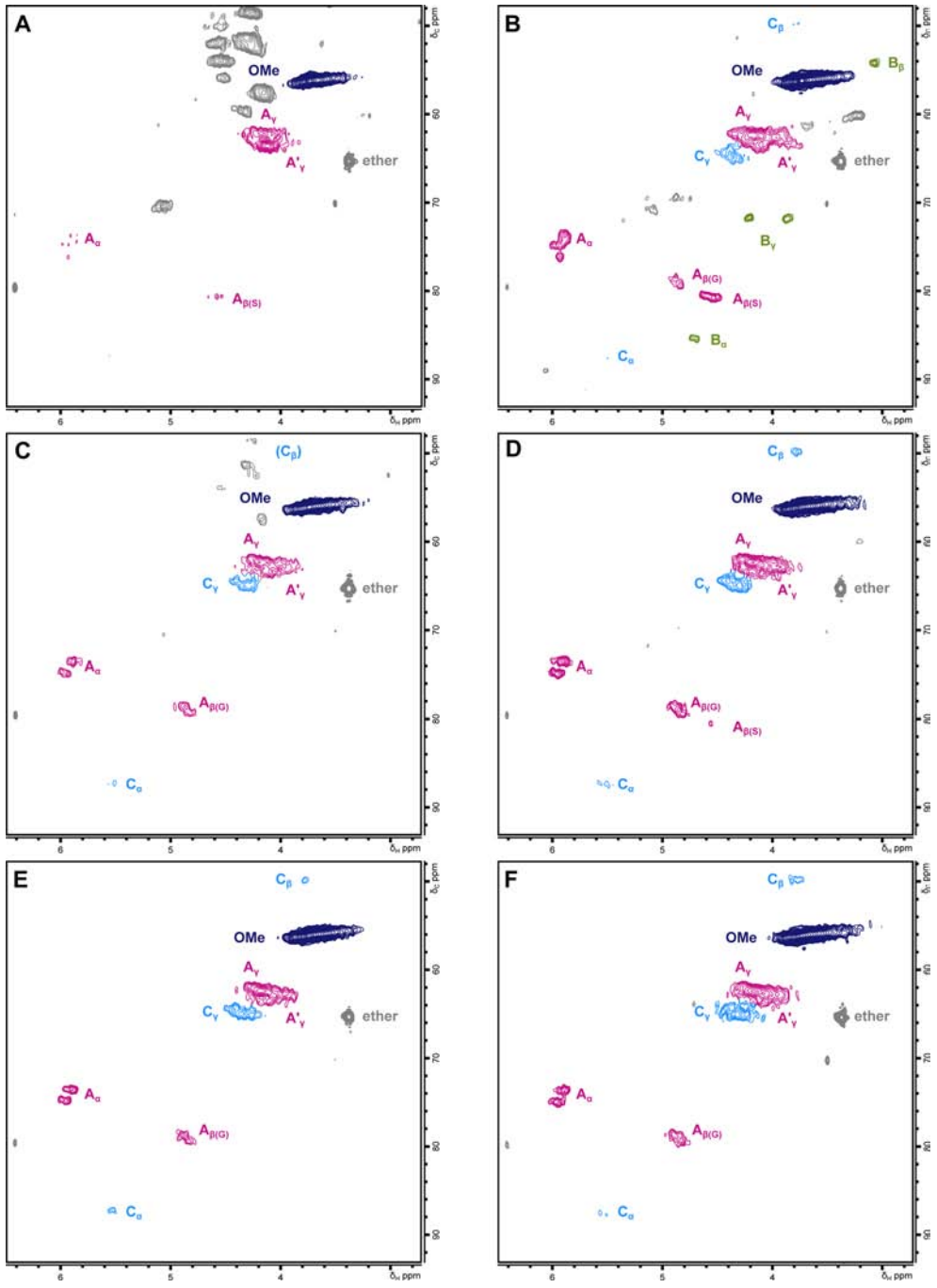


**Figure 3.** Side-chain regions of $^{13}C-^{1}H$ cross-signals in HSQC spectra of acetylated lignins: (A) lignin from leaves (HR); (B) lignin from stems (HR); (C) lignin from segment membranes (HR); (D) lignin from granulated juice sacs (HR); (E) lignin from granulated juice sacs (GX); (F) lignin from granulated juice sacs (SH). The cross-peaks are color coded according to the structures shown in Figure 5.

7.06, respectively, were observed. Despite the weak signals of *p*-hydroxyphenyl (**H**) units, we were able to verify the structures using heteronuclear multiple-bond correlation (HMBC) and heteronuclear single-quantum coherence–total correlation spectroscopy (HSQC-TOCSY) NMR (data not shown). Finally, the cross-signals at $\delta_C/\delta_H$ 121.6/6.97 and 130.50/7.24 of $C_{3,5}-H_{3,5}$ and $C_{2,6}-H_{2,6}$ were assigned to **H** units, respectively. The $^{13}C-^{1}H$ cross-signals at $\delta_C/\delta_H$ 126.63/7.16, 128.34/7.22, and 129.54/7.22 could not be clearly identitied. The chemical shifts and HMBC and HSQC-TOCSY data appeared to suggest a phenyl connected to alkyl chains (**X**) as a potential candidate structure. The three cross-signals were assigned to $C_4-H_4$, $C_{2,6}-H_{2,6}$, and $C_{3,5}-H_{3,5}$ of the **X** structure, respectively. The **X** structure was none of the three basic lignin units and was therefore excluded from abundance calculations.

The composition of **S**, **G**, and **H** units presented big differences among tissues. The lignin of leaves was predominantly composed of **H** (55.81%) and **S** (44.19%) units, whereas that of stems contained all three units with a large amount of **S** units (58.57%), followed by a lower amount of **G** units (38.73%) and traces of **H** units (2.7%). The **G** units were predominant in the lignin from segment membranes and granulated juice sacs, with the abundances of 92.45 and 91.13–96.82%, respectively. Of note, **S** and **H** units were not detected


dx.doi.org/10.1021/jf5041349 | *J. Agric. Food Chem.* 2014, 62, 12082–12089

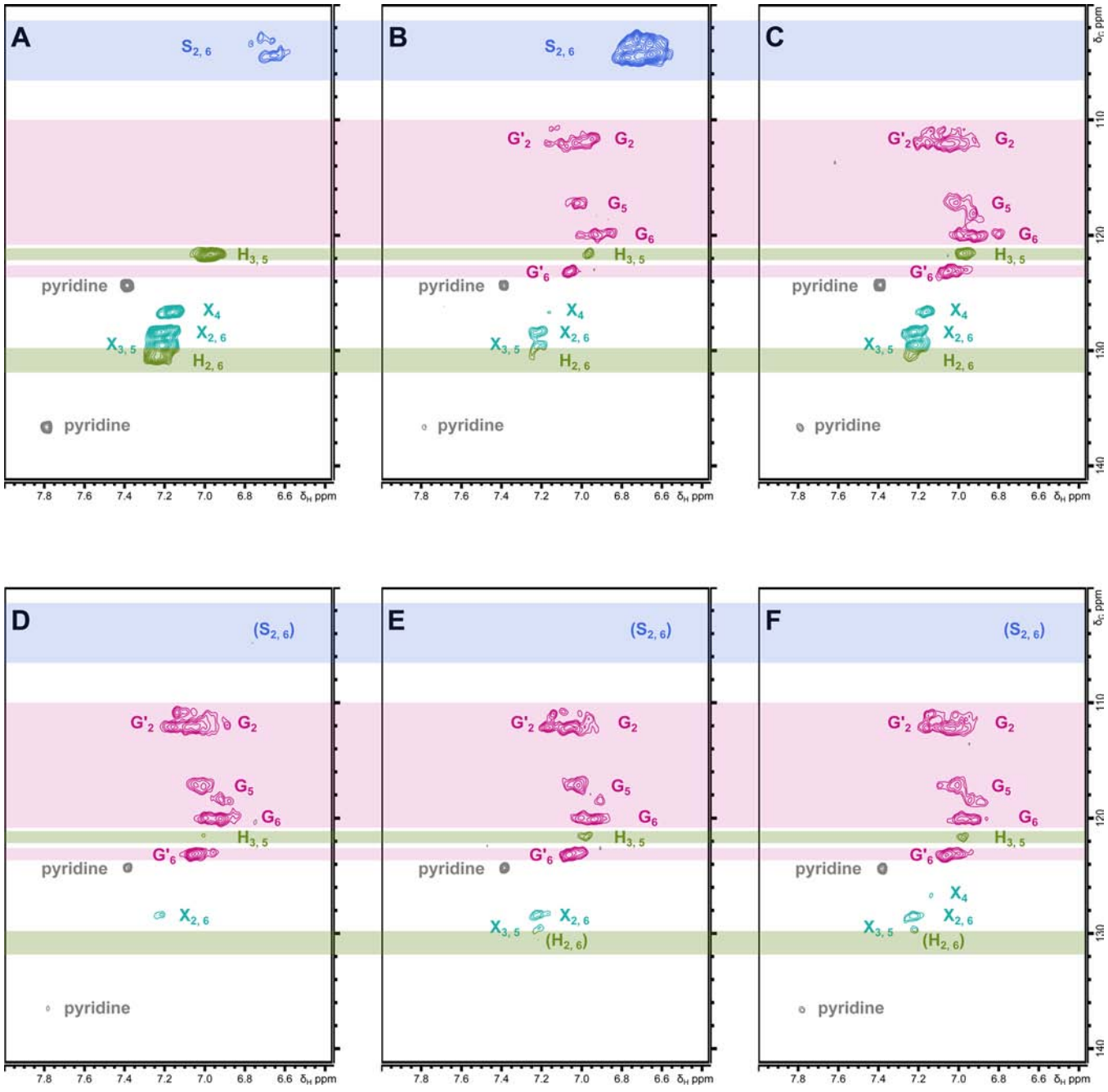


**Figure 4.** Aromatic regions of $^{13}C-^{1}H$ cross-signals in HSQC spectra of acetylated lignins: (A) lignin from leaves (HR); (B) lignin from stems (HR); (C) lignin from segment membranes (HR); (D) lignin from granulated juice sacs (HR); (E) lignin from granulated juice sacs (GX); (F) lignin from granulated juice sacs (SH). The cross-peaks are color coded according to the structures shown in Figure 5.

in the lignin from segment membranes and HR, respectively, and barely observed in other tissues. The **G**/**S** ratio was high in the lignin from granulated juice sacs but varied among cultivars: ratios of 30.45, 18.19, and 66.94% were obtained for HR, GX, and SH, respectively.

## DISCUSSION

Because lignin metabolism is closely associated with the juice sac granulation of pummelo fruits, it deserves careful attention and thorough analysis. To our knowledge, no study concerning lignin metabolism in juice sac granulation has been published. Therefore, it is of particular importance to carry out studies that reveal the mechanisms underlying juice sac granulation.

Although MWL is a common method used in lignin extraction, it was not adopted in this research due to its low yield, modifications during milling, and potential "contaminating" compounds such as lignin-linked carbohydrates (LLC).[11,16] The improved organic solvent extraction method used in this work was suitable for the isolation of lignin from pummelo fruits: the resulting products were relatively pure, and yields were high enough for various analyses. According to the NMR results, the signals of LLC linkages and other carbohydrates were not detected, unlike data obtained after MWL extraction, in which lignin signals are often overlapping with those of carbohydrates.[11,15,26,30] Without the overlapping carbohydrate signals, we were able to distinguish the various

**Table 1. Assignments of Main Lignin $^{13}C-^{1}H$ Cross-Signals in HSQC Spectra Shown in Figures 3 and 4**

| label | $\delta_C/\delta_H$ | assignment |
|---|---|---|
| $C_\beta$ | 49.80/3.78 | $C_\beta-H_\beta$ in $\beta$-5′ substructures (**C**) |
| $B_\beta$ | 54.19/3.07 | $C_\beta-H_\beta$ in $\beta$-$\beta$′ substructures (**B**) |
| OMe | 56.17/3.73 | C−H in methoxyls (**OMe**) |
| $A_\gamma$ | 62.37/3.96−4.29 | $C_\gamma-H_\gamma$ in $\beta$-O-4′ substructures (**A**) |
| $A_\gamma$ | 63.60/3.90−4.26 | $C_\gamma-H_\gamma$ in $\gamma$-acylated $\beta$-O-4′ substructures (**A**′) |
| $C_\gamma$ | 64.63/4.38 | $C_\gamma-H_\gamma$ in $\beta$-5′ substructures (**C**) |
| $B_\gamma$ | 71.77/3.86 | $C_\gamma-H_\gamma$ in $\beta$-$\beta$′ substructures (**B**) |
| $B_\gamma$ | 71.77/4.21 | $C_\gamma-H_\gamma$ in $\beta$-$\beta$′ substructures (**B**) |
| $A_\alpha$ | 73.81/5.88 | $C_\alpha-H_\alpha$ in $\beta$-O-4′ substructures (**A**) (*erythro*) |
| $A_\alpha$ | 74.05/5.96 | $C_\alpha-H_\alpha$ in $\beta$-O-4′ substructures (**A**) (*threo*) |
| $A_{\beta(G)}$ | 78.96/4.86 | $C_\beta-H_\beta$ in $\beta$-O-4′ linked to G (**A**) |
| $A_{\beta(S)}$ | 80.64/4.57 | $C_\beta-H_\beta$ in $\beta$-O-4′ linked to S (**A**) |
| $B_\alpha$ | 85.35/4.71 | $C_\alpha-H_\alpha$ in $\beta$-$\beta$′ substructures (**B**) |
| $C_\alpha$ | 87.29/5.53 | $C_\alpha-H_\alpha$ in phenylcoumaran (**C**) |
| $S_{2,6}$ | 103.92/6.68 | $C_{2,6}-H_{2,6}$ in syringyl units (**S**) |
| $G_2$ | 111.83/6.98 | $C_2-H_2$ in guaiacyl units (**G**) |
| $G'_2$ | 112.11/7.16 | $C_2-H_2$ in oxidized G units (**G**′) |
| $G_5$ | 117.13/7.01 | $C_5-H_5$ in guaiacyl units (**G**) |
| $G_6$ | 120.06/6.93 | $C_6-H_6$ in guaiacyl units (**G**) |
| $H_{3,5}$ | 121.60/6.97 | $C_{3,5}-H_{3,5}$ in H units (**H**) |
| $G'_6$ | 123.10/7.06 | $C_6-H_6$ in oxidized G units (**G**′) |
| $H_{2,6}$ | 130.50/7.24 | $C_{2,6}-H_{2,6}$ in H units (**H**) |

types of lignin structures and determine the lignin composition accurately. As numerous lignin isolation methods have focused mainly on plant samples, especially woody plants that contain high levels of lignins,[17,22,24,34−36] the method described here might be useful for studies assessing lignin from plant materials with relatively low lignin levels. In addition, as an aromatic polymer, lignin has a strong ultraviolet absorption; the shape and absorption coefficient of the peak are determined by the type and content of lignin units and its functional groups.[13,28,37] Although different lignin contents were obtained for the tested tissues, the ultraviolet absorption data have provided useful information for the characterization of lignins in various tissues. Indeed, the different absorption peaks among tissues might indicate the distinct lignin types that they contain. However, for a given tissue, the similar lignin absorption peaks for different cultivars might indicate similar lignin composition. These findings were consistent with the HSQC NMR data.

As expected, the $\beta$-O-4′ linkage (**A**) was the most frequent interunit linkage in our samples. This linkage is the easiest to chemically cleave compared with other bonds.[9] According to previous papers,[9,11] the relative abundances of different interunit linkages depend largely on changes in monolignol availability during the polymerization process of lignin. Lignins composed mainly of **G** units contain more $\beta$-5′ linkages (**C**) than those made of **S** units, which show an abundance of $\beta$-$\beta$′ linkages (**B**). This view is in line with our results. As **G** units increased in the lignin samples from leaves, stems, to segment membranes and juice sacs, the $\beta$-5′ linkages (**C**) increased despite the variations observed in juice sac samples from different cultivars. Meanwhile, $\beta$-$\beta$′ linkages (**B**) were detected only in lignin samples from stems, in which the **S** units were more abundant than in other tissues. In addition, the **G**/**S** ratio was found to reflect the degree and nature of polymeric cross-linking. The high **G** content is known to yield more highly cross-linked lignins characterized by a great proportion of biphenyls and other carbon−carbon bonds, whereas **S** units are typically linked by more labile ether bonds. Therefore, **G**-rich lignins depolymerize with more difficulty compared with those rich in **S** units.[38,39] In addition, plant cell walls rich in guaiacyl lignins thicken more rapidly than those rich in syringyl lignins.[40] The high **G**/**S** ratio obtained in the lignin from granulated juice sacs indicated that the specific lignin accumulated may be tightly integrated and not easily degradable; in addition, the cell walls in granulated juice sacs may thicken more quickly. Other linkages and units reported in previous studies[16,31,33,35,41−43] were not detected in our samples; conversely, certain linkages and units found here have not been detected by other groups. This might be due to the insufficient time for NMR procedures and/or their low abundances in the tested tissues.

The cause of lignin formation and accumulation in juice sac granulation is unknown. According to previous studies, lignin deposition not only follows a developmental process but can also be triggered by several biotic and abiotic stresses.[5] As shown above, the lignin deposited in granulated juice sacs was different from that present in other tissues. However, the composition of lignin linkages and interunits did not change significantly among cultivars. This observation suggests a similar mechanism for juice sac granulation among cultivars. The particularly high **G**/**S** ratio of the lignin in SH showed that the lignified juice sacs in this cultivar were stiffer than those in GX and HR; therefore, the juice sac granulation occurring in SH might be more severe. Consequently, cultivar SH could be used as an important material for assessing juice sac granulation. Besides, the **G**/**S** ratio of the lignin in GX was much lower than those obtained for HR and SH, which had darker fruits (Figure 1). This suggests that juice sac granulation might be associated with fruit pigmentation. In addition, the extremely high abundances of **G** units in the lignin of

**Table 2. Relative Abundances of Main Linkages and Units of Lignin from Pummelo**

| characteristic | leaf | stem | segment membrane | HR | GX | SH |
|---|---|---|---|---|---|---|
| linkages (% side chains involved) | | | | | | |
| $\beta$-O-4′ ary ether (**A**, **A**′) | 100 | 76.48 | 81.04 | 78.76 | 81.76 | 87.65 |
| $\beta$-$\beta$′ resinols (**B**) | nd[a] | 14.88 | nd | nd | nd | nd |
| $\beta$-5′ phenylcoumarans (**C**) | nd | 8.64 | 18.96 | 21.24 | 18.24 | 12.35 |
| lignin units (%) | | | | | | |
| **H** | 55.81 | 2.7 | 7.55 | nd | 3.86 | 2.84 |
| **G** | nd | 38.73 | 92.45 | 96.82 | 91.13 | 95.73 |
| **S** | 44.19 | 58.57 | nd | 3.18 | 5.01 | 1.43 |
| **G**/**S** ratio | 0 | 0.66 | 100 | 30.45 | 18.19 | 66.94 |

[a]nd, not detected.

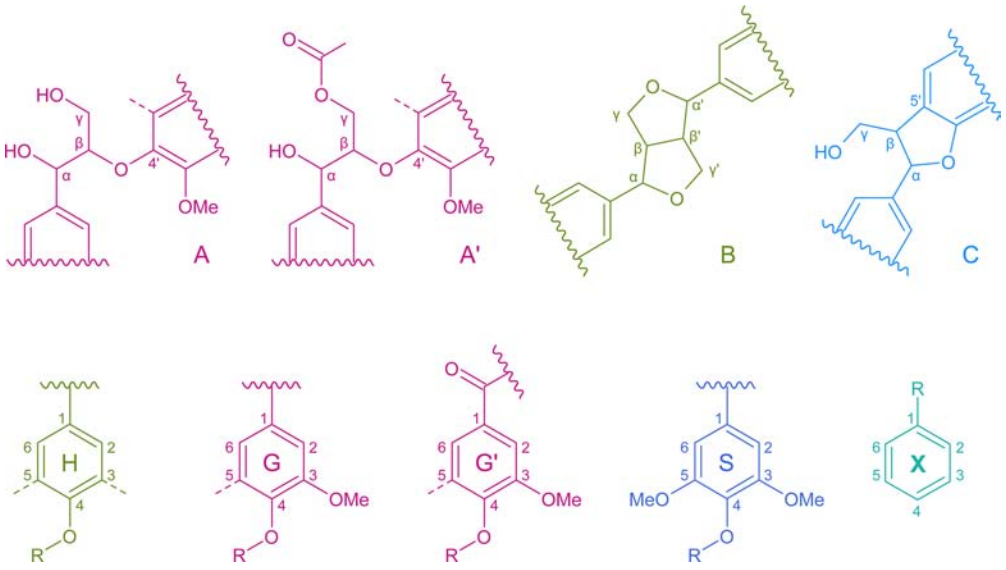


**Figure 5.** Main structures identified in Figures 3 and 4: (**A**) $\beta$-O-4′ linkages; (**A′**) $\gamma$-acetylated $\beta$-O-4′ substructures; (**B**) resinol substructures formed by $\beta$-$\beta'$/$\alpha$-O-$\gamma'$/$\gamma$-O-$\alpha'$ linkages; (**C**) phenylcoumaran substructures formed by $\beta$-5′/$\alpha$-O-4′ linkages; (**H**) *p*-hydroxyphenyl unit; (**G**) guaiacyl unit; (**G′**) $\alpha$-oxidized guaiacyl unit; (**S**) syringyl unit; (**X**) phenyl connected to alkyl chains.

granulated juice sacs indicated that lignins might have polymerized mainly from coniferyl alcohol. No evidence of factors inducing lignin formation was obtained. We propose that regulators or triggers that participate in the synthesis of **G** units might be the key factors for abnormal lignin accumulation in granulated juice sacs. This hypothesis remains to be tested in subsequent studies.

In this study, we established a method to isolate lignins from pummelo fruits. The lignin isolated from leaves, stems, and segment membranes of HR were compared with those from granulated juice sacs of HR, GX, and SH. To our knowledge, this represents the first report describing the specificity of lignins in granulated juice sacs and the possible metabolic pathway for lignin accumulation in pummelo fruits. Our results provide a new insight for further investigations of the mechanism of juice sac granulation in citrus fruits.

## AUTHOR INFORMATION

### Corresponding Authors

*(D.-M.P.) Phone: 0591-83787126. Fax: 0591-83735681. E-mail: pdm666@126.com.

*(T.-F.P.) Phone: 0591-83789281. Fax: 0591-83735681. E-mail: 40058798@qq.com.

### Funding

This work was supported by the National Key Technology R&D Program of China (2007BAD07B01), the China Spark Program (KH1400530), the Natural Science Foundation of Fujian Province of China (2012J05041), and the Special Foundation for Young Scientists of the Horticultural College of Fujian Agriculture and Forestry University (FAFU2012YY-PY02)

### Notes

The authors declare no competing financial interest.

## ACKNOWLEDGMENTS

We thank Zong-Lie Hong from the University of Idaho and Jian-Jun Chen from the University of Florida for reviewing the manuscript and Yun Lin from the University of Fuzhou for helping with figure preparation.

## ABBREVIATIONS USED

2D-NMR, two-dimensional nuclear magnetic resonance; TA, thioacidolysis; Py-GC-MS, pyrolysis−gas chromatography−mass spectrometry; DFRC, derivatization followed by reductive cleavage; UV−vis, ultraviolet−visible; FT-IR, Fourier transform infrared; G, guaiacyl; H, *p*-hydroxyphenyl; S, syringyl; HSQC, heteronuclear single quantum coherence; MWL, milled wood lignin; CEL, cellulolytic enzyme lignin; DMSO-$d_6$, dimethyl-$d_6$ sulfoxide; TMS, tetramethylsilane; HMBC, heteronuclear multiple-bond correlation; HSQC-TOCSY, heteronuclear single-quantum coherence-total correlation spectroscopy; LLC, lignin-linked carbohydrates

## REFERENCES

(1) Shomer, I.; Chalutz, E.; Vasiliver, R.; Lomaniec, E.; Berman, M. Scierification of juice sacs in pummelo (*Citrus grandis*) fruit. *Can. J. Bot.* **1989**, *67*, 625−632.

(2) Pan, D. M.; Zheng, G. H.; Chen, G. X.; She, W. Q.; Guo, Z. X.; Shi, M. T.; Lin, H. Y. Analysis of the reasons caused granulation of juice sacs in Guanximiyou pomelo variety. *J. Fruit Sci.* **1999**, *16*, 202−209.

(3) She, W. Q. *An analysis on physiological changes and gene differential expressions in the process of pummelo fruit [Citrus grandis (L.) Osbeck] juice sac granulation*. Thesis, Fujian Agriculture and Forestry University, Fuzhou, China, 2009.

(4) Xu, Y. *Cloning and expression of lignin genes in Citrus maxima (Burm.) Merr*. Thesis, Fujian Agriculture and Forestry University, Fuzhou, China, 2014.

(5) Cesarino, I.; Araujo, P.; Domingues, A. P.; Mazzafera, P. An overview of lignin metabolism and its effect on biomass recalcitrance. *Braz. J. Bot.* **2012**, *35*, 303−311.

(6) Vogt, T. Phenylpropanoid biosynthesis. *Mol. Plant* **2010**, *3*, 2−20.

(7) Vanholme, R.; Morreel, K.; Ralph, J.; Boerjan, W. Lignin engineering. *Curr. Opin. Plant Biol.* **2008**, *11*, 278−285.

(8) Baucher, M.; Halpin, C.; Petit-Conil, M.; Boerjan, W. Lignin: genetic engineering and impact on pulping. *Crit. Rev. Biochem. Mol. Biol.* **2003**, *38*, 305−350.

(9) Boerjan, W.; Ralph, J.; Baucher, M. Lignin biosynthesis. *Annu. Rev. Plant Biol.* **2003**, *54*, 519−546.

(10) Weng, J. K.; Chapple, C. The origin and evolution of lignin biosynthesis. *New Phytol.* **2010**, *187*, 273−285.

(11) Rencoret, J.; Gutiérrez, A.; Nieto, L.; Jiménez-Barbero, J.; Faulds, C. B.; Kim, H.; Ralph, J.; Martínez, Á. T.; José, C. Lignin composition and structure in young versus adult *Eucalyptus globulus* plants. *Plant Physiol.* **2011**, *155*, 667−682.
(12) Ralph, J.; Lu, F. The DFRC method for lignin analysis. 6. A simple modification for identifying natural acetates on lignins. *J. Agric. Food Chem.* **1998**, *46*, 4616−4619.
(13) Jahan, M. S.; Chowdhury, D. A.; Islam, M. K.; Moeiz, S. M. Characterization of lignin isolated from some nonwood available in Bangladesh. *Bioresour. Technol.* **2007**, *98*, 465−469.
(14) Hu, G.; Cateto, C.; Pu, Y.; Samuel, R.; Ragauskas, A. J. Structural characterization of switchgrass lignin after ethanol organosolv pretreatment. *Energy Fuels* **2011**, *26*, 740−745.
(15) Wen, J. L.; Sun, S. L.; Xue, B. L.; Sun, R. C. Recent advances in characterization of lignin polymer by solution-state nuclear magnetic resonance (NMR) methodology. *Materials* **2013**, *6*, 359−391.
(16) Martínez, Á. T.; Rencoret, J.; Marques, G.; Gutiérrez, A.; Ibarra, D.; Jiménez-Barbero, J.; del Río, J. C. Monolignol acylation and lignin structure in some nonwoody plants: a 2D NMR study. *Phytochemistry* **2008**, *69*, 2831−2843.
(17) Lachenal, D.; Mortha, G.; Sevillano, R. M.; Zaroubine, M. Isolation of residual lignin from softwood kraft pulp. Advantages of the acetic acid acidolysis method. *C. R. Biol.* **2004**, *327*, 911−916.
(18) Su, T. F.; Gao, Y. Z.; Liu, X.; Zhou, B.; Gong, C. R. Review of determination of lignin. *J. Henan Agric. Univ.* **2007**, *41*.
(19) Hu, W. R.; Zhang, F.; Bai, J.; Cao, S. Y.; Fan, L. Extraction of lignin from cotton fiber with organic solvents. *Xinjiang Agric. Sci.* **2011**, *48*, 1701−1703.
(20) Jarrell, T. M.; Marcum, C. L.; Sheng, H.; Owen, B. C.; O'Lenick, C. J.; Maraun, H.; Bozell, J. J.; Kenttamaa, H. I. Characterization of organosolv switchgrass lignin by using high performance liquid chromatography/high resolution tandem mass spectrometry using hydroxide-doped negative-ion mode electrospray ionization. *Green Chem.* **2014**, *16*, 2713−2727.
(21) Bozell, J. J.; Black, S. K.; Myers, M.; Cahill, D.; Miller, W. P.; Park, S. Solvent fractionation of renewable woody feedstocks: Organosolv generation of biorefinery process streams for the production of biobased chemicals. *Biomass Bioenergy* **2011**, *35*, 4197−4208.
(22) Del Río, J. C.; Rencoret, J.; Prinsen, P.; Martínez, Á. T.; Ralph, J.; Gutiérrez, A. Structural characterization of wheat straw lignin as revealed by analytical pyrolysis, 2D-NMR, and reductive cleavage methods. *J. Agric. Food Chem.* **2012**, *60*, 5922−5935.
(23) Wang, Z. L.; Xu, J. H.; Feng, H.; Qi, H. S. Fractal kinetic analysis of polymers/nonionic surfactants to eliminate lignin inhibition in enzymatic saccharification of cellulose. *Bioresour. Technol.* **2011**, *102*, 2890−2896.
(24) Rencoret, J.; Marques, G.; Gutiérrez, A.; Nieto, L.; Jiménez-Barbero, J.; Martínez, Á. T.; del Río, J. C. Isolation and structural characterization of the milled-wood lignin from *Paulownia fortunei* wood. *Ind. Crops Prod.* **2009**, *30*, 137−143.
(25) Müse, G.; Schindler, T.; Bergfeld, R.; Ruel, K.; Jacquet, G.; Lapierre, C.; Speth, V.; Schopfer, P. Structure and distribution of lignin in primary and secondary cell walls of maize coleoptiles analyzed by chemical and immunological probes. *Planta* **1997**, *201*, 146−159.
(26) Wen, J. L.; Xue, B. L.; Xu, F.; Sun, R. C. Unveiling the structural heterogeneity of bamboo lignin by in situ HSQC NMR technique. *BioEnergy Res.* **2012**, *5*, 886−903.
(27) Villaverde, J. J.; Li, J.; Ek, M.; Ligero, P.; de Vega, A. Native lignin structure of *Miscanthus* × *giganteus* and its changes during acetic and formic acid fractionation. *J. Agric. Food Chem.* **2009**, *57*, 6262−6270.
(28) Li, H. T.; Yao, K.; Jia, D. Y.; He, Q. The detecting techniques of content of lignin. *Leath. Sci. Eng.* **2011**, *21*, 31−34.
(29) Sette, M.; Lange, H.; Crestini, C. Quantitative HSQC analyses of lignin: a practical comparison. *Comput. Struct. Biotechnol. J.* **2013**, *6*, 1−7.
(30) Rencoret, J.; Marques, G.; Gutiérrez, A.; Nieto, L.; Santos, J. I.; Jiménez-Barbero, J.; Martínez, Á. T.; del Río, J. C. HSQC-NMR analysis of lignin in woody (*Eucalyptus globulus* and *Picea abies*) and non-woody (*Agave sisalana*) ball-milled plant materials at the gel state. *Holzforschung* **2009**, *63*, 691−698.
(31) Ralph, J.; Akiyama, T.; Kim, H.; Lu, F.; Schatz, P. F.; Marita, J. M.; Ralph, S. A.; Reddy, M. S.; Chen, F.; Dixon, R. A. Effects of coumarate 3-hydroxylase down-regulation on lignin structure. *J. Biol. Chem.* **2006**, *281*, 8843−8853.
(32) Kim, H.; Ralph, J.; Akiyama, T. Solution-state 2D NMR of ball-milled plant cell wall gels in DMSO-d6. *BioEnergy Res.* **2008**, *1*, 56−66.
(33) Kim, H.; Ralph, J. Solution-state 2D NMR of ball-milled plant cell wall gels in DMSO-d6/pyridine-d5. *Org. Biomol. Chem.* **2010**, *8*, 576−591.
(34) Orlandi, M. A multi-analytical study of degradation of lignin in archaeological waterlogged wood. *Talanta* **2009**, *80*, 61−70.
(35) Li, M. F.; Sun, S. N.; Xu, F.; Sun, R. C. Microwave-assisted organic acid extraction of lignin from bamboo: structure and antioxidant activity investigation. *Food Chem.* **2012**, *134*, 1392−1398.
(36) Björkman, A. Isolation of lignin from finely divided wood with neutral solvents. *Nature* **1954**, *174*, 1057−1058.
(37) Ren, M. M.; Lv, H. S.; Zhang, M. H. Supercritical extraction and characterization of corn stover lignin. *Chem. Ind. Eng.* **2012**, *29*, 53−57.
(38) Ferrer, J. L.; Austin, M. B.; Stewart, C., Jr.; Noel, J. P. Structure and function of enzymes involved in the biosynthesis of phenylpropanoids. *Plant Physiol. Biochem.* **2008**, *46*, 356−370.
(39) Ziebell, A.; Gracom, K.; Katahira, R.; Chen, F.; Pu, Y.; Ragauskas, A.; Dixon, R. A.; Davis, M. Increase in 4-coumaryl alcohol units during lignification in alfalfa (*Medicago sativa*) alters the extractability and molecular weight of lignin. *J. Biol. Chem.* **2010**, *285*, 38961−38968.
(40) Donaldson, L. A. Lignification and lignin topochemistry − an ultrastructural view. *Phytochemistry* **2001**, *57*, 859−873.
(41) Samuel, R.; Foston, M.; Jiang, N.; Allison, L.; Ragauskas, A. J. Structural changes in switchgrass lignin and hemicelluloses during pretreatments by NMR analysis. *Polym. Degrad. Stab.* **2011**, *96*, 2002−2009.
(42) Sun, S. N.; Li, M. F.; Yuan, T. Q.; Xu, F.; Sun, R. C. Sequential extractions and structural characterization of lignin with ethanol and alkali from bamboo (*Neosinocalamus affinis*). *Ind. Crops Prod.* **2012**, *37*, 51−60.
(43) Yamamura, M.; Noda, S.; Hattori, T.; Shino, A.; Kikuchi, J.; Takabe, K.; Tagane, S.; Gau, M.; Uwatoko, N.; Mii, M. Characterization of lignocellulose of *Erianthus arundinaceus* in relation to enzymatic saccharification efficiency. *Plant Biotechnol.* **2013**, *30*, 25−35.

humans. The present study investigated effects of natural product EGCG on photodegradation of CTL in aqueous solutions and photodegradation pathways and mechanisms.

## 2. MATERIALS AND METHODS

**2.1. Chemicals and Reagents.** All chemicals and reagents were used as received. Chlorothalonil (99.1%), CTL−OH (99%), EGCG (98%), and *N*,*N*-dimethyl-*p*-nitrosoaniline (PNDA, 98%) were purchased from J&K Chemical Ltd. (Shanghai, China). Acetonitrile (Assay ⩾99.9%, HPLC/Spectro) and methanol (Assay ⩾99.9%, HPLC/Spectro) were purchased from Tedia Co. (Fairfield, USA).

**2.2. Photodegradation Experiments.** CTL standard stock solution was 1.0 g/L (3.76 mmol/L) in acetonitrile. To determine the effect of EGCG on CTL photodegradation in aqueous solution, CTL standard stock solution was transferred into 100 mL flasks followed by addition of EGCG aqueous solution at a mole to mole ratio (CTL: EGCG) of 1:0.6, 1:2.9, 1:5.8, 1:11.6, 1:29.0, and 1:58.1 (CTL is 0.00376 mmol/L). The mixture was then diluted with double-distilled water and subjected to brief ultrasonication. An aliquot of a 10 mL reaction solution of CTL and EGCG was transferred to a quartz cuvette, which was covered with a stopper, and placed under different light sources for photodegradation experiments. The light intensity was 10000−11000 lx for a high-pressure mercury lamp (HPML) (emission line spectrum at 365 nm) and 100000−120000 lx for direct sunlight (N31°52′, E117°17′). The distance between the quartz tube and the HPML was 15 cm. The temperature of the reaction system was maintained at 25 ± 1 °C except for the sunlight treatment which temperatures varied between 25 and 30 °C. A rotary water bath was used to maintain the temperature for the mercury lamp illumination, and the quartz tube was tilted at a 30° angle with the ground to face the sun directly.

Paddy, reservoir, and pond waters were used to determine the effect of EGCG on CTL photodegradation in natural water. The paddy water had turbidity 1.8 FTU, conductivity 0.29 ms/cm, pH 7.42, hardness 264 mg/L, DO 4 mg/L, COD 342 mg/L, $BOD_5$ 2.4 mg/L, TOC 15.08 mg/L, $F^{-1}$ 1.49 mg/L, $Cl^{1-}$ 46.4 mg/L, $NO_2^{-1}$ 0.59 mg/L, $SO_4^{2-}$ 75.98 mg/L. The reservoir water had turbidity 1.4 FTU, conductivity 0.15 ms/cm, pH 7.09, hardness 124 mg/L, DO 15.2 mg/L, COD 8 mg/L, $BOD_5$ 6.4 mg/L, TOC 9.62 mg/L, $F^{-1}$ 0.49 mg/L, $Cl^{1-}$ 14.61 mg/L, $NO_2^{-1}$ 0.53 mg/L, $SO_4^{2-}$ 27.99 mg/L. The pond water had turbidity 2.3 FTU, conductivity 0.32 ms/cm, pH 7.38, hardness 140 mg/L, DO 4.8 mg/L, COD 72 mg/L, $BOD_5$ 2.4 mg/L, TOC 27.82 mg/L, $F^{-1}$ 1.15 mg/L, $Cl^{1-}$ 52.1 mg/L, $NO_2^{-1}$ 0.57 mg/L, $SO_4^{2-}$ 72.54 mg/L. An aliquot of a 10 mL reaction solution of CTL and EGCG (CTL: EGCG of 1:2.9, CTL is 0.00376 mmol/L) was transferred to a quartz cuvette, which was covered with a stopper, and placed under sunlight for photodegradation experiments. The quartz tube was tilted at a 30° angle with the ground to face the sun directly. The light intensity was 82000−88000 lx for direct sunlight (N31°52′, E117°17′), and the temperature of the water solution varied between 40 and 45 °C.

**2.3. Analysis of CTL and Chloride Ion in Photolysis Mixtures.** An appropriate amount of CTL standard stock solution was transferred to a 100 mL volumetric flask, and EGCG was added at a mole to mole ratio of 1:5.8 (CTL is 0.00188 mmol/L). The mixture solution was diluted with double-distilled water and subjected to brief ultrasonication. Controls contained no EGCG. Twenty mL of the mixture was transferred to a quartz tube with a stopper and exposed to HPML. Afterward, samples were taken at different times to measure the concentrations of CTL and chloride ion. A dark control was the flasks completely covered with aluminum foil, while the other conditions remained the same as the treatments. The samples were taken at different time intervals, and each treatment was repeated twice.

**2.4. Detection of Hydroxyl Free Radicals (•OH).** PNDA has a yellow colored sensitive absorption band at 440 nm, and its adsorption decreases when it is reacted with •OH.[15] The reduction of PNDA by •OH thus reflects the amount of •OH it captures. PNDA was used as the •OH scavenger to indicate the changes in the amount of •OH generated by $H_2O_2$ in aqueous solutions under the HPML irradiation. PNDA standard stock solution was transferred to a 100 mL flask, followed by addition of EGCG and $H_2O_2$ at a mole ratio of 1:1.64:1324 and 1:3.28:1324, respectively. The mixture solution was diluted with double-distilled water and subjected to ultrasonic solubilization. A control was prepared without adding EGCG. The reaction solution (10 mL) was transferred to a quartz tube with a stopper and placed under a HPML for the illumination treatment. Samples were taken at different time intervals to measure absorbance at 440 nm using a UV spectrophotometer (UV-1800, Shimadzu Corp.). The results were used to calculate the residual concentration of PNDA at each time interval to reflect •OH changes.

**2.5. Analysis of CTL, CTL−OH, and EGCG.** CTL was analyzed on an Agilent 1200 HPLC system equipped with an Agilent HC-C18 column (4.6 mm × 250 mm, 5 μm) at a detection wavelength of 236 nm (Agilent Technologies, USA). The mobile phase was 80% aqueous acetonitrile at a flow rate of 1.0 mL/min. The column temperature was 30 °C. The injection volume was 10 μL. The limit of detection (LOD) for CTL was 0.01 mg/L.

The HPLC conditions for CTL−OH and EGCG were the same as CTL except the following differences: CTL−OH, detection at 248 nm, acetonitrile/0.5% phosphoric acid mobile phase (60:40 v/v), and injection volume of 20 μL. EGCG, detection at 280 nm, acetonitrile/0.1% citric acid mobile phase (20:80 v/v), and injection volume of 20 μL. The LOD for CTL−OH and EGCG was 0.01 and 0.05 mg/L, respectively.

**2.6. Analysis of Photolytic Products of CTL and Photopolymerization Products of EGCG.** Photolytic products of CTL and photopolymerization products of EGCG were analyzed on an Waters Xevo TQ MS ultra performance liquid chromatograph triple quadrupole tandem mass spectrometer (UPLC-MS/MS; Waters, USA) with an Acquity BEH $C_{18}$ column (1.7 μm × 2.1 mm × 100 mm). The mobile phases were a mixture of water, methanol, and formic acid (98:2:0.1 v/v/v, A) and methanol and formic acid (100:0.1 v/v, B). The gradient elution program was 0−0.25 min 90% A+10% B, 0.25−6 min 0% A+100% B, 6−11 min 0% A+100% B, 11−12 min 90% A+10% B, and 12−15 min 90% A+10% B. The flow rate was 0.35 mL/min. The column temperature was 40 °C. The MS was operated at electrospray ionization (ESI) mode with simultaneous detection of positive and negative ions, cone voltage of 30 V, mass range of 150−1000 ($m/z$), ion source temperature of 150 °C, capillary voltage of 1.5 kV, desolvation gas flow of 800 L/h ($N_2$), and desolvation temperature of 400 °C.

**2.7. Analysis of Chloride Ion ($Cl^-$).** Chloride ion was analyzed on a Dionex ICS 1100 ion chromatograph system equipped with an isocratic pump, an AS-DV automatic injector, a Dionex ASRS-300 suppressor, and a DS6 heated conductivity cell. A mixture of 4.5 mM $Na_2CO_3$ and 0.8 mM $NaHCO_3$ aqueous solution was used as mobile phase at a constant flow rate of 0.5 mL/min. An IonPac AG23 (50 mm × 4 mm) guard column and an IonPac AS23 (250 mm × 4 mm) analytical column (Dionex, Sunnyvale, CA, USA) were employed for separation of target ions. The LOD for $Cl^-$ was 0.2 μg/L.

**2.8. Calculation Methods.** Photodegradation rate was calculated with eq 1

$$\text{photodegradation rate}\ (\%) = [(a - b)/a] \times 100 \quad (1)$$

where $a$ was the residual concentration of CTL in the dark control, and $b$ was the residual concentration of CTL in the light treatment.

Photodegradation half-life ($T_{1/2}$) was calculated with eq 2

$$T_{1/2} = \ln 2/k \quad (2)$$

where $k$ was the photodegradation rate constant and was calculated with eq 3

$$C_t = C_0 \cdot e^{-kt} \quad (3)$$

where $C_0$ and $C_t$ were residual concentrations at time zero and time $t$ after the light treatment, respectively.

Photosensitization efficiency was calculated with eq 4

$$\text{photosensitization efficiency (\%)} = [(k_1 - k_0)/k_0] \times 100 \quad (4)$$

where $k_1$ was the reaction rate constant of CTL with EGCG, and $k_0$ was the reaction rate constant of CTL without EGCG.

## 3. RESULTS AND DISCUSSION

**3.1. Photosensitization Effects of EGCG on Chlorothalonil Degradation in Water.** The photolysis rate constant of CTL without EGCG under HPML illumination (0.0187 $min^{-1}$) was 1.6-fold greater than that (0.0117 $min^{-1}$) under sunlight irradiation (Table 1). The maximum absorption wavelength of CTL was 233 nm. The HPML may contain shortwave light that could be adsorbed by chlorothalonil to facilitate its photodegradation, although the maximum emission spectrum wavelength of HPML was 365 nm.[12] However, sunlight consisted primarily of visible light,[16] consequently, CTL was degraded more slowly than that under HPML illumination. Ferrioxalate is a visible light-responsive photocatalyst. Ferrioxalate/$H_2O_2$ could photosensitize degradation of chlorothalonil in aqueous solution by solar irradiation.[17]

EGCG strongly photosensitized CTL photodegradation under both sunlight and HPML light. The photosensitization efficiency under sunlight was much greater than that under HPML illumination. As the concentrations of EGCG increased, the photosensitization efficiency also increased. The rate constant increased 4-fold under HPML illumination at a molar ratio of CTL to EGCG of 1:11.6, whereas it increased approximately 12-fold under sunlight at a molar ratio of CTL to EGCG of 1:29.0. A maximum rate constant occurred at a ratio of CTL:EGCG 1:11.6 and 1:29.0 under HPML illumination and sunlight irradiation, respectively (Table 1). When the concentration of EGCG further increased, the rate constants decreased. It is noteworthy that EGCG can readily undergo oxidative polymerization and form polymers under irradiation.[13,18] In general, polymers could block light and slowdown

**Table 1. Effects of EGCG on Photodegradation of Chlorothalonil in Water under HPML and Sunlight Irradiation**

| | | kinetic equations | | |
|---|---|---|---|---|
| light sources | mole ratio (CTL/EGCG) | $k$ ($min^{-1}$) | $R^2$ | $T_{1/2}$ (min) |
| HPML | 1:0 | 0.0187 | 0.9796 | 37.1[a] |
| | 1:0.6 | 0.0252 | 0.9949 | 27.5[b] |
| | 1:2.9 | 0.04 | 0.997 | 17.3[c] |
| | 1:5.8 | 0.0575 | 0.9975 | 12.1[d] |
| | 1:11.6 | 0.0755 | 0.9918 | 9.2[d] |
| | 1:29.0 | 0.0515 | 0.9950 | 13.5[d] |
| | 1:58.1 | 0.0326 | 0.9977 | 21.3[c] |
| sunlight | 1:0 | 0.0117 | 0.9690 | 59.2[a] |
| | 1:0.6 | 0.0288 | 0.9747 | 30.4[b] |
| | 1:2.9 | 0.077 | 0.9967 | 9[c] |
| | 1:5.8 | 0.1022 | 0.9948 | 6.8[c] |
| | 1:11.6 | 0.1265 | 0.9987 | 5.5[c] |
| | 1:29.0 | 0.1585 | 0.9940 | 4.4[c] |
| | 1:58.1 | 0.1469 | 1.0000 | 4.7[c] |

[a-d]Different letters indicate significant difference at 0.05 level ($P < 0.05$).

**Table 3. Quenching of Hydroxyl Free Radicals by EGCG as Determined with PNDA in Water Solution under HPML Irradiation**

| | | concns of PNDA (mg/L) at different irradiation times (min) | | | |
|---|---|---|---|---|---|
| experimental group | mole ratio | 0 | 10 | 20 | 30 |
| PNDA | | 1.02 | 1.01 | 1.01 | 0.99 |
| PNDA/$H_2O_2$ | 1:1324 | 1.01 | 0.59 | 0.45 | 0.36 |
| PNDA/EGCG/$H_2O_2$ | 1:1.64:1324 | 1.01 | 1.01 | 1.00 | 0.99 |
| PNDA/EGCG/$H_2O_2$ | 1:3.28:1324 | 1.01 | 1.01 | 0.99 | 0.98 |

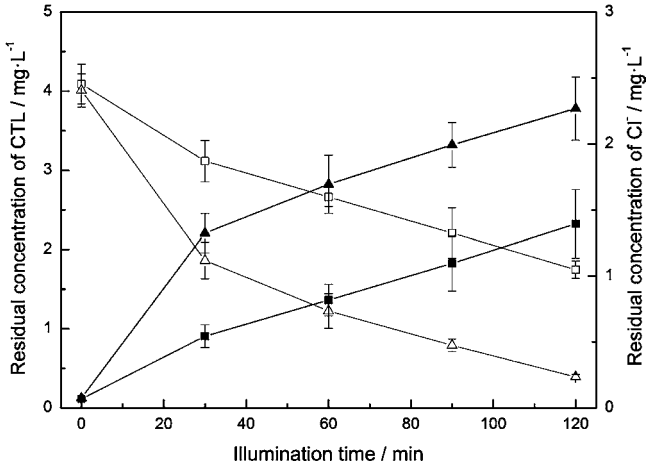


**Figure 1.** Concentrations of CTL and $Cl^-$ in water under HPML illumination. △ The residual concentration of CTL in the control (5 mg/L CTL). ▲ The residual concentration of $Cl^-$ in the control (5 mg/L CTL). □ The residual concentration of CTL in treatment A mixture of CTL and EGCG at a mole ratio of 1:5.8. ■ The residual concentration of $Cl^-$ in treatment A mixture of CTL and EGCG at a mole ratio of 1:5.8. Vertical bars represent the standard errors of the means.

**Table 2. Enhancement Effects of CTL on Degradation of EGCG in Water under HPML and Sunlight Irradiation**

| | initial concns (mg/L) | | concns of EGCG (mg/L) after different irradiation times (min) | | | | | |
|---|---|---|---|---|---|---|---|---|
| light sources | EGCG | CTL | 0 | 15 | 30 | 45 | 60 | decrease of EGCG after 60 min (%)[a] |
| HPML | 2 | 0 | 1.97 | 1.81 | 1.67 | 1.44 | 1.30 | 33.8 ± 3.2 |
| | 2 | 1 | 1.96 | 0.83 | 0.37 | 0.28 | 0.21 | 89.4 ± 7.7 |
| | 5 | 0 | 4.88 | 4.56 | 4.35 | 4.07 | 3.77 | 22.6 ± 1.9 |
| | 5 | 1 | 4.90 | 2.03 | 1.42 | 1.16 | 0.85 | 82.6 ± 6.8 |
| sunlight | 2 | 0 | 1.97 | 1.71 | 1.50 | 1.35 | 1.19 | 39.3 ± 3.1 |
| | 2 | 1 | 1.96 | 0.64 | 0.27 | 0.18 | 0.11 | 94.3 ± 9.2 |
| | 5 | 0 | 4.87 | 4.33 | 4.26 | 3.94 | 3.63 | 25.4 ± 3.1 |
| | 5 | 1 | 4.90 | 1.76 | 1.24 | 1.08 | 0.56 | 88.5 ± 8.3 |

[a]Data were expressed as the mean ± SE of triplicate determinations.

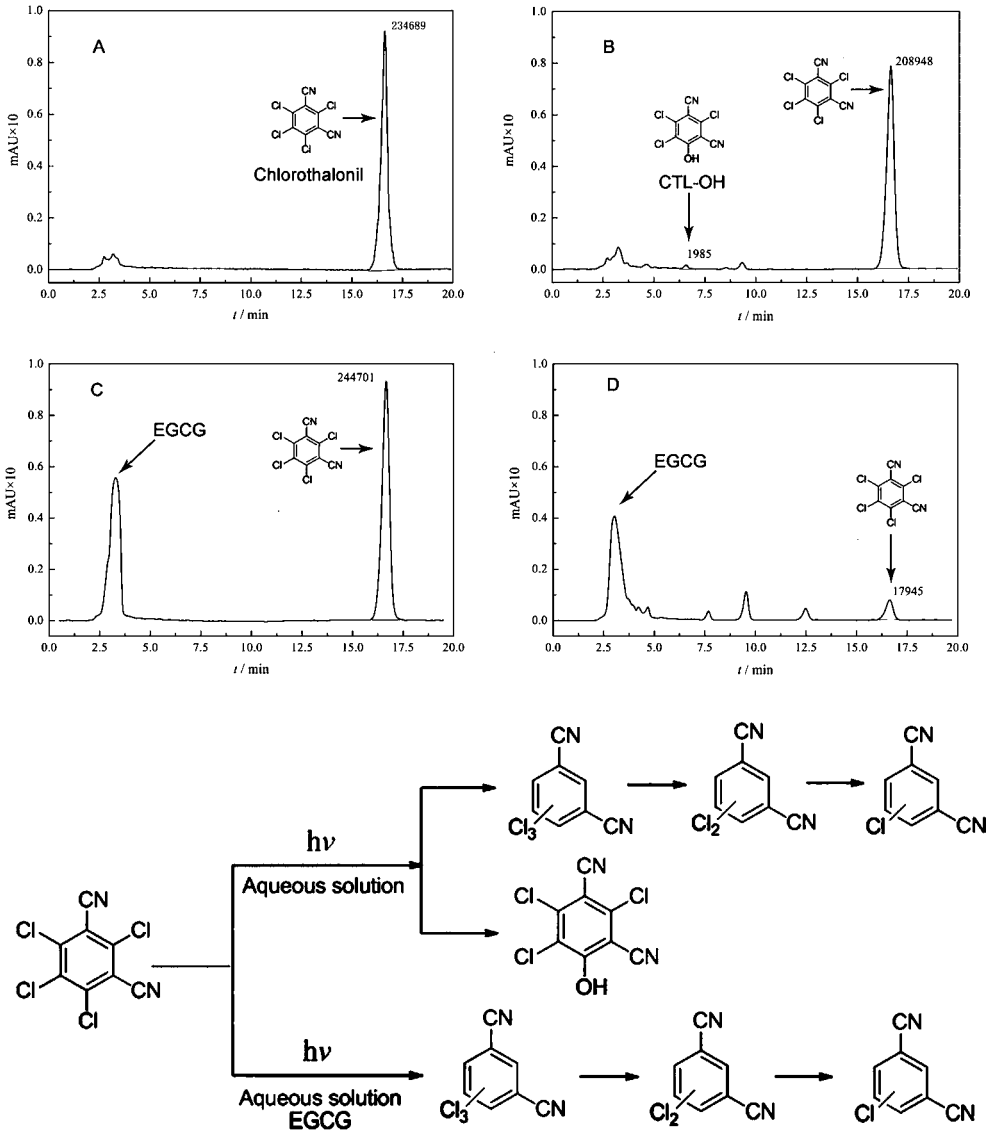


**Figure 2.** HPLC chromatograms of CTL with no EGCG in the dark (**A**) and under HPML (**B**), with EGCG (CTL: EGCG of 1:11.6) in the dark (**C**) and with EGCG under HPML (**D**) for 60 min and proposed step-wide photosensitized degradation pathways of CTL in the presence of and without EGCG (bottom).

**Table 4. Inhibitory Effects of EGCG on Generation of CTL−OH from CTL (2 mg/L) in Water under HPML Irradiation**

| | | concns (mg/L) at different irradiation times (min) | | | |
|---|---|---|---|---|---|
| concns of EGCG (mg/L) | test compds | 0 | 30 | 60 | 90 |
| 0 | CTL | 1.80 | 1.31 | 1.06 | 0.57 |
| | CTL−OH | 0 | 0.022 | 0.03 | 0.031 |
| 20 | CTL | 1.78 | 0.19 | 0.03 | 0.01 |
| | CTL−OH | <LOD | <LOD | <LOD | <LOD |

photodegradation. Therefore, polymers formed at high concentrations of EGCG may partially prevent CTL photodegradation.

**3.2. Mechanism of Photosensitization Effects of EGCG on Chlorothalonil Degradation.** To investigate the photosensitization mechanism of EGCG on CTL degradation, EGCG concentrations under the two light sources irradiation were analyzed (Table 2). The residual concentrations of EGCG gradually declined as irradiation time increased (Table 2), which is probably due to oxidative polymerization of EGCG.[13]

Concentrations of $^{\bullet}OH$ in natural waters are approximately $1.5 \times 10^{-18}$–$5 \times 10^{-16}$ mol/L.[19] Hydroxyl free radicals ($^{\bullet}OH$) can degrade organics via free radical reactions. To further confirm the reduction ability of EGCG, PNDA was used as a free radical trapping agent to detect $^{\bullet}OH$. The residual concentrations of PNDA decreased apparently when $H_2O_2$ was added, indicating generation of $^{\bullet}OH$ from $H_2O_2$ (Table 3). However, when EGCG was added into the mixture of PNDA and $H_2O_2$, the residual concentrations of PNDA did not change, suggesting that EGCG quenched $^{\bullet}OH$. The results indicate EGCG photosensitized reductive photolysis of CTL rather than photooxidation by $^{\bullet}OH$ free radicals.

**3.3. Effects of EGCG on CTL Photodegradation Pathways and Minimizing Toxic Metabolite Formation.** Concentrations of both CTL and chloride ion in the reaction mixture were monitored to further confirm the role of EGCG on CTL photodegradation through reductive dechlorination. Upon illumination for 120 min under HPML, 65% of CTL (5


dx.doi.org/10.1021/jf504565b | J. Agric. Food Chem. 2014, 62, 12090−12095

Table 5. Effects of EGCG on Photodegradation of Chlorothalonil in Natural Water under Sunlight Irradiation

| | | kinetic equations | | | |
|---|---|---|---|---|---|
| natural water | molar ratio (CTL/EGCG) | $k$ ($min^{-1}$) | $R^2$ | $T_{1/2}$ (min) | photosensitization efficiency of EGCG (%) |
| reservoir water | 1:0 | 0.0351 | 0.9295 | 19.7 | |
| | 1:2.9 | 0.0429 | 0.9897 | 16.2 | 22.2 |
| pond water | 1:0 | 0.0257 | 0.9575 | 27.0 | |
| | 1:2.9 | 0.044 | 0.985 | 15.8 | 71.2 |
| paddy water | 1:0 | 0.0421 | 0.8741 | 16.5 | |
| | 1:2.9 | 0.0508 | 0.9459 | 13.6 | 20.7 |

mg/L) was degraded, which was $2.5 \times 10^{-4}$ mmol of CTL (Figure 1), while $5.8 \times 10^{-4}$ mmol of $Cl^-$ ion was detected in this solution. When EGCG was added, 92% of CTL was degraded, which was $3.5 \times 10^{-4}$ mmol of CTL, while $10.3 \times 10^{-4}$ mmol of $Cl^-$ ion was detected, suggesting enhanced dechlorination of CTL after EGCG addition. The apparent increase in $Cl^-$ ion production during CTL photodegradation in the presence of EGCG indicated the photosensitization effect of EGCG on CTL degradation. It is interesting that EGCG promoted the reductive dechlorination of CTL.

The HPLC chromatograms of CTL in the presence of EGCG and without EGCG in the dark and under HPML for 60 min were shown in Figure 2. CTL and CTL−OH were identified by comparison of their retention times and mass spectra with those of their corresponding standards. The other two degradation products shown in Figure 2 were tentatively identified according to their retention times and mass spectra. The one having $m/z$ ($ESI^-$) 195.75, 197.52, and 199.59 with a relative isotope abundance of 9:6:1 may be the molecular ion ($M^+$) of dichloride-1,3-isophthalic nitrile. The peak showing $m/z$ ($ESI^-$) 160.73, 162.77 is possibly $[M-H]^+$ of dichloride-1,3-isophthalic nitrile ($[M-H]^+$, 161.00). CTL−OH ($[M-H]^+$, 245.92) gave $m/z$ ($ESI^-$) 244.82, 246.73, and 248.77 with a relative isotope abundance of 1:1:0.3. The results indicated that CTL mainly underwent step-wide photoreductive dechlorination, and EGCG promoted the dechlorination of CTL.

CTL−OH is one of the main metabolites of CTL photodegradation.[19] Effects of EGCG on the production of CTL−OH were thus studied. The results showed that the concentrations of CTL−OH increased as the illumination time increased to 90 min (Table 4). However, under the same conditions, no CTL−OH was detected in the reaction solution when EGCG was added at a level of 20 mg/L (Figure 2). Chlorinated *m*-dicyanobenzene instead of CTL−OH was produced from CTL photodegradation. EGCG is a polyphenol and a strong antioxidant which can quench free radical reactions[18] in the process of EGCG-catalyzed CTL photodegradation. EGCG not only promoted the reductive photodegradation of CTL but also reduced CTL−OH formation. CTL−OH is greater than 60-fold more toxic than CTL.[20] We concluded that EGCG not only significantly enhances the CTL photodegradation rate but also alters the photodegradation pathways, avoiding the production of the highly toxic CTL−OH. Therefore, EGCG showed a high potential as a natural photosensitizer, which could be of importance in aquatic pollution management.

**3.4. Effects of EGCG on CTL Photodegradation in Nature Water.** Under the sunlight irradiation, EGCG significantly photosensitized CTL photolysis in the three different natural waters. The photodegradation half-lives of CTL in the reservoir, pond, and paddy waters were 19.7, 27.0, and 16.5 min, respectively, while they were 16.2, 15.8, and 13.6 min when EGCG was added (Table 5). We found that EGCG significantly photosensitized CTL degradation in natural waters under sunlight. It indicates that EGCG may be useful in water treatment for cleaning up CTL agricultural pollution via photodegradation. The results warrant further assessments in economic aspects and potential impacts of EGCG on the environment.

## AUTHOR INFORMATION


### Corresponding Author

*Phone: 86 551 65786320. Fax: 86 551 65786296. E-mail: rimaohua@ahau.edu.cn.

### Author Contributions

§These authors contributed equally.



### Funding

This project was supported in part by the National Natural Science Foundation of China (No. 30972053), the National Science and Technology Infrastructure Program of China (2012BAK17B12), National quality & safety risk assessment of Agro-products Program of China (GJFP2014004, GJFP2014011), and the Public sector (Agriculture) research Program of China (201303088-11).


### Notes

The authors declare no competing financial interest.

## REFERENCES


(1) Stallard, D. E.; Wolf, A. L. *The fate of 2,4,5,6-tetrachloroisophthalonitrile (Daconil 2787) in soil*; Diamond Shamrock Chemical Co. Report; 1967.

(2) Motonaga, K.; Takagi, K.; Matumoto, S. Biodegradation of chlorothalonil in soil after suppression of degradation. *Biol. Fertil. Soils* **1996**, *23*, 340−345.

(3) Wan, J.; Xue, M.; Chen, X. X.; Wang, Y. P.; Li, X.-R.; Xie, Y.-S.; Huang, Z.-J. Chlorothalonil residues in greenhouse growing vegetables and corresponding impact resulted from different treatments. *J. Saf. Environ.* **2005**, *5*, 79−82.

(4) Xiao, Y.; Zhang, Z. Y.; Sun, S. L. Residual dynamics of chlorothalonil on shed strawberry. *Agrochemicals* **2007**, *46*, 548−550.

(5) Chaves, A.; Shea, D.; Danehower, D. Analysis of chlorothalonil and degradation products in soil and water by GC/MS and LC/MS. *Chemosphere* **2008**, *71*, 629−638.

(6) Kazos, E. A.; Nanos, C. G.; Stalikas, C. D.; et al. Simultaneous determination of chlorothalonil and its metabolite 4-hydroxychlorothalonil in greenhouse air: dissipation process of chlorothalonil. *Chemosphere* **2008**, *72*, 1413−1419.

(7) Monadjemi, S.; Roz, M. E.; Richard, C.; et al. Photoreduction of chlorothalonil fungicide on plant leaf models. *Environ. Sci. Technol.* **2011**, *45*, 9582−9589.

(8) Rouchaud, J.; Roucourt, P. Hydrolytic biodegradation of chlorothalonil in the soil and in cabbage crops. *Toxicol. Environ. Chem.* **1988**, *17*, 59−68.

(9) Sato, K.; Tanaka, H. Degradation and metabolites of a fungicide, 2,4,5,6-tetra- chloroisophthalonitrile (TPN) in soil. *Biol. Fertil. Soils* **1987**, *3*, 205−209.

(10) Putnam, R. A.; Nelson, J. O.; Clark, J. M. The persistence and degradation of chlorothalonil and chlorpyrifos in a cranberry bog. *J. Agric. Food Chem.* **2003**, *51*, 170−176.
(11) Shi, X. Z.; Guo, R. J.; Takagi, K.; et al. Chlorothalonil degradation by *Ochrobactrum lupini* strain TP-D1 and identification of its metabolites. *World J. Microbiol. Biotechnol.* **2011**, *27*, 1755−1764.
(12) Tan, Y. Q.; Xiong, H. X.; Hua, R. M.; et al. Photosensitizing effects of nanometer $TiO_2$ on chlorothalonil photodegradation in aqueous solution and on the surface of pepper. *J. Agric. Food Chem.* **2013**, *61*, 5003−5008.
(13) Fang, Y. C.; Yin, N.; Mei, C. X. The application prospect of tea polyphenols. *China Food Addit.* **1999**, *4*, 35.
(14) Chen, H. H.; Fu, D. H.; Shi, L.; et al. The research of the stabilities of catechins. *Food Res. Dev.* **2009**, *30*, 10−12.
(15) Grimm, J. H.; Bessarabov, D. G.; Simon, U.; et al. Characterization of doped tin dioxide anodes prepared by a sol-gel technique and their application in an SPE-reactor. *J. Appl. Electrochem.* **2000**, *30*, 293−302.
(16) Li, X. D.; Hua, R. M.; Yue, Y. D.; et al. Photochemical degradation of chlorothalonil in aqueous solution. *Chin. J. Polym. Sci.* **2006**, *17*, 1091−1094.
(17) Chaudhuri, M.; Zuhali, H.; Affam, A. C. Degradation of pesticide chlorothalonil by visible light-responsive photocatalyst ferrioxalate and $H_2O_2$ under solar irradiation. *Int. J. Photoenergy* **2013**, DOI: 10.1155/2013/435017.
(18) Li, C. M.; Xie, B. J. Separation of tea catechin oxy-polymers by high performance liquid chromatography. *J. Tea Sci.* **2001**, *21*, 69−71.
(19) Helz, G. R.; Zepp, R. G.; Crosby, D. G. *Aquatic and Surface Photochemistry*; Lewis Publishers: Boca Raton, FL, 1994; pp 149−161.
(20) Onduka, T.; Kakuno, A.; Kono, K.; et al. Toxicity of chlorothalonil to marine organisms. *Fish Ecol.* **2012**, *78*, 1301−1308.

plasma.[22,23] The ionization efficiency possibly differs even between the respective time-course plasma samples in which the concentrations of Hyp-containing peptides dramatically vary after the oral ingestion of gelation hydrolysate.

To ensure the quantitative accuracy of MS analysis, many studies have used stable isotope-labeled internal standards for quantification of bioactive peptides in plasma.[24−28] The labeled internal standards are identical to the target analytes in all respects except for the mass and thus can compensate for the matrix effects in MS analysis. In general, stable isotopically heavy internal standard peptides are provided commercially or are synthesized by using labeled amino acids. However, labeled Hyp-containing peptides and even labeled Hyp are not commercially available. We have to custom-synthesize the internal standards of Hyp-containing peptides one by one with labeling on other constituent peptide amino acids.

Recently, we developed a novel tool for highly accurate collagen analyses using LC-MS, including quantification of type-specific collagen, total collagen, and collagen post-translational modifications.[29] We produced a stable isotope-labeled collagen named "SI-collagen" in the culture of human embryonic lung (HEL) fibroblasts, which were metabolically labeled with stable isotopically heavy Pro, Lys, and Arg. By mixing SI-collagen into collagen samples as an internal standard, any errors due to downstream experimental procedures and ionization efficiency changes in MS can be eliminated. Furthermore, we showed that the acid hydrolysate of SI-collagen can be used as internal standards of post-translationally modified amino acids, such as 4-Hyp. In this study, we aimed to expand the applicability of SI-collagen to quantification of the Hyp-containing peptides in blood by preparing internal standards of those analytes. Relatively long peptides (four or more amino acids long) can be generated from collagen/gelatin using a single protease,[30,31] and Gly-X-Y type tripeptides are also available after collagenase digestion.[32] However, it was difficult to comprehensively generate various types of Hyp-containing di- and tripeptides. To achieve this objective, we examined the digestion using trypsin/chymotrypsin and dialyzed plasma by mimicking the protein degradation pathways in the body. The serial digestion allowed efficient generation of all the Hyp-containing peptides identified in blood. Using our method with the digest of SI-collagen (SI-digest) as an internal standard mixture, plasma concentrations of Hyp and 13 Hyp-containing peptides were simultaneously quantified by LC-MS with high accuracy and reproducibility.

## MATERIALS AND METHODS

**Chemicals.** SILAC DMEM, dialyzed FBS, $^{13}C_6$-Lys, and $^{13}C_6{}^{15}N_4$-Arg were purchased from Thermo Scientific (Hudson, NH, USA). Pepsin−agarose, *trans*-4-hydroxy-L-proline, heparin sodium salt, and Dulbecco's phosphate-buffered saline (DPBS) with calcium chloride and magnesium chloride were purchased from Sigma-Aldrich (St. Louis, MO, USA). L-Ascorbic acid phosphate magnesium salt *n*-hydrate and ammonium bicarbonate were purchased from Wako Chemicals (Osaka, Japan), and trypsin and chymotrypsin were purchased from Promega (Madison, WI, USA). $^{13}C_5{}^{15}N_1$-Pro was purchased from Cambridge Isotope Laboratories (Andover, MA, USA), and PicoTag sample tubes were purchased from Waters (Milford, MA, USA). Pro-Hyp, Hyp-Gly, and Gly-Pro-Hyp were purchased from Bachem (Bubendorf, Switzerland), and other synthetic peptides were purchased from Anygen (Kwangju, Korea). All other chemicals were purchased from Sigma-Aldrich. Pepsin-solubilized type I collagen was prepared from bovine skin as described previously.[29]

**Preparation of SI-Collagen.** SI-collagen was prepared from the culture of HEL cells as reported previously.[29] In brief, HEL cells were labeled using SILAC DMEM supplemented with 0.5% dialyzed FBS, 100 mg/L $^{13}C_6$-Lys, 100 mg/L $^{13}C_6{}^{15}N_4$-Arg, 200 mg/L $^{13}C_5{}^{15}N_1$-Pro, and 200 μM L-ascorbic acid phosphate in 100 mm dishes. The culture medium from the first 3 days was discarded, and then collection and changing of the labeling medium were performed every 3 days. The collected culture medium was digested by pepsin−agarose (0.1 mg/mL in 0.1 N HCl) with gentle mixing at 4 °C for 16 h. After removal of the immobilized pepsin by centrifugation, salt precipitation was performed with 1 M NaCl for 3 h on ice. SI-collagen was precipitated by centrifugation at 16000*g* for 10 min at 4 °C and dissolved in 5 mM acetic acid after it had been extensively washed with 1 M NaCl in 0.1 N HCl and 95% ethanol.

**Preparation of Time-Course Plasma Samples after Oral Ingestion of Gelatin Hydrolysate.** The human study was performed according to the Helsinki Declaration under the control of medical doctors. The experimental protocol was approved by the experimental ethical committee of Nippi Research Institute of Biomatrix. A healthy volunteer fasted for 12 h before the experiment and was given 25 g of fish-scale gelatin hydrolysate (FCP; Nippi, Tokyo, Japan), which was prepared by enzymatic hydrolysis and has an average molecular weight of 3000−5000 Da. After oral ingestion of the gelatin hydrolysate, venous blood was collected from the cubital vein before (0 h) and 0.5, 1, 2, 4, and 6 h after the ingestion. Plasma was prepared by centrifugation of the blood at 10000*g* for 10 min at 4 °C and stored at −80 °C until used for analysis.

**Quantification of Free Hyp and Peptide-Form Hyp Using the Acid Hydrolysate of SI-Collagen.** Twenty micrograms of SI-collagen was hydrolyzed by acid to generate $^{13}C_5{}^{15}N_1$-Hyp, which was used as an internal standard of 4-Hyp. After SI-collagen solution in PicoTag sample tubes had been dried with a centrifugal evaporator CVE-3100 (EYELA, Tokyo, Japan), acid hydrolysis was performed with 6 N HCl/1% phenol at 110 °C for 20 h in the gas phase under $N_2$. The acid hydrolysate of SI-collagen was dissolved in 1000 μL of distilled water, and 10 μL of the solution was mixed into 20 μL of the human plasma samples and calibration standards of 4-Hyp. Proteins in the plasma samples were precipitated by adding 3 volumes of ethanol followed by centrifugation at 10000*g* for 10 min at 4 °C. Ten microliters of each ethanol-soluble fraction was diluted 20-fold with 0.1% formic acid/50% acetonitrile, and 5 μL of the solution was directly subjected to quantification of free Hyp. In parallel, 50 μL of the ethanol-soluble fraction was subjected to acid hydrolysis for quantification of total Hyp (sum of free Hyp and peptide-form Hyp). The acid hydrolysate was dissolved in 200 μL of 0.1% formic acid/50% acetonitrile, and 2 μL of the solution was used for the quantification. Analysis was performed on a hybrid triple-quadrupole/linear ion trap 3200 QTRAP mass spectrometer (AB Sciex, Foster City, CA, USA) equipped with an electrospray ionization source. The instrument was coupled to an Agilent 1200 series HPLC system (Agilent Technologies, Palo Alto, CA, USA). The samples were loaded onto a ZIC-HILIC column (5 μm particle size, L × i.d. 150 mm × 2.1 mm; Merck Millipore, Billerica, MA, USA) at a flow rate of 200 μL/min and separated by a binary gradient as follows: 90% solvent B (100% acetonitrile) for 5 min, linear gradient of 10−95% solvent A (0.1% formic acid) for 10 min, 95% solvent A for 5 min, and 90% solvent B for 5 min. Analyst 1.6.2 (AB Sciex) was used to perform data acquisition and analysis, and quantification of Hyp and $^{13}C_5{}^{15}N_1$-Hyp was performed in MRM mode. The MRM transitions are shown in Table S1 in the Supporting Information. Capillary voltage was 3 kV, declustering potential was 26 V, heater gas temperature was 600 °C, curtain gas was 15 psi, nebulizer gas was 80 psi, and heater gas was 80 psi. Quantitation of Hyp was calculated with or without correction using $^{13}C_5{}^{15}N_1$-Hyp. Plasma concentrations of peptide-form Hyp were estimated by subtracting the concentration of free Hyp from total Hyp as described in previous studies.[2,3]

**Preparation of SI-Digest.** Plasma was prepared from male ICR mice (Japan SLC, Shizuoka, Japan). The diet of the mice was replaced with AIN-93 M (Oriental Yeast, Tokyo, Japan) which does not contain collagen, at least a day before the procedure. Whole blood was

collected from the heart with heparin and immediately centrifuged at 10000*g* for 10 min at 4 °C. The obtained plasma was dialyzed against DPBS at 4 °C overnight to completely exclude Hyp and Hyp-containing peptides. The dialysate that contains plasma proteases was used to generate stable isotope-labeled Hyp and Hyp-containing peptides from SI-collagen in the next step.

Fifty micrograms of SI-collagen was denatured at 60 °C for 30 min and digested by trypsin and chymotrypsin (1:50 enzyme/substrate ratio) in 100 mM ammonium bicarbonate/1 mM $CaCl_2$ at 37 °C for 16 h. After the reaction, the enzymes were deactivated by heating at 100 °C for 5 min. The solution was dried using the centrifugal evaporator, and then digestion by 100 μL of the freshly prepared dialyzed plasma was performed at 37 °C for 24 h. After ethanol precipitation, the supernatant was dried using the centrifugal evaporator and reconstituted in 400 μL of distilled water. A portion of the prepared SI-digest was mixed with a standard mixture of Hyp and Hyp-containing peptides, and the absolute concentrations of respective labeled Hyp and Hyp-containing peptides were calculated from the relative peak areas of labeled analytes compared to nonlabeled ones in MRM analysis described below.

**Quantification of Hyp and Hyp-Containing Peptides Using SI-Digest.** Two microliters of SI-digest was first mixed into 10 μL of the human plasma samples and calibration mixtures of Hyp and Hyp-containing peptides. Then, the plasma samples were subjected to ethanol precipitation and subsequently dried using the centrifugal evaporator. The samples were dissolved in 50 μL of 10 mM ammonium acetate, and 10 μL of the solution was subjected to MRM analysis. The samples were loaded onto an Ascentis Express F5 HPLC column (5 μm particle size, L × i.d. 250 mm × 4.6 mm; Supelco, Bellefonte, PA, USA) at a flow rate of 400 μL/min and separated by a binary gradient as follows: 100% solvent A (10 mM ammonium acetate) for 7.5 min, linear gradient of 0−99% solvent B (100% acetonitrile) for 12.5 min, 99% solvent B for 5 min, and 100% solvent A for 5 min. Capillary voltage was 3 kV, declustering potential was 15 V, heater gas temperature was 700 °C, curtain gas was 15 psi, nebulizer gas was 80 psi, and heater gas was 80 psi. The light and heavy MRM transitions of 16 Hyp-containing peptides are shown in Table S1 in the Supporting Information. Plasma concentrations of Hyp and Hyp-containing peptides were estimated using the external calibration curves with correction using stable isotope-labeled analytes from SI-digest as internal standards. The area under the plasma concentration−time curve ($AUC_{0-6\,h}$) was calculated using the trapezoidal rule.

**Statistical Analysis.** Data are expressed as the mean ± standard deviation (SD), and coefficient of variation (CV) was calculated for $AUC_{0-6\,h}$ of Hyp and Hyp-containing peptides quantified using SI-digest. The mean values of total plasma concentrations of Hyp-containing peptides estimated by two different approaches using SI-collagen were applied for the statistical analysis. Quantitative values of peptide-form Hyp and total of Hyp-containing peptides were compared using Student's *t* test (Microsoft Excel) at each time point.

## RESULTS AND DISCUSSION

**Effect of Plasma on Quantitative Accuracy of LC-MS Analysis.** We first examined the quantitative accuracy of LC-MS analysis of plasma samples with and without an internal standard. The acid hydrolysate of SI-collagen, in which Pro, Lys, Arg, and their post-translational modifications were all labeled with stable isotope, was first mixed into the human plasma samples as an internal standard of 4-Hyp. Free Hyp was directly quantified following ethanol deproteinization of the samples. Peptide-form Hyp, which corresponds to the total of Hyp-containing peptides, was quantified by subtracting the free Hyp from total Hyp analyzed following acid hydrolysis of the deproteinized plasma. As shown in Figure 1, both free and peptide-form Hyp dramatically increased in plasma after oral ingestion of gelatin hydrolysate. The plasma concentrations reached a maximum at 1−2 h and returned to close to the initial level at 6 h after the ingestion as reported previously.[4] Although similar concentration profiles were observed between quantifications with and without the internal standard, the concentrations estimated without the internal standard were significantly lower than those estimated with the internal standard. At 1 h after the ingestion, the plasma concentrations of total Hyp and free Hyp were 150 ± 10 and 131 ± 9 nmol/mL without the internal standard, respectively, and 315 ± 15 and 219 ± 4 nmol/mL with the internal standard, respectively. Furthermore, the concentration values of peptide-form Hyp fell into the minus range at some time points without the internal standard. We confirmed that the presence of plasma critically suppressed the ionization efficiency in LC-MS both during the analysis of free and peptide-form Hyp even after the deproteinization (Figure S1 in the Supporting Information). In addition, it was hard to completely and quantitatively dissolve burnt plasma samples after acid hydrolysis. These factors could account for the underestimated results without the internal standard, especially in the case of the quantification using acid hydrolysis where the minus values of peptide-form Hyp were observed. Taken together, we concluded that the internal standard is indispensable to ensure the quantitative accuracy of LC-MS analysis of plasma samples. To achieve highly accurate quantification of respective Hyp-containing

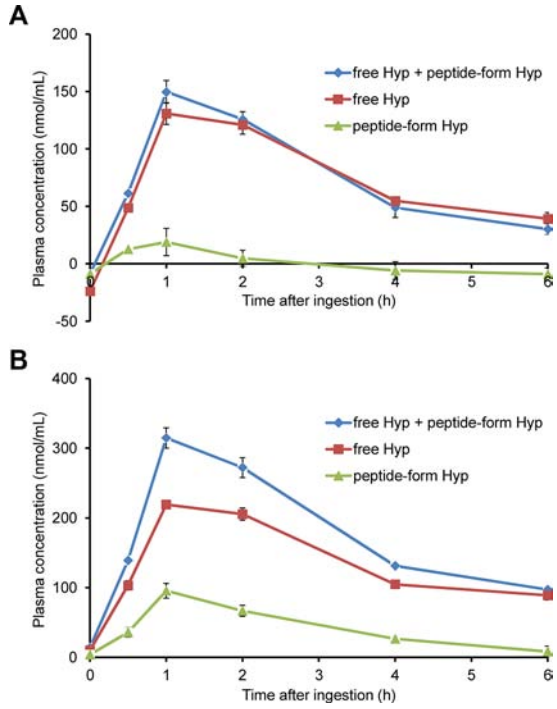


**Figure 1.** Quantification of free Hyp and peptide-form Hyp in human blood after oral ingestion of fish gelatin hydrolysate with or without the acid hydrolysate of SI-collagen. The acid hydrolysate of SI-collagen was first mixed into human plasma samples and calibration standards of 4-Hyp. After ethanol precipitation, part of each ethanol-soluble fraction of the plasma samples was directly analyzed by LC-MS in MRM mode for quantification of free Hyp, and the remaining samples were subjected to acid hydrolysis for quantification of total Hyp (sum of free Hyp and peptide-form Hyp). The plasma concentrations of Hyp were calculated using the calibration curve of 4-Hyp (A) without or (B) with $^{13}C_5{}^{15}N_1$-Hyp from the acid hydrolysate of SI-collagen as an internal standard. The data represent the mean ± SD of three separate measurements on each set of time-course samples from one human subject.

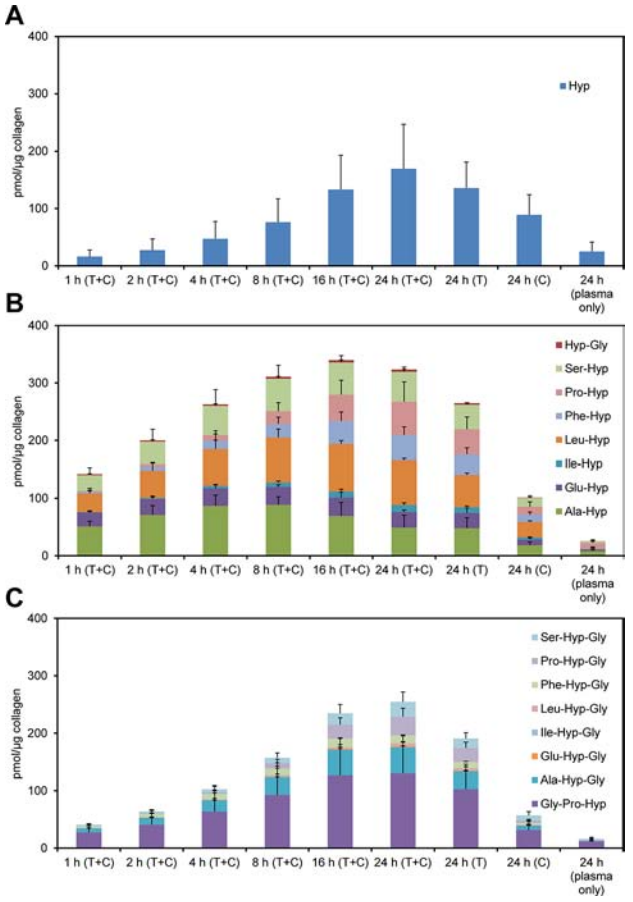


**Figure 2.** Generation of Hyp and Hyp-containing peptides by plasma proteases over various reaction times in combination with trypsin and/or chymotrypsin predigestion. Denatured bovine type I collagen was digested by trypsin and/or chymotrypsin at 37 °C for 16 h. After drying the samples, dialyzed mouse plasma was added to subsequent digestion of the collagen at 37 °C for 1−24 h. The generated (A) Hyp, (B) Hyp-containing dipeptides, and (C) Hyp-containing tripeptides were quantified by MRM analysis. The data represent the mean ± SD of three separate experiments. T indicates trypsin, and C indicates chymotrypsin.

peptides, we prepared internal standards of those peptides from SI-collagen using serial protease digestion as described in the following section.

**Generation of Hyp-Containing Peptides Using Serial Protease Digestion.** Ingested gelatin hydrolysate is first processed through gastrointestinal digestion by trypsin, chymotrypsin, and other proteases. Subsequently, the generated di- and tripeptides are absorbed from the intestine[33,34] and further digested in the blood, which contains many proteases.[35] Herein, we used trypsin/chymotrypsin and plasma proteases to generate various types of Hyp-containing peptides from collagen by mimicking the protein degradation pathways. Plasma prepared from ICR mice was dialyzed to remove non-negligible amounts of Hyp and Hyp-containing peptides, which were detected even after the diet was replaced with a non-collagen-containing one (data not shown). To estimate the generation of Hyp-containing peptides, bovine type I collagen was digested by the dialyzed plasma following trypsin and/or chymotrypsin digestion (Figure 2). Hyp-containing peptides were not detected in heat-denatured collagen, and subsequent digestion using trypsin and/or chymotrypsin did not generate

**Table 1. Content and Labeling Index of Stable Isotopically Labeled Hyp and Hyp-Containing Peptides in SI-Digest[a]**

| | mol wt | content (pmol/μg SI-collagen) | content (ng/μg SI-collagen) | labeling index (%) |
|---|---|---|---|---|
| Hyp | 137 | 190 | 26.0 | 98.1 |
| Ala-Hyp | 208 | 9.20 | 1.91 | 97.6 |
| Glu-Hyp | 266 | 14.9 | 3.95 | 98.2 |
| Ile-Hyp | 250 | 7.96 | 1.99 | 97.7 |
| Leu-Hyp | 250 | 29.3 | 7.33 | 98.3 |
| Phe-Hyp | 284 | 27.7 | 7.88 | 98.1 |
| Pro-Hyp | 240 | 47.7 | 11.5 | 99.4 |
| Ser-Hyp | 224 | 10.6 | 2.37 | 98.1 |
| Hyp-Gly | 194 | 1.82 | 0.353 | 98.9 |
| Gly-Pro-Hyp | 297 | 73.4 | 21.8 | 99.5 |
| Ala-Hyp-Gly | 265 | 31.5 | 8.34 | 98.4 |
| Glu-Hyp-Gly | 323 | 3.36 | 1.08 | 98.2 |
| Ile-Hyp-Gly | 307 | 0.129 | 0.0396 | 98.5 |
| Leu-Hyp-Gly | 307 | 2.56 | 0.786 | 97.8 |
| Phe-Hyp-Gly | 341 | 6.13 | 2.09 | 98.1 |
| Pro-Hyp-Gly | 297 | 17.9 | 5.30 | 99.6 |
| Ser-Hyp-Gly | 281 | 19.5 | 5.49 | 98.3 |
| total | | | 108 | |

[a]Underscoring indicates a stable isotopically labeled site. Labeling index was estimated as peak areas of the labeled analytes relative to the sum of the peak areas of the labeled and nonlabeled ones from MRM analysis.

the oligopeptides (data not shown). Whereas only trace amounts of Hyp-containing peptides were detected by 24 h of plasma sole digestion, the peptide generation was dramatically enhanced by predigestion with trypsin and/or chymotrypsin, especially by the double digestion (Figure 2B,C). The enhancement of peptide generation was especially significant for Hyp-Gly, which showed relatively lower peptide generation (0.181 pmol/μg by 24 h plasma sole digestion, 0.699 pmol/μg with chymotrypsin, 2.84 pmol/μg with trypsin, and 3.95 pmol/μg with trypsin/chymotrypsin). Concomitantly with the oligopeptide generation, Hyp was also generated as an end-product (Figure 2A). Whereas almost all Hyp-containing peptides increased with increasing plasma digestion time, some peptides showed different profiles. For example, Ala-Hyp increased until 8 h of plasma digestion, and then it decreased. The amount of Ala-Hyp is considered to depend on the balance between degradation from other long peptides and further degradation to Ala and Hyp. The X-Pro (Hyp) bond is generally resistant to proteases,[36,37] and Hyp-containing peptides (Pro-Hyp and Hyp-Gly) have been reported to be highly stable in serum.[3,5] However, excess exposure to plasma proteases led to further degradation at least for some Hyp-containing peptides.

**Preparation of Internal Standards of Hyp and Hyp-Containing Peptides.** On the basis of the above data, we adopted the 24 h plasma digestion with trypsin/chymotrypsin predigestion to prepare internal standards of Hyp and Hyp-containing peptides from SI-collagen. The resultant Hyp-

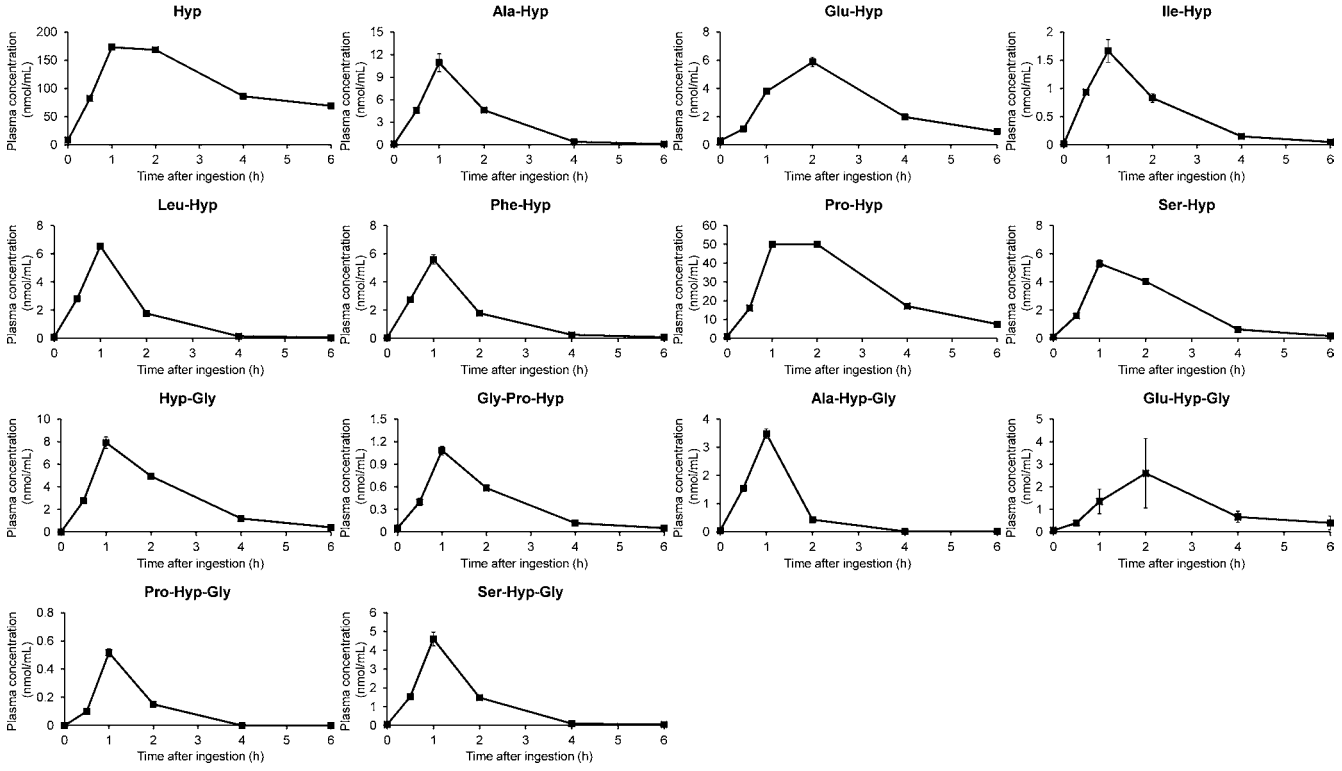


**Figure 3.** Quantification of Hyp and 13 Hyp-containing peptides in human blood after oral ingestion of fish gelatin hydrolysate using SI-digest. SI-digest was first mixed into the human plasma samples and calibration mixtures of 4-Hyp and Hyp-containing peptides. After ethanol precipitation, the supernatants were concentrated using the centrifugal evaporator and subjected to MRM analysis. The plasma concentrations of Hyp and Hyp-containing peptides were calculated using the calibration curves corrected with stable isotope-labeled internal standards of those analytes from SI-digest. The data represent the mean ± SD of three separate measurements on each set of time-course samples from one human subject.

**Table 2. $AUC_{0-6\ h}$ of Hyp and Hyp-Containing Peptides in Human Blood after Oral Ingestion of Fish Gelatin Hydrolysate**

| | $AUC_{0-6\ h}$ (nmol/mL·h) | CV (%) |
|---|---|---|
| Hyp | 668 ± 30 | 4.50 |
| Ala-Hyp | 18.3 ± 0.9 | 5.12 |
| Glu-Hyp | 17.2 ± 0.8 | 4.81 |
| Ile-Hyp | 3.32 ± 0.23 | 6.94 |
| Leu-Hyp | 9.33 ± 0.09 | 1.01 |
| Phe-Hyp | 8.85 ± 0.56 | 6.29 |
| Pro-Hyp | 163 ± 1 | 0.79 |
| Ser-Hyp | 12.3 ± 0.4 | 3.49 |
| Hyp-Gly | 17.5 ± 0.5 | 2.60 |
| Gly-Pro-Hyp | 2.18 ± 0.08 | 3.50 |
| Ala-Hyp-Gly | 4.10 ± 0.22 | 5.29 |
| Glu-Hyp-Gly | 6.86 ± 2.51 | 36.6 |
| Pro-Hyp-Gly | 0.663 ± 0.022 | 3.27 |
| Ser-Hyp-Gly | 6.70 ± 0.37 | 5.46 |

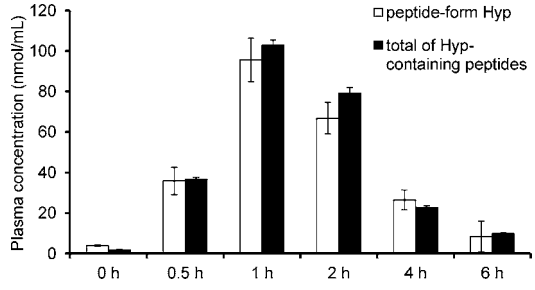


**Figure 4.** Comparison of results obtained with two different approaches using SI-collagen. The data of "peptide-form Hyp" are from Figure 1B, and the data of "total of Hyp-containing peptides" are calculated by integrating the respective values of 13 Hyp-containing peptides from Figure 3. There was no statistically significant difference between "peptide-form Hyp" and "total of Hyp-containing peptides" at each time point, except for 0 h ($p < 0.05$).

containing peptides in the protease digest of SI-collagen (SI-digest) are shown in Table 1. All of the reported Hyp-containing peptides were detected with labeling with stable isotope at Pro and Hyp. The labeling indices were extremely high (>97% for Hyp and all the peptides and >99% for peptides having two labeling sites), which enables highly accurate quantitative analysis. MRM chromatograms of the labeled Hyp and Hyp-containing peptides in the SI-digest are shown in Figure S2 in the Supporting Information. The total of the generated Hyp and Hyp-containing peptides was 10.8% (w/w) of the digested SI-collagen. Considering the Hyp content in collagen (approximately 100 residues/1000 total residues), the digestion procedures appear to efficiently generate the Hyp-containing peptides. Although the abundance of some peptides, such as Hyp-Gly, was relatively low, it was sufficient as an internal standard for LC-MS analysis. We previously confirmed that the linearity and precision of quantification using SI-collagen were excellent, ranging from 1:300 to 30:1 of the internal standard to sample peak area ratio.[29] In the following experiment, SI-digest was mixed into plasma samples appropriately so that all of the heavy to light ratios of respective Hyp-containing peptides fall within the optimum range. SI-digest prepared from SI-collagen from a 3 day culture


dx.doi.org/10.1021/jf5039597 | J. Agric. Food Chem. 2014, 62, 12096−12102

in a 100 mm dish can be used to analyze approximately 100 plasma samples even by conventional LC-MS.

**Quantitative Analysis Using SI-Digest.** To evaluate the usefulness of SI-digest as an internal standard mixture, we reanalyzed the plasma samples measured in Figure 1. The samples were first mixed with SI-digest and subjected to MRM analysis following ethanol deproteinization. As shown in Figure 3, 13 Hyp-containing peptides were detected with a wide range of plasma concentrations after the ingestion of gelatin hydrolysate. The $AUC_{0-6\ h}$ of each Hyp-containing peptide was calculated as ranging from 0.663 ± 0.022 nmol/mL·h for Pro-Hyp-Gly to 163 ± 1 nmol/mL·h for Pro-Hyp (Table 2). The $AUC_{0-6\ h}$ of Pro-Hyp was significantly higher than those of other Hyp-containing peptides, consistent with the previous observations.[3,4,21] To quantify hard-to-detect minor peptides, we concentrated the samples after ethanol precipitation. Although the procedure increases the detection limit of the analytes, it potentially induces increased matrix effects leading to impaired quantitative accuracy. By using SI-digest as the internal standard mixture, we were able to overcome the quantitative limitations and detect previously unreported Hyp-containing peptides (Glu-Hyp, Ser-Hyp, Glu-Hyp-Gly). In addition, high reproducibility of the quantification of respective Hyp-containing peptides was shown by the triplicate measurements with <7% CV (Table 2) except for Glu-Hyp-Gly, the peak intensity of which was near the detection limit.

The estimated values of Hyp-containing peptides were compared between the two different approaches using SI-collagen (Figure 4). The total concentrations of Hyp-containing peptides integrating the respective values from Figure 3 closely matched those of peptide-form Hyp from Figure 1B at each time point, which indicates the high accuracy of the two approaches using the acid hydrolysate or protease digest of SI-collagen. Furthermore, the results can be interpreted as evidence that the 13 di- or tripeptides measured in this study largely account for Hyp-containing peptides appearing in blood after the ingestion of gelation hydrolysate. On the triplicate measurements of peptide-form Hyp, there was a relatively large margin of error. Because the amount of peptide-form Hyp was calculated by subtracting free Hyp from total Hyp, the two-step approach including acid hydrolysis potentially causes quantitative errors. Conversely, the approach using SI-digest showed high reproducibility also for determining the total concentrations of Hyp-containing peptides, probably because of the simple analytical process.

In this study, SI-digest prepared by serial protease digestion of SI-collagen was demonstrated to enable highly accurate and reproducible quantification of Hyp-containing peptides in blood by LC-MS. Thirteen Hyp-containing peptides were able to be simultaneously quantified in human blood after oral ingestion of gelatin hydrolysate using this method. Moreover, we have now additionally detected Leu-Hyp-Gly and Phe-Hyp-Gly in mouse blood (data not shown). Our results in Figure 4 suggested that unidentified major Hyp-containing peptides do not exist at least in the blood analyzed in this study. However, the quantity and structure of Hyp-containing peptides in blood are reported to differ with the animal source of the ingested gelatin hydrolysate.[4] Similarly, we have observed that the quantity and structure also vary with the substrate specificity of the enzyme used to prepare the gelatin hydrolysate (data not shown). Other unidentified Hyp-containing peptides expected to have a beneficial function may still exist in blood and should be suitable targets of our method. In addition, although we have focused on peptides containing Hyp, SI-digest can be also applied to the analysis of other collagen-derived oligopeptides, such as Gly-Pro, which is reported to have an antihypertensive effect.[38]

Over the past decade, many studies have explored functional properties of the oral intake of collagen/gelatin hydrolyzed with enzyme.[39] Tracing the collagen-derived bioactive peptides in the body is important in estimating the effects of the ingestion of gelatin hydrolysate. Our method is useful for quantification of the extent of the absorption and metabolism of orally ingested gelatin hydrolysate and, thus, can facilitate the investigation of biological activity of collagen-derived peptides and the development of functionally characterized gelatin hydrolysate.

## ■ ASSOCIATED CONTENT

### Ⓢ Supporting Information

Figures S1 and S2 and Table S1. This material is available free of charge via the Internet at http://pubs.acs.org.

## ■ AUTHOR INFORMATION

### Corresponding Author

*(Y.T.) Phone: +81-297-71-3046. Fax: +81-297-71-3041. E-mail: y-taga@nippi-inc.co.jp.

### Notes

The authors declare no competing financial interest.

## ■ ABBREVIATIONS USED

Hyp, hydroxyproline; LC-MS, liquid chromatography−mass spectrometry; MRM, multiple reaction monitoring; HEL, human embryonic lung; DPBS, Dulbecco's phosphate-buffered saline; AUC, area under the plasma concentration−time curve; SD, standard deviation; CV, coefficient of variation

## ■ REFERENCES

(1) Berg, R. A.; Prockop, D. J. The thermal transition of a non-hydroxylated form of collagen. Evidence for a role for hydroxyproline in stabilizing the triple-helix of collagen. *Biochem. Biophys. Res. Commun.* **1973**, *52*, 115−120.

(2) Prockop, D. J.; Keiser, H. R.; Sjoerdsma, A. Gastrointestinal absorption and renal excretion of hydroxyproline peptides. *Lancet* **1962**, *2*, 527−528.

(3) Iwai, K.; Hasegawa, T.; Taguchi, Y.; Morimatsu, F.; Sato, K.; Nakamura, Y.; Higashi, A.; Kido, Y.; Nakabo, Y.; Ohtsuki, K. Identification of food-derived collagen peptides in human blood after oral ingestion of gelatin hydrolysates. *J. Agric. Food Chem.* **2005**, *53*, 6531−6536.

(4) Ohara, H.; Matsumoto, H.; Ito, K.; Iwai, K.; Sato, K. Comparison of quantity and structures of hydroxyproline-containing peptides in human blood after oral ingestion of gelatin hydrolysates from different sources. *J. Agric. Food Chem.* **2007**, *55*, 1532−1535.

(5) Shigemura, Y.; Akaba, S.; Kawashima, E.; Park, E. Y.; Nakamura, Y.; Sato, K. Identification of a novel food-derived collagen peptide, hydroxyprolyl-glycine, in human peripheral blood by pre-column derivatisation with phenyl isothiocyanate. *Food Chem.* **2011**, *129*, 1019−1024.

(6) Shigemura, Y.; Iwai, K.; Morimatsu, F.; Iwamoto, T.; Mori, T.; Oda, C.; Taira, T.; Park, E. Y.; Nakamura, Y.; Sato, K. Effect of prolyl-hydroxyproline (Pro-Hyp), a food-derived collagen peptide in human blood, on growth of fibroblasts from mouse skin. *J. Agric. Food Chem.* **2009**, *57*, 444−449.

(7) Nakatani, S.; Mano, H.; Sampei, C.; Shimizu, J.; Wada, M. Chondroprotective effect of the bioactive peptide prolyl-hydroxyproline in mouse articular cartilage in vitro and in vivo. *Osteoarthritis Cartilage* **2009**, *17*, 1620−1627.

(8) Ohara, H.; Ichikawa, S.; Matsumoto, H.; Akiyama, M.; Fujimoto, N.; Kobayashi, T.; Tajima, S. Collagen-derived dipeptide, proline-hydroxyproline, stimulates cell proliferation and hyaluronic acid synthesis in cultured human dermal fibroblasts. *J. Dermatol.* **2010**, *37*, 330−338.
(9) Minaguchi, J.; Tometsuka, C.; Koyama, Y.; Kusubata, M.; Nagayasu, A.; Sawaya, S.; Shiga, T.; Shima, H.; Hara, T.; Takehana, K. Effects of collagen-derived oligopeptide prolylhydroxyproline on differentiation of mouse 3T3-L1 preadipocytes. *Food Sci. Technol. Res.* **2012**, *18*, 593−599.
(10) Murad, S.; Grove, D.; Lindberg, K. A.; Reynolds, G.; Sivarajah, A.; Pinnell, S. R. Regulation of collagen synthesis by ascorbic acid. *Proc. Natl. Acad. Sci. U.S.A.* **1981**, *78*, 2879−2882.
(11) Shigemura, Y.; Kubomura, D.; Sato, Y.; Sato, K. Dose-dependent changes in the levels of free and peptide forms of hydroxyproline in human plasma after collagen hydrolysate ingestion. *Food Chem.* **2014**, *159*, 328−332.
(12) Aito-Inoue, M.; Ohtsuki, K.; Nakamura, Y.; Park, E. Y.; Iwai, K.; Morimatsu, F.; Sato, K. Improvement in isolation and identification of food-derived peptides in human plasma based on precolumn derivatization of peptides with phenyl isothiocyanate. *J. Agric. Food Chem.* **2006**, *54*, 5261−5266.
(13) Langrock, T.; Czihal, P.; Hoffmann, R. Amino acid analysis by hydrophilic interaction chromatography coupled on-line to electrospray ionization mass spectrometry. *Amino Acids* **2006**, *30*, 291−297.
(14) Pataridis, S.; Eckhardt, A.; Mikulikova, K.; Sedlakova, P.; Miksik, I. Identification of collagen types in tissues using HPLC-MS/MS. *J. Sep Sci.* **2008**, *31*, 3483−3488.
(15) Weis, M. A.; Hudson, D. M.; Kim, L.; Scott, M.; Wu, J. J.; Eyre, D. R. Location of 3-hydroxyproline residues in collagen types I, II, III, and V/XI implies a role in fibril supramolecular assembly. *J. Biol. Chem.* **2010**, *285*, 2580−2590.
(16) Ishikawa, Y.; Vranka, J. A.; Boudko, S. P.; Pokidysheva, E.; Mizuno, K.; Zientek, K.; Keene, D. R.; Rashmir-Raven, A. M.; Nagata, K.; Winand, N. J.; Bachinger, H. P. Mutation in cyclophilin B that causes hyperelastosis cutis in American Quarter Horse does not affect peptidylprolyl cis-trans isomerase activity but shows altered cyclophilin B-protein interactions and affects collagen folding. *J. Biol. Chem.* **2012**, *287*, 22253−22265.
(17) Sricholpech, M.; Perdivara, I.; Yokoyama, M.; Nagaoka, H.; Terajima, M.; Tomer, K. B.; Yamauchi, M. Lysyl hydroxylase 3-mediated glucosylation in type I collagen: molecular loci and biological significance. *J. Biol. Chem.* **2012**, *287*, 22998−23009.
(18) Taga, Y.; Kusubata, M.; Ogawa-Goto, K.; Hattori, S., Development of a novel method for analyzing collagen O-glycosylations by hydrazide chemistry. *Mol. Cell Proteomics* **2012**, *11*, M111.010397.
(19) Taga, Y.; Kusubata, M.; Ogawa-Goto, K.; Hattori, S. Site-specific quantitative analysis of overglycosylation of collagen in osteogenesis imperfecta using hydrazide chemistry and SILAC. *J. Proteome Res.* **2013**, *12*, 2225−2232.
(20) Lange, V.; Picotti, P.; Domon, B.; Aebersold, R. Selected reaction monitoring for quantitative proteomics: a tutorial. *Mol. Syst. Biol.* **2008**, *4*, 222.
(21) Ichikawa, S.; Morifuji, M.; Ohara, H.; Matsumoto, H.; Takeuchi, Y.; Sato, K. Hydroxyproline-containing dipeptides and tripeptides quantified at high concentration in human blood after oral administration of gelatin hydrolysate. *Int. J. Food Sci. Nutr* **2010**, *61*, 52−60.
(22) Matuszewski, B. K.; Constanzer, M. L.; Chavez-Eng, C. M. Matrix effect in quantitative LC/MS/MS analyses of biological fluids: a method for determination of finasteride in human plasma at picogram per milliliter concentrations. *Anal. Chem.* **1998**, *70*, 882−889.
(23) Dams, R.; Huestis, M. A.; Lambert, W. E.; Murphy, C. M. Matrix effect in bio-analysis of illicit drugs with LC-MS/MS: influence of ionization type, sample preparation, and biofluid. *J. Am. Soc. Mass Spectrom.* **2003**, *14*, 1290−1294.
(24) Stokvis, E.; Rosing, H.; Lopez-Lazaro, L.; Schellens, J. H.; Beijnen, J. H. Switching from an analogous to a stable isotopically labeled internal standard for the LC-MS/MS quantitation of the novel anticancer drug Kahalalide F significantly improves assay performance. *Biomed. Chromatogr.* **2004**, *18*, 400−402.
(25) van Platerink, C. J.; Janssen, H. G.; Horsten, R.; Haverkamp, J. Quantification of ACE inhibiting peptides in human plasma using high performance liquid chromatography-mass spectrometry. *J. Chromatogr., B Anal. Technol. Biomed. Life Sci.* **2006**, *830*, 151−157.
(26) Fonteh, A. N.; Harrington, R. J.; Harrington, M. G. Quantification of free amino acids and dipeptides using isotope dilution liquid chromatography and electrospray ionization tandem mass spectrometry. *Amino Acids* **2007**, *32*, 203−212.
(27) Mesmin, C.; Dubois, M.; Becher, F.; Fenaille, F.; Ezan, E. Liquid chromatography/tandem mass spectrometry assay for the absolute quantification of the expected circulating apelin peptides in human plasma. *Rapid Commun. Mass Spectrom.* **2010**, *24*, 2875−2884.
(28) Inoue, K.; Ikemura, A.; Tsuruta, Y.; Tsutsumiuchi, K.; Hino, T.; Oka, H. On-line solid-phase extraction LC-MS/MS for the determination of Ac-SDKP peptide in human plasma from hemodialysis patients. *Biomed. Chromatogr.* **2012**, *26*, 137−141.
(29) Taga, Y.; Kusubata, M.; Ogawa-Goto, K.; Hattori, S. Stable isotope-labeled collagen: a novel and versatile tool for quantitative collagen analyses using mass spectrometry. *J. Proteome Res.* **2014**, *13*, 3671−368.
(30) Mendis, E.; Rajapakse, N.; Kim, S. K. Antioxidant properties of a radical-scavenging peptide purified from enzymatically prepared fish skin gelatin hydrolysate. *J. Agric. Food Chem.* **2005**, *53*, 581−587.
(31) Li-Chan, E. C.; Hunag, S. L.; Jao, C. L.; Ho, K. P.; Hsu, K. C. Peptides derived from atlantic salmon skin gelatin as dipeptidyl-peptidase IV inhibitors. *J. Agric. Food Chem.* **2012**, *60*, 973−978.
(32) Fujita, A.; Kawakita, H.; Saito, K.; Sugita, K.; Tamada, M.; Sugo, T. Production of tripeptide from gelatin using collagenase-immobilized porous hollow-fiber membrane. *Biotechnol. Prog.* **2003**, *19*, 1365−1367.
(33) Aito-Inoue, M.; Lackeyram, D.; Fan, M. Z.; Sato, K.; Mine, Y. Transport of a tripeptide, Gly-Pro-Hyp, across the porcine intestinal brush-border membrane. *J. Pept. Sci.* **2007**, *13*, 468−474.
(34) Watanabe-Kamiyama, M.; Shimizu, M.; Kamiyama, S.; Taguchi, Y.; Sone, H.; Morimatsu, F.; Shirakawa, H.; Furukawa, Y.; Komai, M. Absorption and effectiveness of orally administered low molecular weight collagen hydrolysate in rats. *J. Agric. Food Chem.* **2010**, *58*, 835−8341.
(35) Granelli-Piperno, A.; Reich, E. A study of proteases and protease-inhibitor complexes in biological fluids. *J. Exp. Med.* **1978**, *148*, 223−234.
(36) Rodriguez, J.; Gupta, N.; Smith, R. D.; Pevzner, P. A. Does trypsin cut before proline? *J. Proteome Res.* **2008**, *7*, 300−305.
(37) Yang, C.; Park, A. C.; Davis, N. A.; Russell, J. D.; Kim, B.; Brand, D. D.; Lawrence, M. J.; Ge, Y.; Westphall, M. S.; Coon, J. J.; Greenspan, D. S. Comprehensive mass spectrometric mapping of the hydroxylated amino acid residues of the $\alpha$1(V) collagen chain. *J. Biol. Chem.* **2012**, *287*, 40598−40610.
(38) Ichimura, T.; Yamanaka, A.; Otsuka, T.; Yamashita, E.; Maruyama, S. Antihypertensive effect of enzymatic hydrolysate of collagen and Gly-Pro in spontaneously hypertensive rats. *Biosci., Biotechnol., Biochem.* **2009**, *73*, 2317−2319.
(39) Gómez-Guillén, M. C.; Giménez, B.; López-Caballero, M. E.; Montero, M. P. Functional and bioactive properties of collagen and gelatin from alternative sources: a review. *Food Hydrocolloids* **2011**, *25*, 1813−1827.

There are two types of leaf extracts: full extracts and standardized extracts. The full extracts are usually prepared with alcohol and thus contain all constituents soluble in alcohol. The standardized extracts constitute the major commercial ginkgo products and contain 6% TTLs, 24% flavonol glycosides, and trace amount of ginkgolic acid. Such extracts are prepared in a multistep process, in which some compounds are enriched (TTLs and flavonoids) while others (biflavones and ginkgolic acids) are removed. Because of the significant risk factors of the ginkgolic acids, the content of these undesirable components in standardized extracts of *G. biloba* are currently limited to <5 ppm in the European and U.S. pharmacopoeia.[17,18]

Thus, it is desirable to have a simple, sensitive, validated analytical method for the detection and quantification of each of the alkylphenols in commercial products, such as herbal medicines and dietary supplements. Numerous analytical techniques have previously been proposed for the analysis of GAs including HPLC, GC, HPTLC, ELISA, and NMR. Comprehensive reviews of the chemical analysis (including alkylphenols) of *G. biloba* leaves, extracts, and phytopharmaceuticals by van Beek critiqued the various analytical approaches for GAs up through 2009.[3,19] The major challenges for the analysis of GAs are (i) the low concentrations (<5 ppm) imposed by regulation for standardized extracts, (ii) the complex matrix of *G. biloba* plant samples and dietary supplements, (iii) the difficulties of obtaining pure, authentic standards for identification and quantification purposes, and (iv) the rigorous resolution requirements for the analysis of double bond positional isomers of the alkylphenols. Often only the total concentration of all GAs in a given sample is determined; however, the exact roles of the various isomeric GAs in the pharmacological effects of *G. biloba* have never been determined. Thus, any attempt to correlate a given pharmacological effect with a specific GA isomer will require an analytical method that allows the quantitation of all GA isomers.

Liquid chromatography is currently the analytical method of choice for GAs.[20] The major problem with HPLC techniques is the inadequate resolution of GAs differing by carbon number and unsaturation, such as C13:0 and C15:1 or C15:0 and C17:1, as well as the inability to resolve double bond positional isomers. Lee et al.[21] used column switching (heart cutting) to minimize matrix effects and improve resolution. The method was validated, and the LOD and LOQ for the C15:1 and C17:1 GAs were 10 and 40 ppb with a diode array detector. Negative mode ESI/MS/MS was used for identification of the GAs. Udrescu et al.[22,23] developed an RPLC/UV method that avoided the time-consuming solvent evaporation step involved in most HPLC analysis methods for GAs. The method involved an acidified methanol/water extraction followed by LLE with hexane (20:1) for one standardized extract of *G. biloba*. A large volume (50 $\mu$L) of the hexane was injected into the RPLC column with a very steep gradient. The method was validated, and the LOQ for GAs was 1 ppm. Again, the GAs were confirmed by $MS^2$ methods, and collision-induced fragmentation schemes were presented. Gawron-Gzella et al.[24] used HPLC to analyze several pharmaceuticals and dietary supplements for GAs. The total concentrations of GAs ranged from 2 to 8000 ppm.

Gas−liquid chromatography has been used for GAs analysis; however, these methods suffer from the need for derivatization of the alkylphenols. Wang et al.[25,26] introduced a chemothermolysis with trimethylsulfonium hydroxide or tetramethylammonium hydroxide injection system to avoid the pretreatment schemes required for other chromatographic methods. This method was used to resolve seven GAs and three cardanols including C13:0, C15:0 as well as double bond positional isomers C15:1 Δ8 and Δ10, C17:1 Δ8 and Δ12 along with one GA with two unsaturation sites, viz., C17:2. No C17:0 or C17:1 Δ10 isomers were detected. Possible reaction schemes for the electron impact fragmentation of the methylated GAs were discussed. In earlier work, Schotz[16] developed a GC/MS method for the analysis of the silyl derivatives of a standardized extract EGb 761. Five GAs, viz., C13:0, C15:0, C15:1 (Δ8 and Δ10), and C17:1 (Δ12), were identified.

In 2004, Choi et al.[27] reported an NMR method for the analysis of GAs. This spectroscopic method did not require derivatization of the GAs or calibration standards. The peaks associated with the aromatic protons in GAs were individually integrated to give the total GA concentration rather than individual components. This method, however, was not sufficiently sensitive and suffered interference problems when applied for the analysis of commercial samples.

Very recently, van Beek's group addressed the problem of the lack of pure standards of ginkgolic acids.[28] Magnetic nanoparticles were used to selectively adsorb GAs from petroleum ether extracts of ginkgo leaves. The mixed acids were subsequently desorbed with strong acid or base and isolated by prep-scale LC on a $C_8$ column. Significant quantities of eight GAs were isolated by this novel procedure.

The objectives of the present study were to develop and validate a high-resolution gas chromatographic method for the analysis of the individual isomers of C13, C15, and C17 GAs in ginkgo leaves, extracts, and commercial products. In addition, the double bond position and the concentration of each isomer will be determined. This information may improve our understanding of the GA isomer distribution in various plant parts. The accuracy of the GC method will be assessed by comparison with the accepted HPLC methods. Additionally, the veracity of the extracts in dietary supplements will be established by detection of the marker compounds for *G. biloba,* TTLs and flavonol glycosides, by UHPLC/MS analysis.

## MATERIALS AND METHODS

**Sample Information.** A total of 19 plant samples and reference standards including leaves, seeds, leaf extracts, and sarcotesta, and 21 commercial herbal dietary supplements containing extracts of *G. biloba* leaves were analyzed. The dietary supplement samples were purchased at food supermarkets, local retail pharmacies, or online resources. The detailed information for the plant samples and herbal dietary supplements are given in Tables 1 and 2, respectively. Specimens of all samples are deposited at the botanical repository of the National Center for Natural Products Research (NCNPR), University of Mississippi (documented with NCNPR accession code).

**Reagents and Standards.** Four ginkgolic acid standards, viz., C13:0, C15:0, C15:1, and C17:1, as well as the internal standard anthracene were purchased from Sigma-Aldrich (St. Louis, MO). HPLC grade methanol and methylene chloride were purchased from Fisher Scientific (Pittsburgh, PA). GC grade *n*-hexane, formic acid, and the derivatization reagent trimethylsulfonium hydroxide solution (~0.25 M in methanol, for GC derivatization) were obtained from Sigma-Aldrich.

**Sample Preparation.** The plant materials and the dietary supplements were ground and homogenized to obtain a uniform matrix. The dietary supplements were in the form of capsules or tablets. Ten capsules or tablets were weighed for each sample, and the average was taken for the weight of each capsule or tablet of the sample. About 500 mg of plant sample or equivalent amount for the dietary

**Table 1. *Ginkgo biloba* Plant Materials**

| accession code | parts | samples[a] | form |
|---|---|---|---|
| 580 | leaves | A | whole |
| 1095 | leaves | A | powder |
| 2837 | leaves | A | whole |
| 2909 | leaves | A | cut and shifted |
| 8551 | leaves | A | powder |
| 9245 | leaves | A | whole |
| 15212 | leaves | A | powder |
| 16746 | leaves | A | powder |
| 628 | seeds | A | whole |
| 3539 | seeds | C | powder |
| 9604 | seeds | A | whole |
| 9605 | seeds | A | whole |
| 9606 | seeds | A | whole |
| 6049 | seeds | A | pieces |
| 2892 | leaf extracts | C | powder |
| 9335 | leaf extracts | C | powder |
| 16747 | leaf extracts | B | solid |
| 16748 | leaf extracts | B | powder |
| 11637 | sarcotesta | A | whole |

[a]A: authenticated samples. B: botanical reference materials from NIST and ChromaDex. C: commercial samples.

supplement sample was sonicated and centrifuged three times with ca. 15 mL of a 1:1 mixture of methanol and 10% formic acid. The combined supernatant layers were extracted three times with *n*-hexane. The *n*-hexane was evaporated to dryness, and the residue was then dissolved in 250 μL of methylene chloride and 150 μL of methanol. Fifty microliters of internal standard (25.64 μg/mL) and 50 μL of trimethylsulfonium hydroxide were added to the solution. Duplicate samples were extracted, and two injections were made for each sample. The content of each ginkgolic acid was reported as a mean value of the test results.

**Chromatography Instruments and Conditions.** *GC/MS Analysis.* Gas chromatographic analysis was performed on an Agilent 7890 GC instrument equipped with an Agilent 7693 autosampler (Santa Clara, CA). A fused silica capillary column (30 m, 0.25 mm i.d.) coated with a 0.20 μm film of cross-linked (88% cyanopropyl) aryl-polysiloxane (J&W HP-88, Santa Clara, CA) was used with helium as the carrier gas at a flow rate of 1 mL/min. In a typical analysis, the oven was held for 2 min at 150 °C, then programmed at 8 °C/min to 220 °C and 3 °C/min to 250 °C, and held for 2 min. The injector temperature was kept at 260 °C. The split ratio was set to 25:1.

Mass spectrometric analysis was carried out with an Agilent 5975C mass specific detector. The instrument was operated to collect scan and selected ion monitor (SIM) data sequentially within a given run. For the scan measurements, the spectra were recorded at 70 eV from $m/z$ 40 to 500. The ions of $m/z$ 161 and $m/z$ 178 were selected in the SIM mode to monitor GAs and internal standard, respectively. Compound identification involved comparison of the spectra with the databases (Wiley and NIST) using a probability-based matching algorithm. Further identification was based on the relative retention indices (RI) compared with literature and the standard references isolated in-house or purchased from commercial sources.

The method was validated in terms of selectivity, linearity, limits of detection and quantitation, as well as intra- and interday precision and accuracy.

**Table 2. Information of Herbal Dietary Supplements Containing Extracts of *Ginkgo biloba* Leaves Provided by the Manufacture Labels**

| accession code | form | extract form | amount of extract/(capsule/tablet, mg) | average content (mg) | daily serving size | preparation in addition to *Ginkgo biloba* leaf extracts |
|---|---|---|---|---|---|---|
| 15713 | tablets | standardized extract | 60 | 308.4 | 2 | cellulose, dicalcium phosphate, croscarmellose, silica, natural palm leaf glaze, vegetable magnesium stearate, and vegetable stearic acid |
| 15714 | capsules | standardized extract (50:1 leaf) | 120 | 450.5 | 1 | modified cellulose, dicalcium phosphate dehydrate, stearic acid, magnesium stearate, croscarmellose sodium, and color coat ingredients |
| 15907 | capsules | standardized extract | 120 | 138.6 | 2 | hydroxypropylmethylcellulose, and microcrystalline cellulose |
| 15908 | capsules | standardized extract | 120 | 364.9 | 1 | rice flour, gelatin, vegetable magnesium stearate, and silica |
| 15909 | tablets | standardized extract | 60 | 315.3 | 2 | cellulose, dicalcium phosohate, silica, vegetable magnesium stearate, and vegetable stearic acid |
| 15910 | capsules | standardized extract (50:1 leaf extract) | 120 | 542.8 | 1 | rice powder, gelatin capsule, vegetable magnesium, stearate and silica |
| 15911 | capsules | leaf extract | 120 | 602.3 | 1 | rice flour, gelatin, water, and magnesium stearate |
| 15912 | capsules | standardized extract | 60 | 395.1 | 2−4 | plant-derived capsule |
| 15913 | capsules | leaves | 500 | 424.9 | 1 | magnesium stearate and gelatin |
| 15914 | capsules | leaf extract | 120 | 435.6 | 1 | modified cellulose, cellulose, and silicon dioxide |
| 15915 | capsules | standardized extract | 30 | 397.8 | 6 | cellulose gel, gelatin, stearic acid, and water |
| 15916 | capsules | standardized extract | 60 | 276.3 | 2 | microcrystalline cellulose and gelatin |
| 15917 | capsules | standardized extract | 120 | 333.1 | 1 | gluten-free rice concentrate (non-GMO) and vegetarian capsule (non-GMO plant cellulose) |
| 15918 | capsules | certified extract | 120 | 199.2 | 1 | microcrystalline cellulose, vegetable cellulose, and vegetable stearate |
| 15919 | capsules | extract | 60 | 334.3 | 1−2 | rice flour and vegetarian capsule |
| 15920 | capsules | standardized extract (50:1 leaf extract) | 120 | 293.6 | 1 | cellulose, magnesium stearate, and silicon dioxide |
| 15921 | capsules | standardized extract (50:1 concentrate) | 120 | 471.3 | 2 | rice bran, oat fiber, vegetable cellulose, silicon dioxide, magnesium silicate, and magnesium stearate |
| 15922 | capsules | leaf extract | 60 | 442.5 | 2−4 | hpmc (veggie capsule, microcrystalline cellulose, silica, and magnesium stearate |
| 15923 | tablets | standardized extract | 60 | 353.6 | 2−4 | cellulose, starch, modified cellulose, modified cellulose gum, magnesium stearate, silica, titanium dioxide, stearic acid, caramel, and wax |
| 15924 | capsules | standardized extract | 120 | 337.9 | 1 | gelatin, cellulose, stearic acid, and magnesium stearate |
| 15925 | tablets | leaf extract | 120 | 303.5 | 1 | sorbital, stearic acid, and silica |

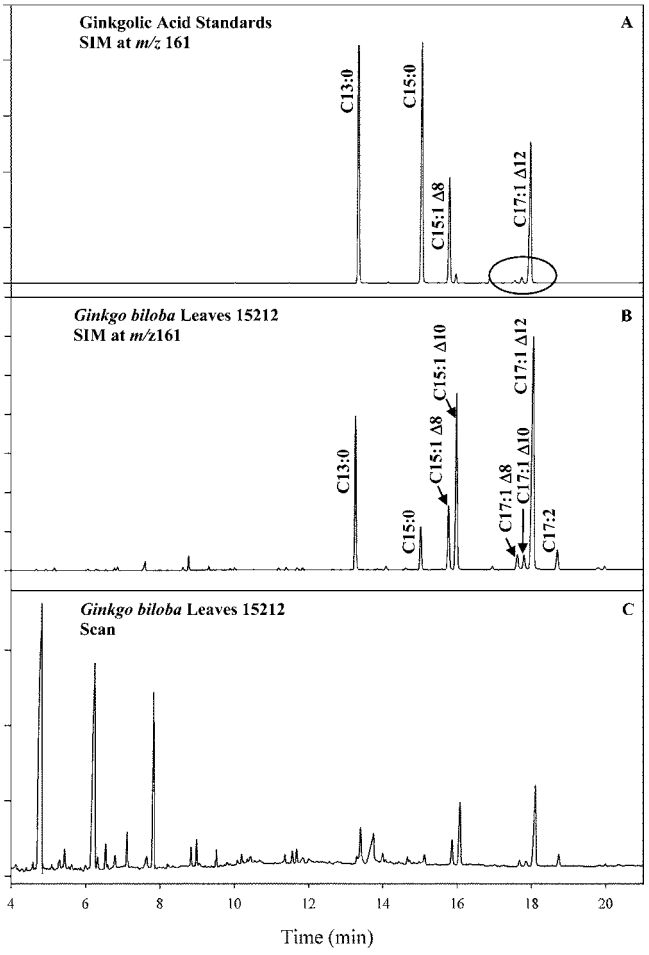


**Figure 2.** SIM and scan GC/MS chromatograms of GA standards and sample 15212 (*Ginkgo biloba* leaves).

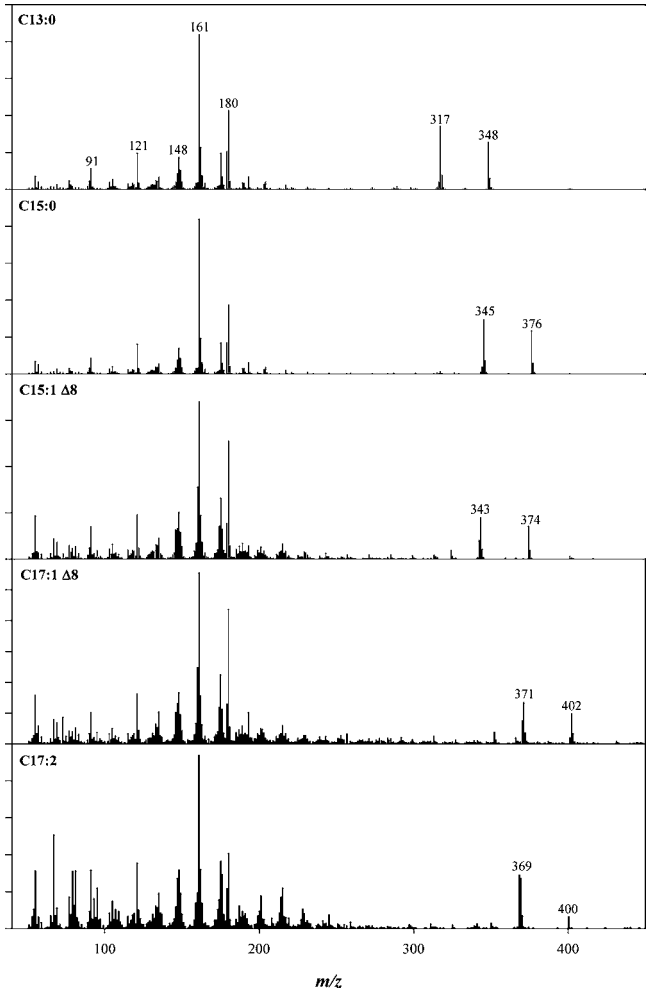


**Figure 3.** EI-MS spectra of the Ginkgolic acids.

*Validation of GC/MS Method with Standard HPLC Technique.* The HPLC system consisted of an Agilent 1290 Infinity series HPLC with a diode array detector, ALS, and thermostated column compartment (Santa Clara, CA). The LC instrument was coupled to an Agilent 6120 quadrupole mass spectrometer with an ESI interface. The column was an Agilent Rapid Resolution Zorbax SB-C8 (2.1 × 100 mm, 1.8 $\mu$m, Santa Clara, CA). The column temperature was 30 °C. The flow rate was 0.4 mL/min. The eluent was 50% acetonitrile (0.1% formic acid) programmed to 100% acetonitrile in 20 min. The ESI was scanned in a mass range from 100 to 500 amu. The fragmentor was set at 120 V; capillary voltage was 3000 V. The SIM was operated to monitor $[M - H]^-$ 319, 347, 345, and 373 for GA C13:0, C15:0, C15:1, and C17:1, respectively. The diode array detector was set to 310 nm.

*UHPLC–MS Analysis of Ginkgo Products.* A published UHPLC-MS method[29] was used for the simultaneous analysis of sesquiterpene lactones and flavonoids from various ginkgo products to confirm the presence of *G. biloba* leaf extracts in the botanical dietary supplements. This method involved the use of $[M + H]^+$ ions of five sesquiterpene lactones and three flavonoids which were observed at $m/z$ 425.2 (ginkgolide J, ginkgolide B), $m/z$ 441.2 (ginkgolide C), $m/z$ 327.3 (bilobalide), $m/z$ 409.2 (ginkgolide A), $m/z$ 303.1 (quercetin), $m/z$ 287.1 (kaempferol), and $m/z$ 317.1 (isorhamnetin). The compound identification was based on retention times and MS in comparison with standard compounds.

**Ozonolysis.** The double bond positions in the C15:1 and C17:1 standards were determined by standard ozonolysis procedures. Each individual C15:1 and C17:1 standard (1.0 mg/mL) was derivatized as described in the sample preparation section. The standard solution was dried. The residue was dissolved in 0.5 mL of methylene chloride. Ozone used for the reaction was generated using a Triozone generator and bubbled through the solution at −78 °C until a blue color was observed indicating ozone saturation. The reaction mixture was stirred for 4 h and then quenched by addition of dimethyl sulfide (200 $\mu$L). The solution allowed to warm to room temperature before analyzed by GC/MS using the method described previously.

## RESULTS AND DISCUSSION

**GC/MS Method Development and Validation.** The selected ion chromatograms (SIC) at $m/z$ 161 for a mixture of four GAs standards (A) and the plant sample 15212 (ginkgo leaves) (B), as well as the total ion chromatogram for the 15212 sample (scan from 40 to 500 amu) (C), are shown in Figure 2. The component pairs that proved difficult to resolve by HPLC, viz., C13:0/C15:1 and C15:0/C17:1, were clearly resolved. The electron impact spectra of eight analyzed GAs are shown in Figure 3. The fragment ions from the salicylic acid moieties ($m/z$ 180, 161, 148, 121, and 91) are identical for all of the ginkgolic acids. The fragment ion at $m/z$ 161 was chosen for selective ion monitoring because it (i) is generally the base peak in the mass spectrum, (ii) is common to all ginkgolic acid components, and (iii) serves as a very sensitive and specific SIM probe ion for all GAs. Possible fragmentation mechanisms different from previous literature[16,26] are given in Figure 4.

A full method validation was performed according to the ICH guidelines[30] by evaluating selectivity, linearity, limits of detection and quantitation, and intra- and interday precision and accuracy.

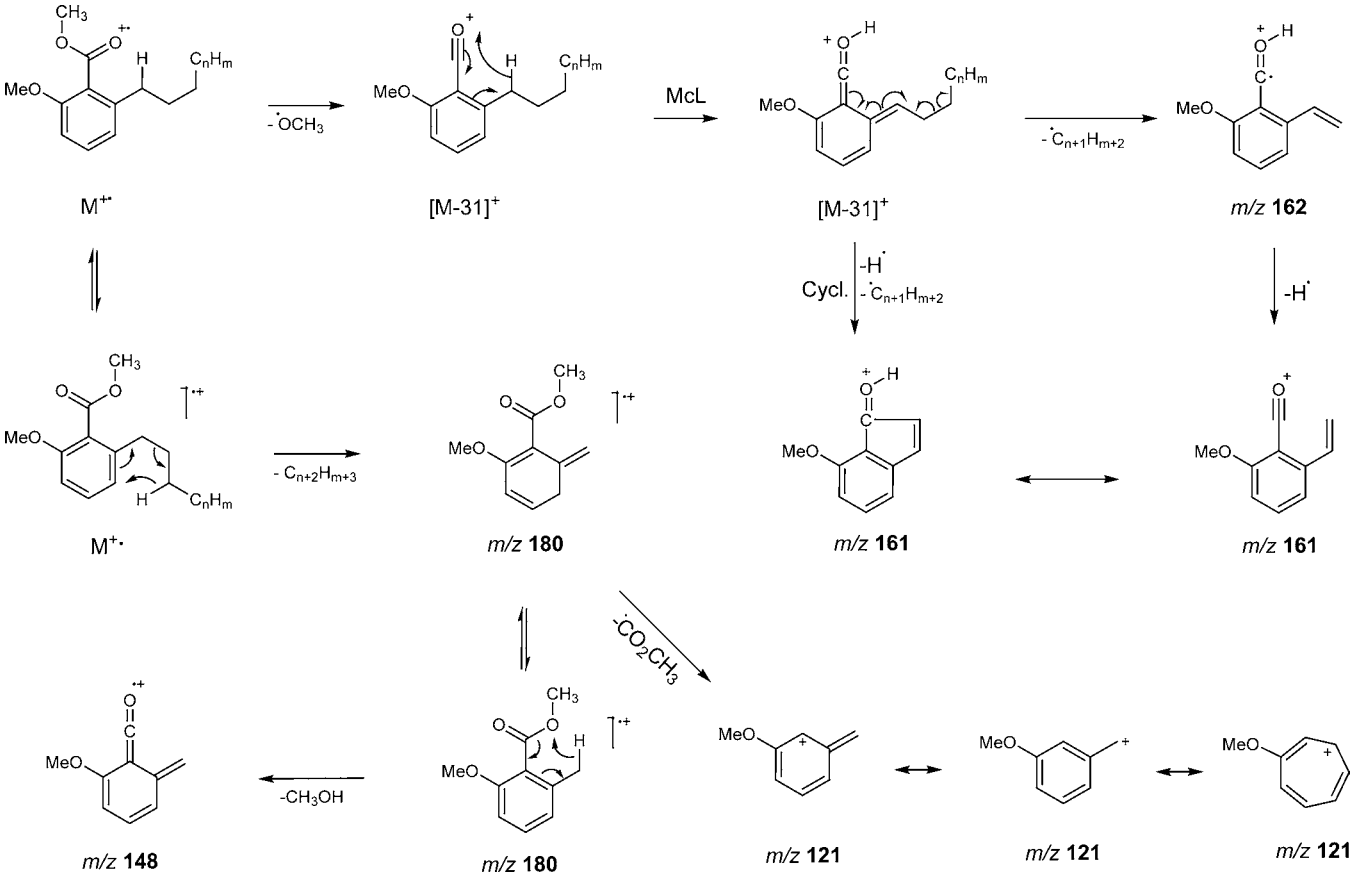


**Figure 4.** Possible EI-MS fragmentation patterns for GAs ($m = 2n + 1$ for C13:0 and C15:1 GAs. $m = 2n$ for C15:1 and C17:1 GAs). McL: McLafferty rearrangement. Cycl: Cyclization.

*Selectivity.* The quantitation analyses were carried out in selected ion monitor mode at $m/z$ 161 for all the GAs. No other components or contaminants were detected at this $m/z$ for the retention time window available for the GAs.

*Accuracy.* The accuracy of the method was determined by spiking ginkgo leaf sample (1095) with a known amount of GA standards. The plant sample was exhaustively extracted six times by following the extraction method described in the experiment section. The sample was dried and then spiked with 40.0 μg/mL C13:0, C15:1, C17:1 and 45.6 μg/mL C15:0 GA standard solutions. The samples were then extracted, derivatized with TMSH, and analyzed under optimized conditions. The percentage recoveries were determined to be 87.7%, 89.5%, 95.4%, and 89.2% for C13:0, C15:0, C15:1, and C17:1, respectively.

*Linearity.* The calibration plots were linear over the range of 5−250 μg/mL with correlation coefficients of >0.99.

*Precision.* The relative standard deviation for triplicate intraday analyses was 1.3−2.1%. The interday variation for nine analyses was 3.8%.

*Limit of Detection (LOD) and Limit of Quantification (LOQ).* The LOD was determined from the signal-to-noise ratio of 3:1 to be 0.5 μg/mL. The LOQ was determined to be 1.5 μg/mL for all of the GAs.

**Localization of the Double Bond in GA Standards.** To date, the exact roles of the various isomeric GAs in the pharmacological effects of *G. biloba* have never been determined. Thus, localization of the double bond position of ginkgolic acids in *G. biloba* is crucial for the determination of biochemical properties, as well as important in structure elucidation of the GA isomers. However, common instrument-based methods cannot elucidate the double bond position and especially clarify the ambiguity of the double bond position for C17:1 GA. To improve our understanding of the GA isomer distribution in various plant parts, ozonolysis of both the C15:1 and C17:1 standards was performed. The reaction products were examined by the same GC/MS method used to analyze the ginkgolic acid samples. All of the reaction products were esters with labile methoxy groups. The electron impact mass spectra of the GAs never contained a molecular ion peak; however, the M-31 peak was prominent in all of the product spectra. Figure 5 illustrates the possible structures of the GAs and the ozonolysis products for the C15:1 and C17:1 standards. The C15:1 standard **3** clearly showed mass peaks corresponding to the loss of methoxy for products **3a**−**c**. The aliphatic ester **3a** resulted from the degradation of the electron-rich aromatic ring of the GAs under the experimental ozonoylsis conditions. Compound **3b** represents a decarboxylated product of **3a**. This confirmed the label claim that the C15:1 standard was Δ8. The results for the C17:1 standard **4**, on the other hand, showed M-31 peaks in the EI spectra for products **4a**−**c**, i.e., the products expected for the C17:1 Δ12 isomer, not the Δ10 positional isomer. The chromatographic results implied that the double bond in C17:1 standard was Δ12 rather than Δ10 as indicated by the CAS number given on the container label.

In addition to the pentanoic acid methyl ester shown in Figure 5, the C17:1 standard also produced heptanoic and nonanoic acid methyl esters as shown in Figure 6. The relative


dx.doi.org/10.1021/jf503980f | J. Agric. Food Chem. 2014, 62, 12103−12111

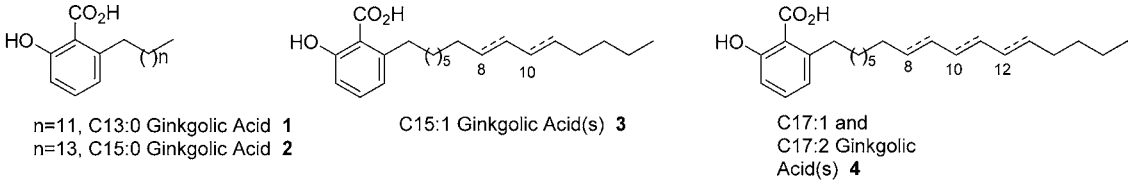


Ozonolysis of Ginkgolic Acids:

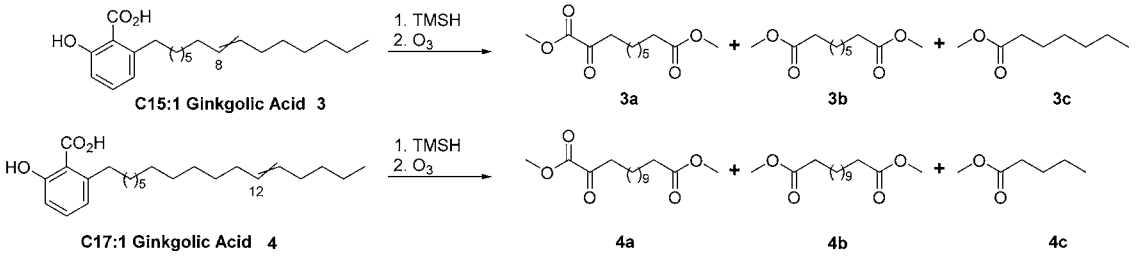


**Figure 5.** Structures of the ginkgolic acids and ozonolysis products for the C15:1 and C17:1 standards.

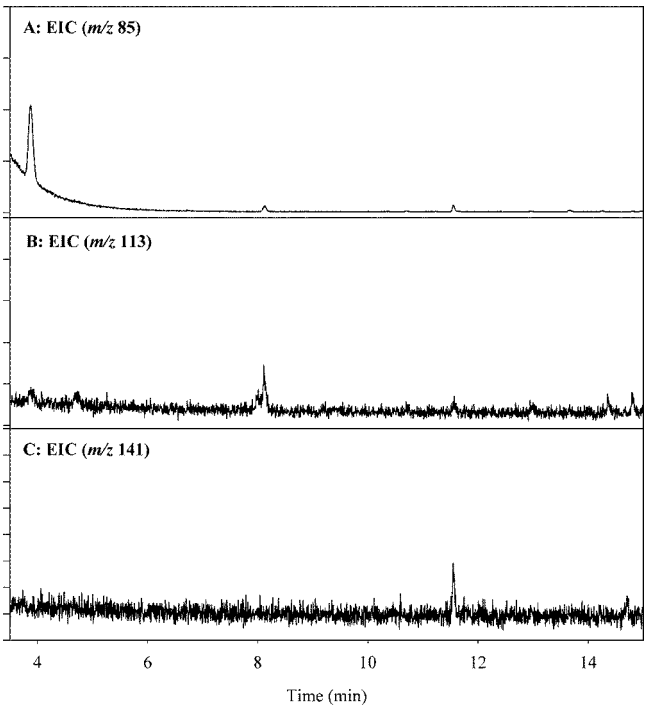


**Figure 6.** Extracted ion chromatograms [M − 31] for the ozonolysis products of the C17:1 standard. A: Pentanoic acid methyl ester. B: Heptanoic acid methyl ester. C: Nonanoic acid methyl ester.

abundance of the three esters agrees with the relative peak areas for the C17:1 isomers circled in Figure 2. Thus, the C17:1 standard was a mixture of isomers with the C17:1 Δ12 isomer accounting for more than 90% of the material. Therefore, in the analyses of plant and dietary supplements, it was assumed that the standard C17:1 contained a double bond at the C12 position (C17:1 Δ12).

**Analysis of Ginkgo Plant Samples.** The plant extracts were complex as shown in Figures 2 B and C. The major peaks with retention times less than 10 min represented methyl esters of saturated fatty acid, viz., palmitic and stearic, as well as unsaturated fatty acids, such as linolenic and linoleic. The compound eluting at ca. 13.8 min was an alkylmethyl ether of unknown structure. Another compound often detected in the plant samples was α-tocopherol with a retention time of 14 min and an $m/z$ of 444 amu. These were the only two contaminants with retention times within the 13−19 min window used for the detection of the GAs. Both contaminants were well resolved from the C13:0 GA, and neither formed an EI fragment at $m/z$ 161.

Nineteen plant samples of *G. biloba* were extracted and analyzed. The samples included seeds, sarcotesta, leaves, and dried alcoholic extracts of leaves. The samples were extracted and injected in duplicate for a total of four analyses. The results for the average analysis are given in Table 3.

The total concentration of GAs in the plant samples varied dramatically. The seed samples contained the lowest concentrations of GAs in the range from 4 to 39 ppm. The sarcotesta sample contained 143 ppm. The dried extracts were in the range of 3−47 ppm. The leaf samples displayed a large range from 42 to 534 ppm with no systematic pattern.

Prior literature results for the analysis of GAs in plant samples are ambiguous. Van Beek[3] cites values of 0.5−4.8% (5000−48 000 ppm) for *G. biloba* leaves and 28 000−53 500 ppm in sarcotesta samples in a 2009 review. Wang et al. reported total GA concentration of 42 000 and 46 000 ppm in sarcotesta samples by GLC and HPLC,[26] 10 000 ppm by GC, and 5000−18 000 ppm by HPLC.[25] On the other hand, Choi et al.[27] used an NMR technique to determine the GA concentration in a single leaf sample to be 16 ppm in agreement with 16 ppm determined by GLC. In 1996, Irie et al.[31] used HPLC methods to determine the concentrations of GAs in ginkgo leaves (17 ppm) and sarcotesta (35 ppm). ELISA techniques were also used to determine the GA concentration in *G. biloba* leaves to be in the range of 12−48 ppm.[32] A sarcotesta sample was found to have a higher concentration of ca. 128 ppm. This large disparity (12−128 000 ppm) for a single species plant is unusual and probably reflects the variations in extraction schemes and analytical techniques (GLC, HPLC, and ELISA) along with collection, production, storage, and environmental variations.

To date, gas chromatography is the only analytical technique for the determination of GAs that is capable of resolving the double bond positional isomers of the GAs. In most of the

**Table 3. Quantitative Analysis of *Ginkgo biloba* Plant Materials and Dietary Supplement Purported To Contain *Ginkgo biloba* Leaves or Leaf Extracts[a]**

| | | | | GA15:1 (ppm) | | | GA17:1 (ppm) | | | | |
|---|---|---|---|---|---|---|---|---|---|---|---|
| type | accession code | GA13:0 (ppm) | GA15:0 (ppm) | Δ8 | Δ10[b] | ratio Δ10/Δ8 | Δ8[c] | Δ10[c] | Δ12 | GA17:2[d] (ppm) | total (ppm) |
| leaves | 580 | 37.6 | 12.1 | 48.4 | 111.7 | 2.3 | 3.3 | 3.2 | 85.1 | 5.4 | 306.8 |
| | 1095 | 19.0 | 2.4 | 19.0 | 29.7 | 1.6 | 1.5 | 2.3 | 33.1 | 1.5 | 108.5 |
| | 2837 | 35.9 | 4.1 | 29.5 | 70.5 | 2.4 | 1.7 | 1.5 | 40.8 | 3.0 | 187.0 |
| | 2909 | 20.4 | 1.5 | 16.0 | 26.6 | 1.7 | 0.7 | 0.7 | 11.4 | 0.5 | 77.8 |
| | 8551 | 10.0 | 1.1 | 6.9 | 15.5 | 2.2 | DUL | DUL | 7.3 | 0.8 | 41.6 |
| | 9245 | 86.4 | 8.0 | 157.5 | 172.7 | 1.1 | 3.1 | 16.5 | 82.6 | 7.1 | 533.9 |
| | 15212 | 4.9 | 1.9 | 10.1 | 29.7 | 2.9 | 1.7 | 1.5 | 30.6 | 2.2 | 82.6 |
| | 16746 | 16.6 | 2.9 | 53.3 | 107.9 | 2.0 | 1.3 | 2.1 | 46.3 | 3.1 | 233.5 |
| leaf extract | 2892 | 7.7 | DUL | 11.4 | 24.4 | 2.1 | ND | ND | 2.1 | 0.9 | 46.5 |
| | 9335 | 4.2 | DUL | 5.9 | 9.8 | 1.7 | DUL | DUL | 6.3 | DUL | 26.2 |
| | 16747 | 0.5 | DUL | 0.8 | 1.2 | 1.5 | ND | ND | 0.7 | ND | 3.2 |
| | 16748 | 0.5 | DUL | 1.0 | 2.4 | 2.4 | ND | ND | DUL | ND | 3.9 |
| seeds | 628 | 0.6 | DUL | 3.1 | DUL | | ND | DUL | DUL | ND | 3.7 |
| | 3539 | 4.6 | 1.1 | 17.0 | 7.9 | 0.5 | 0.7 | 1.2 | 5.8 | 0.6 | 38.9 |
| | 9604 | 0.3 | DUL | 5.1 | 7.0 | 1.4 | DUL | DUL | 1.5 | 0.6 | 14.5 |
| | 9605 | 3.7 | DUL | 9.4 | 2.4 | 0.3 | DUL | 0.9 | 1.4 | DUL | 17.8 |
| | 9606 | 1.1 | DUL | 4.0 | 0.5 | 0.1 | ND | DUL | DUL | ND | 5.6 |
| | 6049 | 1.4 | DUL | 7.6 | 2.0 | 0.3 | DUL | DUL | 1.0 | DUL | 12.0 |
| sarcotesta | 11637 | 16.6 | 2.6 | 76.9 | 16.5 | 0.2 | 1.7 | 7.2 | 19.8 | 1.9 | 143.2 |
| dietary supplements | 15713 | DUL | DUL | DUL | DUL | | ND | ND | DUL | ND | DUL |
| | 15714 | 0.6 | 0.8 | 0.6 | 1.5 | 2.5 | ND | ND | 1.5 | ND | 5.0 |
| | 15907 | DUL | DUL | DUL | 0.8 | | DUL | DUL | 0.7 | ND | 1.5 |
| | 15908 | DUL | DUL | DUL | DUL | | DUL | DUL | DUL | ND | DUL |
| | 15909 | 0.9 | 0.4 | 1.1 | 3.3 | 3.0 | DUL | DUL | 5.1 | ND | 10.8 |
| | 15910 | DUL | ND | DUL | ND | | ND | ND | ND | ND | DUL |
| | 15911 | DUL | DUL | DUL | DUL | | ND | ND | DUL | ND | DUL |
| | 15912 | 1.0 | 0.5 | 0.6 | 0.8 | 1.3 | DUL | DUL | 0.7 | ND | 3.6 |
| | 15913 | 16.8 | 1.1 | 14.5 | 15.0 | 1.0 | 0.4 | 0.9 | 6.2 | 0.6 | 55.5 |
| | 15914 | 0.7 | 0.8 | 0.6 | 1.5 | 2.5 | ND | ND | 0.4 | ND | 4.0 |
| | 15915 | 0.5 | DUL | 0.4 | 0.7 | 1.8 | ND | ND | DUL | ND | 1.6 |
| | 15916 | 1.8 | 0.1 | 2.0 | 3.9 | 2.0 | ND | ND | 1.1 | DUL | 8.9 |
| | 15917 | 0.7 | 0.3 | 0.4 | 0.8 | 2.0 | ND | ND | ND | 0.7 | 2.9 |
| | 15918 | 0.6 | DUL | DUL | 0.5 | | ND | ND | DUL | ND | 1.1 |
| | 15919 | ND | ND | ND | ND | | ND | ND | ND | ND | ND |
| | 15920 | DUL | DUL | DUL | 0.9 | | DUL | DUL | 1.4 | ND | 2.3 |
| | 15921 | 1.1 | 0.2 | 1.0 | 1.7 | 1.7 | DUL | DUL | 1.6 | ND | 5.6 |
| | 15922 | DUL | DUL | DUL | 0.5 | | ND | ND | DUL | ND | 0.5 |
| | 15923 | DUL | ND | ND | ND | | ND | ND | DUL | ND | DUL |
| | 15924 | DUL | DUL | DUL | DUL | | ND | ND | DUL | ND | DUL |
| | 15925 | 9.3 | 0.6 | 6.2 | 12.0 | 1.9 | ND | ND | 1.4 | 0.7 | 30.2 |

[a]DUL: Detected under the limit of quantification. ND: Not detected. [b]Assuming the response factor for Δ10 is equivalent to that for the Δ8 standard. [c]Assuming the response factors for Δ8 and Δ10 are equivalent to that of the Δ12 standard. [d]Assuming the response factors for C17:2 and C17:1 are equivalent.

samples described in Table 3, either C15:1 Δ10 or Δ8 was the major GA component present in every type of plant sample. One interesting observation involves the ratio of the concentrations of these two C15:1 isomers, also given in Table 3. The Δ10/Δ8 ratio for all of the leaf or leaf extract samples was in the range of 1−3. Conversely, the same ratios for the seed and sarcotesta samples were in the range of 0.1−0.5 with the single exception of sample 9604. In other GC analyses, Wang et al.[25,26] found this ratio to be 1.7−1.8 for leaf samples and 0.05 for sarcosta samples. This simple test allows the distinction of samples and products derived from different plant parts. All of the dietary supplements that contained detectable amount of both Δ8 and Δ10 isomers displayed ratios between 1 and 3 indicating that the commercial products were all derived from ginkgo leaves, not seeds or sarcotesta. The C15:1 Δ8 and Δ10 isomers are the only pairs that appear consistently in all of the plant samples. The presence or absence of a single probe component cannot be used to distinguish plant parts because of the wide variation in the GA component concentrations in the ginkgo samples. Gas chromatographic methods are the only technique for the resolution and quantitation of the Δ8 and Δ10 isomers of the C15:1 ginkgolic acid esters.

**GC/MS and LC/MS Analysis and Validity of Ginkgo Dietary Supplement Samples.** Twenty-one dietary supplements in the form of capsules, liquids, or tablets were analyzed

using the developed GC/MS method. In summary, one sample contained no detectable GAs, six samples contained GAs below the limit of quantitation, eight samples contained detectable amounts but less than 5 ppm, and six samples contained >5 ppm GAs ranging from 5 to 56 ppm. The two samples (15913 and 15925) containing the highest concentrations of GAs (56 and 30 ppm, respectively) were both leaf extracts, not standardized extracts. The major active components of *G. biloba* leaf extracts are the flavonoids and sesquiterpenes lactones.[33,34] Standardized commercial extracts usually contain >6% ginkgolides (A, B, C, and J) and bilobalide and 24% flavonoids (quercetin, kaempferol, and isorhamnetin). In order to confirm the presence of *G. biloba* leaf extracts in the botanical dietary supplements, all of the dietary supplements shown in Table 2 were analyzed by a previously published method[29] involving the use of $[M + H]^+$ ions of five sesquiterpene lactones and three flavonoids which were observed at $m/z$ 425.2 (ginkgolide J and ginkgolide B), $m/z$ 441.2 (ginkgolide C), $m/z$ 327.3 (bilobalide), $m/z$ 409.2 (ginkgolide A), $m/z$ 303.1 (quercetin), $m/z$ 287.1 (kaempferol), and $m/z$ 317.1 (isorhamnetin). Based on the retention times and mass spectra in comparison with standard compounds, all commercial ginkgo preparations analyzed were found to contain all eight compounds indicating that all of the analyzed dietary supplements contained ginkgo leaf extracts.

**Confirmation with Standard HPLC Technique.** HPLC with a $C_8$ column, acetonitrile eluent and UV detection at 310 nm is a commonly accepted method for the analysis of GAs without distinction between the double bond positional isomers.[3,20,23,28,35] One leaf sample, 1095, was analyzed in a derivatized form by GC/MS and in the acid form by HPLC. The underivatized 1095 sample was analyzed by LC using three detection schemes, viz., UV at 310 nm, MS scan and MS SIM at $m/z$ 319, 347, 345, and 373 for C13:0, C15:0, C15:1 and C17:1, respectively. The results for the quantitation of GAs in the ginkgo leaf sample (1095) are given in Table 4.

**Table 4. Comparison of HPLC-UV-MS and GC/MS Results for GAs in a Leaf Sample (1095)[a]**

| ginkgolic acid | HPLC SIM | UV 310 nm | average HPLC | GC/MS[b] (from Table 3) |
|---|---|---|---|---|
| C13:0 | 22.3 | 35.1 | 28.7 | 19.0 |
| C15:0 | 8.2 | 8.2 | 8.2 | 2.4 |
| C15:1 | 39.8 | 40.6 | 40.2 | 48.7 |
| C17:1 | 29.8 | 26.9 | 28.4 | 36.9 |
| total | 100.1 | 110.8 | 105.5 | 107.0 |

[a]The concentrations are expressed in ppm. [b]The elution order for a HPLC $C_8$ column is C13:0, C15:1, C15:0, and C17:1. The elution order for a GC-HP88 column is C13:0, C15:0, C15:1, and C17:1.

The GC/MS results agree within experimental error with the standard HPLC analyses. The variation between results obtained with different detection schemes in the HPLC analyses is comparable to the differences between the average GC and HPLC results.

In conclusion, GC/MS methods using selected ion monitoring at $m/z$ 161 can be used to analyze various samples for ginkgolic acid components with detection and quantitation limits of 0.5 and 1.5 ppm, respectively. Gas chromatography allowed the resolution of the double bond positional isomers of the C15:1 and C17:1 ginkgolic acids. This type of resolution could not be achieved with common HPLC techniques. Quantitative analysis results obtained with the GC method were comparable with results achieved by a commonly accepted HPLC method.

The ratios of the concentrations of C15:1 Δ10 to Δ8 observed for leaf samples of ginkgo were in the range of 1−3, whereas the same ratio in the seed samples was always <0.5 with a single exception. This type of test may prove useful in determining the plant parts used to produce ginkgo samples and commercial products. All of the dietary supplements analyzed in this study that contained detectable amounts of GAs displayed a ratio of 1−2.5 indicating that they were probably derived from ginkgo leaves rather than seeds. The seeds and leaves have different functions, metabolic processes, and metabolite distributions resulting in different chemical profiles.

The double bond position in a commercial sample of C17:1 ginkgolic acid was determined to be Δ12 rather than Δ10 by the analysis of the reaction products from an ozonolysis reaction.

A previously developed HPLC method for the analysis of terpene trilactones and flavonol glycosides was used to confirm the presence of *Ginkgo biloba* in all of the commercial dietary supplement samples.

## AUTHOR INFORMATION


### Corresponding Author

*Tel: +1-662-915-7821. Fax:+1-662-915-7062. E-mail: ikhan@olemiss.edu.


### Notes

The authors declare no competing financial interest.

## ACKNOWLEDGMENTS

This research is supported in part by "Science Based Authentication of Dietary Supplements" funded by the Food and Drug Administration grant number 1U01FD004246-03, the United States Department of Agriculture, Agricultural Research Service, Specific Cooperative Agreement No. 58-6408-1-603-04. The authors thank Agilent Technologies for provision of the analytical instrumentation and Dr. Vijayasankar Raman for authentication of the ginkgo plant samples.

## REFERENCES


(1) van Beek, T. A. *Ginkgo biloba*; Taylor & Francis: London, U.K., 2000.

(2) Rimmer, C. A.; Howerton, S. B.; Sharpless, K. E.; Sander, L. C.; Long, S. E.; Murphy, K. E.; Porter, B. J.; Putzbach, K.; Rearick, M. S.; Wise, S. A.; Wood, L. J.; Zeisler, R.; Hancock, D. K.; Yen, J. H.; Betz, J. M.; NguyenPho, A.; Yang, L.; Scriver, C.; Willie, S.; Sturgeon, R.; Schaneberg, B.; Nelson, C.; Skamarack, J.; Pan, M.; Levanseler, K.; Gray, D.; Waysek, E. H.; Blatter, A.; Reich, E. Characterization of a suite of ginkgo-containing standard reference materials. *Anal. Bioanal. Chem.* **2007**, *389*, 179−196.

(3) van Beek, T. A.; Montoro, P. Chemical analysis and quality control of *Ginkgo biloba* leaves, extracts, and phytopharmaceuticals. *J. Chromatogr., A* **2009**, *1216* (11), 2002−2032.

(4) Elsabagh, S.; Hartley, D. E.; File, S. E. Limited cognitive benefits in stage +2 postmenopausal women after 6 weeks of treatment with *Ginkgo biloba*. *J. Psychopharmacol.* **2005**, *19* (2), 173−81.

(5) Kanowski, S.; Hoerr, R. *Ginkgo biloba* extract EGb 761 in dementia: Intent-to-treat analyses of a 24-week, multi-center, double-blind, placebo-controlled, randomized trial. *Pharmacopsychiatry* **2003**, *36* (6), 297−303.

(6) Wang, S.-J.; Chen, H.-H. Ginkgolide b, a constituent of *Ginkgo biloba*, facilitates glutamate exocytosis from rat hippocampal nerve terminals. *Eur. J. Pharmacol.* **2005**, *514* (2−3), 141−149.

(7) Kalkunte, S. S.; Singh, A. P.; Chaves, F. C.; Gianfagna, T. J.; Pundir, V. S.; Jaiswal, A. K.; Vorsa, N.; Sharma, S. Antidepressant and

antistress activity of GC−MS characterized lipophilic extracts of *Ginkgo biloba* leaves. *Phytother. Res.* **2007**, *21* (11), 1061−1065.
(8) Chen, Z.; Zhang, Q. Adverse drug interactions between *Ginkgo biloba* leaf agents and chemicals. *Shanghai Yiyao* **2012**, *33* (5), 16−18.
(9) Koch, E.; Noeldner, M.; Leuschner, J. Reproductive and developmental toxicity of the *Ginkgo biloba* special extract EGb 761 in mice. *Phytomedicine* **2013**, *21* (1), 90−97.
(10) Posadzki, P.; Watson, L.; Ernst, E. Herb−drug interactions: An overview of systematic reviews. *Br. J. Clin. Pharmacol.* **2013**, *75* (3), 603−618.
(11) Zhang, H.; Luo, C.; Xu, H. Investigation and analysis of adverse drug reactions of six traditional chinese medicine injections. *Yaowu Liuxingbingxue Zazhi* **2012**, *21* (7), 346−349.
(12) Ahlemeyer, B.; Selke, D.; Schaper, C.; Klumpp, S.; Krieglstein, J. Ginkgolic acids induce neuronal death and activate protein phosphatase type-2c. *Eur. J. Pharmacol.* **2001**, *430* (1), 1−7.
(13) Itokawa, H.; Totsuka, N.; Nakahara, K.; Maezuru, M.; Takeya, K.; Kondo, M.; Inamatsu, M.; Morita, H. A quantitative structure−activity relationship for antitumor activity of long-chain phenols from *Ginkgo biloba* L. *Chem. Pharm. Bull.* **1989**, *37* (6), 1619−21.
(14) Koch, E.; Jaggy, H.; Chatterjee, S. S. Evidence for immunotoxic effects of crude *Ginkgo biloba* L. Leaf extracts using the popliteal lymph node assay in the mouse. *Int. J. Immunopharmacol.* **2000**, *22* (3), 229−236.
(15) Westendorf, J.; Regan, J. Induction of DNA strand-breaks in primary rat hepatocytes by ginkgolic acids. *Pharmazie* **2000**, *55* (11), 864−865.
(16) Schotz, K. Quantification of allergenic urushiols in extracts of *Ginkgo biloba* leaves, in simple one-step extracts and refined manufactured material (EGb 761). *Phytochem. Anal.* **2004**, *15* (1), 1−8.
(17) European Pharmacopoeia 7.0. Monograph: Ginkgo dry extract. Refined and quantified. 2010. European Directorate for the Quality of Medicines & Healthcare, Strasbourg, France.
(18) United States Pharmacopeia. Thirty-Fourth Revision: Powdered Ginkgo Extract. 2010. The United States Pharmacopeial Convention, Rockville, Md.
(19) van Beek, T. A. Chemical analysis of *Ginkgo biloba* leaves and extracts. *J. Chromatogr., A* **2002**, *967*, 21−55.
(20) Fuzzati, N.; Pace, R.; Villa, F. A simple HPLC−UV method for the assay of ginkgolic acids in *Ginkgo biloba* extracts. *Fitoterapia* **2003**, *74*, 247−256.
(21) Lee, H.; Lim, H.; Yang, J.; Hong, J. Rapid determination of ginkgolic acids in *Ginkgo biloba* leaf using online column switching high-performance liquid chromatography−diode array detection and confirmation by liquid chromatography−tandem mass spectrometry. *Bull. Korean Chem. Soc.* **2013**, *34* (12), 3629−3634.
(22) Udrescu, S.; Medvedovici, A.; David, V. Effect of large volume injection of hydrophobic solvents on the retention of less hydrophobic pharmaceutical solutes in RP-LC. *J. Sep. Sci.* **2008**, *31* (16−17), 2939−2945.
(23) Udrescu, S.; Sora, I. D.; David, V.; Medvedovici, A. Large volume injection of hexane solutions in RPLC/UV to enhance on sensitivity of the assay of ginkgolic acids in *Ginkgo biloba* standardized extracts. *J. Liq. Chromatogr. Relat. Technol.* **2010**, *33*, 133−149.
(24) Gawron-Gzella, A.; Marek, P.; Chanaj, J.; Matlawska, I. Comparative analysis of pharmaceuticals and dietary supplements containing extracts from the leaves of *Ginkgo biloba* L. *Acta Polym. Pharm.* **2010**, *67* (4), 335−343.
(25) Wang, L.; Jia, Y.; Pan, Z.; Mo, W.; Hu, B. Direct analysis of alkylphenols in *Ginkgo biloba* leaves by thermochemolysis-gas chromatography/mass spectrometry in the presence of tetramethylammonium hydroxide. *J. Anal. Appl. Pyrolysis* **2009**, *85* (1 + 2), 66−71.
(26) Sun, Y.; Tang, C.; Wu, X.; Pan, Z.; Wang, L. Characterization of alkylphenol components in *Ginkgo biloba* sarcotesta by thermochemolysis−gas chromatography/mass spectrometry in the presence of trimethylsulfonium hydroxide. *Chromatographia* **2012**, *75* (7−8), 387−395.
(27) Choi, Y. H.; Choi, H.-K.; Peltenburg-Looman, A. M. G.; Lefeber, A. W. M.; Verpoorte, R. Quantitative analysis of ginkgolic acids from ginkgo leaves and products using $^{1}$H-NMR. *Phytochem. Anal.* **2004**, *15* (5), 325−330.
(28) Li, R.; Shen, Y.; Zhang, X.; Ma, M.; Chen, B.; van Beek, T. A. Efficient purification of ginkgolic acids from *Ginkgo biloba* leaves by selective adsorption on $Fe_3O_4$ magnetic nanoparticles. *J. Nat. Prod.* **2014**, *77*, 571−575.
(29) Avula, B.; Wang, Y.-H.; Smillie, T. J.; Khan, I. A. Column liquid chromatography/electrospray ionization-time of flight-mass spectrometry and ultraperformance column liquid chromatography/mass spectrometry methods for the determination of ginkgolides and bilobalide in the leaves of *Ginkgo biloba* and dietary supplements. *J. AOAC Int.* **2009**, *92*, 645−652.
(30) ICH, Validation of analytical procedures: Text and methodology Q2(R1). ICH Harmonized tripartite guidelines. International Conference on Harmonization, Geneva, Switzerland, 2005.
(31) Irie, J.; Murata, M.; Homma, S. Glycerol-3-phosphate dehydrogenase inhibitors, anacardic acids, from *Ginkgo biloba*. *Biosci., Biotechnol., Biochem.* **1996**, *60* (2), 240−3.
(32) Loungratana, P.; Tanaka, H.; Shoyama, Y. Production of monoclonal antibody against ginkgolic acids in *Ginkgo biloba* Linn. *Am. J. Chin. Med.* **2004**, *32* (1), 33−48.
(33) Nishida, S.; Satoh, H. Comparative vasodilating actions among terpenoids and flavonoids contained in *Ginkgo biloba* extract. *Clin. Chim. Acta* **2004**, *339* (1−2), 129−33.
(34) DeFeudis, F. V.; Drieu, K. Ginkgo biloba extract (EGb 761) and cns functions: Basic studies and clinical applications. *Curr. Drug Targets* **2000**, *1* (1), 25−58.
(35) Yang, X.-M.; Zhang, X.-L.; Chen, Y.-C.; Liu, F. LC method for determination of ginkgolic acids in mice plasma and its application to a pharmacokinetic study. *Chromatographia* **2009**, *69*, 593−596.

binding phase in the DGT sampler, has been applied to the measurement of dissolved Cr(VI).[33,34] In this paper, A DGT technique with a dialysis membrane as the diffusive phase and a PQAS aqueous solution as the binding phase (PQAS DGT) was investigated for the sampling of DRP in water. The influences of solution pH and ionic strength on the properties of PQAS DGT were studied. The PQAS DGT performance for the sampling of DRP was investigated under laboratory conditions and then deployed in wastewater and natural water. PQAS DGT will be applied for the assessment of P bioavailability in soils, which, in turn, will help effective fertilization tactics and lessen the danger of environmental pollution, owing to excessive fertilization. When PQAS DGT is applied to evaluating bioavailable P in soils, a relation will be established between the plant response to P manure and the concentration of P in soil determined by PQAS DGT, and PQAS DGT can provide a more accurate suggestion of P fertilizer needs. The study of PQAS DGT for the sampling of DRP in water will lay the foundation for the assessment of P bioavailability in soils, and the assessment of P bioavailability in soils by PQAS DGT will be reported later.

## MATERIALS AND METHODS

**Materials.** Cellulose acetate dialysis membrane (CDM, ~14 000 or greater retain) was bought from Shanghai Yuanju Bio-Tech Co., Ltd., Shanghai, China. Cellulose nitrate membrane (0.45 $\mu$m) was bought from Dikma (Tianjin, China). Poly(quaternary ammonium salt) (PQAS; $M_w = 2 \times 10^4$) was obtained from Henan Titaning Chemical Technology Co., Ltd., Zhengzhou, China. Potassium dihydrogen phosphate, antimony potassium tartrate, ammonium molybdate, hydrochloric acid, sodium hydroxide, and sodium nitrate were bought from Sinopharm Chemical Reagent Co., Ltd., Shanghai, China.

**Apparatus.** Ultraviolet−visible (UV−vis) spectroscopy (Beijing Royleigh Analytical Instrument Co., Ltd., China) was used for measurements of the absorbance of PQAS binding solutions containing phosphates at a wavelength of 700 nm by the ammonium molybdate spectrophotometric (AMS) method based on the National Standard of the People's Republic of China (GB 11893-89).[35] A PB-10 digital pH-meter (Sartorius, Germany) equipped with a combined glass electrode was used for the measurements of pH.

**Preprocessing of the Diffusive Phase and the Binding Phase.** Cellulose acetate dialysis membrane has been used as the diffusive phase of the DGT sampler.[17,18] The dialysis membrane was preprocessed according to the procedures suggested by Li et al.[17] The treated diffusive phase was kept in deionized water.

A 50.0 g PQAS solution was put in a dialysis membrane bag prepared as mentioned above, which was immersed in deionized water for 72 h with the water regularly supplemented.[17] This method effectually got rid of all of the low-molecular-weight PQAS that went through the dialysis membrane.

**Capacity of PQAS DGT.** The binding capacity of PQAS DGT was examined by immersing PQAS DGT for 24 h in 10 L $KH_2PO_4$ solutions containing 0.01 M $NaNO_3$. The concentrations of $KH_2PO_4$ were in the range of 0.1−1.2 mg of P $L^{-1}$.

**Measurement of the Diffusion Coefficient.** The diffusion coefficient of $H_2PO_4^-$ in the dialysis membrane in contact with synthetic water containing 0.01 M $NaNO_3$ at pH 7 was measured using a diffusion cell.[17] The cell was made of two perspex chambers linked by a 2.0 cm diameter hole. A 3.0 cm diameter and 85 $\mu$m thickness disc of the new pretreated diffusive phase was put on the opening between the chambers, assuring that the diffusive phase was the only mass transmission medium. A total of 50 mL of 0.01 mol $L^{-1}$ $NaNO_3$ solution containing 30 mg $L^{-1}$ P ($KH_2PO_4$) was put into the source solution chamber, and a total of 50 mL of 0.01 mol $L^{-1}$ $NaNO_3$ solution containing 0.050 mol $L^{-1}$ PQAS, an optimum concentration of PQAS solution, was put into the receptor solution chamber. Both chambers were mixed constantly using a magnetic stirring apparatus. Samples were taken out from both chambers at a 30 min span up to 180 min and measured by the AMS method.

Diffusion coefficients, $D$ ($cm^2$ $s^{-1}$), were calculated from the slope of a linear plot of measured mass of DRP diffused through the diffusive phase versus time, using eq 1, where $A$ is the exposed area of the diffusive phase, $\Delta g$ is the thickness of the dialysis membrane, and $C$ is the concentration of DRP originally existing in the source chamber of the diffusion cell.[36,37]

$$D = \frac{\text{slope}\ \Delta g}{CA} \tag{1}$$

The diffusion coefficients of DRP at different temperatures can be calculated by the Stokes−Einstein equation below (eq 2)

$$\frac{D_1\eta_1}{T_1} = \frac{D_2\eta_2}{T_2} \tag{2}$$

where $D_1$ and $D_2$ are the diffusion coefficients at temperatures $T_1$ and $T_2$ and $\eta_1$ and $\eta_2$ are the viscosities of water at those temperatures.[38]

**Validation of DGT Performance in the Laboratory.** A verification test for the binding phase of DGT was carried out following the programs stated previously.[17] The DGT samplers were installed according to the procedures described by Chen et al.[24] The samplers were immersed in 30 L of 0.01 mol $L^{-1}$ $NaNO_3$ spiked with 50 $\mu$g $L^{-1}$ P ($KH_2PO_4$) at 20 °C; triplicate samplers were taken out at 4, 8, 12, 16, 24, 36, and 48 h. The PQAS solutions in the DGT samplers were removed at each time point and analyzed by the AMS method.

The concentration gradient formed within the diffusive phase allows for the amount of analyte, $M$, that is enriched in the binding phase from a solution, after passing through a diffusive membrane of area ($A$) and thickness ($\Delta g$) with diffusive coefficient ($D$), over a deployment time ($t$), to be related directly to the concentration of analyte in the bulk solution measured by DGT ($C_{DGT}$).[6]

$$M = \frac{DAC_{DGT}t}{\Delta g} \tag{3}$$

PQAS DGT samplers are verified by investigating the relationship between the mass of analyte enriched in the binding phase ($M$) and the deployment time ($t$) with a solution of known concentration. The performance of PQAS DGT is also evaluated by calculating the percentage uptake ($U$%), defined by the following equation:[25]

$$U\% = \frac{C_{DGT}}{C_{bulk}} \times 100\% \tag{4}$$

where $C_{bulk}$ is the total concentration of DRP in the bulk solution directly measured by the AMS method.[37]

**Effect of Solution pH and Ionic Strength on the DGT Performance.** To evaluate the influence of various pH values (2, 3, 4, 5, 6, 7, 8, 9, and 10) and ionic strengths (0.0001, 0.001, 0.01, 0.1, and 1.0 mol $L^{-1}$ as $NaNO_3$) on the PQAS DGT performance, the PQAS DGT samplers were deployed in solutions containing 50 $\mu$g $L^{-1}$ P ($KH_2PO_4$) at various pH values and ionic strengths for the deployment time from 4 to 48 h. The pH values of the bulk solutions were modulated using 2% NaOH or $HNO_3$. The ionic strengths of the solutions were modulated with the proper addition of $NaNO_3$ at pH ~7.

**Field Deployment of the DGT Samplers in Wastewater and Natural Water.** PQAS DGT samplers were deployed in triplicate in a wastewater canal (Jinzhou, China); triplicate samplers were taken out at 24, 48, 72, 96, and 120 h. The PQAS solutions were removed from the PQAS DGT samplers at each time point and measured by the AMS method, and 0.45 $\mu$m filtered grab samples were gathered daily and measured directly by the AMS method.

PQAS DGT samplers were immersed in triplicate in local natural waters (Nuer River, Ling River, and North Lake, Jinzhou, China); triplicate samplers were taken out at 24, 48, 72, 96, and 120 h. The PQAS solutions were removed from the PQAS DGT samplers at each time point and measured by the AMS method, and 0.45 $\mu$m filtered

grab samples were gathered daily and measured directly by the AMS method.

## RESULTS AND DISCUSSION

**Capacity of PQAS DGT.** There is a trend for the binding phase to become saturated because of the high cumulation of the analytes when the sampling is conducted over a long term (weeks or months) or in an environment with high-concentration analytes. The DGT capacity may be a restrictive factor for such applications. The DGT capacity was studied by immersing DGT samplers in stirred solutions with phosphate concentrations in the range of 0.1−1.2 mg of P $L^{-1}$. A linear response ($y = 35.99x + 4.50$; $r^2 = 0.9985$) was gained with the concentration up to 0.8 mg of P $L^{-1}$ (Figure 1). The effective

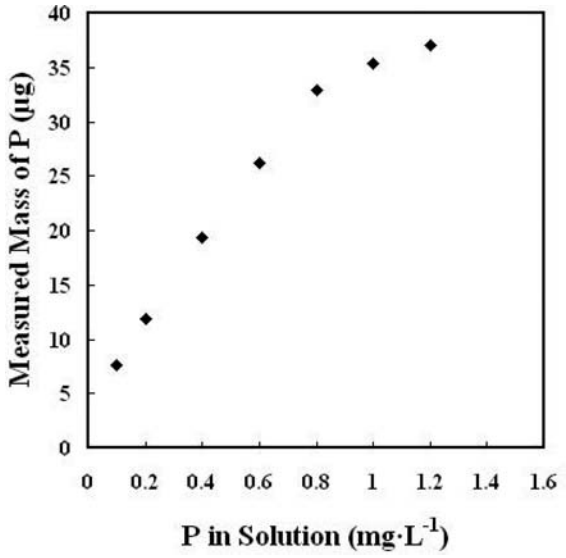


**Figure 1.** Dependence of accumulated mass of phosphorus on the solution concentration for 24 h exposure of a DGT sampler.

binding capacity of PQAS DGT containing 2.0 mL of 0.05 mol $L^{-1}$ PQAS solution was estimated as 9.9 $\mu$g $cm^{-2}$ on the basis of Figure 1 compared to the binding gels used for phosphates reported in the literature, such as ferrous oxide gel (~2 $\mu$g $cm^{-2}$),[26] titanium dioxide gel (~12 $\mu$g $cm^{-2}$),[30] and zirconium oxide gel (~100 $\mu$g $cm^{-2}$).[31] It can be estimated that, if the mean concentration of DRP in a water was 10 $\mu$g $L^{-1}$, DGT could be deployed for up to 54 days. Furthermore, by increasing the volume of the PQAS solution, extended hours of deployment can be expected.

**Diffusion Coefficient of DRP in the Dialysis Membrane.** The diffusion coefficient of DRP through the dialysis membrane in 0.01 mol $L^{-1}$ $NaNO_3$ solutions at 20 °C was $(1.95 \pm 0.17) \times 10^{-6}$ $cm^2$ $s^{-1}$, lower than the value of $D$ in the synthetic polyacrylamide hydrogel ($6.05 \times 10^{-6}$ $cm^2$ $s^{-1}$ at 25 °C). This can be explained by the structure of the dialysis membrane with lower porosity and lower water content.[26,39]

**Validation of the DGT Performance for the Measurement of DRP.** The DGT performance is evaluated in two aspects. First, a linear relationship between the mass of analyte enriched in the binding phase ($M$) and the deployment time ($t$) should be expected, if the DGT sampler works in principle. Second, the percentage uptake of the DGT sampler should be in the range of 90−110%.[40] The uptake of DRP by PQAS in the synthetic solution containing 50 $\mu$g of P $L^{-1}$ increased linearly with time up to 48 h ($r^2 = 0.9993$; $U$% = 98.7%; Figure 2). These results demonstrated that PQAS DGT worked well

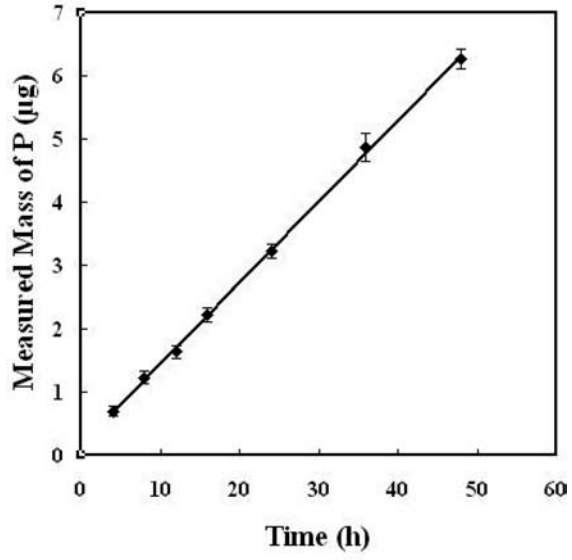


**Figure 2.** Mass of phosphorus accumulated by PQAS DGT in a synthetic solution. Concentration of P ($KH_2PO_4$), 50 $\mu$g $L^{-1}$; ionic strength, 0.01 mol $L^{-1}$ $NaNO_3$; pH, 7; deployment time, from 4 to 48 h; and temperature, 20 °C.

according to the DGT principle and PQAS satisfies the conditions of the DGT binding agent for the sampling of DRP. Therefore, DRP can be measured quantitatively by PQAS DGT.

DRP can be enriched in the PQAS binding phase because of the electrostatic attraction between PQAS and DRP. PQAS is a water-soluble cationic polymer and can interact with anionic substances present in aqueous solutions, whereas DRP exists as various hydrophilic anionic species, such as $H_2PO_4^-$ and $HPO_4^{2-}$, in a water environment and can interact with cationic substances present in aqueous solutions.[32] DRP in water can go through the diffusive phase into the binding phase of the DGT sampler and bind with PQAS quickly; a diffusive gradient of DRP is thereby formed within the dialysis membrane between water and the interface with the binding phase, resulting in an accumulation of DRP in the binding phase.

**Effect of the pH.** The DGT measurements of DRP were not dependent upon solution pH over the pH range of 3−10, which covers most of the pH conditions in natural water (Figure 3), consistent with the earlier findings that DGT measurements of anions were not dependent upon pH.[11,33,41] With the increase of solution pH, more $H_2PO_4^-$ was transferred into $HPO_4^{2-}$ that can be combined by PQAS more strongly because of electrostatic interaction. However, with the increase of solution pH, more competing hydroxide anions must hinder the combination of PQAS and $HPO_4^{2-}$. It was the above two opposite factors that resulted in no significant difference between the bindings of PQAS and anionic species of DRP that existed over the pH range of 3−10. The $U$% values increased significantly at pH 2 probably because PQAS can combine DRP more strongly with the increase of the hydrogen ion concentration.

**Effect of the Ionic Strength.** The binding behavior of PQAS DGT for DRP was investigated in $KH_2PO_4$ aqueous solutions containing various ionic strengths (0.0001, 0.001,

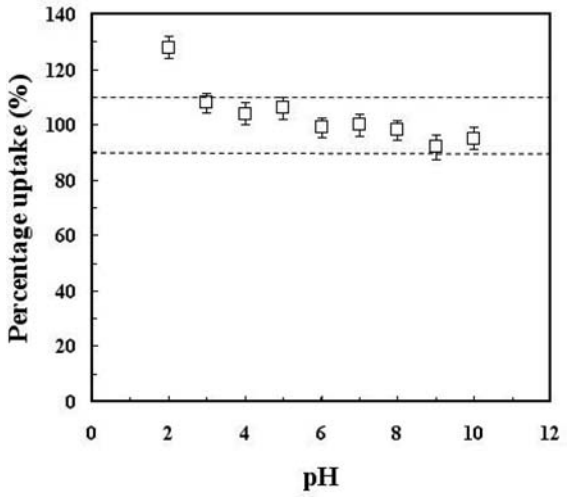


**Figure 3.** Effect of pH on the performance of PQAS DGT by plotting percentage uptake of DRP versus the pH, Concentration of P ($KH_2PO_4$), 50 $\mu$g $L^{-1}$; ionic strength, 0.01 mol $L^{-1}$ $NaNO_3$; deployment time, from 4 to 48 h; and temperature, 20 °C.

0.01, 0.1, and 1.0 mol $L^{-1}$ as $NaNO_3$; Figure 4). The *U*% value of DRP increased with the increase of the ionic strength range

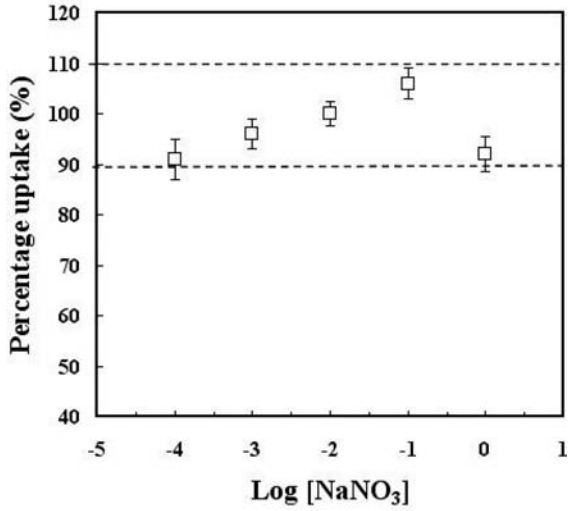


**Figure 4.** Influence of the ionic strength on the performance of PQAS DGT by plotting percentage uptake of DRP versus the $NaNO_3$ concentration. Concentration of P ($KH_2PO_4$), 50 $\mu$g $L^{-1}$; pH, 7; deployment time, from 4 to 48 h; and temperature, 20 °C.

from 0.0001 to 0.1 mol $L^{-1}$, consistent with the experimental results reported by Panther and co-workers and Lucas and co-workers.[42,43] Panther and co-workers found that the diffusion coefficients of As(V) in the negatively charged Nafion membrane increased with the increase of the ionic strength.[42] Lucas and co-workers also found that the diffusion coefficients of Au(III) in a diffusive gel increased with the increase of the ionic strength.[43] The *U*% values decreased at 1.0 mol $L^{-1}$ solution of $NaNO_3$ probably because the competitive diffusion between $NO_3^-$ and DRP in the diffusive phase was strengthened at high ionic strength.[33] However, accumulation was quantitative and consistent in the ionic strength range of 0.001−1.0 mol $L^{-1}$, with *U*% values between 90 and 110%. These results suggest that PQAS DGT can be applied for sampling DRP in the majority of natural fresh and marine waters, although a further study in seawater is essential to guarantee that competing anions other than nitrate do not disturb the measurement of DRP by PQAS DGT.

**Field Deployment.** PQAS DGT samplers were put in a local wastewater canal up to 5 days to investigate the robustness of the technique further. The concentrations of DRP in the wastewater were collected daily and measured directly by the AMS method. The concentration of DRP in the wastewater measured by PQAS DGT was 32.9 ± 0.9 $\mu$g $L^{-1}$, and the $C_{DGT}$ value is in good agreement with the average 0.45 $\mu$m filtered measurement obtained from grab samples ($C_{sol}$), as shown in Table 1. Therefore, DRP in the wastewater can be sampled and measured by PQAS DGT.

**Table 1. Comparison of DRP Measurement by PQAS DGT and Directly by the AMS Method in Wastewater and Natural Waters**

| water sample | $C_{DGT}$[a] ($\mu$g $L^{-1}$) | $C_{sol}$[b] ($\mu$g $L^{-1}$) |
|---|---|---|
| wastewater | 32.9 ± 0.9 | 33.5 ± 1.8 |
| Nuer River | 4.9 ± 0.4 | ND[c] |
| Ling River | 4.6 ± 0.3 | ND |
| North Lake | 6.1 ± 0.5 | ND |

[a]Measured by PQAS DGT. [b]Average value from 0.45 $\mu$m of filtered grab samples. [c]ND = not detected.

PQAS DGT samplers were deployed in natural waters up to 5 days for sampling DRP in the natural water. The concentrations of DRP measured by PQAS DGT in Nuer River, Ling River, and North Lake were 4.9 ± 0.4, 4.6 ± 0.3, and 6.1 ± 0.5 $\mu$g $L^{-1}$, respectively (Table 1). However, the concentrations of DRP in the natural waters cannot be detected directly by the AMS method because they are below the detection limit (Table 1).

This work has demonstrated the feasibility of using PQAS solution as a binding phase for *in situ* sampling and measurement of DRP in water. PQAS is suitable as a liquid binding agent of the DGT technique for sampling DRP. The advantages of PQAS DGT include no requirement of the elution steps and direct concentration measurements of the binding phase. The measurement of DRP in a synthetic solution by PQAS DGT over a 48 h deployment period demonstrated high consistency with the concentration of DRP in the synthetic solution measured directly by the AMS method. A future study should focus on the application of this new technique to the sampling and measurement of DRP in soils and sediments.

## AUTHOR INFORMATION

### Corresponding Author

*Telephone: +86-416-3400008. Fax: +86-416-3400159. E-mail: lijr6491@163.com.

### Funding

This study was supported by the National Key Technologies Research and Development Program of China during the 12th Five-Year Plan Period (2012BAD29B06), the Public-Interest Scientific Research Fund of Liaoning Province (2012003001), and the Food Safety Key Laboratory of Liaoning Province (LNSAKF2011038).

### Notes

The authors declare no competing financial interest.

## ■ ACKNOWLEDGMENTS

The authors thank Henan Titaning Chemical Technology Co., Ltd. for supplying binding agent.

## ■ REFERENCES

(1) Maher, W.; Woo, L. Procedures for the storage and digestion of natural waters for the determination of filterable reactive phosphorus, total filterable phosphorus and total phosphorus. *Anal. Chim. Acta* **1998**, *375*, 5−47.

(2) Monbet, P.; McKelvie, I. D. Phosphates. In *Handbook of Water Analysis*, 2nd ed.; Nollet, L. M. L., Ed.; CRC Press: Boca Raton, FL, 2007.

(3) Worsfold, P. J.; Gimbert, L. J.; Mankasingh, U.; Omaka, O. N.; Hanrahan, G.; Gardolinski, P.; Haygarth, P. M.; Turner, B. L.; Keith-Roach, M. J.; McKelvie, I. D. Sampling, sample treatment and quality assurance issues for the determination of phosphorus species in natural waters and soils. *Talanta* **2005**, *66*, 273−293.

(4) Gardolinski, P.; Hanrahan, G.; Achterberg, E. P.; Gledhill, M.; Tappin, A. D.; House, W. A.; Worsfold, P. J. Comparison of sample storage protocols for the determination of nutrients in natural waters. *Water Res.* **2001**, *35*, 3670−3678.

(5) Jarvie, H. P.; Withers, P. J. A.; Neal, C. Review of robust measurement of phosphorus in river water: Sampling, storage, fractionation and sensitivity. *Hydrol. Earth Syst. Sci.* **2002**, *6*, 113−131.

(6) Davison, W.; Zhang, H. *In situ* speciation measurements of trace components in natural waters using thin-film gels. *Nature* **1994**, *367*, 546−548.

(7) Sui, D. P.; Fan, H. T.; Li, J.; Li, Y.; Li, Q.; Sun, T. Application of poly(ethyleneimine) solution as a binding agent in DGT technique for measurement of heavy metals in water. *Talanta* **2013**, *114*, 276−282.

(8) Hutchins, C. M.; Panther, J. G.; Teasdale, P. R.; Wang, F.; Stewart, R. R.; Bennett, W. W.; Zhao, H. Evaluation of a titanium dioxide-based DGT technique for measuring inorganic uranium species in fresh and marine waters. *Talanta* **2012**, *97*, 550−556.

(9) Liang, S.; Guan, D. X.; Ren, J. H.; Zhang, M.; Luo, J.; Ma, L. Q. Effect of aging on arsenic and lead fractionation and availability insoils: Coupling sequential extractions with diffusive gradients in thin-films technique. *J. Hazard. Mater.* **2014**, *273*, 272−279.

(10) Mongin, S.; Uribe, R.; Puy, J.; Cecília, J.; Galceran, J.; Zhang, H. Key role of the resin layer thickness in the lability of complexes measured by DGT. *Environ. Sci. Technol.* **2011**, *45*, 4869−4875.

(11) Panther, J. G.; Stewart, R. R.; Teasdale, P. R.; Bennett, W. W.; Welsh, D. T.; Zhao, H. Titanium dioxide-based DGT for measuring dissolved As(V), V(V), Sb(V), Mo(VI) and W(VI) in water. *Talanta* **2013**, *105*, 80−86.

(12) Li, W.; Zhao, H.; Teasdale, P. R.; John, R.; Wang, F. Metal speciation measurement by diffusive gradients in thin films technique with different binding phases. *Anal. Chim. Acta* **2005**, *533*, 193−202.

(13) Liu, J. L.; Feng, X. B.; Qiu, G. L.; Anderson, C. W. N.; Yao, H. Prediction of methyl mercury uptake by rice plants (*Oryza sativa* L.) using the diffusive gradient in thin films technique. *Environ. Sci. Technol.* **2012**, *46*, 11013−11020.

(14) Huynh, T.; Zhang, H.; Noller, B. Evaluation and application of the diffusive gradients in thin films technique using a mixed-binding gel layer for measuring inorganic arsenic and metals in mining impacted water and soil. *Anal. Chem.* **2012**, *84*, 9988−9995.

(15) Li, W.; Li, C.; Zhao, J.; Cornett, R. J. Diffusive gradients in thin films technique for uranium measurements in river water. *Anal. Chim. Acta* **2007**, *592*, 106−113.

(16) Panther, J. G.; Bennett, W. W.; Teasdale, P. R.; Welsh, D. T.; Zhao, H. DGT measurement of dissolved aluminum species in waters: Comparing Chelex-100 and titanium dioxide-based adsorbents. *Environ. Sci. Technol.* **2012**, *46*, 2267−2275.

(17) Li, W.; Teasdale, P. R.; Zhang, S.; John, R.; Zhao, H. Application of a poly(4-styrenesufonate) liquid binding layer for measurement of $Cu^{2+}$ and $Cd^{2+}$ with the diffusive gradients in thin-films technique. *Anal. Chem.* **2003**, *75*, 2578−2583.

(18) Li, W.; Zhao, H.; Teasdale, R. P.; Wang, F. Trace metal speciation measurements in waters by the liquid binding phase DGT device. *Talanta* **2005**, *67*, 571−578.

(19) Fan, H. T.; Sun, T.; Li, W.; Sui, D. P.; Jin, S.; Lian, X. J. Sodium polyacrylate as a binding agent in diffusive gradients in thin-films technique for the measurement of $Cu^{2+}$ and $Cd^{2+}$ in waters. *Talanta* **2009**, *79*, 1228−1232.

(20) Chen, H.; Dong, J.; Niu, Y. X.; Sun, T. Determination of $Ni^{2+}$ in waters with sodium polyacrylate as a binding phase in diffusive gradients in thin-films. *Chem. Res. Chin. Univ.* **2011**, *27*, 703−707.

(21) Fan, H. T.; Bian, Y. Q.; Sui, D. P.; Tong, G. F.; Sun, T. Measurement of free copper(II) ions in water samples with polyvinyl alcohol as a binding phase in diffusive gradients in thin-films. *Anal. Sci.* **2009**, *25*, 1345−1349.

(22) Fan, H.; Sun, T.; Xue, M.; Tong, G.; Sui, D. Preparation of thiol−polyvinyl alcohol and its application to diffusive gradients in thin-films technique. *Chin. J. Anal. Chem.* **2009**, *37*, 1379−1381.

(23) Liu, Y.; Chen, H.; Bai, F.; Gu, J.; Liu, L. Application of sodium poly(aspartic acid) as a binding phase in the technique of diffusive gradients in thin films. *Chem. Lett.* **2012**, *41*, 1471−1472.

(24) Chen, H.; Guo, L.; Zhang, M. H.; Zhong, K. L.; Gu, J. L.; Bo, L.; Li, J. Determination of lead in soybean sauce by the diffusive gradients in thin films technique. *Food. Chem.* **2014**, *165*, 9−13.

(25) Fan, H. T.; Liu, J. X.; Sui, D. P.; Yao, H.; Yang, F.; Sun, T. Use of polymer-bound Schiff base as a new liquid binding agent of diffusive gradients in thin-films for the measurement of labile Cu, Cd, and Pb. *J. Hazard. Mater.* **2013**, *260*, 762−769.

(26) Zhang, H.; Davison, W.; Gadi, R.; Kobayashi, T. *In situ* measurement of dissolved phosphorus in natural waters using DGT. *Anal. Chim. Acta* **1998**, *370*, 29−38.

(27) Menzies, N. W.; Kusumo, B.; Moody, P. W. Assessment of P availability in heavily fertilized soils using the diffusive gradients in thin films (DGT) technique. *Plant Soil* **2003**, *269*, 1−9.

(28) Monbet, P.; McKelvie, I. D.; Worsfold, P. J. Combined gel probes for the *in situ* determination of dissolved reactive phosphorus in porewaters and characterization of sediment reactivity. *Environ. Sci. Technol.* **2008**, *42*, 5112−5117.

(29) Pichette, C.; Zhang, H.; Sauve, S. Using diffusive gradients in thin-films for *in situ* monitoring of dissolved phosphate emissions from freshwater aquaculture. *Aquaculture* **2009**, *286*, 198−202.

(30) Panther, J. G.; Teasdale, P. R.; Bennett, W. W.; Welsh, D. T.; Zhao, H. Titanium dioxide-based DGT technique for *in situ* measurement of dissolved reactive phosphorus in fresh and marine waters. *Environ. Sci. Technol.* **2010**, *44*, 9419−9424.

(31) Ding, S.; Xu, D.; Sun, Q.; Yin, H.; Zhang, C. Measurement of dissolved reactive phosphorus using the diffusive gradients in thin films technique with a high-capacity binding phase. *Environ. Sci. Technol.* **2010**, *44*, 8169−8174.

(32) Mazoniene, E.; Zemaitaitiene, R. J.; Buika, G.; Zemaitaitis, A. Interaction of polyquaternary ammonium salt and persulfate. *Colloid Polym. Sci.* **2004**, *282*, 209−214.

(33) Chen, H.; Zhang, Y. Y.; Zhong, K. L.; Guo, L. W.; Gu, J. L.; Bo, L.; Zhang, M. H.; Li, J. R. Selective sampling and measurement of Cr(VI) in water with polyquaternary ammonium salt as a binding agent in diffusive gradients in thin-films technique. *J. Hazard. Mater.* **2014**, *271*, 160−165.

(34) Guo, L. W.; Chen, H.; Zhang, Y. Y.; Bo, L.; Li, J. R. Determination of chromium speciation in tap water using diffusive gradients in thin film technique. *Chem. Lett.* **2014**, *43*, 849−850.

(35) National Standards of the People's Republic of China. *Water Quality−Determination of Total Phosphorus−Ammonium Molybdate Spectrophotometric Method*; National Standards of the People's Republic of China: Beijing, China, 1989; GB 11893-89.

(36) Scally, S.; Davison, W.; Zhang, H. Diffusion coefficients of metals and metal complexes in hydrogels used in diffusive gradients in thin films. *Anal. Chim. Acta* **2006**, *558*, 222−229.

(37) Chen, H.; Sun, T.; Sui, D. P.; Dong, J. Effective concentration difference model to study the effect of various factors on the effective

diffusion coefficient in the dialysis membrane. *Anal. Chim. Acta* **2011**, *698*, 27−35.
(38) Dorsey, N. E. *Properties of Ordinary Water-Substance in All Its Phases: Water-Vapor/Water and All Ices*; Reinhold Publishing Corporation: New York, 1940.
(39) Bryan, N. D.; Hesketh, N.; Livens, F. R.; Tippinge, E.; Jones, M. N. Metal ion−humic substance interaction: A thermodynamic study. *J. Chem. Soc., Faraday Trans.* **1998**, *94*, 95−100.
(40) Li, W.; Zhao, H.; Teasdale, P. R.; John, R. Preparation and characterization of a poly(acrylamidoglycolic acid-*co*-acrylamide) hydrogel for selective binding of Cu and application to diffusive gradients in thin films measurement. *Polymer* **2002**, *43*, 4803−4809.
(41) Mason, S.; Hamon, R.; Nolan, A.; Zhang, H.; Davison, W. Performance of a mixed binding layer (MBL) for measuring anions and cations in a single assay using the diffusive gradients in thin films technique. *Anal. Chem.* **2005**, *77*, 6339−6346.
(42) Panther, J. G.; Stillwell, K. P.; Powell, K. J.; Downard, A. J. Perfluorosulfonated ionomer-modified diffusive gradients in thin films: tool for inorganic arsenic speciation analysis. *Anal. Chem.* **2008**, *80*, 9806−9811.
(43) Lucas, A.; Rate, A.; Zhang, H.; Salmon, S. U.; Radford, N. Development of the diffusive gradients in thin films technique for the measurement of labile gold in natural waters. *Anal. Chem.* **2012**, *84*, 6994−7000.

al.,[28] and Kane et al.[9] In these publications, the phylogenetic relationship in the genus *Theobroma* is analyzed using isolated DNA from fresh leaf material. The publication by Yang et al.[28] deserves particular mention in this context, because of its similarity to this study. Yang et al. used sequencing to identify SNPs and microsatellites in the plastid genome to identify the origin of Trinitario cultivars.

All cited publications are based on a similar question, and similar DNA-based methods are being used. Although Ecuadorian cocoa types are often objects of publications,[17] the type CCN-51 and the possible mixture of Arriba with the more low-cost CCN-51, in particular, were never mentioned before. The present study combines various approaches of other publications, whereas the sequencing method corresponding to Kane et al. is of particular mention. It was possible to sequence the plastid genome of CCN-51 for the first time. The problem complex of parallel cultivation and, thus, a resulting mixture of the two cocoa types in Ecuador, resulting in interest of the analytical differentiation of Arriba and CCN-51, were also never addressed before.

Other groups who have been involved in work concerning the genome of cocoa are Saski et al.[29] and Argout et al.[1]

## MATERIALS AND METHODS

**CCN-51 and Arriba Samples.** Cocoa bean and leaf samples of CCN-51, Arriba, the parents of CCN-51 (ICS-95, Canelo, and IMC-67), and Criollo were used in this study. A total of 23 leaf samples and 51 bean samples were used. The 8 CCN-51 leaf samples were obtained from the Instituto Nacional de Investicaciones Agropecuarias (INIAP, Guayaquil, Ecuador) and from farms in Naranjal, Ecuador (C1, C2, and C3), from the International Cocoa Germplasm Database (ICGD, University of Reading, England, C4), from the Botanical Garden, Hamburg, Germany (C5 and C6), and from the Centro Agronómico Tropical de Investigación y Enseñanza (CATIE), Cartago, Costa Rica (C7 and C8). The 8 Arriba leaf samples (A1, EET-19; A2, EET-48; A3, EET-62; A4, EET-95; A5, EET-96; A6, EET-103; A7, EET-544; and A8, EET-558) were obtained from the INIAP. The CCN-51 parent samples ICS-95 (E1 and E2) and Canelo (E3 and E4) originated from farms in Naranjal, Ecuador, while the IMC-67 sample (E5) originated from the INIAP. A total of 13 of the 15 CCN-51 bean samples were obtained from the INIAP or were collected on Ecuadorian cocoa farms, and 2 of the 15 CCN-51 bean samples were obtained from the CATIE. All of the 35 Arriba bean samples and 1 of the Criollo bean samples originated from Ecuadorian farms or were contributed by different cocoa producers, such as Lindt & Sprüngli GmbH, Schwartauer Werke GmbH & Co., H.D. Cotterell GmbH & Co. KG, Schlüter & Maack GmbH, Quast & Cons. GmbH & Co. KG, Fassbender & Rausch GmbH, and Alfred Ritter GmbH & Co. KG. The bean samples were obtained fermented, unroasted, and unshelled. The leaf samples were freshly picked, stored, and transported in deep-freeze conditions.

Furthermore, Arriba and bulk chocolate samples were analyzed.

**Chemicals.** In this study, the following chemicals are used: acetonitrile (Merck Millipore, Darmstadt, Germany), agarose (Serva Electrophoresis GmbH, Heidelberg, Germany), bovine serum albumin (BSA) solution (New England Biolabs, Ipswich, MA, USA), bromopenol blue (Merck Millipore, Darmstadt, Germany), cetyl trimethyl ammonium bromide (CTAB) (Sigma-Aldrich GmbH, Seelze, Germany), ethanol (Merck KGaA, Darmstadt, Germany), ethidium bromide (Sigma-Aldrich GmbH, Seelze, Germany), glycerine (Carl Roth GmbH & Co KG, Karlsruhe, Germany), isopropanole (Merck KGaA, Darmstadt, Germany), hydrochloric acid (HCl) (Merck Millipore, Darmstadt, Germany), liquid nitrogen (Linde AG, Hamburg, Germany), sodium acetate (Carl Roth GmbH & Co KG, Karlsruhe, Germany), trichloro-methane (VWR International, Darmstadt, Germany), triethylammonium acetate (Transgenomic, Ltd., Glasgow, UK), tris-(hydroxymethyl)aminomethane (Tris) (Carl Roth GmbH & Co KG, Karlsruhe, Germany), and xylene cyanol (Merck Millipore, Darmstadt, Germany).

**DNA Extraction.** The DNA extraction from beans differs from that of leaves.

*Beans and Chocolate.* A total of 100 mg of crushed beans or chocolate were weighed into a 2 mL Eppendorf tube, and two defatted and autoclaved steel beads ($^1/_8$ in.) were added. The material was processed for 5 min at 30 Hz in a TissueLyser (Qiagen, Hilden, Germany). A total of 1 mL of extraction buffer (55 mM CTAB, 1.4 M NaCl, 0.1 M Tris, and 20 mM $Na_2EDTA$ in double-distilled $H_2O$, adjusted to pH 8.0 with HCl) was added, and the material was processed in the TissueLyser for further 5 min at 30 Hz. After incubation for 30 min at 65 °C in a water bath, 500 μL of chloroform was added. The mixture was vortexed and centrifuged for 5 min at 10000*g*. The supernatant was transferred in a new 2 mL Eppendorf tube. After the addition of 500 μL of isopropanol and vortexing, the mixture was incubated for 30 min at 4 °C. Subsequently, the mixture was centrifuged for 5 min at 10000*g*. The supernatant was decanted and rejected, and isopropanol was removed in the vacuum desiccator for 20 min at 160 mbar. The DNA was solved with 50 μL of double-distilled water and

**Table 1. Primer Sequences Used in This Study**

| sequences for the PCR−RFLP analysis | |
|---|---|
| name | sequence (5′−3′) |
| $8C_{PsiI}$ | Fw: CACCGAAGAACCCTATTTAGAGTCCG |
| | Re: GAGTGGACTAAAGCGTCGGATTGC |
| $17C_{PsiI/AEcoRI}$ | Fw: CGGTGGACAAAGCAAATCTCTTCATC |
| | Re: CGGATTTGAACCGATGACTTACGC |
| $21C_{AseI}$ | Fw: CTCCCTCGGCAAAACTGGGATAAAG |
| | Re: CAGGTGGTTTGGCCAATAGTAGGC |
| $43A_{EcoRI}$ | Fw: GAACCAAAGTTCCAGATTCGATATAG |
| | Re: CATATACTTATGGATCACCATTCCAAG |
| $44C_{EcoRV}$ | Fw: CTCAATCTCGGCCTTATTTCTAAGACAAAAG |
| | Re: CGAAATAGAGTCAATCAACACTATATGGCTC |
| **sequences for the analysis of the $(TAAAG)_n$ repeat** | |
| name | sequence (5′−3′) |
| $(TAAAG)_n$ | Fw: GCAGCACCTTAGGATGGCATAGC |
| | Re: CTCTGGGTGCCTAGGTATCCAC |

**Table 2. Experimental Conditions for the RFLP**

| restriction site | $8C_{PsiI}$ | $17C_{PsiI}$ | $17A_{EcoRI}$ | $21C_{AseI}$ | $43A_{EcoRI}$ | $44C_{EcoRV}$ |
|---|---|---|---|---|---|---|
| enzyme | *Psi*I | *Psi*I | *Eco*RI | *Ase*I | *Eco*RI | *Eco*RV |
| enzyme buffer | 4.1 | 4.1 | *Eco*RI | 3.1 | *Eco*RI | 3.1 |
| enzyme solution | 1.5 μL (7.5 units) | 1.0 μL (5 units) | 1.0 μL (20 units) | 3.0 μL (30 units) | 3.0 μL (60 units) | 4.0 μL (80 units) |
| 1 μL of enzyme solution accords | 5 units | 5 units | 20 units | 10 units | 20 units | 20 units |
| 10× enzyme buffer | 2.5 μL | 2.5 μL | 2.5 μL | 2.5 μL | 2.5 μL | 2.5 μL |
| amplicon | 5.0 μL | 5.0 μL | 5.0 μL | 5.0 μL | 5.0 μL | 5.0 μL |
| ad. double-distilled water | 25 μL | | | | | |


dx.doi.org/10.1021/jf504258w | J. Agric. Food Chem. 2014, 62, 12118−12127

incubated for 1 h at room temperature. After centrifugation for 5 min at 10000*g*, the solution was transferred to a new 2 mL Eppendorf tube.

*Leaves.* The isolation of DNA from leaves was performed using the DNeasy Plant Mini Kit (Qiagen, Hilden, Germany), including all buffers. The leaves were washed, dried, and pestled using liquid nitrogen. A total of 100 mg of the pulverized material was weighed into a 2 mL Eppendorf tube. Two defatted and autoclaved steel beads were added, and the tube was kept in liquid nitrogen for 30 s. The material was processed for 1 min at 30 Hz in a TissueLyser and kept in liquid nitrogen again for 30 s. The material was processed for a further 1 min at 30 Hz in the TissueLyser, vortexed, and centrifuged for 1 min at 18000*g*. A total of 400 μL of buffer AP1 and 4 μL of RNase A stock solution were added, and the mixture was vortexed. After the mixture was incubated for 10 min at 65 °C in a water bath (meanwhile vortexing 2−3 times), 400 μL of buffer A2 was added and the mixture was vortexed. Incubation on ice for 5 min was followed by centrifugation for 5 min at 16000*g*. The supernatant was transferred into a QIAshredder Mini spin column and centrifuged for 5 min at 18000*g*. The flow through was transferred into a new 2 mL tube without disturbing the pellet, and 1.5 volumes of Buffer AW1 was added. The components were mixed by pipetting. A total of 650 μL of this mixture were transferred into a DNeasy Mini spin column placed in a 2 mL collection tube. The mixture was centrifuged for 1 min at 6000*g*, and the flow through was discarded. This step was repeated with the remaining sample. The spin column was placed into a new 2 mL collection tube; 500 μL of buffer AW2 was added; and the sample was centrifuged for 1 min at 6000*g*. The flow through was discarded. Another 500 μL of buffer AW2 was added, and the sample was centrifuged for 2 min at 16000*g*. The spin column was transferred to a new 2 mL tube, and 100 μL of buffer AE was added for elution. The sample was incubated for 5 min at room temperature and centrifuged for 1 min at 6000*g*. The last step was repeated with 50 μL of buffer AE.

For bigger amounts of leaf material, we used the DNeasy Plant Maxi Kit (Qiagen, Hilden, Germany) in the same way according to the protocol of the manufacturer.

**DNA Purity.** The purity of DNA extracts was measured by the 260/280 nm extinction ratio using the SpectraMax M2 fluorimeter (Molecular Devices, Ismaning, Germany). Quotients between 1.7 and 1.9 are typical for pure DNA.[30]

**DNA Concentration.** The DNA concentration of the DNA extracts was measured fluorimetrically using SYBR Green I (Invitrogen, Eugene, OR) diluted 1:6250 in 1× TAE buffer (40 mM Tris and 2 mM EDTA, adjusted to pH 8.2 with HCl) in 96 fluorescence well plates using a SpextraMax M2 fluorimeter (Molecular Devices, Ismaning, Germany). The chosen excitation wavelength was 495 nm, and the detection wavelength was 535 nm.

For the measurement, 90 μL of the diluted SYBR Green I solution was placed into each well and completed with the sample or the calibration solution to a final volume of 100 μL. The calibration stock solution was a plasmid solution with a concentration of 10 ng/μL. A calibration curve (1, 2, 4, 6, 8, and 10 ng/μL) was obtained by corresponding dilution.

The DNA extracts were adjusted with water to a final concentration of 5 ng/μL for PCR and 20−25 ng/μL for sequencing, respectively.

**Qualitative PCR.** A total of 2 μL of the DNA extracts (final concentration of 5 ng/μL) was used for PCR. The PCR reactions were carried out in a final volume of 40 μL. The PCR reaction mix contained 4 μL of 10× buffer [5 mM Tris, 1 mM $MgCl_2$, 25 mM KCl, and 1% Triton X-100 (m/v), adjusted to pH 8.8 with HCl], 3.2 μL of dNTPs [10/2.5 mM each (Bioline GmbH, Luckenwalde, Germany)], 0.4 μL of forward primer, 0.4 μL of reverse primer [100 μM (Life Technologies, Darmstadt, Germany)], and 0.4 μL of 30 unit *Taq* polymerase (Fermentas GmbH, Sankt Leon-Rot, Germany). The PCR reaction mix for the PCR−RFLP also contained 0.4 μL of BSA solution (10 mg/mL). PCR conditions were 94 °C for 5 min, followed by 35 cycles of 94 °C for 40 s, 55 °C for 40 s, 72 °C for 40 s, 72 °C for 1 min, and holding at 4 °C. The PCR was performed in a T3 thermocycler (Biometra, Göttingen, Germany). The primer sequences are given in Table 1.

**Electrophoresis.** The resulting PCR products were mixed with about 1 μL of loading buffer (40 mM Tris, 2 mM EDTA, 50% glycerine, 0.25% bromophenol blue, and 0.25% xylene cyanol, adjusted to pH 8.2) and separated on 3% agarose gel in TAE buffer (40 mM Tris-acetate and 2 mM EDTA, adjusted to pH 8.2) at 170 V for about 20 min. The separated PCR products were stained using ethidium bromide (0.001%) and visualized under ultraviolet (UV) light with a wavelength of 312 nm.

**Sequence Analysis: Whole Chloroplast Genome.** DNA was isolated from deep-frozen leaf material using the DNeasy Plant Mini or Maxi Kit (Qiagen, Hilden, Germany); see DNA Extraction for Leaves. The DNA extracts were purified by ethanol precipitation: the extract was mixed with 0.1 vol of 3 M sodium acetate solution and 3 vol of absolute ethanol. After incubation for 12−16 h at −20 °C, the mixture was pelletized for 60 min at 15000*g* and 4 °C. The supernatant was discarded. The pellet was washed with cold ethanol (4 °C) and centrifuged for 10 min at 15000*g* and 4 °C. The supernatant was discarded. The pellet was dried for 15 min at 37 °C and solved with water by incubation with gentle agitation for 10 min at 50 °C. The DNA concentration of the isolates was adjusted to 200 ng/μL by diluting or simple concentration at the speed vac. Sequencing was carried out by GATC Biotech AG, Konstanz, Germany. The obtained sequences (FASTA format) were compared using VectorNTI. In addition, we compared the sequences to all cholorplast genome sequences available at the National Center for Biotechnology Information (NCBI).

**Sequence Analysis: $(TAAAG)_n$.** PCR was performed using the primer pair $(TAAAG)_n$ (see Table 1) using the conditions for qualitative PCR, as described above. PCR products were purified using the peqGOLDGel Extraction Kit (PEQLAB Biotechnologie GmbH, Erlangen, Germany) according to the instructions of the manufacturer. The DNA concentrations of the PCR products were adjusted to 20−25 ng/μL using a speed vac. Sanger sequencing was carried out by GATC Biotech AG, Konstanz, Germany.

**Sequence Analysis: IRR.** PCR was performed using the primer pairs described by Dhingra et al.[31] and using the conditions for qualitative PCR, as described above. PCR products were prepared for the sequencing by an enzymatic degeneration of the primer and the dNTPs: 40 μL of the PCR product were mixed with 4 μL of *Exo*I and 8 μL of FastAP. The mixture was incubated for 15 min at 37 °C and then for 15 min at 85 °C. Sequencing was carried out by GATC Biotech AG, Konstanz, Germany. The obtained sequences were compared together and with the sequences of the published chloroplast genomes up to this point in time (accession numbers NC_014676 and HQ336404).

**dHPLC.** For the detection of PCR products by dHPLC (using a Wave Nucleic Acid Fragment Analysis System, Transgenomic, Glasgow, U.K.), 10 μL of the solution was filled into caps and carried over in the chilled rack. The run was performed using the gradient for the running buffers A [0.05% triethylammonium acetate (TEAA) solution] and B (0.05% TEAA and 0.25% acetonitrile solution). Experimental conditions for the buffer composition for the dHPLC analysis are 0.0 min: A, 50.2%; B, 49.8%; 0.7 min: A, 41.8%; B, 58.2%; 3.8 min: A, 41.8%; B, 58.2%; 4.0 min: A, 38.2%; B, 61.8%; 4.1 min: A, 40.8%; B, 59.2%; 4.2 min: A, 41.8%; B, 58.2%; and 4.3 min: A, 55.0%; B, 45.0%.

**CGE.** Detection of PCR products by CGE was carried out with an Experion System (Bio-Rad Laboratories GmbH, Munich, Germany) according to the instructions of the manufacturer using the Experion DNA 1K Analysis Kit (Bio-Rad Laboratories GmbH, Munich, Germany).

**PCR−RFLP.** Primers for the corresponding enzymes are given in Table 1. The PCR was performed as described above (qualitative PCR), and the PCR products were analyzed by AGE (see above). The restriction enzymes *Psi*I, *Eco*RI, *Ase*I, and *Eco*RV were obtained from New England Biolabs GmbH (Frankfurt, Germany) and used along with the supplied buffer. The amounts of restriction enzyme for the digestion of 5 μL of PCR products with 2.5 μL of corresponding NEB buffer are shown in Table 2. The PCR reaction mix was incubated at 37 °C for 3 h in a final reaction volume of 25 μL. The restriction enzyme was then heat-inactivated for 20 min at 65 °C.

Plastid DNA can not only be identified in the cocoa leaves but also in the cocoa beans. That means all DNA-based methods can be carried out not only in fresh plant materials. DNA is that stable, that it can be amplified by PCR also after technological treatments e.g. fermentation and roasting. This fact is highly important for the application of the methods described above for quality control in the food industry.

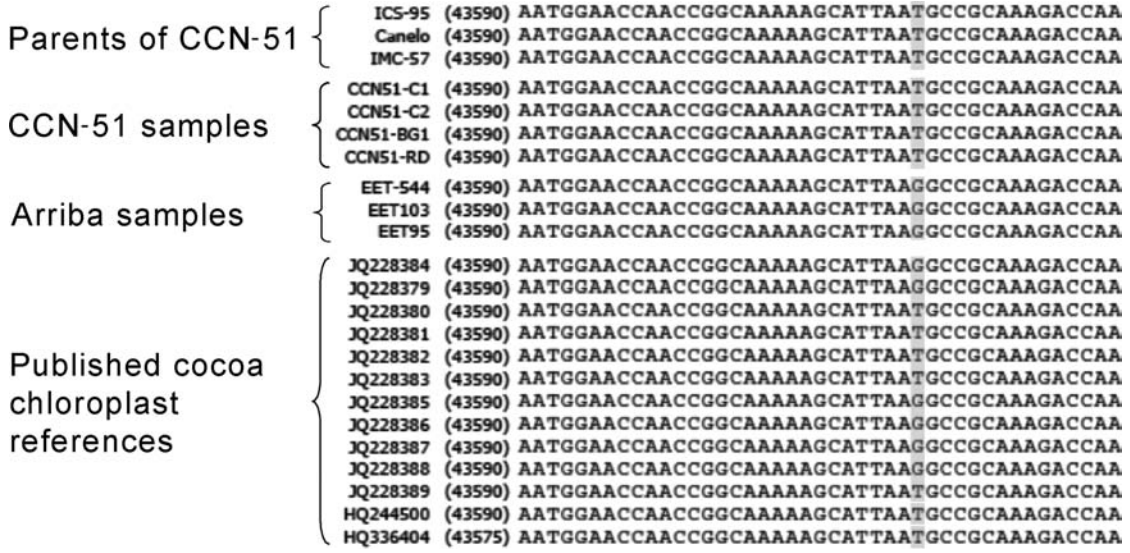


**Figure 1.** Section of the alignment of 10 chloroplast genomes of Arriba, CCN-51, the parents of CCN-51 sequenced in this study, and 13 published cocoa chloroplast genomes: Criollo-22 (JQ228379), Amelonado (JQ228380), ICS-01 (JQ228381), Scavina-6 (JQ228382), ICS-06 (JQ228383), EET-64 (JQ228384), Stahel (JQ228385), Pentagonum (JQ228386), ICS-39 (JQ228387), *T. grandiflorum* (JQ228388), JQ228389, HQ336404, and Scavina-6 (HQ244500).

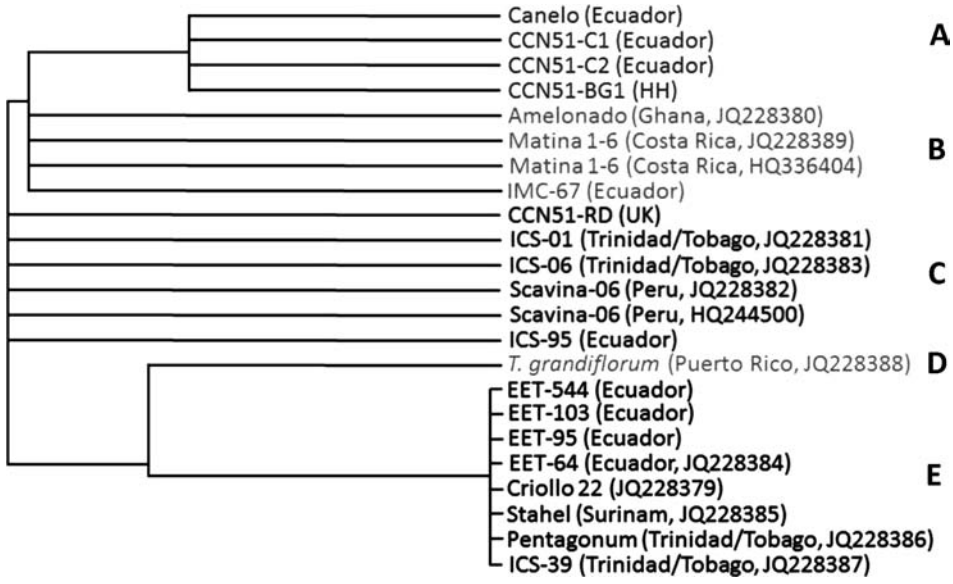


**Figure 2.** Phylogenetic tree of cocoa types based on the alignment of the chloroplast genomes of different cocoa types.

## RESULTS AND DISCUSSION

**Cocoa Samples and DNA Extracts.** The DNA of 23 leaf and 51 bean samples from a number of sources was isolated by two methods: one for leaves and one for beans (see above). Both DNA extraction methods were successful; i.e., it was possible to isolate DNA. The DNA yields of the leaf sample were much higher than those of the bean samples; the purity of both were similar (about $E_{260\ nm}/E_{280\ nm}$ = 1.6). The DNA yield of the extracts varied across a large range (between $c$ = 20 and 900 ng/$\mu$L), which did not influence the PCR.

**Sequencing of 10 Chloroplast Genomes of *T. cacao*.** DNA is a suitable biomarker because of the fact that it is unique for each organism and stable within the time frame relevant for food analysis. As indicated above, besides the nuclear DNA, plant cells contain plastid DNA.[32] In this sort of DNA, a higher genetic variability is assumed,[33] which is an advantage for the discrimination between two very closely related organisms, such as CCN-51 and Arriba cocoa varieties.

To find a difference in the chloroplast genome between CCN-51 and Arriba, the sequence of the genome must be known; therefore, the whole genome must be sequenced. Usually, the plastid DNA must be isolated from the nuclear DNA. Efforts to separate plastid DNA from nuclear DNA using the Chloroplast Isolation Kit (Sigma-Aldrich, Hamburg, Germany) according to the descriptions in other publications were not successful.[34,35] Chloroplasts were isolated from cocoa leaves, and the DNA was extracted from them in correspondence with the DNA extraction of beans. However, the yield of DNA was not sufficient (less than 5 $\mu$g), and nuclear DNA was co-extracted.

Kane et al. described a method for sequencing the whole chloroplast genome by next-generation sequencing, despite the presence of nuclear DNA. It is called "low-coverage whole

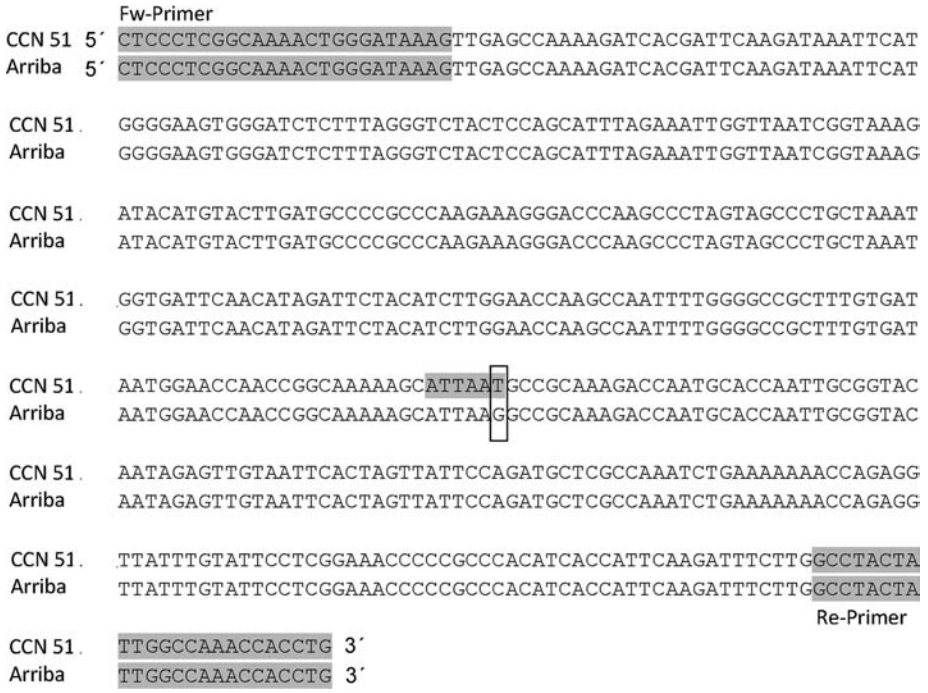


**Figure 3.** Schematic figure of a CCN-51-specific restriction site. This cocoa type includes the recognition sequence for the restriction enzyme *Ase*I. In the cocoa type Arriba, this recognition sequence is disturbed by a SNP. The *Ase*I recognition site is highlighted gray, and the SNP is boxed.

genome shotgun sequencing".[9] In a plant cell, the nuclear genome appears in the cell nucleus in a defined copy number, while the plastid genome occurs in the chloroplasts at a higher copy number. A *T. cacao* cell contains about three to four chloroplasts,[36,37] and each chloroplast disposes of about 70 copies of the plastid genome. At a size of about 160 kbp, the cocoa plastid genome is significantly smaller than the nuclear genome, which has a size of about 330 Mbp.[1] However, as a consequence of low coverage during sequencing, the high copy fraction (the plastid genome) becomes sequenced.

On the basis of this method, the whole chloroplast genome sequences for 10 leaf samples were obtained: 4 CCN-51 samples (2 from Naranjal, Ecuador, 1 from the ICGD, and 1 from the Botanical Garden, Hamburg), 3 Arriba samples (EET-95, EET-103, and EET-544 from the INIAP), and 3 parents of CCN-51 (IMC-67 from the INIAP and ICS-95 and Canelo from Naranjal, Ecuador). The 10 obtained sequences were aligned with 13 already published sequences of the cocoa chloroplast genome. Types of the already published sequences are Criollo-22 (JQ228379), Amelonado (JQ228380), ICS-01 (JQ228381), Scavina-6 (JQ228382), ICS-06 (JQ228383), EET-64 (JQ228384), Stahel (JQ228385), Pentagonum (JQ228386), ICS-39 (JQ228387), and *Theobroma grandiflorum* (JQ228388).

This alignment served as a basis for a search for sequence differences between CCN-51 and Arriba to allow for differentiation between the two types. Figure 1 shows a detail of the obtained data file.

This alignment was also the basis for the development of a phylogenetic tree with which the degree of relationship of the different cocoa types was analyzed. The developed phylogenetic tree is shown in Figure 2. The sequenced Arriba samples form one group with other samples (group E). Similarly, the sequenced CCN-51 samples form a group with one of the parents of CCN-51 Canelo (group A), with the exception of one sample. This CCN-51 sample is located in the group of another parent of CCN-51 (ICS-95). Reasons for this are discussed in the next section.

**SNPs in the Chloroplast Genome.** After analyzing the alignment, we could not find differences between Arriba and CCN-51 that extended over several neighboring base pairs; therefore, the development of a PCR with specific primers was not possible. The only distinctions between the two cocoa types were SNPs. Approximately 30−50 SNPs were determined, corresponding to about 0.03% of the 160 kbp of the chloroplast genome of the cocoa. These SNPs can be used to develop a PCR−RFLP[30,38−40] for differentiation. In this context, it is of vital importance that about five to seven of the 30−50 SNPs are located in the recognition sequences of restriction enzymes. Because of the fact that the method development focused on detecting CCN-51, a SNP that was located in a recognition sequence in the PCR product of CCN-51 was chosen.

We developed five PCR−RFLPs based on five SNPs, which are found in the recognition sequence of a restriction enzyme. Three of these five PCR−RFLP were CCN-51-specific (numbers 8, 21, and 44); one was Arriba-specific (number 43); and one was CCN-51-specific as well as Arriba-specific (number 17). This means that there were two recognition sequences for two restriction enzymes around the SNP and that, depending upon the restriction enzyme used, both CCN-51 (*Psi*I as the applied enzyme) or Arriba (*Eco*RI as the applied enzyme) could be detected. Figure 3 exemplifies one of the CCN-51-specific SNPs, which matches the ATTAAT recognition sequence of the *Ase*I restriction enzyme. Using this enzyme, the PCR product with a size of 436 bp is digested to two smaller fragments of 265 and 171 bp (see Figure 4), whereas the PCR product of Arriba with the size of 436 bp is detected just as before the RFLP (see Figure 4).

The detection limit of the method (carried out with the enzyme *Ase*I) could be determined using well-defined mixtures; even when constituting only 1% in the mixture, CCN-51 was detected.

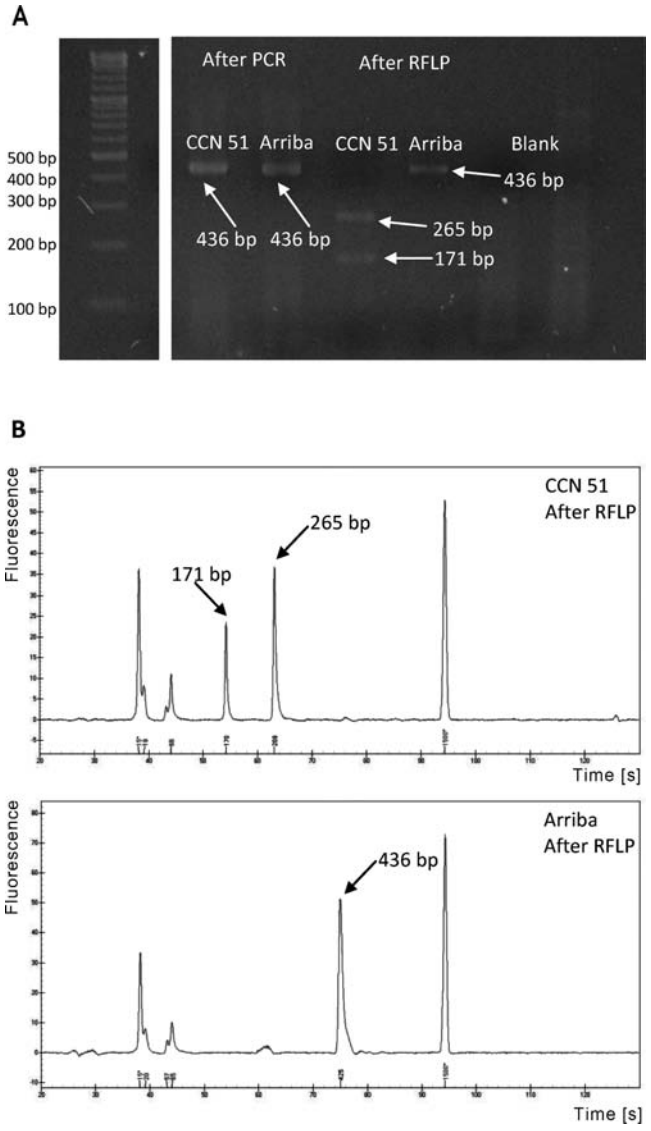


**Figure 4.** Different methods for detecting the amplicons and fragments of Arriba (A) and CCN-51 (C): A, AGE; B, CGE after the PCR–RFLP based on SNPs in the chloroplast genome. PCR product of CCN-51 and Arriba with a size of 436 bp, which includes a SNP, is digested using the restriction enzyme *Ase*I. The CCN-51 DNA fragment includes the correct recognition sequence, leading to two fragments of 265 and 171 bp. The recognition site for *Ase*I is not present in the Arriba sequence, which is why the PCR product is not digested by this enzyme.

The method development was carried out with one Arriba and one CCN-51 leaf sample and was verified using a total of 16 leaf samples and 51 bean samples. Within the leaf samples, 7 of 8 CCN-51 samples showed the expected CCN-51-specific result and 1 CCN-51 sample showed the Arriba-specific result. A total of 6 of 8 Arriba samples showed the expected Arriba-specific result, and 2 Arriba samples showed the CCN-51-specific result. Within the bean samples, 15 of 16 CCN-51 samples showed the expected CCN-51-specific result and 1 CCN-51 sample showed the Arriba-specific result. A total of 16 of 35 Arriba bean samples showed the expected Arriba-specific result and 19 showed the CCN-51-specific result.

In general, the leaf samples showed more homogeneous results than the bean samples, which is assumed to have one main reason: the origin of the leaves can be determined with 100%

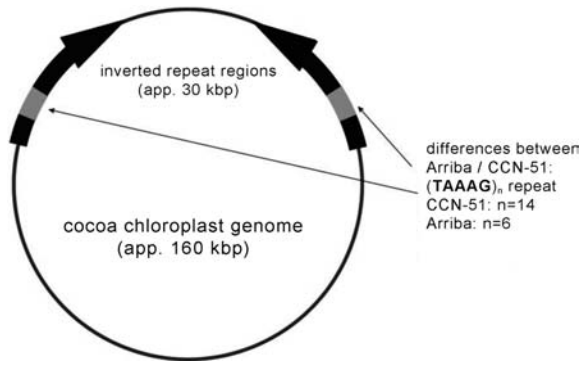


**Figure 5.** Schematic figure of the IRR in the cocoa chloroplast genome, in which the $(TAAAG)_n$ repeat with its different repetitions in CCN-51 ($n$ = 14) and Arriba ($n$ = 6) can be found.

certainty because they were picked by hand from trees that could be classified morphologically as CCN-51 or Arriba. This was different for the bean samples: they were provided to us by cocoa-processing or cocoa-trading companies after several processing steps, such as fermentation and drying. Because of the fact that we did not take the bean samples from the tree, we cannot be sure that they were pure Arriba or pure CCN-51 samples as declared. In fact, our analyses show the relevance of the research field because already the samples seem to be mixtures of both cocoa types or rather Arriba adulterated with CCN-51.

The bean samples from Costa Rica were an exception. Their origin can be considered assured because the raw beans were taken from a fresh fruit whose origin was definitely a CCN-51 tree. Unexpected results within the leaf and the bean samples from Costa Rica must have other reasons. Deviations in Arriba samples may stem from their partially sexual reproduction during which SNPs can develop naturally. This could cause an Arriba sample to behave like a CCN-51 sample. However, this does not apply to CCN-51 samples because this organism is a clone, which is vegetatively reproduced using grafting. Hence, all samples should have an identic genome, and there should not be any differences within the results of CCN-51 samples. It is therefore open to discussion whether the organism CCN-51 really is a pure clone. This question will be verified using the analysis of microsatellites discussed. Microsatellites are short and non-coding sequences that repeat on the same locus present in the chloroplast and in the nuclear genome.[19,41−43]

All five sample of the parents of CCN-51 (ICS-95, Canelo, and IMC-67) showed the CCN-51-specific result for all PCR–RFLP methods, except for one little incident, in which, for only PCR–RFLP number 17, the ICS-95 and IMC-67 samples showed the Arriba-specific result. Because of the accordance of the results of the parents and the CCN-51 samples, it is becoming clear that the SNPs originate from the parents and were not developed during their cultivation in the 1960s. Hence, these SNPs can be valuated as stable traits with a high value as a marker for CCN-51.

**$(TAAAG)_n$ Repeat in the IRR.** Another aberration detected in the sequence of the chloroplast genome between Arriba and CCN-51 is located in the so-called IRR and is represented in Figure 5. The IRR is a sequence that is reverse opposite complementary to another sequence that is located in the same genome. The IRR is typical for chloroplasts and in the cocoa chloroplast genome, and the IRR has a size of about 30 kbp,[31] corresponding to a percentage of about 37%.

**Figure 6.** Alignment of the $(TAAAG)_n$ repeat in the two cocoa types CCN-51 and Arriba. The 5 bp repeat is repeated 14 times in CCN-51 and 6 times in Arriba.

Analyzing the number of repeats using ultra-barcoding at a given target genome is not possible; therefore, we sequenced the IRR separately from the whole chloroplast genome. First, this region was partially sequenced for one CCN-51 and one Arriba sample according to the publication by Dhingra et al., using 27 primer pairs.[31] The obtained two sequences of CCN-51 and Arriba were aligned. We discovered a difference that is shown in the alignment in Figure 6. The IRR includes a sequence 5 bp long, the $(TAAAG)_n$ repeat, which is repeated with varying frequency. In the sequence of the CCN-51 sample, the $(TAAAG)_n$ repeat is repeated 14 times. In that of the Arriba sample, the $(TAAAG)_n$ repeat is repeated 6 times. The obtained result was verified by partial sequencing. A PCR was carried out with the isolates of the CCN-51 and Arriba leaf samples, in which the primer pair flanks the $(TAAAG)_n$ repeat (see Table 1). After sequencing the amplicons, we determined that the $(TAAAG)_n$ repeat appeared 6 times out of 8 Arriba leaf samples. In 6 of 6 CCN-51 leaf samples, the $(TAAAG)_n$ repeat appeared 14 times. This result corresponds to our expectations, because it is congruent with the result of the sequencing of the single CCN-51 and Arriba samples according to the publication by Dhingra et al. (see above and Figure 6). For this reason, the different repetition of the $(TAAAG)_n$ repeat was evaluated as a suitable basis for the development of a method for discrimination between the two cocoa types. PCR products were generated for both cocoa types using a PCR region with a broad margin around the $(TAAAG)_n$ repeat (primer sequences; see Table 1) . In the following step, the obtained PCR products were detected by AGE, CGE, or dHPLC.[13] Dependent upon the cocoa type, one can observe amplicons that differ by 40 bp (CCN-51, 151 bp; Arriba, 111 bp) because the 5 bp long sequence $(TAAAG)_n$ is repeated 14 times in CCN-51 $[(TAAAG)_{14}]$ and 6 times in Arriba $[(TAAAG)_6]$. The three different detection methods AGE, CGE, and dHPLC for the amplicons of CCN-51 and Arriba are shown in Figure 7. The specific bands and peaks for Arriba and CCN-51 appear in the graphic.

The developed method with the three different detection methods for the amplicons was applied to a large volume of sample material. The summarized results are shown in Tables 3 and 4. Within the leaf samples, 5 of 6 CCN-51 samples showed the CCN-51-specific result with an amplicon of 151 bp as expected and 8 of 8 Arriba samples showed the expected result with an amplicon of 111 bp. A total of 3 of the 5 parent samples of CCN-51 showed the Arriba-characteristic result (111 bp), and the other 2 showed the CCN-51-specific result. Therefore, maternal inheritance of plastids[44] could be taken into consideration by the cocoa type Canelo, which shows the CCN-51-specific result. For the Criollo sample, the Arriba-characteristic amplicon was observed. Within the bean samples, 7 of 8 CCN-51 samples showed the CCN-51-specific amplicon of 151 bp and 1 sample showed the Arriba-characteristic result (111 bp). A total of 12 of 13 Arriba bean samples showed the Arriba-specific amplicon (111 bp), and 1 Arriba sample showed the CCN-51-characteristic amplicon (151 bp). For the Criollo sample, the Arriba-characteristic amplicon was observed. For both cocoa types, we detected one exception within the bean samples. The reasons for this are the same as those described for the PCR−RFLP methods based on SNPs in the chloroplast genome. Polymorphisms within the Arriba samples can be explained by sexual reproduction. Polymorphisms should not appear within CCN-51 samples because CCN-51 is defined by the breeders to be a clone. For this organism, all samples should produce the same result. A closer examination of this phenomenon is described in the conclusion.

In a number of PCR experiments and the following detection of the $(TAAAG)_n$ repeat, an additional band/peak with a size of about 100−105 bp was detected. This additional band/peak can be explained by stuttering or slipping of the polymerase during the replication.[45] Nevertheless, the identification of the cocoa types was successful because the CCN-51- or Arriba-specific bands/peaks at 111 and 151 bp were visible, despite the appearance of this more or less broad band/peak.

**Quantitation.** Having established the two methods for qualitative differentiation of the two cocoa types, their ability to quantitate the content of CCN-51 in mixtures of both types was assessed. For this, selected mixtures of both cocoa types with a content of 10, 30, 50, 70, and 90% CCN-51 were analyzed with both methods, on the one hand, with the method based on the $(TAAAG)_n$ repeat in the IRR and, on the other hand, with the PCR−RFLP method based on SNPs in the chloroplast genome.

However, it was not possible to determine the exact content of CCN-51 in the mixture. Only semi-quantitative estimations were possible. The major problem with quantitation using the $(TAAAG)_n$ repeat was the described additional stutter band at about 100−105 bp. This band could not be attributed to either of the two cocoa types and was not consistently intense. Using the PCR−RFLP method, a correct tendency could be established; with an increasing content of CCN-51, the peak area of the two

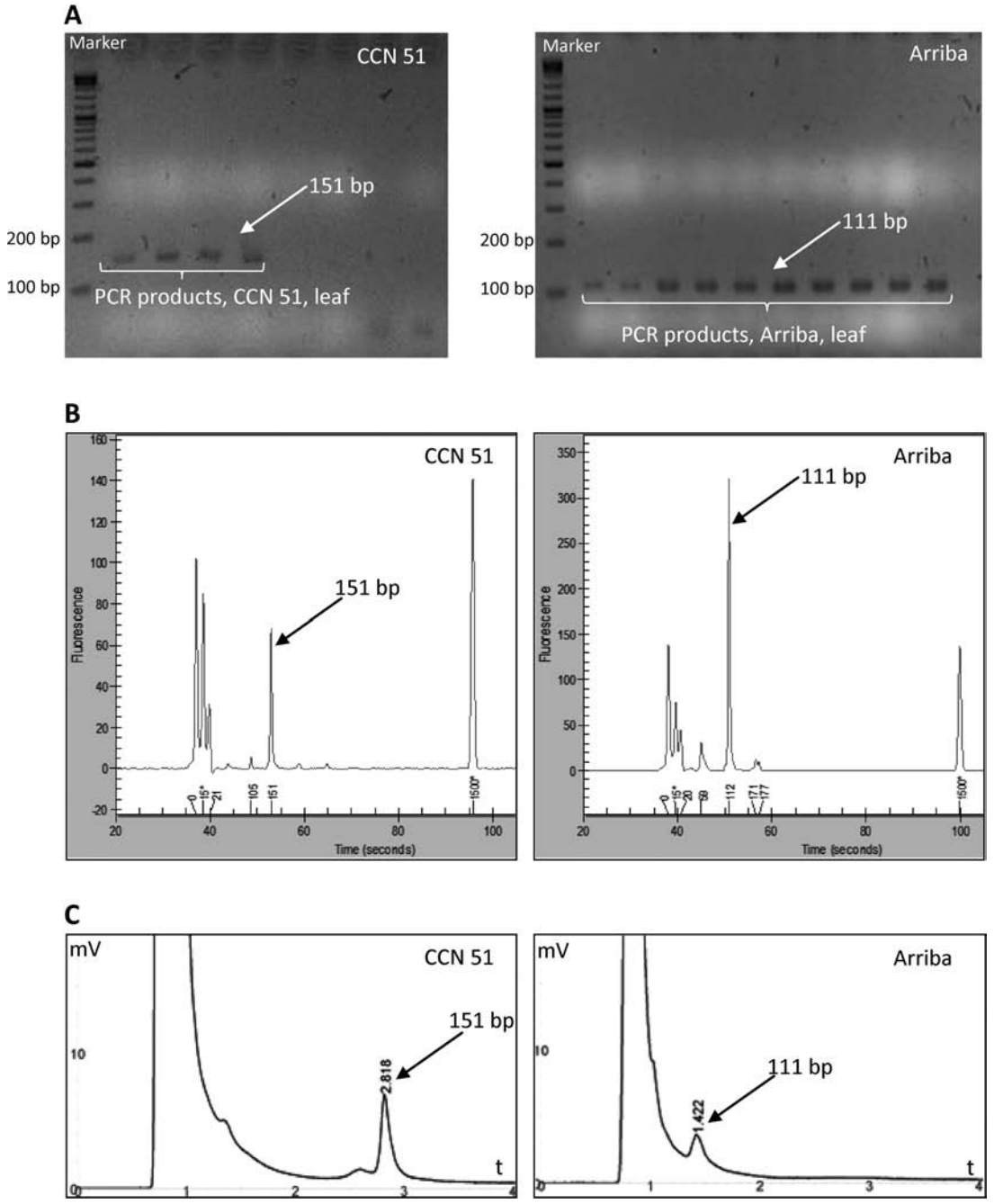


**Figure 7.** Different methods for detecting the amplicons of Arriba and CCN-51: A, AGE; B, CGE; and C, dHPLC. Because of the fact that the $(TAAAG)_n$ is repeated 14 times in CCN-51 and 6 times in Arriba, the size of the amplicons differs by 40 bp: band or peak for CCN-51, 151 bp; band or peak for Arriba, 111 bp.

CCN-51 characteristic fragments rose. However, a quantitation of the exact CCN-51 content was not possible. One reason for this was an inconsistent formation of heteroduplexes,[14] the peak area of which amounted to 15−30%. Another reason why this method is not appropriate for quantitation could be the yield from the isolation of DNA and the grinding of the sample material. It cannot be guaranteed that these two processes are always carried out to an equal extent for CCN-51 and Arriba. This issue is relevant for the cocoa beans and the cocoa liquor made from them, the sample material focused on by the analytics. Neither of the methods can serve as a basis for quantitation of the CCN-51 content in mixtures of both cocoa types. However, a semi-quantitative estimation is possible.

## AUTHOR INFORMATION

### Corresponding Author

*Telephone/Fax: +49-40-428384342. E-mail: markus.fischer@chemie.uni-hamburg.de.

### Funding

This research project was supported by the German Ministry of Economics and Technology (via AiF) and the FEI (Forschungskreis der Ernährungsindustrie e.V., Bonn). Project AiF 16796 N.

### Notes

The authors declare no competing financial interest.

**Table 3. Results of the Analysis of the Leaf Samples of CCN-51 (C) and Arriba (A) Concerning the Repetition of the $(TAAAG)_n$ Repeat in the IRR**

| leaf samples | | | | | |
|---|---|---|---|---|---|
| sample | sort | results of AGE | results of CGE | results of dHPLC | accordance |
| C1 | C | C | C | C | yes |
| C2 | C | C | C | C | yes |
| C3 | C | C | C | C | yes |
| C4 | C | C | C | C | yes |
| C5 | C | C | C | C | yes |
| C6 | C | C | C | C | yes |
| A1 | A | A | A | A | yes |
| A2 | A | A | A | A | yes |
| A3 | A | A | A | A | yes |
| A4 | A | A | A | A | yes |
| A5 | A | A | A | A | yes |
| A6 | A | A | A | A | yes |
| A7 | A | A | A | A | yes |
| A8 | A | A | A | A | yes |
| E1 | ICS-95 | A | A | A | yes |
| E2 | ICS-95 | A | A | A | yes |
| E3 | Canelo | C | C | C | yes |
| E4 | Canelo | C | C | C | yes |
| E5 | IMC-67 | A | A | A | yes |
| Cr1 | Criollo | A | A | A | yes |

**Table 4. Results of the Analysis of the Bean Samples of CCN-51 (C) and Arriba (A) Concerning the Repetition of the $(TAAAG)_n$ Repeat in the IRR**

| bean samples | | | | | |
|---|---|---|---|---|---|
| sample | sort | results of AGE | results of CGE | results of dHPLC | accordance |
| C1 | C | C | C | C | yes |
| C2 | C | C/A | C | C/A | mix |
| C3 | C | C | C | C | yes |
| C4 | C | A | A | A/C | no |
| C5 | C | C | C | C | yes |
| C6 | C | C | C | C | yes |
| C7 | C | C | C | C | yes |
| C8 | C | C | C | C | yes |
| A1 | A | A | A | A | yes |
| A2 | A | C | C | C/A | no |
| A4 | A | A/C | A/C | A/C | mix |
| A5 | A | A | A | A | yes |
| A6 | A | A | A | A | yes |
| A7 | A | A | A | A | yes |
| A8 | A | A | A | A | yes |
| A9 | A | A | A | A | yes |
| A10 | A | A | A | A | yes |
| A11 | A | A/C | A/C | A/C | mix |
| A12 | A | A | A | A | yes |
| A13 | A | A | A | A | yes |
| A14 | A | A/C | A/C | A/C | mix |
| Cr1 | Criollo | A | A | A | yes |

## ■ ACKNOWLEDGMENTS

Cocoa leaf material was obtained from the INIAP, from the CATIE, from the Botanical Garden, Hamburg, and from the ICGD. Cocoa bean material was kindly provided by Lindt & Sprüngli GmbH, Aachen, Germany; Hachez Chocolade GmbH & Co. KG, Bremen, Germany; Alfred Ritter GmbH & Co. KG, Waldenbuch, Germany; Fassbender & Rausch GmbH, Berlin, Germany; Schlüter & Maack GmbH, Hamburg, Germany; Transmar Group/Euromar Commidities GmbH, Fehrbellin, Germany; H. D. Cotterell GmbH & Co. KG, Hamburg, Germany; Quast & Cons. GmbH & Co. KG, Hamburg, Germany; and H.C.C.O. GmbH, Hamburg, Germany. Further, we greatly acknowledge the Stiftung der Deutschen Kakao- und Schokoladenwirtschaft, Bonn, Germany; the LCI des Bundesverbandes der Deutschen Süßwarenindustrie e. V., Köln, Germany; the BDSI e. V., Bonn, Germany; and the giz GmbH, Bonn, Germany. We thank R. Matissek for helpful discussion.

## ■ ABBREVIATIONS USED

AFLP, amplified fragment length polymorphic; AGE, agarose gel electrophoresis; CCN-51, Colección Castro Naranjal 51; CGE, capillary gel electrophoresis; dHPLC, denaturating high-performance liquid chromatography; DNA, deoxyribonucleic acid; IRR, inverted repeat region; PCR, polymerase chain reaction; RAPD, random amplified polymorphic DNA; RFLP, restriction fragment length polymorphism; SNP, single nucleotide polymorphism; SSR, simple sequence repeats; TEAA, triethylammonium acetate

## ■ REFERENCES

(1) Argout, X.; Salse, J.; Aury, J. M.; Guiltinan, M. J.; Droc, G.; Gouzy, J.; Allegre, M.; Chaparro, C.; Legavre, T.; Maximova, S. N.; Abrouk, M.; Murat, F.; Fouet, O.; Poulain, J.; Ruiz, M.; Roguet, Y.; Rodier-Goud, M.; Barbosa-Neto, J. F.; Sabot, F.; Kudrna, D.; Ammiraju, J. S.; Schuster, S. C.; Carlson, J. E.; Sallet, E.; Schiex, T.; Dievart, A.; Kramer, M.; Gelley, L.; Shi, Z.; Bérard, A.; Viot, C.; Boccara, M.; Risterucci, A. M.; Guignon, V.; Sabau, X.; Axtell, M. J.; Ma, Z.; Zhang, Y.; Brown, S.; Bourge, M.; Golser, W.; Song, X.; Clement, D.; Rivallan, R.; Tahi, M.; Akaza, J. M.; Pitollat, B.; Gramacho, K.; D'Hont, A.; Brunel, D.; Infante, D.; Kebe, I.; Costet, P.; Wing, R.; McCombie, W. R.; Guiderdoni, E.; Quetier, F.; Panaud, O.; Wincker, P.; Bocs, S.; Lanaud, C. The genome of *Theobroma cacao*. *Nat. Genet.* **2011**, *43*, 101−108.

(2) International Cocoa Organization (ICCO). *International Cocoa Agreement*; ICCO: London, U.K., 2010.

(3) International Cocoa Organization (ICCO). *ICCO Annual Report 2010/2011*; ICCO: London, U.K., 2011.

(4) Kakaoverein. *Geschäftsbericht 2011/2012*; Kakaoverein: Hamburg, Germany, 2012.

(5) Cook, L. R. *Chocolate Production and Use*; Harcourt: San Diego, CA, 1982; Vol. *1*.

(6) Stern, J. G. *The History of CCN-51 in Ecuador*, 2011; www.jeffreygstern.com.

(7) Sütterlin, S. *Eine Frage des Geschmacks*; Berliner Zeitung: Berlin, Germany, 2006.

(8) Herrmann, R. G. Multiple amounts of DNA related to the size of chloroplasts I. An autoradiographic study. *Planta* **1970**, *90*, 80−96.

(9) Kane, N.; Sveinsson, S.; Dempewolf, H.; Yang, J. Y.; Zhang, D.; Engels, J. M. M.; Cronk, Q. Ultra-barcoding in cacao (*Theobroma* spp.; Malvaceae) using whole chloroplast genomes and nuclear ribosomal DNA. *Am. J. Bot.* **2012**, *99*, 320−329.

(10) McBride, E. K.; Stalker, M. D. Increased expression in plant plastid. WO Patent 1995024493 A1, 1995.

(11) Marino, A. M.; Turni, L. A.; Del Rio, S. A.; Williams, P. E. Molecular size determinations of DNA restriction fragments and polymerase chain reaction products using capillary gel electrophoresis. *J. Chromatogr. A* **1994**, *676*, 185−189.

(12) Zhang, X.; McGown, L. B. Sequence-based separation of single-stranded DNA using nucleotids in capillary electrophoresis: Focus on phosphate. *Electrophoresis* **2013**, *34*, 1778−1786.

(13) Goldenberg, O.; Herrmann, S.; T, A.; Marjoram, G.; Hong, G.; Göbel, U. B.; Graf, B. Use of denaturating high-performance liquid

chromatography for rapid detection and identification of seven *Candida* species. *J. Clin. Microbiol.* **2005**, *43*, 5912−5915.
(14) Xiao, W.; Oefner, P. J. Denaturating high-performance liquid chromatography—A review. *Hum. Mutat.* **2001**, *17*, 439−474.
(15) Botstein, D.; White, R. L.; Skolnick, M.; Davis, R. W. Construction of a genetic linkage map in man using restriction fragment length polymorphisms. *Am. J. Hum. Genet.* **1980**, *32*, 314−331.
(16) Williams, P. E.; Marino, M. A.; Del Rio, S. A.; Turni, L. A.; Devaney, J. M. Analysis of DNA restriction fragments and polymerase chain reaction products by capillary electrophoresis. *J. Chromatogr.* **1994**, *680*, 525−540.
(17) Lerceteau, E.; Flipo, S.; Quiroz, J.; Soria, J.; Pétiard, V.; Crouzilat, D. Genetic differentiation among Ecuadorian *Theobroma cacao* L. accessions using DNA and morphological analyses. *Euphytica* **1997**, 95.
(18) Lerceteau, E.; Robert, T.; Pétiard, V.; Crouzilat, D. Evaluation of the extent of genetic variability among *Theobroma cacao* accessions using RAPD and RFLP markers. *Theor. Appl. Genet.* **1997**, 95.
(19) Lanaud, C.; Risterucci, A. M.; Pieretti, I.; Falque, M.; Bouet, A.; Lagoda, P. J. L. Isolation and characterization of microsatellites in *Theobroma cacao* L. *Mol. Ecol.* **1999**, *8*, 2141−2152.
(20) Saunders, J. A.; Hemeida, A. A.; Mischke, S. USDA DNA fingerprinting programme for identification of *Theobroma cacao* accessions. Bekele, F. L., End, M., Eskes, A., Eds.; *Proceedings of the International Workshop on New Technologies and Cocoa Breeding*; INGENIC Press: London, U.K., 2001; pp 108−114.
(21) Jones, P. G.; Allaway, D.; Gilmour, D. M.; Harris, C.; Rankin, D.; Retzel, E. R.; Jones, C. A. Gene discovery and microarray analysis of cacao (*Theobroma cacao* L.) varieties. *Planta* **2002**, *216*, 255−264.
(22) Alves, R. M.; Artero, A. S.; Sebbenn, A. M.; Figueira, A. Mating system in a natural population of *Theobroma grandiflorum* (Willd. ex Spreng.) Schum. by microsatellite markers. *Genet. Mol. Biol.* **2003**, *26*, 373−379.
(23) Pugh, T.; Follet, C.; Risterucci, A. M.; Brottier, P.; Deletrez, C.; Courtois, B.; Clément, D.; Lamande, P.; N'Goran, J. A. K.; Lanaud, C. A new cacao linkage map based on codominant markers: Development and integration of 201 new microsatellite markers. *Theor. Appl. Genet.* **2004**, *108*, 1151−1161.
(24) Pugh, T. Étude du déséqulilibre de liaison chez le cacaoyer appartenant aux groupes Criollo/Trinitario. Application auu marquage génétique d'intérêt pour la selection. Ph.D. Thesis, École National upérieur d'Argonomie, Montpellier, France, 2005.
(25) Charters, Y. M.; Wilkinson, M. J. The use of self-pollinated progenies as "in-groups" for the genetic characterization of cocoa germplasm. *Theor. Appl. Genet.* **2000**, *100*, 160−166.
(26) Haase, I.; Fischer, M. Differenzierung von *Theobroma cacao* und *Theobroma grandiflorum* mittels PCR. *J. Consum. Prot. Food Saf.* **2007**, *2*, 422−428.
(27) Borrone, J. W.; Kuhn, D. N.; Schnell, R. J. Isolation, characterization, and development of WRKY genes as useful genetic markers in *Theobroma cacao*. *Theor. Appl. Genet.* **2004**, *109*, 495−507.
(28) Yang, J. Y.; Scascitelli, M.; Motilal, L. A.; Sveinsson, S.; Engels, J. M. M.; Kane, N. C.; Dempewolf, H.; Zhang, D.; Maharaj, K.; Cronk, Q. Complex origin of Trinitario-type *Theobroma cacao* (Malvaceae) from Trinidad and Tobago revealed using plastid genomics. *Tree Genet. Genomes* **2013**, *9*, 829−840.
(29) Saski, C. A.; Feltus, F. A.; Staten, M. E.; Blackmon, B. P.; Ficklin, S. P.; Kuhn, D. N.; Schnell, R. J.; Shapiro, H.; Motamayor, J. C. A genetically anchored physical framework for *Theobroma cacao* cv. Matina 1-6. *BMC Genomics* **2011**, *12*, 413.
(30) Mülhardt, C. *Der Experimentator: Molekularbiologie/Genomics*; Spektrum Akademischer Verlag GmbH: Heidelberg, Germany, 2009; Vol. *6*.
(31) Dhingra, A.; Folta, K. M. ASAP: Amplification, sequencing & annotation of plastomes. *BMC Genomics* **2005**, *6*, 176.
(32) Knippers, R. *Molekulargenetik*; Georg Thieme Verlag KG: Stuttgart, Germany, 2006; Vol. *9*.
(33) Jansen, R. K.; Saski, C.; Lee, S.; Hansen, A. K.; Daniell, H. Complete plastid genome sequences of three rosid (*Castaneae*, *Prunus*, *Theobroma*): Evidence for at least two independent transfers of rpl22 to the nucleus. *Mol. Biol. Evol.* **2010**, *28*, 835−847.
(34) Rödiger, A.; Baudisch, B.; Klösgen, R. B. Simultaneous isolation of intact mitochondria and chloroplasts from a single pulping of plant tissue. *J. Plant Physiol.* **2010**, *167*, 620−624.
(35) Storchová, H.; Hrdlicková, R.; Chrtek, J.; Tetera, M.; Fitze, D.; Fehrer, J. An improved method of DNA isolation from plants collected in the field and conserved in saturated NaCl/CTAB solution. *Taxon* **2000**, *49*, 79−84.
(36) Baker, N. R.; Hardwick, K.; KJones, P. Biochemical and physiological aspects of leaf development on cocoa (*Theobroma cacao*). *New Phytol.* **1975**, *75*, 513−518.
(37) Yeoh, H. H.; Chung, D. K.; Fritz, P. J. *Theobroma cacao* chloroplast DNA: Isolation, molecular cloning, an characterization. *Cafe, Cacao, The* **1990**, 173−178.
(38) Motamayor, J. C.; Risterucci, A. M.; Lopez, P. A.; Ortiz, C. F.; Moreno, A.; Lanaud, C. Cacao domestication I: The origin of the cacao cultivated by the Mayas. *Heredity* **2002**, *89*, 380−386.
(39) Löffler, G. *Basiswissen Biochemie*; Springer Verlag: Heidelberg, Germany, 2008; Vol. *7*.
(40) Motamayor, J. C.; Risterucci, A. M.; Heath, M.; Lanaud, C. Cacao domestication II: Progenitor germplasm of the Trinitario cacao cultivar. *Heredity* **2003**, *91*, 322−330.
(41) Saunders, J.; Mischke, S.; Leamy, E. A.; Hemeida, A. A. Selection of international molecular standards for DNA fingerprinting of *Theobroma cacao*. *Theor. Appl. Genet.* **2004**, *110*, 41−47.
(42) Smulders, M. J. M.; Esselink, D.; Amores, F.; Ramos, G.; Sukha, D. A.; Butler, D. R.; Vosman, B.; van Loo, E. N. Identification of cocoa (*Theobroma cacao* L.) varieties with different quality attributes and parentage analysis of their beans. *IGENIC Newsl.* **2012**, *12*, 1−13.
(43) Yang, J. Y.; A, M. L.; Dempewolf, H.; Maharaj, K.; Cronk, Q. C. B. Chloroplast microsatellite primers for cacao (*Theobroma cacao*) and other Malvaceae. *Am. J. Bot.* **2011**, e372−e374.
(44) Svab, Z.; Maliga, P. Exceptional transmission of plastids and mitochondria from the transplastomic pollen parent and its impact on transgene containment. *Proc. Natl. Acad. Sci. U. S. A.* **2007**, *104*, 7003−7008.
(45) Hausmann, S.; Garcin, D.; Delenda, C.; Kolakofsky, D. The versatility of paramyxovirus RNA polymerase stuttering. *J. Virol.* **1999**, *73* (7), 5568−5576.

collected and decolorized by adding 30% (v/v) aqueous $H_2O_2$. The solution was concentrated under vacuum and precipitated with 3 volumes of 95% (v/v) aqueous ethanol and then incubated at 4 °C overnight. Polysaccharide precipitates were obtained by centrifugation at 4000 rpm for 10 min and washed sequentially with acetone and ether. The polysaccharide extract was dried using nitrogen gas and stored in a desiccator for further FT-IR analysis.

**Oxygen Radical Absorbance Capacity (ORAC) Assay.** Determination of the oxygen radical absorbance capacity of the polysaccharides was performed as previously reported[16] using an Infinite F200 PRO microplate reader (Tecan, Switzerland). Samples and Trolox standards were prepared in DMSO, and all other reagents were prepared in 75 mM phosphate buffer (pH 7.4). Briefly, each well in a 96-well plate contained 30 μL of sample (or DMSO for the blank control), and 225 μL of 81.63 nM fluorescein. The plate was covered and incubated at 37 °C for 20 min, and 25 μL of 0.36 M 2,2′-azobis(2-amidinopropane) hydrochloride (AAPH) was added to each well to start the reaction, resulting in a final total volume of 280 μL. The fluorescence was recorded every 5 min for 1 h (ex/em, 485/538 nm) at 37 °C. Trolox equivalents were calculated from the relative area under the curve compared to a Trolox standard curve prepared under the same experimental conditions. Reactions were conducted in triplicate, and results are expressed as micromoles of Trolox equivalents per gram of polysaccharides.

**Ferric Reducing Antioxidant Power (FRAP) Assay.** The ferric reducing antioxidant power assay is based on the reduction of $Fe^{3+}$-tripyridyltriazine (TPTZ) to a blue-colored $Fe^{2+}$-TPTZ.[17,18] The FRAP reagent was prepared by mixing 300 mM acetate buffer (pH 3.6), 10 mM TPTZ, and 20 mM ferric chloride in a ratio of 10:1:1 (v/v/v). Then, 3 mL of FRAP reagent was added to 20 μL of sample or Trolox and incubated at 37 °C for 30 min. Absorbance was measured at 590 nm using an Infinite F200 PRO microplate reader (Tecan, Switzerland). Trolox was used as a standard, and the appropriate sample dilutions were determined. Reactions were conducted in triplicate, and results are reported as Trolox equivalents (TE) per gram of polysaccharides.

**Acid Hydrolysis.** Polysaccharides were hydrolyzed using two approaches. For complete acid hydrolysis, polysaccharides (10 mg) were hydrolyzed in 2 mL of 2 M trifluoroacetic acid (TFA) in an ampule sealed under a nitrogen atmosphere and incubated at 110 °C for 5 h. For partial acid hydrolysis, 2 mL of 0.05 M TFA was added and incubated at 110 °C for only 2 h. After cooling to room temperature, reactions were centrifuged at 4000 rpm for 5 min, and supernatants were dried at reduced pressure. Methanol was twice added and evaporated under vacuum to remove residual TFA.

**FT-IR Spectroscopy and Chemometric Analysis.** FT-IR spectra of nonhydrolyzed polysaccharides were obtained using a PerkinElmer Spectrum 100 FT-IR spectrometer. Spectra were recorded in absorbance mode from 4000 to 400 $cm^{-1}$ at a resolution of 4 $cm^{-1}$. Four replicate spectra were collected for each sample. Spectra from each batch of ZJ samples were exported to Excel 2010 to calculate the mean chromatograph. The Pearson correlation coefficient $r$ ($-1 \leq r \geq 1$) was calculated to evaluate the similarity of fingerprints using eq 1.[13]

$$r = \frac{\sum_{i=1}^{n}(x_i - \bar{x})(y_i - \bar{y})}{\sqrt{\sum_{i=1}^{n}(x_i - \bar{x})^2 \sum_{i=1}^{n}(y_i - \bar{y})^2}} \quad (1)$$

$x_i$ and $y_i$ are the $i$th elements of $x$ and $y$ (from two fingerprints), $n$ is the number of variables in the fingerprints, $\bar{x}$ and $\bar{y}$ are means or averages of the ZJ sample set and SC or FJ samples. The calculation was performed using the Pearson function in Excel 2010 (Microsoft).

**Preparation of PMP Derivatives after Complete Acid Hydrolysis.** Monosaccharide standards or hydrolyzed polysaccharide samples were dissolved in 10 mL of dd-water. The standards or hydrolyzed samples (0.2 mL) were mixed with 0.2 mL of a 0.5 M methanol solution of 1-phenyl-3-methyl-5-pyrazolone (PMP) and 0.2 mL of 0.3 M NaOH and stirred at 70 °C for 60 min. Following cooling to room temperature, reactions were neutralized with 0.2 mL of 0.3 M HCl, and 1 mL of chloroform was added and stirred for 30 s before centrifugation at 2000 rpm for 5 min. The chloroform phase was discarded, and the extraction process was repeated a further two times to remove the excess PMP reagent. The aqueous layer was collected, made up to 5 mL with dd-water, and filtered through a 0.45 μm membrane.

**Preparation of PMP Derivatives after Partial Acid Hydrolysis.** Partially hydrolyzed polysaccharides were dissolved in 2 mL of dd-water, and 0.5 mL was mixed with 0.2 mL of a 0.5 M methanol solution of 1-phenyl-3-methyl-5-pyrazolone (PMP) and 0.2 mL of 0.3 M NaOH and stirred. Subsequent steps were as described above for complete acid hydrolysis.

**HPLC Analysis.** Analysis of PMP derivatives was carried out on an Agilent 1260 HPLC system (Agilent Technologies, USA). Separation was achieved using reverse phase elution on a 5 μm Shim-pack VP-ODS column (4.6 mm × 250 mm, 5 μm, Shimadzu, Kyoto, Japan) fitted with a 4.6 mm × 10 mm Shim-pack GVP-ODS guard column (Shimadzu). The chromatographic conditions were as follows: flow rate = 0.8 mL/min; sample injection volume = 20 μL; column temperature = 30 °C. The mobile phase consisted of 82% (v/v) 0.05 M sodium phosphate (pH 6.8) containing 18% (v/v) acetonitrile for isocratic elution. Spectra were collected at a wavelength of 245 nm.

**Data Analysis.** Antioxidant activity data are reported as means ± standard deviation. One-way ANOVA and the LSD test at the level of 0.05 were used to identify differences in means using SPSS for Windows (version rel. 10.05, 1999, SPSS Inc., Chicago, IL, USA). All material pretreatment, extraction, processing, and spectroscopic/chromatographic fingerprinting and data handling were performed as presented on the flowchart (Figure 1). The similarity of FT-IR fingerprints was determined using the Pearson correlation coefficient $r$ calculated using Excel 2010. The similarity of HPLC fingerprints was determined using the Similarity Evaluation System for Chromatographic Fingerprint of Traditional Chinese Medicine version 2004A (Chinese Pharmacopoeia Committee), which was designed specifically for similarity analyses of LC and GC fingerprints and has been recommended by the State Food and Drug Administration of China.[19,20] The correlation coefficients of complete chromatographic profiles of samples were calculated. The chemical fingerprints of polysaccharides from 12 batches of *F. velutipes* fruiting bodies were analyzed by similarity analysis, and principal component analysis (PCA) was performed using SIMCA-P 11.5 (Umetrics AB, Umea, Sweden).

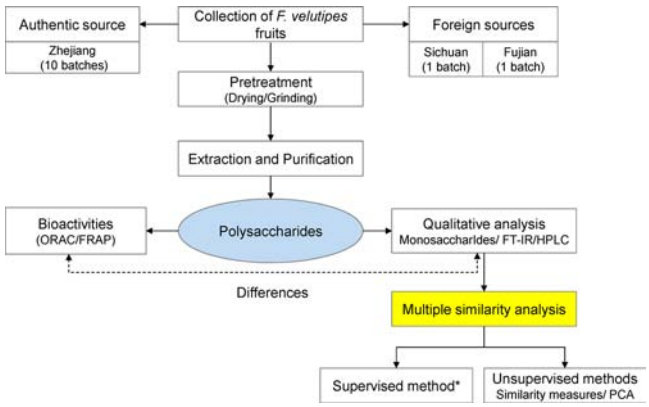


**Figure 1.** Flowchart of material pretreatment, extraction, processing, spectroscopic and chromatographic fingerprinting, and data handling. (*) Similarity Evaluation System for Chromatographic Fingerprint of Traditional Chinese Medicine.

## RESULTS AND DISCUSSION

**Antioxidant Activity of Polysaccharides from *F. velutipes* Fruiting Bodies.** Oxygen radical absorbance capacity (ORAC) and ferric reducing antioxidant power (FRAP) assays were performed to investigate the antioxidant activity of polysaccharide samples and to determine whether

different radical systems influenced the results. Polysaccharides from the authentic source (samples ZJ-1−ZJ-10) and the foreign sources (samples SC and FJ) contributed to the observed ORAC and reducing power in Figure 2. The influence

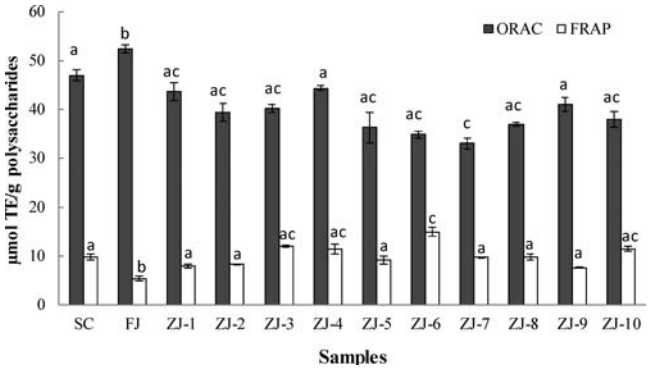


**Figure 2.** ORAC and FRAP values of polysaccharides from *F. velutipes* fruiting bodies. Gray columns indicate ORAC values, and white columns represent FRAP values. ZJ-1−ZJ-10 represent antioxidant values of 10 batches of the authentic source; SC and FJ are the antioxidant values of each of two foreign sources, respectively. Results are expressed as micromoles of Trolox equivalents (TE) per gram of polysaccharides. Tests were conducted in triplicate for each batch, with mean values shown and standard deviations depicted by vertical bars. Shown in the same color, columns marked with different letters are significantly different ($p < 0.05$).

of *F. velutipes* polysaccharides on reactive oxygen species (Figure 2) showed that the antioxidant capacity was highest in fruiting bodies from FJ, and similar in SC and most of the ZJ samples ($p > 0.05$), with ORAC values between 32 and 52 $\mu$mol TE/g polysaccharides. The reducing power serves as a significant indicator of potential antioxidant activity, and this was found to be similar in fruiting bodies from most ZJ samples and SC and to be the lowest in FJ ($p > 0.05$), in the range of 5−11 $\mu$mol TE/g polysaccharides. Variation in antioxidant activities of extracts from different sources of *F. velutipes* fruiting bodies indicated a structural dissimilarity of polysaccharides, which might affect other biological activities of *F. velutipes* fruiting bodies.[9,10]

The quality of polysaccharides in fruiting bodies cannot be determined from mushroom appearance alone, and existing high-throughput methods are unable to differentiate between authentic and foreign sources because distinguishing between complex polysaccharide structures is highly challenging. Therefore, alternative approaches are needed for quality control of *F. velutipes* fruiting bodies.

**FT-IR Fingerprinting: Similarity Analysis and PCA.** The spectroscopic fingerprints of nonhydrolyzed polysaccharide extracts from 10 batches of qualified ZJ samples were analyzed by FT-IR, and the ZJ-7 fingerprint is shown as an example (Figure 3A). The absorption peaks at 3400, 2944, and 1420 $cm^{-1}$ correspond to O−H, C−H, and carboxyl C−O group stretching, whereas the band in the region of 1246 $cm^{-1}$ results from a O−H deformation vibration. Stretching peaks at 934, 885, and 882 $cm^{-1}$ may derive from $\beta$-glycosidic linkages between the sugars, and water molecules bound to the polysaccharides contributed to the absorption band at 1643 $cm^{-1}$. FT-IR chromatograms of SC and FJ samples (Figure 3B,C) were similar to that of ZJ, but key differences in the transmission percent of some peaks were apparent.

The similarity of 12 separate batches of *F. velutipes* fruiting bodies from various sources was evaluated by calculating the correlation coefficient with the original data. All spectra were exported to Excel 2010, and the correlation coefficient $r$ was calculated. The fingerprints of SC and FJ were compared with the standard profiles derived from ZJ samples. A value of 1 indicates a perfect correlation with the standard profile.[13] For 10 batches of ZJ samples, $r$ values varied between 0.973 and 0.996, indicating a high degree of similarity ($r > 0.9$). The $r$ values for SC and FJ samples were 0.788 and 0.828, respectively, indicating significant differences from the ZJ samples.

PCA was applied to confirm the discrimination of sources of *F. velutipes* fruiting bodies based on FT-IR fingerprint data of raw polysaccharide extracts. On the basis of Kaiser's stopping rule, only factors with eigenvalues >1 were considered in the analysis.[21] The 10 characteristic chromatographic peaks (Figure 3) were processed using PCA, and factors 1 and 2 had eigenvalues of 8.60 and 1.07, representing 96.7% of the cumulative variance. Therefore, factors 1 and 2 were used to visualize data inhomogeneity. A two-dimensional PCA plot of IR spectroscopic fingerprints after data pretreatment was constructed in Figure 4. Scattered small triangles representing PCA scores showed that the authentic samples (ZJ-1−ZJ-10) were clustered closely, whereas the SC and FJ samples were more diffuse. This suggests that PCA of IR fingerprint data could be used to discriminate authentic and foreign sources of *F. velutipes* fruiting bodies.

**HPLC Fingerprinting: Similarity Analysis and PCA.** The monosaccharide composition of polysaccharides of *F. velutipes* fruiting bodies was investigated using HPLC following a complete acid hydrolysis and revealed the presence of glucose, mannose, galactose, ribose, and xylose (Figure 5). This profile differed significantly from mycelial tissue, in which glucose was the only monosaccharide identified.[14] Glucose, with a molar ratio of 85.04%, was the predominant monosaccharide, followed by mannose (6.81%), galactose (6.09%), xylose (1.65%), and ribose (0.39%). The fruiting bodies of *F. velutipes* were also previously reported to contain arabinose[22] and fructose.[23]

Similarity analyses were applied to HPLC fingerprints following partial acid hydrolysis because there were too few peaks in the HPLC fingerprints after complete acid hydrolysis. The HPLC profiles of 12 batches of *F. velutipes* fruiting bodies and the mean chromatogram from the 10 ZJ batches (Figure 6A) revealed 17 characteristic peaks suitable for similarity analysis. The correlation coefficients of the 10 ZJ batches were calculated using the Similarity Evaluation System for Chromatographic Fingerprint of Traditional Chinese Medicine software and ranged from 0.930 to 0.998. The $r$ values for SC and FJ samples were 0.955 and 0.982, respectively (Figure 6B,C), suggesting the similarity software was not able to discriminate between the sources.

PCA was applied to the HPLC profiles from precolumn PMP derivatization after partial acid hydrolysis. The relative peak area of 17 characteristic chromatographic peaks (Figure 6) was used for PCA, and three factors had eigenvalues of 7.18, 2.22, and 1.49, representing 90.7% of the cumulative variance. Therefore, a three-dimensional PCA plot of HPLC chromatographic profiles was constructed in Figure 7. Scattered dots representing the PCA scores showed that the qualified samples (ZJ-1−ZJ-10) were clustered closely in geometric space, whereas the SC and FJ samples were more diffuse. This

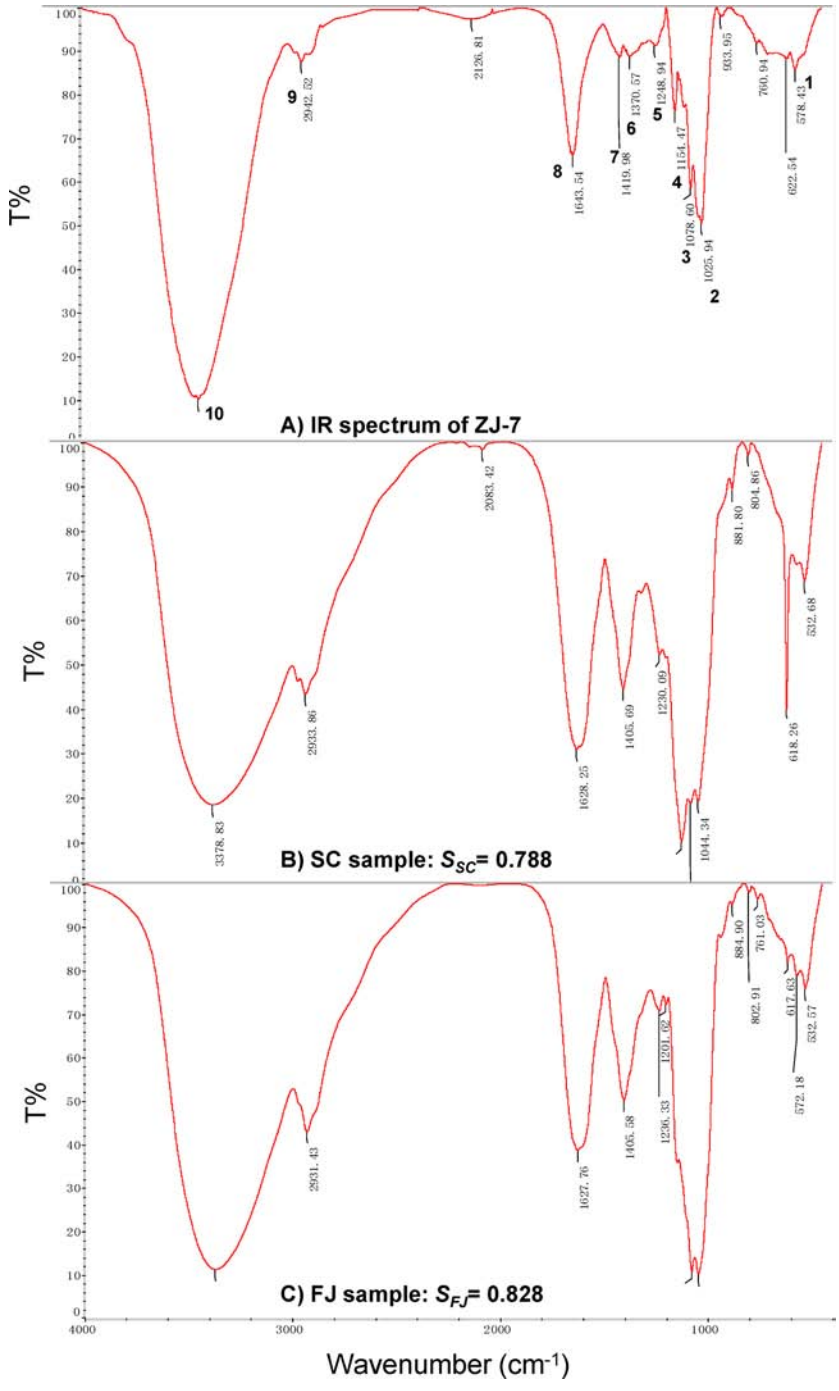


**Figure 3.** Comparison of FT-IR fingerprints of SC and FJ samples (foreign sources) with the mean FT-IR spectra of raw polysaccharide extracts of ZJ samples (authentic source): (A) ZJ-7 sample; (B) SC sample; (C) FJ sample. Peaks 1−10 in (A) were chosen for principal component analysis. $S_{SC}$ and $S_{FJ}$ are similarity values between SC and FJ, respectively, compared with ZJ.

suggests that PCA of partially hydrolyzed PMP derivatives could be used to discriminate between authentic and foreign sources of *F. velutipes* fruiting bodies.

Spectroscopic and chromatographic fingerprints using supervised/unsupervised data analysis techniques including similarity parameters (i.e., correlation coefficient) and PCA have been applied to detect foreign sources of *F. velutipes* fruiting bodies. IR spectroscopic fingerprints using correlation coefficient and PCA proved capable of discriminating sources of *F. velutipes* fruiting bodies. HPLC chromatographic fingerprints using the TCM-supervised method could not discriminate between sources, but PCA of HPLC fingerprints could detect the foreign sources. Generally, IR fingerprinting with unsupervised chemometrics is a reliable identification and qualification method suitable for quality control of *F. velutipes* fruiting bodies. PCA is a widely used mathematical approach for reducing the dimensionality of original data by introducing a small number of underlying factors without losing too much information. In this study, PCA is practicable for analyzing both IR spectroscopic and HPLC fingerprint data to determine the quality of polysaccharides between different sources of *F. velutipes* fruiting bodies. These findings should be taken into


dx.doi.org/10.1021/jf504349r | *J. Agric. Food Chem.* 2014, 62, 12128−12133

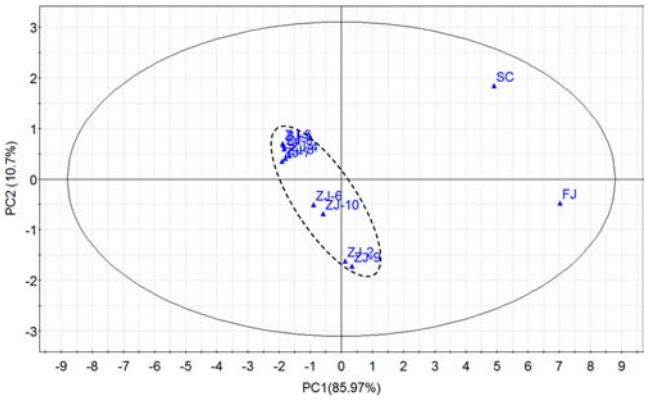


**Figure 4.** Plot of PCA scores from FT-IR fingerprints of non-hydrolyzed polysaccharides. Batches ZJ-1−ZJ-10 were the authentic reference source. SC and FJ refer to foreign sources.

account for quality control of *F. velutipes* fruiting bodies or foods rich in bioactive polysaccharides.

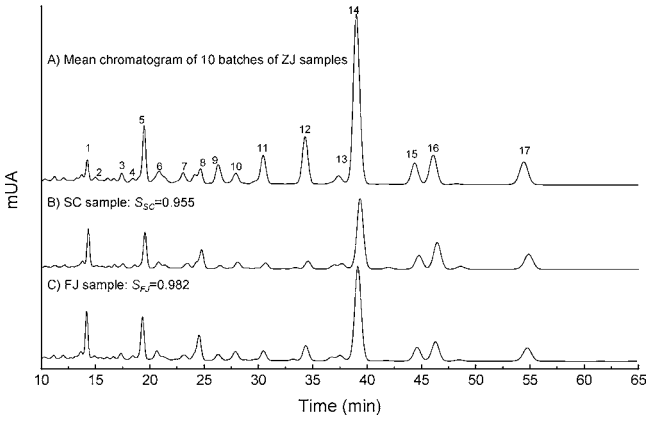


**Figure 6.** Comparison of HPLC fingerprints of SC and FJ samples (foreign sources) with the mean FT-IR chromatograph of hydrolyzed ZJ polysaccharides (authentic source): (A) mean chromatograph of 10 batches of ZJ samples; (B) SC sample; (C) FJ sample. $S_{SC}$ and $S_{FJ}$ are similarity values of SC and FJ, respectively, compared with ZJ. Peaks 1−17 in (A) were chosen for PCA.

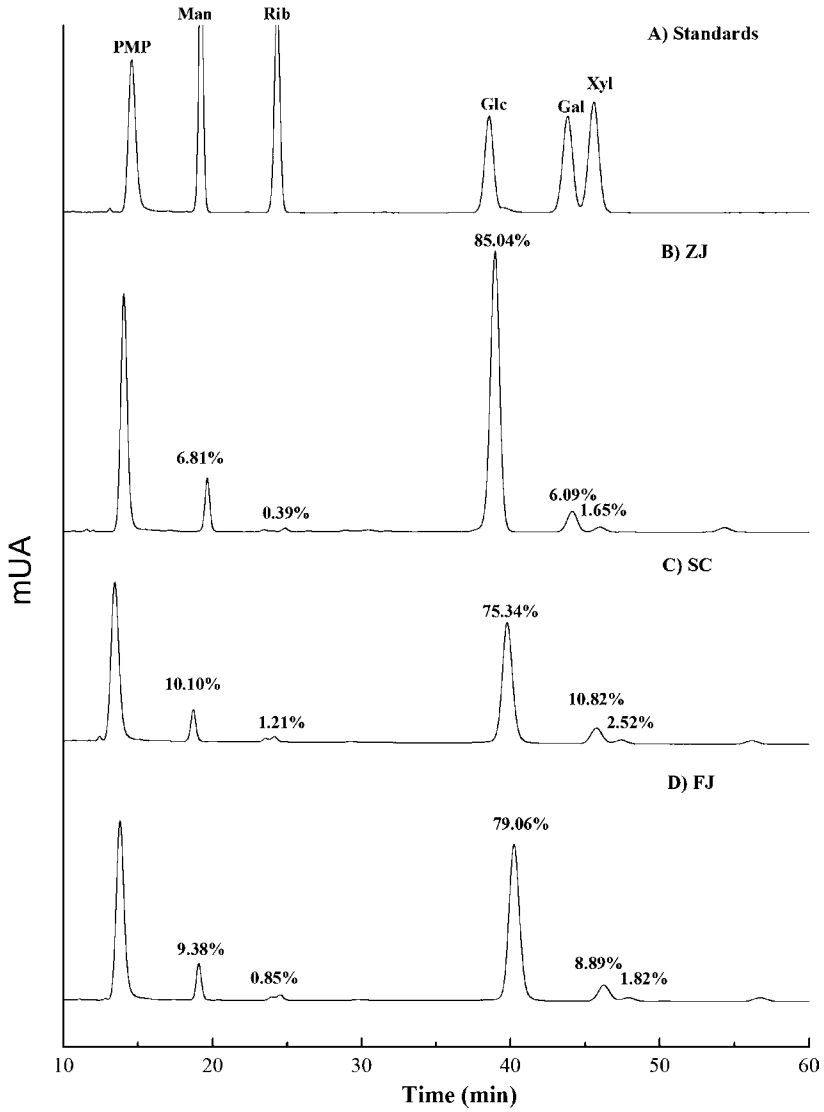


**Figure 5.** Monosaccharide composition of polysaccharides from *F. velutipes* fruiting bodies: (A) monosaccharide standards; (B) ZJ samples (authentic source, average of ZJ-1−ZJ-10); (C) SC sample (foreign source); (D) FJ sample (foreign source). The molar ratios of each monosaccharide are shown as percentages. Tests were conducted in triplicate for each batch.


dx.doi.org/10.1021/jf504349r | *J. Agric. Food Chem.* 2014, 62, 12128−12133

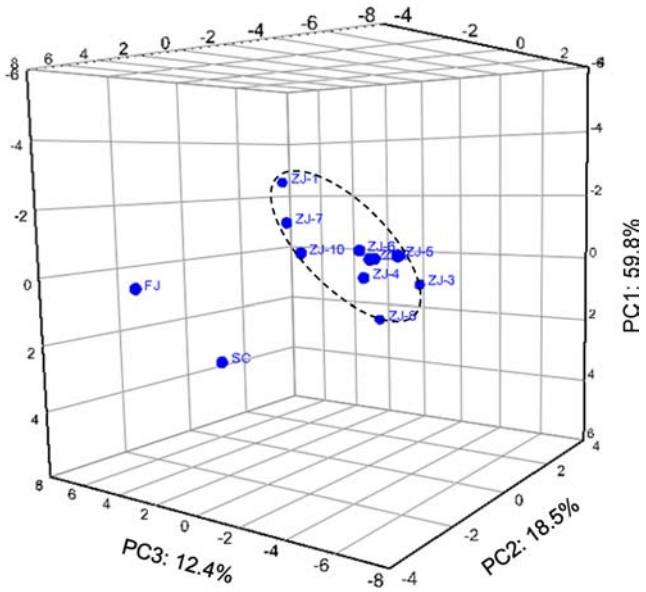


**Figure 7.** Plot of PCA scores from HPLC fingerprints of hydrolyzed polysaccharide PMP derivatives. Batches ZJ-1−ZJ-10 were the authentic reference source. SC and FJ refer to foreign samples.

## AUTHOR INFORMATION


### Corresponding Author

*(L.-H.S.) Phone: +86-2134205717. E-mail: lihuas@sjtu.edu.cn.



### Funding

This study was funded by the National Nature Science Foundation of China (Grant 31371756).

### Notes

The authors declare no competing financial interest.


## REFERENCES


(1) Leifa, F.; Pandey, A.; Soccol, C. R. Production of *Flammulina velutipes* on coffee husk and coffee spent-ground. *Braz. Arch. Biol. Technol.* **2001**, *44*, 205−212.

(2) Song, H. F.; Zhang, Q. B.; Zhang, Z. S.; Wang, J. In vitro antioxidant activity of polysaccharides extracted from *Bryopsis plumosa*. *Carbohydr. Polym.* **2010**, *80*, 1057−1061.

(3) Ma, L.; Chen, H.; Zhang, Y.; Zhang, N.; Fu, L. Chemical modification and antioxidant activities of polysaccharide from mushroom Inonotus obliquus. *Carbohydr. Polym.* **2012**, *89*, 371−378.

(4) Thetsrimuang, C.; Khammuang, S.; Sarnthima, R. Antioxidant activity of crude polysaccharides from edible fresh and dry mushroom fruiting bodies of *Lentinus* sp. strain RJ-2. *Int. J. Pharmacol.* **2011**, *7*, 58−65.

(5) Fukushima, M.; Ohashi, T.; Fujiwara, Y.; Sonoyama, K.; Nakano, M. Cholesterol-lowering effects of maitake (*Grifola frondosa*) fiber, shiitake (*Lentinus edodes*) fiber, and enokitake (*Flammulina velutipes*) fiber in rats. *Exp. Biol. Med.* **2001**, *226*, 758−765.

(6) Wu, D. M.; Duan, W. Q.; Liu, Y.; Cen, Y. Anti-inflammatory effect of the polysaccharides of golden needle mushroom in burned rats. *Int. J. Biol. Macromol.* **2010**, *46*, 100−103.

(7) Yin, H.; Wang, Y.; Chen, T.; Tang, H.; Wang, M. Purification, characterization and immuno-modulating properties of polysaccharides isolated from *Flammulina velutipes* mycelium. *Am. J. Chinese Med.* **2010**, *38*, 191−204.

(8) Leung, M. Y. K.; Fung, K. P.; Choy, Y. M. The isolation and characterization of an immunomodulatory and anti-tumor polysaccharide preparation from *Flammulina velutipes*. *Immunopharmacology* **1997**, *35*, 255−263.

(9) Alban, S.; Schauerte, A.; Franz, G. Anticoagulant sulfated polysaccharides: part I. Synthesis and structure−activity relationships of new pullulan sulfates. *Carbohydr. Polym.* **2002**, *47*, 267−276.

(10) Zhang, M.; Cui, S. W.; Cheung, P. C. K.; Wang, Q. Antitumor polysaccharides from mushrooms: a review on their isolation process, structural characteristics and antitumor activity. *Trends Food Sci. Technol.* **2007**, *18*, 4−19.

(11) *WHO General Guidelines for Methodologies on Research and Evaluation of Traditional Medicine*, http://whqlibdoc.who.int/hq/2000/WHO_EDM_TRM_2000.1.pdf (Aug 1).

(12) Man, Y. B. C.; Rohman, A.; Mansor, T. S. T. Differentiation of lard from other edible fats and oils by means of Fourier transform infrared spectroscopy and chemometrics. *J. Am. Oil Chem. Soc.* **2011**, *88*, 187−192.

(13) Goodarzi, M.; Russell, P. J.; Vander Heyden, Y. Similarity analyses of chromatographic herbal fingerprints: a review. *Anal. Chim. Acta* **2013**, *804*, 16−28.

(14) Pang, X. B.; Yao, W. B.; Yang, X. B.; Xie, C.; Liu, D.; Zhang, J.; Gao, X. D. Purification, characterization and biological activity on hepatocytes of a polysaccharide from *Flammulina velutipes* mycelium. *Carbohydr. Polym.* **2007**, *70*, 291−297.

(15) Staub, A. M. Removal of protein − Sevag method. *Methods Carbohydr. Chem.* **1965**, *5*, 5−6.

(16) Cao, G.; Alessio, H. M.; Cutler, R. G. Oxygen-radical absorbance capacity assay for antioxidants. *Free Radical Biol. Med.* **1993**, *14*, 303−311.

(17) Benzie, I. F. F.; Strain, J. J. The ferric reducing ability of plasma (FRAP) as a measure of "antioxidant power": the FRAP assay. *Anal. Biochem.* **1996**, *239*, 70−76.

(18) Jing, P.; Ye, T.; Shi, H. M.; Sheng, Y.; Slavin, M.; Gao, B. Y.; Liu, L. W.; Yu, L. L. Antioxidant properties and phytochemical composition of China-grown pomegranate seeds. *Food Chem.* **2012**, *132*, 1457−1464.

(19) Kong, W. J.; Wang, J. B.; Zang, Q. C.; Xing, X. Y.; Zhao, Y. L.; Liu, W.; Jin, C.; Li, Z. L.; Xiao, X. H. Fingerprint-efficacy study of artificial *Calculus bovis* in quality control of Chinese materia medica. *Food Chem.* **2011**, *127*, 1342−1347.

(20) Liang, X. R.; Wu, H.; Su, W. K. A rapid UPLC-PAD fingerprint analysis of *Chrysanthemum morifolium* Ramat combined with chemometrics methods. *Food Anal. Methods* **2014**, *7*, 197−204.

(21) Kaiser, H. F. The application of electronic computers to factor analysis. *Educ. Psychol. Measurement* **1960**, *20*, 141−151.

(22) Otagiri, K.; Ohkuma, T.; Ikekawa, T.; Tanaka, S. Intensification of antitumor-immunity by protein-bound polysaccharide EA6, derived from *Flammulina velutipes* (Curt. ex Fr) Sing. combined with murine leukemia L1210 vaccine in animal experiments. *J. Pharm. Dyn.* **1983**, *6*, 96−104.

(23) Mukumoto, T.; Yamaguchi, H. The chemical structure of a mannofucogalactan from the fruit bodies of *Flammulina velutipes* (Fr.) Sing. *Carbohydr. Res.* **1997**, *59*, 614−621.

**Table 1. DNA Market Jellyfish Products Identified in a Previous Study[22] and Used in This Study for the Validation of the Pentaplex PCR Assay[a]**

| | | | BLAST (Max identity) | | |
|---|---|---|---|---|---|
| samples | city and place of collection | sequence length and code | bold | GenBank | Pentaplex PCR results |
| RE-2 | Prato/M | 658, HF930536 | 100% *N. nomurai* | | × 143 bp |
| RE 3 | Prato/M | 658, HF930537 | 100% *N. nomurai* | | × 143 bp |
| RE-5 | Milan/M | 658, HF930538 | 100% *N. nomurai* | | × 143 bp |
| RE-6 | Milan/M | 658, HF930539 | 99% *N. nomurai* | | × 143 bp |
| RE-8 | Prato/M | 658, HF930540 | 100% *N. nomurai* | | × 143 bp |
| RE-9 | Prato/M | 658, HF930541 | 99% *N. nomurai* | | × 143 bp |
| RE-10 | Florence/M | 658, HF930542 | 99% *N. nomurai* | | × 143 bp |
| RE-11 | Rome/M | 658, HF930543 | 100% *N. nomurai* | | × 143 bp |
| RE-12 | Rome/M | 658, HF930544 | 100% *N. nomurai* | | × 143 bp |
| RE-13 | Rome/M | 658, HF930545 | 100% *N. nomurai* | | × 143 bp |
| RE-14 | Rome/R | 658, HF930546 | NM | 100% *R. esculentum* | × 101 bp |
| RE-15 | Rome/M | 658, HF930547 | 100% *N. nomurai* | | × 143 bp |
| RE-19 | Rome/M | 658, HF930548 | 99% *N. nomurai* | | × 143 bp |
| RE-21 | Florence/M | 658, HF930549 | 100% *N. nomurai* | | × 143 bp |
| RE-24 | Florence/R | 658, HF930550 | NM | 100% *R. esculentum* | × 101 bp |
| RE-27 | Milan/M | 658, HF930551 | 99% *N. nomurai* | | × 143 bp |
| RE-40 | Prato/M | 658, HF937280 | 99% *N. nomurai* | | × 143 bp |
| RE-43 | Prato/R | 658, HF937281 | 99% *N. nomurai* | | NB |
| RE-44 | Prato/R | 658, HF937282 | NM | 100% *R. esculentum* | × 101 bp |
| RE-48 | Florence/M | 658, HF937283 | 100% *N. nomurai* | | × 143 bp |
| RE-28 | Milan/M | 206, HF937294 | 100% *N. nomurai* | | × 143 bp |
| RE-29 | Milan/M | 206, HF937295 | 100% *N. nomurai* | | × 143 bp |
| RE-34 | Prato/M | 206, HF937296 | 100% *N. nomurai* | | × 143 bp |
| RE-38 | Prato/M | 206, HF937297 | 100% *N. nomurai* | | × 143 bp |
| RE-39 | Prato/M | 206, HF937298 | 100% *N. nomurai* | | × 143 bp |
| RE-41 | Prato/M | 206, HF937299 | 100% *N. nomurai* | | × 143 bp |
| RE-42 | Prato/M | 206, HF937300 | 100% *N. nomurai* | | NB |
| RE-45 | Florence/M | 206, HF937301 | 100% *N. nomurai* | | NB |
| RE-46 | Florence/M | 206, HF937302 | 100% *N. nomurai* | | × 143 bp |
| RE-47 | Florence/M | 206, HF937303 | 99% *N. nomurai* | | × 143 bp |
| RE-4 | Prato/M | 206, HF937288 | 100% *N. nomurai* | | NB |
| RE-16 | Rome/M | 206, HF937289 | 100% *N. nomurai* | | × 143 bp |
| RE-20 | Florence/M | 206, HF937290 | 100% *N. nomurai* | | × 143 bp |
| RE-23 | Florence/M | 206, HF937292 | 100% *N. nomurai* | | × 143 bp |
| RE-22 | Florence/M | 206, HF937291 | 100% *N. nomurai* | | × 143 bp |
| RE-26 | Prato/M | 206, HF937293 | 100% *N. nomurai* | | × 143 bp |
| RE-30 | Milan/M | 145, HF937318 | 100% *N. nomurai* | | × 143 bp |
| RE-31 | Milan/M | 145, HF937319 | 100% *N. nomurai* | | × 143 bp |
| RE-32 | Prato/M | 145, HF937320 | 100% *N. nomurai* | | × 143 bp |
| RE-33 | Prato/M | 145, HF937321 | 100% *N. nomurai* | | × 143 bp |
| RE-35 | Prato/M | 145, HF937322 | 100% *N. nomurai* | | NB |
| RE-36 | Prato/M | 145, HF937323 | 100% *N. nomurai* | | × 143 bp |
| RE-37 | Prato/M | 145, HF937324 | 100% *N. nomurai* | | × 143 bp |
| RE-1 | Prato/M | 145, HF937313 | 100% *N. nomurai* | | NB |
| RE-7 | Milan/M | 145, HF937314 | 100% *N. nomurai* | | NB |
| RE-17 | Rome/M | 145, HF937315 | 100% *N. nomurai* | | × 143 bp |
| RE-18 | Rome/M | 145, HF937316 | 100% *N. nomurai* | | × 143 bp |
| RE-25 | Prato/M | 145, HF937317 | 100% *N. nomurai* | | × 143 bp |
| CP-7 | Prato/M | 658, HF937284 | 99% *N. nomurai* | | NB |
| CP-8 | Prato/M | 658, HF937285 | 100% *N. nomurai* | | 143 bp |
| CP-24 | Zhejiang (PRC)/M | 658, HF937287 | NM | 100% *R. esculentum* | 101 bp |
| CP-13 | Rome/M | 658, HF937286 | NM | 99% *R. pulmo* | 203 bp |
| CP-30 | Jangsu (PRC)/M | 658, XX | 99% *N. nomurai* | | 143 bp |
| CP-10 | Florence/M | 206, HF937305 | 100% *N. nomurai* | | NB |
| CP-9 | Prato/M | 206, HF937304 | NM | 100% *R. esculentum* | NB |
| CP-11 | Rome/M | 206, HF937306 | NM | 100% *R. esculentum* | × 101 bp |
| CP-15 | Rome/M | 206, HF937308 | 100% *N. nomurai* | | × 143 bp |
| CP-12 | Rome/M | 206, HF937307 | 100% *N. nomurai* | | × 143 bp |

**Table 1. continued**

| samples | city and place of collection | sequence length and code | BLAST (Max identity) bold | BLAST (Max identity) GenBank | Pentaplex PCR results |
|---|---|---|---|---|---|
| CP-18 | Florence/M | 206, HF937309 | 99% *N. nomurai* | | × 143 bp |
| CP-21 | Prato/M | 206, HF937310 | NM | 86% *R. nomadica* | NB |
| CP-27 | Zhejiang (PRC)/M | 206, HF937311 | NM | 100% *P. noctiluca* | × 165 bp |
| CP-28 | Zhejiang (PRC)/M | 206, HF937312 | NM | 100% *P. noctiluca* | NB |
| CP-1 | Prato/M | 145, HF937325 | NM | 100% *R. esculentum* | × 101 bp |
| CP-2 | Prato/M | 145, HF937326 | NM | 100% *R. pulmo* | × 203 bp |
| CP-3 | Prato/M | 145, HF937327 | 99% *N. nomurai* | | NB |
| CP-4 | Prato/M | 145, HF937328 | 99% *N. nomurai* | | × 143 bp |
| CP-5 | Prato/M | 145, HF937329 | NM | 100% *R. esculentum* | NB |
| CP-6 | Prato/M | 145, HF937330 | 100% *N. nomurai* | | × 143 bp |
| CP-14 | Rome/M | 145, HF937331 | NM | 100% *P. noctiluca* | NB |
| CP-16 | Rome/M | 145, HF937332 | NM | 100% *P. noctiluca* | NB |
| CP-17 | Rome/M | 145, HF937333 | NM | 100% *R. esculentum* | × 101 bp |
| CP-19 | Prato/M | 145, HF937334 | 100% *N. nomurai* | | × 143 bp |
| CP-20 | Prato/M | 145, HF937335 | NM | 85% *C. stuhlmanni* | × NB |
| CP-22 | Prato/M | 145, HF937336 | NM | 85% *C. stuhlmanni* | × NB |
| CP-23 | Zhejiang (PRC)/M | 145, HF937337 | NM | 100% *P. noctiluca* | NB |
| CP-25 | Zhejiang (PRC)/M | 145, HF937338 | NM | 100% *P. noctiluca* | × 165 bp |
| CP-26 | Zhejiang (PRC)/M | 145, HF937339 | NM | 100% *P. noctiluca* | NB |
| CP-29 | Jangsu (PRC)/M | 145, XX | NM | 100% *R. esculentum* | × 101 bp |

[a]RE: ready-to-eat. CP: classical products. NB: no bands. ×: expected band obtained.

Polymerase chain reaction (PCR), the technique of choice for species identification, is often coupled with sequencing, which is used to determine the precise order of nucleotides in a DNA molecule.[16,18] FINS (Forensically Informative Nucleotide Sequencing) combines DNA sequencing with a phylogenetic analysis.[19] The development of the DNA Barcoding, an evolution of the FINS method, has determined the increase of use of the cytochrome c oxidase I gene (*COI*) as a genetic marker for species identification.[20,21] In a previous work,[12] we showed that a specific pre-DNA extraction treatment, coupled with FINS of a 142 bp *COI* gene fragment, allowed the molecular identification of jellyfish species, also in case of salted products, in which the DNA is heavily degraded.

Considering that FINS is often limited by high costs and long-time of execution, in this work an alternative method to be used with screening purposes was developed to minimize expenses and save time. This new method, a Pentaplex PCR assay, is capable to identify two Asian jellyfish commonly used as food, such as *N. nomurai* and *R. esculentum*, and another three species distributed in the Mediterranean Sea, such as *R. pulmo*, *P. noctiluca*, and *C. tuberculata*, which could represent a novel business for the industry. This is possible by using a common forward primer together with 5 specific reverse primers, capable to amplify five regions with different size of the *COI* gene. This method can be used as rapid test for checking commercial samples, in which the diagnostic morphological characteristics have been lost.

## 2. MATERIALS AND METHODS

**2.1. Jellyfish Reference (RS) and Market Samples (MS) Collection.** Nine samples belonging to the species *Aurelia* sp., *C. tuberculata*, and *P. noctiluca* were kindly provided by the Institute of Sciences of Food Production of the National Research Council of Lecce (Supporting Information Table 1SI).

**2.2. DNA Extraction.** All the jellyfish RS were extracted according to the protocol proposed by Armani et al.[22] The amount of DNA was determined with a NanoDrop ND-1000 spectrophotometer (NanoDrop Technologies, Wilmington, DE, U.S.A.) by measuring the absorbance at 260 nm. DNA samples obtained from 57 RS jellyfish (Supporting Information Table 1SI) and 78 MS (Table 1), all of them molecularly identified in a previous work,[22] were also used to develop and validate the Pentaplex PCR. Finally, three DNA samples of *R. luteum* from the study of Prieto et al.[23] and six DNA samples of *P. benovici* from the study of Piraino et al.[24] were used.

**2.3. Amplification of *COI* and *28SrRNA* Genes.** *2.3.1. COI.* All the DNA reference samples extracted in this study from jellyfish were initially amplified using the primers FFDL and FRDL2[12] to obtain the first 655 bp of the *mtCOI* gene. The samples that failed the amplification were subsequently amplified using internal reverse primers[12] in combination with the same forward primer. The DNA was amplified according to the following PCR protocol: 20 μL of reaction volume containing 2 μL of 10× buffer (5Prime, Gaithersburg, MD, U.S.A.), 200 μM of each dNTP (dNTPmix, Euroclone S.p.A-Life Sciences Division, Pavia, Italy), 300 nM of primers, 25 ng/μL of BSA (Purified BSA 100× , New England BIOLABS Inc., Ipswich, MA, U.S.A.), 1.25 U of PerfectTaq DNA Polymerase (5Prime, Gaithersburg, MD, U.S.A.), 100 ng of DNA and DNase free water (Water Mol. Bio. Grade, DNase−RNase and Protease free, 5Prime GmbH, Hamburg, Germany), with the following cycling program: denaturation at 94 °C for 3 min; 40 cycles at 94 °C for 30 s, 51 °C for 30 s, and 72 °C for 35 s; final extension at 72 °C for 5 min. PCR products (5 μL) were checked by gel electrophoresis on a 2% agarose gel and the presence of fragments of the expected length was assessed by a comparison with the standard marker SharpMass50-DNA ladder (Euroclone, Wetherby, U.K.). Double-stranded PCR products were purified with the Illustra ExoProStar 1-Step Enzimatic PCR and Sequencing Clean-Up (GE Healthcare U.K. Limited, Amersham Place Little Chalfont Buckinghamshire, U.K.) following the manufacturer's instruction and then sequenced by GATC Biotech (Germany). The obtained sequences were analyzed using ClustalW in MEGA 5.0.[25] Fine adjustments were manually made after visual inspection. All the sequences were used to run a BLAST analysis on GenBank (http://blast.ncbi.nlm.nih.gov/Blast.cgi) and analyzed using the Identification System (IDS) on BOLD (Species Level Barcode Records) (http://www.boldsystems.org/index.php/IDS_OpenIdEngine). Finally, the sequences were deposited on GenBank via EBI (Supporting Information Table 1SI).

*2.3.2. 28S rDNA.* The *28SrRNA* gene sequences belonging to the Order Rhizostomeae and Semaestomeae produced in the work of

Table 2. Primers Designed for Setting up the Pentaplex PCR Assay[a]

| primers code | sequence 5′−3′ | bp | MT | AL |
|---|---|---|---|---|
| FJ1 | CAAACCATAAAGAYATWGG | 19 | 49.1 | |
| **FJ2** | **CAAACCATAAAGAYATTGGWAC** | **22** | **53.7** | |
| RHIZ1 | ACCTCCTATCAACACTG | 17 | 50.4 | **203** |
| **RHIZ1-1** | **ACGTCCTATCAACACTG** | **17** | **50.4** | |
| RHIZ1-2 | ACGTCGTATCAACACTG | 17 | 50.4 | |
| **PEL1** | **TTATTAGGGCGTGAGC** | **16** | **49.2** | **165** |
| **NEMO1** | **AACTACGTTATAAAGTTGG** | **19** | **50.2** | **143** |
| RHOP1 | ACCTGATAGTTCTAATCTA | 19 | 48 | **101** |
| **RHOP1-1** | **ACGCGATAGTTCTAATCTA** | **19** | **50.2** | |
| COT1 | GCCGGCACCTATAATT | 16 | 49.2 | 68 |
| **COT2** | **GGCACCTATAATTCCG** | **16** | **49.2** | **72** |
| **28sfor55** | **TGGTTACAACGGGTGA** | **16** | **49.2** | **55** |
| **28srev55** | **TCTCAGGCTCCCTCT** | **15** | 50.6 | |
| **F28s** | **ACTGTGAAACTGCGAATG** | **18** | **52.4** | **1598** |
| **R28s** | **CCATTCAATCGGTAGTAGC** | **19** | **51.1** | |

[a]Boldface, primers finally selected. bp = base pair; MT = melting temperature; AL= amplicon length.

Bayha et al.[26] were downloaded from GenBank and aligned using Clustal W in MEGA 5.0. The overall mean distance was calculated using the Kimura 2-parameter model[27] on a fragment of 1480 bp. Then, a new couple of primers (F28S and R28S) (Table 2) were designed for the amplification of a fragment of ∼1600 bp from the DNA of *N. nomurai* using the same PCR mix described for the *COI* gene, with the following cycling program: denaturation at 94 °C for 3 min; 40 cycles at 94 °C for 30 s, 51 °C for 30 s, and 72 °C for 35 s; final extension at 72 °C for 10 min. The sequences were analyzed as reported in Section 2.3.1. and were deposited on GenBank via EBI (Supporting Information Table 1SI).

**2.4. Primer Design for the Pentaplex PCR Assay.** *2.4.1. Specie-Specific Primers Targeting the COI Gene.* *mtCOI* sequences (666) belonging to 24 species (Table 3) were aligned with Clustal W in MEGA 5.0. Then, two hypothetical common forward primers were designed (FJ1 and FJ2, Table 2) by modifying the primer FFDL designed in a previous work.[12] The reverse primers were designed on highly polymorphic regions for the amplification of fragments of different length in the range 50−200 bp. Primers score were calculated with the software Beacon designer 7.0 (Premier Biosoft International, Palo Alto, CA) and with the software available on the Eurofins MWG Operon (Ebersberg, Germany) Web page (http://www.eurofinsgenomics.eu/). The number of mismatches between the reverse primers and the annealing region of the no-target species (Supporting Information Table 2SI) was also taken into consideration as a criterion to select specie-specific primers. In total, 11 primers, 2 forward and 9 reverse, were synthesized by the Eurofins MWG Operon.

*2.4.2. Control PCR Primers Targeting the 28SrRNA Gene.* With the aim of amplifying in all the species, a control fragment of 55 bp together with the species-specific fragment, two primers (28sfor55 and 28srev55) (Table 2) were designed on highly conserved regions using the software Beacon designer 7.0 after aligning the *28SrRNA* gene sequences (Order Rhizostomeae and Semaestomeae) produced in the work of Bayha et al.[26] with the sequences of *N. nomurai* produced in this study.

**2.5. PCR Reaction Optimization.** The two forward primers were tested on the DNA of all the reference species in single reaction with each of the reverse primers designed (Supporting Information Table 1SI). The primers capable to amplify the target sequence without producing unspecific bands were selected (Table 2).

All the primers were tested in combination in the same PCR reaction mix using different concentrations (from 100 to 400 nM), in the presence of increasing concentration of $MgCl_2$ (1, 2, and 5 mM) and nucleotides (from 200 to 600 μM). We also tested different amount of total DNA (from 1 to 200 ng) and of Taq polymerase (1× and 2×). The optimal annealing temperature was selected after trials in the range of 47 to 51 °C, on a PeqStar 96 Universal Gradient, PEQLAB BiotechnologieGmgH (Euroclone, Wetherby, U.K.). The control PCR primers were initially tested on all the reference DNA samples and then included in the multiplex reaction. The reaction protocol that showed the best amplification performances was tested on 10 samples of not degraded DNA extracted from 5CP and 5RE to verify the output of the Pentaplex method in case of degraded and low quality DNA.

**2.6. Final Pentaplex PCR Protocol and Analysis of Commercial Samples.** The following final protocol: 10 μL of reaction volume containing 1 μL of 10× buffer (Fisher Molecular Biology, Trevose PA, U.S.A.), 400 μM of each dNTP (dNTPmix, Euroclone S.p.A-Life Sciences Division, Pavia, Italy), 300 nM of FJ2, 200 nM of COT2, 200 nM of RHOP1-1, 225 nM of NEMO1, 200 nM of PEL1, 216 and 100 nM of RHIZ1-1 reverse primers, 100 nM of 28sfor55 and 28srev55 control primers, 25 ng/μL of BSA (Purified BSA 100× , New England BIOLABS Inc. Ipswich, MA, U.S.A.), 1 U of SubTherm TAQ Polymerase (Fisher Molecular Biology, Trevose, PA, U.S.A.), 3 mM of $MgCl_2$, 50 ng of DNA and DNase free water with the following cycling conditions: denaturation at 95 °C for 3 min; 40 cycles at 95 °C for 25 s, 49 °C for 5 s, and 72 °C for 5 s; final extension at 72 °C for 5 min. The electrophoresis was performed using a 4% agarose gel. In case of MS DNA, the length of the specific bands obtained with the multiplex PCR was compared to the results of the BLAST analysis performed on the same samples in a previous article[12] (Table 1), with the aim to assess the efficiency and specificity of the assay in case of low quality DNA.

## 3. RESULTS AND DISCUSSION

Seafood species identification has gained increasing importance in the current global market context. In fact, many studies, carried out in different geographical areas, have highlighted that almost one-third of the commercialized seafood is made of a different species with respect to what declared on the label.[20,21] In some cases, the substitution rate can reach alarming levels, as in the case of jellyfish products.[12]

In this light, the diagnostic techniques, particularly those based on DNA analysis, may assist both private companies and official agencies in ensuring a fair commerce in the light of the traceability regulations. Among the available methods, the multiplex PCR has the advantage to allow considerable saving of time and labor. These methods have been successfully used for several different purposes of identification, fish species included.[28,29]

Table 3. Reference Sequences Used in This Work for the Projecting of the Primers for the Pentaplex PCR Assay[a]

| species | sequences | |
|---|---|---|
| | number | accession code |
| *Aurelia aurita* | 40 | AY903093−95; AY903117−18 AY903208−12; **HF968752** JQ353726−28; JQ623914 JX995329; KC311384−85 KC440127; KC789074−93 |
| *Cassiopea andromeda* | 24 | AB563739−40; AY319448−62 AY319471−73; AY331593−95; **HF930521** |
| *Cassiopea frondosa* | 5 | AY319467; AY319469−70 HF930515; HF930520 |
| *Cassiopea xamachana* | 5 | AY319463−66; AY319468 |
| *Catosylus mosaicus* | 70 | AY319476; AY737184−247 **HF548537−39; HF968746−47** |
| *Cotylorhiza tuberculata* | 5 | **HF930531−35** |
| *Crambionella orsini* | 2 | EU363343−44 |
| *Cyanea annaskala* | 7 | AY902912−17; AY902923 |
| *Cyanea capillata* | 21 | AY902911; AY902924; HF930525−26; JX995329−46 |
| *Cyanea lamarckii* | 14 | JX995347−57; JX995360−62 |
| *Cyanea rosea* | 5 | AY902918−22 |
| *Drymonema dalmatinum* | 5 | HQ234614−17; HQ234621 |
| *Drymonema larsoni* | 9 | HQ234610−13; HQ234618−20 HQ234622; HQ234650 |
| *Lychnorhiza lucerna* | 5 | **HF930522; HF968748−51** |
| *Mastigias sp.* | 132 | AY902925−99; AY903000−51 EU363340; JN215543−46 |
| *Nemopilema nomurai* | 15 | AB243416; EU373728; GU145135 **HF536563−70;** HM045296 JX845348; JQ353746−47 |
| *Pelagia noctiluca* | 183 | GQ120093−96; GQ375903−6025 HE591457; **HF930527−30** HM358383- 403; JQ697960−74 JX235428−42 |
| *Phyllorhiza punctata* | 3 | EU363341−42; GQ120101 |
| *Rhizostoma luteum* | 3 | **HF937340−41; HF545309** |
| *Rhizostoma octopus* | 63 | HQ425417−79 |
| *Rhizostoma pulmo* | 24 | GQ999568−71; **HF536559−62 HF545304−08; HF930513;** HG931669; HQ902114−22 |
| *Rhopilema esculentum* | 12 | EU373722−24; **HF536571−74 HF930514−15;** JQ353756−57 JX845347 |
| *Rhopilema nomadica* | 5 | JN378391; HG931668; HF930516−18 |

[a]Sequences in bold have been produced in this or previous studies.[22,23]

### 3.1. Selection of the Species and of the DNA Target.

*3.1.1. Species Selection.* *R. esculentum* and *N. nomurai* are the Asian species most exploited for human consumption.[10,12]

Regarding the other species selected as target for the Pentaplex PCR, the *R. pulmo* was chosen due to the fact that it is one of the largest and most abundant jellyfish exclusively distributed in the Mediterranean Sea and adjacent areas.[30] The potential utilization of this Mediterranean jellyfish for food preparation was suggested in the work of Muhammed and Sultana[31] and by the fact that an Italian company has recently started to process *R. pulmo* for exportation to the Japanese market (author's note). Finally, Chinese people use to collect jellyfish that have run aground on beaches and to buy jellyfish from fishermen along the Tyrrhenian coast of Italy.[12] *C. tuberculata* and *P. noctiluca* are also widely distributed in the Mediterranean Sea.[32,33] They may likely be used as food products owing to their anatomical features and wide distribution.[35] In support of this, the molecular analyses carried out in a previous work[12] have identified the presence of the species *P. noctiluca* in some commercial products.

*3.1.2. DNA Target Selection.* The selection of a mitochondrial molecular marker is based on its several advantages with respect to the nuclear markers, such as the higher number of copies and the greater resistance to degradation induced by chemical-physical treatments. Moreover, the higher degree of interspecific variability is particularly useful for discrimination of species very close from a phylogenetic point of view.[16,18] Among the mitochondrial markers most used for seafood authentication (*COI*, *16srDNA*, and *cytb*), in this study, the *COI* gene was chosen due the availability of a higher number of reference sequences (Table 3). In fact, the creation of the Barcode of Life Data Systems database (BOLD) (http://www.

boldsystems.org/) has gained the attention of many researchers worldwide making the first 650 bp of the *COI* region one the most targeted mtDNA region for species identification,[20,21,34]. Furthermore, the *COI* gene was found to be informative enough to allow the identification of edible jellyfish species.[12]

**3.2. Primer Design.** *3.2.1. Specie-Specific Primers Targeting the COI Gene.* One of the main points to take into consideration during primers designing is the nature of the sample to be analyzed. In fact, a net difference exists between fresh and processed products: technological treatments, such as heating, acidification, pressurization, or their combination, may negatively influence the integrity of DNA and hence the PCR outputs.[18] In particular, heat treatments and sharp shifts of pH were identified as the main DNA degrading factors in food.[36]

In a previous work,[12] we found that jellyfish products were characterized by very low pH values: ∼4 and ∼6 in CP and RE, respectively. Despite a certain level of DNA degradation, we were able to amplify bands of about 700 bp in the 75% of the DNA extracted from RE samples and in the 44% of the DNA extracted from CP samples. However, in 100% of the DNA extracted from both kind of products, it was possible to obtain amplicons of ∼200 bp. For this reason, in this work the primers were designed to produce amplicons with a maximum length of 200 bp (Table 2).

With the aim to decrease the probability of template-independent primer interactions during amplification, which is greater in a multiplex PCR than in a uniplex, we decided to design a common forward primer (FJ2). This approach was successfully used to develop other methods based on multiplex PCR.[28,29] Considering the high variability of the *COI* gene, which makes difficult to find a common conserved region among five different species, we decided to design a degenerated primer. This was designed by modifying the forward primers proposed in a previous work,[12] while the reverse primers were designed on a polymorphic region of the *COI* gene. Once tested in single and multiplex reactions, the reverse primers PEL1, NEMO1 showed a high specificity for their target species (*P. noctiluca* and *N. nomurai*), producing the expected amplicon of 165 and 143 bp, respectively. No bands were obtained in case of DNA samples belonging to other jellyfish species of the Rhizostomeae and Semaestomeae order (Supporting Information Table 1SI). Interestingly, the primer PEL1 was able to amplify the DNA of *P. noctiluca* but not the DNA of *P. benovici*, a new *Pelagia* species recently described by Piraino et al.[24] For these reasons the reverse PEL1, NEMO1 were selected without modifications, which, on the contrary, were necessary for RHIZ1, RHOP1, and COT1.

The original RHIZ1 reverse primer gave the expected amplicon of 203 bp on all the species belonging to the genus *Rhizostoma*, which, according to Russell,[30] is composed of *R. pulmo*, *R. octopus*, and *R. luteum*. While a recent study of Prieto et al.,[23] on the basis of morphological and molecular results, confirmed that *R. luteum* is a distinct species with respect to the other two, the status of *R. octopus* is still controversial. In fact, Kramp[37] considered *R. luteum* as a variant of *R. pulmo* and Holst et al.[38] advocated that detailed morphological studies and molecular analyses are needed to better define the relationships among *Rhizostoma* species. For these reason, the pairwise Kimura 2-parameter molecular divergence between *R. pulmo* and *R. octopus COI* sequences (Table 3) was calculated. The low values found (6%) suggest that *R. pulmo* and *R. octopus* cannot be unquestionably considered as distinct species by a molecular point of view, supporting the theory of Kramp.[37] In fact, the literature suggests that 10−20% *COI* sequence divergence may be a suitable benchmark value to define species.[39]

In the light of these considerations, the reverse primer RHIZ1 was improved: two new primers were produced (Table 2) by introducing single (RHIZ1-1) and multiple (RHIZ1-2) base modification at different positions, with the aim to create additional mismatches on the annealing region of *R. luteum COI* sequence. RHIZ1-2 was discarded due to its inability to amplify the DNA of both *Rhizostoma* species, while the reverse RHIZ1-1 was selected for its specificity in uniquely amplifying the DNA of *R. pulmo*.

The primer RHOP1 produced the 101 bp amplicon from the DNA of *P. benovici*, other than of *R. esculentum*, due to the presence of only one difference on the annealing sequence of the two species. For these reason, the primer RHOP1 was modified (RHOP1-1) near to the 3′-end. In fact, mismatch at or near the terminal 3′ base of a primer affects PCR more dramatically than those single mismatches located internally or at 5′ end.[40] The new primer RHOP1-1 gave the expected amplicon only in the presence of DNA of *R. esculentum*. Likely, selectivity of amplification using these primers has been increased by the stringent conditions adopted for the amplification protocol (see section 2.6). In fact, to avoid unspecific amplification we used an annealing time of only 5 s.

Finally, even though specific, the reverse primers COT1 was redesigned (COT2) due to its low amplification performance.

*3.2.2. Control PCR Primers Targeting 28SrRNA Gene.* The extraction of DNA contaminated by inhibitors is one of the main obstacles associated with PCR application in complex matrices, such as food. In fact, the inhibitors can interfere with the reaction, even leading to a complete amplification inhibition.[18] In our previous study,[12] we found that $Al^{3+}$ ions may contribute to the overall DNA amplification failure. In fact, the initial concentration of the aluminum in jellyfish food products is extremely different,[12,41] and even though the pre-extraction procedure can reduce its concentration, it is impossible to predict the residual amount in different DNA samples. Therefore, considering that inhibition may be the cause of false-negative reactions, we decided to introduce a reaction control. This consideration, together with the high degradation level of the DNA extracted from MS, led us to design control primers for the amplification of a short DNA fragment of 55 bp.

Ribosomal genes, such as the *16sRNA* gene, are characterized by a low mutation rate.[42] In this study, the overall mean distance calculated on a fragment of 1480 bp belonging to the *28S rDNA* gene sequences (those produced by Bayha et al.[26] together with the sequence of *N. nomurai* produced in this study) was 2%. In the light of these results and taking into consideration that in a previous study[28] the high degree of conservation has played a decisive role for designing primers to be used for the amplification of many species at once, the *28SrRNA* gene was selected as target for designing the control primers.

**3.3. Pentaplex PCR Assay: Development and Final Protocol.** The optimization of a multiplex PCR can imply several difficulties. In fact, the presence of more than one primer pair in the reaction increases the chance of obtaining spurious amplification products and may increase the possibility to obtain the formation of primer dimers. Increasing the concentration of PCR reagents during the optimization step can increase the likelihood of mispriming, with subsequent

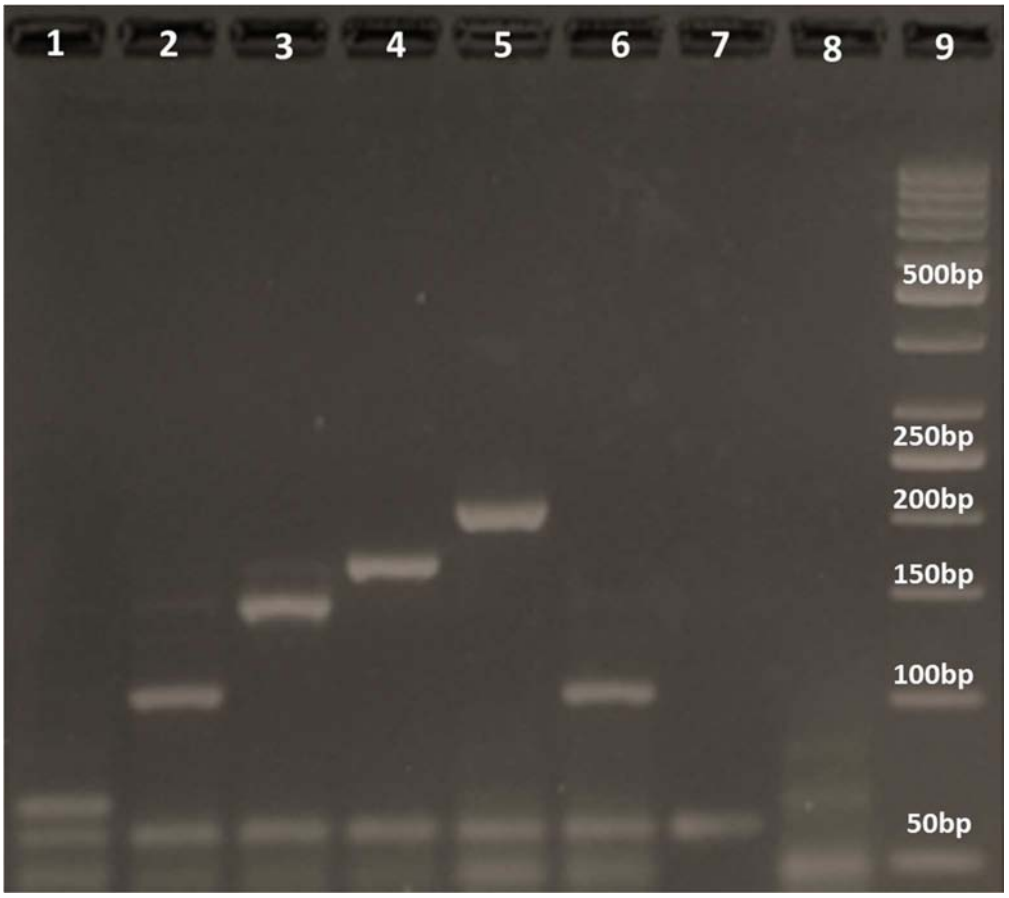


**Figure 1.** Electrophoresis on agarose gel (4%) of the five species of jellyfish selected as target after the Pentaplex PCR. Lane 1, *C. tuberculata* (72 bp); lane 2, *R. esculentum* (101 bp); lane 3, *N. nomurai* (143 bp); lane 4, *P. noctiluca* (165 bp); lane 5, *R. pulmo* (203 bp); lane 6, DNA from RE product; lane 7, DNA from CP product; lane 8, $H_2O$. DNA ladder band size: 1000 bp, 900 bp, 800 bp, 700 bp, 600 bp, 500 bp, 400 bp, 300 bp, 250 bp, 200 bp, 150 bp, 100 bp, 50 bp.

production of nonspecific amplification.[43] However, optimization of these components is usually beneficial. For the aforesaid reasons the final reaction protocol was selected through a process in which different concentration of primers, $MgCl_2$, nucelotides, and Taq polymerase were tested. Meanwhile, the best cycling conditions were selected by testing different temperatures and times.

*3.3.1. Primers and DNA Template Amount.* The primers were used at the same concentration during the first trials (100 nM). Subsequently, the concentrations were modified with the aim to obtain bands of similar intensity. In general, due to the good efficiency of the reverse primers, the concentration was maintained in the range 100−200 nM. Only the degenerated forward primer was used at a higher concentration (300 nM). Overall, primers' concentrations were lower than those at which the formation of considerable amount of primer−dimer (~500 nM) was observed.[43] We found that the introduction of the control primers (28sfor55; 28srev55) reduced the amplification efficiency of some specific primers (PEL1 and NEMO1), even when used at low concentration (50, 100 nM). For this reason, both nucleotides and Taq polymerase concentration were increased (see Section 3.3.3).

Another fundamental step for obtaining of a specific amplification, strictly connected with primers concentration, is the selection of an adequate DNA template concentration. In fact, if the primer-to-template ratio is too low, specific products will not accumulate exponentially while primer dimers may be amplified more efficiently than the desired target.[43,44] In this study, the utilization of total DNA quantities between 50 and 200 ng per reaction did not bring any significant difference regarding bands intensity. On the contrary, DNA quantities over 100 ng negatively affected the background of the gel after electrophoresis, especially in case of DNA extracted from market samples. In fact, when degradation of DNA occurs, small DNA fragments may unspecifically be involved in the reaction, producing spurious amplification products. For this reason, 50 ng were used as working concentration.

*3.3.2. $MgCl_2$, Nucelotides and Taq Polymerase.* To test the influence of $MgCl_2$ different trials were performed keeping the dNTP concentration constant and gradually increasing magnesium chloride from 1 to 5 mM. Using the standard concentration of dNTP (200 $\mu$M), the amplification became more specific and the products acquired comparable intensities at 3 mM: further increases showed a detrimental effect. Then, considering that in a multiplex PCR more amplicons are simultaneously amplified and the pool of enzymes and nucleotides becomes a limiting factor,[45] and in the light of the results obtained after the addition to the reaction mixture of the control primers, we decided to test double concentration of these reagents (400 $\mu$M of dNTP and 1U of TAQ Polymerase). The reaction efficiency was significantly improved and, even though dNTPs directly chelate a proportional number of $Mg^{2+}$ ions, we did not find any advantage using higher concentration of $MgCl_2$.

Table 4. Amplification Rate of DNA Extracted from Market Samples Using the Pentaplex PCR Method

| | sequence length (with primers) | | | | | | | |
|---|---|---|---|---|---|---|---|---|
| | 709 bp | | 256 bp | | 193 bp | | total | |
| | RE | CP | RE | CP | RE | CP | RE | CP |
| tested samples | 20 | 5 | 16 | 9 | 12 | 16 | 48 | 30 |
| positive samples | 19 | 4 | 13 | 5 | 9 | 8 | 41 | 17 |
| percentage of positive samples | 95% | 80% | 81% | 55.5% | 75% | 37.5% | 85.4% | 57% |

*3.3.3. Cycling Condition.* All the primer pairs used in a multiplex PCR should enable similar amplification efficiencies for their respective targets. This may be achieved through the utilization of primers with very similar optimum annealing temperatures. In this work, the average melting temperature of the species-specific reverse primers was 50.5 °C, while the degenerated reverse has a melting temperature of 53.7 °C. Even though our primers produced the expected amplicon in the range of 47−51 °C, an annealing temperature of 49 °C was selected. This temperature facilitate the annealing of the degenerated FJ2 primer and increased the specificity of the reverse primers. This has probably enhanced the specificity of our Pentaplex method allowing to avoid unspecific amplification even in case of close species.

**3.4. Validation of the Pentaplex PCR Assay Using Market Samples DNA.** Once optimized on DNA extracted from RS and from part of the MS (Figure 1), the final Pentaplex PCR protocol was applied to all the DNA samples extracted from MS identified by FINS in a previous work.[12] In particular, 48 RE and 30 CP DNA samples were tested. The results of the amplification are reported in Table 1, while the percentages of successful amplification are summarized in Table 4. Overall, in the case of RE, the Pentaplex PCR was capable to specifically amplify 85.4% of DNA. The higher percentage of amplification (95%) was obtained using those DNA samples from which a sequence of 658 bp (amplicon including primers of 709 bp) was previously amplified, while lower percentages were obtained in case of more degraded DNA samples (Table 4). In case of DNA extracted from CP, the Pentaplex PCR was less effective. Overall, it was able to correctly amplify ∼60% of tested samples. Moreover, the absence of specific amplicons in 3 CP sample that have not been identified at the species level by the phylogenetical analysis (identity value of 86% with *N. nomadica* and 85% with *C. stuhlmanni*) can be considered as a further demonstration of the specificity of the proposed method.

The lower rate of success in case of CP with respect to RE could be attributed to the presence of strongly degraded DNA extracted from products characterized by lower pH values (see Section 3.2.1), rather than to the action of inhibitors, such as aluminum. In fact, in all the DNA from which the specie-specific band was not obtained, the 55 bp control amplicon was always visible (Figure 1). Furthermore, in a previous study,[12] we found that the inhibitory effects affected more the longer than the shorter amplicons.

These results might seem to be in contrast with those obtained in our previous study,[12] in which an amplicon of 145 bp was amplified even from the most degraded DNA from market samples. One possible explanation could be related to the more stringent cycling conditions adopted to increase specificity. In PCR protocols using degenerated primers, the difference between the melting (MT) and the annealing temperature (AT) should be between 10 and 20 °C.[46] In the previous work, in which only degenerated primers were used, AT was 9 °C lower than the mean MT of the primers. In this Pentaplex PCR, the low difference (4.7 °C) between MT and AT of primers could have led to a more difficult annealing. Finally, multiplex PCRs are proven to be less sensitive than single PCR reactions.[47]

**3.5. Jellyfish Labeling: Issues and Outlooks.** All the jellyfish recorded in FAO statistics belong to the order Rhizostomeae and in particular to the genus *Rhopilema*.[48] These statistics are quite questionable considering that at least 11 species in 5 families are known to be exploited worldwide.

Most of the Asian jellyfish are exported to Japan and the remainder are sold to South Korea, Taiwan, Singapore, Hong Kong, U.S.A.,[10,49] and Europe.[11,12] While in eastern Asian countries jellyfish food products are usually categorized in eight types based on the color, form, texture, and size of the semidried products,[49] the Western Countries have tried to regulate the commercialization of these products by establishing a specific labeling.

In U.S.A., the acceptable market name of jellyfish has been associated with all the species belonging to the genus *Rhopilema*.[50] In Italy, the Ministry of Agriculture Food and Forestry Policies (MIPAFF) has adopted the provisional commercial denomination of "Asian jellyfish" for the species *R. esculentum*. At present, to the best of our knowledge, no other EU member Countries has defined a commercial denomination for jellyfish species.

We hypothesize that, due to the impossibility to identify the species in the commodity by a visual inspection, some traceability information, as for example the commercial and scientific denomination, have been deduced at official level from the importation documents. In fact, animal products from third countries outside the EU must be imported via a port or an airport with a Border Inspection Post (BIP), the official office authorized by the Ministry of Health in performing the control according to the European legislation. In fact, the official controls should include at least a systematic documentary check, a random identity check, and, where appropriate, a physical check. However, physical checks, which could include checks on the means of transport, on the packaging, labeling, temperature, the sampling for analysis and laboratory testing, and any other check necessary to verify compliance with the food laws, are performed with a frequency which depends on the risks associated with different foods, the history of compliances with the requirements for the product concerned of the third country, the controls that the food business operator importing the product has carried out, and, finally, the guarantees that the competent authority of the third country of origin has given.[51]

In the U.S., the absence of adequate documentation of fish products entering the market is a serious impediment to establishing the legal origin.[52] Moreover, the incredible rate of adulteration of fish products found in the U.S. market reflected not only the weak collaboration among FDA (Food and Drug Administration), CBP (Customs and Border Protection), and

NMFS (National Marine Fisheries Service) but also the inadequate attention on this issue from FDA.[53] Therefore, new food products coming on the market may be not properly identified.

The hypothesis that, in Italy, the commercial name adopted for Asian jellyfish is not correct seems to be confirmed by one molecular survey previously carried out in our laboratory,[12] which highlighted how most of jellyfish food products sold in Italy were *N. nomurai* instead of *R. esculentum*. Moreover, the identification of other species such as *R. pulmo* and *P. noctiluca* put in evidence the need of a revision of the commercial denomination proposed for these products. For example, the denomination of "Asian jellyfish" should be extended also to the species *N. nomurai* and a new denomination for the Mediterranean species *R. pulmo* should be defined.

It follows that, as specified by the Regulation (EU) No. 1379/2013:[14] "*the available technologies, including DNA-testing, should be used to protect the consumer and in order to deter operators from falsely labeling catches*". In particular, considering the strategic position of the BIPs in the international commerce framework, it could be very important, especially in case of new products (species), to establish a standardized checking procedure to be used during the inspection, to correctly verify the labeling information. This could allow not only to avoid the commercialization of mislabeled products, but to also clearly assess the seafood product characteristics before proposing new official commercial denominations. In fact, in the case of Italy, the number of these denominations has already exceeded nine hundred.[21]

Jellyfish populations appear to be increasing in the majority of the world's coastal ecosystems and seas. Since jellyfish populations can have an important impact on human activities and marine ecosystems but, at the same time, they represent a valuable source of food, it is very important to increase the knowledge regarding the edible species actually exploited worldwide. Although the DNA sequencing appears to be the most commonly applied approach for fish species identification across European laboratories,[17] this procedure needs expensive equipment and long-times of execution. On the countrary, the Multiplex PCR assay developed in this work represents an useful test for the screening of samples and allows to speed up the analysis flow and to reduce costs. Finally, this method represents a useful tool to enforce the law on traceability and to prevent mislabeling in the seafood chain.

## ■ ASSOCIATED CONTENT

### Supporting Information

Table 1SI. Reference samples obtained in this study (highlighted in gray) and in previous studies[22,23] used for the development of the Pentaplex PCR assay. Table 2SI. Mismatches between the reverse specie-specific primers selected for the target jellyfish species and the sequences of other species. This material is available free of charge via the Internet at http://pubs.acs.org.

## ■ AUTHOR INFORMATION

### Corresponding Author

*Tel: +390502210207. Fax: +390502210213. E-mail: andrea.armani@unipi.it.

### Notes

The authors declare no competing financial interest.

## ■ ACKNOWLEDGMENTS

The authors sincerely thank Antonella Leone, Stefano Piraino, and Giorgio Aglieri, who kindly provided reference tissues of jellyfish.

## ■ REFERENCES

(1) Purcell, J. E.; Uye, S. I.; Lo, W. T. Anthropogenic causes of jellyfish blooms and direct consequences for humans: A review. *Mar. Ecol.: Prog. Ser.* **2007**, *350*, 153−174.

(2) Richardson, A. J.; Bakun, A.; Hays, G.; Gibbons, M. J. The jellyfish joyride: Causes, consequences and management responses to a more gelatinous future. *Trends Ecol. Evol.* **2009**, *24* (6), 312−322.

(3) Boero, F. Review of jellyfish blooms in the Mediterranean and Black Sea. Studies and Reviews. General Fisheries Commission for the Mediterranean. FAO 2013, No. 92 (http://www.fao.org/docrep/017/i3169e/i3169e.pdf) (Last accessed on Sept. 22, 2014).

(4) Kang, C.; Munawir, A.; Cha, M.; Sohn, E. T.; Lee, H.; Kim, J. S.; Yoon, W. D.; Lim, D.; Kim, E. Cytotoxicity and hemolytic activity of jellyfish *Nemopilema nomurai* (Scyphozoa: Rhizostomeae) venom. *Comp. Biochem. Phys. C* **2009**, *150*, 85−90.

(5) Yu, H.; Liu, X.; Dong, X.; Li, C.; Xing, R.; Liu, S.; Li, P. Insecticidal activity of proteinous venom from tentacle of jellyfish *Rhopilema esculenta* kishinouye. *Bioorg. Med. Chem. Lett.* **2005**, *15*, 4949−4952.

(6) Ayed, Y.; Bousabbeh, M.; Mabrouk, H. B.; Morjen, M.; Marrakchi, N.; Bacha, H. Impairment of the cell-to-matrix adhesion and cytotoxicity induced by the Mediterranean jellyfish *Pelagia noctiluca* venom and its fractions in cultured glioblastoma cells. *Lipids Health Dis.* **2012**, *28*, 11−84.

(7) Leone, A.; Lecci, R. M.; Durante, M.; Piraino, S. Extract from the zooxanthellate jellyfish *Cotylorhiza tuberculata* modulates gap junction intercellular communication in human cell cultures. *Mar. Drugs* **2013**, *11*, 1728−1762.

(8) Exposito, J. Y.; Larroux, C.; Cluzel, C.; Valcourt, U.; Lethias, C.; Degnan, B. M. Demosponge and sea anemone fibrillar collagen diversity reveals the early emergence of A/C clades and the maintenance of the modular structure of type V/XI collagens from sponge to human. *J. Biol. Chem.* **2008**, *283* (42), 28226−28235.

(9) Addad, S.; Exposito, J. Y.; Faye, C.; Ricard-Blum, S.; Lethias, C. Isolation, characterization, and biological evaluation of jellyfish collagen for use in biomedical applications. *Mar. Drugs* **2011**, *9*, 967−983.

(10) Hsieh, Y. H. P.; Fui-Ming Leong, F. M.; Rudloe, J. Jellyfish as food. *Hydrobiologia* **2001**, *451*, 11−17.

(11) Armani, A.; D'Amico, P.; Castigliego, L.; Sheng, G.; Gianfaldoni, D.; Guidi, A. Mislabeling of an "unlabelable" seafood sold on the European market: The jellyfish. *Food Control* **2012**, *26*, 247−251.

(12) Armani, A.; Tinacci, L.; Giusti, A.; Castigliego, L.; Gianfaldoni, D.; Guidi, A. What is inside the jar? Forensically informative nucleotide sequencing (FINS) of a short mitochondrial *COI* gene fragment reveals a high percentage of mislabeling in jellyfish food products. *Food Res. Int.* **2013**, *54*, 1383−1393.

(13) Commission Regulation (EC) No. 2065/2001 of 22 October 2001. Laying down detailed rules for the application of Council Regulation (EC) No. 104/2000 as regards informing consumers about fishery and aquaculture products. *OJ L*; Oct. 23, 2001; Vol. *278*, pp 6−8.

(14) Regulation (EU) No. 1379/2013 of the European Parliament and of the Council of 11 December 2013 on the common organisation of the markets in fishery and aquaculture products, amending Council Regulations (EC) No. 1184/2006 and (EC) No. 1224/2009 and repealing Council Regulation (EC) No. 104/2000. *OJ L*; Dec. 28, 2013; Vol *354*, pp 1−21.

(15) D'Amico, P.; Armani, A.; Castigliego, L.; Sheng, G.; Gianfaldoni, D.; Guidi, A. Seafood traceability issues in Chinese food business activities in the light of the European provisions. *Food Control* **2014**, *35* (1), 7−13.

(16) Armani, A.; Castigliego, L.; Guidi, A. Fish fraud: The DNA challenge. *CAB Rev.* **2012**, *7* (71) 10.1079/PAVSNNR20127071.
(17) Griffiths, A. M.; Sotelo, C. G.; Mendesc, R.; Perez Martin, R. I.; Schröderd, U.; Shorten, M.; Silva, H. A.; Verrez-Bagnis, V.; Mariani, S. Current methods for seafood authenticity testing in Europe: Is there a need for harmonisation? *Food Control* **2014**, *45*, 95−100.
(18) Teletchea, F.; Maudet, C.; Hanni, C. Food and forensic molecular identification: Update and challenges. *Trends Biotechnol.* **2005**, *7*, 360−366.
(19) Bartlett, S. E.; Davidson, W. S. FINS (forensically informative nucleotide sequencing): A procedure for identifying the animal origin of biological specimens. *Biotechniques* **1992**, *12* (3), 408−411.
(20) Cawthorn, D. M.; Steinman, H. A.; Witthuhn, R. C. DNA barcoding reveals a high incidence of fish species misrepresentation and substitution on the South African market. *Food Res. Int.* **2012**, *46*, 30−40.
(21) Armani, A.; Guardone, L.; Castigliego, L.; D'Amico, P.; Messina, A.; Malandra, R.; Gianfaldoni, D.; Guidi, A. DNA and Mini-DNA Barcoding for the identification of *Porgies* species (family Sparidae) of commercial interest on the international market. *Food Control* **2014**, DOI: 10.1016/j.foodcont.2014.09.025.
(22) Armani, A.; Tinacci, L.; Xiong, X.; Titarenko, E.; Guidi, A.; Castigliego, L. Development of a simple and cost-effective bead-milling method for DNA extraction from fish muscles. *Food Anal. Methods* **2014**, 7 (4), 946−955.
(23) Prieto, L.; Armani, A.; Macias, D. Recent stranding of the giant jellyfish *Rhizostoma luteum* Quoy and Gaimard, 1827 (Cnidaria: Schyphozoa: Rhizostomeae) on the Atlantic and Mediterranean coasts. *Mar. Biol.* **2013**, *160*, 3241−3247.
(24) Piraino, S.; Aglieri, G.; Martell, L.; Mazzoldi, C.; Melli, V.; Milisenda, G.; Scorrano, S.; Boero, F. *Pelagia benovici* sp. nov. (Cnidaria, Scyphozoa): A new jellyfish in the Mediterranean Sea. *Zootaxa* **2014**, *3794* (3), 455−468.
(25) Tamura, K.; Peterson, D.; Peterson, N.; Stecher, G.; Nei, M.; Kumar, S. MEGA5: Molecular evolutionary genetics analysis using maximum likelihood, evolutionary distance, and maximum parsimony methods. *Mol. Biol. Evol.* **2005**, *28*, 2731−2739.
(26) Bayha, K. M.; Dawson, M.; Collins, A. G.; Barbeitos, M. S.; Haddock, S. H. Evolutionary relationship among Scyphozoan jellyfish families based on complete taxon sampling and phylogenetic analyses of 18s and 28s ribosomal DNA. *Integr. Comp. Biol.* **2010**, *50* (3), 436−455.
(27) Kimura, M. A. simple method for estimating evolutionary rate of base substitutions through comparative studies of nucleotide sequences. *J. Mol. Evol.* **1980**, *16*, 111−120.
(28) Armani, A.; Castigliego, L.; Tinacci, L.; Gianfaldoni, D.; Guidi, A. Multiplex conventional and real-time PCR for fish species identification of Bianchetto (juvenile form of *Sardina pilchardus*), Rossetto (*Aphia minuta*), and Icefish in fresh, marinated, and cooked products. *Food Chem.* **2012**, *133* (1), 184−192.
(29) Castigliego, L.; Armani, A.; Tinacci, L.; Gianfaldoni, D.; Guidi, A. Two alternative multiplex PCRs for the identification of the seven species of anglerfish (*Lophius* spp.) using an end-point or a melting curve analysis real-time protocol. *Food Chem.* **2015**, *166* (1), 1−9.
(30) Russell, F. S. The medusae of the British Isles II. Pelagic Scyphozoa with a supplement to the first volume on hydromedusae. *Int. Rev. Gesamten Hydrobiol. Hydrogr.* **1971**, *56* (4), 686 DOI: 10.1002/iroh.19710560438.
(31) Muhammed, F.; Sultana, R. New record of edible jellyfish *Rhizostoma pulmo* (Cnidaria: Scyphozoa: Rhizostomatidae) from Pakistani waters. *Mar. Biodivers. Rec.* **2008**, *1*, e67 DOI: 10.1017/S1755267207007294.
(32) Mariottini, G. L.; Giacco, E.; Pane, L. The mauve stinger *Pelagia noctiluca* (Forsskål, 1775). Distribution, ecology, toxicity and epidemiology of stings. A review. *Mar. Drugs.* **2008**, *6* (3), 496−51.
(33) Brotz, L.; Pauly, D. Jellyfish populations in Mediterranean Sea. *Acta Adriac.* **2012**, *53* (2), 213−232.
(34) Barbuto, M.; Galimberti, A.; Ferri, E.; Labra, M.; Malandra, R.; Galli, P.; Casiraghi, M. DNA barcoding reveals fraudulent substitutions in shark seafood products: The Italian case of "palombo" (Mustelus spp.). *Food Res. Int.* **2010**, *43*, 376−381.
(35) Meduse buone anche in cucina e contro l'ipertensione. *La Gazzetta del Mezzogiornio*; 2013. Available online: http://www.lagazzettadelmezzogiorno.it/notizie-nascoste/meduse-buone-anche-in-cucina-e-contro-l-ipertensione-no619007/ (accessed Sept. 15, 2014).
(36) Bauer, T.; Weller, P.; Hammes, W. P.; Hertel, C. The effect of processing parameters on DNA degradation in food. *Eur. Food Res. Technol.* **2003**, *217*, 338−343.
(37) Kramp, P. L. Synopsis of the medusae of the world. *J. Mar. Biol. Assoc. U.K.* **1961**, *40*, 469.
(38) Holst, S.; Sotje, I.; Tiemann, H.; Jarms, G. Life cycle of the rhizostome jellyfish *Rhizostoma octopus* (L.) (Scyphozoa, Rhizostomeae), with studies on cnidocysts and statoliths. *Mar. Biol.* **2007**, *151*, 1695−1710.
(39) Dawson, M. N.; Jacobs, D. K. Molecular evidence for cryptic species of Aurelia aurita (Cnidaria, Scyphozoa). *Biol, Bull.* **2001**, *200*, 92−96.
(40) Lindeman, R.; Hu, S. P.; Volpato, F.; Trent, R. J. PCR mutagenesis enabling rapid non-radioactive detection of common β-thalassemia mutations in Mediterraneans. *Br. J. Hamaetol.* **1991**, *78*, 100−4.
(41) Wong, W. W. K.; Chung, S. W. C.; Kwong, K. P.; Yin, H. Y.; Xiao, Y. Dietary exposure to aluminium of the Hong Kong population. *Food Addit. Contam.* **2010**, *27* (4), 457−463.
(42) Kochzius, M.; Seidel, C.; Antoniou, A.; Kumar Botla, S.; Campo, D.; Cariani, A.; et al. Identifying fishes through DNA barcodes and microarrays. *PLoS One* **2010**, *5*, e12620.
(43) Markoulatos, P.; Siafakas, N.; Moncany, M. Multiplex Polymerase Chain Reaction: A Practical Approach. *J. Clin. Lab. Anal.* **2002**, *16*, 47−51.
(44) Ruano, G.; Fenton, W.; Kidd, K. K. Biphasic amplification of very dilute DNA samples via "booster" PCR. *Nucleic Acids Res.* **1989**, *17*, 5407.
(45) Henegariu, O.; Heerema, N. A.; Dlouhy, S. R.; Vance, G. H.; Vogt, P. H. Multiplex PCR: critical parameters and step-by-step protocol. *Biotechniques* **1997**, *23* (3), 504−511.
(46) Pelt-Verkuil, E.; van Belkum, A.; Hays, J. P. *Principles and Technical Aspects of PCR Amplification*; Springer Science + Business Media B.V.: New York, 2008; p 325.
(47) McClatchey, K. D. *Clinical Laboratory Medicine*, 2nd ed.; Lippincott Williams & Wilkins: Philadelphia, 2002; p 1693.
(48) Barnes, M.; Gibson, R. N.; Gibson, R. I. *Oceanography and Marine Biology: An Annual Review*; CRC Press: Boca Raton, FL, 2003; Vol. *38*, p 439.
(49) Omori, M.; Nakano, E. Jellyfish fisheries in Southeast Asia. *Hydrobiologia* **2001**, *451* (1−3), 19−26.
(50) The Seafood List; U.S. Food and Drug Administration; http://www.accessdata.fda.gov/scripts/fdcc/?set=seafoodlist&id=%3Ci%3ERhopilema%3C/i%3E%20spp.&sort=SLSN&order=ASC&startrow=1&type=basic&search=jellyfish (accessed Sept. 15, 2014).
(51) Regulation (EC) No. 882/2004 of the European Parliament and of the Council of 29 April 2004, On official controls performed to ensure the verification of compliance with feed and food law, animal health and animal welfare rules. *OJ L*; May 28, 2004; Vol. *191*, pp 1−141.
(52) Pramod, G.; Nakamura, K.; Pitcher, T. J.; Delagran, L. Estimates of illegal and unreported fish in seafood imports to the U.S.A. *Mar. Policy* **2014**, *48*, 102−113.
(53) Timme, K.; Lowell, B.; Hirshfield, M. Oceana study reveals seafood fraud nationwide. *Oceana*, 2013. Available at http://oceana.org/sites/default/files/National_Seafood_Fraud_Testing_Results_Highlights_FINAL.pdf.

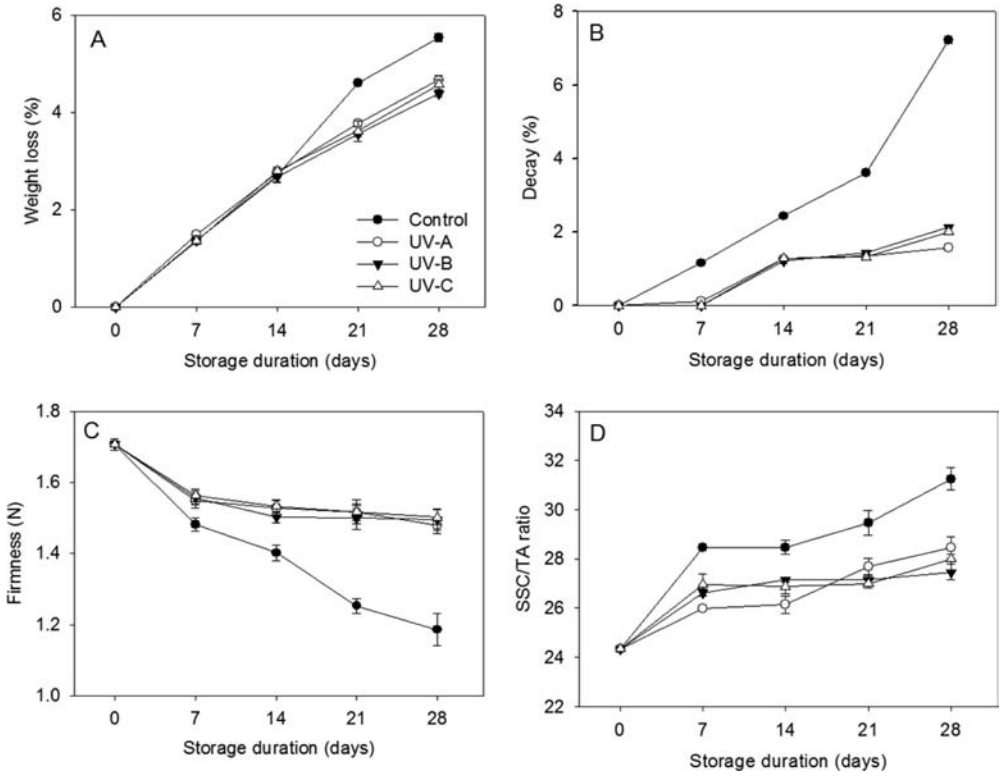


**Figure 1.** Effects of prestorage UV-A, -B, and -C treatments on fruit quality attributes of full-ripe 'Duke' blueberries during subsequent cold storage at 0 °C. Data are the mean ± SE of three replications.

device was equipped with nine 40-W UV lamps and three analog timers.[22] The lamp types of UV-A, -B, and -C were G40TBL ($\lambda_{max}$ = 352 nm), G40T10E ($\lambda_{max}$ = 306 nm), and G40T10 ($\lambda_{max}$ = 254 nm) (Sankyo Denki, Kanagawa, Japan), respectively. The distance of the UV lamp from the fruits was adjusted to obtain the required intensity (10 W/m$^2$) by using a KH-97503 photometer (Cole-Parmer, Vernon Hills, IL, USA). The fruits (about 2 kg) were placed in a mesh bag and radiated for 10 min each on the top and bottom side of the container until the fruits received a radiation dose of 6 kJ/m$^2$. For the control, fruits were not treated with any UV lights. We have selected the 6 kJ/m$^2$ dose from our preliminary study with 1.6, 4.0, and 6.0 kJ/m$^2$, where a dose of 6 kJ/m$^2$ remarkably reduced fruit decay of full-ripe blueberries without surface damage.

**Storage Conditions.** Upon UV treatments, blueberries (200 g) were placed in polyethylene containers (15 × 10 × 10 cm) without covers and stored at 0 °C with 95% relative humidity for 28 days. Experimental fruits were collected at 3 h after UV treatment (AT) and at 7, 14, 21, and 28 days during cold storage. Blueberries from the initial harvest were used as 0 day samples. Three replicates (200 g/container as a replicate) were employed for the experimental analysis.

**Evaluation of Fruit Quality.** Weight loss (%) was determined by the weight changes of samples between the start of the experiment and each sampling date. The values were shown as the percent of weight loss/the initial fruit weight. The decay (%) was calculated by the infected fruit number. The fruit firmness (N) was tested using a texture tester (TA.XT2, Stable Micro Systems, Scarsdale, NY, USA), and a 2 mm flat probe was used. Thirty fruits were randomly selected from each container, and individual fruits were penetrated at a speed of 0.5 mm/s.

Titratable acidity (TA) and soluble solids content (SSC) were determined using fruit juice that was extracted from a 50 g blueberry sample per each container. TA (%) was analyzed using a Fisher Titrimeter (model 35, Pittsburgh, PA, USA) and calculated as percent citric acid. The juice was titrated with sodium hydroxide (0.1 N) until the pH was 8.2. SSC (°Brix) was tested using a Atago PR-32 hand refractometer. The ratio of SSC/TA was expressed by dividing the SSC by the TA values.

**Total Phenolic and Total Anthocyanin Contents.** Blueberries (about 50 g) in bags were blended with 0.5% hydrochloric acid (1:1, w/v) using a home blender. Slurry sample (5 g) was taken and mixied with 30 mL of 80% (v/v) acetone and then centrifuged at 15000*g* for 30 min at 4 °C. The collected supernatants were kept at −80 °C before experiment.

Total phenolics were measured at 765 nm according to the Folin−Ciocalteu method[23] and calculated as milligrams of gallic acid equivalents (GAE) per 100 g of fresh weight. Total anthocyanins were measured using the differences between their absorbance at 515 nm ($A_{515}$) and 700 nm ($A_{700}$) in buffer solution at pH 1.0 and 4.5, where $A = [(A_{515} - A_{700})_{pH\ 1.0} - (A_{515} - A_{700})_{pH\ 4.5}]$.[24] The values were shown as milligrams of cyanidin-3-glucoside chloride equivalents per 100 g of fresh weight.

**2,2-Di-(4-*tert*-octylphenyl)-1-picrylhydrazyl (DPPH) Assay.** The scavenging capacity of the DPPH radicals was determined by a spectrophotometric method[25] with slight modifications. Twenty-four milligrams of DPPH was dissolved in 100 mL of 80% ethanol (v/v), and the solution was kept at −20 °C until the day of the experiment. Ten milliliters of DPPH solution was mixed with 45 mL of 80% ethanol (v/v) to obtain 1.1 ± 0.02 absorbance at 515 nm.

Blueberries were uniformly blended using a home mixer, and fruit slurry was prepared for DPPH and ABTS assays. Five gram samples were homogenized with 25 mL of 80% acetone (v/v), and 150 μL of this homogenate was reacted with the DPPH solution (2.85 mL) for 40 min in total darkness. The absorbance was determined using a Shimadzu UV-2401 spectrophotometer at 515 nm. The standard graph was constructed from 0 to 1.0 μmol of Trolox. The data were calculated as the Trolox equivalent antioxidant capacity (TE) per gram of fresh weight.

**2,2′-Azinobis(3-ethylbenzothiazoline-6-sulfonic acid) (ABTS) Assay.** The ABTS assay was experimented according to the methodof ref 26 with some modifications. A stock of ABTS solution (7.0 mM) was mixed with potassium persulfate (2.45 mM) to make ABTS cation radicals (ABTS$^{\bullet+}$) and was enabled to react for 12 h at 24 °C in total darkness. The ABTS stock solution was diluted with 80% of ethanol (v/v) until the absorbance was 0.7 ± 0.01 at 734 nm. Slurry

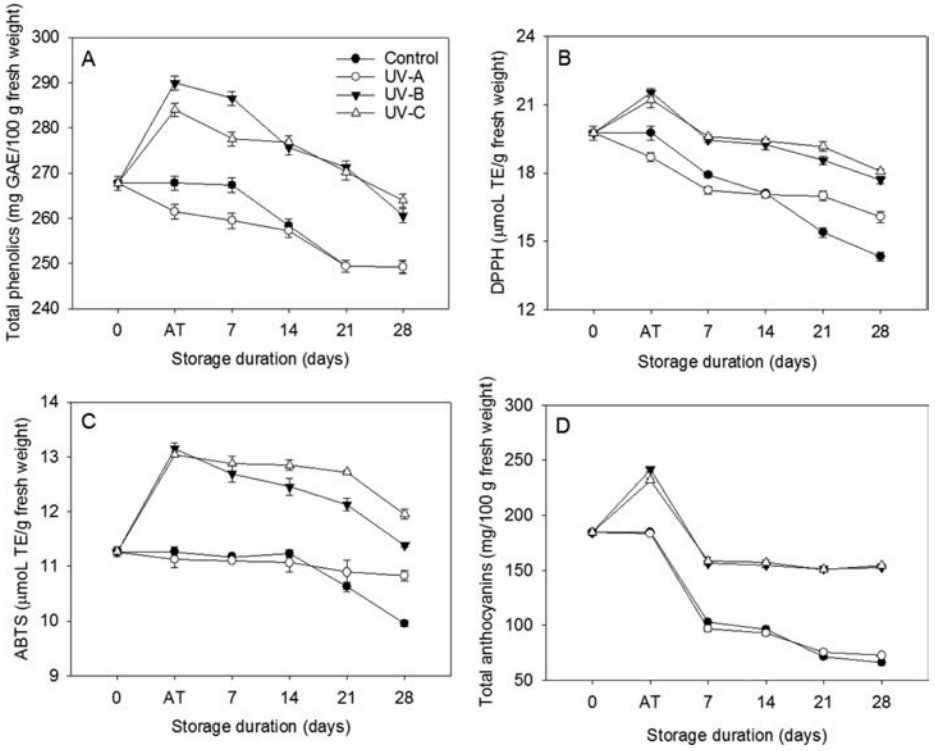


**Figure 2.** Effects of prestorage UV-A, -B, and -C treatments on total phenolics (A), antioxidant activities according to the DPPH (B) and ABTS (C) assays, and total anthocyanins (D) of full-ripe 'Duke' blueberries during subsequent cold storage at 0 °C. AT, measured at 3 h after UV treatments. Data are the mean ± SE of three replications.

samples (5 g) were homogenized with 80% acetone (30 mL). Twenty microliters of fruit extract was combined with $ABTS^{\bullet+}$ solution (3 mL) and kept in total darkness. After 15 min, the absorbance was measured at 734 nm. The Trolox standard curve between 0 and 1.0 μmol was constructed to measure the antioxidant activity, and the activities were shown as TE per gram of fresh weight.

**Extraction and Analysis of Individual Anthocyanins.** Three grams of blueberries was macerated in 20 mL of 80% acetone using a Polytron P-10 tissue homogenizer (Brinkmann, NY, USA). The extracts were filtered and concentrated using a rotary evaporator NN series (EYELA, Tokyo, Japan) in a water bath at 38 °C and then completely dissolved in 3% formic acid in water (v/v). All samples were passed through a $C_{18}$ Sepak cartridge (Waters, Milford, MA, USA). The anthocyanins were then recovered with absolute methanol (2 mL) consisting of 3% formic acid. Ten microliters of sample was separated by high-performance liquid chromatography (HPLC) after passing through a 0.42 μm membrane filter.

Mixed or individual anthocyanin standards were analyzed for the confirmation of anthocyanins extracted from blueberries. Three milligrams of cyanidin-3-glucoside chloride as an external standard was separately dissolved in 2% hydrogen chrolide in methanol (v/v). The individual anthocyanin content was calculated as milligrams of cyanidin-3-glucoside chloride equivalents per gram of fresh weight.

Anthocyanins were analyzed using a YL 9100 HPLC system (YoungLin, Anyang, Korea) consisting of a YL9111 binary pump, a YL9160 diode array detector, and a YL9150 autosampler. An analytical column of Phenomenox Bondclon $C_{18}$ (4.6 × 250 mm, 10 μm) was used. Mobile solvents were 5% formic acid in water (v/v) and acetonitrile (ACN), respectively. The solvent system was programmed from 5% ACN to 20% ACN for 50 min and flushed with 100% ACN for 5 min. The flow rate was 1 mL/min. Ten microliters of sample was injected. Anthocyanins were detected at 520 nm, and spectral data between 200 and 700 nm were collected at a time.

**Identification of Individual Anthocyanins.** Mass identification of anthocyanins was performed on a Surveyor HPLC system (ThermoFinnigan, San Jose, CA, USA). The system was fitted with an LCQ-DECA XP plus quadruple mass spectrometer (ThermoFinnigan). An analytical column of Inno ODS-N-120 (4.6 × 240 mm, 5 μm) was used. As mobile solutions, water and ACN, which both contained 5% formic acid, were eluted. The gradient started at 8% ACN and reached 40% ACN within 50 min. Positive electrospray ionization was performed by applying 5 kV. The temperature of the capillary was held at 275 °C. The Xcalibur 2.0 software package was used to monitor the LC−mass system as well as to process the collected data. Identities were determined by comparison to authentic standards and previous studies.[27,28]

**Statistical Analysis.** The experiment was carried out using a completely randomized design. Measurements and analysis were repeated in triplicate. The means were expressed with standard errors. Descriptive statistics and correlation matrix between studied variables of data from UV-C treatment were analyzed using SAS 9.3 software, and statistically significant levels were considered at $P \leq 0.001$, 0.01, and 0.05, respectively. The figures were generated using Sigma Plot 10.0 (SPSS, Chicago, IL, USA).

## RESULTS AND DISCUSSION

**Quality of Fruits.** The weight loss (%) was comparable for all experimental treatments throughout the storage period, but the control showed ∼1.3% higher rates compared to the UV treatments after 21 days (Figure 1A). A significant reduction in fruit decay was found in the UV treatments, and these differences became greater toward the end of the storage time (Figure 1B). At 28 days, the decay of the control was the highest (7.2%). The decay rate of the UV treatments ranged between 1.3 and 2.1% during storage of 28 days. UV lights effectively inhibited the softening compared with the control; however, differences were not found in fruit firmness between the UV treatments (Figure 1C). The control started to show softening after 7 days. The UV lights delayed further ripening of the fruits as seen by the SSC/TA ratio (Figure 1D) compared with the control. During the storage period, fruits in

the control showed lower acidity and higher sweetness compared with those in the UV treatments. However, there were no differences between UV treatments.

The benefits of low-dose UV lights on fresh fruits have been found in other studies, particularly with UV-C from 0.25 to 8 kJ/m$^2$. Low-dose UV-C promoted the synthesis of phytoalexins[29] or delayed the weight loss and softening of fruits during storage.[30,31] With UV-C treatment between 1 and 4 kJ/m$^2$, the decay in blueberries decreased by 10%.[8] However, a high dose of UV-B treatment from 15 to 30 kJ/m$^2$ induced damage to living organisms, because cellular compounds such as proteins and nucleic acid absorbed the energy-rich radiation.[32] In our experiment, all UV lights of 6 kJ/m$^2$ effectively maintained fruit quality by reducing the weight loss, decay, and ripening of blueberries during subsequent cold storage for 28 days (Figure 1). Therefore, we concluded that the UV treatments regardless of UV light type were beneficial to maintaining fruit qualities of blueberries during cold storage.

**Changes of Total Phenolics.** The total phenolics of blueberries during cold storage were greatly affected by the prior UV treatments. There was a ~17 mg GAE/100 g fresh weight increase in the total phenolics due to the UV-B and -C treatments after 3 h, whereas UV-A showed a slight reduction (Figure 2A). Although the total phenolics gradually declined with storage time, the content in blueberries in the UV-B and -C treatments always remained higher than the control and UV-A treatment. Similarly, the UV-C treatment significantly increased all major individual phenolics as well as the flavonoid compounds in blueberries, but there were no compositional changes of individual anthocyanins.[9] These beneficial effects of UV-C were linked to the PAL activation.[15] In our study, UV-B also showed an effect similar to that of UV-C; however, the total phenolics of blueberries with UV-B and -C decreased quickly with storage time.

**Changes in Antioxidant Activities.** The antioxidant activity measured by the DPPH assay in UV-B- and -C-treated blueberries immediately increased after UV treatments. Contrary to an increased antioxidant activity in the UV-B and -C treatments, there was a slight reduction in the UV-A treatment at 3 h (Figure 2B). The activities determined by the ABTS assay in the UV-B and -C treatments were also much higher than in both the control and UV-A treatment (Figure 2C). This trend did not change throughout the duration of the cold storage. The control showed the lowest antioxidant levels at 28 days.

**Changes in Total Anthocyanins.** The total anthocyanin changes during storage are shown in Figure 2D. The total anthocyanins remarkably increased by UV-B and -C treatments in 3 h, but sharply decreased at 7 days. After the sharp decrease, the contents of total anthocyanins steadily stabilized. The total anthocyanins in UV-B and -C treatments were still ~88 mg/100 g higher than the control and UV-A treatment at 28 days. We have observed that the anthocyanin contents were rapidly increased by the UV-B and -C treatments, then rapidly decreased in 7 days, and a steady decrease thereafter. The initial differences in the increases were maintained during cold storage.

The total anthocyanin contents increased with the treatments of 2 or 4 kJ/m$^2$ UV-C in 'Bluecrop' blueberries, particularly immediately after treatment.[9] UV-B also showed a rapid increase after treatment, and the contents were nearly identical to those for UV-C treatment during storage. These trends were simmilar to those of the total phenolics and antioxidant activities shown in Figure 2A–C. The UV-A treatment did not show any differences compared with the control and thus was considered not to be as effective in the promotion of anthocyanin synthesis.

The anthocyanin contents were rapidly decreased in the cold storage, regardless of prior treatments, and the initial difference was maintained for 28 days. The control and UV-A treatment, having lower anthocyanin contents, showed higher fruit discoloration (data not shown) and decay rates (Figure 1B), as compared to UV-B and -C treatments. We assume that anthocyanins might be rapidly degraded by an increased activity of the anthocyanase catalyzing the anthocyanin–polyphenol reaction during the storage.[33]

**Analysis of Individual Anthocyanins.** The typical HPLC and LC-MS profiles of anthocyanins in blueberry extracts are presented in Figure 3A,B, and the peak number, retention time, and exact mass of each anthocyanin are listed in Table 1. We have obtained similar anthocyanin profiles by HPLC and LC-

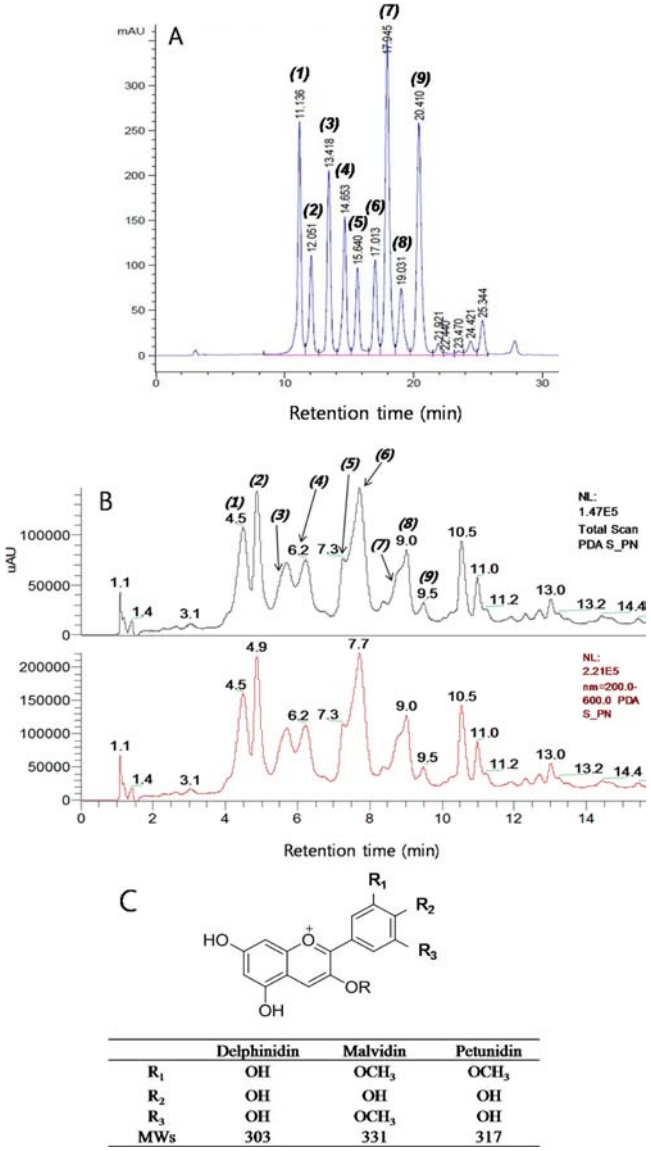


| | Delphinidin | Malvidin | Petunidin |
|---|---|---|---|
| $R_1$ | OH | $OCH_3$ | $OCH_3$ |
| $R_2$ | OH | OH | OH |
| $R_3$ | OH | $OCH_3$ | OH |
| MWs | 303 | 331 | 317 |

**Figure 3.** Typical HPLC (A) and LC-MS (B) profiles of anthocyanins in full-ripe 'Duke' blueberry extracts that were detected at 520 nm and their chemical structures (C). The compounds are listed in Table 1.


dx.doi.org/10.1021/jf504366x | J. Agric. Food Chem. 2014, 62, 12144–12151

**Table 1. Peak Retention Time (RT), Identification, and Molecular Mass of Anthocyanins in Full-Ripe 'Duke' Blueberries**

| peak | RT (min) | anthocyanin (abbreviation) | $M^+$ | fragment |
|---|---|---|---|---|
| 1 | 11.1 | delphinidin-3-galactoside (Del-3-Gal) | 465.07 | 303.25 |
| 2 | 12.0 | delphinidin-3-glucoside (Del-3-Glu) | 465.07 | 303.25 |
| 3 | 13.4 | delphinidin-3-arabinoside (Del-3-Ara) | 435.09 | 303.17 |
| 4 | 14.6 | petunidin-3-galactoside (Pet-3-Gal) | 479.07 | 317.22 |
| 5 | 15.6 | petunidin-3-glucoside (Pet-3-Glu) | 479.07 | 317.22 |
| 6 | 17.0 | petunidin-3-arabinoside (Pet-3-Gal) | 449.07 | 317.22 |
| 7 | 17.9 | malvidin-3-galactoside (Mal-3-Gal) | 493.07 | 331.21 |
| 8 | 19.0 | malvidin-3-glucoside (Mal-3-Glu) | 493.07 | 331.03 |
| 9 | 20.4 | malvidin-3-arabinoside (Mal-3-Ara) | 463.05 | 331.25 |

MS analysis and detected nine major anthocyanins in the full-ripe 'Duke' blueberries. Three major anthocyanins of full-ripe blueberries were malvidin-3-galactoside, delphinidin-3-galactoside, and petunidin-3-galactoside (Figure 4A,D,G).

In our samples, delphinidin-, malvidin-, and petunidin-based anthocyanins were detected as major compounds and those based on cyanidin, pelargonidin, and peonidin were not detected or were in very little amounts. In another study, cyanidin-3-galactoside and malvidin-3-galactoside were the main compounds in the same 'Duke' cultivar,[9] but the cyanidin-based anthocyanins were not detected or the minor compounds in our study. In highbush 'Bergitta' cultivar, dephinidin-, malvidin-, and petunidin-based anthocyanins were detected as major compounds and cyanidin-based anthocyanins were minor.[34] The anthocyanin composition in berries could be different according to cultivar,[24] species,[28,35] or fruit development stage.[36] Therefore, the difference from or similarity to other studies seemed to be due to wide variation in the composition of individual anthocyanins or their contents among the cultivars and locations of production.

**Changes in Individual Anthocyanins in Blueberries.** Changes in the individual anthocyanins during cold storage are shown in Figure 4. All of the individual anthocyanins increased significantly within 3 h when treated with UV-B and -C. This increase was especially distinct in the UV-B treatment. These effects diminished as the storage time increased, although there were apparent UV-induced effects in the UV-B and -C treatments. The contents of all individual anthocyanins in the UV-B and -C treatments were higher than those in the control

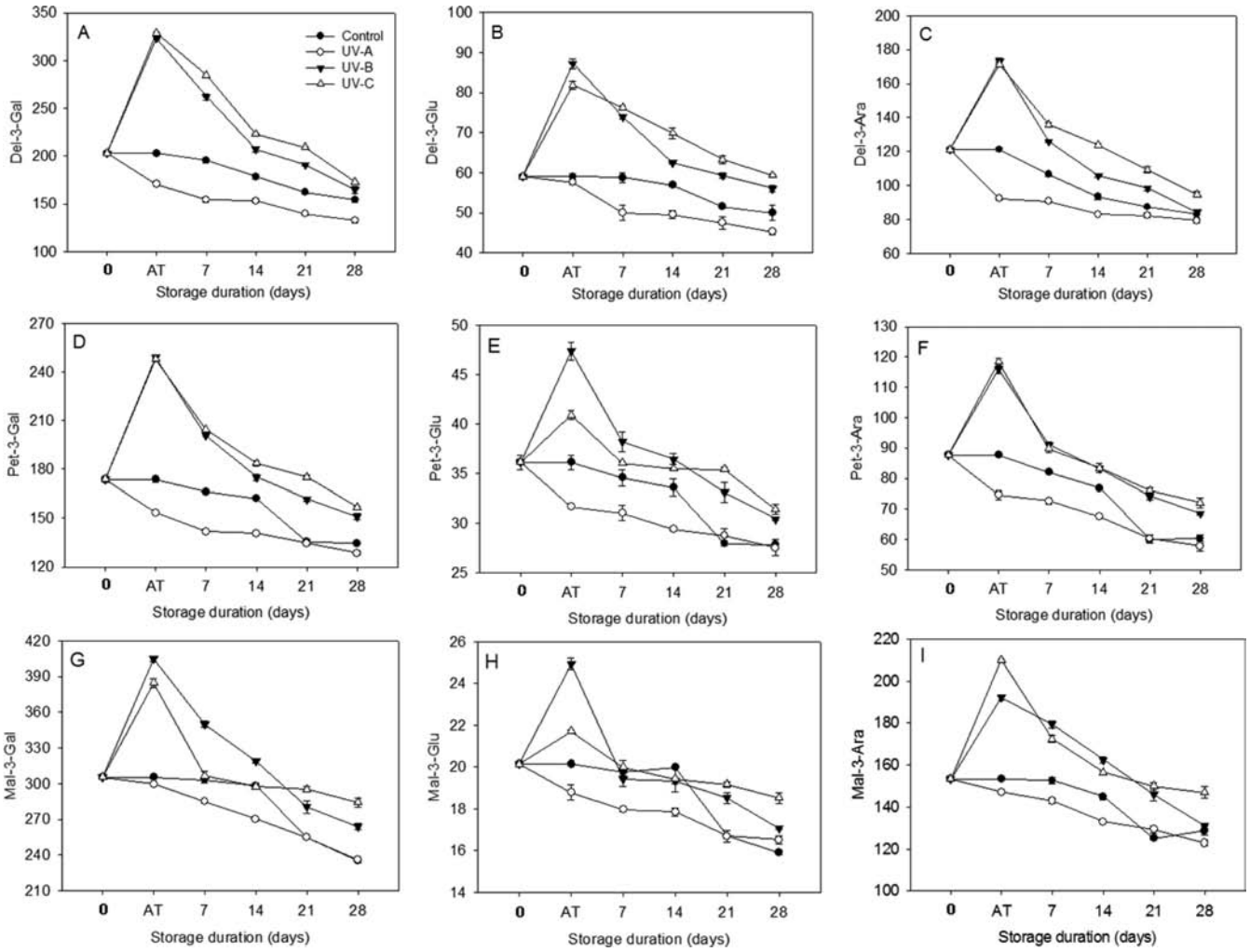


**Figure 4.** Effects of prestorage UV-A, -B, and -C treatments on individual anthocyanin changes ($\mu$g/g fresh weight) of full-ripe 'Duke' blueberries during subsequent cold storage at 0 °C. AT, measured at 3 h after UV treatments. The data are expressed as cyanidin-3-glucoside chloride equivalents. Data are the mean ± SE of three replications.

Table 2. Descriptive Statistics and Correlation Matrix between Studied Variables[a]

| | Del-3-Gal | Del-3-Glu | Del-3-Ara | Pet-3-Gal | Pet-3-Glu | Pet-3-Ara | Mal-3-Gal | Mal-3-Glu | Mal-3-Ara | TPs[b] | DPPH | ABTS | TAs[c] |
|---|---|---|---|---|---|---|---|---|---|---|---|---|---|
| Del-3-Gal | 1.00 | | | | | | | | | | | | |
| Del-3-Glu | 0.96** | 1.00 | | | | | | | | | | | |
| Del-3-Ara | 0.96** | 0.89* | 1.00 | | | | | | | | | | |
| Pet-3-Gal | 0.98*** | 0.93** | 0.98*** | 1.00 | | | | | | | | | |
| Pet-3-Glu | 0.87* | 0.77ns | 0.95** | 0.92** | 1.00 | | | | | | | | |
| Pet-3-Ara | 0.90* | 0.81* | 0.98*** | 0.96** | 0.93** | 1.00 | | | | | | | |
| Mal-3-Gal | 0.86* | 0.77ns | 0.93** | 0.94** | 0.91* | 0.98*** | 1.00 | | | | | | |
| Mal-3-Glu | 0.87* | 0.75ns | 0.96** | 0.92** | 0.96** | 0.98*** | 0.94** | 1.00 | | | | | |
| Mal-3-Ara | 0.95** | 0.90* | 0.96** | 0.98*** | 0.87* | 0.97** | 0.96** | 0.91* | 1.00 | | | | |
| TPs[b] | 0.93** | 0.97** | 0.92** | 0.93** | 0.85* | 0.83* | 0.78ns | 0.79ns | 0.87* | 1.00 | | | |
| DPPH | 0.66ns | 0.80ns | 0.51ns | 0.62ns | 0.45ns | 0.39ns | 0.41ns | 0.29ns | 0.54ns | 0.78ns | 1.00 | | |
| ABTS | 0.86* | 0.76ns | 0.96** | 0.91* | 0.99*** | 0.95** | 0.91* | 0.98*** | 0.88* | 0.84* | 0.38ns | 1.00 | |
| TAs[c] | 0.98*** | 0.81** | 0.83** | 0.96*** | 0.85* | 0.91* | 0.97*** | 0.94** | 0.89* | 0.56ns | −0.02ns | 0.90* | 1.00 |

[a]Abbreviations of anthocyanins are presented in Table 1. Correlations are significant at the (***) 0.001 level, (**) 0.01 level, and (*) 0.05 level or are (ns) nonsignificant. [b]Total phenolic contents. [c]Total anthocyanin contents.

and UV-A during cold storage but not for delphinidin- and malvidin-3-arabinoside at 28 days.

UV-light induced anthocyanin accumulation in plant tissues via the activation of anthocyanin biosynthetic genes.[36,37] In addition to PAL induction, UV radiation also increased the activity of other flavonoid synthesis enzymes, such as chalcon synthase/isomerase or dihydroflavonol-4-reductase.[38] In apples, anthocyanin synthesis was regulated by UV-B.[39] Anthocyanins are one of the most common pigments in plants. However, the effect of UV-A, -B, and -C radiation on anthocyanin biosynthetic genes in harvested blueberries is very little understood. However, we could assume that the nature of UV-induced anthocyanin accumulation in blueberries would be very similar to that of previous reports in other crops.[36,38] In our study, we found that most individual anthocyanins in blueberries were induced by UV-B and -C light and subsequently decreased in the same manner during cold storage.

Our study showed that doses of UV-B and -C at 6 kJ/m$^2$ maintained the postharvest quality of blueberries better than the control, as indicated in Figure 1, and greatly enhanced the total phenolics and antioxidant activities by accumulating phytonutrients in the blueberries (Figure 2). These positive effects of UV-light appeared immediately (in 3 h) after the treatments and gradually diminished during the subsequent cold storage time. The degradation of these compounds in full-ripe blueberries was possibly slowed by the cold temperature, but could not be stopped.

**Correlations between Studied Variables.** The correlation analysis between studied variables is shown in Table 2. Most anthocyanins had a high correlation coefficient with each other, except delphinidin-3-glucoside with petunidin-3-glucoside ($r$ = 0.77), malvidin-3-galactoside ($r$ = 0.77), and malvidin-3-glucoside ($r$ = 0.75). Some pairs had a significant correlation ($r$ = 0.98) at the 0.001 level, such as delphinidin- and petunidin-based anthocyanins, as well as petunidin- and malvidin-based anthocyanins. Total phenolic content also had a significant correlation with most individual anthocyanins, except malvidin-3-galactoside ($r$ = 0.78) and malvidin-3-glucoside ($r$ = 0.79). Although all of the anthocyanins had no significant correlation with the antioxidant activity by the DPPH assay, they had a close correlation in the ABTS assay, except delphinidin-3-glucoside ($r$ = 0.76). The total anthocyanins had a significant correlation with delphinidin-3-galactoside ($r$ = 0.98), petunidin-3-glactoside ($r$ = 0.96), and malvidin-3-galactoside ($r$ = 0.97), which were highly abundant anthocyanins in blueberries. In addition, the antioxidant activity determined by the ABTS analysis had significant correlations with the total phenolics ($r$ = 0.84) and total anthocyanins ($r$ = 0.9) at the 0.05 level, respectively.

The antioxidant capacity, total phenolics, and total anthocyanins in blueberries were highly correlated, from 0.87 to 0.99.[40] Our study also demonstrated that the total phenolic contents were strongly correlated with all individual anthocyanins except malvidin-based anthocyanins. Malvidin-based anthocyanins showed higher antioxidant activities, as measured by the oxygen radical absorbance capacity assay, compared to petunidin- or cyanidin-based anthocyanins.[41] The results from Table 2 showed that all individual anthocyanins except delphinidin-3-glucoside were correlated significantly with total phenolics and antioxidant activity in blueberries, as measured by the ABTS assay. The correlations between delphinidin-based anthocyanins and ABTS assay were relatively low compared to the other anthocyanin compounds. The antioxidant activity in blueberries according to the DPPH assay did not show significant correlations with any of the studied variables. We concluded that the ABTS assay represents the antioxidant activity better than the DPPH assay in individual anthocyanins in blueberry extracts.

The antioxidant activities of anthocyanins are influenced by hydroxylation and glycosylation patterns of their chemical structures.[42,43] The OH group on the positions of both 3′ and 4′ of the B ring contributed to the high antioxidant activity except for delphinidin-based anthocyanins.[42] On the basis of these criteria, anthocyanin compounds with 3′,4′-di-OH substitution in the B ring such as cyanidin- or petunidin-based anthocyanins had high antioxidant capacities compared than the malvidin-based anthocyanins, which show only one OH group in the B ring.[42] In our data, delphinidin-based anthocyanins showed low correlations with ABTS assay compared to the other anthocyanin compounds, but those based on petunidin were correlated significantly with ABTS assay.

There were differences in the response of blueberries to the three types of UV light (A, B, and C). The synthesis of phytonutrient compounds and associated antioxidant activities

were stimulated or maintained by a prestorage UV-B or -C treatment during subsequent cold storage. UV-A had little ability to improve or maintain fruit quality during cold storage. UV-B and -C at 6 kJ/m$^2$ were effective in inhibiting the loss of fruit weight, the development of fruit decay, and the decreases of anthocyanins and antioxidant activities. The UV-B and -C treatments were also effective in the stimulation of individual anthocyanins in 'Duke' blueberries, and the persistence of UV-induced effects was maintained during the cold storage. Our results also showed a strong correlation between these increased individual anthocyanins in blueberries and total phenolics, total anthocyanins, and the antioxidant ability tested by the ABTS assay. Further studies on the dynamics of UV-mediated structural or regulatory gene expression levels involved in anthocyanin biosynthesis in blueberries would elucidate more detailed biosynthesis processes.

## AUTHOR INFORMATION


### Corresponding Author

*(E.J.L.) E-mail: ejinlee3@snu.ac.kr. Phone: (+82)-2-880-4565. Fax: (+82)-2-873-2056.



### Funding

This work was funded by the Basic Science Research Program through the National Research Foundation of Korea funded by the Ministry of Education, Science, and Technology (NRF-2013R1A1A1057658) and by the Cooperative Research Program for Agricultural Science and Technology Development (Project PJ009765), Rural Development Administration, Republic Korea.


### Notes

The authors declare no competing financial interest.

## REFERENCES


(1) Beattie, J.; Crozier, A.; Duthie, G. G. Potential health benefits of berries. *Curr. Nutr. Food Sci.* **2005**, *1*, 71−86.

(2) Huang, W. Y.; Zhang, H. C.; Liu, W. X.; Li, C. Y. Survey of antioxidant capacity and phenolic composition of blueberry, blackberry, and strawberry in Nanjing. *J. Zhejiang Univ. Sci. B* **2012**, *13*, 94−102.

(3) Brouillard, R. The *in vivo* expression of anthocyanin color in plants. *Phytochemistry* **1983**, *22*, 1311−1323.

(4) Wu, X.; Beecher, G. R.; Holden, J. M.; Haytowitz, D. B.; Gebhardt, S. E.; Prior, R. L. Concentrations of anthoyanins in common foods in the United States and estimation of normal consumption. *J. Agric. Food Chem.* **2006**, *54*, 4069−4075.

(5) Francis, F. J.; Markakis, P. C. Food colorants: anthocyanins. *Crit. Rev. Food Sci. Nutr.* **1989**, *28*, 273−314.

(6) Sarkis, J. R.; Jaeschke, D. P.; Tessaro, I. C.; Marczak, L. D. F. Effects of ohmic and conventional heating on anthocyanin degradation during the processing of blueberry pulp. *LWT−Food Sci. Technol.* **2012**, *51*, 79−85.

(7) Heinonen, I. M.; Meyer, A. S.; Frankel, E. N. Antioxidant activity of berry phenolics on human low-density lipoprotein and liposome oxidation. *J. Agric. Food Chem.* **1998**, *46*, 4107−4112.

(8) Perkins-Veazie, P.; Collins, J. K.; Howard, L. Blueberry fruit response to postharvest application of ultraviolet radiation. *Postharvest Biol. Technol.* **2008**, *47*, 280−285.

(9) Wang, C. Y.; Chen, C. T.; Wang, S. Y. Changes of flavonoid content and antioxidant capacity in blueberries after illumination with UV-C. *Food Chem.* **2009**, *117*, 426−431.

(10) Cote, S.; Rodoni, L.; Miceli, E.; Concellón, A.; Civello, P. M.; Vicente, A. R. Effect of radiation intensity on the outcome of postharvest UV-C treatments. *Postharvest Biol. Technol.* **2013**, *83*, 83−89.

(11) El Ghaouth, A.; Wilson, C. L.; Callahan, A. M. Induction of chitinase, β-1,3-glucanase, and phenylalanine ammonia lyase in peach fruit by UV-C treatment. *Phytopathology* **2003**, *93*, 349−355.

(12) Liu, L. H.; Zabaras, D.; Bennett, L. E.; Aguas, P.; Woonton, B. W. Effects of UV-C, red light and sun light on the carotenoid content and physical qualities of tomatoes during post-harvest storage. *Food Chem.* **2009**, *115*, 495−500.

(13) González-Aguilar, G. A.; Wang, C. Y.; Buta, J. G.; Krizek, D. T. Use of UV-C irradiation to prevent decay and maintain postharvest quality of ripe 'Tommy Atkins' mangoes. *Int. J. Food Sci. Technol.* **2001**, *36*, 767−773.

(14) Yoo, K. S.; Lee, E. J.; Patil, B. S. Changes in quercetin glucoside concentrations of onion bulbs by scales, during storage, and in sprouting leaves exposed to UV. *Postharvest Biol. Technol.* **2013**, *83*, 65−71.

(15) Pan, J.; Vicente, A. R.; Martínez, G. A.; Chaves, A. R.; Civello, P. M. Combined use of UV-C irradiation and heat treatment to improve postharvest life of strawberry fruit. *J. Sci. Food Agric.* **2004**, *84*, 1831−1838.

(16) Terry, L. A.; Joyce, D. C. Elicitors of induced disease resistance in postharvest horticultural crops: a brief review. *Postharvest Biol. Technol.* **2004**, *32*, 1−13.

(17) Ben-Yehoshua, S.; Rodov, V.; Peretz, J. Constitutive and induced resistance of citrus fruit against pathogens. *ACIAR Proc.* **1998**, *80*, 78−92.

(18) Bintsis, T.; Litopoulou-Tzanetaki, E.; Robinson, R. K. Existing and potential applications of ultraviolet light in the food industry − a critical review. *J. Sci. Food Agric.* **2000**, *80*, 637−645.

(19) Teramura, A. H. Effects of ultraviolet-B radiation on the growth and yield of crop plants. *Physiol. Plant.* **1983**, *58*, 415−427.

(20) Huyskens-Keil, S.; Eichholz, I.; Kroh, L. W.; Rohn, S. UV-B induced changes of phenol composition and antioxidant activity in black currant fruit (*Ribes nigrum* L.). *J. Appl. Bot. Food Qual.* **2007**, *81*, 140−144.

(21) Hagen, S. F.; Borge, G. I. A.; Bengtsson, G. B.; Bilger, W.; Berge, A.; Haffner, K.; Solhaug, K. A. Phenolic contents and other health and sensory related properties of apple fruit (*Malus domestica* Borkh., cv. Aroma): effect of postharvest UV-B irradiation. *Postharvest Biol. Technol.* **2007**, *45*, 1−10.

(22) Kim, S. K.; Bae, R. N.; Chun, C. H. Changes in bioactive compounds contents of 'Maehyang'and 'Seolhyang' strawberry fruits by UV light illumination. *Kor. Soc. Hortic. Sci.* **2011**, *29*, 172−180.

(23) Slinkard, K.; Singleton, V. L. Total phenol analysis: automation and comparison with manual methods. *Am. J. Enol. Vitic.* **1977**, *28*, 49−55.

(24) Prior, R. L.; Cao, G.; Martin, A.; Sofic, E.; McEwen, J.; O'Brien, C.; Lischner, N.; Ehlenfeldt, M.; Kalt, W.; Krewer, G.; Mainland, M. Antioxidant capacity as influenced by total phenolic and anthocyanin content, maturity, and variety of *Vaccinium* species. *J. Agric. Food Chem.* **1998**, *46*, 2686−2693.

(25) Brand-Williams, W.; Cuvelier, M. E.; Berset, C. Use of a free-radical method to evaluate antioxidant activity. *LWT−Food Sci. Technol.* **1995**, *28*, 25−30.

(26) Arnao, M. B.; Cano, A.; Acosta, M. The hydrophilic and lipophilic contribution to total antioxidant activity. *Food Chem.* **2001**, *73*, 239−244.

(27) Gavrilova, V.; Kajdžanoska, M.; Gjamovski, V.; Stefova, M. Separation, chracterization and quantification of phenolic compounds in blueberries and red and black currants by HPLC-DAD-ESI-MS$^n$. *J. Agric. Food Chem.* **2011**, *59*, 4009−4018.

(28) Wu, X.; Prior, R. L. Systematic identification and characterization of anthocyanins by HPLC-ESI-MS/MS in common foods in the United States: fruits and berries. *J. Agric. Food Chem.* **2005**, *53*, 2589−2599.

(29) Shama, G.; Alderson, P. UV hormesis in fruits: a concept ripe for commercialization. *Trends Food Sci. Technol.* **2005**, *16*, 128−136.

(30) Barka, E. A.; Kalantari, S.; Makhlouf, J.; Arul, J. Impact of UV-C irradiation on the cell wall-degrading enzymes during ripening of

tomato (*Lycopersicon esculentum* L.) fruit. *J. Agric. Food Chem.* **2000**, *48*, 667−671.
(31) Erkan, M.; Wang, S. Y.; Wang, C. Y. Effect of UV treatment on antioxidant capacity, antioxidant enzyme activity and decay in strawberry fruit. *Postharvest Biol. Technol.* **2008**, *48*, 163−171.
(32) Smirinoff, N. Plant resistance to environmental stress. *Curr. Opin. Biotechnol.* **1998**, *9*, 214−219.
(33) Zhang, Z.; Pang, X.; Ji, Z.; Jiang, Y. Role of anthocyanin degradation in litci pericarp browning. *Food Chem.* **2001**, *75*, 217−221.
(34) Wang, J.; Kalt, W.; Sporns, P. Comparison between HPLC and MALDO-TOF MS analysis of anthocyanins in highbush blueberries. *J. Agric. Food Chem.* **2000**, *48*, 3330−3335.
(35) Määttä-Riihinen, K. R.; Kamal-Eldin, A.; Törrönen, A. R. Identification and quantification of phenolic compounds in berries of *Fragaria* and *Rubus* species (family Rosaceae). *J. Agric. Food Chem.* **2004**, *52*, 6178−6187.
(36) Jaakola, L.; Määttä, K.; Pirttilä, A. M.; Törrönen, R.; Kärenlampi, S.; Hohtola, A. Expression of genes involved in anthocyanin biosynthesis in relation to anthocyanin, proanthocyanidin, and flavonol levels during bilberry fruit development. *Plant Physiol.* **2002**, *130*, 729−739.
(37) Mol, J.; Jenkins, G.; Schäfer, E.; Weiss, D.; Walbot, V. Signal perception, transduction, and gene expression involved in anthocyanin biosynthesis. *Crit. Rev. Plant Sci.* **1996**, *15*, 525−557.
(38) Tomás-Barberán, F. A.; Espín, J. C. Phenolic compounds and related enzymes as determinants of quality in fruits and vegetables. *J. Sci. Food Agric.* **2001**, *81*, 853−876.
(39) Arakawa, O. Photoregulation of anthocyanin synthesis in apple fruit under UV-B and red light. *Plant Cell Physiol.* **1998**, *29*, 1385−1389.
(40) Connor, A. M.; Luby, J. J.; Tong, C. B. S. Variability in antioxidant activity in blueberry and correlations among different antioxidant activity assays. *J. Am. Soc. Hortic. Sci.* **2002**, *127*, 238−244.
(41) Wang, S. Y.; Chen, H.; Camp, M. J.; Ehlenfeldt, M. K. Flavonoid constituents and their contribution to antioxidant activity in cultivars and hybrids of rabbiteye blueberry (*Vaccinium ashei* Reade). *Food Chem.* **2012**, *132*, 855−864.
(42) Bors, W.; Heller, W.; Michel, C.; Saran, M. Flavonoids as antioxidants; determination of radical-scavenging efficiencies. *Methods Enzymol.* **1990**, *186*, 343−355.
(43) Wang, H.; Cao, G.; Prior, R. Oxygen radical absorbing capacity of anthocyanins. *J. Agric. Food Chem.* **1997**, *45*, 304−309.

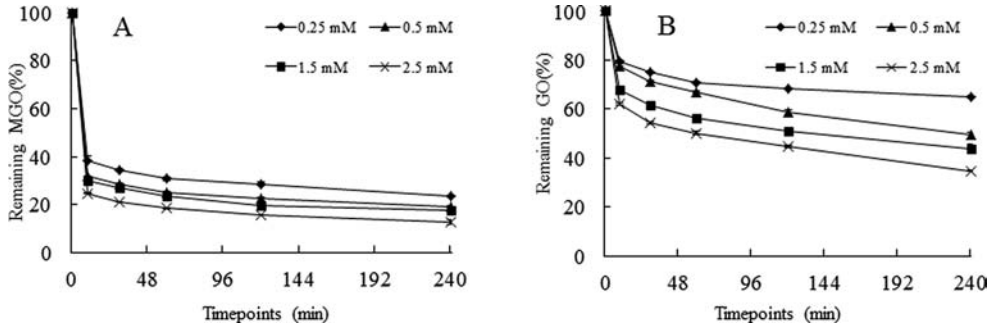


**Figure 1.** Trapping of (A) MGO and (B) GO simultaneously by quercetin under physiological conditions (pH 7.4, 37 °C). MGO (0.5 mM) and GO (0.5 mM) were incubated with quercetin (0.25, 0.5, 1.5, and 2.5 mM) in pH 7.4 phosphate buffer solutions at 37 °C for 10, 30, 60, 120, and 240 min. Data are presented as the means ± SD of three replications.

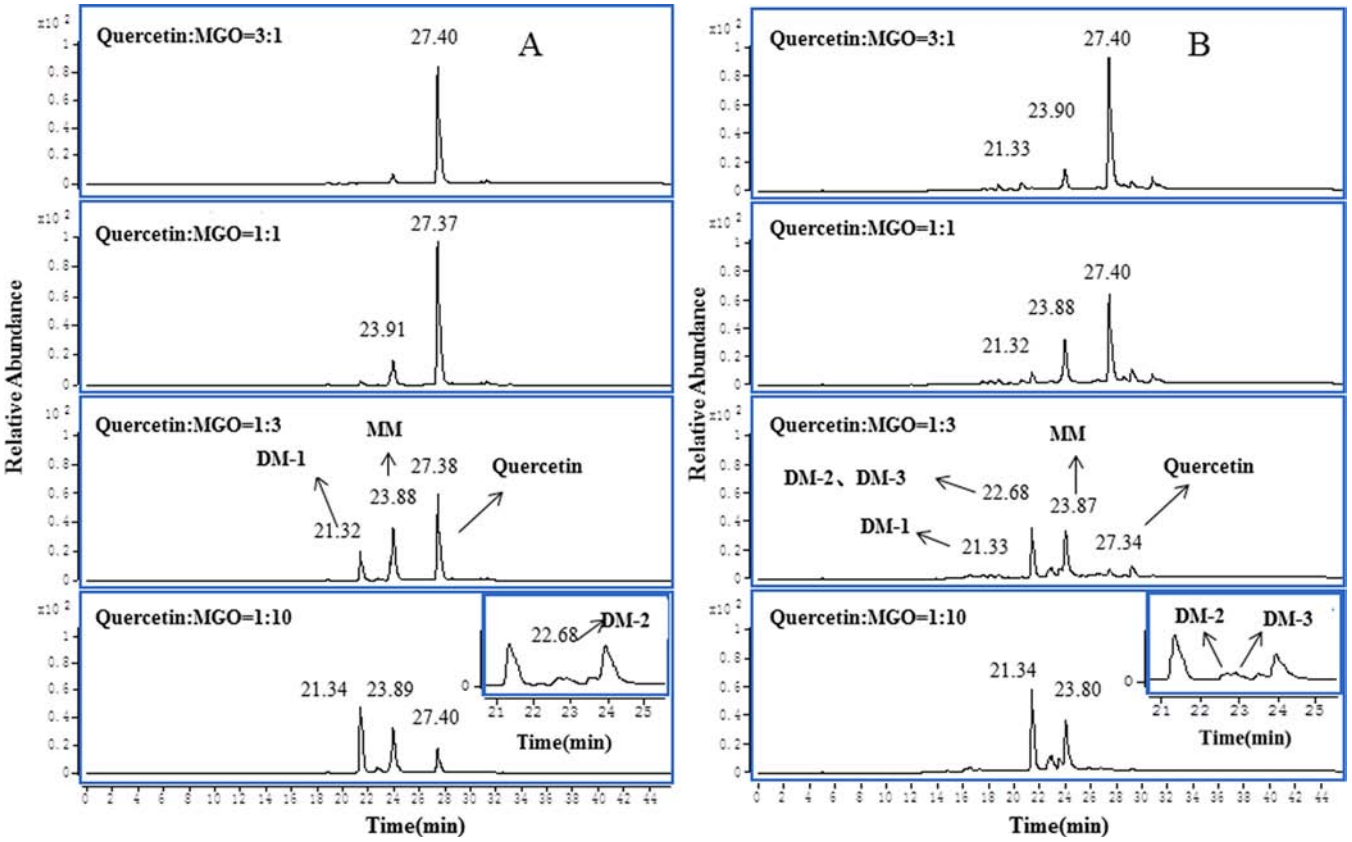


**Figure 2.** LC chromatograms of quercetin after incubation with different ratios of MGO (3:1, 1:1, 1:3, and 1:10) for 4 h (A) and 24 h (B), respectively.

## MATERIALS AND METHODS

**Materials.** Quercetin was obtained from Nanjing Guangrun Biological Products Co., Ltd. (Nanjing, Jiangsu, China). MGO (40% in water), GO (40% in water), 1,2-diaminobenzene (DB), and 2,3-butanedione were purchased from Sigma-Aldrich (St. Louis, MO, USA). Bovine serum albumin (BSA), DMSO, and streptomycin and penicillin mixed solution were purchased from Shanghai Sangon Biological Engineering Technology Co., Ltd. (Shanghai, China). HPLC grade solvents and other reagents were obtained from Shanghai Sinopharm Chemical Reagent Co., Ltd. (Shanghai, China). HPLC grade water was prepared using a Millipore Milli-Q purification system (Bedford, MA, USA).

**Determination of the MGO and GO Trapping Capacity of Quercetin by GC.** MGO (0.5 mM) and GO (0.5 mM) were incubated with quercetin (0.25, 0.5, 1.5, and 2.5 mM) in PBS buffer (pH 7.4, 100 mM) at 37 °C for 0, 10, 30, 60, 120, or 240 min. At each time point, the reaction was stopped by adding 10 μL of acetic acid. The samples were then stored at −80 °C for further use.

**Preparation of Samples.** One milliliter of 100 mM DB was added to 1 mL of sample and then mixed with 0.5 mL of 2,3-butanedione (internal standard) at 1 mM. The reaction mixture was kept at 60 °C for 10 min. Then, 1 mL of 1 M acetaldehyde was added and incubated at 60 °C for 15 min to remove the unreacted DB. The mixture was extracted twice with 2 mL of methylene chloride. The organic phase was combined and concentrated to 0.5 mL. One microliter of this sample was injected directly into the GC. The remaining percentage of MGO and GO was calculated using the equation

$$\text{remaining}\,(\%) = \text{amount of MGO (GO) in test compound (as quinoxalines)/amount of MGO (GO) in control (as quinoxalines)} \times 100$$


dx.doi.org/10.1021/jf504132x | J. Agric. Food Chem. 2014, 62, 12152−12158

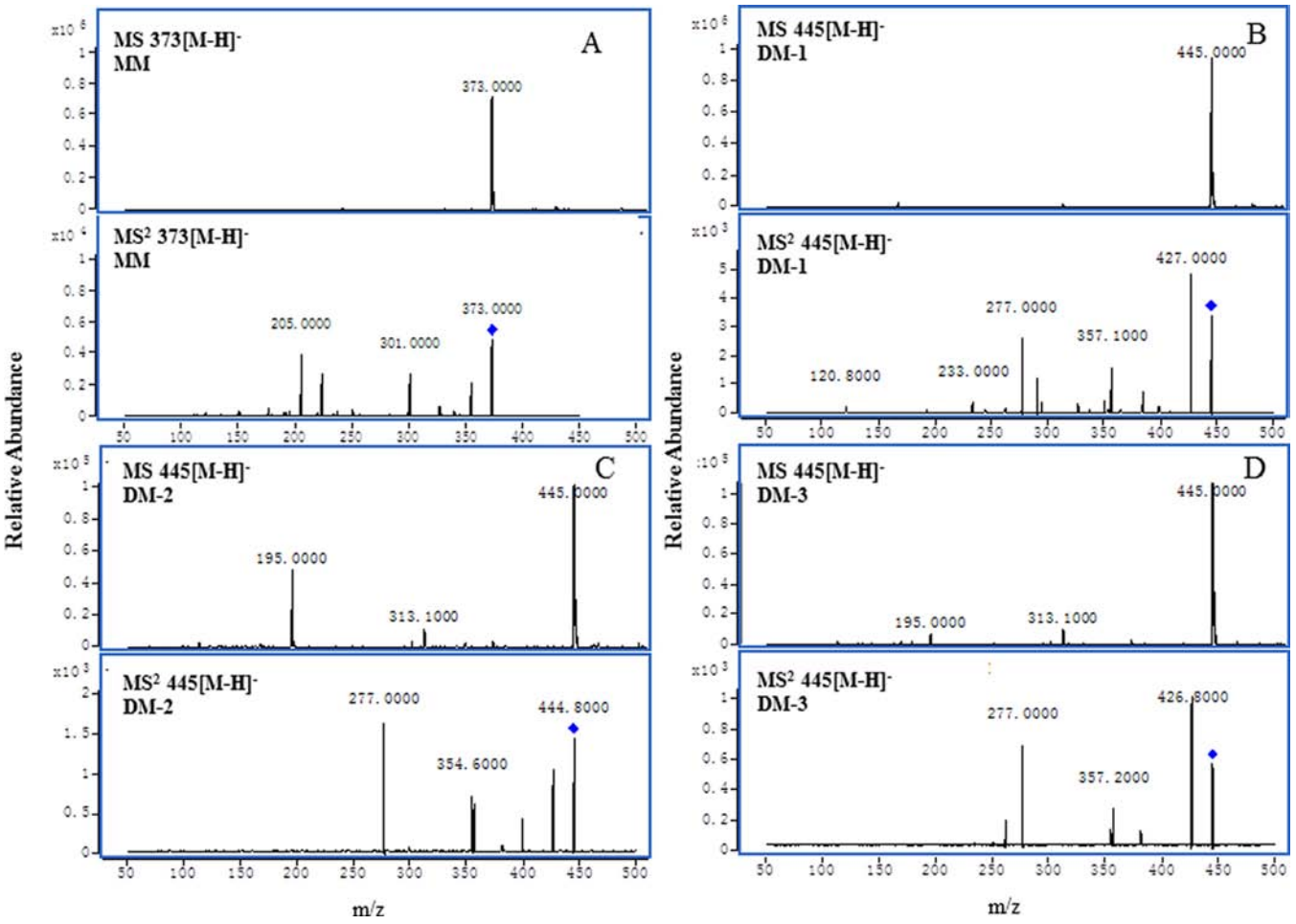


**Figure 3.** Tandem MS/MS spectra of mono-MGO adducts (A) and di-MGO adducts (B–D) of quercetin.

**GC Analysis.** The levels of methylquinoxaline and quinoxaline were analyzed with an Agilent gas chromatograph (7820 series, Agilent Technologies, Palo Alto, CA, USA) equipped with a flame ionization detector (FID). The column was an HP-5 MS (5%-phenyl)-methylpolysiloxane silica capillary (30 m × 0.32 mm i.d., film thickness = 0.25 $\mu$m, Agilent, Wilmington, DE, USA). The injector temperature was 250 °C, and the detector temperature was 280 °C with hydrogen, air, and nitrogen flow rates at 30.0, 300, and 5.0 mL/min, respectively. The injector was in 1:1 split mode. The flow rate of constant carrier gas (nitrogen) was set to be 2.0 mL/min. The GC oven temperature was programmed as follows: the initial oven temperature of 40 °C was held for 1 min, increased to 140 °C at a rate of 5 °C/min, held for 1 min, then increased to 250 °C at a rate of 50 °C/min, and held for 1 min. The total run time was 25.2 min. All of the solvents were filtered with a 0.2 $\mu$m Nylaflo membrane filter. The injection volume was 1 $\mu$L for each sample solution.

**Inhibitory Effects of Quercetin on the Formation of AGEs.** BSA (1.5 mg/mL) was incubated with MGO (500 $\mu$M) or GO (500 $\mu$M) in PBS buffer, pH 7.4, in the presence or absence of quercetin (1.5 mM) at 37 °C. Streptomycin and penicillin (0.3 mL) was added to the solution to prevent bacterial growth. The reaction mixture (500 $\mu$L) was collected and frozen at designated time points (0, 4, 8, 12, 72, 144, 288, 432, and 720 h). The amount of AGEs was determined using fluorescence at an excitation/emission wavelength of 370/440 nm.

**LC-MS Analysis.** LC-MS analysis was performed using an Agilent Masshunter System consisting of a 1290 G4220A BinPump, a 1290 G4226A Wellplate sampler, a G4212A fiode array detector, and a 6460 QQQ mass detector (Agilent, Santa Clara, CA, USA) incorporated with electrospray ionization (ESI) interfaces. A 250 × 4.6 mm i.d., 5 $\mu$m, ZORBAX Eclipse XDB-$C_{18}$ column (Agilent) was used for separation at a flow rate of 0.5 mL/min. The column was eluted with 90% solvent B (water with 0.1% formic acid) for 5 min, followed by linear increases in A (acetonitrile with 0.1% formic acid) to 60% from 5 to 40 min, to 10% from 40 to 41 min, and then with 90% B from 41 to 46 min. The column was then re-equilibrated with 90% B for 5 min. The LC eluent was introduced into the ESI interface. The negative ion polarity mode was set for ESI ion source. The typical operating parameters were as follows: spray needle voltage, 5 kV; nitrogen sheath gas, 45 (arbitrary units); auxiliary gas, 5 (arbitrary units). The structural information on quercetin and the major MGO and GO adducts was obtained by tandem mass spectrometry (MS/MS) through collision-induced dissociation (CID) with a relative collision energy setting of 35%. Data acquisition was performed with Qualitative Analysis of Masshunter (Agilent).

**LC-MS Analysis of MGO or GO Adducts of Quercetin in the BSA–MGO (or GO) System.** The procedure of BSA incubation with MGO/GO and quercetin is the same as the inhibition effect method described above. Samples were collected at designated time points (0, 1, 2, 4, and 8 h) from the quercetin-treated BSA–MGO (or GO) system, and mono- and di-MGO conjugated quercetin was detected using the LC-MS method described above.

## RESULTS

**Trapping of MGO and GO Simultaneously by Quercetin under Physiological Conditions.** The results shown in Figure 1 suggest that quercetin can trap both MGO and GO simultaneously and efficiently under physiological conditions. More than 26.0% of GO and 69.0% of MGO were trapped within 60 min by 0.5 mM quercetin, and the trapping efficiency could be up to 50.5 and 80.1%, respectively, when

Table 1. Percentage[a] of Quercetin−MGO Products for 4 and 24 h at Different Ratios

| | DM-1 | | DM-2 + DM-3 | | MM | | quercetin | |
|---|---|---|---|---|---|---|---|---|
| quercetin/MGO | 4 h | 24 h | 4 h | 24 h | 4 h | 24 h | 4 h | 24 h |
| 3:1 | –[b] | – | – | – | 4.59 | 10.91 | 95.41 | 89.09 |
| 1:1 | 12.28 | 7.87 | – | – | 11.43 | 30.38 | 76.29 | 61.75 |
| 1:3 | 16.89 | 45.33 | – | 10.07 | 33.87 | 38.68 | 49.24 | 5.92 |
| 1:10 | 54.05 | 56.17 | 3.85 | 12.90 | 29.82 | 30.93 | 12.28 | – |

[a]Percent (%) = peak area of each product at 4 or 24 h at each ratio/total sum of peak areas of products at 4 or 24 h at each ratio. [b]–, not detected.

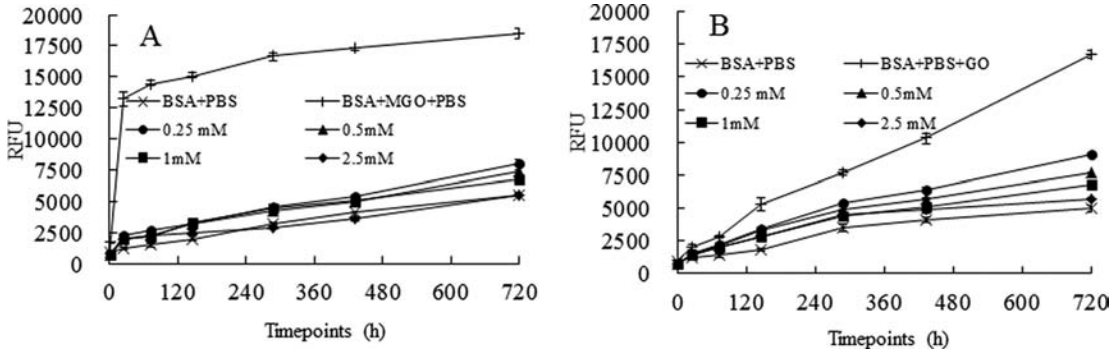


Figure 4. Inhibitory effect of the formation of AGEs by quercetin in the BSA−MGO (or GO) assay: (A) MGO; (B) GO. Data are presented as the means ± SD of three replications.

using 2.5 mM quercetin. Quercetin appeared to trap MGO much more efficiently than GO when both GO and MGO occurred in the same system.

**Analyzing the Formation of MGO or GO Adducts of Quercetin Using LC-MS.** We further identified the quercetin−MGO and quercetin−GO adducts using LC-MS after incubation of quercetin with MGO or GO at four different ratios (3:1, 1:1, 1:3, and 1:10) (Figure 2; Supplemental Figure 1 in the Supporting Information). Under selective ion monitoring (SIM) mode, the structural information on these products was achieved using tandem mass analysis (Figure 3 and Supplemental Figure 2). After 4 h of incubation of quercetin with MGO (ratio = 1:1), one product peak ($t_R$ 23.91 min) appeared in the LC chromatogram as shown in Figure 2A. This peak had the molecular ion $m/z$ 373 $[M - H]^-$ and fragment ion $m/z$ 301 $[M - 72 - H]^-$, indicating the loss of one MGO ($m/z$ 72) molecule, suggesting this product was a mono-MGO conjugated quercetin (MM) (Figure 3A). When quercetin and MGO at a 1:3 ratio were incubated for 4 h, another peak appeared at 21.32 min. This peak had the molecular ion $m/z$ 445 $[M - H]^-$, which was 142 mass units heavier than that of the quercetin, indicating that this peak was a di-MGO adduct of quercetin (DM-1) (Figure 3B). The third new peak appeared at 22.68 min (Figure 2A), with the addition of MGO at the ratio of 1:10 for 4 h, which had the same molecular ion as DM-1, indicating that this peak was also a di-MGO adduct of quercetin (DM-2) (Figure 3C). Under the ratio of 1:3, both mono- and di-MGO adducts were the major products, and the amount of unreacted quercetin dramatically reduced to 12.28% (Table 1), whereas when quercetin and MGO at a 1:10 ratio were incubated for 24 h, di-MGO adducts became the dominant products (Table 1), and one additional peak corresponding to di-MGO adduct (DM-3) was observed (Figure 2B). This peak could not be separated fully from the peak of DM-2 (Figure 2B). When quercetin and GO were incubated at a 1:10 ratio for 24 h, two new peaks were observed at 22.02 and 23.98 min (Supplemental Figure 1). They had the same molecular ion $m/z$ 359 $[M - H]^-$, which was 58 mass units heavier than that of quercetin, indicating both of them are mono-GO adducts of quercetin (Supplemental Figure 2A,B). However, only tiny amounts of mono-GO adducts were detected even when quercetin and GO were incubated at a 1:10 ratio for 24 h, and di-GO adducts were not detectable (Supplemental Figure 1A,B).

**Inhibitory Effects of Quercetin on the Formation of AGEs.** We found that quercetin significantly inhibited the formation of AGEs in the BSA−MGO/GO system (Figure 4). This result is consistent with our observation on the trapping efficacy of MGO/GO by quercetin. When quercetin (0.25 mM) was present in the incubation mixture, the inhibition efficiency could be up to 91.0% at 24 h in the BSA−MGO system (Figure 4A), whereas in the quercetin−BSA−GO system, the inhibitory effect of quercetin on the formation of AGEs seems less than that of the BSA−MGO system, only 76.8% within 30 days (Figure 4B). This may be related to the fact that the formation of AGEs by GO was slow.

**Determining the Adduct Formation of Quercetin in the BSA−MGO or BSA−GO System by LC-MS.** To clarify whether trapping of MGO (or GO) by quercetin is the major mechanism to prevent the formation of AGEs, LC-MS was used to determine the existence of the mono- and di-MGO/GO conjugated quercetin in the samples, which were collected after incubation of quercetin with BSA and MGO or of quercetin with BSA and GO.

As shown in Figure 5, the mono-MGO adduct could be detected after 1 h of incubation, and the di-MGO adduct could be detected after 2 h of incubation. They had retention times and MS/MS spectra identical to those of the mono- and di-MGO adducts in the reaction mixture between quercetin and MGO, but in the BSA−GO system, only mono-GO adducts were detectable at very low levels (Supplemental Figure 3).

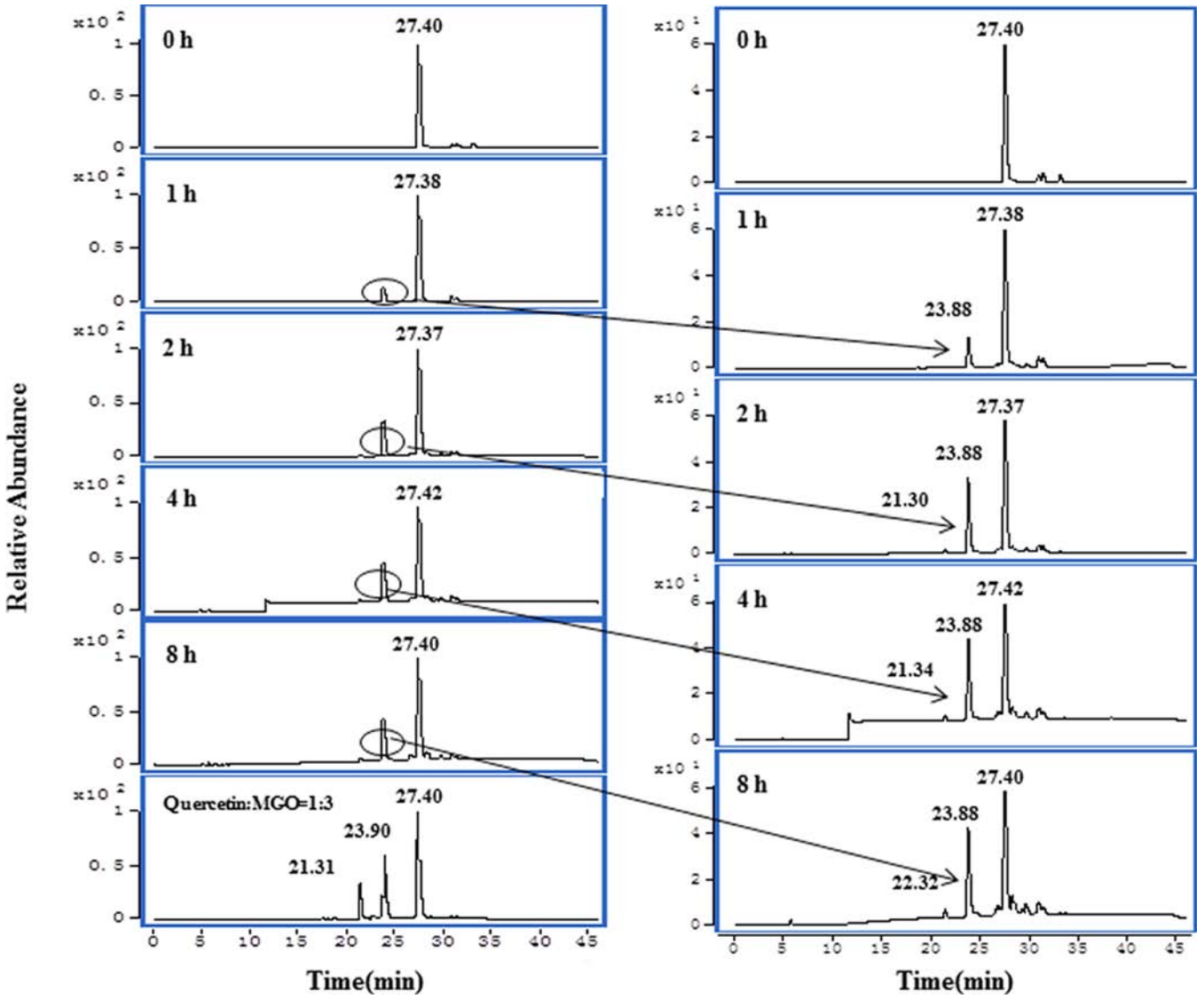


**Figure 5.** LC chromatograms of quercetin and mono- and di-MGO adducts of quercetin after incubation of quercetin in the BSA−MGO assay for 1, 2, 4, and 8 h as well as after the incubation of quercetin with MGO at a 1:3 ratio for 4 h.

## DISCUSSION

Our results revealed that quercetin can rapidly trap MGO and then inhibit the formation of AGEs through forming of mono- and di-MGO adducts under neutral and alkaline conditions in vitro. In this assay, both mono- and di-MGO adducts of quercetin were detected, and the di-MGO adducts became the dominant products during prolonged incubation, whereas only a tiny amount of mono-GO adducts of quercetin was detectable in the reaction mixtures of quercetin and GO.

$\alpha$-Dicarbonyl compounds are known as important precursors of AGEs, which can be generated endogenously through either degradation of glucose or early glycation products. Rising levels of dietary fructose in the Western diet have been associated with an increase of serum MGO and GO.[32] In our study, quercetin efficiently trapped MGO and GO simultaneously under physiological conditions, as MGO and GO appear in the same system. Furthermore, we found that quercetin preferred trapping of MGO to that of GO. The potential reason may be that in aqueous solution GO exists mainly as the hydrated monomer, dimer, or trimer, the conversion of which to free GO is slowed by the trapping reaction between quercetin and GO.[33] Similar results have been reported for EGCG[26] and phloretin;[27] both of them appeared to trap for GO much more slowly than for MGO.

To further study whether quercetin can inhibit the formation of AGEs via trapping MGO/GO, we analyzed the inhibitory effect of quercetin on the formation of AGEs in the BSA−MGO/GO system and then determined the formation of MGO (GO) adducts of quercetin by LC-MS. We demonstrated that quercetin can inhibit the formation of AGEs via trapping MGO and GO. The amount of AGEs rose dramatically with time during incubation with MGO until reaching a plateau. Although no plateau appeared during incubation with GO, the parameter increased progressively with time. Results of this study are consistent with previous reports that MGO rather than GO is the main dicarbonyl compound responsible for albumin glycation.[34] Moreover, the inhibitory activity on the formation of AGEs by quercetin was much higher in the BSA−MGO system than in the BSA−GO system; one of the major causes was that the glycation was dragged down by the conversion among hydrated monomer, dimer, and trimer to free GO.

Flavonoids, consisting of two hydroxy-substituted aromatic rings joined by a three-carbon link (a C6−C3−C6 configuration), can be categorized into flavones, flavanones, isoflavones, chalcones, anthocyanidins, and flavonols according to different C-ring chemical structures. It has been reported that the mechanism of inhibition of AGEs is done via trapping MGO for EGCG[26] (flavanols), genistein[25] (isoflavones), phloretin[27] (chalcones), and proanthocyanidins[35] (oligomers of flavanols). In view of this fact, we investigated quercetin (flavonols) inhibition of the formation of AGEs via trapping MGO and GO. With respect to the structure of these flavonoids, EGCG, genistein, phloretin, and quercetin have the same A ring. The same mechanism for trapping reactive dicarbonyl species and forming mono- and di-MGO adducts at the A ring may be predicted. After quercetin and MGO (1:3) were incubated for 24 h, the MS/MS spectrum of the most abundant daughter ion $m/z$ 373 of the mono-MGO ($t_R$ 27.34 min) adduct had the typical breakdown of the C ring ($m/z$ 150) and a loss of one $H_2O$ to generate the fragment ion 205 $[M - H_2O - 150]^-$ (Figures 3A and 6), which indicates that

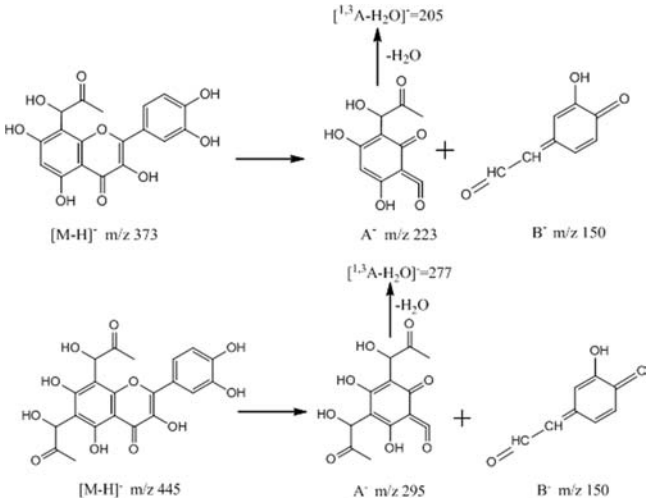


**Figure 6.** Formation pathway of the major fragments of mono- and di-MGO adducts of quercetin.

the MGO conjugates at the A ring of quercetin. Similarly, the MS/MS spectrum of the three di-MGO adducts had the same fragment patent to generate the daughter ion 277 $[M - H_2O - 150]^-$ (Figures 3B−D and 6). Therefore, we could determine that positions 6 and 8 on the A ring of quercetin were the major active sites for trapping MGO (Figure 6), which comprise the essential structural requirement for flavonoids to scavenge methylglyoxal.[36] Quercetin is the major representative of the flavonoid subclass flavonols.[37] It is widely distributed in nature, existing in foods such as apples, onions, tea, berries, red wine, and some herbs. Quercetin is a strong antioxidant,[38] and also possesses antihistamine and anti-inflammatory properties.[39,40] It has been reported that dietary flavonoids including luteolin, rutin, EGCG, and quercetin show effective inhibition on MGO-mediated AGE formation by 82.2, 77.7, 69.1, and 65.3%, respectively.[41] Our results demonstrate the reaction kinetics for quercetin trapping MGO and GO simultaneously, as well as the mechanism of quercetin inhibiting the formation of AGEs in the BSA−MGO/GO system.

In conclusion, using the food-borne flavonoid quercetin intervention to scavenge these dicarbonyl compounds is likely to be an effective strategy to inhibit the formation of AGEs and prevent AGE-mediated processes linked to disease.

## ■ ASSOCIATED CONTENT

### Ⓢ Supporting Information

Supplemental Figures 1−3. This material is available free of charge via the Internet at http://pubs.acs.org.

## ■ AUTHOR INFORMATION

### Corresponding Author

*(L.L.) Phone: +86 25 83598286. Fax: +86 25 83707623. E-mail: lishuanglv@126.com or lulishuang@njnu.edu.cn.

### Funding

This work was supported by NSF of Jiangsu province of China (Project BK2012850), Program of Natural Science Research of Jiangsu Higher Education Institution of China (Project 12KJB5500005), and Natural Science Foundation of Zhejiang province of China (Project LY12C15001).

### Notes

This article does not contain any studies with human or animal subjects.

The authors declare no competing financial interest.

## ■ REFERENCES

(1) The effect of intensive treatment of diabetes on the development and progression of long-term complications in insulin-dependent diabetes mellitus. The Diabetes Control and Complications Trial Research Group. *New Engl. J. Med.* **1993**, *329*, 977−986.

(2) Ahmed, N. Advanced glycation endproducts − role in pathology of diabetic complications. *Diabetes Res. Clin. Practice* **2005**, *67*, 3−21.

(3) Vlassara, H.; Palace, M. R. Diabetes and advanced glycation endproducts. *J. Intern. Med.* **2002**, *251*, 87−101.

(4) Wu, C.-H.; Huang, S.-M.; Lin, J.-A.; Yen, G.-C. Inhibition of advanced glycation endproduct formation by foodstuffs. *Food Funct.* **2011**, *2*, 224−234.

(5) Thornalley, P. J. Use of aminoguanidine (Pimagedine) to prevent the formation of advanced glycation endproducts. *Arch. Biochem. Biophys.* **2003**, *419*, 31−40.

(6) Brownlee, M. Advanced protein glycosylation in diabetes and aging. *Annu. Rev. Med.* **1995**, *46*, 223−234.

(7) Shibamoto, T. Analytical methods for trace levels of reactive carbonyl compounds formed in lipid peroxidation systems. *J. Pharm. Biomed. Anal.* **2006**, *41*, 12−25.

(8) Aldini, G.; Dalle-Donne, I.; Facino, R. M.; Milzani, A.; Carini, M. Intervention strategies to inhibit protein carbonylation by lipoxidation-derived reactive carbonyls. *Med. Res. Rev.* **2007**, *27*, 817−868.

(9) Beisswenger, P.; Howell, S.; Nelson, R.; Mauer, M.; Szwergold, B. α-Oxoaldehyde metabolism and diabetic complications. *Biochem. Soc. Trans.* **2003**, *31*, 1358−1363.

(10) Lo, T.; Westwood, M. E.; McLellan, A. C.; Selwood, T.; Thornalley, P. J. Binding and modification of proteins by methylglyoxal under physiological conditions. A kinetic and mechanistic study with *N*-α-acetylarginine, *N*-α-acetylcysteine, and *N*-α-acetyllysine, and bovine serum albumin. *J. Biol. Chem.* **1994**, *269*, 32299−32305.

(11) Shamsi, F. A.; Partal, A.; Sady, C.; Glomb, M. A.; Nagaraj, R. H. Immunological evidence for methylglyoxal-derived modifications in vivo determination of antigenic epitopes. *J. Biol. Chem.* **1998**, *273*, 6928−6936.

(12) Klöpfer, A.; Spanneberg, R.; Glomb, M. A. Formation of arginine modifications in a model system of *N*-α-*tert*-butoxycarbonyl (Boc)-arginine with methylglyoxal. *J. Agric. Food Chem.* **2010**, *59*, 394−401.

(13) Gao, Y.; Wang, Y. Site-selective modifications of arginine residues in human hemoglobin induced by methylglyoxal. *Biochemistry* **2006**, *45*, 15654−15660.

(14) Kang, J. H. Oxidative damage of DNA induced by methylglyoxal in vitro. *Toxicology Lett.* **2003**, *145*, 181−187.
(15) Kilhovd, B. K.; Juutilainen, A.; Lehto, S.; Rönnemaa, T.; Torjesen, P. A.; Hanssen, K. F.; Laakso, M. Increased serum levels of methylglyoxal-derived hydroimidazolone-AGE are associated with increased cardiovascular disease mortality in nondiabetic women. *Atherosclerosis* **2009**, *205*, 590−594.
(16) Thomas, M.; Baynes, J.; Thorpe, S.; Cooper, M. The role of AGEs and AGE inhibitors in diabetic cardiovascular disease. *Curr. Drug Targets* **2005**, *6*, 453−474.
(17) Cervantes-Laurean, D.; Schramm, D. D.; Jacobson, E. L.; Halaweish, I.; Bruckner, G. G.; Boissonneault, G. A. Inhibition of advanced glycation end product formation on collagen by rutin and its metabolites. *J. Nutr. Biochem.* **2006**, *17*, 531−540.
(18) Peyroux, J.; Sternberg, M. Advanced glycation endproducts (AGEs): pharmacological inhibition in diabetes. *Pathol. Biol.* **2006**, *54*, 405−419.
(19) Webster, J.; Urban, C.; Berbaum, K.; Loske, C.; Alpar, A.; Gärtner, U.; De Arriba, S. G.; Arendt, T.; Münch, G. The carbonyl scavengers aminoguanidine and tenilsetam protect against the neurotoxic effects of methylglyoxal. *Neurotoxicity Res.* **2005**, *7*, 95−101.
(20) Schurman, L.; McCarthy, A.; Sedlinsky, C.; Gangoiti, M.; Arnol, V.; Bruzzone, L.; Cortizo, A. Metformin reverts deleterious effects of advanced glycation end-products (AGEs) on osteoblastic cells. *Exp. Clin. Endocrinol. Diabetes* **2008**, *116*, 333−340.
(21) Beisswenger, P.; Ruggiero-Lopez, D. Metformin inhibition of glycation processes. *Diabetes Metab.* **2003**, *29*, 6S95−6S103.
(22) Price, D. L.; Rhett, P. M.; Thorpe, S. R.; Baynes, J. W. Chelating activity of advanced glycation end-product inhibitors. *J. Biol. Chem.* **2001**, *276*, 48967−48972.
(23) Romagnolo, D. F.; Selmin, O. I. Flavonoids and cancer prevention: a review of the evidence. *J. Nutr. Gerontol. Geriatrics* **2012**, *31*, 206−238.
(24) Morimitsu, Y.; Yoshida, K.; Esaki, S.; Hirota, A. Protein glycation inhibitors from thyme (*Thymus vulgaris*). *Biosci., Biotechnol., Biochem.* **1995**, *59*, 2018−2021.
(25) Lv, L.; Shao, X.; Chen, H.; Ho, C.-T.; Sang, S. Genistein inhibits advanced glycation end product formation by trapping methylglyoxal. *Chem. Res. Toxicol.* **2011**, *24*, 579−586.
(26) Sang, S.; Shao, X.; Bai, N.; Lo, C.-Y.; Yang, C. S.; Ho, C.-T. Tea polyphenol (−)-epigallocatechin-3-gallate: a new trapping agent of reactive dicarbonyl species. *Chem. Res. Toxicol.* **2007**, *20*, 1862−1870.
(27) Shao, X.; Bai, N.; He, K.; Ho, C.-T.; Yang, C. S.; Sang, S. Apple polyphenols, phloretin and phloridzin: new trapping agents of reactive dicarbonyl species. *Chem. Res. Toxicol.* **2008**, *21*, 2042−2050.
(28) Wang, W.; Yagiz, Y.; Buran, T. J.; Nunes, C. d. N.; Gu, L. Phytochemicals from berries and grapes inhibited the formation of advanced glycation end-products by scavenging reactive carbonyls. *Food Res. Int.* **2011**, *44*, 2666−2673.
(29) Sengupta, B.; Uematsu, T.; Jacobsson, P.; Swenson, J. Exploring the antioxidant property of bioflavonoid quercetin in preventing DNA glycation: a calorimetric and spectroscopic study. *Biochem. Biophys. Res. Commun.* **2006**, *339*, 355−361.
(30) Wang, Y.; Ho, C. T. Flavour chemistry of methylglyoxal and glyoxal. *Chem. Soc. Rev.* **2012**, *41*, 4140−4149.
(31) Hsieh, C.-L.; Lin, Y.-C.; Yen, G.-C.; Chen, H.-Y. Preventive effects of guava (*Psidium guajava* L.) leaves and its active compounds against α-dicarbonyl compounds-induced blood coagulation. *Food Chem.* **2007**, *103*, 528−535.
(32) Lee, O.; Bruce, W. R.; Dong, Q.; Bruce, J.; Mehta, R.; O'Brien, P. J. Fructose and carbonyl metabolites as endogenous toxins. *Chem.−Biol. Interact.* **2009**, *178*, 332−339.
(33) European Commission. Scientific Committee on Consumer Products (SCCP) Opinion on Glyoxal, the 4th plenary of June 2005, http://ec.europa.eu/health/ph_risk/committees/04_sccp/docs/sccp_o_023.pdf.
(34) Sadowska-Bartosz, I.; Galiniak, S.; Bartosz, G. Kinetics of glycoxidation of bovine serum albumin by methylglyoxal and glyoxal and its prevention by various compounds. *Molecules* **2014**, *19*, 4880−4896.
(35) Peng, X.; Cheng, K.-W.; Ma, J.; Chen, B.; Ho, C.-T.; Lo, C.; Chen, F.; Wang, M. Cinnamon bark proanthocyanidins as reactive carbonyl scavengers to prevent the formation of advanced glycation endproducts. *J. Agric. Food Chem.* **2008**, *56*, 1907−1911.
(36) Shao, X.; Chen, H.; Zhu, Y.; Sedighi, R.; Ho, C.-T.; Sang, S. Essential structural requirements and additive effects for flavonoids to scavenge methylglyoxal. *J. Agric. Food Chem.* **2014**, *62*, 3202−3210.
(37) Hertog, M. G.; Hollman, P. C.; Katan, M. B.; Kromhout, D. Intake of potentially anticarcinogenic flavonoids and their determinants in adults in The Netherlands. *Nutr. Cancer* **1993**, *20*, 21−29.
(38) Afanas'ev, I. B.; Dcrozhko, A. I.; Brodskii, A. V.; Kostyuk, V. A.; Potapovitch, A. I. Chelating and free radical scavenging mechanisms of inhibitory action of rutin and quercetin in lipid peroxidation. *Biochem. Pharmacol.* **1989**, *38*, 1763−1769.
(39) Murray, M. Quercetin: nature's antihistamine. *Better Nutr.* **1998**, *60*, 10−14.
(40) Comalada, M.; Camuesco, D.; Sierra, S.; Ballester, I.; Xaus, J.; Galvez, J.; Zarzuelo, A. In vivo quercitrin anti-inflammatory effect involves release of quercetin, which inhibits inflammation through down-regulation of the NF-κB pathway. *Eur. J. Immunol.* **2005**, *35*, 584−592.
(41) Wu, C. H.; Yen, G. C. Inhibitory effect of naturally occurring flavonoids on the formation of advanced glycation endproducts. *J. Agric. Food Chem.* **2005**, *53*, 3167−3173.

fermentations. The primary fermentation may take 1−2 weeks in the presence of grape skins, which are responsible for color development of red wines. Furthermore, the primary fermentation is carried out by yeast cells, and their ability to absorb phenolic compounds may result in a higher or lower phenolic content in the wine and in its byproduct. The secondary step is conducted by bacterial fermentation, in the absence of grape skins, which are removed in the process. Thus, grape skins have no influence in the secondary fermentation.

Reactive oxygen species (ROS) are detrimental to health as they take part in oxidative processes both in vivo and in vitro.[12] ROS are involved in cell damage, cancer development, inflammation, and heart disease. Furthermore, ROS play an important role in aging and the development of Parkinson's disease. ROS are constantly generated via mitochondrial metabolism, which can worsen with unhealthy habits such as smoking. High-lipid foods are also affected by ROS generation, which can be influenced by heating, UV light, and $\gamma$-irradiation, leading to sensory changes, decreasing the shelf life of products and becoming an economic burden.[13] Hydrogen peroxide generates hydroxyl radicals in the presence of ferrous ion or via UV light dissociation. Although generation of the highly reactive short-lived hydroxyl radicals is of much concern as it induces DNA damage and lipid and protein oxidation, the presence of $H_2O_2$ itself causes enzyme inactivation and cell damage. The scavenging activity of phenolics against $H_2O_2$ is attributed to electron donation, but neutralization of $H_2O_2$ to $H_2O$ is also contemplated.[12] Moreover, ferric ion catalyzes the oxidation of proteins and lipids, thus being detrimental to food and biological systems.

The present study focused on the unraveling of the phenolic profile of grape byproducts and the contribution of each fraction to potential bioactivity as well as differences between byproducts generated by the juice- and winemaking industries. Total phenolic content (TPC), proanthocyanidin content (PC), scavenging activities against 2,2-diphenyl-1-picrylhydrazyl (DPPH), 2,2′-azinobis(3-ethylbenzothiazoline-6-sulfonic acid) diammonium salt (ABTS), and $H_2O_2$, and reducing power (RP) were evaluated. The detailed phenolic profile was investigated using HPLC-DAD-ESI-MS$^n$, and the potential health benefits of the extracts were evaluated against copper-induced LDL-cholesterol oxidation and peroxyl radical induced DNA strand breakage.

## MATERIALS AND METHODS

Grape juice (BRS Cora and Isabel) byproducts were donated by Embrapa Semiárido (Petrolina, Pernambuco state, Brazil). Syrah and Tempranillo (winemaking byproducts) were donated by Ouro Verde Farm, Grupo Miolo (Casa Nova, Bahia state, Brazil) and Santa Maria winery (Lagoa Grande, Pernambuco state, Brazil), respectively. Original grapes used in the grape juice- and winemaking processes had 20 and 22 °Brix, respectively. Brazilian grape juice is mainly produced using the Isabel cultivar, due to its large production. BRS Cora, hereafter named Cora, is a Brazilian variety developed by Embrapa through crossing between 'Muscat Belly A' and 'H.65.9.14' varieties. Cora and Isabel grapes were grown in Petrolina, Pernambuco state, Brazil. Syrah grape was grown in Casa Nova, Bahia state, Brazil, and Tempranillo was grown in Lagoa Grande, Pernambuco state, Brazil.

Folin−Ciocalteu's reagent, vanillin, DPPH, ABTS, mono- and dibasic potassium phosphates, hydrogen peroxide, potassium ferricyanide, ferric chloride, copper sulfate, human LDL-cholesterol, ethylenediaminetetraacetic acid trisodium salt ($Na_3EDTA$), tris acetate, 2,2′-azobis(2-methylpropionamidine) dihydrochloride (AAPH), agarose, bromophenol blue, xylene cyanol, glycerol, trolox, caffeic, gallic, protocatechuic, and *p*-coumaric acids, (+)-catechin, and (−)-epicatechin were purchased from Sigma-Aldrich Canada Ltd. (Oakville, ON, Canada). Sodium carbonate, sodium hydroxide, sodium chloride, potassium persulfate, trichloroacetic acid, diethyl ether, ethyl acetate, hexane, acetone, methanol, acetonitrile, formic acid, hydrochloric acid, sodium hydroxide, and pBR 322 from *Escherichia coli* were purchased from Fisher Scientific Ltd. (Ottawa, ON, Canada). SYBR safe gel stain was purchased from Probes (Invitrogen, Eugene, OR, USA).

**Extraction of Phenolic Compounds.** Grape byproducts were freeze-dried at −48 °C and 30 × $10^{-3}$ mbar (Freezone 6, model 77530, Labconco, Co., Kansas City, MO, USA) and ground using a coffee bean grinder (model CBG5 series, Black & Decker, Canada, Inc., Brockville, ON, Canada). The powder so obtained was passed through a mesh 16 (sieve opening 1 mm, Tyler test sieve, Mentor, OH, USA) sieve. Ground samples were defatted three times using hexane (solid/solvent, 1:5, w/v) in a Waring blender (model 33BL73, Waring Products Division Dynamics Co. of America, New Hartford, CT, USA). Defatted samples were then stored at −20 °C until used for the extraction of phenolic compounds within 1 week.

Defatted samples (2.5 g) were extracted with 70% acetone (100 mL) in a gyrotory water bath shaker (model G76, New Brunswick Scientific Co. Inc., New Brunswick, NJ, USA) at 30 °C for 20 min. After centrifugation at 4000*g* (IEC Centra MP4, International Equipment Co., Needham Heights, MA, USA), the upper layer was collected and extraction was repeated twice. The combined supernatants were evaporated to remove the organic solvent, and the residue in water was acidified to pH 2 using 6 M HCl. Free phenolic compounds were extracted five times with diethyl ether and ethyl acetate (1:1, v/v). Combined supernatants were evaporated in vacuo at 40 °C (Buchi, Flawil, Switzerland). The remaining water phase was mixed with 4 M NaOH and hydrolyzed while stirring under nitrogen for 4 h at room temperature (23−25 °C) to release esterified phenolics. This was followed by acidification to pH 2 using 6 M HCl, five extractions with diethyl ether and ethyl acetate (1:1, v/v), and evaporation of combined supernatants in vacuo at 40 °C. Free phenolics and those released from their esterified form were separately reconstituted in HPLC grade methanol and stored at −20 °C until used for further analysis within 3 months.

To the solid residue remaining after the first set of extractions, 4 M NaOH was added and hydrolyzed with stirring under nitrogen for 4 h at room temperature (23−25 °C). The resulting slurry was acidified to pH 2 with 6 M HCl. Phenolics released from their insoluble-bound form were then extracted with diethyl ether and ethyl acetate (1:1, v/v) and reconstituted in HPLC grade methanol, as explained above.

**Total Phenolic Contents.** TPC were determined according to the Folin−Ciocalteu method[14] with slight modifications, as previously described by de Camargo et al.[15] The phenolic extracts were used in concentrations ranging from 3 to 30 mg/mL. First, the extracts with appropriate dilutions (0.5 mL), deionized water (4 mL), and Folin−Ciocalteu's reagent (0.5 mL) were added into flasks and mixed thoroughly. After 3 min, a saturated solution of sodium carbonate (0.5 mL) was added, and the mixture was kept in the dark at room temperature (23−25 °C) for 2 h. Finally, the absorbance was read at 760 nm using an Agilent diode array spectrophotometer (Agilent 8453, Palo Alto, CA, USA). The results were expressed as milligram gallic acid equivalents per gram of dry weight of defatted sample.

**Proanthocyanidin Content.** Total proanthocyanidins (condensed tannins) were determined according to the method of Price et al.[16] as explained by de Camargo et al.[3] Briefly, phenolic extracts were diluted in methanol (10−100 mg/mL), and 1 mL of the extracts so obtained was added to 5 mL of a 0.5% (w/v) vanillin solution prepared in 4% (v/v) HCl in methanol. The mixture was incubated in a gyrotory water bath shaker (model G76, New Brunswick Scientific Co., New Brunswick, NJ, USA) at 30 °C for 20 min. Finally, the absorbance was read at 500 nm using an Agilent diode array spectrophotometer (Agilent 8453). The results were expressed as milligram catechin equivalents per gram of dry weight of defatted sample.

**ABTS Radical Cation Scavenging Activity.** The ABTS assay[17] was performed using a modified version of the method described by de

Camargo et al.[3] The ABTS radical, which was generated by oxidation with potassium persulfate, was prepared in 100 mM phosphate buffer saline solution (PBS) (pH 7.4, 0.15 M sodium chloride). The ABTS stock solution consisted of potassium persulfate (2.45 mM) and ABTS (7.00 mM) in PBS. At the time of analysis, the working solution of ABTS was prepared by diluting its stock solution in PBS to reach an absorbance value of 0.70 (734 nm). Phenolic extracts were diluted in PBS (10−30 mg/mL). Diluted phenolic extracts (20 μL) were added to 2 mL of ABTS radical cation solution, and the absorbance was read at 734 nm after 6 min using an Agilent diode array spectrophotometer (Agilent 8453). ABTS radical scavenging activity was calculated using the equation

$$\text{ABTS radical scavenging activity (\%)} = [(\text{Abs}_{\text{control}} - \text{Abs}_{\text{sample}})/(\text{Abs}_{\text{control}})] \times 100$$

where $\text{Abs}_{\text{control}}$ is the absorbance of ABTS radical + PBS and $\text{Abs}_{\text{sample}}$ is the absorbance of ABTS radical cation + phenolic extract or trolox. The results were expressed as micromoles of trolox equivalents per gram of dry weight of defatted sample.

**DPPH Radical Scavenging Activity (DRSA).** The DPPH assay was carried out using a modified version of the method explained by Chandrasekara and Shahidi.[18] The phenolic extracts were used at different concentrations of 10−50 mg/mL. Two milliliters of a methanolic solution of DPPH (0.5 mM) were added to 500 μL of the extracts diluted in methanol. After 10 min, the mixture was passed through the capillary tubing that guides the sample through the sample cavity of a Bruker e-scan electron paramagnetic resonance (EPR) spectrophotometer (Bruker E-Scan, Bruker Biospin Co., Billercia, MA, USA). The spectrum was recorded using the following parameters: $5.02 \times 10^2$ receiver gain, 1.93 G modulation amplitude, 2.62 s sweep time, 8 scans, 100.000 G sweep width, 3495.258 G center field, 5.12 ms time constant, 9.793220 GHz microwave frequency, and 86.00 kHz modulation frequency. The DPPH scavenging activity of the extracts was calculated using the equation

$$\text{DPPH scavenging activity (\%)} = [(\text{EPR}_{\text{control}} - \text{EPR}_{\text{sample}})/(\text{EPR}_{\text{control}})] \times 100$$

where $\text{EPR}_{\text{control}}$ is the signal intensity of DPPH radical + methanol and $\text{EPR}_{\text{sample}}$ is the signal intensity of DPPH radical + phenolic extract or trolox. The results were expressed as micromoles of trolox equivalents per gram of dry weight of defatted sample.

**Hydrogen Peroxide Scavenging Activity.** The hydrogen peroxide scavenging activity of extracts of grape byproducts was evaluated as explained elsewhere.[12] Phenolic extracts (4−40 mg/mL) and 0.4 mM hydrogen peroxide solution were prepared in 0.1 M phosphate buffer (pH 7.4). The extracts (0.4 mL) were mixed with hydrogen peroxide solution (0.6 mL), and the final volume was made to 2 mL with the same buffer. The samples were kept in a gyrotory water bath shaker (model G76, New Brunswick Scientific Co. Inc.) for 40 min, and the absorbance was read at 230 nm using an Agilent diode array spectrophotometer (Agilent 8453). Blanks devoid of hydrogen peroxide (added by phosphate buffer) were prepared for background corrections. The results were expressed as micromoles of trolox equivalents per gram of dry weight of defatted sample.

The scavenging activity was calculated with the equation

$$\text{H}_2\text{O}_2 \text{ scavenging activity (\%)} = [(\text{Abs}_{\text{control}} - \text{Abs}_{\text{sample}})/(\text{Abs}_{\text{control}})] \times 100$$

where $\text{Abs}_{\text{control}}$ is the absorbance of $H_2O_2$ radical + phosphate buffer and $\text{Abs}_{\text{sample}}$ is the absorbance of $H_2O_2$ + phenolic extract extract or trolox.

**Reducing Power.** The RP assay was conducted according to the method described by Alasalvar et al.[19] The extracts (2−20 mg/mL) were diluted in phosphate buffer (pH 6.6, 0.2 mM). Extracts (1 mL) were then further mixed with phosphate buffer (2.5 mL) and 1% (w/v) potassium ferricyanide solution (2.5 mL), followed by their incubation in a gyrotory water bath shaker (model G76, New Brunswick Scientific Co. Inc.) at 50 °C for 20 min, after which a 10% (w/v) solution of trichloroacetic acid was added (2.5 mL). The mixture was subsequently centrifuged at 1750*g* for 10 min, and the supernatant (2.5 mL) was added to distilled water (2.5 mL) and 0.1% (w/v) ferric chloride solution (0.5 mL). The absorbance was read at 700 nm using an Agilent diode array spectrophotometer (Agilent 8453). A calibration curve was prepared using trolox as a standard, and results were expressed as trolox equivalents per gram of dry weight of defatted sample.

**Copper-Induced Human LDL-Cholesterol Oxidation.** The LDL-cholesterol oxidation method described by Shahidi et al.[4] was slightly modified to evaluate the potential inhibitory effect of phenolic extracts of grape byproducts. The solution of LDL-cholesterol was dialyzed overnight against PBS (10 mM, 0.15 M NaCl, pH 7.4) at 4 °C under a flow of nitrogen. The resulting ethylenediaminetetraacetic acid (EDTA)-free LDL-cholesterol was diluted in PBS to reach a concentration of 0.04 mg/mL. Methanol was removed from grape byproduct extracts under a stream of nitrogen followed by their resuspension in PBS to obtain 100 ppm of total phenolic equivalents in relation to the final volume assay (1 mL). This was calculated on the basis of TPC as evaluated by HPLC-DAD-ESI- $MS^n$ (Figure 1).

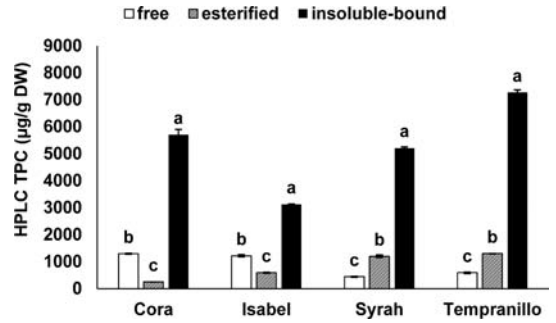


**Figure 1.** HPLC-DAD-ESI-$MS^n$ total phenolic content (HPLC TPC) of different fractions of juice (Cora and Isabel) and winemaking (Syrah and Tempranillo) byproducts. Data represent the mean ± standard deviation of each sample ($n = 3$). Means with different letters indicate significant differences ($p < 0.05$) among fractions within the same grape variety.

Phenolic extracts (100 μL) and LDL-cholesterol (800 μL) were added into Eppendorf tubes and incubated at 37 °C for 15 min, after which the peroxidation was induced by the addition of a 100 μM solution of $CuSO_4$ (100 μL). The reaction was incubated for 24 h at 37 °C, and the conjugated dienes (CD) were assayed at 234 nm using an Agilent diode array spectrophotometer (Agilent 8453). Blanks devoid of LDL-cholesterol and $CuSO_4$ were prepared for background subtraction. A positive control was prepared with catechin (100 ppm), and the results were expressed as percent inhibition according to the equation

$$\text{inhibition of formation of CD (\%)} = [(\text{Abs}_{\text{oxidized}} - \text{Abs}_{\text{sample}})/(\text{Abs}_{\text{oxidized}} - \text{Abs}_{\text{native}})] \times 100$$

where $\text{Abs}_{\text{oxidized}}$ is the absorbance of LDL-cholesterol with $CuSO_4$, $\text{Abs}_{\text{sample}}$ is the absorbance of LDL-cholesterol with extract or catechin and $CuSO_4$, and $\text{Abs}_{\text{native}}$ is the absorbance of LDL-cholesterol without $CuSO_4$.

**Inhibition of Peroxyl Radical Induced Supercoiled Plasmid DNA Strand Breakage.** The supercoiled plasmid DNA strand breakage inhibition was evaluated using a slightly modified version of the method explained by Shahidi et al.[4] Methanol was removed from phenolic extracts under a stream of nitrogen followed by resuspension in water to achieve a concentration of 1−5 mg/mL. An aliquot (2 μL) was pipetted in Eppendorf tubes, and the remaining reagents were added in the following order: 2 μL of PBS (0.5 M, pH 7.4, 0.15 M sodium chloride), 2 μL of supercoiled plasmid DNA pBR 322 from *Escherichia coli* RRI diluted in PBS (50 μL/mL), and 4 μL of a 7 mM

**Table 1. Phenolic Compounds Identified in Grape Byproducts**

| | juice byproducts[a] | | winemaking byproducts[a] | | | | | |
|---|---|---|---|---|---|---|---|---|
| | Cora | Isabel | Syrah | Tempranillo | | MW | $[M-H]^-$ | other product ions ($m/z$) |
| | | | | | **Phenolic Acids**[b] | | | |
| 1 | E, B | B | F, B | F, E, B | protocatechuic acid* | 154 | 153 | 109 |
| 2 | F, E, B | F, E, B | E, B | F, E, B | *p*-coumaric acid* | 164 | 163 | 119 |
| 3 | F, E, B | F, E, B | F, E, B | F, E, B | gallic acid* | 170 | 169 | 125 |
| 4 | F, E, B | F, E, B | E, B | E, B | caffeic acid* | 180 | 179 | 135 |
| 5 | E | F, E | | F | ferulic acid* | 194 | 193 | 177, 149, 134 |
| 6 | | | | E | hydroxycaffeic acid | 198 | 197 | 179, 135 |
| 7 | E | E, B | F | B | ellagic acid* | 302 | 301 | 283, 257 |
| 8 | F | F | | F | caftaric acid | 312 | 311 | 179, 135 |
| 9 | F, E, B | F, E, B | F, E, B | F, E, B | monogalloyl glucose | 332 | 331 | 169, 125 |
| | | | | | **Flavonoids/Proanthocyanidins**[b] | | | |
| 10 | F, E, B | F, E, B | F, E, B | F, E, B | (+)-catechin* | 290 | 289 | 245, 205, 179 |
| 11 | F, E, B | F, E, B | F, E, B | F, E, B | (−)-epicatechin* | 290 | 289 | 245, 205, 179 |
| 12 | F, B | F | F, B | F, B, E | quercetin* | 302 | 301 | 179, 151, 107 |
| 13 | E | B | E, B | F, E, B | isorhamnetin | 316 | 315 | 271 |
| 14 | F, B | F, B, E | F, B, E | F, B, E | epicatechin gallate | 442 | 441 | 289, 169, 125 |
| 15 | F, B, E | F, B, E | F | F | kaempferol hexoside | 448 | 447 | 285 |
| 16 | F, E, B | F, E, B | F, E, B | F | quercetin hexoside | 464 | 463 | 301, 179, 151 |
| 17 | F, E, B | F, E, B | F, E, B | F, E, B | quercetin glucuronide | 478 | 477 | 301, 179, 151 |
| 18 | F, B | F | F, E, B | F, E, B | isorhamnetin hexoside | 478 | 477 | 315, 271 |
| 19 | F, B | F, E | F | F | myricetin hexoside | 480 | 479 | 317, 179, 151 |
| 20 | B | B | | B | procyanidin dimer A | 576 | 575 | 449, 423, 407, 289, 285 |
| 21 | F, B | F, E, B | F, E, B | F, E, B | procyanidin dimer B | 578 | 577 | 451, 425, 289 |
| 22 | F | | B | B | prodelphinidin dimer A | 592 | 591 | 573, 465, 451, 421, 303, 285 |
| 23 | F, E | F, E, B | E, B | B | prodelphinidin dimer B | 594 | 593 | 575, 456, 449, 423, 303, 289, 285 |
| 24 | | F, E, B | F, E, B | F, E, B | galloyled procyanidin dimer | 730 | 729 | 577, 425, 407, 289 |
| 25 | B | F, E, B | F, E | F, E | procyanidin trimer C | 866 | 865 | 739, 695, 575, 407, 289, 287 |

[a]F, E, and B are free, esterified, and insoluble-bound phenolics, respectively. [b]*, compounds identified with authentic standards.

AAPH solution. The mixture was incubated at 37 °C for 1 h in the dark, after which 1 μL of loading dye (0.25% bromophenol blue, 0.25% xylene cyanol, 50% glycerol in distilled water) was added. The samples were loaded onto 0.7 (w/v) agarose gel prepared in Tris−acetic acid−EDTA (TAE) buffer consisting of 40 mM Tris acetate and 1 mM EDTA, pH 8.5. The gel was stained with SYBR safe (100 μL/L). The procedure was conducted at 80 V for 90 min using a submarine gel electrophoresis apparatus (VWR, Radnor, PA, USA). The images were acquired with a Sony digital camera under UV light and analyzed using AlphaEase stand-alone software (Alpha Innotech Co., San Leandro, CA, USA). The inhibition percentage was calculated as follows: inhibition of DNA strand breakage = [(intensity of supercoiled DNA in the presence of oxidant and extract/intensity of supercoiled DNA devoid of oxidant and extract) × 100]. Results were expressed as percentage retention of supercoiled DNA achieved with 1 mg/mL of defatted sample.

**HPLC-DAD-ESI-MS$^n$ Analysis.** Identification of major phenolics in the free, esterified, and insoluble-bound fractions of grape byproducts was carried out using an Agilent 1100 system equipped with a G1311A quaternary pump, a G1379A degasser, a G1329A ALS automatic sampler, a G1130B ALS Therm, a G1316 Colcom column compartment, A G1315B diode array detector (DAD), and a system controller linked to a ChemStation Data handling system (Agilent). Separations were conducted with a SUPERLCOSIL LC-18 column (4.6 × 250 mm × 5 μm, Merck, Darmstadt, Germany). The binary mobile phase consisted of 0.1% formic acid (A) and 0.1% formic acid in acetonitrile (B). The flow rate of mobile phase was 0.5 mL/min, and the elution gradient used was as follows: 0 min, 100% A; 5 min, 90% A; 35 min, 85% A; 45 min, 60% A; held at 60% A from 45 to 50 min. Afterward mobile phase A was increased to 100% at 55 min, followed by column equilibration from 55 to 65 min. The compounds were detected at 280 nm, and the samples were filtered before injection using a 0.45 μm PTFE membrane syringe filter (Thermo Scientific, Rockwood, TN, USA).

HPLC-ESI-MS$^n$ analysis was carried out under the same conditions as described above using an Agilent 1100 series capillary liquid chromatography−mass selective detector (LC-MSD) ion trap system in electrospray ionization (ESI) in the negative mode. The data were acquired and analyzed with Agilent LC-MSD software. The scan range was set from $m/z$ 50 to 1200, using smart parameter setting, drying nitrogen gas at 350 °C, flow of 12 L/min, and nebulizer gas pressure of 70 psi. Phenolic acids, namely, protocatechuic, *p*-coumaric, gallic, ferulic, and ellagic acids, and flavonoids (+)-catechin, (−)-epicatechin, and quercetin were identified by comparing their retention times and ion fragmentation patterns with coded and authentic standards under the same conditions as the samples. Hydroxycaffeic and caftaric acids and monogalloyl glucose as well as isorhamnetin, epicatechin gallate, kaempferol hexoside, quercetin hexoside, quercetin glucuronide, isorhamnetin hexoside, myricetin hexoside, and dimers through tetramers of proanthocyanidins were tentatively identified using tandem mass spectrometry (MS$^n$), UV spectral, and literature data.

**Statistical Analysis.** The experimental design was randomized with three replications, and the results were analyzed using Tukey's test ($p < 0.05$) and SAS software. The correlation analysis ($p < 0.01$ and $p < 0.05$) was carried out using the ASSISTAT 7.6 program.

## RESULTS AND DISCUSSION

**HPLC-DAD-ESI-MS$^n$ Analysis.** In the present study, phenolics from grape juice- and winemaking byproducts were extracted in different fractions (free, esterified, and insoluble-bound) to fill the apparent gap in the existing knowledge and to offer new information on the subject. The MS spectra of free, esterified, and insoluble-bound phenolic fractions of grape

Table 2. Contents ($\mu$g/g of Dry Weight) of Free, Esterified, and Insoluble-Bound Phenolic Compounds of Grape Byproducts[a]

| | juice byproducts | | winemaking byproducts | |
|---|---|---|---|---|
| | Cora | Isabel | Syrah | Tempranillo |
| **Protocatechuic Acid** | | | | |
| free | nd[b] | nd | tr[c] | 3.01 ± 0.0b |
| esterified | 9.96 ± 0.2b | nd | nd | 4.24 ± 0.3b |
| insoluble-bound | 44.0 ± 1.2a | 41.5 ± 0.8 | 33.5 ± 0.8 | 226 ± 8.0a |
| ***p*-Coumaric Acid** | | | | |
| free | tr | 3.71 ± 0.3c | nd | 0.70 ± 0.0b |
| esterified | 69.5 ± 0.5b | 81.4 ± 2.2b | 168 ± 3.8b | 176 ± 3.3a |
| insoluble-bound | 192 ± 4.6a | 193 ± 3.3a | 243 ± 7.4a | 172 ± 12a |
| **Gallic Acid** | | | | |
| free | 7.06 ± 0.7b | 5.73 ± 0.6c | 8.39 ± 0.2c | 16.9 ± 0.3c |
| esterified | 13.8 ± 0.2b | 165 ± 1.2b | 130 ± 0.5b | 236 ± 0.2b |
| insoluble-bound | 1081 ± 44a | 799 ± 21a | 343 ± 17a | 301 ± 20a |
| **Caffeic Acid** | | | | |
| free | 6.54 ± 0.7c | 6.86 ± 0.8c | nd | nd |
| esterified | 54.1 ± 0.1b | 56.5 ± 1.3b | 95.7 ± 2.6b | 75.3 ± 1.2b |
| insoluble-bound | 628 ± 19a | 636 ± 7.7a | 449 ± 0.9a | 234 ± 3.4a |
| **Ferulic Acid** | | | | |
| free | nd | tr | nd | tr |
| esterified | tr | 4.19 ± 0.2 | nd | nd |
| insoluble-bound | nd | nd | nd | nd |
| **Hydroxycaffeic Acid** | | | | |
| free | nd | nd | nd | nd |
| esterified | nd | nd | nd | 8.73 ± 0.4 |
| insoluble-bound | nd | nd | nd | nd |
| **Ellagic Acid** | | | | |
| free | nd | nd | 1.75 ± 0.2 | nd |
| esterified | 0.70 ± 0.1 | tr | nd | nd |
| insoluble-bound | nd | 0.54 ± 0.1 | nd | 8.00 ± 0.7 |
| **Caftaric Acid** | | | | |
| free | 152 ± 14 | 101 ± 5.8 | nd | 1.83 ± 0.1 |
| esterified | nd | nd | nd | nd |
| insoluble-bound | nd | nd | nd | nd |
| **Monogalloyl Glucose** | | | | |
| free | 10.9 ± 0.7c | 8.14 ± 0.4c | 2.27 ± 0.2b | 2.13 ± 0.0b |
| esterified | 15.7 ± 0.3b | 21.1 ± 0.9b | 3.20 ± 0.3ab | 4.73 ± 0.5a |
| insoluble-bound | 27.5 ± 1.6a | 27.1 ± 1.3a | 3.61 ± 0.6a | 4.00 ± 0.4a |
| **Catechin** | | | | |
| free | 190 ± 11b | 114 ± 15b | 12.8 ± 0.5c | 21.6 ± 0.6c |
| esterified | 9.66 ± 0.9c | 82.1 ± 10c | 111 ± 1.8b | 209 ± 5.8b |
| insoluble-bound | 896 ± 48a | 530 ± 2.8a | 874 ± 28a | 506 ± 34a |
| **Epicatechin** | | | | |
| free | 89.4 ± 0.2b | 149 ± 11a | 10.8 ± 1.7c | 15.3 ± 0.6c |
| esterified | tr | 26.3 ± 2.3b | 46.0 ± 7.8b | 73.0 ± 2.6b |
| insoluble-bound | 173 ± 10a | 157 ± 25a | 162 ± 2.3a | 105 ± 12a |
| **Quercetin** | | | | |
| free | 2.29 ± 0.0b | 3.45 ± 0.4 | 1.29 ± 0.3b | 6.85 ± 0.3b |
| esterified | nd | nd | nd | 2.39 ± 0.5c |
| insoluble-bound | 4.77 ± 0.2a | nd | 14.6 ± 1.6a | 9.07 ± 0.6a |
| **Isorhamnetin** | | | | |
| free | nd | nd | tr | 11.1 ± 0.2b |
| esterified | 53.4 ± 0.8 | nd | nd | tr |
| insoluble-bound | nd | tr | tr | 515 ± 48b |
| **Epicatechin Gallate** | | | | |
| free | 38.7 ± 2.3b | 35.3 ± 2.8b | 45.0 ± 1.7c | 25.7 ± 4.2c |
| esterified | nd | 16.4 ± 2.9c | 64.5 ± 5.7b | 65.3 ± 3.3b |
| insoluble-bound | 163 ± 1.1a | 144 ± 5.4a | 136 ± 1.6a | 253 ± 3.7a |
| **Kaempferol Hexoside** | | | | |
| free | 13.3 ± 1.0b | 6.13 ± 0.9 | 11.4 ± 0.8 | 6.46 ± 0.5 |
| esterified | tr | tr | nd | nd |


dx.doi.org/10.1021/jf504185s | J. Agric. Food Chem. 2014, 62, 12159−12171

**Table 2. continued**

| | juice byproducts | | winemaking byproducts | |
|---|---|---|---|---|
| | Cora | Isabel | Syrah | Tempranillo |
| | | **Kaempferol Hexoside** | | |
| insoluble-bound | 37.7 ± 6.0a | tr | nd | nd |
| | | **Quercetin Hexoside** | | |
| free | 94.2 ± 5.4a | 187 ± 7.2a | 20.9 ± 1.1b | 35.0 ± 1.9 |
| esterified | 11.2 ± 0.2c | 15.1 ± 0.6c | 29.9 ± 3.4a | nd |
| insoluble-bound | 64.2 ± 4.0b | 48.3 ± 4.1b | 9.46 ± 1.9c | nd |
| | | **Quercetin Glucuronide** | | |
| free | 242 ± 2.0a | 187 ± 7.2a | 20.9 ± 1.1b | 35.0 ± 1.6a |
| esterified | 6.10 ± 0.8c | 5.49 ± 0.2c | 28.3 ± 2.6a | 28.7 ± 1.5b |
| insoluble-bound | 84.5 ± 4.5b | 48.3 ± 4.1b | 26.7 ± 1.7a | 13.3 ± 1.1c |
| **Isorhamnetin Hexoside** | | | | |
| free | 17.5 ± 1.2a | 11.6 ± 2.3 | 29.4 ± 0.7b | 30.1 ± 0.6a |
| esterified | nd | nd | 25.6 ± 1.3a | 9.92 ± 0.8b |
| insoluble-bound | 70.6 ± 2.1b | nd | tr | tr |
| | | **Myricetin Hexoside** | | |
| free | 190 ± 0.9a | 16.2 ± 1.1a | tr | 3.97 ± 0.08 |
| esterified | nd | 8.20 ± 0.1b | nd | nd |
| insoluble-bound | 143 ± 7.9b | nd | nd | nd |
| | | **Procyanidin Dimer B** | | |
| free | 384 ± 26b | 313 ± 22a | 127 ± 12c | 206 ± 1.1b |
| esterified | tr | 24.2 ± 2.9c | 333 ± 25b | 254 ± 7.2b |
| insoluble-bound | 687 ± 26a | 124 ± 3.0c | 2126 ± 3.5a | 4108 ± 46a |
| | | **Procyanidin Dimer A** | | |
| free | nd | nd | nd | nd |
| esterified | nd | nd | nd | nd |
| insoluble-bound | 915 ± 18 | 63.2 ± 7.4 | nd | 376 ± 12 |
| | | **Prodelphinidin A** | | |
| free | 23.2 ± 3.9 | nd | nd | tr |
| esterified | nd | nd | nd | nd |
| insoluble-bound | nd | nd | 518 ± 12 | 16.7 ± 1.4 |
| | | **Prodelphinidin B** | | |
| free | tr | tr | nd | nd |
| esterified | tr | 74.8 ± 5.1a | 26.8 ± 3.2b | nd |
| insoluble-bound | nd | 47.2 ± 3.0b | 126 ± 10a | 263 ± 20 |
| | | **Galloyled Procyanidin** | | |
| free | nd | 17.8 ± 1.3 | 66.2 ± 6.1c | 50.4 ± 0.8b |
| esterified | nd | tr | 105 ± 6.9b | 151 ± 7.1a |
| insoluble-bound | nd | tr | 147 ± 17a | 38.0 ± 4.4c |
| | | **Procyanidin Trimer C** | | |
| free | nd | 50.8 ± 7.3b | 81.7 ± 12a | 115 ± 14a |
| esterified | nd | 15.5 ± 1.4c | 28.7 ± 2.1b | tr |
| insoluble-bound | 491 ± 49 | 269 ± 19a | nd | 123 ± 1.6a |

[a]Data represent mean values for each sample ± standard deviations ($n = 3$). Means followed by the same letter within a column are not significantly different ($p > 0.05$). [b]nd, nondetected. [c]tr, trace.

byproducts are shown in Table 1. Compounds **1**−**5**, **7**, and **10**−**12** were identified by comparison of their retention times and ion fragmentation patterns with authentic standards. Compound **6** gave deprotonated ions at $m/z$ 197 and $MS^2$ at $m/z$ 179, due to loss of water $[M - H - 18]^-$, and at $m/z$ 135. This ion fragmentation pattern is typical for caffeic acid, as confirmed using a commercial standard, and thus tentatively identified as hydroxycaffeic acid. In the present study, hydroxycaffeic was found only in the esterified fraction of the Tempranillo variety. Hydroxycaffeic acid, which is found in blackberries and blueberries,[20] has not been reported in grapes, possibly because few varieties may contain it or it may be esterified to other components present.

Compound **8**, which was present in the free fraction of Cora, Isabel, and Tempranillo varieties, showed an $m/z$ at 311 in MS followed by 179 and 135 in $MS^2$ and was tentatively identified as caftaric acid.[21] Monogalloyl glucose (compound **9**) was also tentatively identified due to its $m/z$ of 331 in MS and $m/z$ of 169 and 125 in $MS^2$, both typical of gallic acid.[8] Furthermore, monogalloyl glucose was present in all fractions of all samples tested.

Compound **13** gave deprotonated ion $[M - H]^-$ at $m/z$ 315 and at $m/z$ 271 in $MS^2$, which is compatible with the isorhamnetin dissocitation pattern.[22] Compound **14** was tentatively identified as epicatechin gallate (galloylated flavan-3-ol) due to its deprotonated molecular ion at $m/z$ 441 followed by $m/z$ at 289 and 245 in $MS^2$, showing

decarboxylation of epicatechin $[M - H - 44]^-$, at $m/z$ 169 and 125, the last one from decarboxylated gallic acid.[10]

Compound **15** with a deprotonated ion at $m/z$ 447 gave product ions at $m/z$ 285 (kaempferol) in $MS^2$, showing loss of hexose $[M - H - 162]^-$, thus being tentatively identified as kaempferol hexoside.[8] Compound **16** ($m/z$ 463) also showed loss of hexoside and its typical quercetin dissociation at $m/z$ 179 and 151 in $MS^2$, which was confirmed by quercetin standard, indicating its identity as quercetin hexoside.

Quercetin glucuronide was tentatively identified as compound **17**, which gave a deprotonated ion at $m/z$ 477 and $MS^2$ at 301, 179, and 151.[8] Compound **19** showed $[M - H]^-$ at $m/z$ 477, such as quercetin glucuronide, but its $MS^2$ gave product ions at $m/z$ 315 and 271, enabling its tentative identification as isorhamnetin hexoside.[8] Myricetin hexoside was also tentatively identified according to its deprotonated ion at $m/z$ 479, followed by loss of hexose,[10] which gave signals at $m/z$ 317, 179, and 151, the last ones confirmed by using an authentic standard.

With the exception of galloylated procyanidin dimer,[8] the remaining proanthocyanidins were tentatively identified according to the studies of Sarnoski et al.[23] and de Camargo et al.[24] Procyanidins B1−B8 are currently known;[25] thus, some peaks were identified with the same ionization pattern, which has been common for proanthocyanidins isomers. However, accurate stereoisomer identification requires nuclear magnetic resonance (NMR) analysis; thus, for quantification purposes total value was reported.

The quantification data for the phenolics identified are shown in Table 2. Although anthocyanins have been reported in grape byproducts, the HPLC-DAD acquisition data set at 520 nm, which is typical for anthocyanins, did not show major compounds (data not show); thus, the present study focused on phenolic acids, flavonoids, and proanthocyanidins. Varietal differences in phenolics are well documented in the literature;[1,11,26] thus, statistical treatment was carried out among the free, esterified, and insoluble-bound fractions. With very few exceptions, the insoluble-bound fraction had the highest content of individual phenolics.

The HPLC-DAD-ESI-$MS^n$ evaluation demonstrated that gallic and caffeic acids were the major phenolic acids accounting for up to 20 and 14% of the total, respectively. Gallic acid has previously been reported as being the major phenolic acid in grape seeds.[27] Catechin was the major monomeric flavonoid (up to 17%), and procyanidin dimer B was the main proanthocyanidin, with a content of up to 52%. Several factors such as climatic and stress conditions as well as soil quality play important roles in the content of phenolics; thus, a direct comparison with the literature data is not possible, but some trends may be discernible

The present study reveals similarities with the data reported by Ćurko et al.,[28] in which catechin and procyanidin B were the major monomeric flavonoid and proanthocyanidin, respectively. Interestingly, a high concentration of procyanidin dimer A, which has not been commonly reported for grape and its byproducts, was found in the present study. However, Cheng et al.[1] also reported the presence of procyanidin dimer A in grape byproducts (skins, seeds, and pomace). Furthermore, according to these authors, the highest procyanidin dimer A concentration was found in the seeds.

Total phenolics, as evaluated by HPLC-DAD-ESI-$MS^n$, hereafter named HPLC TPC, are shown in Figures 1 and 2. The HPLC TPC were present in the order insoluble-bound > free > esterified for both juice byproducts and insoluble-bound > esterified > free for both winemaking byproducts, which suggests that the process type influences this distribution. The HPLC TPC were in the decreasing order Tempranillo > Cora > Syrah > Isabel (Figure 2), with insoluble-bound fraction representing up to 12 and 23 times the content of the free and esterified fractions, respectively. This is important because most of the available information is focused only on the soluble phenolics (free plus esterified). Finally, Figure 3 shows the percent contribution of soluble and insoluble-bound phenolics in the samples. Insoluble-bound phenolics accounted for 63−79% of the total, thus demonstrating their dominance as a major source of bioactive compounds in grape byproducts.

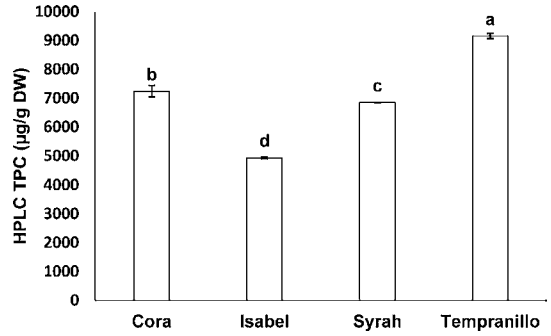


**Figure 2.** HPLC-DAD-ESI-$MS^n$ total phenolic content (HPLC TPC) representing free plus esterified plus insoluble-bound phenolics of juice (Cora and Isabel) and winemaking (Syrah and Tempranillo) byproducts. Data represent the mean ± standard deviation of each sample ($n$ = 3). Means with different letters indicate significant differences ($p < 0.05$).

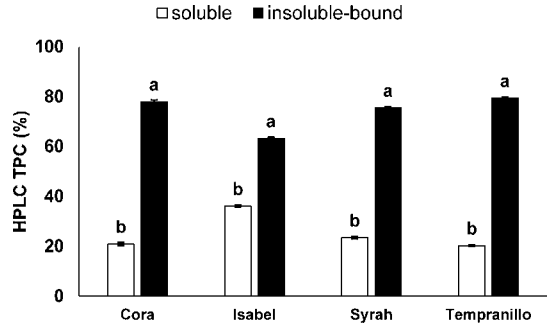


**Figure 3.** HPLC-DAD-ESI-$MS^n$ total phenolic content (HPLC TPC) of soluble and insoluble-bound fractions of juice (Cora and Isabel) and winemaking (Syrah and Tempranillo) byproducts. Means with different letters indicate significant differences ($p < 0.05$) within the same grape variety.

As can be noted by both identification and quantification, a wide range of phenolics was present in the samples. Furthermore, each fraction and grape variety had its own fingerprint; thus, in the following sections, one should bear in mind that this difference may affect each assay to different extents, depending on the operative mechanisms.

**Total Phenolic Contents.** The TPC of grape juice- and winemaking byproducts are given in Table 3. The differences in the TPC, due to different grape varieties, are well documented.[1,11] The TPC of free, esterified, and insoluble-bound fractions were in the ranges of 45.8−124, 48.6−124, and 171−339 mg GAE/g dry weight of fat-free sample, respectively. These data are in accordance with a previous study on soluble

**Table 3. Total Phenolic Content (TPC), Proanthocyanidin Content (PC), Antiradical Scavenging Capacity, and Reducing Power (RP) of Free, Esterified, and Insoluble-Bound Phenolic Compounds from Juice (Cora and Isabel) and Winemaking (Syrah and Tempranillo) Byproducts[a]**

| | juice byproducts | | winemaking byproducts | |
|---|---|---|---|---|
| | Cora | Isabel | Syrah | Tempranillo |
| **Total Phenolic Content (mg GAE/g DW)** | | | | |
| free | 124 ± 1.3Ab | 112 ± 3.4Bb | 45.8 ± 0.2Db | 69.5 ± 1.9Cc |
| esterified | 48.6 ± 1.4Cc | 69.3 ± 2.6Bc | 65.0 ± 2.7Bb | 124 ± 4.2Ab |
| insoluble-bound | 209 ± 5.9BCa | 171 ± 12Ca | 213 ± 14Ba | 339 ± 23Aa |
| **Total Proanthocyanidin (mg CAT/g DW)** | | | | |
| free | 26.6 ± 0.9Bb | 68.1 ± 2.3Ab | 20.2 ± 2.2Cc | 23.0 ± 0.7BCc |
| esterified | 7.22 ± 0.3Dc | 17.1 ± 0.9Cc | 25.0 ± 1.4Bb | 45.6 ± 0.8Ab |
| insoluble-bound | 142 ± 5.7Aa | 91.3 ± 4.0Ba | 85.7 ± 1.8Ba | 145 ± 14Aa |
| **ABTS Radical Cation Scavenging Activity (μmol TE/g DW)** | | | | |
| free | 75.5 ± 6.2Ab | 74.3 ± 8.2Ab | 31.7 ± 1.5Dc | 50.8 ± 0.4Cc |
| esterified | 34.6 ± 2.8Cc | 52.5 ± 1.7Bc | 53.5 ± 3.9Bb | 99.7 ± 4.2Ab |
| insoluble-bound | 283 ± 7.9Ca | 175 ± 8.4 Da | 561 ± 9.3Ba | 738 ± 14Aa |
| **DPPH Radical Scavenging Activity (μmol TE/g DW)** | | | | |
| free | 137 ± 4.7Ab | 79.3 ± 3.6Bb | 36.9 ± 1.3Dc | 56.2 ± 1.6Cc |
| esterified | 55.0 ± 1.0Cc | 72.3 ± 1.1Bb | 61.0 ± 3.1Cb | 91.4 ± 4.1Ab |
| insoluble-bound | 233 ± 3.9Ca | 185 ± 7.8 Da | 554 ± 13Ba | 801 ± 18Aa |
| **$H_2O_2$ Scavenging Activity (μmol TE/g DW)** | | | | |
| free | 143 ± 0.2Bb | 167 ± 0.3Ab | 75.8 ± 1.2Cb | 43.2 ± 0.6Dc |
| esterified | 95.9 ± 1.6Bc | 111 ± 1.7Ac | 71.7 ± 0.1Cb | 60.2 ± 0.1Db |
| insoluble-bound | 304 ± 3.1Aa | 224 ± 14Ba | 261 ± 28Ba | 250 ± 1.7Ba |
| **Reducing Power (μmol TE/g DW)** | | | | |
| free | 56.1 ± 14ABb | 67.5 ± 1.9Ab | 39.9 ± 1.0BCc | 33.7 ± 3.2Cc |
| esterified | 43.0 ± 1.4Db | 52.9 ± 1.6Cc | 90.3 ± 2.7Ab | 71.5 ± 1.0Bb |
| insoluble-bound | 276 ± 10Ca | 186 ± 7.0 Da | 484 ± 26Aa | 358 ± 19Ba |

[a]Data represent the mean values for each sample ± standard deviation ($n$ = 3). Means followed by the same capital letters within a row are not significantly different ($p$ > 0.05). Means followed by the same lower case letters within a column are not significantly different ($p$ > 0.05). CE, catechin equivalents; TE, trolox equivalents; DW, dry weight of defatted sample.

**Table 4. Pearson's Correlation between Total Phenolic Content (TPC), Proanthocyanidin Content (PC), or Phenolic Compounds and Scavenging Activities, Reducing Power, or Induced LDL-Cholesterol Oxidation Inhibition, or Supercoiled Plasmid DNA Strand Breakage Inhibition[a]**

| | ABTS[1] | DPPH | $H_2O_2$ | RP | LDL | DNA |
|---|---|---|---|---|---|---|
| TPC | 0.9319** | 0.9239** | 0.8181** | 0.8384** | 0.6606* | 0.8807** |
| PC | 0.7945** | 0.7496** | 0.8887** | 0.7807** | 0.7495** | 0.8506** |
| protocatechuic acid | 0.8213* | 0.8581* | 0.4973 ns | 0.5212 ns | 0.2419 ns | 0.5876 ns |
| *p*-coumaric acid | 0.5819* | 0.5382 ns | 0.5622 ns | 0.7322** | 0.7720** | 0.6815* |
| gallic acid | 0.3700 ns | 0.2925 ns | 0.7417** | 0.5395 ns | 0.8010** | 0.6128* |
| caffeic acid | 0.4517 ns | 0.3727 ns | 0.7939** | 0.6696** | 0.7308** | 0.7338** |
| ellagic acid | 0.9500* | 0.9527* | 0.5826 ns | 0.8390 ns | 0.5178 ns | 0.5058 ns |
| monogalloyl glucose | −0.1151 ns | −0.1460 ns | 0.4534 ns | 0.0279 ns | 0.3199 ns | 0.1654 ns |
| catechin | 0.7323** | 0.6650* | 0.9066** | 0.8983** | 0.8634** | 0.8337** |
| epicatechin | 0.5034 ns | 0.4530 ns | 0.8703** | 0.6642* | 0.6904* | 0.8212** |
| quercetin | 0.7839* | 0.7540* | 0.5373 ns | 0.8589** | 0.3045 ns | 0.7494* |
| epicatechin gallate | 0.8867** | 0.8662** | 0.7819** | 0.8186** | 0.6653* | 0.8605** |
| kaempferol hexoside | 0.9529* | 0.9050* | 0.8583 ns | 0.9620** | 0.9500* | 0.7157 ns |
| quercetin hexoside | −0.1648 ns | −0.1637 ns | 0.1946 ns | −0.1860 ns | 0.0434 ns | 0.1357 ns |
| isorhamnetin hexoside | 0.7958* | 0.6877 ns | 0.6917 ns | 0.8500* | 0.7192 ns | 0.4240 ns |
| myricetin hexoside | 0.5157 ns | 0.7752 ns | 0.5610 ns | 0.4714 ns | 0.7710 ns | 0.5710 ns |
| procyanidin dimer B | 0.9544** | 0.9733** | 0.5560 ns | 0.7706** | 0.3296 ns | 0.6692* |
| prodelphinidin B | 0.9113* | 0.9360* | 0.6348 ns | 0.6413 ns | 0.2539 ns | 0.5229 ns |
| galloyled procyanidin | 0.0529 ns | 0.0071 ns | −0.0578 ns | 0.2869 ns | 0.5994 ns | 0.1229 ns |
| procyanidin trimer C | 0.2864 ns | 0.1921 ns | 0.7534* | 0.5935 ns | 0.8543** | 0.5192 ns |

[a]**, significant at $p$ < 0.01; *, significant at $p$ < 0.05; ns, nonsignificant. ABTS, ABTS radical cation scavenging activity; DPPH, DPPH radical scavenging activity; $H_2O_2$, $H_2O_2$ scavenging activity; RP, reducing power; LDL, copper-induced LDL-cholesterol oxidation; DNA, supercoiled plasmid DNA strand breakage inhibition. Correlations for ferulic acid, hydroxycaffeic acid, caftaric acid, procyanidin dimer A, and prodelphinidin A were not calculated due to insufficient data.

phenolics (free plus esterified) from winemaking byproducts, in which 10 grape varieties were evaluated.[11]

In the present study, byproducts of the juice industry (Cora and Isabel) showed the highest TPC in the free phenolic fraction in comparison with the winery byproducts (Syrah and Tempranillo). The lower TPC in the free fraction of winemaking byproducts in comparison with those of grape juice byproducts may be explained by different grape variety, their maturation, and crop production area; however, the process influence is also possible. Polyphenols have been shown to provide a better affinity to alcoholic solvents; thus, grape skins and seeds of the winemaking process may lose their soluble phenolics to the liquid medium, which mimics a solvent system. Moreover, a clear cluster can be noted in relation to free and soluble esterified phenolics (e.g., grape juice- vs winemaking byproducts). Cora and Isabel, which are grape juice byproducts, had free phenolics in the range of 62−72%, in relation to total soluble phenolics (free plus esterified), whereas Syrah and Tempranillo, which are winery byproducts, had those in the range of 36−41%. The opposite trend was found for the TPC of the fraction containing phenolics released from their esterified form. This can also be noted when the TPC is evaluated by HPLC (Figure 1). TPC of the insoluble-bound fractions did not indicate the same influence of the process as statistical analysis did not allow their grouping into different clusters (e.g., grape juice- or winemaking byproducts), suggesting that the noted differences were due to varietal influences.

The extraction of insoluble-bound phenolics was conducted via hydrolysis using 4 M NaOH for 4 h. Meanwhile, a simple contact with the medium (e.g., grape juice or wine) would hardly be sufficient to release insoluble-bound phenolics during the grape juice- or winemaking manufacture. Only this would enable their loss to the liquid medium. As this is unlikely, it is possible to suggest that the differences found in the fraction containing insoluble-bound phenolics are due to grape variety, their maturation, and crop production area. The distribution of phenolic compounds among all forms (free, esterified, and insoluble-bound) depends not only on the feedstock but also on the variety and field conditions. Although further studies are necessary to confirm this assumption, the present study indicates a possible influence of the process (e.g., grape juice vs wine) in their distribution.

**Proanthocyanidin Content.** Proanthocyanidins, also known as condensed tannins, consist of flavan-3-ol units, ranging from dimers to higher oligomers. Grapes have a high content of proanthocyanidins, especially procyanidin dimer B, which consists exclusively of catechin and epicatechin units; however, prodelphinidins, which have (epi)gallocatechin in their structures, are also found in grapes, as demonstrated before (Table 1). The method for estimating the PC used here showed better correlation with low molecular weight proanthocyanidins (2−4 units);[29] however, the PC showed a significant and positive correlation ($p < 0.01$) with all antioxidant assays carried out in the present study (Table 4), indicating the quality of the results.

The PC is shown in Table 3; the results presented are in good agreement with those reported for soluble phenolics (free plus esterified) of winemaking byproducts.[11] In accordance with TPC in the present study, the highest PC was found in the insoluble-bound fraction, and its content was up to 6-fold higher than that found in the free fraction. Furthermore, winemaking byproducts (Syrah and Tempranillo) had the highest esterified PC in comparison with the juice byproducts (Cora and Isabel), suggesting that the grape juice process influence on PC takes place in the esterified fraction.

The juice process in the present study was carried out at 85 °C and pH 3.5 for 60 min. Meanwhile, no heat was applied during the winemaking process. Acid hydrolysis (95 °C, 45 min) has been used to release phenolics from their glycosidic bonds.[30] Flavanone 3-hydroxylase is the first enzyme in the biosynthesis of proanthocyanidins. Its optimum temperature is 30−40 °C.[31,32] The remaining enzymes also have low optimum temperature (e.g., dihydroflavonol reductase, 30−45 °C; leucoanthocyanidin reductase, 30−37 °C; and anthocyanidin reductase, 45−55 °C).[33−35] High temperature and time used during the juice process may denature all enzymes present. Thus, heating and acidic condition may release phenolics from their esters during juice making. Furthermore, enzyme inactivation probably occurs, which affects further biosynthesis. Thus, both factors lower the content of esterified proanthocyanidins and the remaining phenolics in the juice byproducts as compared to the winemaking ones.

Supporting the findings of the present study, higher contents of soluble proanthocyanidins (free plus esterified) were found in grape skin and seeds produced in winemaking with a longer fermentation process.[36] It is noteworthy that the highest PC in the esterified fraction of winemaking byproducts is supported by the highest procyanidin B content, the major proanthocyanidin present, as evaluated by HPLC-DAD-ESI-MS$^n$ (Table 2). Interestingly, both catechin and epicatechin, which are subunits of procyanidins, were found in higher concentrations in the esterified fraction of the winemaking byproducts in the present study.

**ABTS Radical Cation Scavenging Activity.** In the present study, no difference was found between the ABTS antioxidant activity (Table 3) of the free phenolic extracts from Cora and Isabel (juice byproducts), which had the highest scavenging activities in comparison with those of the winemaking byproducts (Syrah and Tempranillo). On the other hand, the Tempranillo variety showed the highest scavenging activity for esterified and insoluble-bound fractions. Furthermore, the Syrah cultivar exhibited the highest difference between the scavenging activity of the soluble (free plus esterified) and insoluble-bound fractions, the latter contributing up to 6.5-fold higher scavenging activity than the soluble counterpart. Gallic acid is a potent antioxidant, and grapes contain a high amount of gallic acid and polyphenols bearing galloyl groups (Table 2), which may explain the large difference in scavenging activity between soluble and insoluble-bound fractions, despite the relatively low difference found in their TPC, which was not higher than 1.9-fold (Table 3). In accordance with TPC and PC, the highest scavenging activity for all grape byproducts was found for the insoluble-bound fraction.

**DPPH Radical Scavenging Activity Using Electron Paramagnetic Resonance.** The DRSA results (Table 3) showed a trend similar to those for the free phenolic fraction in both ABTS and TPC determinations, for which grape juice byproducts (Cora and Isabel) demonstrated higher values. However, Cora had the highest DRSA, different from that observed in the ABTS assay, which exhibited no significant difference between both juice byproducts. Different results, depending on the method used, may be obtained due to different chemical structures as well as synergistic, additive, or antagonistic interaction effects. Furthermore, pro-oxidant

effects are also possible depending on the reaction mechanism and polyphenol concentration, among other factors,[37,38]

**Hydrogen Peroxide Scavenging Activity.** The scavenging activity of hydrogen peroxide by grape byproducts is shown in Table 3. Similar to other antioxidant assays, the insoluble-bound fraction exhibited a higher efficacy in scavenging hydroxyl radicals. Interestingly, for the first time in the present study, insoluble-bound phenolics from Cora variety exhibited the most antioxidant effectiveness, suggesting the presence of a particular polyphenol or a synergistic effect among some polyphenols that renders a higher protective influence to Cora against ROS. The remaining results for the free fraction followed a similar trend to TPC, rendering a different cluster, grape juice byproducts (Cora and Isabel) being the most effective in the free phenolic fraction. Furthermore, different from other antioxidant assays, the esterified fraction of grape juice byproducts also displayed the highest effect against $H_2O_2$. Grape byproducts have shown scavenging activity against superoxide anion and peroxyl and hydroxyl radicals.[1,8,39]

**Reducing Power.** The RP of grape byproducts is summarized is Table 3, indicating the ability of polyphenols present to reduce the ferric ion to the ferrous ion. The comparison of reducing power within the free fraction showed that Cora and Isabel, which are grape juice byproducts, had the highest efficacy in reducing ferric to ferrous ions, compared to winemaking byproducts (Syrah and Tempranillo). On the other hand, in the esterified fraction, the winemaking byproducts accounted for the highest RP in comparison to grape juice byproducts, which was also found for the insoluble-bound fraction. Finally, the comparison among free, esterified, and insoluble-bound phenolic fractions confirmed the highest potential bioactivity for the insoluble-bound fraction in all grape varieties. Other studies[8,11] provide information supporting the reducing ability of grape byproducts; however, a direct comparison is not possible due to different units used to report the results and the methods employed in these determinations. Most studies have been using ferric reducing antioxidant power assay (FRAP) at pH 3.6, which is different from the pH 6.6 used in this study. The antioxidant/reducing power of phenolic compounds is known to be dependent on the pH of the medium.[40]

**Copper-Induced LDL-Cholesterol Oxidation.** The presence of oxidized LDL-cholesterol at high levels constitutes a risk factor for atherosclerosis. In the present study, copper-induced oxidation of human LDL-cholesterol was inhibited by all phenolic extracts (Figure 4) and the highest effect was rendered by the insoluble-bound fraction. A recent study demonstrated that nonextractable polyphenols are the major contributors to the Spanish diet.[41] Consumption of commodities containing phenolic acids, monomeric flavonoids, and proanthocyanidins has been correlated with a decrease in the level of oxidized cholesterol in high-risk cardiovascular patients.[42] Grapes have a high content of procyanidin B and monomeric flavonoids as well as gallic acid as their major phenolics, the latter being an antioxidatively potent phenol. The presence of this broad range of bioactive compounds may be responsible for the ability of grape products to prevent LDL-cholesterol oxidation and potentially the development of heart disease.

**Inhibition of Peroxyl Radical Induced Supercoiled Plasmid DNA Strand Breakage.** ROS oxidize the native form of DNA, which can be evaluated by its conversion to a nicked circular or linear form via single- or double-strand

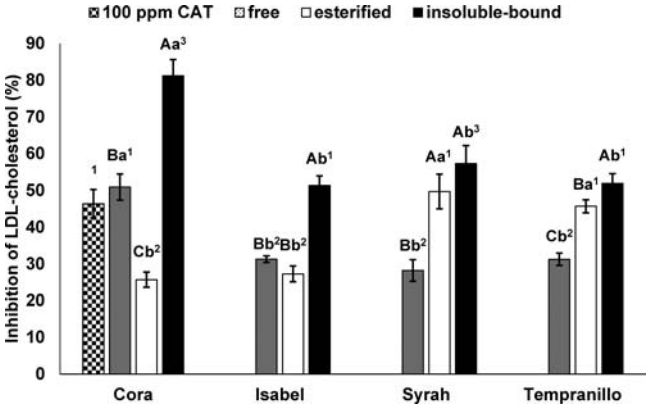


**Figure 4.** Biological activity of free, esterified, and insoluble-bound phenolics of juice (Cora and Isabel) and winemaking (Syrah and Tempranillo) byproducts against LDL-cholesterol induced oxidation. Data represent the mean ± standard deviation of each sample ($n$ = 3). Means with different letters indicate significant differences ($p$ < 0.05) compared to 100 ppm catechin (CAT). Extracts were assayed in concentration of 100 ppm of total phenolic content equivalent (as evaluated by HPLC-DAD-ESI-MS$^n$). Means with different capital letters indicate significant differences ($p$ < 0.05) among fractions within the same grape variety. Means with different lower case letters indicate significant differences ($p$ < 0.05) among grape varieties within the same fraction.

breaks, respectively. Such a process affects DNA replication and transcription, causing mutagenesis and cancer initiation. The present study evaluated the ability of different grape processing byproducts in inhibiting peroxyl radical induced supercoiled plasmid DNA strand breakage (Figures 5−7). Peroxyl radicals

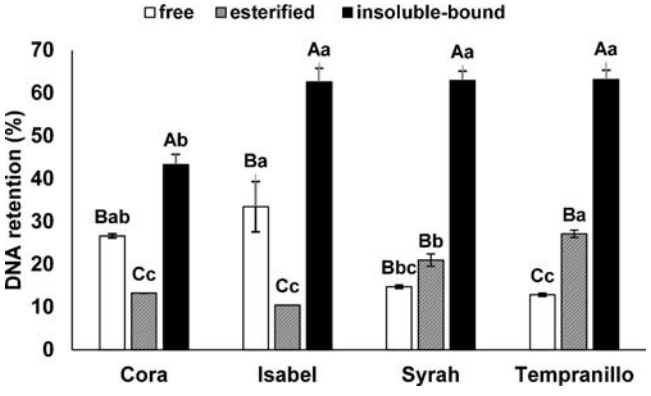


**Figure 5.** Supercoiled plasmid DNA strand breakage inhibition of free, esterified, and insoluble phenolic fractions from juice (Cora and Isabel) and winemaking (Syrah and Tempranillo) byproducts. Data represent the mean ± standard deviation of each sample ($n$ = 3). Means with different capital letters indicate significant differences ($p$ < 0.05) among fractions within the same grape variety. Means with different lower case letters indicate significant differences ($p$ < 0.05) among grape varieties within the same fraction. Results were transformed for concentrations of 1 mg/mL of defatted sample. Representative raw data are given in Figures 3 and 4.

have a relatively long half-life, and therefore their detrimental effects may not only take place at a cellular level but also be extended to biological fluids. All grape extract phenolics rendered a DNA protective effect against peroxyl radicals.

Insoluble-bound phenolics had the highest protective action against peroxyl radical induced supercoiled plasmid DNA

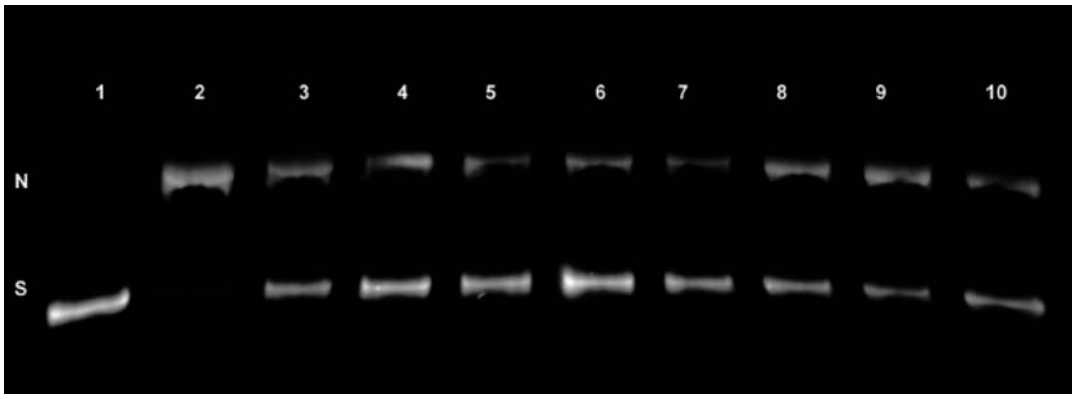


**Figure 6.** Representative raw data of supercoiled plasmid DNA strand breakage inhibition of the free and esterified phenolic fraction of juice (Cora and Isabel) and winemaking (Syrah and Tempranillo) byproducts. Lanes: 1, control (DNA only); 2, DNA + AAPH; 3, free phenolics from Cora (2.5 mg/mL; 53 ± 1% DNA retention); 4, free phenolics from Isabel (2.5 mg/mL; 67 ± 12% DNA retention); 5, free phenolics from Syrah (5.0 mg/mL; 74 ± 2% DNA retention); 6, free phenolics from Tempranillo (5.0 mg/mL; 64 ± 2% DNA retention); 7, esterified phenolics from Cora (5.0 mg/mL; 66 ± 0.3% DNA retention); 8, esterified phenolics from Isabel (5.0 mg/mL; 52 ± 0.2% DNA retention); 9, esterified phenolics from Syrah (2.5 mg/mL; 42 ± 3% DNA retention); 10, esterified phenolics Tempranillo (2.5 mg/mL; 54 ± 2% DNA retention). Data represent the mean ± standard deviation of each sample ($n$ = 3). S and N are supercoiled and nicked plasmid DNA strands, respectively.

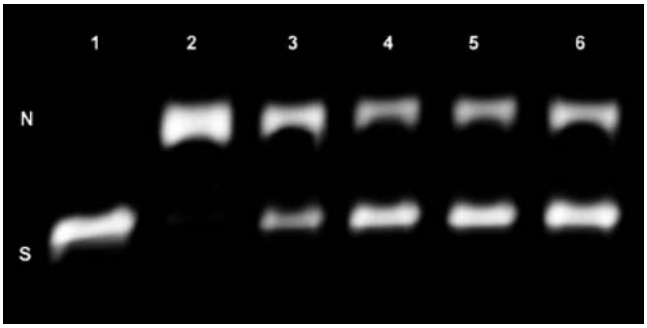


**Figure 7.** Representative raw data of supercoiled plasmid DNA strand breakage inhibition of the insoluble-bound phenolic fraction of juice (Cora and Isabel) and winemaking (Syrah and Tempranillo) byproducts. Insoluble-bound phenolics were assayed in concentration of 1 mg/mL of defatted sample for all varieties. Lanes: 1, control (DNA only); 2, DNA + AAPH; 3, insoluble-bound phenolics from Cora (43 ± 2% DNA retention); 4, insoluble-bound phenolics from Isabel (63 ± 3% DNA retention); 5, insoluble-bound phenolics from Syrah (63 ± 2% DNA retention); 6, insoluble-bound phenolics from Tempranillo (63 ± 2% DNA retention). Data represent the mean ± standard deviation of each sample ($n$ = 3). S and N are supercoiled and nicked plasmid DNA strands, respectively.

strand breakage, showing supercoiled DNA retention of up to 63%. The concentration used for this fraction was equivalent to 1 mg/mL of defatted sample (8 ppm of phenolic compounds as evaluated by HPLC-DAD-ESI-MS$^n$), showing that even a very low concentration of insoluble-bound phenolics of grape byproducts may have health benefits. Minor differences among cultivars were found in the insoluble-bound fraction, thus suggesting little varietal influence on polyphenols liberated from cell walls via hydrolysis. Varietal differences in the free and esterified fractions were in accordance with other antioxidant assays, showing a clear cluster between juice (Cora and Isabel) and winemaking (Syrah and Tempranillo) byproducts, in which, generally, juice byproducts had higher free phenolic content than winemaking byproducts and the opposite was found for their esterified counterparts.

**Correlation of Analyses.** Correlation analyses were carried out between TPC, PC, and the bioactivity evaluations (Table 4). Correlations of individual phenolics quantified were also evaluated to better understand their contribution on each activity. All antioxidant assays were correlated with either TPC and PC, and only the correlation between TPC and inhibition of LDL-cholesterol oxidation demonstrated a lower significance ($p < 0.05$), whereas the remaining results exhibited a higher significance ($p < 0.01$). Most antioxidant assays evaluated (ABTS, DPPH, RP, and supercoiled plasmid DNA strand breakage inhibition) demonstrated a higher correlation with TPC, suggesting that phenolic compounds other than proathocyanidins may play an important role in preventing oxidation-related diseases.

Catechin and epicatechin gallate were the only compounds showing significant correlations with all antioxidant assays. *p*-Coumaric acid, caffeic acid, epicatechin, quercetin, kaempferol hexoside, and procyanidin dimer B had correlations in four of six assays conducted, being positively correlated to 67% of the methods used. In general, epicatechin gallate had higher correlations with the antioxidant assays as compared with epicatechin itself. This suggests that galloyl groups had positive effects on the antioxidant activities of the grape byproducts studied here. Epicatechin has only four hydroxyl groups, whereas epicatechin with a gallic acid attached (epicatechin gallate) has eight. In fact, both the stereochemistry and number of hydroxyl groups may influence the activity of phenolic compounds. *p*-Coumaric acid, gallic acid, caffeic acid, catechin, epicatechin, and epicatechin gallate were positively and significantly correlated with both biological model systems (inhibition of copper-induced human LDL-cholesterol oxidation and peroxyl radical-induced DNA strand breakage), whereas some compounds correlated only with the inhibition of peroxyl-induced DNA strand breakage (quercetin and procyanidin dimer B) or inhibition of copper-induced human LDL-cholesterol oxidation (kaempferol hexoside and procyanidin trimer C). Catechin and epicatechin have also been found to protect against *N*-nitrosodibutylamine- and *N*-nitrosopiperidine-induced DNA damage in human hepatoma cells in vitro.[43] Catechin and caffeic acid also prevented human LDL-cholesterol oxidation.[37]

In summary, the present contribution demonstrated the distribution of free, esterified, and insoluble-bound phenolics in juice- and winemaking byproducts. Although further studies are

necessary for confirmation, it is possible to assume that differences in the distribution of soluble free and esterified phenolics (Figure 1) are due to the process (juice- vs winemaking). Insoluble-bound phenolics must be included in all studies due to their major contribution and efficacy in the byproducts tested. Twenty-five phenolic compounds were positively or tentatively identified by HPLC-DAD-ESI-MS$^n$. Gallic and caffeic acids were the major phenolic acids, catechin was the major monomeric flavonoid, and procyanidin dimer B was the major proanthocyanidin. Procyanidin dimer A was found only in the insoluble-bound fraction, which contained the highest concentration of phenolics, reflecting a higher scavenging activity, reducing power, and inhibition of copper-induced human LDL-cholesterol oxidation and peroxyl-induced DNA strand breakage. Catechin and epicatechin gallate showed significant and positive correlations with all antioxidant assays.

## AUTHOR INFORMATION


### Corresponding Author

*(F.S.) E-mail: fshahidi@mun.com.



### Funding

A.C.C. acknowledges CNPq (National Council for Scientific and Technological Development, Brazil) for granting an international Ph.D. internship through the Science without Borders program (Process 242589/2012-0). This research was also supported by the doctoral scholarship granted by FAPESP (São Paulo Research Foundation) to the same author in Brazil (Process 2012/17683-0). F.S. acknowledges partial financial support from the Natural Sciences and Engineering Research Council (NSERC) of Canada in the form of a Discovery Grant.


### Notes

The authors declare no competing financial interest.

## ACKNOWLEDGMENTS


Ouro Verde Farm (Grupo Miolo) and Santa Maria winery are acknowledged for donating Syrah and Tempranillo byproducts, respectively.


## REFERENCES


(1) Cheng, V. J.; Bekhit, A. E. A.; McConnell, M.; Mros, S.; Zhao, J. Effect of extraction solvent, waste fraction and grape variety on the antimicrobial and antioxidant activities of extracts from wine residue from cool climate. *Food Chem.* **2012**, *134* (1), 474−482.

(2) Chandrasekara, A.; Shahidi, F. Antiproliferative potential and DNA scission inhibitory activity of phenolics from whole millet grains. *J. Funct. Foods* **2011**, *3* (3), 159−170.

(3) de Camargo, A.; Vieira, T.; Regitano-D'Arce, M.; Calori-Domingues, M.; Canniatti-Brazaca, S. Gamma radiation effects on peanut skin antioxidants. *Int. J. Mol. Sci.* **2012**, *13* (3), 3073−3084.

(4) Shahidi, F.; Alasalvar, C.; Liyana-Pathirana, C. M. Antioxidant phytochemicals in hazelnut kernel (*Corylus avellana* L.) and hazelnut byproducts. *J. Agric. Food Chem.* **2007**, *55* (4), 1212−1220.

(5) Lee, N.; Jo, C.; Sohn, S.; Kim, J.; Byun, M. Effects of gamma irradiation on the biological activity of green tea byproduct extracts and a comparison with green tea leaf extracts. *J. Food Sci.* **2006**, *71* (4), C269−C274.

(6) Llobera, A.; Canellas, J. Dietary fibre content and antioxidant activity of Manto Negro red grape (*Vitis vinifera*): pomace and stem. *Food Chem.* **2007**, *101* (2), 659−666.

(7) Shirahigue, L.; Plata-Oviedo, M.; de Alencar, S.; d'Arce, M.; Vieira, T.; Oldoni, T.; Contreras-Castillo, C. Wine industry residue as antioxidant in cooked chicken meat. *Int. J. Food Sci. Technol.* **2010**, *45* (5), 863−870.

(8) Jara-Palacios, M. J.; Gonzalez-Manzano, S.; Escudero-Gilete, M. L.; Hernanz, D.; Duenas, M.; Gonzalez-Paramas, A. M.; Heredia, F. J.; Santos-Buelga, C. Study of Zalema grape pomace: phenolic composition and biological effects in *Caenorhabditis elegans*. *J. Agric. Food Chem.* **2013**, *61* (21), 5114−5121.

(9) Evans, M.; Wilson, D.; Guthrie, N. A randomized, double-blind, placebo-controlled, pilot study to evaluate the effect of whole grape extract on antioxidant status and lipid profile. *J. Funct. Foods* **2014**, *7*, 680−691.

(10) Sandhu, A. K.; Gu, L. W. Antioxidant capacity, phenolic content, and profiling of phenolic compounds in the seeds, skin, and pulp of *Vitis rotundifolia* (Muscadine grapes) as determined by HPLC-DAD-ESI-MS*n*. *J. Agric. Food Chem.* **2010**, *58* (8), 4681−4692.

(11) González-Centeno, M. R.; Jourdes, M.; Femenia, A.; Simal, S.; Rosselló, C.; Teissedre, P.-L. Proanthocyanidin composition and antioxidant potential of the stem winemaking byproducts from 10 different grape varieties (*Vitis vinifera* L.). *J. Agric. Food Chem.* **2012**, *60* (48), 11850−11858.

(12) Wettasinghe, M.; Shahidi, F. Scavenging of reactive-oxygen species and DPPH free radicals by extracts of borage and evening primrose meals. *Food Chem.* **2000**, *70* (1), 17−26.

(13) de Camargo, A. C.; Vieira, T. M. F. S.; Regitano-D'Arce, M. A. B.; de Alencar, S. M.; Calori-Domingues, M. A.; Canniatti-Brazaca, S. G. Gamma radiation induced oxidation and tocopherols decrease in in-shell, peeled and blanched peanuts. *Int. J. Mol. Sci.* **2012**, *13* (3), 2827−2845.

(14) Swain, T.; Hillis, W. E. The phenolic constituents of *Prunus domestica*. I. The quantitative analysis of phenolic constituents. *J. Sci. Food Agric.* **1959**, *10* (1), 63−68.

(15) de Camargo, A. C.; Vieira, T. M. F. S.; Regitano-d'Arce, M. A. B.; de Alencar, S. M.; Calori-Domingues, M. A.; Spoto, M. H. F.; Canniatti-Brazaca, S. G. Gamma irradiation of in-shell and blanched peanuts protects against mycotoxic fungi and retains their nutraceutical components during long-term storage. *Int. J. Mol. Sci.* **2012**, *13* (9), 10935−10958.

(16) Price, M. L.; Hagerman, A. E.; Butler, L. G. Tannin content of cowpeas, chickpeas, pigeon peas, and mung beans. *J. Agric. Food Chem.* **1980**, *28* (2), 459−461.

(17) Re, R.; Pellegrini, N.; Proteggente, A.; Pannala, A.; Yang, M.; Rice-Evans, C. Antioxidant activity applying an improved ABTS radical cation decolorization assay. *Free Radical Biol. Med.* **1999**, *26* (9−10), 1231−1237.

(18) Chandrasekara, N.; Shahidi, F. Effect of roasting on phenolic content and antioxidant activities of whole cashew nuts, kernels, and testa. *J. Agric. Food Chem.* **2011**, *59* (9), 5006−5014.

(19) Alasalvar, C.; Karamac, M.; Kosinska, A.; Rybarczyk, A.; Shahidi, F.; Amarowicz, R. Antioxidant activity of hazelnut skin phenolics. *J. Agric. Food Chem.* **2009**, *57* (11), 4645−4650.

(20) Zadernowski, R.; Naczk, M.; Nesterowicz, J. Phenolic acid profiles in some small berries. *J. Agric. Food Chem.* **2005**, *53* (6), 2118−2124.

(21) Lago-Vanzela, E. S.; Rebello, L. P. G.; Ramos, A. M.; Stringheta, P. C.; Da-Silva, R.; García-Romero, E.; Gómez-Alonso, S.; Hermosín-Gutiérrez, I. Chromatic characteristics and color-related phenolic composition of Brazilian young red wines made from the hybrid grape cultivar BRS Violeta ("BRS Rúbea" × "IAC 1398-21"). *Food Res. Int.* **2013**, *54* (1), 33−43.

(22) Hanhineva, K.; Rogachev, I.; Kokko, H.; Mintz-Oron, S.; Venger, I.; Kärenlampi, S.; Aharoni, A. Non-targeted analysis of spatial metabolite composition in strawberry (*Fragaria* × *ananassa*) flowers. *Phytochemistry* **2008**, *69* (13), 2463−2481.

(23) Sarnoski, P. J.; Johnson, J. V.; Reed, K. A.; Tanko, J. M.; O'Keefe, S. F. Separation and characterisation of proanthocyanidins in Virginia type peanut skins by LC-MS*n*. *Food Chem.* **2012**, *131* (3), 927−939.

(24) de Camargo, A. C.; Vidal, C. M. M.; Canniatti-Brazaca, S. G.; Shahidi, F. Fortification of cookies with peanut skin: effects on the composition, polyphenols, antioxidant properties and sensory quality. *J. Agric. Food Chem.* **2014**, *62* (46), 11228−11235.

(25) Saint-Cricq de Gaulejac, N.; Provost, C.; Vivas, N. Comparative study of polyphenol scavenging activities assessed by different methods. *J. Agric. Food Chem.* **1999**, *47* (2), 425−431.
(26) Weidner, S.; Powałka, A.; Karamać, M.; Amarowicz, R. Extracts of phenolic compounds from seeds of three wild grapevines − comparison of their antioxidant activities and the content of phenolic compounds. *Int. J. Mol. Sci.* **2012**, *13* (3), 3444−3457.
(27) Weidner, S.; Rybarczyk, A.; Karamać, M.; Król, A.; Mostek, A.; Grębosz, J.; Amarowicz, R. Differences in the phenolic composition and antioxidant properties between *Vitis coignetiae* and *Vitis vinifera* seeds extracts. *Molecules* **2013**, *18* (3), 3410−3426.
(28) Ćurko, N.; Kovačević Ganić, K.; Gracin, L.; Đapić, M.; Jourdes, M.; Teissedre, P. L. Characterization of seed and skin polyphenolic extracts of two red grape cultivars grown in Croatia and their sensory perception in a wine model medium. *Food Chem.* **2014**, *145*, 15−22.
(29) Vrhovsek, U.; Mattivi, F.; Waterhouse, A. L. Analysis of red wine phenolics: comparison of HPLC and spectrophotometric methods. *Vitis* **2001**, *40* (2), 87−91.
(30) Chandrasekara, A.; Shahidi, F. Determination of antioxidant activity in free and hydrolyzed fractions of millet grains and characterization of their phenolic profiles by HPLC-DAD-ESI-MS*n*. *J. Funct. Foods* **2011**, *3* (3), 144−158.
(31) Flachowsky, H.; Halbwirth, H.; Treutter, D.; Richter, K.; Hanke, M.-V.; Szankowski, I.; Gosch, C.; Stich, K.; Fischer, T. C. Silencing of flavanone-3-hydroxylase in apple (*Malus* × *domestica* Borkh.) leads to accumulation of flavanones, but not to reduced fire blight susceptibility. *Plant Physiol. Biochem.* **2012**, *51*, 18−25.
(32) Owens, D. K.; Crosby, K. C.; Runac, J.; Howard, B. A.; Winkel, B. S. J. Biochemical and genetic characterization of *Arabidopsis* flavanone 3*β*-hydroxylase. *Plant Physiol. Biochem.* **2008**, *46* (10), 833−843.
(33) Xie, D.-Y.; Jackson, L. A.; Cooper, J. D.; Ferreira, D.; Paiva, N. L. Molecular and biochemical analysis of two cDNA clones encoding dihydroflavonol-4-reductase from *Medicago truncatula*. *Plant Physiol.* **2004**, *134* (3), 979−994.
(34) Pfeiffer, J.; Kühnel, C.; Brandt, J.; Duy, D.; Punyasiri, P. A. N.; Forkmann, G.; Fischer, T. C. Biosynthesis of flavan 3-ols by leucoanthocyanidin 4-reductases and anthocyanidin reductases in leaves of grape (*Vitis vinifera* L.), apple (*Malus* × *domestica* Borkh.) and other crops. *Plant Physiol. Biochem.* **2006**, *44* (5−6), 323−334.
(35) Xie, D.-Y.; Sharma, S. B.; Dixon, R. A. Anthocyanidin reductases from *Medicago truncatula* and *Arabidopsis thaliana*. *Arch. Biochem. Biophys.* **2004**, *422* (1), 91−102.
(36) Cerpa-Calderón, F. K.; Kennedy, J. A. Berry integrity and extraction of skin and seed proanthocyanidins during red wine fermentation. *J. Agric. Food Chem.* **2008**, *56* (19), 9006−9014.
(37) Meyer, A. S.; Heinonen, M.; Frankel, E. N. Antioxidant interactions of catechin, cyanidin, caffeic acid, quercetin, and ellagic acid on human LDL oxidation. *Food Chem.* **1998**, *61* (1−2), 71−75.
(38) Wanasundara, U. N.; Shahidi, F. Antioxidant and pro-oxidant activity of green tea extracts in marine oils. *Food Chem.* **1998**, *63* (3), 335−342.
(39) Yilmaz, Y.; Toledo, R. T. Major flavonoids in grape seeds and skins: antioxidant capacity of catechin, epicatechin, and gallic acid. *J. Agric. Food Chem.* **2004**, *52* (2), 255−260.
(40) Paiva-Martins, F.; Gordon, M. H. Effects of pH and ferric ions on the antioxidant activity of olive polyphenols in oil-in-water emulsions. *J. Am. Oil Chem. Soc.* **2002**, *79* (6), 571−576.
(41) Arranz, S.; Silván, J. M.; Saura-Calixto, F. Nonextractable polyphenols, usually ignored, are the major part of dietary polyphenols: a study on the Spanish diet. *Mol. Nutr. Food Res.* **2010**, *54* (11), 1646−1658.
(42) Khan, N.; Monagas, M.; Andres-Lacueva, C.; Casas, R.; Urpi-Sarda, M.; Lamuela-Raventos, R. M.; Estruch, R. Regular consumption of cocoa powder with milk increases HDL cholesterol and reduces oxidized LDL levels in subjects at high-risk of cardiovascular disease. *Nutr. Metab. Cardiovasc. Dis.* **2012**, *22* (12), 1046−1053.
(43) Delgado, M. E.; Haza, A. I.; García, A.; Morales, P. Myricetin, quercetin, (+)-catechin and (−)-epicatechin protect against *N*-nitrosamines-induced DNA damage in human hepatoma cells. *Toxicol. in Vitro* **2009**, *23* (7), 1292−1297.

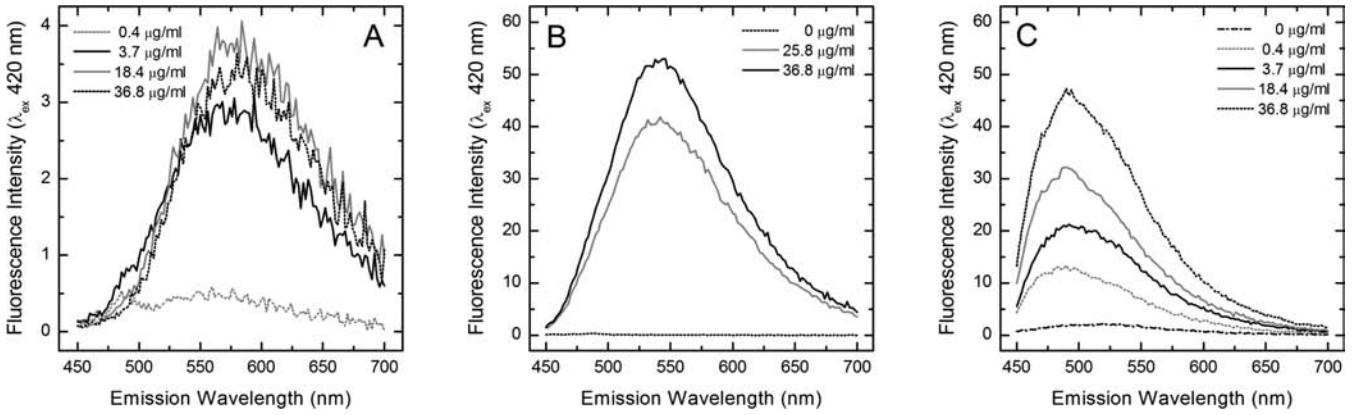


**Figure 1.** Fluorescence spectra of curcuminoids in (A) 2% (v/v) EtOH; (B) a dispersion of $\beta$-glucan (0.28% TS, w/w) in 2% (v/v) EtOH; and (C) a dispersion of oat fiber (1% TS, w/w) in 2% (v/v) EtOH.

dispersions were sonicated in an ultrasonic bath (Unisonic Australia Pty, Brookvale, NSW, Australia) at 20 kHz and 30 °C for 10 min followed by homogenization at 13 500 rpm for 10 min with an Ultra Turax T25 homogenizer (Crown Scientific Pty, Murrarie, QLD, Australia).

**Preparation of Stock Solution and Dispersions for Partitioning and Binding Experiments.** Freshly prepared dispersions (pH 6.8 ± 0.1) of curcuminoids (25.8 $\mu$g/mL) with oat fiber (1% TS, w/w) were used for the partitioning experiments. The curcuminoids were solubilized in 100% EtOH prior to addition to the oat fiber dispersion. The EtOH concentration in the final dispersions was 2% v/v.

To separate the soluble from insoluble fractions of the dispersions, samples were ultracentrifuged (20 400 g, 20 min, 22 °C) to obtain a soluble fraction (supernatant) and an insoluble fraction (precipitate). Each fraction was weighed. The supernatant and precipitate compositions were analyzed separately for total solids, protein, and $\beta$-glucan content. Curcuminoids were also extracted from the supernatant by mixing 5 g of the supernatant with 100% EtOH to obtain an extract in 80% (v/v) EtOH. The dispersion was stirred for 20 min and then centrifuged at 12 100 g at 22 °C for 20 min. A second extraction was carried out, and the supernatants from the first and second extractions were combined and used for fluorescence measurements. For the extraction of curcuminoids in the precipitate, 0.2 g of the precipitated fraction was mixed with 1.6 mL of 80% v/v EtOH. The extraction was repeated twice with 1.6 mL of 80% v/v EtOH. After each extraction, the dispersion was stirred for 45 min and centrifuged at 12 100 g and 22 °C for 20 min, and the supernatant was collected from each extraction and combined for analysis. The concentration of curcuminoids from the extracts was analyzed by fluorescence spectroscopy. The curcuminoid concentration was quantified using a calibration curve of curcuminoids in 80% v/v EtOH at concentrations of 0.4−5.5 $\mu$g/mL. Spiking experiments with a known amount of curcuminoids were also carried out to confirm the recovery of curcuminoids from each fraction. The results showed a recovery of ∼93%.

**Preparation of Curcuminoids−$\beta$-Glucan Dispersion in 2% EtOH.** $\beta$-glucan (84 mg) was dispersed in 29.08 mL of Milli-Q water, and an aliquot of 0.6 mL of the curcuminoid stock solution (1280 $\mu$g/mL) in pure EtOH was added to this dispersion to obtain the final mixtures of curcuminoid (25.8 $\mu$g/mL)−$\beta$-glucan (0.28% TS, w/w) in 2% v/v EtOH. A 0.28% w/w $\beta$-glucan concentration was equivalent to the amount of $\beta$-glucan present in a 1% w/w oat fiber dispersions used to examine the interaction of oat fiber with curcuminoids in this work. The dispersions were sonicated, homogenized, and centrifuged as previously described. The pH value of the mixtures was 7.0. The amount of curcuminoids in the supernatant was analyzed by fluorescence measurements after extraction.

**Fluorescence Measurements.** The fluorescence spectra of curcuminoids, oat fiber dispersion (1% TS w/w), curcuminoid−oat fiber dispersions (1% TS, w/w), and curcuminoid−$\beta$-glucan dispersions (0.28% TS, w/w), all in aqueous EtOH (2% v/v), were measured using a spectrofluorometer (Varioskan Flash microplate reader, Thermo Fisher Scientific Inc., Waltham, MA, USA). Samples (350 $\mu$L) were loaded into a 96-well microplate (OptiPlate-96, PerkinElmer, Santa Clara, CA, USA). The fluorescence emission spectra were recorded from 450−700 nm at a fixed excitation wavelength ($\lambda_{ex}$) of 420 nm.[11,12]

To probe the quenching of the intrinsic fluorescence of proteins in oat fiber dispersions, emission spectra were recorded from 315−600 nm at an excitation wavelength ($\lambda_{ex}$) of 280 nm.[20]

**X-ray Diffraction.** The powdered curcumin (1 g) and the precipitate (1.36 g) obtained after centrifugation of the curcuminoid (25.8 $\mu$g/mL)−oat fiber (1% TS, w/w) dispersions in aqueous EtOH (2% v/v) were analyzed by an X-ray (D8 Advance) diffractometer (Bruker AXS Inc., Madison, WI, USA) with Cu K$\alpha$ radiation. The machine was equipped with backgroundless sample holders. The X-ray diffraction (XRD) scanning was performed at a rate of 0.02 degrees step size and 5 s per step with the scanned angle set from $10° \leq 2\theta \geq 70$. Measurements were performed at a voltage of 40 kV and 30 mA.

**Storage Stability of Curcuminoids.** The storage stability of curcuminoids in the curcuminoids (25.8 $\mu$g/mL)−oat fiber (1% TS, w/w) dispersions in 2% (v/v) EtOH and the supernatant fraction obtained upon centrifugation at 20 400 g (Beckman J2-MC, Ramsey, MN, USA) for 20 min at 22 °C was determined. The curcuminoids content in the precipitated fraction was obtained by difference. Sodium azide was added to all samples (0.02% w/w) to prevent microbial spoilage. Samples (5 g) were placed in glass vials and were stored at 25 °C for 11 days. Samples were taken at intervals for the analysis of curcuminoids. Curcuminoids were extracted using EtOH, and the curcuminoid concentration was estimated using fluorescence spectroscopy as previously outlined.

## RESULTS AND DISCUSSION

**Fluorescence Measurements.** *Fluorescence of Curcuminoids in 2% v/v EtOH.* The florescence intensity of curcuminoid (0−36.8 $\mu$g/mL) in 2% (v/v) EtOH is shown in Figure 1A. The maximum emission wavelength was at 566 nm. The fluorescence intensity of samples containing 3.7, 18.4, and 36.8 $\mu$g/mL were 2.7, 4.0, and 3.6, respectively. One factor that may contribute to the nonlinear increase in fluorescence intensity with increased curcuminoids concentrations from 3.7−18.4 $\mu$g/mL is the supersaturation of curcumin at high concentrations. In addition, with increasing curcuminoid concentration in 2% v/v EtOH, there is likely to be self-quenching of curcuminoids. Self-quenching is particularly prevalent at higher concentrations. Self-quenching of polyphenols compounds has been previously observed.[21]

*Fluorescence of Curcuminoids in the Presence of Pure $\beta$-Glucan in 2% v/v EtOH.* The fluorescence spectra of

curcuminoids in the presence of pure $\beta$-glucan (0.28% TS, w/w) are shown in Figure 1B. There was a blue shift in the position of the maxima when curcuminoids were dispersed in the presence of $\beta$-glucan in 2% v/v EtOH (542 nm) compared to curcuminoids in 2% v/v EtOH alone (566 nm). At an equivalent concentration of added curcuminoid (36.8 $\mu$g/mL), the fluorescent intensity of the curcuminoid−$\beta$-glucan dispersions in 2% v/v EtOH was greater than that in 2% v/v EtOH alone (Figure 1A,B). These observations may be interpreted as an increased solubility of curcuminoids due to binding to the $\beta$-glucan, possibly due to hydrogen bonding and complexation of the phenolic groups of curcumin to $\beta$-glucan.[22]

*Fluorescence of Curcuminoids in the Presence of Oat Fiber in 2% v/v EtOH.* In curcuminoids−oat fiber (1% TS, w/w) dispersions containing 2% v/v EtOH, a blue shift in the wavelength of maximum emission was observed from about 566 nm for curcuminoids in 2% v/v EtOH (Figure 1A) to about 490 nm in oat fiber dispersions with 2% EtOH (Figure 1C). This blue shift in the emission wavelength is consistent with a transfer of the curcuminoids into a less polar microenvironment. At corresponding levels of added curcuminoids (36.8 $\mu$g/mL), the fluorescence intensity of the curcuminoids in the presence of oat fiber in 2% v/v EtOH was approximately 47, whereas it was only approximately 3.6 in 2% v/v EtOH (Figure 1a,c). Blue shifts in the emission spectra of curcuminoids have been observed in mixtures containing casein micelles,[11] hydrophobically modified starch,[14] $\beta$-casein,[23] and $\beta$-lactoglobulin,[24] and for liposomal curcumin preparations,[25] and are consistent with the transfer of curcuminoids into a less polar environment. It was not possible to ascribe the relative binding affinities of the various curcuminoids to components of the oat fiber from the fluorescence spectra obtained in this study.

*Fluorescence of Proteins in Curcuminoids−Oat Fiber Mixtures.* The quenching of the intrinsic fluorescence of proteins within the curcuminoids−oat fiber mixture and the blue shift in the wavelength of maximum emission (Figure 2) are evidence of binding of the curcuminoids to protein. An increase in the curcuminoid concentration from 0−44.2 $\mu$g/mL resulted in a progressive increase in quenching, but there was no further increase when the concentration was raised to 55.3 $\mu$g/mL (Figure 2). Quenching has been observed for binding of curcuminoids to various types of proteins including milk proteins,[12] soy protein,[13] and plasma proteins.[26]

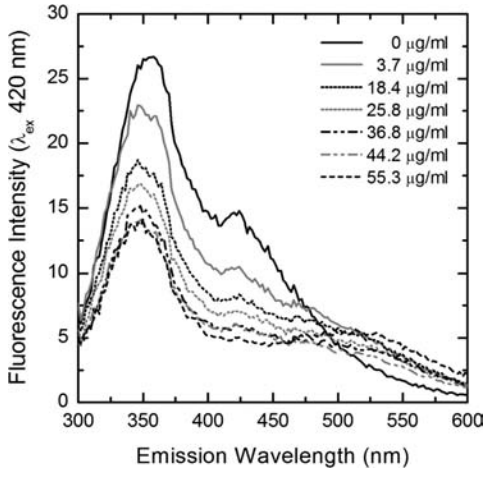


**Figure 2.** Protein fluorescence spectra of curcuminoid−oat fiber (1% TS, w/w) dispersions in 2% (v/v) EtOH at $\lambda_{ex}$ = 280 nm.

**Partitioning of Oat Fiber Components and Curcuminoids between Soluble and Insoluble Fractions upon Centrifugation.** *Partitioning of Oat Fiber Components.* The partitioning of oat fiber components and curcuminoids in the supernatant and precipitated fractions of curcuminoid−oat fiber dispersions was examined to estimate the distribution of curcuminoids in the soluble and insoluble fraction. For these experiments, we used 25.8 $\mu$g/mL curcuminoids in a 1% TS (w/w) oat fiber dispersion in 2% v/v EtOH.

Upon centrifugation of the oat fiber dispersion (1% TS, w/w) in 2% v/v EtOH, a supernatant (soluble) fraction (95.3% w/w, 0.28% TS) and a precipitated (4.7% w/w, 0.73% TS) fraction were obtained (Table 1). Of the total protein in the oat fiber dispersion, 38% partitioned into the supernatant, while 62% partitioned into the precipitate. Most of the $\beta$-glucan (61% of the total $\beta$-glucan) partitioned into the supernatant, with 39% found in the precipitated fraction (Table 1). Both soluble and insoluble proteins and $\beta$-glucans present in unprocessed oats are expected to be present in the oat fiber ingredient used in our experiments. The solubility of the proteins and $\beta$-glucan components and their distribution between the soluble and insoluble phases will depend on the isolation methods used to extract and process the oat fiber ingredient. Oat proteins comprise globulins, albumins, prolamins, and glutenins, and of these, the albumins are the most water-soluble proteins.[27] The insoluble $\beta$-glucans have lower molecular mass than the soluble $\beta$-glucan but remain in the insoluble fiber fraction because of entanglement with arabinoxylan.[28]

*Partitioning of Curcuminoids.* The curcuminoids were approximately equally partitioned between the supernatant and precipitated fractions obtained upon centrifugation of the curcuminoid (25.8 $\mu$g/mL)−oat fiber (1% TS, w/w) dispersion (pH 6.8 ± 0.1) in aqueous 2% v/v EtOH. The supernatant contained 38.6 ± 2.7%, and the precipitated fraction contained 41.1 ± 2.15% of the total added curcuminoids. Thus, the total amount recovered from both the supernatant and precipitated fractions accounted for approximately 79.7% of the total curcuminoids originally added (Table 1). Analysis of the washings from the preparation apparatus (i.e., sample container and the probe used for homogenization) recovered an additional 13.4 ± 0.7% of the total added curcuminoids, which amounts to a total curcuminoids recovery of 93.1%.

**Solubility of Curcuminoids.** *Solubility in 2% v/v EtOH.* Measurement of the supernatant fractions obtained upon centrifugation of 25.8 $\mu$g/mL curcuminoids dispersed in 2% v/v EtOH without oat fiber showed that the highest concentration of curcuminoids in the supernatant was 4.1 $\mu$g/mL. This result showed that the solubility of curcuminoids in aqueous EtOH (2% v/v) exceeds that of the reported solubility of curcumin in aqueous media (11 ng/mL, pH 5).[29]

*Solubility in the Presence of Oat Fiber (1% TS, w/w) in 2% v/v EtOH.* The solubility of the curcuminoids in the oat fiber dispersion was taken as the concentration of curcuminoids in the supernatant. An increase in the concentration of curcuminoids in the oat fiber dispersion from 0 to ∼220 $\mu$g/mL resulted in an increased amount of curcuminoids in the supernatant after centrifugation (Figure 3). However, an increase in the amount of curcuminoids in the dispersion beyond 220 $\mu$g/mL did not result in a further increase of curcuminoids in the supernatant, which indicates a saturation of the sites in the soluble components (i.e., soluble protein and $\beta$-

**Table 1. Composition of Fractions Obtained upon Ultracentrifugation (20 400 g, 20 min, 22 °C) of Curcuminoid (25.8 μg/mL)−Oat Fiber 1% (w/w) Dispersion in 2% EtOH[a]**

| component | supernatant | precipitate | total (supernatant + precipitate) |
|---|---|---|---|
| wt fraction (g) | 95.25 ± 0.13 | 4.74 ± 0.15 | 99.99 |
| total solid (g/100 g dispersion) | 0.28 ± 0.03 | 0.73 ± 0.03 | 1.01 |
| protein (g/100g) | 0.11 ± 0.02 | 0.18 ± 0.01 | 0.29 |
| β-glucan (g/100g) | 0.17 ± 0.01 | 0.11 ± 0.02 | 0.28 |
| curcuminoids (%) | 38.63 ± 2.7 | 41.10 ± 2.15 | 79.7[b] |

[a]Data are the mean of three determinations ± standard deviation. [b]An additional 13.4 ± 0.7% of curcuminoids added was recovered from the washings from the beaker and the probe used for homogenization.

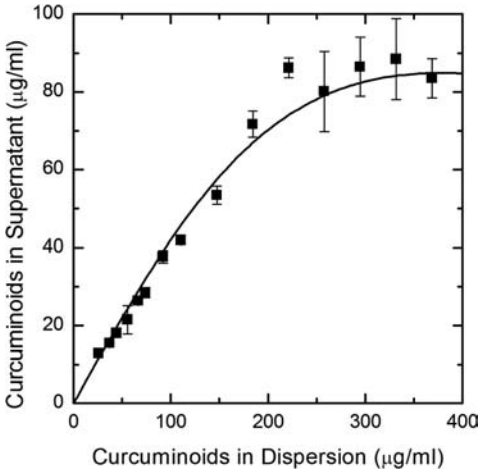


**Figure 3.** Concentration of curcuminoids in supernatant of 1% (w/w) oat fiber dispersion in 2% (v/v) EtOH as a function of total added curcuminoids in initial dispersion.

glucan components) of oat fiber. The highest amount of curcuminoids extracted from the supernatant corresponded to a concentration of ∼88 μg/mL (Figure 3). The solubility of curcuminoids in the soluble supernatant component of the oat fiber dispersion (in 2% v/v EtOH) increased by a factor of 21 over that in 2% v/v EtOH (4.1 μg/mL; this work) without oat fiber. This concentration of curcuminoids in the supernatant is also much higher than that of the reported solubility of curcumin in aqueous media (11 ng/mL, pH 5).[29] This result clearly demonstrated the ability of the soluble oat fiber components to carry curcuminoids in an aqueous system. The combined effects of hydrophobic interactions and hydrogen bonding that govern these reported interactions are likely responsible for the interactions with oat fiber and increased solubility observed.

The increase in curcuminoid solubility in the presence of biopolymers and synthetic polymers has been reported. For example, the addition of curcumin to soy protein (5% (w/v) in water) increased the curcumin solubility by 812-fold because of the formation of a complex, driven by hydrophobic interactions.[13] Micelles of hydrophobically modified starch have also been used to encapsulate curcumin, which resulted in a 1670-fold increase in curcumin solubility.[14] It was suggested that this increase in curcumin solubility was due to the combined effects of the transfer of curcumin into a more hydrophobic environment and hydrogen bonding between curcumin and the starch. Synthesized chemical polymers, including hydroxypropylated derivatives of β (HP-β-CD) and γ (HP-γ-CD) cyclodextrin (CD), also increased the solubility of curcumin to about 1700- and 4700-fold, respectively.[30] The

**Table 2. Comparison of Major Reflections Observed in the XRD Spectra of Curcumin Crystals and Encapsulated Curcumin Preparations from Various Studies[a]**

| this study | | Pan et al.[32] | | Zi et al.[33] | | Patel et al.[34] | | Mohan et al.[35] | |
|---|---|---|---|---|---|---|---|---|---|
| 2θ (deg) | intensity | 2θ (deg) | intensity | 2θ (deg) | intensity | 2θ (deg) | intensity | 2θ (deg) | intensity |
| 7.9 | 94 | ∼7 | ∼490 | - | - | - | - | - | - |
| 8.9 | 191 | ∼8−9 | ∼1500 | 8.84 | ∼12500 | 8.90 | ∼500 | - | - |
| 12.2 | 127 | ∼12−13 | ∼1350 | 12.10 | ∼2500 | 12.26 | ∼350 | 12 | - |
| 14.5 | 139 | ∼15 | ∼2000 | 14.39 | ∼3000 | 14.54 | ∼490 | 14.3 | - |
| 15.1 | 93 | - | - | - | - | - | - | - | - |
| 15.8 | 92 | - | - | - | - | - | - | - | - |
| 16.3 | 80 | ∼16 | ∼1300 | - | - | - | - | - | - |
| 17.3 | 197 | ∼17−18 | ∼4200 | 17.20 | ∼13000 | 17.24 | ∼1100 | 17.1 | - |
| 18.2 | 148 | ∼18 | ∼3000 | - | - | - | - | 18.2 | - |
| 19.5 | 107 | ∼19 | ∼1600 | - | - | - | - | 18.6 | - |
| 21.2 | 108 | ∼21 | ∼2250 | - | - | - | - | 21 | - |
| 23.4 | 138 | ∼23 | ∼3600 | 23.30 | ∼2800 | 23.33 | ∼600 | 23 | - |
| 24.6 | 153 | ∼25 | ∼3400 | 24.50 | ∼2200 | 24.60 | ∼800 | 24.4 | - |
| 25.6 | 152 | ∼26 | ∼4100 | 25.52 | ∼2000 | 25.52 | ∼790 | 25.5 | - |
| 26.1 | 120 | - | - | - | - | - | - | - | - |
| 26.8 | 107 | - | - | - | - | - | - | - | - |
| 27.4 | 131 | ∼27 | ∼3300 | - | - | - | - | 27.2 | - |
| 29.0 | 110 | ∼28 | ∼2800 | 28.87 | ∼1500 | - | - | - | - |

[a]Note: "−" in the table refers to peaks that were not detected or reported.

solubilization of curcumin with various materials appears to be related to the binding of curcumin to hydrophobic regions of molecules. Compared to hydrophobically modified starch and soy protein, oat fiber is less hydrophobic in nature. CDs have a hydrophobic cavity and form inclusion complexes with curcumin.[29] The reduced availability and affinity of hydrophobic sites in oat fiber for curcumin compared to hydrophobically modified starch, soy protein, and CDs possibly explains the lower ability of curcumin to bind to oat fiber and hence its reduced ability to solubilize curcumin.

**Crystallinity of Curcuminoids by X-ray Diffraction.** Wide-angle XRD studies on the precipitated fraction obtained upon centrifugation of the curcuminoid (25.8 $\mu$g/mL)−oat fiber (1% w/w TS) dispersion in aqueous EtOH (2% v/v) were carried out to investigate if crystalline curcuminoid was entrapped in the precipitated fraction.

A powder dispersion of curcuminoid has characteristic peaks between 7 and 30 degrees, which suggest that the powder contains crystalline components (Table 2). The major reflection at ∼17 degrees and relative intensities of reflections are largely consistent with previous reports of curcuminoids in a crystalline form (Table 2). The differences observed are possibly due to the different preparations of curcuminoids used in the various studies.

The XRD spectrum of the precipitate obtained upon centrifugation of the curcuminoids−oat fiber dispersion has an absence of sharp peaks (Figure 4), which suggests that

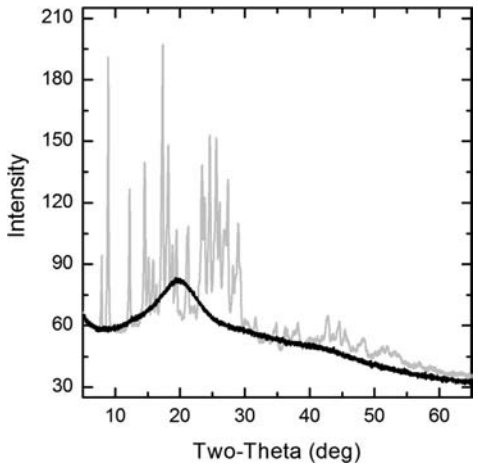


**Figure 4.** XRD spectra of curcuminoids present in the precipitate obtained upon centrifugation of a curcuminoid (25.8 $\mu$g/mL)−oat fiber (1% TS, w/w) dispersion (black) and spectra of the original curcuminoid powder (gray).

curcuminoids in the precipitate were less crystalline in character than the original curcuminoids powder. The broad reflection observed in the precipitated fraction of the curcuminoids−oat fiber dispersions at ∼19 degrees is a typical pattern of a more amorphous substance. The results suggest that the curcumin is in the form of an amorphous solid dispersion. Others have shown that amorphous solid dispersions are formed in a range of cellulose derivative matrices.[31] The curcuminoids in an amorphous form are desirable from a delivery viewpoint as it improves bioavailability.[31]

The position of the reflection ($2\theta$ value) observed for curcuminoids in the presence of oat fiber was at 19.4 deg. The corresponding values for curcumin/curcuminoids encapsulated with various materials were 11−12 and 10−20 deg with sodium caseinate,[32] 19 and 23 deg with soy protein,[33] 8 and 19 deg with zein,[34] and 16 and 22 deg with CD,[35] which show similar trends for the XRD spectrum of encapsulated curcuminoid in different encapsulant materials.

*Storage Stability.* Figure 5 shows the stability of curcuminoids in the presence of the whole curcuminoids−oat

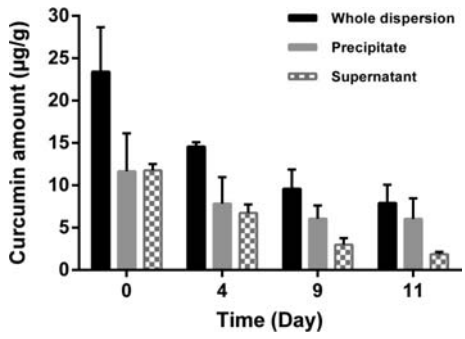


**Figure 5.** Amount of curcuminoids remaining during storage at 25 °C in the dispersion of curcuminoids−oat fiber (1% TS, w/w) and in the supernatant and precipitated fractions obtained upon centrifugation. Values are expressed as the content per g of the original dispersion.

fiber dispersion in 2% (v/v) EtOH and the supernatant and precipitated fractions of this dispersion during 11 days of storage at 25 °C. The concentration of curcuminoids decreased from 23.42 to 8.27 $\mu$g/mL in the whole oat fiber dispersion after 11 days. The degradation of the curcuminoids in the supernatant was faster than that in the precipitate (Figure 5). It is suggested that the difference between the stability of curcuminoid in the precipitate and supernatant is due to the insoluble curcuminoids in the amorphous state in precipitate. Others have shown that curcumin is stabilized against degradation when it is in the amorphous state.[31]

In conclusion, this study showed that both protein and $\beta$-glucan components of oat fiber are able to interact with curcuminoids and increase solubility in an aqueous solution of 2% v/v EtOH. It is possible that curcuminoids also interact with proteins and dietary fibers in the precipitated fraction. These findings illustrate the potential for the curcuminoid carrying capacity of oat fiber to be capitalized upon in the fortification of food with curcuminoids.

## AUTHOR INFORMATION

### Corresponding Author

*E-mail: maryann.augustin@csiro.au. Phone: +63 3 9731 3486.

### Funding

S.S. has an International Postgraduate Research Scholarship and an Australian postgraduate award from the Australian federal government. S.G. is supported by the ARC Dairy Innovation Hub and the Particulate Fluids Processing Centre at The University of Melbourne.

### Notes

The authors declare no competing financial interest.

## ACKNOWLEDGMENTS

The authors thank Laura Elizabeth Gordon for the assistance in the XRD data collection.

## REFERENCES

(1) Arts, I. C. W.; Hollman, P. C. H. Polyphenols and disease risk in epidemiologic studies. *Am. J. Clin. Nutr.* **2005**, *81*, 317−325.

(2) Yang, C. S.; Landau, J. M.; Huang, M. T.; Newmark, H. L. Inhibition of carcinogenesis by dietary polyphenolic compounds. *Annu. Rev. Nutr.* **2001**, *21*, 381−406.
(3) Landete, J. M. Updated knowledge about polyphenols: Functions, bioavailability, metabolism, and health. *Crit. Rev. Food Sci. Nutr.* **2012**, *52*, 936−948.
(4) Pandey, K. B.; Rizvi, S. I. Plant polyphenols as dietary antioxidants in human health and disease. *Oxid. Med. Cell. Longevity* **2009**, *2*, 270−278.
(5) Visioli, F.; Lastra, C. A. D. L.; Andres-Lacueva, C.; Aviram, M.; Calhau, C.; Cassano, A.; D'Archivio, M.; Faria, A.; Favé, G.; Fogliano, V.; Llorach, R.; Vitaglione, P.; Zoratti, M.; Edeas, M. Polyphenols and human health: A prospectus. *Crit. Rev. Food Sci. Nutr.* **2011**, *51*, 524−546.
(6) Munin, A.; Levy, F. E. Encapsulation of natural polyphenolic compounds: A review. *Pharmaceutics* **2011**, *3*, 793−829.
(7) Fang, Z.; Bhandari, B. Encapsulation of polyphenols—A review. *Trends Food Sci. Technol.* **2010**, *21*, 510−523.
(8) Aggarwal, B. B.; Kumar, A.; Bharti, A. C. Anticancer potential of curcumin: Preclinical and clinical studies. *Anticancer Res.* **2003**, *23*, 363−398.
(9) Beevers, C. S.; Huang, S. Pharmacological and clinical properties of curcumin. *Botanics: Targets and Therapy* **2011**, *1*, 5−18.
(10) Anand, P.; Kunnumakkara, A. B.; Newman, R. A.; Aggarwal, B. B. Bioavailability of curcumin: Problems and promises. *Mol. Pharmaceutics* **2007**, *46*, 807−818.
(11) Sahu, A.; Kasoju, N.; Bora, U. Fluorescence study of the curcumin−casein micelle complexation and its application as a drug nanocarrier to cancer cells. *Biomacromolecules* **2008**, *9*, 2905−2912.
(12) Rahimi Yazdi, S.; Corredig, M. Heating of milk alters the binding of curcumin to casein micelles. A fluorescence spectroscopy study. *Food Chem.* **2012**, *132*, 1143−1149.
(13) Tapal, A.; Tiku, P. K. Complexation of curcumin with soy protein isolate and its implications on solubility and stability of curcumin. *Food Chem.* **2012**, *130*, 960−965.
(14) Yu, H.; Huang, Q. Enhanced in vitro anticancer activity of curcumin encapsulated in hydrophobically modified starch. *Food Chem.* **2010**, *119*, 669−674.
(15) Im, K.; Ravi, A.; Kumar, D.; Kuttan, R.; Maliakel, B. An enhanced bioavailable formulation of curcumin using fenugreek-derived soluble dietary fibre. *J. Funct. Foods* **2012**, *4*, 348−357.
(16) Fu, S.; Shen, Z.; Ajlouni, S.; Ng, K.; Sanguansri, L.; Augustin, M. A. Interactions of buttermilk with curcuminoids. *Food Chem.* **2014**, *149*, 47−53.
(17) AOAC official method 995.16, *β*-D-glucan in oats. *AACC−AOAC Methods. Official Method 32.2.10*; AOAC International: Gaithersburg, MD, 2005.
(18) General methods and principles - Determination of fat, gravimetric method. *Australian Standard Method AS 2300.1.3*; Standards Australia: Sydney, Australia, 2008.
(19) International official methods of analysis. Solids (Total) in Milk By Direct Forced Air Oven Drying. *AACC−AOAC Methods. Official Method 990.20*; AOAC International: Gaithersburg, MD, 1993.
(20) Lakowicz, J. R. Introduction to fluorescence. In *Principles of Fluorescence Spectroscopy*, 3rd ed.; Lakowicz, J. R., Ed.; Springer: New York, 2006; p 12.
(21) Liang, L.; Tajmir-Riahi, H. A.; Subirade, M. Interaction ofbeta-lactoglobulin with resveratrol and its biological implications. *Biomacromolecules* **2008**, *9*, 50−56.
(22) Wu, Z.; Ming, J.; Gao, R.; Wang, Y.; Liang, Q.; Yu, H.; Zhao, G. Characterization and antioxidant activity of the complex of tea polyphenols and oat *β*-glucan. *J. Agric. Food Chem.* **2011**, *59*, 10737−10746.
(23) Esmaili, M.; Ghaffari, S. M.; Moosavi-Movahedi, Z.; Atri, M. S.; Sharifizadeh, A.; Farhadi, M.; Yousefi, R.; Chobert, J.-M.; Haertlé, T.; Moosavi-Movahedi, A. A. Beta casein-micelle as a nanovehicle for solubility enhancement of curcumin; food industry application. *LWT—Food Sci. Technol.* **2011**, *44*, 2166−2172.
(24) Sneharani, A. H.; Karakkat, J. V.; Singh, S. A. Interaction of curcumin with *β*-lactoglobulin—Stability, spectroscopic analysis, and molecular modeling of the complex. *J. Agric. Food Chem.* **2010**, *58*, 11130−11139.
(25) Niu, Y.; Wang, X.; Chai, S.; Chen, Z.; An, X.; Shen, W. Effects of curcumin concentration and temperature on the spectroscopic properties of liposomal curcumin. *J. Agric. Food Chem.* **2012**, *60*, 1865−1870.
(26) Leung, M. H. M.; Kee, T. W. Effective stabilization of curcumin by association to plasma proteins: Human serum albumin and fibrinogen. *Langmuir* **2009**, *25*, 5773−5777.
(27) Ma, C. Y.; Harwalkar, V. R. Chemical characterization and functionality assessment of oat protein fractions. *J. Agric. Food Chem.* **1984**, *32*, 144−149.
(28) Johansson, L.; Tuomainen, P.; Ylinen, M.; Ekholm, P.; Virkki, L. Structural analysis of water-soluble and -insoluble *β*-glucans of whole-grain oats and barley. *Carbohydr. Polym.* **2004**, *58*, 267−274.
(29) Tønnesen, H. H.; Másson, M.; Loftsson, T. Studies of curcumin and curcuminoids. XXVII. Cyclodextrin complexation: Solubility, chemical, and photochemical stability. *Int. J. Pharm.* **2002**, *244*, 127−135.
(30) Baglole, K. N.; Boland, P.; Wagner, B. D. Fluorescence enhancement of curcumin upon inclusion into parent and modified cyclodextrins. *J. Photochem. Photobiol., A* **2005**, *173*, 230−237.
(31) Li, B.; Konecke, S.; Weigel, L. A.; Taylor, L. S.; Edgar, K. J. Both solubility and chemical stability of curucmin are enhanced by solid disperion in cellulose derivative matrices. *Carbohdyr. Polym.* **2013**, *98*, 1108−1116.
(32) Pan, K.; Zhong, Q.; Baek, S. J. Enhanced dispersibility and bioactivity of curcumin by encapsulation in casein nanocapsules. *J. Agric. Food Chem.* **2013**, *61*, 6036−6043.
(33) Zi, T.; Yangchao, L.; Wang, Q. Nanoparticles synthesized from soy protein: Preparation, characterization, and application for nutraceutical encapsulation. *J. Agric. Food Chem.* **2012**, *60*, 2712−2720.
(34) Patel, A.; Hu, Y.; Tiwari, J. K.; Velikov, K. P. Synthesis and characterisation of zein−curcumin colloidal particles. *Soft Matter* **2010**, *6*, 6192−6199.
(35) Mohan, P. R. K.; Sreelakshmi, G.; Muraleedharan, C. V.; Joseph, R. Water-soluble complexes of curcumin with cyclodextrins: Characterization by FT−Raman spectroscopy. *Vib. Spectrosc.* **2012**, *62*, 77−84.

Moreover, the egg of SST has been deemed a valuable aquaculture product, and large-scale farming of SST is common in Taiwan due to its high export revenues. Recently, a few reports demonstrated the antihypertensive effect of enzymatic hydrolysate derived from SST;[10,11] however, the active components have not been well characterized.

In our previous study, we isolated a potent ACE-inhibitory (ACEI) peptide generated from a thermolysin digest of soft-shelled turtle egg white (SSTEW), identified as IVRDPNGMGAW (IW-11), which belongs to the protein lysozyme C.[8] According to the simulated gastrointestinal digestion in that study, IW-11 was partly hydrolyzed (approximately 30% of the initial IW-11 was hydrolyzed in 3 h) by trypsin. Interestingly, ACEI activity of the peptide mixture (IW-11 and its hydrolyzed products) increased, and its $IC_{50}$ value improved from 4.39 ± 0.31 $\mu$M (pure form of IW-11) to 2.42 ± 0.09 $\mu$M, which implied that one of the hydrolyzed products shows better ACEI activity than IW-11. IW-11 is expected to be further cut by trypsin to give IVR and DPNGMGAW, and IVR is postulated as the more efficient ACEI component. Because of its excellent ACEI activity and easy digestibility, the aim of this study was to isolate and characterize the ACEI peptide generated by gastrointestinal enzyme hydrolysis of the previously identified IW-11 and also prove its ACEI activity and antihypertensive effect. It is believed that peptides with two and three amino acid residue lengths could be absorbed directly from the digestive tract into the blood circulatory system.[12] In this study, the release of ACE inhibitory peptide from IW-11 and SSTEW by trypsin was demonstrated. The potent ACE-inhibitory tripeptide was subjected to in vivo study on spontaneously hypertensive rats (SHRs), and its binding mechanism was determined through molecular docking simulations. The results of this study may provide valuable information for determining the potential application of SSTEW as a component of antihypertensive functional foods.

## MATERIALS AND METHODS

**Materials and Chemical Reagents.** Unfertilized soft-shelled turtle eggs were obtained from a local farm, Pingtung City, Pingtung County. Chemicals such as acetonitrile (ACN), ammonium bicarbonate (ABC), boric acid, formic acid (FA), sodium chloride (NaCl), and sodium hydroxide (NaOH) were obtained from J. T. Baker (Phillipsburg, NJ); hippuric acid (HA), hippuryl-L-histidyl-L-leucine (HLL), and trifluoroacetic acid (TFA) were purchased from Sigma Chemical Co. (St. Louis, MO). Enzymes such as ACE from rabbit lungs, trypsin (from bovine pancreas), and thermolysin (from *Bacillus thermoproteolyticus rokko*) were purchased from Sigma Chemical Co. All synthetic peptides (IVRDPNGMGAW, DPNGMGAW, and IVR) used in this study were obtained from MDBio, Inc. (Taipei, Taiwan). Water used in this study was produced from a Milli-Q water purification system (Millipore, Billerica, MA). Ultrafiltration membranes (3 kDa molecular weight cutoff (MWCO)) were purchased from Millipore (Bedford, MA). All other chemicals used in this study were of analytical grade.

**One-Stage and Two-Stage Enzymatic Hydrolysis of SSTEW.** For the one-stage strategy, the lyophilized SSTEW was dispersed in ammonium bicarbonate buffer (ABC; 50 mM, pH 8.5) and digested using trypsin with an enzyme to substrate ratio of 1:100. After 24 h of incubation, the tryptic digest was ultracentrifuged using the 3 kDa MWCO membrane; then the resulting filtrate was lyophilized and kept at −20 °C prior to identification and quantification. For the two-stage approach, the first-stage hydrolysis was performed using thermolysin under an optimized condition as previously described by Rawendra et al.[8] Briefly, lyophilized SSTEW was dispersed in 50 mM ABC (pH 8.5) to obtain a 10% (w/v) protein slurry. The SSTEW was digested using thermolysin with an enzyme to substrate ratio of 1:200 at a constant temperature of 60 °C for 3 h. The resulting digest was centrifuged using the 3 kDa MWCO ultrafiltration membrane (14000*g*, 10 min, 4 °C) to give IW-11 as the major product in the filtrate. However, to avoid any loss of the desired peptide, in this study, the crude thermolysin digest was directly subjected to second-stage digestion using trypsin without 3 kDa MWCO ultrafiltration. The trypsin digestion was performed using an enzyme to substrate ratio of 1:50 at a constant temperature of 37 °C for 24 h. The enzyme was inactivated by adding 5% formic acid; then the mixture was lyophilized prior to identification and ACE assay.

**Isolation and Quantification of ACE-Inhibitory Tripeptide IVR.** A freeze-dried trypsin digest of IW-11 dissolved in 5% ACN and 0.2% TFA in deionized water (v/v) was purified using a HYPERSEP Retain-PEP SPE column containing $C_{18}$ resin (Thermo Scientific, United States). After the column was washed with 0.1% TFA (1 mL), the tripeptide IVR was eluted out using 1 mL of 10% ACN in 0.1% TFA. The eluate was collected and freeze-dried to give purified IVR. The abundance of IVR generated from one-stage or two-stage digestion of SSTEW was determined using LC−MS/MS in the selected reaction monitoring (SRM) mode. Standard IVR solutions for the establishment of calibration curves were prepared at concentrations of 0.1, 0.25, 0.5, 1, 5, 10, and 25 ng/$\mu$L. The standard with known concentration was injected into an ODS Hypersil column (Thermo Scientific, 150 mm length, 2.1 mm i.d., 5 $\mu$m particle size) and separated at a flow rate of 350 $\mu$L/min using a mobile phase of 5% acetonitrile containing 0.1% formic acid (solvent A) and 95% acetonitrile containing 0.1% formic acid (solvent B), with a gradient of 0−30% solvent B over 10 min, kept in 30% solvent B from 10 to 15 min, increased to 80% solvent B from 15 to 16 min, kept in 80% solvent B from 16 to 26 min, and then decreased back and equilibrated in 100% solvent A. The MS/MS analysis was performed using an HESI-II ion source and analyzed by a TSQ triple-quadrupole mass analyzer (Quantum Access MAX, Thermo Scientific) in multiple reaction monitoring (MRM) mode. The HESI-II source conditions in the positive ionization mode were as follows: spray voltage, 3.5 kV; tube lens offset, 127 V; skimmer offset, 0 V; capillary temperature, 320 °C; sheath gas pressure (arb), 40; auxiliary gas pressure (arb), 5. The SRM transition for IVR was set as $m/z$ 387.4 > $m/z$ 175.1 under the optimized collision-induced dissociation (CID) energy of 30 V. The hydrolysate was subjected to LC−MS/MS analysis using the same parameters as for the IVR standard. The concentration for IVR was determined on the basis of its calibration curve. Experiments were done in triplicate, and data are expressed as the mean ± standard error (SE).

**Identification of ACE-Inhibitory Tripeptide IVR Using LC−MS/MS.** The peptide identification was carried out according to our previous report.[8] Briefly, freeze-dried peptides dissolved in 5% ACN and 0.1% FA were loaded onto a BioBasic $C_{18}$ column (150 × 2.1 mm, particle size 5 $\mu$m). The peptide mixture was separated using a gradient going from 5% to 70% ACN in 0.1% FA over 90 min at a flow rate of 200 $\mu$L/min. The separated peptides were analyzed online using a mass spectrometer (Thermo LCQ DECA XP MAX system) coupled with an electrospray ionization (ESI) source (Thermo Scientific). The parameters for MS analysis were summarized as follows: flow rate for sheath gas, 50 arb; spray voltage, 4 kV; capillary voltage, 20 V; capillary temperature, 300 °C; MS scan range, from $m/z$ 100 to $m/z$ 1000. The MS/MS raw data were acquired using Thermo-XCalibur (Thermo Scientific) and then converted to MGF files using Mascot Distiller v2.3.2.0 (Matrix Science, London). The database-assisted peptide identification was performed using the Mascot search engine v2.3 (Matrix Science) with the following search parameters: (1) the database option was Testudines (a homemade database established from the combined Fasta files of Testudines); (2) the enzyme option was no enzyme; (3) the mass tolerances for precursor and product ions were 2 and 1 Da, respectively; (4) the significance threshold was $p < 0.05$. In addition to database matching, the peptide sequence was also characterized manually using de novo sequencing based on the peptide's MS/MS spectrum. Finally, the identity of IVR was further confirmed using synthetic IVR.

**ACE-Inhibitory Activity Assay and Determination of $IC_{50}$.** The assay of ACE-inhibitory activity was measured by the method of Cushman et al. with slight modifications.[13] The assay mixture was composed of the following components: 10 $\mu$L of IVR (at different concentrations) was added to 20 $\mu$L of ACE (100 mU/mL) and 30 $\mu$L of HLL (1 mM). The control sample was exactly the same as in the IVR case with only the lack of inhibitor. The reaction mixture was incubated at 37 °C for 30 min without mixing, followed by mixing at the same

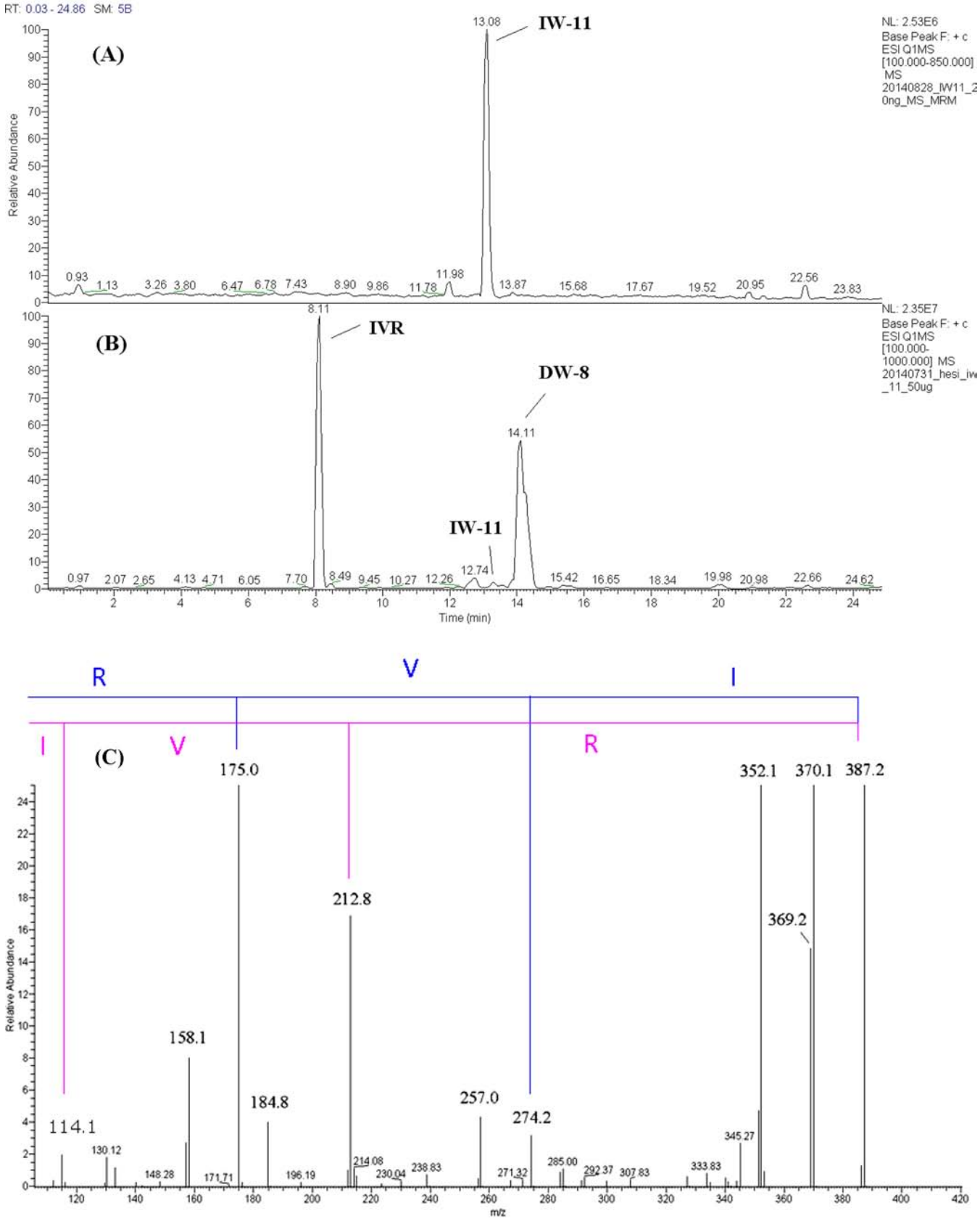


**Figure 1.** (A) LC−MS chromatogram of IW-11. (B) LC−MS chromatogram of the tryptic digest of IW-11 (after 24 h of digestion using trypsin). (C) MS/MS spectrum assignment of IVR. IW-11 represents the peptide IVRDPNGMGAW; DW-8 represents DPNGMGAW.

temperature for the same amount of time in a thermostatically controlled shaker incubator (200 rpm). The reaction was terminated by adding 70 $\mu$L of 1 M HCl, followed by centrifugation at 1500*g* for 5 min. HA and HHL were separated by RP-HPLC in a $C_{18}$ column


dx.doi.org/10.1021/jf504734g | J. Agric. Food Chem. 2014, 62, 12178−12185

(4.6 mm × 250 mm, particle size 5 μm, Thermo Scientific). The mixture was eluted using an isocratic gradient at a flow rate of 1 mL/min with 79% solvent A (5% ACN and 0.1% TFA in deionized water) and 21% solvent B (95% ACN and 0.1% TFA in deionized water) for 15 min. The absorbance was monitored with a UV detector at 228 nm. The degree of ACE-inhibitory activity (%) was calculated according to the following equation:

$$\text{ACE-inhibitory activity (\%)} = [1 - (\Delta A_{\text{sample}}/\Delta A_{\text{blank}})] \times 100$$

where $\Delta A$ is the peak area formed in the sample with or without inhibitor (blank). The definition of $IC_{50}$ is the peptide concentration required to inhibit half or 50% of the ACE activity. The $IC_{50}$ was calculated using linear interpolation of ACE inhibition (%) from five different concentrations of inhibitory peptide.

**Determination of Inhibitory Kinetics.** To characterize the ACE inhibition pattern of IVR, the kinetic study of ACE inhibition was established at different concentrations of substrates according to a previous report.[14] The Lineweaver–Burk plot was used to determine the inhibition type of the peptides, which were competitive, noncompetitive, or uncompetitive. Linear interpolation was plotted at various HHL concentrations (0.5, 1, 2, 3.5, and 6 mM) as the independent variable ($x$-axis) with the production of HA as the dependent variable ($y$-axis). The $x$-axis was proposed in the absence and presence of inhibitor (0.5 and 1 μM). The Lineweaver–Burk plot indicates correlation between $1/V$ and $1/[S]$ with an intercept line between the absence and presence of inhibitor. The slope represents $K_m$, while the $y$-intercept represents $V_{max}$. The dissociation constant ($K_i$) was determined by plotting the slope versus the inhibitor concentration. In the resulting linear regression, the intercept was equal to $K_m/V_{max}$ and the slope was $K_m/(V_{max}K_i)$, and therefore, $K_i$ was equal to the intercept/slope ratio.

**Molecular Docking Simulation.** Docking studies were performed using Molegro Virtual Docker (MVD version 6.0). The conformations of the ACEI peptide were generated using Accelrys Discovery Studio Visualizer version 3.0, and their energies were minimized by the CHARMm program. Crystallographic structures of native human ACE were downloaded from the Protein Data Bank (PDB code 1O8A) and represented the human testicular ACE–lisinopril complex at 2.0 Å resolution.[14,15] The binding site was close to the location of lisinopril, the reference ligand. According to the report by Jimsheena et al., lisinopril can be redocked in this site perfectly using MVD, indicating that this software is feasible to simulate the ACE–ligand docking.[16] Because the binding site and whole C-terminal domain of testicular ACE (tACE) are identical to the catalytic C-terminal domain of the dual-domain human somatic ACE (sACE), the structure of tACE was used to mimic sACE in this study, although sACE is thought to be more important for blood pressure control.[17] Water molecules and lisinopril were removed before the docking simulation. The docking simulation was defined by the presence of cofactors (zinc and chloride ions) using five-cavity detection with a radius of 20 Å with the coordinates $x$ = 37.53, $y$ = 35.24, and $z$ = 45.22.[18] Evaluation of the molecular docking was monitored according to the docking energy, and the best pose of IVR interacted with ACE. Molecular docking was carried out for three runs, and the return data for the 10 best poses obtained in each run were based on the minimum of the affinity energy with a population size of 100 and 10 000 maximum interactions. Hydrogen bonds, $\pi$–$\pi$ interactions, and hydrophobic interactions between peptides and ACE were visualized using Accelrys Discovery Studio Visualizer version 3.0.

**In Vivo Assay of the Antihypertensive Effect.** Male SHRs (10 months old, specific pathogen-free, 250–290 g body weight) with tail systolic blood pressure (SBP) over 200 mmHg were purchased from the National Laboratory Animal Center (Taipei, Taiwan). SHRs were grouped into four groups, and each group consisted of four SHRs. The 16 SHRs resided at room temperature with a 12 h light/dark cycle in clean standard cages. They were fed ad libitum with tap water and a standard diet for rats (LabDiet 5001 rodent diet). Each dose of ACE inhibitors was dissolved in 0.5 mL by following the examined groups: control (saline), positive control (captopril, 2.0 mg/kg), IVR (0.1 mg/kg), IVR (1.0 mg/kg), and IW-11 (1.0 mg/kg). Solutions were given orally by gastric intubation between 10 and 11 a.m. The effect on SBP was measured by the tail-cuff method (NP-NIBP model MK-2000ST, Three Dian Technology Co., Ltd.) 0, 2, 4, 6, 8, and 24 h after administration.

**Statistical Analysis.** In vivo data for SBP were analyzed by one-way analysis of variance (ANOVA) with Dunnett's multiple comparison as postanalysis. Statistical analysis was performed by GraphPad Prism 6.0 software (La Jolla, CA).

## RESULTS AND DISCUSSION

**Isolation and Identification of IVR from the Tryptic Digest of IW-11.** IW-11 (IVRDPNGMGAW) was the first ACEI peptide identified from the enzymatic hydrolysate of SSTEW.[8] Due to the existence of an internal Arg residue, IW-11 is expected to be further cut by trypsin to give IVR and DPNGMGAW during gastrointestinal digestion. In our previous study, the tryptic digest of IW-11 showed an improved ACE inhibition compared to native IW-11. This inspired us to isolate and identify the shorter and better ACEI peptide derived from the IW-11 digest. After 24 h of trypsin digestion at 37 °C, the mixture was analyzed using LC–MS/MS. Two major fragments with $t_R$ = 8.1 and 14.1 min were observed in the LC–MS chromatogram (Figure 1B), and their $m/z$ values were 387 and 847, which matched those of the two predicted fragments IVR (IR-3) and DPNGMGAW (DW-8), respectively. The sequence of IVR was further confirmed by the MS/MS spectrum of the $m/z$ 387 ion, as shown in Figure 1C. To isolate pure forms of IVR and DW-8, the digest was further separated using a C18 SPE column. IVR was isolated in 10% ACN fraction, whereas DW-8 was collected in 50% ACN fraction, without any tedious purification procedure. The ACEI activities of isolated DW-8 and IVR were further examined by ACE-inhibitory assay.

**ACE -Inhibitory Activity and Inhibition Type of IVR.** The ACE inhibitory activities of IW-11, DW-8, and IVR were assessed using the synthetic substrate HHL. IVR showed significantly improved ACE-inhibitory activity, compared to IW-11 (4.39 ± 0.31 μM) and its degradation product DPNGMGAW (14.43 ± 0.21 μM) (data not shown), with an $IC_{50}$ value of 0.81 ± 0.03 μM, as shown in Figure 2. The majority of food protein

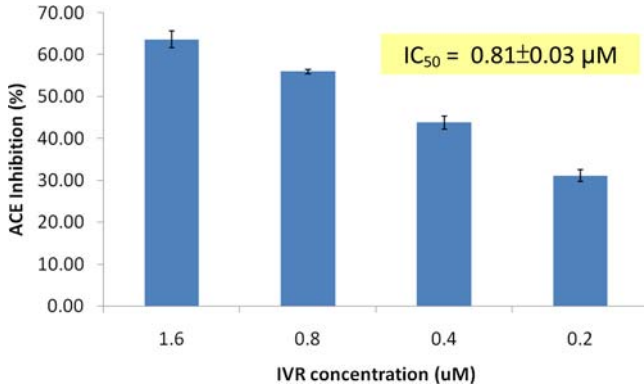


**Figure 2.** Inhibition activities of IVR at various concentrations. Linear regression analysis was used to calculate the $IC_{50}$ value. Data represent the mean ± SD of five independent experiments with three replicates each.

derived ACE-inhibitory peptides typically have moderate inhibitory potencies in the high micromolar range.[19] IVR showed a greater ACE-inhibitory potency compared to other reported peptides derived from milk,[20] eggs,[21] or fish proteins.[22] Tripeptides were reported to have stronger ACE-inhibitory activity compared to longer chain peptides.[23] Notably, the $IC_{50}$ value of IVR (0.81 ± 0.03 μM) is greater than that of lactotripeptide IPP (5 μM)


dx.doi.org/10.1021/jf504734g | J. Agric. Food Chem. 2014, 62, 12178–12185

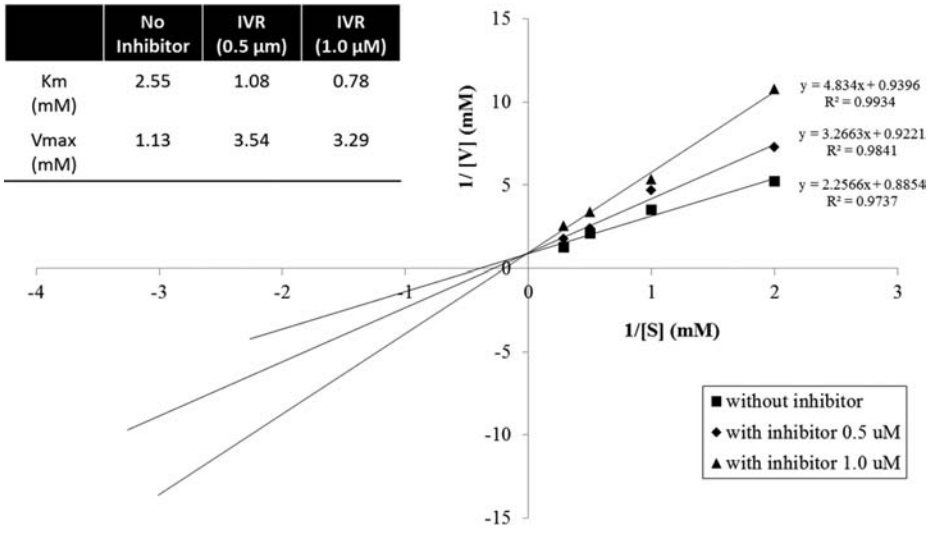


**Figure 3.** Lineweaver–Burk plots of IVR inhibition toward ACE. The ACE-inhibitory activities were measured in the presence or absence of synthetic peptide. $1/[S]$ and $1/V_i$ represent the reciprocal substrate concentration and velocity, respectively. The intersection on the vertical axis indicates that the peptide was a competitive inhibitor.

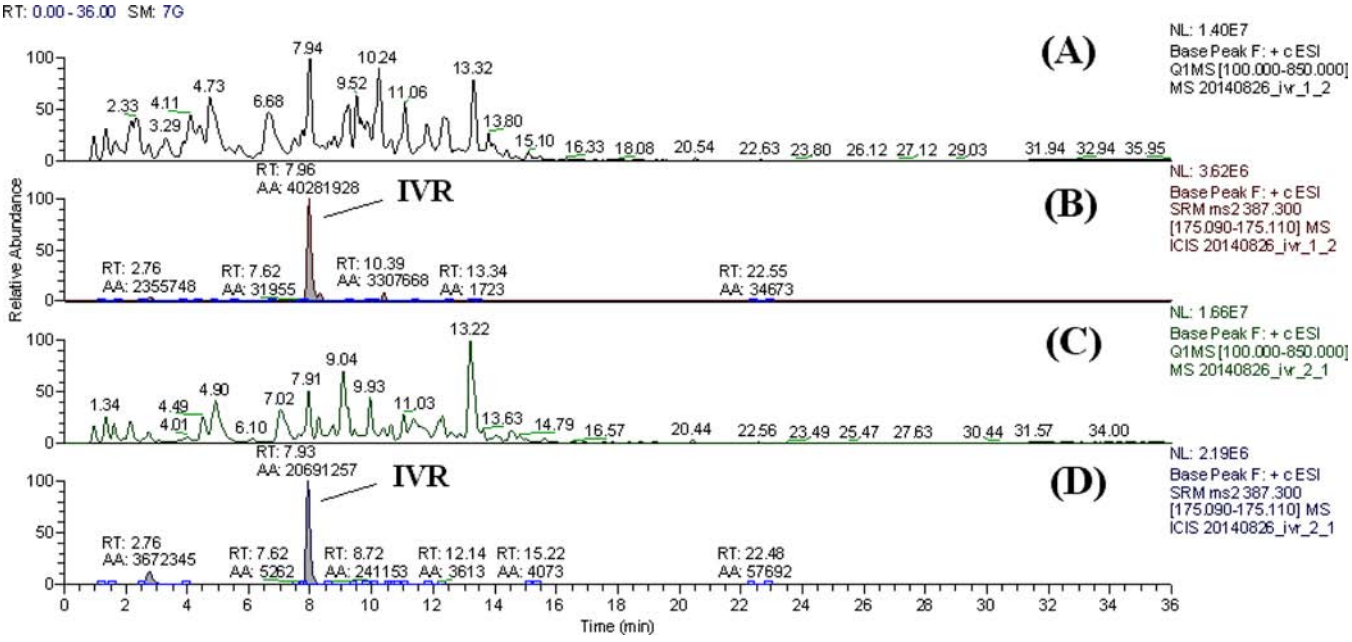


**Figure 4.** Efficacy comparison of IVR production using two-stage and one-stage digestion: (A) LC–MS chromatogram of the crude hydrolysate obtained using thermolysin followed by trypsin digestion. (B) SRM chromatogram of IVR in the crude digest from (A). (C) LC–MS chromatogram of the crude hydrolysate obtained using only trypsin digestion. (D) SRM chromatogram of IVR in the crude digest from (C).

and VPP (9 $\mu$M), well-characterized ACE inhibitor peptides found in fermented milk, currently on the market.[24] The amino acid residues at the N-terminal, internal, and C-terminal positions play significant roles in the ACE-inhibitory effects of the tripeptide. An aromatic residue (e.g., phenylalanine, tryptophan, histidine, and tyrosine) at the C-terminal and a hydrophobic amino acid residue (e.g., valine, isoleucine, and leucine) at the N-terminal had been reported to have a strong ACE-inhibitory activity.[23,25] The N-terminal branched aliphatic isoleucine of IVR perfectly matched one of the requirements. However, our result showed that a tripeptide consisting of a basic C-terminal residue (arginine) also has a strong ACE-inhibitory activity. This result is consistent with the structure–activity correlation proposed by Fujita et al., in which the positive charge on the guanidine or $\varepsilon$-amino group of the C-terminal arginine and lysine side chains, respectively, contributes substantially to the inhibitory potency.[26,27] The effect of a central or an internal amino acid residue of tripeptide IVR on ACE-inhibitory activity is also in accordance with the previous reports. Chen et al.,[28] reported that tripeptides with low electronic properties and hydrophilicity and bulky side amino acid residues such as valine, proline, alanine, and methionine have strong ACE inhibition activities. The ACE inhibition pattern of the active peptide was analyzed by the Lineweaver–Burk plot as shown in Figure 3. The Lineweaver–Burk of the peptide converged at the $y$-intercept with that of the reaction containing no inhibitor. In the presence of peptide, the slope changed while the $y$-intercept of $1/V$ remained unchanged. This suggests that IVR serves as a competitive inhibitor by competing for the binding site on ACE, thus preventing substrate

binding. The $K_i$ value of IVR was determined to be 0.84 $\mu$M, as shown in Figure S1 in the Supporting Information. The Lineweaver−Burk plot indicates that IVR competes with HHL for the binding sites of ACE. Competitive ACE inhibitors have been frequently reported; Rao et al. previously reported competitive ACE-inhibitory peptides from hen egg white lysozyme.[14] The competitive inhibitors can bind to the active site to block substrate−enzyme interaction or to alter the enzyme conformation so that the substrate cannot approach the active site.

**Quantitative Determinations of IVR in SSTW Hydrolysates under Different Conditions.** According to the full sequence of SST (*P. sinensis*) lysozyme reported in the NCBI database and our previous result, the ACEI peptide IVR was expected to be generated from lysozyme in SSTEW using direct trypsin digestion or thermolysin followed by trypsin digestion.[8] To examine the efficacies of one-stage and two-stage digestion conditions, the SRM mode of LC−MS/MS was used to quantitatively determine the amounts of IVR in SSTEW hydrolysates. The SRM calibration curve with a linear regression equation ($y = 697909x - 41441$) and coefficient of determination ($R^2 = 0.999$) was established using the synthetic peptide of IVR with a transition of $m/z$ 387.4 > $m/z$ 175.1, as shown in Figure S2 in the Supporting Information. The full MS chromatogram of the crude digest after the digestion using thermolysin followed by trypsin digestion is shown in Figure 4A; the SRM chromatogram of IVR is shown in Figure 4B. The signal of IVR ($t_R$ = 7.96 min) is the base peak in Figure 4A, which indicates IVR is the most abundant peptide in the crude digest derived from two-stage digestion of SSTEW. The full MS chromatogram of SSTEW hydrolysate when the single enzyme trypsin was used is shown in Figure 4C, and the SRM chromatogram of IVR derived from this crude digest is shown in Figure 4D. The SRM experiments indicated that the contents of IVR obtained from 1 g of SSTEW using direct trypsin digestion and thermolysin followed by trypsin digestion were 1.31 ± 0.12 and 3.14 ± 0.17 mg, respectively. The yield of IVR production using two-stage digestion was more than 2 times that obtained using single-stage digestion. This result may be explained by the fact that trypsin-only digestion may leave some missed cleavage sites due to the proteins' incomplete defolding during the hydrolysis process while multiple enzymes (thermolysin followed by trypsin digestion) can provide more complete hydrolysis and hence give a higher yield of IVR.[29]

**Binding Mechanisms of IVR to tACE Rationalized by Molecular Docking.** Molecular docking simulations of the tripeptide IVR with tACE (PDB 1O8A) were carried out to correlate the ACE-inhibitory potential with their three-dimensional interactions. Molegro Dock, a docking algorithm that uses a cavity prediction alogarthm,[18] was used to elucidate the interaction between tACE and IVR and predict its binding affinity. Through such docking simulation, the most favorable binding of IVR to tACE was given by the best pose (pose 00) on the basis of a binding mode in a manner that mimics the binding of lisinopril. Figure 5 presents the best pose for the docking study of IVR with the most favorable affinity energy (−9.61 kJ/mol) at the catalytic site of tACE in the presence of Zn(II). Zn(II) has been included in the docking simulation as it was found in the active site of ACE.[15] The complexation between zinc(II) and the key motif HEXXH on ACE plays an important role in the activity of this dipeptidyl carboxypeptidase. Additionally, this pose was stabilized by H-bonds, $\pi-\pi$ interactions, and hydrophobic interactions with tACE. Table 1 lists the ACE residues which form hydrogen bonds with lisinopril, and if any of those residues form hydrogen bonds with IVR, then the corresponding

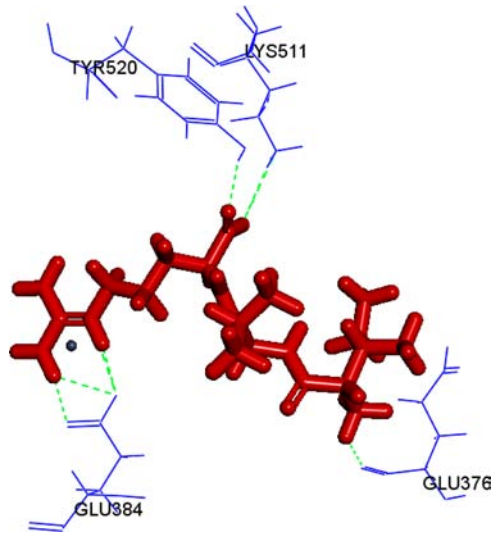


**Figure 5.** Predicted binding mode between ACE and IVR after IVR was docked at the ACE active site. Peptides are shown in a red stick model. ACE residues are shown in blue. Zn(II) and hydrogen bond interactions are represented as a black circle and green dashed lines, respectively. The image was obtained with Accelrys Discover Studio Visualizer.

**Table 1. Hydrogen Bond Contacts of tACE with the IVR Drug Lisinopril and the Best Peptide Pose Obtained from Docking Simulation**[a]

| ACE residue in H-bonding | atom | lisinopril | distance (Å) | IVR (pose 00) | distance (Å) |
|---|---|---|---|---|---|
| Glu 162 | OE2 | √ | 3.4 | X | |
| His 353 | NE2 | √ | 2.8 | X | |
| Ala 354 | O | √ | 2.9 | X | |
| Glu 384 | OE2 | √ | 2.7 | √ | 2.21 |
| Lys 511 | NZ | √ | 2.9 | √ | 3.15 |
| His 513 | NE2 | √ | 3.1 | X | |
| Tyr 520 | OH | √ | 2.6 | √ | 2.02 |
| Tyr 523 | OH | √ | 2.8 | X | |

[a]"√" represents the existence of hydrogen bonding; "X" represents the nonexistence of hydrogen bonding.

hydrogen bond distances are recorded there. Similar to lisinopril, this tripeptide is buried deep inside the active site channel as in the lisinopril−tACE complex. The observed H-bond interactions with Glu384, Lys511, and Tyr520 indicate that IVR is accommodated in the active pocket of a significant and solitary inhibitor registration for the C-terminal carboxylic group of lisinopril,[15] with distances of 2.21, 3.15, and 2.02 Å, respectively. Compared to lisinopril, fewer H-bonds between IVR and the key ACE residues were predicted. However, the H-bonds of IVR with Glu384 (which was located at zinc(II) complexation motif HEXXH) and Tyr520 are shorter than those reported for lisinopril as shown in Figure 5. A shorter distance or closer proximity will greatly favor a stronger interaction between tACE and IVR and obviously contribute as a key factor to the ACE-inhibitory activity of IVR.

**In Vivo ACE-Inhibitory Effects of Peptides in SHR.** The inhibitory potencies of active peptides on ACE activity do not always correlate with their antihypertensive effects.[30] To evaluate IVR's antihypertensive effect, an in vivo experiment using SHRs was further performed in this study. Two doses, 0.1 and 1.0 mg/kg of body weight (BW), were selected to check the dose-dependent antihypertensive effect of IVR. SBP measured by the tail-cuff


dx.doi.org/10.1021/jf504734g | J. Agric. Food Chem. 2014, 62, 12178−12185

method in awake SHRs was 223 ± 3.0 mmHg ($n$ = 16). Oral administration of IVR at 0.1 and 1.0 mg/kg induced significant reductions in SBP, the time courses of which are shown in Figure 6,

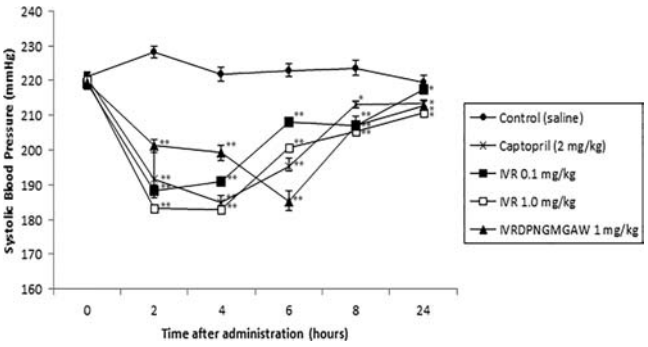


**Figure 6.** Effect of single oral administration of physiological saline alone, captopril (2.0 mg/kg), and IVR (0.1 and 1.0 mg/kg) on systolic blood pressure in SHRs. Blood pressures are expressed in absolute values (mmHg). Data are the mean ± SEM from 12 determinations and were subjected to ANOVA with Dunnett's multiple comparison test as postanalysis. Key: *, significantly different from the control, $P < 0.05$; **, significantly different from the control, $P < 0.01$.

in comparison to the lack of an effect of oral saline and the antihypertensive effect of captopril (2 mg/mL), a common antihypertensive drug, and IW-11 (1 mg/kg), a larger peptide from SST egg white with a higher in vitro $IC_{50}$ value. Maximum antihypertensive activities were shown at 2 h postadministration of 1 mg/kg IVR (183 ± 1.3 mmHg) and 2 h postadministration of 0.1 mg/kg IVR (188 ± 1.79 mmHg), whereas 1.0 mg/kg IW-11 produced its maximum effect at 6 h (185 ± 2.88 mmHg). Notably, IVR at either 0.1 or 1.0 mg/kg reached its maximum effect faster than captopril with a dosage of 2 mg/kg (4 h). The antihypertensive effect remained significant for 0.1 and 1.0 mg/kg IVR up to 8 h postadministration, which is comparable with that of commercially available lactotripeptide VPP/IPP[31] and almost equivalent to that of captopril, a positive control. Interestingly, IW-11 showed its maximum antihypertensive effect in a prolonged period, which implies that the conversion of IW-11 to IVR occurred in the digestive tract of SHRs first and then the resulting more efficient IVR was absorbed and exhibited its ACE inhibition in vivo and therefore decreased the blood pressure. To the best of our knowledge, this is the first report of a potent antihypertensive tripeptide generated from the egg of soft-shelled turtle.

## ■ ASSOCIATED CONTENT

### Ⓢ Supporting Information

Determination of $K_i$ and calibration curve of IVR established using SRM peak areas at 14 different concentrations. This material is available free of charge via the Internet at http://pubs.acs.org.

## ■ AUTHOR INFORMATION

### Corresponding Author

*Phone: 886-8-7703202, ext 5197. Fax: 886-8-7740550. E-mail: jlhsu@mail.npust.edu.tw.

### Funding

This work was financially supported by Taiwan National Science Council (NSC) grants (NSC 102-2113-M-020-001-MY2 and NSC 102-2923-B-020-001-MY2).

### Notes

The authors declare no competing financial interest.

## ■ ACKNOWLEDGMENTS

We appreciate the helpful suggestion from Prof. Robert J. Doerksen of the Department of Medicinal Chemistry and Research Institute of Pharmaceutical Sciences, University of Mississippi. We also gratefully acknowledge the LC−MS/MS support by the Research Center for Active Natural Products Development of the National Pingtung University of Science and Technology.

## ■ REFERENCES

(1) Basu, S.; Millett, C. Social epidemiology of hypertension in middle-income countries: Determinants of prevalence, diagnosis, treatment, and control in the WHO SAGE study. *Hypertension* **2013**, *62*, 18−26.

(2) Quist, E. E.; Phillips, R. D.; Saalia, F. K. Angiotensin converting enzyme inhibitory activity of proteolytic digests of peanut (*Arachis hypogaea* L.) flour. *LWT—Food Sci. Technol.* **2009**, *42*, 694−699.

(3) Katzung, B. G.; Masters, S. B.; Trevor, A. J. *Basic and Clinical Pharmacology*; McGraw-Hill: New York, 2012.

(4) Aleixandre, A.; Miguel, M.; Muguerza, B. Peptides with antihypertensive activity obtained from milk and egg proteins. *Nutr. Hosp.* **2008**, *23*, 313−318.

(5) Iwaniak, A.; Minkiewicz, P.; Darewicz, M. Food-originating ACE inhibitors, including antihypertensive peptides, as preventive food components in blood pressure reduction. *Compr. Rev. Food Sci. Food Saf.* **2014**, *13*, 114−134.

(6) Martinez-Maqueda, D.; Miralles, B.; Recio, I.; Hernandez-Ledesma, B. Antihypertensive peptides from food proteins: A review. *Food Funct.* **2012**, *3*, 350−361.

(7) Nalinanon, S.; Benjakul, S.; Kishimura, H.; Shahidi, F. Functionalities and antioxidant properties of protein hydrolysates from the muscle of ornate threadfin bream treated with pepsin from skipjack tuna. *Food Chem.* **2011**, *124*, 1354−1362.

(8) Rawendra, R. D. S.; Aisha; Chang, C. I.; Aulanni'am; Chen, H. H.; Huang, T. C.; Hsu, J. L. A novel angiotensin converting enzyme inhibitory peptide derived from proteolytic digest of Chinese soft-shelled turtle egg white proteins. *J. Proteomics* **2013**, *94*, 359−369.

(9) Yu, H. L.; Li, Y.; Wang, J. B.; Zheng, L. P.; Yan, W. X. Chinese soft-shelled turtle egg powder lowers serum cholesterol, increases faecal neutral steroids and bile acid excretion, and up-regulates liver cytochrome P450 mRNA level in rats. *Br. J. Nutr.* **2005**, *94*, 315−320.

(10) Chiu, L. H.; Hsu, G. S. W.; Lu, Y. F. Antihypertensive capacity of defatted soft-shelled turtle powder after hydrolysis by gastrointestinal enzymes. *J. Food Biochem.* **2006**, *30*, 589−603.

(11) Liu, L.; Lu, B.; Gong, L.; Liu, L.; Wu, X.; Zhang, Y. Studies on bioactive peptide from Chinese soft-shelled turtle (*Pelodiscus sinensis*) with functionalities of ACE inhibition and antioxidation. *Afr. J. Biotechnol.* **2012**, *11*, 6723−6729.

(12) Mathews, D.; Adibi, S. Peptide absorption. *Gastroenterology* **1976**, *71*, 151−161.

(13) Cushman, D. W.; Cheung, H. S.; Sabo, E. F.; Ondetti, M. A. Design of potent competitive inhibitors of angiotensin-converting enzyme. Carboxyalkanoyl and mercaptoalkanoyl amino acids. *Biochemistry* **1977**, *16*, 5484−5491.

(14) Rao, S. Q.; Ju, T.; Sun, J.; Su, Y. J.; Xu, R. R.; Yang, Y. J. Purification and characterization of angiotensin I-converting enzyme inhibitory peptides from enzymatic hydrolysate of hen egg white lysozyme. *Food Res. Int.* **2012**, *46*, 127−134.

(15) Natesh, R.; Schwager, S. L.U.; Sturrock, E. D.; Acharya, K. R. Crystal structure of the human angiotensinconverting enzyme-lisinopril complex. *Nature* **2003**, *421*, 551−554.

(16) Jimsheena, V. K.; Gowda, L. R. Arachin derived peptides as selective angiotensin-I converting enzyme (ACE) inhibitors: Structure-activity relationship. *Peptides* **2010**, *31*, 1165−1176.

(17) Masuyer, G.; Akif, M.; Czarny, B.; Beau, F.; Schwager, S. L.; Sturrock, E. D.; Isaac, R. E.; Dive, V.; Acharya, K. R. Crystal structures of highly specific phosphinic tripeptide enantiomers in complex with the angiotensin-I converting enzyme. *FEBS J.* **2014**, *281*, 943−956.

(18) Thomsen, R.; Christensen, M. H. MolDock: A new technique for high-accuracy molecular docking. *J. Med. Chem.* **2006**, *49*, 3315−3321.
(19) De Leo, F.; Panarese, S.; Gallerani, R.; Ceci, L. R. Angiotensin converting enzyme (ACE) inhibitory peptides: Production and implementation of functional food. *Curr. Pharm. Des.* **2009**, *15*, 3622−3643.
(20) Ricci, I.; Artacho, R.; Olalla, M. Milk protein peptides with angiotensin i-converting enzyme inhibitory (ACEI) activity. *Crit. Rev. Food. Sci. Nutr.* **2010**, *50*, 390−402.
(21) Miguel, M.; Recio, I.; Gómez-Ruiz, J.; Ramos, M.; López-Fandiño, R. Angiotensin I-converting enzyme inhibitory activity of peptides derived from egg white proteins by enzymatic hydrolysis. *J. Food Prot.* **2004**, *67*, 1914−1920.
(22) Fujita, H.; Yoshikawa, M. LKPNM: A prodrug-type ACE-inhibitory peptide derived from fish protein. *Immunopharmacology* **1999**, *44*, 123−127.
(23) Wu, J.; Aluko, R. E.; Nakai, S. Structural requirements of angiotensin I-converting enzyme inhibitory peptides: Quantitative structure−activity relationship study of di- and tripeptides. *J. Agric. Food Chem.* **2006**, *54*, 732−738.
(24) Nakamura, Y.; Yamamoto, N.; Sakai, K.; Okubo, A.; Yamazaki, S.; Takano, T. Purification and characterization of angiotensin I-converting enzyme inhibitors from sour milk. *J. Dairy Sci.* **1995**, *78*, 777−783.
(25) Cheung, H. S.; Wang, F. L.; Ondetti, M. A.; Sabo, E. F.; Cushman, D. W. Binding of peptide substrates and inhibitors of angiotensin-converting enzyme. Importance of the COOH-terminal dipeptide sequence. *J. Biol. Chem.* **1980**, *255*, 401−407.
(26) Fujita, H.; Yokoyama, K.; Yoshikawa, M. Classification and antihypertensive activity of angiotensin I-converting enzyme inhibitory peptides derived from food proteins. *J. Food Sci.* **2000**, *65*, 564−569.
(27) Murray, B. A.; FitzGerald, R. J. Angiotensin I-converting enzyme inhibitory peptides derived from food proteins and their physiological and pharmacological effects. *Curr. Pharm. Des.* **2007**, *13*, 773−791.
(28) Chen, J.; Wang, Y.; Zhong, Q.; Wu, Y.; Xia, W. Purification and characterization of a novel angiotensin-I converting enzyme (ACE) inhibitory peptide derived from enzymatic hydrolysate of grass carp protein. *Peptides* **2012**, *33*, 52−58.
(29) Choudhary, G.; Wu, S. L.; Shieh, P.; Hancock, W. S. Multiple enzymatic digestion for enhanced sequence coverage of proteins in complex proteomic mixtures using capillary LC with ion trap MS/MS. *J. Proteome Res.* **2003**, *2*, 59−67.
(30) Saito, T.; Nakamura, T.; Kitazawa, H.; Kawai, Y.; Itoh, T. Isolation and structural analysis of antihypertensive peptides that exist naturally in gouda cheese. *J. Dairy Sci.* **2000**, *83*, 1434−1440.
(31) Nakamura, Y.; Yamamoto, N.; Sakai, K.; Takano, T. Antihypertensive effect of sour milk and peptides isolated from it that are inhibitors to angiotensin I-converting enzyme. *J. Dairy Sci.* **1995**, *78*, 1253−1257.

During the past decade, a variety of microbial GADs were expressed and characterized,[34−37] and several crystal structures were determined to investigate the pH dependence of catalytic activity.[12] Consequently, it was found that the N-termini and/or the C-termini of GAD might be responsible for the pH-induced conformational change for the regulation of catalytic activity in the acidic environment. Herein, we overexpressed the *gadB* gene encoding GAD from *Lactobacillus plantarum* in *E. coli* and characterized it. Subsequently, on the basis of the model structure and computational analysis of *L. plantarum* GAD, we attempted to generate C-terminally truncated mutant enzymes and investigated the pH dependence of enzyme activity, underlying the important role of C-terminal region for the GAD activity at low pH values.

## MATERIALS AND METHODS

**Materials.** Restriction enzymes, prime star DNA polymerase, deoxynucleotide triphosphates, and chemicals for PCR were obtained from Takara Biomedicals (Takara Co., Shiga, Japan). The pTOPV2 blunt vector for cloning was obtained from Enzynomics (Daejeon, Korea). The pET-28a expression vector and a His-bind resin kit were obtained from Novagen (Madison, WI, USA). Genomic-tip, gel extraction, PCR purification, and plasmid miniprep kit were obtained from Qiagen (Hilden, Germany). Electrophoresis reagents were obtained from Bio-Rad (Hercules, CA, USA). All chemicals used for enzyme assays and characterization were obtained from Sigma (St. Louis, MO, USA). Oligonucleotides were synthesized by Bioneer (Daejeon, Korea).

**Bacterial Strains and Culture Conditions.** *L. plantarum* ATCC 14917 was obtained from American Type Culture Collection (ATCC). The strain was grown in De Man, Rogosa, and Sharpe (MRS) medium at 30 °C for 72 h. *E. coli* strain DH5$\alpha$ was used as a host for the construction of expression vector. *E. coli* BL21 (DE3) was used as an expression host for GAD from *L. plantarum*. Both *E. coli* strains were grown in Luria−Bertani (LB) medium with kanamycin (50 $\mu$g/mL) in a rotary shaker at 37 and 25 °C, respectively. Plasmid pTOPV2 blunt vector was used as a cloning and sequencing vector, and pET-28a was used for expression.

**Cloning and Expression of *L. plantarum* GAD.** From a search of the microbial genome sequences in GenBank (accession no. CCC80401.1), we found a *gadB*-encoding gene in *L. plantarum*. Genomic DNA was isolated from *L. plantarum* and purified using a genomic DNA extraction kit (Qiagen) according to the manufacturer's instructions. The gene-encoding GAD was amplified by PCR from *L. plantarum* genomic DNA using the forward/reverse primer pair 5′-CATATGGCAATGTTATACGGTAAACAC-3′ and 5′-GAATTCTCAGTGTGTGAATCCGTATTTC-3′. A *Nde*I site was incorporated into the forward primer and an *Eco*RI site into the reverse primer for cloning into pET-28a. PCR was performed in 10× prime star buffer containing 2 mM $MgCl_2$, 20 ng of DNA, 10 pmol of each primer, 200 $\mu$M dNTP mix, and 2.5 U of prime star DNA polymerase in a total volume of 50 $\mu$L. After initial denaturation for 4 min at 94 °C, DNA was amplified over 30 cycles (30 s of denaturation at 94 °C, 30 s of annealing at 57 °C, and 1 min of extension at 72 °C), followed by a final extension step of 5 min at 72 °C. The PCR product was cloned into the pTOPV2-blunt vector and transformed into *E. coli* DH5$\alpha$. Transformants containing the pTOPV2-blunt vector harboring the *L. plantarum gadB* gene were selected on LB medium−ampicillin plates. Plasmid DNA isolated from cells containing the gene was digested with *Nde*I and *Eco*RI. The released *gadB* gene was then ligated into the *Nde*I and *Eco*RI sites of the pET-28a vector, which directs the formation of fusion proteins with N-terminus polyhistidine (6× His) to generate pET-28a-GAD. For expression of the recombinant enzyme, *E. coli* BL21(DE3) cells transformed with pET-28a-GAD were grown in an LB medium (0.5 L) containing 50 $\mu$g of kanamycin per milliliter at 25 °C induced at midexponential phase ($A_{600} \sim 0.6$) with 1 mM IPTG, grown for an additional 12 h, and harvested by centrifugation (10000*g*, 20 min, 4 °C). Bacterial pellets were stored at −70 °C until use.

**Purification of Recombinant *L. plantarum* GAD.** Bacterial pellets were thawed and resuspended in 50 mL of 1× His-binding buffer (0.5 M NaCl, 20 mM Tris, 5 mM imidazole; pH 7.9) and disrupted by sonication. The lysate was centrifuged at 14000*g* for 20 min to remove cell debris, and the supernatant was loaded on a His-bind resin column (5 mL) equilibrated with the 1× His-binding buffer. The column was washed with 10 column volumes of wash buffer (0.5 M NaCl, 20 mM Tris, 60 mM imidazole, pH 7.9), and 250 mM imidazole was applied to elute the recombinant protein. The fractions containing enzyme activity were pooled and dialyzed against 10 mM sodium acetate buffer (pH 7.0). To remove the His-tag from the fusion protein, we added 7 U of thrombin (HTI, USA) to the dialyzed fusion proteins (~10 mg) for 16 h to yield intact GAD without any 6× His tag. For further purification, the reaction mixture was subjected to a HiLoad 16/60 Superdex 200 gel filtration column (GE Healthcare, USA) pre-equilibrated with 50 mM Tris-HCl (pH 7.5, 150 mM NaCl). Protein concentrations were determined by the bicinchoninic acid (BCA) method, with bovine serum albumin as the standard. Enzyme fractions were analyzed by 12% sodium dodecyl sulfate−polyacrylamide gel electrophoresis (SDS-PAGE) and visualized with Coomassie brilliant blue.[38]

**Construction of GAD Truncation Mutants.** GAD truncation mutants were generated by PCR using pET-28a-GAD as a template. Reverse primers containing the mutation were used: 5′-GAATTCTCATCCGTATTTCTTAGGTGC-3′ (for GAD Δ3) and 5′-GAATTCTCAATFATGATAGACAATGTG-3′ (for GAD Δ11). The forward primers were the same as those used to clone the *gadB* gene originally (see above). PCR was performed as described above. The amplified plasmid was digested with *Nde*I and *Eco*RI and transformed into *E. coli* DH5$\alpha$ cells. Clones were sequenced to verify the presence of the mutation. The cloned plasmids were transformed into *E. coli* BL21(DE3) cells and expressed. The truncated mutants (Δ3 and Δ11) expressed in *E. coli* were purified and characterized as described above.

**Enzyme Activity Assay and Statistical Analysis.** Enzyme activity was determined by measuring the amount of GABA produced by GAD through HPLC analysis. The reaction mixture (100 $\mu$L) contained 0.022 mM PLP, 15 mM glutamate, and an appropriate amount of GAD (≈10 $\mu$g) in 100 mM sodium acetate buffer (pH 5.0) or 100 mM piperazine-*N*,*N*′-bis(2-ethanesulfonic acid) (PIPES) buffer (pH 7.0). After a 20 min incubation at 37 °C, the enzyme reaction was stopped by the addition of ice-chilled 100% EtOH (600 $\mu$L) to the reaction mixture. After a centrifugation at 15000*g* for 5 min at 4 °C, the resulting supernatant (120 $\mu$L) was mixed with 380 $\mu$L of *o*-phthalaldehyde (OPA) solutions (pH 9.3) comprising 1.0 mL of methanolic OPA (20 mM OPA in 50% (v/v) methanol), 250 $\mu$L of borate buffer (the 1:1 (v/v) ratio of 0.2 M NaOH and 0.2 M boric acid dissolved in 0.2 M KCl, pH 9.9), and 25 $\mu$L of 2-mercaptoethanol. To detect the amine group, the reaction mixture was further incubated at room temperature for 8 min and then analyzed using the Waters Alliance HPLC system (model 2695; Milford, MA, USA) equipped with a Dual $\lambda$ absorbance detector (model 2487; Waters) with a $C_{18}$ column (SPColumn, 250 × 4.6 mm, 5 $\mu$m particle size). The mobile phase was a 20% (v/v) acetonitrile solution containing 20 mM sodium acetate and 0.02% (v/v) triethylamine. The column temperature was set at 25 °C and eluted at 0.8 mL/min. The reaction products (i.e., GABA) were monitored by measuring the $A_{338\ nm}$, and the amount of GABA was estimated from the integrated peak area based on the HPLC data. One unit of GAD activity is defined as the amount of enzyme that produces 1 $\mu$mol of product per minute under the assay conditions. All experiments were carried out in duplicate.

For kinetic studies, the kinetic parameters of GAD were determined in 100 mM sodium acetate buffer (pH 5.0) or 100 mM PIPES buffer (pH 7.0), by varying the substrate concentration (1−300 mM) for 5 min at 40 °C. Kinetic data were analyzed using Michaelis−Menten equations by fitting data with the Origin 8.0 program.

**Biochemical Characterization of *L. plantarum* GAD.** To determine the effect of temperature on the enzyme activity, the enzyme was incubated in 100 mM sodium acetate (pH 5.0) containing 15 mM glutamate for 20 min at a temperatures from 30 to 60 °C. For a

thermostability test, the enzyme was incubated at various temperatures (40−90 °C) in the presence of 100 mM sodium acetate (pH 5.0) for different periods of time (0−9 h). The residual activity was measured under the same conditions as described above. The pH optimum of the enzyme was determined using the 100 mM sodium acetate buffer and 100 mM PIPES buffer at pH levels from 3.5 to 5.5 and from 5.5 to 6.0, respectively, at 37 °C. To determine pH stability, the enzyme solution was preincubated in each buffer at room temperature for different periods of time (0−96 h), and the residual activity was measured under same conditions as described above. All experiments were performed in triplicate.

**Sequence Alignment and Homology Modeling of GAD Proteins.** In a search of the microbial genome sequences in NCBI, we obtained the amino acid sequence of *L. plantarum* GAD (NCBI protein database accession no. CCC80401.1). The sequence was used to find a suitable template for homology modeling from the Brookhaven Protein Data Bank (PDB) using the software BLAST, revealing that *L. plantarum* GAD had an amino acid sequence identity of 42.6% (similarity of 57.2%) to the crystal structure of *E. coli* GAD (PDB ID 1PMO).[12] On the basis of the *E. coli* GAD structure as a template, homology modeling of *L. plantarum* GAD was performed using the program Modeler[39] in the Homology module of Insight II (Accelrys Inc., San Diego, CA, USA) on a Silicon Graphics R10000 workstation. The dimeric model of *L. plantarum* GAD thus built was subjected to energy minimization by CG using the program DISCOVER (MSI/Accelrys) with the consistent-valence force field (CVFF) until the structure reached the final derivative of 0.001 kcal/mol. To study the interaction between *L. plantarum* GAD and glutamate as the substrate, the crystal structure (PDB code 1PMO) of glutamate bound to GAD was used. The model of glutamate was subjected to energy refinement using the program DISCOVER with CVFF until the structure reached the final derivative of 0.001 kcal/mol. The model of *L. plantarum* GAD was then docked to the glutamate using the Patchdock server.[40] The docked structures that yielded the best score were selected and analyzed visually using the software Insight II. Molecular dynamics (MD) simulations were performed on the docked structures to predict the favorable binding interactions. The docked complexes of *L. plantarum* GAD and glutamate were solvated by a 10 Å water layer by the program SOAK of Insight II. The resulting systems were subsequently energy minimized using Steepest Descent (SD) and DISCOVER. The minimized systems were equilibrated for a period of 210 ps with constant volume and temperature (NVT ensemble, at 298 K) through the velocity verlet integrator.[41] The time step for integration was 1 fs using the RATTLE algorithm, a velocity version of SHAKE.[42] The last 120 ps trajectories were analyzed, saving the coordinates at 0.2 ps intervals. All of the simulations were performed with CVFF force fields; for nonbonded calculations, the cell multipole method along with a dielectric constant of 1 was used. The stereochemical qualities of the final structures were analyzed with PROCHECK. To elucidate the interactions responsible for the dimerization of the protein as well as between the protein and its substrate (i.e., GAD and its substrate glutamate), the What If software package[40] and the Biopolymer module of Insight II were used.

**Thin-Layer Chromatography Analysis.** TLC analysis of monosodium glutamate (Glu) and GABA was performed in *n*-butanol/acetic acid/water (5:3:2 by volume) as a solvent for separation by the ascending technique on 0.2 mm, silica gel-coated, aluminum sheets (type 60; Merck, Deamstadt, Germany). The plate was sprayed with 60% (w/v) ninhydrin and then heated to visualize the spots.[43]

## RESULTS AND DISCUSSION

**Cloning, Expression, and Purification of *L. plantarum* GAD.** The *gadB* gene encoding GAD was amplified by PCR from *L. plantarum* ATCC 14917 genomic DNA and cloned into the pTOPV2 blunt cloning vector. For expression in *E. coli* BL21(DE3) as well as to facilitate subsequent purification, the *gadB* gene was cloned into the pET-28a expression vector, resulting in pET-28a-GAD. The cloned gene was successfully expressed as an N-terminal hexa-histidine-tagged fusion protein

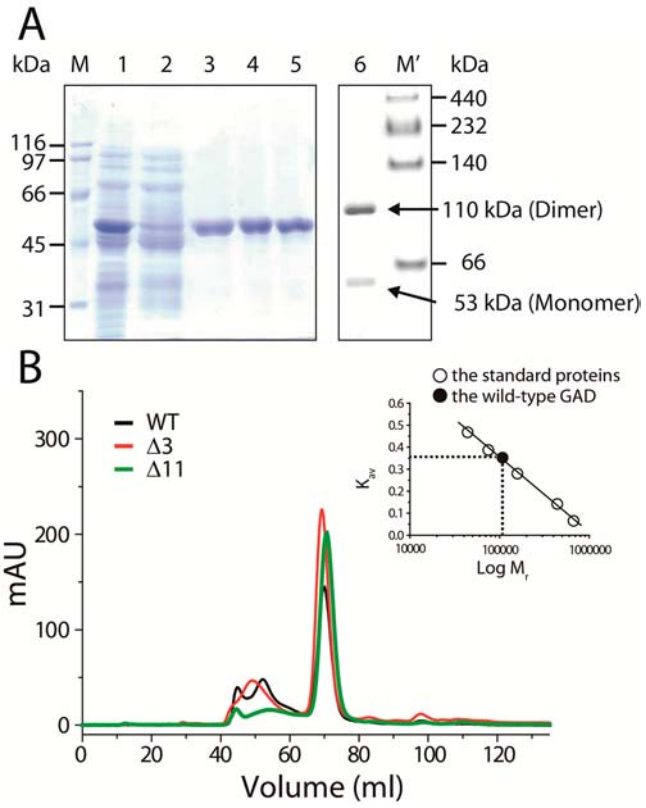


**Figure 1.** Purification of the recombinant *L. plantarum* GADs. Purified wild-type GAD and its truncated mutants were analyzed by SDS-PAGE (left panel) and native-PAGE (right) (A) and by gel filtration chromatography (B). Lanes: M, molecular weight markers (reduced); 1, whole-cell proteins; 2, cytosolic fractions; 3, purified *L. plantarum* GAD; 4, purified *L. plantarum* GAD (Δ3); 5, purified *L. plantarum* GAD (Δ11); 6, purified *L. plantarum* GAD (nonreduced); M′, molecular weight markers (nonreduced). Gel filtration chromatography was performed using a Superdex 200 16/60 column, which was run at a flow rate of 1 mL/min, and the elution profile was monitored at 280 nm. The column was calibrated with blue dextran (2000 kDa), thyroglobulin (669 kDa), ferritin (440 kDa), aldolase (158 kDa), conalbumin (75 kDa), and ovalbumin (44 kDa) as standards.

upon induction with IPTG (Figure 1A). A single $Ni^{2+}$ chelate affinity chromatography step served to purify the expressed *L. plantarum* GAD protein to >95% purity. After removal of the His-tag from the fusion protein by treatment with thrombin, we further purified the intact GAD through gel filtration chromatography (Figure 1B). The apparent $M_r$ of the fusion protein was estimated to be 53 kDa by SDS-PAGE, consistent with the $M_r$ (53 749 Da) calculated from the presumptive amino acid sequence (Figure 1A). However, native-PAGE analysis and gel filtration chromatography on Superdex 200 demonstrated that the purified enzyme was estimated to be about 110 kDa, suggesting a homodimeric structure (Figure 1B). On the basis of the fact that both truncated mutant enzymes were also observed as homodimers, we concluded that truncated mutation did not affect the oligomeric state of both mutant GADs.

**Biochemical Characterization of *L. plantarum* GAD.** The temperature and pH dependences of the recombinant GAD were determined by using HPLC after a 20 min incubation at various temperatures and pH values. Purified GAD had optimal activity at pH 5.0, and its optimum temperature for GAD activity was 40 °C (Figure 2). To investigate the effects of pH on the stability of *L. plantarum* GAD, the purified enzyme

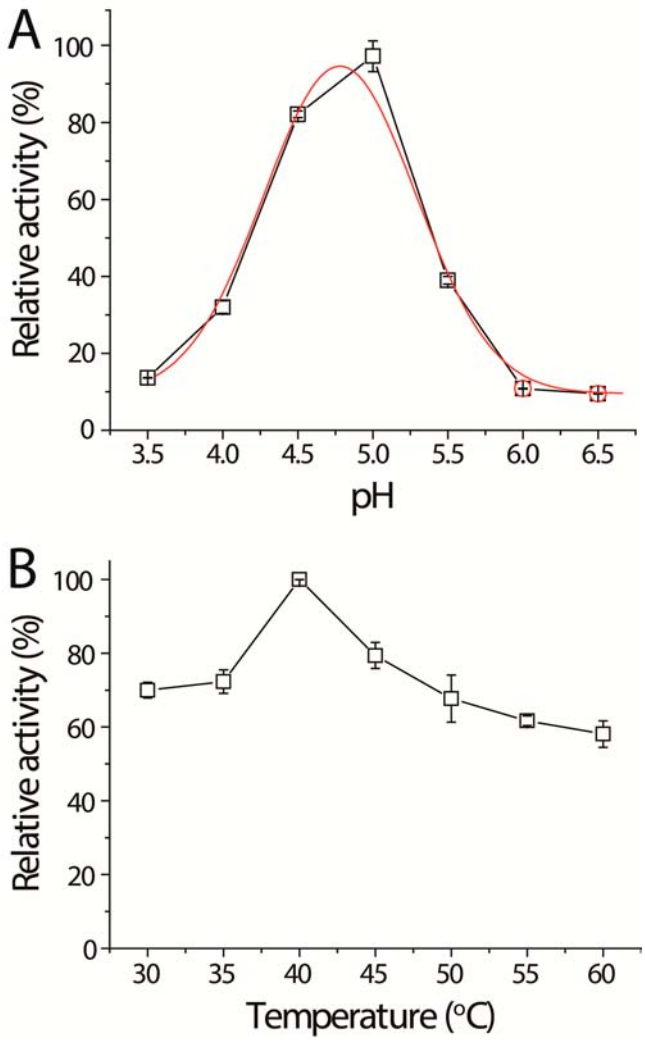


**Figure 2.** Effects of pH (A) and temperature (B) on *L. plantarum* GAD activity. (A) *L. plantarum* GAD activity was measured in 100 mM sodium acetate buffer at pH 3.5−5.5 and 100 mM piperazine-*N*,*N*′-bis(2-ethanesulfonic acid) (PIPES) buffer at pH 6.0−7.0, respectively. (B) *L. plantarum* GAD activity was determined at various temperatures (30−60 °C) in 50 mM sodium acetate buffer at pH 5.0. All experiments were performed in triplicate. Error bars indicate the standard deviation.

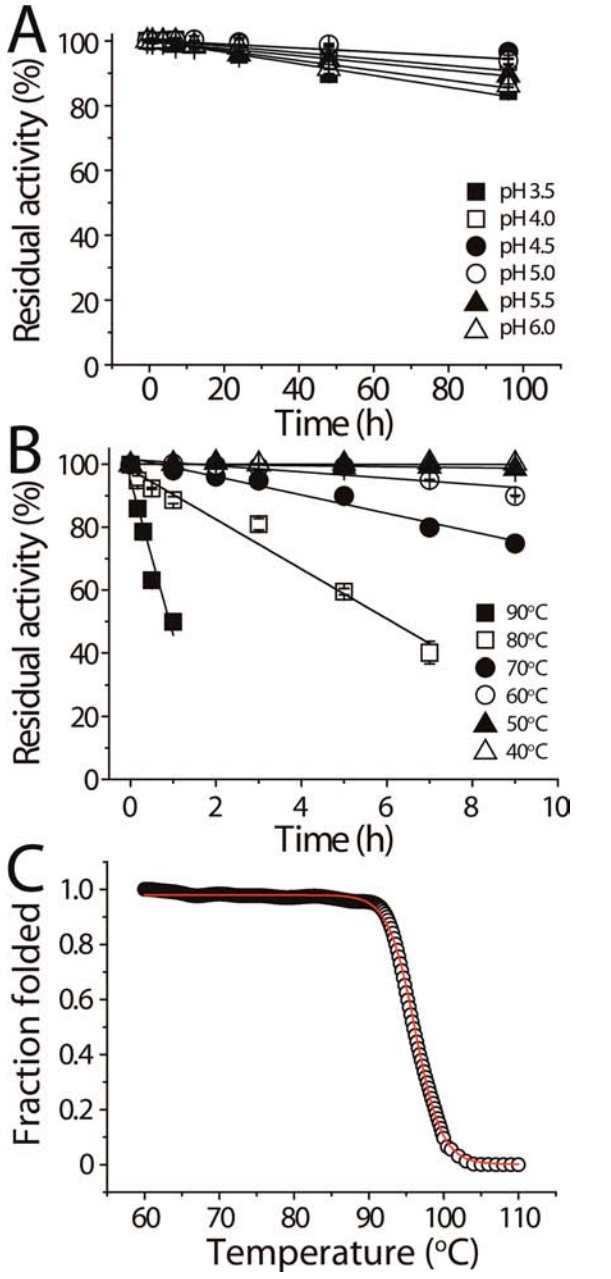


**Figure 3.** Effects of pH (A) and temperature (B, C) on the stability of *L. plantarum* GAD. (A) The purified *L. plantarum* GAD enzyme was preincubated in buffers of various pH values at room temperature for different periods of time (0−96 h) prior to determination of enzyme activity. (B) The purified *L. plantarum* GAD enzyme was incubated at various temperatures (40−90 °C) in 100 mM sodium acetate (pH 5.0) for different periods of time (0−9 h) prior to assessment of the enzyme activity. (C) Irreversible thermal unfolding of *L. plantarum* GAD was monitored by circular dichroism (CD) ellipticity at 222 nm in a 1.0 cm light path quartz glass cuvette at various temperatures ranging from 25 to 110 °C at a heating rate of 1 °C/min. CD measurements were carried out in a Jasco J-810 spectropolarimeter with a Peltier temperature-controlled cuvette holder. Protein concentration was 1 mg/mL in 50 mM sodium acetate buffer. The ratio of denatured and total protein in the transition range, $f_d = (\varepsilon_N - \varepsilon)/(\varepsilon_N - \varepsilon_U)$, was calculated from their CD signal $\varepsilon$ relative to the signal of the native and unfolded baseline $\varepsilon_N$ and $\varepsilon_U$. Melting temperature ($T_m$) is defined as the midpoint transition of unfolding of GAD.

was preincubated at various pH values ranging from pH 3.5 to 6.0 for 96 h at 37 °C, and then their residual activities were measured (Figure 3A). For thermostability, purified enzymes were preincubated at various temperatures ranging from 40 to 90 °C, and the residual activity was also determined under the standard assay conditions (Figure 3B). As expected, incubation of *L. plantarum* GAD at pH values in the range of pH 4.0−5.5 caused no significant loss of GAD activity after a 96 h incubation (>90% of original activity). After a 9 h incubation of *L. plantarum* GAD at various temperatures in the range from 40 to 60 °C, the recombinant enzyme retained >95% of original activity, indicating that *L. plantarum* GAD is thermostable. Indeed, the recombinant enzyme with a thermal half-life of 46 min at 90 °C retained approximately 70% of initial activity even after incubation at 70 °C for 9 h, whereas the enzyme was rapidly inactivated at 100 °C. Therefore, these data indicated that the *gadB* gene from *L. plantarum* encodes a thermostable GAD, the structure of which is quite stable at acidic pH and elevated temperatures.

To further investigate the effect of temperature on the stability of *L. plantarum* GAD in more detail, we performed

**Table 1. Biochemical Properties and Kinetic Parameters of *L. plantarum* and Other Microbial GADs[a]**

| microorganism | $T_{opt}$ (°C) | $pH_{opt}$ | $K_m$ (mM) | $k_{cat}$[b] ($min^{-1}$) | $k_{cat}/K_m$ ($mM^{-1}$ $min^{-1}$) | ref |
|---|---|---|---|---|---|---|
| *Lactobacillus plantarum* | 40 | 4.5 | 22.8 ± 1.1[a] | 1304.8 ± 23.3 | 57.2 ± 1.8 | this study |
| *Lactobacillus brevis* IFO 12005 | 30 | 4.2 | 9.3 | 390 | 42 | 19 |
| *Lactobacillus brevis* 877G | 45 | 5.2 | 3.6 | 17.7 | 4.9 | 34 |
| *Lactobacillus paracasei* | 50 | 5 | 5 | 428 | 85.5 | 36 |
| *Lactococcus lactis* | 30 | 4.7 | 0.5 | | | 45 |
| *Neurospora crassa* | | 5.0 | 2.2 | | | 46 |
| *Escherichia coli* | | 4.4 | 1.0 | | | 44 |

[a]Data are means ± standards deviations. [b]$k_{cat}$ is the number of substrate molecules reacted per active site per minute.

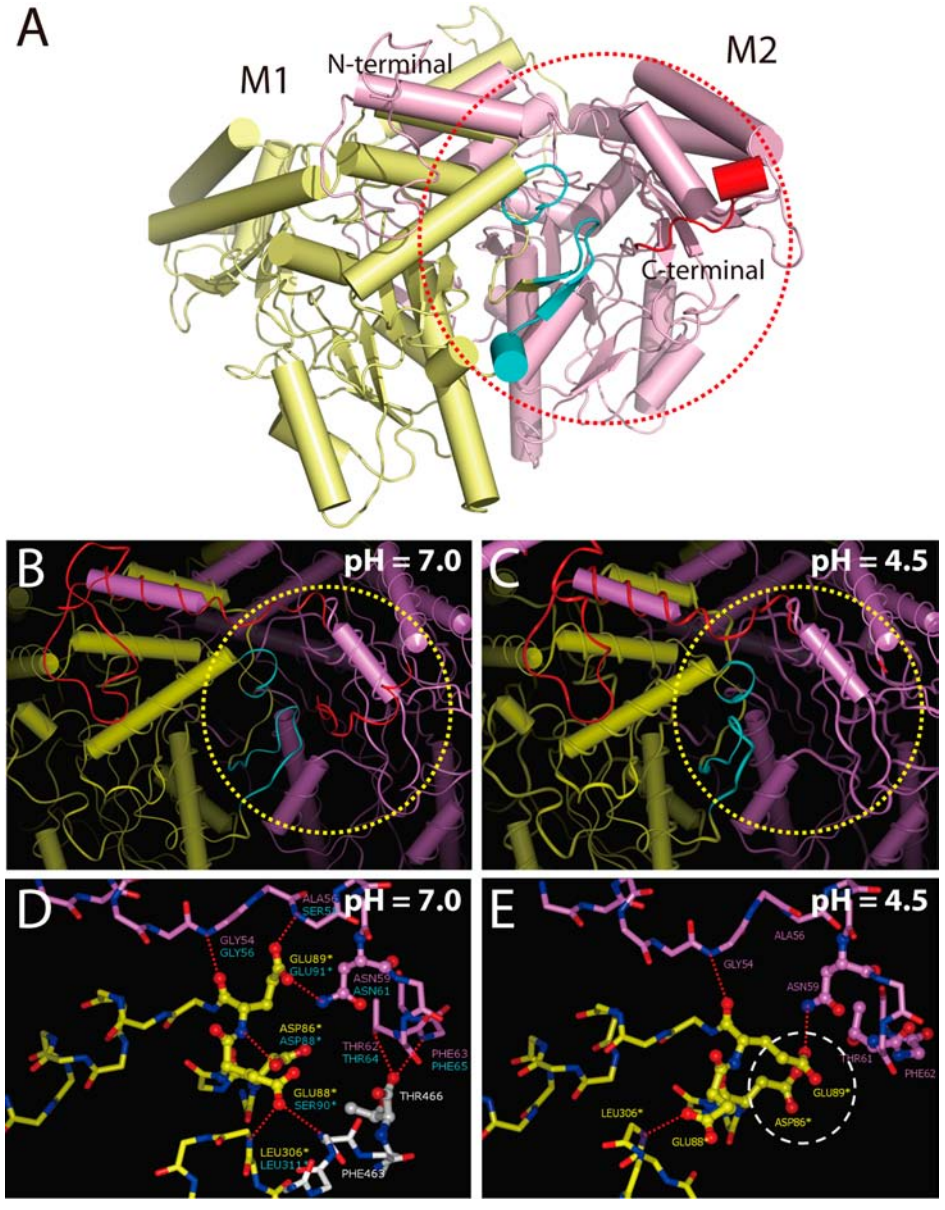


**Figure 4.** Model structure of the dimeric *L. plantarum* GAD and its detailed views. (A) The dimeric *L. plantarum* GAD is shown using cylindrical representations. The modeled structure of *L. plantarum* GAD was generated on the basis of the crystal structure of *E. coli* GAD (PDB code 1PMO) using the SWISS-MODEL program. One monomer (M1, left) is in pale yellow, whereas the other monomer (M2, right) is in pale pink. (B, C) Close-up view of the intersubunit contact regions between the two monomers. N-terminal (1−60 residues, *E. coli* numbering) and C-terminal (Pro452−Thr466, *E. coli* numbering) regions of the monomer (M2) of the *L. plantarum* GAD are in red, and the loop regions (Ile85−Tyr90 and Val300−Phe313, *E. coli* numbering) of the other monomer (M1) are in cyan. (D) The conformation of GAD at normal pH (i.e., pH 7.0) involves C-terminal residues of the protein (colored white) occupying the substrate binding site. Amino acid residues in *L. plantarum* GAD are in blue. (E) At low pH (i.e., pH 4.5), GAD undergoes a conformational change. Red dotted lines indicate hydrogen bonds. Amino acids with asterisks refer to residues specific to the *L. plantarum* GAD sequence.

thermal unfolding experiments using circular dichroism (CD). Thermal unfolding of enzyme was initiated at temperatures beyond the optimal temperature for growth of the corresponding bacterium. Consequently, *L. plantarum* GAD had the apparent melting temperature ($T_m$) of 95 °C (Figure 3C). Together with the thermostability data above, this unfolding experiment clearly demonstrated that *L. plantarum* GAD is not only acidophilic but also thermostable.

To determine the kinetic parameters of *L. plantarum* GAD for glutamate as the substrate, we measured GAD activity after 5 min of incubation at 40 °C as described above. As a result, the $K_m$ for glutamate was 22.8 mM, and the $V_{max}$ was 24.4 U/mg. The catalytic efficiency ($k_{cat}/K_m$) for glutamate was 57.2 $mM^{-1}$ $min^{-1}$ (Table 1). As expected, *L. plantarum* GAD also showed very similar physicochemical properties (i.e., $T_{opt}$ and $pH_{opt}$), in comparison with other microbial GADs including *E. coli* GAD.[44] However, *L. plantarum* GAD had at least a $k_{cat}$ value that is about 3 times higher than for other GADs (Table 1).

**Homology Modeling and Truncation Mutagenesis of *L. plantarum* GAD.** Comparative sequence analysis between *E. coli* and *L. plantarum* GADs was performed by FASTA. *L. plantarum* GAD showed sequence similarity of about 57% with *E. coli* GAD encoded by the *gadB* gene. To provide a structural basis for further investigations of the *L. plantarum* GAD, a homology-based structural modeling was performed as described above (Figure 4). Because the active forms of other microbial GADs derived from *Lactobacillus* strains as well as *E. coli* GadB are known as a dimer and a hexamer, respectively,[12,36] we generated the dimeric model of the *L. plantarum* GAD by superimposing two monomeric models separately into the corresponding monomeric units of *E. coli* GAD and subsequently merging them together by the Biopolymer module of Insight II. To study the interaction between *L. plantarum* GAD and glutamate as the substrate, the crystal structure (PDB code 1PMO) of glutamate bound to GAD was used.

Previously, it has been reported that *E. coli* GAD undergoes a pH-dependent conformational change and exhibits optimal activity at low pH.[12] The GAD enzyme is localized exclusively to the cytoplasm at neutral pH but is recruited to the membrane when pH levels fall. Indeed, our structural modeling by the Insight II program suggested that the Ile85−Tyr90 (*E. coli* numbering) region in M1 adjacent to the other GAD subunit (M2) is where conformational changes occur by mainly Asp86 and Glu89 (*E. coli* numbering) residues in a pH-dependent manner (Figure 4). Intriguingly, such a pH-induced conformational change is accompanied by displacement of the loop region (Val300−Phe313 residues, *E. coli* numbering) away from the entrance site for the substrate at low pH values. Simultaneously, the C-terminal loop region (Pro452−Thr466, *E. coli* numbering) was also pushed away to open the entrance for the substrate binding site at low pH, resulting in the formation of active GAD (Figure 4B,C). On the other hand, both the 300−313 region in M1 and the C-terminal Pro452−Thr466 loop region in M2 occupy the substrate binding site tunnel at neutral pH, resulting in the inactive GAD. These simulation data strongly suggested that the C-terminal loop region may play an important role in the regulation of GAD activity through pH-induced conformational changes. Therefore, we examined whether the C-terminal loop region is mainly involved in the regulation of GAD activity through pH-dependent conformational change. For this, we generated two C-terminally truncated mutants (i.e., GAD Δ3 and GAD Δ11), which contain deletions of 9 and 33 nucleotides, respectively. Notably,

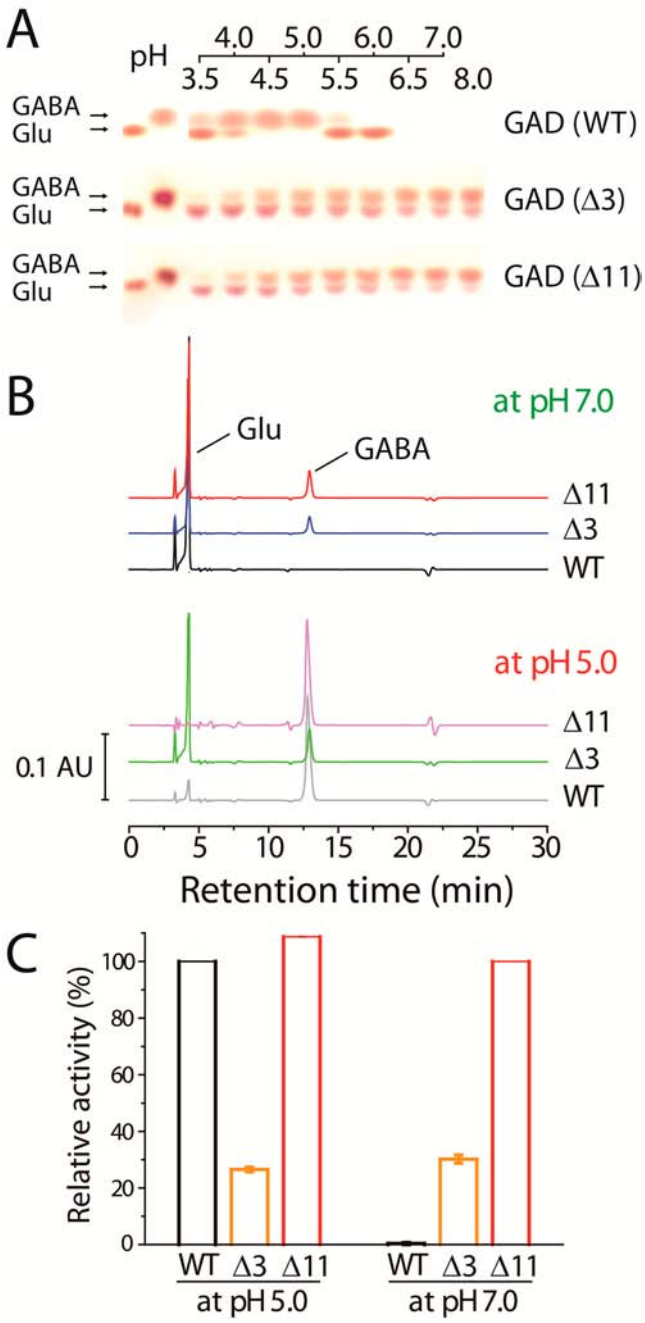


**Figure 5.** pH dependence of catalytic activity for *L. plantarum* GAD and its truncated mutants. After incubation of the wild-type *L. plantarum* GAD and its C-terminally truncated mutants (Δ3 and Δ11) with monosodium glutamate (Glu) as a substrate at different pH values, reaction mixtures were analyzed by (A) TLC and (B) HPLC. (C) Comparison of relative enzyme activities for the wild-type and mutant GADs at pH 5 and 7. The specific activities for the wild-type (8.9 U/mg) and the mutant Δ11 (1.3 U/mg) were set at 100% at pH 5 and 7, respectively.

it was found that the expression level of both truncated mutants in *E. coli* at 25 °C was much higher than that at 37 °C (data not shown). Thus, we purified both mutant enzymes expressed in *E. coli* at 25 °C. After purification of those mutants, their enzymatic activities were then determined on the basis of the production of GABA in a pH range of 3.5−8.0 as judged by thin-layer chromatography. As shown in Figure 5A, the wild-type GAD showed its GABA conversion activity under acidic conditions, indicating that it became an active form at low pH


dx.doi.org/10.1021/jf504656h | J. Agric. Food Chem. 2014, 62, 12186−12193

Table 2. Kinetic Parameters for the Wild-Type GAD and Its Truncated Mutants[a]

| enzyme | pH | $V_{max}$ (U/mg) | $K_m$ (mM) | $k_{cat}$[b] ($min^{-1}$) | $k_{cat}/K_m$ ($mM^{-1}$ $min^{-1}$) |
|---|---|---|---|---|---|
| WT | 5.0 | 24.4 ± 0.4 | 22.8 ± 1.1 | 1304.8 ± 23.3 | 57.2 ± 1.8 |
| | 7.0 | nd[c] | 122.1 ± 3.8 | 0.91 ± 0.01 | nd |
| Δ11 | 5.0 | 45.1 ± 2.9 | 33.8 ± 4.3 | 2415.2 ± 156.5 | 72.1 ± 4.6 |
| | 7.0 | 1.3 ± 0. 1 | 137.1 ± 11.2 | 29.1 ± 0.9 | 0.2 ± 0.1 |

[a]Data are means ± standards deviations. The kinetic parameters were obtained by fitting the experimental data with the Michaelis−Menten equation as follows: $v = V_{max}[S]/K_m + [S]$. [b]$k_{cat}$ is the number of substrate molecules reacted per active site per minute. [c]nd, not determined.

values (pH 3.5−5.0). However, the enzyme did not show any activity at pH 5.5−6.0. On the other hand, both GAD Δ3 and GAD Δ11 exhibited pronounced enzyme activity in the broader pH range of 3.5−8.0. On the basis of these qualitative results, we also performed a HPLC analysis to compare the GAD activities for the wild-type and mutant enzymes (Figure 5B). At pH 5, both truncated enzymes showed lower activities than the wild-type enzyme, as expected. However, although the wild-type enzyme exhibited little activity, both mutants had pronounced GABA peaks at pH 7. Indeed, the amounts of GABA produced by Δ11 and Δ3 mutants were much higher than that of the wild-type enzyme (Figure 5C). These data clearly indicated that deletion of the Ile454−Thr468 region (corresponding to Pro452−Thr466 in *E. coli* GAD) at the C-terminus of *L. plantarum* GAD caused loss of sensitivity to change in pH values. In addition, together with the prediction data, these observations strongly suggested that the C-terminal region might function as a lid for the entrance of glutamate as the substrate, thereby regulating the GAD activity.

**Comparison of the pH Dependence of GAD Activity with Its Truncated Mutants.** To further investigate the pH dependence of the C-terminal domain for GAD activity, we determined the kinetic parameters for the wild-type GAD and its Δ11 mutant at pH 5 and 7. As described in Table 2, the wild-type enzyme showed the $V_{max}$ value of 24.4 at pH 5, whereas its enzyme activity was negligible at pH 7 as expected and described elsewhere.[22] GAD Δ11 showed higher activity than the wild-type at pH 5 (Figure 5C), which is clearly supported by the kinetic values (Table 2). This might be ascribed to the deletion of the C-terminal loop region, where glutamate is more freely accessible to the substrate binding site of GAD. Indeed, even at pH 7 at which there is no activity detected from the wild-type enzyme, the GAD Δ11 mutant showed a prominent level of enzyme activity (0.54 U/mg) with an unusually high $k_{cat}$ value (Table 2), although it had lower levels of activity than those of the wild-type and mutant enzymes at pH 5. To date, it has been noted that the critical feature of microbial GADs is the conformational change of a calmodulin (CaM)-binding domain in the C-terminal region of *Saccharomyces cerevisiae* and the N-termini of *E. coli* GadB for the acidic pH optimum.[12,37] Therefore, our HPLC analysis and kinetic data clearly demonstrated that the C-terminus of *L. plantarum* GAD plays an important role in the regulation of enzyme activity for the pH alteration of environments. These data also provide biochemical evidence for the involvement of protein in functioning as a molecular switch for acid resistance as described in refs 12, 29, 37, and 44.

In this study, we expressed the *gadB* gene-encoding GAD from *L. plantarum* as the generally recognized as safe (GRAS) strain and characterized the recombinant enzyme. Characterization of its physicochemical properties (i.e., the $pH_{opt}$, $temp_{opt}$, thermostability, $V_{max}$, $k_{cat}$, etc.) demonstrated that this *L. plantarum* GAD has properties (i.e., an acidic pH optimum of 5.0 for enzymatic activity) very similar to those of other microbial GADs in terms of the pH dependence of enzyme activity. Its 3D structural model suggested that the C-terminal loop region may be critical for the pH dependence of enzyme activity at low pH. Such a pH-induced GAD activity through conformational changes such as the molecular switch can be a useful engineering target for altering the $pH_{opt}$ of GAD, which allows us to create GAD mutants that are resilient to pH fluctuations. Therefore, this feature might be beneficial for engineering GAD with the broad range of pH optimum for its catalytic activity in the immobilization of the enzyme for the production of GABA.

## AUTHOR INFORMATION


### Corresponding Author

*(D.-W. L.) Phone: +82-53-950-5718. Fax: +82-53-953-7233. E-mail: leehicam@knu.ac.kr.

### Author Contributions

‖S.-M.S. and H.K. contributed equally to the work.



### Funding

This work was supported by the National Agenda Program for Agricultural R&D (PJ0097672014) from the Rural Development Administration and the Basic Science Research Program through the National Research Foundation of Korea (NRF-2012R1A1A2042114), South Korea.

### Notes

The authors declare no competing financial interest.


## ACKNOWLEDGMENTS


We greatly appreciate Do-Yoon Kim's critical contribution to 3D modeling and structural analysis.


## REFERENCES


(1) Foster, A. C.; Kemp, J. A. Glutamate- and GABA-based CNS therapeutics. *Curr. Opin. Pharmacol.* **2006**, *6*, 7−17.

(2) Kakee, A.; Takanaga, H.; Terasaki, T.; Naito, M.; Tsuruo, T.; Sugiyama, Y. Efflux of a suppressive neurotransmitter, GABA, across the blood-brain barrier. *J. Neurochem.* **2001**, *79*, 110−118.

(3) Khakhalin, A. S. Questioning the depolarizing effects of GABA during early brain development. *J. Neurophysiol.* **2011**, *106*, 1065−1067.

(4) Mihic, S. J.; Ye, Q.; Wick, M. J.; Koltchine, V. V.; Krasowski, M. D.; Finn, S. E.; Mascia, M. P.; Valenzuela, C. F.; Hanson, K. K.; Greenblatt, E. P.; Harris, R. A.; Harrison, N. L. Sites of alcohol and volatile anaesthetic action on GABA(A) and glycine receptors. *Nature* **1997**, *389*, 385−389.

(5) Jeng, K. C.; Chen, C. S.; Fang, Y. P.; Hou, R. C.; Chen, Y. S. Effect of microbial fermentation on content of statin, GABA, and polyphenols in pu-erh tea. *J. Agric. Food Chem.* **2007**, *55*, 8787−8792.

(6) Di Cagno, R.; Mazzacane, F.; Rizzello, C. G.; De Angelis, M.; Giuliani, G.; Meloni, M.; De Servi, B.; Gobbetti, M. Synthesis of γ-aminobutyric acid (GABA) by *Lactobacillus plantarum* DSM19463: functional grape must beverage and dermatological applications. *Appl. Microbiol. Biotechnol.* **2010**, *86*, 731−741.

(7) Chiu, T. H.; Tsai, S. J.; Wu, T. Y.; Fu, S. C.; Hwang, Y. T. Improvement in antioxidant activity, angiotensin-converting enzyme inhibitory activity and in vitro cellular properties of fermented pepino milk by *Lactobacillus* strains containing the glutamate decarboxylase gene. *J. Sci. Food Agric.* **2013**, *93*, 859−866.
(8) Lee, S.; Ahn, J.; Kim, Y. G.; Jung, J. K.; Lee, H.; Lee, E. G. γ-Aminobutyric acid production using immobilized glutamate decarboxylase followed by downstream processing with cation exchange chromatography. *Int. J. Mol. Sci.* **2013**, *14*, 1728−1739.
(9) Binh, T.; Ju, W.-T.; Jung, W.-J.; Park, R.-D. Optimization of γ-amino butyric acid production in a newly isolated *Lactobacillus brevis*. *Biotechnol. Lett.* **2014**, *36*, 93−98.
(10) Stromeck, A.; Hu, Y.; Chen, L.; Gänzle, M. G. Proteolysis and bioconversion of cereal proteins to glutamate and γ-aminobutyrate (GABA) in rye malt sourdoughs. *J. Agric. Food Chem.* **2011**, *59*, 1392−1399.
(11) Mazuelos, A.; Moreno, J. M.; Carranza, F.; Palomino, C.; Torres, A.; Villalobo, E. Biotic factor does not limit operational pH in packed-bed bioreactor for ferrous iron biooxidation. *J. Ind. Microbiol. Biotechnol.* **2012**, *39*, 1851−1858.
(12) Capitani, G.; De Biase, D.; Aurizi, C.; Gut, H.; Bossa, F.; Grutter, M. G. Crystal structure and functional analysis of *Escherichia coli* glutamate decarboxylase. *EMBO J.* **2003**, *22*, 4027−4037.
(13) De Biase, D.; Tramonti, A.; Bossa, F.; Visca, P. The response to stationary-phase stress conditions in *Escherichia coli*: role and regulation of the glutamic acid decarboxylase system. *Mol. Microbiol.* **1999**, *32*, 1198−1211.
(14) Castanie-Cornet, M. P.; Penfound, T. A.; Smith, D.; Elliott, J. F.; Foster, J. W. Control of acid resistance in *Escherichia coli*. *J. Bacteriol.* **1999**, *181*, 3525−3535.
(15) Cotter, P. D.; Gahan, C. G.; Hill, C. A glutamate decarboxylase system protects *Listeria monocytogenes* in gastric fluid. *Mol. Microbiol.* **2001**, *40*, 465−475.
(16) Sanders, J. W.; Leenhouts, K.; Burghoorn, J.; Brands, J. R.; Venema, G.; Kok, J. A chloride-inducible acid resistance mechanism in *Lactococcus lactis* and its regulation. *Mol. Microbiol.* **1998**, *27*, 299−310.
(17) Teixeira, J. S.; Seeras, A.; Sanchez-Maldonado, A. F.; Zhang, C.; Su, M. S.-W.; Gänzle, M. G. Glutamine, glutamate, and arginine-based acid resistance in *Lactobacillus reuteri*. *Food Microbiol.* **2014**, *42*, 172−180.
(18) Ma, D.; Lu, P.; Shi, Y. Substrate selectivity of the acid-activated glutamate/γ-aminobutyric acid (GABA) antiporter GadC from *Escherichia coli*. *J. Biol. Chem.* **2013**, *288*, 15148−15153.
(19) Ueno, Y.; Hayakawa, K.; Takahashi, S.; Oda, K. Purification and characterization of glutamate decarboxylase from *Lactobacillus brevis* IFO 12005. *Biosci., Biotechnol., Biochem.* **1997**, *61*, 1168−1171.
(20) Meng, S. Y.; Bennett, G. N. Nucleotide sequence of the *Escherichia coli* cad operon: a system for neutralization of low extracellular pH. *J. Bacteriol.* **1992**, *174*, 2659−2669.
(21) Blankenhorn, D.; Phillips, J.; Slonczewski, J. L. Acid- and base-induced proteins during aerobic and anaerobic growth of *Escherichia coli* revealed by two-dimensional gel electrophoresis. *J. Bacteriol.* **1999**, *181*, 2209−2216.
(22) Feehily, C.; Karatzas, K. A. Role of glutamate metabolism in bacterial responses towards acid and other stresses. *J. Appl. Microbiol.* **2013**, *114*, 11−24.
(23) Kieboom, J.; Abee, T. Arginine-dependent acid resistance in *Salmonella enterica* serovar Typhimurium. *J. Bacteriol.* **2006**, *188*, 5650−5653.
(24) Park, Y. K.; Bearson, B.; Bang, S. H.; Bang, I. S.; Foster, J. W. Internal pH crisis, lysine decarboxylase and the acid tolerance response of *Salmonella typhimurium*. *Mol. Microbiol.* **1996**, *20*, 605−611.
(25) Alvarez-Ordonez, A.; Fernandez, A.; Bernardo, A.; Lopez, M. Arginine and lysine decarboxylases and the acid tolerance response of *Salmonella* Typhimurium. *Int. J. Food Microbiol.* **2010**, *136*, 278−282.
(26) Blethen, S. L.; Boeker, E. A.; Snell, E. E. Argenine decarboxylase from *Escherichia coli*. I. Purification and specificity for substrates and coenzyme. *J. Biol. Chem.* **1968**, *243*, 1671−1677.
(27) Hersh, B. M.; Farooq, F. T.; Barstad, D. N.; Blankenhorn, D. L.; Slonczewski, J. L. A glutamate-dependent acid resistance gene in *Escherichia coli*. *J. Bacteriol.* **1996**, *178*, 3978−3981.
(28) Smith, D. K.; Kassam, T.; Singh, B.; Elliott, J. F. *Escherichia coli* has two homologous glutamate decarboxylase genes that map to distinct loci. *J. Bacteriol.* **1992**, *174*, 5820−5826.
(29) Feehily, C.; O'Byrne, C. P.; Karatzas, K. A. Functional γ-aminobutyrate shunt in *Listeria monocytogenes*: role in acid tolerance and succinate biosynthesis. *Appl. Environ. Microbiol.* **2013**, *79*, 74−80.
(30) Shi, F.; Li, Y. Synthesis of γ-aminobutyric acid by expressing *Lactobacillus brevis*-derived glutamate decarboxylase in the *Corynebacterium glutamicum* strain ATCC 13032. *Biotechnol. Lett.* **2011**, *33*, 2469−2474.
(31) De Biase, D.; Tramonti, A.; John, R. A.; Bossa, F. Isolation, overexpression, and biochemical characterization of the two isoforms of glutamic acid decarboxylase from *Escherichia coli*. *Protein Expr. Purif.* **1996**, *8*, 430−438.
(32) Lin, J.; Lee, I. S.; Frey, J.; Slonczewski, J. L.; Foster, J. W. Comparative analysis of extreme acid survival in *Salmonella typhimurium*, *Shigella flexneri*, and *Escherichia coli*. *J. Bacteriol.* **1995**, *177*, 4097−4104.
(33) Lin, J.; Smith, M. P.; Chapin, K. C.; Baik, H. S.; Bennett, G. N.; Foster, J. W. Mechanisms of acid resistance in enterohemorrhagic *Escherichia coli*. *Appl. Environ. Microbiol.* **1996**, *62*, 3094−3100.
(34) Seo, M. J.; Nam, Y. D.; Lee, S. Y.; Park, S. L.; Yi, S. H.; Lim, S. I. Expression and characterization of a glutamate decarboxylase from *Lactobacillus brevis* 877G producing γ-aminobutyric acid. *Biosci., Biotechnol., Biochem.* **2013**, *77*, 853−856.
(35) Park, J. Y.; Jeong, S. J.; Kim, J. H. Characterization of a glutamate decarboxylase (GAD) gene from *Lactobacillus zymae*. *Biotechnol. Lett.* **2014**, *36*, 1791−1799.
(36) Komatsuzaki, N.; Nakamura, T.; Kimura, T.; Shima, J. Characterization of glutamate decarboxylase from a high γ-aminobutyric acid (GABA)-producer *Lactobacillus paracasei*. *Biosci., Biotechnol., Biochem.* **2008**, *72*, 278−285.
(37) Coleman, S. T.; Fang, T. K.; Rovinsky, S. A.; Turano, F. J.; Moye-Rowley, W. S. Expression of a glutamate decarboxylase homologue is required for normal oxidative stress tolerance in *Saccharomyces cerevisiae*. *J. Biol. Chem.* **2001**, *276*, 244−250.
(38) Laemmli, U. K. Cleavage of structural proteins during the assembly of the head of bacteriophage T4. *Nature* **1970**, *227*, 680−685.
(39) Eswar, N.; Webb, B.; Marti-Renom, M. A.; Madhusudhan, M. S.; Eramian, D.; Shen, M. Y.; Pieper, U.; Sali, A. Comparative protein structure modeling using Modeller. *Curr. Protoc. Bioinformatics* **2006**, Chapter 5, Unit 5-6.
(40) Vriend, G. WHAT IF: a molecular modeling and drug design program. *J. Mol. Graph.* **1990**, *8* (52−56), 29.
(41) Verlet, L. Computer "experiments" on classical fluids. I. Thermodynamical properties of Lennard-Jones molecules. *Phys. Rev.* **1967**, *159*, 98−103.
(42) Ryckaert, J. P.; Ciccotti, G.; Berendsen, H. J. C. Numerical integration of the cartesian equations of motion of a system with constraints: molecular dynamics of n-alkanes. *J. Comput. Phys.* **1977**, *23*, 327−341.
(43) Holdiness, M. R. Chromatographic analysis of glutamic acid decarboxylase in biological samples. *J. Chromatogr.* **1983**, *277*, 1−24.
(44) Fonda, M. L. L-Glutamate decarboxylase from bacteria. *Methods Enzymol.* **1985**, *113*, 11−16.
(45) Nomura, M.; Nakajima, I.; Fujita, Y.; Kobayashi, M.; Kimoto, H.; Suzuki, I.; Aso, H. *Lactococcus lactis* contains only one glutamate decarboxylase gene. *Microbiology* **1999**, *145* (Part 6), 1375−1380.
(46) Hao, R.; Schmit, J. C. Purification and characterization of glutamate decarboxylase from *Neurospora crassa conidia*. *J. Biol. Chem.* **1991**, *266*, 5135−5139.

Table 1. Polymerase Chain Reaction (PCR) Primers Used for Metabolite Gene Screening

| primer | target | sequence (5′−3′)[a] |
|---|---|---|
| GBF | PKS | RTRGAYCCNCAGCAICG[5] |
| GBR | PKS | VGTNCCNGTGCCRTG[5] |
| GCF | PKS | GCSATGGAYCCSCARCARCGSVT[31] |
| GCR | PKS | GTSCCSGTSCRTGSSCYTCSAC[31] |
| KSDPOOF | PKS | MGNGARGARGCNNWNSMNATGGAYCCNCARCANMG[5] |
| KSHGTGr | PKS | GGRTCNCCNARNSWNGTNCCNGTNCCRTG[5] |
| KS11f | PKS | GCIATGGAYCCICARCARMGIVT[31] |
| KS12r | PKS | GTICCIGTICCRTGISCYTCIAC[31] |
| MTF | PKS | GCNGGYGGYGCNTAYGTNCC[32] |
| MTR | PKS | CCNCGDATYTTNACYTG[32] |

[a]The superscript numbers indicate the references.

experiments. Standard pulse sequences were used for DEPT, $^1$H−$^1$H COSY, and two-dimensional NOESY, HMQC, and HMBC experiments. Liquid chromatography−mass spectrometry experiments were performed on an Applied Biosystems QTrap 2000 (Applied Biosystems, Darmstadt, Germany) coupled to an Agilent 1100 HPLC system (Agilent, Waldbronn, Germany) using a Luna 5 μm C18 column (100 A, 100 × 4.6 mm, Phenomenex, Aschaffenburg, Germany) or a Luna 3 μm C18 column (100 A, 50 × 1.0 mm, Phenomenex) and a gradient of solvents A (0.1% HCOOH) and B ($CH_3CN$ + 0.1% HCOOH, gradient 0% B to 100% B in 10 min) with a flow rate of 1.5 mL/min or 60 μL/min, respectively. ESI-MS spectra were acquired in the positive and negative modes with a turboionspray voltage, curtain gas, turbo temperature, and nebulizer gas of −4500 V, 30 psi, 500 °C, and 50 psi (flow rate at 1.5 mL/min), respectively. The microbial strains *Vibrio harveyi* MTCC 3438, and *Vibrio vulnificus* MTCC 1146 were procured from the Microbial Type Culture Collection Centre of Institute of Microbial Technology, Chandigarh, India, whereas *Vibrio parahemolyticus* ATCC 17809 was procured from the American Type Culture Collection, Manassas, VA, USA. The solvents used for preparing samples were of analytical grade (E-Merck, Darmstadt, Germany) and were redistilled in an all-glass system. Doubly distilled water was used throughout this work. All of the reagents used in this study were of analytical grade and purchased from E-Merck.

**Isolation of Antagonistic Bacterial Isolates Associated with Seaweeds.** Intertidal seaweeds belonging to Phaeophyceae and Rhodophyceae were collected by scuba diving from the intertidal zone of Mandapam situated at 9° 17′ 0″ N, 79° 7′ 0″ E, Gulf of Mannar region along the southeastern coast of India. The brown seaweeds collected were *Anthophycus longifolius*, *Sargassam myriocystum*, *Padina gymnospora*, *Turbinaria ornata*, and *Dictyota dichomata*, whereas red seaweeds were *Hypnea valentiae* and *Laurentiae pappilosa*. Seaweed samples were processed and the associated bacterial strains were isolated as described earlier.[1] The isolated strains were assayed for antagonistic activity against pathogens including food pathogens *Vibrio parahemolyticus* (ATCC 17802), *Vibrio parahemolyticus* MTCC451, *Vibrio vulnificus* MTCC1145, *Aeromonas hydrophilla*,*Vibrio angullarum*, and *Vibrio alginolyticus*. The inhibitory activity was assayed by a spot over lawn assay as described earlier.[6] Briefly the pathogens were grown to the log phase in nutrient broth with 1% sodium chloride ($10^8$ CFU/mL). They were then swabbed on Mueller−Hinton agar (HiMedia) with 1% NaCl over which the purified isolates were spotted (3 mm diameter) under sterile conditions. The plates were then incubated at 30 °C for 24−72 h, and the zone of inhibition observed around the isolates was recorded. The bacteria showing antibacterial activity were preserved in nutrient agar slants and in 20% glycerol stocks at −80 °C until further use.

**Identification of the Active Isolates.** Bacteria with antagonistic properties were identified using classical biochemical methods followed by 16S rRNA gene sequencing. DNA was extracted from the bacterial isolates showing inhibitory activity against test bacteria. Extraction was conducted from bacterial cultures grown in nutrient broth using the phenol−chloroform extraction method.[10] The DNA samples were examined by gel electrophoresis and concentrations estimated using a Biophotometer (Eppendorf, Germany). PCR was performed in a total volume of 25 μL containing 1× reaction buffer with $MgCl_2$ (Sigma), 0.25 mM of each dNTP (Fermentas), 0.5 mM of each primer (Sigma), 1 ng of DNA, and 0.3 U of Taq DNA polymerase (Sigma). The following cycling conditions were used: initial denaturation at 94 °C for 5 min, followed by 30 cycles of 95 °C for 1 min, 58 °C for 1 min, and 72 °C for 2 min, with a final extension 72 °C for 5 min (Bio-Rad, Hercules, CA, USA). The primers used were AGAGTTTGATCCTGGCTCAG (forward) and ACGGCTACCTTGTTACGACTT (reverse).[11] The molecular sizes of the amplified fragments were estimated by comparison with a 1 kb ladder on a 1.5% (w/v) agarose gel using 1× TAE buffer at 80 V. Fragments with the expected size were gel-purified using a GelElute gel extraction kit (Sigma) following the manufacturer's protocol and sequenced. Sequence data were deposited in GenBank and compared with existing sequences using the blastn search program. Sequences were aligned against reference sequences with CLUSTALW software of the Bioedit program, and the aligned data set was used as input for phylogenetic analysis program. The evolutionary history was inferred using the neighbor-joining method based on the Kimura two-parameter model and bootstrap analysis with 1000 replications.[12,13] Evolutionary analyses were conducted in MEGA6.[14]

**Screening of Metabolite Genes.** Different sets of degenerate primers targeting genes encoding *pks-I* and *nrps* were used to screen the biosynthetic potential of the bacterial isolates to elicit bioactive polyketide compounds and nonribosomal peptides. The primers are listed in Table 1. PCR was performed in a total volume of 25 μL containing 1× reaction buffer with $MgCl_2$ (Sigma), 0.25 mM of each dNTP (Fermentas), 0.5 mM of each primer (Sigma), 1 ng of DNA, and 0.3 U of Taq DNA polymerase (Sigma). The PCR process was set as initial denaturation 5 min at 94 °C followed by 35 cycles of 1 min at 95 °C, 1 min at 45 °C, 1 min at 72 °C, and a final extension of 5 min at 72 °C. All of the amplification products were examined by 1.5% agarose gel electrophoresis, and bands of 700−800 and 1000−1400 bp were classified as products of *pks-I* and *nrps* genes, respectively. Polymerase chain reaction amplicons were separated by agarose gel electrophoresis, and the bands of expected size were gel-purified using electrophoresis; bands of 700−800 bp (*pks-I*) and 1000−1400 bp (*nrps*) were gel-purified using a Gel Elute Gel Extraction Kit (Sigma) and cloned into the pGET-Blunt M13 vector (Fermentas) following the manufacturer's instructions and transformed into chemocompetent *Escherichia coli* cells. The positive recombinants were screened by ampicillin-resistant recombinant selection method assisted with colony PCR with M13 specific primers. Positive clones were used for plasmid isolation using a GenJET Plasmid isolation kit (Fermentas) and sequenced using M13 F and M13 R primers. Forward and reverse sequences of the PKS gene amplified product were assembled using Dna Baser v2.exe, and the vector sequences were removed using Vescreen (NCBI). The sequence data were subjected to GenBank searches with the blastx algorithm. Nucleotide sequences were translated into peptide sequences by EMBOSS Transeq (EMBL-EBI), and blastp searches of deduced amino acid sequences were also

Table 2. NMR Spectroscopic Data of 7-*O*-Methyl-5′-hydroxy-3′-heptenoate−Macrolactin in $CDCl_3$[a]

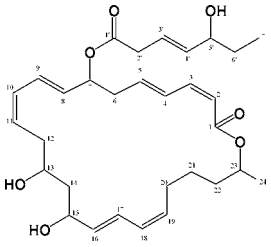

| carbon | $^{13}$C NMR (DEPT) | H | $\delta^1$H NMR[b] (int, mult, *J* in Hz) | $^1$H−$^1$H COSY | HMBC ($^1$H−$^{13}$C) |
|---|---|---|---|---|---|
| 1 | 165.16 (C) | | | | |
| 2 | 116.11 (CH) | 2H | 5.60 (d, *J* = 11.2) | | |
| 3 | 143 (CH) | 3H | 6.74 (t, *J* = 11.1) | H-2, H-4 | C-4 |
| 4 | 127 (CH) | 4H | 7.25 (dd, 15.2, 11.1) | | |
| 5 | 142.7 (CH) | 5H | 6.19 (dt, *J* = 15.3, 7.1) | | |
| 6 | 42.69 ($CH_2$) | 6H$^a$, 6H$^b$ | 6H$^a$ at 2.60 (m), 6H$_b$ at 2.04 (m) | H-7 | |
| 7 | 73.2 (CH) | 7H | 5.05 (td) | H-8, H-6 | C-1$^1$, C-8 |
| 8 | 139 (CH) | 8H | 5.71 (dd, *J* = 15.2, 6.1) | H-9 | |
| 9 | 125.02 (CH) | 9H | 6.40 (dd, 15.1, 11.3) | | |
| 10 | 130.308 (CH) | 10H | 6.17 (m) | H-11 | |
| 11 | 127 (CH) | 11H | 5.71 (dt, *J* = 10.6, 8.4) | H-12, H-10 | |
| 12 | 38.08 ($CH_2$) | 12 H$^a$, 12H$^b$ | 12 H$^a$ at 2.68 (m), 12H$^b$ at 2.33 (m) | H-13 | C-14 |
| 13 | 67.5 (CH) | 13H | 3.42 (dd) (4.02, OH) | H-14 | |
| 14 | 45.41 ($CH_2$) | 14H$^a$, 14H$^b$ | 14H$^a$ at 1.94 (m), 14H$^b$ at 1.78 (m) | | |
| 15 | 67.5 (CH) | 15H | 4.84 (dt, *J* = 6.1, 6.1) (3.79, OH) | | C-13, C-16 |
| 16 | 135.20 (CH) | 16H | 5.80 (dd, *J* = 15.4, 6.2) | H-17 | |
| 17 | 127 (CH) | 17H | 6.29 (dd, *J* = 15.1, 10.6) | | |
| 18 | 130.3 (CH) | 18H | 6.1 9 (t, 10.6) | H-19 | |
| 19 | 135 (CH) | 19H | 5.72 (ddd, *J* = 14.2, 7.0, 6.7) | | |
| 20 | 31.9 ($CH_2$) | 20H$^a$, 20H$^b$ | 20H$^a$ at 2.07 (m), 20H$^b$ at 1.96 | | |
| 21 | 24.30 ($CH_2$) | 21H$^a$, 21H$^b$ | 21H$^a$ at 1.60 (m), 21H$^b$ at 1.81 (dt, 11.2, 5.2) | H-22 | C-1, C-24, C-23 |
| 22 | 35.93($CH_2$) | 22H$^a$, 22H$^b$ | 22H$^a$ at 1.54 (m), 22H$^b$ at 1.43 (m) | | |
| 23 | 71.72 (CH) | 23H | 4.99 (ddq, *J* = 4.5, 7.1, 5.1) | H-24 | |
| 24 | 20.10 ($CH_3$) | | 1.30 (d, *J* = 6.1) | | |
| 1$^1$ | 169.54 (C) | | | | |
| 2$^1$ | 50.8 ($CH_2$) | H$^a$, H$^b$ | H$^a$ at 2.26, H$^b$ at 2.35 | H-3$^1$ | |
| 3$^1$ | 139 (CH) | | 4.06 (dt, *J* = 15.6, 7.4) | H-4$^1$, H-2$^1$ | |
| 4$^1$ | 147 (CH) | | 6.18 (dd, *J* = 17.4, 7.2) | H-3$^1$ | |
| 5$^1$ | 75.4 (CH) | | 4.94 (m) (3.16, OH) | H-4$^1$ | |
| 6$^1$ | 31.94 ($CH_2$) | | 1.21 (m) | H-7$^1$ | C-4 $^1$, C-7 $^1$ |
| 7$^1$ | 14.1 ($CH_3$) | | 0.81 (t) | | C-6 $^1$ |

[a]NMR spectra recorded on a Bruker AVANCE III 500 MHz (AV 500) spectrometer (Bruker, Karlsruhe, Germany) in $CDCl_3$ as aprotic solvent at ambient temperature with TMS as the internal standard ($\delta$ 0). [b]Values in ppm, multiplicity and coupling constants (*J*1/4 Hz) are indicated in parentheses. Assignments were made with the aid of the $^1$H−$^1$H COSY, HMQC, and HMBC experiments.

performed. Partial 16S rRNA gene sequences were deposited under accession numbers KC559432−KC559434, KC510279−KC510286, and JX203227−JX203230, and partial PKS sequences were deposited under accession numbers KC589396−KC589400 and KC607821−KC607823.

**Purification and Characterization of 7-*O*-Methyl-5′-hydroxy-3′-heptenoate−Macrolactin from Seaweed-Associated *Bacillus subtilis* MTCC 10403.** The antibiotic-producing bacterium SWI 2 (*Bacillus subtilis* MTCC 10403) was isolated from *Anthophycus longifolius*. The preparation and recovery of secondary metabolites were carried out by a surface culturing method over solid nutrient agar plates. The adsorbed products were subsequently extracted with ethyl acetate by agitation followed by hot extraction at 40 °C. Evaporation of the solvent under reduced pressure yielded the ethyl acetate extract (230 mg) from the total culture volume of 4 L. The pooled ethyl acetate extract (2.3 g) was fractionated by chromatography over silica gel (180−230 mesh) in a flash column chromatograph (Biotage SP, SP1-B1A, Biotage AB, Sweden), with a stepwise gradient of $CH_2Cl_2$/MeOH (0−100% MeOH) using the flash silica gel cartridge (Biotage no. 25+M 0489-1) at a collection UV wavelength at 236 nm to provide 43 fractions (12 mL, F1−23). Fractions F13−17 as eluted by $CH_2Cl_2$/MeOH (3:2 to 1:1, v/v) were pooled together (81.8 mg) and further applied to a silica gel column (80−120 mesh) to yield four subfractions ($F13_1$−$F13_4$). Subfraction $F13_3$ was purified by preparatory TLC ($CH_2Cl_2$/MeOH, 4:1, v/v) to afford 7-*O*-methyl-5′-hydroxy-3′-heptenoate−macrolactin (99% purity, 10.2 mg). Evaporation of solvents from the fractions followed by TLC over precoated silica gel $GF_{254}$ (particle size = 15 mm, E-Merck) using $CH_2Cl_2$/MeOH (99:1, v/v) supported the purity. 7-*O*-Methyl-5′-hydroxy-3′-heptenoate−macrolactin: amorphous solid; UV (MeOH) $\lambda_{max}$ (log $\varepsilon$) 226 nm (3.72) and 248 nm (3.21); TLC (Si gel $GF_{254}$ 15 mm; $CH_2Cl_2$/MeOH 1:99, v/v) $R_f$ 0.70; Rt 6.22 min; IR $\nu_{max}$ (KBr) $cm^{-1}$ 970 (trans C═C oop bending), 1073.71 (unsaturated secondary alcohol C—O str), 1121.80 (C—O—C symmetrical str), 1282.20 (CH—OH in plane bending), 1376.96 (O═C—$CH_2$, C—H bending), 1461.43 (C—H asym-bending), 1640.23 (C═C str), 1753.96 ($\alpha,\beta$-unsaturated C═O str), 2854.74 (−O—$CH_2$ sym C—H str), 2923.22 (alkane C—H str), 3014 (asym alkene C−H str),

**Table 3. Antimicrobial Spectrum of Candidate Strains and Occurrence of Metabolite Genes**

| | | | antimicrobial activity (mm) against test pathogens[a] | | | | | | | presence of metabolite gene[b] | |
|---|---|---|---|---|---|---|---|---|---|---|---|
| strain | seaweed host | seaweed-associated strains[c] | *V. parahemolyticus* ATCC 17802 | *V. parahemolyticus* MTCC 451 | *V. vulnificus* MTCC 1145 | *A. hydrophilla* | *V. harveyi* | *V. angullarum* | *V. alginolyticus* | *pks* | *nrps* |
| SWI 1 | *Anthophycus longifolium* | *B. cereus* MTCC 10404 | 17 ± 1.00 | 17 ± 1.00 | 12 ± 2.50 | 12 ± 1.00 | 8 ± 1.15 | ND | ND | N | N |
| SWI 2 | *Anthophycus longifolium* | *B. subtilis* MTCC 10403 | 20 ± 2.00 | 22 ± 2.50 | 17 ± 0.20 | 13 ± 1.00 | 14 ± 1.53 | 12 ± 2.00 | 14 ± 1.50 | P[a] | N |
| SWI 3 | *Padina gymnospora* | *B. subtilis* MTCC 10403[B] | 15 ± 1.15 | 17 ± 1.50 | 22 ± 1.50 | 12 ± 2.00 | 15 ± 1.00 | 11.3 ± 1.20 | 15 ± 1.00 | P[b] | N |
| SWI 4A | *Laurentia papillosa* | *B. subtilis* MTCC 10402 | 13 ± 1.15 | 15 ± 1.20 | 18 ± 1.50 | 14 ± 1.00 | 13 ± 1.15 | 11.3 ± 1.20 | 13 ± 1.20 | N | N |
| SWI 4B | *Laurentia papillosa* | *B. amyloliquefacens* MTCC 10456[C] | 16 ± 1.53 | 14 ± 1.50 | 18 ± 1.00 | 15 ± 3.00 | ND | ND | ND | P[c] | N |
| SWI 5 | *Turbinaria ornata* | *B. amyloliquefacens* MTCC 10456 | 18 ± 1.15 | 14 ± 0.60 | 16 ± 1.00 | 14 ± 2.00 | 14 ± 0.58 | 12.3 ± 0.60 | 13 ± 1.20 | P[d] | N |
| SWI 6 | *Hypnea valentiae* | *B. amyloliquefacens* MTCC 10456[D] | 14 ± 0.58 | 15 ± 1.00 | 18 ± 0.60 | 14 ± 0.00 | 13 ± 0.58 | 11.3 ± 1.20 | 14 ± 0.60 | P[e] | N |
| SWI 7 | *Padina gymnospora* | *B. amyloliquefacens* MTCC 10456[B] | 19 ± 1.53 | 16 ± 0.60 | 17 ± 1.00 | 12 ± 1.00 | 12 ± 2.00 | 11.3 ± 1.20 | 9.7 ± 0.60 | P[f] | N |
| SWI 8 | *Laurentia papillosa* | *B. subtilis* MTCC 10407[B] | 5 ± 2.08 | 12 ± 0.60 | 16 ± 1.00 | 2 ± 2.00 | ND | ND | ND | N | N |
| SWI 9 | *Hypnea valentiae* | *S. algae* MTCC 10455[B] | 17 ± 5.03 | 16 ± 0.60 | 22 ± 3.00 | ND | 18 ± 0.58 | ND | ND | N | N |
| SWI 10 | *Laurentia papillosa* | *S. algae* MTCC 10609 | 14 ± 3.21 | 14 ± 1.00 | 24 ± 3.20 | ND | ND | ND | ND | N | N |
| SWI 11 | *Padina gymnospora* | *S. algae* MTCC 10608 | 19 ± 2.65 | 5 ± 0.60 | 21 ± 2.10 | ND | 15 ± 0.58 | ND | ND | N | N |
| SWI 12 | *Hypnea valentiae* | *S. algae* MTCC 10455 | 19 ± 2.00 | ND | 17 ± 1.50 | ND | ND | ND | ND | N | N |
| SWI 12B | *Hypnea valentiae* | *V. alginolyticus*[d] | ND | ND | 12 ± 2.00 | ND | 3 ± 0.58 | 4.67 ± 0.60 | ND | N | N |
| SWI 13 | *Padina gymnospora* | *S. algae* MTCC 10609[B] | 17 ± 1.15 | ND | ND | ND | 20 ± 1.53 | ND | ND | N | N |
| SWI 14 | *Anthophycus longifolium* | *S. algae* MTCC 10608[B] | 17 ± 0.58 | 5 ± 0.60 | 11 ± 1.20 | ND | 21 ± 1.15 | ND | ND | N | N |
| SWI 16A | *Anthophycus longifolium* | *B. subtilis* MTCC 10407 | 17 ± 1.15 | 14 ± 1.50 | ND | 12 ± 2.00 | ND | ND | ND | N | N |
| SWI 16B | *Anthophycus longifolium* | *B. subtilis* MTCC 10402[B] | 15 ± 1.53 | 13 ± 1.20 | 16 ± 1.20 | 12 ± 2.00 | 14 ± 0.58 | 11.3 ± 1.20 | 12 ± 2.10 | P[g] | N |
| SWI 17 | *Dictyota dichomata* | *S. algae* MTCC 10609[C] | 19 ± 2.08 | ND | 17 ± 1.00 | ND | 10 ± 0.58 | 8.67 ± 0.60 | ND | N | N |
| SWI 18 | *Dictyota dichomata* | *S. algae* MTCC 10608[C] | 14 ± 2.00 | ND | 13 ± 1.20 | ND | 5 ± 0.58 | ND | 2.3 ± 0.60 | N | N |
| SWI 19 | *Sargassam myriocystum* | *B. subtilis* MTCC 10407[C] | 17 ± 0.58 | 11 ± 0.60 | 17 ± 1.00 | 11 ± 1.00 | 16 ± 0.58 | 11 ± 1 | 11 ± 1.20 | P[h] | N |
| SWI 20 | *Laurentia papillosa* | *Vibrio sp*[d] | ND | ND | 13 ± 1.00 | ND | ND | ND | ND | N | N |
| SWI 21 | *Laurentia papillosa* | *P. putida* MTCC 10458 | ND | ND | 12 ± 2.00 | ND | 4 ± 0.58 | 2.67 ± 0.60 | ND | N | N |

[a]Data are expressed as mean +standard deviation of three replicates. ND, no detectable activity. [b]GenBank number for the sequenced amplicons: (a) KC589397, (b) KC607823. (c) KC607821, (d) KC589396, (e) KC607822, (f) KC589396, (g) KC589400, and (h) KC589398. (P) signifies positive and (N), negative. [c]Superscripts A–D signify different strains belonging to similar species. [d]Not deposited.



dx.doi.org/10.1021/jf504845m | J. Agric. Food Chem. 2014, 62, 12194−12208

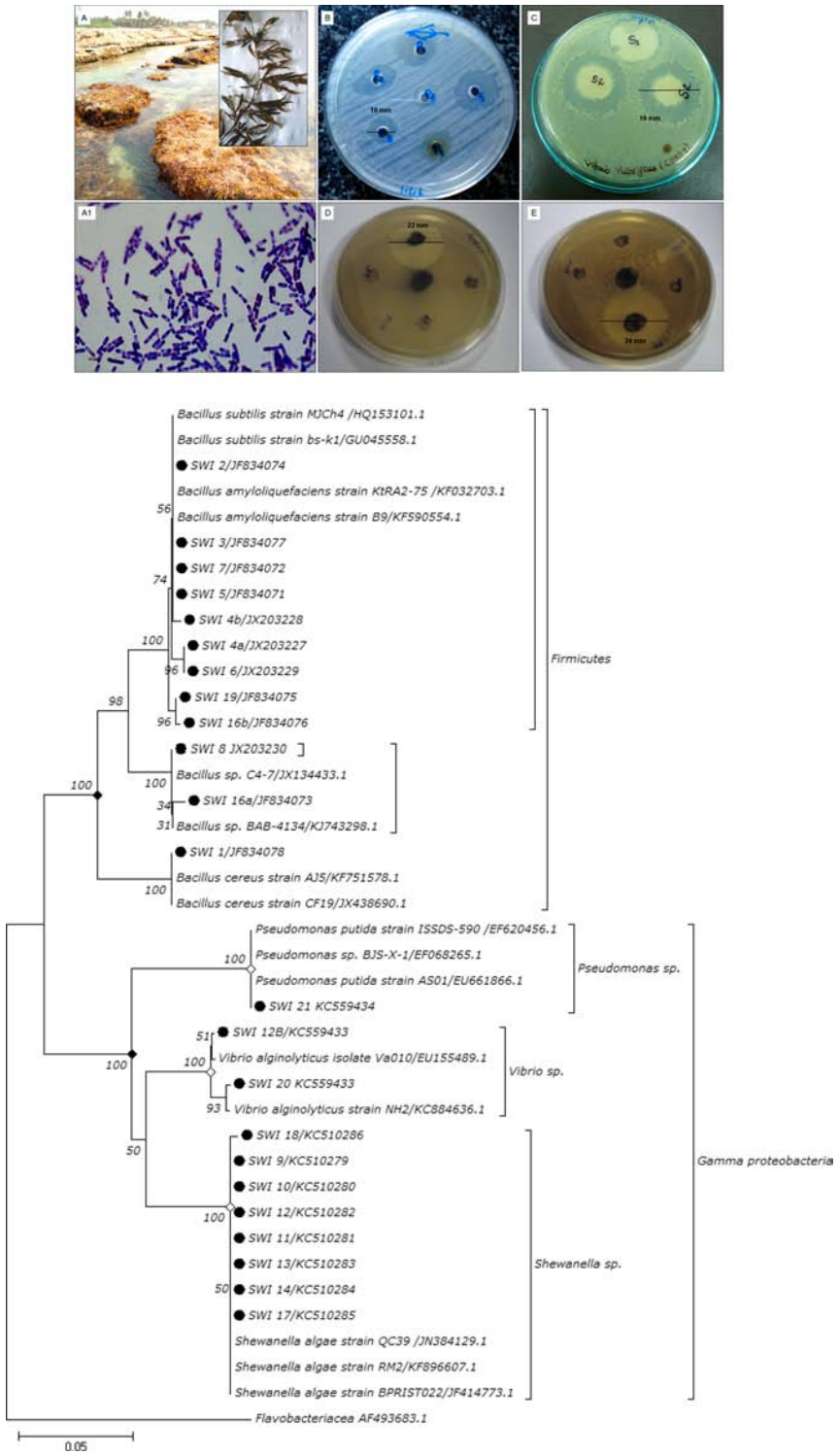


**Figure 1.** (A) Seaweeds at harvest location; (inset) brown seaweed *Anthophycus longifolius* used to isolate (A1) *Bacillus subtilis* MTCC10403 (SWI2). (B) Well diffusion of culture SWI2 supernatant against *V. vulnificus* MTCC 1145; spot over lawn assay of culture SWI2 against (C) *V. vulnificus* MTCC 114, (D) *V. parahemolyticus* ATCC 17802, and (E) *V. parahemolyticus* MTCC 451. The clearance zones realized by the isolates signify the antibacterial activity. Antagonistic activity was recorded as the diameter of inhibition zones determined as a distance of ≥1 mm between the circular area (= lawn of the isolate) and the end of the clear zone bounded by the lawn of the test strain. (Bottom) Phylogenetic tree derived from 16S rRNA gene sequences, showing evolutionary history of the antagonistic bacterial isolates associated with seaweeds. The evolutionary history was inferred using the neighbor-joining method.[12] The analysis involved 40 nucleotide sequences. All positions containing gaps and missing data were eliminated. There were a total of 569 positions in the final data set. Evolutionary analyses were conducted in MEGA6.[14]

3437.24 $cm^{-1}$ (O−H str); $^{1}H$ ($CDCl_3$, 500 MHz, $\delta$) and $^{13}C$ NMR ($CDCl_3$, $\delta$) data, see Table 2; HRMS (ESI) $m/z$ calcd for $C_{31}H_{45}O_7$ 529.6422, found 529.6894 $[M + H]^+$.

**Determination of Antibacterial Activities by Agar Diffusion Method.** Sterile disks (HiMedia, India) containing 10 $\mu$L of crude extract or 10 $\mu$L of purified macrolactin in methanol (the methanol

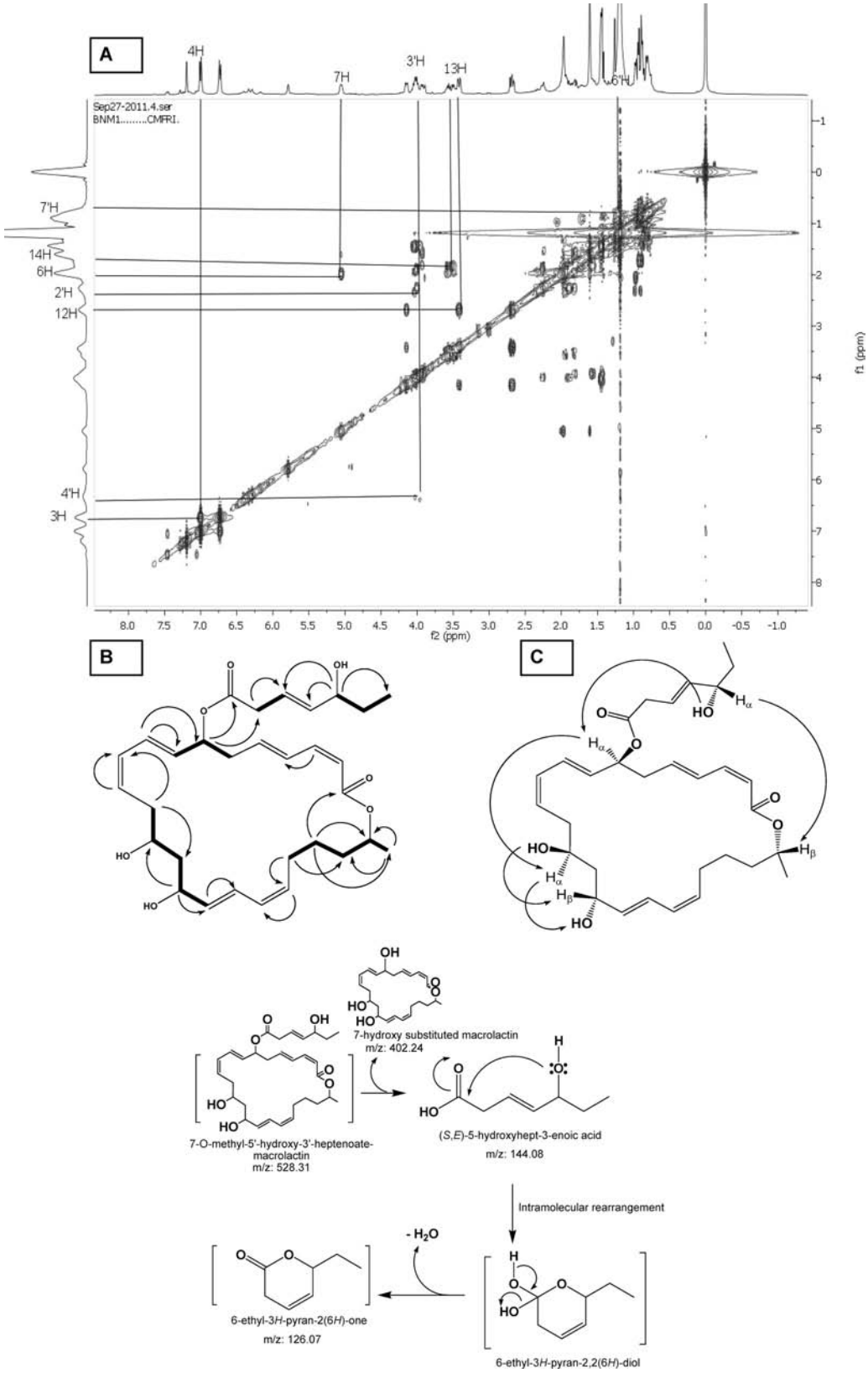


**Figure 2.** 2D NMR correlations in 7-*O*-methyl-5′-hydroxy-3′-heptenoate−macrolactin: (A) key $^{1}$H−$^{1}$H COSY couplings; (B) $^{1}$H−$^{1}$H COSY couplings represented by bold face bonds. The HMBC couplings are indicated as double-barbed arrows; (C) key NOESY correlations. (Bottom) Mass fragmentation pattern of 7-*O*-methyl-5′-hydroxy-3′-heptenoate−macrolactin.

traces were removed by drying in nitrogen, and the final compound concentration on the disk was 100 $\mu$g) were placed on fresh plates of Mueller−Hinton agar (Difco) seeded with suspensions ($10^5$ CFU/mL) of overnight cultures of the test microorganisms. The diameters of the zones of inhibition of growth around the disks were measured after incubation periods of 18 h at 37 °C. Antibiotic disk for Gram-


dx.doi.org/10.1021/jf504845m | *J. Agric. Food Chem.* 2014, 62, 12194−12208

negatives, namely, Octodiscs G-I minus (OD005) (HiMedia, India), was used to compare the results. The antibiotics used were ampicillin (A, 10 μg/disk), ciprofloxacin (Cf, 10 μg/disk), colistin (Cl, 10 μg/disk), cotrimoxazole (Co, 25 μg/disk), gentamicin (G, 10 μg/disk), nitrofurantoin (Nf, 300 μg/disk), streptomycin (S, 10 μg/disk), and tetracycline (T, 30 μg/disk).

## RESULTS

**Isolation and Identification of Bacterial Isolates Associated with Seaweeds.** About 22% of the bacterial isolates showed inhibition against at least one pathogen used in the study, with 9% of these showing broad-spectrum activity against the pathogen screened (Table 3). Figure 1A shows the indicative diagram for activity spectrum of culture isolates from seaweeds. Candidate strains were identified with the aid of biochemical and FAME analyses (data not shown). The bacterial isolates have been submitted to the Microbial Type Culture Collection and Gene Bank (MTCC) of the Institute of Microbial Technology (Chandigarh, India), an International Depository Authority under the Budapest Treaty. The identifications were confirmed through 16S rRNA gene based molecular evolutionary analysis using the neighbor-joining method.[12] The optimal tree with the sum of branch length of 0.80792901 is shown (Figure 1B). The percentage of replicate trees in which the associated taxa clustered together in the bootstrap test (1000 replicates) is shown next to the branches.[15] The evolutionary distances were computed using the Kimura two-parameter method.[13] Evolutionary analyses were conducted in MEGA6.[14] PCR primers used for metabolite gene screening are listed in Table 1. None of the isolates were positive for *nrps* genes, whereas a few *Bacillus* strains could amplify the *pks* gene products (Table 3). Although specific prediction of products of *nrps* and *pks* genes according to the obtained sequences was problematic, because only small gene fragments were amplified, an attempt was made to correlate the structural properties of produced secondary metabolites with the presence of *nrps* and *pks* genes.

**Structural Characterization of Antibacterial Metabolite from *Bacillus subtilis* MTCC 10403.** 7-*O*-Methyl-5′-hydroxy-3′-heptenoate−macrolactin (Figure 2A), a new derivative of the macrolactin, was isolated as an amorphous solid upon chromatography over silica columns. The IR absorption band (in MeOH) at 3014 $cm^{-1}$ was due to −CH stretching vibrations. The −OH group in the skeleton exhibited free −OH stretching vibrations near 3437 $cm^{-1}$. The bending vibration bands near 1753 $cm^{-1}$ denoted the ester carbonyl absorption. The olefinic (C═C), and ether (C—O—C) groups have been symbolized by the absorption bands at 1640 and 1073 $cm^{-1}$. The IR spectrum revealed a broad absorption band at $\nu_{max}$ 3500−3000 $cm^{-1}$, attributed to a hydroxyl functionality and to an olefinic system (1200, 1121 $cm^{-1}$). The ultraviolet absorbances at $\lambda_{max}$ (log e) 226 (3.72) and 248 (3.21) nm were assigned to a chromophore with extended conjugation. Its mass spectrum exhibited a molecular ion peak at $m/z$ 528 (HRESIMS $m/z$ 529.689 $[M + H]^+$; D 0.0 amu), which in combination with its $^1H$ and $^{13}C$ NMR data (Table 2) indicated the elemental composition of $C_{31}H_{44}O_7$ as 7-*O*-methyl-5′-hydroxy-3′-heptenoate−macrolactin with 10 degrees of unsaturation (Figure 2A): 7 degrees of unsturation from double bonds of macrolactin ring, 2 degrees of unsturation from double bonds of the substitution as (*S*,*E*)-methyl 5-hydroxyhept-3-enoate ($C_8H_{14}O_3$), and 1 degree from the ring of macrolacin were demonstrated. The molecular ion peak at $m/z$ 528 appeared to undergo elimination of (5-hydroxyhept-3-enoic acid ($C_7H_{12}O_3$, $m/z$ 144.1708) to yield 7-hydroxy-substituted macrolactin at $m/z$ 402.2450 ($C_{24}H_{34}O_5$), which underwent dehydration ($-H_2O$) to afford a fragment with $m/z$ 386.2580 ($C_{24}H_{34}O_4$). The appearance of the fragment at $m/z$ 126.1507 indicated the presence of a 6-ethyl-3*H*-pyran-2(6*H*)-one moiety ($C_7H_{10}O_2$), resulting from the intramolecular rearrangement and dehydration of 5-hydroxyhept-3-enoic acid via the intermediate 6-ethyl-3*H*-pyran-2,2(6*H*)-dial (Figure 2B).

The $^1H$ NMR in conjugation with $^{13}C$ NMR recorded the presence of two methyl signals at $\delta$ 0.81 and 1.30. The former was assigned to be due to the terminal methyl group at the side-chain 5-hydroxyhept-3-enoate moiety, whereas the methyl group at $\delta$ 1.30 shifted downfield due to the acrylate moiety (−OC(═O)—C═C−) at the $\beta$-position with respect to the deshielded methyl group. The methylene group protons at $\delta$ 2.60 and 2.04 were assigned to be at the 6-carbon position of the macrolactin ring structure, and the downfield shift (about $\delta$ 0.5) was due to the presence of the conjugated butadiene moiety at one side and the side-chain acetate group (−OC(═O)—C) attached to the macrolactin ring at its 7-carbon position. Three methylene groups have been assigned to occupy at the C20−22 positions of the macrolactin ring structure as heptenyl formate moiety. The protons of the $-CH_2-$ group at $\delta$ 1.45 and 1.43 were at C22 and were deshielded due to the presence of the acrylate moiety (−OC(═O)—C═C−) at the $\beta$-position with respect to the deshielded methyl group. The methyl group protons at $\delta$ 2.07 and 1.96 (C-20) also appeared to be deshielded due to the conjugated double-bond structure (butadiene) spanning from position C16 to C19 of the macrolactin ring. The methylene protons at the C21 position appeared at $\delta$ 1.81 and 1.60. The $-CH_2-$ protons appearing at $\delta$ 1.94 and 1.78 were due to the presence of the propanediol group and have been assigned to be present at the C14 position in the macrolactin ring structure. The protons at $\delta$ 2.68 and 2.33 shifted downfield due to the presence of a −C═C− group at its $\alpha$-position and a $\beta$-OH group. The methylene protons at $\delta$ 2.35 and 2.26 have been assigned to be present at the side-chain 5-hydroxyhept-3-enoate moiety, and their downfield shift was due to the ester functionality at the $\alpha$-position of the methylene protons and −C═C− at its $\beta$-position. The other $-CH_2-$ group at $\delta$ 1.21 was a part of the terminal ethyl group of 5-hydroxyhept-3-enoate. The methine protons at $\delta$ 3.42 and 4.84 were assigned to be present at the C13 and C15 positions in the macrolactin ring structure. The downfield shift appeared to be due to the propane-1,3-diol moiety at C13−C15. The methine proton at $\delta$ 4.84 appeared to be deshielded due to the presence of a $\beta$-olefinic group extended by further conjugated structure. The carboxyl ester group at the C1 position of the macrolactin ring resulted in strong deshielding of the −CH− proton at $\delta$ 4.99 and, therefore, has been assigned to be present at the C23 position of the macrolactin ring structure. The methine proton (given a triplet of the doublet) at $\delta$ 5.05 is characteristic of the junction point of the macrolactin ring (C-7) to that of the side-chain 5-hydroxyhept-3-enoate moiety. The $^1H$ NMR spectrum showed three exchangeable hydroxyl protons at $\delta$ 4.23 (1H, bs in $CDCl_3$), $\delta$ 3.79 (1H, bs in $CDCl_3$), and $\delta$ 3.16 (1H, bs in $CDCl_3$), which disappeared upon addition of $D_2O$.

The $^{13}C$ NMR spectrum of the purified compound in combination with DEPT experiments indicated the occurrence of 31 carbon atoms in the molecule, including 2 ester carbonyl

carbons at $\delta$ 165.16 and 168.2, 14 methine carbons between $\delta$ 116.1 and 146 assigned to 7 double bonds, 5 oxygenated methine carbons between $\delta$ 67.5and 75.4, and 10 aliphatic carbons between $\delta$ 20.10 and 50.8. The $^{13}$C NMR spectrum displayed two quaternary carbons ($\delta$ 165.16 and 169.54) atoms bearing the carbonyl groups. The low-field quaternary signals ($^{13}$C NMR) were in agreement with that to a quaternary carbon signal carrying the carbonyl groups at C-1 of the macrolactin ring structure and C-1′ of the side chain (5-hydroxyhept-3-enoate) attached to the macrolactin framework at the 7-C position of the ring. This was supported by the relative downfield shift of the H2, 23 signals ($\delta$ 5.60 t and 4.99 ddq, respectively) and methylene signals at C-2′ ($\delta$ 2.26 and 2.35), which referred to a possible oxygenation in its vicinity. The side chain is substituted at C-7 with either an $\alpha$- or a $\beta$-oriented hydroxyl group at the 5′ position.

The position of the hydroxyl group at C-5′ was further confirmed from the $^{1}$H−$^{1}$H COSY, HSQC, NOESY, and HMBC spectra. In the $^{1}$H−$^{1}$H COSY spectrum, the couplings were apparent between H-7/H-6,8; H-13/H-12, 14; H-15/H-14,16; and H-20/H-21/H-22/H-23, which support the presence of a macrolactin skeleton. The point of cyclization of the ester in the macrolactone ring was indicated by the low-field shift of H-23 at $\delta$ 4.99, which has been coupled with the H-24 methyl group at $\delta$ 1.30 (d, $J$ = 6.1 Hz), which also gives clear $^{1}$H−$^{1}$H COSY correlation. Also, the $^{1}$H−$^{1}$H COSY correlations between H′-5/H-6/H-7 supported the presence of the terminal propanol moiety at the 5-hydroxyhept-3-enoate side chain. The proton and carbon connectivity deduced from HSQC and HMBC experiments confirmed the marolactin framework attached to the side-chain 5-hydroxyhept-3-enoate moiety at the seventh position of the macrolactin. The H−H and C−H connectivity apparent in the $^{1}$H−$^{1}$H COSY and HMBC spectra, respectively, indicate that one of the three unsaturations was due to the macrolactin ring framework (Table 2). In the HMBC spectrum, it was observed that H-12/C-10,14; H15/C-13,16; H-20/C-19,22; and H-21/C-1,23,24 were correlated with each other. In addition, a methine proton (H-7) was coupled to the olefinic tertiary carbon (C-9) and methine H-15 with C-16,17. This indicated that these protons (H-7 and H-15) were connected to the olefinic tertiary carbon atoms. The proton at C-21 appeared to demonstrate long-range HMBC correlation with ester carbonyl carbon at $\delta$ 165.16 (C-1). The proton at C-7 realized HMBC correlation at $\delta$ 169.54, which belongs to the second ester carbon. The HMBC analysis revealed that the carbon at $\delta$ 75.4 (C-5′), bearing the hydroxyl group, correlated with a primary methyl proton $\delta$ 0.81 (H′-7).

The HMQC spectrum of the purified compound also revealed connections of the protons (H-2′) to the methylene carbon at $\delta$ 50.8. Placement of the 5-hydroxyhept-3-enoic acid group at C-7 was confirmed by the downfield shift of H-7 ($\delta$ 5.05) in the compound as compared to the baseline value ($\delta$ 4.34) and also by the long-range correlation of H-7 to the carbonyl carbon at $\delta$ 169.54 (C-1′) in the HMBC spectrum.[16] The HMBC spectrum demonstrated long-range correlations of the methine proton (H-5′) to the vinylic carbon at $\delta$ 139.0 (C-3′) and methyl carbon at $\delta$ 14.1 (C-7′). These observed spectral data were indicative of the presence of the hydroxyheptenoic acid half-ester moiety, which was supported by the IR spectral data exhibiting intensely broad hydroxyl absorption from 3500 to 3000 cm$^{-1}$ and ester carbonyl absorption at 1710 cm$^{-1}$. The geometric isomerisms of the olefinic protons have been established by the $^{1}$H coupling constants suitable for the geometries ($Z$ and $E$ forms). The relative stereochemistry of the chiral centers, particularly that of C-13 and -15 carrying the hydroxyl group of the macrolactin framework and that of C′-5, was deduced from the NOESY spectrum of the compound and the $J$ values. NOE couplings were observed between H$\alpha$-13/H$\alpha$-7, thus indicating that these groups must be equatorial and on the $\alpha$-side of the molecule. NOE correlations between H$\beta$-23/H$\beta$-15/H$\beta$-20 and those among H-5′/H-15/H-23 indicated the close proximity of these groups and their $\beta$-disposition. Therefore, the C-1 carboxyl group is equatorial and $\alpha$-oriented. The methine proton at the C′-5 group did not exhibit NOE interactions with H-7 and H-13 and the methylene proton at C-14 ($\delta$ 1.78, m), which is in the $\alpha$-face of the molecule, thereby indicating that H-7 is at the equatorial disposition. An interaction through the space of the hydroxyl protons at C-5′ ($\delta$ 3.16,1H, bs) and C-15 ($\delta$ 3.79, 1H, bs) with H-7 ($\delta$ 5.05, td) and H$\alpha$-14 ($\delta$ 1.94, m in $CDCl_3$) is only possible for the $\alpha$-orientation of the tertiary hydroxyl group on C-5′ and C-15. The stereochemistry at the tertiary alcohol at C-15 position was established by the fact that H-15 has mutual NOE correlations with H-23, which had been shown to be in the $\beta$-face of the molecule (axial configuration) under observation, and the secondary alcohol group that appeared as a broad singlet (at $\delta$ 4.23) has NOE interactions with H-13 and H-7 in the molecule. This is only possible if the C-15 hydroxyl group lies on the $\alpha$-side of the molecule.

**Determination of Antibacterial Activities by Agar Diffusion Method.** The disk diffusion method was used to compare the antimicrobial activities of the crude extract from strain *Bacillus subtilis* MTCC10403, the purified macrolactin, and the clinically important antibiotics against different food pathogenic strains used in the study. The purified macrolactin exhibited a good qualitative inhibitory spectrum to the tested isolates. The crude extract from *Bacillus subtilis* MTCC 10403 was found to possess antibacterial activity against pathogenic *Aeromonas* and *Vibrio* (inhibitory zone diameter >20 mm, 100 $\mu$g on disk). However, 7-*O*-methyl-5′-hydroxy-3′-heptenoate−macrolactin purified from the crude extract showed an inhibitory zone diameter of 18 mm against *Aeromonas hydrophila* and 16 mm against *V. parahemolyticus* ATCC 17802 at a concentration of 100 $\mu$g on disk (Table 4).

## DISCUSSION

Seaweeds are potential sources of bioactive compounds producing bacterial isolates when compared to other marine sources such as seawater and sediments.[17] A greater percentage of active isolates (22%) in this study found good agreement with the literature where the relative proportions of antimicrobial-producing culturable isolates were reported to be >16% from intertidal seaweeds.[3] The pathogens used include reported human pathogens such as *Aeromonas hydrophila*, *Vibrio vulnificus*, and *Vibrio parahemolyticus*. These food pathogens are present in the freshwater and marine environments and were reported to cause gastroenteritis and wound infections in healthy individuals or fatal cases of septicemia in individuals with impaired immune systems or various malignancies.[18] These candidate isolates under study were tested against these food pathogenic bacteria and were found to have a broad-spectrum activity (Table 3).

The taxonomic classifications showed that a higher proportion of the marine isolates belonged to the Firmicutes genera belonging to *Bacillus* sp. Manmadan et al. reported a greater level of epibiotic bacterial isolates belonging to *Bacillus*

Table 4. In Vitro Antibacterial Activities of Crude Extract and the Purified 7-*O*-Methyl-5′-hydroxy-3′-heptenoate−Macrolactin Isolated from Seaweed-Associated *Bacillus subtilis* MTCC 10403 vis-à-vis the Reference Antibiotics

| | inhibition zone[a] (mm) | | | | | | | | | |
|---|---|---|---|---|---|---|---|---|---|---|
| strain | crude extract[b] | purified macrolactin | ampicillin[c] | ciprofloxacin[c] | colistin[c] | co-trimoxazolex[d] | gentamicin[c] | nitrofurantoin[e] | streptomycin[c] | tetracycline[f] |
| *V. parahemolyticus* ATCC 17802 | 25 ± 1. 00 | 16.00 ± 1.00 | 17.67 ± 0.58 | 22.00 ± 0.00 | 12.33 ± 0.58 | 17.33 ± 0.58 | 14.00 ± 0.00 | 15.00 ± 1.00 | 14.33 ± 0.58 | 19.33 ± 0.58 |
| *Vibrio vulnificus* | 21.67 ± 0.58 | 14.3 ± 0.58 | 16.00 ± 0.00 | 22.00 ± 0.00 | 15.00 ± 1.00 | 18.00 ± 0.00 | 14.33 ± 0.58 | 16.00 ± 0.00 | 14.00 ± 0.00 | 19.67 ± 0.58 |
| *Aeromonas hydrophilla* | 26.53 ± 0.58 | 18.67 ± 0.58 | 12.33 ± 0.58 | 24.67 ± 0.58 | 17.67 ± 0.58 | 21.67 ± 0.58 | 18.00 ± 0.00 | 21.67 ± 0.58 | 15.67 ± 0.58 | 16.00 ± 0.00 |

[a]Data are expressed as the mean ± standard deviation of three replicates. [b]100 μg. [c]10 μg. [d]25 μg. [e]300 μg. [f]30 μg.

with antibiotic activity from the surface of nine species of seaweeds of Japan.[1] *Bacillus* strains were also isolated from the surface of coralline seaweed *Jania rubens* (southern Mediterranean Sea).[8] Recent advances in genome sequencing have highlighted the genus *Bacillus* as a potential source of antibiotic-like compounds such as polyketides, nonribosomal peptide, and bacteriocins as well as other unusual compounds.[19] The remaining isolates in our study belong to γ-proteobacteria.

Polyketides have found application as bioactive leads in pharmaceutical products for use against pathogenic microorganisms and various immunocompromising diseases. Rapamycin, epothilone B, and erythromycin are the common polyketides of industrial importance with immunosuppressant, anticancer, and antibiotic properties, respectively. Lovostatin is the popular anticholesterol drug, which also bears the polyketide backbone. *Bacillus* and *Actinomycetes* have been recognized to contain various PKS gene clusters and bioactive molecules bearing the polyketide backbone. It may be assumed that a genome with a greater number of biosynthetic gene clusters is more likely to result in a positive hit in an *nrps/pks* gene-screening approach. The highly conserved sequences of β-ketoacyl synthase (KS) domains are shared among all *pks*, and therefore the KS domains are useful in the screening for PKS genes in bacteria. Similarly, the most conserved adenylation (A) domain can be used for PCR primer design to survey *nrps* gene diversity. Therefore, positive results in a PCR-based screening for *nrps* and *pks*-II genes not only provide evidence of the production of corresponding metabolites but also may indicate the existence of further metabolic pathways of secondary metabolite synthesis.

Although several studies have investigated the antibacterial activity of seaweed-associated bacteria, the chemical characterization of the isolates for their active metabolites are relatively limited.[1,6−8] In the present study the secondary metabolite of *Bacillus subtilis* MTCC 10403 with potent antibacterial activity against bacterial pathogens was demonstrated to possess the polyketide backbone and was identified as 7-*O*-methyl-5′-hydroxy-3′-heptenoate−macrolactin that represents the scaffold of *pks1* gene-encoded products.

The crude extract from strain *B. subtilis* MTCC10403, the purified macrolactin, and commercial antibiotics (as control) were analyzed against human opportunistic pathogens *V. parahemolyticus*, *V. vulnificus*, and *A. hydrophilla*. 7-*O*-Methyl-5′-hydroxy-3′-heptenoate−macrolactin showed a good qualitative inhibitory spectrum to the tested isolates (Table 4; Figure 3B). It is significant to note that the antibacterial activities of the crude extract against the test pathogens were greater than those exhibited by the pure macrolactin with 5-hydroxyhept-3-enoate moiety at the side chain C-7 position of the macrolactin ring system (Table 4). It is apparent that there might be other bioactive compounds along with the purified macrolactin, which acted synergistically to impart greater antibacterial activities against the test food pathogenic bacteria used in this study.

The macrolactins possess a 24-member lactone ring with three isolated diene elements and have been originally isolated from deep sea bacterium and *Actinomadura* sp.[20,21] A total of 16 macrolactins have been chemically characterized.[20,22] Macrolactin A was found to be the most active compound in this series with potent antiviral properties and was reported to possess antibacterial and anticancerous activities.[16,20] 7-*O*-Succinyl macrolactin F and 7-*O*-succinyl macrolactin A were isolated from the ethyl acetate extract of the marine *Bacillus* sp.

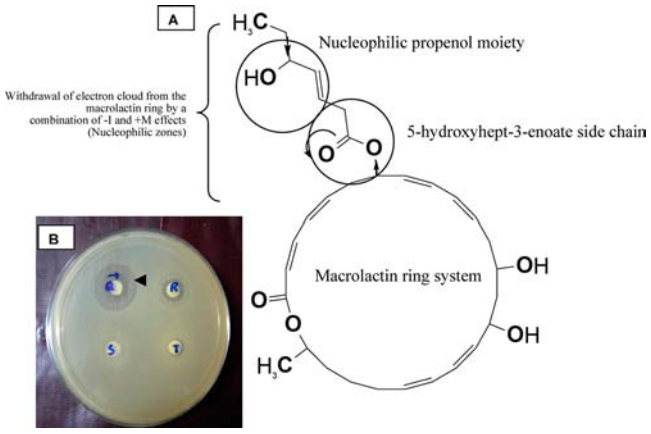


**Figure 3.** (A) Sketch model of 7-O-methyl-5′-hydroxy-3′-heptenoate-macrolactin showing structure−activity correlation. Induction of bioactivity is directly proportional to the inductive (field/polar effect) and resonance effects of the 5-hydroxyhept-3-enoate side chain attached to the macrolactin ring system at C-7. The 5-hydroxyhept-3-enoate moiety with electronegative acetyl group withdraw the electron cloud by a combination of inductive (-I effect) and mesomeric effect (+M-effect) from the substituted macrolactin ring, thus acting as the nucleophilic center of the molecule resulting in a greater level of activity. (B) Antibacterial activity of 7-O-methyl-5′-hydroxy-3′-heptenoate-macrolactin against *V. parahemolyticus* ATCC 17802. The inhibition zone is indicated by an arrow.

SC026 and were reported as antiviral.[16] The antibacterial activities of the macrolactins have been compared by Nagao et al., who reported that the $C_{15}$−OH group is responsible for the target bioactivity of this group of compounds.[21] However, there were no studies regarding the effects of the side chain attached at the $C_7$−OH position of the macrolactin ring system.

The physicochemical parameters of bioactive molecules such as polarizability, steric, and hydrophobic descriptors (lipophilicity, partition coefficients) have a major role in influencing biological activities.[23,24] The ability of any molecule to penetrate biological membranes is a primary factor in controlling the interaction of compounds with biological systems and is dependent on lipophilicity factors as determined by the partition coefficient between 1-octanol and water (log *P*). It is of note that the terminal functional group as the 5-hydroxyhept-3-enoate moiety at the side chain C-7 position of the macrolactin ring system increases lipophilicity. The increased lipophilicity (log *P* 4.43) of 7-*O*-methyl-5′-hydroxy-3′-heptenoate−macrolactin as compared to the parent compound (log *P* 3.28) affords better penetration of the former through the lipoidal membrane barrier to arrive at the receptor site, thereby resulting in greater antibacterial activity of 7-*O*-methyl-5′-hydroxy-3′-heptenoate−macrolactin than the parent compound. The lipophilicity factors of the related compounds have been compared to demonstrate the lesser log *P* value of 7-*O*-methyl-5′-hydroxy-3′-heptenoate−macrolactin than of 7-*O*-succinyl−macrolactin (log *P* 3.24) with a succinate side chain (−C(=O)$CH_2CH_2$COOH) and 7-*O*-malonyl−macrolactin (log *P* 3.18) with a malonyl side chain (−C(=O)$CH_2$COOH) are lesser than 7-*O*-methyl-5′-hydroxy-3′-heptenoate−macrolactin (log *P* 4.43) with a 5-hydroxyhept-3-enoate side chain. 7-*O*-Methyl-5′-hydroxy-3′-heptenoate−macrolactin exhibited significantly greater activity against test pathogens (at a concentration of 20 μg per disk) than the parent macrolactin apparently due to the presence of more polarizable (polarizability 59.91 × $10^{-24}$ $cm^3$) C-7,5-hydroxyhept-3-enoate group as compared to the less polarizable succinate or malonate groups ((52−24) × $10^{-24}$ $cm^3$). It can be inferred that the 5-hydroxyhept-3-enoate moiety with highly electronegative acetyl and olefinic groups withdraws the electron cloud by a combination of inductive (−I effect) and mesomeric effect (+M effect) from the substituted macrolactin ring of 7-*O*-methyl-5′-hydroxy-3′-heptenoate−macrolactin, thus acting as the nucleophilic center of the molecule, resulting in a high level of activity (Figure 3A). This lead demonstrated in the present study will be significant in explaining the pharmacophore-fit in the macromolecular receptor site and exploring the primary site and mode of action of this class of the substituted macrolactone analogues.

The elongation module of type-I PKS harbors the acyl carrier protein (ACP), acyltransferase, (AT) and ketosynthase (KS) domains that synergistically catalyze a series of decarboxylative Claisen condensation involving malonyl units to result in the elongation of the polyketide chain affording the formation of the intermediate biosynthetic product as β-ketoacyl-S-ACP. A series of condensation, dehydration, reduction, and hydrolysis of the intermediate polyketides results in the biosynthesis of 7-*O*-methyl-5′-hydroxy-3′-heptenoate−macrolactin (Figure 4A). It is, however, of note that the ketoreductase (KR), dehydratase (DH), and enoyl reductase (ER) are active in a few steps to reduce the carbonyl group to −OH, olefinic double bond, or a fully reduced end product.

The correlations of metabolite genes such as *pks* with secondary metabolites belonging to polyketides and their putative biosynthesis pathway in related bacteria were reported in earlier studies.[25,26] The *pks* gene has been assigned to the biosynthesis of bacillaene, a polyketide product in the *Bacillus amyloliquefaciens* FZB42 genome. The *pks* gene cluster was identified from *B. amyloliquefaciens* CH12, a genetically engineered strain, and the putitive biosynthetic pathway of bacillane was demonstrated. A bacillaene multienzyme complex of *trans*AT PKSs with *pks*-like chemistry was characterized in an earlier study, where introduction of the β-branch and subsequent incorporation of olefinic bonds into the non-canonical bimodules have been comprehended.[25] The *pksX* polyketide synthase (PKS) genes were also reported in *Bacillus subtilis*.[26] A stepwise aldol addition of acetyl-ACP and Grob fragmentation on the enzymatically loaded acyl carrier proteins were demonstrated to result *pks*-derived antibacterial metabolites bacillaene and curacin.[27,28] Mupirocin H, a novel metabolite resulting from mutation of the HMG-CoA synthase analogue, *mupH* in *Pseudomonas fluorescens*, has been reported.[29] Previous work demonstrated that unlike fatty acid biosynthesis, the biosynthesis of polyketide products does not follow a rigid sequence.[30] Instead, some or none of these steps and reduction reactions occur in different biosynthetic steps to result in various combinations of structural diversity of the PKS products. It is of note that some of the domains remain inactive at one or more steps of macrolactin biosynthesis, thereby leading to the formation of conjugation at three positions (C2−5, C8−11, and C16−19 of the macrolactin ring system) and three hydroxyl groups of the intermediate polyketide product (S-ACP-7,13,15,23-tetrahydroxytetracosa-2,4,8,10,16,18-hexaenethioate). The latter undergoes intramoleculear cyclization by the nucleophilic attack of the terminal hydroxy group on the thioester-activated carbonyl to result in the formation of a −C(=O)—O− linkage in the 24-member macrolactin ring location system with the elimination of ACP-SH.

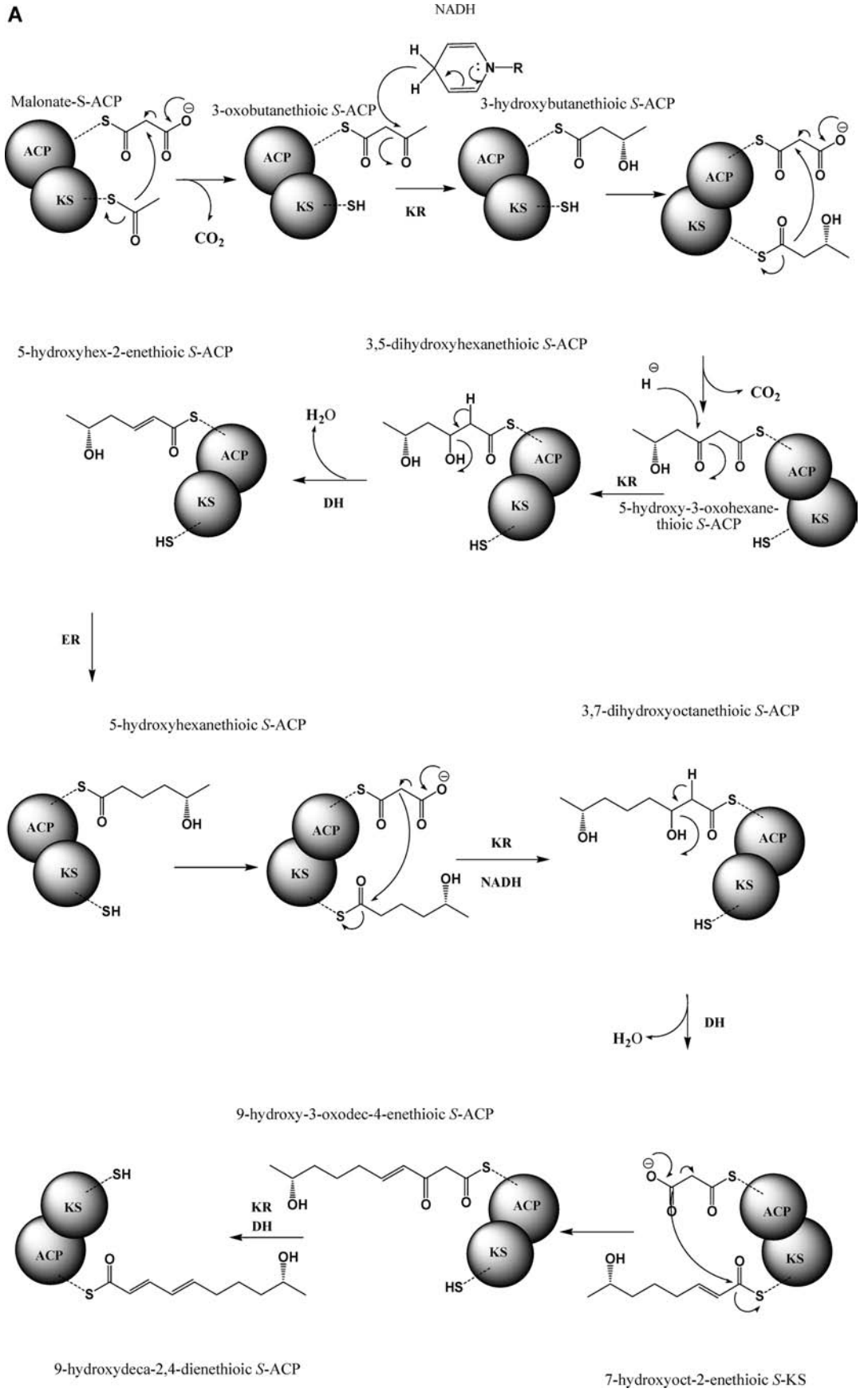


**Figure 4.** continued


dx.doi.org/10.1021/jf504845m | J. Agric. Food Chem. 2014, 62, 12194−12208

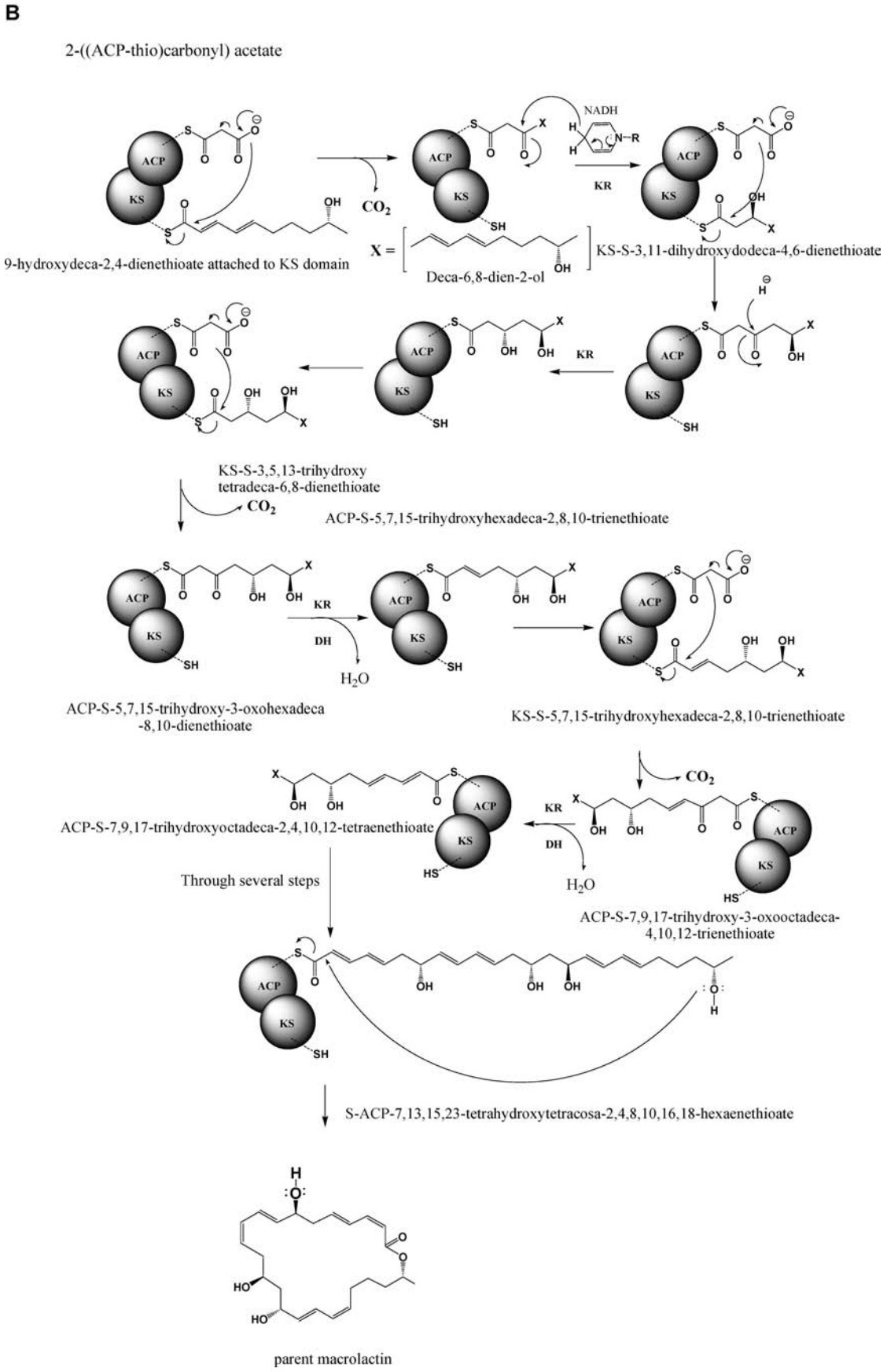


**Figure 4.** continued


dx.doi.org/10.1021/jf504845m | J. Agric. Food Chem. 2014, 62, 12194−12208

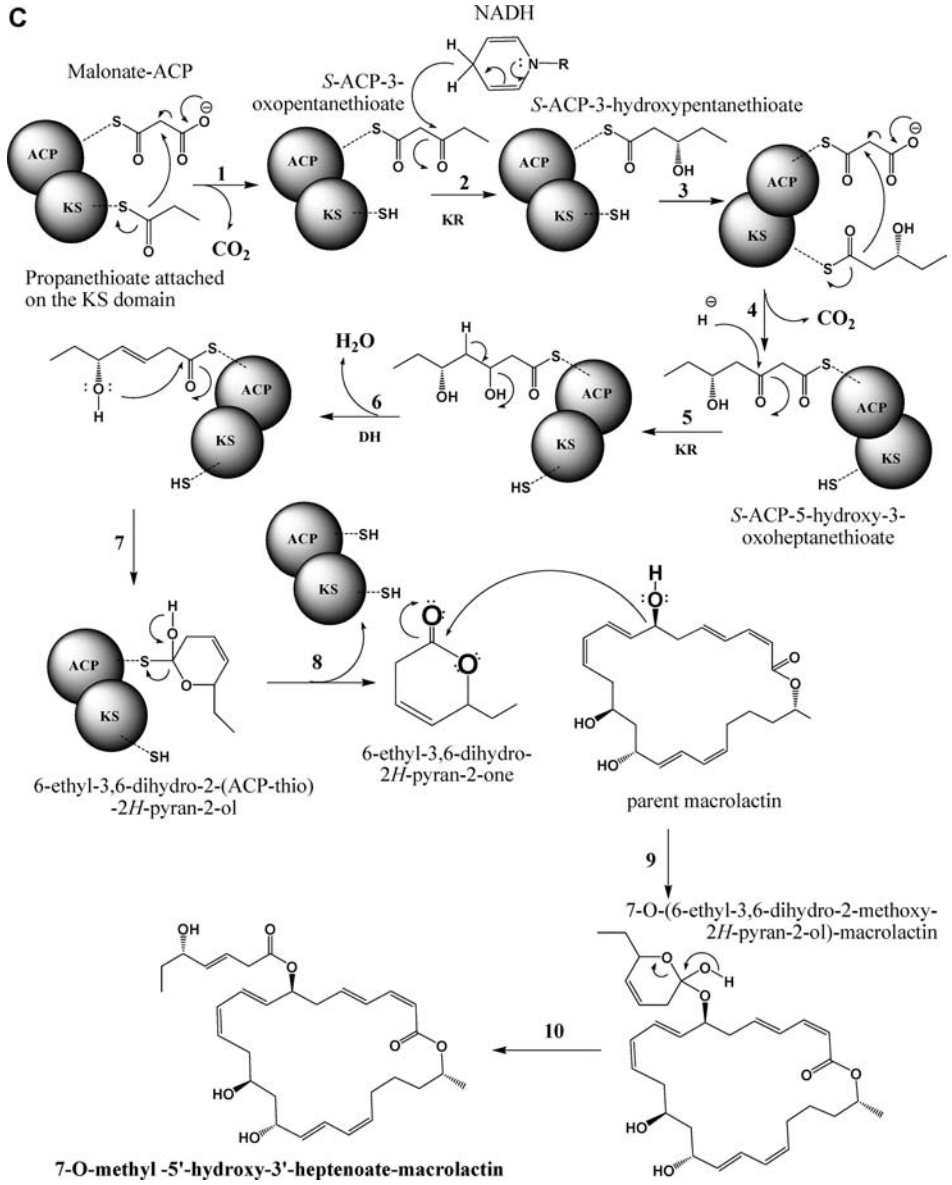


**Figure 4.** (A) Hypothetical biosynthetic pathways of 7-*O*-methyl-5′-hydroxy-3′-heptenoate−macrolactin, showing the loading, decarboxylation, and elongation steps catalyzed by PKS-1. Both enzymes build their products from an acetate starter unit and malonate extender units. The intermediates shown bound to the PKSs are hypothetical, but consistent with experimental results. (B, C) Sequences of events in the biosynthesis of side chain 5-hydroxyhept-3-enoate moiety attached to the macrolactin ring system at C-7, and the final PKS product as 7-*O*-methyl-5′-hydroxy-3′-heptenoate−macrolactin. (1) Chain extension is initiated by decarboxylation of malonyl-ACP to propanoyl-ACP by the KS domain. (2) The propanoate group is then passed from the ACP to the active site cysteine of the KS. (3) The ACP is loaded with another unit of malonate, and then KS-catalyzed condensation takes place, resulting in *S*-5-hydroxy-3-oxohaptanethoate-ACP. (4) The ketoester is then transferred back to the KS, and another cycle of chain extension can begin. The biosynthetic route starts from propanethioate attached on the KS domain and is accomplished by two alternate steps of decarboxylative Claisen condensations and ketoreduction. (5) DH catalyzes the elimination of the water molecule in the intermediate KR product S-ACP-3,5-dihydroxyheptanethioate to afford S-ACP-5-hydroxyhept-3-enethioate. The nucleophilic attack of the terminal hydroxy group (as butanol moiety) on the thioester-activated carbonyl carbon atom of S-ACP-5-hydroxyhept-3-enethioate results in the formation of a cyclic polyketide product as 6-ethyl-3,6-dihydro-2-(ACP-thio)-2*H*-pyran-2-ol in the six-membered pyran ring lactone system. A subsequent elimination of ACP-SH afforded 6-ethyl-3,6-dihydro-2*H*-pyran-2-one. The carbonyl carbon atom of the latter undergoes nucleophilic attack by the 7-OH group in the macrolactin ring system followed by ring opening yielding the final PKS product as 7-*O*-methyl-5′-hydroxy-3′-heptenoate−macrolactin.

The post-biosynthetic modifications of the macrolactin ring at the C7 position of macrolactin has been reported in earlier literature.[16] In general, type I PKSs use malonyl/methylmalonyl/ethylmalonyl derivatives of CoA and hydroxymalonyl/aminomalonyl/methoxymalonyl ACP extender units to biosynthesize diverse natural products bearing the polyketide backbone.[16] It is of note that in the biosynthetic route leading to the formation of the side-chain 5-hydroxyhept-3-enoate moiety is also a polyketide biosynthetic product. A model for biosynthesis of 5-hydroxyhept-3-enoate can be proposed (Figure 4B), which accounts for the fact that propanethioate/malonate as the starting building blocks instead of acetate/malonate in the biosynthesis of this polyketide backbone. Accordingly, the biosynthetic route starts from propanethioate (KS—S—C(=O)$C_2H_5$) attached with the KS domain and is accomplished by two alternate steps of decarboxylative Claisen

condensations and ketoreduction. Finally, DH catalyzes the elimination of the water molecule in the intermediate KR product S-ACP-3, 5-dihydroxyheptanethioate, to afford the S-ACP-5-hydroxyhept-3-enethioate. The nucleophilic attack of the terminal hydroxyl group (as butanol moiety) on the thioester-activated carbonyl carbon atom of S-ACP-5-hydroxyhept-3-enethioate results in the formation of a cyclic polyketide product as 6-ethyl-3,6-dihydro-2-(ACP-thio)-2*H*-pyran-2-oil in the 6-member pyran ring location system. A subsequent elimination of ACP-SH afforded 6-ethyl-3,6-dihydro-2*H*-pyran-2-one. The carbonyl carbon atom of the latter undergoes a nucleophilic attack by the 7-OH group in the macrolactin ring system followed by ring opening, yielding the final PKS product as 7-*O*-methyl-5′-hydroxy-3′-heptenoate−macrolactin (Figure 4C). It is apparent from this study that various combinations of the starter and elongation units used for polyketide biosynthesis lead to the formation of multiple stereocenters and structurally diverse polyketide backbone.

The past decade witnessed the discovery of various polyketide leads from bacterial sources with tremendous importance in food control and from a human health perspective. The newly evolving antibacterials bearing the polyketide backbone will be increasingly important keeping in mind the development of multidrug-resistant bacteria and pathogenic microorganisms against the existing antibiotics and related molecules. In this study, we described a new variant of macrolactin, 7-*O*-methyl-5′-hydroxy-3′-heptenoate−macrolactin. This novel polyketide product holds promise for the development of a new generation of drug candidates for use against the multiresistant microbial pathogens. We have also provided evidence for a biosynthetic route of this compound, and this may lead to the identification of a new target for antimicrobial lead molecule discovery programs. The results of this screening led to the conclusion that these polyene antibiotics are widespread metabolites of seaweed-associated bacterial populace particularly belonging to *Bacillus* species. The present work may have an impact on the exploitation of macrolactins for food, pharmaceutical, and biotechnological applications.

## AUTHOR INFORMATION


### Corresponding Author

*(K.C.) Phone: +91-484-2394867. Fax: +91-484-2394909. E-mail: kajal_cmfri@yahoo.com.


### Notes

The authors declare no competing financial interest.

## REFERENCES


(1) Manmadhan, K.; Hideaki, S.; Shinichi, N. Phylogenetic identification of epibiotic bacteria possessing antimicrobial activities isolated from red algal species of Japan. *World J. Microbiol. Biotechnol.* **2008**, *24*, 2315−2321.

(2) Meklat, A.; Sabaou, N.; Zitouni, A.; Mathieu, F.; Lebrihi, A. Isolation, taxonomy, and antagonistic properties of halophilic actinomycetes in Saharan soils of Algeria. *Appl. Environ. Microbiol.* **2011**, *77*, 6710−6714.

(3) Lemose, M. L.; Toranzo, A. E.; Barja, J. L. Antibiotic activity of epiphytic bacteria isolated from intertidal seaweeds. *Microb. Ecol.* **1985**, *11*, 149−163.

(4) Chakraborty, K.; Lipton, A. P.; Paulraj, R.; Chakraborty, R. D. Guaiane sesquiterpenes from seaweed *Ulva fasciata* Delile and their antibacterial properties. *Eur. J. Med. Chem.* **2010**, *45*, 2237−2244.

(5) Zhang, W.; Zhang, F.; Li, Z.; Miao, X.; Meng, Q.; Zang, X. Investigation of bacteria with polyketide synthase genes and antimicrobial activity isolated from South China Sea sponges. *J. Appl. Microbiol.* **2009**, *107*, 1364−5072.

(6) Kumar, V.; Rao, D.; Thomas, T.; Kjelleberg, S.; Egan, S. Antidiatom and antibacterial activity of epiphytic bacteria isolated from *Ulva lactuca* in tropical waters. *World J. Microbiol. Biotechnol.* **2011**, *27*, 1543−1549.

(7) Gomez, V. L. J.; Soria-Mercado, I. E.; Rivas, G. G.; Ayala-Sánchez, N. E. Antibacterial and anticancer activity of seaweeds and bacteria associated with their surface. *Rev. Biol. Mar. Oceanogr.* **2010**, *45*, 267−275.

(8) Ben Ali, A. I.; Bour, M. E.; Ktari, L.; Bolhuis, H.; Ahmed, M.; Boudabbous, A.; Stal, L. J. *Jania rubens*-associated bacteria: molecular identification and antimicrobial activity. *J. Appl. Phycol.* **2012**, *24*, 525−534.

(9) Goecke, F.; Labes, A.; Wiese, J.; Imhoff, J. F. Chemical interactions between marine macroalgae and bacteria. *Mar. Ecol.: Prog. Ser.* **2010**, *409*, 267−300.

(10) Sambrook, J.; Russell, D. W. *Molecular Cloning: A Laboratory Manual*, 3rd ed.; Cold Spring Harbor Laboratory: Cold Spring Harbor, NY, 2011; 999 pp, ISBN 0879695773.

(11) Weisburg, W. G.; Barns, S. M.; Pelletier, D. A.; Lane, D. J. 16S ribosomal DNA amplification for phylogenetic study. *J. Bacteriol.* **1991**, *173*, 697−703.

(12) Saitou, N.; Nei, M. The neighbor-joining method: a new method for reconstructing phylogenetic trees. *Mol. Biol. Evol.* **1987**, *4*, 406−425.

(13) Kimura, M. A simple method for estimating evolutionary rate of base substitutions through comparative studies of nucleotide sequences. *J. Mol. Evol.* **1980**, *16*, 111−120.

(14) Tamura, K.; Stecher, G.; Peterson, D.; Filipski, A.; Kumar, S. MEGA6: Molecular Evolutionary Genetics Analysis version 6.0. *Mol. Biol. Evol.* **2013**, *30*, 2725−2729.

(15) Felsenstein, J. Confidence limits on phylogenies: an approach using the bootstrap. *Evolution* **1985**, *39*, 783−791.

(16) Jaruchoktaweechai, K.; Suwanborirux, S.; Tanasupawatt, P.; Kittakoop, P.; Menasveta, P. New macrolactins from a marine *Bacillus* sp. SC026. *J. Nat. Prod.* **2000**, *63*, 984−986.

(17) Wilson, G. S.; Raftos, D. A.; Corrigan, S. L.; Nair, S. V. Diversity and antimicrobial activities of surface-attached marine bacteria from Sydney Harbour, Australia. *Microbiol. Res.* **2010**, *165*, 300−311.

(18) Dedicated website: http://www.fda.gov/food/foodborneillnesscontaminants/causesofillnessbadbugbook/ucm070523.htm, Food and Drug Administration (accessed Aug 9, 2014).

(19) Fickers, P. Antibiotic compounds from *Bacillus*: why are they so amazing? *Am. J. Biochem. Biotechnol.* **2012**, *8*, 40−46.

(20) Gustafson, K.; Roman, M.; Fenical, W. The macrolactins, a novel class of antiviral and cytotoxic macrolides from a deep-sea marine bacterium. *J. Am. Chem. Soc.* **1989**, *111*, 7519−7524.

(21) Nagao, T.; Adachi, K.; Sakai, M.; Nishijima, M.; Sano, H. Novel macrolactins as antibiotic lactones from a marine bacterium. *J. Antibiot. (Tokyo)* **2001**, *54*, 333−339.

(22) Marino, J. P.; McClure, M. S.; Holub, D. P.; Comasseto, J. V.; Tucci, F. C. Stereocontrolled synthesis of (−)-macrolactin A. *J. Am. Chem. Soc.* **2002**, *124*, 1664−1668.

(23) Chakraborty, K.; Paulraj, R. Enrichment of eicosapentaenoic acid from sardine oil with Δ5-olefinic bond specific lipase from *Bacillus licheniformis* MTCC 6824. *J. Agric. Food Chem.* **2008**, *56* (4), 1428−1433.

(24) Cinq-Mars, C. D.; Hu, C.; Kitts, D. D.; Li-Chan, E. C. Y. Investigations into inhibitor type and mode, simulated gastrointestinal digestion, and cell transport of angiotensin I converting enzyme-inhibitory peptides in pacific hake (*Meriuccius productus*) fillet hydrolysate. *J. Agric. Food Chem.* **2008**, *56* (2), 410−419.

(25) Moldenhauer, J.; Chen, X. H.; Borriss, R.; Piel, J. Biosynthesis of the antibiotic bacillaene, the product of a giant polyketide synthase complex of the trans-AT family. *Angew. Chem.* **2007**, *119*, 1−4.

(26) Scotti, C.; Piatti, M.; Cuzzoni, A.; Perani, P.; Tognoni, A.; Grandi, G.; Galizzi, A.; Albertini, A. M. A *Bacillus subtilis* large ORF

coding for a polypeptide highly similar to polyketide synthases. *Gene* **1993**, *130* (1), 65−71.
(27) Calderone, C. T.; Kowtoniuk, W. E.; Kelleher, N. L.; Walsh, C. T.; Dorrestein, P. C. Convergence of isoprene and polyketide biosynthetic machinery: isoprenyl-S-carrier proteins in the *pksX* pathway of *Bacillus subtilis*. *Proc. Natl. Acad. Sci. U.S.A.* **2006**, *103*, 8977−8982.
(28) Gu, L. C.; Jia, J. Y.; Liu, H. C.; Hakansson, K.; Gerwick, W. H.; Sherman, D. H. Metabolic coupling of dehydration in the curacin A pathway: functional identification of a mechanistically diverse enzyme pair. *J. Am. Chem. Soc.* **2006**, *128*, 9014−9015.
(29) Wu, J.; Cooper, S. M.; Cox, R. J.; Crosby, J.; Crump, M. P.; Hothersall, J.; Simpson, T. J.; Thomas, C. M.; Willis, C. L. Mupirocin H, a novel metabolite resulting from mutation of the HMG-CoA synthase analogue, *mupH* in *Pseudomonas fluorescens*. *Chem. Commun.* **2007**, *28* (20), 2040−2042.
(30) Weissman, K.; Leadlay, P. F. Combinatorial biosynthesis of reduced polyketides. *Nat. Rev. Microbiol.* **2005**, *3*, 925−936.
(31) Schirmer, A.; Sabaou, N.; Gadkari, R.; Reeves, C. D.; Ibrahim, F.; Delong, E. F.; Hutchinson, C. R. Metgenomic analysis reveals diverse polyketide synthase gene clusters in microorganisms associated with the marine sponge *Discodermia dissoluta*. *Appl. Environ. Microbiol.* **2005**, *71*, 4840−4849.
(32) Zhao, J.; Yang, N.; Zeng, R. Phylogenetic analysis of type I polyketide synthase and nonribosomal peptide synthetase genes in Antarctic sediment. *Extremophiles* **2008**, *12*, 97−105.

honeys,[15] and flavonoid glycosides containing the aglycone quercetin, kaempferol, or isorhamnetin were reported in *T. carbonaria* honeys from suburban areas of Queensland.[18] Whether these stingless bees collect *Leptospermum* nectars to produce "jellybush-sugarbag" honeys was unknown.

The study of antimicrobial natural products in honeys is important to determine honey varieties with medicinal potential and for clinical applications. Bioactive natural products found in honeys can be derived from plant nectars or other plant materials such as propolis.[19] Propolis is a resinous mixture that the bees produce by mixing their beeswax, salivary secretions, and plant resins. Whether propolis can contribute to the composition of stingless bee honey was yet to be ascertained. Therefore, the natural products, MGO levels, and peroxide content were investigated in this study to assess the contribution of these factors to the antimicrobial effects reported in *T. carbonaria* honeys.[17]

Chemical investigations of Meliponini honeys require an appropriate sample preparation. The complex matrix rich in polar compounds including sugars and proteins can complicate the sample preparation and analysis.[20] Moreover, a high content of flavonoid glycosides that are not hydrolyzed by the bee salivary $\beta$-glucosidases can be expected.[19] Therefore, a combination of methodologies of extraction techniques has proven successful in honey analyses including solid-phase extraction methods and liquid chromatography−mass spectrometry to analyze nonvolatile compounds in extracts.[19,21,22] Other analytical paper have indicated gas chromatography−mass spectrometry to screen the volatiles with a chemotaxonomical relevance in honeys from Australian honeybees foraging on *Leptospermum* spp.[23] A combination of analytical techniques was applied to a dereplication approach for the characterization of natural products in Australian *T. carbonaria* honeys in this study.

The aims were to characterize the natural products, levels of MGO, and peroxide contents in *T. carbonaria* honeys, to determine if these honeys originate from *Leptospermum* nectars using known phytochemical markers, and to assess the in vitro antibacterial activities of their concentrated phenolic fractions and peroxide contents.

## MATERIALS AND METHODS

**Chemicals.** Methanol, acetonitrile, ethanol, and ethyl acetate of analytical grade were purchased from Merck Pty Ltd. (Kilsyth, VIC, Australia). Milli-Q water was obtained from an in-house Milli-Q Ultrapure Water System. Muller−Hinton nutrient broth (MHB) and agar (MHA) media, 3-[4,5-dimethylthiazol-2-yl-]-2,5-diphenyltetrazolium bromide (MTT), hexadecane, phenol standard (>99.5%), *N*,*O*-bis(trimethylsilyl)trifluoroacetamide (BSTFA), *O*-(2,3,4,5,6-pentafluorobenzyl)hydroxylamine−HCl (PFBHA), hydroxyacetone (HA), methylglyoxal (MGO), dihydroxyacetone (DHA), hydroxymethylfurfural (HMF), gallic acid, quercetin hydrate, 3-phenyllactic acid, *o*-dianisidine, horseradish peroxidase type IV, and hydrogen peroxide were purchased from Sigma-Aldrich (Castle Hill, NSW, Australia).

**Beehive Products.** Stingless bee *T. carbonaria* honeys were produced in beehives using wooden compartments (honeysupers) of 25 × 15 cm. Three sites were used for the apiaries ($n$ = 6 beehives each). Two sites contained plants of *L. polygalifolium* and *L. liversidgii* at high density in the coastal area of Tyagarah, NSW (site 1) and heathland of East Beerwah, QLD (site 2). The third and control site was in heathland of West Beerwah, QLD (site 3), and did not contain *Leptospermum* spp. The honeys were produced between September 2012 and April 2013 during *Leptospermum* nectar flow. The honeys from beehives within the same site were pooled to yield one representative batch per each site. The three batches were labeled as honeys 1, 2, and 3 (control).

The honeys were harvested from honeypots and sieved using a metal drainer to remove other hive materials including propolis, bees, and pollen particles. Honey aliquots (200 mL) were centrifuged at 1000 rpm at room temperature for 5 min to recover the supernatants for later analyses. Propolis from the same honeypots of site 2 was extracted by maceration in absolute methanol (5% w/v) for 24 h at room temperature, filtered, and evaporated to dryness under vacuum to yield the propolis extract.

**Liquid−Liquid Extraction for the Phenolics Concentrates.** The raw honeys (ca. 50 g) were extracted in absolute ethanol (20 mL, 40% v/w) at around 60 °C and allowed to cool at 24 °C for 2 h and then at 4 °C for 2 h, followed by storage at −18 °C overnight. The supernatants were decanted, and the sugar precipitates were extracted again following the same protocol. The combined supernatants were evaporated to dryness under reduced pressure. Three cycles of solvent extractions were repeated to precipitate the carbohydrates of the honey matrices and to concentrate the phenolic fractions into ethanolic extracts. The last step of extraction used acetone/ethanol (1:1) followed by evaporation to dryness and freeze-drying to yield three honey phenolic concentrates (2.40, 2.70, and 3.70 mg). Aliquots of the three dry extracts were reconstituted in methanol for the liquid chromatography analyses and in ethanol for the antibacterial assays.

A further extraction involved raw honeys (ca. 50 g) in deionized water/ethyl acetate (2:1) using a modified protocol.[24] The mixture was warmed at 50 °C in a water bath for 5 min and vortexed to homogeneity. The ethyl acetate extracts were transferred into clean test tubes and dried using anhydrous $Na_2SO_4$ (70 mg each) for 5 min. Aliquots of the final solutions were subjected to gas chromatography.

**GC-MS Analyses.** Equipment was a PerkinElmer Clarus580 GC-EI-MS fitted with an Elite-5MS column ($L$ = 30 m, i.d. = 0.25 mm, DF - 0.25 $\mu$m, PerkinElmer) operated at 70 eV ionization. The ethyl acetate extracts (1.0 $\mu$L) were injected at 260 °C into the gas chromatograph, split ratio of 10:1, and the oven temperature was ramped from 50 to 315 °C at 5 °C/min and held for 5 min, for a total run time of 47 min. A solution of *n*-alkane standards ($C_8$−$C_{40}$) was also analyzed for the calculation of retention indices. The mass spectrometer acquisition was set in the range of $m/z$ 50−650.

A further protocol required the analyses of trimethylsilyl (TMS) derivatives after BSTFA derivatization of honey extract. The ethyl extracts were treated with BSTFA (50 $\mu$L) for 2 h at 60 °C and analyzed under the same GC-MS conditions.

**UPLC-UV-ESI-HR-MS Analyses.** Samples of the three honeys and one propolis extract were reconstituted in MeOH (2 mg/mL) and injected onto an Eclipse Plus C18 UPLC column (2.1 × 100 mm, 1.8 $\mu$m particle size). The equipment (Thermo Scientific, New Zealand) included a Dionex Ultimate 3000 UPLC pump linked in series with eluent from the column into the photodiode array detector and then into the qExactive Mass Spectrometer (qEMS). The ESI module was a heated ESI (HESI). The qEMS resolution was set at 140,000, and separate UPLC runs were done for positive and negative ionization modes. Mobile phase A (MPA) consisted of 0.1% acetic acid in water, and mobile phase B (MPB) consisted of 0.1% acetic acid in acetonitrile. The flow rate was 0.4 mL/min. The gradient was 2.5% MPB at $t$ = 0.5 min to 20% MPB at 15 min and 100% MPB at 25 min, held for 2.5 min. A photodiode array detector was coupled to the LC and set at 205, 260, 290, and 340 nm. The spray voltage was set to 3.5 kV with the source temperature at 100 °C.

Quantitation of individual compounds was performed by HPLC-DAD at 205 nm on a HPLC series 200 with a Flexar DAD (PerkinElmer) equipped with an RP-C18 column, 75 $\mu$m, 4.6 × 4 mm (Phenomenex Synergi Fusion), with a flow rate of 1.2 mL/min and the same analytical conditions of mobile phases and gradient method as indicated for the UPLC analyses. Accurate ethanolic solutions of the phenolic extracts were analyzed against a standard calibration curve ($R^2$= 0.9984) of gallic acid (0−0.6 mg/mL), and signals were interpolated to yield gallic acid equivalents (GAE) per 100 mg of phenolic extract. Quantifications were performed at 205 nm, mean values, $n$ = 2.

**Table 1. Phenolic Extracts of Honeys by LC-UV-HR-ESI-MS**

| | | | | | | | abundances[a] (%) | | |
|---|---|---|---|---|---|---|---|---|---|
| no. | $t_R$ (min) | identification | $UV_{max}$ (nm) | formula for $[M-H]^-$ | | other HR-MS fragments ($m/z$) | 1 | 2 | 3 |
| 8[b] | 10.91 | 3-phenyllactic acid | 288 | $C_9H_9O_3$ | 165.0551 | (−) 147 $[M-H_2O]$, 119 | 3.7 | 12.7 | 5.9 |
| 1 | 12.48 | quercetin-6,8-di-*O*-glucoside | 210, 263, 347 | $C_{27}H_{29}O_{17}$ | 625.1423 | (+) 627.1562 $[M+H]^+$, (+) 465.1032 $[M+H-162]^+$ | tr | tr | 2.3 |
| | | | | | | (+) 303.0501 (aglycone) $[M+H-162-162]^+$ | | | |
| 2 | 13.39 | quercetin-3-*O*-glucosyl-*O*-pentose | 248, 292, 362 | $C_{26}H_{27}O_{16}$ | 595.1319 | (+) 597.1453 $[M+H]^+$, (+) 465.1031 $[M+H-132]^+$ | tr | tr | 2.2 |
| | | | | | | (+) 303.0500 $[M+H-162]^+$ | | | |
| 3 | 13.62 | tricetin-3-*O*-rhamnose-*O*-glucoside | 224, 289 | $C_{27}H_{29}O_{16}$ | 609.1474 | (+) 611.1609 $[M+H]^+$, (+) 465.1031 $[M+H-146]^+$ | tr | 1.1 | 3.0 |
| | | | | | | (+) 303.0500 (aglycone) $[M+H-146-162]^+$ | | | |
| 4 | 13.76 | kaempferol-3-*O*-diglucoside | 250, 285, 348 | $C_{26}H_{27}O_{17}$ | 609.1476 | (+) 611.1268 $[M+H]^+$, (+) 450.1116 $[M+2H-162]^+$ | 3.1 | 2.8 | 6.6 |
| | | | | | | (+) 287.0552 (aglycone) $[M+H-162-162]^+$ | | | |
| 5 | 14.56 | isorhamnetin-3-*O*-rhamnose-*O*-glucoside | 260, 290, 340 | $C_{28}H_{31}O_{16}$ | 623.1626 | (+) 625.1768 $[M+H]^+$, (+) 479.1189 $[M+H-146]^+$ | 1.6 | 43.7 | 22.6 |
| | | | | | | (+) 317.0658 ($C_{16}H_{13O7}$) $[M+H-146-162]^+$ | | | |
| 6 | 14.87 | luteolin-3-*O*-rhamnose-*O*-glucoside | 299 | $C_{26}H_{27}O_{16}$ | 595.1319 | (+) 595.1661 $[M+H]^+$, (+) 449.1082 $[M+H-146]^+$ | tr | 1.1 | 12.7 |
| | | | | | | (+) 287.0551 (aglycone) $[M+H-146-162]^+$ | | | |
| 9 | 15.12 | 13-hydroxyabscisic acid | 260 | $C_{15}H_{19}O_5$ | 279.1242 | (−) 168.0787 ($C_9H_{12}O_3$), 139.0758 ($C_8H_{11}O_2$) | | | tr |
| 7 | 15.30 | isorhamnetin-3-*O*-rhamnose-*O*-glucoside isomer | 248, 295, 358 | $C_{28}H_{31}O_{16}$ | 623.1628 | (+) 625.1767 $[M+H]^+$, (+) 479.1188 $[M+H-146]^+$ | | 0.3 | tr |
| | | | | | | (+) 317.0657 (aglycone) $[M+H-146-162]^+$ | | | |
| 10[b] | 15.50 | unedone | nd[c] | | | (+) 241.1436 ($C_{13}H_{21}O_4$) $[M+H]^+$, 197.0010 $[M+H-CO_2]^+$ | | | tr |
| 12[b] | 16.65 | lumichrome | 260, 340 | $C_{12}H_9N_4O_2$ | 241.0733 | (−) 223 $[M-H-H_2O]^-$, (−) 198.0667 ($C_{11}H_8N_3O$) $[M-H-HNCO]^-$ | tr | | |
| | | | | | | (+) 243.0879 $[M+H]^+$ | | | |
| 11[b] | 19.20 | abscisic acid (*cis*,*trans*) | 260 | $C_{15}H_{19}O_4$ | 263.1293 | (−) 219.1390 ($C_{14}H_{19}O_2$) $[M-COOH]^-$, 151.0758 ($C_9H_{11}O_2$) | | tr | |
| | 19.54 | methylflavanone | 260, 290 | $C_{15}H_9O_7$ | 301.0358 | (−) 285.0409 $[M-H-CH_3]^-$ | | | tr |
| | 20.17 | flavonol | 260, 340 | $C_{15}H_{11}O_5$ | 271.0618 | (+) 273.0760 $[M+H]^+$ | tr | | |
| | 20.69 | flavonol | 290, 340 | $C_{16}H_{13}O_6$ | 301.0724 | (+) 303.0865 $[M+H]^+$ | tr | | |
| - | 21.61 | flavonol | 290, 340 | $C_{17}H_{15}O_5$ | 299.0931 | | tr | | |
| | 22.03 | pinocembrin[d,e] | 290 | $C_{15}H_{11}O_4$ | 255.0666 | | | tr | |
| | 22.78 | cryptostrobin[d,e] | 290, 340 | $C_{16}H_{13}O_4$ | 269.0824 | (+) 271.0966 $[M+H]^+$ | 1.6 | 1.7 | 0.1 |
| | 26.88 | acylphloroglucinol[e] | 260 | $C_{25}H_{37}O_3$ | 385.2757 | (+) 387.2893 $[M+H]^+$ | tr | tr | tr |
| | 27.42 | phloroglucinol-flavanone[e] | nd | $C_{31}H_{35}O_7$ | 519.2399 | (−) 471, 339, 325, 255, 181 | tr | tr | tr |

[a]Quantitative amounts were measured as mg/100 mg of gallic acid equivalents at 205 nm. Mean values, $n = 2$. tr, traces <1%. [b]See structures in Figure 2. [c]nd, not determined. [d]Matched with references. [e]Identified in propolis from the same honeypots of honey 2.

**MGO Protocols.** The calibration of standards MGO, DHA, and HMF was undertaken against the internal standard HA (3.0 mg/mL) according to known protocols.[25,26] The internal standard HA (250 μL) was added to raw honey samples (ca. 0.3 g) and diluted with water (600 μL) before being mixed thoroughly. The solutions were derivatized with 1200 μL of PFBHA (0.02 g/mL in 0.1 M, pH 4, citrate buffer) for 1 h at room temperature, and then acetonitrile was added (2 mL). Solutions were diluted with water (1 mL) and mixed. Aliquots (10 μL) were chromatographed by HPLC-DAD at 263 nm.[25,26] This procedure was repeated in triplicate for batches harvested in 2013.

**Antibacterial Assays.** Two bacterial strains were available at the University of the Sunshine Coast laboratory. Inocula of *Staphylococcus aureus* ATCC 25923 or *Klebsiella pneumoniae* ATCC 13883 were cultured in MHB overnight at 37 °C and used at lag phase as determined by optical density to be 0.500−0.550 OD. Fresh media were inoculated with culture suspensions to the final concentration of $10^5$ CFU/mL in plates. Controls were absolute ethanol and the phenol standard (>99.5% purity) solution in ethanol. The negative control showed no bacterial inhibition. The positive control phenol solution showed mean zones of inhibition of 9.78−28.55 mm used to construct the calibration curves for the concentrations of 0.5−8% (w/v) that were tested against the two bacterial strains. Samples were raw honeys or phenolic concentrates reconstituted in absolute ethanol. Two methodologies were applied for the assays.

In the agar diffusion assay, agar plates of 20 × 20 cm were prepared with MHA inoculated media. Samples were dispensed to wells of 8 mm diameter: aliquots (100 μL) of raw honeys or phenolic solutions (at final weights of 100−800 μg) were delivered to MHA plates. The plates were incubated at 37 °C for 16 h in a humidified incubator. Results of growth inhibition by the samples were reported as the mean zone of inhibition (mm) and calibrated by values of phenol equivalents in the range of 0−8% (w/v).

In the broth dilution assay, 96-well microplates were filled with 170 μL of inoculated MHB. Aliquots (10 μL) of raw honeys or phenolic solutions (at final concentrations up to 3.3 mg/mL) were added to wells of microplates. Absolute ethanol (10 μL) yielded a final concentration of 5.5% v/v. Phenol standard solution ranged between 0.02 and 0.2% (w/v). The microplates were incubated at 37 °C for 16 h in a humidified incubator. The MTT tetrazolium dye was used to visualize the inhibition of bacterial growth, showing a yellow coloration for full inhibition. Minimum inhibitory concentrations (MICs) were replated using cotton swabs on fresh agar plates that were incubated for 24 h at 37 °C. The bactericidal effects were assessed for >99% lack of bacterial growth.

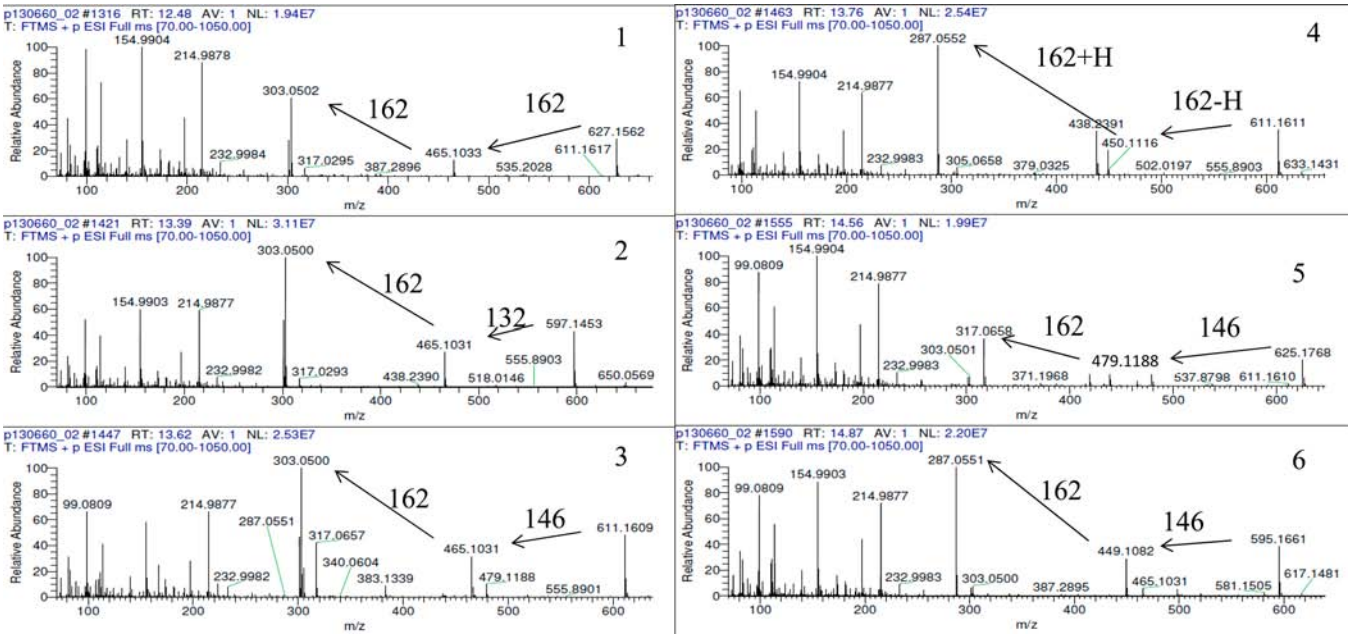


**Figure 1.** Full mass spectra of the glycosylated flavonoids (**1**) quercetin-6,8-di-*O*-glucoside; (**2**) quercetin-3-*O*-glucosyl-*O*-pentose; (**3**) tricetin-3-*O*-rhamnose-*O*-glucoside; (**4**) kaempferol-3-*O*-diglucoside; (**5**) isorhamnetin-3-*O*-rhamnose-*O*-glucoside; and (**6**) luteolin-3-*O*-rhamnose-*O*-glucoside, as identified in honey 2 by UPLC-ESI-(+)-MS. Characteristic fragmentation patterns showed the diagnostic mass losses for hexose moieties of 162 Da for a glucose unit, 146 Da for a rhamnose unit, and 132 Da for the internal cleavage of a *C*-pentosyl unit in **2**.

**Peroxide Quantitation.** Quantitative concentrations of hydrogen peroxide in honey were determined from a modified protocol.[3] Briefly, 135 $\mu$L of a buffer containing 50 $\mu$g/mL of *o*-dianisidine and 20 $\mu$g/mL of horseradish peroxidase type IV (Sigma-Aldrich, Australia) were dispensed to wells of a 96-well microplate. The negative control was deionized water. The positive control was a standard solution of hydrogen peroxide at concentrations of 1 $\mu$M−1 mM used for calibration curves. The assay measured the product formation after horseradish peroxidase catalysis of hydrogen peroxide in the presence of *o*-dianisidine. The absorbance values were read at 540 nm at intervals of 5, 15, 30, and 60 min using a Versa Max Tunable Microplate Reader (Associates of Cape Cod Int. Inc., Liverpool, UK). The enzymatic assays were conducted at 24 °C. Standard and honeys were analyzed in duplicate. Mean values (± standard error) were averaged for the three honeys to show common levels of hydrogen peroxide in undiluted and diluted stingless bee honeys.

Peroxide assays were undertaken using undiluted and diluted honeys to compare the accumulation of hydrogen peroxide. Aliquots (40 $\mu$L) of raw honeys were added to wells containing the reagents for 5 min, and the absorbances were read at the conditions indicated above. A further test employed honeys diluted in water (44%) for 1 h, and aliquots (40 $\mu$L) were transferred to wells containing the reagents for 5 min before the absorbance was monitored at the time intervals aforementioned.

**Data and Statistical Analyses.** GC-MS results were interpreted against NIST library, mass spectra of chemical references, and the literature on norisoprenoids and other volatiles from honeys and nectars including *Leptospermum* sources.[2327,28]

The quantitation of compounds was undertaken by the internal standard method using hexadecane $C_{16}$ (stock 8.89 $\mu$g/100 mL) in the GC-MS analyses. The peak areas were standardized to hexadecane areas to the mass ($\mu$g/g) of individual components in honey. A response factor of 1 was assumed for all constituents.

The HR-MS data were analyzed using Thermo Xcalibur (v. 3.0.63). Accurate mass measurements and elemental compositions were used to generate chemical formula using http://www.chemcalc.org/.[29] Constituents were dereplicated using SciFinder (https://scifinder.cas.org/) against available literature. Known natural products were searched using ESI-MS marker ions in the positive mode at *m/z* 550−700 for glycosyl flavonoids. Other ESI-MS markers were searched at *m/z* 165 for 3-phenyllactic acid and at *m/z* 243 for lumichrome.[30] *Leptospermum* markers of mānuka and jellybush honeys were searched for methyl syringate (MYSR),[7] leptosin,[31] unedone,[10] and MGO.[8] Propolis constituents were identified in honeys from the same honeypots by comparing retention times of individual peaks and their ESI-UV-MS against known data.[32]

MGO, HMF, and DHA were identified by comparison of their retention times and UV spectra against those of commercial standards (Sigma-Aldrich, NSW) showing distinct retention times and UV spectra for DHA ($t_R$, 9.82; $UV_{max}$, 201, 256), HA ($t_R$, 13.27; $UV_{max}$, 199, 259), HMF ($t_R$, 14.45; $UV_{max}$, 276), and MGO ($t_R$, 18.39; $UV_{max}$, 201, 242). Linear regression curves (MGO, $R^2$ = 0.998, $n$ = 3; DHA, $R^2$ = 0.9999, $n$ = 3; HMF, $R^2$ = 0.9996, $n$ = 3) were used for quantitation.

Quantitative amounts of hydrogen peroxide were measured in undiluted (raw) and 44% diluted honeys by interpolating the absorbance readings of samples at 30 min of enzymatic activity against linear regressions of standard peroxide ($R^2$ = 0.9989).

The antibacterial concentration curves from the agar diffusion assay against *S. aureus* were fitted with centered second-order polynomial equations (quadratic curve-fits) using GraphPad Prism 6.0. Phenol equivalents were calculated against calibrated curves of phenol standard solutions tested in the same plate (mean values, $n$ = 3, standard error).

## RESULTS

**Glycosyl Flavonoids and Propolis Phenolics.** The UPLC-UV-HR-ESI-MS(+) analyses of the three phenolic extracts showed the high content of flavonoid glycosides **1**−**7** with MW of 596−626 (Table 1; Figure 1). Their UV maxima were in the ranges of 220−264 nm for flavonoids that could be distinguished at subclass level between flavones for the band I's absorption at 335−350 nm or flavonols at 360−390 nm. The ESI-MS(+) fragmentation patterns of the protonated molecular ions showed diagnostic mass losses of 162 Da for a hexosyl residue and 146 Da for a deoxyhexosyl (most likely rhamnose) residue. Therefore, **1**−**7** were identified to be *O*-glycosylated flavonoids containing two glycosidic residues (Table 1; Figure

1). The ESI-MS(+) fragmentation of **2** showed a mass loss of 132 Da that was indicative of an internal cleavage of a *C*-pentosyl unit. The aglycones were determined from the protonated base peaks with accurate mass measurements at $m/z$ 286 ($C_{15}H_{11}O_6$) for **4** and **6**, at $m/z$ 302 ($C_{15}H_{11}O_7$) for **1**−**3**, and at $m/z$ 317 ($C_{16}H_{13}O_7$) for **5** and **7**: identifications were kaempferol, quercetin, and isorhamnetin, respectively. The base peaks were detected as the deprotonated aglycones of compounds **2**−**4**, **6**, and **7** (Figure 1).

Comparison of UPLC-ESI(−)-MS analyses of the extracts obtained from honey 2 and propolis from the same honeypots showed some common constituents (Figure S1). Trace amounts of flavonoid aglycones pinocembrin and cryptostrobin and of two phloroglucinols were found in the late eluting regions of honey extracts (Table 1). The glycosyl flavonoids were found only in honeys and eluted at 12−17 min by LC. Gallic acid (a phenolic acid) and a catechin (a polar flavonoid aglycone) were found only in propolis by LC.

**Norisoprenoids.** The LC-MS analyses detected three norisoprenoids **9**−**11**, namely, abscisic acid, unedone, and 13-hydroxyabscisic acid, by dereplicating the accurate mass measurements of their deprotonated MS ions (Table 1) for structural identification (Figure 2). The *cis,trans* isomerism of **11** was identified by the diagnostic fragment ion at $m/z$ 151 (Figure S2) as previously reported.[33] The GC-MS analyses of the ethyl acetate extracts of *T. carbonaria* honeys contained 3-oxo-$\alpha$-ionone **13** and related norisoprenoids **14** and **15** that were tentatively identified against entries of the NIST library (Table 2; Figure 2).

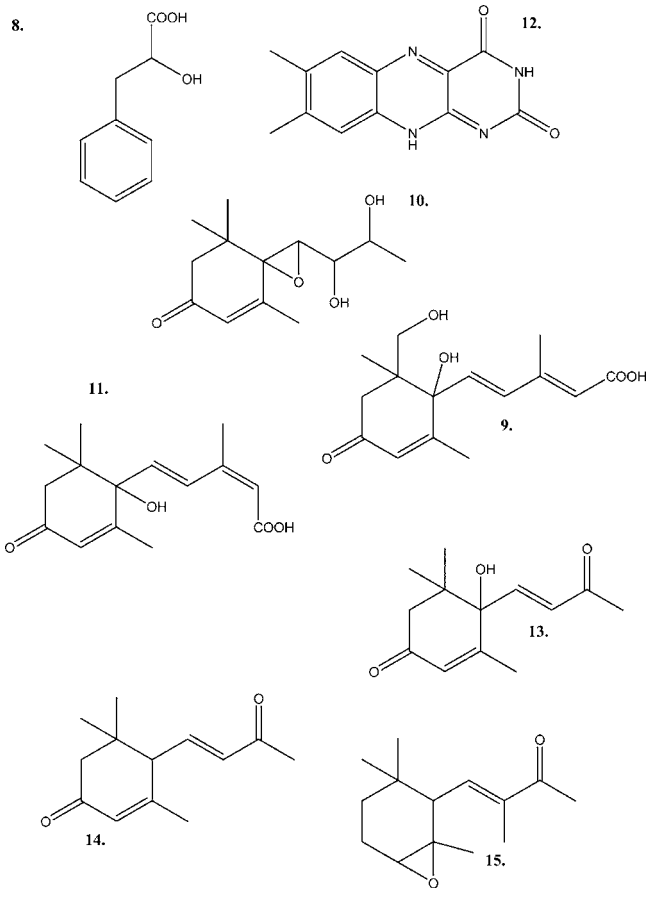


**Figure 2.** Structures of dereplicated honey constitutents: (**8**) 3-phenyllactic acid; (**12**) lumichrome; (**9**) 13-hydroxyabscisic acid; (**11**) abscisic acid; (**13**) 6-hydroxy-3-oxo-$\alpha$-ionone; (**14**) 3-oxo-$\alpha$-ionone; (**15**) oxabicycloheptanyl.

**Lumichrome and Aromatics.** Lumichrome (7,8-dimethylalloxazine, **12**) was identified in trace amounts in honey 1 (Table 1). In the negative mode of ESI-MS, the accurate mass measurement of the deprotonated ion at $m/z$ 241.0733 yielded the elemental composition of $C_{12}H_9N_4O_2$ and $m/z$ 198.0667 ($C_{11}H_8N_3O$) due to the loss of HNCO (Figure S3) and confirmed the interpretations reported previously.[30]

3-Phenyllactic acid (**8**) was found in the three honeys by UPLC-ESI-MS and also by GC-MS (Tables 1 and 2). It showed the same UV spectra with maxima at 224sh and 283 nm of the reference compound (Sigma-Aldrich, NSW). Its deprotonated fragmented ESI-MS ions (Figure S4) were dereplicated against the literature.[30]

In the attempt to determine whether *Leptospermum* nectars contributed to the composition of multifloral sugarbag honeys, samples 1 and 2 were obtained from two sites where these plant species were predominant during *Leptospermum* nectar flow. Results indicated that no MGO or phenolics recommended as *Leptospermum* markers were found within the *T. carbonaria* honeys analyzed in this study.

**Peroxide Content in Honeys and Antibacterial Activity of Standard.** Levels of hydrogen peroxide accumulated to 155.8 ± 10.0 and 91.5 ± 11.3 $\mu$M (mean values, standard error) in undiluted and 44% diluted honeys, respectively. The standard peroxide showed to be bactericidal at 760 $\mu$M in broth dilution, and mean zones of inhibition were up to 43.86 mm against *S. aureus* ATCC 25923 and up to 42.63 against *K. pneumoniae* ATCC 13883 at concentrations of 0−5.5 mM in agar diffusion (Table 3).

**Antimicrobial Effects of Phenolic Concentrates from Honeys.** In agar diffusion, the raw honeys (100 $\mu$L) were active against both bacterial strains (Table 3; Figure S5). However, the phenolic extracts (100 $\mu$g) inhibited only *S. aureus* growth with diameters of inhibition ranging from 10.18 to 19.87 mm with phenol equivalents of 1.0−5.1% (w/v) (Table 3). The phenolic extracts up to 100 $\mu$g did not inhibit *K. pneumoniae* ATCC 13883. The positive control phenol solution showed mean zones of inhibition of 10.00−10.75 mm at the concentration of 1% (w/v) against the two strains (Table 3).

In broth dilution, the raw honeys and phenolic concentrates were active against both strains at the dilution used. The raw honeys in MHB were used at the dilution of 5.5% (v/v) showing bactericidal effects after 16 h of incubation. The phenolic concentrates had bactericidal MIC values ranging from 1.2 to 1.8 mg/mL. The control phenol standard yielded a MIC value of 0.18% (w/v) against both bacterial strains (Table 3).

## DISCUSSION

**Chemotaxonomical Composition and Significance.** The liquid−liquid extraction methodologies applied in this study proved successful in recovering the phytochemicals and concentrating them in phenolic extracts for the chromatographic analyses and the antibacterial assays. The soft ionization of ESI coupled to MS interpretation allowed for the characterization of the aglycone type, the number of sugar units, and the type of *O*-glycosidic flavonoids. The high abundances of the mass-to-charge ions of the aglycone moieties indicated that the glycosidic residues were possibly attached on a single position of the flavonoid core.[19,34] The sugar residues

**Table 2. GC-MS Analyses of the Ethyl Acetate Extracts of Honeys[a]**

| | | | | | | μg/g | | |
|---|---|---|---|---|---|---|---|---|
| no. | $t_R$ (min) | identification | EI-MS ($m/z$) | M*[b] | KI[c] | 1 | 2 | 3 |
| | 6.65 | β-pinene | 93 (BP), 136 | 136 | 980 | 4.9 | 0.7 | 6.9 |
| | 18.06 | lactic acid diTMS | 73, 147 (BP), 189, 233, 261, 303 | 318 | 1476 | 1241.5 | 682.1 | 1398.9 |
| **8**[d] | 18.73 | 3-phenyllactic acid[f] | 65, 91 (BP), 103, 148, 166 | 166 | 1508 | - | 25.3 | - |
| | 20.69 | alkylated phloroglucinol[e] | 70 (BP), 137, 179, 207, 250 | 250 | 1605 | 0.8 | - | - |
| | 21.21 | 2-hydroxyisocaproic, diTMS[g] | 73, 147 (BP), 189, 275, 303 | 360 | 1631 | 0.8 | 0.8 | 0.9 |
| **14**[d] | 21.46 | 3-oxo-α-ionone | 73, 180, 150, 172 | 206 | 1644 | 3.5 | 1.3 | 3.4 |
| | 23.38 | succinate, diTMS[g] | 73 (BP), 147, 289 | 346 | 1743 | 44.8 | 11.7 | 11.9 |
| **13**[d] | 24.01 | 6-hydroxy-3-oxo-α-ionone | 75, 124 (BP), 149, 166, 207 | 222 | 1777 | 4.4 | 0.9 | 9.3 |
| **15**[d] | 25.73 | oxabicycloheptanyl | 93 (BP), 123, 137, 153, 166 | 222 | 1880 | 0.8 | 0.8 | 0.9 |
| | 27.06 | hexadeconoic acid[f] | 73 (BP), 129, 171213, 227, 256 | 256 | 1961 | 17.3 | 5.1 | 6.5 |
| | 28.01 | 3-phenyllactic, diTMS[g] | 147 (BP), 73, 189, 309 | 310 | 2015 | 20.6 | 45.2 | 22.8 |
| | 29.79 | linoleic acid[f] | 67 (BP), 81, 95, 109, 123, 280 | 280 | 2133 | 0.7 | 8.4 | 5.5 |
| | 29.89 | α-linoleic acid[f] | 67, 79 (BP), 95, 108, 222, 280 | 280 | 2140 | 0.7 | 8.4 | 5.5 |
| | 33.68 | acylphloroglucinol | 69, 91, 135, 191, 245 (BP), 386 | 386 | 2302 | 10.0 | 2.3 | 9.2 |
| | 35.04 | hydroxybenzoic, diTMS ester[g] | 73 (BP), 193, 439, 480 | 496 | 2504 | 4.7 | 0.8 | 6.4 |
| | 35.39 | cryptostrobin[h] | 69, 138 (BP), 166, 193, 270 | 270 | 2531 | 5.2 | 3.5 | 44.2 |
| | 35.53 | stroboponin[h] | 69, 138, 166 (BP), 193, 270 | 270 | 2542 | 4.5 | 0.8 | 0.9 |
| | 37.28 | docadosene | 55 (BP), 67, 97, 308 | 322 | 2581 | 0.8 | 0.8 | 0.9 |
| | 40.85 | lupeol | 69, 207 (BP), 281, 341, 408 | 426 | 2886 | 15.2 | 0.3 | 6.7 |

[a]Compounds were quantitated in honey (μg/g) using peak areas against the internal standard hexadecane in underivatized and silylated extracts. Mean values, $n = 2$. [b]M*, molecular ion [c]KI, Kovats indices. [d]BP, base peak. [e]See structures in Figure 2. [f]Identified only in underivatized, nonsilylated extracts. [g]BSTFA was used in derivatizing for trimethylsilyl (TMS) groups. [h]Identified against purified references.

**Table 3. Antibacterial Effects of Honeys and Their Phenolic Extracts**

| | *S. aureus* ATCC 25923 | | *K. pneumoniae* ATCC 13883 | |
|---|---|---|---|---|
| sample | MID[a] (phen equiv[b]) | MIC[c] | MID[a] (phen equiv[b]) | MIC |
| raw honey 1 | 19.87 ± 0.02[a] (5.1) | | 17.39 ± 0.01[a] (4.0) | |
| raw honey 2 | 17.45 ± 0.44[a] (4.0) | | 15.41 ± 0.01[a] (3.3) | |
| raw honey 3 | 15.15 ± 0.02[a] (2.8) | | 15.42 ± 0.07[a] (3.3) | |
| phenolics 1 | 10.60 ± 0.05[a] (1.2) | 1.2[e] | *a* | 1.2[e] |
| phenolics 2 | 10.18 ± 0.03[a] (1.0) | 1.8[e] | *a* | 1.2[e] |
| phenolics 3 | 10.27 ± 0.15[a] (1.1) | 1.2[e] | *a* | 1.2[e] |
| $H_2O_2$ standard | 12.37 ± 0.01[d] (1.8) | 760.0[f] | 11.20 ± 2.31[d] (1.6) | 760.0[f] |
| phenol standard | 10.75 ± 0.01[g] (1.0) | 0.18[b] | 10.00 ± 0.0[g] (1.0) | 0.18[b] |

[a]MID (mean inhibition diameter, mm) for samples at 100 μg in 100 μL. Mean value ± standard error ($n = 3$). [b]Phenol equivalents % (w/v). [c]MIC, minimum inhibitory concentrations. [d]At 300 μM. [e]mg/mL. [f]μM. [g]1% (w/v).

could be possibly positioned on C-3 or C-7,[18] and previous reports of *T. carbonaria* honeys were identified to be 3-*O*-glycosides.[15,18] For instance, the ESI-MS in positive mode of compounds **2**−**4**, **6**, **7** showed the base peaks of the protonated aglycones after two glycosidic losses, and thus these compounds were identified to be flavonol *O*-diglycosides (Table 1; Figure 1). Compounds **1** and **5** showed low relative abundances of the aglycone ions (Table 1; Figure 1), as previously reported in flavonoid di-*O*-glucosides.[34]

The first-order ESI-MS technique of this study suggested a (1→2) interglycosidic linkage as it was identified on the basis of the high relative abundance (10−35%) of the moieties containing one sugar-*O*-aglycone after the loss of one glucosidic (162 Da) or rhamnosyl (146 Da) unit.[34] Further tandem $MS^n$ studies are warranted to carry out the sequential fragmentation of parent molecular ions and daughter ions to confirm the type of interglycosidic linkage of flavonoids of this study.[19,35] Using ESI-tandem $MS^n$, the interglycosidic linkages on flavonoids were characterized previously.[18,19,35] For instance, the ESI-MS fragmentation in positive mode of a dihexoside flavonol with interglycosidic linkage 1→2 was reported in Argentinean honeybee honeys.[36]

The presence of several *O*-glycosylated flavonoids **1**−**7** and of few flavonoid aglycones was consistent with previous papers describing the honey composition due to Meliponini bees lacking β-glucosidases.[18,19] On the contrary, Australian honeys from honeybees were reported to be low in glycosidic flavonoids and high in flavonoid aglycones,[21] especially myricetin, tricetin, and luteolin that were detected in *Eucalyptus* honeys from Australia and Europe.[37,38] These aglycones were not found in *T. carbonaria* honeys. Aglycones of flavonols **1**−**7** matched previous identifications in sugarbag pot-honeys.[18]

Compounds **3** and **5**−**7** showed a rhamnosyl residue (loss of 146 Da) and were indicative of floral nectars rich in flavonoid rhamnosides that are not hydrolyzed by *T. carbonaria* bees salivary enzymes. Similar observations were reported on flavonoid rhamnosides found in European honeys of honeybees foraging on *Robinia pseudoacacia*.[19] Therefore, sugarbag honeys of *T. carbonaria* bees have a particular profile high in *O*-glycosidic flavonoids including rhamnosides and lower in flavonoid aglycones than that of Australian *A. mellifera* honeybees.[18]

Some flavonoid aglycones and phloroglucinols were found in honey. These natural products are widely distributed in plant materials and are likely to have originated from floral nectars converted into honeys. These compounds were also tracked in propolis extracts from the same honeypots (Figure S4); hence,

it is possible that they were obtained from propolis during honey maturation and harvest.[18] However, a highly polar catechin of propolis was not traced in honey (Figure S4) and was expected to be transferred into the polar matrix of honey from propolis. Therefore, the extent to which propolis can contribute to the phytochemical profiles of honeys remains to be confirmed. Nevertheless, the presence of flavonoids and phloroglucinols in honeys is of interest because these compounds were reported for their in vitro antistaphylococcal activities of stingless bee propolis extracts.[32]

The local flora included several *Eucalyptus* species that were visited by the *T. carbonaria* bees of this study. The monoterpenoid eucalyptol (MW 154) was not found in the ethyl acetate extracts of stingless bee honeys, although it was reported as one abundant compound of honeybee *Eucalyptus* honeys.[39] However, *Eucalyptus* as a source for nectars collected by stingless bees was supported by the presence of norisoprenoids among the volatiles.[23] Norisoprenoids derive from carotenoid degradation.[39] Oxo-$\alpha$-ionone (**14**) together with related norisoprenoids **13** and **15** are chemical markers of honeys from *Eucalyptus*.[39] Other identified norisoprenoids of Australian stingless bee honeys were unedone (**10**), abscisic acid (**12**), and derivative **9** and were previously described in *Apis* honeys originating from Sardinian strawberry-tree (*Arbutus unedo* L., Ericaceae) that was used in medicinal preparations by ancient Greeks and Romans.[33,40] Abscisic acids are plant hormones that help regulate stressful conditions via control of stomatal closure.[33] In the subtropical areas of eastern Australia, water-stress conditions are likely to induce a production of abscisic acid and its derivatives.

Lumichrome was found in trace amounts in *T. carbonaria* honeys. This compound was reported in mānuka honey by German researchers Oelschlägel et al.,[10] as well as in Mediteranean thistle (*Galactites tomentosa* Moench) honeys along with phenyllactic acid.[30] Lumichrome and its carboxyl derivative were indicated as characteristic floral markers of cornflower (*Centaurea cyanus*) honeys from Romania and Germany.[5] Lumichrome is a breakdown product of riboflavin, and it is formed under photochemical-induced conditions, is a plant-growth regulator, and is a constituent of unifloral honeys from Dalmatian sage (*Salvia officinalis* L.).[41] It was not found in previous analyses of *Eucalyptus* monofloral honeys of honeybees, and therefore its botanical origin in Australian stingless bee honeys remains to be determined.

3-Phenyllactic acid is a compound commonly found in honey, including *Leptospermum* mānuka varieties.[10,30] This phenolic is also common in kanuka honey from New Zealand *Kunzea ericoides* (Myrtaceae)[8] and in Australian leatherwood honeys (*Eucryphia lucida*);[27] it was linked to the sensorial notes of thistle honey[30] and found across the three investigated honeys, although being a predominant marker in honey 2.

Investigations of *Leptospermum* varieties of jellybush-sugarbag honeys were attempted using *T. carbonaria* stingless bees in two sites of this study. However, no diagnostic chemical markers of *Leptospermum* nectars were detected in *T. carbonaria* honeys: MGO and DHA levels[26] were nil, and the phenolic markers MYSR,[7] leptosin,[31] and flavonoids pinobanksin, galangin, and chrysin were absent.[9] Traces of unedone were detected in the investigated honeys, but this norisoprenoid is a common phytochemical in honeys from Myrtaceae, that is, *Eucalyptus*, and therefore not specific to *Leptospermum* species.[10] When compared to previous chemical analyses of Australian honeybee jellybush honey,[13] the chemical markers reported for this honey were not found in Australian stingless bee honeys of this study. It was concluded that *T. carbonaria* stingless bees might not collect these nectars for their honey production.

Commercial honeys processed through heating or their improper storage can cause the formation of the undesirable cyclic aldehyde HMF. HMF is mutagenic, and thus a limit of 40 mg/kg is warranted for commercialization to reduce the health hazard to food consumers.[25] In stingless bee honeys of this study, HMF levels were nil; therefore, this bee product can suit future uses for food and medicinal purposes.

**Bioactive Constituents of the Extracts.** *T. carbonaria* raw honeys and their phenolic extracts showed in vitro antibacterial effects (Table 3) that were within the reported ranges of 9.7−23.3 mm and 2.3−8.9% (w/v) of phenol equivalents.[16] However, higher values of 26.3% (w/v) were indicated for other *T. carbonaria* honeys and compared to 18.0% for manuka honeys and 13.4% for other *A. mellifera* honeys.[12] Nevertheless, *T. carbonaria* honey at 5.5% (v/v) inhibited the microbial growth consistently with the reported dilution factor of <10%.[16] As the phenolic fractions contributed to an average of 1.1% phenol equivalents against the Gram-positive *S. aureus*, the identified phytochemicals can be considered as one antimicrobial factor linked to the nonperoxide effects of Australian stingless bee honeys.[12,17]

Different results were observed from the antibacterial testing with the two methods used (Table 3). All raw honeys inhibited the bacterial growth when tested by agar diffusion, but no bactericidal effects were observed in broth dilution at the concentrations used. The broth dilution method indicated that the raw honeys were active via bacteriostatic effects on the bacterial strains tested. This method also seemed more sensitive than the agar diffusion method in detecting the bactericidal activity of the phenolic extracts against *K. pneumoniae*. The phenolic extracts did not stop the bacterial growth in agar testing, possibly due to the limited diffusion of phenolic extracts through the hydrophobic agar media. It is possible that such limited diffusion could be affected by the high molecular weight of the glycosylated flavonoids as well as the reduced hydrophilicity of less polar flavonoid aglycones. When tested in broth dilution, the bactericidal effects of the phenolic extracts were attained possibly from the direct exposure of the compounds to the bacterial cells, because there was no physical limitation to the diffusion as experienced in the agar tests. The phenolic extracts proved to be bactericidal against both strains, therefore indicating that the phenolic fractions contribute to the total antibacterial activities of *T. carbonaria* honeys.

The peroxide content in *T. carbonaria* honeys accumulated up to 155 $\mu$M (Table 3) in undiluted and diluted (44.4% v/v) honeys. However, a minimum concentration of 760 $\mu$M $H_2O_2$ was required for bactericidal effects (Table 3). As a comparison, a higher content of 5.62 mM was reported in medical grade honey of *A. mellifera* bees.[6] Therefore, the total antimicrobial effects of *T. carbonaria* honeys were partly ascribed to the peroxide content, and other factors could be accounted for the nonperoxide activity, including the presence of phytochemicals as previously mentioned.

No MGO was detected in *T. carbonaria* honeys of this study; thus, the nonperoxide antimicrobial activity might be derived from other factors. For instance, one peptide called bee defensin-1, also known as royalisin, was previously linked to the nonperoxide activity of honeys.[6] This cationic peptide with bactericidal properties was reported in medical grade honeys,[42]

but not found in mānuka varieties.[6] It remains to be investigated in Australian stingless bee honeys in future work.

## ■ ASSOCIATED CONTENT

### Supporting Information

Full ESI-MS chromategrams of the three honeys' phenolic extract and of propolis from the same honeypots; mass spectra of (**11**) abscisic acid, (**2**) lumichrome, and (**8**) 3-phenyllactic acid; dose−response curves of antistaphylococcal inhibition by the three phenolic extracts. This material is available free of charge via the Internet at http://pubs.acs.org.

## ■ AUTHOR INFORMATION


### Corresponding Author

*(C.F.M.) Phone:+61415031483. E-mail:cfmassaro@gmail.com.



### Funding

This study and CFM received financial help through studentships and in-kind support from the University of the Sunshine Coast.


### Notes

The authors declare that the experiments described in this paper comply with the current laws for the conduct of scientific research in Australia.

The authors declare no competing financial interest.

## ■ ACKNOWLEDGMENTS


We thank Michael Howes at Tyagarah Apiaries, Dieter Horstmann at Eagle Farm Tyagarah, and Valley Bees members GlenBo Craigg, Chris Fueller, and Robert Luttrell for their help in beekeeping. We are grateful to Terry Braggins at Analytica Laboratories Ltd., New Zealand, for running the HR-UV-MS analyses at that laboratory.


## ■ REFERENCES


(1) Blair, S.; Carter, D. The potential for honey in the management of wounds and infection. *Healthcare Infect.* **2005**, *10*, 24−31.

(2) Ortiz-Vázquez, E.; Cuevas-Glory, L.; Zapata-Baas, G.; Martínez-Guevara, J.; Ramón-Sierra, J. Which bee honey components contribute to its antimicrobial activity? A review. *Afr. J. Microbiol. Res.* **2013**, *7*, 5758−5765.

(3) Kwakman, P. H.; Zaat, S. A. Antibacterial components of honey. *IUBMB Life* **2012**, *64*, 48−55.

(4) Brudzynski, K.; Abubaker, K.; St-Martin, L.; Castle, A. Re-examining the role of hydrogen peroxide in bacteriostatic and bactericidal activities of honey. *Front. Microbiol.* **2011**, *2* DOI: 10.3389/fmicb.2011.00213.

(5) Oelschlaegel, S.; Pieper, L.; Staufenbiel, R.; Gruner, M.; Zeippert, L.; Pieper, B.; Koelling-Speer, I.; Speer, K. Floral markers of cornflower (*Centaurea cyanus*) honey and its peroxide antibacterial activity for an alternative treatment of digital dermatitis. *J. Agric. Food Chem.* **2012**, *60*, 11811−11820.

(6) Kwakman, P. H.; te Velde, A. A.; de Boer, L.; Speijer, D.; Vandenbroucke-Grauls, C. M.; Zaat, S. A. How honey kills bacteria. *FASEB J.* **2010**, *24*, 2576−82.

(7) Inoue, K.; Murayama, S.; Seshimo, F.; Takeba, K.; Yoshimura, Y.; Nakazawa, H. Identification of phenolic compound in manuka honey as specific superoxide anion radical scavenger using electron spin resonance (ESR) and liquid chromatography with coulometric array detection. *J. Sci. Food Agric.* **2005**, *85*, 872−878.

(8) Stephens, J. M.; Schlothauer, R. C.; Morris, B. D.; Yang, D.; Fearnley, L.; Greenwood, D. R.; Loomes, K. M. Phenolic compounds and methylglyoxal in some New Zealand manuka and kanuka honeys. *Food Chem.* **2010**, *120*, 78−86.

(9) Chan, C. W.; Deadman, B. J.; Manley-Harris, M.; Wilkins, A. L.; Alber, D. G.; Harry, E. Analysis of the flavonoid component of bioactive New Zealand mānuka (*Leptospermum scoparium*) honey and the isolation, characterisation and synthesis of an unusual pyrrole. *Food Chem.* **2013**, *141*, 1772−1781.

(10) Oelschlaegel, S.; Gruner, M.; Wang, P.-N.; Boettcher, A.; Koelling-Speer, I.; Speer, K. Classification and characterization of manuka honeys based on phenolic compounds and methylglyoxal. *J. Agric. Food Chem.* **2012**, *60*, 7229−7237.

(11) Lu, J.; Carter, D. A.; Turnbull, L.; Rosendale, D.; Hedderley, D.; Stephens, J.; Gannabathula, S.; Steinhorn, G.; Schlothauer, R. C.; Whitchurch, C. B. The effect of New Zealand kanuka, manuka and clover honeys on bacterial growth dynamics and cellular morphology varies according to the species. *PLoS One* **2013**, *8*, No. e55898.

(12) Irish, J.; Blair, S.; Carter, D. A. The antibacterial activity of honey derived from Australian flora. *PLoS One* **2011**, *6*, No. e18229.

(13) Beitlich, N.; Koelling-Speer, I.; Oelschlaegel, S.; Speer, K. Differentiation of manuka honey from kanuka honey and from jelly bush honey using HS-SPME-GC/MS and UHPLC-PDA-MS/MS. *J. Agric. Food Chem.* **2014**, *62*, 6435−6444.

(14) Vit, P.; Pedro, S. R.; Roubik, D. *Pot-Honey: A Legacy of Stingless Bees*; Springer: Berlin, Germany, 2013.

(15) Oddo, L. P.; Heard, T. A.; Rodríguez-Malaver, A.; Pérez, R. A.; Fernández-Muiño, M.; Sancho, M. T.; Sesta, G.; Lusco, L.; Vit, P. Composition and antioxidant activity of *Trigona carbonaria* honey from Australia. *J. Med. Food* **2008**, *11*, 789−794.

(16) Boorn, K.; Khor, Y. Y.; Sweetman, E.; Tan, F.; Heard, T.; Hammer, K. Antimicrobial activity of honey from the stingless bee *Trigona carbonaria* determined by agar diffusion, agar dilution, broth microdilution and time-kill methodology. *J. Appl. Microbiol.* **2010**, *108*, 1534−1543.

(17) Irish, J.; Carter, D. A.; Blair, S. E.; Heard, T. A. Antibacterial activity of honey from the Australian stingless bee *Trigona carbonaria*. *Int. J. Antimicrob. Agents* **2008**, *32*, 89−90.

(18) Tomás-Barberán, F. A.; Truchado, P.; Ferreres, F. Flavonoids in stingless-bee and honey-bee honeys. In *Pot-Honey*; Vit Olivier, P., Roubik, D. W., Pedro, S. R., Eds.; Springer: Berlin, Germany, 2013; pp 461−474.

(19) Truchado, P.; Vit, P.; Ferreres, F.; Tomas-Barberan, F. Liquid chromatography-tandem mass spectrometry analysis allows the simultaneous characterization of *C*-glycosyl and *O*-glycosyl flavonoids in stingless bee honeys. *J. Chromatogr., A* **2011**, *1218*, 7601−7607.

(20) Guerrini, A.; Bruni, R.; Maietti, S.; Poli, F.; Rossi, D.; Paganetto, G.; Muzzoli, M.; Scalvenzi, L.; Sacchetti, G. Ecuadorian stingless bee (Meliponinae) honey: a chemical and functional profile of an ancient health product. *Food Chem.* **2009**, *114*, 1413−1420.

(21) Yao, L.; Datta, N.; Tomás-Barberán, F. A.; Ferreres, F.; Martos, I.; Singanusong, R. Flavonoids, phenolic acids and abscisic acid in Australian and New Zealand *Leptospermum* honeys. *Food Chem.* **2003**, *81*, 159−168.

(22) Zhou, J.; Yao, L.; Li, Y.; Chen, L.; Wu, L.; Zhao, J. Floral classification of honey using liquid chromatography-diode array detection-tandem mass spectrometry and chemometric analysis. *Food Chem.* **2014**, *145*, 941−949.

(23) D'arcy, B. R.; Rintoul, G. B.; Rowland, C. Y.; Blackman, A. J. Composition of Australian honey extractives. 1. Norisoprenoids, monoterpenes, and other natural volatiles from blue gum (*Eucalyptus leucoxylon*) and yellow box (*Eucalyptus melliodora*) honeys. *J. Agric. Food Chem.* **1997**, *45*, 1834−1843.

(24) da Silva, I. A. A.; da Silva, T. M. S.; Camara, C. A.; Queiroz, N.; Magnani, M.; de Novais, J. S.; Soledade, L. E. B.; Lima, E. d. O.; de Souza, A. L.; de Souza, A. G. Phenolic profile, antioxidant activity and palynological analysis of stingless bee honey from Amazonas, northern Brazil. *Food Chem.* **2013**, *141*, 3552−3558.

(25) Windsor, S.; Kavazos, K.; Brooks, P. The quantitation of hydroxymethylfurfural in Australian *Leptospermum* honeys. *J. Pharmacogn. Phytother.* **2013**, *5*, 21−25.

(26) Windsor, S.; Pappalardo, M.; Brooks, P.; Williams, S.; Manley-Harris, M. A convenient new analysis of dihydroxyacetone and

methylglyoxal applied to Australian *Leptospermum* honeys. *J. Pharmacogn. Phytother.* **2012**, *4*, 6−11.
(27) Rowland, C. Y.; Blackman, A. J.; D'Arcy, B. R.; Rintoul, G. B. Comparison of organic extractives found in leatherwood (*Eucryphia lucida*) honey and leatherwood flowers and leaves. *J. Agric. Food Chem.* **1995**, *43*, 753−763.
(28) Windsor, S.; Brooks, P. Essential oils from *Leptospermums* of the Sunshine Coast and Northern Rivers regions. *Chem. Centr. J.* **2012**, *6*, 1−7.
(29) Patiny, L.; Borel, A. ChemCalc: a building block for tomorrow's chemical infrastructure. *J. Chem. Inf. Model.* **2013**, *53*, 1223−1228.
(30) Tuberoso, C.; Bifulco, E.; Caboni, P.; Sarais, G.; Cottiglia, F.; Floris, I. Lumichrome and phenyllactic acid as chemical markers of thistle (*Galactites tomentosa Moench*) honey. *J. Agric. Food Chem.* **2010**, *59*, 364−369.
(31) Kato, Y.; Umeda, N.; Maeda, A.; Matsumoto, D.; Kitamoto, N.; Kikuzaki, H. Identification of a novel glycoside, leptosin, as a chemical marker of manuka honey. *J. Agric. Food Chem.* **2012**, *60*, 3418−3423.
(32) Massaro, C.; Katouli, M.; Grkovic, T.; Vu, H.; Quinn, R. J.; Heard, T. A.; Carvalho, C.; Manley-Harris, M.; Wallace, H.; Brooks, P. Anti-staphylococcal activity of *C*-methyl flavanones from propolis of Australian stingless bees (*Tetragonula carbonaria*) and fruit resins of *Corymbia torelliana* (Myrtaceae). *Fitoterapia* **2014**, *95*, 247−257.
(33) Tuberoso, C.; Bifulco, E.; Caboni, P.; Cottiglia, F.; Cabras, P.; Floris, I. Floral markers of strawberry tree (*Arbutus unedo* L.) honey. *J. Agric. Food Chem.* **2009**, *58*, 384−389.
(34) Ferreres, F.; Llorach, R.; Gil-Izquierdo, A. Characterization of the interglycosidic linkage in di-, tri-, tetra- and penta-glycosylated flavonoids and differentiation of positional isomers by liquid chromatography/electrospray ionization tandem mass spectrometry. *J. Mass Spectrom.* **2004**, *39*, 312−321.
(35) Ferreres, F.; Gil-Izquierdo, A.; Vinholes, J.; Grosso, C.; Valentão, P.; Andrade, P. B. Approach to the study of *C*-glycosyl flavones acylated with aliphatic and aromatic acids from Spergularia rubra by high-performance liquid chromatography-photodiode array detection/electrospray ionization multi-stage mass spectrometry. *Rapid. Commun. Mass. Spectrom.* **2011**, *25*, 700−712.
(36) Truchado, P.; Tourn, E.; Gallez, L. M.; Moreno, D. A.; Ferreres, F.; Tomás-Barberán, F. A. Identification of botanical biomarkers in Argentinean *Diplotaxis* honeys: flavonoids and glucosinolates. *J. Agric. Food Chem.* **2010**, *58*, 12678−12685.
(37) Martos, I.; Cossentini, M.; Ferreres, F.; Tomás-Barberán, F. A. Flavonoid composition of Tunisian honeys and propolis. *J. Agric. Food Chem.* **1997**, *45*, 2824−2829.
(38) Martos, I.; Ferreres, F.; Yao, L.; D'Arcy, B.; Caffin, N.; Tomás-Barberán, F. A. Flavonoids in monospecific *Eucalyptus* honeys from Australia. *J. Agric. Food Chem.* **2000**, *48*, 4744−4748.
(39) Alissandrakis, E.; Tarantilis, P. A.; Pappas, C.; Harizanis, P. C.; Polissiou, M. Investigation of organic extractives from unifloral chestnut (*Castanea sativa* L.) and eucalyptus (*Eucalyptus globulus* Labill.) honeys and flowers to identification of botanical marker compounds. *LWT−Food Sci. Technol.* **2011**, *44*, 1042−1051.
(40) Bianchi, F.; Careri, M.; Musci, M. Volatile norisoprenoids as markers of botanical origin of Sardinian strawberry-tree (*Arbutus unedo* L.) honey: characterisation of aroma compounds by dynamic headspace extraction and gas chromatography-mass spectrometry. *Food Chem.* **2005**, *89*, 527−532.
(41) Tuberoso, C. I. G.; Jerković, I.; Bifulco, E.; Marijanovic, Z.; Congiu, F.; Bubalo, D. Riboflavin and lumichrome in Dalmatian sage honey and other unifloral honeys determined by LC-DAD technique. *Food Chem.* **2012**, *135*, 1985−1990.
(42) Weston, R. J.; Brocklebank, L. K.; Lu, Y. Identification and quantitative levels of antibacterial components of some New Zealand honeys. *Food Chem.* **2000**, *70*, 427−435.

roasted under atmospheric pressure.[24] Approximately 79% of AA in coffee beans is removed by a two-step method, in which the first step involves producing a high amount of AA in coffee beans by pre-roasting and the second step involves decreasing the AA by supercritical $CO_2$ extraction.[25]

The purpose of the present study is to investigate how to decrease the AA content in canned coffee using heat treatment used for sterilization during the manufacturing process of canned coffee. This study might provide us with useful insights for producing healthy and safe coffee drinks.

## MATERIALS AND METHODS

**Materials and Reagents.** L-Cysteine (lot M1P3255), L-alanine (lot M1K9848), glycine (lot M6T9022), L-glutamic acid (lot M1M1635), L-glutamine (lot M1R7813), L-arginine (lot M1M1478), L-asparatic acid (lot M1N2683), L-asparagine (lot M2F9008), L-lysine (lot M1H0151), L-histidine (lot M1R4253), L-serine (lot M1H0189), L-leucine (lot M1T9167), L-isoleucine (lot M2A1588), L-valine (lot M1T1361), L-methionine (lot M4G1363), L-(−)-proline (lot M1N2357), L-threonine (lot M1R4350), L-tryptophan (lot M1H0273), L-tyrosine (lot M1H005), L-phenylalanine (lot M1H2655), dithiothreitol (lot M2A6379), L-(−)-cystine (lot M1R4150), *myo*-inositol (lot M7R9559), L-(+)-ascorbic acid (lot M7T9666), β-cyclodextrin (lot M2P9788), hexane (lot V1K6074), acetone (lot V9P1472), and methanol (lot M2E7208) were purchased from Nacalai Tesque (Kyoto, Japan). Catechin mixture from green tea (lot CDR4267), casein phosphopeptide (lot TSM1329), casein sodium (lot TSH4729), 1 mol/L sodium thiosulfate solution (lot STK4553), 0.05 mol/L bromine solution (lot STH6224), hydrobromic acid (STG0833), potassium bromide (lot HLH7661), AA standard solution (1 mg/mL methanol solution) (lot DCQ3733), and AA (1,2,3-$^{13}C_3$) (1 mg/mL in methanol) (lot SDBF-014) were purchased from Wako Pure Chemicals (Osaka, Japan). D-(+)-Glucose (lot 011W2262) and ethyl acetate (lot 401U1600) were from Kanto Chemical (Tokyo, Japan). Strata-X-C (33 μm, cation mixed-mode polymeric sorbent) and Strata C18-E were from Phenomenex (Torrance, CA). InertSep slim-J active carbon (400 mg) was from GL Science (Tokyo, Japan). Canned coffee and roasted barley tea beverages were purchased at local markets and stored in a refrigerator at 4 °C before use.

**Heat Treatment.** A total of 190 g of the canned coffee and various amounts of the additives were put into a 200 mL flask and mixed at room temperature. The mixture was placed into a new stainless-steel can. A stainless-steel lid was placed on the can containing the mixture and was sealed using a seamer (M-2 semi-automatic seamer, Toyo Seikan, Tokyo, Japan). Next, the can was treated by a retort sterilization apparatus (RCS-40RTGN, Hisaka Works, Osaka, Japan) at 121 °C for 6 min. This process is commonly undertaken in manufacturing canned coffee. The heat-treated cans were immediately cooled in an ice water bath and stored in a refrigerator at 4 °C until further use.

**Preparation of Brominated Samples for the Analysis of AA.** A total of 100 g of the sample was put into a 100 mL flask, followed by the addition of 5 μL of 100 ppm of internal standard solution ($^{13}C_3$-AA prepared in methanol). The combined mixture was applied to a column connected to a Strata C18-E column and an InertSep slim-J active carbon column, and the solution passed through the column was discarded. Only the InertSep slim-J active carbon column was removed from the connected column, and it was dried under reducing pressure at 35 °C for 30 min using an evaporator. The absorption was eluted by the addition of 7 mL of acetone and collected in a 15 mL spitz tube. Subsequently, 300 μL of deionized water was added to the spitz tube and dried under reducing pressure at 35 °C for 5 min using an evaporator to remove the acetone. The solution volume in the spitz tube was adjusted to 1 mL with deionized water. Then, the solution (1 mL) was applied to a Strata-X-C column. Subsequently, 4 mL of deionized water was applied to the column. The first 1 mL of the eluate was discarded, and the subsequent 3 mL was collected in the spitz tube. The collected solution (3 mL) was mixed with 2 mL of a bromination reagent (a mixture of 15 g of KBr, 1.2 mL of HBr, 7.5 mL of $Br_2$ solution, and 30 mL of deionized water) and incubated in the dark for 1 h. The bromination reaction was stopped by adding 100 μL of 1 M sodium thiosulfate solution, and the volume of the reaction mixture was adjusted to 6 mL with deionized water. After 2 mL of hexane was added to the mixture and agitated vigorously, the hexane layer was discarded and the aqueous layer was collected in the spitz tube. A total of 1 g of NaCl was then added to the tube. After 2 mL of ethyl acetate was added to the tube and stirred vigorously, the ethyl acetate layer was collected in another spitz tube. This operation to recover the ethyl acetate layer was performed 3 times with the spitz tube. The spitz tube containing the ethyl acetate layer was placed in a block heater (dry thermo unit DTU-1C, Taitec, Tokyo, Japan), and the volume of the mixture in the tube was reduced with a nitrogen gas purge to less than 0.3 mL and then adjusted to 0.5 mL with acetone.

**Analysis of AA in Brominated Samples.** The AA content was analyzed according to the procedures previously reported,[11,23] with slight modifications. $^{13}C_3$-AA is used as the internal standard. The quantification of AA in the brominated samples was performed using gas chromatography−mass spectrometry (GCMS-QP2010, Shimadzu, Kyoto, Japan) equipped with a split−splitless injector and a Zebron ZB-1 capillary column (30 m × 0.32 mm inner diameter, 1.0 μm film thickness, Phenomenex). A total of 2 μL of the brominated sample was injected into the GC−MS system using the splitless flow control mode and then splitting by a ratio of 1:13.5. The flow of the helium carrier gas was maintained at 55 cm/s using a constant linear velocity mode. The temperatures of the ion source, interface, and vaporization chamber were set at 230, 270, and 270 °C, respectively. The temperature of the column oven was programmed as follows: isothermal at 70 °C for 1 min, increasing from 70 to 120 °C at a rate of 12 °C/min, increasing from 120 to 160 °C at a rate of 5 °C/min, increasing from 160 to 300 °C at a rate of 20 °C/min, and then subjected to isothermal conditions at 300 °C for 5 min. Analysis was performed using the electric impact mode at 70 eV and the single ion monitoring (SIM) mode. The SIM ions selected for identification of 2,3-dibromopropionamide and $^{13}C_3$-dibromopropionamide were $m/z$ 150, 106, and 152 and $m/z$ 155, 110, and 153, respectively. The recovery of AA from canned black coffee was 90.7 ± 2.6% in triplicate experiments. The lowest level of detection (LOD) and the lowest level of quantification (LOQ) for AA were 0.03 and 0.1 ppb, respectively.

## RESULTS AND DISCUSSION

**Effect of the Heat Treatment with the Addition of Additives on the AA in Canned Black Coffee.** The AA content in the commercially available canned black coffee investigated in this study was 6.2 ± 0.2 ppb with three different samples (Figure 1). Previous studies on approximately 30 types of canned coffee in Japan have shown results for the AA content in the range of 5−14 ppb,[22] and our result was in this range. The AA content in major foods is reported to be in the ranges of 170−3700 ppb for potato chips and crisps, 200−12 000 ppb for French fries, and 64−457 ppb for nuts.[26] Commercially available canned coffee contains AA. However, the levels are significantly less than those in other processed foods mentioned above. The AA contents in ground coffee and coffee brews were reported to be in the range of 210−330 and 6−66.7 ppb, respectively.[27,28] It has been reported that AA in coffee beans is extracted approximately 100% by brewing.[29] Therefore, we can conclude that the difference in the AA content in canned coffee and coffee brews might be caused by the dilution by water during the preparation process.

The AA content in canned black coffee after heat treatment at 121 °C for 6 min decreased slightly to be 6.0 ± 0.1 ppb (Figure 1). The heat treatment process used in this experiment is typical of the heat sterilization process used in manufacturing canned coffee. Recently, it has been reported that the AA

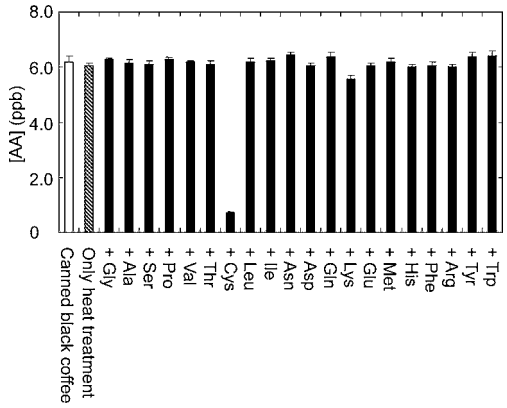


**Figure 1.** AA content in canned black coffee after heat treatment with and without the addition of amino acid at 121 °C for 6 min: (open bar) canned black coffee, (hatched bar) canned black coffee after the heat treatment at 121 °C for 6 min, and (closed bar) 190 g of canned black coffee after heat treatment with 200 mg of each amino acid at 121 °C for 6 min. The AA content in canned black coffee is defined as 100% (control). Each bar represents the mean and standard deviation of triplicate experiments.

content in coffee decreases in the reaction of melanoidins in coffee with AA at 180 °C for 2−12 min.[30] In addition, it has been reported that the residual ratios of AA after heat treatment of 2.8 mM AA aqueous solution for 2 h at 160, 180, and 200 °C are 95, 90, and 80%, respectively.[31] Therefore, it is considered that AA in canned coffee is decreased by heat treatment at 121 °C for 6 min, accompanying with thermal decomposition of AA or conversion to other compounds by combining AA with other components, such as melanoidins.

A total of 200 mg of each amino acid, out of 18 amino acids, except lysine (Lys) and cysteine (Cys), was added to 190 g of canned black coffee. Then, the mixture was treated at 121 °C for 6 min. The relative values of the AA contents contained in the canned coffee after the heat treatment with these amino acids were in the range of 97−104% to that (6.2 ± 0.1 ppb as 100%) in the canned coffee heat treated without amino acids (Figure 1). On the other hand, the relative AA content in the canned coffee after heat treatment with 200 mg of Lys at 121 °C for 6 min decreased to approximately 90% to be 5.6 ± 0.1 ppb (Figure 1). In addition, when 200 mg of Cys was added, the relative AA content decreased remarkably to approximately 10% to be 0.7 ± 0.0 ppb. It was already reported that the AA content was decreased by amino acids, including Cys, Gly, Lys, Arg, Asp, Gln, Glu, Ser, Ala, Tyr, and Val, when 50 mM of each amino acid was added to olive oil juice, followed by heat treatment at 121 °C for 30 min.[32] In this report, the AA-decreasing effect of Cys was the highest. However, the effects of Gly, Gln, and Val are different from our results (Figure 1). The effects of Arg, Asp, Glu, Ser, Ala, and Tyr were not significant, and the residual AA contents for the canned coffee heat treated with these amino acids were almost equivalent to those without amino acids. Of the 20 amino acids examined in this experiment, Cys gives the greatest AA-decreasing effect, followed closely by Lys (Figure 1). The AA-decreasing effects by heat treatment with the addition of Cys and Lys at 121 °C for 6 min were similar to the effects found in the previous study on olive oil juice.[32] It is reported that AA disappears as a result of the nucleophilic attack of a $NH_2$ group of Lys and a SH group of Cys to the C═C double bond of AA.[31,33,34]

The residual AA content in 190 g of canned black coffee after the heat treatment at 121 °C for 6 min with adding 200 mg of dithiothreitol having 2 SH groups was 2.8 ± 0.2 ppb, representing 55 ± 3% of the initial AA content (Figure 2).

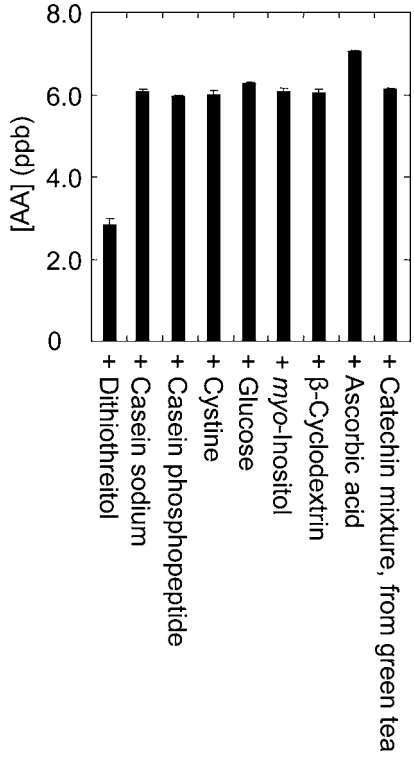


**Figure 2.** AA content in canned black coffee after heat treatment at 121 °C for 6 min with the addition of 200 mg of each compound to 190 g of the canned coffee. Each bar represents the mean and standard deviation of triplicate experiments.

The AA content after the heat treatment with 200 mg of cystine, in which two Cys molecules are combined by a disulfide bond, was substantially the same as that of the coffee that underwent the heat treatment without additives (Figures 1 and 2). From these results, we can conclude that SH groups play an important role in decreasing the AA content in coffee. The content after the heat treatment with 200 mg of ascorbic acid was 7.0 ± 0.1 ppb, being 10% higher than that of the initial value (Figure 2). It has been reported that 14.7 μg of AA is generated when a dried mixture, which was prepared by drying 5 mL of the Asp solution (10 mg/mL) containing ascorbic acid (10 mg/mL) and starch (1 g/mL) as a carrier substance at 110 °C for 30 min, was heated at 170 °C for 1 h in a drying oven.[35] In the same study, it has been also reported that the amount of AA generated by the dried mixture without ascorbic acid is 9.8 μg, being lower than that generated by the mixture prepared with ascorbic acid. In addition, 0.66 μg of AA is generated when a dried mixture, which was prepared by drying 5 mL of an ascorbic acid solution (10 mg/mL) containing ammonium acetate (5 mg/mL) as a source for amino nitrogen and starch (1 g/mL) at 110 °C for 30 min, was heated at 170 °C for 1 h in a drying oven. On the other hand, it has been reported that the AA content decreases by 23.4 and 27.1% by the treatment of a mixture of 2.8 mM AA and 2.8 or 5.8 mM ascorbic acid at 180 °C for 2 h.[31] Future studies are required to clarify the effect of ascorbic acid on the generation of AA examined under different

conditions, investigating the effects of reaction time, temperatures, additives, etc.

**Effects of Cys, Lys, and Arg on Decreasing the AA Content in Canned Coffee.** Figure 3 shows the AA-decreasing effects of heat treatment with the addition of Cys, Lys, and Arg at 121 °C for 6 min in canned coffee. The AA contents in the heat-treated canned coffee decreased with increasing the concentration of these amino acids (Figure 3). The amounts of Cys required to decrease the AA content by 50% was 69.3 ± 1.9 mg. The AA content after the heat treatment with 300 mg of Cys decreased to 0.3 ± 0.1 ppb. Although no countries have placed regulations on the AA content in food and beverages, the maximum safe level of AA in tap water has been set to 0.5 ppb by the WHO. It has been suggested that the AA content in canned black coffee can be decreased to the level below this value by the heat treatment at 121 °C for 6 min with 300 mg of Cys. Similarly, the AA content after the heat treatment with 200 and 300 mg of Lys decreased to 5.6 ± 0.2 and 5.2 ± 0.1 ppb, respectively (Figure 3). The contents after the heat treatment with 200 and 300 mg of Arg were similar as 6.0 ± 0.1 and 5.9 ± 0.1 ppb, respectively (Figure 3). The AA-decreasing effect of Cys is much greater than that of Lys and Arg.

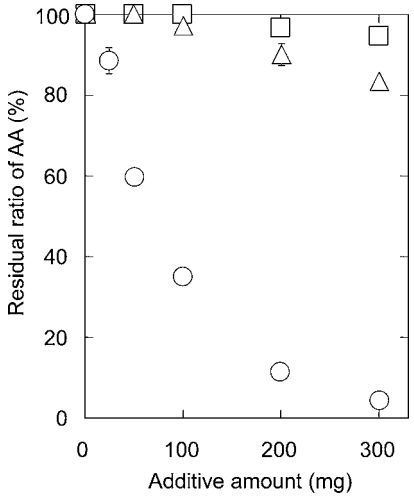


**Figure 3.** Dependence of the concentrations of Cys, Lys, and Arg upon AA decreasing in 190 g of canned black coffee after the heat treatment with the addition of them at 121 °C for 6 min: (○) Cys, (△) Lys, and (□) Arg. Each bar represents the mean and standard deviation of triplicate experiments.

The AA content in medium-roasted coffee beans manufactured under vacuum pressure is approximately 50% less than that in medium-roasted beans manufactured under atmospheric pressure.[24] Approximately 79% of AA in coffee beans can be removed using a two-step method, which consists of the first step producing a high amount of AA in coffee beans by roasting and the second step reducing AA from the coffee beans by supercritical $CO_2$ extraction.[25] The AA content in instant coffee is decreased by 70% with the addition of sucrose and baker's yeast with fermentation at 30 °C for 2 days.[36] These methods are effective but costly and less practical, with special processes being required. These processes are not for the typical manufacturing of canned coffee. Our method can be implemented using normal manufacturing processes and provides an economical benefit to manufacturers. The only cost associated with our method is the raw material cost of Cys, and the heat-treatment time is short. Therefore, we believe that our method is one of the effective means for decreasing AA in canned coffee. However, there are subjects to be investigated further. It is considered that AA might be decreased in the heat treatment with the addition of Cys by converting to cystein-*S*-*β*-propionamide and others, in which Cys and AA are combined by the Michael addition reaction.[31] It has been reported that 0.1, 0.7, and 7.1% (w/w) of AA are generated after heat treatment of cysteine-*S*-*β*-propionamide for 2 h at 60, 120, and 180 °C, respectively.[31] It is necessary to verify about regeneration of AA in the heat-treated canned coffee by our method. In particular, verification of AA regeneration in long-term storage at low temperatures (4−25 °C) is important, because canned coffee is usually drank as refrigerated goods and stored at refrigerated or room temperature. In addition, it is needed to evaluate the toxicity of these products.

**Effect of the Heat Treatment with the Addition of Cys on AA in Canned Milk Coffee and Roasted Barley Tea.** Figure 4 shows the AA-decreasing effects of the heat treatment with the addition of 200 mg of Cys at 121 °C for 6 min to 190 g of commercially available canned milk coffee. The initial AA content was 6.2 ± 0.2 ppb, and the content after the heat treatment with 200 mg of Cys was 0.2 ± 0.0 ppb (Figure 4). It was shown that our method can be applicable to canned milk coffee as well as black coffee. The content in commercially roasted barley tea was 3.9 ± 0.1 ppb and decreased to 0.2 ± 0.0 ppb after the heat treatment with 200 mg of Cys at 121 °C for 6 min (Figure 4). The treatment is also effective for roasted barley tea. It has been reported that approximately 90% of AA can be removed but acrylic acid is generated when roasted green tea containing *Aspergillus oryzae* KBN1010 or *A. oryzae* No. 100 is incubated at 30 °C for 3 days.[37] Our method might be more simple and easier to carry out than the above-mentioned method using *A. oryzae*.

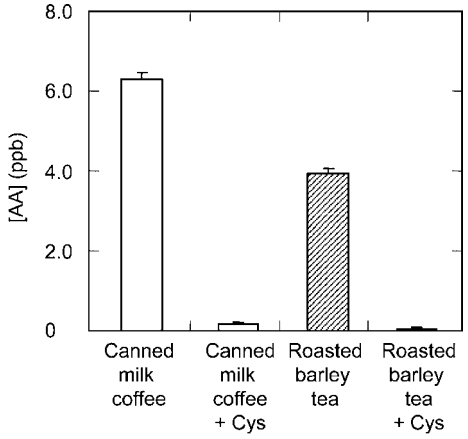


**Figure 4.** AA content in canned milk coffee and roasted barley tea before and after heat treatment with the addition of 200 mg of Cys at 121 °C for 6 min to 190 g of samples: (open bar) 190 g of canned milk coffee before and after heat treatment with the addition of 200 mg of Cys at 121 °C for 6 min and (hatched bar) 190 g of roasted barley tea before and after heat treatment with the addition of 200 mg of Cys at 121 °C for 6 min. Each bar represents the mean and standard deviation of triplicate experiments.

## AUTHOR INFORMATION


### Corresponding Author

*Telephone: +81-75-753-6268. Fax: +81-75-753-6265. E-mail: inouye@kais.kyoto-u.ac.jp.


### Notes

The authors declare no competing financial interest.

## REFERENCES


(1) Smith, E. A.; Oehme, F. W. Acrylamide and polyacrylamide: A review of production, use, environmental fate and neurotoxicity. *Rev. Environ. Health* **1991**, *9*, 215−218.

(2) Miller, M. S.; Spencer, P. S. The mechanisms of acrylamide axonopathy. *Annu. Rev. Pharmacol. Toxicol.* **1985**, *25*, 643−666.

(3) Dearfield, K. L.; Abernathy, C. O.; Ottley, M. S.; Brantner, J. H.; Hayes, P. F. Acrylamide: Its metabolism, developmental and reproductive effects, genotoxicity, and carcinogenicity. *Mutat. Res.* **1988**, *195*, 45−77.

(4) International Agency for Research on Cancer (IARC). Acrylamide. *Monographs on the Evaluation of Carcinogenic Risk to Humans: Some Industrial Chemicals*; IARC: Lyon, France, 1994; Vol. *60*, pp 389−433.

(5) Abou-Donia, M. B.; Ibrahim, S. M.; Corcoran, J. J.; Lack, L.; Friedman, M. A.; Lapadula, D. M. Neurotoxicity of glycidamide, an acrylamide metabolite, following intraperitoneal injections in rats. *J. Toxicol. Environ. Health* **1993**, *39*, 447−464.

(6) Sumner, S. C. J.; Fennell, T. R.; Moore, T. A.; Chanas, B.; Gonzalez, F.; Ghanayem, B. I. Role of cytochrome P450 2E1 in the metabolism of acrylamide and acrylonitrile in mice. *Chem. Res. Toxicol.* **1999**, *12*, 1110−1116.

(7) Ghanayem, B. I.; McDaniel, L. P.; Churchwell, M. I.; Twaddle, N. C.; Snyder, R.; Fennell, T. R.; Doerge, D. R. Role of CYP2E1 in the epoxidation of acrylamide to glycidamide and formation of DNA and hemoglobin adducts. *Toxicol. Sci.* **2005**, *88*, 311−318.

(8) Besaratinia, A.; Pfeifer, G. P. Genotoxicity of acrylamide and glycidamide. *J. Natl. Cancer Inst.* **2004**, *96*, 1023−1029.

(9) Moldoveanu, S. C.; Gerardi, A. R. Acrylamide analysis in tobacco, alternative tobacco products, and cigarette smoke. *J. Chromatogr. Sci.* **2011**, *49*, 234−242.

(10) Tareke, E.; Rydberg, P.; Karlsson, P.; Eriksson, S.; Tornqvist, M. Analysis of acrylamide, a carcinogen formed in heated foodstuffs. *J. Agric. Food Chem.* **2002**, *50*, 4998−5006.

(11) Mizukami, Y.; Kohata, K.; Yamaguchi, Y.; Hayashi, N.; Sawai, Y.; Chuda, Y.; Ono, H.; Yada, H.; Yoshida, M. Analysis of acrylamide in green tea by gas chromatography−mass spectrometry. *J. Agric. Food Chem.* **2006**, *54*, 7370−7377.

(12) Vinci, R. M.; Mestdagh, F.; De Meulenaer, B. Acrylamide formation in fried potato products—Present and future, a critical review on mitigation strategies. *Food Chem.* **2012**, *133*, 1138−1154.

(13) Mottram, D. S.; Wedzicha, B. L.; Dodson, A. T. Acrylamide is formed in the maillard reaction. *Nature* **2002**, *419*, 448−449.

(14) Robert, F.; Vuataz, G.; Pollien, P.; Saucy, F.; Alonso, M.-I.; Bauwens, I.; Blank, I. Acrylamide formation from asparagine under low-moisture maillard reaction conditions. 1. Physical and chemical aspects in crystalline model systems. *J. Agric. Food Chem.* **2004**, *52*, 6837−6842.

(15) van Dam, R. M.; Feskens, E. J. M. Coffee consumption and risk of type 2 diabetes mellitus. *Lancet* **2002**, *360*, 1477−1478.

(16) Turati, F.; Galeone, C.; La Vecchia, C.; Garavello, W.; Tavani, A. Coffee and cancers of the upper digestive and respiratory tracts: Meta-analyses of observational studies. *Ann. Oncol.* **2011**, *22*, 536−544.

(17) Iwai, K.; Narita, Y.; Fukunaga, T.; Nakagiri, O.; Kamiya, T.; Ikeguchi, M.; Kikuchi, Y. Study on the postprandial glucose responses to a chlorogenic acid-rich extract of decaffeinated green coffee beans in rats and healthy human subjects. *Food Sci. Technol. Res.* **2012**, *18*, 849−860.

(18) Narita, Y.; Inouye, K. Kinetic analysis and mechanism on the inhibition of chlorogenic acid and its components against porcine pancreas $\alpha$-amylase isozymes I and II. *J. Agric. Food Chem.* **2009**, *57*, 9218−9225.

(19) Narita, Y.; Inouye, K. Inhibitory effects of chlorogenic acids from green coffee beans and cinnamate derivatives on the activity of porcine pancreas $\alpha$-amylase isozyme I. *Food Chem.* **2011**, *127*, 1532−1539.

(20) Narita, Y.; Iwai, K.; Fukunga, T.; Nakagiri, O. Inhibitory activity of chlorogenic acids in decaffeinated green coffee beans against porcine pancreas lipase and effect of a decaffeinated green coffee bean extract on an emulsion of olive oil. *Biosci., Biotechnol., Biochem.* **2012**, *76*, 2329−2331.

(21) Guenther, H.; Anklam, E.; Wenzl, T.; Stadler, R. H. Acrylamide in coffee: Review of progress in analysis, formation and level reduction. *Food Addit. Contam.* **2007**, *24*, 60−70.

(22) Yamazaki, K.; Isagawa, S.; Kibune, N.; Urushiyama, T. A method for the determination of acrylamide in a broad variety of processed foods by GC−MS using xanthydrol derivatization. *Food Addit. Contam.* **2012**, *29*, 705−715.

(23) Alves, R. C.; Soares, C.; Casal, S.; Fernandes, J. O.; Oliveira, M. B. P. P. Acrylamide in espresso coffee: Influence of species, roast degree and brew length. *Food Chem.* **2010**, *119*, 929−934.

(24) Anese, M.; Nicoli, M. C.; Verardo, G.; Munari, M.; Mirolo, G.; Bortolomeazzi, R. Effect of vacuum roasting on acrylamide formation and reduction in coffee beans. *Food Chem.* **2014**, *145*, 168−172.

(25) Banchero, M.; Pellegrino, G.; Manna, L. Supercritical fluid extraction as a potential mitigation strategy for the reduction of acrylamide level in coffee. *J. Food Eng.* **2013**, *115*, 292−297.

(26) Friedman, M. Chemistry, biochemistry, and safety of acrylamide. A review. *J. Agric. Food Chem.* **2003**, *51*, 4504−4526.

(27) Dias Soares, C. M.; Alves, R. C.; Casal, S.; Oliveira, M. B. P. P.; Fernandes, J. O. Development and validation of a matrix solid-phase dispersion method to determine acrylamide in coffee and coffee substitutes. *J. Food Sci.* **2010**, *75*, T57−T63.

(28) Andrzejewski, D.; Roach, J. A. G.; Gay, M. L.; Musser, S. M. Analysis of coffee for the presence of acrylamide by LC−MS/MS. *J. Agric. Food Chem.* **2004**, *52*, 1996−2002.

(29) Lantz, I.; Ternite, R.; Wilkens, J.; Hoenicke, K.; Guenther, H.; van der Stegen, G. H. D. Studies on acrylamide levels in roasting, storage and brewing of coffee. *Mol. Nutr. Food Res.* **2006**, *50*, 1039−1046.

(30) Pastoriza, S.; Rufian-Henares, J. A.; Morales, F. J. Reactivity of acrylamide with coffee melanoidins in model systems. *LWT—Food Sci. Technol.* **2012**, *45*, 198−203.

(31) Adams, A.; Hamdani, S.; Van Lancker, F.; Mejri, S.; De Kimpe, N. Stability of acrylamide in model systems and its reactivity with selected nucleophiles. *Food Res. Int.* **2010**, *43*, 1517−1522.

(32) Casado, F. J.; Sanchez, A. H.; Montano, A. Reduction of acrylamide content of ripe olives by selected additives. *Food Chem.* **2010**, *119*, 161−166.

(33) Hidalgo, F. J.; Delgado, R. M.; Zamora, R. Role of mercaptans on acrylamide elimination. *Food Chem.* **2010**, *122*, 596−601.

(34) Hidalgo, F. J.; Delgado, R. M.; Zamora, R. Positive interaction between amino and sulfhydryl groups for acrylamide removal. *Food Res. Int.* **2011**, *44*, 1083−1087.

(35) Weisshaar, R.; Gutsche, B. Formation of acrylamide in heated potato products—Model experiments pointing to asparagine as precursor. *Deut. Lebensm.-Rundsch.* **2002**, *98*, 397−400.

(36) Akillioglu, H. G.; Gokmen, V. Mitigation of acrylamide and hydroxymethyl furfural in instant coffee by yeast fermentation. *Food Res. Int.* **2014**, *61*, 252−256.

(37) Wakaizumi, M.; Yamamoto, H.; Fujimoto, N.; Ozeki, K. Acrylamide degradation by filamentous fungi used in food and beverage industries. *J. Biosci. Bioeng.* **2009**, *108*, 391−393.

(IR) spectroscopy which is limited by the strong IR absorbance of water. The objective of this study is to use Raman spectroscopy with a range of external and internal standards to identify and quantify the calcium phosphate that forms in response to $CaCl_2$ addition to bovine milk. The study combines the Raman analysis with standard wet chemical analyses to determine the re-distribution of calcium, phosphate, and the major inorganic milk constituents in response to $CaCl_2$ addition to milk and compares this to the solubility product of the calcium phosphate minerals.

## MATERIALS AND METHODS

**Chemicals.** All water used in the experiments was Milli-Q water with a resistivity of 18.2 MΩ·cm. The $CaCl_2$, NaOH, trichloroacetic acid (TCA), and $LaCl_3{\cdot}7H_2O$ were purchased from Sigma-Aldrich. The $NH_4OH$, $(NH_4)_2HPO_4$, $Na_2HPO_4$, $CaCl_2{\cdot}2H_2O$, $H_3PO_4$, and boric acid were purchased from AJAX Finechem while the $NaNO_3$ was from Fluka.

**Milk Samples.** The milk was prepared from a low-heat skim milk powder sample supplied by Westland Co-operative Dairy Co. Ltd., Hokitika, New Zealand, and had a composition of 35.5% protein and 1.25% fat. A stock skim milk was prepared with 20% (w/w) skim milk powder in Milli-Q water and was stirred for 2 h on a magnetic stirrer to ensure complete dispersal of the powder. Calcium fortification between 5 and 50 mM was achieved by adding the appropriate amounts of 0.2 M $CaCl_2$ solution to the milk. After 3 h at room temperature, the pH was adjusted back to 6.7, water was added to take the milk to 11.1% (w/w) solids, and this was left overnight at room temperature. The pH was again adjusted to 6.7 and water added to produce the final milk with 10% (w/w) solids. Changes in pH over time were manually corrected, and the sample was held until there was no further drift in pH. To achieve phase separation between the micellar and serum phases, the milk samples were ultracentrifuged at 20 °C and 38000*g* for 1 h using an Avanti-J-30I instrument with JA-25.50 rotor (Beckman Coulter, Brea, CA, USA). The supernatants were immediately collected by decantation and centrifuged again at 3000 rpm for 30 min in Vivaspin Turbo 15 containing poly(ether sulfone) membranes with molecular weight cutoff inferior to 10 kDa (Sartorius Stedim Biotech GmbH, Goettingen, Germany). These samples are termed the milk sera, and the pellets remaining after ultracentrifugation are the milk pellet samples.

**Preparation of Reference Calcium Phosphate Phases.** Standard methods were used to prepare the reference calcium phosphate phases. Amorphous calcium phosphate was prepared by rapidly adding a calcium solution (46.3 g of $Ca(NO_3)_2{\cdot}4H_2O$ in 550 mL of water containing 40 mL of 28% $NH_4OH$) to a phosphate solution (27.2 g of $(NH_4)_2HPO_4$ in 1,300 mL of water containing 40 mL of 28% $NH_4OH$).[15] The resulting precipitate was immediately filtered, washed, and freeze-dried. Dicalcium phosphate dihydrate (DCPD, $CaHPO_4{\cdot}2H_2O$) was prepared by rapidly adding a calcium solution (4.014 g of $CaCl_2{\cdot}2H_2O$ in 200 mL of water at pH 5.5) to a phosphate solution (0.825 g of $KH_2PO_4$ in 700 mL of water and then addition of 3.01 g of $Na_2HPO_4$, pH 7.4), aging for 80 min, and then filtration and drying at 65 °C.[16] The $\beta$-tricalcium phosphate ($\beta$-TCP, $\beta$-$Ca_3(PO_4)_2$) was prepared by dropwise addition of a calcium solution (71.9 g of $Ca(NO_3)_2{\cdot}4H_2O$ in 250 mL of water at pH 6.30) to a phosphate solution (27.0 g of $(NH_4)_2HPO_4$ in 250 mL of water at pH 8.28) over 150 min while vigorously stirring and maintaining the pH at 8 by manually adding NaOH.[17] The suspension was stirred for 12 h, and solids were filtered, washed, dried at 80 °C, and then calcined at 700 °C for 2 h. Octacalcium phosphate (OCP, $Ca_8H_2(PO_4)_6{\cdot}5H_2O$) was prepared by adding 11.69 g of concentrated $H_3PO_4$ and 13.3 g of $CaCO_3$ to 1 L of water, stirring for 6 h at 60 °C, and followed by filtration and drying at 60 °C.[18] Hydroxylapatite (HAP, $Ca_5OH(PO_4)_3$) was prepared by dropwise addition of a phosphate solution (25.87 g of $(NH_4)_2HPO_4$ in 150 mL of water, pH to 11 with ≈80 mL of $NH_4OH$ and then dilution to 320 mL) to a vigorously stirred calcium solution (43.15 g of $Ca(NO_3)_2{\cdot}4H_2O$ in 90 mL of water, pH to 11 with ≈4 mL of 28% $NH_4OH$ and followed by dilution to 180 mL) over 30−40 min.[19] The resultant suspension was stirred for 24 h and centrifuged at 2000 rpm for 10 min and then the solid washed with water and recentrifuged. The resultant white pellet was vacuum filtered for ≈3 h, and then the filter cake was dried at 90 °C.

**Solid Phase Characterization.** Raman spectra were measured using a Renishaw Raman Imaging Microscope System 1000 equipped with a confocal Leica microscope and CCD detector. Spectra were collected using either the 785 or the 488 nm laser as discussed in Results and Discussion. The instrument was calibrated daily using the 1086 $cm^{-1}$ calcite peak. To allow for quantitative information from the spectra, a range of compounds were assessed for suitability as internal standards. The ideal internal standard should have a strong Raman signal but have no peaks in the 910−1110 $cm^{-1}$ region of the spectrum where the characteristic calcium phosphate phases are observed. The internal standard should not interfere with the chemistry of the system, for example by acting as a ligand toward $Ca^{2+}$. Powder X-ray diffraction (XRD) patterns were measured using a Model D5000 Siemens instrument with a Cu K$\alpha$ source operating at 40 kV and 30 mA. Solid samples were crushed to a fine powder and mounted in an aluminum well. XRD data were collected between 2 and 70° 2$\theta$ with a step size of 0.02° 2$\theta$. The morphology and topography were examined using the environmental scanning electron microscopy (ESEM; FEI Quanta 200F, Hillsboro, OR, USA) with large-field detector (LFD) at 0.58 Torr pressure. Samples were mounted on black carbon tape and sputter coated with platinum (Pt) for 15 min using a Quorum Q150RS at 20 mA current and $1 \times 10^{-1}$ mBar chamber pressure.

**Solution Phase Characterization.** Prior to cation analysis, the milk and milk sera samples were treated using the procedure from Fox et al.[20] Initially 1 mL of 24% TCA was added to 2 mL of a 10-fold diluted sample and the mixture shaken for 30 min. Following this, 1 mL of 5% $LaCl_3{\cdot}7H_2O$ was added as an ionization suppressor for the atomic absorption measurement and the samples were diluted to 50.0 mL with water. All samples were centrifuged at 3500 rpm for 30 min, and the resultant supernatants were collected for measurement. Calcium and magnesium were quantified using atomic absorption spectroscopy (AAS) while atomic emission spectroscopy (AES) was used for sodium and potassium. All measurements were made using an air−acetylene flame and parameters described by de la Fuente and Juarez[21] on a Varian AA-1275 series atomic absorption spectrophotometer (Varian Techron Pty. Ltd., Springvale, Australia). The standards for AAS and AES were prepared from TraceCERT grade 1000 ppm reference standards that were diluted and pretreated using the same method as the samples. Phosphorus in the sera was quantified using a colorimetric method based on that by Allen.[22] Initially protein was precipitated by adding 2.5 mL of 24% TCA to 5 mL of a 10-fold diluted sample and the mixture shaken for 30 min, then diluted to 25 mL, and centrifuged at 3500 rpm for 30 min. Supernatant (18 mL) was removed and to this was added 1.17 mL of 70% $HNO_3$, 2 mL of amidol reagent (2 g of 2,4-diaminophenol dihydrochloride and 40 g of sodium bisulphite in 200 mL water) and 1 mL of an 8.3% (w/v) ammonium molybdate reagent. Samples were mixed for 5 min and left to stand for 15 min, and then absorbance was measured at 695 nm and compared to matrix matched standards.

All milk samples were prepared in duplicate, and the error bars on the figures represent one standard deviation. The milk pellet samples with the internal standard for Raman analysis were prepared in duplicate, and the relationship between Raman band intensity and the amount of phosphate removed from the serum was determined by regression analysis using the Data Analysis Tools facility in EXCEL and a 95% confidence interval.

**Modeling the Serum Chemistry.** The distribution of calcium and $P_i$ in the milk without added $CaCl_2$ was modeled using the framework from Holt.[3] The model input concentrations for fat were 0 g $L^{-1}$, while lactose, total protein, and casein were the measured values of 50.1, 35.5, and 27.3 g $L^{-1}$, respectively, and the total concentration of phosphate centers (PCs) was 1.51 mM based on the distribution of phosphate centers per mole of each casein from Holt.[3] The ratios of $Ca^{2+}$, $P_i$, $Mg^{2+}$, and citrate per PC in the nanoclusters were 13.2, 6.5, 1.0, and 0.637, respectively. The model input total cation

concentrations for $Mg^{2+}$, $Na^{+}$, and $K^{+}$ were the measured values of 4.29, 13.9, and 31.3 mM, respectively, while the total anion concentrations for phosphate, sulfate, citrate, and a generic carboxylate ($ROO^{-}$) were 17.2, 0.12, 4.66, and 3.1 mM, respectively. The calcium and chloride values varied with the added $CaCl_2$, the pH was 6.7, and the partial pressure of $CO_2$ was set at 0. Activity coefficients were calculated using the Davies equation except in the cases of $Ca^{2+}$, $Mg^{2+}$, $H^{+}$, and the −3 charged citrate anion where the ion specific Truesdell−Jones equation was used. The solution phase complexation and protonation constants are from Holt.[3]

## RESULTS AND DISCUSSION

**Serum Chemistry.** *Serum Chemistry without Added $Ca^{2+}$.* The measured total concentrations of calcium and $P_i$ in the milk were 28.0 ± 0.8 mM and 17.2 ± 0.1 mM, respectively. These values are at the low end or slightly below the typical ranges of 26−32 mM and 19−23 mM for total calcium and $P_i$, respectively.[23] In the serum phase the corresponding measured concentrations were 7.0 ± 0.5 mM for calcium and 7.5 ± 0.2 mM for the $P_i$ which represent concentrations inferior to 10 kDa fraction. While some of the nondiffusible calcium will be associated with nonmiscellar proteins, the "great majority of the nondiffusible salts are in the form of colloidal calcium phosphate"[3] indicating that approximately 21 mM calcium and 10 mM $P_i$ were contained within the calcium phosphate nanoclusters. The 2:1 ratio of calcium to $P_i$ in the nanoclusters is typical[3] of milk CPNs but does not reflect the calcium phosphate phase because of the inclusion of the casein based phosphorylated serine residues with the structure. The distribution of calcium and $P_i$ between the serum and the CPN was in good agreement with the ion activity product (IAP) of Holt[3] which is $(Ca^{2+})(HPO_4^{2-})^{0.7}(PO_4^{3-})^{0.2}$ where (X) is the activity of species X and the IAP has a value of $10^{-6.80}$, whereas the value calculated from the measured parameters in this work was $10^{-6.81}$. Based on the PC concentration in the milk (1.51 mM) and the Ca:$P_i$:PC ratio in the CPN (13.2:6.5:1), almost 100% of the PCs are incorporated into the CPNs in the milk without added $CaCl_2$.

It is instructive to consider this system with regard to the individual terms in the equation prior to discussing the systems with added calcium. The 7.5 mM $P_i$ in the serum is predominantly present as either $H_2PO_4^{-}$ (4.3 mM) or as complexes with the group I or II cations present in the milk (1.7 mM). The calculated concentration of $HPO_4^{2-}$ is 1.3 mM and the activity coefficient ($\gamma_2$) = 0.45 so $((HPO_4^{2-})^{0.7})$ = $10^{-2.26}$. Because the pH of the milk (6.7) is much lower than the p$K_a$ of $HPO_4^{2-}$ (12.4), the calculated concentration of $PO_4^{3-}$ is very low at 7.4 nM. The activity coefficient ($\gamma_3$) is 0.15 so $((PO_4^{3-})^{0.2})$ = $10^{-1.8}$. In the case of the 7.0 mM serum calcium approximately 3 mM is complexed by citrate while another 1 mM is complexed by inorganic ligands including $HPO_4^{-}$ and $Cl^{-}$. This leaves 3.5 mM free $Ca^{2+}$ in solution and with a $\gamma_2$ of 0.45 the $(Ca^{2+})$ = $10^{-2.80}$. Therefore, the presence of citrate in the serum approximately doubles the solubility of calcium.

Table SI1 (Supporting Information (SI)) gives the algebraic expressions and values for $K_{SP}$ and the calculated serum IAP for each of the calcium phosphate phases. The milk serum is oversaturated with respect to all of the main crystalline calcium phosphate phases and is most oversaturated with respect to HAP with a ratio of the IAP to the $K_{SP}$ of $10^{10.7}$. This means that, all else being equal, the $(Ca^{2+})$ would have to be 140 times lower, i.e., $(10^{10.7})^{0.2}$, for the solution to be saturated with respect to HAP. The failure of HAP to precipitate from the milk serum contrasts with inorganic ACP in an aqueous suspension for which the transformation to HAP can occur on the time scale of minutes to hours. Table SI1 (SI) also gives the $K_{SP}$ and IAP for two ACP phases from Christoffersen et al.,[24] where mixing $CaCl_2$ and $K_2HPO_4$ solutions initially formed an amorphous phase denoted ACP1 followed after a few minutes by formation of a less soluble amorphous phase termed ACP2. The milk is undersaturated with respect to ACP1 but is oversaturated with respect to ACP2.

*Serum Chemistry in Response to Added Calcium.* The measured concentrations of calcium and $P_i$ in the sera of milk with added $CaCl_2$ are shown in Figure 1a. In response to $CaCl_2$

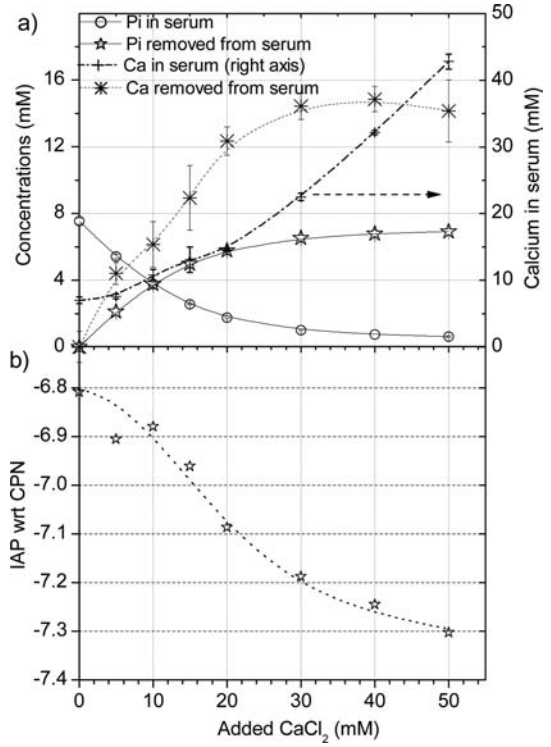


**Figure 1.** Response of milk sera to added $CaCl_2$: (a) measured calcium and Pi in the <10 kDa fraction of the sera and the amount removed from the <10 kDa fraction in response to adding $CaCl_2$ (error bars are 1 standard deviation); (b) calculated ion activity product of the sera with respect to CPN as $CaCl_2$ is added to the milk.

addition to the milk, calcium phosphate is removed from the sera and the $P_i$ concentration in the sera decreases asymptotically toward 0 M. Figure 1a also shows the amount of calcium and $P_i$ that is removed from the sera in response to $CaCl_2$ addition. After 5 mM $CaCl_2$ was added to the milk, 4.4 mM of this added calcium is removed from the sera along with 2.1 mM $P_i$ giving a Ca/$P_i$ ratio removed of 2.1, and this does not change appreciably as more $CaCl_2$ is added. Figure 1b shows the sera IAP with respect to CPN which decreases as $CaCl_2$ is added, falling even after the first 5 mM $CaCl_2$ were added. This presumably reflects the fact that without added $CaCl_2$ essentially all of the PCs were incorporated into the CPNs. Therefore, the addition of just 5 mM $CaCl_2$ results in a change from a CPN system which is thermodynamically stable[12] to the precipitation of metastable calcium phosphate phases. The serum IAP with respect to ACP2 decreases from $10^{-10.8}$ to $10^{-11.1}$ as $CaCl_2$ is added to the milk, and this IAP approaches the ACP2 $K_{SP}$ of $10^{-11.4}$.

**Solid Phase.** *Characterization of the Pure Calcium Phosphate Phases.* The XRD patterns, for the five reference calcium phosphate phases, are shown in Figure SI1 in the Supporting Information. All of the peaks in the XRD patterns correspond to the expected peaks for the synthetic phases with the exception of a small HAP peak present in the XRD pattern for DCPD in addition to a small DCPD peak present in the XRD pattern OCP. As expected for a material with very little long-range order, the ACP has only a very broad weak peak which is present at 30° 2$\theta$ with a very low signal-to-noise ratio. It is clear that XRD will not be useful for detecting the presence of ACP in milk solids. Of the crystalline phases the DCPD had the highest signal-to-noise ratio and the narrowest peaks consistent with the SEM images of the phases (SI Figure SI2) which show that the DCPD had the largest particles with micrometer sized platy crystals. In contrast, the HAP primary particles were not clearly discernible in the SEM and the HAP XRD pattern had the lowest signal-to-noise ratio and the widest peaks. The TCP morphology had sub-micrometer nodules while the OCP had a platy morphology but with smaller plates than the DCPD. The signal-to-noise ratio and the peak widths of the TCP and OCP XRD were, like the particle size, intermediate between those of DCPD and HAP.

The Raman spectra for the five phases (Figure 2) are dominated by the stretching modes of the $PO_4^{3-}$ groups with

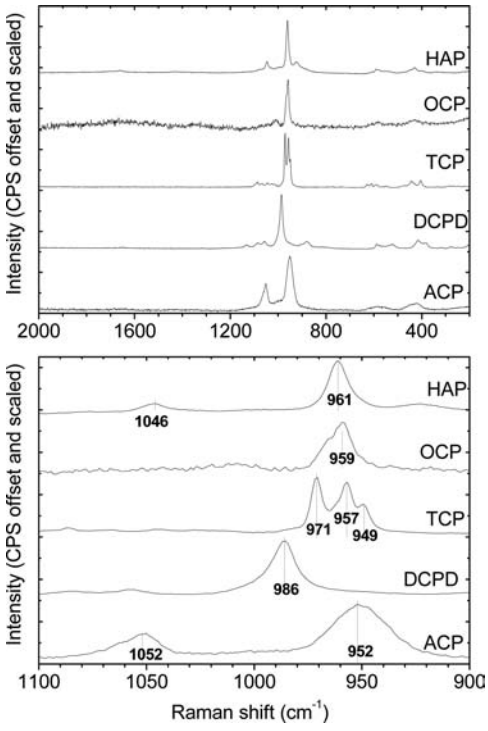


**Figure 2.** Raman spectra measured for the five synthetic calcium phosphate phases using the 488 nm laser. The lower panel has the same spectra with an expanded $x$ axis.

bands between 950 and 1050 $cm^{-1}$. The position and number of bands in the Raman spectra are a reflection of the local environment around the $PO_4^{3-}$ groups in each phase. The Raman spectra of the five phases agree with previously reported spectra,[25−27] and there was little difference in the peak positions or the relative intensities of peaks in spectra measured with a 785 or 488 nm excitation laser. It is clear the ACP Raman spectrum is distinctive, and unlike the XRD patterns, allows for the definitive identification of the phase. With a combination of Raman and XRD, all of the possible phases can be distinguished.

*Characterization of the Calcium Phosphate Phase in Milk.* The XRD patterns of freeze-dried milk pellets obtained from ultracentrifugation of the milk and milk with 40 mM $CaCl_2$ added both have a broad peak at 20° 2$\theta$ as the main feature, and there are no peaks indicative of crystalline calcium phosphate phases. To explore the limits of crystalline phase detection by XRD, samples of freeze-dried pellets were prepared into which known amounts of each synthetic crystalline calcium phosphate standard had been added and homogenized by grinding in a ball mill at −80 °C. The mass of each phase added was the same as the amount of calcium phosphate precipitated in response to $CaCl_2$ addition as calculated from the decrease in $P_i$. For each of the milk pellets with an added crystalline phase there were peaks corresponding with the major peaks of the added standard clearly present in the diffraction patterns. This suggests that crystalline calcium phosphate phases are not formed in response to $CaCl_2$ addition.

The Raman spectra of freeze-dried samples of milk and milk with 40 mM $CaCl_2$ that were measured with the 785 nm laser are shown in Figure 3. The spectra were baseline corrected to

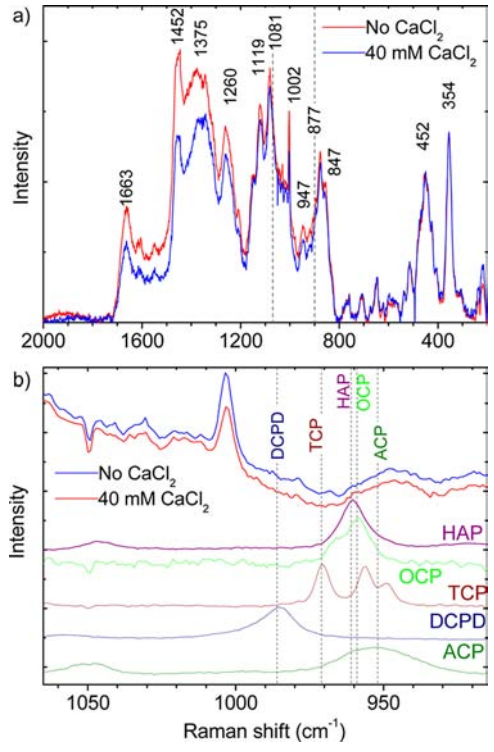


**Figure 3.** Raman spectra measured for the freeze-dried milk and milk with 40 mM of added $CaCl_2$. The main peaks are assigned in SI Table SI2. Panel b shows the $PO_4^{3-}$ stretching region of the spectra with the spectra for five synthetic crystalline calcium phosphate phases.

remove fluorescence, and the intensities of the two spectra were normalized to the lactose band at 354 $cm^{-1}$ because the lactose content in freeze-dried samples will be independent of the added calcium. The main peaks present in the spectra are assigned as previously described, and details are given in Table SI2 (Supporting Information). In the $PO_4^{3-}$ stretching region of both spectra there is a large narrow band at 1002 $cm^{-1}$ which

is due to the phenylanaline ring breathing mode.[28] In addition there is a small broad feature centered at 947 $cm^{-1}$ which is not symmetric and may contain more than one band, one of which could be ACP (Figure 3b). The height of the 947 $cm^{-1}$ feature does not appear to increase with the addition of $CaCl_2$; however, no additional peaks were observed in this region, indicating that no additional phases were detected. Overall, however, the spectra are not particularly convincing regarding the nature of the calcium phosphate removed from the serum in response to $CaCl_2$ addition.

*Raman with an Internal Standard.* The Raman spectra in Figure 3 were of freeze-dried milk which therefore includes the entire content of the serum which precipitates during the drying process. This was done so that the lactose present in milk could serve as an internal reference for the quantification of peaks in the spectra. An internal standard is required because the intensity of peaks in Raman spectra are not directly proportional to the sample composition because of a dependence on factors that affect the scattering phenomena of the sample. However, there are many constituents in the serum that will make the spectra more complex. To avoid the confounding effect of sera contents on the spectra, it is desirable to take spectra of pellets collected by ultracentrifugation. The lactose peaks in these spectra were very small which necessitated the addition of an internal standard. The ideal internal standard needs to meet many criteria such as being water soluble and chemically inert in relation to the $P_i$, calcium, and caseins in the system. The standard needs to have an intense Raman band for referencing peak heights to but also needs to have no bands in the $PO_4^{3-}$ region of the spectra. The compound cannot be volatile or prone to hydrolysis or oxidation. Many small organic molecules were investigated, including D-(+)-galactose, $\beta$-D-fructose, D-glucose, sorbitol, mannitol, and bis tris, HEPES, but these invariably had peaks in the 950−1050 $cm^{-1}$ region of the spectra. Boric acid is a small symmetrical molecule with a simple Raman spectrum which was considered promising with a strong peak at 881 $cm^{-1}$. However, $H_3BO_3$ reacts with the vicinal diols of sugars and therefore could not be used for the milk system.

For these reasons sodium nitrate was used as the internal standard. The $NaNO_3$ Raman spectrum has two strong bands at 1068 and 186 $cm^{-1}$ and weak bands at 726 and 1387 $cm^{-1}$. The nitrate anion is a very weak ligand and does not appreciably coordinate to cations such as $Ca^{2+}$. The only shortcoming of using $NaNO_3$ as an internal standard in this system is that it will raise the ionic strength of the milk and this will affect the solubility of the solid phases by decreasing the activity coefficient of the ions in solution. Therefore, the $NaNO_3$ was added to the milk just before the ultracentrifugation step, and the serum calcium of the systems with added $NaNO_3$ was monitored to determine the effect of the $NaNO_3$ on solubility.

Milk samples having 0, 20, or 40 mM added $CaCl_2$ were prepared with $NaNO_3$ as an internal standard. The Raman spectra of freeze-dried pellets collected by ultracentrifugation of milks with 0.4 M added $NaNO_3$ are shown in Figure 4 with the intensity scale normalized to the height of the $NO_3^-$ peak at 1045 $cm^{-1}$. The spectra are much simpler (i.e., contain less peaks) than the spectra of freeze-dried milk, particularly in the region at <1000 $cm^{-1}$. Because the Raman spectra are collected with a microscope objective, it is important to verify the homogeneity of the internal standard at this spatial resolution. Therefore, spectra were measured at several positions on the sample, and the ratios of the areas of the $NO_3^-$ peak at 1045 $cm^{-1}$ and phenylanaline ring breathing peak at 1002 $cm^{-2}$ were compared. Across the various sample positions the average peak area ratio was 4.1 with a $\sigma$ = 0.2, suggesting a homogeneity within 5% which is adequate for this study.

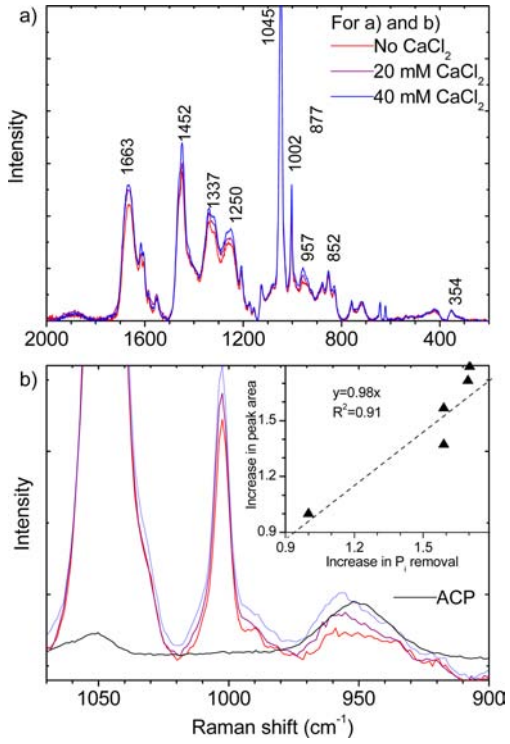


**Figure 4.** Raman spectra measured for the freeze-dried pellets from ultracentrifuged milk with 0, 20, or 40 mM added $CaCl_2$. Panel b shows the $PO_4^{3-}$ stretching region of the spectra with the spectra for the synthetic ACP calcium phosphate phase. Insert: Proportional increase in the area of the $PO_4^{3-}$ stretching band and the amount of $P_i$ removed from solution after 0, 20, or 40 mM $CaCl_2$ addition.

In the lower panel of Figure 4 the $PO_4^{3-}$ stretching region of the spectra is shown, again with the intensity normalized to the $NO_3^-$ band at 1045 $cm^{-1}$. In this view it is clear that the shape and position of the band at 957 $cm^{-1}$ is close to that of the ACP Raman spectrum. In addition as $CaCl_2$ is added to the system and calcium phosphate precipitates, the size of this band increases. In the milk with no added $CaCl_2$ the total concentration of $P_i$ was 17.2 ± 0.1 with 7.5 ± 0.2 $P_i$ in the serum, and adding $CaCl_2$ reduced the serum $P_i$ concentration to almost 0 mM, meaning that there would be 70% more calcium phosphate in the solid phase. If all of the calcium phosphate that precipitated in response to $CaCl_2$ addition is present as ACP, it would be expected that the area of the band centered at 957 $cm^{-1}$ would also increase by 70%. To test this, the areas of the bands were calculated using a baseline from 920 to 975 $cm^{-1}$ and the proportional increase in band area due to added $CaCl_2$ was plotted against the calculated proportional increase in calcium phosphate precipitate. The six data points from replicates with 0, 20, and 40 mM added $CaCl_2$ had a linear relation with a slope of 0.98 ± 0.03 and an $R^2$ = 0.91 and are shown in the insert in Figure 4b. This is reasonably convincing evidence that the calcium phosphate that precipitates in response to $CaCl_2$ addition is in fact an amorphous phase much like the phase that is present in milk with no added $CaCl_2$. Therefore, this work has for the first time demonstrated

the application of Raman spectroscopy using internal and external standards to the qualitative and quantitative determination of the calcium phosphate that forms in response to $Ca^{2+}$ fortification of bovine milk.

## ■ ASSOCIATED CONTENT

### Supporting Information

Tables listing expressions for the solubility product and the calculated ion activity product for the main calcium phosphate minerals and band assignments of milk powder Raman spectra and figures showing XRD patterns for the five synthetic calcium phosphate phases and SEM images of the four crystalline synthetic calcium phosphate phases. This material is available free of charge via the Internet at http://pubs.acs.org.

## ■ AUTHOR INFORMATION

### Corresponding Author

*Fax: 64-9-3737-422. Phone: 64-9-923-4296. E-mail: p.swedlund@auckland.ac.nz.

### Notes

The authors declare no competing financial interest.

## ■ ACKNOWLEDGMENTS

We are extremely grateful to Carl Holt for providing the original computer program for performing the speciation of minerals in milks and helping us understand it.

## ■ REFERENCES

(1) Little, E. M.; Holt, C. An equilibrium thermodynamic model of the sequestration of calcium phosphate by casein phosphopeptides. *Eur. Biophys. J. Biophys. Lett.* **2004**, *33*, 435−447.

(2) Baum, F.; Ebner, J.; Pischetsrieder, M. Identification of Multiphosphorylated Peptides in Milk. *J. Agric. Food Chem.* **2013**, *61*, 9110−9117.

(3) Holt, C. An equilibrium thermodynamic model of the sequestration of calcium phosphate by casein micelles and its application to the calculation of the partition of salts in milk. *Eur. Biophys. J. Biophys. Lett.* **2004**, *33*, 421−434.

(4) Pan, K.; Zhong, Q. Improving Clarity and Stability of Skim Milk Powder Dispersions by Dissociation of Casein Micelles at pH 11.0 and Acidification with Citric Acid. *J. Agric. Food Chem.* **2013**, *61*, 9260−9268.

(5) Tercinier, L.; Ye, A.; Anema, S. G.; Singh, A.; Singh, H. Interactions of Casein Micelles with Calcium Phosphate Particles. *J. Agric. Food Chem.* **2014**, *62*, 5983−5992.

(6) Fox, P. F.; McSweeney, P. L. H. *Dairy Chemistry and Biochemistry*; Blackie Academic & Professional: London, 1998.

(7) de Kruif, C. G.; Huppertz, T. Casein Micelles: Size Distribution in Milks from Individual Cows. *J. Agric. Food Chem.* **2012**, *60*, 4649−4655.

(8) Dalgleish, D. G.; Spagnuolo, P. A.; Goff, H. D. A possible structure of the casein micelle based on high-resolution field-emission scanning electron microscopy. *Int. Dairy J.* **2004**, *14*, 1025−1031.

(9) Holt, C.; de Kruif, C. G.; Tuinier, R.; Timmins, P. A. Substructure of bovine casein micelles by small-angle X-ray and neutron scattering. *Colloids Surf., A* **2003**, *213*, 275−284.

(10) de Kruif, C. G.; Holt, C. Casein micelle structure, functions and interactions. In *Advanced Dairy Chemistry*; Fox, P. F., McSweeney, P. L. H., Eds.; Kluwer Academic/Plenum: New York, 2003; Vol. *1A*, pp 675−698.

(11) Holt, C. Unfolded phosphoproteins enable soft and hard tissues to coexist in the same organism with relative ease. *Curr. Opin. Struct. Biol.* **2013**, *23*, 420−425.

(12) Holt, C.; Sorensen, E. S.; Clegg, R. A. Role of calcium phosphate nanoclusters in the control of calcification. *FEBS J.* **2009**, *276*, 2308−2323.

(13) Motoyama, M.; Chikuni, K.; Narita, T.; Aikawa, K.; Sasaki, K. In Situ Raman Spectrometric Analysis of Crystallinity and Crystal Polymorphism of Fat in Porcine Adipose Tissue. *J. Agric. Food Chem.* **2012**, *61*, 69−75.

(14) Santos, P. M.; Pereira-Filho, E. R.; Rodriguez-Saona, L. E. Application of Hand-Held and Portable Infrared Spectrometers in Bovine Milk Analysis. *J. Agric. Food Chem.* **2013**, *61*, 1205−1211.

(15) Somrani, S.; Banu, M.; Jemal, M.; Rey, C. Physico-chemical and thermochemical studies of the hydrolytic conversion of amorphous tricalcium phosphate into apatite. *J. Solid State Chem.* **2005**, *178*, 1337−1348.

(16) Mandel, S.; Tas, A. C. Brushite ($CaHPO_4{\cdot}2H_2O$) to octacalcium phosphate ($Ca_8(HPO_4)_2(PO_4)_4{\cdot}5H_2O$) transformation in DMEM solutions at 36.5 °C. *Mater. Sci. Eng., C* **2010**, *30*, 245−254.

(17) Bahman, M.; Behzadb, M.; Nayereha, A. Synthesis of nano-sized $\beta$-tricalcium phosphate via wet precipitation. *Process. Appl. Ceram.* **2011**, *5*, 193−198.

(18) Kamitakahara, M.; Ohtsuki, C.; Takahashi, A.; Tanihara, M. Effect of Silane-Coupling Treatment on Thermal Decomposition of Octacalcium Phosphate. *J. Soc. Mater. Sci., Jpn.* **2006**, *55*, 881−884.

(19) Jarcho, M.; Bolen, C. H.; Thomas, M. B.; Bobick, J.; Kay, J. F.; Doremus, R. H. Hydroxylapatite synthesis and characterization in dense polycrystalline form. *J. Mater. Sci.* **1976**, *11*, 2027−2035.

(20) Fox, K. K.; Holsinger, V. H.; Posati, L. P.; Pallansch, M. J. Separation of $\beta$-Lactoglobulin from Other Milk Serum Protein by Trichloroacetic Acid. *J. Dairy Sci.* **1967**, *50*, 1363−1367.

(21) de la Fuente, M. A.; Juarez, M. Rapid Determination of Calcium, Magnesium, Sodium and Potassium in Milk by Flame Atomic Spectrometry After Microwave Oven Digestion. *Analyst* **1995**, *120*, 107−111.

(22) Allen, R. J. L. The estimation of phosphorus. *Biochem. J.* **1940**, *34*, 858−865.

(23) Gaucheron, F. The minerals of milk. *Reprod., Nutr., Dev.* **2005**, *45*, 473−483.

(24) Christoffersen, M. R.; Christoffersen, J.; Kibalczyc, W. Apparent solubilities of two amorphous calcium phosphates and of octacalcium phosphate in the temperature-range 30−42°C. *J. Cryst. Growth* **1990**, *106*, 349−354.

(25) Sauer, G. R.; Zunic, W. B.; Durig, J. R.; Wuthier, R. E. Fourier-Transform Raman Spectroscopy of Synthetic and Biological Calcium Phosphates. *Calcif. Tissue Int.* **1994**, *54*, 414−420.

(26) de Aza, P. N.; Santos, C.; Pazo, A. Vibrational Properties of Calcium Phosphate Compounds. 1. Raman Spectrum of $\beta$-Tricalcium Phosphate. *Chem. Mater.* **1997**, *9*, 912−915.

(27) Xu, J.; Gilson, D. F. R.; Butler, I. S. FT-Raman and high-pressure FT-infrared spectroscopic investigation of monocalcium phosphate monohydrate, $Ca(H_2PO_4)_2{\cdot}H_2O$. *Spectrochim. Acta, Part A* **1998**, *54*, 1869−1878.

(28) McGoverin, C. M.; Clark, A. S. S.; Holroyd, S. E.; Gordon, K. C. Raman spectroscopic quantification of milk powder constituents. *Anal. Chim. Acta* **2010**, *673*, 26−32.

Acetonitrile and methanol (chromatographic grade) were purchased from Merck (Darmstadt, FR, Germany).

**Materials.** Ripe Pu-er tea, produced from the crude green tea prepared with leaves of *C. sinensis* var. *assamica*, was provided by Menghai Tea Factory, Yunnan Province, China, in 2007. These materials were identified by Prof. Ying-Jun Zhang, Kunming Institute of Botany, Chinese Academy of Sciences.

**Extraction and Isolation.** Ripe Pu-er tea (1.0 kg) was extracted with hot water (10 L, 100 °C for 30 min) for three times and filtered. The combined filtrate was concentrated to small volume (2 L) and then partitioned with $CHCl_3$, EtOAc, and *n*-BuOH, consecutively. The *n*-BuOH fraction (56.8 g) was applied to a MCI gel CHP20P column chromatography (CC), eluting with water containing increased proportions of MeOH (10% stepwise gradient, each 700 mL) to give six fractions 1−6. Fraction 2 (4.7 g) was chromatographed over MCI gel CHP20P (0−20% MeOH), Toyopearl HW-40F (0−40% MeOH), and Sephadex LH-20 (100% EtOH) columns to afford compound **20** (10.0 mg). Fraction 3 (6.0 g) was chromatographed over MCI gel CHP20P (0−20% MeOH) to yield five subfractions, Fr.3−1 to Fr.3−5. Fr.3−2 was repeatedly subjected to CC over Toyopearl HW-40F (0−20% MeOH) and MCI gel CHP20P (0−20% MeOH) to yield compound **21** (7.0 mg). Fr.3−4 was subjected to CC over Toyopearl HW-40F (0−20% MeOH) and MCI gel CHP20P (0−20% MeOH) to yield compound **18** (7.0 mg). Fr.3−5 was chromatographed over MCI gel CHP20P (30%−100% MeOH) and Toyopearl HW-40F (0−20% MeOH) to yield compound **19** (7.0 mg). Fraction 4 (14.3 g) was chromatographed over Sephadex LH-20 (0−50% MeOH) to yield six subfractions, Fr.4−1 to Fr.4−6.Fr.4−3 was chromatographed repeatedly over MCI gel CHP20P (10%−60% MeOH) and Toyopearl HW-40F (0−20% MeOH) to yield compounds **6** (26.0 mg), **7** (52.0 mg). and **8** (6.0 mg). Fr.4−4, 4−5 and 4−6 were repeatedly subjected to CC over Toyopearl HW-40F (0−30% MeOH), MCI gel CHP 20P (10%−30% MeOH), and semipreparative HPLC (26% MeOH) to yield compounds **1** (5.0 mg), **2** (3.0 mg), **3** (10.0 mg), **4** (60.0 mg), and **5** (9.0 mg). Fraction 5 (14.8 g) was chromatographed over Sephadex LH-20 (30−100% MeOH) to yield four subfractions, Fr.5−1 to Fr.5−4. Fr.5−1 was subjected to CC over Toyopearl HW-40F (40−70% MeOH), MCI gel CHP20P (30−70% MeOH) and silica gel ($CHCl_3$−MeOH−$H_2O$, 8:2:0.2−7.5:2.5:0.2) to yield compounds **9** (18.0 mg), **10** (9.0 mg), and **11** (10.0 mg). Fr.5−2 was repeatedly subjected to CC over Sephadex LH-20 (100% MeOH), MCI gel CHP20P (30−70% MeOH) and silica gel ($CHCl_3$−MeOH−$H_2O$, 8:2:0.2) to yield compounds **12** (24.0 mg), **13** (3.0 mg), and **22** (7.0 mg). Fr.5−4 was subjected to CC over MCI gel CHP20P (30−70% MeOH), and Toyopearl HW-40F (60−100% MeOH) to yield two mixtures of compounds **14** and **15** (24.0 mg), and **16** and **17** (22.0 mg).

*8-Carboxymethyl-(+)-Catechin (**1**).* A white amorphous powder; $[\alpha]_D^{16}$ +22.0° (*c* 0.18, MeOH); UV (MeOH), $\lambda_{max}$ (log$\varepsilon$): 282 (3.65), 204 (4.67) nm; IR (KBr) $\nu_{max}$ 3425, 2929, 2857, 1619, 1527, 1458, 1385, 1285, 1117 $cm^{-1}$; $^1H$ (600 MHz, acetone-$d_6$) and $^{13}C$ NMR (150 MHz, acetone-$d_6$) data, see Tables 1 and 2, respectively; ESIMS (negative ion mode) *m*/*z* 347 $[M-H]^-$, HRESIMS *m*/*z* 347.0768 $[M-H]^-$ (calcd for $C_{17}H_{15}O_8$, 347.0772).

*8-Carboxymethyl-(+)-Catechin Methyl Ester (**2**).* A white amorphous powder; $[\alpha]_D^{16}$ +21.6° (*c* 0.12, MeOH); UV (MeOH), $\lambda_{max}$ (log$\varepsilon$): 281 (3.67), 204 (4.76) nm; IR (KBr) $\nu_{max}$ 3442, 2927, 1621, 1526, 1457, 1383, 1284, 1202, 1115 $cm^{-1}$; $^1H$ (500 MHz, acetone-$d_6$) and $^{13}C$ NMR (125 MHz, acetone-$d_6$) data, see Tables 1 and 2, respectively; ESIMS (negative ion mode) *m*/*z* 361 $[M-H]^-$; HRESIMS *m*/*z* 361.0925 $[M-H]^-$ (calcd for $C_{18}H_{17}O_8$, 361.0928).

*6-Carboxymethyl-(+)-Catechin (**3**).* A white amorphous powder; $[\alpha]_D^{16}$ +7.6° (0.09, MeOH); UV (MeOH), $\lambda_{max}$ (log$\varepsilon$): 282 (3.68), 204 (4.71) nm; IR (KBr) $\nu_{max}$ 3440, 2926, 2854, 1618, 1528, 1454, 1385, 1286, 1198, 1118 $cm^{-1}$; $^1H$ (600 MHz, acetone-$d_6$) and $^{13}C$ NMR (150 MHz, acetone-$d_6$) data, see Tables 1 and 2, respectively; ESIMS (negative ion mode) *m*/*z* 347 $[M-H]^-$; HRESIMS *m*/*z* 347.0768 $[M-H]^-$ (calcd for $C_{17}H_{15}O_8$, 347.0772).

*6-Carboxyl-(−)-Gallocatechin (**4**).* A white amorphous powder; $[\alpha]_D^{16}$ −10.8° (*c* 0.19, MeOH); UV (MeOH), $\lambda_{max}$ (log$\varepsilon$): 260 (4.15), 217 (4.63), 195 (4.39) nm; IR (KBr) $\nu_{max}$ 3442, 2924, 2853, 1637, 1834, 1043 $cm^{-1}$; $^1H$ (500 MHz, acetone-$d_6$) and $^{13}C$ NMR (125 MHz, acetone-$d_6$) data, see Tables 1 and 2, respectively; ESIMS (negative ion mode) *m*/*z* 349 $[M-H]^-$; HRESIMS *m*/*z* 349.0552 $[M-H]^-$ (calcd for $C_{16}H_{13}O_9$, 349.0559).

**Table 1. $^1H$ NMR Spectroscopic Data for 1−4 (in Acetone-$d_6$)**

| position | 1 | 2 | 3 | 4 |
|---|---|---|---|---|
| 2 | 4.61 (d, 7.5) | 4.56 (d, 7.5) | 4.49 (d, 7.9) | 4.42 (d, 8.0) |
| 3 | 3.92 (ddd, 8.0, 7.5, 5.4) | 3.92 (ddd, 8.2, 7.5, 5.3) | 3.97 (ddd, 8.3, 7.9, 5.5) | 3.93 (dd, 8.7, 4.9) |
| 4 | 2.82 (dd, 16.0, 5.4) | 2.78 (dd, 16.1, 5.3) | 2.84 (dd, 15.8, 5.5) | 2.67 (dd, 15.6, 4.9) |
| | 2.52 (dd, 16.0, 8.0) | 2.47 (dd, 16.1, 8.2) | 2.50 (dd, 15.8, 8.3) | 2.27 (dd, 15.6, 8.7) |
| 6 | 6.10 (s) | 6.05 (s) | | |
| 8 | | | 5.94 (s) | 5.68 (s) |
| 2′ | 6.87 (d, 1.9) | 6.80 (s) | 6.82 (d, 2.0) | 6.42 (s) |
| 5′ | 6.75 (d, 8.2) | 6.74 (d, 8.2) | 6.74 (d, 8.2) | |
| 6′ | 6.71 (dd, 8.2, 1.9) | 6.65 (d, 8.2) | 6.42 (dd, 8.2, 2.0) | 6.42 (s) |
| $-CH_2-$ | 3.51 (d, 16.7) | 3.47 (d, 16.7) | 3.49 (s) | |
| | 3.43 (d, 16.7) | 3.37 (d, 16.7) | | |
| $-CH_3$ | | 3.48 (s) | | |

**Table 2. $^{13}C$ NMR Spectroscopic Data for 1−4 (in Acetone-$d_6$)**

| position | 1 | 2 | 3 | 4 |
|---|---|---|---|---|
| 2 | 82.4 | 81.9 | 81.9 | 81.6 |
| 3 | 68.3 | 67.8 | 67.8 | 67.0 |
| 4 | 28.5 | 28.0 | 28.6 | 26.8 |
| 5 | 155.5 | 155.1 | 154.5 | 160.0 |
| 6 | 95.9 | 95.5 | 103.3 | 98.1 |
| 7 | 155.4 | 154.9 | 155.2 | 160.1 |
| 8 | 101.3 | 100.6 | 95.7 | 94.0 |
| 9 | 154.5 | 154.1 | 154.8 | 157.9 |
| 10 | 100.3 | 100.0 | 101.1 | 99.4 |
| 1′ | 132.1 | 131.6 | 131.5 | 130.4 |
| 2′ | 115.0 | 114.9 | 115.3 | 107.7 |
| 3′ | 145.6 | 145.2 | 145.4 | 145.7 |
| 4′ | 145.6 | 145.2 | 145.3 | 133.0 |
| 5′ | 115.7 | 115.7 | 115.9 | 145.7 |
| 6′ | 119.6 | 119.3 | 119.8 | 107.7 |
| $-CH_2-$ | 29.0 | 28.8 | 29.8 | |
| −COOR | 174.8 | 174.3 | 176.3 | 177.3 |
| $-CH_3$ | | 51.9 | | |

**HPLC Analysis for Identification of the Constituents.** The optimal mobile phase for analysis of fractions of *n*-BuOH fraction of Pu-er tea was a binary gradient elution system consisting of solvent A (Aceonitrile) and solvent B (Water containing 0.34% phosphoric acid). The gradient program used started from 4 to 40% of solvent A in solvent B within 40 min at a flow rate of 0.8 mL/min. The injection volume was 10 $\mu$L. The UV detection wavelength was monitored at 210 nm. The peaks were confirmed by the UV absorptions and retention times of authentic samples, which were 6.9 (**22**), 7.5 (gallic acid), 15.0 (**7**), 21.2 (**9**), 21.9 (**10**), 23.0 (**14**), 23.8 (**11**), 24.4 (**12**), 25.5 (**16**), and 26.9 (**13**) min, respectively (Figure 1).

**Insulin Sensitivity Assay.** Insulin sensitivity assays were performed using the method as reported previously.[7−9]

## RESULTS AND DISCUSSION

Repeated column chromatography over MCI gel CHP20P, Sephadex LH-20, Toyopearl HW-40F and semi-preparative

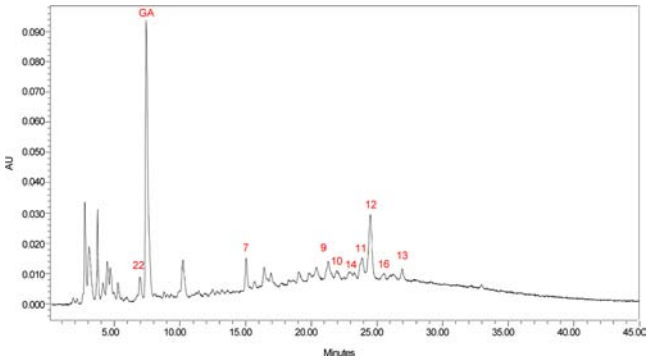


**Figure 1.** HPLC profile of *n*-BuOH-soluble fraction of ripe Pu-er tea (GA: gallic acid).

HPLC led to the isolation of four new flavan-3-ol derivatives **1**−**4** from the thearubigin (*n*-BuOH-soluble) fraction of the commercial ripe Pu-er tea. Moreover, 18 known compounds (**5**−**22**) were identified as three catechin derivatives, 8-carboxyl-(+)-catechin (**5**),[10] (+)-catechin-8-*C*-*β*-D-glucopyranoside (**6**),[11] and (−)-epicatechin-8-*C*-*β*-D-glucopyranoside (**7**),[11] 10 flavonoid glycosides, vicenin-2 (**8**),[12] isoschaftoside (**9**),[13] 2″-*O*-*β*-D-glucopyranosylvitexin (**10**),[14] quercetin 4′-*O*-*α*-L-rhamnopyranosyl-3-*O*-*α*-L-rhamnopyranosyl-(1 → 6)-*β*-D-glucopyranoside (**11**),[15] rutin (**12**),[16] nicotifiorin (**13**),[17] myricetin 3-*O*-*β*-D-glucopyranoside (**14**),[18] myricetin 3-*O*-*β*-D-galactopyranoside (**15**),[19] quercetin 3-*O*-*β*-D-glucopyranoside (**16**),[20] and quercetin 3-*O*-*β*-D-galactopyranoside (**17**),[21] two hydrolyzable tannins, 2-*O*-galloyl-D-glucose (**18**)[22] and 1-*O*-galloyl-*β*-D-glucopyranose (**19**),[23] two quinic acid derivatives, 3-*O*-galloylquinic acid (**20**)[24] and 3-*O*-caffeoylquinic acid (**21**),[25] and one purine alkaloid, 7-methylxanthine (**22**),[26] respectively, by comparing the spectra and physical data with those reported in the literature.

8-Carboxymethyl-(+)-catechin (**1**) was obtained as a white amorphous powder. Its molecular formula $C_{17}H_{16}O_8$ was established on the basis of the HRESIMS at *m*/*z* 347.0768 $[M-H]^-$ (calcd for $C_{17}H_{15}O_8$, 347.0772). The $^1H$ NMR spectrum of **1** showed the presence of three ABX coupled aromatic protons [*δ* 6.87 (d, *J* = 1.9 Hz, H-2′), 6.75 (d, *J* = 8.2 Hz H-5′), and 6.71 (dd, *J* = 8.2, 1.9 Hz, H-6′)], one aromatic singlet proton [*δ* 6.10 (*s*, H-6)], four catechin characteristic aliphatic protons [*δ* 4.61 (d, *J* = 7.5 Hz, H-2), 3.92 (ddd, *J* = 8.0, 7.5, 5.4 Hz, H-3), 2.82 (dd, *J* = 16.0, 5.4 Hz, H-4a), 2.52 (dd, *J* = 16.0, 8.0 Hz, H-4b)], and two mutually coupled aliphatic protons [*δ* 3.51, 3.43 (each 1H, *d*, *J* = 16.7, Hz)]. In $^{13}C$ NMR spectrum, 17 carbon signals were observed, and were further classified as two methylenes ($\delta_C$ 28.5, 29.0), four $sp^2$ methines ($\delta_C$ 95.9, 115.0, 115.7, 119.6), two $sp^3$ methines ($\delta_C$ 68.3, 82.4), one carboxylic carbon ($\delta_C$ 174.8) and other eight $sp^2$ quaternary carbons by HSQC and DEPT experiments. Comparison the $^1H$ and $^{13}C$ NMR data of **1** (Tables 1 and 2) with those of catechin,[27] indicated the presence of an additional carboxymethyl group in **1**, which should be substituted at C-6 or C-8 of the A-ring. The position of substitution was further identified by 2D NMR experiments. In the HMBC spectrum (Figure 2), the correlations from H-2 ($\delta_H$ 4.61) to C-9 ($\delta_C$ 154.5), and from H-4 ($\delta_H$ 2.82, 2.52) to C-5 ($\delta_C$ 155.5) and C-9, clearly assigned the signals of C-5 and C-9. The correlations of the additional methylene protons ($\delta_H$ 3.51, 3.43) with C-7 ($\delta_C$ 155.4), C-8 ($\delta_C$ 101.3), C-9 and the carboxylic carbon ($\delta_C$ 174.8) confirmed that the location of carboxymethyl unit was at

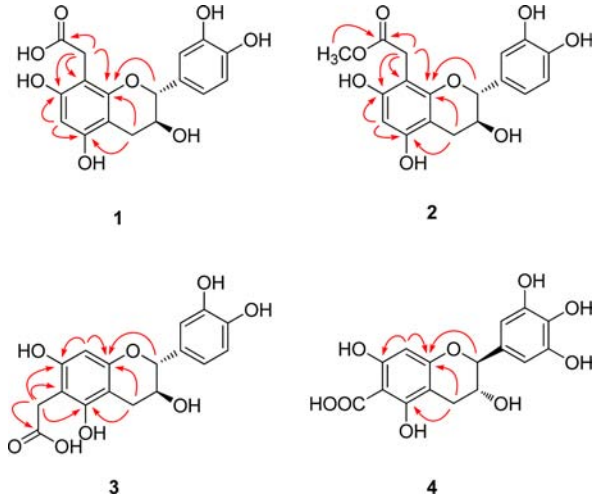


**Figure 2.** Key HMBC correlations (H → C) of **1**−**4**.

C-8. Other 2D NMR experiments further confirmed the planar structure of **1**, as shown in Figure 3. The coupling constant (7.5 Hz) between H-2 and H-3 indicated a 2,3-*trans* configuration. Further comparison the $[\alpha]_D$ of **1** ($[\alpha]_D^{16}$+ 22.0° (*c* 0.18, MeOH)) with (+)-catechin ($[\alpha]_D^{24}$ +15.5°(*c* 1.0, acetone))[27] and (−)-catechin ($[\alpha]_D$ −17.5° (*c* 0.16, MeOH))[28] revealed the 2*R*,3*S* absolute configurations in **1**. This can be confirmed by the CD spectrum, in which compound **1** gave a high-amplitude positive Cotton effect (CE) near 240 nm (Supporting Information Figure S17), corresponding to the $^1L_a$ electronic transition of the flavan-3-ols, consistent with 3*S*-configuration.[29] Based on the above evidence, the structure of **1** was determined to be 8-carboxymethyl-(+)-catechin.

8-Carboxymethyl-(+)-catechin methyl ester (**2**) was obtained as a white amorphous powder, possessing a molecular formula of $C_{18}H_{18}O_8$, as deduced from the HRESIMS measurement at *m*/*z* 361.0925 $[M-H]^-$ (calcd for $C_{18}H_{17}O_8$, 361.0928). The $^1H$ and $^{13}C$ NMR spectra of **2** (Tables 1 and 2) were closely resembled to those of **1**, except for an additional methoxy group ($\delta_H$ 3.48, $\delta_C$ 51.9) in **2**. In the HMBC spectrum of **2**, correlations of H-2 ($\delta_H$ 4.56, d, *J* = 7.5 Hz) with C-9 ($\delta_C$ 154.1), and the methylene protons ($\delta_H$ 3.47, 3.37) with C-7 ($\delta_C$ 154.9), C-8 ($\delta_C$ 100.6), C-9, and the carboxylic carbon ($\delta_C$ 174.3) confirmed that the carboxylmethyl group was attached to C-8. Moreover, the additional methoxy protons ($\delta_H$ 3.48) showed HMBC correlation with the carboxylic carbon ($\delta_C$ 174.3), revealing its linkage to the carboxyl group. Finally, the large coupling constant (7.5 Hz) between H-2 and H-3 in **2**, and the similar $[\alpha]_D$ value ($[\alpha]_D^{16}$ +21.6° (*c* 0.12, MeOH)) with **1**, suggested that **2** possesses the same 2*R*,3*S* configurations to **1**. In the CD spectrum, **2** showed a positive CE near 240 nm supported that **2** has a 2*R*,3*S*-configuration. Accordingly, compound **2** was determined as 8-carboxymethyl-(+)-catechin methyl ester.

6-Carboxymethyl-(+)-catechin (**3**), obtained as a white amorphous powder, has a same molecular formula of $C_{17}H_{16}O_8$ to **1**, as established by the HRESIMS (*m*/*z* 347.0768 $[M-H]^-$). The $^1H$ and $^{13}C$ NMR spectra of compound **3** were also closely resembled to those of **1**. In the HMBC spectrum of **3**, H-2 ($\delta_H$ 4.49) showed correlation with C-9 ($\delta_C$ 154.8), while H-4 ($\delta_H$ 2.84, 2.50) displayed correlations with C-5 ($\delta_C$ 154.5) and C-9 ($\delta_C$ 154.8). These led to the assignments of C-5 ($\delta_C$ 154.5), C-9 ($\delta_C$ 154.8), and C-7


dx.doi.org/10.1021/jf5036959 | J. Agric. Food Chem. 2014, 62, 12229−12234

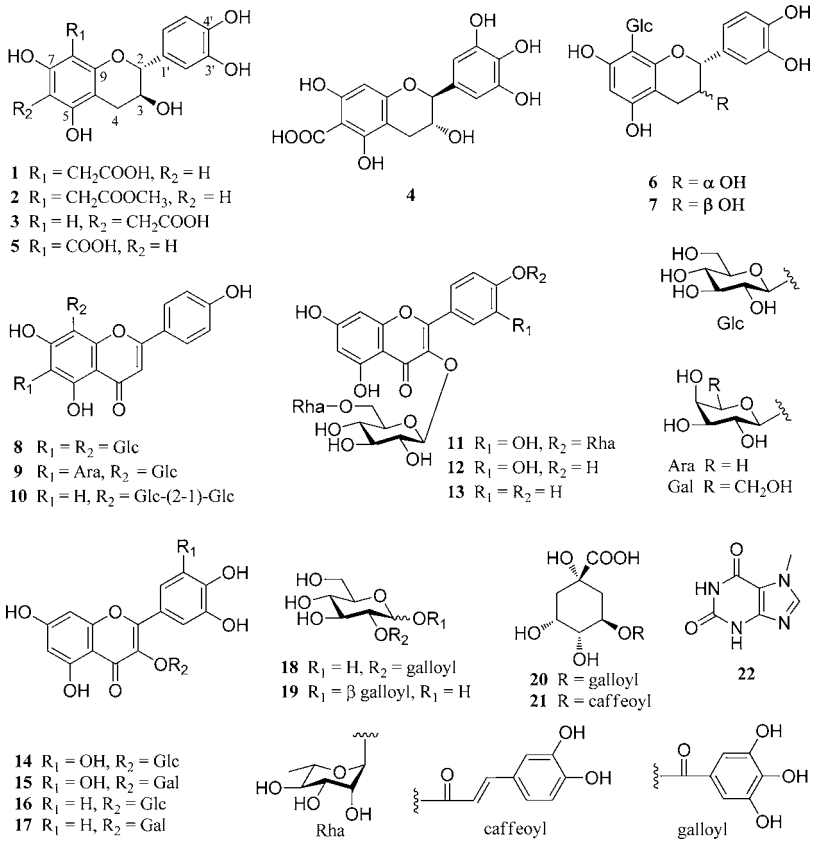


**Figure 3.** Compounds isolated from ripe Pu-er tea.

($\delta_C$ 155.2) clearly. Moreover, the HMBC correlations of the carboxymethyl ($\delta_H$ 3.49) with C-5 ($\delta_C$ 154.5), C-7 ($\delta_C$ 155.2), and the carboxylic carbon ($\delta_C$ 176.3) revealed that the carboxymethyl group in **3** was attached to C-6 (Figure 2). Further analysis of HSQC and HMBC spectra of **3** confirmed its structure as shown in Figure 3. The similar $[\alpha]_D$ of **3** ($[\alpha]_D^{16}$ +7.6° (*c* 0.09, MeOH)) with **1**, together with the positive CE near 240 nm confirmed that **3** has the same 2*R*,3*S* configurations to **1**. Therefore, compound **3** was determined to be 6-carboxymethyl-(+)-catechin, the isomer of compound **1**.

6-Carboxyl-(−)-gallocatechin (**4**), obtained as a white amorphous powder, gave a quasi-molecular ion peak at *m*/*z* 349.0552 $[M-H]^-$ on the HRESIMS, corresponding to a molecular formula of $C_{16}H_{14}O_9$ for **4**. The molecular weight of **4** is 44 mass units larger than that of gallocatechin, corresponding to a carboxyl group. The $^1H$ and $^{13}C$ NMR data of **4** were very similar to those of gallocatechin,[27] except for the disappearance of one aromatic proton and the appearance of an additional carboxyl carbon ($\delta_C$ 177.3) signal. The above data suggested that one of the aromatic protons in gallocatechin was substituted by a carboxyl group in **4**. The position of substitution was identified by HMBC experiment. The HMBC correlations of H-2 ($\delta_H$ 4.42, d, *J* = 8.0 Hz) with the carbon at $\delta_C$ 157.9, and H-4 [$\delta_H$ 2.67 (dd, *J* = 15.6, 4.9 Hz), 2.27 (dd, *J* = 15.6, 8.7 Hz)] with the carbons at $\delta_C$ 160.0 and 157.9 could assign unambiguously these carbon signals as C-5 ($\delta_C$ 160.0) and C-9 ($\delta_C$ 157.9). Thus, an unresolved signal at $\delta_C$ 160.1 must be arisen from C-7. The HMBC correlations of aromatic proton at $\delta_H$ 5.68 with the C-7($\delta_C$ 160.1) and C-9 ($\delta_C$ 157.9) indicated the position of aromatic proton to be H-8. Therefore, the carboxyl group was located on the C-6 position. A $J_{2,3}$ coupling constant of 8.0 Hz confirmed a 2,3-*trans* configuration. Further comparison the $[\alpha]_D$ of **4** ($[\alpha]_D^{16}$ −10.8° (*c* 0.19, MeOH)) with those of (−)-gallocatechin ($[\alpha]_D^{24}$ −11.2° (*c* 1.0, acetone))[27] and (+)-gallocatechin ($[\alpha]_D^{20}$ +150° (*c* 0.1, MeOH))[30] suggested that compound **4** has the same absolute configuration with (−)-gallocatechin, namely, 2*S*,3*R*-configuration. Moreover, **4** gave a high-amplitude negative CE near 240 nm, consistent with 3*R*-configuration. On the basis of the above evidence, the structure of **4** was deduced as 6-carboxyl-(−)-gallocatechin.

Thearubigin, having relative molecular weights between 700−4000 Da, is the main pigments in black tea considered generally as the *n*-BuOH soluble fraction. This fraction is presumed to be the polymers of catechins and/or theaflavins.[31] Inspired by concept of thearubigin in black tea, the *n*-BuOH soluble fraction of ripe Pu-er tea, the relative polar fraction after sequential solvent partitions, was qualitatively analyzed by HPLC analysis. As shown in Figure 1, compounds **7**, **9**−**14**, **16**, **22** and gallic acid (GA) were identified from the *n*-BuOH soluble fraction of ripe Pu-er tea, by comparison the retention time and UV profile with those of authentic samples under the same HPLC condition. The isolates constitute only a small portion of the *n*-BuOH-soluble ripe Pu-er tea pigments, albeit the visible peaks under wavelength of 210 nm in HPLC trace. The large unknown polymer pigments need to be further exploited.

Tea polyphenols from ripe Pu-er tea are reported to be active in antiobesity and antidiabetes,[32] of which, catechins are showing antiobesity and antidiabetes activities.[33] Most of the isolates, **4**, **6**−**17**, and **21**−**22** were tested for their acute activities on insulin sensitivity in differentiated 3T3-L1 adipocytes, but no significant activities were observed in these


dx.doi.org/10.1021/jf5036959 | J. Agric. Food Chem. 2014, 62, 12229−12234

compounds at a concentration of 10 $\mu$M. The above results suggested that the antidiabetes activity of catechins may not undergo the increasing insulin sensitivity.

In conclusion, the isolated phenolic compounds **1**−**21** could be divided into three groups, flavan-3-ol derivatives (**1**−**7**), flavonoid glycosides (**8**−**17**), and simple hydrolyzable tannins (**18**−**21**). Of them, **1**−**3** have additional carboxymethyl group in comparison with catechin. Compounds **4** and **5** are presumed to be formed through enzymatic Kolbe-Schmitt reaction from catechin.[34] Flavonoid glycosides **8**−**11** are reported from tea plants for the first time. Compound **11** have only been reported from *Zizyphus lotus* previously.[15] Simple hydrolyzable tannins (**18** and **19**) and quinic acid derivatives (**20** and **21**) were common constituents reported from green tea. The 7-methylxanthine (**22**) is the precursor of caffeine.[26] The *n*-BuOH-soluble fraction of ripe Pu-er tea was qualitatively analyzed by HPLC, from which nine compounds, **7**, **9**−**14**, **16**, **22** and gallic acid were identified by comparison the retention time and UV profile with those of authentic samples under the same HPLC condition, and gallic acid was found to be the major component. However, the compounds identified in HPLC trace only account for a small portion of *n*-BuOH-soluble fraction of ripe Pu-er tea pigment. The structure and function of the largely unknown polymer pigments are yet to be unveiled.

## ■ ASSOCIATED CONTENT

### Supporting Information

The $^{1}$H, $^{13}$C, HSQC, HMBC, and CD spectra of compounds **1**−**4** in acetone-$d_6$ are available free of charge via the Internet at http://pubs.acs.org.

## ■ AUTHOR INFORMATION


### Corresponding Author

*Tel: +86-871-65223235. Fax: +86-871-65223235. E-mail: zhangyj@mail.kib.ac.cn.

### Author Contributions

§L.-W.T. and M.-K.T. contributed equally to this paper.



### Funding

This work was partly supported by the NSFC 21172224 and the 973 Program of Science and Technology of P. R. China (2011CB915503).


### Notes

The authors declare no competing financial interest.

## ■ ACKNOWLEDGMENTS

The authors are grateful to the staffs of the analytical group at State Key Laboratory of Phytochemistry and Plant Resources in West China, Kunming Institute of Botany, Chinese Academy of Sciences, for measuring the spectroscopic data.

## ■ REFERENCES


(1) Yang, C. R.; Chen, K. K.; Zhang, Y. J. Classification of tea and definition of Pu-er tea. *Chaye Kexue Jishu* **2006**, *2*, 37−38 in Chinese.

(2) Drynan, J. W.; Clifford, M. N.; Obuchowicz, J.; Kuhnert, N. The chemistry of low molecular weight black tea polyphenols. *Nat. Prod. Rep.* **2010**, *27*, 417−462.

(3) Zhang, L.; Li, N.; Ma, Z. Z.; Tu, P. F. Comparison of the chemical constituents of aged pu-erh tea, ripened pu-erh tea, and other teas using HPLC-DAD-ESI-MSn. *J. Agric. Food Chem.* **2011**, *59*, 8754−8760.

(4) Jiang, H. Y.; Shii, T.; Matsuo, Y.; Tanaka, T.; Jiang, Z. H.; Kouno, I. A new catechin oxidation product and polymeric polyphenols of post-fermented tea. *Food Chem.* **2011**, *129*, 830−836.

(5) Zhou, Z. H.; Zhang, Y. J.; Xu, M.; Yang, C. R. Puerins A and B, two new 8-C substituted flavan-3-ols from Pu-er tea. *J. Agric. Food Chem.* **2005**, *53*, 8614−8617.

(6) Chen, H. F.; Takashi, T.; Gen Ichiro, N.; Toshihiro, F.; Kunihide, M. Phenylpropanoid-substituted catechins from *Castanopsis hystrix* and structure revision of cinchonains. *Phytochemistry* **1993**, *33*, 183−187.

(7) Prasad, C. N. V.; Anjana, T.; Banerji, A.; Gopalakrishnapillai, A. Gallic acid induces GLUT4 translation and glucose uptake activity in 3T3-L1 cells. *FEBS Lett.* **2010**, *584*, 531−536.

(8) Tan, M. J.; Ye, J. M.; Turner, N.; Hohnen-Behrens, C.; Ke, C. Q.; Tang, C. P.; Chen, T.; Weiss, H. C.; Gesing, E. R.; Rowland, A.; James, D. E.; Ye, Y. Antidiabetic activities of triterpenoids isolated from bitter melon associated with activation of the AMPK pathway. *Chem. Biol.* **2008**, *15*, 263−73.

(9) Xiong, W. Y.; Jordens, I.; Gonzalez, E.; McGraw, T. E. GLUT4 issorted to vesicles whose accumulation beneath and insertion into the plasma membrane are differentially regulated by insulin and selectively affected by insulin resistance. *Mol. Biol. Cell* **2010**, *21*, 1375−1386.

(10) Ballenegger, M. E.; Weith, A. J.; Rimbault, C. G.; Albert, A. I.; Courbat, P.; Tyson, R. G.; Thompson, D. G.; Palmer, D. R. Pharmceutical preparations containing (+)-cyanidan-3-ol derivatives, the use thereof, novel substituted (+)-cyanidan-3-ol derivatives, and processes for producing them. *Eur. Pat. Appl.* 96007A2. Dec. 7, 1983.

(11) Stark, T.; Hofmann, T. Application of a molecular sensory science approach to alkalized cocoa (*Theobroma cacao*): Structure determination and sensory activity of nonenzymatically *C*-glycosylated flavan-3-ols. *J. Agric. Food Chem.* **2006**, *54*, 9510−9521.

(12) Lu, Y. R.; Yeap Foo, L. Flavonoid and phenolic glycosides from *Salvia officinalis*. *Phytochemistry* **2000**, *55*, 263−267.

(13) Hilsenbeck, R. A.; Wright, S. J.; Mabry, T. J. *C*-Glycosylflavones from *Yeatesia viridiflora*. *J. Nat. Prod.* **1984**, *47*, 312−315.

(14) Segelman, A. B.; Segelman, F. P.; Star, A. E.; Wagner, H.; Seligmann, O. Structure of two *C*-diglycosylflavones from *Cannabis sativa*. *Phytochemistry* **1978**, *17*, 824−826.

(15) Maciuk, A.; Ghedira, K.; Thepenier, P.; Lavaud, C.; Zeches-Hanrot, M. A new flavonol glycoside from leaves of *Zizyphus lotus*. *Pharmize* **2003**, *58*, 158−159.

(16) Akbay, P.; Basaran, A. A.; Undeger, U.; Basaran, N. In vitro immunomodulatory activity of flavonoid glycosides from *Urtica dioica* L. *Phytother. Res.* **2003**, *17*, 34−37.

(17) Lee, H. B.; Kim, E. K.; Park, S. J.; Bang, S. G.; Kim, T. G.; Chung, D. W. Isolation and characterization of nicotiflorin obtained by enzymatic hydrolysis of two precursors in tea seed extract. *J. Agric. Food Chem.* **2010**, *58*, 4808−4813.

(18) Scharbert, S.; Holzmann, N.; Hofmann, T. Identification of the astringent taste compounds in black tea infusions by combining instrumental analysis and human bioresponse. *J. Agric. Food Chem.* **2004**, *52*, 3498−3508.

(19) Ye, G.; Huang, C. G. Flavonoids of *Limonium aureum*. *Chem. Nat. Compd.* **2006**, *42*, 232−234.

(20) Beck, M. A.; Haberlein, H. Flavonol glycosides from *Eschscholtzia californica*. *Phytochemistry* **1999**, *50*, 329−32.

(21) Yasukawa, K.; Takido, M. A flavonol glycoside from *Lysimachia Mauritiana*. *Phytochemistry* **1987**, *26*, 1224−1226.

(22) Haslam, E.; Uddin, M. The synthesis of 2- and 3-galloyl derivatives of arbutin. *Tetrahedron* **1968**, *24*, 4015−4020.

(23) Saijo, R.; Nonaka, G.-i.; Nishioka, I. Gallic acid esters of bergenin and norbergenin from *Mallotus japonicus*. *Phytochemistry* **1990**, *29*, 267−270.

(24) Zhou, Z. H.; Yang, C. R. Chemical constituents of crude green tea, the material of Pu-er tea in Yunnan. *Acta Bot. Yunnan.* **2000**, *22*, 343−350 in Chinese.

(25) Morishita, H.; Iwahashi, H.; Osaka, N.; Kido, R. Chromatographic separation and identification of naturally occurring chlorogenic acids by $^{1}$H nuclear magnetic resonance spectroscopy and mass spectrometry. *J. Chromatogr. A* **1984**, *315*, 253−260.

(26) Ashihara, H.; Sano, H.; Crozier, A. Caffeine and related purine alkaloids: Biosynthesis, catabolism, function, and genetic engineering. *Phytochemistry* **2008**, *69*, 841−856.
(27) Seto, R.; Nakamura, H.; Nanjo, F.; Hara, Y. Preparation of epimers of tea catechins by heat treatment. *Biosci. Biotechnol. Biochem.* **1997**, *61*, 1434−1439.
(28) Cefarelli, G.; D'Abrosca, B.; Fiorentino, A.; Izzo, A.; Mastellone, C.; Pacifico, S.; Piscopo, V. Free-radical-scavenging and antioxidant activities of secondary metabolites from reddened cv. Annurca apple fruits. *J. Agric. Food Chem.* **2006**, *54*, 803−809.
(29) Slade, D.; Ferreira, D.; Marais, J. P. Circular dichroism, a powerful tool for the assessment of absolute configuration of flavonoids. *Phytochemistry* **2005**, *66*, 2177−215.
(30) Tian, Y. J.; Luo, Y. G.; Li, B. G.; Zhang, G. L. Chemical study on *Dendrobenthamia capitata* (Wall.) Hutch. *Nat. Prod. Res. Dev.* **2002**, *14*, 18−20.
(31) Haslam, E. Thoughts on thearubigins. *Phytochemistry* **2003**, *64*, 61−73.
(32) Zhang, D. Y.; Liu, Z. H.; Shi, Z. P.; Liu, Y. L.; Fu, D. H. Study on blood glucose-depressing and blood lipid-depressing function of Pu-er tea by high through screening method. *Chaye Kexue* **2005**, *26*, 49−53 in Chinese.
(33) Murase, T.; Misawa, K.; Haramizu, S.; Hase, T. Catechin-induced activation of the LKB1/AMP-activated protein kinase pathway. *Biochem. Pharmacol.* **2009**, *78*, 78−84.
(34) Kirimura, K.; Gunji, H.; Wakayama, R.; Hattori, T.; Ishii, Y. Enzymatic Kolbe−Schmitt reaction to form salicylic acid from phenol: Enzymatic characterization and gene identification of a novel enzyme, Trichosporon moniliiforme salicylic acid decarboxylase. *Biochem. Biophys. Res. Commun.* **2010**, *394*, 279−84.

carbohydrate structure (chain length; pentose/hexose) on the efficiency of these inhibitors have not been studied.

The aim of the present study was to investigate the effects of selected Maillard reaction inhibitors, including aminoguanidine, cysteine, pyridoxamine, and sodium bisulfite, on the production of potato patatin (PTT)−galactose/xylose/galactooligosaccharides (GOS)/xylooligosaccharides (XOS)/galactan/xylan conjugates with specific functionalities. PTT has previously demonstrated numerous biological and functional properties including lipid acyl hydrolase activity,[18] antiproliferative activity on mouse melanoma cells, and antioxidant activity,[19] which makes it an interesting candidate for carbohydrate conjugation. The effectiveness of the investigated inhibitors to control the glycation of PTT was assessed by monitoring the glycation extent and the protein cross-linking along with the formation of dicarbonyl compounds. The PTT−carbohydrate conjugates were produced using the effective inhibitors and their digestibility was assessed.

## MATERIALS AND METHODS

**Materials.** Solanic 206P (≈75% PTT, ≈25% protease inhibitors) was kindly provided by Solanic (Foxhol, Netherlands). Potato galactan (∼280 kDa) and endo-1−4-$\beta$-D-galactanase from *Aspergillus niger* were purchased from Megazyme (Wicklow, Ireland). Furosine standard was purchased from Neosystem Lab (Strasbourg, France). Biogel P2 extra fine, Bradford reagent and broad range SDS-PAGE standards were purchased from Bio-Rad (Philadelphia, PA, U.S.A.). XOS was obtained from Shandong Longlive Biotech (Yucheng, China). Xylan from beechwood (≥90%) and all other chemicals were purchased from Sigma Chemical Co. (St. Louis, MO, U.S.A.).

**Production of Conjugates.** Potato proteins (Solanic 206P) in sodium phosphate buffer (50 mM, pH 7) were ultrafiltered using a stirred ultrafiltration unit (Amicon system, Millipore, Billerica, MA, U.S.A.) fitted with a 30 kDa molecular mass cutoff membrane to remove the protease inhibitors. The protein profile of the purified PTT revealed that the collected retentate was 90% composed of PTT.[20] Galactose, xylose, GOS, XOS, potato galactan, and soluble xylan were investigated as selected carbohydrates for the preparation of conjugates. GOS, with an average molar mass of 1990.9 g/mol, was produced according to Seo et al.[9] Mixtures of enriched PTT and selected carbohydrates at a molar ratio of 1:7 were prepared. The appropriate Maillard reaction inhibitor (aminoguanidine/cysteine/pyridoxamine or sodium bisulfite) was added to the mixtures at a protein to inhibitor ratio of 1:0.2 (w/w). The mixtures were freeze-dried and incubated at 48 °C for 1, 3, 5, and 7 days at $a_w$ of 0.65 (saturated potassium iodide). The collected mixtures were kept at −20 °C.

**Determination of Glycation Extent.** The glycation extent of PTT was determined through the measurement of the furosine amount, formed upon the acid hydrolysis, and of the total amount of available lysine according to the method of Seo et al.[20]

The final percentage of blocked lysine was indirectly estimated from the furosine content, considering that the Amadori compound tagatosyl−lysine formed during the Maillard reaction between lysine residues and galactose moieties generate about 42% furosine upon 8 M hydrochloric acid hydrolysis.[21] Although the amount of furosine formed from xylulosyl−lysine to furosine is unknown, the difference between the amount of furosine formed upon acid hydrolysis from different carbohydrates has been demonstrated to be smaller at stronger acid hydrolysis conditions used in this study.[21] Therefore, the same correction factor for the conversion of tagtosyl−lysine to furosine was used for the estimation of xylulosyl−lysine. The furosine content and the total available lysine content before glycation were used for the estimation of the percentage of blocked lysine that was due to the glycation and not to the protein cross-linking according to the following equation.

$$\%\text{blocked lysine} = (1/0.42 \times \text{furosine}) \times 100/\text{total lysine} \quad (1)$$

Experimental results are presented as averages of triplicates and the standard deviations are ≤5%.

**Determination of the Level of Protein Cross-Linking.** *Advanced Glycation Reaction Index of Glycoforms.* The advanced glycation reaction index was estimated by measuring spectrophotometrically the turbidity/browning of protein−carbohydrate mixtures (10 mg/mL) at 600 nm. All assays were run in triplicates and the presented values are their averages.

*Molecular Weight Distribution of PTT Glycoforms.* The glycated sample mixtures were subjected to size exclusion chromatography on Superdex 200 5/150 (GE Healthcare, Piscataway, NJ, U.S.A.) column on ÄKTA purifier system (GE Healthcare). The isocratic elution was run with potassium phosphate buffer (50 mM, pH 7) containing 0.15 M sodium chloride (3CV) at a flow rate of 0.3 mL/min. The fractions were detected at 280 nm. Selected proteins, including $\beta$-amylase, albumin, chymotrypsinogen A, and lysozyme, were used as standards for calibration. The results are presented as averages of duplicate measurements.

*Particle Size Distribution of PTT Glycoforms.* To estimate the distribution of the protein aggregates, the particle size was estimated through dynamic light scattering (DLS) measurements by Delsa Nano C system (Beckman Coulter) at 25 °C. The means of intensity distributions were obtained from 70 measurements.

**Quantitation of $\alpha$-Dicarbonyls.** The quantitation of $\alpha$-dicarbonyls was carried out according to the method of Marceau and Yaylayan.[22] Glycated samples (20 mg/mL) were suspended in 0.5% (w/v) solution of *o*-phenylenediamine solution and incubated overnight in darkness at 25 °C. After centrifugation (5000*g*, 5 min), the quantitation of $\alpha$-dicarbonyls was performed with a Beckman HPLC system equipped with a programmable solvent module (model 126), a photodiode array detector and 32 Karat software for data collection. The separation was performed on a Zorbax SB-C18 (4.6 × 150 mm, 5 $\mu$m, Agilent Technologies, Palo Alto, CA, U.S.A.) at 25 °C. The elution of the derivatized samples (20 $\mu$L) was carried out with an isocratic mobile phase of methanol/water/formic acid (55:45:0.1, v/v/v) at 0.7 mL/min. The detection was done at 312 nm, and the spectrum was recorded from 200 to 400 nm. The unglycated proteins/carbohydrate mixtures with and without inhibitor were run as controls. To assess the presence of any side derivatization reactions due to the presence of protein, carbohydrate, and/or inhibitors, control reactions were run with each of these glycation components separately. Glyoxal, methylglyoxal, and 2,3-butanedione were used as standards for the identification of the formed dicarbonyls. The derivatization of these standards at selected concentration varying from 8.33 to 300 $\mu$g/mL was carried out as discussed here above. The identification of deoxyosone was done based on the characteristic two absorption maxima of the quinoxaline derivatives (∼250 nm, ∼330 nm) and on the RP-HPLC elution order characterized by Marceau and Yaylayan.[22] Experimental results are presented as averages of triplicates and the standard deviations are ≤5%.

**Simulated Gastric Digestion of PTT and its Glycoforms.** The simulated gastric digestion of PTT and its corresponding glycoforms was performed according to the modified method of Moreno et al.[23] The glycated and nonglycated PTT samples (1 mg/mL) were suspended in 20% (v/v) simulated gastric fluid (0.75 M sodium chloride, pH 2.2). To initiate the enzymatic digestion, porcine pepsin (7 mg/mL, ≥ 2,500 units/mg protein) at a ratio of 1:50 (v/v) was added. After 2 h incubation at 37 °C, the pH of the mixture was raised to 7.5 with ammonium carbonate (0.125 M). The following solutions were added to slightly lower the pH and to simulate a duodenal environment: (1) 10 $\mu$L bile salt mixture consisting of 0.025 M sodium taurocholate, 0.25 M sodium glycodeoxycholic acid, 0.4 M calcium chloride, and 0.5 M Bis-Tris; (2) 6 $\mu$L of porcine trypsin (3 mg/mL, ≥6000 units/mg protein) and 10 $\mu$L of bovine $\alpha$-chymotrypsin (4.77 mg/mL, ≥39 units/mg protein). The sample was then incubated at 37 °C for 1 h. The reaction was stopped by heating the samples in boiling water for 5 min. The control without the incubation steps was prepared as the unhydrolyzed control, and the native PTT was used as hydrolyzed control. All assays were done in triplicate.

**Table 1. Progress of the Maillard Reaction at 48°C at $a_w$ of 0.65**

| | | percent blocked lysine[a,d,e] | | | | | advanced reaction index[b,d,e] | | | | | reaction control ratio[c,d] | | | | |
|---|---|---|---|---|---|---|---|---|---|---|---|---|---|---|---|---|
| PTT mixtures | incubation time | N | A | C | P | S | N | A | C | P | S | N | A | C | P | S |
| PTT−galactose | 1 | 7.7 | 3.5 | 0.0 | 3.8 | 0.0 | 0.6 | 0.1 | 0.8 | 0.4 | 0.1 | 12.8 | 35.0 | 0.0 | 9.5 | 0.0 |
| | 3 | 97.9 | 4.0 | 18.0 | 2.9 | 4.3 | 1.2 | 0.2 | 1.7 | 0.8 | 0.1 | 81.6 | 20.0 | 10.6 | 3.6 | 43.0 |
| | 5 | 18.2 | 0.0 | 15.4 | 1.8 | 21.0 | 4.7 | 0.7 | 0.1 | 0.1 | 0.1 | 3.9 | 0.0 | 154.0 | 18.0 | 210.0 |
| | 7 | 1.0 | 0.8 | 12.4 | 2.8 | 2.9 | 3.2 | 0.6 | 1.4 | 0.1 | 0.1 | 0.3 | 1.3 | 8.9 | 28.0 | 29.0 |
| PTT−xylose | 1 | 0.0 | 0.0 | 3.6 | 0.0 | 0.8 | 3.9 | 0.1 | 0.4 | 0.1 | 0.1 | 0.0 | 0.0 | 9.0 | 0.0 | 8.0 |
| | 3 | 2.4 | 3.5 | 13.7 | 1.7 | 0.0 | 3.6 | 0.1 | 1.0 | 2.4 | 0.1 | 0.7 | 35.0 | 13.7 | 0.7 | 0.0 |
| | 5 | 13.0 | 6.4 | 0.4 | 0.0 | 1.7 | 3.3 | 3.7 | 6.1 | 9.8 | 1.7 | 3.9 | 1.7 | 0.1 | 0.0 | 1.0 |
| | 7 | 0.0 | 16.0 | 0.0 | 0.0 | 0.0 | 4.5 | 0.1 | 4.3 | 4.5 | 2.1 | 0.0 | 160.0 | 0.0 | 0.0 | 0.0 |
| PTT−GOS | 1 | 0.8 | 0.0 | 0.0 | 0.0 | 0.0 | 0.5 | 3.0 | 0.1 | 0.1 | 0.1 | 1.6 | 0.0 | 0.0 | 0.0 | 0.0 |
| | 3 | 1.3 | 0.0 | 66.3 | 0.0 | 0.0 | 1.0 | 6.0 | 0.1 | 0.1 | 0.1 | 1.3 | 0.0 | 663.0 | 0.0 | 0.0 |
| | 5 | 0.0 | 0.0 | 0.0 | 0.0 | 0.0 | 0.9 | 2.5 | 1.8 | 0.1 | 0.4 | 0.0 | 0.0 | 0.0 | 0.0 | 0.0 |
| | 7 | 6.1 | 0.0 | 0.0 | 1.2 | 0.0 | 1.6 | 3.1 | 0.1 | 0.1 | 0.1 | 3.8 | 0.0 | 0.0 | 12.0 | 0.0 |
| PTT−XOS | 1 | 0.0 | 0.0 | 3.2 | 0.0 | 0.0 | 1.5 | 0.2 | 0.4 | 3.1 | 0.1 | 0.0 | 0.0 | 8.0 | 0.0 | 0.0 |
| | 3 | 0.4 | 14.3 | 6.9 | 2.3 | 0.0 | 1.1 | 0.1 | 0.1 | 11.6 | 0.1 | 0.4 | 143.0 | 69.0 | 0.2 | 0.0 |
| | 5 | 11.7 | 7.8 | 1.2 | 0.5 | 2.7 | 0.6 | 0.1 | 0.1 | 12.0 | 0.1 | 19.5 | 78.0 | 12.0 | 0.0 | 27.0 |
| | 7 | 3.0 | 2.9 | 3.6 | 7.3 | 0.9 | 1.0 | 0.1 | 0.8 | 14.5 | 1.0 | 3.0 | 29.0 | 4.5 | 0.5 | 0.9 |
| PTT−galactan | 1 | 0.2 | 1.7 | 0.0 | 0.0 | 2.0 | 0.1 | 3.8 | 0.1 | 9.3 | 0.1 | 2.0 | 0.4 | 0.0 | 0.0 | 20.0 |
| | 3 | 1.2 | 2.5 | 2.7 | 0.7 | 2.2 | 0.1 | 4.0 | 0.1 | 14.5 | 0.1 | 12.0 | 0.7 | 27.0 | 0.0 | 22.0 |
| | 5 | 4.3 | 2.0 | 7.1 | 4.6 | 2.2 | 0.1 | 4.1 | 0.1 | 16.9 | 0.1 | 43.0 | 0.5 | 71.0 | 0.3 | 22.0 |
| | 7 | 2.2 | 0.9 | 5.7 | 1.5 | 0.3 | 1.7 | 10.8 | 0.1 | 17.0 | 0.1 | 1.2 | 0.1 | 57.0 | 0.1 | 3.0 |
| PTT−xylan | 1 | 3.1 | 1.5 | 16.6 | 2.2 | 0.7 | 2.0 | 0.9 | 4.6 | 9.0 | 0.4 | 1.0 | 1.7 | 3.6 | 0.2 | 1.8 |
| | 3 | 3.9 | 2.4 | 1.6 | 7.0 | 3.8 | 2.9 | 0.7 | 2.4 | 11.7 | 1.0 | 1.3 | 3.4 | 0.7 | 0.6 | 3.8 |
| | 5 | 8.2 | 15.0 | 2.9 | 8.4 | 16.7 | 3.6 | 2.1 | 3.1 | 16.3 | 1.3 | 2.3 | 7.1 | 0.9 | 0.5 | 12.8 |
| | 7 | 16.5 | 3.0 | 2.5 | 3.4 | 5.4 | 6.5 | 6.6 | 4.6 | 18.5 | 5.7 | 2.5 | 0.5 | 0.5 | 0.2 | 0.9 |

[a]Percentage of blocked lysine was calculated from furosine content and total free amino groups. [b]Turbidity/browning measurement at 600 nm. [c]Reaction control ratio = percent blocked lysine/advanced reaction index. [d]Mixture containing different Maillard reaction inhibitiors: no inhibitor (N), aminoguanidine (A), cysteine (C), pyridoxamine (P), sodium bisulfite (S). [e]Experimental results are averages of triplicates and the standard deviations are less than 5%.

The analysis of hydrolysates was performed by HPLC using a Beckman HPLC system equipped with a programmable solvent module (model 126), a photodiode array detector, and 32 Karat software for data collection. The separation was performed on a Zorbax SB-C8 (4.6 × 150 mm, 5 $\mu$m) at 25 °C. The hydrolyzed sample (20 $\mu$L) was injected in triplicates. The absorbance was measured at 214 nm. A linear gradient at a flow of 0.5 mL/min was used using water/acetonitrile/formic acid (90:10:0.1, v/v/v) as solvent A and water/acetonitrile/formic acid (10:90:0.07, v/v/v) as solvent B. The elution gradient was as follows: 1−45 min, 50% B; 45−50 min, 100% B; 50−55 min, 58% B; 55−60 min, 0% B, 60−80 min, 0% B. The unhydrolyzed control was used as a standard to quantitate the unhydrolyzed PTT in the samples. Percent hydrolysis was calculated as follows:

$$\text{percent protein digestion} = 100 - (\text{peak area of unhydrolyzed PPT}/\text{peak area of the PPT control}) \times 100 \quad (2)$$

## RESULTS AND DISCUSSION

**Effects of the Inhibitors on the Progress of the Maillard Reaction.** *Changes in the Glycation Level of PTT with Galactose/Xylose in the Presence of Inhibitors.* To investigate the effects of inhibitors on the level of PTT glycation and protein cross-linking, the percent blocked lysine, the advanced reaction index, and their ratio (reaction control index) were estimated (Table 1). The Maillard reaction was conducted at 48 °C to prevent the denaturation of PTT during incubation. The results show a faster glycation reaction rate of PTT with galactose (3 to 5 days) than with xylose (3 to 7 days). Similar findings were reported by Hofmann[24] where the low glycation rate of L-alanine with pentoses was attributed to the higher degradation of pentoses as compared to hexoses, limiting their availability. In addition, higher advanced reaction index values of PTT−xylose conjugates (0.1−9.8) were obtained as compared to those of PTT−galactose conjugates (0.1−4.7). These results may be due to the formation of more reactive dicarbonyls with xylose rather than with galactose.[24] As compared to other inhibitors, the highest percent blocked lysine of PTT−galactose conjugates (21.0%) and the lowest advanced reaction index (0.1) was achieved in the presence of sodium bisulfite, while aminoguanidine inhibitor resulted in the highest percent blocked lysine of PTT−xylose conjugates (16.0%) with the lowest advanced reaction index (0.1). As compared to the reaction without inhibitor (maximum blocked lysine of 97.9%, day 3), the presence of sodium bisulfite limited both the glycation rate and the conjugation level of PTT with galactose achieving maximum percent blocked lysine of 21.0% upon 5 days of incubation. On the other hand, the aminoguanidine lowered the glycation rate of PTT with xylose, without affecting the maximum conjugation level, which was slightly higher as compared to the reaction without inhibitor (maximum blocked lysine of 13.0%, day 5). Such effect of sodium bisulfite may be attributed to its ability to trap the free-radicals and the reactive dicarbonyls formed during the reaction through its sulfite ion.[16] Conflicting results have been reported in the literature regarding the inhibitory effect of aminoguanidine at the early stage of the reaction. Edelstein and Brownlee[12] have shown that, in the presence of excess of carbohydrates, aminoguanidine had no effect on the conjugate

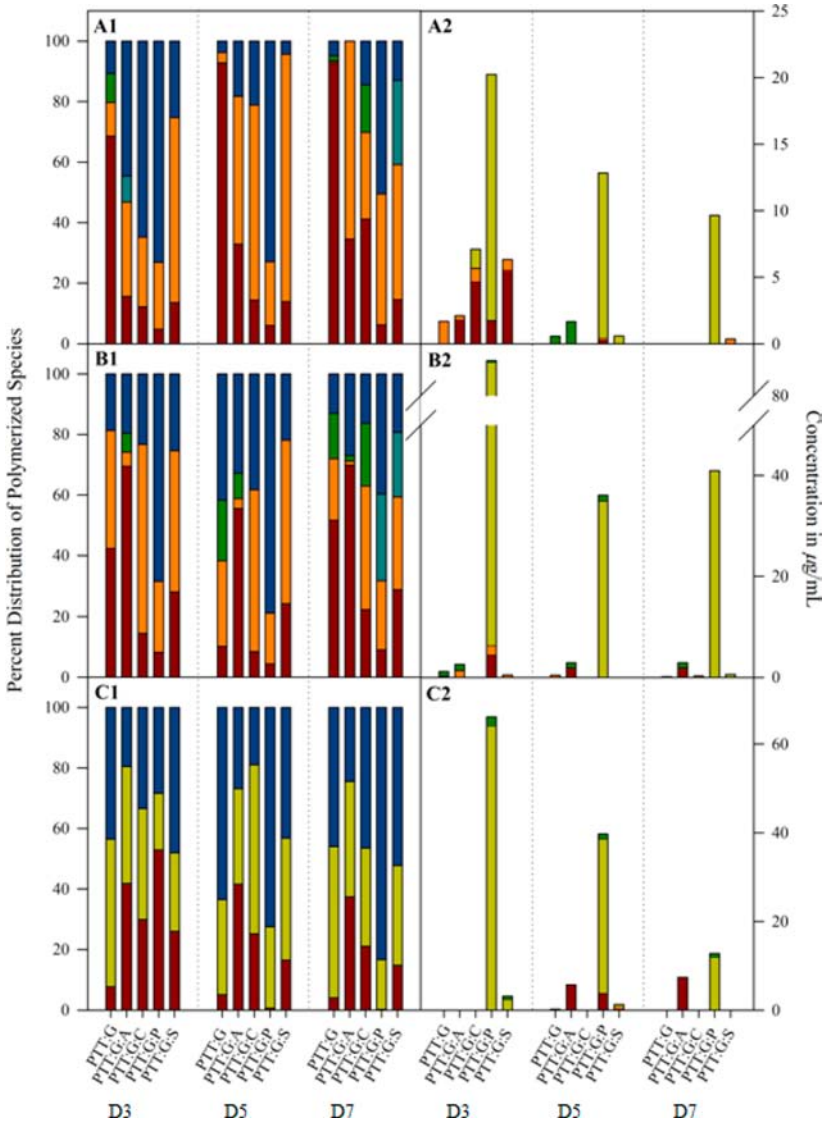


**Figure 1.** Effect of inhibitors on the degree of polymerization of proteins during the reaction between PTT and galactose (A1), GOS (B1), galactan (C1) at days 3, 5, and 7: extensive polymerization (red), degree of polymerization >10 (orange), 8−10 (yellow), 5−7 (green), 3−4 (cyan), <3 (blue). Quantitation of $\alpha$-dicarbonyls present in the incubated mixtures of PTT−galactose (A2), PTT−GOS (B2), PTT−galactan (C2) estimated by measuring quinoxalines derivatized with *o*-phenylenediamine: deoxyosone (red), glyoxal (orange), methylglyoxal (yellow), 2,3-butanedione (green). Inhibitors used: aminoguanidine, A; cysteine, C; pyridoxamine, P; sodium bisulfite, S.

formation and inhibited the Maillard reaction at the advanced stage. On the other hand, Requena et al.[25] have reported that, at concentrations of aminoguanidine similar to the concentration used in this study, the early glycation reaction of albumin with glucose was inhibited. For both PTT−galactose and PTT−xylose conjugates, pyridoxamine did not lead to any improvement in their reaction control ratio (0.0−28.0). These results may be due to the fact that the primary amino group of pyridoxamine competes with protein lysine residues for the carbonyl group of the carbohydrate as demonstrated by the important browning/aggregate formation was found (0.3−2.2, data not shown) in our controls containing only pyridoxamine and galactose/xylose.

*Changes in the Glycation Levels of PTT with XOS/GOS in the Presence of Inhibitors.* XOS (maximum blocked lysine of 11.7%, day 5) exhibited more or less the same reactivity toward the glycation of PTT as its corresponding monosaccharide, xylose (Table 1). However, GOS showed a much slower rate of glycation with the $\varepsilon$-amino groups of PTT lysine residues, reaching a maximum percent blocked lysine of 6.1% after 7 days. The lower reactivity of longer chain carbohydrates has been previously reported.[26] Furthermore, at the early stage of the reaction (1−3 days), the low percentage of blocked lysine of PTT−GOS (0.8−1.3%) and PTT−XOS (0.0−0.4%) conjugates was accompanied by high advanced reaction index (0.5−1.5); these results reveal that the high advanced reaction index values were not significantly due to the degradation of the Amadori products, but to the initial degradation of the oligosaccharides through autoxidation/glycoxidation leading to protein cross-linking.[27] As compared to GOS, the higher maximum glycation level of XOS is probably due to the high release of the degradation products that may have promoted the glycation.[28] As compared to other inhibitors, the highest percent blocked lysine of PTT−GOS conjugates and the lowest advanced reaction index (0.1) were achieved in the presence of cysteine (66.3%, 3 days). These results may be due to the

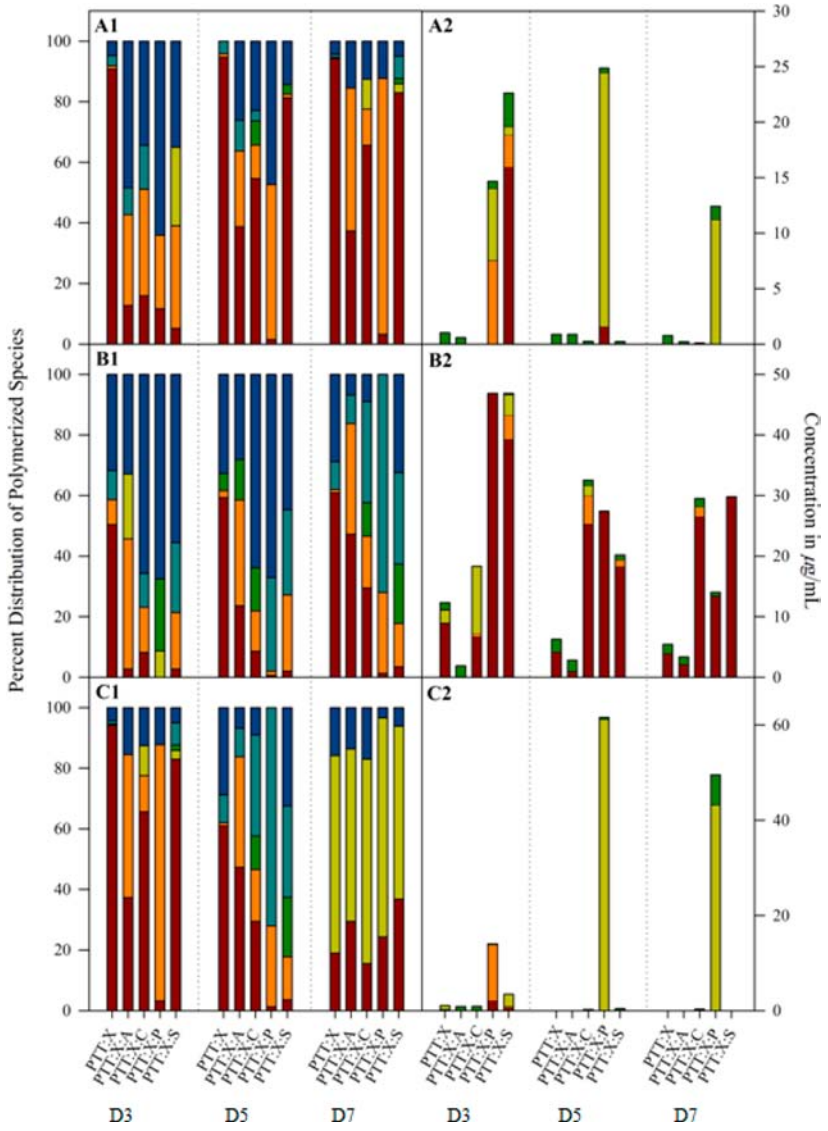


**Figure 2.** Effect of inhibitors on the degree of polymerization of proteins during the reaction between PTT and xylose (A1), XOS (B1), xylan (C1) at days 3, 5, and 7: extensive polymerization (red), degree of polymerization >10 (orange), 8−10 (yellow), 5−7 (green), 3−4 (cyan), <3 (blue). Quantitation of $\alpha$-dicarbonyls present in the incubated mixtures of PTT−xylose (A2), PTT−XOS (B2), PTT−xylan (C2) estimated by measuring quinoxalines derivatized with *o*-phenylenediamine: deoxyosone (red), glyoxal (orange), methylglyoxal (yellow), 2,3-butanedione (green). Inhibitors used: aminoguanidine, A; cysteine, C; pyridoxamine, P; sodium bisulfite, S.

reaction of cysteine with GOS leading to the accumulation of reactive species that increased the affinity of GOS toward PTT glycation binding sites. As compared to PTT−GOS conjugates, cysteine led to lower percent blocked lysine of PTT−XOS conjugates (6.9% at 3 days). This demonstrates the lower reactivity of cysteine toward XOS and its high scavenging of the reactive species generated upon XOS degradation. Aminoguanidine was the most efficient in improving the reaction control ratio of PTT−XOS conjugates (143.0), with a maximum percent blocked lysine of 14.3% at 3 days and an advanced reaction index of 0.1. The accumulation of reactive species produced as precursors at the early stage seems to be important for the initiation of Schiff base formation and hence favoring the glycation of PTT with GOS/XOS.

*Changes in the Glycation Level of PTT with Xylan/Galactan in the Presence of Inhibitors.* Similarly to their oligosaccharides counterpart, xylan (maximum blocked lysine of 16.5%, day 7) resulted in higher percent blocked lysine of PTT as compared to galactan (4.3%, day 5). As compared to PTT−galactan conjugates (0.1−1.7), the higher advanced reaction index values of PTT−xylan conjugates (2.0−6.5) demonstrate the high extent of side autoxidation/glycoxidation reactions of xylan.[24] These results may be due to the presence of arabinose, an intermediate during the autoxidation/glycoxidation of monosaccharides, on the side chains of the soluble xylan.[29−31] Contrary to the reaction with its oligosaccharide counterpart (XOS), the use of Maillard reaction inhibitors with xylan was less effective at inhibiting the formation of protein aggregates and the browning compounds at the intermediate and advanced stages. Nevertheless, the highest reaction control ratio (12.8) of PTT−xylan conjugates was obtained in the presence of sodium bisulfite with a percent blocked lysine of 16.7% (5 days). These results reveal that the use of sodium bisulfite did not inhibit the conjugation of PTT with xylan at the early stages, but slightly prevented the protein cross-linking from occurring. Similarly, Scaman et al.[17] have


dx.doi.org/10.1021/jf502497r | J. Agric. Food Chem. 2014, 62, 12235−12243

reported that the use of sodium bisulfite did not inhibit the percent glycation of lysozyme with dextran at pH 8.5 at 40 °C but prevented protein cross-linking. Similarly to PTT−GOS conjugates, the highest reaction control ratio (71.0) of PTT−galactan conjugates was achieved in the presence of cysteine after 5 days, where the highest percent blocked lysine of 7.1% and the lowest advanced reaction index of 0.1 were obtained.

**Protein Cross-Linking and Formation of Reactive Carbonyl Species in the Presence of Selected Inhibitors.** Selected reactive carbonyl species, including methylglyoxal, glyoxal, 2,3-butanedione, and deoxyosone, can lead to protein cross-linking at different rates and, as a result, to the formation of aggregates.[32] The reactive dicarbonyl compounds can be formed during the autoxidation/glycoxidation of carbohydrates and/or from the Schiff base, the initial condensation product of a reducing carbohydrate and an amino compound, via the so-called Namiki pathway under oxidative conditions.[33] In addition, the Amadori products, although fairly stable in foods with low water activity, may undergo several degradation reactions leading to the formation of dicarbonyls.[34] Some authors have identified the methylglyoxal as the important intermediate in the formation of protein cross-linking products.[4,7] Others have identified glyoxal, deoxyosone, and methylglyoxal as the key intermediates.[30] To elucidate the protein cross-linking inhibition mechanism in the presence of aminoguanidine, cysteine, pyridoxamine, or sodium bisulfite, the molecular distribution of polymerized species of PTT conjugates and the formation of dicarbonyls' *o*-phenylenediamine derivatives were investigated. The comparison of protein polymerization degree and the quantity of dicarbonyls' *o*-phenylenediamine derivatives can reveal the effectiveness of inhibitors to scavenge the reactive dicarbonyls. Mild protein aggregation of PTT occurred upon incubation at 48 °C forming dimers (59.9%) with some oligomerized species (27.2%) (data not shown). The Maillard reaction between PTT and galactose (Figure 1A1) and xylose (Figure 2A1) led to the formation of a high proportion of extensively polymerized species of 68.5 and 90.8%, respectively, at day 3. At day 3, the presence of inhibitors led to a lower proportion of extensively polymerized species of PTT−galactose/xylose conjugates (4.7−16.0%) and to a higher proportion of its mono/dimer (34.4−73.1%). As compared to other inhibitors, the cross-linking of PTT−galactose/xylose conjugates in the presence of pyridoxamine exhibited the lowest rate, which can be attributed to the low amount of percent blocked lysine. The effectiveness of pyridoxamine as an inhibitor of protein cross-linking occurring during the Maillard reaction has already been demonstrated by Corzo-Martinez et al.,[1] where they have observed lower poly oligomer formation within the reaction between $\beta$-lactoglobulin and galactose/tagatose in the presence of pyridoxamine.

The only $\alpha$-dicarbonyls formed in the reaction with galactose (Figure 1A2) or xylose (Figure 2A2) without inhibitor was glyoxal (1.7 $\mu$g/mL) and butanedione (1.1 $\mu$g/mL), respectively. Glyoxal was found to be formed during the degradation of monosaccharide by retroaldol condensation reactions activated by deprotonation of the 2- or 3-hydroxy groups,[32] which supports the higher amount of glyoxal found in galactose reactions. Butanedione is a well-known sugar fragmentation product, which could arise from xylose fragmentation.[35] The major dicarbonyl formed in the presence of aminoguanidine, cysteine, and sodium bisulfite was deoxyosone for the reactions with galactose, and butanedione and deoxyosone for the reactions with xylose. As compared to methylglyoxal and glyoxal, the lower reactivity of deoxyosone and butanedione[4,7] toward Maillard reaction inhibitors and toward the lysine/arginine residues of the protein may explain the accumulation of these dicarbonyls. The reaction between PTT and galactose/xylose in the presence of pyridoxamine led to more methyglyoxal formation. From our results, it seems possible that pyridoxamine only reacted with one of the two carbonyl groups of methylglyoxal leaving the other carbonyl group available to react with the lysine residues found on the protein preventing its cross-linking. The decrease in lysine residues and pyridoxamine led to the accumulation of unreacted methylglyoxal in the system (Scheme 1, adapted from Miller et al.,[7]). The inhibitors identified previously (Table 1), sodium bisulfite for galactose (day 5) and aminoguanidine for xylose (day 7), which led to the highest reaction control ratios, resulted in the release of low amounts of total unreacted dicarbonyls (0.6 and 0.2 $\mu$g/mL, respectively) and in lower proportions of extensive polymerized species (13.9 and 37.3%, respectively) as compared to the reaction without inhibitor, demonstrating the efficiency of these inhibitors to modulate the reaction progress.

**Scheme 1. Possible Reaction Pathway for Methylglyoxal's Reaction with Lysine Residues on PTT in the Presence of Pyridoxamine**[a]

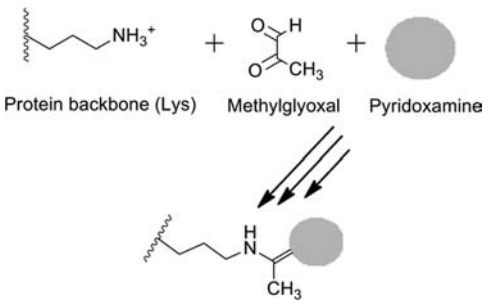


[a]Adapted with permission from Miller et al.[7] Copyright 2003, Elsevier B.V.

The reaction between PTT and GOS or XOS (Figure 1B1, 2B1) without inhibitor led to higher formation of oligomerized species (18.7 and 41.3%; < 3, 3−4, 5−7) at day 3 as compared to their monosaccharide counterparts (galactose and xylose). In the PTT−GOS/XOS reaction systems, all investigated inhibitors limited the rate of protein cross-linking over 7 days of reaction time, with the exception of aminoguanidine. Similarly to the reaction of PTT with galactose/xylose, the most effective inhibitor for the prevention of protein cross-linking during the reaction of PTT with GOS and XOS was pyridoxamine, leading to only 9.0 and 1.3% of extensively cross-linked polymers, respectively, after 7 days of incubation. The best identified inhibitors, leading to the highest reaction control ratio for PTT−GOS (cysteine, day 3) and PTT−XOS (aminoguanidine, day 5) (Table 1) systems resulted in low amounts of total unreacted dicarbonyls (0.0 and 2.8 $\mu$g/mL) and in lower proportions of extensive polymerized species (14.4 and 23.6%) as compared to the reaction without inhibitor (1.1−6.3 $\mu$g/mL; 42.4−59.3%).

PTT−xylan reaction system without inhibitor (Figure 2C1) exhibited a higher proportion of extensively polymerized species (94.2%) than in the presence of inhibitors (3.2−82.9%) after 3 days of incubation. In contrast, PTT−galactan reaction system (Figure 1C1) showed a lower proportion of

extensively polymerized species (7.7%) than in the presence of inhibitors (26.0−52.9%). However, the decrease in the proportion of extensively polymerized species of PTT−xylan with an increase in incubation time reveals the noncovalent interactions of these species. Indeed, the decrease in the hydrophobicity of PTT upon glycation may have decreased its affinity to interact with xylan and to form large noncovalent complexes (Figure 2C1) through low energy interactions, such as hydrogen bonding and hydrophobic bonding.[36] The lower protein cross-linking observed with galactan may be attributed to its ability to depress the protein polymerization associated with the advanced Maillard reaction.[8] However, as compared to the system without inhibitor, the higher proportion of extensively polymerized species observed at day 3 in the PTT−galactan reaction system containing aminoguanidine (41.8%) or pyridoxamine (52.9%) could be due to the higher reactivity of galactan toward these inhibitors. Methylglyoxal (34.9−41.0 μg/mL) was identified as the main unreacted dicarbonyl with galactan/xylan (Figures 1C2 and 2C2) in the presence of pyridoxamine as with their monosaccharide counterparts (Figures 1A2 and 2A2), except for the reaction with xylan at day 3 of incubation. The best identified inhibitors, leading to the highest reaction control ratio, for PTT−galactan (cysteine, day 5) and PTT−xylan (sodium bisulfite, day 5) (Table 1) systems resulted in lower amounts of total unreacted dicarbonyls (0.0 μg/mL) for the galactan reaction system and in lower proportions of extensive polymerized species (3.5%) for the xylan reaction system as compared to the reaction without inhibitor (0.0−0.2 μg/mL; 5.1−60.9%).

**Particle Size and Digestibility of the Conjugates Produced Using Selected Inhibitors.** Cysteine and aminoguanidine were identified as the best inhibitors for galactose-type or xylose-type PTT conjugates, respectively, favoring high glycation levels and limiting protein cross-linking to a certain extent during the advanced stages of the Maillard reaction. Although pyridoxamine was the most efficient in inhibiting protein cross-linking, it exhibited an inhibition effect on the PTT conjugation by limiting or delaying the formation of Amadori product (Table 1). PTT conjugates were produced using the identified inhibitors and their particle size distribution and digestibility were investigated (Figure 3). These conjugates produced with or without inhibitor were compared to the native PTT on the basis of their relative percent digestibility and their increase in average particle size per 5.0% blocked lysine to normalize the effect of the different levels of glycation on these parameters. The average particle size and the total digestibility of the incubated PTT controls were 321.3−347.2 nm and 59.6−60.2%, respectively (data not shown). PTT−galactose conjugates showed more or less similar increase in the particle size of their aggregates, per 5.0% blocked lysine, in the presence (44.0 nm) or in the absence (45.9 nm) of cysteine inhibitor. In contrast, a significantly smaller increase in the particle size distribution of PTT−xylose conjugates, per 5.0% blocked lysine, was obtained in the presence of aminoguanidine (16.3 nm) as compared to without inhibitor (2640.6 nm). Due to the higher cross-linking level of PTT−xylose conjugates produced without inhibitor, their relative digestibility (43.1%) was lower than that of PTT−galactose (94.8%). However, the use of cysteine and aminoguanidine as inhibitors resulted in an increase in the relative digestibility of PTT−galactose and PTT−xylose conjugates by 0.4 and 8.2%, respectively, as compared to without inhibitor. The relative digestibility of PTT−xylose conjugates was nonconcomitantly increased, upon

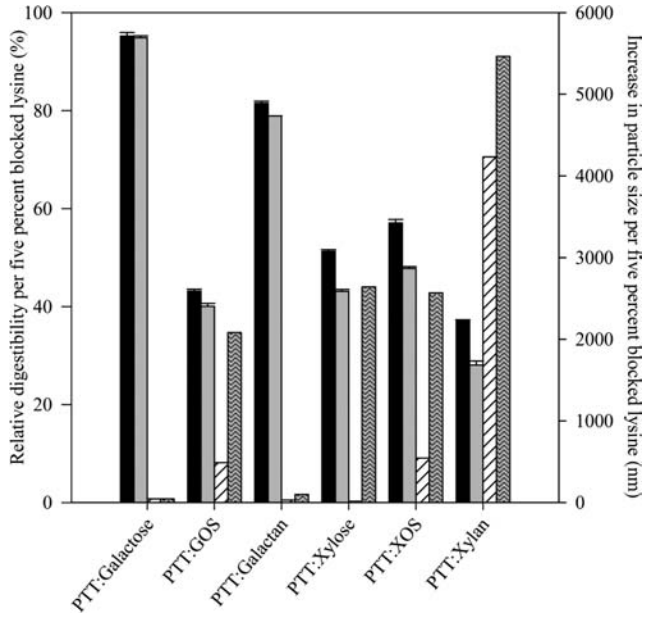


**Figure 3.** Relative digestibility and the increase in particle size, per 5% blocked lysine, of the PTT−galactose/GOS/galactan:cysteine incubated mixtures and of the PTT−xylose/XOS/xylan:aminoguanidine incubated mixtures compared to the reaction mixture without inhibitors: digestibility with (black) and without inhibitors (gray), and the particle size with (white diagonal stripes) and without inhibitors (gray zigzag stripes). The error bars represent the standard deviations of triplicate measurements. The particle size is an average of 70 measurements and the polydispersity index of each sample was ≤0.5.

the use of aminoguanidine, as compared to the large decrease of their particle size demonstrating that the large particle size of PTT−xylose conjugates produced without inhibitor was largely due to their noncovalent aggregation. The results also show the high increase of the average particle size, per 5.0% blocked lysine, of PTT−GOS conjugates (2080.8 nm) produced without inhibitor. As expected, the use of cysteine dropped the increase in the average particle size of PTT−GOS conjugates to 487.3 nm. The increase in average particle size of PTT−XOS conjugates, per 5.0% blocked lysine, produced with and without aminoguanidine was 544.0 and 2567.3 nm, respectively. As a result of the lower level of protein cross-linking, PTT−GOS and PTT−XOS conjugates produced in the presence of the inhibitors showed 3.1 and 9.3% increases in their percent digestion, respectively. The experimental findings also show that PTT−galactan conjugates produced in the presence of cysteine (29.9 nm) had a smaller increase in the average particle size of its aggregates, per 5.0% blocked lysine, than without cysteine (100.2 nm). Contrary to PTT−galactan conjugates, the average particle size of PTT−xylan conjugate aggregates increased significantly (5,463.4 nm) per 5.0% blocked lysine, and the use of aminoguanidine as inhibitor limited slightly this increase to 4,231.6 nm. The use of cysteine or aminoguanidine as inhibitors for the production of PTT−xylan or PTT−galactan conjugates led to 2.6 and 9.0% increase in the percent digestion. These increases are in good agreement with the decrease in the particle size of the conjugate aggregates. To the best of our knowledge, this is the first study where the effect of Maillard reaction inhibitors on the improvement of digestibility of protein−carbohydrate conjugates has been investigated.

**Conclusion.** The effect of selected Maillard reaction inhibitors on the production of PTT−carbohydrate conjugates was investigated. Sodium bisulfite (galactose, xylan), aminoguanidine (xylose, xylooligosaccharides), and cysteine (GOS, galactan) were the inhibitors that led to the highest glycation level of the conjugates. These glycation levels were mostly similar or even higher than those of the conjugates produced without inhibitors. The use of these inhibitors led to lower proportions of extensive polymerized species or to lower amounts of total unreacted dicarbonyls. By using cysteine for the production of PTT−galactose/GOS/galactan conjugates, and by using aminoguanidine for the production of PTT−xylose/XOS/xylan conjugates, the particle size distribution of the conjugates was lowered and the digestibility of the conjugates was improved. The use of the Maillard reaction inhibitors to limit the protein cross-linking, associated with the intermediate and advanced stages, will allow the production of protein−carbohydrate conjugates with improved properties as potential functional ingredients.

## AUTHOR INFORMATION

### Corresponding Author

*Tel.: +1-514-398-8666. Fax: +1-514-398-7977. E-mail: salwa.karboune@mcgill.ca.

### Notes

The authors declare no competing financial interest.

## ACKNOWLEDGMENTS

We gratefully acknowledge Solanic (Avebe) for providing us with the potato proteins. This research is supported by funds from The Natural Sciences and Engineering Research Council (NSERC) of Canada. Financial infrastructure support from the Canada Foundation for Innovation (CFI) is grateful acknowledged.

## ABBREVIATIONS USED

CV, column volume; GOS, galactooligosaccharides; PTT, patatin; XOS, xylooligosaccharides

## REFERENCES

(1) Corzo-Martínez, M.; Moreno, F. J.; Olano, A.; Villamiel, M. Role of pyridoxamine in the formation of the Amadori/Heyns compounds and aggregates during the glycation of β-lactoglobulin with galactose and tagatose. *J. Agric. Food Chem.* **2010**, *58*, 500−6.

(2) Huang, M.; Liu, P.; Song, S.; Zhang, X.; Hayat, K.; Xia, S.; Jia, C.; Gu, F. Contribution of sulfur-containing compounds to the color-inhibiting effect and improved antioxidant activity of Maillard reaction products of soybean protein hydrolysates. *J. Sci. Food Agric.* **2011**, *91*, 710−20.

(3) Mauron, J. Influence of processing on protein quality. *J. Nutr. Sci. Vitaminol.* **1990**, *36*, S57−69.

(4) Meade, S. J.; Miller, A. G.; Gerrard, J. A. The role of dicarbonyl compounds in non-enzymatic crosslinking: A structure−activity study. *Bioorg. Med. Chem.* **2003**, *11*, 853−62.

(5) Nagaraj, R. H.; Shipanova, I.; Faust, F. M. Protein cross-linking by the Maillard reaction. Isolation, characterization, and in vivo detection of a lysine−lysine cross-link derived from methylglyoxal. *J. Biol. Chem.* **1996**, *271*, 19338−45.

(6) Degenhardt, T. P.; Thorpe, S. R.; Baynes, J. W. Chemical modification of proteins by methylglyoxal. *Cell. Mol. Biol.* **1998**, *44*, 1139−45.

(7) Miller, A. G.; Meade, S. J.; Gerrard, J. A. New insights into protein crosslinking via the Maillard reaction: Structural requirements, the effect on enzyme function, and predicted efficacy of crosslinking inhibitors as anti-ageing therapeutics. *Bioorg. Med. Chem.* **2003**, *11*, 843−52.

(8) Seo, S.; Karboune, S.; L'Hocine, L.; Yaylayan, V. Characterization of glycated lysozyme with galactose, galactooligosaccharides, and galactan: Effect of glycation on structural and functional properties of conjugates. *LWT—Food Sci. Technol.* **2013**, *53*, 44−53.

(9) Seo, S.; Karboune, S.; Yaylayan, V. A.; L'Hocine, L. Glycation of lysozyme with galactose, galactooligosaccharides, and potato galactan through the Maillard reaction and optimization of the production of prebiotic glycoproteins. *Process Biochem.* **2012**, *47*, 297−304.

(10) Oliver, C. M.; Melton, L. D.; Stanley, R. A. Creating proteins with novel functionality via the Maillard reaction: A review. *Crit. Rev. Food Sci. Nutr.* **2006**, *46*, 337−350.

(11) Thornalley, P. J.; Yurek-George, A.; Argirov, O. K. Kinetics and mechanism of the reaction of aminoguanidine with the α-oxoaldehydes glyoxal, methylglyoxal, and 3-deoxyglucosone under physiological conditions. *Biochem. Pharmacol.* **2000**, *60*, 55−65.

(12) Edelstein, D.; Brownlee, M. Mechanistic studies of advanced glycosylation end product inhibition by aminoguanidine. *Diabetes* **1992**, *41*, 26−9.

(13) Huang, M. G.; Zhang, X. M.; Eric, K.; Abbas, S.; Hayat, K.; Liu, P.; Xia, S. Q.; Jia, C. S. Inhibiting the color formation by gradient temperature-elevating Maillard reaction of soybean peptide−xylose system based on interaction of L-cysteine and Amadori compounds. *J. Pept. Sci.* **2012**, *18*, 342−9.

(14) Adrover, M.; Vilanova, B.; Frau, J.; Muñoz, F.; Donoso, J. The pyridoxamine action on Amadori compounds: A reexamination of its scavenging capacity and chelating effect. *Bioorg. Med. Chem.* **2008**, *16*, 5557−69.

(15) Booth, A. A.; Khalifah, R. G.; Todd, P.; Hudson, B. G. In vitro kinetic studies of formation of antigenic advanced glycation end products (AGEs). Novel inhibition of post-Amadori glycation pathways. *J. Biol. Chem.* **1997**, *272*, 5430−7.

(16) Friedman, M.; Molnar-Perl, I. Inhibition of browning by sulfur amino acids. 1. Heated amino acid-glucose systems. *J. Agric. Food Chem.* **1990**, *38*, 1642−7.

(17) Scaman, C.; Nakai, S.; Aminlari, M. Effect of pH, temperature, and sodium bisulfite or cysteine on the level of Maillard-based conjugation of lysozyme with dextran, galactomannan, and mannan. *Food Chem.* **2006**, *99*, 368−80.

(18) Anderson, C.; Pinsirodom, P.; Parkin, K. L. Hydrolytic selectivity of patatin (lipid acyl hydrolase) from potato (*Solanum tuberosum* L.) tubers toward various lipids. *J. Food Biochem.* **2002**, *26*, 63−74.

(19) Sun, Y.; Jiang, L.; Wei, D. Partial characterization, in vitro antioxidant and antiproliferative activities of patatin purified from potato fruit juice. *Food Funct.* **2013**, *4*, 1502−11.

(20) Seo, S.; L'Hocine, L.; Karboune, S. Allergenicity of potato proteins and of their conjugates with galactose, galactooligosaccharides, and galactan in native, heated, and digested forms. *J. Agric. Food Chem.* **2014**, *62*, 3591−3598.

(21) Krause, R.; Knoll, K.; Henle, T. Studies on the formation of furosine and pyridosine during acid hydrolysis of different Amadori products. *Eur. Food Res. Technol.* **2003**, *216*, 277−83.

(22) Marceau, E.; Yaylayan, A. V. Profiling of α-dicarbonyl content of commercial honeys from different botanical origins: Identification of 3,4-dideoxyglucoson-3-ene (3,4-DGE) and related compounds. *J. Agric. Food Chem.* **2009**, *57*, 10837−44.

(23) Moreno, F. J.; Quintanilla-Lopez, J. E.; Lebron-Aguilar, R.; Olano, A.; Sanz, M. L. Mass spectrometric characterization of glycated β-lactoglobulin peptides derived from galacto-oligosaccharides surviving the in vitro gastrointestinal digestion. *J. Am. Soc. Mass Spectrom.* **2008**, *19*, 927−37.

(24) Hofmann, T. Quantitative studies on the role of browning precursors in the Maillard reaction of pentoses and hexoses with L-alanine. *Eur. Food Res. Technol.* **1999**, *209*, 113−21.

(25) Requena, J. R.; Vidal, P.; Cabezas-Cerrato, J. Aminoguanidine inhibits protein browning without extensive Amadori carbonyl blocking. *Diabetes Res. Clin. Pract.* **1993**, *19*, 23−30.

(26) Corzo-Martínez, M.; Moreno, F. J.; Villamiel, M.; Harte, F. M. Characterization and improvement of rheological properties of sodium caseinate glycated with galactose, lactose, and dextran. *Food Hydrocolloids* **2010**, *24*, 88−97.
(27) Hollnagel, A.; Kroh, L. W. Degradation of oligosaccharides in nonenzymatic browning by formation of α-dicarbonyl compounds via a "Peeling off" mechanism. *J. Agric. Food Chem.* **2000**, *48*, 6219−26.
(28) Yeboah, F. K.; Alli, I.; Yaylayan, V. A.; Konishi, Y.; Stefanowicz, P. Monitoring glycation of lysozyme by electrospray ionization mass spectrometry. *J. Agric. Food Chem.* **2000**, *48*, 2766−74.
(29) Teleman, A.; Tenkanen, M.; Jacobs, A.; Dahlman, O. Characterization of *O*-acetyl-(4-*O*-methylglucurono)xylan isolated from birch and beech. *Carbohydr. Res.* **2002**, *337*, 373−7.
(30) Usui, T.; Yanagisawa, S.; Ohguchi, M.; Yoshino, M.; Kawabata, R.; Kishimoto, J.; Arai, Y.; Aida, K.; Watanabe, H.; Hayase, F. Identification and determination of α-dicarbonyl compounds formed in the degradation of sugars. *Biosci. Biotechnol. Biochem.* **2007**, *71*, 2465−72.
(31) Wells-Knecht, K. J.; Zyzak, D. V.; Litchfield, J. E.; Thorpe, S. R.; Baynes, J. W. Mechanism of autoxidative glycosylation: Identification of glyoxal and arabinose as intermediates in the autoxidative modification of proteins by glucose. *Biochem.* **1995**, *34*, 3702−9.
(32) Thornalley, P. J.; Langborg, A.; Minhas, H. S. Formation of glyoxal, methylglyoxal, and 8-deoxyglucosone in the glycation of proteins by glucose. *Biochem. J.* **1999**, *344*, 109−16.
(33) Hayashi, T.; Namiki, M. Formation of two-carbon sugar fragment at an early stage of the browning reaction of sugar with amine. *Agr. Biol. Chem. Tokyo* **1980**, *44*, 2575−80.
(34) Henle, T. Protein-bound advanced glycation endproducts (AGEs) as bioactive amino acid derivatives in foods. *Amino Acids* **2005**, *29*, 313−22.
(35) Ames, J. M.; Apriyantono, A. Volatile reaction products from a heated xylose−lysine model system. *Food Chem.* **1993**, *48*, 271−7.
(36) Turgeon, S. L.; Schmitt, C.; Sanchez, C. Protein−polysaccharide complexes and coarcervates. *Curr. Opin. Colloid Interface Sci.* **2007**, *12*, 166−78.

Chemicals were purchased from Merck (Darmstadt, Germany) or Sigma-Aldrich (St. Louis, MO, USA), unless otherwise specified. Fruit bodies of *G. tsugae* were washed, wiped by a paper towel, and then cut into small piece. Deionized water was added (500 mL per 7.5 g of dry solid). The mixture was crumbled for 5 min by a Waring blender (Blender 7012S, Waring Commercial, Stamford, CT, USA) and then was pulverized by using a high-speed blender (Polytron PT 3000, Kinematica AG, Switzerland) at 12000 rpm for 5 min. The resulting material was designated the blended suspension.

**Proximate Composition.** Small pieces of *G. tsugae* were used for composition analysis. The contents of moisture, ash, crude fat, and crude protein were determined, according to the methods of the Association of Official Analytical Chemists (AOAC).[21] Moisture and dry matter were presented on the basis of wet weight; others were reported on a dry weight basis.

**Hot-Water Extraction.** The blended suspension was placed in a hot water bath at 99 °C for extraction of 3 h. Then, the suspension was cooled and filtered through Whatman no. 1 filter paper. The filtrate was collected and designated the hot-water extract. Micro-organisms were removed by filtration using a 0.45 μm membrane for cell cultures. The filtrate was designated the S-extract.

**Media Milling.** A two-step milling was employed to prepare nano/submicrometer *G. tsugae* suspension using a media mill (MiniPur, NETZCH-Feinmahltechnik GmbH, Germany) with a driving motor of 0.94 kW. Media (yttria-stabilized tetragonal zirconia, YTZ) of 0.8 or 0.3 mm were loaded in the milling chamber (200 mL) at 70% v/v filling ratio. The blended suspension was placed into a jacket-cooling tank and then fed at a flow rate of 220 mL/min into the milling chamber by a circulation pump. During milling, particles smaller than the gap of the media separator were brought out into the stirred tank for cooling by the circulation system. The temperature of the suspension was thus maintained below 35 °C during milling. The milling was conducted with 0.8 mm media for 1 h with an agitation speed of 2700 rpm, and then 0.3 mm media were employed for 2 h with an agitation speed of 3000 rpm. Total milling time was 3 h. Samples, designated the milled suspension, were taken at 0, 1, 2, and 3 h for particle size distribution measurement and SEM observation.

Large particles and aggregated clusters in 3 h milled suspension were removed by centrifuge (4 °C, 10000*g*, 10 min) (Rotina 35R Hettich Zentrifugen, Tuttlingen, Germany). The supernatant, designated the nano/submicrometer *G. tsugae*, was collected for determining particle size distribution and further studies. The nano/submicrometer *G. tsugae* was filtered through a 0.45 μm membrane for removing micro-organisms. The filtrate was designated the S-supernatant.

**Particle Size Analysis.** The particle size distributions were determined by using a static laser diffraction particle size analyzer (LS230, Beckman Coulter, Brea, CA, USA) with a detection range of 0.04−2000 μm. The instrument was calibrated with deionized water. All samples were pretreated by violently shaking (1 min in a Vortex-Genie 2, Scientific Industries, Inc., Bohemia, NY, USA) and degassed by ultrasound. Average diameters of particles were obtained using the equations

$$\text{by volume,}\quad D_V = \sum_i \frac{n_i d_i^4}{n_i d_i^3}$$

$$\text{by number,}\quad D_N = \sum_i \frac{n_i d_i}{n_i}$$

where $n_i$ is the number of $i$ particles with diameter of $d_i$. All of the measurements were done in triplicate, and the average data were reported.

**Morphology.** The morphology of suspended particles in *G. tsugae* samples was examined by scanning electron microscope (SEM) (Hitachi S-800, Hitachi Co. Ltd., Tokyo, Japan). Critical-point drying was employed to prepare samples for SEM. Sample (3 mL) was mixed with 27 mL of 75% ethanol and evaporated to 3 mL at 60 mmHg. Two more replacement processes were conducted by using 95% ethanol. After a final replacement using 99% ethanol, solids were suspended in 3 mL of 99% ethanol. The suspensions were further dried using liquid $CO_2$ in a critical-point drying apparatus (Hitachi HCP-2, Hitachi Co. Ltd., Tokyo, Japan) at 31.1 °C and 73.9 bar. After being dried, the sample was attached on an SEM stub using double-backed cellophane tape. The stub and sample were coated with gold−palladium and then were examined and photographed at 10 kV.

**Total Carbohydrate Content.** The method of phenol−sulfuric acid reaction[22] was used to determine the total carbohydrate content. Sample (0.2 mL) was mixed with 0.2 mL of 5% phenol in a test tube. Subsequently, 1 mL of concentrated sulfuric acid was added rapidly to the mixture. After allowing the test tubes to stand for 10 min, they were vortexed for 30 s and placed for 20 min in a water bath at 25 °C for color development. Then, optical density at 490 nm was recorded on a spectrophotometer. The content of glucose was determined against a standard curve. Glucose solutions with concentrations from 0 to 100 μg/mL were employed as the standard.

**Protein Content.** The protein content was determined by following the method of Bradford.[23] A protein assay kit was purchased from Bio-Rad (Hercules, CA, USA). The protein solution (20 μL), containing 0.05−0.5 mg protein, was pipetted into each well of 96-well plates. The reagent (dye) was diluted by deionized water at 5 times of volume. The diluted dye (200 μL) was pipetted into each sample well, mixed, and reacted at 25 °C for 5 min. The optical density at 595 nm was determined by an ELISA reader (iMark microplate and Microplate Manager 6 software, Bio-Rad). The standard curve was established by using bovine serum albumin (BSA) solutions at different concentrations.

**Content of (1→3)-β-D-Glucan.** Aniline blue assay[24] was employed to determine the content of (1→3)-β-D-glucan. Sample was mixed with 1 N NaOH (1:1 by volume) and stirred at 25 °C for at least 30 min for complete dissolution of polysaccharides The pH of the mixture was adjusted to 11.5 ± 0.1 by adding 1 N HCl, and the volume was then made up to 10 mL by using $Na_2HPO_4$−NaOH buffer (pH 11.5 and containing 0.5 M NaCl). Sample aliquot (2 mL) was reacted with 0.2 mL of 0.1% (w/v) aniline blue (Ferak, Berlin, Germany) for 2 h at 25 °C. The fluorescence intensity was read by a fluorescence spectrophotometer (Hitachi F4500, Tokyo, Japan). The excitation and emission wavelengths of the fluorescence spectrophotometer were set at 395 and 495 nm, respectively. A standard curve was established by using laminarin at concentrations from 0 to 50 μg/mL. The branching of 1→3-β-D-glucan was not determined in this study.

**Mutagenicity Assay.** By following the method of Mortelmans and Zeiger[18] with slight modification, the Ames test was conducted with five *Salmonella* Typhimurium tester strains of TA98, TA100, TA102, TA1535, and TA1537, with or without S9 mix. For each tester strain, a specific positive control was always used to test. Without S9 mix, 4NQO was used as a positive control for TA98, SA was used for TA100 and TA1537, MMC was used for TA102, and 9AA was used for TA1537; benzo[*a*]pyrene (B[a]p) (for TA98) and 2-aminoanthracene (2AA) (for others) were used as positive controls with metabolic activation.

We added 500 μL of S9 mix (or 500 μL of phosphate buffer), 100 μL of test solution at designated concentration, and 100 μL of cell suspension from an overnight culture together. The mixtures were incubated at 37 °C for 20 min with shaking at 100 rpm. The admixtures were diluted using 2 mL of molten top agar and then poured on minimum salts agar. Plates were incubated at 37 °C for 48 h, and the revertant bacterial colonies on each plate were counted. Positive controls and negative controls (distilled water) were maintained concurrently. Three independent assays were performed for statistical analysis. A positive response for mutagenicity was defined as a reproducible 2-fold increase in revertant number with dose−response relationship.[25,26]

**Primary Cell Viability.** Male BALB/c mice were purchased from the National Laboratory Animal Center of Ministry of Science and Technology (Taipei, Taiwan) and domesticated in an air-conditioned room at 23 ± 2 °C with a relative humidity of 40−60% and a 12 h interval light/dark cycle. The organ tissues, including stomach, intestines, colon, liver, and kidney of mice, were collected after

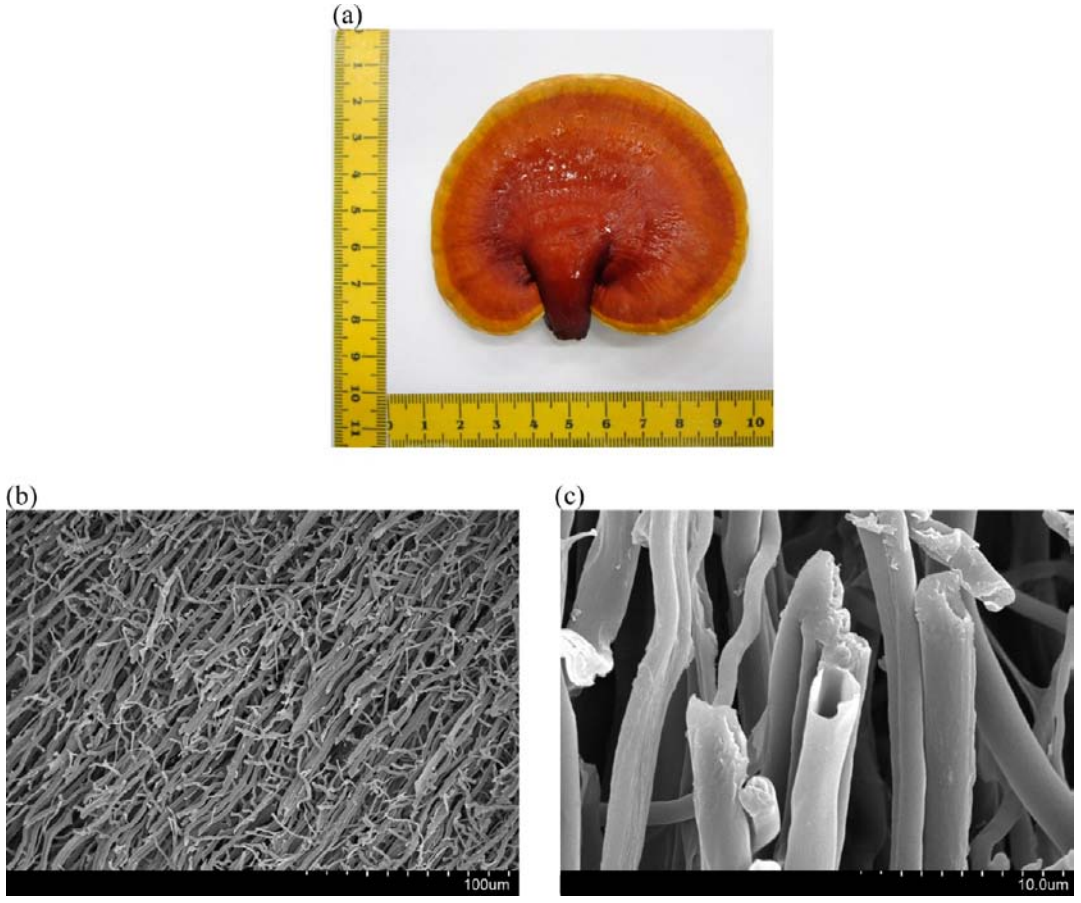


**Figure 1.** (a) Fruit body, (b) hyphae, and (c) enlargement of hyphae of *G. tsugae*.

euthanization. Cell suspensions were prepared according to the method of Park et al.[27] with slight modification. Organ tissues were moistened with RPMI 1640 medium (BI, Biological Industries, Kibbutz Beit Haemek, Israel) containing 10% fetal bovine serum (FBS, BI) and were smashed through a 70 $\mu$m screen filter (BD) in RPMI 1640 medium. Cells were collected, and red blood cells were removed by treatment with a hypotonic solution (8.29 g of $NH_4Cl$, 37.2 mg of $Na_2EDTA$, and 1.0 g of $KHCO_3$). After being washed twice in RPMI 1640 medium, the cells were resuspended in RPMI 1640 with 10% heat-inactivated FBS. Cell suspension was added into the trypan blue on plate to count cell numbers by microscope, and then the cell suspension was adjusted to contain $4 \times 10^5$ cells/mL for MTT assay.

An MTT colorimetric assay[28] with slight modification was employed to determine cell viability. The cell suspensions ($2 \times 10^4$ cells/well) in RPMI 1640 medium supplemented with 10% FBS were treated with *G. tsugae* samples (S-extract or S-supernatant at 0−500 $\mu$g/mL) in a 96-well plate. The control group was treated with an equivalent volume of sterilized deionized water. The 96-well plates were then placed in an incubator (5% $CO_2$, 37 °C) for 24, 48, and 72 h. Then, 25 $\mu$L of 3-[4,5-dimethylthiazol-2-yl]-2,5-diphenyltetrazolium bromide (MTT) (2 mg/mL) was added to each well and incubated for 3 h. After incubation, 50 $\mu$L of DMSO was added to each well, and the optical density at 570 nm was measured by an ELISA reader.

**Statistical Analysis.** Data were reported as the mean of measurements in triplicate. One-way analysis of variance (ANOVA) was used to determine the significance of treatment using the Statistical Analysis System (SAS version 9.1; SAS Institute Inc., Cary, NC, USA), followed by a Duncan's new multiple-range test. Differences were considered as statistically significant when the $P$ value was <0.05.

## RESULTS AND DISCUSSION

**Morphology and Particle Size Distribution.** The appearance of the fresh fruit body of *G. tsugae* is illustrated in Figure 1a, which was similar to the report of Wang et al.[29] Both the contents of ash and crude fat were lower than 2% (dry basis). Crude protein (14.5%) and carbohydrate (81.8%) were two major components. It was woody and rigid even with a water content of 73.9% due to the compounded structure of hyphae (Figure 1b), which appeared to be a hollow tube (Figure 1c). Cao and Yuan[30] have observed hyphae similar to a tube by using a light microscope. This confirmed the microstructure of hyphae by using SEM. Most hyphae had a diameter of about 3 $\mu$m with a few smaller than 0.9 $\mu$m, which could be recognized as natural nanotubes.

Particle size distributions of samples after the treatments are illustrated in Figure 2. The size (in volume) of blended *G. tsugae* ranged from 1.75 to 905 $\mu$m with a volume-mean diameter of 248.50 ± 2.12 $\mu$m (Figure 2a and Table 1). The size distribution was quite wide with multiple peaks. Nevertheless, the size distribution became monomodal in terms of number (Figure 2b) with a range of 1.45−23.8 $\mu$m and a number-mean diameter of 3.38 ± 0.03 $\mu$m (Table 1). The data showed that all of the particles were in micrometer scale. After 3 h of media milling, the largest particle was reduced from 905 to 23.8 $\mu$m (in volume) (Figure 2c). In addition, there existed about 22% of particles smaller than 1 $\mu$m. When counted by number, all of the particles were smaller than 1 $\mu$m with a number-mean diameter of 0.11 $\mu$m (Figure 2d and Table 1). There were about 62% of particles smaller than 0.1 $\mu$m. The

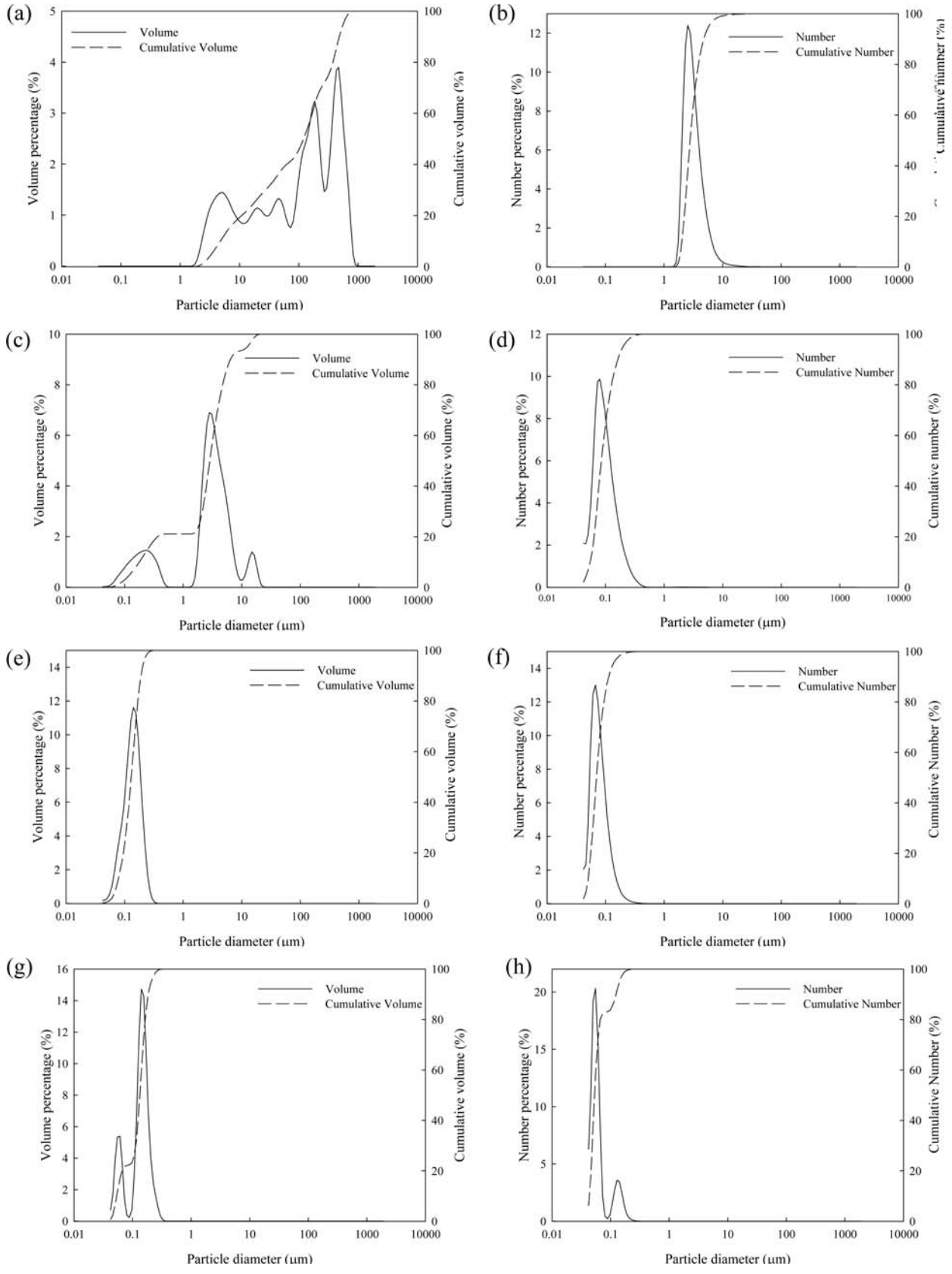


**Figure 2.** continued


dx.doi.org/10.1021/jf503898y | *J. Agric. Food Chem.* 2014, 62, 12244−12255

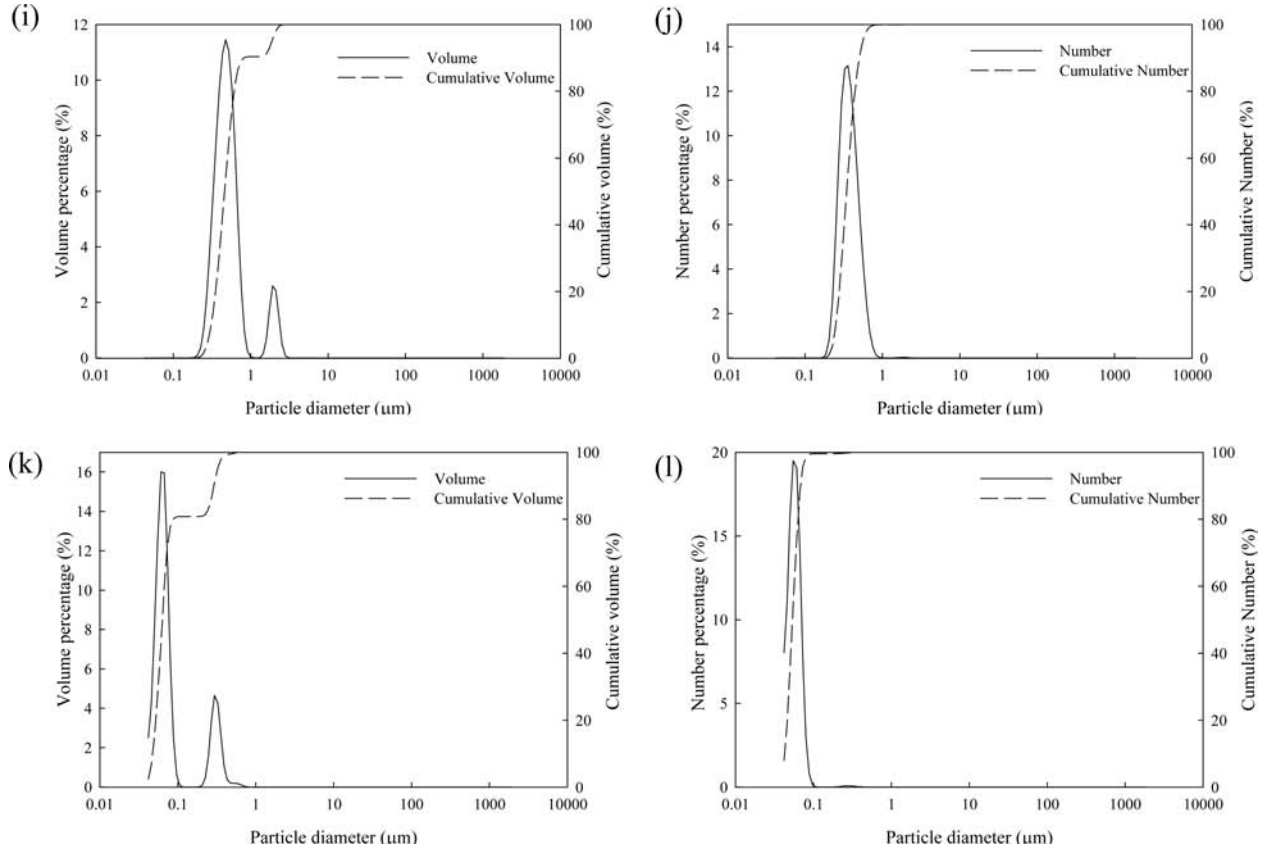


**Figure 2.** Particle size distribution of blended *G. tsugae* in (a) volume and (b) number, 3 h media-milled *G. tsugae* in (c) volume and (d) number, supernatant of centrifuged media-milled (nano/submicrometer) *G. tsugae* in (e) volume and (f) number, filtered media-milled *G. tsugae* (S-supernatant) in (g) volume and (h) number; *G. tsugae* hot-water extract in (i) volume and (j) number, filtered *G. tsugae* hot-water extract (S-extract) in (k) volume and (l) number.

**Table 1. Mean Diameters ($D_v$, $D_n$)[a] of *G. tsugae* Samples with Different Treatments[b]**

| sample | $D_v$ ($\mu$m) | $D_n$ ($\mu$m) |
|---|---|---|
| blended | 248.50 ± 2.12a | 3.38 ± 0.03a |
| media milled 1 h | 10.26 ± 0.47b | 0.10 ± 0.00c |
| media milled 2 h | 6.40 ± 0.75c | 0.10 ± 0.00c |
| media milled 3 h | 3.70 ± 0.23d | 0.11 ± 0.00d |
| supernatant | 0.14 ± 0.02e | 0.08 ± 0.00cd |
| S-supernatant | 0.14 ± 0.00e | 0.07 ± 0.01d |
| hot-water extract | 0.62 ± 0.02e | 0.38 ± 0.01b |
| S-extract | 0.11 ± 0.01e | 0.06 ± 0.00d |

[a] $D_v$, volume mean diameter; $D_n$, number mean diameter. [b] Mean ± standard deviation ($n$ = 3). Values in the same column with different lower case letters (a–e) are significantly different by Duncan's new multiple-range test ($P$ < 0.05).

data indicated that 3 h of media milling resulted in most of the particles being smaller than 1 $\mu$m with a few particles greater than 1 $\mu$m.

After centrifugation (10000 *g*, 10 min), particles in the supernatant (nano/submicrometer *G. tsugae*) ranged from 0.042 to 0.393 $\mu$m with a mean diameter of 0.14 $\mu$m (in volume) (Figure 2e and Table 1). There were 21% of particles smaller than 0.1 $\mu$m. The size distribution of particles was shifted to smaller ones in terms of number (Figure 2f). The percentages of particles smaller than 0.1 $\mu$m were increased to 82%. The centrifugation resulted in a more uniform size distribution by removing large particles. Filtration resulted in bimodal size distribution (Figure 2g,h). The ranges of particle size in volume and number were similar. There were about 84% of particles smaller than 0.1 $\mu$m in terms of number. All of the particles in nano/submicrometer *G. tsugae* and S-supernatant fell in the nano/submicrometer scale. As illustrated in Figure 2i, particles in the hot-water extract ranged from 0.17 to 3.06 $\mu$m with a volume-mean diameter of 0.624 ± 0.019 $\mu$m (Table 1). When counted by number, the size distribution (Figure 2j) was similar to that counted by volume, but no particles were greater than 1 $\mu$m. The data indicated that there existed a more uniform size distribution for the hot-water extract than for media-milled samples. After filtration, all of the particles were smaller than 1 $\mu$m in terms of both volume and number (Figure 2k,l). There were about 99.5% (in number) of particles smaller than 0.1 $\mu$m. The size of both the hot-water extract and the S-extract fell in the nano/submicrometer scale.

After blending, fibrous structure was observed as shown in Figure 3a. An enlargement (Figure 3b) of the image indicated that blending only tore off the fibrous structure of hyphae. This confirmed that there were no nanoparticles in the blended sample. One hour of media milling generated abrasion on the surface of the fibrillar structure and resulted in the reduction of the diameter of filamentous materials (Figure 3c) and the presence of nanoparticles (Figure 3d). There existed few fine particles on the surface of fibrillar structure. From the size measurement, the volume-mean diameter was counted as 10.26 ± 0.47 $\mu$m (Table 1) with a number-mean diameter of 0.1 $\mu$m. Continuous milling (2 h) reduced the volume-mean diameter to 6.40 ± 0.75 $\mu$m (Table 1) with no significant change in

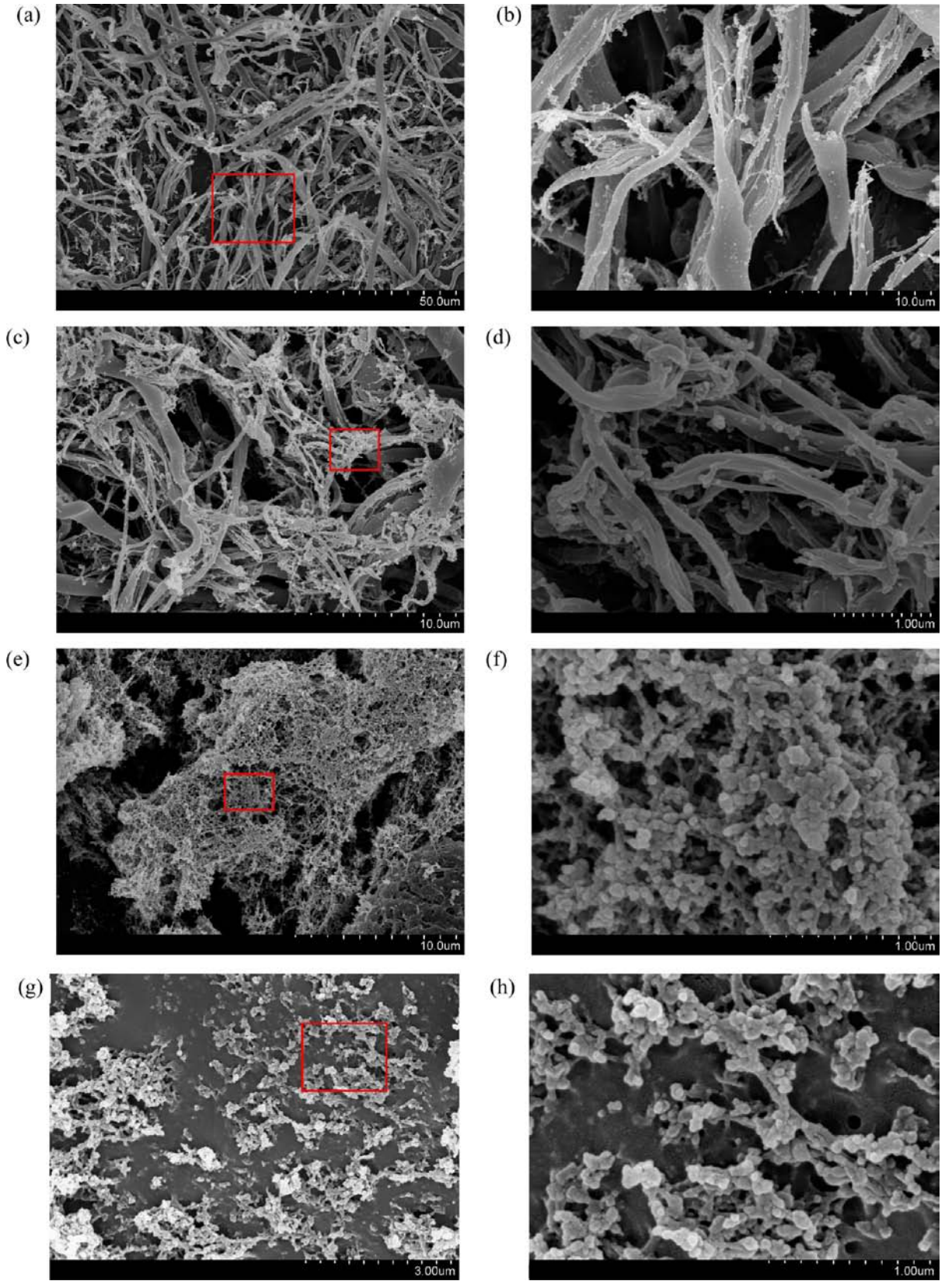


**Figure 3.** continued


dx.doi.org/10.1021/jf503898y | *J. Agric. Food Chem.* 2014, 62, 12244−12255

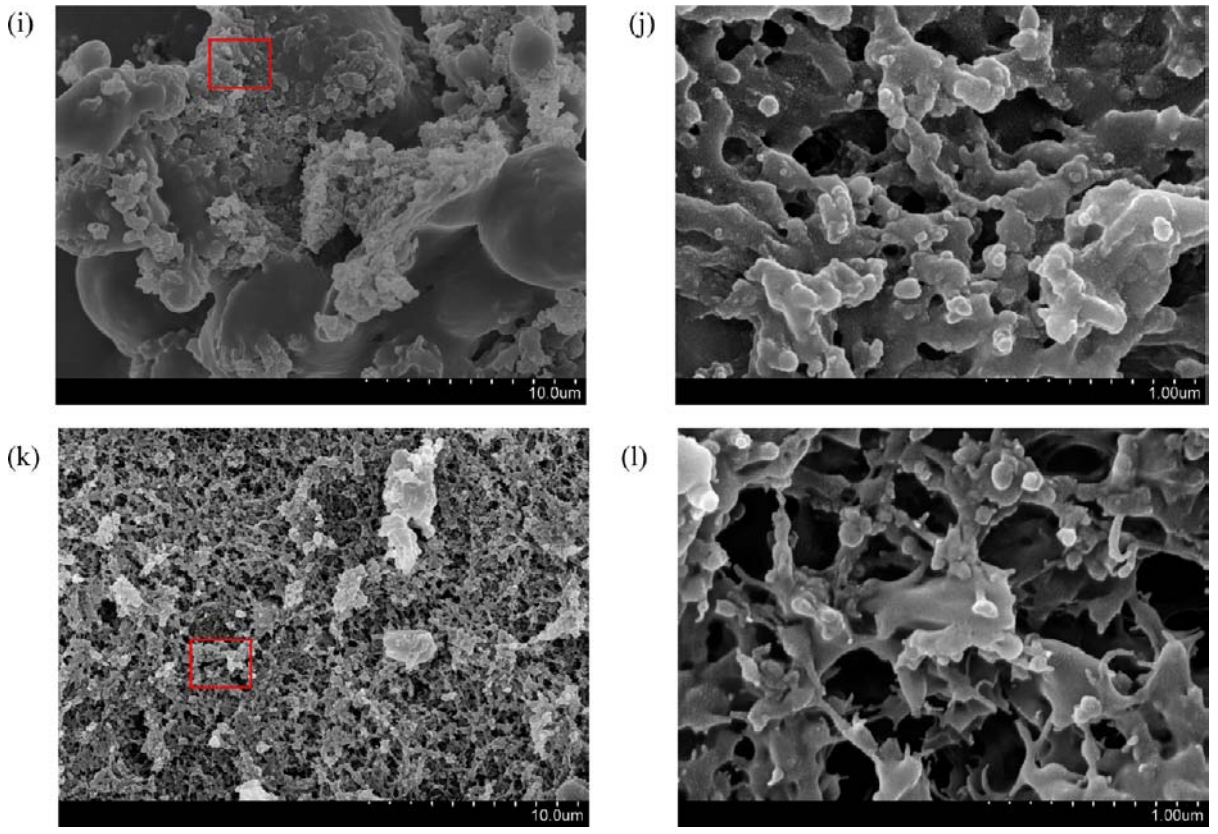


**Figure 3.** SEM of (a, b) blended, (c, d) 1-h media milled, (e, f) 3-h media-milled, and (g, h) filtered media-milled (S-supernatant) *G. tsugae* and (i, j) hot-water extract and (k, l) filtered hot-water extract (S-extract) of *G. tsugae*.

number-mean diameter. The volume-mean diameter was slightly reduced to 3.70 ± 0.23 μm (Table 1) with extended milling (3 h). No fibrillar structures were observed (Figure 3e), and most of the particles were in nano scale (Figure 3f). The observation concurred with the size measurement. Nevertheless, particles aggregated due to lack of dispensers, which would result in the presence of large particles during size measurement.

Filtration removed large particles (Figure 3g) and resulted in finer particles (Figure 3h) with a volume-mean diameter of 0.14 μm and a number-mean diameter of 0.07 μm (Table 1). There existed a few large particles (mostly smaller than 10 μm) in the hot-water extract (Figure 3i). Most of the particles were smaller than 1 μm (Figure 3j) and aggregated similarly to media-milled sample. It was not surprising to see large particles being removed by filtration (Figure 3k), which resulted in a volume-mean diameter of 0.11 μm and a number-mean diameter of 0.06 μm (Table 1). Again, an enlargement of the image illustrated the presence of nanoparticles (Figure 3l). The SEM confirmed that both 3 h media-milled samples and *G. tsugae* hot-water extract consisted of nanoparticles.

Figure 4 summarizes the morphological change in *G. tsugae* during the milling process. Before treatments, native hyphae had a diameter of about 3 μm with few less than 0.9 μm (Figure 4a). Once physical forces were imparted by blending, the surface of hyphae was threaded off and few small particles (smaller than 0.1 μm) were generated (Figure 4b). It appeared that hyphae were torn off by further milling, which resulted in more fine particles (Figure 4c). A mixture of threads and ultrafine particles (Figure 4d) was formed after extended milling. Most of the particles aggregated to form tiny threads, probably due to van der Waals forces and no emulsifiers.

**Composition and Solid Content.** Total carbohydrate, protein, and 1→3-β-D-glucan are three important components in *G. tsugae*. As discussed previously, filtration removed large particles. Nevertheless, filtration did not result in significant difference in the content of total carbohydrate, 1→3-β-D-glucan, and solid for both media-milled samples and hot-water extract (Table 2). The contents of solid and 1→3-β-D-glucan were similar to the report of Lin et al.,[31] who used three different sizes of media. The data indicated that the percentages (in terms of weight) of large particles were small. Thus, the removal of large particles did not significantly affect the solid content. The solid content in S-supernatant was 61% more than in S-extract. The contents of total carbohydrate, protein, and 1→3-β-D-glucan in S-supernatant were >3 times those in S-extract. For example, the content of 1→3-β-D-glucan in S-supernatant was about 3.5-fold that in S-extract. The data indicated that media milling exerted abrasive forces, which was helpful for releasing bioactive compounds from *G. tsugae*. Media milling would be an attractive method for replacing extraction.

**Mutagenicity.** In both non-S9 and S9 conditions, the mutagen in positive control induced the mutation of *Salmonella* Typhimurium strains with high readings of revertant colonies (Tables 3 and 4). Without S9, the $His^+$ revertants of six different concentrations of S-supernatant and S-extract were not significantly different from those of the spontaneous revertants among five tester strains (Table 3). With S9, the $His^+$ revertants of six different concentrations of S-supernatant and S-extract were not significantly greater than those for the

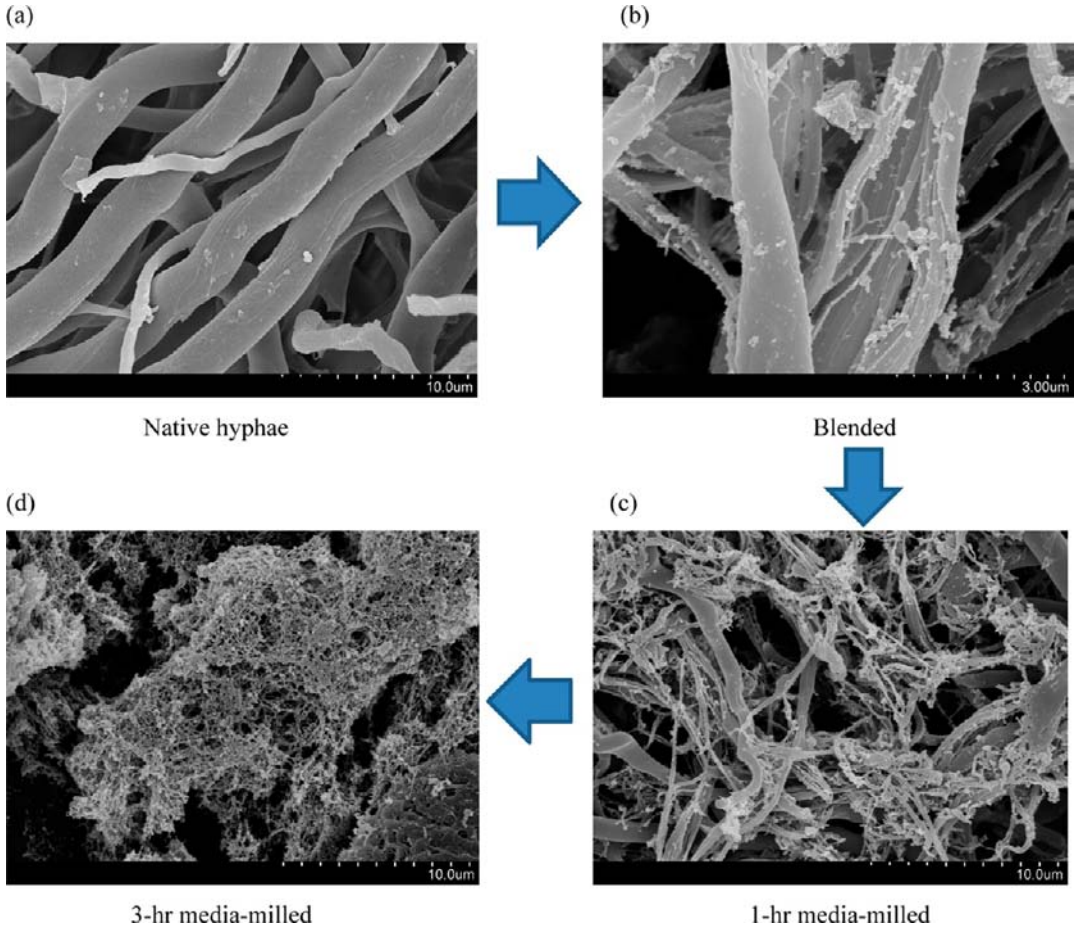


**Figure 4.** Structural change of hyphae from (a) native to (b) blended, (c) 1 h media-milled, and (d) 3 h media-milled.

**Table 2. Total Carbohydrate,[a] Protein, and 1→3-β-D-Blucan Contents of Nano/Submicromemter *G. tsugae*, S-Supernatant,[b] *G. tsugae* Hot-Water Extract, and S-Extract[c]**

| sample | total carbohydrate (μg/mL) | protein (μg/mL) | 1→3-β-D-glucans (μg/mL) | solid content (mg/mL) |
|---|---|---|---|---|
| nano/submicrometer *G. tsugae* | 1528.3 ± 139.4a | 155.5 ± 24.4a | 62.6 ± 8.8a | 3.8 ± 0.4a |
| S-supernatant | 1444.2 ± 150.8a | 132.5 ± 21.0b | 59.8 ± 8.5a | 3.7 ± 0.4a |
| *G. tsugae* hot-water extract | 394.9 ± 38.7b | 22.0 ± 4.7c | 17.9 ± 5.5b | 2.4 ± 0.1b |
| S-extract | 383.1 ± 32.0b | 17.2 ± 4.7c | 17.3 ± 5.b8 | 2.3 ± 0.2b |

[a]Mean ± standard deviation ($n$ = 3).Values in the same column with different lower case letters (a−c) are significantly different by Duncan's new multiple-range test ($p < 0.05$). [b]S-supernatant: nano/submicrometer *G. tsugae* solution filtered by 0.45 μm membrane. [c]S-extract: hot-water extract solution filtered by 0.45 μm membrane.

spontaneous revertants among four strains of TA98, TA102, TA1535, and TA1537. For S-extract, $His^+$ revertants were significant greater than the spontaneous revertants on TA100 strain at three concentrations (25, 100, and 200 μg/mL), but not dose dependent. As pointed out in the literature,[27,28] a compound exhibited mutagenic potencies when $His^+$ revertants were more than doubled the control group with dose dependency. Thus, S-extract did not exhibit mutagenic potencies. The toxicity test against *Salmonella* Typhimurium strains showed the maximum concentrations of S-supernatant and S-extract (300 and 240 μg/mL, respectively) were not toxic at non-S9 and S9 conditions (Tables 3 and 4). Mutation in *Salmonella* (SAL) has been recognized as the most predictive for carcinogenicity among in vitro genetic toxicity in short-term tests. When chemicals exhibit mutagenicity to SAL, 89% of those chemicals have been found to be carcinogenic in rodents.[32] The data indicated that neither S-supernatant nor S-extract exhibited mutagenic potencies.

**Viability of Primary Cells.** S-supernatant did not exhibit any inhibition on the viability of primary cells from the mouse alimentary canal (Figure 5a−c). Once the concentrations of S-supernatant were no less than 250 μg/mL, the viability of primary cells (stomach, intestines, and colon) was significantly greater than the control. The data indicated that S-supernatant was good for the growth of primary cells. Similar results were obtained for S-extract. For intestine cells, there existed a decrease in cell viability when S-extract was employed at 5−100 μg/mL. Nevertheless, the viability remained greater than 100% when the addition levels were no less than 250 μg/mL (Figure 5b-2). Both S-supernatant and S-extract were not toxic to the primary cells from mouse alimentary canal. Both S-supernatant and S-extract exhibited similar effects on the growth of primary cells from liver and kidney (Figure 5d,e) and thus did not

Table 3. Mutagenicity[a,b] of S-Supernatant[c] and S-Extract[d] in *Salmonella* Typhimurium Tester Strains

| | *Salmonella* Typhimurium | | | | |
|---|---|---|---|---|---|
| | TA98 | TA100 | TA102 | TA1535 | TA1537 |
| test item concn revertant colonies (CFU[e]/plate) | | | | | |
| positive control (mutagen) | 261 ± 9a | 445 ± 27a | 1419 ± 66a | 449 ± 24a | 130 ± 6a |
| spontaneous revertants | 8 ± 3b | 41 ± 5b | 140 ± 15bc | 10 ± 3b | 7 ± 4b |
| S-supernatant (μg/plate) | | | | | |
| 5 | 6 ± 1b | 42 ± 1b | 158 ± 6bc | 6 ± 4b | 6 ± 4b |
| 25 | 11 ± 3b | 43 ± 5b | 151 ± 12bc | 9 ± 3b | 7 ± 2b |
| 50 | 7 ± 2b | 49 ± 10b | 150 ± 20bc | 8 ± 3b | 6 ± 2b |
| 100 | 11 ± 3b | 47 ± 3b | 153 ± 4bc | 8 ± 1b | 4 ± 1b |
| 200 | 9 ± 4b | 48 ± 10b | 157 ± 14c | 9 ± 1b | 6 ± 3b |
| 300 | 11 ± 3b | 57 ± 7b | 163 ± 35bc | 7 ± 5b | 6 ± 4b |
| S-extract (μg/plate) | | | | | |
| 5 | 8 ± 6b | 50 ± 10b | 130 ± 13c | 7 ± 3b | 7 ± 3b |
| 25 | 10 ± 2b | 48 ± 6b | 142 ± 21bc | 7 ± 3b | 5 ± 2b |
| 50 | 12 ± 3b | 60 ± 3b | 155 ± 12bc | 8 ± 1b | 7 ± 3b |
| 100 | 12 ± 5b | 51 ± 10b | 184 ± 8 | 9 ± 1b | 8 ± 2b |
| 200 | 11 ± 1 | 55 ± 10b | 169 ± 8bc | 9 ± 1b | 6 ± 2b |
| 240 | 8 ± 6b | 57 ± 7b | 163 ± 21bc | 9 ± 3b | 7 ± 5b |

[a]Mean ± standard deviation ($n$ = 3). Values in the same column with different lower case letters (a−c) are significantly different by Duncan's new multiple-range test ($p$ < 0.05). [b]Mutagenicity: the ratio of (number of His+ revertants)/ (number of spontaneous revertants) >2 means mutagenic potencies. [c]S-supernatant: nano/submicrometer *G. tsugae* solution filtered by 0.45 μm membrane. [d]S-extract: hot-water extract solution filtered by 0.45 μm membrane. [e]CFU:-colony forming unit.

Table 4. Mutagenicity[a,b] of S-Supernatant[c] and S-Extract[d] in *Salmonella* Typhimurium Tester Strains (+S9)

| | *Salmonella* Typhimurium | | | | |
|---|---|---|---|---|---|
| | TA98 | TA100 | TA102 | TA1535 | TA1537 |
| test item concn revertant colonies (CFU[e]/plate) | | | | | |
| positive control (mutagen) | 362 ± 9a | 155 ± 18a | 278 ± 24a | 208 ± 14a | 358 ± 3a |
| spontaneous revertants | 16 ± 3b | 62 ± 4e | 116 ± 5b | 12 ± 3b | 7 ± 0b |
| S-supernatant (μg/plate) | | | | | |
| 5 | 11 ± 1b | 71 ± 21cde | 138 ± 5b | 11 ± 1b | 7 ± 1bcd |
| 25 | 19 ± 2b | 72 ± 6cde | 137 ± 23b | 9 ± 1b | 6 ± 2bcd |
| 50 | 15 ± 3b | 66 ± 7de | 109 ± 12b | 9 ± 2b | 8 ± 1bcd |
| 100 | 21 ± 3b | 71 ± 5cde,[e] | 146 ± 8b | 10 ± 6b | 6 ± 3bcd |
| 200 | 12 ± b3 | 75 ± 7bcde | 116 ± 11b | 12 ± 2b | 4 ± 4d |
| 300 | 17 ± 2b | 88 ± 14bcde | 124 ± 7b | 11 ± 1b | 6 ± 2bcd |
| S-extract (μg/plate) | | | | | |
| 5 | 11 ± 5b | 72 ± 11cde | 118 ± 13b | 8 ± 2b | 10 ± 4b |
| 25 | 18 ± 6b | 90 ± 18bcd | 142 ± 15 | 9 ± 2b | 9 ± 2bcd |
| 50 | 13 ± 2b | 89 ± 5bcde | 123 ± 13b | 7 ± 3b | 8 ± 2bcd |
| 100 | 13 ± 1b | 100 ± 20b | 118 ± 10b | 9 ± 2b | 11 ± 4bc |
| 200 | 13 ± 3b | 97 ± 24bc | 137 ± 14b | 13 ± 2b | 4 ± 4d |
| 240 | 17 ± 4b | 88 ± 13bcde, | 129 ± 8b | 11 ± 3b | 5 ± 3cd |

[a]Mean ± standard deviation ($n$ = 3). Values in the same column with different lower case letters (a−e) are significantly different by Duncan's new multiple-range test ($p$ < 0.05). [b]Mutagenicity: the ratio of (number of His+ revertants)/(number of spontaneous revertants) >2 means mutagenic potencies. [c]S-supernatant: nano/submicrometer *G. tsugae* solution filtered by 0.45 μm membrane. [d]S-extract: hot-water extract solution filtered by 0.45 μm membrane. [e]CFU: colony-forming unit.

restrain the cells. These might be due to some nutrients present in samples, which resulted in more cell proliferation. In the control group, sterilized deionized water was added to the medium (RPMI 1640, 10% FBS) and resulted in dilution of nutrients. The addition of S-supernatant or S-extract might bring nutrients into the culture. Thus, the enhancement on cell proliferation was concentration dependent. To check this concept, a positive control (not shown in this study) was conducted by adding medium (RPMI 1640, 10% FBS) instead of sterilized deionized water or samples. In other words, there were no concentration changes in culture. There was about a 150−250% increase in cell viability compared with the control group. It appeared that the nutrient concentration in the control group was the least one. In addition, polysaccharides have been found to stimulate cell proliferation via the *c-myc* gene.[33] Nevertheless, the mechanism of the increase in cell proliferation needs further studies. Some nanoparticles have been found to exhibit cytotoxic and genotoxic potential, such as copper oxide nanoparticles[34] and methyl parathion and parathion.[35] Unlike metallic material and insecticide, both S-supernatant and S-extract (containing nano/submicrometer-scaled particles) originated from the edible resource of *G. tsugae*

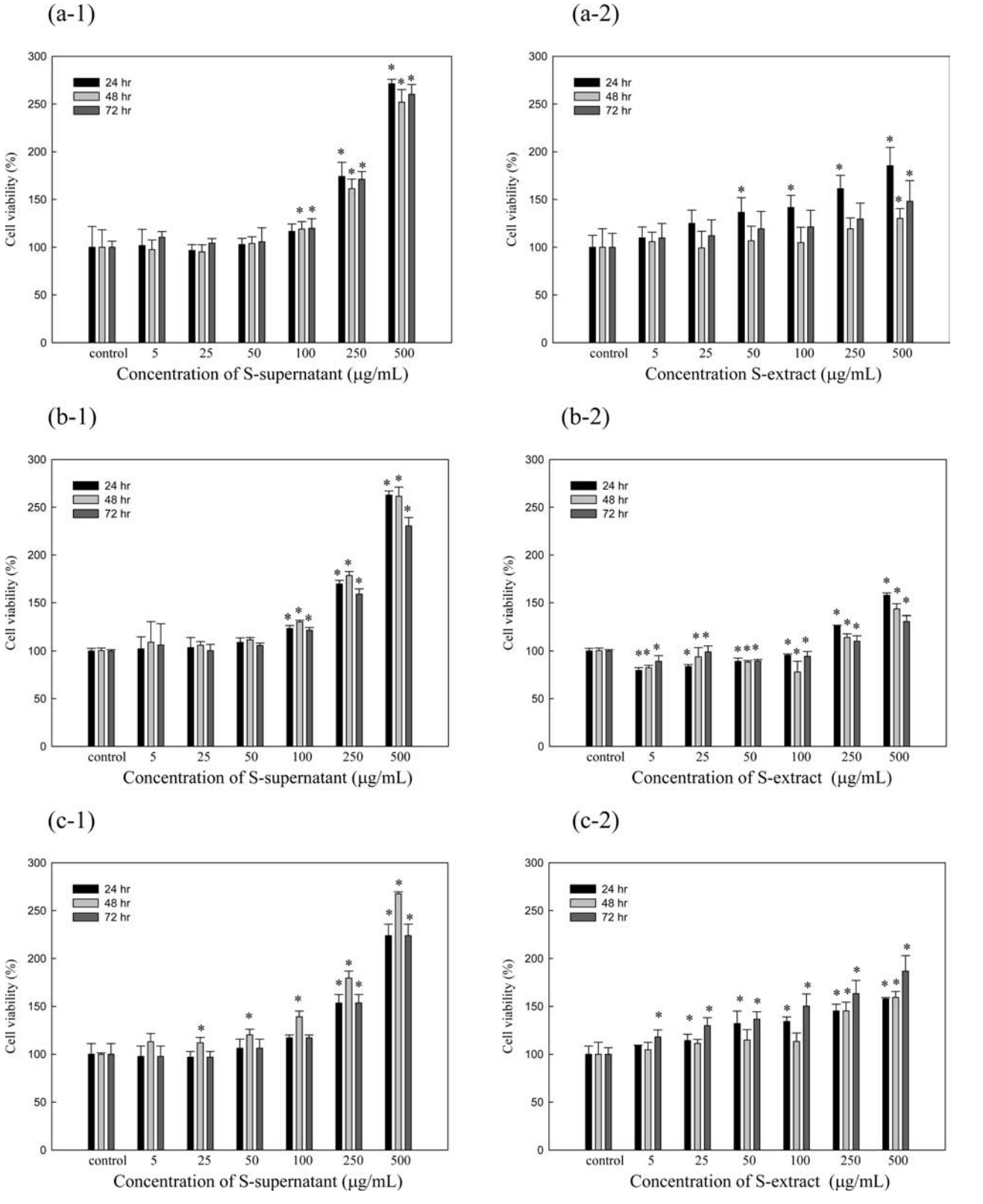


**Figure 5.** continued


dx.doi.org/10.1021/jf503898y | J. Agric. Food Chem. 2014, 62, 12244−12255

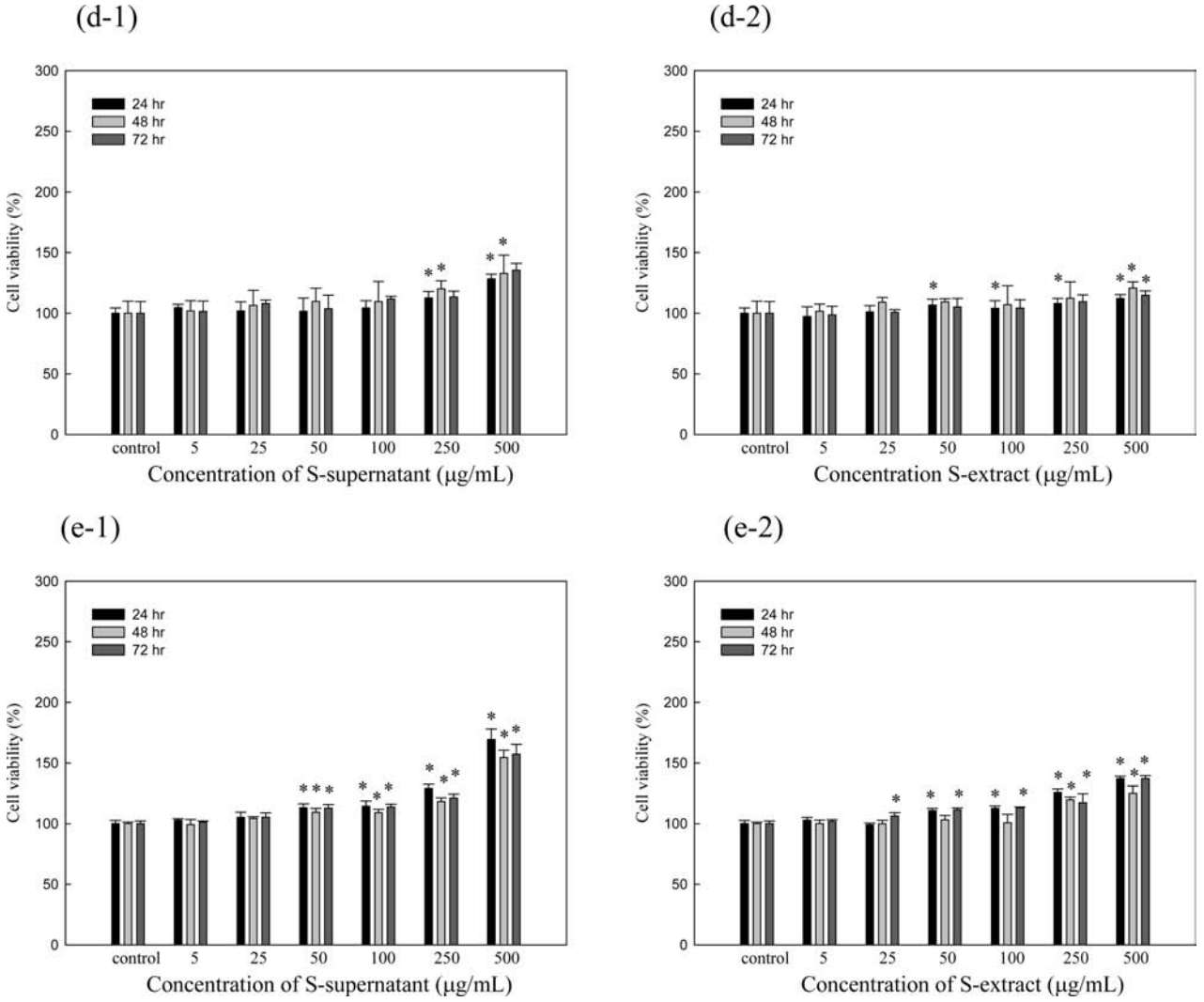


**Figure 5.** Viability of mouse primary cells of (a) stomach, (b) intestines, (c) colon, (d) liver, and (e) kidney treated with S-supernatant (1) and S-extract (2) for 24−72 h. The asterisk (*) indicates the datum was significantly different from the control group by Duncan's new multiple-range test ($p < 0.05$).

and did not exhibit toxicity to the primary cells of the alimentary canal and metabolism organs of the mouse.

## AUTHOR INFORMATION


### Corresponding Author

*(A.-I.Y.) Mail: Graduate Institute of Food Science and Technology, National Taiwan University, 1 Roosevelt Road, Section 4, Taipei 10617, Taiwan. Phone: +886-2-3366-4121. Fax: +886-2-2362-0849. E-mail: yehs@ntu.edu.tw.



### Funding

This study (Project NSC 99-2313-B-002-032MY2) has been financially supported by the Ministry of Science and Technology of Taiwan.


### Notes

The authors declare no competing financial interest.

## ABBREVIATIONS USED

2AA, 2-aminoanthracene; 9AA, 9-aminoacridine; ANOVA, analysis of variance; B[a]P, benzo[*a*]pyrene; BSA, bovine serum albumin; DMSO, dimethyl sulfoxide; FBS, fetal bovine serum; MMC, mitomycin C; MTT, 3-[4,5-dimethylthiazol-2-yl]-2,5-diphenyltetrazolium bromide; 4NQO, 4-nitroquinoline-*N*-oxide; rpm, rounds per minute; S-extract, hot-water extract solution filtered by 0.45 μm membrane; S-supernatant, nano/submicrometer *G. tsugae* solution filtered by 0.45 μm membrane; SA, sodium azide; SAS, Statistical Analysis System; SEM, scanning electron microscopy; YTZ, yttria-stabilized tetragonal zirconia

## REFERENCES


(1) Wang, G.; Zhang, J.; Mizuno, T.; Zhuang, C.; Ito, H.; Mayuzumi, H.; Okamoto, H.; Li, J. Antitumor active polysaccharides from the Chinese mushroom songshan lingzhi, the fruiting body of *Ganoderma tsugae*. *Biosci., Biotechnol., Biochem.* **1993**, *57*, 894−900.

(2) Chen, M. L.; Lin, J. Y.; Lin, B. F. The immunomodulatory effects of *Ganoderma tsugae* supplementation on immune responses of BALB/c mice. *Taiwan. J. Agric. Chem. Food Sci.* **2006**, *44*, 243−249.

(3) Mau, J. L.; Tsai, S. Y.; Tseng, Y. H.; Huang, S. J. Antioxidant properties of hot water extracts from *Ganoderma tsugae* Murrill. *LWT−Food Sci. Technol.* **2005**, *38*, 589−597.

(4) Liao, C. H.; Hsiao, Y. M.; Hsu, C. P.; Lin, M. Y.; Wang, C. H.; Huang, Y. L.; Ko, J. L. Transcriptionally-mediated inhibition of telomerase of fungal immunomodulatory protein from *Ganoderma tsugae* in A549 human lung adenocarcinoma cell line. *Mol. Carcinogen.* **2006**, *45*, 220−229.

(5) Liao, C. H.; Hsiao, Y. M.; Lin, C. H.; Yeh, C. S.; Wang, C. H.; Ni, C. H.; Hsu, C. P.; Ko, J. L. Induction of premature senescence in human lung cancer by fungal immunomodulatory protein from *Ganoderma tsugae*. *Food Chem. Toxicol.* **2008**, *46*, 1851−1859.
(6) Ko, H. H.; Hung, C. F.; Wang, J. P.; Lin, C. N. Antiinflammatory triterpenoids and steroids from *Ganoderma lucidum* and *G. tsugae*. *Phytochemistry* **2008**, *69*, 234−239.
(7) Tseng, Y. H.; Mau, J. L. Antioxidant properties of cold water extracts from *Ganoderma tsugae*. *Fung. Sci.* **2007**, *22*, 13−23.
(8) Mizuno, T.; Sakai, T.; Chihara, G. Health foods and medicinal usages of mushrooms. *Food Rev. Int.* **1995**, *11*, 69−81.
(9) Zong, A.; Cao, H.; Wang, F. Anticancer polysaccharides from natural resources: a review of recent research. *Carbohydr. Polym.* **2012**, *90*, 1395−1410.
(10) Liu, Y. J.; Shen, J.; Xia, Y. M.; Zhang, J.; Park, H. S. The polysaccharides from *Ganoderma lucidum*: are they always inhibitors on human hepatocarcinoma cells? *Carbohydr. Polym.* **2012**, *90*, 1210−1215.
(11) Kuo, H. Y.; Chen, S. H.; Yeh, A. I. Preparation and physicochemical properties of whole-bean soymilk. *J. Agric. Food Chem.* **2014**, *62*, 742−749.
(12) Shinohara, K.; Golman, B.; Uchiyama, T.; Otani, M. Fine-grinding characteristics of hard materials by attrition mill. *Powder Technol.* **1999**, *103*, 292−296.
(13) Tian, Y.; Wang, X.; Xi, R.; Pan, W.; Jiang, S.; Li, Z.; Zhao, Y.; Gao, G.; Liu, D. Enhanced antitumor activity of realgar mediated by milling it to nanosize. *Int. J. Nanomed.* **2014**, *9*, 745−757.
(14) Lin, N. C.; Lin, J. C.; Chen, S. H.; Ho, C. T.; Yeh, A. I. Effect of goji (*Lycium barbarum*) on expression of genes related to cell survival. *J. Agric. Food Chem.* **2011**, *59*, 10088−10096.
(15) Chiang, L. H.; Chen, S. H.; Yeh, A. I. Preparation of nano/submicrometer yam and its benefits on collagen secretion from skin fibroblast cells. *J. Agric. Food Chem.* **2012**, *60*, 12332−12340.
(16) Cockburn, A.; Bradford, R.; Buck, N.; Constable, A.; Edwards, G.; Haber, B.; Hepburn, P.; Howlett, J.; Kampers, F.; Klein, C.; Radomski, M.; Stamm, H.; Wijnhoven, S.; Wildeman, T. Approaches to the safety assessment of engineered nanomaterials (ENM) in food. *Food Chem. Toxicol.* **2012**, *50*, 2224−2242.
(17) Maron, D. H.; Ames, B. N. Revised methods for the *Salmonella typhimurium* mutagenicity test. *Mutat. Res.* **1983**, *113*, 173−215.
(18) Mortelmans, K.; Zeiger, E. The Ames *Salmonella*/microsome mutagenicity assay. *Mutat. Res.* **2000**, *445*, 29−60.
(19) Magnuson, B. A.; Jonaitis, T. S.; Card, J. W. A brief review of the occurrence, use, and safety of food-related nanomaterials. *J. Food Sci.* **2011**, *76*, 126−133.
(20) Roberts, J. C.; Bhalgat, M. K.; Zera, R. T. Preliminary biological evaluation of polyamidoamine (PAMAM) starburst dendrimers. *J. Biomed. Mater. Res.* **1996**, *30*, 53−65.
(21) *Official Methods of Analysis of AOAC International*, 19th ed.; AOAC International: Gaithersburg, MD, USA, 2012.
(22) Dubois, M.; Gilles, K. A.; Hamilton, J. K.; Rebers, P. A.; Smith, F. Colorimetric method for determination of sugars and related substances. *Anal. Chem.* **1956**, *28*, 350−356.
(23) Bradford, M. M. Rapid and sensitive method for the quantitation of microgram quantities of protein utilizing the principle of protein-dye binding. *Anal. Chem.* **1976**, *72*, 248−254.
(24) Chang, Y. W.; Lu, T. J. Molecular characterization of polysaccharides in hot-water extracts of *Ganoderma lucidum* fruiting bodies. *J. Food Drug Anal.* **2004**, *12*, 59−67.
(25) Vargas, V. M. F.; Motta, V. E. P.; Henriques, J. A. P. Mutagenic activity detected by the Ames test in river water under the influence of petrochemical industries. *Mutat. Res.* **1993**, *319*, 1−45.
(26) Vargas, V. M. F.; Guidobono, R. R.; Jordao, C.; Henriques, J. A. P. Use of two short-term tests to evaluate the genotoxicity of river water treated with different concentration/extraction procedures. *Mutat. Res.* **1995**, *343*, 31−52.
(27) Park, J. H.; Lee, J. K.; Kim, H. S.; Chung, S. T.; Eom, J. H.; Kim, K. A.; Chung, S. J.; Paik, S. Y.; Oh, H. Y. Immunomodulatory effect of caffeic acid phenethyl ester in Balb/c mice. *Int. Immunopharmacol.* **2004**, *4*, 429−436.
(28) Mosmann, T. Rapid colorimetric assay for cellular growth and survival: application to proliferation and cytotoxicity assays. *J. Immunol. Methods* **1983**, *65*, 55−63.
(29) Wang, X. C.; Xi, R. J.; Li, Y.; Wang, D. M.; Yao, Y. J. The species identity of the widely cultivated *Ganoderma*, '*G. lucidum*' (Ling-zhi), in China. *PLoS One* **2012**, *7*, 1−12.
(30) Cao, Y.; Yuan, H. S. *Ganoderma mutabile* sp. *nov.* from southwestern China based on morphological and molecular data. *Mycol. Prog.* **2013**, *12*, 121−126.
(31) Lin, Y. S.; Cheng, W. C.; Chen, S. H.; Yeh, A. I. Preparation of nano/submicron *Ganoderma tsugae* and its stability. *J. Food Drug Anal.* **2012**, *20* (4), 900−907.
(32) Zeiger, E.; Haseman, J. K.; Shelby, M. D.; Margolin, B. H.; Tennant, R. W. Evaluation of four in vitro genetic toxicity tests for predicting rodent carcinogenicity: confirmation of earlier results with 41 additional chemicals. *Environ. Mol. Mutagen.* **1990**, *18*, 1−14.
(33) Sun, L. X.; Chen, L. H.; Lin, Z. B.; Qin, Y.; Zhang, J. Q.; Yang, J.; Ma, J.; Ye, T.; Li, W. D. Effects of *Ganoderma lucidum* polysaccharides on IEC-6 cell proliferation, migration and morphology of differentiation benefiting intestinal epithelium healing in vitro. *J. Pharm. Pharmacol.* **2011**, *63*, 1595−1603.
(34) Bucchianico, S. D.; Fabbrizi, M. R.; Misra, S. K.; Eugenia, V. J.; Berhanu, D.; Reip, P.; Bergamaschi, E.; Migliore, L. Multiple cytotoxic and genotoxic effects induced in vitro by differently shaped copper oxide nanomaterials. *Mutagenesis* **2013**, *28*, 287−299.
(35) Falicia, L. E.; Clement, G. Y.; Paul, B. T. Involvement of oxidative stress in methyl parathion and parathion-induced toxicity and genotoxicity to human liver carcinoma (HepG2) cells. *Environ. Toxicol.* **2013**, *28*, 342−348.

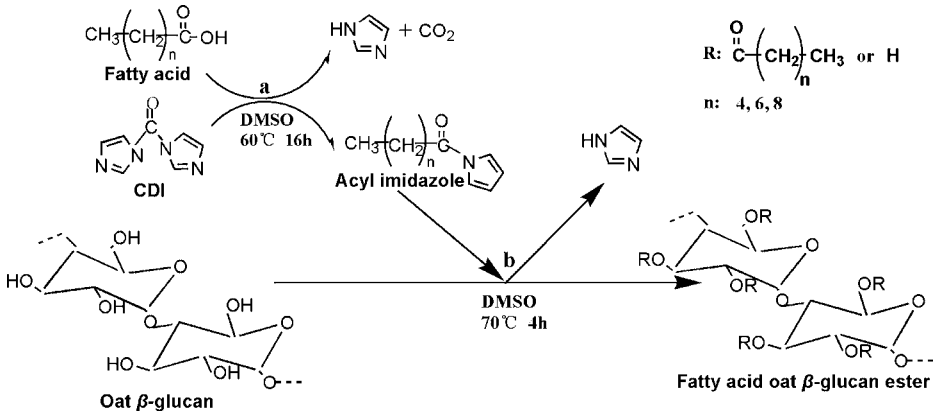


**Figure 1.** Synthetic scheme for fatty acid oat $\beta$-glucan ester (FAOGE). The fatty acid was first activated by reacting with carbonyl-di-imidazole (CDI) and converted into its acyl imidazole (a). The latter reacted with native oat $\beta$-glucan to produce FAOGE (b).

**Table 1. Box–Behnken Design Matrix (in Coded and Uncoded Levels of Three Variables) and Experimental and Predicted Values for the Degree of Substitution (DS) of Fatty Acid Oat $\beta$-Glucan Esters (FAOGEs)**

| | coded and uncoded values | | | DS | |
|---|---|---|---|---|---|
| trial | acyl chain length ($A$) | $M_w$ of $\beta$-glucan ($B$, $\times 10^4$ g/mol) | addition of acyl imidazole ($C$, mL/g $\beta$-glucan) | experimental | predicted |
| 1 | (−1) 6 | (−1) 7.4 | (0) 3.5 | 0.035 ± 0.002 | 0.037 |
| 2 | (1) 10 | (−1) 7.4 | (0) 3.5 | 0.041 ± 0.003 | 0.043 |
| 3 | (−1) 6 | (1) 16.8 | (0) 3.5 | 0.015 ± 0.001 | 0.013 |
| 4 | (1) 10 | (1) 16.8 | (0) 3.5 | 0.020 ± 0.001 | 0.018 |
| 5 | (−1) 6 | (0) 12.1 | (−1) 2.0 | 0.015 ± 0.002 | 0.013 |
| 6 | (1) 10 | (0) 12.1 | (−1) 2.0 | 0.022 ± 0.004 | 0.020 |
| 7 | (−1) 6 | (0) 12.1 | (1) 5.0 | 0.041 ± 0.003 | 0.043 |
| 8 | (1) 10 | (0) 12.1 | (1) 5.0 | 0.045 ± 0.002 | 0.047 |
| 9 | (0) 8 | (−1) 7.4 | (−1) 2.0 | 0.032 ± 0.003 | 0.032 |
| 10 | (0) 8 | (1) 16.8 | (−1) 2.0 | 0.011 ± 0.001 | 0.015 |
| 11 | (0) 8 | (−1) 7.4 | (1) 5.0 | 0.073 ± 0.004 | 0.069 |
| 12 | (0) 8 | (1) 16.8 | (1) 5.0 | 0.035 ± 0.001 | 0.035 |
| 13 | (0) 8 | (0) 12.1 | (0) 3.5 | 0.059 ± 0.001 | 0.061 |
| 14 | (0) 8 | (0) 12.1 | (0) 3.5 | 0.058 ± 0.002 | 0.061 |
| 15 | (0) 8 | (0) 12.1 | (0) 3.5 | 0.061 ± 0.002 | 0.061 |
| 16 | (0) 8 | (0) 12.1 | (0) 3.5 | 0.064 ± 0.001 | 0.061 |
| 17 | (0) 8 | (0) 12.1 | (0) 3.5 | 0.063 ± 0.002 | 0.061 |

chain length, $M_w$ of $\beta$-glucan, and addition of acyl imidazole were investigated. On the basis of the structural features and aqueous self-assembly behavior of the products characterized by FT-IR, $^1$H NMR, and TEM, the structure–curcumin loading capacity (CLC) relationship of FAOGEs was investigated.

## MATERIALS AND METHODS

**Materials.** A commercial soluble $\beta$-glucan (80 wt % $\beta$-glucan content) extracted from oats was bought from Zhangjiakou Yikang Biological Technology Co., Ltd. (Zhangjiakou, China). Methyl decanoate, methyl octanoate, methyl hexanoate, *N*,*N*′-carbonyl-di-imidazole (CDI), and curcumin (98%) were purchased from Adamas Reagent Co. (Shanghai, China). Hexanoic acid, octanoic acid, decanoic acid, isopropanol, dimethyl sulfoxide (DMSO), acetonitrile, and formic acid were bought from KeLong Reagent Co,. Ltd. (Chengdu, China). Potassium bromide (KBr) of infrared spectroscopy grade was obtained from GuangFu Reagent Chemical Co., Ltd. (Tianjin, China). All chemical reagents were commercially available and used as received.

**Preparation of Oat $\beta$-Glucan Hydrolysates.** Two hydrolysates of oat $\beta$-glucan (denoted OG1 and OG2) were prepared according to a previously described method with slight modifications.[19] In detail, oat $\beta$-glucan (2.0 g) was dispersed in 1 L of distilled water and heated at 80 °C with magnetic stirring for 2 h. The resulting solution was cooled to room temperature and then centrifuged at 3000*g* for 10 min to obtain oat $\beta$-glucan solution. One milliliter (OG1) or 3 mL (OG2) of hydrochloric acid (6 M) was mixed with 500 mL of the above-prepared oat $\beta$-glucan solution. Then, the mixture was incubated at 50 °C for 10 min to allow the intended hydrolysis. After hydrolysis completed, the hydrolysates were rapidly cooled to room temperature and neutralized (pH 6–7) with 2 M NaOH. The mother $\beta$-glucan solution and its hydrolysates were precipitated by respectively mixing them with 2 volumes of ethanol and lyophilized. The $M_w$ values of oat $\beta$-glucan, OG1, and OG2 were determined as $16.8 \times 10^4$, $12.1 \times 10^4$, and $7.4 \times 10^4$ g/mol, respectively, on a high-performance size-exclusion (HPSEC) system.[20]

**FAOGE Synthesis.** To synthesize FAOGE, a two-step reaction was carried out according to the method reported in the literature (Figure 1).[21] For the first step, fatty acid (0.031 mol) and CDI (5.02 g, 0.031 mol) were dissolved in 50 mL of DMSO. The resultant solution was kept at 60 °C for 16 h to realize the activation of fatty acid in the form of acyl imidazole. In the next step, oat $\beta$-glucan (1 g) was dissolved in DMSO (20 mL) at 70 °C with continuous stirring for 30 min. Then the non-isolated acyl imidazole was added dropwise into the oat $\beta$-glucan solution, and the resultant solution was kept at 70 °C under continuous agitation for 4 h to produce FAOGE. The DS of the products was monitored by the addition of acyl imidazole. The product was precipitated from reacting solution by mixing with 2 volumes of isopropanol. It was recovered by vacuum filtration through an 80 mm diameter Buchner funnel and washed five times with

Table 2. Analysis of Variance (ANOVA) for the Effects of Acyl Chain Length ($A$), $M_w$ of $\beta$-Glucan ($B$), Addition of Acyl Imidazole ($C$), and Their Quadratic Terms ($A^2$, $B^2$, $C^2$) and Interactive Terms ($AB$, $AC$, $BC$) on the Degree of Substitution (DS) of Fatty Acid Oat $\beta$-Glucan Esters (FAOGEs)

| source | sum of squares | degree of freedom | mean square | $F$ value | $P$ value |
|---|---|---|---|---|---|
| model | 0.0062 | 9 | 0.00068 | 48.73 | <0.0001 |
| $A$ | 0.000061 | 1 | 0.000061 | 4.30 | 0.077 |
| $B$ | 0.0013 | 1 | 0.0013 | 88.83 | <0.0001 |
| $C$ | 0.0016 | 1 | 0.0016 | 115.45 | <0.0001 |
| $AB$ | 0.00000025 | 1 | 0.00000025 | 0.018 | 0.90 |
| $AC$ | 0.0000023 | 1 | 0.0000023 | 0.16 | 0.70 |
| $BC$ | 0.000072 | 1 | 0.000072 | 5.13 | 0.058 |
| $A^2$ | 0.0017 | 1 | 0.0017 | 121.19 | <0.0001 |
| $B^2$ | 0.00073 | 1 | 0.00073 | 51.55 | 0.0002 |
| $C^2$ | 0.00043 | 1 | 0.00043 | 30.68 | 0.0009 |
| residual | 0.000099 | 7 | 0.000014 | | |
| lack of fit | 0.000073 | 3 | 0.000024 | 3.72 | 0.12 |
| pure error | 0.000026 | 4 | 0.0000065 | | |
| cor total | 0.0063 | 16 | | | |
| $R^2$ | 0.98 | CV (%) = 9.24 | | | |

Table 3. Box–Behnken Design Matrix (in Coded and Uncoded Levels of Three Variables) and Experimental and Predicted Values for the Curcumin Loading Capacity (CLC) of Fatty Acid Oat $\beta$-Glucan Esters (FAOGEs)

| | coded and uncoded values | | | CLC ($\mu$g/mg) | |
|---|---|---|---|---|---|
| trial | $M_w$ of $\beta$-glucan ($X_1$, $\times 10^4$ g/mol) | degree of substitution ($X_2$) | acyl chain length ($X_3$) | experimental | predicted |
| 1 | (−1) 7.4 | (−1) 0.0090 ± 0.0004 | (0) 8 | 0.55 ± 0.03 | 0.49 |
| 2 | (1) 16.8 | (−1) 0.0090 ± 0.0005 | (0) 8 | 1.09 ± 0.06 | 1.14 |
| 3 | (−1) 7.4 | (1) 0.0291 ± 0.0012 | (0) 8 | 1.04 ± 0.12 | 0.99 |
| 4 | (1) 16.8 | (1) 0.0287 ± 0.0008 | (0) 8 | 2.14 ± 0.09 | 2.20 |
| 5 | (−1) 7.4 | (0) 0.0219 ± 0.0008 | (−1) 6 | 1.25 ± 0.17 | 1.44 |
| 6 | (1) 16.8 | (0) 0.0214 ± 0.0010 | (−1) 6 | 1.68 ± 0.07 | 1.75 |
| 7 | (−1) 7.4 | (0) 0.0198 ± 0.0015 | (1) 10 | 2.37 ± 0.04 | 2.30 |
| 8 | (1) 16.8 | (0) 0.0197 ± 0.0022 | (1) 10 | 4.04 ± 0.07 | 3.85 |
| 9 | (0) 12.1 | (−1) 0.0105 ± 0.0012 | (−1) 6 | 0.75 ± 0.08 | 0.63 |
| 10 | (0) 12.1 | (1) 0.0301 ± 0.0011 | (−1) 6 | 1.17 ± 0.11 | 1.03 |
| 11 | (0) 12.1 | (−1) 0.0108 ± 0.0008 | (1) 10 | 1.60 ± 0.02 | 1.74 |
| 12 | (0) 12.1 | (1) 0.0309 ± 0.0023 | (1) 10 | 2.77 ± 0.13 | 2.89 |
| 13 | (0) 12.1 | (0) 0.0186 ± 0.0010 | (0) 8 | 1.79 ± 0.11 | 1.93 |
| 14 | (0) 12.1 | (0) 0.0201 ± 0.0007 | (0) 8 | 1.91 ± 0.06 | 1.93 |
| 15 | (0) 12.1 | (0) 0.0212 ± 0.0006 | (0) 8 | 2.09 ± 0.10 | 1.93 |
| 16 | (0) 12.1 | (0) 0.0196 ± 0.0009 | (0) 8 | 1.89 ± 0.05 | 1.93 |
| 17 | (0) 12.1 | (0) 0.0208 ± 0.0004 | (0) 8 | 1.97 ± 0.09 | 1.93 |

isopropanol (300 mL) to completely eliminate the unreacted regents. The precipitate was dissolved in distilled water and successively dialyzed against tap water (24 h) and distilled water (24 h) in a dialysis bag (MD44-14, Union Carbide Co., Seadrift, TX, USA) with a size exclusion of 14000 g/mol for globular molecules.[22,23] Finally, the dialysate was lyophilized to obtain FAOGE. The effects of synthesis parameters on the reaction efficiency, in terms of DS, were investigated using a response surface methodology (RSM). The observed parameters included $A$, acyl chain lengths; $B$, $M_w$ of $\beta$-glucan; and $C$, addition of acyl imidazole. The independent factors, levels, and experimental design in terms of coded and uncoded values are shown in Table 1.

**Determination of Degree of Substitution.** The DS of FAOGEs was determined according to a previously described method with slight modifications.[24] The sample (30 mg) dissolved in 0.5 mL of DMSO was mixed with 1 mL of 0.07 M sodium methoxide in methanol. The mixture was then hermetically heated to 80 °C and kept for 60 min. After the mixture was completely cooled, 1 mL of deionized water and 1 mL of $n$-heptane were added. The mixture was shaken for 1 min and left to settle. The top organic phase could be subjected to GC analysis with methyl laurate as an internal standard.[25] A gas chromatography (GC) system (GC-2010, Shimadzu, Kyoto, Japan) equipped with a DB-WAX capillary column (30 m × 0.25 mm i.d.; SGE Inc., Austin, TX, USA) and a flame ionization detector (FID) was applied. Nitrogen was supplied as carrier gas, and the column oven temperature was equilibrated at 100 °C for 3 min, ramped at 10 °C/min to 220 °C, and maintained at 220 °C for 3 min. The DS of the fatty acid ester was calculated using the equation previously reported by Singh et al.[5]

**FAOGE Characterization.** The esterification of oat $\beta$-glucan with fatty acids were evidenced with the aid of $^1$H NMR and Fourier transform infrared spectroscopy (FT-IR). $^1$H NMR spectra of the samples in DMSO-$d_6$ were recorded on a Bruker AV 600 MHz (Bruker Corp., Fallanden, Switzerland). Chemical shifts were given in parts per million (ppm) from tetramethylsilane. FT-IR spectra were acquired on a PerkinElmer Spectrum 2000 Fourier transform IR spectrometer (Shelton, CT, USA) using KBr disks prepared from powdered samples mixed with dry KBr in a weight ratio of 1:30. The morphology of nanoparticles of FAOGE in aqueous solution was observed at 200 kV using a JEOL JEM-2100 instrument (JEOL, Japan) equipped with a Gatan 94 Ultrascan 1k charge-coupled device camera.[15,26] The behavior of the aqueous solution of FAOGE was characterized by fluorescence spectroscopy.[27] Meanwhile, the size of

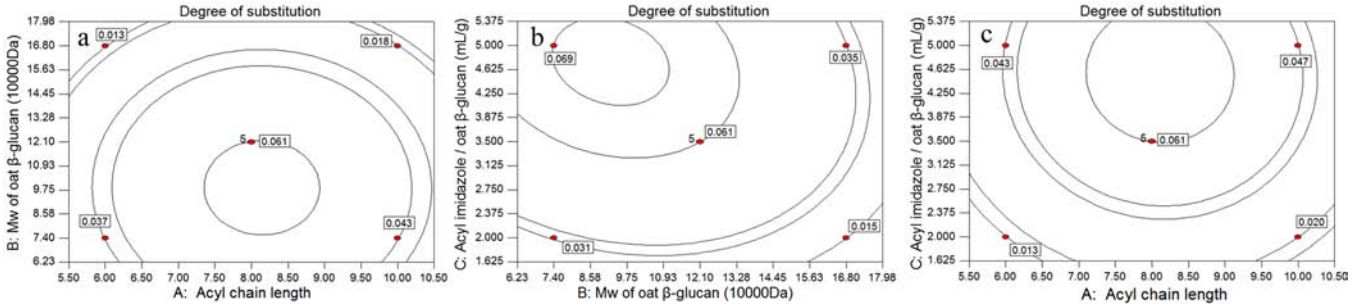


**Figure 2.** Response surface plots showing the interactive effects of acyl chain length ($A$), $M_w$ of oat $\beta$-glucan ($B$), and addition of acyl imidazole ($C$) on the degree of substitution of fatty acid oat $\beta$-glucan esters (FAOGEs).

the self-aggregates formed by FAOGE was determined by dynamic light scattering (DLS) with a Malvern Zetasizer, Nano ZS90 (Malvern Instruments Limited, Malvern, Worcestershire, UK).[28] Finally, the solubilizing or loading capacity of FAOGE for curcumin, a representive of hydrophobic phytochemicals, was determined according to a previously reported method.[16] With the aid of RSM, the structure−CLC of FAOGEs was explored by using CLC as dependent and $M_w$ of $\beta$-glucan, acyl chain length, and DS as variables. The experimental design in terms of coded and uncoded values is shown in Table 3.

**Statistical Analysis.** All results were expressed as means with standard deviations of at least three measurements. Statistical significance of difference between groups was tested by one-way analysis of variance (ANOVA) using SPSS 19.0 (SPSS Inc., Chicago, IL, USA). In all statistical analyses, $P < 0.05$ was considered significant.

## RESULTS AND DISCUSSION

**FAOGE Synthesis.** The design of RSM and the determined and predicted results of 17 designed experimental runs are depicted in Table 1. ANOVA (Table 2) was used to attest the effects of the acyl chain length ($A$), $M_w$ of $\beta$-glucan ($B$), addition of acyl imidazole ($C$), and their quadratic terms ($A^2$, $B^2$, $C^2$) and interactive terms ($AB$, $AC$, $BC$) on the DS of FAOGE. The results indicated that $M_w$ of $\beta$-glucan ($B$), addition of acyl imidazole ($C$), and all three quadratic terms ($A^2$, $B^2$, $C^2$) generated significant effects on DS, whereas the DS values of FAOGEs were independent of acyl chain length ($A$) and all three interactive terms ($AB$, $AC$, $BC$). Together, these results indicate that the three selected factors are vital to FAOGE synthesis. Comparatively, $M_w$ of $\beta$-glucan ($B$) and the addition of acyl imidazole ($C$) are of more importance than the acyl chain length ($A$) in terms of their effects on DS.

To reflect the effect tendencies of selected factors on DS, the isoresponse curves are plotted as a function of two factors, whereas the third is maintained at its central level (0) (Figure 2). Panels a and b of Figure 2 reveal that the DS of FAOGEs with the same acyl significantly decreased with the $M_w$ of $\beta$-glucan. With regard to the plausible reason for the effects of $M_w$ on DS of modified $\beta$-glucan, the increase in the number of hydroxyl groups resulting from acid hydrolysis was first considered. However, on the basis of the number-average molecular weights of native $\beta$-glucan ($13.95 \times 10^4$), OSG1 ($3.93 \times 10^4$), and OSG2 ($2.71 \times 10^4$), the number of hydroxyl groups per mole of OSG1 and OSG2 increased by approximately 0.27 and 0.40% in contrast to that of native $\beta$-glucan, whereas the DS of their modified products with octanoic acid substantially increased by 154.6 and 168.2%. Therefore, the increased number of hydroxyl groups is not the sole explanation for the increased DS of modified $\beta$-glucan with lowered $M_w$. To make the truth clearer, differences in the average reactivity, steric hindrance, and solution viscosity of $\beta$-glucans with varied $M_w$ should be addressed. In acid hydrolysis of $\beta$-glucan, the cleavage of a 1,3- or 1,4-glycosidic bond generated a new $C_1$−OH and a $C_3$− or $C_4$−OH. Commonly, the reactivity of hydroxyl groups decreased in a position sequence of $C_4 < C_3 < C_2 < C_6 < C_1$.[29−31] In this context, the newly derived hydroxyl groups by acid hydrolysis possessed a higher reactivity than those in native $\beta$-glucan. Obviously, hydrolyzed $\beta$-glucans were certainly smaller than native $\beta$-glucan and possessed more flexible chains,[32] which substantially decreased the steric hindrance of backbone chains[30] and consequently increased the regent accessibility.[33] In addition, decreased solution viscosity of $\beta$-glucans was always accompanied by the decrease in their molecular weight.[34] The decreased viscosity denoted more vivid Brownian movements of substrates and, as a result, an increase in their contact frequency was obtained, which finally facilitated the expected etherification.[35]

Panels a and c of Figure 2 reveal that the DS of FAOGEs first increased and then decreased with the acyl chain length within an insignificant level. Similarly, according to the research of Aburto et al., under the same reaction conditions, the DS of fatty acid starch esters prepared with octanoyl and decanoyl were equivalent.[36] Fang et al. also reported that no obvious differences were observed on the DS of fatty acid starch esters when gelatinized potato starch was reacted under the same conditions with butyryl chloride, capryloyl chloride, and lauroyl chloride.[37] Consequently, the present results implied the hexanoyl imidazole, octanoyl imidazole, and decanoyl imidazole presented analogous reactivity with oat $\beta$-glucan.

Panels b and c of Figure 2 illustrate that the DS of FAOGEs sharply increased with the addition of acyl imidazole. This was obviously due to the fact that the increase in acyl imidazole concentration brought about a higher contact frequency between acyl imidazole and $\beta$-glucan. The enhanced contact frequency improved the reaction efficiency of esterification.[38]

According to the results of RSM, the dependence of DS on the acyl chain length ($A$), $M_w$ of $\beta$-glucan ($B$), and addition of acyl imidazole ($C$) could be described by the following equation:

$$DS = 0.061 + 0.0028A - 0.013B + 0.014C - 0.02A^2 - 0.013B^2 - 0.01C^2 - 0.00025AB - 0.00075AC - 0.0043BC$$

This equation could be used as a model to provide a solid support in synthesizing water-soluble FAOGEs with required DS by modulating the addition of acyl imidazole in the reaction system. The good performance of this model is attested by Table 2 in terms of the significance of the model ($P$ value), the coefficient of determination ($R^2$), "lack of fit", and the coefficient of variation (CV). The present $P$ value (<0.0001)

and "lack of fit" ($P$ value = 0.12) indicated the equation was accurate enough to represent the actual relationship between DS and the addition of acyl imidazole. A high value of $R^2$ (0.98) implied a heavy dependence of DS on the addition of acyl imidazole. In other words, when specific oat $\beta$-glucan (with known $M_w$) and fatty acid (with known chain length) were used as substrates, 98% of the variability in DS could be explained by the variation in the addition of acyl imidazole.[39] Furthermore, a small value in CV (9.24%), not higher than 10%, indicated a good reproducibility of this model in controlling FAOGE synthesis.[40] To validate this model, a FAOGE with an expected DS of 0.030 was synthesized in triplicate in our laboratory with native oat $\beta$-glucan ($M_w$ = 16.8 × $10^4$ g/mol) and octanoic acid. The obtained results (0.028, 0.030, 0.029) gave an average DS of 0.029, which was comparative to the expected value.

**FAOGE Characterization.** The structural characteristic changes of oat $\beta$-glucan induced by the esterification with fatty acids were evidenced by FT-IR and $^1$H NMR analysis. The native oat $\beta$-glucan and its octoates with varied DS were compared as representatives. Figure 3 compares the FT-IR

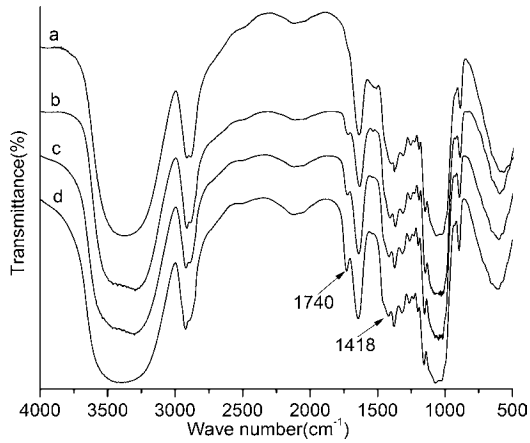


**Figure 3.** FT-IR spectra of native $\beta$-glucan (a) and $\beta$-glucan octoates with degrees of substitution of 0.011 (b), 0.021 (c), and 0.034 (d).

spectra of $\beta$-glucan octoates with that of native $\beta$-glucan. Obviously, the differences between FT-IR spectra of $\beta$-glucan octoates and native $\beta$-glucan were mainly related to the presence of a peak at 1740 $cm^{-1}$ and the peak intensity at 1418 $cm^{-1}$. With regard to peak at 1740 $cm^{-1}$, it was unlimitedly observed for $\beta$-glucan octoates but absent from the FT-IR spectrum of native $\beta$-glucan. Moreover, the intensity of this peak increased with the DS of $\beta$-glucan octoates. On the basis of the related references, this peak could be assigned to C═O stretching vibration of octanoyl groups and evidenced the successful synthesis of FAOGE.[18,41] With regard to the peak at 1418 $cm^{-1}$ attributed to the C—H scissoring vibration of $CH_2$ groups,[42] $\beta$-glucan octoates presented stronger intensity than native $\beta$-glucan. Therefore, the increased number of $CH_2$ groups by the introduction of acyl groups revealed the truth.

The $^1$H NMR spectra of native oat $\beta$-glucan (Figure 4a), oat $\beta$-glucan octoates with DS of 0.011 (Figure 4b), 0.021 (Figure 4c), and 0.034 (Figure 4d) are depicted in Figure 4. Obviously, the $^1$H NMR spectra of oat $\beta$-glucan octoates showed significant differences from that of native oat $\beta$-glucan. The most relevant changes were observed in the scope of 0.80−2.30 ppm. The important signals in the $^1$H NMR spectra were assigned according to previously reported data in the literature. The prominent peaks at 3.33 and 2.49 ppm resulted from the solvents, that is, $H_2O$ and DMSO, respectively.[43] Peaks around 5.39, 5.26, and 4.65 ppm were assigned to chemical shifts of 3-OH, 2-OH, and 6-OH, respectively.[8] Compared to native $\beta$-glucan, $^1$H NMR signals at 2.31, 1.49, 1.24, and 0.85 ppm arose in the $^1$H NMR spectra of $\beta$-glucan octoates as protons of octanoyl groups suggested that the oat $\beta$-glucan were substituted by octanoyl groups during the esterification process. The triplet peak (peak 5 in Figure 4), centered at 0.85 ppm, was assigned to the three protons in the terminal methyl group of the octanoyl chain.[41] Another triplet peak (peak 4 in Figure 4) located around 1.24 ppm was associated with the four methylene groups adjacent to the terminal methyl group.[18] The weak peak (peak 3 in Figure 4) at 1.49 ppm was related to the second methylene group in the octanoyl chain. Finally, the proton resonance at 2.31 ppm (peak 2 in Figure 4) was linked to the methylene group directly attached to the carbonyl group.[44]

When the intensity of peaks at 1.49, 1.24, and 0.85 ppm was correlated to the DS of oat $\beta$-glucan octoates, high correlation coefficients of 0.9781, 0.9866, and 0.9739 were obtained, respectively. This confirmed that $^1$H NMR spectroscopy is a reliable method for determining the DS of fatty acid polysaccharide esters.[45]

As is well-known, water-soluble amphiphilic molecules can spontaneously self-assemble in aqueous solution and form self-aggregates, such as micelles and vesicles.[3] The solution behavior of FAOGEs was investigated with a soluble oat $\beta$-glucan octoate (DS = 0.021) as the substrate. The present study evidenced the self-aggregate formation of oat $\beta$-glucan octoate with the aid of TEM (Figure 5a). This figure also depicted that the self-aggregates were spherical with diameters ranging from 100 to 400 nm. To obtain more information on the formation of the self-aggregate, the behavior of $\beta$-glucan octoate in aqueous solution was investigated by fluorometry and its CAC was determined. As shown in Figure 5b, the $I_{373}/I_{384}$ ratio was approximately 1.80 at low concentration of oat $\beta$-glucan octoate (0.0003−0.03 mg/mL). However, it was gradually decreased with further increase in oat $\beta$-glucan octoate concentration, suggesting the onset of $\beta$-glucan octoate micellization.[46] Accordingly, the CAC of oat $\beta$-glucan octoate (DS = 0.021) was determined as 0.144 mg/mL, which was comparative to the previous results obtained for octenylsuccinated oat $\beta$-glucan in our laboratory.[15] Furthermore, the size distribution of the self-aggregate was characterized by DLS. The obtained DLS curves gave two peaks, that is, a smaller peak located around 100 nm and a bigger one centered at a larger size (300−600 nm). The smaller peak was related to polymeric micelles, and the bigger one was ascribed to the larger self-aggregates.[47] By comparing two curves in Figure 5c, it was concluded that the average size of the self-aggregate increased with the concentration of $\beta$-glucan octoate. This was possibly due to the increased viscosity of the $\beta$-glucan octoate solution resulting from high concentration.[15]

**Structure−CLC Relationship of FAOGE.** The self-aggregate of an amphiphilic polymer in aqueous media possessed a hydrophobic inner core surrounded by a hydrophilic outer shell.[3] The former guaranteed its ability to capture the hydrophobic agents, and the latter was responsible for its solubility in water. Therefore, the self-aggregates of amphiphilic polymers could be used as a tool to increase the solubility, stability, and bioavailability of small hydrophobic

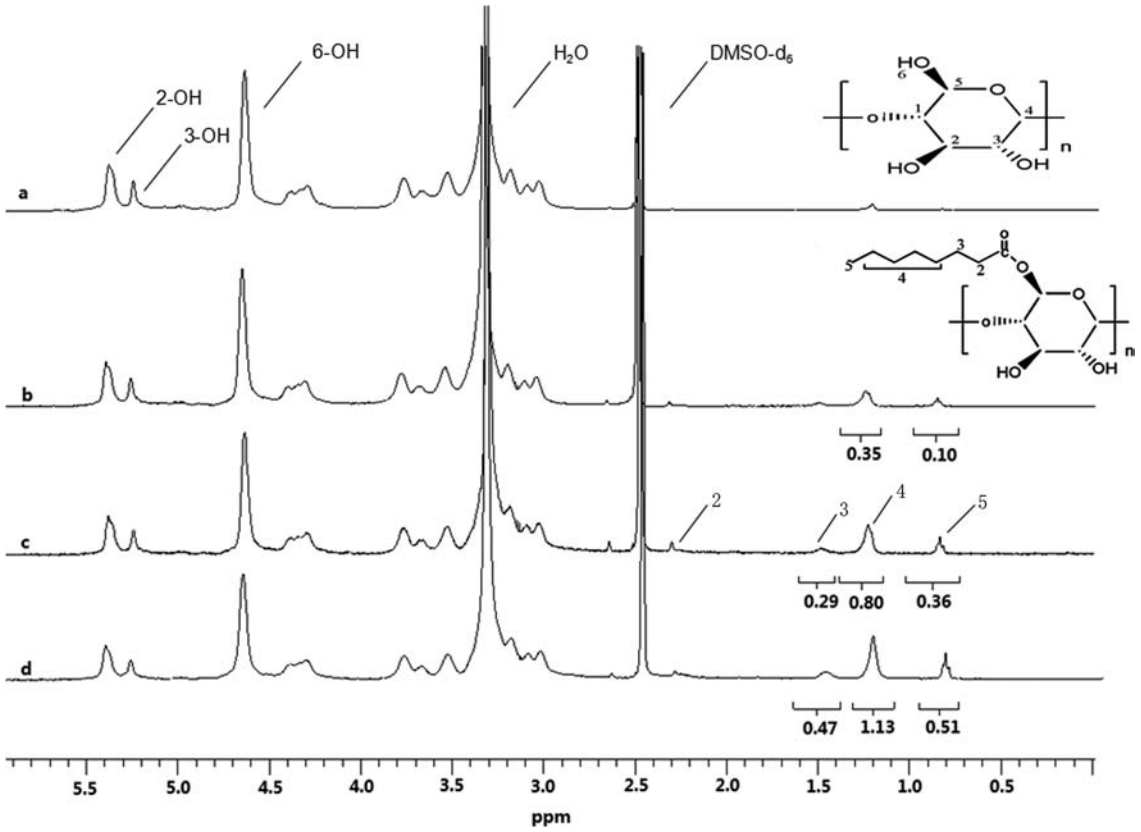


**Figure 4.** [1]H NMR spectra of native $\beta$-glucan (a) and $\beta$-glucan octoates with degrees of substitution of 0.011 (b), 0.021 (c), and 0.034 (d). The data located beneath a peak correspond to its intensity.

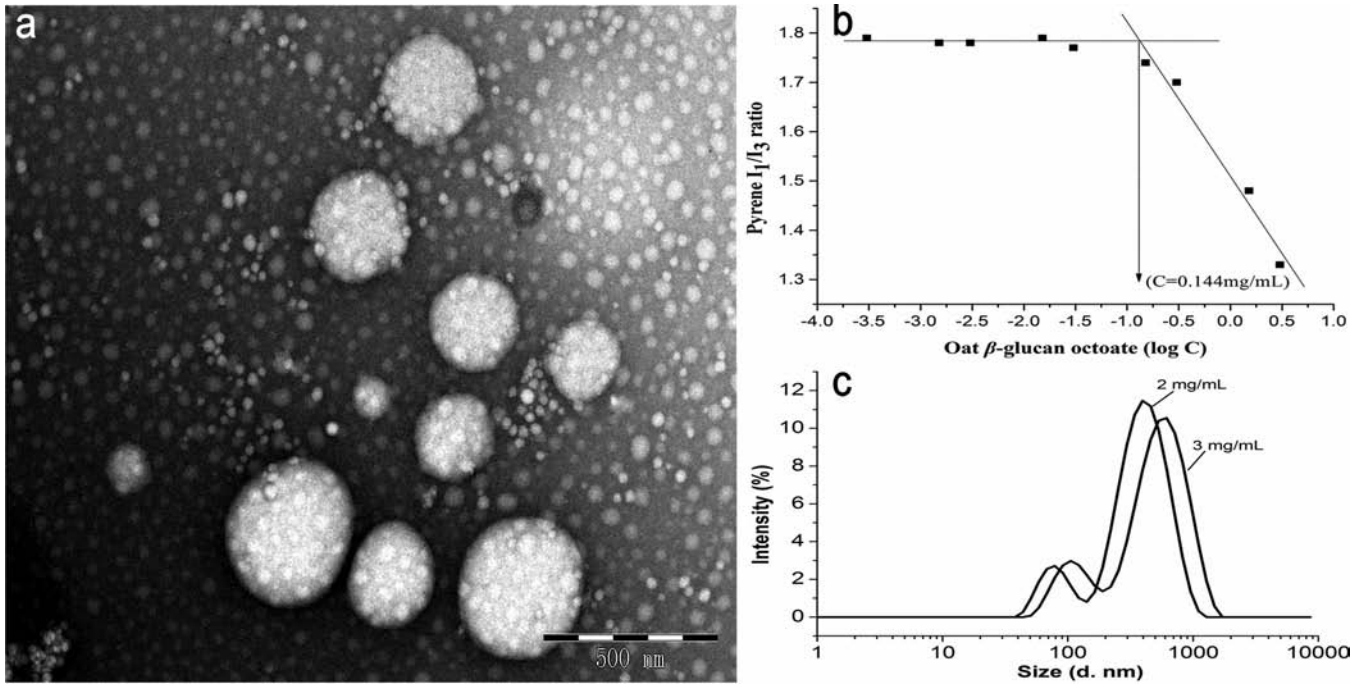


**Figure 5.** Morphology (a), critical aggregation concentration (b), and size distribution (c) of self-aggregates of oat $\beta$-glucan octoate (DS = 0.021) determined or recorded by transmission electron micrograph, fluorescence spectroscopy, and dynamic light scattering, respectively.

compounds.[4] Basically, the solubilizing or loading capacity of a specific hydrophobic agent by micelles formed with an amphiphilic polymer was heavily dependent on its structure parameters.[48] Accordingly, the effects of key structural parameters of FAOGEs, namely $M_w$ of $\beta$-glucan, DS, and acyl chain length, on hydrophobic agent loading capacity by its micelle were explored. This investigation was performed with RSM by using curcumin as an example hydrophobic agent and

**Table 4. Analysis of Variance (ANOVA) for the Effects of $M_w$ of $\beta$-Glucan ($X_1$), DS ($X_2$), Acyl Chain Length ($X_3$), and Their Quadratic Terms ($X_1^2$, $X_2^2$, $X_3^2$) and Interactive Terms ($X_1X_2$, $X_1X_3$, $X_2X_3$) on Curcumin Loading Capacity (CLC) of Fatty Acid Oat $\beta$-Glucan Esters (FAOGEs)**

| source | sum of squares | degree of freedom | mean square | $F$ value | $P$ value |
|---|---|---|---|---|---|
| model | 10.81 | 9 | 1.20 | 40.39 | <0.0001 |
| $X_1$ | 1.75 | 1 | 1.75 | 58.79 | 0.0001 |
| $X_2$ | 1.22 | 1 | 1.22 | 41.18 | 0.0004 |
| $X_3$ | 4.40 | 1 | 4.40 | 147.80 | <0.0001 |
| $X_1X_2$ | 0.078 | 1 | 0.078 | 2.64 | 0.1485 |
| $X_1X_3$ | 0.38 | 1 | 0.38 | 12.93 | 0.0088 |
| $X_2X_3$ | 0.14 | 1 | 0.14 | 4.73 | 0.0662 |
| $X_1^2$ | 0.00148 | 1 | 0.00148 | 0.050 | 0.8298 |
| $X_2^2$ | 2.33 | 1 | 2.33 | 78.32 | <0.0001 |
| $X_3^2$ | 0.63 | 1 | 0.63 | 21.12 | 0.0025 |
| residual | 0.21 | 7 | 0.030 | | |
| lack of fit | 0.16 | 3 | 0.053 | 4.35 | 0.0946 |
| pure error | 0.049 | 4 | 0.012 | | |
| cor total | 11.02 | 16 | | | |
| $R^2$ | 0.98 | CV (%) = 9.74 | | | |

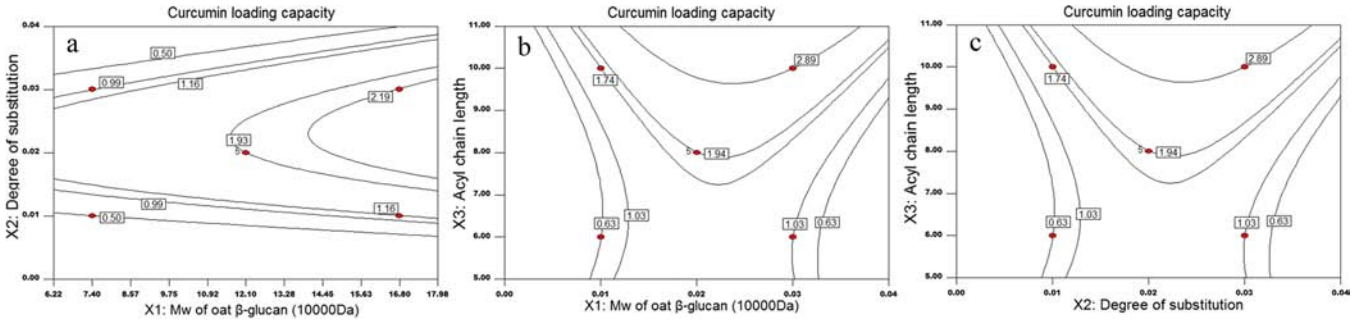


**Figure 6.** Response surface plots showing the interactive effects of $M_w$ of $\beta$-glucan ($X_1$), degree of substitution ($X_2$), and acyl chain length ($X_3$) on the curcumin loading capacity of fatty acid oat $\beta$-glucan ester (FAOGE) micelles.

the above-mentioned structural parameters as variables. The design of RSM and the determined and predicted loading capacities of 17 designed experimental runs are depicted in Table 3. The 17 subjects required for the experiment of structure−capacity relationship (with known $M_w$ of $\beta$-glucan, specific acyl chain length) were synthesized by modulating the addition of acyl imidazole using the above-obtained model. The subjects were validated by judging whether their DS located in the scope of uncoded value ±0.002. The structure−CLC relationship was obtained by multiple regression analysis. The effects of $M_w$ of $\beta$-glucan ($X_1$), DS ($X_2$), and acyl chain length ($X_3$) on the dependent variable CLC ($Y$) could be described by the following model:

$$Y = 1.93 + 0.47X_1 + 0.39X_2 + 0.74X_3 + 0.14X_1X_2 + 0.31X_1X_3 + 0.19X_2X_3 + 0.019X_1^2 - 0.74X_2^2 + 0.39X_3^2$$

The ANOVA (Table 4) results showed that the quadratic polynomial model was statistically significant ($P < 0.0001$) together with an $R^2$ value of 0.98. This indicated that the obtained regression model is effective in explaining the effects of three selected structural parameters on CLC and could be used as a tool to quantitatively predict the resulting changes in CLC when any of the considered parameters had been changed. The "lack of fit $P$ value" of 0.0946 implied the "lack of fit" was not significant relative to the pure error. The small value of CV (9.74%) indicated the considerable precision and reliability of the obtained model. From Table 4, it was also observed that $M_w$ of $\beta$-glucan ($X_1$), DS ($X_2$), acyl chain length ($X_3$), the quadratic terms ($X_2^2$, $X_3^2$), and the interactive terms ($X_1X_3$) had significant effects on the CLC of FAOGE micelles ($P < 0.05$), whereas the quadratic term of $M_w$ of $\beta$-glucan ($X_1^2$), the interactive term of $M_w$ of $\beta$-glucan and DS ($X_1X_2$), and the interactive term of DS and acyl chain length ($X_2X_3$) presented little effect on the CLC of FAOGE micelles ($P > 0.05$).

The effect tendencies of selected factors on CLC were studied by plotting the isoresponse curves (Figure 6) as a function of two factors, whereas the third is fixed at zero level. Panels a and b of Figure 6 reveal that the CLC of FAOGE micelles increased with the $M_w$ of $\beta$-glucan. The similar tendencies were observed in loading curcumin in octenylsuccinate oat $\beta$-glucan,[16] pluronic block copolymer,[49] and poly(ethylene oxide)-*b*-poly($\varepsilon$-caprolactone).[50]

For the effects of DS on CLC of FAOGE micelles, a typical parabola pattern was observed (Figure 6a,c). In other words, CLC values maximized at a medium DS. In lower DS scope (0.01−0.024), CLC increased with DS. This could be ascribed to the following reasons: (1) the increase in DS improved the self-aggregating ability of FAOGEs and resulted in a significant increase in the number of micelles for cucurmin solubilization; (2) the increase in DS enhanced the molecular interaction between cucurmin and FAOGE and facilitated the cucurmin solubilization. Oppositely, in higher DS scope (0.024−0.03), CLC decreased with DS. This could be explained as the (1) further increase in DS decreasing the micelle size significantly, leading to less accommodation for curcumin loading;[15] or (2)

the presence of too much acyl group in the hydrophobic core of the formed micelles impeding the loading of curcumin. The similar tendencies in the effects of DS on loading capacity were observed for complexing steroids by sulfoalkyl ether β-cyclodextrins[51] and loading curcumin in octenylsuccinate oat β-glucan micelles.[16]

With regard to acyl chain length, its increase was always accompanied by an increase in CLC (Figure 6b,c). With the similar DS, the FAOGE with a longer acyl chain length was more hydrophobic than the counterpart with a shorter acyl chain length.[52] As reported previously, hydrophobic interaction is the driving force for the FAOGE micelle to encapsulate curcumin.[16] Thus, the longer the acyl chain length, the more curcumin entrapped in the micelles.

Theoretically, according to the obtained model, a maximum CLC (4.01 μg/mg) could be achieved when a FAOGE with structural parameters of $M_w$ = 16.8 × $10^4$ g/mol, acyl chain length = 10, and DS = 0.0243 was applied. At a FAOGE concentration of 2 mg/mL and solubilizing procedure duration of 24 h, the maximum CLC was validated as 4.05 ± 0.26 μg/mg (Supporting Information).

In summary, with an aim to prepare a novel amphiphilic polymer, FAOGEs were first synthesized in the present study by reacting oat β-glucan with CDI-activated fatty acids in DMSO. RSM was used to analyze the effects of three key reaction parameters (acyl chain length, $M_w$ of β-glucan, addition of acyl imidazole) on the synthesis efficiency, that is, DS. The results indicated that the DS of product increased with the addition of acyl imidazole but decreased with $M_w$ of β-glucan. Meanwhile, the acyl chain length was not significantly related to DS. As a result, with known $M_w$ of β-glucan and fatty acid, a precise model was obtained to control the DS of product by modulating the addition of acyl imidazole in the reaction system. In view of the chemical structure, the FT-IR and $^1$H NMR spectra evidenced the successful synthesis of FAOGE. Finally, the effects of structural parameters of FAOGE ($M_w$ of β-glucan, acyl chain length, and DS) on CLC were investigated by using RSM. As a result, a quadratic polynomial model was obtained to quantitatively describe the structure−CLC relationship of FAOGEs. However, this study is only the first small step toward exploring the application possibility of FAOGEs in solubilizing hydrophobic compounds. Further works on the toxicology, stability, and bioavailability of cucurmin-loaded FAOGE micelles should be addressed.

## ■ ASSOCIATED CONTENT

### Ⓢ Supporting Information

Supplementary figure. This material is available free of charge via the Internet at http://pubs.acs.org.

## ■ AUTHOR INFORMATION

### Corresponding Author

*(G.Z.) Mail: College of Food Science, Southwest University, Tiansheng Road 2, Chongqing 400715, China. Phone: +86 23 68 25 19 02. Fax: +86 23 68 25 19 47. E-mail: zhaogh@swu.edu.cn.

### Funding

We acknowledge financial support from the National Natural Science Foundation of China (31371737).

### Notes

The authors declare no competing financial interest.

## ■ ACKNOWLEDGMENTS

We acknowledge the staff at Beijing ZKBC Testing and Technology Co., Ltd., for their kind support and assistance with $^1$H NMR and TEM.

## ■ REFERENCES

(1) Huang, Q.; Yu, H.; Ru, Q. Bioavailability and delivery of nutraceuticals using nanotechnology. *J. Food Sci.* **2009**, *75*, 50−56.
(2) Hu, H.; Huang, Q. Enhanced in vitro anti-cancer activity of curcumin encapsulated in hydrophobically modified starch. *Food Chem.* **2010**, *119*, 669−674.
(3) Gonçalves, C.; Martins, J. A.; Gama, F. M. Self-assembled nanoparticles of dextrin substituted with hexadecanethiol. *Biomacromolecules* **2007**, *8*, 392−398.
(4) Lei, D.; Liu, J.; Ye, F.; Chen, F.; Zhao, G. Synthesis, characterization and aqueous self-assembly of octenylsuccinic corn dextrin ester with high molecular weight. *Food Hydrocolloids* **2014**, *41*, 250−256.
(5) Singh, A. V.; Nath, L. K. Evaluation of acetylated moth bean starch as a carrier for controlled drug delivery. *Int. J. Biol. Macromol.* **2012**, *50*, 362−368.
(6) Zhong, L.; Gao, Y.; Wu, Y.; Zhang, L. Preparation of amphiphilic cellulose carrier and study of its drug release performance. *Mater. Res. Innovations* **2013**, *17*, 79−82.
(7) Huo, M.; Zhang, Y.; Zhou, J.; Zou, A.; Yu, D.; Wu, Y.; Li, J.; Li, H. Synthesis and characterization of low-toxic amphiphilic chitosan derivatives and their application as micelle carrier for antitumor drug. *Int. J. Pharm.* **2010**, *394*, 162−173.
(8) Kokubun, S.; Ratcliffe, I.; Williams, P. A. Synthesis, characterization and self-assembly of biosurfactants based on hydrophobically modified inulins. *Biomacromolecules* **2013**, *14*, 2830−2836.
(9) Kaewprapan, K.; Tuchinda, P.; Marie, E.; Duend, A.; Inprakon, P. pH-imprinted lipase catalyzed synthesis of dextran fatty acid ester. *J. Mol. Catal. B−Enzym.* **2007**, *47*, 135−142.
(10) Eenschooten, C.; Guillaumie, F.; Kontogeorgis, G. M.; Stenby, E. H.; Schwach-Abdellaoui, K. Preparation and structural characterisation of novel and versatile amphiphilic octenyl succinic anhydride-modified hyaluronic acid derivatives. *Carbohydr. Polym.* **2010**, *79*, 597−605.
(11) van den Broek, L. A.; Boeriu, C. G. Enzymatic synthesis of oligo- and polysaccharide fatty acid esters. *Carbohydr. Polym.* **2013**, *93*, 65−72.
(12) Kondaveeti, S.; Chejara, D. R.; Siddhanta, A. K. Synthesis of self-assembly of agarose-fatty acid ester nanoparticles. *Indian J. Chem.* **2014**, *54*, 679−687.
(13) Wu, Z.; Ming, J.; Gao, R.; Wang, Y.; Liang, Q.; Guan, Y.; Zhao, G. Characterization and antioxidant activity of the complex of tea polyphenols and oat β-glucan. *J. Agric. Food Chem.* **2011**, *59*, 10737−10746.
(14) Bartlomiej, S.; Justyna, R.; Ewa, N. Bioactive compounds in cereal grains − occurrence, structure, technological significance and nutritional benefits − a review. *Food Sci. Technol. Int.* **2012**, *18*, 559−568.
(15) Liu, J.; Li, J.; Ma, Y.; Chen, F.; Zhao, G. Synthesis, characterization and aqueous self-assembly of octenyl-succinate oat β-glucan. *J. Agric. Food Chem.* **2013**, *61*, 12683−12691.
(16) Liu, J.; Chen, F.; Tian, W.; Ma, Y.; Li, J.; Zhao, G. Optimization and characterization of curcumin loaded in octenylsuccinate oat β-glucan micelles with an emphasis on degree of substitution and molecular weight. *J. Agric. Food Chem.* **2014**, *62*, 7532−7540.
(17) European Food Safety Authority Panel on Food Additives and Nutrient Sources added to Food (ANS).. Scientific Opinion on the safety of sucrose esters of fatty acids prepared from vinyl esters of fatty acids and on the extension of use of sucrose esters of fatty acids in flavourings on request from the European Commission. *EFSA J.* **2010**, *3*, 1512.

(18) Wu, C.; Chu, B.; Kuang, L.; Meng, B.; Wang, X.; Tang, S. Synthesis of β-1,3-glucan esters showing nanosphere formation. *Carbohydr. Polym.* **2013**, *98*, 807−812.
(19) Tosh, S. M.; Wood, P. J.; Wang, Q.; Weisz, J. Structural characteristics and rheological properties of partially hydrolyzed oat β-glucan: the effects of molecular weight and hydrolysis method. *Carbohydr. Polym.* **2004**, *55*, 425−436.
(20) Lazaridou, A.; Biliaderis, C. G.; Izydorczyk, M. S. Molecular size effect on rheological properties of oat β-glucans in solution and gels. *Food Hydrocolloids* **2003**, *17*, 693−712.
(21) Gref, R.; Rodrides, J.; Couvreur, P. Polysaccharieds grafted with polyesters: novel amphiphilic copolymers for biomedical applications. *Macromolecules* **2002**, *35*, 9861−9867.
(22) Han, J.; Borjihan, G.; Bai, R.; Sun, Z.; Bao, N.; Chen, X.; Jing, X. Synthesis and anti-hyperlipidemic activity of a novel starch piperinic ester. *Carbohydr. Polym.* **2008**, *71*, 441−447.
(23) Liebert, T.; Kulicke, W. M.; Heinze, T. Novel aprroach towards hydrolytically stable starch acetates for physiological applications. *React. Funct. Polym.* **2008**, *68*, 1−11.
(24) Alissandratos, A.; Baudendistel, N.; Flitsch, S. L.; Hauer, B.; Halling, P. J. Lipase-catalysed acylation of starch and determination of the degree of substitution by methanolysis and GC. *BMC Biotechnol.* **2010**, *10*, 1−8.
(25) Arijaje, E. O.; Wang, Y.; Shinn, S.; Shah, U.; Andrew, P. Effects of chemical and enzymatic modifications on starch-stearic acid complex formation. *J. Agric. Food Chem.* **2014**, *62*, 2963−2972.
(26) Zhu, Y.; Liu, L.; Du, J. Probing into homopolymer self-assembly: how does hydrogen bonding influence morphology? *Macromolecules* **2013**, *46*, 194−203.
(27) Aguiar, J.; Carpena, P.; Molina-BolÍvar, J. A.; Ruiz, C. On the determination of the critical micelle concentration by the pyrene 1:3 ratio method. *J. Colloid Interface Sci.* **2003**, *258*, 116−122.
(28) Luo, Y.; Teng, Z.; Wang, Q. Development of zein nanoparticles coated with carboxymethyl chitosan for encapsulation and controlled release of vitamin D3. *J. Agric. Food Chem.* **2012**, *60*, 836−843.
(29) van Dijk-Wolthuis, W. N. E.; Kettenes-van den Bosch, J. J.; van der Kerk-van Hoof, A.; Hennink, W. E. Reaction of dextran with glycidyl methacrylate: an unexpected transesterification. *Macromolecules* **1997**, *30*, 3411−3413.
(30) Tupa, M.; Maldonadoa, L.; Vazqueza, A.; Foresti, M. L. Simple organocatalytic route for the synthesis of starch esters. *Carbohydr. Polym.* **2013**, *98*, 349−357.
(31) Riva, S.; Nonini, M.; Ottolina, G.; Danieli, B. Subtilisin-catalyzed esterification of di- and oligosaccharides containing a D-fructose moiety. *Carbohydr. Res.* **1998**, *314*, 259−266.
(32) Ryu, J.; Lee, S.; You, S.; Shim, J.; Yoo, S. Effects of barley and oat β-glucan structures on their rheological and thermal characteristics. *Carbohydr. Polym.* **2012**, *89*, 1238−1243.
(33) Puri, V. Effect of crystallinity and degree of polymerization of cellulose on enzymatic sacchrification. *Biotechnol. Bioeng.* **1984**, *26*, 1219−1222.
(34) Zhang, M.; Zhang, L.; Wang, Y.; Cheung, P. C. K. Chain conformation of sulfated derivatives of β-glucan from sclerotia of *Pleurotus tuber-regium*. *Carbohydr. Res.* **2003**, *338*, 2863−2870.
(35) Johansson, L.; Virkki, L.; Anttila, H.; Esselström, H.; Tuomainen, P.; Sontag-Strohm, T. Hydrolysis of β-glucan. *Food Chem.* **2006**, *97*, 71−79.
(36) Aburto, J.; Hamaili, H.; Mouysset-Baziard, G.; Senocq, F.; Alric, I.; Borredon, E. Free-solvent synthesis and properties of higher fatty esters of starch − part 2. *Starch/Staerke* **1999**, *51*, 302−307.
(37) Fang, J. M.; Fowler, P. A.; Tomkinson, J.; Hill, C. A. S. The preparation and characterisation of a series of chemically modified potato starches. *Carbohydr. Polym.* **2002**, *47*, 245−252.
(38) Singh, J.; Kaur, L.; McCarthy, O. J. Factors influencing the physico-chemical, morphological, thermal and rheological properties of some chemically modified starches for food applications − a review. *Food Hydrocolloids* **2007**, *21*, 1−22.
(39) Zhao, H.; Liu, J.; Lv, F.; Ye, R.; Bie, X.; Zhang, C. Enzymatic synthesis of lard-based ascorbyl esters in a packed-bed reactor: optimization by response surface methodology and evaluation of antioxidant properties. *LWT−Food Sci. Technol.* **2014**, *57*, 393−399.
(40) Hajar, M.; Shokrollahzadeh, S.; Vahabzadeh, F.; Monazzami, A. Solvent-free methanolysis of canola oil in a packed-bed reactor with use of Novozym 435 plus loofa. *Enzyme Microb. Technol.* **2009**, *45*, 188−194.
(41) Lu, X.; Luo, Z.; Fu, X.; Xiao, Z. Two-step method of enzymatic synthesis of starch laurate in ionic liquids. *J. Agric. Food Chem.* **2013**, *61*, 9882−9891.
(42) Nagasoe, Y.; Ichiyanagi, N.; Okabayashi, H.; Nave, S.; Eastoe, J.; O'Connor, C. J. Infrared absorption spectra of Aerosol-OT homologous sodium dialkylsulfosuccinates and the effect of crystal polymorphism on the environment of the succinate segment. *Colloid Polym. Sci.* **1999**, *277*, 1051−1057.
(43) Barriosa, S. E.; Giammancoa, G.; Contrerasa, J. M.; Laredob, E.; Lopez-Carrasquero, F. Characterization of esterified cassava starch with long alkyl side chains and different substitution degrees. *Int. J. Biol. Macromol.* **2013**, *59*, 384−390.
(44) Tizzotti, M. J.; Sweedman, M. C.; Tang, D.; Schaefer, C.; Gilbert, R. G. New $^{1}$H NMR procedure for the characterization of native and modified food-grade starches. *J. Agric. Food Chem.* **2011**, *59*, 6913−6919.
(45) Elomaa, M.; Asplund, T.; Soininen, P.; Laatikainen, R.; Peltonen, S.; Hyvarinen, S.; Urtti, A. Determination of the degree of substitution of acetylated starch by hydrolysis, 1H NMR and TGA/IR. *Carbohydr. Polym.* **2004**, *57*, 261−267.
(46) Vieira, N. A. B.; Moscardini, M. S.; de Oliveira Tiera, V. A.; Tiera, M. J. Aggregation behavior of hydrophobically modified dextran in aqueous solution: a fluorescence probe study. *Carbohydr. Polym.* **2003**, *53*, 137−143.
(47) Hause, G.; Kressler, J.; Mäder, K. Hydrophobically modified hydroxyethyl starch: synthesis, characterization, and aqueous self-assembly into nano-sized polymeric micelles and vesicles. *Biomacromolecules* **2007**, *8*, 359−367.
(48) Xu, Y.; Du, Y. Effect of molecular structure of chitosan on protein delivery properties of chitosan nanoparticles. *Int. J. Pharm.* **2003**, *250*, 215−226.
(49) Sahu, A.; Kasoju, N.; Goswami, P.; Bora, U. Encapsulation of curcumin in pluronic block copolymer micelles for drug delivery applications. *J. Biomater. Appl.* **2011**, *25*, 619−639.
(50) Ma, Z.; Haddadi, A.; Molavi, O.; Lavasanifar, A.; Lai, R.; Samuel, J. Micelles of poly(ethylene oxide)-*b*-poly(ε-caprolactone) as vehicles for the solubilization, stabilization, and controlled delivery of curcumin. *J. Biomed. Mater. Res., Part A* **2008**, *86*, 300−310.
(51) Zia, V.; Rajewski, R. A.; Bornancini, E. R.; Luna, E. A.; Stella, V. J. Effect of alkyl chain length and degree of substitution on the complexation of sulfoalkyl ether β-cyclodextrins with steroids. *J. Pharm. Sci.* **1997**, *86*, 220−224.
(52) van Kempen, S. E. H. J.; Schols, H. A.; van der Linden, E.; Sagis, L. M. C. Effect of variations in the fatty acid chain on functional properties of oligofructose fatty acid esters. *Food Hydrocolloids* **2014**, *40*, 22−29.

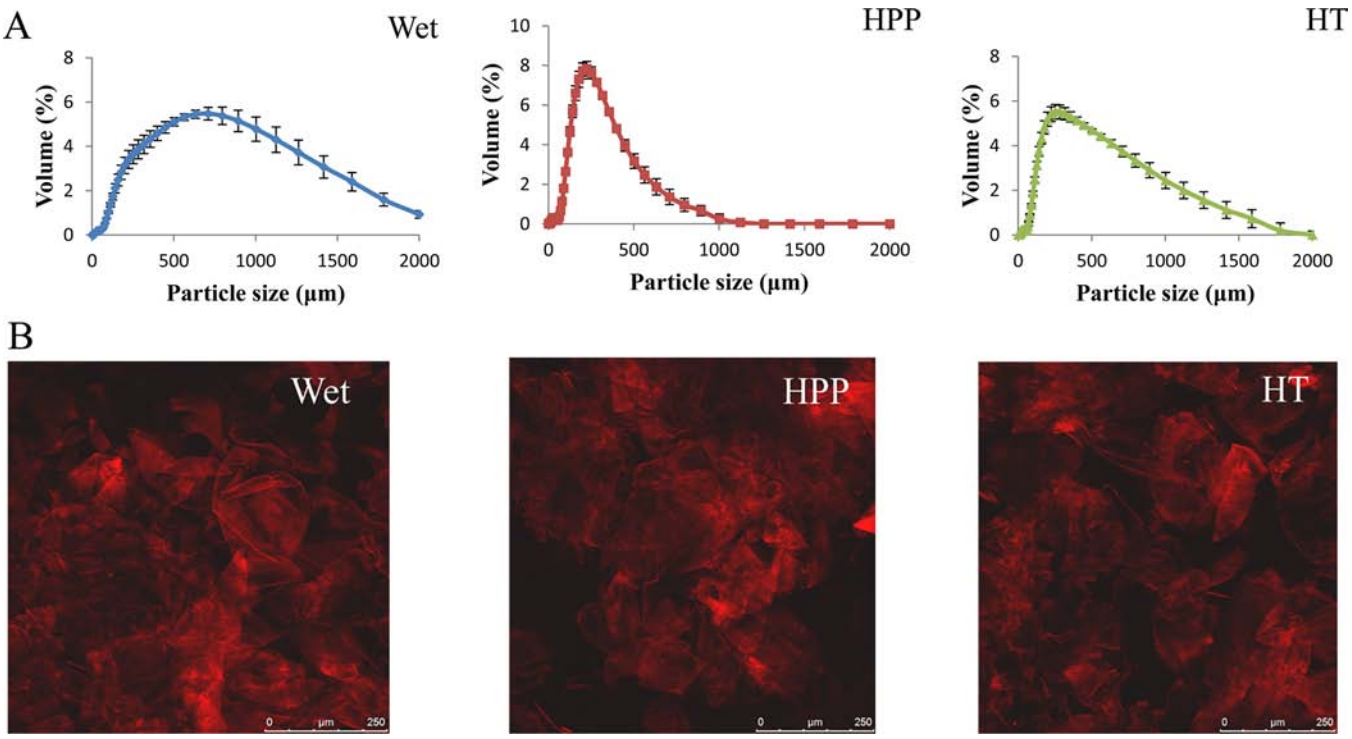


**Figure 1.** (A) Particle size distribution and (B) confocal laser images of wet, HPP, and HT apple pomace.

121 °C for 5 min using an autoclave (Centenary Series, Atherton Company, Victoria, Australia). The processed pomace was stored at 4 °C and used within 1 week of preparation. The moisture contents of the wet, HPP, and HT apple pomace, as determined using the MA-30 moisture meter (Sartorius, GER), were 76.8 ± 0.4, 76.6 ± 0.8, and 76.4 ± 0.5% (w/w), respectively. The pH of the apple pomace after HPP and HT was 4.2 ± 0.2. Unless otherwise stated, EGCG, porcine pancreatin, pepsin, and other chemicals were purchased from Sigma-Aldrich Chemical Co. (St. Louis, MO). High-performance liquid chromatography (HPLC)-grade acetonitrile was from Fisher Scientific Company (Waltham, MA).

**Particle Size Distribution.** The particle size distribution of the apple pomace was measured using a laser diffraction analyzer (Mastersizer 2000, Malvern Instruments, Ltd., U.K.). The apple pomace samples were diluted with water until an obscuration reading ranging from 13 to 17%. A general purpose model (on the basis of Mie and Fraunhofer scattering) was used to fit the particle size data, using a refractive index of 1.533 in the calculation. Analyses were carried out in triplicate on the diluted samples in distilled water.

**Confocal Laser Microscopy.** The fresh frozen wet, HPP, and HT apple pomace were assessed using a Leica SP5 confocal laser scanning microscope (Leica Microsystems, Wetzlar, Germany). The sample was stained with a drop of fluorescent Congo red dye (0.2%, w/v) to stain polysaccharides. Observation was conducted at room temperature (~22 °C) using a HC PL APO 20× objective, and excitation was achieved with the use of a 488 nm argon laser.

**Adsorption Kinetic Studies.** Samples of pomace (0.50 g equivalent dry weight; pH 4.2 ± 0.2) were added to 100 mL of EGCG solution (200 mg of EGCG $L^{-1}$) in separate conical flasks. The conical flasks were sealed by parafilm (Pechiney Plastic Packaging, Inc., Chicago, IL) and placed in a shaking water bath at 120 rpm at 25 °C. Aliquots (1.0 mL) were taken at specific time intervals (5, 15, 30, 60, 120, 180, 300, and 480 min) and subjected to HPLC analysis. The amount of EGCG adsorbed at time $t$, $q_t$ (mg $g^{-1}$), was calculated using the following equation:

$$q_t = \frac{(C_0 - C_t)V}{W}$$

where $C_0$ and $C_t$ (mg $L^{-1}$) are the EGCG concentrations of the liquid phase initially and at time $t$, $V$ (L) is the volume of the solution, and $W$ (g) is the dry mass of adsorbent used. The experiment was carried out in duplicate.

***In Vitro* Digestion Simulation.** A total of 10 mL of EGCG aqueous solution (10 g $L^{-1}$) was mixed with 40 g of apple pomace, and the mixture was blended with a mixer (BSB-380, Breville Pty Ltd., Botany, New South Wales, Australia) for 1 h. Then 1 g of mixture was taken for *in vitro* digestion simulation. For the control, 1 mL of 2 g $L^{-1}$ EGCG solution was used. *In vitro* digestions were carried out in simulated gastric fluids with or without added enzymes according to a published method.[19]

*Preparation of Simulated Gastric Fluid (SGF) and Simulated Intestinal Fluid (SIF).* For the preparation of SGF, 2.0 g of sodium chloride was dissolved in 500 mL of deionized water. To this solution was added 7 mL of 36% (w/v) hydrochloric acid and 3.2 g of pepsin (800−2500 units/mg of protein), and the mixture was made up to a volume of 1000 mL using deionized water. The pH was adjusted to1.2 using 1.0 M hydrochloric acid.

For the preparation of SIF, 13.6 g of potassium dihydrogen phosphate was dissolved in 800 mL of deionized water. To this solution was added 154 mL of 0.2 M sodium hydroxide and 2.5 g of 8× USP pancreatin. The mixture was made up to a volume of 1000 mL using deionized water and stirred at 4 °C overnight. The final pH was adjusted to 6.8 using a few drops of 1.0 M sodium hydroxide.

*Sequential Gastric and Intestinal Digestion in Vitro.* For each treatment, 22 digestion tubes were prepared and subjected to *in vitro* digestion. For each tube, apple pomace (1.0 g) was mixed with 10 mL of SGF, vortexed, placed into a glass tube, and held at 37 °C in a shaking water bath (120 rpm for 2 h). Following gastric digestion, the pH was adjusted from pH 1.2 to 6.8 and 10 mL of SIF was added. The tube was then placed in a shaking water bath (120 rpm for 3 h) at 37 °C. Samples were removed at 30 min intervals during the digestion for analysis of remaining EGCG. For each time point, two samples were removed for analysis.

**Extraction and Preparation of Samples for HPLC Analysis.** For samples containing apple pomace, the contents of the whole tubes containing EGCG−apple pomace sample were used for extraction of EGCG. For EGCG−apple pomace samples exposed to simulated

gastric fluid, the whole sample was mixed with 10 mL of ethanol and stirred for 3 h prior to centrifugation. Extraction of samples at time $t$ = 0 min showed that the amount extracted was the same as that originally added into the sample, showing that the extraction protocol was adequate. For EGCG−apple pomace samples exposed to sequential gastric and simulated intestinal fluids, the whole sample was mixed with 20 mL of ethanol, the pH was then adjusted to ∼3.5 to stabilize the EGCG against degradation, and the mixture was stirred for 3 h prior to centrifugation. All ethanol extracts were centrifuged at 10 000 rpm and 4 °C for 10 min, and the supernatant was used for HPLC analysis. For the control, where only EGCG solutions were added into gastrointestinal fluids (without apple pomace), samples were centrifuged at 10 000 rpm and 4 °C for 10 min and then the supernatant was used for HPLC analysis. The amount recovered at $t$ = 0 min was also the same as that originally added.

**HPLC Analysis.** The concentration of EGCG in the supernatants was determined following the method that we previously used.[15] The HPLC [Surveyor system with photodiode array (PDA) detector and mass spectrometry (MS) pump, Thermo Finningan, NJ] conditions were as follows: injection volume, 10 μL; VYDAC $C_{18}$ monomeric 238EV52 column (250 × 2.1 mm inner diameter × 5 μm particle size); column temperature, 28 °C; mobile phase A, acetonitrile + 0.08% trifluoroacetic acid; mobile phase B, water + 0.1% trifluoroacetic acid; and linear gradient elution, from 2% A/98% B to 24% A/76% B within 45 min and then change to 2% A/98% B until 50 min, with a flow rate of 200 μL/min. The ultraviolet−visible (UV−vis) detector wavelength was set at 280 nm. For quantification of EGCG, peak areas were compared to an external standard solution of EGCG. When an extract from apple pomace alone was analysed, there was no EGCG peak detected at the expected retention time for EGCG, confirming the absence of EGCG in the original apple pomace used.

**Data Analysis.** All experiments were carried out at least in duplicate, and the data were analyzed using Origin 8.0 (Origin Lab, Inc., Northampton, MA) for a one-way analysis of variation (ANOVA). Duncan's multiple range test was used to determine whether significant difference ($p < 0.05$) existed between mean values.

## RESULTS AND DISCUSSION

**Effect of Processing Treatments on the Particle Size and Structure.** The particle size distributions of the wet, HPP, and HT apple pomace are given in Figure 1A, and the confocal images of the corresponding samples are shown in Figure 1B.

The characteristics of the size distribution were different for the three samples, with the high-pressure-treated apple pomace having the narrowest size distribution (Figure 1A). The particle size distribution of the wet apple pomace was wider, and particles were larger compared to those of high-pressure-treated or heat-treated pomace. The $d(0.5)$ for high-pressure-treated pomace was 227 ± 3 μm, while those for the heat-treated and original wet apple pomace were 329 ± 2 and 563 ± 12 μm, respectively. There was a broad distribution of particles in fresh frozen wet apple pomace, with a peak observed at approximately 800 μm (Figure 1A) and particles larger than 800 μm, which may be particles comprising clusters of undissociated cells and also smaller particles existing, which may be ascribed to fragments of broken cells. As for HPP apple pomace, there was a narrow size distribution with a peak at ∼200 μm (Figure 1A), which may be individual cells because of the separation of cell clusters as a consequence of HPP. In heated apple pomace, the distribution centered around 300 μm, indicating that the parenchyma may have been disrupted and separated into small pieces of clusters during heat processing. The fact that processing treatments including thermal processing separate cell clusters and disrupt the apple cell wall into fragments has been previously observed.[20,21] The confocal laser images of the wet, HPP, and HT pomace are shown in Figure 1B. Although there were differences in the particle size distribution obtained using particle sizing data from light scattering (Figure 1A), the differences between the treatments of the apple pomace were not that obvious (Figure 1B).

**Adsorption of EGCG onto Apple Pomace.** The adsorption capacity of EGCG onto wet apple pomace was significantly higher than that for HPP or HT ($p < 0.05$) processed apple pomace at 25 °C (Figure 2). In the initial stages, there were sufficient available adsorption sites on the surface of apple pomace, resulting in rapid adsorption of EGCG onto the pomace. There was subsequent plateauing with increasing time because of the saturation of available adsorption sites.

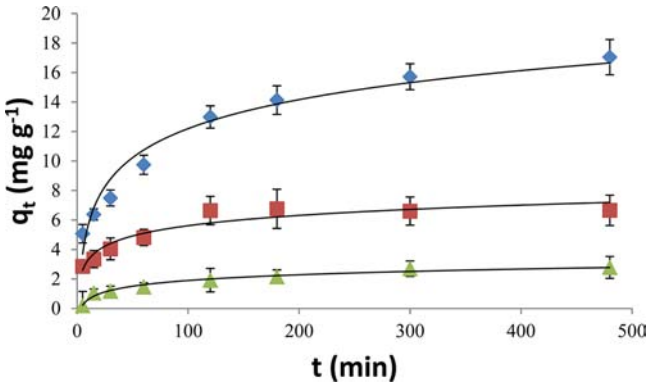


**Figure 2.** Adsorption of EGCG onto wet (blue diamonds), HPP (red squares), and HT (green triangles) apple pomace in sequential contact time at 25 °C. Initial [EGCG] = 200 mg L$^{-1}$.

The apple pomace consists of insoluble fiber, such as lignin and cellulose. Hence, there are a large number of hydroxyl groups in these polymers that could potentially associate with EGCG through hydrogen bonding. Various processing treatments, such as heating and HPP, may cause multiple structural changes at the molecular, microstructural, and macroscopic levels and change the characteristics of the dispersed phase of the processed material.[22] All of these changes are likely to impact on the adsorption capacity of small molecules, such as bioactive molecules, and the kinetics of the adsorption.

**Gastric and Intestinal Digestion *in Vitro*.** The total EGCG in EGCG−apple pomace samples and EGCG alone exposed to gastrointestinal fluids is shown in Table 1 and Figure 3.

*Digestion in the Presence of Enzymes.* As there is no EGCG in apple pomace, any EGCG detected in the system will be due to EGCG carried by the apple pomace. Upon exposure to SGF, there was minimal degradation of EGCG (<10% degradation), irrespective of whether EGCG was delivered in combination with apple pomace or on its own. However, there was a marked decrease in the amount of EGCG in all systems in SIF, with only 16−35% EGCG remaining at the end of SGF−SIF exposure. These results are similar to other studies which showed that the major degradation of tea polyphenols occurs in intestinal fluids.[13,23] The pH-dependent stability of EGCG observed in this study is consistent with the reported EGCG degradation at near neutral or alkaline pH.[11,13]

At the end of the digestion process, only 16% EGCG was recovered in the control sample without apple pomace in our study (Table 1), which is of a similar order to the recovery of

**Table 1. Measured EGCG Contents in the Sample before and after Exposure to SGF and Sequential Exposure to SGF + SIF *in Vitro*[a]**

| system | initial EGCG (mg) | after exposure to SGF (2 h) | | after sequential exposure to SGF (2 h) + SIF (3 h) | |
|---|---|---|---|---|---|
| | | amount of EGCG (mg) | percentage of initial EGCG (%) | amount of EGCG (mg) | percentage of initial EGCG (%) |
| EGCG alone | 2.01 ± 0.02 a | 1.84 ± 0.06 a | 92 | 0.33 ± 0.19 b | 16 |
| EGCG−wet apple pomace | 1.99 ± 0.10 a | 1.82 ± 0.03 a | 91 | 0.40 ± 0.06 b | 20 |
| EGCG−HPP apple pomace | 2.04 ± 0.08 a | 1.94 ± 0.05 a | 95 | 0.71 ± 0.02 a | 35 |
| EGCG−HT apple pomace | 2.05 ± 0.10 a | 1.90 ± 0.02 a | 93 | 0.56 ± 0.13 a | 27 |

[a]The data are the average ± standard deviation (SD) of the measured values. The same amount of EGCG (2 mg) was used initially in all samples. Different letters between treatments in the same column denote that there are significant differences ($p < 0.05$).

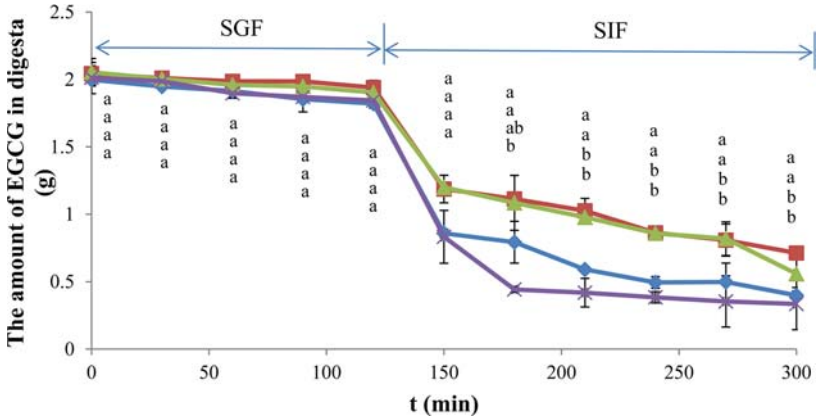


**Figure 3.** Amount of EGCG that remained in wet (blue diamonds), HPP (red squares), and HT (green triangles) apple pomace and EGCG solution alone (purple crosses) exposed to SGF and SIF *in vitro* in the presence of enzymes. The letters in the same column represent the significant difference ($p < 0.05$) at the same time point between HPP apple pomace, HT apple pomace, wet apple pomace, and EGCG alone (from top to bottom).

EGCG obtained in other studies.[24,25] The protection to EGCG provided by the apple pomace follows the order: HPP = HT > wet apple pomace. The recovery of EGCG in EGCG−HPP and EGCG−HT apple pomace mixtures was significantly higher ($p < 0.05$) than that of control and that for EGCG−wet apple pomace at the end of intestinal digestion. This demonstrates the ability of apple pomace to protect EGCG against degradation at ∼ neutral pH.

Although the measured adsorption of EGCG to apple pomace follows the order of wet > HPP > HT apple pomace under equilibrium conditions when apple pomace is mixed with EGCG (Figure 2), it is possible for the binding affinity to change with pH of the gastrointestinal fluids. This was not measured in our study. However, the observation that apple pomace protects EGCG against degradation in SIF suggests that the protection afforded to EGCG may in part be due to the binding of EGCG to the pomace. It is also likely that the differences in the microstructure of the pomace may also have had an influence on degradation of bound EGCG. It is conceivable that a physical barrier to contact with the external environment provided by the apple pomace may contribute to the stabilization of EGCG. Other studies have suggested that processing treatments on plant tissue (e.g., tomato and potato) that alter structure affect the bioaccessibility of bioactives.[26]

*Effect of the Enzyme.* To determine if intestinal enzymes contributed to the rate of degradation of EGCG in simulated gastrointestinal conditions, the EGCG degradation in the absence and presence of enzymes (pepsin and pancreatin) was compared. Figure 4 shows the comparison of the digestion system with or without enzyme. The effect of the enzyme was significantly different ($p < 0.05$) when only EGCG was delivered as an aqueous solution during intestinal digestion (Figure 4A). In contrast, the presence of enzyme did not have a marked effect on the EGCG−pomace mixtures during gastrointestinal digestion (panels B−D of Figure 4). In the presence of apple pomace, there already exists an interaction between EGCG and the pomace. It is not understood why there was a significant effect of the enzyme in EGCG only solutions (Figure 4 A) but not when EGCG was delivered in the presence of pomace (panels B−D of Figure 4). However, the effect of the enzyme, although significant, is small in comparison to the effect of pH on EGCG solutions (Figure 4A). Overall, the results suggest that pH had the overriding effect on the rate of EGCG degradation.

In the *in vitro* system examined, the EGCG−pomace mixture markedly decreased the extent of degradation of EGCG during intestinal digestion. The enzyme had an effect on the digestion of EGCG solution, but the main factor influencing the degradation of EGCG was the pH. The observations that apple pomace protects EGCG against degradation implies that apple pomace could be considered as a suitable carrier for EGCG and polyphenols, with the potential to enhance the stability and bioavailability of polyphenolic compounds. The use of apple pomace as a carrier for EGCG is an alternative to use of encapsulation of EGCG in liposomes or biopolymeric nanopartricles for protecting EGCG against degradation in the gastrointestinal tract. Comparative studies between the efficacy of apple pomace as a carrier for EGCG compared to the use of encapsulation systems would be of interest. Experiments *in vivo* with humans are needed to validate the effects of apple pomace

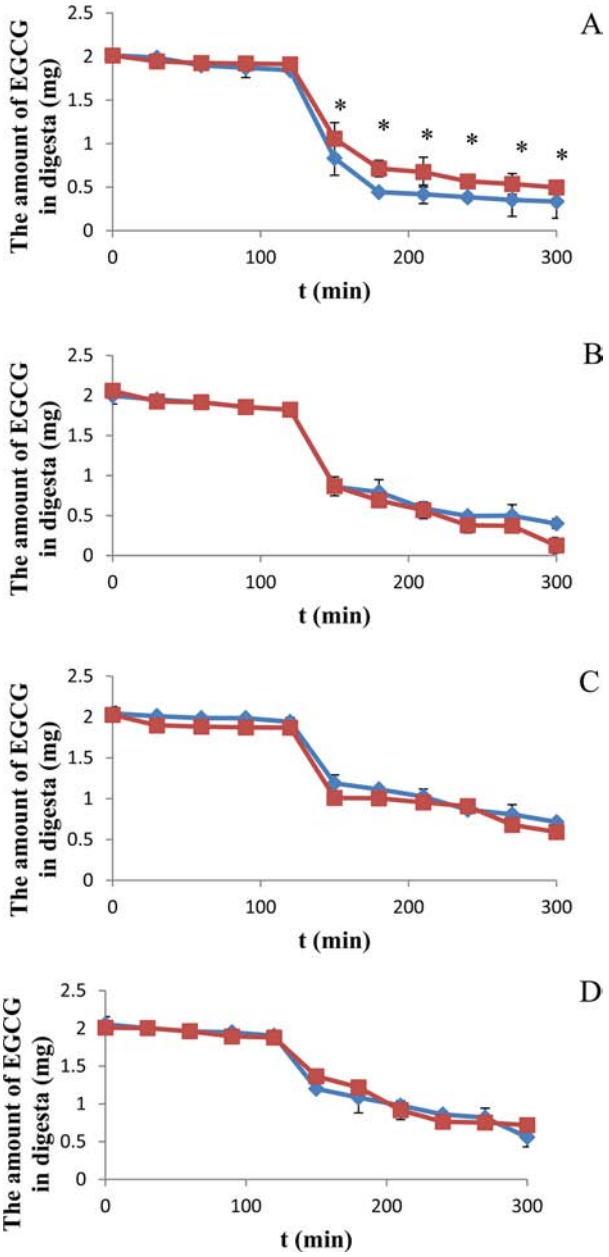


**Figure 4.** Amount of EGCG digested with (blue diamonds) or without (red squares) enzyme during the gastrointestinal digestion simulation, with the asterisks indicating that there is a significant difference ($p < 0.05$) at the same time point: (A) EGCG alone, (B) EGCG–wet apple pomace, (C) EGCG–HPP apple pomace, (D) EGCG–HT apple pomace.

on the bioavailability of polyphenols and to determine whether this can be translated to the achievement of desirable physiological properties.

## AUTHOR INFORMATION

### Corresponding Author

*Telephone: +61-3-9731-3486. Fax: +613-9731-3201. E-mail: maryann.augustin@csiro.au.

### Funding

This work was funded in part by the Natural Science Foundation of Fujian Province (2014J01082) and the Doctoral Program of Higher Education China (20123515120007) awarded to Liangyu Wu.

### Notes

The authors declare no competing financial interest.

## REFERENCES

(1) Na, H. K.; Surh, Y. J. Modulation of Nrf2-mediated antioxidant and detoxifying enzyme induction by the green tea polyphenol EGCG. *Food Chem. Toxicol.* **2008**, *46*, 1271–1278.

(2) Ying, Z.; Chao-Mei, M.; Shahidi, F. Antioxidant and antiviral activities of lipophilic epigallocatechin gallate (EGCG) derivatives. *J. Funct. Foods* **2012**, *4*, 87–93.

(3) Ikigai, H.; Nakae, T.; Hara, Y.; Shimamura, T. Bactericidal catechins damage the lipid bilayer. *Biochim. Biophys. Acta, Bioenerg.* **1993**, *1147*, 132–136.

(4) Caturla, N.; Vera-Samper, E.; Villalain, J.; Mateo, C. R.; Micol, V. The relationship between the antioxidant and the antibacterial properties of galloylated catechins and the structure of phospholipid model membranes. *Free Radical Biol. Med.* **2003**, *34*, 648–662.

(5) Nakayama, M.; Suzuki, K.; Toda, M.; Okubo, S.; Hara, Y.; Shimamura, T. Inhibition of the infectivity of influenza virus by tea polyphenols. *Antivir. Res.* **1993**, *21*, 289–299.

(6) Pang, J. Y.; Zhao, K. J.; Wang, J. B.; Ma, Z. J.; Xiao, X. H. Green tea polyphenol, epigallocatechin-3-gallate, possesses the antiviral activity necessary to fight against the hepatitis B virus replication *in vitro*. *J. Zhejiang Univ., Sci., B* **2014**, *15*, 533–539.

(7) Long, H.; Zhu, Y.; Cregor, M.; Tian, F.; Coury, L.; Kissinger, C. B.; Kissinger, P. T. Liquid chromatography with multi-channel electrochemical detection for the determination of epigallocatechin gallate in rat plasma utilizing an automated blood sampling device. *J. Chromatogr. B: Biomed. Sci. Appl.* **2001**, *763*, 47–51.

(8) Ullmann, U.; Haller, J.; Decourt, J.; Girault, N.; Girault, J.; Richard-Caudron, A.; Pineau, B.; Weber, P. A single ascending dose study of epigallocatechin gallate in healthy volunteers. *J. Int. Med. Res.* **2003**, *31*, 88–101.

(9) Yoshino, K.; Suzuki, M.; Sasaki, K.; Miyase, T.; Sano, M. Formation of antioxidants from (−)-epigallocatechin gallate in mild alkaline fluids, such as authentic intestinal juice and mouse plasma. *J. Nutr. Biochem.* **1999**, *10*, 223–229.

(10) Hirun, S.; Roach, P. D. A study of stability of (−)-epigallocatechin gallate (EGCG) from green tea in a frozen product. *Int. Food Res. J.* **2011**, *18*, 1261–1264.

(11) Zhu, Q. Y.; Zhang, A.; Tsang, D.; Huang, Y.; Chen, Z. Y. Stability of green tea catechins. *J. Agric. Food Chem.* **1997**, *45*, 4624–4628.

(12) Dube, A.; Nicolazzo, J. A.; Larson, I. Assessment of plasma concentrations of (−)-epigallocatechin gallate in mice following administration of a dose reflecting consumption of a standard green tea beverage. *Food Chem.* **2011**, *128*, 7–13.

(13) Krook, M. A.; Hagerman, A. E. Stability of polyphenols epigallocatechin gallate and pentagalloyl glucose in a simulated digestive system. *Food Res. Int.* **2012**, *49*, 112–116.

(14) Lavelli, V.; Kerr, W. Apple pomace is a good matrix for phytochemical retention. *J. Agric. Food Chem.* **2012**, *60*, 5660–5666.

(15) Wu, L.; Melton, L. D.; Sanguansri, L.; Augustin, M. A. The batch adsorption of the epigallocatechin gallate onto apple pomace. *Food Chem.* **2014**, *160*, 260–265.

(16) Yen, G. C.; Lin, H. T. Comparison of high pressure treatment and thermal pasteurization effects on the quality and shelf life of guava puree. *Int. J. Food Sci. Technol.* **1996**, *31*, 205–213.

(17) Abid, M.; Jabbar, S.; Hu, B.; Hashim, M. M.; Wu, T.; Wu, Z. W.; Khan, M. A.; Zeng, X. X. Synergistic impact of sonication and high hydrostatic pressure on microbial and enzymatic inactivation of apple juice. *LWT—Food Sci. Technol.* **2014**, *59*, 70–76.

(18) Vercammen, A.; Vanoirbeek, K. G. A.; Lemmens, L.; Lurquin, I.; Hendrickx, M. E. G.; Michiels, C. W. High pressure pasteurization of apple pieces in syrup: Microbiological shelf-life and quality evolution during refrigerated storage. *Innovative Food Sci. Emerging Technol.* **2012**, *16*, 259–266.

(19) Kosaraju, S. L.; Weerakkody, R.; Augustin, M. A. *In-vitro* evaluation of hydrocolloid-based encapsulated fish oil. *Food Hydrocolloids* **2009**, *23*, 1413−1419.
(20) Espinosa, L.; To, N.; Symoneaux, R.; Renard, C. M. G. C.; Biau, N.; Cuvelier, G. Effect of processing on rheological, structural and sensory properties of apple puree. *Procedia Food Sci.* **2011**, *1*, 513−520.
(21) Espinosa-Muñoz, L.; Renard, C. M. G. C.; Symoneaux, R.; Biau, N.; Cuvelier, G. Structural parameters that determine the rheological properties of apple puree. *J. Food Eng.* **2013**, *119*, 619−626.
(22) Moelants, K. R. N.; Cardinaels, R.; Van Buggenhout, S.; Van Loey, A. M.; Moldenaers, P.; Hendrickx, M. E. A review on relationship between processing, food structure, and rheological properties of plant-tissue-based food suspensions. *Compr. Rev. Food Sci. Food Saf.* **2014**, *13*, 241−260.
(23) Record, I. R.; Lane, J. M. Simulated intestinal digestion of green and black teas. *Food Chem.* **2001**, *73*, 481−486.
(24) Green, R. J.; Murphy, A. S.; Schulz, B.; Watkins, B. A.; Ferruzzi, M. G. Common tea formulations modulate *in vitro* digestive recovery of green tea catechins. *Mol. Nutr. Food Res.* **2007**, *51*, 1152−1162.
(25) Neilson, A. P.; Hopf, A. S.; Cooper, B. R.; Pereira, M. A.; Bomser, J. A.; Ferruzzi, M. G. Catechin degradation with concurrent formation of homo- and heterocatechin dimers during *in vitro* digestion. *J. Agric. Food Chem.* **2007**, *55*, 8941−8949.
(26) Panozzo, A.; Lemmens, L.; Van Loey, A.; Manzocco, L.; Nicoli, M. C.; Hendrickx, M. Microstructure and bioaccessibility of different carotenoid species as affected by high pressure homogenisation: A case study on differently coloured tomatoes. *Food Chem.* **2013**, *141*, 4094−4100.

JOURNAL OF AGRICULTURAL AND FOOD CHEMISTRY

Addition/Correction

pubs.acs.org/JAFC

# Correction to Efficient Hydrolysis of Cellulose over a Novel Sucralose-Derived Solid Acid with Cellulose-Binding and Catalytic Sites

Shuanglan Hu, Thomas John Smith, Wenyong Lou,* and Minhua Zong

*J. Agric. Food Chem.* **2014**, *62* (8), 1905−1911. DOI: 10.1021/jf405712b

An incorrect version of Figure 4 was published. The correct version is below.

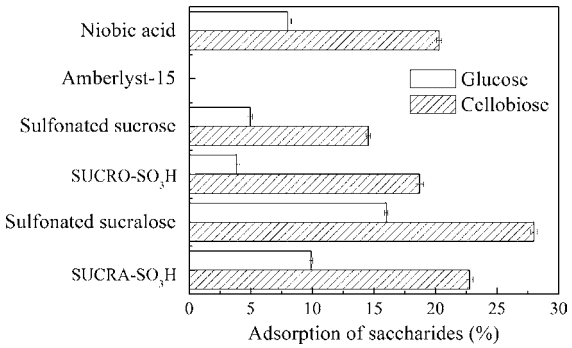


**Figure 4.** The adsorption capacity of the tested catalysts. 100% adsorption would correspond to binding of 50 mg of carbohydrate to 100 mg of catalyst in a volume of 1 mL.

**Published:** December 2, 2014

ACS Publications © 2014 American Chemical Society

**Table 1. Volatiles Detected at Day 3, 8, or 15 from ex Situ Cactus Plugs by HS-SPME over the 2 Week Period and from the Three Abiotic Treatments**

| | | detected in treatment[a] | | | | | | | | |
|---|---|---|---|---|---|---|---|---|---|---|
| | | day 3 | | | day 8 | | | day 15 | | |
| compound identity | RI[b] | Δ | ∫ | ≈ | Δ | ∫ | ≈ | Δ | ∫ | ≈ |
| α-pinene[c] | 1019 | | X | | X | X | | X | X | |
| α-fenchene[c,d] | 1052 | X | | | X | | | X | X | |
| camphene[c] | 1058 | X | | X | | | | X | X | |
| hexanal | 1076 | | X | | | X | | | X | |
| isobutyl alcohol[d] | 1095 | | | X | | | X | | | X |
| β-pinene | 1106 | | X | | | X | | | X | |
| limonene | 1197 | | X | | | X | | | X | |
| 3-methyl-1-butanol | 1209 | | | X | | | X | | | X |
| 3-octanone | 1251 | | | X | | | | | | |
| p-cymene[c] | 1265 | | X | | X | X | | X | X | |
| cyclohexanone[d] | 1285 | | | | | X | | | X | |
| conophthorin | 1286 | | | | | | X | | | X |
| unknown | 1300 | | | | | X | | | X | |
| 6-methyl-5-heptene-2-one | 1334 | | | X | | X | | | X | |
| (Z)-chalcogran | 1348 | | | | | | X | | | X |
| (E)-chalcogran | 1353 | | | | | | X | | | X |
| unknown sesquiterpene | 1356 | | | | | | X | | | X |
| unknown | 1368 | | | | | | X | | | X |
| nonanal | 1391 | | | | | X | | | X | |
| 3-hepten-1-yl acetate[d] | 1435 | | | X | | | X | | | |
| 1-octen-3-ol | 1451 | | | X | | | X | | | |
| 2-ethyl-1-hexanol | 1491 | | X | X | | X | X | X | X | X |
| benzaldehyde | 1515 | | X | X | X | | | | X | |
| guaiacol[d] | 1853 | | | X | | | X | | | X |
| 2-phenylethanol | 1907 | | | X | | | X | | | X |

[a]Key: Δ = control (room temperature); ∫ = −15 °C; ≈ = −15 °C to room temperature; control samples were monitored on days 2, 7, and 14. [b]Retention indices relative to *n*-alkanes on DB-Wax column for compound identification including comparison of retention times and mass fragmentation to authentic samples. [c]Volatiles detected at day 0 in all treatments. [d]Tentatively identified.

performed in five replicates. Collected volatiles were analyzed using a method identical to previously published protocols[9] on a DB-Wax column, 60 m × 0.32 mm i.d. × 0.25 μm (J&W Scientific, Folsom, CA, USA) installed on a 6890 gas chromatograph coupled to an HP-5973 mass selective detector (Agilent, Palo Alto, CA, USA). Retention index (RI) values were calculated using a homologous series of *n*-alkanes on the DB-Wax column. The identities of the reported volatiles were determined by comparison of fragmentation patterns to NIST and Wiley databases, as well as verified by injection of authentic samples and comparison of retention times and fragmentation patterns. Sources of compounds for GC-MS authentication were identical to those in a recent publication.[16] Compounds not verified by authentication are listed as tentative in Table 1.

**Statistical Analysis.** Volatiles were only considered for analysis if they were detected within three of the five replicates at any time point. Relative peak areas were log transformed. Principal component analyses (PCA) were performed on the data using BioNumerics 4.6 (Applied Maths, Austin, TX, USA) where the three treatments (five replicates per treatment, $n = 15$) were compared at each of the three time points.

## RESULTS AND DISCUSSION

The volatiles α-pinene, α-fenchene, camphene, and *p*-cymene were detected from the cactus tissue samples in all treatments at day 0 (Table 1). The compounds α-pinene, β-pinene, and *p*-cymene have been reported from the headspace of intact *Opuntia stricta*;[17] however, the previously reported cymene was the meta-isomer, whereas we detected and report the para-isomer. Additionally, we report the monoterpene camphene as a component of *O. humifusa* plugs, whereas camphene was not detected in the previous study of *O. stricta*. In an additional note regarding volatiles from cacti, Flath et al.[18] report numerous compounds of various classes from their hydrodistillation of prickly pear fruit. However, the differences of method extraction and tissue studied[18] do not allow for comparison to either the present study or the headspace analysis performed by Pophof et al.[17]

PCA showed three distinct clusters representing the three treatments (control, cold, and shock) at days 3 and 8, respectively (Figure 2A,B), thus supporting the overall difference in volatile emissions from the tissues as shown in Table 1. From the PCA for day 3, the volatiles α-pinene, hexanal, β-pinene, and limonene in the cold treatment and 3-octanone, 3-hepten-1-yl acetate, and 1-octen-3-ol in the shock treatment were most responsible for the distinct clustering of the shock (red ellipse) and cold (blue ellipse) treatments (Figure 2A).

The volatiles 3-octanone and 1-octen-3-ol on day 3 from the shock tissue are characteristic of fungal metabolism of fatty acids,[9,19] as well as the volatiles 3-hepten-1-yl acetate and 2-ethyl-1-hexanol. Both of these latter volatiles have reported plant origins,[20,21] but the compound 2-ethyl-1-hexanol is also thought to be a contaminant.[22] Whereas we found no reported semiochemical activity of either 3-hepten-1-yl acetate or 2-ethyl-1-hexanol, it should be noted that 3-octanone and 1-octen-3-ol elicited high electrophysiological responses from both male and female *Amyelois transitella* (Lepidoptera: Pyralidae) moth antennae.[16]

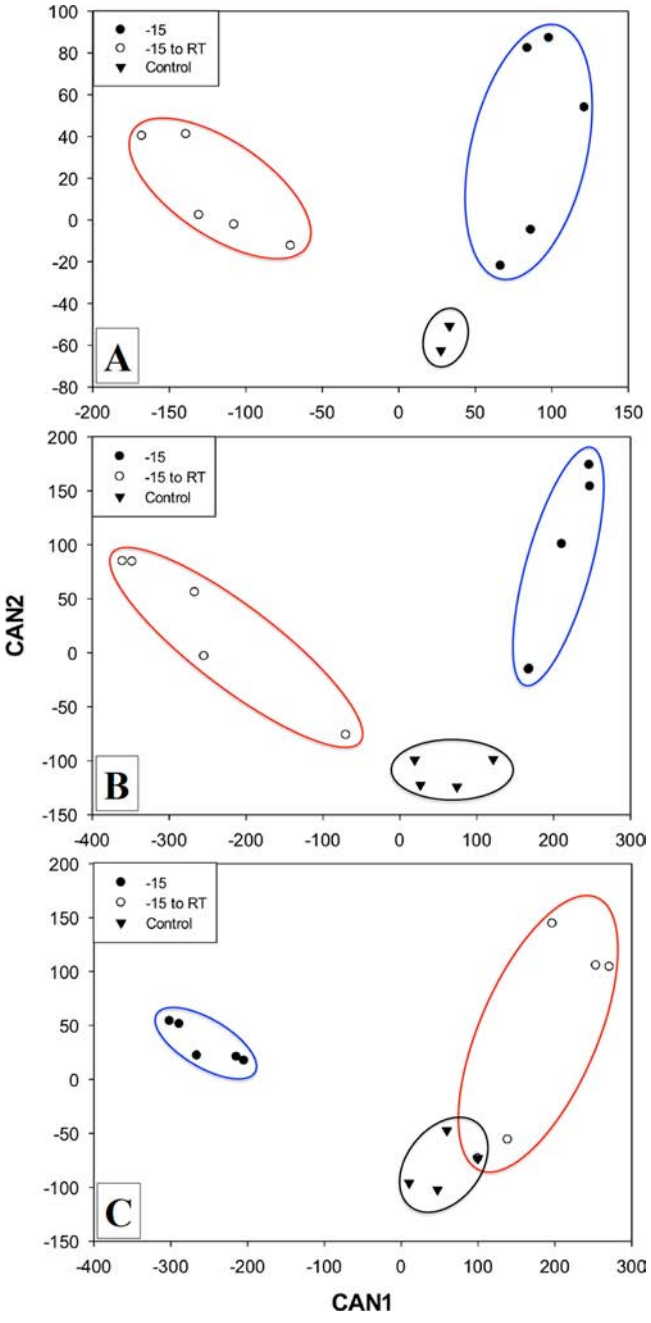


**Figure 2.** Principal component analysis of data from the five replicates of all treatments at (A) day 3, (B) day 8, and (C) day 15. Control treatments are shown in black ellipses, cold treatments in blue ellipses, and shock treatments in red ellipses.

The shock and cold treatments at day 8 produced a number of new compounds not found in the control samples (Figure 2B and Table 1). The volatile composition of the cold treatment cactus tissue (blue ellipse) is suggestive of tissue stress with detection of hexanal, a fatty acid breakdown product,[5,23] as well as a sudden increase in monoterpenes, such as $\beta$-pinene, limonene, and *p*-cymene, which are not seen in the control or shock treatments. This latter phenomenon may contribute to the plants' production of certain terpenoids as a defense mechanism against oxidation,[4] as well as to the inhibition of fungal germination.[24] An interesting finding was the detection of benzaldehyde (days 8 and 15) and nonanal (day 15) in the later days of cold treatment. These aldehydes, among other compounds, have been reported as fungistatics produced by plant bacteria,[25] although the reason for their presence in this tissue and this particular treatment is presently unknown. Therefore, the increase in volatiles with these notable activities in the cold treatment at day 8 warrants further investigation regarding the role of extended cold on plant tissue volatile emissions.

The shock tissue at day 8 produced a diverse range of compounds (Table 1) not detected in the control and cold tissue treatment and resulted in the separation of the shock treatment (red ellipse) relative to the other treatments as seen in the PCA (Figure 2B). The most striking and a primary reason for this paper was the production of a number of compounds that have elicited noteworthy electrophysiological and behavioral responses in other lepidopteran[11,16] and coleopteran[13,14] insects. Most notable among these were the spiroketals conophthorin (**1**) and chalcogran (**2**), the origin of which has been directly associated with developing fungal spores.[9]

Aside from guaiacol, the volatiles from the day 8 shock treatment have associations with fungi and damaged tissue,[9,26] semiochemical activity in Coleoptera,[27] and elicition of electrophysiological responses from navel orangeworm moth antennae.[16] In particular, the volatile 2-phenylethanol elicited a very strong response from male navel orangeworm antennae (Lepidoptera).[16] Additionally, 2-phenylethanol has been reported as a yeast-produced volatile that inhibited aflatoxin-producing genes in the fungus *Aspergillus flavus*,[28] thus raising a possible secondary role for signaling among fungi. Furthermore, a recent report[29] described the semiochemical activity of conophthorin for the ambrosia beetle (Coleoptera) and the emission of conophthorin from stressed and weakened deciduous tree hosts. Given our findings[9,10] concerning the apparent spirogenesis from fungal spores, it would be of interest to determine if the condition of the tree and the beetle's attraction to it are a result of fungal emissions.

Conspicuously absent from the day 8 and 15 shock treatment volatiles were the monoterpenes, which have been implicated in antifungal activity.[24,25] The differences in volatile profiles of the shock and cold treatments raise numerous questions regarding the effect of cold on ex situ plant tissue, either as a preservation and defensive mechanism (sustained cold) or as brief instance (tissue shock). These differences also suggest a subsequent effect on the microbial community within the plant tissue and a consequential effect toward possible insect−microbe mutualisms.

The results described in this paper address a number of important issues in several ongoing investigations: (1) the identification of potential semiochemicals from *O. humifusa* of the insect pest cactus moth (*Cactoblastis cactorum*), a highly invasive pest that has spread across the southeastern portions of the United States, threatening native *Opuntia* species that are important agricultural, ecological, and ornamental plants;[30] (2) the role of abiotic stress on plant tissue, its resident microbes, and the resultant volatiles in either insect−microbe or microbe−microbe interactions; and (3) the expanding role of the spiroketals conophthorin and chalcogran in the possible mutualism between certain insects and fungal spores. The results also highlight several important new findings and include a unique tissue source of the spiroketals; the implication of abiotic cold-shock stress as a trigger for spiroketal production; and, given our previous findings of spirogenesis,[9,10] the possibility of spore involvement as a

biosynthetic origin of the spiroketals. Likewise, these findings have important implications regarding fungal volatile emissions when plants may be vulnerable to insect pests.

**John J. Beck***[,†]
**Nausheena Baig**[†]
**Daniel Cook**[‡]
**Noreen E. Mahoney**[†]
**Travis D. Marsico**[§]

[†]Foodborne Toxin Detection and Prevention, Western Regional Research Center, Agricultural Research Service, U.S. Department of Agriculture, 800 Buchanan Street, Albany, California 94710, United States

[‡]Poisonous Plant Research Laboratory, Agricultural Research Service, U.S. Department of Agriculture, 1150 East 1400 North, Logan, Utah 84341, United States

[§]Department of Biological Sciences, Arkansas State University, State University, Arkansas 72467, United States

## AUTHOR INFORMATION

### Corresponding Author

*(J.J.B.) Phone: (510) 559-6154. Fax: (510) 559-6493. E-mail: john.beck@ars.usda.gov.

### Funding

Research was performed under USDA-ARS CRIS Project 5325-42000-037.

### Notes

The authors declare no competing financial interest.

## ACKNOWLEDGMENTS

We thank W. S. Gee (USDA-ARS) and A. M. W. Cooper (ASU) for their assistance.

## REFERENCES

(1) Bruce, T. J. A.; Wadhams, L. J.; Woodcock, C. M. Insect host location: a volatile situation. *Trends Plant Sci.* **2005**, *10*, 269−274.

(2) Das, A.; Lee, S.-H.; Hyun, T. K.; Kim, S.-W.; Kim, J.-Y. Plant volatiles as method of communication. *Plant Biotechnol. Rep.* **2013**, *7*, 9−26.

(3) Davis, T. S.; Crippen, T. L.; Hofstetter, R. W.; Tomberlin, J. K. Microbial volatile emissions as insect semiochemicals. *J. Chem. Ecol.* **2013**, *39*, 840−859.

(4) Vickers, C. E.; Gershenzon, J.; Lerdau, M. T.; Loreto, F. A unified mechanism of action for volatile isoprenoids in plant abiotic stress. *Nat. Chem. Biol.* **2009**, *5*, 283−291.

(5) Holopainen, J. K.; Gershenzon, J. Multiple stress factors and the emission of plant VOCs. *Trends Plant Sci.* **2010**, *15*, 176−184.

(6) Loreto, F.; Schnitzler, J.-P. Abiotic stresses and induced BVOCs. *Trends Plant Sci.* **2010**, *15*, 154−166.

(7) Niinemets, U.; Kännaste, A.; Copolovici, L. Quantitative patterns between plant volatile emissions induced by biotic stresses and the degree of damage. *Front. Plant Sci.* **2013**, *4*, 262, DOI: 10.3389/fpls.2013.00262.

(8) Junker, R. R.; Tholl, D. Volatile organic compound mediated interactions at the plant-microbe interface. *J. Chem. Ecol.* **2013**, *39*, 810−825.

(9) Beck, J. J.; Mahoney, N. E.; Cook, D.; Gee, W. S. Generation of the volatile spiroketals conophthorin and chalcogran by fungal spores on polyunsaturated fatty acids common to almonds and pistachios. *J. Agric. Food Chem.* **2012**, *60*, 11869−11876.

(10) Beck, J. J. Conophthorin from almond host plant and fungal spores and its ecological relation to navel orangeworm: a natural products chemist's perspective. *J. Mex. Chem. Soc.* **2013**, *57*, 69−72.

(11) Beck, J. J.; Higbee, B. S.; Light, D. M.; Gee, W. S.; Merrill, G. B.; Hayashi, J. M. Hull split and damaged almond volatiles attract male and female navel orangeworm. *J. Agric. Food Chem.* **2012**, *60*, 8090−8096.

(12) Mahoney, N. E.; Gee, W. S.; Higbee, B. S.; Beck, J. J. *Ex situ* volatile survey of ground almond and pistachio hulls for the emission of spiroketals: analysis of hull fatty acid composition, water content, and water activity. *Phytochem. Lett.* **2014**, *7*, 225−230.

(13) Francke, W.; Bartels, J.; Meyer, H.; Schroder, F.; Kohnle, U.; Baader, E.; Vite, J. P. Semiochemicals from bark beetles: new results, remarks, and reflections. *J. Chem. Ecol.* **1995**, *21*, 1043−1063.

(14) Jaramillo, J.; Torto, B.; Mwenda, D.; Troeger, A.; Borgemeister, C.; Poehling, H.-M.; Francke, W. Coffee berry borer joins bark beetles in coffee klatch. *PLoS One* **2013**, *8*, No. e74277.

(15) Rowley, E. R.; Mockler, T. C. Plant abiotic stress: insights from the genomics era. In *Abiotic Stress Response in Plants − Physiological, Biochemical and Genetic Perspectives*; Shanker, A., Ed.; Intech: Rijeka, Croatia, 2011; pp 221−268.

(16) Beck, J. J.; Light, D. M.; Gee, W. S. Electrophysiological responses of male and female *Amyelois transitella* antennae to pistachio and almond host plant volatiles. *Entomol. Exp. Appl.* **2014**, *153*, 217−230.

(17) Pophof, B.; Stange, G.; Abrell, L. Volatile organic compounds as signals in a plant-herbivore system: electrophysiological responses in olfactory sensilla of the moth *Cactoblastis cactorum*. *Chem. Senses* **2005**, *30*, 51−68.

(18) Flath, R. A.; Takahashi, J. M. Volatile constituents of prickly pear (*Opuntia ficus indica* Mill., de Castilla variety). *J. Agric. Food Chem.* **1978**, *26*, 835−837.

(19) Miyamoto, K.; Murakami, T.; Kakumyan, P.; Keller, N. P.; Matsui, K. Formation of 1-octen-3-ol from *Aspergillus flavus* conidia is accelerated after disruption of cells independently of Ppo oxygenases, and is not the main cause of inhibition of germination. *Peer J.* **2014**, *2*, No. e395.

(20) Irwin, R. E.; Dorsett, B. Volatile production by buds and corollas of two sympatric, confamilial plants, *Ipomopsis aggregata* and *Polemonium foliosissimum*. *J. Chem. Ecol.* **2002**, *28*, 565−578.

(21) Pontes, M.; Pereira, J.; Câmara, J. S. Dynamic headspace solid-phase microextraction combined with one-dimensional GC-MS as a powerful tool to differentiate banana cultivars based on their volatile metabolite profile. *Food Chem.* **2012**, *134*, 2509−2520.

(22) Ackman, R. G. 2-Ethyl-1-hexanol: contaminant or sex pheromone in *Arenicola marina*? *Mar. Ecol.* **1997**, *No. 152*, 311−312.

(23) Beck, J. J.; Mahoney, N. E.; Cook, D.; Gee, W. S. Volatile analysis of ground almonds contaminated with naturally occurring fungi. *J. Agric. Food Chem.* **2011**, *59*, 6180−6187.

(24) Kelpzig, K. D.; Smalley, E. B.; Raffa, K. F. Combined chemical defenses against an insect-fungal complex. *J. Chem. Ecol.* **1996**, *22*, 1367−1388.

(25) Bitas, V.; Kim, H.-S.; Bennett, J. W.; Kang, S. Sniffing on microbes: diverse roles of microbial volatile organic compounds in plant health. *Mol. Plant−Microbe Interact.* **2013**, *26*, 835−843.

(26) Beck, J. J.; Higbee, B. S.; Merrill, G. B.; Roitman, J. N. Comparison of volatile emissions from undamaged and mechanically damaged almonds. *J. Sci. Food Agric.* **2008**, *88*, 1363−1368.

(27) Pierce, A. M.; Pierce, H. D.; Borden, J. H.; Oehlschlager, A. C. Fungal volatiles: semiochemicals for stored-product beetles (Coleoptera: Cucujidae). *J. Chem. Ecol.* **1991**, *17*, 581−597.

(28) Hua, S. S. T.; Beck, J. J.; Sarreal, S. B. L.; Gee, W. S. The major volatile compound 2-phenylethanol from the biocontrol yeast, *Pichia anomala*, inhibits growth and expression of aflatoxin biosynthetic genes of *Aspergillus flavus*. *Mycotoxin Res.* **2014**, *30*, 71−78.

(29) Ranger, C. M.; Gorzlancyk, A. M.; Addesso, K. M.; Oliver, J. B.; Reding, M. E.; Schultz, P. B.; Held, D. W. Conophthorin enhances the electroantennogram and field behavioural response of *Xylosandrus germanus* (Coleoptera: Curculionidae) to ethanol. *Agric. For. Entomol.* **2014**, *16*, 327−334.

(30) Hight, S. D.; Carpenter, J. E. Flight phenology of male *Cactoblastis cactorum* (Lepidoptera: Pyralidae) at different latitudes in the southeastern United States. *Fla. Entomol.* **2009**, *92*, 208−216.

**Table 1. Structures and Properties of SGPMs Used in Sorption Studies**

| Name | Structure | CAS Number | MW (g/mol) | log$K_{ow}$ | Estimated[a] Solubility (mg/L) |
|---|---|---|---|---|---|
| Trenbolone Acetate (TBA) | 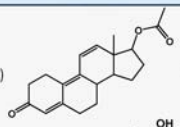 | 10161349 | 312.4 | 4.21[b] | 7.9 |
| 17β-trenbolone (17β-TBOH) | 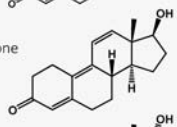 | 10161338 | 270.4 | 3.08[c]/3.09[b] | 320 |
| 17α-trenbolone (17α-TBOH) | 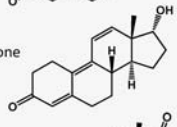 | 80657176 | 270.4 | 2.72[c] | 320 |
| Trendione (TBO) | 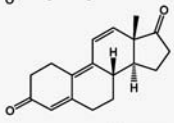 | 4642959 | 268.4 | 2.63[c] | 280 |
| Melengestrol Acetate (MGA) | 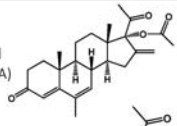 | 2919666 | 396.5 | 3.93[c] | 0.55 |
| Melengestrol | 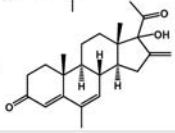 | 5633181 | 354.5 | 3.39[b] | 10.2 |
| Zeranol | 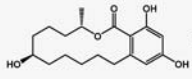 | 26538443 | 322.4 | 3.88 | 2.9 |
| β-zearalanol | 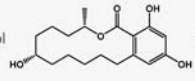 | 42422684 | 322.4 | 3.29 | 2.9 |
| Zearalanone | 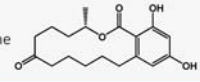 | 5975780 | 320.4 | 4.10 | 2.5 |

[a]Aqueous solubilities were estimated via the U.S. EPA EPISuite using WSKOW (v. 1.41).[36] [b]Experimentally measured in this study. [c]Value reported by Card et al.[9]

oxides,[17] via mechanisms including electrostatic interactions and surface complexation. Alternatively, they may represent reactive substrates able to promote transformation reactions. For example, MGA and the zeranol family have hydrolyzable functionalities, whereas the 4,9,11-triene structure of trenbolone includes several electron-deficient carbon centers possibly susceptible to nucleophilic attack. Although hydrolysis is reportedly slow at near-neutral pH values for SGPMs,[18−20] metal oxides common to soil can catalyze hydrolysis, and presumably nucleophilic addition, via the formation of surface complexes that leave carbon centers more favorable to attack by $H_2O$ or $OH^-$ than the freely dissolved molecule.[21] Furthermore, manganese oxides and some iron oxides can oxidize species structurally analogous to SGPMs[22,23] including estrone and 17$\beta$-estradiol. Although such mineral-promoted transformation pathways remain uncharacterized, we suspect some SGPMs are highly reactive toward inorganic phases routinely encountered in soil.

Here, we explore the abiotic pathways influencing SGPM fate in soils. The rate and extent of SGPM sorption were considered in sterilized (with azide) systems using a model, organic-rich soil (Pahokee Peat, 43% organic carbon) and several commercially available model soils exhibiting a range of soil organic carbon (1.0−5.9% OC). Sorption kinetics and isotherms were used to examine trends both within (e.g., 17$\alpha$-TBOH, 17$\beta$-TBOH, and TBO) and across SGPM families (e.g., comparing TBA metabolites, MGA and melengestrol, and metabolites), explore the nature of chemical interactions (e.g., specific or hydrophobic) contributing to uptake, and establish the extent to which SGPM sorption is reversible. We emphasize that in all model soil systems, solvent (i.e., methanol) extraction of equilibrated soils was used to recover the mass of sorbed SGPM, and loss of mass over time in our experimental systems was interpreted as evidence for abiotic transformation processes (i.e., reaction with inorganic mineral phases). To further explore the potential for such abiotic transformations, experiments also monitored the stability of select SGPMs (17$\beta$-TBOH, MGA, and zeranol) in suspensions of metal oxides (e.g., manganese, iron, and silica oxides) representative of those naturally occurring in soil. Results from this study will help to characterize more fully the environmental fate and mobility of SGPMs in subsurface environments, thereby improving our ability to predict the risk posed to ecosystems by this emerging pollutant class.

## MATERIALS AND METHODS

**Reagents.** A complete reagent list is provided in the Supporting Information (SI).

**Measurement of $K_{ow}$ Values for Select SGPMs.** Octanol−water partitioning coefficients ($K_{ow}$ values) were measured for SGPMs without published values available in the literature. These were trenbolone acetate, melengestrol, zearalanone, and $\beta$-zeralanol. Details of our method, which was adapted from that of Khan et al.,[8] are provided in the SI. To assess the accuracy of our approach, we also measured the $K_{ow}$ value for 17$\beta$-trenbolone so that our experimental value could be compared to a reference value available in the literature.

**Model Soils and Mineral Oxides.** Seven commercial, model soils exhibiting a range of soil OC content were used in sorption studies. Pahokee Peat (43% OC) was purchased from the International Humic Substances Society (IHSS), whereas other soils with various textures and OC contents were acquired from AGVISE Laboratories (Benson, MN, USA). These include two sandy loams (referred to as PVPF and LBLS with OC contents of 5 and 3%, respectively), two loams (PVLPF and EL-7 with OC contents of 5.9 and 2.8%, respectively), a clay loam (DUL; 3.3% OC content), and a loamy sand (RMN; 1% OC content). The OC content of Pahokee Peat was determined by Test America via the Lloyd Kahn method,[24] whereas the OC values of all other soils were provided by AGVISE Laboratories and quantified by loss-on-ignition methods.[25] Also explored were several mineral phases representative of naturally occurring metal oxides including a commercially available silica dioxide ($SiO_2$; Sigma-Aldrich, 99%), ferrihydrite synthesized via the method of Burleson and Penn,[26] and an amorphous manganese dioxide ($MnO_2$) synthesized according to the method of Murray.[27] Synthesis details are provided in the SI.

**Sorption Experiments.** Soils were first sterilized by adding sodium azide ($NaN_3$) as described by Wolf et al.,[28] with the exception that the dose was increased to 30.8 mmol $NaN_3$/kg soil.[29] Additional details and our rationale for sterilizing with azide as opposed to other methods are provided in the SI. Batch sorption experiments were then conducted at pH 7.0 in a 5 mM phosphate buffer. The rate of SGPM sorption was explored using initial concentrations between 2 and 5 $\mu$M and a soil loading between 2 and 10 g/L. Sorption isotherms were collected over a range of initial concentrations (1−10 $\mu$M) using a constant sorbent (i.e., soil sample or metal oxide) loading of 2 g/L at room temperature. Although these initial concentrations are higher than environmental relevance, they were necessary to facilitate SGPM analysis via high-pressure liquid chromatography with diode array detection (HPLC-DAD), which was the preferred method for processing the large number of samples generated experimentally. In

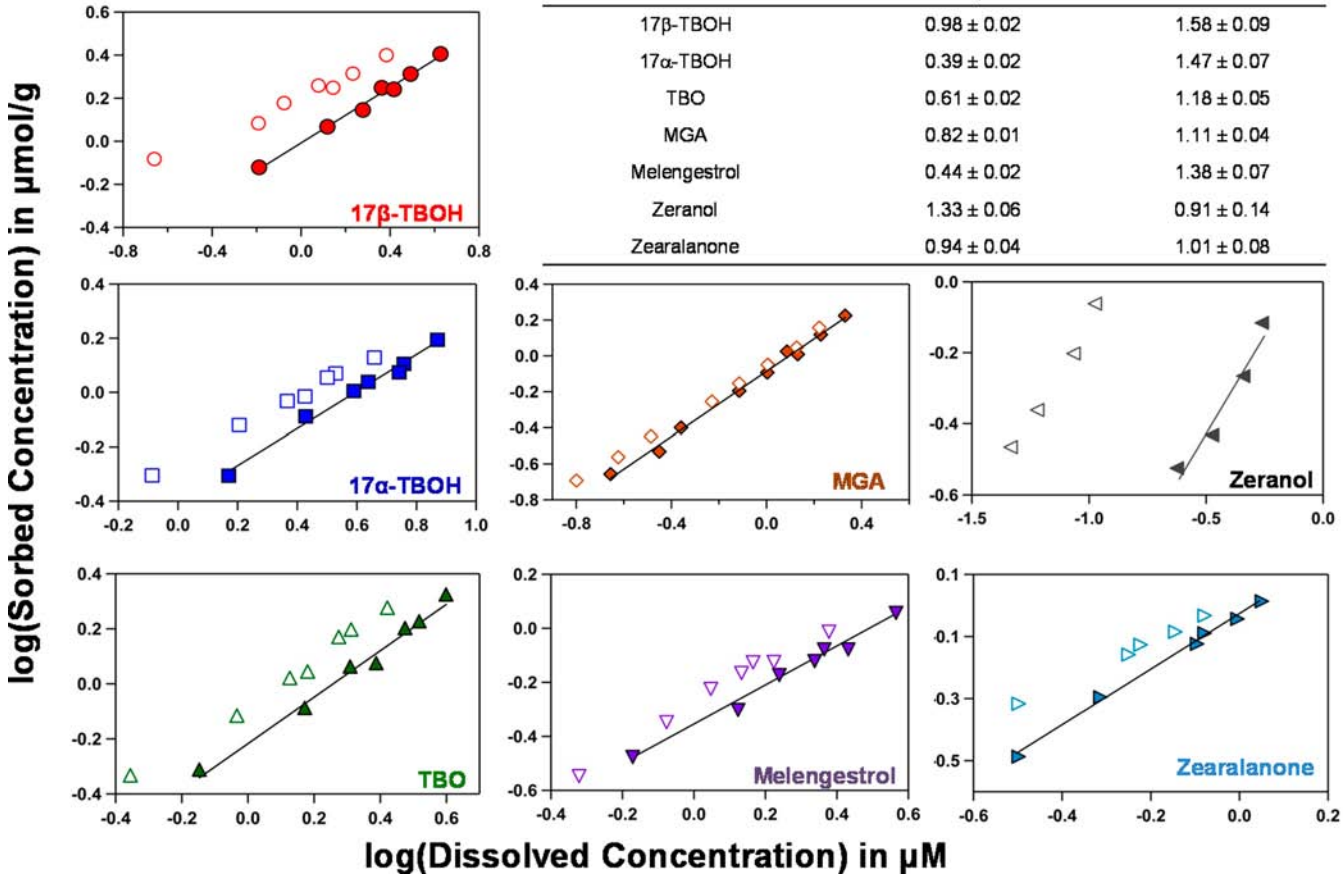


| SGPM | $K_f$ | $n$ |
|---|---|---|
| 17β-TBOH | 0.98 ± 0.02 | 1.58 ± 0.09 |
| 17α-TBOH | 0.39 ± 0.02 | 1.47 ± 0.07 |
| TBO | 0.61 ± 0.02 | 1.18 ± 0.05 |
| MGA | 0.82 ± 0.01 | 1.11 ± 0.04 |
| Melengestrol | 0.44 ± 0.02 | 1.38 ± 0.07 |
| Zeranol | 1.33 ± 0.06 | 0.91 ± 0.14 |
| Zearalanone | 0.94 ± 0.04 | 1.01 ± 0.08 |

**Figure 1.** Linearized Freundlich isotherms for SGPMs on Pahokee Peat (please note the difference in the *x*- and *y*-axes scales for each species). Solid symbols indicate measured concentrations after 3 days (sufficient to achieve sorption equilibrium), whereas open symbols correspond to data collected to test the reversibility of sorption according to the protocol described in the text. Linear regression and resulting best-fit parameters for values of $K_f$ (in $\mu$mol$^{(1-(1/n))}$ $L^{(1/n)}$ g$^{-1}$) and $n$ (unitless) are provided, along with 95% confidence intervals associated with the regression analysis. Experimental details are provided in the text.

all cases, the highest initial concentration used for each SGPM was below aqueous solubility (based upon reported values of 1330, 2.6, and 15 $\mu$M for 17$\alpha$-trenbolone, MGA, and zeranol, respectively;[18−20] estimated aqueous solubilities are provided for all SGPMs in Table 1). Nevertheless, control experiments were conducted in the absence of soil to ensure the aqueous phase stability of the SGPMs at these concentrations.

To initiate sorption experiments, a small volume (2−18 $\mu$L) of SGPM methanolic stock solution was added to a suspension of sterilized soil via syringe to achieve the desired initial concentration. In all cases, this approach resulted in no more than 0.1% of methanol by volume in our reactors, below the threshold likely to induce cosolute effects.[30] To avoid sorption losses to vial septa (which was observed for some species in preliminary experiments), all experiments were conducted in 20 mL glass beakers, and the contents were well-mixed via a glass-coated, magnetic stir bar and electronic stir plate. We note that initial experiments using Teflon-coated stir bars revealed losses of some SGPMs in controls, presumably due to sorption on the stir bar. Over the duration of the experiments, reactors were sealed with Parafilm to slow evaporation and covered in Al foil to prevent photoreactions.

Sorption rate studies were typically conducted over 1 week, with sample collection at predetermined time intervals to monitor the change in SGPM solution concentration over time. For sorption isotherms, equilibrium was typically established after 3 days, at which time samples were collected to monitor the mass of SGPM remaining in solution. The extent to which sorption was reversible was considered as follows. After 3 days, the entire equilibrated suspension (18 mL) was centrifuged (3000 rpm for 5 min), and a fixed volume (typically 8 mL) of supernatant was replaced by fresh buffer to perturb the sorption equilibrium. The altered suspension was then allowed to re-equilibrate for another 3 days, at which time the aqueous phase SGPM concentration was once again measured.

Reactor samples were centrifuged, and the supernatant was analyzed immediately on HPLC-DAD to quantify dissolved phase concentrations. Centrifugation was chosen for solid removal rather than filtration because most commercially available filters (PTFE or nylon) resulted in some loss of SGPMs during application. Using this approach, the amount of SGPM sorbed to the soil was quantified via mass balance from the difference in the initial SGPM concentration in the reactor and the aqueous phase concentration of SGPM present in solution at equilibrium.

At the conclusion of sorption experiments, the mass of SGPM sorbed on the soil sample was quantified via extraction with organic solvent.[8] The entire suspension was centrifuged, the supernatant was removed, and 3 mL of methanol was added to the soil. The resulting suspension was sonicated for 5 min, which was found to be sufficient for recovery of the sorbed mass. After sonication, the suspension was centrifuged once again to separate the methanol from the solid, and the solvent phase was analyzed by HPLC-DAD.

**SGPM Reactivity toward Metal Oxides.** Reactions with metal oxides $SiO_2$ and ferrihydrite were conducted at pH 7.0 in 5 mM phosphate buffer at room temperature. For $MnO_2$, we observed reactivity inhibition in phosphate buffer; thus, experiments were conducted in 5 mM $NaClO_4$ at either pH 6 or 7. Experiments with metal oxides were conducted over a range of solid loadings (1−10 g/

L) and SGPM initial concentrations (1−5 μM). The oxide suspensions were allowed to equilibrate with the buffer/electrolyte solution for 20 min, after which the pH of the system was adjusted (if necessary) back to the desired initial value using 1 M HCl or NaOH. Once the pH was stabilized, a small volume of methanolic stock solution delivered the SGPM to the suspension. The suspension was well-mixed using a glass-coated magnetic stir bar and stir plate, and reactors were covered by Al foil to prevent photoreaction. Over time, 1 mL aliquots of suspension were collected and centrifuged to separate the metal oxide from the aqueous phase, and the supernatant then was transferred to an amber autosampler vial for immediate HPLC-DAD analysis.

**Analytical Methods.** Aqueous samples were analyzed on a 1200 series Agilent HPLC-DAD equipped with an Eclipse XBD-C18 column (4.6 × 150 mm, 5 μm particle size) according to the methods presented in our earlier work[31] and also detailed in the SI. All soils and metal oxides were characterized via powder X-ray diffraction using a Rigaku MiniFlex II with a Co Kα source.

## RESULTS AND DISCUSSION

**SGPM Sorption Isotherms on Organic-Rich Pahokee Peat.** Sorption rate experiments suggested that most SGPMs, with the exception of β-zearalanol (see SI), achieved steady state (i.e., no further decrease in solution phase concentration over time) in Pahokee Peat suspensions within 3 days (at 2 g/L Pahokee Peat and ∼5 μM initial SGPM; Figure S1). Accordingly, sorption isotherms collected after 3 days are shown in Figure 1, in which data are presented on a log−log scale. Also shown are fits in which sorption is assumed to follow the Freundlich isotherm model (eqs 1 and 2).

$$C_s = K_f C_w^{1/n} \quad (1)$$

$$\log C_s = \log K_f + 1/n \log C_w \quad (2)$$

In eqs 1 and 2, $C_s$ is the sorbed SGPM concentration and $C_w$ is the aqueous phase concentration at equilibrium (after 3 days). The Freundlich adsorption capacity parameter, $K_f$, and the Freundlich adsorption intensity parameter, $1/n$, were obtained from linear regression analysis of experimental data (according to eq 2), as summarized in Figure 1 for each SGPM.

These model fit parameters were used to explore trends in SGPM sorption on Pahokee Peat. For example, $K_f$ values indicate the magnitude of sorption,[32] and correlations between $K_f$ values and metrics of sorbate hydrophobicity (e.g., $K_{ow}$ values) have occasionally been suggested as evidence for hydrophobic interactions driving sorption.[33] Here, the largest $K_f$ values (with units of $\mu mol^{(1-(1/n))}\ L^{(1/n)}\ g^{-1}$) were measured for zeranol (1.33 ± 0.06) and its metabolite zearalanone (0.94 ± 0.04), 17β-TBOH (0.98 ± 0.02), and MGA (0.82 ± 0.01). However, across families of growth promoters, octanol−water partitioning coefficients ($K_{ow}$ values) were a weak predictor for sorption on Pahokee Peat (Figure S2a). Moreover, we failed even to observe clear trends in $K_f$ values within SGPM families; trendione exhibited greater sorption than 17α-TBOH despite its lower $K_{ow}$ value.

A notable and important distinction across SGPMs in Pahokee Peat systems was that some isotherms were essentially linear. The greatest degrees of nonlinearity, based on model fit values of $n$, were observed for 17β-TBOH, 17α-TBOH, and melengestrol, whereas the slopes of isotherms for zeranol and zearalanone were statistically equivalent to unity (i.e., their isotherms were linear). Linear isotherms are most often observed when hydrophobic interactions drive uptake and an excess of such hydrophobic sorption sites exists.[30] In contrast, nonlinear isotherms are typically observed for more polar compounds, for which specific interactions will also contribute to sorption.[30] SGPM sorption appears consistent with these scenarios, with linear isotherms most frequently observed for more hydrophobic SGPMs (based on reported or measured $K_{ow}$ values; Figure S2b). Thus, the linear isotherms for zeranol and zearalanone suggest an excess of hydrophobic sites on Pahokee Peat suitable for partitioning, behavior likely linked to the aromatic functionalities of zeranol and it metabolites. In contrast, nonlinear isotherms for 17β-TBOH, 17α-TBOH, and melengestrol are evidence that more limited, specific sites on Pahokee Peat also contribute to sorption.

We also interpret trends in $n$ values within a family of compounds as evidence of the functional groups involved in such specific interactions. Specifically, isotherms for 17β-TBOH and 17α-TBOH exhibited greater nonlinearity than TBO, whereas the isotherm for melengestrol exhibited greater nonlinearity than that of MGA. In each of these cases, therefore, the presence of an −OH group at the C17 position increased the degree of specific interactions. We attribute this observation to the ability of this hydroxyl group to promote sorption via hydrogen bonding with functionalities of Pahokee Peat.

**Reversibility of SGPM Sorption on Organic-Rich Pahokee Peat.** A final consideration for SGPM sorption in Pahokee Peat systems is the extent to which the process is reversible. Data pertaining to sorption reversibility are also presented in Figure 1. Open symbols represent data collected after system equilibrium was first disrupted after 3 days and then once again allowed to achieve steady state over an additional 3 days. In Figure 1, therefore, overlap between open and solid symbols indicates a sorption process that is entirely reversible.

MGA was the only SGPM to sorb onto Pahokee Peat reversibly (see overlap in Figure 1 of open and solid symbols), whereas sorption of 17α-TBOH, TBO, melengestrol, and zearalanone was partially reversible. Sorption of zeranol and 17β-TBOH was essentially irreversible, as evidenced by the nearly identical concentration of adsorbed species after system equilibrium was perturbed (i.e., open symbols are horizontally, but not vertically, offset from their solid counterparts). Notably, we were able to recover completely all of the sorbed mass via extraction with methanol. Measured percent recoveries in Pahokee Peat systems were 110 (±8), 99 (±7), 165 (±10), 125 (±0.12), 105 (±9), and 124 (±11) for 17β-TBOH, 17α-TBOH, MGA, melengestrol, zeranol, and zearalanone, respectively. Values represent the mean and standard deviation for at least $n$ = 3 extractions (we note that only one instance of trendione extraction was completed, resulting in 115% recovery). Thus, concentration changes in Pahokee Peat systems occur via sorption and not from processes such as abiotic transformation reactions or biodegradation.

Several trends in the reversibility of SGPM sorption are noteworthy, if not surprising. MGA and zeranol have comparable log$K_{ow}$ values, and both produced linear isotherms, collectively suggesting that hydrophobic interactions govern their sorption. However, the nature of these hydrophobic interactions must be fundamentally different because MGA uptake was entirely reversible, whereas zeranol sorption was essentially irreversible. Likewise, 17β-TBOH is among the more polar of SGPMs considered herein, and the presumed specific interactions (e.g., hydrogen bonding) associated with its sorption are typically considered relatively weak. Nevertheless, the irreversible nature of 17β-TBOH sorption implies rather

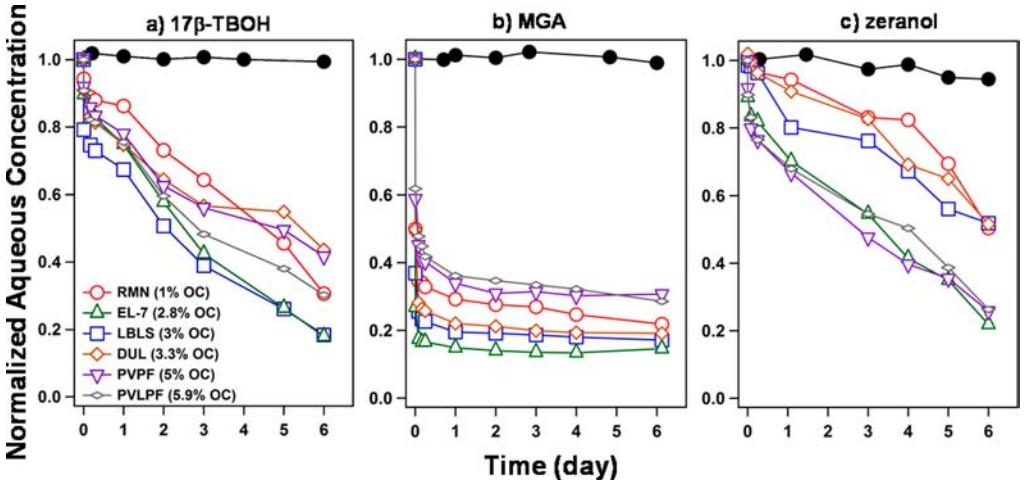


**Figure 2.** Change in aqueous phase concentration over time for (a) 17$\beta$-TBOH, (b) MGA, and (c) zeranol in 4 g/L suspensions of azide-treated model soils. Results from soil-free controls are shown as solid black symbols. All experiments were conducted in 5 mM phosphate buffer at pH 7. The initial concentrations were 4, 2, and 2 $\mu$M for 17$\beta$-TBOH, MGA, and zeranol, respectively.

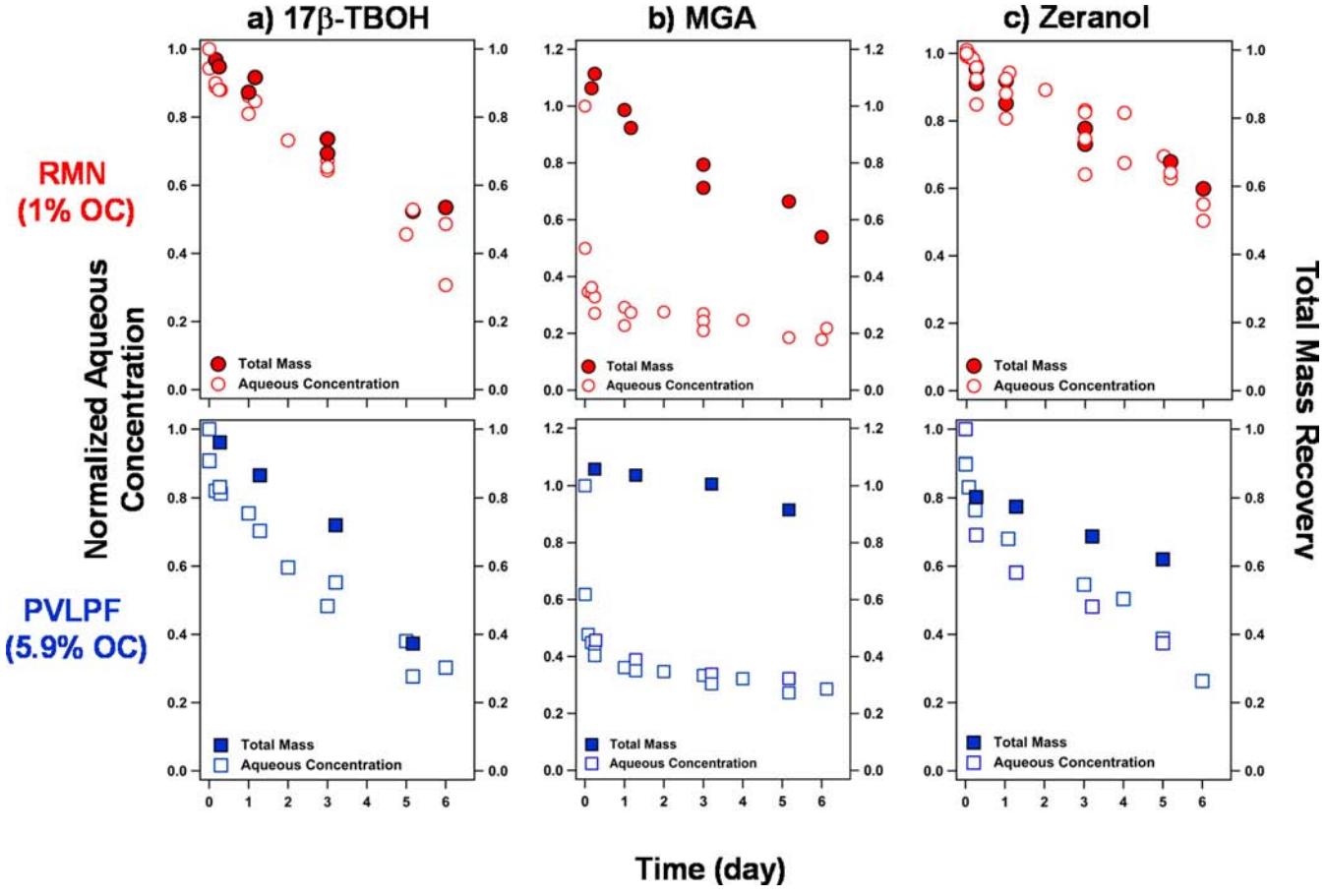


**Figure 3.** Aqueous phase concentration change over time for (a) 17$\beta$-TBOH, (b) MGA, and (c) zeranol in suspensions (4 g/L at pH 7) of two model soils, RMN (red; top) and PVLPF (blue; bottom), which represent those with the lowest (1%) and highest (5.9%) organic carbon content. Also presented (solid symbols) are data pertaining to the total mass of each species in the systems over time, which also includes the mass that was recoverable from extraction of solids with methanol.

strong binding with Pahokee Peat, perhaps suggesting multiple sorption mechanisms occurring in parallel (e.g., hydrogen bonding in combination with electron donor−acceptor interactions) to strengthen the overall degree of interaction. Ultimately, these findings complicate prediction of SGPM mobility in soils and the subsurface; not only do log$K_{ow}$ values fail to reasonably predict the extent of sorption onto soil organic matter either within or across SGPM families, but they also appear to have little correlation with the extent to which sorption is reversible.

**SGPM Sorption on Model Soils.** Initial experiments with 17$\beta$-TBOH, MGA, and zeranol explored the time scales


dx.doi.org/10.1021/jf5035527 | J. Agric. Food Chem. 2014, 62, 12277−12286

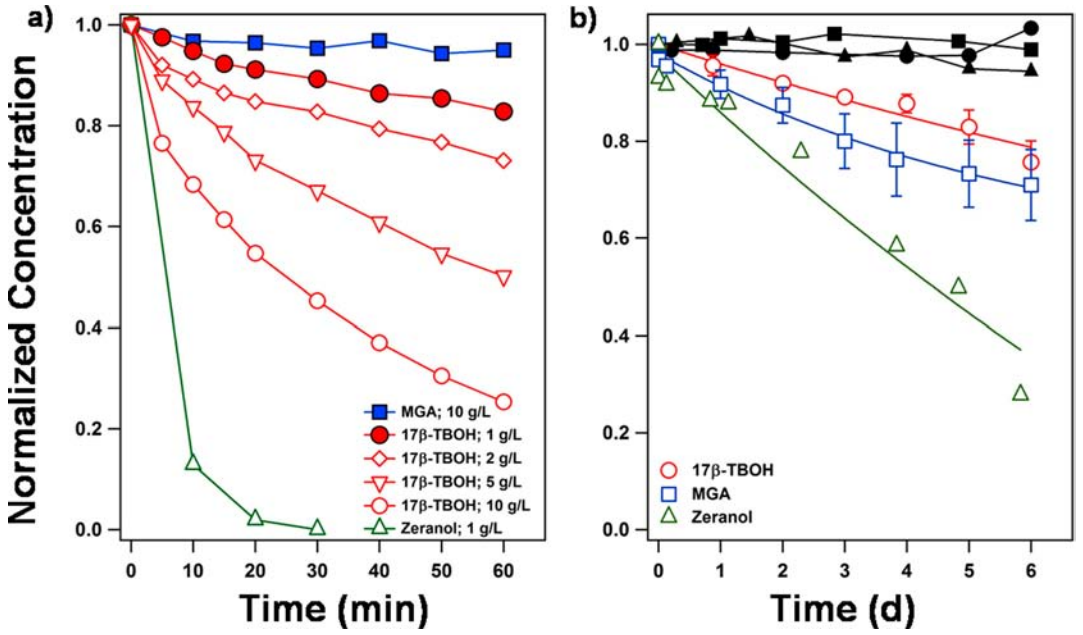


**Figure 4.** (a) Aqueous phase concentration change over time of MGA, 17$\beta$-TBOH, and zeranol in suspensions of $MnO_2$. For 17$\beta$-TBOH, data are shown for several $MnO_2$ solid loadings. All experiments were conducted in 5 mM $NaClO_4$ at pH 6. The initial concentrations of 17$\beta$-TBOH, MGA, and zeranol were 10, 2, and 2 $\mu$M, respectively. All SGPMs were stable in $MnO_2$-free controls (data not shown). (b) Aqueous phase concentration change of 17$\beta$-TBOH, MGA, and zeranol in ferrihydrite suspensions (5 g/L). Reactions were conducted in 5 mM phosphate buffer at pH 7. Lines are exponential decay model fits from which half-lives were estimated. Data are also presented from control systems conducted in the absence of solid (shown as corresponding solid black symbols).

necessary to achieve sorption equilibrium in suspensions of azide-sterilized model soils (Figure 2). Over 6 days, the MGA appeared to reach steady state; after an initially sharp, nearly immediate drop, aqueous phase MGA concentration was essentially stable over the remainder of the 6 day period for all soils. However, the amount of MGA lost from solution did not scale with soil organic carbon content. Rather, if anything, we observed an approximately inverse relationship, in which soils with the highest OC content (PVPF with 5.0% and PVLPF with 5.9%) tended to produce the smallest amount of MGA loss from solution.

Unlike MGA, the solution phase concentrations of 17$\beta$-TBOH and zeranol failed to achieve steady state, even after 6 days of mixing with soils (whereas soil-free controls were stable over the same time scale). For 17$\beta$-TBOH, there was no apparent relationship between the rate of disappearance and soil OC content, whereas zeranol loosely exhibited behavior expected if hydrophobic interactions were driving sorption in these suspensions (i.e., rates and extent of loss were generally greatest in higher OC soils). However, zeranol's inability to achieve sorption equilibrium in these model soil suspensions was notable; whereas equilibrium was readily achieved with high OC Pahokee Peat, the lack of equilibrium in lower OC content soils implies that other, nonconservative, processes may be contributing to the loss of solution phase zeranol.

Additional experiments with select model soils suggest that sorption occurs concurrently with abiotic chemical transformation of SGPMs. Figure 3 shows dissolved concentration versus time plots for 17$\beta$-TBOH, MGA, and zeranol for low (RMN; 1% OC) and high (PVLPF; 5.9% OC) OC content soils, which are identical to the data previously shown in Figure 2 for these soils. However, also provided for comparison are data corresponding to the total mass in these systems over time (i.e., dissolved + sorbed concentration), in which sorbed concentration was determined via methanol extraction of soils at each sampling point (recall that this extraction technique successfully recovered all sorbed mass from Pahokee Peat during our isotherm experiments).

In nearly all systems, we observed loss in total SGPM mass, and the extent of this loss generally increased over time. For 17$\beta$-TBOH and zeranol, there was little, if any, difference in the measured aqueous concentration and the total recoverable mass, and equivalent behavior was observed for both soil systems considered. The agreement in aqueous concentration and total mass profiles is consistent with all 17$\beta$-TBOH and zeranol loss in these soil systems being attributable to some nonconservative process (e.g., reaction) rather than sorption. Because systems were sterilized, we propose that this loss is due to mineral-promoted surface reactions such as hydrolysis or oxidation occurring on underlying inorganic phases in these soils. We note, however, that no products were detected using LC-DAD methods, suggesting that such products either are too polar to be separated on C-18 columns with our existing analytical method or are no longer chromophoric.

Results with MGA may elucidate factors controlling the rate at which SGPMs are degraded in soil systems via such nonconservative processes (i.e., transformation reactions). For both soils in Figure 3, the aqueous phase concentration of MGA showed nearly identical profiles; about 60−70% of the solution concentration disappeared within the first day, after which it remained relatively constant over the experiment's 6 day duration. In contrast, the total mass profiles were distinct for each soil system. For high OC PVLPF, the total mass of MGA in suspension was relatively stable and ∼90% remained after 5 days, consistent with most if not all of the MGA loss from solution being due to sorption. In contrast, total MGA mass decreased steadily over time in the low OC soil RMN, with only 50% remaining after 6 days. However, the rapid,

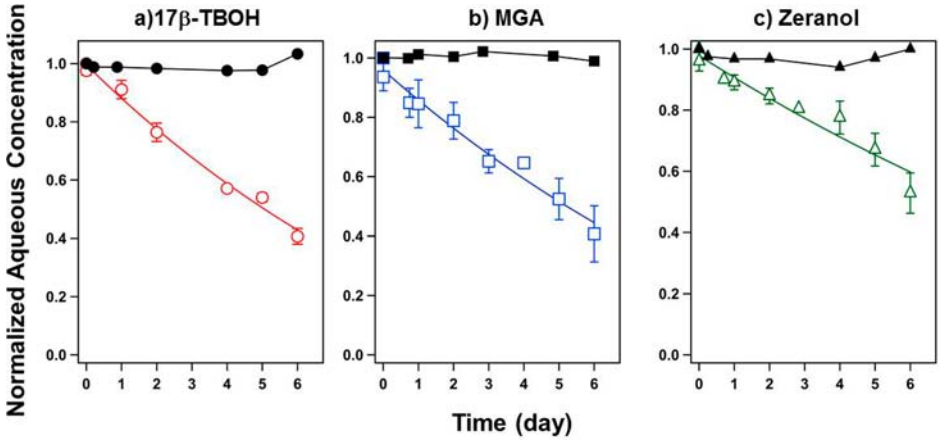


**Figure 5.** Reaction of 17$\beta$-TBOH, MGA, and zeranol with 10 g/L $SiO_2$ at pH 7. Lines represent exponential decay model fits from which half-lives were estimated. Experiments were conducted in 5 mM phosphate buffer at pH 7 and used initial concentrations of 4, 2, and 2 $\mu$M for 17$\beta$-TBOH, MGA, and zeranol, respectively.

initial MGA loss from solution appears to result entirely from sorption, as the total mass recovery for the RMN system was nearly 100% over the short time scales associated with this initial, steep decrease in aqueous concentration. Then, although there was relatively little change in the solution phase concentration of MGA between days 2 and 6, the total MGA mass in the system decreased by ~50%. This suggests that transformation processes in RMN suspensions involve the initially sorbed MGA mass.

One potential explanation for our MGA results is a two-step process for its mineral-promoted transformation in low-to-moderate OC-containing soils. The MGA first sorbs to the organic layer coating the particle, through which it must then diffuse to react at the surface of the underlying inorganic phase, which we assume is the same reactive mineral in both RMN and PVLPF systems. Because MGA has a relatively high $K_{ow}$ value and its isotherm with Pahokee Peat is consistent with hydrophobic partitioning, it is not surprising that the extent of its mass loss from reaction is highly dependent upon soil OC content. Specifically, for high OC content PVLPF (5.9%) MGA is more tightly and/or frequently bound to the organic phase, ultimately making it less available for transformation at the underlying mineral interface. In contrast, the smaller reservoir for hydrophobic partitioning on lower OC RMN (1%) allows MGA to more readily access reactive sites on the surface of the inorganic phase.

When this scenario is extended to 17$\beta$-TBOH and zeranol, their relative rates of organic partitioning (sorption) versus surface transformation (reaction) must be considered. Notably, instances when losses in total mass and solution phase concentration are equivalent (e.g., as we observed for 17$\beta$-TBOH and zeranol) imply that the rate of surface reaction is much faster than that of organic partitioning, thereby limiting the amount of sorbed mass that can accumulate in the system. Unfortunately, without greater understanding of the differences in OC composition and/or the nature of the reacting species in these two soil systems, it is difficult to more fully explain why 17$\beta$-TBOH and zeranol behave so distinctly from MGA.

**Reactivity of SGPMs toward Inorganic Mineral Phases.** The preceding discussion is predicated on the reactivity of SGPMs toward naturally occurring mineral phases. To assess the potential for such mineral-promoted transformations, additional experiments were conducted with several metal oxides representative of those naturally occurring in soil. Figure 4a shows the reactivity of amorphous manganese oxide (hereafter $MnO_2$), a known oxidant of certain steroids,[22] toward 17$\beta$-TBOH, MGA, and zeranol at pH 6. Zeranol was most reactive, undergoing nearly complete transformation over the course of 0.5 h at a relatively low $MnO_2$ loading (1 g/L). Although not as reactive as zeranol, the rate of 17$\beta$-TBOH decay increased with $MnO_2$ solid loading (from 1 to 10 g/L), behavior that is consistent with loss via surface reaction. Also, HPLC-DAD analysis of samples from these 17$\beta$-TBOH suspensions provided evidence of product formation. We note that these products, although not yet structurally identified, are considerably more polar than the monohydroxylated photoproducts of 17$\beta$-TBOH we have elucidated,[31,34,35] which is consistent with highly oxidized products resulting from 17$\beta$-TBOH oxidation by $MnO_2$. Interestingly, MGA is essentially unreactive toward $MnO_2$, exhibiting stability in 10 g/L at pH 6. In fact, we observed evidence of only limited MGA transformation under far more extreme suspension conditions (20 g/L at pH 4).

Iron oxides such as amorphous ferrihydrite are weaker oxidants than $MnO_2$ but may also promote other processes including hydrolysis[21] or, similarly, nucleophilic (e.g., $H_2O$ or $OH^-$) addition. Indeed, a modest amount of 17$\beta$-TBOH and MGA loss (~25%) was observed over approximately 1 week in ferrihydrite suspensions (5 g/L, pH 7) (Figure 4b), whereas zeranol was most reactive. These losses in ferrihydrite suspensions correspond to half-lives of 5 days for zeranol and roughly 15 days for 17$\beta$-TBOH and MGA. Furthermore, attempts to recover any SGPM mass sorbed to the ferrihydrite surface via methanol extraction were unsuccessful, consistent with a nonconservative process being responsible for SGPM loss. However, the relative reactivity of MGA and17$\beta$-TBOH is far different from the trend observed for $MnO_2$, which is reasonably assumed as an oxidant. Thus, we believe the data from ferrihydrite suspensions are evidence of a nonredox, surface-promoted reaction for SGPMs, although reaction products were not detected. This is particularly noteworthy for MGA, as melengestrol, a plausible hydrolysis product easily detected via our analytical methods, was not observed.

Finally, the stability of 17$\beta$-TBOH, MGA, and zeranol was examined in suspensions (10 g/L, pH 7) of $SiO_2$ (Figure 5). $SiO_2$ is not a viable oxidant, so it would be expected to promote

only nonredox pathways (e.g., hydrolysis or nucleophilic addition). Solution phase concentrations of 17$\beta$-TBOH, MGA, and zeranol decreased over time in these suspensions, and once again we were unable to recover any of this lost mass via methanol extraction of the $SiO_2$ at the conclusion of the experiment. Similar to observations with ferrihydrite, 17$\beta$-TBOH and MGA exhibited comparable rates of decay in $SiO_2$ (half-lives of 4.9 and 5.3 days, respectively), seemingly supporting a shared transformation pathway between iron and silica oxide systems. In fact, because 17$\beta$-TBOH and MGA share identical structures in the steroid A ring, we propose these similar time scales indicate A-ring susceptibility to hydroxylation via surface-promoted nucleophilic addition rather than hydrolysis. Zeranol, which has a hydrolyzable ester group, decays at a slightly slower rate compared to the other SGPMs ($t_{1/2}$ of ~8 days).

Although work is ongoing to better characterize SGPM reactivity and fate in these metal oxide systems, these data clearly support the surface-promoted transformation of SGPMs in model soils. Oxidation by manganese oxide appears viable for the TBA and zeranol families, whereas all SGPMs are susceptible to hydrolysis or nucleophilic addition on iron and silica oxides. As for the primary reactive inorganic phase in our model soil systems, our data appear to implicate $SiO_2$. Assuming exponential decay in our model $SiO_2$ systems, the relative rate of transformation for 17$\beta$-TBOH, MGA, and zeranol is 1:1.1:1.6. Notably, if we apply a similar exponential decay model to the total SGPM mass data obtained in our low OC model soil (i.e., RMN; see Figure 3), we find an equivalent trend in relative reactivity for 17$\beta$-TBOH, MGA, and zeranol (1:1.1:1.5). Consistent with these identical trends in relative reactivity, silica was the only mineral phase detected during X-ray diffraction analysis of model soils, although we cannot rule out that iron and manganese oxides were present at levels below the limit of analytical detection. We note that reactivity differences observed in the high OC content soil (PVLPF; 5.9% OC) may indicate a combination of reactive oxides (e.g., $SiO_2$ and $MnO_2$) at play or simply reflect an influence of the organic matter coating on transformation rates by concentrating the SGPMs at the interface of the reactive mineral phase.

**Environmental Implications.** Consistent with initial expectations, our results indicate that the fate of SGPMs in soil is likely far more complex than currently appreciated. Although sorption and biodegradation have long been thought to dominate SGPM fate in soil, we provide converging lines of evidence that abiotic transformation reactions promoted by naturally abundant mineral surfaces, including quartz (i.e., $SiO_2$), can occur over time scales comparable to those previously reported for biotransformation.[7] These transformation pathways likely will influence the persistence of SGPMs in soil while also producing novel, yet uncharacterized, transformation products.

Collectively, our findings highlight the challenges in accurately predicting SGPM fate in soil as a result of their many competing fate pathways (e.g., sorption, biotransformation, mineral-promoted transformation). Generally, we can conclude that SGPM sorption will dominate only in soil systems with very high OC content. For example, the Pahokee Peat systems used herein may indeed be a reasonable approximation of organic-rich agricultural topsoil or land-applied manure, both of which would then be expected to effectively retain SGPMs. However, the extent and reversibility of SGPM uptake do not appear easily predictable from traditional metrics of compound hydrophobicity (e.g., $K_{ow}$ values), which are typically used as a starting point to assess soil partitioning. In particular, more polar species (i.e., those with functionalities capable of specific binding interactions such as hydrogen bonding) will be most difficult to model, as their interactions with organic-rich soil will be influenced heavily by soil organic carbon properties responsible for such specific binding interactions.

A clear need arising from this work is a closer examination of mineral-promoted transformation pathways of SGPMs. This includes identifying the key properties and constituents of soils most likely to promote such reactions, especially because prior studies with these compound classes in model soils (e.g., Card et al.[9]) have failed to observe similar evidence of transformation. Another priority is the structural identification of products generated via mineral-promoted reactions. Whereas the structure of some products may be inferred on the basis of the presence of reactive moieties in the parent structure (e.g., the hydrolyzable ester functionality in zeranol), such mechanistic details remain less obvious in other cases. For example, there are several electron-deficient carbon centers within the trienone structure of trenbolone that could be prone to surface-promoted hydroxylation, although our initial assessment suggests this reaction may proceed through the A ring.

We contend that identification of trenbolone transformation products is a particular priority on the basis of our prior findings regarding trenbolone photolysis. Recently, we reported[35] on the formation of metastable photoproducts of trenbolone, C5 and C12 hydroxylated species, that unexpectedly decompose, or revert, into the parent metabolite from which they were generated. Mineral-promoted nucleophilic addition, as we have proposed, will also likely yield hydroxylated products. We believe that if such hydroxlyation occurs within or adjacent to trenbolone's unique trienone moiety, such products may also be prone to similar transformations to yield novel steroidal byproducts with unknown implications for ecosystem health. We reiterate, however, that all evidence to date suggests that products of mineral-promoted reactions with trenbolone are different from those generated photolytically. Furthermore, changes in solution conditions that promote product-to-parent reversion in photoproduct mixtures (e.g., lowering solution pH to promote acid-catalyzed reversion) have thus far failed to regenerate parent trenbolone metabolites in reacted mineral suspensions.

## ■ ASSOCIATED CONTENT

### Supporting Information

Additional experimental details including the reagent list, sterilization protocol for model soil systems, methodology for measurement of octanol−water partitioning coefficients, and synthesis methods of ferrihydrite and manganese oxide; additional results and discussion regarding the fate of synthetic growth promoters and their metabolites (SGPMs) in model soil and metal oxide systems. This material is available free of charge via the Internet at http://pubs.acs.org.

## ■ AUTHOR INFORMATION

### Corresponding Author

*(D.M.C.) E-mail: david-cwiertny@uiowa.edu. Phone: (319) 335-1401. Fax: (319) 335-5660.

## Funding

This work is supported through a USDA Agriculture Food Research Initiative (AFRI) Water and Watersheds grant (2010-65102-20425).

## Notes

The authors declare no competing financial interest.

## ■ ACKNOWLEDGMENTS

We acknowledge Matthew Tarnoff, who assisted in experiments with inorganic metal oxides. We thank Dale Swenson of the Department of Chemistry at the University of Iowa for assistance with the X-ray diffraction analysis of all synthesized metal oxides. We also acknowledge the anonymous reviewers whose comments greatly improved the quality of this work.

## ■ REFERENCES

(1) California Environmental Contaminant Biomonitoring Program (CECBP) Scientific Guidance Panel (SGP). *Synthetic Hormones in Animal Husbandry*, 2008; available at http://oehha.ca.gov/multimedia/biomon/pdf/120408synhormonesdoc.pdf.

(2) Biswas, S.; Shapiro, C. A.; Kranz, W. L.; Mader, T. L.; Shelton, D. P.; Snow, D. D.; Bartelt-Hunt, S. L.; Tarkalson, D. D.; van Donk, S. J.; Zhang, T. C.; Ensley, S. Current knowledge on the enviromental fate, potential impacts, and management of growth-promoting steroids used in the US beef cattle industry. *J. Soil Water Conserv.* **2013**, *68*, 325−336.

(3) Khan, S. J.; Roser, D. J.; Davies, C. M.; Peters, G. M.; Stuetz, R. M.; Tucker, R.; Ashbolt, N. J. Chemical contaminants in feedlot wastes: concentrations, effects and attenuation. *Environ. Int.* **2008**, *34*, 839−859.

(4) Bartelt-Hunt, S. L.; Snow, D. D.; Kranz, W. L.; Mader, T. L.; Shapiro, C. A.; van Donk, S. J.; Shelton, D. P.; Tarkalson, D. D.; Zhang, T. C. Effect of growth promotants on the occurrence of endogenous and synthetic steroid hormones on feedlot soils and in runoff from beef cattle feeding operations. *Environ. Sci. Technol.* **2012**, *46*, 1352−1360.

(5) Gall, H. E.; Sassman, S. A.; Lee, L. S.; Jafvert, C. T. Hormone discharges from a midwest tile-drained agroecosystem receiving animal wastes. *Environ. Sci. Technol.* **2011**, *45*, 8755−8764.

(6) Schiffer, B.; Daxenberger, A.; Meyer, K.; Meyer, H. H. The fate of trenbolone acetate and melengestrol acetate after application as growth promoters in cattle: environmental studies. *Environ. Health Perspect.* **2001**, *109*, 1145−1151.

(7) Khan, B.; Lee, L. S.; Sassman, S. A. Degradation of synthetic androgens 17$\alpha$- and 17$\beta$-trenbolone and trendione in agricultural soils. *Environ. Sci. Technol.* **2008**, *42*, 3570−3574.

(8) Khan, B.; Qiao, X.; Lee, L. S. Stereoselective sorption by agricultural soils and liquid−liquid partitioning of trenbolone (17$\alpha$ and 17$\beta$) and trendione. *Environ. Sci. Technol.* **2009**, *43*, 8827−8833.

(9) Card, M. L.; Chin, Y.-P.; Lee, L. S.; Khan, B. Prediction and experimental evaluation of soil sorption by natural hormones and hormone mimics. *J. Agric. Food Chem.* **2012**, *60*, 1480−1487.

(10) Neal, P. A.; Escher, B. I.; Schafer, A. I. pH dependence of steroid hormone-organic matter interactions at environmental concentrations. *Sci. Total Environ.* **2009**, *407*, 1164−1173.

(11) Yamamoto, H.; Liljestrand, H. M. The fate of estrogenic compounds in the aquatic environment: sorption onto organic colloids. *Water Sci. Technol.* **2003**, *47*, 77−84.

(12) Mashtare, M. L.; Khan, B.; Lee, L. S. Evaluating stereoselective sorption by soils of 17$\alpha$-estradiol and 17$\beta$-estradiol. *Chemosphere* **2011**, *82*, 847−852.

(13) Yamamoto, H.; Liljestrand, H. M.; Shimizu, Y.; Morita, M. Effects of physical-chemical characteristics on the sorption of selected endocrine disruptors by dissolved organic matter surrogates. *Environ. Sci. Technol.* **2003**, *37*, 2646−2657.

(14) Qiao, X.; Carmosini, N.; Li, F.; Lee, L. S. Probing the primary mechanisms affecting the environmental distribution of estrogen and androgen isomers. *Environ. Sci. Technol.* **2011**, *45*, 3989−3995.

(15) Schiffer, B.; Totsche, K. U.; Jann, S.; Kögel-Knabner, I.; Meyer, K.; Meyer, H. H. D. Mobility of the growth promoters trenbolone and melengestrol acetate in agricultural soil: column studies. *Sci. Total Environ.* **2004**, *326*, 225−237.

(16) Jones, G. D.; Benchetler, P. V.; Tate, K. W.; Kolodziej, E. P. Mass balance approaches to characterizing the leaching potential of trenbolone acetate metabolites in agro-ecosystems. *Environ. Sci. Technol.* **2014**, *48*, 3715−3723.

(17) Shareef, A.; Angove, M. J.; Wells, J. D.; Johnson, B. B. Sorption of bisphenol A, 17$\alpha$-ethynylestradiol and estrone to mineral surfaces. *J. Colloid Interface Sci.* **2006**, *297*, 62−69.

(18) Mallinckrodt Veterinary, Inc. *Environmental Assessment for Zeranol*, 1994; available at http://www.fda.gov/ucm/groups/fdagov-public/@fdagov-av-gen/documents/document/ucm071898.pdf.

(19) Upjohn Co. *Environmental Assessment: Melengestrol Acetate (MGA) for Suppression of Estrus for Heifers Intended for Breeding*, 1996; available at http://www.fda.gov/ucm/groups/fdagov-public/@fdagov-av-gen/documents/document/ucm071903.pdf.

(20) Syntex Animal Health. *Synovex Plus (Trenbolone Acetate and Estradiol Benzoate) Implant Environmental Assessment*, 1995; available at http://www.fda.gov/ucm/groups/fdagov-public/@fdagov-av-gen/documents/document/ucm072347.pdf.

(21) Torrents, A.; Stone, A. T. Hydrolysis of phenyl picolinate at the mineral/water interface. *Environ. Sci. Technol.* **1991**, *25*, 143−149.

(22) Xu, L.; Xu, C.; Zhao, M.; Qiu, Y.; Sheng, G. D. Oxidative removal of aqueous steroid estrogens by manganese oxides. *Water Res.* **2008**, *42*, 5038−5044.

(23) Zhang, H.; Huang, C. Adsorption and oxidation of fluoroquinolone antibacterial agents and structurally related amines with goethite. *Chemosphere* **2007**, *66*, 1502−1512.

(24) Kahn, L. Determination of total organic carbon in sediment (Lloyd Kahn method). In *Region II*; U.S. Environmental Protection Agency: Edison, NJ, USA, 1988; Vol. 5p.

(25) Dean, W. E., Jr. Determination of carbonate and organic matter in calcareous sediments and sedimentary rocks by loss on ignition: comparison with other methods. *J. Sediment. Petrol.* **1974**, *44*, 242−248.

(26) Burleson, D. J.; Penn, R. L. Two-step growth of goethite from ferrihydrite. *Langmuir* **2005**, *22*, 402−409.

(27) Murray, J. W. The surface chemistry of hydrous manganese dioxide. *J. Colloid Interface Sci.* **1974**, *46*, 357−371.

(28) Wolf, D. C.; Dao, T. H.; Scott, H. D.; Lavy, T. L. Influence of sterilization methods on selected soil microbiological, physical, and chemical properties. *J. Environ. Qual.* **1989**, *18*, 39−44.

(29) Yang, Y.; Hunter, W.; Tao, S.; Gan, J. Relationships between desorption intervals and availability of sediment-associated hydrophobic contaminants. *Environ. Sci. Technol.* **2008**, *42*, 8446−8451.

(30) Schwarzenbach, R. P.; Gschwend, P. M.; Imboden, D. M. *Environmental Organic Chemistry*; Wiley: New York, 2003.

(31) Qu, S.; Kolodziej, E. P.; Cwiertny, D. M. Phototransformation rates and mechanisms for synthetic hormone growth promoters used in animal agriculture. *Environ. Sci. Technol.* **2012**, *46*, 13202−13211.

(32) Allen-King, R. M.; McKay, L. D.; Trudell, M. R. Organic carbon dominated trichloroethene sorption in a clay-rich glacial deposit. *Ground Water* **1997**, *35*, 124−130.

(33) Zhang, Y.; Wei, D.; Huang, R.; Yang, M.; Zhang, S.; Dou, X.; Wang, D.; Vimonses, V. Binding mechanisms and QSAR modeling of aromatic pollutant biosorption on *Penicillium oxalicum* biomass. *Chem. Eng. J.* **2011**, *166*, 624−630.

(34) Kolodziej, E. P.; Qu, S.; Forsgren, K.; Long, S.; Gloer, J.; Jones, G.; Schlenk, D.; Baltrusaitis, J.; Cwiertny, D. Identification and environmental implications of photo-transformation products of trenbolone acetate metabolites. *Environ. Sci. Technol.* **2013**, *47*, 5031−5041.

(35) Qu, S.; Kolodziej, E. P.; Long, S. A.; Gloer, J. B.; Patterson, E. V.; Baltrusaitis, J.; Jones, G. D.; Benchetler, P. V.; Cole, E. A.;

Kimbrough, K. C.; Tarnoff, M. D.; Cwiertny, D. M. Product-to-parent reversion of trenbolone: unrecognized risks for endocrine disruption. *Science* **2013**, *342*, 347−351.
(36) U.S. EPA. *Estimation Programs Interface Suite for Microsoft® Windows*, v 4.11; U.S. Environmental Protection Agency: Washington, DC, USA, 2012.

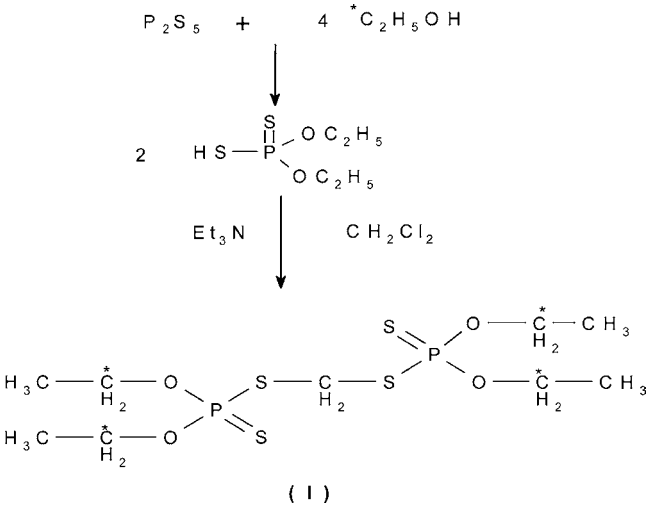


**Figure 1.** Pathway of $^{14}$C-ethion synthesis.

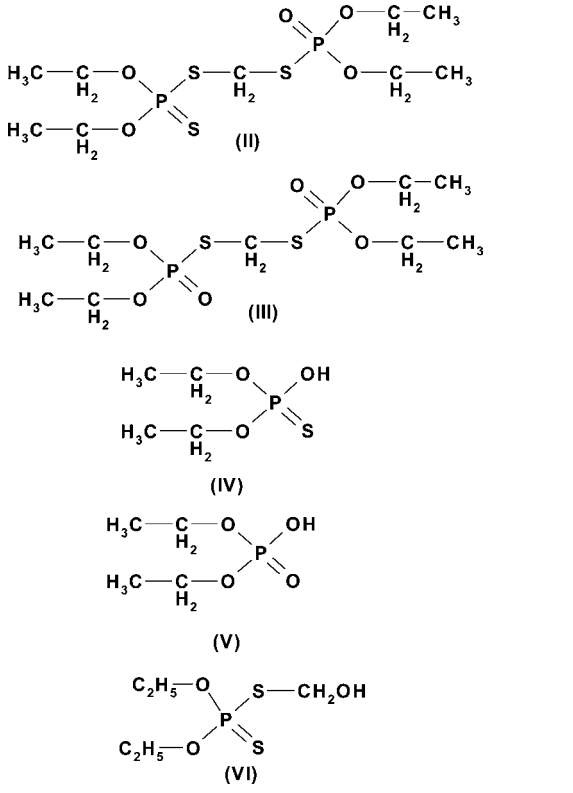


**Figure 2.** Main degradation products of ethion insecticide.

**Field Experiments.** *Treatment of Plants with Pesticides.* Pesticide-free *G. hirsutum* L. seeds (var. Giza 86) were obtained from the Agricultural Research Centre, Cairo. The seeds were cleaned from any dockage and impurities before cultivation. Sound whole seeds of cotton were cultivated under normal field conditions in a controlled, isolated field area. Irrigation, fertilization, and hand weeding were performed, and soil management was conducted as usually practiced in the field. A control field plot of similar soil characteristics to the experimental plot was cultivated as in the experimental plot and kept untreated with pesticides. Shortly at flowering stage, leaves of plants were treated twice, 21 days apart, with $^{14}$C-ethion alone (8 mg/plant) and in the presence of deltamethrin (3.6 mg/plant) and dimilin (1.6 mg/plant) pesticides. Samples of cotton plant were collected manually at harvest time. The cotton seed samples were air-dried and delinted to get cotton seed for preparation of oil and cake and determination of radioactivity.

*Extraction of Cotton Seeds.* The analysis procedures for $^{14}$C-residues in cotton seeds are shown in Figure 3. Dry cotton seeds were crushed and extracted with *n*-hexane for 12 h using a Soxhlet apparatus. After evaporation of hexane under reduced pressure, radioactivity in the cotton oil was measured. The residue remaining after extraction (cake A) was further extracted with ethanol (Figure 3). Aliquots of the hexane extract (oil) and the ethanol extract were determined for radioactivity.

The remaining cake (cake B) was air-dried and digested by adding 1 mL of Solusol (tissue and gel solubilizer); samples were digested at 40−50 °C until the tissue dissolved and then decolorized with 30% $H_2O_2$ (1 mL). Seventy microliters of glacial acetic was added to eliminate chemiluminescence.[12] The radioactivity was determined using a liquid scintillation counter.

*Removal of Pesticide Residues from Oils.* Oil processing was conducted in four steps, namely, alkali refining, bleaching, winterization, and deodorization, as previously reported.[5]

*Neutralization (Alkali Refining).* Samples of the crude cotton oil (17.5 g) were heated at 85 °C with continuous stirring for 30 min and then neutralized by adding 2 N NaOH ,and stirring was continued for another 30 min. The mixture was then centrifuged at 3000 rpm for 10 min. After the oil had been separated from the soap stock, i was washed with 100 mL of hot distilled water several times using a separating funnel until the washings were neutral. This process removed free fatty acids and other acidic material from the oil. The $^{14}$C-activity of the oil was determined.

*Bleaching.* Bleaching clay performs not only color removal but also the removal of trace metals and the adsorption of phospholipids, soap, and decomposition of oxidation products such as peroxides. Neutralized oil was heated to 60 °C and fuller earth (Tonsil, 0.15 g) was added. The mixture was then heated to 100−110 °C on an oil bath for 30 min with continuous stirring. The oil was centrifuged at 3000 rpm for 10 min, and $^{14}$C-residue levels were determined.

*Winterization.* The clear dry oil was winterized (cooled) at 5 °C for 3 days, and the high saturated glycosides that separated were removed by filtration or centrifuged at 3000 rpm for 10 min; $^{14}$C-residue levels were determined.

*Deodorization.* Deodorization is the last major processing step in the refining of edible oil and is responsible for removing undesirable ingredients. The winterized oil was heated at 200−220 °C on an oil bath while superheated steam passed. The deodorization was continued for 3 h. The oil was then separated, and $^{14}$C-residue levels were determined.

*Bioavailability of Bound Residues in Rats.* Three-month-old, sexually mature white male rats (derived from Sprague−Dawlay strain) weighing 150 ± 10 g were purchased from animal house colony, Dokki, Giza Egypt. The animals were individually housed in glass metabolism cages that allowed separate collection of feces, urine, and expired air. The rats were conditioned for 2 days to a daily diet consisting of standard feed mixed with extracted untreated cotton seeds for acclimatization under the laboratory conditions (29 ± 3 °C). The animals were kept without food for 24 h and then fed the diet containing bound $^{14}$C-ethion residues for 3 days. To make the feed palatable, the extracted seeds were mixed thoroughly with an equal amount of white cheese, and the paste was left to dry.

The respiratory carbon dioxide was trapped in a 10% NaOH solution. Urine, feces, and $^{14}CO_2$ were collected separately for 3 days and assayed for radioactivity. After the end of 3 days, each rat was lightly anaesthetized with ether and blood removed from the pumping heart. The animal was then killed with an overdose of ether, and samples from liver, kidney, fat, blood, lung, and brain were collected and kept frozen until analysis of radioactivity by digestion and LSC.

*Isolation and Characterization of $^{14}$C-Residues.* Analysis of radioactive compounds was achieved by thin layer chromatography (TLC). Samples of crude oil at harvest time and after each refining process were partitioned between acetonitrile and hexane to remove the oil. The radioactive residues were almost completely retained in

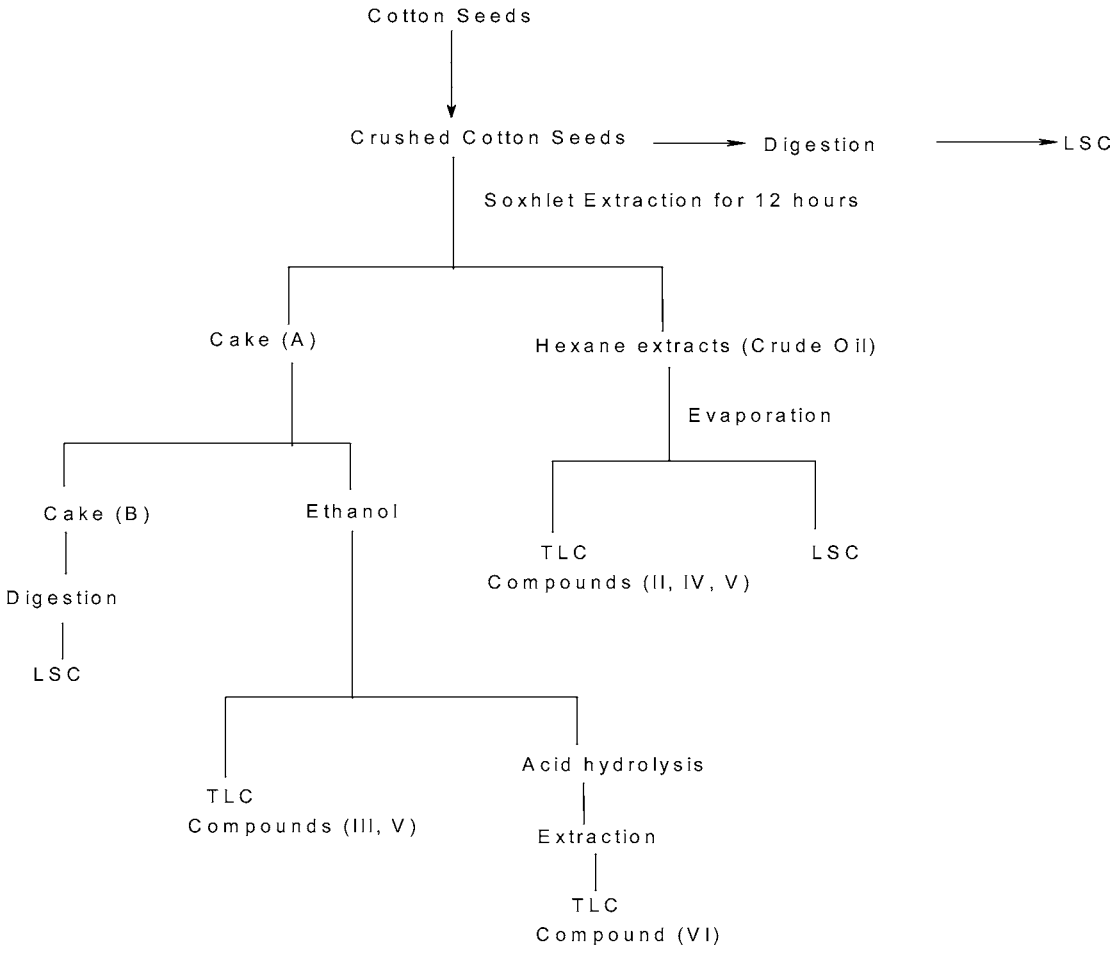


**Figure 3.** Analysis procedures for $^{14}$C-residues in cotton seeds and oils.

the acetonitrile layer. Analysis of crude and refined oil extracts were achieved by TLC.

Urine was extracted with chloroform (chloroform 1), and the aqueous layer was then acidified with 2 N HCl and heated for 2 h at 100 °C on a water bath and reextracted with chloroform three times. The combined chloroform was dried over anhydrous sodium sulfate, filtered off, and evaporated under vacuum (chloroform 2) to obtain the conjugated metabolites. Aliquots from both chloroform 1 and 2 and ethanol layers (after hexane extraction) were analyzed by TLC on silica gel plates using suitable solvents.

Residues were characterized by TLC on silica gel plates (20 × 20 cm; 0.25 mm thickness) with fluorescent indicator (Kiesel gel 60 $F_{254}$, Merck, Darmstadt, Germany) using these solvent systems: system 1, toluene/xylene 50:50 (v/v); system 2, dioxane/xylene/petrolum ether 20:40:40 (v/v/v); system 3, *n*-hexane/ethyl acetate 98:2 (v/v).

Authentic samples were run alongside as references, and spots were viewed under UV light at 254 nm and by spraying the plates with a freshly prepared Hans–Isherwood reagent,[13] or after preliminary spraying with $PdCl_2$ solution, the plates were subjected to $I_2$ vapor to detect the compound by color.[14,15]

*Radioactivity Measurements.* Radioactivity in oil (acetonitrile extracts), ethanol extracts, urine, and other liquid samples was measured directly by LSC using a Packard Tri-Carb liquid scintillation spectrometer (model 2300, PerkinElmer Life Science, Boston, MA, USA) in vials using a dioxane-based scintillation cocktail composed of dioxane (1 L), naphthalene (100 g), 2,5-diphenyloxazole (PPO; 10 g), and 1,4-di[2-(5-phenyloxazolyl)]benzene (POPOP; 0.25 g).

Cake, feces, ground cotton, and animal tissues (100 mg) were assayed for radioactivity by digestion using [1 mL of Solusol (tissue and gel solubilizer), 1 mL of 30% $H_2O_2$, and 70 μL of glacial acetic at 40–50 °C]. The radioactivity was determined using a LSC. The internal standard technique was used for quench correction. Thin layer plates were divided in 1 cm increments, scraped into vials, eluted with methanol, covered with scintillator, and counted.

## RESULTS AND DISCUSSION

**$^{14}$C-Residues in Seeds, Oil, and Cake.** The $^{14}$C-residues in dry cotton seeds obtained from $^{14}$C-ethion-treated plants amounted to 0.11% of the applied dose at harvest time. The percentage of residues decreases to 0.08 and 0.05% in the presence of deltamethrin and dimilin pesticides, respectively (Table 1). The insecticide was absorbed and translocated very slowly from the treated leaves to the seeds of investigated plant due to enzyme metabolic activity.[5,16] Following foliar application of soybean plants with $^{14}$C-pirimiphos-methyl,[17] and cotton plants with $^{14}$C-malathion,[18] the aged insecticide

**Table 1. $^{14}$C-Residues in Seeds after Treatment of Cotton Plants with $^{14}$C-Ethion in the Presence of Deltamethrin and Dimilin Pesticides at Harvest Time**

| sample[a] | weight (g) | average $^{14}$C-residues[b] (ppm) | %[c] |
|---|---|---|---|
| ethion | 88.7 | 0.59 ± 0.051 | 0.11 |
| ethion and deltamethrin | 81.8 | 0.47 ± 0.024 | 0.08 |
| ethion and dimilin | 93.0 | 0.27 ± 0.011 | 0.05 |

[a]At harvest time. [b]Results are expressed as the mean ± SD for three determinations of ethion residue level for each sample. [c]Percent of applied dose.

Table 2. $^{14}$C-Residues in Extracted Seeds after Treatment of Cotton Plants with $^{14}$C-Ethion in the Presence of Deltamethrin and Dimilin Pesticides at Harvest Time

| sample[a] | oil hexane[b] (ppm) | ethanol[b] (ppm) | cake[b] (ppm) | % recovery |
|---|---|---|---|---|
| ethion | 0.280 ± 0.025 | 0.063 ± 0.005 | 0.220 ± 0.015 | 95.4 |
| ethion and deltamethrin | 0.280 ± 0.018 | 0.098 ± 0.003 | 0.038 ± 0.002 | 88.5 |
| ethion and dimilin | 0.140 ± 0.004 | 0.083 ± 0.002 | 0.028 ± 0.001 | 92.9 |

[a]After the second application. [b]Results are expressed as the mean ± SD for three determinations of ethion residue level for each sample.

residues in seeds amounted to 0.37 and 0.11% of the applied dose, respectively. The data obtained are in agreement with those reported by Singh et al.[19] in their studies on the persistence of ethion residues on cucumber. Although persistent insecticides are beneficial for controlling pests for extended periods, their residues in consumable parts of the crops may be harmful to the consumers when they exceed the maximum residue limit (MRL) values.[20]

About 47.5% of $^{14}$C-activity in dry seeds was found to be associated with oil (hexane extract). The ethanol-soluble $^{14}$C-residues accounted for 10.6% of the total seed residues, whereas the cake contained about 37.3% of the total residues as nonextractable or bound residues in the case of ethion only. The percentage of bound residues decreases when deltamethrin or dimilin pesticide was used in combination with ethion and amounted to 8.1 and 10.4%, respectively. The recovery percent of the applied radioactivity ranged from 88.5 to 95.4% as shown in Table 2. When two compounds are mixed, there are basically four types of interactions that change the efficacy of pesticide combinations; they can either be additive effects or synergistic responses (potentiating) or antagonism or enhancement in an insect species. If a mixture is potentiating, it is a useful tool in enhancing control efficacy and combating insecticide resistance. If a mixture is antagonistic, it should not be used, because it will reduce the efficiency of pest control and aggravate the resistance problem.[1,21] It is worth mentioning that Zayed et al.[22] found that repeated applications of pesticides might enhance the release of $^{14}$C-bound residues in their study on the impact of repeated pesticide applications on the binding and release of methyl $^{14}$C-monocrotophos and U-ring-labeled $^{14}$C-carbaryl to soil matrices under field conditions.

**Effect of Refining Processes.** Simulated commercial processing procedures resulted in a gradual decrease in the total amount of $^{14}$C-residues in oils with aged residues (Table 3). This decrease could be attributed to alkali hydrolysis, effect of adsorption, effect of heat, or evolution of $^{14}CO_2$ gas. The deodorization processes proved to be the most effective step in reducing $^{14}$C-ethion residues, as they eliminated 95% of the residues originally present in crude oil. On the other hand, the alkali treatment, bleaching, and winterization eliminated 30, 75, and 82% of the originally present radioactivity in oil, respectively. These results agree with Miyahara and Saito,[23] who found that in some organophosphorus insecticides, such as malathion, dichlorvos, and chlorpyrifos, the deodorizing process was effective in removing pesticide residues due to decomposition and volatilization. This also agreed with the findings of Ruiz Méndez et al.,[24] who reported that pesticide residues (simazine) were highly eliminated in olive oil during the deodorizing step. Zayed et al.[17,25] showed that the amounts of both $^{14}$C-carbofuran and $^{14}$C-pirimiphos-methyl residues in soybean oil decreased to 16 and 25%, respectively, through the refining processes. Hegazi et al.[26] found that the sunflower oil obtained from treated sunflower plants lost about 64% of the total $^{14}$C-zineb residues in crude oil through refining processes. Abdel-Gawad and Hegazi[5] noted that the refined oil from canola seeds treated with prothiofos lost about 69% of the total $^{14}$C-residues in crude oil through the processing procedures. Also, Abdel-Gawad et al.[6,7] reported that the refined oil from maize and soybean seeds treated with ethion lost about 70 and 62.5% of the total $^{14}$C-residues in crude oil, respectively, through refining processes.

Table 3. Effect of Refining Processes on $^{14}$C-Ethion Residues in Cottonseed Oil

| sample | $^{14}$C-residues[a] (ppm) | % reduction[b] |
|---|---|---|
| crude oil | 0.280 ± 0.025 | 0.0 |
| neutralized oil | 0.196 ± 0.017 | 30 |
| bleached oil | 0.070 ± 0.004 | 75 |
| winterized oil | 0.050 ± 0.003 | 82 |
| deodorized oil | 0.014 ± 0.001 | 95 |

[a]Results are expressed as the mean ± SD for three determinations of ethion residue level for each sample. [b]Percent reduction = [(crude oil − each step)/crude oil] × 100.

**Identification and Characterization of Radioactive Degradation Products in Oil.** The $R_f$ values and the average concentration of $^{14}$C-ethion and its metabolites in cotton oil extract at harvest time are shown in Table 4. Chromatographic analysis of cotton oil extracts (acetonitrile layer) revealed the presence of ethion monooxon (**II**), *O*,*O*-diethyl phosphorothioate (**IV**), and *O*,*O*-diethyl phosphoric acid (**V**) in addition to one unknown compound in the case of ethion alone and ethion and dimilin. The same degradation products are found in the case of ethion and deltamethrin besides ethion dioxon (**III**).

The ethanol-extractable residues contain the hydrophilic compounds ethion dioxon (**III**) and *O*,*O*-diethyl phosphoric acid (**V**) as free metabolites, in addition to an unknown compound. Acid hydrolysis of the ethanol extract with 2 N HCl at 100 °C followed by extraction with chloroform yielded *O*,*O*-diethyl *S*-hydroxymethyl phosphorodithioate (**VI**).

The residues in refined cottonseed oil were identified as ethion monooxon (**II**), *O*,*O*-diethyl phosphorothioate (**IV**), and *O*,*O*-diethyl phosphoric acid (**V**) in addition to one unknown compound. Their amounts decreased during the refining steps (Table 5). Abdel-Gawad et al.[11] studied the distribution and elimination of $^{14}$C-ethion in chamomile flowers and found the presence of the parent compound together with four metabolites, which were identified as ethion monooxon, ethion dioxon, *O*,*O*-diethyl phosphorothioate, and *O*-ethyl phosphorothioate.

The suggested metabolic fate of ethion labeled with $^{14}$C-ethyl groups in cotton seeds and oil after double application to leaves in the presence of deltamethrin and dimilin pesticides at harvest time is shown in Figure 4. Three pathways are suggested for the degradation of $^{14}$C-ethion in cotton seeds. The first is oxidation of P═S to P═O, yielding ethion monooxon (**II**) and ethion

**Table 4. $^{14}$C-Ethion and Its Degradation Products in the Presence of Deltamethrin and Dimilin Pesticides in Extracts of Cottonseed Oil (Crude Oil) at Harvest Time**

| substance | $R_f$ in system[a] | | | metabolites concentration (ppm) | | |
|---|---|---|---|---|---|---|
| | 1 | 2 | 3 | ethion | ethion and deltamethrin | ethion and dimilin |
| ethion (**I**) | 0.75 | 0.80 | 0.75 | 0.000 | 0.000 | 0.000 |
| ethion monooxon (**II**) | 0.88 | 0.92 | 0.65 | 0.060 | 0.035 | 0.027 |
| ethion dioxon (**III**) | 0.69 | 0.56 | 0.55 | 0.000 | 0.037 | 0.000 |
| *O,O*-diethyl phosphorothioate (**IV**) | 0.33 | 0.23 | 0.42 | 0.036 | 0.053 | 0.024 |
| *O,O*-diethyl phosphoric acid (**V**) | 0.61 | 0.71 | 0.82 | 0.071 | 0.031 | 0.022 |
| unknown | 0.10 | 0.15 | 0.00 | 0.095 | 0.119 | 0.056 |

[a]System 1, toluene/xylene 50:50 (v/v); system 2, dioxane/xylene/petrolum ether 20:40:40 (v/v/v); system 3, *n*-hexane/ethyl acetate 98:2 (v/v).

**Table 5. $R_f$ Values and Concentrations of $^{14}$C-Ethion and Its Degradation Products in Cottonseed Oil after Subjection to Commercial Processing Procedures**

| substance | $R_f$ in system[a] | | | metabolites concentration[b] (ppm) | | |
|---|---|---|---|---|---|---|
| | 1 | 2 | 3 | crude oil | A | D |
| ethion (**I**) | 0.75 | 0.80 | 0.75 | 0.000 | 0.000 | 0.000 |
| ethion monooxon (**II**) | 0.88 | 0.92 | 0.65 | 0.060 | 0.010 | 0.001 |
| *O,O*-diethyl phosphorothioate (**IV**) | 0.33 | 0.23 | 0.42 | 0.036 | 0.020 | 0.006 |
| *O,O*-diethyl phosphoric acid (**V**) | 0.61 | 0.71 | 0.82 | 0.071 | 0.060 | 0.003 |
| unknown | 0.10 | 0.15 | 0.00 | 0.095 | 0.091 | 0.003 |

[a]System 1, toluene/xylene 50:50 (v/v); system 2, dioxane/xylene/petrolum ether 20:40:40 (v/v/v); system 3, *n*-hexane/ethyl acetate 98:2 (v/v). [b]A, neutralization; D, deodorization.

dioxon (**III**). The second is cleavage of the P−S−alkyl to yield *O,O*-diethyl phosphorothioate (**IV**) and *O,O*-diethyl phosphoric acid (**V**). The third is hydrolysis to yield *O,O*-diethyl *S*-hydroxymethyl phosphorodithioate (**VI**). Katagi and Mikami[27] noted that the metabolism of organophosphorus pesticides in plants has revealed cleavage of the P−O−aryl linkage and *O*-dealkylation to be among the most predominant metabolic pathways. Ethion is converted via desulfuration in the liver by cytochrome P-450 enzymes to its active oxygen analogue, ethion monooxon.[28]

**Bioavailability in Rats.** Elimination and distribution of $^{14}$C-ethion residues following the feeding of rats with the extracted cotton seeds (cake containing 13.2 $\mu$g equiv per rat) are shown in Table 6. Most of the radioactivity was eliminated via urine (60%), whereas residues in feces and expired air were 9 and 10% of the ingested $^{14}$C-activity, respectively. Appreciable amounts of $^{14}$C-residues (11%) were also detected in the liver, kidney, blood, lung, brain, and fat. Bound $^{14}$C-ethion in cotton

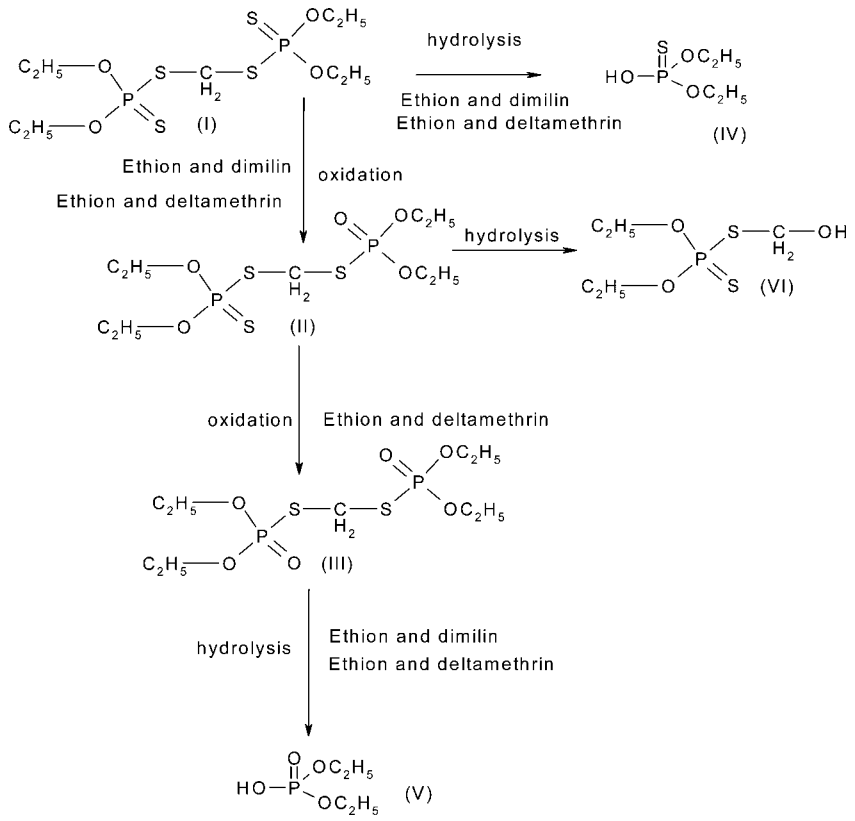


**Figure 4.** Metabolic pathway of $^{14}$C-ethion in cottonseed oil and in the presence of deltamethrin and dimilin.

**Table 6. Excretion and Distribution of $^{14}$C-Bound Ethion Residues in Cotton Seed after Feeding to Rats for 72 h**

| sample | insecticide[a] equivalent ($\mu$g) | % of administered dose |
|---|---|---|
| carbon dioxide | 1.30 ± 0.11 | 10 |
| urine | 7.90 ± 0.680 | 60 |
| faces | 1.20 ± 0.070 | 9 |
| liver | 0.50 ± 0.020 | 4 |
| kidney | 0.10 ± 0.008 | 1 |
| fat | 0.20 ± 0.009 | 1.5 |
| blood | 0.40 ± 0.010 | 3 |
| lung | 0.10 ± 0.007 | 1 |
| brain | 0.07 ± 0.003 | 0.5 |
| total recovery | 11.77 | 90 |

[a]Administered dose = (13.2 $\mu$g equivalent per rat) 100%. Results are expressed as the mean ± SD for three determinations of ethion residue level for rats.

seeds proved to be highly bioavailable to rats. Similar observations were reported from studies on the bioavailability of soybean-bound residues of dichlorovos[29] and fenitrothion.[30] Also, the data obtained are in line with many other studies that indicate a moderate to high bioavailability of grain-bound $^{14}$C-pesticide residues in experimental animals.[5,31,32]

Chromatographic analysis of urine extracts (chloroform layer) revealed the presence of three metabolites, which were identified as ethion dioxon (**III**), *O*,*O*-diethyl phosphorothioate (**IV**), and *O*,*O*-diethyl phosphoric acid (**V**) as free metabolites in addition to one uknown substance. Compound *O*,*O*-diethyl *S*-hydroxymethyl phosphorodithioate (**VI**) was detected as a conjugated metabolite, and its concentration was 0.004 ppm (Table 7). This result agrees with some previous studies,[5,33,34]

**Table 7. $^{14}$C-Ethion and Its Degradation Products in Urine of Male Rats Fed with Cake Containing Ethion-Bound Residues after 72 h**

| | $R_f$ in system[a] | | | |
|---|---|---|---|---|
| metabolite | 1 | 2 | 3 | urine extract chloroform layer[b] (ppm) |
| **III** | 0.69 | 0.56 | 0.55 | 0.042 ± 0.0040 |
| **IV** | 0.33 | 0.23 | 0.42 | 0.015 ± 0.0011 |
| **V** | 0.24 | 0.50 | 0.71 | 0.033 ± 0.0028 |
| unknown | 0.10 | 0.15 | 0.00 | 0.038 ± 0.0031 |

[a]System 1, toluene/xylene 50:50 (v/v); system 2, dioxane/xylene/petrolum ether 20:40:40 (v/v/v); system 3, *n*-hexane/ethyl acetate 98:2 (v/v). [b]Results are expressed as the mean ± SD for three determinations of ethion residue level for rats.

which noted that in adult rats, prothiofos gave prothiofos oxon, *O*-ethyl phosphoric acid, and 2,4-dichlorophenole. Fenitrothion insecticide was converted to phosphorothioate and dimethyl-phosphate. Malathion insecticide was converted to malathion monocarboxylic acid and malathion dicarboxylic acid. Carbofuran, on the other hand, gave carbofuran phenol and 3-hydroxycarbofuran. Ethion is converted via desulfuration in the liver by cytochrome P-450 enzymes to its active oxygen analogue, ethion monooxon.[28]

**Conclusion.** The joint action of deltamethrin and dimilin in combination with the organophosphate ethion was studied on cotton plants by using radiolabeled insecticide. Ethion produced a good potentiation with deltamethrin and dimilin, respectively. The residues of ethion in cotton oil included both free and conjugated metabolites. The $^{14}$C-ethion residues decrease in the presence of deltamethrin and dimilin pesticides. The number of degradation products increases in the presence of deltamethrin more than with dimilin. The bound residues decrease in the presence of deltamethrin and dimilin pesticides as compared with ethion alone. The major part of the insecticide residues (about 95%) could be eliminated during processing of the oil. Refining processes led to progressive degradation of the parent insecticide. The deodorization was found to be an efficient step for reduction of the insecticide residues. Alkali treatment, bleaching, and winterization led to significant losses of the pesticide residues in oil as well. The removal efficiency during the refining processes seems to depend upon the nature of the residue present. The data obtained emphasize the importance of studying the effect of oil refinement on reduction or elimination of aged pesticide residues in edible oils. The present results obtained indicate that cotton-bound $^{14}$C-ethion residues are highly bioavailable to rats. It should be stressed that the presence of bound pesticide residues can no longer be ignored in the evaluation of toxicological hazards.

## AUTHOR INFORMATION


### Corresponding Author

*(A.-G.H.) E-mail: abdelgawadhassan@hotmail.com.


### Notes

The authors declare no competing financial interest.

## REFERENCES


(1) Ahmad, M. Potentiation/antagonism of deltamethrin and cypermethrins with organophosphate insecticides in the cotton bollworm, *Helicoverpa armigera* (Lepidoptera: Noctuidae). *Pestic. Biochem. Physiol.* **2004**, *80*, 31−42.

(2) Guo, X. L.; Xu, Y. J.; Zhang, F. H.; Yu, S.; Han, L. J. Chlormequat residues and dissipation rates in cotton crops and soil. *Ecotoxicol. Environ. Saf.* **2010**, *73*, 642−646.

(3) Hibert, G.; Lillemark, L.; Balchen, S.; Schriver-Hojskov, C. Reduction of organochlorine contaminants from fish oil during refining. *Chemosphere* **1998**, *37*, 1241−1252.

(4) Zayed, S. M. A. D.; Farghaly, M.; Mahdy, F. Effect of commercial processing procedures on carbofuran residues in soybean oil. *Food Chem.* **1998**, *6*, 265−268.

(5) Abdel-Gawad, H.; Hegazi, B. Fate of $^{14}$C-ethyl prothiofos insecticide in canola seeds and oils. *J. Environ. Sci. Health B* **2010**, *45*, 116−122.

(6) Abdel-Gawad, H.; Abdel-Hameed, R. M.; Witczak, A. Residues of $^{14}$C-ethion along the extraction and refining process of maize oil, and the bioavailability of bound residues in the cake for experimental animals. *Bull. Environ. Contam. Toxicol.* **2013**, *91* (2), 240−245.

(7) Abdel-Gawad, H.; Taha, H.; Abdel-Hameed, R. M.; Hegazi, B. $^{14}$C-Ethion residues in soybean seeds: metabolic pathway, effect of processing, bioavailability, toxicity and protective action of artichoke leaf powder towards rats. *Toxicol. Environ. Chem.* **2013**, *95* (2), 288−303.

(8) EPA guidance for the registration of pesticide products containing ethion as the active ingredient. U.S. Environmental Protection Agency, Washington, DC, Sept 29, 1989.

(9) Sine, C. *Farm Chemicals Handbook*; Meister Publishing, Willoughby, OH, USA, 1993; p 141.

(10) Tomlin, C. D. S. Ethion. In *The Pesticide Manual: A World Compendium*, 11th ed.; British Crop Protection Council Publications and the Royal Society of Chemistry: Surry, UK, 1997; pp 480−482.

(11) Abdel-Gawad, H.; Abdelhameed, R. M.; Elmesalamy, A. M.; Hegazi, B. Distribution and elimination of $^{14}$C-ethion insecticide in chamomile flowers and oil. *Phosphorous, Sulfur, Silicon Relat. Elements* **2011**, *186* (10), 2122−2134.

(12) Ono, C.; Takao, A.; Atsumi, R. Absorption, distribution, and excretion of DJ-927, a Novel orally effective taxane, in mice, dogs, and monkeys. *Biol. Pharm. Bull.* **2004**, *27* (3), 345−351.
(13) Hanes, C. A.; Isherwood, F. A. Separation of the phosphoric esters on the filter paper chromatogram. *Nature* **1949**, *164*, 1107−1112.
(14) Iqbal, Z. M.; Menzer, R. E. Metabolism of *O*-ethyl *S*,*S*-dipropyl phosphorodithioate in rats and liver microsomal systems. *Biochem. Pharmacol.* **1972**, *21*, 1569−1584.
(15) Hirashima, A.; Leader, H.; Holden, I.; Casida, J. E. Resolution and stereoselective action of sulprofos and related *S*-propyl phosphorothiolates. *J. Agric. Food Chem.* **1984**, *32*, 1302−1307.
(16) Fakhr, I. M. I.; Hegazi, B.; Abdel-Gawad, H. Residues of $^{14}$C-ethyl profenofos in sugar beet plants and the effect of processing according to industrial practice. *Isotope Radiat. Res.* **2001**, *33*, 85−96.
(17) Zayed, S. M. A. D.; Farghaly, M.; Mahdy, F. Efficiency of the refining processes in removing $^{14}$C-pirimiphos-methyl residues in soybean oil. *Bull. NRC Egypt* **2003**, *28*, 567−575.
(18) Zayed, S. M. A. D.; Farghaly, M.; Mahdy, F. Effect of refining processes on magnitude and nature of malathion and carbofuran residues in cotton seed oil. *Arab J. Nucl. Sci. Appl.* **2005**, *38*, 277−288.
(19) Singh, G.; Singh, B.; Battu, R. S.; Jyot, G.; Singh, B.; Joia, B. S. Persistence of ethion residues on cucumber, *Cucumis sativus* (Linn.) using gas chromatography with nitrogen phosphorus detector. *Bull. Environ. Contam. Toxicol.* **2007**, *79*, 437−439.
(20) Bhatnagar, A.; Gupta, A. Chlorpyriphos, quinalphos, and lindane residues in sesame seed and oil (*Sesamum indicum* L.). *Bull. Environ. Contam. Toxicol.* **1998**, *60*, 596−600.
(21) Petroff, R., Pesticide Education Specialist, Montana State University. *Pesticide Interactions and Compatibility*; OVS: McMinnville, OR, USA, 2008; www.ovs.com.
(22) Zayed, S. M. A. D.; Farghaly, M.; Mahdy, F.; Soliman, S. M. Impact of repeated pesticide applications on the binding and release of methyl $^{14}$C-monocrotophos and U-ring labelled $^{14}$C-carbaryl to soil matrices under field conditions. *J. Environ. Sci. Health B* **2008**, *43*, 595−604.
(23) Miyahara, M.; Saito, Y. Pesticide removal efficiencies of soybean oil refining processes. *J. Agric. Food Chem.* **1993**, *41*, 731−734.
(24) Ruiz Méndez, M. V.; Pérez de la Rosa, I.; Jiménez Márquez, A.; Uceda Ojeda, M. Elimination of pesticides in olive oil by refining using bleaching and deodorization. *Food Addit. Contam.* **2005**, *22*, 23−30.
(25) Zayed, S. M. A. D.; Farghaly, M.; Mahdy, F. Effect of commercial processing procedures on carbofuran residues in soybean oil. *Food Chem.* **1998**, *6*, 265−268.
(26) Hegazi, B.; Abdel-Gawad, H.; Afifi, L. M. $^{4}$C-Zineb residues in sunflower seeds and oils and the effect of processing. *Arab J. Nucl. Sci. Appl.* **2003**, *36*, 345−354.
(27) Katagi, T.; Mikami, N. *Metabolism of Agrochemicals in Plants*; Roberts, T., Ed.; Wiley: New York, 2000, Chapter 3, pp 43−106.
(28) Rao, S. L. N.; McKinley, W. P. Metabolism of organophosphorus insecticides by liver homogenates from different species. *Can. J. Biochem.* **1969**, *47* (12), 1155−1159.
(29) Mahdy, F.; Taha, H. Toxicity of bound $^{14}$C-dichlorvos residues in stored soybeans and their bioavailability to rats. *Bull. NRC Egypt* **2007**, *32*, 125−137.
(30) Farghaly, M.; El-Maghraby, S. Toxicological evaluation and bioavailability of $^{14}$C-fenitrothion bound residues on soybeans towards experimental animals. *Food Chem. Toxicol.* **2008**, *46*, 3111−3115.
(31) Khan, S. U.; Kacew, S.; Matthews, W. A. Bioavailability to rats of bound $^{14}$C-pirimiphos-methyl in stored wheat. *J. Environ. Sci. Health B* **1992**, *27*, 355−367.
(32) Abdel-Gawad, H.; Taha, H. Bioavailability and toxicological potential of sunflower-bound residues of $^{14}$C-chlorpyrifos insecticide in rats. *J. Environ. Sci. Health B* **2011**, *46* (8), 683−690.
(33) Sultatos, L. G. Mammalian toxicology of organophosphorus pesticides. *J. Toxicol. Environ. Health* **1994**, *43*, 271−289.
(34) Farghaly, M.; Mahdy, F.; Zayed, S. M. A. D. Bioavailability to rats of bound residues of $^{14}$C-malathion and $^{14}$C-carbofuran in soybean seeds. *Bull. NRC Egypt* **2002**, *27*, 351−359.

## NOTE ADDED AFTER ASAP PUBLICATION

This paper published ASAP on December 3, 2014, with changes made to two authors' names. The corrected version was reposted on December 9, 2014.

Table 1. Analysis of Volatile Aroma Compounds of Soy Sauce in China

| code | type | compound | code | type | compound |
|---|---|---|---|---|---|
| v1 | alcohol | ethanol | v15 | phenol | phenylacetaldehyde |
| v2 | alcohol | 3-methyl-1-butanol | v16 | phenol | 2-methoxyphenol |
| v3 | alcohol | 1-octen-3-ol | v17 | phenol | phenol |
| v4 | alcohol | 2,3-butanediol | v18 | phenol | 4-ethyl-2-methoxyphenol |
| v5 | alcohol | 2-furylmethanol | v19 | phenol | 2,4-bis(1,1-dimethylethyl)-phenol |
| v6 | alcohol | 3-methylthio-1-propanol | v20 | ester | ethyl phenylacetate |
| v7 | alcohol | 2-ethyl-1-hexanol | v21 | ester | ethyl hexadecanoate |
| v8 | alcohol | phenethyl alcohol | v22 | furan | 2-pentylfuran |
| v9 | acid | benzoic acid | v23 | furan | 2-acetyl-5-methylfuran |
| v10 | acid | acetic acid | v24 | ketone | 2-methyl 3-octanone |
| v11 | furan | furfural | v25 | sulfur-containing | dimethyl trisulfide |
| v12 | aldehyde | 2-methylbutyraldehyde | v26 | alcohol | cedrol |
| v13 | aldehyde | 3-methylbutyraldehyde | v27 | pyrrole | 1-(1*H*-pyrrol-2-yl)ethan-1-one |
| v14 | aldehyde | benzaldehyde | v28 | furan | dihydro-5-pentyl-2(3*H*)-furanone |

commercial-grade and obtained from Sinopharm Chemical Reagent Co., Ltd. (Shanghai, China).

All used reagents were analytical-grade, and all dilutions and samples were prepared using deionized water. Fermented and deep-colored soy sauce samples were analyzed because they are the most popular types in China. These samples represented different fermentation processes and geographic regions.

**Isolation of Volatile Aroma Compounds.** Divinylbenzene/carboxen/polydimethylsiloxane (DVB/CAR/PDMS) 50/30 $\mu$m fiber from Supelco Company (Bellefonte, PA) was used to extract volatile components. The fiber was preconditioned as recommended by the manufacturer. Soy sauce (10 g) was pipetted into a conical screw-cap test tube by a polytetrafluoroethylene (PTFE)/silicone septum. The headspace in the vial was stabilized by equilibration for 15 min at 60 °C before extraction. The extraction efficiency is a function of both the temperature and extraction time to obtain the maximum extraction yield. DVB/CAR/PDMS was exposed at 30 °C for 60 min with magnetic stirring (200 rpm).

**Gas Chromatography with Mass Spectrometric Detection.** A HP 5890 II gas chromatograph with a HP 5971A mass selective detector was used for GC−MS. After the extraction, injections provided the fiber thermal desorption into GC. Sample injection was performed in splitless mode. A fused silica HP-5MS capillary column (30 m × 0.32 mm × 0.25 $\mu$m) was employed with the following temperature program: 35 °C (0.5 min), 4 °C/min, and 220 °C. Helium was used as the carrier gas (linear velocity of 25 cm/s), and the ionization energy was 70 eV. The selected compounds were identified by comparing the spectral pattern to the NIST08 MS spectral database or using reference materials and published retention indices. Further instrumental details are described in the literature.[12]

A total of 28 volatile aroma compounds were detected in all soy sauce samples. These volatile aroma compounds represented the flavor compounds of soy sauces in China. In total, 78 soy sauce samples were included in the data set (three geographic regions and two fermentations) for analysis. Hence, the data tables should be 78 × 28 (row × column). A complete data table is needed; however, only 28 variables involving the concentrations of volatile aroma compounds in the table columns were used and surveyed in Table 1. These volatile aroma compounds include alcohols, acids, furans, aldehydes, phenols, esters, ketone, sulfocompound, and pyrrole.

**Identification and Quantification.** Identification was based on the retention indices and mass spectra of reference standards matching in the standard National Institute of Standards and Technology (NIST) 08 library. Positive identifications were achieved by matching linear retention indices and mass spectra to those of standard reference compounds analyzed under the same experimental conditions. When reference standards were not available, tentative identification was conducted in accordance with the mass spectra and retention indices matched in the NIST 08 Standard Reference Database and Wiley library. Retention indices were calculated by using a $C_6$−$C_{33}$ *n*-alkane series (Supelco) under the same chromatographic conditions.

A series of concentrations of standard compounds with 2-octanol (1 mg/L compound solutions) as an internal standard was prepared. For key volatile compound quantification, a five-point calibration curve was developed for each of the identified key volatile compounds. The calibration curve was drawn by plotting the concentration ratio of a standard compound to the internal standard against the corresponding peak area of the standard compound to that of the internal standard. The concentration of each compound was calculated on the basis of the standard curve derived from the area ratio and the concentration ratio of each compound.

**ANNs.** ANNs are computational models inspired by the central nervous systems of animals that are capable of machine learning and pattern recognition. A back-propagation (BP) neural network was used for neural network training on the basis of the data set of varying input−output pairs with input, output, and hidden layers. In accordance with the previous layer, the processing of each layer data, multiplied by the corresponding weight, obtaining the sum value, adopting nonlinear or linear activation function ($f$), and adding the bias, can be mathematically expressed as

$$y_j = \sum_{i=1}^{n} f(w_{ij}x_i) + b_j \quad (1)$$

where $x$ and $y$ are the input and output of the neuron, respectively, and are the number of inputs to the neurons, which is the weight of the connection between neurons $i$ and $j$, and $b$ is the bias associated with jet neuron.

$$E = \sum_{i=1}^{t} E_i = \sum_{i=1}^{t} (y_i - d_i)^2 \quad (2)$$

The aim of the neural network training is to minimize the error $E$ by changing the weights and offsets, where $r$ is the number of input−output vector pairs in the training set, $d_i$ is the respective component of the required output vector, and $y_i$ is the response to the adequate component $x_i$ of the input vector. The error $E$ is usually minimized by the steepest descent method or another gradient method.

**Genetic Algorithm (GA).** The GA was employed in accordance with the fitness function and was operated by selection, crossover, and mutation. Superiority of winner beings is due to their individual characteristics that normally depend upon their genes. Individuals were screened; superior individuals were reserved, and inferior individuals were eliminated. The optimal fitness individuals were identified through selection, crossover, and mutation. The selection operation is the first to choose the best individuals according to the roulette wheel and fitness function. On the basis of mutation probability, the mutation operation randomly alters the element of the individual. Mutation improves the GA ability by random search and global mutation, which allows the GA to avoid learning into local

**Table 2. Sensitivity Analysis: $p$ Values and the Corresponding Ranks of the Volatile Aroma Compounds Selected for China Soy Sauce Classification by Fermentation and Geographic Regions**

| | | sensitivity analysis, $p$ value[a] | | | | | sensitivity analysis, the rank of the variable | | | | |
|---|---|---|---|---|---|---|---|---|---|---|---|
| code | type | LSFSS | HLFSS | eastern | southern | northern | LSFSS | HLFSS | eastern | southern | northern |
| v1 | alcohol | 0.48311 | 0.50276 | $1.6742 \times 10^{-16}$ | $1.0101 \times 10^{-15}$ | $3.4801 \times 10^{-18}$ | 2 | 4 | 28 | 28 | 28 |
| v2 | alcohol | $1.3324 \times 10^{-15}$ | $2.2313 \times 10^{-15}$ | 0.01814 | 0.01376 | 0.00306 | 28 | 28 | 9 | 11 | 2 |
| v3 | alcohol | $1.3337 \times 10^{-15}$ | $2.2317 \times 10^{-15}$ | 0.01763 | 0.01759 | 0.00027 | 27 | 27 | 10 | 9 | 18 |
| v4 | alcohol | 0.35458 | 0.49979 | 0.01423 | 0.01346 | 0.0006 | 9 | 7 | 12 | 12 | 12 |
| v5 | alcohol | $1.3387 \times 10^{-15}$ | $2.2324 \times 10^{-15}$ | 0.23752 | 0.23931 | 0.00039 | 26 | 26 | 1 | 1 | 15 |
| v6 | alcohol | $1.3401 \times 10^{-15}$ | $2.2333 \times 10^{-15}$ | 0.00193 | 0.00041 | 0.00084 | 25 | 25 | 20 | 19 | 9 |
| v7 | alcohol | $1.3424 \times 10^{-15}$ | $2.2347 \times 10^{-15}$ | $1.6821 \times 10^{-16}$ | $1.0243 \times 10^{-15}$ | $3.4951 \times 10^{-18}$ | 24 | 24 | 27 | 27 | 27 |
| v8 | alcohol | 0.22129 | 0.35011 | 0.01084 | 0.01204 | 0.00042 | 14 | 14 | 15 | 13 | 13 |
| v9 | acid | 0.12006 | 0.03667 | 0.01227 | 0.01181 | 0.0004 | 15 | 15 | 13 | 15 | 14 |
| v10 | acid | 0.46714 | 0.49973 | $1.6846 \times 10^{-16}$ | $1.0256 \times 10^{-15}$ | $3.5112 \times 10^{-18}$ | 6 | 8 | 26 | 26 | 26 |
| v11 | furan | $1.3507 \times 10^{-15}$ | $2.2351 \times 10^{-15}$ | $1.6904 \times 10^{-16}$ | $1.0341 \times 10^{-15}$ | $3.5135 \times 10^{-18}$ | 23 | 23 | 25 | 25 | 25 |
| v12 | aldehyde | $1.3515 \times 10^{-15}$ | $2.2357 \times 10^{-15}$ | 0.00311 | 0.00314 | $3.0143 \times 10^{-5}$ | 22 | 22 | 19 | 20 | 22 |
| v13 | aldehyde | $1.3536 \times 10^{-15}$ | $2.2378 \times 10^{-15}$ | 0.01567 | 0.01451 | 0.00083 | 21 | 21 | 11 | 10 | 10 |
| v14 | aldehyde | $1.3579 \times 10^{-15}$ | $2.2379 \times 10^{-15}$ | 0.02183 | 0.02046 | 0.00105 | 20 | 20 | 8 | 8 | 7 |
| v15 | phenol | 0.42123 | 0.48657 | 0.02928 | 0.02966 | 0.00022 | 7 | 10 | 6 | 5 | 19 |
| v16 | phenol | 0.42123 | 0.47923 | 0.02855 | 0.02556 | 0.00227 | 8 | 12 | 7 | 7 | 3 |
| v17 | phenol | $1.3581 \times 10^{-15}$ | $2.2382 \times 10^{-15}$ | $1.714 \times 10^{-16}$ | $1.0404 \times 10^{-15}$ | $3.5312 \times 10^{-18}$ | 19 | 19 | 24 | 24 | 24 |
| v18 | phenol | $1.3599 \times 10^{-15}$ | $2.2384 \times 10^{-15}$ | 0.03232 | 0.02833 | 0.00321 | 18 | 18 | 5 | 6 | 1 |
| v19 | phenol | 0.29744 | 0.43173 | 0.00699 | 0.00972 | 0.00122 | 12 | 13 | 18 | 16 | 5 |
| v20 | ester | 0.34523 | 0.51031 | 0.04598 | 0.04747 | $8.2396 \times 10^{-5}$ | 11 | 1 | 4 | 4 | 21 |
| v21 | ester | 0.35059 | 0.48362 | 0.01018 | 0.01198 | 0.00071 | 10 | 11 | 16 | 14 | 11 |
| v22 | furan | 0.44683 | 0.50363 | $1.7271 \times 10^{-16}$ | $1.0565 \times 10^{-15}$ | $3.5461 \times 10^{-18}$ | 6 | 2 | 23 | 23 | 23 |
| v23 | furan | 0.46949 | 0.50182 | 0.05086 | 0.05476 | 0.00092 | 4 | 5 | 3 | 3 | 9 |
| v24 | ketone | 0.48761 | 0.50262 | 0.07776 | 0.08013 | 0.00014 | 1 | 3 | 2 | 2 | 20 |
| v25 | sulfur | $1.3601 \times 10^{-15}$ | $2.2391 \times 10^{-15}$ | $6.1311 \times 10^{-5}$ | 0.00259 | 0.00125 | 17 | 17 | 22 | 21 | 4 |
| v26 | alcohol | 0.29364 | 0.38413 | 0.00176 | 0.00115 | 0.00032 | 13 | 9 | 21 | 22 | 17 |
| v27 | pyrrole | $1.3622 \times 10^{-15}$ | 0.49536 | 0.00149 | 0.00962 | 0.00115 | 16 | 16 | 14 | 17 | 6 |
| v28 | furan | 0.47091 | 0.50165 | 0.00742 | 0.00842 | 0.00038 | 3 | 6 | 17 | 18 | 16 |

[a]The $p$ value expresses the probability that the variable is insignificant for the classification by fermentation and geographic region.

optima. These three operations are repeated until the optimal or near-optimal convergence of the solutions is achieved.[13] The ANN modeling and GA optimization in the present study were set in a NeuroSolution (version number 5.07) environment.

**Feature Selection or Detection of the Best Variables for Sensitive Analysis.** The importance of an individual variable and the concentration of a selected volatile compound differ and depend upon the classification criteria, namely, fermentation and geographic region. Therefore, new chemical information on the classified samples is obtained by detecting the most useful variables for soy sauce classification. The process is generally called feature selection, which aims to eliminate redundant variables and, thus, avoids problems with overfitting in the ANN application.

Feature selection can be implemented in ANN in several ways: (1) sensitivity analysis, (2) forward feature selection, and (3) backward feature selection. We have used the first way, which is frequently used in multivariate data analysis, discriminant analysis, or logistic regression. A sensitivity analysis was conducted to select features that exert the largest contribution to the network. The elimination of irrelevant inputs reduces the data collection cost and can sometimes improve the performance of a network. Furthermore, sensitivity analysis will provide insights into the underlying relationships between volatile compounds and the classification by fermentation and geographic region.

**Building Neural Networks.** A total of 78 samples of three geographic regions and two fermentation processes were used in this study. Of the 78 samples, 28 were accepted as final variables for the training process. The soy sauce samples were classified through the ANN technique by fermentation (two classes: HLFSS and LSFSS) and geographic region (three classes: southern, northern, and eastern).

The numbers of input and output neurons were set by the numbers of variables and classes (two for fermentation and three for geographic region), respectively. The training of the BP networks was terminated after a maximum of 1000 iterations or until no increase in mean square error (MSE) was observed. For each cross-validation, the network with the minimum MSE from the cross-validations was calculated to identify the best network. The learning rule in which weights and biases were adjusted was BP through the network. In this work, the hyperbolic tangent function of S type was used in the hidden layer, whereas a linear function was applied in the output layer. The Levenberg−Marquardt algorithm served as a training algorithm.

For convergence and avoidance of overlearning of the ANN, the available training data (78 samples) were split into two subsets: training (62 samples) and testing (15 samples) data. The Kennard−Stone algorithm is well-known in the field of sample selection and has already found many applications. For ANN modeling, 15 samples were selected from the 78 samples using the Kennard−Stone algorithm. The training data set was used to train the network, and the testing data set was used to evaluate the performance of the network on new data that did not appear during the training.

**Classification by Linear Discriminant Analysis (LDA) and ANN.** Two discrimination methods, namely, LDA and non-parametric K-nearest neighbor (KNN) methods, were used and compared to ANN. The KNN algorithm simply works on the basis of the minimum distance from the query instance to the training samples to determine the KNN. This algorithm classifies a new object on the basis of attributes and training samples. Under the test, the nearest neighbor was a set of five with the best performance. LDA was used in pattern recognition to find a linear combination of features, which characterizes or separates two or more classes of objects or events. It uses high-dimensional projection mode samples to the best vector space to extract classified information and the effect of the compression feature space dimension. It guarantees mode samples after projections in the new subspace of minimum and maximum distances between clusters

Table 3. Summary of Optimized Network Architecture Using the Genetic Algorithm

| | hidden layer | | | output layer | |
|---|---|---|---|---|---|
| | number of neurons | learning rate | momentum | learning rate | momentum |
| network information (fermentation) | 7 | 0.645 | 0.896 | 0.457 | 0.343 |
| network information (geographic region) | 6 | 0.431 | 0.565 | 0.125 | 0.835 |

from within a class. That is, the model separability in that space is the best. The leave-one-out validation technique was used to improve the performance of LDA and KNN. A total of 78 samples were created, of which 77 were used in the modeling set and the remaining sample was used to establish a test set; hence, each soy sauce sample was used only once as the test set.

**Optimizing the Parameters of ANNs through the GA.** Rules for determining the parameters of ANNs are inadequate; thus, the GA is used to develop the parameters of the BP network. These parameters include learning rate, momentum, and hidden layer number. To apply the GA to the ANN, the parameter values of chromosomes were translated into the predefined ANN, and the network was trained with the training data set. Learning rate and momentum influenced the prediction accuracy and convergence rate of the ANN. Using a very small value causes a long training time, and applying a very large learning rate may result in a non-convergent training. The range of neuron numbers in hidden layers, step size, and momentum was set to 3−21, 0−1, and 0−1, respectively, to determine the neural network with the best performance by trial and error. The generation number was set to 100 on the basis of the termination criterion. The set of crossover and mutation parameters was reported.[14] The resulting values were based on computational experiences and a literature review. Uniform crossover and mutation operators with a mixing ratio of 0.5 were used, and the probabilities of crossover and mutation operators were adjusted at 0.9 and 0.01, respectively. Increasing the population size positively influenced model fitness but prolonged the training time. Thus, the best generation number was determined to be 50.[15] Therefore, the termination criterion of 40 was chosen.

## RESULTS AND DISCUSSION

**Contribution Assessment of Volatile Compounds by Sensitivity Analysis.** Table 2 shows the contribution of each of the 28 selected volatile compounds in China soy sauce classification. The calculation by sensitivity analysis only considered the volatile compounds and disregarded other volatile compounds.

Furans represented the variables with the greatest contribution in classifying soy sauce samples by fermentation. However, furans are not among the influential variables for China soy sauce classification by geographic region. Ketones and alcohols also played important roles for soy sauce classification by fermentation, whereas phenols and alcohols represented the variables with the greatest contribution in classifying soy sauce samples by geographic region.

The most important compounds for soy sauce class differentiation were as follows: (1) 2-furylmethanol for the classification by geographic region of eastern and southern, (2) 4-ethyl-2-methoxyphenol for the classification by geographic region of northern, (3) 2-methyl 3-octanone for the classification by fermentation of LSFSS, and (4) ethyl phenylacetate for the classification by fermentation of HLFSS.

**Classification of Soy Sauce Using GA−ANN.** On the basis of a successfully performed feature selection, which agreed with the sensitivity analysis results, we used the volatile compounds for ANN training. Calculations for the factors of fermentation and geographic region, followed by sensitivity analysis, were performed in a similar way as described above. The optimum network architecture was 22−6−3 and 15−7−2, as determined on the basis of the MSE by the GA. BP networks were trained with one hidden layer and different neuron numbers. The best network with the lowest MSE was selected after training with different hidden layers, neuron numbers, momentums, and step sizes by trial and error. Table 3 summarizes the different parameters of the developed network using the GA for fermentation and geographic region. The optimum network architecture was selected using all soy sauce samples after GA optimization. As shown in Table 4, the success rate of the classification by fermentation and geographic region was 100% for the 15 test samples. The best fitness, in which the MSE is the lowest across all of the networks within the corresponding generation, is decreased crosswise generations until it becomes relatively constant after 10 generations.

Table 4. Selection of Soy Sauce Samples That Create the Test Data Set and Classification Performance by GA−ANN for Two Classification Criteria

| network | performance (%) | eliminated variables |
|---|---|---|
| fermentation classification | 100.0 | v2, v3, v5, v6, v7, v11, v12, v13, v14, v17, v18, v25, and v27 |
| 15 × 7 × 2 | | |
| geographic region classification | 100.0 | v1, v7, v10, v11, v17, and v22 |
| 22 × 6 × 3 | | |

After variable selection based on the Kennard−Stone algorithm, 15 samples were also used to estimate the performance of LDA and ANN. Under the described leave-one-out technique, the 15 test data were classified using LDA and KNN, and the results are shown in Table 5. LDA and KNN yield good classification results; however, the results of GA−ANN are better than those of LDA and KNN.

Table 5. Classification Performance by KNN and LDA Using Testing Data Set

| classification criterion | KNN | LDA |
|---|---|---|
| fermentation test data | 86.7 | 73.3 |
| geographic region test data | 80.0 | 86.7 |

It has been demonstrated that ANN can be a very useful tool for China soy sauce classification. An ANN with single hidden layer architecture of feed forward type was designed and trained using the BP algorithm to classify soy sauce by fermentation and geographic region. The optimal variable selection was performed by sensitivity analysis. The results of the sensitivity analysis are independent of volatile compound correlations and, thus, can be used complementarily with the ANN results. Therefore, GA−ANN proved to be a dependable software tool for identifying the characteristic volatile compounds of soy sauce. The results of this study can be further used to establish a database of the flavors of soy sauce from different fermentation processes and geographic regions.

## AUTHOR INFORMATION

### Corresponding Author

*Telephone: 13986093482. E-mail: dongshengli86@163.com.

### Funding

This work was supported by the Natural Science Foundation of Hubei Province, China (No.2013CFB032, No.2013CFA096), Wuhan Planning Project of Science and Technology, China (No.20130205010173), and Doctoral scientific research foundation of Hubei University of Technology (No.BSQD12147), China.

### Notes

The authors declare no competing financial interest.

## REFERENCES

(1) Yan, L.; Zhang, Y.; Tao, W.; Wang, L.; Wu, S. Rapid determination of volatile flavor compounds in soy sauce using head space solid-phase microextraction and gas chromatography−mass spectrometry. *Chin. J. Chromatogr.* **2008**, *26*, 285−291.

(2) Gao, X.; Cui, C.; Zhao, H. F.; Zhao, M. M.; Yang, L.; Ren, J. Y. Changes in volatile aroma compounds of traditional Chinese-type soy sauce during moromi fermentation and heat treatment. *Food Sci. Biotechnol.* **2010**, *19*, 889−898.

(3) Sun, S. Y.; Jiang, W. G.; Zhao, Y. P. Profile of volatile compounds in Chinese soy sauces produced by a high-salt-diluted state fermentation. *J. Inst. Brew.* **2012**, *116*, 316−328.

(4) Zhang, Y. F.; Tao, W. Y. Flavor and taste compounds analysis in Chinese solid fermented soy sauce. *Afr. J. Biotechnol.* **2010**, *8*, 673−681.

(5) Iizuka, K.; Aishima, T. Soy sauce classification by geographic region based on NIR sepectra and chemomterics pattern recognition. *J. Food Sci.* **1997**, *62*, 101−104.

(6) Aishima, T. Object evaluation of soy sauce by statistical analysis of GC profiles. *Agric. Biol. Chem.* **1979**, *43*, 1935−1943.

(7) Dehghani, A. A.; Mohammadi, Z. Z.; Maghsoudlou, Y.; Mahoonak, A. S. Intelligent estimation of the canola oil stability using artificial neural networks. *Food Bioprocess Technol.* **2012**, *5*, 533−540.

(8) Bardot, I.; Martin, N.; Trystram, G.; Hossenlopp, J.; Rogeaux, M.; Bochereau, L. A new approach for formulation of beverages. Part II: Interactive automatic method. *LWT—Food Sci. Technol.* **1994**, *27*, 513−521.

(9) Dornier, M.; Decloux, M.; Trystram, G.; Lebert, A. Dymamic modeling of crossflow microfiltration using neural networks. *J. Membr. Sci.* **1995**, *98*, 263−273.

(10) Kruzlicova, D.; Mocak, J.; Balla, B.; Petka, J.; Farkova, M.; Havel, J. Classification of Slovak white wines using artificial neural networks and discriminant techniques. *Food Chem.* **2009**, *112*, 1046−1052.

(11) Llave, Y. A.; Hagiwara, T.; Sakiyama, T. Artificial neural network model for prediction of cold spot temperature in retort sterilization of starch-based foods. *J. Food Eng.* **2012**, *109*, 553−560.

(12) Feng, Y. Z.; Cai, Y.; Su, G. W.; Zhao, H. F.; Wang, C. X.; Zhao, M. M. Evaluation of aroma differences between high-salt liquid-state fermentation and low-salt solid-state fermentation soy sauces from China. *Food Chem.* **2014**, *145*, 126−134.

(13) Shankar, T.; Sokhansanj, S.; Bandyopadhyay, S.; Bawa, A. A case study on optimization of biomass flow during single-screw extrusion cooking using genetic algorithm and response surface method. *Food Bioprocess Technol.* **2010**, *3*, 498−510.

(14) Mohebbi, M.; Fathi, M.; Shahidi, F. Genetic algorithm−artificial neural network modeling of moisture and oil content of pretreated fried mushroom. *Food Bioprocess Technol.* **2011**, *4*, 603−609.

(15) Saemi, M.; Ahmadi, M.; Varjani, A. Y. Design of neural networks using genetic algorithm for the permeability estimation of the reservoir. *J. Pet. Sci. Eng.* **2007**, *59*, 97−105.

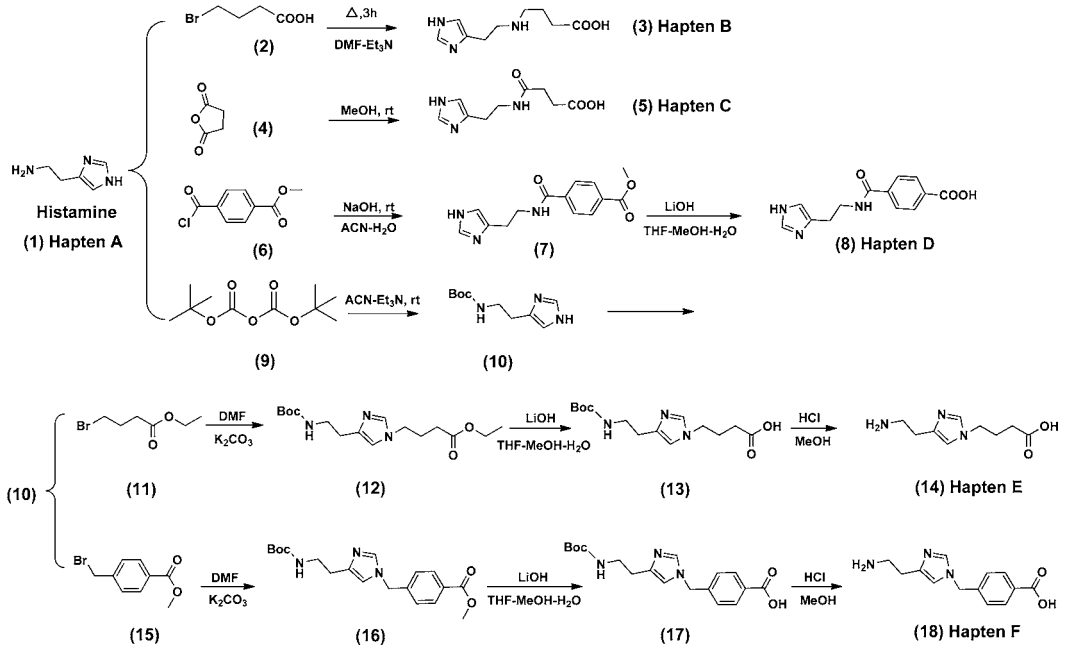


**Figure 1.** Synthetic route for haptens.

chemical residues. However, the development of a high affinity antibody against HA is not easy, and has puzzled immunochemists for some time due to the simple structure of HA (MW, 111 Da).[25] In general, all reported antibody methods used for immunoassay determination of HA in foods can be classified into three categories. (1) An antibody that specifically recognized the *p*-benzoquinone−histamine conjugate was initially reported in 1986.[26] Based on this conjugate, ELISAs were proposed for HA detection in foodstuffs, using a preanalysis HA derivatization step with *p*-benzoquinone.[27,28] But drawbacks did exist for this strategy. The derivatization reaction between HA and *p*-benzoquinone was complicated due to side reactions, and the product was unstable. (2) A second antibody was developed against a modified HA by coupling succinylated HA to BSA grafted with a glycyl residue.[29] The obtained antibody also showed no binding affinity for free histamine, but it had high binding affinity for modified HA which was formed through the reaction between HA and *N*-hydroxysuccinimide ester−succinyl-glycinamide (NHS-SGA). However, the synthesis of the derivatization reagent, NHS-SGA, was laborious with multisteps, making this reagent costly. (3) The only antibody developed that was able to recognize intact HA was developed by coupling HA to KLH via glutaraldehyde, and then the conjugate was used as an immunogen to immunize New Zealand white rabbits.[30] However, the repeatability of this strategy is poor, and four attempts using this strategy to produce an antihistamine antibody have failed in our group.

This study aimed at finding a reliable strategy for producing an antihistamine antibody, as well as the development of a competitive indirect enzyme-linked immunosorbent assay (ciELISA) for HA determination in foods based on the obtained antibody. For this purpose, several haptens were synthesized in attempts to obtain an antibody with specific histamine affinity or derivatized histamine affinity. Although, the development of an antibody against free HA failed, a highly specific polyclonal antibody produced against *p*-nitrobenzoylated HA (NPHA) was used to develop a ciELISA for derivatized HA in foods. Because HA can be efficiently and quantitatively converted to NPHA by PNBA-OSu under mild basic conditions at room temperature, a ciELISA was developed here for the analysis of HA in food samples via a preanalysis HA derivatization step. This work also fully optimized the assay conditions. In addition, the immunoassay results were validated by comparison with LC−MS/MS results.

## MATERIALS AND METHODS

**Animals and Reagents.** Histamine dihydrochloride, L-histidine, L-tryptophan, tryptamine hydrochloride, tyramine hydrochloride, phenethylamine hydrochloride, and cadaverine hydrochloride were obtained from Heowns Biochem Technologies Co. Ltd. (Tianjin, China). Methyl 4-(chlorocarbonyl)benzoate, *p*-nitrobenzoic acid, *N*-hydrosuccinimide, dicyclohexylcarbodiimide (DCC), and triethylamine were obtained from Aladdin Chemical Technology Co., Ltd. (Shanghai, China). Histamine, 3,3′,5,5′-tetramethylbenzidine (TMB), glutaraldehyde (50%, v/v), complete and incomplete Freund's adjuvants, keyhole limpet hemocyanin (KLH), bovine serum albumin (BSA), ovalbumin (OVA), horseradish peroxidase, and peroxidase-labeled goat anti-rabbit IgG (secondary antibody) were obtained from Sigma-Aldrich (St. Louis, MO, USA). *N*,*N*-Dimethylformamide (DMF), acetonitrile (ACN), Tween-20, ethanol, methanol (MeOH), ethyl acetate (EtOAc), tetrahydrofuran (THF), and chloroform ($CHCl_3$) were obtained from Damao Chemical Reagent Co., Ltd. (Tianjin, China). New Zealand white rabbits were raised at the Guangdong Medical Experimental Animal Centre. 96-Well polystyrene microplates were obtained from Shenzhen Jinchanhua Industrial Co. Ltd. (Shenzhen, China). All other reagents were of analytical reagent grade or higher purity.

**Instruments.** ELISA plates were washed in a Multiskan MK2 microplate washer (Thermo Scientific, Hudson, NH, USA). Absorbance was measured at a wavelength of 450 nm using a Multiskan MK3 microplate reader (Thermo Scientific). Ultraviolet spectrometry (UV) was recorded on a UV-3010 spectrophotometer (Hitachi, Tokyo, Japan). LC−MS/MS analysis was carried out by using the 1200 series LC system (Agilent Technologies) equipped with the Agilent 6410 Triple Quad LC−MS system (Agilent Technologies). Nuclear magnetic resonance (NMR) spectra were achieved with either a DRX-400 or DRX-600 NMR spectrometer (Bruker, Rheinstetten, Germany).

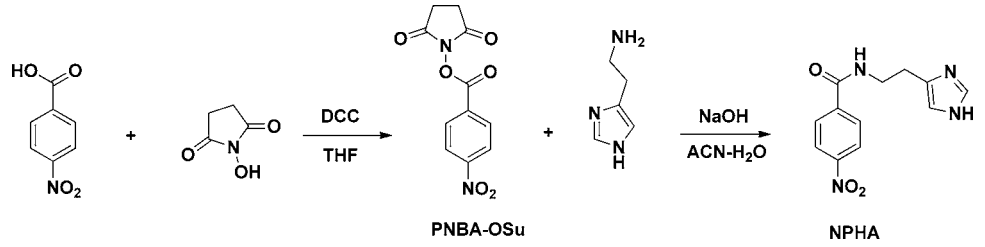


**Figure 2.** Synthetic route for the derivatizing reagents, PNBA-OSu and NPHA.

**Buffers and Solutions.** The following were the buffers and solutions used in this study: (1) Borate buffer (0.2 mol/L, pH 9.0) was used for histamine chemical derivatization; (2) 50 mmol/L carbonate buffer (pH 9.6) was used for coating antibody on plates; (3) $PBST_1$ (10 mmol/L phosphate-buffered saline (PBS) with Tween-20 (0.05%), pH 7.4) was used for washing plates and secondary antibody dilution and was the working buffer used in the nonoptimized ciELISA; (4) $PBST_2$ (20 mmol/L PBS, Tween 20 (0.05%), pH 7.4) was used for the working buffer in the optimized ciELISA; (5) 0.1 mol/L sodium acetate (pH 5.5) was used for the substrate buffer; (6) 2 mol/L $H_2SO_4$ was used for the stop reagent; and (7) HA stock standard solution (1 mg/mL HA in distilled water (d.w.)).

**Synthesis and Verification of Histamine Derivatives.** Five histamine derivatives (haptens B–F) were synthesized by introduction of different spacer arms containing a carboxyl group at histamine's primary amine or by substitution of H on the ring NH group (Figure 1). Figure 2 shows the synthetic route to produce the derivatization reagents PNBA-OSu and NPHA. The following is a detailed description of the synthetic procedure and characterization of these compounds.

*Hapten A, HA (**1**).* Hapten A is intact HA. Histamine was conjugated to the carrier protein via glutaraldehyde according to previous work.[30]

*Hapten B, 4-((2-(1H-Imidazol-4-yl)ethyl)amino)butanoic Acid (**3**).* Histamine dihydrochloride (1.84 g, 10 mmol) and triethylamine (6 mL) were added to DMF (20 mL) containing 4-bromobutanoic acid (**2**, 1.65 g, 10 mmol). The mixture was stirred at room temperature for 1 h and then refluxed at 80 °C for 3 h, after which time the solvent was evaporated under vacuum, leaving a gummy residue. The residue was purified on a silica gel column, using $CHCl_3$/MeOH/$NH_4OH$ (10:5:1) as the eluent, and then crystallized from ethanol (10 mL) to afford hapten B (**3**, 832 mg, 4.2 mmol): ESI analysis (positive ion) $m/z$ 198 $[M + H]^+$; $^1H$ NMR (600 MHz, $D_2O$) $\delta$ 8.84 (s, 1H), 7.57 (s, 1H), 3.11 (t, $J$ = 5.2 Hz, 2H), 2.94 (t, $J$ = 5.2 Hz, 2H), 2.62 (t, $J$ = 7.7 Hz, 2H), 2.34 (t, $J$ = 8.2 Hz, 2H), 1.86 (t, $J$ = 7.9 Hz, 2H).

*Hapten C, 4-((2-(1H-Imidazol-4-yl)ethyl)amino)-4-oxobutanoic Acid (**5**).* Succinic anhydride (**4**, 500 mg, 5 mmol) was added to a solution of histamine dihydrochloride (920 mg, 5 mmol) in methanol (15 mL) and stirred at room temperature for 4 h, and the solvent was removed by evaporation. The residue was redissolved in ethanol (20 mL) and kept at 4 °C overnight, and then hapten C (**5**, 650 mg, 3.1 mmol) was crystallized: ESI analysis (negative ion) $m/z$ 210 $[M - H]^-$; $^1H$ NMR (600 MHz, $D_2O$) $\delta$ 8.54 (s, 1H), 7.26 (s, 1H), 3.45 (t, $J$ = 6.3 Hz, 2H), 2.89 (t, $J$ = 6.4 Hz, 2H), 2.44–2.35 (m, 4H).

*Hapten D, 4-((2-(1H-Imidazol-4-yl)ethyl)carbamoyl)benzoic Acid (**8**).* A solution of methyl 4-(chlorocarbonyl)benzoate **6** (198 mg, 1 mmol) in 5 mL of ACN was added dropwise to a solution of histamine dihydrochloride (184 mg, 1 mmol) in 1 M NaOH (5 mL). The mixture was stirred at room temperature for 3 h, and then the ACN was removed by rotoevaporation under vacuum. A yellow precipitate was filtered and washed three times with 0.1 M HCl and dried to yield intermediate **7** (232 mg, 0.84 mmol). A solution of intermediate **7** (232 mg, 0.84 mmol) in a mixture of THF/MeOH/$H_2O$ (1:1:1, 15 mL) was treated with LiOH·$H_2O$ (84 mg, 2.0 mmol) and refluxed at 40 °C overnight. The organic solvent was evaporated under vacuum, and the aqueous layer was acidified with 1 M HCl until a white precipitate formed. The precipitate was filtered off and washed with 0.1 M HCl, and dried to yield hapten D (**8**, 196 mg, 0.75 mmol): ESI analysis (negative ion) $m/z$ 258 $[M - H]^-$; $^1H$ NMR (400 MHz, methanol-$d_4$) $\delta$ 8.54 (d, $J$ = 1.4 Hz, 1H), 8.12–8.05 (m, 2H), 7.90–7.82 (m, 2H), 7.27 (d, $J$ = 1.3 Hz, 1H), 3.72 (t, $J$ = 6.8 Hz, 2H), 3.04 (t, $J$ = 6.8 Hz, 2H).

*Hapten E, 4-(4-(2-Aminoethyl)-1H-imidazol-1-yl)butanoic Acid (**14**).* Histamine dihydrochloride (3.68 g, 20 mmol) and triethylamine (56 mL, 40 mmol) were mixed in acetontrile (150 mL), then di-*tert*-butyl dicarbonate (**9**, 4.36 g, 20 mmol) was added. The mixture was stirred at room temperature overnight and then filtered. The filtrate was evaporated under vacuum, and the residue was washed with petroleum ether (100 mL). The undissolved substance was treated with d.w. (100 mL), and the mixture was filtered. The aqueous solution was saturated with NaCl and extracted with ethyl acetate. The organic layer was dried over anhydrous $Na_2SO_4$ and evaporated under vacuum, leaving an oil. The residue was crystallized from ether/petroleum ether to afford the intermediate **10** (2.3 g, 10.8 mmol). Ethyl 4-bromobutanoate (**11**, 386 mg, 2 mmol), the intermediate (**10**, 422 mg, 2 mmol), and DMF (20 mL) were mixed, and then $K_2CO_3$ (500 mg, 3.6 mmol) and tetrabutyl ammonium bromide (5 mg, 0.016 mmol) were added. The mixture was stirred under reflux at 80 °C overnight and then was concentrated by rotoevaporation under vacuum. The crude product was purified on a silica gel column, using EtOAc/MeOH (20:1) as eluent to afford **12** (334 mg, 1.02 mmol). Compound **13** was synthesized from **12** by subjection of **12** to the same hydrolysis step as previously used to convert **7** to **8**. The resulting mixture was concentrated by rotoevaporation under vacuum and purified on a silica gel column using EtOAc/MeOH (4:1) as eluent to give **13** (280 mg, 0.94 mmol). Compound **13** was dissolved in methanol (20 mL), and concentrated hydrochloric acid (5 mL) was added. The mixture was stirred on an ice bath for 1 h and then concentrated by rotoevaporation under vacuum to give hapten E (**14**, 262 mg, 0.78 mmol, in its hydrochloride form): ESI analysis (negative ion) $m/z$ 196 $[M - H]^-$; $^1H$ NMR (600 MHz, methanol-$d_4$) $\delta$ 8.97 (s, 1H), 7.61 (s, 1H), 4.30–4.26 (m, 2H), 3.30–3.28 (m, 1H), 3.14 (t, $J$ = 7.5 Hz, 2H), 2.45 (t, $J$ = 7.2 Hz, 2H), 2.21–2.18 (m, 2H).

*Hapten F, 4-((4-(2-Aminoethyl)-1H-imidazol-1-yl)methyl)benzoic Acid (**18**).* The synthetic route of hapten F (**18**) was similar to hapten E (**14**), except the initial ester, ethyl 4-bromobutanoate (**11**), was replaced with 4-((4-(2-aminoethyl)-1*H*-imidazol-1-yl)methyl)benzoic acid (**15**) (see Figure 1): ESI analysis (positive ion) $m/z$ 246 $[M + H]^+$; $^1H$ NMR (600 MHz, methanol-$d_4$) $\delta$ = 9.05 (s, 1H), 8.03 (t, $J$ = 5.3, 2H), 7.54 (s, 1H), 7.50 (t, $J$ = 6.6, 2H), 5.47 (s, 2H), 3.24 (t, $J$ = 7.6, 2H), 3.07 (t, $J$ = 7.5, 2H).

*Derivatization Reagent (PNBA-OSu) and N-(2-(1H-Imidazol-4-yl)ethyl)-4-nitrobenzamide (NPHA).* PNBA-OSu was synthesized as previously described:[31] ESI analysis (positive ion) $m/z$ 306 $[M + ACN]^+$; $^1H$ NMR (600 MHz, $CDCl_3$) $\delta$ 8.37 (d, $J$ = 9.0 Hz, 2H), 8.33 (d, $J$ = 9.0 Hz, 2H), 2.94 (s, 4H). A solution of PNBA-OSu (700 mg, 2.65 mmol) in ACN (20 mL) was added dropwise (with stirring) to a solution of histamine dihydrochloride (460 mg, 2.5 mmol) in 1 M NaOH (10 mL). The resulting mixture was stirred at room temperature for 2 h, and then the organic solvent was removed by evaporation under vacuum. The yellow precipitate that formed was filtered off and washed with 0.1 M NaOH and dried to give NPHA (588 mg, 2.25 mmol): ESI analysis (positive ion) $m/z$ 261 $[M + H]^+$; $^1H$ NMR (400 MHz, methanol-$d_4$) $\delta$ 8.54 (d, $J$ = 1.1 Hz, 1H), 8.09 (d, $J$ = 8.5 Hz, 2H), 7.86 (d, $J$ = 8.5 Hz, 2H), 7.27 (s, 1H), 3.72 (t, $J$ = 6.8 Hz, 2H), 3.04 (t, $J$ = 6.8 Hz, 2H).


dx.doi.org/10.1021/jf504689x | *J. Agric. Food Chem.* 2014, 62, 12299–12308

**Synthesis of Immunogen and Coating Antigen.** Histamine (hapten A) was coupled to KLH via glutaraldehyde for the immunogen and to OVA for the coating antigen.[30] Haptens B−F were conjugated to BSA with 1-ethyl-3-(3-dimethylaminopropyl)-carbodiimide hydrochloride (EDC) and used as the immunogen, and they were conjugated to OVA and used for the coating antigen according to previous work, with modifications.[32] Briefly, a hapten (0.1 mmol) and carrier protein (10 mg) were dissolved in the conjugation buffer (PBS, pH 6.0, 5 mL). The resulting solution was cooled on an ice bath, and EDC (32 mg) was added with stirring. The mixture was held at 0 °C overnight with stirring, and then the conjugation mixture was dialyzed against 10 mM PBS (4 × 5 L) at 4 °C for 72 h, and finally stored at −20 °C until used. UV−vis spectral data was used to confirm the structures of final conjugates, and the hapten density was estimated by the TNBS method.[33]

**Immunization and Polyclonal Antibody Production.** Twelve New Zealand white rabbits were housed and maintained at the Guangdong Medical Laboratory Animal Center. All animal experiments were performed in compliance with the protective and administrative laws for laboratory animals of China and conducted with the approval of the Institutional Authority for Laboratory Animal Care, South China Agricultural University, Guangzhou, China. The rabbits (10-wk-old, 1.5−2.0 kg) were equally divided into six groups for the six immunogens, and each was intradermally and intramuscularly immunized with 1 mL of an emulsion (1:1) containing 0.5 mg/mL of an immunogen in PBS and complete Freund's adjuvant. Four booster immunizations using the same amount of immunogen emulsified in incomplete Freund's adjuvant were given monthly. Ten days after the fourth booster injection, the rabbits were exsanguinated and their blood was collected. The obtained antiserum was stored at −20 °C until purified by saturated ammonium sulfate precipitation.[34] Serum was collected from the marginal ear vein from each rabbit prior to the first immunization and used as the negative controls.

**Antibody Screening and Characterization.** A ciELISA was used to evaluate the antiserums for binding ability to the analytes (histamine or its derivatives). Briefly, the coating antigens (1 mg/L, 100 μL/well) in carbonate buffer were added to 96-well polystyrene ELISA plates and incubated at 4 °C overnight, and then the wells were washed twice with $PBST_1$ solution prior to adding 5% skimmed milk in $PBST_1$ (100 μL/well) to block the uncoated sites for 3 h at 37 °C and dried at 37 °C for 1 h. Histamine standards or other competitors in PBS (50 μL) and the diluted antiserum (50 μL) in $PBST_1$ were added to each well and incubated at 37 °C for 40 min, and then the wells were washed five times with $PBST_1$. The secondary antibody diluted 1:10000 in $PBST_1$ (100 μL/well) was then added to the wells and incubated for 40 min at 37 °C. The wells were washed again five times with $PBST_1$ before the TMB solution was added to the wells (100 μL/well) and incubated for 10 min. Finally, 50 μL of 2 M $H_2SO_4$ was added to quench the reaction and the optical density was measured at 450 nm. The percent inhibition of antibody binding used to characterized the binding ability of antibodies was expressed as follow: inhibition (%) = $[1 - (B/B_0)] \times 100$; $B_0$ was the mean absorbance of the wells in the absence of a competitor; $B$ was the mean absorbance of wells in the presence of a competitor.

**Optimization of ELISA Conditions.** To improve performance of the ELISA, heterology in the chemical structure of the coating hapten was used, and optimization was performed of the physicochemical parameters considered to have significant effects on immunoassay performance,[35] such as antibody dilution/coating concentration, and working buffer (concentration of Tween 20, ionic strength, and pH). For each condition, NPHA was used as the competitor analyte to construct inhibition curves ($n$ = 3). The maximum value of the inhibition curve (Amax) and competitor analyte concentration leading to a 50% decrease in Amax ($IC_{50}$) were calculated from these curves. The optimal conditions were confirmed by evaluating the ratio of Amax to $IC_{50}$. Higher value of Amax/$IC_{50}$ equates to better assay performance under such conditions.

**Preparation of Food Samples.** Fish, red wine, and yoghurt samples were purchased from a local supermarket in Guangzhou, China. For fish, an equivalent weight of d.w. was added to the muscles and homogenized, and then d.w. (8 mL) and the homogenate (2 g) were mixed and shaken vigorously for 1 min. The mixture was centrifuged at 3000$g$ for 10 min, and the supernatant was then diluted 20-fold in d.w. and subjected to the derivatization procedure as follows: 200 μL of diluted supernatant, 400 μL of borate buffer (pH 9.0), and 400 μL of PNBA-OSu solution (2 mg/mL in ACN) were successively added to a 1.5 mL conical tube and vortexed for 10 s. The reaction mixture was kept at room temperature (25 °C) for 20 min, and 100 mg of NaCl was added to separate the organic layer (ACN) from the aqueous layer. The organic layer was diluted (10-fold) in $PBST_2$ (optimized working buffer) for ciELISA analysis, and in a mixture of MeOH/$H_2O$ (v/v, 10:90) for analysis by LC−MS/MS. For red wine and yoghourt, d.w. (9 mL) was added to the samples (1 mL or 1 g) and shaken for 1 min, and then centrifuged at 3000$g$ for 10 min. The supernatant was directly subjected to the same derivatization process as were the fish samples above, and then analyzed by ciELISA and LC−MS/MS. All prepared samples were filtered through a 0.22 μm membrane before LC−MS/MS analysis.

**Histamine Assay.** Each prepared sample was split and subjected to histamine analysis by both ciELISA and LC−MS/MS methods.

*ciELISA.* A calibration curve was constructed as follows: 200 μL serial dilutions of HA from the HA stock solution were subjected to the derivatization procedure as described above, 50 μL of the resulting solution was used as competitor in the ciELISA, and then the calibration curve was obtained by plotting the percent binding of antibodies in the wells ($B/B_0 \times 100$) against the logarithm of the HA concentration. For sample analysis, 50 μL of the prepared samples, as described above, were used as competitor in the ciELISA, and the determined $B/B_0 \times 100$ was used to calculate the HA concentration from the calibration curve.

*LC−MS/MS.* The results from the ciELISA were confirmed by the LC−MS/MS method (completed by the Zhongshan Quality Supervision & Inspection Institute of Agricultural Products of Guangdong Province, Zhongshan, China). A 5 μL portion of the prepared samples was injected into the LC system (Agilent 1200-6410) equipped with an Agilent ZORBAX SB-C18 column (2.1 mm × 150 mm, 3.5 μm) and separated at a 0.4 mL/min flow rate (mobile phase A, 0.1% acetic acid; mobile phase B, ACN) in the following gradient profile: 0−3 min, 8%−15% B; 3−5 min, 15%−30% B; 5−5.01 min, 30%−90% B; 5.01−8 min, 90% B. Analytes were determined by an Agilent 6410 Triple Quad mass spectrometer (Agilent Technologies, Lexington, MA, USA) using ESI-MS/MS in the positive ion mode. The MS parameters were as follows: capillary voltage at 4.0 kV; desolvation temperature at 350 °C; desolvation gas ($N_2$), flow rate at 10 L/min; ion spray voltage at 4000 V. The analytes were identified by parent/daughter ions as well as peak retention times in comparison to the standards. The $[M + H]^+$ at $m/z$ 261.0 was the parent ion of NPHA. The daughter ion at $m/z$ 95.1 was used for quantitation, and the daughter ion at $m/z$ 68.1 was selected as a qualitative ion (see Figure S1 in the Supporting Information).

A calibration curve for HA analysis by LC−MS/MS was constructed as follows: Serial concentrations (10−1000 ng/mL) of HA standard solutions in d.w. were prepared from the HA stock solution, and were subjected to the derivatization and treatment steps as described above. The treated solutions (5 μL) were injected into the instrument and analyzed. The responses of the mass spectrometer were plotted against the concentration of HA, which resulted in the calibration curve.

## RESULTS AND DISSCUSSION

**Hapten Synthesis and Antibody Production.** It cannot be underestimated how big a key role the proper hapten design plays in antibody production and immunoassay development, especially for a compound like HA having an extremely simple structure. As can be seen from the structure of HA (Figure 1), the structure consists of two parts, an imidazole ring and a side chain (amino ethyl) containing a primary amino group. The only previously reported antibody that could specifically recognize free HA was produced by conjugating HA to KLH

**Table 1. Evaluation of Antiserum Binding Ability To Free Histamine under Homologous and Heterologous Coating Format**

| coating antigen | antiserum A | | antiserum B | | antiserum C | | antiserum D | | antiserum E | | antiserum F | |
|---|---|---|---|---|---|---|---|---|---|---|---|---|
| | titer[a] ($\times 10^3$) | inhibn[b] (%) | titer ($\times 10^3$) | inhibn (%) | titer ($\times 10^3$) | inhibn (%) | titer ($\times 10^3$) | inhibn (%) | titer ($\times 10^3$) | inhibn (%) | titer ($\times 10^3$) | inhibn (%) |
| hapten A-OVA | 4 | 2.1 | <1 | –[c] | <1 | – | <1 | – | <1 | – | <1 | – |
| hapten B-OVA | <1 | – | 4 | −7.6 | <1 | – | <1 | – | <1 | – | <1 | – |
| hapten C-OVA | <1 | – | <1 | – | 8 | 6.4 | 16 | 10.2 | <1 | – | <1 | – |
| hapten D-OVA | <1 | – | <1 | – | 1 | 3.1 | 512 | 7.1 | <1 | – | <1 | – |
| hapten E-OVA | <1 | – | <1 | – | <1 | – | <1 | – | 4 | −4.0 | 8 | −4.5 |
| hapten F-OVA | <1 | – | <1 | – | <1 | – | <1 | – | 1 | 2.7 | 128 | 6.9 |

[a]Titer is defined as dilution factor of antiserum with the abosorbance at 450 nm being situated at about 1.0 at coating concentration of 1.0 mg/L. [b]Percentage inhibition was expressed as follow: inhibition (%) = $[1 - (B/B_0)] \times 100$. $B_0$ was mean absorbance of the wells in the absence of competitor; $B$ was mean absorbance of the wells in the presence of certain concentration of competitor (50 mg/L histamine). [c]Not calculated.

via the primary amino group using the glutaraldehyde method.[30] Initially, our laboratory attempted the same strategy using intact HA as hapten (hapten A). Meanwhile, two carboxyl groups containing spacer arms were also introduced via the primary amino group, forming hapten B and hapten C. To maintain functionality around the primary amino group, a carboxyl group containing a 4-carbon length spacer arm (hapten E) and a carboxyl group containing a benzene ring in the spacer arm (hapten F) were introduced in the ring at N-1. These haptens were conjugated to KLH (hapten A) or BSA (haptens B, C, E, and F) and used to immunize rabbits, while no antisera against these haptens were found to contain antibodies specific against free HA (Table 1). The failure in production of an antibody that possessed the desired affinity and specificity for HA using the above immunogens probably resulted from the extreme simplicity of HA's structure and lack of a sufficient epitope to be identified by the T helper or naive (virgin) B cells. This result revealed the necessity for chemical derivatization of HA for immunoanalysis of HA, which was similar to most of the past studies on immunoanalysis of histamine.[26−29] However, derivatization of histamine by *p*-benzoquinone did not meet the requirements necessary for immunoanalysis due to the reaction's complexity with side reactions and instability of the target analyte.[26,27] In work by Morel et al.,[29] synthesis of the derivatization reagent, NHS-SGA, was laborious, requiring multiple steps, making this reagent quite costly. However, the use of the *N*-hydroxysuccinimide ester, PNBA-OSu, in our work can preferentially and efficiently acylate primary amino groups under mild conditions.[36] HA can smoothly and rapidly convert to NPHA by the interaction with PNBA-OSu under mild conditions (Figure 2). It can be seen from the structure of NPHA (Figure 2) that the structure of benzoylated histamine exhibits more than a 100% increase in mass compared to histamine and contains a benzene ring. Thus, NPHA should substantially improve the rate of successful generation of specific antibody. Therefore, hapten D, benzoylated histamine, with a carboxyl group para to the amido bond was synthesized according to the synthetic route shown in Figure 1, and then coupled to BSA to form an immunogen. As expected, the corresponding antiserum showed high binding affinity to NPHA, and no binding affinity to free histamine (Table 2). Thus, a ciELISA based on antiserum D could be used to quantitate histamine by introducing a quick preanalysis derivatization of the samples.

**Table 2. Evaluation of Antiserum D against NPHA[a] under Heterologous and Homologous Coating Formats**

| coating antigen | antiserum D | |
|---|---|---|
| | titer ($\times 10^3$) | inhibn (%) |
| hapten A-OVA (hetero-)[b] | <1 | –[c] |
| hapten B-OVA (hetero-) | <1 | – |
| hapten C-OVA (hetero-) | 16 | 96.2 |
| hapten D-OVA (homo-) | 512 | 72.4 |
| hapten E-OVA (hetero-) | <1 | – |
| hapten F-OVA (hetero-) | <1 | – |

[a]Analyte, 0.5 mg/L NPHA. [b]The coating antigen format is indicated as being heterologous or homologous. [c]Not calculated.

**Optimization of the ciELISA.** The effect from the degree of heterology in the chemical structure of the coating antigen on ELISA performance was investigated. As shown in Table 2, the obtained antibody exhibited a much lower affinity for the heterologous coating antigen (hapten C-OVA, titer 1:16000) than for the homologous coating (hapten D-OVA, titer 1:512000), and no affinity for coating antigens with a high degree of heterology (haptens A, B, E, and F, titer >1:1000). However, there was about 20 times improvement in assay sensitivity when using hapten C-OVA ($IC_{50}$ = 9.1 ng/mL) as the coating antigen compared to using hapten D-OVA ($IC_{50}$ = 174.6 ng/mL) based on the $IC_{50}$ obtained from the inhibition curves (Figure 3). Hapten C possesses the *N*-acetylated HA moiety, which has a partial structure of the target analyte NPHA. The result of this work is consistent with conclusions obtained in our previous studies:[37,38] that using a partial structure of the target molecule as the coating hapten may be a good strategy to improve assay sensitivity. Therefore, coating antigen hapten C-OVA was chosen for further experimentation.

Effects of the physicochemical parameters on ELISA performance are summarized in Table S1 (see Supporting Information). To determine the coating concentration and antibody dilution, a preliminary checkerboard titration was employed to screen several combinations of coating concentration and antibody dilution, while keeping the Amax value at about 1.0. The highest sensitivity was achieved when the coating concentration and antibody dilution were at 125 ng/mL and 1:2000, respectively. For the working buffer, PBS with different $PO_4^{3-}$ concentrations (10−100 mmol/L), Tween-20 concentrations (0−0.2%), and pH values (6.6−8.5) was

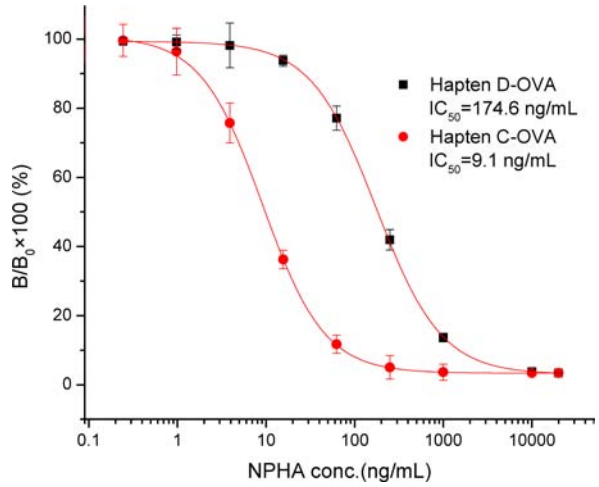


**Figure 3.** Dose-dependent competitive indirect ELISA curves for NPHA with heterologous coating (hapten C-OVA) and homologous coating (hapten D-OVA) ($n$ = 3).

evaluated. The results indicated that a $PO_4^{3-}$ concentration of 20 mmol/L, a Tween-20 concentration of 0.05%, and a pH value of 7.4 were the most suitable for improving assay sensitivity.

**Optimization of Derivatization Conditions.** The chemical structure of PNBA-OSu and its reaction with HA are depicted in Figure 2. In order to achieve the maximum derivatization yield, factors influencing the efficiency of derivatization were optimized, including pH of the buffer, reaction time, and concentration of derivatization reagent. Since this is a nucleophilic substitution reaction, alkaline conditions are important. LC−MS/MS was used to monitor the process of the reaction with borate buffer over the pH range of 7.4−9.6. Figure 4 shows that the reaction proceeds more quickly with a

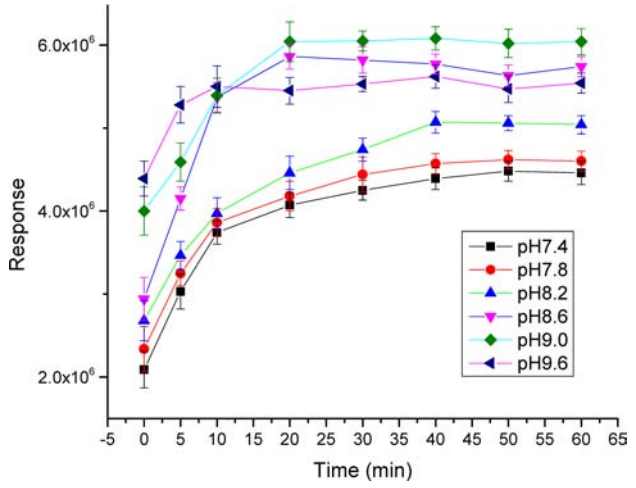


**Figure 4.** Effect of pH on the reaction process of histamine conversion to NPHA ($n$ = 3).

borate buffer of higher pH values, and a maximum yield was observed at 20 min when the pH of the buffer solution was at 9.0. Thus, the HA derivatization conditions with the borate buffer at pH 9.0 and 20 min reaction time were selected. The concentration effect of the derivatization reagent on assay performance was investigated by comparing the inhibition curves obtained by using different concentrations (1−16 mg/mL) of PNBA-OSu. High concentrations of PNBA-OSu (exceeding 2 mg/mL) were detrimental to assay sensitivity (Figure 5). But to guarantee that the HA in high level HA

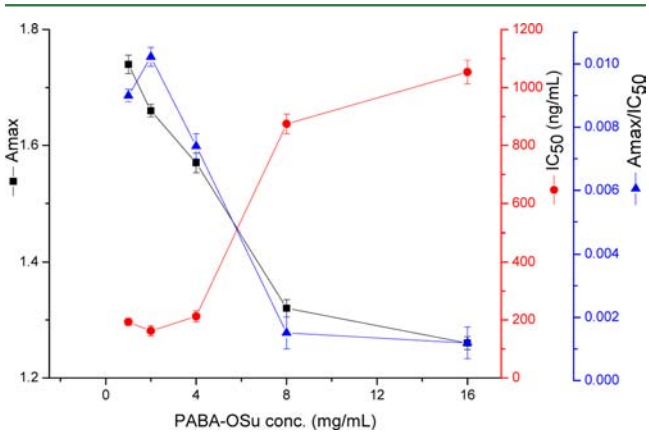


**Figure 5.** Concentration effect of PNBA-OSu on ciELISA performance.

samples was completely derivatized, 2 mg/L of PNBA-OSu was selected. Since the reaction can efficiently proceed at room temperature (25 °C), room temperature was chosen for the reaction temperature without further optimization.

**Sensitivity and Specificity of the ciELISA.** The calibration curve for histamine constructed under the optimal conditions is shown in Figure 6. The assay demonstrated an $IC_{50}$ of 153.2 ng/mL and a limit of detection (LOD) of 9.4 ng/mL (the HA concentration which inhibits 10% of the binding of the antibody, $IC_{10}$) for histamine, whereas the quantification linear range was 12.7−1853.1 ng/mL ($y$ = 126.37 − 34.09$x$). The assay specificity, cross-reactivity (CR) of related compounds including some biogenic amines and amino acids commonly found in foods, was examined, and the results are summarized in Table 3. Since L-histidine has a high degree of similarity to HA and may be contained in foods at high concentration levels, a small CR may interfere with the analysis of HA and would be unacceptable. However, no CR was observed to all the related compounds tested, including L-histidine. This result demonstrated the excellent specificity of the developed ciELISA to HA, which probably results from the high specificity of the antibody to NPHA.

**Detection of Histamine in Spiked Foods.** Sample preparation is the process of sample cleanup and matrix effect elimination and plays a significant part in development of the analytical procedure. To study the matrix effect, a matrix-matched inhibition curve for HA was constructed by diluting the stock solution of HA with blank sample extracts. Since HA is a compound commonly occurring in meat and fermented foods and is spontaneously formed, it is impossible to find blank samples containing no HA for fish, red wine, and yoghurt. Therefore, fresh fish and yoghurt containing HA at a level below the LOD of LC−MS/MS was considered a blank sample. The matrix effect was assessed by comparing the matrix-matched inhibition curves with standard inhibitory curves. It was found that the yoghurt matrix-matched inhibition curve was similar to the solvent inhibition curve, indicating the effectiveness of the yoghurt sample preparation method; while a 20-fold dilution of fish extracts was required to minimize the matrix effect. Therefore, blank fish samples were fortified with relatively higher levels of HA (5.0, 10.0, and 50.0 mg/L) than

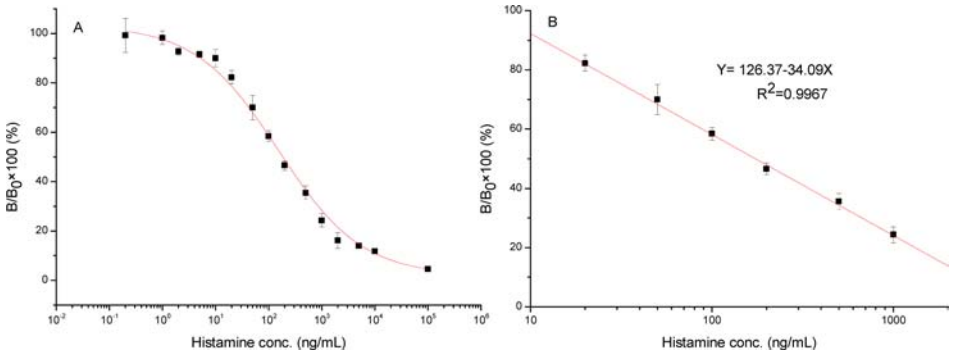


**Figure 6.** (A) Calibration curve and (B) ciELISA calibration curve in the linear range for histamine.

**Table 3. Cross-Reactivity of Related Compounds in ciELISA (under Optimized Conditions)**

| Compound | Structure | CR[a](%) |
|---|---|---|
| Histamine | 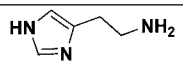 | 100 |
| L-Histidine | 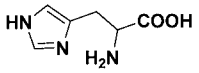 | <0.01% |
| L-Tryptophan | 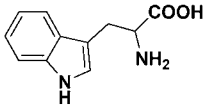 | <0.01% |
| Trytamine | 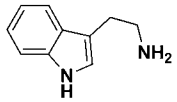 | <0.01% |
| Tryamine | 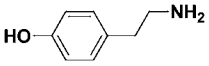 | <0.01% |
| Phenethylamine | 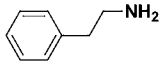 | <0.01% |
| Cadaverine | 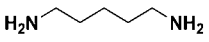 | <0.01% |

[a]CR, cross-reactivity. The percentage of CR was calculated by the following equation: CR (%) = [$IC_{50}$ (histamine, mmol/L)/$IC_{50}$ (cross-reactant, mmol/L)] × 100.

the blank yoghurt samples (0.5, 2.0, and 5.0 mg/L). For red wine, a blank sample was not found. The HA level in red wine samples was initially analyzed by LC−MS/MS, and then the sample was spiked in the linear range of the ciELISA at three levels (0.5, 2.0, 5.0 mg/L). Average recoveries were observed from 80.9% to 110.1% with the coefficient of variance (CV) ranging from 8.4% to 16.3% after all the spiked samples were analyzed by ciELISA (Table 4), which indicated that the matrix effect of these three types of samples was negligible using the sample preparation method. The LOD of the developed ciELISA in fish, red wine, and yoghurt was estimated as the LOD of the calibration curve multiplied by the dilution factor required during sample preparation, which was 1.8 mg/kg, 93.6 μg/L, and 93.6 μg/kg, respectively. Taking the maximum residue limits (MRLs) set for HA in fish (50−300 mg/L) and recommended upper limits for HA in wine (2−10 mg/L)[39] into consideration, the ciELISA was sensitive enough for HA analysis in these food samples.

To confirm the reliability of the developed ciELISA, spiked food samples were subjected to HA analysis by LC−MS/MS which had a LOD of 2.9 ng/mL (LOD is defined as the lowest concentration level that produces a signal-to-noise ratio of 3, S/N = 3) and good linearity over the HA range of 10−1000 ng/mL, with a correlation coefficient of 0.996 (see Figure S2 in Supporting Information). Average recoveries obtained by LC−MS/MS ranged from 92.0% to 105.4% with CVs between 5.2% and 10.7% (Table 4). The results of the ciELISA were in good agreement with those of LC−MS/MS with a correlation coefficient ($R^2$) of 0.978 (Figure 7), revealing good reliability and accuracy for this ciELISA.

**Analysis of Blind Samples.** The developed ciELISA was then applied to detect HA in blind samples to assess its effectiveness. Four fish samples having different degrees of

Table 4. Recoveries of Histamine from Spiked Food Samples by ciELISA and LC−MS/MS ($n$ = 4)[a]

| | | ciELISA | | | LC−MS/MS | | |
|---|---|---|---|---|---|---|---|
| sample | spiked (mg/kg or mg/L) | measd (mg/kg or mg/L) (mean ± SD[b]) | recovery (%) | CV[c] (%) | measd (mg/kg or mg/L) (mean ± SD) | recovery (%) | CV (%) |
| fish | 0 | ND[d] | — | — | ND | — | — |
| | 5.0 | 4.2 ± 0.7 | 83.0 | 15.3 | 4.8 ± 0.37 | 96.7 | 7.3 |
| | 10.0 | 9.1 ± 1.2 | 91.2 | 11.9 | 9.7 ± 0.72 | 97.0 | 7.2 |
| | 50.0 | 47.9 ± 6.9 | 95.7 | 8.8 | 46.4 ± 6.5 | 92.9 | 6.2 |
| red wine | 0 | 2.44 ± 0.43 | — | 15.8 | 2.03 ± 0.37 | — | 10.7 |
| | 0.5 | 2.95 ± 0.21 | 110.1 | 16.3 | 2.46 ± 0.08 | 82.6 | 9.4 |
| | 2.0 | 4.27 ± 0.39 | 93.5 | 13.1 | 4.24 ± 0.38 | 102.0 | 8.7 |
| | 5.0 | 6.85 ± 0.16 | 89.1 | 8.4 | 6.83 ± 0.23 | 100.4 | 5.2 |
| yoghurt | 0 | ND | — | — | ND | — | — |
| | 0.5 | 0.405 ± 0.05 | 80.9 | 13.0 | 0.46 ± 0.04 | 92.0 | 7.6 |
| | 2.0 | 2.07 ± 0.16 | 103.6 | 11.4 | 2.11 ± 0.14 | 105.4 | 7.2 |
| | 5.0 | 4.69 ± 0.69 | 93.7 | 9.8 | 4.74 ± 0.60 | 94.8 | 5.9 |

[a]For one concentration, four samples were spiked and determined by ELISA and LC−MS/MS. [b]SD, standard deviation. [c]CV, coefficient of variance, which was obtained from intra-assay. [d]ND, not detected. Data were below the LOD of the assay in corresponding sample.

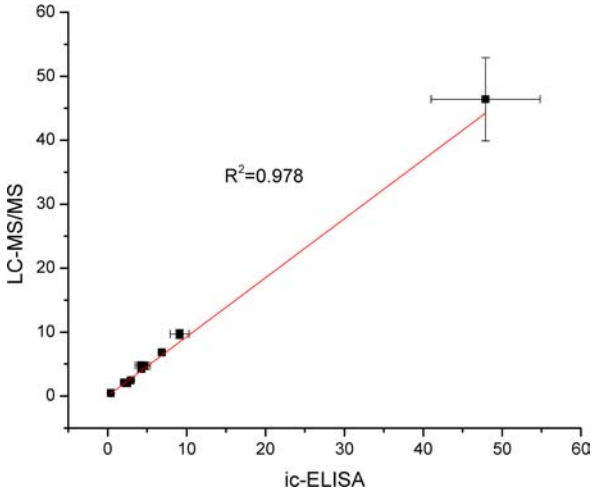


Figure 7. Correlation of LC−MS/MS results with ciELISA results.

Table 5. Comparison of the Blind Analysis Results for Histamine Content in Foods by ciELISA and LC−MS/MS ($n$ = 4)

| | content (mg/L or mg/kg) | |
|---|---|---|
| sample | ciELISA (mean ± SD) | LC−MS/MS (mean ± SD) |
| fish 1 | 3.4 ± 0.6 | 3.2 ± 0.5 |
| fish 2 | 11.2 ± 1.1 | 9.7 ± 0.8 |
| fish 3 | ND[a] | ND |
| fish 4 | 5.6 ± 0.5 | 6.3 ± 0.3 |
| yoghurt 1 | 0.13 ± 0.02 | 0.11 ± 0.01 |
| yoghurt 2 | ND | ND |
| yoghurt 3 | 0.17 ± 0.02 | 0.20 ± 0.02 |
| yoghurt 4 | ND | ND |
| red wine 1 | 2.14 ± 0.14 | 2.36 ± 0.12 |
| red wine 2 | 0.72 ± 0.06 | 0.63 ± 0.04 |
| red wine 3 | 1.33 ± 0.07 | 1.54 ± 0.05 |
| red wine 4 | 2.71 ± 0.18 | 2.98 ± 0.13 |

[a]ND, not detected. Data were below the LOD of the assay in the corresponding samples.

freshness, four red wine samples, and four yoghurt samples were randomly collected from a local supermarket and analyzed by the ciELISA and LC−MS/MS. As shown in Table 5, a good correlation was observed between the results of the ciELISA and those of the LC−MS/MS, demonstrating the effectiveness and applicability of the developed ciELISA for HA analysis in these foods.

In summary, a ciELISA for the determination of HA in foods was developed based on a highly specific antibody against the NPHA derivative. All attempts to generate a specific antibody for free HA with enough affinity for the required HA analysis failed. Thus, a preanalysis chemical derivatization of HA was used in a similar manner as in the previously reported immunoanalysis of HA. However, the novel HA chemical derivatization involved in this assay was ideally suited for the requirements of a rapid immunoassay for HA, for rapidity, simplicity, and low cost. Rapidity: Conversion of HA to the NPHA derivative was efficient (completed in 20 min) under mild conditions (room temperature in borate buffer). Simplicity: Owing to the high hydrophobicity of NPHA, it can easily be extracted by organic solvent (ACN) from aqueous solutions containing high ionic strength and separated from most interfering substances, and then directly analyzed by dilution with working buffer ($PBST_2$). Low cost: Compared with the derivatization reagent SGA-NHS, which was used for derivatization of HA in a previous report,[29] PNBA-OSu is easily accessible by a one-step synthesis between $p$-nitrobenzoic acid and $N$-hydroxysuccinimide, which are cheap and easily available. The developed ciELISA exhibited the required sensitivity for detection of HA with LOD values of 1.8 mg/kg, 93.6 μg/L, and 93.6 μg/kg for fish, red wine, and yoghurt samples, respectively. Excellent recoveries (ranging from 80.9% to 110.1%) from HA-spiked food samples and a satisfactory correlation ($R^2$ = 0.978) between the results of ciELISA analysis and those of LC−MS/MS analysis were observed. Overall, the ciELISA described in this study was ideally suited as a screening tool for routine HA monitoring in large numbers of food samples.

## ■ ASSOCIATED CONTENT

### Supporting Information

Total ionization chromatogram and mass spectrometry of NPHA standard during LC−MS/MS analysis (Figure S1), calibration curve for histamine in LC−MS/MS (Figure S2), and optimization of physicochemical parameters of ciELISA

(Table S1). This material is available free of charge via the Internet at http://pubs.acs.org.

## AUTHOR INFORMATION


### Corresponding Authors

*(Y.-M.S.) No. 483, Wushan Road, Tianhe District, Guangzhou, 510642, China. Tel: +86 20 8528 3448. Fax: +86 20 8528 0270. E-mail: gzsyming@163.com.

*(Y.-D.S.) No. 483, Wushan Road, Tianhe District, Guangzhou, 510642, China. Tel: +86 20 8528 3448. Fax: +86 20 8528 0270. E-mail: shenyudong@scau.edu.cn.

### Author Contributions

‡L.L. and Z.-L.X made equal contributions.



### Funding

This work was supported by the National Basic Research Program of China (973 Program, 2012CB720803), the Excellent Young Teachers Program on Higher Education of Guangdong Province (Zhen-Lin Xu), and the Guangdong Provincial Project of Science and Technology (2013B040402006 and 2012A020100002).


### Notes

The authors declare no competing financial interest.

## REFERENCES


(1) ten Brink, B.; Damink, C.; Joosten, H. M. L. J.; Huis in't Veld, J. H. J. Occurrence and formation of biologically active amines in foods. *Int. J. Food Microbiol.* **1990**, *11*, 73−84.

(2) Shalaby, A. R. Significance of biogenic amines to food safety and human health. *Food Res. Int.* **1996**, *29*, 675−690.

(3) Santos, M. H. S. Biogenic amines: their importance in foods. *Int. J. Food Microbiol.* **1996**, *29*, 213−231.

(4) Bodmer, S.; Imark, C.; Kneubühl, M. Biogenic amines in foods: Histamine and food processing. *Inflammation Res.* **1999**, *48*, 296−300.

(5) Lehane, L.; Olley, J. Histamine fish poisoning revisited. *Int. J. Food Microbiol.* **2000**, *58*, 1−37.

(6) Beaven, M. A. Histamine: Its role in physiological and pathological processes. *Monogr. Allergy* **1978**, *13*, 1−113.

(7) Taylor, S. L.; Eitenmiller, R. R. Histamine food poisoning: Toxicology and clinical aspects. *Crit. Rev. Toxicol.* **1986**, *17*, 91−128.

(8) Tsai, Y.-H.; Hsieh, H.-S.; Chen, H.-C.; Cheng, S.-H.; Chai, T.-j.; Hwang, D.-F. Histamine level and species identification of billfish meats implicated in two food-borne poisonings. *Food Chem.* **2007**, *104*, 1366−1371.

(9) Hwang, D.-F.; Chang, S.-H.; Shiau, C.-Y.; Cheng, C.-C. Biogenic amines in the flesh of sailfish (*Istiophorus platypterus*) responsible for scombroid poisoning. *J. Food Sci.* **1995**, *60*, 926−928.

(10) Tsai, Y.-H.; Kung, H.-F.; Lee, T.-M.; Chen, H.-C.; Chou, S.-S.; Wei, C.-I.; Hwang, D.-F. Determination of histamine in canned mackerel implicated in a food borne poisoning. *Food Control* **2005**, *16*, 579−585.

(11) Jastrzębska, A.; Kurzawa, M.; Piasta, A.; Szlyk, E. Determination of histamine in some foods by isotachophoretic method with simple sample preparation. *Food Anal. Methods* **2012**, *5*, 1079−1087.

(12) Commission Regulation (EC). No. 2073/2005 of 15 November 2005 on microbiological criteria for foodstuffs; *Official Journal of the European Union*; L338/1−26.

(13) Talon, R.; Leroy, S. Diversity and safety hazards of bacteria involved in meat fermentations. *Meat Sci.* **2011**, *89*, 303−309.

(14) Department of Health and Human Services, Public Health Service, Food and Drug Administration, Center for Food Safety and Nutrition. *Fish and Fishery Products Hazards and Controls Guidance*, 4th ed.; 2011, April.

(15) GB2733-2005 Hygienic standard for fresh and marine products of animal origin.

(16) Ough, C. S. Measurement of histamine in California wines. *J. Agric. Food Chem.* **1971**, *19*, 241−244.

(17) Chin, K. D. H.; Koehler, P. E. Identification and estimation of histamine, tryptamine, phenylethylamine and tyramine in soy sauce by thin-layer chromatography of dansyl derivatives. *J. Food Sci.* **1983**, *48*, 1826−1828.

(18) Numanoğlu, E.; Boyaci, İ. H.; Topcu, A. Simple determination of histamine in cheese by capillary electrophoresis with diode array detection. *J. Food Drug Anal.* **2008**, *16*, 74−80.

(19) Tamim, N. M.; Bennett, L. W.; Shellem, T. A.; Doerr, J. A. High-performance liquid chromatographic determination of biogenic amines in poultry carcasses. *J. Agric. Food Chem.* **2002**, *50*, 5012−5015.

(20) Romero-González, R.; Alarcón-Flores, M. I.; Vidal, J. L. M.; Frenich, A. G. Simultaneous determination of four biogenic and three volatile amines in anchovy by ultra-high-performance liquid chromatography coupled to tandem mass spectrometry. *J. Agric. Food Chem.* **2012**, *60*, 5324−5329.

(21) Antoine, F. R.; Wei, C.-I.; Otwell, W. S.; Sims, C. A.; Littell, R. C.; Hogle, A. D.; Marshall, M. R. Gas chromatographic analysis of histamine in mahi-mahi (*Coryphaena hippurus*). *J. Agric. Food Chem.* **2002**, *50*, 4754−4759.

(22) Hwang, B.-S.; Wang, J.-T.; Choong, Y.-M. A rapid gas chromatographic method for the determination of histamine in fish and fish products. *Food Chem.* **2003**, *82*, 329−334.

(23) Young, J. A.; Jiang, X.; Kirchhoff, J. R. Amperometric detection of histamine with a pyrroloquinoline-quinone modified electrode. *Electroanalysis* **2013**, *25*, 1589−1593.

(24) Pérez, S.; Bartrolí, J.; Fàbregas, E. Amperometric biosensor for the determination of histamine in fish samples. *Food Chem.* **2013**, *141*, 4066−4072.

(25) Morel, A.; Darmon, M.; Delaage, M. Recognition of imidazole and histamine derivatives by monoclonal antibodies. *Mol. Immunol.* **1990**, *27*, 995−1000.

(26) Guesdon, J.-L.; Chevrier, D.; Mazié, J.-C.; David, B.; Avrameas, S. Monoclonal anti-histamine antibody: Preparation, characterization and application to enzyme immunoassay of histamine. *J. Immunol. Methods* **1986**, *87*, 69−78.

(27) Serrar, D.; Brebant, R.; Bruneau, S.; Denoyel, G. A. The development of a monoclonal antibody-based ELISA for the determination of histamine in food: Application to fishery products and comparison with the HPLC assay. *Food Chem.* **1995**, *54*, 85−91.

(28) Rauch, P.; Rychetsky, P.; Hochel, I.; Bilek, R.; Guesdon, J. L. Enzyme immunoassay of histamine in foods. *Food Agric. Immunol.* **1992**, *4*, 67−72.

(29) Morel, A. M.; Delaage, M. A. Immunoanalysis of histamine through a novel chemical derivatization. *J. Allergy Clin. Immunol.* **1988**, *82*, 646−654.

(30) Schneider, E.; Usleber, E.; Märtlbauer, E. Production and characterization of antibodies against histamine. In *Immunoassays for Residue Analysis: Food Safety*; Beier, R. C., Stanker, L. H., Eds.; ACS Symposium Series 621; American Chemical Society: Washington, DC, 1996; pp 413−420.

(31) Rubin, H.; Cockrell, J.; Morgan, J. B. Scalable synthesis of *N*-acylaziridines from *N*-tosylaziridines. *J. Org. Chem.* **2013**, *78*, 8865−8871.

(32) Mahon, W. A.; Ezer, J.; Wilson, T. W. Radioimmunoassay for measurement of gentamycin in blood. *Antimicrob. Agents Chemother.* **1973**, *3*, 585−589.

(33) Habeeb, A. F. S. A. Determination of free amino groups in proteins by trinitrobenzenesulfonic acid. *Anal. Biochem.* **1966**, *14*, 328−336.

(34) Page, M.; Thorpe, R. Purification of IgG by precipitation with sodium sulfate or ammonium sulfate. In *The Protein Protocols Handbook*; Springer: 1996; pp 721−722.

(35) Xu, Z.-L.; Sun, W.-J.; Yang, J.-Y.; Jiang, Y.-M.; Campbell, K.; Shen, Y.-D.; Lei, H.-T.; Zeng, D.-P.; Wang, H.; Sun, Y.-M. Development of a solid-phase extraction coupling chemiluminescent enzyme immunoassay for determination of organophosphorus pesticides in environmental water samples. *J. Agric. Food Chem.* **2012**, *60*, 2069−2075.

(36) Cline, G. W.; Hanna, S. B. The aminolysis of *N*-hydroxysuccinimide esters. A structure-reactivity study. *J. Am. Chem. Soc.* **1987**, *109*, 3087−3091.
(37) Shen, Y.-D.; Xu, Z.-L.; Zhang, S.-W.; Wang, H.; Yang, J.-Y.; Lei, H.-T.; Xiao, Z.-L.; Sun, Y.-M. Development of a monoclonal antibody-based competitive indirect enzyme-linked immunosorbent assay for furaltadone metabolite AMOZ in fish and shrimp samples. *J. Agric. Food Chem.* **2012**, *60*, 10991−10997.
(38) Xu, Z.-L.; Shen, Y.-D.; Zheng, W.-X.; Beier, R. C.; Xie, G.-M.; Dong, J.-X.; Yang, J.-Y.; Wang, H.; Lei, H.-T.; She, Z.-G.; Sun, Y.-M. Broad-specificity immunoassay for *O,O*-diethyl organophosphorus pesticides: Application of molecular modeling to improve assay sensitivity and study antibody recognition. *Anal. Chem.* **2010**, *82*, 9314−9321.
(39) Lehtonen, P. Determination of amines and amino acids in wine—A review. *Am. J. Enol. Vitic.* **1996**, *47*, 127−133.

quantification and limits of detection of Robusta that may be too high. Also, a DNA-based food authenticity assay was recently proposed[16] that is able to detect 5% Robusta in Arabica coffee.

The content of 16-OMC remains a valuable option for detection of Robusta additions to Arabica blends, but a fast, reliable, and sensitive method is needed. The aim of the present work is to report an analytical method based on nuclear magnetic resonance (NMR) spectroscopy that could be used as an alternative to the DIN standard and that could guarantee the authenticity of 100% Arabica blends by detecting possible commercial frauds in a rapid and dependable way. NMR spectra can be acquired in a very short time; the technique is inherently reproducible and provides quantitative and structural information. These features combined with the minimal sample preparation required and the absence of any derivatization step make NMR a promising choice for our purposes.

## MATERIALS AND METHODS

**Chemicals and Materials.** Deuterated chloroform ($CDCl_3$, 99.96% D, stabilized with silver, Sigma-Aldrich), deuterated water (≥99.96% D, Eurisotop), *N*,*N*-dimethylformamide [DMF, ≥99.99% (GC), Fluka-Sigma-Aldrich], 16-OMC (phyproof References Substances, PhytoLab), 5 mm precision glass NMR tubes (535-pp, Wilmad), and coaxial insert (wgs-5bl, Wilmad) were used.

**Coffee Samples.** *C. canephora* from Ivory Coast, India, and Uganda, hereafter named R1, R2, and R3, respectively, were roasted to a medium roasting degree in a lab roaster (Probat). The *C. arabica* sample came from Brazil. Several commercial roasted coffee samples (in whole beans) were purchased in local markets. These samples were named CB0, ..., CB*n*.

**Sample Treatment.** Coffee powder was obtained by grinding the roasted coffee beans in liquid nitrogen. Extraction of ca. 0.45 g of powder (accurately weighed) was carried out by vortexing for 15 min with 1.5 mL of $CDCl_3$. Samples were then quickly filtered through a cotton wool filter directly into the NMR tube. All of the operations were conducted at about 4 °C to minimize solvent evaporation. A $^1$H NMR spectrum was acquired immediately after filtration.

**Preparation of the External Standard Solution.** To quantify absolute concentrations, a coaxial insert filled with a DMF solution in $D_2O$ was placed inside the NMR tube. This standard was chosen because of its long-term stability that allows for a large set of samples to be measured and quantified with respect to the same reference solution. The solution was prepared by accurately weighing DMF and the $D_2O$ solvent for a final concentration of the standard in the capillary tube of 5.99 mM to provide a S/N ratio comparable to that of the test substance.

**NMR Spectroscopy.** The assignment of $^1$H and $^{13}$C of the standard 16-OMC was achieved using one-dimensional (1D) and two-dimensional (2D) spectra. The complete assignment of the esterified form of 16-OMC was also achieved using 2D NMR experiments performed directly on the extracts and by comparison to the NMR data of the standard 16-OMC. A Bruker (Rheinstetten, Germany) Avance DMX600 spectrometer operating at 599.90 MHz for $^1$H and equipped with a 5 mm TXI xyz-triple gradient probe was used. The 1D spectra were acquired in deuterated chloroform using a common one-pulse sequence with a spectral width of 6000 Hz, with 32 768 data points; the receiver gain ranged from 64 to 128; and scans varied from 32 to 64 depending upon the 16-OMC concentration.

Two-dimensional total correlation spectroscopy (TOCSY), heteronuclear multiple-quantum coherence (HMQC), heteronuclear multiple-bond coherence (HMBC), and nuclear Overhauser effect spectroscopy (NOESY) spectra were recorded at 298 K using standard Bruker pulse programs. Chemical shifts are reported in $\delta$ values using the residual signal of $CHCl_3$ set to 7.27 and 77.00 ppm as reference for $^1$H and $^{13}$C, respectively.

The ACD software (ACD labs 12.0) was used to process the spectra. Fourier transformation was performed after exponential line broadenings of 0.2−0.4 Hz. Integrations were manually obtained after careful manual phase and baseline correction.

**Quantification.** To determine the total concentration of the 16-OMC esters, a scale factor of 0.108 was used, corresponding to the ratio between the volume of the coaxial insert ($V_c$) and the volume occupied by the sample in the outer part of the NMR tube ($V_t$), calculated as reported by Rastrelli et al.[17] The absolute concentration of 16-OMC esters ($C_a$) was determined by comparing the integral value of the area of the methyl protons at position 21 ($I_a$) and that of the methyl protons of DMF at 3.02 ppm ($I_s$), using the relationship

$$C_a\ (\mathrm{mol/L}) = (I_a/I_s)(V_c/V_t)C_s$$

where $C_s$ is the concentration of the external standard. These methyl protons fall in a free region in all of the analyzed samples.

The following formula gives the concentration of the free 16-OMC in mg/kg:

$$C_{16\text{-OMC}}\ (\mathrm{mg/kg}) = C_a \mathrm{MW}_{16\text{-OMC}} V_{extr}\ (\mathrm{mL})/m_{coffee}\ (\mathrm{kg})$$

where $\mathrm{MW}_{16\text{-OMC}}$ is the molecular weight of 16-OMC, $V_{extr}$ is the $CDCl_3$ volume used in the extraction, and $m_{coffee}$ is the weight of the coffee powder.

The longitudinal relaxation time $T_1$ of all signals of interest was determined in the matrices, in the standard solutions, and in chloroform using the inversion−recovery sequence. To produce quantitative data, the relaxation delay was at least 5 times the longest measured $T_1$, corresponding to one of the methyl signals of DMF in $D_2O$, which determined a relaxation delay of 43 s.

**Method Validation.** To verify the linearity of the proposed method with respect to the concentration of 16-OMC, 12 coffee blends with increasing content of Robusta were prepared. For each mixture, the $CDCl_3$ extraction was performed in triplicate and a $^1$H NMR spectrum of each sample was acquired using identical experimental conditions. The integrals of the non-overlapping signals of esterified 16-OMC (i.e., protons 17 and 21) were plotted versus the nominal concentration of 16-OMC.

To calculate the limit of detection (LoD) and limit of quantification (LoQ), a signal-to-noise ratio of 3 and 10 was used, respectively. These limits were determined by plotting the S/N value versus the 16-OMC amount using a concentration range of 0−450 mg/kg. The coffee powder/solvent ratio chosen was 0.3 g/mL (see the Method Development section), and the spectra were acquired with 64 scans for a total acquisition time of about 48 min.

**Extraction Efficiency.** To assess the extraction efficiency of the proposed method, three different samples were extracted twice. Specifically, after the first extraction, the residual solvent remaining on the ground beans was evaporated and the solid residue was subjected to a second extraction procedure. The amount of esterified 16-OMC recovered in the second extraction was calculated taking into account the amount of esterified 16-OMC present in the solvent that was not recovered during the first filtration. The following equations were used:

$$n^1_{16\text{-OMC}} = V_1^{add} C^1_{16\text{-OMC}}$$

$$n^2_{16\text{-OMC}} = V_2^{add} C^2_{16\text{-OMC}} - (V_1^{add} - V_1^{rec}) C^1_{16\text{-OMC}}$$

where $n^1_{16\text{-OMC}}$ and $n^2_{16\text{-OMC}}$ are the moles of 16-OMC recovered in the first and second extraction, respectively, $V_1^{add}$ and $V_2^{add}$ are the volumes of $CDCl_3$ used in the first and second extraction, respectively, $C^1_{16\text{-OMC}}$ and $C^2_{16\text{-OMC}}$ are the concentrations of 16-OMC determined in the first and second extraction, respectively, and $V_1^{rec}$ is the volume recovered in the first extraction. The value of $n^2_{16\text{-OMC}}$ is taken as a measure of the efficiency of the first extraction.

## RESULTS AND DISCUSSION

**Analysis of Spectra.** The $CDCl_3$ extraction of coffee powder provides a mixture of the main components of coffee

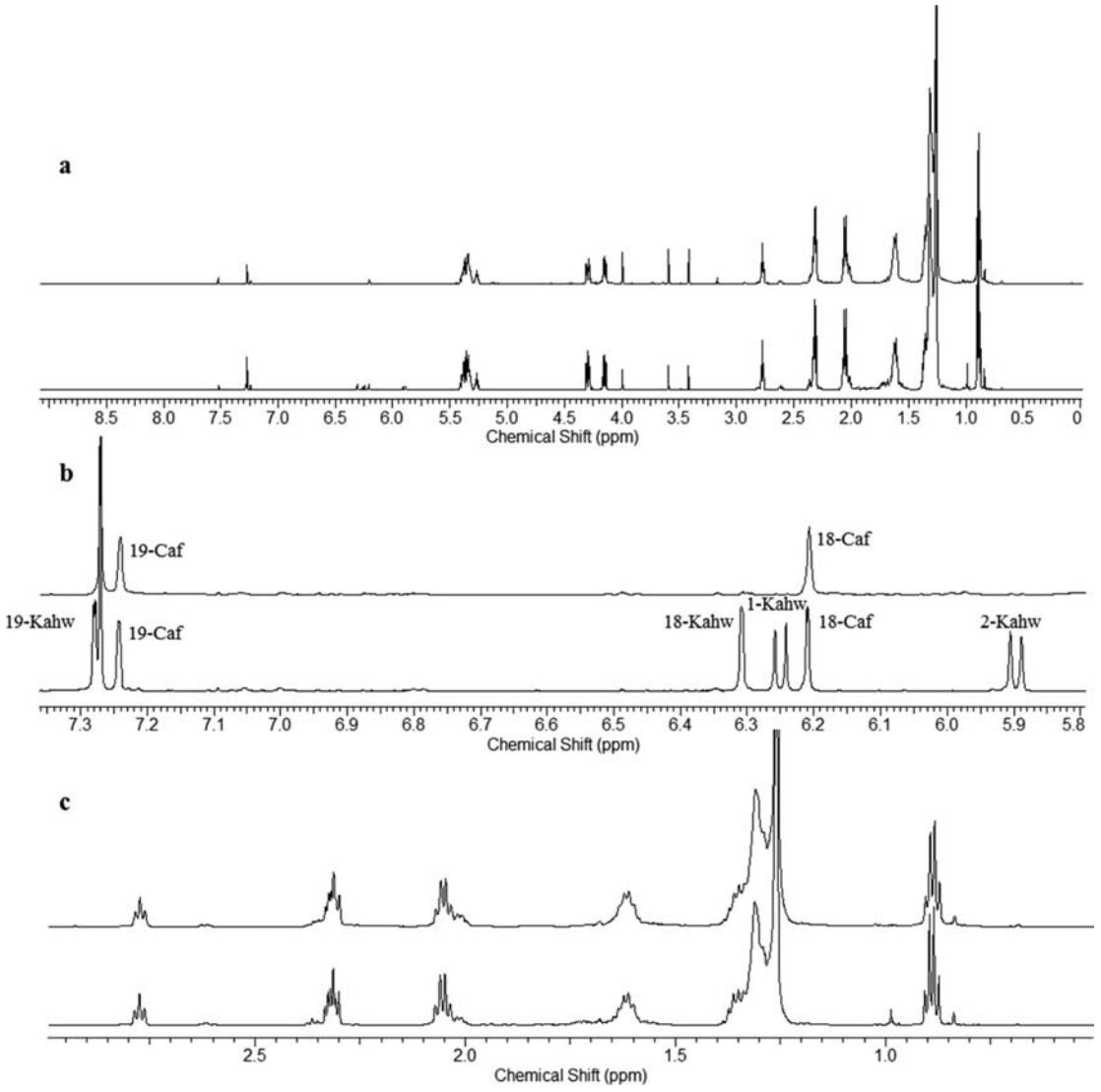


**Figure 1.** (a) $^{1}$H NMR of samples extracted from 100% Arabica (bottom) and 100% Robusta (top) roasted coffee powder. (b) Expanded region containing the olefinic proton resonances of cafestol and kaweol. The olefinic protons of 16-OMC and those of cafestol are overlapped. (c) NMR profile of the fatty acid proton region.

oil, i.e., fatty acids, caffeine, diterpenes (principally present as esters of fatty acids[18]), and other less concentrated species (see Figure 1). Identification of the $^{1}$H and $^{13}$C signals of the marker (i.e., esterified 16-OMC) was carried out using the assignment of free 16-OMC, which was compared to that reported in the literature[19] as an aid, and it is reported in Table 1. The chemical structures of esterified 16-OMC, cafestol, and kahweol are shown in Figure 2.

In Figure 3a, the diagnostic region (protons 17 and 21) of 16-OMC in a Robusta extract is shown. Protons 21 in esterified 16-OMC resonate as a singlet at 3.17 ppm, slightly shifted with respect to the free form (3.18 ppm; see Figure 3c). Protons 17 form a second-order system at 3.78 ppm in the free form, while, in the ester, two doublets are obtained at 4.28 and 4.45 ppm, respectively, with a scalar coupling constant $J_{AM}$ = 12.8 Hz. Only the doublet at 4.45 ppm is well-resolved in the spectrum, while the other doublet is partially overlapping the signals of the glycerol moiety of triglycerides. The same region in a $^{1}$H spectrum of Arabica is shown in Figure 3b. As expected, the signals of protons 17 and 21 from the 16-OMC unit are absent.

The free form of 16-OMC is generally present in trace amounts, visible in some samples, as shown in the inset of Figure 3.

As a first consideration, a visual inspection of the spectrum allows for an immediate distinction of a 100% Arabica coffee from a mixture with Robusta. Specifically, the protons 21 of esterified 16-OMC immediately reveal the presence of Robusta, while the signals attributed to kahweol (18, 19, 1, and 2 of Figure 1b) that almost disappear in the Robusta sample reveal the presence of Arabica.

**Method Development.** We optimized a very fast and simple procedure that requires only a few steps using a deuterated solvent directly. The selection of $CDCl_3$ as the solvent for extraction was based on the observation that the diterpenes are very soluble in this solvent and that it is not expensive. Also, the residual signal of the protonated form does not overlap with important peaks to integrate. The coffee powder/solvent ratio was optimized to obtain an easily filterable solution and a well-resolved spectrum. The best solid/liquid ratio was found to be $\leq$0.3 g/mL.

**Table 1. $^{1}H$ and $^{13}C$ Resonances of Esterified 16-OMC in the Chloroform Extract of Robusta Roasted Coffee Beans[a]**

| | esterified 16-OMC (esterified cafestol) | |
|---|---|---|
| | $\delta^{1}H^{b}$ | $\delta\ ^{13}C^{b}$ |
| 1 | 1.25, 2.07 | 33.8 |
| 2 | 2.63 | 21.4 |
| 3 | | 149 |
| 4 | | 120.1 |
| 5 | 2.29 | 43.1 |
| 6 | 1.81, 1.85 | 22.7 |
| 7 | 1.57−1.67 | 41 |
| 8 | - | |
| 9 | 1.19 | 53.1 |
| 10 | - | 38.5 |
| 11 | 1.57−1.67 | 19.8 |
| 12 | 1.57−1.67 | 22.9 |
| 13 | 2.26 (2.10) | 45.6 (46.8) |
| 14 | 1.48, 2.00 | 38.34 |
| 15 | 1.57, 1.67 (1.54, 1.58) | 55.3 (53.0) |
| 16 | - | 84.58 (79.9) |
| 17 | 4.24, 4.44 (4.27−4.29) | 62.72 (68.37) |
| 18 | 6.24 | 107.83 |
| 19 | 7.24 | 140.52 |
| 20 | 0.83 | 14.16 |
| 21 | 3.17 (-) | 49.84 (-) |
| CO fatty acid | | 173.72 |

[a]Only the cafestol assignments that differ from those of 16-OMC are reported in parentheses. [b]$\delta$ is in parts per million. NMR solvent was $CDCl_3$.

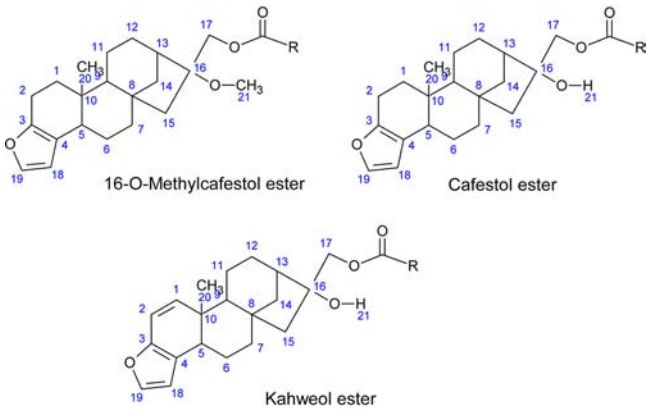


**Figure 2.** Chemical structure and atom numbering of esterified diterpenes: 16-OMC, cafestol, and kahweol.

**Quantification of 16-OMC.** 16-OMC was quantified by integrating the resolved peaks at 3.17 ppm (protons 21) and the signal of one of the protons in position 17 (4.45 ppm) of the analyte compared to the integral of the methyl signal of DMF at 3.02 ppm, which did not present any overlap in any of the samples studied. The proximity of the methyl 21 peaks of the free and esterified forms allowed us to integrate them together; therefore, the value of 16-OMC that is obtained is always referring to the total amount.

**Linearity, Precision, and Sensitivity of the Analytical Procedure.** Good linearity was achieved for both signals, as indicated by the equation shown in Figure 4 for concentrations ranging from 5 to at least 1500 mg/kg, with a satisfactory determination coefficient $R^2$. Because a higher $R^2$ value was obtained for the methyl singlet at 3.17 ppm, this signal was used for quantification of 16-OMC. The values of the relative standard deviation (RSD) ranged from 2 to 5% and confirm the suitability of the proposed method.

By plotting the S/N versus nominal concentration ($R^2$ = 0.9906, data not shown), the sensitivity of the method was assessed in terms of LoD and LoQ, which were 5 and 20 mg/kg, respectively. These LoD and LoQ values are satisfactory; by considering the reported range of the 16-OMC content found in Robusta green beans (0.8−2.5 g/kg of dry weight, with both the median and mean values equal to approximately 1.7 g/kg of dry weight[3]), this method allows for the detection of the presence of Robusta at percentages lower than 0.9% and down to 0.2%. This level is lower than that reported by the DIN method (about 2%).

**Extraction Efficiency.** For all three of the samples investigated, the corrected amount of marker ($n^{2}_{16\text{-OMC}}$) recovered from the second extraction was lower than 2% with respect to the first extraction. This indicates that the first extraction is practically quantitative. Interestingly, by grinding at room temperature with a coffee mill, according to the DIN recommendations, a lower extraction efficiency was obtained for all examined samples (73−82%, data not shown). Therefore, grinding at a low temperature seems to be crucial.

**Comparison to the DIN Method.** The method presented here is able to detect and to quantify 16-OMC in roasted coffee samples without complex sample manipulation and in a few minutes. Exploiting the power of NMR to determine the presence and amount of a substance in a complex mixture, this method avoids long Soxhlet extractions, a saponification step, and chromatographic procedures to isolate and separate the analyte of interest. In addition to easy detection, the method that we propose permits the quantification of 16-OMC and, in principle, determines the content of Robusta ingredients in roasted coffee blends.

To evaluate the accuracy of the proposed method, the entire procedure was repeated twice on the same sample and the quantities of 16-OMC found were compared to that determined by the DIN method. In Table 2, a comparison between the 16-OMC content determined by the two methods is reported. The agreement between the two different determinations is satisfactory, although the values obtained by the DIN method are often lower than those determined by NMR. An underestimation of the 16-OMC content by the DIN method is possibly related to the complex manipulation necessary to perform the analysis, while the much simpler sample preparation of our procedure avoids the danger of loss of analyte. Therefore, the small amounts of sample required, the rapidity, precision, and accuracy, and the low detection limit of the analysis make the NMR method promising for screening purposes.

The wide range of the 16-OMC concentration in different Robusta samples poses a serious obstacle for the quantification of Robusta percentage in roasted coffee blends. This problem is common to every method that exploits 16-OMC and makes the determination of this molecular marker more appropriate for authentication of 100% Arabica blends. This point, however, could be the subject of further investigation. In this regard, a large database might help in better defining the real range of the 16-OMC concentration in different Robusta samples and in a possible correlation with geographical origin and agronomical practices.

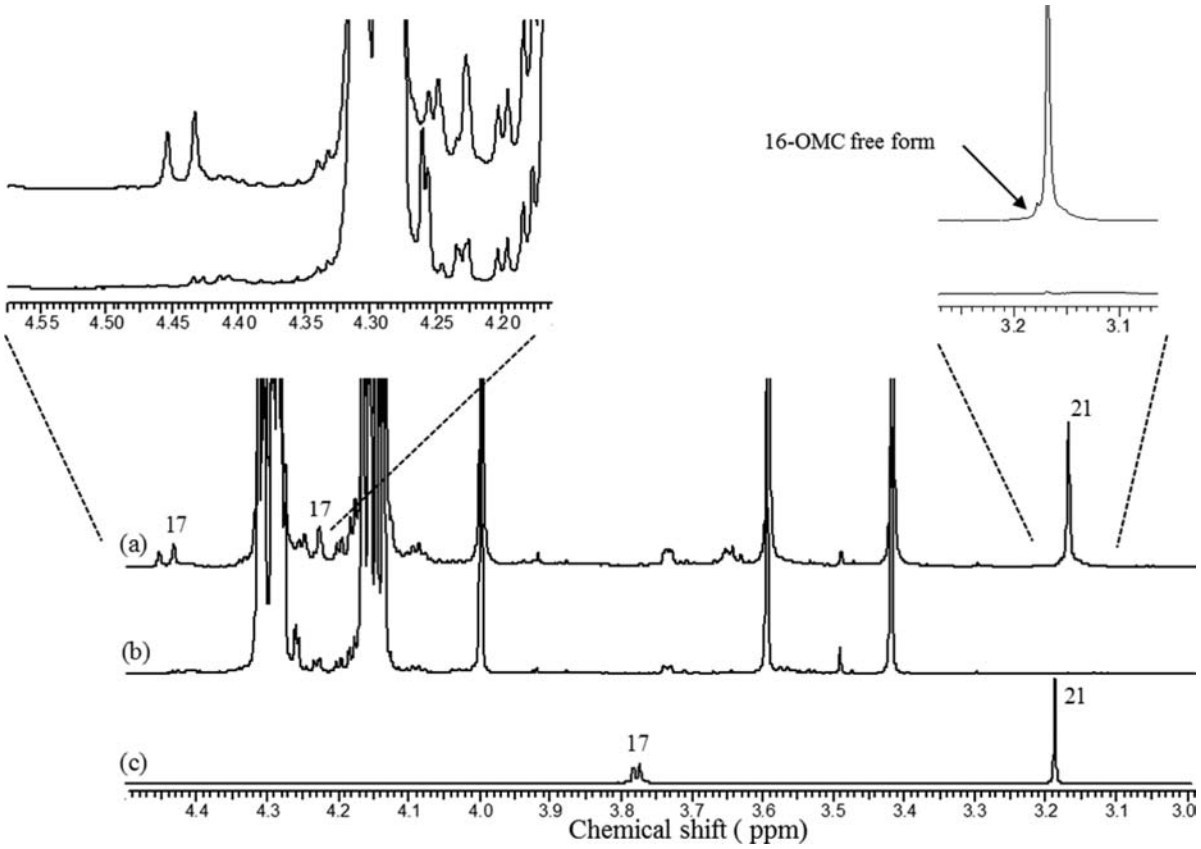


**Figure 3.** Expanded region of the $^{1}$H NMR spectrum showing the diagnostic resonances of protons 17 and 21: (a) 100% Robusta sample, (b) 100% Arabica sample, and (c) 16-OMC standard. In the insets on the top of the figure, the signals of 17 and 21 protons of 16-OMC ester are enlarged. They are clearly visible in the Robusta sample (top), but they are absent from the Arabica sample. The arrow shows the weak methyl signals in position 21 of 16-OMC in its free form.

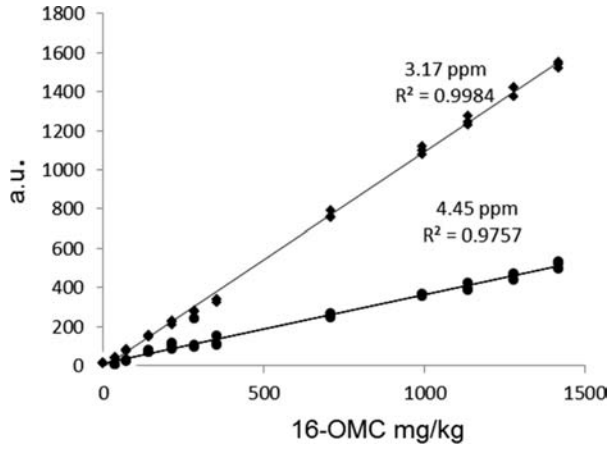


**Figure 4.** Plot of the integrals of non-overlapping signals of esterified 16-OMC (i.e., protons 17 and 21) versus nominal 16-OMC content of 12 coffee blends with increasing content of Robusta. For each mixture, the $CDCl_3$ extraction was performed in triplicate.

**Table 2. 16-OMC Content in Commercial Roasted Coffee Samples**

| | | 16-OMC (mg/kg) | |
|---|---|---|---|
| | blend | NMR[a] | DIN[a] |
| R1[b] | 100% R | 1841 (36) | 1980 (100) |
| R2[b] | 100% R | 1770 (43) | 1630 (240) |
| R3[b] | 100% R | 1490 (40) | 1008 (200) |
| CB0 | 100% R | 1442 (44) | 1428 (18) |
| CB1 | 100% R | 1739 (14) | 1450 (18) |
| CB2 | A/R | 1160 (24) | 1193 (51) |
| CB3 | nd[c] | 619 (2) | 434 (9) |
| CB4 | nd | 284 (2) | 130 (40) |
| CB5 | nd | 736 (31) | 945 (100) |
| CB6 | 100% R | 1750 (7) | 1279 (230) |
| CB7 | A/R | 1537 (14) | 1135 (14) |
| CB8 | nd | 1348 (61) | 1305 (80) |
| CB9 | nd | 32 (2) | <50 |
| CB10 | nd | 591(11) | 388 (45) |

[a]Values are averages of duplicate analysis ± standard error. [b]Samples are from a single geographical origin. [c]nd = not declared.

An aspect that we have not pursued in this work but that is naturally present in the NMR analysis is the possibility to detect and to quantify also kahweol in Robusta samples. This feature may provide the opportunity to trace, on a very large number of samples, the content of kahweol in Robusta. Beside those typical of 16-OMC and kahweol, other resonances may be useful to discriminate Arabica from Robusta samples and could be used to detect the percentage of the latter in 100% Arabica commercial blends in a more precise way. Indeed, caffeine, chlorogenic acids, and other markers were used in multivariate approaches for the botanical and geographical characterization of green or exotic coffee.[20−22] Our extraction method could be applied to a large database in an untargeted metabolomics investigation.

The validation of the quantitative NMR method in conformity with the Eurachem guidelines[23] and the NMR characterization of other coffee diterpenes will constitute the grounds for further studies.

## AUTHOR INFORMATION


### Corresponding Author

*Telephone: +39-049-827-5742. Fax: +39-049-8275050 and/or 0498275135. E-mail: elisabetta.schievano@unipd.it.


### Notes

The authors declare no competing financial interest.

## ABBREVATIONS USED

16-OMC, 16-*O*-methylcafestol; DMF, *N*,*N*-dimethylformamide

## REFERENCES


(1) Deutsches Institut für Normung e.V. (DIN). *Standard DIN 10779, Analysis of Coffee and Coffee Products—Determination of 16-O-Methyl Cafestol Content of Roasted Coffee—HPLC Method*; DIN: Berlin, Germany, 2011.

(2) D'Amelio, N.; De Angelis, E.; Navarini, L.; Schievano, E.; Mammi, S. Green coffee oil analysis by high-resolution nuclear magnetic resonance spectroscopy. *Talanta* **2013**, *110*, 118−127.

(3) Kölling-Speer, I.; Kurzrock, T.; Speer, K. Diterpenes in green coffees harvested in different years. *Proceedings of the 21th ASIC Colloquium*; Montpellier, France, Sept 11−15, 2006; pp 197−199.

(4) Naidoo, N.; Chen, C.; Rebello, S. A.; Speer, K.; Tai, E. S.; Lee, J.; Buchmann, S.; Koelling-Speer, I.; van Dam, R. M. Cholesterol-raising diterpenes in types of coffee commonly consumed in Singapore, Indonesia and India and associations with blood lipids: A survey and cross sectional study. *Nutr. J.* **2011**, *10*, 48.

(5) Martin, M. J.; Pablos, F.; Gonzalez, A. G.; Valdenebro, M. S.; Leon-Camacho, M. Fatty acid profiles as discriminant parameters for coffee varieties differentiation. *Talanta* **2001**, *54*, 291−297.

(6) Gonzalez, A. G.; Pablos, F.; Martin, M. J.; Leon-Camacho, M.; Valdenebro, M. S. HPLC analysis of tocopherols and triglycerides in coffee and their use as authentication parameters. *Food Chem.* **2001**, *73*, 93−101.

(7) Carrera, F.; Leòn-Camacho, M.; Pablos, F.; Gonzalès, A. G. Authentication of green coffee varieties according to their sterolic profile. *Anal. Chim. Acta* **1998**, *370*, 131−139.

(8) Mariani, C.; Fedeli, E. Sterols of coffee grain of Arabica and Robusta species. *Riv. Ital. Sostanze Grasse* **1991**, *68*, 111−115.

(9) Valdenebro, M. S.; Leòn-Camacho, M.; Pablos, F.; Gonzalès, A. G.; Martin, M. J. Determination of the Arabica/Robusta composition of roasted coffee according to their sterolic content. *Analyst* **1999**, *124*, 999−1002.

(10) Pacetti, D.; Boselli, E.; Balzano, M.; Frega, N. G. Authentication of Italian espresso coffee blends through the GC peak ratio between kahweol and 16-*O*-methylcafestol. *Food Chem.* **2012**, *135*, 1569−1574.

(11) Silva, J. A.; Borges, N.; Santos, A.; Alves, A. Method validation for cafestol and kahweol quantification in coffee brews by HPLC−DAD. *Food Anal. Methods* **2012**, *5*, 1404−1410.

(12) Pizarro, C.; Esteban-Diez, I.; Gonzalez-Saiz, J. M. Mixture resolution according to the percentage of robusta variety in order to detect adulteration in roasted coffee by near infrared spectroscopy. *Anal. Chim. Acta* **2007**, *585*, 266−276.

(13) Keidel, A.; von Stetten, D.; Rodrigues, C.; Maguas, C.; Hildebrandt, P. Discrimination of green Arabica and Robusta coffee beans by Raman spectroscopy. *J. Agric. Food Chem.* **2010**, *58*, 11187−11192.

(14) Wermelinger, T.; D'Ambrosio, L.; Klopprogge, B.; Yeretzian, C. Quantification of the Robusta fraction in a coffee blend via Raman spectroscopy: Proof of principle. *J. Agric. Food Chem.* **2011**, *59*, 9074−9079.

(15) El-Abassy, R. M.; Donfack, P.; Materny, A. Discrimination between Arabica and Robusta green coffee using visible micro Raman spectroscopy and chemometric analysis. *Food Chem.* **2011**, *126*, 1443−1448.

(16) Christopoulos, T.; Trantakis, I.; Spaniolas, S.; Kalaitzis, P.; Ioannou, P.; Tucker, G. Dipstick test for DNA-based food authentication. Application to coffee authenticity assessment. *J. Agric. Food Chem.* **2012**, *60*, 713−717.

(17) Rastrelli, F.; Schievano, E.; Bagno, A.; Mammi, S. NMR quantification of trace components in complex matrices by band-selective excitation with adiabatic pulses. *Magn. Reson. Chem.* **2009**, *47*, 868−872.

(18) Speer, K.; Kolling-Speer, I. The lipid fraction of coffee bean. *J. Plant Physiol.* **2006**, *18*, 201−216.

(19) Scharnhop, H.; Winterhalter, P. Isolation of coffee diterpenes by means of high-speed countercurrent chromatography. *J. Food Compos. Anal.* **2009**, *22*, 233−237.

(20) Serra, F.; Guillou, C. G.; Reniero, F.; Ballarin, L.; Cantagallo, M. I.; Wieser, M.; Iyer, S. S.; Héberger, K.; Vanhaecke, F. Determination of the geographical origin of green coffee by principal component analysis of carbon, nitrogen and boron stable isotope ratios. *Rapid Commun. Mass Spectrom.* **2005**, *19*, 2111−2186.

(21) Alonso-Salces, R.; Serra, F.; Reniero, F.; Héberger, K. Botanical and geographical characterization of green coffee (*Coffea arabica* and *Coffea canephora*): Chemometric evaluation of phenolic and methylxanthine contents. *J. Agric. Food Chem.* **2009**, *57*, 4224−4235.

(22) Jumhawan, U.; Putri, S. P.; Yusianto; Marwanni, E.; Bamba, T.; Fukusaki, E. Selection of discriminant markers for authentication of Asian palm civet coffee (Kopi Luwak): A metabolomics approach. *J. Agric. Food Chem.* **2013**, *61*, 7994−8001.

(23) Eurachem. *Quantifying Uncertainty in Analytical Measurement*, 3rd ed.; Eurachem: Leoben, Austria, 2012; https://www.eurachem.org/index.php/publications/guides/quam.

proteasomal degradation of the modified protein, whereas the K63 polyubiquitin chain or linear polyubiquitination can promote the protein−protein interactions and signal transduction.[7] On the other hand, the ubiquitination process can be reversed by DUB enzyme, which, through cleaving the ubiquitin chains from their substrates, leads to the termination of NF-κB signaling.[8]

Among the known DUBs, TNF-α-induced protein 3 (TNFAIP3), also known as A20, has been recognized as a potent modulator of NF-κB signaling. TNFAIP3 has typical deubiquitinating activity with its ovarian tumor (OTU) domain at its amino terminus. Also, a carboxy-terminal zinc finger (ZnF) domain endows it with E3 ubiquitin ligase activity.[9] In most cell types, TNFAIP3 serves as a negative feedback regulator of the NF-κB-driven response, either by directly removing ubiquitin moieties from the signaling molecule of TRAF6 or through binding to TRAF6 to prevent its interactions with Ubc13, an E2-conjugating enzyme.[10,11] Consequently, TNFAIP3-null cells appear to be highly activated and secrete excessive pro-inflammatory cytokines. TNFAIP3-deficient mice die prematurely from multiorgan inflammation. Moreover, the clinical relevance of TNFAIP3 is underscored by the fact that a loss-of-function mutation within the TNFAIP3 gene is closely associated with certain inflammatory and autoimmune diseases, such as rheumatoid arthritis (RA), systemic lupus erythematosus (SLE), inflammatory bowel disease (IBD), psoriasis, and type I diabetes.[12,13]

In the respiratory system, maintaining TNFAIP3 levels is essential for tissue homeostasis. TNFAIP3 acts as a checkpoint to prevent the production of the pro-inflammatory cytokine interleukin-8 (IL-8) and down-regulate TLR2- and TLR4-induced inflammation in healthy human bronchial airway epithelial cells.[14] Loss of TNFAIP3 resulted in the amplification of pro-inflammatory responses and exaggerated lung inflammation and injury, and its levels showed to be negatively associated with the number of inflammatory cells infiltrated and the levels of pro-inflammtory cytokines.[15] Recently, a study showed that TNFAIP3 levels were substantially lower in patients with cystic fibrosis (CF), a type of lung disease with intrinsically dysregulated inflammation, and that TNFAIP3 levels were proportional to forced expiratory volume in 1s (FEV1), indicative of lung function. Additionally, a nonfunctional form of TNFAIP3 has been found in inflamed airway epithelial cells, which was unable to colocalize with TRAF6 and failed to prevent or diminish NF-κB activation.[16] Consistent with these findings, the clinic data critically implicated aberrant expression or dysfunction of TNFAIP3 in the pathogenesis of inflammatory lung disorders such as asthma, CF, and chronic obstructive pulmonary disease (COPD).[17] Thus, TNFAIP3 is emerging as a potent diagnostic marker as well as therapeutic target in these diseases, and the endeavor to search for novel TNFAIP3-targed treatment is currently under way.

Daphnetin is a natural product extracted from plants of the genus *Daphne* and belongs to the coumarin family. It has been shown to possess a variety of biological properties, including anti-inflammation, antihypoxia, antimicrobial, and anticancer properties.[18,19] The traditional Chinese medicine Zushima, primarily composed of daphnetin, has been used to treat inflammatory diseases in clinic. It can alleviate collagen-induced arthritis as revealed by suppressed synovial hyperplasia, joint destruction, and chondrocyte degeneration, and accompanying this, the infiltration of inflammatory cells and production of interleurin 1β (IL-1β), tumor necrosis factor α (TNF-α), and macrophage migration inhibitory factor (MIF) were significantly repressed by daphnetin treatment.[20] In addition, daphnetin exhibited the ability to blunt the differentiation of inflammatory Th17 and Th1 cells and promote the development of regulatory T (Treg) cells, thus alleviating T cell-mediated immunopathology in the inflammatory autoimmune disorders.[21] It is noted that daphnetin has been used to treat inflammatory airway diseases such as bronchitis and demonstrated to be a promising alternative for these disorders with little side effect.[18] However, the protective efficacy of daphnetin in inflammatory pulmonary disorders has not yet been fully explored and, particularly, the ability of daphnetin to antagonize the inflammatory signaling and the molecular mechanism underlying its action remain to be determined.

In the present study, we, for the first time, reveal the significant protective effect of daphnetin against lung inflammation and injury. By impairing the key signaling events involved in NF-κB activity, daphnetin negatively regulated the TLR-triggered inflammatory response. Moreover, TNFAIP3 was identified as a target of daphnetin to modulate the K63-linked ubiquitination of TRAF6 and thereby NF-κB-driven pro-inflammatory signaling. This finding provides an insight into the action mode of daphnetin in the inflammatory context and has profound implications for its use as a protective or even therapeutic agent in ALI and related compliance.

## MATERIALS AND METHODS

**Reagents.** Daphnetin (7,8-dihydroxycoumarin), with a purity >99.4%, was obtained from Tauto Biotech Co., Ltd. (Shanghai, China). Dimethyl sulfoxide (DMSO), LPS (055:B5), 3-(4,5-dimethylthiazol-2-yl)-2,5-diphenyltetrazolium bromide (MTT), Griess reagent, and 4′,6-diamidino-2-phenylindole (DAPI) were purchased from Sigma-Aldrich Co. (St. Louis, MO, USA). All antibodies, unless otherwise indicated, were obtained from Cell Signaling. Antibodies against β-actin were obtained from Sigma-Aldrich, and the pRL-TK plasmids were purchased from Promega. All cell culture reagents and media were obtained from Life Technologies.

**Cell Lines and Generation of Peritoneal Macrophages.** The A549 and RAW264.7 cell lines were obtained from the American Type Culture Collection and grown in RPMI 1640 medium containing 10% (v/v) heat-inactivated fetal bovine serum. To prepare murine peritoneal macrophages, 8−10-week-old mice were injected intraperitoneally (ip) with 3% thioglycolate broth. After 72 h, the peritoneal cells were harvested, and macrophages were enriched by quick adhesion. All cells were grown at 37 °C in a humidified atmosphere in the presence of 5% $CO_2$.

**Cell Viability Assay.** Cell viability was determined using an MTT reduction assay. In brief, RAW264.7 cells were treated with various concentrations of daphnetin or vehicle for 24 or 48 h. Then the culture supernatants were replaced with MTT (0.5 mg/mL) and the resulting dark blue crystals were dissolved with DMSO. The absorbance values were read at 550 nm and obtained by replication in at least three independent experiments.

**RNA Isolation and Quantitative RT-PCR.** Total RNA was isolated using TRIzol reagent (Takara) following the manufacturer's protocol. SYBR Green PCR Master Mix (Bio-Rad) was used to detect mRNA levels, and relative expression levels were determined by applying the ΔΔCt method using β-actin as the endogenous control. The following primers were used: TNF-α, forward 5′-AAGGCCGGGGTGTCCTGGAG-3′ and reverse 5′-AGGCCAGGTGGGGACAGCTC-3′; IL-6, forward 5′-CCACTTCACAAGTCGGAGGCTTA-3′ and reverse 5′-AGTGCATCATCGTTGTTCATAC-3′; IL-1β, forward 5′-AACCTCACCTACAGGGCGGACTTCA-3′ and reverse 5′-TGTAATGAAAGACGGCACACC-3′; and inducible nitric oxide synthase (iNOS), forward 5′-CCCTTCCGAAGTTTCTGGCAGCAGCG-3′ and reverse 5′-GGCTGTCAGAGCCTCGTGGCTTTGG-3′.

**Bronchoalveolar Lavage, Differential Cell Counts, and Histological Analysis.** Briefly, the trachea was exposed through a midline incision and cannulated with a sterile 22-gauge needle. Bronchoalveolar lavage fluid (BALF) was obtained by flushing three times with 1 mL of 0.5 mM EDTA/PBS. After centrifugation, the supernatants were stored at −80 °C until use. The total cell numbers in the BALF were counted with a hemocytometer, and differential cell counts were determined on cytospin preparations with Diff-Quick staining (IMEB). Alternatively, neutrophils and macrophages in the BALF were assessed through immunostaining and subsequent flow cytometry. For histological analyses, mouse lung samples were washed thoroughly in PBS, fixed in 4% (wt/vol) formalin, and embedded in paraffin; 5 $\mu$M sections were then stained with hematoxylin and eosin (H&E) using standard procedures.[22]

**Plasmid Transfection and Luciferase Reporter Assays.** To investigate NF-$\kappa$B reporter activity, the mouse PGL3-NF-$\kappa$B reporter plasmid was transfected into peritoneal macrophages or RAW264.7 cells using Jet-ENDO transfection reagents (Polyplus). After 24 h, the cells were treated with DMSO or daphnetin at different concentrations (20, 40, 60, 80, and 100 $\mu$M, respectively) followed by stimulation with LPS (100 ng/mL) for 6 h. The cells were then collected and lysed for dual luciferase assays (Promega).

**RNA Interference.** Small interference RNA (siRNA) targeting TNFAIP3 and scramble siRNA were synthesized by GIMA Co. (Shanghai, China). siRNA duplexes were transfected into macrophages using INTERFERin-HTS according to standard protocols (Polyplus). For the in vivo knockdown of TNFAIP3, 60 $\mu$g of siRNA per mouse was administered intratracheally.[23] The knockdown efficacy was determined through RT-PCR or Western blotting.

**Animal Experiments.** All procedures were conducted in accordance with university guidelines and approved by the ethical committee for Animal Care and the Use of Laboratory Animals, Hangzhou Normal University. The mice were anesthetized ip with ketamine hydrochloride (100 mg/kg) and xylazine (10 mg/kg). Daphnetin was injected at 5 mg/kg (ip) for a total of 100 $\mu$L into each mouse, and 1 h later, a total volume of 50 $\mu$L of PBS or LPS (1 mg/kg) was instilled intratracheally.[24] For mortality studies, C57BL/6 mice were injected with daphnetin (5 or 10 mg/kg, ip) or DMSO 1 h before LPS injection (25 mg/kg, ip). Survival was monitored twice daily for up to 6 days.

**Determination of Cytokines and MPO Levels.** The levels of TNF-$\alpha$, IL-6, and IL-1$\beta$ were measured in the culture supernatants or BALF by ELISA (R&D Systems). Lung myeloperoxidase (MPO) levels were determined using mouse MPO ELISA (Hycult Biotech) following the manufacturer's instructions.[25]

**Immunofluorescence Staining and Confocal Microscopy.** RAW264.7 cells, seeded on slides at 30% confluence, were pretreated with daphnetin (160 $\mu$M) or DMSO 30 min prior to LPS stimulation. After the indicated time, the cells were collected, fixed with 100% methanol, washed, and permeabilized in 0.2% saponin. Upon blocking with 5% bovine serum, the cells were stained with primary rabbit anti-p65 overnight at 4 °C and then stained with goat anti-rabbit IgG conjugated to Texas Red (Invitrogen). The nuclei were labeled with DAPI (Invitrogen). The cells were finally mounted in Vectashield and detected through fluorescence confocal microscopy (LSM confocal microscope, Carl Zeiss, Inc.).[26]

**Immunoprecipitation and Immunoblotting.** Briefly, cell lysates were prepared, and the protein concentrations were determined using a bicinchoninic acid (BCA) protein assay (Thermo Fisher Scientific). For the immunoprecipitation of polyubiquitinated proteins with linkage-specific Abs, the cells were lysed at room temperature in buffer containing 1% Triton-X-100, 6 M urea, and 2 mM *N*-ethylmaleimide (NEM). Cell lysates were precleared and then incubated overnight with a specific primary antibody, followed by the incubation of protein A/G plus agarose beads. After extensive washing, the bead-bound complexes and cell lysates were resolved on 10% SDS-PAGE gels and finally immunoblotted with the appropriate monoclonal antibodies.[27] Targeted proteins were visualized using an ECL Western blotting kit (Millipore).

**Statistical Analyses.** The data are presented as the mean ± SD of independent experiments. The statistical significance between two groups was analyzed using Student's *t* test. Survival data were analyzed with the Kaplan−Meier method and the log-rank test. Differences with a *p* value of ≤0.05 were considered significant.

## RESULTS

**Daphnetin Confers Protection against LPS-Induced Lung Inflammation and Injury.** Daphnetin is a natural plant-derived product with the chemical structure of 7,8-dihydroxycoumarin, which was shown to have no notable effect on cell survival as revealed in our study (Figure 1). It has long been used in the treatment of inflammatory disorders and is therefore considered to have the potential to regulate the immune response. To further understand the biological activity of daphnetin, we used a prototypical model of LPS-induced lung inflammation and injury, which has been widely used to investigate the mechanisms of ALI.[28,29] Histopathological examination revealed that, compared with the control mice, the animals pretreated with daphnetin exhibited lessened alveolar damage and inflammation, characterized by reduced interstitial edema and debris deposit, less inflammatory cell recovery, and decreased MPO activity in lung tissues (Figure 2A−C). Moreover, protein leakage into the BALF and production of pro-inflammatory cytokines including IL-6, TNF-$\alpha$, and IL-1$\beta$ were repressed by daphnetin (Figure 2D,E). On the basis of these results, daphnetin appeared to protect against endotoxin-induced lung inflammation and injury.

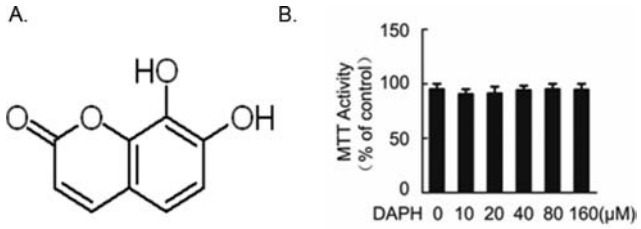


**Figure 1.** Chemical structure and effect of daphnetin on macrophage survival: (A) chemical structure of daphnetin; (B) viability of RAW264.7 cells that were treated with daphnetin (DAPH) at the dose indicated for 48 h, analyzed by the MTT assay. Data represent the mean ± SD of three independent experiments.

To further understand its protective role in the inflammatory setting, we evaluated the effect of daphnetin in sepsis-induced mortality. The mice were preinstilled with daphnetin (5 or 10 mg/kg, ip) or vehicle and then challenged with lethal doses of LPS. Animal survival was monitored for up to 6 days. As shown in Figure 2F, the mice treated with daphnetin exhibited significantly prolonged survival compared with the animals pretreated with the vehicle, and greater protection was conveyed by daphnetin at the higher dose relative to the lower dose.

**Daphnetin Negatively Regulates the Inflammatory Response.** Given the importance of macrophages in the pathogenesis of lung inflammation and injury, we then assessed the effect of daphnetin in the LPS-stimulated macrophage response. As expected, LPS stimulation in macrophages caused a remarkable production of pro-inflammatory cytokines, including IL-6, TNF-$\alpha$, and IL-1$\beta$, at the mRNA and protein levels, which nevertheless was significantly repressed by

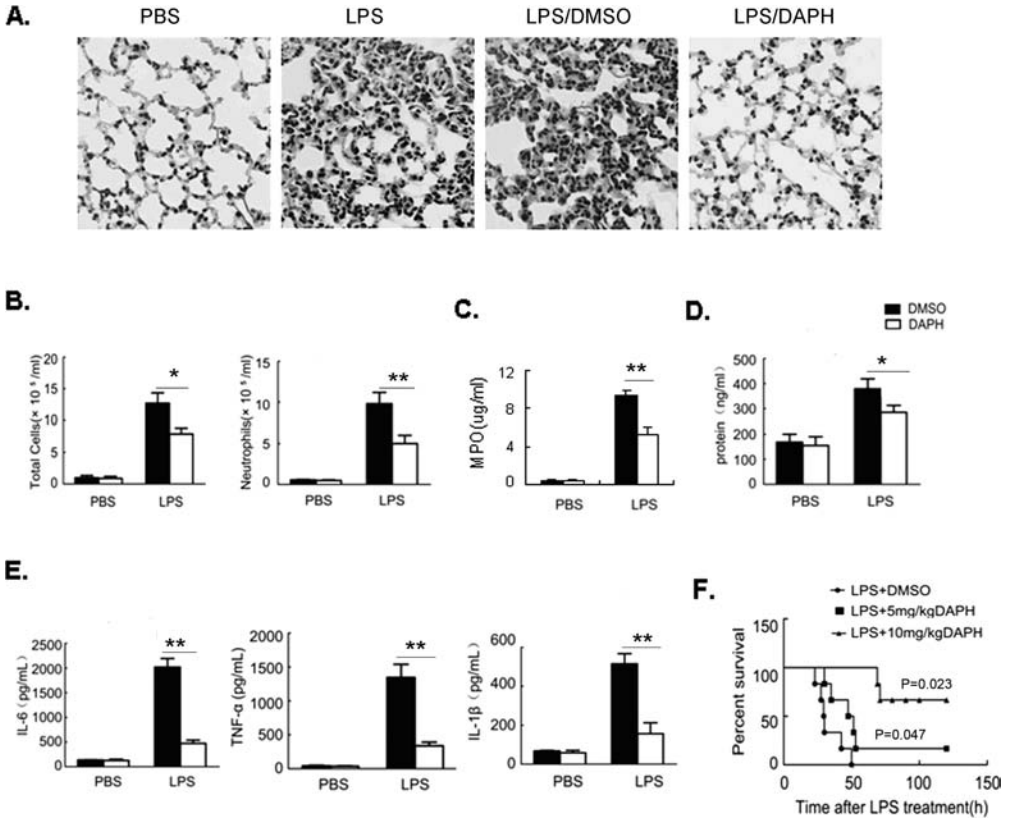


**Figure 2.** Daphnetin renders the mice resistant to LPS-induced inflammation and acute lung injury. (A–E) Age- and sex-matched C57BL/6 mice (5 mice/group) were pretreated with DAPH (5 mg/kg, ip) or DMSO as a vehicle and then intratracheally challenged with LPS (1 mg/kg) or PBS. Twelve hours later the animals were sacrificed for the analysis: (A) representative H&E staining of lung tissues; (B) BAL fluid cell recovery; (C) MPO activity of lung tissues; (D) protein and (E) cytokine levels in BAL fluid. Original magnification, ×200. All results are expressed as the mean ± SD: (∗)$p < 0.05$ and (∗∗)$p < 0.01$ by Student's $t$ test. (F) Mice were injected with DAPH (5 or 10 mg/kg, ip) or DMSO 1 h before LPS administration (25 mg/kg, ip). Kaplan–Meier survival plots are depicted, and comparisons were made with the log-rank statistic ($n$ = 10 per group).

daphnetin in a dose- and time-dependent manner (Figure 3A,B). Because nitric oxide (NO) is a well-known mediator in ALI pathogenesis, we examined the expression of inducible nitric-oxide synthase (iNOS), the enzyme required for NO production. The results showed a profound reduction in iNOS expression in daphnetin-treated macrophages (Figure 3C), suggesting a general effect of daphnetin on the production of the inflammatory mediators. Unexpectedly, expression of IL-10, an anti-inflammatory cytokine, was also found to be repressed (Figure 3D). Furthermore, we extended the study to A549 cells, human alveolar epithelial cells critically involved in lung inflammation. The results showed that LPS-induced expression of IL-6 and TNF-$\alpha$ in A549 cells was also markedly suppressed by daphnetin (Figure 2E). Together, the data defined a crucial role for daphnetin in the negative regulation of TLR-triggered innate and inflammatory responses.

**Daphnetin Modulates NF-κB and MAPK Signaling.** It is known that NF-κB and MAPK signaling are essential for the expression of pro-inflammatory genes in response to TLR stimulation. To investigate the molecular mechanism through which daphnetin controls inflammatory cytokine production, we analyzed the key signaling events involved. As shown in Figure 4A, phosphorylation of MAPKs, including p38, ERK, and JNK kinases, was down-regulated by daphnetin. In addition, daphnetin suppressed LPS-stimulated NF-κB activation, and the critical signaling events including phosphorylation of RelA/NF-κB, phosphorylation and degradation of IκBα, and activation of the upstream kinase IKK were substantially impaired by daphnetin treatment in murine macrophages (Figure 4B–D). Consistent with these results, NF-κB-driven transcriptional activity in RAW264.7 and A549 cells was also repressed by daphnetin in a dose-dependent manner (Figure 4E). Additionally, considering that derepression of Rel/NF-κB from the restraint of IκBα and the translocation of RelA into the nuclear constitutes the key step for the pro-inflammatory gene transcription, we thus detected the impact of daphnetin on LPS-initiated nuclear translocation of RelA. The result clearly showed that a robust nuclear translocation of RelA induced by LPS was remarkably affected in daphnetin-treated macrophages, particularly at the early stage of activation (Figure 5A,B). Together, daphnetin profoundly modulated the key signals required for the expression of pro-inflammatory genes, which might contribute to its anti-inflammatory property and protective effect in ALI.

**TNFAIP3 Is Targeted by Daphnetin during the Inflammatory Response.** Next, we sought to obtain further insights into the mechanism used by daphnetin to regulate NF-κB and MAPK signaling. TAK1, a member of the MAP3 kinase family, is presumed to be a key intermediate that transmits signals to the downstream IKK and MAPKs.[30] Our present study showed that TAK1 phosphorylation was remarkably attenuated in daphnetin-treated macrophages as compared with that in the control cells (Figure 6A). We then questioned whether TRAF6, which is known to associate with TAK1 and has the potential to regulate its activity, was affected by daphnetin in LPS-stimulated macrophages. TRAF6 is a RING

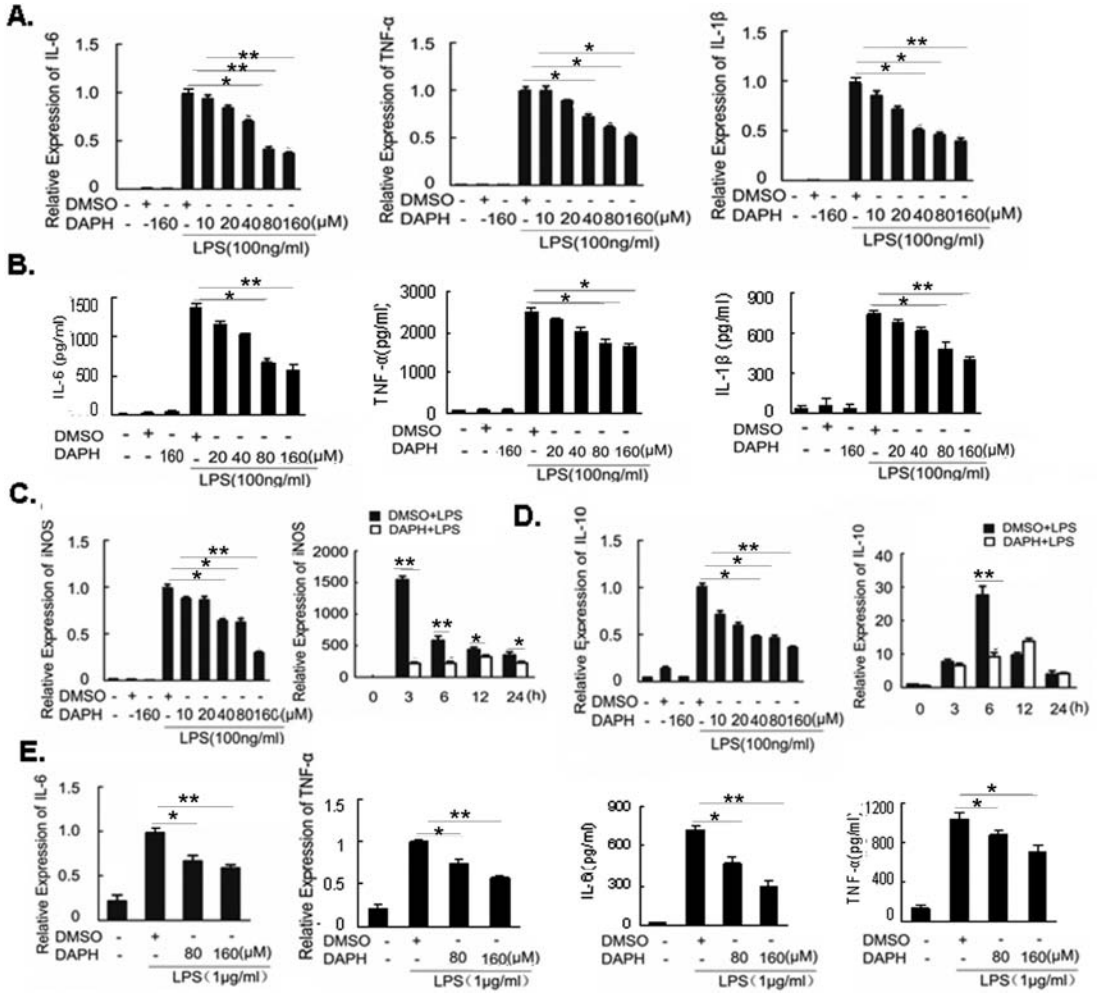


**Figure 3.** Daphnetin inhibits LPS-triggered production of pro-inflammatory cytokines. (A–D) RAW264.7 cells were pretreated with DMSO or DAPH for 30 min at the dose indicated and followed by LPS (100 ng/mL) stimulation for 6 h (for the mRNA) or 24 h (for the protein). Expression of IL-6, TNF-$\alpha$, and IL-1$\beta$, at the mRNA level (A) and protein level (B) was assessed by quantitative real-time PCR and ELISA, respectively. (C, D) iNOS and IL-10 expression was time- and dose-dependently inhibited by daphnetin. (E) Production of IL-6 and TNF-$\alpha$ in A549 cells was induced by LPS with pretreatment of DAPH (160 $\mu$M) or DMSO. Data are the mean ± SD of three independent experiments: (*) $p < 0.05$ and (**) $p < 0.01$ by Student's $t$ test.

domain ubiquitin ligase that mediates the assembly of K63-linked poly-Ub chains required for TAK1 and the subsequent IKK activation. As depicted in Figure 6B, our data showed that TRAF6 level was not altered upon daphnetin treatment. However, K63-linked ubiquitination of TRAF6 triggered by LPS was substantially suppressed in daphnetin- but not vehicle-treated cells. We next wondered what drove the daphnetin-induced modulation of TRAF6 ubiquitination. As protein ubiquitination is a dynamic process tightly regulated by ubiquitinating and deubiquitinating enzymes, our attention was focused on the impact of daphnetin on TNFAIP3, a ubiquitin-editing enzyme with the ability to cleave K63-linked polyubiquitination of TRAF6 and thereby counteract NF-$\kappa$B signaling. Indeed, in a dose- and time-dependent manner, treating macrophages with daphnetin caused a significant increase in TNFAIP3 expression, at either mRNA or protein levels (Figure 6C,D). Also, the mice pretreated with daphnetin exhibited enhanced expression of TNFAIP3 in lung tissues following LPS challenge when compared with the control animals (Figure 6E,F). The data thus implicated TNFAIP3 activity in daphnetin-mediated regulation on the inflammation and lung injury.

**TNFAIP3 Is Required for Daphnetin-Mediated Anti-inflammatory Activity.** To further relate TNFAIP3 to the action mode of daphnetin, we knocked down TNFAIP3 in macrophages using specific siRNA. As expected, TNFAIP3 deficiency in macrophages led to enhanced I$\kappa$B$\alpha$ phosphorylation and degradation (Figure 7A), indicative of augmented activation of NF-$\kappa$B activity. NF-$\kappa$B transcriptional activity in response to LPS was consistently strengthened upon TNFAIP3 loss. Strikingly, specific interference of TNFAIP3 in daphnetin-treated cells elevated NF-$\kappa$B transcriptional activity to a level comparable to that in DMSO-treated cells, indicating that daphnetin-driven down-regulation of NF-$\kappa$B activity was largely abrogated by TNFAIP3 deletion (Figure 7B). Consistent with these data, defective production of IL-6, TNF-$\alpha$, and IL-1$\beta$ upon daphnetin administration was, to varying degrees, restored by TNFAIP3 knockdown (Figure 7C,D). The data thus established the importance of TNFAIP3 in the anti-inflammatory activity of daphnetin in macrophages. Furthermore, TNFAIP3 protein in murine lungs was knocked down through the intratracheal delivery of the specific siRNA prior to daphnetin treatment, and the response of the mice to the endotoxin was evaluated.[23] As shown in Figure 8A, there

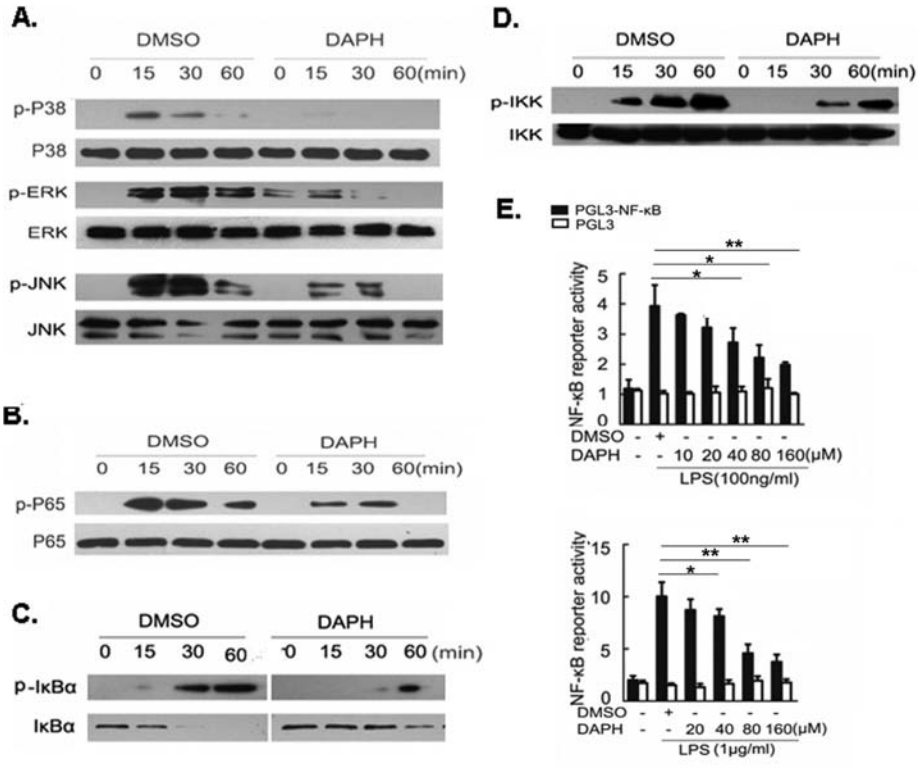


**Figure 4.** Daphnetin suppresses NF-κB-dependent signaling. Peritoneal macrophages were pretreated with either DMSO or DAPH (80 μM) 30 min prior to LPS stimulation. Levels of total and phosphorylated p38, ERK, and JNK (A), p65 (B), IκBα(C), and IKK (D) were measured by immunoblotting. Results are representative of three individual experiments. (E) NF-κB-driven promoter activity in response to LPS was analyzed in RAW264.7 cells (upper) or A549 cells (lower). Cells were transfected with pGL3-NF-kB or the control pGL3 plasmid. After 24 h of transfection, cells were pretreated with DMSO or DAPH (80 μM) and then subjected to LPS stimulation. Six hours later, cells were collected for luciferase activity analysis. Data are the mean ± SD of three independent experiments: (∗)$p < 0.05$ and (∗∗) $p < 0.01$ by Student's $t$ test.

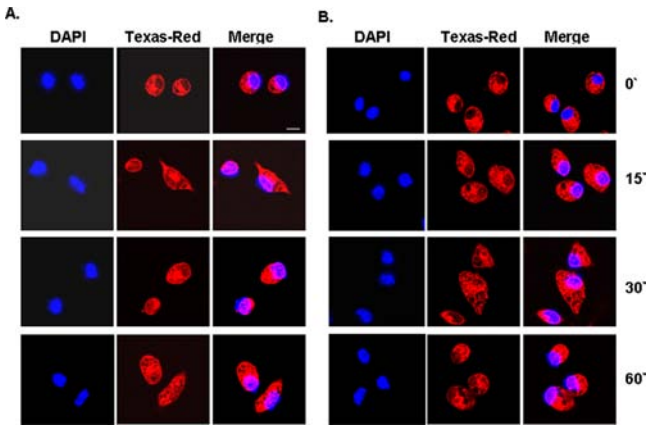


**Figure 5.** Daphnetin blocks LPS-triggered RelA/NF-κB nuclear translocation. RAW264.7 cells were pretreated with either DMSO (A) or 80 μM DAPH (B) 30 min prior to LPS stimulation. Nuclear translocation of RelA was analyzed by confocal fluorescence microscopy. Immunoreactivity of RelA is shown in red, and the nuclei are stained with DAPI (blue). Scale bar = 10 μm. Representative results from three independent experiments are depicted.

occurred about 80% less TNFAIP3 protein in the mice given TNFAIP3-specific siRNA relative to control siRNA at 48 h post delivery. The symptoms of lung inflammation and injury induced by LPS in TNFAIP3 siRNA-treated mice were significantly greater than those of their counterparts instilled with nonspecific siRNA (Figure 8B). Also, the repressed activation of p65/NF-κB by daphnetin was elevated by TNFAIP3 siRNA treatment, and production of inflammatory cytokines, protein leakage, and MPO activity showed to be exaggerated by TNFAIP3 silence in daphnetin-treated mice, as compared with the animals receiving nonspecific siRNA (Figure 8C−F). The data thus suggested that TNFAIP3-mediated negative regulation of pro-inflammatory signaling contributed substantially to the anti-inflammatory activity and protective effect of daphnetin in ALI.

## DISCUSSION

Unrestrained activation of leukocytes and persistent lung inflammation are presumed to be the major reasons for excessive lung injury or acute respiratory distress (ARDS). Despite pharmacological developments over the past several decades, inflammation-associated pulmonary diseases still result in high morbidity and mortality rates. Exploring effective treatments is therefore of critical importance. Using a prototypical model of LPS-induced inflammation and lung injury, we for the first time have established the protective effect of daphnetin in inflammatory airway disorders and suggest a novel promising therapy for these conditions. In particular, we demonstrated that daphnetin alleviated the symptoms of lung injury, blocked the infiltration of inflammatory cells, and dampened the expression of pro-inflammatory cytokines such as IL-6, TNF-α, and IL-1β, which are highly expressed in patients with severe pulmonary inflammatory diseases.[31] In addition, animals treated with daphnetin displayed a remarkable survival advantage in endotoxin shock, highlighting its beneficial effect in the inflammation-associated disorders. More impor-

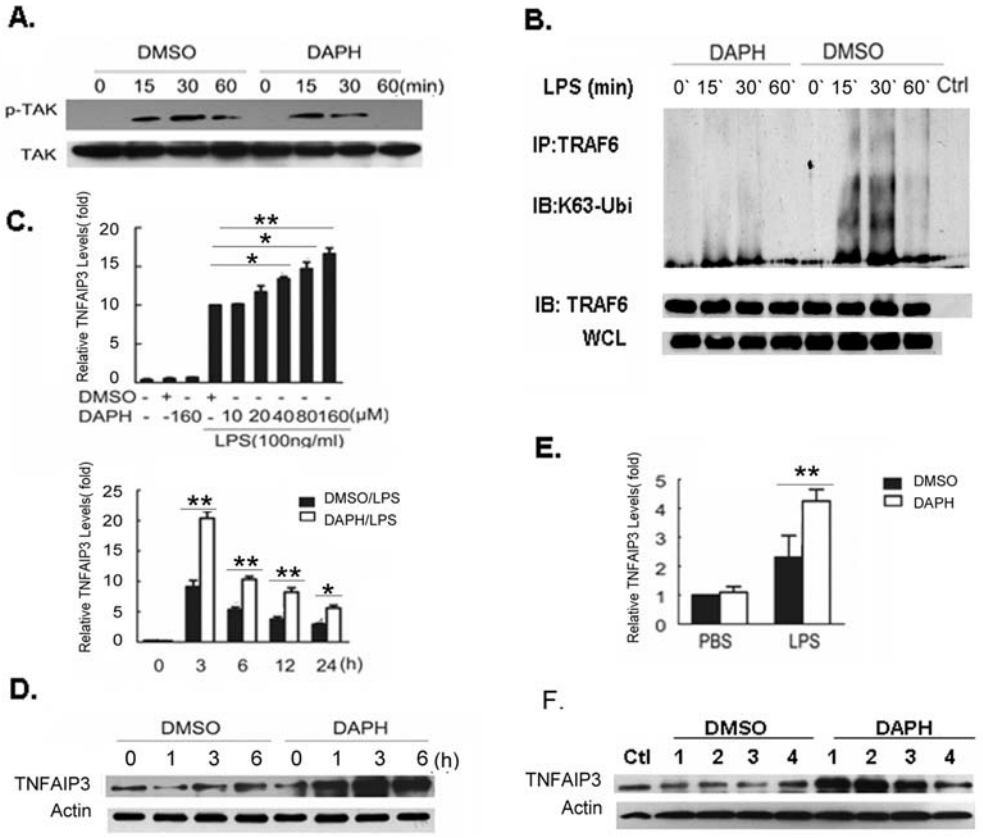


**Figure 6.** TNFAIP3 is involved in daphnetin-mediated negative regulation of NF-κB signaling. RAW264.7 cells were pretreated with DMSO or DAPH (80 μM) 30 min prior to LPS (100 ng/mL) stimulation. (A) Levels of total and phosphorylated TAK1 were measured by immunoblotting. (B) Immunoprecipitation (IP) of TRAF6 by immunoblotting (IB) for K63-linkage ubiquitin in the cells. IP with immunoglobulin (IgG) serves as an IP control (Ctrl), and IB of TRAF6 in whole cell lysates (WCL) serves as a loading control. Data were confirmed in at least three biological replicates. (C) Time- and dose-dependent induction of TNFAIP3 production by daphnetin was tested in murine peritoneal macrophages. Cells were pretreated with DMSO or DAPH at the concentration indicated (or 160 μM in the lower lane) and then stimulated with LPS. (D) TNFAIP3 protein levels upon DMSO or DAPH (160 μM) treatment were analyzed by Western blot in LPS-treated macrophages. (E) Real-time PCR and (F) Western blot analysis illustrate TNFAIP3 levels in lung tissues from LPS-challenged mice that were pretreated with DAPH or DMSO. Ctl, no treatment prior to LPS instillation. Representative results are depicted. All data are the mean ± SD of three independent experiments: (*) $p < 0.05$ and (**) $p < 0.01$ by Student's $t$ test.

tantly, we demonstrate that daphnetin targeted the DUB TNFAIP3 and selectively reversed TRAF6 ubiquitination to limit the NF-κB-driven pro-inflammatory signaling. The study thus revealed the action mode of daphnetin in counteracting inflammatory response, providing insights into the biological properties and protective applications of this naturally occurring coumarin compound.

The NF-κB signaling pathway is essential in the transcription of most pro-inflammatory cytokines and other effector molecules, thereby contributing to an excessive inflammatory response and tissue injury when uncontrollably activated. Enhanced and prolonged NF-κB activation has been described in chronic inflammatory lung diseases.[32,33] In keeping with its therapeutic effect in LPS-induced pulmonary inflammation and injury, daphnetin exhibited the ability to potentially modulate NF-κB signaling mostly by disturbance of the major events in this cascade. We have shown that daphnetin reduced the phosphorylation and degradation of IκBα, retarding the release of NF-κB and the subsequent nuclear translocation, the presumed determinant for the initiation of transcription of pro-inflammaotry genes. In addition, we revealed a role for daphnetin in modulating the TAK1/IKK axis upon LPS stimulation. TAK1 is a master kinase that mediates the activation of IKK and MAPKs.[28−30] Upon stimulation, TAK1 forms ternary complexes with its adaptor molecule TAK1-binding proteins (TABs), conveying the signaling to IKK and promoting phosphorylation and proteasome-mediated degradation of IκBα.[34] TAK1 thus becomes a key point in TLR-triggered inflammatory signaling and is vulnerable to multiple layers of modulation, particularly to the post-translational mechanism. For example, it has been revealed that phosphorylation of Thr-184/187 in the activation loop of TAK1 correlates with its kinase activity.[35] Our data showed that daphnetin significantly repressed TAK1 phosphorylation at Thr-184/187, which might account for the down-regulation of IKK and MAPKs by daphnetin. Additionally, TAK1 was previously reported to be regulated by ubiquitination, methylation, or O-GlcNAcylation.[36] The DUB cylindromatosis (CYLD) proved to physically interact with TAK1 and inhibit its ubiquitination and the resultant catalytic activity.[37] In our present study, we demonstrated that modulation of TAK1 by daphnetin in LPS-stimulated macrophages was most likely through down-regulation of TRAF6 activity. Despite the previous proposal that TAK1 exerted an effect on the activity JNK and p38 MAPKs downstream of MKK6 signaling, a recent investigation indicated that TAK1 also modulated ERK activity


dx.doi.org/10.1021/jf503667v | J. Agric. Food Chem. 2014, 62, 12315−12325

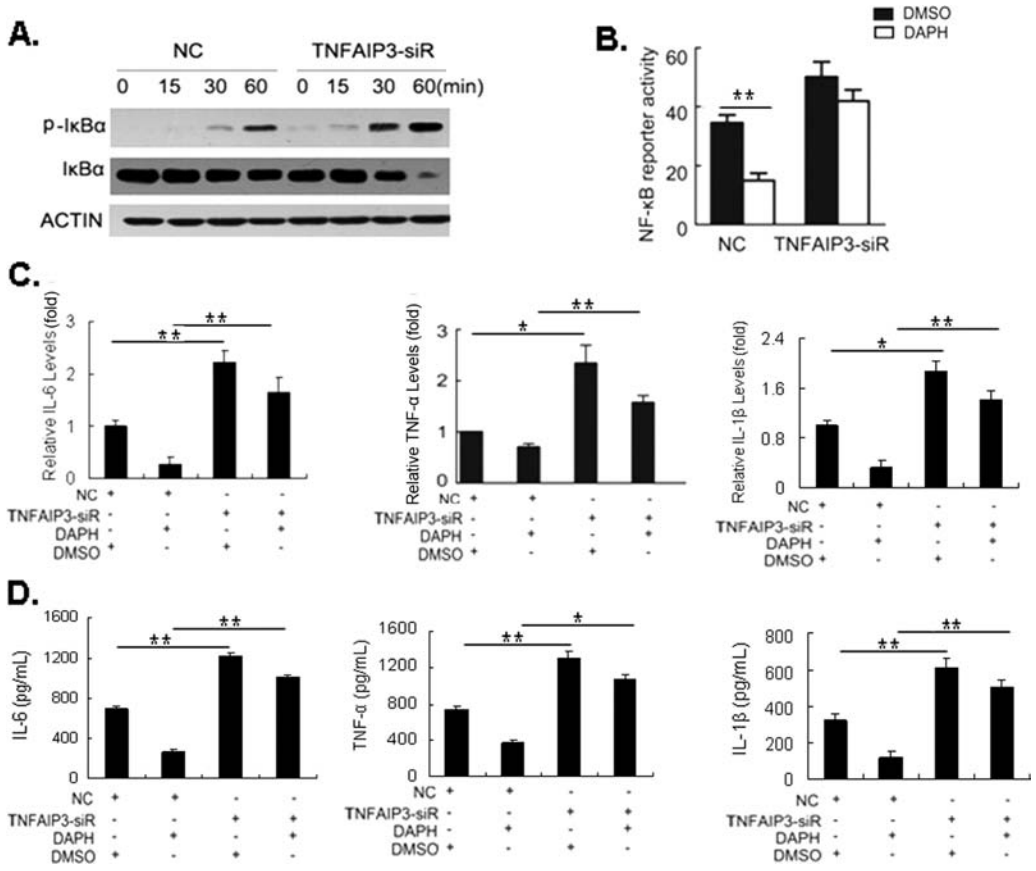


**Figure 7.** TNFAIP3 is required for anti-inflammatory action of daphnetin. (A) Macrophages were transfected with TNFAIP3 siRNA or scramble siRNA for 24 h and then subjected to LPS stimulation. Levels of total and phosphorylated IκBα were measured by immunoblotting. Results are representative of three individual experiments. (B) NF-κB-driven promoter activity in response to LPS was analyzed in DAPH- or DMSO-treated macrophages. RAW264.7 cells were transfected with pGL3-NF-κB or pGL3 for 24 h and were transfected with TNFAIP3 siRNA or scramble siRNA (NC). Twelve hours later, cells were administered DMSO or DAPH followed by LPS stimulation. (C, D) RAW264.7 cells were transfected with TNFAIP3 siRNA or scramble siRNA for 24 h and then treated with DMSO or DAPH followed by LPS stimulation. Levels of IL-6, TNF-α, and IL-1β were analyzed 12 h after the exposure. Data are the mean ± SD: (∗) $p < 0.05$ and (∗∗) $p < 0.01$ by Student's $t$ test.

via regulation of IKK-β activity.[38] This agrees with our finding that, along with the defective TAK1 activity in daphnetin-treated macrophage, LPS-induced MAPK activation was also profoundly affected. Together, our data indicated that daphnetin might act on TAK1 or the upstream kinase to disrupt IKK and MAPKs for termination of the inflammatory signaling.

Protein ubiquitination is a process that has been suggested to play important roles in a variety of cellular events, including DNA repair, signal transduction, and receptor endocytosis.[39] Modification of TRAF6 by the addition of K-63-linked polyubiquitin (polyUb) chains is essential for the TLR-induced inflammatory response. The RING type E3 ligase TRAF6 can promote K63-linked ubiquitination within the kinase domain, facilitating TAK1 phosphorylation and hence IKK-NF-κB activation and transcription of pro-inflammatory cytokine gene expression.[40] We herein revealed that daphnetin impaired K63-linked ubiquitination of TRAF6 in LPS-stimulated macrophages without altering TRAF6 protein level, thereby implicating the modulation of the nondegradative polyubiquitination of TRAF6 in the anti-inflammatory action of daphnetin. Given the key role for TRAF6 in NF-κB-driven signaling, it can be expected that aberrant expression or dysfunction of TRAF6 might cause the inflammation-associated disorders,[41] and understanding of the mechanism responsible for TRAF modulation should be helpful in the search for novel treatments. One important finding in the present study is the identification of TNFAIP3 as a target by daphnetin in regulating the inflammatory response. TNFAIP3 has been recognized as a key regulator that dampens NF-κB signaling mostly by removing K63-linked polyubiquitin chains from TRAF6.[13,42] Our study revealed that daphnetin enhanced TNFAIP3 expression in macrophages as well as in lung tissues following LPS challenge. Using TNFAIP3-specific siRNA, we showed that TNFAIP3 deletion in macrophages overcame the daphnetin-elicited suppression of IκBα degradation and, hence, NF-κB transcriptional activity. Thus, the reduced expression of IL-6 and TNF-α caused by daphnetin was almost abolished. Most strikingly, when TNFAIP3 was knocked down in the airway prior to endotoxin challenge, the protective effect of daphnetin appeared to be, at least partially, abrogated. These results thereby establish a critical role for TNFAIP3 in the protective effect of daphnetin and suggest a promising treatment for inflammatory lung disorders. Indeed, the beneficial effect of TNFAIP3 in counteracting airway inflammation has been documented. It has been found that TNFAIP3 expression in bronchial airway epithelial cells or other innate immune cells is required for the restricted NF-κB activation upon engagement of TLRs, IL-1R, IL-33R, and even high-affinity IgE receptor (FcεRI).[43,44] In addition, TNFAIP3

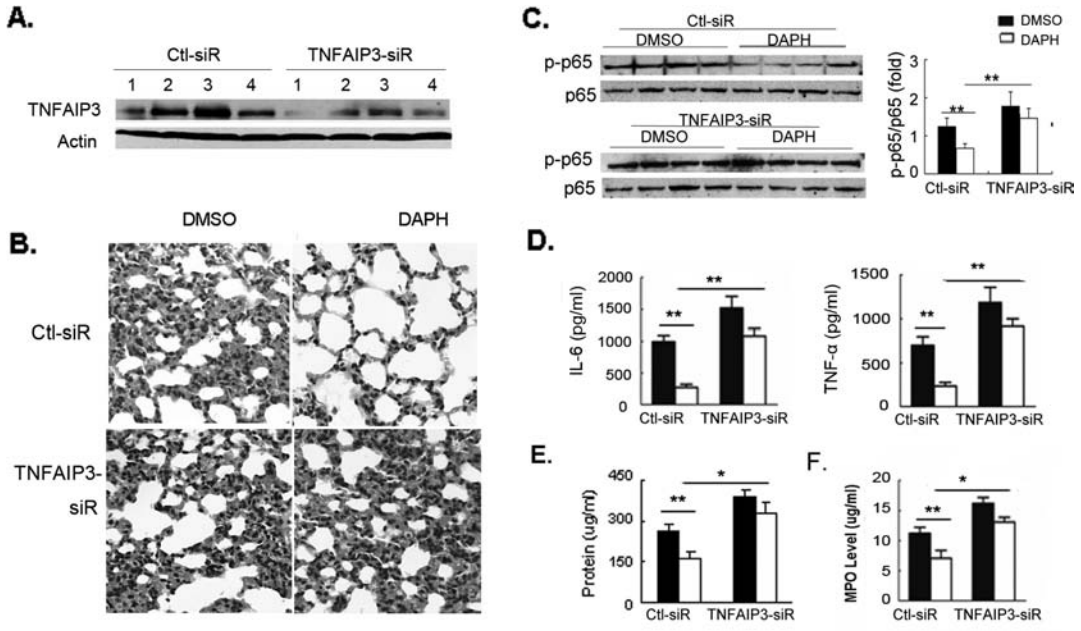


**Figure 8.** Loss of TNFAIP3 abrogates the protective effect of daphnetin in endotoxin-induced lung injury and inflammation. C57BL/6 mice were instilled with TNFAIP3 siRNA or scramble siRNA (60 $\mu$g/mice, i.t.) for 12 h and then administered DMSO or DAPH (5 mg/kg, ip) followed by intratracheal inoculation of LPS (1 mg/kg). Twelve hours later mice were sacrificed: (A) immunoblot analysis of TNFAIP3 in lungs from the mice ($n$ = 4 per group) injected with TNFAIP3 siRNA or control siRNA (Ctl-siR); (B) representative H&E staining performed on the lung sections (original magnification, ×200); (C) immunoblot analysis of phosphorylated and total p65 in lungs from the mice (relative density was obtained by densitometry of the corresponding band); (D) cytokine secretion and (E) protein lavage in BAL fluid and (F) MPO activity in lung tissues. Data are the mean ± SD: (∗) $p < 0.05$ and (∗∗) $p < 0.01$ by Student's $t$ test.

contributed substantially to the relief of lung immunopathology caused by infection of *Pseudomonas aeruginosa* or influenza virus.[45,46] Recently, a trial on TNFAIP3-targeted gene therapy was conducted in allergic asthma mice via the adenoviral transfer method, which showed that, compared with controls, the animals with enforced TNFAIP3 expression can decrease the production of mucin and inflammatory cytokines and attenuate the airway hyper-responsiveness.[47] These findings highlight the potential of TNFAIP3-targeted treatment in inflammatory lung disorders that are largely associated with exaggerated NF-$\kappa$B activity. However, the strategy by gene transfer of functional TNFAIP3 into the airway may be limited by ethical issues. Pharmaceutical induction of TNFAIP3 or members of the TNFAIP3 ubiquitin-editing complex has yet to be developed and will require a significant financial and time investment. In view of the established low toxicity, relatively low cost, and availability in herbal plants, the natural compound daphnetin and other similar plant derivatives might have implications in treating inflammatory respiratory diseases.[48,49] However, we should note that daphnetin pretreatment, in the absence of TNFAIP3, did not fully abolish its protection of the mice from LPS-induced lung injury and inflammation, suggesting that daphnetin might also act via other anti-inflammatory mechanisms.

In conclusion, we provide the first evidence to establish a beneficial effect of daphnetin in LPS-induced inflammation and pulmonary injury and elucidate a molecular mechanism through which daphnetin dampens NF-$\kappa$B-dependent inflammatory signaling. Our results might serve as a basis for the development of new approaches to lessen the severity of inflammation through use of the naturally occurring coumarin derivative.

## AUTHOR INFORMATION


### Corresponding Author

*(L.S.) Phone: +86-571-28865632. Fax: +86-571-28865632. E-mail: shi_liyun@msn.com.



### Funding

This work was supported by the National Key Scientific Research Project (2012CB911200), National Natural Scientific Funds (81270066 and 30872262), funds from the Ministry of Education (201070, NCET-08-0927), and Provincial and Municipal Funds (2011R10027, LY12H1007, 2012C37052, and 20100633B11).


### Notes

The authors declare no competing financial interest.

## ACKNOWLEDGMENTS


We thank Hongping Ying (Center of Medical Research, Hangzhou Normal University) for histological analysis of lung tissues.


## ABBREVIATIONS USED

TNFAIP3, TNF-$\alpha$-induced protein 3; ALI, acute lung injury; MAPK, mitogen-activated protein kinase; DAPH, daphnetin; DMSO, dimethyl sulfoxide; TRAF6, TNF receptor-associated factor; I$\kappa$B, inhibitor of $\kappa$B; NF-$\kappa$B, nuclear factor-$\kappa$B; iNOS, inducible NO synthase; DUB, deubiquitinating enzyme; TLR, Toll-like receptor; JNK, c-Jun NH2-terminal protein kinase; ERK, extracellular signal-regulated kinase; MPO, myeloperoxidase; WT, wild type; KO, knockout; PRR, pattern recognition receptor; BALF, bronchoalveolar lavage fluid; TNFR, tumor necrosis factor receptor; MyD88, myeloid differentiation factor88

## REFERENCES


(1) Wheeler, A. P.; Bernard, G. R. Acute lung injury and the acute respiratory distress syndrome: a clinical review. *Lancet* **2007**, *369* (9572), 1553−1564.

(2) Rubenfeld, G. D.; Caldwell, E.; Peabody, E.; Weaver, J.; Martin, D. P.; Neff, M.; Stern, E. J.; Hudson, L. D. Incidence and outcomes of acute lung injury. *N. Engl. J. Med.* **2005**, *353* (16), 1685−1693.

(3) Karin, M.; Lin, A. NF-κB at the crossroads of life and death. *Nat. Immunol.* **2002**, *3* (3), 221−227.

(4) Hoffmann, A.; Levchenko, A.; Scott, M. L.; Baltimore, D. The IκB-NF-κB signaling module: temporal control and selective gene activation. *Science* **2002**, *298* (5596), 1241−1245.

(5) Medzhitov, R.; Horng, T. Transcriptional control of the inflammatory response. *Nat. Rev. Immunol.* **2009**, *9* (10), 692−703.

(6) Hochstrasser, M. Biochemistry. All in the ubiquitin family. *Science* **2000**, *289* (5479), 563−564.

(7) Hochstrasser, M. Lingering mysteries of ubiquitin-chain assembly. *Cell* **2006**, *124* (1), 27−34.

(8) Reiley, W. W.; Zhang, M.; Jin, W.; Losiewicz, M.; Donohue, K. B.; Norbury, C. C.; Sun, S. C. Regulation of T cell development by the deubiquitinating enzyme CYLD. *Nat. Immunol.* **2006**, *7* (4), 411−417.

(9) Sun, S. C. Deubiquitylation and regulation of the immune response. *Nat. Rev. Immunol.* **2008**, *8* (7), 501−511.

(10) Mabilleau, G.; Chappard, D.; Sabokbar, A. Role of the A20-TRAF6 axis in lipopolysaccharide-mediated osteoclastogenesis. *J. Biol. Chem.* **2011**, *286* (5), 3242−3249.

(11) Shembade, N.; Ma, A.; Harhaj, E. W. Inhibition of NF-κB signaling by A20 through disruption of ubiquitin enzyme complexes. *Science* **2010**, *327* (5969), 1135−1139.

(12) Vereecke, L.; Beyaert, R.; van Loo, G. The ubiquitin-editing enzyme A20 (TNFAIP3) is a central regulator of immunopathology. *Trends Immunol.* **2009**, *30* (8), 383−391.

(13) Wang, J.; Ouyang, Y.; Guner, Y.; Ford, H. R.; Grishin, A. V. Ubiquitin-editing enzyme A20 promotes tolerance to lipopolysaccharide in enterocytes. *J. Immunol.* **2009**, *183* (2), 1384−1392.

(14) Gon, Y.; Asai, Y.; Hashimoto, S.; Mizumura, K.; Jibiki, I.; Machino, T.; Ra, C.; Horie, T. A20 inhibits toll-like receptor 2- and 4-mediated interleukin-8 synthesis in airway epithelial cells. *Am. J. Respir. Cell Mol. Biol.* **2004**, *31* (3), 330−336.

(15) Onose, A.; Hashimoto, S.; Hayashi, S.; Maruoka, S.; Kumasawa, F.; Mizumura, K.; Jibiki, I.; Matsumoto, K.; Gon, Y.; Kobayashi, T.; Takahashi, N.; Shibata, Y.; Abiko, Y.; Shibata, T.; Shimizu, K.; Horie, T. An inhibitory effect of A20 on NF-κB activation in airway epithelium upon influenza virus infection. *Eur. J. Pharmacol.* **2006**, *541* (3), 198−204.

(16) Kelly, C.; Williams, M. T.; Elborn, J. S.; Ennis, M.; Schock, B. C. Expression of the inflammatory regulator A20 correlates with lung function in patients with cystic fibrosis. *J. Cyst. Fibros.* **2013**, *12* (4), 411−415.

(17) Kelly, C.; Shields, M. D.; Elborn, J. S.; Schock, B. C. A20 regulation of nuclear factor-κB: perspectives for inflammatory lung disease. *Am. J. Respir. Cell Mol. Biol.* **2011**, *44* (6), 743−748.

(18) Venugopala, K. N.; Rashmi, V.; Odhav, B. Review on natural coumarin lead compounds for their pharmacological activity. *Biomed. Res. Int.* **2013**, *2013*, No. 963248.

(19) Fylaktakidou, K. C.; Hadjipavlou-Litina, D. J.; Litinas, K. E.; Nicolaides, D. N. Natural and synthetic coumarin derivatives with anti-inflammatory/antioxidant activities. *Curr. Pharm. Des.* **2004**, *10* (30), 3813−3833.

(20) Tu, L.; Li, S.; Fu, Y.; Yao, R.; Zhang, Z.; Yang, S.; Zeng, X.; Kuang, N. The therapeutic effects of daphnetin in collagen-induced arthritis involve its regulation of Th17 cells. *Int. Immunopharmacol.* **2012**, *13* (4), 417−423.

(21) Yao, R.; Fu, Y.; Li, S.; Tu, L.; Zeng, X.; Kuang, N. Regulatory effect of daphnetin, a coumarin extracted from *Daphne odora*, on the balance of Treg and Th17 in collagen-induced arthritis. *Eur. J. Pharmacol.* **2011**, *670* (1), 286−294.

(22) Bosmann, M.; Grailer, J. J.; Zhu, K.; Matthay, M. A.; Sarma, J. V.; Zetoune, F. S.; Ward, P. A. Anti-inflammatory effects of β2 adrenergic receptor agonists in experimental acute lung injury. *FASEB J.* **2012**, *26* (5), 2137−2144.

(23) Dela, C. C.; Liu, W.; He, C. H.; Jacoby, A.; Gornitzky, A.; Ma, B.; Flavell, R.; Lee, C. G.; Elias, J. A. Chitinase 3-like-1 promotes *Streptococcus pneumoniae* killing and augments host tolerance to lung antibacterial responses. *Cell Host Microbe* **2012**, *12* (1), 34−46.

(24) Liu, G.; Friggeri, A.; Yang, Y.; Park, Y. J.; Tsuruta, Y.; Abraham, E. miR-147, a microRNA that is induced upon Toll-like receptor stimulation, regulates murine macrophage inflammatory responses. *Proc. Natl. Acad. Sci. U.S.A.* **2009**, *106* (37), 15819−15824.

(25) Hsu, L. C.; Liang, Y. H.; Hsu, Y. W.; Kuo, Y. H.; Pan, T. M. Anti-inflammatory properties of yellow and orange pigments from *Monascus purpureus* NTU 568. *J. Agric. Food Chem.* **2013**, *61* (11), 2796−2802.

(26) Kang, Y.; Wang, F.; Lu, Z.; Ying, H.; Zhang, H.; Ding, W.; Wang, C.; Shi, L. MAPK kinase 3 potentiates Chlamydia HSP60-induced inflammatory response through distinct activation of NF-κB. *J. Immunol.* **2013**, *191* (1), 386−394.

(27) Yang, M.; Wang, C.; Zhu, X.; Tang, S.; Shi, L.; Cao, X.; Chen, T. E3 ubiquitin ligase CHIP facilitates Toll-like receptor signaling by recruiting and polyubiquitinating Src and atypical PKCζ. *J. Exp. Med.* **2011**, *208* (10), 2099−2112.

(28) Do-Umehara, H. C.; Chen, C.; Urich, D.; Zhou, L.; Qiu, J.; Jang, S.; Zander, A.; Baker, M. A.; Eilers, M.; Sporn, P. H.; Ridge, K. M.; Sznajder, J. I.; Budinger, G. R.; Mutlu, G. M.; Lin, A.; Liu, J. Suppression of inflammation and acute lung injury by Miz1 via repression of C/EBP-δ. *Nat. Immunol.* **2013**, *14* (5), 461−469.

(29) Islam, M. N.; Das, S. R.; Emin, M. T.; Wei, M.; Sun, L.; Westphalen, K.; Rowlands, D. J.; Quadri, S. K.; Bhattacharya, S.; Bhattacharya, J. Mitochondrial transfer from bone-marrow-derived stromal cells to pulmonary alveoli protects against acute lung injury. *Nat. Med.* **2012**, *18* (5), 759−765.

(30) Sato, S.; Sanjo, H.; Takeda, K.; Ninomiya-Tsuji, J.; Yamamoto, M.; Kawai, T.; Matsumoto, K.; Takeuchi, O.; Akira, S. Essential function for the kinase TAK1 in innate and adaptive immune responses. *Nat. Immunol.* **2005**, *6* (11), 1087−1095.

(31) Park, W. Y.; Goodman, R. B.; Steinberg, K. P.; Ruzinski, J. T.; Radella, F. N.; Park, D. R.; Pugin, J.; Skerrett, S. J.; Hudson, L. D.; Martin, T. R. Cytokine balance in the lungs of patients with acute respiratory distress syndrome. *Am. J. Respir. Crit. Care Med.* **2001**, *164* (10 Part 1), 1896−1903.

(32) Lim, J. H.; Stirling, B.; Derry, J.; Koga, T.; Jono, H.; Woo, C. H.; Xu, H.; Bourne, P.; Ha, U. H.; Ishinaga, H.; Xu, H.; Andalibi, A.; Feng, X. H.; Zhu, H.; Huang, Y.; Zhang, W.; Weng, X.; Yan, C.; Yin, Z.; Briles, D. E.; Davis, R. J.; Flavell, R. A.; Li, J. D. Tumor suppressor CYLD regulates acute lung injury in lethal *Streptococcus pneumoniae* infections. *Immunity* **2007**, *27* (2), 349−360.

(33) Deng, J. C.; Cheng, G.; Newstead, M. W.; Zeng, X.; Kobayashi, K.; Flavell, R. A.; Standiford, T. J. Sepsis-induced suppression of lung innate immunity is mediated by IRAK-M. *J. Clin. Invest.* **2006**, *116* (9), 2532−2542.

(34) Wang, C.; Deng, L.; Hong, M.; Akkaraju, G. R.; Inoue, J.; Chen, Z. J. TAK1 is a ubiquitin-dependent kinase of MKK and IKK. *Nature* **2001**, *412* (6844), 346−351.

(35) Yu, Y.; Ge, N.; Xie, M.; Sun, W.; Burlingame, S.; Pass, A. K.; Nuchtern, J. G.; Zhang, D.; Fu, S.; Schneider, M. D.; Fan, J.; Yang, J. Phosphorylation of Thr-178 and Thr-184 in the TAK1 T-loop is required for interleukin (IL)-1-mediated optimal NFκB and AP-1 activation as well as IL-6 gene expression. *J. Biol. Chem.* **2008**, *283* (36), 24497−24505.

(36) Sakurai, H. Targeting of TAK1 in inflammatory disorders and cancer. *Trends Pharmacol. Sci.* **2012**, *33* (10), 522−530.

(37) Ahmed, N.; Zeng, M.; Sinha, I.; Polin, L.; Wei, W. Z.; Rathinam, C.; Flavell, R.; Massoumi, R.; Venuprasad, K. The E3 ligase Itch and deubiquitinase Cyld act together to regulate Tak1 and inflammation. *Nat. Immunol.* **2011**, *12* (12), 1176−1183.

(38) Bhattacharyya, S.; Ratajczak, C. K.; Vogt, S. K.; Kelley, C.; Colonna, M.; Schreiber, R. D.; Muglia, L. J. TAK1 targeting by

glucocorticoids determines JNK and IκB regulation in Toll-like receptor-stimulated macrophages. *Blood* **2010**, *115* (10), 1921−1931.
(39) Chen, B. B.; Coon, T. A.; Glasser, J. R.; McVerry, B. J.; Zhao, J.; Zhao, Y.; Zou, C.; Ellis, B.; Sciurba, F. C.; Zhang, Y.; Mallampalli, R. K. A combinatorial F box protein directed pathway controls TRAF adaptor stability to regulate inflammation. *Nat. Immunol.* **2013**, *14* (5), 470−479.
(40) Deng, L.; Wang, C.; Spencer, E.; Yang, L.; Braun, A.; You, J.; Slaughter, C.; Pickart, C.; Chen, Z. J. Activation of the IκB kinase complex by TRAF6 requires a dimeric ubiquitin-conjugating enzyme complex and a unique polyubiquitin chain. *Cell* **2000**, *103* (2), 351−361.
(41) Song, Z.; Yao, C.; Yin, J.; Tong, C.; Zhu, D.; Sun, Z.; Jiang, J.; Shao, M.; Zhang, Y.; Deng, Z.; Tao, Z.; Sun, S.; Bai, C. Genetic variation in the TNF receptor-associated factor 6 gene is associated with susceptibility to sepsis-induced acute lung injury. *J. Transl. Med.* **2012**, *10*, 166.
(42) Boone, D. L.; Turer, E. E.; Lee, E. G.; Ahmad, R. C.; Wheeler, M. T.; Tsui, C.; Hurley, P.; Chien, M.; Chai, S.; Hitotsumatsu, O.; McNally, E.; Pickart, C.; Ma, A. The ubiquitin-modifying enzyme A20 is required for termination of Toll-like receptor responses. *Nat. Immunol.* **2004**, *5* (10), 1052−1060.
(43) Heger, K.; Fierens, K.; Vahl, J. C.; Aszodi, A.; Peschke, K.; Schenten, D.; Hammad, H.; Beyaert, R.; Saur, D.; van Loo, G.; Roers, A.; Lambrecht, B. N.; Kool, M.; Schmidt-Supprian, M. A20-deficient mast cells exacerbate inflammatory responses in vivo. *PLoS Biol.* **2014**, *12* (1), No. e1001762.
(44) Zhao, J.; Wei, J.; Mialki, R. K.; Mallampalli, D. F.; Chen, B. B.; Coon, T.; Zou, C.; Mallampalli, R. K.; Zhao, Y. F-box protein FBXL19-mediated ubiquitination and degradation of the receptor for IL-33 limits pulmonary inflammation. *Nat. Immunol.* **2012**, *13* (7), 651−658.
(45) Tiesset, H.; Pierre, M.; Desseyn, J. L.; Guery, B.; Beermann, C.; Galabert, C.; Gottrand, F.; Husson, M. O. Dietary (n-3) polyunsaturated fatty acids affect the kinetics of pro- and antiinflammatory responses in mice with *Pseudomonas aeruginosa* lung infection. *J. Nutr.* **2009**, *139* (1), 82−89.
(46) Maelfait, J.; Roose, K.; Bogaert, P.; Sze, M.; Saelens, X.; Pasparakis, M.; Carpentier, I.; van Loo, G.; Beyaert, R. A20 (Tnfaip3) deficiency in myeloid cells protects against influenza A virus infection. *PLoS Pathog.* **2012**, *8* (3), No. e1002570.
(47) Kang, N. I.; Yoon, H. Y.; Lee, Y. R.; Won, M.; Chung, M. J.; Park, J. W.; Hur, G. M.; Lee, H. K.; Park, B. H. A20 attenuates allergic airway inflammation in mice. *J. Immunol.* **2009**, *183* (2), 1488−1495.
(48) Lee, M. S.; Kwon, M. S.; Choi, J. W.; Shin, T.; No, H. K.; Choi, J. S.; Byun, D. S.; Kim, J. I.; Kim, H. R. Anti-inflammatory activities of an ethanol extract of *Ecklonia stolonifera* in lipopolysaccharide-stimulated RAW 264.7 murine macrophage cells. *J. Agric. Food Chem.* **2012**, *60* (36), 9120−9129.
(49) Kontogiorgis, C.; Detsi, A.; Hadjipavlou-Litina, D. Coumarin-based drugs: a patent review (2008−present). *Expert. Opin. Ther. Pat.* **2012**, *22* (4), 437−454.

examined the histological changes of this organ related to toxicity of nitrite. Nitrite is an intermediate compound in bacterial nitrification and denitrification processes; therefore, an imbalance in these processes can lead to a built up of nitrite in aquatic habitats.[19]

Red shrimp *P. muelleri* has a large distribution area in southwest Atlantic waters from 20° S, Espíritu Santo, Brazil, to 50° S, Santa Cruz, Argentina. This shrimp has acquired great interest on account of its potential use in culture in temperate areas; therefore, it is important to determine the optimal culture conditions to have healthy individuals.

The aim of this research was to investigate the interaction between the astaxanthin concentration in the feed and antioxidant response to exposure to nitrite in postlarvae of *P. muelleri*. For this purpose, the effects of these compounds on growth, survival, free radical scavenging, and functional morphology of the midgut gland were evaluated.

## MATERIALS AND METHODS

**Chemicals.** The DPPH standard was obtained from Aldrich. Astaxanthin (98%) was obtained from Sigma and stored in the dark at 253 K. Sodium nitrite ($NaNO_2$) and all other reagents were analytical-grade. The solvents were from Merck, and they were carefully purified following the literature method to have them free of alkenes and carbonyl compounds. All solvents used were dried conveniently.

**Experimental Animals.** Specimens of *P. muelleri* were reared from hatchery-raised postlarvae (15 ± 0.004 mg initial weight) at Nágera Station, Marine Science Department, Mar del Plata National University, Mar del Plata, Argentina. Feeds were tested in three replicate groups of 90 individuals each for 30 days. Shrimps were stocked at a density of 10 per 0.1 $m^2$ in aquaria with continuous aeration, and filtered seawater (to 5 $\mu$m) was exchanged at a rate of 50% per day. The experimental conditions were as follows: photoperiod, 12 h light/12 h dark; temperature, 20 ± 0.8 °C; salinity, 33 g $L^{-1}$; and pH, 7.

The treatments consisted of three feeds (37% protein and 7.5% lipids) supplemented with astaxanthin at concentrations of 0 mg of astaxanthin $kg^{-1}$ of diet ($C_0$), 100 mg of astaxanthin $kg^{-1}$ of diet ($C_{100}$), and 300 mg of astaxanthin $kg^{-1}$ of diet ($C_{300}$). Feeds were freshly prepared every 2 weeks to avoid carotenoid decomposition during storage (at −20 °C). Measurements confirmed the stability of the carotenoids within this period of time by scanning the spectrum between 200 and 750 nm using an ultraviolet−visible (UV−vis) spectrophotometer. Formulations of feed were made according to the chemical composition results of the byproduct meal to obtain isoproteic and isolipidic feeds.[20] All ingredients, from a local feed manufacturer, were mixed and cold-pelleted (<50 °C) by extrusion[21] and were oven-dried for 24 h at 50 °C (Table 1).

All groups of animals were fed *ad libitum* once a day. Upon completion of the feeding trial, surviving postlarvae from each treatment were weighed and transferred to glass jars with four postlarvae of each in triplicate for the static test of acute toxicity nitrite ($NO_2Na$). Nitrite test solutions were prepared with seawater at concentrations of 0, 10, 20, 40, 80, 100, 120, 160, and 200 mg $L^{-1}$. Animals were not fed during experimental trial. Shrimp behavior and death were monitored at 24 h intervals up to 96 h.

At the end of the static test, some postlarvae from each treatment and control individuals were fixed in Davidson fluid for 24 h and processed using routine techniques for light microscopy.[22] The fixed tissues were dehydrated in ascending concentrations of ethyl alcohol and embedded in paraffin. The tissue sections were cut to ∼5 $\mu$m and stained with hematoxylin and eosin (H&E).

**EPR Sample Preparation.** About 25 mg of lyophilized tissue of postlarvae from each treatment and control individuals was mixed with 1 mL of chloroform under an argon atmosphere. Each reaction mixture contained 50 $\mu$L of the tissue solution and 50 $\mu$L of DPPH ($2.8 \times 10^{-5}$ M) solution. Control or blank preparations, containing 50 $\mu$L of DPPH in chloroform solvent, remained unaltered after a long period of time. Samples for EPR measurements were prepared in quartz tubes with an internal diameter of 4 mm to achieve an adequate tuning at a constant room temperature of 293 K and were analyzed at fixed time intervals for 60 min. DPPH proved to be a very stable free radical;[9] the intensity of the signal decays with time and represents the radical−tissue reaction.

**Table 1. Percent Composition of the Control Feed**

| ingredients (g 100 $g^{-1}$) | $C_0$ |
|---|---|
| fish meal (65% crude protein)[a] | 48.0 |
| soybean meal (42% crude protein)[b] | 17.0 |
| corn starch | 20.0 |
| squid protein concentrate | 1.0 |
| wheat bran | 8.5 |
| fish oil | 2.0 |
| fish soluble | 2.0 |
| soybean lecithin | 0.5 |
| cholesterol | 0.5 |
| vitamin supplement[c] | 0.5 |

[a]Agustinier S.A., Mar del Plata, Argentina. [b]Melrico S.A., Buenos Aires, Argentina. [c]Cholecalciferol, 1.8 g/kg; thiamin, 8.2 g/kg; riboflavin, 7.8 g/kg; pyridoxine, 10.7 g/kg; calcium panthothenate, 12.5 g/kg; biotin, 12.5 g/kg; niacin, 25.0 g/kg; folic acid, 1.3 g/kg; $B_{12}$ HCl, 1.0 g/kg; ascorbic acid (Rovimix Stay C), 39.1 g/kg; menadione, 1.7 g/kg; inositol, 0.3 g/kg; choline chloride, 0.2 g/kg; $\alpha$-tocopherol acetate, 75 g/kg; and vitamin A acetate, 5.0 g/kg.

**EPR Measurements.** Potential antioxidant activity of postlarvae extracts was determined on the basis of the scavenging activity of the stable free radical DPPH using EPR with a Bruker ELEXSYS E 500 T spectrometer, operating at X-band. Amplitude signals were transformed in radical concentrations by comparing the area under the EPR absorption spectrum of the sample to that of a chloroform solution of the concentration standard, DPPH. All data were recorded at the same acquisition parameters: microwave power, 12.93 mW; microwave frequency, 9.71 GHz; modulation frequency, 100 kHz; attenuation, 12 dB; modulation amplitude, 100 mT; magnetic field center, 346.5 mT; sweep width, 10 mT; and sweep time, 60 s for three scans.[25] Measurements were repeated at least 3 times to minimize random errors. The standard plotting program Origin Pro was used to fit all sets of points whenever necessary.

**Statistical Analysis.** The analysis of variance and least significant difference tests were conducted to identify differences among means. Data were reported as the mean ± standard deviation. The concentration of nitrite lethal to 50% of the test organisms in a specified time period ($LC_{50}$) values were derived from regression of Probit-transformed mortalities against the log concentration[23] with the computer software XLSTAT 2010. The estimated Probit line and the results of a $\chi^2$ test for goodness of fit were computed. In all cases, significance was set as $p < 0.05$.[24]

## RESULTS AND DISCUSSION

After 30 days of rearing trial with feeds $C_0$, $C_{100}$, and $C_{300}$, percent weight gain ranged from 172 to 190%, with no significant differences between treatments. In most cases, there is no positive effect observed on growth of crustacean penaeoids fed with carotenoid-supplemented feeds.[26,27] Some studies showed that dietary astaxanthin has a positive effect on shrimp survival. In the study by Niu et al.,[28] growth performance and survival in *Litopenaeus vannamei* were significantly higher when fed diets with supplemental astaxanthin (100−400 mg $kg^{-1}$) related to shrimp fed with the control diet and there were no significant differences among the three dietary treatments supplemented with astaxanthin. However, in *Marsupenaeus japonicus*, similar survival between shrimp fed at different concentrations of pigmented feeds was

observed, indicating that carotenoid supplemented at 100 mg $kg^{-1}$ had no extra benefit on the survival of shrimp when compared to 50 mg $kg^{-1}$.[27]

In *P. muelleri*, survival was between 71 and 82%, with no significant differences among them, even with feeds supplemented with astaxanthin; the use of carotenoids as a nutritional additive would not be necessary for this species if they are fed diets containing animal meals, such as fish or squid, or vitamin A as a supplement.

The $LC_{50}$ values of nitrite N (mg $L^{-1}$) at 96 h estimated for shrimps by the Probit statistical method were 76.3, 89.7, and 157 mg $L^{-1}$ fed with $C_0$, $C_{100}$, and $C_{300}$, respectively (Table 2).

**Table 2. $LC_{50}$ of Nitrite to *P. muelleri* Fed with Experimental Feeds after 96 h of Exposure**

| | | confidence intervals (95%) | | |
|---|---|---|---|---|
| feed | $LC_{50}$ (mg $L^{-1}$) | low limit | upper limit | $\chi^2$ |
| $C_0$ | 76.3 | 51.1 | 61.5 | 0.28 |
| $C_{100}$ | 89.7 | 13.1 | 55.4 | 0.46 |
| $C_{300}$ | 157 | 9.4 | 57.8 | 0.51 |

Research in fish and other aquatic animals have disclosed that nitrite is a disrupter of multiple physiological functions, including ion balance, respiratory, cardiovascular, endocrine, and excretory processes.[19] Enhancement of resistance to environmental stress in penaeoid shrimp postlarvae was associated with an increase in dietary and body astaxanthin.[8] Present results showed that astaxanthin improves shrimp health in terms of resistance against nitrite stress; the median lethal concentration of nitrite increases with higher astaxanthin dietary concentrations. In the trial testing nitrite N tolerance, it was determined that the 96 h $LC_{50}$ values for shrimps fed with $C_0$, $C_{100}$, and $C_{300}$ were significantly lower than the results reported by Lin and Chen[29] for *L. vannamei* juveniles (322 mg $L^{-1}$) but higher than those found for freshwater prawn *Macrobrachium rosenbergii*, with values between 8.8 and 12.9 mg $L^{-1}$. When the toxicological effects of nitrite in aquatic ecosystems are checked, it can be concluded that seawater animals are more tolerant to nitrite toxicity than freshwater animals, probably because of the improving effect of chloride ions on the tolerance of aquatic animals.[30]

Figure 1 shows the histology of the midgut gland of *P. muelleri*. Control treatment (no addition of nitrite) shows normal morphology of the midgut gland, composed of many tubules lined by a simple epithelium with clearly differentiated cells, namely, embryonic (E), fibrillar (F), absortive (R), and blister-like (B). Individuals of all nitrite treatments showed tissular alterations compared to the initial histological conditions. The main histopathological alteration was the retraction of the epithelium within the layer of laminar connective tissue that surrounds each tubule. Some tubules had a reduction in the number and size of store lipid vacuoles, while other tubules were completely devoid of epithelial cells and with tubular lumen dilated. Both types of tubules contained sloughed epithelial cells and cellular debris. Histological structure analysis of shrimps from treatment groups with elevated nitrite levels displayed varying degrees of tissue pathology in the midgut gland. It was observed in the sample of animals fed with astaxanthin and submitted at the highest concentration of nitrite that the general structure of the organ studied was less affected than the sample of those fed $C_0$. This allows for the inference that the addition of astaxanthin in feed

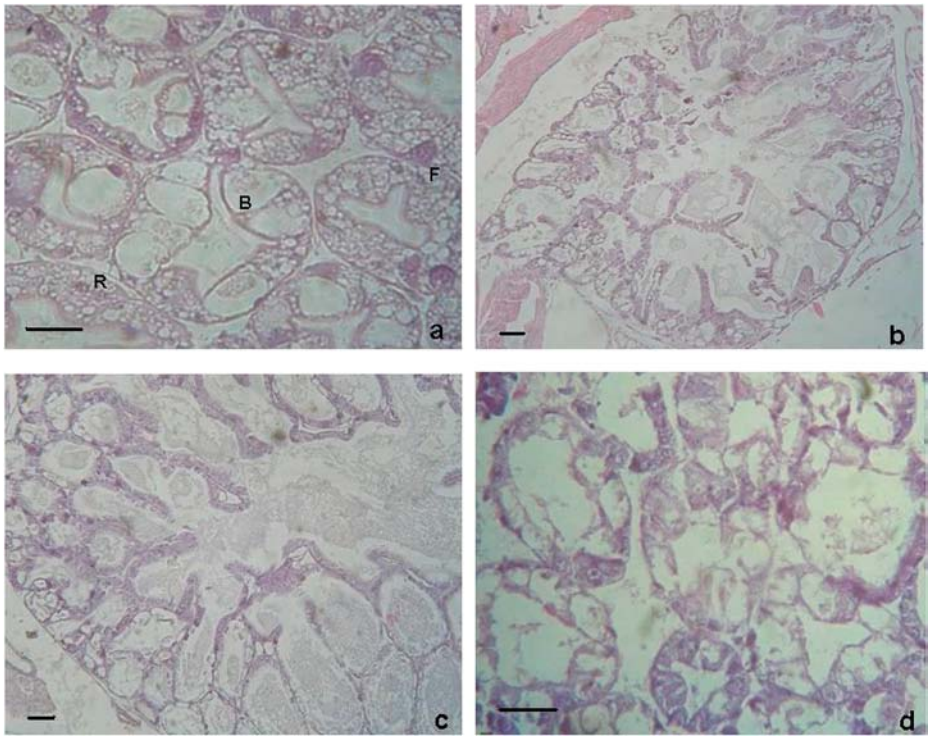


**Figure 1.** Transverse section through the midgut gland from postlarvae *P. muelleri* stained with H&E: (a) control treatment (no addition of nitrites) showing normal tubules, with B, B cell; F, F cell; and R, R cell, with a scale bar of 50 $\mu$m; (b) treatment with $C_{300}$ and 80 mg/L nitrite, with a scale bar of 200 $\mu$m; (c) treatment $C_0$ with 10 mg/L nitrite, with a scale bar of 100 $\mu$m; and (d) treatment $C_0$ with 80 mg/L nitrite, with a scale bar of 50 $\mu$m.

avoids the damage in the animals subjected to concentrations of 80 mg $L^{-1}$ nitrite. All of these changes suggest that elevated nitrite levels negatively affect the health of the shrimp even if outward signs are no evident, such as growth and survival. According to Vogt,[31] the process of desquamation in the midgut gland of *P. monodon* starts with the cell lysis, particularly R cells, and the neighboring cells protrude in small basolateral extensions, pushing the damaged cells into the tubular lumen, generating ulcerations. In the present work, degenerative desquamation of the tubular epithelium in the midgut gland of *P. muelleri* was a pathological feature observed with all nitrite concentrations tested. This alteration was also observed in marine crustaceans acclimatized to low salinities, such as *Artemesia longinaris*[32] and *P. muelleri*,[33] and freshwater prawn *Palaemonetes argentinus* under hypersaline conditions.[34] The increased desquamation produced by different stressors resulted in a high rate of cell loss that does not make possible the restitution of the damage tissue. The midgut gland plays an important role in lipid metabolism; alterations observed in R cells suggest that the shrimp not metabolizing feeds normally might be due to the enhanced energy demand in response to stress by high concentrations of nitrite.[35]

In Figure 2, the kinetics of the DPPH reaction of tissue homogenates of shrimp fed with $C_0$ and $C_{300}$ exposed at different sublethal concentrations of nitrite (0, 20, 40, and 80 mg $L^{-1}$) can be observed. Figure 2a ($C_0$) shows that free radical scavenging activity was detected at all tested nitrite concentrations; the signal decayed between 34 and 52% at 30 min. Similar kinetic curves were observed for control and 20 mg $L^{-1}$ nitrite, and the lowest activity was at 80 mg $L^{-1}$ nitrite. Higher contents of carotenoids in the feed (300 mg $kg^{-1}$) promoted production of protective substances, thereby increasing the quenching free radical in the system (Figure 2b). There exist some mechanistic explanations for the radical scavenging reactions of carotenoids *in vitro*,[36] but it is difficult to be certain which antioxidant role that carotenoids play in biological systems and the possible interference of toxic stressors, such as nitrite. The extracts of individuals exposed at 80 mg $L^{-1}$ nitrite concentration for all feed treatments showed DPPH scavenging capacity, although some differences were noted among shrimp fed with $C_0$ (43%) and those fed with $C_{100}$ and $C_{300}$, which had the greatest activity to quench DPPH (62 and 59%, respectively) (Figure 3).

Carotenoids have been reported to be the most efficient quenchers of singlet oxygen ($^1O_2$). Astaxanthin as a member of the carotenoid family reduces the oxidation rate;[37] for this reason, it plays an important role in animal health as an antioxidant through inactivation of the free radical produced from normal cellular activity and various stressors.[38] A previous work on *P. muelleri* demonstrated that the postlarval stages (with higher carotenoid concentrations) promoted a greater percentage of decay of DPPH over time, because radicals are consumed in the tissue at a speed that depends upon the amount of protective substances.[25] The long-standing controversy of function of carotenoids as antioxidants may be related to extrapolation of properties determined in homogeneous solution to more complex biological systems, where other factors, such as spatial organization and interaction between antioxidants, become important.[39] Nitrite exerts part of its toxicity through the formation of reactive oxygen intermediates (ROIs) that are able to attack almost all biomolecules present in their vicinity, causing protein modification, lipid peroxidation, and DNA damage. Activities

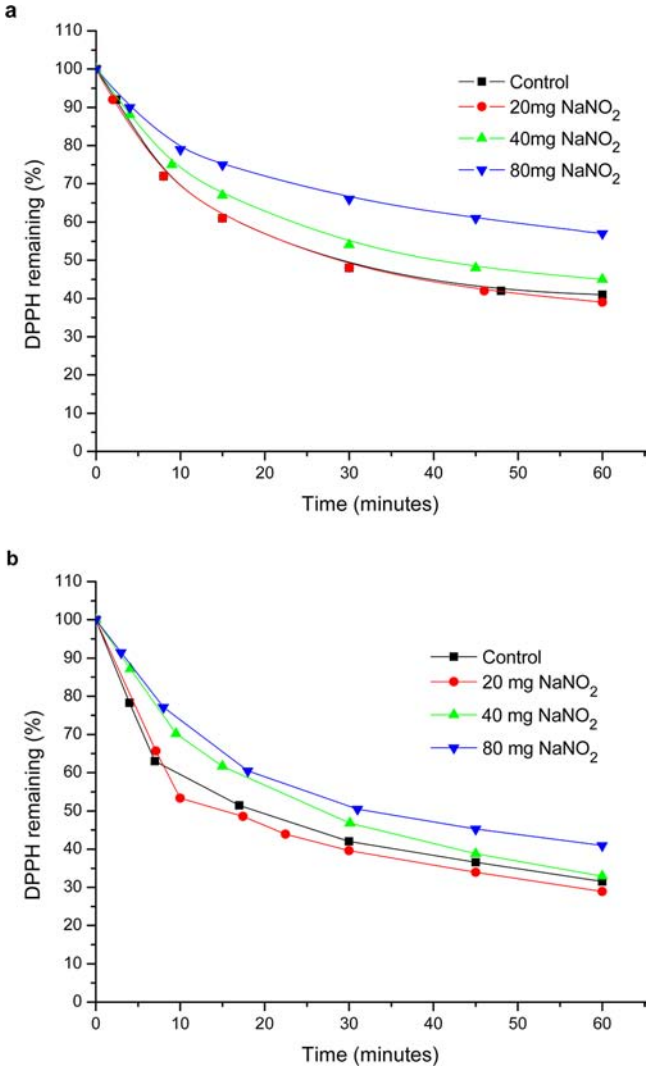


**Figure 2.** Reaction kinetics of tissue with the DPPH radical. Tissue extracts were tested for a pool of animals exposed at different concentrations of nitrite, by mixing 0.025 g of tissue with 50 $\mu$L of DPPH solution ($2.8 \times 10^{-5}$ M). All tests were conducted in triplicate, and the means are used: (a) animals fed with $C_0$ (without astaxanthin) and (b) animals fed with $C_{300}$.

of the three major antioxidant enzymes (glutathione peroxidase, superoxide dismutase, and catalase) responsible for combating the effects of ROIs diminished significantly in response to levels of ambient nitrite in *L. vannamei*.[40] Polar carotenoids, such as astaxanthin, are localized perpendicularly in the plasma membrane, consequently, allowing for the protection of the unsaturated lipids from the adverse effects of the oxidants.[41]

Results of the present work show a relationship between the carotenoid feed supplementation and the protective capacity of the homogenate against the nitrite concentration. Chien et al.[8] suggest that astaxanthin is a "semi-essential" nutrient for *P. monodon*, mainly when the animal is under physiological stress. Because an enhancement of antioxidant capacity by dietary astaxanthin in *P. muelleri* was observed. One of the most important aspects of this study is to optimize culture techniques for this species. The use of bioactive substances, such as nutritional additives, to improve performance in shrimp farming is receiving increasing attention, and efforts are being made to define the role of astaxanthin as a dietary supplement. The

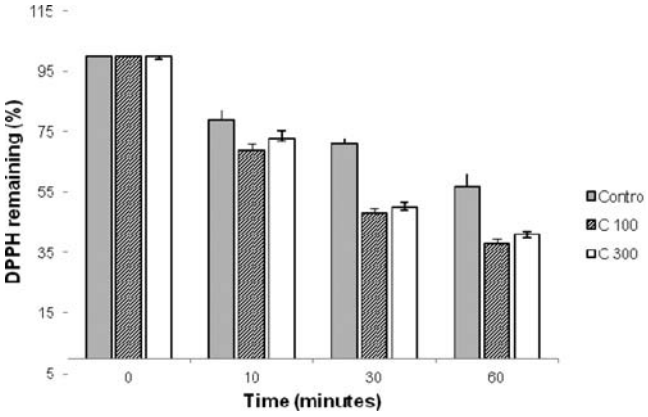


**Figure 3.** DPPH scavenging effect followed up to 60 min. Midgut gland extracts for a pool of animals exposed at 80 mg of nitrite and fed with different diets were tested by mixing 0.025 g of tissue with 100 $\mu$L of DPPH solution ($2.8 \times 10^{-5}$ M). Vertical bars represent the standard deviation of each data point ($n$ = 3).

addition of carotenoid pigments as bioactive additives, which affect physiological and molecular processes under controlled conditions, is more evident as a result of not be synthesized *de novo*. It can be concluded that these compounds act as protectors of ambient nitrite under culture conditions. Further studies are necessary to identify the free radicals that contribute to total antioxidant activities of carotenoids under different physiological conditions and to determine the relationship between their radical scavenging properties and their biological effects.

## AUTHOR INFORMATION

### Corresponding Author

*Telephone/Fax: 54-223-4753150. E-mail: acdiaz@mdp.edu.ar.

### Funding

This research was funded by Grant PIP 11201101-0515 from CONICET, Argentina.

### Notes

The authors declare no competing financial interest.

## REFERENCES

(1) Supamattaya, K.; Kiriratnikom, S.; Boonyaratpalin, M.; Borowitzka, L. Effect of a *Dunaliella* extract on growth performance, health condition, immune response and disease resistance in black tiger shrimp (*Penaeus monodon*). *Aquacult. Nutr.* **2005**, *248*, 207−216.

(2) Stahl, W.; Sies, H. Antioxidant activity of carotenoids. *Mol. Aspects Med.* **2003**, *24*, 345−351.

(3) Blasko, A.; Belagyi, J.; Dergez, T.; Deli, J.; Papp, G.; Papp, T.; Vagvolgyi, C.; Pesti, M. Effect of polar and non-polar carotenoids on *Xanthophylomyces dendrorhous* membranes by EPR. *Eur. Biophys. J.* **2008**, *37*, 1097−1104.

(4) Okada, S.; Nur-E-Borhan, S. A.; Yamaguchi, K. Carotenoid composition in the exoskeleton of commercial black tiger prawns. *Fish. Sci.* **1994**, *60*, 213−215.

(5) Plaza, M.; Herrero, M.; Cifuentes, A.; Ibañez, E. Innovative natural functional ingredients from microalgae. *J. Agric. Food Chem.* **2009**, *57*, 7159−7170.

(6) Torrissen, O. J.; Christiansen, R. Requirements of carotenoids in fish diets. *J. Appl. Ichthyol.* **1995**, *11*, 225−230.

(7) Paibulkichakul, C.; Piyatiratitivorakul, S.; Sorgeloos, P.; Menasveta, P. Improved maturation of pond-reared, black tiger shrimp (*Penaeus monodon*) using fish oil and astaxanthin feed supplements. *Aquaculture* **2008**, *282*, 83−89.

(8) Chien, Y. H.; Pan, C. H.; Hunter, B. The resistance to physical stresses by *Penaeus monodon* juveniles fed diets supplemented with astaxanthin. *Aquaculture* **2003**, *216*, 177−191.

(9) Díaz, A. C.; Fernández Giménez, A. V.; Mendiara, S. N.; Fenucci, J. L. Antioxidant activity in hepatopancreas of the shrimp (*Pleoticus muelleri*) by electron paramagnetic spin resonance spectrometry. *J. Agric. Food Chem.* **2004**, *52* (10), 3189−3193.

(10) Winston, G. W.; Lemaire, G. E.; Lee, R. F. Antioxidants and total oxyradical scavenging capacity during grass shrimp, *Palaemonetes pugio*, embryogenesis. *Comp. Biochem. Physiol., Part C: Toxicol. Pharmacol.* **2004**, *139*, 281−288.

(11) Paital, B.; Chainy, G. B. N. Antioxidant defenses and oxidative stress parameters in tissues of mud crab (*Scylla serrata*) with reference to changing salinity. *Comp. Biochem. Physiol., Part C: Toxicol. Pharmacol.* **2010**, *151*, 142−151.

(12) Yordanov, N. Quantitative EPR spectrometry "state of the art". *Appl. Magn. Reson.* **1994**, *6*, 241−257.

(13) Al-Mohanna, S. Y.; Nott, J. A. Functional cytology of the hepatopancreas of *Penaeus semisulcatus* (Crustacea: Decapoda) during the moult cycle. *Mar. Biol.* **1989**, *101*, 535−544.

(14) Bautista, M. N.; Lavilla-Pitogo, C.; Subosa, P. F.; Benigno, E. T. Aflatoxin B1 contamination of shrimp feeds and its effect on growth and hepatopancreas of preadult *Penaeus monodon*. *J. Sci. Food Agric.* **1994**, *65*, 5−11.

(15) Rosas, C.; Bolongaro-Crevenna, A.; Sánchez, A.; Gaxiola, G.; Soto, L.; Escobar, E. Role of the digestive gland in energetic metabolism of *Penaeus setiferus*. *Biol. Bull.* **1995**, *189*, 168−174.

(16) Flores, M.; Díaz, F.; Medina, R.; Re, A. D.; Licea, A. Physiological, metabolic and haematological responses in white shrimp *Litopenaeus vannamei* (Boone) juveniles fed diets supplemented with astaxanthin acclimated to low-salinity water. *Aquacult. Res.* **2007**, *38*, 740−747.

(17) Díaz, A. C.; Souza, L. G.; Petriella, A. M. Morfología e histología del aparato digestivo en diferentes estadios de vida de los camarones peneidos. In *Estado Actual y Perspectivas de la Nutrición de los Camarones Peneidos Cultivados en Iberoamerica*, 1st ed.; Rosas, C., Carrillo, O., Wilson, R., Andreatta, E. R., Eds.; Publidisa Mexicana: Mexico City, Mexico, 2006; pp 10−26.

(18) Fenucci, J. L.; Díaz, A. C.; Fernández Giménez, A. V. A review on the status of protein nutrition of Argentine penaeoid shrimp: Comparisons and contrasts within the penaeidae. In *The Rising Tide Proccedings of the Special Session on Sustainble Shrimp Farming*; Browdy, C. L., Jory, D. E., Eds.; World Aquaculture Society: Baton Rouge, LA, 2009; pp 148−160.

(19) Jensen, F. B. Nitrite disrupts multiple physiological functions in aquatic animals. *Comp. Biochem. Physiol., Part A: Mol. Integr. Physiol.* **2003**, *135*, 9−24.

(20) AOAC International. *Official Methods of Analysis of AOAC International*, 16th ed.; Cuniff, P., Ed.; AOAC International: Gaithersburg, MD, 1997.

(21) Díaz, A. C.; Fenucci, J. L. Comparative evaluation of different animal protein source in juvenile of *Pleoticus muelleri* (Crustacea, Penaeoidea). In *Modern Approaches to the Study of Crustacea*; Escobar-Briones, E., Alvarez, F., Eds.; Kluwer Academic/Plenum Publisher: New York, 2002; pp 75−78.

(22) Bell, T. A.; Lightner, D. V. *A Handbook of Normal Penaeid Shrimp Histology*; World Aquaculture Society: Baton Rouge, LA, 1988.

(23) Finney, D. J. *Probit Analysis*, 3rd ed.; Cambridge University Press: New York, 1971.

(24) Sokal, R.; Rohlf, J. *Biometry, the Principles and Practice of Statistics in Biological Research*, 3rd ed.; W. H. Freeman and Company: New York, 1995.

(25) Díaz, A. C.; Velurtas, S. M.; Mendiara, S. N.; Fenucci, J. L. Correlation between radical scavenging capacity and carotenoid profile during larval development of *Pleoticus muelleri*. *Invertebr. Reprod. Dev.* **2013**, *51* (1), 43−48.

(26) Pan, C. H.; Chien, Y. H.; Cheng, J. H. Effects of light regime, algae in the water, and dietary astaxanthin on pigmentation, growth,

and survival of black tiger prawn *Penaeus monodon* post-larvae. *Zool. Stud.* **2001**, *40*, 371−382.
(27) Chien, Y. H.; Shiau, W. C. The effects of dietary supplementation of algae and synthetic astaxanthin on body astaxanthin, survival, growth, and low dissolved oxygen stress resistance of kuruma prawn, *Marsupenaeus japonicus* Bate. *J. Exp. Mar. Biol. Ecol.* **2005**, *318*, 201−211.
(28) Niu, J.; Tian, L.; Liu, Y.; Yang, H.; Ye, C.; Gao, W.; Mai, K. Effect of dietary astaxanthin on growth, survival, and stress tolerance of postlarval shrimp, *Litopenaeus vannamei*. *J. World Aquacult. Soc.* **2009**, *40*, 795−802.
(29) Lin, Y. C.; Chen, J. C. Acute toxicity of nitrite on *Litopenaeus vannamei* (Boone) juveniles at different salinity levels. *Aquaculture* **2000**, *224*, 193−201.
(30) Camargo, J. A.; Alonso, A. Ecologycal and toxicological effects of inorganic nitrogen pollution in aquatic ecosystems: A global assessment. *Environ. Int.* **2006**, *32*, 831−849.
(31) Vogt, G. Pathology of midgut gland cells of *Penaeus monodon* postlarvae after *Leucaena leucocephala* feeding. *Dis. Aquat. Org.* **1990**, *9* (1), 45−61.
(32) Masson, I.; Díaz, A. C.; Petriella, A. M. Effect of salinity changes on the midgut gland of *Artemesia longinaris* (Decapoda, Penaeidae). *Lat. Am. J. Aquat. Res.* **2012**, *40* (2), 358−366.
(33) Cuartas, E. I.; Díaz, A. C.; Petriella, A. M. Modificaciones del hepatopáncreas del langostino *Pleoticus muelleri* (Crustacea, Penaedoidea) por efecto de la salinidad. *Biociencias* **2003**, *11* (1), 53−59.
(34) Díaz, A. C.; Sousa, L. G.; Petriella, A. M. Functional cytology of the hepatopancreas of *Palaemonetes argentinus* (Crustacea, Decapoda, Caridea) under osmotic stress. Changes induced by the posterior acclimation to freshwater. *Braz. Arch. Biol. Technol.* **2010**, *53* (3), 599−608.
(35) Kuhn, D. D.; Smith, S. A.; Boardman, G. D.; Angier, M. W.; Marsh, L.; Flick, G. J., Jr. Chronic toxicity of nitrate to Pacific white shrimp, *Litopenaeus vannamei*: Impacts on survival, growth, antennae length, and pathology. *Aquaculture* **2010**, *309*, 109−114.
(36) Mendiara, S. N.; Baquero, R. P.; Katunar, M. R.; Mansilla, A. Y.; Perissinotti, L. J. Reaction of $\beta$-carotene with nitrite anion in a homogeneous acid system. An electron paramagnetic resonance and ultraviolet−visible study. *Appl. Magn. Reson.* **2009**, *35*, 549−567.
(37) Pu, J.; Bechtel, P. J.; Sathivel, S. Extraction of shrimp astaxanthin with flaxseed oil: Effects on lipid oxidation and astaxanthin degradation rates. *Biosyst. Eng.* **2010**, *107*, 364−371.
(38) Chew, B. P. Antioxidant vitamins affect food animal immunity and health. *J. Nutr.* **1995**, *125*, 1804S−1808S.
(39) Liang, J.; Tian, Y.; Yang, F.; Zhang, J.; Skibsted, L. H. Antioxidant synergism between carotenoids in membranes. Astaxanthin as a radical transfer bridge. *Food Chem.* **2008**, *115*, 1437−1442.
(40) Wang, W.; Wang, A.; Zhang, Y. Effect of dietary higher level of selenium and nitrite concentration on the cellular defense response of *Penaeus vannamei*. *Aquaculture* **2006**, *256*, 558−563.
(41) Skibsted, L. H. Carotenoids in antioxidant networks. Colorants or radical scavengers. *J. Agric. Food Chem.* **2012**, *60*, 2409−2417.

Table 1. Name, Origin, and Total Polyphenols of Sour Cherry Cultivars Used in This Study

| cultivars | origin | | | TP (mg/100 g dm) |
|---|---|---|---|---|
| | parents | country | date of harvest | |
| Agat | Łutówka x Nefris | Poland | June 30 | 2278.92 |
| Ametyst | Łutówka x Nefris | Poland | July 14 | 2270.15 |
| Cesarzowa Eugenia | unknown | France | July 14 | 2261.91 |
| Dradem | Łutówka x Northstar | Poland | July 14 | 2748.75 |
| Erdi Botermo | Pandy Meggy 38 x Nagy Angol | Hungary | June 30 | 2244.24 |
| Erdi Nagygyümöscu | unknown | Hungary | June 22 | 1539.43 |
| Fanal | selected from local cherry, origin unknown | Germany | July 7 | 2366.25 |
| Fortuna | unknown | Germany | June 22 | 1687.22 |
| Groniasta z Ujfehertoi | unknown | Hungary | July 7 | 1672.68 |
| Karneol | Kerezer x Schattenmorelle | Germany | July 14 | 1894.68 |
| Kelleris 14 | Ostheimska x Marchijska | Denmark | July 14 | 2292.73 |
| Książęca | unknown | unknown | June 22 | 2193.17 |
| Lucyna | Łutówka x Shirpotreb | Poland | July 7 | 1880.89 |
| Łutówka | unknown | France or Holand | July 21 | 2286.99 |
| Meteor Korai | unknown | Hungary | June 22 | 2679.22 |
| Morina | Kerezer x Reinharts Ostheimer | Germany | July 7 | 2733.46 |
| Nana | Crisina x Morello Neagra | Rumunia | July 14 | 2251.07 |
| Northstar | English Morello x Serbian pie | USA | July 7 | 2427.49 |
| Pandy 103 | clone cv Pondy | Hungary | July 7 | 2349.43 |
| Sabina | Łutówka x Shirpotreb | Poland | June 30 | 2449.25 |
| Safir | Schattenmorelle x Fanal | Germany | July 7 | 2842.41 |
| Stevensbaer | clone *P. ceraus* | Denmark | July 14 | 2572.28 |
| Topas | Fanal x Kelleris 16 | Germany | July 7 | 2651.91 |
| Turgieniewka | seedling cv Żukowskaja | Rosja | July 7 | 2608.20 |
| Wanda | Neferis x Wołyńska | Poland | June 30 | 2160.74 |
| Wiblek | selected from local cherries, origin unknown | Poland | July 14 | 2112.77 |
| Wider (syn. Skierka) | selected from local cherries, origin unknown | Poland | June 30 | 2543.59 |
| Wifor | selected from local cherries, origin unknown | Poland | July 21 | 1709.04 |
| Wilena | selected from local cherries, origin unknown | Poland | July 7 | 2046.32 |
| Wilga | selected from local cherries, origin unknown | Poland | July 14 | 1685.01 |
| Winer | selected from local cherries, origin unknown | Poland | July 21 | 2485.18 |
| Wisok | selected from local cherries, origin unknown | Poland | July 21 | 2982.51 |
| Wołyńska (syn. Morelka) | selected from local cherries, origin unknown | Poland | July 14 | 2288.72 |

## MATERIALS AND METHODS

**Chemicals.** 2,2′-azinobis(3-ethylbenzothiazoline-6-sulfonic acid) (ABTS), 6-hydroxy-2,5,7,8-tetramethylchroman-2-carboxylic acid (Trolox), 2,4,6-tri(2-pyridyl)striazine (TPTZ), 2,2′-azobis (2-amidino-propane) dihydrochloride (AAPH), fluorescein disodium (FL), potassium persulfate, acetic acid, phloroglucinol, and methanol were purchased from Sigma-Aldrich (Steinheim, Germany). (−)-Epicatechin, (+)-catechin, procyanidins B1, *p*-coumaric acid, quercetin and kaempferol-3-*O*-glucoside, cyanidin-3-*O*-sophoroside, cyanidin-3-*O*-glucoside, cyanidin-3-*O*-rutinoside, peonidin-3-*O*-rutinoside, and pelargonidin-3-*O*-glucoside were purchased from Extrasynthese (Lyon, France). Chlorogenic acid, neochlorogenic acid, cryptochlorogenic acid, and 3,5-dicaffeoylquinic acid were purchased from TRANS MIT GmbH (Giessen, Germany). Acetonitrile for ultra-phase liquid chromatography (UPLC; Gradien grade) and ascorbic acid were from Merck (Darmstadt, Germany). UPLC grade water, prepared by HLP SMART 1000s system (Hydrolab, Gdańsk, Poland), was additionally filtrated through a 0.22 $\mu$m membrane filter immediately before use.

**Plant Materials.** Thirty-three sour cherries cultivars ('Agat', 'Ametyst', 'Cesarzowa Eugenia', 'Dradem', 'Erdi botermo', 'Erdi Nagygyümöscu', 'Fanal', 'Fortuna', 'Groniasta', 'Karneol', 'Kelleris 14', 'Książęca', 'Lucyna', 'Łutówka', 'Meteor korai', 'Morina', 'Nana', 'Northstar', 'Pandy 103', 'Sabina', 'Safir', 'Skierka', 'Stevensbaer', 'Topas', 'Turgieniewka', 'Wanda', 'Wiblek', 'Wifor', 'Wilena', 'Wilga', 'Winer', 'Wisok', and 'Wołyńska', Table 1) were used in this research; all of them were appropriate for food manufacturing and widely grown in Poland. The fruits were harvested at the Research Station for Cultivar Testing in Zybiszów near Wrocław (51° 3′ 51.11″ N, 16° 54′ 43.56″ E). The sour cherries were collected at "ready-to-eat" ripening stage, evaluated by means of change in ground color from green to red. Since sour cherries quality shows variablility within tree, fruit sampling under the following conditions: middle vigor trees, south exposure, external part of the tree. In the course of the measurements, five replications (each 100 g randomly chosen fruits) from three trees, i.e., 15 replications per cultivar, were established.

The fruit mass, dry matter, soluble solids, pH and titratable acidity, sugars, and ascorbic acid content were measured on fresh berries soon after harvest. For polyphenolic compounds and antioxidant activity analyses, the whole fruits were cut directly to liquid nitrogen and crushed by laboratory mill for homogeneous powder in liquid nitrogen (IKA 11A; Staufen, Germany) and freeze-dried (24 h; Alpha 14 LSC; Martin Christ GmbH, Osterode am Harz, Germany). The samples were stored in a freezer (−70 °C; Frilabo; Lyon, France) until analysis, no longer than 2 weeks.

**Physicochemical Analyses.** Fruit weight was evaluated in triplicate from a 10 whole fruit sample (fruit and seed). The sour cherry seeds were manually removed. Titratable acidity (TA) was determined by titration aliquots of homogenate of fresh fruits by 0.1 N NaOH to an end point of pH 8.1 using an automatic pH titration system (pH-metr typ IQ 150; Warsav, Polska) and expressed as g of malic acid. The pH was measured with the same equipment used for TA, while the soluble solids content (SSC) was determined in fresh juices with a refractometer (Atago Rx 5000, Atago Co. Ltd., Japan) and expressed as °Brix. Total and directly reducing sugars was determined by the Lane−Eynon method (PN-90/A-75101/07).

**Identification of Polyphenols by the LC-PDA-MS Method.** The extract of polyphenols for analysis was prepared as described previously by Wojdyło et al.[13] Identification and quantification of polyphenols of sour cherry extracts was carried out using an Acquity ultraperformance LC system equipped with a photodiode detector (PDA; UPLC) with binary solvent manager (Waters Corp., Milford, MA, USA) series with a mass detector G2 QTof Micro mass spectrometer (Waters, Manchester, UK) equipped with an electrospray ionization (ESI) source operating in negative and positive modes. Separations of polyphenols were carried out using a UPLC BEH C18 column (1.7 $\mu$m, 2.1 × 100 mm; Waters Corp., Milford, MA, USA) at 30 °C. Samples (5 $\mu$L) were injected, and elution was completed within 15 min using a sequence of elution modes: linear gradients and isocratic. The flow rate was 0.45 mL/min. The mobile phase was composed of solvent A (4.5% formic acid) and solvent B (100% of acetonitrile). The program began with isocratic elution with 99% A (0−1 min), and then a linear gradient was used until 12 min, lowering A to 0%; from 12.5 to 13.5 min, returned to the initial composition (99% A), and then held constant to re-equilibrate the column. Analysis was carried out using full scan, datadependent MS scanning from $m/z$ 100 to 1000. The mass tolerance was 0.001 Da, and the resolution was 5.000. Leucine enkephalin was used as the mass reference compound at a concentration of 500 pg/$\mu$L at a flow rate of 2 $\mu$L/min, and the $[M - H]^-$ ion at 554.2615 Da was detected over 15 min of analysis during ESIMS accurate mass experiments, which was permanently introduced via the LockSpray channel using a Hamilton pump. The lock mass correction was ±1.000 for Mass Window. The mass spectrometer was operated in a negative ion mode, set to the base peak intensity (BPI) chromatograms, and scaled to 12 400 counts per second (= 100%). The optimized MS conditions were as follows: capillary voltage of 2500 V, cone voltage of 30 V, source temperature of 100 °C, desolvation temperature of 300 °C, and desolvation gas (nitrogen) flow rate of 300 L/h. Collision-induced fragmentation experiments were performed using argon as collision gas, with voltage ramping cycles from 0.3 to 2 V. The characterization of the single components was carried out via the retention time and the accurate molecular masses. Hydroxycinnamic acids, flavan-3-ols, and flavonols were optimized to its estimated molecular mass $[M - H]^-$ in the negative mode before and after fragmentation and for anthocyanidin compounds optimized to its estimated molecular mass $[M + H]^+$ in the positive mode. The data obtained from LCMS were subsequently entered into MassLynx 4.0 ChromaLynx Application Manager software. On the basis of these data, the software is able to scan different samples for the characterized substances.

**Determination of Polyphenols by UPLC Coupled to PDA and FL Detector.** The analysis of polyphenolic compounds was carried out on a UPLC system Acquity (Waters Corp., Milford, MA, USA) consisting of a binary solvent manager, sample manager, PDA (model $\lambda$e), and fluorescence detector (FL). Empower 3 software was used for chromatographic data collection and integration of chromatograms. The UPLC analyses were performed on a BEH Shield C18 analytical column (2.1 mm × 50 mm; 1.7 $\mu$m). The flow rate was 0.45 mL/min. A partial loop injection mode with a needle overfill was set up, enabling 5 $\mu$L injection volumes when a 10 $\mu$L injection loop was used. Acetonitrile (100%) was used as a strong wash solvent and acetonitrile−water (10%) as a weak wash solvent.

**Analysis of Polyphenol Compounds.** Five milliliters of the resultant extract were centrifuged for 10 min at 15000$g$ at 4 °C. The analytical column was kept at 30 °C by column oven, whereas the samples were kept at 4 °C. The mobile phase was composed of solvent A (4.5% formic acid) and solvent B (acetonitrile). Elution was as follows: 0−5 min, linear gradient from 1 to 25% B; 5.0−6.5 min, linear gradient from 25 to 100%; 6.5−7.5 min, column washing; and reconditioning for 0.5 min. PDA spectra were measured over the wavelength range of 200−600 nm in steps of 2 nm. The runs were monitored at the following wavelengths: flavan-3-ols at 280 nm, hydroxycinnamates at 320 nm, flavonol glycosides at 360 nm, and anthocyanins at 520 nm. Retention times and spectra were compared with those of pure standards. Calibration curves at concentrations ranging from 0.05 to 5 mg/mL ($r^2 \leq 0.9998$) were made from (−)-epicatechin, (+)-catechin, chlorogenic acid, neochlorogenic acid, 3,5-dicaffeoylquinic acid, quercetin-3-$O$-glucoside, quercetin-3-$O$-rutinoside, kaempferol-3-$O$-rutinoside, cyanidin-3,5-$O$-diglucoside, cyanidin-3-$O$-glucoside, cyanidin-3-$O$-rutinoside, peonidin-3-$O$-rutinoside, and pelargonidin-3-$O$-rutinoside as standards. 3-$p$-Coumarylquinic acid was expressed as $p$-coumaric acid, and quercetin derivatives was expressed as quercetin-3-$O$-glucoside, kaempferol derivatives was expressed as kaempferol-3-$O$-rutinoside, and derivatives of apigenin were expressed as quercetin-3-$O$-glucoside. All determination were done in triplicate. Results were expressed as milligrams per 100 g of dry matter (dm).

**Analysis of Proanthocyanidins by the Phloroglucinolysis Method.** Direct phloroglucinolysis of freeze dried sour cherry varieties was performed as described previously by Wojdyło et al.[13] Portions (0.05 g) of powder were precisely measured into 2 mL Eppendorf vials, then 0.8 mL of the methanolic solution of phloroglucinol (75 g/L) and ascorbic acid (15 g/L) was added. After the addition of 0.4 mL of methanolic HCl (0.3 mol/L), the vials were closed and incubated for 30 min at 50 °C with continuous vortexing using a thermo shaker (TS100; BIOSAN, Lithuania). The reaction was stopped by placing the vials in an ice bath; 0.5 mL of the reaction medium was drawn out and diluted with 0.5 mL of 0.2 mol/L sodium acetate buffer. Next the vials were cooled in ice water and centrifuged immediately at 20000$g$ for 10 min at 4 °C. The analytical column was kept at 15 °C by column oven, whereas the samples were kept at 4 °C. The mobile phase was composed of solvent A (2.5% acetic acid) and solvent B (acetonitrile). Elution was as follows: 0−0.6 min, isocratic 2% B; 0.6−2.17 min, linear gradient from 2 to 3% B; 2.17−3.22 min, linear gradient from 3 to 10% B; 3.22−5.00 min, linear gradient from 10 to 15% B; 5.00−6.00 min, column washing; and reconditioning for 1.50 min. The fluorescence detection was recorded at an excitation wavelength of 278 nm and an emission wavelength of 360 nm. The calibration curves, which were based on peak area, were established using (+)-catechin, (−)-epicatechin, and procyanidin B1 after phloroglucinol reaction as (+)-catechin and (−)-epicatechin−phloroglucinol adduct standards. The average degree of polymerization was calculated as the molar ratio of all the flavan-3-ol units (phloroglucinol adducts + terminal units) to (−)-epicatechin and (+)-catechin, which correspond to terminal units. All determinations were done in triplicate. Results were expressed as milligrams per 100 g dm.

**L-Ascorbic Acid Analysis.** L-Ascorbic acid was analyzed according to the method described previously by Oszmiański et al.[15] Fresh fruits (3−4 g) were mixed with 50 mL of 0.1 M phosphoric acid and centrifuged at 20000$g$ for 10 min. The estimation of ascorbic acid was carried out using a Waters liquid chromatograph with a tunable absorbance detector (Waters 486) and a quaternary pump with a Waters 600 Controller apparatus (Waters Associates). A 20 $\mu$L sample was injected into a Chromolith Performance RP18e column (100 × 4.6 mm) (Merck, Darmstadt, Germany). The elution was carried out using 0.1 M phosphoric acid at the flow rate of 1.0 mL/min. The absorbance was monitored at 254 nm. Ascorbic acid was identified by comparison with the standard. The calibration curve was prepared by plotting different concentrations of the standard versus the area measurements in HPLC. All determination were done in triplicate. Results were expressed as milligrams per 100 g dm.

**Analysis of Antioxidant Activity.** The solvent for analysis of polyphenols was prepared as described previously by Wojdyło et al.[14] The ORAC, ABTS$^{\circ+}$, and FRAP assay were determined as previously described by Ou et al.,[16] Re et al.,[17] and Benzie et al.,[18] respectively. All antioxidant activity were expressed as millimoles of Trolox per 100 g of dry matter (dm). ORAC assay was performed using a RF5301 PC spectrofluorometer (Shimadzu, Kyoto, Japan). Determinations by ABTS and FRAP methods were performed using a UV2401 PC spectrophotometer (Shimadzu, Kyoto, Japan).

**Statistical Analysis.** Results are given as the mean of three independent determinations. Principal Components Analysis (PCA) was carried out using the Statistica version 10 software (StatSoft, Krakow, Poland).

**Table 2. Four Groups of Phenolic Compounds Identified by LC/MS in Sour Cherry Fruits**

| compound | $t_R$ (min) | $\lambda_{max}$ (nm) | $[M - H]^-$ ($m/z$) | |
|---|---|---|---|---|
| | | | MS | MS/MS[b] |
| **Anthocyanins** | | | | |
| cyanidin-3-*O*-diglucoside-5-glucoside | 3.46 | 279/515 | 773.2294+[a] | 579.1520/305.0685/**287.0536** |
| cyanidin-3-*O*-sophoroside | 3.69 | 242/278/515 | 611.1564+ | 449.1063/**287.0536** |
| cyanidin-3-*O*-(2′-glucosyl)rutinoside | 3.89 | 242/278/517 | 757.2184+ | 611.1614/433.1125/**287.0536** |
| cyanidin-3-*O*-glucoside | 4.01 | 242/516 | 449.1063+ | **287.0571** |
| cyanidin-3,5-pentoside-hexoside | 4.03 | 241/277/517 | 581.1671+ | **287.0571** |
| cyanidin-3-*O*-(xylosyl)rutinoside | 4.09 | 242/278/513 | 727.2052+ | 581.1573/363.7898/**287.0571** |
| cyanidin-3-*O*-rutinoside | 4.31 | 242/279/517 | 595.1664+ | 499.1063/**287.0571** |
| pelargonidin-3-*O*-(2′-glucosyl)rutinoside | 4.66 | 241/282/310/506 | 741.2279+ | 579.1520/**271.0601** |
| peonidin-3-(6′-*p*-coumaroylglucoside)glucoside | 4.98 | 241/277/517 | 771.2365+ | 577.1355/**301.0730** |
| peonidin-3-*O*-rutinoside | 5.45 | 241/279/517 | 609.1857+ | **301.0730**/463.9432 |
| cyanidin-3-(6′-*p*-coumaroyl)glucoside | 6.36 | 241/278/513 | 595.1664+ | **287.0571** |
| **Hydroxycinnamic Acids** | | | | |
| neochlorogenic acid (3-*O*-caffeoylquinic acid) | 2,09 | 323 | 353.0840 | **191.0524** |
| 3-*p*-coumarylquinic acid | 2.92 | 310 | 337.0899 | **191.0524**/183.0112 |
| chlorogenic acid (5-*O*-caffeoylquinic acid) | 3.20 | 324 | 353.0879 | **191.0553** |
| 4-*O*-caffeoylquinic acid | 4.85 | 320 | 353.0840 | **191.0581**/183.0140 |
| 3,5-dicaffeoylquinic acid | 7.65 | **326** | 515.1196 | 353.0879/**191.0524**/173.0446 |
| **Flavan-3-ols** | | | | |
| (+)-catechin | 3.15 | 279 | 289.0688 | |
| procyanidin B1 | 3.88 | 278 | 577.1349 | **289.0758** |
| procyanidins, tetramer | 3.99 | 279 | 1153.2776 | **577.1349**/275.0286 |
| procyanidins, dimer | 4.23 | 280 | 577.1398 | 275.0286 |
| (−)-epicatechin | 4.59 | 278 | 289.0723 | |
| procyanidins, trimer | 5.02 | 278 | 865.1967 | **577.1349**/289.0758 |
| procyanidins, trimer | 5.25 | 278 | 865.1967 | 577.1349/**289.0758** |
| procyanidins, trimer | 5.32 | 278 | 865.1967 | 577.1349/**289.0758** |
| procyanidins, trimer | 5.45 | 278 | 865.1967 | 577.1349/**289.0758** |
| procyanidins, trimer | 5.52 | 278 | 865.1967 | 577.1349/**289.0758** |
| procyanidins, tetramer | 5.62 | 278 | 1153.2776 | 577.1349/**289.0758** |
| procyanidins, trimer | 5.75 | 278 | 865.1967 | 577.1349/**289.0758** |
| procyanidins, dimer | 7.19 | 278 | 577.1349 | **289.0758** |
| procyanidins, trimer | 7.30 | 278 | 865.1967 | 577.1349/**289.0758** |
| **Flavonols and Flavon** | | | | |
| kaempferol-trihexose | 3.42 | 242/337 | 773.2153 | 488.2101/**285.0394** |
| quercetin-3-*O*-rutinoside-glucoside | 5.25 | 253/351 | 771.1962 | 609.1438/**301.0277** |
| quercetin-3-*O*-glucoside-dirhamnoside | 5.95 | 241/351 | 755.2006 | **301.0319**/183.0140 |
| quercetin-3-*O*-rutinoside | 6.61 | 254/352 | 609.1483 | 577/407/**301.0319** |
| quercetin-3-*O*-galactoside | 6.73 | 251/350 | 463.0887 | **301.0319** |
| isorhamnetin-3-rutinoside-7-rhamnoside | 6.90 | 241/351 | 769.2195 | **315.0457**/183.0140/229.0226 |
| dihydrokaempferol-dihexoside | 7.09 | 275/346 | 611.2565 | **285.0252** |
| apigenin-7-*O*-glucoside | 7.26 | 241/340 | 431.0994 | 183.0140/**269.0435**/137.0086 |
| kaempferol-3-*O*-rutinoside | 7.72 | 264/347 | 593.1507 | **285.0394** |
| isorhamnetin-3-*O*-rutinoside | 7.98 | 253/352 | 623.1598 | **315.0512**/183.0167 |
| dihydrokaempferol-glucoside | 8.20 | 242/278/348 | 449.2017 | **285.0252** |

[a] $[M + H]^+$ ($m/z$) for anthocyanins were obtained in the positive ion mode. [b] The $m/z$ values of the predominant ions are given in bold type.

## RESULTS AND DISCUSSION

**Identification and Quantification of Phenolic Compounds in the Sour Cherry Fruits.** *Total Polyphenol (TP).* Table 2 shows the data after LC/MS QTOF analysis. The LC/MS analysis of different sour cherry cultivars allowed for a characterization of 41 compounds. These can be classified into four groups of phenolic compounds: anthocyanins, hydroxycinnamic acids, flavonols and flavons, and flavan-3-ols (monomer, dimers, and polymeric procyanidins).

The concentration range of total phenolics (TP) determined for different sour cherry cultivars is presented in Table 1. The TP contents ranged from 2982.51 to 1539.43 mg/100 g dm for the 'Wisok' and 'Erdi Nagygyümöscu' cultivars, respectively (Table 1). The average TP content of 33 sour cherry cultivars analyzed was 2278.69 mg/100 g dm and depended significantly on the cultivar. High TP levels (>2500 mg/100 g dm) were found in 'Meteor Korali', 'Skierka', 'Turgieniewka', 'Morina', 'Topas', 'Safir', 'Dradem', and 'Stevensbaer', but 'Wifor', 'Wilga', 'Lucyna', 'Groniasta', 'Groniasta z Ujfehertoi', 'Fortuna', and 'Karneol' revealed <1900 mg/100 g dm of polyphenols.

Considerably variable amounts of TP were reported previously.[19,20] It is difficult to compare them with our results, because different methods of extraction and determination were used, but the proportions of individual phenolics seem to be

similar. The highest polyphenol content was measured in a Polish cultivar, 'Wisok', but many other cultivars contained significantly less polyphenols. Variability in the content of phenolic compounds in fruits depends on many factors, such as degree of maturity at harvest, environmental conditions during fruit development, etc.[21] However, the production of fruit with high content of nutritional components and extensive antioxidant properties depends to a much greater degree on their genetic background than on the climatic conditions and agricultural practices. Additionally, the total content of polyphenolic compounds in red-colored fruits increases at the last ripening stage, due to maximal accumulation of anthocyanins and flavonols.[22]

*Flavan-3-ols.* Based on the LC/MS technique, 12 additional compounds belonging to flavan-3-ols were detected and identified in the sour cherry fruits (Table 2). These compounds included three procyanidin dimers with $m/z$ 577, one of which was identified compared to standards as procyanidin B1, seven procyanidin trimers with $[M - H]^-$ at $m/z$ 865, and two procyanidin tetramers with $[M - H]^-$ at $m/z$ = 1153. All the detected procyanidins had the characteristic fragmentation pattern of a negatively charged molecular ion $[M - H]^-$ at $m/z$ = 577 and/or 289.

The difference between the content of (−)-epicatechin and (+)-catechin was significant. Concentrations of (−)-epicatechin ranged from 18.12 to 282.87 mg/100 g dm and of (+)-catechin from 4.27 to 115.72 mg/100 g dm. The highest monomer levels were found in 'Dradem', 'Meteor Koral', and 'Winer' fruits, while the lowest were found in 'Wanda', 'Lucyna', and 'Wifor' fruits (Table 3).

Previous studies by Serra et al.,[23] Toydemir et al.,[24] and Diaz-Garcia et al.,[25] concerning flavan-3-ols profiles of sour and sweet cherry, suggested that the major compounds in this group were (−)-epicatechin and (+)-catechin. However, Kołodziejczyk et al.[26] suggested, based on HPLC/MS analysis, that the sour cherry pomace extract contained different polymeric procyanidins, up to pentamers. Similarly, Tomas-Barberan et al.[27] reported the presence of (−)-epicatechin and procyanidin dimers and trimers in plums, peaches, and nectarines that belong to the same plant family.

Individual concentration of polymeric procyanidins in the sour cherry fruits was difficult to estimate, and to this end the phloroglucinol method was employed to determine their quantity in different cultivars. Phloroglucinol degradation of sour cherry procyanidins released (+)-catechin and (−)-epicatechin as the only free flavan-3-ols and (−)-epicatechin phloroglucinol as the main flavan-3-ol adduct, suggesting that these procyanidins essentially consisted of (−)-epicatechin units with (+)-catechin present only in a very low proportion as a terminal unit.

Regarding the polymeric procyanidin levels, the investigated cultivars can be classified into three groups: the first group with levels ranging >1000 mg/100 g dm ('Agat', 'Skierka', Fanal', 'Wilena', 'Karneol', 'Stevensbaer', and 'Łutówka' cvs), the second group with intermediate levels between 700 and 1000 mg/100 g dm ('Lucyna', 'Morina', 'Pandy', 'Groniasta', 'Nordstar', 'Topas', 'Safir', 'Nana', 'Wilbek', 'Dradem', 'Keleris 14', 'Ametyst', 'Wilga', 'Wołyńska', 'Wifor', 'Winer', and 'Wisok' cvs), and the third group with much lower levels below 700 mg/100 g dm ('Książęca', 'Erdi Nagygyümöscu', 'Fortuna', 'Meteor Korai', 'Sabina', 'Wanda', 'Erdi botermo', 'Turgieniewka', and 'Cesarzowa Eugenia' cvs). An analysis of the polymeric procyanidins content in sour cherry fruit revealed significant differences between Polish cultivars.

A degree of polymerization (DP; number of flavan-3-ol units) modulates the physicochemical properties of procyanidins. The DP of the sour cherry polymeric fraction ranged from 2.6 to 6.6. The highest DP was found in 'Groniasta' cultivar, and the other cultivars were characterized by lower DP values of about 3.2−4.4. According to the literature data, the DP was similar for blue honeysuckle berries (2.5−6.1),[13] but lower than for chokeberry fruits (23),[28] lowbush blueberry (∼15),[29] and quince fruits (8.3−11.2).[14] Lower DP value means that the sour cherry fruits are characterized by lower astringency than other fruits. Bitterness and astringency in fruits and fruit-based products depend on the flavonol content, DP, and residual pectin.[30]

*Anthocyanins.* Red color of the sour cherry is mainly due to anthocyanins. A total of 11 anthocyanins were detected across all the investigated fruits, including 8 cyanidins, 1 pelargonidin, and 2 peonidins (Table 2). However, the profile was not the same for all the cultivars. Five main anthocyanins, i.e., cyanidin-3-*O*-sophoroside, cyanidin-3-*O*(2′-glucosyl)rutinoside, cyanidin-3-*O*-glucoside, cyanidin-3-*O*-rutinoside, and peonidin-3-*O*-rutinoside, detected in the studied sour cherry cultivars, were the same as those identified in different cultivars by other authors.[8,12,31,32]

This is the first time that acylated anthocyanins such as *p*-coumaric acid (peonidin-3-(6′-*p*-coumaroylglucoside)glucoside with $[M + H]^+$ at $m/z$ = 771 and cyanidin-3-(6′-*p*-coumaroyl)glucoside with $[M + H]^+$at $m/z$ = 595) have been identified. The rest of the anthocyanins were non-acylated compounds; however, there were mono- and diglucosides (cyanidin-3-*O*-diglucoside-5-glucoside with $[M + H]^+$ at $m/z$ = 773; cyanidin-3,5-pentoside-hexoside with $m/z$ = 581; cyanidin-3-*O*-(xylosyl)-rutinoside with $[M + H]^+$ at $m/z$ = 727; pelargonidin-3-*O*-(2′-glucosyl)-rutinoside) with $[M + H]^+$ at $m/z$ = 741, and peonidin-3-*O*-rutinoside with $[M + H]^+$ at $m/z$ = 609). The main sour cherry anthocyanins were glycosides of cyanidin ($[M + H]^+$ at $m/z$ = 287), and among 8 various cyanidin derivatives, cyanidin-3-*O*-(2′-glucosyl)-rutinoside and cyanidin-3-*O*-rutinoside were the most abundant.

Total anthocyanin levels ranged from 994.00 mg/100 g dm in 'Sabina' cultivar to 844.77 mg/100 g dm in 'Wisok' cultivar. 'Safir', 'Książęca', 'Fortuna', 'Erdi botermo', and 'Nana' cultivars also showed high content of anthocyanins, but it was low in 'Karneol' (91.40 mg/100 g dm), 'Wilena' (199.71 mg/100 g dm), 'Pandy' (292.05 mg/100 g dm), and 'Groniasta' (238.01 mg/100 g dm) (Table 3). The fruits of 'Karneol' cultivar were typically the lightest in color, and therefore their anthocyanin content was lower than in the other examined cultivars.

Total anthocyanin levels in our study were comparable to those reported for other fruits and berries. The total anthocyanin content of sweet cherry cultivars was 7.56−94.20 mg/100 g of fresh weight (fw),[20] in red grape it was 316−1911 mg/100 g fw,[33] in black currant 1044−1568 mg/100 g dm,[34] in blackberry 126−152 mg/100 g fw,[35] and in blueberries 650−2290 mg/100 g fw.[36] Some of our results were comparable with these outcomes, and it can be concluded that the sour cherry cultivars were found to be a good source of anthocyanins among fruit species. The anthocyanin content and their composition in fruits depend on environmental factors, as

**Table 3. Concentrations of Anthocyanins, Flavan-3-ols, Hydroxycinnamic Acids, and Flavonols and Flavons (in mg/100 g dm) in the Fruit of Sour Cherry Cultivars, Estimated by UPLC[a]**

| | anthocyanins | | | | | | | | | | | flavan-3-ols | | |
|---|---|---|---|---|---|---|---|---|---|---|---|---|---|---|
| cultivar | A1 | A2 | A3 | A4 | A5 | A6 | A7 | A8 | A9 | A10 | A11 | C | E | PP |
| Agat | 0.69 | 108.60 | 342.54 | 0.21 | 18.09 | 111.35 | nd | nd | nd | 5.74 | nd | 5.12 | 117.52 | 1123.02 |
| Ametyst | 0.60 | 81.09 | 215.98 | 0.10 | 13.13 | 55.95 | nd | 0.52 | nd | 9.31 | nd | 38.54 | 70.55 | 799.23 |
| Cesarzowa Eugenia | 0.64 | 71.04 | 382.50 | 0.24 | 19.88 | 99.96 | nd | nd | nd | 8.49 | nd | 40.20 | 128.40 | 606.89 |
| Dradem | 0.57 | 17.93 | 200.45 | 0.08 | 8.76 | 88.53 | nd | 1.07 | nd | 9.46 | 0.02 | 16.22 | 187.57 | 903.10 |
| Erdi Botermo | 3.22 | 655.15 | 592.99 | 0.38 | 48.71 | 100.37 | nd | 1.90 | nd | 10.83 | nd | 22.11 | 282.87 | 525.68 |
| Erdi Nagygyümöscu | nd | 62.91 | 299.07 | 0.12 | 13.53 | 126.28 | nd | nd | 0.01 | nd | 0.01 | 4.27 | 62.85 | 449.69 |
| Fanal | 1.37 | 69.80 | 331.13 | 0.12 | 16.64 | 78.03 | nd | nd | nd | 5.40 | nd | 9.31 | 142.62 | 1075.99 |
| Fortuna | 0.67 | 391.64 | 281.04 | 0.06 | 17.30 | 48.03 | nd | nd | nd | 4.60 | nd | 10.78 | 54.51 | 444.14 |
| Groniasta | 0.33 | 41.01 | 158.05 | 0.05 | 7.52 | 22.60 | nd | 0.39 | nd | 8.07 | 0.02 | 26.37 | 100.18 | 754.04 |
| Karneol | 0.12 | 3.36 | 59.11 | 0.02 | 2.97 | 23.21 | nd | 0.11 | nd | 2.51 | nd | 27.20 | 131.86 | 1108.01 |
| Kelleris 14 | 0.48 | 54.66 | 252.28 | 0.21 | 12.58 | 92.44 | nd | 0.34 | nd | 8.35 | nd | 34.75 | 105.95 | 931.36 |
| Książęca | 0.35 | 407.36 | 213.92 | nd | 30.59 | 94.39 | nd | nd | nd | 5.38 | 0.02 | 41.07 | 101.71 | 403.57 |
| Lucyna | 0.58 | 43.54 | 202.12 | 0.06 | 13.30 | 53.91 | nd | 0.25 | nd | 0.23 | nd | 37.25 | 19.05 | 839.27 |
| Łutówka | 0.69 | 77.91 | 273.04 | 0.17 | 14.20 | 70.45 | nd | 1.03 | nd | 8.07 | nd | 27.36 | 90.52 | 1167.27 |
| Meteor Korai | 0.44 | 59.23 | 187.88 | 0.02 | 13.63 | 143.62 | nd | nd | nd | 10.06 | 0.03 | 62.31 | 129.50 | 655.09 |
| Morina | 0.52 | 30.98 | 204.40 | 0.06 | 12.42 | 65.58 | nd | nd | nd | 6.57 | nd | 62.16 | 30.29 | 924.84 |
| Nana | 0.71 | 134.54 | 391.24 | 0.37 | 28.22 | 135.39 | nd | 1.85 | nd | 12.24 | nd | 21.84 | 51.79 | 819.39 |
| Northstar | 0.40 | 96.65 | 362.24 | 0.20 | 25.89 | 144.18 | nd | nd | nd | 26.18 | nd | 29.22 | 112.25 | 866.05 |
| Pandy 103 | 0.45 | 26.50 | 187.59 | 0.06 | 8.87 | 61.92 | nd | nd | nd | 6.66 | nd | 51.16 | 120.95 | 835.43 |
| Sabina | 1.28 | 334.15 | 524.06 | 0.61 | 32.26 | 100.64 | nd | 1.00 | nd | nd | nd | 28.53 | 75.36 | 676.55 |
| Safir | 0.64 | 216.69 | 386.55 | 0.29 | 39.98 | 138.90 | nd | nd | nd | 10.68 | nd | 25.12 | 47.89 | 989.31 |
| Skierka | 0.98 | 124.64 | 323.05 | 0.31 | 14.11 | 37.21 | nd | 0.97 | nd | 3.30 | 0.02 | 6.33 | 82.15 | 1215.67 |
| Stevensbaer | 0.63 | 84.73 | 305.67 | 0.25 | 22.31 | 115.99 | nd | 0.34 | nd | 10.18 | 0.01 | 21.60 | 122.38 | 1119.66 |
| Topas | 0.81 | 131.74 | 379.12 | 0.30 | 17.32 | 107.63 | nd | nd | nd | 6.31 | nd | 30.15 | 73.01 | 744.73 |
| Turgieniewka | 0.96 | 138.91 | 402.69 | 0.32 | 18.29 | 114.34 | nd | nd | nd | 6.73 | nd | 40.50 | 29.54 | 628.21 |
| Wanda | 0.44 | 125.29 | 191.30 | 0.09 | 16.43 | 81.49 | nd | 0.32 | nd | 0.26 | nd | 31.49 | 18.12 | 537.16 |
| Wiblek | 0.75 | 28.17 | 264.52 | 0.15 | 12.29 | 74.70 | nd | 0.17 | nd | 5.44 | nd | 39.16 | 66.21 | 842.39 |
| Wifor | 0.78 | 30.44 | 215.21 | 0.10 | 12.70 | 74.38 | 0.28 | 0.35 | nd | 0.45 | nd | 30.17 | 31.66 | 724.71 |
| Wilena | 0.18 | 27.19 | 130.58 | 0.06 | 6.25 | 28.02 | nd | 0.50 | nd | 6.94 | 0.1 | 58.62 | 77.13 | 1058.34 |
| Wilga | 0.74 | 105.12 | 344.78 | 0.26 | 26.57 | 98.12 | nd | 1.77 | nd | 7.79 | nd | 19.86 | 75.52 | 731.16 |
| Winer | 0.52 | 75.33 | 376.42 | 0.36 | 25.77 | 161.23 | 0.72 | 0.33 | nd | 15.32 | 0.03 | 39.42 | 144.94 | 798.99 |
| Wisok | 2.02 | 282.47 | 474.78 | 0.45 | 14.27 | 56.97 | 9.53 | 1.03 | nd | 3.26 | nd | 115.72 | 28.40 | 913.36 |
| Wołyńska | 0.79 | 58.18 | 283.63 | 0.14 | 16.01 | 115.69 | nd | 0.52 | 0.02 | 7.85 | nd | 28.17 | 136.35 | 878.57 |
| *minimum* | 0.00 | 3.36 | 59.11 | 0.00 | 2.97 | 9.53 | 0.00 | 0.00 | 0.00 | 0.00 | 0.00 | 4.27 | 18.12 | 403.57 |
| *maximum* | 3.22 | 655.15 | 592.99 | 0.61 | 48.71 | 161.23 | 9.53 | 1.90 | 0.02 | 26.18 | 0.1 | 115.72 | 282.87 | 1215.67 |
| *mean* | 0.74 | 127.18 | 295.16 | 0.19 | 18.21 | 87.09 | 3.51 | 0.45 | 0.02 | 7.05 | 0.03 | 33.09 | 92.41 | 820.93 |



dx.doi.org/10.1021/jf504023z | J. Agric. Food Chem. 2014, 62, 12332−12345

**Table 3. continued**

| | hydroxycinnamic acids | | | | | flavonols | | | | | | | | | flavons |
|---|---|---|---|---|---|---|---|---|---|---|---|---|---|---|---|
| cultivar | Nch | 3pc | 4cq | Ch | 3,5cq | QR | QRG | QGRR | QG | Kh | KR | IRR | IR | dKG+H | AG |
| Agat | 87.73 | 96.57 | 0.21 | 67.08 | 7.28 | 51.18 | 11.69 | nd | 6.69 | 6.71 | 53.97 | 8.90 | 33.75 | 2.32 | 1.99 |
| Ametyst | 500.12 | 37.74 | nd | 199.53 | 26.83 | 37.10 | 4.20 | 0.80 | 5.95 | 4.64 | 56.39 | 13.89 | 93.39 | 2.15 | 2.42 |
| Cesarzowa Eugenia | 205.38 | 122.88 | nd | 311.88 | 39.94 | 51.76 | 7.69 | 0.78 | 5.56 | nd | 66.94 | 9.51 | 78.38 | 2.99 | nd |
| Dradem | 239.14 | 296.68 | nd | 522.45 | 50.02 | 25.79 | 10.08 | 1.17 | 4.48 | 13.05 | 72.20 | 8.05 | 61.59 | 2.41 | 7.92 |
| Erdi Botermo | 496.70 | 593.33 | nd | 287.49 | 21.67 | 134.02 | 28.95 | 3.08 | 27.84 | nd | 81.90 | 16.76 | 76.93 | 4.68 | 5.24 |
| Erdi Nagygyümöscu | 175.41 | 6.77 | nd | 139.54 | 17.66 | 40.06 | 16.19 | nd | 1.05 | 3.74 | 110.38 | 7.70 | nd | 2.23 | nd |
| Fanal | 155.45 | 134.82 | nd | 160.43 | 22.49 | 40.88 | 8.00 | 1.59 | 4.45 | 5.34 | 48.72 | 13.14 | 34.20 | 2.73 | 3.61 |
| Fortuna | 152.02 | 7.94 | nd | 114.71 | 11.59 | 40.06 | 2.08 | nd | 9.04 | nd | 31.15 | 7.11 | 58.77 | nd | nd |
| Groniasta | 184.48 | 10.15 | nd | 190.39 | nd | 17.27 | 6.21 | 0.87 | 8.12 | 1.57 | 31.15 | 6.77 | 95.78 | 1.33 | nd |
| Karneol | 142.17 | 61.74 | 9.85 | 91.55 | 19.47 | 42.76 | 3.37 | nd | 2.02 | 10.29 | 73.00 | 9.76 | 64.09 | 1.21 | 4.93 |
| Kelleris 14 | 243.57 | 116.03 | nd | 160.96 | 19.85 | 48.87 | 4.61 | 1.10 | 5.45 | 5.22 | 69.28 | 12.50 | 100.02 | 3.56 | 8.31 |
| Książęca | 620.60 | 55.70 | nd | 87.78 | 17.65 | 34.14 | 12.01 | 0.67 | 14.11 | nd | 28.30 | 5.49 | 18.39 | nd | nd |
| Lucyna | 403.11 | 41.73 | nd | 128.67 | 15.21 | 22.63 | 5.70 | nd | nd | nd | 42.88 | 5.11 | 4.26 | 1.51 | 0.54 |
| Łutówka | 137.98 | 87.41 | nd | 182.28 | 25.04 | 38.76 | 4.65 | 0.43 | 4.22 | nd | 33.11 | 3.06 | 36.99 | 2.06 | nd |
| Meteor Korai | 794.82 | 75.54 | 7.93 | 181.72 | 36.10 | 24.75 | 14.14 | nd | nd | nd | 136.33 | 23.20 | 118.57 | 4.34 | nd |
| Morina | 938.55 | 37.46 | nd | 199.23 | 25.65 | 16.16 | 11.69 | 1.82 | 6.04 | 3.50 | 69.95 | 13.41 | 67.77 | 2.52 | 1.89 |
| Nana | 116.44 | 145.08 | nd | 161.72 | 21.71 | 66.72 | 4.36 | nd | 6.62 | 4.13 | 63.19 | 9.14 | 69.75 | 2.66 | nd |
| Northstar | 225.49 | 83.84 | nd | 76.48 | 23.30 | 59.24 | 12.13 | 3.16 | 13.17 | 16.43 | 83.73 | 25.62 | 125.70 | 3.55 | 11.98 |
| Pandy 103 | 702.38 | 28.40 | nd | 134.25 | 21.17 | 12.72 | 10.81 | 1.48 | 5.16 | 3.34 | 58.24 | 12.28 | 55.70 | 2.13 | 1.79 |
| Sabina | 165.33 | 78.46 | 3.43 | 192.26 | 22.55 | 78.19 | 19.03 | nd | 3.47 | 1.46 | 97.39 | 11.58 | nd | 1.68 | nd |
| Safir | 168.35 | 200.49 | nd | 258.63 | 25.12 | 71.80 | 4.74 | 1.08 | 7.46 | 3.11 | 101.76 | 23.76 | 115.78 | 3.26 | 1.02 |
| Skierka | 176.67 | 183.85 | nd | 164.95 | 10.25 | 57.01 | 3.55 | nd | 5.01 | 9.55 | 53.27 | 8.94 | 54.08 | 2.44 | 5.27 |
| Stevensbaer | 124.10 | 142.06 | nd | 207.32 | 24.21 | 55.89 | 5.18 | 0.82 | 5.33 | nd | 86.80 | 13.93 | 100.57 | 2.35 | nd |
| Topas | 339.59 | 261.65 | nd | 271.53 | 22.62 | 54.82 | 8.76 | 2.38 | 6.50 | 15.41 | 83.48 | 10.83 | 70.57 | 3.62 | 9.01 |
| Turgieniewka | 362.10 | 275.66 | nd | 286.48 | 25.16 | 57.85 | 9.14 | 2.43 | 6.88 | 16.28 | 88.07 | 9.81 | 75.00 | 3.65 | 9.20 |
| Wanda | 438.37 | 23.41 | nd | 66.24 | 13.65 | 24.29 | 10.35 | 0.98 | 1.71 | 0.70 | 104.78 | 16.37 | 2.51 | 1.37 | 1.89 |
| Wiblek | 368.98 | 8.96 | nd | 100.86 | 30.56 | 33.05 | 7.30 | 2.63 | 4.87 | 2.74 | 58.12 | 10.23 | 79.33 | 2.08 | 2.66 |
| Wifor | 320.09 | 29.94 | nd | 106.99 | 14.38 | 24.30 | 6.59 | 0.86 | 1.18 | nd | 47.57 | 5.77 | 4.95 | 1.43 | nd |
| Wilena | 436.25 | 15.22 | 11.71 | 119.51 | 18.03 | 18.27 | 4.79 | 0.86 | 5.11 | 1.87 | 44.42 | 7.90 | 81.72 | 1.27 | nd |
| Wilga | 123.54 | 119.55 | nd | 175.58 | 19.78 | 70.14 | 4.24 | 0.98 | 6.46 | nd | 71.59 | 14.58 | 92.27 | 2.38 | nd |
| Winer | 133.96 | 193.07 | nd | 249.58 | 21.95 | 53.52 | 5.74 | 1.17 | 4.61 | nd | 79.35 | 12.80 | 88.15 | 1.94 | nd |
| Wisok | 266.00 | 332.58 | nd | 262.15 | 11.81 | 107.33 | nd | 0.58 | 8.83 | nd | 40.20 | 3.95 | 37.96 | 3.74 | 5.15 |
| Wołyńska | 151.36 | 132.91 | nd | 123.58 | 23.28 | 64.23 | 9.34 | 1.07 | 4.96 | nd | 133.30 | 19.37 | 95.72 | 3.69 | nd |
| *minimum* | 87.73 | 6.77 | 0.21 | 66.24 | 0.00 | 12.72 | 0.00 | 0.00 | 0.00 | 0.00 | 28.30 | 3.06 | 0.00 | 0.00 | 0.00 |
| *maximum* | 938.55 | 593.33 | 11.71 | 522.45 | 50.02 | 134.02 | 28.95 | 3.16 | 27.84 | 16.43 | 136.33 | 25.62 | 125.70 | 4.68 | 11.98 |
| *mean* | 246.40 | 122.35 | 6.63 | 181.33 | 22.06 | 47.74 | 8.40 | 0.99 | 6.13 | 3.91 | 69.72 | 11.55 | 63.41 | 2.40 | 2.57 |

[a]Values are means of three repetitions. Abbreviations: A1, cyanidin-3-*O*-diglucoside-5-glucoside; A2, cyanidin-3-*O*-spohoroside; A3, cyanidin-3-*O*-glucosylrutinoside; A4, cyanidin-3-*O*-glucoside; A5, cyanidin-3,5-pentoside-hexoside; A6, cyanidin-3-*O*-rutinoside; A7, cyanidin-3-*O*-xylosyl-rutinoside; A8, pelargonidin-3-*O*-(2′-glucosyl)rutinoside; A9, peonidin-3-(6′-*p*-coumaroylglucoside)glucoside; A10, peonidin-3-*O*-rutinoside; A11, cyanidin-3-(6′-*p*-coumaroyl)glucoside; C, (+)-catechina; E, (−)-epicatechina; PP, polymeric procyanidins; Nch, neochlorogenic acid; 3pc, 3-*p*-coumarylquinic acid; 4cq, 4-*O*-caffeoylquinic acid; Ch, chlorogenic acid; 3,5cq, 3,5-dicaffeoylquinic acid; QR, quercetin-3-*O*-rutinoside; QRG, quercetin-3-*O*-rutinoside-glucoside; QGRR, quercetin-3-glucoside-dirhamnoside; QG, quercetin-3-*O*-galactoside; Kh, kaempferol-trihexose; AG, apigenin-7-*O*-glucoside; KR, kaempferol-3-*O*-rutinoside; IRR, isorhamnetin-3-rutinoside-7-rhamnoside; IR, isorhamnetin-3-*O*-rutinoside; dKG+H, dihydrokaempferol-glucoside + dihydrokaempferol-dihexoside; nd, not detected.



dx.doi.org/10.1021/jf504023z | J. Agric. Food Chem. 2014, 62, 12332−12345

well as on postharvest processing conditions and analytical methods.[37]

Concerning anthocyanin distribution, there were significant differences ($p < 0.05$) in the content of individual anthocyanins among the examined cultivars (Table 3). In general, cyanidin-3-*O*-(2′-glucosyl)-rutynoside was a predominant compound in the sour cherry fruits, with a mean range of 57% of the total anthocyanins. The next most abundant was cyanidin-3-*O*-spohoroside with a mean range of 20%, and finally cyanidin-3-*O*-rutinoside, with a mean range of 19%. The other anthocyanins were of minor importance. Cyanidin-3-*O*-xylosyl-rutinoside was detected and quantified only in some Polish cultivars, i.e., 'Wifor', 'Winer', and 'Wisok'. These anthocyanins are typically present in red currant berries.[35,38]

*Hydroxycinnamic Acids.* Hydroxycinnamic acids were the next major group of sour cherry polyphenols. The identification of hydroxycinnamic acid derivatives and their conjugates is presented in Table 2. Tentative identifications were made according to the UV/vis spectra, MS and MS/MS spectra, and molecular ions $[M - H]^-$. Retention times compared with standards were identified for four derivatives of caffeoylquinic acid: noechlorogenic acid, chlorogenic acid, 4-*O*-caffeoylquinic acid with $[M - H]^-$ at $m/z = 353$, and 3,5-dicaffeoylquinic acid with $[M - H]^-$ at $m/z = 515$ (Table 2). The presence of 4-*O*-caffeoylquinic acid and 3,5-dicaffeoylquinic acids has not been reported in sour cherry fruits until now. In addition, one ion was identified $[M - H]^-$ at $m/z = 337$ as corresponding to *p*-coumarylquinic acid derivatives, one of which was classified as 3-*p*-coumarylquinic acid. Similar configuration of these compounds was described in plum fruits,[39] belonging to the same family.

Contrary to anthocyanidins, the same hydroxycinnamic acid compounds were present in each cultivar, but there were differences in their relative levels. In almost all cultivars, neochlorogenic acid (~47%) was the major hydroxycinnamic acid derivative, followed by chlorogenic acid (~30%) and *p*-coumaroylquinic acid (~19%). The highest concentration of hydroxycinnamic acids was found in 'Morina' and 'Dradem' cultivars (1200.90 and 1108.29 mg/100 g dm, respectively), and the lowest in 'Agat' and 'Fortuna' cultivars (258.86 and 286.26 mg/100 g dm, respectively).

In some sour cherry cultivars, such as 'Sabina', 'Fanal', 'Safir', 'Wilena', 'Nana', 'Dradem', 'Cesarzowa Eugenia', 'Wilga', 'Stevensbaer', 'Łutówka', and 'Winer', the levels of chlorogenic acid were found to be higher than those of neochlorogenic acid. Additionally, in the cultivars such as 'Agat', 'Erdi botermo', 'Skierka', Nana', 'Dradem', 'Stevensbaer', 'Winer', and 'Wisok', the levels of 3-*p*-coumarylquinic acid were found to be higher than those of neochlorogenic acid. However, for many other cultivars the content of this acid was lower than 50 mg/100 g dm. The content of 3,5-dicaffeoylquinic acid was very stable (except in 'Groniasta' cv), and in all the analyzed cultivars it ranged between 7.28 and 50.02 mg/100 g dm (Table 3). Mozetic et al.[40] demonstrated that the levels of hydroxycinnamic derivatives changed during ripening. A change in the ratio of neochlorogenic acid and *p*-coumaroylquinic acid could also be due to the hydroxylation of *p*-coumarylquinic acid to neochlorogenic acid during biosynthesis pathways.

In the present study, the concentrations of hydroxycinnamic acid derivatives were higher than in sweet cherry[20,41−43] blue honeysuckle[13] or plums,[39] lower than in quince fruits,[14] and comparable to black currant fruits.[35,38] The concentration of phenolic acids, especially of chlorogenic acid, is very important, because these compounds are the precursors of flavor.[44]

*Flavonols and Flavon.* Three types of flavonol derivatives with a fragment at $m/z$ 301, 285, and 315, characteristic for quercetin, kaempferol, and rhamnetin derivatives, respectively, were found in the sour cherry fruits (Table 2).

In this study, four quercetins, i.e., 3-*O*-rutinoside-glucoside ($[M - H]^-$ at $m/z = 771$), 3-*O*-glucosidedirhamoside ($[M - H]^-$ at $m/z = 755$), 3-*O*-rutinoside ($[M - H]^-$ at $m/z = 609$), and 3-*O*-galactoside ($[M - H]^-$at $m/z = 463$) were found, at a wavelength characteristic for these compounds $\lambda_{max} = 350$ nm. Similar results were obtained for kaempferol derivatives, which were identified as trihexose with $[M - H]^-$ at $m/z = 773$; dihydrokaempferol-dihexoside, and dihydrokaempferol-glucoside with $[M - H]^-$ at $m/z = 611$ and 449, respectively, and kaempferol-3-*O*-rutinoside with $[M - H]^-$at $m/z = 593$ at $\lambda_{max} = 340$ nm. Additionally, two derivatives of isorhamnetin, i.e., -3-rutinoside-7-rhamnoside and -3-*O*-rutinoside, were identified with $[M - H]^-$at $m/z = 769$ and 623, respectively. Some of these compounds were previously reported in sour cherry pomace by Kolodziejczyk et al.[26] However, neither naringenin nor genistin was found by these authors.

Additionally, one flavon was identified as apigenin derivative, according to its UV spectrum and MS fragmentation. This compound was apigenin aglycone $[M - H]^-$ at $m/z = 269$, in a negative mode at 7.26 min, with $[M - H]^-$ at $m/z = 431$, and characteristic $\lambda_{max} = 241$ and 340 nm of apigenin-7-*O*-glucoside. Chaovanalikit et al.[31] suggested the presence of this flavon compound in the sour cherry. This is the first time the identification and quantification of so many flavonol and flavon derivatives were performed in the sour cherry fruit. Previous work by Serra et al.[23] indicated the presence of quercetin-3-*O*-rutinoside and quercetin-3-*O*-glucoside. Kirakosyan et al.[32] claimed quercetin, kaempferol, and isorhamnetin rutinoside to be the main flavonol compounds in the tart cherry. Quercetin derivatives even than rarely the major polyphenolic compounds of fruits, they are very important for human health.[45] Flavonols are also effective antioxidants. Their high antioxidant potential is due to 3′,4′-dihydroxy substitution in B-ring and conjugation between A and B rings. In general, flavones have higher antioxidant activity as compared with anthocyanins with the same hydroxylation patterns measured with ORAC assay.[46]

Among the five groups of phenolic compounds identified is the sour cherry fruits, flavonols and flavon were found to be the least abundant. Major compounds in this group were quercetin-3-*O*-rutinoside (8−52% of total flavonol+flavon) > kaempferol-3-*O*rutinoside (18−64%) > isorhamnetin-3-*O*-rutinoside (0−57%); less abundant compounds included quercetin-3-glucoside-dirhamnoside (2−10%) and isorhamnetin-3-rutinoside-7-rhamnoside (0−11%), but the other compounds were present in trace amounts and not in all cultivars (Table 3). Total content of flavonols in the sour cherry samples ranged from 82.07 to 374.17 mg/100 g dm. The cultivars showing the highest content of flavonols were 'Erdi botermo', 'Norstar', 'Wołyńska', 'Meteor Korali', and 'Safir', whereas 'Wifor' and 'Lucyna' cultivars were characterized by the lowest flavonoid content. Kirakosyan et al.[32] reported comparable amounts of flavonols in the sour cherry cultivars to those presented in this study. The concentration of apigenin-7-*O*-glucoside amounted to 11.98 mg/100 g dm for the 'Nordstar', but it was detected in only 17 other cultivars.

**Antioxidant Activity in Sour Cherry Fruits.** Three in vitro assays, based on the scavenging activity of the stable oxygen radical absorbance capacity (ORAC) assay, ABTS radical scavenging capacity assay, and ferric reducing antioxidant potential (FRAP) assay, were used as complementary methods to evaluate the potential antioxidant activity of sour cherry fruits (Table 4). Significant differences were observed among the cultivars with reference to these three assays, but all the cultivars revealed the same trend. Antioxidant activity of the sour cherry evaluated using the ORAC assay was 8.13−38.11 mmol TE/100 g dm; for ABTS assay it was 3.72−18.40 mmol TE/100 g dm, and for FRAP assay it amounted to 1.93−12.95 mmol TE/100 g dm. 'Książęca', 'Erdi Nagygyümöscu', and 'Groniasta' cultivars showed the lowest antioxidant potential, and 'Łutówka', 'Fanal', 'Topaz', and 'Wołyńska' were characterized by the highest antioxidant activity among all the investigated cultivars across all the assays.

**Table 4. Antioxidant Activity of Sour Cherry Cultivars Measured by ABTS, FRAP, and ORAC Methods, Expressed as mmol Trolox/100 g dm[a]**

| cultivar | ABTS | FRAP | ORAC |
|---|---|---|---|
| Agat | 14.73 | 9.36 | 23.86 |
| Ametyst | 13.10 | 9.14 | 19.88 |
| Cesarzowa Eugenia | 12.81 | 9.40 | 20.64 |
| Dradem | 11.34 | 6.70 | 20.91 |
| Erdi Bötermo | 9.04 | 6.26 | 13.98 |
| Erdi Nagygyümöscu | 3.72 | 9.67 | 8.13 |
| Fanal | 18.40 | 12.77 | 38.11 |
| Fortuna | 6.99 | 9.67 | 24.71 |
| Groniasta | 8.84 | 5.71 | 17.57 |
| Karneol | 14.94 | 10.37 | 30.44 |
| Keleris 14 | 14.50 | 9.90 | 27.59 |
| Książęca | 5.38 | 8.10 | 9.21 |
| Lucyna | 13.41 | 9.14 | 30.74 |
| Łutówka | 16.38 | 10.35 | 32.91 |
| Meteor Korai | 4.79 | 1.93 | 17.66 |
| Morina | 14.70 | 10.31 | 32.86 |
| Nana | 11.64 | 7.39 | 19.69 |
| Nordstar | 12.84 | 8.94 | 31.91 |
| Pandy | 11.93 | 7.71 | 20.69 |
| Sabina | 11.39 | 7.68 | 21.29 |
| Safir | 15.40 | 10.64 | 35.72 |
| Skierka | 9.20 | 12.95 | 24.23 |
| Stevensbaer | 14.77 | 9.85 | 31.40 |
| Topas | 16.71 | 12.93 | 36.30 |
| Turgieniewka | 11.68 | 7.97 | 25.12 |
| Wanda | 10.94 | 7.85 | 16.68 |
| Wiblek | 10.94 | 7.36 | 21.72 |
| Wifor | 12.37 | 8.82 | 27.06 |
| Wilena | 18.02 | 11.84 | 31.22 |
| Wilga | 12.55 | 8.51 | 21.15 |
| Winer | 11.83 | 8.96 | 26.84 |
| Wisok | 13.27 | 8.89 | 32.24 |
| Wołyńska | 16.65 | 11.55 | 35.00 |
| *minimum* | 3.72 | 1.93 | 8.13 |
| *maximum* | 18.40 | 12.95 | 38.11 |
| *mean* | 12.28 | 9.05 | 25.07 |

[a]Values are means of three repetitions.

Literature data[16,24,35,47,48] indicate that not only the total content of polyphenolic compounds played a very important role in antioxidant activity, but also the type of phenolic compounds, i.e. anthocyanins, was essential. Our results suggest that antioxidant activity of the sour cherry is not related to the presence of anthocyanins, but may be ascribed to polymeric procyanidins. Significant positive correlations were found only between the results of total antioxidant assays and polymeric procyanidins (Pearson correlation = 0.742, 0.692, and 0.482 for ORAC, ABTS, and FRAP, respectively). Our results indicated that these compounds markedly contributed to the total antioxidant capacity in the investigated fruits.

Rice-Evans et al.[47] discussed the relationship between the antioxidant potential of polyphenols and their chemical structure and claimed that hydroxylation of B ring and glycosylation had a strong influence on the antioxidant potential of phenolic compounds. Bandoniene et al.[48] tested kinetic behaviors of different antioxidants present in apple and apple extract with the HPLC/DPPH method and showed that the antioxidant activity was to the greatest extent influenced by polyphenolic compounds from the group of flavan-3-ols, such as (+)-catechin and (−)-epicatechin, as well as their oligomers, i.e., procyanidin dimer and trimer (B1, B2, and C1). Khoo et al.[6] pointed out that the sour cherry biologically active antioxidants involved not only anthocyanins, but colorless phenolics also exerted an important antioxidant impact by affecting the plant biological performance. Usenik et al.[42] reported that the relationship between antioxidant activity and total anthocyanin content varied between cultivars from $r^2$ = 0.01 to 0.99. According to these authors, antioxidant activity depended on different chemical attributes and was cultivar-specific. Their study showed that some cultivars of sweet cherry ('Ferrador' cv) contained low levels of phenolic compounds and anthocyanins, but exhibited very high antioxidant activity. Comparable results was observed in our study for 'Książęca' cultivar. Goncalves et al.[49] found that the antioxidant activity of sour cherries correlated with the content of *p*-coumaroylquinic acid and also tended to correlate with catechin monomer concentration.

**L-Ascorbic Acid in Sour Cherry Fruits.** Fruits are generally a good source of ascorbic acid (vitamin C). The content of ascorbic acid in individual sour cherry cultivars differed greatly, ranging from 5.45 to 22.11 mg/100 g fw (Table 5). The highest ascorbic acid content (up to 18 mg) was detected in 'Morina', 'Meteor Korai', 'Erdi botermo', 'Wilena', and 'Stevensbaer' cultivars. Ascorbic acid content in most of the analyzed variations was lower than 10 mg, as was the case in e.g. 'Książęca', Erdi Nagygyümöscu', 'Fortuna', 'Sabina', 'Skierka', 'Nordstar', 'Turgieniewka', 'Safir', 'Nana', 'Karneol', 'Keleris 14', Ametyst', 'Łutówka', and 'Wifor' cultivars. In addition, ascorbic acid concentration in these cultivars was lower than in other fruits, well known for their high ascorbic acid content, such as kiwi (29−80 mg/100 g fw)[50] or cornelian cherries (31−112 mg/100 g fw).[51] However, the content of ascorbic acid found in this study was comparable with quinces (6−26 mg/100 g fw),[14] nectarines (4.8−13.2 mg/100 g fw),[52] peaches (3.6−12.6 mg/100 g fw),[52] plums (2.5−10.2 mg/100 g fw),[52] and blue honeysuckle (4.86−20.69 mg/100 g fw).[53] Additionally, we found no significant correlation between the results of total antioxidant activity assays and vitamin C content.

**Fruit Weight, Dry Matter, Soluble Solids, pH, Total Acidity, and Total and Reducing Sugar in Sour Cherries Fruits.** The main physicochemical characteristics of 33 sour

Table 5. Nutritional and Chemical Components in Different Sour Cherry Cultivars[a]

| cultivar | FW | dm | SSC | pH | TA | TS | RS | MI | A | P | AA |
|---|---|---|---|---|---|---|---|---|---|---|---|
| Agat | 3.34 | 15.85 | 14.2 | 3.27 | 1.87 | 9.96 | 9.27 | 7.93 | 0.37 | 0.51 | 13.70 |
| Ametyst | 3.14 | 18.96 | 17.85 | 3.20 | 2.29 | 11.82 | 10.57 | 13.51 | 0.40 | 0.0 | 6.21 |
| Cesarzowa Eugenia | 4.20 | 18.10 | 16.65 | 3.55 | 1.47 | 11.15 | 10.21 | 8.54 | 0.60 | 0.26 | 8.89 |
| Dradem | 4.29 | 19.69 | 18.30 | 3.42 | 1.89 | 11.78 | 10.83 | 8.94 | 0.48 | 0.19 | 10.38 |
| Erdi Botermo | 5.34 | 17.92 | 16.65 | 3.54 | 1.14 | 11.64 | 10.96 | 15.28 | 0.60 | 0.62 | 18.59 |
| Erdi Nagygyümöscu | 6.02 | 14.37 | 13.25 | 3.27 | 1.02 | 10.77 | 9.29 | 13.66 | 0.59 | 0.41 | 7.21 |
| Fanal | 4.75 | 19.25 | 17.45 | 3.25 | 2.17 | 11.26 | 9.91 | 8.43 | 0.45 | 0.54 | 10.23 |
| Fortuna | 3.78 | 13.71 | 12.90 | 3.30 | 1.04 | 9.09 | 8.33 | 12.40 | 0.61 | 0.24 | 6.46 |
| Groniasta | 3.67 | 15.89 | 14.30 | 3.37 | 1.71 | 9.91 | 9.52 | 8.77 | 0.48 | 0.38 | 13.02 |
| Karneol | 5.56 | 16.49 | 14.70 | 3.38 | 1.72 | 9.89 | 8.85 | 9.53 | 0.51 | 0.14 | 8.17 |
| Kelleris 14 | 4.65 | 16.84 | 15.40 | 3.55 | 1.28 | 9.87 | 9.02 | 12.62 | 0.75 | 0.38 | 5.45 |
| Książęca | 6.10 | 14.71 | 13.50 | 3.36 | 0.94 | 10.39 | 9.23 | 15.08 | 0.61 | 0.42 | 9.80 |
| Lucyna | 3.74 | 20.07 | 18.35 | 3.26 | 2.17 | 12.96 | 11.83 | 8.87 | 0.36 | 0.35 | 15.87 |
| Łutówka | 3.96 | 17.22 | 16.30 | 3.31 | 1.76 | 11.06 | 10.10 | 7.90 | 0.46 | 0.37 | 5.91 |
| Meteor Korai | 2.35 | 19.18 | 18.30 | 3.14 | 1.68 | 13.02 | 11.33 | 10.89 | 0.68 | 0.25 | 18.54 |
| Morina | 3.42 | 21.89 | 20.25 | 3.26 | 2.15 | 13.25 | 12.25 | 9.88 | 0.56 | 0.55 | 22.18 |
| Nana | 3.77 | 21.31 | 19.20 | 3.35 | 2.12 | 12.97 | 12.01 | 11.70 | 0.50 | 0.29 | 8.88 |
| Northstar | 3.95 | 15.60 | 14.80 | 3.24 | 2.09 | 10.37 | 8.95 | 7.40 | 0.37 | 0.14 | 9.50 |
| Pandy 103 | 4.66 | 18.57 | 16.95 | 3.38 | 1.59 | 11.86 | 10.87 | 11.19 | 0.45 | 0.34 | 14.30 |
| Sabina | 4.90 | 16.88 | 15.60 | 3.27 | 1.87 | 10.65 | 9.93 | 8.72 | 0.28 | 0.47 | 7.25 |
| Safir | 5.41 | 15.56 | 15.00 | 3.22 | 1.81 | 10.34 | 9.16 | 8.67 | 0.40 | 0.63 | 7.68 |
| Skierka | 2.45 | 15.28 | 14.50 | 3.32 | 1.97 | 9.20 | 8.42 | 7.36 | 0.35 | 0.58 | 8.64 |
| Stevensbaer | 2.10 | 25.96 | 25.15 | 3.40 | 2.21 | 16.33 | 14.41 | 10.11 | 1.84 | 0.37 | 18.27 |
| Topas | 6.07 | 16.23 | 15.35 | 3.04 | 2.79 | 9.61 | 8.82 | 5.76 | 0.20 | 0.43 | 10.06 |
| Turgieniewka | 4.15 | 17.70 | 16.30 | 3.41 | 1.61 | 11.08 | 9.95 | 10.62 | 0.50 | 0.45 | 6.74 |
| Wanda | 4.10 | 19.02 | 18.05 | 3.23 | 1.94 | 12.15 | 11.56 | 9.76 | 0.29 | 0.65 | 10.97 |
| Wiblek | 2.60 | 19.78 | 18.15 | 3.40 | 1.99 | 11.88 | 10.85 | 9.93 | 0.55 | 0.29 | 11.38 |
| Wifor | 2.25 | 17.15 | 16.10 | 3.40 | 1.88 | 10.84 | 9.78 | 11.92 | 0.53 | 0.26 | 8.79 |
| Wilena | 2.20 | 21.33 | 20.55 | 3.34 | 2.19 | 13.27 | 12.10 | 9.83 | 0.58 | 0.72 | 18.08 |
| Wilga | 3.57 | 20.37 | 19.10 | 3.32 | 2.31 | 12.40 | 11.30 | 11.89 | 0.82 | 0.43 | 12.93 |
| Winer | 4.29 | 18.36 | 17.25 | 3.29 | 2.03 | 10.92 | 9.89 | 10.15 | 0.44 | 0.31 | 11.11 |
| Wisok | 2.27 | 20.69 | 19.40 | 3.34 | 2.33 | 11.93 | 10.84 | 10.16 | 0.74 | 0.30 | 13.08 |
| Wołyńska | 2.37 | 20.88 | 19.75 | 3.39 | 2.04 | 12.56 | 11.38 | 8.66 | 1.01 | 0.63 | 14.41 |
| *minimum* | 2.10 | 13.71 | 12.90 | 3.04 | 0.94 | 9.09 | 8.33 | 5.76 | 0.20 | 0.00 | 5.45 |
| *maximum* | 6.10 | 25.96 | 25.15 | 3.55 | 2.79 | 16.33 | 14.41 | 15.28 | 1.84 | 0.72 | 22.18 |
| *mean* | 3.92 | 18.20 | 16.96 | 3.32 | 1.85 | 11.40 | 10.36 | 10.18 | 0.56 | 0.39 | 11.29 |

[a]Values are means of three repetitions. Abbreviations and units: FW, fruits weight (g); dm, dry matter (%); SSC, total soluble solids content (°Brix); TA, total titratable acidity (g malic acid/100 g); TS, total sugars (mg/100 g); RS, reducing sugars (mg/100 g); MI, maturity index (−); A, ash (%); P, pectins (%); AA, ascorbic acid (mg/100 g).

cherry cultivars were evaluated in this study. Some of these cultivars ('Agat', 'Ametyst', 'Dradem', 'Lucyna', 'Sabina', 'Wanda', 'Wible', 'Wifor', 'Wilena', 'Wilga', 'Winer', 'Wisok') were new Polish cultivars, investigated for the first time (Tables 1 and 5).

Fruit size is a varietal characteristic that may fluctuate depending on climatic and agricultural conditions. Fruit weight depends on fruit load, agricultural conditions, and fruit maturity stage.[53] Average fruit weight in our study ranged from 2.10 g ('Stevensbaer') to 6.10 g ('Ksiażęca') (Table 5). Many of the investigated cultivars had larger fruits than the mean value of 4.15 g. Especially interesting were 'Keleris 14', 'Pandy', 'Fanal', 'Sabina', 'Erdi botermo', 'Safir', 'Karneol', 'Erdi Nagygyümöscu', and 'Topas' cultivars, characterized by the largest fruits (Table 5). In contrast, new Polish cultivars, such as 'Wilbek', 'Wołyńska', 'Wisok', and 'Wilena', were characterized by rather small fruits, lighter than 3.00 g. The above-mentioned variability of weight parameter of sour cherry fruits is important for industrial processing effectiveness and for efficient depitting procedure, especially in the case of products where the shape of the fruit should be retained after processing. Additionally, the weight and size of berries play important roles in the evaluation of fruit quality and clearly affect consumers' acceptance.

Differences were found among the analyzed sour cherry cultivars in dry matter, total soluble solids (SSC), pH, total titratable acidity (TA), reducing sugars, and maturity index (MI) (Table 5).

The lowest dry matter and SSC values were determined for 'Fortuna' (13.71% and 12.9°Brix, respectively), 'Erdi Nagygyümöscu' (14.37% and 13.3°Brix, respectively), and 'Książęca' cultivars (14.71% and 13.5°Brix, respectively). The highest dry matter and SSC content were observed in 'Morina' (21.89% and 20.3°Brix, respectively), 'Wilena' (21.33% and 20.6°Brix, respectively), 'Stevensbaer' (25.96% and 25.2°Brix, respectively), and 'Wołyńska' cultivars (20.88% and 19.8°Brix, respectively). Compared to other fruits, SSC content in sour cherry was similar to that in pomegranate (10.0−16.5°Brix)[54,55] and cornelian cherry (14.4%),[51] but higher than in raspberry (7.1−8.8°Brix).[58]

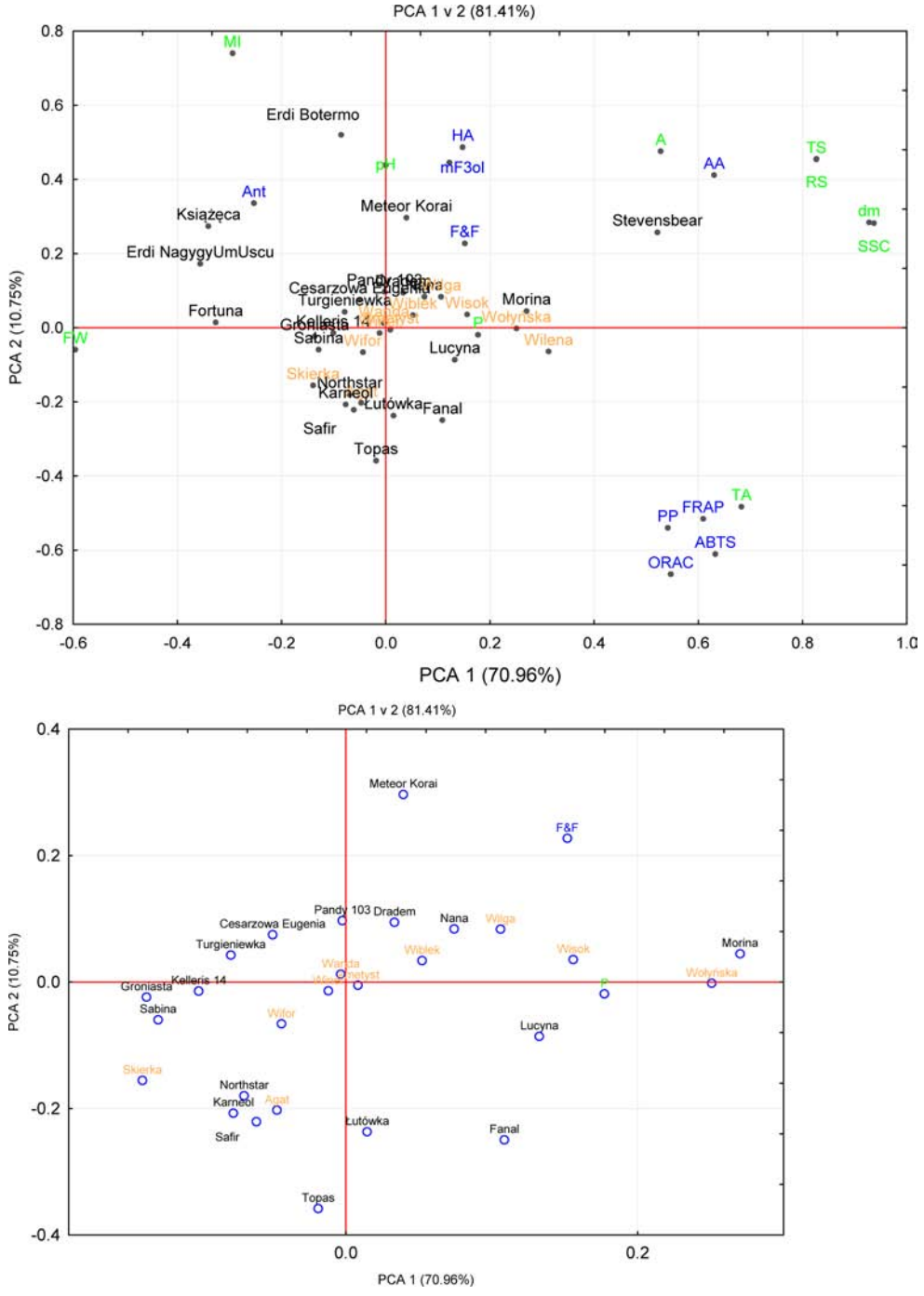


**Figure 1.** PCA map (top, and bottom, zoom) showing the relationship among phytochemical profile and health-related compounds of sour cherry fruits.

pH values of the sour cherry ranged from 3.04 in 'Topas' and the highest pH of 3.55 was recorded in both 'Keleris 14' and 'Cesarzowa Eugenia' cultivars. 'Książęca', 'Erdi Nagygyümöscu', and 'Fortuna' cultivars were the least acidic, with TA value of 0.90, 0.97, and 0.96 g of malic acid/100 g fw, while the fruits of 'Topas', 'Wilga', 'Stevensbaer', and 'Wisok' cultivars were the most acidic, with TA value of 2.67, 2.21, 2.11, and 2.23 g of malic acid/100 g fw, respectively. These pH and TA values were lower than reported for the sweet cherry.[20] However, these results were in agreement with other data reported in the literature for blue honeysuckle,[13] pomegranate,[55] or cornelian cherry.[51] In general, sour cherry fruits are rich in organic acids, and this characteristic confers a distinct sour taste of these fruits.

Maturity index (MI = SSC/TA) appears to be a key factor responsible for the taste and flavor of fruits and the factor influencing consumers' preference and acceptance. Some authors[13,21,55] used the maturity index to classify fruit cultivars as sour, sour-sweet, and sweet. MI in the analyzed sour cherry cultivars varied considerably from 5.7 in 'Topas' to 15.3 in 'Erdi botermo' and 'Książęca'. According to a classification established for the analyzed fruits, most of the cultivars were soursweet rather than only sour or only sweet.


dx.doi.org/10.1021/jf504023z | J. Agric. Food Chem. 2014, 62, 12332−12345

Total sugar content in the sour cherry cultivars varied between 9.09 and 16.33%, and reducing sugar between 8.33 and 14.41%. The lowest level of total and reducing sugars was detected in 'Fortuna' (9.09% and 8.33%), 'Skierka' (9.20% and 8.42%), 'Topas' (9.61% and 8.82%), and 'Karnelo' (9.89% and 8.85%), and the highest in 'Nana' (12.97% and 12.01%), 'Wilena' (13.27 % and 12.10%), 'Morina' (13.25% and 12.25%), and 'Stevensbaer' cultivars (16.33% and 14.41%) (Table 5). The content of total sugars in sour cherry fruit was lower than in apples,[56] but higher than in cornelian cherry.[51]

The investigated sour cherry cultivars differed in their ash composition. Mineral composition of fruits depends not only on the species or cultivars, but also on the growing conditions, such as soil and climate-related factors.[57] Only in 'Stevensbaer' and 'Wołyńska' cultivars was the content of ash higher than in the other analyzed fruits. The rest of analyzed cultivars were characterized low ash content, especially 'Topas', 'Groniasta', 'Sabina', 'Wanda', 'Łutówka', 'Lucyna', 'Turgieniewka', 'Safir', and 'Winer' (< 0.50% ash content).

Fruits are essential dietary components and a good source of pectins. The highest pectin level was found in 'Wilena' cultivar (0.72%), while extremely low content was detected in 'Northstar', 'Karneol' (0.14%), and 'Dradem' cultivars (0.19 %). Some cultivars of raspberry[58] and blue honeysuckle berries[13] contained more pectins than sour cherry fruits.

Many of the discussed factors depend on the cultivar, but also on a number of environmental conditions.[57,59]

**Principal Component Analysis (PCA).** To better understand the trends and relationships among the 43 different sour cherry cultivars, principal component analysis (PCA) was applied (see Figure 1). When considering the first two dimensions of the biplot (PCA1 and PCA2), quality parameters and contents of bioactive compounds explained 81.41% of the variation. The results obtained from PCA, using the linkage method among groups, indicated the presence of four clusters:

(1) 'Fanal', 'Wołyńska', 'Ametyst', 'Lucyna', 'Wilena', and 'Łutówka' cultivars, characterized by high content of polymeric procyanidins (PP) and high total antioxidant activity (e.g., ABTS, FRAP, and ORAC). Additionally, high levels of total acid (TA) and pectins (P) were detected in these cultivars.

(2) 'Stevensbaer', 'Meteor Korai', 'Morina', 'Wołyńska', 'Wisok', 'Wilga', 'Nana', 'Wibek', 'Dradem' cultivars, characterized by high content of polyphenols (hydroxycinnamic acid (HA), stotal amount of (+)-catechin, and (−)-epicatechin (mF3ol), flavonols and flavon (F&F), and L-ascorbic acid (AA). Fruits in these cultivars were scored high in such parameters as dry matter (dm), total soluble solids (SSC), total and reducing sugars (TS and RS), and ash (A).

(3) 'Erdi Botermo', 'Książęca', 'Erdi Nagygyumuscu', 'Fortuna', 'Cesarzowa Eugenia', 'Pandy 103', 'Turgieniewka', 'Keleris 14' and 'Wanda' cultivars, characterized by high content of anthocyanins (Ant). Fruits located in this cluster high correlated with maturity index (MI).

(4) 'Groniasta', 'Keleris 14', 'Winer', 'Skierka', 'Sabina', 'Northstar', 'Karneol', 'Agat', 'Safir', and 'Topas' cultivars, with typically high fruits weight but additionally positive correlation with antioxidant activity (ABTS, FRAP, ORAC) and content of polymeric procyanidins (PP) but negative correlations with other phenolic compounds such as HA, mF3ol, and F&F.

In this study, fruit quality parameters and chemical properties of 33 sour cherry cultivars grown in Poland were evaluated. The results confirm the correlation between a cultivar and the content of bioactive compounds and antioxidant activity of sour cherry fruits, which possibly affect dietary choices. Therefore, the sour cherry cultivars used as progenitors in a breeding program are vital for generating new cultivars with high content of bioactive compounds. On the other hand, a high number of evaluated cultivars, from different genetic origins and with large phenotypic variability, constitutes a considerable contribution on sour cherry species, especially for breeding purposes. New Polish cultivars, particularly 'Wider', 'Winer', 'Wilena', 'Wisok', and 'Ametyst', are promising, but they should be constantly improved through breeding programs to refine their functional properties.

## AUTHOR INFORMATION

### Corresponding Author

*Tel: (+48) 71 3207706. Fax: (+48) 71 3207707. E-mail: aneta.wojdylo@up.wroc.pl.

### Funding

This work was financially supported by the National Science Centre UMO2011/01/B/NZ9/07139.

### Notes

The authors declare no competing financial interest.

## ACKNOWLEDGMENTS

We are grateful to Kamili Strong, Marii Bortkiewicz and Elżbiecie Buckiej for their technical assistance.

## REFERENCES

(1) Food and Agriculture Organization of the United Nations, 2012; http://faostat.fao.org.

(2) Damar, I.; Eksi, A. Antioxidant capacity and anthocyanin profile of sour cherry (*Prunus cerasus L.*) juice. *Food Chem.* **2012**, *135*, 2910−2914.

(3) Kim, D. O.; Padilla-Zakour, O. I. Jam processing effect on phenolics and antioxidant capacity in anthocyanin-rich fruits: cherry, plum, and raspberry. *J. Food Sci.* **2004**, *69*, S395−400.

(4) Wojdyło, A.; Figiel, A.; Lech, K.; Nowicka, P.; Oszmiański, J. Effect of convective and vacuum-microwave drying on the bioactive compounds, colour and antioxidant activity of sour cherries. *Food Bioprocess Technol.* **2014**, *7*, 829−841.

(5) Sumic, Z.; Tepic, A.; Vidovic, S.; Jokic, S.; Malbasa, R. Optimization of frozen sour cherries vacuum drying process. *Food Chem.* **2013**, *136*, 55−63.

(6) Khoo, G. M.; Clausen, M. R.; Pedersen, H.; Larsen, E. Bioactivity and total phenolic content of 34 sour cherry cultivars. *J. Food Comp. Anal.* **2001**, *24*, 772−776.

(7) Wang, H.; Nair, M. G.; Strasburg, G. M.; Chang, Y. C.; Booren, A. M.; Gray, J. I.; DeWitt, D. L. Antioxidant and antiinflamatory activities of anthocyanins and their aglycon, cyanidin from tart cherries. *J. Nat. Prod.* **1999**, *62*, 294−296.

(8) Mulabagal, V.; Lang, G. A.; Dewitt, D. L.; Dalavoy, S. S.; Nair, M. G. Anthocyanin 526 content, lipid peroxidation and cyclooxygenase enzyme inhibitory activities of sweet and sour cherries. *J. Agric. Food Chem.* **2009**, *57*, 1239−1246.

(9) Seymour, E. M.; Singer, A. A. M.; Kirakosyan, A.; Urcuyo-Llanes, D. E.; Kaufman, P. B.; Bolling, S. F. Altered hyperlipidemia, hepatic steatosis, and hepatic peroxisome proliferator-activated receptors in rats with intake of tart cherry. *J. Med. Food* **2008**, *11*, 252−259.

(10) Burkhardt, S.; Tan, D. X.; Manchester, L. C.; Hardeland, R.; Reiter, R. J. Detection and quantification of the antioxidant melatonin in Montmorency and Balaton tart cherries (*Prunus cerasus*). *J. Agric. Food Chem.* **2001**, *49*, 4898−4902.

(11) Papp, N.; Szilvassy, B.; Szabo, Z.; Nyeki, J.; Stefanovits-Banyai, E.; Hegedus, A. Antioxidant capacity, total phenolics and mineral element contents in fruits of Hungarian sour cherry cultivars. *Acta Horticulturae* **2008**, *14*, 59−64.
(12) Bonerz, D.; Wurth, K.; Dietrich, H.; Will, F. Analytical characterization and the impact of aging on anthocyanin composition and degradation in juices from five sour cherry cultivars. *Eur. Food Res. Technol.* **2007**, *224*, 355−364.
(13) Wojdyło, A.; Nuncio Jauregui, P. N.; Carbonell-Barrachina, A. A.; Oszmiański, J.; Golis, T. Variability of phytochemical properties and content of bioactive compounds in *Lonicera caerulea* L. var. kamtschatica berries. *J. Agric. Food Chem.* **2013**, *61*, 12072−12084.
(14) Wojdyło, A.; Oszmiański, J.; Bielicki, P. Polyphenolic composition, antioxidant activity, and polyphenol oxidase (PPO) activity of quince (*Cydonia oblonga* Miller) varieties. *J. Agric. Food Chem.* **2013**, *61*, 2762−2772.
(15) Oszmiański, J.; Wojdyło, A. Effects of blackcurrant and apple pulp blended on phenolics, antioxidant capacity and colour of juices. *J. Czech Food Technol.* **2009**, *27*, 338−351.
(16) Ou, B.; Huang, D.; Hampsch-Woodill, M.; Flanagan, J. A.; Deemer, E. K. Analysis of antioxidant activities of common vegetables employing oxygen radical absorbance capacity (ORAC) and ferric reducing antioxidant power (FRAP) assay: a comparative study. *J. Agric. Food Chem.* **2002**, *50*, 3122−3128.
(17) Re, R.; Pellegrini, N.; Proteggente, A.; Pannala, A.; Yang, M.; Rice-Evans, C. Antioxidant activity applying an improved ABTS radical cation decolorization assay. *Free Radical Biol. Med.* **1999**, *26*, 1231−1237.
(18) Benzie, I. F. F.; Strain, J. J. Ferric reducing ability of plasma (FRAP) as a measure of antioxidant power: The FRAP assay. *Anal. Biochem.* **1996**, *239*, 70−76.
(19) Wu, X.; Gu, L.; Prior, R. L.; McKay, S. Characterization of anthocyanins and proanthocyanins in some cultivars of Ribes, Aronia and Sambucus and their antioxidant capacity. *J. Agric. Food Chem.* **2004**, *52*, 7846−7856.
(20) Ballistreri, G.; Continella, A.; Gentile, A.; Amenta, M.; Fabroni, S.; Rapisarda, P. Fruit quality and bioactive compounds relevant to human health of sweet cherry (*Prunus avium* L.) cultivars grown in Italy. *Food Chem.* **2013**, *140*, 630−638.
(21) Zadernowski, R.; Naczk, M.; Nesterowicz, J. Phenolic acid profiles in some small berries. *J. Agric. Food Chem.* **2005**, *53*, 2118−2124.
(22) Gerasopoulos, D.; Stavroulakis, G. Quality characteristics of four mulberry (*Morus spp.*) cultivars in the area of Chania Greece. *J. Sci. Food Agric.* **1997**, *73*, 261−264.
(23) Serra, A. T.; Duarte, R. O.; Bronze, M. R.; Duarte, C. M. M. Identification of bioactive response in traditional cherries from Portugal. *Food Chem.* **2011**, *125*, 318−325.
(24) Toydemir, G.; Capanoglu, E.; Gomez Roldan, M. V.; De Vos, R. C. H.; Boyacioglu, D.; Hall, R. D.; Beekwilder, J. Industrial processing effects on phenolic compounds in sour cherry(*Prunus cerasus* L.) fruit. *Food Res. Int.* **2013**, *53*, 218−225.
(25) Diaz-Garcia, M. C.; Obon, J. M.; Castellar, M. R.; Collado, J.; Alacid, M. Quantification by UHPLC of total individual polyphenols in fruit juices. *Food Chem.* **2013**, *138*, 938−949.
(26) Kołodziejczyk, K.; Sojka, M.; Abadias, M.; Vinas, I.; Guyot, S.; Baron, A. Polyphenol composition, antioxidant capacity, and antimicrobial activity of the extracts obtained from industrial sour cherry pomace. *Ind. Crops Prod.* **2013**, *51*, 279−288.
(27) Tomas-Barberan, F. A.; Gil, M. I.; Cremin, P.; Waterhouse, A. L.; Hess-Pierce, B.; Kader, A. A. HPLC−DAD−ESIMS analysis of phenolic compounds in nectarines, peaches, and plums. *J. Agric. Food Chem.* **2001**, *49*, 4748−60.
(28) Oszmiański, J.; Wojdyło, A. *Aronia melanocarpa* phenolics and their antioxidant activity. *Eur. Food Res. Technol.* **2005**, *221*, 809−813.
(29) Gu, L.; Kelm, M.; Hammerstone, J. F.; Beecher, G.; Cunningham, D.; Vannozzi, S.; Prior, R. L. Fractionation of polymeric procyanidins from lowbush blueberry and quantification of procyanidins in selected foods with an optimized normal-phase HPLC-MS fluorescent detection method. *J. Agric. Food Chem.* **2002**, *50*, 4852−4860.
(30) Vidal, S.; Francis, L.; Noble, A.; Kwiatkowski, M.; Cheynier, V.; Waters, E. Taste and mouth feel properties of different types of tannin-like polyphenolic compounds and anthocyanins in wine. *Anal. Chim. Acta* **2004**, *513*, 57−65.
(31) Chaovanalikit, A.; Wrolstad, R. E. Total anthocynains and total phenolics of fresh and processed cherries and their antioxidant properties. *J. Food Sci.* **2004**, *69*, 67−72.
(32) Kirakosyan, A.; Seymour, E. M.; Urcuyo Llanes, D. E.; Kaufman, P. B.; Bolling, S. F. Chemical profile and antioxidant capacities of tart cherry products. *Food Chem.* **2009**, *115*, 20−25.
(33) Liang, Z.; Yang, Y.; Cheng, L.; Zhong, G.-Y. Polyphenolic composition and content in the ripe berries of wild Vitis species. *Food Chem.* **2012**, *132*, 730−738.
(34) Wojdyło, A.; Oszmiański, J.; Milczarek, M.; Wietrzyk, J. Phenolic profile, antioxidant and antiproliferative activity of black and red currants (Ribes spp.) from organic and conventional cultivation. *Int. J. Food Sci. Technol.* **2013**, *48*, 715−726.
(35) Pantelidis, G. E.; Vasilakakis, M.; Manganaris, G. A.; Diamantidis, G. Antioxidant capacity phenol, anthocyanin and ascorbic acid contents in raspberries, blackberries, red currants, gooseberries and Cornelian cherries. *Food Chem.* **2007**, *102*, 777−783.
(36) Howard, L. R.; Clark, J. R.; Brownmiller, C. Antioxidant capacity and phenolic content in blueberries as affected by genotype and growing season. *J. Sci. Food Agric.* **2003**, *83*, 1238−1247.
(37) Benvenuti, S.; Pellati, F.; Melegari, M.; Bertelli, D. Polyphenols, anthocyanins, ascorbic acid and radical scavenging activity of Rubus, Ribes, and Aronia. *J. Food Sci.* **2004**, *69*, 164−169.
(38) Anttonen, M. J.; Karjalainen, R. O. High-Performance liquid chromatography analysis of black currant (*Ribes nigrum* L.) fruit phenolics grown either conventionally or organically. *J. Agric. Food Chem.* **2006**, *54*, 7530−7538.
(39) Jaiswal, R.; Karakose, H.; Ruhmann, S.; Goldner, K.; Neumuller, M.; Treutter, D.; Kuhnert, N. Identification of phenolic compounds in plum fruits (*Prunus salicina* L. and *Prunus domestica* L.) by High-Performance Liquid Chromatography/Tandem Mass Spectrometry and characterization of varieties by quantitative phenolic fingerprints. *J. Agric. Food Chem.* **2013**, *61*, 12020−12031.
(40) Mozetic, B.; Trebse, P.; Hribar, J. Determination and quantification of anthocyanins and hydroxycinnamic acid in different cultivars of sweet cherries (*Prunus avium* L.) from Nova Gorica region (Slovenia). *Food Technol. Biotechnol.* **2002**, *40*, 207−212.
(41) Gonzalez-Gomez, D.; Lozano, M.; Fernandez-Leon, M. F.; Bernalte, M. J.; Ayuso, M. C.; Rodriguez, A. B. Sweet cherry phytochemicals: Identification and characterization by HPLC DAD/ESI-MS in six sweet-cherry cultivars grown in Valle del Jerte (Spain). *J. Food Comp. Anal.* **2010**, *23*, 533−539.
(42) Usenik, V.; Fabcic, J.; Stampar, F. Sugars, organic acids, phenolic composition and antioxidant activity of sweet cherry (*Prunus avium* L.). *Food Chem.* **2008**, *107*, 185−192.
(43) Kelebek, H.; Selli, S. Evaluation of chemical constituents and antioxidant activity of sweet cherry (*Prunus avium* L.) cultivars. *International J. Food Sci. Technol.* **2011**, *46*, 2530−2537.
(44) Guyot, S.; Marnet, M.; Laraba, D.; Sanoner, P.; Drilleau, J. F. Reversed-phase HPLC following thiolysis for quantitative estimation and characterization of the four main classes of phenolic compounds in different tissue zones of a French cider apple variety (*Malus domestica* var. Kermerrien). *J. Agric. Food Chem.* **1998**, *46*, 1698−1705.
(45) Knekt, P.; Isotupa, S.; Rissanen, H.; Heliovaara, M.; Jarvinen, R.; Hakkinen, S.; Aroma, A.; Reunanen, A. Quercetin intake and the incidence of cerebrovascular disease. *Eur. J. Clin. Nutr.* **2000**, *54*, 415−417.
(46) Wang, S. Y.; Chen, C. T.; Sciarappa, W.; Wang, C. Y.; Camp, M. J. Fruit quality, antioxidant capacity, and flavonoid content of organically and conventionally grown blueberries. *J. Agric. Food Chem.* **2008**, *56*, 5788−5794.

(47) Rice-Evans, C. A.; Miller, N. J.; Paganga, G. Structure-antioxidant activity relationships of flavonoids and phenolic acids. *Free Radical Biol. Med.* **1996**, *20*, 933−965.
(48) Bandoniene, D.; Murkovic, M. On-line HPLC-DPPH screening method for evaluation of radical scavenging phenols extracted from apples (*Malus domestica* L.). *J. Agric. Food Chem.* **2002**, *50*, 2482−2487.
(49) Goncalves, B.; Landbo, A. K.; Let, M.; Silva, A. P.; Rosa, E.; Meyer, A. S. Storage affects the phenolic profiles and antioxidant activities of cherries (*Prunus avium* L.) on human low-density lipoproteins. *J. Sci. Food Agric.* **2004**, *84*, 1013−1020.
(50) Nishiyama, I.; Yamashita, Y.; Yamanaka, M.; Shimohashi, A.; Fukuda, T.; Oota, T. Varietal difference in vitamin C content in the fruit of kiwifruit and other Actinidia species. *J. Agric. Food Chem.* **2004**, *52*, 5472−5475.
(51) Yilmaz, K. U.; Ercisli, S.; Zengin, Y.; Sengul, M.; Kafkas, E. Y. Preliminary characterisation of cornelian cherry (*Cornus mas* L.) genotypes for their physico-chemical properties. *Food Chem.* **2009**, *114*, 408−412.
(52) Gil, M. I.; Tomas-Barberan, F. A.; Hess-Pierce, B.; Kader, A. A. Antioxidant capacities, phenolic compounds, carotenoids, and vitamin C contents of nectarine, peach, and plum cultivars from California. *J. Agric. Food Chem.* **2002**, *50*, 4976−4982.
(53) Ochmian, I.; Skupień, K.; Grajkowski, J.; Smolik, M.; Ostrowska, K. Chemical composition and physical characteristics of fruits of two cultivars of blue honeysuckle (*Lonicera caerulea* L.) in relation to their degree of maturity and harvest date. *Not. Bot. Hortic. Agrobot.* **2012**, *40*, 155−162.
(54) Fadavi, A.; Barzegar, M.; Azizi, M. H.; Bayat, M. Physicochemical composition of 10 pomegranate cultivars (*Punica granatum* L.) grown in Iran. *Food Sci. Technol. Int.* **2005**, *11*, 113−119.
(55) Tehranifar, A.; Zarei, M.; Nemati, Z.; Esfandiyari, B.; Vazifeshenas, M. R. Investigation of physico-chemical properties and antioxidant activity of twenty Iranian pomegranate (*Punica granatum* L.) cultivars. *Sci. Hortic.* **2010**, *126*, 180−185.
(56) Hofer, M.; Grill, D.; Hecke, K.; Herbinger, K.; Keppel, H.; Monschein, S.; Stampar, F.; Keppel, H.; Grill, D. Inhaltsstoffe alter apfelsorten unter diatetischem aspekt-schwerpunkt diabetes. *J. Ernahrungsmed.* **2005**, *7*, 30−33.
(57) Ercisli, S.; Orhan, E. Chemical composition of white (*Morus alba*), red (*Morus rubra*) and black (*Morus nigra*) mulberry fruits. *Food Chem.* **2007**, *103*, 1380−1384.
(58) Wojdyło, A.; Oszmiański, J.; Rozpara, E. Biological composition, phenolic compounds, and antioxidant capacity of organic and conventional grown raspberry (*Rubus ideaus*). In *Monografia: The Impact of Organic Production Methods on The Vegetable Product Quality*; Rembiałkowska, E., Ed.; Warsaw, 2010; pp 245−258.
(59) Hardisson, A.; Rubio, C.; Martin, M.; Alvarez, R.; Diaz, E. Mineral composition of the banana (*Musa acuminata*) from the island of Tenerife. *Food Chem.* **2001**, *73*, 153−161.

## MATERIALS AND METHODS

**Animals and Samples Preparation.** Forty, 47 week-old Single Comb Hy-Line Brown Leghorn hens, purchased from Sangol Egg Farm (Sancheong, Korea), were housed in individual cages in a room with a light regimen of 15 h light and 9 h dark (lights on at 6:00 AM) and an ambient temperature of 20 ± 2 °C during the entire experimental period. A commercial layer diet and tap water were provided *ad libitum*. This study was approved by the Institutional Animal Use and Care Committee of Gyeongsang National University (GAR-101020-X0007).

After adaptation to the experimental environment for the first 14 days, hens were divided into two groups, each of which was provided for the next 14 days with either ethanol (Control) or corticosterone (Stress)-containing diet at 30 mg/kg.[3,14] A commercial layer diet (Nonghyup Feed Co., Ltd., Seoul, Korea), which was used as a basal diet for the adaptation, was mixed for 30 min in a mixer with ethanol (95%) with or without corticosterone (92%, Sigma) at 2.61 mg/mL to produce either Stress or Control diet, respectively. Therefore, ethanol in the diet (12.5 mL/kg) was completely evaporated at the end of the 30 min mixture.

For each hen, feed intake, egg production and egg weight were monitored daily in the morning and body weight measured weekly throughout the experimental period. Eggs, laid by the same laying hens on 0 and 5 days (days 0 vs 5) after the initiation of providing hens with the experimental diets, were selected for the ongoing proteomic analysis as egg production started to decrease around day 5 by 30% (Figure 1). Immediately after being manually separated from the egg

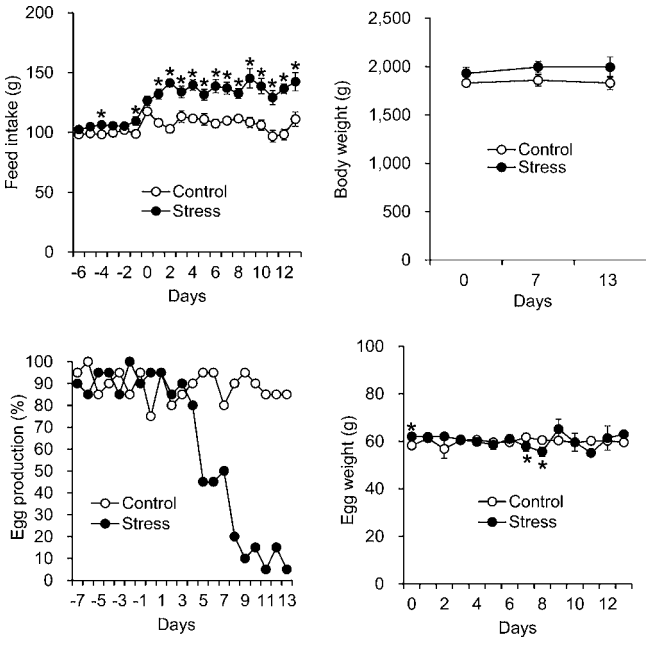


**Figure 1.** Feed intake (g), body weight (g), egg production (%), and egg weight (g) in laying hens. Hens were acclimatized to the experimental environment for the first 2 weeks (days −14 to 0) and then were divided into two groups to receive either ethanol- (Control) or corticosterone- (Stress) containing diet at 30 mg/kg for the next 2 weeks (days 0−14), respectively. Data are means ± SEM ($n$ = 20 per group). *$P \leq 0.05$ vs Control.

yolk, the egg white was freeze-dried using a lyophilization freeze-dryer (#PVTFD50A, Ilshin Bio Base, Dongduchen, Korea) and then stored at −80 °C. Hens, which had a mean egg production of higher than 90% and their egg weights of being higher than 60 g during the adaptation period (63.4 ± 0.46 g in average), were selected for the study.

At the end of the entire experimental period (day 14), hens were killed using a guillotine and blood was collected from the trunk into 10 mL tubes treated with sodium heparin (BD, Franklin Lakes, NJ, USA) followed by centrifugation at 2 000*g*, 4 °C for 10 min. Plasma obtained was stored at −80 °C for further analysis. Organs including the oviduct were sectioned off, frozen in liquid nitrogen, and stored at −80 °C for later analysis. The magnum was cut into three parts of similar length before being stored at −80 °C, and the middle one was used for subsequent analysis.

**Corticosterone Assay.** Corticosterone concentrations in plasma were determined in duplicates each sample by ELISA using a kit (#ADI-901−097, Enzo Life Sciences, Farmingdale, NY, USA), according to the manufacture's instruction. Optical density was measured at 405 nm using a Multiskan FC Microplate Photometer (#51119000, Thermo Scientific, Waltham, MA, USA). Inter- and intra-assay coefficients of variations of this assay were 8.2% and 8.4%, respectively.

**Reagents and Apparatus.** Sodium dodecyl sulfate (SDS), phenyl methanesulfonyl fluoride (PMSF), tris(hydroxymethyl)aminomethane (Tris), urea, thiourea, 3-[(3-cholamidopropyl)dimethylammonio]-1-propanesulfonate hydrate (CHAPS), dithiothreitol (DTT), glycerol, bromophenol blue, isopropanol, silver nitrate, sodium thiosulfate pentahydrate and iodoacetamide were purchased from Amresco (Cochran, GA, USA); protease inhibitor cocktail from Roche (Indianapolis, IN, USA); agarose from GeorgiaChem (Suwanee, GA, USA); trypsin from Promega (Fitchburg, WI, USA); potassium ferricyanide, ammonium bicarbonate (ABC), ∂-cyano-4-hydroxycinnamic acid (CHCA), trifluoroacetic acid (TFA), formaldehyde and ethidium bromide (EtBr) from Sigma (St. Louis, MO, USA); 2-D Quant kit and immobilized pH gradient (IPG) buffer from GE Healthcare Life Sciences (Little Chalfont, UK); PrimeScript first strand cDNA synthesis kit from Takara (Ootsu, Japan); SYBR Green PCR Master Mix and Sequazyme Peptide Mass Standard Kit (Calibration 1) from Applied Biosystems (ABI, Foster City, CA, USA); IPG strip (pH 4−10 Nonlinear (NL), 180 × 3 × 0.5 mm) from Genomine (Pohang, Korea); Gradi-Gel II gradient PAGE analysis kit from Elpis (Daejeon, Korea); methanol, acetic acid and acetonitrile (ACN) from DaeJung (Siheumg, Korea); and Easy-spin total RNA extraction kit from Intron (Sungnam, Korea).

**Extraction of Solubilized Proteins from Egg White for Proteomics.** Lysis buffer A consisted of 1% SDS, 1 mM PMSF, protease inhibitor cocktail, and 100 mM Tris-HCl (pH 6.8), and lysis buffer B of 7 M urea, 2 M thiourea, 4% CHAPS, 0.1 M DTT, and 40 mM Tris-HCl (pH 6.8). One gram of dried egg white was ground into fine powder using a mortar and a pestle. Twenty mg of powdered egg white was dissolved in 25-fold volume lysis buffer A of the weight of egg white (v/w) and then dissolved in the same volume of lysis buffer B as lysis buffer A. The solution was shaken gently at room-temperature (RT) for 1 h, followed by sonication with a 2 s-on and 9 s-off cycle for five times. After incubation at RT for 1 h, this solution was centrifuged at 15 000*g*, 4 °C for 20 min to remove debris. The supernatant was incubated at 4 °C for 1 h and then the process was repeated twice to remove debris. The solubilized protein extracts were quantified using a 2-D Quant kit (#80-6483-56, GE).

**SDS-PAGE.** Egg white protein (10 μg) was diluted in a buffer (2% SDS, 10% glycerol, and 125 mM Tris-HCl (pH 6.8)), which was loaded on 4−20% premade SDS polyacrylamide gels (#84713, Thermo Scientific) at 20 mA, RT for 3 h until the bromophenol blue dye, containing a standard protein marker (#161-0374, Bio-Rad, Hercules, CA, USA) of 10−250 kDa, disappeared from the bottom of the gel.

**Two-Dimensional Electrophoresis (2DE).** Egg white protein (200 μg) was mixed in rehydration buffer (7 M urea, 2 M thiourea, 4% CHAPS, 2.5% DTT, 10% isopropanol, 5% glycerol, and 2% IPG buffer) to a total volume of 450 μL. The sample was loaded onto a swelling tray in which IPG strips (pH 4−10 NL) were allowed to be rehydrated overnight. The first dimensional isoelectric focusing (IEF) was then performed using an IEF unit (#28926930, Ettan IPGphor 3, GE) at 20 °C, 50 V for 30 min, 100 V for 30 min, 250 V for 1 h, 8 000 V gradient for 9 h and 8 000 V for 6 h. The IPG strips were placed for 15 min in an equilibration solution (6 M urea, 30% glycerol, and 2% SDS, and 50 mM Tris-HCl (pH 8.8)) containing 1% DTT, and then

**Table 1. Primer Information Used in the Present Study**

| Full name (protein and gene names) | Gene symbols | Accession no. | Forward (5′ → 3′)<br>Reverse (5′ → 3′) | Size |
|---|---|---|---|---|
| Ovalbumin | SERPINB14 | NM_205152.1 | TTCCTGGGTAGAAAGTCAGACAAAT | 100 |
| | | | GACAATGGCATTAACCAGAACCA | |
| Ovalbumin-related protein Y (OVAY) | SERPINB14B | NM_001031001.1 | TGGCCTTGGGAATGACAGA | 100 |
| | | | GAACACCCCATGGACAGCAT | |
| Ovotransferrin | Ovotransferrin | NM_205304.1 | CAGTGATGGCAGAACGATATGAC | 112 |
| | | | TTCCAGTTGACGTTGCTGTCTT | |
| Extracellular fatty acid -binding protein (Ex-FABP) | EX-FABP | NM_205422.1 | GGAGGACCTTGCACATGATGA | 100 |
| | | | GTGTAGTTCCGCTCCCTAGCA | |
| Transiently expressed in neural precursors (TENP) | TENP | NM_205026.1 | CCAAACGAGCAGCTGATGTC | 103 |
| | | | TGCCCTGCTTGGAGAACAC | |
| Ovoinhibitor | OIH | NM_001030612.1 | ACCAGCGTTGCCAAAAAGC | 111 |
| | | | GCAGGCCACCACCTGTCT | |
| Hemopexin (HPX) | Hemopexin | M37319.1 | AGCGCGTGGACTTGACAAA | 107 |
| | | | GCAGCAGGTAGATGCCATCA | |

treated with the same equilibration solution containing 2.5% iodoacetamide for 15 min. The second dimensional separation was performed on 7.5% SDS polyacrylamide gels using a Gradi-Gel II gradient PAGE analysis kit (#EBA-1056, Elpis). The gels were placed into a Protean II XL for 2DE (#165−3188, Bio-Rad) at 20 mA, RT for 18 h until the bromophenol blue dye, with the standard protein marker of 10−250 kDa (Bio-Rad), disappeared from the bottom of the gel. After the electrophoresis, the gels were fixed in a fixation solution (38% water, 50% methanol, and 12% acetic acid) overnight and stained in a silver nitrate solution as previously described.[15] Gel images were scanned using an imaging densitometer (#GS-800, Bio-Rad), and the intensity of protein spots from 3 gel images each group was processed using an image master (#28−9380−55, Image Master 2D Plantinum, v.7.0, GE), followed by the determination of molecular weights of the spots.

**Matrix-Assisted Laser Desorption−Ionization Time-of-Flight/Time-of-Flight Mass Spectrometry/Mass Spectrometry (MALDI-TOF/TOF MS/MS).** Selected spots were excised out from 2DE gels and subjected to in-gel digestion with trypsin as previously described.[15] Shortly, each of the spots predetermined by the image analysis was repeatedly picked up using a pipet tip into a 1.5 mL tube, and a destaining process was performed to remove the silver dye. Individual protein spots, 50 μL of 30 mM potassium ferricyanide, and 50 μL of 0.1 M sodium thiosulfate pentahydrate were vortexed for 1 min and spun down to remove the supernatant. To break the disulfide bonds, the samples were incubated in 0.1 mL of 10 mM DTT in 0.1 M ABC at 56 °C for 45 min and then the supernatant was removed after centrifugation. For alkylation, they were incubated again in 0.1 mL of 55 mM iodoacetamide in 0.1 M ABC at RT for 30 min, and then spun down to remove the supernatant. Individual precipitates were incubated with 5 μL of 50 ng trypsin in order to cleave peptide chain mainly at the carboxyl side of the amino acids lysine or arginine in 25 mM ABC at 37 °C overnight for in-gel digestion and spun down to collect the supernatant. The digested products were then dried using a vacuum concentrator (Ecospin 3180C, Hanil Science Industrial, Incheon, Korea) and stored at −20 °C. The peptides, dissolved in 1 μL of matrix solution (0.05 g CHCA in 0.1% TFA/50% ACN), were eluted onto a MALDI plate (#1016629, ABI), and was air-dried in a clean bench. MS and MS/MS analyses were performed on an ABI 4800 Plus TOF-TOF Mass spectrometer (ABI) using a mass standard kit (calibration mixture 1, ABI), according to the method described by Kwon et al.[15] The spectrometer used a 200 Hz ND:YAG laser operating at 355 nm and air as a collision gas. At least, ten most intensive ionized peptides per MALDI spot, with signal/noise ratios >25, were selected for subsequent MS/MS analysis in 1 kV mode and 1 000−1 500 consecutive laser shots. MS/MS spectrum data were searched against the UniProt Knowledgebase (UniProtKB) by ProteinPilot (v.3.0) in combination with MASCOT as the database search engine and with peptide and fragment ion mass tolerance of 50 ppm. Both carbamidomethylation of cysteine and oxidation of methionine were taken into account during the search of the peptides. High confidence identifications had statistically significant search scores which were equivalent to the expected values on the MASCOT at $P \leq 0.05$ and were consistent with the pI and MW of the individual proteins, which accounted for the majority of ions present in the mass spectra.

**mRNA and Protein Expression Analysis of the Magnum.** Total RNA was isolated from homogenized magnum tissue using an Easy-spin total RNA extraction kit (#17221, Intron), according to the manufacturer's protocol. One hundred mg of frozen magnum tissue was homogenized in 1 mL of lysis buffer (Intron). Each of the homogenized samples was mixed with 200 μL of chloroform and then centrifuged at 13 000 rpm, 4 °C for 10 min to harvest the supernatant. Four hundred μL of the supernatant was mixed with 400 μL of a binding buffer (Intron) by inverting and spun down, which was incubated at RT for 1 min and loaded into a spin column (Intron). The spin column was centrifuged at 13 000 rpm, RT for 30 s, and the eluted buffer was discarded. Seven hundred μL of washing buffer (Intron) was loaded into each column and centrifuged again in the same way as before. After washing, the column membrane was dried by centrifugation at 13 000 rpm, RT for 1 min, soaked with 50 μL of the elution buffer (Intron) and then centrifuged at 13 000 rpm to extract RNA. The total amount of RNA was determined by measuring optical density at 260 nm using a Nanodrop2000C spectrophotometer (Thermo Scientific). RNA quality was assessed by loading 2.5 μg of each RNA sample on a 1% agarose gel with formaldehyde and EtBr to visualize the bands of 28S and 18S rRNA.

For magnum tissues, proteomics was performed based on the methods similar to those for egg white with some modification: magnum tissues (100−200 mg) were homogenized in lysis buffers A and B of 10-fold magnum volume, followed by incubation, sonication and centrifugation to obtain solubilized protein. Protein (150 ug) was loaded onto IPG strip (pH 4−7 L) and 12% SDS polyacrylamide gels, followed by MALDI-TOF/TOF MS/MS analysis.

**Reverse Transcription (RT) and Real-Time Quantitative PCR (qPCR).** Relative expressions of each gene encoding the proteins differentially expressed in the egg white were determined in the magnum of the oviduct. Primer sequences, shown in Table 1, were designed with software (Primer Express, v. 3.0.1, ABI), in which glyceraldehyde-3-phosphate dehydrogenase (GAPDH) served as a housekeeping gene. Two μg of RNA was reverse-transcripted using a PrimeScript first strand cDNA synthesis kit (#6110A, Takara) in a final volume of 20 μL according to the manufacturer's protocol. qPCR was then performed using a Step One Plus Real-Time PCR System (ABI) with Power SYBR Green PCR Master Mix (#4368702, ABI). Thermal cycling had 3 stages which were 1) activation of DNA polymerase at 95 °C for 10 min, 2) fluorescent detection of amplification by 40 cycles at 95 °C for 15 s and at 60 °C for 1 min, and 3) fluorescent

detection of melting curve at 95 °C for 15 s, 60 °C for 1 min, with a heating rate of 0.5 °C/s between 60 °C ~ 95 °C, and 95 °C for 15 s.

**Statistical Analysis.** All experimental data were represented as mean ± SEM. Student's *t*-test was performed using Microsoft Excel program to assess differences between Control and Stress at $P \leq 0.05$. Feed intake, body weight and egg production were measured in 20 hens each group to estimate mean values of each parameter. For corticosterone concentrations, mean values were calculated from 8 hens each group. For 2DE analysis, mean values of each spot were calculated from triplicated data in egg white samples and magnum tissues. Protein spots, which were differentially expressed at least 1.2 fold between days 0 and 5 in each group, were selected from 2DE gels, and statistically analyzed by a *t*-test ($P \leq 0.05$). Relative mRNA expression in magnum samples collected from 8 hens each group was measured in duplicates based on the $2^{-\Delta\Delta CT}$ method, and differences between both groups were analyzed by *t*-test.

## RESULTS

**Animal Study.** No hens were found dead from any of the dietary treatments during the whole period of the experiment. During the adaption period (days −7−0), feed intake, egg production, and egg weight were relatively constant. Stress resulted in significant increase in mean-daily feed intake compared with Control (days 1−7: 109 ± 1 g for Control vs 136 ± 2 g for Stress, $P \leq 0.0001$; days 8−13: 105 ± 2 g for Control vs 137 ± 2 g for Stress, $P \leq 0.0001$). No differences were, however, detected in body weight between the two groups although it was slightly higher in the Stress group throughout the entire experimental period (Figure 1). Egg production was drastically decreased to approximately 30% in Stress on day 5 while Control had about 90% (days 1−7: 89 ± 3% for Control vs 70 ± 8% for Stress, $P \leq 0.05$; days 8−13: 88 ± 2% for Control vs 12 ± 2% for Stress, $P \leq 0.0001$). Dietary corticosterone resulted in a significant decrease in the number of follicles equal to or greater than 10 mm in diameter and in increased corticosterone concentrations in plasma ($P \leq 0.05$) (Figure 2).

**Differential Protein Abundance in Egg White of Treated and Untreated Hens (Day 5 after Treatment).** Because egg production was sharply reduced around 4 days (45%) after hens started to consume dietary corticosterone while no changes were detected between the two groups during the adaptation period (Control: 89 ± 3% vs Stress: 92 ± 2%, $P \leq 0.47$, for the second week of the adaptation period), eggs produced on day 5 were used for subsequent proteomic analysis. Protein profiles of the egg white were significantly changed in the eggs laid between days 0 and 5 in Stress whereas they remained unchanged in Control (Figures 3−5). SDS-PAGE analysis showed a drastic reduction in protein bands between 37 and 50 kDa and between 50 and 75 kDa on day 5 compared with day 0 in Stress, whereas such changes were not seen in Control (Figure 5). These findings were confirmed using 2DE analysis (Figure 4).

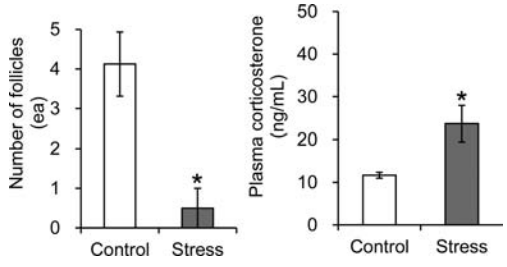


**Figure 2.** Number of follicles (≥10 mm in diameter) and plasma concentrations of corticosterone (ng/mL) in laying hens. Laying hens were acclimatized to the experimental environment for the first 2 weeks (days −14 to 0) and then were divided into two groups to receive either ethanol- (Control) or corticosterone- (Stress) containing diet at 30 mg/kg for the next 2 weeks (days 0−14), respectively. The number of follicles equal to or greater than 10 mm in diameter was counted at the end of the experiment ($n$ = 8 per group), and blood obtained from the trunk of the hens was determined for plasma corticosterone concentrations by ELISA ($n$ = 8 per group). Data are means ± SEM. *$P \leq 0.05$ vs Control.

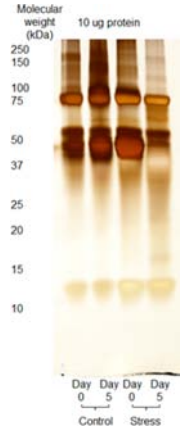


**Figure 3.** SDS-PAGE analysis of egg white proteins of hens. Laying hens were acclimatized to the experimental environment for the first 2 weeks (days −14 to 0) and then were divided into two groups to receive either ethanol- (Control) or corticosterone- (Stress) containing diet at 30 mg/kg for the next 2 weeks (days 0−14), respectively. Eggs laid by the same hens on days 0 and 5 in each group were used for proteomic study. Egg white protein samples (10 μg) were loaded on 4−20% SDS polyacrylamide premade gel and stained with silver nitrate staining.

Thirty-four protein spots in Stress were up- or down-expressed at least 1.2-fold compared with Control (Figure 4). Eight protein spots (#6−12 and 18) were significantly up-expressed on day 5 ($P \leq 0.05$) but six (#2, 15, 22, 27, 28, and 29) were down-expressed ($P \leq 0.05$) in Stress. By contrast, such change was detected in the only one protein spot (#19) from Control, which was up-expressed on day 5 compared with day 0 ($P \leq 0.05$).

From 34 protein spots, 9 proteins were identified through MALDI-TOF/TOF MS/MS analysis and the data mining based on subsequent bioinformatics: ovoinhibitor, ovalbumin-related protein X (OVAX), transiently expressed in neural precursors (TENP), hemopexin (HPX), ovotransferrin, IgY-Fc$\upsilon$3-4, extracellular fatty acid-binding protein (Ex-FABP), ovalbumin-related protein Y (OVAY), and ovalbumin. Of nine spots (#3−11) that were estimated as ovoinhibitor, 6 spots (#4−8 and 11) were determined as ovoinhibitor. While expression of this protein was significantly increased over 5 days in egg white in Stress ($P \leq 0.05$), no such significant changes were detected in Control (Tables 2 and 3). Three spots (#12, 18, and 24) were determined as OVAX, and corticosterone-treatment resulted in significant increase in 2 spots ($P \leq 0.05$) whereas no significant changes were detected in Control. Eight spots were considered to be TENP: among them, 4 spots (#17, 18, 27, and 28) were confirmed as TENP. Corticosterone treatment up-regulated 1 spot (#18) and down-regulated the other three spots (#17, 27, and 28) but no

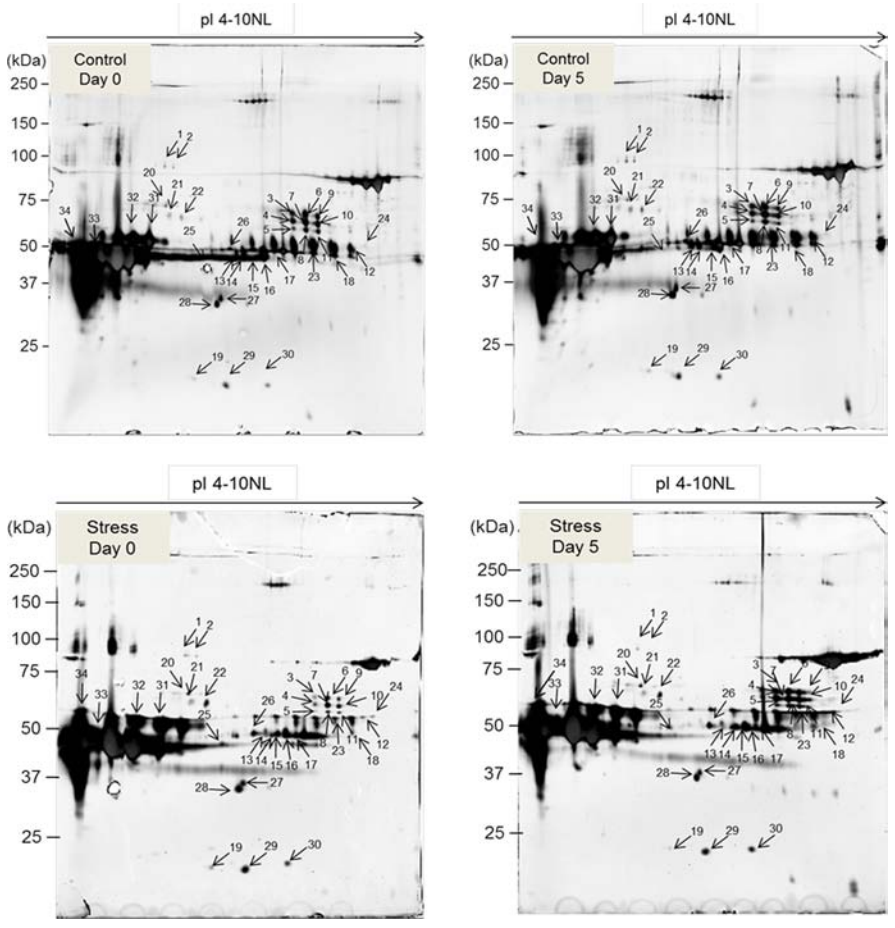


**Figure 4.** Representative two-dimensional electrophoresis (2DE) of hen's egg white proteins. Laying hens were acclimatized to the experimental environment for the first 2 weeks (days −14 to 0) and then were divided into two groups to receive either ethanol- (Control) or corticosterone- (Stress) containing diet at 30 mg/kg for the next 2 weeks (days 0−14), respectively. Eggs laid by the same hens on days 0 and 5 in each group were used for proteomic study. The 2DE gel images of egg white were obtained from eggs laid on days 0 and 5 by the same laying hens treated with Control or Stress. Egg white protein samples (200 $\mu$g) were loaded on 7.5% SDS polyacrylamide gels using a Gradi-Gel II gradient PAGE analysis kit and stained with silver nitrate staining. Protein spots determined are ovoinhibitor (#4−8 and 11), OVAX, ovalbumin-related protein X (#12, 18, and 24), TENP, transiently expressed in neural precursors (#17, 18, 27, and 28), HPX, hemopexin (#21 and 22), ovotransferrin (#24), IgY-Fc$\upsilon$3-4 (#27), Ex-FABP, extracellular fatty acid-binding protein (#29), OVAY, ovalbumin related protein Y (#31 and 32) and ovalbumin (#33 and 34), whereas spots are estimated for ovoinhibitor (#3, 9, and 10), TENP (#13, 14, 15, and 16), OVAY (#23 and 26), CAL, chondrogenesis-associated lipocalin (#19 and 30), and HPX (#20) based on recent publications. However, estimation for proteins was not possible for spots #1, 2, and 25, due to either lack of reference data or ambiguity of reference.

significant change was found in Control. Of three spots estimated as HPX, 2 spots (#21 and 22) were confirmed. HPX expression was significantly reduced by Stress on days 5 over 0 ($P \leq 0.05$), but no such changes were seen in Control. One spot (#27) was identified as IgY-Fc$\upsilon$3-4, expression of which was significantly reduced in Stress ($P \leq 0.05$) but not in Control. Similarly, another spot (#29) corresponding with Ex-FABP was significantly down-expressed by corticosterone-treatment ($P \leq 0.05$) but not by control. Among 4 spots which were estimated as OVAY, two spots (#31 and 32) were verified as OVAY, and one (#32) spot was significantly increased in Control ($P = 0.06$), but not in Stress. Although 2 spots (#33 and 34) were identified to be ovalbumin protein, no significant changes were found in both groups over 5 days. Two spots (#19 and 30), which were estimated to be chondrogenesis-associated lipocalin (CAL), were significantly increased in Control ($P \leq 0.05$) but not in Stress. One spot (#24), which was determined as ovotransfferin, was detected in Stress but not in Control.

Proteins "determined" were identified based on proteomic analysis in the present study (Table 3) whereas proteins "estimated" were found to have similar molecular weight (MW) and pH in the 2DE gels to those reported in recent papers.[16,17] Spots #18, #24, and #27 were determined to contain each of two different proteins (OVAX and TENP; OVAX and ovotransferrin; and TENP and IgY-Fc$\upsilon$3-4, respectively) (Tables 2 and 3).

Some of the proteins show differences between the theoretical (MWt) and observed (MWo) molecular weights (Table 2). The latter was based on the analysis of 2D gels using an image analyzer. The MWo values for some proteins were nearly the same as (#4, 5, 7, 8, 11, 17, 18, and 29), much smaller than (#24, 27, 28, and 34), or much larger than (#6, 12, 18, 21, 22, 24, 27, 31, 32, and 33) those of MWt.

**Differential Protein Abundance in Magnum of Treated and Untreated Hens (Day 14).** Of the proteins differentially abundant in the egg white on day 5 there were 6 proteins (ovalbumin, ovoinhibitor, ovotransferrin, hemopexin, IgY-Fc$\upsilon$3-4, and OVAY) which were also differently abundant

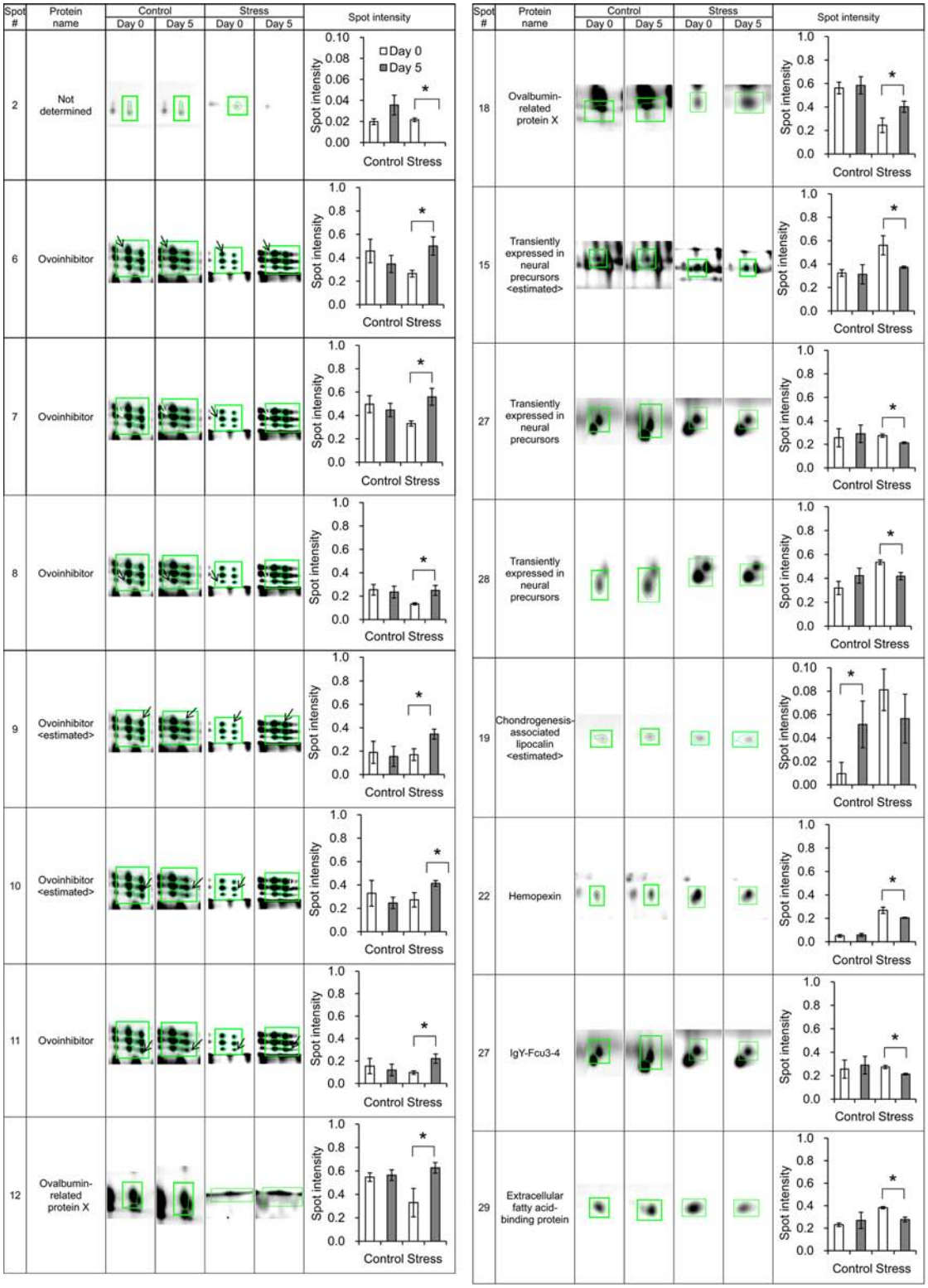


**Figure 5.** Differential expression of egg white proteins in spots derived from two-dimensional electrophoresis (2DE). Laying hens were acclimatized to the experimental environment for the first 2 weeks (days −14 to 0) and then were divided into two groups to receive either ethanol- (Control) or corticosterone- (Stress) containing diet at 30 mg/kg for the next 2 weeks (days 0−14), respectively. Eggs laid by the same hens on days 0 and 5 in each group were used for proteomic study. The 2DE gel images of egg white were obtained from eggs laid on days 0 and 5 by the same laying hens treated with Control or Stress. Individual spots on the gels were matched between the 2 days and between two treatments, and their intensities equal to or greater than 1.2-fold in expression were compared between days 0 and 5 in each treatment and were shown in graphs. The spot numbers are the same as those specified in Figure 4. Data are means ± SEM ($n$ = 3 per day per group). *All spots identified show statistically significant differences at $P \leq 0.05$ by $t$-test.


dx.doi.org/10.1021/jf504469t | J. Agric. Food Chem. 2014, 62, 12346−12359

**Table 2. Proteins Identified by Two-Dimensional Electrophoresis (2DE), and Matrix-Assisted Laser Desorption-Ionization Time-of-Flight/Time-of-Flight Mass Spectrometry/Mass Spectrometry (MALDI-TOF/TOF MS/MS) Followed by Bioinformatics**

| Spot no.[a] | Protein name[b] | Accession no.[c] | MWt[d] /MWo[e] (kDa) | pI | Score[f] | Coverage (%)[g] | Matched peptides[h] | Matched peptide sequences[i] |
|---|---|---|---|---|---|---|---|---|
| 4 | Ovoinhibitor | P10184 | 52/59 | 6.2 | 58 | 32 | 14 | K.DGTSWVACPR.N/R.NLKPVCGTDGSTYSNECGICLYNR.E/R.EHGANVEK.E/K.HVTIDCSPYLQVVR.D/R.DGNTMVACPR.I/K.LHDGECK.L/R.TLVACPR.I/R.ILSPVCGTDGFTYDNECGICAHNAEQR.T/R.QEIPEIDCDQYPTR.K/K.VSPICTMEYVPHCGSDGVTYSNR.C/R.CFFCNAYVQSNR.T |
| 5 | Ovoinhibitor | P10184 | 52/54 | 6.2 | 47 | 23 | 14 | K.DGTSWVACPR.N/R.EHGANVEK.E/K.HVTIDCSPYLQVVR.D/R.DGNTMVACPR.I/K.LHDGECK.L/R.TLVACPR.I/R.QEIPEIDCDQYPTR.K/R.CREEVPELDCSK.Y/K.VSPICTMEYVPHCGSDGVTYSNR.C/R.CFFCNAYVQSNR.T |
| 6 | Ovoinhibitor | P10184 | 52/63 | 6.2 | 46 | 22 | 13 | K.DGTSWVACPR.N/R.NLKPVCGTDGSTYSNECGICLYNR.E/R.EHGANVEK.E/K.HVTIDCSPYLQVVR.D/R.DGNTMVACPR.I/K.LHDGECK.L/R.TLVACPR.I/R.QEIPEIDCDQYPTR.K/R.CREEVPELDCSK.Y/R.CEEDITK.E |
| 7 | Ovoinhibitor | P10184 | 52/58 | 6.2 | 362[d] | 33 | 19 | K.DGTSWVACPR.N/R.NLKPVCGTDGSTYSNECGICLYNR.E/K.HVMIDCSPYLQVVR.D/R.DGNTMVACPR.I/R.TLVACPR.I/R.ILSPVCGTDGFTYDNECGICAHNAEQR.T/K.CRQEIPEIDCDQYPTR.K/R.QEIPEIDCDQYPTRK.T/R.CREEVPELDCSK.Y/K.VSPICTMEYVPHCGSDGVTYSNR.C/R.CFFCNAYVQSNR.T |
| 8 | Ovoinhibitor | P10184 | 52/54 | 6.2 | 46 | 17 | 10 | K.DGTSWVACPR.N/R.EHGANVEK.E/K.HVTIDCSPYLQVVR.D/R.DGNTMVACPR.I/K.LHDGECK.L/R.TLVACPR.I/K.SHDGRCK.E/K.VSPICTMEYVPHCGSDGVTYSNR.C/R.CFFCNAYVQSNR.T |
| 11 | Ovoinhibitor | P10184 | 52/53 | 6.2 | 37 | 20 | 11 | K.DGTSWVACPR.N/R.NLKPVCGTDGSTYSNECGICLYNR.E/R.EHGANVEK.E/K.HVTIDCSPYLQVVR.D/R.DGNTMVACPR.I/K.LHDGECK.L/R.TLVACPR.I/R.QEIPEIDCDQYPTR.K/R.CFFCNAYVQSNR.T / |
| 12 | OVAX | P01013 | 26/52 | 5.1 | 79 | 30 | 7 | K.TAFNAEDTREMPFHVTK.Q/K.ILELPFASGDLSMLVLLPDEVSDLER.I/K.VYLPQMK.I/K.HSPESEQFR.A/K.HNPTNTIVYFGR.Y |
| 17 | TENP | O42273 | 47/51 | 5.5 | 39 | 13 | 6 | K.VADLWLSVVPEAGLR.L/R.LGIEVELR.V/R.VAPLHAVPMPVR.I |
| 18 | TENP | O42273 | 47/50 | 5.5 | 147[d] | 23 | 10 | R.APDCGGILTPLGLSYLAEVSKPHAEVVLR.Q/K.VADLWLSVIPEAGLR.L/R.LGIEVELR.I/K.ITQVGSLYHEDLPITLSAALR.S/R.VVLEEGR.A/R.MMISTAVIEDAELSLAASNVGLVR.A / |
| 18 | OVAX | P01013 | 26/50 | 5.1 | 103[d] | 27 | 8 | K.TAFNAEDTREMPFHVTK.Q/K.ILELPFASGDLSMLVLLPDEVSDLER.I/K.VYLPQMK.I/K.HSPESEQFR.A/K.HNPTNTIVYFGR.Y |
| 21 | HPX | Q90WR3 | 30/60 | 5.9 | 35 | 24 | 9 | R.ERPWLDAGPCDAALR.W/R.YYCLQGTQFYR.F/R.FRPHSWEVLPGYPR.D/R.DLRDYFIPCPGR.G/R.GGHQLVEGYPR.A |
| 22 | HPX | Q90WR3 | 30/61 | 5.9 | 340[d] | 48 | 18 | R.ERPWLDAGPCDAALR.W/R.YYCLQGTQFYR.F/R.FRPHSWEVLPGYPR.D/R.DLRDYFIPCPGR.G/R.DYFIPCPGR.G/R.MYLIQGSQVSIYVSGR.G/R.GGHQLVEGYPR.A/K.ADAAFTCPGSAELYVITGDR.M/R.HADEPQPLPYDGVDGAMCTADGIYLLR.G |
| 24 | OVAX | P01013 | 26/52 | 5.1 | 108[d] | 27 | 8 | K.TAFNAEDTREMPFHVTK.Q/K.ILELPFASGDLSMLVLLPDEVSDLER.I/K.HSPESEQFR.A/K.HNPTNTIVYFGR.Y |
| 24 | Ovotransferrin | P02789 | 78/52 | 6.7 | 63 | 21 | 10 | R.SAGWNIPIGTLLHR.G/K.AQSDFGVDTKSDFHLFGPPGK.K/K.GEADAVALDGGLVYTAGVCGLVPVMAER.Y/K.TDERPASYFAVAVAR.K/R.TAGWVIPMGLIHNR.T/R.TGTCNFDEYFSEGCAPGSPPNSR.L/K.YFGYTGALR.C/K.NLQMDDFELLCTDGR.R/K.DLTKCLFK.V |
| 27 | TENP | O42273 | 47/38 | 5.6 | 246[d] | 24 | 10 | M.GALLALLDPVQPTR.A/K.VADLWLSVIPEAGLR.L/K.ITQVGSLYHEDLPITLSAALR.S/R.VVLEEGR.A/R.MMISTAVIEDAELSLAASNVGLVR.A/R.AALLEELFLAPVCQQVPAWMDDVLR.E |
| 27 | IgY-Fc$\upsilon$3-4 | UPI000 18BF9C1 | 25/38 | 5.6 | 112[d] | 30 | 4 | R.NTGPTTPPLIYPFAPHPEELSLSR.V/R.AVPATEFVTTAVLPEER.T |
| 28 | TENP | O42273 | 47/36 | 5.6 | 232[d] | 20 | 13 | K.VADLWLSVIPEAGLR.L/K.ITQVGSLYHEDLPITLSAALR.S/R.VVLEEGR.A/R.MMISTAVIEDAELSLAASNVGLVR.A/R.AALLEELFLAPVCQQVPAWMDDVLR.E |
| 29 | Ex-FABP | P21760 | 20/24 | 5.6 | 351[d] | 52 | 17 | R.SEVAGKWYIVALASNTDFFLR.E/K.WYIVALASNTDFFLREK.G/R.ISFLGEDELEVSYAAPSPK.G/K.SYAVIFATR.V/R.TLHMMR.L/R.SREVSPTAMAIFR.K/R.EVSPTAMAIFR.K/R.ERNYTDEMVAVLPSQEECSVDEV.- |
| 31 | OVAY | P01014 | 44/52 | 5.2 | 638[d] | 40 | 16 | K.FCFDVFNEMK.V/K.VHHVNENILYCPLSILTALAMVYLGAR.G/K.VLHFDSITGAGSTTDSQCGSSEYVHNLFK.E/K.TFSVLPEYLSCAR.K/R.KFYTGGVEEVNFK.T/K.IAFNTEDTR.E/K.ILELPYASGDLSMLVLLPDEVSGLER.I/K.HSLELEEFRADHPFLFFIR.Y/R.ADHPFLFFIR.Y/R.YNPTNAILFFGR.Y |
| 32 | OVAY | P01014 | 44/52 | 5.2 | 645[d] | 44 | 20 | K.FCFDVFNEMK.V/K.VHHVNENILYCPLSILTALAMVYLGAR.G/K.VLHFDSITGAGSTTDSQCGSSEYVHNLFK.E/K.LYVDKTFSVLPEYLSCAR.K/R.KFYTGGVEEVNFK.T/R.QLINSWVEK.E/K.IAFNTEDTR.E/K.ILELPYASGDLSMLVLLPDEVSGLER.I/K.HSLELEEFRADHPFLFFIR.Y/R.ADHPFLFFIR.Y/R.YNPTNAILFFGR.Y |
| 33 | Ovalbumin | P01012 | 43/49 | 5.2 | 645[d] | 38 | 19 | R.DILNQITKPNDVYSFSLASR.L/R.YPILPEYLQCVK.E/R.GGLEPINFQTAADQAR.E/R.ELINSWVESQTNGIIR.N/K.AFKDEDTQAMPFR.V/R.VTEQESKPVQMMYQIGLFR.V/K.LTEWTSSNVMEER.K/K.ISQAVHAAHAEINEAGR.E/R.ADHPFLFCIK.H/K.HIATNAVLFFGR.C |
| 34 | Ovalbumin | P01012 | 43/21 | 5.2 | 488[d] | 38 | 19 | R.DILNQITKPNDVYSFSLASR.L/R.LYAEERYPILPEYLQCVK.E/R.GGLEPINFQTAADQAR.E/R.ELINSWVESQTNGIIR.N/K.AFKDEDTQAMPFR.V/R.VTEQESKPVQMMYQIGLFR.V/K.LTEWTSSNVMEERK.I/K.ISQAVHAAHAEINEAGR.E/R.ADHPFLFCIK.H/K.HIATNAVLFFGR.C |



dx.doi.org/10.1021/jf504469t | J. Agric. Food Chem. 2014, 62, 12346−12359

Table 2. continued

[a]Spot numbers correspond to the labels in Figure 4. Spots #1, 2, 3, 9, 10, 13, 14, 15, 16, 19, 20, 23, 25, 26, and 30 were not determined due to the limit of either database availability or instrumental detection. [b]Abbreviations: OVAX, ovalbumin-related protein X; TENP, transiently expressed in neural precursors; HPX, hemopexin; Ex-FABP, extracellular fatty acid-binding protein; and OVAY, ovalbumin related protein Y. [c]Accession numbers are from the UniProt Knowledgebase (UniProtKB) databases. [d]Molecular weights in theory. [e]Calculated molecular weights from 2D gels using by ImageMaster 2D Platinum 7.0. [f]Score (MOWSE), used in MASCOT PMF (peptide mass fingerprint), represents MS data from the UniProtKB database. Scores greater than 84 are significant ($P \leq 0.05$). [g]Sequence coverage. [h]The number of both ionized and nonionized peptides identified using MALDI-TOF/TOF MS/MS were matched with the whole peptides. [i]The sequences of peptides identified using MALDI-TOF/TOF MS/MS were matched with the whole sequences.

in the magnum of Stress ($P \leq 0.05$) on day 14, whereas no significant changes were detected for Ex-FABP and TENP (Figure 6). Ovoinhibitor, ovalbumin, and IgY-Fc$\upsilon$3-4 had at least two different spots which were significantly increased or decreased in the magnum whereas the expression of ovotransferrin and hemopexin was up-regulated. OVAY was decreased ($P \leq 0.05$), and no significant changes of both Ex-FABP and TENP were detected (Figure 6).

**Differential Gene Expression in Magnum of Treated and Untreated Hens (Day 14).** The genes, whose proteins were significantly up- or down-expressed in the egg white proteomic study ($P \leq 0.05$), were analyzed using qPCR in protein extracts of the magnum of the oviduct on day 14 (Figure 7). The seven genes encoding the proteins ovalbumin, OVAY, ovotransferrin, Ex-FABP, TENP, ovoinhibitor, and HPX were significantly down-expressed ($P \leq 0.0001$) in the magnum of laying hens treated with corticosterone compared with Control. One twenty-ninths for ovalbumin, 1/46 for OVAY, 1/12 for ovotransferrin, 1/23 for Ex-FABP, 1/33 for TENP, 1/16 for ovoinhibitor, and 1/49 for HPX genes were down-expressed in Stress against Control. The expressions of both the genes and proteins for HPX, TENP, Ex-FABP, OVAY, and ovalbumin were equally decreased. The gene for ovoinhibitor was down-regulated but its protein up-regulated.

## DISCUSSION

**Corticosterone Decreases Egg Production.** Corticosterone, the primary stress hormone in avian species including chickens, stimulates gluconeogenesis for survival to provide the body with energy when chickens are under stress.[2,4] Stress can affect performance in quantitative and qualitative manners as well as health by causing endocrine, metabolic, physiological, and behavioral changes in chickens.[5,7] The results of the present study show that although laying hens treated with corticosterone consumed more feed and had higher plasma corticosterone concentrations than did control hens, body weight was not significantly different from Control ($P = 0.11$). In a sharp contrast to the current results, corticosterone treatments show different effects in laying hens: corticosterone injected subcutaneously at 2 mg/kg body weight twice a day caused significant reduction in feed intake and body weight,[18] whereas dietary corticosterone at 1.5 mg/bird/day enhanced feed intake while reducing body weight gain.[19] Administration of corticosterone via drinking water at 20 mg/L for 1 week at 7, 11, and 15 weeks of age resulted in reduced body weight in laying hens.[3] ACTH, which stimulates the secretion of corticosterone from the adrenal and was delivered via osmotic pumps, increased feed intake and body weight in laying hens.[5] The controversy among these results may have resulted from different methods such as age of birds and delivery and dosage of corticosterone.

In the present study Stress caused significant reduction in egg production with relatively constant egg weight while increasing plasma corticosterone concentrations. The reduced egg production can be accounted for in part by decreased numbers of ovarian follicles (≥10 mm in diameter) in this study and by increased numbers of atretic follicles and reduced weights of the oviduct and ovary.[3,5] A strong negative relationship has been reported between elevated corticosterone concentrations and reduced egg production in studies in which hens were treated with ACTH via osmotic pumps,[5] subcutaneous corticosterone injections,[18] or corticosterone administration by way of either feed[19] or drinking water.[3] Indeed, stressful

**Table 3. Relative protein abundances that were increased (+) or decreased (−) in the egg white produced on day 5 by the same laying hens treated with Control or Stress, compared with those on day 0**

| | | | Control | | Stress | |
|---|---|---|---|---|---|---|
| Protein name[a] | Spot no. | Determined or estimated[b] | Relative change[c] | *P*-value | Relative change | *P*-value |
| Ovoinhibitor | 3 | Estimated | +1.1 | 0.21 | +2.3 | 0.17 |
| | 4 | Determined | −1.1 | 0.30 | +2.6 | 0.14 |
| | 5 | Determined | −1.1 | 0.28 | +2.0 | 0.18 |
| | 6 | Determined | −1.3 | 0.20 | +1.9 | 0.02 |
| | 7 | Determined | −1.1 | 0.30 | +1.7 | 0.02 |
| | 8 | Determined | −1.1 | 0.39 | +1.9 | 0.03 |
| | 9 | Estimated | −1.2 | 0.40 | +2.0 | 0.03 |
| | 10 | Estimated | −1.3 | 0.26 | +1.5 | 0.05 |
| | 11 | Determined | −1.3 | 0.35 | +2.3 | 0.02 |
| OVAX | 12 | Determined | +1.1 | 0.39 | +1.9 | 0.04 |
| | 18[d] | Determined | +1.1 | 0.40 | +1.6 | 0.05 |
| | 24[d] | Determined | - | - | +1.9 | 0.16 |
| TENP | 13 | Estimated | +1.4 | 0.10 | −1.5 | 0.13 |
| | 14 | Estimated | - | - | −1.6 | 0.25 |
| | 15 | Estimated | −1.1 | 0.45 | −1.5 | 0.04 |
| | 16 | Estimated | +1.3 | 0.14 | −1.5 | 0.08 |
| | 17 | Determined | −1.1 | 0.39 | −1.3 | 0.12 |
| | 18[d] | Determined | +1.1 | 0.40 | +1.6 | 0.05 |
| | 27[d] | Determined | +1.1 | 0.38 | −1.3 | 0.01 |
| | 28 | Determined | +1.3 | 0.13 | −1.3 | 0.02 |
| HPX | 20 | Estimated | +1.1 | 0.38 | −1.2 | 0.37 |
| | 21 | Determined | +1.3 | 0.22 | −1.2 | 0.30 |
| | 22 | Determined | +1.2 | 0.33 | −1.3 | 0.04 |
| IgY-Fc$\upsilon$3-4 | 27[d] | Determined | +1.1 | 0.38 | −1.3 | 0.01 |
| Ex-FABP | 29 | Determined | +1.2 | 0.31 | −1.4 | 0.01 |
| OVAY | 23 | Estimated | +1.1 | 0.14 | +1.3 | 0.17 |
| | 26 | Estimated | +1.2 | 0.26 | −1.3 | 0.10 |
| | 31 | Determined | +1.1 | 0.33 | −1.2 | 0.10 |
| | 32 | Determined | +1.1 | 0.06 | −1.2 | 0.11 |
| Ovalbumin | 33 | Determined | −1.1 | 0.40 | −1.4 | 0.28 |
| | 34 | Determined | +1.1 | 0.30 | −1.3 | 0.19 |
| Ovotransferrin | 24[d] | Determined | - | - | +1.9 | 0.16 |
| CAL | 19 | Estimated | +5.4 | 0.05 | −1.4 | 0.21 |
| | 30 | Estimated | +1.9 | 0.13 | −1.3 | 0.22 |

[a]Abbreviations: OVAX, ovalbumin-related protein X; TENP, transiently expressed in neural precursors; HPX, hemopexin; Ex-FABP, extracellular fatty acid-binding protein; OVAY, ovalbumin related protein Y; and CAL, chondrogenesis-associated lipocalin. [b]Proteins "Determined" were those identified based on MALDI TOF/TOF MS/MS analysis followed by bioinformatics in the present study. In contrast, proteins "Estimated" have not been identified due to the detection limit of the mass spectrometry. Proteins of these spots were estimated based on both those reported in recent papers[16,17] and the observational molecular weight (MWo) from the 2D gels of the current study using an image master. Ovoinhibitor (#3, 9, and 10): 64, 61, and 56 kDa; TENP (#13−16): 51 kDa; HPX (#20): 66 kDa; OVAY (#23 and 26): 52 and 51 kDa; CAL (#19 and 24): 24 and 25 kDa, respectively. [c]Relative changes of proteins show the spot intensity of any given protein on day 5 against those on day 0 under the same treatment. [d]Spots #18 (OVAX and TENP), #24 (OVAX and ovotransferrin,) and #27 (TENP and IgY-Fcu3-4) were determined as two different proteins.

environment caused reduced plasma concentrations of testosterone, progesterone, and estrogen,[1] which resulted in decrease ovarian function[1] and low-quality offspring.[2] This proclivity suggests that various environmental stimuli enhancing the release of corticosterone in plasma can contribute to decreased egg production and quality.

**Corticosterone Modulates Egg White Protein.** The present study is the first to present evidence suggesting that dietary corticosterone can not only contribute to decreased egg production and quality but also modify the expression of proteins in the egg white. We found several proteins that differentially expressed in the egg white in response to dietary corticosterone: ovoinhibitor and OVAX were significantly increased while TENP, Ex-FABP, HPX, and IgY-Fc$\upsilon$3-4 were decreased. With the exception of OVAY, however, such changes were not seen in Control, suggesting that the changes are treatment-specific.

The present results of proteomic analysis show that some spots were identified as two or more different proteins. There is one spot (#18) that was identified as both OVAX and TENP. As shown in Table 3, expression of the spots that were determined as OVAX protein was consistently increased in the egg white associated with stress. With the exception of spot #18, which was positively expressed, those that were determined as TENP protein were consistently negatively regulated. Therefore, it is plausible to consider, based on these data and the literature,[16] that spot #18 is OVAX protein rather than TENP. However, the spot (#24), which was determined as both OVAX and ovotransferrin, was positively expressed in the egg white by Stress whereas the spot (#27), which was

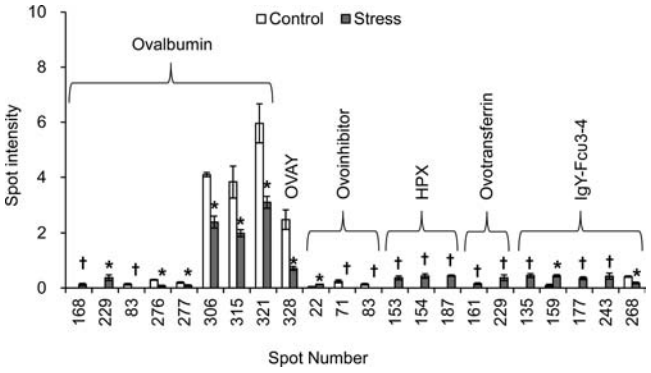


**Figure 6.** Differential expression of proteins in the magnum of the oviduct in hens. Laying hens were acclimatized to the experimental environment for the first 2 weeks (days −14 to 0) and then were divided into two groups to receive either ethanol- (Control) or corticosterone- (Stress) containing diet at 30 mg/kg for the next 2 weeks (days 0−14), respectively. The magnum obtained on day 14 was used for proteomic analysis. After individual protein spots on the gels derived from two-dimensional electrophoresis (2DE) were matched between two groups, their intensity was quantified and compared to identify protein spots that expressed equal to or greater than 1.2-fold, and is shown in graphs. Data are means ± SEM ($n$ = 3 per group). Spots identified by ∗ show significant differences at $P \leq 0.05$ by $t$-test, and those identified by † were detected in only one group. Abbreviations: OVAY, ovalbumin related protein Y; and HPX, hemopexin.

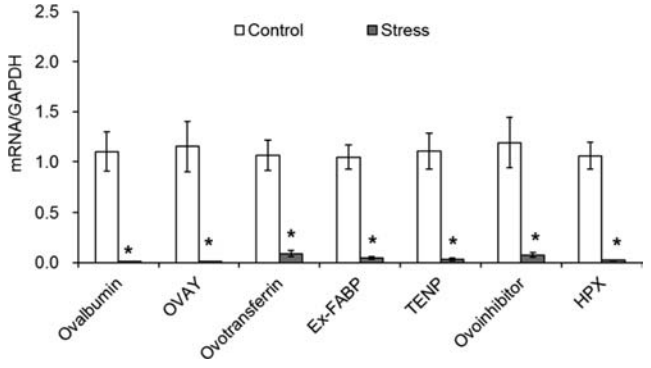


**Figure 7.** mRNA expression of ovalbumin, OVAY, ovotransferrin, Ex-FABP, TENP, ovoinhibitor, and HPX genes in the magnum of the oviduct in laying hens. Laying hens were acclimatized to the experimental environment for the first 2 weeks (days −14 to 0) and then were divided into two groups ($n$ = 20 each) to receive either ethanol- (Control) or corticosterone- (Stress) containing diet at 30 mg/kg for the next 2 weeks (days 0−14), respectively. Hens were killed using a guillotine, and the magnum was cut off at the end of the entire experimental period. Relative mRNA expression of individual genes against GAPDH was determined in duplicate using qPCR. Data are means ± SEM ($n$ = 8 birds each group). *$P \leq 0.0001$ vs Control. Abbreviations: OVAY, ovalbumin related protein Y; Ex-FABP, extracellular fatty acid-binding protein; and HPX, hemopexin.

determined as both TENP and IgY-Fc$\upsilon$3-4, was negatively expressed. Due to the limit of data available, whether or not each of these spots has a single protein or includes two different proteins remains to be determined.

In the present study, MWo values for some spots were similar to, lower than, or higher than those for MWt, suggesting their possible degradation or polymerization during the preparation of proteins for the 2DE analysis, which is consistent with those reported by Guerin-Dubiard et al.[16] and Wang et al.[17]

**Corticosterone Modulates Protein and Gene Expression in Magnum.** Several differential proteins, with the exception of Ex-FABP, TENP, and OVAX, were common between the egg white and oviductal magnum of hens administered with dietary corticosterone. Furthermore, we also found that mRNA expression of the genes encoding these proteins was significantly modified in the magnum.

There are different patterns of expression among proteins in the egg white and genes and proteins in the magnum in the current study. This could be attributable to the differences in collection time between eggs and the oviduct: eggs laid on days 0 and 5 were used for proteomic analysis whereas mRNA and protein expression was determined using the oviduct obtained at the conclusion of the whole experiment (day 14), thus being highly likely to reflect different physiological and cellular events from those on day 5. The oviduct was visually regressed in these hens treated with dietary corticosterone for 14 days in this study, and differential expression of genes[9,10] and proteins[20] has been reported in the oviduct of hens subject to molting. Another explanation is that the time and process of transcription may be different among individual genes, after which translation for protein biosynthesis would occur.[21]

**Ovoinhibitor.** Ovoinhibitor is one of the 4 proteinase inhibitors found in the egg white that are ovostatin, ovomucoid, ovoinhibitor, and cystatin.[11] Distinct expression of ovoinhibitor mRNA was detected in the liver, magnum, and uterus of chickens, and the protein was up-regulated in the liver of prelaying hens (14−16 weeks of age) compared with laying hens (41 weeks).[22] Ovoinhibitor has MW of 48.6−49 kDa,[11] consists of 1.5% of total egg white protein,[11] and inhibits serine proteinase such as trypsin, chymotrypsin, and elastase.[23] Synthesis and secretion of ovoinhibitor are controlled by estrogen and progesterone,[11] as seen in other enzymes in the oviduct and ovary.[11]

In the current study, ovoinhibitor was significantly up-expressed ($P \leq 0.05$) in the egg white produced from hens treated with corticosterone, but its gene expression was down-regulated in the magnum by Stress ($P \leq 0.001$). Significant changes of this protein were also seen in the oviduct. Estrogen increases the transcription rate of ovoinhibitor in the liver,[11] although concentrations of estrogen were not measured in this study. A recent study shows that expression of 6 ovoinhibitor precursor spots was strongly increased in fertilized egg white on 7 days after hatching.[24] Discrepancy in expression patterns between the gene and protein of ovoinhibitor remains to be solved.

**Ovalbumin, Ovalbumin-Related Protein X (OVAX), and Ovalbumin-Related Y (OVAY).** Ovalbumin is the major protein in the egg white, consisting of 54% egg white protein.[25] Ovalbumin, OVAX, and OVAY proteins are encoded by three distinct genes, the ovalbumin, ovalbumin X, and ovalbumin Y genes, respectively, belonging to the ovalbumin gene family located within a 40 kDa region.[26] Ovalbumin is composed of 386 amino acids, alternatively named as allergen Gal d II, egg albumin, plakalbumin, or allergen=Gal d 2 (UniProtKB ID: P01012); OVAX of 232 amino acids, alternatively named as gene X protein (UniProtKB ID: P01013); and OVAY of 388 amino acids, alternatively named as gene Y protein (UniProtKB ID: P01014). According to the nomenclature guidelines of serpin, ovalbumin, gene X, and gene Y are named as serpinb14, serpinb14c, and serpinb14b, respectively.[26] OVAX has been

shown to be similar to OVAY in the amino acid sequence and structure.[8,27] OVAY is present in the yolk,[28] and OVAX is approximately 2.4 mg/mL in average in egg white and seems to show antimicrobial activity.[29]

Glucocorticoids (e.g., cortisol and corticosterone) increase the expression of ovalbumin mRNA and protein in the chicken oviductal magnum.[30,31] Study showed that ovalbumin gene expression and protein synthesis in the magnum were increased in chicks administered with glucocorticoid at 2 mg/chick every 6 h, but decreased in those treated with 10 mg of glucocorticoid.[31] Synthesis and secretion of ovalbumin are also controlled by estrogen.[32] Corticosterone treatment reduces plasma concentrations of estrogen[1] and expression of its gene and protein.[30,31] Stress such as molting can also decrease plasma concentrations of estrogen[33] and reduce ovalbumin protein expression in egg shell.[34]

In the present study, OVAX protein abundance was significantly increased in the egg white of hens treated with dietary corticosterone at 30 mg/kg diet but not in Control. Expression of ovalbumin and OVAY proteins remained unchanged in both groups. On the other hand, gene expression of ovalbumin and OVAY was significantly decreased in the magnum of Stress. Together, these findings suggest that expression of these genes and proteins is differentially regulated by glucocorticoids depending on hormone concentrations and severity of stress.

**Transiently Expressed In Neural Precursors (TENP).** Protein TENP is a member of BPIFB subfamilies which belong to the bactericidal permeability-increasing protein (BPI) fold-containing (BPIF) superfamily,[35] and it consists of 440 amino acids.[36] The full name of the gene encoding this protein, known as TENP, is BPI fold containing family B, member 7, the official symbol of which is BPIFB7 (NCBI gene ID: 395882). As indicated in its name "transiently expressed in neural precursors", TENP was originally reported to be temporarily expressed only in the retina and brain of embryonic chicks being hatched but not in the other organs such as the heart, liver, and kidney.[36] mRNA expression diminished over time in the brain and retina of the chicken embryo but up-regulated in adult birds.[37] TENP has been now well-known to be present in the extraneural organs/tissues such as the oviductal magnum and appears to be avian specific, expressing almost exclusively in the magnum of adult birds.[37] In fact, protein TENP has been shown to be detected in the egg: the egg white[16,27] and yolk[28] of unfertilized chicken eggs and in emu egg white,[38] suggesting that expression of this protein is independent of fertilization and avian species.

Protein TENP consists of 0.1−0.5% of dried egg white protein[27] with MW of 47−50 kDa.[16] In the present study, TENP in the egg white was down-regulated by Stress while no such changes were seen in Control, and we even failed to detect TENP expression in the magnum. A recent study has shown that TENP mRNA was largely increased in the magnum of the oviduct in laying hens compared with nonlaying hens and in juvenile chicks administrated with either estrogen or progesterone, and was site-specifically expressed in the magnum of adult chickens and ducks,[37] suggesting gonadal regulation of TENP expression. The roles of TENP are not clear in chickens but appear to be associated with natural defense of avian eggs and embryonic development.[36]

**Hemopexin (HPX).** HPX is a plasma glycoprotein which is mainly expressed in the liver and less abundantly in the central and peripheral nervous systems, and it has a high binding affinity to heme in an equimolar ratio to protect the body from oxidative damage.[39] HPX increases the resistance of proteolytic digestion when it binds to heme.[40] HPX belongs to the acute phase protein and is increased by inflammation and stress.[39] Avian serum HPX is a 52 kDa $\alpha_1$-glycoprotein and can be detected from a few days before the egg hatches.[40] HPX concentrations in 4-day-old chicks were half those of adults (3.5 months old), and its concentrations in plasma were gradually increased after hatching.[41] HPX protein concentrations in plasma are significantly increased by immune challenge such as injection of lipopolysaccharide.[42] Both full length (IgY) and truncated isoforms (Fc) of IgY were isolated from ducks vaccinated against *Escherichia coli* (*E. coli*) and used to make *E. coli*-Ig immune complexes. When IgY and IgY (Fc) were injected intravenously into naive Mallard ducks, plasma HPX concentrations were higher in ducks given either 0:100 ratio or 100:0 ratio than in those given 50:50 or *E. coli* alone.[43] HPX has been recently shown in a variety of eggs produced from different raising conditions in nutrients or hens' strains, which suggests that its abundance can be affected by hens' strain, nutrients, or housing conditions.[17]

In the present study we found that HPX protein in the egg white and its gene in the magnum were significantly down-expressed in laying hens treated with corticosterone whereas HPX protein was increased in the magnum. Considering the findings that HPX concentrations are increased by acute stress such as inflammation,[39] it is notable in the current study that both HPX protein and gene expressions were different depending on what was investigated, which is worthy of further study.

**IgY-Fc$\upsilon$3-4.** Yolk proteins occupy approximately 16% of the total weight of egg yolk in fresh eggs.[23] Livetin fraction is a type of egg yolk proteins including $\alpha$-, $\beta$-, and $\gamma$-livetin. Both yolk $\alpha$-livetin and chicken serum albumin are the same protein.[23] $\beta$-Livetin is a D-2-glycoprotein with a MW of 45 kDa. A third protein, $\gamma$-livetin, is IgY with a MW of approximately 167 kDa.[23] Avian IgY is closely related to the ancestors of mammalian IgG and IgE.[44] The predominant serum immunoglobulin (Ig) in chickens has been proposed to be called IgY rather than IgG.[45] IgY consists of two heavy and two light chains,[46] and IgY-Fc$\upsilon$3-4 is an IgY-Fc fragment containing heavy chain constant domains 3 (C$\upsilon$3) and 4 (C$\upsilon$4).[44,46]

As IgY in the egg has passive immunity granted from the mother, it is transported into the yolk by receptors from blood, and its amount in the yolk is related to plasma IgY concentrations.[47] IgY was detected in 3.26−6.02 mg per 1 mL of hen's plasma and in 1.15−2.26 mg per 1 mL of the egg yolk.[47] Human (h) IgG was increased to maximum in the yolk on 5 days after laying hens were administered with hIgG.[48] Although hIgA, but not hIgG, was detected from egg albumen,[48] the current results, showing the presence of IgY-Fc$\upsilon$3-4 in the egg white of hens treated with corticosterone, suggest the presence of IgY in the egg white. Indeed, IgY has been shown to be detected in the egg white (3.57−9.58 $\mu$g/mL), at a much lower concentration than that in the yolk (1.15−2.26 mg/mL).[47] When some of the hens were infected with pathogen, IgY concentrations were increased in the circulation, which in turn resulted in an elevation of IgY in the egg.[49] In the present study, the abundance of IgY-Fc$\upsilon$3-4 was rather decreased in the egg white, which cannot be accounted for by possible infection of the hens. Furthermore, these hens had an increased feed intake during the entire treatment period (Figure 1). Thus, down-expression of IgY-Fc$\upsilon$3-4 in the egg

white means that the eggs of hens treated with corticosterone or raised under stressful environment are highly likely to have less amount of antibody than those in normal environment. In other words, if breeder hens are being raised under stress, their offspring produced are likely to be susceptible to diseases.[7] Concentrations of IgY in egg yolk and white were not determined in this study.

**Extracellular Fatty Acid-Binding Protein (Ex-FABP).** Fatty acids are present in complex with binding proteins rather than free form in order to be dissolved and transported in biological fluids for metabolism because fatty acid is hydrophobic. Ex-FABP is identified for the first time from the bone and cartilage of the developing chicken embryo[50] and then was also detected in muscle fibers and blood granulocytes in chickens.[50] It is also called protein Ch21, quiescence-specific protein, p20K (UniProtKB ID: P21760), or chondrogenesis-associated lipocalin, and it belongs to the chondrogenesis-associated lipocalin superfamily.[50] Ex-FABP is transported in the extracellular fluid and serum following binding to long-chain unsaturated fatty acids.[50] Ex-FABP is involved in heart development, fatty acid transport, and lipid metabolism, and it supposedly acts as a cell survival protein that protects cells from toxic lipid accumulation of fat.[51] Expression of Ex-FABP is enhanced in the liver of embryonic chickens by inflammatory agents such as lipopolysaccharide,[52] and it plays a role as an acute phase protein that is reduced by treatment with anti-inflammatory agents.[52,53] Ex-FABP gene expression is significantly increased in the lung, liver, and spleen of 3-week-old White Leghorn chicks infected with *E. coli*.[52,53] Growth inhibition of *E. coli* was observed in the presence of Ex-FABP,[54] suggesting that this protein possesses an antibacterial activity. On the other hand, suppressing gene expression of Ex-FABP resulted in increased apoptosis, decreased differentiation, and proliferation of cells.[52]

The results of the present study show that both Ex-FABP in the egg white and its gene in the magnum were significantly down-regulated in hens treated with dietary corticosterone. We failed however to detect Ex-FABP expression in the magnum using 2DE plus MALDI-TOF/TOF MS/MS. Although the relationship between Ex-FABP expression in the egg white and gene expression of Ex-FABP in the lung or liver has not been investigated in the present study, the present findings in the egg and magnum show an inverse relationship with protein and gene expressions in other organs (e.g., embryo, lung, liver, and spleen) of chickens infected.[52−54] Together, these results suggest that the reduced expression of Ex-FABP in the egg white may have resulted from the reduced expression of its gene, specifically in the magnum, but not the lung, liver, or spleen. From this perspective, a recent proteomic study,[55] which shows that the amount of an Ex-FABP precursor was gradually decreased in the egg white as the storage temperature of eggs was increased, implies that Ex-FABP can be used as an indicator for the evaluation of egg quality.

**Ovotransferrin.** Ovotransferrin is a 78 kDa, disulfide-rich (15 disulfide bonds) single-chain glycoprotein consisting of 686 amino acids and accounts for 13% of total egg white proteins.[25] Ovotransferrin is a member of the transferrin family that has high ability to bind two $Fe^{3+}$ ions (iron-binding capacity) and can be transferred into the egg white through the oviduct of hens.[56] Ovotransferrin and its hydrolysates have been shown to exert antimicrobial, antiviral, and antioxidant activities and to play as markers for stress and metabolic diseases in chickens infected with various pathogens.[56] Concentrations of ovotransferrin are increased in serum of chickens infected with pathogens or treated with inflammatory agents.[56] As ovotransferrin is regulated by inflammatory or microbial stress,[56] its concentrations in blood could be used as a diagnostic marker of chickens subject to infection or inflammation. Glucocorticoids (e.g., cortisol and corticosterone) stimulate enhanced synthesis of ovotransferrin mRNA and protein in the chicken magnum in vivo.[31] We found in the current study that ovotransferrin was slightly but not significantly up-regulated in the egg white by corticosterone and was significantly increased in the magnum while its gene expression was significantly reduced in the magnum. Others showed that gene and protein expression was increased in the magnum of chicks administrated with glucocorticoid at 2 mg/chick in every 6 h but decreased in chicks at 10 mg,[31] suggesting that their expression depends upon its concentrations used.

In summary, the results of the present study show that dietary corticosterone modulates the expression of proteins in the egg white. Similar findings were observed in the expression of proteins and genes of the magnum. Recent studies have shown, by proteomics, that expression of egg white proteins are affected by egg storage conditions, time, or fertilization.[55,57] In other words, the quantity of individual proteins consisting of the egg white can be changed in response to environmental conditions, which can have a direct impact on the quality of eggs. Egg quality can be affected by various factors, such as nutrients, ambient temperature, housing conditions, and stressful conditions, under which hens are raised,[58−60] and by the age and strain of hens.[58−60] Thus, egg quality has been evaluated based on external and internal aspects of the egg as well as on a food safety perspective that has long been a subject of public concern, having been linked to hens' welfare. Therefore, egg white proteins could be used as markers which help estimate the state of animal welfare or housing environment at the time of laying the egg. In conclusion, the findings from the current study provide evidence for the first time that dietary corticosterone modulates protein abundance in the egg white in laying hens, and suggest that environmental stress can differentially modify expression of egg white proteins in laying hens.

## AUTHOR INFORMATION

### Corresponding Author

*Address: Department of Animal Science. E-mail address: yhchoi@gnu.ac.kr. Tel.: +82-55-772-1946. Fax.: +82-55-772-1949.

### Funding

This study was supported in part by an NGB21 grant (PJ008049) from RDA, and by a grant from NRF (0014786) of Korea. J.K. was supported in part by a scholarship from the BK21Plus Program, the Ministry of Education, Republic of Korea.

### Notes

The authors declare no competing financial interest.

## ACKNOWLEDGMENTS

Part of this study was presented at the Poultry Science Association 101st Annual Meeting (#229), held on July 9−12, 2012, at the University of Georgia, Athens, GA. The authors would like to thank Dr. Dong-Won Bae and Young Sang Kwon for their assistance with proteomic analysis, and Yeon-Hwa Kim

and HyungSook Yoon for their technical assistance with the animal studies. The authors are grateful to the anonymous reviewers for their criticism and comments on the manuscript.

## REFERENCES

(1) Henriksen, R.; Groothuis, T. G.; Rettenbacher, S. Elevated plasma corticosterone decreases yolk testosterone and progesterone in chickens: linking maternal stress and hormone-mediated maternal effects. *PLoS One* **2011**, *6*, e23824.

(2) Saino, N.; Romano, M.; Ferrari, R. P.; Martinelli, R.; Møller, A. P. Stressed mothers lay eggs with high corticosterone levels which produce low-quality offspring. *J. Exp. Zool., Part A* **2005**, *303*, 998−1006.

(3) Shini, S.; Shini, A.; Huff, G. R. Effects of chronic and repeated corticosterone administration in rearing chickens on physiology, the onset of lay and egg production of hens. *Physiol. Behav.* **2009**, *98*, 73−77.

(4) Okuliarova, M.; Sarnikova, B.; Rettenbacher, S.; Skrobanek, P.; Zeman, M. Yolk testosterone and corticosterone in hierarchical follicles and laid eggs of Japanese quail exposed to long-term restraint stress. *Gen. Comp. Endrocrinol.* **2010**, *165*, 91−96.

(5) Mumma, J. O.; Thaxton, J. P.; Vizzier-Thaxton, Y.; Dodson, W. L. Physiological stress in laying hens. *Poult. Sci.* **2006**, *85*, 761−769.

(6) Schmidt, J. B.; Satterlee, D. G.; Treese, S. M. Maternal corticosterone reduces egg fertility and hatchability and increases the numbers of early dead embryos in eggs laid by quail hens selected for exaggerated adrenocortical stress responsiveness. *Poult. Sci.* **2009**, *88*, 1352−1357.

(7) Henriksen, R.; Rettenbacher, S.; T, G. G. G. Maternal corticosterone elevation during egg formation in chickens (Gallus gallus domesticus) influences offspring traits, partly via prenatal undernutrition. *Gen. Comp. Endrocrinol.* **2013**, *191C*, 83−91.

(8) Rozenboim, I.; Tako, E.; Gal-Garber, O.; Proudman, J. A.; Uni, Z. The effect of heat stress on ovarian function of laying hens. *Poult. Sci.* **2007**, *86*, 1760−1765.

(9) Ariyadi, B.; Isobe, N.; Yoshimura, Y. Differences in the mucosal surface barrier formed by mucin in the lower oviductal segments between laying and molting hens. *Poult. Sci.* **2012**, *91*, 1173−1178.

(10) Sundaresan, N. R.; Anish, D.; Sastry, K. V.; Saxena, V. K.; Mohan, J.; Saxena, M. Differential expression of lipopolysaccharide-induced TNF-alpha factor (LITAF) in reproductive tissues during induced molting of white leghorn hens. *Anim. Reprod. Sci.* **2007**, *102*, 335−342.

(11) Saxena, I.; Tayyab, S. Protein proteinase inhibitors from avian egg whites. *Cell. Mol. Life Sci.* **1997**, *53*, 13−23.

(12) Hager, L. J.; McKnight, G. S.; Palmiter, R. D. Glucocorticoid induction of egg white mRNAs in chick oviduct. *J. Biol. Chem.* **1980**, *255*, 7796−7800.

(13) Rories, C.; Lau, C. K.; Fink, K.; Spelsberg, T. C. Rapid inhibition of c-myc gene expression by a glucocorticoid in the avian oviduct. *Mol. Endocrinol.* **1989**, *3*, 991−1001.

(14) Lin, H.; Sui, S. J.; Jiao, H. C.; Jiang, K. J.; Zhao, J. P.; Dong, H. Effects of diet and stress mimicked by corticosterone administration on early postmortem muscle metabolism of broiler chickens. *Poult. Sci.* **2007**, *86*, 545−554.

(15) Kwon, Y. S.; Ryu, C. M.; Lee, S.; Park, H. B.; Han, K. S.; Lee, J. H.; Lee, K.; Chung, W. S.; Jeong, M. J.; Kim, H. K.; Bae, D. W. Proteome analysis of Arabidopsis seedlings exposed to bacterial volatiles. *Planta* **2010**, *232*, 1355−1370.

(16) Guerin-Dubiard, C.; Pasco, M.; Molle, D.; Desert, C.; Croguennec, T.; Nau, F. Proteomic analysis of hen egg white. *J. Agric. Food Chem.* **2006**, *54*, 3901−3910.

(17) Wang, J.; Liang, Y.; Omana, D. A.; Kav, N. N.; Wu, J. Proteomics analysis of egg white proteins from different egg varieties. *J. Agric. Food Chem.* **2012**, *60*, 272−282.

(18) Liu, L.; Song, Z.; Sheikhahmadi, A.; Jiao, H.; Lin, H. Effect of corticosterone on gene expression of feed intake regulatory peptides in laying hens. *Comp. Biochem. Physiol., B: Biochem. Mol. Biol.* **2012**, *162*, 81−87.

(19) El-lethey, H.; Jungi, T. W.; Huber-Eicher, B. Effects of feeding corticosterone and housing conditions on feather pecking in laying hens (Gallus gallus domesticus). *Physiol. Behav.* **2001**, *73*, 243−251.

(20) Ariyadi, B.; Isobe, N.; Yoshimura, Y. Induction of mucin expression by estrogen and lipopolysaccharide in the lower oviductal segments in hens. *Poult. Sci.* **2013**, *92*, 3205−3213.

(21) Nilsen, T. W.; Graveley, B. R. Expansion of the eukaryotic proteome by alternative splicing. *Nature* **2010**, *463*, 457−463.

(22) Bourin, M.; Gautron, J.; Berges, M.; Attucci, S.; Le Blay, G.; Labas, V.; Nys, Y.; Rehault-Godbert, S. Antimicrobial potential of egg yolk ovoinhibitor, a multidomain Kazal-like inhibitor of chicken egg. *J. Agric. Food Chem.* **2011**, *59*, 12368−12374.

(23) Huopalahti, R.; López-Fandiño, R.; Anton, M.; Schade, R. *Bioactive egg compounds*; Springer: 2007.

(24) Liu, Y.; Qiu, N.; Ma, M. Comparative proteomic analysis of hen egg white proteins during early phase of embryonic development by combinatorial peptide ligand library and matrix-assisted laser desorption ionization-time of flight. *Poult. Sci.* **2013**, *92*, 1897−1904.

(25) Guerin-Dubiard, C.; Pasco, M.; Hietanen, A.; Quiros del Bosque, A.; Nau, F.; Croguennec, T. Hen egg white fractionation by ion-exchange chromatography. *J. Chromatogr., A* **2005**, *1090*, 58−67.

(26) Benarafa, C.; Remold-O'Donnell, E. The ovalbumin serpins revisited: perspective from the chicken genome of clade B serpin evolution in vertebrates. *Proc. Natl. Acad. Sci. U. S. A.* **2005**, *102*, 11367−11372.

(27) Mann, K. The chicken egg white proteome. *Proteomics* **2007**, *7*, 3558−3568.

(28) Farinazzo, A.; Restuccia, U.; Bachi, A.; Guerrier, L.; Fortis, F.; Boschetti, E.; Fasoli, E.; Citterio, A.; Righetti, P. G. Chicken egg yolk cytoplasmic proteome, mined via combinatorial peptide ligand libraries. *J. Chromatogr., A* **2009**, *1216*, 1241−1252.

(29) Rehault-Godbert, S.; Labas, V.; Helloin, E.; Herve-Grepinet, V.; Slugocki, C.; Berges, M.; Bourin, M. C.; Brionne, A.; Poirier, J. C.; Gautron, J.; Coste, F.; Nys, Y. Ovalbumin-related protein X is a heparin-binding ov-serpin exhibiting antimicrobial activities. *J. Biol. Chem.* **2013**, *288*, 17285−17295.

(30) Dean, D. M.; Jones, P. S.; Sanders, M. M. Regulation of the chicken ovalbumin gene by estrogen and corticosterone requires a novel DNA element that binds a labile protein, Chirp-1. *Mol. Cell. Biol.* **1996**, *16*, 2015−2024.

(31) Le Bouc, Y.; Groyer, A.; Cadepond, F.; Groyer-Schweizer, G.; Robel, P.; Baulieu, E. E. Effects of progesterone and tamoxifen on glucocorticosteroid-induced egg-white protein synthesis in the chick oviduct. *Endocrinology* **1985**, *116*, 2384−2392.

(32) Dougherty, D. C.; Sanders, M. M. Estrogen action: revitalization of the chick oviduct model. *Trends Endocrinol Metab.* **2005**, *16*, 414−419.

(33) Berry, W. D. The physiology of induced molting. *Poultry Science* **2003**, *82*, 971−980.

(34) Ahmed, A. M.; Rodriguez-Navarro, A. B.; Vidal, M. L.; Gautron, J.; Garcia-Ruiz, J. M.; Nys, Y. Changes in eggshell mechanical properties, crystallographic texture and in matrix proteins induced by moult in hens. *Br. Poult. Sci.* **2005**, *46*, 268−279.

(35) Bingle, C. D.; Seal, R. L.; Craven, C. J. Systematic nomenclature for the PLUNC/PSP/BSP30/SMGB proteins as a subfamily of the BPI fold-containing superfamily. *Biochem. Soc. Trans.* **2011**, *39*, 977−983.

(36) Yan, R. T.; Wang, S. Z. Identification and characterization of tenp, a gene transiently expressed before overt cell differentiation during neurogenesis. *J. Neurobiol.* **1998**, *34*, 319−328.

(37) Whenham, N.; Wilson, P. W.; Bain, M. M.; Stevenson, L.; Dunn, I. C. Comparative biology and expression of TENP, an egg protein related to the bacterial permeability-increasing family of proteins. *Gene* **2014**, *538*, 99−108.

(38) Maehashi, K.; Matano, M.; Irisawa, T.; Uchino, M.; Itagaki, Y.; Takano, K.; Kashiwagi, Y.; Watanabe, T. Primary Structure of Potential

Allergenic Proteins in Emu (Dromaius novaehollandiae) Egg White. *J. Agric. Food Chem.* **2010**, *58*, 12530−12536.
(39) Tolosano, E.; Altruda, F. Hemopexin: structure, function, and regulation. *DNA Cell Biol.* **2002**, *21*, 297−306.
(40) Goldfarb, V.; Trimble, R. B.; De Falco, M.; Liem, H. H.; Metcalfe, S. A.; Wellner, D.; Muller-Eberhard, U. An avian serum alpha 1-glycoprotein, hemopexin, differing significantly in both amino acid and carbohydrate composition from mammalian (beta-glycoprotein) counterparts. *Biochemistry* **1986**, *25*, 6555−6562.
(41) Grieninger, G.; Liang, T. J.; Beuving, G.; Goldfarb, V.; Metcalfe, S. A.; Muller-Eberhard, U. Hemopexin is a developmentally regulated, acute-phase plasma protein in the chicken. *J. Biol. Chem.* **1986**, *261*, 15719−15724.
(42) Buyse, J.; Swennen, Q.; Niewold, T. A.; Klasing, K. C.; Janssens, G. P.; Baumgartner, M.; Goddeeris, B. M. Dietary L-carnitine supplementation enhances the lipopolysaccharide-induced acute phase protein response in broiler chickens. *Vet. Immunol. Immunopathol.* **2007**, *118*, 154−159.
(43) Humphrey, B. D.; Calvert, C. C.; Klasing, K. C. The ratio of full length IgY to truncated IgY in immune complexes affects macrophage phagocytosis and the acute phase response of mallard ducks (Anas platyrhynchos). *Dev. Comp. Immunol.* **2004**, *28*, 665−672.
(44) Taylor, A. I.; Fabiane, S. M.; Sutton, B. J.; Calvert, R. A. The crystal structure of an avian IgY-Fc fragment reveals conservation with both mammalian IgG and IgE. *Biochemistry* **2009**, *48*, 558−562.
(45) Leslie, G. A.; Clem, L. W. Phylogen of immunoglobulin structure and function. 3. Immunoglobulins of the chicken. *J. Exp. Med.* **1969**, *130*, 1337−1352.
(46) Warr, G. W.; Magor, K. E.; Higgins, D. A. IgY: clues to the origins of modern antibodies. *Immunol. Today* **1995**, *16*, 392−398.
(47) Hamal, K. R.; Burgess, S. C.; Pevzner, I. Y.; Erf, G. F. Maternal antibody transfer from dams to their egg yolks, egg whites, and chicks in meat lines of chickens. *Poult. Sci.* **2006**, *85*, 1364−1372.
(48) Mohammed, S. M.; Morrison, S.; Wims, L.; Trinh, K. R.; Wildeman, A. G.; Bonselaar, J.; Etches, R. J. Deposition of genetically engineered human antibodies into the egg yolk of hens. *Immunotechnology* **1998**, *4*, 115−125.
(49) Yang, Y. E.; Wen, J.; Zhao, S.; Zhang, K.; Zhou, Y. Prophylaxis and therapy of pandemic H1N1 virus infection using egg yolk antibody. *J. Virol. Methods* **2014**, *206*, 19−26.
(50) Cancedda, F. D.; Malpeli, M.; Gentili, C.; Di Marzo, V.; Bet, P.; Carlevaro, M.; Cermelli, S.; Cancedda, R. The developmentally regulated avian Ch21 lipocalin is an extracellular fatty acid-binding protein. *J. Biol. Chem.* **1996**, *271*, 20163−20169.
(51) Gentili, C.; Tutolo, G.; Zerega, B.; Di Marco, E.; Cancedda, R.; Cancedda, F. D. Acute phase lipocalin Ex-FABP is involved in heart development and cell survival. *J. Cell Physiol.* **2005**, *202*, 683−689.
(52) Di Marco, E.; Sessarego, N.; Zerega, B.; Cancedda, R.; Cancedda, F. D. Inhibition of cell proliferation and induction of apoptosis by ExFABP gene targeting. *J. Cell Physiol.* **2003**, *196*, 464−473.
(53) Cermelli, S.; Zerega, B.; Carlevaro, M.; Gentili, C.; Thorp, B.; Farquharson, C.; Cancedda, R.; Cancedda, F. D. Extracellular fatty acid binding protein (Ex-FABP) modulation by inflammatory agents: ″physiological″ acute phase response in endochondral bone formation. *Eur. J. Cell Biol.* **2000**, *79*, 155−164.
(54) Garénaux, A.; Houle, S.; Folch, B.; Dallaire, G.; Truesdell, M.; Lépine, F.; Doucet, N.; Dozois, C. M. Avian lipocalin expression in chickens following Escherichia coli infection and inhibition of avian pathogenic Escherichia coli growth by Ex-FABP. *Vet. Immunol. Immunopathol.* **2013**, *152*, 156−167.
(55) Qiu, N.; Ma, M.; Zhao, L.; Liu, W.; Li, Y.; Mine, Y. Comparative Proteomic Analysis of Egg White Proteins under Various Storage Temperatures. *J. Agric. Food Chem.* **2012**, *60*, 7746−7753.
(56) Giansanti, F.; Leboffe, L.; Pitari, G.; Ippoliti, R.; Antonini, G. Physiological roles of ovotransferrin. *Biochim. Biophys. Acta* **2012**, *1820*, 218−225.
(57) Qiu, N.; Ma, M.; Cai, Z.; Jin, Y.; Huang, X.; Huang, Q.; Sun, S. Proteomic analysis of egg white proteins during the early phase of embryonic development. *J. Proteomics* **2012**, *75*, 1895−1905.
(58) Scott, T. A.; Silversides, F. G. The effect of storage and strain of hen on egg quality. *Poult. Sci.* **2000**, *79*, 1725−1729.
(59) Choi, Y.-H. Conjugated linoleic acid as a key regulator of performance, lipid metabolism, development, stress and immune functions, and gene expression in chickens. *Asian-Aust. J. Anim. Sci.* **2009**, *22*, 448−458.
(60) Singh, R.; Cheng, K. M.; Silversides, F. G. Production performance and egg quality of four strains of laying hens kept in conventional cages and floor pens. *Poult. Sci.* **2009**, *88*, 256−264.

## MATERIALS AND METHODS

**Materials.** Bamboo (*Dendrocalamus membranaceus* Munro) was kindly provided by a pulp and papermaking factory (Yunnan, China). Bamboo was first ground into powder, and the powder between 60 and 80 mesh was collected for subsequent experimentation. The bamboo powder was dewaxed by refluxing in a Soxhlet apparatus with toluene-ethanol (2:1, v/v) for 6 h to remove extractives. The extractive-free bamboo powder was consisted of cellulose (36.6%), acid insoluble lignin (30.4%), hemicelluloses (19.7%) and ash (5.5%) according to the method of NREL.[14] All chemicals used were of analytical grade and purchased from Aladdin-Reagent.

**Methods.** Schematic illustration of the experimental procedure is shown in Scheme 1. In this study, all experiments were conducted in a batch reactor equipped with heating module (SLM 50, Beijing Century Senlong experimental apparatus Co., Ltd., Beijing, China), which was made of 316L stainless steel (50 mL nominal capacity, internal diameter = 35 mm; height = 80 mm). The hydrothermal processes were carried out using 1.0 g of extractive-free bamboo powder dispersed in 50 mL of distilled water. Magnetic stirring was used and the agitation was set at 500 rpm. The reactor was purged five times with nitrogen to remove the inside air, and finally the pressure was released to normal pressure. Then the mixture was heated up to designed temperature (180−240 °C) and maintained at this temperature for 3−60 min. The pressure in the reactor was equal to the saturated vapor pressure of water at the operating temperature. Upon completion of the reaction, the reactor was cooled down first by fan and then immersed into cold water. The reaction mixture was separated by filtration. The filtrates were collected in plastic bottles for further analysis. The solid residues were extracted with acetone to collect the acetone-soluble samples (setting the volume to 50 mL). Then, the solid residues (SR) were dried in a vacuum oven at 60 °C overnight. The water in the filtrate was evaporated under vacuum to recover the water-soluble (WS) fractions. The acetone extractives were also evaporated under vacuum to obtain the acetone-soluble (AS) fractions. WS, AS, and SR fractions were weighed, and each product yield was calculated according to the equations below based on the initial weight of bamboo. The gaseous products and loss (GL) was calculated by determining the weight change between the initial weights of bamboo and recovered weights of solids (SR, WS, and AS). SR, WS, and AS samples were collected for further analysis.

**Scheme 1. Illustration of the Experimental Procedure**

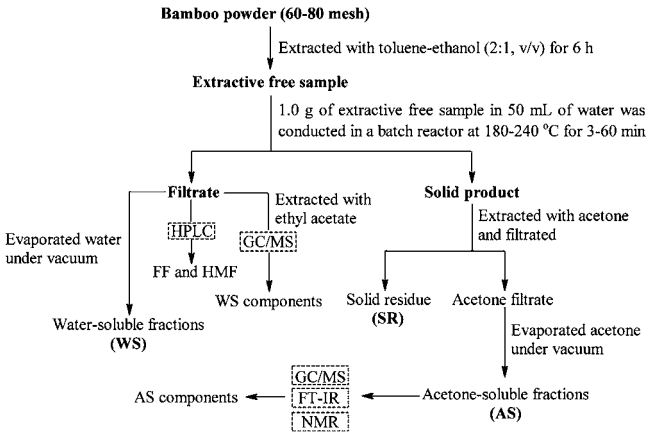


$$SR + WS + AS + GL = \frac{m_r}{m_b} + \frac{m_{w-s}}{m_b} + \frac{m_{a-s}}{m_b} + GL = 1 \quad (1)$$

where $m_b$ is the initial weight of dried bamboo, $m_r$ is the weight of hydrothermal solid residue after acetone extracting, $m_{w\text{-}s}$ is the weight of the water-soluble fractions, and $m_{a\text{-}s}$ is the weight of the acetone-soluble fractions.

**Characterizations of Hydrothermal Solid Residues, WS, and AS Fractions.** The major compositions of these hydrothermally treated bamboo samples were determined according to the method of NREL.[14] These compositions, acid-insoluble fractions (AIF), cellulose (Cel), and hemicelluloses (Hem) were all calculated based on the initial weight of bamboo.

As illustrated in Scheme 1, the ethyl acetate extractives (WS fractions) and acetone extractives (AS fractions) were treated with anhydrous $MgSO_4$ to remove the residual water. Equal volumes of WS filtrates and acetone extractives were employed and treated exactly the same to guarantee their comparability. These samples were determined on an Agilent 7890/5975 GC/MS (Agilent Technologies, U.S.A.) with a DB-5 ms column (30 m × 250 μm, J&W Scientific). The injector temperature was kept at 250 °C. For WS, the oven temperature was programmed from 40 °C (2 min) to 280 °C (5 min) with a heating rate of 5 °C/min. For AS fractions, the oven temperature was programmed from 40 °C (10 min) to 280 °C (10 min) with a heating rate of 5 °C/min. Helium (99.999%) was used as the carrier gas with a constant column flow rate of 1 mL/min and a split ratio of 1:10. The mass spectra were obtained from $m/z$ 30 to 500. The chromatographic peaks were identified by comparison with the NIST05 library.

FT-IR spectra of AS samples were recorded on a Bruker spectrophotometer (Bruker Tensor 27, Germany) in the range of 4000−400 $cm^{-1}$ with a resolution of 4 $cm^{-1}$. KBr disc containing 1% finely ground sample was used for measurement. $^1H$ NMR spectra of AS fractions were carried on a Bruker DRX-400 spectrometer (Bruker, Germany) in acetone-$d_6$ solution operating at 400.12 MHz at 25 °C.

Furfural (FF) and 5-hydroxymethyl furfural (HMF) contents in the filtrates were quantified by an Agilent 1100 series HPLC (Agilent Technologies, U.S.A.) with a Platisil ODS C18 column (250 × 4.6 $mm^2$, 5 μm) and a UV/vis detector at 277 and 285 nm, respectively. The sample loop had a volume of 50 μL, and the column temperature was maintained at 30 °C. Methanol and water (30/70, v/v) were used as the eluents at a flow rate of 1.0 mL/min.

## RESULTS AND DISCUSSION

**Product Distributions.** HTC is considered as a simple, convenient, inexpensive, and environmentally friendly method to upgrade lignocellulose into various valuable products. During the hydrothermal progress, lignocellulose can be transformed into solid, liquid, or gaseous products. Some loss is inevitable in the following separation and recovery of these products. Since lignocellulose hydrolysis and formation of gases were slow under subcritical water conditions (below 374 °C),[15] the major loss was likely caused by the substance attached on the surface of the reactor and the weight losses of WS and AS fractions during drying process. Therefore, gaseous products and loss (GL) were integrated to determine the product loss during the hydrothermal process. Figure 1 shows the hydrothermal product distributions of bamboo and the product loss under different hydrothermal conditions. The hydrothermal products were mainly composed of 37.11−89.98% of SR, 4.51−20.41% of WS, and 4.23−16.17% of AS. Obviously, a decrease of SR content indicated that more lignocellulosic components were decomposed and transferred into WS, AS, and GL fractions with the elevation of temperature and the elongation of time. The WS fraction ranged from 4.51% to 20.41%, and the maximum value was obtained at 200 °C for 3 min. The proportion of WS increased with the elongation of time at 180 °C, while as the temperature rose to 200 °C, the WS value started to decrease with the elongation of time. As the temperature further increased to 220−240 °C, the WS values were relatively stable. Additionally, considerable amounts of AS fractions (4.23−16.17%) were extracted from the hydrothermal residues of bamboo. The AS content gradually increased with

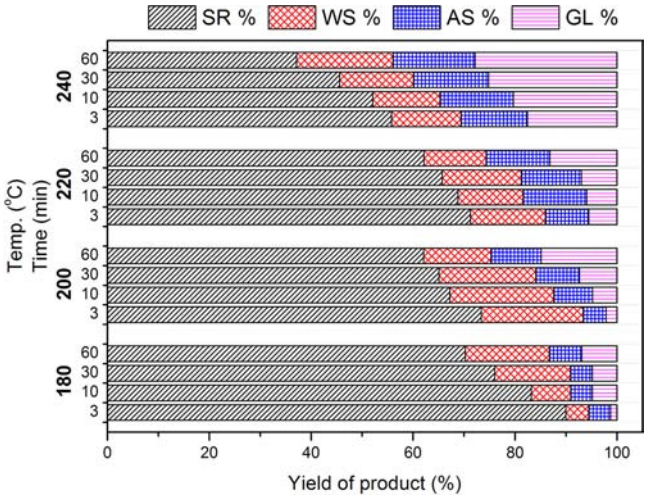


**Figure 1.** Hydrothermal products distributions of bamboo and the product loss under different hydrothermal conditions.

the increase of temperature and time. It was assumed that partial WS fractions were likely converted into AS fractions during the HTC process. In addition to the decomposition of bamboo into WS fractions, a lot of AS fractions were produced and attached to the hydrothermal solid residue, which might finally lead to the formation of hydrochar via dehydration, aromatization, condensation, etc. Additionally, 1.25−27.82% of GL were observed and the GL also gradually increased with the increase of temperature and time.

**Composition of SR from Different Hydrothermal Conditions.** To clearly illustrate the composition variation of bamboo under different hydrothermal conditions, the yield and chemical composition of the hydrothermally treated bamboo are shown in Table 1. It should be noted that the contents of acid-insoluble fractions (AIF), cellulose (Cel), and hemicelluloses (Hem) were all calculated based on the initial weight of bamboo instead of SR. As can be seen, all of these three compositions showed a declined tendency with the increase of the hydrothermal severity, suggesting that the degradations of lignin, cellulose, and hemicelluloses were more severe under high temperatures or extended periods. Among these three major compositions, the decompositions of hemicelluloses were much easier than those of cellulose and lignin. Only 5.9% of hemicelluloses could be detected at 180 °C for 60 min as compared with the initial 19.7%. When the bamboo was hydrothermally treated at 220 °C for 10 min or treated under more severe conditions, only less than 1.0% of hemicelluloses were retained. For cellulose, it was relatively stable at 180−220 °C and only a small quantity of cellulose was degraded as the reaction time increased. However, as the temperature further increased to 240 °C, the degradation of cellulose became obvious. It was in line with the results found by Sasaki et al.,[16] who reported that hemicelluloses and lignin could be mainly converted into a water-soluble fraction at 200−230 °C, while cellulose was hydrolyzed at hydrothermal temperatures higher than 230 °C. In this study, only 15.5% of cellulose was retained at 240 °C for 60 min, as compared with 36.6% of cellulose in the initial bamboo material. Most hemicelluloses and cellulose would be initially decomposed into their corresponding oligosaccharides and monomers, and then further degraded into small molecular compounds, especially FF and HMF.[17] For AIF, the content of AIF decreased gradually with the increase of reaction temperature and time, and about half of AIF was retained at 240 °C for 30 min. Due to the high stability of aromatic structures, most products derived from lignin are phenolic compounds, such as 2-methoxy-phenol, 4-methyl-phenol, benzenediol, etc.[18] The degradation products of these compositions were analyzed to further investigate the degradation pathway of lignocellulose.

**Table 1. Yield and Chemical Composition of the Hydrothermally Treated Bamboo**

| temp. (°C) | $t$ (min) | yield[a] (%) | AIF (%)[b] | Cel (%)[b] | Hem (%)[b] |
|---|---|---|---|---|---|
| | | | 30.4 | 36.6 | 19.7 |
| 180 | 3 | 90.0 | 29.5 | 34.3 | 18.3 |
| | 10 | 83.2 | 27.4 | 34.3 | 15.6 |
| | 30 | 76.0 | 24.5 | 34.1 | 11.5 |
| | 60 | 70.3 | 24.5 | 32.5 | 5.9 |
| 200 | 3 | 73.4 | 24.7 | 32.7 | 9.4 |
| | 10 | 67.2 | 22.8 | 32.0 | 4.1 |
| | 30 | 65.1 | 23.2 | 29.8 | 2.3 |
| | 60 | 62.1 | 21.9 | 30.6 | 1.5 |
| 220 | 3 | 71.2 | 23.5 | 32.4 | 2.4 |
| | 10 | 68.8 | 21.5 | 31.5 | 0.7 |
| | 30 | 65.7 | 22.1 | 30.5 | 0.5 |
| | 60 | 62.1 | 21.9 | 29.1 | 0.2 |
| 240 | 3 | 55.8 | 18.3 | 29.0 | 0.3 |
| | 10 | 52.1 | 17.4 | 24.8 | 0.1 |
| | 30 | 45.6 | 13.8 | 19.9 | 0.1 |
| | 60 | 37.1 | 14.6 | 15.5 | |

[a]Solid residue yield. [b]AIF, acid insoluble fractions; Cel, cellulose; Hem, hemicellulose; The contents of AIF, Cel, and Hem were all based on the initial weight of dried bamboo.

**GC/MS Analysis of WS Fractions.** To identify the degradation products in WS fractions, the WS solutions extracted with ethyl acetate were further analyzed using GC/MS (Supporting Information, SI, Figure S1). The compositions in the WS solutions were checked against NIST mass spectral library and their structures are shown in SI Figure S2. The absolute areas of these identified compositions are illustrated in SI Table S1. Among these identified compounds, high concentrations of FF and HMF were always detected in the hydrothermal liquid of hemicelluloses and cellulose, respectively.[19,20] Generally, FF and HMF were considered as typical degradation products derived from the dehydration of pentose and hexose, especially xylose and glucose. In consideration of the especial phenyl-propane structures of lignin, these phenolic compounds in the hydrothermal liquid are likely originated from the degradation of lignin. Previous literature also reported that lots kinds of phenolic compounds were observed in the hydrothermal liquid of lignin.[21] Therefore, according to their origins, these identified chemicals were further classified into hemicelluloses derivatives (Hem-D), cellulose derivatives (Cel-D), and lignin derivatives (Lig-D).

The integral area of hydrothermal products derived from hemicelluloses, cellulose, and lignin in water-soluble fractions are shown in Figure 2. The integral area of Hem-D increased rapidly as a function of time at 180 and 200 °C. However, as the temperature further increased to 220 °C, the increase of Hem-D started to slow down, which was observed obviously as the reaction time increased from 30 to 60 min. According to data in Table 1, it was likely that the formation rate of Hem-D decreased dramatically with the exhaustion of hemicelluloses. As the temperature further increased to 240 °C, the area of

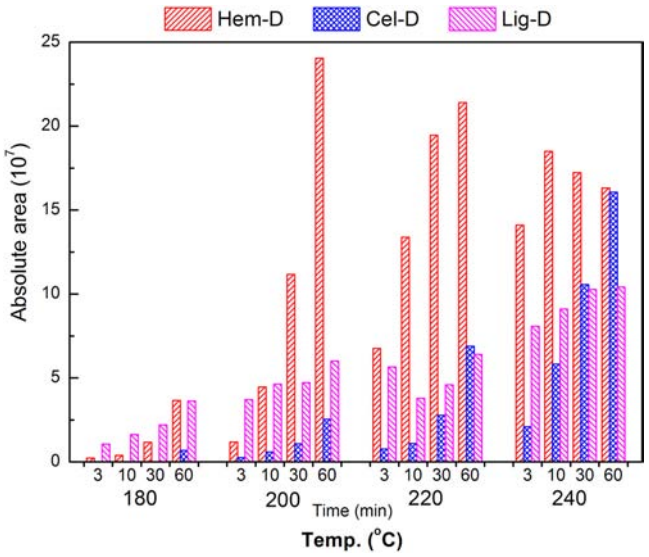


**Figure 2.** Integral area of hydrothermal products derived from hemicelluloses, cellulose, and lignin in water-soluble fractions.

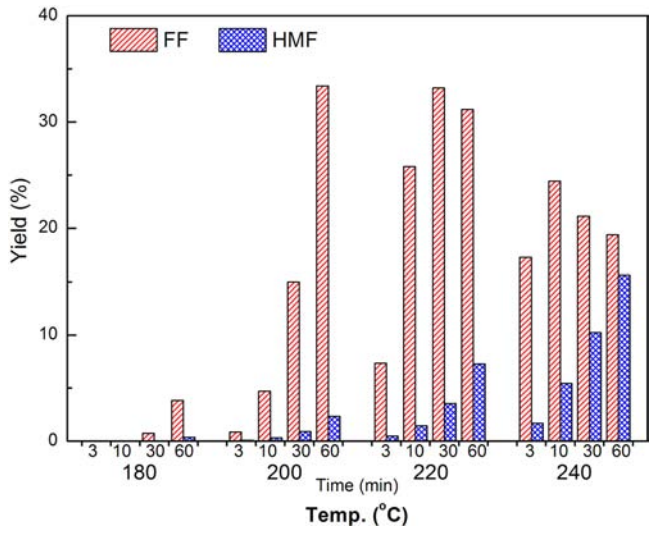


**Figure 3.** Yields of FF and HMF in water-soluble fractions.

Hem-D showed a trend to decrease with the extension of time, suggesting the server decomposition or condensation of FF at such high temperature.[21] For Cel-D, the area of Cel-D increased steadily with the temperature and time in this study. Since lignin is a heterogeneous, cross-linked three-dimensional phenylpropane polymer, the formation of most phenolic compounds originates from the decomposition of lignin. As can be seen in SI Table S1, many phenols with different substitution groups were detected in the WS fractions. Furthermore, the area of Lig-D was higher than that of Cel-D in most cases. Since chromatographic peak area of compound is considered linear with its quantity,[22] it was assumed that the hydrothermal stabilities of the three major components in the bamboo material were likely in the order of cellulose > lignin > hemicelluloses over the temperature range of this study, which was in line with the data in Table 1.

**HPLC Analysis of FF and HMF in WS Fractions.** As we know, FF and HMF are the characteristic degradation products of xylan and cellulose, respectively. To quantitatively study the degradation products of hemicelluloses and cellulose in bamboo material during the HTC process, the yields of FF and HMF as functions of hydrothermal temperature and time are illustrated in Figure 3. The HPLC chromatograms of partial WS fractions are shown in SI Figure S3. As can be seen, the yield variations of FF and HMF showed very similar trends to the area changes of Hem-D and Cel-D measured by GC/MS. FF and HMF were first observed at 180 °C for 30 and 60 min, respectively. It suggested that both hemicelluloses and cellulose could be converted into FF and HMF at 180 °C, but the formation rate of HMF was much lower than that of FF. As the hydrothermal temperature rose to 200 °C, the yield of FF increased dramatically from 0.9% to 33.4% as the reaction time increased from 3 to 60 min, while the corresponding yield of HMF increased gradually from 0.1% to 2.3%, which was much lower than that of FF. At 220 °C, the yield of FF displayed a rapid upward trend as the reaction time extended from 3 to 10 min, which increased dramatically from 7.3% to 25.8% within 7 min. The highest yield of FF at 220 °C was 33.2% for 30 min, which was very close to that obtained at 200 °C for 60 min (33.4%). As the reaction time further increased to 60 min, the yield of FF began to decline. When the hydrothermal temperature increased to 240 °C, 17.2% of FF could be obtained for 3 min, which was much higher than that at 220 °C (7.3%). The highest yield of FF at 240 °C could be obtained at 10 min (24.4%), and then it started to decrease gradually. The yield of HMF gradually increased with the elevation of temperature and the elongation of time, and the highest yield of HMF (15.6%) could be obtained at 240 °C for 60 min. Furthermore, no visible yield decrease of HMF was observed from Figure 3 over the temperature and time range. Previous studies reported that the decomposition rates of xylose and glucose were significantly higher than those of FF and HMF under the same condition.[21,23] However, as the content of xylose or glucose decreased and the degradation of FF or HMF increase, the yield of FF or HMF would start to decline with increasing time. Therefore, there was always an initial increase and then decrease in the yield for FF and HMF during the HTC process. The optimum temperature to produce FF without catalysts was mainly located at 200−220 °C, while the highest yield of HMF was observed at 240 °C.

**GC/MS, FT-IR, and $^1$H NMR Analyses of AS Fractions.** In order to identify the degradation products in AS fractions, the AS solutions were also analyzed by using GC/MS and their total ion chromatograms (TIC) are shown in SI Figure S4. A broad and strong peak at around 9.7 min was found in all the chromatograms, which originated from 4-hydroxy-4-methyl-2-pentanone. It was reported that 4-hydroxy-4-methyl-2-pentanone could exist in the AS fractions as the major product.[24,25] Furthermore, 4-hydroxy-4-methyl-2-pentanone was also observed in the bio-oils from fast pyrolysis of some energy crops.[23] Previous studies showed that phenolic compounds, such as 2-methoxyphenol and 4-methylphenol, likely existed in the AS fractions.[18,27] However, phenolic compounds, like 2-methoxyphenol or 4-methylphenol, were hardly found in the AS fractions in our study. The signals appearing after 48 min were mostly unrecognizable compounds with high boiling points. Two relatively strong signals at 54.7 and 56.4 min are assigned to a complex aromatic compound with two benzene rings and column packing material, respectively. In addition to these peaks, almost no peak with large area was found in these chromatograms. Therefore, FT-IR

and $^1$H NMR were used to further investigate the components in AS fractions.

The FT-IR spectra of these AS samples were recorded and illustrated in SI Figure S5. Very similar spectra were observed among these samples, indicating that these AS fractions obtained at different hydrothermal conditions had similar composition. Peak at around 1701 $cm^{-1}$ is assigned to the carbonyl group in 4-hydroxy-4-methyl-2-pentanone. Four sharp peaks observed at 1603, 1514, 1462, and 1427 $cm^{-1}$ are characteristic absorption peaks of substituted benzene. The strong signals at 3423 and 1271 (1217) $cm^{-1}$ are assigned to the O—H stretching and O—H and C—O combination band of phenolic compounds, respectively. Furthermore, signals at 1121 (1032) and 833 $cm^{-1}$ are originated from the C—H in-plane and out-of-plane bending of 1,2- or 1,4-disubstituted benzene. Obviously, the major aromatic compounds in AS fractions are originated from the decomposition of lignin.[18,24,27]

Additionally, $^1$H NMR of AS sample in acetone-*d*6 was also recorded and shown in SI Figure S6. These sharp peaks appearing at around 1.06 (s), 1.96 (t), and 2.47 (s) ppm are assigned to 4-hydroxy-4-methyl-2-pentanone, while the broad peaks observed at around 3.68 and 6.66 ppm originate from methoxy groups on the benzene ring and aromatic hydrogens, respectively. The broad signals of methoxy groups and aromatic hydrogens indicated that the aromatic products in the AS fractions consisted of many similar phenolic compounds. Therefore, according to the results from GC/MS, FT-IR, and $^1$H NMR, it was assumed that 4-hydroxy-4-methyl-2-pentanone and complex aromatic compounds with multibenzene rings were likely the major components of the AS fractions.

In this study, the major products of bamboo hydrothermally treated at 180−240 °C for 3−60 min, and their distributions were comparatively studied. More lignocellulose components were transformed into hydrothermal products with the increase of hydrothermal severity. Besides 4.51−20.41% of lignocellulose was converted into water-soluble fractions, considerable amounts of acetone-soluble fractions (4.23−16.17%) were extracted from the hydrothermally treated solid residue. The products in WS fractions mainly consisted of furfural (FF), 5-hydroxymethylfurfural (HMF), and phenolic compounds, while the products in AS fractions were mainly 4-hydroxy-4-methyl-2-pentanone and complex aromatic compounds with multibenzene rings. Additionally, various kinds of hydrothermal products with relatively low yields were observed in the noncatalytic HTC process. The utilization of appropriate catalyst may be helpful to convert lignocellulose into valuable products with high energy efficiency and atom economy.

## ■ ASSOCIATED CONTENT

### Supporting Information

(Figure S1) Total ion chromatograms (TIC) of partial water-soluble fractions; (Figure S2) compounds in water-soluble fractions identified by GC/MS; (Figure S3) HPLC chromatograms (TIC) of partial water-soluble fractions; (Figure S4) total ion chromatograms (TIC) of partial acetone-soluble fractions; (Figure S5) FT-IR spectra of partial acetone-soluble fractions; (Figure S6) the 1H NMR spectrum of acetone-soluble sample (obtained at 220 °C for 60 min) in acetone-d6; and (Table S1) the integral area of the compounds in the water-soluble fractions identified by GC/MS. This material is available free of charge via the Internet at http://pubs.acs.org.

## ■ AUTHOR INFORMATION

### Corresponding Authors

*Phone/Fax: +86-20-87111861; e-mail: lxzhong0611@scut.edu.cn.

*Phone/Fax: +86-20-87111861; e-mail: rcsun3@bjfu.edu.cn.

### Notes

The authors declare no competing financial interest.

## ■ ACKNOWLEDGMENTS

The authors are extremely grateful for financial support from the State Key Program of National Natural Science Foundation of China (No. 21336002), Research Fund for the Doctoral Program of Higher Education (20130172120024), and Science and Technology Project of Guangzhou City in China (2014J2200063).

## ■ REFERENCES

(1) Binder, J. B.; Raines, R. T. Simple chemical transformation of lignocellulosic biomass into furans for fuels and chemicals. *J. Am. Chem. Soc.* **2009**, *131*, 1979−1985.

(2) Zhou, C. H.; Xia, X.; Lin, C. X.; Tong, D. S.; Beltramini, J. Catalytic conversion of lignocellulosic biomass to fine chemicals and fuels. *Chem. Soc. Rev.* **2011**, *40*, 5588−5617.

(3) McKendry, P. Energy production from biomass (part 1): Overview of biomass. *Bioresour. Technol.* **2002**, *83*, 37−46.

(4) Fisher, J. R.; Barnes, H. L. Ion-product constant of water to 350°. *J. Phys. Chem.* **1972**, *76*, 90−99.

(5) Wang, Y.; Deng, W.; Wang, B.; Zhang, Q.; Wan, X.; Tang, Z.; Wang, Y.; Zhu, C.; Cao, Z.; Wang, G.; Wan, H. Chemical synthesis of lactic acid from cellulose catalysed by lead(II) ions in water. *Nat. Commun.* **2013**, *4*, 2141.

(6) Ji, N.; Zhang, T.; Zheng, M. Y.; Wang, A. Q.; Wang, H.; Wang, X. D.; Chen, J. G. G. Direct catalytic conversion of cellulose into ethylene glycol using nickel-promoted tungsten carbide catalysts. *Angew. Chem., Int. Ed.* **2008**, *47*, 8510−8513.

(7) Luo, C.; Wang, S. A.; Liu, H. C. Cellulose conversion into polyols catalyzed by reversibly formed acids and supported ruthenium clusters in hot water. *Angew. Chem., Int. Ed.* **2007**, *46*, 7636−7639.

(8) Gao, P.; Li, G.; Yang, F.; Lv, X. N.; Fan, H.; Meng, L.; Yu, X. Q. Preparation of lactic acid, formic acid and acetic acid from cotton cellulose by the alkaline pre-treatment and hydrothermal degradation. *Ind. Crops Prod.* **2013**, *48*, 61−67.

(9) Pavlovič, I.; Knez, Ž.; Škerget, M. Hydrothermal reactions of agricultural and food processing wastes in sub- and supercritical water: A review of fundamentals, mechanisms, and state of research. *J. Agric. Food Chem.* **2013**, *61*, 8003−8025.

(10) Tekin, K.; Karagoez, S. Non-catalytic and catalytic hydrothermal liquefaction of biomass. *Res. Chem. Intermed.* **2013**, *39*, 485−498.

(11) Chheda, J. N.; Huber, G. W.; Dumesic, J. A. Liquid-phase catalytic processing of biomass-derived oxygenated hydrocarbons to fuels and chemicals. *Angew. Chem., Int. Ed.* **2007**, *46*, 7164−7183.

(12) Srokol, Z.; Bouche, A. G.; van Estrik, A.; Strik, R. C. J.; Maschmeyer, T.; Peters, J. A. Hydrothermal upgrading of biomass to biofuel; studies on some monosaccharide model compounds. *Carbohydr. Res.* **2004**, *339*, 1717−1726.

(13) Sevilla, M.; Fuertes, A. B. Chemical and structural properties of carbonaceous products obtained by hydrothermal carbonization of saccharides. *Chem.—Eur. J.* **2009**, *15*, 4195−4203.

(14) Sluiter, A.; Hames, B.; Ruiz, R.; Scarlata, C.; Sluiter, J.; Templeton, D.; Crocker, D. Determination of structural carbohydrates and lignin in biomass. *Laboratory Analytical Procedure*; 2008.

(15) Elliott, D. C. Catalytic hydrothermal gasification of biomass. *Biofuel. Bioprod. Bior.* **2008**, *2*, 254−265.

(16) Sasaki, M.; Adschiri, T.; Arai, K. Fractionation of sugarcane bagasse by hydrothermal treatment. *Bioresour. Technol.* **2003**, *86*, 301−304.

(17) Makishima, S.; Mizuno, M.; Sato, N.; Shinji, K.; Suzuki, M.; Nozaki, K.; Takahashi, F.; Kanda, T.; Amano, Y. Development of continuous flow type hydrothermal reactor for hemicellulose fraction recovery from corncob. *Bioresour. Technol.* **2009**, *100*, 2842−2848.
(18) Karagöz, S.; Bhaskar, T.; Muto, A.; Sakata, Y. Comparative studies of oil compositions produced from sawdust, rice husk, lignin and cellulose by hydrothermal treatment. *Fuel* **2005**, *84*, 875−884.
(19) Yemiş, O.; Mazza, G. Acid-catalyzed conversion of xylose, xylan and straw into furfural by microwave-assisted reaction. *Bioresour. Technol.* **2011**, *102*, 7371−7378.
(20) Yin, S.; Pan, Y.; Tan, Z. Hydrothermal Conversion of Cellulose to 5-Hydroxymethyl Furfural. *Int. J. Green Energy.* **2011**, *8*, 234−247.
(21) Jing, Q.; LÜ, X. Kinetics of non-catalyzed decomposition of D-xylose in high temperature liquid water. *Chin. J. Chem. Eng.* **2007**, *15*, 666−669.
(22) Watanabe, M.; Aizawa, Y.; Iida, T.; Nishimura, R.; Inomata, H. Catalytic glucose and fructose conversions with $TiO_2$ and $ZrO_2$ in water at 473 K: Relationship between reactivity and acid−base property determined by TPD measurement. *Appl. Catal. A-Gen.* **2005**, *295*, 150−156.
(23) Jing, Q.; LÜ, X. Kinetics of non-catalyzed decomposition of glucose in high-temperature liquid water. *Chin. J. Chem. Eng.* **2008**, *16*, 890−894.
(24) Bhaskar, T.; Sera, A.; Muto, A.; Sakata, Y. Hydrothermal upgrading of wood biomass: Influence of the addition of $K_2CO_3$ and cellulose/lignin ratio. *Fuel* **2008**, *87*, 2236−2242.
(25) Yan, X.; Jin, F.; Tohji, K.; Moriya, T.; Enomoto, H. Production of lactic acid from glucose by alkaline hydrothermal reaction. *J. Mater. Sci.* **2007**, *42*, 9995−9999.
(26) Shen, Z.; Jin, F.; Zhang, Y.; Wu, B.; Kishita, A.; Tohji, K.; Kishida, H. Effect of alkaline catalysts on hydrothermal conversion of glycerin into lactic acid. *Ind. Eng. Chem. Res.* **2009**, *48*, 8920−8925.
(27) Karagöz, S.; Bhaskar, T.; Muto, A.; Sakata, Y. Hydrothermal upgrading of biomass: Effect of $K_2CO_3$ concentration and biomass/water ratio on products distribution. *Bioresour. Technol.* **2006**, *97*, 90−98.

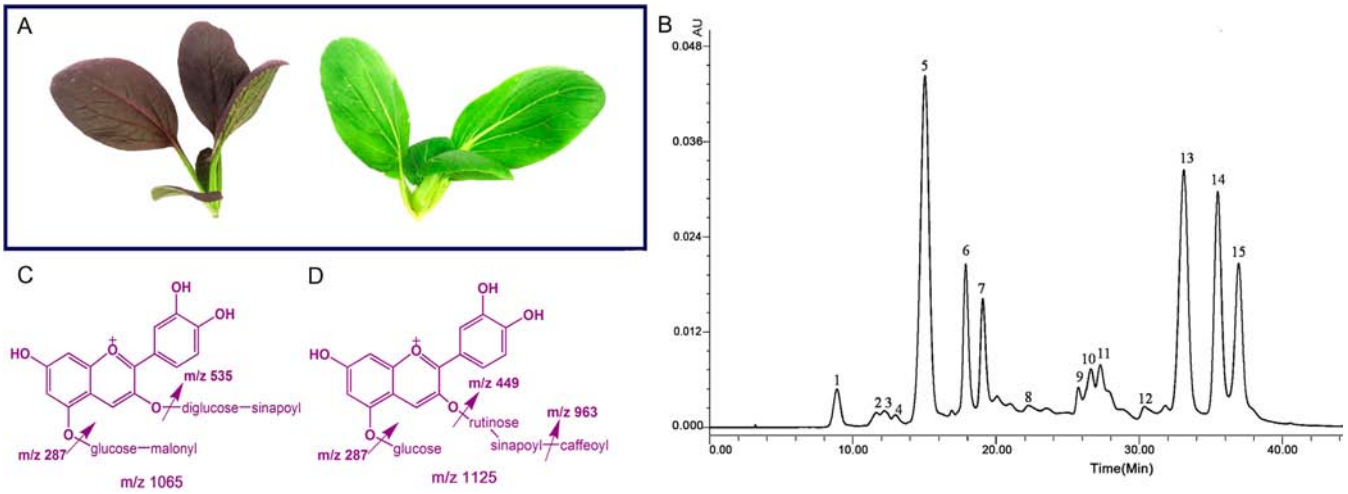


**Figure 1.** Anthocyanin component analysis of bok choy: (A) photographs of the two bok choy cultivars (Zi He on the left and Su Zhouqing on the right) used in this study; (B) HPLC profiles of anthocyanins of the leaves from the purple cultivar (Zi He) (peak numbers refer to the anthocyanins listed in Table 1); (C) structures and major cleavage of cyanidin 3-(sinapoyl) diglucoside-5-(malonyl) glucoside in reference to peak 5 of panel B; (D) structures and major cleavage of cyanidin 3-caffeoyl (sinapoyl) rutinoside-5-glucoside in reference to peak 13 of panel B.

**Table 1. Anthocyanins Identified in Edible Leaves of the Purple Bok Choy (Zi He)**

| no.[a] | RT[b] (min) | $[M + M]^+$ ($m/z$) | MS/MS ($m/z$) | anthocyanin |
|---|---|---|---|---|
| 1 | 8.87 | 979 | 449/287 | Cy[c] 3-(sinapoyl)-diglucoside-5-glucoside |
| 2 | 11.64 | 611 | 449/287 | Cy 3,5-diglucoside |
| 3 | 12.16 | 859 | 535/287 | Cy 3-diglucoside-5-(malonyl)glucoside |
| 4 | 15.02 | 1051 | 535/287 | Cy 3-(hydroxyferuloyl)diglucoside-5-(malonyl)glucoside |
| 5 | 17.87 | 1065 | 535/287 | Cy 3-(sinapoyl)diglucoside-5-(malonyl)-glucoside |
| 6 | 19.07 | 641 | 479/317 | petunidin 3,5-diglucoside |
| 7 | 20.04 | 1035 | 757/535/287 | Cy 3-(malonoyl)glucoside(*p*-hydroxybenzoyl)arabinoside-5-(malonoyl)glucoside |
| 8 | 25.73 | 1211 | 535/287 | Cy 3-feruloyl(sinapoyl)diglucoside -5-(malonyl)glucoside |
| 9 | 26.61 | 1005 | 757/535/287 | Cy 3- hydroxysinapoyl (malonyl)-glucoside-5-(malonyl)glucoside |
| 10 | 27.26 | 1021 | 773/535/287 | Cy 3- dihydroxysinapoyl(malonyl)-glucoside-5-(malonyl)glucoside |
| 11 | 30.35 | 949 | 787/449/287 | Cy 3-(feruloyl)diglucoside-5-glucoside |
| 12 | 31.82 | 1227 | 535/287 | Cy 3-sinapoyl(glucoside)diglucoside-5-(malonyl)glucoside |
| 13 | 33.11 | 1125 | 963/449/287 | Cy 3-caffeoyl (sinapoyl) rutinoside-5-glucoside |
| 14 | 35.48 | 1241 | 993/535/287 | Cy 3-malonyl(glucoside)-*p*-hydroxybenzoyl(feruloyl) glucoside-5-(malonyl)-glucoside |
| 15 | 36.94 | 1181 | 933/535/287 | Cy 3-malonyl(glucoside)-*p*-hydroxybenzoyl(*p*-coumaroyl) arabinoside-5-(malonyl)glucoside |

[a]Number corresponds to the elution order by HPLC analysis in Figure 1 B. [b]RT, retention time. [c]Cy, cyanidin.

**Table 2. Anthocyanin Content (Milligrams per Gram Dry Weight) in the Leaves of the Two Bok Choy Cultivars ($n$ = 3)**

| no.[a] | anthocyanin | green[b] | purple[b] |
|---|---|---|---|
| 1 | Cy[c] 3-(sinapoyl)-diglucoside-5-glucoside | nd[d] | 0.07 ± 0.00 |
| 2 | Cy 3,5-diglucoside | nd | 0.02 ± 0.00 |
| 3 | Cy 3-diglucoside-5-(malonyl)glucoside | nd | 0.02 ± 0.00 |
| 4 | Cy 3-(hydroxyferuloyl)diglucoside-5-(malonyl)-glucoside | nd | 0.01 ± 0.00 |
| 5 | Cy 3-(sinapoyl)diglucoside-5-(malonyl)-glucoside | nd | 0.91 ± 0.06 |
| 6 | petunidin 3,5-diglucoside | nd | 0.23 ± 0.02 |
| 7 | Cy 3-(malonoyl)glucoside(*p*-hydroxybenzoyl)-arabinoside-5-(malonoyl)glucoside | nd | 0.18 ± 0.01 |
| 8 | Cy 3-feruloyl(sinapoyl)diglucoside-5-(malonyl)-glucoside | nd | 0.02 ± 0.00 |
| 9 | Cy 3-hydroxysinapoyl(malonyl)glucoside-5-(malonyl)glucoside | nd | 0.07 ± 0.00 |
| 10 | Cy 3-dihydroxysinapoyl(malonyl)glucoside-5-(malonyl)glucoside | nd | 0.04 ± 0.00 |
| 11 | Cy 3-(feruloyl)diglucoside-5-(malonyl)glucoside | nd | 0.03 ± 0.00 |
| 12 | Cy 3-(sinapoyl)diglucoside-5-(malonyl) diglucoside | nd | 0.02 ± 0.00 |
| 13 | Cy 3-caffeoyl(sinapoyl)rutinoside-5-glucoside | nd | 0.69 ± 0.03 |
| 14 | Cy 3-(hydroxybenzoyl)feruloyl(malonyl)-diglucoside-5-(malonyl)glucoside | nd | 0.49 ± 0.02 |
| 15 | Cy 3-malonyl(glucoside)-*p*-hydroxybenzoyl(*p*-coumaroyl)arabinoside-5-(malonyl)glucoside | nd | 0.33 ± 0.02 |
| total | | nd | 3.13 ± 0.16 |

[a]Number corresponds to the elution order by HPLC analysis in Figure 1 B. [b]Green bok choy cultivar (Su Zhouqing); purple bok choy cultivar (Zi He). [c]Cy, cyanidin. [d]Nd, not detected.

transcription of the corresponding genes immediately.[18] Extensive studies showed that abundant anthocyanin accumulation in certain tissues of some purple fruits and vegetables arises from the spatiotemporal transcriptional activation of R2R3MYB or bHLH transcription factors.[8,19−23] On the other hand, light, which acts as an essential environmental stimulus, also modulates the intensity of the pigment through the regulation of anthocyanin structural genes.[24] It is known that a basic leucine zipper (bZIP) type of transcription factor LONG HYPOCOTYL 5 (HY5) plays a central role in the biological process of the coordination of light signals and the adjustment of appropriate gene expression. Furthermore, HY5 has also been demonstrated to positively regulate anthocyanin biosynthesis by directly binding to the promoters of *CHS* and *F3H* in *Arabidopsis*.[25,26]

As a variant cultivar of the turnip, bok choy (*Brassica rapa* var. *chinensis*) was originally cultivated in China and distinct from another leafy vegetable, Chinese cabbage, which usually forms a compact head in winter. Being winter-hardy, bok choy is widely


dx.doi.org/10.1021/jf503453e | J. Agric. Food Chem. 2014, 62, 12366−12376

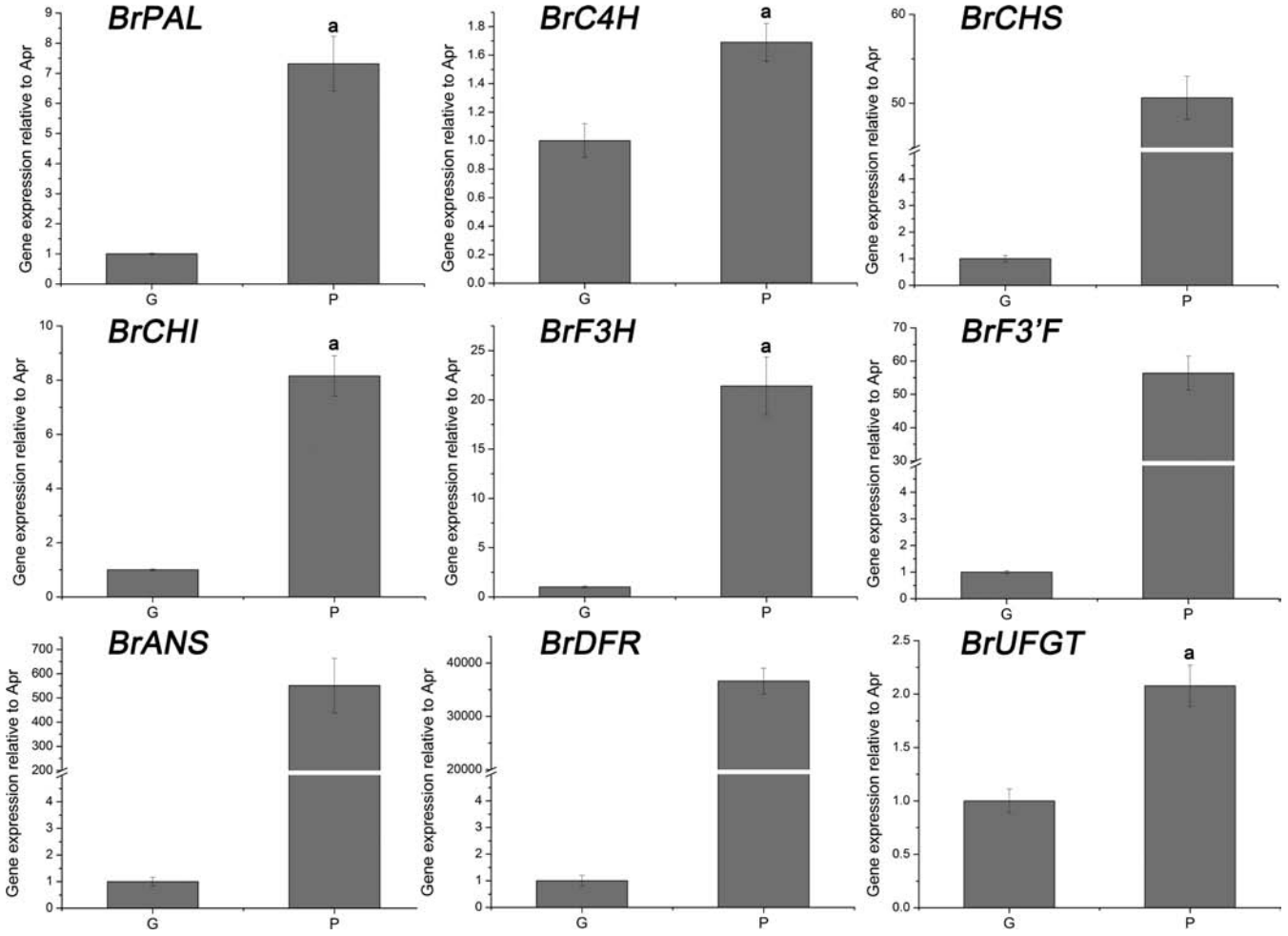


**Figure 2.** Expression analysis of anthocyanin biosynthetic genes in edible leaves of the two bok choy cultivars. P and G represent purple edible leaves and green edible leaves separately. Error bars represent the standard error of the mean ($n = 3$). Statistical significance of the differences between samples was calculated with ANOVA by paired-group comparisons. Different letters indicate significance at $P < 0.05$.

cultivated and consumed in China and northeastern Asia and is increasingly grown in northern Europe and North America. Furthermore, the purple bok choy receives more attention from the public than green cultivars for high levels of anthocyanin accumulation in mature leaves besides the well-known health benefits of cruciferous vegetables.[27,28] However, being an economically important crop, the composition of anthocyanins and molecular mechanisms of anthocyanin biosynthesis in purple bok choy remain unknown. In this paper, we characterize the components of anthocyanin production in the purple cultivar (Zi He) with high-performance liquid chromatography–electrospray ionization tandem mass spectrometry (HPLC-ESI-MS/MS). For the purpose of investigating the molecular mechanisms underlying anthocyanin accumulation in the purple edible leaves, the expression level of anthocyanin biosynthetic and regulatory genes was analyzed by quantitative real-time polymerase chain reaction (qRT-PCR) in corresponding tissues of the purple and green cultivars. Because the production of anthocyanins in seedlings of Zi He is strictly dependent on lightness, the expression profiles of anthocyanin biosynthesis associated genes were further analyzed in seedlings of different developmental stages under light and dark conditions. These results certainly expanded our understanding about the mechanisms of anthocyanin accumulation in purple bok choy at both the metabolic and transcriptional levels.

## MATERIALS AND METHODS

**Chemicals and Solvents.** Anthocyanin (cyanidin 3,5-diglucoside) for external standards was purchased from Phytolab (Germany). High-performance liquid chromatography (HPLC) grade formic acid and methanol (MeOH) were bought from Sigma. All other solvents were provided from Aldrich (St. Louis, MO, USA).

**Plant Materials and Culture Conditions.** Bok choy (*B. rapa* var. *chinensis*) seeds of green cultivar (Su Zhouqing) and purple cultivar (Zi He) were obtained from the Chongqing Academy of Agriculture Sciences. The samples used for HPLC-ESI-MS/MS and qRT-PCR analysis were collected from edible leaves of green and purple cultivars that were grown in a greenhouse with a 16 h photoperiod at 25 °C. The samples used for total anthocyanin and qRT-PCR analysis were collected from seedlings of green and purple cultivars that were generated by follow procedures. Bok choy seeds were surface-sterilized with 70% ethanol for 30 s and with a 4% (v/v) bleach solution for 15 min and then rinsed several times in sterile water. These seeds were then placed on half-strength sterilized Murashige–Skoog medium (1/2 MS) solidified with 0.8% agar. The two cultivars were germinated in a growth chamber under light/dark (16/8 h) or dark conditions at 25 °C and approximately 60% humidity. Samples were harvested after 3, 6, 9, and 12 days, measured for their length and fresh weight, frozen in liquid nitrogen, and stored at −80 °C until other analysis.

**RNA Extraction and qRT-PCR Analysis.** The samples of the two bok choy cultivars were ground into powder in liquid nitrogen. Total RNA was isolated from various tissues for three biological repeats using RNAiso reagent according to the manufacturer's instruction

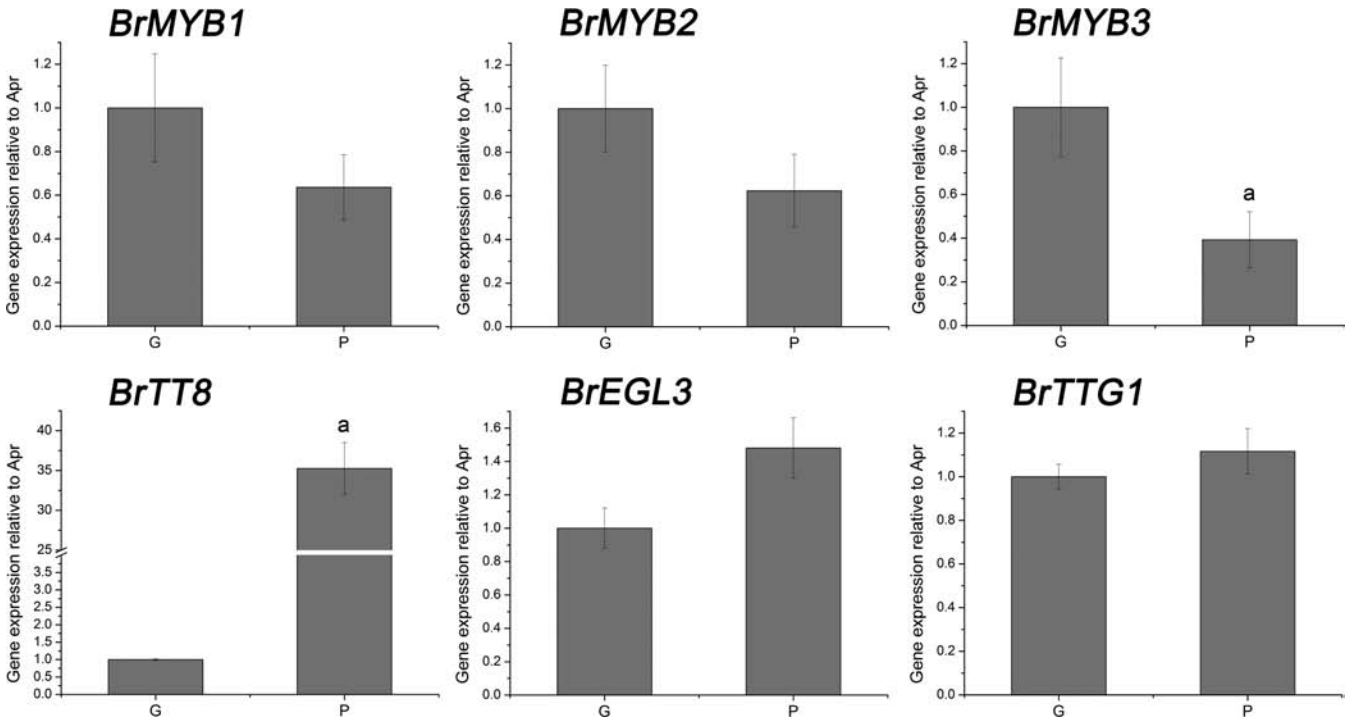


**Figure 3.** Expression analysis of anthocyanin biosynthesis regulatory genes in edible leaves of the two bok choy cultivars. P and G represent purple edible leaves and green edible leaves separately. Error bars represent the standard error of the mean ($n = 3$). Statistical significance of the differences between samples was calculated with ANOVA by paired-group comparisons. Different letters indicate significance at $P < 0.05$.

(Takara, Dalian, China). RNA samples (1 $\mu$g) were reverse transcripted into complementary DNA (cDNA) with an oligo(dT)20 primer and M-MLV reverse transcriptase (Promega, Madison, WI, USA) following the manufacturer's protocol. The synthesized cDNAs were diluted five times in $H_2O$ for qRT-PCR analysis.

qRT-PCR was carried out using the CFX96 Real-Time System (C1000 thermal cycler). All reactions were performed using the GoTaq qPCR Master Mix according to the manufacturer's instructions. Reactions were performed in triplicate using 5 $\mu$L of Master Mix, 0.25 $\mu$M of each primer, 1 $\mu$L of diluted cDNA, and DNase-free water to a final volume of 10 $\mu$L. The PCR amplification was as follows: 1 cycle of 3 min at 95 °C, 40 cycles of denaturation for 15 s at 95 °C, annealing for 30 s at 60 °C, and elongation for 15 s at 72 °C. Amplification was followed by a melting curve analysis with continual fluorescence data acquisition during the 60−95 °C melt. Melt curve analysis of qPCR samples revealed that there was only one product for each gene primer reaction. The primers used for qPCR analysis of bok choy were designed by Primer Premier 5 and are listed in Supplementary Table 1 (Supporting Information). In addition, primers used for qPCR analysis for regeneration shoots of tomato are listed in Supplementary Table 2 (Supporting Information). The PCR products were sequenced to confirm the specific amplifications. The gene expression was normalized to *BrApr* and *SlCAC* as a reference gene for bok choy and tomato, respectively.[29,30] Values reported here were calculated from three biological repeats for each sample.

**Anthocyanin Extraction and HPLC-ESI-MS/MS Analysis.** Anthocyanin extraction of bok choy was carried out in the same way as for radish.[31] The extract was filtered through a 0.2 $\mu$m PTFE syringe filter. The samples were then analyzed by an Agilent Technologies 1200 series HPLC (Agilent Technologies, Palo Alto, CA, USA), equipped with an Agilent 1200 HPLC variable-wavelength detector. The results were analyzed by Agilent 1200 HPLC ChemStation software. The chromatographic separation was performed on a Zorbax Stablebond Analytical SB-C18 column (4.6 mm × 250 mm, 5 $\mu$m, Agilent Technologies, Rising Sun, MD, USA). The injection sling was 5 $\mu$L. Elution was performed using mobile phase A (aqueous 2% formic acid solution) and mobile phase B (methanol). The detection was at 520 nm, and the column oven temperature was set at 40 °C. The flow rate was 0.6 mL/min. The gradient program is described as follows: 0−2 min, 10−20% B; 2−40 min, 20−55% B; 40−41 min, 55−80% B; 41−45 min, 80% B; 45−50 min, 80−10% B; 50−55 min, 10% B. Quantification of the different anthocyanins was based on peak areas and calculated as equivalents of the standard compounds. All contents were expressed as milligrams per gram dry weight. Low-resolution electrospray mass spectrometry was performed with a solariX ion trap mass spectrometer (Bruker Daltoniks, Billerica, MA, USA). The experimental conditions were as follows: ESI interface, nebulizer, 50 psi; dry gas, 15.0 psi; dry temperature, 320 °C; MS/MS, scan from $m/z$ 200 to 1500; ion trap, scan from $m/z$ 200 to 1500; source accumulation, 50 ms; ion accumulation time, 300 ms; flight time to acquisition cell, 1 ms; smart parameter setting (SPS), compound stability, 50%; trap drive level, 60%.

**Total Anthocyanin Analysis.** Spectrophotometric differential pH method was used for the total anthocyanin measurement of bok choy following the procedure of Yuan et al.[15]

**Gene Cloning and Sequence Analyses.** The primers used for BrMYB1, BrMYB2, BrMYB3, and BrTT8 were designed from the sequences of known orthologous sequences (Supplementary Table S3 in the Supporting Information). Then, the PCR products were cloned into a T-Blunt vector (Takara) and sequenced. Sequence similarities were calculated with DNAMAN version 5.2.2. The phylogenetic and molecular evolutionary analysis was used with MEGA (Molecular Evolutionary Genetics Analysis) version 3.1.

**Statistical Analyses.** SPSS, version 17.0 (SPSS Inc., Chicago, IL, USA), was used for the data analysis. One-way analysis of variance (ANOVA) followed by pairwise comparisons was performed with post hoc Tukey's honestly significant different (HSD) test, with significance set at $P < 0.05$.

**Vector Construction and Transformation of Tomato.** The complement DNA was synthesized with total RNA with M-MLV (Promega) as the recommendation of manufacturer. The full-length coding sequence of *BrTT8* was cloned into pBI121 for the replacement of GUS to obtain the construct pBI121-BrTT8. Primers used for amplification of *BrTT8* were *BrTT8*-con-F, TCTAGATACAGGTTT-TCATCTCGGG, and *BrTT8*-con-R, GAGCTCCATTAAGGTTAG-AATCTCGGAA. The binary vector pBI121-*BrTT8* containing the *BrTT8* cDNA driven by the 35S promoter was transferred into

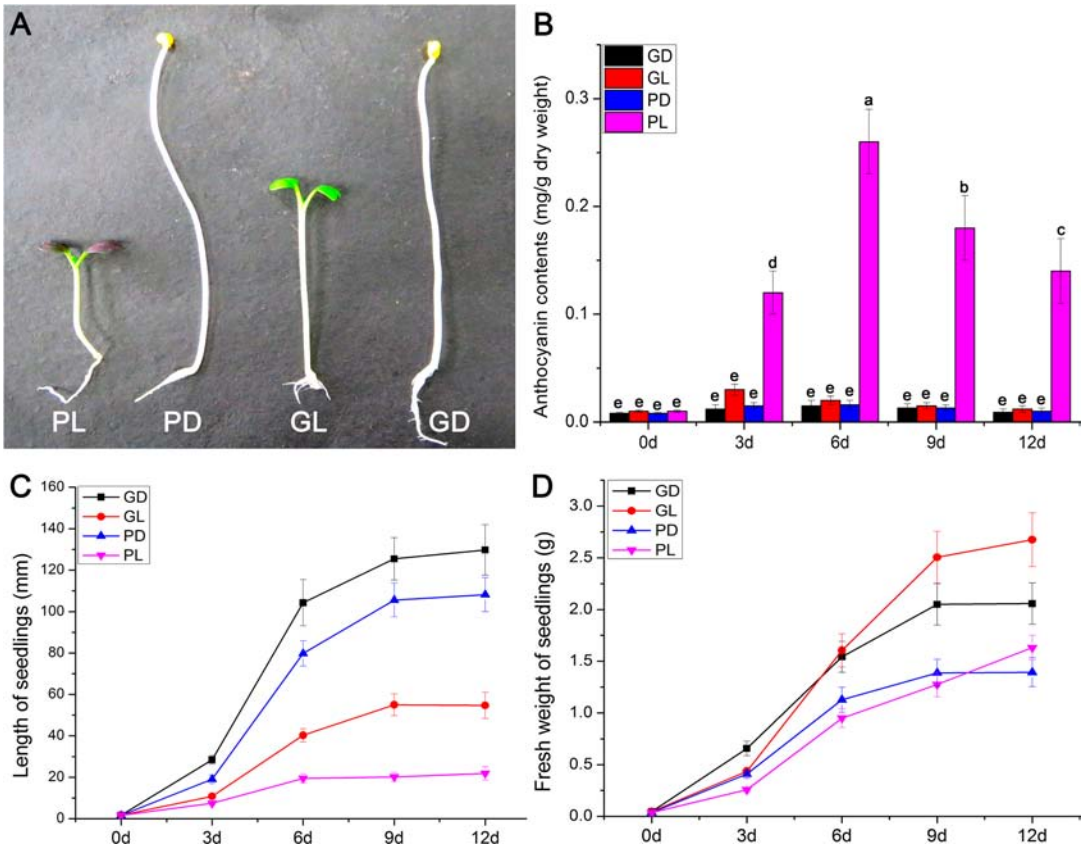


**Figure 4.** Phenotype of bok choy seedlings grown under dark and light conditions: (A) photographs of the two bok choy cultivars 6 days after sowing under dark and light conditions; (B) anthocyanin contents (mg/g dry weight) during the development of bok choy seedlings under dark and light conditions; (C) average length of seedlings of bok choy from 0 to 12 days after sowing ($n$ = 30 per treatment); (D) average fresh weight of seedlings of bok choy from 0 to 12 days after sowing ($n$ = 30 per treatment). PL, purple light; PD, purple dark; GL, green light; GD, green dark. Error bars represent the standard error of the mean ($n$ = 3). Statistical significance of the differences between samples was calculated with ANOVA by paired-group comparisons. Different letters indicate significance at $P < 0.05$.

*Agrobacterium tumefaciens* strain LBA4404 by the freeze−thaw method. Tomato (*Solanum lycopersicum* Mill. cv. Ailsa Craig) was used for the generation of transgenic shoots by *Agrobacterium*-mediated transformation, using the protocol previously reported.[32]

## RESULTS AND DISCUSSION

**Identification and Quantitative Analyses of Anthocyanins.** By analyzing the extracts from edible leaves of Zi He (purple cultivar) and Su Zhouqing (green cultivar) with the method of HPLC-ESI-MS/MS, a total of 15 anthocyanins were separated and characterized (Figure 1A,B). To verify the identity of anthocyanins in the purple cultivar, fragmentation patterns of MS/MS ($m/z$) were used to compare with those radical groups emerged in a previous study.[33] As the results show in Table 1, some new anthocyanins such as cyanidin 3-(sinapoyl) diglucoside-5-(malonyl) glucoside never reported in plants were identified in purple bok choy. Moreover, cyanidin was characterized as the major anthocyanidin in the purple bok choy with the absence of pelargonidin (Table 1). Obviously, acylated cyanidin of anthocyanidins is the most common modification of anthocyanins except for cyanidin 3,5-diglucoside. Broadly, the composition of anthocyanins identified in purple bok choy is similar to those of the other cruciferous vegetables except radish reported so far.[15,31,34]

Total anthocyanin content was found to be 3.13 mg/g dry weight for edible leaves from Zi He (Table 2). However, there were no obvious anthocyanins detected in mature leaves of Su Zhouqing. Furthermore, the anthocyanins showing the highest levels were cyanidin 3-(sinapoyl) diglucoside-5-(malonyl) glucoside and cyanidin 3-caffeoyl (sinapoyl) rutinoside-5-glucoside at 0.91 and 0.69 mg/g dry weight, respectively (Figure 1C,D; Table2). Nevertheless, a trace amount of petunidin 3,5-diglucoside was detected in HPLC profiles of anthocyanins in Zi He. This kind of anthocyanin has not been reported in the species of *Brassica* up to now. Previously published papers showed that accumulation of petunidin needs further hydroxylation at the 3′- and 5′-positions in the B-ring of naringenin;[35] that is to say, isoenzymes which share the same catalytic activity with F3′5′H probably exist in bok choy.

**Expression Analysis of Anthocyanin Biosynthesis Associated Genes in Edible Leaves of Different Cultivars.** To investigate the molecular mechanisms underlying the pigment accumulation in purple leaves of Zi He, the transcripts of anthocyanin biosynthetic and regulatory genes were examined by qRT-PCR. The expression levels of *BrPAL*, *BrC4H*, *BrCHS*, *BrCHI*, *BrF3H*, *BrF3′H*, *BrANS*, *BrDFR*, and *BrUFGT* are shown in Figure 2. In the edible leaves, all of the genes in the anthocyanin biosynthetic pathway were significantly up-regulated in the purple bok choy. Compared with the green cultivar, the expression levels of *BrDFR* and *BrANS* were especially up-regulated to at least 500-fold in the purple leaves. As the early studies reported, trace amounts of transcripts of all the anthocyanin biosynthetic genes were always observed despite the absence of visible pigment accumulation in the corresponding

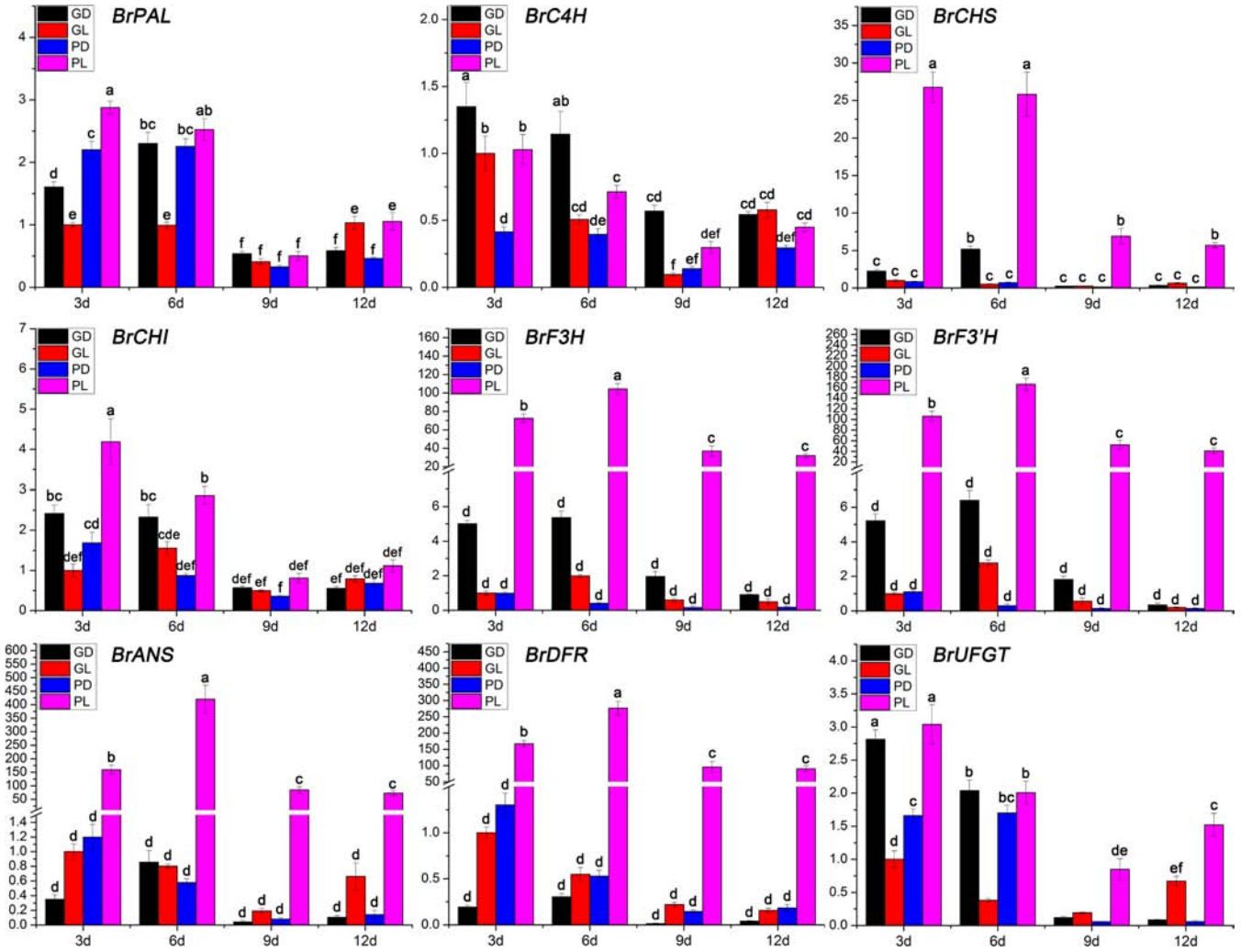


**Figure 5.** Expression analysis of anthocyanin biosynthetic genes during the development of bok choy seedlings under dark and light conditions. GD, green dark; GL, green light; PD purple dark; PL, purple light. The longitudinal axis indicates the expression levels of genes relative to the level of *BrApr*. Error bars represent the standard error of the mean ($n = 3$). Statistical significance of the differences between samples was calculated with ANOVA by paired-group comparisons. Different letters indicate significance at $P < 0.05$.

tissues.[15] These results indicate that adequate transcripts of some vital structural genes are essential for a large sum of anthocyanin biosynthesis. It is worth mentioning that the drastic increment of F3′H should make a complete conversion of DHK to dihydroquercetin because of the absence of pelargonidin-based anthocyanins.

To investigate the mechanisms about transcriptional regulation of structural genes that are responsible for pigmentation production, the transcripts of some anthocyanin biosynthesis regulatory orthologous genes of *Arabidopsis*, *BrMYB1*, *BrMYB2*, *BrMYB3*, *BrTT8*, *BrEGL3*, and *BrTTG1* were examined by qRT-PCR. It is worth mentioning that the three MYB genes (*BrMYB1*, *BrMYB2*, and *BrMYB3*) share high similarity with *AtPAP1* and *AtPAP2*, which regulate anthocyanin biosynthesis by activating the transcription of structural genes directly in a bHLH- and TTG1-dependent manner.[18,36] However, the up-regulation of bHLH transcription factors accounts for visible pigment accumulation in certain tissues of some species.[23,37,38] As the data show in Figure 3, *BrTT8* was the only transcription factor that is found to be significantly up-regulated in the leaves of the purple cultivar. The deduced amino acid sequences of BrTT8 were aligned with other bHLH transcription factors, which were known to regulate the anthocyanin biosynthesis in diverse species. BrTT8 exhibited highest sequence similarities with other bHLH proteins within the bHLH domain and the N-terminal MYB interaction domain (Supplementary Figure 1). Phylogenetic analysis divided bHLH regulators into two different clades. BrTT8 was placed in the same cluster with TT8 from *Arabidopsis*, NtAn1a and NtAn1b from tobacco, MdbHLH3 from apple, and PhAn1 from petunia (Supplementary Figure 2). Ectopic expression of *NtAN1a*, *NtAN1b*, and *MdbHLH3* activated the transcription of anthocyanin biosynthetic genes efficiently, whereas ectopic expression of *PhAN1* failed to activate the expression of DFR.[23,39,40] As the mechanism of anthocyanin biosynthesis pathway genes regulated by the MBW complex directly is widely found in many species, the different background expression levels of R2R3MYB transcription factors in respective species might explain the discrepancy observed above. These results suggest that the dramatically increased expression of BrTT8 might account for the anthocyanin accumulation in edible leaves of Zi He by activating the transcription of structural genes upon the formation of MBW complex with sufficient amounts of R2R3MYB and WD40 proteins.

**Growth of Bok Choy Seedlings under Light and Dark Conditions.** To evaluate the effects of light on seedling development


dx.doi.org/10.1021/jf503453e | J. Agric. Food Chem. 2014, 62, 12366−12376

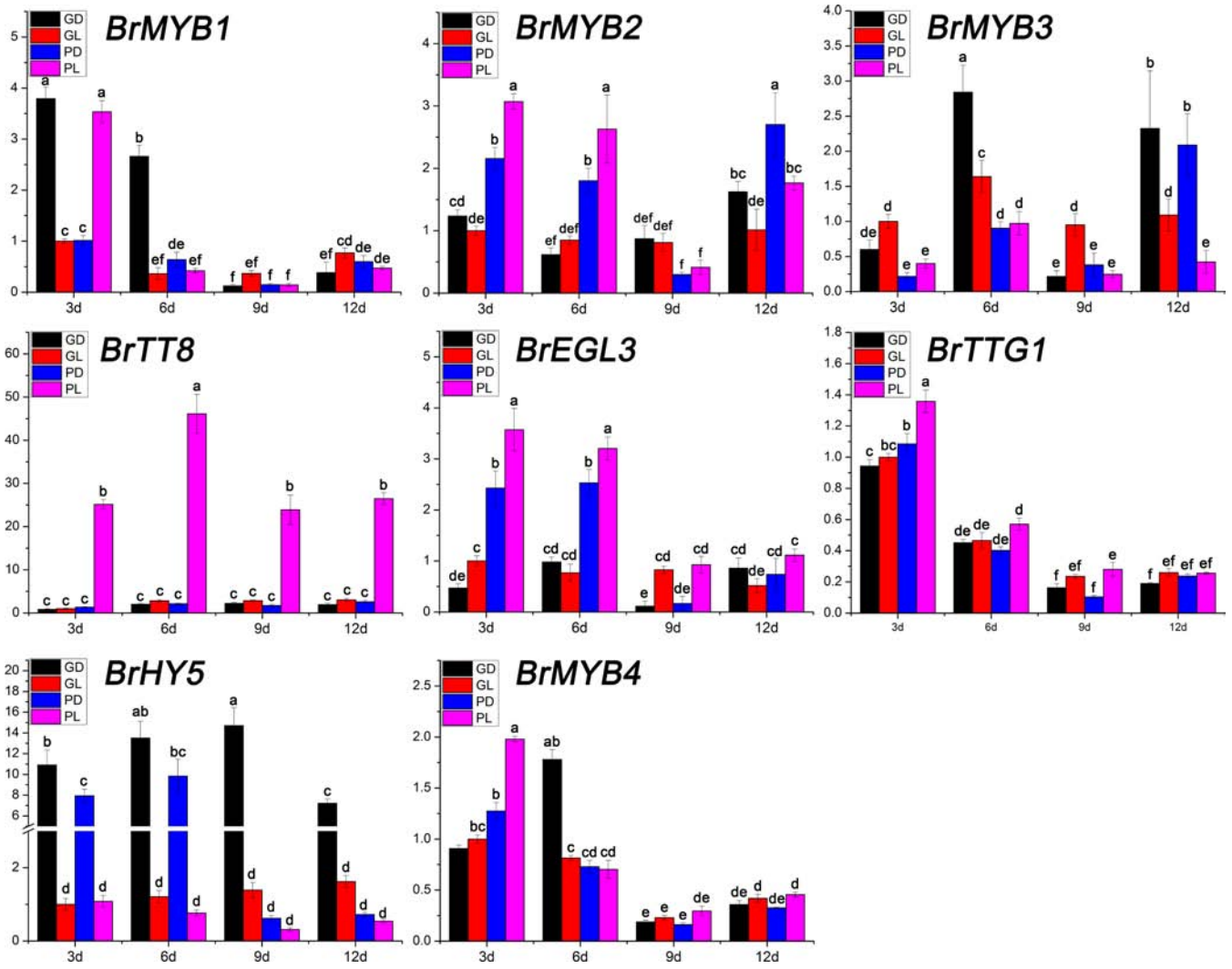


**Figure 6.** Expression analysis of anthocyanin biosynthesis regulatory genes during the development of bok choy seedlings under dark and light conditions. The longitudinal axis indicates the expression levels of genes relative to the level of *Apr*. Error bars represent the standard error of the mean ($n = 3$). Statistical significance of the differences between samples was calculated with ANOVA by paired-group comparisons. Different letters indicate significance at $P < 0.05$.

and anthocyanin accumulation, the length, fresh weight, and total pigment content of seedlings of both cultivars under light and dark conditions were examined every 3 days until 12 days after sowing (DAS) (Figure 4). Compared with the seedlings grown under light, the seedlings of both cultivars grown in darkness were all long and yellow (Figure 4A,C). The fresh weights of seedlings grown in dark conditions of both Zi He and Su Zhouqing were all obviously higher than those of the cultivars grown under light initially. However, the fresh weight of seedlings of both cultivars grown under light exceeded that of the seedlings grown in dark conditions gradually. Interestingly, the seedlings of Zi He grown in light took about 10 days to exceed the seedlings grown in darkness at the level of fresh weight, whereas the seedlings of Su Zhouqing took only 6 days to exceed the seedlings grown in darkness (Figure 4D). The growth rate of seedlings of the purple cultivar under light seems apparently lower than that of green cultivars. One reasonable explanation for this phenomenon is that the pigments synthesized in the cotyledon of Zi He reduced the efficiency of photosynthesis by inhibiting the light capture of chlorophyll.[24] Moreover, a large amount of anthocyanin production might consume a certain amount of energy and nutrients of plant cell and interfere with the normal metabolic activities in the plant itself. Although extensive studies showed that an adequate amount of anthocyanin production provides photoprotective function against excess visible light during the early development of young leaves and facilitates nutrient recovery in autumn by shielding leaves from potentially damaging light levels,[41−43] the results displayed above strongly suggest that constant anthocyanin accumulation in leaves might be a burden during the process of development, especially in seedlings.

**Expression Profiles of Anthocyanin Biosynthetic and Regulatory Genes in Seedlings of Different Cultivars under Light and Dark Conditions.** The expression profiles of anthocyanin pathway genes in the four groups of materials collected at different DAS were examined by qRT-PCR. As the results show in Figure 5, the transcript levels of *BrCHS*, *BrF3H*, *BrANS*, and *BrDFR* were greatly up-regulated in light-grown seedlings of Zi He, in contrast to the other three materials. In addition, the expression levels of these structural genes reached the maximum at 6 DAS in purple light-grown seedlings of different stages. The expression profiles of these structural genes

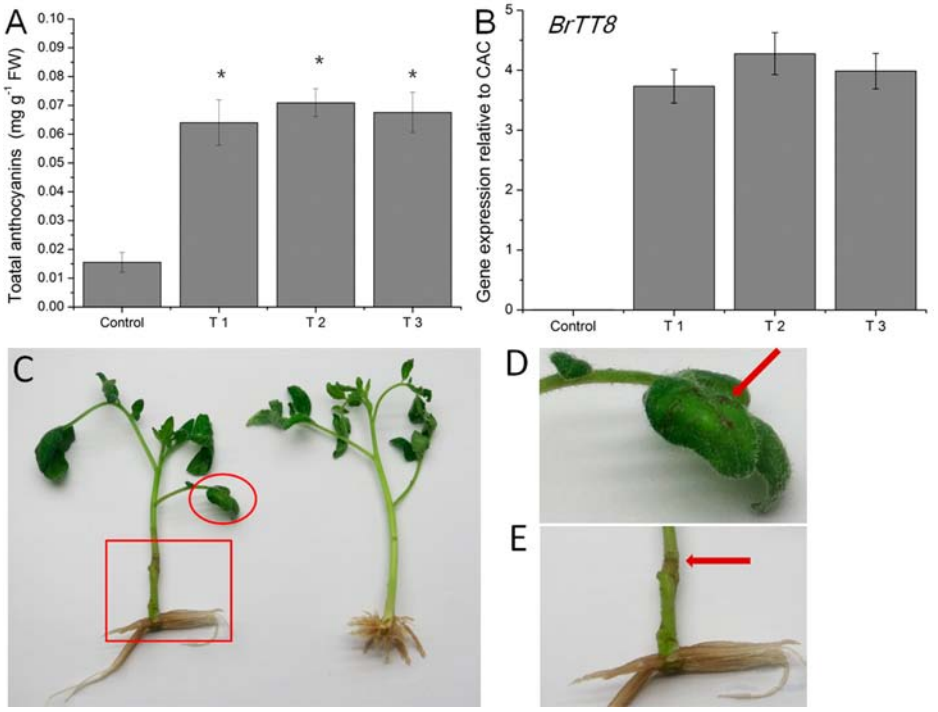


**Figure 7.** Heterologous expression of *BrTT8* in regenerating shoots of tomato promotes the biosynthesis of anthocyanins: (A) anthocyanin content in different lines of shoots; (B) transcriptional analysis of *BrTT8* in different regeneration shoots; (C) transformants (the T0 generation) of tomato transformed by pBI121-BrTT8 (left) and empty vector (right), respectively; (D) anthocyanins accumulated as small purple spots in leaves of transgenic seedlings; (E) anthocyanins accumulated visibly in the lower part in stems of transgenic seedlings. T1, T2, and T3 indicate independent regenerating shoot lines transformed with pBI121-BrTT8, whereas control indicates regenerating shoots transformed with empty vector. Asterisks above each column indicate a significant difference ($P < 0.05$) between control and transgenic lines.

were highly in accordance with the patterns of anthocyanin accumulation in seedlings of bok choy (Figure 4B). That is, it was the significantly increased expression of *BrCHS*, *BrF3H*, *BrANS*, and *BrDFR* that activates visible pigmentation production in seedlings of Zi He under light.

As we have speculated above, a bHLH transcription factor, *BrTT8*, probably regulates the anthocyanin biosynthesis by activating the transcription of structural genes in purple edible leaves with MYB and WD40 proteins. To investigate the molecular mechanisms of light-dependent anthocyanin accumulation in purple seedlings of bok choy, the transcripts of related regulatory genes were examined in the four serials of materials referred above. As Figure 6 shows, only the expression profile of *BrTT8* agreed well with those of *BrCHS*, *BrF3H*, *BrANS*, and *BrDFR*. Therefore, it is reasonable to speculate that the light-induced expression of *BrTT8* plays an important role in the anthocyanin biosynthesis activation in seedlings of Zi He under light. As the results show, *BrHY5* is greatly up-regulated in the seedlings of Zi He and Su Zhouqing under dark conditions. The high-level expression of *BrHY5* should be important for the inhibition of excessive elongation of hypocotyls of bok choy seedlings grown in darkness.[25,44] Besides, the increased expression of *BrHY5* might account for the slight up-regulation of *BrCHS* and *BrF3H* in early stages of Su Zhouqing despite no visible pigment accumulation in corresponding tissues. Nevertheless, the functions *BrHY5* plays during light-induced anthocyanin accumulation in seedlings of Zi He need further studies. In addition, *BrMYB4*, which is a potential transcriptional repressor of *BrC4H*, shows no significant changes at the mRNA level under visible light, in contrast with the seedlings grown in darkness.[45]

**Heterologous Expression of *BrTT8* in Transgenic Tomato Promotes the Expression of Partial Anthocyanin Biosynthetic Genes.** Phylogenetic and sequence analysis shows that BrTT8 lays in the same cluster with the anthocyanin synthesis activators *AmDEL*, *MdbHLH1*, *NtAN1a*, and *NtAN1b* (Supplementary Figures 1 and 2). To further study the function of the *BrTT8* gene, the full-length coding sequence of *BrTT8* driven by 35S promoter was expressed in the callus of tomato. Compared with the seedlings (the T0 generation) of tomato transformed by empty vector, the transgenic seedlings, which show high expression levels of the *BrTT8* gene, display visible anthocyanin accumulation as small purple spots in leaves and the lower part in stems (Figure 7). Furthermore, the expression level of anthocyanin biosynthetic genes in regeneration shoots was confirmed by qRT-PCR. The heterologous expression of *BrTT8* was in accordance with a coordinated increase in transcript levels of *SlPAL*, *SlCHS2*, *SlF3H*, and *Sl3GT* (Figure 8). In addition, SlCHS2 and SlF3H were significantly up-regulated in regeneration shoots. which showed visible accumulation of anthocyanins. These results suggest that the up-regulation of some vital structural genes is able to enhance the anthocyanin biosynthesis in shoots of transgenic tomato. As indicated before, the overexpression of NtAN1a and NtAN1b was able to enhance the accumulation of anthocyanin in petals of transgenic tobacco.[39] Furthermore, the purple spots in transgenic leaves resembled the phenotype observed in leaves of transgenic tomato that showed high expression of a heterologous gene *AmDEL* from snapdragon.[37] These results prove that heterologous expression of *BrTT8* in tomato is able to promote anthocyanin biosynthesis by activating the transcription of some vital anthocyanin structural genes.


dx.doi.org/10.1021/jf503453e | J. Agric. Food Chem. 2014, 62, 12366−12376

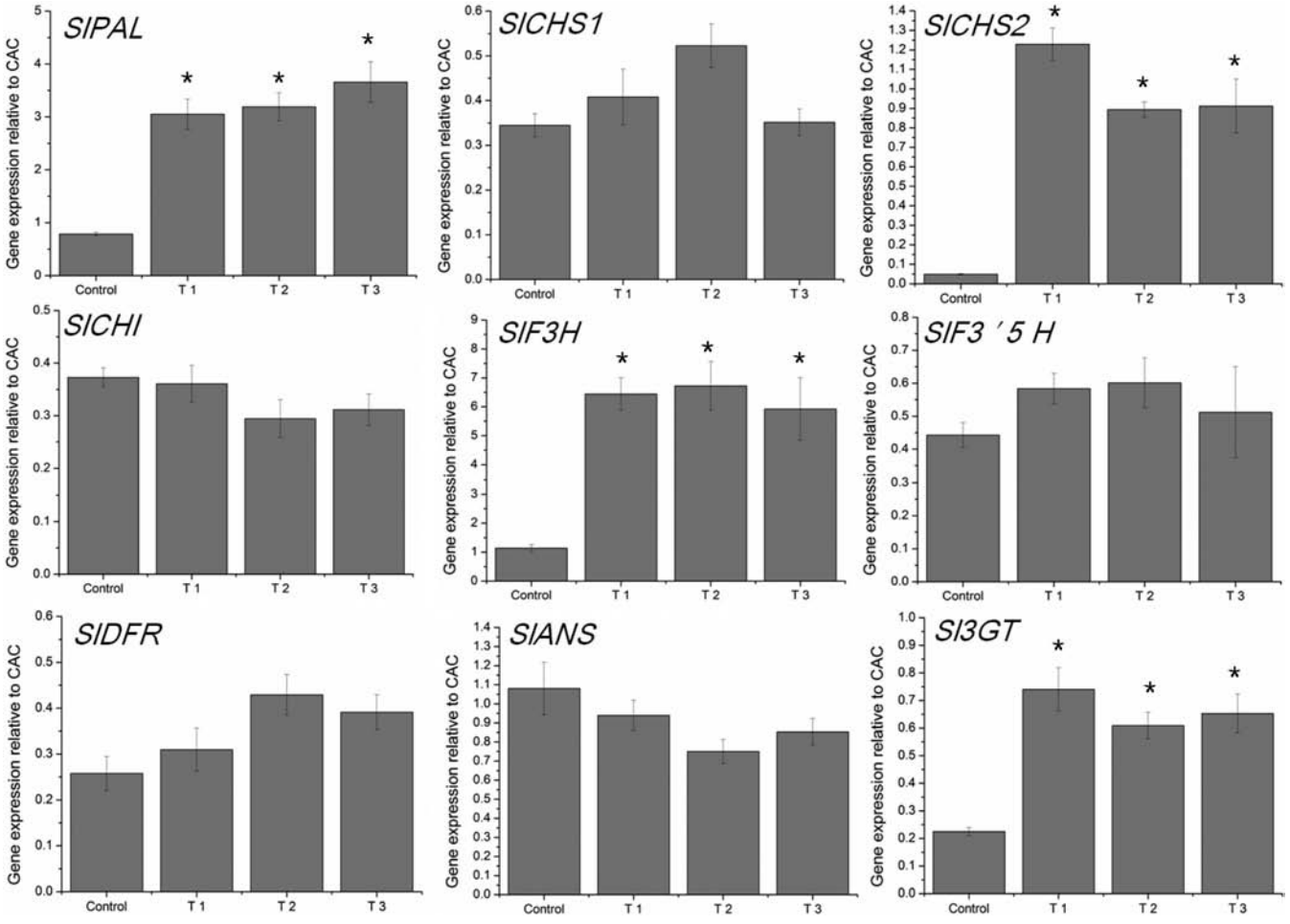


**Figure 8.** Expression analysis of structural genes of anthocynanin pathway in regeneration shoots of transgenic tomato. The longitudinal axis indicates the expression levels of genes relative to the level of *SlCAC*. Asterisks above each column indicate a significant difference ($P < 0.05$) from the control.

In this paper, the mechanisms of anthocyanin accumulation in bok choys were analyzed at both molecular and metabolic levels using the methods of HPLC-ESI-MS/MS and qRT-PCR. Cyanidin 3-(hydroxyferuloyl) diglucoside-5-(malonyl) glucoside and cyanidin 3-caffeoyl (sinapoyl) rutinoside-5-glucoside were identified as the major anthocyanins in edible leaves of Zi He. Moreover, the solely up-regulated transcription factors *BrTT8* in both edible leaves and seedlings under light probably contribute to the onset of anthocyanin biosynthesis by activating the transcription of structural genes in purple bok choy. Similarity and phylogenetic analysis of BrTT8 with other bHLH proteins from different species suggests that *BrTT8* may probably be a functional anthocyanin biosynthesis activator in purple bok choy. Furthermore, the anthocyanins detected in the regeneration shoots of tomato transformed by pBI121-BrTT8 confirmed the hypothesis we speculated above. As we have mentioned before, the large amount of anthocyanin accumulation in leaves inevitably counts against the growth of purple cultivars. This explanation agrees well with the facts that the growth rates of plants with excessive purple pigment accumulation are always significantly lower than those of the green cultivars.[24,41] However, a large amount of anthocyanin production is an important contributor to nutrition and consumer preference for bok choy. One possible solution for this conflict is the breeding of new cultivars with anthocyanin accumulation activators spatiotemporal specific expressed in edible parts during harvesting time like the strategy used in transgenic tomato.[5] Thence, the elucidation of the primary transcriptional control of anthocyanin accumulation in bok choy provides an important basis for the breeding of new purple cultivars of bok choy with more excellent agronomic characteristics.

## ■ ASSOCIATED CONTENT

### Ⓢ Supporting Information

Table of primers used for qPCR analysis of anthocyanin biosynthetic genes in bok choy, table of primers used for qPCR analysis of anthocyanin biosynthetic genes in tomato, table of primers used for gene cloning, figure showing multiple alignment of deduced amino acid sequences of *BrTT8* with bHLH homologues, and figure depicting phylogenetic analysis of BrTT8 and other bHLHs. This material is available free of charge via the Internet at http://pubs.acs.org.

## ■ AUTHOR INFORMATION

### Corresponding Author

*(Z.H.) Phone: 0086 23 65112674. Fax: 0086 23 65112674. E-mail: huzongli@cqu.edu.cn.

### Funding

This work was supported by the National Natural Science Foundation of China (30871709, 31100089, 31101546) and the Graduate Science and Technology Innovation Fund (CDJXS12230001).

### Notes

The authors declare no competing financial interest.

## ■ ABBREVIATIONS USED

PAL, phenylalanine ammonia-lyase; C4H, cinnamate 4-hydroxylase; 4CL, 4-coumarateCoA ligase; CHS, chalcone synthase; CHI, chalcone isomerase; F3H, flavone 3-hydroxylase; F3′H, flavonoid 3′-hydroxylase; F3′5′H, flavonoid 3′,5′-hydroxylase; DFR, dihydroflavonol reductase; ANS, anthocyanidin synthase; UFGT, flavonoid-3-*O*-glucosyltransferase; DHK, dihydrokaempferol; HPLC, high-performance liquid chromatography; ESI-MS/MS, elctrospray ionization tandem mass spectrometry; qRT-PCR, quantitative real-time PCR

## ■ REFERENCES


(1) Holton, T. A.; Cornish, E. C. Genetics and biochemistry of anthocyanin biosynthesis. *Plant Cell* **1995**, *7*, 1071−1083.

(2) Harborne, J. B.; Williams, C. A. Advances in flavonoid research since 1992. *Phytochemistry* **2000**, *55*, 481−504.

(3) Williams, R. J.; Spencer, J. P.; Rice-Evans, C. Flavonoids: antioxidants or signalling molecules? *Free Radical Biol. Me.* **2004**, *36*, 838−849.

(4) Guarnieri, S.; Riso, P.; Porrini, M. Orange juice vs vitamin C: effect on hydrogen peroxide-induced DNA damage in mononuclear blood cells. *Br. J. Nutr.* **2007**, *97*, 639−643.

(5) Butelli, E.; Titta, L.; Giorgio, M.; Mock, H. P.; Matros, A.; Peterek, S.; Schijlen, E. G.; Hall, R. D.; Bovy, A. G.; Luo, J.; Martin, C. Enrichment of tomato fruit with health-promoting anthocyanins by expression of select transcription factors. *Nat. Biotechnol.* **2008**, *26*, 1301−1308.

(6) de Pascual-Teresa, S.; Moreno, D. A.; Garcia-Viguera, C. Flavanols and anthocyanins in cardiovascular health: a review of current evidence. *Int. J. Mol. Sci.* **2010**, *11*, 1679−1703.

(7) Paredes-Lopez, O.; Cervantes-Ceja, M. L.; Vigna-Perez, M.; Hernandez-Perez, T. Berries: improving human health and healthy aging, and promoting quality life − a review. *Plant Foods Hum. Nutr.* **2010**, *65*, 299−308.

(8) Butelli, E.; Licciardello, C.; Zhang, Y.; Liu, J.; Mackay, S.; Bailey, P.; Reforgiato-Recupero, G.; Martin, C. Retrotransposons control fruit-specific, cold-dependent accumulation of anthocyanins in blood oranges. *Plant Cell* **2012**, *24*, 1242−1255.

(9) Winkel-Shirley, B. Flavonoid biosynthesis. A colorful model for genetics, biochemistry, cell biology, and biotechnology. *Plant Physiol.* **2001**, *126*, 485−493.

(10) Sparvoli, F.; Martin, C.; Scienza, A.; Gavazzi, G.; Tonelli, C. Cloning and molecular analysis of structural genes involved in flavonoid and stilbene biosynthesis in grape (*Vitis vinifera* L.). *Plant Mol. Biol.* **1994**, *24*, 743−755.

(11) Lo Piero, A. R.; Puglisi, I.; Rapisarda, P.; Petrone, G. Anthocyanins accumulation and related gene expression in red orange fruit induced by low temperature storage. *J. Agric. Food Chem.* **2005**, *53*, 9083−9088.

(12) Zhao, Z. C.; Hu, G. B.; Hu, F. C.; Wang, H. C.; Yang, Z. Y.; Lai, B. The UDP glucose:flavonoid-3-*O*-glucosyltransferase (UFGT) gene regulates anthocyanin biosynthesis in litchi (*Litchi chinesis* Sonn.) during fruit coloration. *Mol. Biol. Rep.* **2012**, *39*, 6409−6415.

(13) Piero, A. L.; Consoli, A.; Puglisi, I.; Orestano, G.; Recupero, G.; Petrone, G. Anthocyaninless cultivars of sweet orange lack to express the UDP-glucose flavonoid 3-*O*-glucosyl rransferase. *J. Plant Biochem. Biotechnol.* **2005**, *14*, 9−14.

(14) Grotewold, E. The genetics and biochemistry of floral pigments. *Annu. Rev. Plant Biol.* **2006**, *57*, 761−780.

(15) Yuan, Y.; Chiu, L. W.; Li, L. Transcriptional regulation of anthocyanin biosynthesis in red cabbage. *Planta* **2009**, *230*, 1141−1153.

(16) Broun, P. Transcriptional control of flavonoid biosynthesis: a complex network of conserved regulators involved in multiple aspects of differentiation in *Arabidopsis*. *Curr. Opin. Plant Biol.* **2005**, *8*, 272−279.

(17) Koes, R.; Verweij, W.; Quattrocchio, F. Flavonoids: a colorful model for the regulation and evolution of biochemical pathways. *Trends Plant Sci.* **2005**, *10*, 236−242.

(18) Gonzalez, A.; Zhao, M.; Leavitt, J. M.; Lloyd, A. M. Regulation of the anthocyanin biosynthetic pathway by the TTG1/bHLH/Myb transcriptional complex in *Arabidopsis* seedlings. *Plant J: Cell Mol. Biol.* **2008**, *53*, 814−827.

(19) Espley, R. V.; Hellens, R. P.; Putterill, J.; Stevenson, D. E.; Kutty-Amma, S.; Allan, A. C. Red colouration in apple fruit is due to the activity of the MYB transcription factor, MdMYB10. *Plant J.: Cell Mol. Biol.* **2007**, *49*, 414−427.

(20) Chiu, L. W.; Zhou, X.; Burke, S.; Wu, X.; Prior, R. L.; Li, L. The purple cauliflower arises from activation of a MYB transcription factor. *Plant Physiol.* **2010**, *154*, 1470−1480.

(21) Chiu, L. W.; Li, L. Characterization of the regulatory network of BoMYB2 in controlling anthocyanin biosynthesis in purple cauliflower. *Planta* **2012**, *236*, 1153−1164.

(22) Zhang, Y.; Hu, Z.; Chu, G.; Huang, C.; Tian, S.; Zhao, Z.; Chen, G. Anthocyanin accumulation and molecular analysis of anthocyanin biosynthesis-associated genes in eggplant (*Solanum melongena* L.). *J. Agric. Food Chem.* **2014**, *62*, 2906−2912.

(23) Xie, X. B.; Li, S.; Zhang, R. F.; Zhao, J.; Chen, Y. C.; Zhao, Q.; Yao, Y. X.; You, C. X.; Zhang, X. S.; Hao, Y. J. The bHLH transcription factor MdbHLH3 promotes anthocyanin accumulation and fruit colouration in response to low temperature in apples. *Plant, Cell Environ.* **2012**, *35*, 1884−1897.

(24) Feng, S.; Wang, Y.; Yang, S.; Xu, Y.; Chen, X. Anthocyanin biosynthesis in pears is regulated by a R2R3-MYB transcription factor PyMYB10. *Planta* **2010**, *232*, 245−255.

(25) Zhang, Y.; Zheng, S.; Liu, Z.; Wang, L.; Bi, Y. Both HY5 and HYH are necessary regulators for low temperature-induced anthocyanin accumulation in *Arabidopsis* seedlings. *J. Plant Physiol.* **2011**, *168*, 367−374.

(26) Lee, J.; He, K.; Stolc, V.; Lee, H.; Figueroa, P.; Gao, Y.; Tongprasit, W.; Zhao, H.; Lee, I.; Deng, X. W. Analysis of transcription factor HY5 genomic binding sites revealed its hierarchical role in light regulation of development. *Plant Cell* **2007**, *19*, 731−749.

(27) Murillo, G.; Mehta, R. G. Cruciferous vegetables and cancer prevention. *Nutr. Cancer* **2001**, *41*, 17−28.

(28) Keck, A. S.; Finley, J. W. Cruciferous vegetables: cancer protective mechanisms of glucosinolate hydrolysis products and selenium. *Integrative Cancer Ther.* **2004**, *3*, 5−12.

(29) Qi, J.; Yu, S.; Zhang, F.; Shen, X.; Zhao, X.; Yu, Y.; Zhang, D. Reference gene selection for real-time quantitative polymerase chain reaction of mRNA transcript levels in chinese cabbage (*Brassica rapa* L. ssp. *pekinensis*). *Plant Mol. Biol. Rep.* **2010**, *28*, 597−604.

(30) Exposito-Rodriguez, M.; Borges, A. A.; Borges-Perez, A.; Perez, J. A. Selection of internal control genes for quantitative real-time RT-PCR studies during tomato development process. *BMC Plant Biol.* **2008**, *8*, 131.

(31) Park, N. I.; Xu, H.; Li, X.; Jang, I. H.; Park, S.; Ahn, G. H.; Lim, Y. P.; Kim, S. J.; Park, S. U. Anthocyanin accumulation and expression of anthocyanin biosynthetic genes in radish (*Raphanus sativus*). *J. Agric. Food Chem.* **2011**, *59*, 6034−6039.

(32) Sun, H. J.; Uchii, S.; Watanabe, S.; Ezura, H. A highly efficient transformation protocol for Micro-Tom, a model cultivar for tomato functional genomics. *Plant Cell Physiol.* **2006**, *47*, 426−431.

(33) Wu, X.; Prior, R. L. Identification and characterization of anthocyanins by high-performance liquid chromatography-electrospray ionization-tandem mass spectrometry in common foods in the United States: vegetables, nuts, and grains. *J. Agric. Food Chem.* **2005**, *53*, 3101−3113.

(34) Lin, L. Z.; Sun, J.; Chen, P.; Harnly, J. UHPLC-PDA-ESI/HRMS/MS($n$) analysis of anthocyanins, flavonol glycosides, and hydroxycinnamic acid derivatives in red mustard greens (*Brassica juncea* Coss variety). *J. Agric. Food Chem.* **2011**, *59*, 12059−12072.

(35) Han, Y.; Vimolmangkang, S.; Soria-Guerra, R. E.; Rosales-Mendoza, S.; Zheng, D.; Lygin, A. V.; Korban, S. S. Ectopic expression of apple F3′H genes contributes to anthocyanin accumulation in the

*Arabidopsis* tt7 mutant grown under nitrogen stress. *Plant Physiol.* **2010**, *153*, 806−820.
(36) Teng, S.; Keurentjes, J.; Bentsink, L.; Koornneef, M.; Smeekens, S. Sucrose-specific induction of anthocyanin biosynthesis in *Arabidopsis* requires the MYB75/PAP1 gene. *Plant Physiol.* **2005**, *139*, 1840−1852.
(37) Mooney, M.; Desnos, T.; Harrison, K.; Jones, J.; Carpenter, R.; Coen, E. Altered regulation of tomato and tobacco pigmentation genes caused by the delila gene of *Antirrhinum*. *Plant J.* **1995**, *7*, 333−339.
(38) Bai, Y.; Pattanaik, S.; Patra, B.; Werkman, J. R.; Xie, C. H.; Yuan, L. Flavonoid-related basic helix-loop-helix regulators, NtAn1a and NtAn1b, of tobacco have originated from two ancestors and are functionally active. *Planta* **2011**, *234*, 363−375.
(39) Bai, Y.; Pattanaik, S.; Patra, B.; Werkman, J. R.; Xie, C. H.; Yuan, L. Complexity and robustness of the flavonoid transcriptional regulatory network revealed by comprehensive analyses of MYB-bHLH-WDR complexes and their targets in Arabidopsis seed. *New Phytol.* **2014**, *202*, 132−144.
(40) Spelt, C.; Quattrocchio, F.; Mol, J. N.; Koes, R. anthocyanin1 of petunia encodes a basic helix-loop-helix protein that directly activates transcription of structural anthocyanin genes. *Plant Cell* **2000**, *12*, 1619−1632.
(41) Feild, T. S.; Lee, D. W.; Holbrook, N. M. Why leaves turn red in autumn. The role of anthocyanins in senescing leaves of Red-Osier dogwood. *Plant Physiol.* **2001**, *127*, 566−574.
(42) Hoch, W. A.; Singsaas, E. L.; McCown, B. H. Resorption protection. Anthocyanins facilitate nutrient recovery in autumn by shielding leaves from potentially damaging light levels. *Plant Physiol.* **2003**, *133*, 1296−1305.
(43) Karageorgou, P.; Manetas, Y. The importance of being red when young: anthocyanins and the protection of young leaves of *Quercus coccifera* from insect herbivory and excess light. *Tree Physiol.* **2006**, *26*, 613−621.
(44) Chattopadhyay, S.; Ang, L. H.; Puente, P.; Deng, X. W.; Wei, N. Arabidopsis bZIP protein HY5 directly interacts with light-responsive promoters in mediating light control of gene expression. *Plant Cell* **1998**, *10*, 673−683.
(45) Jin, H.; Cominelli, E.; Bailey, P.; Parr, A.; Mehrtens, F.; Jones, J.; Tonelli, C.; Weisshaar, B.; Martin, C. Transcriptional repression by AtMYB4 controls production of UV-protecting sunscreens in Arabidopsis. *EMBO J.* **2000**, *19*, 6150−6161.

extracted with ethanol (100 mL) after soaking at room temperature for 24 h. The ethanol solution was filtered through filter paper, and then the filtrate was then evaporated under reduced pressure at 40 °C. The purple residue after vacuum desiccation resulted in a gummy product (237 mg, 4.7%). 5,7-DMF and 5,7,4′-TMF were isolated according to the published method.[11] Flavonoids used for the reactivity study were purchased from Indofine Chemical Company (Hillsborough, NJ). Gifu anaerobic medium (GAM) from Nissui Pharmaceutical Co. (Tokyo, Japan) was used for isolation and growth media. GAM broth was prepared according to the instructions of the manufacturer, and GAM plates were prepared by the addition of 1.5% agar to the GAM broth.

**PMF Biotransformation with Fecal Samples.** The experiment was performed in compliance with the Bioethics and Safety Act enforced by the Korean government and the policies of the Chung-Ang University Institutional Research Board (CAU-IRB). Fresh fecal samples from a healthy 34-year-old female were collected directly once in deoxygenated GAM broth (4 mL), covered with sterilized mineral oil, and placed immediately in an anaerobic chamber (5% $CO_2$, 10% $H_2$, and 85% $N_2$) at 37 °C. The inoculated medium was stabilized for 2 h after filtration through sterilized gauze, and a portion of the medium was stored in liquid $N_2$ for further investigation. For the biotransformation of PMFs, 100 μL of the medium was inoculated in GAM broth (2 mL) and grown for 17 h at 37 °C. PMFs obtained from the ethanol extraction of krachaidum were dissolved in DMF at the concentration of 3 mg/mL, and then 2 μL was added to the 200 μL of bacterial culture and reacted for 3 days at 37 °C. After 3 days, ethyl acetate (1 mL) was added to each tube to stop the reaction and the mixture was vortexed for 20 s. After centrifugation at 10770*g* for 10 min, 800 μL of the organic supernatant was taken and the solvent was evaporated with a centrifugal evaporator (Micro-Cenvac NB-503CIR, N-Biotek, Gyeonggi, Korea). The residue was redissolved in 10 μL of methanol for further analysis. For thin-layer chromatography (TLC) analysis, 1 μL each of the methanol extract and the PMFs were applied on a silica gel TLC plate (Merck silica gel 60 F254). The TLC plate was developed in a mixture of hexanes/acetone (1:1, vol/vol). For HPLC analysis, the Finnigan Surveyor Plus high-performance liquid chromatography (HPLC) system (Thermo Scientific, Waltham, MA) equipped with a photodiode array detector (PDA Plus) and a $C_{18}$ reverse-phase column (Hypersil GOLD 5 μm, 4.6 × 100 mm, Thermo Scientific, Waltham, MA) was employed. The mobile phase was composed of 0.1% acetic acid in water (A) and 0.1% acetic acid in methanol (B). The solvent gradient profile started with 45% solvent B for 1 min and then increased from 45 to 55% solvent B over 14 min, from 55 to 60% solvent B over 9 min, and from 60 to 65% solvent B over 8 min, after which it decreased to 60% solvent B for 5 min at the flow rate of 1.0 mL/min.

**Isolation of PMF-Metabolizing Bacterium and Culture Conditions.** Strain MRG-PMF1 was isolated from the fecal samples, which showed PMF bioconversion activity. The mixed cell culture (360 μL) prepared from fecal samples was diluted to $10^{-4}$ with GAM broth after the addition of 3.6 μL of the PMF solution (3.0 mg/mL in DMF). The diluted solution was spread on GAM agar plates for isolation. After incubation for 2 days at 37 °C, single colonies were picked from the plates, transferred into 500 μL of GAM broth, and incubated overnight. The PMF-metabolizing activity was checked by TLC and HPLC, as described above. Subcultures and activity checks were repeated until a pure bacterium was obtained.

**16S rRNA Gene Sequencing and Phylogeny Analysis.** 16S rRNA gene sequence analysis of the isolated bacterium was performed for identification of the bacterial strain. The bacterium was streaked on GAM agar plates in an anaerobic chamber and grown for 2 days at 37 °C. The 16S rRNA gene was amplified by PCR with universal bacteria primers 27F (5′-AGAGTTTGATCMTGGCTCAG-3′) and 1492R (5′-GGYTACCTTGTTACGACTT-3′), and sequencing was performed via the sequencing service at Solgent, Inc. (Daejeon, Korea). The 16S rDNA sequences were analyzed using the BLASTN tool of the National Center for Biotechnology Information (NCBI) to identify bacterial strains with sequence similarity.[12] Phylogenetic trees were constructed by the neighbor-joining method using the MEGA 6 program.[13]

**Bacterial Growth and pH Changes.** The bacterial culture stored in liquid nitrogen was thawed in an anaerobic chamber, and 100 μL was then transferred to 2 mL of GAM broth. When the optical density at 600 nm ($OD_{600}$) reached 0.7, 400 μL of the cell culture was transferred to 20 mL of fresh GAM broth. Bacterial growth was monitored by measuring $OD_{600}$ with the ultraviolet−visible (UV−vis) spectrophotometer S-3100 (Scinco, Seoul, Korea), and the pH of the medium was also measured by the Laqua pH meter F-74BW (Horiba Scientific, Kyoto, Japan) every 30 min.

**Biotransformation of 5,7-DMF and 5,7,4′-TMF.** 5,7-DMF and 5,7,4′-TMF were used for the study of biotransformation kinetics in an anaerobic chamber and the identification of the intermediates. When the growth of the bacteria in GAM broth reached $OD_{600}$ of 0.8, each substrate was added to the reaction media (1.5 mL, 100 μM) to initiate biotransformation. Aliquots of the reaction mixtures (100 μL) were taken and allocated into Eppendorf tubes every 3 h. The allocated media were extracted with 1 mL of ethyl acetate, and the supernatant (800 μL), collected after vortexing and centrifugation (10770*g* for 10 min), was dried under vacuum. The residue was dissolved in 100 μL of methanol and analyzed by HPLC. The solvent gradient profile for 5,7-DMF biotransformation started with 53% solvent B for 1 min and then increased from 53 to 55% solvent B over 14 min and from 55 to 70% solvent B over 3 min. The solvent gradient profile for 5,7,4′-TMF biotransformation started with 45% solvent B for 1 min and then increased from 45 to 55% solvent B over 9 min, from 55 to 61% solvent B over 3 min, and finally from 61 to 70% over 2 min.

**Structural Analyses of 5,7-DMF and 5,7,4′-TMF Metabolites.** 5,7-DMF and 5,7,4′-TMF metabolites were analyzed by a Dionex Ultimate 3000 HPLC system (Thermo Scientific, Waltham, MA) equipped with a $C_{18}$ reversed-phase column (Kinetex, 100 × 2.1 mm, 1.7 μm, Phenomenex, Torrance, CA) and a diode array detector (DAD). A Thermo Fisher Scientific LCQ fleet instrument (Thermo Scientific, Waltham, MA) was coupled to the HPLC system for electrospray ionization mass spectrometry (ESI−MS) analysis. The mobile phase was a gradient of water with 0.1% formic acid (A) and acetonitrile with 0.1% formic acid (B). The initial composition of the mobile phase was 33% solvent B for 1 min. In linear gradients, the composition changed to 45% solvent B over 2 min and then 50% solvent B over 8 min, where it stayed for 10 min at the flow rate of 0.2 mL/min. ESI−MS analyses were performed in positive-ion mode within the $m/z$ range of 50−500 and processed with Xcalibur software (Thermo Scientific, Waltham, MA). ESI conditions: spray voltage, 5.4 kV; sheath gas, 15 arbitrary units; auxiliary gas, 5 arbitrary units; heated capillary temperature, 275 °C; capillary voltage, 27 V; and tube lens, 100 V.

For the isolation of intermediate A produced during the biotransformation of 5,7-DMF, 1 mL of GAM medium containing MRG-PMF1 ($OD_{600}$ of 0.6) was added to 200 mL of GAM medium. When the $OD_{600}$ of the GAM medium reached 0.8, 5,7-DMF (10 mg, 5 mL of 5 mM DMF) was added to the reaction medium and reacted in an anaerobic chamber. The conversion of 5,7-DMF was monitored by TLC analysis of the medium. After 58 h, the reaction medium was centrifuged (10770*g* for 20 min) and the supernatant was extracted with EtOAc (100 mL × 3). The combined organic layer was dried with anhydrous $MgSO_4$, and the organic solvent was removed under reduced pressure by a rotatory evaporator. After vacuum desiccation of the residue, the fraction containing intermediate A (2 mg) was isolated by vacuum liquid chromatography.[14] Intermediate A was further purified by preparative TLC (0.5 mg, isolation yield of 2.4%), and the proton nuclear magnetic resonance ($^1$H NMR) spectrum was recorded in MeOH-$d_4$ on a Varian VNS (600 MHz, Palo Alto, CA). Chemical shift ($\delta$) was reported in parts per million (ppm). Intermediate A (5-methylchrysin): UV ($\lambda_{max}$, nm), 264, 314; $^1$H NMR (600 MHz, $CD_3OD$) $\delta$, 7.92 (*m*, 2H, H-2′, H-6′), 7.52 (*m*, 2H, H-3′, H-5′), 7.51 (*m*, H, H-4′), 6.64 (*s*, 1H, H-3), 6.56 (*d*, 1H, $J$ = 2.2 Hz, H-6), 6.41 (*d*, 1H, $J$ = 2.2 Hz, H-8), 3.96 (*s*, 3H, −$OCH_3$).

**Reactivity Study of PMF-Metabolizing Bacterium.** To study the substrate specificity of flavonoid biotransformation, the isolated bacterium was reacted with 100 μM of various substrates. In detail,

bacteria were grown to $OD_{600}$ of 0.7 in 495 μL of GAM broth in an anaerobic chamber at 37 °C, after which 5 μL of each substrate (10 mM in DMF) was added. After incubation for 15 min and 1, 2, 3, and 7 days, 100 μL of reaction media was taken from each culture and 1 mL of ethyl acetate was added to stop the biotransformation. The mixture was then vortexed for 20 s and centrifuged (10770*g* for 10 min). The supernatant (800 μL) was taken and dried under reduced pressure. The residue was dissolved in 100 μL of methanol, and a 10 μL aliquot was injected for HPLC. The solvent gradient profile started with 20% solvent B for 1 min and then increased from 20 to 50% solvent B over 9 min and from 50 to 70% solvent B over 5 min at the flow rate of 1.0 mL/min. The reaction products were detected and identified from comparison to the expected standard flavonoids.

## RESULTS

**PMF Biotransformation by Human Fecal Sample and the Isolation of Strain MRG-PMF1.** The PMF mixture obtained by ethanol extraction of krachaidum was completely metabolized by the fecal sample obtained from a healthy 34-year-old female (see Figure S1 of the Supporting Information). From the diluted fecal samples showing PMF-metabolizing activity, 75 single colonies were isolated and further tested for activity. An obligatory anaerobic Gram-positive coccobacilli, which can metabolize PMFs was isolated under anaerobic conditions (see Figure S1 of the Supporting Information) and successfully subcultured on GAM plates without losing the PMF-metabolizing activity. The 16S rRNA gene of the isolate was sequenced for identification and deposited in GenBank under accession number KJ078647. The partial 16S rRNA gene sequence (1361 bp) was most closely related with *Blautia producta* ATCC 27340T (X94966), showing 99.85% similarity. Other strains in the family Lachnospiraceae and genus *Blautia*, particularly *Blautia coccoides* ATCC 29236T (M59090, 99.70% similarity), *Blautia stercoris* GAM6-1T (HM626177, 95.39% similarity), *Blautia hansenii* DSM 20583T (ABYU01000028, 95.37% similarity), *Blautia stercoris* SJTU C 02 47 (EF403927, 95.30% similarity), *Blautia schinkii* BT (X94965, 95.13% similarity), *Blautia faecis* M25T (HM626178, 95.00% similarity), and *Blautia glucerasea* HFTH-1T (AB439724, 94.77% similarity), also showed high sequence similarity to the isolated bacterium (Figure 1). Therefore, the isolated PMF-metabolizing anaerobic bacterium was identified as *Blautia* sp. MRG-PMF1.

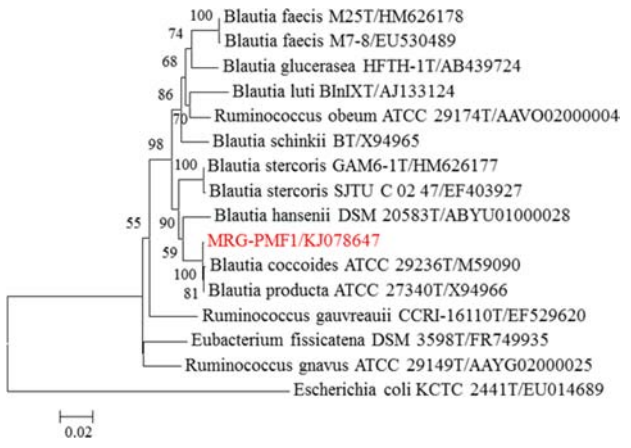


**Figure 1.** Molecular phylogenetic tree analysis of *Blautia* sp. MRG-PMF1. Numbers at the branching points indicate bootstrap values greater than 50% based on 1000 samplings. *Escherichia coli* was used as an out group. Bar, 0.02 nucleotide substitutions per position.

The PMF biotransformation by strain MRG-PMF1 was studied by HPLC analysis. The ethanol extract of krachaidum is known to contain 11 PMFs, for which TLC and HPLC analyses of the compositional changes were reported before.[11] The mixture of PMFs used herein for the reaction with fecal samples contained 5,7-DMF (10%), 5,7,4′-TMF (12%), and 3,5,7,3′,4′-pentamethoxyflavone (3,5,7,3′,4′-PMF, 20%) as the major compounds. Along with these three compounds, 3,5,7,4′-tetramethoxyflavone (3,5,7,4′-TMF, 6%) and 5-hydroxy-3,7,4′-trimethoxyflavone (5-OH-3,7,4′-TMF, 6%) were also abundant.[9] After the 3 day reaction with MRG-PMF1, biotransformation products of the PMFs were analyzed by HPLC (Figure 2). Chrysin (5,7-dihydroxyflavone) and apigenin (5,7,4′-trihydroxyflavone) were identified by comparing their retention times and UV spectra to the standard compounds. The other metabolites 3-*O*-methylquercetin and 3-*O*-methylkaempferol were assigned on the basis of the HPLC retention times and published UV spectra.[15] From analysis of the biotransformation of PMFs by MRG-PMF1 (Figure 3), it was found that the methyl group at the C-3 position of flavone was not hydrolyzed even after 3 days of incubation.

A growth curve of the isolated bacteria in GAM medium under anaerobic conditions was obtained by monitoring the changes in $OD_{600}$. *Blautia* sp. MRG-PMF1 reached the stationary phase in 9 h after a lag phase of 3.5 h at 37 °C (see Figure S2 of the Supporting Information). After the stationary phase, a decrease in $OD_{600}$ was observed. The growth of MRG-PMF1 showed good correlation with the pH changes of the media. The initial pH of the medium was pH 6.9, and a decrease to pH 5.4 was observed during exponential cell growth of the strain.

**Biotransformation of 5,7-DMF and 5,7,4′-TMF and Kinetics Study.** Biotransformation of 5,7-DMF and 5,7,4′-TMF by *Blautia* sp. MRG-PMF1 produced chrysin and apigenin, respectively, through the hydrolysis of methyl aryl ether functional groups of the substrates (Figure 2). In the time-dependent study, *Blautia* sp. MRG-PMF1 was found to metabolize completely 0.1 mM 5,7-DMF and 5,7,4′-TMF within 30 h (see Figure S3 of the Supporting Information). Furthermore, biotransformation intermediates were observed for both PMFs via TLC (see Figure S4 of the Supporting Information) and HPLC (Figure 4) analyses. During the biotransformation of 5,7-DMF, an intermediate A was identified on the HPLC chromatogram. The HPLC retention time and UV spectrum of intermediate A were different from 7-methoxychrysin, another PMF found in krachaidum extract.[11] The UV absorption at 264 and 314 nm was the same as the reported data for 5-methoxychrysin.[16] The molecular ion $[M + H]^+$ peak of intermediate A was found at $m/z$ 269.23 from the ESI−MS spectrum, which was smaller than that of 5,7-DMF ($m/z$ 283.24) by 14 Da and larger than that of chrysin by 14 Da (see Figure S5 of the Supporting Information). Between two possible demethylation intermediates of 5,7-DMF, intermediate A was assigned as 5-methoxychrysin by comparison of the HPLC retention times and electronic spectra. The molecular structure of intermediate A was confirmed by $^1$H NMR spectroscopy. Two methoxy groups of 5,7-DMF are found at $\delta$ 3.96 ppm (5-$OCH_3$) and $\delta$ 3.92 ppm (7-$OCH_3$),[11] but the peak corresponding to the 7-methoxy group disappeared from the $^1$H NMR spectrum of intermediate A. Two metabolic intermediates B and C were observed during the biotransformation of 5,7,4′-TMF, which were assigned as 7-OH-5,4′-DMF and thevetiaflavone, respectively (Figure 5).

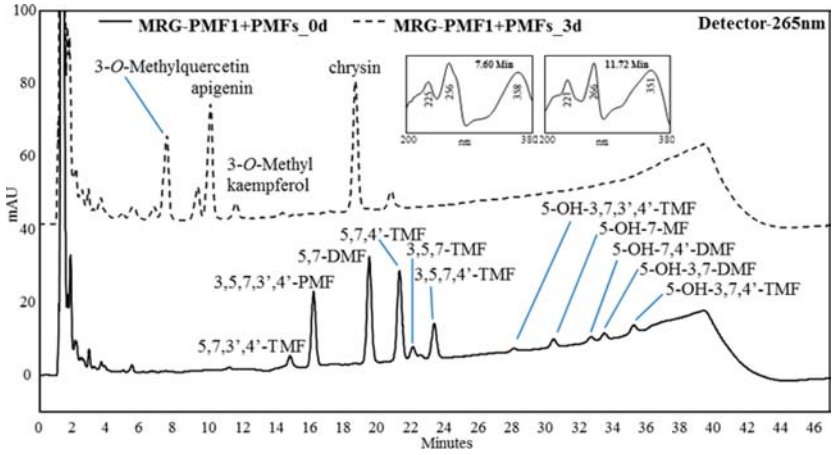


**Figure 2.** HPLC analysis of PMF metabolism by fecal sample. The solid and dotted lines represent PMFs before and after 3 days of reaction, respectively. (Inset) PDA UV spectra and the retention times of metabolites from the 3 day reaction data were used for the identification of 3-*O*-methylquercetin and 3-*O*-methylkaempferol. Abbreviations: 5,7,3′,4′-TMF, 5,7,3′,4′-tetramethoxyflavone; 3,5,7,3′,4′-PMF, 3,5,7,3′,4′-pentamethoxyflavone; 3,5,7-TMF, 3,5,7-trimethoxyflavone; 3,5,7,4′-TMF, 3,5,7,4′-tetramethoxyflavone; 5-OH-3,7,3′,4′-TMF, 5-hydroxy-3,7,3′,4′-tetramethoxyflavone; 5-OH-7-MF, 5-hydroxy-7-methoxyflavone; 5-OH-7,4′-DMF, 5-hydroxy-7,4′-dimethoxyflavone; 5-OH-3,7-DMF, 5-hydroxy-3,7-dimethoxyflavone; and 5-OH-3,7,4′-TMF, 5-hydroxy-3,7,4′-trimethoxyflavone.

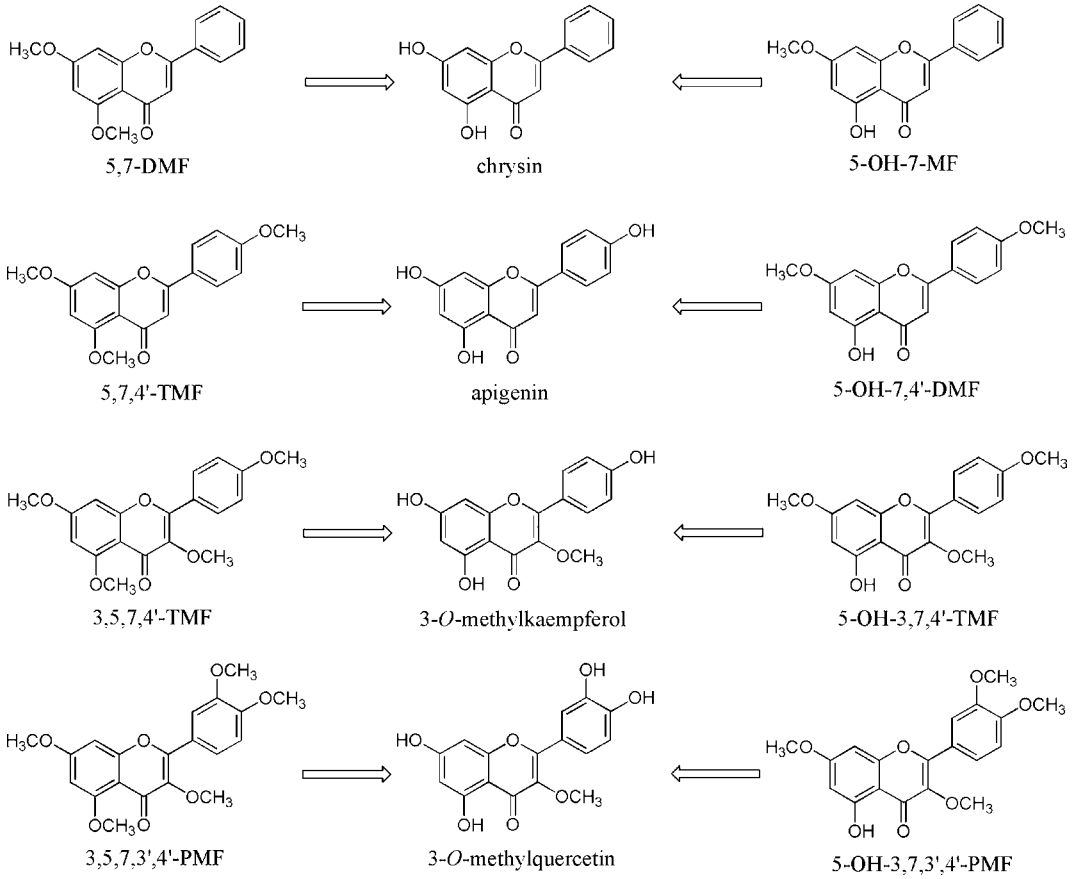


**Figure 3.** Bioconversion of the PMF mixture by *Blautia* sp. MRG-PMF1.

**Biotransformation of Other Flavonoids by *Blautia* sp. MRG-PMF1.** *Blautia* sp. MRG-PMF1 was tested for the ability to metabolize other flavonoids (Table 1). The metabolites, except for eriodictyol (5,7,3′,4′-tetrahydroxyflavanone), were identified by comparison to the retention times and UV spectra of the standard compounds by HPLC. The other two metabolites were confirmed by comparing the UV spectrum to the published data.[17] Along with PMF-metabolizing activity, *Blautia* sp. MRG-PMF1 also showed flavone *O*-glucose and flavone *O*-rutinose hydrolysis activities. Apigetrin and rutin were converted to apigenin and quercetin, respectively. Various isoflavones, except for puerarin, were also metabolized by *Blautia* sp. MRG-PMF1. For example, daidzin, genistin, glycitin, ononin, and sissotrin were converted to their aglycones, daidzein, genistein, glycitein, formononetin, and biochanin A, respectively, because of the *O*-glucose and *O*-methyl hydrolysis

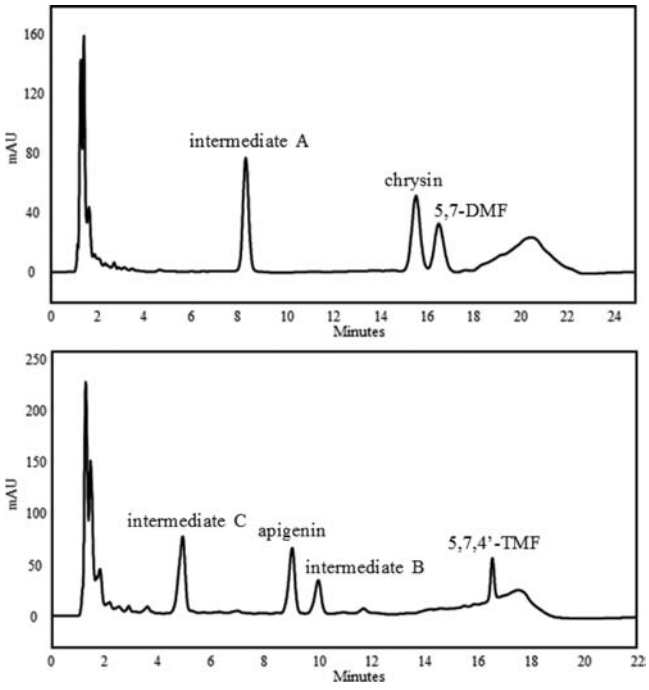


**Figure 4.** HPLC chromatograms (265 nm) of *Blautia* sp. MRG-PMF1 biotransformation products obtained from 5,7-DMF (18 h, above) and 5,7,4′-TMF (21 h, below).

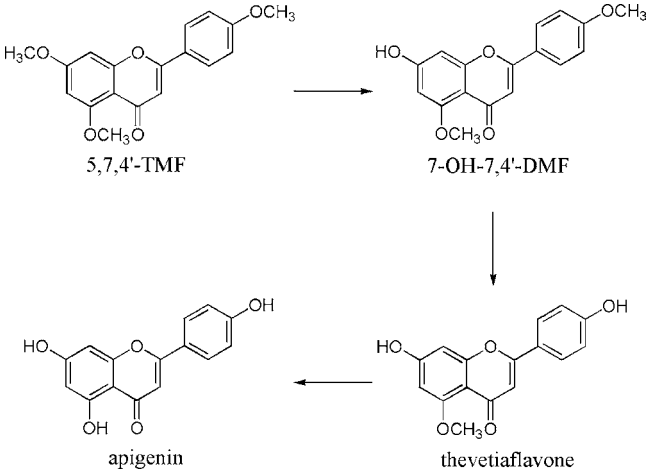


**Figure 5.** Metabolic pathway of 5,7,4′-TMF biotransformation.

activities. Glycitein biotransformation by human fecal flora was reported to produce the metabolite 6,7,4′-trihydroxyisoflavone.[18] However, strain MRG-PMF1 did not show *C*-glucoside-hydrolyzing activity.[19] Flavone and isoflavone *C*-glucosides, such as puerarin and vitexin, were not metabolized by *Blautia* sp. MRG-PMF1. Flavanones with methoxy groups, hesperidin and hesperetin, were metabolized, but naringin was not.

## DISCUSSION

Although dietary polyphenols, including flavonoids, are known to exhibit various biological activities, there is accumulating evidence that it is their metabolites, produced by human intestinal bacteria, which contribute more significantly to human health.[20,21] PMFs are a group of bioactive flavonoids that exhibit a broad spectrum of biological activities, including anticancer and anti-inflammatory properties. To investigate PMF metabolism in the human intestine, PMFs were reacted with human fecal samples herein for the first time. Demethylated metabolites of the PMFs from the fecal samples of rats to which krachaidum extract was orally administered were reported previously.[8] Although PMFs were considered to be stable bioactive compounds because of the chemical stability of the methyl aryl ether functional group, the robust biotransformation of PMFs was observed by a human fecal sample at room temperature under anaerobic conditions. The chemical cleavage of ether bonds usually requires high temperatures in the presence of strong acid or base.[22] As shown in Figure 2, the PMF biotransformation by MRG-PMF1 produced chrysin, apigenin, 3-methylkeampferol, and 3-methylquercetin. It is interesting to note that these compounds are reported to be present in propolis.[23] Therefore, different flavonoids were produced by demethylation of the PMFs, and new biological effects of these metabolites are expected to be observed in humans. In the case of nobiletin, the metabolites 3′-demethylnobiletin, 4′-demethylnobiletin, and 3′,4′-bisdemethylnobiletin, were reported to exhibit stronger anti-inflammatory and anticarcinogenic properties.[24]

From the time-dependent biotransformation of 5,7-DMF and 5,7,4′-TMF, the metabolic pathways of 5,7-DMF → 5-methylchrysin → chrysin and 5,7,4′-TMF → 5,4′-dimethoxy-7-hydroxyflavone → thevetiaflavone → apigenin were elucidated, respectively. Demethylation was faster for the 7-methoxy group and slower for the 5-methoxy group. From biotransformation of the mixture of PMF, *Blautia* sp. MRG-PMF1 was found not to be able to hydrolyze the 3-methoxy group of flavone. There are surprisingly few reports on the biotransformation intermediates identified herein, such as 5-methylchrysin, 5,4′-dimethoxy-7-hydroxyflavone, and thevetiaflavone. Most PMF metabolites and their intermediates were reported from bee products.[23] In addition to the PMFs, various flavonoids were also observed to be biotransformed by *Blautia* sp. MRG-PMF1 (Table 1). Through the tested substrates, it was found that MRG-PMF1 exhibited hydrolysis activity for methyl ether, *O*-glucose, and *O*-rutinose functional groups of flavone, isoflavone, and flavanone. The only exception of this finding was naringin, but it was not clear whether or not naringin metabolites have antibacterial activity against MRG-PMF1.

Although bioinformatic approaches using high-throughput sequencing contribute significantly to the areas of food and clinical microbiology, it is evident from our previous work that the biotransformation of bioactive flavonoids by human intestinal bacteria can produce new bioactive compounds that may not exist in the human diet and that cannot be biosynthesized in the body.[25] For example, the new metabolic intermediates, *R*-DHD,[26] (3*S*,4*R*)-THD,[27] and *R*-*O*-DMA[28] were discovered from the biosynthetic study of *S*-equol.

Besides, the isolation of new intestinal bacteria and characterization of metabolites are of great significance to the discovery of novel enzymes and leading bioactive compounds. Identification of bioactive metabolites produced by specific intestinal bacteria is also important and is a prerequisite to investigating microbiota−host interactions at the molecular level. Furthermore, the structural characterization of various metabolites formed from dietary flavonoids can provide valuable data for the metabolomic study in human microbiome research.[29] The unprecedented PMF demethylation activity of *Blautia* sp. MRG-PMF1 will expand our understanding of

**Table 1. Flavonoid Metabolism by *Blautia* sp. MRG-PMF1**

| substrate | product | activity | time |
|---|---|---|---|
| | Flavone | | |
| apigetrin | apigenin | *O*-glucose hydrolysis | <24 h |
| rutin | quercetin | *O*-rutinose hydrolysis | <3 days |
| vitexin | nc[a] | | |
| | Isoflavone | | |
| daidzin | daidzein | *O*-glucose hydrolysis | <24 h |
| genistin | genistein | *O*-glucose hydrolysis | <24 h |
| glycitin | glycitein | *O*-glucose hydrolysis | <24 h |
| | 6,7,4′-trihydroxyisoflavone | *O*-methyl hydrolysis | |
| glycitein | 6,7,4′-trihydroxyisoflavone | *O*-methyl hydrolysis | <24 h |
| ononin | formononetin | *O*-glucose hydrolysis | <24 h |
| | daidzein | *O*-methyl hydrolysis | |
| formononetin | daidzein | *O*-methyl hydrolysis | >7 days |
| sissotrin | biochanin A | *O*-glucose hydrolysis | <24 h |
| | genistein | *O*-methyl hydrolysis | |
| biochanin A | genistein | *O*-methyl hydrolysis | >7 days |
| puerarin | nc | | |
| | Flavanone | | |
| hesperidin | hesperetin | *O*-rutinose hydrolysis | <24 h |
| | eriodictyol | *O*-methyl hydrolysis | |
| hesperetin | eriodictyol | *O*-methyl hydrolysis | <24 h |
| naringin | nc | | |

[a]nc = no conversion.

flavonoid metabolism in the human intestine and could lead to the development of novel bioactive compounds.

## ■ ASSOCIATED CONTENT

### Supporting Information

Screening of PMF metabolizing colony by TLC analysis and microscopic image of isolated bacterium (Figure S1), growth curve and pH changes of *Blautia* sp. MRG-PMF1 (Figure S2), biotransformation kinetics of 5,7-DMF and 5,7,4′-TMF by *Blautia* sp. MRG-PMF1 (Figure S3), TLC analysis of 5,7-DMF and 5,7,4′-TMF metabolites (Figure S4), and LC/ESI−MS analysis of 5,7-DMF and 5,7,4′-TMF biotransformation intermediates (Figure S5). This material is available free of charge via the Internet at http://pubs.acs.org.

## ■ AUTHOR INFORMATION


### Corresponding Author

*Telephone: +82-31-670-4830. Fax: +82-31-675-1381. E-mail: jaehongh@cau.ac.kr.



### Funding

This work was supported by the National Research Foundation of Korea (NRF) grants funded by the Ministry of Science, Information and Communications Technology (ICT) and Future Planning (MSIP) of the Korean government (2012R1A2A2A01013356) and the Ministry of Education, Science and Technology (MEST) of the Korean government (2012R1A1A3011925).


### Notes

The authors declare no competing financial interest.

## ■ REFERENCES


(1) Walker, A. W.; Duncan, S. H.; Louis, P.; Flint, H. J. Phylogeny, culturing, and metagenomics of the human gut microbiota. *Trends Microbiol.* **2014**, *22*, 267−274.

(2) Yuan, J. P.; Wang, J. H.; Liu, X. Metabolism of dietary soy isoflavones to equol by human intestinal microflora—Implications for health. *Mol. Nutr. Food Res.* **2007**, *51*, 765−781.

(3) Kim, M.; Han, J.; Kim, S. U. Isoflavone daidzein: Chemistry and bacterial metabolism. *J. Appl. Biol. Chem.* **2008**, *51*, 253−261.

(4) Setchell, K. D. R.; Clerici, C. Equol: Pharmacokinetics and biological actions. *J. Nutr.* **2010**, *140*, 1363S−1368S.

(5) Kim, M.; Kim, S. I.; Han, J.; Wang, X. L.; Song, D. G.; Kim, S. U. Stereospecific biotransformation of dihydrodaidzein into (3*S*)-equol by the human intestinal bacterium *Eggerthella* strain Julong 732. *Appl. Environ. Microbiol.* **2009**, *75*, 3062−3068.

(6) Li, S. M.; Lo, C. Y.; Dushenkov, S.; Ho, C. T. Polymethoxyflavones: Chemistry, biological activity, and occurrence in orange peel. In *Dietary Supplements*; Ho, C. T., Simon, J. E., Shahidi, F., Shao, Y., Eds.; American Chemical Society (ACS): Washington, D.C., 2008; ACS Symposium Series, Vol. *987*, Chapter 13, pp 191−210.

(7) Lu, W. C.; Sheen, J. F.; Hwang, L. S.; Wei, G. J. Identification of 5,7,3′,4′-tetramethoxyflavone metabolites in rat urine by the isotope-labeling method and ultrahigh-performance liquid chromatography−electrospray ionization−mass spectrometry. *J. Agric. Food Chem.* **2012**, *60*, 8123−8128.

(8) Mekjaruskul, C.; Jay, M.; Sripanidkulchai, B. Pharmacokinetics, bioavailability, tissue distribution, excretion, and metabolite identification of methoxyflavones in *Kaempferia parviflora* extract in rats. *Drug Metab. Dispos.* **2012**, *40*, 2342−2353.

(9) Wongsrikaew, N.; Kim, H.; Vichitphan, K.; Cho, S. K.; Han, J. Antiproliferative activity and polymethoxyflavone composition analysis of *Kaempferia parviflora* extracts. *J. Korean Soc. Appl. Biol. Chem.* **2012**, *55*, 813−817.

(10) Kim, Y. U.; Han, J. Steroid 5α-reductase inhibition by polymethoxyflavones. *J. Korean Soc. Appl. Biol. Chem.* **2013**, *56*, 469−471.

(11) Wongsrikaew, N.; Woo, H. C.; Vichitphan, K.; Han, J. Supercritical $CO_2$ for efficient extraction of polymethoxyflavones in *Kaempferia parviflora*. *J. Korean Soc. Appl. Biol. Chem.* **2011**, *54*, 1008−1011.

(12) Altschul, S.; Gish, W.; Miller, W.; Myers, E.; Lipman, D. Basic local alignment search tool. *J. Mol. Biol.* **1990**, *215*, 403−410.

(13) Tamura, K.; Stecher, G.; Peterson, D.; Filipski, A.; Kumar, S. MEGA6: Molecular evolutionary genetics analysis version 6.0. *Mol. Biol. Evol.* **2013**, *30*, 2725−2729.
(14) Coll, J. D.; Bowden, B. F. The application of vacuum liquid chromatography to the separation of terpene mixtures. *J. Nat. Prod.* **1986**, *49*, 934−936.
(15) Moiseev, D. V.; Buzuk, G. N.; Shelyuto, V. L. Identification of flavonoids in plants by HPLC. *Pharm. Chem. J.* **2011**, *45*, 47−50.
(16) Pellati, F.; Orlandini, G.; Pinetti, D.; Benvenuti, S. HPLC−DAD and HPLC−ESI−MS/MS methods for metabolite profiling of propolis extracts. *J. Pharm. Biomed. Anal.* **2011**, *55*, 934−948.
(17) Sanz, M.; Cadahia, E.; Esteruelas, E.; Munoz, A. M.; Simon, B. F. D.; Hernandez, T.; Estrella, I. Phenolic compounds in cherry (*Prunus avium*) heartwood with a view to their use in cooperage. *J. Agric. Food Chem.* **2010**, *58*, 4907−4914.
(18) Rüfer, C. E.; Maul, R.; Donauer, E.; Fabian, E. J.; Kulling, S. E. *In vitro* and *in vivo* metabolism of the soy isoflavone glycitein. *Mol. Nutr. Food Res.* **2007**, *51*, 813−823.
(19) Kim, M.; Lee, J.; Han, J. Deglycosylation of isoflavone *C*-glycosides by newly isolated human intestinal bacteria. *J. Sci. Food Agric.* **2014**, DOI: 10.1002/jsfa.6900.
(20) Jacobs, D. M.; Gaudier, E.; van Duynhoven, J.; Vaughan, E. E. Non-digestible food ingredients, colonic microbiota and the impact on gut health and immunity: A role for metabolomics. *Curr. Drug Metab.* **2009**, *10*, 41−54.
(21) Jin, M. J.; Kim, I. S.; Kim, D. H.; Yoo, H. H. Effects of intestinal microbiota on the bioavailability of geniposide in rats. *J. Agric. Food Chem.* **2014**, *62*, 9632−9636.
(22) Ryu, I.; Matsubara, H.; Yasuda, S.; Nakamura, H.; Curran, D. P. Phase-vanishing reactions that use fluorous media as a phase screen. facile, controlled bromination of alkenes by dibromine and dealkylation of aromatic ethers by boron tribromide. *J. Am. Chem. Soc.* **2002**, *124*, 12946−12947.
(23) Gómez-Caravaca, A. M.; Gómez-Romero, M.; Arráez-Román, D.; Segura-Carretero, A.; Fernández-Gutiérrez, A. Advances in the analysis of phenolic compounds in products derived from bees. *J. Pharm. Biomed. Anal.* **2006**, *41*, 1220−1234.
(24) Li, S.; Wang, Z.; Sang, S.; Huang, M. T.; Ho, C. T. Identification of nobiletin metabolites in mouse urine. *Mol. Nutr. Food Res.* **2006**, *50*, 291−299.
(25) Possemiers, S.; Bolca, S.; Verstraete, W.; Heyerick, A. The intestinal microbiome: A separate organ inside the body with the metabolic potential to influence the bioactivity of botanicals. *Fitoterapia* **2011**, *82*, 53−66.
(26) Park, H. Y.; Kim, M.; Han, J. Stereospecific microbial production of isoflavanones from isoflavones and isoflavone glucosides. *Appl. Microbiol. Biotechnol.* **2011**, *91*, 1173−1181.
(27) Kim, M.; Marsh, E. N. G.; Kim, S. U.; Han, J. Conversion of (3*S*,4*R*)-tetrahydrodaidzein to (3*S*)-equol by THD reductase: Proposed mechanism involving a radical intermediate. *Biochemistry* **2010**, *49*, 5582−5587.
(28) Kim, M.; Han, J. Chiroptical study and absolute configuration of (−)-*O*-DMA produced from daidzein metabolism. *Chirality* **2014**, *26*, 434−437.
(29) Nicholson, J. K.; Holmes, E.; Kinross, J.; Burcelin, R.; Gibson, G.; Jia, W.; Pettersson, S. Host−gut microbiota metabolic interactions. *Science* **2012**, *336*, 1262−1267.

Table 1. Primer Sequences Used in Full-Length Cloning and Heterologous Expression of *C. nobilis* Fads2 and Elovl4[a]

| aim | primer | primer sequence |
|---|---|---|
| RACE PCR | DEB31 | CACTGCACAGGCTCAAGCTGGATGG |
| | DEB32 | GGCCATATAAAGGGTGCCTCTTCCC |
| | DEB51 | CATAATCATGTTGAGACCATCCAGC |
| | DEB52 | AGTTCCACCAGTGGGAAGAGGCACC |
| | E431 | ATATCAGCATATAGAGCGGGGTACAGT |
| | E432 | TGACCCTAATGAAATGAATATTGCCTC |
| | E451 | GATAATTGTGACACCGTACACTAAG |
| | E452 | ACAGACTTTGAAATCCATACACCATC |
| ORF cloning | D8EF1 | TGGCCTTTTCAGGCTGAAGTCA |
| | D8ER1 | TGGCCTTTTCAGGCTGAAGTCA |
| | D8EF2 | CCCAAGCTTAGAATGGGGAAAGGTGGA |
| | D8ER2 | TGCTCTAGACTATCCTTCATATCGGGC |
| | E4EF1 | CTGATCGGTAGATTGGATTTAGGGA |
| | E4EF2 | CCCAAGCTTTCAAGATGGAAGTCATACAAGACAA |
| | E4ER1 | TGCTCTAGAGTATACTGACCAACAACCTTAGTGT |

[a]Restriction sites for *Hin*dIII and *Xba*I are underlined in primer D8XF2, D8XR2, E4XF2, and E4XR1 sequences.

termed Elovl4 were cloned and functionally characterized. The preference for n−6 PUFA substrates of these enzymes implied an advanced adaptation of noble scallop to the marine environment. The results increased our knowledge of the relationship between LC-PUFA biosynthesis pathways and the habitat and feeding habit of mollusk species.

## MATERIALS AND METHODS

**Cloning of a Putative Desaturase cDNA.** The noble scallops maintained at Nan'ao Island of Guangdong Province, China, were sacrificed. Female gonad was sampled to extract total RNA using TRIzol reagent (Invitrogen, Grand Island, NY). The first fragment of scallop Fads2 and Elovl4 was obtained by BLASTX searching against noble scallop transcriptome data set (Accession: SRX253988). 3′ and 5′ RACE PCRs were carried out using the SMART RACE cDNA amplification kit (Clontech, USA) according to the instructions. The preparation methods of cDNA and amplification conditions of RACE PCRs were both conducted as suggested by the manufacturers. Positive fragments were obtained by two-round PCR based on the known partial sequences using RACE PCR primers, then cloned into pMD18-T vector (TaKaRa, Guangzhou, China), and sequenced (Sangon Biotech, Shanghai, China). Full lengths of the two genes were obtained by aligning the 3′-end fragment with 5′-end fragment.

**Sequence and Phylogenetic Analyses.** The multiple sequence alignment was performed using ClustalX 2.1, and phylogenetic trees were made using the neighbor-joining method in the MEGA 4.1 package on the basis of putative protein sequence of desaturase or elongase from the scallop and other organisms. Confidence in the resulting phylogenetic tree branch topology was measured by bootstrapping through 1,000 iterations.

**Heterologous Expression of Desaturase ORFs in Yeast and Fatty Acid Analysis by GC.** The open reading frames (ORFs) encoding Fads2 or Elovl4 were amplified from scallop gonad cDNA using the high-fidelity *Pfu* DNA polymerase (Tiangen, Beijng, China). D8EF1 and D8ER1 were used to perform the first round PCR, and D8EF2 and D8ER2 were used to perform the second PCR to get Fads2 ORF. Similarly, a two-round PCR approach was used to amplify Elovl4 ORF, with the first round performed with primers E4EF1 and E4ER1, and second with primers E4EF2 and E4ER1 (Table 1). All PCR amplifications involved an initial denaturation step at 95 °C for 2 min, followed by 30 cycles of denaturation at 95 °C for 30 s, annealing at 57 °C for 30 s, and extension at 72 °C for 90 s. After PCR, the DNA fragments were purified, digested with restrictive enzyme, and ligated into similarly digested yeast expression vector pYES2.0 (Invitrogen). The recombinant plasmids with right sequence were transformed into yeast accordingly to the method of Liu et al.[25] Recombinant yeast was cultivated in minimal medium minus uracil (SCMM−uracil) broth using galactose for induction of gene expression as described previously.[27] Cultures with Fads2 were supplemented with one of the following PUFA substrates: 18:2n−6, 18:3n−3, 20:2n−6, 20:3n−3, 20:3n−6, 20:4n−3, 22:5n−3, and 22:4n−6. Cultures with Elovl4 were supplemented with 20:4n−6 or 20:5n−3. Total lipids of yeast cells were extracted by homogenization in chloroform/methanol (2:1, vol/vol), containing 0.01% butylated hydroxytoluene (Sigma-Aldrich) as the antioxidant. Fatty acid methyl esters (FAMEs) were prepared, extracted, and purified by TLC on a 20 cm × 20 cm × 0.25 mm silica gel 60 plate (Merck, Germany), accordingly to the method of Liu et al.[25] FAMEs were analyzed using gas chromatography (GC-17A, Shimadzu, Kyoto, Japan) equipped with a hydrogen flame ionization detector and a capillary column (30 m × 0.25 mm × 0.25 μm, VF-23ms, Varian, USA). When analyzing FAMEs from cultures with Fads2, the column was temperature-programmed from 50 to 170 °C at 40 °C/min and 170 to 230 °C at 3 °C/min. When analyzing FAMEs from cultures with Elovl4, the column was temperature-programmed from 50 to 170 °C at 40 °C/min and 170 to 230 °C at 10 °C/min. Hydrogen was used as carrier gas at flow rate of 1.1 mL/min. Both detector and injection port were set at 250 °C. Individual methyl ester was identified by comparison to authentic standards (Sigma-Aldrich). The proportion of substrate fatty acid converted to desaturation product or elongation product was calculated from the gas chromatograms as 100 × [product area/(product area + substrate area)].

**Fatty Acids Composition of Tissues in Scallop.** Scallops at 14 months old were cultured in a 500 L plastic bucket and fed daily using about 15−20 cells/mL of *Platymonas subcordiformis*. The temperature was 19.0 ± 0.5 °C, and the salinity was 31 ± 0.5 ppt. Four weeks later, viscera, adductor, mantle, and gonad from 10 scallops were sampled after 12 h starvation. The scallop tissues and *P. subcordiformis* cells were dried in a vacuum freeze-drying machine and ground to fine powder in mortars. Lipid extraction and preparation of FAMEs were as described above. The column was temperature-programmed from 50 to 170 °C at 40 °C/min and 170 to 230 °C at 3 °C/min for analysis of FAMEs. Individual fatty acids were identified by comparison against commercial standards (Sigma-Aldrich), and the results are presented as area percent FAME composition (%).

## RESULTS

**Identification and Characterization of Scallop Fad and Elovl4.** BLASTX analysis of scallop transcriptome revealed a transcript whose putative amino acid sequence was different from previously cloned Δ5 Fad, but highly homologous to Δ6 Fads2 of vertebrate origin. Another transcript was also identified whose putative amino acid sequence was highly homologous to that of vertebrate Elovl4.

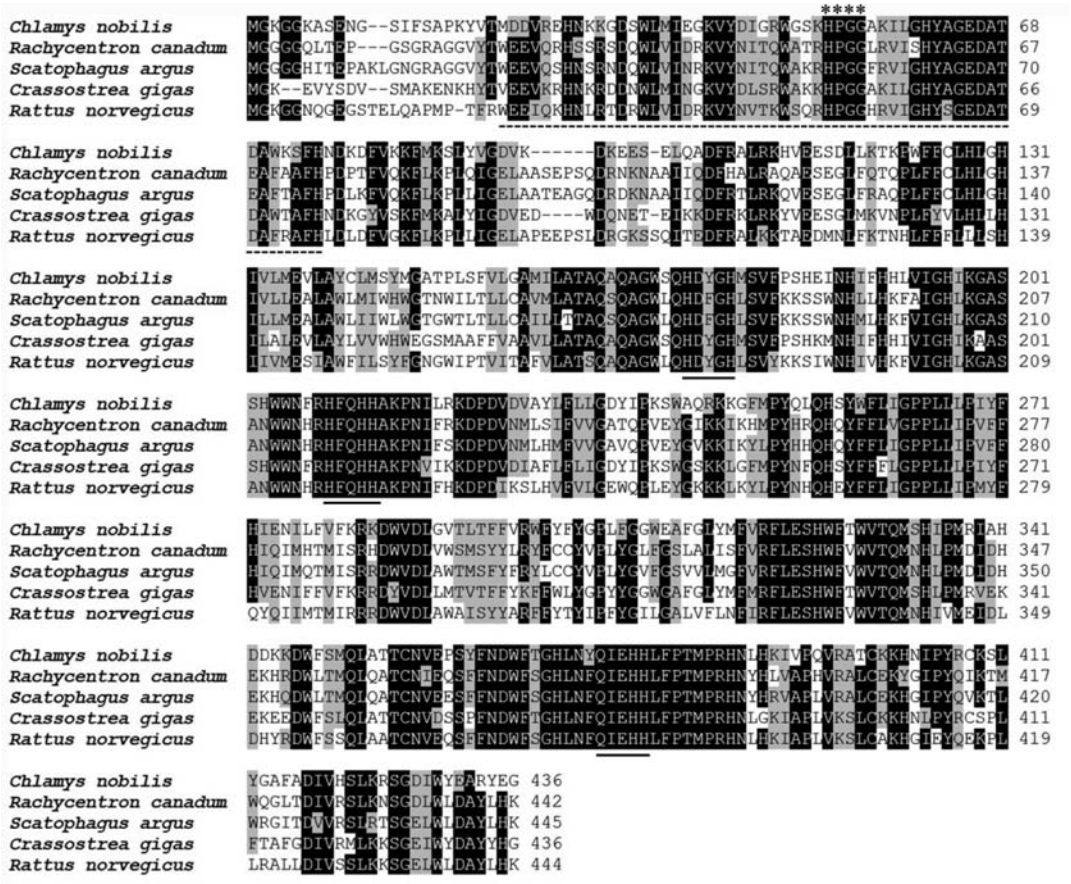


**Figure 1.** ClustalW2 alignment of the deduced amino acid sequence of noble scallop Fads2 with *Rachycentron canadum* (ACJ65149), *Scatophagus argus* (AHA62794), *Crassostrea gigas* (EKC33620), and *Rattus norvegicus* (NP_112634) Fad. Identical residues are shaded black and similar residues are shaded gray based on the BLOSUM62 matrix, and the cutoff for shading was 75%. The dotted line indicates the cytochrome b5 domain, with asterisks above to indicate the heme-binding motif. The solid underlines indicates the three histidine boxes (HXXXH, HXXHH, and QXXHH).

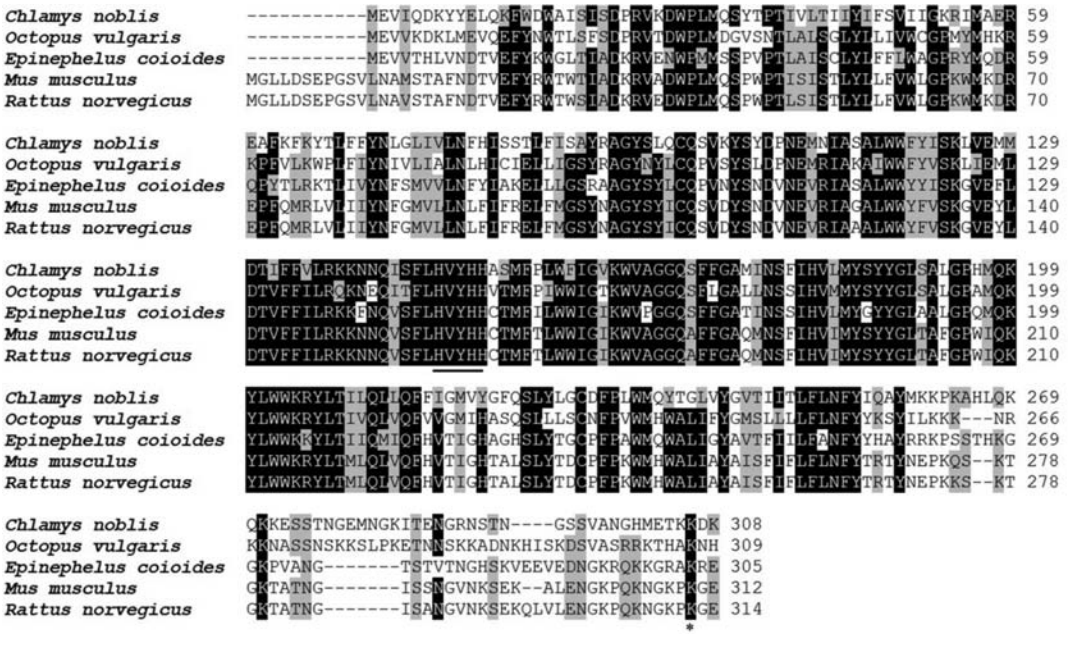


**Figure 2.** ClustalW2 alignment of the deduced amino acid sequences of noble scallop Elovl4 with *Octopus vulgaris* (AIA58679), *Epinephelus coioides* (AHI17192), *Mus musculus* (NP_683743), and *Rattus norvegicus* (NP_001178725) Elovl4. Identical residues are shaded black and similar residues are shaded gray based on the BLOSUM62 matrix, and the cutoff for shading was 75%. The solid underline is the conserved histidine box motif. An asterisk indicates the lysine or arginine residuals proposed to function as ER retrieval signals.


dx.doi.org/10.1021/jf504648f | *J. Agric. Food Chem.* 2014, 62, 12384−12391

Full lengths of the two genes were obtained by using RACE PCR based on partial fragments.

Thus, the putative Fad, designated as CnFads2, containing an ORF of 436 amino acid, shared 52% identity with functionally characterized Δ6 Fad from *Rachycentron canadum* (ACJ65149), *Scatophagus argus* (AHA62794), and *Rattus norvegicus* (NP_112634). It was also 68% similar to a putative protein of the Pacific oyster *C. gigas* (EKC33620) which was not functionally characterized. The newly cloned scallop Fads2 possessed three diagnostic histidine boxes, a cytochrome b5-like domain, and a heme-binding motif that are characteristic of PUFA desaturase (Figure 1). Phylogenetic analysis showed that CnFads2 was not grouped with mollusk Fad, but instead clustered with vertebrate Fad (Figure 3).

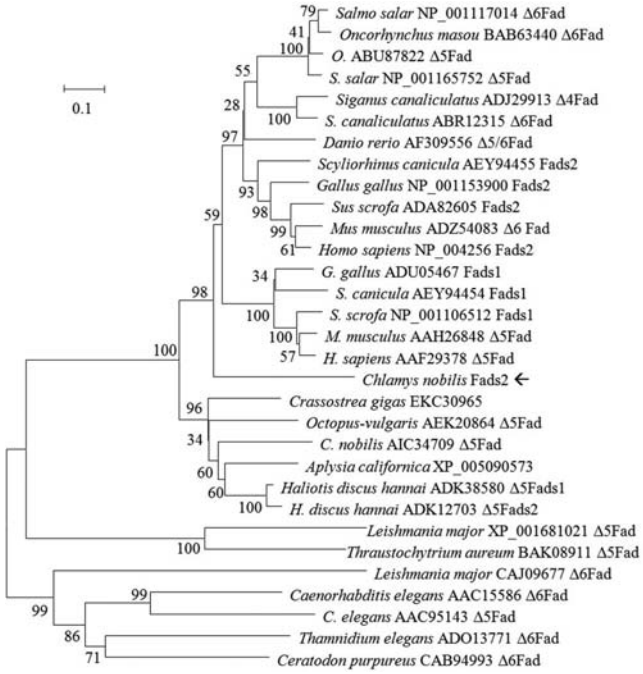


**Figure 3.** Phylogenetic tree comparing the deduced aa sequences of *C. nobilis* Fads2 with Fad proteins from mollusk and other organisms. The alignment was generated by the Clustal W program, and the tree was constructed using the neighbor joining method with MEGA4 software. The horizontal branch length is proportional to aa substitution rate per site. The numbers represent the frequencies with which the tree topology presented was replicated after 1,000 iterations.

The putative scallop Elovl4 contained an ORF of 308 amino acid which was 56% similar to Elovl4 of mollusk octopus (AIA58679), while sharing 49−51% identify with functionally characterized Elovl4 from teleosts such as *Epinephelus coioides* (AHI17192), *R. canadum* (ADG59898), *Siganus canaliculatus* (ADZ73580), and *S. argus* (AHX22600), and mammals such as *Mus musculus* (NP_683743) and *R. norvegicus* (NP_001178725). Scallop Elovl4 was characterized for containing a histidine box of HXXHH motif (Figure 2), which was conserved in all elongases.[28] Phylogenetic analysis comparing a variety of elongase from Elovl1 to Elovl7 showed that scallop Elovl4 could be clustered first to vertebrate Elovl4, and then grouped with Elovl2/5 (Figure 4).

**Functional Characterization.** The putative scallop Fads2 and Elovl4 were functionally characterized by determining the FA profiles of yeast *Saccharomyces cerevisiae* transformed with

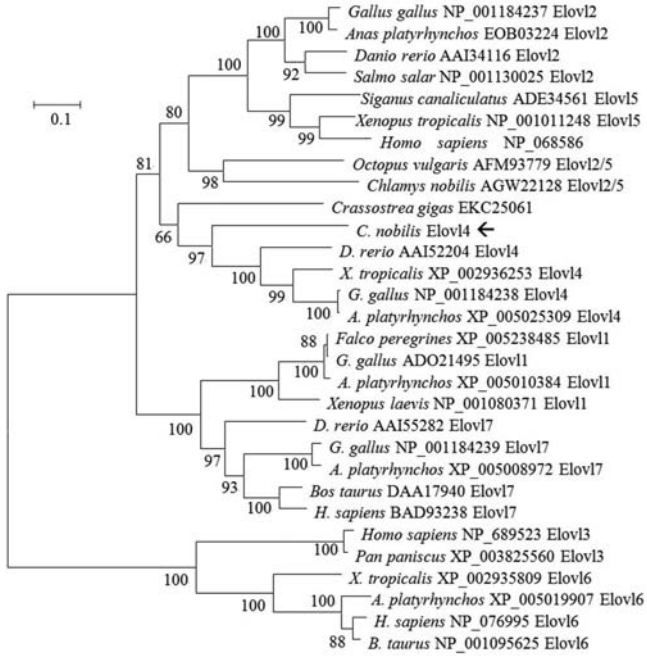


**Figure 4.** Phylogenetic tree comparing the deduced aa sequences of *C. nobilis* Elovl4 with Elovl proteins from mollusk and other organisms. The alignment was generated by the Clustal W program, and the tree was constructed using the neighbor joining method with MEGA4 software. The horizontal branch length is proportional to aa substitution rate per site. The numbers represent the frequencies with which the tree topology presented was replicated after 1,000 iterations.

pYES2 vector alone or containing Fads2 and Elovl4 cDNA ORF. The FA composition in yeast with empty plasmid was characterized of essentially only C16:0, C16:1n−7, C18:0, and C18:1n−9 (peaks 1−4).[27] Yeast transformed with pYES2-Fads2 recombinant plasmid was grown in the presence of Δ6-(18:3n−3 and 18:2n−6), Δ5- (20:4n−3), Δ4- (22:5n−3 and 22:4n−6), and Δ8-desaturation (20:3n−3 and 20:2n−6) substrates. Thus, only exogenously added 20:2n−6 (peak 7; Figure 5D) and 20:3n−3 (peak 9; Figure 5D) were converted into 20:3n−6 (peak 8; Figure 5D) and 20:4n−3 (peak 10; Figure 5E) respectively, indicating that the noble scallop Fads2 possessed Δ8-desaturation activity. 29% of 20:2n−6 and 13% of 20:3n−3 were desaturated to 20:3n−6 and 20:4n−3 respectively (Table 2), indicating that Fads2 desaturated n−6 PUFA substrates more efficiently than n−3 substrates. No additional desaturated products were detected when Δ6 (18:3n−3 and 18:2n−6), Δ5 (20:3n−6), or Δ4 (22:5n−3 and 22:4n−6) were used as the substrates, indicating that the new cloned Fads2 possessed no Δ6-, Δ5-, or Δ4-desaturation activity.

In order to assess the role of scallop Elovl4 in PUFA biosynthesis, yeast transformed with Elovl4 ORF was incubated with ALA, LA, EPA, and AA substrates. Thus, 41% of exogenously added AA (peak 13; Figure 5I) was elongated to 22:4n−6 (peak 11; Figure 5I) and 24:4n−6 (peak 14; Figure 5I); while 23% of exogenously added EPA (peak 15; Figure 5J) was elongated to 22:5n−3 (peak 12; Figure 5J) and 24:5n−3 (peak 16; Figure 5J). In addition, 9% of 22:4n−6 and 5% of 22:5n−3 were elongated to 24:4n−6 and 24:5n−3 respectively. The elongase elongated n−6 PUFA substrates more actively than their homologous n−3 substrates. No FA with C26 or


dx.doi.org/10.1021/jf504648f | J. Agric. Food Chem. 2014, 62, 12384−12391

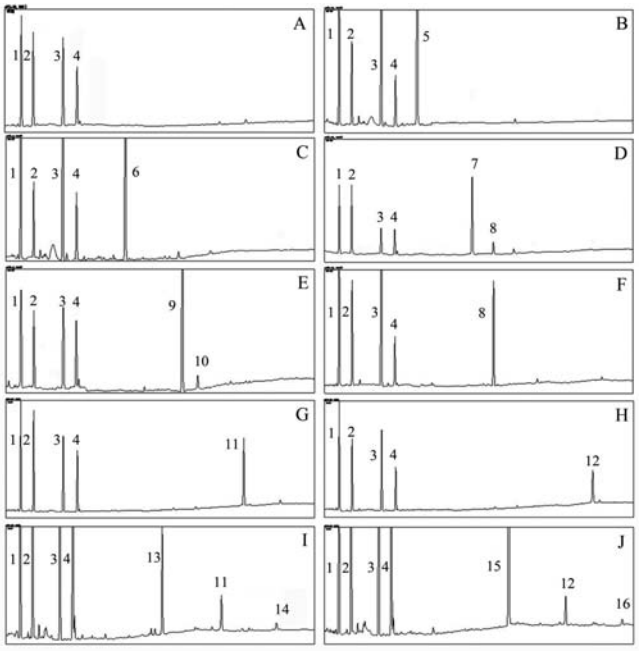


**Figure 5.** Functional characterization of the *C. nobilis* putative Fads2 and Elovl4 in transgenic yeast (*S. cerevisiae*). FAMEs were extracted from yeast transformed with pYES2 vector alone (A) or pYES2-Fads2 (B–H) and pYES2-Elovl4 (I, J), and grown in the presence of FA substrates (peak number) 18:2n−6 (5), 18:3n−3 (6), 20:2n−6 (7), 20:3n−6 (8), 20:3n−3 (9), 22:4n−6 (11), 22:5n−3 (12), 20:4n−6 (13), and 20:5n−3 (15). Peaks 1–4 represent main endogenous FAs of *S. cerevisiae*, namely, 16:0, 16:1, 18:0, and 18:1n−9, respectively. Based on retention times, PUFA productions were identified as 20:3n−6 (D, 8), 20:4n−3 (E, peak 10), 22:4n−6 (I, peak 11), 22:5n−3 (J, peak 12), 24:4n−6 (I, peak 14) and 24:5n−3 (J, peak 16). Vertical axis: FID response. Horizontal axis: retention time.

**Table 2. Functional Characterization of *C. nobilis* Fads2 and Elovl4 in Yeast *S. cerevisiae*[a]**

| enzyme | FA substrate | product | conversion rate (%) | activity |
|---|---|---|---|---|
| Fads2 | 18:2n−6 | 18:3n−6 | 0 | Δ6 |
| | 18:3n−3 | 18:4n−3 | 0 | Δ6 |
| | 20:2n−6 | 20:3n−6 | 29 ± 4 A | Δ8 |
| | 20:3n−3 | 20:4n−3 | 13 ± 1 B | Δ8 |
| | 20:3n−6 | 20:4n−6 | 0 | Δ5 |
| | 22:4n−6 | 22:5n−6 | 0 | Δ4 |
| | 22:5n−3 | 22:6n−3 | 0 | Δ4 |
| Elovl4 | 18:2n−6 | 20:3n−6 | 0 | 18 → 20 |
| | 18:3n−3 | 20:3n−3 | 0 | 18 → 20 |
| | 20:4n−6 | 22:4n−6 | 32 | 20 → 22 |
| | | 24:4n−6 | 9 | 22 → 24 |
| | | 26:4n−6 | 0 | 24 → 26 |
| | | total | 41 ± 10 A | |
| | 20:5n−3 | 22:5n−3 | 18 | 20 → 22 |
| | | 24:5n−3 | 5 | 22 → 24 |
| | | 26:5n−3 | 0 | 24 → 26 |
| | | total | 23 ± 3 B | |

[a]Conversion rates represent the proportion of substrate fatty acid converted to desaturated fatty acid product, calculated from gas chromatograms as 100 × [product area/(product area + substrate area)]. Uppercase letter indicates comparison of conversion rate exhibited by the same enzyme, and different letter means significant difference by one-way ANOVA test.

more carbon was detected. No elongation production was detected in the presence of ALA and LA.

**Fatty Acid Profile of Scallop Tissues.** Some fatty acids are important intermediates which could give some clues on how PUFA was biosynthesized. For example, 18:4n−3 and 20:4n−3 were usually the intermediates of major route pathway, while 20:2n−6 and 20:3n−3 might indicate a "Δ8 pathway".

Fatty acid profile in microalgae *P. subcordiformis* and scallop tissues including the viscera, adductor, mantle, and gonad were determined (Table 3). Microalga *P. subcordiformis* was

**Table 3. Fatty Acids Composition (% of Area) of Microalgae and Scallop**

| | | noble scallop | | | |
|---|---|---|---|---|---|
| fatty acid | *Platymonas helgolandica* | viscera | adductor | mantle | gonad |
| 14:00 | 1.67 | 2.90 | 1.30 | 2.06 | 5.68 |
| 15:00 | –[a] | 0.54 | 0.38 | 0.64 | 0.70 |
| 16:00 | 35.15 | 19.86 | 23.59 | 21.78 | 35.98 |
| 17:00 | – | 0.82 | 1.19 | 1.34 | 2.50 |
| 18:00 | 2.93 | 9.51 | 16.52 | 21.74 | 15.16 |
| 20:00 | 0.69 | 0.11 | 0.15 | 0.12 | 0.18 |
| 16:1n−7 | 6.16 | 7.63 | 2.20 | 2.44 | 10.81 |
| 18:1n−7 | 6.75 | 5.35 | 1.66 | 1.97 | 1.37 |
| 18:1n−9 | 12.25 | 3.19 | 3.58 | 3.87 | 5.21 |
| 18:2n−6 | 6.02 | 1.05 | 0.96 | 0.93 | 1.02 |
| 18:3n−3 | 18.51 | 1.62 | 0.42 | 0.22 | 0.30 |
| 18:4n−3 | 4.37 | 4.24 | <0.10 | <0.10 | <0.10 |
| 20:1n−9 | 1.24 | 3.31 | 2.54 | 4.62 | 2.90 |
| 20:2n−6 | – | <0.10 | 0.30 | 0.21 | 0.44 |
| 20:3n−6 | 0.62 | 0.21 | 0.28 | 0.19 | 0.21 |
| 20:3n−3 | – | – | 0.15 | 0.21 | 0.10 |
| 20:4n−3 | <0.1 | 0.76 | – | – | – |
| 20:4n−6 | 0.41 | 1.79 | 4.45 | 6.06 | 2.03 |
| 20:5n−3 | 3.22 | 22.29 | 14.39 | 7.73 | 7.62 |
| 22:4n−6 | – | 0.15 | 0.82 | 1.13 | 0.48 |
| 22:5n−6 | – | 0.31 | <0.10 | <0.10 | <0.10 |
| 22:5n−3 | – | 1.82 | 2.40 | 1.36 | 1.38 |
| 22:6n−3 | – | 10.52 | 22.71 | 21.37 | 5.92 |
| unidentified1[b] | – | 0.53 | – | – | – |
| unidentified2[c] | – | 1.48 | – | – | – |

[a]Not detected. [b]Unidentified1 showed 3 double bands and 16 carbons when being tested in GC–MS. [c]Unidentified2 showed 4 double bands and 16 carbons when being tested in GC–MS.

characterized of relatively high percent of intermediate fatty acid 18:4n−3 with predominant fatty acid of 16:0, 18:1n−9, and 18:3n−3. EPA accounts for 3.22% while no DHA was detected. Scallop viscera was characterized of high percent of 20:5n−3, and the interesting point was that DHA was occupied 10.52%, which was absent in diet microalgae. In addition, 20:4n−3 and 22:5n−3 were also detected, implying biosynthesis activity of DHA through major route pathway in viscera.

The adductor and mantle were characterized as having a high degree of unsaturated FAs encompassing high percentages of n−3 PUFA (22:6n−3 and 20:5n−3), while the gonad displayed high percent of saturated FAs. In these three tissues, 16:0 was the most abundant among the six saturated FAs, followed by 18:0 and 14:0. Further, four MUFAs including 16:1n−7, 18:1n−7, 18:1n−9, and 20:1n−9 were detected. As for PUFAs, EPA and DHA followed by AA were among the most

represented. 20:2n−6 and 20:3n−6, which were absent or quite lacking in diet microalgae and viscera, suggested a possible "Δ8 pathway" in noble scallop.

## DISCUSSION

The ability of PUFA biosynthesis in mollusks has also been investigated in some marine species by using $^{14}$C-labeled radioactive FAs,[16,29−32] resulting in the functional characterization of several genes/enzymes involved in the PUFA biosynthesis pathway. The Δ5 desaturase reported in common octopus represents the first molecular proof of the existence of enzyme that is involved in PUFA biosynthesis in mollusk species.[21] Subsequently, an elongase from common octopus[22] and two Δ5 Fad in abalone *Haliotis discus hannai*[23] have been successively characterized. However, whether mollusk could de novo synthesize important LC-PUFAs such as AA, EPA, and DHA is still ambiguous due to the lack of desaturase with Δ6 or Δ8 activity. In noble scallop *C. nobilis*, an elongase has been found to elongate 18:2n−6 and 18:3n−3 to 20:2n−6 and 20:3n−3 respectively, providing Δ8 FA substrates.[26] Further, a desaturase with Δ5 activity has been recently reported to desaturate 20:3n−6 and 20:4n−3 to AA and EPA.[25] In this study, a second Fad (Fads2) was cloned and functionally characterized to display Δ8 activity, providing the first compelling evidence that marine mollusks could at least de novo biosynthesize EPA and AA via the alternative "Δ8 pathway" of elongation−Δ8-desaturation−Δ5-desaturation. Consistent with the PUFA biosynthesis pathway observed in vitro, the FA profiles of scallop tissues indicated the existence of the alternative pathway accounting for the production of intermediates FAs 20:2n−6 and 20:3n−3 (Table 3).

The alternative pathway using Δ8-desaturase has been mainly reported in unicellular organisms,[33−35] and some mammalian Δ6-desaturases also show a Δ8 activity.[11] Using yeast expression system, Óscar et al. have demonstrated that Δ8 desaturase activity is a common feature of vertebrate Δ6 Fad from a range of freshwater, diadromous, and marine teleost fish, and marine species display far higher Δ8 activity than mammal.[36] Different from vertebrate Δ6 Fad with bifunctional activity, scallop Fads2 reported in this study displayed only a Δ8 activity. Based on our results, we speculated that the alternative "Δ8-pathway" was actually the major route of PUFA biosynthesis in some marine bivalves.

Oyster *C. gigas* has been reported to be able to elongate and desaturate n−3 FAs to produce EPA and DHA,[16] whereas clam *Mesodes mamactroides* displays no ability to produce 20:5n−3,[30] indicating that the ability to de novo biosynthesize PUFAs varies among bivalves. Different from oyster or clam, noble scallop could biosynthesize EPA but had quite limited ability to synthesize DHA from EPA due to the lack of desaturase with Δ4 or Δ6 activity. It seems impossible for noble scallop to synthesize DHA through the alternative "Δ8 pathway" by elongating EPA to 26:5n−3, then desaturating to 26:6n−3 with Δ8 Fad, followed by two steps of $\beta$-oxidation, because the newly cloned Elovl4 had quite limited efficiency to elongate 20:5n−3 to 24:5n−3, and no production of 26:5n−3 was detected. Additionally, two elongases and two desaturases, which had been isolated from this species, might represent the complete set of enzymes necessary for the synthesis of LC-PUFA from precursors, because no more PUFA elongase or desaturase could be found in the scallop transcriptome database. Therefore, noble scallop possibly had quite limited ability to de novo synthesize DHA, and heavily relied on dietary supplied DHA to optimize health.

PUFA biosynthesis genes/enzymes have been functionally characterized in many species, most of which show more activity toward n−3 PUFA substrates in vertebrates.[4−9] Contrarily, study on conversion rate of four scallop PUFA biosynthesis genes/enzymes reveals that scallop Elovl2/5,[26] Elovl4, and Fads2 tended to be more active toward n−6 substrates than n−3 substrates (Figure 5D,E,I,J); only Δ5 Fad1 shows similar activity toward n−3 and n−6 substrates.[25] Similar results have also been reported in the common octopus, whose elongase has more activity toward n−6 FA substrates,[22] while Δ5 Fad shows equal activity toward n−3 and n−6 FA substrates.[21] The marine ecosystem is characterized by high levels of n−3 LC-PUFA, particularly EPA and DHA,[37] produced by marine microalgae, which then are passed on to high trophic mollusks through the food chain. Compared to abundant n−3 PUFAs, n−6 PUFAs are relatively insufficient in the marine ecosystem. Higher conversion of n−6 FA substrates than n−3 FA substrates displayed by noble scallop PUFA biosynthesis genes/enzymes indicates a greater efficacy to de novo biosynthesize n−6 PUFAs, which could compensate shortage of n−6 PUFAs in the natural diet. Meanwhile, the low conversion rate of 20:3n−3 to 20:4n−3 exhibited by Fads2 and 20:4n−3 to 20:5n−3 by Fads1 indicated that noble scallop had low efficiency to de novo biosynthesize EPA. Furthermore, noble scallop had limited capability to produce DHA due to lack of enzymes with Δ6 or Δ4 activity, implying that noble scallop would heavily rely on dietary DHA to optimize its health. These results indicate that noble scallop is highly adapted to the marine environment.

In summary, our result provided compelling evidence that noble scallop had the capability to endogenously produce EPA and AA from PUFA precursors, but limited ability to synthesis DHA from EPA. Preference of PUFA biosynthesis enzymes indicated that noble scallop relied on diet supplied n−3 PUFA and showed an advanced adaptation to the marine environment.

## AUTHOR INFORMATION

### Corresponding Author

*Tel: 0086-754-865003285. Fax: 0086-754-86500614. E-mail: hpzheng@stu.edu.cn.

### Funding

Funding for this research was provided by National Natural Science Foundation of China (31372528), Ministry of Education of P. R. China (20114402110001), China Modern Agro-industry Technology Research System (CARS-48), National Basic Research Program of China (973 Program, 2010CB126402), Knowledge Innovation Program of the Chinese Academy of Sciences (SIDSSE-QN-201407), Department of Education (2050205-95), Department of Science & Technology (2013B020503061), and Oceanic and Fisheries Administrator (B201300B06) of Guangdong Province, China.

### Notes

The authors declare no competing financial interest.

## ACKNOWLEDGMENTS

We thank Prof. Chiju Wei (Multidisciplinary Research Center, Shantou University) for reviewing our manuscript.

## REFERENCES


(1) Graham, I.; Cirpus, P.; Rein, D.; Napier, J. The use of very long chain polyunsaturated fatty acids to ameliorate metabolic syndrome: transgenic plants as an alternative sustainable source to fish oils. *Nutr. Bull.* **2004**, *29*, 228−233.

(2) Nugent, A. P. The metabolic syndrome. *Nutr. Bull.* **2004**, *29*, 36−43.

(3) Richardson, A. J. Omega-3 fatty acids in ADHD and related neurodevelopmental disorders. *Int. Rev. Psychiatry* **2006**, *18*, 155−172.

(4) Zheng, X.; Seiliez, I.; Hastings, N.; Tocher, D. R.; Panserat, S.; Dickson, C.; Bergot, P.; Teale, A. Characterization and comparison of fatty acyl Δ6 desaturase cDNAs from freshwater and marine teleost fish species. *Comp. Biochem. Physiol., Part B: Biochem. Mol. Biol.* **2004**, *139*, 269−279.

(5) Zheng, X.; Ding, Z.; Xu, Y.; Monroig, O.; Morais, S.; Tocher, D. R. Physiological roles of fatty acyl desaturases and elongases in marine fish: Characterisation of cDNAs of fatty acyl Δ6 desaturase and *elovl5* elongase of cobia (*Rachycentron canadum*). *Aquaculture* **2009**, *290*, 122−131.

(6) Tocher, D. R.; Zheng, X.; Schlechtriem, C.; Hastings, N.; Dick, J. R.; Teale, A. J. Highly unsaturated fatty acid synthesis in marine fish: Cloning, functional characterization, and nutritional regulation of fatty acyl Δ6 desaturase of Atlantic cod (*Gadus morhua* L.). *Lipids* **2006**, *41*, 1003−1016.

(7) Morais, S.; Monroig, O.; Zheng, X.; Leaver, M. J.; Tocher, D. R. Highly unsaturated fatty acid synthesis in Atlantic salmon: characterization of ELOVL5-and ELOVL2-like elongases. *Mar. Biotechnol.* **2009**, *11*, 627−639.

(8) Carmona-Antoñanzas, G.; Monroig, Ó.; Dick, J. R.; Davie, A.; Tocher, D. R. Biosynthesis of very long-chain fatty acids (C> 24) in Atlantic salmon: Cloning, functional characterisation, and tissue distribution of an Elovl4 elongase. *Comp. Biochem. Physiol., Part B: Biochem. Mol. Biol.* **2011**, *159*, 122−129.

(9) Hastings, N.; Agaba, M. K.; Tocher, D. R.; Zheng, X.; Dickson, C. A.; Dick, J. R.; Teale, A. J. Molecular cloning and functional characterization of fatty acyl desaturase and elongase cDNAs involved in the production of eicosapentaenoic and docosahexaenoic acids from α-linolenic acid in Atlantic salmon (*Salmo salar*). *Mar. Biotechnol.* **2004**, *6*, 463−474.

(10) Agaba, M. K.; Tocher, D. R.; Zheng, X.; Dickson, C. A.; Dick, J. R.; Teale, A. J. Cloning and functional characterisation of polyunsaturated fatty acid elongases of marine and freshwater teleost fish. *Comp. Biochem. Physiol., Part B: Biochem. Mol. Biol.* **2005**, *142*, 342−352.

(11) Park, W. J.; Kothapalli, K. S.; Lawrence, P.; Tyburczy, C.; Brenna, J. T. An alternate pathway to long-chain polyunsaturates: the FADS2 gene product Δ8-desaturates 20:2n-6 and 20:3n-3. *J. Lipid Res.* **2009**, *50*, 1195−1202.

(12) Williams, C. M.; Burdge, G. Long-chain n−3 PUFA: plant v. marine sources. *Proc. Nutr. Soc.* **2006**, *65*, 42−50.

(13) Bimbo, A. P. Current and future sources of raw materials for the long-chain omega-3 fatty acid market. *Lipid Technol.* **2007**, *19*, 176−179.

(14) Naylor, R. L.; Goldburg, R. J.; Primavera, J. H.; Kautsky, N.; Beveridge, M. C.; Clay, J.; Folke, C.; Lubchenco, J.; Mooney, H.; Troell, M. Effect of aquaculture on world fish supplies. *Nature* **2000**, *405*, 1017−1024.

(15) Deutsch, L.; Gräslund, S.; Folke, C.; Troell, M.; Huitric, M.; Kautsky, N.; Lebel, L. Feeding aquaculture growth through globalization: Exploitation of marine ecosystems for fishmeal. *Global Environ. Change* **2007**, *17*, 238−249.

(16) Waldock, M.; Holland, D. Fatty acid metabolism in young oysters, *Crassostrea gigas*: polyunsaturated fatty acids. *Lipids* **1984**, *19*, 332−336.

(17) Zhukova, N. V. The pathway of the biosynthesis of non-methylene-interrupted dienoic fatty acids in molluscs. *Comp. Biochem. Physiol., Part B: Biochem. Mol. Biol.* **1991**, *100B*, 801−804.

(18) Zhukova, N.; Svetashev, V. Non-methylene-interrupted dienoic fatty acids in molluscs from the sea of Japan. *Comp. Biochem. Physiol., Part B: Biochem. Mol. Biol.* **1986**, *83B*, 643−646.

(19) Caers, M.; Coutteau, P.; Sorgeloos, P.; Gajardo, G. Impact of algal diets and emulsions on the fatty acid composition and content of selected tissues of adult broodstock of the Chilean scallop *Argopecten purpuratus* (Lamarck, 1819). *Aquaculture* **2003**, *217*, 437−452.

(20) Da Costa, F.; Nóvoa, S.; Ojea, J.; Martínez-Patiño, D. Effects of algal diets and starvation on growth, survival and fatty acid composition of *Solen marginatus* (Bivalvia: Solenidae) larvae. *Sci. Mar.* **2012**, *76*, 527−537.

(21) Monroig, Ó.; Navarro, J. C.; Dick, J. R.; Alemany, F.; Tocher, D. R. Identification of a Δ5-like fatty acyl desaturase from the cephalopod *Octopus vulgaris* (Cuvier 1797) involved in the biosynthesis of essential fatty acids. *Mar. Biotechnol.* **2012**, *14*, 411−422.

(22) Monroig, Ó.; Guinot, D.; Hontoria, F.; Tocher, D. R.; Navarro, J. C. Biosynthesis of essential fatty acids in *Octopus vulgaris* (Cuvier, 1797): Molecular cloning, functional characterisation and tissue distribution of a fatty acyl elongase. *Aquaculture* **2012**, *360*, 45−53.

(23) Li, M.; Mai, K.; He, G.; Ai, Q.; Zhang, W.; Xu, W.; Wang, J.; Liufu, Z.; Zhang, Y.; Zhou, H. Characterization of two $\Delta^5$ fatty acyl desaturases in abalone (*Haliotis discus hannai* Ino). *Aquaculture* **2013**, *416*, 48−56.

(24) Zheng, H.; Liu, H.; Zhang, T.; Wang, S.; Sun, Z.; Liu, W.; Li, Y. Total carotenoid differences in scallop tissues of *Chlamys nobilis* (Bivalve: Pectinidae) with regard to gender and shell colour. *Food Chem.* **2010**, *122*, 1164−1167.

(25) Liu, H.; Guo, Z.; Zheng, H.; Wang, S.; Wang, Y.; Liu, W.; Zhang, G. Functional characterization of a Δ5-like fatty acyl desaturase and its expression during early embryogenesis in the noble scallop *Chlamys nobilis* Reeve. *Mol. Biol. Rep.* **2014**, DOI: 10.1007/s11033-014-3633-4.

(26) Liu, H.; Zheng, H.; Wang, S.; Wang, Y.; Li, S.; Liu, W.; Zhang, G. Cloning and functional characterization of a polyunsaturated fatty acid elongase in a marine bivalve noble scallop *Chlamys nobilis* Reeve. *Aquaculture* **2013**, *416*, 146−151.

(27) Hastings, N.; Agaba, M.; Tocher, D. R.; Leaver, M. J.; Dick, J. R.; Sargent, J. R.; Teale, A. J. A vertebrate fatty acid desaturase with Δ5 and Δ6 activities. *Proc. Natl. Acad. Sci. U.S.A.* **2001**, *98*, 14304−14309.

(28) Jakobsson, A.; Westerberg, R.; Jacobsson, A. Fatty acid elongases in mammals: their regulation and roles in metabolism. *Prog. Lipid Res.* **2006**, *45*, 237−249.

(29) Chu, F.-L.; Greaves, J. Metabolism of palmitic, linoleic, and linolenic acids in adult oysters, *Crassostrea virginica*. *Mar. Biol.* **1991**, *110*, 229−236.

(30) De Moreno, J. E.; Moreno, V. J.; Brenner, R. R. Lipid metabolism of the yellow clam, *Mesodesma mactroides*: 2-polyunsaturated fatty acid metabolism. *Lipids* **1976**, *11*, 561−566.

(31) Zhukova, N. V. Lipid classes and fatty acid composition of the tropical nudibranch mollusks *Chromodoris* sp. and *Phyllidia coelestis*. *Lipids* **2007**, *42*, 1169−1175.

(32) Zhukova, N. V. The pathway of the biosynthesis of non-methylene-interrupted dienoic fatty acids in molluscs. *Comp. Biochem. Physiol., Part B: Biochem. Mol. Biol.* **1991**, *100*, 801−804.

(33) Vrinten, P.; Mavraganis, I.; Qiu, X.; Senger, T. Biosynthesis of long chain polyunsaturated fatty acids in the marine ichthyosporean *Sphaeroforma arctica*. *Lipids* **2013**, *48*, 263−274.

(34) Sayanova, O.; Haslam, R.; Qi, B.; Lazarus, C. M.; Napier, J. A. The alternative pathway $C_{20}$ Δ8-desaturase from the non-photosynthetic organism *Acanthamoeba castellanii* is an atypical cytochrome $b_5$-fusion desaturase. *FEBS Lett.* **2006**, *580*, 1946−1952.

(35) Chu, F.-L. E.; Lund, E. D.; Harvey, E.; Adlof, R. Arachidonic acid synthetic pathways of the oyster protozoan parasite, *Perkinsus marinus*: evidence for usage of a delta-8 pathway. *Mol. Biochem. Parasitol.* **2004**, *133*, 45−51.

(36) Monroig, Ó.; Li, Y.; Tocher, D. R. Delta-8 desaturation activity varies among fatty acyl desaturases of teleost fish: high activity in delta-6 desaturases of marine species. *Comp. Biochem. Physiol., Part B: Biochem. Mol. Biol.* **2011**, *159*, 206−213.

(37) Monroig, Ó.; Tocher, D. R.; Navarro, J. C. Biosynthesis of polyunsaturated fatty acids in marine invertebrates: Recent advances in molecular mechanisms. *Mar. Drugs* **2013**, *11*, 3998−4018.

**Table 1. Primers Used for the Construction of the pUC18−VHb Expression Cassette and the PCR Analysis of the VHb Gene**

| primer | sequence (5′ to 3′)[a] | inserted restriction site |
|---|---|---|
| V1F | GGAGGGCCCTCATGATAGACCAGCAAA | *Apa*I |
| V1R | ATGCTGCAGTTTTTTATGTCCTGAA | *Pst*I |
| PF | AGAGGTACCAATTTTAGGCCCCCCACT | *Kpn*I |
| PR | AGACCATGGTGTTGGTGGTGTTGT | *Nco*I |
| V2F | GGGTCAACCGCTTGAGCGTAC | N/A |
| PUCr | AGCGGATAACAATTTCACACAGGAA | N/A |
| TF | CATGGCCAAGTTGACCAGTGC | N/A |
| TR | CAATCTAGAGGTACCAGACATGATAAGATACATTG | *Xba*I |
| V3F | TTGAAGGAGCATGGCGTTAC | N/A |
| V3R | GCGTACAAATCTGCTTCCACT | N/A |

[a]Underlined positions indicate the inserted restriction site.

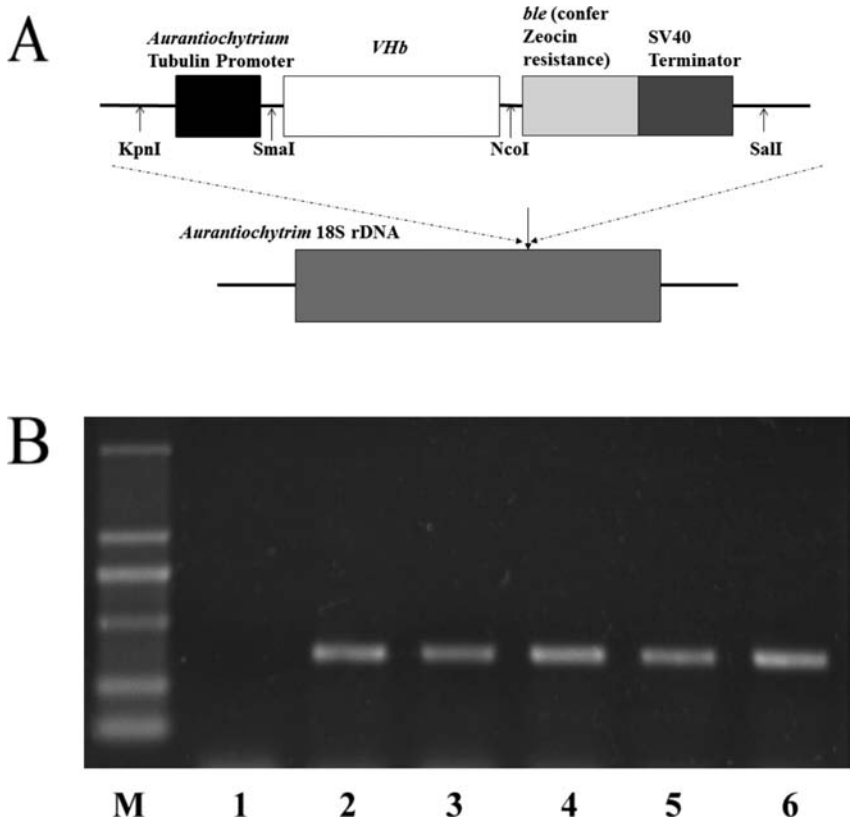


**Figure 1.** Expression construct and PCR detection of transformants: (A) schematic diagram of pUC18-SK4 tubulin promotor−*VHb*−*ble*−SV40 teminator; (B) genomic PCR detection of VHb in transformants resistance to zeocin generated by transformation with the above construct. The PCR product corresponding to VHb is 370 bp. Lanes: M, 250 bp marker; 1, MP4; 2, TMP4−VHb1; 3, TMP4−VHb10; 4, TMP4−VHb24; 5, TSK4−VHb2; 6, positive control (with plasmid containing VHb as a template).

*V. stercoraria* ATCC 15218 was cultured in tryptic soy broth (15 g/L tryptone, 5 g/L soytone, 5 g/L sodium chloride, pH 7.3) at 26 °C.

*Aurantiochytrium* sp. MP4 and SK4 were maintained in glucose−yeast extract agar plates (1 g/L glucose, 15‰ artificial seawater (v/v), 1 g/L yeast extract, 1 g/L peptone, and 15 g/L bacto agar, pH 5.5). The innoculum of each *Aurantiochytrium* sp. strain was prepared by culturing the cells in a 250 mL Erlenmeyer flask, which contained 50 mL of 15‰ artificial seawater (v/v) with 10 g/L glucose and 1 g/L yeast extract at pH 5.5. The flasks were incubated in an orbital shaker set at 200 rpm at 25 °C in the dark.

**Genomic DNA Isolation from *V. stercoraria* and *Aurantiochytrium* sp. SK4.** The standard phenol/chloroform method was used to extract genomic DNA from *V. stercoraria* ATCC 15218 and *Aurantiochytrium* sp. SK4, respectively, at the late exponential phase.[23]

**Cloning of the VHb Gene.** The primers used in the study are listed in Table 1. VHb gene was amplified from the genomic DNA of *V. stercoraria* ATCC 15218 with the standard polymerase chain reaction (PCR), using the primers V1F and V1R. The amplified fragment was ligated to the correponding restriction sites on the pTZ57R plasmid for cloning in *Escherichia coli*.

The expression cassette shown in Figure 1 was constructed. It was then cloned into the *Xba*I and *Sal*I restiction sites of an *Aurantiochytrium* 18S rDNA fragment cloned in a pUC18 vector. This was for the homologous recombination of the expression cassette into the genome of *Aurantiochytrium* sp. MP4 and SK4.

The tubulin promoter was amplified from the genomic DNA of *Aurantiochytrium* sp. SK4 with PCR with the primers PF and PR. VHb gene was amplified from the plasmid pTZ57R−VHb cloned in the previously transformed *E. coli*, using the primers V2F and PUCr. Moreover, the fragment with the *ble* gene and the SV40 terminator was amplified from the plasmid pcDNA3.1/zeo(−) (Invitrogen, Carlsbad, CA, USA), with the primers TF and TR. The VHb, tubulin promoter, and *ble*−SV40 terminator fragments were cloned sequen-


dx.doi.org/10.1021/jf5048578 | J. Agric. Food Chem. 2014, 62, 12392−12398

tially into the pUC18-18s rDNA vector through the ligation at the complementary restriction sites. Restriction enzyme cutting and sequencing were used to confirm the correct construct for transformation into *Aurantiochytrium* sp. MP4 and SK4.

**Transformation of *Aurantiochytrium* sp.** *Aurantiochytrium* sp. was transformed with the construct described under Cloning of the VHb Gene by electroporation using the Micropulser Electroporator (Bio-Rad, Hercules, CA, USA). The parameters of electroporation were set as 1.8 kV, 300 Ω, and 50 μF. Cells of each electroporated strain were resuspended in 15 mL of 15‰ artificial seawater (v/v) with 10 g/L glucose and 1 g/L yeast extract. The cells were allowed to recover for 24 h in an orbital shaker at 150 rpm at 25 °C in the dark. Then they were selected on glucose−yeast extract agar plates with 50 μg/mL zeocin. The colonies resistant to zeocin were isolated and cultured for subsequent analysis. The presence of the VHb gene and its expression were varified by PCR with primers V3F and V3R and the carbon monoxide (CO) difference spectra.[24]

**Growth of VHb-Expressing *Aurantiochytrium* sp. in Flask Cultures.** The innocula of the VHb-expressing MP4 and SK4 and their corresponding wild types were prepared. Five percent of each exponentially growing inoculum was used to inoculate 100 mL of glucose−yeast extract (GYE) medium (20 g/L glucose, 15‰ artificial seawater (v/v), 10 g/L yeast extract, pH 5.5) in 250 mL Erlenmeyer flasks. The culture of each strain was separated into two batches, each in triplicates: the flask opening was covered with a filter in one batch to allow free air diffusion, whereas it was covered with a rubber plug in the other batch to block air diffusion. The condition was aerobic when free air diffusion was allowed, as the DO level was above 2% saturation (data not shown). In constrast, it was defined as microaerobic when free air diffusion was blocked, as the DO level was below 0.5% saturation (data not shown). All flasks were incubated in an orbital shaker set at 200 rpm at 25 °C in the dark. Growth of the VHb-expressing MP4 and SK4 and their correponding wild type controls was measured by the optical density (OD) at 660 nm.

**GC Analysis on the Fatty Acid Content.** Freeze-dried samples of VHb-expressing MP4 and SK4 and their wild type controls (from aerobic flask cultures) were collected at day 3 (for TMP4−VHb24 and MP4) or day 7 (for TSK4−VHb2 and SK4) of growth in GYE medium. They were treated by direct transmethylation with sulfuric acid in methanol to convert the fatty acids in the samples to fatty acid methyl esters (FAMEs). Briefly, 20 mg of each freeze-dried sample was weighed and incubated with 2 mL of 1% sulfuric acid in methanol (v/v) and 0.8 mL of the internal standard, nonadecanoic acid (C19:0) (1 mg/mL hexane), in 1 mL of toluene at 50 °C for 12 h. The upper hexane layer with FAMEs was washed with 5% sodium chloride solution (w/v) and 2% potassium hydrogen carbonate solution (w/v) sequentially and then dried by passing nitrogen gas. The FAMEs extracted were then redissolved in 1 mL of hexane and analyzed by a Hewlett-Packard (HP) 6890 capillary gas chromatography (GC) system with a flame ionization detector (FID) and a HP-INNOwax capillary column (30 m × 0.32 mm) (Agilent Technologies, Santa Clara, CA, USA). The carrier gas was nitrogen, and the column temperature was programmed to rise from 170 to 230 °C at 1 °C/min. Two microliters of sample was injected under the splitless mode through the injector, which was kept at 250 °C while the FID was kept at 270 °C. Individual FAMEs were identified by comparsion to the retention time of the peak with that of each pure standard, and they were quantified by the peak area of the internal standard C19:0 fatty acid, which was injected in a known amount. The analysis was done in triplicates for each strain.

**HPLC Analysis on the Carotenoid Contents.** VHb-expressing SK4 and its wild type control were collected at day 9 of growth (from aerobic and microaerobic cultures prepared as under Growth of VHb-Expressing Aurantiochytrium sp. in Flask Cultures) in a modified By+ medium (30 g/L glucose, 1 g/L yeast extract, 1 g/L peptone, and 15‰ artificial seawater (v/v)). Samples were freeze-dried for the extraction of the carotenoid pigments from the biomass. Twenty milligrams of each sample was ground in liquid nitrogen, and the carotenoids released were dissolved in acetone, which were blown to dryness with nitrogen gas and then redissolved in 200 μL of acetone for analysis.

The extracted pigments were then analyzed by a high-performance liquid chromatography (HPLC) system of Waters 2695 separation module (Waters, Milford, MA, USA). They were separated through a Waters Spherisorb ODS2 analytical column (5 μm, 4.6 × 250 mm). Two solvents were used as the mobile phase: solvent A (acetonitrile/methanol/0.1 M Tris-HCl (pH 8.0), 84:2:14, v/v/v) and solvent B (methanol/ethyl acetate, 68:32, v/v). The extracted pigments were eluted through the column with a linear gradient from 100% solvent A to 100% solvent B at a flow rate of 1.2 mL/min over 15 min and then 10 min of 100% solvent B at the same flow rate. The absorption spectra between 250 and 700 nm were recorded with a Waters 2996 photodiode array detector. The carotenoids were qualified and quantified by the comparing the retention times and peak areas of the individual absorption spectra with those of pure carotenoid standards. The analysis was done in duplicates for each strain.

**Statistical Analysis.** Statistical analyses were performed with the SPSS statistical package. Paired-samples *t* test was applied. The experimental results were considered statistically significant when $p < 0.05$.

## RESULTS AND DISCUSSION

**Transformation of *Aurantiochytrium* sp. by VHb-ble.** A linear DNA fragment of VHb-ble (Figure 1A) was introduced

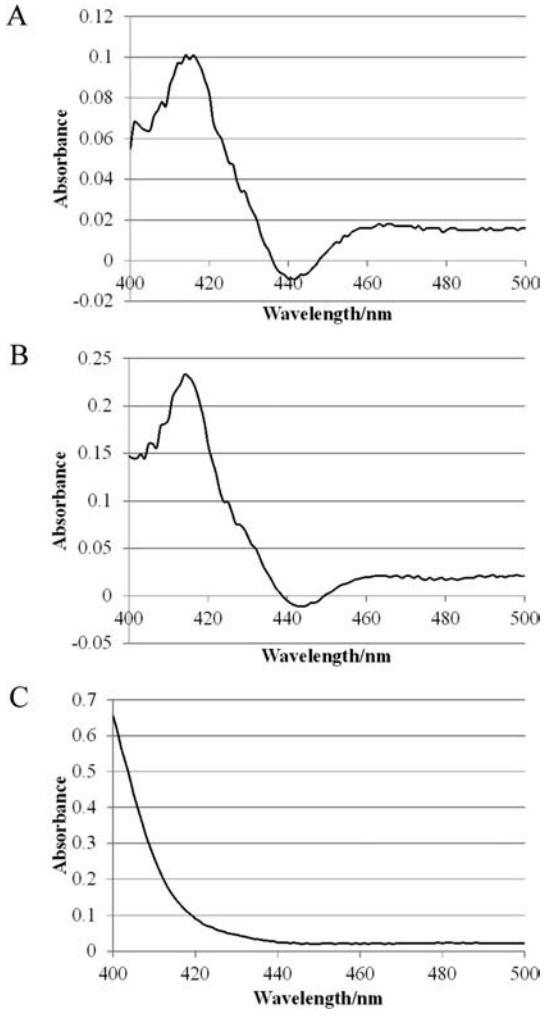


**Figure 2.** CO difference spectrum of wild type and VHb-expressing *Aurantiochytrium* sp.: (A) TMP4−VHb24; (B) *Aurantiochytrium* sp. TSK4−VHb2; (C) MP4.

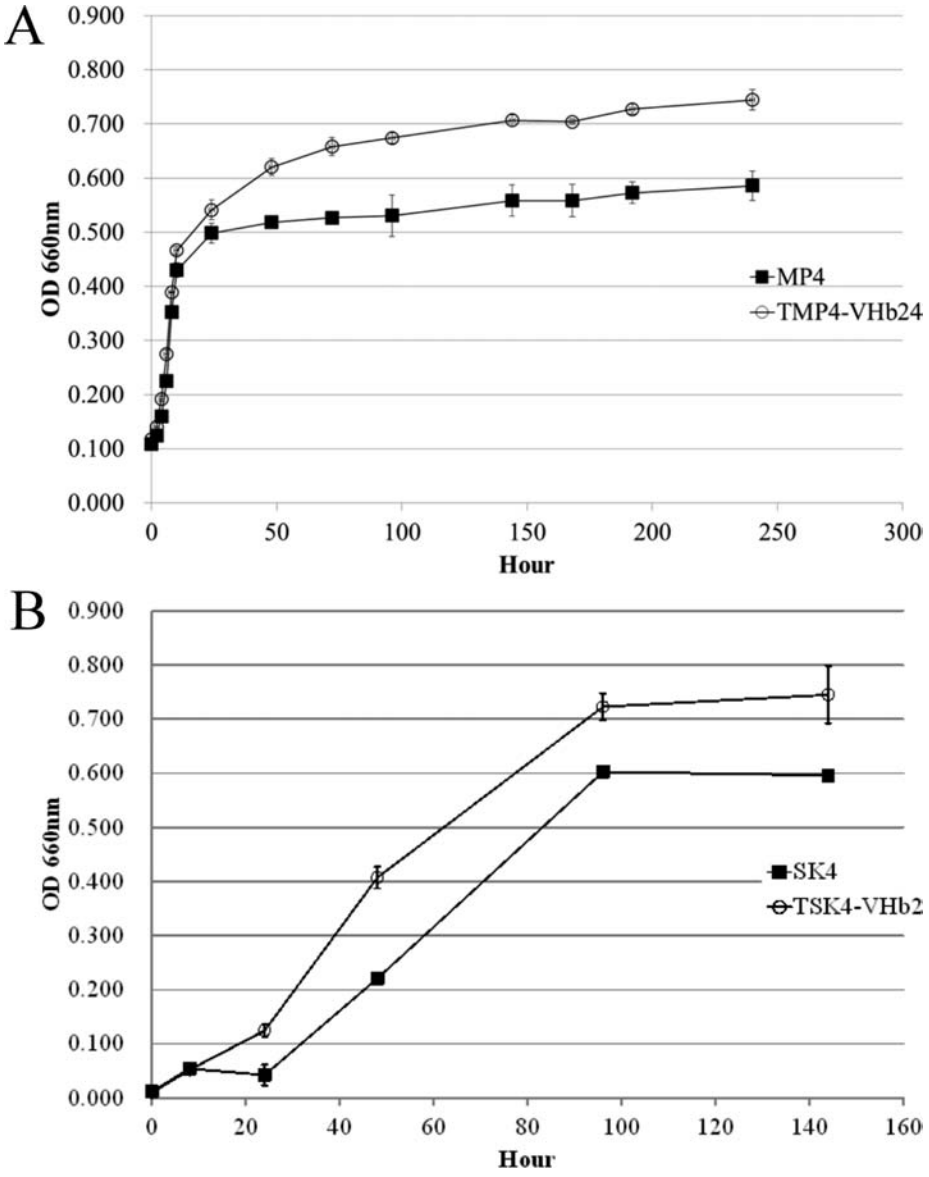


**Figure 3.** Growth curve of *Aurantiochytrium* sp. cultured in microaerobic conditions, measured in terms of OD at 660 nm: (A) MP4 and TMP4−VHb24; (B) SK4 and TSK4−VHb2. Data are expressed as the mean ± standard deviation of triplicates.

into *Aurantiochytrium* sp. MP4 and SK4 by electroporation. The *Ble* gene conferring zeocin resistance was used as a selective marker to screen positive transformants of *Aurantiochytrium* sp. Generally 50−100 zeocin-resistant colonies were obtained on a 9 cm Petri dish, suggesting the feasibility of the electroporation approach for the introduction of foreign genes into *Aurantiochytrium*. The presence of VHb was verified by genomic PCR amplification (Figure 1B). Three MP4 transformants (namely, TMP4−VHb1, TMP4−VHb10, and TMP4−VHb24) and one SK4 transformant (namely, TSK4−VHb2) were selected for further investigation. To verify the expression of VHb, the carbon monoxide (CO) difference spectra of both transformants and wild types were measured, and the results are shown in Figure 2. The VHb-specific CO difference spectrum, a maximal absorbance peak at about 419 nm, was observed in the CO-treated crude extracts of TMP4−VHb24 (Figure 2A) and TSK4−VHb2 (Figure 2B) but not in the control (Figure 2C). These results clearly show that biologically active VHb was produced in the PCR-verified transformants.

**Growth of VHb-Expressing *Aurantiochytrium* sp.** The effect of VHb expression on the growth of *Aurantiochytrium* sp. was studied in both microaerobic and aerobic conditions. Significant improvement of cell growth was observed in TMP4−VHb24 (Figure 3A) and TSK4−VHb2 (Figure 3B) in microaerobic conditions. The effects of VHb led to 27 and 24% higher maximum OD values achieved in TMP4−VHb24 and TSK4−VHb2, respectively, when compared with the corresponding wild type controls. In contrast, the effects of VHb on cell growth in aerobic conditions were not significant, possibly due to the sufficient supply of oxygen in both transgenic cells and control cells as well as a relatively low cell density achieved (data not shown). Dissolved oxygen concentrations decline as cell density increases in fed-batch processes. Our results support the feasibility of VHb to economically solve the common problem of limited DO occurring in high-cell density fermentation.

Table 2. Fatty Acid Composition and Content of *Aurantiochytrium* sp. MP4, TMP4−VHb24, SK4, and TSK4−VHb24, Respectively[a]

| | % total fatty acids | | | |
|---|---|---|---|---|
| fatty acid | MP4 | TMP4−VHb24 | SK4 | TSK4−VHb2 |
| C12:0 | 0.20 ± 0.02 | 0.26 ± 0.19 | 0.00 ± 0.00 | 0.00 ± 0.00 |
| C13:0 | 0.35 ± 0.30* | 1.19 ± 0.34* | 0.63 ± 0.43 | 1.14 ± 0.12 |
| C14:0 | 4.66 ± 0.88 | 6.78 ± 1.33 | 5.58 ± 1.03 | 4.57 ± 0.46 |
| C15:0 | 19.35 ± 1.07* | 27.59 ± 0.71* | 17.17 ± 1.57** | 23.26 ± 1.29** |
| C16:0 | 46.25 ± 3.48 | 41.45 ± 0.65 | 28.07 ± 2.57** | 21.18 ± 0.69** |
| C17:0 | 2.73 ± 0.12* | 4.55 ± 0.10* | 4.31 ± 0.86** | 7.07 ± 0.56** |
| C18:0 | 0.83 ± 0.03* | 0.77 ± 0.01* | 0.54 ± 0.13 | 0.62 ± 0.02 |
| C18:1n9 | 0.67 ± 0.11* | 0.06 ± 0.01* | 0.00 ± 0.00 | 0.00 ± 0.00 |
| C20:3n6 | 1.18 ± 0.14* | 0.58 ± 0.01* | 3.43 ± 0.28 | 3.12 ± 0.09 |
| C20:4n6 (AA) | 0.36 ± 0.04* | 0.23 ± 0.01* | 0.10 ± 0.17** | 0.52 ± 0.06** |
| C20:5n3 (EPA) | 0.53 ± 0.06* | 0.41 ± 0.01* | 6.86 ± 0.67 | 6.82 ± 0.34 |
| CC22:5n3 (DPA) | 2.53 ± 0.01* | 2.25 ± 0.05* | 10.66 ± 2.09** | 7.17 ± 0.46** |
| C22:6n3 (DHA) | 16.74 ± 1.40* | 11.60 ± 0.34* | 19.82 ± 2.50 | 20.17 ± 0.65 |
| others | 3.62 ± 1.73 | 2.28 ± 1.38 | 2.82 ± 0.31 | 4.36 ± 0.66 |
| SFA[b] (%) | 74.37 ± 3.03* | 82.59 ± 1.73* | 56.30 ± 5.19 | 57.84 ± 1.70 |
| MUFA[c] (%) | 0.67 ± 0.11* | 0.06 ± 0.01* | 0.00 ± 0.00 | 0.00 ± 0.00 |
| PUFA[d] (%) | 21.34 ± 1.64* | 15.07 ± 0.40* | 40.88 ± 5.34 | 37.80 ± 1.23 |
| TFA[e] (mg/g dry cell wt) | 454.86 ± 5.96* | 500.72 ± 25.65* | 86.30 ± 8.07** | 124.57 ± 9.23** |
| % fatty acids (% dry cell wt) | 45.48 ± 0.60* | 50.07 ± 2.57* | 8.63 ± 0.81** | 12.46 ± 0.92** |

[a]Data are expressed as the mean ± standard deviation of triplicates; data indicated by * in the same fatty acid category are significantly different from each other ($p < 0.05$), same case for data indicated by **. AA, arachidonic acid; EPA, eicosapentaenoic acid; DPA, docosapentaenoic acid; DHA, docosahexaenoic acid. [b]SFA, saturated fatty acids. [c]MUFA, monounsaturated fatty acids. [d]PUFA, polyunsaturated fatty acids. [e]TFA, total fatty acids.

**Fatty Acid Biosynthesis of VHb-Expressing *Aurantiochytrium* sp.** DO levels are a critical factor not only for cell growth but also for fatty acid productivity in *Aurantiochytrium*.[12] To determine the effect of VHb expression on fatty acid biosynthesis, TMP4−VHb24 and TSK4−VHb2 were surveyed on the fatty acid composition and content under normal culture conditions (see GC Analysis on the Fatty Acid Content). In aerobic conditions, the total cellular fatty acid content in TMP4−VHb24 was 500.72 mg/g, which is 10% higher than the value of 454.86 mg/g in nontransformed control (Table 2). *Aurantiochytrium* sp. SK4 accumulated much less total fatty acids than strain MP4[21](Table 2). However, the expression of VHb in this strain resulted in a greater increase of total fatty acids by 44% from the value of 86.30 mg/g in SK4 to 124.57 mg/g in TSK4−VHb2 (Table 2). In addition, the expression of VHb also induced significant changes in the fatty acid composition, especially to the ratio of saturated and polyunsaturated fatty acids (Table 2). Generally the effect of VHb led to increases of saturated fatty acids (SFAs) and decreases of polyunsaturated fatty acids (PUFAs) with a lower effect on strain SK4.

**Carotenoid Biosynthesis of VHb-Expressing *Aurantiochytrium* sp.** In addition to accumulating significant amounts of fatty acids, *Aurantiochytrium* sp. SK4 also synthesizes carotenoids, with $\beta$-carotene being the prominent pigment, and echeninon, canthaxanthin, adonirubin, and astaxanthin the minor ones[21] (Figure 4A). The effect of VHb led to great changes of carotenoid profiles, making astaxanthin the major pigment and all of its precursors, including $\beta$-carotene, the minor ones (Figure 4B.) The carotenoid compositions and contents of TSK4−VHb2 and SK4 grown in aerobic conditions were measured, and the results are shown in Figure 4C. The cellular astaxanthin content of TSK4−VHb2 was 131.09 $\mu$g/g, which is about 10-fold that in SK4 (14.47 $\mu$g/g), suggesting that the conversion of $\beta$-carotene to astaxanthin was greatly promoted in the transformant. Such a promotion might result from the increased DO levels due to the effect of VHb expression because the biosynthesis of astaxanthin strongly depends on oxygen accessibility. Similar results were achieved in an astaxanthin-producing bacterium that simultaneously expressed a hemoglobin gene.[25] The authors suggested that possibly the heterologous hemoglobin improved the activity of the oxygen-requiring enzymes involved in astaxanthin biosynthesis. Wang et al.[26] suggested that VHb improved the oxygen-required metabolism and antioxidant biosynthesis through up-regulating the mRNA levels of $\beta$-carotene hydroxylase, which converts $\beta$-carotene to zeaxanthin and canthaxanthin to astaxanthin.

Previously, the biosynthetic pathway of astaxanthin in thraustochytrids was proposed to be ketolating $\beta$-carotene first to form canthaxanthin via echinenone followed by hydroxylation reactions.[8] This study demonstrated that a similar pathway existed in *Aurantiochytrium* sp. SK4 according to the existence of the intermediates and changes of carotenoid profiles between TSK4−VHb2 and SK4. In addition, *Aurantiochytrium* sp. SK4 and its transformant accumulate astaxanthin in free form rather than esterified form as in some green algae, such as *Haematococcus pluvialis* and *Chlorella zofingiensis*. *Aurantiochytrium* sp. SK4 accumulates much less astaxanthin than the green algae, which may result from its failure to store astaxanthin in esterified form.

The effect of VHb not only significantly improved the growth of *Aurantiochytrium* sp. under microaerobic conditions (Figure 2) but also enhanced the biosynthesis of both fatty acid (Table 2) and astaxanthin (Figure 4) under aerobic conditions. Therefore, VHb expression may serve as an approach to solve the problem of limited DO occurring in high-cell density fermentation with controlled air pumping and agitation rate to provide DO > 2%, which is the range of DO levels in the aerobic flask cultures in this study. This is not a relatively high

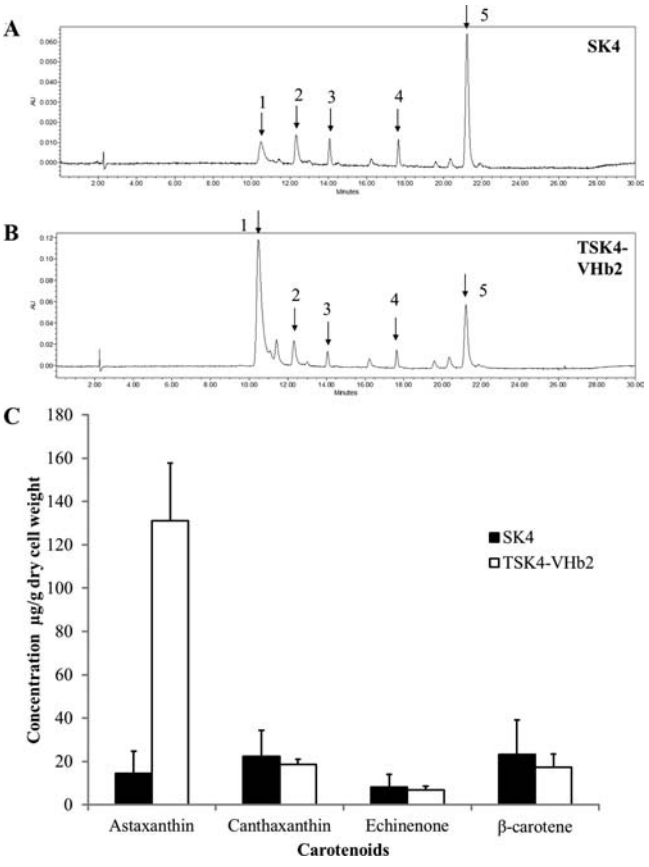


**Figure 4.** Analysis of carotenoids from wild type and VHb-expressing *Aurantiochytrium* sp. SK4: HPLC chromatogram of the carotenoid from *Aurantiochytrium* sp. SK4 (A) and TSK4−VHb2 (B) in flask cultures with free air diffusion. Peaks: 1, astaxanthin; 2, adonirubin (phoenicoxanthin); 3, canthaxanthin; 4, echineone; 5, $\beta$-carotene. (C) Composition and content of carotenoids in *Aurantiochytrium* sp. SK4 and TSK4−VHb2 in flask cultures with free air diffusion. Data are expressed as the mean ± standard deviation of duplicates.

DO level to achieve in a fermenter, and therefore the energy consumption to maintain it will not be too high. In this condition, the action of VHb can relieve the limitation of low oxygen availability to cell growth at high density, whereas the fatty acid or astaxanthin production can also be improved.

In conclusion, the effect of VHb expression in *Aurantiochytrium* sp. was studied. VHb expression led to improved growth under microaerobic conditions and enhanced productions of total fatty acids and astaxanthin in the thraustochytrid cells under aerobic conditions. This study highlights the potential of VHb to enhance cell growth and the production of value-added metabolites by large-scale high-cell density fermentation.

## AUTHOR INFORMATION


### Corresponding Authors

*(F.C.) Phone: +86-10-82529003. E-mail: sfchencoe@pku.edu.cn.

*(J.H.) E-mail: huangjc@mail.kib.ac.cn.

### Author Contributions

‖Y.L.S and H.T. contributed equally.



### Funding

This study was partially supported by the "985" Project of Peking University, the 19 State Oceanic Administration of China, and the "863" Plan of the Ministry of Science 20 and Technology of China (2012AA02A707).

### Notes

The authors declare no competing financial interest.


## REFERENCES


(1) Raghukumar, S. Thraustochytrid marine protists: production of PUFAs and other emerging technologies. *Mar. Biotechnol.* **2008**, *10*, 631−640.

(2) Yokoyama, R.; Honda, D. Taxonomic rearrangement of the genus *Schizochytrium* sensu lato based on morphology, chemotaxonomic characteristics, and 18S rRNA gene phylogeny (Thraustochytriaceae, Labyrinthulomycetes): emendation for *Schizochytrium* and erection of *Aurantiochytrium* and *Oblongichytrium* gen. nov. *Mycoscience* **2007**, *48*, 199−211.

(3) Yokoyama, R.; Salleh, B.; Honda, D. Taxonomic rearrangement of the genus *Ulkenia* sensu lato based on morphology, chemotaxonomical characteristics, and 18S rRNA gene phylogeny (Thraustochytriaceae, Labyrinthulomycetes): emendation for *Ulkenia* and erection of *Botryochytrium*, *Parietichytrium*, and *Sicyoidochytrium* gen. nov. *Mycoscience* **2007**, *48*, 329−341.

(4) Johnson, M. B.; Wen, Z. Y. Production of biodiesel fuel from the microalga *Schizochytrium limacinum* by direct transesterification of algal biomass. *Energy Fuels* **2009**, *23*, 5179−5183.

(5) Lee Chang, K. J.; Dunstan, G. A.; Abell, G. C.; Clementson, L. A.; Blackburn, S. I.; Nichols, P. D.; Koutoulis, A. Biodiscovery of new Australian thraustochytrids for production of biodiesel and long-chain omega-3 oils. *Appl. Microbiol. Biotechnol.* **2012**, *93*, 2215−2231.

(6) Song, X.; Tan, Y.; Liu, Y.; Zhang, J.; Liu, G.; Feng, Y.; Cui, Q. Different impacts of short-chain fatty acids on saturated and polyunsaturated fatty acid biosynthesis in *Aurantiochytrium* sp. SD116. *J. Agric. Food Chem.* **2013**, *61*, 9876−9881.

(7) Iwasaka, H.; Aki, T.; Adachi, H.; Watanabe, K.; Kawamoto, S.; Ono, K. Utilization of waste syrup for production of polyunsaturated fatty acids and xanthophylls by *Aurantiochytrium*. *J. Oleo Sci.* **2013**, *62*, 729−736.

(8) Aki, T.; Hachida, K.; Yoshinaga, M.; Katai, Y.; Yamasaki, T.; Kawamoto, S.; Kakizono, T.; Maoka, T.; Shigeta, S.; Suzuki, O.; Ono, K. Thraustochytrid as a potential source of carotenoids. *J. Am. Oil Chem. Soc.* **2003**, *80*, 789−794.

(9) Yamasaki, T.; Aki, T.; Shinozaki, M.; Taguchi, M.; Kawamoto, S.; Ono, K. Utilization of Shochu distillery wastewater for production of polyunsaturated fatty acids and xanthophylls using thraustochytrid. *J. Biosci. Bioeng.* **2006**, *102*, 323−327.

(10) Quilodran, B.; Hinzpeter, I.; Hormazabal, E.; Quiroz, A.; Shene, C. Docosahexaenoic acid (C22:6n-3, DHA) and astaxanthin production by *Thraustochytriidae* sp. AS4-A1 a native strain with high similitude to *Ulkenia* sp.: evaluation of liquid residues from food industry as nutrient sources. *Enzyme Microb. Technol.* **2010**, *47*, 24−30.

(11) Chen, G.; Fan, K. W.; Lu, F. P.; Li, Q.; Aki, T.; Chen, F.; Jiang, Y. Optimization of nitrogen source for enhanced production of squalene from thraustochytrid *Aurantiochytrium* sp. *Nat. Biotechnol.* **2010**, *27*, 382−389.

(12) Huang, T. Y.; Lu, W. C.; Chu, I. M. A fermentation strategy for producing docosahexaenoic acid in *Aurantiochytrium* limacinum SR21 and increasing C22:6 proportions in total fatty acid. *Bioresour. Technol.* **2012**, *123*, 8−14.

(13) Nakazawa, A.; Matsuura, H.; Kose, R.; Kato, S.; Honda, D.; Inouye, I.; Kaya, K.; Watanabe, M. M. Optimization of culture conditions of the thraustochytrid *Aurantiochytrium* sp. strain 18W-13a for squalene production. *Bioresour. Technol.* **2012**, *109*, 287−291.

(14) Konz, J. O.; King, J.; Cooney, C. L. Effects of oxygen on recombinant protein expression. *Biotechnol. Prog.* **1998**, *14*, 393−409.

(15) Wu, G.; Wainwright, L. M.; Poole, R. K. Microbial globins. *Adv. Microb. Physiol.* **2003**, *47*, 255−310.

(16) Zhang, L.; Li, Y. J.; Wang, Z. N.; Xia, Y.; Chen, W. S.; Tang, K. X. Recent developments and future prospects of *Vitreoscilla*

hemoglobin application in metabolic engineering. *Biotechnol. Adv.* **2007**, *25*, 123−136.
(17) Geckil, H.; Barak, Z.; Chipman, D. M.; Erenler, S. O.; Webster, D. A.; Stark, B. C. Enhanced production of acetoin and butanediol in recombinant *Enterobacter aerogenes* carrying *Vitreoscilla* hemoglobin gene. *Bioprocess Biosyst. Eng.* **2004**, *26*, 325−330.
(18) Sanny, T.; Arnaldos, M.; Kunkel, S. A.; Pagilla, K. R.; Stark, B. C. Engineering of ethanolic *E. coli* with the *Vitreoscilla* hemoglobin gene enhances ethanol production from both glucose and xylose. *Appl. Microbiol. Biotechnol.* **2010**, *88*, 1103−1112.
(19) Arnaldos, M.; Kunkel, S. A.; Wang, J.; Pagilla, K. R.; Stark, B. C. *Vitreoscilla* hemoglobin enhances ethanol production by *Escherichia coli* in a variety of growth media. *Biomass Bioenergy* **2012**, *37*, 1−8.
(20) Sakaguchi, K.; Matsuda, T.; Kobayashi, T.; Ohara, J.; Hamaguchi, R.; Abe, E.; Nagano, N.; Hayashi, M.; Ueda, M.; Honda, D.; Okita, Y.; Taoka, Y.; Sugimoto, S.; Okino, N.; Ito, M. Versatile transformation system that is applicable to both multiple transgene expression and gene targeting for thraustochytrids. *Appl. Environ. Microbiol.* **2012**, *78*, 3193−3202.
(21) Fan, K. W.; Jiang, Y.; Ho, L. T.; Chent, F. Differentiation in fatty acid profiles of pigmented and nonpigmented *Aurantiochytrium* isolated from Hong Kong mangroves. *J. Agric. Food Chem.* **2009**, *57*, 6334−6341.
(22) Fan, K. W.; Jiang, Y.; Faan, Y. W.; Chen, F. Lipid characterization of mangrove thraustochytrid − *Schizochytrium mangrovei*. *J. Agric. Food Chem.* **2007**, *55*, 2906−2910.
(23) Sambrook, J. *Molecular Cloning: A Laboratory Manual*, 2nd ed.; Cold Spring Harbor Laboratory: Cold Spring Harbor, NY, 1989.
(24) Lamba, P.; Webster, D. A. Effect of growth-conditions on yield and heme content of *Vitreoscilla*. *J. Bacteriol.* **1980**, *142*, 169−173.
(25) Tao, L.; Sedkova, N.; Yao, H.; Ye, R. W.; Sharpe, P. L.; Cheng, Q. Expression of bacterial hemoglobin genes to improve astaxanthin production in a methanotrophic bacterium *Methylomonas* sp. *Appl. Microbiol. Biotechnol.* **2007**, *74*, 625−633.
(26) Wang, Z. N.; Xiao, Y.; Chen, W. S.; Tang, K. X.; Zhang, L. Functional expression of *Vitreoscilla* hemoglobin (VHb) in *Arabidopsis* relieves submergence, nitrosative, photo-oxidative stress and enhances antioxidants metabolism. *Plant Sci.* **2009**, *176*, 66−77.

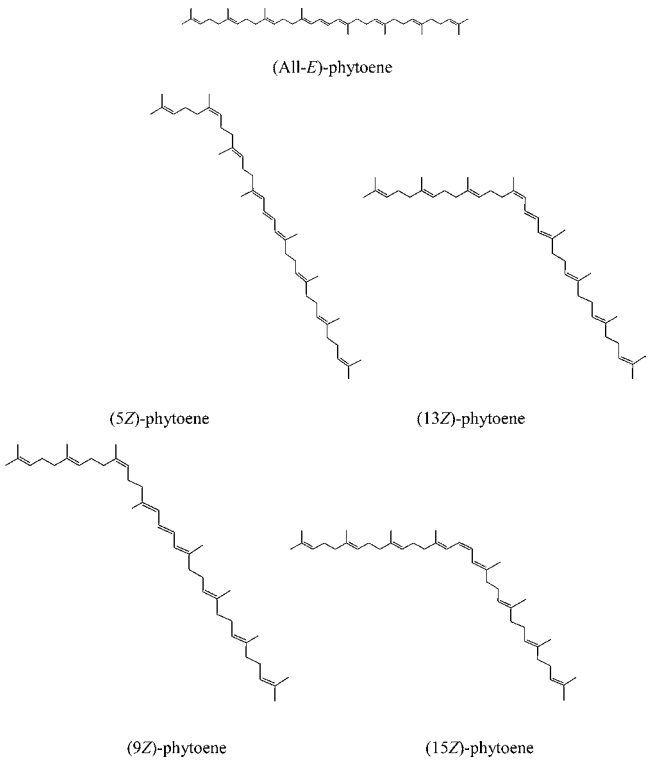


**Figure 1.** Representation of the chemical structures of geometrical isomers of phytoene.

standpoints. In this study, lycopene, phytoene, and phytofluene from a natural extract of lycopene-rich tomatoes have been stereomutated following two different methodologies. We have compared the different isomeric sets at the equilibrium and obtain information about kinetically and thermodynamically favored compounds. Furthermore, we carried out *in silico* studies on the relative stability of different lycopene, phytoene, and phytofluene isomers. This information is useful to gain further insight into the meaning of the existence of certain (*Z*)-lycopene isomers in foods, plasma, tissues, and other matrices. More importantly, it led us to hypothesize the isomeric mixtures of phytoene and phytofluene (two largely understudied carotenoids) that can be expected in certain foods, plasma, and tissues.

## MATERIALS AND METHODS

**Isolation of Carotenoid Standards.** The carotene standards (phytoene, phytofluene, and lycopene) were isolated by open column chromatography according to standard procedures[15] from a natural extract of lycopene-rich tomatoes (Lycomato). This was kindly provided by LycoRed Ltd. (Beer Sheva, Israel). Briefly, the Lycomato material was dissolved in hexane and gently poured into the column, which was packed with MgO:HyfloSupercel (1:1). Phytoene, phytofluene, and lycopene were eluted with hexane, 2% diethyl ether in hexane, and acetone, respectively. Fractions containing mixtures of phytoene and phytofluene were further purified by HPLC by collecting the fractions of the corresponding peaks.

**Stereomutation Conditions.** *Thermal Isomerization.* The fractions of pure carotenoids obtained were evaporated at room temperature by flushing nitrogen. Solutions of carotenoids in toluene (0.1 mg/mL, 5 mL) were heated in a thermoblock at 75 °C. Aliquots were taken at times 0, 15, 30, 60, 90, 120, 240, 480, and 1440 min, evaporated to dryness by flushing nitrogen, redissolved in ethyl acetate, and injected on the HPLC system. After every sampling, the tube was flushed gently with nitrogen. The experiments were carried out in duplicate on two consecutive days (one experiment each day).

*Iodine-Catalyzed Isomerization.* A 10 μL portion of a 1 mg/mL iodine solution in toluene was added to 0.1 mg/mL solutions of carotenoids in toluene placed in transparent glass tubes. These were exposed to illumination (conventional fluorescent bulbs) for 24 h at a distance of 50 cm. Aliquots were taken at times 0, 15, 30, 60, 90, 120, 240, 480, and 1440 min, evaporated to dryness, redissolved in ethyl acetate, and injected on the HPLC system. After every sampling, the tube was flushed gently with nitrogen. The experiments were carried out at room temperature in duplicate on two consecutive days (one experiment each day).

**HPLC Analysis and Identification of Isomers.** The HPLC conditions and criteria for the identification of geometrical isomers are explained in detail.[16] Briefly, the separations were carried out on an YMC C30 column, (3 μm, 4.6 mm × 150 mm, YMC America, Inc., Allentown, PA) kept at 25 °C. Methanol (MeOH, containing 0.1% of ammonium acetate) and methyl-*tert*-butyl ether (MTBE) were used for the separations according to the following gradient.

| time (min) | % MeOH | % MTBE | curve |
|---|---|---|---|
| 0 | 100 | 0 | |
| 45 | 85 | 15 | lineal |
| 55 | 40 | 60 | lineal |
| 60 | 30 | 70 | lineal |
| 65 | 30 | 70 | lineal |
| 70 | 100 | 0 | lineal |

The tentative identification of the lycopene isomers was carried out by comparing the spectroscopic data with those reported in previous studies.[17,18]

*In Silico Study.* The MOE suite 2010.11 software version (Molecular Operating Environment (MOE 2007.09), Chemical Computing Group, Inc. Montreal, Quebec, Canada) was used for the analyses. The three-dimensional (3D) structures of the (all-*E*)-isomers of lycopene, phytofluene, and phytoene (Figure 2), as well as of their mono- (*Z*)-isomers,

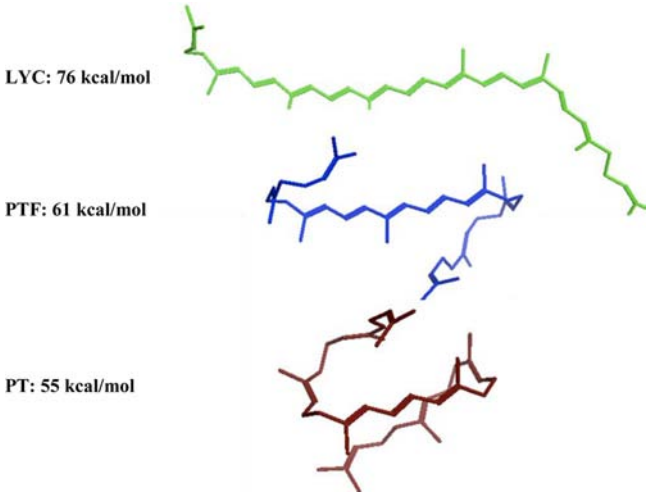


**Figure 2.** Energy-minimized three-dimensional representations of lycopene (LYC), phytofluene (PTF), and phytoene (PT) in the all-*E* configuration.

were built. Their energies were subsequently evaluated and minimized using the MMF94x force field method. In this, the potential energy of a molecular system is a function of the atomic coordinates:

$$E(\chi) = E_{str} + E_{ang} + E_{oop} + E_{tor} + E_{vdw} + E_{ele} + E_{sol} + E_{res}$$

Each of the energy terms is itself a sum involving particular kinds of atomic interactions like stretching (str), angle bending (ang), out of plane (oop), torsional (tor), van der Waals (vdw), electrostatic (ele), solvation (sol), or restriction (res).


dx.doi.org/10.1021/jf5041965 | J. Agric. Food Chem. 2014, 62, 12399−12406

In a second step, all the structures were energy minimized. Energy minimization consists of finding a set of atomic coordinates that correspond to a local minimum of the molecular energy function (such as the potential energy model). This is done by applying large-scale nonlinear optimization techniques. The goal is to calculate a conformation close to the starting geometry for which the forces on the atoms are zero. Nonlinear optimization algorithms typically have a sequence of four steps: a test for convergence, the compute to stablish the search direction $p_k$, the evaluation of the step size, and the advance.

As a third step, all putative conformations were systematically searched for each energy-minimized model. The systematic search method generates molecular conformations by rotating nonring bonds in a molecule by discrete dihedral increments. All possible combinations of the dihedral increments are produced. Each dihedral angle combination is subjected to dihedral angle energy minimization to relieve gross strain due to atom overlap, followed by an all-atom energy minimization. As we aimed to find all putative conformations of the geometrical isomers, a restriction to maintain the corresponding (*Z*)- and (all-*E*)-conformations was added. We obtained conformational databases of the above 50 conformations for each geometrical isomer, with a total of 1200 conformations (data not shown).

As a fourth step, the MMFF94x potential energy was minimized again for all the conformations of all the geometrical isomers and the lowest energy conformation of each was selected. A new database of isomers was finally obtained and ranked by their torsional potential energies (Figure 3).

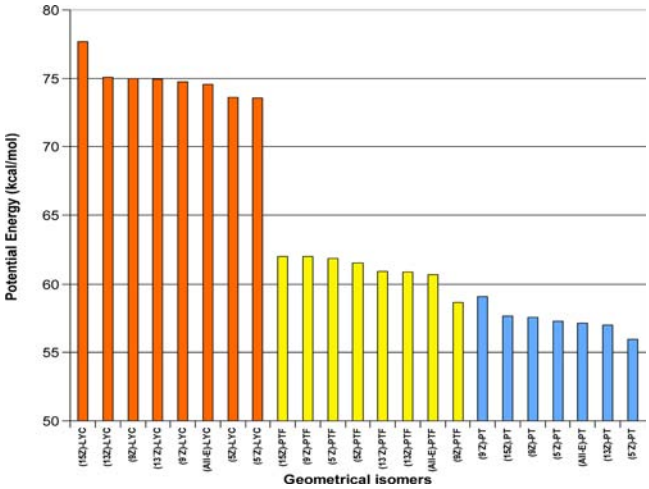


**Figure 3.** Torsional potential energies (kcal/mol) of different geometrical isomers of lycopene (LYC), phytofluene (PTF), and phytoene (PT).

**Statistical Analyses.** The results of the isomerization reactions were expressed as the mean and standard deviation of the two independent determinations.

## RESULTS AND DISCUSSION

**Isomerization Reactions.** An isomerization reaction for carotenoids can be kinetically or thermodynamically controlled. In the first case, the composition of the set of all the geometrical isomers formed (stereoisomeric set) is determined by the relative rate of formation for each one. Kinetically controlled isomerizations of carotenoids can be easily achieved by gentle heating. In the case of thermodynamically controlled reactions, the composition of the stereoisomeric set at the equilibrium is dependent on the relative stability of each isomer. These reactions have been traditionally carried out by using iodine as catalyst.[19]

Chromatograms corresponding to the stereochemical sets of lycopene, phytofluene, and phytoene at the thermodynamic equilibrium are shown in Figure 4. Chromatographic and UV−vis spectroscopic data are summarized in Supporting Information Table 1.

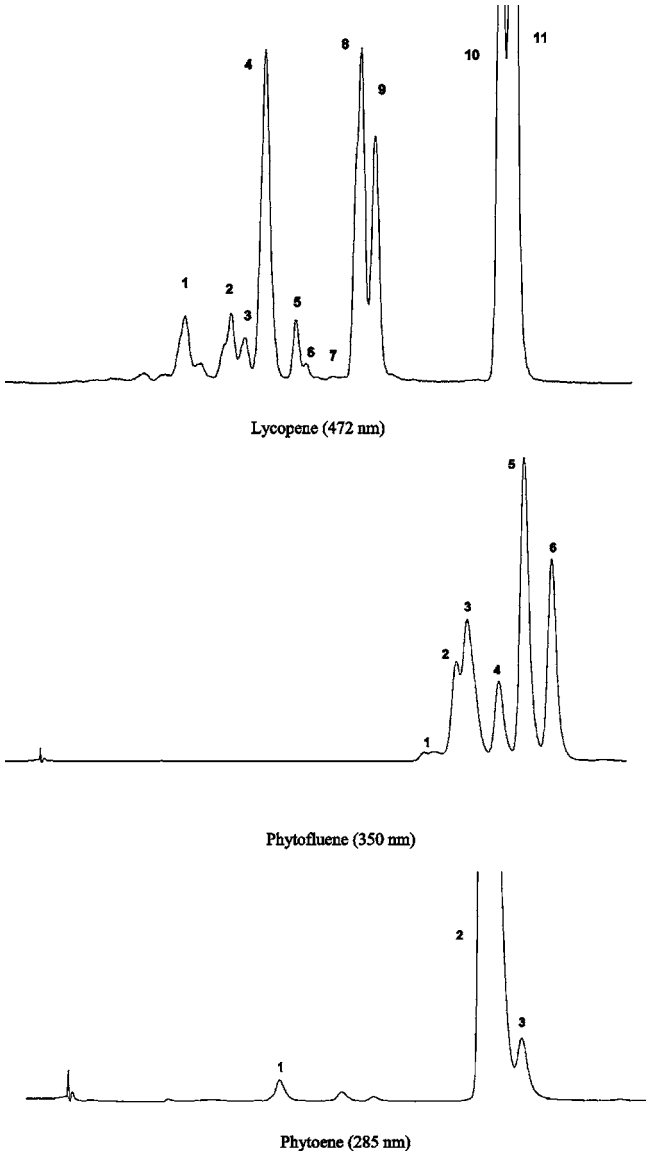


**Figure 4.** Chromatograms corresponding to the stereochemical sets of lycopene, phytofluene, and phytoene at the thermodynamic equilibrium. Chromatographic and UV−vis spectroscopic details are summarized in Supporting Information Table 1.

The time-course changes in the proportions (calculated as a function of chromatographic peak area) of their different geometrical isomers as a function of the stereomutation method used are represented in Figure 5.

The results indicated that the equilibrium in the thermal isomerization of lycopene was already achieved at time (*t*) = 60 min, as the relative proportions of the isomers remained almost constant from this time point. At 60 min the relative proportions of the major compounds were as follows: (5*Z*)-lycopene (approximately 33%), (all-*E*)-lycopene (approximately 22%), lycopene isomers 8 (tentatively identified as (9*Z*)-lycopene) (approximately 13%), lycopene isomer 4 (tentatively identified as (15*Z*)-lycopene) (approximately 13%), and lycopene isomer 9 (tentatively identified as (5*Z*,9*Z*)-lycopene) (approximately 8.5%). In a recent study the thermal isomerization at 50 °C


dx.doi.org/10.1021/jf5041965 | J. Agric. Food Chem. 2014, 62, 12399−12406

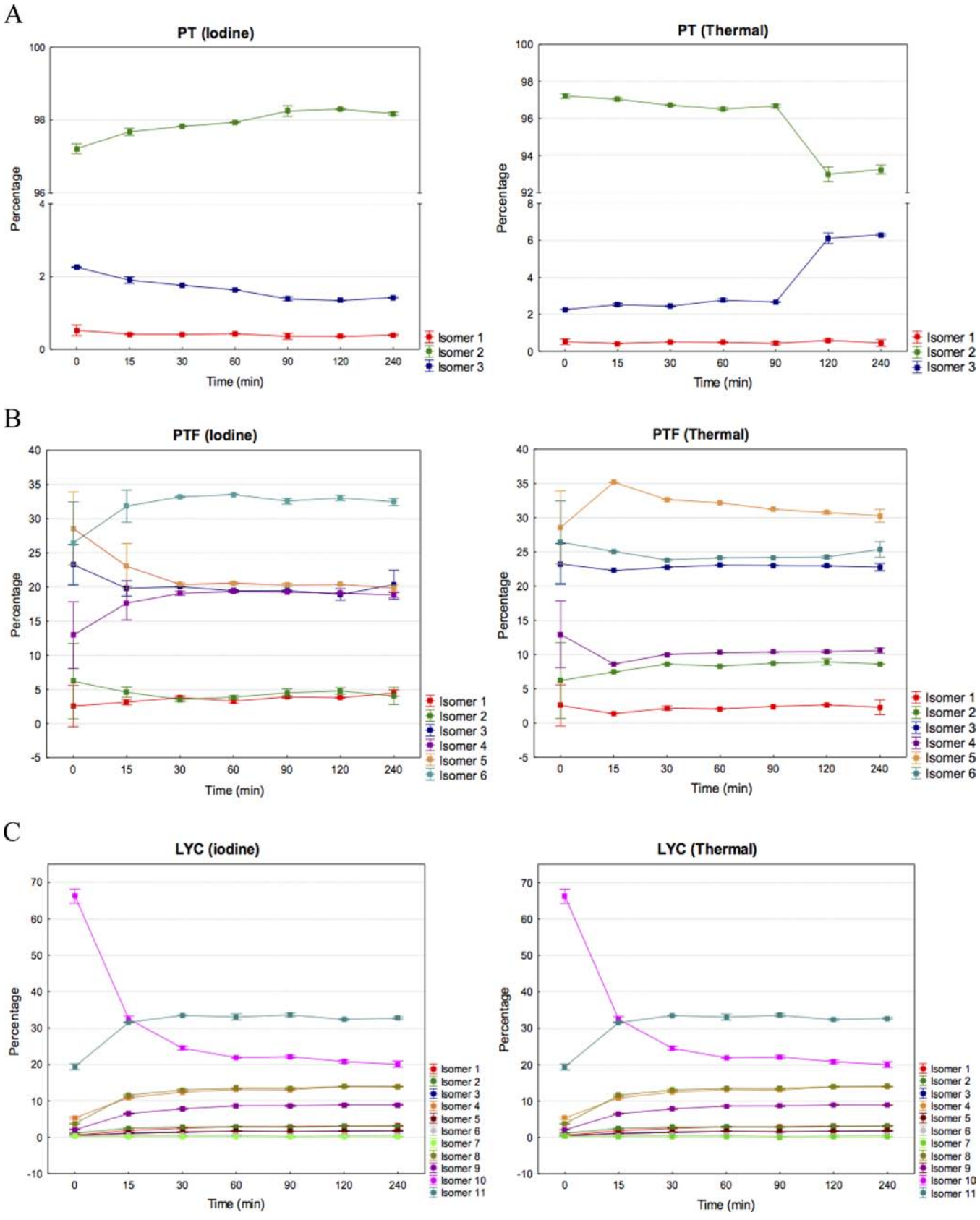


**Figure 5.** Time-course changes in the proportions of the different geometrical isomers of phytoene (PT, part A), phytofluene (PTF, part B), and lycopene (LYC, part C) as a function of the stereomutation method used.

of lycopene in both hexane and benzene was evaluated. In the case of the reaction in hexane, the levels of (5*Z*)-lycopene were the highest from 96 h up to the end of the test period (192 h). In the case of the reaction in benzene, its levels increased steadily


dx.doi.org/10.1021/jf5041965 | *J. Agric. Food Chem.* 2014, 62, 12399−12406

from time 0 until the end of the test period, which was only 96 h in this case. (13*Z*)-Lycopene was identified as the first (*Z*)-isomer to be formed as a result of the heating of (all-*E*)-lycopene[20]

Considering the iodine-catalyzed isomerization, the equilibrium was also achieved at $t$ = 60 min. At that time the major compounds were the same as those observed in the thermal stereomutation. Interestingly, their relative proportions were also almost the same (Figure 5).

Concerning phytofluene, the equilibrium of the thermal stereomutation was already achieved at $t$ = 30 min. The major isomers at that point were the isomer tentatively identified (please see Supporting Information Table 1 and Figure 4) as (all-*E*)-phytofluene (approximately 33%, peak 5), phytofluene isomer 6 (approximately 24%, peak 6), and phytofluene isomer 3 (approximately 23%, peak 3). The isomeric set at the equilibrium achieved with the iodine catalyzed isomerization ($t$ = 30 min) was different in quantitative terms. The relative proportions of the major isomers were the following: isomer 6 (approximately 33%, peak 6), isomer 5 (approximately 20%, peak 5), isomer 3 (approximately 20%, peak 3), and isomer 4 (approximately 19%, peak 4).

The changes in the relative proportions of geometrical isomers of phytoene as a result of the isomerization reactions were less noticeable. As a result of the thermal treatment the equilibrium was already achieved at $t$ = 120 min. The relative proportion of (15*Z*)-phytoene was approximately 93% and that of (all-*E*)-phytoene approximately 6%. The photoisomerization catalyzed by iodine led to a different isomeric set at the equilibrium ($t$ = 90 min). Specifically, the relative proportions of (15*Z*)-phytoene and (all-*E*)-phytoene were approximately 98% and 1.5%, respectively.

Altogether, the experiments indicated that, regardless of the compound and the stereomutation procedure, the levels of (*Z*)-isomers clearly predominated over their all-*E* counterparts at the equilibrium. Except in the case of lycopene, noticeable differences were observed in the isomeric sets at the equilibrium as a function of the stereomutation method followed. Considering that the photochemical isomerization catalyzed by iodine leads to a thermodynamic equilibrium, it appears that both (5*Z*)-lycopene and (15*Z*)-phytoene are more stable than their (all-*E*)-isomer. In addition, the compound identified as phytofluene isomer 6 seems to be more stable than the isomer tentatively identified as (all-*E*)-phytofluene.

On the other hand, heating leads to a kinetic equilibrium. In the light of our results it seems that such equilibrium favors (5*Z*)-lycopene and (15*Z*)-phytoene over their (all-*E*)-counterparts. Likewise, the equilibrium favors (all-*E*)-phytofluene over phytofluene isomer 6.

**In Silico Study of the Relative Stability of Isomers.** To gain further insight into the relative thermodynamic stability of geometrical isomers, *in silico* studies were performed. As a first step, the (all-*E*)-isomers of the three carotenoids were modeled and their minimal energies calculated. As it can be readily observed in Figure 2, the shapes of the three (all-*E*)-isomers are markedly different. In the case of lycopene, the longh chromophore of 11 conjugated double bonds (cdb) prevents the molecule from folding to a great extent. Phytoene and phytoene (with 5 and 3 cdb, respectively) can fold more freely and adopt less rigid shapes. Consequently, the torsional potential energies (kcal/mol) increased in the following order: phytoene < phytofluene < lycopene. The same trend was observed after the conformational analysis once the (*Z*)-isomers were included, the phytoene isomers being the least energetic due to their increased flexibility (Figure 3).

In the case of lycopene it was observed that the energy of the (5*Z*)-isomer (73.6 kcal/mol) was lower than that of (all-*E*)-lycopene (74.6 kcal/mol). This agrees with a previous study on the relative stability of several lycopene isomers.[21]

Concerning phytofluene, the energy of the modeled (9*Z*)-isomer was lower (58.7 kcal/mol) than that of (all-*E*)-phytofluene (60.7 kcal/mol). Regarding phytoene, the modeled (5*Z*)- and (13*Z*)-isomers were found to be less energetic (55.9 and 57.0 kcal/mol) than (all-*E*)-phytoene (57.1 kcal/mol). This finding is in disagreement with the observation that (15*Z*)-phytoene is the major isomer in the equilibria achieved by the stereomutation methods used in this study and in carotenogenic organisms in general. Altogether the results of the *in silico* studies indicate that, in the case of the major tomato carotenes, all of which are linear (i.e., they do not contain rings), the (all-*E*)-isomers are not the most stable thermodynamically. However, it should be noted that the energy differences between isomers were very low in some cases.

Interestingly the calculated energy of apparently symmetrical isomers (for example (5*Z*)- and (5′*Z*)-lycopene) was slightly different (Figure 3).

**Technological Implications.** *Presence of (Z)-Carotene Isomers in Tomato Fruits and Products.* Lycopene is largely in the (all-*E*) configuration in most red tomato genotypes whereas phytoene occurs largely as the (15*Z*)-isomer.[22] Information on the main configuration of phytofluene in tomatoes is not as conclusive. Different geometrical isomers of phytofluene in tomato were separated by HPLC on a calcium hydroxide column[23] and from the tomato source used in the present study (Figure 6). Some of these phytofluene isomers have also been observed in other studies,[16] although their conclusive annotation remains obscure.

(*Z*)-Lycopene isomers proportions ranging from 8% to 21% of total lycopene have been reported in processed tomato products, with (5*Z*)-lycopene being the predominant (*Z*)-isomer.[24] The mean proportions of (*Z*)-lycopene isomers in tomato and tomato products reported in that study were very similar (13% and 14%, respectively), and agreed well with data reported by Schierle et al.[25] This proportion is lower than that found in the thermodynamic or kinetic equilibria, indicating that the conditions of the industrial processing and the food matrix play an important role in the isomerization. These results further support that lycopene from tomato is relatively stable to isomerization during industrial processing. In contrast to lycopene, the occurrence of different isomers of phytoene and phytofluene in commercial tomato products has not been specifically studied previously.

*Effect of Thermal Treatments on the Isomerization of Tomato Carotenes.* Industrial thermal treatments are not expected to result in an extensive isomerization of (all-*E*)-lycopene to (*Z*)-isomers.[26−29] Some studies indicate that long times and very high temperatures are required to markedly increase lycopene (*Z*)-isomers. Colle et al. (2010)[30] concluded that 140 °C for 30 min was needed to cause noticeable increases in (*Z*)-isomers. The impact of thermal processing in the levels of tomato phytoene and phytofluene has not been studied in detail.

*Isomerization of Tomato Lycopene, Phytoene, and Phytofluene: Technological Implications.* Considering the large proportions of lycopene (*Z*)-isomers achieved in our experiments (approximately 80%), it appears that they (particularly the (5*Z*)-isomer) are favored both thermodinamically

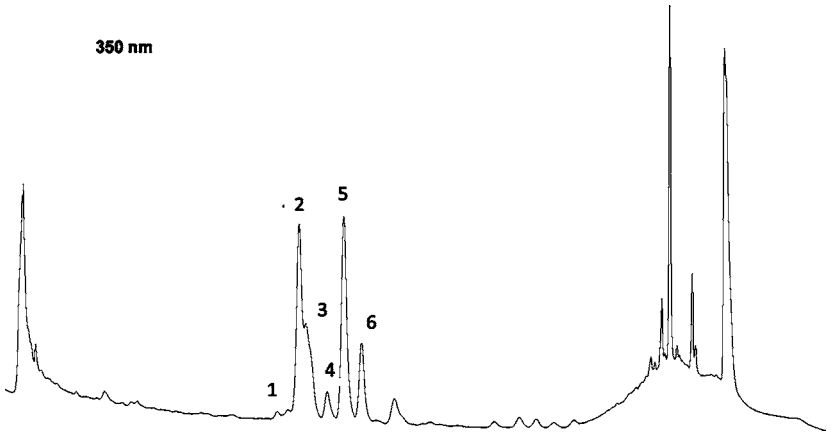


**Figure 6.** Chromatogram at 350 nm of the tomato extract used for the isolation of pure carotenoids. Major phytofluene isomers detected are indicated (peaks 1−6).

and kinetically in the equilibria. The fact that such a proportion does not match those observed in processed tomato products is striking. However, it is well-known that (all-*E*)-lycopene aggregates into crystalline structures in tomato chromoplasts,[9] and lycopene molecules in crystalline structures are not expected to participate in isomerization reactions.[31] There is evidence that the addition of oil results in an increase of the levels of (*Z*)-lycopene isomers,[29,32] attributable to the solubilization of the crystals. Thus, van het Hof et al. (1998)[33] reported a proportion of (*Z*)-isomers approximately 55% when a tomato product was thermally treated in the presence of 10% maize oil, such proportion being lower (approximately 35%) with 5% oil addition and in the absence of oil (approximately 5%).

Phytoene occurs mainly (typically >95%) as the (15*Z*)-isomer in tomatoes.[22] The data obtained in the present study indicated that (15*Z*)-isomer is (>94%) the predominant isomer in the equilibria. (*Z*)-Isomers are thought to show less tendency to form crystals. In fact, phytoene crystals in tomato have not been described. Consequently, it is unlikely to expect high levels of other phytoene isomers as a result of the thermal treatment and/or addition of oil to tomato products. In the untreated phytofluene extract for the stereomutation experiments, up to 6 isomers were detected, with proportions ranging from approximately 2.5% to approximately 28% ($t$ = 0, Figure 5). Consequently, it can be deduced that the (all-*E*)-isomer was in a lower proportion that the sum of the (*Z*)-isomers independent of the procedure followed. The aggregation of tomato phytofluene into crystals has not been described, and the presence of 3−4 predominant geometrical isomers of phytofluene as a result of tomato processing can be expected. Presently the impact of oil addition on the isomerization of both phytoene and phytofluene is sparsely studied.

**Nutritional Implications.** Stahl and Sies (1992)[34] hypothesized that lycopene (*Z*)-isomers may be better absorbed than the (all-*E*)-isomer and that there may be *in vivo* isomerization mechanisms. Several studies reported that lycopene (*Z*)-isomers predominate in human samples[25,35] and that the absorption of those isomers was possibly favored.[36,37] Other investigators concluded that (all-*E*)-lycopene remains largely in that isomeric form during digestion and that the intestinal cells may be a key location for its isomerization.[38] Unlu et al. (2007)[37] concluded that the hypothesis of the preferential absorption of lycopene (*Z*)-isomers could not explain their increased proportion in human samples suggesting that additional *in vivo* isomerization may take place. Richelle et al. (2010)[38] observed that in their *in vitro* and *in vivo* models the lycopene isomeric profiles were comparable, suggesting that the ability of "low" and "high" lycopene absorbers for the isomerization of lycopene is very similar. The formation of lycopene isomers may therefore depend to a great extent on factors like their relative thermodynamic stability or formation rate. Evidence for this hypothesis was obtained in a study[39] where meals containing high proportions (approximately 70%) of different lycopene (*Z*)-isomers were provided to humans and high proportions of the (5*Z*)- and (all-*E*)-isomers were found in the triglyceride-rich lipoproteins. These observations agreed well with the data reported in the present study indicating that the thermodynamic stability and formation rates of (5*Z*)- and (all-*E*)-lycopene are higher in comparison to other geometrical isomers. Interestingly, Clinton et al. (1996)[40] reported proportions of lycopene (*Z*)-isomers in human serum and prostate sample tissues resembling those found at the equilibrium (approximately 80%) in the present study.

Although there are studies that report the presence of both phytoene and phytofluene in the plasma and tissues of mammals (including humans),[5,41,42] data on their isomeric profile are very scarce. In a recent study, the presence of large amounts of (15*Z*)-phytoene and several isomers of phytofluene in samples from mammals has been reported.[16]

In conclusion, the results of the stereomutations and the *in silico* studies performed in this study indicate that certain (*Z*)-isomers of lycopene, phytoene, and phytofluene are favored thermodynamically and kinetically. Although these observations cannot be extrapolated to biological systems directly, they can aid in understanding the findings of some nutritional studies, where high levels of lycopene (*Z*)-isomers are consistently found in human plasma and tissues. The results also enlighten why the concentration of lycopene (*Z*)-isomers can increase when oil is added to tomato products. The data on the proportions of different isomers of the colorless carotenes, phytoene, and phytofluene in the equilibria is useful to forecast their expected isomeric mixtures in foods and human tissues and biological fluids. According to the results of this study, phytoene could be expected to occur largely as the (15*Z*)-isomer in humans and phytofluene as a mixture of several geometrical isomers. Finally, on the basis of our results, the use of geometrical isomers of lycopene and phytofluene on their own or as mixtures are recommended in the *in vitro*, *ex vivo*, and *in vivo* future studies aimed at assessing their possible biological activities. Likewise, it is recommended to use (15*Z*)-phytoene in such studies.

## ■ ASSOCIATED CONTENT

### Supporting Information

Additional table. Chromatographic and UV−vis spectroscopic data of phytoene, phytofluene, and lycopene geometrical isomers. This material is available free of charge via the Internet at http://pubs.acs.org.

## ■ AUTHOR INFORMATION


### Corresponding Author

*Phone: +34 954556495. Fax: +34 954557017. E-mail: ajmelendez@us.es.



### Funding

A.J.M.-M. acknowledges funding from the Spanish State Secretariat of Research, Development and Innovation (Ministry of Economy and Competitiveness, CAROTFUNCT project ref AGL2012−37610, cofunded by FEDER) and the Andalusian Coundil of Economy, Innovation, Science and Employment (project ref CAROTINCO-P12-AGR-1287). A.J.M.-M., M.P., C.M.S., and P.M.-B. are members of the IBERCAROT network, funded by CYTED (ref 112RT0445).


### Notes

The authors declare no competing financial interest.

## ■ ACKNOWLEDGMENTS


The authors are grateful to LycoRed Ltd. (Beer Sheva, Israel) for the supply of Lycomato.


## ■ REFERENCES


(1) Britton, G.; Liaaen-Jensen, S.; Pfander, H. *Carotenoids. Vol. 4: Natural Functions*; Birkhäuser: Basel, Switzerland, 2008.

(2) Krinsky, N.; Mayne, S. T.; Sies, H. *Carotenoids in Health and Disease*; Marcel Dekker: New York, 2004.

(3) Britton, G.; Liaaen-Jensen, S.; Pfander, H. *Carotenoids. Vol. 5: Nutrition and Health*; Birkhäuser: Basel, Switzerland, 2009.

(4) Giovannucci, E. A review of epidemiologic studies of tomatoes, lycopene, and prostate cancer. *Exp. Biol. Med.* **2002**, *227*, 852−859.

(5) Khachik, F.; Carvalho, L.; Bernstein, P. S.; Muir, G. J.; Zhao, D. Y.; Katz, N. B. Chemistry, distribution, and metabolism of tomato carotenoids and their impact on human health. *Exp. Biol. Med.* **2002**, *227*, 845−851.

(6) Meléndez-Martínez, A. J.; Fraser, P. D.; Bramley, P. M. Accumulation of health promoting phytochemicals in wild relatives of tomato and their contribution to in vitro antioxidant activity. *Phytochemistry.* **2010**, *71*, 1104−1114.

(7) Engelmann, N. J.; Clinton, S. K.; Erdman, J. W. Nutritional aspects of phytoene and phytofluene, carotenoid precursors to lycopene. *Adv. Nutr.* **2011**, *2*, 51−61.

(8) Zechmeister, L. *Cis-Trans Isomeric Carotenoids, Vitamins A and Arylpolyenes*; Spring-Verlag: Wien, Austria, 1962.

(9) Britton, G. Structure and properties of carotenoids in relation to function. *FASEB J.* **1995**, *9*, 1551−1558.

(10) Hu, K. Q.; Liu, C.; Ernst, H.; Krinsky, N. I.; Russell, R. M.; Wang, X. D. The biochemical characterization of ferret carotene-9 ′,10 ′-monooxygenase catalyzing cleavage of carotenoids in vitro and in vivo. *J. Biol. Chem.* **2006**, *281*, 19327−19338.

(11) Lian, F.; Smith, D. E.; Ernst, H.; Russell, R. M.; Wang, X. D. Apo-10′-lycopenoic acid inhibits lung cancer cell growth in vitro, and suppresses lung tumorigenesis in the A/J mouse model in vivo. *Carcinogenesis* **2007**, *28*, 1567−1574.

(12) Lian, F.; Wang, X. D. Enzymatic metabolites of lycopene induce Nrf2-mediated expression of phase II detoxifying/antioxidant enzymes in human bronchial epithelial cells. *Int. J. Cancer* **2008**, *123*, 1262−1268.

(13) Böhm, V.; Puspitasari-Nienaber, N. L.; Ferruzzi, M. G.; Schwartz, S. J. Trolox equivalent antioxidant capacity of different geometrical isomers of α-carotene, β-carotene, lycopene, and zeaxanthin. *J. Agric. Food Chem.* **2002**, *50*, 221−226.

(14) Müller, L.; Goupy, P.; Fröhlich, K.; Dangles, O.; Caris-Veyrat, C.; Böhm, V. Comparative Study on Antioxidant Activity of Lycopene (Z)-Isomers in Different Assays. *J. Agric. Food Chem.* **2011**, *59*, 4504−4511.

(15) Rodriguez-Amaya, D. B. *A Guide to Carotenoid Analysis in Foods*; ILSI Press: Washington, DC, 2001.

(16) Meléndez-Martínez, A. J.; Stinco, C. M.; Liu, C.; Wang, X. D. A simple HPLC method for the comprehensive analysis of cis/trans (Z/E) geometrical isomers of carotenoids for nutritional studies. *Food Chem.* **2013**, *138*, 1341−1350.

(17) Fröhlich, K.; Conrad, J.; Schmid, A.; Breithaupt, D. E.; Böhm, V. Isolation and structural elucidation of different geometrical isomers of lycopene. *Int. J. Vitam. Nutr. Res.* **2007**, *77*, 369−375.

(18) Hengartner, U.; Bernhard, K.; Meyer, K.; Englert, G.; Glinz, E. Synthesis, isolation, and NMR-spectroscopic characterization of fourteen (Z)-isomers of lycopene and of some acetylenic didehydro- and tetradehydrolycopenes. *Helv. Chim. Acta* **1992**, *75*, 1848−1865.

(19) Liaaen-Jensen, S.; Lutnæs, B. F. E/Z Isomers and Isomerization. In *Carotenoids. Vol. 4*, 4th ed.; Britton, G., Liaaen-Jensen, S. v., Pfander, H., Eds.; Birkhäuser: Basel, Switzerland, 2008; pp 15−36.

(20) Takehara, M.; Nishimura, M.; Kuwa, T.; Inoue, Y.; Kitamura, C.; Kumagai, T.; Honda, M. Characterization and thermal isomerization of (all-E)-lycopene. *J. Agric. Food Chem.* **2014**, *62*, 264−269.

(21) Chasse, G. A.; Mak, M. L.; Deretey, E.; Farkas, I.; Torday, L. L.; Papp, J. G.; Sarma, D. S. R.; Agarwal, A.; Chakravarthi, S.; Agarwal, S.; Rao, A. V. An ab initio computational study on selected lycopene isomers. *THEOCHEM* **2001**, *571*, 27−37.

(22) Fraser, P. D.; Bramley, P. M. The biosynthesis and nutritional uses of carotenoids. *Prog. Lipid Res.* **2004**, *43*, 228−265.

(23) Schmitz, H. H.; Emenhiser, C.; Schwartz, S. J. HPLC separation of geometric carotene isomers using a calcium hydroxide stationary phase. *J. Agric. Food Chem.* **1995**, *43*, 1212−1218.

(24) Stinco, C. M.; Rodríguez-Pulido, F. J.; Escudero-Gilete, M. L.; Gordillo, B.; Vicario, I. M.; Meléndez-Martínez, A. J. Lycopene isomers in fresh and processed tomato products: Correlations with instrumental color measurements by digital image analysis and spectroradiometry. *Food Res. Int.* **2013**, *50*, 111−120.

(25) Schierle, J.; Bretzel, W.; Bühler, I.; Faccin, N.; Hess, D.; Steiner, K.; Schüep, W. Content and isomeric ratio of lycopene in food and human blood plasma. *Food Chem.* **1997**, *59*, 459−465.

(26) Nguyen, M. L.; Schwartz, S. J. Lycopene stability during food processing. *Proc. Soc. Exp. Biol. Med.* **1998**, *218*, 101−105.

(27) Abushita, A. A.; Daood, H. G.; Biacs, P. A. Change in carotenoids and antioxidant vitamins in tomato as a function of varietal and technological factors. *J. Agric. Food Chem.* **2000**, *48*, 2075−2081.

(28) Nguyen, M.; Francis, D.; Schwartz, S. Thermal isomerisation susceptibility of carotenoids in different tomato varieties. *J. Sci. Food Agric.* **2001**, *81*, 910−917.

(29) Seybold, C.; Fröhlich, K.; Bitsch, R.; Otto, K.; Bõhm, V. Changes in contents of carotenoids and vitamin E during tomato processing. *J. Agric. Food Chem.* **2004**, *52*, 7005−7010.

(30) Colle, I.; Lemmens, L.; Van Buggenhout, S.; Van Loey, A.; Hendrickx, M. Effect of thermal processing on the degradation, isomerization, and bioaccessibility of lycopene in tomato pulp. *J. Food Sci.* **2010**, *75*, C753−C759.

(31) Lambelet, P.; Richelle, M.; Bortlik, K.; Franceschi, F.; Giori, A. M. Improving the stability of lycopene Z-isomers in isomerised tomato extracts. *Food Chem.* **2009**, *112*, 156−161.

(32) Agarwal, A.; Shen, H.; Agarwal, S.; Rao, A. V. Lycopene content of tomato products: Its stability, bioavailability and in vivo antioxidant properties. *J. Med. Food* **2001**, *4*, 9−15.

(33) Van het Hof, K. H.; Gärtner, C.; West, C. E.; Tijburg, L. B. Potential of vegetable processing to increase the delivery of carotenoids to man. *Int. J. Vitam. Nutr. Res.* **1998**, *68*, 366−370.

(34) Stahl, W.; Sies, H. Uptake of Lycopene and Its Geometrical Isomers Is Greater from Heat-Processed than from Unprocessed Tomato Juice in Humans. *J. Nutr.* **1992**, *122*, 2161−2166.

(35) Ferruzzi, M. G.; Nguyen, M. L.; Sander, L. C.; Rock, C. L.; Schwartz, S. J. Analysis of lycopene geometrical isomers in biological microsamples by liquid chromatography with coulometric array detection. *J. Chromatogr. B: Biomed. Sci. Appl.* **2001**, *760*, 289−299.
(36) Failla, M. L.; Chitchumroonchokchai, C.; Ishida, B. K. In vitro micellarization and intestinal cell uptake of cis isomers of lycopene exceed those of all-trans lycopene. *J. Nutr.* **2008**, *138*, 482−486.
(37) Unlu, N. Z.; Böhn, T.; Francis, D. M.; Nagaraja, H. N.; Clinton, S. K.; Schwartz, S. J. Lycopene from heat-induced cis-isomer-rich tomato sauce is more bioavailable than from all-trans-rich tomato sauce in human subjects. *Br. J. Nutr.* **2007**, *98*, 140−146.
(38) Richelle, M.; Sánchez, B.; Tavazzi, I.; Lambelet, P.; Bortlik, K.; Williamson, G. Lycopene isomerisation takes place within enterocytes during absorption in human subjects. *Br. J. Nutr.* **2010**, *103*, 1800−1807.
(39) Richelle, M.; Lambelet, P.; Rytz, A.; Tavazzi, I.; Mermoud, A. F.; Juhel, C.; Borel, P.; Bortlik, K. The proportion of lycopene isomers in human plasma is modulated by lycopene isomer profile in the meal but not by lycopene preparation. *Br. J. Nutr.* **2012**, *107*, 1482−1488.
(40) Clinton, S. K.; Emenhiser, C.; Schwartz, S. J.; Bostwick, D. G.; Williams, A. W.; Moore, B. J.; Erdman, J. W. cis-trans lycopene isomers, carotenoids, and retinol in the human prostate. *Cancer Epidemiol., Biomarkers Prev.* **1996**, *5*, 823−833.
(41) Khachik, F.; Spangler, C. J.; Smith, J. C., Jr.; Canfield, L. M.; Steck, A.; Pfander, H. Identification, quantification and relative concentrations of carotenoids and their metabolites in human milk and serum. *Anal. Chem.* **1997**, *69*, 1873−1881.
(42) Aust, O.; Stahl, W.; Sies, H.; Tronnier, H.; Heinrich, U. Supplementation with tomato-based products increases lycopene, phytofluene, and phytoene levels in human serum and protects against UV-light-induced erythema. *Int. J. Vitam. Nutr. Res.* **2005**, *75*, 54−60.

are also explored in relation with their concentrations to evalute their contribution to the antioxidant capacity of calafate. This research is a contribution to promote, from a scientific perspective, the potential of this underexploited fruit, complementing previous work about anthocyanins and hydroxycinnamic acids now with flavonol and alkaloid levels and antioxidant capacity.

## MATERIALS AND METHODS

**Reagents, Standards, and Extraction Materials.** Commercial standards of quercetin-3-rutinoside (<94%), quercetin-3-galactoside (>97%), quercetin-3-glucoside (>90%), quercetin-3-rhamnoside (85%), quercetin-3-*O*-(6″malonyl)-D-*β*-glucoside (85%), berbamine dihydrochloride, and berberine hydrochloride (<90%) were obtained from Sigma (Steinheim, Germany). Quercetin-3-glucoside (99%), jatrorrhizine hydrochloride (99.71%), palmatine hydrochloride (96.98%), and canadine (99.99%) were provided by Phytolab (Vestenbergsreuth, Germany), and oxyacanthine was from Extrasynthese (Genay, France). Formic acid, ammonia (25%), dichloromethane, hydrochloric acid, and HPLC grade solvents (acetonitrile, methanol, and water) were provided by Merck (Darmstadt, Germany). Flavonol cleanup was accomplished using a 150 mg Oasis MCX 6 $cm^3$ mixed phase SPE cartridges from Waters (Milford, MA, USA) and alkaloid recovery by using organic extracts from Extrelut NT 20 columns from Merck.

**Plant Material.** Flavonols and alkaloids were studied in 65 mature calafate samples and in 16 mature samples of other endemic *Berberis* species including *B. empetrifolia*, *B. darwinii*, *Berberis ilicifolia*, *Berberis montana*, and the introduced *Berberis vulgaris*. All of the fruits were collected from Chilean Patagonia, between the Araucanía and Magallanes regions (37−54° S and 74−69° W) in 2010 and 2011, with the exception of *B. vulgaris*, which was obtained in the Bio Bio region (36° 49′ S; 73° 02′ W). Other samples of roots, leaves, branches, and fruits were obtained from six different *Berberis* plants (*B. microphylla* G. Forst, *B. ilicifolia*, and *B. vulgaris*) to study the distribution of alkaloids in the plants. Additionally, calafate berry samples collected with three different phenological stages from one plant from sector Barranco Amarillo, Magallanes (53° 05′ S; 70° 52′ W) were included to study their influence on flavonol and alkaloid profiles and concentrations. The study of flavonol profile and concentrations in skin, pulp, and seed obtained from two composed calafate samples, one from Magallanes and other from Aysen, was also accomplished. All samples were kept frozen (−20 °C) before their analyses, and all their classifications were made by a taxonomy expert compared with specimens from the University of Concepcion Herbarium.

**Instruments.** An analytical balance of Denver Instrument Co. (New York, USA), an ultrasonic bar homogenizer Cole Palmer Series 4710 (Chicago, IL, USA), a mechanical shaker Stuart S01 Bibby Sterilin LTD (Stanford, UK), a centrifuge Sigma 3-16p Christ, (Osterode, Germany), and a rotavapor complemented with a vacuum pump V-700 and controller system V-850, Büchi (Flawil, Switzerland) were used for sample preparation. A microplate reader (Epoch, Biotek Instruments, Winooski, VT, USA) was used for antioxidant assays.

The HPLC-DAD-ESI-MS/MS analyses for flavonol and alkaloid identification were carried out by using a Shimadzu Nexera UHPLC/HPLC system (Kyoto, Japan) equipped with a quaternary LC-30AD pump, a DGU-20A5R degasser unit, a Prominence CTO-20 AC oven, an SIL-30AC autosampler, and an SPD-M20A UV−vis photodiode array spectrophotometer detector coupled in tandem with a LC-MS/MS detector QTrap 3200 MDS Sciex (USA). Instrument control and the data collection system were carried out using CLASS-VP DAD Shimadzu Chromatography Data System (Kyoto, Japan) and Analyst software version 1.5.2 for MS/MS analysis AB Sciex (Framingham, MA, USA).

Quantitative analyses of alkaloids were carried out using a HPLC with fluorescence detector composed of a LaChrom Elite L-2130 pump, an L-2200 autosampler, and an L-7485 detector from Hitachi High Technologies Co, (Tokyo, Japan), with a CTO-10AVP oven Shimadzu (Kyoto, Japan). The data collection was done using an interactive software graphics version 6.2 Varian Inc. (Palo Alto, CA, USA).

**Sample Pretreatments.** *Flavonols.* Whole extract preparation and cleanup were carried out on the basis of the methods described by Ruiz et al. and Castillo-Muñoz et al.[2,11] with minor modifications. Five grams of whole fruit was ground in a stainless steel mixer with 10 mL of methanol/water (93:7% v/v); the extract was treated for 45 s with the ultrasonic bar, followed by 16 h of mechanical shaking under darkness. After centrifugation, the separated supernatant was transferred, and the residual solid was washed three times with 5 mL of the same solvent by mechanical shaking for 15 min. Cleanup of the combined extracts (25 mL) was made by using Oasis MCX cartridges, to eliminate the interfering anthocyanins. One milliliter of crude extract was dried in a rotary evaporator and reconstituted in 1.0 mL of 0.1 N hydrochloric acid. This solution was loaded on a MCX cartridge previously conditioned with 5.0 mL of methanol and 5.0 mL of water. A washing step, using 5.0 mL of 0.1 N hydrochloric acid and 5.0 mL of water, was necessary to remove sugars. The flavonol fraction was eluted with 3 × 5.0 mL of methanol and, finally, the solvent was distilled off by vacuum evaporation and the residue was redissolved in 1 mL of the mobile phase (0.1% formic acid in water/acetonitrile 85:15%v/v) for its chromatographic analysis. This fraction also contained the hydroxycinnamic acids.

In the study of flavonol distribution in different parts of the fruits (seeds, pulp, and skin), frozen berries were peeled, the pulp was separated from the seed, and all were carefully dried with paper toweling. Each was separately ground before the same extraction procedure as described above was applied.

*Alkaloids.* The method was adapted from a procedure described for alkaloid extraction of lupine seeds and plants,[9] which was based on the method proposed by Wink,[10] with modifications: 1 g of calafate sample (fruit, seeds, leaves, branches, or roots) was extracted with 8 mL of 0.1 N HCl with the assistance of an ultrasonic bar for 45 s and mechanical shaking for 10 min. After centrifugation, the supernatant was transferred to a 25 mL volumetric flask, and the solid residues were washed three times with 5 mL of the same solvent (in the case of fruits, seeds, and leaves) and 8 mL (in the case of roots and branches). The whole extract was neutralized using $NH_4OH$ and completed to 25 mL. Twenty milliliters of extract was transferred to an Extrelut NT-20 column, to carry out the liquid−liquid extraction, using dichloromethane as the elution solvent (4 × 25 mL). After that, the solvent was evaporated at reduced pressure (30 °C) and finally redissolved in 1 mL of mobile phase (0.1% of formic acid in water/acetonitrile 20:80% v/v) and filtered before its chromatographic analysis.

**Flavonol Analyses.** *HPLC-DAD.* Three $C_{18}$ columns were evaluated for flavonol HPLC separation: (A) $C_{18}$ column (Kromasil $C_{18}$ 100 A, 5 $\mu$m, 250 × 4.6 mm) with a $C_{18}$ precolumn (Nova-Pak Waters, 4 $\mu$m, 22 × 3.9 mm); (B) $C_{18}$ core−shell column (Kinetex $C_{18}$ 100 A, 2.6 $\mu$m, 150 × 4.6 mm) with a $C_{18}$ precolumn for UHPLC columns (Phenomenex AJ0-9000, 2.2 $\mu$m, 22 × 3.9 mm); (C) $C_{18}$ UHPLC column (Shim-pack XR-ODS III, 2.2 $\mu$m, 150 × 2.0 mm) without a precolumn. The chromatographic separation conditions were optimized for each column and were carried out at 30 °C using 0.1% of formic acid in water (A) and acetonitrile (B) as mobile phase. The optimized separation using column A was carried out at a flow rate of 1 mL/min, with a gradient starting with 80% A for 6.5 min, from 80 to 76% in 6 min, from 76 to 60% in 2.5 min, and from 60 to 0% in 0.5 min, maintaining the proportion for 6.5 min, and a final stabilization step of 10 min at 80% A. The injection volume was 10 $\mu$L.

The separation using column B was carried out also at 1 mL/min with a gradient starting with 85% A for 0.1 min, from 85 to 80% in 5 min, from 80 to 70% in 2.5 min, from 70 to 0% in 0.5 min, maintaining the proportion for 2 min, and with a final stabilization step of 5 min at 85% A. The injection volume was 5 $\mu$L.

Finally, the separation in column C was carried out at a flow rate of 0.5 mL/min, with a gradient starting with 85% A for 12 min, from 85 to 60% in 3 min, from 60 to 0% in 0.5 min, maintaining the proportion for 5 min, and with a final stabilization step of 7 min at 85% A. The injection volume in this case was also 5 $\mu$L.

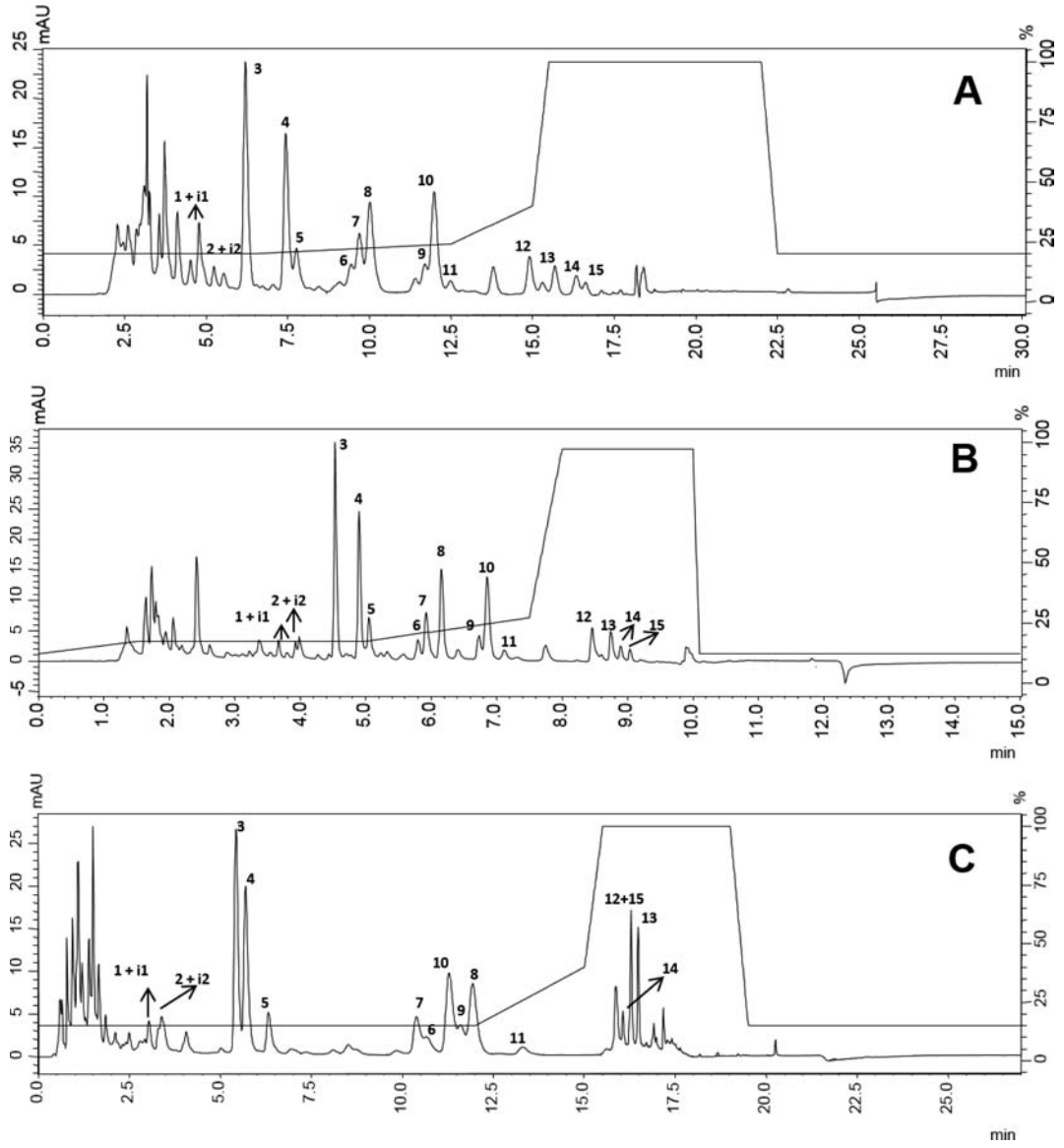


**Figure 1.** Chromatograms of flavonols extract of *B. microphylla* G. Forst fruit (from Reserva Forestal Magallanes) using different columns: (A) classical column; (B) core−shell column; (C) UHPLC column. Chromatographic conditions are described in the text.

Flavonol quantitation was performed through a DAD chromatogram extracted at 360 nm by external calibration using quercetin-3-rhamnoside, quercetin-3-rutinoside, quercetin-3-galactoside, and quercetin-3-glucoside. Because of the lack of pure standards, 3-rutinoside derivatives were quantitated using the quercetin-3-rutinoside calibration curve. The other detected flavonols were quantitated using the quercetin-3-glucoside curve, based on the similitude between their molar absorptivities.[12] Results were expressed as micromoles per gram FW to compare values obtained using different standards.

*HPLC-DAD-ESI-MS/MS.* The identification by MS/MS was carried out using the same chromatographic condition for core−shell columns (B) with 0.5 mL/min as mobile phase flow. Negative ionization mode was as follows: −20 V declustering potential, −5 V collision energy, −4000 V ionization voltage, capillary temperature at 450 °C, and $N_2$ nebulizer at 15 psi. The identity assignation of analytes was carried out by comparison of their retention time ($t_R$) with those of their respective commercial standards and also by comparison of characteristic spectral data (MS/MS and UV).

In the context of the study of antioxidant capacity, hydroxycinnamic acid derivatives and total phenolics were quantitated by HPLC-DAD according to methods described by Ruiz in 2013 and 2010, respectively.[2,3] Total phenolics were determined as the sum of flavonols, hydroxycinnamic acid derivatives, and anthocyanins present in the whole extracts.

**Alkaloid Analyses.** *Separation and Quantitation.* A $C_{18}$ column (Kromasil C18 XDB, 5 $\mu$m, 250 × 4.6 mm) with a $C_{18}$ precolumn (Nova-Pak Waters, 4 $\mu$m, 22 × 3.9 mm) was used. The separation was carried out at 30 °C at a flow rate of 1 mL/min, by using a mobile phase constituted by 0.1% of formic acid in water (A) and acetonitrile (B), with a gradient starting with 80% A for 1 min, from 80 to 50% for 11 min, from 50 to 0% for 1 min, maintaining the proportion for 5 min, and with a final stabilization step of 10 min at 80% A. The injection volume was 25 $\mu$L, and the detection by fluorescence used 350 and 530 nm as excitation and emission wavelengths, respectively. The quantitative analysis was carried out by external calibration with berberine standard.

*Identification.* Using the same separation conditions described in the preceding paragraph, identification was carried out using the following MS/MS conditions: positive ionization mode, 60 V declustering potential, 10 V collision energy, 5000 V ionization voltage, capillary temperature at 500 °C, and $N_2$ nebulizer at 30 psi. Analyte identity was by comparison of their $t_R$ with those of reference compounds and by comparison of MS/MS and UV spectra.

Table 1. Identity Assignment of Flavonols in *B. microphylla* G. Forst Extracts by HPLC-DAD-ESI-MS/MS

| flavonol | peak identification | $t_R$ (min) | $\lambda_{max}$ (nm) | $[M - H]^-$ | product ion |
|---|---|---|---|---|---|
| myricetin-3-rutinoside + unknown (i1) | 1+i1 | 6.56 | 336 | 625.7 | 316.3 |
| myricetin-3-glucoside + unknown (i2) | 2+i2 | 6.99 | 350 | 479.0 | 316.3 |
| quercetin-3-rutinoside | 3 | 7.97 | 354 | 609.8 | 300.8 |
| quercetin-3-galactoside | 4 | 8.70 | 354 | 463.5 | 300.4 |
| quercetin-3-glucoside | 5 | 8.97 | 351 | 463.6 | 300.4 |
| quercetin-3-malonylgalactoside | 6 | 10.34 | 351 | 463.5 | 301.3 |
| quercetin-3-malonylglucoside | 7 | 10.57 | 354 | 505.6 | 300.3 |
| isorhamnetin-3-rutinoside | 8 | 10.86 | 352 | 623.6 | 315.4 |
| isorhamnetin-3-galactoside | 9 | 11.98 | 351 | 477.5 | 314.3 |
| quercetin-3-rhamnoside | 10 | 12.22 | 347 | 447.5 | 300.4 |
| isorhamnetin-3-glucoside | 11 | 12.65 | 351 | 477.5 | 314.4 |
| isorhamnetin-3-malonylgalactoside | 12 | 15.02 | 351 | 519.5 | 314.3 |
| isorhamnetin-3-malonylglucoside | 13 | 15.72 | 351 | 519.6 | 314.4 |
| quercetin-hexoside + 100 uma | 14 | 16.08 | 352 | 563.5 | 300.3 |
| kaempferol-deoxyhexoside | 15 | 16.46 | 340 | 431.5 | 284.3 |
| kaempferol[a] | 16 | 20.00 | - | 283.6 | - |

[a]Detected only with MS/MS detection.

**$TEAC_{CUPRAC}$ and $TEAC_{ABTS}$ Assays.** $TEAC_{CUPRAC}$ assays were conducted in 96-well microplates. To each well was added with 50 $\mu$L of solution constituted by 10 mM copper(II) solution, neocuproine solution (7.5 mM), and buffer (1 M, pH 7). Microplates were incubated at 37 °C for 15 min before 100 $\mu$L of TROLOX solution or sample was added, and then the plates were incubated at 37 °C for 30 min, after which absorbance was determined at 450 nm using a microplate reader. To evaluate intrinsic absorbance of samples, copper(II) solution and neocuproine solution were replaced by 100 $\mu$L of Milli-Q water. ABTS assay was performed as explained by Ruiz et al.[2] Antioxidant capacity of whole calafate extracts was compared with the SPE fractions (containing flavonols/hydroxycinnamic acids), obtained as previously described.

## RESULTS AND DISCUSSION

**HPLC of Flavonols.** Flavonol separation in the calafate extract is a complex task due to the high diversity of flavonols and other compounds, such as phenolic acids, which coelute on reversed phase columns. As described under Materials and Methods, three reversed phase C-18 columns were evaluated to obtain a better separation of this complex sample. The first column (A) was a classic HPLC column (250 × 4.6 mm, 5 $\mu$m), which allows a higher sample load; the second was a core−shell column (B), with the same internal diameter but a shorter length (150 mm) and smaller particle size 2.6 $\mu$m; and the last one was an UHPLC column (C) with the same length (150 mm) but smaller internal diameter (2 mm) and particle size 2.2 $\mu$m, allowing reduction of solvent consumption.[13] The respective chromatograms obtained for each under optimal conditions are presented in Figure 1.

The best separation was reached using the core−shell column (B). This is a sub-3-$\mu$m particle size column, with higher permeability due to the external layer of porous silica bonded to the stationary phase. This type of stationary phase has diminished eddy diffusion coefficients in the van Deemter equation, a decreased axial diffusion by diminution of intraparticle porosity, and a reduced mass transference by decreasing diffusion into the particles of stationary phase.[14] This improved the chromatographic efficiency, with the advantage of working at a much lower pressure and obtaining a more acceptable resolution. All subsequent flavonol analyses were carried out by using the core−shell column (B).

**Flavonol Identification in Calafate Extract.** A great diversity of flavonols was found in calafate samples, with 16 flavonol derivatives being detected in the methanolic calafate extract. The results are summarized in Table 1 and are in accordance with those previously described for a reduced number of samples.[2] However, some exceptions were found. Traces of isorhamnetin malonyl-hexoside, quercetin and kaempferol derivatives, and kaempferol aglycone were observed, with the last one being detected at 20 min by only the MS/MS detector. The low intensity of these signals may have hindered their identification in the previous study by Ruiz et al.[2] On the other hand, 3-rutinoside-7-galactosides of myricetin, quercetin, and isorhamnetin, which have been previously described as present in trace amounts in calafate,[2] were not detected in any of the current samples. Additionally, the higher hydrophilic characteristic of these flavonols, under the separation condition used in this method, could have resulted in the coelution with other interfering compounds in the first part of the chromatogram, mainly hydroxycinnamic acids (see Figure 1B).

The identities of quercetin-3-galactoside (peak 4) and quercetin-3-glucoside (peak 5) were assigned by comparison with retention time of standards. Their identity was confirmed on the basis of their fragmentation pattern, where both compounds showed a quasi-molecular ion of $m/z$ 463, with a product ion of $m/z$ 300. In the case of 3-galactoside and 3-glucoside derivatives of isorhamnetin (peaks 9 and 11), their identities were assigned according to data on flavonol glycosides from the literature.[15]

Signals 6 and 7 showed the same fragmentation pattern, with a quasi-molecular ion of $m/z$ 505 and a product ion of $m/z$ 300, which may be the acetyl hexoside of quercetin. However, the presence of a minor signal of $m/z$ 549 suggested the presence of a malonyl derivate instead. Retention time and mass spectra were compared against a commercial standard of quercetin-3-*O*-(6″-malonyl)-D-$\beta$-glucoside, confirming the identity of this compound. In Figure 2 are presented the mass spectra of the standard and signal 7, showing the same fragmentation patterns. According to the elution order described by Cho et al.,[15] where galactoside showed a shorter retention time in reversed phase chromatography than glucoside derivatives because of their higher polarity, signal 6 was assigned as the

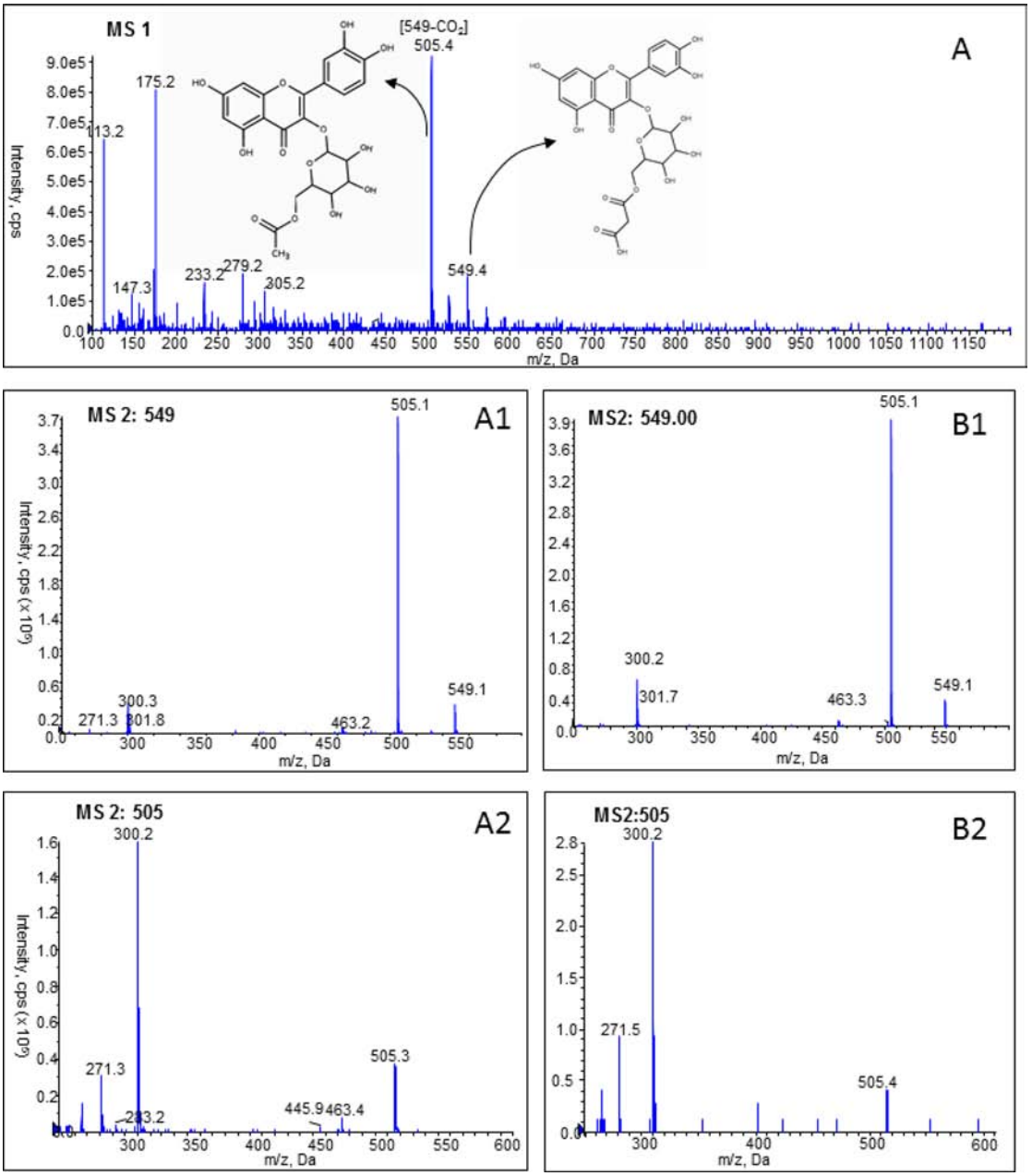


**Figure 2.** (A) Mass spectra of quercetin-3-malonyl glucoside standard; (A1, A2) $MS^2$ of $m/z$ 549 and 505, respectively, of the standard (peak 7); (B1, B2) $MS^2$ of $m/z$ 549 and $m/z$ 505, respectively, of calafate sample (peak 7).

galactoside derivate of this compound. Similar mass spectra were observed for signals 12 and 13 showing a quasi-molecular ion of $m/z$ 519 and a product ion of $m/z$ 314 corresponding to an isorhamnetin. The same criterion was used to assign the malonylgalactoside and malonylglucoside derivatives, respectively, being in this case tentatively identified because no commercial standards were available.

The deoxyhexoside derivatives of quercetin and kaempferol (peaks 10 and 15) were assigned on the basis of their MS/MS spectra. In both cases, a neutral loss of 146, consistent with a rhamnose, was detected.[15] Peak 10 was confirmed as quercetin-3-rhamnoside by comparison with their respective standard.

Another quercetin derivative, with a quasi-molecular ion of $m/z$ 563 and two product ions of $m/z$ 463 and 300, was detected. This compound was assigned as a quercetin-glucoside derivative according to the fragmentation pattern. Finally, peaks 1 and 2 coeluted with interfering signals (i1 and i2, respectively). Their MS/MS identification, as well as that of peaks 3 and 10, was consistent with the previous study.[2]

**Quantitative Analytical Parameters for Flavonol Analyses.** The quantitative method validation included the efficiency of the flavonol extraction, which was evaluated using a calafate sample subjected to seven successive extraction steps, to ensure exhaustive extraction. The quantitative results were obtained for each of them. After seven steps, no further increase in flavonol concentration was detected, and the total concentration of the seven steps was considered to be 100% extraction. The results showed that by applying four extraction steps, >95% of the flavonols were extracted, which is a good compromise between extraction efficiency and extraction time. The internal precision of flavonol determination in calafate samples, considering the whole method including liquid−solid

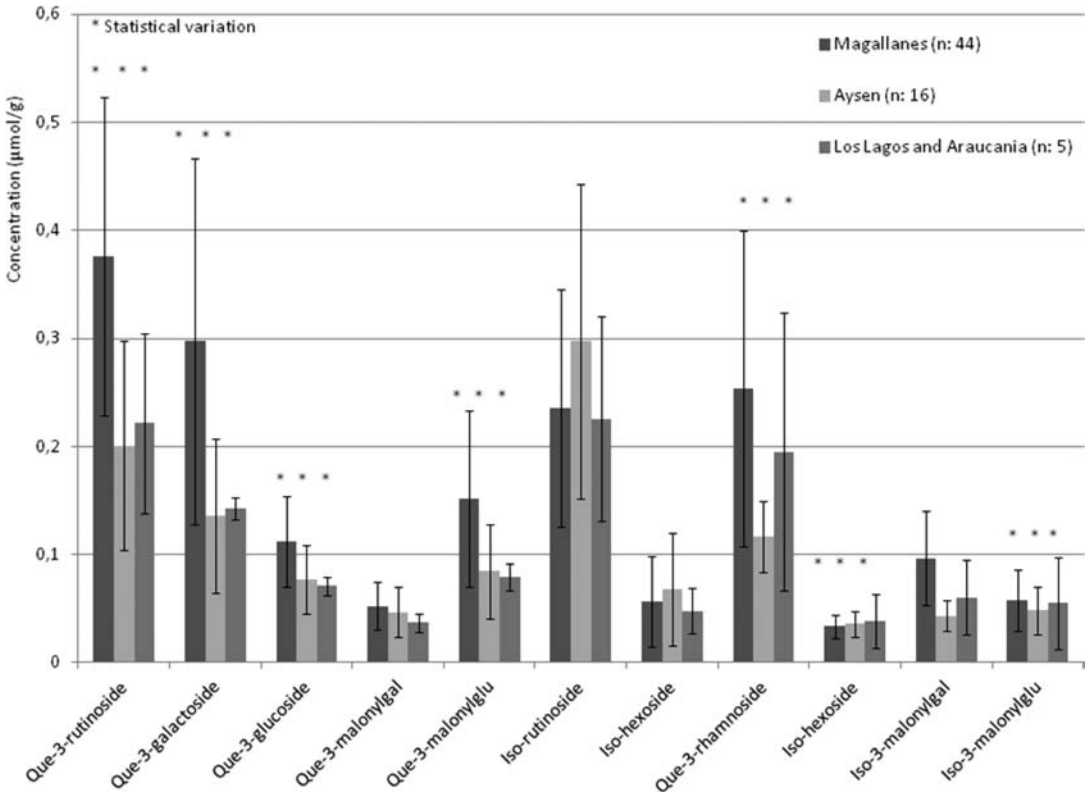


**Figure 3.** Individual flavonol concentrations in 65 samples of *B. microphylla* G. Forst obtained in Magallanes, Aysen, and Los Lagos and Araucania.

extraction, SPE cleanup steps, and chromatographic separation, was 7.9%, and the extracts were stable for 7 months at −20 °C. The analytical response and other analytical parameters for the main flavonols are summarized in the Supporting Information. Total flavonols were determined by the sum of individual flavonols detected over the limit of quantitation of the method.

**Flavonol Quantitation in Calafate and Other *Berberis* Berries.** Sixty-five samples of calafate berries obtained at different latitudes in Patagonia were analyzed. In all of them, 16 flavonol derivates were detected. The most abundant was quercetin-3-rutinoside, showing a mean concentration of 0.32 ± 0.15 μmol/g FW, with a range from traces to 0.74 μmol/g FW. Quercetin-3-galactoside, quercetin-3-rhamnoside, and isorhamnetin-3-rutinoside also showed interesting concentrations of 0.24 ± 0.16, 0.25 ± 0.12, and 0.24 ± 0.14 μmol/g FW, respectively. For the other quercetin and isorhamnetin derivates, their mean concentrations were <0.10 μmol/g FW. The myricetin and kaempferol derivatives were detected only at trace levels. In Figure 3 are summarized and compared the quantitative results for each quantifiable flavonol in relation to its origins. By ANOVA (Tukey−Kramer test), statistical variations in concentrations of flavonols in calafate from different regions were evaluated. The most significant differences were observed in quercetin derivatives (quercetin-3-rutinoside, quercetin-3-galactoside, and quecetin-3-rhamnoside), the most abundant flavonols in calafate, whereas no significant differences were observed for isorhamnetin derivatives, except isorhamnetin-3-malonylglucoside, which presented lower concentrations in samples from the Aysen region.

For all quantifiable flavonols, the total concentration, expressed as a mean of all studied samples ($n$ = 65), was 1.33 ± 0.54 μmol/g FW, with a range between 0.27 ± 0.01 and 2.89 ± 0.05 μmol/g FW; no significant difference was observed between samples obtained in 2011 and 2012 (1.34 ± 0.55 and 1.32 ± 0.49 μmol/g FW, respectively). Samples from more southerly latitudes (Magallanes 51−54° S) showed higher concentrations than those from the northern ones (Aysen 43−47° S) and Chiloe Main Island (42° S). This trend is similar to that observed for hydroxycinnamic acid derivates,[3] in which a decrease in their concentrations was observed from south to north. However, in the flavonol study, an exception was observed for four samples obtained further north, in Gorbea (39° 06′ S; 72° 40′ W in the Araucanía region), which showed similar mean concentrations to the Magallanes samples. The quantitative results by region are summarized in Table 2.

The profile and concentration of flavonols in mature samples of calafate (*B. microphylla*) were compared with those for mature berry samples of other endemic *Berberis* species obtained in the same study zone (between Bio-Bio and Magallanes regions). The respective flavonol chromatograms for the *Berberis* species are presented in Figure 4.

The results showed different profiles for the species, especially for *B. empetrifolia*, *B. ilicifolia*, and *B. darwinii*, in comparison with *B. microphylla*. In the first one, only three flavonols (rutinoside, galactoside, and glucoside derivatives of quercetin) predominated, only traces of other flavonols being observed (isorhamnetin-3-rutinoside, isorhamnetin-3-galactoside, and isorhamnetin-3 malonylglucoside). In *B. ilicifolia*, isorhamnetin-3-rutinoside predominated, whereas quercetin-3-rhamnoside, quercetin-malonyl derivatives, and the other isorhamnetin malonyl derivatives were absent. In *B. darwinii*, the absence of isorhamnetin-3-rutinoside and isorhamnetin-3-galactoside was noted, with a similar proportion of the other flavonols to *B. microphylla*. *B. montana* and *B. vulgaris* presented flavonol profiles similar to that of calafate, with similar proportions of them. This observation is interesting because

**Table 2. Total Concentration of Flavonols in *B. microphylla* G. Forst Berries**

| sample location | | *n* | median (μmol/g) | range (μmol/g) |
|---|---|---|---|---|
| **Magallanes region (between 51−55° S and 69−74° W)** | | **44** | **1.53 ± 0.40** | **0.50−2.89** |
| Tierra del Fuego | Lago Fagnano | 5 | 1.35 ± 0.91 | 0.77−2.89 |
| | Lago Blanco | 2 | 1.16 ± 0.48 | 0.82−1.50 |
| | Laguna Deseada | 1 | 1.38 ± 0.00 | |
| | Bosque alto Rasmusen | 1 | 2.04 ± 0.00 | |
| | Parque Karukinka | 1 | 1.15 ± 0.00 | |
| | Cameron | 3 | 1.07 ± 0.14 | 0.91−1.16 |
| | Camino Porvenir. Km 25 | 1 | 1.44 ± 0.00 | |
| Punta Arenas | Camino Faro San Isidro | 1 | 1.49 ± 0.00 | |
| Nearby | Río San Luis | 2 | 1.15 ± 0.25 | 0.97−1.32 |
| | Fuerte Bulnes | 3 | 1.97 ± 0.24 | 1.75−2.22 |
| | Camino Parrillar | 2 | 2.48 ± 0.22 | 2.19−2.63 |
| | Reserva Forestal Magallanes | 1 | 2.19 ± 0.00 | |
| | Parque Chabunco | 1 | 0.94 ± 0.00 | |
| | Sector Aeropuerto | 4 | 1.16 ± 0.17 | 0.94−1.33 |
| | Punta Prat | 2 | 1.70 ± 0.14 | 1.61−1.80 |
| | Seno Otway | 6 | 1.75 ± 0.38 | 1.25−2.09 |
| | Kampenaike | 4 | 1.71 ± 0.24 | 1.37−1.90 |
| Puerto Natales | Estancia El Valle | 2 | 1.71 ± 0.10 | 1.64−1.78 |
| Nearby | Estancia Dos Lagunas | 1 | 1.47 ± 0.00 | |
| | Estancia El Chingue | 1 | 1.20 ± 0.00 | |
| **Aysen region (between 43−47° S and 71−73° W)** | | **16** | **0.88 ± 0.23** | |
| | Puerto Tranquilo | 4 | 0.71 ± 0.33 | 0.27−0.97 |
| | Ceballo | 2 | 0.87 ± 0.51 | 0.51−1.20 |
| | Chile Chico | 4 | 0.83 ± 0.10 | 0.74−0.94 |
| | Santa Elena | 3 | 0.92 ± 0.71 | 0.71−1.24 |
| | Valle Simpson | 2 | 1.04 ± 0.29 | 0.83−1.24 |
| | Lago Rosselot | 1 | 0.94 ± 0.00 | |
| **Los Lagos region (Chiloé main island 42° 28′ S and 73° 46′ W)** | | **1** | **0.77 ± 0.00** | |
| **Araucania region (Gorbea 39° 06′ S and 72° 40′ W** | | **4** | **1.52 ± 0.10** | **1.38−1.58** |

*B. montana* and *B. microphylla* are taxonomically similar,[1] which could explain their similar profiles. However, *B. vulgaris* is an introduced species, which is used as an ornamental plant in gardens and is very different from *B. microphylla*.

The quantitative results of the 16 samples of other *Berberis* species were compared with the results for calafate samples summarized in Table 2. The total flavonol concentration of *B. microphylla* was less than that observed for *B. montana* samples ($n$ = 4), showing 1.33 ± 0.54 and 1.61 ± 0.64 μmol/g FW, respectively, and for *B. empetrifolia* (2.01 μmol/g FW, $n$ = 1), but was higher than that observed for *B. ilicifolia* (0.71 ± 0.18 μmol/g FW, $n$ = 1), *B. darwinii* (1.04 ± 0.31 μmol/g FW, $n$ = 6), and the only available sample of *B. vulgaris* (0.72 μmol/g FW), which was obtained from University of Concepción gardens.

The flavonol concentration in different parts of the calafate fruit (skin, pulp, and seeds) was determined in two composed samples, one of them from Magallanes and the other from the Aysen region. The results were similar for samples from both regions. Flavonol concentrations were lower in the seeds than in the pulp and skin. Quercetin-3-rutinoside and quercetin-3-galactoside were the predominant flavonols in skin and pulp, followed by isorhamnetin-3-rutinoside. Quercetin-3-rhamnoside was detected only in seeds, being the main flavonol found in this structure (>60% of the total flavonols in seed). It is important to note that this flavonol is one of the predominant flavonols in calafate. This distribution within the different structures of the fruit is very interesting and must be explained by the calafate plant metabolism; however, this has not been studied until now.

The profile and concentrations of flavonols in different phenological stages was evaluated using berry samples obtained from the same plant in the stages of fruit setting, green fruit, and full-colored fruit. The samples were taken on December 15, 2011; January 15, 2012; and February 15, 2012, respectively. Results showed that the flavonol profile changed in this process. Quercetin-3-malonylglucoside decreased, whereas quercetin-3-rhamnoside increased, and the overall flavonol concentration decreased to 75% of the initial level. These results are presented in Figure 5. These observations are similar to those previously obtained for hydroxycinnamic acid derivatives in calafate[3] and are correlated with those observed by Arena et al.[16] for total polyphenol and flavonoid contents in calafate. The phenolic content decrease has also been observed for other berries, including different cultivars of the blueberry,[17] in which a change in the pool of total phenolics toward anthocyanin synthesis, with an overall decline in the content of other phenolic components, is observed during ripening.

These findings about flavonols in calafate are very relevant because of the enhancement of calafate and other *Berberis* from a nutraceutical point of view. They also contributed to finding the optimal growing time and conditions.

**Reducing Capacity of Whole and SPE Fractions Calafate Extracts.** Four previously quantitated fractions obtained by SPE were subjected to in vitro antioxidant capacity assays ($TEAC_{CUPRAC}$ and $TEAC_{ABTS}$). This was carried out to evaluate the contribution of these anthocyanin free fractions on the antioxidant capacity of calafate. These fractions contained mainly flavonols and hydroxycinnamic acids. Two of these samples (C1 and C2) had low concentrations of these compounds, whereas the other two were included due to its high concentrations (C3 and C4). In Table 3 are summarized these results. High $TEAC_{CUPRAC}$ and $TEAC_{ABTS}$ values were observed for whole extracts with high total phenolics (C1 and C4). This is explained mainly due to the high anthocyanin concentrations present in these extracts. Also, it is possible to observe a trend of higher $TEAC_{CUPRAC}$ and $TEAC_{ABTS}$ values for SPE fractions with high flavonol−hydroxycinnamic acid concentrations (C3 and C4), compared with the fraction with minor concentrations of this compounds (C1 and C2); however, this trend is less clear than those observed for whole extracts. The antioxidant capacities obtained for flavonol plus hydroxycinnamic acid fractions represent 15 ± 5 and 5 ± 4% of $TEAC_{CUPRAC}$ and $TEAC_{ABTS}$ values, respectively, in comparison with the values obtained for the whole extracts. This shows that flavonols and hydroxycinnamic acids have a notable incidence in the antioxidant capacity of calafate, despite its lower concentration in comparison with anthocyanins.

**Alkaloid Identification and Quantitation in Calafate and Other *Berberis* Berries.** Alkaloid determination was done with the objective of guaranteeing the innocuousness of *Berberis*. The identification of alkaloids in calafate and other

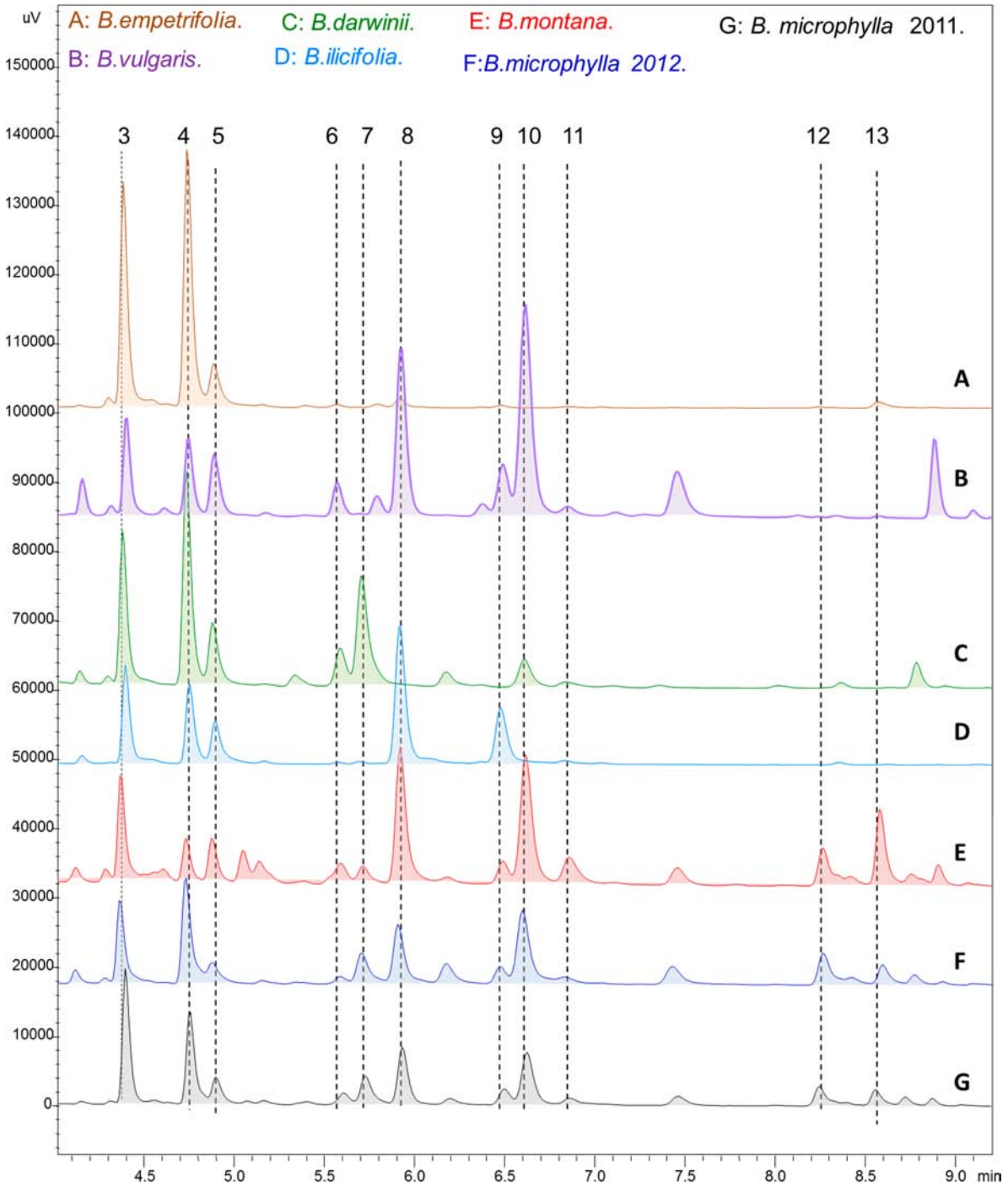


**Figure 4.** Chromatographic profiles of flavonols extract of different *Berberis* species, by HPLC-DAD using core−shell column: (A) *B. empetrifolia* (sample from Parque Pinguino Rey, Provenir, Tierra del Fuego); (B) *B. vulgaris* (sample from gardens of University of Concepción, Concepción); (C) *B. darwinii* (sample from Gorbea, Temuco); (D) *B. ilicifolia* (sample from Lago Deseado, Porvenir, Magallanes); (E) *B. montana* (sample from Valle Las Trancas, Chillan); ( (F) *B. microphylla* 2012 (sample from Lago Fagnano, Magallanes); (G) *B. microphylla* 2011 (sample from Seno Otway, Magallanes).

*Berberis* species was done by comparison of $t_R$ with commercial standards. The identity confirmation was based on their MS/MS and UV−vis spectra. Table 4 presents spectroscopic characteristics of alkaloids detected in different *Berberis* structures. In all calafate fruits analyzed in this part of the research ($n$ = 62), only berberine was detected. However, jatrorrhizine and palmatine were detected at trace levels in calafate leaves. The alkaloid coridaline was assigned to a signal found in fruits of *B. ilicifolia* based on the MS/MS spectra, in accordance with Wang et al.[18]

Quantitative analysis of berberine was carried out by HPLC with fluorescence detection using an external calibration curve, which was performed by triplicate injection at six levels of berberine standard concentration. The calibration curve showed a low level of dispersion, with a regression coefficient of 0.9993 and an equation of ($y$ = 560704.27$x$ − 80514.59). Fluorescence detection showed a high sensitivity and low

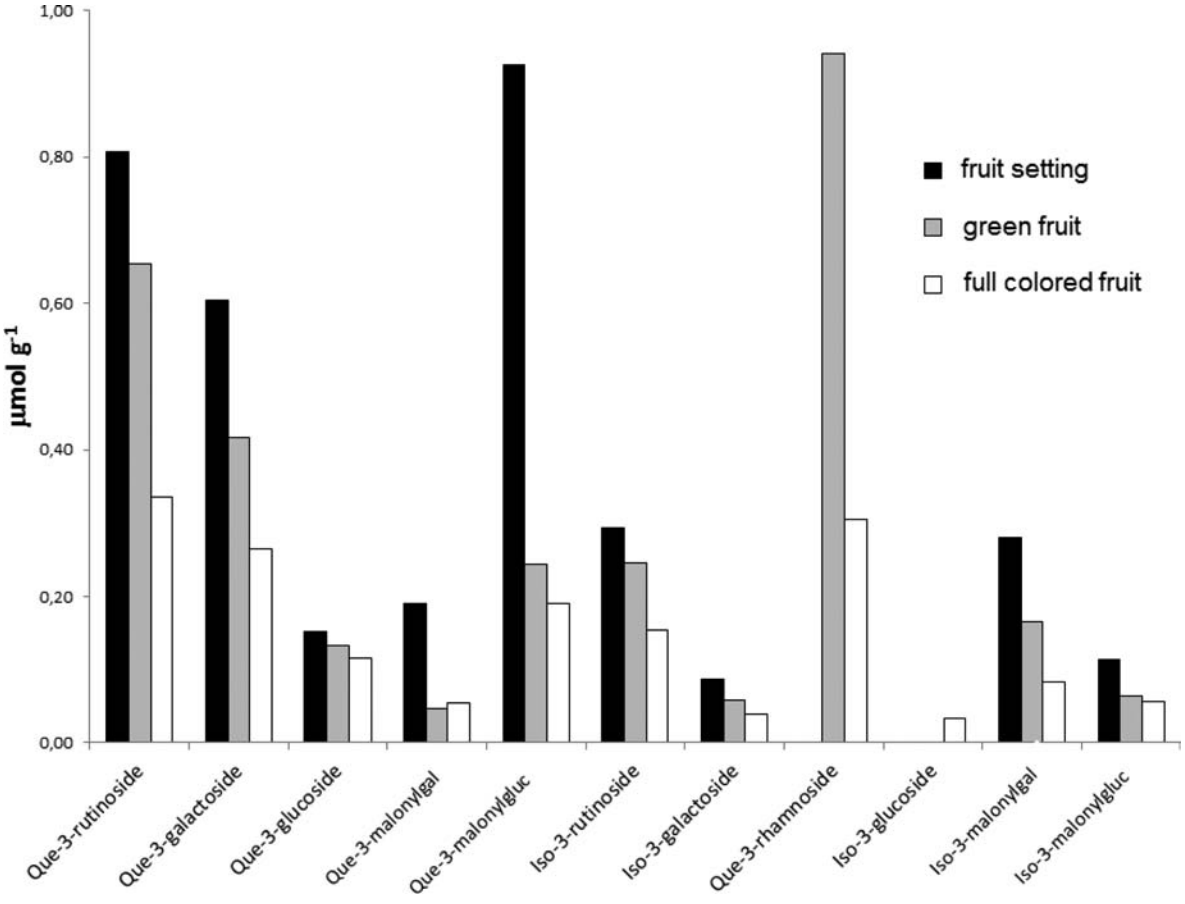


**Figure 5.** Flavonols profile and concentration during the maturation process of *B. microphylla* G. Forst (sample from Sector Barranco Amarillo, Magallanes).

**Table 3. In Vitro Antioxidant Capacity ($TEAC_{CUPRAC}$ and $TEAC_{ABTS}$) of SPE Fractions and Whole Extracts of *B. microphylla* G. Forst[a]**

| | whole calafate extracts | | | |
|---|---|---|---|---|
| | total phenolic concn ($\mu$mol/g FW) | $TEAC_{CUPRAC}$ ($\mu$mol TE/g FW) | $TEAC_{ABTS}$ ($\mu$mol TE/g FW) | |
| calafate 1 | 32.63 ± 0.14 | 405.95 ± 33.01 | 105.48 ± 4.43 | |
| calafate 2 | 3.06 ± 0.04 | 179.61 ± 12.12 | 71.56 ± 0.12 | |
| calafate 3 | 11.56 ± 0.03 | 224.68 ± 12.19 | 106.92 ± 15.92 | |
| calafate 4 | 37.68 ± 0.54 | 577.73 ± 35,.5 | 133.47 ± 3.17 | |
| | SPE fractions (flavonols + HCADs) | | | |
| | flavonols concn ($\mu$mol/g FW) | HCADs concn ($\mu$mol/g FW) | $TEAC_{CUPRAC}$ ($\mu$mol TE/g FW) | $TEAC_{ABTS}$ ($\mu$mol TE/g FW) |
| calafate 1 | 0.26 ± 0.01 | 0.68 ± 0.00 | 34.87 ± 7.44 | 4.69 ± 0.14 |
| calafate 2 | 1.56 ± 0.04 | 0.89 ± 0.00 | 35.79 ± 0.69 | 5.29 ± 0.14 |
| calafate 3 | 0.97 ± 0.01 | 4.21 ± 0.02 | 42.88 ± 11.39 | 5.68 ± 0.18 |
| calafate 4 | 1.44 ± 0.03 | 4.88 ± 0.00 | 66.85 ± 11.27 | 11.45 ± 0.44 |

[a]The identifications of each sample are, respectively, calafate 1, Puerto tranquilo, Aysen; calafate 2, Gorbea, Temuco; calafate 3, Rio San Luis, Magallanes; calafate 4, Camino Provenir. Km 25, Magallanes. HCADs, hydroxycinnamic acids.

detection and quantitation limits (0.6 and 1.5 nmol/g, respectively). Repeatability and intermediate precision were also evaluated, giving RSD values of 8.9 and 10.9%, respectively. The quantitative method validation included the efficiency of the extraction, and it was evaluated in the same manner as that of flavonols. The results showed that with three extractions, a recovery of >90% of berberine was obtained, reaching 94.3% when four steps were carried out. Three extractions were considered optimal as a good compromise between accuracy and time/cost of analysis.

Berberine levels were evaluated in fruits of different *Berberis* species, showing low concentrations; however, some variations between the different samples were observed. The highest concentration of berberine was detected in *B. ilicifolia* ($n$ = 3) with 160.0 nmol/g FW. In calafate fruits (*B. microphylla*) collected in the year 2011 ($n$ = 45) levels of berberine were between 1.8 and 126.9 nmol/g FW, whereas in samples collected in 2012 ($n$ = 18) concentrations between 3.3 and 152.8 nmol/g FW were determined. Higher contents of berberine were found in *B. ilicifolia* (55.9−160.5 nmol/g FW)

Table 4. Spectroscopic Characteristic of Alkaloidd Found in *Berberis* Genera from Patagony by HPLC-DAD-MS/MS

| | $t_R$ (min) | $\lambda_{max}$ (nm) | $[M + H]^+$ | product ions | detected in |
|---|---|---|---|---|---|
| berbamine[a] | 6.7 | 274 | 609 | 566, 305, 535, 552 | |
| coridaline | 11.99 | 345 | 370 | 322, 192, 307 | *B. ilicifolia* (fruits) |
| berberine | 12.88 | 347 | 337 | 321, 292, 278, 306 | *B. microphylla* (fruits, leaves, seeds, branches, and roots), *B. montana*, *B. ilicifolia*, *B. empetrifolia*, *B. vulgaris* |
| jatrorrhizine | 11.96 | 344 | 338 | 323, 294 | *B. microphylla* (only in leaves) |
| palmatine | 12.66 | 344 | 352 | 337, 308 | *B. microphylla* (only in leaves) |

[a]Not detected in the *Berberis* samples studied. Data were obtained for a standard solution.

and *B. darwinii* (57.7−156.1 nmol/g FW), whereas the upper concentrations are in berries of *B. microphylla*. In two samples of *B. vulgaris* collected from the University of Concepcion gardens, lower levels of berberine (1.8−3.3 nmol/g FW) were observed. The only *B. montana* analyzed contained 8.3 nmol/g FW berberine. The observed variations could be explained by different factors that can contribute to the biosynthesis of alkaloids in plants, such as the *Berberis* species, the place of collection, climate conditions, and number of seeds per fruit, as well as insect and disease attack.[19]

The distribution of berberine in calafate plants and fruit was evaluated using four samples. The results showed that berberine levels decreased with the distance of the analyzed structure from the roots. The highest levels were detected in the roots (4655.7 ± 1067.3 nmol/g FW), followed by the branches (1343.8 ± 981.1 nmol/g FW), and much lower levels in their fruits (32.7 ± 11.9 nmol/g FW) and leaves (35.7 ± 8.9 nmol/g FW). On the other hand, in two of these fruit samples, it was possible to analyze the berberine distribution, showing a higher level in the seeds (between 55.0 and 121.3 nmol/g FW) than in a sample of pulp mixed with the skin (between 3.6 and 6.2 nmol/g FW). Seeds are principally responsible of berberine content in the edible part of calafate fruits. This implies that in calafate products such as juices or jams, which are produced without seeds, berberine levels will be even lower than in whole fresh berries.

Berberine levels were also studied in fruits with different phenological stages, using the same methods as in the flavonol study. A low concentration of berberine in the first stage (fruit setting) was observed (6.8 nmol/g FW), which increased toward maturation, reaching concentrations of 47.0 and 41.9 nmol/g FW in green berry and colored berry, respectively. This is consistent with the maturation process, if one of the functions of the seeds is to provide chemical protection to the plant during germination.

$LD_{50}$ of berberine has been previously reported in mice.[20] According to these data and assuming a 7 times lower metabolic rate in humans,[8,21] a consumption of 139 kg of calafate fruits, assuming the highest level of berberine detected in calafate berries in the present study, is necessary to reach the $LD_{50}$ in humans. The berberine concentrations in calafate fruits suggest that they are innocuous for human consumption. On the other hand, considering the beneficial biological effect attributed by several authors to this molecule,[22,6] its low presence in calafate fruit would not be relevant from a nutraceutical point of view; however, calafate roots and branches constitute an interesting source of this compound. It mediates the chemical defense of plants against viruses, bacteria, fungi, other plants, insects, and vertebrates,[23] protecting the vegetative part of the plant and the seeds, but not the edible part of the berry, facilitating the dissemination of the species, that is, by birds.

Finally, the distribution of these phytochemicals in the calafate berries, the effect of the maturity process, the different growing latitudes, and the antioxidant capacity of the extract have influence on the nutraceutical potential of this wild and underexploited fruit.

## ■ ASSOCIATED CONTENT

### Supporting Information

Analytical parameters for flavonol quantification. This material is available free of charge via the Internet at http://pubs.acs.org.

## ■ AUTHOR INFORMATION


### Corresponding Author

*(C.M.) Phone: 56-41-2204598. Fax: 56-41-2226382. E-mail: cmardone@udec.cl.



### Funding

We thank FONDECYT (Grant 1100944) and CONICYT, Chile (doctoral fellowship).


### Notes

The authors declare no competing financial interest.

## ■ ACKNOWLEDGMENTS

We thank Prof. Dr. Roberto Rodriguez, Director of Herbario CONC, and the Department of Botany, University of Concepción, for botanical classification of the *Berberis* samples.

## ■ REFERENCES


(1) Marticorena, C.; Rodríguez, R. *Flora de Chile Vol. 2: Berberidaceae−Betulaceae*, 1st ed.; Universidad de Concepción: Concepción, Chile, 2003.

(2) Ruiz, A.; Hermosin-Gutierrez, I.; Mardones, C.; Vergara, C.; Herlitz, E.; Vega, M.; Dorau, C.; Winterhalter, P.; von Baer, D. Polyphenols and antioxidant activity of calafate (*Berberis microphylla*) fruits and other native berries from southern Chile. *J. Agric. Food Chem.* **2010**, *58*, 6081−6089.

(3) Ruiz, A.; Mardones, C.; Vergara, C.; Hermosín-Gutiérrez, I.; von Baer, D.; Hinrichsen, P.; Rodríguez, R. Analysis of hydroxycinnamic acids derivatives in calafate (*Berberis microphylla* G. Forst) berries by liquid chromatography with photodiode array and mass spectrometry detection. *J. Chromatogr., A* **2013**, *1281*, 38−45.

(4) Ruiz, A.; Mardones, C.; Vergara, C.; von Baer, D.; Gómez-Alonso, S.; Gómez, M. V.; Hermosín-Gutiérrez, I. Isolation and structural elucidation of anthocyanidin 3,7-$\beta$-*O*-diglucosides and caffeoyl-glucaric acids from calafate berries. *J. Agric. Food Chem.* **2014**, *62*, 6918−6925.

(5) Mokhber-Dezfuli, N.; Saeidnia, S.; Reza-Gohari, A.; Kurepaz-Mahmoodabadi, M. Phytochemistry and pharmacology of *Berberis* species. *Pharmacogn. Rev.* **2014**, *8*, 8−15.

(6) Fajardo, V. *Alcaloides en Especies del Género Berberis en Chile, Química de la Flora de Chile*, 1st ed.; Universidad de Chile: Santiago, Chile, 1992.
(7) Kheir, M.; Wang, Y.; Hua, L.; Hu, J.; Li, L.; Lei, F.; Dua, L. J. Acute toxicity of berberine and its correlation with the blood concentration in mice. *Food Chem. Toxicol.* **2010**, *48*, 1105−1110.
(8) Tillhon, M.; Ortiz, L. M. G.; Lombardi, P.; Scovassi, A. I. Berberine: new perpective for old remedies. *Biochem. Pharmacol.* **2012**, *84*, 1260−1267.
(9) Marivil, P. *Variación del perfil de alcaloides durante el crecimiento de L. albus y en semillas de L. angustifolius*. Tesis para optar al título de Bioquímico, Universidad de Concepción, Concepción, Chile, 1995.
(10) Wink, M.; Meißner, C.; Witte, L. Patterns of quinolizidine alkaloids in 56 species of the genus *Lupinus*. *Phytochemistry* **1995**, *38*, 139−153.
(11) Castillo-Muñoz, N.; Gomez-Alonso, S.; Garcia-Romero, E.; Hermosin-Gutierrez, I. Flavonol profiles of *Vitis vinifera* red grapes and their single-cultivar wines. *J. Agric. Food Chem.* **2007**, *55*, 992−1002.
(12) Hungria, M.; Joseph, C.; Phillips, D. Anthocyanidins and flavonols, major *nod* gene inducers from seeds of a black-seeded common bean (*Phaseolus vulgaris* L.). *Plant Physiol.* **1991**, *97*, 751−758.
(13) Meyer, V. *Practical High-Performance Liquid Chromatography*, 4th ed.; Wiley: Hoboken, NJ, USA, 2005.
(14) Guiochon, G.; Gritti, F. Shell particles, trials, tribulations and triumphs. *J. Chromatogr., A* **2011**, *1218*, 1915−1938.
(15) Cho, M. J.; Howard, L.; Prior, R.; Clark, J. Flavonol glycosides and antioxidant capacity of various blackberry and blueberry genotypes determined by high-performance liquid chromatography/mass spectrometry. *J. Sci. Food Agric.* **2005**, *85*, 2149−2158.
(16) Arena, M. E.; Postemsky, P.; Curvetto, N. R. Flavonol glycosides and antioxidant capacity of various blackberry and blueberry genotypes determined by high-performance liquid chromatography/mass spectrometry. *N. Z. J. Bot.* **2002**, *50*, 15−28.
(17) Rodarte Castrejon, A. D.; Eichholz, I.; Rohn, S.; Kroh, L. W.; Huyskens-Keil, S. Phenolic profile and antioxidant activity of highbush blueberry *Vaccinium corymbosum* L. during fruit maturation and ripening. *Food Chem.* **2008**, *109*, 564−572.
(18) Wang, Y.; Huang, Y.; Yiming, L.; Aimin, X. Berberine prevents hyperglycemia-induced endothelial injury and enhances vasodilatation via adenosine monophosphate-activated protein kinase and endothelial nitric oxide synthase. *Cardiovasc. Res.* **2009**, *82*, 484−492.
(19) Roberts, M. F.; Wink, M. *Alkaloids: Biochemistry, Ecology, and Medical Applications*, 1st ed.; Plenum Press: New York, 1998.
(20) Yi, J.; Ye, X.; Wang, D.; He, K.; Yang, Y.; Liu, X.; Li, X. Safety evaluation of main alkaloids from *Rhizoma coptidis*. *J. Ethnopharmacol.* **2012**, *145*, 303−310.
(21) Terpstra, A. H. M. Differences between humans and mice in efficacy of the body fat lowering effect of conjugated linoleic acid: role of metabolic rate. *J. Nutr.* **2001**, *131*, 2067−2068.
(22) Chen, C.; Xu, X. M.; Chen, Y.; Xu, M. Y.; Wen, F. Y.; Zhang, H. Identification, quantitation and antioxidant activity of acylated flavonol glycosides from sea buckthorn (*Hippophae rhamnoides* ssp. *sinensis*). *Food Chem.* **2013**, *141*, 1573−1579.
(23) Schmeller, T.; Latz-Brüning, B.; Wink, M. Biochemical activities of berberine, palmatine and sanguinarine mediating chemical deference against microorganisms and herbivores. *Phytochemistry* **1997**, *44*, 257−266.

turonase.[15,16] We have previously found that the general pattern and extent of uronic acid solubilization and depolymerization showed high similarity in firm and soft cherries.[9] However, soft cherries had lower total cell wall content (alcohol-insoluble residue, AIR) and higher branching of tightly bound pectins than firm fruit. Unfortunately, almost all studies looking at cherry genotypes with contrasting firmness have compared a single firm cultivar to a soft genotype, making it difficult to determine whether or not the changes observed are valid in broader contexts. In order to explore further this, we have extended the chemical study by analyzing the changes in cell wall polysaccharides on five cherry cultivars ('Sunburst', 'Regina', 'Chelan', 'Sumele', and 'Brooks') at two developmental stages (immature and ripe). Pectin evaluations were complemented by their analysis by ultraviolet matrix-assisted laser desorption/ionization time-of-flight (UV-MALDI-TOF) mass spectrometry.

## MATERIALS AND METHODS

**Plant Material.** Cherry fruit cultivars 'Chelan', 'Brooks', 'Sumele', 'Sunburst', and 'Regina' were randomly picked from trees located in the Río Negro Upper Valley, Argentina (39° 01′ 32′′ S, 67° 44′ 22′′ W, 242 m above sea level). Samples of about 1.5 kg of each genotype were collected in 2009 at two different developmental stages, namely immature (I) ('Sumele', 45 days after anthesis (DAA); 'Regina' and 'Chelan', 47 DAA; 'Brooks' and 'Sunburst', 49 DAA) and ripe (R) ('Sumele', 73 DAA; 'Brooks' and 'Chelan', 75 DAA; 'Sunburst', 84 DAA; 'Regina', 90 DAA).

**Firmness, Soluble Solids Content, Titratable Acidity, Surface Color, Dry Matter, and Cracking Index.** Firmness was measured at 20 °C for each cultivar on 20 randomly selected fruits, by measuring the force required to compress the fruit over the equatorial zone (distance, 0.5 mm; speed, 50 mm/s) using a Durofel texture analyzer (Güss FTA, Strand, South Africa). Given the average diameter of the fruit (25−27 mm), this test yielded only a small compression (ca. 2%) For soluble solids measurements, juice samples obtained by squeezing ten cherries were evaluated with a hand-held temperature-compensated refractometer (Atago Co., Tokyo, Japan). Measurements were done in triplicate. Titratable acidity (TA) was determined by titrating a 10 mL juice sample (out of 20 cherries) with 0.1 mol/L NaOH to an end point of pH 8.2, and expressed as g malic acid/100 g juice (% w/w). Three replicates per condition were evaluated. Fruit surface color measurements were taken with a CR-300 chroma meter (Minolta, Osaka, Japan) using D65 illuminant lighting conditions, in 20 cherries per cultivar. Dry matter was determined on ten cherries by drying in an oven at 45−55 °C until constant weight (ca. 7 d). The cracking index (CI) was determined after leaving 50 cherries per condition in deionized water at 20 °C. After 2, 4, and 6 h, the fruit was checked for wounds or exocarp/skin leaks, and those unaffected were submerged again. The index was calculated as

$$\mathrm{CI} = \frac{5n_{2h} + 3n_{4h} + n_{6h}}{250} \times 100$$

where $n_{xh}$ is the number of affected fruit after $x$ hours.[17]

**Alcohol Insoluble Residue (AIR).** After removal of the core and peduncle, the pulp was treated as described by Ponce et al.[18] in order to obtain the AIR. Briefly, about 100 g of pulp were put in cool 80% ethanol (4 mL/g fruit) and blended in an Omni Mixer homogenizer (Omni International, Kennesaw, GA). The homogenate was boiled for 30 min, cooled, and filtered through glass filter paper (Whatman GF/C). The retentate was thoroughly washed with 95% (v/v) ethanol. The solids were then resuspended in a mixture of chloroform:methanol (1:1, 3 mL/g fruit), stirred for 15 min, and filtered. The retentate was washed with the same solvent mixture. The insoluble material was washed with acetone, yielding the crude cell wall extract (AIR). The AIR was air-dried in a hood and in a vacuum desiccator overnight and weighed.

**Cell Wall Fractionation.** AIR fractionation was performed as previously described[18] with minor modifications. Briefly, 1 g of AIR was stirred for 4 h at room temperature with 100 mL of 0.02% (w/v) thimerosal aqueous solution and filtered. The suspension was filtered, and the filtrate was saved and designated as water-soluble fraction (WSF). Sequential extraction of the pellet with 0.05 mol/L *trans*-1,2-diaminocyclohexane-*N*,*N*,*N*′,*N*′-tetraacetic acid (CDTA) in 0.05 M NaOAc/HOAc buffer, pH 6, containing 0.02% (w/v) thimerosal (24 h), 0.1 mol/L $Na_2CO_3$ containing 0.02 mol/L $NaBH_4$ (24 h), 1 mol/L KOH containing 0.02 mol/L $NaBH_4$ (24 h), and 4 mol/L KOH containing 0.02 mol/L $NaBH_4$ (24 h), yielded the CDTA-soluble fraction (CSF), $Na_2CO_3$-soluble fraction (NSF), and 1 and 4 mol/L KOH-soluble fractions (1KSF and 4KSF), respectively. The supernatants were recovered after centrifugation at 13100*g* at 6 °C for 40 min. In the case of the KOH-soluble fractions, pH was adjusted to 5 with glacial acetic acid. All fractions were dialyzed (molecular weight (MW) cutoff 6000−8000 Da) against tap water for 2 days and against distilled water for 1 day at 4 °C. The fractions were freeze-dried and stored until analysis.

**Uronic Acids, Total Carbohydrate, and Neutral Sugar Measurements.** Uronic acids (UAs) were quantitated with the *m*-hydroxybiphenyl method[19] using galacturonic acid as standard, and expressed as anhydro units. Total carbohydrates were determined by the phenol−$H_2SO_4$ method[20] using glucose as standard. The proportion of neutral sugars (NSs) was determined after subtracting the UA content from that of total carbohydrates. For this purpose, the phenol−$H_2SO_4$ reaction was also carried out with a galacturonic acid standard, which showed an absorbance ratio of 0.28 against the same glucose weight.[18]

**Size-Exclusion Chromatography (SEC).** To examine the size distributions of polymers in CSF and NSF, ca. 3 mg of lyophilized samples from each fraction were dissolved in 0.8 mL of 0.4 mg/mL imidazole, to which 0.2 mL of 1 mol/L ammonium acetate (pH 5) was added. The samples were centrifuged, and the supernatants were chromatographed on a low-pressure SEC by employing a 300 mm × 9 mm i.d. Sepharose CL-2B column (Sigma Chemical Co., St. Louis, MO). Samples were eluted at room temperature with 0.2 mol/L ammonium acetate, pH 5. Fractions were collected, and aliquots were assayed for total carbohydrates.[20] Samples from the WSF, 1KSF, and 4KSF were dissolved in 0.1 mol/L NaOH, cleaned up by centrifugation, and chromatographed on a 300 mm × 9 mm i.d. Sepharose CL-6B column (Sigma Chemical Co., St. Louis, MO) eluted at room temperature with 0.1 mol/L NaOH. Fractions were collected, and aliquots were assayed for total carbohydrates.[20]

**Neutral Sugar Composition.** Each fraction (ca. 3 mg) was hydrolyzed with 1 mL of 2 mol/L trifluoroacetic acid (TFA) for 90 min at 120 °C in closed-cap vials. The TFA was eliminated by evaporation, and the resulting monosaccharides were reduced to alditols using $NaBH_4$, converted to alditol acetates, and subsequently analyzed using a Hewlett-Packard 5890 gas chromatograph (Agilent Technologies Inc., Santa Clara, CA) fitted with a capillary column (30 m × 0.25 mm i.d. × 0.20 μm, SP-2330, Supelco Inc., Bellefonte, PA) and equipped with a flame ionization detector (FID) operated at 240 °C. The injector temperature was 240 °C, and the oven temperature was kept isothermally at 220 °C. Nitrogen was used as the carrier gas at a head pressure of 1.05 bar. Samples were injected with a split ratio of 80:1. *Myo*-inositol was used as the internal standard, and the different alditol acetates were identified by comparison with authentical standards. The percentage of the different monosaccharides was calculated by considering that the integrated FID responses are proportional to the MW of the alditol acetates.

**UV-MALDI-TOF Mass Spectrometry.** Solutions of pectin samples (1 mg/mL) were prepared in Milli-Q water with the aid of sonication at 20 kHz (3 × 20 min). Two different matrices were used: nor-harmane (9-*H*-pyrido-[3,4*b*]indole) and gentisic acid (2,5-dihydroxybenzoic acid). The stock solutions of the matrices were prepared by dissolving 2 mg of the selected compound in 1 mL of methanol (HPLC-grade)/water (75:25, v/v). In order to prepare the analyte−matrix sample the thin-film layer method (sandwich method[21]) was used. Typically 0.5 μL of the matrix solution was

Table 1. Soluble Solids Content (SSC), Acidity, Weight, Lightness (L*), Firmness, and Cracking Index of Ripe 'Sunburst', 'Brooks', 'Chelan', 'Sumele', and 'Regina' Cherries[a]

| cultivar | SSC (% w/w) | acidity (% w/w) | weight (g) | $L^*$ | firmness (g/mm) | cracking index |
|---|---|---|---|---|---|---|
| Sunburst | 22 ± 3 a | 1.29 ± 0.03 a | 7.8 ± 0.9 c | 24.3 ± 0.04 e | 415 ± 2 e | 68 ± 2 b |
| Brooks | 20 ± 1 ab | 0.92 ± 0.01 c | 9.2 ± 0.8 b | 31.9 ± 0.02 a | 440 ± 2 d | 98 ± 5 a |
| Chelan | 20 ± 2 ab | 0.98 ± 0.05 b | 7.9 ± 1.1 c | 29.6 ± 0.04 b | 475 ± 1 c | 15 ± 2 d |
| Sumele | 19 ± 1 b | 0.96 ± 0.04 b | 8.0 ± 1.1 c | 28.6 ± 0.03 d | 492 ± 3 b | 71 ± 4 b |
| Regina | 20 ± 2 ab | 1.01 ± 0.06 b | 10.3 ± 1.0 a | 28.8 ± 0.01 c | 561 ± 1 a | 34 ± 3 c |

[a]Different letters within a column indicate differences based on a Tukey test at a level of significance of $P < 0.05$.Values are expressed as means ± SD ($n$ = 50 for cracking index, 30 for weight, 20 for firmness and lightness, 3 for SSC and acidity).

placed on the sample probe tip and air-dried at room temperature. Subsequently, 0.5 μL of the analyte solution were placed on the sample probe tip, covering the matrix and partially dissolving it, and air-dried. Then, two additional portions (0.5 μL) of matrix solution were deposited on the same sample probe tip, producing a partial dissolution of the previously deposited thin-film, and air-dried. The matrix-to-analyte ratio was 3:1 (v/v), and the matrix and analyte solution loading sequence was (i) matrix, (ii) analyte, (iii) matrix, and (iv) matrix. Comparative experiments were also conducted preparing the analyte−matrix sample by the mixture method. The pre-prepared mixture was done mixing the matrix and analyte solutions in 3:1 (v/v) and 1:1 (v/v) ratios. Three portions (0.5 μL) of the mixture were successively loaded on the probe, and air-dried as described above. Similar results were obtained with both sample preparation methods. Spectra were recorded on a BrukerUltraflex II TOF/TOF, controlled by the FlexControl 3.0 software (BrukerDaltonics, Bremen, Germany). Desorption/ionization was performed using a frequency-tripled Nd:YAG laser emitting at 355 nm with a 100 Hz shot frequency. All mass spectra were taken in the positive linear and reflectron modes. Experiments were performed first using the full range setting for laser firing position in order to select the optimal position for data collection, and second fixing the laser firing position in the sample sweet spots. The laser power was adjusted to obtain high signal-to-noise ratio while ensuring minimal fragmentation of the parent ions, and each mass spectrum was generated by averaging 500 laser pulses per spot. Spectra were obtained and analyzed with the programs FlexControl and FlexAnalysis, respectively. MTP plate steel with 384 circular spots, 3.5 mm diameter, was used (Bruker, Bremen, Germany).

**Statistical Analysis.** Statistical significance was determined by one-way ANOVA with the Stratgraphic software package (Manugistics Inc., Rockville, MD). The model assumptions of homogeneity of variance and normality were probed by means of Levene's and Shapiro-Wilk's tests, respectively. When these assumptions were not satisfied, data were transformed into ranks for further analysis. When a significant $F$-value was found, treatment means were compared using the Tukey's studentized range test ($P < 0.05$).

## RESULTS AND DISCUSSION

**Fruit Size, Soluble Solids Content, Acidity, Color, Firmness, Dry Matter, and Cracking Susceptibility.** Quality attributes of ripe fruit of the five varieties are shown in Table 1. 'Brooks', 'Sumele', 'Chelan', and 'Regina' showed similar levels of soluble solids (19−20% w/w) and acidity (0.92−1.01% w/w) upon ripening. 'Sunburst' presented slightly higher SSC (22% w/w) and titratable acidity (1.29% w/w). 'Regina' and 'Brooks' yielded fruit having higher weight (Table 1) and size (ca. 27 mm), whereas the remaining three cultivars produced the lighter and smaller cherries (ca. 25 mm). Fruit lightness ($L^*$) was highest in 'Brooks', with minimum values in 'Sunburst'. The dry matter content varied between 21 and 23% with no association to the cultivar firmness.

Firmness showed a large inter-cultivar variation. 'Regina' cherries were the firmest followed by 'Sumele', 'Chelan', and 'Brooks'. Soft cherries were produced by 'Sunburst'. The genotypes with the extreme firmness values were studied previously, on another batch.[10] Although prior work on strawberry showed that for a given cultivar, larger fruit tended to be softer,[22] in the current study no correlation was found between fruit size and firmness. This indicates that fruit size is not a major factor contributing to the genotypic differences in cherry texture. The cultivars also showed large differences in their cracking susceptibility. 'Chelan' fruit manifested relatively low cracking incidence, as opposed to 'Brooks' which was highly susceptible. Firmness as measured in compression tests was not related to the susceptibility of the fruit to cracking. The variations in cracking incidence and severity may be more highly associated with differences in cuticle thickness and composition.[23] Variations in the cell wall composition yielding changes in tissue physical properties under tension may be also important.

**Cell Wall Yield and Fractionation.** To further characterize the wall composition of the cultivars with contrasting firmness, the cell walls (AIR) were obtained after treatment of the fruit tissue with ethanol and chloroform/methanol, and further dehydration with acetone. The AIR was later fractionated into five different fractions, corresponding to pectins which are loosely bound (WSF), ionically bound (CSF), covalently bound (NSF), and loosely bound (1KSF) and strongly bound (4KSF) cross-linking glycans (hemicelluloses). Their yields for the five cultivars and two ripening stages are shown in Figure 1. The overall yield of non-cellulosic biopolymers from AIR was above 50% for immature cherries, and usually much less (<40%, with the exception of 'Sumele') for ripe cherries. The yields of the cell wall preparations dropped during ripening in all cultivars (Figure 1). No association between the accumulated yield of the different cell wall fractions and cultivar firmness was found at the immature or ripe stages, differing from previous reports.[9]

Growth and ripening change the architecture of fruit cell wall.[24] Although soluble polysaccharides usually accumulate during ripening[8] and some studies have associated softening of cherry with high levels of water-soluble polysaccharides, this does not seem to be a general feature, but rather a cultivar-dependent response. In fact, in the present study the yield of WSF increased with ripeness in 'Sunburst' and 'Regina', whereas no marked variation was detected in 'Brooks' and 'Sumele'. Moreover, a decrease in the WSF yield was found in 'Chelan'. It is also worth noting that the fraction of loosely bound polysaccharides represented for all cultivars (even at the ripe stage) less than 5% of the total wall non-cellulosic polysaccharides.

Tightly bound pectins (NSF) comprised the most abundant cell wall fraction in the five cultivars regardless of the ripening stage. The drop in polysaccharide yield accompanying ripening was in all cases due to the decrease of the NSF (Figure 1). A

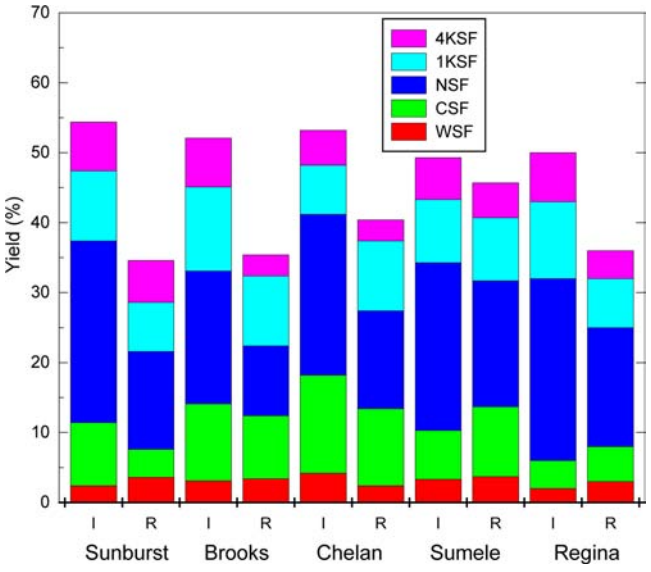


**Figure 1.** Accumulated yields of the water-, CDTA-, $Na_2CO_3$-, 1 M KOH-, and 4 M KOH-soluble fractions (WSF, CSF, NSF, 1KSF, 4KSF) of immature (I) and ripe (R) 'Brooks', 'Chelan', 'Sumele', 'Sunburst', and 'Regina' cherry fruit. Data represent an average of two independent weight measurements.

similar trend was previously observed on cherries,[8,9] grapes,[25] raspberries,[26] among other fruit species.[27]

**Depolymerization of Pectins and Cross-linking Glycans.** The MW distribution of all the isolated samples was determined by SEC, using Sepharose CL-6B for fractions WSF, 1KSF, and 4KSF, and Sepharose CL-2B for CSF and NSF. The WSF of immature cherries showed a wide profile of MWs in most cultivars. Depolymerization of pectins with ripening is highly variable among fruit species. Pectin downshifts were very limited in strawberry[28] and apple,[29] moderate in tomato[30] and peach,[31] but extensive in avocado.[32] Even within a single species, large variations have been reported depending on the cultivar.[33] In the present work a clear shift of the WSF profile toward lower MWs was observed as ripening proceeded. Firm 'Regina' cherries showed little or no depolymerization. In contrast, a downshift trend was observed in the WSF of the remaining cultivars. No association between firmness and pectin size was observed in these four genotypes indicating that the extent of fruit softening is not directly dependent on the degree of polymerization of loosely bound polyuronides.

The CSF showed a broad distribution of pectin MWs from early development, with no major changes occurring during ripening. A slight loss of high-MW polysaccharides was evident in soft 'Sunburst' fruit. The highly abundant NSF showed some unexpected features considering the traditional direct association that has been made between depolymerization and softening in several fruits. Indeed, the firmest genotype showed a lower degree of polymerization than soft 'Sunburst' cherries. Thus, the intermolecular interactions between polymers or their preferential distribution within the cell wall may be more relevant than their individual polymerization degree. No marked depolymerization was observed in this fraction as ripening progressed with the exception of relatively firm 'Sumele' fruit.

As occurs in blueberry,[34] and in contrast to raspberry[26] depolymerization of matrix glycans was related to ripening. For both loosely and tightly bound cross-linking glycans, soft 'Sunburst' cherries showed a greater reduction in polymer size than firm 'Regina' fruit. However, it is important to note that the firmest cultivar ('Regina') presented unripe cross-linking glycans with a relatively low MW. The 1KSF profile was characterized by a second, sharper peak with relatively high MW upon ripening, already observed for prunes and in previous work on cherries.[9,18] Overall, results from low-pressure SEC of pectin and hemicelluloses suggest that cherries show some depolymerization of WSF and 1KSF. However, with a few exceptions, the degree of polymerization of non-cellulosic

**Table 2. Neutral Sugar Composition (mol/100 mol) of the Water-, CDTA-, and $Na_2CO_3$-Soluble Fractions in Immature (I) and Ripe (R) 'Sunburst', 'Brooks', 'Chelan', 'Sumele', and 'Regina' Cherries**[a]

| | | monosaccharide | | | | | | | | | | | | | |
|---|---|---|---|---|---|---|---|---|---|---|---|---|---|---|---|
| | | Rha | | Fuc | | Ara | | Xyl | | Man | | Gal | | Glc | |
| fraction | cultivar | I | R | I | R | I | R | I | R | I | R | I | R | I | R |
| WSF | Sunburst | 8 | 10 | – | 1 | 31 | 40 | 11 | 7 | 12 | 9 | 26 | 18 | 12 | 15 |
| | Brooks | 8 | 7 | – | 1 | 40 | 40 | 6 | 7 | 9 | 10 | 27 | 20 | 10 | 15 |
| | Chelan | 9 | 10 | – | 1 | 44 | 30 | 8 | 8 | 10 | 11 | 20 | 23 | 9 | 17 |
| | Sumele | 9 | 8 | 1 | 1 | 44 | 35 | 5 | 7 | 10 | 11 | 24 | 24 | 7 | 15 |
| | Regina | 6 | 9 | 1 | 1 | 31 | 36 | 12 | 5 | 12 | 12 | 23 | 22 | 13 | 16 |
| CSF | Sunburst | 13 | 12 | 3 | 1 | 64 | 66 | 5 | 3 | 3 | 3 | 10 | 11 | 2 | 3 |
| | Brooks | 12 | 11 | 1 | 1 | 59 | 80 | 3 | 1 | 4 | 1 | 17 | 4 | 5 | 2 |
| | Chelan | 11 | 12 | 1 | 1 | 73 | 70 | 1 | 2 | tr | 1 | 13 | 10 | 1 | 4 |
| | Sumele | 10 | 14 | 1 | 2 | 53 | 70 | 6 | 3 | 8 | 1 | 19 | 9 | 3 | 2 |
| | Regina | 9 | 12 | 1 | 1 | 64 | 67 | 4 | 4 | 6 | 2 | 11 | 10 | 6 | 4 |
| NSF | Sunburst | 8 | 8 | tr | tr | 69 | 84 | – | 2 | – | tr | 23 | 5 | – | 1 |
| | Brooks | 10 | 8 | tr | tr | 75 | 81 | 1 | 1 | – | tr | 13 | 7 | tr | 2 |
| | Chelan | 10 | 7 | tr | 1 | 76 | 83 | 1 | 2 | tr | tr | 12 | 5 | 1 | 2 |
| | Sumele | 10 | 8 | 1 | 1 | 70 | 77 | 2 | 3 | tr | 1 | 16 | 9 | 1 | 1 |
| | Regina | 10 | 8 | tr | tr | 66 | 78 | 1 | 2 | tr | tr | 19 | 8 | 3 | 3 |

[a]The average value is indicated ($n$ = 2–3).


dx.doi.org/10.1021/jf504357u | J. Agric. Food Chem. 2014, 62, 12418–12427

**Table 3. Neutral Sugar Composition (mol/100 mol) of the 1 M KOH- and 4 M KOH-Soluble Fractions of Immature (I) and Ripe (R) 'Sunburst', 'Brooks', 'Chelan', 'Sumele', and 'Regina' Cherries**[a]

| | | monosaccharide | | | | | | | | | | | | | |
|---|---|---|---|---|---|---|---|---|---|---|---|---|---|---|---|
| | | Rha | | Fuc | | Ara | | Xyl | | Man | | Gal | | Glc | |
| fraction | cultivar | I | R | I | R | I | R | I | R | I | R | I | R | I | R |
| 1KSF | Sunburst | 5 | 4 | 1 | 1 | 52 | 55 | 21 | 16 | 2 | 1 | 11 | 11 | 8 | 11 |
| | Brooks | 5 | 4 | 1 | 1 | 50 | 60 | 17 | 12 | 4 | 4 | 12 | 7 | 11 | 11 |
| | Chelan | 5 | 4 | 1 | 1 | 46 | 57 | 23 | 15 | 4 | 4 | 11 | 9 | 11 | 10 |
| | Sumele | 3 | 4 | 1 | 1 | 57 | 59 | 22 | 16 | 3 | 4 | 8 | 8 | 7 | 8 |
| | Regina | 3 | 4 | tr. | 1 | 56 | 56 | 24 | 13 | 1 | 5 | 9 | 12 | 7 | 9 |
| 4KSF | Sunburst | 4 | 5 | 3 | 2 | 34 | 36 | 24 | 18 | 6 | 5 | 15 | 20 | 14 | 14 |
| | Brooks | 3 | 4 | 2 | 2 | 36 | 33 | 21 | 22 | 5 | 4 | 13 | 11 | 20 | 24 |
| | Chelan | 4 | 5 | 2 | 1 | 29 | 30 | 23 | 20 | 7 | 8 | 11 | 13 | 25 | 24 |
| | Sumele | 3 | 6 | 2 | 2 | 37 | 37 | 23 | 17 | 5 | 4 | 10 | 9 | 19 | 24 |
| | Regina | 4 | 6 | 2 | 2 | 27 | 38 | 26 | 14 | 5 | 9 | 10 | 13 | 26 | 18 |

[a]The average value is indicated ($n$ = 2–3).

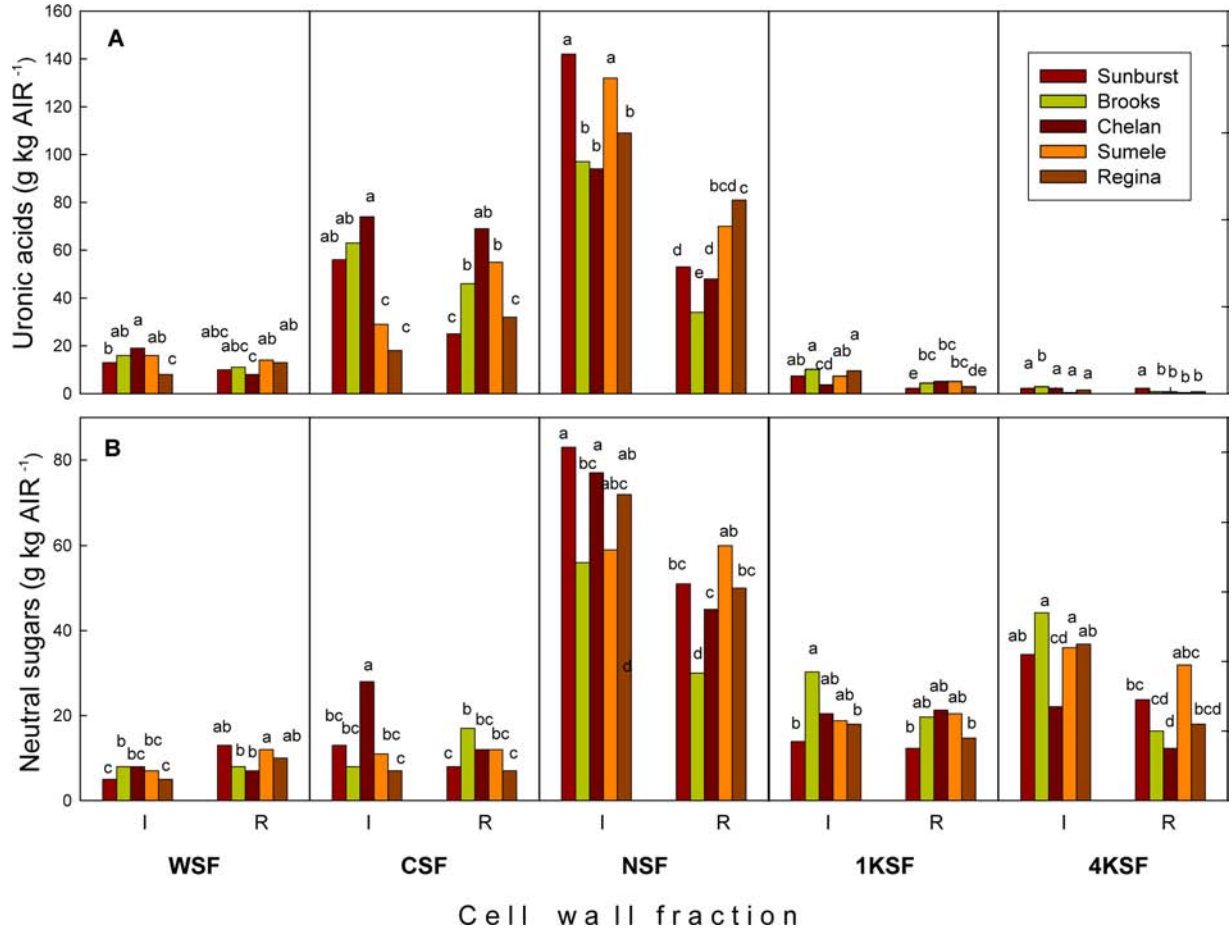


**Figure 2.** Uronic acids (A) and neutral sugars (B) in the water- (WSF), CDTA- (CSF), $Na_2CO_3$- (NSF), 1 M KOH- (1KSF), and 4 M KOH-soluble fractions (4KSF) of immature (I) or ripe (R) 'Brooks', 'Chelan', 'Sumele', 'Sunburst', and 'Regina' cherries during development. Different letters indicate significant differences between cultivars and stages based on a Tukey test at a level of significance of $P \leq 0.05$.

polysaccharides at immature stages and its variation during ripening do not correlate with genotype firmness.

**Polysaccharide Neutral Sugar Composition.** The NS compositions of the different cultivars were surprisingly similar. Arabinose was the most abundant monosaccharide in all pectic fractions and cultivars (Table 2). Arabinose represented 31% of total NSs in the WSF. Its level increased to ca. 60% in the CSF and 65–76% in the NSF. In pear, arabinose was rather lost,[35] but in cherries this sugar increases its proportion with ripening. Galactose and rhamnose were also present in substantial amounts, indicating the presence of RG-I in all three pectic fractions and cultivars. Xylose, glucose, and mannose only appeared in considerable levels in the WSF, whereas the most abundant pectic NSF fraction only showed low proportions of

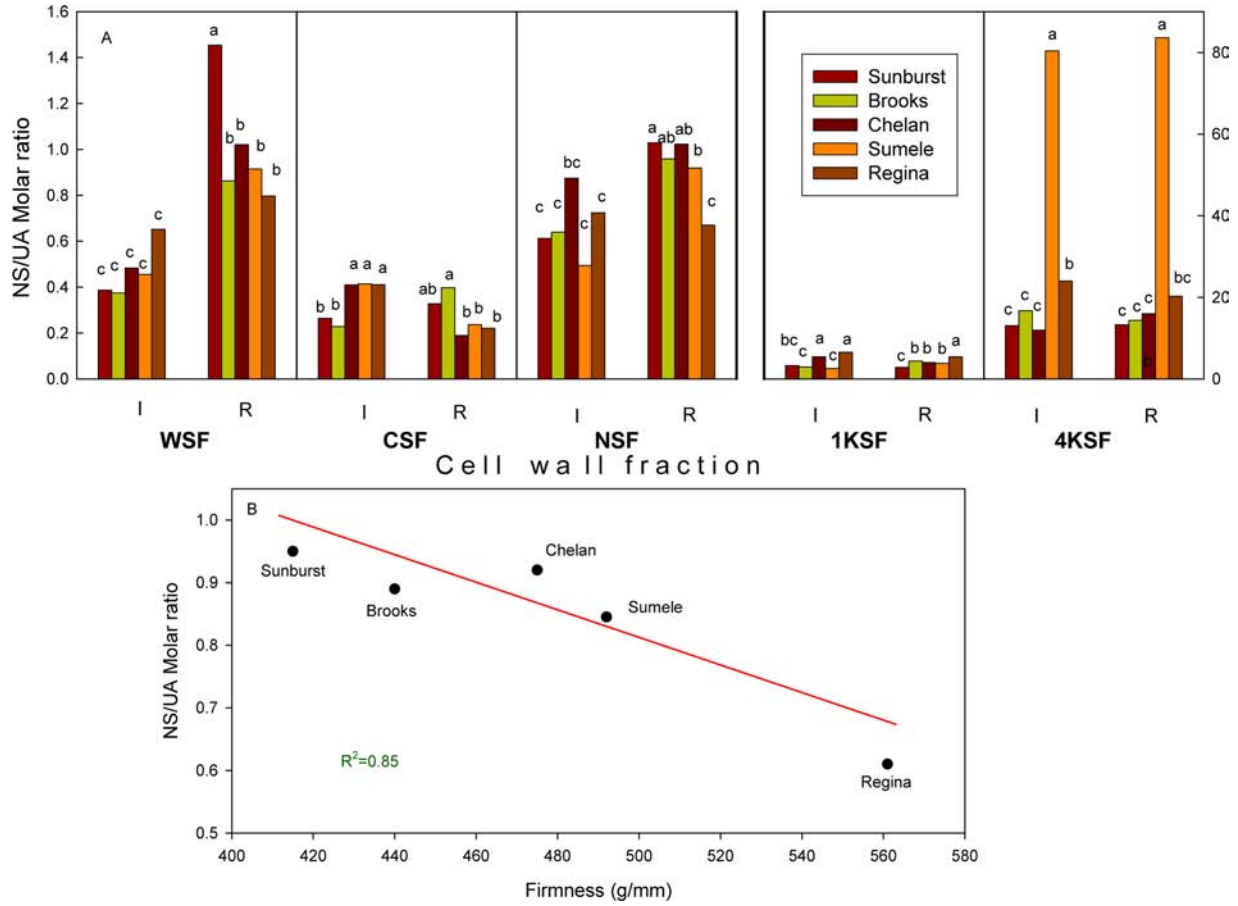


**Figure 3.** (A) Neutral sugars-to-uronic acids molar ratios calculated for the water- (WSF), CDTA- (CSF), $Na_2CO_3$- (NSF), 1 M KOH- (1KSF), and 4 M KOH-soluble fractions (4KSF) of immature (I) and ripe (R) 'Brooks', 'Chelan', 'Sumele', 'Sunburst', and 'Regina' cherry fruit during development. Different letters indicate differences based on a Tukey test at a level of significance of $P \leq 0.05$. Note the different scale for the two last figures. (B) Association between the NS/UA ratio and firmness from the NSF of ripe 'Brooks', 'Chelan', 'Sumele', 'Sunburst', and 'Regina' cherries.

these residues (Table 2). The proportion of arabinose in the WSF varied with ripening in a different fashion depending on the cultivar. This fraction also showed some increase in glucose proportion at the ripe stage.

No marked enrichment or drop of a specific NS was observed during ripening in the ionically bound pectins (CSF), regardless of the cultivar. The UA/rhamnose ratio may be indicative of the relative proportion of RG-I to homogalacturonan (HG) in the pectic fractions, with higher values being expected in fractions enriched in HG. The NSF showed lower UA/rhamnose ratios (10−20) than the other pectic fractions, suggesting a higher prevalence of RG-I. The proportion of arabinose in this fraction increased in all the cultivars during ripening, with a corresponding reduction in galactose. This points out to a preferential cleavage of galactan side chains from RG-I, or from an arabinose enrichment originated in material associated with cross-linking glycans or cellulose. Loss of galactose is important in some species but not in others.[35−38]

Although hemicelluloses are usually considered to be predominant in the KOH-soluble fractions, arabinose still represented 50% of total NS in the 1KSF. The residual pectins present in the cross-linking glycan fraction 1KSF show considerably lower ratios (UA/rhamnose = 4−12) than those of the pectin-richer fractions. The ratio is even lower (<2) for the 4KSF, suggesting that these residual pectins are RG-I-rich and that tight association through side-chain interactions exists between hemicelluloses and RG-I regardless of the cultivar[39,40] (Table 3). Xylose was the second most abundant sugar, but its proportion (ca. 20%) dropped upon ripening. The presence of xylose in levels exceeding those of glucose, suggests that besides some xyloglucan, xylans may be present. This may also contribute to the relatively high arabinose levels which could be, at least in part, in the form of arabinoxylans.

Arabinose proportion was, as expected, lower in the 4KSF, but, differently from other fruit species, it still represented the most abundant NS, closely followed by xylose and glucose. As for the 1KSF, the level of xylose tended to decrease with ripening. Noteworthy, the presence of small but constant levels of rhamnose and UA suggests that some RG-I still remains in this fraction, possibly entangled to the cellulose-xyloglucan/arabinoxylan network.

**Pectin and Hemicellulose Solubilization.** At the immature stage UAs were ca. 2- and 7-fold higher in the NSF than in the CSF and WSF (Figure 2A). The UA of the tightly bound pectin showed a marked decrease during ripening. This has also been observed in other fruits.[27] The drop of UA in the NSF did not occur with a concomitant accumulation in the water or CDTA-soluble fractions, suggesting that it was caused by the action of exo-acting galacturonate hydrolases yielding free galacturonic acid, which may be possibly lost in the ethanol washings of the AIR. At the ripe stage, firmer 'Regina' cherries maintained higher levels of tightly bound UA (Figure 2A). However, the absolute level of $Na_2CO_3$-soluble polyuronides showed no high association with

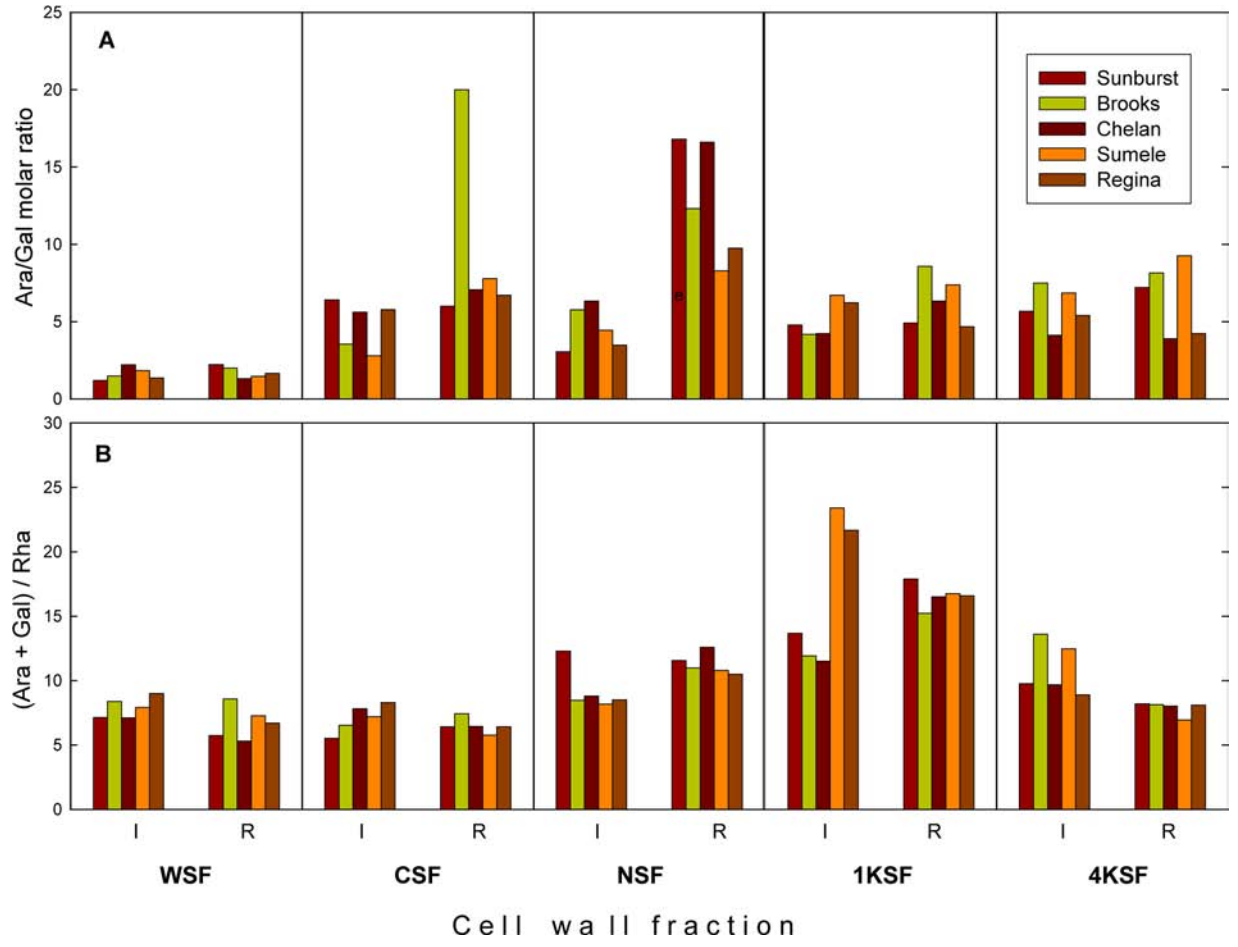


**Figure 4.** (A) Ara/Gal and (B) (Ara+Gal)/Rha molar ratios calculated for the water- (WSF), CDTA- (CSF), $Na_2CO_3$- (NSF), 1 M KOH- (1KSF), and 4 M KOH-soluble fractions (4KSF) of immature (I) and ripe (R) 'Brooks', 'Chelan', 'Sumele', 'Sunburst', and 'Regina' cherry fruit during development. Different letters indicate differences based on a Tukey test at a level of significance of $P \leq 0.05$.

cultivar firmness. For the CSF, a more erratic behavior of the UA content changes with ripening was observed; they increased with ripening in 'Sumele' and diminished in 'Sunburst'. The strong interaction between pectic and hemicellulosic matrices by covalent linkages[39,40] was also evident in cherry by the fact that alkali-soluble fractions still contained considerable amounts of UA. These polyuronides showed a progressive loss between early ripening stages and commercial maturity.

Analysis of the fate of the NSs on ripening (Figure 2B) showed small quantitative variations for WSF, an erratic behavior for CSF, but a decreasing tendency in the remaining fractions. The sum of NSs diminished clearly on ripening for all cultivars excluding 'Sumele', where it remained unchanged. The decrease ranged from 28% in 'Regina' and 'Sunburst' to 37% in 'Chelan' and 'Brooks'.

**Relationship between Cell-Wall Polysaccharides.** By considering the neutral sugars-to-uronic acids molar ratio (NS/UA) (Figure 3A), an outline of the proportion of branching on RG-I can be assessed on pectic fractions, as well as the hemicellulose/pectin ratios on cross-linking glycan fractions. Pectin fractions WSF, CSF, and NSF were enriched in UAs, and thus gave relatively low NS/UA ratios (0.2−1.4). The glycan fractions 4KSF gave high values (12−84), whereas intermediate levels were observed in the 1KSF (3−6). No major variations in the NS/UA molar ratio with ripening were observed for the cross-linking glycan fractions 1KSF and 4KSF. However, some inter-cultivar differences could be depicted (Figure 3A). For WSF, a significant increase in the NS/UA ratio with ripening was observed (Figure 3A) in all varieties. A lower but still significant increase was also found in the NSF fraction of three varieties. On the other hand, the CSF fractions showed the lowest ratio among the pectic fractions (Figure 3A), suggesting that they are HG-rich. Only a small variation with ripening was observed in this fraction. For the most abundant NSF, a high negative correlation ($R^2$ = −0.85) was found between the NS/UA ratio and cultivar firmness (Figure 3B). Firm cherries presented pectic polymers with lower NS/UA ratio, suggesting that the branching of polyuronides or the proportion of branched RG-I to HG may contribute to the differences in firmness between cultivars.

The Ara/Gal molar ratio allows an estimate of the relative importance of these monosaccharides in RG-I side chains. These ratios (Figure 4A) were always well above 1. The lowest ratios were found in the WSF (i.e., the most galactose-rich RG-I). For the CSF, the arabinose/galactose ratios for immature fruit were at or below 5, but they increased for ripe fruit, especially in 'Brooks'. The NSF showed a clear increase in this ratio upon ripening for all cultivars. This suggests that during ripening, higher loss of galactan or arabinogalactan chains occurs as compared to those of arabinans, regardless of the cultivar. However, since cherries show overlap between growth and ripening, *de novo* deposition of polysaccharides may occur

providing more complexity to the interpretation of the results. The Ara/Gal ratios in the cross-linking glycan fractions (Figure 4A) showed a more or less constant value, close to 5, regardless of the ripening stage, and changes were more dependent upon the variety.

As these Ara and Gal moieties are mostly part of the side chains of RG-I, their ratios relative to Rha estimate the degree of branching on RG-I. These results are shown in Figure 4B. A small decrease of these ratios upon ripening was observed in WSF and CSF, but for NSF these ratios became larger and increased further at the ripe stage. Ripe fruit showed (Ara +Gal)/Rha ratios in these fractions close to 11−12, regardless of the cultivar. This suggests that the variation in NS/UA ratio of the tightly bound pectin was more likely due to different proportions of HG and RG-I. The independent presence of HG and RG has been questioned by some authors. Vincken et al.[41] proposed a molecular brush model in which HG, (arabino) galactan, and arabinan occur as side chains of RG-I. Considering this model and the results found herein, firm cherry fruit would have a brush structure richer in HG side chains than soft cultivars. Overall, our results suggest that branching of polyuronide occurs early in development, and that the proportion of branched RG-I to HG may contribute to the differences in firmness between cherry cultivars. Studies evaluating differences in the levels of enzymes involved in pectin biosynthesis (e.g., rhamnosyl, galactosyl and arabinosyl transferases) could be of great interest for further work.

Few studies have analyzed changes in turgor pressure during fruit ripening, but early reports suggested that turgor pressure may be also an important contributor to fruit texture.[42] Recent work[43] has shown that turgor pressure drops during cherry fruit development. Thus, the potential role of differences in turgor pressure on cultivar texture could not be ruled out.

**UV-MALDI-TOF Mass Spectrometry of Pectins.** Determination of changes in polymer composition attracts the interest of researchers in the field of plant cell wall carbohydrates synthesis and degradation. Even with only a limited number of monosaccharides used as building blocks, variations in sequence, linkage, branching, side-chain distribution, and functional group modifications result in a wide structural diversity. No single analytical method alone is capable of resolving carbohydrate structures, especially when present in complex mixtures. Mass spectrometry is a selective and powerful technique to identify and obtain structural information and quick profiles on compounds present in complex mixtures.[44,45] Since it requires only small amounts of sample, it is an excellent tool for researchers interested in detecting changes in composition of complex plant carbohydrates. Nevertheless, detection of native non-derivatized polysaccharides by UV-MALDI MS is still a challenge due to the shortage of adequate matrices.[44−49] So far, there have been only a few studies reported for detection of native polysaccharides with MW > 40 000 Da[44,45,49−51] In the current work, our challenge was to observe if the association of this pattern of depolymerization with firmness and development among cultivars can be foreseen in a different fashion using UV-MALDI-MS than that found by traditional size exclusion chromatography.

In the current work, we have found that 2,5-dihydroxybenzoic acid[46] and 9*H*-pyrido[3,4*b*]indole (nor-harmane)[48] are good matrices for MALDI-MS analysis of native polysaccharides with high MWs and broad mass ranges ($m/z$ 40 000−160 000).

In order to further characterize the cell wall changes occurring on development and to identify putative factors associated with firmness variation in cherry fruit genotypes, we performed a detailed evaluation of the UV-MALDI-TOF mass spectra of the different pectin fractions WSF, CSF, and NSF for the five cultivars. Experiments were conducted with two different matrices, nor-harmane and gentisic acid, in order to get complementary information, and in five independent experiments. In this analysis, the intensity of the signals, the signal-to-noise ratio (S/N), and the number of signals with intensities higher than a given threshold (S/N > 2) in all the $m/z$ region analyzed were taken into account. Although each mass spectrum appears as a bidimensional image (intensity vs $m/z$), the number of "true" signals in each $m/z$ region yields additional data. These three variables (intensity, number of signals, and $m/z$) were taken into account for the comparative analysis of all the extracts studied. In the range $m/z$ 80 000−200 000, a large number of pectin signals originated in the WSF fractions from immature fruit were very conspicuous by this technique, showing clear spectra. The CSF gave much poorer spectra with very low S/N, whereas for the NSF almost no signals were observed in this $m/z$ range. As an example, the results obtained for cv. Regina using nor-harmane as matrix are shown in Figure 5. From ripe cherries, WSF showed poor

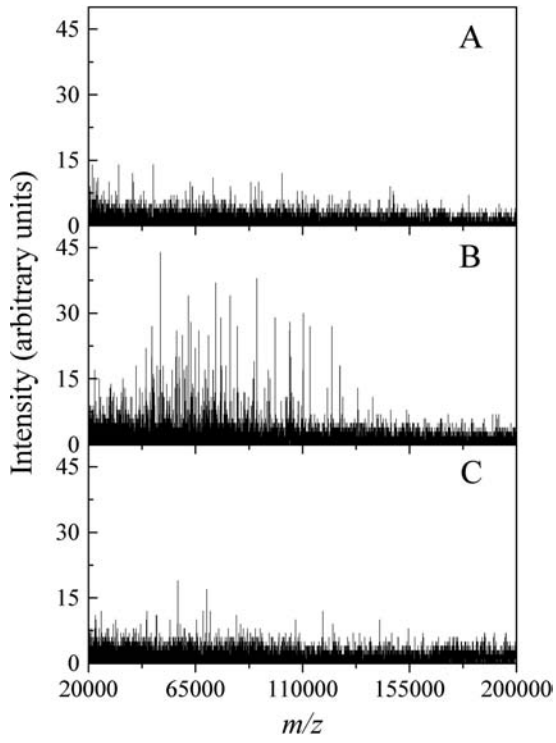


**Figure 5.** UV-MALDI-MS analysis of 'Regina' fractions in positive ion mode using nor-harmane as matrix. Characteristic profiles obtained for WSF from ripe fruit (A), WSF from immature fruit (B), and CSF from immature fruit (C).

spectra in the range $m/z$ 20 000−150 000 (no signals with intensity >15 arbitrary units and S/N > 2 (Figure 5A). In contrast, WSF of immature cherries showed clear profiles with abundant high-intensity ion signals (Figure 5B) in the same $m/z$ range. Poor spectra with very few signals at the $m/z$ range 40 000−80 000 with the stated intensity and S/N were obtained when the corresponding CSF was analyzed (Figure

5C). The differences observed in the spectra agree with the facts that complex mixtures of polysaccharides were analyzed and with the possibility that ion source decomposition occurs.[44,45] Similar characteristic profiles were obtained for immature WSF from the other four varieties studied.

In this work, we have focused on the evaluation of the changes in cell wall polysaccharides of five cherry cultivars ('Chelan', 'Sumele', 'Brooks', 'Sunburst', and 'Regina') with contrasting firmness at two developmental stages, showing that, contrary to what is usually shown in most fruits, cherry softening could occur is some cultivars without marked increases in water-soluble pectin. The degree of pectin or hemicellulose depolymerization or the solubilization of polyuronides is not directly associated with fruit firmness. The tightly bound polyuronides represented the most abundant cell wall fraction in all cultivars. A high negative correlation was found between the NS-to-UA ratio in this fraction and tissue texture, causing firm cultivars to exhibit lower NS/UA than soft cherries. The similar molar ratio of arabinose and galactose relative to rhamnose [(Ara+Gal)/Rha] suggests that the cultivars differed in their relative proportion of homogalacturonan and rhamnogalacturonan I rather than in the size of RG side chains, with greater proportions of HG in firmer cherries. Finally, we showed that UV-MALDI-TOF mass spectrometry may be a powerful analytical approach to complement traditional methods used to study polysaccharides contributing to improve our understanding of cell wall catabolism, as the mass spectra allowed immature to be distinguished from ripe fruits. WSF of immature cherries showed clear profiles with abundant ion signals in the range $m/z$ 20 000−150 000, but poor spectra with very few signals in the range $m/z$ 40 000−80 000 were obtained when CSF was analyzed. On the contrary, from ripe cherries WSF showed poor spectra with either matrix at the former $m/z$ region.

## ■ ASSOCIATED CONTENT

### Supporting Information

NS composition of the fractions expressed in g/kg AIR; SEC profiles of all the fractions; and UV-MALDI-MS analysis of selected fractions. This material is available free of charge via the Internet at http://pubs.acs.org.

## ■ AUTHOR INFORMATION

### Corresponding Author

*Phone/fax (+5411)-4576-3346; e-mail stortz@qo.fcen.uba.ar.

### Author Contributions

§N.M.A.P., M.L.S., A.R.V., R.E.-B., and C.A.S. are Research Members of the Consejo Nacional de Investigaciones Científicas y Técnicas (CONICET), Argentina.

### Funding

The authors thank the Consejo Nacional de Investigaciones Científicas y Técnicas (PIP 0559/10 and 0400/10) and the Universidad de Buenos Aires (UBACyT Program) for financial support.

### Notes

The authors declare no competing financial interest.

## ■ ABBREVIATIONS USED

AIR, alcohol-insoluble residue; CDTA, *trans*-1,2-diaminocyclohexane-*N*,*N*,*N*′,*N*′-tetraacetic acid; CSF, CDTA-soluble fraction; DAA, days after anthesis; HG, homogalacturonan; 1KSF, 1 M KOH-soluble fraction; 4KSF, 4 M KOH-soluble fraction; NS, neutral sugar; NSF, $Na_2CO_3$-soluble fraction; RG-I, rhamnogalacturonan I; SEC, size-exclusion chromatography; S/N, signal-to-noise ratio; SSC, soluble solids content; TFA, trifluoroacetic acid; UA, uronic acid; WSF, water-soluble fraction

## ■ REFERENCES

(1) Young, K. Cherries of the World 2014, 2014; http://www.freshfruitportal.com/wp-content/uploads/2013/12/cherries_of_the_world_2014.pdf (accessed Nov 13, 2014).

(2) FAOSTAT, 2014; http://faostat.fao.org/ (accessed Oct 22, 2014).

(3) Cittadini, E. D. Sweet cherries from the end of the world: options and constrains for fruit production systems in South Patagonia, Argentina. Ph.D. Thesis, Wageningen University, The Netherlands, 2007.

(4) Mitcham, E. J.; Crisosto, C. H.; Kader, A. A. Cherry: Recommendations for maintaining postharvest quality, 1996; http://postharvest.ucdavis.edu/PFfruits/Cherry/ (accessed Nov 13, 2014).

(5) Cantu, D.; Vicente, A. R.; Greve, L. C.; Dewey, F. M.; Bennett, A. B.; Labavitch, J. M.; Powell, A. L. T. The intersection between cell wall disassembly, ripening, and fruit susceptibility to *Botrytis cinerea*. *Proc. Natl. Acad. Sci. U.S.A.* **2008**, *105*, 859−864.

(6) Looney, N. E.; Webster, A. D.; Kupferman, E. M. Harvest and handling sweet cherries for the fresh market. In *Cherries: crop physiology, production and uses*; Webster, A. D., Looney, N. E., Eds.; CAB International: Wallingford, UK, 1996; pp 411−441.

(7) Mattheis, J.; Fellman, J.. Cherry (sweet). In *USDA, ARS Agriculture Handbook Number 66*, 2004; http://www.ba.ars.usda.gov/hb66/contents.html (accessed Nov 13, 2014).

(8) Choi, C.; Toivonen, P.; Wiersma, P. A.; Kappel, F. Differences in levels of pectic substances and firmness in fruit from six sweet cherry genotypes. *J. Am. Pomol. Soc.* **2002**, *56*, 197−201.

(9) Salato, G. S.; Ponce, N. M. A.; Raffo, M. D.; Vicente, A. R.; Stortz, C. A. Developmental changes in cell wall polysaccharides from sweet cherry (*Prunus avium* L.) cultivars with contrasting firmness. *Postharvest Biol. Technol.* **2013**, *84*, 66−73.

(10) Basanta, M. F.; de Escalada Plá, M. F.; Stortz, C. A.; Rojas, A. M. Chemical and functional properties of cell wall polymers from two cherry varieties at two developmental stages. *Carbohydr. Polym.* **2013**, *92*, 830−841.

(11) Batisse, C.; Buret, M.; Coulomb, P. J. Biochemical differences in cell wall of cherry fruit between soft and crisp fruit. *J. Agric. Food Chem.* **1996**, *44*, 453−457.

(12) Batisse, C.; Buret, M.; Coulomb, P. J.; Coulomb, C. Ultrastructure of different textures of Bigarreau Burlat cherries during maturation. *Can. J. Bot.* **1996**, *74*, 1974−1981.

(13) Fils-Lycaon, B.; Buret, M. Loss of firmness and changes in the pectic fractions during ripening and overripening of sweet cherry. *HortScience* **1990**, *25*, 777−778.

(14) Kondo, S.; Danjo, C. Cell wall polysaccharide metabolism during fruit development in sweet cherry 'Satohnishiki' as affected by gibberellic acid. *J. Jpn. Soc. Hortic. Sci.* **2001**, *70*, 178−184.

(15) Andrews, P. K.; Shulin, L. Cell wall hydrolytic enzyme activity during development of nonclimateric sweet cherry (*Prunus avium* L.) fruit. *J. Hortic. Sci. Biotechnol.* **1995**, *70*, 561−567.

(16) Barrett, D. M.; Gonzalez, C. Activity of softening enzymes during cherry maturation. *J. Food Sci.* **1994**, *59*, 574−577.

(17) Christensen, J. V. Cracking in cherries. III. Determination of cracking susceptibility. *Acta Agric. Scand.* **1972**, *22*, 128−136.

(18) Ponce, N. M. A.; Ziegler, V. H.; Stortz, C. A.; Sozzi, G. O. Compositional changes in cell wall polysaccharides from Japanese plum (*Prunus salicina* Lindl.) during growth and on-tree ripening. *J. Agric. Food Chem.* **2010**, *58*, 2562−2570.

(19) Filisetti-Cozzi, T. M. C. C.; Carpita, N. C. Measurement of uronic acids without interference from neutral sugars. *Anal. Biochem.* **1991**, *197*, 157−162.

(20) Dubois, M.; Gilles, K. A.; Hamilton, J. K.; Robers, P. A.; Smith, F. Colorimetric method for determination of sugars and related substances. *Anal. Chem.* **1956**, *28*, 350−356.
(21) Monge, M. E.; Negri, R. M.; Kolender, A. A.; Erra-Balsells, R. Structural characterization of native highly-methoxylated pectin using UV-MALDI-TOF mass spectrometry. Comparative use of 2,5-dihydroxybenzoic acid and nor-harmane as UV-MALDI matrices. *Rapid Commun. Mass Spectrom.* **2007**, *21*, 2638−2646.
(22) Jiménez-Bermúdez, S.; Redondo-Nevado, J.; Muñoz-Blanco, J.; Caballero, J. L.; López-Aranda, J. M.; Valpuesta, V.; Pliego-Alfaro, F.; Quesada, M. A.; Mercado, J. A. Manipulation of strawberry fruit softening by antisense expression of a pectate lyase gene. *Plant Physiol.* **2002**, *128*, 751−759.
(23) Alkio, M.; Jonas, U.; Sprink, T.; van Nocker, S.; Knoche, M. Identification of putative candidate genes involved in cuticle formation in *Prunus avium* (sweet cherry) fruit. *Ann. Bot.* **2012**, *110*, 101−112.
(24) Vicente, A. R.; Saladié, M.; Rose, J. K.; Labavitch, J. M. The linkage between cell wall metabolism and fruit softening: looking to the future. *J. Sci. Food Agric.* **2007**, *87*, 1435−1448.
(25) Nunan, K. J.; Sims, I. M.; Bacic, A.; Robinson, S. P.; Fincher, G. B. Changes in cell wall composition during ripening of grape berries. *Plant Physiol.* **1998**, *118*, 783−792.
(26) Vicente, A. R.; Ortugno, C.; Powell, A. L. T.; Greve, L. C.; Labavitch, J. M. Temporal sequence of cell wall disassembly events in developing fruits. 1. Analysis of raspberry (*Rubus idaeus*). *J. Agric. Food Chem.* **2007**, *55*, 4119−4124.
(27) Brummell, D. A. Cell wall disassembly in ripening fruits. *Funct. Plant Biol.* **2006**, *33*, 103−119.
(28) Huber, D. J. Strawberry (*Fragaria ananassa*) fruit softening, the potential roles of polyuronides and hemicelluloses. *J. Food Sci.* **1984**, *49*, 1310−1315.
(29) Yoshioka, H.; Aoba, K.; Kashimura, Y. Molecular weight and degree of methoxylation in cell wall polyuronide during softening in pear and apple fruit. *J. Am. Soc. Hortic. Sci.* **1992**, *117*, 600−606.
(30) Huber, D. J.; O'Donoghue, E. M. Polyuronides in avocado (*Persea americana*) and tomato (*Lycopersicon esculentum*) fruits exhibit markedly different patterns of molecular weight downshifts during ripening. *Plant Physiol.* **1993**, *102*, 473−480.
(31) Brummell, D. A.; Dal Cin, V.; Crisosto, C. H.; Labavitch, J. M. Cell wall metabolism during maturation, ripening and senescence of peach fruit. *J. Exp. Bot.* **2004**, *55*, 2029−2039.
(32) Sakurai, N.; Nevins, D. J. Relationship between fruit softening and wall polysaccharides in avocado (*Persea americana* Mill) mesocarp tissues. *Plant Cell Physiol.* **1997**, *38*, 603−610.
(33) Rosli, H. G.; Civello, P. M.; Martínez, G. A. Changes in cell wall composition of three *Fragaria* x *ananassa* cultivars with different softening rate during ripening. *Plant Physiol. Biochem.* **2004**, *42*, 823−831.
(34) Vicente, A. R.; Ortugno, C.; Rosli, H.; Powell, A. L.; Greve, L. C.; Labavitch, J. M. Temporal sequence of cell wall disassembly events in developing fruits. 2. Analysis of blueberry (*Vaccinium* species). *J. Agric. Food Chem.* **2007**, *55*, 4125−4130.
(35) Gross, K. C.; Sams, C. E. Changes in cell wall neutral sugar composition during fruit ripening: a species survey. *Phytochemistry* **1984**, *11*, 2457−2461.
(36) Peña, M. J.; Carpita, N. C. Loss of highly branched arabinans and debranching of rhamnogalacturonan I accompany loss of firm texture and cell separation during prolonged storage of apples. *Plant Physiol.* **2004**, *135*, 1305−1313.
(37) Redgwell, R. J.; Melton, L. D.; Brasch, D. J. Cell wall changes in kiwifruit following postharvest ethylene treatment. *Phytochemistry* **1990**, *29*, 399−407.
(38) Redgwell, R. J.; Mac Rae, E.; Hallett, I.; Fischer, M.; Perry, J.; Harker, R. *In vivo* and *in vitro* swelling of cell walls during fruit ripening. *Planta* **1997**, *203*, 162−173.
(39) Zykwinska, A. W.; Ralet, M. C. J.; Garnier, C. D.; Thibault, J. F. J. Evidence for *in vitro* binding of pectin side chains to cellulose. *Plant Physiol.* **2005**, *139*, 397−407.
(40) Thompson, J. E.; Fry, S. C. Evidence of covalent linkage between xyloglucan and acidic pectins in suspension-cultured rose cells. *Planta* **2000**, *211*, 275−286.
(41) Vincken, J. P.; Schols, H. A.; Oomen, R. J. F. J.; McCann, M. C.; Ulvskov, P.; Voragen, A. G. J.; Visser, R. G. F. If homogalacturonan were a side chain of rhamnogalacturonan I. Implications for cell wall architecture. *Plant Physiol.* **2003**, *132*, 1781−1789.
(42) Shackel, K.; Greve, C.; Labavitch, J. M.; Ahmadi, A. Cell turgor changes associated with ripening in tomato pericarp tissue. *Plant Physiol.* **1991**, *97*, 814−816.
(43) Knoche, M.; Grimm, E.; Schlegel, H. J. Mature sweet cherries have low turgor. *J. Am. Soc. Hort. Sci.* **2014**, *139*, 3−12.
(44) Harvey, D. J. Matrix-assisted laser desorption/ionization mass spectrometry of carbohydrates. *Mass Spectrom. Rev.* **1999**, *18*, 349−451.
(45) Harvey, D. J. Analysis of carbohydrates and glycoconjugates by matrix-assisted laser desorption/ionization mass spectrometry: An update covering the period 2007−2008. *Mass Spectrom. Rev.* **2012**, *31*, 183−211.
(46) Stahl, B.; Steup, M.; Karas, M.; Hillenkamp, F. Analysis of neutral oligosaccharides by matrix-assisted laser desorption ionization mass spectrometry. *Anal. Chem.* **1991**, *63*, 1463−1466.
(47) Mohr, M. D.; Olaf Börnsen, K.; Widmer, H. M. Matrix-assisted laser desorption/ionization mass spectrometry: Improved matrix for oligosaccharides. *Rapid Commun. Mass Spectrom.* **1995**, *9*, 809−814.
(48) Nonami, H.; Fukui, S.; Erra-Balsells, R. $\beta$-Carboline alkaloids as matrices for Matrix-assisted ultraviolet laser desorption time-of flight mass spectrometry of proteins and sulfated oligosaccharides: a comparative study using phenylcarbonyl compounds, carbazoles and classical matrices. *J. Mass Spectrom.* **1997**, *32*, 287−296.
(49) Hsu, N. Y.; Yang, W. B.; Wong, C. H.; Lee, Y. C.; Lee, R. T.; Wang, Y. S.; Chen, C. H. Matrix-assisted laser desorption/ionization mass spectrometry of polysaccharides with 2,4,6-trihydroxyacetophenone as matrix. *Rapid Commun. Mass Spectrom.* **2007**, *21*, 2137−2146.
(50) Nonami, H.; Tanaka, K.; Fukuyama, Y.; Erra-Balsells, R. $\beta$-Carboline alkaloids as matrices for UV-Matrix-assisted laser desorption/ionization time-of-flight mass spectrometry in positive and negative ion modes. Analysis of proteins of high molecular mass, and of cyclic and acyclic oligosaccharides. *Rapid Commun. Mass Spectrom.* **1998**, *12*, 285−296.
(51) Erra-Balsells, R.; Kolender, A.; Matulewicz, M. C.; Nonami, H.; Cerezo, A. S. Matrix-assisted ultraviolet laser desorption-ionization time of-flight mass spectrometry of sulfated mannans from the red seaweed *Nothogenia fastigiata*. *Carbohydr. Res.* **2000**, *329*, 157−167.

based studies have been complemented with electron spin resonance (ESR) spectroscopy for detection of radical-related reactions, and oxygen consumption for monitoring the overall extent of lipid oxidation in emulsions.

## MATERIALS AND METHODS

**Materials.** Medium-chain triglyceride (MCT) oil was obtained from Cognis GmbH, Ludwigshafen, Germany, and used as received. Linseed oil (LSO) and sunflower oil (SFO) were purchased from a local supermarket and purified of peroxyl radicals, trace metals, and tocopherols by alumina column chromatography according to Yoshida et al.[7] with few changes: the oil was mixed with hexane 1:1 and extracted from hexane by rotaty evaporation (Büchi Rotavapor R-144, Labortechnik AG, Flawil, Switzerland). The probe (*E*,*E*)-3,5-bis(4-phenyl-1,3-butadienyl)-4,4-difluoro-4-bora-3a,4a-diaza-*s*-indacene (BODIPY$^{665/676}$, B-3932) was purchased from Life Technologies Corp. N-*tert*-Butyl-α-phenylnitrone (PBN), methyl linoleate, methyl oleate, and Tween-20 were purchased from Sigma−Aldrich Inc., St. Louis, MO. Di-*tert*-butyl peroxide (DTBP) was purchased from Merck Schuchardt OHG, Hohenbrunn, Germany, and 2,2′-azobis(2,4-dimethyl)valeronitrile (AMVN) was purchased from Santa Cruz Biotechnology Inc., Dallas, TX.

**Radical-Initiated Fluorometric Studies.** *UV-Irradiation-Induced Radical Reactions.* Fluorometric measurements of UV-irradiation-induced radical reactions were performed with a 1 cm path length quartz cuvette on a spectrofluorometer (PerkinElmer Instruments, LS55 luminescence spectrometer, Seer Green, U.K.). UV irradiation was conducted with a Rayonet miniphotochemical reactor (model RMR-500, The Southern New England Ultraviolet Co., Hamden, CT) using four 300 nm UV lamps as described earlier.[6] Briefly, a sample in a quartz cuvette was placed in the middle of the minireactor, and UV light was exposed from four sides, making the irradiation uniform throughout the whole sample. The irradiation procedure was carried out on a control (oil with 1 μM BODIPY$^{665/676}$) and a sample (oil with 1 μM BODIPY$^{665/676}$ and 5.7 μM DTBP) for specific periods of time. Subsequently, the fluorescence spectra at excitation wavelengths ($\lambda_{ex}$) 675 and 580 nm were measured. Samples included MCT oil and linseed oil (LSO). In the case of LSO, handling of the oil was carried out under a nitrogen atmosphere. The extent of oxidation was quantified as a relative decrease of the fluorescence intensity measured at $\lambda_{ex}$ 675 nm, and a relative increase of the fluorescence intensity at $\lambda_{ex}$ 580 nm in the samples compared to the nonirradiated controls. The measurements were conducted in triplicate.

*Fluorescence Studies of Radical Reactions in Oils.* Fluorometric measurements of heat-induced radical reactions were performed with a 1 cm path length quartz cuvette on a luminescence spectrometer (Aminco-Bowman Series 2, Thermo Fisher Scientific, Waltham, MA). Heating in a thermo chamber at 37 °C was carried out on the control (oil with 1 μM BODIPY$^{665/676}$) and on the sample (oil with 1 μM BODIPY$^{665/676}$ and 13 mM AMVN) for 3 h. Fluorescence spectra were recorded at 1 min intervals at $\lambda_{ex}$ 580 nm. Samples included MCT oil, sunflower oil (SFO), mixtures of MCT oil and SFO in various ratios, MCT oil mixed with methyl linoleate (10 wt %), and MCT oil mixed with methyl oleate (10 wt %). The samples containing unsaturated fatty acids were handled under a nitrogen atmosphere. The extent of oxidation was quantified as percentage of increase of the fluorescence at $\lambda_{ex}$ 580 nm in irradiated samples compared to the nonirradiated controls. The measurements were conducted in triplicate.

**Electron Spin Resonance Spectroscopic Studies.** The rate of radical formation in oils containing radical initiator AMVN (6 mM) and spin trap PBN (20 mM) were determined by electron spin resonance (ESR). The oil phase was kept on ice while AMVN was dissolved, and subsequently PBN was added. The intensity of the generated spin adducts was recorded with an ESR spectrometer (Miniscope MS200, Magnettech, Berlin, Germany). The samples in the ESR measuring cavity were heated at 37 °C by using a temperature controller (temperature controller M01, Magnettech, Berlin, Germany). The oil samples included MCT oil, sunflower oil (SFO), and blends of MCT oil and SFO in various ratios. The samples containing unsaturated fatty acids were handled under a nitrogen atmosphere. The settings in all ESR measurements were as follows: sweep width 99.63 G, sweep time 30 s, modulation 1000 mG, and microwave attenuation 10 dB. The peak-to-peak amplitudes of the center doublet peaks of the ESR spectra were used to quantify the amount of spin adducts, and all results were expressed as an initial rate of radical formation calculated from the slopes of the initial linear parts of plots of spin adduct ESR intensities as a function of heating time. However, in the case of MCT oil mixed with 10 wt % methyl linoleate, MCT oil, and MCT oil blended with SFO in the ratios of 7:3 and 9:1, the plots were fitted to exponential curves from which the initial rates of spin adduct formation were calculated. The measurements were conducted at least in duplicate.

**Oil-in-Water Tween-20-Stabilized Emulsions.** Oil-in-water emulsions stabilized by Tween-20 were made according to Berton et al.[8] Emulsions consisted of 30 wt % MCT oil or sunflower oil (SFO), 0.5 wt % Tween-20, and 69.5 wt % sodium acetate−acetic acid buffer (pH = 4.65). Homogenization was done with Ultra Turrax T25 (IKA Works GmbH & Co. KG, Staufen, Germany) at 8000 rpm and with a dispersion element of 8 mm in diameter. The fluorescent probe BODIPY$^{665/676}$ and the radical initiator AMVN were added to the oil phases prior to homogenization. In the case of added AMVN, the emulsion preparation and homogenization were done on ice. When SFO was used, the whole mixing process was additionally carried out under a nitrogen atmosphere.

**Confocal Laser Scanning Microscopic Studies of Radical Reactions in Oil-in-Water Emulsions.** A series of emulsions were made as described above containing oil (MCT or SFO), radical initiator (with AMVN or without) and a fluorescent probe (with BODIPY$^{665/676}$ and without). Mixtures of two different emulsions were made such that each combination contained AMVN (6 mM) and BODIPY$^{665/676}$ (1 μM), although not necessarily present in the same lipid droplet of the original emulsions (Table 1). The controls were single emulsions and consisted only of oil, emulsifier, and aqueous phase. Radicals were generated by unimolecular decomposition of AMVN upon heating samples in a water bath at 37 °C during specific periods of time. The measurements were conducted with a confocal Leica TCS SP5-X MP microscope. The objective was an oil immersion 40× HCX PL APO CS, NA 1.30, pinhole 1 AU, and image resolution 1024 × 1024. The samples were scanned with a supercontinuum white light laser either at $\lambda_{ex}$ 580 nm, with signal detection by a hybrid detector at the emission band of 585−620 nm, or at $\lambda_{ex}$ 670 nm, with signal detection at the emission band of 675−785 nm. Droplets loaded with BODIPY$^{665/676}$ were selected to study the changes in fluorescence emission intensities at $\lambda_{ex}$ 580 and 670 nm, and droplets without BODIPY$^{665/676}$ were selected to establish background intensities. Droplets with BODIPY$^{665/676}$ and droplets without BODIPY$^{665/676}$ were discernible at both excitation wavelengths, $\lambda_{ex}$ 580 and 670 nm, due to emitted fluorescence of BODIPY$^{665/676}$-loaded droplets and simultaneous use of transmitted light mode. For each combination of

**Table 1. Combinations of Emulsions (1:1) Investigated by CLSM Studies**[a]

| | emulsion II | | | |
|---|---|---|---|---|
| emulsion I | SFO + AMVN + BODIPY$^{665/676}$ | SFO + AMVN | SFO + BODIPY$^{665/676}$ | SFO |
| MCT oil + AMVN + BODIPY$^{665/676}$ | | | | X |
| MCT oil + AMVN | | | X | |
| MCT oil + BODIPY$^{665/676}$ | | X | | X |
| MCT oil | X | | X | |

[a]MCT, medium-chain triglyceride; SFO, sunflower oil; BODIPY$^{665/676}$, (*E*,*E*)-3,5-bis(4-phenyl-1,3-butadienyl)-4,4-difluoro-4-bora-3a,4a-diaza-*s*-indacene; AMVN, 2,2′-azobis(2,4-dimethyl)valeronitrile.

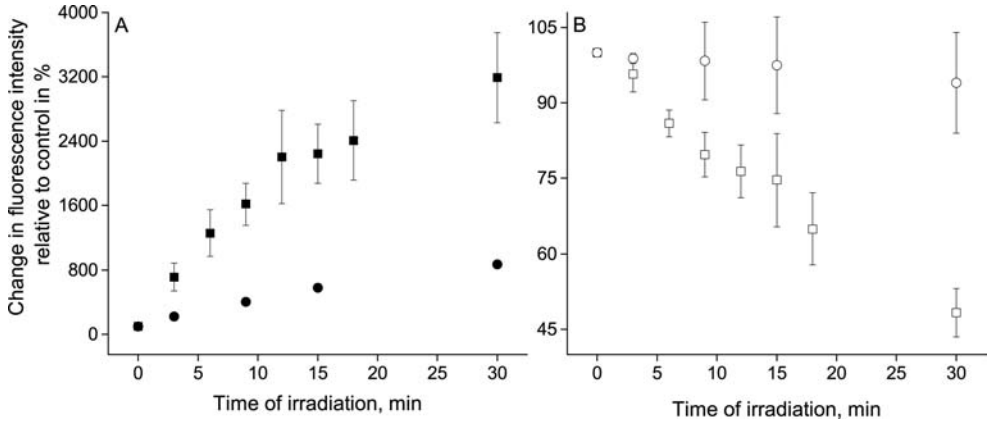


**Figure 1.** Fluorescence intensity changes of BODIPY$^{665/676}$ in (□, ■) MCT oil and (○, ●) LSO. The oils contained DTBP (5.7 $\mu$M) and BODIPY$^{665/676}$ (1 $\mu$M) and were irradiated with 300 nm UV lamps. The fluorescence intensity was measured (A) at $\lambda_{ex}$ 580 nm (closed symbols) and (B) at $\lambda_{ex}$ 670 nm (open symbols). The fluorescence changes are reported relative to the nonirradiated control.

emulsions, five droplets loaded with BODIPY$^{665/676}$ and five droplets without BODIPY$^{665/676}$ were quantified. For that purpose, a region of interest (ROI) for about $^4/_5$ the diameter of the droplet, excluding the border regions, was drawn; average intensity of the ROI was acquired; and changes in the fluorescence intensities were expressed relative to the unexposed controls.

**Oxygen Consumption Measurements of Emulsions.** A Clark-type oxygen electrode (Radiometer, Copenhagen, Denmark) was used to determine the oxygen concentration in emulsions. The data were recorded by use of a Unisense picoammeter (Unisense PA2000, Aarhus, Denmark) by a method described earlier.[2] Briefly, a sample was transferred into a 2.7 mL glass vessel with a ground glass stopper, a capillary-size hole through the center, and a magnetic stirring bar and was then placed in a water bath at 37 °C. Oxygen concentrations were recorded every 30 s. The rates of oxygen consumption were calculated as slopes of the linear part of plots of percent oxygen concentration as a function of time in minutes. The samples studied included (1) MCT oil emulsion, (2) SFO emulsion, (3) SFO emulsion containing BODIPY$^{665/676}$, and (4) blended oil emulsions with MCT oil and SFO blended in weight ratios 3:7 or 7:3. Various concentrations of AMVN (0, 1.8, 4.2, or 6 mM) were added to oils prior to mixing of the emulsions. In addition, MCT oil and SFO emulsions mixed in ratios 3:7 and 7:3 were studied, where only one of the two original emulsions contained AMVN.

**Statistical Analysis.** All data shown are presented as the mean value and standard deviation of at least three measurements. Box and whisker diagrams (Figure 5) illustrate mean values, ranges of scores between 25% and 75%, and outliers.

## RESULTS

**BODIPY$^{665/676}$ as Radical Probe in Bulk Triglyceride Oils.** The effect of radicals on the fluorescence of BODIPY$^{665/676}$ was tested in purified unsaturated linseed oil (LSO), where lipid oxidation after initial formation of radicals can be maintained through radical chain reactions. The probe has been demonstrated to be able to detect radicals in saturated medium-chain triglyceride (MCT) oil.[6] The bulk LSO samples contained di-*tert*-butyl peroxide (DTBP), which upon irradiation with 300 nm UV light generates alkoxyl radicals that can initiate lipid autoxidation. The relatively low concentration of added DTBP (5.7 $\mu$M) was chosen on the basis of previous experiments to provide an adequate radical flux, to ensure propagation of radical-induced processes, and reduce the effect of terminating bimolecular radical reactions.[6] The UV irradiation was carried out in 3 min intervals during the initial 18 min of irradiation, and a final measurement was carried out after a total of 30 min of irradiation. The fluorescence of BODIPY$^{665/676}$ was measured at $\lambda_{ex}$ 675 and 580 nm (Figure 1). Control experiments with saturated MCT oil showed that the fluorescence intensity at $\lambda_{ex}$ 580 nm increased initially linearly with irradiation time, but after the first 12 min of irradiation, the increase in the fluorescence intensity began to level off. For MCT oil the total $\lambda_{ex}$ 580 nm fluorescence intensity increased around 3000% relative to a nonirradiated control sample, whereas the $\lambda_{ex}$ 675 nm fluorescence intensity decreased around 50% in comparison with the unexposed control (Figure 1B). Accordingly, the change in fluorescence intensity measured at $\lambda_{ex}$ 675 nm was not as pronounced as in the case of $\lambda_{ex}$ 580 nm. The experiments with bulk LSO gave a linear increase in the fluorescence intensity of BODIPY$^{665/676}$ at $\lambda_{ex}$ 580 nm with irradiation time (Figure 1A). However, the maximum intensity reached only 900% relative to the unexposed control, and the variations between the repetitions were smaller with LSO than with MCT oil. Also, with LSO the fluorescence measured at $\lambda_{ex}$ 675 nm was constant, in contrast to MCT oil, where it decreased during irradiation (Figure 1B).

The fluorescence changes of BODIPY$^{665/676}$ in the two oils were not in agreement with the expected levels of oxidation, because highly unsaturated LSO should be oxidatively unstable and be able to sustain pronounced radical-chain lipid oxidation. The response of BODIPY$^{665/676}$ toward lipid oxidation was therefore tested in an alternative set of experiments based on the temperature-dependent lipid-soluble radical initiator AMVN in blends of oxidatively stable MCT oil and purified unsaturated sunflower oil (SFO). Oil samples containing BODIPY$^{665/676}$ were heated at 37 °C, and the rate of fluorescence change was measured as the initial change of fluorescence intensity with heating time (Figure 2). The blends of oils with high levels of SFO gave low rates of fluorescence changes in comparison with the pure MCT oil, where the rates were substantially higher. In addition, blends of MCT oil with 10 wt % methyl oleate and MCT oil with 10 wt % methyl linoleate were included in the experiment, and these blends gave similar high rates of changes in fluorescence intensity as the pure MCT oil.

The two sets of experiments with different unsaturated oils and different modes of radical generation both indicated that BODIPY$^{665/676}$ was most sensitive toward radicals in pure saturated MCT oil, while the response in unsaturated LSO and SFO was low. To further understand the underlying mechanism of radical reactions and differences in radical sensitivity of the

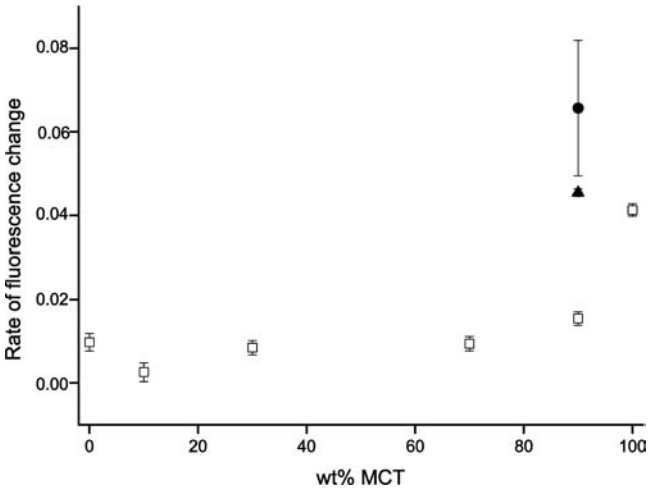


**Figure 2.** Rate of fluorescence change of BODIPY$^{665/676}$ in blends of MCT oil and sunflower oil (SFO) measured at $\lambda_{ex}$ 580 nm. The samples of oil blends contained AMVN (13 mM) and were subjected to heating at 37 °C for 3 h. The rate of fluorescence intensity change is presented as a function of weight percent MCT oil in the oil blend. (□) Various blends of MCT oil and SFO, (●) blend of 90 wt % MCT oil and 10 wt % methyl linoleate, (▲) blend of 90 wt % MCT and 10 wt % methyl oleate.

probe, electron spin resonance (ESR) spectroscopy was used to evaluate the level of radical reactions initiated by AMVN in the oils and their blends (Figure 3). The detection of radicals was

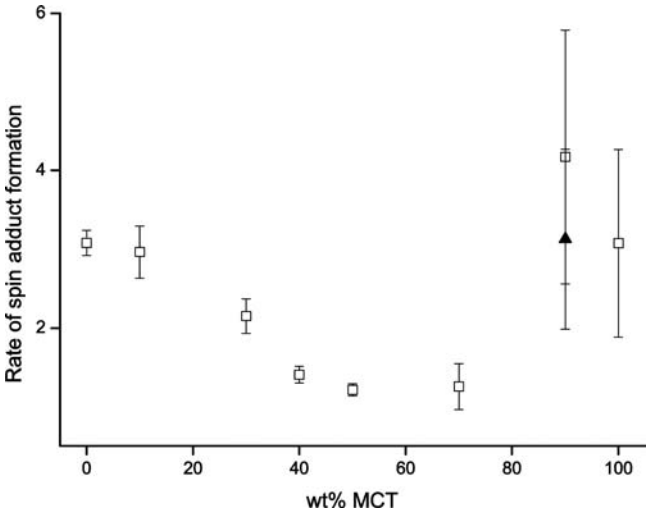


**Figure 3.** Rate of spin adduct formation in blends of MCT oil and SFO. The samples of oil blends contained the spin trap PBN (20 mM) and radical initiator AMVN (6 mM) and were subjected to heating at 37 °C. The rate of spin adduct formation is calculated as an increase of the spin adduct signal detected by ESR as a function of heating time and is reported as a function of weight percent MCT oil in the oil blend. (□) Blends of MCT oil and SFO in various concentrations; (▲) blend of 90 wt % MCT oil and 10 wt % methyl linoleate.

based on the formation of long-lived spin adducts with the spin trap PBN, which traps radicals generated directly from AMVN as well as radicals formed during radical-chain lipid oxidation reactions. The ESR experiments demonstrated that rates of spin adduct formation in the oil blends decreased with increasing concentration of MCT oil up to 70 wt %. However, at MCT oil concentrations above 70 wt %, rates of spin adduct formation increased to levels similar to that of pure SFO. The high rate of spin adduct formation in SFO was expected, since the high degree of unsaturation should give a high level of oxidative chain reactions, thus sustaining a high steady-state concentration of radicals.[9,10] At the same time, the high rate of spin adduct formation in MCT oil was surprising. A blend of MCT oil with 10 wt % methyl linoleate gave the same high rate of spin adduct formation as the MCT oil blend with 10 wt % SFO.

**Oxidation in Emulsions.** Confocal laser scanning microscopy (CLSM) together with BODIPY$^{665/676}$ was used to study the progression of oxidation in emulsion systems on the scale of single oil droplets. The fluorescent probe BODIPY$^{665/676}$ has been shown not to diffuse between oil droplets, and remaining localized in the droplets where it has been initially dissolved during preparation of the emulsion.[6] In order to study the transfer of radicals between oil droplets, a series of experiments were carried out where two Tween-20-stabilized emulsions made from different oils were mixed in a way so that the temperature-dependent radical initiator AMVN was present in some oil droplets and the fluorescent probe BODIPY$^{665/676}$ was present in the same droplets, or in the droplets without AMVN, or no AMVN was present at all (Table 1). When the respective combinations were investigated under a confocal microscope, the images showed that droplets loaded with BODIPY$^{665/676}$ were easily recognizable by their fluorescence at $\lambda_{ex}$ 670 nm, while droplets without BODIPY$^{665/676}$ could be detected and located in the transmitted light mode. In the case when no radicals were released (samples not heated), no fluorescence was seen at $\lambda_{ex}$ 580 nm. Therefore, no differentiation based on fluorescence between the two emulsions could be made, and the droplets were visible and could be defined only in transmitted light. Upon heating of the AMVN-containing mixtures of emulsions, an increase in the fluorescence at $\lambda_{ex}$ 580 nm could be noticed in the BODIPY$^{665/676}$-loaded oil droplets, indicating the presence of radicals. During the heating of the samples and consequent constant generation of radicals for up to 60 min, it was seen that the fluorescence intensities were rising independent of the location of the radical initiator AMVN and the probe BODIPY$^{665/676}$ (Figure 4). Extended heating for more than 60 min resulted in a drop in the fluorescence intensity of the mixtures of emulsions, where SFO droplets contained the probe, while in the combination where MCT oil droplets were loaded with BODIPY$^{665/676}$ a further increase was measured up to 120 min. Regardless of the oil medium of the droplets carrying the probe, the oil droplets without the probe showed no increase in fluorescence during the experiments (Figure 4).

The combination of SFO emulsion containing AMVN and BODIPY$^{665/676}$ mixed with MCT oil emulsion had a high level of fluorescence (~100 fluorescence units, FU) already before heating. This resulted in a stable initial fluorescence, which did not change during the heating (data not shown). No change in the fluorescence intensity was seen in the two emulsion combinations that did not contain AMVN, serving as internal controls. Similarly, MCT oil emulsion with BODIPY$^{665/676}$ and control experiments on emulsions without BODIPY$^{665/676}$ did not show any changes in the fluorescence intensities upon heating (data not shown). The presence of radicals also influenced the fluorescence intensities at $\lambda_{ex}$ 670 nm. At this wavelength, a weaker contrast between the BODIPY$^{665/676}$-loaded droplets and their counterparts was seen. The fluorescence decrease in oil droplets observed at $\lambda_{ex}$ 670 nm

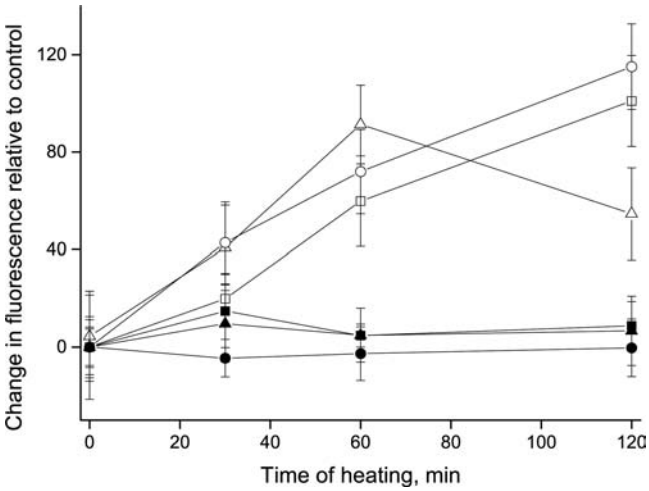


**Figure 4.** Changes in fluorescence intensity at $\lambda_{ex}$ 580 nm of single oil droplets in mixtures of emulsions observed with CLSM. The following systems were studied: (○, ●) MCT oil emulsion containing AMVN (6 mM) and BODIPY$^{665/676}$ (1 $\mu$M) mixed with SFO emulsion; (□, ■) MCT oil emulsion containing BODIPY$^{665/676}$ (1 $\mu$M) mixed with SFO emulsion containing AMVN (6 mM); and (Δ, ▲) SFO emulsion containing BODIPY$^{665/676}$ (1 $\mu$M) mixed with MCT emulsion containing AMVN (6 mM). The combinations were heated at 37 °C. Open symbols depict the fluorescence intensities of droplets in the combinations of emulsions containing BODIPY$^{665/676}$, and closed symbols show the fluorescence intensities of droplets where BODIPY$^{665/676}$ was absent. The fluorescence intensities are reported relative to unexposed control samples.

correlated with the increases of fluorescence observed at $\lambda_{ex}$ 580 nm for all the studied emulsions (data not shown).

The effect of location of the radical initiator AMVN in the mixtures of emulsions on lipid oxidation was also studied on a macroscopic scale by measuring rates of oxygen consumption (Figure 5). The rates of oxygen consumption in MCT oil emulsions both with and without added AMVN were very low (Figure 5A). Mixing MCT emulsion containing AMVN with SFO emulsion gave rates of oxygen consumption even higher than the rates of oxygen consumption in a pure SFO emulsion without AMVN (Figure 5A,B). The level of oxidation in these combinations increased with the amount of SFO from 30 to 70 wt %, although the total concentration of AMVN decreased, from 4.2 to 1.8 mM at the same time. These results demonstrate that oxidation was accelerated in the mixed emulsions.

SFO emulsions with different concentrations of AMVN gave rates of oxygen consumption very similar when 6 mM or 4.2 mM AMVN was used, whereas in the case of 1.8 mM AMVN the rate of oxygen consumption was significantly lower (Figure 5B). Moreover, the presence of BODIPY$^{665/676}$ with AMVN in the SFO emulsion slightly increased the oxidation rate indicating that BODIPY$^{665/676}$ did not inhibit the progression of lipid oxidation as it has been reported earlier.[11,12]

Experiments were also carried out where the total concentration of AMVN in the mixed emulsions was kept constant at either 4.2 or 1.8 mM but the localization of AMVN within the oil droplets, either in MCT oil or SFO, was different (Figure 5C). The rates of oxygen consumption in the samples, which contained a combination of two SFO emulsions, were similar when AMVN was located with a higher local concentration in either 70 or 30 wt % of the droplets as compared to being present in all droplets (Figure 5C). The mixture of SFO emulsion containing AMVN with MCT emulsion gave a lower rate of oxygen consumption in the case of a total concentration of 4.2 mM AMVN. However, the combinations, where MCT oil and SFO emulsions with added AMVN were mixed in a ratio of 7:3 (corresponding to a total concentration of 1.8 mM AMVN) seemed to have a critical combination of components, and despite several repeated measurements, a rather large variation of the oxygen consumption rates was observed.

Oxygen consumption was also measured in emulsions made with blended MCT and SFO oils (Figure 6). Emulsions based on blended oils with 70 wt % MCT oil gave very low rates of oxygen consumption independent of the concentration of AMVN, whereas the emulsions made with 30 wt % MCT oil gave high rates of oxygen consumption, and the emulsion with 4.2 mM AMVN gave the highest rate. These results correspond to the evaluation of radical formation in bulk oil blends by ESR, where higher level of radicals were observed in the 30 wt % MCT oil blend than in the 70 wt % MCT oil blend (Figure 3).

## ■ DISCUSSION

The lipophilic fluorescent probe BODIPY$^{665/676}$ has previously been shown to be suitable for oxidation studies in single droplets of oil-in-water emulsions made with saturated MCT oil, since it does not diffuse between droplets and its fluorescence changes in the presence of radicals.[6] In the present work, it was found that the fluorescence of BODIPY$^{665/676}$ changed more in oxidatively stable saturated MCT oil than in oxidation-sensitive unsaturated linseed oil (LSO) and sunflower oil (SFO). The fluorescence changes were low in oil blends with high levels of SFO, and only at high levels of MCT did the rate of fluorescence intensity change increase. These experiments were based on the radical initiator AMVN, which produces radicals at a constant rate. The amounts of radicals generated in the different oil blends can therefore be assumed to be similar. The experiments with BODIPY$^{665/676}$ in the various blends of MCT oil and SFO, taken together with the concentration of radicals evaluated by ESR, suggest that BODIPY$^{665/676}$ was most sensitive to the initial radicals generated from AMVN and less sensitive to bulky lipid autoxidation-derived radicals. It has been reported that probes belonging to the C11 class, including BODIPY$^{665/676}$ and BODIPY$^{581/591}$ C-11, overestimate the oxidation of lipids due to their own high susceptibility to oxidation.[11,13] Moreover, Yoshida et al.[12] reported that the rates of reaction between unsaturated fatty acids and peroxyl radicals were half the reaction rates between BODIPY$^{581/591}$ C-11 and peroxyl radicals, which suggests that BODIPY$^{665/676}$ will react with radicals even more readily since it is more sensitive toward peroxyl radicals than BODIPY$^{581/591}$ C-11.[14] In the experiments based on the radical initiator DTBP, radicals in MCT oil interacted directly with the probe, mainly because the probe was the only available substance prone to oxidation. In LSO, on the other hand, probably due to the competition between BODIPY$^{665/676}$ and the unsaturated lipids, fewer radicals attacked the radical-sensitive fluorescent probe. Fluorometric experiments with fatty acid methyl esters in MCT oil gave higher rates of fluorescence intensity changes than in LSO, indicating that the reaction between the lipid-derived radicals and BODIPY$^{665/676}$ was affected by steric effects and thus mitigated the response to oxidation reported by the probe.

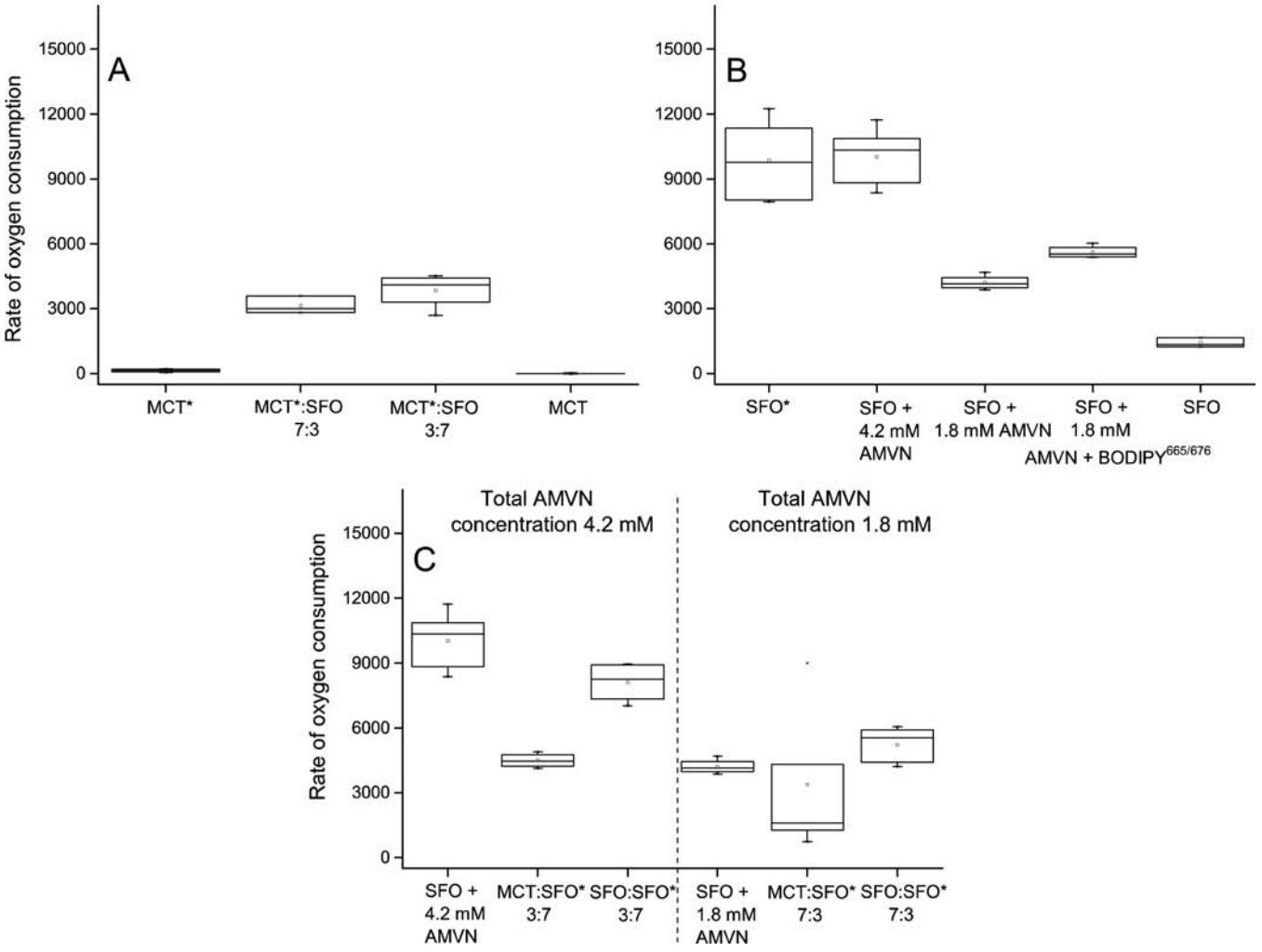


**Figure 5.** Rate of oxygen consumption in Tween-20-stabilized emulsions and mixtures of emulsions measured at 37 °C, and presented as percent of oxygen consumption per minute. (A) Experiments with MCT oil emulsion containing AMVN (6 mM) and MCT oil emulsion mixed with SFO emulsion. MCT emulsion without AMVN was included as a control. (B) Experiments with SFO emulsions with different concentrations of AMVN and SFO emulsion with AMVN (1.8. mM) and BODIPY$^{665/676}$ (1 $\mu$M). (C) Experiments with SFO emulsions containing AMVN and combinations of MCT oil emulsion and SFO emulsions. An asterisk indicates the original emulsion that contained 6 mM AMVN.

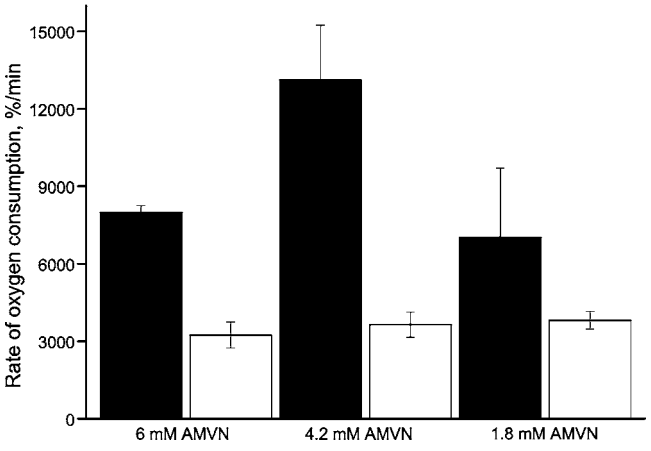


**Figure 6.** Rate of oxygen consumption in Tween-20-stabilized emulsions made with blended oils and with various concentrations of added AMVN measured at 37 °C, presented as percent of oxygen consumption per minute. Solid bars: blends of 30 wt % MCT oil and 70 wt % SFO. Open bars: blends of 70 wt % MCT and 30 wt % SFO.

The spin trap PBN also gave varying levels of detectable spin adducts in different oil blends. The decrease of spin adduct formation when the level of MCT oil was increased up to 50 wt % in oil blends could be due to dilution of the unsaturated SFO, which is in agreement with the notion that the level of oxidation decreases with decreasing level of unsaturation. In these oil blends, trapping of lipid oxidation-derived radicals is dominant.[15] Under the present experimental conditions at 37 °C, the PBN spin adducts with peroxyl radicals are very unstable, and thus PBN formed detectable stable adducts probably with alkoxyl and alkyl radicals.[16−19] The high levels of spin adduct formation at high concentrations of MCT in oil blends were surprising and suggest PBN was more efficiently reacting with the initial radicals generated from AMVN when the extent of competing reactions between AMVN-derived radicals and unsaturated fatty acids were low, due to low levels of unsaturation.

Experiments with oil blends illustrate that the fluorescence intensity changes of BODIPY$^{665/676}$ can be used for detecting reactive radicals in triglyceride systems; however, the structure of the radicals can significantly affect the level of intensity changes: bulky triglyceride-derived radicals apparently give

smaller changes due to steric effects. The degree of unsaturation should therefore always be taken into consideration when spectral changes of BODIPY$^{665/676}$ are compared between different triglyceride blends. In addition, a low level of intensity changes in highly unsaturated oil cannot be directly interpreted as indicative of a low level of lipid oxidation.

In confocal microscopy studies of two mixed Tween-20-stabilized emulsions with different compositions of oil phase, the probe BODIPY$^{665/676}$ gave a clear indication of transfer of radicals between oil droplets. Having BODIPY$^{665/676}$ and the radical initiator AMVN localized within the same droplets led, as expected, to changes of fluorescence spectra measured at $\lambda_{ex}$ 580 and 670 nm. However, more interestingly, when BODIPY$^{665/676}$ and AMVN were located in separate droplets, the fluorescence intensity of the probe also changed, showing that radicals could be detected in droplets neighboring the AMVN-loaded droplets. The concentration of Tween-20 was higher than the critical micelle concentration, and the emulsifier micelles could potentially solubilize smaller compounds, including AMVN and AMVN-derived radicals, providing transporter mechanism for radical reactions.[20,21] The escape of AMVN-derived radicals from lipid-containing particles has been observed in the case of LDL particles, where it was found that they could initiate lipid oxidation in neighboring particles.[22,23] Krainev and Bigelow[24] found that negligible amounts of AMVN-derived radicals were able to leave the lipophilic environment of rabbit skeletal sarcoplasmic reticulum membranes and egg phosphatidylcholine liposomes.

The hypothesis that radicals are able to move between the oil droplets, either by transporter mechanisms or by diffusion, was supported by determining the rates of oxygen consumption in the mixtures of emulsions. Oxygen consumption was expected to reflect the overall extent of lipid oxidation, and accordingly the rates of oxygen consumption were very low in MCT emulsions, even in the presence of AMVN, whereas the rates were very high in SFO emulsions. Experiments with combinations of emulsions showed that AMVN located in MCT oil droplets led to increased oxidation when mixed with SFO droplets, indicative of the transfer of radicals between droplets. A mixture of SFO emulsion containing 6 mM AMVN and MCT oil emulsion in the ratio 7:3 decreased the rate of oxygen consumption compared to SFO emulsion with added 4.2 mM AMVN. Furthermore, a combination of SFO emulsion containing 6 mM AMVN and SFO emulsion in the ratio 7:3 gave rates of oxygen consumption comparable to those of SFO emulsion with added 4.2 mM AMVN. Since the total concentration of AMVN in all these mixed systems was the same and identical amounts of radicals were generated, the presence of MCT oil must have had an effect on the level of oxidation, as has previously been observed with mixed mayonnaises.[2] This suggests the transfer of radicals from radical-loaded SFO droplets to saturated MCT oil droplets may inhibit the efficiency of radical transfer to other SFO droplets, and therefore may lead to reduction of the overall rate of oxidation in the mixture of emulsions, since MCT oil droplets are not expected to be able to sustain the transfer of radicals.

In conclusion, BODIPY$^{665/676}$ is a useful lipophilic fluorescent probe for detecting and studying radical reactions in bulk oils and oil-in-water emulsions. However, the structure of radicals can significantly affect the level of fluorescence intensity changes, and a low level of BODIPY$^{665/676}$ intensity change cannot be directly interpreted as indicative of a low level of lipid oxidation. Studies of mixed emulsions by confocal laser scanning microscopy with BODIPY$^{665/676}$ as a fluorescent probe, supplemented by oxygen consumption studies, demonstrated that radicals can be transferred between oil droplets and lipid autoxidation can spread between neighboring oil droplets.

The possibility of radical transfer between oil droplets will have to be taken into account when discussing the mechanisms of lipid autoxidation in oil-in-water emulsions. Radical-driven lipid autoxidation is not taking place as an isolated event in individual droplets but can spread between emulsion droplets. Although it is expected that radicals mainly are generated by metal-catalyzed mechanisms in the aqueous phase, the present results suggest that radicals generated in the interior of oil droplets can contribute to the initiation of autoxidation in neighboring droplets. Such transfer of radicals between droplets could be the main mechanism of initiating and spreading lipid autoxidation at higher temperatures, where generation of radicals by cleavage of preformed lipid hydroperoxides inside oil droplets may begin to play a significant role. The design of emulsion protection schemes based on surface-active antioxidants would accordingly have to consider that radicals may be able to both enter and exit droplets.

## AUTHOR INFORMATION

### Corresponding Author

*E-mail mola@food.ku.dk; phone +45 35333262.

### Funding

This work was funded by the Danish Agency of Science, Technology and Innovation. The CLSM work was carried out at the Center for Advanced Bioimaging (CAB), University of Copenhagen, Denmark.

### Notes

The authors declare no competing financial interest.

## ABBREVIATIONS

AMVN, 2,2′-azobis(2,4-dimethyl)valeronitrile; BODIPY$^{665/676}$, (*E*,*E*)-3,5-bis(4-phenyl-1,3-butadienyl)-4,4-difluoro-4-bora-3a,4a-diaza-*s*-indacene; CLSM, confocal laser scanning microscopy; DTBP, di-*tert*-butyl peroxide; ESR, electron spin resonance; FU, fluorescence units; LSO, linseed oil; MCT, medium-chain triglyceride; PBN, *N*-*tert*-butyl-$\alpha$-phenylnitrone; SFO, sunflower oil; $\lambda_{ex}$, excitation wavelength

## REFERENCES

(1) Coupland, J. N.; McClements, D. J. Lipid oxidation in food emulsions. *Trends Food Sci. Technol.* **1996**, *7*, 83−91.

(2) Raudsepp, P.; Brüggemann, D. A.; Lenferink, A.; Otto, C.; Andersen, M. L. Oxidative stabilization of mixed mayonnaises made with linseed oil and a saturated medium-chain triglycerides oil. *Food Chem.* **2014**, *152*, 378−385.

(3) Chen, X.; Zhong, Z.; Xu, Z.; Chen, L.; Wang, Y. 2′,7′-Dichlorodihydrofluorescein as a fluorescent probe for reactive oxygen species measurements: Forty years of application and controversy. *Free Radical Res.* **2010**, *44*, 587−604.

(4) Folkes, L. K.; Patel, K. B.; Wardmann, P.; Wrona, M. Kinetics of reaction of nitrogen dioxide with dihydrorhodamine and the reaction of the dihydrorhodamine radical with oxygen: Implications for quantifying peroxynitrite formation in cells. *Arch. Biochem. Biophys.* **2009**, *484*, 122−126.

(5) Kervinen, M.; Pätsi, J.; Finel, M.; Hassinen, I. E. Lucigenin and coelenterazine as superoxide probes in mitochondrial and bacterial membranes. *Anal. Biochem.* **2004**, *324*, 45−51.

(6) Raudsepp, P.; Brüggemann, D. A.; Andersen, M. L. Detection of radicals in single droplets of oil-in-water emulsions with the lipophilic

fluorescent probe BODIPY$^{665/676}$ and confocal laser scanning microscopy. *Free Radical Biol. Med.* **2014**, *70*, 233−240.
(7) Yoshida, H.; Kondo, I.; Kajimoto, G. Participation of free fatty acids in the oxidation of purified soybean oil during microwave heating. *J. Am. Oil Chem. Soc.* **1992**, *69*, 1136−1140.
(8) Berton, C.; Genot, C.; Ropers, M. H. Quantification of unadsorbed protein and surfactant emulsifiers in oil-in-water emulsions. *J. Colloid. Interfac. Sci.* **2011**, *354*, 739−748.
(9) Coupland, J. N.; Zhu, Z.; Wan, H.; McClements, D. J.; Nawar, W. W.; Chinachoti, P. Droplet composition affects the rate of oxidation of emulsified ethyl linoleate. *J. Am. Oil Chem. Soc.* **1996**, *73*, 795−801.
(10) Miyashita, K.; Nara, E.; Ota, T. Oxidative stability of polyunsaturated fatty-acids in an aqueous-solution. *Biosci. Biotechnol. Biochem.* **1993**, *57*, 1638−1640.
(11) McDonald, M. L.; Murray, I. V. J.; Axelsen, P. H. Mass spectrometric analysis demonstrated that BODIPY581/591 C11 overestimated and inhibits oxidative lipid damage. *Free Radical Biol. Med.* **2007**, *42*, 1392−1397.
(12) Yoshida, Y.; Shimakawa, S.; Itoh, N.; Niki, E. Action of DCFH and BODIPY as a probe for radical oxidation in hydrophilic and lipophilic domain. *Free Radical Res.* **2003**, *37*, 861−872.
(13) Itoh, N.; Cao, J.; Chen, Z.-H.; Yoshida, Y.; Niki, E. Advantages and limitation of BODIPY as probe for the evaluation of lipid peroxidation and its inhibition by antioxidants in plasma. *Biorg. Med. Chem. Lett.* **2007**, *17*, 2059−2063.
(14) Naguib, Y. M. A. Antioxidant activities of astaxanthin and related carotenoids. *J. Agric. Food Chem.* **2000**, *48*, 1150−1154.
(15) Velasco, J.; Andersen, M. L.; Skibsted, L. H. Evaluation of oxidative stability of vegetable oils by monitoring the tendency to radical formation. A comparison of electron spin resonance spectroscopy with the Rancimat method and differential scanning calorimetry. *Food Chem.* **2004**, *85*, 623−632.
(16) Barclay, L. R. C.; Vinqvist, M. R. Do spin traps also act as classical chain-breaking antioxidants? A quantitative kinetic study of phenyl tert-butylnitrone (PBN) in solution and in liposomes. *Free Radical Biol. Med.* **2000**, *28*, 1079−1090.
(17) Dikalov, S. I.; Mason, R. P. Reassignment of organic peroxyl radical adducts. *Free Radical Biol. Med.* **1999**, *27*, 864−872.
(18) Pfab, J. Alkylperoxynitroxides in the photo-oxidation of nitrosoalkanes and the 'spin trapping' of peroxy radicals by C-nitroso-compounds. *Tetrahedron Lett.* **1978**, *19*, 843−846.
(19) Janzen, E. G.; Krygsman, P. H.; Lindsay, D. A.; Haire, D. L. Detection of alkyl, alkoxyl, and alkylperoxyl radicals from the thermolysis of azobis(isobutyronitrile) by ESR/spin trapping. Evidence for double spin adducts from liquid-phase chromatography and mass spectroscopy. *J. Am. Chem. Soc.* **1990**, *112*, 8279−8284.
(20) Kiralan, S. S.; Doğu-Baykut, E.; Kittipongpittaya, K.; McClements, D. J.; Decker, E. A. Increased antioxidant efficacy of tocopherols by surfactant solubilization in oil-in-water emulsions. *J. Agric. Food Chem.* **2014**, *62*, 10561−10566.
(21) Panya, A.; Laguerre, M.; Bayrasy, C.; Lecomte, J.; Villeneuve, P.; McClements, D. J.; Decker, E. A. An investigation of the versatile antioxidant mechanisms of action of rosmarinate alkyl esters in oil-in-water emulsions. *J. Agric. Food Chem.* **2012**, *60*, 2692−2700.
(22) Ingold, K. U.; Bowry, V. W.; Stocker, R.; Walling, C. Autoxidation of lipids and antioxidation by $\alpha$-tocopherol and ubiquinol in homogeneous solution and in aqueous dispersions of lipids: Unrecognized consequence of lipid particle size as exemplified by oxidation of human low density lipoprotein. *Proc. Natl. Acad. Sci. U.S.A.* **1993**, *90*, 45−49.
(23) Bowry, V. W.; Stocker, R. Tocopherol-mediated peroxidation. The prooxidant effect of vitamin E on the radical-initiated oxidation of human low-density lipoprotein. *J. Am. Chem. Soc.* **1993**, *115*, 6029−6044.
(24) Krainev, A. G.; Bigelow, D. J. Comparison of 2,2′-azobis(2-amidinopropane) hydrochloride (AAPH) and 2,2′-azobis(2,4-dimethylvaleronitrile (AMVN) as free radical initiators: A spin-trapping study. *J. Chem. Soc., Perkin Trans. 2* **1996**, 747−754.

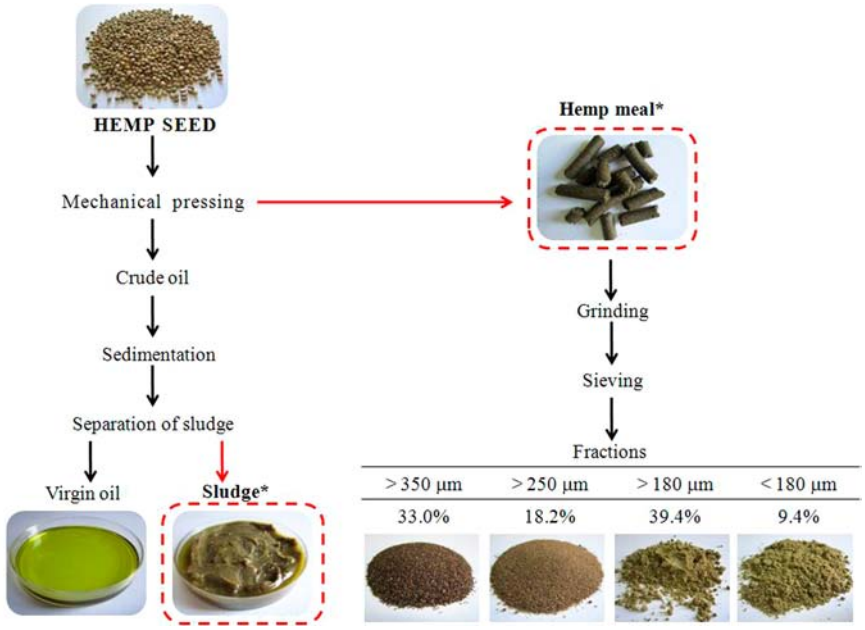


**Figure 1.** Simplified processing flow diagram for mechanical hemp oil pressing indicating byproducts generated during processing and the yield of hemp meal fractions.

## MATERIALS AND METHODS

**Chemicals.** 1,1-Diphenyl-2-picrylhydrazyl (DPPH), Folin-Ciocalteu's reagent, gallic acid, protocatechuic acid, caffeic acid, vanillic acid, chlorogenic acid, syringic acid, ferulic acid, rutin, myricetin, rosmarinic acid, *trans*-cinnamic acid, naringenin, luteolin, kaempferol, apigenin, phytic acid dodecasodium salt, (+)-catechin, vanillin, BAPA (*N*-benzoyl-DL-arginine *p*-nitroanilide hydrochloride), trypsin, sinigrin hydrate, ecteola cellulose, Supelco 37 component fatty acid methyl ester mix, 2,2′-bipyridine, palladium(II) chloride, ammonium iron(III) sulfate dodecahydrate, and tris(hydroxymethyl) aminomethane were purchased from Sigma−Aldrich GmbH (Sternheim, Germany). Methanol (HPLC, gradient-grade), quercetin, formic acid (HPLC-grade), *n*-heptane (GC-grade), and 50% boron(III) fluoride in methanol were purchased from Merck (Darmstadt, Germany). Anhydrous methanol and sodium chloride were obtained from Avantor Materials (Gliwice, Poland). Thioglycolic acid was purchased from Kemika (Zagreb, Croatia). Calcium chloride dehydrate, dimethyl sulfoxide, methanol, and other chemicals used for proximate composition were of p.a. (pro analysis) quality and obtained from Lach-Ner (Neratovice, Czech Republic). Water used throughout the experiments was purified on a Millipore Elix UV and simplicity water purification system (Milford, MA).

**Materials.** Hemp meal, a byproduct remaining after cold mechanical pressing of hemp seeds, was supplied by the company Svet Konoplje (Kisač, Serbia). Cannabinoid-free hemp variety Helena, bred by the Institute of Field and Vegetable Crops, Novi Sad, Serbia, was grown in 2013 in the South Bačka district in the northern part of Serbia. Hemp flour was obtained by grinding hemp meal in a laboratory mill, Foss Knifetec 1095 (Foss, Hillerød, Denmark), fitted with tubing to allow circulation of water to cool the sample during milling. Ground hemp meal was separated into four fractions of different particle size by use of a universal laboratory sifter (Bühler AG, Uzwil, Switzerland) equipped with a stack of sieves of decreasing mesh size (>350 $\mu$m, >250 $\mu$m, >180 $\mu$m, and <180 $\mu$m). Along with the individual fractions, the whole ground hemp meal was analyzed.

The hemp meal extracts were prepared for subsequent determination of DPPH$^{\bullet}$ free radical scavenging activity and phenolic compounds by an HPLC method as follows: hemp meal was extracted with methanol/water mixture (80:20 v/v), with the ratio of raw materials to methanol solution 1:80. After treatment in an ultrasonic bath at room temperature for 10 min, the extracts were macerated for 2 h, filtered through a filter paper (Whatman, grade 4 Chr), and dried by vacuum evaporation at 40 °C. The dried extracts were redissolved in methanol (HPLC-grade) and stored at −4 °C until further use.

**Color Measurements.** Color measurements were carried out in five replicates on a Minolta Chroma Meter CR 400 colorimeter equipped with accessories for granular materials attachment CR-A50 (glass light-protection tube with plate 40 mm CR-A33b; Konica Minolta Sensing Inc., Japan). The instrument was calibrated against a standard light white reference tile, and the measurements were conducted under standard illuminant D65. The results were recorded according to the CIELab color system, where the determined parameters were expressed as $L^*$ describing lightness ($L^* = 0$ for black, $L^* = 100$ for white), $a^*$ describing intensity in greenness/redness ($a^* < 0$ for green, $a^* > 0$ for red), and $b^*$ describing intensity in blueness/yellowness ($b^* < 0$ for blue, $b^* > 0$ for yellow). Moreover, the total color difference ($\Delta E$) between whole hemp meal and separated hemp meal fractions was expressed as

$$\Delta E = \sqrt{\Delta L^2 + \Delta a^2 + \Delta b^2}$$

where $\Delta L$ is the lightness difference, $\Delta a$ is the redness/greenness difference, and $\Delta b$ is the yellowness/blueness difference. For $\Delta E < 1$, color differences were not considered obvious to the human eye; for $1 < \Delta E < 3$, color differences were not considered appreciated by the human eye; and for $\Delta E > 3$, color differences were considered obvious to the human eye.[13]

**Chemical Composition.** The moisture content of hemp meal fractions was determined by oven-drying to a constant mass at 105 °C. Crude protein, crude lipid, crude fiber, ash, and total sugars content were determined according to AOAC standard methods.[14]

**DPPH$^{\bullet}$ Free Radical Scavenging Activity.** Free radical scavenging activity against the stable DPPH$^{\bullet}$ (1,1-diphenyl-2-picrylhydrazyl) radical was determined spectrophotometrically following the procedure of Espin et al.[15] The $IC_{50}$ value (milligrams per milliliter), defined as the mass concentration of an antioxidant extract that was required to quench 50% of the initial DPPH$^{\bullet}$ under the given experimental conditions, was obtained by interpolation from linear regression analysis.

**Separation and Determination of Phenolic Compounds.** Determination of phenolic compounds was performed by a single rapid resolution reverse phase HPLC method as previously described by Mišan et al.[16]

**Fatty Acid Determination.** Fatty acid composition of the samples was expressed as fatty acid methyl esters (FAMEs). Lipids were


dx.doi.org/10.1021/jf5044426 | J. Agric. Food Chem. 2014, 62, 12436−12442

**Table 1. Color Parameters of Different Hemp Meal Fractions[a]**

| color parameter[b] | hemp meal fractions | | | | whole meal |
|---|---|---|---|---|---|
| | >350 μm | >250 μm | >180 μm | <180 μm | |
| $L^*$ | 28.7 ± 1.11 a | 39.9 ± 1.02 b | 49.9 ± 0.23 d | 53.5 ± 0.23 e | 46.0 ± 0.67 c |
| $a^*$ | 3.68 ± 0.19 c | 3.92 ± 0.14 c | 1.59 ± 0.14 b | 1.15 ± 0.01 a | 1.22 ± 0.09 a |
| $b^*$ | 7.44 ± 0.29 a | 12.6 ± 0.46 b | 20.5 ± 0.30 d | 21.3 ± 0.30 d | 17.1 ± 0.59 c |
| $\Delta E$ | 19.9 ± 1.72 b | 8.00 ± 1.94 a | 5.28 ± 0.85 a | 8.61 ± 0.93 a | |

[a]Values are means ± SD. Means in the same row followed by different letters are significantly different ($P < 0.05$). [b]$L^*$, lightness; $a^*$, greenness/redness; $b^*$, blueness/yellowness, $\Delta E$, total color difference between whole meal and single fraction.

**Table 2. Proximate Analysis of Hemp Meal Fractions[a]**

| | hemp meal fractions | | | | whole meal |
|---|---|---|---|---|---|
| | >350 μm | >250 μm | >180 μm | <180 μm | |
| moisture content (%) | 6.98 ± 0.01 b | 6.63 ± 0.04 a | 7.39 ± 0.04 c | 7.34 ± 0.02 c | 7.88 ± 0.06 d |
| protein content (%) | 10.6 ± 0.10 a | 20.3 ± 0.25 b | 41.2 ± 0.04 d | 44.4 ± 0.02 e | 27.9 ± 0.12 c |
| lipid content (%) | 8.26 ± 0.02 a | 10.0 ± 0.05 b | 15.1 ± 0.02 d | 18.6 ± 0.04 e | 11.8 ± 0.01 c |
| total sugar content (%) | <0.05 a | 0.56 ± 0.08 a | 4.96 ± 0.11 d | 3.46 ± 0.08 c | 1.49 ± 0.08 b |
| ash content (%) | 3.46 ± 0.02 a | 5.51 ± 0.06 b | 9.60 ± 0.01 d | 9.83 ± 0.01 e | 6.74 ± 0.02 c |
| crude fiber content (%) | 29.5 ± 0.04 e | 21.3 ± 0.03 d | 7.13 ± 0.04 b | 4.96 ± 0.01 a | 17.3 ± 0.03 c |

[a]Values are means ± SD. Means in the same row followed by different letters are significantly different ($P < 0.05$).

extracted with chloroform/methanol (2:1 v/v) mixture following the Folch extraction procedure,[17] and the obtained extracts were dried by vacuum evaporation at 40 °C. Methyl esters were prepared from the extracted lipids by transesterification with 14% boron(III) fluoride in methanol.[18] The obtained samples were analyzed by a GC Agilent 7890A system with flame-ionization detector (FID), autoinjection module for liquid samples, equipped with fused silica capillary column (DB-WAX 30 m, 0.25 mm, 0.50 μm). Helium was used as a carrier gas (purity >99.9997 vol %, flow rate = 1.26 mL/min). The fatty acids peaks were identified by comparison of retention times with retention times of standards from Supelco 37 component fatty acid methyl ester mix (Sigma–Aldrich) and with data from an internal data library based on previous experiments. Results were expressed as the mass of fatty acid or fatty acid group (grams) in 100 g of fatty acids.

**Antinutritional Factors.** Phytic acid was extracted from defatted flour with 0.2 M HCl and determined according to Haug and Lantzsch.[19] Tannins were extracted from defatted material with 70% acetone, evaporated to dryness, and then resuspended in methanol. Condensed tannins were determined by the vanillin method (absorbance at 500 nm) with catechin as a standard.[20] Trypsin inhibitors were extracted from defatted flour with 0.01 M NaOH (pH adjusted to 8.4–10.0). Trypsin inhibitor activity was measured according to Hamerstrand et al.[21] with *N*-benzoyl-DL-arginine *p*-nitroanilide hydrochloride (BAPA) as a substrate for trypsin. One unit of trypsin inhibitor was defined as 0.01 decrease in absorbance at 410 nm under the assay conditions compared with the control (without inhibitor).The glucosinolates content was determined according to MSZ-08-1908.[22] The assay is based on measurement of absorbance of Pd–glucosinolate complex at 425 nm. A standard curve was constructed with synigrine as a standard.

**Statistical Analysis.** The results were analyzed by one-way analysis of variance with Fisher's least significant difference (LSD), which was performed by Statistica 12.0 (Statsoft, Tulsa, OK). The significance of differences among the mean values is indicated at the 95% confidence level.

## RESULTS AND DISCUSSION

**Physical Characteristics of Hemp Meal Fractions.** Hemp seed oil is a niche market product, mainly produced in small-scale artisan-type plants by mechanical pressing with a screw press. Although this type of oil production does not involve any refining procedures, the oil is purified by simple sedimentation to remove contaminants, such as fine pulp, resins, and water. Although this type of processing appears to be rather simple, the disposal of waste generated throughout the processing can pose a number of problems to the processors having not enough resources to cope with it.

Figure 1 shows the simplified processing flow diagram of mechanical hemp oil pressing. During the cold oil processing, different byproducts could be distinguished: sludge or sediment and press cake or meal. The sludge represents a complex mixture comprising small pieces of pressed seed and hull as well as phospholipids, oil, waxes, and minor amounts of other constituents like phytosterols, tocopherols, pigments, and fatty acids. Hemp seed press cake or meal is a byproduct obtained after the seeds are pressed to extract the oil.

The obtained hemp meal was milled with simultaneous sample cooling to avoid the decomposition of thermolabile components. Subsequently, it was fractionated by sieving, which enabled the separation on the basis of the differences in particle size. Generally, two groups of fractions were identified: coarse fractions of particle sizes >350 and >250 μm, containing hull particles, and fine fractions of particle sizes >180 and <180 μm, containing predominantly cotyledon particles. The yield of these fractions was determined relative to the amount of starting material (Figure 1). The fraction with the highest yield (39.4%) was that with particle size in the range 180–250 μm, which, according to the appearance and structure was predominantly composed of ground cotyledon particles, while sieving yielded 33.0% coarse fraction consisting of hulls. Different particle size distribution was due to different grinding behavior of cotyledons and hulls, which were of higher elasticity due to higher content of structural carbohydrates. which made them more resistant to the grinding.[23] The obtained fractions were clearly separated according to their color, which was quantified by total color difference (Table 1).

The obtained results indicated the existence of a significant difference in lightness ($L^*$), ranging from 28.74 for the coarsest fraction (>350 μm) to 53.46 for the finest fraction (<180 μm). The difference in lightness can be attributed to the difference in scattering effect by the particles of various sizes. Thus the finest fraction, with the smallest particles and increased surface area, scattered more light and appeared to be lighter, unlike the

fractions with larger particle size.[24] The redness of the separated fractions increased with increasing the particle size and varied between 1.15 for the finest fraction (<180 $\mu$m) and 3.92 for the medium coarse fraction (>250 $\mu$m). Conversely, the yellowness of the fractions increased with decreasing particle size, being highest for the finest fraction (<180 $\mu$m). Significant differences in redness ($a^*$) and yellowness ($b^*$) were observed between coarse and fine fractions. The increase in greenness with decreasing particle size could be associated with the presence of chlorophyll pigments, which were found to be abundant in hemp oil.[25] Namely, fractions with smaller particle size (>180 $\mu$m and <180 $\mu$m) had significantly higher oil content in comparison to other meal fractions (Table 2), which resulted in increased chlorophyll content and thus led to pronounced green color of these fractions. Consequently, the increase in yellowness of the fractions rich in oil (lipid; Table 2) could be related to high content of $\gamma$-tocopherol present in hemp oil.[25] In order to quantify the difference in the appearance between separated fractions, the total color difference was calculated relative to the whole hemp meal. Since the total color difference was greater than 3 between all the fractions and the whole hemp meal, an indication of the perception of a color difference by human eye was confirmed.

**Proximate Composition of Hemp Meal Fractions.** The proximate composition of hemp meal is primarily determined by the quality of starting raw material, itself dependent on variety, locality, applied agrotechnical measures, weather conditions, and processing parameters. The proximate composition of hemp meal fractions is shown in Table 2. The moisture content of hemp meal fractions varied between 6.98% and 7.88%, being significantly the lowest ($p < 0.05$) for hull-containing fractions. When it is considered that the cotyledons are the main reserve of proteins, carbohydrates, and oils, cotyledon fractions (of particle size <250 $\mu$m) appeared to be of the richest nutritive composition. More specifically, protein content of hemp meal fractions varied between 10.62% for the coarsest fraction and 44.36% for the finest cotyledon fraction. The same trend was observed for oil and total sugar content, ranging between 8.26% and 18.60% and between 0.00% and 4.96%, respectively. Differentiation of hemp meal fractions in relation to protein, fat, total sugar, ash, and crude fiber content was achieved by sieving as previously indicated by Maaroufi et al.[23] for pea flour and Sreerama et al.[26] for chickpea and horse gram flours.

The protein content in the whole meal was lower than that reported by Callaway[4] and Tang et al.[27] in hemp meal, but it progressively increased in cotyledon-containing fractions. The protein content in whole meal was also lower than that determined in defatted soy flour, as reported by Sudha et al.[28] as well as in rapeseed and soybean meal.[29] The results of crude fiber content (which comprise only insoluble fibers) and ash content in hemp meal were in accordance with the results obtained for hemp seed residue after oil extraction reported by Anwar et al.[30] Crude fiber content varied from 4.96% to 29.54% between the hemp meal fractions. Large quantities of crude fibers were found in coarse meal fractions and consequently were significantly lower in cotyledon fractions. Oil content in the whole meal was consistent with the results reported by Callaway.[4]

**Antioxidant Compounds and Activities of Hemp Meal Fractions.** The radical-scavenging capacities ($IC_{50}$ values) of fraction extracts are presented in Figure 2. $IC_{50}$ values significantly differed ($p < 0.05$) between hemp meal fractions,

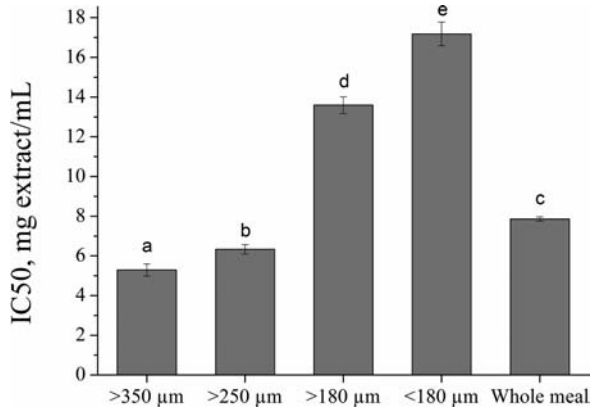


**Figure 2.** Radical scavenging capacities ($IC_{50}$ values) of fraction extract.

the lowest being the coarsest fraction (>350 $\mu$m), indicating the strongest radical-scavenging activity (5.29 mg/mL), unlike that of the finest cotyledon fraction (<180 $\mu$m), which appeared to have the weakest radical-scavenging activity (17.18 mg/mL). Although reported for selected pulses, the same distribution of the radical-scavenging capacity was observed by Duenas et al.[31] and Sreerama et al.[32] Moreover, fractions originating from the peripheral parts of soybean seed manifested higher antioxidant capacity than those originating from cotyledons.[33]

The antioxidant potential of hemp oil has been recently reported, as it has been recognized as one of the nontraditional vegetable oils not so long ago introduced to the market.[34] Literature data on phenolic profile of hemp products other than hemp oil are very limited, except that published by Chen et al.,[35] who reported only phenolic compounds with major significance. Phenolic compounds of hemp meal fractions are presented in Table 3. Apart from *N-trans*-caffeoyltyramine and cannabisin B, identification of phenolic compounds in crude extracts was performed by comparing the retention times and spectra of phenolic compounds of extracts with those of the corresponding external standards. *N-trans*-caffeoyltyramine (UV $\lambda_{max}$ in MeOH 220, 294, 318 nm) and cannabisin B (UV $\lambda_{max}$ in MeOH 220, 245, 283, 335 nm) were identified on the basis of their spectral characteristics, as they were previously isolated and identified as phenolic compounds with predominant radical-scavenging activity in hemp seed.[35] The identification of *N-trans*-caffeoyltyramine and cannabisin B within the present research, solely based on UV spectral characteristics, has been only tentative. However, the presence of previously known and new lignanamides and cannabisins was recently reported by Lesma et al.,[6] who performed a thorough investigation of the metabolic content of hemp seeds in various cultivars, making an important contribution to their NMR spectroscopic characterization. Quantification of phenolic compounds was based on external standards calibration except for *N-trans*-caffeoyltyramine and cannabisin B, which were expressed in *trans*-cinnamic acid equivalents due to the lack of corresponding external standards. The determination of distribution of *N-trans*-caffeoyltyramine and cannabisin B between our hemp meal fractions revealed that they were abundantly present in the hull-containing fractions, in accordance with the results of Chen et al.[35] Apart from those, important phenolic compounds detected in defatted hemp meal were catechin and *p*-hydroxybenzoic acid in the cotyledon fractions, and ferulic and sinapic acid in the hull

**Table 3. Phenolic Compounds of Hemp Meal Fractions[a]**

| | hemp meal fractions | | | | |
|---|---|---|---|---|---|
| phenolic compd | >350 μm | >250 μm | >180 μm | <180 μm | whole meal |
| gallic acid | 0.43 ± 0.06 a | 0.63 ± 0.05 b | 0.79 ± 0.04 c | 1.06 ± 0.05 d | 0.82 ± 0.08 c |
| protocatechuic acid | 14.5 ± 1.67 a | 22.2 ± 1.88 b | 31.7 ± 2.28 cd | 36.0 ± 2.04 d | 28.2 ± 2.47 c |
| *p*-hydroxybenzoic acid | 33.3 ± 3.20 a | 29.8 ± 1.64 a | 129 ± 8.56 c | 124 ± 6.47 c | 78.6 ± 8.00 b |
| catechin | 107 ± 12.4 a | 221 ± 13.0 b | 744 ± 22.2 e | 313 ± 12.4 c | 498 ± 35.9 d |
| vanillic acid | 0.41 ± 0.04 ab | 0.43 ± 0.02 b | 0.55 ± 0.03 c | 0.54 ± 0.03 c | 0.35 ± 0.04 a |
| ferulic acid | 88.4 ± 6.05 c | 82.0 ± 6.26 c | 9.67 ± 0.74 a | 4.72 ± 0.55 a | 47.4 ± 5.37 b |
| sinapic acid | 66.8 ± 5.48 d | 58.3 ± 2.39 c | 26.4 ± 2.21 b | 17.3 ± 1.45 a | 22.2 ± 1.89 ab |
| *N-trans*-caffeoyltyramine[b] | 287 ± 23.1 d | 267 ± 15.9 d | 54.6 ± 3.17 b | 41.7 ± 3.42 a | 152 ± 11.2 c |
| cannabisin B[b] | 153 ± 8.62 e | 117 ± 3.22 d | 25.7 ± 1.15 b | 4.27 ± 0.39 a | 64.9 ± 1.94 c |

[a]Values are means ± SD and are given in milligrams per kilogram dry sample. Means in the same row followed by different letters are significantly different ($P < 0.05$). [b]Expressed in *trans*-cinnamic acid equivalents.

**Table 4. Fatty Acid Composition in Different Hemp Meal Fractions[a]**

| | hemp meal fractions | | | | |
|---|---|---|---|---|---|
| fatty acid | >350 μm | >250 μm | >180 μm | <180 μm | whole meal |
| 16:0 | 6.48 ± 0.01 a | 6.54 ± 0.03 ab | 7.05 ± 0.08 d | 6.90 ± 0.01 c | 6.63 ± 0.03 b |
| 18:0 | 3.26 ± 0.04 b | 3.18 ± 0.01 a | 3.86 ± 0.02 d | 3.69 ± 0.01 d | 3.30 ± 0.03 b |
| 18:1 n9c | 13.9 ± 0.08 c | 12.7 ± 0.02 a | 13.6 ± 0.51 bc | 13.9 ± 0.01 c | 13.0 ± 0.47 ab |
| 18:2 n6c | 54.6 ± 0.32 ab | 55.4 ± 0.01 c | 54.2 ± 0.26 ab | 54.1 ± 0.03 a | 54.8 ± 0.30 b |
| 20:0 | 1.04 ± 0.01 b | 1.00 ± 0.01 a | 1.40 ± 0.01 e | 1.31 ± 0.01 d | 1.10 ± 0.01 c |
| 18:3 n6 | 2.64 ± 0.02 b | 2.75 ± 0.01 c | 2.57 ± 0.02 a | 2.61 ± 0.01 a | 2.76 ± 0.01 c |
| 18:3 n3 | 17.6 ± 0.09 b | 18.4 ± 0.01 c | 17.3 ± 0.13 a | 17.5 ± 0.04 b | 18.4 ± 0.10 c |

[a]Values are means ± SD and are given in grams per 100 g total fatty acids. Means in the same row followed by different letters are significantly different ($P < 0.05$).

**Table 5. Content and Ratio of Saturated and Unsaturated Fatty Acids in Different Hemp Meal Fractions[a]**

| | hemp meal fractions | | | | |
|---|---|---|---|---|---|
| fatty acid fraction[b] | >350 μm | >250 μm | >180 μm | <180 μm | whole meal |
| SFA | 10.8 ± 0.07 a | 10.7 ± 0.03 a | 12.3 ± 0.09 d | 11.9 ± 0.01 c | 11.0 ± 0.07 b |
| MUFA | 14.3 ± 0.49 c | 12.7 ± 0.02 a | 13.6 ± 0.51 abc | 13.9 ± 0.01 bc | 13.0 ± 0.47 ab |
| PUFA | 74.9 ± 0.42 a | 76.6 ± 0.02 b | 74.1 ± 0.42 a | 74.2 ± 0.01 a | 76.0 ± 0.40 b |
| UFA | 89.2 ± 0.07 d | 89.3 ± 0.03 d | 87.7 ± 0.09 a | 88.1 ± 0.01 b | 89.0 ± 0.07 c |
| PUFA/SFA ratio | 6.94 | 7.14 | 6.02 | 6.24 | 6.88 |

[a]Values are means ± SD and are given as grams per 100 g total fatty acids. Means in the same row followed by different letters are significantly different ($P < 0.05$). [b]SFA, saturated fatty acids; MUFA, monounsaturated fatty acids; PUFA, polyunsaturated fatty acids; UFA, unsaturated fatty acids.

fractions. The content of gallic acid, protocatechuic acid, *p*-hydroxybenzoic acid, vanillic acid, and catehin increased from hull fraction to cotyledon fraction, thus disproving the fact that hull is necessarily the main source of natural antioxidants (Table 3). Conversely, the content of ferulic and sinapic acids in the hull fractions was significantly higher than that of cotyledon fractions. However, the content of ferulic and gallic acid was lower than those determined in defatted flaxseed.[36] The content of *p*-hydroxybenzoic acid in all hemp meal fractions was higher than that of coconut, cottonseed, sesame, flax, and peanut flours as reported by Dabrowski and Sosulski.[37] Furthermore, whole hemp meal and cotyledon fractions contained higher content of *p*-hydroxybenzoic acid than that of rapeseed and sunflower flours and a similar level as soybean flour. The content of all determined phenolic compounds was higher than that determined for cold-pressed hemp oil, wherein protocatechuic acid was not detected in hemp oil.[34] The content of sinapic acid was lower than that determined in canola meal.[38]

**Fatty Acid Composition of Hemp Meal Fractions.** Fatty acid compositions of different hemp meal fractions are provided in Table 4. According to obtained data, fatty acid distribution was mainly uniform across different fractions. The main fatty acids were linoleic (54.09−55.42%), linolenic (17.31−18.42%), and oleic (12.96−13.93%) acids, followed by palmitic (6.48−7.90%), stearic (3.18−3.86%), and γ-linolenic (2.61−2.76%) acids. Similar results were obtained for hemp seed oil according to Teh and Birch[25] and Da Porto et al.[7] Moreover, high content of polyunsaturated acids, especially of linoleic (18:2 n6c) as well as ω-3 linolenic acid in the ratio of approximately 3:1, indicated a positive nutritional profile of all hemp meal fractions. Similar results were reported for fatty acid composition of hemp seed oil.[7]

Results presented in Table 5 show relatively high content of polyunsaturated fatty acids (PUFA) in all fractions. Hemp meal fraction with coarse particles (>250 μm) was characterized by higher content of polyunsaturated fatty acids and consequently lower level of monounsaturated fatty acids (MUFA) in comparison to other hemp meal fractions. Moreover, slightly

Table 6. Distribution of Major Antinutrients in Different Fractions of Hemp Meal[a]

| | hemp meal fractions | | | | |
|---|---|---|---|---|---|
| antinutrient | >350 μm | >250 μm | >180 μm | <180 μm | whole meal |
| trypsin inhibitor (TIU/mg of protein) | 1.39 ± 0.00 a | 1.96 ± 0.04 b | 3.70 ± 0.02 d | 3.90 ± 0.07 e | 2.88 ± 0.09 c |
| phytic acid (mg/g) | 4.36 ± 0.05 a | 18.35 ± 0.57 b | 21.2 ± 0.11 c | 21.4 ± 0.11 c | 22.5 ± 0.07 d |
| glucosinolates (μmol/g) | 3.14 ± 0.20 a | 3.66 ± 0.08 ab | 5.33 ± 0.17 c | 5.64 ± 0.30 c | 3.80 ± 0.27 b |
| condensed tannins (mg/g) | 0.19 ± 0.04 a | 0.33 ± 0.05 b | 0.25 ± 0.00 a | 0.26 ± 0.00 ab | 0.23 ± 0.01 a |

[a]Values are means ± SD. Means in the same row followed by different letters are significantly different ($P < 0.05$).

higher content of saturated fatty acids was found in fine hemp meal fractions (>180 μm and <180 μm). Saturated fatty acids (SFA) have been labeled as a possible cause of cancer and coronary heart diseases when present in excessive amounts in human diet. The mean ratio of PUFA/SFA recommended by the British Department of Health is more than 0.45, and WHO/FAO experts have reported guidelines for a "balanced diet" in which the suggested ratio of PUFA/SFA is above 0.40.[39,40] In this respect, all investigated meal fractions exhibited a favorable PUFA/SFA ratio (from 6.02 to 7.14).

**Antinutritive Factors in Hemp Meal Fractions.** The concentrations of antinutrients in different hemp meal fractions are shown in Table 6. Considerable variability in trypsin inhibitor activity between hemp meal fractions was evident, the lowest being in the fraction containing mainly husk (>350 μm) and the highest for cotyledon fraction. These results were higher than those obtained for watermelon, pumpkin, and paprika seed flour reported by El-Adawy and Taha.[41] Considerable variability in phytic acid content between hemp meal fractions was observed, being the highest in the fine fractions (Table 6). The coarsest fraction (>350 μm) appeared to have the lowest phytic acid content. The phytic acid content was lower than that of canola meal reported by Bell[42] and those determined in hemp seed meal of Italian and French varieties.[43] The presence of certain antinutrients (condensed tannins, polyphenols, trypsin, chymotrypsin, α-amylase inhibitors, oligosaccharides, trypsin inhibitors, phytic acid, tannins, glucosinolates, and saponins) may limit their conversion into edible-grade products and utilization in human nutrition as they influence protein digestibility, organoleptic properties, and bioavailability of macro- and microelements. However, in recent decades an increasing trend of reutilization of plant byproducts in food, cosmetic, and pharmaceutical industries has been observed.[2,29] Apart from the well-known harmful effects of antinutrients, certain health-promoting and disease-preventing properties also have been attributed to them. A preventive impact of phytic acid, phenolics, saponins, protease inhibitors, phytoestrogens, and lignans on diabetes, cardiovascular diseases, and cancer has been demonstrated.[44,45]

Finally, it can be concluded that fractionation by sieving can be used as a processing operation in order to preserve and concentrate target valuable compounds from hemp meal, a byproduct of hemp oil processing. While certain fractions might be used as food functional ingredients, the other fractions, due to increased antinutritive factors, could be used as a substrate for recovery of valuable compounds or in cosmetic and pharmaceutical industries.

## AUTHOR INFORMATION


### Corresponding Author

*Telephone +381 214853811; fax +381 21450725; e-mail miroslav.hadnadjev@fins.uns.ac.rs.



### Funding

This work was financially supported by the Ministry of Education, Science and Technological Development, Republic of Serbia (Grant III46001).


### Notes

The authors declare no competing financial interest.

## REFERENCES


(1) Galanakis, C. M. Recovery of high added-value components from food wastes: Conventional, emerging technologies and commercialized applications. *Trends Food Sci. Technol.* **2012**, *26*, 68−87.

(2) Oreopoulou, V.; Tzia, C. Utilization of plant by-products for the recovery of proteins, dietary fibers, antioxidants, and colorants. In *Utilization of By-Products and Treatment of Waste in the Food Industry*; Oreopoulou, V., Russ, W., Eds.; Springer Science+Business Media, LLC: New York, 2007; pp 209−232.

(3) Zanetti, F.; Monti, A.; Berti, M. T. Challenges and opportunities for new industrial oilseed crops in EU-27: A review. *Ind. Crops Prod.* **2013**, *50*, 580−595.

(4) Callaway, J. C. Hempseed as a nutritional resource: An overview. *Euphytica* **2004**, *140*, 65−72.

(5) Montserrat-de la Paz, S.; Marín-Aguilar, F.; García-Giménez, M. D.; Fernández-Arche, M. A. Hemp (*Cannabis sativa* L.) seed oil: Analytical and phytochemical characterization of the unsaponifiable fraction. *J. Agric. Food Chem.* **2014**, *62*, 1105−1110.

(6) Lesma, G.; Consonni, R.; Gambaro, V.; Remuzzi, C.; Roda, G.; Silvani, A.; Vece, V.; Visconti, G. L. Cannabinoid-free *Cannabis sativa* L. grown in the Po valley: Evaluation of fatty acid profile, antioxidant capacity and metabolic content. *Nat. Prod. Res.* **2014**, *28*, 1801−1807.

(7) Da Porto, C.; Decorti, D.; Tubaro, F. Fatty acid composition and oxidation stability of hemp (*Cannabis sativa* L.) seed oil extracted by supercritical carbon dioxide. *Ind. Crops Prod.* **2012**, *36*, 401−404.

(8) Wang, X. S.; Tang, C. H.; Yang, X. Q.; Gao, W. R. Characterization, amino acid composition and in vitro digestibility of hemp (*Cannabis sativa* L.) proteins. *Food Chem.* **2008**, *107*, 11−18.

(9) Kim, J.-J.; Lee, M.-Y. Isolation and characterization of edestin from Cheungsam hempseed. *J. Appl. Biol. Chem.* **2011**, *54*, 84−88.

(10) Schwab, U. S.; Callaway, J. C.; Erkkilä, A. T.; Gynther, J.; Uusitupa, M. I. J.; Jarvinen, T. Effects of hempseed and flaxseed oils on the profile of serum lipids, serum total and lipoprotein lipid concentrations and haemostatic factors. *Eur. J. Nutr.* **2006**, *45*, 470−477.

(11) Wang, Y.-Y.; Norajit, K.; Kim, M.-H.; Kim, Y.-H.; Ryu, G.-H. Influence of extrusion condition and hemp addition on wheat dough and bread properties. *Food Sci. Biotechnol.* **2013**, *22*, 89−97.

(12) Radočaj, O.; Dimić, E.; Tsao, R. Effects of hemp (*Cannabis sativa* L.) seed oil press-cake and decaffeinated green tea leaves (*Camellia sinensis*) on functional characteristics of gluten-free crackers. *J. Food Sci.* **2014**, *79*, C318−C325.

(13) Francis, F. J., Clydesdale, F. M. *Food Colorimetry: Theory and Applications*; Avi Publishing: Westport, CT, 1975.

(14) *AOAC Official Methods of Analysis*, 15th ed.; Association of Official Analytical Chemists: Washington, DC, 1990; Vol. *I* and *II*.

(15) Espin, J. C.; Soler-Rivas, C.; Wichers, H. J. Characterization of the total free radical scavenger capacity of vegetable oils and oil fractions using 2,2-diphenyl-1-picrylhydrazyl radical. *J. Agric. Food Chem.* **2000**, *48*, 648−656.

(16) Mišan, A.Č.; Mimica-Dukić, N. M.; Mandić, A. I.; Sakač, M. B.; Milovanović, I. Lj.; Sedej, I. J. Development of a rapid resolution HPLC method for the separation and determination of 17 phenolic compounds in crude plant extracts. *Cent. Eur. J. Chem.* **2011**, *9*, 133−142.
(17) Folch, J.; Lees, M.; Stanley, G. H. S. A simple method for the isolation and purification of total lipids from animal tissues. *J. Biol. Chem.* **1957**, *226*, 497−509.
(18) Karlović, Đ., Andrić, N. *Kontrola kvaliteta semena uljarica*; Tehnološki fakultet: Novi Sad, Serbia, 1996.
(19) Haug, W.; Lantzsch, H.-J. Sensitive method for the rapid determination of phytate in cereals and cereal products. *J. Sci. Food Agric.* **1983**, *34*, 1423−1426.
(20) Butler, E. J.; Pearson, A. W.; Fenwick, G. R. Problems which limit the use of rapeseed meal as a protein source in poultry diets. *J. Sci. Food Agric.* **1982**, *33*, 866−875.
(21) Hamerstrand, G. E.; Black, L. T.; Glover, J. D. Trypsin inhibitors in soy products: Modification of the standard analytical procedure. *Cereal Chem.* **1981**, *58*, 42−45.
(22) MSZ-08-1908. Determination of the glucosinolate content of rapeseeds and rapeseed meals. Magyar köztársaság Mezógazdasági és Élelmezésügyi Ágazati Szabvány, MSZH Nyomda és Kiadó Kft: Budapest, 1989.
(23) Maaroufi, C.; Melcion, J. P.; de Monredon, F.; Giboulot, B.; Guibert, D.; Le Guen, M. P. Fractionation of pea flour with pilot scale sieving. I. Physical and chemical characteristics of pea seed fractions. *Anim. Feed Sci. Technol.* **2000**, *85*, 61−78.
(24) Joshi, P. Colour measurement of foods by colour reflectance. In *Colour in Food: Improving Quality*; MacDougall, D. B., Ed.; Woodhead Publishing Limited and CRC Press LLC: Cambridge, U.K., 2002; pp 80−114.
(25) Teh, S.-S.; Birch, J. Physicochemical and quality characteristics of cold-pressed hemp, flax and canola seed oils. *J. Food Compos. Anal.* **2013**, *30*, 26−31.
(26) Sreerama, Y. N.; Neelam, D. A.; Sashikala, V. B.; Pratape, V. M. Distribution of nutrients and antinutrients in milled fractions of chickpea and horse gram: Seed coat phenolics and their distinct modes of enzyme inhibition. *J. Agric. Food Chem.* **2010**, *58*, 4322−4330.
(27) Tang, C.-H.; Ten, Z.; Wang, X.-S.; Yang, X.-Q. Physicochemical and functional properties of hemp (*Cannabis sativa* L.) protein isolate. *J. Agric. Food Chem.* **2006**, *54*, 8945−8950.
(28) Sudha, M. L.; Rajeswari, G.; Venkateswara Rao, G. Influence of defatted soy flour and whey protein concentrate on dough rheological characteristics and quality of instant vermicelli. *J. Texture Stud.* **2011**, *42*, 72−80.
(29) Rodrigues, I. M.; Coelho, J. F. J.; Carvalho, M. G. V. S. Isolation and valorisation of vegetable proteins from oilseed plants: Methods, limitations and potential. *J. Food Eng.* **2012**, *109*, 337−346.
(30) Anwar, F.; Latif, S.; Ashraf, M. Analytical characterization of hemp seed oil from different agro-ecological zones of Pakistan. *J. Am. Oil Chem. Soc.* **2006**, *83*, 323−329.
(31) Duenas, M.; Hernandez, T.; Estrella, I. Assessment of in vitro antioxidant capacity of the seed coat and the cotyledon of legumes in relation to their phenolic contents. *Food Chem.* **2006**, *98*, 95−103.
(32) Sreerama, Y. N.; Sashikala, V. B.; Pratape, V. M. Variability in the distribution of phenolic compounds in milled fractions of chickpea and horse gram: Evaluation of their antioxidant properties. *J. Agric. Food Chem.* **2010**, *58*, 8322−8330.
(33) Xu, B. J.; Chang, S. K. C. Antioxidant capacity of seed coat, dehulled bean, and whole black soybeans in relation to their distributions of total phenolics, phenolic acids, anthocyanins, and isoflavones. *J. Agric. Food Chem.* **2008**, *56*, 8365−8373.
(34) Siger, A.; Nogala-Kalucka, M.; Lampart-Szczapa, E. The content and antioxidant activity of phenolic compounds in cold-pressed plant oils. *J. Food Lipids* **2008**, *15*, 137−149.
(35) Chen, T.; He, J.; Zhang, J.; Li, X.; Zhang, H.; Hao, J.; Li, L. The isolation and identification of two compounds with predominant radical scavenging activity in hempseed (seed of *Cannabis sativa* L.). *Food Chem.* **2012**, *134*, 1030−1037.
(36) Kajla, P.; Sharma, A.; Sood, D. R. Flaxseed: a potential functional food source. *J. Food Sci. Technol.* **2014**, DOI: 10.1007/s13197-014-1293-y.
(37) Dabrowski, K. J.; Sosulski, F. W. Composition of free and hydrolyzable phenolic acids in defatted flours of ten oilseeds. *J. Agric. Food Chem.* **1984**, *32*, 128−130.
(38) Cai, R.; Arntfield, S. D. A rapid high-performance liquid chromatographic method for the determination of sinapine and sinapic acid in canola seed and meal. *J. Am. Oil Chem. Soc.* **2001**, *78*, 903−910.
(39) Wood, J. D.; Enser, M.; Fisher, A. V.; Nute, G. R.; Sheard, P. R.; Richardson, R. I.; Huges, S. I.; Whittington, F. M. Fat deposition, fatty acid composition and meat quality: A review. *Meat Sci.* **2008**, *78*, 343−358.
(40) Department of Health. Nutritional aspects of cardiovascular disease. Report on Health and Social Subject No 46; HMSO: London, 1994.
(41) El-Adawy, T. A.; Taha, K. Characteristics and composition of different seed oils and flours. *Food Chem.* **2001**, *74*, 47−54.
(42) Bell, J. M. Factors affecting the nutritional value of canola meal: A review. *Can. J. Anim. Sci.* **1993**, *73*, 679−697.
(43) Russo, R.; Reggiani, R. Variability in antinutritional compounds in hempseed meal of Italian and French varieties. *Plant* **2013**, *1*, 25−29.
(44) Thompson, L. U. Potential health benefits and problems associated with antinutrients in foods. *Food Res. Int.* **1993**, *26*, 131−149.
(45) Jacobs, D. R., Jr.; Steffen, L. M. Nutrients, foods, and dietary patterns as exposures in research: A framework for food synergy. *Am. J. Clin. Nutr.* **2003**, *78*, 508S−513S.

**Scheme 1. Genipin Reacted with Amino Groups in CS and Peptide To Yield Two Main Cross-Linking Reactions (Taking CS, for Example)**

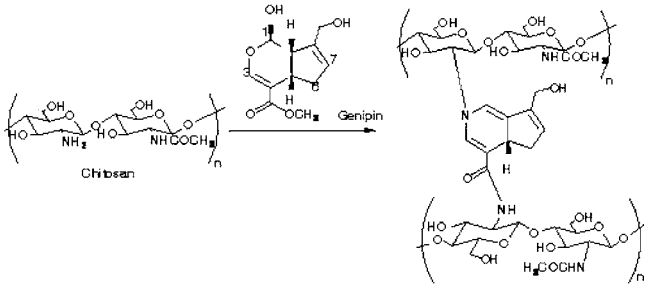


synthetic chemicals as cross-linking agents, such as glutaraldehyde, ethylene glycol, diglycidyl ether, and diisocyanate.[20]

Herein, the CPP−CS (NPs) were cross-linked with genipin, and the critical centrifuge parameters for purification of the biopolymer nanoparticles were optimized. The morphology, particle size, and surface charge of the nanoparticles before and after the centrifugal purification were characterized using TEM, DLS, and electrophoretic mobility ($\zeta$-potential) measurements. The cross-linking reaction was confirmed and characterized by FT-IR. The structure behaviors of the nanoparticles, including morphology, particle size, and surface charge, as well as the controlled release profile of EGCG, from the nanoparticles under different digestion pH and enzyme conditions were investigated systematically. EGCG is the most abundant and bioactive polyphenol in green tea. However, the bioavailability of EGCG is very low.[21] The anticancer activities of the EGCG-loaded CPP−CS nanoparticles cross-linked with genipin were investigated by in vitro cell assays.

## MATERIALS AND METHODS

**Materials.** CS of molecular weight 100 kDa with a 90% deacetylation degree, derived from crab shell, was obtained from Golden-Shell Biochemical Co. Ltd. (Hangzhou, China). CPPs were prepared and identified with HPLC-MS-MS as described in our previous study.[22] EGCG (purity > 98%) and trypan blue were purchased from Sigma-Aldrich Co. (St. Louis, MO, USA). Genipin (purity > 98%) was purchased from Linchuan Zhixin Biotechnology Co., Ltd. (Jiangxi, China). High-purity grade pepsin with activity of 3000−3.5 NF U/mg and trypsin with activity of >250 NF U/mg were purchased from Beijing Solarbio Science and Technology Co., Ltd. (Beijing, China). Dimethyl sulfoxide (DMSO) and acetic acid were obtained from Sinopharm Chemical Reagent Co., Ltd. (Shanghai, China). Human gastric BGC823 and liver HepG2 cancer cells were obtained from the Cell Bank of Shanghai Institute of Cell Biology (Shanghai, China). Dulbecco's modified Eagle's medium (DMEM) and fetal bovine serum were purchased from Wisent Biotechnology (Wisent Inc., Quebec, Canada). All other chemicals were of analytical grade.

**General Procedure for Preparation of CPP−CS NPs and EGCG-Loaded CPP−CS NPs.** CPP−CS NPs were prepared according to our previously reported procedure.[22] Briefly, CS was dissolved in 1% (w/v) acetic acid solution with sonication until the solution was transparent. The aqueous solution of CPP was obtained at a suitable concentration. Both CS and CPP solutions were adjusted to pH 6.2 with 1.0 N HCl or NaOH solution. Subsequently, CS solution was added to CPP solution under stirring at room temperature. For the preparation of EGCG-loaded CPP−CS NPs, an aqueous solution of EGCG was added to a CPP solution before the addition of CS solution. The formation of CPP−CS NPs started spontaneously via the CPP-initiated ionic gelation mechanism.

**Cross-Linking of CPP−CS NPs and EGCG-Loaded CPP−CS NPs with Genipin.** For the preparation of genipin-cross-linked CPP−CS NPs, different amounts of genipin were added to the CPP−CS nanoparticle suspension, forming different final genipin concentrations of 0, 0.031, 0.063, 0.125, 0.250, 0.500, 1.000, and 2.000 mg/mL. The reaction mixture was incubated at 37 °C for different times of 3, 6, 12, and 24 h. The cross-linking reaction of the CPP−CS NPs was terminated by separating the nanoparticles from the residual free genipin in the reaction system using a centrifugal purification method that was optimized in following section. The genipin-cross-linked nanoparticles were washed three times using deionized water, precipitated, and collected. Cross-linking of the EGCG-loaded CPP−CS NPs with genipin was operated using the same procedure as described above.

**Purification of CPP−CS NPs and Genipin-Cross-Linked CPP−CS NPs.** The CPP−CS NPs and the genipin-cross-linked CPP−CS NPs were purified from their parental reaction suspension by centrifugation using an Avanti J-25 high-speed centrifuge (Beckman Coulter, Inc., Brea, CA, USA), with different centrifugal forces (25000, 10000, 7500, 5000, and 2500$g$) and various duration times (15, 30, 45, and 60 min) to optimize the critical centrifuge parameters, under which the nanoparticles could be just precipitated and then recovered to nanoparticle suspension after redispersion. The redispersion property of the nanoparticle precipitate was preliminarily observed by checking whether there were visible particles in the redispersed colloid solution. The nanoparticles were washed three times using deionized water and redispersed to the same volume as that before centrifugation. The size distribution, surface charge, and surface morphology of the purified nanoparticle suspension and their parental ones were characterized by DLS, zeta-potential measurement, and TEM.

**Nanoparticle Stability and Structure Behavior in Simulated GI pH and Enzyme Environments.** Equal amounts of the precipitates of the CPP−CS NPs and the genipin-cross-linked CPP−CS NPs were first redispersed in pH 1.2 (0.1 N HCl), pH 6.2, and pH 7.4 (10 mM PBS) solutions for 2 h, respectively, simulating the pH environments of the GI tract. The size distribution, surface charge, and morphology of the nanoparticles at these distinct pH conditions were characterized by DLS, zeta-potential measurement, and TEM. The nanoparticles that withstood the GI pH environments were further dispersed in 50 mL of 0.1 N HCl (pH 1.2) containing 0.1% pepsin as the simulated gastric fluid (SGF) and 50 mL of 10 mM PBS (pH 7.4) with 1.0% trypsin as the simulated intestinal fluid (SIF) for 2 h, respectively. The samples after gastric and intestinal digestion were isolated from the SGF and SIF, washed, and redispersed in deionized water for the determinations of size distribution, surface charge, and morphology.

**Cytotoxicity of the EGCG-Loaded CPP−CS NPs Cross-Linked with Genipin against Cancer Cells.** Cytotoxicity was measured using the trypan blue dye exclusion test. Human liver HepG2 cells or human gastric BGC823 cells (100,000) were seeded in 6-well plates, in 2.5 mL of medium per well. After 24 h, supernatants were discarded and replaced by fresh EGCG, CPP−CS NPs cross-linked with genipin, or the EGCG-loaded CPP−CS NPs cross-linked with genipin dilutions in cell culture medium in a range of concentrations from 12.5 to 200 $\mu$g/mL (0.0273−0.437 mmol/L) for EGCG and from 12.5 to 200 $\mu$g/mL (0.0273−0.437 mmol/L) for the nanoparticles. After 24 h of exposure, supernatants were discarded and cells rinsed twice with PBS. Cells exposed to EGCG, CPP−CS NPs cross-linked with genipin, or the EGCG-loaded CPP−CS NPs cross-linked with genipin were harvested with 1× trypsin. Cells were mixed with an aqueous solution of trypan blue 0.4% in PBS (pH 7.0) according to a method previously described.[23] Cell counting was performed using Kova counting chambers (Kova Glasstic Slide, Hycor Biomedical) by microscopy. The cell viability was calculated as the ratio between uncolored cells and total cells. All measurements were performed in triplicate.

**Statistical Analysis.** Data were expressed as the mean ± standard deviation (SD) of at least triplicates. The least significant difference (LSD) test and one-way analysis of variance (ANOVA) were used for multiple comparisons by SPSS 16.0. Difference was considered to be statistically significant at $p < 0.05$.

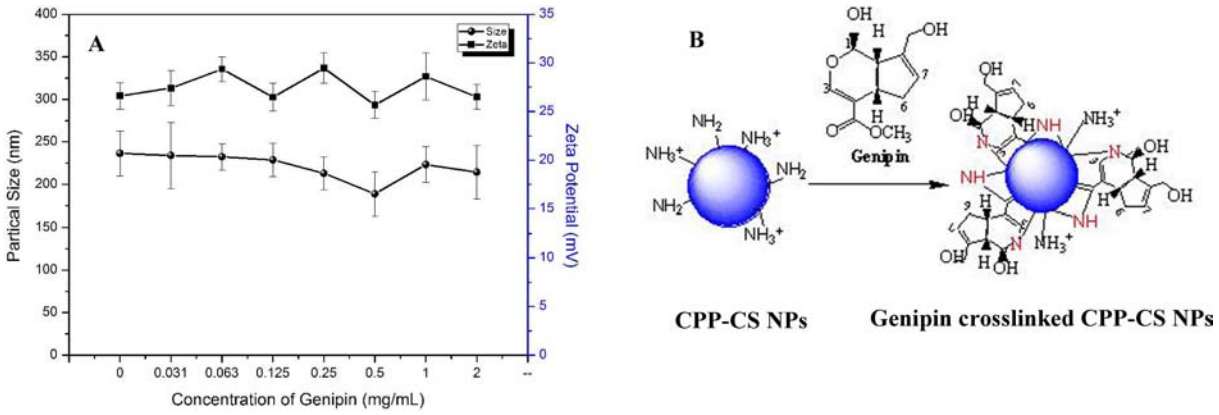


**Figure 1.** (A) Particle size and surface charge of the genipin cross-linked CPP−CS nanoparticles (NPs) with different concentrations of genipin; (B) schematic plot of the intra-cross-linkage of the CPP−CS NPs.

## RESULTS AND DISCUSSION

**Cross-Linking the CPP−CS NPs with Genipin.** Covalent cross-linking of the CPP−CS NPs with genipin took place spontaneously when genipin was added to the parental suspension. The appearance of blue coloration in the reaction mixture was traditionally considered as rapid evidence that the cross-linking reaction was taking place.[17] The cross-linking reaction occurred by means of a complex mechanism.[24] When the CPP−CS NPs were submitted to cross-linking with genipin, a nucleophilic attack by the amino groups of CS (peptide) on the olefinic carbon atom at C-3 in genipin occurred, followed by opening the dihydropyran ring and attack by the secondary amino group on the newly formed aldehydo group (Scheme 1). Genipin could form multiple cross-linkings among CS and CPP. In the product, short chains of condensed genipin acted as cross-linking bridges. The cross-linking reaction of the CPP−CS NPs with genipin could be further characterized by FT-IR, which will be presented and discussed later.

Theoretically, genipin might cause intra- and inter-cross-linkage of the CPP−CS NPs, leading to changes in particle size and surface charge. Therefore, the effect of different genipin concentrations on the physicochemical properties of the CPP−CS NPs was first investigated. Figure 1A shows the particle size and surface charge of the CPP−CS NPs and the covalently cross-linked CPP−CS NPs with different genipin concentrations. The particle size of CPP−CS NPs before cross-linking was 236.5 ± 26.3 nm ($n$ = 3) with a polydispersity index (PDI) of 0.152 ± 0.032 ($n$ = 3), which indicated a homogeneous dispersion of nanoparticles. Zeta-potential analysis revealed a surface charge of 26.6 ± 1.4 mV ($n$ = 3). After cross-linking with different genipin concentrations at 37 °C for 24 h, no significant change in particle size and surface charge of the nanoparticles could be observed. It could be found that the particle size decreased slightly with the increase of genipin concentrations, which might be related to the tighter cross-linking of the nanoparticles at higher concentration of genipin. The PDIs of the genipin cross-linked CPP−CS NPs were in the range of 0.108−0.204, which also indicated a homogeneous dispersion of nanoparticles. Therefore, it could be concluded that genipin mainly produced intra-cross-linkage of the CPP−CS NPs (Figure 1B), leading to little influence on their physicochemical properties.

**Purification of Nanoparticles.** CS-based polyelectrolyte nanoparticles are some of the most widely utilized engineered nanocarriers in bioimaging and biomedical therapeutics.[10,25] However, scarce data on purification of the CS-based nanoparticles from the reaction systems have been reported. Excess free CS, the corresponding negative polyelectrolytes, and the unloaded free cargoes are expected to remain in the product solution and should be removed before use, which otherwise could cause misleading results, such as in fluorescence labeling experiments. Furthermore, purification of the polymer nanoparticles is essential for further modification of nanoparticle surface properties, such as conjugating with functional groups, layer by layer coating with multilayers, and tests of the polymer nanoparticles' effects on biological tissues. In the present study, separation of the covalently cross-linked CPP−CS NPs from the free genipin, CS, and CPP remaining in the reaction system was of primary importance to terminate the spontaneous cross-linking reaction and to characterize the physicochemical and biological properties of the nanoparticles.

Centrifugation is most commonly used to separate nanoparticles, probably because of the easy availability of the instrument.[26] This purification method also offers more flexibility to vary the final volume of the treated nanoparticle suspension.[27] However, during centrifugation, the polymer nanoparticles are prone to cluster and mesh, leading to precipitation, even a polymer film that can never be redispersed as nanoparticle suspension. Therefore, a critical centrifuge parameter has to be optimized, under which the nanoparticles could just be precipitated and could also be recovered to nanoparticle suspension with similar physicochemical properties as the original ones. We summarized the centrifuge speed and duration employed in various studies to purify the CS-based nanoparticles (Supporting Information, Table S1) and found that the use of different parameters (e.g., rpm vs $g$-force) in the papers challenged attempts to cross-compare the studies. Even if a similar unit expression was adopted, the centrifuge forces and durations were seemingly selected arbitrarily (Supporting Information, Table S1).

To address the above-mentioned issues, in the present study, the critical centrifuge parameters for purification of the CPP−CS NPs and the genipin-cross-linked CPP−CS NPs were optimized with different centrifuge forces (25000, 10000, 7500, 5000, and 2500$g$) and various centrifugal times (15, 30, 45, and 60 min). The $g$-force ($g$) can be widely used and cross-compared, independent of different types of centrifuge equipment. As different genipin concentrations had little impact on the physicochemical properties of the nanoparticles,

we first took the cross-linked CPP−CS NPs with a genipin concentration of 0.125 mg/mL as the test sample. The redispersion properties of the nanoparticle precipitate were preliminarily checked whether there were visible particles in the redispersed colloid solution. Eventually, it was found that, under a centrifuge force of 2500*g* for 45 min, the nanoparticles could be just fully precipitated (Figure 2A) and then redispersed without visible particles (Figure 2B). The purified nanoparticles were washed and centrifuged three times before further characterization.

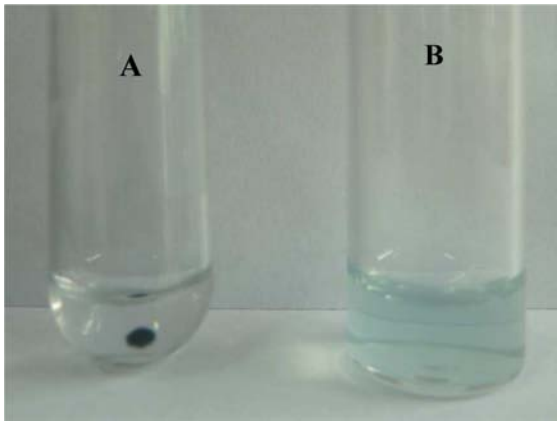


**Figure 2.** Centrifugation and redispersion of the genipin cross-linked CPP−CS NPs operating at a centrifuge force of 2500*g* and duration of 45 min (genipin concentration = 0.125 mg/mL).

Figure 3 shows the structure and morphology of the CPP−CS nanoparticle and the genipin-cross-linked CPP−CS nanoparticle samples before and after centrifugal purification at 2500*g* for 45 min, which were characterized using TEM. It can be seen that the parental CPP−CS NPs (Figure 3A) and genipin cross-linked CPP−CS NPs (Figure 3C) were regularly spherical in shape, dispersed homogeneously, and surrounded with free polymers. According to our previous study, it was mainly the excess free CS that was around the nanoparticles, allowing adsorption of free CS onto the surface of the nanoparticles and desorption of CS from the nanoparticles to reach equilibrium.[22] In addition, CS aggregates including certain crystal structures (marked with red arrows) could be observed in the background of the TEM images of the nanoparticle sample before centrifugation (Figure 3A,C). Comparatively, after centrifugal purification, in the TEM images of both the CPP−CS NPs (Figure 3B) and the genipin-cross-linked CPP−CS NPs (Figure 3D), the free CS surrounding the nanoparticles and the CS aggregates in the background disappeared, and the background of the images became clear. This phenomenon indicated that the CPP−CS NPs and genipin-cross-linked CPP−CS NPs had been successfully separated from the reaction system by the centrifugal purification method. The purified nanoparticles were regular spheres as well and dispersed homogeneously without aggregations (Figure 3B,D). No significant variations in the nanoparticle structure and morphology can be found by comparing the CPP−CS NPs with the genipin-cross-linked CPP−CS NPs themselves.

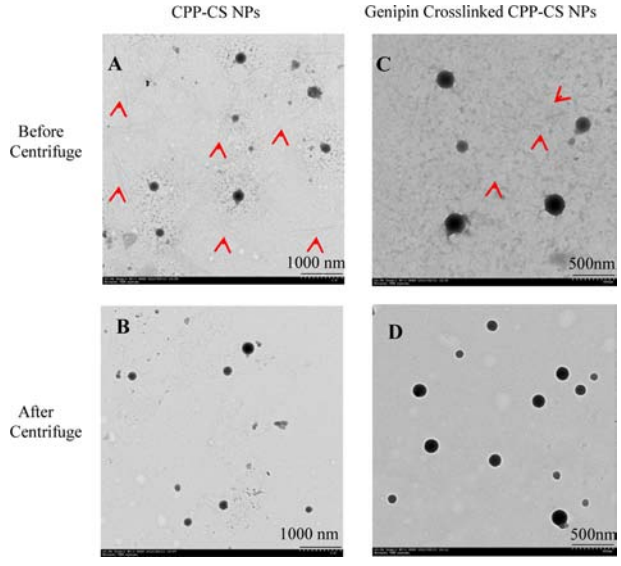


**Figure 3.** TEM images of CPP−CS NPs (A, B) and genipin-cross-linked CPP−CS NPs (C, D) before (A, C) and after (B, D) purification with centrifugation at a centrifuge force of 2500*g* and duration of 45 min (genipin concentration = 0.125 mg/mL).

The particle size and surface charge of the CPP−CS nanoparticle and genipin-cross-linked CPP-CS nanoparticle samples before and after centrifugal purification were further determined by DLS and zeta-potential measurement, which are shown in Figure 4. The mean particle size of the parental CPP−CS NPs and genipin-cross-linked CPP−CS NPs before centrifugation were 269.2 ± 19.6 nm (Figure 4A) and 246.2 ± 17.0 nm (Figure 4C), with PDIs of 0.165 and 0.142, respectively, indicating that the nanoparticles dispersed homogeneously. After centrifugation and redispersion, the particles size of the purified CPP−CS NPs (279.4 ± 21.1 nm) and genipin-cross-linked nanoparticles (245.3 ± 18.3 nm) were almost the same as that of their parental nanoparticles before centrifugation. This result was in accordance with the TEM result (Figure 3). After centrifugation, the surface charge of both the CPP−CS NPs and the genipin-cross-linked CPP−CS NPs increased from 20.3 ± 1.5 to 25.9 ± 3.8 mV and from 24.3 ± 3.5 to 32.4 ± 6.1 mV, respectively. This phenomenon might be related to the removal of the shielding effect caused by the excess free CS around the nanoparticles (Figure 3).

Therefore, operation at 2500*g* for 45 min was the critical centrifuge parameter for purification of the CPP−CS NPs and the genipin-cross-linked CPP−CS NPs for terminating the cross-linking reaction and for further separating the nanoparticles from the simulated GI fluids. The nanoparticles themselves maintained their structure and physicochemical properties after centrifugal purification. The CPP−CS NPs and the genipin-cross-linked CPP−CS NPs with different genipin concentrations (0.063, 0.125, and 0.250 mg/mL) and various reaction times (3, 6, 12, and 24 h) were purified by the centrifuge method and lyophilized for further FT-IR analysis.

**FT-IR Analysis.** To characterize the cross-linking reaction, we acquired the FT-IR spectra of the purified CPP−CS NPs and genipin-cross-linked nanoparticles with different genipin concentrations and reaction times (Figure 5). In Figure 5A, the covalently cross-linked CPP−CS NPs were obtained after cross-linking reaction for 3 h with different genipin concentrations of 0.063, 0.125, and 0.250 mg/mL. In Figure 5B, the genipin cross-linked nanoparticles with a fixed genipin concentration of 0.125 mg/mL were purified at different reaction times of 3, 6, 12, and 24 h. The main characteristic

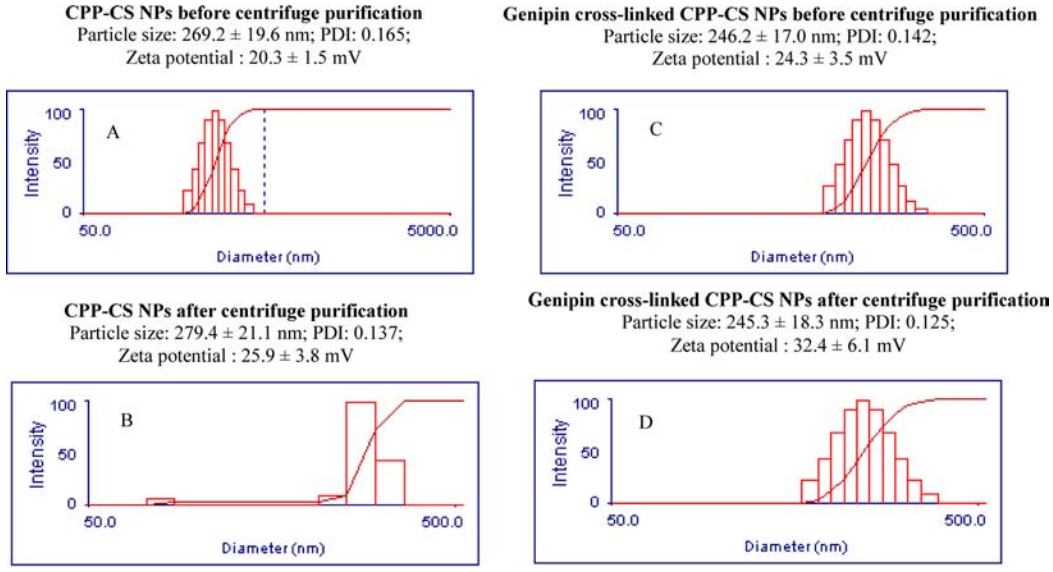


**Figure 4.** Particle size distribution of the CPP−CS NPs (A, B) and the genipin cross-linked CPP−CS NPs (C, D) before and after centrifugal purification at a centrifuge force of 2500*g* and duration of 45 min (genipin concentration = 0.125 mg/mL).

absorption bands of the CPP−CS NPs appeared at 1625, 1518, and 1150−1040 $cm^{-1}$, which corresponded to amide I and amide II groups and glycosidic linkage (C—O—C), respectively.[28] The amide I bands originated from C═O stretching vibrations coupled to N—H bending vibration. The amide II bands arise from the N—H bending vibrations coupled to C—N stretching vibrations. After cross-linking with genipin, the characteristic absorption band of amide I at 1625.15 $cm^{-1}$ shifted to 1636.80 $cm^{-1}$ with the increase of genipin concentration from 0.063 to 0.250 mg/mL, indicating the formation of secondary amides as a result of the reaction between the ester groups on genipin and the amino groups on CS.[29] A similar phenomenon also appeared in Figure 5B; the absorption band of amide I at 1624.72 $cm^{-1}$ shifted to 1634.92 $cm^{-1}$ with the increase of reaction time from 3 to 24 h. Furthermore, in both panels A and B of Figure 5, two new very weak absorptions at 1719 and 1700 $cm^{-1}$ appeared after cross-linking with genipin, and the intensity of these two absorptions increased with the elevation of the genipin concentration and prolonged reaction time.

The appearance and increased absorption of the peak at 1719 $cm^{-1}$ corresponded to the formation of aldehydo that was the reaction product between the carboxymethyl group of genipin and the amino groups on the surface of CPP−CS NPs[30] (insets of Figure 5). The absorption at lower wavenumber (1700 $cm^{-1}$) represented the aldehydo that formed intermolecular hydrogen bonding with other groups. After cross-linking with genipin, there were still many amino groups available on the surface of the CPP−CS NPs, which could be used as reaction sites for further surface modification.

**Stability of Nanoparticles under Simulated GI pH Conditions.** To study the stability of nanoparticles under simulated GI pH conditions, equal amounts of the purified CPP−CS nanoparticle and genipin-cross-linked CPP−CS nanoparticle precipitates were redispersed in pH 1.2 (0.1 N HCl), pH 6.2, and pH 7.4 buffers (PBS), respectively, for 2 h. Then, the samples in different pH conditions were submitted to characterization of particle size and morphology using DLS and TEM. The particle size and PDI of the CPP−CS NPs and the genipin-cross-linked CPP−CS NPs in different pH conditions are summarized in Table 1. It can be seen that, under pH 6.2, the CPP−CS NPs and the genipin-cross-linked CPP−CS NPs (reaction for 3 or 24 h) had similar particle sizes with PDI ranging from 0.095 to 0.189. After dispersion in 0.1 N HCl for 2 h, stimulating the pH environment in the stomach, the average count rate (ACR) of the CPP−CS nanoparticle suspension under laser decreased sharply from 342.8 kcps (pH 6.2) to 3.6 kcps (pH 1.2), indicating the disappearance of the nanoparticles under pH 1.2. ACR is a parameter that is influenced by the number and size of the particles in a suspension. In the experimental condition used in the present study, the detected particle size values were legal and reasonable only when the ACR value was in the range of 100−500 kcps. Therefore, under an ACR of 3.6 kcps, the detected particle size was illegal, which was recorded as "nd" in Table 1. Dispersed in pH 7.4 PBS buffer for 2 h, the particle size of the CPP−CS NPs was 310.6 ± 24.9 nm, which was larger than that under pH 6.2. Comparatively, after cross-linking with genipin (reaction for both 3 and 24 h), the CPP−CS NPs became very stable with just slight changes in particles size and PDI values under different simulating GI fluid pH values (pH 1.2, 6.2, and 7.4). The morphology and structure of the samples under different pH conditions were further investigated by TEM.

Figure 6 shows the structure and morphology of the CPP−CS NPs and the corresponding genipin cross-linked CPP−CS NPs (reaction for 3 h) after they were dispersed in pH 1.2, 6.2, and 7.4 buffers for 2 h, respectivley. Both the CPP−CS NPs (Figure 6B) and the genipin-cross-linked nanoparticles (Figure 6B′) were regular spheres and dispersed well under pH 6.2. Under pH 1.2 (Figure 6A), it can be seen that the CPP−CS NPs were dissoved with cloudy morphology and the release of the inner composition peptides (black dots marked with arrows), which was consistent with the DLS result of the sharp decrease of ACR value. This phenomenon was caused by the strong repusion among the highly protonated amino groups in CS under strong acidic condition, leading to the burst of the CPP−CS NPs. On the other hand, under pH 7.4, the CS capping on the surface of the nanoparticles seemed to precipitate in the insoluble state, which could be seen clearly

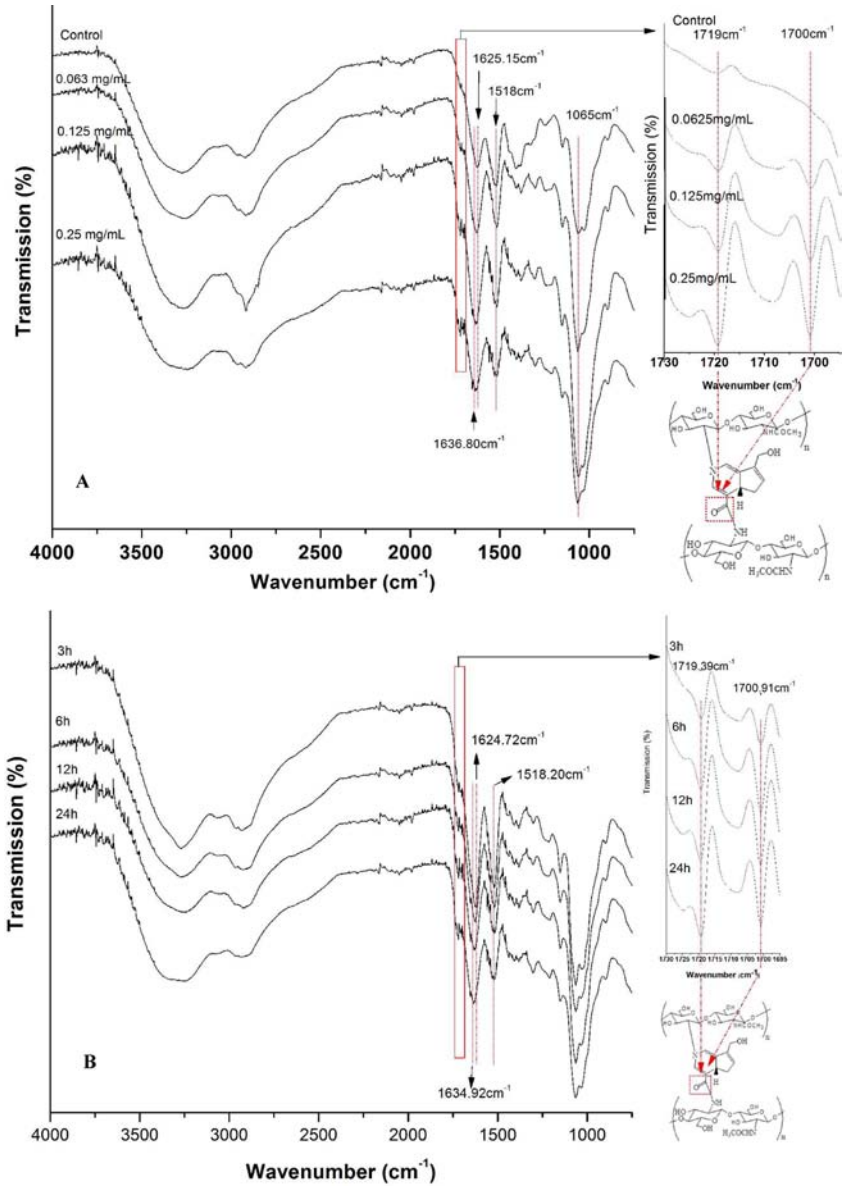


**Figure 5.** FT-IR spectra of the purified genipin cross-linked nanoparticles with different genipin concentrations (A) and reaction times (B).

**Table 1. Effects of pH on Particle Size and Polydispersity Index (PDI) Values of the CPP−CS NPs and the Genipin-Cross-Linked CPP−CS NPs[a]**

| | CPP−CS NPs | | G-CPP−CS NPs for 3 h[b] | | G-CPP−CS NPs for 24 h[c] | |
|---|---|---|---|---|---|---|
| pH value | particle size (nm) | PDI | particle size (nm) | PDI | particle size (nm) | PDI |
| 1.2 | nd | nd | 289.4 ± 18.2 | 0.099 | 276.1 ± 8.5 | 0.141 |
| 6.2 | 269.4 ± 15.2 | 0.095 | 266.4 ± 13.3 | 0.189 | 268.1 ± 18.9 | 0.143 |
| 7.4 | 310.6 ± 24.9 | 0.174 | 269.4 ± 16.6 | 0.143 | 266.9 ± 16.9 | 0.129 |

[a]Genipin concentration was 0.125 mg/mL. Values are expressed as the mean ± standard deviation ($n$ = 3). [b]The parental CPP−CS nanoparticle suspension was incubated with genipin for 3 h. Then, the cross-linked NPs were purified by the centrifugal purification method. [c]The parental CPP−CS nanoparticle suspension was incubated with genipin for 24 h. Then, the cross-linked NPs were purified by the centrifugal purification method.

in the inset image of Figure 6C. A similar result was also reported by Tang et al.[31] As the p$K_a$ value of the amine groups on CS is approximately pH 6.5, CS precipitates at neutral pH due to deprotonation of amine groups. This property of CS suggests that the CS NPs can be effective as a mucoadhesive agent and an absorption enhancer only in a limited area of the intestinal lumen where the pH values are below or close to its p$K_a$. In contrast, after cross-linking with genipin, no significant changes on structure and morphology of the CPP−CS NPs could be observed after they were dispersed in pH 1.2, 6.2, and 7.4 buffers for 2 h, respectively (Figure 6A′,B′,C′), which was consistent with the DLS results in Table 2. This meant that cross-linking with genipin, a simple and green method, could significantly enhance the stability of the CPP−CS NPs and successfully extend their effective scope in GI fluid, which was

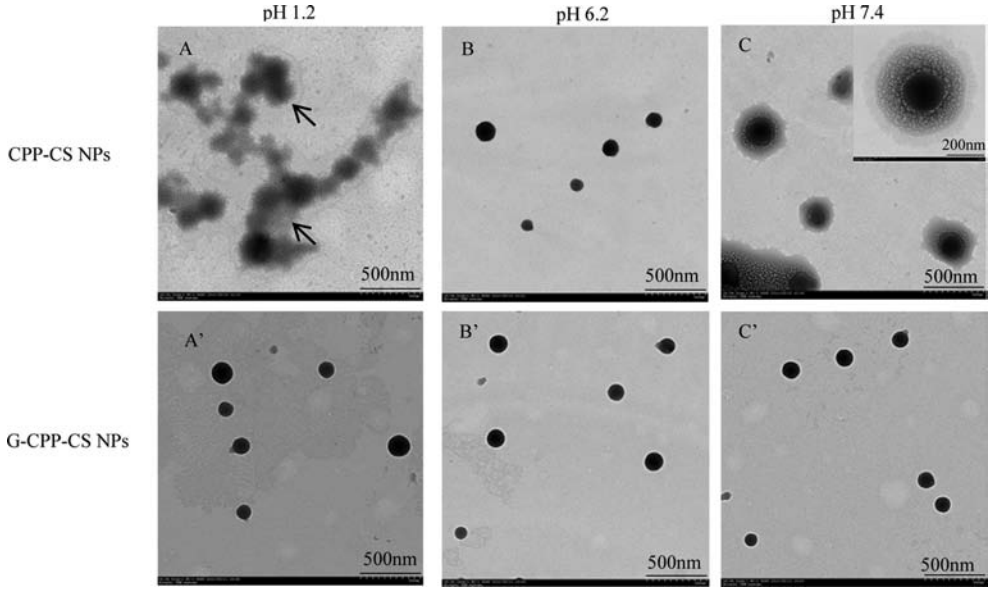


**Figure 6.** TEM images of the CPP−CS NPs (A, B, C) and genipin cross-linked CPP−CS NPs (A′, B′, C′) under different simulated GI pH environments.

**Table 2. Effects of Digestion Enzymes on Particle Size, Polydispersity index (PDI) Value, and Surface Charge (Zeta Potential) of the Genipin Cross-Linked CPP−CS NPs (G-CPP−CS NPs)[a]**

| sample | mean particle size (nm) | PDI | zeta potential (mV) |
|---|---|---|---|
| G-CPP−CS NPs | 245.3 ± 18.3 | 0.125 | 32.4 ± 6.1 |
| G-CPP−CS NPs incubated with SGF for 30 min | 262.7 ± 25.1 | 0.097 | 29.6 ± 11.5 |
| G-CPP−CS NPs incubated with SGF for 120 min | 251.8 ± 31.3 | 0.176 | 32.6 ± 7.5 |
| G-CPP−CS NPs incubated with SIF for 30 min | 523.8 ± 62.9 | 0.104 | 34.4 ± 5.6 |
| G-CPP−CS NPs incubated with SIF for 120 min | 1388.9 ± 152.1 | 0.285 | 32.1 ± 5.3 |

[a]Genipin concentration was 0.125 mg/mL. Values are expressed as mean ± standard deviation ($n$ = 3).

the prerequirement for intestinal mucosal delivery of therapeutics.

**Structure of Nanoparticles under Simulated GI Enzyme Conditions.** Despite the genipin-cross-linked CPP−CS NPs were able to maintain their stability under the GI pH environments, the presence of digestion enzymes was another big challege for them. To investigate the effects of digestion enzymes on the physicochemical properties of the polymer nanoparticles, equal amounts of the purified genipin-cross-linked CPP−CS NPs were incubated in SGF and SIF for 2 h, respectively. After incubation for 30 and 120 min, the nanoparticle samples were isolated from the SGF and SIF according to the centrifugal purification method as mentioned above. Their structure were characterized by TEM, DLS, and zeta-potential measurement. After incubation with SGF for either 30 or 120 min, no significant changes could be observed in the particle size, PDI value, and zeta potential of the genipin-cross-linked CPP−CS NPs compared with those of the original ones (Table 2).

It can be seen from Figure 7A,B that the nanoparticles remained stable and dispersed well after incubation with the SGF for either 30 and 120 min, which was consistent with the DLS results. In fact, the stability of nanocarriers in gastic fluid has attracted a lot of attention in the rational design of oral delivery nanodevices. It was found that the negatively charged nanodevices, such as poly(lactic acid) (PLA) nanoparticle and [32] $\beta$-lactoglobulin ($\beta$-lg)-stabilized emulsions,[33,34] underwent aggregation or flocculation in gastric conditions, which were mainly caused by neutralization of their surface charge. Comparatively, in the present study, the genipin-cross-linked CPP−CS NPs were stable and well dispersed in SGF, which

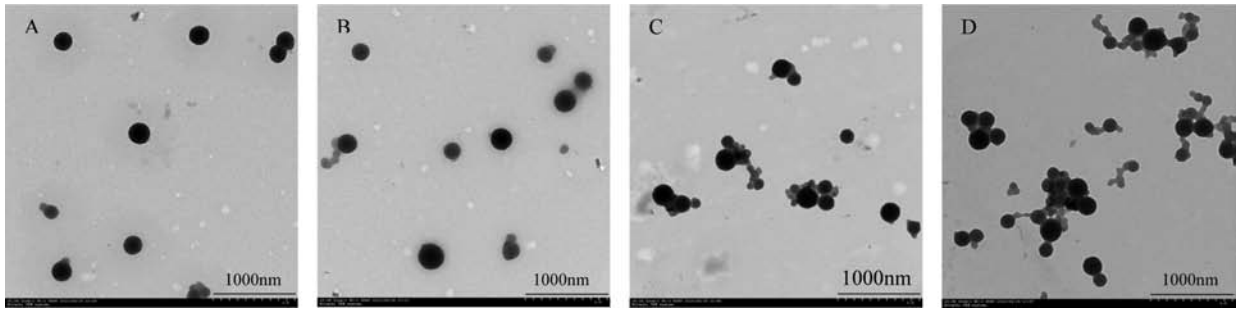


**Figure 7.** TEM images of the genipin-cross-linked CPP−CS NPs under simulated gastric fluid for 30 min (A) and 120 min (B) and under simulated intestinal fluid for 30 min (C) and 120 min (D).


dx.doi.org/10.1021/jf5046766 | J. Agric. Food Chem. 2014, 62, 12443−12452

should be mainly attributed to their highly positive surface charge. It could be concluded that pepsin in the stomach had little impact on the colloid structure and physicochemical properties of the genipin-cross-linked CPP−CS NPs.

After incubation with the SIF for 30 min, the particle size increased from 245.3 ± 18.3 to 523.8 ± 62.9 nm and further sharply to 1388.9 ± 152.1 nm when the incubation time was prolonged to 120 min (Table 2). Meanwhile, the PDI of the nanoparticle suspension increased to 0.285 (Table 2) with the incubation time of 120 min, which indicated the increased heterogeneity of the nanoparticle suspension. Observed with TEM (Figure 7C), it could be seen that aggregations of the genipin-cross-linked CPP−CS NPs appeared after the nanoparticles were incubated with SIF for 30 min. The degree of aggregation increased with prolonged incubation time. When the nanoparticles were incubated with SIF for 120 min, much bigger clusters of the nanoparticles could be seen (Figure 7D), compared with those with an incubation time of 30 min (Figure 7C). The nanoparticles inside the aggregations/clusters were still integral and compact. Therefore, it could be concluded that the increase of particle size was mainly caused by the aggregation of the nanopaticles, rather than the swelling of the nanoparticles. Similar results were also reported by Tobío et al., that PLA nanoparticles interacted with the digestive enzymes, thus leading to their agglomeration in the incubation medium.[35]

**In Vitro Release Profile of EGCG from the CPP−CS NPs and the Genipin-Cross-Linked CPP−CS NPs in Simulated GI Environments.** The encapsulation efficiencies of EGCG in the CPP−CS NPs and genipin-cross-linked CPP−CS NPs were around 71% in the present stduy, which was consistent with our previous result.[21] The in vitro release of EGCG from the CPP−CS NPs and the genipin-cross-linked CPP−CS NPs in simulated gastric and intestinal environments is shown in Figure 8. Compared with the non-cross-linked nanoparticles, cross-linking the CPP−CS NPs with genipin significantly ($p < 0.05$) reduced the burst release or leakage of EGCG from the CPP−CS NPs either in simulated gastric or in intestinal environments. It should be related to the significantly enhanced structure stability of the nanoparticles in simulated gastric and intestinal environments after cross-linking with genipin (Figure 6). Furthermore, for the genipin-cross-linked CPP−CS NPs, the release of EGCG from the nanoparticles slowed significantly ($p < 0.05$) to a much more controllable manner with the increase of the cross-linking degree. This meant that the controlled release profile of the EGCG from the nanoparticles could be modulated effectively through changing the genipin cross-linking degree. For the genipin-cross-linked nanoparticles, the release rate of EGCG in the simulated intestinal environment was higher than that in the gastric environment, which should be caused by the instability and aggregation of the nanoparticles under intestinal conditions (Figure 7). This release profile was especially desirable for oral delivery systems. In Figure 8B, the decrease of the measured release rate after 120 min was mainly caused by the instability and degradation of the EGCG under neutral and alkaline environments,[36,37] which also indicated it was necessary to encapsulate EGCG in polymer nanoparticles. Preventing the burst release of loading drugs, especially small molecular and hydrophilic drugs, from the delivery systems in the GI tract is important. The results in the present study indicated that the release profile of the payloads from the genipin-cross-linked CPP−CS NPs could be adjusted through changing the genipin cross-linking degree, which would favor the controlled release of the payloads at the sites of their action.

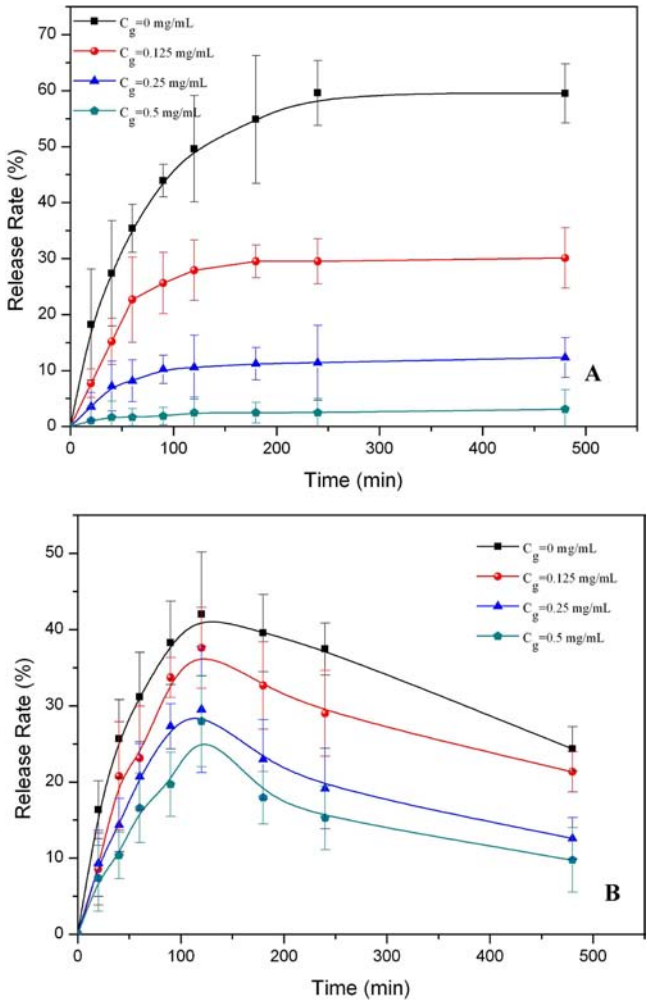


**Figure 8.** Release profile of EGCG from the CPP−CS NPs and the genipin-cross-linked CPP−CS NPs in simulated gastric (A) and intestinal (B) environments.

**Anticancer Activities of the EGCG-Loaded CPP−CS NPs Cross-Linked with Genipin.** The cytotoxicity of the EGCG-loaded CPP−CS NPs cross-linked with genipin against gastrointestinal cancer cells (human gastric BGC823 cells) and human liver HepG2 cells was investigated. In our previous studies, it had been found that the CPP−CS NPs could significantly enhance the intestinal absorption of EGCG in an in vitro cell assay, and the uptake of the nanoparticles played an important role in this process.[12] Generally, the oral drugs and delivery systems would first transport to the liver. To evaluate the anticancer potential of the EGCG-loaded CPP−CS NPs cross-linked with genipin, we conducted a trypan blue assay to determine gastric cell and live cell density. The viable cells could exclude the trypan blue dye, which could not be stained. The trypan blue assay showed that the EGCG-loaded CPP−CS NPs cross-linked with genipin exhibited cell growth inhibition similar to that of EGCG (Figure 9). The naked CPP−CS NPs cross-linked with genipin did not show cytotoxicity against the cells. In BGC823 cancer cells, the $IC_{50}$ values of the EGCG-loaded CPP−CS NPs cross-linked with genipin and free EGCG were 0.107 and 0.123 mmol/L (calculated in terms of EGCG concentration), respectively, which in HepG2 cells were 0.208

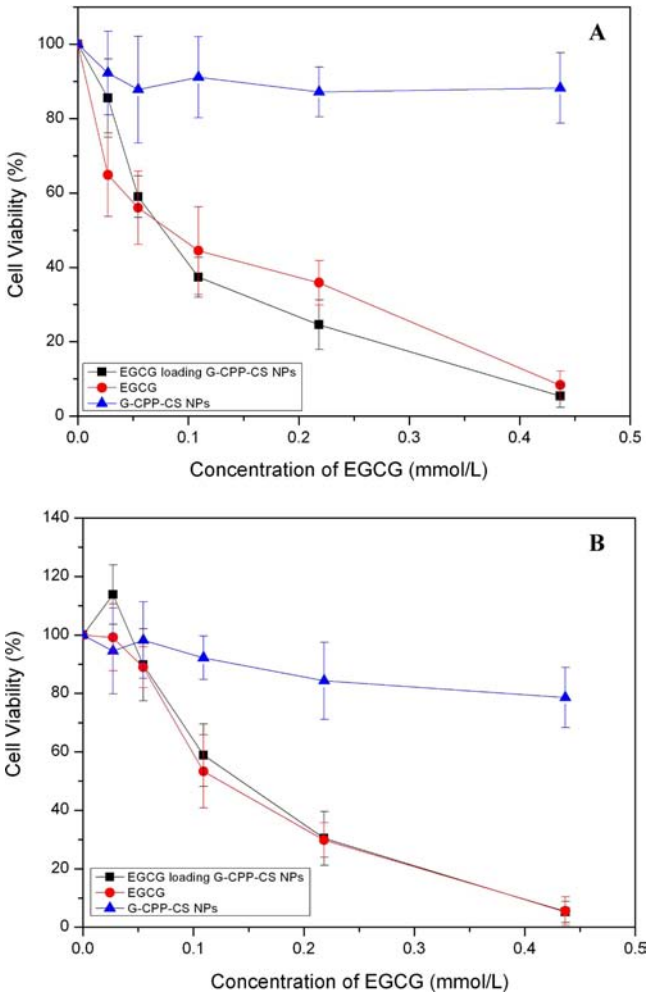


**Figure 9.** Cell viability of the human gastric BGC24 (A) and liver HepG2 (B) cancer cells incubated with the CPP−CS NPs cross-linked with genipin (G-CPP−CS NPs), EGCG, and EGCG-loaded CPP−CS NPs cross-linked with genipin (EGCG loading G-CPP−CS NPs).

and 0.193 mmol/L, respectively. This meant that encapsulation of EGCG in the nanoparticles maintained its anticancer activities. Similar results in the cytotoxicity of the polyphenol-loaded nanoparticles against cancer cells were also reported in previous studies. Majumdar et al. found that nano-luteolin encapsulated in PLA−polyethylene glycol ether (PEG) nanoparticles showed anticancer activities similar to those of the free luteolin.[38] Shutava et al. reported that encapsulation of EGCG in the gelatin-based nanoparticles with a surrounding layer-by-layer shell retained its biological activity as potently as free EGCG.[39] The animal studies about the in vivo bioavailability and cancer prevention functions of the EGCG-loaded CPP−CS NPs cross-linked with genipin will be further investigated in our following studies.

In conclusion, novel biopolymer nanoparticles with significantly improved stability and adjustable release profile in simulated GI environments were successfully developed through cross-linking the CPP−CS NPs with genipin at different cross-linking degrees. Genipin cross-linking represented an efficient, simple, and green method to enhance the stability of the amine-group-containing biopolymer nanoparticles and to adjust their release profile under harsh GI environments, which favors the controlled release of the payloads at the sites of their action. The structure behaviors of the biopolymer nanoparticles under simulated GI conditions were thoroughly characterized, providing basic information for the rational design of oral delivery nanoparticles. In addition, the established centrifugal purification method will provide technical reference for further purification of other polymer nanoparticles. The EGCG-loaded CPP−CS NPs cross-linked with genipin demonstrated significant anticancer activities, similar to that of free EGCG. Therefore, the novel polymer nanoparticles showed promise as an efficient oral delivery vehicle of polyphenols.

## ■ ASSOCIATED CONTENT

### Supporting Information

Methods for characterization of nanoparticles and determination of encapsulation efficiency and in vitro release profile of EGCG.; summary of the centrifuge parameters used to prepare chitosan-based nanoparticles in previous studies. This material is available free of charge via the Internet at http://pubs.acs.org.

## ■ AUTHOR INFORMATION

### Corresponding Authors

*(B.H.) E-mail: hubing212002@njau.edu.cn. Phone: (+86)-13915983201.

*(X.Z.) E-mail: zengxx@njau.edu.cn. Phone: (+86)-25-84396791. Fax: (+86)-25-84396791.

### Funding

This work was supported by The Natural Science Foundation of Jiangsu Province, China (BK2012367), Project Funded by the Priority Academic Program Development of Jiangsu Higher Education Institutions, Specialized Research Fund for the Doctoral Program of Higher Education of China (20120097120001), and an Undergraduate Student Research Trainning (SRT) program from Nanjing Agricultural University (1318A05).

### Notes

The authors declare no competing financial interest.

## ■ REFERENCES

(1) Ting, Y. W.; Jiang, Y. K.; Ho, C.-T.; Huang, Q. R. Common delivery systems for enhancing in vivo bioavailability and biological efficacy of nutraceuticals. *J. Funct. Foods* **2014**, *7*, 112−128.

(2) Yi, J.; Lam, T. I.; Yokoyama, W.; Cheng, L. W.; Zhong, F. Controlled release of $\beta$-carotene in $\beta$-lactoglobulin-dextran-conjugated nanoparticles' in vitro digestion and transport with Caco-2 monolayers. *J. Agric. Food Chem.* **2014**, *62*, 8900−8907.

(3) Acosta, E. Bioavailability of nanoparticles in nutrient and nutraceutical delivery. *Curr. Opin. Colloid Interface Sci.* **2009**, *14*, 3−15.

(4) Gamboa, J. M.; Leong, K. W. *In vitro* and *in vivo* models for the study of oral delivery of nanoparticles. *Adv. Drug Delivery Rev.* **2013**, *65*, 800−810.

(5) Ensign, L. M.; Cone, R.; Hanes, J. Oral drug delivery with polymeric nanoparticles: the gastrointestinal mucus barriers. *Adv. Drug Delivery Rev.* **2012**, *64*, 557−570.

(6) Evans, D. F.; Pye, G.; Bramley, R.; Clark, A. G.; Dyson, T. J.; Hardcastle, J. D. Measurement of gastrointestinal pH profiles in normal ambulant human subjects. *Gut* **1988**, *29*, 1035−1041.

(7) O'Neill, M. J.; Bourre, L.; Melgar, S.; O'Driscoll, C. M. Intestinal delivery of non-viral gene therapeutics: physiological barriers and preclinical models. *Drug Discovery Today* **2011**, *16*, 203−218.

(8) Chiu, Y. L.; Ho, Y. C.; Chen, Y. M.; Peng, S. F.; Ke, C. J.; Chen, K. J.; Mi, F. L.; Sung, H. W. The characteristics, cellular uptake and intracellular trafficking of nanoparticles made of hydrophobically-modified chitosan. *J. Controlled Release* **2010**, *146*, 152−159.

(9) Nam, H. Y.; Kwon, S. M.; Chung, H.; Lee, S. Y.; Kwon, S. H.; Jeon, H.; Kim, Y.; Park, J. H.; Kim, J.; Her, S.; Oh, Y. K.; Kwon, I. C.;

Kim, K.; Jeong, S. Y. Cellular uptake mechanism and intracellular fate of hydrophobically modified glycol chitosan nanoparticles. *J. Controlled Release* **2009**, *135*, 259−267.
(10) Chen, M.-C.; Mi, F.-L.; Liao, Z.-X.; Hsiao, C.-W.; Sonaje, K.; Chung, M.-F.; Hsu, L.-W.; Sung, H.-W. Recent advances in chitosan-based nanoparticles for oral delivery of macromolecules. *Adv. Drug Delivery Rev.* **2013**, *65*, 865−879.
(11) Hu, B.; Ting, Y. W.; Yang, X. Q.; Tang, W. P.; Zeng, X.; Huang, Q. R. Nanochemoprevention by encapsulation of (−)-epigallocatechin-3-gallate with bioactive peptides/chitosan nanoparticles for enhancement of its bioavailability. *Chem. Commun.* **2012**, *48*, 2421−2423.
(12) Tian, J. S.; Shi, B. Y.; Xiang, H.; Gao, S.; Qin, X. M.; Du, G. H. $^1$H-NMR-based metabonomic studies on the anti-depressant effect of genipin in the chronic unpredictable mild stress rat model. *PLoS One* **2013**, *8*, No. e75721.
(13) Koo, H. J.; Lim, K. H.; Jung, H. J.; Park, E. H. Anti-inflammatory evaluation of gardenia extract, geniposide and genipin. *J. Ethnopharmacol.* **2006**, *103*, 496−500.
(14) He, Q.; Kong, X.; Wu, G.; Ren, P.; Tang, H.; Hao, F. H.; Huang, R. L.; Li, T. J.; Tan, B.; Li, P.; Tang, Z. R.; Yin, Y. L.; Wu, Y. N. Metabolomic analysis of the response of growing pigs to dietary L-arginine supplementation. *Amino Acids* **2009**, *37*, 199−208.
(15) Kim, B. C.; Kim, H. G.; Lee, S. A.; Lim, S.; Park, E. H.; Kim, S. J.; Lim, C. Genipin-induced apoptosis in hepatoma cells is mediated by reactive oxygen species/c-Jun $NH_2$-terminal kinase-dependent activation of mitochondrial pathway. *J. Biochem. Pharmacol.* **2005**, *70*, 1398−1047.
(16) Muzzarelli, R. A. A. Genipin-crosslinked chitosan hydrogels as biomedical and pharmaceutical aids. *Carbohydr. Polym.* **2009**, *77*, 1−9.
(17) Macaya, D.; Ng, K. K.; Spector, M. Injectable collagen−genipin gel for the treatment of spinal cord injury: in vitro studies. *Adv. Funct. Mater.* **2011**, *21*, 4788−4797.
(18) Chen, M. C.; Liu, C. T.; Tsai, H. W.; Lai, W. Y.; Chang, Y.; Sung, H. W. Mechanical properties, drug eluting characteristics and *in vivo* performance of a genipin-crosslinked chitosan polymeric stent. *Biomaterials* **2009**, *30*, 5560−5571.
(19) Chen, S. C.; Wu, Y. C.; Mi, F. L.; Lin, Y. H.; Yu, L. C.; Sung, H. W. A novel pH-sensitive hydrogel composed of *N*,*O*-carboxymethyl chitosan and alginate cross-linked by genipin for protein drug delivery. *J. Controlled Release* **2004**, *96*, 285−300.
(20) Hillberg, A. L.; Holmes, C. A.; Tabrizian, M. Effect of genipin crosslinking on the cellular adhesion properties of layer-by-layer assembled polyelectrolyte films. *Biomaterials* **2009**, *30*, 4463−4470.
(21) Hu, B.; Ting, Y. W.; Zeng, X.; Huang, Q. R. Bioactive peptides/chitosan nanoparticles enhance cellular antioxidant activity of (−)-epigallocatechin-3-gallate. *J. Agric. Food Chem.* **2013**, *61*, 875−881.
(22) Hu, B.; Wang, S. S.; Li, J.; Zeng, X. X.; Huang, Q. R. Assembly of bioactive peptide−chitosan nanocomplexes. *J. Phys. Chem. B* **2011**, *115*, 7515−7523.
(23) Grabowski, N.; Hillaireau, H.; Vergnaud, J.; Santiago, L. A.; Kerdine-Romer, S.; Pallardy, M.; Tsapis, N.; Fattal, E. Toxicity of surface-modified PLGA nanoparticles toward lung alveolar epithelial cells. *Int. J. Pharm.* **2013**, *454*, 686−694.
(24) Butler, M. F.; Ng, Y. F.; Pudney, P. D. A. Mechanism and kinetics of the crosslinking reaction between biopolymers containing primary amine groups and genipin. *J. Polym. Sci., Polym. Chem.* **2003**, *41*, 3941−3953.
(25) Mizrahy, S.; Peer, D. Polysaccharides as building blocks for nanotherapeutics. *Chem. Soc. Rev.* **2012**, *41*, 2623−2640.
(26) Akbulut, O.; Mace, C. R.; Martinez, R. V.; Kumar, A. A.; Nie, Z. H.; Patton, M. R.; Whitesides, G. M. Separation of nanoparticles in aqueous multiphase systems through centrifugation. *Nano Lett.* **2012**, 4060−4064.
(27) Balasubramanian, S. K.; Yang, L. M.; Yung, L. Y. L.; Ong, C. N.; Ong, W. Y.; Yu, L. E. Characterization, purification, and stability of gold nanoparticles. *Biomaterials* **2010**, *31*, 9023−9030.
(28) Pawlak, A.; Mucha, A. Thermogravimetric and FTIR studies of chitosan blends. *Thermochim. Acta* **2003**, *396* (1−2), 153−166.
(29) Chen, H. M.; Wei, O. Y.; Bisi, L. Y.; Martoni, C.; Prakash, S. Reaction of chitosan with genipin and its fluorogenic attributes for potential microcapsule membrane characterization. *J. Biomed. Mater. Res., Part A* **2005**, *75A*, 917−927.
(30) Mi, F. L.; Shyu, S. S.; Peng, C. K. Characterization of ring-opening polymerization of genipin and pH-dependent Crosslinking reactions between chitosan and genipin. *J. Polym. Sci., Polym. Chem.* **2005**, *43*, 1985−2000.
(31) Tang, D. W.; Yu, S. H.; Ho, Y. C.; Mi, F. L.; Kuo, P. L.; Sung, H. W. Heparinized chitosan/poly($\gamma$-glutamic acid) nanoparticles for multi-functional delivery of fibroblast growth factor and heparin. *Biomaterials* **2010**, *31*, 9320−9332.
(32) Lazzari, S.; Moscatelli, D.; Codari, F.; Salmona, M.; Morbidelli, M.; Diomede, L. Colloidal stability of polymeric nanoparticles in biological fluids. *J. Nanopart. Res.* **2012**, *14*, 920.
(33) Sarkar, A.; Goh, K. K. T.; Singh, R. P.; Singh, H. Behaviour of an oil-in-water emulsion stabilized by $\beta$-lactoglobulin in an *in vitro* gastric model. *Food Hydrocolloids* **2009**, *23*, 1563−1569.
(34) Golding, M.; Wooster, T. J. The influence of emulsion structure and stability on lipid digestion. *Curr. Opin. Colloid Interface Sci.* **2010**, *15*, 90−101.
(35) Tobio, M.; Sanchez, A.; Vila, A.; Soriano, I.; Evora, C.; Vila-Jato, J. L.; Alonso, M. The role of PEG on the stability in digestive fluids and in vivo fate of PEG-PLA nanoparticles following oral administration. *J. Colloids Surf. B* **2000**, *18*, 315−323.
(36) Hong, J.; Lu, H.; Meng, X. F.; Ryu, J. H.; Hara, Y.; Yang, C. S. Stability, cellular uptake, biotransformation, and efflux of tea polyphenol (−)-epigallocatechin-3-gallate in HT-29 human colon adenocarcinoma cells. *Cancer Res.* **2002**, *62*, 7241−7246.
(37) Yoshino, K.; Suzuki, M.; Sasaki, K.; Miyase, T.; Sano, M. Formation of antioxidants from (−)-epigallocatechin gallate in mild alkaline fluids, such as authentic intestinal juice and mouse plasma. *J. Nutr. Biochem.* **1999**, *10*, 223−229.
(38) Majumdar, D.; Jung, K.-H.; Zhang, H. Z.; Nannapaneni, S.; Wang, X.; Amin, A. R. M. R.; Chen, Z. J.; Chen, Z. G.; Shin, D. M. Luteolin nanoparticle in chemoprevention: in vitro and in vivo anticancer activity. *Cancer Prev. Res.* **2014**, *7*, 65−73.
(39) Lvov, Y. M.; Shutava, T. G.; Balkundi, S. S.; Vangala, P.; Steffan, J. J.; Bigelow, R. L.; Cardelli, J. A.; O'Neal, D. P.; Lvov, Y. M. Layer-by-layer-coated gelatin nanoparticles as a vehicle for delivery of natural polyphenols. *ACS Nano* **2009**, *3*, 1877−1885.

Table 1. Experiment Design and Chemical and Fatty Acid Composition of the Diet Groups (Based on Original Matter)[23]

| | $LSM_{SEM}$ ($n$ = 8)[a] | | | | |
|---|---|---|---|---|---|
| | HPD-SO | HPD-LO | RPD-SO | RPD-LO | CON |
| start wt (kg) | $68.84_{1.60}$ | $69.69_{1.60}$ | $69.36_{1.60}$ | $69.01_{1.60}$ | $69.24_{1.60}$ |
| live wt at slaughter (kg) | $120.56_{0.75}$ a[b] | $121.38_{0.75}$ a | $123.19_{0.75}$ a | $120.62_{0.75}$ a | $117.80_{0.75}$ b |
| | | Chemical Composition[c] | | | |
| dry matter | 90.0 | 88.7 | 89.8 | 89.6 | 89.3 |
| crude protein | 19.6 | 19.4 | 15.7 | 15.0 | 17.4 |
| crude fat | 5.2 | 5.7 | 5.9 | 6.3 | 3.4 |
| crude fiber | 4.7 | 4.6 | 5.3 | 5.5 | 4.2 |
| crude ash | 4.9 | 4.9 | 4.8 | 5.0 | 4.8 |
| starch | 36.9 | 36.2 | 40.0 | 40.7 | 40.1 |
| ME (MJ/kg) | 13.7 | 13.7 | 13.5 | 13.5 | 13.2 |
| | | Amino Acids[c] | | | |
| lysine | 0.93 | 0.95 | 0.82 | 0.82 | 0.96 |
| methionine | 0.26 | 0.27 | 0.22 | 0.22 | 0.24 |
| cysteine | 0.31 | 0.31 | 0.26 | 0.27 | 0.30 |
| threonine | 0.60 | 0.61 | 0.48 | 0.45 | 0.56 |
| | | Fatty Acids (%)[d] | | | |
| 16:0 | 10.30 | 10.03 | 9.89 | 9.52 | 12.44 |
| 18:0 | 3.38 | 3.84 | 3.43 | 3.75 | 1.84 |
| 18:1*cis*-9 | 22.81 | 17.29 | 22.96 | 18.01 | 32.46 |
| 18:2*n*-6 | 52.94 | 29.43 | 51.69 | 31.77 | 39.07 |
| 18:3*n*-3 | 6.66 | 36.11 | 8.10 | 33.80 | 6.74 |

[a]LSM: Least-squares mean. SEM: Standard error of the LSM. HPD-SO: High protein diet with sunflower oil. HPD-LO: High protein diet with linseed oil. RPD-SO: Reduced protein diet with sunflower oil. RPD-LO: Reduced protein diet with linseed oil. CON: Control. [b]a, b: significant effect of diet. [c]Percent based on original matter. [d]Proportion of total fatty acids.

acid biosynthesis and fat partitioning. Recently, our research group described the effect of RPD in combination with *n*-3/*n*-6 PUFA-containing plant oils, linseed oil (lipids high in *n*-3 PUFA), and sunflower seed oil (lipids high in *n*-6 PUFA) on carcass traits, meat quality, and fatty acid profile in porcine muscle of Landrace pigs.[23] We hypothesize that RPD in combination with *n*-3/*n*-6 PUFA-containing plant oil supplementation led to an increase of IMF contents including higher accumulation of precursor and de novo synthesized long-chain PUFA in muscle associated with minor effect on back fat tissue of pigs. The focus of the present study was to investigate protein expression levels of transcription factors and lipogenic enzymes related to the contents of fatty acid products in muscle, back fat, and liver of pigs fed RPD/high protein diet (HPD) supplemented with plant oils (linseed oil/sunflower seed oil).

## MATERIALS AND METHODS

**Experiment.** In total 40 male Landrace pigs (castrates) were used in the diet experiment. The animals were individually housed and allocated into five feeding groups (each $n$ = 8) at a live weight of approximately 60 kg (Table 1). The pigs were fed ad libitum from 60 to 100 kg live weight and restricted to 2.8 kg/day until 120 kg. The animals in the experimental groups (1−4, Table 1) were fed with two different levels of protein and two different types of vegetable oil. The animals in the control group were fed with a normal pig diet without plant oil supplementation. The chemical and fatty acid composition of the diet of the five groups (HPD-SO, HPD-LO, RPD-SO, RPD-LO, and CON) are presented in Table 1 (Hohburg Mineralfutter, Lossatal, Germany). The diet experiment was previously described in detail.[23] Briefly, the HPD was formulated to contain 19.6% crude protein, and the RPD was formulated to contain 15.5% crude protein. Sunflower oil was used in the diet groups HPD-SO and RPD-SO and linseed oil in diet groups HPD-LO and RPD-LO as fat sources. The diets contained the same level of metabolizable energy (ME) of approximately 13.6 MJ/kg. The feed intake acquisition data was performed for each single animal. The pigs were weighed during the diet experiment once a week. The pig experiment was carried out at the facilities of University of Rostock (Germany), Faculty of Agricultural and Environmental Sciences. All experiments were conducted simultaneously to avoid seasonal effects between the different feeding groups. All animals were slaughtered at an average live weight of 120 kg in the abattoir of the Leibniz Institute for Farm Animal Biology in Dummerstorf (Germany). The slaughter and dressing procedures were in accordance with EU specifications. Immediately after slaughtering, tissue samples were collected from the right side of the carcass. *Longissimus* muscles and back fat, directly located over the muscle, were taken from the 13th/14th rib, snap-frozen, and stored at −80 °C until analysis. The liver samples were taken from the top of the Spigelian lobe, snap-frozen, and stored at −80 °C until analysis.

**Protein Expression Analysis via Western Blotting.** Proteins were extracted by homogenizing muscle, liver, and back fat samples in ice-cold lysis buffer (1 g/L Triton X-100, 50 mmol/L HEPES/Tris, 4 mmol/L EGTA, 10 mmol/L EDTA, 100 mmol/L $\beta$-glycerophosphate, 15 mmol/L tetrasodium pyrophosphate, 5 mmol/L sodium orthovanadate, 2.5 mmol/L sodium fluoride with protease and phosphatase inhibitors, pH 7.4) using TissueRuptor (Quiagen, Hilden, Germany). After centrifugation (1000*g*, 10 min, 4 °C), clear protein supernatant aliquots (10 $\mu$g) were collected, analyzed for protein concentration (Bio-Rad protein assay cat. no. 500-0006, Munich, Germany) by using microtiter plates and a plate reader (SynergyMx, Biotek, Germany), and stored at −20 °C until further analysis. Post a denaturing protein sample pretreatment [thawing of protein samples, adding blue loading buffer (Cell Signaling Technology, Boston, USA), at 94 °C 4 min], proteins (10 $\mu$g/lane) were separated by using self-prepared SDS−PAGE Maxi Gels (Maxi gel casting module; Roth, Karlsruhe, Germany) (7.5% Tris-HCl, 1.0 mm, 43 well) in a Maxi Buffer tank with gel running buffer (cat. no. 3060.1; Roth, Karlsruhe, Germany) with electrophoresis constant power supply (Consort, Turnhout, Belgium). Subsequently, proteins were transferred (90 min, 1.0 mA/cm$^2$) to a PVDF membrane (Roth, Karlsruhe, Germany) with a semidry blotting unit (Hoefer, San Francisco, CA, USA). Nonspecific binding sites were blocked with skim milk powder in TBST (w/v = 5%). For the recognition of pSREBP-1c (125 kDa) the PVDF

membrane was incubated with specific primary antibody (sc-367, Santa Cruz Biotechnology, Santa Cruz, CA, USA), and for mSREBP-1c (68 kDa) the specific primary antibody (sc-366, Santa Cruz Biotechnology, Santa Cruz, CA, USA) was used, overnight at 6 °C. After washing, the PVDF membrane was probed with the secondary antibody goat anti-rabbit IgG-HRP (Santa Cruz Biotechnology, Santa Cruz, CA, USA) during 90 min incubation at room temperature, followed by washing three times with TBST and water. For visualization, membranes were developed with SuperSignal West FEMTO chemiluminescent agent (ThermoScientific, Schwerte, Germany). Membranes were scanned with a Chemiluminescence Imager (Intas Science Imaging Instruments, Goettingen, Germany) and band intensities were densitometrically evaluated using LabImage 1D L340 Electrophoresis Software (Kapelan Bio-Imaging, Leipzig, Germany). For recognition of ACC, the primary antibody (ab72046, abcam, Cambridge, U.K.) for FAS (SC-20140, Santa Cruz Biotechnology, Santa Cruz, CA, USA) and for SCD-1 (PAB9094, Abnova, Taipei, Taiwan) was used. For each protein, the same procedure with the same secondary antibody (Rabbit TrueBlot anti-Rabbit IgG HRP, 18-8816, eBioscience, San Diego, CA, USA) was performed as for the SREBP-1c. Western blot analyses were performed in triplicate, applying all 40 individual protein samples per tissue of all five diet groups per gel. To exclude chemiluminescent protein signal intensity differences between the three repeated blots as factors influencing protein expression data, individual protein expression values were normalized to tubulin intensity for all investigated protein expression values per blot. Statistical evaluation was performed as described in the statistical analysis section.

**Lipid Extraction and Fatty Acid Analysis.** Samples of muscle (approximately 2.0 g), liver (approximately 2.0 g), and back fat (approximately 0.5 g) were thawed at 4 °C. The detailed sample preparation procedure has been previously described by Nuernberg et al.[3] Briefly, after homogenization (Ultra Turrax, IKA, Staufen, Germany; T25, 3 × 15 s, 12,000 rpm) and the addition of the fatty acid C19:0 as an internal standard, the total lipids were extracted in duplicate using chloroform/methanol (2:1, v/v) at room temperature. All of the solvents contained 0.005% (w/v) of *tert*-butylhydroxytoluene (BHT) to prevent the oxidation of PUFAs. The extraction mixture was stored at 5 °C for 18 h in the dark and subsequently washed with 0.02% aqueous $CaCl_2$. The organic phase was dried with $Na_2SO_4$ and $K_2CO_3$ (10:1, w/w), and the solvent was subsequently removed under nitrogen at room temperature. The lipid extracts were redissolved in 300 μL of toluene, and a 25 mg aliquot was used for methyl ester preparation. Next, 2 mL of 0.5 M sodium methoxide in methanol was added to the samples, which were shaken in a 60 °C water bath for 10 min. Subsequently, 1 mL of 14% boron trifluoride ($BF_3$) in methanol was added to the mixture, which was then shaken for an additional 10 min at 60 °C. Saturated $NaHCO_3$ (2 mL) was added, and the fatty acid methyl esters (FAMEs) were extracted three times in 2 mL of *n*-hexane. The solvent containing the FAMEs was reduced to dryness under an oxygen-free nitrogen stream, and the FAMEs were resuspended in 100 μL of *n*-hexane and stored at −18 °C until used for gas chromatography (GC) analysis. The FAMEs were evaporated under an oxygen-free nitrogen stream and dissolved in *n*-heptane for GC analysis. The fatty acid analysis of the muscle lipids was performed using capillary GC with a CP-Sil 88 CB column (100 m × 0.25 mm, Chrompack-Varian, Lake Forest, CA, United States) that was installed in a PerkinElmer gas chromatograph Autosys XL with a flame ionization detector and split injection (PerkinElmer Instruments, Shelton, CT, United States). The detailed GC conditions were recently described by Shen et al.[24] Briefly, the initial oven temperature was 150 °C, which was held for 5 min; subsequently, the temperature was increased to 175 °C and then to 200 °C at a rate of 2 °C $min^{-1}$ and held for 10 min. Finally, the temperature was increased to 225 °C at a rate of 1.5 °C $min^{-1}$ and held for 25 min. Hydrogen was used as the carrier gas at a flow rate of 1 mL $min^{-1}$. The split ratio was 1:20, and the injector and detector were set at 260 and 280 °C, respectively.

**Statistics.** The effects of the RPD in combination with vegetable oils on protein expression and fatty acid concentrations were estimated by one-way analysis of variance with fixed factor group (groups 1 to 5) using the GLM procedure of the SAS software system (SAS Systems, Release 9.2, SAS Institute Inc., Cary, NC). The least-squares means (LSMs) and the standard errors (SEM) of the LSMs are given in the tables. All post hoc tests were performed at a significance level of $p \leq 0.05$ using the Tukey−Kramer correction for multiple tests.

## RESULTS

**Protein Expression.** Protein expression of the transcription factor SREBP-1c precursor (pSREBP-1c) in muscle of the present study was not affected by diet; however the active nuclear form of SREBP-1c (mSREBP-1c) was significantly increased in muscle of HPD-SO-fed pigs compared to the pigs of the other diet groups (Figure 1). For SCD-1, the protein expression in *longissimus* muscle of pigs was not affected by different dietary protein level or linseed/sunflower seed oil supplementation. The expression of the cytosolic enzymes in pig muscle, ACC and FAS, was low, and no abundances were detected in the total muscle extract. In back fat, the expression

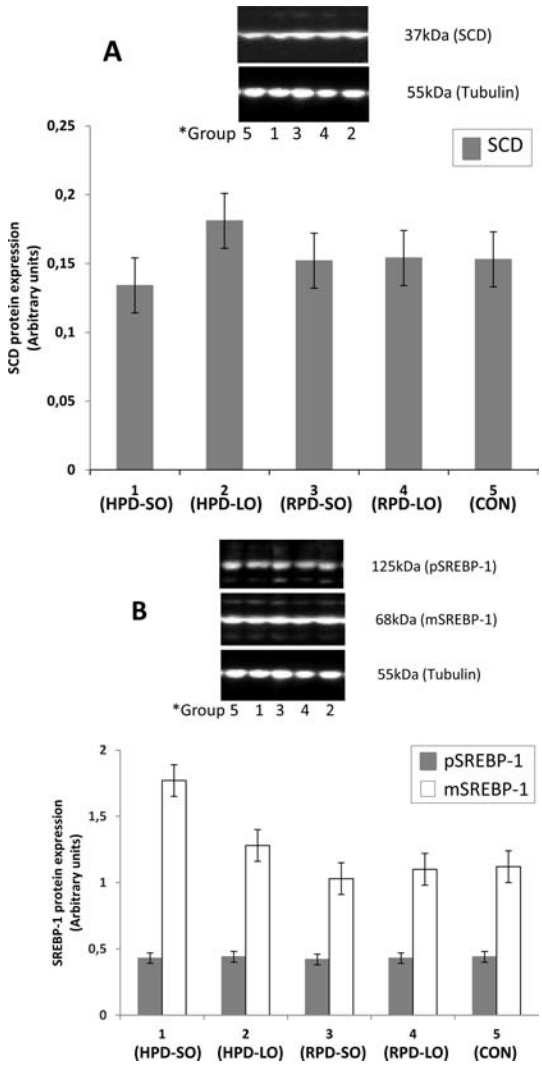


**Figure 1.** Protein expression of SCD (A) and pSREBP-1 and mSREBP-1 (B) in *longissimus* muscle of pigs fed different diets (normalized to tubulin); a, b: significant effect of diet, <0.05, *one selected sample per diet group. HPD-SO: High protein diet with sunflower oil. HPD-LO: High protein diet with linseed oil. RPD-SO: Reduced protein diet with sunflower oil. RPD-LO: Reduced protein diet with linseed oil. CON: Control.

of SREBP-1c precursor (pSREBP-1c) was not affected by different diets. RPD supplemented with linseed/sunflower seed oil significantly increased the mSREBP-1c expression in back fat compared with the control group, and showed a higher level compared with HPD groups; however the values did reach statistical significance (Figure 2). For ACC, FAS, and SCD-1, the protein expression in back fat of Landrace pigs was not affected by different dietary protein level or linseed/sunflower seed oil supplementation. In liver, the expression of transcription factors pSREBP-1c and mSREBP-1c and expression of the lipogenic enzyme SCD-1 were not affected by different dietary protein level or linseed/sunflower seed oil supplementation. Both ACC and FAS expression in liver of pigs in the control group was significantly higher compared with protein expression of RPD/HPD groups in combination with linseed oil or sunflower oil (Figure 3).

**Fatty Acid Concentrations.** The fatty acid concentrations of *longissimus* muscle, back fat, and liver in Landrace pigs fed diets with RPD/HPD supplemented with vegetables oils (sunflower seed oil/linseed oil) are shown in Tables 2, 3, and 4, respectively. In *longissimus* muscle, the sum concentration of all fatty acids (IMF) was not affected by diet and ranged between 1.29 and 1.52 g/100 g (Table 2). RPD in combination with linseed oil (RPD-LO) did not affect single and sum concentrations of MUFA and *n*-3 or *n*-6 PUFA in muscle of pigs compared with HPD in combination with linseed oil (HPD-LO). Furthermore, RPD in combination with sunflower oil (RPD-SO) did not affect single and sum fatty acids in muscle compared with HPD in combination with sunflower oil (HPD-SO). However, different plant oil supplementations resulted in significant changes in single and sum *n*-3 or *n*-6 PUFA concentrations in muscle as well as in RPD and HPD groups (Table 2). Linseed oil supplementation caused significantly higher single (18:3*n*-3, 20:5*n*-3, 22:5*n*-3) and sum *n*-3 fatty acid concentrations up to 113 mg/100 g in porcine muscle of RPD and HPD groups compared to sunflower oil supplemented RPD and HPD groups, except 22:6*n*-3. In muscle, diet did not affect the concentration of single SFA (14:0, 16:0, and 18:0). In back fat, the sum concentration of all fatty acids (fat content) was not affected by diet and ranged between 71.9 and 76.1 g/100 g (Table 3). As was shown for muscle, RPD in combination with linseed oil or sunflower seed oil (RPD-LO, RPD-SO) did not affect single and sum concentrations of SFA, MUFA, and *n*-3 or *n*-6 fatty acids in back fat of pigs compared to HPD in combination with linseed oil or sunflower seed oil (HPD-LO/HPD-SO). Different vegetable oil supplementations resulted in significant changes in single and sum MUFA, PUFA, and *n*-3 or *n*-6 fatty acid concentrations in back fat as well as in RPD and HPD groups (Table 3), expect for 22:6*n*-3. Linseed oil supplementation significantly decreased the *n*-6/*n*-3 PUFA ratio in back fat of RPD and HPD group compared to sunflower oil supplemented RPD and HPD groups from 6.4 to 7.2 to 1.3, respectively. As was shown in muscle and back fat, the sum concentrations of all fatty acids (fat content) in pig liver were not affected by diet and ranged between 3.04 and 3.30 g/100 g, and RPD in combination with linseed oil or sunflower oil (RPD-LO, RPD-SO) did not affect single and sum concentrations of SFA, MUFA, and *n*-3 or *n*-6 fatty acids in liver of pigs compared to high protein diet in combination with linseed oil (HPD-LO) (Table 4). Linseed oil supplementation caused significantly higher single (18:3*n*-3, 20:5*n*-3, 22:5*n*-3) and sum *n*-3 fatty acid concentrations up to 743 mg/100 g in porcine

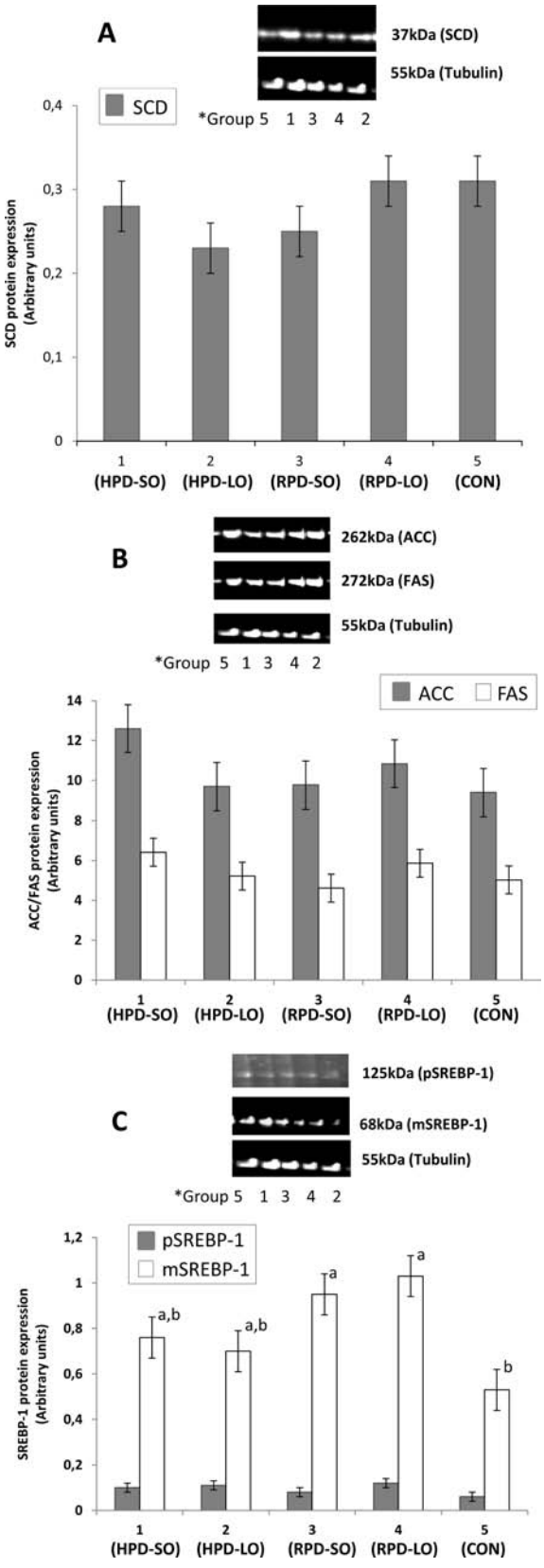


**Figure 2.** Protein expression of SCD (A), FAS and ACC (B), and pSREBP-1 and mSREBP-1 (C) in back fat of pigs fed different diets (normalized to tubulin); a, b: significant effect of diet, <0.05, *one selected sample per diet group. HPD-SO: High protein diet with sunflower oil. HPD-LO: High protein diet with linseed oil. RPD-SO: Reduced protein diet with sunflower oil. RPD-LO: Reduced protein diet with linseed oil. CON: Control.

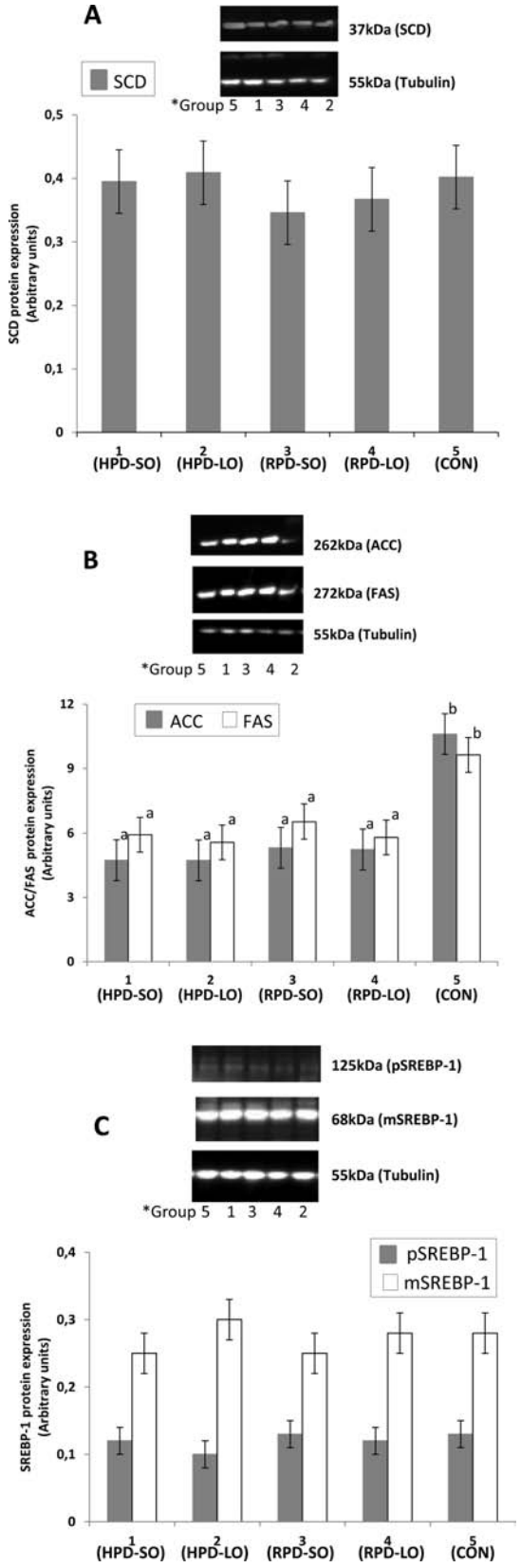


**Figure 3.** Protein expression of SCD (A), FAS and ACC (B), and pSREBP-1 and mSREBP-1 (C) in liver of pigs fed different diets (normalized to tubulin); a, b: significant effect of diet, <0.05, *one selected sample per diet group. HPD-SO: High protein diet with sunflower oil. HPD-LO: High protein diet with linseed oil. RPD-SO: Reduced protein diet with sunflower oil. RPD-LO: Reduced protein diet with linseed oil. CON: Control.

liver of RPD and HPD groups compared to sunflower oil supplemented RPD and HPD groups, except 22:6*n*-3.

## DISCUSSION

A number of studies have revealed that IMF and adipose tissue (back fat) contents in pigs might be affected independently by dietary means. Previous studies indicated that RPD intervention increased the IMF contents with much smaller/no effects on back fat content in pigs.[20,25−27] However, the mechanisms regulating de novo fatty acid synthesis and fat partitioning in different tissues in pigs are not completely understood.[17,18,20] Inadequate dietary protein and/or lysine limit protein synthesis and increase the amount of energy available for fat deposition, resulting in higher IMF. In addition, the IMF content varies in different pig breeds, fatty and lean pigs, fed RPD diet compared with control diets.[16,17,28] One explanation for higher IMF contents fed RPD in pigs might be the tissue-specific activation of expression of lipogenic enzymes which may lead to the increase of synthesis of de novo fatty acids in the muscle tissues. It is generally known that one of the key factors regulating the de novo synthesis of fatty acids and fat deposition is expression of lipogenic enzymes. The key enzyme involved in MUFA biosynthesis is stearoyl-CoA-desaturase (SCD-1).[20] SCD-1 is under control of transcription factors like SREBP-1c. It has been previously demonstrated that the increase of IMF content under RPD conditions was accompanied by increased SCD-1 expression levels in crossbred pigs.[18,20,25] In contrast to crossbreds, recent published results showed that the IMF content of Alentejana purebred (fatty) pigs did not respond to any dietary treatment.[17] Furthermore, different dietary amino acid levels (reduced lysine and/or high arginine and leucine contents) were reported to increase the IMF contents in pigs mediated via the upregulation of SCD-1 gene expression.[17,18,29] Madeira et al.[18] observed that dietary arginine supplementation did not affect the IMF content in male crossbred pigs (Duroc × Pietrain × Large White × Landrace) but increased amount of subcutaneous fat. In the same RPD study, with/without leucine supplementation elevated IMF contents were observed possibly caused by increased FAS and SCD-1 gene expression levels.[18] The hypothesis of the present study was that RPD in combination with *n*-3/*n*-6 PUFA containing plant oils (linseed oil/sunflower seed oil) could lead to an increase of IMF contents accompanied by a higher accumulation of de novo synthesized long-chain *n*-3/*n*-6 PUFA in pig muscle. This hypothesis rested on recent findings, which suggest that RPD results in elevated IMF deposition in pigs based on activated expression of lipogenic enzymes.[16,17,25] However, the results of the present study did not confirm the starting hypothesis and showed that the IMF contents in the lean Landrace pigs fed RPD/HPD (approximately 15.3% vs 19.5% of CP) combined with *n*-3/*n*-6 PUFA-containing plant oil supplementation were not affected by diet. Indeed, the muscle fatty acid concentrations of the present study appeared to be significantly affected by the diet, resulting in significantly higher single and sum *n*-3 PUFA concentrations (sum *n*-3 PUFA up to 113 mg/100 g muscle) in linseed oil-containing RPD/HPD groups compared to sunflower seed oil diet fed groups. However, this effect seems to be only caused by the use of different plant oil (linseed oil vs sunflower seed oil) and was not depending on RPD vs HPD intervention. As a result, the single and sum *n*-3/*n*-6 PUFA concentrations in muscle of RPD-LO/RPD-SO fed pigs showed no significant differences compared with the

**Table 2. Fatty Acid Concentrations (mg/100 g *longissimus* Muscle) of Landrace Pigs Fed Different Diets**

| | LSM$_{SEM}$ ($n$ = 8)[a] | | | | | |
|---|---|---|---|---|---|---|
| | HPD-SO | HPD-LO | RPD-SO | RPD-LO | CON | signif |
| sum FA (IMF) | $1404.1_{150.4}$ | $1518.1_{150.4}$ | $1487.1_{150.4}$ | $1411.3_{150.4}$ | $1293.5_{150.4}$ | 0.852 |
| 14:0 | $16.8_{2.76}$ | $20.5_{2.76}$ | $19.2_{2.76}$ | $16.9_{2.76}$ | $15.1_{2.76}$ | 0.667 |
| 16:0 | $331.8_{40.15}$ | $368.2_{40.15}$ | $354.2_{40.15}$ | $321.0_{40.15}$ | $302.9_{40.15}$ | 0.792 |
| 16:1*cis*-9 | $38.7_{6.45}$ | $44.2_{6.45}$ | $41.4_{6.45}$ | $37.9_{6.43}$ | $37.6_{6.42}$ | 0.941 |
| 18:0 | $162.9_{19.13}$ | $183.5_{19.13}$ | $183.3_{19.13}$ | $164.3_{19.13}$ | $154.5_{19.13}$ | 0.761 |
| 18:1*cis*-9 | $475.3_{61.02}$ | $508.4_{61.02}$ | $500.6_{61.02}$ | $469.4_{61.02}$ | $467.4_{61.02}$ | 0.980 |
| 18:2*n*-6 | $201.3_{10.70}$ a[b] | $148.2_{10.70}$ b | $203.9_{10.70}$ a | $163.0_{10.70}$ a,b | $139.3_{10.70}$ b | <0.001 |
| 18:3*n*-3 | $13.1_{4.05}$ a | $65.2_{4.05}$ b | $16.8_{4.05}$ a | $66.8_{4.05}$ b | $10.3_{4.05}$ a | <0.001 |
| 20:4*n*-6 | $43.4_{1.01}$ a | $29.4_{1.01}$ b | $41.4_{1.01}$ a | $29.9_{1.01}$ b | $39.9_{1.01}$ a | <0.001 |
| 20:5*n*-3 | $4.4_{0.54}$ a | $17.9_{0.54}$ b | $5.1_{0.54}$ a | $19.7_{0.54}$ b | $6.3_{0.54}$ a | <0.001 |
| 22:4*n*-6 | $4.8_{0.14}$ a | $2.3_{0.14}$ b | $4.6_{0.14}$ a | $2.0_{0.14}$ b | $4.3_{0.14}$ a | <0.001 |
| 22:5*n*-3 | $8.5_{0.29}$ a | $13.8_{0.29}$ b | $9.4_{0.29}$ a | $14.0_{0.29}$ b | $8.9_{0.29}$ a | <0.001 |
| 22:6*n*-3 | $3.7_{0.23}$ | $3.5_{0.23}$ | $3.6_{0.23}$ | $3.6_{0.23}$ | $4.7_{0.23}$ | 0.005 |
| sum SFA[c] | $524.3_{62.84}$ | $587.9_{62.84}$ | $570.2_{62.84}$ | $515.9_{62.84}$ | $486.8_{62.84}$ | 0.785 |
| sum MUFA[d] | $584.2_{76.42}$ | $629.8_{74.42}$ | $614.2_{76.42}$ | $575.7_{76.42}$ | $578.5_{76.44}$ | 0.982 |
| sum PUFA[e] | $294.9_{15.27}$ a | $299.6_{15.27}$ a | $301.9_{15.27}$ a | $319.0_{15.27}$ a | $227.6_{15.27}$ b | 0.002 |
| sum *n*-3 FA[f] | $32.4_{5.19}$ a | $108.9_{5.19}$ b | $38.4_{5.19}$ a | $113.0_{5.19}$ b | $32.2_{5.19}$ a | <0.001 |
| sum *n*-6 FA[g] | $262.5_{11.30}$ a | $190.7_{11.30}$ b | $263.5_{11.30}$ a,b | $206.0_{11.30}$ b | $195.4_{11.30}$ a,b | <0.001 |
| ratio *n*-6/*n*-3 FA | $8.2_{0.12}$ a | $1.8_{0.12}$ a,b | $6.9_{0.12}$ a,b | $1.8_{0.12}$ a,b | $6.1_{0.12}$ b | <0.001 |
| SCD index[h] | $50.0_{0.73}$ a | $48.4_{0.73}$ b | $48.9_{0.73}$ b | $50.1_{0.73}$ a | $51.6_{0.73}$ a | 0.040 |

[a]LSM: Least-squares mean. SEM: Standard error of the LSM. [b]a, b: Significant diet effect ($p < 0.05$). [c]Sum SFA: 10:0 + 11:0 + 12:0 + 13:0 + 14:0 + 15:0 + 16:0 + 17:0 + 18:0 + 20:0 + 21:0 + 22:0 + 23:0 + 24:0. [d]Sum MUFA: 14:1 + 15:1+ 16:1 + 17:1 + 18:1*t* + 18:1*c*9 + C18:1*c*11 + C22:1 + C24:1. [e]Sum PUFA: 18:2*t* + 18:2*n*-6 + 18:3*n*-3 + 18:4*n*-3 + 20:3*n*-6 + 20:4*n*-6 + 20:5*n*-3 + 22:1 + 22:4*n*-6 + 22:5*n*-3 + 22:6*n*-3 + c9,tr11CLA + 18:3*n*-6 + 20:2*n*-6 + 20:3*n*-3 + 22:2*n*-6. [f]Sum *n*-3 FA: 20:3*n*-3 + 22:6*n*-3 + 22:5*n*-3 + 20:5*n*-3 + 18:4*n*-3 + 18:3*n*-3. [g]Sum *n*-6 FA: 22:2*n*-6 + 20:2*n*-6 + 18:3*n*-6 + 22:4*n*-6 + 20:3*n*-6 + 18:2*n*-6 + 20:4*n*-6. [h]SCD: Calculated index (14:1 + 16:1 + 18:1*cis*-9 + 18:1*trans*-11 + 17:1/14:1 + 16:1 + 18:1*cis*-9 + 18:1*trans*-11 + 17:1 + 14:0 + 16:0 + 17:0 + 18:0) × 100.

**Table 3. Fatty Acid Concentrations (mg/100 g) in Back Fat of Landrace Pigs Fed Different Diets[a]**

| | LSM$_{SEM}$ ($n$ = 8) | | | | | |
|---|---|---|---|---|---|---|
| | HPD-SO | HPD-LO | RPD-SO | RPD-LO | CON | signif |
| sum FA | $75412.1_{2162}$ | $75693.3_{2162}$ | $71914.5_{2162}$ | $76098.4_{2162}$ | $73251.5_{2162}$ | 0.5984 |
| 14:0 | $908.5_{34.72}$ | $930.6_{34.72}$ | $856.2_{34.72}$ | $848.4_{34.72}$ | $886.6_{34.72}$ | 0.4233 |
| 16:0 | $15641.4_{509.9}$ | $15437.1_{509.9}$ | $14606.0_{509.9}$ | $14683.7_{509.9}$ | $15581.2_{509.9}$ | 0.4332 |
| 16:1 | $1274.8_{69.77}$ | $1379.3_{69.77}$ | $1206.5_{69.77}$ | $1352.5_{69.77}$ | $1467.9_{69.77}$ | 0.1076 |
| 18:0 | $8104.4_{359.3}$ | $8200.3_{359.3}$ | $7571.1_{359.3}$ | $7473.2_{359.3}$ | $8032.3_{359.3}$ | 0.5056 |
| 18:1*cis*-9 | $27457.8_{853.2}$ a | $26949.9_{853.2}$ a | $25659.0_{853.2}$ a | $27468.4_{853.2}$ a | $31397.1_{853.2}$ b | 0.0006 |
| 18:2*n*-6 | $14538.4_{479.5}$ a | $9452.6_{479.5}$ b | $14532.9_{479.5}$ a | $10200.9_{479.5}$ a,b | $8336.9_{479.5}$ b | <0.0001 |
| 18:3*n*-3 | $1968.3_{172.6}$ a | $7274.5_{172.6}$ b | $2216.0_{172.6}$ a | $7901.8_{172.6}$ b | $1265.1_{172.6}$ a | <0.0001 |
| 20:4*n*-6 | $210.7_{6.45}$ a | $146.8_{6.45}$ b | $197.0_{6.45}$ a | $142.8_{6.45}$ b | $177.3_{6.45}$ a,b | <0.0001 |
| 20:5*n*-3 | $34.3_{3.49}$ a | $110.4_{3.49}$ b | $42.0_{3.49}$ a | $129.6_{3.49}$ b | $34.2_{3.49}$ a | <0.0001 |
| 22:4*n*-6 | $78.9_{2.70}$ a | $43.0_{2.70}$ b | $68.4_{2.70}$ a | $38.9_{2.70}$ b | $58.0_{2.70}$ a | <0.0001 |
| 22:5*n*-3 | $132.2_{7.11}$ a | $257.9_{7.11}$ b | $141.9_{7.11}$ a | $256.9_{7.11}$ b | $125.1_{7.11}$ a | <0.0001 |
| 22:6*n*-3 | $62.4_{4.77}$ | $75.4_{4.77}$ | $67.5_{4.77}$ | $77.9_{4.77}$ | $75.4_{4.77}$ | 0.1400 |
| sum SFA | $25295.6_{853.0}$ | $25232.3_{853.0}$ | $23636.6_{853.0}$ | $23609.0_{853.0}$ | $25303.7_{853.0}$ | 0.3586 |
| sum MUFA | $32176.8_{960.0}$ a | $32496.7_{960.2}$ a | $30118.1_{960.2}$ a | $33078.9_{960.2}$ a | $37253.2_{960.2}$ b | 0.0002 |
| sum PUFA | $17893.3_{628.5}$ a | $17907.8_{628.5}$ a | $18114.9_{628.5}$ a | $19356.2_{628.5}$ a | $10645.4_{628.5}$ b | <0.0001 |
| sum *n*-3 FA | $2209.6_{177.8}$ a | $7728.2_{177.8}$ b | $2474.1_{177.8}$ a,b | $8373.9_{177.8}$ b | $1517.4_{177.8}$ a | <0.0001 |
| sum *n*-6 FA | $15683.7_{507.4}$ a | $10179.6_{507.4}$ b | $15640.8_{507.4}$ a | $10982.6_{507.4}$ a,b | $9128.0_{507.4}$ a,b | <0.0001 |
| ratio *n*-6/*n*-3 FA | $7.2_{0.15}$ a | $1.3_{0.15}$ b | $6.4_{0.15}$ a,b | $1.3_{0.15}$ b | $6.0_{0.15}$ a,b | <0.0001 |

[a]For footnotes see Table 2.

corresponding concentrations of HPD-LO/HPD-SO fed animals. The results of the present study are not in line with those of Teye et al.,[30] who reported that PRD in combination with palm kernel, palm, or soybean oil supplementation led to significantly decreased single *n*-3/*n*-6 PUFA and sum PUFA contents in muscle of crossbreds (Duroc × Large White × Landrace). RPD intervention per se resulted in increased single *n*-3 PUFA and sum PUFA contents in muscle of Wujin pigs,[31] but in significantly lower contents of single *n*-3/*n*-6 PUFA and sum PUFA in muscle of crossbred pigs (Landrace × Large White).[8,18] It has been previously demonstrated that the expression/activity of lipogenic enzymes have decisive control on IMF deposition in pigs. SREBP-1c, a key transcription factor, regulates the expression of lipogenic enzymes including

Table 4. Fatty Acid Concentrations (mg/100 g) in Liver of Landrace Pigs Fed Different Diets[a]

| | LSM$_{SEM}$ ($n$ = 8) | | | | | |
|---|---|---|---|---|---|---|
| | HPD-SO | HPD-LO | RPD-SO | RPD-LO | CON | signif |
| sum FA | $3063.6_{121.8}$ | $3041.4_{121.8}$ | $3057.8_{121.8}$ | $3301.8_{121.8}$ | $3213.1_{121.8}$ | 0.4706 |
| 14:0 | $8.1_{1.03}$ | $7.0_{1.03}$ | $7.5_{1.03}$ | $8.5_{1.03}$ | $6.3_{1.03}$ | 0.5973 |
| 16:0 | $397.0_{19.23}$ | $347.6_{19.23}$ | $369.2_{19.23}$ | $355.2_{19.23}$ | $410.9_{19.23}$ | 0.1172 |
| 16:1 | $14.0_{1.56}$ | $14.1_{1.56}$ | $12.8_{1.56}$ | $15.5_{1.56}$ | $17.7_{1.56}$ | 0.2370 |
| 18:0 | $717.9_{25.65}$ | $761.7_{25.65}$ | $735.4_{25.65}$ | $809.9_{25.65}$ | $755.9_{25.65}$ | 0.1450 |
| 18:1*cis*-9 | $304.7_{23.28}$ a | $268.6_{23.28}$ a | $287.2_{23.28}$ a | $315.1_{23.28}$ b | $378.6_{23.28}$ b | 0.0236 |
| 18:2*n*-6 | $571.0_{20.91}$ a | $465.7_{20.91}$ b | $591.0_{20.91}$ a | $523.7_{20.91}$ b | $414.2_{20.91}$ b | <0.0001 |
| 18:3*n*-3 | $30.7_{12.84}$ a | $165.2_{12.84}$ b | $39.8_{12.84}$ a | $209.3_{12.84}$ b | $21.9_{12.84}$ a | <0.0001 |
| 20:4*n*-6 | $629.0_{22.76}$ a | $349.1_{22.76}$ b | $610.5_{22.76}$ a | $363.9_{22.76}$ b | $644.3_{22.76}$ a | <0.0001 |
| 20:5*n*-3 | $41.0_{9.76}$ a | $301.6_{9.76}$ b | $56.6_{9.76}$ a | $334.0_{9.76}$ b | $86.6_{9.76}$ a | <0.0001 |
| 22:4*n*-6 | $26.7_{1.18}$ a | $7.5_{1.18}$ b | $22.7_{1.18}$ a | $6.6_{1.18}$ b | $24.2_{1.18}$ a | <0.0001 |
| 22:5*n*-3 | $94.4_{5.65}$ a | $132.4_{5.65}$ b | $98.5_{5.65}$ a | $126.6_{5.65}$ b | $107.8_{5.65}$ a | <0.0001 |
| 22:6*n*-3 | $50.7_{4.43}$ a | $41.0_{4.43}$ a | $52.5_{4.43}$ a | $47.8_{4.43}$ a | $102.7_{4.43}$ b | <0.0001 |
| sum SFA | $1186.3_{44.26}$ | $1174.5_{44.26}$ | $1172.4_{44.26}$ | $1231.5_{44.26}$ | $1278.8_{44.26}$ | 0.3830 |
| sum MUFA | $371.7_{27.72}$ a | $333.1_{27.72}$ a | $350.4_{27.72}$ a | $385.0_{27.72}$ a | $472.8_{27.72}$ a,b | 0.0111 |
| sum PUFA | $1504.3_{58.28}$ | $1532.4_{58.28}$ | $1533.9_{58.28}$ | $1684.0_{58.28}$ | $1460.3_{58.28}$ | 0.1020 |
| sum $n$-3 FA | $221.1_{21.75}$ a | $662.7_{21.75}$ b | $254.2_{21.75}$ a | $743.4_{21.75}$ b | $322.3_{21.75}$ a | <0.0001 |
| sum $n$-6 FA | $1281.5_{43.12}$ a | $868.7_{43.12}$ b | $1278.8_{43.12}$ a | $939.4_{43.12}$ b | $1136.6_{43.12}$ a | <0.0001 |
| ratio $n$-6/$n$-3 FA | $5.8_{0.12}$ a | $1.3_{0.12}$ b | $5.1_{0.12}$ b | $1.3_{0.12}$ b | $3.5_{0.12}$ b | <0.0001 |

[a]For footnotes see Table 2.

ACC, FAS, and SCD-1.[18,20] The protein expression of the SREBP-1c precursor (pSREBP-1c) in muscle of the present study was not affected by RPD compared with HPD and control diet, except increased expression level of SREBP-1c (mSREBP-1c) in muscle of HPD-SO-fed pigs compared to the other diet groups. Based on the regulatory function of SREBP-1c for expression of lipogenic enzymes, also the protein expression levels of SCD-1 in muscle of the present study highlighted no significant differences between RPD and HPD intervention. It has been shown that $n$-3 PUFA can inhibit transcription of lipogenic genes by suppressing SREBP-1c gene expression or inhibiting the proteolytic release of nuclear SREBP-1c in bovine muscle and adipose tissues.[32] It is generally known that $n$-3 and $n$-6 PUFA as ligands/modulators for nuclear receptors suppress de novo fatty acid synthesis; $n$-3 PUFA seems to be more potent than $n$-6 PUFA.[33] Based on present results, we assume that the unaffected SCD-1 expression in muscle of Landrace pigs fed RPD in combination with $n$-3/$n$-6 PUFA-containing plant oils may be explained by the mentioned opposite effects of RPD and $n$-3/$n$-6 PUFA supplementation with respect to protein expression levels. This can potentially result in their canceling out the effects of each other. This is reflected in SCD-1 expression levels and single and sum MUFA muscle concentrations of the present study resulting in both unchanged SCD-1 expression levels and unchanged MUFA concentrations within the RPD and HPD groups. Intervention studies using RPD intervention without $n$-3/$n$-6 PUFA-containing plant oil supplementation revealed increased single and sum MUFA contents in pig muscle caused by enhanced SCD expression levels, the key enzyme involved in MUFA biosynthesis, compared with control diets.[18,30,31] Furthermore, the protein expression of the lipogenic enzymes ACC and FAS, key rate limiting enzymes in the de novo pathway of fatty acid synthesis in pig muscle of the present study, seems to be on a quite low level and no abundances were detected in the total muscle extract. The corresponding concentrations of single SFA, e.g., 14:0, 16:0, and 18:0, and sum SFA were not affected by either the protein content or the type of oil supplementation. Madeira et al.[17] showed that RPD intervention per se resulted in significantly higher SFA contents relative to control diet in pig muscle of Alentejana and commercial crossbred (Large White × Landrace × Pietrain), despite no significant effect of RPD on relative mRNA level of key genes controlling fatty acid deposition, such as ACC and FAS and also fatty acid-binding protein 4 (FABP4), lipoprotein lipase (LPL), PPAR alpha (PPARa), and PPARg. In addition, Doran et al.[20] fed RPD in combination with palm kernel, palm, or soybean oil supplementation to crossbred pigs and reported elevated muscle concentrations of 14:0, 16:0, and total SFAs caused by increased ACC and FAS protein expression level in RPD compared with control intervention.

It has been previously demonstrated that increases in the de novo biosynthesis of fatty acids caused by RPD are accompanied by rather low effects on back fat tissue in pigs. This seems to be due to tissue-specific activation of expression of lipogenic enzymes based on RPD.[17,18,20] These findings are consistent with results of the present study, that RPD intervention led to an increase of protein expression of the active nuclear form of SREBP-1c (mSREBP-1c) in back fat of pigs, but not in muscle compared to the control diet. This is in agreement with results of Zhao et al.,[22] who investigated the impact of dietary protein on lipid metabolism in back fat of different old Wujin pigs. Both the relative mRNA level and protein expression of SREBP-1c in 60 and 100 kg pigs were increased by RPD (14% CP) diet compared with HPD (18% CP). In contrast, Madeira et al.[17,18] reported in two studies investigating the effect of RPD on lipid metabolism in back fat of Alentejana purebred and/or Large White × Landrace × Pietrain crossbred pigs that dietary protein level did not significantly affect the relative mRNA level of SREBP-1c and other genes controlling the fatty acid metabolism, e.g., ACC, FAS, LPL, PPARa, FABP4. Even lower dietary protein level (6% CP in dry matter) compared to before discussed RPD studies induced only modest variations in the adipose tissue proteome of newborn Landrace piglets.[34] Also in the present study, besides SREBP-1c, the protein expression of the

lipogenic enzymes of SCD-1, ACC, and FAS was not affected by dietary protein level or type of *n*-3/*n*-6 PUFA-containing plant oil in back fat of Landrace pigs. Consequently, the concentrations of single and sum SFA in back fat of pigs were not affected by RPD or HPD compared with the control group. Furthermore, based on unchanged SCD-1 expression levels, the single and sum MUFA concentrations in back fat of Landrace pigs were not diet affected, with the exception of increased sum MUFA concentrations in the back fat of the control group compared with the RPD/HPD groups. In contrast, Zhao et al.[22] reported that the relative mRNA abundances for ACC and FAS in back fat of 60 and 100 kg Wujin pigs were significantly increased by RPD compared with HPD intervention. This also suggests differences in response of different dietary protein levels on lipid metabolism in adipose tissues between lean pigs (Landrace) and fatty pigs (Wujin) and also crossbred pigs. The tissue-specific response of RPD vs HPD of the present study is also reflected by the protein expression of SCD-1, FAS, ACC, pSREBP-1c, and mSREBP-1c in liver of pigs. In contrast to muscle and back fat, both dietary protein level and type of *n*-3/*n*-6 PUFA-containing plant oil revealed no significant differences in protein expression of SCD-1, FAS, ACC, pSREBP-1c, and mSREBP-1c in the liver of pigs. In addition, independent of dietary interventions the overall expression levels of SCD-1, FAS, ACC, pSREBP-1c, and mSREBP-1c in muscle, back fat, and liver tissues of the present study were different and tissue-specific. The highest pSREBP-1c and mSREBP-1c expression levels (based on arbitrary units) were detected in muscle and the lowest ones in liver. In back fat, there were found the highest ACC expression levels (based on arbitrary units), and the highest SCD-1 expression levels (based on arbitrary units) were measured in liver tissue compared to muscle of pigs.

Our hypothesis that RPD in combination with *n*-3/*n*-6 PUFA-containing plant oils would lead to an increase of IMF contents including higher accumulation of de novo synthesized *n*-3/*n*-6 PUFA in muscle was not confirmed in Landrace pigs. The protein expression level of lipogenic enzymes in muscle was not increased as expected. One explanation of unchanged IMF contents in pigs could be based on mutual effects of RPD intervention and *n*-3/*n*-6 PUFA-containing plant oil supplementation on de novo fatty acid synthesis and IMF deposition. Further studies should clarify if (i) an RPD-based diet intervention increases expression of lipogenic enzymes and (ii) an *n*-6/*n*-3 PUFA supplementation suppresses the lipogenic enzyme expressions, and subsequently if the effects cancel each other out using a combination of RPD and *n*-6/*n*-3 PUFA supplementation in Landrace pigs. In the literature there exists a discrepancy of results feeding RPD with respect to lipid metabolism in muscle and adipose tissues in pigs. This might be also explained by different genetic backgrounds which are expressed also in different results in studies of purebred vs crossbred pigs and should be further investigated.

## AUTHOR INFORMATION

### Corresponding Author

*Leibniz-Institute for Farm Animal Biology, Institute Muscle Biology and Growth, Function of bioactive lipids Unit, Wilhelm-Stahl-Allee 2, 18196 Dummerstorf, Germany. Tel: + 49 (38208) 68884. Fax: + 49 (38208) 68852. E-mail: dannenberger@fbn-dummerstorf.de.

### Notes

The authors declare no competing financial interest.

## ACKNOWLEDGMENTS

The authors wish to thank B. Jentz and M. Dahm of the Department of Muscle Biology and Growth, who collaborated in the sample preparation, GC measurements, and Western blot analysis of transcription factors and lipogenic enzymes.

## REFERENCES

(1) *Agriculture, forestry and fishery statistics*, 2013 edition; Eurostat Pocketbooks; Publications Office of the European Union: Luxembourg, 2013; ISBN 978-92-79-33005-6.

(2) Duran-Montge, P.; Realini, C. E.; Barroeta, A. C.; Lizardo, R. G.; Esteve-Garcia, E. De novo fatty acid synthesis and balance of fatty acids of pigs fed different fat sources. *Livest. Sci.* **2010**, *132*, 157−164.

(3) Nuernberg, K.; Nuernberg, G.; Dannenberger, D. Effect of extruded linseed on growth and lipids of muscle and back fat in pigs. *Fleischwirtschaft* **2011**, *91*, 88−92.

(4) Ross, G. R.; Van Nieuwenhove, C. P.; Nelina, S. Fatty acid profile of pig meat after probiotic administration. *J. Agric. Food Chem.* **2012**, *60*, 5974−5978.

(5) Turner, T. D.; Mapiye, C.; Aalhus, J. L.; Beaulieu, A. D.; Patience, J. F.; Zijlstra, R. T.; Dugan, M. E. R. Flaxseed fed pork: n-3 fatty acid enrichment and contribution to dietary recommendations. *Meat Sci.* **2014**, *96*, 541−547.

(6) Young, J. F.; Rosenvold, K.; Stagsted, J.; Nielsen, J. H.; Andersen, H. J. Significance of Vitamin E supplementation, dietary content of polyunsaturated fatty acids, and preslaughter stress on oxidative status in pig as reflected in cell integrity and antioxidative enzyme activities in porcine muscle. *J. Agric. Food Chem.* **2005**, *53*, 745−749.

(7) Wood, J. D.; Enser, M.; Fisher, A. V.; Nute, G. R.; Sheard, P. R.; Richardson, R. I.; Hughes, S. I.; Whittington, F. M. Fat deposition, fatty acid composition and meat quality: A review. *Meat Sci.* **2008**, *78*, 343−358.

(8) Alonso, A.; Campo, M. M.; Provincial, L.; Roncales, P.; Beltran, J. A. Effect of protein level in commercial diets on pork meat quality. *Meat Sci.* **2010**, *85*, 7−14.

(9) Calder, P. C.; Dangour, A. D.; Diekman, C. Essential fats for future health. Proceedings of the 9th Unilever Nutrition Symposium. *Eur. J. Clin. Nutr.* **2010**, *64*, S1−S13.

(10) Simopoulos, A. P.; Bourne, P. G.; Faergeman, O. Bellagio Report on Healthy Agriculture, Healthy Nutrition, Healthy People. *Nutrients* **2013**, *5*, 411−423.

(11) Hoenselaar, R. Saturated fat and cardiovascular disease: The discrepancy between the scientific literature and dietary advice. *Nutrition* **2012**, *28*, 118−123.

(12) McNeill, S.; Van Elswyk, M. E. Red meat in global nutrition. *Meat Sci.* **2012**, *92*, 166−173.

(13) Wyness, L.; Weichselbaum, E.; O'Connor, A.; Williams, E. B.; Rilex, H.; Stanner, S. Red meat in the diet: an update. *Nutr. Bull.* **2011**, *36*, 34−77.

(14) Nuernberg, K. Optimizing the nutritional profile of beef. In *Improving the sensory and nutritional quality of fresh meat*; Kerry, J. P., Ledward, D., Eds.; Woodhead Publishing: Cambridge, United Kingdom, 2009; pp 321−341.

(15) Duan, Y.; Li, F.; Li, L.; Fan, J.; Sun, X.; Yin, Y. N-6:n-3 PUFA ratio is involved in regulating lipid metabolism and inflammation in pigs. *Br. J. Nutr.* **2014**, *111*, 445−451.

(16) Marins, A. P.; Lopes, P. A.; Madeira, M. S.; Martins, S. V.; Santos, N. C.; Moura, T. F.; Prates, J. A. M.; Soveral, G. Differences in lipid deposition and adipose membrane biophysical properties from lean and obese pigs under dietary protein restriction. *Biochem. Biophys. Res. Commun.* **2012**, *423*, 170−175.

(17) Madeira, M. S.; Pires, V. M. R.; Alfaia, C. M.; Costa, A. S. H.; Luxton, R.; Doran, O.; Bessa, R. J. B.; Prates, J. A. M. Differential effects of reduced protein diets on fatty acid composition and expression in muscle and subcutaneous adipose tissue of Alentejana purebred and Large White x Landrace x Pietrain crossbred pigs. *Br. J. Nutr.* **2013**, *110*, 216−229.

(18) Madeira, M. S.; Pires, V. M. R.; Alfaia, C. M.; Luxton, R.; Doran, O.; Bessa, R. J. B.; Prates, J. A. M. Combined effect of dietary arginine, leucine and protein levels on fatty acid composition and gene expression in the muscle and subcutaneous adipose tissue of crossbred pigs. *Br. J. Nutr.* **2014**, *111*, 1521−1535.
(19) Gondret, F.; Lebret, B. Feeding intensity and dietary protein level affect adipocyte cellularity and lipogenic capacity of muscle homogenates in growing pigs, without modification of the expression of sterol regulatory element binding protein. *J. Anim. Sci.* **2002**, *80*, 3184−3193.
(20) Doran, O.; Moule, S. K.; Teye, G. A.; Whittington, F. M.; Hallett, K. G.; Wood, J. D. A reduced protein diet induces stearoyl-CoA desaturase protein expression in pig muscle but not in subcutaneous adipose tissue: relationship with intramuscular lipid formation. *Br. J. Nutr.* **2006**, *95*, 609−617.
(21) Bergen, W. G.; Mersmann, H. J. Comparative aspects of lipid metabolism: impact on contemporary research and use of animal models. *J. Nutr.* **2006**, *135*, 2499−2502.
(22) Zhao, S. M.; Wang, J.; Song, X.; Zhang, X.; Ge, C.; Gao, S. Impact of dietary protein on lipid metabolism-related gene expression in porcine adipose tissue. *Nutr. Metab.* **2010**, *7* (6), 13.
(23) Dannenberger, D.; Nuernberg, K.; Nuernberg, G.; Priepke, A. Different dietary protein and PUFA intervention alters the fatty acid concentrations, but not the meat quality of porcine muscle. *Nutrients* **2012**, *4*, 1237−1246.
(24) Shen, X.; Dannenberger, D.; Nuernberg, K.; Nuernberg, G.; Zhao, R. Trans-18:1 and CLA isomers in rumen and duodenal digesta of bulls fed n-3 and n-6 PUFA-based diets. *Lipids* **2011**, *46*, 831−841.
(25) Guo, X.; Tang, R.; Wang, W.; Dayu, L.; Wang, K. Effects of dietary protein/carbo-hydrate ratio on fat deposition and gene expression of peroxisome proliferator activated receptor $\gamma$ and heart fatty acid-binding protein of finishing pigs. *Livest. Sci.* **2011**, *140*, 111−116.
(26) Wood, J. D.; Lambe, N. R.; Walling, G. A.; Whitney, H.; Jagger, S.; Fullarton, P. J.; Bayton, J.; Hallet, K.; Bünger, L. Effects of low protein diets on pigs with lean genotype. 1. Carcass composition measured by dissection and muscle fatty acid composition. *Meat Sci.* **2013**, *95*, 123−128.
(27) Tan, B. E.; Yin, Y. L.; Liu, Z. Q.; Tang, W. J.; Xu, H. J.; Konga, X. F.; Li, X. G.; Yao, K.; Gu, W. T.; Smith, S. B.; Wu, G. Y. Dietary L-arginine supplementation differentially regulates expression of fat-metabolic genes in porcine adipose tissue and skeletal muscle. *J. Nutr. Biochem.* **2011**, *22*, 441−445.
(28) Zhao, S. M.; Ren, L. J.; Chen, L.; Zhang, X.; Cheng, M. L.; Li, W. Z.; Zhang, Y. Y.; Gao, S. Z. Differential expression of lipid metabolism related genes in porcine muscle tissue leading to different intramuscular fat deposition. *Lipids* **2009**, *44*, 1029−1037.
(29) D'Souza, D. N.; Pethick, D. W.; Dunshea, F. R.; Pluske, J. R.; Mullan, B. P. Reducing the lysine to energy content in the grower growth phase diet increases intramuscular fat and improves the eating quality of the longissimus thoracis muscle of gilts. *Aust. J. Exp. Agric.* **2008**, *48*, 1105−1109.
(30) Teye, G. A.; Sheard, P. R.; Whittington, F. M.; Nute, G. R.; Stewart, A.; Wood, J. D. Influence of dietary oils and protein level on pork quality. 1. Effects on muscle fatty acid composition, carcass, meat and eating quality. *Meat Sci.* **2006**, *73*, 157−165.
(31) Wang, J.; Zhao, S. M.; Song, X. L.; Pan, H. B.; Li, W. Z.; Zhang, Y. Y.; Gao, S. Z.; Chen, D. W. Low protein diet up-regulate intramuscular lipogenic gene expression and down-regulate lipolytic gene expression in growth-finishing pigs. *Livest. Sci.* **2012**, *148*, 119−128.
(32) Hiller, B.; Herdmann, A.; Nuernberg, K. Dietary n-3 fatty acids significantly suppress lipogenesis in bovine muscle and adipose tissue: A functional genomic approach. *Lipids* **2011**, *46*, 557−567.
(33) Schmitz, G.; Ecker, J. The opposing effects of *n*-3 and *n*-6 PUFA. Prog. *Lipid Res.* **2008**, *47*, 147−155.
(34) Sarr, O.; Louveau, I.; Kalbe, C.; Metges, C. C.; Rehfeldt, C.; Gondret, F. Prenatal exposure to maternal low or high protein diets induces modest changes in the adipose tissue proteome of newborn piglets. *J. Amin. Sci.* **2010**, *88*, 1626−1641.

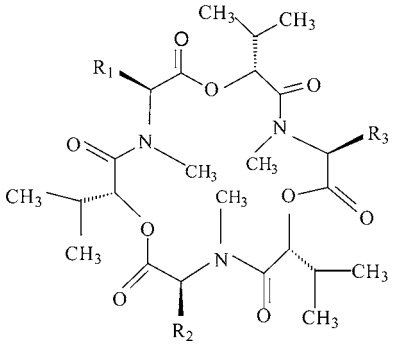

| | $R_1$ | $R_2$ | $R_3$ |
|---|---|---|---|
| **BEA** | Phenyl-methyl | Phenyl-methyl | Phenyl-methyl |
| **ENA** | *sec*-butyl | *sec*-butyl | *sec*-butyl |
| **$ENA_1$** | *sec*-butyl | *sec*-butyl | *iso*-propyl |
| **ENB** | *iso*-propyl | *iso*-propyl | *iso*-propyl |
| **$ENB_1$** | *iso*-propyl | *iso*-propyl | *sec*-butyl |

**Figure 1.** Structure of BEA and ENs. ENA, enniatin A; $ENA_1$, enniatin $A_1$; ENB, enniatin B; $ENB_1$, enniatin $B_1$; BEA, beauvericin.

Because of the susceptibility to mycotoxin contamination in mixed feeds and the presence of these mycotoxins in animal tissues, the aim of this work was to develop a new rapid, sensitive, and reproducible analytical strategy for the determination of ENs and BEA in feeds for farmed fish and fish tissues by LC-MS/MS-LIT.

## MATERIALS AND METHODS

**Chemical and Reagents.** All solvents (acetonitrile and methanol) were purchased from Merck (Darmstadt, Germany). Deionized water (<18 MΩ cm resistivity) was obtained from a Milli-Q water purification system (Millipore Corp., Bedford, MA, USA). Ammonium formate ($HCO_2NH_4$, 97%) was supplied by Sigma-Aldrich (St. Louis, MO, USA). All solvents were passed through a 0.22 μm cellulose filter from Membrane Solutions (Dallas, TX, USA).

The stock standard of BEA was purchased from Sigma-Aldrich. EN toxin solutions were provided by Biopure (Tulln, Austria). Individual stock solutions of BEA, ENA, $ENA_1$, ENB, and $ENB_1$ with concentrations of 1000 mg/L were prepared in methanol. They were stored in glass-stoppered bottles and darkness in security conditions at −20 °C. These stock solutions were then diluted with pure methanol to obtain the appropriate working solutions (ranging from 0.01 to 100 μg/kg) and were stored in darkness at 4 °C.

**Sampling.** *Feed for Farmed Fish.* Twenty samples of fish feed were purchased from Valencian hatcheries. Feed samples analyzed included, as nutrient composition, crude protein (36−49%), crude fat (18−26%), ashes (7−10%), crude fiber (1−4% as cellulose), and total phosphorus (1−2%). Their composition included vegetable products (21%), such as roasted soybeans, decorticated sunflower meal, soy protein concentrate, colza oil, and vegetable protein extract; cereal products (28%), such as corn and wheat gluten and wheat flour; fish and fish products (14%) such as fishmeal, fish oil, fish protein concentrate (14%), molluscs, and crustaceans (6%); algae (19%); and eggs and egg products (1%).

*Fish Samples.* Twenty fish (*Dicentrarchus labrax* ($n$ = 10) and *Sparus aurata* ($n$ = 10)) were purchased from different supermarkets located in Valencia (Spain), all of them from hatcheries. These species were selected for the study because they are two of the most important farmed Mediterranean fish species.[31] The origins of the sea bass and sea bream samples were Spain (Cartagena, Murcia) and Greece (Argolis). The nutrient compositions of both are similar, but the fat contents (concentrated mainly in liver) differ (1.3 g/100 g of edible portion in sea bass and 2.7 g/100 g of edible portion in sea bream).[32] These contents can differ between wild and farmed species and can also differ between seasons in wild species. Thus, cultured sea bass and sea bream contain higher lipid content than their wild counterparts (3 and 2 times higher in cultured fish, respectively).[33,34]

For the analysis, all samples were stored in a dark and dry place at −20 °C until analysis. After their packages had been opened, they were put into specific glass food containers and analyzed the same day.

**Mycotoxin Extraction.** *Extraction with Ultra-Turrax.* For feed samples, a 5 g aliquot was homogenized with 50 mL of acetonitrile during 5 min using an IKA T18 basic Ultra-Turrax (Staufen, Germany).The extract was centrifuged at 3540*g* for 15 min at 5 °C. The supernatant was purified using $C_{18}$ cartridges (Waters, Milford, MA, USA) by applying a slight vacuum. Cartridges were previously conditioned with 5 mL of MeOH and 5 mL of deonized water, washed with 5 mL of water, and then vacuum-dried for 5 min. Finally, mycotoxins were eluted with 5 mL of AcN/MeOH 50:50 v/v (MeOH with 20 mM ammonium formate). The extract was evaporated to dryness at 30 °C using a Büchi Rotavapor R-200 (Flawil, Switzerland). Then, the solution was reconstituted with 10 mL of AcN/MeOH 50:50 v/v (MeOH with 20 mM of ammonium formate) and evaporated to dryness at 30 °C using a multisample Turbovap LV Evaporator (Zymark, Hopkinton, MA, USA). The solution was reconstituted in 1 mL of AcN/MeOH 50:50 v/v (MeOH with 20 mM of ammonium formate) and filtered through a 13 mm/0.22 μm nylon filter prior injection into the LC-MS/MS-LIT system. The samples were extracted in triplicate.

*Extraction with Ultrasonic Bath.* For fish samples, a 10 g aliquot was homogenized with 50 mL of acetonitrile for 30 min at 30 °C using a Branson 5200 ultrasonic bath (Branson Ultrasonic Corp., Danbury, CT, USA). The extract was centrifuged at 3540*g* for 15 min at 5 °C. The supernatant was purified using $C_{18}$ cartridges (Waters) by applying a slight vacuum. Cartridges were previously conditioned with 5 mL of MeOH and 5 mL of deonized water, washed with 5 mL of water, and then vacuum-dried for 5 min. Finally, mycotoxins were eluted with 5 mL of AcN/MeOH 50:50 v/v (MeOH with 20 mM ammonium formate). The extract was evaporated to dryness at 30 °C using a Büchi Rotavapor R-200. The solution was reconstituted in 10 mL of AcN/MeOH 50:50 v/v (MeOH with 20 mM of ammonium formate) and transferred to a 15 mL conical tube to be evaporated to dryness at 30 °C using a multisample Turbovap LV Evaporator (Zymark). After solvent evaporation, the solution was reconstituted with 1 mL of AcN/MeOH 50:50 v/v (MeOH with 20 mM of ammonium formate) and placed again in the ultrasonic bath (30 min, 30 °C). Then, the solution was washed with hexane to eliminate fat particles in liver and viscera samples and filtered through a 13 mm/0.22 μm nylon filter (Membrane Solutions) prior to injection into the LC-MS/MS-LIT system. The samples were extracted in triplicate.

*Extraction with Microwave.* Fish samples (5 g) were extracted with 50 mL of acetonitrile during 3 min at 250 W using a microwave Saivod WP700P17-2 (Manisa, Turkey). The extract was centrifuged at 3540*g* for 15 min at 5 °C. The supernatant was purified using $C_{18}$ cartridges (Waters) by applying a slight vacuum. Cartridges were previously conditioned with 5 mL of MeOH and 5 mL of deonized water, washed with 5 mL of water, and then vacuum-dried for 5 min. Finally, mycotoxins were eluted with 5 mL of AcN/MeOH 50:50 v/v (MeOH with 20 mM ammonium formate). The extract was evaporated to dryness at 30 °C using a Büchi Rotavapor R-200. Then, the solution was reconstituted with 10 mL of AcN/MeOH 50:50 v/v (MeOH with 20 mM of ammonium formate) and evaporated to dryness at 30 °C using a multisample Turbovap LV evaporator (Zymark). The solution was reconstituted in 1 mL of AcN/MeOH 50:50 v/v (MeOH with 20 mM ammonium formate) and filtered through a 13 mm/0.22 μm nylon filter (Membrane Solutions) prior to injection into the LC-MS/MS-LIT system. The samples were extracted in triplicate.

**Instrumental and Chromatographic Conditions.** LC-MS/MS-LIT analyses were conducted on a system consisting of an Agilent

1200 chromatographic system (Agilent Technologies, Palo Alto, CA, USA) coupled to a 3200 QTRAP mass spectrometer (AB Sciex, Foster City, CA, USA) equipped with a turbo electrospray ionization (ESI) interface. The QTRAP analyzer combines a fully functional triple-quadrupole and a linear ion trap mass spectrometer within the same instrument. Separation of analytes was performed using a Gemini-NX LC-column (Phenomenex, Aschaffenburg, Germany) (150 mm × 4.6 mm, 5 $\mu$m of particle size) preceded by a guard column utilizing the same packing material. The flow rate was set to 0.8 mL $min^{-1}$, and the oven temperature was 40 °C, with eluent A water (mobile phase A) slightly acidified with 0.1% formic acid and 5 mM ammonium formate and eluent B (mobile phase B) methanol with 5 mM ammonium formate and 0.1% formic acid. The elution gradient started with 0% of eluent B, increased to 100% in 10 min, decreased to 80% in 5 min and, finally, decreased to 70% in 2 min. During the subsequent 6 min, the column was cleaned, readjusted to the initial conditions, and equilibrated for 7 min. The volume of the injections was 20 $\mu$L.

The analyses were performed using the Turbo V ionspray in positive ionization mode (ESI+). Nitrogen served as the nebulizer and collision gas. The operating conditions for the analysis were the following: ion spray voltage, 5500 V; curtain gas, 20 (arbitrary units); GS1 and GS2, 50 and 50 psi, respectively; probe temperature (TEM), 450 °C. MRM experiments were performed to obtain the maximum sensitivity for the detection of target molecules.

## RESULTS AND DISCUSSION

**Method Validation of the LC-MS/MS-LIT Analysis.** Before the MS/MS conditions were optimized, full scan and daughter scan under positive and negative mode have been used. In addition, each compound was also characterized by the retention time. The criteria adopted for accepting the analysis was a retention time deviation <2.5% compared to the standard.

The optimization of MS parameters as declustering potential (DP), collision energy (CE), and collision cell entrance potential (CEP) was performed by flow injection analysis for each standard mycotoxin; entrance potential (EP) and collision cell exit potential (CXP) were set at 10 and 4 V, respectively, for all analytes (Table 1). The MS was operated in multiple reaction monitoring (MRM) mode and with the resolution set to unit resolution for $Q_1$ and $Q_3$.

Method validation was carried out according to the guidelines established by the European Commission.[35] The method validation included the determination of linearity, limits of detection (LODs), limits of quantification (LOQs), recoveries, repeatabilities (intraday precision), reproducibilities (interday precision), and matrix effects.

Good sensitivity was obtained for selected mycotoxins when the ESI+ mode was applied: the base peak observed was $[M + NH_4]^+$ for all of the mycotoxins studied. Table 1 shows the optimum parameter values for each analyte and the two most relevant MRM transitions: the first transition was used for quantification purposes, whereas the second transition was used to confirm the presence of target compounds in the sample.

To determine the linearity, calibration curves for each studied mycotoxin were constructed from the standards prepared in methanol and from the standards prepared in the extract of blank sample (fish from extractive fishing). All mycotoxins exhibited good linearity over the working range (10LOQ and 100LOQ), and the regression coefficient of calibration curves was >0.992. For the evaluation of matrix effects, a mixture of blank extracts of different fish was prepared as blank sample. A suppression of the signal for all mycotoxins was observed (ranging from 7 to 40%). Therefore, to minimize these matrix effects and for a selective and reliable mycotoxin quantification in different fish samples, the employment of liquid chromatography coupled to mass spectrometry with linear ion trap (LC-MS/MS-LIT) required matrix-matched calibration standards prepared with fish samples.

**Table 1. Product Ions Obtained in Product Ion Scan Mode for Selected Mycotoxins and Multiple Reaction Monitoring Optimized Parameters**

| mycotoxin[a] | retention time (min) | precursor ion | product ions[b] | DP[c] (V) | CE[d] (V) | CXP[e] (V) |
|---|---|---|---|---|---|---|
| ENA | 16.4 | 699.4 | $210^{Q}$ | 76 | 35 | 14 |
| | | | $228^{q}$ | 76 | 59 | 16 |
| $ENA_1$ | 15.7 | 685.4 | $210^{Q}$ | 66 | 37 | 8 |
| | | | $214^{q}$ | 66 | 59 | 10 |
| ENB | 14.9 | 657.3 | $196^{Q}$ | 51 | 39 | 8 |
| | | | $214^{q}$ | 51 | 59 | 10 |
| $ENB_1$ | 15.5 | 671.2 | $214^{Q}$ | 66 | 61 | 10 |
| | | | $228^{q}$ | 66 | 57 | 12 |
| BEA | 15.3 | 801.2 | $784^{Q}$ | 116 | 27 | 10 |
| | | | $244^{q}$ | 116 | 39 | 6 |

[a]ENA, enniatin A; $ENA_1$, enniatin $A_1$; ENB, enniatin B; $ENB_1$, enniatin $B_1$; BEA, beauvericin. [b]Product ions. "Q" indicates quantification transition, and "q" indicates qualification transition. [c]DP, declustering potential. [d]CE, collision energy. [e]CXP, collision cell exit potential.

The LODs and LOQs were estimated from an extract of a blank sample, fortified with decreasing concentrations of the analytes. Additions were performed from three different blank samples ($n$ = 18), to the estimated concentrations for each mycotoxin. The LODs and LOQs were calculated using the criterion of S/N ≥ 3 or S/N ≥ 10 for LOD and LOQ, respectively (Table 2).

The recoveries, intraday precisions, and interday precisions were evaluated by spiking different levels of standard analyte to samples at two spiked levels (10 times LOQ and 100 times LOQ) (Table 2). According to Commission Decision (2002), recoveries were within the relative standard deviation (<20%).[35]

**Extraction Procedures.** For the optimization procedure, different parameters depending on the extraction method were tested. All experiments were carried out in triplicate using blank sample of fish fillet (hake from extractive fishing) spiked at two levels (10LOQ and 100LOQ) of ENs and BEA. The extraction efficiency was evaluated in terms of recovery. In Table 2 are shown the results for the parameters tested.

Ultra-Turrax extraction was used for feed samples. However, this method could not be used for fish sample extraction. For this reason, two extraction methods (ultrasonic and microwave extraction) were tested for fish samples.

**Ultra-Turrax Optimization.** This extraction method was employed only for feed samples. Critical parameters tested were the nature of the solvent, the volume of solvent (10, 20, 50 mL), and the weight of sample (2, 5, 10 g). Solvents tested with different polarities were AcN, a mixture of AcN/MeOH 50:50 v/v (MeOH with 20 mM ammonium formate), and ethyl acetate (EtOAc). Using the mixture of AcN/MeOH 50:50 v/v (MeOH with 20 mM ammonium formate), mean recoveries were not acceptable for ENA, $ENA_1$, and BEA (<70%) (data not shown). Mean recoveries for all mycotoxins when EtOAc was used as extraction solvent were lower than AcN ones. Recoveries obtained with 50 mL of AcN and 5 g of feed sample were acceptable

Table 2. Analytical Parameters Obtained in the Validation of the Method: Limits of Detection (LODs), Limits of Quantification (LOQs), Matrix Effects (ME), Recoveries, and Intraday and Interday Precisions for Feed (Ultra-Turrax Extraction) and Fish (Ultrasonic Bath Method), Both with AcN

| | LOD (μg/kg) | | LOQ (μg/kg) | | ME (%) | | recovery (%) ± RSD[a] | | | | | | | |
|---|---|---|---|---|---|---|---|---|---|---|---|---|---|---|
| | | | | | | | intraday precision | | | | interday precision | | | |
| | | | | | | | feed | | fish | | feed | | fish | |
| | feed | fish | feed | fish | feed | fish | 10LOQ | 100LOQ | 10LOQ | 100LOQ | 10LOQ | 100LOQ | 10LOQ | 100LOQ |
| ENA | 0.15 | 3.00 | 0.50 | 10.00 | 13.00 | 7.00 | 92.00 ± 6.00 | 91.00 ± 5.30 | 86.00 ± 7.20 | 88.00 ± 8.90 | 89.00 ± 7.30 | 90.00 ± 7.00 | 86.00 ± 11.50 | 93.60 ± 9.00 |
| $ENA_1$ | 0.08 | 0.30 | 0.25 | 1.00 | 19.00 | 23.00 | 80.00 ± 10.20 | 85.00 ± 6.10 | 85.00 ± 6.30 | 91.00 ± 7.80 | 82.00 ± 13.00 | 87.00 ± 9.00 | 84.00 ± 12.00 | 82.30 ± 13.00 |
| ENB | 0.03 | 0.30 | 0.10 | 1.00 | 11.00 | 7.00 | 87.00 ± 9.20 | 88.00 ± 11.30 | 82.00 ± 5.30 | 84.00 ± 7.50 | 85.00 ± 11.00 | 90.00 ± 7.00 | 81.00 ± 10.90 | 89.70 ± 11.00 |
| $ENB_1$ | 0.03 | 0.30 | 0.10 | 1.00 | 16.00 | 12.00 | 88.00 ± 7.20 | 91.00 ± 6.80 | 78.00 ± 9.60 | 82.00 ± 7.40 | 87.00 ± 7.80 | 86.00 ± 7.00 | 82.00 ± 7.00 | 89.60 ± 8.00 |
| BEA | 0.02 | 3.00 | 0.10 | 10.00 | 29.00 | 40.00 | 85.00 ± 5.30 | 86.00 ± 6.50 | 83.00 ± 7.20 | 86.00 ± 7.70 | 83.00 ± 6.70 | 86.00 ± 7.00 | 85.00 ± 12.10 | 83.00 ± 8.90 |

[a]RSD, standard deviation (calculated by injecting samples in triplicate).

(ranging from 80 to 92%) according to the European Commission Decision.[35] For recovery assay a sample of feed destinated to other species (but with similar composition as feed for farmed fish) was used because all samples analyzed were positive for all mycotoxins analyzed in this study. The results obtained are presented in Table 2.

This extraction method is efficient and quick; however, it is not possible to use it for fish samples because fish tissue filaments were trapped in the Ultra-Turrax, eliminating the correct mixture and contact between the solid and liquid phases.

**Microwave Optimization.** Critical parameters tested were the time, potency, and nature of the extraction solvent. This study was performed with three solvents: AcN, a mixture of AcN/MeOH 50:50 v/v (MeOH with 20 mM ammonium formate), and MeOH. EtOAc was discarded due to its high volatility. The temperature applied was as low as possible because $ENA_1$ presents a melting point lower (66−67 °C) than those of the other ENs.[7] In fact, when the extraction was performed using high potency (500−1000 W), temperature was higher than the solvent boiling point, so a continuous potency of 250 W was used for the extraction procedure. The solvent volume was determined according to results previously described for Ultra-Turrax optimization, but the weight of sample was 10 g. Recoveries obtained with 10 g of sample and 50 mL of AcN were acceptable (ranging from 70 to 89%); however, the extracts were not clean, probably due to increased solubility of several compounds during the thermal treatment.

**Ultrasonic Bath Optimization.** Critical parameters tested were the nature of the extraction solvent, the temperature, and time of sonication. The best recoveries were obtained when the temperature applied was 30 °C (to prevent mycotoxin melting) and the sonication time applied was 30 min. As discussed above, solvents tested were AcN, a mixture of AcN/MeOH 50:50 v/v (MeOH with 20 mM ammonium formate), and EtOAc. The tested solvent with the best result was AcN: the extract was clear, the amount of fat in the extract was easy to eliminate, and recoveries were the highest. Results are presented in Table 2 and Figure 2. It can be observed that samples containing a large

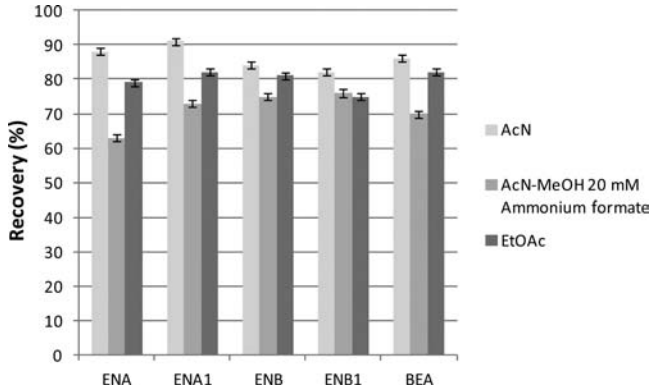


**Figure 2.** Recoveries with different solvents tested for fish samples by ultrasonic extraction. ENA, enniatin A; $ENA_1$, enniatin $A_1$; ENB, enniatin B; $ENB_1$, enniatin $B_1$; BEA, beauvericin. AcN, acetonitrile; MeOH, methanol with 20 mM ammonium formate; EtOAc, ethyl acetate. Standard deviation was obtained by analysis performance in triplicate.

fraction of AcN are appropriate for the extraction of most of the analytes. With regard to the results, this extraction method was selected for fish samples.

**Optimization of Liver and Viscera Preparation Conditions.** For animal origin samples, lipids may cause the main interference in the analysis of low-polarity contaminants in biological materials. Thus, the presence of lipids in the extracts must be avoided or reduced as much as possible to improve detection and quantification limits.[36] The main difference between edible muscle and liver is the lipid content, concentrated mainly in the liver, as mentioned under Materials and Methods. For this reason, for liver and viscera sample preparation, some variations were necessary: before the concentration on the turbovap evaporator, the extract was reconstituted with 3 mL of *n*-hexane (the third part of the total volume) and 6 mL of MeOH (total volume = 9 mL) and ultrasonicated for 30 min at room temperature. Two different phases appeared: the lipidic and the methanolic. The lipidic phase was discarded, and the methanolic phase was collected and evaporated. This procedure was carried out in triplicate. Finally, samples were reconstituted in 1 mL of AcN/MeOH 50:50 v/v (MeOH with 20 mM of ammonium formate) and filtered through a 13 mm/0.22 $\mu$m nylon filter (Membrane Solutions) prior to injection. Recoveries obtained were acceptable (ranging from 72 to 88%).

**Cleanup Procedure.** To obtain maximum extraction recoveries and to reduce the presence of compounds that may interfere in the determination, the extract purification was performed with cartridges with different types of dispersing agent to evaluate cleanup efficiency. Dispersing agents tested for fish samples were $C_8$, silica, and $C_{18}$. Results are shown in Figure 3. The best dispersing agent for obtaining the best performances in fish samples was $C_{18}$. Cartridges were previously conditioned with 5 mL of MeOH and 5 mL of deonized water, washed with 5 mL of watern and then vacuum-dried for 5 min. Finally, mycotoxins were eluted with 5 mL of AcN/MeOH 50:50 v/v (MeOH with 20 mM ammonium formate).

**Occurrence of ENs and BEA in Analyzed Samples.** *Feed for Farmed Fish.* All of the samples analyzed were contaminated with emerging *Fusarium* mycotoxins. Results are shown in Table 3. Concentrations in positive samples ranged from 0.19 to 3.40 $\mu$g/kg for ENA, from 0.24 to 6.50 $\mu$g/kg for $ENA_1$, from 0.11 to 3.20 $\mu$g/kg for ENB, from 0.15 to 10 $\mu$g/kg for $ENB_1$, and from 0.13 to 6.60 $\mu$g/kg for BEA.

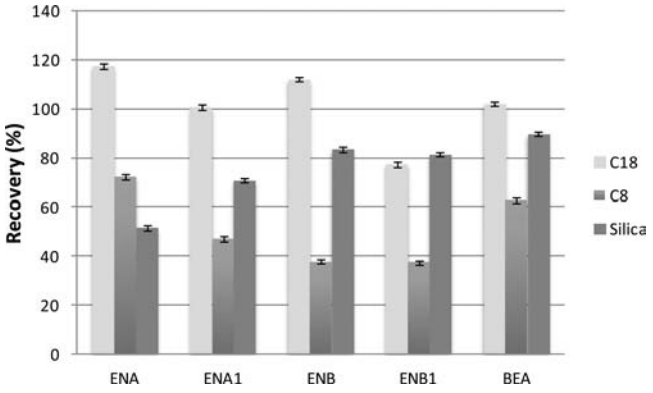


**Figure 3.** Recovery assays with different dispersing agents ($C_{18}$, $C_8$, silica) tested in fish samples by ultrasonic extraction with acetonitrile. Standard deviations were obtained by analysis of performance in triplicate.

The results obtained in this work are according to contents reported in different feed studies: in a study conducted by Warth et al.[37] in 10 feed samples from Burkina Faso and Mozambique, ENB and $ENB_1$ showed the highest contents (2.2−114 and 0.1−94.4 $\mu$g/kg, respectively), and BEA was present in 100% of the samples analyzed (3.3−418.4 $\mu$g/kg). Contents for ENA ranged from 0.6 to 7.9 $\mu$g/kg and for $ENA_1$, from 3.4 to 43.9 $\mu$g/kg.

These results are also according to those reported by Jurjevic et al.,[38] in which BEA was present in 19 of 209 corn samples and with those reported by Lee et al.[39] about the occurrence of *Fusarium* mycotoxin BEA in animal feeds from Korea: 27% of feed ingredients were contaminated with BEA at levels of 10−1800 $\mu$g/kg (mean = 480 $\mu$g/kg). The mean concentration of BEA was higher in bran feeds, followed by vegetable protein feeds, and grain feeds. In compound feeds, 33% of samples were contaminated with BEA at levels of 10−4660 $\mu$g/kg. BEA was not found in any of the 19 animal byproduct feed samples (fat meal, fish meal, and fish soluble) analyzed.

**Table 3. Occurrence (Micrograms per Kilogram) of Enniatins and Beauvericin in Feed for Farmed Fish and in Fish Samples**

| | | incidence (positives/total) | | | | | concentration range (mean of positives) | | | | |
|---|---|---|---|---|---|---|---|---|---|---|---|
| sample analyzed | | ENA | $ENA_1$ | ENB | $ENB_1$ | BEA | ENA | $ENA_1$ | ENB | $ENB_1$ | BEA |
| feed | | 20/20 | 20/20 | 20/20 | 20/20 | 19/20 | 0.6−3.4 (0.9) | 0.3−6.5 (1.1) | 0.1−3.2 (0.89) | 0.15−10 (1.77) | 0.1−6.6 (1.4) |
| total fish | muscle | 0/20 | 8/20 | 13/20 | 10/20 | 0/20 | nd[a] | 1.7−7.5 (4.2) | 1.3−44.6 (13.5) | 1.4−31.5 (10.9) | nd |
| | liver | 1/20 | 4/20 | 3/20 | 3/20 | 0/20 | 84.0 (84.0) | 1.01−9.9 (5.1) | 6.6−17.7 (12.6) | 2.7−6.8 (5.3) | nd |
| | head | 0/20 | 4/20 | 5/20 | 5/20 | 0/20 | nd | 1.7−30.5 (11.1) | 2.0−29.7 (13.0) | 1.1−75.4 (19) | nd |
| | viscera | 0/20 | 2/20 | 3/20 | 3/20 | 0/20 | nd | 9.9−45.0 (27.4) | 1.9−72.3 (30.6) | 2.8−119.0 (42.7) | nd |
| sea bass | muscle | 0/10 | 5/10 | 9/10 | 7/10 | 0/10 | nd | 1.7−6.9 (4.3) | 1.3−44.6 (12.8) | 1.4−31.5 (10.2) | nd |
| | liver | 1/10 | 3/10 | 2/10 | 2/10 | 0/10 | 84.0 (84.0) | 1.0−9.9 (5.6) | 6.6−17.7 (12.1) | 2.7−6.4 (4.5) | nd |
| | head | 0/10 | 2/10 | 3/10 | 3/10 | 0/10 | nd | 9.3−30.5 (19.9) | 2.0−29.7 (13.5) | 1.1−75.4 (28.9) | nd |
| | viscera | 0/10 | 2/10 | 2/10 | 3/10 | 0/10 | nd | 9.9−45.0 (27.4) | 17.7−72.3 (45.0) | 2.8−119.0 (42.7) | nd |
| sea bream | muscle | 0/10 | 3/10 | 4/10 | 3/10 | 0/10 | nd | 2.1−7.5 (4.0) | 1.3-21.6 (14.9) | 7.1−19.0 (12.7) | nd |
| | liver | 0/10 | 1/10 | 1/10 | 1/10 | 0/10 | nd | 3.2 | 13.4 | 6.8 | nd |
| | head | 0/10 | 2/10 | 2/10 | 2/10 | 0/10 | nd | 1.7−3.0 (2.3) | 8.4−15.9 (12.1) | 2.8−5.2 (4.0) | nd |
| | viscera | 0/10 | 0/10 | 1/10 | 0/10 | 0/10 | nd | nd | 1.9 | nd | nd |

[a]nd, not detectable.


dx.doi.org/10.1021/jf5036838 | J. Agric. Food Chem. 2014, 62, 12462−12470

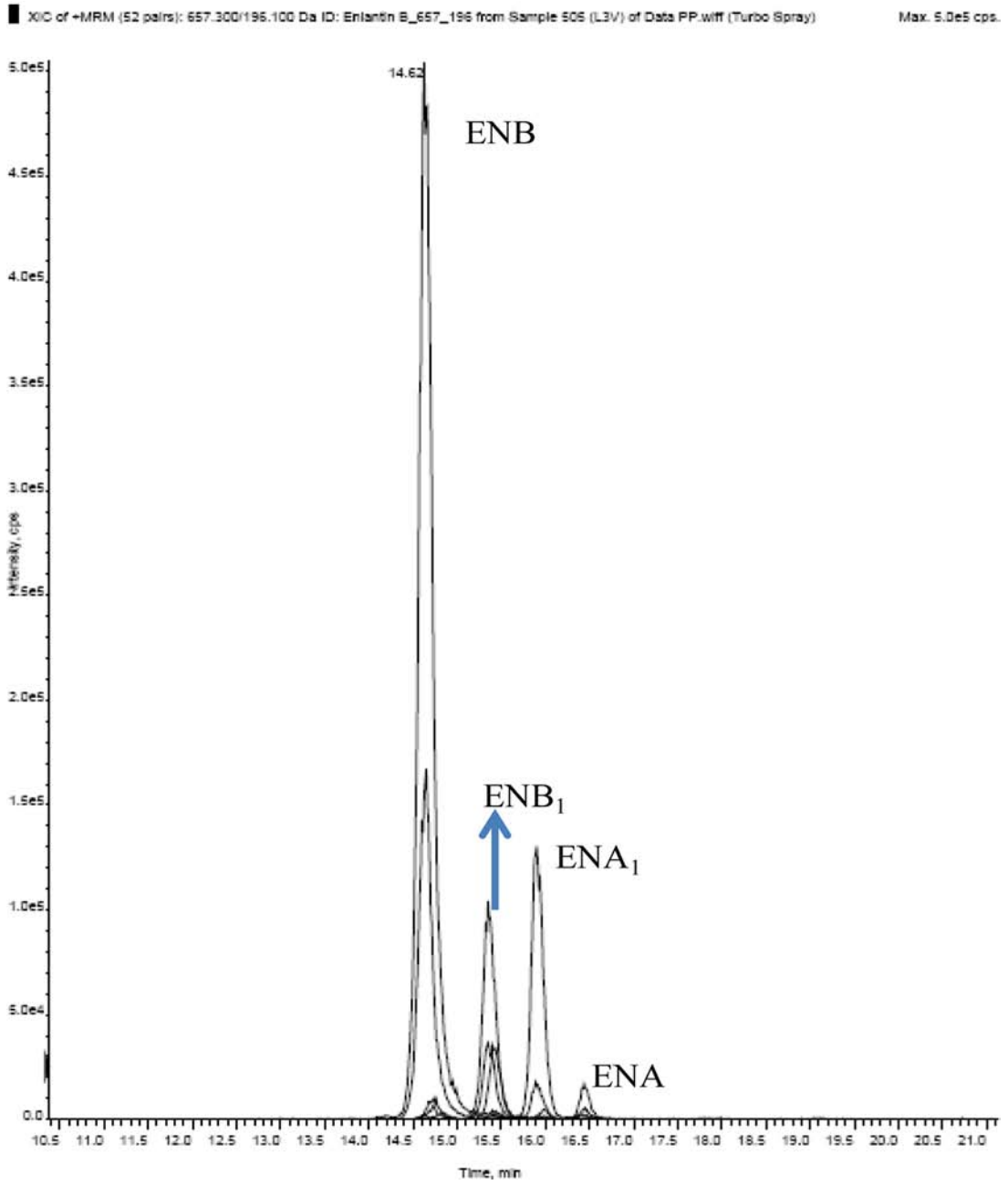


**Figure 4.** Chromatogram obtained from a sea bass tissue sample analyzed (contents were as follows: ENA, trace levels; $ENA_1$, 7 $\mu$g/kg; ENB, 7 $\mu$g/kg; and $ENB_1$, 18 $\mu$g/kg). BEA retention time = 15.3 min.

Mycotoxins can be present in processed feed due to the their resistance to treatments applied in feed processing (heat, chemical and mechanical extraction, and dehydration). These processes eliminate most of the original contaminating mycoflora; however, fungi spores and heat-stable toxins present in spores and mycelium can remain until more favorable conditions are reached.[40]

*Farmed Fish.* To determine the differences in mycotoxin contents in different fish tissues, samples were separated into four parts (liver, viscera, tissue, and head) and analyzed separately. Results are shown in Table 3.

The incidence of positive samples was lower than the incidence in feed, but the contents obtained were higher. These results suggest that contents depend on the time of withdrawal of the toxins from the diet. In this way, in a study conducted by Wu,[41] mycotoxin concentration in tissues decreased by 95−99% within 3 days after withdrawal of $AFB_1$ and OTA. In a pilot toxicokinetic study of $ENB_1$ in pigs, Devreese et al.[42] observed that $ENB_1$ is rapidly absorbed after oral administration and rapidly distributed and eliminated. The absolute oral bioavailability is high.

For the total fish samples analyzed, the highest incidence was obtained in muscle samples: 65% of samples (9 sea bass and 4 sea bream) were positive for ENB, 50% of samples (7 sea bass and 3 sea bream) were positive to $ENB_1$, and 40% of samples (5 sea bass and 3 sea bream) were positive for $ENA_1$. Thus, the highest incidence was found for ENB. The results obtained showed that the incidences for $ENA_1$, ENB, and $ENB_1$ in muscle samples were higher for sea bass samples than for sea bream samples. Figure 4 shows a chromatogram of a positive sea bass sample (tissue).

For $ENA_1$, the highest incidence was found in muscle and liver samples (40 and 20% of positive sample, respectively), whereas


dx.doi.org/10.1021/jf5036838 | J. Agric. Food Chem. 2014, 62, 12462−12470

Table 4. Estimated Daily Intake (EDI) of $ENA_1$, ENB, and $ENB_1$ for Spanish Fish Consumers

| mycotoxin | mean levels (nd = LOD[a]) (μg/kg) | mean levels (positive samples) (μg/kg) | EDI (μg/kg bw/day) | |
|---|---|---|---|---|
| | | | mean levels (nd = LOD) | mean levels (positive samples) |
| $ENA_1$ | 2.000 | 4.201 | 0.003 | 0.005 |
| ENB | 8.803 | 13.500 | 0.011 | 0.016 |
| $ENB_1$ | 5.100 | 10.902 | 0.006 | 0.013 |
| co-occurrence (sum of ENs) | 15.903 | 28.603 | 0.020 | 0.034 |

[a]nd, not detectable; LOD, limit of detection.

for ENB and $ENB_1$, the highest incidence was found in muscle (65 and 50%, respectively) and head samples (25%).

In the head samples analyzed, the percentages of positive samples were 20% for $ENA_1$ and 25% for ENB and $ENB_1$. In liver, 20% of samples analyzed were positive for $ENA_1$, whereas 15% of samples were positive for ENB and $ENB_1$. In viscera, 15% of samples were positive for ENB and $ENB_1$, whereas only 10% of samples were positive for $ENA_1$.

The mean contents obtained in muscle samples were higher in sea bream than in sea bass. This suggests differences in the mycotoxin intake and/or mycotoxin metabolism. Contents obtained for sea bass were similar in the four parts analyzed. However, for sea bream, higher contents were found in muscle and lower contents were obtained in viscera (Table 3).

With respect to different parts analyzed in sea bass and sea bream, in analyzed samples of sea bass head, the percentage of positive samples were 20% for $ENA_1$ and 30% for ENB and $ENB_1$, whereas for sea bream samples, the percentages were 20% for $ENA_1$, ENB, and $ENB_1$. In sea bream samples, the highest content was found for ENB (15.9 μg/kg). However, for sea bass, $ENB_1$ showed the highest content (75.4 μg/kg).

In liver samples of sea bass, 30% of analyzed samples were positive for $ENA_1$, whereas 20% of samples were positive for ENB and $ENB_1$. With regard to sea bream samples, only 10% of them were positive for $ENA_1$, ENB, and $ENB_1$. Only one sample of sea bass liver was positive for ENA, with 84.0 μg/kg. The highest content in both species analyzed was detected for ENB (17.7 and 13.4 μg/kg for sea bass and sea bream, respectively).

In viscera samples of sea bass, 30% of samples were positive for $ENB_1$ and 20% of samples were positive for ENB and $ENA_1$. The highest content was obtained for $ENB_1$ (119.0 μg/kg). In viscera samples from sea bream, only one sample was positive for ENB (1.9 μg/kg).

No more data are available for the toxicokinetic and bioavailability of the emerging mycotoxins in fish, but in the literature consulted is reported the presence of other mycotoxins in fish tissues. In this way, results of this survey are according to those reported by El Sayed and Khalil,[43] who reported 4.2 ± 0.8 μg/kg of $AFB_1$ in edible muscle of sea bass, and Nomura et al.[44], who reported $AFB_1$ concentrations in liver higher than in muscle, suggesting that AFs from feed were more highly accumulated in liver than in muscle. Deng et al.[45] reported that no detectable $AFB_1$ residues were found in muscle, whereas quite high residues were determined in liver.

*Daily Intake Estimation for Mycotoxins.* To determine an approximation to exposure assessment related to the intake of ENs and BEA in the Spanish adult population, the estimated daily intake (EDI) was calculated by relating the presence of mycotoxins in samples analyzed with the consumption data of fish by the Spanish population (26.84 kg per capita from January to December 2013).[46]

From these consumption data and the mean concentrations obtained (only from muscle samples analyzed), the estimated daily intake for Spanish consumers was calculated. Table 4 shows the mean concentration data for all samples (positives and negatives, criteria of nd = LOD) and only for positive samples and the EDI for each mycotoxin and also the sum of ENs (co-occurrence), because the obtained results are considered as the total exposure to mycotoxins found in samples analyzed at the same time.

With the data evidenced it is not possible to confirm that ENs represent a risk for the Spanish population, because a provisional maximum tolerable daily intake (PMTDI) has been not established by the Joint Expert Committee on Food Additives (JECFA). For this reason, approximation to the risk assessment was carried out according to the safety guidelines established for other *Fusarium* mycotoxins. In this way, results obtained were compared with the PMTDI values established for nivalenol (NIV) (1 μg/kg bw/day), DON (0.7 μg/kg bw/day), the sum of HT-2/T-2 toxins (0.1 μg/kg bw/day), and the sum of $FB_1$ and $FB_2$ (2 μg/kg bw/day).[47] It can be observed that the calculated EDIs for fish at mean levels (for positive samples and for all samples) were lower than the tolerable daily intakes (TDIs) for NIV, DON, $FB_1$/$FB_2$, and HT-2/T-2.

Although more information about toxicological data is necessary, special attention should be paid to these results, because some authors reported that DON cytotoxicity was not significantly different from that of ENs and BEA. These results indicated that ENs may have an underestimated toxic potential.[6]

## AUTHOR INFORMATION

### Corresponding Author

*(J.T.) E-mail: josefa.tolosa@uv.es. Phone: 0034 963 54 49 58. Fax: 0034 963 54 49 54.

### Funding

This work was supported by th Projects AGL2013/43194/P (Spanish Ministry of Economy and Competitiveness), PLAT/2009-012 (Valencian government, Spain), and Universitat de València (UV-BI-12-007).

### Notes

The authors declare no competing financial interest.

## ABBREVIATIONS USED

Ens, enniatins; BEA, beauvericin; ENA, enniatin A; $ENA_1$, enniatin $A_1$; ENB, enniatin B; $ENB_1$, enniatin $B_1$; LC-MS/MS/LIT, liquid chromatography−mass spectrometry with linear ion trap; TC, trichothecenes; ZEN, zearalenone; FUM, fumonisins; ROS, reactive oxygen species; LPO, lipid peroxidation oxidative; OTA, ochratoxin A; AFs, aflatoxins; AcN, acetonitrile; MeOH, methanol; EtOAc, ethyl acetate; LOQ, limit of quantification; LOD, limit of detection; ME, matrix effect; DP, declustering potential; CE, collision energy; CEP, collision cell entrance

potential; EP, entrance potential; CXP, collision cell exit potential; $AFB_1$, aflatoxin $B_1$; DON, deoxynivalenol; EDI, estimated daily intake; PMTDI, provisional maximum tolerable daily intake; TDI, tolerable daily intake; JECFA, Joint Expert Committee on Food Additives

## REFERENCES


(1) Milićević, D. R.; Škrinjar, M.; Baltić, T. Real and perceived risks for mycotoxin contamination in foods and feeds: challenges for food safety control. *Toxins* **2010**, *2*, 572−592.

(2) Serrano, A. B.; Font, G.; Ruiz, M. J.; Ferrer, E. Co-occurrence and risk assessment of mycotoxins in food and diet from Mediterranean area. *Food Chem.* **2012**, *135*, 423−442.

(3) Tolosa, J.; Font, G.; Mañes, J.; Ferrer, E. Nuts and dried fruits: natural occurrence of emerging *Fusarium* mycotoxins. *Food Control* **2013**, *33*, 215−220.

(4) Santini, A.; Meca, G.; Uhlig, S.; Ritieni, A. Fusaproliferin, beauvericin and enniatins: occurrence in food − a review. *World Mycotoxin J.* **2012**, *5*, 71−81.

(5) Prosperini, A.; Juan-García, A.; Font, G.; Ruiz, M. J. Reactive oxygen species involvement in apoptosis and mitochondrial damage in Caco-2 cells induced by enniatins A, $A_1$, B and $B_1$. *Toxicol. Lett.* **2013**, *222*, 36−44.

(6) Ivanova, L.; Skjerve, E.; Eriksen, G. S.; Uhlig, S. Cytotoxicity of enniatins A, $A_1$, B, $B_1$, $B_2$ and $B_3$ from *Fusarium avenaceum*. *Toxicon* **2006**, *47*, 868−876.

(7) Jestoi, M. Emerging fusarium-mycotoxins fusaproliferin, beauvericin, enniatins, and moniliformin − a review. *Crit. Rev. Food Sci. Nutr.* **2008**, *48*, 21−49.

(8) Manyes, L.; Escrivá, L.; Serrano, A. B.; Rodríguez-Carrasco, Y.; Tolosa, J.; Meca, G.; Font, G. A preliminary study in Wistar rats with enniatin A contaminated feed. *Toxicol. Mech. Methods* **2014**, *24*, 179−190.

(9) Juan, C.; Manyes, L.; Font, G.; Juan-García, A. Evaluation of immunologic effect of enniatin A and quantitative determination in feces, urine and serum on treated Wistar rats. *Toxicon* **2014**, *87*, 45−53.

(10) Devreese, M.; De Baere, S.; De Backer, P.; Croubels, S. Quantitative determination of the *Fusarium* mycotoxins beauvericin, enniatin A, $A_1$, B and $B_1$ in pig plasma using high performance liquid chromatography−tandem mass spectrometry. *Talanta* **2013**, *106*, 212−219.

(11) Ivanova, L.; Fæste, C. K.; Van Pamel, E.; Daeseleire, E.; Callebaut, A.; Uhlig, S. Presence of enniatin B and its hepatic metabolites in plasma and liver samples from broilers and eggs from laying hens. *World Mycotoxin J.* **2014**, *7*, 167−175.

(12) Zinedine, A.; Mañes, J. Occurrence and legislation of mycotoxins in food and feed from Morocco. *Food Control* **2009**, *20*, 334−344.

(13) Hooft, J. M.; Elmor, A. E. H. I.; Encarnação, P.; Bureau, D. P. Rainbow trout (*Oncorhynchus mykiss*) is extremely sensitive to the feed-borne *Fusarium* mycotoxin deoxynivalenol (DON). *Aquaculture* **2011**, *311*, 224−232.

(14) Binder, E. M. Managing the risk of mycotoxins in modern feed production. *Anim. Feed Sci. Technol.* **2007**, *133*, 149−166.

(15) Tan, D. C.; Flematti, G. R.; Ghisalberti, E. L.; Sivasithamparam, K.; Chakraborty, S.; Obanor, F.; Barbetti, M. J. Mycotoxins produced by *Fusarium* species associated with annual legume pastures and sheep feed refusal disorders in Western Australia. *Mycotoxin Res.* **2011**, *27*, 123−135.

(16) Fraga, M.; Curvello, F.; Gatti, M.; Cavaglieri, L.; Dalcero, A.; Da Rocha Rosa, C. Potential aflatoxin and ochratoxin A production by *Aspergillus* species in poultry feed processing. *Vet. Res. Commun.* **2007**, *31*, 343−353.

(17) Santacroce, M. P.; Narracci, M.; Acquaviva, M. I.; Cavallo, R. A.; Zacchino, V.; Centoducati, G. New development in aflatoxin research: from aquafeed to marine cells. *Aflatoxins* **2009**, *2*, 209−234.

(18) Rosa, C.; Keller, K.; Keller, L.; González Pereyra, M.; Pereyra, C.; Dalcero, A.; Cavaglieri, L.; Lopes, C. Mycological survey and ochratoxin A natural contamination of swine feedstuffs in Rio de Janeiro State, Brazil. *Toxicon* **2009**, *53*, 283−288.

(19) Püssa, T. Toxicological issues associated with production and processing of meat. *Meat Sci.* **2013**, *95*, 844−853.

(20) Martins Almeida, I. F.; Martins, H. M. L.; Santos, S. M. O.; Freitas, M. S.; Nunes da Costa, J. M. G. Mycobiota and aflatoxin B1 in feed for farmed sea bass (*Dicentrarchus labrax*). *Toxins* **2011**, *3*, 163−171.

(21) Pietsch, C.; Kersten, S.; Burkhardt-Holm, P.; Valenta, H.; Dänicke, S. Occurrence of deoxynivalenol and zearalenone in commercial fish feed: an initial study. *Toxins* **2013**, *5*, 184−192.

(22) Bakos, K.; Kovács, R.; Staszny, Á.; Sipos, D. K.; Urbányi, B.; Müller, F.; Csenki, Z.; Kovács, B. Developmental toxicity and estrogenic potency of zearalenone in zebrafish (*Danio rerio*). *Aquatic Toxicol.* **2013**, *136*, 13−21.

(23) Jakić-Dimić, D.; Jeremić, S.; Nešić, K.; Radosavljević, V. The influence of mycotoxins in food on fish health status. *Proc. Nat. Sci. Matica Srpska* **2005**, *109*, 73−79.

(24) Labarta, U. The development of agriculture in Spain. *Arbor* **2007**, *182*, 669−685.

(25) FAO El estado mundial de la pesca y la acuicultura 2012, ISBN 978-92-5-307225-5, http://www.fao.org/docrep/016/i2727s/i2727s.pdf (accessed May 26, 2014).

(26) Bahurmiz, O. M.; Ng, W. K. Effects of dietary palm oil source on growth, tissue fatty acid composition and nutrient digestibility of red hybrid tilapia, *Oreochromis* sp., raised from stocking to marketable size. *Aquaculture* **2007**, *262*, 382−392.

(27) Ivić, D.; Domijan, A. M.; Peraica, M.; Miličević, T.; Cvjetković, B. *Fusarium spp.* contamination of wheat, maize, soybean and pea grain in Croatia. *Arh. Hig. Rada Toksikol.* **2009**, *60*, 435−442.

(28) Accensi, F.; Abarca, M.; Cabañes, F. Occurrence of *Aspergillus* species in mixed feeds and component raw materials and their ability to produce ochratoxin A. *Food Microbiol.* **2004**, *21*, 623−627.

(29) Binder, E.; Tan, L.; Chin, L.; Handl, J.; Richard, J. Worldwide occurrence of mycotoxins in commodities, feeds and feed ingredients. *Anim. Feed. Sci. Technol.* **2007**, *137*, 265−282.

(30) Caruso, D.; Talamond, P.; Moreau, Y. Mycotoxines et pisciculture: un risque oublié? *Cah. Agric.* **2013**, *22*, 165−173.

(31) Grigorakis, K. Compositional and organoleptic quality of farmed and wild gilthead sea bream (*Sparus aurata*) and sea bass (*Dicentrarchus labrax*) and factors affecting it: a review. *Aquaculture* **2007**, *272*, 55−75.

(32) Mataix, J.; Mañas, M.; Llopis, J.; Martínez de Victoria, E.; Juan, J.; Borregón, A. *Tablas de Composición de Alimentos Españoles*; Universidad de Granada: Granada, Spain, 1998; ISBN 9788433849809.

(33) Alasalvar, C.; Taylor, K. D. A.; Zubcov, E.; Shahidi, F.; Alexis, M. Differentiation of cultured and wild sea bass (*Dicentrarchus labrax*): total lipid content, fatty acid and trace mineral composition. *Food Chem.* **2002**, *79*, 145−150.

(34) Mnari, A.; Bouhlel, I.; Chraief, I.; Hammami, M.; Romdhane, M. S.; El Cafsi, M.; Chaouch, A. Fatty acids in muscles and liver of Tunisian wild and farmed gilthead sea bream, *Sparus aurata*. *Food Chem.* **2007**, *100*, 1393−1397.

(35) European Commission, Decision 2002/657/EC of 12 August 2002, implementing Council Directive 96/23/EC concerning the performance of analytical methods and the interpretation of results. *Off. J. Eur. Union* **2002**, *L221*, 8−36.

(36) Ballesteros-Gómez, A.; Rubio, S.; Pérez-Bendito, D. Analytical methods for the determination of bisphenol A in food. *J. Chromatogr., A* **2009**, *1216*, 449−469.

(37) Warth, B.; Parich, A.; Atehnkeng, J.; Bandyopadhyay, R.; Schuhmacher, R.; Sulyok, M.; Krska, R. Quantitation of mycotoxins in food and feed from Burkina Faso and Mozambique using a modern LC-MS/MS multitoxin method. *J. Agric. Food Chem.* **2012**, *60*, 9352−9363.

(38) Jurjevic, Z.; Solfrizzo, M.; Cvjetkovic, B.; De Girolamo, A.; Visconti, A. Occurrence of beauvericin in corn from Croatia. *Food Technol. Biotechnol.* **2002**, *40*, 91−94.

(39) Lee, K. E.; Kim, B. H.; Lee, C. Occurrence of *Fusarium* mycotoxin beauvericin in animal feeds in Korea. *Anim. Feed Sci. Technol.* **2010**, *157*, 190−194.

(40) Çakmak, M. N.; Kazim, A. Mycological and bacteriological survey on fish feed ingredients and mixed feeds in Elazing Province (online). *J. Biol. Sci.* **2002**, *2*, 757−758.
(41) Wu, F. Retention of diet-related mycotoxins in tissues of channel catfish. *Dissertation Abstr. Int. Part B: Sci. Eng.* **1999**, *59*, 3791.
(42) Devreese, M.; Broekaert, N.; De Mil, T.; Fraeyman, S.; De Backer, P.; Croubels, S. Pilot toxicokinetic study and absolute oral bioavailability of the *Fusarium* mycotoxin enniatin B1 in pigs. *Food Chem. Toxicol.* **2014**, *63*, 161−165.
(43) El-Sayed, Y. S.; Khalil, R. H. Toxicity, biochemical effects and residue of aflatoxin $B_1$ in marine water-reared sea bass (*Dicentrarchus labrax*). *Food Chem. Toxicol.* **2009**, *47*, 1606−1609.
(44) Nomura, H.; Ogiso, M.; Yamashita, M.; Takaku, H.; Kimura, A.; Chikasou, M. Uptake by dietary exposure and elimination of aflatoxins in muscle and liver of rainbow trout (*Oncorhynchus mykiss*). *J. Agric. Food Chem.* **2011**, *59*, 5150−5158.
(45) Deng, S.; Tian, L.; Liu, F.; Jin, S.; Liang, G.; Yang, H. Toxic effects and residue of aflatoxin $B_1$ in tilapia (*Oreochromis niloticus* × *O. aureus*) during long-term dietary exposure. *Aquaculture* **2010**, *307*, 233−240.
(46) MAGRAMA. Ministry of Agriculture, Food and Environment. Data on food consumption, 2014, http://www.magrama.gob.es/es/alimentacion/temas/consumo-y-comercializacion-y-distribucion-alimentaria/panel-de-consumo-alimentario/base-de-datos-de-consumo-en-hogares/consulta10.asp (accessed July 2, 2014).
(47) SCF. Opinion of the Scientific Committee on Food on *Fusarium* toxins. Parts 6: Group evaluation of T-2 toxin, HT-2 toxin, nivalenol and deoxynivalenol. Scientific Committee on Food: SCF/CS/CNTM/MYC/27 Final.n., 2002.

**Scheme 1. Schematic Illustration of the SPR Sensor for Detecting MEL**

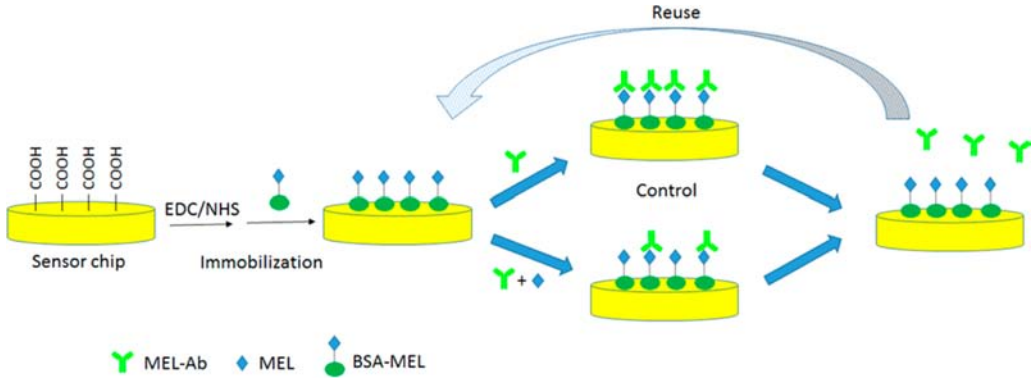


triazin-2-yl)methyl)thio)propanoic acid, with BSA. MEL−Ab was generated against MEL hapten−ovalbumin (OVA) immunogen.

**Instrumentation.** The GE BIAcore X100 and the sensor chips (CM-5, which contain a carboxymethylated dextran matrix on a thin gold surface) were purchased from GE Healthcare (Tianjin, China). A BIAcore X100 system contains two flow cells in a sequential array. One of the cells was used for the test, and another one was treated as a blank cell. A centrifugal machine (Sigma, 3-30K) and an ultrafine filter (Sartorius, Germany) were used for sample preparation.

**Sensor Platform Preparation.** The MEL−BSA conjugates were immobilized onto the sensor chip using the EDC/NHS method. Briefly, a CM 5 sensor chip was activated by injecting 170 $\mu$L of 0.4 mol/L EDC and 0.1 mol/L NHS (1:1, v/v) into the flow cell at a flow rate of 30 $\mu$L/min. After a rinse with HBS at 30 $\mu$L/min (5 min), 175 $\mu$L of MEL−BSA (9 $\mu$g/mL) in acetate buffer, pH 4.5, was injected into the flow cell for immobilization. Any unreacted sites were deactivated by applying 126 $\mu$L of ethanolamine solution (61.08 mg/mL, pH 8.5) on the sensor surface. Finally, the chip surface was rinsed and stored at 4 °C before use.

**Preparation of MEL and Its Analogue Standards.** Standard stock solutions of MEL and its analogues (cyanuric acid, cyanuric chloride, and atrazine) were prepared by dissolving an appropriate amount of each chemical in HBS buffer to make a final concentration of $1.0 \times 10^3$ $\mu$g/mL. For atrazine, methanol was utilized to enhance the dissolution and make the refraction index changes (RIU). The individual stock solutions were stored in glass amber vials at 4 °C. The working standards were prepared by diluting the stock solutions in the assay buffer just before use.

**Measuring Procedure of MEL.** One hunder and ninety microliter MEL working standards at different concentrations (0, $0.5 \times 10^{-3}$, $1 \times 10^{-3}$, $5 \times 10^{-3}$, 0.01, 0.05, 0.10, 0.15, and 0.20 $\mu$g/mL) were prepared in HBS and incubated with 10 $\mu$L of MEL−Ab (100 $\mu$g/mL) for 10 min. Following this, 200 $\mu$L of each MEL/MEL−Ab mixture was injected into the flow cell (30 $\mu$L/min) for 3 min individually to allow the un-MEL-bound antibodies to bind with the immobilized MEL−BSA conjugates. The schematic diagram is shown in Scheme 1.

**Sensor Regeneration.** Gly−HCl, NaOH, SDS, and HCl at different concentrations and pH were tested to disassociate the combination of the antibody−analyte without removing the MEL−BSA conjugates from the sensor surface. After the each detection, 60 $\mu$L of the tested solution above was injected into the flow cell at 30 $\mu$L/min and rinsed with HBS.

**Cross-Reactivity.** The specificity of the assay was evaluated using selected structurally related MEL analogues in the concentration range of 0−0.20 $\mu$g/mL. These were cyanuric chloride, cyanuric chloride, cyanuric acid, cyromazine, and atrazine. Percent cross-reactivity (% CR) was calculated at $IC_{50}$:

$$\text{cross-reactivity (\%) at } IC_{50} = \left( \frac{IC_{50}\ \text{MEL}}{IC_{50}\ \text{test compound}} \right) \times 100$$

$IC_{50}$ is defined as the concentration of a test compound at which the corresponding absorbance is equal to half of the maximum absorbance.

**Sample Preparation and Spiking Method.** The milk products and pet food samples were obtained from a local supermarket and known to be MEL free.

*Full-Cream Milk.* Ten milliliters of milk sample was spiked with MEL stock solution to make final concentrations of 0.5, 2.0, and 10.0 $\mu$g/mL. After centrifugation (14243*g*, 30 min), the supernatant was 10-fold diluted and ultrafiltered. Finally, the supernatant was collected and diluted another 10 times with HBS buffer before it was loaded on the SPR sensor.

*Skim Milk Powder.* A 1.53 g sample of the skim milk powder was spiked with MEL and left overnight before it was dissolved into 10 mL of ultrapure water. The final concentrations of MEL were 0.5, 2.0, and 10.0 $\mu$g/mL. After centrifugation (14243*g*, 30 min), the supernatant was ultrafiltered and 10-fold diluted with ultrapure water for ultrafiltration. The diluted sample was ultrafiltered and diluted another 10 times with HBS buffer before use.

*Infant Formula.* Similarly to skim milk powder, the infant formula (1.53 g) was spiked with MEL. After overnight incubation, the spiked samples were dissolved into 10 mL of ultrapure water to make final concentrations of 0.5, 2.0, and 10.0 $\mu$g/mL. The samples were centrifuged (14243*g*, 30 min) to collect the supernatant. Following this, the supernatant was 10-fold diluted with ultrapure water and ultrafiltered before another 10-fold dilution with HBS.

*Cat Food and Dog Food.* In the spiking experiment, the cat food (or dog food) sample was crushed with triturator, then 1.0 g of sample was spiked with MEL stock solution and allowed to stand at room temperature overnight. Following this, the spiked sample was homogenized and immersed in 10 mL of ultrapure water to final concentrations of MEL at 0.5, 2.0, and 10.0 $\mu$g/mL. After being sonicated for 30 min, the sample was centrifuged (14243*g*, 15 min) and the supernatant was collected and diluted 100-fold with HBS before the SPR analysis.

## RESULTS AND DISCUSSION

**Fabrication of the Immunosensor Surface.** The immobilization strategy was to covalently bind MEL−BSA with activated carboxyl dextran using the EDC/NHS method. In this study, the acetate buffer at different pH values (4.0, 4.5, 5.0, and 5.5) was used to prepare MEL−BSA solution at the concentration of 9.0 $\mu$g/mL for optimizing the MEL−BSA conjugate immobilization condition. The MEL−BSA stock solution ($1.0 \times 10^{-3}$ $\mu$g/mL) was diluted to 9.0 $\mu$g/mL and injected into the flow cell at the rate of 30 $\mu$L/min for 3 min.

All of the immobilization process was performed by the instrument and is demonstrated in Figure S1 in the Supporting Information. In the immobilization pH-scouting procedure, MEL−BSA diluted in coupling buffer with different pH values was immobilized onto the sensor surface using electrostatic adsorption. The amount of immobilized MEL−BSA increased as the buffer pH decreased during the immobilization process

(Supporting Information, Figure S2). The relative response at pH 5.0 was only one-third of that at pH 4.5. The reason was that when the pH of the coupling buffer was in the range of 3.5−4.7 (the isoelectric point of BSA), the dextran on the sensor surface was negatively charged and the MEL−BSA conjugate was positively charged, causing MEL−BSA to favor covalent immobilizatiom on the sensor surface. However, at pH 4.0, a saturation point was observed, which implied the amount of MEL−BSA conjugate was overloaded; even the relative response was much higher than the one under pH 4.5. Therefore, by comparison of all the results of regeneration conditions, the acetate buffer at pH 4.5 was selected as the coupling buffer for the further experiment.

**Optimization of the Regeneration Procedure.** Regeneration is the process of removing bound MEL−Ab from the chip surface without damaging the MEL−BSA layer after one sample analysis in preparation for the next analysis cycle. The regeneration procedure was optimized in this study to improve the stability and reusability of the sensor.

Different regeneration conditions were tested including 0.01 mol/L Gly−HCl (pH 1.5, 2.0, and 2.5), the NaOH solution (0.05, 0.04, 0.03, and 0.02 mol/L), 5% SDS, and 0.1 mol/L HCl. The change of baseline response and response after immobilization of MEL−BSA (sample response) were compared (Supporting Information, Figure S3).

In the Gly, SDS, and NaOH condition, the baseline was continuously growing, whereas the sample response was decreasing under the influence. This indicated that the bound MEL−Ab was hardly removed from the sensor surface by these regeneration solutions. However, when HCl was used, there was no significant change in baseline and sample response, indicating there was no damage to the MEL−BSA layer. Thus, 0.1 mol/L HCl was selected as the regeneration solution for the chip.

The reusability of the sensor was evaluated by several replicate analyses in 1 month. With 5 $\mu$g/mL MEL−Ab injected in the flow cell, the relative response was reduced only <5% after 500 analysis cycles, which showed the high stability and reusability of the sensor surface.

**Detection of MEL by SPR Immunosensor.** The principle for detecting MEL was based on the inhibition assay. Briefly, 5 $\mu$g/mL of MEL−Ab was mixed with different concentrations of MEL (0, $0.5 \times 10^{-3}$, $1 \times 10^{-3}$, $5 \times 10^{-3}$, 0.01, 0.05, 0.10, 0.15, and 0.20 $\mu$g/mL), respectively. After 10 min of inhibition, the mixture was injected into the sensor chip by series system from channel 2 to channel 1. Channel 1 was used as blank to reduce the nonspecific adsorption and control the bulk effects, which may be caused by the different refractive indices of the instrument buffer and the sample solution.

The standard curve for MEL is illustrated in Figure 1. Under the optimal condition, the linearity region for measuring MEL had a wide range of $1.40 \times 10^{-3}$−0.1729 $\mu$g/mL. The LOD at a signal-to-noise ratio of 3.0 (S/N = 3.0) and the limit of quantitation (LOQ, S/N = 10.0) were $1.40 \times 10^{-3}$ and $2.32 \times 10^{-2}$ $\mu$g/mL, respectively. Higher sensitivity of MEL was achieved by SPR sensor than the reported measurement methodologies.[28]

**Specificity Research.** To validate the specificity of the sensor, percent cross-reactivity (%CR) for MEL was tested using four MEL analogues (cyanuric acid, cyromazine, atrazine, and cyanuric chloride). Table 1 exhibits the %CR of the SPR sensor calculated at $IC_{50}$ values.

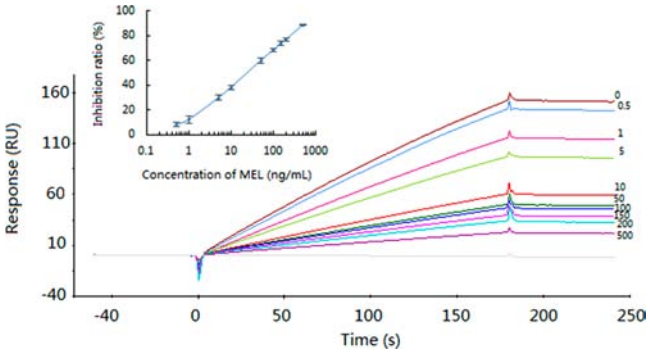


**Figure 1.** Response results corresponding with MEL−Ab mixed with different concentrations of MEL and the standard curve of SPR for MEL.

%CRs for most of the MEL analogues (cyanuric chloride, cyanuric acid, and atrizine) were <0.01% except cyromazine, which was up to 599%. This result was similar to that in a previous study.[29] The electronic configuration to MEL and the MEL hapten were more similar. The extra lone pair of electrons from the hydroxyl group in ammeline was able to inhibit binding with MEL−Ab.[29] However, because MEL was the major metabolite of cyromazine, the high %CR was not a detrimental feature of the assay.[30]

**Matrix Effect.** Matrix interferences such as pigment, protein, fat, and excess salt or sugar in foods can cause false positives by interfering with the antigen−antibody interaction.[31] For the milk products and pet food samples that contain protein and fat, the matrix interference could be simply minimized by the centrifugation, dilution, and ultrafiltration. The standard curves in the HBS buffer and the food samples shown in Figure 2 were overlapped, indicating there was no sample matrix effect. The sensitivities of the assay in full-cream milk, skim milk powder, infant formula, dog food, and cat food were higher than in the other studies,[28,32,33] which were $2.57 \times 10^{-2}$ $\mu$g/mL, $2.32 \times 10^{-2}$ $\mu$g/kg, $2.51 \times 10^{-2}$ $\mu$g/kg, $2.66 \times 10^{-2}$ $\mu$g/kg, and $2.68 \times 10^{-2}$ $\mu$g/kg, respectively. They were much lower than the MRLs for MEL set by the U.S. Food and Drug Administration (FDA) (1.0 mg/kg for infant formula and 2.5 mg/kg for normal milk, milk products, and animal feed).

**Recovery Studies of Food Samples.** Full-cream milk sample was spiked to $5 \times 10^{-3}$, 0.02, and 0.1 $\mu$g/mL MEL. Infant formula, skim milk powder, cat food, and dog food were spiked to $5 \times 10^{-3}$, 0.02, and 0.1 $\mu$g/kg MEL. The data shown in Table 2 represented the recoveries of MEL: 76.4−105.0% for full-cream milk, 97.9−99.9% for skim milk powder, 79.0−113.5% for infant formula, 86.0−113.3% for dog food, and 73.5−109.4% for cat food. In general, most of the recoveries were within a reasonable range of 73.5−113.5%. The recovery result in skim milk powder was better than the others. The reason may be that the residual fat may have a little influence on the responses of the SPR sensor. As above, the SPR method used to detect samples in milk products and pet food was feasible with precise quantitative and qualitative analysis by a simple preparation.

In summary, a SPR biosensor based on competitive format with MEL−BSA immobilized onto a gold surface was developed to monitor MEL in food samples. The optimized assay was proved to detect MEL with high rapidity, sensitivity, and stability. The cycle of sample detection could finish in 15 min including binding of 180 s and regeneration of 60 s. A good

Table 1. CR of SPR Sensor Calculated at $IC_{50}$ Values[a]

| compound | structural formula | $IC_{50}$ (ng/mL) | cross-reactivity (%) |
|---|---|---|---|
| MEL hapten | 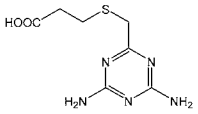 | - | - |
| MEL | 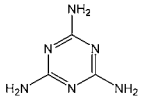 | 23.2 | 100 |
| cyanuric chloride | 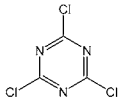 | >1000 | <0.01 |
| cyanuric acid | 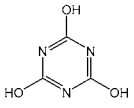 | >1000 | <0.01 |
| atrizine | 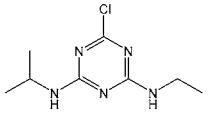 | >1000 | <0.01 |
| cyromazine | 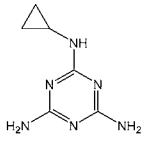 | 3.87 | 599 |

[a]–, no data shown.

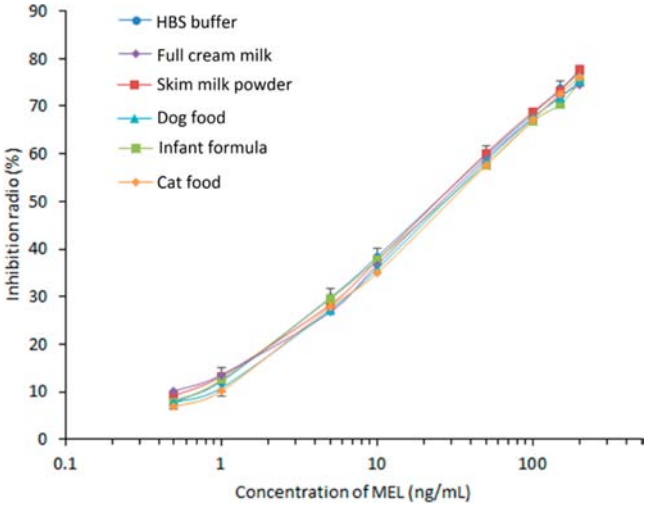


**Figure 2.** Calibration curves of MEL in different samples.

liner range from $1.40 \times 10^{-3}$ to 0.1729 $\mu$g/mL and a detection limit of $1.40 \times 10^{-3}$ $\mu$g/mL (S/N = 3.0) were obtained for the detection of MEL with SPR. The SPR chip was reused in a favorable stability, with response attenuation of <5% after 500

**Table 2. Recovery Studies of Five Samples at Three Concentration Levels by SPR Biosensor**

| sample | spiked (ng/mL) | average ± SD (ng/mL) | recovery (%) |
|---|---|---|---|
| skim milk powder | 5 | 5.0 ± 0.1 | 99.2 |
| | 20 | 19.6 ± 0.9 | 97.9 |
| | 100 | 99.9 ± 1.7 | 99.9 |
| infant formula | 5 | 4.0 ± 0.2 | 80.9 |
| | 20 | 15.8 ± 0.8 | 79.0 |
| | 100 | 113.5 ± 5.5 | 113.5 |
| milk | 5 | 3.8 ± 0.3 | 76.4 |
| | 20 | 21.0 ± 1.8 | 105.0 |
| | 100 | 92.8 ± 5.1 | 92.8 |
| dog food | 5 | 4.3 ± 0.4 | 86.0 |
| | 20 | 17.3 ± 2.1 | 86.5 |
| | 100 | 113.3 ± 6.9 | 113.3 |
| cat food | 5 | 3.7 ± 0.1 | 74.0 |
| | 20 | 14.7 ± 1.2 | 73.5 |
| | 100 | 109.4 ± 6.0 | 109.4 |


dx.doi.org/10.1021/jf504055g | J. Agric. Food Chem. 2014, 62, 12471−12476

analysis cycles. The recovery results for infant formula, skim milk powder, full-cream milk, dog food, and cat food using this SPR assay ranged from 73.5 to 113.5%. On the basis of the SPR assay, the proposed method was found to have wide potential applications and rapid detection of various contaminants in food safety.

## ■ ASSOCIATED CONTENT

### Supporting Information

Figures S1−S3. This material is available free of charge via the Internet at http://pubs.acs.org.

## ■ AUTHOR INFORMATION


### Corresponding Author

*(S.W.) Phone: (86 22) 60601430. Fax: (86 22) 60601332. E-mail: s.wang@tust.edu.cn.

### Author Contributions

‖Y.L. and Y.X. contributed equally to this work as the first authors.



### Funding

This work is financially supported by the Ministry of Science and Technology of the People's Republic of China (2013BAD18B11), Industry of Quality Public Welfare Scientific Research (201310146-3), the program for Changjiang Scholars and Innovative Research Team in University (IRT1166), and the Student Lab Innovations Fund project from Tianjin University of Science and Technology (Project 1414A209).


### Notes

The authors declare no competing financial interest.

## ■ REFERENCES


(1) Sugita, T.; Ishiwata, H.; Yoshihira, K. Release of formaldehyde and melamine from tableware made of melamine-formaldehyde resin. *Food Addit. Contam.* **1990**, *7*, 7−21.

(2) Ehling, S.; Tefera, S.; Ho, I. P. High-performance liquid chromatographic method for the simultaneous detection of the adulteration of cereal flours with melamine and related triazine by-products ammeline, ammelide, and cyanuric acid. *Food Addit. Contam.* **2007**, *24*, 1319−1325.

(3) Yang, S. P.; Ding, J. H.; Zheng, B.; Hu, J.; Li, H.; Chen, Z.; Zhou, X. Detection of melamine in milk products by surface desorption atmospheric pressure chemical ionization mass spectrometry. *Anal. Chem.* **2009**, *81*, 2426−2436.

(4) Huang, G. M.; Ouyang, Z.; Cooks, R. G. High-throughput trace melamine analysis in complex mixtures. *Chem. Commun.* **2009**, *5*, 556−558.

(5) Yardley, J.; Barboza D. Despite warnings (2008), China's regulators failed to stop milk; http://www.heraldtribune.com/article/20080927/ZNYT03/809270413/1006/SPORTS?Title=Despite_Warnings__China__x2019_s_Regulators_Failed_to_Stop_Milk (accessed Aug 25, 2014).

(6) Brown, C. A.; Jeong, K.-S.; Poppenga, R. H.; Puschner, B.; Miller, D. M.; Ellis, A. E.; Kang, K.-II; Sum, S.; Cistola, A. M.; Brown, S. A. Outbreaks of renal failure associated with melamine and cyanuric acid in dogs and cats in 2004 and 2007. *J. Vet. Diagn. Invest.* **2007**, *19*, 525−531.

(7) Puschner, B.; Poppenga, R. H.; Lowenstine, L. J.; Filigenzi, M. S.; Pesavento, P. A. Assessment of melamine and cyanuric acid toxicity in cats. *J. Vet. Diagn. Invest.* **2007**, *19*, 616−624.

(8) Richard, S. China accused over contaminated baby milk, 2008; http://www.telegraph.co.uk/news/worldnews/asia/china/2963808/China-accused-over-contaminated-baby-milk.html (accessed Aug 25, 2014).

(9) Chan, E. Y. Y.; Griffiths, S. M.; Chan, C. W. Public-health risks of melamine in milk products. *Lancet* **2008**, *372*, 1444−1445.

(10) Zhou, Y.; Li, C. Y.; Li, Y. S.; Ren, H. L.; Lu, S.-Y.; Tian, X.-L.; Hao, Y.-M.; Zhang, Y.-Y.; Shen, Q.-F.; Liu, Z.-S.; Meng, X.-M.; Zhang, J.-H. Monoclonal antibody based inhibition ELISA as a new tool for the analysis of melamine in milk and pet food samples. *Food Chem.* **2012**, *135*, 2681−2686.

(11) Lei, H. T.; Su, R.; Haughey, S. A.; Wang, Q.; Xu, Z.; Yang, J.; Shen, Y.; Wang, H.; Jiang, Y.; Sun, Y. Development of a specifically enhanced enzyme-linked immunosorbent assay for the detection of melamine in milk. *Molecules* **2011**, *16*, 5591−5603.

(12) Liu, J. X.; Zhong, Y. B.; Liu, J.; Zhang, H. C.; Xi, J. Z.; Wang, J. P. An enzyme linked immunosorbent assay for the determination of cyromazine and melamine residues in animal muscle tissues. *Food Control* **2010**, *21*, 1482−1487.

(13) Desmarchelier, A.; Cuadra, M. G.; Delatour, T.; Mottier, P. Simultaneous quantitative determination of melamine and cyanuric acid in cow's milk and milk-based infant formula by liquid chromatography-electrospray ionization tandem mass spectrometry. *J. Agric. Food Chem.* **2009**, *57*, 7186−7193.

(14) Goscinny, S.; Hanot, V.; Halbardier, J. F.; Michelet, J. Y.; Van Loco, J. Rapid analysis of melamine residue in milk, milk products, bakery goods and flour by ultra-performance liquid chromatography/tandem mass spectrometry from food crisis to accreditation. *Food Control* **2011**, *22*, 226−230.

(15) MacMahon, S.; Begley, T. H.; Diachenko, G. W.; Stromgren, S. A. A liquid chromatography-tandem mass spectrometry method for the detection of economically motivated adulteration in protein-containing foods. *J. Chromatogr., A* **2012**, *1220*, 101−107.

(16) Tyan, Y. C.; Yang, M. H.; Jong, S. B.; Wang, C. K.; Shiea, J. Melamine contamination. *Anal. Bioanal. Chem.* **2009**, *395*, 729−735.

(17) Squadrone, S.; Ferro, G. L.; Marchis, D.; Mauro, C.; Palmegiano, P.; Amato, G.; Genin, E. P.; Abete, M. C. Determination of melamine in feed: validation of a gas chromatography-mass spectrometry method according to 2004/882/CE regulation. *Food Control* **2010**, *21*, 714−718.

(18) Hsu, Y. F.; Chen, K. T.; Liu, Y. W.; Hsieh, S. H.; Huang, H. Y. Determination of melamine and related triazine by-products ammeline, ammelide, and cyanuric acid by micellar electrokinetic chromatography. *Anal. Chim. Acta* **2010**, *673*, 206−211.

(19) Du, X. B.; Chu, H. Y.; Huang, Y. W.; Zhao, Y. P. Qualitative and quantitative determination of melamine by surface-enhanced raman spectroscopy using silver nanorod array substrates. *Appl. Spectrosc.* **2010**, *64*, 781−785.

(20) Vaclavik, L.; Rosmus, J.; Popping, B.; Hajslova, J. Rapid determination of melamine and cyanuric acid in milk powder using direct analysis in real time-time-of-flight mass spectrometry. *J. Chromatogr., A* **2010**, *1217*, 4204−4211.

(21) Campbell, J. A.; Wunschel, D. S.; Petersen, C. E. Analysis of melamine, cyanuric acid, ammelide, and ammeline using matrix-assisted laser desorption ionization/time-of-flight mass spectrometry (MALDI/TOFMS). *Anal. Lett.* **2007**, *40*, 3107−3118.

(22) WHO. International experts limit melamine levels in food, 2010; http://www.who.int/mediacentre/news/releases/2010/melamine_food_20100706/en/ (accessed Aug 25, 2014).

(23) Liu, Y.; Todd, E. E. D.; Zhang, Q.; Shi, J. R.; Liu, X. J. Recent developments in the detection of melamine. *Biomed. Biotechnol.* **2012**, *13*, 525−532.

(24) Homola, J. Present and future of surface plasmon resonance biosensors. *Anal. Bioanal. Chem.* **2003**, *377*, 528−539.

(25) Haasnoot, W.; Olieman, K.; Cazemier, G.; Verheijen, R. Direct biosensor immunoassays for the detection of nonmilk proteins in milk powder. *J. Agric. Food Chem.* **2001**, *49*, 5201−5206.

(26) Spadavecchia, J.; Manera, M. G.; Quaranta, F.; Siciliano, P.; Rella, R. Surface plamon resonance imaging of DNA based biosensors for potential applications in food analysis. *Biosens. Bioelectron.* **2005**, *21*, 894−900.

(27) Shi X. W. *Development of Enzyme-Linked Immunoseorbent Assay for the Determination of Melamine*. M.S. thesis, Tianjin University of Science and Technology, 2012.

(28) Guo, H.; Zhou, X.; Zhang, Y.; Song, B.; Liu, L.; Zhang, J.; Shi, H. Highly sensitive and rapid detection of melamine in milk products by planar waveguide fluorescence immunosensor (PWFI). *Sensor. Actuat. B—Chem.* **2014**, *194*, 114—119.
(29) Fodey, T. L.; Thompson, C. S.; Traynor, I. M.; Haughey, S. A.; Kennedy, D. G.; Crooks, S. R. H. Development of an optical biosensor based immunoassay to screen infant formula milk samples for adulteration with melamine. *Anal. Chem.* **2011**, *83*, 5012—5016.
(30) Caldas, E. D. Cyromazine, 2010; http://www.fao.org/fileadmin/templates/agphome/documents/Pests_Pesticides/JMPR/Evaluation07/Cyromazine.pdf (accessed Jan 29, 2010).
(31) Lu, Y.; Peterson, J. R.; Gooding, J. J.; Lee, N. A. Development of sensitive enzyme-linked immunosorbent assays (ELISAs) for monitoring of bisphenol-A in foods and beverages. *Anal. Bioanal. Chem.* **2012**, *403*, 1607—1618.
(32) Fodey, T. L.; Thompson, C. S.; Traynor, I. M.; Simon, A. H.; Kennedy, D. G.; Crooks, S. R. H. Development of an optical biosensor based immunoassay to screen infant formula milk samples for adulteration with melamine. *Anal. Chem.* **2011**, *83*, 5012—5016.
(33) Wu, H. N.; Li, H. Y.; Chua, F. Z.-H.; Li, S. F. Y. Rapid detection of melamine based on immunoassay using portable surface plasmon resonance biosensor. *Sensor. Actuat. B—Chem.* **2013**, *178*, 541—546.

investigation has been conducted to identify chemical triggers for the enhanced lipid accumulation in *C. cohnii*.

In this study, we first evaluated effects of two antioxidant chemical triggers on lipid accumulation in *C. cohnii*. The results showed a differential effect of different antioxidants on lipid accumulation in *C. cohnii*, with BHA enhancing lipid content by 8.80%, while another antioxidant propyl gallate (PG) inhibiting lipid accumulation in *C. cohnii*. Currently, little is known about mode of action (MOA) of antioxidants on lipid production in microalgae, although various possible biological effects, such as modulation of photooxidative stress pathways and therefore enhance photosynthetic efficiency, have been proposed.[14] To determine the MOA, we first applied a metabolomics approach integrating both GC-MS and LC-MS to reveal time-series responses of *C. cohnii* to the antioxidant BHA. As a measurement and study of the small-molecule metabolites that constitute biochemical networks, metabolomics has recently been applied to studies of various microalgae[15−17] and was demonstrated as a valuable tool in analyzing cell metabolism.[18] Second, we constructed a metabolic network using a weighted gene coexpression network analysis (WGCNA)[19] to reveal metabolic modules and hub metabolites significantly associated with BHA supplementation. The study provided an overview of the metabolomics basis of the BHA stimulation effect of lipid accumulation in *C. cohnii*.

## MATERIALS AND METHODS

**Chemicals.** Antioxidant BHA and PG were purchased from Sigma-Aldrich (Taufkirchen, Germany) and stored at 4 °C until use. A stock solution of 10 mM BHA or PG in dimethyl sulfoxide (DMSO) was made in amber glass vials and stored in the dark at −20 °C.

**Strains and Cultivation.** *Crypthecodinium cohnii* ATCC 30772 was obtained from American Type Culture Collection (ATCC) and grown in 50 mL of basal medium (pH 6.5) consisting of 9 g/L glucose, 2 g/L yeast extract (OXOID, Basingstoke, UK), and 25 g/L sea salt (Sigma-Aldrich, USA) in 250 mL Erlenmeyer flasks at 25 °C and 180 rpm. The seed cultures were cultivated for 2 days after reaching exponential growth phase and then used to inoculate the fermentation flasks at an inoculum size of 10% (v/v). Two control cultures, one with 0.4% DMSO (v/v) and another without DMSO, were established in parallel with the chemical-spiked cultures. Varying concentrations of chemicals in 0.4% DMSO (v/v) were added at the beginning of the cultivation. Three biological replicates were established for each concentration. Cell density was measured on a UV-1750 spectrophotometer (Shimadzu, Japan) at $OD_{490}$. Cell number was determined by direct counting under microscope.

**Lipid Analysis and Extraction.** Two methods were used to determine the lipid accumulation under various chemicals in *C. cohnii* cells. The first protocol involves fluorescence intensity measurements at 510/585 nm after Nile Red staining.[20−22] A fluorescence spectrophotometer (F-2700FL, HITACHI) was used for the assay. The second protocol involves direct lipid extraction using a modified method described previously.[23] Briefly, *C. cohnii* cells were collected at 72 h by centrifugation (3500*g*) and then freeze-dried to generate a lyophilized algal powder. For lipid extraction, 15−25 mg of lyophilized algal powder was used for extraction using a chloroform/methanol solution (2:1, v/v). The extraction process was repeated three to four times, and then all organic solvents were combined and dried using a vacuum concentrator system (ZLS-1, Hunan, China).

**GC-MS and LC-MS Based Metabolomic Analysis.** All chemicals used for metabolome isolation and GC-MS and LC-MS analyses were obtained from Sigma-Aldrich (Taufkirchen, Germany). For metabolomic analysis, cells were collected by centrifugation at 8,000*g* for 10 min at 4 °C (Eppendorf 5430R, Hamburg, Germany) at three time points (i.e., 24, 48, and 72 h corresponding to exponential, transition, and stationary phases). The cell pellets were immediately frozen in liquid nitrogen and then stored at −80 °C before use. GC-MS metabolomic analysis was preformed according to methods described previously.[24,25] Briefly, the protocol included (i) metabolome extraction with cold 10:3:1 (*v*/*v*/*v*) methanol/chloroform/$H_2O$ solution (MCW); (ii) sample derivatization according to the two-stage technique;[26] (iii) GC-MS analysis on a GC-MS system-GC 7890 coupled to an MSD 5975 (Agilent Technologies, Inc., Santa Clara, CA) equipped with a HP-5MS capillary column (30 m × 250 mm id); (iv) data processing and statistical analysis using the automated massspectral deconvolution and identification system (AMDIS) to identify the compounds by matching the data with Fein Library and the mass spectral library of the National Institute of Standards and Technology (NIST). All metabolomic profile data were first normalized by the internal control and the cell numbers of the samples, and then subjected to partial least-squares-discriminant analyses (PLS-DA) using software SIMCA-P 11.5.

LC-MS metabolomic analysis was performed according to a previous publication with minor modifications.[27] Briefly, the protocol included: (i) Metabolome extraction by quenching quickly and methanol extraction;[28] (ii) LC-MS analysis using an Agilent 1260 series binary HPLC system (Agilent Technologies, Waldbronn, Germany) coupled to an Agilent 6410 triple quadrupole mass analyzer equipped with an electronic spray ion (ESI) source. A Synergi Hydro-RP (C18, 150 mm × 2.0 mm I.D., 4 μm 80 Å particles, Phenomenex, Torrance, CA) column was used for the separation of metabolites. Mobile phase A (MPA) was an aqueous 10 mM tributylamine solution adjusted to pH 4.95 with acetic acid, and Mobile phase B (MPB) was 100% HPLC grade methanol. Constant flow rate was maintained at 0.2 mL/min; (iii) Data processing and statistical analysis using Agilent Mass Hunter workstation LC/QQQ acquisition software (version B.04.01) and analyzed using Agilent Mass Hunter workstation qualitative analysis software (version B.04.00). The MS was operated in negative mode for multiple reaction monitoring (MRM) development, method optimization, and sample analysis. Injected sample volume for all cases was 10 μL; capillary voltage was 4000 V; and nebulizer gas flow rate and pressure were 10 L/min and 50 psi, respectively. Nitrogen nebulizer gas temperature was 300 °C. Metabolomic data was normalized by interior control and cell number, and then submitted to principal component analysis (PCA) using SIMCA-P 11.5.[29] A heatmap were created using MultiExperiment Viewer software available publically at http://www.tm4.org/.

**WGCNA Network Construction.** A metabolic correlation network was constructed from the metabolomic data, first by calculating weighted Pearson correlation matrices corresponding to metabolite abundance, and then by following the standard procedure of WGCNA to create the networks.[19,30] Hierarchical clustering based on topological overlap (TO) was used to group metabolites with highly similar correlation relationships into modules. The associated modules with correlation coefficient $r > 0.6$ and a statistical significance $p$-value less than 0.05 were extracted for further analysis. Hub metabolites were screened by high connectivity with other metabolites (≥5) in the modules strongly associated with phenotype.

## RESULTS AND DISCUSSION

**Screening Chemical Enhancers for Lipid Accumulation.** Based on previous results of antioxidant effects on lipid accumulation,[13] two antioxidant chemicals, BHA and PG were selected for evaluation of their effects on lipid accumulation in *C. cohnii*. In a previous study, BHA has been found to be an efficient lipophilic antioxidant in plants.[31] The roles of PG in lipid accumulation is not clearly defined yet, with one early study showing that PG can inhibit lipid accumulation in *C. cohnii*,[32] while another study showing that it can enhance lipid accumulation in *N. salina*.[14] Since both BHA and PG were dissolved in DMSO, two control cultures were established: one with 0.4% DMSO and another without. In the screening process, we determined the changes of growth and lipid content in cells, first in 96-well cultivation plates with Nile Red staining and then confirmed in 250 mL flask cultivation with

lipids extracted for more accurate quantitation. Multiple concentrations were evaluated for each chemical. The results showed that neither antioxidant of BHA and PG was found to affect cell growth under the tested conditions (Supporting Information, Figure S1); meanwhile, both antioxidants were found affecting lipid accumulation in *C. cohnii* (Table 1 and Supporting Information, Figure S2). Interestingly, BHA had positive effects on lipid accumulation at a concentration range of 40 nM to 30 $\mu$M, while PG issued no visible effect at low concentration but negative effects at high concentration (>30 $\mu$M) on lipid accumulation (Supporitng Information, Figure S2), consistent with the early study.[32] In addition, cell morphology of *C. cohnii* under various chemicals was also compared using microscopic analyses, and no significant difference was observed between treatments and controls (data not shown). Moreover, the opposite roles of antioxidant BHA and PG on lipid accumulation in *C. cohnii* found in this study suggested that the mechanisms in which antioxidants are involved in microalgae may be more complicated than previously proposed.[14] Finally, quantitative determination of DHA in the lipid was also conducted, and the results showed that although BHA can enhance total lipid content, it did not change the proportion of DHA in the total lipid (data now shown).

**Table 1. Lipid Content under Different BHA Concentrations**

| BHA concn | lipid content (mean) (%) | increasing proportion (%) |
|---|---|---|
| 40 $\mu$M | 46.11 | 0.72 |
| 30 $\mu$M | 49.81 | 8.80 |
| 4 $\mu$M | 49.17 | 7.40 |
| 400 nM | 48.79 | 6.57 |
| 40 nM | 48.34 | 5.59 |
| $C_{DMSO}$ | 46.25 | 1.03 |
| control | 45.78 | 0.00 |

**LC-MS Metabolomics Analysis.** Considering its low cost,[14] BHA could be a very useful chemical enhancer for lipid accumulation in large-scale fermentation of *C. cohnii*, so it is worth further investigating its enhancement mechanism on lipid accumulation. In the experiments, *C. cohnii* was cultivated with or without BHA for 3 days, and samples were collected at 24, 48, and 72 h, which correspond to exponential, transition, and stationary phases of the batch cultures, respectively. To exclude possible effects of DMSO since the BHA was dissolved and introduced as a DMSO solution, additional controls were also established for *C. cohnii* supplemented with 0.4% DMSO only. We then applied LC-MS based metabolomics to quantify the time series changes of selected metabolites related to central carbohydrate and energy metabolism in the *C. cohnii* cells with and without 30 $\mu$M BHA. Using the optimized protocol modified from a previous method for photosynthetic cyanobacteria,[26] reproducible analyses of 24 selected intracellular metabolites was achieved for *C. cohnii*, including acetyl coenzyme A (Ac-CoA), NADPH, NADP, NADH, NAD, ADP, UDP, ATP, ADP, Coenzyme A hydrate (CoA), AMP, D-fructose 1,6-bisphosphate (FBP), D-ribulose 1,5-bisphosphate (RuBP), D-fructose 6-phosphate (F6P), D-glucose 6-phosphate (G6P), D-ribose 5-phosphate (R5P), D-3-phosphoglyceric acid (3PG), dihydroxyacetone phosphate (DHAP), DL-glyceraldehyde 3-phosphate (GAP), phosphor-(enol)-pyruvic acid (PEP), L-glutamic acid (Glu), $\alpha$-ketoglutaric acid (AKG), oxaloacetic acid (OXA), and fumarate dibasic (FUM), mostly of which are unstable metabolites (Supporting Information, Table S1). Quantitative analyses of these targeted intracellular metabolites in samples collected at three time points (i.e., 24, 48, and 72 h) were conducted, each with three biological replicates and two analytical replicates, which led to time-series metabolomic profiles of *C. cohnii* with or without BHA. The quality of the LC-MS analysis was demonstrated from the following aspects (Figure 1): (i) all 24 metabolites were successfully detected in replicate samples of all time points and treatments; (ii) a PCA analysis of all samples showed an obvious clustering pattern for cell samples of the same time point and condition; (iii) samples of time points (i.e., 24, 48, and 72 h) were well separated; in addition, a clear moving trend of metabolomic profiles along the time courses was observed, suggesting the gradual change of the metabolic status; moreover, the analysis suggested that growth time may be a key distinguishing component which

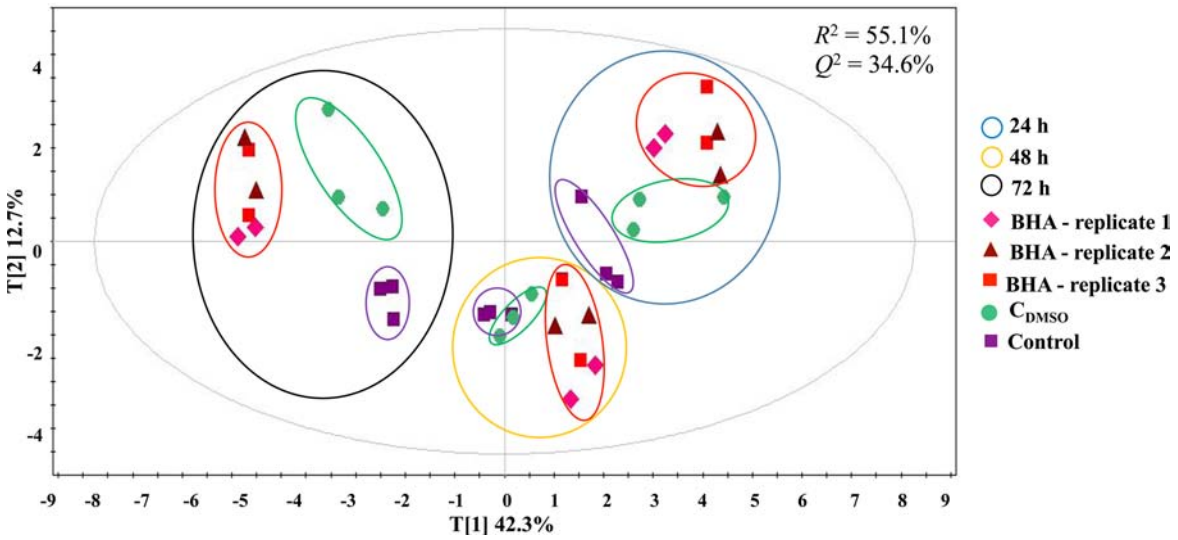


**Figure 1.** PCA analysis of LC-MS metabolomic profiles. Score plot of cell samples collected at 24, 48, and 72 h. BHA represents a microalgal cell sample grown in media supplemented with 30 $\mu$M BHA in 0.4% (v/v) DMSO. $C_{DMSO}$ represents a microalgal cell sample grown in media supplemented only with 0.4% (v/v) DMSO. Control represents a microalgal cell sample grown in media without DMSO or BHA.

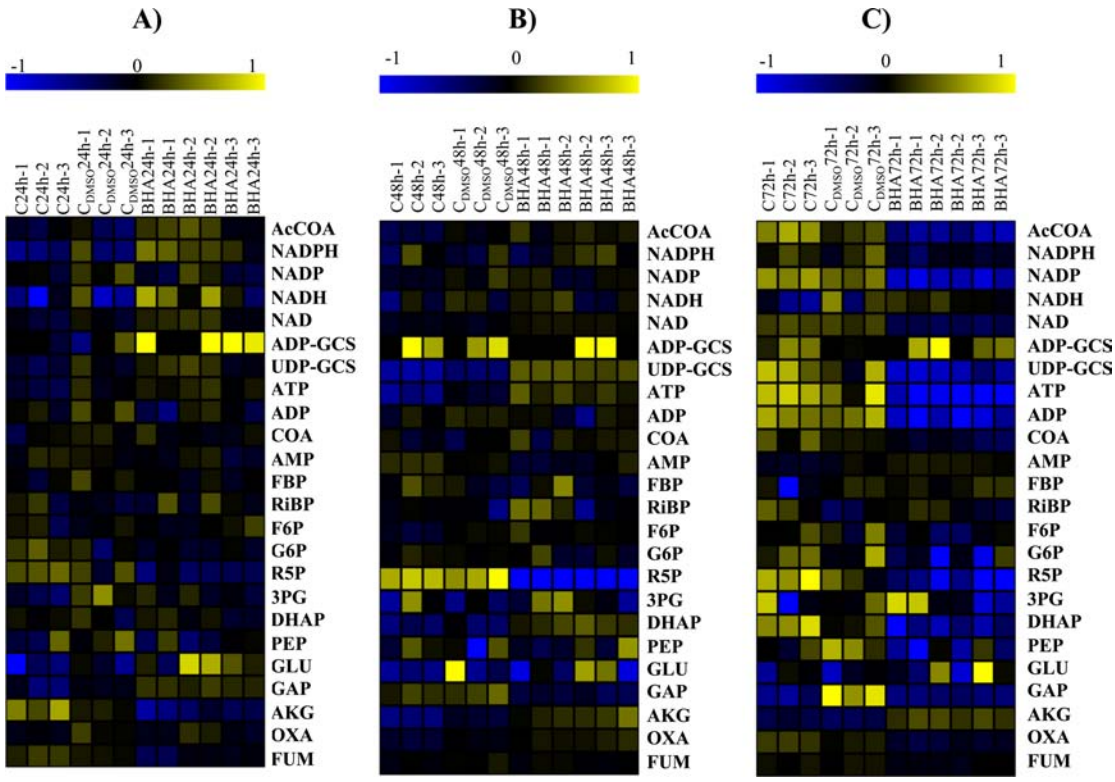


**Figure 2.** Heat maps of LC-MS metabolomic profiles. C represents control media, D represents media supplemented only with 0.4% (v/v) DMSO, and B represents BHA-spiked media. The number represents biological replicates. (A) 24 h; (B) 48 h; and (C) 72 h.

contributed significantly to the difference between samples; (iv), the samples with or without BHA can also be separated at any time point, suggesting differential metabolic changes in cells with or without BHA. Overall, the results demonstrated that the LC-MS methodology used in the study provided a good analytical resolution to distinguish various samples (Figure 1). In addition, variation of detected metabolites among biological replicates was also calculated, and a reasonably small variation was also observed, suggesting in general good quality of the LC-MS metabolomic analysis (Supporting Information, Table S2).

Heat maps of 24 metabolites in the cells with or without BHA treatment at 24, 48, and 72 h were generated (Figure 2). In the analysis, ratio of a given metabolite was calculated between the concentration of the metabolite in a given condition and the average concentration of the metabolite in all samples; a similar approach has been successfully applied in transcriptomic analysis.[33] Although the fold changes were relatively small, the results showed a clear up-regulation of ADP, NADH, NADPH, and PEP at 24 h and ATP, UDP, and GAP at 48 h. Among the BHA-induced metabolites, NADPH is an essential reducing agent for fatty acid biosynthesis, for example, it is estimated that the formation of one C18 fatty acid requires 54 NADPH from oxygenic photosynthesis in a microalgal *Phaeodactylum tricornutum*.[34] In addition, the NADPH supply has been found crucial for the DHA production in *Schizochytrium* sp. HX-308, where a reinforced acetyl-CoA and NADPH supply increased DHA content of total fatty acids from 35 to 60%.[35] Moreover, biochemical studies with the *N. salina* indicated that lipid accumulation is controlled by the availability of NADPH.[36] However, no significant increase of NADPH was observed at late stages after BHA treatment, suggesting that the effects may be related to fast growth of the cells. Interestingly, our LC-MS analysis showed that acetyl-CoA, which was considered as the major precursor for fatty acid biosynthesis, was not significantly regulated in BHA-treated samples, suggesting that the enhanced lipid synthesis by BHA may not be directly due to improved supply of the precursor acetyl-CoA.

Heat maps showed that AKG was down-regulated at 24 h but up-regulated at 72 h; and R5P was down-regulated at all three time points. Meanwhile, at 72 h of the stationary phase, most of the metabolites except AKG, PEP, and ADP, were significantly down-regulated, consistent with the slowed central carbohydrate and energy metabolisms in the aging cells. AKG is an important microbial metabolic intermediate in the citric acid cycle, a key node connecting the intracellular carbon−nitrogen metabolism.[37] Previous studies showed that in the oleaginous yeast *Yarrowia lipolytica*, AKG can behave as potent inhibitors of the malic enzyme that has been suggested as a key path to generate NADPH.[38] The down-regulation of AKG at the early phases (i.e., 24 h) and the up-regulation of AKG at the later phase (i.e., 72 h) may thus be consistent with the increased NADPH at the early phase, and the decreased NADPH at the later phase, respectively. R5P is an intermediate of the pentose phosphate pathway. In a recent study examining induction of lipid accumulation by nitrogen starvation in the green microalga *Chlamydomonas reinhardtii*, the pentose phosphate pathway was found down-regulated after lipid accumulation started.[39]

**GC-MS Metabolomic Analysis.** GC-MS based metabolomics has become a popular approach in recent years since it can achieve good coverage of polar metabolites and allow analysis of a wide range of chemical metabolite classes in a single run.[40,41] In the previous study, we developed an optimized protocol characterizing the time-series metabolic

responses for metabolite isolation and MS analysis, and achieved identification of more than 65 and 60 chemically classified metabolites from *Escherichia coli*[23] and *Synechocystis* sp. PCC 6803,[42] respectively. In this study, we first evaluated the protocol for *C. cohnii* and found that more than a hundred metabolites can be identified with good reproducibility (Supporting Information, Table S3), demonstrating that the GC-MS metabolomics approach can be applied to the study of *C. cohnii*. Following the same experimental design as LC-MS analysis described above, cells with or without 30 $\mu$M BHA treatments were collected 24, 48, and 72 h, and an extra control of only DMSO was also established as described above. Each condition carried three biological replicates, generating a total of 24 samples for GC-MS analysis. The results showed that a good separation of intracellular metabolites was achieved on the GC column, and further MS analysis allowed the chemical classification of 96 intracellular metabolites in all *C. cohnii* samples, including large number of amino acids, sugars, and organic acids (Supporting Information, Table S3). The metabolites were excluded from the list if it was detected in only one out of three replicates. The number of metabolites identified in *C. cohnii* is almost double that detected in *E. coli* and *Synechocystis*,[23,42] indicating possibly more abundant metabolites in *C. cohnii* cells. Supervised PLS-DA plots were applied to evaluate the similarities and differences between a total of 24 metabolomic profiles (Figure 3). Within each time point, BHA-treated samples were well separated from the controls at all time points. In addition, most biological replicate samples tended to be clustered together, demonstrating an overall good reproducibility.

**WGCNA Correlation Network Construction.** To further decipher mode of action of BHA in *C. cohnii*, we applied a WGCNA network analysis to the GC-MS metabolomic data sets. WGCNA is a correlation-based and unsupervised computational method to describe and visualize correlation patterns of data points[18] and was successfully applied to metabolomic data to define metabolic modules.[23,43] Following the standard protocol, we constructed unsigned networks using the GC-MS metabolomic data sets of three time points (i.e., 24, 48, and 72 h) and then localized the correlated metabolites into various metabolic modules; in addition, the association of each distinguished metabolic module with BHA treatment was also determined, as highly associated modules indicated on the plots (Figure 4). Setting a minimal number of metabolites in any module greater than 3, a cutoff of correlation coefficients ($r$ value) between module and treatment condition greater than 0.6 and their statistical confidence ($p$ value) less than 0.05, the WGCNA analysis identified 4, 2, and 2 distinct metabolic modules highly associated with BHA at 24, 48, and 72 h, respectively (Figure 4). Member metabolites clustered into each of the BHA-responsive modules are provided in Table 2. Among all eight BHA-responsive modules, it worth noting that only three modules were positively associated with BHA treatment (i.e., module M-24 h-4 at 24 h and module M-48 h-1 and M-48 h-2 at 48 h), and no module positively associated with BHA was found at 72 h. Analysis of the metabolites within the three modules showed a similar trend of high content of amino acids and sugar, such as alanine, glycine, glyceric acid, isoleucine, proline, isomaltose, lactose, maltose L-sorbose, and D-lyxose (Table 2). It may be worth further investigating whether these metabolites directly contribute to the enhanced lipid accumulation in *C. cohnii*.

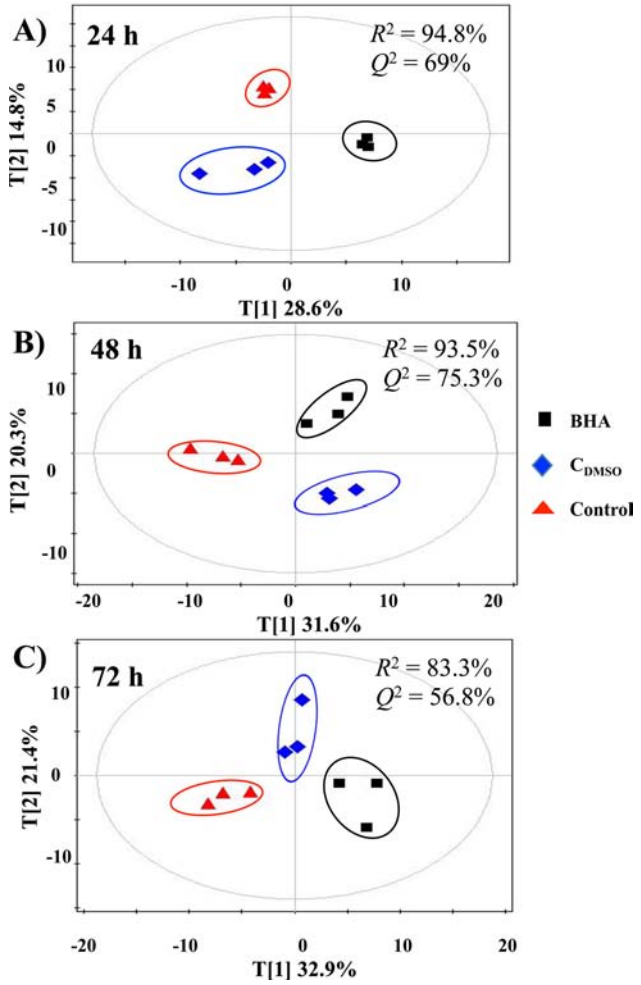


**Figure 3.** PLS-DA of GC-MS metabolomic profiles. (A) 24 h; (B) 48 h; and (C) 72 h. Each dot represents one biological sample, while the dots of the same color are biological replicates. Three conditions: control, DMSO control, and BHA treatment are indicated by different colors.

Hub metabolites have a high degree of connectivity in biological interaction networks and are thus supposed to have high biological importance.[44] Assuming hub metabolites with connectivity greater than 5, from the WGCNA network we were able to identify 3, 5, and 1 hub metabolites significantly associated with BHA at 24, 48, and 72 h, respectively (Figure 4). At 24 h, the first hub metabolite, isomaltose, was located in module M-24 h-1 negatively associated with BHA treatment ($r$ = −0.67, $p$ = 0.05); and adenosine and hydroquinone were located in module M-24 h-2 negatively associated with BHA treatment ($r$ = −0.89, $p$ = 0.002). At 48 h, three hub metabolites, 3-hydroxypropanoic-acid, L-isoleucine, and L-proline, were located in module M-48 h-1 positively associated with BHA treatment ($r$ = 0.89, $p$ = 0.001). Although never reported for any role in microalga, a chemical analogue of 3-hydroxypropanoic-acid, 2-hydroxypropanoic-acid extracted from grass *Lolium multiflorum*, was found increasing the lipid accumulation in 3T3-L1 cells.[45] At 48 h, two hub metabolites, methylmyristate and methyloleate were located in module M-48 h-2 positively associated with BHA treatment ($r$ = 0.67, $p$ = 0.05), which may be consistent with their roles as free fatty acids that can be incorporated into lipids.[46] At 72 h, one hub metabolite, malonic acid, was located in module M-72 h-2

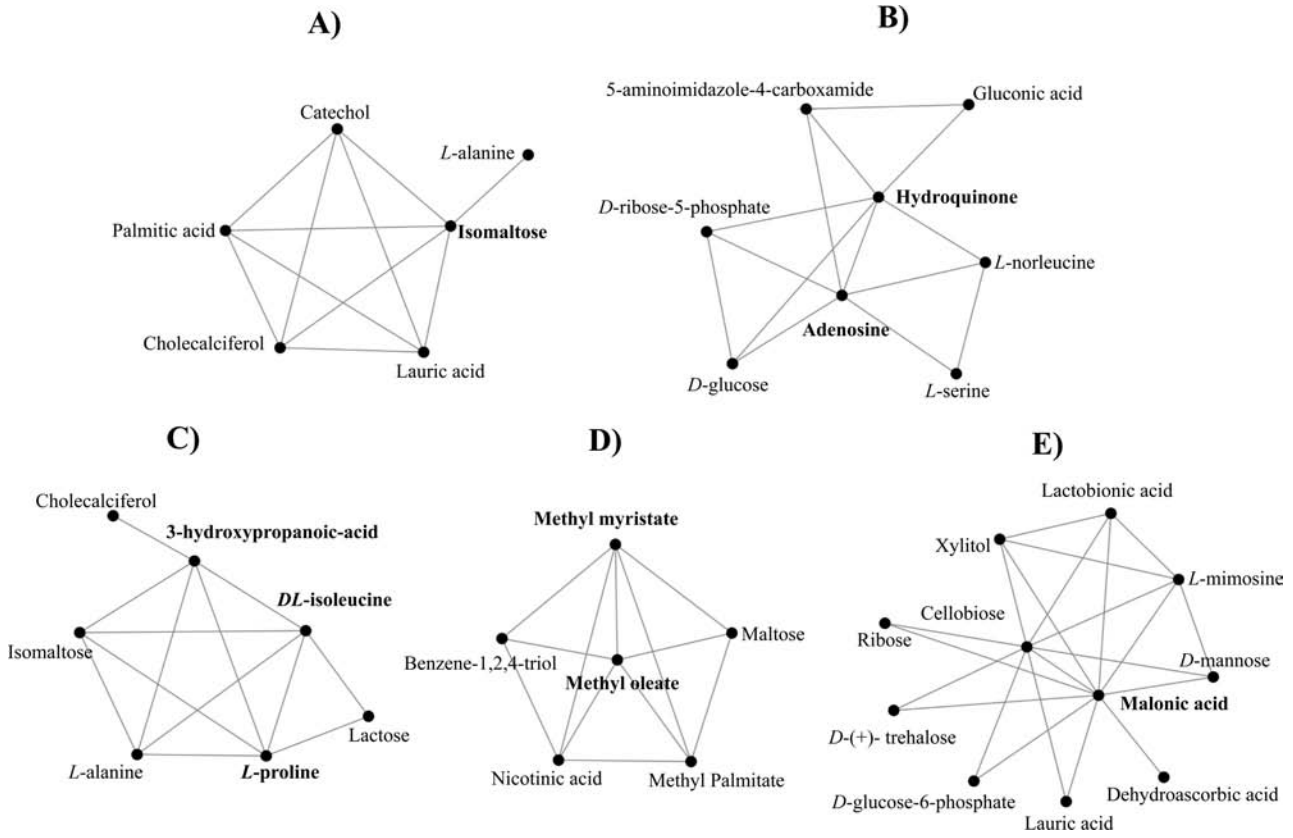


**Figure 4.** Hub metabolites and their metabolic profiles as represented by a node and edge graph. (A) Hub metabolites and associated network from module M-24 h-1; (B) hub metabolites and associated network from module M-24 h-2; (C) hub metabolites and associated network from module M-48 h-1; (D) hub metabolites and associated network from module M-48 h-2; (E) hub metabolites and associated network from module M-72 h-2.

**Table 2. Member Metabolites Clustered into Each of the BHA-Responsive Modules**[a]

| module | association | *p* value | metabolites |
|---|---|---|---|
| M-24 h-1 | $r = -0.67$ | $p = 0.05$ | catechol, cholecalciferol, L-alanine, L-allothreonine, isomaltose, nicotinic acid |
| M-24 h-2 | $r = -0.89$ | $p = 0.002$ | 3-hydroxypyridine, 5-aminoimidazole-4-carboxamide, adenosine, D-glucose, D-ribose-5-phosphate, DL-isoleucine, gluconic acid, hydroquinone, L-(+)-lactic acid, L-leucine, L-norleucine, maltose, urea |
| M-24 h-3 | $r = -0.74$ | $p = 0.02$ | benzoic acid, methyl laurate, nicotinamide, tagatose, uracil |
| M-24 h-4 | $r = 0.85$ | $p = 0.004$ | D-lyxose, ribose, glyceric acid, glycine, squalene |
| M-48 h-1 | $r = 0.89$ | $p = 0.001$ | 3-hydroxypropanoic acid, cholecalciferol, DL-isoleucine, L-alanine, L-proline, lactose, isomaltose |
| M-48 h-2 | $r = 0.67$ | $p = 0.05$ | benzene-1,2,4-triol, Maltose, L-sorbose, methyl myristate, methyl oleate, methyl palmitate, nicotinic acid |
| M-48 h-3 | $r = -0.64$ | $p = 0.06$ | D-ribose-5-phosphate, methyl-beta-D-galactopyranoside, L-alanine, linoleic acid |
| M-72 h-2 | $r = -0.87$ | $p = 0.002$ | catechol, cellobiose, dehydroascorbic acid, dioctyl phthalate, D-(+)-trehalose, D-mannose, D-glucose-6-phosphate, hydroquinone, itaconic acid, glycolic acid, lactobionic acid, lactose, lauric acid, L-mimosine, malonic acid, maltose, nicotinic acid, ribose, sucrose, uracil, xylitol |

[a]GC-MS metabolomic data set was used for this analysis.

negatively associated with BHA treatment ($r = -0.87$, $p = 0.002$). The coenzyme A derivative of malonic acid, malonyl-CoA, is an important precursor in lipid biosynthesis, and a previous study has found that malonic acid can enhance astaxanthin accumulation in *Haematococcus pluvialis*.[47] It is thus unexpected that malonic acid was negatively associated with BHA treatment, although another plausible explanation was that malonic acid is a well-known competitive inhibitor of succinate dehydrogenase and TCA cycle.[48] This negative association at 72 h may be due to cell aging and death occurring in the same phase.

A recent study demonstrated that the lipid accumulation in several microalga could be increased by antioxidant molecules in nanomolar concentration.[13] In this study, we studied the effects of selected antioxidants on lipid accumulation in *C. cohnii*. The efforts led to the discovery of an antioxidant BHA that could increase lipid content by 8.80% at a final concentration of 30 $\mu$M. To further explore the enhancing mechanism, we employed an integrated LC-MS and GC-MS metabolomic approach to determine the metabolic changes in cells treated with BHA, which allowed identification of 24 and 96 intracellular metabolites from the *C. cohnii* cells, respectively. In addition, analysis of metabolic networks constructed using a WGCNA approach uncovered eight distinguished metabolic modules and nine hub metabolites highly associated with BHA treatment. The metabolomic overview of cellular status under BHA treatment could be a useful knowledge base to further understand the molecular mechanisms of BHA and to discover relevant chemical enhancers for lipid accumulation in *C. cohnii*. Finally, as the first metabolomic study of DHA-producing *C.*

*cohnii*, the study demonstrated that the technology is a powerful tool in deciphering mode of action of chemical enhancers and could be useful in guiding optimization of lipid and DHA production in microalgae.

## ■ ASSOCIATED CONTENT

### Supporting Information

Growth of *C. cohnii* under various conditions; lipid accumulation in *C. cohnii* supplemented with PG; WGCNA analysis of GC-MS metabolomic profiles; compound-specific collisional mass spectrometric parameters used in MRM; LC-MS metabolomics data and reproducibility tests; and GC-MS metabolomic data obtained in this study. This material is available free of charge via the Internet at http://pubs.acs.org.

## ■ AUTHOR INFORMATION

### Corresponding Author

*Tel: 0086-22-2740-6394. Fax: 0086-22-27406364. E-mail: wwzhang8@tju.edu.cn.

### Funding

This research was supported by grants from the National High-tech R&D Program ("863" program, project No. 2012AA02A707), the National Basic Research Program of China ("973" program, project No. 2011CBA00803, No. 2014CB745101, and No. 2012CB721101), and the Doctoral Program of Higher Education of China (Nos. 20120032110020 and 20130032120022).

### Notes

The authors declare no competing financial interest.

## ■ ABBREVIATIONS USED

3PG, D-3-phosphoglyceric acid; Ac-CoA, acetyl coenzyme A; AKG, $\alpha$-ketoglutaric acid; ATCC, American Type Culture Collection; AMDIS, Automated MassSpectral Deconvolution and Identification System; BHA, butylated hydroxyanisole; CoA, coenzyme A hydrate; DHA, docosahexaenoic acid; DHAP, dihydroxyacetone phosphate; DMSO, dimethyl sulfoxide; EGCG, epigallocatechin gallate; ESI, electronic spray ion; F6P, D-fructose 6-phosphate; FBP, D-fructose 1,6-bisphosphat; FUM, fumarate dibasic; G6P, D-glucose 6-phosphate; GAP, DL-glyceraldehyde 3-phosphate; GC-MS, gas chromatography−mass spectrometry; Glu, L-glutamic acid; LC-MS, Liquid Chromatography−Mass Spectrometry; MCW, methanol/chloroform/$H_2O$ solution; MPA, mobile phase A; MPB, mobile phase B; NIST, National Institute of Standards and Technology; OXA, oxaloacetic acid; PCA, principal component analysis; PEP, phosphor-(enol)-pyruvic acid; PG, propyl gallate; PLS-DA, partial least-squares-discriminant analysis; R5P, D-ribose 5-phosphate; RuBP, D-ribulose 1,5-bisphosphate; WGCNA, Weighted Gene Coexpression Network Analysis

## ■ REFERENCES

(1) Oh, R. Practical applications of fish oil (Ω-3 fatty acids) in primary care. *J. Am. Board Fam. Pract.* **2005**, *18*, 28−36.

(2) Glaser, C.; Lattka, E.; Rzehak, P.; Steer, C.; Koletzko, B. Genetic variation in polyunsaturated fatty acid metabolism and its potential relevance for human development and health. *Matern. Child Nutr.* **2011**, *7*, 27−40.

(3) Russell, F. D.; Bürgin-Maunder, C. S. Distinguishing health benefits of eicosapentaenoic and docosahexaenoic acids. *Mar. Drugs* **2012**, *10*, 2535−2559.

(4) Sijtsma, L.; De Swaaf, M. Biotechnological production and applications of the $\omega$-3 polyunsaturated fatty acid docosahexaenoic acid. *Appl. Microbiol. Biotechnol.* **2004**, *64*, 146−153.

(5) Jiang, Y.; Chen, F.; Liang, S. Production potential of docosahexaenoic acid by the heterotrophic marine dinoflagellate *Crypthecodinium cohnii*. *Process Biochem.* **1999**, *34*, 633−637.

(6) de Swaaf, M. E.; T, P. J.; Sijtsma, L. Fed-batch cultivation of the docosahexaenoic-acid-producing marine alga *Crypthecodinium cohnii on ethanol*. *Appl. Microbiol. Biotechnol.* **2003**, *61*, 40−43.

(7) da Silva, T. L.; Reis, A. The use of multi-parameter flow cytometry to study the impact of n-dodecane additions to marine dinoflagellate microalga *Crypthecodinium cohnii* batch fermentations and DHA production. *J. Ind. Microbiol. Biotechnol.* **2008**, *35*, 875−887.

(8) Harrington, G.; Holz, G., Jr. The monoenoic and docosahexaenoic fatty acids of a heterotrophic dinoflagellate. *Biochim. Biophys. Acta* **1968**, *164*, 137−139.

(9) Ratledge, C. Fatty acid biosynthesis in microorganisms being used for single cell oil production. *Biochimie* **2004**, *86*, 807−815.

(10) de Swaaf, M. E.; De Rijk, T. C.; Eggink, G.; Sijtsma, L. Optimisation of docosahexaenoic acid production in batch cultivations by *Crypthecodinium cohnii*. *Prog. Ind. Microbiol.* **1999**, *35*, 185−192.

(11) de Swaaf, M. E.; Sijtsma, L.; T, P. J. High-cell-density fed-batch cultivation of the docosahexaenoic acid producing marine alga *Crypthecodinium cohnii*. *Biotechnol. Bioeng.* **2003**, *81*, 666−672.

(12) Stockwell, B. R. Exploring biology with small organic molecules. *Nature* **2004**, *432*, 846−854.

(13) Walsh, D. P.; Chang, Y.-T. Chemical genetics. *Chem. Rev.* **2006**, *106*, 2476−2530.

(14) Franz, A. K.; Danielewicz, M. A.; Wong, D. M.; Anderson, L. A.; Boothe, J. R. Phenotypic screening with oleaginous microalgae reveals modulators of lipid productivity. *ACS Chem. Biol.* **2013**, *8*, 1053−1062.

(15) Bölling, C.; Fiehn, O. Metabolite profiling of *Chlamydomonas reinhardtii* under nutrient deprivation. *Plant Physiol.* **2005**, *139*, 1995−2005.

(16) Niino, T.; Harada, T.; Houjou, T.; Yamada, S.; Oonishi, K.; Sato, Y.; Saito, H. Metabolomic approach for assessing the mode of action of bioactive compounds on the green algae *Pseudokirchneriella subcapitata*. *Jpn. J. Environ. Toxicol.* **2008**, *11*, 83−89.

(17) Courant, F.; Martzolff, A.; Rabin, G.; Antignac, J.-P.; Le Bizec, B.; Giraudeau, P.; Tea, I.; Akoka, S.; Couzinet, A.; Cogne, G. How metabolomics can contribute to bio-processes: a proof of concept study for biomarkers discovery in the context of nitrogen-starved microalgae grown in photobioreactors. *Metabolomics* **2013**, *9*, 1286−1300.

(18) Zhang, W.; Li, F.; Nie, L. Integrating multiple 'omics' analysis for microbial biology: application and methodologies. *Microbiology* **2010**, *156*, 287−301.

(19) Zhang, B.; Horvath, S. A general framework for weighted gene co-expression network analysis. *Stat. Appl. Genet. Mol. Biol.* **2005**, *4*, 1128.

(20) de la Jara, A.; Mendoza, H.; Martel, A.; Molina, C.; Nordström, L.; de la Rosa, V.; Díaz, R. Flow cytometric determination of lipid content in a marine dinoflagellate, *Crypthecodinium cohnii*. *J. Appl. Phycol.* **2003**, *15*, 433−438.

(21) Govender, T.; Ramanna, L.; Rawat, I.; Bux, F. BODIPY staining, an alternative to the Nile Red fluorescence method for the evaluation of intracellular lipids in microalgae. *Bioresour. Technol.* **2012**, *114*, 507−511.

(22) Doan, T.-T. Y.; Obbard, J. P. Improved Nile Red staining of *Nannochloropsis* sp. *J. Appl. Phycol.* **2011**, *23*, 895−901.

(23) Yang, S.; Lu, S. H.; Yuan, Y. J. Cerium elicitor-induced phosphatidic acid triggers apoptotic signaling development in *Taxus cuspidata* cell suspension cultures. *Chem. Phys. Lipids* **2009**, *159*, 13−20.

(24) Wang, J.; Chen, L.; Tian, X.; Gao, L.; Niu, X.; Shi, M.; Zhang, W. Global metabolomic and network analysis of *Escherichia coli* responses to exogenous biofuels. *J. Proteome Res.* **2013**, *12*, 5302−5312.

(25) Wang, J.; Zhang, X.; Shi, M.; Gao, L.; Niu, X.; Te, R.; Chen, L.; Zhang, W. Metabolomic analysis of the salt-sensitive mutants reveals changes in amino acid and fatty acid composition important to long-term salt stress in *Synechocystis* sp. PCC 6803. *Funct. Integr. Genomics* **2014**, *14*, 431−440.
(26) Roessner, U.; Luedemann, A.; Brust, D.; Fiehn, O.; Linke, T.; Willmitzer, L.; Fernie, A. R. Metabolic profiling allows comprehensive phenotyping of genetically or environmentally modified plant systems. *Plant Cell* **2001**, *13*, 11−29.
(27) Bennette, N. B.; Eng, J. F.; Dismukes, G. C. An LC−MS-based chemical and analytical method for targeted metabolite quantification in the model cyanobacterium *Synechococcus* sp. PCC 7002. *Anal. Chem.* **2011**, *83*, 3808−3816.
(28) Park, C.; Lee, Y. J.; Lee, S. Y.; Oh, H. B.; Lee, J. Determination of the intracellular concentrations of metabolites in *Escherichia coli* collected during the exponential and stationary growth phases using liquid chromatography-mass spectrometry. *Bull. Korean Chem. Soc.* **2011**, *32*, 524−530.
(29) Rodriguez-Campos, J.; Escalona-Buendía, H.; Orozco-Avila, I.; Lugo-Cervantes, E.; Jaramillo-Flores, M. Dynamics of volatile and non-volatile compounds in cocoa (*Theobroma cacao* L.) during fermentation and drying processes using principal components analysis. *Food Res. Int.* **2011**, *44*, 250−258.
(30) Wang, J.; Wu, G.; Chen, L.; Zhang, W. Cross-species transcriptional network analysis reveals conservation and variation in response to metal stress in cyanobacteria. *BMC Genomics* **2013**, *14*, 112.
(31) Zhang, Z.; Wang, H.; Wang, X.; Bi, Y. Nitric oxide enhances aluminum tolerance by affecting cell wall polysaccharides in rice roots. *Plant Cell Rep.* **2011**, *30*, 1701−1711.
(32) de Swaaf, M.; Rijk, T. d.; Meer, P.; Eggink, G.; Sijtsma, L. Analysis of docosahexaenoic acid biosynthesis in *Crypthecodinium cohnii* by $^{13}C$ labelling and desaturase inhibitor experiments. *J. Biotechnol.* **2003**, *103*, 21−29.
(33) Putri, S. P.; Nakayama, Y.; Matsuda, F.; Uchikata, T.; Kobayashi, S.; Matsubara, A.; Fukusaki, E. Current metabolomics: practical applications. *J. Biosci. Bioeng.* **2013**, *115*, 579−589.
(34) Langfelder, P.; Horvath, S. WGCNA: an *R* package for weighted correlation network analysis. *BMC Bioinformatics* **2008**, *9*, 559.
(35) Yang, Z. K.; Niu, Y. F.; Ma, Y. H.; Xue, J.; Zhang, M. H.; Yang, W.-D.; Liu, J.-S.; Lu, S.-H.; Guan, Y.; Li, H. Y. Molecular and cellular mechanisms of neutral lipid accumulation in diatom following nitrogen deprivation. *Biotechnol. Biofuels* **2013**, *6*, 1−67.
(36) Ren, L. J.; Huang, H.; Xiao, A. H.; Lian, M.; Jin, L. J.; Ji, X. J. Enhanced docosahexaenoic acid production by reinforcing acetyl-CoA and NADPH supply in *Schizochytrium* sp. HX-308. *Bioprocess Biosyst. Eng.* **2009**, *32*, 837−843.
(37) Bellou, S.; Aggelis, G. Biochemical activities in *Chlorella* sp. and *Nannochloropsis salina* during lipid and sugar synthesis in a lab-scale open pond simulating reactor. *J. Biotechnol.* **2012**, *164*, 318−329.
(38) Gupta, V.; Thakur, R. S.; Reddy, C.; Jha, B. Central metabolic processes of marine macrophytic algae revealed from NMR based metabolome analysis. *RCS Adv.* **2013**, *3*, 7037−7047.
(39) Wase, N.; Black, P. N.; Stanley, B. A.; DiRusso, C. C. Integrated quantitative analysis of nitrogen stress response in *Chlamydomonas reinhardtii* using metabolite and protein profiling. *J. Proteome Res.* **2014**, *13*, 1373−1396.
(40) Zhang, H.; Zhang, L.; Chen, H.; Chen, Y. Q.; Ratledge, C.; Song, Y.; Chen, W. Regulatory properties of malic enzyme in the oleaginous yeast, *Yarrowia lipolytica*, and its non-involvement in lipid accumulation. *Biotechnol. Lett.* **2013**, *35*, 2091−2098.
(41) Schwarz, D.; Orf, I.; Kopka, J.; Hagemann, M. Recent applications of metabolomics toward cyanobacteria. *Metabolites* **2013**, *3*, 72−100.
(42) Zhu, H.; Ren, X.; Wang, J.; Song, Z.; Shi, M.; Qiao, J.; Tian, X.; Liu, J.; Chen, L.; Zhang, W. Integrated OMICS guided engineering of biofuel butanol-tolerance in photosynthetic *Synechocystis* sp. PCC 6803. *Biotechnol. Biofuels* **2013**, *6*, 106.
(43) DiLeo, M. V.; Strahan, G. D.; den Bakker, M.; Hoekenga, O. A. Weighted correlation network analysis (WGCNA) applied to the tomato fruit metabolome. *PLoS One* **2011**, *6*, e26683.
(44) Han, J. D. J.; Bertin, N.; Hao, T.; Goldberg, D. S.; Berriz, G. F.; Zhang, L. V.; Dupuy, D.; Walhout, A. J.; Cusick, M. E.; Roth, F. P. Evidence for dynamically organized modularity in the yeast protein−protein interaction network. *Nature* **2004**, *430*, 88−93.
(45) Ilavenil, S.; Arasu, M. V.; Lee, J.-C.; Kim, D. H.; Vijayakumar, M.; Lee, K. D.; Choi, K. C. Positive regulations of adipogenesis by Italian ryegrass [*Lolium multiflorum*] in 3T3-L1 cells. *BMC Biotechnol.* **2014**, *14*, 54.
(46) Feron, G.; Dufossé, L.; Mauvais, G.; Bonnarme, P.; Spinnler, H. E. Fatty acid accumulation in the yeast *Sporidiobolus salmonicolor* during batch production of gamma-decalactone. *FEMS Microbiol. Lett.* **1997**, *149*, 17−24.
(47) Orosa, M.; Franqueira, D.; Cid, A.; Abalde, J. Analysis and enhancement of astaxanthin accumulation in *Haematococcus pluvialis*. *Bioresour. Technol.* **2005**, *96*, 373−378.
(48) Minato, Y.; Fassio, S. R.; Häse, C. C. Malonate inhibits virulence gene expression in *Vibrio cholerae*. *PLoS One* **2013**, *8*, e63336.

Editorial Advisory Board (EAB) members have been aimed at increasing the visibility of *JAFC*. We are soliciting and receiving many more Reviews and Perspectives than in the past, increasing our impact factor, and we now offer a fast-track Letters category for publishing urgent work with a focused, brief format.

The categories that define the scope of *JAFC* have been streamlined and modernized. This is a continuing and evolving task.

Improvements have been made to solidify our leadership position, given that there are now several new journals in agricultural and food sciences. Food, the science behind food, and its importance to good health have caught the attention of the research community as well as the public. Strong chemistry has been at the core of what *JAFC* is about, and it will continue to be a distinguishing feature. The chemistry related to antioxidants has been a major theme since about 1990, so much so that Associate Editor John Finley once quipped that we should change the name of the journal to "Journal of Antioxidant and Food Chemistry".

We have aimed to position *JAFC* for the research challenges of the present and future. The agricultural chemistry behind biofuels and biobased products is an example, as well as increasing focus on biopesticides and nanomaterials. The very recent development of commercial-scale cellulosic ethanol facilities was made possible by research, published in *JAFC* and other outlets. *JAFC* has been a leader in metabolomics, proteomics, and genomics applied to agriculture and food. Nanotechnology is a current focus area for *JAFC*, following on publication by *JAFC* of an ACS Selects on this topic earlier in 2014. This effort to expand coverage of emerging topics while maintaining strength in traditional areas is an ongoing challenge.

I leave the position of Editor-in-Chief with many good feelings toward all in the *JAFC* family, particularly our Associate Editors, EAB members, office staff in Davis (Loreen and Ann), and colleagues in the ACS Publications Division and ACS Divisions of AGFD and AGRO as well as our many authors and reviewers worldwide. I thank USDA's Agricultural Research Service for allowing me to be a federal Senior Executive Service Center Director and also editor of a major journal. The two appointments added value to the work conducted in each area. I look forward to continuing with teaching and service in related areas in my home department at the University of California, Davis, Environmental Toxicology.

The *Journal* will be in good hands with incoming Editor-in-Chief Dr. Thomas Hofmann, and the continuing efforts of our incredibly dedicated and knowledgeable Associate Editors and EAB members. I offer my support to Thomas and the Associate Editor team as they move forward. The *Journal* will continue to pursue excellence in publishing the research of agricultural and food chemistry, building upon a 60 year legacy, made possible by the efforts of thousands of authors, coauthors, and reviewers who share their time and intellect to advance the knowledge of applied chemistry.

**Jim Seiber,** Editor

## AUTHOR INFORMATION

### Notes

Views expressed in this editorial are those of the author and not necessairly the views of the ACS.


dx.doi.org/10.1021/jf5054645 | *J. Agric. Food Chem.* 2014, 62, 12485−12486

*brevibacter ruminantium* cells and of partially purified methyl-CoM reductase with the aim to obtain additional information on the inhibitor's molecular target.

## MATERIALS AND METHODS

Please see the Supporting Information.

## RESULTS AND DISCUSSION

The impact of 2-bromoethanesulfonate on methane production was determined using cultures of *Methanobrevibacter ruminantium* growing in 50 mL serum vessels using a complex medium as described in the Supporting Information and an atmosphere containing 80 mol % of $H_2$ and 20 mol % of $CO_2$ at an initial pressure of 210 kPa. Individual culture vessels were doped with the inhibitor at concentrations extending from 3 nM to 30 $\mu$M. The methane concentration in the overhead space was determined by gas chromatography after incubation for 3 days. The semilogarithmic plot in Figure 1A shows a sigmoidal, essentially symmetrical curve. Evaluation using the software package Dynafit (Biokin) affords an $IC_{50}$ value of 0.8 ± 0.2 $\mu$M.[19]

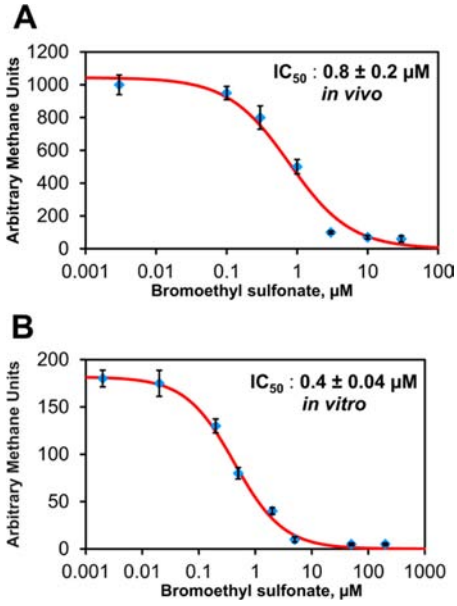


**Figure 1.** Inhibition of methyl-CoM reductase by 2-bromoethanesulfonate: (A) in vivo methane formation at different inhibitor concentrations; (B) in vitro methane formation at different inhibitor concentrations; (blue diamonds) mean of three independent measurements (error bars indicate standard deviation); (red curve) line of best fit.

To measure the in vitro impact of 2-bromoethanesulfonate on methyl-CoM reductase, we cultured *Methanobrevibacter ruminantium* to late log phase under an atmosphere containing 80 mol % of $H_2$ and 20 mol % of $CO_2$ in 1 L Schott flasks. The cells were harvested under anaerobic conditions and were disrupted by sonication. SDS-PAGE analysis of the crude extract revealed prominent bands at 59.8, 47.1, and 28.7 kDa most likely visualizing the $\alpha$, $\beta$, and $\gamma$ subunit types, respectively, of methyl-CoM reductase (not shown). The specific activity of the peak fraction was 6 nmol/mg·min.

The crude cell extract was placed on a column of Sepharose Q that was kept under anaerobic conditions and developed with a gradient of 0.4−1.0 M NaCl in 100 mM MOPS, pH 7.2. Fractions were analyzed for in vitro methane production using methyl-CoM and coenzyme B as substrates (Figures 2 and 3).

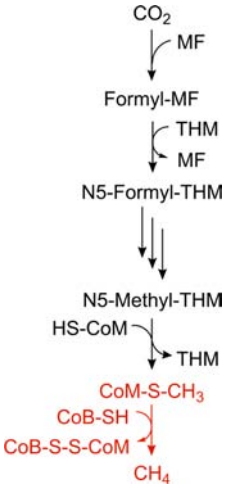


**Figure 2.** Methanogenesis in *Methanobrevibacter ruminantium*; methyl-CoM reductase reaction shown red. MF, methanofuran; THM, tetrahydromethanopterin.

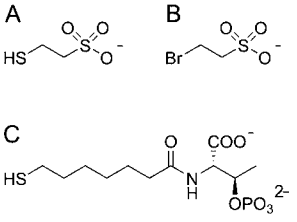


**Figure 3.** (A) Coenzyme M (CoM); (B) 2-bromoethanesulfonate; (C) coenzyme B (CoB).

Under these specific conditions, one molecule of methyl-CoM and one molecule of coenzyme B gave rise to one molecule of methane plus one disulfide (CoM−CoB complex). In vivo, this CoM−CoB complex is subject to reductive cleavage conducive to the regeneration of coenzymes B and M. Because our in vitro assay did not include any enzyme for coenzyme recycling, the mixed disulfide was the final product. Using this assay, active methyl-CoM reductase was shown to be eluted from the column with a retention volume of 30−40 mL. All three subunit types of methyl-CoM reductase were confirmed in the partially purified (about 90%) enzyme preparation as revealed by mass spectrometry.

In line with observations reported for *Methanothermobacter thermoautotrophicus*, the enzyme was subject to rapid activity loss under in vitro conditions.[20] Hence, inhibition assays were carried out immediately after the purification procedure. Figure 1B demonstrates the impact of 2-bromoethanesulfonate on the in vitro formation of methane by the partially purified enzyme. The semilogarithmic plot shows a sigmoid curve with $c_2$ symmetry. Evaluation with the software package Dynafit assigned an $IC_{50}$ of 0.4 ± 0.04 $\mu$M. Thus, methyl-CoM reductase from *Methanobrevibacter ruminantium* appears to be more sensitive to 2-bromoethanesulfonate inhibition than the enzyme from *Methanothermobacter thermoautotrophicus*, for which an $IC_{50}$ of 4 $\mu$M has been reported.[21] Notably, the $IC_{50}$ values obtained with *Methanobrevibacter ruminantium* cultures and with the partially purified *Methanobrevibacter ruminantium* enzyme are numerically similar. This is well in line


dx.doi.org/10.1021/jf505056g | J. Agric. Food Chem. 2014, 62, 12487−12490

with the hypothesis that the terminal enzyme of methanogenesis is the actual target of the inhibitor, which is a structural analogue of coenzyme M. Methyl-CoM reductase has been identified as a potential target for inhibition of methanogenesis.[10] The results of our study unequivocally support this hypothesis and confirm the relevance of using 2-bromoethanesulfonate as a model compound to test the effects of reduced methanogenesis in complex ecosystems such as the rumen or as a positive control to develop compounds working according to the same mode of action while benefiting from more favorable toxicological profiles.

Whereas methyl-CoM reductase from *Methanobrevibacter ruminantium* is not well suited for high-throughput screening, due to the limited storing options, it is, however, possible to directly test potential new inhibitors in our in vivo system. Currently, we are downsizing the required culture volume with the scope to run growth studies in 1.5 mL GC vials.

**Tobias Gräwert**[†]
**Hans-Peter Hohmann**[§]
**Maik Kindermann**[§]
**Stephane Duval**[§]
**Adelbert Bacher**[†]
**Markus Fischer***[,†]

[†]Hamburg School of Food Science, Institute of Food Chemistry, Grindelallee 117, D-20146 Hamburg, Germany
[§]DSM Nutritional Products, Wurmisweg 576, CH-4303 Kaiseraugst, Switzerland

## ■ ASSOCIATED CONTENT

### Ⓢ Supporting Information

Materials and methods, Tables S1−S3, and additional references. This material is available free of charge via the Internet at http://pubs.acs.org.

## ■ AUTHOR INFORMATION

### Corresponding Author

*(M.F.) Phone: +49-40-428384342. Fax: +49-40-428384342. E-mail: markus.fischer@chemie.uni-hamburg.de.

### Funding

We thank the Hans-Fischer-Gesellschaft for funding.

### Notes

The authors declare no competing financial interest.

## ■ ABBREVIATIONS USED

CoB, coenzyme B; CoM, coenzyme M; GC- FID, gas chromatograph−flame ionization detector; $IC_{50}$, half-maximal inhibitory concentration; MF, methanofuran; MOPS, 3-(*N*-morpholino)propanesulfonic acid; THM, tetrahydromethanopterin

## ■ REFERENCES

(1) Myhre, G.; Shindell, D.; Bréon, F.-M.; Collins, W.; Fuglestvedt, J.; Huang, J.; Koch, D.; Lamarque, J.-F.; Lee, D.; Mendoza, B.; Nakajima, T.; Robock, A.; Stephens, G.; Takemura, T.; Zhang, H. Anthropogenic and natural radiative forcing. In *Climate Change 2013: The Physical Science Basis. Contribution of Working Group I to the Fifth Assessment Report of the Intergovernmental Panel on Climate Change*; Stocker, T. F., Qin, D., Plattner, G.-K., Tignor, M., Allen, S. K., Boschung, J., Nauels, A., Xia,Y., Bex, V., Midgley, P. M., Eds.; Cambridge University Press: Cambridge, UK, 2013; pp 659−740.

(2) Hook, S. E.; Wright, A.-D. G.; McBride, B. W. Methanogens: methane producers of the rumen and mitigation strategies. *Archaea* **2010**, 945785, 11 pages.

(3) Janssen, P. H.; Kirs, M. Structure of the archaeal community of the rumen. *Appl. Environ. Microbiol.* **2008**, *74*, 3619−3625.

(4) Johnson, K. A.; Johnson, D. E. Methane emissions from cattle. *J. Anim. Sci.* **1995**, *73*, 2483−2492.

(5) Scheehle, E. A.; Kruger, D. Global anthropogenic methane and nitrous oxide emissions. *Energy J.* **2006**, *3* (Special Issue), 33−44.

(6) Ermler, U. On the mechanism of methyl-coenzyme M reductase. *Dalton Trans.* **2005**, *21*, 3451−3458.

(7) Vermorel, M. Emissions annuelles de méthane d'origine digestive par les bovins en France. *INRA Prod. Anim.* **1995**, *8*, 265−272.

(8) Hristov, A. N.; Oh, J.; Lee, C.; Meinen, R.; Montes, F.; Ott, T.; Firkins, J.; Rotz, A.; Dell, C.; Adesogan, A.; Yang, W. Z.; Tricarico, J.; Kebreab, E.; Waghorn, G.; Dijkstra, J.; Oosting, S. Mitigation of greenhouse gas emissions in livestock production − a review of technical options for non-$CO_2$ emissions. In *FAO Animal Production and Health Paper 177*; Gerber, P., Henderson, B., Makkar, H., Eds.; Food and Agriculture Organization of the United Nations: Rome, Italy, 2013; pp 1−226.

(9) Whitford, M. F.; Teather, R. M.; Forster, R. J. Phylogenetic analysis of methanogens from the bovine rumen. *BMC Microbiol.* **2001**, 1.

(10) Leahy, S. C.; Kelly, W. J.; Altermann, E.; Ronimus, R. S.; Yeoman, C. J.; Pacheco, D. M.; Dong, L.; Zhanhao, K.; McTavish, S.; Sang, C.; Lambie, S. C.; Janssen, P. H.; Dey, D.; Attwood, G. T. The genome sequence of the rumen methanogen *Methanobrevibacter ruminantium* reveals new possibilities for controlling ruminant methane emissions. *PLoS One* **2010**, *5*, e8926.

(11) McAllister, T. A.; Newbold, C. J. Redirecting rumen fermentation to reduce methanogenesis. *Aust. J. Exp. Agric.* **2008**, *48*, 7−13.

(12) Ungerfeld, E. M.; Rust, S. R.; Boone, D. R.; Liu, Y. Effects of several inhibitors on pure cultures of ruminal methanogens. *J. Appl. Microbiol.* **2004**, *97*, 520−526.

(13) Gunsalus, R. P.; Wolfe, R. S. Methyl coenzyme M reductase from *Methanobacterium thermoautotrophicum*. Resolution and properties of the components. *J. Biol. Chem.* **1980**, *255*, 1891−1895.

(14) Rospert, S.; Böcher, R.; Albracht, S. P.; Thauer, R. K. Methyl-coenzyme M reductase preparations with high specific activity from H2-preincubated cells of *Methanobacterium thermoautotrophicum*. *FEBS Lett.* **1991**, *291*, 371−375.

(15) Rospert, S.; Voges, M.; Berkessel, A.; Albracht, S. P.; Thauer, R. K. Substrate-analogue-induced changes in the nickel-EPR spectrum of active methyl-coenzyme-M reductase from *Methanobacterium thermoautotrophicum*. *Eur. J. Biochem.* **1992**, *210*, 101−107.

(16) Gunsalus, R. P.; Romesser, J. A.; Wolfe, R. S. Preparation of coenzyme M analogues and their activity in the methyl coenzyme M reductase system of *Methanobacterium thermoautotrophicum*. *Biochemistry* **1978**, *17*, 2374−2377.

(17) Smith, M. R.; Mah, R. A. Growth and methanogenesis by *Methanosarcina* strain 227 on acetate and methanol. *Appl. Environ. Microbiol.* **1978**, *36*, 870−879.

(18) Nevel, C. J.; Demeyer, D. Feed additives and other interventions for decreasing methane emissions. In *Biotechnology and Animal Feeds and Animal Feeding*; Wallace, R. J., Chesson, A., Eds.; Wiley-VCH Verlag: Weinheim, Germany, 1995; pp 329−349.

(19) Kuzmic, P. Program Dynafit for the analysis of enzyme kinetic data: application to HIV proteinase. *Anal. Biochem.* **1996**, *237*, 260−273.

(20) Bonacker, L. G.; Baudner, S.; Mörschel, E.; Böcher, R.; Thauer, R. K. Properties of the two isoenzymes of methyl-coenzyme M reductase in *Methanobacterium thermoautotrophicum*. *Eur. J. Biochem.* **1993**, *217*, 587−595.

(21) Holliger, C.; Kengen, S. W.; Schraa, G.; Stams, A. J.; Zehnder, A. J. Methyl-coenzyme M reductase of *Methanobacterium thermoautotrophicum* delta H catalyzes the reductive dechlorination of 1,2-

dichloroethane to ethylene and chloroethane. *J. Bacteriol.* **1992**, *174*, 4435−4434.

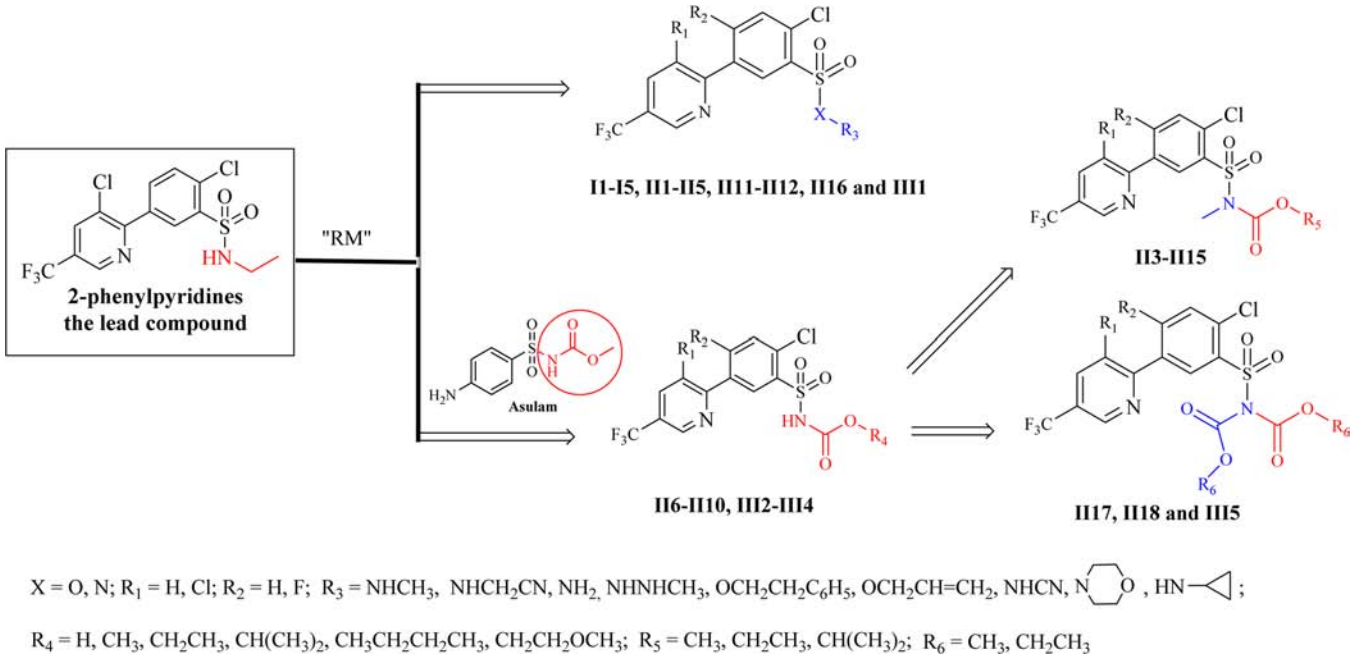


**Figure 1.** Design of 3-(pyridin-2-yl)benzenesulfonamide derivatives. "RM" means "terminal group replacement method".

dimethoxyethane and 550 mL of water were refluxed for 4 h. The mixture was then acidified to pH 4−5 with dilute hydrochloric acid, and dimethoxyethane was removed by distillation. The remaining aqueous phase was extracted with methylene chloride. The combined methylene chloride phased was washed with water, dried over sodium sulfate, and evaporated. The residue was stirred with a little cold *n*-hexane, filtered off with suction, and dried.

*2-(4-Chlorophenyl)-5-(trifluoromethyl)pyridine (**a1**).* Yield: 60% of colorless crystals of melting point 89−90 °C. $^1$H NMR (300 MHz, $CDCl_3$) $\delta_H$ (ppm) = 7.47 (d, *J* = 8.3 Hz, 2H), 7.73 (d, *J* = 8.4 Hz, 2H), 8.04 (d, *J* = 8.5 Hz, 1H), 8.05 (d, *J* = 8.3 Hz, 1H), 8.83 (s, 1H).

*3-Chloro-2-(4-chlorophenyl)-5-(trifluoromethyl)pyridine (**a2**).* Yield: 70% of colorless crystals of melting point 72−74 °C. $^1$H NMR (300 MHz, $CDCl_3$) $\delta_H$ (ppm) = 7.47 (d, *J* = 8.4 Hz, 2H), 7.73 (d, *J* = 8.4 Hz, 2H), 8.04 (s, 1H), 8.83 (s, 1H).

*3-Chloro-2-(4-chloro-2-fluorophenyl)-5-(trifluoromethyl)pyridine (**a3**).* Yield: 76% of colorless crystals of melting point 34−35 °C. $^1$H NMR (300 MHz, $CDCl_3$) $\delta_H$ (ppm) = 7.32 (dd, *J* = 8.3, 2.2 Hz, 2H), 7.43 (d, 1H), 8.05 (s, 1H), 8.86 (s, 1H).

**Synthesis of Intermediate b.** The intermediate **a** (0.033 mol) was added dropwise to chlorosulfonic acid at 0−5 °C, and the mixture was heated at 130 °C for 8 h.[25] The reaction mixture was then cooled to room temperature and was poured into crushed ice with ethyl acetate (3 × 60 mL). The combined extract was washed with water and saturated brine and dried over anhydrous magnesium sulfate, and then filtered and concentrated under reduced pressure to give a pale yellow liquid.

*2-Chloro-5-(5-(trifluoromethyl)pyridin-2-yl)benzene-1-sulfonyl Chloride (**b1**).* Yield: 90%. $^1$H NMR (300 MHz, $CDCl_3$) $\delta_H$ (ppm) = 7.73 (d, *J* = 8.3 Hz, 1H), 7.92 (d, *J* = 8.4 Hz, 1H), 8.05 (d, *J* = 8.3 Hz, 1H), 8.32 (d, *J* = 8.4 Hz, 1H), 8.80 (s, 1H), 8.99 (s, 1H).

*2-Chloro-5-(3-chloro-5-(trifluoromethyl)pyridin-2-yl)benzene-1-sulfonyl Chloride (**b2**).* Yield: 90%. $^1$H NMR (300 MHz, $CDCl_3$) $\delta_H$ (ppm) = 7.68 (d, *J* = 8.4 Hz, 1H), 7.96 (d, *J* = 8.4 Hz, 1H), 8.08 (s, 1H), 8.52 (s, 1H), 8.87 (s, 1H).

*2-Chloro-5-(3-chloro-5-(trifluoromethyl)pyridin-2-yl)-4-fluorobenzene-1-sulfonyl Chloride (**b3**).* Yield: 91%. $^1$H NMR (300 MHz, $CDCl_3$) $\delta_H$ (ppm) = 7.40 (d, *J* = 8.3 Hz, 1H), 8.05 (s, 1H), 8.25 (d, 1H), 8.86 (s, 1H).

**Synthesis of Substituted 3-(pyridin-2-yl)-benzenesulfonamide Compounds.** *2-Chloro-5-(5-(trifluoromethyl)pyridin-2-yl)benzenesulfonamide (**I1**).* The intermediate **b1** (0.01 mol) in 20 mL of THF was added dropwise to $NH_3 \cdot H_2O$ at 0−5 °C, and the mixture was stirred at room temperature. Then the mixture was concentrated under reduced pressure to obtain a pale yellow solid. Yield: 85%. Melting point: 163−165 °C. $^1$H NMR (300 MHz, $CDCl_3$) $\delta_H$ (ppm) = 8.97 (s, 1H), 8.76 (d, *J* = 2.3 Hz, 1H), 8.28 (d, *J* = 8.4 Hz, 1H), 8.04 (s, 1H), 7.93 (s, 1H), 7.70 (d, *J* = 8.3 Hz, 1H), 5.17 (s, 2H). Anal. Calcd (%) for $C_{12}H_8ClF_3N_2O_2S$: C, 42.80; H, 2.39; N, 8.32. Found: C, 42.81; H, 2.42; N, 8.35.

*2-((2-Chloro-5-(5-(trifluoromethyl)pyridin-2-yl)phenyl)sulfonyl)-acetonitrile (**I2**).* 2-amino acetonitrile (3 mmol), the intermediate **b1** (1.5 mmol), and triethylamine in 15 mL of THF were stirred at room temperature. Then the mixture was concentrated under reduced pressure to get the target compound. Yield: 40% of yellow solid of melting point 158−160 °C. $^1$H NMR (300 MHz, $CDCl_3$) $\delta_H$ (ppm) = 8.99 (s, 1H), 8.81 (s, 1H), 8.33 (d, *J* = 8.3 Hz, 1H), 8.05 (s, 1H), 7.93 (d, *J* = 7.9 Hz, 1H), 7.74 (d, *J* = 8.5 Hz, 1H), 5.52 (s, 1H), 4.12 (d, *J* = 6.7 Hz, 2H). Anal. Calcd (%) for $C_{14}H_9ClF_3N_3O_2S$: C, 44.75; H, 2.41; N, 11.18. Found: C, 44.76; H, 2.43; N, 11.16.

**II1**-**II5**, **II11**, **II12**, **II16**, and **III1** were synthesized using the synthetic method of **I2**

*Methyl ((2-Chloro-5-(3-chloro-5-(trifluoromethyl)pyridin-2-yl)-phenyl)sulfonyl)carbamate (**II6**).* Synthesis of 2-chloro-5-(3-chloro-5-(trifluoromethyl)pyridin-2-yl)benzenesulfonamide. The intermediate **b2** (0.01 mol) in 20 mL of THF was added dropwise to $NH_3 \cdot H_2O$ (0.02 mol) at 0−5 °C, and the mixture was stirred at room temperature for 2 h. Then the mixture was concentrated under reduced pressure to obtain a pale yellow solid. Yield: 81%. Melting point: 166−168 °C. $^1$H NMR (300 MHz, $CDCl_3$) $\delta_H$ (ppm) = 5.17(2H, s), 7.69(1H, d), 7.96(1H, d), 8.09(1H, s), 8.57(1H, s), 8.86(1H, s). Synthesis of methyl ((2-chloro-5-(3-chloro-5-(trifluoromethyl)pyridin-2-yl)phenyl)sulfonyl)carbamate. 2-Chloro-5-(3-chloro-5-(trifluoromethyl)pyridin-2-yl)benzenesulfonamide (0.6 g, 1.6 mmol), $K_2CO_3$ (0.31 g, 2.26 mmol), and methyl chloroformate (0.2 g, 1.67 mmol) in 15 mL of acetone were refluxed for 6 h. The mixture was concentrated under reduced pressure. Then the crude product was purified by column chromatography with a mixture of ethyl acetate and petroleum ether (1:3) to get 0.25 g of target compound. Yield: 31% of yellow solid of melting point 144−146 °C. $^1$H NMR (300 MHz, $CDCl_3$) $\delta_H$ (ppm) = 8.90 (s, 1H), 8.77 (d, *J* = 2.2 Hz, 1H), 8.12 (s, 1H), 8.07 (dd, *J* = 8.3, 2.2 Hz, 1H), 7.89 (s, 1H), 7.72 (d, *J* = 8.3 Hz, 1H), 3.75 (s, 3H). $^{13}$C NMR (75 MHz, $CDCl_3$) $\delta$ 156.42, 150.51, 144.57, 144.52, 144.47, 135.76, 135.71, 135.63, 134.27, 133.95, 133.44, 131.81, 127.32, 53.87. Anal. Calcd (%) for


dx.doi.org/10.1021/jf504018z | *J. Agric. Food Chem.* 2014, 62, 12491−12496

**Table 1. Chemical Structures and Herbicidal Activity of Substituted 3-(Pyridin-2-yl)benzenesulfonamide Analogues by Postemergence Treatment in Glasshouse Tests[b]**

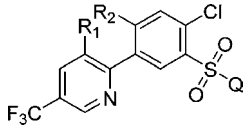

| compounds | $R_1$ | $R_2$ | Q | YOApost- (ga.i./ha) | | | VELpost- (ga.i./ha) | | | FOXpost- (ga.i./ha) | | | BYG post- (ga.i./ha) | | |
|---|---|---|---|---|---|---|---|---|---|---|---|---|---|---|---|
| | | | | 600 | 150 | 37.5 | 600 | 150 | 37.5 | 600 | 150 | 37.5 | 600 | 150 | 37.5 |
| **I1** | H | H | $NH_2$ | **0** | /[a] | / | **0** | / | / | **0** | / | / | **0** | / | / |
| **I2** | H | H | $NHCH_2CN$ | 0 | / | / | 0 | / | / | 0 | / | / | 0 | / | / |
| **I3** | H | H | $NCH(CH_3)_2$ | 0 | / | / | 0 | / | / | 0 | / | / | 0 | / | / |
| **I4** | H | H | $NHOCH_3$ | 0 | / | / | 5 | / | / | 0 | / | / | 0 | / | / |
| **I5** | H | H | $NHCH_3$ | 0 | / | / | 0 | / | / | 0 | / | / | 0 | / | |
| **II1** | Cl | H | $OCH_2CH_2C_6H_5$ | 20 | 10 | 5 | 40 | 25 | 20 | 10 | 5 | 5 | 5 | 5 | 0 |
| **II2** | Cl | H | $OCH_2CH{=}CH_2$ | 50 | 15 | 0 | 60 | 10 | 5 | 20 | 15 | 5 | 10 | 0 | 0 |
| **II3** | Cl | H | HN | / | / | / | 100 | / | / | / | / | / | 40 | / | / |
| **II4** | Cl | H | NHCN | 100 | 98 | 15 | 100 | 80 | 35 | 35 | 15 | 5 | 35 | 20 | 10 |
| **II5** | Cl | H | $NHCH_2CN$ | 100 | 100 | 100 | 100 | 100 | 100 | 100 | 100 | 100 | 100 | 95 | 95 |
| **II6** | Cl | H | $NHCO_2CH_3$ | 100 | 100 | 100 | 100 | 100 | 100 | 100 | 100 | 100 | 100 | 100 | 100 |
| **II7** | Cl | H | $NHCO_2C_2H_5$ | 100 | 100 | 100 | 100 | 100 | 100 | 100 | 100 | 90 | 100 | 100 | 90 |
| **II8** | Cl | H | $NHCO_2CH(CH_3)_2$ | 100 | 100 | 90 | 100 | 100 | 90 | 100 | 100 | 90 | 100 | 100 | 90 |
| **II9** | Cl | H | $NHCO_2CH_2CH_2CH_2CH_3$ | 100 | 100 | 100 | 100 | 100 | 100 | 65 | 45 | 10 | 65 | 50 | 15 |
| **II10** | Cl | H | $NHCO_2CH_2CH_2OCH_3$ | 100 | 100 | 100 | 100 | 100 | 100 | 85 | 55 | 45 | 98 | 65 | 50 |
| **II11** | Cl | H | $NHN(CH_3)_2$ | 100 | 100 | 100 | 100 | 100 | 100 | 95 | 60 | 50 | 98 | 50 | 45 |
| **II12** | Cl | H | $NHNHCH_3$ | 90 | 80 | 40 | 85 | 15 | 5 | 20 | 0 | 0 | 0 | 0 | 0 |
| **II13** | Cl | H | $N(CH_3)CO_2CH_3$ | / | / | / | 85 | / | / | / | / | / | 35 | / | / |
| **II14** | Cl | H | $N(CH_3)CO_2C_2H_5$ | / | / | / | 0 | / | / | / | / | / | 0 | / | / |
| **II15** | Cl | H | $N(CH_3)CO_2CH(CH_3)_2$ | 25 | 20 | 15 | 95 | 50 | 25 | 10 | 10 | 0 | 15 | 10 | 5 |
| **II16** | Cl | H | | 35 | 25 | 20 | 98 | 50 | 35 | 10 | 10 | 5 | 10 | 5 | 5 |
| **II17** | Cl | H | $N(CO_2CH_3)_2$ | 95 | 90 | 85 | 98 | 85 | 90 | 90 | 40 | 60 | 85 | 40 | 20 |
| **II18** | Cl | H | $N(CO_2C_2H_5)_2$ | 45 | 30 | 20 | 50 | 45 | 10 | 30 | 20 | 20 | 20 | 10 | 10 |
| **III1** | Cl | F | $NHCH_2CN$ | 5 | / | / | 0 | / | / | 0 | / | / | 0 | / | / |
| **III2** | Cl | F | $NHCO_2H$ | 100 | 100 | 100 | 100 | 100 | 100 | 100 | 100 | 98 | 100 | 100 | 100 |
| **III3** | Cl | F | $NHCO_2CH_3$ | 100 | 100 | 100 | 100 | 100 | 100 | 100 | 100 | 65 | 100 | 100 | 60 |
| **III4** | Cl | F | $NHCO_2CH_2CH_3$ | 100 | 100 | 100 | 100 | 100 | 100 | 100 | 100 | 100 | 100 | 100 | 100 |
| **III5** | Cl | F | $N(CO_2CH_3)_2$ | 100 | 100 | 95 | 100 | 100 | 100 | 100 | 100 | 80 | 100 | 100 | 50 |
| ***Lead compound*** | *Cl* | *H* | *$NHCH_2CH_3$* | *100* | */* | *20* | *100* | */* | *15* | *30* | */* | *10* | *25* | */* | *10* |
| | | | ***Saflufenacil*** | *100* | *100* | *100* | *100* | *100* | *100* | *100* | *100* | *100* | *100* | *100* | *90* |
| | | | ***95% sulcotrione*** | *95* | *90* | *55* | *95* | *80* | *60* | *98* | *90* | *55* | *100* | *98* | *55* |

[a]Stands for no data. [b]YOApost-, VELpost-, FOXpost-, and BYG post- mean youth-and-old age (*Zinnia elegans Jacq.*), velvet leaf (*Abutilon theophrasti Medic.*), foxtail (*Setaria glauca (L.) Beauv*), and barnyard grass (*Echinochloa crus-galli (L.) Beauv*), respectively.

**Scheme 1. Overview Synthetic Methods of Substituted 3-(Pyridin-2-yl)benzenesulfonamide Derivatives**

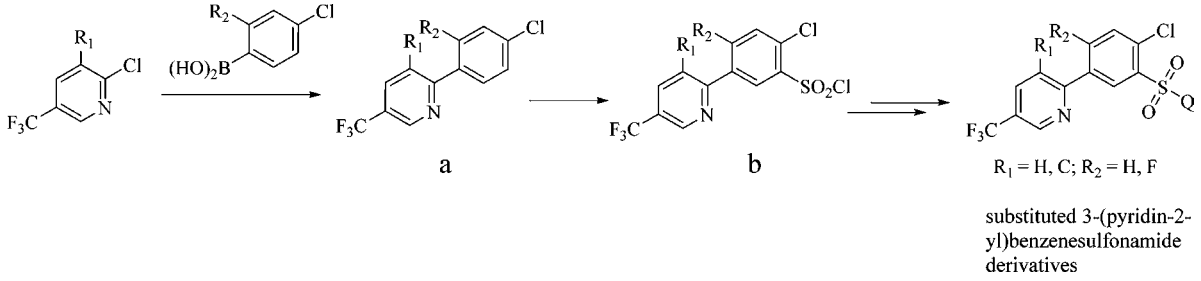


$C_{14}H_9Cl_2F_3N_2O_4S$: C, 39.18; H, 2.11; N, 6.53; Found: C, 39.19; H, 2.15; N, 6.52.

**II7**–**II10**, **II13**–**II15**, **II17**, **II18**, and **III2**–**III5** were synthesized using the synthetic method of **II6**.

**Herbicidal Activity Assay.** *Herbicidal Activity Assay in Glasshouse Tests.* All plant materials were obtained from the Agrochemical Discovery Department in Shenyang Research Institute of Chemical Industry. Plants were grown in plastic flowerpots containing loamy sand with about 3.0% humus as substrate. The seeds of the test plants were sown separately according to species.

The test plants were grown to a height of 3–15 cm, depending on the species, and only then treated with the active ingredients


dx.doi.org/10.1021/jf504018z | J. Agric. Food Chem. 2014, 62, 12491–12496

Table 2. Herbicidal Activity of II5, II6, II7, II10, III2, and III4 by Postemergence Treatment in Glasshouse Tests Employing a Parallel Experiment[a]

| | YOApost- | | | | VELpost- | | | | FOXpost- | | | | BYGpost- | | | |
|---|---|---|---|---|---|---|---|---|---|---|---|---|---|---|---|---|
| compd | 300 | 150 | 37.5 | 18.75 | 300 | 150 | 37.5 | 18.75 | 300 | 150 | 37.5 | 18.75 | 300 | 150 | 37.5 | 18.75 |
| II5 | 100 | 100 | 100 | 100 | 100 | 100 | 100 | 100 | 100 | 100 | 70 | 55 | 100 | 100 | 100 | 75 |
| II6 | 100 | 100 | 100 | 100 | 100 | 100 | 100 | 100 | 100 | 100 | 100 | 100 | 100 | 100 | 100 | 100 |
| II7 | 100 | 100 | 100 | 100 | 100 | 100 | 100 | 100 | 100 | 100 | 100 | 100 | 100 | 100 | 100 | 100 |
| II10 | 100 | 100 | 100 | 100 | 100 | 100 | 100 | 100 | 85 | 55 | 45 | 40 | 100 | 98 | 50 | 45 |
| III2 | 100 | 100 | 100 | 100 | 100 | 100 | 100 | 100 | 100 | 100 | 65 | 50 | 100 | 100 | 60 | 50 |
| III4 | 100 | 100 | 100 | 100 | 100 | 100 | 100 | 90 | 100 | 100 | 80 | 50 | 100 | 100 | 50 | 25 |

[a]YOApost-, VELpost-, FOXpost- and BYG post- mean youth-and-old age (*Zinnia elegans Jacq.*), velvet leaf (*Abutilon theophrasti Medic.*), foxtail (*Setaria glauca (L.) Beauv*), and barnyard grass (*Echinochloa crus-galli (L.) Beauv*), respectively.

suspended or emulsified in water. For this purpose, the test plants were either sown directly or grown in the same vessels or they were germinated separately and transplanted into the test vessels a few days before the treatment. The application rate for postemergence treatment was 600, 150, and 37.5 g/ha active substance.

The plants were kept at 10−25 °C or 20−35 °C depending on the species. The test lasted 2−4 weeks during which the plants were tended and their reaction to the individual treatments was evaluated.

Evaluation was on a scale from 0 to 100, where 100 means no emergence of the plants or complete destruction of at least the above-ground parts and 0 means no damage or normal growth.

The plants used in the glasshouse tests comprised the following species: velvet leaf (*Abutilon Theophrasti Medic.*), youth-and-old age (*Zinnia Elegans Jacq.*), barnyard grass (*Echinochloa crus-galli(L.) Beauv.*), and foxtail (*Setaria Glauca(L.) Beauv.*).

*Herbicidal Activity Assay in Field Tests.* The experiment of the field tests was operated on the basis of field efficacy trials of Chinese pesticide standards (a) GB/T17980.40-2000. The test weeds in rice field were at 2−4 leaf stage. The controlling weeds comprised the following species: dayflower (*commelina tuberosa*) and nightshade (*disambiguation*) in Liaoning and arrowhead (*sagittarian trifolia*) in Heilongjiang. The application rate for treatment was 30 and 60 g/ha active substance. The application rate for treatment of bentazon[46]-(48%, water dispersible granule) which was used as the control in Liaoning was 1440 g/ha active substance, while 24% oxyfluorfen EC was used as the control in Herlongjiang.

Formulas used in these tests are as follows: Control effect (%) = (the number of live weeds in the control area − the number of live weeds in the treated area)/the number of live weeds in the control area × 100%.

## RESULTS AND DISCUSSION

**Chemistry.** The designed substituted 3-(pyridin-2-yl)-benzenesulfonamide compounds were synthesized through critical intermediates (**b**) as shown in Scheme 1. The reactions of the intermediates **b1**, **b2**, and **b3** via the amino compounds and triethylamine using THF as the solvent afforded series I, series II, and series III in considerable yield, respectively. The 28 target compounds and intermediates were characterized by $^1$H NMR and elemental analyses. All spectral and analytical data were consistent with the assigned structures.

**Herbicidal Activity.** The 28 target compounds were evaluated for their herbicidal ability to control the unwanted plants using postemergence treatment in the glasshouse and the field tests. For postemergence treatment in the glasshouse, the designed substituted 3-(pyridin-2-yl)benzenesulfonamide compounds were compared to the lead compounds which were disclosed by researchers at BASF Aktiengesellschaft,[26] saflufenacil[47] and sulcotrione.[48] As shown in Table 1, series **I** compounds which were synthesized through intermediates **b1** could not control unwanted plants at the 600 g/ha active substance, and most compounds of series II and III could efficiently control velvet leaf, youth-and-old age, barnyard grass, and foxtail. Especially, **II6**, **II7**, **II8**, **II9**, **II10**, **II11**, **III2**, **III3**, **III4**, and **III5** showed higher activity than the lead compound which showed detective values of 20, 15, 10, and 10 for velvet leaf, youth-and-old age, barnyard grass, and foxtail at the 37.5 g/ha active substance, respectively. The activity of **II6**, **II7**, **III2**, and **III4** proved roughly equivalent to the saflufenacil and better than 95% sulcotrione at the same concentration. Meanwhile, the other compounds of series **II** and **III** did not show exciting activity.

By comparison of activity of series **I**, series **II**, and series **III**, it may be seen that substituent site $R_1$ is a critical active group, and it could clearly improve the activities once $R_1$ is chlorine. Hydrogen and fluorine were designed to infer the preliminary structure−activity relationship of substituent site $R_2$; **II6** and **III3** which have the same structure except $R_2$ showed similar excellent activity for velvet leaf, youth-and-old age, barnyard grass, and foxtail. However, the activities of **II5** and **III1** differ significantly. **II5** of which $R_2$ is hydrogen could obviously control target weeds, while **III1** of which $R_2$ is fluorine loses the ability to control weeds. Therefore, more compounds should be synthesized to get the structure−activity relationship at site $R_2$. Moreover, it is evident that introduction at substituent position Q of methyl carbamate (**II6**), ethyl carbamate (**II7**), isopropyl carbamate (**II8**), buty carbamate (**II9**) and 2-methoxyethyl carbamate (**II10**) could improve the herbicidal activity, and it seems that the ability to control barnyard grass and foxtail may decrease with the increase in number of carbon of carbamic acid ester.

In order to compare activity of these highly reactive compounds (**II5**, **II6**, **II7**, **II10**, **III2,** and **III4**), a parallel experiment was executed in glasshouse. As shown in Table 2, **II6** and **II7** could excellently control youth-and-old age, velvet leaf, foxtail, and barnyard grass at 18.5 g/ha active substance. **II5**, **II10**, **III2**, and **III4** showed detective values of 100 for youth-and-old age and velvet leaf at 18.5 g/ha active substance and not good enough for foxtail and barnyard grass at low concentration.

Herbicidal activity results in field test (Table 3) showed that **II7** at 60 g/ha active substance showed roughly the same activity with bentazon (48%, water dispersible granule) at 1440 g/ha active substance. The detective value of control effect of **II7** at 60 g/ha active substance is 70% after 7 days treatment and 60% after 15 days treatment. Especially, 10% **II7** OF (oil miscible flowable concentrate) could excellently control arrowhead and showed better activity than 24% oxyfluorfen EC (emulsifiable concentrate). As shown in Table 4, the control effect of 10% **II7** OF showed 95, 100, and 100 at 150

**Table 3. Herbicidal Activity of II7 in Field Tests (Liaoning, China)**

| compd | concn g(a.i./ha) | control effect to dayflower and nightshade (%) | |
|---|---|---|---|
| | | 7 days | 15 days |
| II7 | 30 | 40 | 40 |
| | 60 | 70 | 60 |
| bentazon | 1440 | 70 | 70 |

**Table 4. Herbicidal Activity of II7 in Field Tests (Heilongjiang, China)**

| compd | concn g(a.i./ha) | control effect to arrowhead (%) | | | control effect to rice (%) | | |
|---|---|---|---|---|---|---|---|
| | | 15 days | 30 days | 45 days | 15 days | 30 days | 45 days |
| 10% II7 OF | 100 | 95 | 97 | 95 | 0 | 0 | 0 |
| | 150 | 95 | 100 | 100 | 0 | 0 | 0 |
| 24% oxyfluorfen EC | 180 | 31 | 68 | 69 | 0 | 0 | 0 |

g(a.i./ha) after 15 days, 30 days, and 45 days treatment, respectively, while 24% oxyfluorfen EC showed detective values of 31, 68, and 69 for arrowhead at 180 g(a.i./ha) after 15 days, 30 days, and 45 days treatment, respectively. Meanwhile, **II7** and oxyfluorfen could not control rice and showed high security to rice.

In summary, a series of novel substituted 3-(pyridin-2-yl)benzenesulfonamide compounds were designed and synthesized by intermediate derivatization methods. The compounds (**II6**, **II7**, **II8**, **II9**, **II10**, **II11**, **III2**, **III3**, **III4**, and **III5**) showed higher activity than the lead compound at the 37.5 g/ha active substance using herbicidal activity assay in glasshouse tests, and the activity of **II6**, **II7**, **III2**, and **III4** proved roughly equivalent to the saflufenacil and better than 95% sulcotrione at the same concentration. The result of the herbicidal activity assay in field tests in Liaoning showed that **II7** could effectively control dayflower and nightshade. The activity of **II7** at 60 g/ha active substance proved roughly equivalent to bentazon at 1440 g/ha active substance. Meanwhile, the herbicidal assay in field tests in Heilongjiang showed 10% **II7** OF could excellently control arrowhead. Compound **II7** excited better activity than oxyfluorfen and security to rice. Our results suggest that **II7** may be a novel compound candidate for potential herbicide. This study will be useful for the design of new herbicides for weed control.

## ■ ASSOCIATED CONTENT

### Supporting Information

$^1$H NMR, melting point data, and elemental analyses data for compounds **I3, I5, II1−II5, II7−II18, and III1−III5.** This material is available free of charge via the Internet at http://pubs.acs.org.

## ■ AUTHOR INFORMATION


### Corresponding Author

*Telephone: 86-24-85869078. Fax: 86-24-85869137. E-mail: liuchangling@vip.163.com.



### Funding

The project was supported by the National Key Technology Support Program during the 12th Five-Year Plan Period of China (Grant No. 2011BAE06B03).


### Notes

The authors declare no competing financial interest.

## ■ REFERENCES


(1) Ravichandran, V.; Shalini, S.; Sundram, K.; Sokkalingam, A. D. QSAR study of substituted 1,3,4-oxadiazole naphthyridines as HIV-1 integrase inhibitors. *Eur. J. Med. Chem.* **2010**, *45*, 2791−2797.

(2) Gouliaev, A. H.; Larsen, M.; Varming, T.; Mathiesen, C.; Johansen, T. H.; Scheel-Kruger, J.; Olsen, G. M.; Nielsen, E. O. Preparation of benzothiadiazines, quinazolines, and other aryl-fused heterocycles as positive AMPA-receptor modulators for treatment of memory and learning disorders. WO 9942456, 1999.

(3) Ashweek, N.; Chen, M.; Coon, T. R.; Ewing, T.; Jiang, W.; Moree, W.; Rowbottom, M.; Wade, W.; Zhao, L.; Zhu, Y. F.; Yu, J. H.; Beaton, G. Preparation of benzenesulfonylamide derivatives as Gonadotropin-releasing hormone receptor antagonists. WO 2008124614, 2008.

(4) Su, S. Development and application of pyridine herbicides. *World Pesticides* **2012**, *34*, 4−6.

(5) Yang, J. C.; Diao, J.; Ge, T.; Liu, C. L. Recent research advances on pyridine pesticides. *Agrochemicals* **2007**, *46*, 1−9.

(6) Yang, J. C.; Dai, R. H.; Liu, Y. P.; Wu, Q.; Liu, C. L. Recent advance and synthesis on pesticides of pyridine series. *Agrochemicals* **2011**, *50*, 625−629.

(7) Shimanskaya, M. V.; Leitis, L. Pesticides based on pyridine derivatives. *Khim. Geterotsikl. Soedin.* **1989**, 579−587.

(8) Li, H. P.; Cheng, S. X.; Li, M.; Li, T.; Chen, J. X.; Gao, H. X. A review of neonicotinoid insecticides nitenpyram. *World Pesticides* **2013**, *35*, 20−23 36.

(9) Kagabu, S. Pharmacophore of neonicotinoid insecticides. *J. Pestic. Sci.* **2008**, *33*, 9−13.

(10) Watanabe, E.; Miyake, S.; Yogo, Y. Review of enzyme-linked immunosorbent assays (ELISAs) for analyses of neonicotinoid insecticides in agro-environments. *J. Agric. Food Chem.* **2013**, *61*, 12459−12472.

(11) Sarmah, A. K.; Sabadie, J. Hydrolysis of sulfonylurea herbicides in soils and aqueous solutions: A review. *J. Agric. Food Chem.* **2002**, *50*, 6253−6265.

(12) Tomlin, C. D. S. *The Pesticide Manual*, 16th ed.; British Crop Protection Council: Hampshire, Britain, 2012.

(13) Fu, C.; Pei, J.; Ning, Y.; Liu, M.; Shan, P.; Liu, J.; Li, Y.; Hu, F.; Zhu, Y.; Yang, H.; Zou, X. Synthesis and insecticidal activities of novel pyrazole oxime ether derivatives with different substituted pyridyl rings. *Pest Manage. Sci.* **2014**, *70*, 1207−1214.

(14) Hanai, D.; Matsui, M.; Aoyama, H.; Tanigawa, H. Pyridine compound or salt thereof, pest control agent, insecticide or acaricide, and ectoparasite control agent. JP 2014065209, 2014.

(15) Kaiser, F.; Narine, A.; Dickhaut, J.; Koerber, K.; Bandur, N. G. Preparation and use of pesticidal substituted pyridyl thiazole compounds and derivatives for combating pests. WO 2013186089, 2013.

(16) Liu, X.; Sun, S.; Yang, M.; Tan, C.; Weng, J. Preparation of pyridine-containing 1,3,4-thiadiazoles as pesticides. CN 103626751, 2014.

(17) Maienfisch, P.; Rendler, S.; Pitterna, T. Preparation of pyridine carboxamides as pesticides. WO 2013127768, 2013.

(18) Numata, A.; Iwawaki, Y.; Furukawa, H.; Ando, K. Pyridines and their use for pest control agents. JP 2014208631, 2014.

(19) Numata, A.; Maeda, K.; Saito, F.; Ando, K. Preparation of pyrazole derivatives as pesticides. JP 2014111559, 2014.

(20) Pitterna, T.; Loiseleur, O.; Luksch, T.; Mondiere, R. J. G. Preparation of carboxamides as pesticidal compounds. WO 2014173921, 2014.

(21) Ren, L.; Lou, Y.; Chen, N.; Xia, S.; Shao, X.; Xu, X.; Li, Z. Synthesis and insecticidal activities of tetrahydroimidazo[1,2-a] pyridinones: Further exploration on *cis*-neonicotinoids. *Synth. Commun.* **2014**, *44*, 858−867.

(22) Wang, B.; Zhao, Y.; He, D.; Li, W. Preparation of multi-substituted 1-pyridyl-1*H*-pyrazole-5-carboxamide derivatives as pesticides. CN 104003976, 2014.
(23) Yerkes, C. N.; Mann, R. K. Herbicidal compositions comprising 4-amino-3-chloro-5-fluoro-6-(4-chloro-2-fluoro-3-methoxyphenyl) pyridine-2-carboxylic acid or a derivative thereof and insecticides. U.S. 20140274698, 2014.
(24) Wang, B. L.; Zhu, H. W.; Ma, Y.; Xiong, L. X.; Li, Y. Q.; Zhao, Y.; Zhang, J. F.; Chen, Y. W.; Zhou, S.; Li, Z. M. Synthesis, insecticidal activities, and SAR studies of novel pyridylpyrazole acid derivatives based on amide bridge modification of anthranilic diamide insecticides. *J. Agric. Food Chem.* **2013**, *61*, 5483−5493.
(25) Schaefer, P.; Hamprecht, G.; Puhl, M.; Westphalen, K. O.; Zagar, C. Synthesis and herbicidal activity of phenylpyridines—A new lead. *Chimia* **2003**, *57*, 715−719.
(26) Schaefer, P.; Hamprecht, G.; Heistracher, E.; Koenig, H.; Klintz, R.; Muenster, P.; Rang, H.; Westphalen, K. O.; Gerber, M.; Walter, H. Preparation of substituted 2-phenylpyridine herbicides. DE 4323916, 1995.
(27) Honda, T.; Murata, T. Multilayer composite blow bottles with good appearance and excellent water vapor barrier property and impact resistance and their manufacture by direct blow molding method. JP 2010147917, 2012.
(28) Kuehne, M.; Gallay, J. J. Thiobarbituric acid derivatives. EP 1985810303, 1986.
(29) Boy, P.; Combellas, C.; Thiebault, A. Synthesis of 4-[(trifluoromethyl)pyridyl]phenol derivatives. *Synlett* **1991**, 923−924.
(30) Takeuchi, J.; Ikura, M.; Higashino, M.; Iwahashi, M.; Hashimura, K. Preparation of thiazole-containing urea derivatives as tropomyosin receptor kinase (Trk kinase) inhibitors. WO 2013161919, 2013.
(31) Schaefer, P.; Hamprecht, G.; Heistracher, E.; Klintz, R.; Koenig, H.; Walter, H.; Westphalen, K.-O.; Mislitz, U. Preparation of substituted 2-phenylpyridine herbicides and defoliants. DE 19500760, 1996.
(32) L'Heureux, A.; Hiebert, S.; Hu, C.; Lam, P. Y. S.; Lloyd, J.; Pi, Z.; Qiao, J. X.; Thibeault, C.; Tora, G. O.; Yang, W.; Wang, Y.; Wang, T. C.; Bowsher, M. S.; Ruel, R. Preparation of hydroxyindoline derivatives for use as P2Y1 receptor antagonists. WO 2014022343, 2014.
(33) Narabu, S.; Yoneta, Y.; Yanagi, A.; Shirakura, S.; Ukawa, S.; Ichihara, T.; Nakamura, S.; Hills, M.; Kehne, H.; Dittgen, J.; Feucht, D.; Rosinger, C. Preparation of tetrazolylethoxybenzoylpyrazoles as herbicides. JP 2006279533, 2013.
(34) Liu, C. L. Innovation of pesticide discovery methods and candidate compounds. *High-Technol. Industr.* **2008**, *9*, 79−81.
(35) Liu, C. L. Approach and application of novel agrochemical innovation. *Chin. J. Pestic. Sci.* **2011**, *50*, 20−23.
(36) Guan, A. Y.; Liu, C. L.; Yang, X. P.; Dekeyser, M. Application of the intermediate derivatization approach in agrochemical discovery. *Chem. Rev.* **2014**, *114*, 7079−7107.
(37) Fujii, K.; Fukuda, Y.; Yamanaka, Y. Preparation of aralkylaminopyrimidines as bactericides. JP 04235976, 1992.
(38) Ohata, K.; Adachi, K.; Hashimoto, M.; Kage, A. Fungicidal 3-hydroxyisoxazole derivatives. DE 2032809, 1971.
(39) Vogelbacher, U. J.; Otto, P.; Rack, M. Preparation of β-ketonitriles. WO 2008107397, 2008.
(40) Wong, M.; Blouet, A.; Guckert, A. Effectiveness of SC2053 as a chemical hybridizing agent for winter wheat. Importance of developmental stages and doses of application. *Plant Growth Regul.* **1995**, *16*, 243−248.
(41) Guan, A. Y.; Liu, C. L.; Li, M.; Zhang, H.; Li, Z. N.; Li, Z. M. Design, synthesis and structure−activity relationship of novel coumarin derivatives. *Pest Manage. Sci.* **2011**, *67*, 647−55.
(42) Chai, B. S.; Liu, C. L.; Li, H. C.; Zhang, H.; Liu, S. W.; Huang, G.; Chang, J. B. The discovery of SYP-10913 and SYP-11277: Novel strobilurin acaricides. *Pest Manage. Sci.* **2011**, *67*, 1141−1146.
(43) Li, M.; Liu, C. L.; Yang, J. C.; Zhang, J. B.; Li, Z. N.; Zhang, H.; Li, Z. M. Synthesis and biological activity of new (*E*)-α-(Methoxyimino)benzeneacetate derivatives containing a substituted pyrazole ring. *J. Agric. Food Chem.* **2010**, *58*, 2664−2667.
(44) Guan, A. Y.; Liu, C. L.; Huang, G.; Li, H. C.; Hao, S. L.; Xu, Y.; Li, Z. N. Design, synthesis, and structure−activity relationship of novel aniline derivatives of chlorothalonil. *J. Agric. Food Chem.* **2013**, *61*, 11929−11936.
(45) Golcz, L.; Szulc, W.; Zalecki, R. Chemical control of weeds in the cultivation of Glaucium flavum Cranz. *Herba Pol.* **1981**, *27*, 317−24.
(46) Eldabaa, M. A. T.; Abouziena, H. F.; El-Desoki, E. R.; Abd El Wahed, M. S. A. Efficacy of some chemical weed control treatments on soybean [*Glycine Max (L.) Merr.*] plants and associated weeds in sandy soil. *J. Appl. Sci. Res.* **2012**, *8*, 4678−4684.
(47) Grossmann, K.; Niggeweg, R.; Christiansen, N.; Looser, R.; Ehrhardt, T. The herbicide saflufenacil (Kixor) is a new inhibitor of protoporphyrinogen IX oxidase activity. *Weed Sci.* **2010**, *58*, 1−9.
(48) Beraud, J. M.; Compagnon, J. M. Sulcotrione: A selective postemergence herbicide for corn. *Phytoma* **1993**, *456*, 55−57.

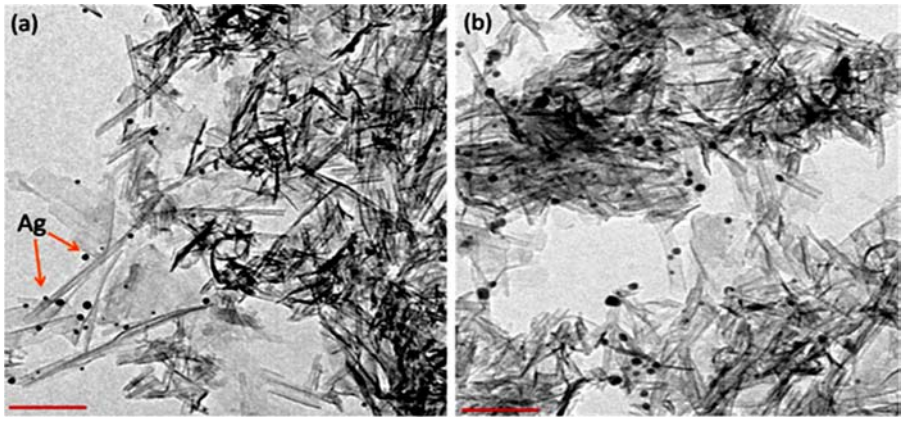


**Figure 1.** (a, b) TEM images for 0.5 wt % Ag photodeposited sodium titanate nanotubes. Scale bar = 100 nm.

## EXPERIMENTAL PROCEDURES

**Materials.** Sodium hydroxide (AR), acetonitirile (HPLC), methanol (GC), ethyl acetate (GC), isopropyl alcohol (AR), silver chloride, and nitric acid were purchased from Loba Chemie. Commercially available P25-$TiO_2$ (size = 30−50 nm, anatase phase = 70%, rutile phase = 30%, surface area = 50 $m^2$ $g^{-1}$) and imidacloprid were obtained from Degussa Corp., Germany, and Ravi Organics Pvt. Ltd. (Mumbai), India, respectively. Standard $CO_2$ gas (200 ppm) with $N_2$ as a base was obtained from Centurion Scientific Pvt. Ltd., New Delhi, India. Sodium nitrite, sodium nitrate, and sodium chloride were used as standards of nitrite, nitrate, and chloride ions, respectively, and were obtained from Sigma-Aldrich. All of the chemicals were used without further purification.

**Synthesis, Characterization, and Photoactivity of Bare and Ag-Loaded TNT.** TNT were prepared through the hydrothermal route using P25-$TiO_2$ as reported[7,8] by our group. Surface modification of TNT by Ag loading (0.2−1.0 wt %) was carried out by irradiating (125 W Hg arc lamp) the deaerated solution (50% v/v isopropyl alcohol) of TNT and $AgNO_3$ (equivalent to 0.2, 0.5, and 1.0 wt % of Ag) as reported[7,8] recently by our group. Catalysts thus obtained are termed 0.2-Ag-TNT, 0.5-Ag-TNT, and 1.0-Ag-TNT, respectively.

The photocatalytic activity of the as-prepared catalysts was carried out in a test tube (rubber capped) by taking 5.0 mg of catalysts and 5 mL (50 ppm) of aqueous solution of imidacloprid under UV light irradiation for various time intervals. The reaction solution was analyzed by HPLC (Agilent-LC1120) equipped with a UV detector (at $\lambda$ = 270 nm) having a C-18 column (BDS, Qualigens) of dimensions 250 mm × 4.6 mm and particle size of 5 $\mu$m using acetonitrile : water :: 80:20 as mobile phase (1 mL/min), at ambient temperature, using a 20 $\mu$L injection volume. The $CO_2$ evolution was determined by injecting 1 mL of gaseous mixture from the reaction vessel (gastight test tube) into a gas chromatograph (GC, NUCON-5765) using a Propak-Q column with nitrogen as carrier gas (30 mL/min) and thermal conductivity detector. The column oven was maintained at 40 °C, whereas the injector and detector were at 70 and 80 °C, respectively. Identification of the intermediates formed during photooxidation of IMI was carried out using a gas chromatograph (45X-GC)−mass spectrometer (MS-Scion-45P), by injecting 1 $\mu$L of extracted sample (Supporting Information, Scheme 1) on a HP-5MS column (15 m × 0.25 mm × 0.25 $\mu$m), with helium gas (1 mL/min) as a carrier. The oven was programmed from 60 °C (5 min hold) to 240 °C at 6 °C/min, whereas the transfer line and injector were kept isothermally at 250 and 275 °C, respectively, and the identified intermediates are termed I-1−I-8 hereafter. The formation of inorganic anions (nitrate, nitrite, and chloride) has been quantitatively estimated by injecting 100 $\mu$L of the sample into an ion chromatograph equipped with a Waters 501 pump, a Waters 431 conductivity detector, and an ion pack (50 mm × 4.6 mm, Metrhom) column using methanol : water :: 60:40 as mobile phase at 0.6 mL/min.

## RESULTS AND DISCUSSION

Morphological analysis of TNT (Figure 1) reveals the formation of open-ended straw-like nanotubes having length (L) = 80−115 nm and diameter (D) = 8−13 nm and has been reported by our group.[7,8] The Ag nanoparticles of narrow size (3−5 nm) distribution at the surface of many TNT particles can be distinctly noted for the 0.5-Ag-TNT sample.

The time course PCA of bare and Ag-loaded TNT in relation to P25 is shown in Figure 2. It is observed that TNT exhibited

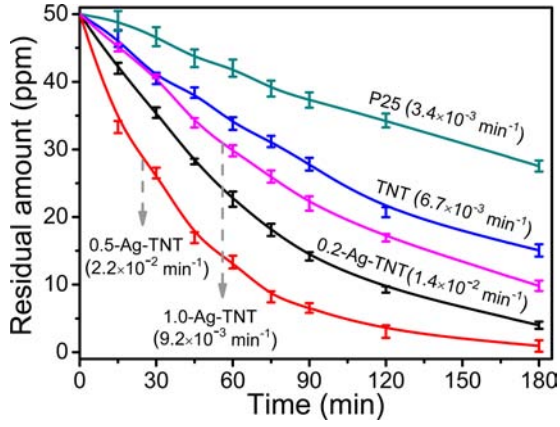


**Figure 2.** Time course study and pseudo-first-order decay constants for photocatalytic degradation of imidacloprid using various catalysts. Error bars represent standard deviation from three replicate experiments.

higher activity than P25 and is consistent with our[7,8] and other previous papers.[3−5] However, Ag-loading increases the activity of TNT up to 0.5 wt % for the degradation of IMI, and thereafter its activity decreases. Photooxidation of IMI was found to follow pseudo-first-order kinetics (Supporting Information, Figure S1) with the highest value of apparent rate constant ($k$) of 2.2 × $10^{-2}$ $min^{-1}$ for 0.5-Ag-TNT catalyst, and the half-life of IMI found (Supporting Information, Table 1) was ∼32 min, notably much lower in relation to that of TNT (∼103 min) or P25 (∼204 min) catalysts, under similar reaction conditions.

Time course GC-MS (Figure 3) analysis showed a gradual decrease in peak height for IMI along with the appearance of some new peaks, each belonging to a different intermediate. Some of these intermediates were identified by their mass spectra (Figure 4). There is a complete disappearance of peak


dx.doi.org/10.1021/jf5041614 | J. Agric. Food Chem. 2014, 62, 12497−12503

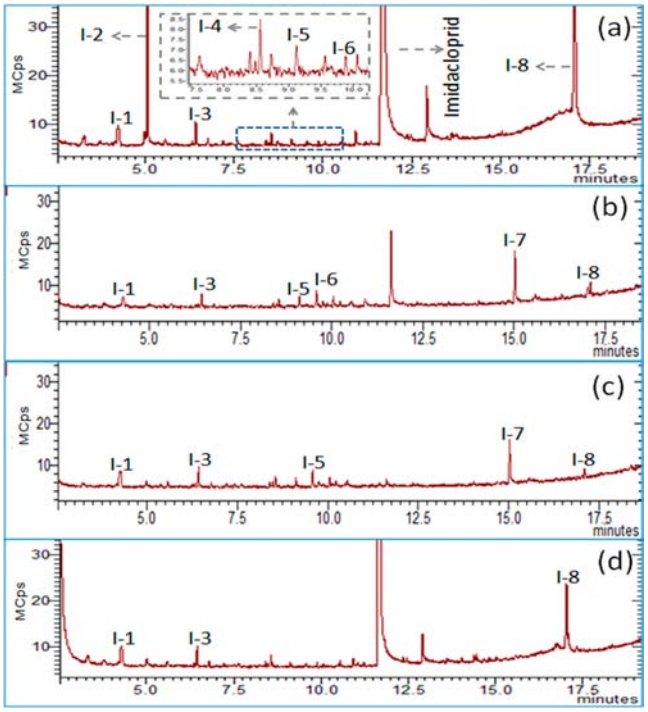


**Figure 3.** Gas chromatograms for identified intermediates (I-1−I-8) obtained after photocatalytic degradation of imidacloprid using 0.5 wt % Ag-photodeposited sodium titanate nanotubes after (a) 30 min, (b) 120 min, and (c) 180 min in comparison to (d) bare sodium titanate nanotubes after 180 min. (Inset) Corresponding enlarged view.

corresponding to IMI (at retention time ($R_t$) = 11.2 min, Figure 3) after 180 min of its photooxidation in the presence of 0.5-Ag-TNT catalyst; however, its presence was observed when studied with bare TNT under similar experimental conditions, confirming the improved activity of the former catalyst.

The quantitative estimation for $CO_2$ formation (Figure 5) during degradation of IMI by various catalysts was found to follow trends similar to those of its photooxidation. The highest amount of $CO_2$ formation (Supporting Information, Table 2) by 0.5-Ag-TNT catalyst with highest ($2.4 \times 10^{-3}$ $min^{-1}$) pseudo-first-order rate constant (Supporting Information, Table 3) corresponds to ∼70% of its actual mineralization despite its complete oxidation. This incomplete mineralization of IMI is because of the existence of some intermediates found (Figures 3 and 4) even after 180 min of its photooxidation.

Investigation for the fate of heteroatoms showed that the amounts of inorganic ions formed (Supporting Information, Figure S2) by 0.5-Ag-TNT are higher than those for P25 (Figure 6). Moreover, the amount of inorganic ions increases with increase in the time of irradiation, again confirming the mineralization of IMI during its photodegradation.

The chemical equation (eq 1) obtained from these results is found to deviate from stoichiometrically balanced eq 2, evidencing incomplete mineralization of IMI. The increase in the amount of nitrate ion formation with irradiation time is probably due to mineralization of the imidazole or pyridine-substituted ring(s). These results are in correlation with a previous study[27] for the dissipation of cyrpoconazole, where the nitrogen atoms present in the triazole moiety were found to decompose to nitrate and ammonium ions.

$$C_9H_{10}N_5O_2Cl + \frac{5}{2}O_2 \xrightarrow[h\nu\ (180\ min)]{0.5\ wt\%\ Ag\text{-}TNT} 2.88CO_2 + 0.04NO_2^- + 0.62NO_3^- + 0.6Cl^- + {}^{\bullet}intermediates \quad (1)$$

$$C_9H_{10}N_5O_2Cl + \frac{33}{2}O_2 \rightarrow 9CO_2 + 5NO_3^- + Cl^- + 6H^+ + 2H_2O \quad (2)$$

The PCA of TNT with Ag depositions was enhanced remarkably, certainly with an optimum amount (0.5 wt %) of the silver. With a greater amount of Ag photodeposition, the metal would rapidly become the recombination center for electron/hole ($e^-/h^+$) pairs and consequently diminish the PCA. Moreover, Ag being a plasmonic[28] nanostructure supports the formation of resonant surface plasmons in response to a photon flux that in turn could yield a high concentration of $e^-/h^+$ pairs in Ag-TNT samples. The formation of such plasmonic nanostructures also allows the selective formation of $e^-/h^+$ pairs at the interface of Ag-TNT, which could readily separate these carriers from each other and easily migrate[28−30] to the surface, where they can carry out PCA. Loaded Ag is well-known[28,31] to improve the adsorption capacity of $TiO_2$ for molecular oxygen; therefore, it can scavenge more conduction band electrons by the formation of highly oxidative superoxide radicals, whereas $h^+$ reacts with absorbed surface −OH groups and/or $H_2O$ molecules to form hydroxyl radicals possessing high oxidizability and causing the improved PCA of Ag-loaded TNT nanoparticles.

The formation of a variety of intermediates during the photooxidation of IMI suggests various possible attack positions for the hydroxyl radical leading to the formation of intermediates (Figure 7). The primary attack sites by the hydroxyl radical during photooxidation of IMI yielded I-2 and I-4 by cleavage of the N−N bond between the N1 and N2 positions and of the C−N bond at the C-1 position. The intermediate I-2 thus formed could be degraded to I-6 via attack of the hydroxyl radical on the C−N bond of the $-CH_2-N-$ moiety. On the other hand, intermediate I-4 (primary alcohol) is oxidized to the corresponding acid (I-5). The formation of carboxylated compounds has been observed during the photocatalytic degradation pesticides such as for cyproconazole[33] (fungicide) that has triazole and chlorobenzene moieties in its structure. Alternatively, hydrolysis, which is often reported[34−36] during the photocatalytic degradation of pesticides, could result (Scheme 1a) in the formation of intermediate I-8. The successive oxidation of I-8 on the methyl group at the C-2 position of the imidazole ring could lead to the formation of I-3. The formation of intermediate I-6 is proposed to be via fragmentation of I-3 and is reported to be an intermediate product[26] of IMI photooxidation. Interestingly, I-7, formed (Scheme 1b) by the removal of Cl and $NO_2$ radicals from IMI, has been identified in the present study using Ag-loaded TNT samples. This could be attributed to the facts that (i) the I-7 intermediate formed remained below the detection limit of GC-MS and (ii) it may have formed/consumed/transformed into some other product during the photooxidation. The formation of I-7 via the proposed radical mechanism is also suggested by Donald et al.[37] during the gas phase fragmentation of IMI. Because there is evolution of $CO_2$ and formation of inorganic ions during the photooxidation of IMI, it is possible that intermediates might further oxidize to

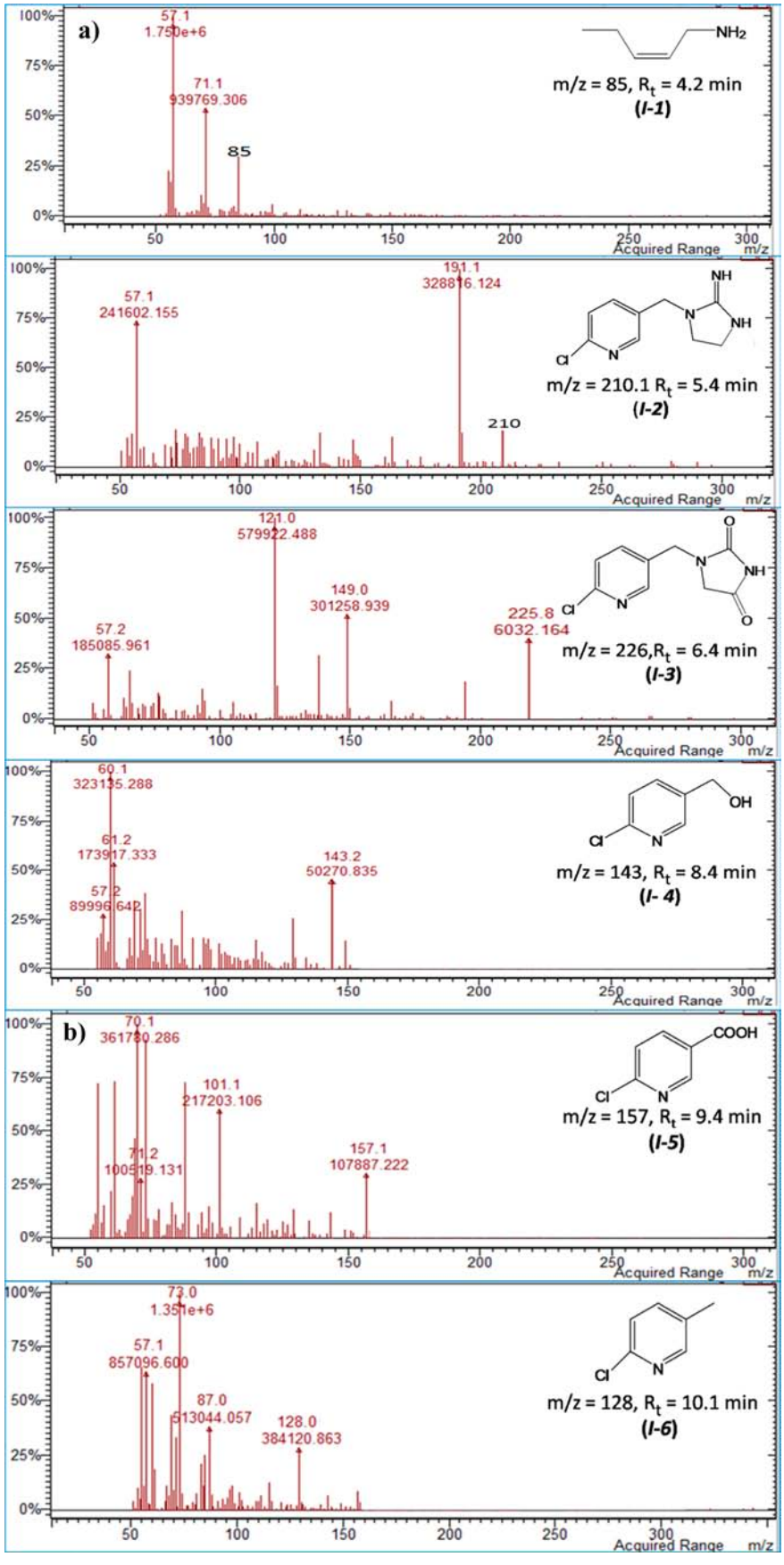


**Figure 4.** continued


dx.doi.org/10.1021/jf5041614 | J. Agric. Food Chem. 2014, 62, 12497−12503

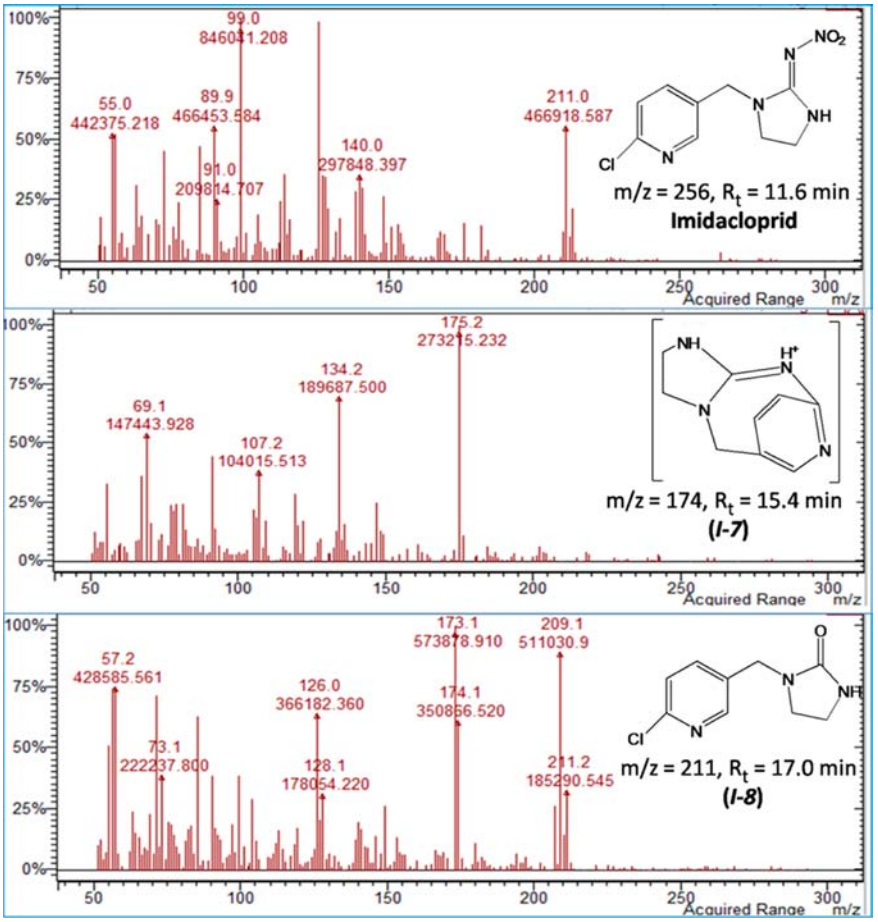


**Figure 4.** Mass spectra for identified intermediates (a, I-1−I-4; b, I-5−I-8). (Inset) Retention time ($R_t$) as per gas chromatograms, molecular structure, and mass/charge ratio ($m/z$).

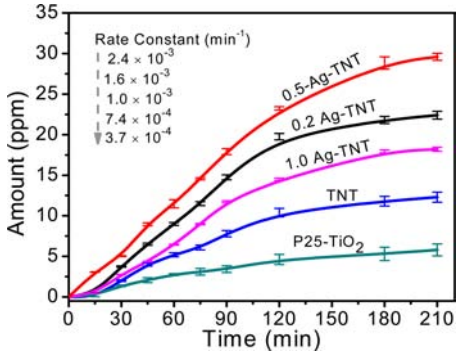


**Figure 5.** Time course of $CO_2$ formation during the photooxidation of imidacloprid by different catalysts. Error bars represents standard deviation from three replicate experiments.

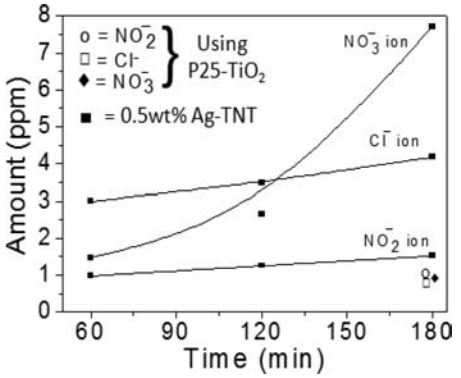


**Figure 6.** Evolution of inorganic ions during photooxidation of imidacloprid by 0.5 wt % Ag-photodeposited TNT and bare P25.

smaller compound(s) and eventually become mineralized. Similar to identified intermediates, previous studies also identified these intermediates[26] during the photooxidation of IMI using P25. However, the extent of IMI mineralization was 14−29%[32] and is 1.7 times less than in the present study, revealing the improved efficiency of as-prepared catalysts relative to P25.

The proposed mechanism is further supported by kinetic analysis of the intermediates (Figure 8) and by relating the ratio of peak area at any time ($area_{(t)}$) to the maximum peak area ($area_{(max)}$), due to the unavailability of authentic intermediates. Intermediates I-2, I-4, and I-8 appear promptly, and the concentration becomes maximum after 30 min before being degraded, whereas their corresponding transformed intermediates, namely, I-1, I-5, I-3, and I-6, were found to be at their maximum level after 15−30 min of photooxidation of I-2, I-4, and I-8 intermediates, respectively. Afterward, intermediates start disappearing and within 180 min of photooxidation are almost leveled off, except for I-2 and I-5. The existence of heteroatoms containing intermediates (I-2 and I-5) even after complete degradation of IMI signifies their stability in the reaction medium and is believed to be a cause for the incomplete mineralization for IMI. The results of the present are also supported by the results of Lhomme et al.[33] and


dx.doi.org/10.1021/jf5041614 | J. Agric. Food Chem. 2014, 62, 12497−12503

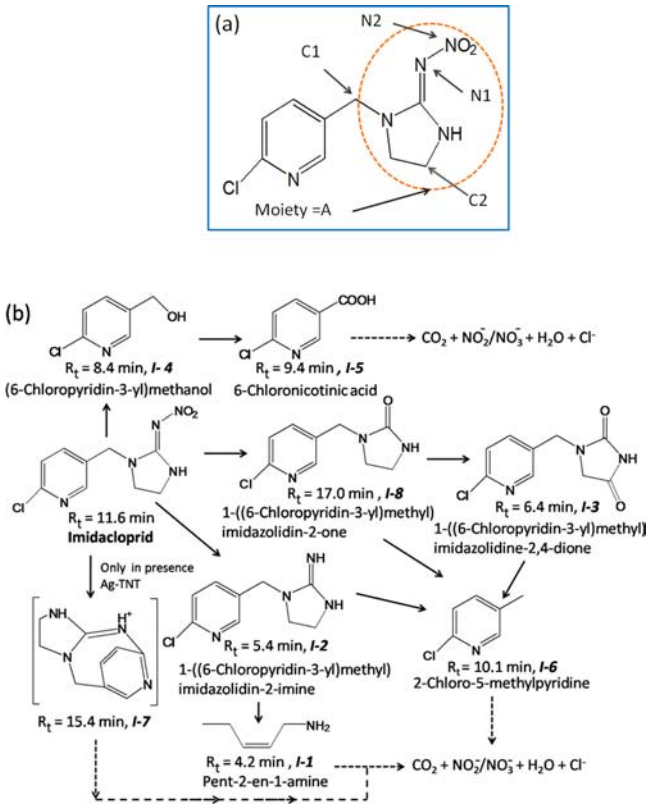


**Figure 7.** (a) Various attack positions by hydroxyl radicals at imidacloprid and (b) probable pathway proposed for the degradation of imidacloprid.

**Scheme 1. Mechanism for Formation of Intermediates (a) I-8 and (b) I-7 after Photooxodation of Imidacloprid**

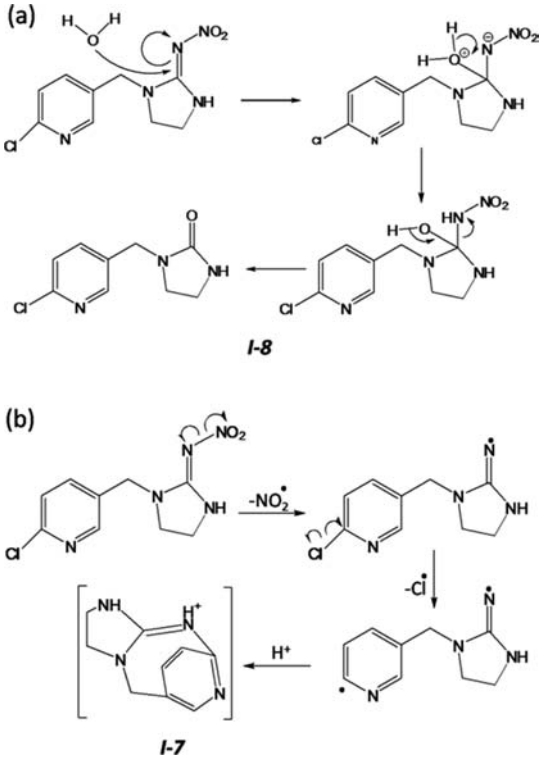


Lambropoulou et al.,[38] suggesting phoromineralization of heteroatoms (present in their moieties) to inorganic ions and

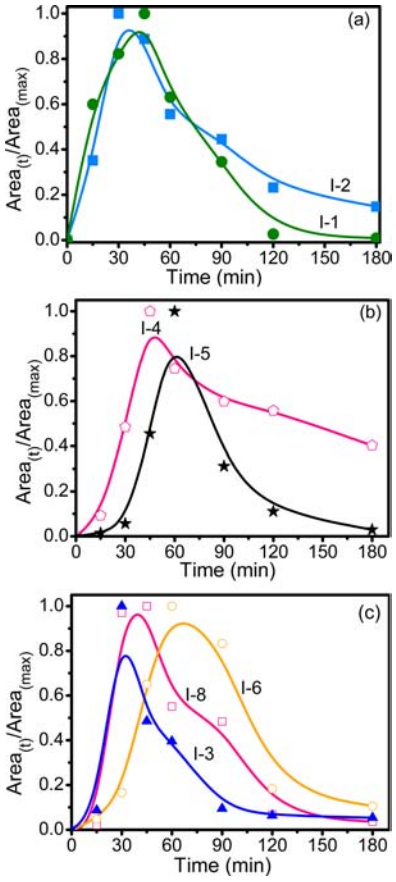


**Figure 8.** (a–c) Time evolution for the intermediates formed during the photooxidation of imidacloprid.

leveling off the intermediates with time during the photocatalytic degradation of cyproconazole and fenhexamid, respectively, in the presence of $TiO_2$.

Thus, Ag-photodeposited TNT is an efficient catalyst for the decomposition of IMI to $CO_2$ and inorganic ions, and it notably reduces the half-life of IMI to that found by most photoactive P25-$TiO_2$. Although structural parameters of TNT were found to play a vital role in the improved decay constants, a detrimental influence of sodium atoms was not observed in the present study. The formation of a number of intermediates identified revealed the complexity of the photocatalytic process, suggesting the existence of various oxidation routes and nonspecific attack of hydroxyl radicals that resulted in multistep and interconnected pathways for decomposition of IMI. The fate of heteroatoms suggests the partial mineralization to inorganic ions and is manifested by the presence of heteroatoms containing persistent intermediates even after the complete degradation of IMI.

## ■ ASSOCIATED CONTENT

### Ⓢ Supporting Information

Scheme 1, Figures Sl and S2, and Tables 1–3.This material is available free of charge via the Internet at http://pubs.acs.org.

## ■ AUTHOR INFORMATION

### Corresponding Author

*(B. Pal) E-mail: bpal@thapar.edu. Phone: +91-175-2393128. Fax: +91-175-2364498.

### Funding

We acknowledge the University Grants Commission and Department of Science and Technology, New Delhi, government of India, for providing financial support.

### Notes

The authors declare no competing financial interest.

## ■ ACKNOWLEDGMENTS

Degussa Corp., Germany, is gratefully acknowledged for the gift sample of $TiO_2$.

## ■ ABBREVIATIONS USED

$e^-$, electron; $h^+$, hole; TNT, sodium titanate nanotubes; 0.2-Ag-TNT, 0.2 wt % Ag deposited sodium titanate nanotubes; 0.5-Ag-TNT, 0.5 wt % Ag deposited sodium titanate nanotubes; 1.0-Ag-TNT, 1.0 wt % Ag deposited sodium titanate nanotubes; P25, commercially available P25-$TiO_2$; MCPS, mega counts per second; IC, ion chromatograph; GC, gas chromatograph; HPLC, high-performance liquid chromatograph; GC-MS, gas chromatograph coupled with mass spectrometer; TEM, transmission electron microscope; I-1−I-8, identified intermediates; IMI, imidacloprid; $t_{1/2}$, half-life time; AR, analytical reagent grade

## ■ REFERENCES

(1) Qamar, M.; Yoon, C. R.; Oh, H. J.; Lee, N. H.; Park, K.; Kim, D. H.; Lee, K. S.; Lee, W. J.; Kim, S. J. *Catal. Today* **2008**, *131*, 3−14.
(2) Qamar, M.; Yoon, C. R.; Jho, H.; Kim, D. H.; Jho, J. H.; Lee, K. S.; Lee, W. J.; Lee, H. G.; Kim, S. J. *Nanotechnology* **2006**, *17*, 5922−5929.
(3) Zhu, H.; Gao, X.; Lan, Y.; Song, D.; Xi, Y.; Zhao, J. *J. Am. Chem. Soc.* **2004**, *126*, 8380−8381.
(4) Antonio, J. A. T.; Jacome, M. A. C.; Cerros, S. L. O.; Palacios, E. M.; Parra, R. S.; Chavez, C. A.; Navarete, J.; Salinas, E. L. *Appl. Catal. B: Environ.* **2010**, *100*, 47−54.
(5) Potari, G.; Madarasz, D.; Nagy, L.; Laszlo, B.; Sapi, A.; Oszko, A.; Kukovecz, A.; Erdohelyi, A.; Konya, Z.; Kiss, J. *Langmuir* **2013**, *29*, 3061−3072.
(6) Morgado, E., Jr.; de-Abreu, M. A. S.; Pravia, O. R. C.; Marinkovic, B. A.; Jardim, P. M.; Rizzo, F. C.; Araujo, A. S. *Solid State Sci.* **2006**, *8*, 888−900.
(7) Grover, I. S.; Singh, S.; Pal, B. *Appl. Surf. Sci.* **2013**, *280*, 366−372.
(8) Grover, I. S.; Singh, S.; Pal, B. *J. Nanosci. Nanotechnol.* DOI: 10.1166/jnn.2014.9072.
(9) Stengl, V.; Bakardjieva, S.; Subrt, J.; Vecernıkova, E.; Szatmary, L.; Klementova, M.; Balek, V. *Appl. Catal. B: Environ.* **2005**, *63*, 20−30.
(10) Bavykin, D. V.; Friedrich, J. M.; Walsh, F. C. *Adv. Mater.* **2006**, *18*, 2807−2824.
(11) Ding, X.; Xu, X. G.; Chen, Q.; Peng, L. M. *Nanotechnology* **2006**, *17*, 5423−5427.
(12) Si, X.; Li, F.; Sun, L.; Xu, F.; Liu, S.; Zhang, J.; Zhu, M.; Ouyang, L. Z.; Sun, D.; Liu, Y. L. *J. Phys. Chem. C* **2011**, *115*, 9780−9786.
(13) Bavykin, D. V.; Lapkin, A. A.; Plucinski, P. K.; Murciano, L. T.; Friedrich, J. M.; Walsh, F. C. *Top. Catal.* **2006**, *39*, 3−4.
(14) Tsai, J. Y.; Chao, J. H.; Lin, C. H. *J. Mol. Catal. A Chem.* **2009**, *298*, 115−124.
(15) Guzsvany, V.; Banic, N.; Papp, Z.; Gaal, F.; Abramovic, B. *React. Kinet. Mech. Catal.* **2010**, *99*, 225−233.
(16) Halm, M. P.; Rortais, A.; Arnold, G.; Tasei, J. N.; Rault, S. *Environ. Sci. Technol.* **2006**, *40*, 2448−2454.
(17) Medrzycki, P.; Montanari, R.; Bortolotti, L.; Sabatini, A. G.; Maini, S.; Porrini, C. *Bull. Insectol.* **2003**, *56*, 59−62.
(18) Wamhoff, H.; Schneider, V. *J. Agric. Food Chem.* **1999**, *47*, 1730−1734.
(19) Philippidis, N.; Sotiropoulos, S.; Efstathiou, A.; Poulios, I. *J. Photochem. Photobiol. A: Chem.* **2009**, *204*, 129−136.
(20) Marugan, J.; Munoz, M. J. L.; Gernjak, W.; Malato, S. *Ind. Eng. Chem. Res.* **2006**, *45*, 8900−8908.
(21) Malato, S.; Caceres, J.; Aguera, A.; Mezcua, M.; Hernando, D.; Vial, J.; Alba, A. F. *Environ. Sci. Technol.* **2001**, *35*, 4359−4366.
(22) Zabar, R.; Komel, T.; Fabjan, J.; Kralj, M. B.; Trebse, M. *Chemosphere* **2012**, *89*, 293−301.
(23) Malev, O.; Klobucar, R. S.; Fabbretti, E.; Trebse, P. *Pestic. Biochem. Physiol.* **2012**, *104*, 178−186.
(24) Jadhav, S. R.; Saharan, V. K.; Pinjari, D.; Sonawane, S.; Saini, D.; Pandit, A. *J. Hazard. Mater.* **2013**, *261*, 139−147.
(25) Liu, W. P.; Zheng, W.; Gan, J. Y. *J. Agric. Food Chem.* **2002**, *50*, 6823−6827.
(26) Redlich, D.; Shahin, N.; Ekici, P.; Friess, A.; Parlar, H. *Clean* **2007**, *35*, 452−458.
(27) Lhomme, L.; Brosillon, S.; Wolbert, D. *Chemosphere* **2008**, *70*, 381−386.
(28) Zhang, X.; Chen, Y. L.; Liu, R. S.; Tsai, D. P. *Rep. Prog. Phys.* **2013**, *76*, 46401−46442.
(29) Inerbaev, T. M.; Hoefelmeyer, J. D.; Kilin, D. S. *J. Phys. Chem. C* **2013**, *117*, 9673−9692.
(30) Balasanthiran, C.; Hoefelmeyer, J. D. *Chem. Commun.* **2014**, *50*, 5721−5724.
(31) Chen, X.; Mao, S. S. *Chem. Rev.* **2007**, *107*, 2891−2959.
(32) Kitsiou, V.; Filippidis, N.; Mantzavinos, D.; Poulios, I. *Appl. Catal. B: Environ.* **2009**, *86*, 27−35.
(33) Lhomme, L.; Brosillon, S.; Wolbert, D. *J. Photochem. Photobiol. A: Chem.* **2007**, *188*, 34−42.
(34) Yadini, A. E.; Marouane, B.; Ahmido, A.; Dunlop, P.; Byrne, J. A.; Azzouzi, M. E.; Hajjaji, S. E. *J. Mater. Environ. Sci.* **2013**, *4*, 973−980.
(35) Konstantinou, I. K.; Sakellarides, T. M.; Sakkas, V. A.; Albanis, T. A. *Environ. Sci. Technol.* **2001**, *35*, 398−405.
(36) Ramesh, A.; Balasubramanian, M. *Food Chem.* **1999**, *47*, 3367−3371.
(37) Donald, W. A.; Leeming, M. G.; O'Hair, R. A. J. *Int. J. Mass Spectrom.* **2012**, *316− 318*, 91−99.
(38) Lambropoulou, D. A.; Konstantinou, I. K.; Albanis, T. A.; Alba, A. R. F. *Chemosphere* **2011**, *83*, 367−378.

Recently, we developed a novel emulsion and biomimetic dual-templating approach to synthesize oil-core silica-shell nanocapsules with tunable shell thickness.[29] Bifunctional SurSi peptide (Ac-MKQLAHSVSRLEHARKKRKKRKKRKKGGGY-$CONH_2$) was designed by modularizing a surface active peptide sequence (Sur module, MKQLAHSVSRLEHA) with a sequence for biosilicification (Si module, RKKRKKRKKR KKGGGY). Typically, oil-in-water (O/W) nanoemulsions are formed with a pharmaceutically safe oil, Miglyol 812, dispersed in the SurSi aqueous solution. Then a silica precursor tetraethoxysilane (TEOS) is added to facilitate the biosilicification at the O/W interfaces forming the oil-core silica-shell nanocapsules under room temperature, and at nearly neutral pH without use of any toxic chemicals. In contrast to the chemical methods mentioned above, our method is more biocompatible and environmentally friendly. An additional advantage of using peptide biosurfactant is the ability to be produced renewably at large scale and relatively low cost using biological expression.[30,31] Furthermore, our dual-templating approach offers easy preloading of active components by simply dissolving in the oil phase with a high loading capacity. It has been demonstrated that fipronil saturated in Miglyol 812 (at 10 $mg{\cdot}mL^{-1}$) was easily encapsulated in silica nanocapsules by a preloading technique and without the need for template removal.[29]

Fipronil (5-amino-1-[2,6-dichloro-4-(trifluoromethyl)-phenyl]-4-[(trifluoromethyl)sulfinyl] pyrazole-3-carbonitrile) is a systemic insecticide commonly used as soil treatment, seed coating, or baits[32] due to its nonrepellent property, broad-spectrum activity against agricultural, forest, pastoral, domestic and veterinary pests,[33] and high specificity for insect pests over mammalians.[34] The biochemical mode of action of fipronil is by blocking $\gamma$-aminobutyric acid (GABA) receptor of the GABA-gated chloride channel, thereby disrupting central nervous system activity and, at a sufficient dose, causing death.[34] It has low water solubility (~2 $\mu g{\cdot}mL^{-1}$ at 25 °C) and low Henry's constant ($6.6 \times 10^{-6}$ $m^3{\cdot}atm{\cdot}mol^{-1}$ at 25 °C), suggesting low volatility, and its soil organic carbon partition coefficient ($K_{oc}$) of 727 indicates low mobility in soil and, hence, low potential for groundwater contamination.[32,35]

In this study, sustained release of fipronil *in vitro* and *in vivo* from biocompatible oil-core silica-shell nanocapsules were investigated and compared. Fipronil-encapsulated silica nanocapsules with different shell thicknesses were synthesized using the dual-templating approach aforementioned. The *in vitro* release of fipronil was studied in water. The efficacy of the fipronil-encapsulated silica nanocapsules was evaluated by conducting *in vivo* laboratory tests, i.e., direct- and feeding-treatments, against economically important subterranean termites (i.e., *Coptotermes acinaciformis*). Subterranean termites cause substantial damages to cultivated plants, wooden structures, pastures, forests and other agricultural crops.[36] Based on the sales estimation of insecticides in 2010, the worldwide annual control and repair costs can reach US$40 billion with subterranean termites accounted for 80% of the costs.[37] This study would thus be expected to bring significant impact in agricultural fields.

## MATERIALS AND METHODS

**Chemicals.** SurSi peptide (Ac-MKQLAHSVSRLEHARKKRKK RKKRKKGGGY-$CONH_2$, $M_w$ 3632 $g{\cdot}mol^{-1}$) was custom synthesized by Peptide 2.0 Inc. (Chantilly, VA, USA) with purity >95% and was lyophilized prior to use. Fipronil in a powder form ($C_{12}H_4Cl_2F_6N_4OS$, $M_w$ 437.15 $g{\cdot}mol^{-1}$, mp 196−201 °C, and $d$ 1.55 $g{\cdot}cm^{-3}$) was of analytical standard obtained from Sigma-Aldrich. Miglyol 812 was purchased from AXO Industry S.A. (Wavre, Belgium) and was passed through heat-activated silica gel (Sigma-Aldrich) prior to use. Termidor (9.1% fipronil in a form of suspension concentrate) was obtained from BASF Australia Ltd. Water with >18.2 MΩ·cm resistivity was obtained from a Milli-Q (Millipore, Australia) system with a 0.22 $\mu$m filter. Other chemicals were of analytical grade purchased from either Sigma-Aldrich or Merck and used as received.

**Synthesis.** Oil-core silica-shell nanocapsules were synthesized using an emulsion and biomimetic dual-templating approach as we previously reported.[29] Briefly, fipronil was dissolved in Miglyol 812 oil at a concentration of 0.05 $mg{\cdot}mL^{-1}$ or 1 $mg{\cdot}mL^{-1}$, and then the fipronil-loaded oil was added into a solution of SurSi peptide (400 $\mu$M) containing $ZnCl_2$ (800 $\mu$M) in sodium 4-(2-hydroxyethyl)-1-piperazine ethanesulfonate (HEPES) buffer (25 mM, pH 7), and the mixture was sonicated at 10 W (Branson Sonifier 450 ultrasonicator) to obtain O/W nanoemulsions which were dialyzed against HEPES buffer (25 mM, pH 7.5) at 4 °C for 20 h to remove residual peptide in the bulk solution. Then the nanoemulsions (pH 7.5) were mixed with tetraethoxysilane (TEOS) at a concentration of 16 $\mu$mol, 32 $\mu$mol or 96 $\mu$mol under stirring at room temperature for 30 h to form fipronil-encapsulated silica nanocapsules having three different shell thicknesses. Subsequently, the nanocapsules were dialyzed against water at 4 °C for 20 h to remove the residual TEOS and prevent further growth of the silica shell.

**Characterization.** *Encapsulation Efficiency.* The suspensions of fipronil-encapsulated silica nanocapsules were freeze-dried for 20 h, subsequently mixed with water and sonicated at 20 W (Branson Sonifier 450 ultrasonicator) for 60 s to finely disperse the nanocapsules. Subsequently, acetonitrile was added into the suspensions with final acetonitrile concentration of 60 v/v%, and vigorously stirred at room temperature for up to 72 h. At different time intervals, the supernatants were collected by centrifugation, then fresh acetonitrile (60 v/v%) was added to the pellets to repeat the release of fipronil from the nanocapsules until no residual fipronil in the supernatants was detected via reversed-phase high-performance liquid chromatography (RP-HPLC).

*Reversed-Phase High-Performance Liquid Chromatography (RP-HPLC).* Concentrations of fipronil were assayed by RP-HPLC using a Shimadzu system equipped with a Jupiter C18 column (5 $\mu$m, 300 Å, 150 mm × 4.6 mm). Mobile phase A was water containing 0.1 v/v% phosphoric acid, while phase B contained 90 v/v% acetonitrile and 0.1 v/v% phosphoric acid. The elution gradient was increased from 50% B to 70% B over 20 min at a monitoring wavelength of 220 nm. The concentration of fipronil was determined based on the peak area at retention time of approximately 14.5 min according to calibration curve obtained from standard solution of fipronil in acetonitrile solution (60 v/v%).

*Fourier Transform-Infrared (FT-IR) Spectroscopy.* Silica nanocapsules without and with fipronil in the oil cores were prepared as described previously. The nanocapsules were washed twice with water and subsequently freeze-dried. FT-IR spectra of lyophilized SurSi peptide and the nanocapsules were determined by using a PerkinElmer Spectrum 100 FT-IR Spectrometer equipped with a universal attenuated total reflection (ATR) attachment. Spectra data were collected in the transmission mode by averaging 135 scans over wavenumber range 4000−600 $cm^{-1}$ at a spectral resolution of 4 $cm^{-1}$.

*Dynamic Light Scattering (DLS).* Size distributions of nanoemulsions and nanocapsules were determined by DLS using Malvern Zetasizer Nano ZS (Malvern Instrument Ltd., UK) at a scattering angle of 173° and a temperature of 25 °C. Samples were diluted by a factor of 100 prior to the measurements to avoid multiple scattering effects.

*Transmission Electron Microscopy (TEM).* Morphology of the fipronil-encapsulated silica nanocapsules was characterized by depositing the suspension (2 $\mu$L) onto Formvar-coated copper grids (ProSciTech Pty Ltd., Australia) and was then visualized via TEM (JEOL 1010, accelerating voltage of 100 kV). Size of the nanocapsules was analyzed using iTEM software (version 3.2, Soft Imaging System

GmbH) equipped with the TEM. Structure of the silica shell was determined using selected area electron diffraction (SAED) technique via high-resolution (HR) TEM (JEOL 2100, accelerating voltage of 200 kV).

***In Vitro* Release Study of Fipronil into Water.** Silica nanocapsules with three different shell thicknesses encapsulating 1 mg·mL$^{-1}$ fipronil in Miglyol 812 were used to study the release profile of fipronil *in vitro*. The releases of fipronil from the silica nanocapsules to water were carried out by stirring the suspensions at room temperature for up to 142 h. At different time intervals, aliquots were taken, replaced with fresh water and centrifuged to obtain clear supernatants which were then analyzed using RP-HPLC.

***In Vivo* Study against Termites.** Termites (*C. acinaciformis*) were collected from field site in Esk (Queensland, Australia). Plastic containers filled with moist wood were inverted (lid off) onto a timber-filled trench known to contain termite infestation, and each container was then covered with insulating material secured with soil. After harvesting, actively moving termites were carefully selected from the containers for *in vivo* tests.

*Direct Treatment.* Six samples, including water, nanoemulsions, silica nanocapsules (encapsulating 0.05 mg·mL$^{-1}$ fipronil in Miglyol 812) with three different shell thicknesses (8, 25, and 44 nm), and Termidor were used in the direct treatment, and they all contained the same final fipronil concentration except for the water sample. Water was used as control, and nanoemulsion was used as nanocapsules with zero silica-shell thickness. All six samples were used in five replicates for the direct treatment. Prior to the treatment, termites were placed in a group of ten termites in a Petri dish (92 mm × 16 mm), and incubated at 2 °C for 2 min to slow their movement. Each of the fipronil formulations or water (5.5 μL) was topically applied on the dorsal thorax of the worker termite. The termites were then transferred to clean Petri dishes containing a filter paper (42.5 mm, Whatman). The Petri dishes were placed into a controlled-environment chamber (65 cm × 47 cm × 37.5 cm) containing a thermometer, a lid and a 11.5-L metal container with water and heater to maintain the temperature at 28 ± 1 °C and high humidity, and, once covered with insulating material, total darkness (except during observation). At different time intervals, the Petri dishes were removed from the chamber, and the lids were opened with the least possible disturbance in order to examine termite response (mortality). A termite was considered dead when it was on its back or side (not supported by legs) and not able to move even after prodding with a soft brush.

*Feeding Treatment.* Silica nanocapsules (encapsulating 1 mg·mL$^{-1}$ fipronil in Miglyol 812) with the thickest shell (44 nm) were used in the feeding treatment. Termidor with the same final fipronil concentration and water were used as controls. Each fipronil formulation and water samples were used in four and two replicates for the feeding treatment, respectively. To mimic natural environment of termite colonies, a 750 mL container was filled with *Nasutitermes magnus* mound material (150 g) which was roasted (200 °C, 60 min), ground and mixed with water (50 g) prior to use. A clear vinyl tubing (150 mm × 6 mm) was connected from the container to a 70 mL feeding vial containing α-cellulose (20 g) bait with a moisture content of 70 w/w%. Then termites (7.5 g ≈ 1500 worker and soldier termites) were placed into the container. Each of the assembled feeding devices was placed into a controlled-environment chamber having dimensions and conditions similar to that in the direct treatment (described above). The termites in the ten assemblies were allowed to acclimatize to these conditions for 4 days and began feeding on the baits as indicated by the presence of enclosed tunnels and chambers built in the baits. Then, 0.5 mL of the sample (water, Termidor or the nanocapsule) was transferred into each feeding vial. The assemblies were removed from the chamber and observed daily with the least possible disturbance in order to detect movement of living termites using a TermatracT3i device (Termatrac Pty Ltd., Australia). Lack of movement indicated 100% mortality of termites and inspections in the containers were conducted to confirm. During the treatment, termite groups in one container connected to Termidor-treated bait and in two containers connected to nanocapsule-treated baits remained alive for up to 8 days as the tube entrances to the vials were blocked with mud built by the termites. These containers were not considered for further study. Therefore, three treatment results were included in the analysis for the Termidor-treated baits and two treatment results for the nanocapsule-treated baits. The termites in two containers connected to water-treated baits survived throughout the study.

## RESULTS AND DISCUSSION

**Encapsulation of Fipronil in Silica Nanocapsules.** Fipronil was easily dissolved in Miglyol 812 due to its high solubility in the oil (i.e., 10 mg·mL$^{-1}$).[29] The fipronil-loaded oil was emulsified in the presence of SurSi peptide via sonication, and nanoemulsions with narrow droplet size distribution were obtained due to the presence of the surface active Sur module[29] (Figure 1) in the emulsifying peptide. Following addition of the

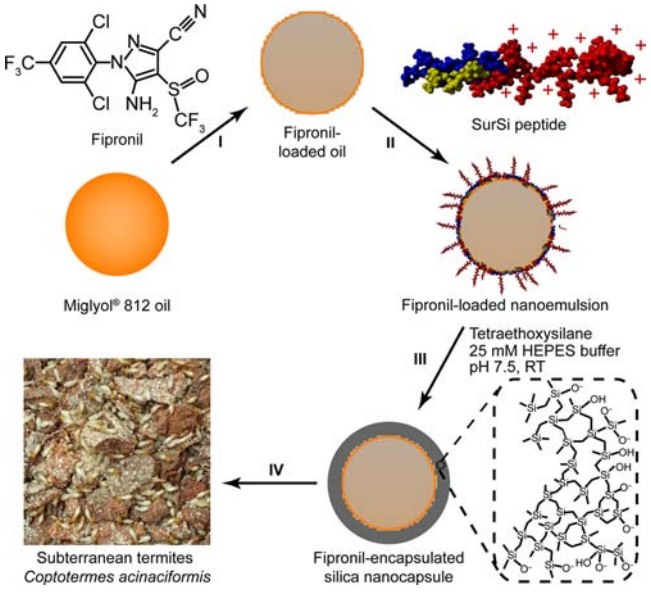


**Figure 1.** Illustration of the synthesis of fipronil-encapsulated silica nanocapsules formed using an emulsion and biomimetic dual-templating approach for sustained-release agroformulations against termites. Step (I), solubilization of fipronil in Miglyol 812 oil; step (II), sonication of the oil in SurSi peptide solution to form fipronil-loaded nanoemulsions; step (III), addition of tetraethoxysilane (TEOS) in the nanoemulsions to form a silica shell encapsulating the nanoemulsion core; step (IV), *in vivo* efficacy tests of the fipronil-encapsulated silica nanocapsules against economically important subterranean termites.

silica precursor tetraethoxysilane (TEOS) to the nanoemulsions, silica shell encasing the nanoemulsion core was formed at near-neutral pH and room temperature without using any toxic chemicals. The biosilicification process at the oil–water interface was due to the catalytic role of densely packed cationic arginine (R) and lysine (K) residues of Si module (RKKRKKRKKRKKGGGY) as well as polar residues of Sur module exposed toward the bulk aqueous solution that could induce hydrolysis of TEOS and interfacial polycondensation of the hydrolysis products i.e., silanol (≡Si–OH) and negatively charged silanolate (≡Si–O$^-$)[29] (Figure 1).

In this study, fipronil dissolved in Miglyol 812 oil at a concentration of 0.05 mg·mL$^{-1}$ or 1 mg·mL$^{-1}$ was encapsulated in silica nanocapsules and used for the sustained release study *in vitro* and *in vivo*. The amount of fipronil encapsulated in silica nanocapsules was determined based on the lethal dose of

fipronil sufficient to eliminate a termite for the *in vivo* tests. It has been reported that the lethal dose of fipronil for *Coptotermes* spp. is in the range of 2−10 ng per termite.[38,39] Based on this consideration, the encapsulated fipronil which was dissolved in Miglyol 812 at concentrations of 0.05 mg·mL$^{-1}$ and 1 mg·mL$^{-1}$ was equivalent to 1 ppm and 20 ppm in the silica nanocapsule suspensions and, at an applied volume, would give fipronil dose of around 6 ng/termite in the direct- and feeding treatments, respectively.

The encapsulation efficiencies (%*EE*) of fipronil in silica nanocapsules were determined by monitoring the concentration of fipronil released in acetonitrile solution (60 v/v%) over a period of time compared to initial concentration of fipronil dissolved in Miglyol 812 oil. Higher solubility of fipronil in acetonitrile (60 v/v%) i.e., 71.5 mg·mL$^{-1}$ than in Miglyol 812 i.e., 10 mg·mL$^{-1}$ promotes easy partition of the fipronil and its diffusion out of the silica nanocapsules. The results of practical encapsulation efficiencies of fipronil were calculated using eq 1:[29]

$$\%EE = \frac{\sum_{j=1}^{n} (C_f V_f)_j}{C_i V_i} \times 100\% \quad (1)$$

where $C_f$ (mg·mL$^{-1}$) and $V_f$ (mL) are the fipronil concentration released in acetonitrile solution and volume of the acetonitrile solution, respectively, $C_i$ (mg·mL$^{-1}$) and $V_i$ (mL) are the initial fipronil concentration in Miglyol 812 and volume of the Miglyol 812, respectively, and $n$ is the number of repeated-release of fipronil. At an initial fipronil concentration of 0.05 mg·mL$^{-1}$, %*EE* of fipronil in silica nanocapsules obtained at reactions with 16 $\mu$mol, 32 $\mu$mol and 96 $\mu$mol of TEOS were 72.8%, 73.2%, and 73.6%, respectively, while similar %*EE* of 71.6%, 72.2%, and 72.9%, respectively, were obtained when initial fipronil concentration of 1 mg·mL$^{-1}$ was used. The encapsulation of fipronil in the silica nanocapsules demonstrated high encapsulation efficiency which is suitable for agricultural applications.

**Characterization of Silica Nanocapsules Containing Fipronil.** To determine the molecular components of fipronil-encapsulated silica nanocapsules, SurSi peptide and silica nanocapsules without and with fipronil in the oil cores were analyzed using Fourier transform-infrared (FT-IR) spectroscopy, and the results were compared in Figure 2. For SurSi peptide, four characteristic peaks of the peptide backbone were observed (Figure 2a) which are assigned to amide A (N−H stretch), amide B (N−H stretch), amide I (C═O stretch), and amide II (C−N stretch and N−H in-plane bend) at 3284, 3071, 1648, and 1542 cm$^{-1}$, respectively.[40] The functional groups of peptide side chains can also be identified (Figure 2a) i.e., peak at 1298 cm$^{-1}$ corresponds to O−H deformation of hydroxyl group of serine (S), shoulder at 1248 cm$^{-1}$ and doublet at 837 and 800 cm$^{-1}$ are associated with C−O stretch and phenyl ring of tyrosine (Y), respectively, and doublet at 1180 and 1130 cm$^{-1}$ can be attributed to $NH_3^+$ rocking of lysine (K).[40,41] FT-IR spectrum of the silica nanocapsules without fipronil (Figure 2b) shows a broad signal centered at 3330 cm$^{-1}$ which reflects the vibration of O−H stretching of silanol group Si−OH. A strong absorption band at about 1060 cm$^{-1}$, with a shoulder at 1160 cm$^{-1}$, and a band at 780 cm$^{-1}$ correspond to asymmetric and symmetric Si−O−Si stretching vibrations of siloxane group, respectively. An absorption shoulder at 960 cm$^{-1}$ arises from the Si−O$^-$ stretching of Si−OH. The major peaks of N−H stretch of peptide and other peptide side chains are

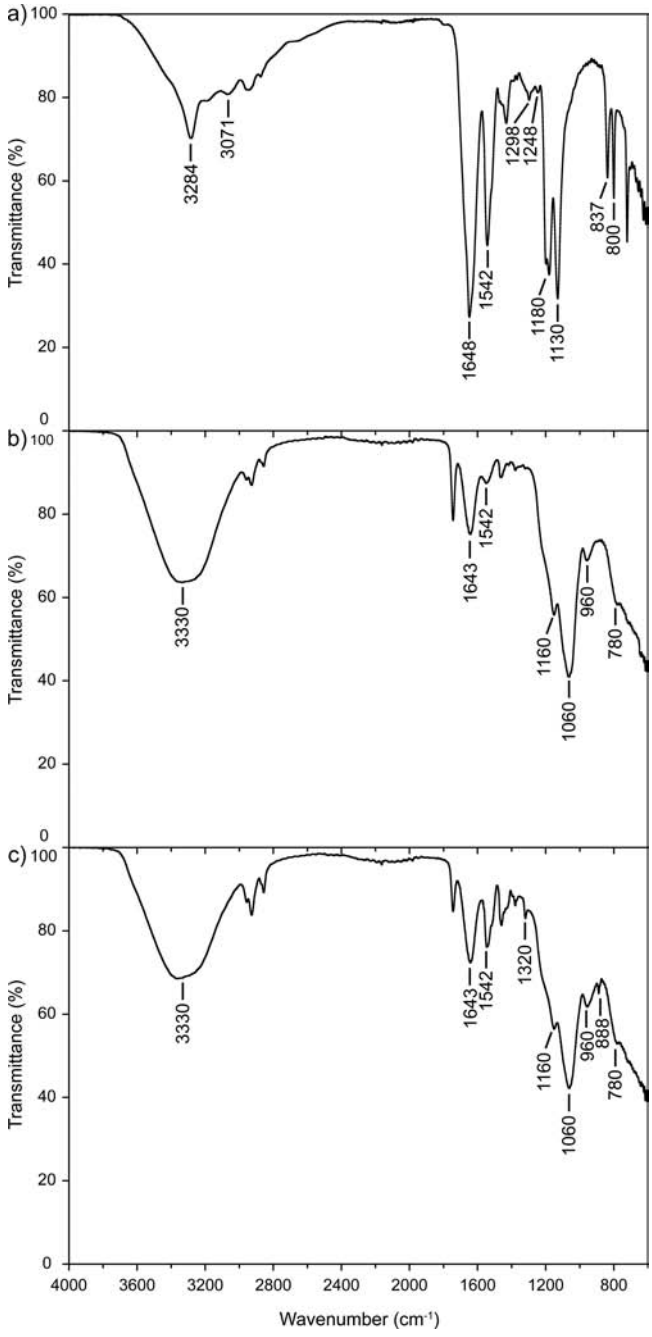


**Figure 2.** FT-IR spectra of (a) SurSi peptide, (b) silica nanocapsules without fipronil in the oil cores, and (c) fipronil-encapsulated silica nanocapsules.

overlapped by the characteristic bands of silica and thus are unobserved (Figure 2b). However, the presence of peptide in the silica nanocapsules can still be characterized by the absorption bands of amide I and amide II although the intensities are significantly reduced. The FT-IR spectrum of fipronil-encapsulated silica nanocapsules (Figure 2c) retained most of the major peaks of the silica nanocapsules without fipronil (Figure 2b). Additionally, new absorption bands appear and are clearly discernible at 1320 and 888 cm$^{-1}$ which can be attributed to $-CF_3$ stretching of trifluoromethyl group and C−H out-of-plane bending of benzene ring[42] of the fipronil molecule, respectively (Figure 2c). These vibrational frequen-


dx.doi.org/10.1021/jf504455x | J. Agric. Food Chem. 2014, 62, 12504−12511

cies further verify the incorporation of fipronil into silica nanocapsules.

Morphology of silica nanocapsules can be visualized by using TEM without the need for staining or cryo-preservation. The TEM images showed morphology of a core−shell structure of fipronil-encapsulated silica nanocapsules having three different shell thicknesses (Figure 3a−c). In contrast, fipronil-loaded

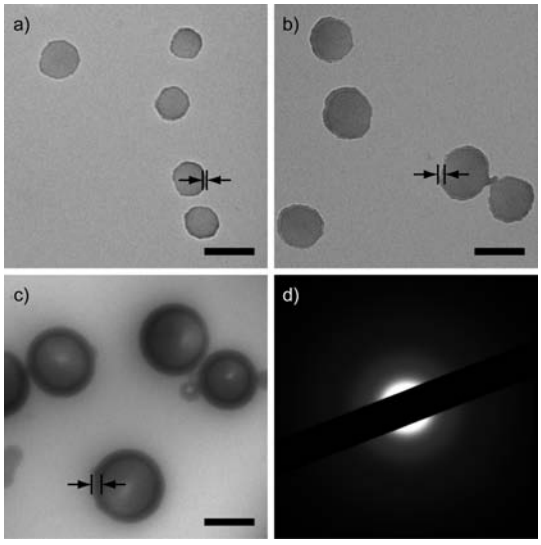


**Figure 3.** Fipronil-encapsulated silica nanocapsules with tunable shell thickness. (a−c) Representative transmission electron microscopy (TEM) images of fipronil-encapsulated silica nanocapsules having (a) 8 nm, (b) 25 nm, and (c) 44 nm shells. Scale bars are 200 nm. Arrows indicate the boundary of the silica shell. (d) Representative selected area electron diffraction (SAED) pattern of silica nanocapsules confirmed the amorphous state of the silica shell.

nanoemulsion having no silica shell was hardly observed in TEM as its structure was prone to disintegrate under high vacuum and electron beam irradiation (data not shown). The measured shell thicknesses, as determined by using TEM, of silica nanocapsules obtained at TEOS concentrations of 16 $\mu$mol, 32 $\mu$mol and 96 $\mu$mol were 8 nm, 25 nm, and 44 nm, respectively, while the outer diameters were 140 nm, 198 nm, and 288 nm, respectively. These values are consistent with our previously reported silica nanocapsules that encapsulated fipronil at concentration of 10 mg·mL$^{-1}$ in Miglyol 812.[29] Additionally, the representative selected area electron diffraction (SAED) of silica nanocapsules shows diffuse ring pattern (Figure 3d), indicating the amorphous structure of the silica shell. The formation of amorphous silica via peptides has also been reported for natural biogenic silica[43,44] and biomimetic silica.[45]

Dynamic light scattering (DLS) confirmed a size increase for silica nanocapsules in comparison with the nanoemulsion template (Figure 4). Furthermore, increasing TEOS concentrations corresponded to an increase in number-averaged diameters of the nanocapsules (Figure 4a−c). The number-weighted size distribution results showed that silica nanocapsules having 8, 25, and 44 nm shells have narrow size distributions (polydispersity index, PDI < 0.350).

**Fipronil Release Study *in Vitro*.** The release profiles of fipronil *in vitro* from silica nanocapsules with three different shell thicknesses encapsulating 1 mg·mL$^{-1}$ fipronil in Miglyol 812 i.e., 1F-NC8, 1F-NC25 and 1F-NC44 are shown in Figure

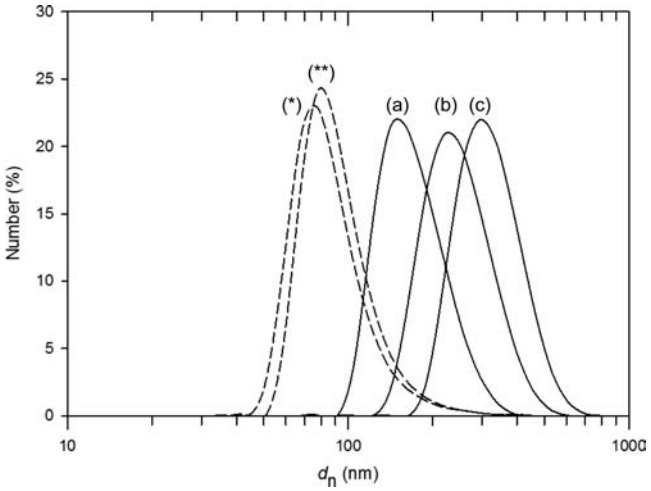


**Figure 4.** Number-weighted size distributions of fipronil-encapsulated silica nanocapsules and the nanoemulsion template. The measured number-averaged diameters ($d_n$) include silica nanocapsules having (a) 8 nm, (b) 25 nm, and (c) 44 nm shells, (*) fipronil-loaded nanoemulsions before reaction with TEOS, and (**) control fipronil-loaded nanoemulsions incubated over the reaction period.

5. The concentration of fipronil released in the water phase was normalized against the saturated concentration of fipronil in

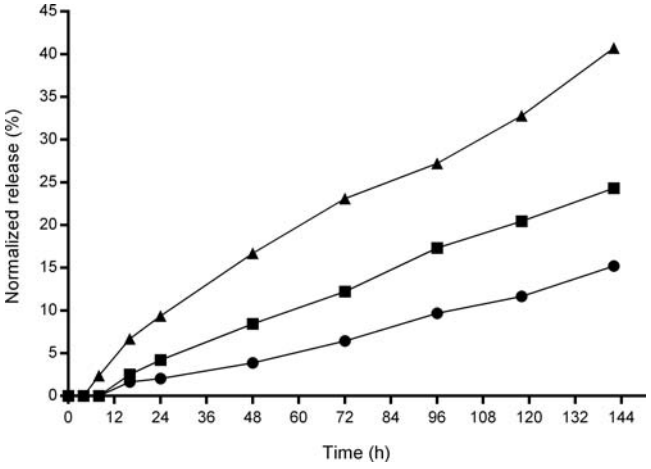


**Figure 5.** *In vitro* release profile of fipronil from silica nanocapsules having 8 nm (1F-NC8, ▲), 25 nm (1F-NC25, ■), and 44 nm (1F-NC44, ●) shells into water.

water considering the low solubility of fipronil in water (2 $\mu$g·mL$^{-1}$). The release of fipronil from 1F-NC8 was detected after 8 h of release study at 2.4%, while a longer lag time of 16 h was observed for fipronil released at 2.5% and 1.6% from silica nanocapsules having thicker shells i.e., 1F-NC25 and 1F-NC44, respectively (Figure 5). After 142 h, fipronil was released at percentages of 40.7%, 24.3% and 15.2% from 1F-NC8, 1F-NC25 and 1F-NC44, respectively. The rates of fipronil released in water show the order of 1F-NC8 > 1F-NC25 > 1F-NC44, demonstrating that increasing shell thickness resulted in an increased diffusion pathway and hence enhanced barrier to diffusion of fipronil across the silica shell, thus the slower release of fipronil.

**Fipronil Release Study *in Vivo*.** Sustained release of fipronil from silica nanocapsules was also investigated *in vivo*

against termites. Two experiments were carried out, including direct treatment and feeding treatment.

Direct treatment was demonstrated by topical application of six different formulations including water, Termidor, nanoemulsions (0.05F-NE), silica nanocapsules with three different shell thicknesses of 8 nm (0.05F-NC8), 25 nm (0.05F-NC25) and 44 nm (0.05F-NC44), on the dorsal thorax of worker termite *C. acinaciformis* (Figure 6). Rapid mortality was

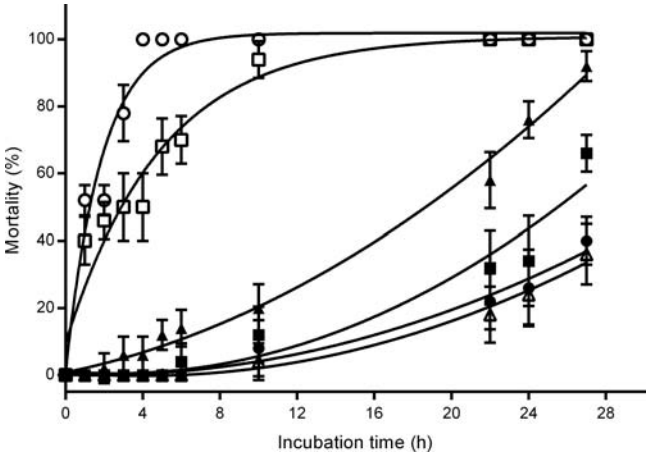


**Figure 6.** *In vivo* efficacy test via topical application on the dorsal thorax of worker termites. Fipronil-encapsulated silica nanocapsules having 8 nm (0.05F-NC8, ▲), 25 nm (0.05F-NC25, ■), and 44 nm (0.05F-NC44, ●) shells are tested in comparison with fipronil-loaded nanoemulsions without silica shells (0.05F-NE, □), Termidor (○), and water containing no fipronil (control, Δ). The lines are drawn to assist in reading the trends.

observed when termites were treated with commercial Termidor or fipronil-loaded nanoemulsions having no silica shells (0.05F-NE). The fipronil penetrated through the cuticle layer on the body surface of worker termites and eventually caused death depending the fipronil doses.[39] Termidor gave burst release of fipronil resulting in 50% mortality within the first hour and 100% mortality at 4 h (Figure 6). Fipronil-loaded nanoemulsions having no silica shells (0.05F-NE) exhibited a two-step release profile; a significant initial burst effect, with mortality of almost 50% within the first 4 h, and then more sustained release over 22 h (Figure 6). In contrast, silica nanocapsules showed sustained release as a result of the silica shell. First mortality was at 4 h (6%), 6 h (4%), and 10 h (8%) for silica nanocapsules having 8 nm (0.05F-NC8), 25 nm (0.05F-NC25) and 44 nm (0.05F-NC44) shells, respectively (Figure 6). Further, the termite mortality gradually increased in a way dependent on shell thickness suggesting that the silica shell provided an effective barrier for the controlled diffusion of the encapsulated fipronil, which corresponds well with the *in vitro* release study. The lag time, which was also observed in *in vitro* experiments, prior to termite mortality in the topical applications of silica nanocapsules strongly evidenced the sustained release of fipronil from the nanocapsules with no indication of burst release. Fipronil-encapsulated silica nanocapsules having 44 nm shell demonstrated the most significant delay in termite mortality and thus was chosen for the subsequent *in vivo* test.

We further evaluated the sustained release performance of fipronil-encapsulated silica nanocapsule having 44 nm shell (1F-NC44) *in vivo* by remote feeding treatment against *C. acinaciformis*. Prior to the treatment, groups of orphaned worker and soldier termites (≈1500) were allowed to adapt to the living conditions maintaining their biological activities in a container filled with nutritious materials at set temperature.[46] Food in the form of α-cellulose was supplied in peripheral feeding vials which were accessible through clear vinyl tubes. After 4 days, we observed that termites built mud and cellulose surrounding the interior space of the connector tubes as well as galleries within the baits, indicating that termites were responding to the α-cellulose. The α-cellulose in the feeding vials was then treated with water containing no fipronil, Termidor or 1F-NC44. As termites foraged in the feeding vials, they acquired and carried the α-cellulose back to the container, and inadvertently transferred it to other termites within the groups. These interactions could be through trophallaxis in which foraging worker termites feed other termites that do not or cannot forage on their own including soldier termites due to their anatomical and behavioral specializations.[47] Termidor-treated α-cellulose caused 100% mortality to termite groups after 3 days, whereas more delayed 100% mortality (6 days) was observed after treatment using nanocapsule-treated α-cellulose (Figure 7). The α-cellulose treated with water

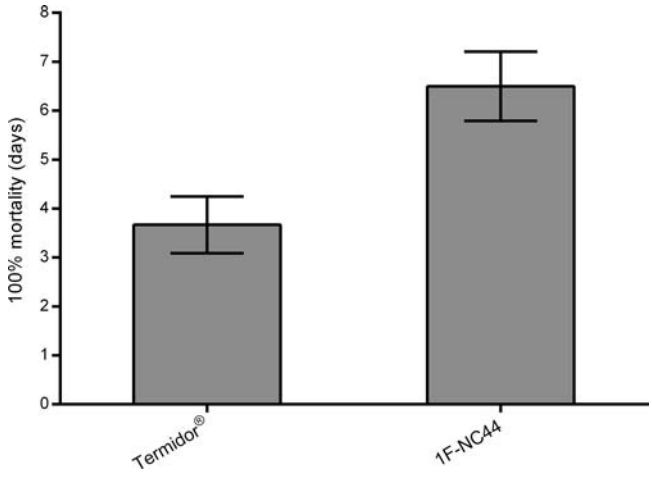


**Figure 7.** *In vivo* efficacy test via feeding treatment against groups of ≈1500 worker and soldier termites. The delayed 100% mortality of the termite groups caused by fipronil-encapsulated silica nanocapsules having a 44 nm shell (1F-NC44) is presented as compared to Termidor.

containing no fipronil in the feeding vials caused negligible termite mortality during the 8 days of the test. The feeding experiment results further confirmed the sustained release property of silica nanocapsules as a result of the presence of silica shell which plays a role as barrier to diffusion of fipronil.

Dead and decaying bodies of termites can elicit avoidance behavior of other termites,[48,49] and consequently any transmission through those termites is ineffective.[39] Therefore, the sustained release property of the fipronil-encapsulated silica nanocapsules is important to ensure constant exposure of fipronil to the termites in the colony until 100% mortality of the colony can be achieved. Furthermore, the more delaying insecticidal effect demonstrated by the silica nanocapsules as compared to the commercial fipronil formulation would be highly desirable, as it increases the likelihood of horizontal transfer of fipronil, hence allowing improved areawide control of larger populations of termite colonies.

## CONCLUSION

Biocompatible oil-core silica-shell nanocapsules synthesized using an emulsion and biomimetic dual-templating approach under environmentally friendly conditions were investigated as nanocarriers for the sustained release of fipronil insecticide. *In vitro* release studies of fipronil showed decreased release rate with increasing the shell thickness. *In vivo* direct treatment experiments using silica nanocapsules with three different shell thicknesses (8, 25, and 44 nm) against worker termites demonstrated that the time interval between the application of the nanocapsules and the occurrence of the termite mortality could be prolonged in a way dependent on silica-shell thickness as compared to the commercial formulation Termidor and fipronil-loaded nanoemulsions having no silica shells. The *in vivo* efficacy of 44-nm-shell nanocapsules against orphaned groups of ≈1500 worker and soldier termites by dispersing the nanocapsules in $\alpha$-cellulose feeding bait proved that the silica nanocapsules could be taken up from the bait vials by foraging workers, transmitted to recipient termites in the groups probably through horizontal transfer, and eventually caused 100% mortality of the termite groups in 6 days after the application, which was 3 days longer than the commercial Termidor. Both the *in vitro* and *in vivo* fipronil-released studies presented in this paper demonstrated the effectiveness of a pesticide delivery system having biocompatibility, high encapsulation efficiency, and sustained release property, which open potential utilities of the silica nanocapsules for other agricultural applications.

## AUTHOR INFORMATION


### Corresponding Authors

* Phone: +61-7-3346-4189. Fax: +61-7-3346-4197. E-mail: z.chunxia@uq.edu.au.

* Phone: +61-7-3346-4189. Fax: +61-7-3346-4197. E-mail: a.middelberg@uq.edu.au.



### Funding

This work was supported by the Australian Research Council (grants DP1093056 and 120103683). D.W. acknowledges a scholarship from The University of Queensland. C.X.Z. acknowledges financial support from the Australian Research Council in the form of an Australian Postdoctoral Fellow (DP110100394). A.P.J.M. acknowledges support from the Queensland Government through award of the 2010 Queensland Premier's Science Fellowship.


### Notes

The authors declare no competing financial interest.

## ACKNOWLEDGMENTS


The authors thank Lei Yu for taking the SAED images as well as the facilities and the scientific and technical assistance of the Australian Microscopy & Microanalysis Research Facility at the Centre for Microscopy and Microanalysis, The University of Queensland. Termatrac Pty Ltd., Beenleigh QLD (Australia), is thanked for the use of the Termatrac T3i device.


## ABBREVIATIONS USED

Ac, acetyl; M, methionine; K, lysine; Q, glutamine; L, leucine; A, alanine; H, histidine; S, serine; V, valine; R, arginine; E, glutamic acid; G, glycine; Y, tyrosine; O/W, oil-in-water; $M_w$, molecular weight; mp, melting point; *d*, density; TEOS, tetraethoxysilane; HEPES, sodium 4-(2-hydroxyethyl)-1-piperazine ethanesulfonate; 0.05F-NE, nanoemulsions loaded with 0.05 mg·mL$^{-1}$ fipronil in Miglyol 812 oil; *x*F-NC*y*, silica nanocapsules (encapsulating *x* mg·mL$^{-1}$ fipronil in Miglyol 812 oil) with shell thickness of *y* nm; TEM, transmission electron microscopy; HR-TEM, high-resolution transmission electron microscopy; SAED, selected area electron diffraction; DLS, dynamic light scattering; FT-IR, Fourier transform-infrared; RP-HPLC, reversed-phase high-performance liquid chromatography

## REFERENCES


(1) Mulqueen, P. Recent advances in agrochemical formulation. *Adv. Colloid Interface Sci.* **2003**, *106*, 83−107.

(2) Ghormade, V.; Deshpande, M. V.; Paknikar, K. M. Perspectives for nano-biotechnology enabled protection and nutrition of plants. *Biotechnol. Adv.* **2011**, *29*, 792−803.

(3) Gogos, A.; Knauer, K.; Bucheli, T. D. Nanomaterials in plant protection and fertilization: current state, foreseen applications, and research priorities. *J. Agric. Food Chem.* **2012**, *60*, 9781−9792.

(4) Rai, M.; Ingle, A. Role of nanotechnology in agriculture with special reference to management of insect pests. *Appl. Microbiol. Biotechnol.* **2012**, *94*, 287−293.

(5) Kah, M.; Hofmann, T. Nanopesticide research: current trends and future priorities. *Environ. Int.* **2014**, *63*, 224−235.

(6) Asrar, J.; Ding, Y. W.; La Monica, R. E.; Ness, L. C. Controlled release of tebuconazole from a polymer matrix microparticle: release kinetics and length of efficacy. *J. Agric. Food Chem.* **2004**, *52*, 4814−4820.

(7) Sopena, F.; Cabrera, A.; Maqueda, C.; Morillo, E. Controlled release of the herbicide norflurazon into water from ethylcellulose formulations. *J. Agric. Food Chem.* **2005**, *53*, 3540−3547.

(8) Stloukal, P.; Kucharczyk, P.; Sedlarik, V.; Bazant, P.; Koutny, M. Low molecular weight poly(lactic acid) microparticles for controlled release of the herbicide metazachlor: preparation, morphology, and release kinetics. *J. Agric. Food Chem.* **2012**, *60*, 4111−4119.

(9) Frederiksen, H. K.; Kristenson, H. G.; Pedersen, M. Solid lipid microparticle formulations of the pyrethroid gamma-cyhalothrin-incompatibility of the lipid and the pyrethroid and biological properties of the formulations. *J. Controlled Release* **2003**, *86*, 243−252.

(10) Garrido-Herrera, F. J.; Gonzalez-Pradas, E.; Fernandez-Perez, M. Controlled release of isoproturon, imidacloprid, and cyromazine from alginate-bentonite-activated carbon formulations. *J. Agric. Food Chem.* **2006**, *54*, 10053−10060.

(11) Ziv, D.; Mishael, Y. G. Herbicide solubilization in micelle-clay composites as a basis for controlled release sulfentrazone and metolachlor formulations. *J. Agric. Food Chem.* **2008**, *56*, 9159−9165.

(12) Chen, Y.; Chen, H.; Shi, J. *In vivo* bio-safety evaluations and diagnostic/therapeutic applications of chemically designed mesoporous silica nanoparticles. *Adv. Mater.* **2013**, *25*, 3144−3176.

(13) Hussain, H. I.; Yi, Z.; Rookes, J. E.; Kong, L. X.; Cahill, D. M. Mesoporous silica nanoparticles as a biomolecule delivery vehicle in plants. *J. Nanopart. Res.* **2013**, *15*.

(14) Martin-Ortigosa, S.; Valenstein, J. S.; Lin, V. S. Y.; Trewyn, B. G.; Wang, K. Gold functionalized mesoporous silica nanoparticle mediated protein and DNA codelivery to plant cells via the biolistic method. *Adv. Funct. Mater.* **2012**, *22*, 3576−3582.

(15) Torney, F.; Trewyn, B. G.; Lin, V. S. Y.; Wang, K. Mesoporous silica nanoparticles deliver DNA and chemicals into plants. *Nat. Nanotechnol.* **2007**, *2*, 295−300.

(16) Ao, M. M.; Zhu, Y. C.; He, S.; Li, D. G.; Li, P. L.; Li, J. Q.; Cao, Y. S. Preparation and characterization of 1-naphthylacetic acid-silica conjugated nanospheres for enhancement of controlled-release performance. *Nanotechnology* **2013**, *24*, 1−8.

(17) Chen, J.; Wang, W.; Xu, Y.; Zhang, X. Slow-release formulation of a new biological pesticide, pyoluteorin, with mesoporous silica. *J. Agric. Food Chem.* **2011**, *59*, 307−311.

(18) Popat, A.; Liu, J.; Hu, Q.; Kennedy, M.; Peters, B.; Lu, G. Q.; Qiao, S. Z. Adsorption and release of biocides with mesoporous silica nanoparticles. *Nanoscale* **2012**, *4*, 970−975.

(19) Wanyika, H.; Gatebe, E.; Kioni, P.; Tang, Z.; Gao, Y. Mesoporous silica nanoparticles carrier for urea: potential applications in agrochemical delivery systems. *J. Nanosci. Nanotechnol.* **2012**, *12*, 2221−2228.
(20) Wanyika, H. Sustained release of fungicide metalaxyl by mesoporous silica nanospheres. *J. Nanopart. Res.* **2013**, *15*.
(21) Wen, L. X.; Li, Z. Z.; Zou, H. K.; Liu, A. Q.; Chen, J. F. Controlled release of avermectin from porous hollow silica nanoparticles. *Pest. Manag. Sci.* **2005**, *61*, 583−590.
(22) Tan, W. M.; Hou, N.; Pang, S.; Zhu, X. F.; Li, Z. H.; Wen, L. X.; Duan, L. S. Improved biological effects of uniconazole using porous hollow silica nanoparticles as carriers. *Pest. Manag. Sci.* **2012**, *68*, 437−443.
(23) Li, Z. Z.; Xu, S. A.; Wen, L. X.; Liu, F.; Liu, A. Q.; Wang, Q.; Sun, H. Y.; Yu, W.; Chen, J. F. Controlled release of avermectin from porous hollow silica nanoparticles: influence of shell thickness on loading efficiency, UV-shielding property and release. *J. Controlled Release* **2006**, *111*, 81−88.
(24) Liu, F.; Wen, L.-X.; Li, Z.-Z.; Yu, W.; Sun, H.-Y.; Chen, J.-F. Porous hollow silica nanoparticles as controlled delivery system for water-soluble pesticide. *Mater. Res. Bull.* **2006**, *41*, 2268−2275.
(25) Qian, K.; Shi, T. Y.; He, S.; Luo, L. X.; Liu, X. L.; Cao, Y. S. Release kinetics of tebuconazole from porous hollow silica nanospheres prepared by miniemulsion method. *Microporous Mesoporous Mater.* **2013**, *169*, 1−6.
(26) Lou, X. W.; Archer, L. A.; Yang, Z. C. Hollow micro-/nanostructures: synthesis and applications. *Adv. Mater.* **2008**, *20*, 3987−4019.
(27) U.S. Food and Drug Administration's Website. *GRN No. 321: Synthetic amorphous silica*, http://www.accessdata.fda.gov/scripts/fcn/gras_notices/GRN000321.pdf (21 May 2014).
(28) Zhu, Y. F.; Shi, J. L.; Shen, W. H.; Dong, X. P.; Feng, J. W.; Ruan, M. L.; Li, Y. S. Stimuli-responsive controlled drug release from a hollow mesoporous silica sphere/polyelectrolyte multilayer core-shell structure. *Angew. Chem., Int. Ed.* **2005**, *44*, 5083−5087.
(29) Wibowo, D.; Zhao, C.-X.; Middelberg, A. P. J. Emulsion-templated silica nanocapsules formed using bio-inspired silicification. *Chem. Commun.* **2014**, *50*, 11325−11328.
(30) Kyle, S.; Aggeli, A.; Ingham, E.; McPherson, M. J. Production of self-assembling biomaterials for tissue engineering. *Trends Biotechnol.* **2009**, *27*, 423−433.
(31) Morreale, G.; Lee, E. G.; Jones, D. B.; Middelberg, A. P. J. Bioprocess-centered molecular design (BMD) for the efficient production of an interfacially active peptide. *Biotechnol. Bioeng.* **2004**, *87*, 912−923.
(32) Tingle, C. C. D.; Rother, J. A.; Dewhurst, C. F.; Lauer, S.; King, W. J. Fipronil: environmental fate, ecotoxicology, and human health concerns. *Rev. Environ. Contam. Toxicol.* **2003**, *176*, 1−66.
(33) Colliot, F.; Kukorowski, K. A.; Hawkins, D. W.; Roberts, D. A. *Fipronil: A New Soil and Foliar Broad Spectrum Insecticide*; British Crop Protection Council: 2000.
(34) Cole, L. M.; Nicholson, R. A.; Casida, J. E. Action of phenylpyrazole insecticides at the gaba-gated chloride channel. *Pestic. Biochem. Physiol.* **1993**, *46*, 47−54.
(35) Ngim, K. K.; Crosby, D. G. Abiotic processes influencing fipronil and desthiofipronil dissipation in California, USA, rice fields. *Environ. Toxicol. Chem.* **2001**, *20*, 972−977.
(36) Rouland-Lefevre, C. Termites as Pests of Agriculture. In *Biology of Termites: A Modern Synthesis*; Bignell, D. E., Roisin, Y., Lo, N., Eds.; Springer: London, U.K., 2011; pp 499−517.
(37) Rust, M. K.; Su, N.-Y. Managing social insects of urban importance. *Annu. Rev. Entomol.* **2012**, *57*, 355−375.
(38) Song, D. L.; Hu, X. P. Effects of dose, donor-recipient interaction time and ratio on fipronil transmission among the Formosan subterranean termite nestmates (Isoptera: Rhinotermitidae). *Sociobiology* **2006**, *48*, 237−246.
(39) Ibrahim, S. A.; Henderson, G.; Fei, H. X. Toxicity, repellency, and horizontal transmission of fipronil in the formosan subterranean termite (Isoptera: Rhinotermitidae). *J. Econ. Entomol.* **2003**, *96*, 461−467.
(40) Krimm, S.; Bandekar, J. Vibrational spectroscopy and conformation of peptides, polypeptides, and proteins. *Adv. Protein Chem.* **1986**, *38*, 181−364.
(41) Hernandez, B.; Pfluger, F.; Derbel, N.; De Coninck, J.; Ghomi, M. Vibrational Analysis of Amino Acids and Short Peptides in Hydrated Media. VI. Amino Acids with Positively Charged Side Chains: L-Lysine and L-Arginine. *J. Phys. Chem. B* **2010**, *114*, 1077−1088.
(42) Gauglitz, G.; Moore, D. S. *Handbook of Spectroscopy*, 2nd ed.; Wiley-VCH: Germany, 2014; Vol. *1*.
(43) Hildebrand, M. Diatoms, biomineralization processes, and genomics. *Chem. Rev.* **2008**, *108*, 4855−4874.
(44) Müller, W. E. G.; Belikov, S. I.; Tremel, W.; Perry, C. C.; Gieskes, W. W. C.; Boreiko, A.; Schröder, H. C. Siliceous spicules in marine demosponges (example *Suberites domuncula*). *Micron* **2006**, *37*, 107−120.
(45) Patwardhan, S. V. Biomimetic and bioinspired silica: recent developments and applications. *Chem. Commun.* **2011**, *47*, 7567−7582.
(46) Spomer, N. A.; Kamble, S. T.; Warriner, R. A.; Davis, R. W. Influence of temperature on rate of uptake and subsequent horizontal transfer of (14)C Fipronil by eastern subterranean termites (Isoptera: Rhinotermitidae). *J. Econ. Entomol.* **2008**, *101*, 902−908.
(47) Buczkowski, G.; Wang, C.; Bennett, G. Immunomarking reveals food flow and feeding relationships in the eastern subterranean termite, Reticulitermes flavipes (Kollar). *Environ. Entomol.* **2007**, *36*, 173−182.
(48) Su, N. Y.; Tamashiro, M.; Yates, J. R.; Haverty, M. I. Effect of behavior on the evaluation of insecticides for prevention of or remedial control of the formosan subterranean termite (Isoptera, Rhinotermitidae). *J. Econ. Entomol.* **1982**, *75*, 188−193.
(49) Fei, H.; Henderson, G. Repellency of formosan subterranean termites (Isoptera: Rhinotermitidae) to dead termites and attraction to 2-phenoxyethanol with and without nonrepellent insecticides. *J. Agr. Urban Entomol.* **2005**, *22*, 159−172.

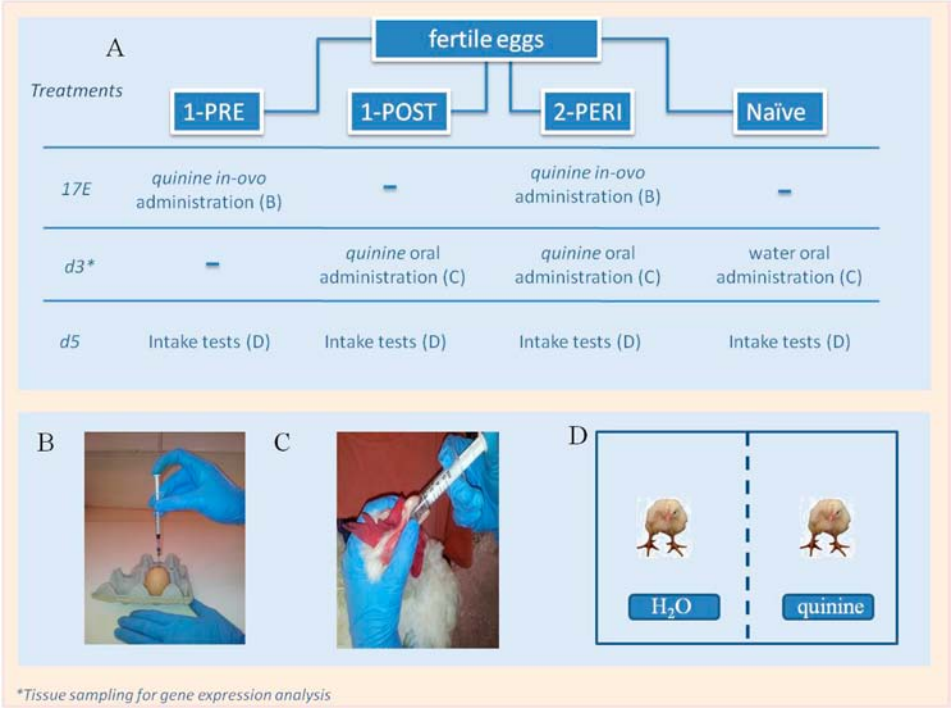


**Figure 1.** Quinine administration procedures and intake taste tests. (A) Groups in the experiment were 1-PRE, 0.6 mL of 2 mM quinine administered prenatally (0.04 μmol quinine/g BW); 1-POST, 1.3 mL of 2 mM quinine administered postnatally (0.04 μmol quinine/g BW); 2-PERI, two perinatal administrations (pre- and postnatal) of 2 mM (in both 0.04 μmol quinine/g BW) quinine and naïve. Intake tests to evaluate bitter tastant consumption were performed for all treatments on day 5. (B) Illustration of in ovo prenatal administration procedure in chicken embryos on embryonic day 17 (E17) delivers the quinine solution into the amnion. (C) Illustration of postnatal administration to chickens into the oral cavity. (D) Illustration of the no-choice intake test, where each chick is offered either water or quinine solution. (*) On day 3 palate and duodenum tissues were removed from all treatment groups for gene expression analysis.

## MATERIALS AND METHODS

**Chemicals.** Quinine (Sigma-Aldrich) was used at 2 mM (dissolved in distilled water) and 30 μM (dissolved in C1 buffer).

C1 buffer consisted of 130 mM NaCl, 5 mM KCl, 10 mM *N*-2-hydroxyethylpiperazine-*N*′-2-ethanesulfonic acid, 2 mM $CaCl_2$, and 10 mM glucose (pH 7.4).

**Functional Expression Procedures.** The expression constructs of chicken ggTas2r1, ggTas2r2, and ggTas2r7, containing the full length coding cDNA of the receptors flanked by an upstream located sequence coding for an sst3-tag and a downstream located sequence coding for a herpes simplex virus glycoprotein D (hsv)-epitope in the vector pcDNA5FRT (Invitrogen) were available from a previous study.[24] For functional analysis, HEK 293T cells stably expressing the G-protein chimera Gα16gust44[25] were transiently transfected with the expression constructs using Lipofectamine2000 (Invitrogen) as detailed before.[8,24] For a negative control, cells were transfected with empty vector (mock). About 24 h after transfection, cells were washed, loaded with the calcium-indicator dye Fluo4-AM in the presence of 2.5 mM probenecid, and subjected to calcium imaging analysis as described previously.[8,24] After automatic application of the stimulus (30 μM quinine in buffer C1), changes in fluorescence were monitored using a fluorometric imaging plate reader (FLIPR, Molecular Devices). The traces of identically treated cells were averaged using the program ScreenWorks 3.1 and exported to the graphics software Corel Photo-Paint X3 to create an overlay picture.

**Birds and Procedures.** Fertile broiler eggs ($n$ = 150; Cobb) were obtained from a maternal flock (32 weeks in lay; Brown Ltd., Hod Hasharon, Israel). The eggs were incubated under standard conditions at the Department of Animal Sciences of the Hebrew University (Rehovot, Israel). The eggs were divided into four groups ($n$ = 30) depending on time of quinine administration (prenatal or postnatal) and number of times administered (once or twice): (1) one prenatal administration (1-PRE); (2) one postnatal administration (1-POST); (3) two administrations, pre- and postnatally (perinatally) (2-PERI); (4) control (naïve). A concentration of 2.0 mM quinine (0.04 μmol/g BW) was chosen on the basis of previous reports of quinine aversion thresholds in chicken.[17] Administration of the bitter quinine molecule to the GIT of animals from the different treatment groups was as follows (see Figure 1): (a) 1-PRE, administration into the amniotic fluid of the embryo on E17 using a 21-gauge needle and 0.6 mL per embryo of sterile 2.0 mM quinine solution by in-ovo feeding procedure, which delivers nutrients to the GIT;[26] (b) 1-POST, oral administration at 3 days of age of 1.3 mL of 2.0 mM quinine per chick (0.04 μmol/g BW) using a 2 mL syringe; (c) 2-PERI, two administrations, on E17, with sterile 2.0 mM quinine solution (0.6 mL/embryo) by in-ovo feeding procedure and oral administration at 3 days of age with 2.0 mM quinine (1.3 mL/chick) using a 2 mL syringe; (d) naïve, oral administration of 1.3 mL of water at 3 days of age using a 2 mL syringe per chick. In addition, a water-injected control was used ($n$ = 30) to assess injection effects as an internal control (not shown). Ages for 1-PERI, 1-POST, and 2-PERI (E17 and day 3) were chosen on the basis of the following previous findings: between E16 and E20 the embryo orally consumes the amniotic fluid;[27] on E17, the embryo's taste buds are already visible, and on E19, they are fully developed and functioning; the number of taste buds peaks on E19 and then remains constant.[11]

**Treatment Procedure.** All eggs from all treatment groups were taken out of incubation (including the naïve group) and kept in a 37 °C room (similar to incubation temperature) during the in-ovo procedure. The eggs (which contained the embryos) were sprayed with 75% ethanol before and after the in-ovo procedure and were placed in hatching trays until hatch. Hatchability was 90% for in-ovo-administered groups (1-PRE and 2-PERI) and 93.3% for 1-POST and naïve. After hatch, chicks were placed in pens in a brooding house (27−28 birds/pen) for the 5 day trial period. Post hatch feed, which was formulated to meet National Research Council (1994) requirements as appropriate, was offered ad libitum, and water was freely

**Table 1. Primers Used for RT-PCR Analysis of Palate, Tongue, Duodenum, Jejunum, and Ileum Gene Expression in Mature Broilers**

| target[a] | accession no. | primer (5′) | primer (3′) | amplicon size (bp) |
|---|---|---|---|---|
| *ggTas2r1* | AB249766.1 | TTGAGTCAGTTGTGGGGCTT | GAAGTTGCTGTGTGCGTTGT | 434 |
| *ggTas2r2* | AB249767.1 | GTCAACGGGGAACTGTGGAG | CCTCAATGCCAGTTTCAGCTT | 415 |
| *ggTas2r7* | NM_001080719 | CTGTGCGCCACGTGGATATA | CCACAGGTTGGAAGAGCTTAAAA | 119 |
| *α-gustducin* | NM_001267811.1 | GCTGTTGGGTGCTGGAGA | CAAATCATTGAGGTAATAGGCTGC | 367 |
| *PLCβ2* | XM_420945.4 | CTGAAGATGCAGCTGAACGC | TCTGGAGACAACTGCCCTCT | 404 |
| *TRPM5* | XM_003641321.2 | AACTACGGCTCGCTTTGGAA | CACAGGACTTCCACTCCACG | 537 |
| *β-actin* | NM_205518.1 | AATGGCTCCGGTATGTGCAA | GGCCCATACCAACCATCACA | 112; intron size 321 |

[a]gg, *Gallus gallus*; PLCβ2, phospholipase Cβ2; TRMP5, transient receptor potential melastatin 5.

**Table 2. Primers Used for Real-Time PCR Analysis of Palate and Duodenum Gene Expression Following Pre-, Post-, and Perinatal Administration of 2.0 mM Quinine**

| target[a] | accession no. | primer (5′) | primer (3′) |
|---|---|---|---|
| *ggTas2r1* | AB249766.1 | TTGAGTCAGTTGTGGGGCTT | GAAGTTGCTGTGTGCGTTGT |
| *ggTas2r2* | AB249767.1 | GTCAACGGGGAACTGTGGAG | CCTCAATGCCAGTTTCAGCTT |
| *ggTas2r7* | NM_001080719 | CTGTGCGCCACGTGGATATA | CCACAGGTTGGAAGAGCTTAAAA |
| *α-gustducin* | NM_001267811.1 | GCTGTTGGGTGCTGGAGA | CAAATCATTGAGGTAATAGGCTGC |
| *PLCβ2* | XM_420945.4 | CTGAAGATGCAGCTGAACGC | TCTGGAGACAACTGCCCTCT |
| *TRPM5* | XM_003641321.2 | AACTACGGCTCGCTTTGGAA | CACAGGACTTCCACTCCACG |
| *B2M*[b] | NM_001001750.1 | GAACGTCCTCAACTGCTTCGT | GGCACGCCATCCTTCATC |
| *Cyc A*[c] | GQ849480.1 | GGCTACAAGGGCTCCTGCTT | CCG TTG TGG CGC GTA AA |

[a]gg, *Gallus gallus*; PLCβ2, phospholipase Cβ2; TRMP5, transient receptor potential melastatin 5; B2M, microglobulin; Cyc A, cyclophilin A. [b]VanHerch et al.[31] [c]Yadgary et al.[54]

available until the intake test was performed. Body weights and intestinal weights were recorded at day of hatch for all treatment groups including water injection group; no significant differences were found. Mortality was recorded and was negligible (1 bird per 100). All experimental procedures followed established guidelines for animal care and handling and were approved by the Hebrew University Institutional Animal Care and Use Committee (OPRR-A01-5011).

**Intake Experiments.** An individual no-choice intake taste test based on Gentle[28] was conducted on all treatment groups following quinine administration experiments (Figure 1). The tests were conducted on day 5 to separate them from the administrations by at least 24 h, thereby avoiding effects of the administrations themselves. One bird from each treatment group, chosen on the basis of the weight-average of all treatment groups, was placed in a separate pen. A water tray filled with either water or 2.0 mM quinine in water was weighed and placed in the pen for 10 min. Then the trays were reweighed and intake was calculated (evaporation was recorded and included in the final calculation). Four repeats (four different birds) were performed for each treatment group.

In all intake experiments, all groups were subjected to restricted water intake and ad libitum feeding for 6 h prior to the intake experiments.[17,28]

**Tissue Sampling and RNA Extraction.** For reverse transcription (RT)-PCR, the upper palate, tongue, and the three segments of small intestine, duodenum, jejunum, and ileum, were removed from a chicken (broiler; day 25) and kept in RNA Save (Biological Industries, Beit Haemek, Israel) according to the manufacturer's instructions.

For real-time PCR, following the 3 day postnatal administrations (in the appropriate treatment groups), four chicks from each treatment group, chosen on the basis of average weight of each treatment group, were terminated. Two tissues, palate and duodenum, were selected for real-time analysis based on (RT)-PCR results with highest expression levels. Upper palate and duodenum were removed and kept in RNA Save (Biological Industries) according to the manufacturer's instructions until RNA isolation. Total RNA for RT-PCR and real-time PCR was isolated from the upper palate and intestinal segments using an Animal Tissue RNA Purification Kit (Norgen Biotek Corp., Ontario, Canada), which includes on-column DNase digestion for elimination of genomic (g)DNA. Fifteen chicks remaining from each treatment group were used for DNA extraction for future studies.

**Primer Design and RT-PCR.** cDNA was synthesized using 1.0 μg total RNA and a Verso RT-PCR Kit (Thermo Fisher Scientific, Waltham, MA, USA) following the manufacturer's protocol. To assess the relative mRNA abundance of *ggTas2r1*, *ggTas2r2*, *ggTas2r7*, *α-gustducin*, *PLCβ2*, *TRPM5*, and the housekeeping gene *β-actin* gene-specific primers were used according to the published cDNA sequences (Table 1). Primers were either designed with the aid of Primer-BLAST[29] or taken from previous work[30,31] and are specified in Table 1. Because *Tas2rs* are exon-only sequences, we used a combination of controls to exclude gDNA contaminating cDNA samples; no-RT (−RT) negative controls were used, as well as chicken gDNA purified from intestinal segments using the GeneJET Genomic DNA purification column and collection tube (Thermo Fisher Scientific) as a negative control with either exon-spanning or intron-including primers (when possible). All PCR products were validated by running samples on a 1.5% agarose gel, excising bands of the correct size for purification using the Gel/PCR DNA Fragment Extraction Kit (Geneaid Biotech, Bade City, Taiwan), and sequencing (at the Weizmann Institute of Science, Rehovot, Israel).

**mRNA Abundance by Real-Time PCR.** Real-time PCR was performed on a Stratagene (Amsterdam, The Netherlands) MX3000P instrument. Specific primers for SYBR green detection were generated as described above for *ggTas2r1*, *ggTas2r2*, *ggTas2r7*, *α-gustducin*, *PLCβ2*, and *TRPM5* according to the published cDNA sequences (Table 2). The PCR mixture consisted of 3.0 μL of cDNA sample diluted 1:5, 200 nM of each primer, and 10 μL of Platinum SYBR Green qPCR super mix-UDG (Invitrogen, Carlsbad, CA, USA) in a final volume of 20 μL. All PCRs were performed in duplicate in ABgene PCR plates (Thermo Fisher Scientific) closed with optically clear flat QPCR caps (Thermo Fisher Scientific) under the following conditions: 50 °C for 2 min, 95 °C for 2 min, and 40 cycles of 95 °C for 30 s and 60 °C for 1 min. In addition, to ensure amplification of a single product, a dissociation curve was determined under the following conditions: 95 °C for 1 min, 55 °C for 30 s, and 95 °C for 30 s. To control for false positives, a nontemplate control was run for each template and primer pair. Single bands with the predicted product size for each gene tested were confirmed by gel electro-

phoresis, excising for purification using a Gel/PCR DNA Fragment Extraction Kit (Geneaid Biotech) and sequencing (Weizmann Institute of Science). Calculations of threshold cycles, amplification efficiencies, and $R_0$ values (the starting fluorescence value, which is proportional to the relative starting template concentration) were performed using the Data Analysis for Real-Time PCR Excel Workbook.[32] The raw fluorescence data for each of the examined genes were exported to the workbook, and the efficiency ($E$) of each individual reaction was determined using linear regression analysis of the fluorescence data from the exponential phase of each amplification. One-way ANOVA detected no significant difference in amplification efficiencies among samples within treatment groups; therefore, the average $E$ value (arithmetical mean of $E$ values of all samples) for each of the genes was used for the $R_0$ calculation in each sample. The $R_0$ values of two housekeeping genes, $\beta$2 microglobulin (*B2M*) and cyclophilin A, were not significantly different ($P > 0.05$) among the different treatments and, therefore, mRNA abundance was normalized for RNA loading to the geometric average of B2M and cyclophilin A as the internal control ([$R_0$ target gene/$R_0$ AVRHKs (geometric average of housekeeping genes)] × 100).

**Statistical Analysis.** Differences among solution intake in the intake test results (Figure 3A) were calculated using Student's $t$ test (results are the mean ± SEM; differences among means between water and quinine intake within each treatment group are marked by the letters a and b). Differences between the Δ consumption (Figure 3B) were subjected to one-way ANOVA, and the mean ± SD for each treatment group was calculated. Differences between means were calculated using the Tukey–Kramer test. Gene-expression data were subjected to one-way ANOVA. Prior to ANOVA, the mean ± SD for each data set was calculated. Heterogeneity of variance (expressed as an increase in SD with the mean) was observed between treatments for *ggTas2r1*, *ggTas2r2*, *ggTas2r7*, *α-gustducin*, *PLCβ2*, and *TRPM5*, and therefore logarithmic (ln) transformation was carried out for these genes' data. Differences among means were tested by Tukey–Kramer HSD (differences in means marked by the letters a and b) and within treatment group contrasts using Student's $t$ test (differences in means marked by *). For log-transformed data, values are presented as the back-transformed mean ± SEM. All statistical analyses were carried out using JMP 7 software (SAS Institute, 2006, Cary, NC, USA).

## RESULTS

**Functional Calcium Imaging.** To verify the activation of the three chicken bitter taste receptors, functional calcium imaging assays were conducted. As evident from our calcium imaging experiments, all three chicken receptors respond to quinine stimulation. The signal amplitudes of cells transfected with chicken Tas2r1and Tas2r2 were similar and higher compared to Tas2r7 transfected cells (Figure 2), in agreement with previously published results.[24]

**Intake of Quinine versus Water.** To evaluate the chicken's behavioral response to the bitter tastant following administration experiments, individual water or quinine solution (2.0 mM) no-choice intake experiments were conducted (Figure 1A,D) on day 5. In the naïve group, a decreasing trend with no significant differences ($P = 0.1049$) was apparent between water and quinine intake weights (7.8 ± 1.0 and 5.2 ± 0.7 g, respectively; Figure 3A). However, the difference in intake was significant for all treated groups: in the 1-PRE group, water-intake weight was 8.8 ± 0.6 g and quinine-intake weight was significantly lower ($P = 0.01$) at 4.6 ± 0.95 g; in the 1-POST group, water-intake weight was 8.8 ± 1.35 g and quinine-intake weight was significantly lower ($P = 0.0031$) at 3.9 ± 0.3 g. In the 2-PERI group, water-intake weight was 9.2 ± 1 g and quinine-intake weight was significantly lower ($P = 0.0049$) at 4.6 ± 1.6 g. The Δ consumption, which represents the difference between water and quinine consumptions during the intake test, was calculated as well and is represented in Figure 3B. No significant differences were found in the Δ consumption between the treatment groups and the naïve group.

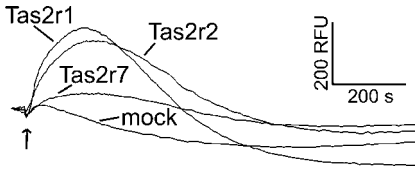


**Figure 2.** Chicken bitter taste receptors respond to quinine. HEK 293T Gα16gust44 cells transiently transfected with expression constructs coding for chicken Tas2r1, Tas2r2, and Tas2r7 respond to stimulation with 30 μM quinine. Traces of fluorescence signals corresponding to changes in intracellular calcium levels after quinine stimulation (arrow) are shown and labeled. Scale: $y$-axis, 200 relative fluorescence units (RFU); $x$-axis, 200 s.

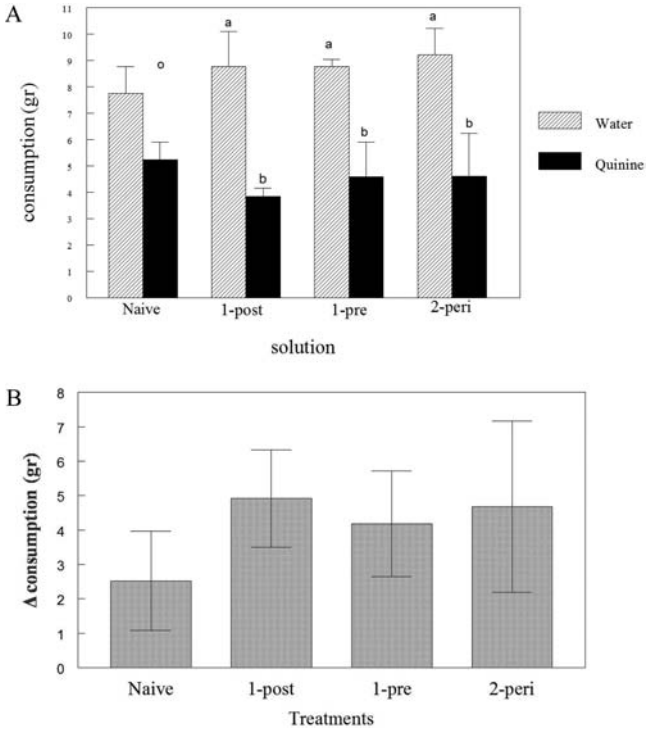


**Figure 3.** No-choice individual intake test following quinine administration. (A) Effect of quinine administration on individual no-choice intake of water or quinine solution. Values are presented as the mean ± SEM intake during 10 min for each treatment group: naïve (control, no quinine administration); 1-PRE (0.6 mL of 2 mM quinine administered prenatally, 0.04 μmol quinine/g BW); 1-POST (1.3 mL of 2 mM quinine administered postnatally, 0.04 μmol quinine/g BW); 2-PERI (two perinatal administrations, pre- and postnatal, of 2 mM quinine). For all treatment groups, $n = 8$ (4 water and 4 quinine solution). Means without a common letter (a, b) differ significantly ($P < 0.05$); o, means differ at $P = 0.1$. (B) Effect of quinine administration on the Δ consumption between water and quinine solution. Values are presented as the mean Δ consumption ± SEM in 10 min for each treatment group, where Δ consumption is (water consumption − quinine solution consumption in g) per each repeat. Treatments were as described for panel A.

***ggTas2rs* and Downstream Signal Transduction Molecules Are Expressed in the Chicken GIT.** RT-PCR analysis was used to determine the gene expression of the three

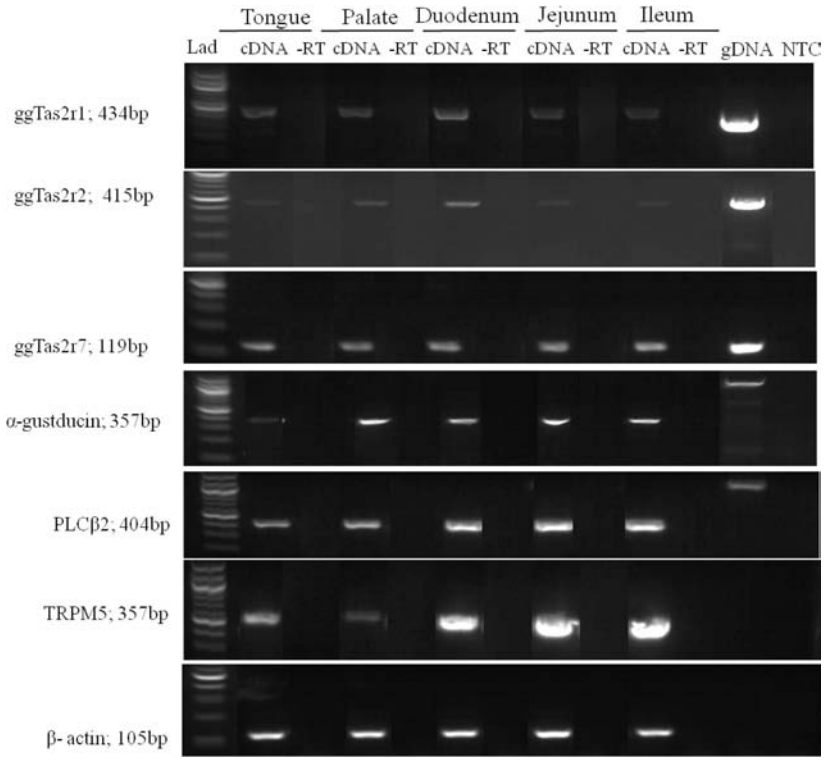


**Figure 4.** RT-PCR demonstrating taste receptors and taste transduction molecules in the chicken GIT. Templates were cDNA prepared from RNA isolated from tongue, palate, duodenum, jejunum, and ileum, as well as a chicken gDNA control. cDNA-amplified products of the expected sizes were obtained for *ggTas2r1* (434 bp), *ggTas2r2* (415 bp), *ggTas2r7* (119 bp), *α-gustducin* (357 bp), *PLCβ2* (404 bp), *TRPM5* (357 bp), and the housekeeping gene *β-actin* (105 bp). RT, negative control reactions without reverse transcriptase. Primers for α-gustducin and PLC*β*2 were designed as intron-inclusion primers (both >1000 bp). Primers for TRPM5 and *β*-actin were designed as exon-spanning, and therefore no product is seen in the gDNA control. PLC*β*2, phospholipase C*β*2; TRMP5, transient receptor potential melastatin 5; NTC, no template control.

chicken *Tas2rs* and three of the downstream effectors, *α*-gustducin, PLC*β*2, and TRPM5, in chicken gustatory tissue (tongue and palate) and extra-gustatory tissue (small intestinal segments duodenum, jejunum, and ileum). All three chicken (*G. gallus*) *Tas2r* genes, *ggTas2r1*, *ggTas2r2*, and *ggTas2r7*, and genes for taste-signaling proteins *α-gustducin*, *PLCβ2*, and *TRPM5*, were found to be expressed in the chicken tongue, palate, and small intestinal segments (Figure 4). Although not quantified, results showed different apparent expression levels of the tested genes among the different sampled tissues.

**ggT2RGene Expression on Day 3.** To test for possible effects of perinatal administration of a bitter tastant on bitter taste related gene expression, real-time PCR was conducted with all treatment groups in comparison to naïve chicks. Overall, and regardless of the treatment, *ggTas2r1* and*ggTas2r7* gave, respectively, 4.0- and 4.6-fold higher relative mRNA abundance values than *ggTas2r2* in the chicken palate and 2.5- and 1.5-fold higher relative mRNA abundance values in the duodenum (Figure 5). In addition, *TRPM5* showed 28-fold higher relative mRNA abundance in the duodenum than in the palate (Figure 6).

Following bitter tastant administration, all treated groups exhibited a trend toward elevated ggTas2rmRNA abundance in the palate on day 3 (Figure 5A). Providing quinine once postnatally caused a significant elevation in *ggTas2r1* and *ggTas2r7* mRNA abundance (6.5- and 4.5-fold, respectively) compared to naïve chicks, and providing quinine twice perinatally caused a significant 4.8-fold elevation in *ggTas2r1* compared to the naïve group.

However, in the duodenum, increasing trends in *ggTas2r* relative mRNA abundance were found in the 1-POST group, but decreasing trends were found in the 2-PERI group, although there were no significant changes in the mRNA abundance levels of the *ggTas2r* genes compared to the naïve group. Within treatment groups, a significant difference was found between 1-POST (higher expression) and 2-PERI (lower expression) for all three *ggTas2rs*.

**Downstream Signal Transduction Gene Expression on Day 3.** In the palate, diverse expression trends were found on day 3 (after quinine administration; Figure 6). Whereas*PLCβ2* relative mRNA abundance decreased significantly in the 1-POST and 2-PERI groups compared to the naïve group (7.2- and 8.2-fold decreases, respectively), *TRPM5* mRNA abundance was significantly elevated in 1-POST (by 3.36-fold) and showed a trend toward elevation in 1-PRE and 2-PERI compared to naïve.

In the duodenum, *α-gustducin* expression was significantly decreased in the 2-PERI compared to naïve and 1-POST groups (by 3.7- and 3.6-fold, respectively). On the other hand, no significant changes were demonstrated in *PLCβ2* and *TRPM5* gene expressions in any of the treatment versus naïve groups.

## DISCUSSION

Expression of *Tas2rs* and taste-signaling components in the GIT was first identified over a decade ago.[33,34] Over the years, *Tas2rs* and downstream signaling components have been identified along the GIT in a variety of different species[35,36] and found to be located in brush cells and enteroendocrine

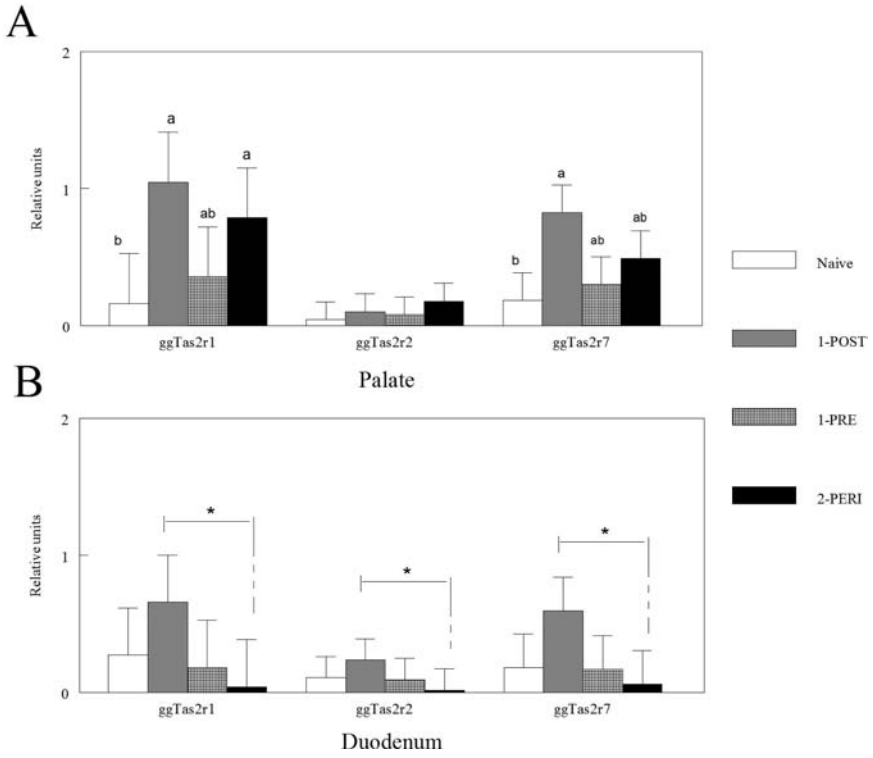


**Figure 5.** Effect of quinine administration on mRNA abundance of the three chicken taste receptors, *ggTas2r1*, *ggTas2r2*, and *ggTas2r7*, in chicken palate (A) and duodenum (B) as shown by relative mRNA abundance in naïve ($n$ = 4), 1-POST ($n$ = 4), 1-PRE ($n$ = 4), 2-PERI ($n$ = 4) treatment groups. Values are presented as back-transformed means (after normalization of RNA loading to the geometric average of B2M and cyclophilin A) ± SEM. Means without a common letter (a, b) differ significantly ($P < 0.05$) between treatments. (*) Means differ significantly when compared individually using each paired Student $t$ test. 1-PRE, 0.6 mL of 2 mM quinine administered prenatally (0.04 μmol quinine/g BW); 1-POST, 1.3 mL of 2 mM quinine administered postnatally (0.04 μmol quinine/g BW); 2-PERI, two perinatal administrations (pre- and postnatal) of 2 mM quinine.

cells[37] as well as in a subset of colonic goblet cells.[38] The exact role of these bitter taste-related genes in the GIT remains unclear, although they have been suggested to be involved in metabolic regulation and feed intake.[39−41] It is only in the past few years that the effect of bitter tastants on these genes' expression and its relationship to bitterness sensitivity and acceptance have begun to be investigated.[42]

The current study provides molecular evidence of gustatory and GIT (extra-gustatory) expression of the three bitter-taste receptors *ggTas2r1*, *ggTas2r2*, *ggTas2r7* and the signaling components *α-gustducin*, *PLCβ2*, and *TRPM5* in chicken, as indicated by RT-PCR; the activation of the three chicken bitter taste receptors by quinine stimuli was illustrated in vitro. Intake tests demonstrate that even a single exposure to quinine during early development (before or after hatch) significantly decreases its intake compared to water, whereas in the naïve group only a trend toward decrease in quinine consumption was evident ($P$ = 0.1). Real-time PCR results indicate that exposure to quinine at an early age affects the later expression of bitter taste transduction genes in both the palate and the duodenum of chicks.

**Quinine-Intake Taste Tests.** Using no-choice intake taste tests, we examined the chicken's behavioral responses to the administration of the bitter tastant quinine following prenatal, postnatal, and perinatal quinine administration treatments. No-choice intake taste tests were chosen for evaluating the animal response because in broiler feeding interface and broiler production, the animals have a no-choice diet.

The individual no-choice taste tests indicated intake in naïve animals encountering the bitter tastant for the first time demonstrated a decrease trend of quinine intake compared to water ($P$ = 0.105). Early exposure to quinine (either prenatally, postnatally, or both) decreases its intake significantly compared to water ($P$ values < 0.05).

Many studies dealing with flavor learning and programming in mammals during the perinatal period make use of repetitive exposure to the aversive tastants during early developmental stages, often leading to adaptation and improved acceptance.[43−47] In the current study, the no-choice taste test results did not indicate adaptation. Rather, the results may suggest a trend toward sensitization to the bitter tastant following early exposure. This can also be seen in Figure 3B, where the Δ consumption (the difference in intake between water and quinine solution) in the three treatment groups does not decrease (rather showing a trend of increase) compared to the Δ consumption of the naïve group.

**Gene Expression.** *ggTas2r1*, *ggTas2r2*, and *ggTas2r7* and the signal transduction components *α-gustducin*, *PLCβ2*, and *TRPM5* were expressed in the tongue, palate, and the three segments of the small intestine, duodenum, ileum and jejunum (Figure 4), as determined by RT-PCR. To the best of our knowledge, the only previous evidence of bitter taste perception-related gene expression in chicken is the expression of *α-gustducin* in taste buds located in the oral cavity.[48]

An important question is the relationship between bitter tastant consumption and bitter taste-related genes' expression. Does administration of quinine also affect the expression of bitter taste-related genes and is there an association between quinine intake and the related genes' expression in the chick GIT?

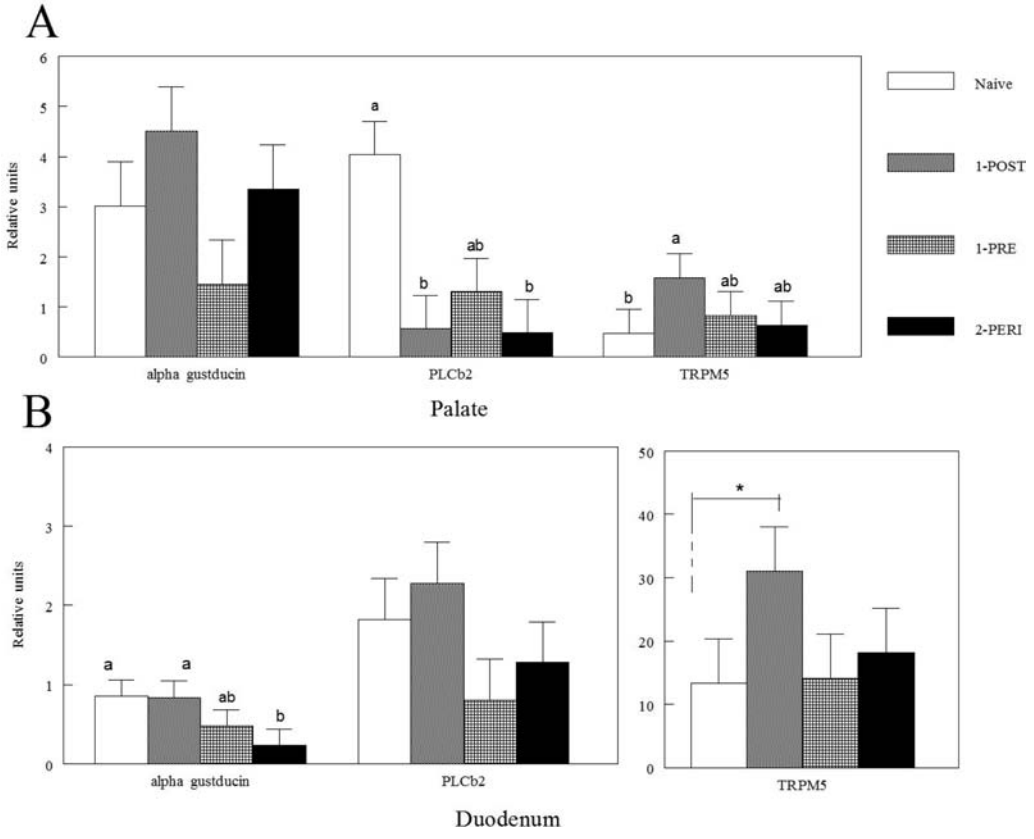


**Figure 6.** Expression of signal transduction molecule-encoding genes following quinine administration in chicken palate (A) and duodenum (B) by real-time PCR as shown by relative mRNA abundance in naïve ($n$ = 4), 1-POST ($n$ = 4), 1-PRE ($n$ = 4), and 2-PERI ($n$ = 4) treatment groups. Values are presented as back-transformed means (after normalization of RNA loading to the geometric average of B2M and cyclophilin (A) ± SEM. Means without a common letter (a, b) differ significantly ($P < 0.05$) between treatments. (*) Means differ significantly when compared individually using each paired Student $t$ test. 1-PRE, 0.6 mL of 2 mM quinine administered prenatally (0.04 $\mu$mol quinine/g BW); 1-POST, 1.3 mL of 2 mM quinine administered postnatally (0.04 $\mu$mol quinine/g BW); 2-PERI, two perinatal administrations (pre- and postnatal) of 2 mM quinine. PLC$\beta$2, phospholipase C$\beta$2; TRMP5, transient receptor potential melastatin 5.

Indeed, exposure to the bitter tastant quinine affects expression in the chicks' palate and duodenum. Our results demonstrate that in the palate, *ggTas2rs* expression is elevated following quinine administration, whereas in the duodenum,*ggTas2rs* and *α-gustducin* response to quinine was treatment-dependent: the one-time postnatal (1-POST) administration caused an increasing trend in all duodenal *ggTas2rs*, whereas two-time perinatal (2-PERI) administration resulted in a decreasing trend for all duodenal*ggTas2rs* (with expression in 1-POST being significantly higher than that in 2-PERI; Figure 5).

The increase in expression change in the palate following administration (all treatment groups showed elevated *ggTas2r1* and *ggTas2r7* expression compared to naïve) is in correlation with lowered quinine intake results. This is not surprising, because in chicken the palate is the major gustatory tissue responsible for bitter sensing.[49] Our findings are in accord with recent studies in humans: Hirai et al.[50] investigated mRNA expression and its association with taste sensitivity and perception and reported that increased T2R expression is related to human taste disorders involving increased bitter taste sensation. More recent research has shown a correlation between human bitter perception and mRNA expression of *TAS2R38*, one of the human bitter taste receptors, in the human fungiform papilla located in the tongue.[42]

Interestingly, gene expression patterns in the duodenum varied between the different treatment groups. The difference seen in the duodenum in *ggTas2r* and *α*-gustducin expression between 1-POST and 2-PERI may be a result of the number of times the chicken was exposed to the tastant (once versus twice). Changes in expression levels of taste transduction genes in the duodenum, following the different treatments, suggest possible extra-gustatory roles for these genes. Previous reports in mammals have also reported expression of *Tas2rs* and the downstream molecules *α-gustducin*, *PLCβ2*, and *TRPM5* located in the mouse GIT,[51] although their expression was not analyzed following bitter tastant administration. The precise participation of taste-signaling genes in these intestinal pathways is yet unclear. Studies performed in rodents suggest that the assumed surveillance of the luminal contents of the GIT by bitter taste receptor signaling may serve roles in metabolic control[52] and satiety regulation,[40] as well as defensive functions.[38,41,53] Following up on this result may help unravel the molecular mechanisms involved in intestinal tastant sensing.

In summary, the results of the present study demonstrate the expression of bitter taste related genes in the chicken's gustatory and extra-gustatory (GIT) tissues. Early developmental stage exposure to a bitter tastant prenatally, postnatally, or both, changes taste related genes' expression in the palate and duodenum and leads to a decreased bitter tastant intake. Our

results pave the way for studying the roles of GIT taste signaling machinery in poultry.

## AUTHOR INFORMATION


### Corresponding Author

*(Z.U.) Phone: 972-89489205. Fax: 972-89489887. E-mail: zehava.uni@mail.huji.ac.il.



### Funding

The Israel Science Foundation (ISF) − The Chief Scientist, Ministry of Agriculture, Israel.

### Notes

The authors declare no competing financial interest.


## ACKNOWLEDGMENTS

We thank U. Redel for excellent technical assistance.

## ABBREVIATIONS USED

GIT, gastrointestinal tract; E, embryonic day; TRPM5, transient receptor potential melastatin 5; PLC$\beta$2, phospholipase C$\beta$2; Tas2r, taste 2 receptor; gDNA, genomic DNA; gg, *Gallus gallus*

## REFERENCES


(1) Lindemann, B. Taste reception. *Physiol. Rev.* **1996**, *76*, 718−766.

(2) Drewnowski, A.; Gomez-Carneros, C. Bitter taste, phytonutrients, and the consumer: a review. *Am. J. Clin. Nutr.* **2000**, *72*, 1424−1435.

(3) Dawid, C.; Hofmann, T. Identification of sensory-active phytochemicals in asparagus (*Asparagus officinalis* L.). *J. Agric. Food Chem.* **2012**, *60*, 11877−11888.

(4) Cattoor, K.; et al. Metabolism of hop-derived bitter acids. *J. Agric. Food Chem.* **2013**, *61*, 7916−7924.

(5) Boland, M. J.; et al. The future supply of animal-derived protein for human consumption. *Trends Food Sci. Technol.* **2013**, *29*, 62−73.

(6) Godfray, H. C.; et al. Food security: the challenge of feeding 9 billion people. *Science* **2010**, *327*, 812−818.

(7) Iwata, S.; Yoshida, R.; Ninomiya, Y. Taste transductions in taste receptor cells: basic tastes and moreover. *Curr. Pharm. Des.* **2013**, *20*, 2684−2692.

(8) Meyerhof, W.; et al. The molecular receptive ranges of human TAS2R bitter taste receptors. *Chem. Senses* **2010**, *35*, 157−170.

(9) Matsunami, H.; Montmayeur, J.-P.; Buck, L. B. A family of candidate taste receptors in human and mouse. *Nature* **2000**, *404*, 601−604.

(10) Yamamoto, K.; Ishimaru, Y. Oral and extra-oral taste perception. *Semin. Cell Dev. Biol.* **2013**, *24*, 240−246.

(11) Ganchrow, J. R.; Ganchrow, D. Taste bud development in chickens (*Gallus gallus domesticus*). *Anat. Rec.* **1987**, *218*, 88−93.

(12) Behrens, M.; Meyerhof, W. Bitter taste receptor research comes of age: from characterization to modulation of TAS2Rs. *Semin. Cell Dev. Biol.* **2013**, *24*, 215−221.

(13) Bachmanov, A. A.; Beauchamp, G. K. Taste receptor genes. *Annu. Rev. Nutr* **2007**, *27*, 389−414.

(14) Shi, P.; Zhang, J. Contrasting modes of evolution between vertebrate sweet/umami receptor genes and bitter receptor genes. *Mol. Biol. Evol.* **2006**, *23*, 292−300.

(15) Gentle, M. J. Gustatory hyposensitivity to quinine hydrochloride following diencephalic lesions in *Gallus domesticus*. *Physiol. Behav.* **1975**, *14*, 265−270.

(16) Ganchrow, J. R.; Steiner, J. E.; Bartana, A. Behavioral reactions to gustatory stimuli in young chicks (*Gallus gallus domesticus*). *Dev. Psychobiol.* **1990**, *23*, 103−117.

(17) Kudo, K.; Shiraishi, J.; Nishimura, S.; Bungo, T.; Tabata, S. The number of taste buds is related to bitter taste sensitivity in layer and broiler chickens. *Anim. Sci. J. (Nihon Chikusan Gakkaiho)* **2010**, *81*, 240−244.

(18) Vince, M. A. Taste sensitivity in the embryo of the domestic fowl. *Anim. Behav.* **1977**, *25*, 797−805.

(19) Gentle, M. J. Sensory involvement in the control of food intake in poultry. *Proc. Nutr Soc.* **1985**, *44*, 313−321.

(20) Behrens, M.; Meyerhof, W. Oral and extraoral bitter taste receptors. *Results Probl. Cell Differ.* **2010**, *52*, 87−99.

(21) Rozengurt, E. Taste receptors in the gastrointestinal tract. I. Bitter taste receptors and alpha-gustducin in the mammalian gut. *Am. J. Physiol. Gastrointest. Liver Physiol.* **2006**, *291*, G171−G177.

(22) Roura, E.; Baldwin, M. W.; Klasing, K. C. The avian taste system. *Aust. Poult. Sci.* **2012**, *7*, 97−104.

(23) Wiener, A.; Shudler, M.; Levit, A.; Niv, M. Y. BitterDB: a database of bitter compounds. *Nucleic Acids Res.* **2012**, *40*, D413−D419.

(24) Behrens, M.; Korsching, S. I.; Meyerhof, W. Tuning properties of avian and frog bitter taste receptors dynamically fit gene repertoire sizes. *Mol. Biol. Evol.* **2014**, DOI: 10.1093/molbev/msu254.

(25) Ueda, T.; Ugawa, S.; Yamamura, H.; Imaizumi, Y.; Shimada, S. Functional interaction between T2R taste receptors and G-protein $\alpha$ subunits expressed in taste receptor cells. *J. Neurosci.* **2003**, *23*, 7376−7380.

(26) Uni, Z.; Ferket, P. R. In-ovo administration method. U.S. Patent, 2003.

(27) Romanoff, A. L. *The Avian Embryo: Structural and Functional Development*; Macmillan: New York, 1960.

(28) Gentle, M. J. Gustatory hyposensitivity to quinine hydrochloride following diencephalic lesions in *Gallus domesticus*. *Physiol. Behav.* **1975**, *14*, 265−270.

(29) Ye, J.; et al. Primer-BLAST: a tool to design target-specific primers for polymerase chain reaction. *BMC Bioinf.* **2012**, *13*, 134.

(30) Cheled-Shoval, S. L.; Amit-Romach, E.; Barbakov, M.; Uni, Z. The effect of in ovo administration of mannan oligosaccharide on small intestine development during the pre- and posthatch periods in chickens. *Poult. Sci.* **2011**, *90*, 2301−2310.

(31) Van Herch, S.; Geysen, S.; Delbaere, J.; Tylzanowski, P.; Darras, V. M. Expression profile and thyroid hormone responsiveness of transporters and deiodinases in early embryonic chicken brain development. *Mol. Cell. Endocrinol.* **2012**, 289−297.

(32) Peirson, S. N.; Butler, J. N.; Foster, R. G. Experimental validation of novel and conventional approaches to quantitative real-time PCR data analysis. *Nucleic Acids Res.* **2003**, *31*, No. e73.

(33) Wu, S. V.; et al. Expression of bitter taste receptors of the T2R family in the gastrointestinal tract and enteroendocrine STC-1 cells. *Proc. Natl. Acad. Sci. U.S.A.* **2002**, *99*, 2392−2397.

(34) Höfer, D.; Püschel, B.; Drenckhahn, D. Taste receptor-like cells in the rat gut identified by expression of $\alpha$-gustducin. *Proc. Natl. Acad. Sci. U.S.A.* **1996**, *93*, 6631−6634.

(35) Gonda, S.; Matsumura, S.; Saito, S.; Go, Y.; Imai, H. Expression of taste signal transduction molecules in the caecum of common marmosets. *Biol. Lett.* **2013**, *9*, No. 20130409.

(36) Rozengurt, E.; Sternini, C. Taste receptor signaling in the mammalian gut. *Curr. Opin. Pharmacol.* **2007**, *7*, 557−562.

(37) Sternini, C.; Anselmi, L.; Rozengurt, E. Enteroendocrine cells: a site of 'taste' in gastrointestinal chemosensing. *Curr. Opin. Endocrinol. Diabetes Obes.* **2008**, *15*, 73−78.

(38) Prandi, S.; et al. A subset of mouse colonic goblet cells expresses the bitter taste receptor Tas2r131. *PLoS One* **2013**, *8*, No. e82820.

(39) Walker, J.; et al. Identification of beer bitter acids regulating mechanisms of gastric acid secretion. *J. Agric. Food Chem.* **2012**, *60*, 1405−1412.

(40) Janssen, S.; et al. Bitter taste receptors and alpha-gustducin regulate the secretion of ghrelin with functional effects on food intake and gastric emptying. *Proc. Natl. Acad. Sci. U.S.A.* **2011**, *108*, 2094−2099.

(41) Glendinning, J. I.; Yiin, Y. M.; Ackroff, K.; Sclafani, A. Intragastric infusion of denatonium conditions flavor aversions and delays gastric emptying in rodents. *Physiol. Behav.* **2008**, *93*, 757−765.

(42) Lipchock, S. V.; Mennella, J. A.; Spielman, A. I.; Reed, D. R. Human bitter perception correlates with bitter receptor messenger RNA expression in taste cells. *Am. J. Clin. Nutr.* **2013**, *98*, 1136−1143.
(43) Mennella, J. A.; Beauchamp, G. K. The effects of repeated exposure to garlic-flavored milk on the nursling's behavior. *Pediatr. Res.* **1993**, *34*, 805−708.
(44) Mennella, J. A. Flavour programming during breast-feeding. *Adv. Exp. Med. Biol.* **2009**, *639*, 113−120.
(45) Mennella, J. A.; Griffin, C. E.; Beauchamp, G. K. Flavor programming during infancy. *Pediatrics* **2004**, *113*, 840−845.
(46) Mennella, J. A.; Jagnow, C. P.; Beauchamp, G. K. Prenatal and postnatal flavor learning by human infants. *Pediatrics* **2001**, *107*, No. E88.
(47) Mennella, J. A.; Pepino, M. Y.; Beauchamp, G. K. Modification of bitter taste in children. *Dev. Psychobiol.* **2003**, *43*, 120−127.
(48) Kudo, K.; Wakamatsu, K.; Nishimura, S.; Tabata, S. Gustducin is expressed in the taste buds of the chicken. *Anim. Sci. J. (Nihon Chikusan Gakkaiho)* **2010**, *81*, 666−672.
(49) Ganchrow, D.; Ganchrow, J. R. Number and distribution of taste buds in the oral cavity of hatchling chicks. *Physiol. Behav.* **1985**, *34*, 889−894.
(50) Hirai, R.; Takao, K.; Onoda, K.; Kokubun, S.; Ikeda, M. Patients with phantogeusia show increased expression of T2R taste receptor genes in their tongues. *Ann. Otol. Rhinol. Laryngol.* **2012**, *121*, 113.
(51) Bezencon, C.; le Coutre, J.; Damak, S. Taste-signaling proteins are coexpressed in solitary intestinal epithelial cells. *Chem. Senses* **2007**, *32*, 41−49.
(52) Dotson, C. D.; et al. Bitter taste receptors influence glucose homeostasis. *PLoS One* **2008**, *3*, No. e3974.
(53) Kaji, I.; Karaki, S.-i.; Fukami, Y.; Terasaki, M.; Kuwahara, A. Secretory effects of a luminal bitter tastant and expressions of bitter taste receptors, T2Rs, in the human and rat large intestine. *Am. J. Physiol. Gastrointest. Liver Physiol.* **2009**, *296*, G971−G981.
(54) Yadgary, L.; Yair, R.; Uni, Z. The chick embryo yolk sac membrane expresses nutrient transporter and digestive enzyme genes. *Poult. Sci.* **2011**, *90*, 410−416.

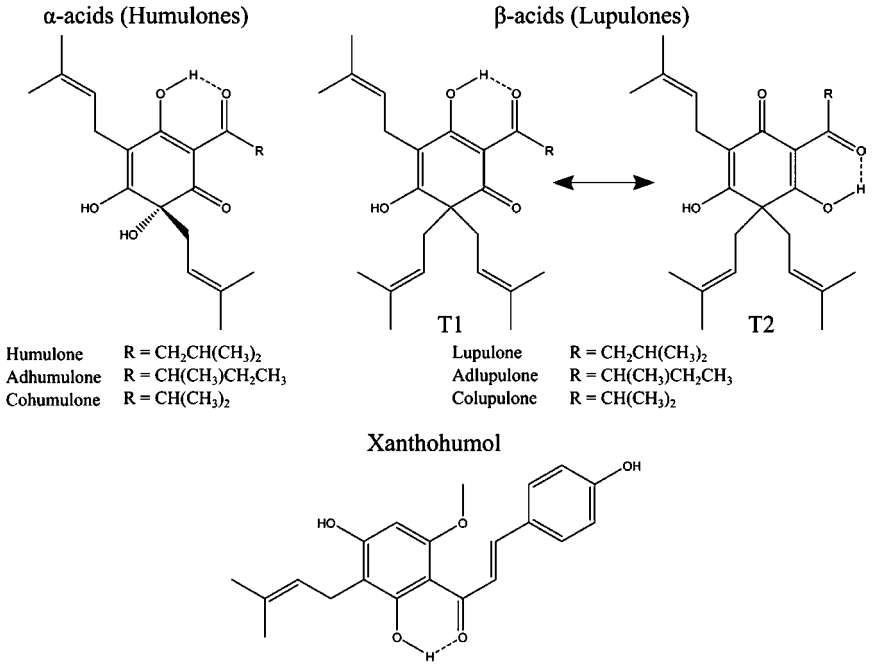


**Figure 1.** Structures of hops bitter acids and xanthohumol.

data, which means that a single spectral matrix can be successively tuned to different reference data using PLS-R.[28] This approach is particularly relevant to hops, where quantitation of the structurally similar $\alpha$- and $\beta$-acids in addition to the bioactive xanthohumol is desirable.

PLS-R has recently been successfully applied to quantitation of iridoid glycosides from *Verbena* by IR and NIR,[24] aspalathin in green rooibos by Raman,[23] and caffeine in roasted coffee beans by NIR.[29] As suggested by these examples, studies generally use only one or two vibrational spectroscopy techniques, a practice that risks missing the most suitable technique. Analysis by all three techniques results in complementary data sets that can be appraised relative to one another and in the context of their performances for a given application. In some cases, analytical challenges have been overcome using "fused" spectroscopic data sets.[30]

To better understand the PLS-R models, cohumulone, colupulone, and xanthohumol were isolated, their Raman and IR spectra were measured, and the vibrational bands were assigned using density functional theory (DFT) calculations. These assignments allowed the interpretation of LVs in the generated PLS-R models, which in turn permitted a more insightful understanding of model performances.

## MATERIALS AND METHODS

**Plant Material.** Hops were grown at Motueka, South Island, New Zealand (41°6′ S, 172°58′ E) in Riwaka silt loam. Advanced selections (139 individual plants encompassing 39 genetic varieties) from hops breeding trials were harvested in March 2013. Hops cones were kiln-dried at ∼60 °C for 8 h followed by determination of residual water content. Subsamples, ∼5 g of cones, were pulverized under $N_2$ (l) and stored at −20 °C prior to the analyses.

**Isolation of Hops Bitter Acids.** An aliquot of the hops International Calibration Extract (ICE-3) was purchased from the American Society of Brewing Chemists (ASBC). A solution containing ∼100 mg mL$^{-1}$ of ICE-3 in MeOH was filtered before it was injected onto an Agilent 1260 Infinity semipreparative HPLC system equipped with a Phenomenex Luna (5 $\mu$) C18 column (10 × 250 mm) with UV detection at 210 nm. Injections (50 $\mu$L) were eluted over 18 min in 87.9:12:0.1 MeOH:$H_2O$:formic acid, with a flow rate of 5 mL min$^{-1}$. Fractions were collected at retention times of 7.3, 8.4, 10.8, and 12.9 min and identified by $^1$H NMR as cohumulone, a mixture of humulone/adhumulone, colupulone, and a mixture of lupulone/adlupulone, respectively, by comparison to published spectra.[6] Using the same methodology, xanthohumol was isolated from a MeOH extract of hops inflorescences. This compound had a retention time of 5.5 min. The compound was identified by $^1$H NMR by comparison to published spectra.[31]

**Quantitation of Bitter Acids by UV Spectrophotometry.** Hops cones (10 g) were added to 100 mL of toluene for extraction in an Omni mixer. Over a 10 min period, samples were sequentially blended and rested for 30 s periods. Samples were filtered, and 50 $\mu$L was diluted to 25 mL with alkaline MeOH. The UV absorbances at 275, 325, and 355 nm were recorded using a UV spectrophotometer, with 50 $\mu$L of toluene in alkaline MeOH (25 mL) as a blank. This was adapted from a standard industry method.[10]

**Quantitation of Bitter Acids and Xanthohumol by HPLC.** Hops were extracted as described above, and 3 mL was transferred to a 50 mL volumetric flask and made to volume with MeOH. Ten $\mu$L of this solution was injected onto a Shimadzu SCL10Avp HPLC system equipped with a 250 mm × 4.6 mm, 5 $\mu$m Kinetix C18 column at 30 °C at a flow rate of 1.5 mL min$^{-1}$. The mobile phase was MeOH:$H_2O$:phosphoric acid:0.1 M EDTA (1700:350:5:1) with UV detection at 270 nm. Run time was 18 min. This was adapted from a standard industry method.[9]

**IR Analysis.** Hops powder (∼10 mg) was deposited directly onto the ATR crystal and compressed by the anvil mechanism. Spectra were acquired using a Bruker ALPHA Platinum Fourier transform infrared (FT-IR) spectrometer equipped with a diamond attenuated total relection (ATR) crystal. Spectra were recorded from 376−4000 cm$^{-1}$ with a spectral resolution of 4 cm$^{-1}$ and were the average of 32 scans. Prior to acquisition of each spectrum, the crystal and anvil were thoroughly cleaned, and a background spectrum was acquired to account for any environmental changes throughout the analysis. Spectral acquisition time was ∼1 min per sample.

**Raman Analysis.** Hops powder (∼50 mg) was packed into aluminum divots for analysis. Spectra were acquired using a FRA 106/5 Bruker Equinox FT-Raman spectrometer equipped with a Nd:YAG laser emitting at 1064 nm, Equinox 55 interferometer, and a germanium detector cooled with $N_2$ (l). The Raman Stokes shift was recorded from 200−3500 cm$^{-1}$ with a spectral resolution of 4

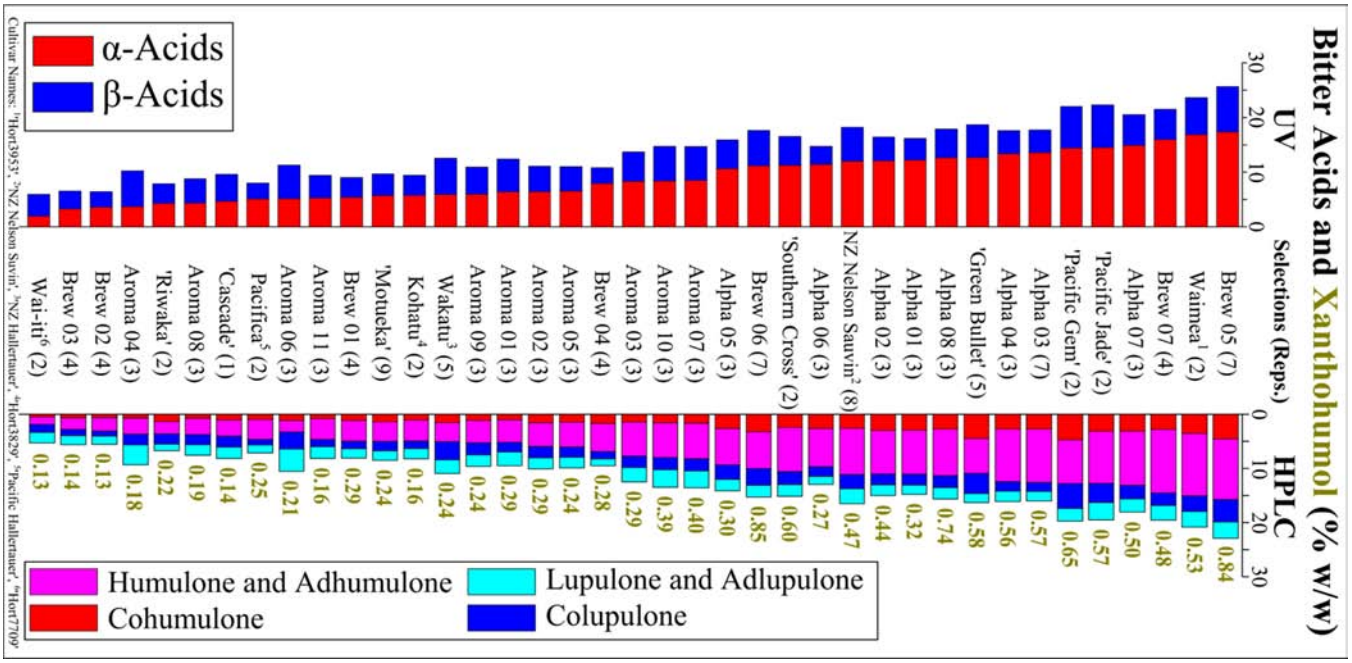


**Figure 2.** Concentrations of $\alpha$-acids, $\beta$-acids, and xanthohumol by HPLC and UV spectrophotometry.

**Table 1. Comparison of Hops Analyses by Vibrational Spectroscopy with UV and HPLC Analyses Using Partial Least-Squares Regression (PLS-R)**

| | | UV analyses | | HPLC analyses | | | |
|---|---|---|---|---|---|---|---|
| spectroscopic technique | PLS-R parameters | total $\alpha$-acids | total acids | alpha | total | cohumulone | xanthohumol |
| IR | | | | | | | |
| | $r^2$ (RMSEC)[a] | 0.92 (1.2) | 0.90 (1.6) | 0.86 (1.4) | 0.90 (1.5) | 0.92 (0.3) | 0.85 (0.09) |
| | $r^2$ (RMSEP)[b] | 0.91 (1.3) | 0.91 (1.8) | 0.89 (1.4) | 0.89 (1.8) | 0.91 (0.4) | 0.88 (0.07) |
| | no. of LVs | 5 | 5 | 3 | 5 | 5 | 5 |
| | RPD[c] | **3.4** | **3.3** | 2.9 | 3.0 | **3.4** | 2.9 |
| Raman | | | | | | | |
| | $r^2$ (RMSEC) | 0.88 (1.5) | 0.87 (1.9) | 0.86 (1.5) | 0.84 (1.9) | 0.90 (0.4) | 0.87 (0.08) |
| | $r^2$ (RMSEP) | 0.91 (1.3) | 0.90 (1.8) | 0.90 (1.3) | 0.90 (1.7) | 0.91 (0.4) | 0.87 (0.08) |
| | no. of LVs | 4 | 4 | 4 | 4 | 7 | 4 |
| | RPD | **3.3** | **3.1** | **3.2** | **3.1** | **3.3** | 2.8 |
| NIR DRIFT | | | | | | | |
| | $r^2$ (RMSEC) | 0.87 (1.5) | 0.91 (1.6) | 0.86 (1.4) | 0.89 (1.6) | 0.82 (0.5) | 0.85 (0.09) |
| | $r^2$ (RMSEP) | 0.91 (1.4) | 0.93 (1.5) | 0.91 (1.2) | 0.92 (1.5) | 0.82 (0.5) | 0.78 (0.10) |
| | no. of LVs | 4 | 4 | 4 | 4 | 5 | 6 |
| | RPD | **3.3** | **3.7** | **3.3** | **3.6** | 2.4 | 2.1 |
| NIR micro | | | | | | | |
| | $r^2$ (RMSEC) | 0.82 (1.8) | 0.85 (2.0) | 0.81 (1.7) | 0.82 (2.0) | 0.76 (0.6) | 0.77 (0.10) |
| | $r^2$ (RMSEP) | 0.88 (1.5) | 0.90 (1.8) | 0.90 (1.3) | 0.91 (1.6) | 0.76 (0.6) | 0.63 (0.13) |
| | no. of LVs | 7 | 7 | 7 | 7 | 7 | 6 |
| | RPD | 3.0 | **3.3** | **3.2** | **3.5** | 2.0 | 1.5 |

[a]Root mean square error of calibration. [b]Root mean square error of prediction. [c]Ratio of prediction to deviation.

$cm^{-1}$, spot size of 0.3 mm, and laser power of 120 mW. Spectra were the average of 256 scans, and the acquisition time was ~8 min per sample. Raman analysis with excitation at 830 and 785 nm could not distinguish Raman bands from raised baselines due to emission. These Raman systems have previously been described in detail.[21]

**NIR Analysis.** Hops powder (~1 g) was added to a sample cup, and the surface was smoothed with gentle compression. Background spectra, consisting of diffusely reflected light from a reflective surface, were taken prior to each sample acquisition. Diffuse reflectance infrared Fourier transform (DRIFT) spectra were recorded using a FRA 106/5 Bruker FT-NIR spectrometer equipped with an Equinox 55 interferometer and germanium detector cooled with $N_2$ (l) from 4000−10000 $cm^{-1}$, with a resolution of 8 $cm^{-1}$ in Kubelka−Munk units. Spectral acquisition time was ~1 min per sample.

**Portable NIR Analysis.** Hops powder (~1 g) were presented to the MicroNIR spectrometer (JDS Uniphase Corporation) in clear, 4 mL glass vials, and reflectance spectra were acquired through the base of the vial. A spectral acquisition time of 1 s was used, and analysis was performed in triplicate by shaking the vial between acquisitions. Two tungsten filaments were used to produce polychromatic radiation, and diffusely reflected light was dispersed with a linear variable filter onto a 128-pixel uncooled InGaAs photodiode array detector. Spectra were recorded from 4545−8696 $cm^{-1}$ (1150−2100 nm) with a spectral resolution of 32 $cm^{-1}$.

**Density Functional Theory Calculations.** The molecular geometries of xanthohumol, cohumulone, and both colupulone conformers (Figure 1) were optimized with DFT using the 6-31+G(d) basis set. A correction factor of 0.960 was applied to the predicted vibrational frequencies to correct for their systematic overestimation.[32−34] The mean absolute deviation between the calculated and experimental vibrational bands was 13 $cm^{-1}$. Quantum chemical calculations were performed using Gaussian 09 and, where possible, initiated from published crystal structures.[31,35]

**Regression Modeling.** *Quantitative IR Spectroscopy.* The IR spectrum of each sample was imported into the multivariate software "The Unscrambler®". A standard normal variate (SNV) transformation was applied to each spectrum to compensate for scattering effects that arise from experimental factors such as varying optical path lengths, sample inhomogeneity, and background effects.[36] Models were generated from the spectral region from 850−1700 $cm^{-1}$ (the spectral region below 850 $cm^{-1}$ and from 1810−2700 $cm^{-1}$ were omitted since IR spectra of purified bitter acids (Figure 3a) did not contain any distinct or intense vibrational bands in these regions, and the spectral region above 2700 $cm^{-1}$ was also omitted because the C−H and O−H stretching vibrations of many biological compounds contribute intensity in this region). One-third of the sample spectra was selected at random to be used as a test set for model validation. The remaining two-thirds were used as a calibration set to generate PLS-R models (noniterative, PLS1[27]) that relate the selected spectral regions to the reference values from the UV and HPLC analyses (Figure 2). This independent "test-set" validation methodology is considered robust.[37] Models were used to predict test-set values from their IR spectra with selected results in Table 1. The number of LVs selected was the optimum for predicting values in the independent validation test set. Data for all models are included in Table S1 of the Supporting Information.

*Quantitative Raman Spectroscopy.* The spectral region from 1050−1750 $cm^{-1}$ was used to generate PLS-R models that relate Raman spectra to UV and HPLC reference values (Figure 2). This spectral region was selected by comparison to the spectra of purified bitter acids (Figure 3b). The same validation methodology was used with the same samples comprising the calibration and test sets. Selected results of the test set analyses are shown in Table 1. Data for all models are included in Table S1 of the Supporting Information.

*Quantitative NIR Spectroscopy.* PLS-R models were generated from 4000−7300 $cm^{-1}$ from the DRIFT NIR spectra. This spectral region was chosen based on visual inspection and correlation loadings, which suggested that the noisy spectral region from 7300−10000 $cm^{-1}$ could not effectively be related to the reference data. For the NIR spectra measured with the portable NIR spectrometer, regression models were generated from the entire spectral range acquired (4545−8696 $cm^{-1}$). In both cases, spectra were subjected to SNV and used to generate PLS-R models relating them to UV and HPLC reference data (Figure 2). The calibration and test sets comprised the same samples used for in the Raman and IR analyses, and selected model performances are presented in Table 1. Data for all models are included in Table S1 of the Supporting Information.

## RESULTS AND DISCUSSION

Thirty-nine hops varieties, with one−nine replicate samples each (139 total) were used in this study, including both well-known commercial varieties and genetically novel selections chosen to encompass broad chemotypical differences. The novel selections were designated sequentially based on their associated breeding trials, that is, Alpha, Aroma, and Brewing (Brew) (Figure 2).

**Reference Analyses.** Bitter acid concentrations for all 139 hops samples were determined by the standard industry methods of HPLC[9] and UV spectrophotometry.[10] The average $\alpha$-acid and $\beta$-acid concentrations for each variety by UV are shown in Figure 2 in addition to HPLC results for the concentrations of the $\alpha$-acids cohumulone and the coeluting adhumulone and humulone, the $\beta$-acids colupulone and the coeluting adlupulone and lupulones, and the chalcone xanthohumol (Figure 1). $\alpha$-Acid concentrations were 2−17% w/w, and $\beta$-acid concentrations were 2−8%, which is close to the full range of values reported for wild and domesticated hops varieties.[17,38] Xanthohumol concentrations of 0.1−0.8% (Figure 2) also covered almost the full reported range.[3]

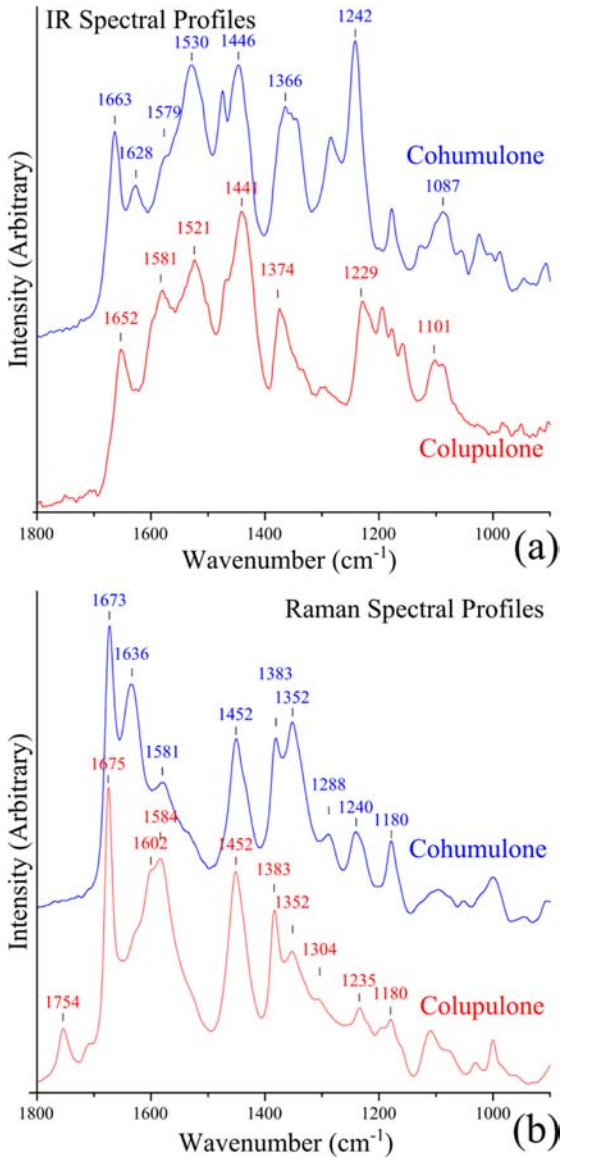


**Figure 3.** IR and Raman spectral profiles of pure cohumulone and colupulone.

Total $\alpha$-acids and total $\beta$-acids measured by the HPLC and UV methods showed good agreement between the results of both analyses, with correlation coefficients of 0.99 and 0.95, respectively. However, the absolute values for $\alpha$- and $\beta$-acids by UV spectrophotometry were, on average, 10% larger than values from HPLC analyses. It has been reported that the UV analysis method is subject to interference from bitter acid oxidation products, which absorb at analytically relevant wavelengths and cause this discrepancy.[39] Total $\alpha$-acid concentrations did not correlate strongly with total $\beta$-acid concentrations: $r^2$ = 0.36 (UV) and 0.39 (HPLC). Likens et al. found that $\alpha$-acid concentrations were negatively correlated to $\beta$-acid concentrations in lupulin from different hops varieties

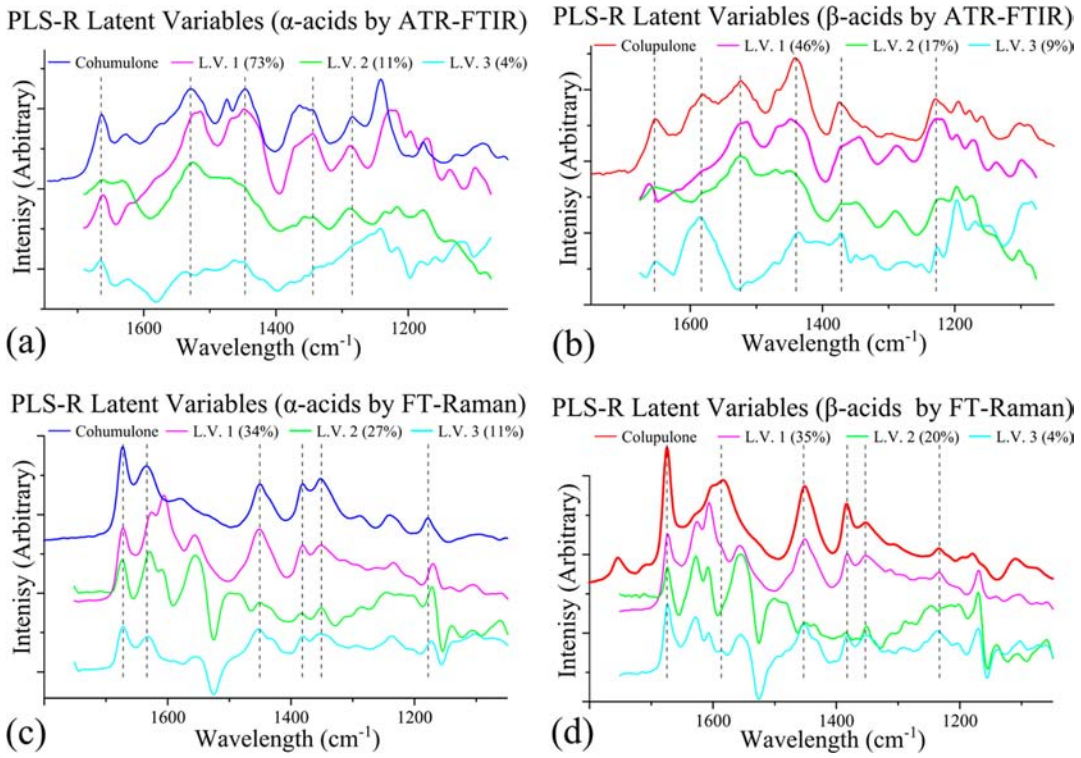


**Figure 4.** Overlay of spectral profiles of the pure bitter acids with latent variables from the Raman and IR PLS-R models predicting $\alpha$-acids (a and b) and $\beta$-acids (c and d) by UV spectrophotometry. Traces are scaled for ease of comparison. Dashed lines highlight discussed bands.

but that the variation in lupulin content between hops varieties confounded this correlation.[39] The key quality indicators for breeding selections, that is, total $\alpha$-acids, total bitter acids ($\alpha$ plus $\beta$), and cohumulone concentrations, were strongly correlated to one another. The correlations for the HPLC results were: total $\alpha$-acids versus total bitter acids, $r^2$ = 0.95; total $\alpha$-acids versus cohumulone, $r^2$ = 0.82. The $\alpha$-acids were the main bitter acids in most hops varieties, and the proportion of cohumulone in the $\alpha$-acids was 17−40% in these varieties (Figure 2).

**Vibrational Spectroscopic Analyses.** These same 139 hops samples were analyzed by the different vibrational spectroscopy techniques of IR, Raman, and NIR (two instruments) to assess which was best suited to the application of rapid screening of bittering hops. PLS-R models were generated, which related spectral matrixes to each of the UV and HPLC reference data, and these models were categorized using the ratio of prediction to deviation (RPD) methodology described by Williams (Table 1).[40] "Prediction" refers to the standard error of prediction (SEP) of the test-set values predicted by the calibration model, and "deviation" refers to the standard deviation of the corresponding reference data. The scale is used to broadly categorize PLS-R models by their fitness for purpose and was useful for our data set, which contained an unwieldy number of models with a large range of performances. The RPD scale defines models with values of $\geq$ 3.1 as suitable for quantitative screening applications.[40] Details of hops models that met this criterion are shown in Table 1. These models predicted the concentrations of the most important chemical values for breeding selections, that is, total $\alpha$-acids, cohumulone, total bitter acids ($\alpha$ plus $\beta$), and the bioactive xanthohumol. Results from the other models can be found in the Supporting Information (Table S1).

The RPD values (Table 1) showed that spectra from all three vibrational spectroscopy techniques could be used to predict total $\alpha$-acids and total bitter acids as determined by industry standard UV analyses. However, the portable NIR analysis, which had a RPD value of 3.0 for total $\alpha$-acids, fell just short of the suitability criterion. The spectroscopic techniques could also be used to predict total $\alpha$-acids and total bitter acids as determined by HPLC analyses, with the exception of the IR models, which fell short of the criterion. The IR spectra could be used to predict concentrations of the minor $\alpha$-acid cohumulone, as could Raman spectra, but NIR spectral analyses failed (Tables 1 and S1).

We had expected that xanthohumol would be readily quantifiable by Raman spectroscopy as the compound was predicted to show strong Raman scattering. However, the RPD values suggested that both Raman and IR spectra would not be appropriate for quantitative analysis (Table 1), which highlights the difficulty of predicting which vibrational spectroscopic technique will be most suitable and illustrates how different vibrational techniques can be appropriate for different analytes. Models that predict total and individual $\beta$-acids failed for all spectroscopic techniques (RPD values 1.0−2.4), but these components are not considered critical for the screening of hops varieties (Table S1, Supporting Information).

**Assignment of IR and Raman Spectra of Bitter Acids and Xanthohumol.** DFT calculations were used to predict the optimized geometries of cohumulone, colupulone, and xanthohumol. The predicted IR and Raman vibrational modes were compared to the experimental IR (Figure 3a) and Raman (Figure 3b) spectra of cohumulone and colupulone. Calculated values were in good agreement with the experimental, with a mean absolute deviation value of 13 $cm^{-1}$ for the assigned bands.

Most of the IR spectral differences occurred in the region from 1700−1000 $cm^{-1}$ (Figure 3a). The ring carbonyl band occurred at 1663 $cm^{-1}$ in cohumulone and at 1652 $cm^{-1}$ in colupulone. These were in good agreement with the DFT calculations, which predicted the bands at 1663 and 1660 $cm^{-1}$, respectively. A medium-intensity band was observed as a shoulder in cohumulone at 1579 $cm^{-1}$, and an equivalent colupulone band was observed at 1581 $cm^{-1}$. These bands were assigned to the keto−enol carbonyl stretching vibration, predicted at 1603 and 1608 $cm^{-1}$ for cohumulone and colupulone, respectively. The relatively low frequencies of these carbonyl bands were consistent with previous vibrational spectroscopic and DFT studies performed on compounds bearing similar intramolecularly hydrogen-bonded groups.[41,42] The intense band at ∼1525 $cm^{-1}$ in both compounds was due to a conjugated mode that involved large displacement of the intramolecularly bonded proton. Lastly, a number of overlapping C−H bending modes gave rise to a strong band at ∼1440 $cm^{-1}$ in both compounds.

Selected regions of the Raman spectra of cohumulone and colupulone are shown in Figure 3, panel b. The prenyl alkene stretching vibration at 1674 ± 1 $cm^{-1}$ was prominent in the spectra of both compounds (predicted at 1681 ± 1 $cm^{-1}$). The cohumulone and colupulone spectra deviated from one another in the region from 1660−1500 $cm^{-1}$ (Figure 3b). Four bands were predicted for each compound in this region with variable intensities. The vibrations are complex and involve displacement throughout the conjugated backbones of the molecules. The bands were loosely assigned at their maxima as diene stretches. The predicted spectrum of the colupulone tautomer (T2) (Figure 1) had no intense vibrational modes in this region, which implied that the lower energy (T1) structure (Figure 1) was abundant in the solid state of the compound. This was consistent with a published crystal structure.[35] The other noteworthy bands in the Raman spectra occurred at 1452, 1383, and 1352 $cm^{-1}$ in both cohumulone and colupulone. These were in good agreement with the calculations for overlapping C−H twisting, wagging, and bending modes.

**IR PLS-R Models Predicting UV Reference Data.** The PLS-R models that predicted total $\alpha$- and $\beta$-acid concentrations (by UV) from IR and Raman spectral data were interpreted visually by comparing the first three LVs of each model to the relevant bitter acid spectra (Figure 4). When a LV is similar to spectra of the pure compound, this implies that the model is spectrally meaningful, but when the LVs no longer contain the features of the analyte, the model may no longer be extracting spectrally relevant information, and overfitting becomes a consideration.[43] This approach complements the standard approach for model interpretation based on statistical data, that is, the validation data (Tables 1 and S1).

In Figure 4, panel a, the IR spectrum of cohumulone is overlaid with the first three LVs from the PLS-R model for $\alpha$-acids by IR spectroscopy. The first LV explained 73% of the reference value variance and was almost identical to the profile of cohumulone—a sure indication of effective modeling. Successive LVs described less variance and deviated increasingly from the spectrum of the pure compound. In Figure 4, panel b, LVs from the IR $\beta$-acids models are overlaid with colupulone. In this case, the first LV did not mimic the colupulone spectrum and explained only 46% of the reference data variance. In particular, one of the key lupulone bands, at 1580 $cm^{-1}$, was almost absent, which made the profile more similar to that of cohumulone. Subsequent LVs related more specifically to $\beta$-acid concentrations and the third LV, which explained 9% of the variance in the reference data, had high loading coefficients around 1580 $cm^{-1}$. This inspection of LVs implied that the $\alpha$-acids, which were nearly always present in greater concentrations (Figure 2), were interfering with chemometric quantitation of $\beta$-acids, which explains the poor performance of these models (Table S1, Supporting Information).

**Raman PLS-R Models Predicting UV Reference Data.** The Raman PLS-R LVs are compared to the relevant IR and Raman spectra in Figure 4, panels c and d. The first LV in the $\alpha$-acid model had high loading coefficients around 1673, 1452, 1382, and 1352 $cm^{-1}$ (Figure 4c). These bands were all observed in the spectrum of cohumulone (Figure 3b), which suggests that the model was extracting spectrally relevant data. However, the first LV also had high loading coefficients around 1608 and 1626 $cm^{-1}$ that were not observed in the spectrum of cohumulone (Figure 3b). Xanthohumol, the conjugated chalcone responsible for the yellow color of lupulin (Figure 1), had intense Raman bands at both of these frequencies (Figure 5) and was present in the hops samples at concentrations ranging from 0.13−0.85% (by HPLC, Figure 2). Despite its relatively low concentration, the contribution of xanthohumol to the Raman spectrum of hops was pronounced due to the large and highly polarizable $\pi$-conjugated system that makes the compound extremely Raman active (Figure 1). The relative intensities of xanthohumol and cohumulone (intensity ×10) are shown in Figure 5 and highlight the extreme Raman activity of the bioactive chalcone. Figure 5 also shows the vibrational displacement vectors of the most intense xanthohumol bands, which highlights the complexity and delocalization of these vibrations.

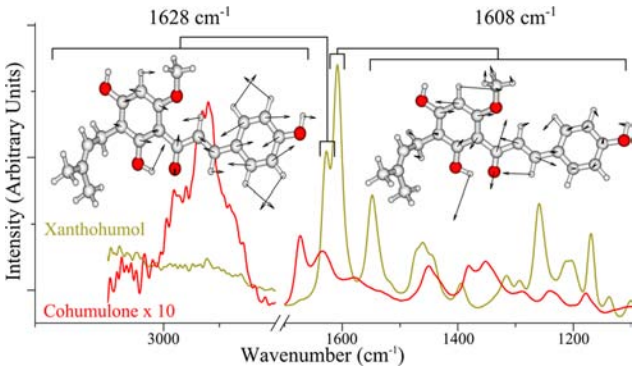


**Figure 5.** Raman spectra of xanthohumol and cohumulone (intensity ×10) with the DFT predicted vibrational displacement vectors of the most intense xanthohumol modes inset (lengths of arrows are proportional to predicted displacements).

After initial studies, it was feared that these intense xanthohumol bands would interfere with PLS-R models and prohibit the use of Raman spectroscopy for the analysis of hops bitter acids. This did not prove to be the case, as evidenced by the performance metrics in Table 1. This was not altogether surprising given the fact that xanthohumol concentrations were correlated to $\alpha$-acids ($r^2$ = 0.68) and total bitter acids ($r^2$ = 0.73). In the case of $\beta$-acids models, xanthohumol had a more detrimental effect since concentrations of these components were poorly correlated to one another ($r^2$ = 0.46). This, in tandem with the interfering $\alpha$-acids, which were more concentrated in nearly all varieties, could explain the poor

performance of the Raman PLS-R models for β-acids (Table S1, Supporting Information).

We have shown that NIR, IR, and Raman spectroscopy could be used to quantitatively screen for the key hops components α-acids, total bitter acids, and cohumulone. It has also been shown that portable NIR technology could be used for this purpose. Some of the limitations of these techniques are also reported, including the fact that quantitation of β-acids is unlikely to be achieved using this approach. Although some analytical challenges have been overcome using "fused" spectroscopic data sets,[30,44] our preliminary investigation suggested that this approach did not improve the performance of the reported models. The spectroscopic techniques required less sample preparation and, in most cases, greatly reduced analysis times compared to traditional analyses. Solvent use was also eliminated. Some vibrational features of cohumulone, colupulone, and xanthohumol have been assigned. Finally, the PLS-R LVs have been related to the pure spectra of the compounds for which they predict, which allows for a more insightful appraisal of the generated PLS-R models.

## ■ ASSOCIATED CONTENT

### Supporting Information

PLS-R model summaries (all models). This material is available free of charge via the Internet at http://pubs.acs.org.

## ■ AUTHOR INFORMATION


### Corresponding Author

*E-mail: Nigel.Perry@plantandfood.co.nz. Phone: +64 3 4798354.



### Funding

This research was supported by a University of Otago Doctoral Scholarship in collaboration with Plant and Food Research Capability Funding.


### Notes

The authors declare no competing financial interest.

## ■ ACKNOWLEDGMENTS

We thank R. Rushton Green, L. Graham, D. Graham, and C. Sansom for their technical assistance and O. Watkins and E. Burgess for their advice.

## ■ REFERENCES


(1) Neve, R. A. *Hops*; Chapman and Hall: London, 1991.

(2) Malowicki, M. G.; Shellhammer, T. H. Isomerization and degradation kinetics of hop (*Humulus lupulus*) acids in a model wort-boiling system. *J. Agric. Food Chem.* **2005**, *53*, 4434−4439.

(3) Stevens, J. F.; Page, J. E. Xanthohumol and related prenylflavonoids from hops and beer: To your good health! *Phytochemistry* **2004**, *65*, 1317−1330.

(4) Zanoli, P.; Zavatti, M. Pharmacognostic and pharmacological profile of *Humulus lupulus* L. *J. Ethnopharmacol.* **2008**, *116*, 383−396.

(5) Molyneux, R. J.; Wong, Y. Nuclear magnetic resonance spectroscopic determination of α- and β-acid homolog composition in hops. *J. Agric. Food Chem.* **1975**, *23*, 1201−1204.

(6) Intelmann, D.; Haseleu, G.; Hofmann, T. LC−MS/MS quantitation of hop-derived bitter compounds in beer using the ECHO technique. *J. Agric. Food Chem.* **2009**, *57*, 1172−1182.

(7) Hughes, P. The significance of iso-α-acids for beer quality—Cambridge prize paper. *J. Inst. Brew.* **2000**, *106*, 271−276.

(8) Beatson, R.; Ansell, K.; Graham, L. Breeding, development, and characteristics of the hop (*Humulus lupulus*) cultivar "Nelson Sauvin". *N. Z. J. Crop Hortic. Sci.* **2003**, *31*, 303−309.

(9) American Society of Brewing Chemists. *Hops 14. α-Acids and β-Acids in Hops and Hop Extracts by HPLC (International Method)*. http://methods.asbcnet.org/summaries/hops-14.aspx, 2010 (accessed 17 December 2014).

(10) American Society of Brewing Chemists. *Hops 6. α-Acids and β-Acids in Hops and Hop Pellets by Spectrophotometry and by Conductometric Titration*. http://methods.asbcnet.org/summaries/hops-6.aspx, 2010 (accessed 17 December 2014).

(11) European Brewery Convention. *EBC 7.7 Alpha- and Beta-acids in hops and hop products by HPLC*; Brussels, Belgium, 2010.

(12) Holtzel, A.; Schlotterbeck, G.; Albert, K.; Bayer, E. Separation and characterisation of hop bitter acids by HPLC−H-1 NMR coupling. *Chromatographia* **1996**, *42*, 499−505.

(13) Hoek, A. C.; Hermans-Lokkerbol, A. C. J.; Verpoorte, R. An improved NMR method for the quantification of α-acids in hops and hop products. *Phytochem. Anal.* **2001**, *12*, 53−57.

(14) Pusecker, K.; Albert, K.; Bayer, E. Investigation of hop and beer bitter acids by coupling of high-performance liquid chromatography to nuclear magnetic resonance spectroscopy. *J. Chromatogr., A* **1999**, *836*, 245−252.

(15) Halsey, S. A. Near-infrared reflectance analysis of whole hop cones. *J. Inst. Brew.* **1987**, *93*, 399−404.

(16) Axcell, B.; Tulej, R.; Murray, J. The determination of alpha-acids and moisture by near-infrared reflectance spectroscopy. *Brew. Dig.* **1981**, *41*, 18−19.

(17) Garden, S. W.; Pruneda, T.; Irby, S.; Hysert, D. W. Development of near-infrared calibrations for hop analysis. *Am. Soc. Brew. Chem.* **2000**, *58*, 73−82.

(18) Foley, W. J.; McIlwee, A.; Lawler, I.; Aragones, L.; Woolnough, A. P.; Berding, N. Ecological applications of near-infrared reflectance spectroscopy—A tool for rapid, cost-effective prediction of the composition of plant and animal tissues and aspects of animal performance. *Oecologia* **1998**, *116*, 293−305.

(19) Carron, K.; Cox, R. Qualitative analysis and the answer box: A perspective on portable Raman spectroscopy. *Anal. Chem.* **2010**, *82*, 3419−3425.

(20) Van Vuuren, J.; Meyer, J.; Claassens, A. Potential use of near-infrared reflectance monitoring in precision agriculture. *Commun. Soil Sci. Plant Anal.* **2006**, *37*, 2171−2184.

(21) Killeen, D. P.; Sansom, C. E.; Lill, R. E.; Eason, J. R.; Gordon, K. C.; Perry, N. B. Quantitative Raman spectroscopy for the analysis of carrot bioactives. *J. Agric. Food Chem.* **2013**, *61*, 2701−2708.

(22) Baranska, M.; Schulz, H.; Siuda, R.; Strehle, M. A.; Rosch, P.; Popp, J.; Joubert, E.; Manley, M. Quality control of *Harpagophytum procumbens* and its related phytopharmaceutical products by means of NIR-FT-Raman spectroscopy. *Biopolymers* **2005**, *77*, 1−8.

(23) Baranska, M.; Schulz, H.; Joubert, E.; Manley, M. In situ flavonoid analysis by FT-Raman spectroscopy: Identification, distribution, and quantification of aspalathin in green rooibos (*Aspalathus linearis*). *Anal. Chem.* **2006**, *78*, 7716−7721.

(24) Schonbichler, S. A.; Bittner, L. K. H.; Pallua, J. D.; Popp, M.; Abel, G.; Bonn, G. K.; Huck, C. W. Simultaneous quantification of verbenalin and verbascoside in *Verbena officinalis* by ATR-IR and NIR spectroscopy. *J. Pharm. Biomed. Anal.* **2013**, *84*, 97−102.

(25) Santos, J. R.; Sarraguça, M. C.; Rangel, A. O.; Lopes, J. A. Evaluation of green coffee beans quality using near-infrared spectroscopy: A quantitative approach. *Food Chem.* **2012**, *135*, 1828−1835.

(26) Geladi, P.; Kowalski, B. R. Partial least-squares regression—A tutorial. *Anal. Chim. Acta* **1986**, *185*, 1−17.

(27) Wold, S.; Sjöström, M.; Eriksson, L. PLS-regression: A basic tool of chemometrics. *Chemom. Intell. Lab. Syst.* **2001**, *58*, 109−130.

(28) Perez-Marin, D.; Garrido-Varo, A.; Guerrero, J. Non-linear regression methods in NIRS quantitative analysis. *Talanta* **2007**, *72*, 28−42.

(29) Zhang, X.; Li, W.; Yin, B.; Chen, W.; Kelly, D. P.; Wang, X.; Zheng, K.; Du, Y. Improvement of near-infrared spectroscopic (NIRS) analysis of caffeine in roasted Arabica coffee by variable selection method of stability competitive adaptive reweighted sampling (SCARS). *Spectrochim. Acta., Part A* **2013**, *114*, 350−356.

(30) Khaleghi, B.; Khamis, A.; Karray, F. O.; Razavi, S. N. Multisensor data fusion: A review of the state-of-the-art. *Inf. Fusion* **2013**, *14*, 28−44.
(31) Chadwick, L. R.; Nikolic, D.; Burdette, J. E.; Overk, C. R.; Bolton, J. L.; van Breemen, R. B.; Frohlich, R.; Fong, H. H. S.; Farnsworth, N. R.; Pauli, G. F. Estrogens and congeners from spent hops (*Humulus lupulus*). *J. Nat. Prod.* **2004**, *67*, 2024−2032.
(32) Andersson, M. P.; Uvdal, P. New scale factors for harmonic vibrational frequencies using the B3LYP density functional method with the triple-ζ basis set 6-311 + G (d, p). *J. Phys. Chem. A* **2005**, *109*, 2937−2941.
(33) Clarke, T. M.; Gordon, K. C.; Officer, D. L.; Hall, S. B.; Collis, G. E.; Burrell, A. K. Theoretical and spectroscopic study of a series of styryl-substituted terthiophenes. *J. Phys. Chem. A* **2003**, *107*, 11505−11516.
(34) Scott, A. P.; Radom, L. Harmonic vibrational frequencies: An evaluation of Hartree−Fock, Møller−Plesset, quadratic configuration interaction, density functional theory, and semiempirical scale factors. *J. Phys. Chem.* **1996**, *100*, 16502−16513.
(35) Archer, R. P.; Tyrrell, E.; Singh, K. Colupulone. *Acta Crystallogr., Sect. E: Struct. Rep. Online* **2007**, *63*, o1511−o1512.
(36) Barnes, R. J.; Dhanoa, M. S.; Lister, S. J. Standard normal variate transformation and detrending of near-infrared diffuse reflectance spectra. *Appl. Spectrosc.* **1989**, *43*, 772−777.
(37) Snee, R. D. Validation of regression models: Methods and examples. *Technometrics* **1977**, *19*, 415−428.
(38) Krofta, K. Comparison of quality parameters of Czech and foreign hop varieties. *Plant Soil Environ.* **2003**, *49*, 261−268.
(39) Likens, S.; Nickerson, G.; Haunold, A.; Zimmermann, C. Relationship between alpha acids, beta acids, and lupulin content of hops. *Crop Sci.* **1978**, *18*, 380−386.
(40) Williams, P. C. Variables affecting near-infrared reflectance spectroscopic analysis. In *Near-Infrared Technology in the Agriculture and Food Industries*; Hill, L., Ed.; Am. Cereal Assoc. Cereal Chem.: St. Paul, MN, 1987; Vol. 2, pp 145−169.
(41) Teslova, T.; Corredor, C.; Livingstone, R.; Spataru, T.; Birke, R. L.; Lombardi, J. R.; Canamares, M. V.; Leona, M. Raman and surface-enhanced Raman spectra of flavone and several hydroxy derivatives. *J. Raman Spectrosc.* **2007**, *38*, 802−818.
(42) Galasso, V. Probing the molecular and electronic structure of the lichen metabolite usnic acid: A DFT study. *Chem. Phys.* **2010**, *374*, 138−145.
(43) Hawkins, D. M. The problem of overfitting. *J. Chem. Inf. Comput. Sci.* **2004**, *44*, 1−12.
(44) Biancolillo, A.; Bucci, R.; Magrì, A. L.; Magrì, A. D.; Marini, F. Data fusion for multiplatform characterization of an Italian craft beer aimed at its authentication. *Anal. Chim. Acta* **2014**, *820*, 23−31.

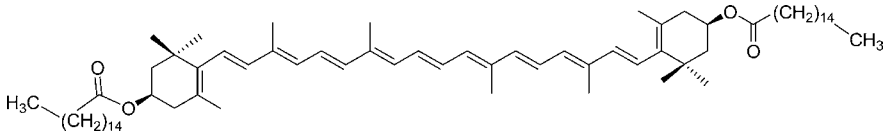

Figure 1. Structure of zeaxanthin dipalmitate.

was to develop a quality control method for goji berry that could be applied in the industry to give fast and reliable results.

## MATERIALS AND METHODS

**Fruits and Sample Preparation.** Nine commercial samples of dried fruits of *L. barbarum* were used (S1−S9) along with five juices (S10−S15) and one jam (S16). Samples S1−S3 were of Chinese origin (S1-Shroeger, lot 950276; S2-Hebei Meiwei Chinese Herb, lot 110313; S3-Shenzhou, lot 0040, art. no MEDBOOM 30177; S4−S9 were purchased on the Italian market (herbalists'shops, pharmacies, supermarkets) and consisted of the entire dried fruits. The juices (samples S10−S15) were concentrated juice obtained from the fresh fruits and in some cases with the addition of other juices (pear, acer, etc.).

**Optimized Extraction of Carotenoids from the Dried Fruit.** Ten grams of each sample of goji was weighed and ground with a mortar and pestle in liquid $N_2$. Approximately 500 mg of the ground fruits was ultrasonicated with 50 mL of distilled water for 15 min. The sample was centrifuged, and the supernatant was discarded. The samples were washed with 20 mL of absolute ethanol and centrifuged, and the supernatant was again discarded. The residue was ultrasonicated for 15 min with 20 mL of hexane/acetone 50:50 and centrifuged, and the supernatant was collected. The procedure was repeated until the supernatant remained colorless (four to five times in total). The extracts were combined, concentrated partially under vacuum (at 20 °C), and adjusted to 50.0 mL using hexane/acetone 40:60. The solutions were filtered and immediately injected.

**Extraction of Carotenoids from Juices.** Ten milliliters of a well-shaken juice was added in a volumetric flask of 50 mL, and the volume was adjusted with distilled water. Two milliliters of this solution was transferred to a separator funnel, a small quantity of NaCl was added, and the aqueous phase was extracted with hexane/EtOAc until the upper layer was colorless (three to five times, depending on the sample). Extracts were combined, concentrated partially under vacuum (at 20 °C), and adjusted to 10.0 mL using hexane/acetone 40:60. The samples were filtered and immediately injected.

**Chemicals.** All solvents used for HPLC analysis were of HPLC grade; $CH_3CN$ and MeOH for HPLC were purchased from Sigma-Aldrich (Amersham, Sweden). Water was purified by a Milli-Qplus system from Millipore (Bedford, MA, USA). All laboratory chemicals used in this study in the isolation protocol were of reagent grade. Sephadex LH-20 was purchased from Sigma-Aldrich. The Sep Pak C18 cartridge (Vac35 $cm^3$) was from Waters (Milford, MA, USA). Nylon filters (0.45 $\mu$m pore size) were from Agilent (Agilent Technologies, Palo Alto, CA, USA).

**Standards.** $\beta$-Carotene (98% purity) was purchased from Extrasynthèse (Genay, France). About 5 mg of $\beta$-carotene was accurately weighed and dissolved in 25 mL of hexane 100%. This stock solution was kept at −20 °C. A series of dilutions was prepared in acetone 100% each time immediately before analysis.

**Preparation of Zeaxanthin Dipalmitate Enriched Extract and Isolation of Zeaxanthin Dipalmitate (Figure 1).** The above-described extraction scheme was employed using a higher amount of herbal drug (5−10 g). The extract was subjected to size exclusion chromatography on Sephadex LH-20 (15 × 3 cm) using MeOH/acetone 50:50 as elution solvent and afforded 10 fractions. Fractions were monitored using HPLC-DAD and combined accordingly. The fraction containing zeaxanthin dipalmitate was then subjected to a fast RP column chromatography on Sep Pak using mixtures of acetone/MeOH of descending polarity. The fraction obtained with 70% acetone contained zeaxanthin dipalmitate 85% pure. This fraction was used to perform the precision and accuracy of the HPLC method. The zeaxanthin dipalmitate enriched extract was obtained as above without the use of Sep Pak. Fractions containing zeaxanthin dipalmitate were combined to afford the enriched extract. This extract was used to estimate the accuracy of the overall method, as matrix spike. The protocol described above was fast to ensure minimum exposure of the carotenoid to light and heat.

**Instrumentation.** The centrifuge used was a Hermle Labortechnik Z323 K operating at 5 °C, and 5000 rpm. A Bandelin Sonorex RK 100 H (Germany) sonicator was operated at a medium operating frequence of 35 kHz.

**HPLC-DAD-MS Analysis Instrumentation.** Analysis was carried out using an Agilent 1200 liquid chromatograph equipped with a DAD detector and an Agilent 6410 triple-quadrupole equipped with dual mode APCI-electrospray source operated in APCI mode and managed by Masshunter software (Agilent Technologies). The column was a Luna RP-C18 (150 mm × 4.6 mm) with a particle size of 5 $\mu$m (Phenomenex) maintained at 20 °C. An isocratic system was used, acetone/MeOH 55:45 (v/v) with a flow rate of 1.4 mL/min. After the DAD detector, the flow was split 1:4 to meet the flow requirements for maximal sensitivity of the dual mode source. The injected volume of the samples was 5 $\mu$L. The UV−vis spectra were recorded between 220 and 650 nm, and the chromatographic profiles were registered at 350, 430, 450, and 480 nm. Carotenoids were detected by positive ionization mode, scan spectra from $m/z$ 100 to 1500; fragmentors were 135 and 200 V, gas temperature was 350 °C, nitrogen flow rate was 12 L/min, nebulizer pressure was 30 psi, quadrupole temperature was 100 °C, and corona needle voltage was 4000 V.

**Linearity, LOD, LOQ, Precision, and Accuracy of the HPLC Method.** The linearity range of responses of the standard was determined on six concentration levels with three injections for each level. Calibration graphs for HPLC were recorded with sample amounts ranging from 2.6 ng to 0.35 $\mu$g. Stock solutions of the standards (LOQ included) were prepared at different concentrations ranging from $0.18 \times 10^{-3}$ $8.9 \times 10^{-3}$ mg/mL and were injected into HPLC (injection volumes varying from 2 to 20 $\mu$L). The limits of detection (LOD) and quantification (LOQ) under the chromatographic conditions were determined by injecting a series of standard solutions until the signal-to-noise (S/N) ratio was 3 for LOD and 10 for LOQ. To evaluate the repeatability of the HPLC method on real sample (S3 sample), extracts were analyzed at three different concentration levels (200, 100, and 50%) in the range of the calibration curve. For the intraday variability test, the sample was analyzed in six replicates within 1 day. For the interday variability test, the sample was examined in triplicate for three consecutive days. The contents of zeaxanthin dipalmitate were evaluated to calculate the relative standard deviation (RSD). For the accuracy test of the HPLC method, the spiking method was applied. A known amount of freshly prepared standard solution (zeaxanthin dipalmitate of 85% purity) in three different concentration levels (in the range of the calibration curve) was added into a certain amount of sample. The samples were measured in triplicates, and the amount of the standards added was calculated by subtraction (in total, 12 injections).

**Precision and Accuracy of the Overall Method (Including Extraction Process).** To check the repeatability of the method over a broad range of concentrations, amounts of herbal drug corresponding to 150 100, and 50% (750, 500, and 250 mg) of the expected analyte were analyzed. Six different extracts for each concentration level were prepared according to the method described above and injected twice in the HPLC. The mean, standard deviation, and relative standard deviation were calculated on the basis of zeaxanthin dipalmitate. Results are expressed as RSD. For the accuracy study of the overall

method the recovery experiment was modified as described previously in the literature.[18] As the amount of the purified zeaxanthin dipalmitate was too little to perform this analysis, an enriched extract was prepared and used as a matrix spike solution. Different stock solutions of this extract were prepared and added (2, 1 mL) to 500 mg of herbal drug in to obtain three different concentration levels (120, 140, and 200%) of the main analyte. Samples were left for a few minutes under $N_2$ to dry and were extracted according to the method. Extractions were repeated three times for each concentration level, and samples were injected twice. Results are presented in Table 4.

**Qualitative and Quantitative Determination of Zeaxanthin Dipalmitate.** Identification of zeaxanthin dipalmitate was done by HPLC-APCI-MS ($m/z$ 1045.8 $[M + H]^+$, 789.6 $[M -$ palmitoyl $+ H]^+$). Due to the presence of triglycerides in the fruits, suppression of the ionization was observed in the positive ion mode.[19] For the quantitative determination of zeaxanthin dipalmitate, the method of external standard was applied using $\beta$-carotene as standard. The regression curve was obtained by measuring each point in triplicate. Measurements were performed at 450 nm, which is the maximum absorbance for $\beta$-carotene and zeaxanthin dipalmitate. Results were adjusted using a molecular weight correction factor (molecular weight of zeaxanthin dipalmitate 1045.8 vs 536.8 for $\beta$-carotene).

## RESULTS AND DISCUSSION

The fruits of *L. barbarum* have been the subject of many phytochemical and analytical investigations, which have given evidence to a wide variety of secondary metabolites and nutritive elements. Besides polysaccharides, which are responsible for the significant nutritive value and antioxidant activity of goji berry,[4−6] the fruits contain glycerogalactolipids, carotenoids, simple phenolics, flavonoids, and considerable amounts of vitamins, most importantly vitamin C.[15,20,21] Furthermore, the fruit contains free amino acids and especially nonproteinogenic amino acids such as taurine, $\gamma$-aminobutyric acid, and betaine.[2,22] Taurine has been claimed to be responsible for the protective role of goji berry on diabetic retinopathy.[23] All of these groups of constituents cover a wide range of polarity and molecular weight so as to require analytical methods specific for each case. Several analytical protocols have been developed accordingly, which include classic phytochemical separations, enzymatic hydrolysis, HPLC-UV-MS, capillary electrophoresis, size exclusion chromatography, thin layer densitometry characterization by NMR, and IR.[4,5,8,9,15,20−22] A literature survey makes evident that quality control of the fruit cannot be achieved by a single analytical protocol. The methodology described in the current study targeted the carotenoids and especially zeaxanthin dipalmitate. The solvent system used was specific for the extraction of this type of constituent, and other types of constituents were not extracted as observed in our analyses.

**Development of the HPLC Methodology.** Preliminary analyses of the *L. barbarum* fruit nonpolar extracts (hexane/acetone 50:50) showed the predominance of one main constituent, which was identified by its UV and MS data as zeaxanthin dipalmitate. By applying the normalization method at 450 nm, the content of zeaxanthin dipalmitate was estimated to be >80% of total carotenoids. Therefore, the developed assay was based solely on this active/marker constituent.

A typical C18 column was chosen (Luna, 150 × 4.6 mm, 5 $\mu$m) with spherical particles, end-capped, and high carbon load. Due to the nonpolar nature of the main metabolite, mixtures of methanol/acetonitrile or acetonitrile 100% did not provide adequate elution strength. An isocratic mixture of acetone/MeOH 55:45 instead resulted in a well-separated peak of zeaxanthin dipalmitate and afforded pseudomolecular ion in the HPLC-MS analysis. Due to the well-reported low stability of carotenoids, the temperature during the analysis was kept at 20 °C.

**Preparation of the Samples: Sampling−Grinding−Extraction.** Analysis of carotenoid presents many problems that are linked to the uneven distribution of carotenoids within the berry and nature of the matrix in the preparations, instability of carotenoids under light, high temperature, oxygen, metal exposure, and stability in the presence of solvents ($H_2O$, acetone, dichloromethane).[24] Generally, an extraction protocol should be fast and simple and respect the physical and chemical properties of the tested constituents. In the case of goji berry, besides the carotenoid instability, two other issues had to be taken into consideration: the gluey nature of the fruits, which makes their handling difficult, and the variability of the fruits in the same package in terms of different sizes and moisture levels. The first step of this study was to develop a practical and efficient method to overcome these problems.

Due to the gluey nature of the fruits, grinding is very difficult, and during any grinding process the temperature is increased and aggregates are afforded. Therefore, classical mill pulverization is not feasible, whereas a lyophilization step prior to milling does not resolve the problem. The use of a sieve to refine and homogenize the ground material is also not feasible due to the sticky behavior of the grinded pieces. Both methods were tested in our laboratory without success. Zhao et al.[17] described a method during which the fruits are ground together with silica gel micropowder or anhydrous sodium sulfate. This method, however, suffers from low repeatability. Peng et al.[16] succeeded in grinding the material after extraction with water and air-drying. This methodology was also excluded in the present paper due to the long total analysis time (not reported by the authors), which makes the assay not practical over a large number of samples. Instead, liquid $N_2$ with the use of a mortar and pestle was a fast way to reduce the material to smaller pieces of berry, maintaining the samples at low temperature, preserving carotenoids. With this method it is also possible to grind a higher amount of fruits (10 g or more), obtaining a representative and homogenized sample.

The next step was the choice of the most suitable extraction solvent and the method of extraction. Maceration with HEAT (hexane/ethanol/acetone/toluene 10:6:7:7, v/v/v/v) followed or not by saponification in one extraction cycle was reported in the literature.[15,17] When this method was performed in our laboratory without the saponification step, the material was not discolored, and further extraction steps afforded intense yellow extracts, suggesting that the carotenoid extraction is not complete. This extraction protocol along with the extraction solvent mixture was excluded because of the toxicity of toluene. Ultrasonication instead of the previously reported maceration[15,25] gave better results (extracts monitored by LC-UV). Ultrasonication is a fast and efficient way of extracting, favoring the penetration of solvent in plant tissues, and might be useful especially in the case of carotenoids, which are located inside the plant tissues. To avoid raising the temperature during ultrasonication, ice was added into the sonication bath.

Preliminary experiments with goji had shown that the main constituent, zeaxanthin dipalmitate, is more soluble in nonpolar organic solvents, such as petroleum ether and hexane. Therefore, the extraction protocol was designed aiming at the exhaustive extraction of this lipophilic compound. Previously described[24] solvent systems for carotenoids such as THF/methanol or ethanol 100% are not suitable for *L. barbarum*.

Mixtures with hexane such as ethanol/hexane 4:3 or combinations of partition between ethanol and hexane[26] were tested along with a series of mixtures of acetone/hexane and dioxane/hexane (0:100, 25:75, 50:50, 75:25, 100:0, respectively). Acetone is considered a good solvent for its capacity to penetrate the solid matrix and dissolve the range of carotenoids present in the samples. Indeed, mixtures of hexane/acetone gave better results than mixtures of dioxane/hexane. Among different mixtures of hexane/acetone, the best results (controlled by UV-DAD) were obtained using the combination 50:50. It is noteworthy that in all of these experiments no discoloration of the herbal drug was observed, indicating that the extraction was not exhaustive. This fact was attributed to the high content of polysaccharides in the fruits, which form a layer and do not favor the extraction of the carotenoids from the pericarp.[26] A step of ultrasonication with water prior to extraction with our solvent system removed efficiently the polysaccharides, and after four to five cycles of extraction (ultrasonication), the residue had become visually colorless as a sign of the exhaustive extraction of carotenoids (Supporting Information, Figure S1). At this point an additional extraction step was necessary to remove water and because mixtures of acetone/hexane are not miscible with water and carotenoids can be oxidized under humidity. To achieve this, acetone 100% and absolute ethanol were tested as suitable solvent. Six independent experiments were carried out using acetone or ethanol for the water removal, and the amounts of zeaxanthin dipalmitate were calculated. The repeatability of the extraction was better (<5%) when absolute ethanol was used, probably because this solvent removes water without solubilizing the nonpolar zeaxanthin dipalmitate. Quantification of the ethanol fractions obtained with this method showed only a small loss of zeaxanthin dipalmitate ranging from 0.05 to 0.1%.

Other issues taken into consideration during the preparation of the samples were evaporation of solvents in the rotary evaporator and the final adjustment of volume in the volumetric flask. Experiments were carried out in subdued light using amber glassware, and the evaporation was carried out at 20 °C to avoid degradation of carotenoids. Furthermore, the extracts were not evaporated to dryness to avoid adhesion of carotenoids on glassware, whereas the final adjustment of volume was done using hexane/acetone 40:60, instead of acetone 100%, as in this solvent degradation of carotenoids has been reported.[24] Indeed, degradation of zeaxanthin dipalmitate was observed on the second day (Figures S2 and S3 in the Supporting Information) when acetone 100% was used, whereas it remained stable after 1 week (in each case samples kept at 4 °C) when a mixture of hexane/acetone 40:60 was added in the volumetric flask, in complete accordance with Taungbodhitham et al.[27]

**Analysis of the Fruits.** Nine samples of goji fruits were analyzed for their content in zeaxanthin dipalmitate. Results are shown in Table 2. Quantitative differences among samples are linked to the status of conservation and time of harvest. On the basis of these results the mean content of zeaxanthin dipalmitate in fruits of goji is 0.3−0.4% compared to the 0.1−0.2% that is reported in the literature. This difference is attributed to the exhaustive extraction of carotenoids of the developed assay and confirms the method's efficiency. In all samples studied zeaxanthin dipalmitate represents >85% of the total carotenoid content. Quantitative results showed a big variance among investigated samples, which might be due to different sources of the fruits and different harvest times, manufacturing processes, and storage conditions.[28−30] Comparison of our results with those reported in the literature is also not feasible. Besides the variances of the samples, the methodology reported in the literature is completely different, aiming at the whole range of carotenoids, especially when saponification is applied. Nevertheless, from the results given in this study the high content of zeaxanthin dipalmitate in goji berry might be due to the efficient extraction.

According to our results, the amounts of zeaxanthin dipalmitate vary from 28 to 54 mg/10 g of edible portion. Compared to other fruits or vegetables of our daily diet,[31] it can be concluded that goji berry contains remarkable amounts of zeaxanthin dipalmitate and is a rich source of carotenoids. What is more important is that the esterified zeaxanthin has a better solubility and bioavailability in comparison to zeaxanthin alone.[32,33]

**Analysis of Products Based on Goji Berry.** Although the scope of this study was to develop a quality control assay for Fructus Lycii, other types of commercial samples were tested for comparison reasons. Because juices contained residues of the fruit, it was not feasible to filter the samples and inject them as such in the HPLC. Therefore, a small extraction (partition) using hexane/EtOAc was necessary to obtain a zeaxanthin dipalmitate fraction. HPLC analyses showed a great variability in the content of zeaxanthin dipalmitate among juices depending on the source or manufacturing process and probably from the addition of other juices (acer syrup, black cherry juice, pear juice, apple juice, carrot juice). As to the quality of the juices available in the market, some of them showed a high content of zeaxanthin dipalmitate, but the HPLC-DAD analyses clearly indicated that in the aqueous environment of the juice the main carotenoid was isomerized,

**Table 1. Calibration Equations, LOD, LOQ, and Repeatability Calibration Curve for β-Carotene**

| calibration eq | correl coeff | LOD (ng) | LOQ (ng) | repeatability (RSD %) ($n$ = 3) |
|---|---|---|---|---|
| $y = 0.0008x - 0.0052$ | 0.9986 | 0.87 | 2.6 | 0.0004 |

**Table 2. Amounts of Zeaxanthin Dipalmitate in Samples of Goji Berry ($n$ = 3)**

| sample | zeaxanthin dipalmitate,[a] % mg ± SD (RSD) | total carotenoids, % mg ± SD (RSD) | % of zeaxanthin dipalmitate in total carotenoids |
|---|---|---|---|
| S1 | 0.42 ± 0.01 (2.92) | 0.49 ± 0.02 (2.60) | 85 |
| S2 | 0.35 ± 0.01 (2.10) | 0.42 ± 0.01 (2.56) | 83 |
| S3 | 0.42 ± 0.02 (4.13) | 0.43 ± 0.03 (4.10) | 84 |
| S4 | 0.28 ± 0.01 (4.11) | 0.32 ± 0.01 (3.79) | 87.5 |
| S5 | 0.54 ± 0.01 (1.71) | 0.63 ± 0.03 (4.18) | 85.7 |
| S6 | 0.44 ± 0.01 (3.40) | 0.52 ± 0.01 (1.91) | 84.6 |
| S7 | 0.42 ± 0.02 (5.09) | 0.48 ± 0.02 (4.33) | 87.5 |
| S8 | 0.40 ± 0.01 (1.71) | 0.49 ± 0.01 (2.60) | 81.6 |
| S9 | 0.44 ± 0.01 (3.07) | 0.54 ± 0.02 (4.61) | 81.5 |

[a]Zeaxanthin dipalmitate expressed as β-carotene and after application of a molecular weight correction factor.

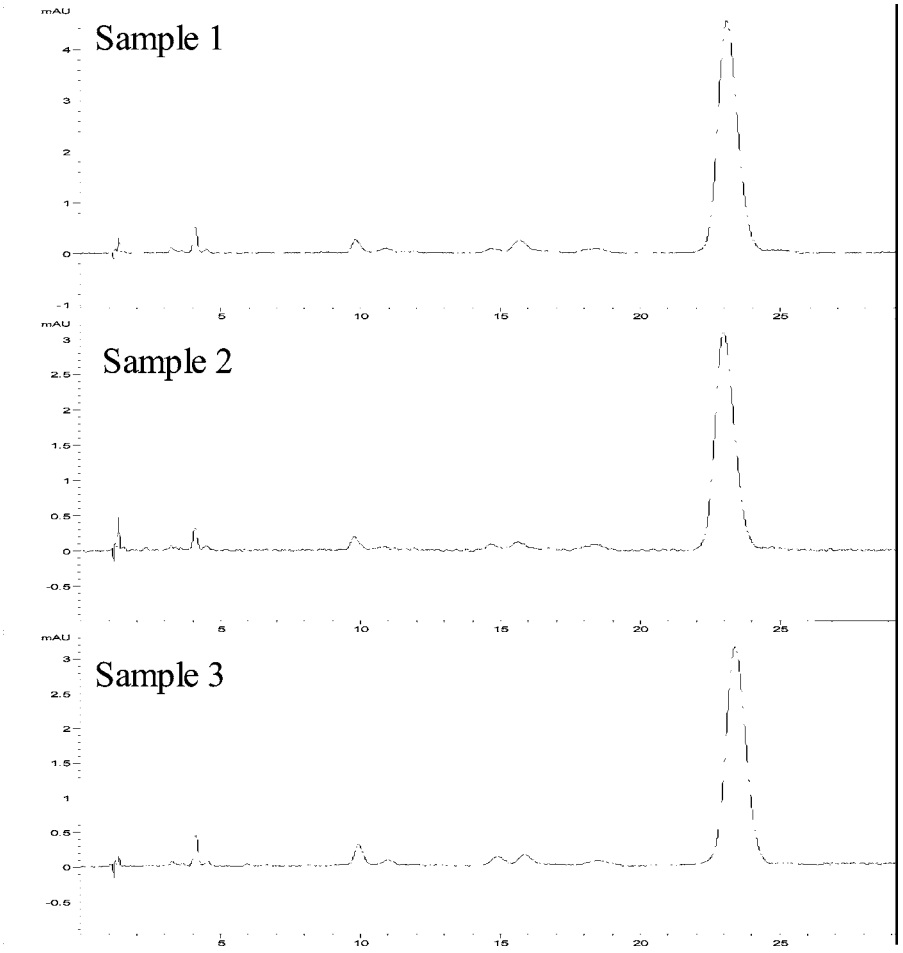


**Figure 2.** Representative chromatograms of the goji berry extracts (samples S1−S3) at 450 nm. Experimental conditions: column, Luna RP-C18 (150 × 4.6 mm); particle size, 5 $\mu$m (Phenomenex) at 20 °C; eluents, isocratic acetone/MeOH 55:45 (v/v); flow rate, 1.4 mL/min; injected volume, 5 $\mu$L solution. Zeaxanthin dipalmitate is the main carotenoid.

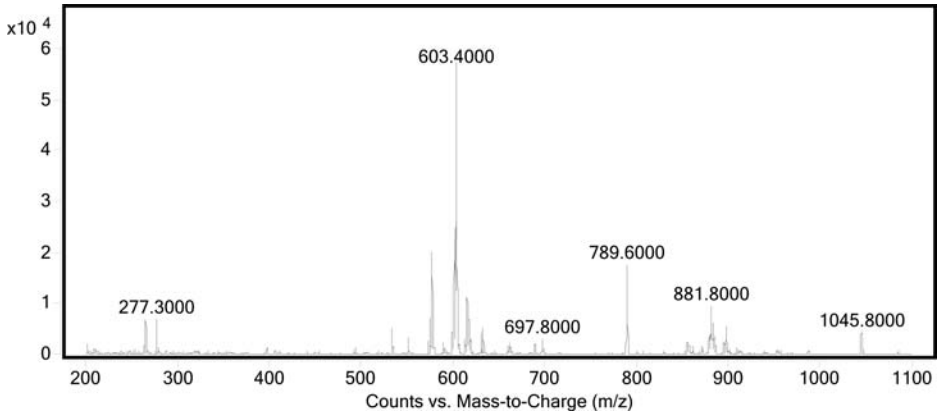


**Figure 3.** Mass spectra (APCI-positive mode) of zeaxanthin dipalmitate. Fragments 881.8 and 603.4 correspond to triglycerides. Fragments $m/z$ 1045.8 $[M + H]^+$ and 789.6 $[M - \text{palmitoyl} + H]^+$ correspond to zeaxanthin dipalmitate.

giving broad peaks in the chromatograms (Figure 2 and Supporting Information, Figure S4).

**Validation Data.** *Linearity, Repeatability on Real Sample, LOD, LOQ, Precision, and Accuracy of both HPLC and Overall Method.* The method had good linearity with $r^2$ value for zeaxanthin dipalmitate of 0.9986 (regression curve: $y = 0.0008x - 0.0052$) (Table 1). The repeatability on real sample was calculated on three individual extracts corresponding to nine different samples. Each was analyzed by HPLC, and the relative standard deviation (% RSD) of the contents of the major constituents was calculated (Table 2). RSD values ranged between 1.71 and 5.01%, 5.01% being calculated only in one sample. Although in some sample RSD values seem to be a little high (4−5%), this is still acceptable if the matrix is taken into consideration. Many of the packages tested had a heterogeneous aspect: fruits of different sizes and moisture

Table 3. Precision and Accuracy Data (HPLC Method) Based on Zeaxanthin Dipalmitate

| | precision, mean (% RSD) | | accuracy | | | |
|---|---|---|---|---|---|---|
| concn level | intraday ($n$ = 6) | interday ($n$ = 3) | added ($\mu$g) | found ($\mu$g) | recovery (%) | RSD (%, $n$ = 3) |
| 200% (1 g) | 0.34 ± 0.01 (0.72) | 0.34 ± 0.01 (0.34) | 0.0543 | 0.0518 | 95.38 | 0.34 |
| 100% (500 mg) | 0.34 ± 0.01 (0.53) | 0.35 ± 0.01 (1.97) | 0.0271 | 0.0278 | 102.26 | 0.42 |
| 50% (250 mg) | 0.36 ± 0.01 (0.64) | 0.35 ± 0.01 (1.52) | 0.0136 | 0.0136 | 99.98 | 1.83 |

Table 4. Precision and Accuracy Data of the Overall Method Based on Zeaxanthin Dipalmitate

| precision | | | | accuracy | | | |
|---|---|---|---|---|---|---|---|
| amount of herbal drug (%) | % mg ± SD | mean (RSD, %) ($n$ = 6) | concn level | added ($\mu$g) | found ($\mu$g) | recovery (%) | RSD (%, $n$ = 3) |
| 150 | 0.4151 ± 0.0160 | 3.86 | high (200%) | 4.2130 | 4.1730 | 99.11 | 1.21 |
| 100 | 0.4215 ± 0.0178 | 4.13 | medium (140%) | 1.6181 | 1.5362 | 94.94 | 1.92 |
| 50 | 0.4243 ± 0.0166 | 3.81 | low (120%) | 0.8426 | 0.9047 | 107.37 | 1.84 |

contents, factors that deeply affect the extraction yield.[26] More robust fruits contain more carotenoids, are well preserved (limited carotenoid loss during the manufacturing process), and have a moisture content that favors efficient extraction. Being highly lipophilic, carotenoids are distributed internally in the tissues. When the water content of the herbal drug is high, the tissues are softer, solvents penetrate more easily into the material, and the whole extraction process is simplified, affording a better and more repeatable result. Samples that had a better macroscopic aspect (bigger, more robust, or less dry) were those that gave the lowest RSD values.

The HPLC method was validated for intra- and interday variation using purified zeaxanthin dipalmitate at three different concentration levels (50, 100, and 200%) in six replicates for the intraday and in three replicates for the interday. For each concentration level mean, standard deviation and RSD were calculated. The accuracy of the HPLC method was also evaluated using the purified zeaxanthin dipalmitate solution, which was spiked to one sample with known content. RSD values were less than 0.72 and 1.97, respectively. Results are displayed in Table 3.

Finally, the overall method (extraction step included) was tested for repeatability (in six independent replicates) and for accuracy at three different concentration levels of the main analyte. Results are displayed in Table 4. The method afforded good repeatability with acceptable RSD (<5%). For the accuracy test a recovery experiment was carried out. It has been stated that the analyte added to a substrate may behave differently from an endogenous analyte, and because it is not protected by plant tissues, it may be more easily extracted, giving an artificially high recovery.[24] This is true in the case of goji berry, for which even after the removal of polysaccharides repeated extractions are needed to obtain a colorless material, indicating distribution of carotenoids in the internal parts of the tissues. In such cases a recovery experiment is of little importance, and it may serve only as a measure of losses (degradation) during analysis. With this concept, a recovery test was carried out at three different concentration levels. The values obtained were between 94 and 107% (with RSD values <2%), which are within the acceptable limits (80−120%) for matrix spike.

It is noteworthy that the assay is based solely on zeaxanthin dipalmitate, but it is very suitable as marker constituent for the quality assays because it represents ≥85% (based on our extraction method) of the total carotenoids, and there are numerous studies in the literature confirming the increased stability of esterified carotenoids compared to their free analogues.[34,35] Therefore, a quality control method based on this constituent provides consistent results. Furthermore, the isocratic system in the HPLC enables work with a single channel, and given the fact that the solvents employed are volatile, it permits a more stable and repeatable HPLC chromatogram throughout the whole analysis period.

## ■ ASSOCIATED CONTENT

### Supporting Information

Figures S1−S4. This material is available free of charge via the Internet at http://pubs.acs.org.

## ■ AUTHOR INFORMATION


### Corresponding Author

*(A.K.) E-mail: anastasiakarioti@yahoo.it.


### Notes

The authors declare no competing financial interest.

## ■ ACKNOWLEDGMENTS

We are grateful to the Mass Spectrometry Center, University of Florence − CISM for recording the HPLC-APCI mass spectra.

## ■ REFERENCES


(1) Potterat, O. Goji (*Lycium barbarum* and *L. chinense*): phytochemistry, pharmacology and safety in the perspective of traditional uses and recent popularity. *Planta Med.* **2010**, *76*, 7−19.

(2) Amagase, H.; Farnsworth, N. R. A review of botanical characteristics, phytochemistry, clinical relevance in efficacy and safety of *Lycium barbarum* fruit (goji). *Food Res. Int.* **2011**, *44*, 1702−1717.

(3) Adams, M.; Wiedenmann, M.; Tittel, G.; Bauer, R. HPLC-MS trace analysis of atropine in *Lycium barbarum* berries. *Phytochem. Anal.* **2006**, *17*, 279−283.

(4) Liang, B.; Jin, M.; Liu, H. Water-soluble polysaccharide from dried *Lycium barbarum* fruits: isolation, structural features and antioxidant activity. *Carbohydr. Polym.* **2011**, *83*, 1947−1951.

(5) Wu, H. T.; He, X. J.; Hong, Y. K.; Ma, T.; Xu, Y. P.; Li, H. H. Chemical characterization of *Lycium barbarum* polysaccharides and its inhibition against liver oxidative injury of high-fat mice. *Int. J. Biol. Macromol.* **2010**, *46*, 540−543.

(6) Gan, L.; Zhang, S. H.; Yang, X. L.; Xu, H. B. Immunomodulation and antitumor activity by a polysaccharide−protein complex from *Lycium barbarum*. *Int. Immunopharmacol.* **2004**, *4*, 563−569.

(7) Amagase, H.; Sun, B.; Borek, C. *Lycium barbarum* (goji) juice improves in vivo antioxidant biomarkers in serum of healthy adults. *Nutr. Res. (N.Y.)* **2009**, *29*, 19−25.

(8) Wang, C. C.; Chang, S. C.; Chen, B. H. Chromatographic determination of polysaccharides in *Lycium barbarum* Linneaus. *Food Chem.* **2009**, *116*, 595−603.

(9) Inbaraj, B. S.; Lu, H.; Kao, T. H.; Chen, B. H. Simultaneous determination of phenolic acids and flavonoids in *Lycium barbarum* Linnaeus by HPLC−DAD−ESIMS. *J. Pharm. Biomed. Anal.* **2010**, *51*, 549−556.
(10) Benzie, I. F. F.; Chung, W. Y.; Wang, J.; Richelle, M.; Bucheli, P. Enhanced bioavailability of zeaxanthin in a milk-based formulation of wolfberry (Gou Qi Zi; *Lycium barbarum* L.). *Br. J. Nutr.* **2006**, *96*, 154−160.
(11) Careri, M.; Bianchi, F.; Corradini, C. Recent advances in the application of mass spectrometry in food-related analysis. *J. Chromatogr., A* **2002**, *970*, 3−64.
(12) Strege, M. A. High-performance liquid chromatographic−electrospray ionization mass spectrometric analyses for the integration of natural products with modern high-throughput screening. *J. Chromatogr., B* **1999**, *725*, 67−78.
(13) Barnes, S.; Birt, D. F.; Cassileth, B. R.; Cefalu, W. T.; Chilton, F. H.; Farnsworth, N. R.; Raskin, I.; van Breemen, R. B.; Weave, C. M. Technologies and experimental approaches at the National Institutes of Health Botanical Research Centers[1−4]. *Am. J. Clin. Nutr.* **2008**, *87* (Suppl.), 476S−480S.
(14) Rodriguez-Amaya, D. B. General procedure and sources of errors in carotenoid analysis. In *A Guide to Carotenoids Analysis in Foods*; ILSI Press − International Life Sciences Institute: Washington, DC, USA, 2001; pp 23−33.
(15) Stephen Inbaraj, B.; Lu, H.; Hung, C. F.; Wu, W. B.; Lin, C. L.; Chen, B. H. Determination of carotenoids and their esters in fruits of *Lycium barbarum* Linnaeus by HPLC-DAD-APCI-MS. *J. Pharm. Biomed. Anal.* **2008**, *47*, 812−818.
(16) Peng, Y.; Ma, C.; Li, Y.; Leung, K. S. Y.; Jiang, Z. H.; Zhao, Z. Quantification of zeaxanthin dipalmitate and total carotenoids in *Lycium* fruits (Fructus Lycii). *Plant Food Hum. Nutr.* **2005**, *60*, 161−164.
(17) Zhao, L.-Q.; Qiu, Z.-Q.; Narasimhamoorthy, B.; Greaves, J. A. Development of a rapid, high-throughput method for quantification of zeaxanthin in Chinese wolfberry using HPLC−DAD. *Ind. Crops Prod.* **2013**, *47*, 51−57.
(18) Dhooghe, L.; Mesia, K.; Kohtala, E.; Tona, L.; Pieters, L.; Vlietinck, A. J.; Apers, S. Development and validation of an HPLC-method for the determination of alkaloids in the stem bark extract of *Nauclea pobeguinii*. *Talanta* **2008**, *76*, 462−468.
(19) Bijttebier, S.; D'Hondt, E.; Noten, B.; Hermans, N.; Apers, S.; Voorspoels, S. Improving method reliability in carotenoid analysis through selective removal of glycerolipid interferences by lipase treatment. *J. Agric. Food Chem.* **2014**, *62*, 3114−3124.
(20) Toyoda-Ono, Y.; Maeda, M.; Nakao, M.; Yoshimura, M.; Sugiura-Tomimori, N.; Fukami, H. 2-*O*-($\beta$-D-Glucopyranosyl)ascorbic acid, a novel ascorbic acid analogue isolated from *Lycium* fruit. *J. Agric. Food Chem.* **2004**, *52*, 2092−2096.
(21) Gao, Z.; Ali, Z.; Khan, I. A. Glycerogalactolipids from the fruit of *Lycium barbarum*. *Phytochemistry* **2008**, *69*, 2856−2861.
(22) Cao, Y.; Zhang, X.; Chu, Q.; Fang, Y.; Ye, J. Determination of taurine in *Lycium barbarum* L. and other foods by capillary electrophoresis with electrochemical detection. *Electroanalysis* **2003**, *15*, 898−902.
(23) Song, M. K.; Salam, N. K.; Roufogalis, B. D.; Huang, T. H. W. *Lycium barbarum* (goji berry) extracts and its taurine component inhibit PPAR-$\gamma$-dependent gene transcription in human retinal pigment epithelial cells: possible implications for diabetic retinopathy treatment. *Biochem. Pharmacol.* **2011**, *82*, 1209−1218.
(24) Rodriguez-Amaya, D. B. Quantitative analysis, in vitro assessment of bioavailability and antioxidant activity of food carotenoids − a review. *J. Food Compos. Anal.* **2010**, *23*, 726−740.
(25) Wang, C. C.; Chang, S. C.; Stephen Inbaraj, B.; Chen, B. H. Isolation of carotenoids, flavonoids and polysaccharides from *Lycium barbarum* L. and evaluation of antioxidant activity. *Food Chem.* **2010**, *120*, 184−192.
(26) Rodriguez, G. A. Extraction, isolation and purification of carotenoids. *Current Protocols in Food Analytical Chemistry*; Wiley: Hoboken, NJ, USA, 2001; pp F2.1.1−F2.1.8.
(27) Taungbodhitham, A. K.; Jones, G. P.; Wahlqvist, M. L.; Briggs, D. R. Evaluation of extraction method for the analysis of carotenoids in fruits and vegetables. *Food Chem.* **1998**, *63*, 577−584.
(28) Piao, M.; Murata, Y.; Zhu, B.; Shimoishi, Y.; Tada, M. Changes in carotenoid content and its composition of fructus lycii fruits during maturation. *Jpn. J. Food Chem.* **2005**, *12*, 35−38.
(29) Ma, W. P.; Li, H.; Ye, L. Q.; Chen, M.; Zhang, S. Changes of the main carotenoids pigment contents during the drying processes at different harvest stage in *Lycium barbarum* L. fruits. *Sci. Agric. Sinica* **2007**, *40*, 1492−1497.
(30) Li, H.; Chen, M.; Ma, W. P.; Wang, J. Y. Law of changes of carotenoids contents in Fructus Lycii of Chinese wolfberry (*Lycium barbarum* L.) at different mature periods. *Sci. Agric. Sinica* **2006**, *39*, 599−605.
(31) Holden, J. M.; Eldridge, A. L.; Beecher, G. R.; Buzzard, I. M.; Bhagwat, S.; Davis, C. S.; Douglass, L. W.; Gebhardt, S.; Haytowitz, D.; Schake, S. Carotenoid content of U.S. foods: an update of the database. *J. Food Compos. Anal.* **1999**, *12*, 169−196.
(32) Breithaupt, D. E.; Weller, P.; Wolters, M.; Hahn, A. Comparison of plasma responses in human subjects after the ingestion of 3*R*,3*R*′-zeaxanthin dipalmitate from wolfberry (*Lycium barbarum*) and nonesterified 3*R*,3*R*′-zeaxanthin using chiral high performance liquid chromatography. *Br. J. Nutr.* **2004**, *91*, 707−713.
(33) Sajilata, M. G.; Singhal, R. S.; Kamat, M. Y. The carotenoid pigment zeaxanthin − a review. *Compr. Rev. Food Sci. Food Saf.* **2008**, *7*, 29−49.
(34) Schweiggert, U.; Kurz, C.; Schieber, A.; Carle, R. Effects of processing and storage on the stability of free and esterified carotenoids of red peppers (*Capsicum annuum* L.) and hot chilli peppers (*Capsicum frutescens* L.). *Eur. Food Res. Technol.* **2007**, *225*, 261−270.
(35) Daood, H. G.; Kapitány, J.; Biacs, P.; Albrecht, K. Drying temperature, endogenous antioxidants and capsaicinoids affect carotenoid stability in paprika (red pepper spice). *J. Sci. Food Agric.* **2006**, *86*, 2450−2457.

noncompetitive indirect ELISA (iELISA) for the detection of horse meat, this approach is again applicable only to raw meats.

The objective of this study was, therefore, to (1) develop horse selective monoclonal antibodies (mAbs) using thermally stable horse muscle proteins as the immunogen and, consequently, (2) develop a suitable mAb-based ELISA for the quantitative detection of horse meat in both raw and heat-processed ground meat samples.

## MATERIALS AND METHODS

**Materials.** Hydrogen peroxide, $\beta$-mercaptoethanol, 2,2′-azinobis(3-ethylbenzthiazoline-6-sulfonic acid (ABTS), and EZblue gel staining reagent were purchased from Sigma-Aldrich Co. (St. Louis, MO, USA). The alkaline phosphates (AP) conjugate substrate kit, goat anti-mouse IgG (H + L) AP (anti-Ig-AP) conjugate, Tris-buffered saline (TBS), 0.5 M Tris-HCl buffer (pH 6.8), 1.5 M Tris-HCl (pH 8.8), *N*,*N*,*N*′,*N*′-tetramethyl-ethylenediamine (TEMED), Precision Plus Protein Kaleidoscope Standards, 30% acrylamide/bis solution, Tris/glycine buffer, Tris/glycine/SDS buffer, supported nitrocellulose membrane (0.2 $\mu$m), and thick blot paper were purchased from Bio-Rad Laboratories Inc. (Hercules, CA, USA). All other chemicals, reagents, filter paper (Whatman no. 1 paper), egg albumin, nonfat dry milk, and polystyrene microplates were purchased from Fisher Scientific (Fair Lawn, NJ, USA). All chemicals and reagents were of analytical grade, and solutions were prepared using distilled deionized pure water (DD water) from a NANOpure DIamond ultrapure water system (Barnstead International, Dubuque, IA, USA). Meat samples, including beef eye of round roast, pork loin, lamb shoulder, whole chicken, whole duck, whole goose, turkey breast, bison, and frozen dressed rabbit were purchased from a local supermarket. Horse meat was obtained from the College of Veterinary Medicine, Auburn University (Auburn, AL, USA). Deer, elk, and African buffalo steak meats were provided by the Fats and Proteins Research Foundation (Bloomington, IL, USA). Porcine and bovine gelatins were provided by GELITA USA Inc. (Sioux City, IA, USA). Kosher fish gelatin, whey protein concentrate (80%), and soy powder were provided by Custom Collagen (Addison, IL, USA), Davisco Foods International, Inc. (Le Sueur, MN, USA), and Soylink (Oskaloosa, IA, USA), respectively.

**Production of mAbs.** Horse meat samples trimmed of visible fat were cut up and ground twice using a household meat grinder. A portion (100 g) of the ground horse lean meat was autoclaved at 121 °C for 1 h at 1.2 bar using the SterileMax benchtop steam sterilizer (Barnstead International) and the autoclaved meat mashed into fine particles. One hundred milliliters of extraction buffer [10 mM phosphate buffer solution containing 0.5 M NaCl (pH 7.0), PB-salt solution] was added to the mashed sample and the mixture homogenized for 2 min at 11000 rpm using the ULTRA-TURRAX T25 basic homogenizer (IKA Works Inc., Wilmington, NC, USA) and kept overnight at 4 °C. The mixture was then centrifuged at 4 °C for 1 h at 3220*g* (Eppendorf 5810R centrifuge, Brinkman Instruments Inc., Westbury, NY, USA), and filtered through Whatman no. 1 filter paper. The filtrate [comprising thermally stable soluble proteins (TSPs)] was dialyzed in 10 mM phosphate-buffered saline (PBS) for 24 h with frequent changes and the dialyzed extract used as the immunogen. The protein concentration of the immunogen was determined by the Bradford method using a protein assay kit (Bio-Rad). The immunization and subsequent hybridoma procedures were performed as previously described.[18] Only those clones secreting the IgG class of antibodies were selected, and mAbs were obtained from the supernatants of the propagated cell cultures. The isotype of each selected mAb was determined using a mouse mAb isotyping kit (ISO-2 1 kit, Sigma) according to the manufacturer's protocol.

**Sample Preparation.** *Meat Extracts.* Lean meat samples (horse, beef, pork, lamb, bison, African buffalo, deer, elk, chicken, turkey, goose, duck, and rabbit) trimmed of visible fat and connective tissues were ground twice, and 5 g of each sample was weighed into a sampling bag. Twenty-five milliliters of PB-salt solution was added to each, and the mixture was blended for 2 min using the Lab-Blender 400 stomacher (Tekmar Co., Cincinnati, OH, USA). Two other sets of 5 g meat samples that had been cooked (immersed in boiling water for 15 min) or autoclaved for 15 min at 121 °C and 1.2 bar using a SterileMax benchtop steam sterilizer (Barnstead International) were mashed into fine particles, 10 mL of PB-salt solution was added, and the mixtures were homogenized (using the ULTRA-TURRAX T25 basic homogenizer) for 2 min. The raw and heat-treated mixtures were then centrifuged and filtered as described above to obtain raw, cooked, and autoclaved meat extracts. The clear extracts were aliquoted into 1.5 mL small tubes and stored at −20 °C until use.

*Spiked Sample Extracts.* Sampling beakers containing 9 g of either ground pork or ground beef with 1 g of ground horse meat were prepared to obtain 10% (w/w) horse meat spiked ground pork or beef samples. These spiked meat samples were then placed in sampling bags, and 50 mL of PB-salt solution was added, after which the mixtures were blended (using the stomacher) and centrifuged as described above to obtain extracts of the 10% (w/w) raw horse meat in either ground pork or beef. A further set of 10% (w/w) horse meat in ground pork or beef in separate beakers was cooked as described above. The cooked samples were mashed, 20 mL of PB-salt solution was added, and the mixture was homogenized, centrifuged, and filtered as described above to obtain extracts of the 10% (w/w) cooked horse meat in either ground pork or beef. Ten percent (w/w) autoclaved horse meat in ground pork and beef extracts was similarly prepared as described for the spiked cooked samples except that the heating involved autoclaving the samples at 121 °C for 15 min at 1.2 bar. The resulting 10% (w/w) spiked samples were mixed with appropriate amounts of the respective unspiked (0%) beef or pork extracts (described above) to obtain 0.1, 0.3, 0.5, 1, and 3% (v/v) concentrations of spiked samples. All of these spiked samples were analyzed immediately.

*Food Protein Extracts.* Extracts of common food proteins (nonfat dry milk, soy powder, whey protein concentrate, bovine serum albumin, egg albumin, porcine gelatin, bovine gelatin, and fish gelatin) were prepared as previously described.[19]

**SDS-PAGE and Western Blot.** Western blot analysis was performed to reveal the approximate molecular weight of the antigenic protein recognized by the raised mAbs. Briefly, soluble proteins (3 $\mu$g of protein in 10 $\mu$L of sample buffer per lane) from the samples were loaded on 5% stacking gel and separated on a 12% polyacrylamide separating gel (at 200 V using the Mini-Protein 3 Electrophoresis Cell, Bio-Rad) in accordance with the method by Laemmli.[20] The separated proteins were transferred electrophoretically (1 h at 100 V, using the Mini Trans-Blot Electrophoretic Transfer Cell, Bio-Rad) as described by Towbin and others,[21] and the membrane was blocked with 1% BSA in TBS, incubated with raised mAbs diluted 1:4 (v/v) in TBST (TBS containing 0.05% (v/v) Tween-20) and secondary antibody (goat anti-mouse IgG (H + L)-AP conjugate diluted 1:3000 (v/v) in 1% BSA in TBST) in succession, and color was developed as previously described.[22] Precision Plus Protein Kaleidoscope standards were used for molecular weight estimation on gels and blots.

**Noncompetitive Indirect ELISA (iELISA).** The selectivity of raised mAbs was characterized using antigen coated iELISA as follows. One hundred microliters of sample extract appropriately diluted in 0.06 M carbonate buffer (pH 9.6) to contain 2 $\mu$g of protein was coated on the wells of a polystyrene microplate alongside controls and incubated at 37 °C for 2 h. The plate was then blocked for 1 h at 37 °C with 200 $\mu$L/well of blocking buffer [1% bovine serum albumin (BSA) in PBS]. Next, 100 $\mu$L of mAbs appropriately diluted in antibody buffer [1% BSA in PBST−PBS containing 0.05% (v/v) Tween 20] was added and the plate incubated for 2 h at 37 °C. At the end of this period, the plate was incubated with 100 $\mu$L of goat anti-mouse IgG (Fc-specific)−peroxidase conjugate diluted 3000 times in antibody buffer for 1 h at 37 °C. Finally, 100 $\mu$L of substrate solution (22 mg of ABTS and 15 $\mu$L of 30% hydrogen peroxide in 100 mL of 0.1 M phosphate−citrate buffer, pH 4.0) was added and the color developed for 20 min at 37 °C. The enzyme reaction was stopped at the end of 20 min by the addition of 0.2 M citric acid solution and the absorbance measured at 415 nm using the PowerWave XS microplate reader (Bio-Tek Instruments, Winooski, VT, USA). The microplate was washed between steps with PBST.

**Epitope Comparison.** The additivity test described by Friguet and others[23] was performed to determine whether pairs of mAbs bind to the same epitope or to different epitopes on the common antigenic protein. Briefly, saturation curves were first generated to determine the dilution of each antibody required to saturate the antigen (cooked horse meat) using iELISA as described above. To perform the additivity test, to one well containing 2 $\mu$g/100 $\mu$L of bound cooked horse meat was added 100 $\mu$L of mAb H3E3 so diluted to saturate the antigen as obtained from the saturation curve. To another well was added 100 $\mu$L of mAb H4E4 similarly diluted. To a third well was added 50 $\mu$L each of appropriately diluted H3E3 and H4E7. Secondary antibody, color substrate, and stop solution were added in succession as previously described, and the absorbance for well 1(mAb H3E3 alone), well 2 (mAb H4E7 alone), and well 3 (mAb H3E3 and mAb H4E7) was recorded as $A_1$, $A_2$, and $A_{1+2}$, respectively. The additivity index (AI) was calculated according to eq 1. AI values between 50 and 100% are deemed to indicate that the two antibodies bind cooperatively.

$$\mathrm{AI} = [(2A_{1+2})/(A_1 + A_2) - 1]\times 100 \quad (1)$$

*Competitive ELISA (cELISA).* The presence of horse meat in raw and cooked ground pork or beef was determined by testing ground meats (pork or beef) spiked with horse meat using cELISA. A series of experiments was utilized to select the optimum concentration of immobilized antigen (cooked horse meat extract) and sample extracts, dilutions of mAbs, and incubation times for antigen and antibody binding. One hundred microliters of cooked horse meat extract appropriately diluted in 0.06 M carbonate buffer to contain 0.5 $\mu$g of protein was coated on the wells of a polystyrene microplate and the plate incubated at 37 °C for 2 h. The plate was then blocked by adding 200 $\mu$L of blocking buffer, and the plate was incubated at 37 °C for 1 h. Next, 50 $\mu$L of undiluted sample extract (cooked horse meat, spiked samples, and common food proteins) was added to the wells alongside 50 $\mu$L of mAbs diluted 200 times in antibody buffer, and the plate was incubated at 37 °C for 2 h. Finally, the plate was incubated in succession with peroxidase-conjugated secondary antibody and substrate solution, and the color was developed and absorbance measured as described above. The microplate was washed between steps with PBST.

*Data Analysis.* All experiments were performed in triplicate and the results analyzed using Microsoft Excel 2007 or OriginPro 9 (OriginLab Corp., Northampton, MA, USA). One-way ANOVA using SPSS software 11.0 for Windows (SPSS Inc., Chicago, IL, USA) was used to compare means for difference among three or more treatment groups. Post hoc analysis was performed using Tukey HSD. Significance was accepted at $P < 0.05$.

## RESULTS AND DISCUSSION

**Production of mAbs.** Meat products may undergo heat processing ranging from mild to severe heat processes such as autoclaving (as in the case of canned meat). Accordingly, to increase the chances of selecting for mAbs that recognize their cognate antigen even when it has been subjected to excessive heat processes such as canning, autoclaved horse meat extract containing soluble heat-stable peptides was used as the immunogen. Although the use of a pure antigen increases the chances of obtaining the desired mAbs, there was no prior knowledge of potentially suitable species-specific and thermally stable horse meat proteins. Therefore, crude thermally stable protein extract of autoclaved horse meat was used as the immunogen to enhance the chances of getting mAbs with desired specificity as each protein in the extract had the potential to induce immune response for antibody production. Only hybridomas that secreted mAbs that reacted both with raw and autoclaved meat extracts were selected for further characterization studies.

**Specificity of mAbs.** Among approximately 80 positive hybridomas, 5 were selected for cloning due to their interesting reaction patterns. The preliminary screening of these five clones against the immunogen (protein extracts of autoclaved meats) showed that three (1A11, 2H5, and 7A2) cross-reacted with other species and only two (H4E7 and H3E3) exhibited a species specificity to horse meat alone. Their subclasses and reactivity patterns are listed in Table 1. On the basis of these results, the immunoreactivity of the two mAbs that demonstrated species specificity, H3E3 (IgG2b) and H4E7 (IgG2a), were examined against raw, cooked (100 °C for 15 min), and autoclaved (121 °C for 15 min at 1.2 bar) meat extracts from a broader range of animal species (horse, beef, pork, elk, deer, lamb, bison, African buffalo, rabbit, turkey, chicken, goose, and duck) using both iELISA and Western blot (WB) to confirm their suitability as probes for the detection of horse meat contamination.

**Table 1. Immunoreactivity of Five Selected Clones Determined by iELISA**

| antibody | subclass | species reactivity |
|---|---|---|
| 3E3 | IgG2b | reacts strongly to raw, cooked and autoclaved horse, and also reacts with raw poultry meats |
| 4E7 | IgG2a | |
| 1A11 | IgG1 | reacts strongly to all raw, cooked, and autoclaved meats |
| 2H5 | IgG1 | reacts strongly to all autoclaved meats; does not react to any cooked meat, but reacts slightly to raw meat |
| 7A2 | IgG1 | reacts strongly to all autoclaved meats but does not react to cooked or raw meats |

The iELISA results showed that both mAbs reacted strongly with raw, cooked, and autoclaved horse meat, with mAb H3E3 consistently exhibiting stronger immunoreactivity than mAb H4E7 (Figure 1). In the case of raw meat, both mAbs H3E3 and 4E7 also exhibited reactivity with raw poultry meat (turkey, chicken, duck, and goose) (Figure 1a). For the cooked and autoclaved meat extracts, both mAbs reacted solely with cooked (Figure 1b) and autoclaved (Figure 1c) horse meat extracts, with no cross-reactivity with other species of meat samples (beef, pork, elk, deer, lamb, bison, African buffalo, rabbit, turkey, chicken, goose, and duck). By comparison of the results for the raw and heat-treated samples, the absorbance readings ($A_{415\ \mathrm{nm}}$) for cooked horse meat for mAbs H3E3 and H4E7 were respectively 2.6 and 2.8 times stronger than those for raw horse meat. Likewise, the absorbance readings ($A_{415\ \mathrm{nm}}$) for autoclaved horse meat were 1.7 and 1.8 times stronger, respectively. In iELISA, antigens adsorbed onto the solid support (microplate) at high concentrations encourage high avidity and bivalent binding, leading to higher reaction signals.[24] The much stronger reaction with heat-treated compared to raw horse meat extracts may therefore be due to the higher concentrations of thermally stable antigens in the heat-treated samples because of insolubilization of most of the thermally labile soluble proteins in the raw extract.

The results from the Western blot analysis revealed that in raw meat samples both mAbs H3E3 (Figure 2a(i)) and H4E7 (Figure 2b(i)) reacted with a 32 kDa protein found not only in horse meat but also in all mammalian meats except beef and rabbit. However, several other higher molecular weight antigenic bands (35−150 kDa for mAb H4E7 and 50−150 kDa for mAb H3E3) that appeared as smeared bands were also present in the horse meat extracts. As was the case with iELISA, both mAbs also reacted with poultry meats, but compared with mammalian meats, the molecular weight for the antigenic

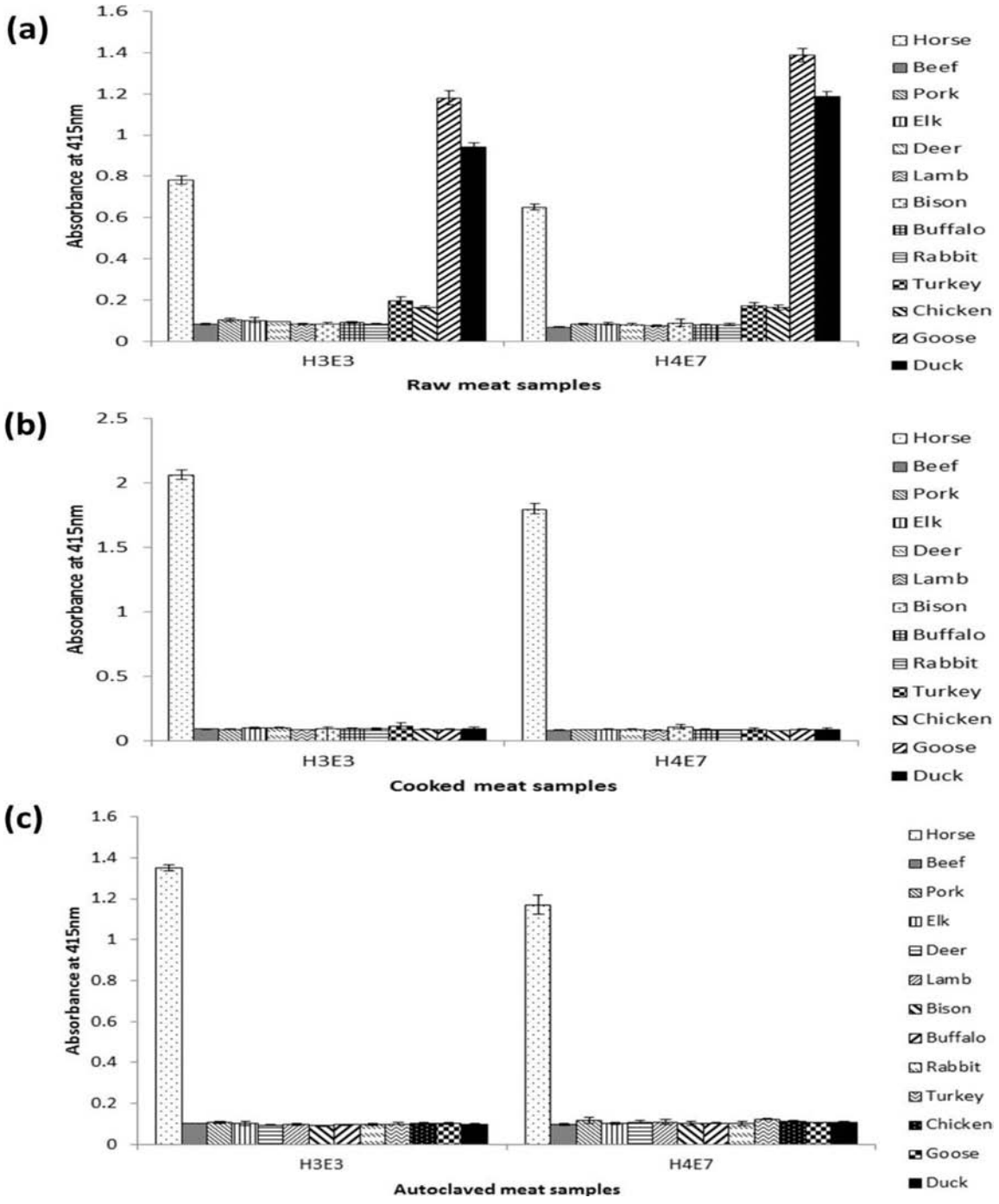


**Figure 1.** Species specificity of mAbs H3E3 and H4E7 with (a) raw, (b) cooked, and (c) autoclaved meats using indirect ELISA. Soluble proteins extracted from raw, cooked and autoclaved meat extracts were coated at 2 $\mu$g/100 $\mu$L. Results are expressed as $A_{415\ nm} \pm$ SD, $n = 3$.

protein in poultry meat had a higher estimated weight of 37 kDa. For the cooked and autoclaved samples, the Western blot analysis showed a positive reaction only with horse meat for both mAbs H3E3 (Figure 2a(ii)) and H4E7 (Figure 2b(ii)), although the bands were smeared as for the raw meat samples. For both antibodies, a 150 kDa band was visible in the cooked samples, but the bands were more smeared in autoclaved samples compared to the raw and cooked meat samples. SDS-PAGE, which involves a prior heat treatment that includes boiling for 5 min, may have denatured the proteins somewhat and hence caused the smeared bands for the raw samples. The progressive increase in the severity of the band smearing for cooked and autoclaved samples may similarly be due to the denaturation of proteins caused by the heat treatment of cooking (100 °C for 15 min) and autoclaving (121 °C for 15 min at 1.2 bar), respectively, and the additional presample treatment of boiling for 5 min.

Unlike the cooked and autoclaved samples, the Western blot results for the raw meat extracts did not agree completely with the results for iELISA, largely because there are many more types of soluble proteins present in raw meat than heated meat extracts. An antibody recognizes a specific feature on the antigen referred to as the epitope, which is usually composed of six to eight amino acids.[25] Epitopes may be either linear


dx.doi.org/10.1021/jf504032j | J. Agric. Food Chem. 2014, 62, 12536−12544

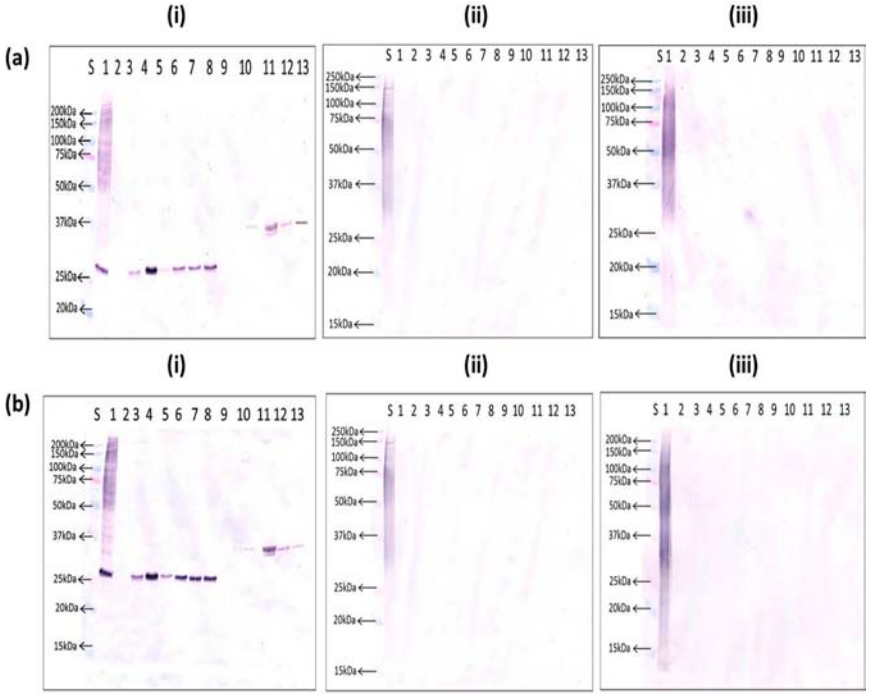


**Figure 2.** Western blot of soluble proteins extracted from (i) raw, (ii) cooked, and (iii) autoclaved meats using (a) mAb H3E3 and (b) mAb H4E7. Protein extracts were loaded at 3 $\mu$g/10 $\mu$L per lane alongside Precision Plus protein kaleidoscope prestained standards. Lanes: S, standard; 1, horse; 2, beef; 3, pork; 4, elk; 5, deer; 6, lamb; 7, bison; 8, African buffalo; 9, rabbit; 10, turkey; 11, chicken; 12, goose; 13, duck.

(formed by contiguous amino acid sequences) or conformational (formed by noncontiguous amino acid sequences).[26] In iELISA, the adsorption of proteins onto the solid support (wells of microplate) happens randomly and is therefore vulnerable to conformational changes that may either totally block or drastically reduce accessibility to the epitope such that recognition by its cognate antibody can be either hampered considerably or completely prevented.[27−29] This is not a factor in Western blot analysis, where the use of SDS ensures that the proteins or polypeptides that have been separated by SDS-PAGE assume a linear conformation,[26] thus exposing otherwise hidden epitopes. These differences in assay formats may explain why both antibodies failed to react with pork, elk, deer, lamb, bison, and African buffalo meat using iELISA but did react with these same meat samples when using Western blot, probably as a result of the exposure of hidden epitopes (in the case of iELISA) from specific or even nonspecific molecules due to the treatment with SDS in the Western blot analysis.

Because the epitopes recognized by antibodies are located in relatively small regions on the antigen, as mentioned above, sometimes antibodies find similar epitopes on related molecules, and this forms the molecular basis for cross-reaction.[24] This may explain why although horse meat extract was used as the immunogen, cross-reactions with raw poultry meat (using both iELISA and Western blot) and all mammalian meats except beef and rabbit (using Western blot) were observed. The lack of binding with heated poultry meat extracts using iELISA may occur because the antigenic protein (37 kDa) in poultry meat that is recognized by these two mAbs may be a different protein that is not as thermally stable as its counterpart in horse meat.

To test for the existence of additional cross-reactions that could lead to false positives, the two mAbs were also tested against extracts of proteins (nonfat dry milk, soy protein, whey protein concentrate, bovine serum albumin, egg albumin, gelatin, soy, whey, etc.) commonly used in food formulations using iELISA. Both mAbs failed to react with any of the proteins tested, producing absorbance readings ($A_{415\ nm}$) of <0.1 for all of the food proteins examined.

**Detection of Horse Meat in Ground Pork and Beef Using mAbs H3E3 and H4E7 Individually in cELISA.** Of all the ELISA formats, sandwich ELISA (sELISA) is often preferred because it is both sensitive and user-friendly. A requirement for developing a sELISA is that the two mAbs used (one as the capturing antibody and the other as the detecting antibody) must bind to different epitopes on the same antigenic protein without inhibiting each other's binding sites. The binding characteristics of these two mAbs were therefore examined for their suitability for use in a sELISA. The results of the additivity test performed as described by Friguet and others[23] to determine whether mAbs H3E3 and H4E7 bind complimentarily on the common antigenic protein revealed an additivity index of 0% (data not shown), indicating that these two antibodies completely inhibited epitope binding of each other on the antigenic protein and therefore were not suitable for use in a sELISA. However, although ruled out for sELISA, the two mAbs could be used individually as probes in cELISA for the quantitative detection of horse meat in raw, cooked, and autoclaved ground pork and beef samples.

In cELISA, an antigen in free form (here, the horse meat present in the spiked samples) competes with a known amount of a bound antigen (cooked extract of horse meat) such that the expected absorbance (OD) for the bound antigen in the absence of the competitor is reduced. This reduction is calculated as the percent inhibition in accordance with eq 2,[30] where 0 and 100% inhibition are controls representing the inhibitions calculated when the competitors are unspiked (0%) horse meat sample (raw, cooked, or autoclaved beef or pork meat) and a cooked horse meat sample (100% horse meat), respectively.

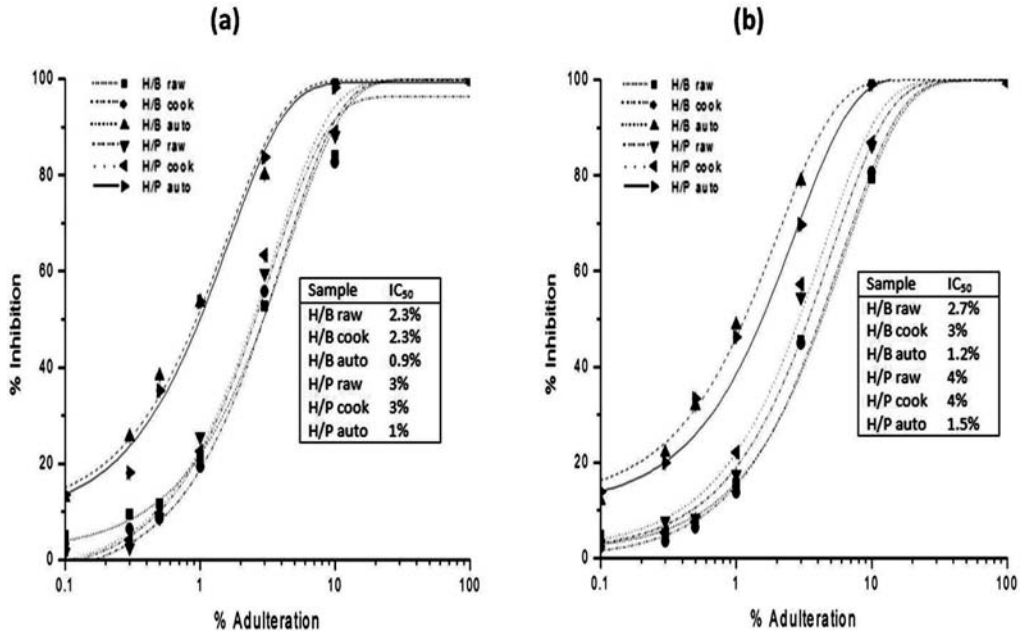


**Figure 3.** Inhibition curves with $IC_{50}$ values of raw, cooked, and autoclaved ground beef and pork adulterated with horse meat using cELISA with (a) mAb H3E3 and (b) mAb H4E7. H/B raw, horse meat in raw ground beef; H/B cook, horse meat in cooked ground beef; H/B auto, horse meat in autoclaved ground beef; H/P raw, horse meat in raw ground pork; H/P cook, horse meat in cooked ground pork; H/P auto, horse meat in autoclaved ground pork.

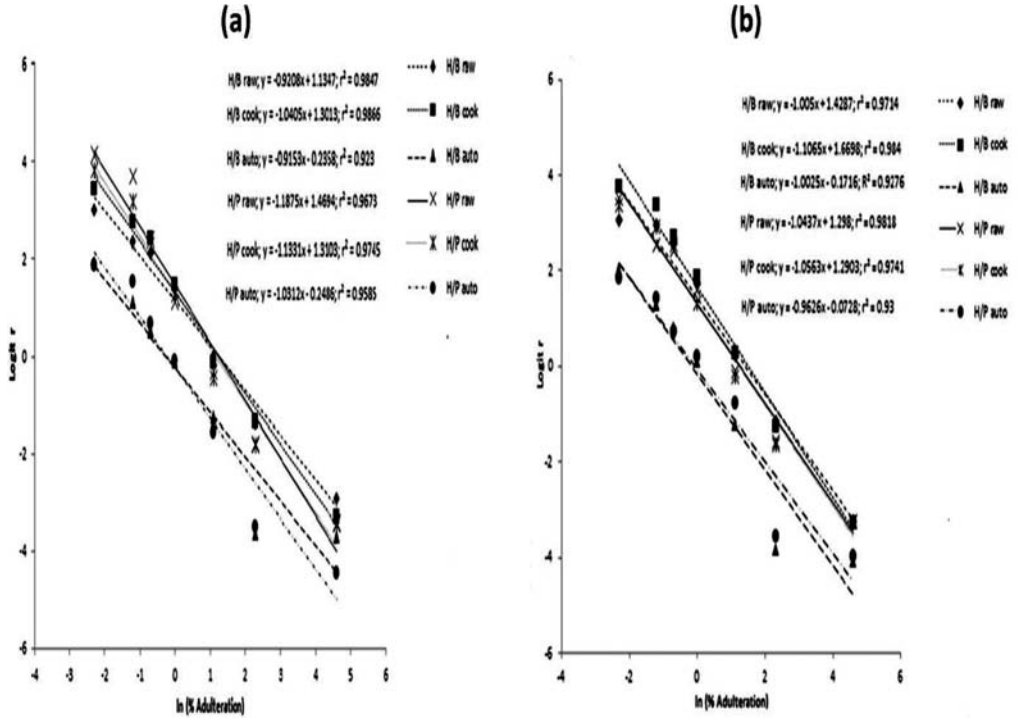


**Figure 4.** Logit-log transformed linear curves of raw, cooked, and autoclaved ground beef and pork spiked with ground horse meat as analyzed by (a) mAb H3E3- and (b) mAb H4E7-based cELISA. H/B raw, horse meat in raw ground beef; H/B cook, horse meat in cooked ground beef; H/B auto, horse meat in autoclaved ground beef; H/P raw, horse meat in raw ground pork; H/P cook, horse meat in cooked ground pork; H/P auto, horse meat in autoclaved ground pork.

$$\%\ \text{inhibition} = 100 - \frac{\text{sample OD} - 100\%\text{inhibition OD}}{0\%\text{inhibition OD} - 100\%\text{inhibition OD}} \times 100 \quad (2)$$

Because the degree of inhibition is proportional to the amount of freely competing antigen in a sample, a standard inhibition curve can be generated by plotting the percent inhibition against known concentrations of the antigen that can be used to quantify the amount of antigen present in an unknown sample. Using the spiked samples described above, six


dx.doi.org/10.1021/jf504032j | J. Agric. Food Chem. 2014, 62, 12536−12544

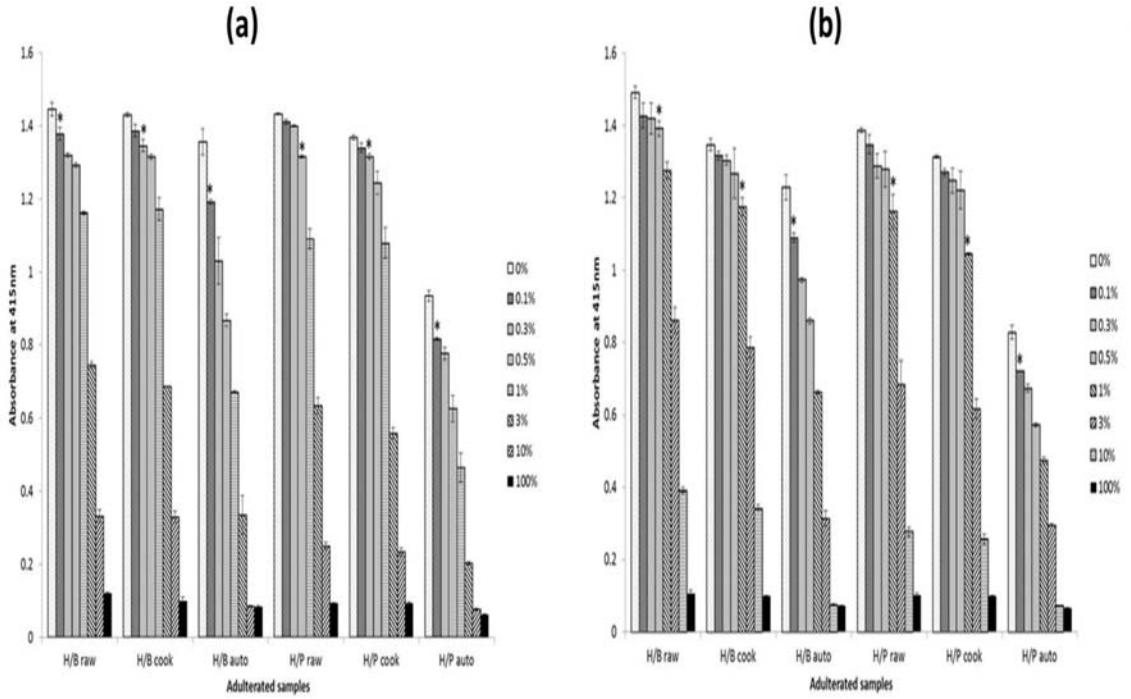


**Figure 5.** Detection limit for raw, cooked, and autoclaved ground beef and pork adulterated with horse meat using (a) mAb H3E3- and (b) mAb H4E7-based cELISA. H/B raw, horse meat in raw ground beef; H/B cook, horse meat in cooked ground beef; H/P auto, horse meat in autoclaved ground beef; H/P raw, horse meat in raw ground pork; H/P cook, horse meat in cooked ground pork; H/P auto, horse meat in autoclaved ground pork. Results are expressed as $A_{415\ nm} \pm SD$, $n = 3$. An asterisk indicates a significant difference ($P < 0.05$).

such inhibition curves were generated for each of the two mAbs, H3E3 (Figure 3a) and mAb H4E7 (Figure 3b), for the quantification of horse meat in test samples and the 50% inhibitory concentrations $IC_{50}$, the competitor concentration at which the OD is halved (50% inhibition) compared to the OD in the absence of a competitor (0% inhibition), determined for each mAb and each type of sample. For mAb H3E3, the $IC_{50}$ values were 2.3% (v/v) for horse meat in both raw and cooked beef and 0.9% (v/v) for horse meat in autoclaved beef (Figure 3a). For adulterated ground pork, the $IC_{50}$ values were 3.0% (v/v) for horse meat in both raw and cooked ground pork and 1.0% for horse meat in autoclaved ground pork (Figure 3a). In the case of the other mAb, H4E7, the $IC_{50}$ values were 2.7, 3.0, and 1.2% (v/v) for horse meat in raw, cooked, and autoclaved ground beef, respectively (Figure 3b). For adulterated ground pork, the $IC_{50}$ values were 4.0% (v/v) for horse meat in both raw and cooked ground pork and 1.5% (v/v) for horse meat in autoclaved ground pork (Figure 3b).

The issue of matrix interference in antigen−antibody interactions is usually determined by comparing the $IC_{50}$ values.[31] The differences in $IC_{50}$ between the two matrices (beef and pork) described above suggest that different matrices do indeed have an effect on the detectability of horse meat. Hence, for accurate quantification of horse meat in different matrices, corresponding matrix-matched sample standards must be analyzed simultaneously. $IC_{50}$ is also a measure of the sensitivity of the assay; the higher the $IC_{50}$ value, the lower the sensitivity of the assay and vice versa. This means that cELISAs using both mAbs will have a higher sensitivity for horse meat in ground beef than for horse meat in ground pork. Our iELISA results revealed that mAb H3E3 exhibited a consistently higher immunoreactivity than mAb H4E7, and these cELISA results also indicate that an assay based on mAb H3E3 will be more sensitive than one based on mAb H4E7, suggesting that mAb H3E3 may have an intrinsically higher affinity for the antigenic protein in horse meat than mAb H4E7.

To obtain a more accurate quantification of the target material (horse meat) in each sample, the dose−response standard inhibition curves were transformed into linear relationships using logit-log transformations for both mAbs H3E3 (Figure 4a) and H4E7 (Figure 4b), as previously described.[32] Both assays exhibited a good linear response over a wide concentration range (0.1−100%) for all of the horse meat spiked samples, with high correlations ($r^2$ = 0.9276−0.9818 for H4E7-based cELISA; $r^2$ = 09230−0.9866 for H3E3-based cELISA) between the horse meat concentrations and ELISA responses. These linear curves can thus serve as a useful standard curve for the quantification of horse meat in different matrices over a wide range of horse meat contaminated samples.

The limit of detection, defined as the smallest amount of the analyte (horse meat) that could be significantly ($P < 0.05$) differentiated from unadulterated samples (0%), was also determined for both assays. The detection limits for the mAb H3E3-based cELISA were 0.1, 0.3, and 0.1% (v/v) for horse meat in raw, cooked, and autoclaved ground beef, respectively; and 0.5% (v/v) for horse meat in both raw and cooked ground pork and 0.1% (v/v) in autoclaved ground pork (Figure 5a). For the mAb H4E7-based cELISA, the detection limits were 0.5% (v/v) for horse meat in raw ground beef, 1% (v/v) for horse meat in cooked ground beef, 0.1% (v/v) for horse meat in autoclaved ground beef, 1% for horse meat in both raw and cooked ground pork, and 0.1% for horse meat in autoclaved ground pork (Figure 5b). The detection limits for the mAb H3E3-based cELISA were lower than for the mAb H4E7-based cELISA for all of the horse meat spiked samples except for

those that had been autoclaved, indicating a higher sensitivity for the former.

For both cELISAs, the detection limit was generally lower for the spiked beef samples compared to those for the corresponding spiked pork samples, indicating a higher sensitivity to horse meat in beef than in pork, which agreed with the $IC_{50}$ values. The observed detection limit for both the new assays was lower than the 5% of horse meat in raw ground beef reported by Lopez-Andreo and others[15] and either comparable to (in the case of mAb H4E7-based cELISA) or lower than (in the case of mAb H3E7-based cELISA) the 1% horse meat in raw ground pork reported by the same group[15] using PCR. The mAb H3E7-based cELISA also performed better than the detection limit of 1% horse meat in raw ground pork and beef reported by Martin and others[16] using a polyclonal antibody-based sELISA. The detection limits of the new assays were, however, higher than the 0.05 and 0.1% horse meat in raw and cooked ground pork and beef achieved by the PCR methods of Xu and others[14] and Kesmen and others,[11] respectively, although both suffered from problems due to an inability to detect amplified fragments with increasing heating temperature or time[14] or guarantee that the assay could be effective against samples cooked to an internal temperatures above 72 °C.[11] In contrast, the new cELISAs reported here were able to detect horse meat down to 1% or lower in ground meat samples that had been boiled for 15 min and to as low as 0.1% for autoclaved samples, which were not considered in either of the earlier studies.

In conclusion, two mAbs (H3E3 and H4E7) were selected from a panel of mAbs raised against partially purified protein in autoclaved horse meat extract to detect the presence of horse meat in cooked and autoclaved samples without exhibiting any cross-reactivity with other meat or food proteins. These two mAbs were used individually to develop cELISAs for the quantitative determination of horse meat content in raw, cooked, and autoclaved beef and pork samples. Although the mAb H3E3-based cELISA was the more sensitive of the two, the cELISA based on mAb H4E7 could detect ≤1% of horse meat in raw and cooked ground beef or pork and down to 0.1% of horse meat in autoclaved ground beef or pork, thus easily satisfying the 1% detection limit required by the European Union. The cELISA based on either mAb H3E3 or mAb H4E7 is therefore expected to become a valuable analytical tool for monitoring horse meat adulteration in meat products to address many health, ethical, and economic issues associated with horse meat contamination in meat products for human consumption. In situations involving raw poultry, the cross-reactivity of these mAbs with raw poultry can be readily eliminated by heating the samples prior to analysis to avoid possible false-positive results.

## AUTHOR INFORMATION

### Corresponding Author

*(Y-H.P.H.) E-mail: yhsieh@fsu.edu. Phone: (850) 644-1744. Fax: (850) 645-5000.

### Funding

This research was financially supported by the Alabama Agricultural Experimental Station, Auburn University, and by the Betty M. Watts Name Professorship funds, Florida State University.

### Notes

The authors declare no competing financial interest.

## ACKNOWLEDGMENTS

The antibody production was performed at Auburn University, and we thank Roger Bridgman for his technical assistance.

## REFERENCES

(1) Meza-Marquez, O. G.; Gallardo-Velazquez, T.; Osorio-Revilla, G. Application of mid-infrared spectroscopy with multivariate analysis and soft independent modeling of class analogies (SIMCA) for the detection of adulterants in minced beef. *Meat Sci.* **2010**, *86*, 511−519.

(2) Hsieh, Y.-H. P.; Woodward, B. B.; Ho, S.-H. Detection of species substitution in raw and cooked meats using immunoassays. *J. Food Prot.* **1995**, *58*, 555−559.

(3) The Japan Times News. Meat Hope Co. files for bankruptcy, http://www.japantimes.co.jp/news/2007/07/18/business/meat-hope-co-files-for-bankruptcy/#.U_FnDvldWT5 (accessed Aug 17, 2014).

(4) The Guardian. Horse meat scandal: where did the 29% horse in your Tesco burger come from? http://www.theguardian.com/uk-news/2013/oct/22/horsemeat-scandal-guardian-investigation-public-secrecy (accessed Aug 17, 2014).

(5) BBC News UK. Veterinary drug found in ASDA budget corned beef, http://www.bbc.com/news/uk-22087123 (accessed Aug 17, 2014).

(6) Touratier, L.; Boireau, P.; Dupouy-Camet, J.; Pages, J. P. Trichinellosis of the horse and its importance in veterinary public health. Facts and consequences. *Bull. Mens. Soc. Vet. Pratique Fr.* **1999**, *83*, 223−264.

(7) Hsieh, Y.-H. P. Meat species identification. In *Handbook of Food Science, Technology, and Engineering*; Hui, Y. H., Ed.; CRC Press: Boca Raton, FL, USA, 2006; Vol. 2, pp 1−19.

(8) Bai, W. B.; Xu, W. T.; Huang, K. L.; Yuan, Y. F.; Cao, S. S.; Luo, Y. B. A novel common primer multiplex PCR (CP-M-PCR) method for the simultaneous detection of meat species. *Food Control* **2009**, *20*, 366−370.

(9) Chisholm, J.; Conyers, C.; Booth, C.; Lawley, W.; Hird, H. The detection of horse and donkey using real-time PCR. *Meat Sci.* **2005**, *70*, 727−732.

(10) Kesmen, Z.; Gulluce, A.; Sahin, F.; Yetim, H. Identification of meat species by TaqMan-based real-time PCR assay. *Meat Sci.* **2009**, *82*, 444−449.

(11) Kesmen, Z.; Sahin, F.; Yetim, H. PCR assay for the identification of animal species in cooked sausages. *Meat Sci.* **2007**, *77*, 649−653.

(12) Koppel, R.; Ruf, J.; Rentsch, J. Multiplex real-time PCR for the detection and quantification of DNA from beef, pork, horse and sheep. *Eur. Food Res. Technol.* **2011**, *232*, 151−155.

(13) Matsunaga, T.; Chikuni, K.; Tanabe, R.; Muroya, S.; Shibata, K.; Yamada, J.; Shinmura, Y. A quick and simple method for the identification of meat species and meat products by PCR assay. *Meat Sci.* **1999**, *51*, 143−148.

(14) Xu, W. T.; Bai, W. B.; Luo, Y. B.; Yuan, Y. F.; Zhang, W.; Guo, X.; Huang, K. L. A novel common single primer multiplex polymerase chain reaction (CSP-M-PCR) method for the identification of animal species in minced meat. *J. Sci. Food Agric.* **2008**, *88*, 2631−2637.

(15) Lopez-Andreo, M.; Garrido-Pertierra, A.; Puyet, A. Evaluation of post-polymerase chain reaction melting temperature analysis for meat species identification in mixed DNA samples. *J. Agric. Food Chem.* **2006**, *54*, 7973−7978.

(16) Martin, R.; Azcona, J. I.; Garcia, T.; Hernandez, P. E.; Sanz, B. Sandwich ELISA for detection of horse meat in raw meat mixtures using antisera to muscle soluble-proteins. *Meat Sci.* **1988**, *22*, 143−153.

(17) Garcia, T.; Martin, R.; Morales, P.; Haza, A. I.; Anguita, G.; Gonzalez, I.; Sanz, B.; Hernandez, P. E. Production of a horse-specific monoclonal-antibody and detection of horse meat in raw meat mixtures by an indirect ELISA. *J. Sci. Food Agric.* **1994**, *66*, 411−415.

(18) Chen, F. C.; Hsieh, Y. H. P.; Bridgman, R. C. Monoclonal antibodies against troponin I for the detection of rendered muscle tissues in animal feedstuffs. *Meat Sci.* **2002**, *62*, 405−412.

(19) Ofori, J. A.; Hsieh, Y. H. Sandwich enzyme-linked immunosorbent assay for the detection of bovine blood in animal feed. *J. Agric. Food Chem.* **2007**, *55*, 5919−5924.
(20) Laemmli, U. K. Cleavage of structural proteins during the assembly of the head of bacteriophage T4. *Nature* **1970**, *227*, 680−685.
(21) Towbin, H.; Staehelin, T.; Gordon, J. Electrophoretic transfer of proteins from polyacrylamide gels to nitrocellulose sheets: procedure and some applications. *Proc. Natl. Acad. Sci. U.S.A.* **1979**, *76*, 4350−4354.
(22) Hsieh, Y. H.; Ofori, J. A.; Rao, Q.; Bridgeman, C. R. Monoclonal antibodies specific to thermostable proteins in animal blood. *J. Agric. Food Chem.* **2007**, *55*, 6720−6725.
(23) Friguet, B.; Djavadi-Ohaniance, L.; Pages, J.; Bussard, A.; Goldberg, M. A convenient enzyme-linked immunosorbent assay for testing whether monoclonal antibodies recognize the same antigenic site. Application to hybridomas specific for the beta 2-subunit of *Escherichia coli* tryptophan synthase. *J. Immunol. Methods* **1983**, *60*, 351−358.
(24) Harlow, E.; Lane, D. *Antibodies: A Laboratory Manual*; Cold Spring Harbor Laboratory Press: Cold Spring Harbor, NY, USA, 1988.
(25) Kajiya, H.; Takekoshi, S.; Takei, M.; Egashira, N.; Miyakoshi, T.; Serizawa, A.; Teramoto, A.; Osamura, R. Y. Selection of buffer pH by the isoelectric point of the antigen for the efficient heat-induced epitope retrieval: re-appraisal for nuclear protein pathobiology. *Histochem. Cell. Biol.* **2009**, *132*, 659−667.
(26) Lodish, H.; Baltimore, D.; Berk, A.; Zipursky, S. L.; Matsudaira, P.; Darnell, J. *Molecular Cell Biology*, 3rd ed.; Scientific American Books: New York, 1995.
(27) Hnasko, R.; Lin, A.; McGarvey, J. A.; Stanker, L. H. A rapid method to improve protein detection by indirect ELISA. *Biochem. Biophys. Res. Commun.* **2011**, *410*, 726−731.
(28) Nakanishi, K.; Sakiyama, T.; Kumada, Y.; Imamura, K.; Imanaka, H. Recent advances in controlled immobilization of proteins onto the surface of the solid substrate and its possible application to proteomics. *Curr. Proteomics* **2008**, *5*, 161−175.
(29) Niveleau, A.; Bruno, C.; Drouet, E.; Brebant, R.; Sergeant, A.; Troalen, F. Grafting peptides onto polystyrene microplates for ELISA. *J. Immunol. Methods* **1995**, *182*, 227−234.
(30) Crowther, J. R. Practical exercises. In *The ELISA Guidebook*; Crowther, J. R., Ed.; Humana Press: Totowa, NJ, USA, 2000; Vol. 149, pp 153−231.
(31) Riley, C. M. *Development and Validation of Analytical Methods*; Elsevier Science: New York, 1996; Vol. 3.
(32) Rao, Q.; Hsieh, Y. H. Competitive enzyme-linked immunosorbent assay for quantitative detection of bovine blood in heat-processed meat and feed. *J. Food Prot.* **2008**, *71*, 1000−1006.

Table 1. Initial Fatty Acid Composition (Area %), Tocopherol Content (mg/kg), Acid Value (mg KOH/g), Peroxide Value (mequiv $O_2$/kg), and *p*-Anisidine Value of Vegetable Oil[a]

| sample | palm oil | camellia oil | sunflower oil | perilla oil |
|---|---|---|---|---|
| palmitic acid | 38.23 ± 1.18a | 7.80 ± 0.01b | 6.27 ± 0.02c | 6.02 ± 0.10c |
| stearic acid | 4.49 ± 0.07a | 2.42 ± 0.07d | 3.94 ± 0.07b | 2.76 ± 0.07c |
| oleic acid | 43.05 ± 0.88b | 80.14 ± 0.08a | 29.50 ± 0.03c | 21.97 ± 0.25d |
| linoleic acid | 10.33 ± 0.35c | 6.98 ± 0.01d | 55.24 ± 0.11a | 12.73 ± 0.12b |
| α-linolenic acid | 0.14 ± 0.01b | 0.22 ± 0.01b | 0.07 ± 0.01b | 54.37 ± 0.29a |
| total SFA | 44.52 ± 1.25a | 10.36 ± 0.05bc | 11.46 ± 0.07b | 9.17 ± 0.25c |
| total MUFA | 43.41 ± 0.88b | 80.89 ± 0.09a | 29.75 ± 0.05c | 22.28 ± 0.14d |
| total PUFA | 10.51 ± 0.35c | 7.22 ± 0.03d | 55.55 ± 0.11b | 67.18 ± 0.41a |
| α-tocopherol | 191.1 ± 2.8b | 199.0 ± 3.5b | 1106 ± 39a | 37.22 ± 4.98c |
| β-tocopherol | nd | nd | nd | nd |
| γ-tocopherol | 2.26 ± 0.07c | nd | 7.63 ± 0.23b | 128.3 ± 2.3a |
| δ-tocopherol | nd | nd | nd | 19.51 ± 0.20 |
| total tocopherol | 193.4 ± 2.8b | 198.7 ± 3.5b | 1113 ± 39a | 185.0 ± 3.8b |
| AV | 0.06 ± 0.02b | 0.04 ± 0.02b | 0.04 ± 0.01b | 0.72 ± 0.04a |
| POV | 5.11 ± 0.57a | 2.89 ± 0.65b | 2.16 ± 0.38b | 0.41 ± 0.06c |
| *p*-AV | 4.07 ± 0.69a | 2.15 ± 0.01b | 3.81 ± 0.05a | 0.22 ± 0.01c |

[a]Data are mean values ± SD, $n = 3$. nd, peak not detected under this analysis condition; SFA, saturated fatty acid; MUFA, monounsaturated fatty acid; PUFA, polyunsaturated fatty acid; AV, acid value; POV, peroxide value; *p*-AV, *p*-anisidine value. Values followed by the same letter in the same row are not significantly different ($p < 0.05$).

(15 μg/mL of each carbonyl) from Supelco Inc. (TO11/IP-6A Mix, Supelco Inc., Bellefonte, PA, USA): formaldehyde, acetaldehyde, acrolein, acetone, propionaldehyde, crotonaldehyde, butyraldehyde, benzaldehyde, isovaleraldehyde, valeraldehyde, *o*-tolualdehyde, *m*-tolualdehyde, *p*-tolualdehyde, hexaldehyde, and 2,5-dimethylbenzaldehyde. Standard fatty acid methyl esters (FAME, GLC-463) were obtained from Nu-Chek Prep Inc. (Elysian, MN, USA). Tocopherol standards (α, β, γ, and δ) were purchased from Sigma (Sigma Chemicals, Shanghai, China). Methanol, *n*-hexane, acetonitrile, and isopropanol (HPLC grade) were purchased from Merck (Darmstadt, Germany). Water was purified using a Milli-Q system from Millipore (Bedford, MA, USA). All other solvents were of analytical reagent grade. Potassium hydroxide, phenolphthalein, ethyl alcohol, acetic acid, isooctane, soluble starch, potassium iodide, sodium thiosulfate, and *p*-anisidine were of analytical grade.

**Measurements of Acid Value (AV), Peroxide Value (POV), and *p*-Anisidine Value (*p*-AV).** AOCS official methods were used to determine acid value (method Cd 3d-63), peroxide value (method Cd 8-53), and *p*-anisidine value (method Cd 18-90) of oil samples.

Total oxidation value (TOTOX) was calculated as follows:[17]

$$\text{TOTOX} = 2\text{POV} + p\text{-AV}$$

**Tocopherols Analysis by HPLC.** The concentration of tocopherols in oil samples was determined according to the method reported by Hu et al.[18] Approximately 1 g of oil sample was put into a volumetric flask and made up to 10 mL with HPLC grade hexane. After filtering through a 0.45 μm filter, 3 μL of sample was directly injected into an Agilent 1100 series HPLC system equipped with a fluorometric detector. The excitation wavelength was set at 295 nm, and the emission wavelength was set at 325 nm. The column was a Hypersil ODS2 C18 column (4.6 mm × 15 cm, 5 μm, Elite, Dalian, China). The mobile phase was methanol/water (98:2, v/v), and the flow rate was 0.8 mL/min. The corresponding standards (α-, β-, γ-, and δ-tocopherol) for identification and quantification were prepared separately in a 100 mL volumetric flask with hexane, and the final concentrations of α-, β-, γ-, and δ-tocopherol were 100, 20, 15, and 80 μg/mL, respectively. Then they were serially diluted to different concentration gradients for generating the standard curves.

**Fatty Acids Analysis by GC.** Fatty acid compositions of vegetable oils were analyzed by gas chromatography. Samples were methylated as described by Cruz-Hernandez et al.[19] The FAMEs were identified using a capillary column of fused silica (100 m × 0.25 mm × 0.20 μm) coated with 100% cyanopropyl polysiloxane (CP-Sil 88, Chrompack, Agilent Technologies, Shanghai, China) equipped with a flame ionization detector. Hydrogen was used as the carrier gas at a flow rate of 30 mL/min. The oven temperature program (86 min in total) was as follows: The initial temperature was set at 45 °C for 4 min, increased to 175 °C at a rate of 13 °C/min, maintained for 27 min, further raised to 215 °C at a rate of 4 °C/min, and finally kept at 215 °C for 35 min.[20] The injector and detector were kept at 250 °C. Analysis of all peaks was accomplished by comparison of their retention time with FAME standards. Area under each fatty acid peak relative to the total area of all fatty acid peaks was used to quantify the fatty acids identified,[21,22] and the obtained results are reported as percentage of fatty acid.

**Accelerated Oxidation Assay.** A Schaal oven test was used to accelerate the oxidation process in different vegetable oils.[23] The modified protocol followed AOCS (1998) Recommended Practice Cg 5-97 (AOCS cg 5-97). In total, 500 g of oils was weighed into 500 mL glass bottles that were loosely capped. Bottles were kept randomly inside an oven maintained at 62 ± 1 °C without light to accelerate the oxidation (WGS201, Hongzhan Products Inc., Shanghai, China). After intervals of 7 days of heating, samples were removed into bottles. Then they were topped immediately with nitrogen, capped tightly, and kept frozen (−20 °C) until analysis. Analyses were conducted on the same day for some sensitive indices such as POV, *p*-AV, and secondary oxidative products or for other indices within 2 days of removal from the oven.

**Synthesis of DNPH Derivatives.** DNPH derivatives of aldehyde/ketone products in oxidized oils were synthesized as follows: Oil sample (0.1−1.0 g) was put into a 10 mL volumetric flask, and the flask was filled to volume with isopropanol containing DNPH (3 g/L) and hydrochloric acid (3%).[8,24] The test tube was shaken and kept at 40 °C for 1 h to accelerate derivatization reaction. Then it was cooled in water and centrifuged at 4200 rpm for 5 min. The sample was then filtered through a 0.22 μm membrane syringe filter and injected into the HPLC column.

**Isolation and Identification of DNPH Derivatives by HPLC-ESI-QqQ-MS.** An Agilent 1260 series HPLC system equipped with a diode array detector (DAD) was used to analyze samples. Separation of DNPH derivatives was achieved on a Zorbax Edipse plus-C18 column (4.6 mm × 25 cm, 5 μm, Agilent Technologies, Shanghai, China). The column was thermostatically controlled at 30 °C. The flow rate was set to 1 mL/min, and the injection volume was 5 μL. The mobile phase consisted of two solvents: methanol (A, 100%) and Milli-Q water (B, 100%). The solvent gradient in volumetric ratios was set as follows: 0−15 min, 70−75% A; 15−45 min, 75−100% A; and held at 100% A for an additional 2 min. There was a 3 min postrun,

which brings it back to the starting condition. The ultraviolet (UV) absorbance values of the peaks were collected between 200 and 620 nm using a DAD and monitored at wavelengths of 360 nm.

A triple-quadrupole mass spectrometer (6430 QqQ LC/MS system; Agilent Technologies) equipped with an orthogonal electrospray ionization (ESI) source was used to identify the derivatives. Negative ion mode was selected for data collection.[25,26] MS parameters were set as follows: sheath gas was nitrogen and collision gas was helium; drying gas flow rate, 11.0 L/min; drying gas temperature, 300 °C; nebulizing gas pressure, 15 psi; capillary voltage, 4 kV. Some of the ketones, alkanals, alkenals, and alkadienals were identified by using standards. Others were tentatively identified according to their retention times, mass spectra, and matching with mass spectra by the software MassHunter Acquisition B.03.01, Qualitative Analysis B.03.01 and Quantitative Analysis B.03.02 (Agilent Technologies).

**Quantification of Carbonyls.** To have a more complete picture of the carbonyls present in the four oils and of their evolution with heating time, their quantification was expressed as peak area per gram of oil acquired by HPLC chromatogram.

**Statistical Analysis.** Data are expressed as the mean value ± standard deviation. One-way ANOVA was used to compare the differences between mean values. A level of probability at $p < 0.05$ was set as statistically significant. Regression analysis was used to determine the correlation of two data sets. All of the data were performed with SPSS 13.0 software for Windows (SPSS Inc., Chicago, IL, USA).

## RESULTS AND DISCUSSION

**Initial Properties of Oils.** Initial fatty acid composition, tocopherol content, acid value, peroxide value, and *p*-anisidine value of oil samples are shown in Table 1. These oils contained the typical proportions of fatty acids: palm oil contained higher percentages of palmitic acid (38.23%) and oleic acid (43.05%); camellia oil was rich in oleic acid (80.14%), whereas sunflower oil and perilla oil were rich in linoleic acid (55.24%) and linolenic acid (54.37%), respectively.

The analysis of tocopherols showed that sunflower oil contained the highest concentration of total tocopherols (the sum of $\alpha$-, $\beta$-, $\gamma$-, and $\delta$-tocopherols), at 1113 mg/kg. Palm, camellia, and perilla oils contained a similar amount of total tocopherols (193.4, 198.7, and 185.0 mg/kg, respectively). Additionally, palm, camellia, and sunflower oils had high proportions of $\alpha$-tocopherol (>98%), whereas perilla oil had 69% of $\gamma$-tocopherol and only 20% of $\alpha$-tocopherol.

Before accelerated oxidation assay, analysis of AV, POV, and *p*-AV showed that the four oil samples were so-called fresh oils. All complied with the legal dietary requirements of China. The maximal AV was 0.72 mg KOH/g in perilla oil, and maximal POV and *p*-AV were 5.11 mequiv $O_2$/kg and 4.07 in palm oil.

**Changes of Total Oxidation Value during Oxidation.** The TOTOX is often used to estimate oxidative deterioration of lipids, as it has the advantage of combining the amounts of primary oxidation products (hydroperoxides) with secondary products (principally alkenals and alkadienals) in fats or oils.[17] As shown in Figure 1, the highest increment of TOTOX at 62 °C with limited air for 35 days was found in sunflower oil (814), rising from 8.12 to 822, followed by camellia oil (247) and perilla oil (223). Palm oil gave rise to the lowest increment of TOTOX, only 155. That means the order of oxidation stability was sunflower oil < camellia oil < perilla oil < palm oil.

**Comparison of Carbonyl Products Generated in Oils.** Identification of carbonyls in these oils heated at 62 °C with limited air for 35 days (Figure 2) showed that camellia oil (20 types), sunflower oil (19 types), and palm oil (19 types) contained numerous nonpolar carbonyl compounds, whereas

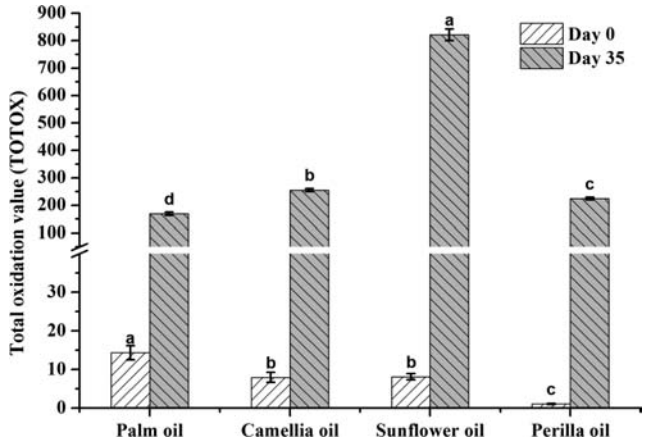


**Figure 1.** Initial and final total oxidation value (TOTOX) for four oils heated at 62 °C with limited air for 35 days. TOTOX = 2POV + *p*-AV. Data are mean values ± SD, $n = 3$. Values followed by the same letter in each set are not significantly different ($p < 0.05$).

perilla oil (14 types) lacked some types of compounds. Twenty carbonyls identified in camellia oil were ranked as retention time of peak: ethanal, 2-propenal, acetone, propanal, pentanal, 2-hexenal, hexanal, 2-hexanone, 2,5-dimethylbenzaldehyde, 2-heptenal, heptanal, 2-octenal, octanal, octanone, 2-nonenal, nonanal, 2-nonanone, 2-decenal, decanal, and decanone, respectively. The above 19 types of nonpolar carbonyls, except 2-decenal, were also detected in palm oil. Sunflower oil contained the most similar components of nonpolar carbonyls to palm oil, but acetone was not detected in sunflower oil and 2,4-decadienal was not detected in palm oil. Fourteen types of carbonyls identified in perilla oil were ethanal, acetone, propanal, butanal, 2-pentenal, 2-hexenal, hexanal, 2,4-heptadienal, 2,5-dimethylbenzaldehyde, 2,4-nonadienal, 2-octenal, octanal, 2-nonenal, and nonanal. These compounds represented groups of secondary oxidation products resulting mainly from the oxidative deterioration of unsaturated fatty acids.[3]

Although the four oil samples contained the most similar components of nonpolar carbonyls, 2-decenal was detected only in camellia oil, and 2,4-decadienal was found only in sunflower oil. Butanal, 2-pentenal, 2,4-heptadienal, and 2,4-nonadienal were observed only in perilla oil. Guillén and Uriarte[5] reported that aldehydes and relative carbonyls generated in lipids during oxidation were substantially different in quantity and type depending on the composition of the lipid matrix. Hence, it was estimated that 2-decenal might be derived mainly from oleic acid, and 2,4-decadienal might be from linoleic acid. Linolenic acid might be the parent fatty acid of butanal, 2-pentenal, 2,4-heptadienal, and 2,4-nonadienal. Similar results have been reported by other researchers.[11,27] For example, there were high levels of 2-decenal in high-oleic rapeseed oil[4] and high-oleic sunflower oil.[28]

The distribution of nonpolar carbonyls in four vegetable oils is shown in Figure 3. Ketones, alkanals, and alkenals were identified in camellia and palm oils during the whole experimental period. Alkanals were the major compounds in camellia oil on the 35th day (72% of total carbonyls), followed by ketones (15%). Both alkanals and alkenals were the main carbonyls in palm oil (49 and 24%) and sunflower oil (45 and 41%). For perilla oil, the major products were alkanals (44%), followed by alkenals (19%) and alkadienals (16%). These carbonyl compounds with different double bonds in samples

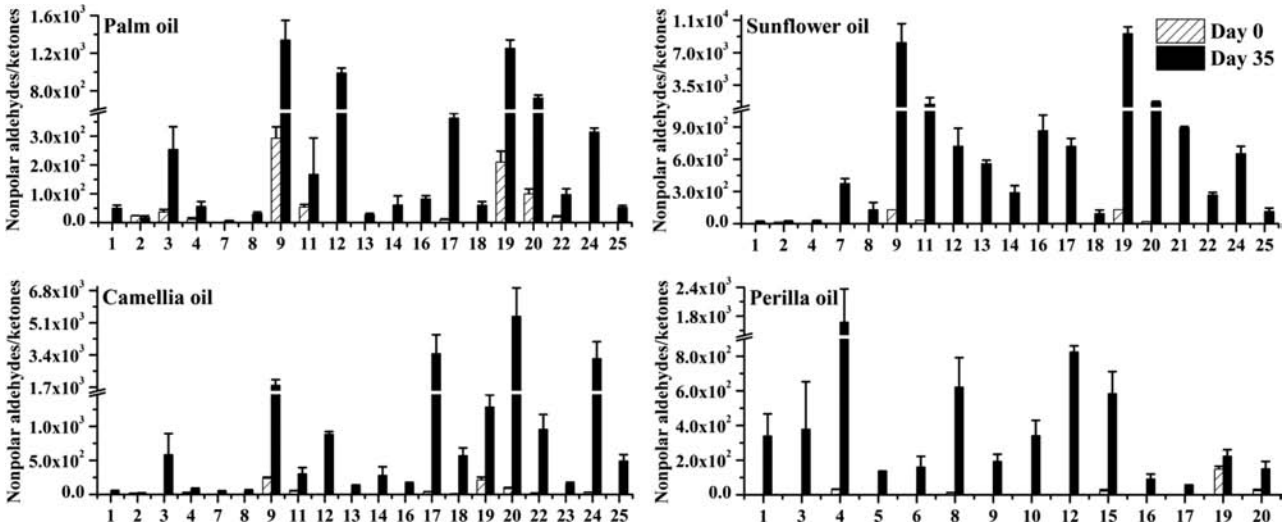


**Figure 2.** Initial and final nonpolar aldehydes/ketones (peak area/g oil) identified for four oils heated at 62 °C with limited air by HPLC-QqQ-MS. 1, ethanal; 2, 2-propenal; 3, acetone; 4, propanal; 5, butanal; 6, 2-pentenal; 7, pentanal; 8, 2-hexenal; 9, hexanal; 10, 2,4-heptadienal; 11, 2-hexanone; 12, 2,5-dimethylbenzaldehyde; 13, 2-heptenal; 14, heptanal; 15, 2,4-nonadienal; 16, 2-octenal; 17, octanal; 18, octanone; 19, 2-nonenal; 20, nonanal; 21, 2,4-decadienal; 22, 2-nonanone; 23, 2-decenal; 24, decanal; 25, decanone. They were ranked as retention time of peak. The identification or quantification was done according to the retention times and the $m/z$ ratio reported in the author's previous paper.[41] Data are mean values ± SD, $n$ = 3.

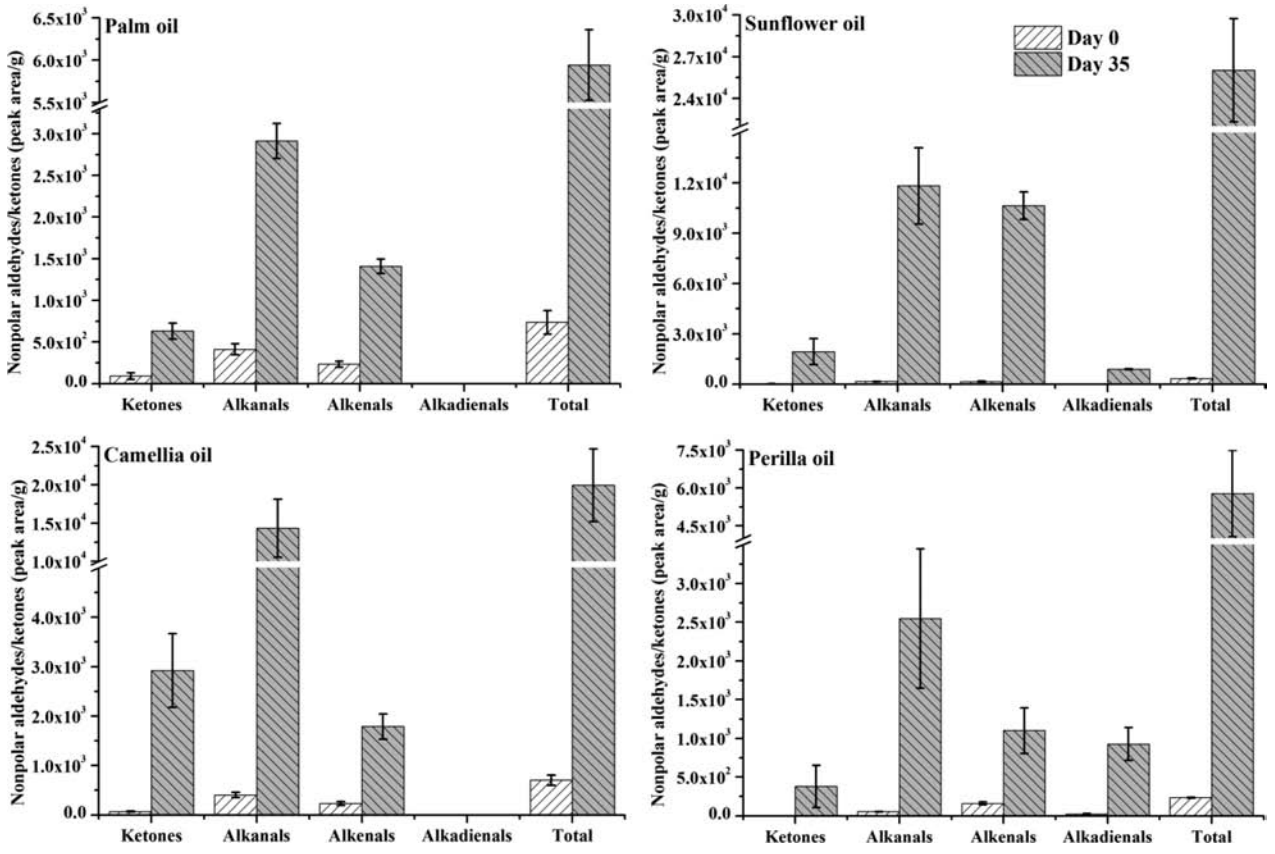


**Figure 3.** Distribution of nonpolar aldehydes/ketones (peak area/g oil) in four oils heated at 62 °C with limited air. Data are mean values ± SD, $n$ = 3.

were mainly owing to the fatty acid chains with different double bonds.[27]

**Possible Pathways of Fatty Acid Decomposition and Aldehyde/Ketone Formation.** The autoxidation of lipid or the reaction of free radical chain mainly includes three steps: initiation, propagation, and termination.[1] Hydroperoxides as the primary oxidation products are first formed. However, they are unstable and rapidly decomposed to a variety of volatile compounds, including aldehydes, ketones, hydrocarbons, and other secondary products.[29,30] Aldehydes, either saturated or

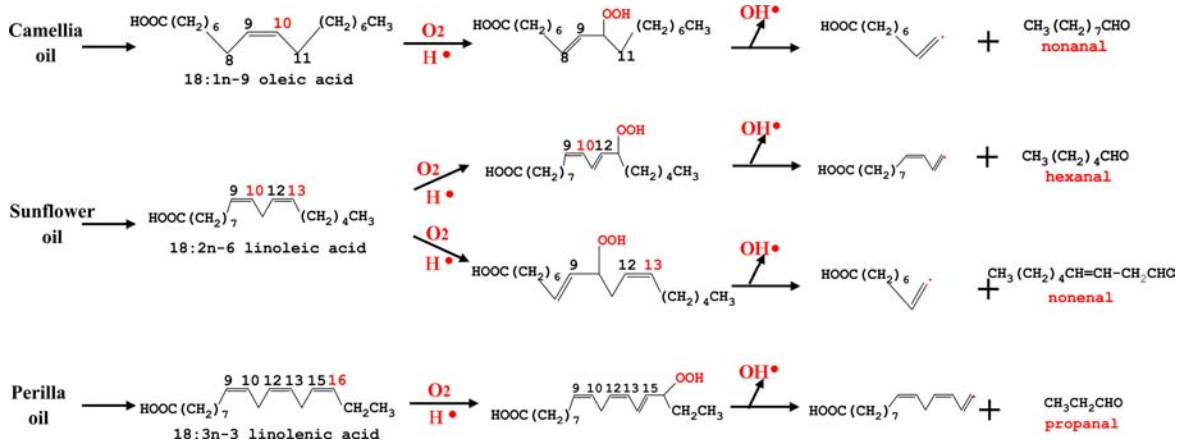


**Figure 4.** Nonanal, hexanal, nonenal, and propanal, from oleic, linoleic, and linolenic acyl group oxidation, identified in the HPLC-QqQ-MS after derivatization.

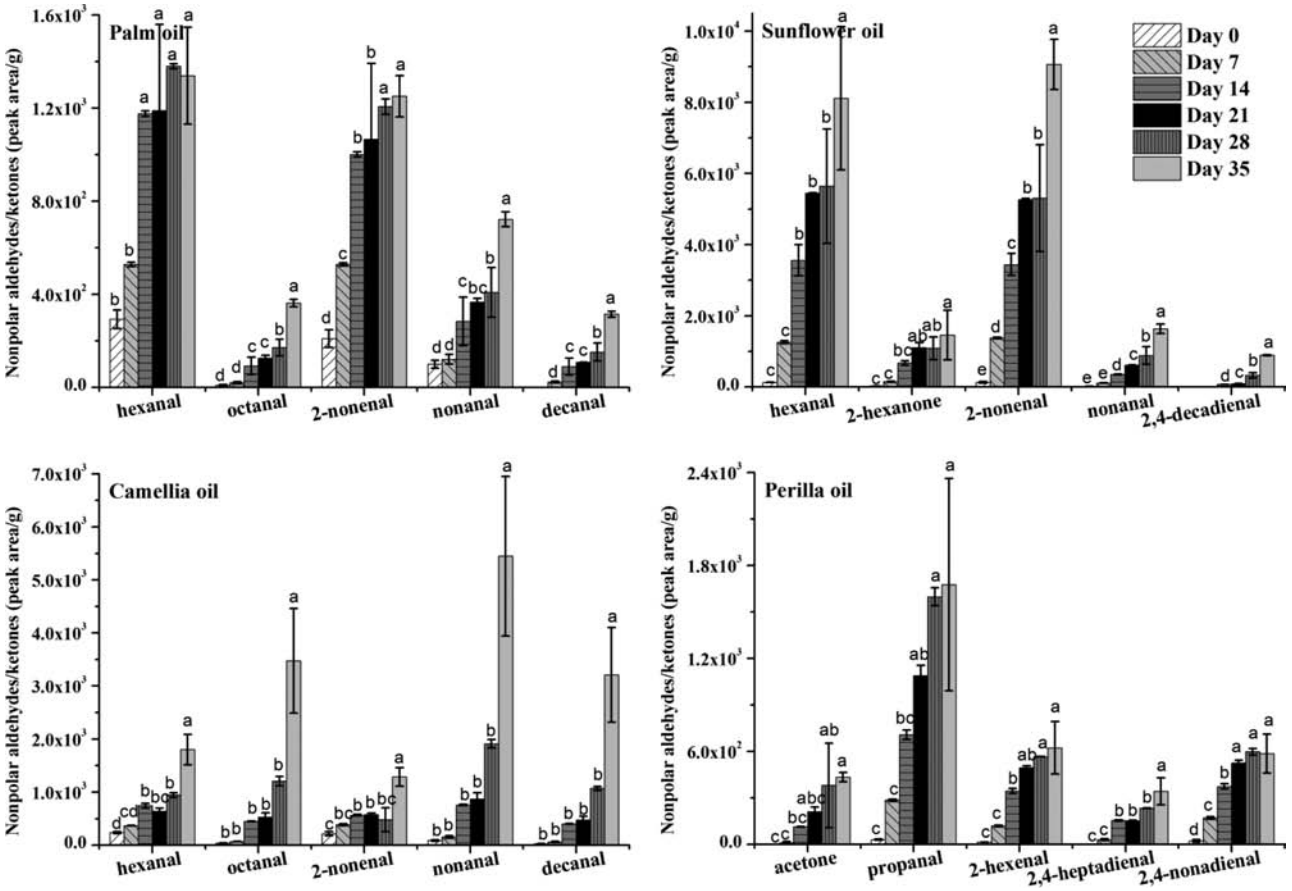


**Figure 5.** Oxidative volatile profiles obtained for four oils by plotting the content of five major carbonyl compounds (chosen from Figure 2) versus time of thermal treatment at 62 °C with limited air. Data are mean values ± SD, $n = 3$. Values followed by the same letter in the same assay are not significantly different ($p < 0.05$).

unsaturated, are considered as the main volatile secondary compounds formed in any oil oxidation process.[6] Vegetable oils are rich in unsaturated fatty acids, especially oleic, linoleic, and linolenic acids, which are the main causes of deterioration. It was reported that the relative oxidation rates of methyl oleate, linoleate, and linolenate were 1:10.3:21.6.[31] Different types of unsaturated fatty acids would generate various types of hydroperoxides and aldehydes/ketones.[32,33] Possible formation pathways of nonanal, propanal, hexanal, and 2-nonenal are shown in Figure 4. Nonanal is produced probably by breakdown of oleate 10-OOH; hexanal and 2-nonenal are probably from linoleate 13- and 10-OOH; propanal is probably by decomposition of linolenate 16-OOH. Additionally, decanal, 2-decenal, and octanal from oleate 8-, 9-, and 11-OOH, heptanal, 2-octenal, and pentanal originated by decomposition of linoleate 11- and 13-OOH; 2-hexenal and 2,4-heptadienal from linolenate 13- or 12-OOH were also produced.[32]

The breakdown of acyl group chains in unsaturated fatty acids was the main formation pathway of aldehydes/ketones. According to the distribution of aldehydes/ketones shown in

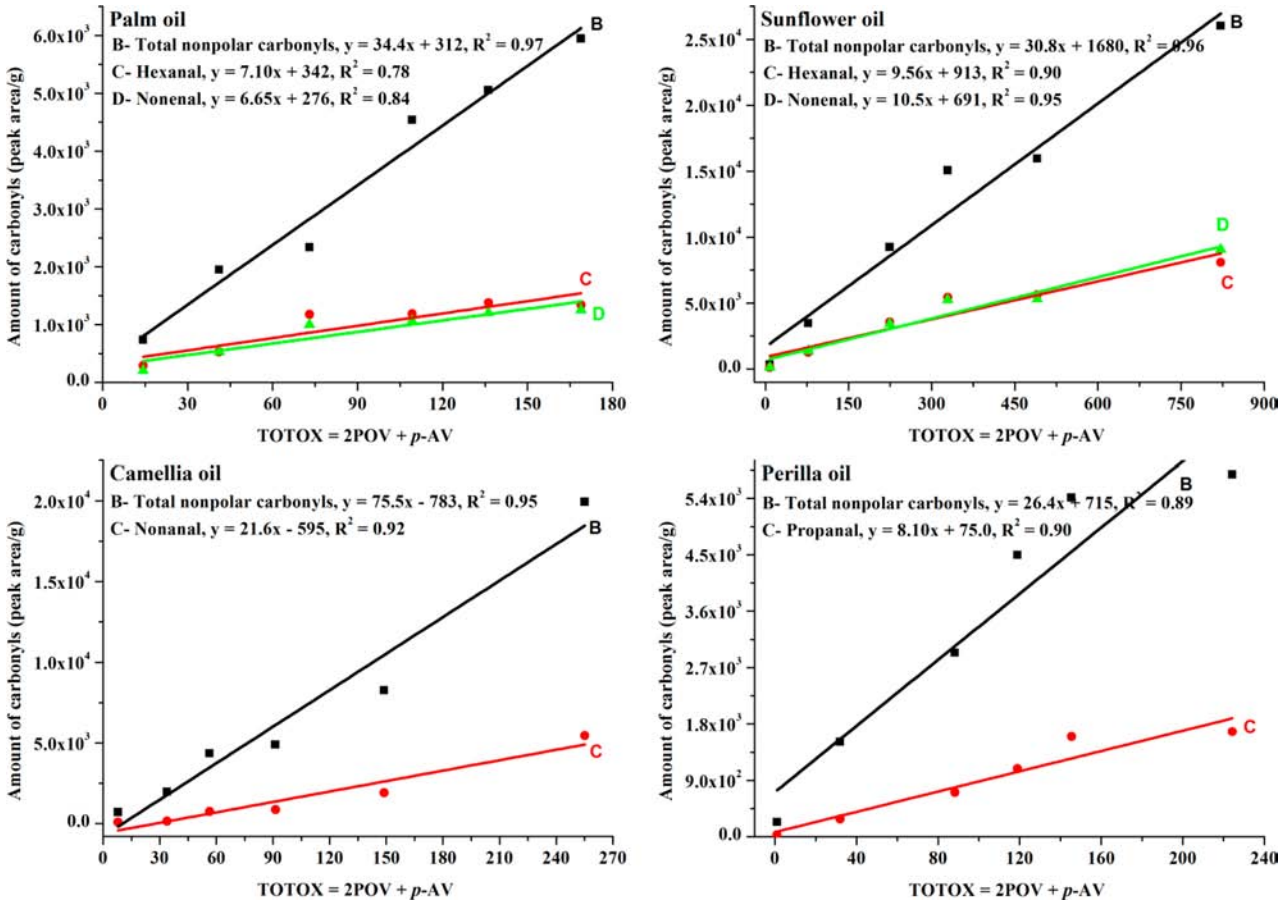


**Figure 6.** Linear correlations of TOTOX versus carbonyl compounds (peak area/g oil) during 35 days of accelerated oxidation at 62 °C.

Figures 2 and 3, these carbonyls derived from linoleic acyl groups showed the highest abundances, followed by those derived from oleic acyl and much lower proportions of those derived from linolenic acyl. Similar results were also found in the studies of many other studies on oil oxidation.[6,34] Additionally, the formation of all secondary products depends not only on the intrinsic property of lipid but also on the conditions under which the process takes place, such as temperature, amount of air, and type of bottle.[35,36]

**Changes of Carbonyls during Oxidation.** Before oxidation assay (day 0), only 10 types of carbonyl compounds in camellia oil and 9 types in palm oil were found, and sunflower and perilla oils showed a lower number of carbonyls, 6 and 5 types, respectively (Figure 2). It is well-known that the thermoxidative degradation of unsaturated fatty acids may result in the presence of many other secondary products, and their concentrations increased with time. As shown in Figure 3, the highest increment of total carbonyls (the sum of all detected aldehydes and ketones) measured as area count during 35 days of oxidation was detected in sunflower oil ($2.57 \times 10^4$) from $3.33 \times 10^2$ to $2.60 \times 10^4$, followed by camellia oil ($1.92 \times 10^4$). By contrast, there were lower increments in perilla oil ($5.54 \times 10^3$) and palm oil ($5.21 \times 10^3$). That means the order of oxidation stability was sunflower oil < camellia oil < perilla oil < palm oil. Interestingly, the order was the same as that in comparison of TOTOX of samples.

Figure 5 shows oxidative volatile profiles obtained for four oils by plotting five major carbonyl compounds' content (chosen from Figure 2) versus time of thermal treatment at 62 °C with limited air. It is very obvious that oil samples with different fatty acid compositions had their characteristic carbonyl compounds. For camellia oil (oleic acid mainly), nonanal was the most abundant carbonyl on the 35th day, followed by octanal and decanal. For sunflower oil (linoleic acid mainly), 2-nonenal and hexanal (measured as area count) showed the highest increments during 35 days of oxidation assay, increasing by $8.93 \times 10^3$ and $7.97 \times 10^3$, respectively. Hence, the two carbonyls might be good oxidation indicators for evaluating the oxidation state of sunflower oil. For perilla oil (linolenic acid mainly), propanal showed a more remarkable growth compared with other products, which might be also the key oxidation marker. Although 2-nonenal and hexanal were the most abundant carbonyls in palm oil, they showed slow increases after 14 days of oxidation. On the other hand, the concentration of nonanal was sharply increased after 14 days of oxidation and showed a high level on the 35th day. The increment tendency of nonanal, octanal, and decanal in palm oil had the same patterns as that in camellia oil. These results indicated linoleic acid was first oxidized and generated 2-nonenal and hexanal and then oleic acid was oxidized and formed nonanal (octanal and decanal) in palm oil.

The changes of the above characteristic carbonyls also played an important role in the evaluation of oil deterioration. By choosing 2-nonenal or hexanal as the oxidation indicators for palm and sunflower oils, nonanal for camellia oil, and propanal for perilla oil, it was found that sunflower oil had the highest indicator increment ($8.93 \times 10^3$ or $7.97 \times 10^3$), followed by camellia oil ($5.36 \times 10^3$), perilla oil ($1.65 \times 10^3$), and palm oil

($1.04 \times 10^3$ or $1.05 \times 10^3$). The order of oxidation stability was sunflower oil < camellia oil < perilla oil < palm oil. Hence, the yield of indicator could be used to demonstrate the oxidation state of oil. Meanwhile, the correct choice of oxidation indicator was necessary.

**Regression Analysis.** As shown in Figure 6, good linear correlations were observed between the total nonpolar carbonyl amount ($y$) and TOTOX ($x$) during 35 days of accelerated oxidation: palm oil ($y = 34.4x + 312$, $R^2 = 0.97$), camellia oil ($y = 75.5x - 783$, $R^2 = 0.95$), sunflower oil ($y = 30.8x + 1680$, $R^2 = 0.96$), and perilla oil ($y = 26.4x + 715$, $R^2 = 0.89$). These linear trends suggested that the amount of nonpolar carbonyls could be used to estimate oxidative deterioration of oils as TOTOX. To our knowledge, this is the first report on this linear relationship between nonpolar carbonyl amount and TOTOX during lipid oxidation. TOTOX was calculated by POV and *p*-AV, and also linear correlations were found between nonpolar carbonyl amount and POV in the four oils ($R^2 = 0.92-0.97$; Supporting Information, Figure S1). In a sense, generation of carbonyl compounds may be closely related to the production of hydroperoxides. Richards et al.[37] established a model relating ln[POV] to the volatile oxidation products: $\ln[\text{POV}] = -2.50 + 0.308 \times \ln[\text{hexanal}] + 0.229 \times \ln[\textit{trans,trans}\text{-2,4-heptadienal}]$, but $R^2$ was much lower (only 0.26). Hence, the total amount of nonpolar carbonyls was a good index for oxidation assessment, despite their difficult and time-consuming determination.

Generally, POV, *p*-AV, and TBARS are the common and foundational oxidation indices in lipid analysis. Actually, hexanal has become a well-known indicator owing to its being a major secondary oxidation product in lipid.[38−40] However, the profile of carbonyl compounds may be closely linked to the fatty acid composition of lipid. In our previous study, we found that oleic, linoleic, and linolenic acids had their characteristic carbonyl compounds during accelerated oxidation.[41] Thus, it is necessary and significant to choose corresponding oxidation indicators for oil samples with different fatty acids.

It was found that both hexanal and 2-nonenal were good oxidation indicators for sunflower and palm oils, as both had good linear relationship with TOTOX (Figure 6): hexanal = 7.10 TOTOX + 342, $R^2 = 0.78$, and nonenal = 6.65 TOTOX + 276, $R^2 = 0.84$ for palm oil; hexanal =9.56 TOTOX + 913, $R^2 = 0.90$, and nonenal = 10.5 TOTOX + 691, $R^2 = 0.95$ for sunflower oil. For camellia oil, nonanal was a good indicator because of the good linear correlation (nonanal = 21.6 TOTOX − 595, $R^2 = 0.92$). Propanal was a good indicator for perilla oil, and also a good linear relationship was found between the amount of propanal and TOTOX: propanal = 8.10 TOTOX + 75.0, $R^2 = 0.90$. Hence, the yield of the indicator was a key index for evaluating the oxidation state of vegetable oil.

In summary, in this work, palm, camellia, sunflower, and perilla oils were selected in oxidation assays in consideration of their typical fatty acid compositions. Camellia (20 types), sunflower (19 types), and palm (19 types) oils were found to have more types of nonpolar carbonyls than perilla oil (14 types) on the 35th day. Besides, alkanal contained a higher proportion of nonpolar carbonyl than alkenal and alkadienal in the four oils. Interestingly, the four oils had their own characteristic carbonyl products, which could be used as markers to monitor the oxidation state of oils. Nonanal was a good oxidation indicator for camellia oil (oleic acid mainly); hexanal and nonenal were good oxidation indicators for sunflower oil (linoleic acid mainly) and palm oil (palmitic and oleic acids mainly); propanal was a good oxidation indicator for perilla oil (linolenic acid mainly). In addition, these indicators had good linear correlations with their corresponding TOTOX and the amounts of total nonpolar carbonyls in oils ($R^2 > 0.8$) during 35 days of accelerated oxidation. According to the change patterns of POV, TOTOX, total nonpolar carbonyls, and oxidation indicator, the corresponding order of oxidation stability was uniformly sunflower oil < camellia oil < perilla oil < palm oil. Hence, the yield of indicator was a key index for evaluating the oxidation state of vegetable oil. In addition, the determination of indicator was a novel approach to monitor oil oxidation. They played an important role as TOTOX or POV in the oxidation assessment of lipid.

## ■ ASSOCIATED CONTENT

### Ⓢ Supporting Information

Figures S1 and S2. This material is available free of charge via the Internet at http://pubs.acs.org.

## ■ AUTHOR INFORMATION


### Corresponding Authors

*(Y.F.) Phone/fax: +86 791 88304402. E-mail: fanyawei@tom.com. Mail: State Key Laboratory of Food Science and Technology, Nanchang University, 235 Nanjing East Road, Nanchang 330047, Jiangxi, China.

*(Z.-Y.D.) E-mail: zeyuandeng@hotmail.com



### Funding

This study was supported by the National Natural Science Foundation of China (31460427; 31071561) and Jiangxi Provincial Natural Science Foundation of China (20132BAB204001).


### Notes

The authors declare no competing financial interest.

## ■ ABBREVIATIONS USED

AV, acid value; POV, peroxide value; *p*-AV, *p*-anisidine value; TOTOX, total oxidation value; DNPH, 2,4-dinitrophenylhydrazine; FAME, fatty acid methyl ester(s); DAD, diode array detector; UV, ultraviolet; ESI, electrospray ionization

## ■ REFERENCES


(1) Choe, E.; Min, D. B. Mechanisms and factors for edible oil oxidation. *Compr. Rev. Food Sci. Food Saf.* **2006**, *5*, 169−186.

(2) Beltrán, A.; Ramos, M.; Grané, N.; Martín, M. L.; Garrigós, M. C. Monitoring the oxidation of almond oils by HS-SPME-GC-MS and ATR-FTIR: application of volatile compounds determination to cultivar authenticity. *Food Chem.* **2011**, *126*, 603−609.

(3) Poyato, C.; Ansorena, D.; Navarro-Blasco, I.; Astiasarán, I. A novel approach to monitor the oxidation process of different types of heated oils by using chemometric tools. *Food Res. Int.* **2014**, *57*, 152−161.

(4) Petersen, K. D.; Kleeberg, K. K.; Jahreis, G.; Busch-Stockfisch, M.; Fritsche, J. Comparison of analytical and sensory lipid oxidation parameters in conventional and high-oleic rapeseed oil. *Eur. J. Lipid Sci. Technol.* **2012**, *114*, 1193−1203.

(5) Guillén, M. D.; Uriarte, P. S. Aldehydes contained in edible oils of a very different nature after prolonged heating at frying temperature: presence of toxic oxygenated $\alpha,\beta$ unsaturated aldehydes. *Food Chem.* **2012**, *131*, 915−926.

(6) Goicoechea, E.; Guillén, M. D. Volatile compounds generated in corn oil stored at room temperature. Presence of toxic compounds. *Eur. J. Lipid Sci. Technol.* **2014**, *116*, 395−406.

(7) Guillen, M. D.; Goicoechea, E. Formation of oxygenated α,β-unsaturated aldehydes and other toxic compounds in sunflower oil oxidation at room temperature in closed receptacles. *Food Chem.* **2008**, *111*, 157−164.
(8) Seppanen, C. M.; Saari Csallany, A. Simultaneous determination of lipophilic aldehydes by high-performance liquid chromatography in vegetable oil. *J. Am. Oil Chem. Soc.* **2001**, *78*, 1253−1260.
(9) Zhu, H.; Li, X.; Shoemaker, C. F.; Wang, S. C. Ultrahigh performance liquid chromatography analysis of volatile carbonyl compounds in virgin olive oils. *J. Agric. Food Chem.* **2013**, *61*, 12253−12259.
(10) Narváez-Rivas, M.; Gallardo, E.; León-Camacho, M. Chemical changes in volatile aldehydes and ketones from subcutaneous fat during ripening of Iberian dry-cured ham. Prediction of the curing time. *Food Res. Int.* **2014**, *55*, 381−390.
(11) Mathew, S.; Grey, C.; Rumpunen, K.; Adlercreutz, P. Analysis of carbonyl compounds in sea buckthorn for the evaluation of triglyceride oxidation, by enzymatic hydrolysis and derivatisation methodology. *Food Chem.* **2011**, *126*, 1399−1405.
(12) Spiteller, G.; Kern, W.; Spiteller, P. Investigation of aldehydic lipid peroxidation products by gas chromatography-mass spectrometry. *J. Chromatogr., A* **1999**, *843*, 29−98.
(13) Wang, S.; Hwang, H.; Yoon, S.; Choe, E. Temperature dependence of autoxidation of perilla oil and tocopherol degradation. *J. Food Sci.* **2010**, *75*, C498−C505.
(14) Iqbal, S.; Bhanger, M. Stabilization of sunflower oil by garlic extract during accelerated storage. *Food Chem.* **2007**, *100*, 246−254.
(15) Kawahara, F.; Dutton, H. Volatile cleavage products of autoxidized soybean oil. *J. Am. Oil Chem. Soc.* **1952**, *29*, 372−377.
(16) Gaddis, A.; Ellis, R.; Currie, G. Carbonyls in oxidizing fat. V. The composition of neutral volatile monocarbonyl compounds from autoxidized oleate, linoleate, linolenate esters, and fats. *J. Am. Oil Chem. Soc.* **1961**, *38*, 371−375.
(17) Shahidi, F.; Wanasundara, U. N. Chapter 14. Methods for measuring oxidative rancidity in fats and oils. In *Food Lipids: Chemistry, Nutrition and Biotechnology*, 2nd ed.; CRC Press: Boca Raton, FL, USA, 2002; pp 387−403.
(18) Hu, J. N.; Zhang, B.; Zhu, X. M.; Li, J.; Fan, Y. W.; Liu, R.; Tang, L.; Lee, K. T.; Deng, Z. Y. Characterization of medium-chain triacylglycerol (MCT)-enriched seed oil from *Cinnamomum camphora* (Lauraceae) and its oxidative stability. *J. Agric. Food Chem.* **2011**, *59*, 4771−4778.
(19) Cruz-Hernandez, C.; Deng, Z. Y.; Zhou, J.; Hill, A. R.; Yurawecz, M. P.; Delmonte, P.; Mossoba, M. M.; Dugan, M. E. R.; Kramer, J. K. G. Methods for analysis of conjugated linoleic acids and trans-18:1 isomers in dairy fats by using a combination of gas chromatography, silver-ion thin-layer chromatography/gas chromatography, and silver-ion liquid chromatography. *J. AOAC Int.* **2004**, *87*, 545−562.
(20) Lei, L.; Li, J.; Luo, T.; Fan, Y. W.; Zhang, B.; Ye, J.; Ye, H.; Sun, Y.; Deng, Z. Y. Predictable effects of dietary lipid sources on the fatty acids compositions of four 1-year-old wild freshwater fish from Poyang Lake. *J. Agric. Food Chem.* **2012**, *61*, 210−218.
(21) Cerretani, L.; Maggio, R. M.; Barnaba, C.; Toschi, T. G.; Chiavaro, E. Application of partial least square regression to differential scanning calorimetry data for fatty acid quantitation in olive oil. *Food Chem.* **2011**, *127*, 1899−1904.
(22) Ramadan, M. F.; Wandan, K. M. M. Blending of corn oil with black cumin (*Nigella sativa*) and coriander (*Coriandrum sativum*) seed oils: impact on functionality, stability and radical scavenging activity. *Food Chem.* **2012**, *132*, 873−879.
(23) Li, H.; Fan, Y. W.; Li, J.; Tang, L.; Hu, J. N.; Deng, Z. Y. Evaluating and predicting the oxidative stability of vegetable oils with different fatty acid compositions. *J. Food Sci.* **2013**, *78*, H633−H641.
(24) Endo, Y.; Li, C. M.; Tagiri-Endo, M.; Fujimoto, K. A modified method for the estimation of total carbonyl compounds in heated and frying oils using 2-propanol as a solvent. *J. Am. Oil Chem. Soc.* **2001**, *78*, 1021−1024.
(25) Pang, X.; Shi, X.; Mu, Y.; He, H.; Shuai, S.; Chen, H.; Li, R. Characteristics of carbonyl compounds emission from a diesel-engine using biodiesel-ethanol-diesel as fuel. *Atmos. Environ.* **2006**, *40*, 7057−7065.
(26) Kölliker, S.; Oehme, M.; Dye, C. Structure elucidation of 2,4-dinitrophenylhydrazone derivatives of carbonyl compounds in ambient air by HPLC/MS and multiple MS/MS using atmospheric chemical ionization in the negative ion mode. *Anal. Chem.* **1998**, *70*, 1979−1985.
(27) Belitz, H. D.; Grosch, W.; Schieberle, P. Chapter 14. Edible fats and oils. In *Food Chemistry*, 4th ed.; Springer: Berlin Heidelberg, Germany, 2009; pp 640−669.
(28) Petersen, K. D.; Kleeberg, K. K.; Jahreis, G.; Fritsche, J. Assessment of the oxidative stability of conventional and high-oleic sunflower oil by means of solid-phase microextraction-gas chromatography. *Int. J. Food Sci. Nutr.* **2012**, *63*, 160−169.
(29) Sjovall, O.; Kuksis, A.; Kallio, H. Tentative identification and quantification of TAG core aldehydes as dinitrophenylhydrazones in autoxidized sunflowerseed oil using reversed-phase HPLC with electrospray ionization MS. *Lipids* **2003**, *38*, 1179−1190.
(30) Guillen, M. D.; Goicoechea, E. Oxidation of corn oil at room temperature: primary and secondary oxidation products and determination of their concentration in the oil liquid matrix from $^{1}$H nuclear magnetic resonance data. *Food Chem.* **2009**, *116*, 183−192.
(31) Fatemi, S. H.; Hammond, E. G. Analysis of oleate, linoleate and linolenate hydroperoxides in oxidized ester mixtures. *Lipids* **1980**, *15*, 379−385.
(32) Morales, M.; Rios, J.; Aparicio, R. Changes in the volatile composition of virgin olive oil during oxidation: flavors and off-flavors. *J. Agric. Food Chem.* **1997**, *45*, 2666−2673.
(33) Wheatley, R. A. Some recent trends in the analytical chemistry of lipid peroxidation. *TrAC−Trends Anal. Chem.* **2000**, *19*, 617−628.
(34) Guillén, M. D.; Uriarte, P. S. Simultaneous control of the evolution of the percentage in weight of polar compounds, iodine value, acyl groups proportions and aldehydes concentrations in sunflower oil submitted to frying temperature in an industrial fryer. *Food Control* **2012**, *24*, 50−56.
(35) Guillén, M. D.; Ruiz, A. Oxidation process of oils with high content of linoleic acyl groups and formation of toxic hydroperoxy- and hydroxyalkenals. A study by $^{1}$H nuclear magnetic resonance. *J. Sci. Food Agric.* **2005**, *85*, 2413−2420.
(36) Guillén, M. D.; Goicoechea, E. Detection of primary and secondary oxidation products by fourier transform infrared spectroscopy (FTIR) and $^{1}$H nuclear magnetic resonance (NMR) in sunflower oil during storage. *J. Agric. Food Chem.* **2007**, *55*, 10729−10736.
(37) Richards, A.; Wijesundera, C.; Salisbury, P. Evaluation of oxidative stability of canola oils by headspace analysis. *J. Am. Oil Chem. Soc.* **2005**, *82*, 869−874.
(38) Sanches-Silva, A.; Rodriguez-Bernaldo de Quiros, A.; López-Hernández, J.; Paseiro-Losada, P. Determination of hexanal as indicator of the lipidic oxidation state in potato crisps using gas chromatography and high-performance liquid chromatography. *J. Chromatogr., A* **2004**, *1046*, 75−81.
(39) Brunton, N. P.; Cronin, D. A.; Monahan, F. J.; Durcan, R. A comparison of solid-phase microextraction (SPME) fibres for measurement of hexanal and pentanal in cooked turkey. *Food Chem.* **2000**, *68*, 339−345.
(40) Panseri, S.; Soncin, S.; Chiesa, L. M.; Biondi, P. A. A headspace solid-phase microextraction gas-chromatographic mass-spectrometric method (HS-SPME-GC/MS) to quantify hexanal in butter during storage as marker of lipid oxidation. *Food Chem.* **2011**, *127*, 886−889.
(41) Cao, J.; Zou, X. G.; Deng, L.; Fan, Y. W.; Li, H.; Li, J.; Deng, Z. Y. Analysis of nonpolar lipophilic aldehydes/ketones in oxidized edible oils using HPLC-QqQ-MS for the evaluation of their parent fatty acids. *Food Res. Int.* **2014**, *64*, 901−907.

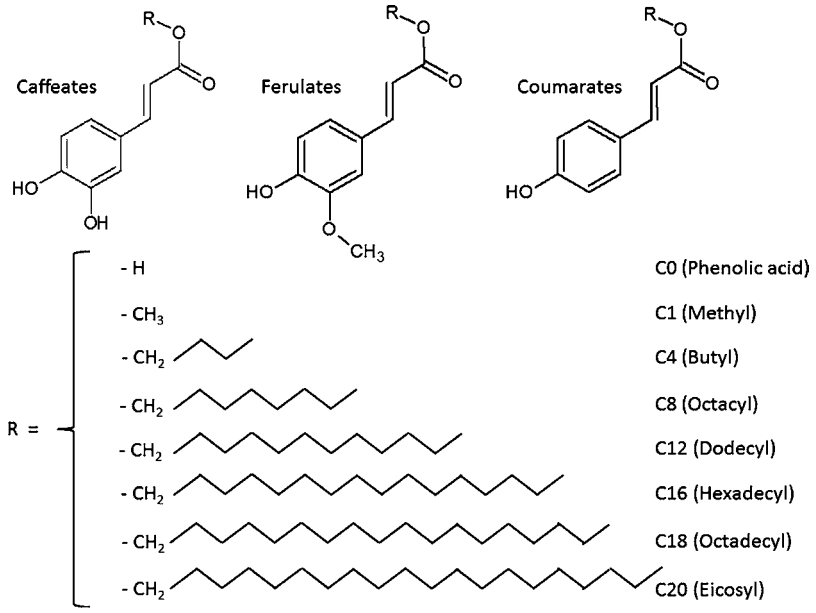


**Figure 1.** Molecular structure of caffeic, ferulic, and coumaric acids and synthesized alkyl caffeates, ferulates and coumarates.

The aim of the study was to evaluate the antioxidant properties of hydroxycinnamic acids with very similar structures and their alkyl esters (phenolipids) using different *in vitro* antioxidant assays. Moreover, the efficacy of the antioxidants was evaluated in a microemulsion using the conjugated autoxidizable triene (CAT) assay. The phenolics selected only differ in one chemical group on the phenolic ring (Figure 1). Caffeic acid has an *o*-dihydroxyl (catechol) group, ferulic acid has a hydroxyl and a methoxyl group, and coumaric acid has one hydroxyl group substituted to the benzene ring. It is hypothesized that the structure will impact antioxidant efficacy and critical chain length for the different phenolipids: caffeates, ferulates, and coumarates.

## MATERIALS AND METHODS

**Materials.** Phenolic acids (caffeic, ferulic, and coumaric), alcohols, Amberlite IR-120H, and molecular sieves were purchased from Sigma-Aldrich (Saint Quentin, France). All solvents used were of HPLC or analytical grade and were purchased from Sigma (Saint Quentin, France). Silica columns for flash chromatography were purchased from Acros organics (Geel, Belgium). Tung oil (872 g/mol), Brij 35 (a nonionic polyoxyethylene surfactant, estimated Mw 1198 g/mol), AAPH (2,2′-azobis-2-methyl-propanimidamide, dihydrochloride), phosphate buffer solution (PBS, pH 7.2), alumina, BHT (butylated hydroxytoluene), and trolox were purchased from Sigma-Aldrich (Steinheim, Germany). EDTA (Titriplex, ethylenedinitrilo-tetraacetic acid disodium salt dehydrate) was purchased from Merck (Darmstadt, Germany).

**Synthesis of Caffeates, Ferulates, and Coumarates (Phenolipids).** Esterification of caffeic, ferulic, and coumaric acids was catalyzed by acid either added as the strongly acidic sulfonic resin Amberlite IR-120H or as pure sulfuric acid to the reaction medium. The composition of the reaction mixtures depending on catalyst applied is described below. Molecular sieves (3 Å, 4−8 mesh, 40 mg/mL, Aldrich, St. Louis, MO, USA) were added to the reaction mixtures to remove water generated during reaction. The reaction mixtures were stirred in an orbital shaker (250 rpm, 55 °C) during the whole reaction time. Samples (20 μL) from the reaction mixtures were regularly withdrawn, mixed with methanol (980 μL), filtered (0.45 μm syringe filter Millex-FH, Millipore Corp., Bedford, MA, USA), and analyzed by reverse phase HPLC with UV detection at 328 nm.

*Methyl Caffeate, Methyl Feulate, and Methyl Coumarate Synthesized with Amberlite IR-120H.* Phenolic acid (3 g, caffeic acid (16.7 mmol), ferulic acid (15.4 mmol), and coumaric acid (18.3 mmol)) were solubilized in methanol (150 mL, 3.7 mol) in a dark, sealed bottle in an orbital shaker. The reaction between phenolic acid and methanol was catalyzed by adding 5% sulfonic resin Amberlite IR-120H (w/w of total weight of both substrates, dried 4 h at 103 °C).

*Phenolipids Synthesized with Sulfuric Acid.* Phenolic acid (caffeic, ferulic, and coumaric acids) was solubilized in THF (tetrahydrofuran) in a dark, sealed bottle in an orbital shaker. THF was applied as a solubilization medium due to the poor solubility of phenolic acids in longer chain alcohols (lipophilic medium). Alcohol was added to the phenolic acid-THF solution in a mole ratio of 1 mol phenolic acid to 3−5 mol of alcohol. Excess of alcohol was reduced as much as possible due to difficulties in the purification of synthesized phenolipids. The purification difficulties were due to the similarity in polarity of synthesized phenolipids and unreacted alcohols. Pure sulfuric acid (5% v/v of total volume of alcohol and THF) was added to the reactants in THF.

**Purification of Synthesized Phenolipids.** Methyl esters were purified one way, and all other phenolipids were purified in different ways depending on the phenolic acid from which they were synthesized. The different ways applied to purify the synthesized phenolipids are described below. The purity of the purified phenolipids was evaluated quantitatively by HPLC-MS[13] and qualitatively by TLC. The HPLC-MS analysis of the synthesized compounds revealed a purity ≥95%.

*Purification of Methyl Caffeate, Ferulate, and Coumarate.* When the reaction was completed (>90% conversion), the reaction was stopped by removal of Amberlite IR-120H and molecular sieves in a centrifugation and filtration step. Then THF and unreacted methanol were evaporated, the mixture was diluted in ethyl acetate, and unreacted phenolic acid was removed by washing the ethyl acetate solution with two different saturated salt solutions (sodium bicarbonate (3 times), sodium chloride (2 times)), and water (2 times). To remove traces of water, the ethyl acetate solution was dried over sodium sulfate. Finally, the purified methyl ester was obtained by evaporating off ethyl acetate.

*Purification of Butyl, Octyl, Dodecyl, Hexadecyl, Octadecyl, and Eicosyl Esters.* When the reaction was completed (>90% conversion), molecular sieves were removed from the reaction mixture in a centrifugation and filtration step. Then, THF was evaporated, and the reaction mixture was diluted in ethyl acetate. To neutralize the reaction mixture in ethyl acetate, this solution was washed with water

several times and dried over sodium sulfate to remove traces of water. Then, the remaining alcohol and phenolic acid were eliminated by flash chromatography (CombiFlash Companion system, Teledyne Isco Inc., Lincoln, NE, USA). Separation was carried out on a silica column (pore size 60 Å, Acros organics, Geel, Belgium) using an elution gradient of two solvents with different polarities. Because of the different polarities of the phenolic acids and their alkyl esters, a different elution gradient was applied for caffeates (chloroform and methanol, 0−100%), ferulates, and coumarates (dichloromethane and ethyl acetate, 5−100%), respectively. For some phenolipids, alcohol was still present after flash chromatography. In these cases, preparative TLC with different migration solvents was applied (caffeates, 96% chloroform and 4% methanol; ferulates, 95% dichloromethane and 5% ethyl acetate; and coumarates, 90% dichloromethane and 10% ethyl acetate).

**Antioxidant Properties.** The antioxidative properties of the phenolic acids and their synthesized alkyl esters were evaluated using three different *in vitro* antioxidant assays: radical scavenging (DPPH), iron chelating activity, and reducing power. All antioxidants were evaluated in 4 concentrations (final concentrations: 50, 100, 200, and 400 $\mu$M) and were measured in triplicate ($n$ = 3). The concentrations were selected based on earlier antioxidant property analysis and storage experiments with similar compounds.[14]

*Radical Scavenging.* Antioxidants were solubilized in methanol in different concentrations, and BHT was included in this assay as a positive control in the same concentrations. The antioxidant solution (150 $\mu$L) was diluted 1:1 (v/v) with 0.1 mM DPPH in ethanol (96%, 150 $\mu$L). Then, 200 $\mu$L of this mixture was transferred to a well in the microplate.[15] The absorbance at 517 nm was measured after 30 min (RT, darkness) in a microplate reader (Synergy 2 BioTek, Winooski, VT, USA). Results are expressed as inhibition percentages.

$$\text{Inhibition } [\%] = \left(1 - \frac{A_s - A_0}{A_b}\right) \times 100$$

where $A_s$ is the measured absorbance after the antioxidant-DPPH reaction, $A_0$ is the measured absorbance of antioxidant in ethanol without DPPH (sample control), and $A_b$ is the absorbance measured of DPPH without the antioxidant added.

*Reducing Power.* Antioxidants were solubilized in methanol in different concentrations, and ascorbic acid was included in this assay as a positive control in the same concentrations. Antioxidant methanolic solutions (200 $\mu$L) were transferred to test tubes, and 0.2 M phosphate buffer (200 $\mu$L) and 1% potassium ferricyanide (200 $\mu$L) were added. These mixtures were incubated at 50 °C for 20 min. After incubation, 10% TCA (trichloroacetic acid, 200 $\mu$L) was added and mixed. This reaction mixture (228 $\mu$L) was transferred to an Eppendorf tube and mixed with an equal amount of water (228 $\mu$L). Ferric chloride (0.1%, 46 $\mu$L) was added to the reaction mixture, and it was incubated for 10 min at RT. After incubation, the reaction mixtures (200 $\mu$L) were transferred to the wells in the microplate,[15] and absorbance was measured at 700 nm in a microplate reader (Synergy 2 BioTek, Winooski, VT, USA). Results are shown relative to ascorbic acid ($Abs_{Sample}/Abs_{Ascorbic\ acid}$).

*Iron Chelating Ability.* Antioxidants were solubilized in warm water in different concentrations. Because of solubility problems with long alkyl chain phenolipids, only caffeic acid, ferulic acid, coumaric acid, and their methyl esters were evaluated for their chelating ability of ferrous chloride. EDTA was included in this assay as a positive control in the same concentrations as the phenols and phenolipids. For further details, refer to Sørensen et al.[14] The absorbance was measured at 562 nm (UV-1800 Shimadzu, Columbia, MD, USA), and results are expressed as chelating activities.

**Antioxidant (Hydroxycinnamic Acids and Their Alkyl Esters)−Iron Interactions.** Interactions between iron and the antioxidant were evaluated using a spectrophotometer according to the method developed by Sørensen et al.[9] Methanolic solutions of caffeic acid, ferulic acid, coumaric acid, and their methyl esters were diluted in a buffer solution: 10 mM sodium acetate−imidazole (pH 7). Moreover, methanolic solutions of caffeic acid and methyl caffeate were also diluted in PBS (pH 7.2). The final concentration of antioxidant was 100 $\mu$M. Iron, as $FeSO_4$, was solubilized in 0.50 M HCl and buffer (1:1, v/v) and added to pure buffer and to the antioxidant−buffer solution. The final concentration of iron was 100 $\mu$M. Each solution was measured using a spectrophotometer (UV-1800, Shimadzu Scientific Instruments, Columbia, MD, USA), and a spectrum was recorded in the UV−vis region (200−800 nm).

**Conjugated Autoxidizable Triene (CAT) Assay.** Stock solutions of the different hydroxycinnamic acids, their alkyl esters, and trolox were prepared in methanol. Various volumes of these antioxidant methanolic solutions were added to 1.8 mL of PBS (pH 7.2) and then filled up to 2 mL with pure methanol. These buffered solutions with antioxidant (50 $\mu$L) were transfered into a microtiterplate, (UV-Star 96-well microplate, Greiner, Frickenhausen, Germany). The microplate was then preheated (37 °C) and stirred in the microplate reader (Synergy 2, BioTek, Winooski, VT, USA) for 5 min at medium speed. Brij 35-PBS (34 $\mu$M, 25 mL) was added to 5 mg of stripped tung oil in a brown glass bottle. Brij 35−PBS−tung oil was premixed for at least 10 s using a vortex apparatus before the mixture was homogenized with a POLYTRON PT1200E (Kinematica AG, Lucerne, Switzerland) at high speed for 4 min. Each well was then filled with 100 $\mu$L of the tung oil-in-PBS microemulsion; the plate was again preheated and stirred for 1 min. The oxidation of tung oil was initiated by adding 50 $\mu$L of 4 mM AAPH in PBS. Finally, each microplate well contained 200 $\mu$L of the following mixture: 115 $\mu$M stripped tung oil, 17 $\mu$M Brij 35, 1 mM AAPH, and various concentrations of phenolics, phenolipids, or trolox (0.2−0.8 $\mu$M). The progress of lipid oxidation was immediately followed by measuring the decrease in absorbance at 273 nm. Measurements were performed each minute for 6 h at 37 °C with 5 s stirring before each measurement. Each antioxidant concentration was measured in triplicate on the plate and via independent measurements (three different microplates), $n$ = 9. Results were expressed as CAT value (mean ± SD). This method was developed by Laguerre et al.[16] For further details about the calculations, see refs 7 and 16 by Laguerre et al.

**Removal of Tocopherols from Tung Oil.** Tung oil was stripped from tocopherols using an alumina packed glass column. A glass column was packed with 25 g of alumina oxide in hexane. The excess of hexane was removed. Tocopherols were removed from the tung oil by passing 25 mL (200 mg/mL) of tung oil in hexane through the packed column. Pure hexane (50 mL) was then loaded to the column to get the loaded tung oil through the column. After passing the tung oil through the column, hexane in the stripped tung oil was removed using a vacuum rotary evaporator. Finally, a trace of hexane in the stripped tung oil was removed under nitrogen. The stripped tung oil was bottled (5 mg/bottle) in brown glass tubes, flushed with nitrogen, and stored at −80 °C until use (CAT Assay). Furthermore, the absence of tocopherols in the stripped tung oil was checked by HPLC according to the AOCS method.[17]

**Data Treatment.** All measurements were performed in triplicate and reported as average ± SD. In the separate method descriptions, calculations are described, or there are references to data treatment.

*Statistics.* The obtained results were analyzed by one-way ANOVA (GraphPad Prism, version 4.03, GraphPad Software Inc.). Bonferroni multiple comparison post-test was used to test differences between samples. For statistics, a significance level of $p < 0.05$ was used. When a significant difference was observed between samples, they are denoted with different lowercase letters in the text, table and figures.

## RESULTS

**Antioxidant Properties.** All the synthesized antioxidants were evaluated for different antioxidant properties as radical scavenger (DPPH), reducing power, and iron chelation in *in vitro* assays.

*Radical Scavenging Properties.* The phenolics and synthesized phenolipids were all able to scavenge free radicals measured by the DPPH assay (Figure 2A−C). Caffeic acid and caffeates had similar radical scavenging activities in the

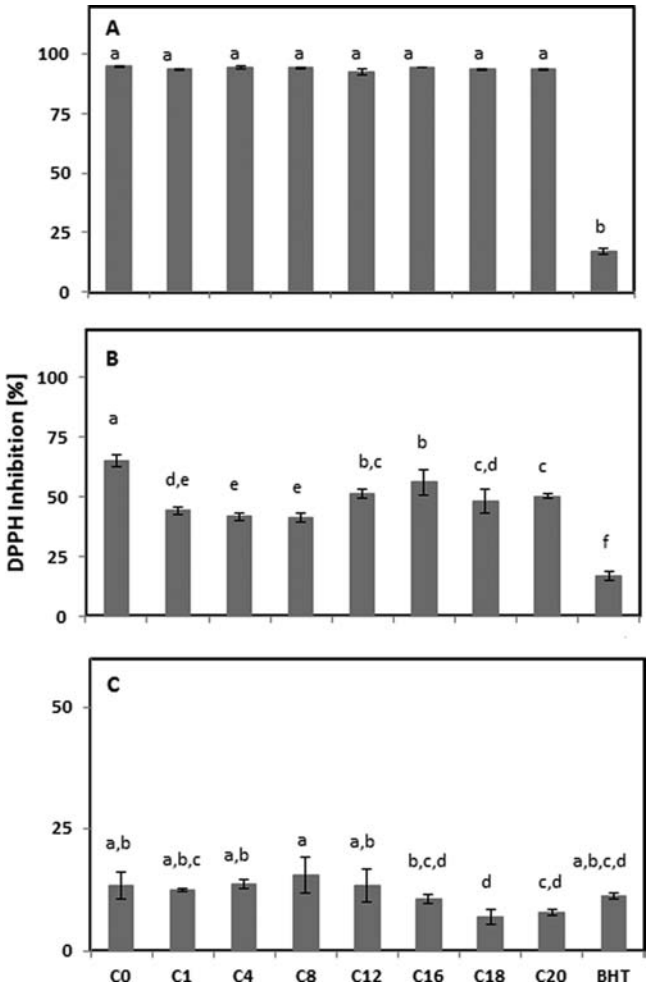


**Figure 2.** Radical scavenging properties of hydroxycinnamic acids and their alkyl esters at 100 $\mu$M calculated as DPPH inhibition [%]. (A) Caffeic acid and caffeates, (B) ferulic acid and ferulates, and (C) coumaric acid and coumarates. BHT was included as a positive control in this assay. C0 is phenolic acid, and C1 to C20 indicate the length of the alkyl chain grafted to the phenolic acids (phenolipids). Error bars indicate the standard deviation ($n$ = 3). Significant differences between different compounds are denoted with different lowercase letters (significance level was $p < 0.05$).

concentration range (50−400 $\mu$M) evaluated (Supporting Information, Figure A). The DPPH inhibition was >85%, and the lowest inhibition was observed for caffeic acid (95%) and caffeates (87−92%) at the lowest concentration (50 $\mu$M) evaluated. At this low concentration, a significantly different DPPH inhibition was observed, although the differences in inhibition were small. In the concentration range of 100−400 $\mu$M, the DPPH inhibition of caffeic acid and alkyl caffeates was not significantly influenced by the applied concentration, and no significant effects of the chain length were observed. Caffeic acid and all alkyl caffeates were more efficient in scavenging DPPH than BHT irrespective of the concentration applied. Ferulic acid appeared to have the highest DPPH inhibition followed by long chain alkyl ferulates > medium, short chain alkyl ferulates, and BHT (Figure 2B). BHT had significantly lower DPPH inhibition than ferulic acid (~1.5−4 fold) and alkyl ferulates (~1.4−3 fold) at the different concentrations, but significant differences in DPPH inhibition between ferulic acid and alkyl ferulates were more unclear. The ranking of ferulic acid and alkyl ferulates was independent of their concentration in the evaluated range (50−400 $\mu$M, Supporting Information, Figure A). Coumaric acid and alkyl coumarates had low DPPH inhibition <25% in the evaluated concentration range (50−400 $\mu$M, Supporting Information, Figure A. Depending upon the concentration evaluated, coumaric acid (50 $\mu$M) or octyl coumarate (100 $\mu$M, Figure 2C) had the highest DPPH inhibition. For high concentrations (200 and 400 $\mu$M), BHT showed significantly higher inhibition percentages compared to those of coumaric acid (~1.5−2-fold) and coumarates (~2.5−3.7-fold). Overall, caffeic acid and alkyl caffeates had the highest radical scavenging activity followed by ferulic acid and alkyl ferulates, whereas coumaric acid and alkyl coumarates were least efficient.

*Reducing Power.* The ability of hydroxycinnamic acids and their alkyl esters to reduce ferric ions ($Fe^{3+}$) to ferrous ions ($Fe^{2+}$) is shown in Figure 3 (100 $\mu$M) and Figure B in the Supporting Information (50−400 $\mu$M). For alkyl caffeates and ferulates, the same trend was observed (Figure 3A and B). Caffeic acid and ferulic acid had the highest reducing power, and an increase in alkyl chain length for caffeates and ferulates significantly decreased the reducing power. The reducing power observed for coumaric acid and alkyl coumarates was different (Figure 3C). At low concentration (50 $\mu$M), coumaric acid had the highest reducing power. Whereas, at 100 $\mu$M and higher concentrations dodecyl coumarate appeared to have the highest reducing power. Its effect was significantly higher than the other alkyl coumarates only at the highest concentration (400 $\mu$M). Overall, the highest reducing power was obtained with caffeic acid and its alkyl esters followed by ferulic acid and its alkyl esters. Lowest reducing effect was observed for coumaric acid and its alkyl esters. As shown in Figure 3, results were calculated relative to ascorbic acid. Increments in concentration of ascorbic acid resulted in increased reducing power (50−400 $\mu$M). Since, the reducing power of coumaric acid and coumarates decreased slightly with increased concentrations, their reducing power increased to a lower extent with increasing concentrations than that of ascorbic acid. In contrast, increasing the concentration of caffeic acid and ferulic acid to 400 $\mu$M resulted in a higher increase in reducing power than that measured for ascorbic acid (Supporting Information, Figure B).

*Iron Chelation Ability.* This assay measured the ability of the antioxidant to chelate iron, and the obtained results are shown in Table 1. Because of decreased solubility in water with increasing alkyl chain length, only the hydroxycinnamic acids and their methyl esters were evaluated in this assay. EDTA is known as a strong iron chelator and was included as a positive control. At all concentrations (50−400 $\mu$M) evaluated, EDTA had significantly higher iron chelating ability than the hydroxycinnamic acids and their methyl esters. For all compounds evaluated, the iron chelating activity increased with increasing concentrations. In general, the structure with two hydroxyl groups in ortho position (a catechol group), i.e., caffeic acid and methyl caffeate, were the most efficient among the evaluated hydroxycinnamic acids and methyl esters followed by ferulic acid and methyl ferulate (Table 1). The least efficient was coumaric acid, which only had minor activity (<5%). However, the esterification of coumaric acid significantly increased its iron chelating ability at concentrations of 200 (~10-fold) and 400 $\mu$M (~6-fold) (Table 1).

*Antioxidant−Iron Interactions.* Interactions between ferric ions ($Fe^{2+}$) and different antioxidants were determined by spectrophotometry. The spectra obtained for iron−caffeic acid

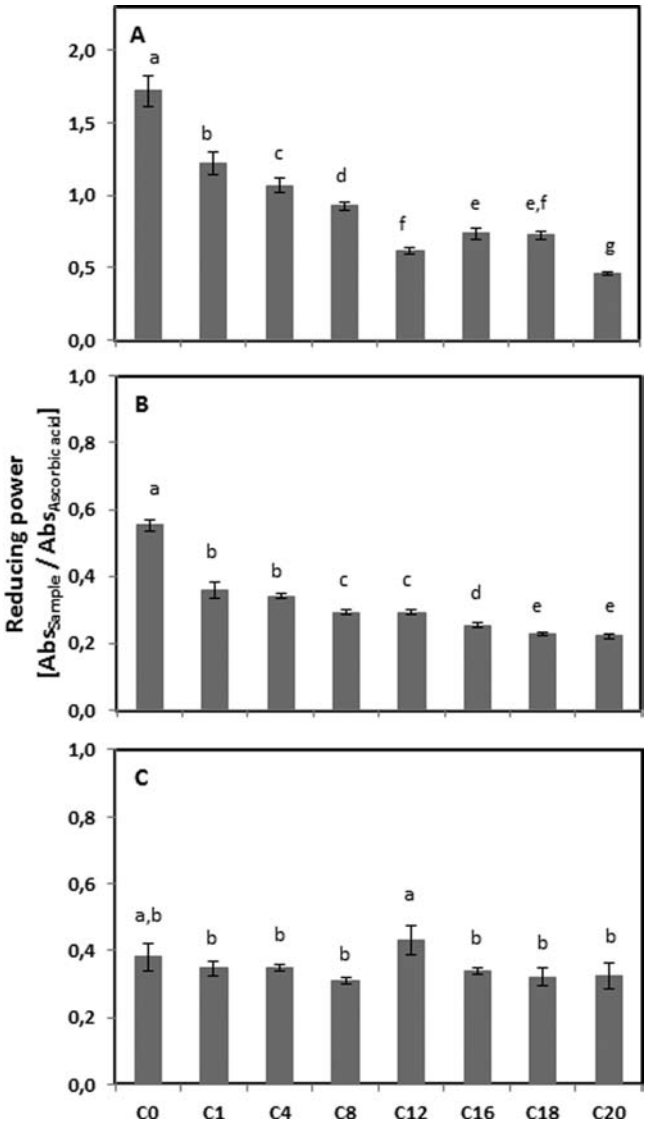


**Figure 3.** Reducing power properties of hydroxycinnamic acids and their alkyl esters at 100 $\mu$M calculated relative to ascorbic acid (positive control in the assay). (A) Caffeic acid and caffeates, (B) ferulic acid and ferulates, and (C) coumaric acid and coumarates. C0 is phenolic acid, and C1 to C20 indicates the length of the alkyl chain grafted to the phenolic acids (phenolipids). Error bars indicate the standard deviation ($n$ = 3). Significant differences between different compounds are denoted with different lowercase letters (significance level was $p < 0.05$).

and iron−methyl caffeate in two different buffers are shown in Figure 4. The absorbance measured was different for the two different buffers used. When either caffeic acid and iron or methyl caffeate and iron were solubilized in phosphate buffer, no absorbance was observed in the visible area, 400−800 nm (Figure 4A and B). In contrast, when the other buffer, sodium acetate−imidazole (10 mM), was used, both the combination of caffeic acid and iron or methyl caffeate and iron resulted in low absorbances in the visible area of the spectrum (Figure 4C and D). Moreover, these solutions changed from no color to blue or black color when iron was added. Phosphate buffer with caffeic acid and with and without iron added had peaks at the same wavelengths; however, when iron was added the absorbance was slightly higher in the UV area than that without iron added (Figure 4A). When methyl caffeate was solubilized in phosphate buffer, the spectra changed when iron was added compared to that when no iron was present (Figure 4B). This may indicate other types of interactions with iron. Furthermore, when iron was added to phosphate buffer without antioxidant, the spectrum changed, whereas iron added to sodium acetate−imidazole buffer did not alter the spectrum (Figure 5). Thus, phosphate buffer may also participate in interactions with the iron added. The other compounds evaluated, ferulic acid, methyl ferulate, coumaric acid, or methyl coumarate solubilized in sodium-acetate imidazole buffer, were not influenced by the addition of iron since similar absorbance spectra were obtained with and without iron addition (data not shown). This indicates that a catechol structure is needed to form a complex with iron, while a monophenol (coumaric acid-like structure) or a monophenol combined to a methoxyl group in ortho position (ferulic acid-like structure) does not allow the formation of such an iron complex. The possible interactions between iron and caffeates will be discussed in more detail later.

**Antioxidant Activity Evaluated by the CAT Assay (o/w Emulsion).** The antioxidant effect of the hydroxycinnamic acids and their alkyl esters was evaluated in the CAT assay. In the CAT assay, lipid oxidation and the effect of the tested antioxidants are evaluated from the decrease in conjugated trienes over time. The results for the three series of homologues are shown in Figure 6. Similar to the other assays evaluated, the highest antioxidant effect was obtained with alkyl caffeates followed by alkyl ferulates with CAT values of 1.3−5.0 and 0.2−1.5, respectively. Coumarates had close to zero antioxidant effect due to the low CAT values measured (0.05−0.36). For caffeic acid and alkyl caffeates, an increase in antioxidant capacity with increasing alkyl chain length up to octyl caffeate ($C_8$) was observed, whereas further increase in the alkyl chain length resulted in a decreased antioxidant

**Table 1. Iron Chelating Ability [%] of Caffeic Acid, Ferulic Acid, Coumaric Acid, and Their Methyl Esters (50−400 $\mu$M)[a]**

| | concentration [$\mu$M] | | | |
|---|---|---|---|---|
| compounds | 50 | 100 | 200 | 400 |
| caffeic acid | 7.37 ± 0.57 b,c | 16.0 ± 0.71 c | 39.8 ± 2.85 c | 78.2 ± 0.73 b |
| methyl caffeate | 11.6 ± 0.44 b | 22.3 ± 1.23 b | 59.3 ± 1.53 b | 75.1 ± 8.79 b |
| ferulic acid | 12.3 ± 0.80 b | 14.4 ± 1.30 c | 24.2 ± 2.64 d | 36.6 ± 2.95 d |
| methyl ferulate | 3.92 ± 1.51 c,d | 13.0 ± 1.85 c | 27.1 ± 3.01 d | 46.0 ± 3.50 c |
| coumaric acid | 0.05 ± 0.22 d | 1.11 ± 0.08 d | 1.47 ± 1.56 f | 4.30 ± 0.60 f |
| methyl coumarate | 0.80 ± 0.35 d | 5.93 ± 0.57 d | 14.7 ± 1.03 e | 26.9 ± 3.16 e |
| EDTA | 65.5 ± 3.26 a | 94.2 ± 2.29 a | 99.3 ± 0.80 a | 100 ± 0.04 a |

[a]EDTA was included as a positive control. The analyses were performed in triplicate ($n$ = 3). When a significant difference was observed between samples (within each column, i.e., concentrations), it is denoted with different lowercase letters (significance level was $p < 0.05$).

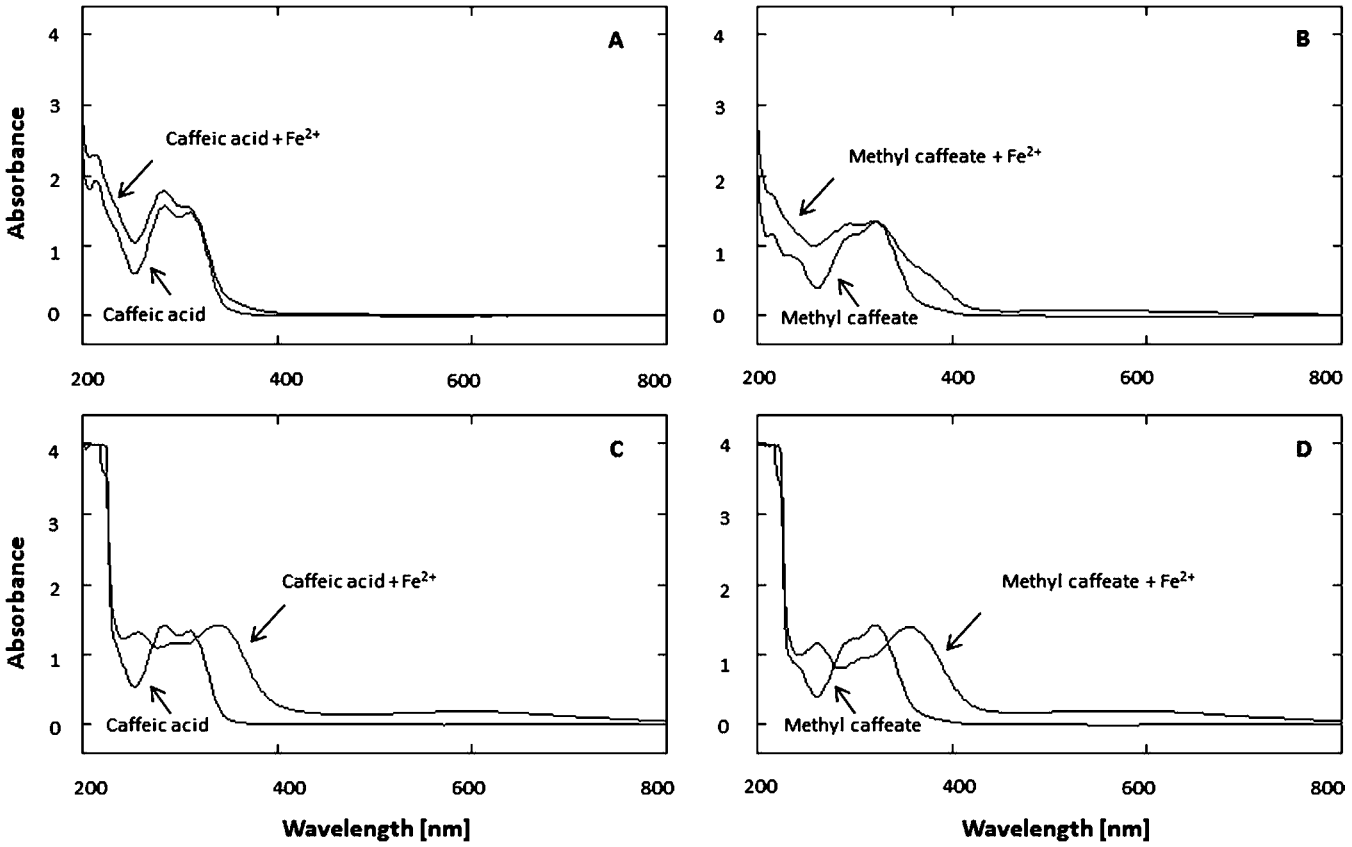


**Figure 4.** UV−vis spectra (200−800 nm) recorded for caffeic acid and methyl caffeate solubilized in different buffers with and without iron addition. (A) Phosphate buffer (pH 7.2), caffeic acid (100 $\mu$M) and ± Fe (100 $\mu$M), (B) phosphate buffer (pH 7.2), methyl caffeate (100 $\mu$M) and ± Fe (100 $\mu$M), (C) sodium acetate−imidazole buffer (10 mM, pH 7.0), caffeic acid (100 $\mu$M) and ± Fe (100 $\mu$M), and (D) sodium acetate−imidazole buffer (10 mM, pH 7.0), methyl caffeate (100 $\mu$M), and ± Fe (100 $\mu$M).

capacity (Figure 6). Thus, the most efficient antioxidant among the alkyl caffeates was octyl caffeate followed by dodecyl caffeate (not significantly different), and a cut-off effect was observed with $C_8$−$C_{12}$ as critical chain length. Octadecyl caffeate and eicosyl caffeate were significantly less efficient antioxidants than caffeic acid. The same clear cut-off effect as that for alkyl caffeates, with octyl caffeate being the best of the homologues series, was not observed for alkyl ferulates and alkyl coumarates, even though a global nonlinear tendency was observed between the CAT values and the alkyl chain lengths. The ranking of the alkyl ferulates was as follows: $C_{12}{}^{a} = C_8{}^{a} = C_4{}^{a} \geq C_1{}^{a,b} \geq C_0{}^{b} = C_{16}{}^{b}$ (Figure 6). Alkyl coumarates had limited antioxidant efficacy in this assay. The most efficient antioxidant among the alkyl coumarates was dodecyl coumarates, and the ranking of the alkyl coumarates according to their antioxidant efficiency was as follows: $C_{12}{}^{a} \geq C_8{}^{a,b} = C_4{}^{a,b} \geq C_0{}^{b} = C_{16}{}^{b} = C_1{}^{b}$ (Figure 6). Even though the antioxidative effects of coumaric acid and alkyl coumarates were limited, an improvement in the efficacy was observed with esterification. Dodecyl coumarate had approximately 5.6 times higher CAT value than coumaric acid.

## DISCUSSION

**Antioxidant Properties and Molecular Structure.** Antioxidant properties depend upon the molecular structure of the compounds.[18] Apart from the different degrees of lipophilization (alkyl chain length), three different molecular structures were evaluated: caffeic acid, ferulic acid, and coumaric acid (Figure 1). The antioxidant activity of phenolic compounds is primarily due to resonance stabilization of the phenoxyl radical and various substitutions, e.g., electronegative hydroxyl groups may increase radical stability. Thus, di- and trihydroxyl substitutions have greater antioxidant activity than monohydroxyl substitution due to greater resonance stabilization.[18,19] Moreover, Dueñas et al.[20] have evaluated antioxidant activities of O-methylation of the catechol group in quercetin and catechins using the FRAP assay (ferric reducing power) and ABTS$^{\bullet+}$ assay (radical scavenging). The O-methylation of one of the hydroxyls in the catechol group reduced the antioxidant activity compared to that of the parent compounds.[20] Thus, destroying the catechol structure lowered the antioxidant activity of the compound. Therefore, the efficacy based on radical scavenging and reducing power assays of the evaluated antioxidants is expected to be highest for caffeic acid followed by ferulic acid and coumaric acid. The obtained results confirmed this ranking in activity of the evaluated hydroxycinnamic acids (Figures 2 and 3). Moreover, Kikuzaki et al.[21] have also reported that caffeic acid had the highest DPPH scavenging activity followed by ferulic acid and coumaric acid. This ranging of the three types of alkyl ester is also observed in another study where short saturated alkyl esters of caffeic and ferulic acids were evaluated.[22] In addition, ester of sinapic acid has shown antioxidant activities in between those of alkyl caffeates and ferulates.[23] In the DPPH assay, caffeic acid and alkyl caffeates showed similar activities, whereas ferulic acid and coumaric acid showed higher activities than their alkyl esters (Figure 2). However, among the alkyl esters there was no clear pattern with respect to the effect of the chain length on the DPPH

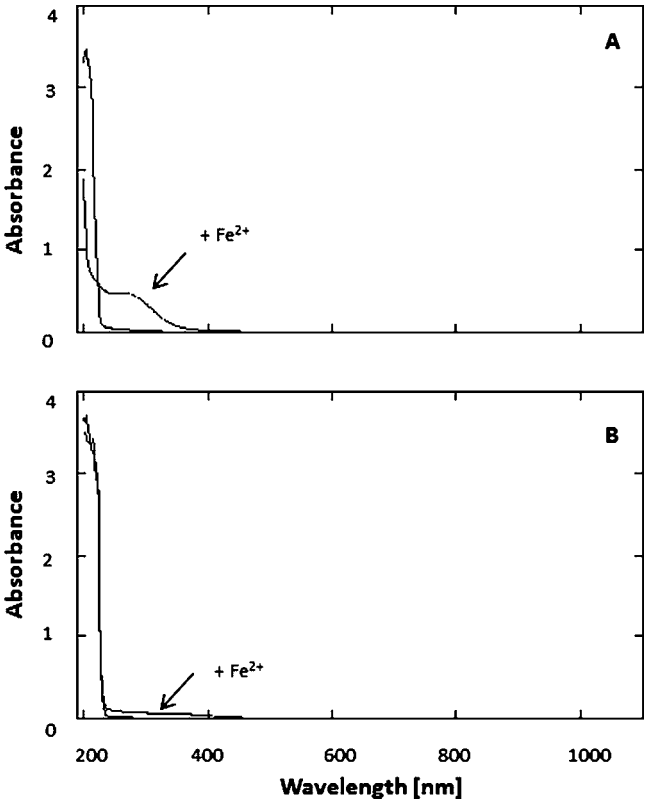


**Figure 5.** Spectra (200−800 nm) recorded for different buffers with and without iron addition. (A) Phosphate buffer (pH 7.2) ± Fe (100 $\mu$M) and (B) sodium acetate−imidazole buffer (10 mM, pH 7.0) ± Fe (100 $\mu$M).

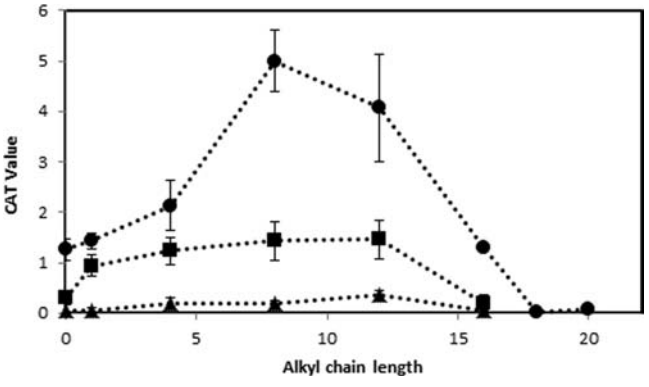


**Figure 6.** Influence of the alkyl chain length of phenolic alkyl esters on their antioxidant activity in stripped tung oil-in-water microemulsions oxidized by AAPH at 37 °C (CAT assay). Symbols: ●, caffeic acid and caffeates; ■, ferulic acid and ferulates; and ▲, coumaric acid and coumarates. Error bars indicate the standard deviation ($n$ = 3).

radical scavenging activity. These findings are similar to observations reported by Garrido and co-workers,[22] who had measured the $IC_{50}$ for different short chain saturated alkyl esters (methyl, ethyl, propyl, and butyl) of caffeic and ferulic acids using the DPPH assay. They reported similar $IC_{50}$ values for caffeic acid (16.6 $\mu$M) and caffeates (13.5−14.5 $\mu$M), whereas ferulic acid (44.6 $\mu$M) was reported with lower $IC_{50}$ than ferulates (56.3−74.7 $\mu$M). For the two evaluated alkyl esters, the efficiency was as follows for caffeates and ferulates: ethyl (lowest $IC_{50}$) > methyl > butyl > propyl and butyl > propyl > ethyl > methyl.[22] In contrast, in the reducing power assay, caffeic and ferulic acids had higher activities than their alkyl esters, and the activities decreased with increasing alkyl chain lengths for alkyl caffeates and alkyl ferulates (Figure 3). However, this is contrary to findings reported by Garrido et al.[22] who used the FRAP assay to measure reducing power, which was similar to the $IC_{50}$ findings, i.e., compounds with low $IC_{50}$ had high reducing power.

Phenylethanoid glycosides are ester derivatives of phenolic acids and are widely distributed in nature. These phenylethanoid glycosides are more lipophilic compounds compared to phenolic acids. Interestingly, some phenylethanoid glycosides of caffeic and ferulic acids, namely, acyl derivatives, have shown lower (∼2-fold) $IC_{50}$ values than those of their corresponding phenolic acid,[24] whereas alkyl esters of caffeic acid showed similar $IC_{50}$ values as those of caffeic acid.[22] Thus, some of these alkyl and glycoside esters of phenolic compounds may serve as good antioxidants in emulsions or other complex systems due to increased lipophilicity, which is important in multiphases systems.

Both antioxidant assays in this study are homogeneous systems; whereas the DPPH assay is measured in ethanol, the reducing power assay is measured in distilled water. Thus, solubility may influence the results obtained. The evaluated compounds are more soluble in solvent than water, i.e., less polar. Therefore, the reduced activity with increased alkyl chain length in the reducing power assay can at least partly be explained by the reduced solubility of the more lipophilic alkyl esters in water. In the DPPH assay, the ethanolic medium did not influence the solubility of the more lipophilic alkyl esters. Additionally, the results obtained in the DPPH assay are in accordance with results obtained earlier by Kikuzaki et al.[21] In their study, ferulic acid also had higher scavenging activity than alkyl ferulates, and no dependency in lipophilicity and antioxidant activity of the different alkyl ferulates was observed.[21] Thus, these data confirm the earlier assumption regarding solubility issues that the ethanolic solution does not have the same impact on the solubility of the more lipophilic alkyl esters as the water solution. In addition, the lower activity observed for alkyl ferulates and alkyl coumarates than their corresponding acids in the DPPH and reducing power assays has also been reported earlier for other phenolipids, namely, dihydrocaffeates[25] and rutin esters.[26] These findings may indicate that the esterification site for the alkyl chain play an active role for the antioxidant properties measured in these assays. Additionally, López-Giraldo et al.[27] have evaluated the kinetics of the reaction of chlorogenic acid and its alkyl esters with the DDPH radical. For the different compounds, strong differences were observed. Hence, pathways of DPPH stabilization were suggested to be different for chlorogenic acid and its alkyl esters, which were confirmed by LC-MS characterization of the reaction products obtained.

Another antioxidant property is chelation of transition metal irons, which are prooxidants. Therefore, if they are chelated their interactions with the lipid substrate or lipid hydroperoxides is supposed to be inactivated.[28] The iron chelating assay can thus reveal the ability of the compounds to chelate iron. This assay is, like the reducing power assay, a homogeneous solution of water wherein the antioxidants are solubilized. Solubility was indeed an issue for this assay. It seemed like the methanolic stock solutions of the different antioxidants interfered with the assay since the results obtained were not reproducible. The assay was repeated with the antioxidant solubilized only in water. Only caffeic acid, ferulic

acid, coumaric acid, and their methyl esters were evaluated. It is known that phenolic compounds containing a catechol group are able to chelate iron in the form of an iron-phenolic complex. Only caffeic acid and its esters contain a catechol group in their molecular structure. Nevertheless, all the evaluated hydroxycinnamic acids and their methyl esters had iron chelating activity (Table 1). UV−vis spectra (200−800 nm) of caffeic acid and methyl caffeate in sodium acetate−imidazole buffer revealed different absorbance patterns when iron was added (Figure 4). Furthermore, absorbance was detected in the visible area when iron was added. Change in the absorbance at 587 and 680 nm has been reported to correspond to iron−gallyl and iron−catechol complexes, respectively.[29] Thus, the obtained spectra indicated the formation of an iron−catechol complex with caffeic acid and methyl caffeate. Moreover, the absorbance spectra for these compounds changed in the area of 250−400 nm upon iron addition. The absorbance spectra in the area of 250−400 nm are characterizing the ring substitutions. Similar results have been reported by Andjelković et al.[30] who evaluated the formation of a complex between caffeic acid and iron in Tris buffer. When EDTA was added to the iron−caffeic acid complex, the absorbance spectrum changed again and was similar to that obtained for caffeic acid solubilized in Tris buffer without iron.[30] On the basis of the results reported by Andjelković et al.[30] with caffeic acid, iron, and EDTA and the fact that the catechol group was a part of the complex formed with iron, the changes in this area of the spectra were due to the formed complex.

Ferulic acid, methyl ferulate, and methyl coumarate had chelating ability but no change in their UV−vis spectra when iron was added. None of these compounds has a catechol or gallyl group. Therefore, the similar spectra obtained with and without iron were expected. The chelating ability measured for those compounds is therefore suggested to be due to other types of interactions with iron. Earlier findings support this suggestion since both caffeic acid and coumaric acid were shown to form nanoparticles in the presence of iron.[9]

Moreover, the complex formed between iron and the catechol group in caffeic acid and methyl caffeate were not formed when sodium acetate−imidazole buffer was substituted with phosphate buffer. A change in the UV region of the spectrum with phosphate buffer upon iron addition was also observed. Thus, this indicated interaction between phosphate and iron that impeded the complex formation between iron and the catechol group. A similar observation for phosphate buffer and iron has also been reported by Andjelković et al.[30] when they evaluated the interaction with iron and different phenolics. Therefore, the choice of buffer is crucial when evaluating the chelating ability of different compounds[30] due to the changed reactivity with different buffers.

Studies have shown that the most efficient antioxidants in limiting lipid oxidation in food emulsions during storage are not always comparable to antioxidant properties measured in *in vitro* antioxidant assays.[31,32] Hence, these antioxidant assays are only indicators of the properties of the compound studied and do not provide information about the efficiency of the antioxidants in emulsions or complex food systems.

**Antioxidant Activity in Emulsions.** In contrast to the above-discussed antioxidant assays, emulsions are heterogeneous systems. In general, the efficacy of antioxidants in food emulsion is dependent on their reactivity, properties, and partitioning in the emulsion.[33,34] These factors are not included in the simple antioxidant assays. Moreover, several components present in the emulsions may interfere with the antioxidants and thus alter their efficacy.

The CAT assay developed by Laguerre et al.[17] measures the antioxidant activity in a microemulsified system with AAPH used as a peroxyradical initiator. This assay gave different results than those obtained with the DPPH (radical) assay. In the CAT assay, there was an effect of the alkyl chain length grafted to caffeic acid, which was not observed in the DPPH assay. The difference between the results obtained with the CAT assay and the DPPH assay is suggested to be due to the influence of the antioxidant partitioning in the microemulsion. However, the influence of the phenolic structure was similar to the findings with the DPPH assay; caffeic acid was the most efficient antioxidant followed by ferulic acid and then with less activity coumaric acid.

For the three homologues series of antioxidants, the trend was that the antioxidant efficiency was highest for the phenolipids with medium chain length. However, only alkyl caffeates showed significant differences between the different chain lengths. Other reported results from the CAT assay have also shown that the CCL was obtained for medium chain length phenolipids. For alkyl chlorogenates and rosmarinates, the antioxidant efficiency was highest with a chain length of 12 and 8 carbon atoms, respectively.[7,11] Moreover, the antioxidant efficiency of alkyl rosmarinates is 3−5 times higher than that of alkyl chlorogenates and caffeates. This is suggested to be due to the substituted groups in the ring structure. Rosmarinic acid has two catechol groups, whereas chlorogenic acid and caffeic acid only have one.

The most efficient alkyl caffeate in the CAT assay was octyl caffeate. Recent studies with alkyl caffeates in food emulsions have shown that the effect of the chain length depended upon the system it was added into. In milk emulsion, the most efficient alkyl ferulate was methyl ferulate (C1),[35] and the most efficient alkyl caffeates were methyl caffeate (C1) and butyl caffeate (C4), whereas in mayonnaise the most efficient were butyl caffeate (C4), octyl caffeate (C8), and dodecyl caffeate (C12).[36] Similarly, the CCL for alkyl rosmarinates has also been shown to be influenced by the different emulsion systems. Despite this, the CCL for alkyl chlorogenates in emulsion and fibroblasts was similar , dodecyl chlorogenate (C12).[37]

In addition, a study reported by Anselmi et al.[38] shows that ferulic acid lipophilized with different saturated unbranched and branched alkyl chain lengths resulted in different three-dimensional structures. Different anchorages of the phenolic with the different alkyl chains were observed, which resulted in a specific folding of some of the alkyl esters. This structure resulted in the highest antioxidative capacity of these molecules (octyl ferulate and dodecyl ferulate) in rat liver microsomes. It was assumed that it was due to the orientation of the phenoxy group outside the membrane surface, which may have favored the radical scavenging in the microsomes.[38] In milk emulsion, octyl and dodecyl ferulate were reported to be intermediate to strong prooxidants.[35] Unfortunately, the three-dimensional structure of the molecules was not analyzed. However, if the alkyl chain has folded toward the ethylenic protons as reported by Anselmi et al.,[38] this is not a favorable structure in milk emulsions due to their prooxidative effects. Hence, CCL can be a variable parameter dependent upon the molecule and its three-dimensional structure, as well as the structure and composition of the emulsion system. Therefore, the effect of

antioxidants has to be studied in each emulsion system where antioxidant protection is needed.

In conclusion, the evaluated hydroxycinnamic acids and their alkyl esters showed antioxidant properties and activity. The antioxidant properties were affected by the molecular structure. Caffeic acid was a stronger iron chelator than ferulic acid and coumaric acid due to its ability to form complexes with iron. Moreover, caffeic acid also had higher radical scavenging activity and reducing power than the other hydroxycinnamic acids. The CCL in the CAT assay was C8−C12 for alkyl caffeates.

Additionally, esterification of caffeic acid with saturated short alkyl chains (methyl, ethyl, propyl, and butyl) was shown to improve the cell protective activity against oxidative stress, whereas caffeic acid, ferulic acid, and alkyl esters of ferulic acid were not able to protect the cells.[22] Moreover, esters of caffeic and ferulic acids have also shown excellent inhibition of tumor cell proliferation.[39]

Thus, the lipophilicity of phenolic compounds is a crucial factor that can determine their efficiency as antioxidants in multiphase systems such as food emulsions and cellular systems.

Hence, the synthesized phenolipids may serve as good antioxidants in food emulsions, especially alkyl caffeates, due to their free radical scavenging properties and antioxidant efficacy. However, their activity will also depend upon the partitioning of the antioxidant in the food emulsion as well as the interaction with other compounds present in the food emulsion. Our present and previous findings seem to suggest that the effect of alkyl esterification on the antioxidant activity may differ from one phenolic compound to another. Thus, antioxidant protection has to be further studied in each specific food emulsion with the different phenolic compounds.

## ■ ASSOCIATED CONTENT

### Supporting Information

Results for the radical scavenging properties and reducing power with all the measured concentrations (50, 100, 200, and 400 $\mu$M). This material is available free of charge via the Internet at http://pubs.acs.org.

## ■ AUTHOR INFORMATION


### Corresponding Author

*E-mail: adms@food.dtu.dk.



### Funding

The study is a part of the project entitled "Phenolipids as Antioxidants in Omega-3 Model and Real Food Systems − Effect of Alkyl Chain Length and Concentration" with project number 10-093655 financed by the Danish Research Council, Technology and Production.


### Notes

The authors declare no competing financial interest.

## ■ ACKNOWLEDGMENTS


We thank Nathalie Barouh for her assistance with the purification of some of the synthesized phenolipids.


## ■ ABBREVIATIONS USED

AAPH, 2,2′-azobis-2-methyl-propanimidaminde dichloride; BHT, butylated hydroxytoluene; $C_0$, phenolic acid; $C_1$, methyl; $C_4$, butyl; $C_8$, octyl; $C_{12}$, dodecyl; $C_{16}$, hexadecyl; $C_{18}$, octadecyl; $C_{20}$, eicosyl; CAT, conjugated autoxidizable triene; CCL, critical chain length; EDTA, ethylenedinitrilo-tetraacetic acid; PBS, phosphate buffer solution; TCA, trichloroacetic acid; THF, tetrahydrofuran

## ■ REFERENCES


(1) Waraho, T.; McClements, D. J.; Decker, E. A. Mechanisms of lipid oxidation in food dispersions. *Trends Food Sci. Technol.* **2011**, *22*, 3−13.

(2) Porter, W. L. Paradoxical behavior of antioxidants in food and biological systems. *Toxicol. Ind. Health* **1993**, *9* (1−2), 93−122.

(3) Frankel, E. N.; Huang, S.-W.; Kanner, J.; German, J. B. Interfacial phenomena in the evaluation of antioxidants: Bulk oils vs emulsions. *J. Agric. Food Chem.* **1994**, *42*, 1054−1059.

(4) Huang, S.-W.; Frankel, E. N.; Schwarz, K.; German, J. B. Effect of pH on the antioxidant activity of $\alpha$-tocopherol and trolox in oil-in-water emulsions. *J. Agric. Food Chem.* **1996**, *44*, 2496−2502.

(5) Huang, S.-W.; Frankel, E. N.; Schwarz, K.; Aeschbach, R.; German, J. B. Antioxidant activity of carnosic acid and methyl carnosate in bulk oils and oil-in-water emulsions. *J. Agric. Food Chem.* **1996**, *44*, 2951−2956.

(6) Frankel, E. N.; Huang, S. W.; Prior, E.; Aeschbach, R. Evaluation of antioxidant activity of rosemary extracts, carnosol and carnosic acid in bulk vegetable oils and fish oil and their emulsions. *J. Sci. Food Agric.* **1996**, *72* (2), 201−208.

(7) Laguerre, M.; Giraldo, L. J. L.; Lecomte, J.; Figueroa-Espinoza, M. C.; Barea, B.; Weiss, J.; Decker, E. A.; Villeneuve, P. Chain length affects antioxidant properties of chlorogenate esters in emulsion: the cutoff theory behind the polar paradox. *J. Agric. Food Chem.* **2009**, *57* (23), 11335−11342.

(8) Lue, B.-M. Enzymatic Lipophilization of Bioactive Compounds in Ionic Liquids. Ph.D. Thesis, Department of Molecular Biology, Aarhus University, Denmark, 2009.

(9) Sørensen, A.-D. M.; Haahr, A.-M.; Becker, E. M.; Skibsted, L. H.; Bergenståhl, B.; Nilsson, L.; Jacobsen, C. Interactions between iron, phenolic compounds, emulsifiers, and ph in omega-3-enriched oil-in-water emulsions. *J. Agric. Food Chem.* **2008**, *56*, 1740−1750.

(10) Yuji, H.; Weiss, J.; Villeneuve, P.; Giraldo, L. J. L.; Figueroa-Espinoza, M.-C.; Decker, E. A. Ability of surface-active antioxidants to inhibit lipid oxidation in oil-in-water emulsion. *J. Agric. Food Chem.* **2007**, *55*, 11052−11056.

(11) Laguerre, M.; Giraldo, L. J. L.; Lecomte, J.; Figueroa-Espinoza, M.-C.; Baréa, B.; Weiss, J.; Decker, E. A.; Villeneuve, P. Relationship between hydrophobocity and antioxidant ability of "phenolipids" in emulsion: a parabolic effect of the chain length of rosmarinate esters. *J. Agric. Food Chem.* **2010**, *58*, 2869−2876.

(12) Laguerre, M.; Sørensen, A.-D. M.; Bayrasy, C.; Lecomte, J.; Jacobsen, C.; Decker, E. A.; Villeneuve, P. Role of Hydrophobicity on Antioxidant Activity in Lipid Dispersions from the Polar Paradox to the Cut-off Theory. In *Lipid Oxidation: Challenges in Food Systems*, 1st ed.; Logan, A., Nienaber, U., Pan, X., Eds.; AOCS Press: Urbana, IL, 2013; pp 261−296.

(13) Giraldo, L. J. L.; Laguerre, M.; Lecomte, J.; Figueroa-Espinoza, M.-C.; Barouh, N.; Barea, B.; Villeneuve, P. Lipase-catalyzed synthesis of chlorogenate fatty acid esters in solvent-free medium. *Enzyme Microb. Technol.* **2007**, *41*, 721−726.

(14) Sørensen, A.-D. M.; Nielsen, N. S.; Yang, Z.; Xu, X.; Jacobsen, C. The effect of lipohilization of dihydrocaffeic acid on its antioxidative properties in fish-oil-enriched emulsion. *Eur. J. Lipid Sci. Technol.* **2012**, *114*, 134−145.

(15) Farvin, K. H. S.; Andersen, L. L.; Nielsen, H. H.; Jacobsen, C.; Jakobsen, G.; Johansson, I.; Jessen, F. Antioxidant activity of cod (*Gadus morhua*) protein hydrolysates: Part 1 - *In vitro* assays and evaluation in 5% fish oil-in-water emulsion. *Food Chem.* **2014**, *149*, 326−334.

(16) Laguerre, M.; Lopez-Giraldo, L. J.; Lecomte, J.; Barea, B.; Cambon, E.; Tchobo, P. F.; Barouh, N.; Villeneuve, P. Conjugated autoxidizable triene (CAT) assay: A novel spectrophotometric method

for determination of antioxidant capacity using triacylglycerol as ultraviolet probe. *Anal. Biochem.* **2008**, *380* (2), 282−290.
(17) AOCS *Official Method Ce 8-89. Determination of Tocopherols and Tocotrienols in Vegetable Oils and Fats by HPLC*. AOCS Press: Champaign, IL, 1997.
(18) Rice-Evans, C. A.; Miller, N. J.; Paganga, G. Antioxidant properties of phenolic compounds. *Trends Plant Sci.* **1997**, *2* (4), 152−159.
(19) Zhou, L.; Elias, R. J. Understanding Antioxidant and Prooxidant Mechanisms of Phenolics in Food Lipids. In *Lipid Oxidation Challenges in Food Systems*, 1st ed.; Logan, A., Nienaber, U., Pan, X., Eds.; AOCS Press: Urbana, IL, 2013; pp 297−321.
(20) Dueñas, M.; González-Manzano, S.; González-Paramás, A.; Santos-Buelga, C. Antioxidant evaluation of *O*-methylated metabolites of catechin, epicatechin and quercetin. *J. Pharm. Biomed. Anal.* **2010**, *51*, 443−449.
(21) Kikuzaki, H.; Hisamoto, M.; Hirose, K.; Akiyama, K.; Taniguchi, H. Antioxidant properties of freulic acid and its related compounds. *J. Agric. Food Chem.* **2002**, *50*, 2161−2168.
(22) Garrido, J.; Gaspar, A.; Garrido, E. M.; Miri, R.; Tavakkoli, M.; Pourali, S.; Saso, L.; Borges, F.; Firuzi, O. Alkyl esters of hydroxycinnamic acids with improved antioxidant activity and lipophilicity protect PC12 cells against oxidative stress. *Biochimie* **2012**, *94*, 961−967.
(23) Menezes, J. C.; Kamat, S. P.; Cavaleiro, J. A. S.; Gaspar, A.; Garrido, J.; Borges, F. Synthesis and antioxidant activity of long chain alkyl hydroxycinnamates. *Eur. J. Med. Chem.* **2011**, *46*, 773−777.
(24) Heilmann, J.; Çalis, I.; Kirmizibekmez, H.; Schühly, W.; Harput, S.; Sticher, O. Radical scavenger activity of phenylethanoid glycosides in FMLP stimulated human polymorphonuclear leukocytes: structure-activity relationships. *Planta Med.* **2000**, *66*, 746−748.
(25) Sabally, K.; Karboune, S.; St-Louis, R.; Kermasha, S. Lipase-catalyzed synthesis of phenolic lipids from fish liver oil and dihydrocaffeic acid. *Biocatal. Biotransform.* **2007**, *25* (2−4), 211−218.
(26) Lue, B.-M.; Nielsen, N. S.; Jacobsen, C.; Hellgren, L.; Guo, Z.; Xu, X. Antioxidant properties of modified rutin esters by DPPH, reducing power, iron chelation and low density lipoprotein assays. *Food Chem.* **2010**, *123* (2), 221−230.
(27) López-Giraldo, L. J.; Laguerre, M.; Lecomte, J.; Figueroa-Espinoza, M.-C.; Baréa, B.; Weiss, J.; Decker, E. A.; Villeneuve, P. Kinetic and stoichiometry of the reaction of chlorogenic acid and its alkyl esters against the DPPH radical. *J. Agric. Food Chem.* **2009**, *57*, 863−870.
(28) Jacobsen, C.; Hartvigsen, K.; Thomsen, M. K.; Hansen, L. F.; Lund, P.; Skibsted, L. H.; Hølmer, G.; Adler-Nissen, J.; Meyer, A. S. Lipid oxidation in fish oil enriched mayonnaise: calcium disodium ethylenediaminetetraacetate, but not gallic acid, strongly inhibited oxidative deterioration. *J. Agric. Food Chem.* **2001**, *49* (8), 1009−1019.
(29) Khokhar, S.; Apenten, R. K. O. Iron binding characteristics of phenolic compounds: some tentative structure-activity relations. *Food Chem.* **2003**, *81*, 133−140.
(30) Andjelkovic, M.; Camp, J. V.; Meulenaer, B. D.; Depaemelaere, G.; Verloo, M.; Verhe, R. Iron-chelation properties of phenolic acids bearing catechol and galloyl groups. *Food Chem.* **2006**, *98*, 23−31.
(31) Sørensen, A.-D. M.; Friel, J.; Winkler-Moser, J. K.; Jacobsen, C.; Huidrom, D.; Reddy, N.; Thiyam-Holländer, U. Impact of endogenous canola phenolics on the oxidative stability of oil-in-water emulsions. *Eur. J. Lipid Sci. Technol.* **2013**, *115*, 501−512.
(32) Alamed, J.; Chaiyasit, W.; McClements, D. J.; Decker, E. A. Relationships between free radical scavenging and antioxidant activity in foods. *J. Agric. Food Chem.* **2009**, *57* (7), 2969−2976.
(33) Frankel, E. N. Antioxidants in lipid foods and their impact on food quality. *Food Chem.* **1996**, *57*, 51−55.
(34) Heins, A.; McPhail, D. B.; Sokolowski, T.; Stockmann, H.; Schwarz, K. The location of phenolic antioxidants and radicals at interfaces determines their activity. *Lipids* **2007**, *42* (6), 573−582.
(35) Sørensen, A.-D. M.; Lyneborg, K. S.; Villeneuve, P.; Jacobsen, C. Alkyl chain length impacts the antioxidative effect of lipophilized ferulic acid in fish oil enriched milk. *J. Funct. Food* **2014**, DOI: 10.1016/j.jff.2014.04.08.
(36) Alemán, M.; Bou, R.; Guardiola, F.; Durand, E.; Villeneuve, P.; Jacobsen, C.; Sørensen, A.-D. M. Antioxidative effect of lipophilized caffeic acid in fish oil enriched mayonnaise and milk. *Food Chem.* **2015**, *167*, 236−244.
(37) Laguerre, M.; Bayrasy, C.; Lecomte, J.; Chabi, B.; Decker, E. A.; Wrutniak-Cabello, C.; Cabello, G.; Villeneuve, P. How to boost antioxidants by lipophilization? *Biochimie* **2013**, *95*, 20−26.
(38) Anselmi, C.; Centini, M.; Granata, P.; Sega, A.; Buonocore, A.; Bernini, A.; Facino, R. M. Antioxidant activity of ferulic acid alkyl esters in heterophasic system: A mechanistic insight. *J. Agric. Food Chem.* **2004**, *52*, 6425−6432.
(39) Jayaprakasam, B.; Vanisree, M.; Zhang, Y.; Dewitt, D. L.; Nair, M. G. Impact of alkyl esters of caffeic and ferulic acids on tumor cell proliferation, cyclooxygenase enzyme, and lipid peroxidation. *J. Agric. Food Chem.* **2006**, *54*, 5375−5381.

The use of organogel as a delivery system is possibly a good choice to enhance the stability of the products. However, its use in water-rich systems may be inconvenient because of its high hydrophobicity. Emulsification of organogel may offer additional benefits and increase its application versatility. To date, the use of modern delivery systems, such as organogel-based nanoemulsions, to encapsulate a hydrophobic compound is very limited. However, Yu and Huang[35] developed a novel curcumin organogel-based nanoemulsion by ultrasonication. The authors have reported that the organogel-based nanoemulsion has contributed to the improvement of the bioavailability of curcumin by enhancing its water solubility. This finding result may give evidence that these systems are very useful in terms of improving the solubility of hydrophobic compounds.

The objective of the current study was to prepare a D-limonene organogel-based nanoemulsion by high-pressure homogenization and investigate the influence of the type and concentration of organogelators and emulsifiers, homogenization pressure, and number of cycles on the formation and stability of the formulation.

## MATERIALS AND METHODS

**Chemicals.** D-Limonene was obtained from Florida Worldwide Citrus Products Group, Inc. (Bradenton, FL). Monostearin and stearic acid were purchased from Aladdin Reagents Co., Ltd. (Shanghai, China). Non-ionic surfactants (Tween 20, 40, 60, 80, and 85) were purchased from the Sinopharm Chemical Reagent Co., Ltd. (Beijing, China). The Tween surfactant structures were composed of a polyoxyethylene headgroup and fatty acid tail group of various lengths, with the two moieties being connected together via a sorbitol molecule. Medium-chain triglyceride (MCT oil) was purchased from Sigma-Aldrich (Shanghai, China).

**Preparation of D-Limonene Organogel and Organogel-Based Nanoemulsion.** D-Limonene organogel was prepared as described by Yu and Huang,[35] with some modifications. Briefly, D-limonene, MCT oil, and stearic acid or monostearin were mixed together followed by heating to ensure complete dissolution of the organogelator. The mixture was set at room temperature, and organogel was formed within a few minutes. D-Limonene organogel-based nanoemulsion preparation was carried out by a high-pressure homogenization procedure. D-Limonene organogel was used as the oil phase, and Milli-Q water containing different types of Tween surfactants was used as the aqueous phase. The organogel-based nanoemulsion formation was performed by mixing the water phase together with the oil phase. Then, the two phases were mixed by a high-blending homogenizer at 24 000 rpm for 5 min to form a coarse emulsion, followed by high-pressure homogenization to form D-limonene organogel-based nanoemulsion. Using the above procedure, several batches were established by varying the organogelator, surfactant type and concentration, homogenization pressure, and cycles to study their effect on the formation and stability of the formulation.

**Particle Size Measurements.** The average particle diameters and particle size distributions of the organogel-based nanoemulsions were determined using dynamic light scattering at 25 °C (Zetasizer Nano-ZS90, Malvern Instruments, Malvern, U.K.). The measurements were carried out at a scattering angle of 90°. Each measurement was recorded in an average of 10 scans. The samples were diluted approximately 1000-fold with Milli-Q water. The particle size of the emulsions was described by the mean particle size diameter, and the size distribution was described by the polydispersity index (PdI).

**Turbidity Measurements.** The turbidity was determined using an ultraviolet−visible (UV−vis) spectrophotometer at 600 nm (Ultraspec 2450, Shimadzu, Ltd., Japan). Distilled water was used as a reference to the blank cells.

**Storage Stability.** The prepared formulations were placed in amber bottles and stored at 4 or 28 °C. The stability was determined by measuring the change of the droplet sizes every 3 days for 2 weeks.

**Statistical Analysis.** All experiments were carried out in triplicate. The data were recorded as the mean ± standard deviation (SD) for the measurements. The data were analyzed by the statistical package (SPSS, version 12.0, for Windows, SPSS, Inc., Chicago, IL).

## RESULTS AND DISCUSSION

**Effects of Organogelators on the D-Limonene Organogel-Based Nanoemulsion Formation.** To investigate the impact of the organogelator type and concentration on the formation of nanoemulsions with small droplet sizes, a series of organogel-based nanoemulsions with a fixed surfactant content and homogenization conditions (10% Tween 80, 10 cycles, and 30 MPa) was prepared using two kinds of organogelators (stearic acid or monostearin) at different concentrations. As shown in Table 1, a large decrease on the mean droplet size was observed, following the addition of the organogelator into the oil phase. The average diameter decreased from $d$ = 133.8 ± 2.03 to 112.8 ± 1.17 and 122.8 ± 1.06 nm, following the addition of 5% stearic acid or monostearin, respectively. This can give evidence that the organogelator has contributed to the decrease of the droplet diameters. In addition, there was a minor change on the droplet diameters after increasing the amount of the organogelators, which means that the amount of the organogelators did not influence the formation of the D-limonene organogel-based nanoemulsion. In comparison of the mean droplet diameters of the formulations prepared by stearic acid or monostearin, stearic acid organogel-based nanoemulsion exhibited the smallest droplet size. Possible reasons are the difference on physicochemical proprieties between this two organogelators or the low molecular weight of stearic acid compared to monostearin. On the other hand, the increase on the stearic acid amount (5, 10, and 15% for $d$ = 112.2, 110.4, and 110.8 nm, respectively) did not contribute to a large change on the mean droplet diameters. For this reason, 5% stearic acid was used as the structuring agent of D-limonene organogel preparation for the following experiments.

**Table 1. Impact of the Organogelator Type and Concentration on the Mean Droplet Formation**

| organogelator type | content of the organogelator in the organogel (%) | mean droplet diameter[a] ($z$ average) |
|---|---|---|
| stearic acid | 0 | 133.8 ± 2.03[b] |
| | 5 | 112.2 ± 1.17[c] |
| | 10 | 110.4 ± 0.95 |
| | 15 | 110.8 ± 1.32 |
| monosearin | 5 | 122.8 ± 1.06[d] |
| | 10 | 125.9 ± 1.65 |
| | 15 | 127.5 ± 0.72 |

[a]Data shown are the mean ± SD. [b]D-Limonene nanoemulsion prepared without the addition of the organogelator. [c]The mean droplet diameter of D-limonene organogel-based nanoemulsion prepared by stearic acid at different amounts. [d]The mean droplet diameter of D-limonene organogel-based nanoemulsion prepared by monostearin at different amounts.

**Effects of the Surfactant Type and Concentration on D-Limonene Organogel-Based Nanoemulsion Formation.** *Effect of the Surfactant Type on the Particle Size.* In this part, a series of organogel-based nanoemulsions with fixed homogenization conditions (10 cycles and 30 MPa) was

formulated using a series of non-ionic surfactants (Tween 20, 40, 60, 80, and 85). Figure 1 shows the particle size parameters

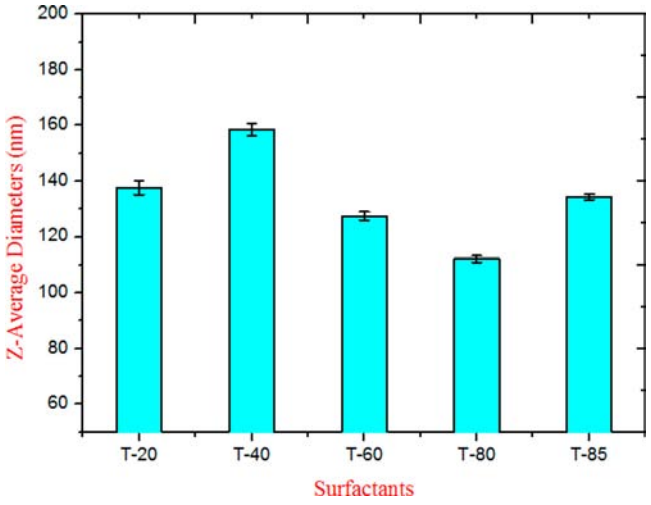


**Figure 1.** Effect of the surfactant type on the mean droplet diameter of D-limonene organogel-based nanoemulsion. Surfactants were Tween 20, 40, 60, 80, and 85, from the left to the right (data shown are the mean ± SD).

of organogel-based nanoemulsion prepared at 10% (w/w) with different Tween surfactants. The mean droplet diameters of the colloidal dispersions were arrayed between 112 and 158 nm with the PdI being in the range of 0.148−0.229. This can give evidence that D-limonene organogel-based nanoemulsions can be formulated using all tested surfactants, with the dispersed droplets in the nanometer scale. Among the five different surfactants tested, Tween 80 produced the smallest mean droplet size ($d$ = 112.2 ± 1.17 nm) with a slightly turbid shape, as presented in panels A and B of Figure 2. In contrast, the largest droplets were produced in the systems prepared by Tween 40 ($d$ = 158.5 ± 2.15 nm). The difference of the mean droplet diameters is maybe due to the hydrophilic−lipophilic balance (HLB) of the surfactants, which is a very important factor for the selection of surfactants having the ability to form

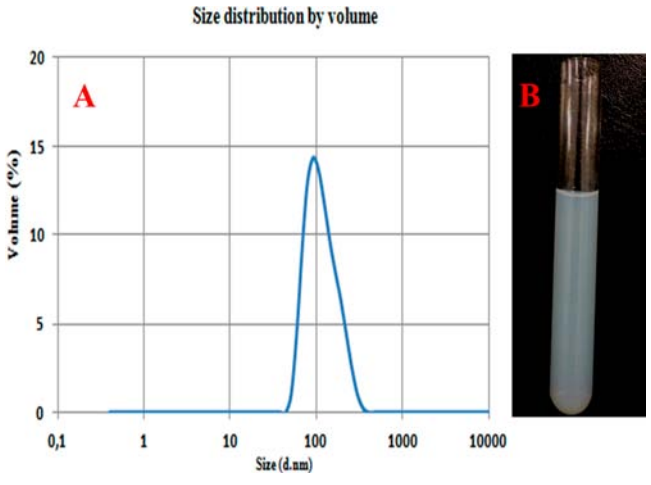


**Figure 2.** (A) Profile of the particle size distribution of D-limonene organogel-based nanoemulsion prepared with Tween 80 at a final concentration of 10% (w/w), 30 MPa, and 10 cycles and (B) its typical picture.

and stabilize the emulsions.[36,37] Surfactants with high HLB values, such as Tween 20 and 40 (HLB = 16.7 and 15.6, with $d$ = 137.7 and 158.5 nm, respectively) or a low HLB value, such as Tween 85 (HLB = 11.0, with $d$ = 134.4 nm) were not able to form D-limonene organogel-based nanoemulsion with the smallest droplet sizes. However, surfactants with a medium HLB value, such as Tween 60 and 80 (HLB = 14.9 and 15.0, with $d$ = 127.5 and 112.2 nm, respectively) could form organogel-based nanoemulsion with the smallest particle sizes. Furthermore, Tween 60 and 80 both have approximately the same HLB value of ≈15, but they have given colloidal dispersions with different droplet size diameters ($d$ = 112.2 and 127.5 nm, respectively). This is maybe due to the molecular geometry of the surfactants, which is known to play an important role in the emulsion production and stability.[38] There is thus far a prominent similarity between the geometric structures of both Tween 60 and 80 (polar headgroup and nonpolar tail), making their HLB approximately the same. However, the nonpolar tails of Tween 60 are saturated, but those of Tween 80 are unsaturated. Those saturated tails may affect the packaging of the surfactant at the oil phase interface, which may cause a disturbance in the formation of small droplets when the oil phase (organogel) and the water phases are mixed together. Moreover, many researchers have reported that the presence of unsaturation on the non-ionic surfactant structures may favor the tiny droplet formation.[36,39]

In the following experiments, Tween 80 was chosen as the appropriate surfactant because it contributes to the formation of an organogel-based nanoemulsion with the smallest mean droplet size diameter.

*Effect of the Surfactant Concentration on the Particle Size Formation.* The effect of the surfactant concentration on the mean droplet size formation and distribution was also investigated. D-Limonene organogel-based nanoemulsions were prepared by Tween 80 at different concentrations with a fixed homogenization condition (30 MPa and 10 cycles). The surfactant concentrations were varied from 2.5 to 20% (w/w). As shown in Figure 3, the surfactant concentration seems to play an efficient role on the formation of the droplets. The mean droplet sizes were found to decrease by increasing the content of surfactant. For example, at 2.5% Tween 80, the mean

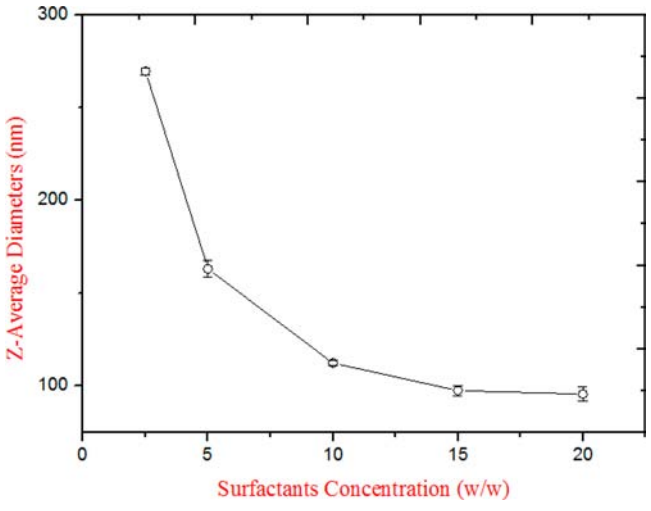


**Figure 3.** Effect of the Tween 80 concentration on the mean droplet diameter of D-limonene organogel-based nanoemulsion (data shown are the mean ± SD).


dx.doi.org/10.1021/jf5032108 | J. Agric. Food Chem. 2014, 62, 12563−12569

droplet size was large ($d$ = 269.7 ± 2.02 nm). In contrast, the amount of surfactant was increased, the droplet size diameters decreased ($d$ = 163.3 ± 4.5, 112.4 ± 1.17, 97.44 ± 2.85, and 95.6 ± 4.03 nm at 5, 10, 15, and 20%, respectively). Our results are in agreements with a previous study reported by Yuan et al.,[40] who found that the droplet sizes of $\beta$-carotene nanomulsions prepared by the high-pressure homogenization method decreased by increasing the amount of surfactant. These results can be explained by a greater amount of Tween 80 being able to completely dissolve the dispersed phase (D-limonene organogel) into the dispersing phase (water). On the other hand, Tween 80 can also form a layer between the two phases, leading to the formation of a minimum interfacial tension, hence promoting the formation of a tiny droplet size with a narrow distribution. It is already known the use of a high amount of surfactants on the nanoemulsion preparation is costly and may have an undesirable taste in commercial formulations. Thus, an intermediate amount of surfactant is maybe more suitable for the preparation of stable nanoemulsions. In this regard, we found it necessary to use 10% Tween 80 in the following experiments.

*Effects of the Homogenization Pressure and Number of Cycles on the Proprieties of D-Limonene Organogel-Based Nanoemulsion.* It is well-known that the homogenization pressure and number of cycles significantly influence the mean droplet size formation and particle distributions.[41] In this part, the influence of the homogenization pressure and number of cycles on the average droplet diameter of D-limonene organogel-based nanoemulsion was investigated (Figure 4).

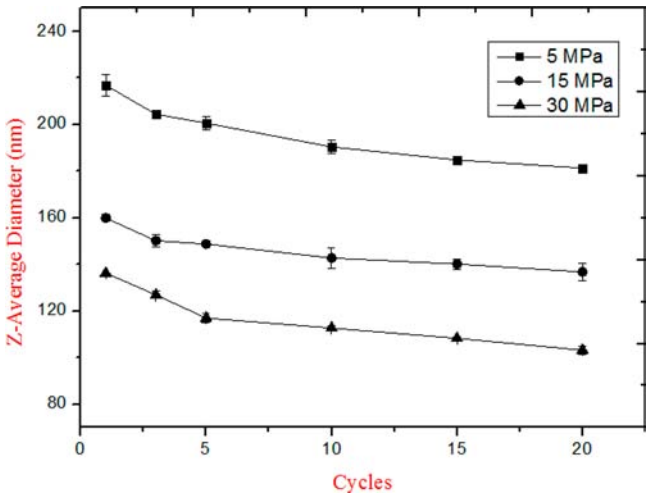


**Figure 4.** Effect of the high-pressure homogenization pressure (5, 15, and 30 MPa) and number of cycles (1, 3, 5, 10, 15, and 20) on the mean droplet diameter of D-limonene organogel-based nanoemulsion (data shown are the mean ± SD).

The mean droplet diameter was decreased by increasing the homogenization pressure and number of cycles. These results are in agreement with previous studies reported by many researchers.[40,42,43] A large decrease of the mean droplet diameter was observed when the coarse emulsions were passed through the high-pressure homogenizer at all pressures studied. For example, the average droplet size decreased from 1340 ± 340 nm before homogenization to 216.9 ± 4.6, 160 ± 1.61, and 136.3 ± 0.45 nm after passing 1 cycle through the high-pressure homogenizer system working at 5, 15, and 30 MPa, respectively. These results showed that organogel-based nanoemulsion can be formed using a high-pressure homogenizer method, and this technique is efficient for preparing organogel-based nanemulsions with small droplet sizes. The average particle size of the organogel-based nanoemulsion continued to decrease by increasing the number of cycles, but the decrease was modest in a certain stage. Organogel-based nanoemulsion prepared at 30 MPa showed the lowest average of the particle size, as it was decreased from 136.3 ± 0.45 after 1 cycle to 103.2 ± 1.84 after 20 cycles. It should be noted that the average particle sizes did not mainly change after about 10 cycles. Therefore, we found it necessary to use this value as a processing condition for our experiments.

*Storage Stability of D-Limonene Organogel-Based Nanoemulsion.* For most commercial applications, it is very important that nanoemulsion-based delivery systems remain physically stable during their shelf life (i.e., there is little change in their particle size diameter during storage). The change on the turbidity of D-limonene organogel-based nanoemulsion was investigated in this part during a storage time of 2 weeks at 4 or 28 °C. As shown in Figure 5, the turbidity of D-limonene organogel-based nanoemulsion increased rapidly throughout the first 6 days and the increase was slight for the remaining storage time.

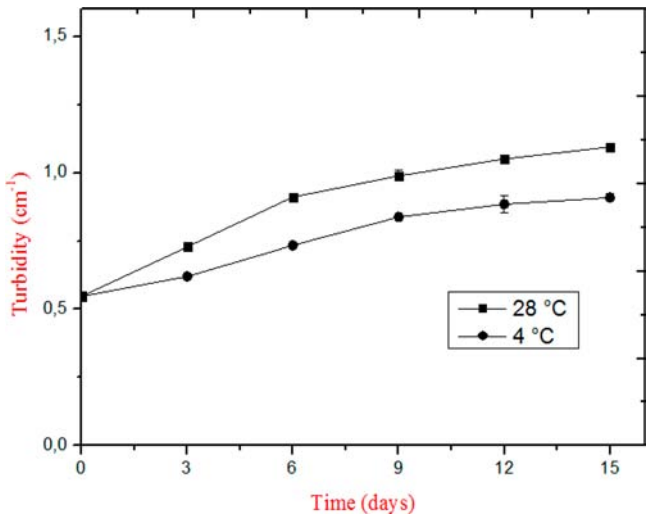


**Figure 5.** Storage turbidity of D-limonene organogel-based nanoemulsion at 4 and 28 °C (data shown are the mean ± SD).

The droplet diameter and size distribution are important parameters affecting nanoemulsion stability.[44] The change of the nanoemulsion droplet sizes is due to numerous physiochemical processes, which include coalescence, flocculation, gravitational separation, and Ostwald ripening.[28] We therefore investigated the influence of the storage time at 4 and 28 °C on the stability of D-limonene organogel-based nanoemulsion for 2 weeks of storage. There was a slight increase in the mean droplet diameters for all samples stored at 4 and 28 °C, respectively (Figure 6). This increase is maybe due to the movement of the dispersed droplet throughout the dispersing phase, which increased the opportunities of droplet collisions.[45] In comparison to conventional emulsions, nanoemulsions are endowed with good stability against phase separation, creaming, and sedimentation because of their small droplet sizes. However, many researchers have reported that Ostwald ripening and/or coalescence are the main mechanisms causing the instability of nanoemulsions.[46] Ostwald ripening

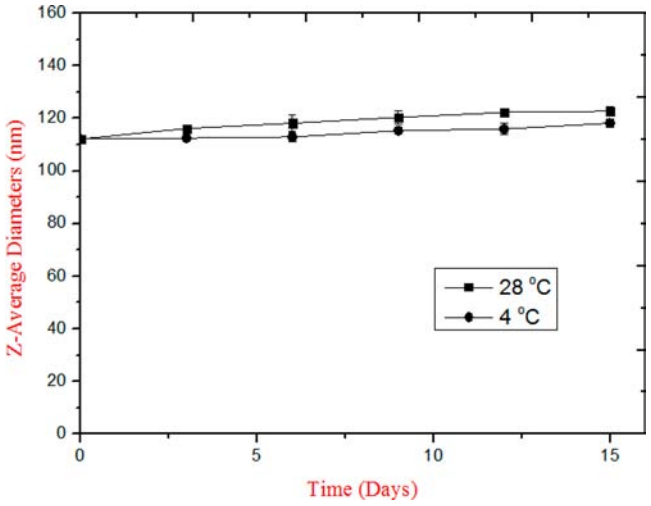


**Figure 6.** Storage stability of D-limonene organogel-based nanoemulsion at 4 and 28 °C (data shown are the mean ± SD).

can occur because of the difference in the chemical potential of the oil phase between the droplets.[47] In this phenomenon, larger droplets grow at the expense of smaller droplets, which is caused by the molecular diffusion through the dispersing phase. In other words, the small droplets become smaller and the larger droplets become bigger. D-Limonene has a slight solubility in water around 13.8 g/L.[48,49] This can increase the susceptibility to the Ostwald ripening process of the nanoemulsion made from it. As demonstrated previously, the Ostwald ripening can be inhibited by incorporating a highly water-insoluble oil into a relatively water-insoluble oil prior to nanoemulsion formation,[50,51] because of the entropy of the mixing effect. Li and Chiang[11] prepared D-limonene nanoemulsion and reported that the main destabilization mechanism of the system was Ostwald ripening. In addition, the droplet growth of the nanoemulsion was large through the storage period of 98 days. In another study, Li et al.[20] reported that Ostwald ripening was also the major destabilization mechanism for D-limonene nanoemulsion. Furthermore, they have mentioned that the growth of the particle size increased at a relatively higher rate to 128 nm at 4 °C and 67 nm at 28 °C during a storage period of 2 weeks, whereas, in our study, the increase of the particle size was 10 nm at 28 °C and 6 nm at 4 °C during a storage period of 2 weeks. In comparison to their results, D-limonene organogel-based nanoemulsion showed an ameliorated stability with a slight increase on the droplet size diameter at the same storage conditions. This improvement is maybe due to the incorporation of D-limonene into the organogel prior to nanoemulsion preparation, which contributed to the decrease of the D-limonene polarity, thereby increasing the stability of the nanoemulsion.

Coalescence is the process in which two or more droplets merge together when they colloid.[52,53] A higher amount of essential oils may lead to the droplet coalescence acceleration, which is caused by the low interfacial tension and the relatively high polarity of this kind of oil.[54] In addition, the polarity of the oil may play an efficient role in the rate of droplet coalescence (i.e., nanoemulsions containing more polar oils occur more rapidly than the nonpolar oils), and this phenomenon is maybe due to the influence of the oil phase proprieties on the optimum curvature.[55,56] The incorporation of D-limonene on the organogel (MCT oil and monostearin) and the preparation conditions seem to have a good benefit on both nanoemulsion formation and storage stability by decreasing the polarity and increasing the interfacial tension, thereby acting as Ostwald ripening and/or coalescence.

In the current study, D-limonene organogel-based nanoemulsion was successfully prepared by high-pressure homogenization technology. The type and concentration of organogelators and emulsifiers, homogenization pressure, and number of cycles on the formation and stability of the nanoemulsions were investigated. It was found that stearic acid was the most suitable structuring agent for small droplet formation. In addition, among the non-ionic emulsifiers tested, Tween 80 at 10% (w/w) was appropriate for the formation of D-limonene organogel-based nanoemulsion with the smallest mean droplet size. The optimum conditions of high-pressure homogenization emulsification of the nanoemulsion were 30 MPa and 10 cycles. The prepared formulation showed good stability in terms of Ostwald ripening and/or coalescence through the storage period at the two different temperatures tested. In summary, our results may have a valuable implication for the design and use of organogel-based nanoemulsion as a delivery system in food and other industries.

## AUTHOR INFORMATION


### Corresponding Authors

*Telephone: +86-10-6443-1557. Fax: +86-10-6443-7610. E-mail: lianghao@mail.buct.edu.cn.

*Telephone: +86-10-6443-7610. Fax: +86-10-6443-7610. E-mail: yuanqp@mail.buct.edu.cn.



### Funding

This project was supported by the National High Technology Research and Development Program of China (863 Program, Grants 2012AA021403 and 2014AA021705) and the Beijing Higher Education Young Elite Teacher Project (YETP0520).

### Notes

The authors declare no competing financial interest.


## REFERENCES


(1) Sun, J. D-Limonene: Safety and clinical applications. *Altern. Med. Rev.* **2007**, *12* (3), 259.

(2) Roberto, D.; Micucci, P.; Sebastian, T.; Graciela, F.; Anesini, C. Antioxidant activity of limonene on normal murine lymphocytes: Relation to $H_2O_2$ modulation and cell proliferation. *Basic Clin. Pharmacol. Toxicol.* **2010**, *106* (1), 38−44.

(3) Van Vuuren, S. F.; Viljoen, A. M. Antimicrobial activity of limonene enantiomers and 1,8-cineole alone and in combination. *Flavour Fragrance J.* **2007**, *22* (6), 540−544.

(4) Chikhoune, A.; Hazzit, M.; Kerbouche, L.; Baaliouamer, A.; Aissat, K. *Tetraclinis articulata* (Vahl) Masters essential oils: Chemical composition and biological activities. *J. Essent. Oil Res.* **2013**, *25* (4), 300−307.

(5) Settanni, L.; Palazzolo, E.; Guarrasi, V.; Aleo, A.; Mammina, C.; Moschetti, G.; Germanà, M. A. Inhibition of food borne pathogen bacteria by essential oils extracted from citrus fruits cultivated in Sicily. *Food Control* **2012**, *26* (2), 326−330.

(6) Crowell, P. L.; Gould, M. N. Chemoprevention and therapy of cancer by D-limonene. *Crit. Rev. Oncog.* **1994**, *5* (1), 1−22.

(7) Crowell, P. L.; Kennan, W. S.; Haag, J. D.; Ahmad, S.; Vedejs, E.; Gould, M. N. Chemoprevention of mammary carcinogenesis by hydroxylated derivatives of D-limonene. *Carcinogenesis* **1992**, *13* (7), 1261−1264.

(8) Wattenberg, L. W.; Coccia, J. B. Inhibition of 4-(methylnitrosamino)-1-(3-pyridyl)-1-butanone carcinogenesis in mice by D-limonene and citrus fruit oils. *Carcinogenesis* **1991**, *12* (1), 115−117.

(9) Murali, R.; Saravanan, R. Antidiabetic effect of D-limonene, a monoterpene in streptozotocin-induced diabetic rats. *Biomed. Prev. Nutr.* **2012**, *2* (4), 269−275.
(10) Soottitantawat, A.; Yoshii, H.; Furuta, T.; Ohkawara, M.; Linko, P. Microencapsulation by spray drying: Influence of emulsion size on the retention of volatile compounds. *J. Food Sci.* **2003**, *68* (7), 2256−2262.
(11) Li, P. H.; Chiang, B. H. Process optimization and stability of D-limonene-in-water nanoemulsions prepared by ultrasonic emulsification using response surface methodology. *Ultrason. Sonochem.* **2012**, *19* (1), 192−197.
(12) Djordjevic, D.; Cercaci, L.; Alamed, J.; McClements, D. J.; Decker, E. A. Chemical and physical stability of protein and gum arabic-stabilized oil-in-water emulsions containing limonene. *J. Food Sci.* **2008**, *73* (3), C167−C172.
(13) Marcuzzo, E.; Debeaufort, F.; Sensidoni, A.; Tat, L.; Beney, L.; Hambleton, A.; Peressini, D.; Voilley, A. Release behavior and stability of encapsulated D-limonene from emulsion-based edible films. *J. Agric. Food Chem.* **2012**, *60* (49), 12177−12185.
(14) Anandaraman, S.; Reineccius, G. A. Stability of encapsulated orange peel oil. *Food Technol.* **1986**, *40* (11), 88−93.
(15) Wyler, L.; Solms, J. Starch flavour complexes III. Stability of dried starch-flavor complexes and other dried flavor preparations. *Lebensm.-Wiss. Technol.* **1982**, *15* (2), 93−97.
(16) Bertolini, A. C.; Siani, A. C.; Grosso, C. R. F. Stability of monoterpenes encapsulated in gum arabic by spray-drying. *J. Agric. Food Chem.* **2001**, *49* (2), 780−785.
(17) Jafari, S. M.; Beheshti, P.; Assadpoor, E. Rheological behavior and stability of D-limonene emulsions made by a novel hydrocolloid (Angum gum) compared with Arabic gum. *J. Food Engineering* **2012**, *109* (1), 1−8.
(18) Mohammadzadeh, H.; Koocheki, A.; Kadkhodaee, R.; Razavi, S. Physical and flow properties of D-limonene-in-water emulsions stabilized with whey protein concentrate and wild sage (*Salvia macrosiphon*) seed gum. *Food Res. Int.* **2013**, *53* (1), 312−318.
(19) Dickinson, E.; Galazka, V. B. Emulsion stabilization by ionic and covalent complexes of β-lactoglobulin with polysaccharides. *Food Hydrocolloids* **1991**, *5* (3), 281−296.
(20) Li, Y.; Zhang, Z.; Yuan, Q.; Liang, H.; Vriesekoop, F. Process optimization and stability of D-limonene nanoemulsions prepared by catastrophic phase inversion method. *J. Food Eng.* **2013**, *119* (3), 419−424.
(21) Mahdi Jafari, S.; He, Y.; Bhandari, B. Nano-emulsion production by sonication and microfluidization—A comparison. *Int. J. Food Prop.* **2006**, *9* (3), 475−485.
(22) Sanguansri, P.; Augustin, M. A. Nanoscale materials development—A food industry perspective. *Trends Food Sci. Technol.* **2006**, *17* (10), 547−556.
(23) Huang, Q.; Yu, H.; Ru, Q. Bioavailability and delivery of nutraceuticals using nanotechnology. *J. Food Sci.* **2010**, *75* (1), R50−R57.
(24) Lee, S. J.; McClements, D. J. Fabrication of protein-stabilized nanoemulsions using a combined homogenization and amphiphilic solvent dissolution/evaporation approach. *Food Hydrocolloids* **2010**, *24* (6), 560−569.
(25) Weiss, J.; Takhistov, P.; McClements, D. J. Functional materials in food nanotechnology. *J. Food Sci.* **2006**, *71* (9), R107−R116.
(26) Tadros, T.; Izquierdo, P.; Esquena, J.; Solans, C. Formation and stability of nano-emulsions. *Adv. Colloid Interface Sci.* **2004**, *108*, 303−318.
(27) Chen, H.; Weiss, J.; Shahidi, F. Nanotechnology in nutraceuticals and functional foods. *Food Technol.* **2006b**, *60* (3), 30−36.
(28) McClements, D. J. Edible nanoemulsions: Fabrication, properties, and functional performance. *Soft Matter* **2011**, *7* (6), 2297−2316.
(29) Weiss, J.; Gaysinsky, S.; Davidson, M.; McClements, J. Nanostructured encapsulation systems: Food antimicrobials. In *Global Issues in Food Science and Technology*; Barbosa-Canovas, G. V., Mortimer, A., Lineback, D., Spiess, W., Buckle, K., Colonna, P., Eds.; Academic Press: Waltham, MA, 2009; Chapter: 24, pp 425−479.
(30) Hughes, N. E.; Marangoni, A. G.; Wright, A. J.; Rogers, M. A.; Rush, J. W. Potential food applications of edible oil organogels. *Trends Food Sci. Technol.* **2009**, *20* (10), 470−480.
(31) Vintiloiu, A.; Leroux, J. C. Organogels and their use in drug delivery—A review. *J. Controlled Release* **2008**, *125* (3), 179−192.
(32) Pernetti, M.; van Malssen, K.; Kalnin, D.; Flöter, E. Structuring edible oil with lecithin and sorbitan tri-stearate. *Food Hydrocolloids* **2007**, *21* (5), 855−861.
(33) Lo Nostro, P. L.; Ramsch, R.; Fratini, E.; Lagi, M.; Ridi, F.; Carretti, E.; Ninham, B. W.; Baglioni, P. Organogels from a vitamin C-based surfactant. *J. Phys. Chem. B* **2007**, *111* (40), 11714−11721.
(34) Motulsky, A.; Lafleur, M.; Couffin-Hoarau, A. C.; Hoarau, D.; Boury, F.; Benoit, J. P.; Leroux, J. C. Characterization and biocompatibility of organogels based on L-alanine for parenteral drug delivery implants. *Biomaterials* **2005**, *26* (31), 6242−6253.
(35) Yu, H.; Huang, Q. Improving the oral bioavailability of curcumin using novel organogel-based nanoemulsions. *J. Agric. Food Chem.* **2012**, *60* (21), 5373−5379.
(36) Wang, L.; Dong, J.; Chen, J.; Eastoe, J.; Li, X. Design and optimization of a new self-nanoemulsifying drug delivery system. *J. Colloid Interface Sci.* **2009**, *330* (2), 443−448.
(37) Gullapalli, R. P.; Sheth, B. B. Influence of an optimized non-ionic emulsifier blend on properties of oil-in-water emulsions. *Eur. J. Pharm. Biopharm.* **1999**, *48* (3), 233−238.
(38) Israelachvili, J. N. *Intermolecular and Surface Forces*, 3rd ed.; Academic Press: Waltham, MA, 2011.
(39) Dai, L.; Li, W.; Hou, X. Effect of the molecular structure of mixed nonionic surfactants on the temperature of miniemulsion formation. *Colloids Surf., A* **1997**, *125* (1), 27−32.
(40) Yuan, Y.; Gao, Y.; Zhao, J.; Mao, L. Characterization and stability evaluation of β-carotene nanoemulsions prepared by high pressure homogenization under various emulsifying conditions. *Food Res. Int.* **2008**, *41* (1), 61−68.
(41) Floury, J.; Desrumaux, A.; Lardieres, J. Effect of high-pressure homogenization on droplet size distributions and rheological properties of model oil-in-water emulsions. *Innovative Food Sci. Emerging Technol.* **2000**, *1* (2), 127−134.
(42) Tan, C. P.; Nakajima, M. Effect of polyglycerol esters of fatty acids on physicochemical properties and stability of β-carotene nanodispersions prepared by emulsification/evaporation method. *J. Sci. Food. Agric.* **2005**, *85*, 121−126.
(43) Tcholakova, S.; Denkov, N. D.; Sidzhakova, D.; Ivanov, I. B.; Campbell, B. Interrelation between drop size and protein adsorption at various emulsification conditions. *Langmuir* **2003**, *19* (14), 5640−5649.
(44) Heurtault, B.; Saulnier, P.; Pech, B.; Benoît, J. P.; Proust, J. E. Interfacial stability of lipid nanocapsules. *Colloids Surf., B* **2003**, *30* (3), 225−235.
(45) Henry, J. V.; Fryer, P. J.; Frith, W. J.; Norton, I. T. Emulsification mechanism and storage instabilities of hydrocarbon-in-water sub-micron emulsions stabilized with Tweens (20 and 80), Brij 96v and sucrose monoesters. *J. Colloid Interface Sci.* **2009**, *338*, 201−206.
(46) Liu, W.; Sun, D.; Li, C.; Liu, Q.; Xu, J. Formation and stability of paraffin oil-in-water nano-emulsions prepared by the emulsion inversion point method. *J. Colloid Interface Sci.* **2006**, *303*, 557−563.
(47) Lifshitz, I. M.; Slyozov, V. V. The kinetics of precipitation from supersaturated solid solutions. *J. Phys. Chem. Solids* **1961**, *19*, 35−50.
(48) National Toxicology Program (NTP). *NTP Chemical Repository Data Sheet: D-Limonene*; NTP: Research Triangle Park, NC, 1991.
(49) National Library of Medicine (NLM). *Hazardous Substances Data Bank (HSDB)*; NLM: Bethesda, MD, 1998; Record 4186.
(50) Ziani, K.; Chang, Y.; McLandsborough, L.; McClements, D. J. Influence of surfactant charge on antimicrobial efficacy of surfactant stabilized thyme oil nanoemulsions. *J. Agric. Food Chem.* **2011**, *59*, 6247−55.

(51) Liang, R.; Xu, S.; Shoemaker, C. F.; Li, Y.; Zhong, F.; Huang, Q. Physical and antimicrobial properties of peppermint oil nanoemulsions. *J. Agric. Food Chem.* **2012**, *60*, 7548−7555.
(52) McClements, D. J. *Food Emulsions: Principles, Practices, and Techniques*, 2nd ed.; CRC Press: Boca Raton, FL, 2005.
(53) Capek, I. Degradation of kinetically-stable o/w emulsions. *Adv. Colloid Interface Sci.* **2004**, *107*, 125−155.
(54) Chanamai, R.; Horn, G.; McClements, D. J. Influence of oil polarity on droplet growth in oil-in-water emulsions stabilized by a weakly adsorbing biopolymer or a nonionic surfactant. *J. Colloid Interface Sci.* **2002**, *247*, 167−176.
(55) Kabalnov, A.; Wennerström, H. Macroemulsion stability: The oriented wedge theory revisited. *Langmuir* **1996**, *12*, 276−292.
(56) Rao, J.; McClements, D. J. Stabilization of phase inversion temperature nanoemulsions by surfactant displacement. *J. Agric. Food Chem.* **2010**, *58*, 7059−7066.

lactate/40% water, Lincolnshire, IL); and anhydrous dibasic sodium succinate was obtained from Spectrum Chemical Corp. (Gardena, CA). A Wheaton Potter−Elvehjem grinder tube with polytetrafluoroethylene pestle, RNase-free D-sucrose, and lactic acid were obtained from Fisher Scientific (Fair Lawn, NJ). Ethylene glycol-bis(β-aminoethyl ether)-N′-N′-N′-N′-tetraacetic acid (EGTA) was obtained from MP Biomedicals (Solon, OH). A Kontes Duall tissue grinder glass tube with polytetrafluoroethylene pestle and centrifuge tubes (DNase, RNase, and endotoxin free) were obtained from VWR (Suwanee, GA). A heavy-duty mechanical drill driver purchased locally was used to drive the pestles for the tissue-grinding procedures.

**Beef Homogenate Preparation and Color Measurements.** A total of 25 g (devoid of fat and connective tissue) of minced bovine skeletal muscle from strip loin ($n$ = 3) was homogenized with 4 times (weight by volume) of 0.04 M MOPS buffer solution containing either 2% (w/v) lactate or 2% (w/v) succinate or only buffer as the control. Samples were homogenized at 5000 rpm with a variable-speed PowerGen homogenizer (model 35, Fisher Scientific, Pittsburgh, PA) for 60 s, and visible lumps of connective tissue were removed. The pH of the homogenate was adjusted to 5.6 ± 0.1, and the homogenate was poured into sterile polystyrene Petri plates (60 × 100 mm, Fisher Scientific, Pittsburgh, PA) and covered with a clear, snug-fitting lid. To this, 200 ppm of ferrous and/or ferric ions was added to achieve the final concentration of RRI between 0 and 60 ppm in the homogenate. The homogenates were gently stirred with a clean glass rod, and the Petri plates were incubated at 37 °C for 30 min.

Post-incubation, the homogenates were stirred and color parameters CIE $L^*$, $a^*$, and $b^*$ and reflectance from 400 to 700 nm using A/10 illuminant (d/8°, LAV, 25 mm port) from HunterLab Miniscan EZ portable spectrophotometer (Hunter Associates Laboratory, Inc., Reston, VA) were measured. The CIE $L^*$, $a^*$, and $b^*$ values and reflectance measurements were recorded in duplicate and averaged for statistical analysis. The relative percent of the Mb redox forms were determined using the absorption and scattering index ($K/S$) values specific to isosbestic wavelengths as described in the American Meat Science Association (AMSA) Meat Color Guidelines.[22]

**Mitochondrial Isolation.** A briefly modified procedure by Tang and colleagues was followed for mitochondrial isolation and oxygen polarographic measurements.[23] Briefly, 50 g of cardiac muscle, free of visible connective tissue and fat was excised and washed twice in the wash solution before mitochondrial isolation. The lean meat was minced and suspended in 200 mL of isolation buffer while being gently stirred with a magnetic stirrer. Bacterial nagarse protease (25 mg/50 g of tissue) was added to this suspension, and the pH was maintained between 7.2 and 7.4. After 20 min of proteolysis, the suspension was allowed to stand and the supernatant was gently decanted. The protease-treated cardiac tissue was washed twice with the isolation buffer to remove the residual protease and resuspended in 500 mL of isolation buffer. This suspension was given three passes each of Kontes Duall grinder and the Wheaton Potter−Elvehjem grinder. The resulting suspension was centrifuged at 1200$g$ for 20 min. The supernatant was filtered through two layers of ultrapure water-washed cheese cloth. This clear solution was further centrifuged at 20000$g$ for 20 min (Sorvall RC 6 centrifuge, Thermo Fisher Scientific, Waltham, MA). The resulting pellets were washed twice with suspension buffer and resuspended in the same. The temperature of the entire mitochondrial isolation operation was maintained between 0 to 4 °C. The protein concentration of the mitochondrial suspension was measured using the Bicinchoninic acid assay (BCA, bicinchoninic acid kit, Sigma-Aldrich, St. Louis, MO).

**Oxygen Consumption of Isolated Mitochondria.** The mitochondrial oxygen consumption was measured using a Clark electrode attached to a model 20 controller (Rank Brothers, Cambridge, U.K.) and PicoLog ADC 20 USB data logger. The data logger was attached to a computer for real-time data acquisition and storage. The temperature of the electrode cell was maintained at 25 °C using a circulating water bath. A 1 cm magnetic flea stirrer was used to keep the cell suspension agitated during oxygen consumption measurements. Iron solutions of suitable concentrations to obtain final concentrations of 5 or 60 nm of iron/mg of mitochondrial protein were added to 1 mL of incubation buffer in the electrode chamber, and it was sealed with a stopper. These levels represent the normal iron concentration and exceptionally high concentration of mitochondrial iron reported in viable cells suffering from mitochondrial dysfunction as in the case of Friedreich's ataxia, respectively.[24] Although iron accumulation of such a high level in beef muscle mitochondria is unlikely, the level was tested as a realistic extremity to understand the iron-mediated changes in mitochondrial respiration.

Additions of mitochondrial suspension, substrates (lactate and succinate), and ADP solutions were made to the electrode cell using Hamilton syringes through the port in the stopper while being continuously stirred. The mitochondrial suspension was added until the protein concentration in the cell chamber achieved 1 mg/mL, which is sufficient to exhibit measurable oxygen consumption. The state IV oxygen consumption rate was calculated as the rate of consumption of atomic oxygen per mg of mitochondrial protein per minute in the presence of substrate alone, and the state III oxygen consumption rate was calculated as the rate of consumption of atomic oxygen per mg of mitochondrial protein per minute in the presence of both the substrate and ADP. The respiratory control ratio (RCR) was calculated as the ratio of state III to state IV oxygen consumption rates. The time of calculation of the slopes varied according to the response given by mitochondria to the substrate and ADP additions.

**Design of Experiments and Statistical Analysis.** For the experiments on beef homogenate, the experimental design was a balanced factorial with three levels of substrate treatment (control, succinate, and lactate) and five levels each of $Fe^{2+}$ and $Fe^{3+}$ ion concentrations (3 × 5 × 5 = 75 × 3 replications = 225 total samples). Data were collected in duplicate samples, and the experiment was repeated 3 times ($n$ = 3) at three different occasions. Type-3 tests of fixed effects were performed using the MIXED procedure of SAS (SAS Institute, Inc., Cary, NC). Least-square means for $F$ tests ($p < 0.05$) were separated using the diff option (least significant differences) and were considered significant at $p < 0.05$.

For the mitochondrial experiments, a complete randomized block design was used. Experimental replication was performed 3 times ($n$ = 3) on three separate occasions. The treatments were applied on the isolated mitochondria within a heart; duplicate samples were used for each treatment application; and data were averaged for statistical analysis. Fixed effects for experiment included a two-way treatment structure consisting of treatments lactate, succinate, and combination of different RRI concentrations. Type-3 tests of fixed effects were performed using the MIXED procedure of SAS (version 9.1, SAS Institute, Inc., Cary, NC). Least-square means were separated using the Pdiff option of SAS and were considered significant at $p < 0.05$. The results were expressed as the least-square mean values of three independent trials.

## RESULTS AND DISCUSSION

**Instrumental Color.** The $a^*$ values of samples containing metabolic substrates in the absence of RRI were higher ($p < 0.05$) than those with added RRI (Figure 1). The addition of lactate and succinate with RRI resulted in a decrease ($p < 0.05$) of $a^*$ values compared to the control. The $a^*$ values did not differ ($p > 0.05$) between samples containing RRI with added lactate and added succinate. However, in the absence of added RRI, the $a^*$ values were higher ($p < 0.05$) for added lactate compared to succinate and the control. The $a^*$ value decreased as concentrations of $Fe^{2+}$ ions ($p < 0.05$) and $Fe^{3+}$ ions ($p < 0.01$; Figure 2) increased.

Lindahl et al.[25] found that the overall pigment content and fraction of MMb were most important in explaining the variation of the $a^*$ value in pork *longissimus dorsi* and *biceps femoris* muscles. Metabolic substrates, lactate and succinate, increase MMb reducing activity by generating NADH and increasing the oxygen consumption, respectively, which reduce MMb to DMb. When exposed to oxygen, DMb is oxygenated

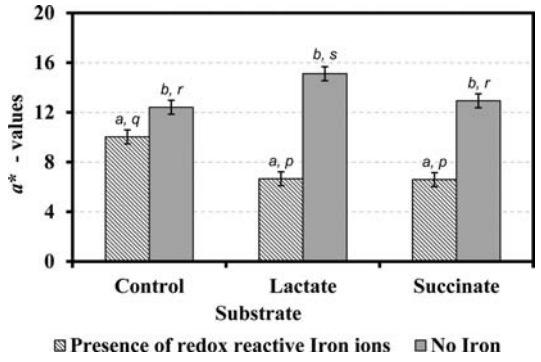


**Figure 1.** Variation of $a^*$ with metabolic substrates, with and without the presence of redox iron ions ($n = 3$). In the absence of redox iron ions, the $a^*$ of lactate-added homogenates was higher ($p < 0.05$) than that of succinate and control. In the presence of redox iron ions, the $a^*$ was lower ($p < 0.05$) for homogenates with added succinate and lactate. Values are expressed as least-square means with standard error of the mean (SEM) = 0.56. Means within a substrate treatment with different letters a and b are different ($p < 0.05$). Means across the substrate treatment with different letters p, q, r, and s are different ($p < 0.05$).

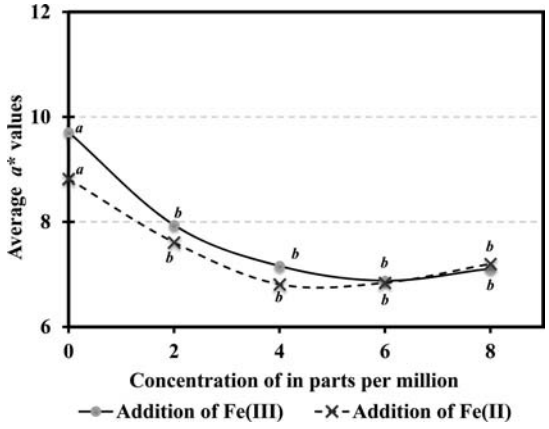


**Figure 2.** Effects of RRI (ferrous or ferric ions) concentration interaction with lactate and succinate on beef skeletal muscle homogenate $a^*$ values. The $a^*$ values of the beef homogenate was measured after the addition of increasing cocentrations of RRI forms (ferrous or ferric) in the presence of either lactate or succinate. Increasing $a^*$ values indicate a redder color, whereas a lower value indicates a less red color with some discoloration. Values are expressed as least-square means with SEM = 0.47. Means not sharing common letters a and b across the iron concentration are different ($p < 0.05$).

to OMb, which gives the desired bright cherry red color appearance to meat.[18,26] In this study, the $a^*$ values for the beef homogenate treated with lactate and succinate, in the absence of added RRI, were higher than that of the control, which was expected because of the color-stabilizing effect of metabolic substrates. However, in the presence of RRI, the homogenates with added lactate and those with added succinate had lower $a^*$ values than that of the control. This reduction in $a^*$ values may be due to oxidation of OMb directly or through other mechanisms, such as lipid oxidation, which might also contribute to reducing the redness indirectly.

Of the two RRI forms used in this work, $Fe^{2+}$ ions are pro-oxidants with well-documented roles in lipid peroxidation in raw muscle foods. This leads to a series of detrimental qualitative changes.[26] $Fe^{3+}$ ions are not soluble at post-mortem meat pH, which is approximately pH 5.6 or more. In the presence of reducing agents, such as ascorbate, NADPH, or cysteine, which are commonly present in raw meat[17] and in an aerobic environment, ferric ions are reduced to ferrous ions. This reaction contributes to lipid peroxidation through reactions 1−3, where AH is an arbitrary reducing agent.

$$Fe^{3+} + AH \rightarrow Fe^{2+} + A^{\bullet} + H^{+} \quad (1)$$

$$Fe^{2+} + O_2 \rightarrow Fe^{3+} + O_2^{\bullet -} \quad (2)$$

$$Fe^{2+} + ROOH \rightarrow Fe^{3+} + RO^{\bullet} + OH^{-} \quad (3)$$

In an acidic environment, the superoxide radicals also combine to form hydrogen peroxide through reaction 4, which further reacts with RRI ions to generate hydroxyl radicals through Fenton reactions 5 and 6. The hydrogen peroxide can further knock out iron from porphyrin in Mb, increasing the inorganic iron content. Overall, the oxidation reactions are self-catalyzing.

$$2O_2^{\bullet -} + 2H^{+} \rightarrow H_2O_2 + O_2 \quad (4)$$

$$Fe^{2+} + H_2O_2 \rightarrow Fe^{3+} + HO^{\bullet} + OH^{-} \quad (5)$$

$$Fe^{3+} + H_2O_2 \rightarrow Fe^{2+} + HO^{\bullet} + HOO^{\bullet} + OH^{-} \quad (6)$$

**Variation in Mb Redox Forms.** The interaction effect of the $Fe^{2+}$ concentration and substrate affected the OMb content ($p < 0.01$; Figure 3). For homogenate samples with added

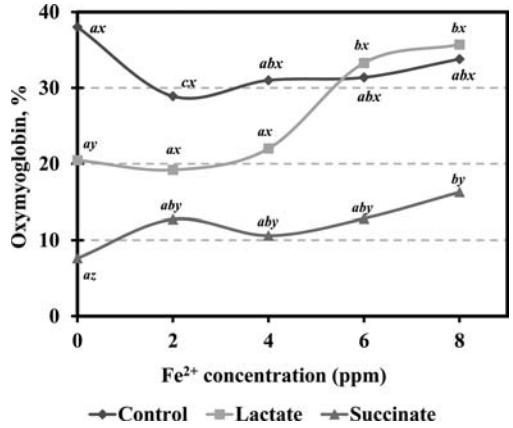


**Figure 3.** Variation of the OMb content with the ferrous ion concentration and different substrates ($n = 3$). The interaction effect between the ferrous ion concentration and substrate was significant ($p < 0.05$). For both lactate- and succinate-added homogenates, the OMb content increased with the ferrous ion concentration ($p < 0.05$). Values are expressed as least-square means with SEM = 6.31. Means not sharing common letters a, b, and c within a substrate are different ($p < 0.05$). Means not sharing common letters x, y, and z across the substrates are different ($p < 0.05$).

lactate and succinate, the OMb content increased ($p < 0.05$) with the ferrous ion concentration. However, the OMb content reduced with the ferrous ion concentration in the absence of lactate or succinate. The ferric ion concentration directly influenced ($p < 0.05$) the relative content of all three Mb redox forms in the homogenate system (Figure 4). The relative DMb and OMb contents decreased ($p < 0.01$) with the $Fe^{3+}$ concentration, and the relative MMb content increased ($p < 0.01$) with $Fe^{3+}$ addition.

A previous study of a buffered model system containing microsomes, purified Mb, and redox iron ions has shown that redox iron along with membranal lipid oxidation causes most

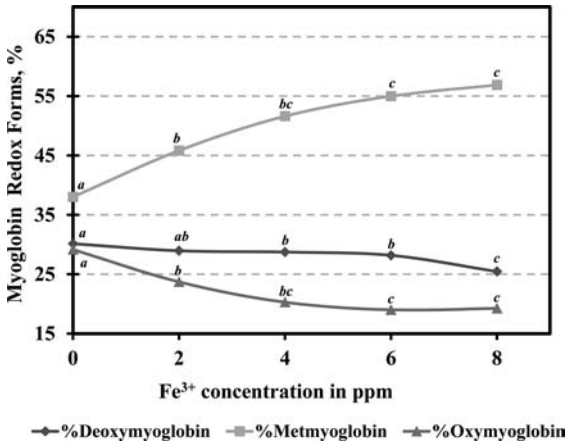


**Figure 4.** Variation in the relative contents of Mb redox forms with the ferric ion concentration ($n$ = 3). With the increase of the ferric ion concentration, the relative MMb content increased ($p$ < 0.05) and DMb and OMb contents decreased ($p$ < 0.05). Values are expressed as least-square means with SEM (DMb, 1.5; OMb, 3.6; and MMb, 3.15). Means not sharing common letters a, b, and c across $Fe^{3+}$ ion concentrations are different ($p$ < 0.05).

oxidation of OMb to MMb. However, the oxidation activity attributed to redox iron alone was very small.[27] The present study involved beef homogenate containing the cell membrane lipids as well as other components inherent to skeletal muscle, which can have both pro- and antioxidant activities. The relative percentage of OMb decreased ($p$ < 0.05) with the ferric concentration (Figure 4), while the percentage of MMb increased ($p$ < 0.05) with the ferric concentration. The results of this study suggest that the extent of OMb oxidation increased with the ferric ion concentration, possibly by the following reaction:

$$\mathrm{Mb{-}Fe^{2+}{-}O_2\ (OMb) + Fe^{3+} \rightarrow Mb{-}Fe^{3+}\ (MMb) + Fe^{2+} + O_2} \quad (7)$$

However, increasing the ferric ion concentration may lead to increased ferrous ion production via reaction 1. This can possibly lead to the formation of hydrogen peroxide, hydroxyl radicals, and perhydroxyl radicals (reactions 2 and 4−6). These can oxidize ferrous Mb through reactions 8 and 9.

$$\mathrm{Mb{-}Fe^{2+} + H_2O_2 \rightarrow Mb{-}Fe^{4+}{=}O + H_2O} \quad (8)$$

$$\mathrm{Mb{-}Fe^{2+} + OH^{\bullet} \rightarrow Mb{-}Fe^{3+} + OH^{-}} \quad (9)$$

Hence, it is difficult to pinpoint the exact route of action of ferric ions on oxidation of DMb and OMb. The underlying presence of either lactate or succinate in this experiment may be significant in the reactions of ferrous ions. Also, it would be worth investigating how RRI ions affect lactate dehydrogenase and succinate dehydrogenase in the beef skeletal muscle environment.

**Mitochondrial Oxygen Consumption.** In the absence of RRI, the addition of succinate to mitochondria isolated from the fresh beef hearts resulted in a much greater ($p$ < 0.05) state III consumption rate (oxygen consumption in the presence of substrate and ADP) than that for lactate, as seen in Table 1. Tang and colleagues[23] have reported that RCR above 2.2 is indicative of functional integrity and active respiration of beef heart mitochondria. In the absence of RRI, the RCR for both succinate (2.87) and lactate (2.38) addition indicated that the mitochondria isolated during the present experiments were functional and actively respiring. Loading with inorganic iron has been reported to negatively influence mitochondrial function, possibly by causing oxidation of cell membrane polyunsaturated fatty acids, loss of activity in thiol-dependent enzymes, and increased fragility of lysosomes.[27−30] When

**Table 1. Effect of Inorganic Iron and Metabolic Substrates on the Oxygen Consumption Rates and Respiratory Control Ratios of Beef Heart Mitochondria, Observed at pH 7.2 and 25 °C ($n$ = 3)[a]**

| Fe(II) concentration (nmol/mg of protein) | Fe(III) concentration (nmol/mg of protein) | state III OCR[c] | state IV OCR[b] | RCR[d] |
|---|---|---|---|---|
| | Substrate = 8 mM Succinate | | | |
| 0 | 0 | 132 ax[e] | 46 cx[e] | 2.9 ax[e] |
| 5 | 0 | 65 cx | 60 bx | 1.1 cdx |
| 60 | 0 | 15 ex | 18 ex | 0.9 dx |
| 0 | 5 | 41 dx | 42 cdx | 1.0 cdx |
| 0 | 60 | 48 dx | 32 dx | 1.5 cx |
| 5 | 5 | 79 bx | 78 ax | 1.0 cdx |
| 60 | 60 | 24 ex | 11 ex | 2.1 bx |
| | Substrate = 8 mM Lactate | | | |
| 0 | 0 | 80 ay | 34 ax | 2.4 abx |
| 5 | 0 | 34 bcy | 21 aby | 1.6 cx |
| 60 | 0 | 42 by | 27 abx | 1.5 cy |
| 0 | 5 | 26 cx | 36 ax | 0.7 dx |
| 0 | 60 | 46 bx | 25 abx | 1.9 bcx |
| 5 | 5 | 45 by | 16 by | 2.8 ay |
| 60 | 60 | 33 bcx | 19 bx | 1.8 bcx |

[a]The iron ion concentrations are expressed as nanomoles of iron per milligram of mitochondrial protein. [b]State IV OCR is the oxygen consumption rate of mitochondria in the presence of substrate alone. The oxygen consumption rates are expressed in nanomoles of atomic oxygen per milligram of protein per minute. [c]State III OCR is the oxygen consumption rate in the presence of both substrate and ADP. The oxygen consumption rates are expressed in nanomoles of atomic oxygen per milligram of protein per minute. [d]RCR is the ratio of state III OCR divided by state IV OCR. Each combination of ferrous and ferric ions is considered as a level of treatment. [e]Within a substrate, values in each column not sharing common letters a−e are significantly different ($p$ < 0.05). Within an iron ion concentration across the two substrates, values in each column not sharing common letters x and y are significantly different ($p$ < 0.05).

succinate was added to the isolated mitochondria treated with 5 nmol/mg of ferrous ions, either alone or in combination with 5 nmol/mg of ferric ions, RCRs near unity were obtained. A similar RCR was observed for 60 nmol/mg of ferrous treatment and succinate. A low RCR of near 1 indicates that the mitochondria are structurally compromised and unresponsive to ADP addition, which would otherwise increase oxygen uptake (i.e., the state III oxygen consumption rate).[23]

For lactate-supported mitochondrial respiration, either ferrous or ferric ions at 60 ppm alone or ferrous and ferric ions together at 60 ppm had a similar effect on both state III and state IV oxygen consumption rates. The three treatments reduced the RCR with respect to the lactate control, although the value was greater than 1, indicating that the mitochondria were actively respiring. Ferric ions at 5 ppm level reduced ($p < 0.05$) the state III OCR and RCR, indicating structural and functional compromise to mitochondria.[23]

The treatment combination of succinate with 60 ppm each of ferrous and ferric ions on mitochondria exhibited RCR greater than 2. Also, a RCR greater than 2 was observed with a combination of lactate with 5 ppm of both ferrous and ferric ions. Both of the treatments, however, reduced ($p < 0.05$) the state III and IV oxygen consumption rates compared to their respective controls.

Lactate as a metabolic substrate has been reported to support mitochondrial activity, because it can enter mitochondria through monocarboxylate shuttles. Mitochondria also contain an isoform of lactate dehydrogenase, which can oxidize lactate to generate NADH. NADH participates in the electron transfer chain and, thus, leads to oxygen consumption.[31,32] The mitochondrial oxygen consumption rates obtained with lactate and succinate fuelled respiration in the absence of iron addition, are similar to those reported in the literature.[33]

Mb and active mitochondria compete for dissolved oxygen in the tissue. Oxygen uptake because of mitochondrial respiration leads to reduction of oxygen partial pressure, causing conversion of OMb to MMb. Through metabolite-mediated enzymatic reduction, MMb can be further reduced to DMb via mitochondrial MMb reduction pathways,[34] thus offering better color stability. Because both lactate and succinate support mitochondrial respiration, their addition would lead to MMb reduction in post-mortem skeletal muscle. Mitochondria have been reported to be actively respiring for up to 45 days post-mortem at refrigeration temperatures.[35] Thus, they can participate in MMb reduction when supplied with suitable substrates. RCR values of near unity for mitochondria treated with inorganic iron are indicative of their compromised structure and function. This seems to indicate that inorganic iron would be detrimental to color stability of raw beef products.

The inorganic iron concentrations employed in this work represented those associated with storage, ingredient addition, and processing of fresh beef. A combination of inorganic ferrous and ferric ions (also termed redox reactive inorganic iron) was observed to reduce redness in raw beef homogenates. Ferric ions showed a concentration-dependent increase in MMb content, resulting in discoloration of the beef homogenates. Mitochondrial respiration was adversely affected by RRI. These findings provide evidence of the detrimental role of inorganic RRI on the color and color stability of raw beef. Specific iron-mediated targeting of mitochondrial components in raw beef skeletal muscles merits further research.

## AUTHOR INFORMATION


### Corresponding Author

*Telephone: +1-706-542-6673. Fax: +1-706-542-9066. E-mail: anandmohan@uga.edu.


### Notes

The authors declare no competing financial interest.

## ACKNOWLEDGMENTS

The authors thank Dr. Ranjith Ramanathan for his technical input and troubleshooting in the experiments on mitochondria. Also, the authors express their gratitude to White Oak Pastures, Bluffton, GA, for donating the beef hearts used in this study.

## REFERENCES


(1) Smith, G.; Belk, K.; Sofos, J.; Tatum, J.; Williams, S.; Decker, E.; Faustman, C.; Lopez-Bote, C. *Economic Implications of Improved Color Stability in Beef*; John Wiley & Sons, Inc.: Hoboken, NJ: 2000; pp 397−426.

(2) Ryan, T. P.; Aust, S. D. The role of iron in oxygen-mediated toxicities. *CRC Crit. Rev. Toxicol.* **1992**, *22*, 119−141.

(3) Welch, K. D.; Davis, T. Z.; Aust, S. D. Iron autoxidation and free radical generation: Effects of buffers, ligands, and chelators. *Arch. Biochem. Biophys.* **2002**, *397*, 360−369.

(4) Ponnampalam, E.; Butler, K.; McDonagh, M.; Jacobs, J.; Hopkins, D. Relationship between muscle antioxidant status, forms of iron, polyunsaturated fatty acids and functionality (retail colour) of meat in lambs. *Meat Sci.* **2012**, *90*, 297−303.

(5) Allen, K. E.; Cornforth, D. P. Myoglobin oxidation in a model system as affected by nonheme iron and iron chelating agents. *J. Agric. Food Chem.* **2006**, *54*, 10134−10140.

(6) Gorelik, S.; Kanner, J. Oxymyoglobin oxidation and membranal lipid peroxidation initiated by iron redox cycle. *J. Agric. Food Chem.* **2001**, *49*, 5939−5944.

(7) Decker, E. A.; Hultin, H. O. Lipid oxidation in muscle foods via redox iron. In *Lipid Oxidation in Food*; St. Angelo, A. J. Ed.; American Chemical Society (ACS): Washington, D.C., 1992; ACS Symposium Series, Vol. *500*, Chapter 3, pp 33−54.

(8) Faustman, C.; Chan, W.; Schaefer, D.; Havens, A. Beef color update: The role for vitamin E. *J. Anim. Sci.* **1998**, *76*, 1019−1026.

(9) Lanari, M.; Cassens, R. Mitochondrial activity and beef muscle color stability. *J. Food Sci.* **1991**, *56*, 1476−1479.

(10) Mészáros, L.; Tihanyi, K.; Horváth, I. Mitochondrial substrate oxidation-dependent protection against lipid peroxidation. *Biochim. Biophys. Acta, Lipids Lipid Metab.* **1982**, *713*, 675−677.

(11) Mohan, A.; Hunt, M. C.; Muthukrishnan, S.; Barstow, T. J.; Houser, T. A. Myoglobin redox form stabilization by compartmentalized lactate and malate dehydrogenases. *J. Agric. Food Chem.* **2010**, *58*, 7021−7029.

(12) Kondo, H.; Miura, M.; Kodama, J.; Ahmed, S. M.; Itokawa, Y. Role of iron in oxidative stress in skeletal muscle atrophied by immobilization. *Pfluegers Arch.* **1992**, *421*, 295−297.

(13) Napier, I.; Ponka, P.; Richardson, D. R. Iron trafficking in the mitochondrion: Novel pathways revealed by disease. *Blood* **2005**, *105*, 1867−1874.

(14) Pierrel, F.; Cobine, P. A.; Winge, D. R. Metal ion availability in mitochondria. *BioMetals* **2007**, *20*, 675−682.

(15) Kim, Y. H.; Hunt, M. C.; Mancini, R. A.; Seyfert, M.; Loughin, T. M.; Kropf, D. H.; Smith, J. S. Mechanism for lactate-color stabilization in injection-enhanced beef. *J. Agric. Food Chem.* **2006**, *54*, 7856−7862.

(16) Mancini, R.; Hunt, M. Current research in meat color. *Meat Sci.* **2005**, *71*, 100−121.

(17) Ramanathan, R.; Mancini, R. Effects of pyruvate on bovine heart mitochondria-mediated metmyoglobin reduction. *Meat Sci.* **2010**, *86*, 738−741.

(18) Mohan, A.; Hunt, M.; Barstow, T.; Houser, T.; Muthukrishnan, S. Effects of malate, lactate, and pyruvate on myoglobin redox stability in homogenates of three bovine muscles. *Meat Sci.* **2010**, *86*, 304−310.
(19) Mancini, R.; Ramanathan, R. Sodium lactate influences myoglobin redox stability *in vitro*. *Meat Sci.* **2008**, *78*, 529−532.
(20) Ramanathan, R.; Mancini, R.; Dady, G. Effects of pyruvate, succinate, and lactate enhancement on beef longissimus raw color. *Meat Sci.* **2011**, *88*, 424−428.
(21) North American Meat Processors Association. *The Meat Buyers Guide*; John Wiley & Sons, Inc.: Hoboken, NJ, 2004.
(22) American Meat Science Association (AMSA). *Guidelines for Meat Color Evaluation*; AMSA: Champaign, IL, 2012.
(23) Tang, J.; Faustman, C.; Hoagland, T. A.; Mancini, R. A.; Seyfert, M.; Hunt, M. C. Postmortem oxygen consumption by mitochondria and its effects on myoglobin form and stability. *J. Agric. Food Chem.* **2005**, *53*, 1223−1230.
(24) Foury, F.; Cazzalini, O. Deletion of the yeast homologue of the human gene associated with Friedreich's ataxia elicits iron accumulation in mitochondria. *FEBS Lett.* **1997**, *411*, 373−377.
(25) Lindahl, G.; Lundström, K.; Tornberg, E. Contribution of pigment content, myoglobin forms and internal reflectance to the colour of pork loin and ham from pure breed pigs. *Meat Sci.* **2001**, *59*, 141−151.
(26) Zhu, J.; Liu, F.; Li, X.; Dai, R. Effect of succinate sodium on the metmyoglobin reduction and color stability of beef patties. *J. Agric. Food Chem.* **2009**, *57*, 5976−5981.
(27) Eaton, J. W.; Qian, M. Molecular bases of cellular iron toxicity. *Free Radical Biol. Med.* **2002**, *32*, 833−840.
(28) Link, G.; Pinson, A.; Hershko, C. Iron loading of cultured cardiac myocytes modifies sarcolemmal structure and increases lysosomal fragility. *J. Lab. Clin. Med.* **1993**, *121*, 127−134.
(29) Link, G.; Pinson, A.; Kahane, I.; Hershko, C. Iron loading modifies the fatty acid composition of cultured rat myocardial cells and liposomal vesicles: Effect of ascorbate and $\alpha$-tocopherol on myocardial lipid peroxidation. *J. Lab. Clin. Med.* **1989**, *114*, 243−249.
(30) Link, G.; Pinson, A.; Hershko, C. Ability of the orally effective iron chelators dimethyl- and diethyl-hydroxypyrid-4-one and of deferoxamine to restore sarcolemmal thiolic enzyme activity in iron-loaded heart cells. *Blood* **1994**, *83*, 2692−2697.
(31) Brooks, G. A.; Dubouchaud, H.; Brown, M.; Sicurello, J. P.; Butz, C. E. Role of mitochondrial lactate dehydrogenase and lactate oxidation in the intracellular lactate shuttle. *Proc. Natl. Acad. Sci. U. S. A.* **1999**, *96*, 1129−1134.
(32) Pallotta, M. L.; Valenti, D.; Iacovino, M.; Passarella, S. Two separate pathways for d-lactate oxidation by *Saccharomyces cerevisiae* mitochondria which differ in energy production and carrier involvement. *Biochim. Biophys. Acta, Bioenerg.* **2004**, *1608*, 104−113.
(33) Ramanathan, R.; Mancini, R. A.; Konda, M. R. Effects of lactate on beef heart mitochondrial oxygen consumption and muscle darkening. *J. Agric. Food Chem.* **2009**, *57*, 1550−1555.
(34) Tang, J.; Faustman, C.; Mancini, R. A.; Seyfert, M.; Hunt, M. C. Mitochondrial reduction of metmyoglobin: Dependence on the electron transport chain. *J. Agric. Food Chem.* **2005**, *53*, 5449−5455.
(35) Mancini, R.; Ramanathan, R. Effects of postmortem storage time on color and mitochondria in beef. *Meat Sci.* **2014**, *98*, 65−70.

## MATERIALS AND METHODS

**Subjects.** Healthy subjects, 12 men and 12 women, were selected to participate in this study. Subjects' characteristics were 27 ± 6 years old, weight 68.3 ± 11.7 kg, and body mass index (BMI) 24 ± 3 kg $m^{-2}$. The subjects were non-smokers and non-vegetarians, and were not currently using hormones or nutritional supplements or taking medication for any gastrointestinal or metabolic diseases. The subjects did not regularly consume alcohol or perform intensive physical exercise. Systolic and diastolic blood pressures were 118 ± 11 and 70 ± 10 respectively, and the levels of triglycerides, total cholesterol, high density lipoprotein cholesterol, glucose and insulin were within normal ranges. The study was approved by the Ethics Committee of the School of Pharmaceutical Sciences, São Paulo State University, and an informed written consent was obtained from each participant before entering the study (protocol no. 00558712.5.0000.5426, The Ministry of Health, Brazil).

**Study Design.** The study was a crossover trial where the subjects received a sequence of two types of orange juice, (1) FOJ and (2) POJ, on two different days separated by a washout period of 30 d. The subjects agreed to refrain from consuming citrus fruits in any form for 3 d before each treatment and to follow a citrus flavonoid free diet. They were given a list of allowed and prohibited foods. Clinical data (anthropometric and blood pressure) were collected on the day before the first treatment.

The fasted subjects arrived at 8 a.m. on each day of the experiment, and a blood sample of 10 mL was collected (time point zero). The subjects were given 11.5 mL/kg body weight of orange juice, FOJ or POJ, in a 10 min period, and after 30 min they had a flavonoid-free standard breakfast. Blood samples of 10 mL were collected at 3, 4, 5, 6, 7, 8, and 24 h after each treatment with a catheter installed in a vein of the arm, and blood was sampled into heparinized vacuum tubes. At 4 h after ingestion of the orange juice the subjects were provided a lunch consisting of skinless chicken breast, rice and beans. After collection of the 7 h blood sample the subjects were provided with a snack similar to breakfast. Water was freely available during the entire day.

The first urine sample was discarded, and the subsequent urine samples were collected in plastic bottles containing 1 g of ascorbic acid, and kept at 4 °C. The subjects were asked to avoid eating any foods that contained polyphenols until after the last time point blood sampling. The subjects returned the following morning and the last blood sample was collected 24 h after ingestion of the orange juice.

**Orange Juices.** Two standard boxes of fresh oranges (Pera Rio sp) and 20 L of commercially extracted processed orange juice (POJ), made from the same batch of fruits, were provided by Citrosuco, Matao, Brazil. The fresh-squeezed orange juice (FOJ) was prepared from fruit extracted with a commercial fresh fruit juicer (MJ-20 Basic, Mulligan Associates, Inc., Jupiter, FL, USA) in the morning 2 h before starting the procedure for each subject. Remaining portions of the FOJ were frozen immediately after administration to the subjects. The POJ was pasteurized at 95 °C for 15 s, frozen, stored in 1 L bottles at −20 °C, and thawed under refrigeration the day before the experiment.

**Extraction of Flavonoids in Orange Juice.** FOJ and POJ were thawed and mixed, and triplicate samples (35 g) were centrifuged at 27000*g* at 4 °C for 30 min. Supernatants were collected and pellets were suspended with 35 mL of deionized water and centrifuged. The final pellets were vacuum-dried for 24 h at 55 °C. Prior to analysis, supernatant samples (1.0 mL) were spiked with 5.4 μg of mangiferin as an internal standard and analyzed without further processing. The vacuum-dried samples were ground to fine powder under liquid nitrogen for sample preparation. The ground pellet (100 mg) was extracted with 3 mL of dimethyl sulfoxide by shaking for 18 h with a platform shaker at 110 rpm at 25 °C. The extracts were centrifuged at 7500*g* for 15 min to remove any solid particulates. The supernatant (1.0 mL) was placed in a vial containing 5.4 μg of mangiferin (internal standard) prior to analysis by high-performance liquid chromatography−mass spectrometry (HPLC-MS).

Analyses of the orange juice flavonoids were done with a Waters 2695 Alliance HPLC (Waters, Medford, MA) connected in parallel with a Waters 996 PDA detector and a Waters/Micromass ZQ single-quadrupole mass spectrometer equipped with an ESI source. Compound separations were achieved with a Waters XBridge C8 column (5 μm, 4.5 × 150 mm) with linear gradients of acetonitrile and 0.5% aqueous formic acid with a flow rate of 0.75 mL/min. Identifications of compounds were done by absorbance and mass spectrometry, and by comparison of retention times of samples and authentic standards (narirutin, hesperidin, didymin, and vicenin-2). Quantitations of the flavanone glycosides and hydroxycinnamates were performed with UV peak integrations at 285 and 330 nm, respectively. The PMFs were quantified using both MS and UV absorbance detection and calibration curves with authentic standards (sinensetin, nobiletin, heptamethoxyflavone, and tangeretin). MS parameters were as follows: ionization mode, positive ESI; capillary voltage, 3.0 kV; extractor voltage, 5 V; source temperature, 100 °C; desolvation temperature, 225 °C; desolvation gas flow, 465 L/h; cone gas flow, 70 L/h; scan range, *m*/*z* 100−900; rate, 1 scan/s; cone voltages, 20 and 40 V. Quantification of flavonoids was done by external calibration curves obtained by injecting different amounts of stock solution containing the internal standard and all the compounds of interest.

**Plasma and Urine Samples Preparation.** Blood samples were collected in heparinized tubes and stored for a maximum of 15 min before centrifugation at 10000*g* for 4 min. Plasma was recovered and stored at −80 °C until processed. Plasma samples (200 μL) were combined with methanol (600 μL), thoroughly mixed, and centrifuged at 10000*g* for 4 min at room temperature. The supernatants were collected and reduced to dryness under vacuum with a Speedvac centrifugal evaporator (Savant, Holbrook, NY). Total urine samples collected in the flasks were homogenized and a 200 mL sample was withdrawn from each bottle. Five C18 Sep Pak (360 mg of resin/cartridge) (Waters, Milford, MA) were series connected and were preconditioned with methanol and water. The metabolites were absorbed onto the Sep Pak cartridges, and then eluted with 80% methanol. The recovered metabolites were dried under vacuum with a Speedvac centrifugal evaporator. Plasma and urine metabolite samples were dissolved in 1.0 mL of methanol/dimethyl sulfoxide (1/1 v/v), and 5.4 μg of mangiferin as internal standard was added.

**Analyses of Flavanone Metabolites in Human Plasma and Urine.** The flavanone metabolites in human plasma and urine samples were analyzed by HPLC-ESI-MS, with a Waters 2695 Alliance HPLC connected in parallel with a 996 photodiode array (PDA) detector and a Micromass ZQ single-quadrupole mass spectrometer equipped with an ESI source. Post-column split to the PDA and mass ZQ detector was 10:1. Compound separations were achieved with a Waters Atlantis dC18 column (2.1 × 100 mm) using linear gradients of aqueous 0.5% formic acid/acetonitrile, initially composed of 90:10 (v/v), and increased in acetonitrile content to 85:15, 80:20, 70:30, 30:70, 30:70 and then decreased to 90:10 (v/v) at 5, 7, 12, 20, 23, and 25 min, respectively, at a flow rate of 0.45 mL/min. Data handling was done with Mass Lynx software ver. 4.1 (Micromass, Division of Waters Corp., Beverly, MA). MS parameters were as follows: ionization mode, negative ESI; capillary voltage, 3.0 kV; extractor voltage, −4 V; source temperature, 100 °C; desolvation temperature, 250 °C; desolvation $N_2$ flow, 550 L/h; cone $N_2$ flow, 100 L/h; cone voltage, 40 V.

Detection and identifications of the metabolites were based on their characteristic UV spectra, molecular masses, and fragmentation patterns as described previously.[20,28] Hesperetin glucuronides were identified by ions at *m*/*z* 477 and 301, hesperetin sulfates at *m*/*z* 381 and 301, mixed sulfo/glucurono hesperetin conjugates at *m*/*z* 301, 477, and 557, and naringenin glucuronides with *m*/*z* ions at 477 and 271. Quantifications of the metabolites in the plasma and urine samples were made with peak area (PA)/μg conversion factors of authentic metabolite standards using integrated mass-extracted peak areas (PA) obtained either in the scan mode (100−900 amu) or in the single ion response (SIR) mode at the $[M-H]^-$ *m*/*z* for each compound. Standards for hesperetin-7-*O*-*β*-glucuronide (product no. HD322), hesperetin-3′-*O*-*β*-glucuronide (HD324), hesperetin-7, 3′-di-*O*-*β*-glucuronide (HD326), and naringenin-7-*O*-*β*-glucuronide (ND329) were obtained from LC Scientific Inc. (Concord, Ontario, Canada). Conversion factors (SIR PA $\mu g^{-1}$) of the metabolite standards were linear over the concentrations in the test urine samples.

**Plasma Metabolite Pharmacokinetics Analysis.** The plasma metabolites' data were plotted versus time (24 h), and the area under curve was calculated by the trapezoidal rule (AUC):

$$\mathrm{AUC} = \frac{1}{2}\sum_{i=1}^{n-1}(m_{i+1} - m_i)(H_{i+1} + H_i)$$

where $m_i$ is the $i$th hour, $H_i$ is the $i$th available concentration value, and $n$ is the number of hours. Plasma bioavailability of metabolites was from 0 to 24 h, and the secondary outcomes were $C_{max}$, i.e., maximum concentration, and $T_{max}$, i.e., time after treatment when reaching $C_{max}$. The pharmacokinetic parameters (AUC, $C_{max}$, and $T_{max}$) were calculated using Microcal Origin (version 6.0).

**Statistical Analysis.** Clinical characteristics were documented by descriptive statistics. All results are expressed as mean ± SD or SEM. The data distributions were tested for normality, and subsequently, a paired $t$ test or Wilcoxon test was applied using Sigma Stat version 3.11 (Systat Software Inc., USA).

## RESULTS

**Phenolic Compounds in FOJ and POJ.** The flavonoids in orange juice occur mainly as flavanone and flavone glycosides and polymethoxylated flavones,[29,30] although other phenolic compounds such as hydroxycinnamates and phenolic alkaloids also occur.[31−33] The concentrations of the main flavonoids in the juices used in this study are summarized in Table 1. Three

**Table 1. Concentrations of Flavanone Glycosides and Polymethoxylated Flavones (μg/mL) in Pasteurized Orange Juice (POJ) and Fresh-Squeezed Orange Juice (FOJ)**

| flavonoids | POJ | FOJ |
|---|---|---|
| Flavanone Glycosides | | |
| narirutin (NR) | 36.5 ± 5.5 | 5.5 ± 0.91 |
| hesperidin (HSP) | 154.6 ± 47.2 | 47.2 ± 4.03 |
| isosakuranetin rutinoside (ISR) | 10.5 ± 4.3 | 4.27 ± 1.34 |
| Polymethoxylated Flavones | | |
| sinensetin (SIN) | 0.60 ± 0.03 | 1.77 ± 0.07 |
| nobiletin (NOB) | 0.84 ± 0.04 | 2.36 ± 0.19 |
| tetramethylscutellarein (TMS) | 0.35 ± 0.03 | 0.86 ± 0.07 |
| 3,5,6,7,8,3′,4′-heptamethoxyflavone (HMF) | 0.35 ± 0.03 | 1.18 ± 0.10 |
| tangeretin (TAN) | 0.11 ± 0.02 | 0.45 ± 0.04 |

of the main flavanone glycosides, hesperidin, narirutin, and isosakuranetin rutinoside (didymin) (Figure 1) were identified by their elution times and characteristic UV and mass spectra matching those of authentic standards. The results show that 3.5 times higher total flavanone glycoside concentrations occurred in the POJ than in the FOJ. The average POJ and FOJ samples (786 ± 135 mL) consumed in this study contained 121.5 ± 37.1 and 37.1 ± 3.1 mg of hesperidin, respectively. For narirutin the average doses contained 28.7 ± 4.3 and 4.3 ± 0.7 mg in the POJ and FOJ, respectively. In sharp contrast, the polymethoxylated flavones occurred at concentrations 2−3 times higher in the FOJ than in the POJ. In the average sample of FOJ the total polymethoxylated flavone content was 4.73 ± 0.18 mg, but only 1.76 ± 0.30 mg in the average sample of POJ. The polymethoxylated flavones occur in orange juice as constituents of the peel oil introduced into the juice by the fruit extraction methods, and consistent with this were differences in the peel oil levels (estimated by limonene content) of the FOJ (0.080 ± 0.004%) and POJ (0.028 ± 0.037%).

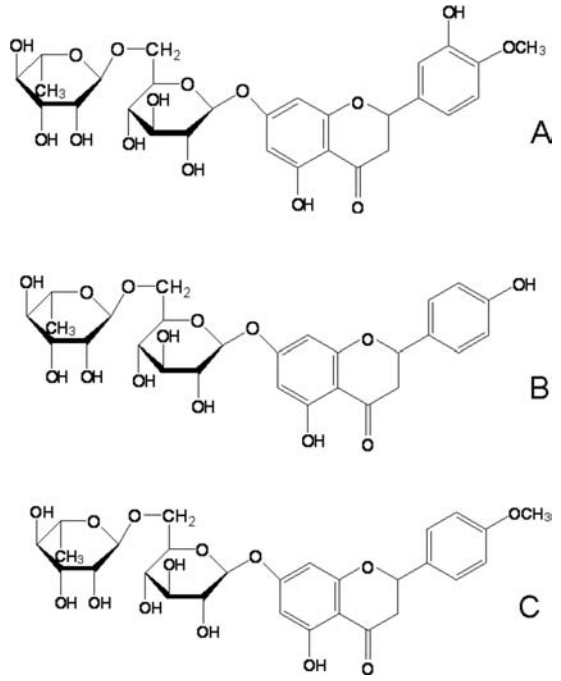


**Figure 1.** Main flavanone glycosides: (A) hesperidin, (B) narirutin, and (C) isosakuranetin rutinoside.

The levels of additional juice compounds in the POJ and FOJ were also analyzed. Concentrations of vicenin-2 (6,8-di-*C*-glucosylapigenin) and feruloylputrescine were 4.5 and 3.3 times higher in the POJ than in the FOJ, respectively (data not shown). Concentrations of the total hydroxycinnamic acids, ferulic, *p*-coumaric, and sinapinic acids in the POJ and FOJ released after saponification of the juices are shown in Table 2.

**Table 2. Contents of Hydroxycinnamic Acids (μg/mL) in Pasteurized Orange Juice (POJ) and Fresh-Squeezed Orange Juice (FOJ) after Saponification**

| hydroxycinnamic acids | POJ | FOJ |
|---|---|---|
| *p*-coumaric acid | 13.1 ± 1.0 | 20.5 ± 0.6 |
| ferulic acid | 66.2 ± 3.1 | 42.1 ± 2.1 |
| sinapinic acid | 15.1 ± 0.6 | 16.0 ± 0.3 |

These compounds occur in orange juice mainly as hydroxycinnamates with glucaric acids.[34] The levels of ferulic and sinapinic acids were nearly the same in POJ compared to FOJ, while the levels of *p*-coumaric acid were higher in FOJ (20.5 ± 0.6 ppm) than in the POJ (13.1 ± 1.0 ppm).

In addition to the differences in total concentrations of the main flavanone glycosides and polymethoxylated flavones in the POJ compared to the FOJ, there were also important differences in the distributions of these compounds occurring soluble in the juice serum or precipitated in the juice cloud. The average flavonoid content (μg) of pellets and sera of POJ and FOJ, along with percent averages in parentheses are listed in Table 3. In the FOJ 98.6% of the hesperidin occurred soluble in solution, whereas in the POJ only 28.6% of the total hesperidin remained soluble. The remaining 71.4% of the hesperidin in the POJ was precipitated in the juice cloud. Similar properties were observed for isosakuranetin rutinoside. In the FOJ 99% of the narirutin occurred soluble in solution and 62.4% soluble in solution for POJ. In this latter aspect, narirutin differed from

**Table 3. Average Flavonoid Content (μg) of Precipitated Pellets and Serum in 35 g of Pasteurized Orange Juice (POJ) and Fresh Orange Juice (FOJ)[a]**

| flavonoids | POJ | | FOJ | |
|---|---|---|---|---|
| | pellet | supernatant | pellet | supernatant |
| Flavanone Glycosides | | | | |
| narirutin (NR) | 255.2 ± 5.7 (37.6) | 423.4 ± 62 (62.4) | 0.6 ± 0.1 (1) | 66.5 ± 5.4 (99) |
| hesperidin (HSP) | 2212.7 ± 69.9 (71.4) | 888.2 ± 140.3 (28.6) | 13.2 ± 4.1 (1.4) | 899.6 ± 116.4 (98.6) |
| isosakuranetin rutinoside (ISR) | 173.9 ± 11.7 (78) | 49.1 ± 10.2 (22) | 0.5 ± 0.1 (4.1) | 11.4 ± 0.2 (95.9) |
| Polymethoxylated Flavones | | | | |
| sinensetin (SIN) | 4.2 ± 0.7 (62.8) | 2.5 ± 0.6 (37.2) | 3.2 ± 0.5 (36.7) | 5.4 ± 0.5 (63.3) |
| nobiletin (NOB) | 4.3 ± 0.4 (51.1) | 4.1 ± 0.8 (48.9) | 9.7 ± 1.8 (33.3) | 19.4 ± 0.6 (66.7) |
| 3,5,6,7,8,3′,4′-heptamethoxyflavone (HMF) | 1.6 ± 0.2 (51.5) | 1.5 ± 0.4 (48.5) | 3.7 ± 0.7 (37.2) | 6.2 ± 0.2 (62.8) |
| tangeretin (TAN) | 1.1 ± 0.1 (71.4) | 0.4 ± 0.1 (28.6) | 3.4 ± 0.7 (72.2) | 1.3 ± 0.2 (27.8) |

[a]Values in parentheses are percent averages.

**Table 4. Pharmacokinetic Parameters for Hesperidin and Narirutin Metabolites in Human Blood Plasma after Ingestion for Fresh-Squeezed (FOJ) and Commercially Processed (POJ) Orange Juice[a]**

| | | | AUC[c] (nmol·h/L) | | $C_{max}$[d] (nmol/L) | | $T_{max}$[e] (h) | |
|---|---|---|---|---|---|---|---|---|
| metabolite | mass ions (amu) | $t_R$[b] (min) | FOJ | POJ | FOJ | POJ | FOJ | POJ |
| hesperetin glucuronide | | | | | | | | |
| **B** | 477/301 | 13.1[f] | 138.0 ± 42.3 | 560 ± 195* | 22.0 ± 5.7 | 87.2 ± 37.3* | 5.00 ± 1.6 | 4.7 ± 1.0 |
| **C** | 477/301 | 13.6[g] | 53.5 ± 18.4 | 67.1 ± 21.8 | 3.1 ± 1.0 | 5.7 ± 1.5 | 3.7 ± 1.2 | 4.5 ± 2.4 |
| hesperetin glucuronide sulfate | | | | | | | | |
| **E** | 557/477/301 | 10.3 | 33.6 ± 11.1 | 25.3 ± 4.8 | 2.2 ± 0.9 | 2.2 ± 1.1 | 5.0 ± 1.9 | 4.3 ± 1.4 |
| **G** | 557/477/301 | 11.2 | 36.6 ± 11.3 | 95.9 ± 66.4* | 7.0 ± 4.5 | 21.5 ± 16.0* | 4.3 ± 1.0 | 5.2 ± 0.8 |
| hesperetin sulfate | | | | | | | | |
| **H** | 381/301 | 15.0 | nd[i] | 15.0 ± 13.4 | nd | 6.6 ± 2.4 | nd | 5.2 ± 1.2 |
| naringenin glucuronide | | | | | | | | |
| **J** | 447/271 | 10.6 | 129 ± 30.4* | 53.0 ± 27.5 | 15.4 ± 2.5 | 15.2 ± 4.7 | 6.3 ± 0.5 | 5.7 ± 1.2 |
| **K** | 447/271 | 12.3[h] | 80.3 ± 77.6 | 192.1 ± 91.9* | 14.1 ± 8.3 | 127.3 ± 15.4* | 4.7 ± 2.7 | 5.0 ± 1.3 |

[a]Values are reported as mean ± standard deviation. Asterisk (*) indicates that values are significantly different ($P < 0.05$). [b]$t_R$, retention time. [c]AUC, area under the curve. [d]$C_{max}$, maximum concentration. [e]$T_{max}$, time at $C_{max}$. [f]Hesperetin-7-*O*-glucuronide. [g]Hesperetin-3′-*O*-glucuronide. [h]Naringenin-7-*O*-glucuronide. [i]nd, not detected.

hesperidin and isosakuranetin rutinoside which occurred mostly in the juice clouds of the POJ. The polymethoxylated flavones also occurred soluble in the serum and precipitated in the juice cloud. Unlike the flavanone glycosides, there were no clear trends in these distributions for these compounds resulting from the different juice extraction methods. An exception was sinensetin, which occurred mainly soluble in the FOJ (63.3%), but mainly precipitated in the juice cloud of the POJ (62.8%).

**Plasma and Urine Metabolites.** Previous reports have shown that metabolites of hesperidin and narirutin in humans occur as glucuronic acid and/or sulfate conjugates of the hesperetin and naringenin aglycones.[20,28] In the present study, the relative bioavailabilty and uptake of hesperidin and narirutin in the POJ and FOJ were studied by HPLC-ESI-MS analyses of extracts of blood plasma and urine samples obtained over a 24 h period for each human subject. Analyses of the plasma and urine samples showed no evidence of the original flavanone glycosides, rather, in plasma, two main metabolites (**B** and **C**) exhibited mass ions at $m/z$ 301 and 477 (Table 4), and in urine two additional minor metabolites (**A** and **D**) also exhibited these mass ions (Table 5). Metabolites **B** and **C** were identified as hesperetin-7-*O*-glucuronide and hesperetin-3′-*O*-glucuronide, respectively, by comparisons with authentic standards. The neutral losses of 176 atomic mass units (amu) associated with these compounds were attributed to cleavages of glucuronic acid units from the $m/z$ 477 deprotonated molecular ions. Two other metabolites (**E** and **G**) also exhibited $m/z$ 477 and 301 ions and also an $m/z$ 557 ion. The 80 amu neutral loss between the 557 and 477 $m/z$ ions was attributed to cleavages of sulfate units from these metabolites. An additional metabolite, **H**, exhibited mass ions at $m/z$ 301 and 381, suggestive of a hesperetin-sulfate conjugate. Two metabolites (**J** and **K**) in the plasma, along with two other minor metabolites (**I** and **L**) in the urine (Table 5) are tentatively attributed to naringenin glucuronide conjugates. Metabolite **K** was identified as naringenin-7-*O*-glucuronide, based on peak overlaps and spectroscopic comparisons with an authentic standard.

**Plasma Kinetic Data.** The pharmacokinetic parameters—area under the curve (AUC), maximum concentration ($C_{max}$), and time of $C_{max}$ ($T_{max}$)—for the hesperidin and narirutin metabolites in the human plasma are listed in Table 4, and the average kinetic curves of the plasma metabolites obtained from the intake of the FOJ and POJ samples are presented in Figure 2. Concentrations of the flavanone metabolites in the blood plasma of subjects consuming POJ were higher than in the plasma of subjects consuming FOJ, with the exception for the tentatively identified naringenin glucuronic acid metabolite **J** (Table 4). In addition, the tentatively identified hesperetin-sulfate metabolite **H** was detected only after POJ intake. Plasma concentrations of the flavanones metabolites started to increase after the ingestion of orange juice and reached maximum

**Table 5. Concentrations of Hesperidin and Narirutin Metabolites Excreted in Human Urine 24 h after Consumption of Fresh-Squeezed (FOJ) and Commercially Processed (POJ) Orange Juice[a]**

| | | | urine metabolite concentrations | |
|---|---|---|---|---|
| metabolite | mass ion (amu) | $t_R$[b] (min) | FOJ | POJ |
| hesperetin glucuronide | | | | |
| **A** | 477/301 | 11.6 | nd[f] | 7.1 ± 2.4 |
| **B** | 477/301 | 13.1[c] | 28.7 ± 10.7 | 65.8 ± 9.2* |
| **C** | 477/301 | 13.6[d] | 91.0 ± 27.0 | 226.3 ± 29.2* |
| **D** | 477/301 | 15.7 | 4.1 ± 0.7 | 7.7 ± 1.7* |
| hesperetin glucuronide sulfate | | | | |
| **E** | 577/477/301 | 10.3 | nd | 3.1 ± 1.4* |
| **F** | 577/477/301 | 10.9 | 6.5 ± 1.4 | 72.2 ± 24.2* |
| **G** | 577/477/301 | 11.2 | 31.1 ± 24.6 | 72.9 ± 11.7* |
| hesperetin sulfate | | | | |
| **H** | 381/301 | 15.0 | 162.3 ± 29.5 | 404.2 ± 75.3* |
| naringenin glucuronide | | | | |
| **I** | 447/271 | 9.6 | 5.2 ± 0.6 | 8.9 ± 1.0* |
| **J** | 447/271 | 10.6 | 21.6 ± 2.0 | 37.6 ± 4.7* |
| **K** | 447/271 | 12.3[e] | 22.3 ± 8.1 | 51.9 ± 8.7* |
| **L** | 447/271 | 12.8 | 20.7 ± 6.7 | 56.2 ± 8.9* |

[a]Values are reported as mean ± standard deviation. Asterisk (*) indicates that values are significantly different ($P < 0.001$). [b]$t_R$, retention time. [c]Hesperetin-7-*O*-glucuronide. [d]Hesperetin-3′-*O*-glucuronide. [e]Naringenin-7-*O*-glucuronide. [f]nd, not detected.

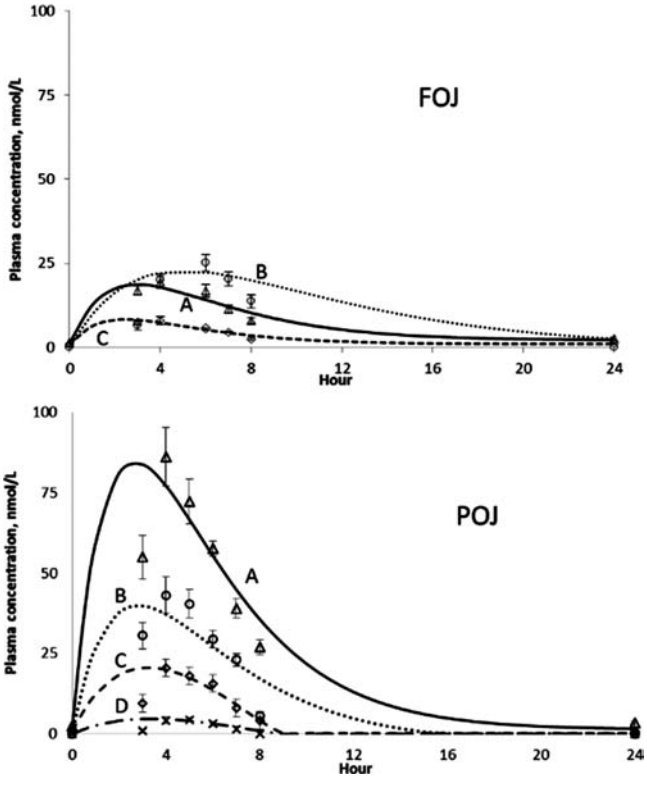


**Figure 2.** Plasma concentrations versus time of flavanones metabolites: (A) hesperetin-7-*O*-glucuronide (13.1 min), (B) hesperetin glucuronide sulfate (11.2 min), (C) naringenin glucuronide (10.6 min), and (D) hesperitin sulfate (15.0 min) after ingestion of FOJ and POJ. Values are expressed as mean ± standard deviation ($n = 24$).

concentrations between 3.7 and 6.3 h ($T_{max}$), and then returned to base values 24 h after orange juice consumption.

The average maximum concentrations ($C_{max}$) of the majority of the metabolites in the plasma were higher after the intake of POJ than after the intake of FOJ. As shown in Table 4, naringenin glucuronide metabolite **K** was 9 times higher in the plasma of subjects consuming the POJ than those consuming the FOJ; the hesperetin glucuronide metabolites **B** and **C** were 4 and 1.8 times higher, respectively, in the plasma of subjects consuming the POJ than those consuming the FOJ; and the hesperetin glucuronide sulfate metabolite **G** was 3.1 times higher in the plasma of subjects consuming the POJ than those consuming the FOJ. The areas under the concentration−time curve (AUC = 0−24) values for the plasma metabolites **K**, **G**, and **B** were 2.4, 2.6, and 4.1 time higher, respectively, for subjects consuming the POJ than for subjects consuming the FOJ. Only the metabolite tentatively identified as a naringenin glucuronide (**J**), was 2.4 times higher in the plasma measurements following intake of FOJ than following the intake of POJ.

**Urine Metabolites.** Analyses of the flavonoid metabolites in the urine samples obtained from the subjects after the consumption of both types of juices showed high concentrations of glucuronic acid and sulfate conjugates (Table 5), and numerous similarities occurred between the plasma and urine metabolite profiles. The metabolite **E**, tentatively identified as a hesperetin glucuronide sulfate was detected in the urine of subjects after consuming POJ, but not after consuming FOJ. Similarly assigned metabolites **F** and **G** were 11 and 2.4 times higher in the urine of subjects consuming the POJ compared to subjects consuming FOJ. The $m/z$ 381 metabolite **H** was detected at 2.5 times higher values in the urine of subjects consuming the POJ compared to subjects consuming FOJ. The naringenin glucuronide metabolites **I**−**L** were present respectively at 1.7, 1.7, 2.3, and 2.7 times higher after ingestion of POJ compared to the ingestion of FOJ. The hesperetin glucuronide metabolite **A** was detected in the urine after intake of POJ, but not after intake of the FOJ. Hesperetin-7-*O*-glucuronide (**B**) and hesperetin-3′-*O*-glucuronide (**C**) were present, respectively, at 2.3 and 2.5 times higher after ingestion of the POJ than after the ingestion of the FOJ. The percent urine excretion and absorption values for the combined hesperetin and naringenin metabolites are shown in Tables 6 and 7, respectively. Also included in Tables 6 and 7 are comparisons of the AUC, $C_{max}$, and $T_{max}$ values of the plasma metabolites reported in this current study as well as other previously reported studies. For our current study, the percent absorptions of the ingested hesperetin doses, measured by the combined urinary hesperetin metabolites were 0.8 and 0.9% after consumption of the POJ and FOJ, respectively (Table 6). The percent urine excretions were 4.13 ± 3.33 and 3.76 ± 2.19% for the POJ and FOJ, respectively. For the narirutin doses, the percent naringenin absorptions were 1.05 and 5.95% after consumption of the POJ and FOJ, respectively (Table 7).

## DISCUSSION

Orange juice has long been known to play important roles in healthy diets, contributing to daily intakes of folic acid, vitamin C, potassium, calcium, and other minerals. Particular benefits of orange juice consumption now focus on cardiovascular health, where orange juice has recently been shown to improve lipid profiles in humans by decreasing low-density lipoprotein cholesterol in hypercholesterolemic subjects, and by improving lipid transfer to high-density lipoprotein.[35−37] Additionally, in spite of its high sugar content, orange juice triggers no inflammatory oxidative responses in humans, rather, the

**Table 6. Percent Urine Excretion and Absorption of Hesperetin Doses of POJ and FOJ and Comparisons with Previous Studies**

| | | | | plasma hesperitin | | | | |
|---|---|---|---|---|---|---|---|---|
| source | vehicle (OJ) | volume OJ (mL) | hesperitin dose (mg) | AUC ($\mu$g·h/L) | $C_{max}$ ($\mu$g/L) | $T_{max}$ (h) | urine excretion (%) | absorption[b] (%) |
| Erlund et al.[47] ($n$ = 8) | commercial juice | 400−760 | 126 ± 26 | 3099 ± 2464 | 655 ± 479 | 5.4 ± 1.6 | 5.30 ± 3.1 | 2.4 |
| Manach et al.[48] ($n$ = 5) | commercial juice | 500 | 110 ± 3.7 | 1266 ± 335 | 139 ± 21 | 5.4 ± 0.40 | 4.13 ± 1.18 | 1.2 |
| | | 1000 | 220 ± 7.4 | 2805 ± 589 | 387 ± 39 | 5.8 ± 0.37 | 6.41 ± 1.32 | 1.3 |
| Mullen et al.[28] ($n$ = 8) | commercial juice w/HSP | 250 | 50.7 ± 0.0 | 1234 ± 873 | 278 ± 67.4 | 4.4 ± 0.5 | 6.30 ± 2.0 | 2.4 |
| Brett et al.[44] ($n$ = 20) | commercial juice | 300 | 71.8 ± 8.1 | 346 ± 363 | 30.9 ± 38 | 6.2 ± 2.0 | 4.63 ± 3.05 | 0.5 |
| | fruit | 150 | 79.7 ± 17.7 | 376 ± 508 | 28.8 ± 37.3 | 7.0 ± 4.23 | 4.53 ± 3.44 | 0.5 |
| Vallejo et al.[20] ($n$ = 10) | commercial OJ (A and B) (reconstituted) | A: 400 | 35.05 | 361 ± 90 | 97.8 ± 19.6 | 4.6 ± 0.7 | 5.4 ± 1.2 | 1.03 |
| | | B: 400 | 77.40 | 286 ± 69 | 110.2 ± 21.0 | 6.4 ± 0.7 | 1.7 ± 0.4 | 0.40 |
| Navarro et al.[27] ($n$ = 18) | fresh hand-squeezed | 400 | 18.8 | nd[c] | nd | nd | 8.1 ± 1.4/ 8.4 ± 1.5 | nd |
| | high-pressure homogenized | | 51.6 | nd | nd | nd | 4.8 ± 1.1/ 10.1 ± 2.4 | nd |
| | pasteurized OJ | | 56.2 | nd | nd | nd | 3.3 ± 0.5/ 7.7 ± 1.1 | nd |
| processed OJ[a] ($n$ = 24) | | 786 ± 135 | 47.5 ± 8.2 | 371 ± 23 | 57.1 ± 5.4 | 4.67 ± 0.82 | 4.13 ± 3.33 | 0.8 |
| fresh OJ[a] ($n$ = 24) | | 786 ± 135 | 14.4 ± 2.5 | 131 ± 5 | 16.2 ± 0.9 | 5.00 ± 1.55 | 3.76 ± 2.19 | 0.9 |

[a]Current study. [b]AUC/HSPTN dose (% absorption). [c]nd, not determined.

consumption of orange juice has been shown to prevent the induced oxidative and inflammatory responses caused by high-fat meals.[38,39] Although complete understandings of the modes of action for these beneficial effects are lacking, results from in vitro and animal trials suggest that the flavonoids in orange juice are at least partly responsible for these effects. In vitro cell culture studies with hesperidin and narirutin provide evidence for the roles of metabolites of the main orange juice flavonoids in cardiovascular protective effects.[40−43]

Many of the orange juice flavonoids, including hesperidin and narirutin, occur both soluble in solution and precipitated in the juice cloud, and a number of studies have now shown that these distributions are influenced by commercial juice processing and storage techniques.[23,24,26,27] In commercially processed orange juice the majority of the flavanone glycosides occur precipitated in the juice cloud.[22] Also associated with the juice cloud are major portions of the polymethoxylated flavones.[26] Under the physiological conditions of the gastrointestinal tract, a high percentage of the flavanones occurs as precipitated chalcones,[24] and the uptake and pharmacokinetics of these compounds are thought to be influenced by the relative distributions of soluble and cloud-precipitated forms. Hand squeezing of the fruit provides a higher content of soluble and permeable hesperidin than industrial extraction, while freezing and cold storage of processed juice decreases hesperidin solubility.[24] No effects on hesperidin solubility were seen with juice pasteurization and concentration.

The orange juices in our study were prepared by commercial industrial processing techniques and by a commercial fresh-squeezed method, and the differences in the flavonoid contents of the juices were consistent with earlier studies. The POJ contained higher total concentrations of the flavanone glycosides than the FOJ, and most occurred precipitated in the cloud fraction. In contrast, nearly all the flavanone glycosides in the FOJ occurred in the soluble form. Preparation of the FOJ introduced a high content of peel oil with a resultant higher polymethoxylated flavone content than in the POJ. These two styles of juices provided very different doses of flavonoids to the human subjects participating in this current study, and were valid systems to test for the influences of precipitated and soluble states of the flavanone glycosides on their absorption and pharmacokinetics in humans.

The metabolites of hesperidin and narirutin detected in the blood plasma and urine of the subjects that consumed the FOJ and POJ agreed with those detected in previous studies. Vallejo et al.[20] reported the detection of naringenin-7-*O*-glucuronide, naringenin-4′-*O*-glucuronide, naringenin and hesperetin sulfates, and hesperetin-7-*O*-glucuronide and hesperetin-3′-*O*-glucuronide as major constituents in human plasma. Other minor-occurring naringenin and hesperetin diglucuronides and sulfoglucoronides were also detected in human plasma.[20,21,28] Similar metabolites have been reported in urine of human subjects post orange juice consumption. We report the detection of hesperetin-7-*O*-glucuronide (**B**), hesperetin-3′-*O*-glucuronide (**C**), two hesperetin-sulfoglucuronides (**E** and **G**), a hesperetin sulfate (**H**), and naringenin-7-*O*-glucuronide (**K**) in the human plasma extracts (Table 4). Additional sulfo/glucurano-metabolites were detected in the concentrated extracts of the human urine samples (Table 5). The above metabolites have also been reported elsewhere.[20,21,28,44] Further metabolism of these compounds by colon microbiota leads to the ring fission of the main flavanone structures, leading to conjugated forms of ferulic and *m*-coumaric acids, phenyl propionic acids, benzoic acids, hippuric acid, and others.[45]

**Table 7. Percent Urine Excretion and Absorption of Naringenin Doses of POJ and FOJ and Comparisons with Previous Studies**

| | | | | plasma naringenin | | | | |
|---|---|---|---|---|---|---|---|---|
| source | vehicle (OJ) | volume OJ (mL) | naringenin dose (mg) | AUC ($\mu$g·h/L) | $C_{max}$ ($\mu$g/L) | $T_{max}$ (h) | urine excretion (%) | absorption[b] (%) |
| Erlund et al.[47] ($n$ = 8) | commercial juice | 400−760 | 23 ± 2 | 719 ± 437 | 175 ± 110 | 5.5 ± 2.9 | 1.1 ± 0.8 | 3.12 |
| Manach et al.[48] ($n$ = 5) | commercial juice | 500 | 22.6 ± 1.9 | 117 ± 46 | 16.0 ± 5 | 4.6 ± 0.60 | 7.1 ± 1.9 | 0.51 |
| | | 1000 | 45.2 ± 4.0 | 351 ± 90 | 54.0 ± 11 | 5.0 ± 0.45 | 7.9 ± 1.7 | 0.77 |
| Mullen et al.[28] ($n$ = 8) | commercial juice w/HSP | 250 | 3.3 ± 0. | nd[c] | nd | nd | 17.7 ± 3.9 | nd |
| Brett et al.[44] ($n$ = 20) | commercial juice | 300 | 9.4 ± 0.7 | 176 ± 170 | 14.3 ± 14.4 | 4.5 ± 2.5 | 10.2 ± 6.8 | 1.87 |
| | fruit | 150 | 11.8 ± 5.5 | 230 ± 230 | 23.0 ± 32.1 | 5.9 ± 1.8 | 12.5 ± 10.6 | 1.95 |
| Bredsdorff et al.[21] ($n$ = 16) | commercial juice | nd | 0.39 | 81.6 ± 54.4 | 32.6 ± 38.1 | 5.2 ± 3.0 | 7.0 ± 3.0 | nd |
| Vallejo et al.[20] ($n$ = 10) | commercial OJ (A and B) (reconstituted) | A: 400 | 12.38 | 18 ± 7.3 | 10.1 ± 2.7 | 4.7 ± 1.1 | 2.6 ± 0.5 | 0.15 |
| | | B: 400 | 15.19 | 200 ± 48.7 | 120.5 ± 29.6 | 5.7 ± 0.7 | 0.7 ± 0.2 | 1.31 |
| Navarro et al.[27] ($n$ = 18) | fresh hand-squeezed | 400 | nd | nd | nd | nd | 11 ± 1.8/ 11.4 ± 1.9 | nd |
| | high-pressure homogenized | | nd | nd | nd | nd | 7.7 ± 1.9/ 9.3 ± 2.3 | nd |
| | pasteurized OJ | | nd | nd | nd | nd | 6.7 ± 1.2/ 8.5 ± 1.6 | nd |
| processed OJ[a] ($n$ = 24) | | 786 ± 135 | 10.5 ± 1.8 | 110 ± 9 | 21.2 ± 2.1 | 5.2 ± 1.2 | 3.8 ± 2.1 | 1.05 |
| fresh OJ[a] ($n$ = 24) | | 786 ± 135 | 1.57 ± 0.27 | 93.4 ± 9.2 | 12.5 ± 0.9 | 5.3 ± 1.0 | 8.7 ± 4.9 | 5.95 |

[a]Current study. [b]AUC/NGNIN dose (% absorption). [c]nd, not determined.

Glucuronic acid conjugates of these metabolites were detected, but not quantified, by Vallejo et al.[20] Similar compounds were detected in our current study, and further analyses of these compounds in the plasma and urine samples are in progress. It is possible that some of these metabolites are also produced from the hydroxycinnamates in the juices consumed in this study.

The bioavailabilities of orange juice flavanones were shown in a previous study to be influenced by the soluble levels of the flavanones, but independent of the total hesperidin (soluble plus precipitated) concentrations in the juices.[20] Yet the pharmacokinetics in our study show that the AUC and $C_{max}$ values, when corrected for differences in dose amounts were not influenced by the soluble/precipitate ratios. Juices with contrasting flavanone profiles were analyzed in our study, where the profiles of these compounds in the POJ appeared to match several of the commercial juices and pulp-enriched juice analyzed by Vallejo et al.[20] The hesperidin in the latter juices contained 78% in the precipitated form in comparison to 71% in our POJ (Table 3). The FOJ analyzed in our study contained less than 2% precipitated hesperidin, and thus contrasted sharply with any of the juices analyzed in the previous study.[20] An important feature of the juices tested in our study was that the levels of soluble hesperidin in the FOJ and POJ were nearly identical at 46.5 and 44.2 $\mu$g/mL, respectively. Yet, the total AUC values for the three main plasma flavanone metabolites in Table 4 (**B**, **G**, and **K**) of subjects consuming the POJ was 848 nmol·h/L, in contrast to 255 nmol·h/L for subjects that consumed FOJ. The difference in these values reflect the differences in total flavanones in these juices (Table 1), and not the soluble flavanone concentrations, as discussed above. Furthermore, the percent hesperidin urinary excretion values measured in the POJ and FOJ trials (Table 6) show no statistically significant difference, thus providing additional evidence that the absorption of the orange juice flavanones was not appreciably influenced by the distributions of soluble and precipitated forms. As shown in Tables 6 and 7, these percent urinary excretion values were similar to values reported in other previous orange juice consumption studies. Hence, while the different styles of orange juices produced different blood plasma concentrations of the main flavanone metabolites, the qualitative aspects of the pharmacokinetics of this metabolism in humans remain similar for the two juices.

However, other factors may also influence flavanone metabolism and bioavailability from orange juice, including differences in the colon microbiota that are essential to flavonoid metabolism. Multiple pathways may exist that produce the abundant flavanone ring-fission products that occur in addition to the intact flavanone metabolites.[45,46] What influence the physical state of flavanones have in controlling these pathways is unknown, although further influences of the colon microbiota on orange juice flavanone bioavailability were recently studied by Navarro et al.[27] in human subjects exhibiting either high (>10% flavanone intact), medium (5−10%), or low (>5%) urinary hesperidin excretion capabilities. Subjects with high capabilities of urinary hesperidin excretion exhibited better absorption of hesperidin from juices with smaller juice cloud particles in contrast to the medium and low capacity hesperidin urinary excretors. Navarro et al.[27] proposed that these differences arise from differences in colon microbiota

and intestinal transporters capable involved in flavanone release and uptake. It is possible, therefore, that differences in colon microbiota may greatly expand the influences of hesperidin solubility and juice cloud interactions on flavanone bioavailability in many individuals.

## AUTHOR INFORMATION

### Corresponding Author

*Phone: 772-462-5930. E-mail: john.manthey@ars.usda.gov.

### Notes

Mention of a trademark or proprietary product is for identification only and does not imply a guarantee or warranty of the product by the U.S. Department of Agriculture.
The authors declare no competing financial interest.

## ACKNOWLEDGMENTS

The authors are grateful to the Brazilian agency CAPES for grant of scholarship to Jacqueline Silveira (Proc. BEX 18493/12-2), and to Citrosuco S/A (Brazil) for supplying oranges and orange juice for this study.

## REFERENCES

(1) Demontry, I.; Lin, Y.; Zebregs, Y. E. M. P.; Vermeer, M. A.; van der Knapp, H. C. M.; Jakel, M.; Trautwein, E. A. The citrus flavonoids hesperidin and naringin do not affect serum cholesterol in moderately hypercholesterolemic men and women. *J. Nutr.* **2010**, *140*, 1615−1620.

(2) Miwa, Y.; Yamada, M.; Sunayama, T.; Mitsuzumi, H.; Tsuzaki, Y.; Chaen, H.; Mishima, Y.; Kibata, M. Effects of glucosyl hesperidin on serum lipids in hyperlipidemic subjects: preferential reduction in elevated serum triglyceride level. *J. Nutr. Sci. Vitaminology* **2004**, *50*, 211−218.

(3) Miwa, Y.; Mitsuzumi, H.; Sunayama, T.; Yamada, M.; Okada, K.; Kubota, M.; Chaen, H.; Mishima, Y.; Kibata, M. Glucosyl hesperidin lowers serum triglyceride level in hypertriglyceridemic subjects through the improvement of very low-density lipoprotein metabolic abnormality. *J. Nutr. Sci. Vitaminology* **2005**, *51*, 460−470.

(4) Morand, C.; Dubray, C.; Milenkovic, D.; Lioger, D.; Martin, J. F.; Scalbert, A.; Mazur, A. Hesperidin contributes to the vascular protective effects of orange juice: a randomized crossover study in human volunteers. *Am. J. Clin. Nutr.* **2011**, *93*, 73−80.

(5) Milenkovic, D.; Deval, C.; Dubray, C.; Mazur, A.; Morand, C. Hesperidin displays relevant role in the nutrigenomic effect of orange juice on blood leukocytes in human volunteers: a randomized controlled cross-over study. *PLoS One* **2011**, *6*, No. e26669.

(6) Yamamoto, M.; Suzuki, A.; Hase, T. Short-term effects of glucosyl hesperidin and hesperetin on blood pressure and vascular endothelial function in spontaneously hypertensive rats. *J. Nutr. Sci. Vitaminology* **2008**, *54*, 95−98.

(7) Ikemuro, M.; Sasaki, Y.; Giddings, J. C.; Yamamoto, J. Preventive effects of hesperidin, glucosyl hesperidin, and naringin on hypertension and cerebral thrombosis in stroke-prone spontaneously hypertensive rats. *Phytother. Res.* **2012**, *26*, 1272−1277.

(8) Kawaguchi, K.; Kikuchi, S.; Hasunuma, R.; Maruyama, H.; Yoshikawa, T.; Kumazawa, Y. A citrus flavonoid hesperidin suppresses infection-induced endotoxin shock in mice. *Biol. Pharm. Bull.* **2004**, *27*, 679−683.

(9) Kawaguchi, K.; Maruyama, H.; Hasunuma, R.; Kumazawa, Y. Suppression of inflammatory responses after onset of collagen-induced arthritis in mice by oral administration of the *Citrus* flavanone naringin. *Immunopharm. Immunotoxicol.* **2011**, *33*, 723−729.

(10) Li, R.; Li, J.; Cai, L.; Hu, C. M.; Zhang, L. Suppression of adjuvant arthritis by hesperidin in rats and its mechanisms. *J. Pharm. Pharmacol.* **2008**, *60*, 221−228.

(11) Yeh, C. C.; Kao, S. J.; Lin, C. C.; Wang, S. D.; Liu, C. J.; Kao, S. T. The immunomodulation of endotoxin-induced acute lung injury by hesperidin in vivo and in vitro. *Life Sci.* **2007**, *80*, 1821−1831.

(12) Bok, S. H.; Lee, S. H.; Park, Y. B.; Bai, K. H.; Son, K. H.; Jeong, T. S.; Choi, M. S. Plasma and hepatic cholesterol and hepatic activities of 3-hydroxy-3-methyl-glutaryl-CoA reductase and acyl CoA:cholesterol transferase are lower in rats fed citrus peel extract or a mixture of citrus bioflavonoids. *J. Nutr.* **1999**, *129*, 1182−1185.

(13) Kurowska, E. M.; Manthey, J. A. Hypolipidemic effects and absorption of citrus polymethoxylated flavones in hamsters with diet-induced hypercholesterolemia. *J. Agric. Food Chem.* **2004**, *52*, 2879−2886.

(14) Jung, U. J.; Lee, M. K.; Park, Y. B.; Kang, M. A.; Choi, M. S. Effect of citrus flavonoids on lipid metabolism and glucose-regulating enzyme mRNA levels in type-2 diabetic mice. *Int. J. Biochem. Cell Biol.* **2006**, *38*, 1134−1145.

(15) Akiyama, S.; Katsumata, S.; Suzuki, K.; Nakaya, Y.; Ishimi, Y.; Uehara, M. Hypoglycemic and hypolipidemic effects of hesperidin and cyclodextrin-clathrated hesperetin in Goto-kakizaki rats with type 2 diabetes. *Biosci. Biotechnol. Biochem.* **2009**, *73*, 2779−2782.

(16) Chiba, H.; Uehara, M.; Wu, J.; Wang, X.; Masuyama, R.; Suzuki, K.; Kanazawa, K.; Ishimi, Y. Hesperidin, a citrus flavonoid, inhibits bone loss and decreases serum and hepatic lipids in ovariectomized mice. *J. Nutr.* **2003**, *133*, 1892−1897.

(17) Chiba, H.; Kim, H.; Matsumoto, A.; Akiyama, S.; ishimi, Y.; Suzuki, K.; Uehara, M. Hesperidin prevents androgen deficiency-induced bone loss in male mice. *Phytother. Res.* **2014**, *28*, 289−295.

(18) Habauzit, V.; Sacco, S. M.; Gil-Izquierdo, A.; Trzeciakiewicz, A.; Morand, C.; Barron, D.; Pinaud, S.; Offord, E.; Horcajada, M. N. Differential effects of two citrus flavanones on bone quality in senescent male rats in relation to their bioavailability and metabolism. *Bone* **2011**, *49*, 1108−1116.

(19) Nielsen, I. L. F.; Chee, W. S. S.; Poulsen, L.; Offord-Cavin, E.; Rasmussen, S. E.; Frederiksen, H.; Enslen, M.; Barron, D.; Horcajada, M. N.; Williamson, G. Bioavailability is improved by enzymatic modification of the citrus flavonoid hesperidin in humans: A randomized, double-blind, crossover trial. *J. Nutr.* **2006**, *136*, 404−408.

(20) Vallejo, F.; Larrosa, M.; Escudero, E.; Zafrilla, M. P.; Cerda, B.; Boza, J.; Garcia-Conesa, M. T.; Espin, J. C.; Tomas-Barberan, F. A. Concentration and solubility of flavanones in orange beverages affect their bioavailability in humans. *J. Agric. Food Chem.* **2010**, *58*, 6516−6524.

(21) Bredsdorff, L.; Nielsen, E. L. F.; Rasmussen, S. E.; Cornett, C.; Barron, D.; Bouisset, F.; Offord, E.; Williamson, G. Absorption, conjugation and excretion of the flavanones, naringenin and hesperetin from a-rhamnosidase-treated orange juice in human subjects. *Br. J. Nutr.* **2010**, *103*, 1602−1609.

(22) Gil-Izquierdo, A.; Gil, M. I.; Ferreres, F.; Tomas-Barberán, F. In vitro availability of flavonoids and other phenolics in orange juice. *J. Agric. Food Chem.* **2001**, *49*, 1035−1041.

(23) Gil-Izquierdo, A.; Gil, M. I.; Ferreres, F. Effect of processing techniques at industrial scale on orange juice antioxidant and beneficial health compounds. *J. Agric. Food Chem.* **2002**, *50*, 5107−5114.

(24) Gil-Izquierdo, A.; Gil, M. I.; Tomas-Barberán, F.; Ferreres, F. Influence of industrial processing on orange juice flavanone solubility and transformation to chalcones under gastrointestinal conditions. *J. Agric. Food Chem.* **2003**, *51*, 3024−3028.

(25) Baker, R. A.; Cameron, R. G. Clouds of citrus juices and juice drink. *Food Technol.* **1999**, *53*, 64−69.

(26) Bai, J.; Manthey, J. A.; Ford, B. L.; Luzio, G.; Cameron, R. G.; Narciso, J.; Baldwin, E. A. Effect of extraction, pasteurization and cold storage on flavonoids and other secondary metabolites in fresh orange juice. *J. Sci. Food Agric.* **2013**, *93*, 2771−2781.

(27) Navarro, M.; Vallejo, F.; Sentandreu, E.; Navarro, J. L.; Tomás-Barberán, F. A. Volunteer stratification is more relevant than technological treatment in orange juice flavanone bioavailability. *J. Agric. Food Chem.* **2014**, *62*, 24−27.

(28) Mullen, W.; Archeveque, M. A.; Edwards, C. A.; Matsumoto, H.; Crozier, A. Bioavailability and metabolism of orange juice flavanones

in humans: Impact of a full-fat yogurt. *J. Agric. Food Chem.* **2008**, *56*, 11157−11164.
(29) Kanes, K.; Tisserat, B.; Berhow, M.; Vandercook, C. Phenolic composition of various tissues of Rutaceae species. *Phytochemistry* **1993**, *32*, 967−974.
(30) Nogata, Y.; Sakamoto, K.; Shiratsuchi, H.; Ishii, T.; Yano, M.; Ohta, H. Flavonoid composition of fruit tissues of citrus species. *Biosci. Biotechnol. Biochem.* **2006**, *70*, 178−192.
(31) Manthey, J. A.; Grohmann, K. Phenols in citrus peel byproducts. Concentrations of hydroxycinnamates and polymethoxylated flavones in citrus peel molasses. *J. Agric. Food Chem.* **2001**, *49*, 3268−3273.
(32) Peleg, H.; Naim, M.; Rouseff, R. L.; Zehavi, U. Distribution of bound and free phenolic acids in oranges and grapefruit. *J. Sci. Food Agric.* **1991**, 417−426.
(33) Baldwin, E.; Plotto, A.; Manthey, J.; McCollum, G.; Bai, J.; Irey, M.; Cameron, R.; Luzio, G. Effect of Liberibacter infection (Huanglongbing disease) of citrus on orange fruit physiology and fruit/fruit juice quality: chemical and physical analyses. *J. Agric. Food Chem.* **2010**, *58*, 1247−1262.
(34) Risch, B.; Herrmann, K.; Wray, V. (*E*)-*O*-*p*-coumaroyl-, (*E*)-*O*-feruloyl-derivatives of glucaric acid in citrus. *Phytochemistry* **1988**, *27*, 3327−3329.
(35) Cesar, T. B.; Aptekmann, N. P.; Araujo, M. P.; Vinagre, C. C.; Maranhao, R. C. Orange juice decreases low-density lipoprotein cholesterol in hypercholesterolemic subjects and improves lipid transfer to high-density lipoprotein in normal and hypercholesterolemic subjects. *Nutr. Res. (N.Y.)* **2010**, *30*, 689−694.
(36) Aptekmann, N. P.; Cesar, T. B. Orange juice improved lipid profile and blood lactate of overweight middle-aged women subjected to aerobic training. *Maturitas* **2010**, *67*, 343−347.
(37) Aptekmann, N. P.; Cesar, T. B. Long-term orange juice consumption is associated with low LDL-cholesterol and apolipoprotein B in normal and moderately hypercholesterolemic subjects. *Lipids Health Dis.* **2013**, *12*, No. 119.
(38) Ghamin, H.; Mohanty, P.; Pathak, R.; Chaudhuri, A.; Sia, C. L.; Dandona, P. Orange juice or fructose intake does not induce oxidative and inflammatory response. *Diabetes Care* **2007**, *30*, 1406−1411.
(39) Ghanim, H.; Sia, C. L.; Upadhyay, M.; korzeniewski, K.; Visswanathan, P.; Abuaysheh, S.; Mohanty, P.; Dandona, P. Orange juice neutralizes the proinflammatory effect of a high-fat high carbohydrate meal and prevents endotoxin increase and Toll-like receptor expression. *Am. J. Clin. Nutr.* **2010**, *91*, 940−949.
(40) Yang, H. L.; Chen, S. C.; Kumar, J. K. S.; Yu, K. N.; Chao, P. D. L.; Tsai, S. Y.; Hou, Y. C.; Hseu, Y. C. Antioxidant and anti-inflammatory potential of hesperetin metabolites obtained from hesperetin-administered rat serum: An ex vivo approach. *J. Agric. Food Chem.* **2012**, *60*, 522−532.
(41) Assini, J. M.; Mulvihill, E. E.; Huff, M. W. Citrus flavonoids and lipid metabolism. *Curr. Opin. Lipidol.* **2013**, *24*, 34−40.
(42) Chanet, A.; Milenkovic, D.; Claude, S.; Maier, J. A. M.; Khan, M. K.; Rakotomanomana, N.; Shinkaruk, S.; Bérard, A. M.; Bennetau-Pelissero, C.; Mazur, A.; Morand, C. Flavanone metabolites decrease monocyte adhesion to TNF-*a*-activated endothelial cells by modulating expression of atherosclerosis-related genes. *Br. J. Nutr.* **2013**, *110*, 587−598.
(43) Yamamoto, M.; Jokura, H.; Hashizume, K.; Ominami, H.; Shibuya, Y.; Suzuki, A.; Hase, T.; Shimotoyodome, A. Hesperidin metabolite hesperetin-7-*O*-glucuronide, but not hesperetin-3′-*O*-glucuronide, exerts hypotensive, vasodilatory and anti-inflammatory activities. *Food Function.* **2013**, *4*, 1346−1351.
(44) Brett, G. M.; Hollands, W.; Needs, P. W.; Teucher, B.; Dainty, J. R.; Davis, B. D.; Brodbelt, J. S.; Kroon, P. A. Absorption, metabolism and excretion of flavanones from single portions of orange fruit and juice and effects of anthropometric variables and contraceptive pill use on flavanone excretion. *Br. J. Nutr.* **2009**, *101*, 664−675.
(45) Booth, A. T.; Jones, F. T.; DeEds, F. Metabolic fate of hesperidin, eriodictyol, homoeriodictyol, and diosmin. *J. Biol. Chem.* **1958**, *230*, 661−668.
(46) Serra, A.; Macla, A.; Romero, M. P.; Reguant, J.; Ortega, N.; Motilva, M. J. Metabolic pathways of the colonic metabolism of flavonoids (flavanols, flavones and flavanones) and phenolic acids. *Food Chem.* **2012**, *130*, 383−393.
(47) Erlund, I.; Meririnne, E.; Alfthan, G.; Aro, A. Plasma kinetics and urinary excretion of the flavanones naringenin and hesperetin in humans after ingestion of orange juice and grapefruit juice. *J. Nutr.* **2001**, *131*, 235−241.
(48) Manach, C.; Morand, C.; Gil-Izquierdo, A.; Bouteloup-Demange, C.; Remesy, C. Bioavailability in humans of the flavanones hesperidin and narirutin after the ingestion of two doses of orange juice. *Eur. J. Clin. Nutr.* **2003**, *57*, 235−242.

trients.[25,26] However, available information on cooking and the effects on phytochemicals and antioxidant properties of lentil is rather scarce. Hence, the present study was conducted to deliver a comprehensive investigation on the effects of domestic boiling without presoaking, as is recommended by Pulse Canada,[27] on phytochemical compositions (in both lipophilic and hydrophilic fractions) and antioxidant activities of lentils.

## MATERIALS AND METHODS

**Plant Materials.** Four lentil cultivars and breeding lines received from Saskatchewan Pulse Growers (Canada) on September 26, 2012, were selected for this study. The four selected lentils included two red lentil cultivars, Blaze and Maxim, and two green cultivars, Greenland and Sovereign. The four cultivars used in the present study were cultured at the same time and location. The whole raw lentil samples were used for cooking or ground into fine powder and stored in sealed plastic bags at −4 °C prior to analysis.

**Domestic Cooking Process.** Whole raw lentils (150 g) were rinsed in a strainer with cold running water for 1 min and then shaken for 30 s to remove excess water. The rinsed lentils were transferred to a pot and boiled with 450 mL of deionized water (seed/water, 1:3, w/v) on a Cimarec hot plate (Fischer Scientific Inc., Waltham, MA, USA). The hot plate was set at 500 °C until boiling and then lowered to 280 °C to simmer the lentils with the pot covered. The lentils were tested for firmness after 30 min of cooking by squeezing lentils between two fingers. Lentils are considered cooked when the seeds have little or no resistance to squeezing. The cooked lentils were allowed to cool and then lyophilized with the boiling water. The cooked lentil samples were ground into fine powder and stored in sealed plastic bags at −4 °C prior to analysis.

**Chemicals and Reagents.** 2,2-Diphenyl-1-picrylhydrazyl radical (DPPH), fluorescein disodium (FL), 2,2′-azobis(2-methylpropionamidine) dihydrochloride (AAPH), Folin−Ciocalteu reagent, gallic acid (GA), catechin, and 6-hydroxy-2,5,7,8-tetramethylchroman-2-carboxylic acid (Trolox) were purchased from Sigma (St. Louis, MO, USA). All standards used in this study were purchased from Sigma. Sodium acetate, ferric chloride hexahydrate, sodium phosphate monobasic, sodium phosphate dibasic, and HPLC grade solvents, including methanol (MeOH), methyl *tert*-butyl ether (MTBE), hexane, isopropanol, formic acid, and hydrochloric acid (HCl) were purchased from Caledon Laboratories (Georgetown, ON, Canada). All other chemical reagents used were of analytical grade.

**Sequential Extraction of Raw and Cooked Lentils.** The lipophilic fraction of lentils was extracted from 1 g of the finely ground raw or cooked samples by using hexane/isopropanol (3:2, v/v) as described in our recent publication.[12] The lipophilic extract was then evaporated under nitrogen stream at room temperature, redissolved in 1 mL of DMSO, and stored at −20 °C before use for different analyses. Subsequently, the residue from lipophilic extraction was air-dried under room temperature and extracted with aqueous methanol to obtain the hydrophilic extractable fraction. In brief, the dried residue was extracted with 20 mL of 70% methanol in 0.1% HCl (v/v) overnight (ca. 15 h) at room temperature with constant rolling on a rotary shaker (Scientific Industries Inc., Bohemia, NY, USA) at 150 rpm and then re-extracted two more times each with 10 mL of the same solvent. The supernatants were combined after centrifugation (Eppendorf centrifuge 5810R, Brinkman Instruments Inc., Westbury, NY, USA), topped up to 40 mL, filtered through a 0.2 μm PTFE membrane filter (VWR International, ON, Canada), and analyzed for extractable hydrophilic phenolics. The resulting residue from this extraction was dried under nitrogen and then hydrolyzed with 2 M NaOH (20 mL) at room temperature overnight on a rotary shaker at 150 rpm. The solution was then acidified to pH 2 with concentrated HCl (ca. 37%, w/w; 12 M) and extracted three times each with 20 mL of ethyl acetate/ethyl ether (1:1, v/v). The organic layer was combined, evaporated to dryness under nitrogen, dissolved in 1 mL of methanol, and analyzed for bound phenolics.

**Fatty Acid Analysis by Gas Chromatography.** The fatty acid compositions of the lipophilic fraction of both raw and cooked lentils were analyzed according to the method described in our recent publication.[12] Fatty acid methyl esters (FAME) were prepared using base-catalyzed reactions. Briefly, 10 mg of lipophilic extract was placed in a 15 mL glass tube equipped with Teflon-lined screw cap and dissolved in 80 μL of toluene. One milliliter of $NaOCH_3$/methanol (0.5 N) was then added for methylation at 50 °C for 30 min. After cooling to room temperature, 1 mL of water was added to the solution, and the esters were extracted with 2 mL of hexane.

**Total Phytochemical Contents by Colorimetric Assays.** *Total Carotenoid Content (TCC).* TCC in the raw and cooked lentil extract was determined according to the method described in our previous publication.[12] In brief, the absorbance of extract diluted appropriately and serial dilutions of lutein standard (0.5−10 μg/mL) were measured at 450 nm using a UV−vis plate reader (EL 340, Bio-Tek Instruments Inc., Winooski, VT, USA). The purity of the lutein standard was based on the manufacturer's information and has not been measured in the present study. The TCC was calculated on the basis of authentic lutein, which is the main carotenoid in lentil, and expressed as micrograms of lutein equivalent per gram of dry weight (DW) of sample.

*Total Phenolic (TPC), Flavonoid (TFC), and Condensed Tannin Content (CTC).* The contents of total phenolics, flavonoids, and condensed tannins in raw and cooked lentil extracts were determined according to our previously reported method.[28] Briefly, TPC was measured using Folin−Ciocalteu's phenol reagent and expressed as milligrams of gallic acid equivalent (GAE) per gram of dry weight of lentil (mg GAE/g DW). TFC was measured by the aluminum chloride ($AlCl_3$) assay by reading the absorbance at 510 nm, and result was expressed as milligrams of catechin equivalents (mg CAE) per gram of DW. CTC was determined according to the vanillin−HCl procedure by reading the absorbance at 500 nm, and the result was expressed as milligrams of catechin equivalents (mg CAE) per gram of DW.

**Phytochemical Composition by HPLC.** *Carotenoids and Tocopherols.* All-*trans*-carotenoids, *cis*-isomers, and tocopherols were separated by HPLC using the method described in our recent publication.[12] Identification of these lipophilic compounds was based on matching retention time, UV−vis spectra, and similarity in elution order with the available commercial standards, as well as by comparison with reported data in the literature.

*Phenolic Compounds.* The phenolic compositions of hydrophilic extracts (extractable and bound) in raw and cooked lentils were analyzed according to a previously reported HPLC method.[28] Briefly, HPLC separation was done in a Kinetex phenyl-hexyl column (100 × 4.60 mm, 2.6 μm) (Phenomenex Inc., Torrance, CA, USA) with a binary mobile phase consisting of 5% formic acid in water (v/v) (solvent A) and 95% methanol/5% acetonitrile (v/v) (solvent B). The gradient program was set as follows: 0−12 min, 0−20% B; 12−25 min, 20% B; 25−50 min, 20−80% B; 50−55 min, 80−100% B; 55−60 min, 100−0% B. The flow rate was 0.7 mL/min, and the data were collected at 280 nm for phenolic compounds. At least 21 phenolic compounds were identified in the lentil hydrophilic extract, all of which were quantified using individual standard curves of external standards or similar compounds of the same phenolic subgroup generated by plotting HPLC peak areas against the concentrations. For instance, catechin glucoside, catechin gallate, procyanidins, and related flavonoid derivatives were expressed as catechin equivalents; epicatechin glucoside and epicatechin gallate were expressed as epicatechin equivalents. Kaempferol glycosides and quercetin glycosides were quantified with the calibration curve of kaempferol and quercetin, respectively.

**Antioxidant Assays.** *DPPH Assay.* The antioxidant activities of both lipophilic and hydrophilic extracts (including extractable and bound phenolics) were estimated by DPPH assay.[12,28] Briefly, aliquots of 200 μL of methanolic solution of DPPH (350 μM) were mixed with 25 μL of the lipophilic lentil extract diluted 5-fold with methanol or the hydrophilic lentil extract or with a series of Trolox standard solutions (62.5−1000 μM) in a 96-well plate and allowed to react for 6 h at room temperature before the absorbance was recorded at 517 nm. Both lipophilic (DPPH-L) and hydrophilic (DPPH-H) DPPH antioxidant activities were calculated as micromoles of Trolox equivalent per gram of dry weight of lentil (μmol TE/g DW).

*Oxygen Radical Absorption Capacity Assay for Lipophilic Extract (ORAC-L).* The ORAC-L assay was conducted according to existing

**Table 1. Effect of Domestic Cooking on the Lipophilic Phytochemical Contents ($\mu$g/g DW) of Lentil Cultivars[a]**

| | lentil cultivars | | | | | | | |
|---|---|---|---|---|---|---|---|---|
| | Blaze | | Maxim | | Greenland | | Sovereign | |
| lipophilic phytochemical | raw | cooked | raw | cooked | raw | cooked | raw | cooked |
| **carotenoids** | | | | | | | | |
| 15-*cis*-lutein | 0.49 ± 0.03 a | 0.53 ± 0.06 a | tr | 0.60 ± 0.04 ab | 0.51 ± 0.03 a | 0.65 ± 0.06 b | tr | 0.55 ± 0.02 a |
| 13-*cis*-lutein | 0.73 ± 0.06 bc | 0.77 ± 0.04 cd | 0.66 ± 0.07 ab | 0.81 ± 0.03 cd | 0.61 ± 0.01 a | 0.75 ± 0.02 bc | 0.70 ± 0.05 b | 0.84 ± 0.02 d |
| 13′-*cis*-lutein | tr | 0.48 ± 0.02 a | tr | 0.55 ± 0.04 ab | 0.62 ± 0.04 bc | 0.77 ± 0.05 d | tr | 0.65 ± 0.04 c |
| all-*trans*-lutein | 5.12 ± 0.14 b | 7.61 ± 0.25 c | 7.11 ± 0.16 c | 9.19 ± 0.26 d | 9.22 ± 0.19 d | 10.33 ± 0.31 e | 4.30 ± 0.11 a | 6.91 ± 0.13 c |
| all-*trans*-zeaxanthin | 0.44 ± 0.02 b | 0.35 ± 0.01 a | 0.80 ± 0.04 d | 1.10 ± 0.05 e | 0.67 ± 0.05 c | 0.99 ± 0.08 e | 0.33 ± 0.02 a | 0.36 ± 0.02 a |
| 9-*cis*-lutein | 0.61 ± 0.05 ab | 0.57 ± 0.02 a | 0.83 ± 0.09 c | 1.19 ± 0.08 d | 0.91 ± 0.02 c | 1.29 ± 0.07 d | 0.69 ± 0.07 b | 0.69 ± 0.05 b |
| 9′-*cis*-lutein | 0.63 ± 0.03 ab | 0.54 ± 0.04 a | 0.96 ± 0.05 d | 0.84 ± 0.05 c | 1.00 ± 0.04 d | 1.26 ± 0.10 e | 0.70 ± 0.03 b | 0.84 ± 0.05 c |
| 9-*cis*-zeaxanthin | tr | 0.09 ± 0.00 a | 0.13 ± 0.02 b | 0.13 ± 0.00 b | 0.23 ± 0.01 d | 0.29 ± 0.02 e | 0.16 ± 0.00 b | 0.19 ± 0.01 c |
| total carotenoids index (TCI)[b] | 8.02 ± 0.33 b | 10.94 ± 0.44 d | 9.69 ± 0.43 c | 12.71 ± 0.55 e | 12.77 ± 0.39 e | 16.33 ± 0.61 f | 6.88 ± 0.28 a | 11.03 ± 0.34 d |
| total carotenoids content (TCC)[c] | 8.34 ± 0.26 b | 12.26 ± 0.14 d | 11.56 ± 0.21 c | 15.88 ± 0.16 f | 16.28 ± 0.28 f | 24.50 ± 0.32 g | 7.24 ± 0.10 a | 14.71 ± 0.24 e |
| **tocopherols** | | | | | | | | |
| $\alpha$-tocopherol | 0.67 ± 0.04 b | 2.01 ± 0.12 d | 1.30 ± 0.08 c | 3.74 ± 0.21 f | 0.81 ± 0.05 b | 1.59 ± 0.11 c | 0.53 ± 0.03 a | 2.57 ± 0.18 e |
| $\gamma$-tocopherol | 54.96 ± 1.07 b | 60.56 ± 2.13 c | 47.94 ± 1.52 a | 57.45 ± 1.74 bc | 65.19 ± 2.33 d | 83.04 ± 4.16 e | 45.68 ± 1.98 a | 55.60 ± 1.61 b |
| $\delta$-tocopherol | 1.59 ± 0.13 c | 1.42 ± 0.09 c | 0.50 ± 0.06 a | 0.58 ± 0.10 ab | 0.67 ± 0.08 b | 0.63 ± 0.05 b | 0.59 ± 0.03 ab | 0.66 ± 0.09 b |
| total tocopherols | 57.22 ± 1.24 b | 63.99 ± 2.34 cd | 49.74 ± 1.66 a | 61.77 ± 2.05 c | 66.67 ± 2.46 d | 85.26 ± 4.32 e | 46.80 ± 2.04 a | 58.83 ± 1.88 b |

[a]Values are the mean ± SD, $n$ = 3. tr, trace, below detection limit. Values followed by different letters in the same row are significantly different ($P < 0.05$). [b]Sum of concentrations of all detected carotenoids. [c]Values are from spectrophotometric analysis.



dx.doi.org/10.1021/jf504181r | J. Agric. Food Chem. 2014, 62, 12585−12594

**Table 2. Effect of Domestic Cooking on the Fatty Acid Composition (Relative Percent) of the Lipophilic Extracts from Lentil Cultivars[a]**

| | lentil cultivars | | | | | | | |
|---|---|---|---|---|---|---|---|---|
| | Blaze | | Maxim | | Greenland | | Sovereign | |
| fatty acid | raw | cooked | raw | cooked | raw | cooked | raw | cooked |
| 14:0 | 0.28 ± 0.01 a | 0.39 ± 0.02 bc | 0.48 ± 0.03 d | 0.34 ± 0.02 b | 0.48 ± 0.05 d | 0.44 ± 0.02 cd | 0.42 ± 0.01 cd | 0.38 ± 0.02 b |
| 15:0 | 0.19 ± 0.01 ab | 0.22 ± 0.01 b | 0.17 ± 0.01 a | 0.17 ± 0.01 a | 0.19 ± 0.01 ab | 0.19 ± 0.01 ab | 0.20 ± 0.01 b | 0.18 ± 0.01 a |
| 16:0 | 14.12 ± 0.12 d | 14.19 ± 0.14 d | 12.21 ± 0.10 b | 12.19 ± 0.09 ab | 11.87 ± 0.22 a | 12.22 ± 0.18 ab | 12.64 ± 0.13 c | 12.40 ± 0.17 bc |
| 16:1 | 0.34 ± 0.03 b | 0.42 ± 0.05 c | 0.34 ± 0.01 b | 0.17 ± 0.01 a | 0.15 ± 0.01 a | 0.14 ± 0.01 a | 0.17 ± 0.01 a | 0.15 ± 0.02 a |
| 17:0 | 0.15 ± 0.01 b | 0.15 ± 0.01 b | 0.20 ± 0.01 c | 0.20 ± 0.01 c | 0.09 ± 0.00 a | 0.09 ± 0.01 a | 0.10 ± 0.01 a | 0.11 ± 0.01 a |
| 17:1 | 0.16 ± 0.00 b | 0.25 ± 0.01 c | 0.17 ± 0.00 b | 0.16 ± 0.01 b | 0.06 ± 0.01 a | 0.08 ± 0.01 a | 0.06 ± 0.01 a | 0.09 ± 0.01 a |
| 18:0 | 1.87 ± 0.05 d | 1.97 ± 0.06 d | 1.59 ± 0.07 c | 1.68 ± 0.04 c | 0.96 ± 0.06 a | 1.00 ± 0.08 ab | 1.11 ± 0.07 b | 1.13 ± 0.08 b |
| 18:1 | 15.36 ± 0.09 a | 15.78 ± 0.21 b | 25.30 ± 0.51 c | 26.30 ± 0.23 d | 26.29 ± 0.71 d | 28.24 ± 0.46 e | 29.24 ± 0.59 f | 29.86 ± 0.65 f |
| 19:0 | 0.05 ± 0.00 b | 0.08 ± 0.00 c | 0.03 ± 0.00 a | 0.04 ± 0.01 ab | 0.02 ± 0.00 a | 0.04 ± 0.00 b | 0.02 ± 0.00 a | 0.03 ± 0.01 a |
| 18:2n-6 | 49.30 ± 0.85 e | 48.65 ± 1.03 de | 44.64 ± 0.78 c | 43.46 ± 1.21 bc | 46.21 ± 1.54 cd | 42.75 ± 1.18 ab | 41.82 ± 1.15 ab | 40.76 ± 1.06 a |
| 20:0 | 0.58 ± 0.04 bc | 0.60 ± 0.01 c | 0.63 ± 0.05 c | 0.53 ± 0.05 ab | 0.48 ± 0.04 a | 0.49 ± 0.02 a | 0.51 ± 0.02 a | 0.49 ± 0.02 a |
| 20:1 | 0.91 ± 0.04 a | 0.90 ± 0.02 a | 0.88 ± 0.03 a | 0.91 ± 0.07 a | 1.02 ± 0.04 b | 1.02 ± 0.06 b | 0.93 ± 0.04 a | 1.04 ± 0.06 b |
| 18:3n-3 | 14.00 ± 0.21 e | 12.61 ± 0.10 d | 11.84 ± 0.24 c | 10.64 ± 0.18 b | 10.29 ± 0.17 b | 9.38 ± 0.20 a | 10.12 ± 0.22 b | 9.10 ± 0.14 a |
| 21:0 | 0.27 ± 0.01 b | 0.32 ± 0.02 c | 0.25 ± 0.01 ab | 0.22 ± 0.02 a | 0.27 ± 0.05 b | 0.30 ± 0.01 bc | 0.27 ± 0.01 b | 0.29 ± 0.02 b |
| 20:2n-6 | 0.14 ± 0.01 b | 0.12 ± 0.01 b | 0.08 ± 0.01 a | 0.08 ± 0.02 a | 0.08 ± 0.01 a | 0.10 ± 0.02 ab | 0.09 ± 0.01 a | 0.09 ± 0.01 a |
| 22:0 | 0.60 ± 0.05 c | 0.65 ± 0.05 c | 0.33 ± 0.01 a | 0.45 ± 0.06 b | 0.44 ± 0.03 b | 0.42 ± 0.01 b | 0.41 ± 0.03 b | 0.41 ± 0.02 b |
| 20:3n-6 | 0.03 ± 0.00 b | 0.04 ± 0.00 b | 0.01 ± 0.00 a | 0.01 ± 0.00 a | 0.01 ± 0.00 a | 0.01 ± 0.00 a | 0.01 ± 0.00 a | 0.01 ± 0.00 a |
| 22:1 | 0.24 ± 0.05 b | 0.19 ± 0.01 b | 0.14 ± 0.01 a | 0.14 ± 0.01 a | 0.16 ± 0.01 a | 0.16 ± 0.02 a | 0.15 ± 0.01 a | 0.14 ± 0.01 a |
| 23:0 | 0.23 ± 0.01 c | 0.25 ± 0.03 c | 0.13 ± 0.01 a | 0.16 ± 0.01 b | 0.14 ± 0.01 a | 0.15 ± 0.02 ab | 0.15 ± 0.02 ab | 0.14 ± 0.01 a |
| 24:0 | 0.31 ± 0.03 bc | 0.35 ± 0.03 c | 0.21 ± 0.04 a | 0.26 ± 0.01 a | 0.23 ± 0.01 a | 0.26 ± 0.03 ab | 0.27 ± 0.02 ab | 0.27 ± 0.03 ab |
| 20:5n-3 | 0.22 ± 0.01 d | 0.03 ± 0.00 b | 0.04 ± 0.01 b | 0.07 ± 0.00 c | 0.01 ± 0.00 a | 0.03 ± 0.01 b | 0.04 ± 0.00 b | 0.04 ± 0.00 b |
| 24:1n-9 | 0.07 ± 0.00 c | 0.05 ± 0.01 b | 0.04 ± 0.00 a | 0.03 ± 0.00 a | 0.04 ± 0.01 a | 0.04 ± 0.00 a | 0.03 ± 0.00 a | 0.03 ± 0.00 a |
| 22:3n-6 | 0.08 ± 0.00 c | 0.11 ± 0.02 d | 0.01 ± 0.00 a | 0.03 ± 0.00 c | 0.02 ± 0.00 b | 0.05 ± 0.02 b | 0.08 ± 0.00 c | 0.09 ± 0.01 c |
| 26:0 | 0.43 ± 0.01 b | 1.27 ± 0.08 c | 0.25 ± 0.02 a | 1.61 ± 0.10 d | 0.46 ± 0.03 b | 2.23 ± 0.15 e | 1.08 ± 0.12 c | 2.58 ± 0.16 e |
| 22:5n-3 | 0.08 ± 0.01 c | 0.21 ± 0.02 e | 0.02 ± 0.00 a | 0.15 ± 0.01 d | 0.04 ± 0.00 b | 0.18 ± 0.07 de | 0.08 ± 0.01 c | 0.17 ± 0.03 de |
| Σ SFA | 19.08 ± 0.35 e | 20.44 ± 0.46 f | 16.48 ± 0.36 ab | 17.85 ± 0.42 cd | 15.63 ± 0.51 a | 17.83 ± 0.54 cd | 17.18 ± 0.45 bc | 18.41 ± 0.55 d |
| Σ MUFA | 17.08 ± 0.21 a | 17.59 ± 0.31 a | 26.87 ± 0.56 b | 27.71 ± 0.33 b | 27.72 ± 0.79 b | 29.68 ± 0.56 c | 30.58 ± 0.66 cd | 31.31 ± 0.75 d |
| Σ PUFA | 63.85 ± 1.09 d | 61.77 ± 1.18 d | 56.64 ± 1.04 c | 54.44 ± 1.42 bc | 56.66 ± 1.72 c | 52.50 ± 1.50 ab | 52.24 ± 1.39 ab | 50.26 ± 1.25 a |
| Σ UFA | 80.93 ± 1.30 ab | 79.36 ± 1.49 a | 83.51 ± 1.60 b | 82.15 ± 1.75 ab | 84.38 ± 2.51 b | 82.18 ± 2.06 ab | 82.82 ± 2.05 ab | 81.57 ± 2.00 ab |

[a]Data are expressed as the mean ± SD, $n = 3$. Values followed by different letters in the same row are significantly different ($P < 0.05$).

protocols described by Li et al.[29] Briefly, samples and Trolox standard were prepared in 7% (w/v) randomly methylated $\beta$-cyclodextrin (RMCD) to ensure the solubility of the lipophilic antioxidants in the reaction mixture. Twenty-five microliters of blank, Trolox standard, or the lipophilic extract was mixed with 200 $\mu$L of fluorescein (0.0868 nM) and incubated for 30 min at 37 °C and then added to 25 $\mu$L of AAPH (153 mM). The fluorescence (excitation wavelength, 485 nm; emission wavelength, 528 nm) was measured every minute for about 120 min until it reached zero in a Bio-Tek fluorescence spectrophotometer equipped with an automatic thermostatic holder (PLX 800, Bio-Tek Instruments, Inc.). The results were expressed as micromoles of Trolox equivalent (TE) per gram of dry weight of sample ($\mu$mol TE/g DW).

*ORAC Assay for Hydrophilic Extract (ORAC-H).* The ORAC assay for the hydrophilic extracts (both extractable and bound fractions) of lentil (ORAC-H) was conducted according to the method of Li et al.[29] The protocol was the same as that described above for the ORAC-L assay except that a phosphate buffer (75 mM, pH 7.4) instead of 7% (w/v) RMCD was used.

**Statistical Analysis.** All assays or tests were conducted in triplicate, and data are expressed as the mean ± standard deviation (SD). One-way analysis of variance (ANOVA) was used to compare the means. Differences were considered significant at $p < 0.05$. All statistical analyses were performed using Statistix for Windows version 9.0 (Analytical Software, Tallahassee, FL, USA).

## RESULTS AND DISCUSSION

**Effect of Domestic Cooking on Lipophilic Phytochemicals.** Concentrations of total and individual lipophilic antioxidants, namely, carotenoids and tocopherols, in tested lentils before and after cooking are summarized in Table 1. The TCC varied from 7.24 to 16.28 $\mu$g/g DW in raw lentils and significantly increased ($P < 0.05$) to 12.26−24.50 $\mu$g/g DW after cooking (increases of 37.37−103.18%). The cooking process also caused significant increases in individual carotenoids; for example, increases of 12.04−60.70% were found for the major carotenoid all-*trans*-lutein among the four varieties after cooking. Another measure for total carotenoids is total carotenoid index (TCI), which is the sum of the concentrations of all detected carotenoids by HPLC. Similar to TCC, TCI also had a 21.80−37.62% increase in cooked lentils as compared with all tested raw samples (Table 1). These results are the first to be reported for lentils but consistent with findings in other carotenoid-rich foods. For instance, the carotenoid content of tomato was found to be markedly higher after thermal processing.[30]

Because tocopherols are considered as one of the most effective lipophilic natural antioxidants, changes in concentration of individual and total tocopherols in lentils before and after cooking were determined by analyzing all tocopherol isomers by HPLC. $\gamma$-Tocopherol was the predominant isomer in lentils, which accounted for 96.38−97.78% of the total tocopherol content, followed by $\alpha$- and $\delta$-tocopherols among all tested raw lentils. Cooking caused the largest increase in $\alpha$-tocopherol level by 187.52−381.78%. Significant increases ($P < 0.05$) in $\gamma$-tocopherol and total tocopherols, but not in $\delta$-tocopherol level, were also observed after cooking (Table 1). This observation,

Table 3. Changes of TPC, TFC, and CTC in the Hydrophilic Extractable and Bound Phenolic Extracts of Lentil before and after Domestic Cooking[a]

| | | TPC[b] | | TFC[b] | | CTC[b] | |
|---|---|---|---|---|---|---|---|
| cultivar | sample | extractable (TPC-E) | bound (TPC-B) | extractable (TFC-E) | bound (TFC-B) | extractable (CTC-E) | bound (CTC-B) |
| Blaze | raw | 4.26 ± 0.18 bc | 0.29 ± 0.01 f | 0.76 ± 0.04 ab | 0.22 ± 0.01 e | 2.76 ± 0.16 c | 0.10 ± 0.00 e |
| | cooked | 3.78 ± 0.12 a | 0.16 ± 0.00 c | 0.68 ± 0.06 a | 0.05 ± 0.00 b | 1.62 ± 0.12 a | 0.01 ± 0.00 a |
| Maxim | raw | 6.96 ± 0.36 e | 0.27 ± 0.02 f | 1.24 ± 0.08 c | 0.18 ± 0.01 d | 5.82 ± 0.48 e | 0.08 ± 0.01 d |
| | cooked | 5.58 ± 0.18 d | 0.17 ± 0.01 cd | 1.16 ± 0.04 c | 0.10 ± 0.01 c | 3.42 ± 0.28 d | 0.03 ± 0.00 c |
| Greenland | raw | 7.80 ± 0.42 f | 0.18 ± 0.00 d | 1.72 ± 0.08 d | 0.03 ± 0.01 a | 6.24 ± 0.42 f | 0.02 ± 0.00 b |
| | cooked | 7.02 ± 0.30 e | 0.11 ± 0.00 a | 1.72 ± 0.12 d | 0.02 ± 0.00 a | 5.52 ± 0.16 e | nd |
| Sovereign | raw | 4.56 ± 0.30 c | 0.20 ± 0.01 e | 0.80 ± 0.04 b | 0.06 ± 0.01 b | 2.52 ± 0.24 c | 0.03 ± 0.00 c |
| | cooked | 4.04 ± 0.12 ab | 0.14 ± 0.01 b | 0.84 ± 0.04 b | 0.05 ± 0.00 b | 1.86 ± 0.08 b | nd |

[a]Values are the mean ± SD, $n = 3$. Values followed by the different letter in the same column are significantly different ($P < 0.05$). nd, not detected. [b]TPC, total phenolic content, expressed as mg GAE/g DW; TFC, total flavonoid content, expressed as mg CAE/g DW; CTC, condensed tannin content, expressed as mg CAE/g DW.

however, is contrary to what was found by others. For instance, Kalogeropoulos et al. reported a 1−2 orders of magnitude decrease in $\alpha$- and $\gamma$-tocopherols realtive to uncooked legumes including lentils.[31] These discrepancies could be attributed to different cooking protocols. Kalogeropoulos et al. removed soaking water before cooking and drained excess water after cooking, which is believed to cause significant loss of tocopherols. However, presoaking is not a normally followed cooking practice for lentil. The present study was carried out according to the cooking protocol recommended by Pulse Canada,[27] that is, one without presoaking and draining of the boiling water. This suggests that the recommended protocol retains the majority of tocopherols and other bioactive phytochemicals.

Results of the present study also suggest that thermal processing such as domestic cooking by boiling can significantly enhance the bioaccessibility of lipophilic bioactives of lentil. Heating is considered to cause cell membranes and cell walls to disrupt, releasing the lipophilic components such as carotenoids and tocopherols from the lentil matrix, thus leading to increased extraction efficiency.[30]

**Effect of Domestic Cooking on Fatty Acid Compositions.** Although lentils contain only 1.5−3% oil, its fatty acid composition had a very favorable omega-3 to omega-6 ratio (1:4).[12] Heating can potentially cause degradation of fatty acids, especially the essential fatty acids.[32,33] The effect of boiling on the fatty acid composition of lentils was investigated, and the results are summarized in Table 2. The lipophilic extracts from raw lentils mainly contained unsaturated fatty acids (UFA) (80.93−84.38%) including monounsaturated fatty acids (MUFA) (17.08−30.58%) and polyunsaturated fatty acids (PUFA) (52.24−63.85%), and an insignificant amount of saturated fatty acids (SFA). Cooking caused significant increases ($P < 0.05$) in SFA in all tested lentils, but had no significant effect on MUFA and PUFA. In terms of individual fatty acids, however, the predominant fatty acid 18:2n-6 decreased significantly ($P < 0.05$), whereas 18:3n-3 decreased only slightly without any statistical significance ($P > 0.05$) upon cooking. The concentration of the major MUFA 18:1 was markedly higher in cooked lentils ($P < 0.05$). These results indicate that the majority of PUFA in lentils remain relatively stable after cooking. Possible explanations may include the relatively low temperature of boiling as compared to other thermal processing techniques that can cause lipid oxidation. It may also be due to the coexistence of tocopherols, which can prevent lipid peroxidation by acting as peroxyl radical scavengers that terminate chain reactions in membranes and lipoprotein particles.[34]

**Effect of Domestic Cooking on Hydrophilic Phytochemicals.** *TPC, TFC, and CTC in Extractable and Bound Phenolic Extracts.* Table 3 shows the total phenolic content, total flavonoid content, and condensed tannin content in the extractable (TPC-E, TFC-E, and CTC-E) and bound phenolic (TPC-B, TFC-B, and CTC-B) fractions from raw and cooked lentils. Significant ($P < 0.05$) decreases in TPC-E and CTC-E were found in the extractable fraction of cooked lentils, whereas no significant change in TFC-E was observed in the same sample. Decreased TPC-E and CTC-E contents in cooked lentils suggest that losses of condensed tannin might be the contributing factor. The losses of condensed tannin could be well explained by the interactions between tannins and starch molecules. Barros et al. recently reported that condensed tannins could interact with starch (forming insoluble complexes) during cooking, particularly with amylose, thus resulting in significant decreases in extractable phenolic content.[35] Interactions between condensed tannins and starch molecules could, however, increase resistant starch content and decrease starch digestibility, thus providing benefits to human health.

Bound phenolics in lentils, both raw and cooked, were low compared to extractable phenolics. As shown in Table 3, bound phenolics (TPC-B, TFC-B, and CTC-B) represented only roughly 5% of the respective extractable phenolic fraction. TPC-B, TFC-B, and CTC-B varied significantly among tested lentils, ranging from 0.18 to 0.29 mg GAE/g DW, from 0.03 to 0.22 mg CE/g DW, and from 0.02 to 0.10 mg CE/g DW in cooked lentils, respectively. Bound phenolics, especially in TFC-B and CTC-B, were significantly higher in tested red lentil cultivars (Blaze and Maxim) than in the tested green cultivars (Greenland and Sovereign), despite the similar concentrations of extractable phenolics. Results that lentils had only a small portion of bound phenolics do not agree with those reported by Han et al., who found concentrations of bound phenolics were higher than extractable phenolics and the former to be the main contributor to total antioxidant activity in pulse seeds including lentils.[20] The discrepancy could be attributed to the different extraction protocol, as well as the genotype of tested lentils. Similar to the extractable phenolics, cooking also significantly decreased the

**Table 4. Effects of Cooking on the Hydrophilic Extractable and Bound Phenolic Contents ($\mu$g/g DW) of Lentil Cultivars[a]**

| | lentil cultivar | | | | | | | |
|---|---|---|---|---|---|---|---|---|
| | Blaze | | Maxim | | Greenland | | Sovereign | |
| phenolic compound | raw | cooked | raw | cooked | raw | cooked | raw | cooked |
| **extractable phenolics** | | | | | | | | |
| dihydroxybenzoic acid | 1.05 ± 0.14 a | 0.94 ± 0.08 a | 2.41 ± 0.11 c | 2.62 ± 0.19 cd | 2.76 ± 0.21 cd | 3.12 ± 0.22 d | 1.24 ± 0.28 ab | 1.58 ± 0.12 b |
| *p*-hydroxybenzolc acid | 3.48 ± 0.36 b | 3.69 ± 0.25 b | 4.11 ± 0.28 bc | 4.58 ± 0.38 c | 5.41 ± 0.30 d | 6.22 ± 0.31 e | 2.33 ± 0.12 a | 3.64 ± 0.24 b |
| catechin-3-glucoside | 124.13 ± 5.11 bc | 108.45 ± 3.46 a | 133.15 ± 6.14 cd | 120.65 ± 4.26 b | 141.72 ± 4.52 d | 128.30 ± 5.26 bc | 119.46 ± 4.58 b | 102.33 ± 3.41 a |
| catechin gallate | 63.19 ± 1.98 d | 55.74 ± 2.04 c | 69.54 ± 2.59 e | 60.88 ± 2.65 d | 78.15 ± 1.96 f | 71.02 ± 3.14 e | 50.26 ± 2.65 b | 39.60 ± 2.16 a |
| epicatechin-3-glucoside | 39.42 ± 2.05 b | 30.27 ± 1.56 a | 51.09 ± 3.01 c | 43.26 ± 2.14 b | 82.48 ± 2.24 e | 70.68 ± 2.95 d | 48.69 ± 1.55 c | 40.23 ± 1.94 b |
| sinapic derivative | 0.53 ± 0.07 a | 0.71 ± 0.05 bc | 0.62 ± 0.05 ab | 0.87 ± 0.06 d | 0.82 ± 0.05 d | 1.05 ± 0.03 e | 0.71 ± 0.07 bc | 0.79 ± 0.05 cd |
| procyanidin dimer 1 | 4.54 ± 0.22 d | 3.85 ± 0.16 c | 3.78 ± 0.24 c | 2.63 ± 0.15 b | 7.48 ± 0.51 f | 5.91 ± 0.32 e | 3.04 ± 0.34 b | 2.11 ± 0.14 a |
| syringic acid | 2.51 ± 0.41 ab | 3.08 ± 0.11 c | 3.24 ± 0.34 cd | 3.75 ± 0.20 d | 4.85 ± 0.39 f | 4.26 ± 0.17 e | 2.12 ± 0.19 a | 2.54 ± 0.20 b |
| *trans-p*-coumaroyl-malic acid | 0.78 ± 0.05 ab | 0.69 ± 0.07 a | 1.55 ± 0.11 d | 2.06 ± 0.12 f | 1.12 ± 0.04 c | 1.78 ± 0.08 e | 0.71 ± 0.05 a | 0.85 ± 0.06 b |
| *trans-p*-coumaric acid | 5.69 ± 0.62 bc | 6.92 ± 0.59 d | 6.12 ± 0.10 c | 8.23 ± 0.48 e | 12.16 ± 0.55 f | 14.11 ± 1.21 g | 4.15 ± 0.13 a | 5.24 ± 0.28 b |
| epicatechin gallate | 1.69 ± 0.05 c | 1.88 ± 0.05 d | 2.42 ± 0.18 f | 1.68 ± 0.08 c | 2.28 ± 0.08 e | 1.64 ± 0.14 c | 1.08 ± 0.06 b | 0.43 ± 0.02 a |
| kaempferol tetraglycoside | 214.72 ± 4.18 a | 231.52 ± 3.98 b | 289.55 ± 3.34 d | 310.24 ± 6.05 e | 302.14 ± 5.09 e | 331.20 ± 5.93 f | 230.15 ± 5.02 b | 251.52 ± 4.21 c |
| kaempferol triglycoside | 94.58 ± 2.54 a | 102.26 ± 2.04 b | 137.49 ± 2.58 de | 146.53 ± 2.59 f | 132.88 ± 2.79 d | 143.86 ± 3.67 e | 91.42 ± 3.57 a | 109.34 ± 3.64 c |
| kaempferol-3-robinoside-7-rhamnoside | 0.84 ± 0.04 a | 0.95 ± 0.06 a | 1.27 ± 0.08 b | 1.56 ± 0.18 c | 1.57 ± 0.11 c | 2.13 ± 0.23 d | 1.21 ± 0.08 b | 1.88 ± 0.13 d |
| quercetin-3-xyloside | 3.95 ± 0.26 a | 5.18 ± 0.51 b | 8.14 ± 0.25 d | 9.45 ± 0.33 e | 10.16 ± 0.23 f | 12.06 ± 1.35 g | 6.05 ± 0.55 b | 7.36 ± 0.42 c |
| procyanidin dimer 2 | 9.38 ± 0.61 c | 6.44 ± 0.32 b | 20.19 ± 1.31 e | 16.17 ± 1.15 d | 35.56 ± 2.65 f | 21.08 ± 1.76 e | 10.82 ± 1.12 c | 5.27 ± 0.29 a |
| procyanidin dimer 3 | 14.11 ± 0.97 c | 10.38 ± 0.86 b | 25.28 ± 1.29 e | 21.34 ± 1.27 d | 40.58 ± 1.54 g | 31.51 ± 2.07 f | 11.32 ± 0.79 b | 7.06 ± 0.35 a |
| quercetin-3-glucoside | 30.16 ± 1.44 a | 32.21 ± 2.13 a | 37.66 ± 1.86 b | 40.12 ± 2.98 b | 59.13 ± 3.09 c | 62.33 ± 1.62 c | 32.15 ± 1.54 a | 38.69 ± 2.44 b |
| flavonoid derivative | 1.97 ± 0.49 a | 2.16 ± 0.36 a | 11.53 ± 0.54 d | 13.58 ± 1.06 e | 11.96 ± 1.12 d | 11.25 ± 1.22 d | 5.09 ± 0.11 c | 4.28 ± 0.27 b |
| flavonoid derivative | 4.52 ± 0.23 e | 4.07 ± 0.31 e | 3.43 ± 0.12 c | 3.97 ± 0.24 d | 2.17 ± 0.08 ab | 2.37 ± 0.11 b | 1.94 ± 0.18 a | 2.41 ± 0.21 b |
| kaempferol-3-glucoside | 5.94 ± 0.21 bc | 5.43 ± 0.28 b | 6.09 ± 0.25 c | 7.23 ± 0.21 c | 8.10 ± 0.24 d | 9.32 ± 0.43 e | 3.47 ± 0.22 a | 4.02 ± 0.38 a |
| total phenolic index (TPI-E) | 627.18 ± 22.03 a | 616.82 ± 19.27 a | 818.66 ± 24.77 b | 821.40 ± 26.77 b | 943.48 ± 27.79 c | 935.20 ± 32.22 c | 627.41 ± 23.20 a | 631.17 ± 20.96 a |
| **bound phenolics** | | | | | | | | |
| gallic acid | 19.18 ± 0.59 f | 5.21 ± 0.26 b | 11.56 ± 0.34 e | 4.70 ± 0.22 a | 8.54 ± 0.34 d | 4.83 ± 0.16 ab | 10.96 ± 0.43 e | 6.64 ± 0.27 c |
| protocatachuic acid | 11.09 ± 0.34 g | 7.24 ± 0.31 e | 8.67 ± 0.18 f | 5.47 ± 0.15 c | 6.39 ± 0.25 d | 4.48 ± 0.20 b | 7.59 ± 0.27 e | 3.68 ± 0.19 a |
| catechin | 71.04 ± 2.35 h | 9.12 ± 0.28 c | 58.05 ± 3.42 g | 19.51 ± 0.69 e | 14.19 ± 0.51 d | 2.16 ± 0.11 a | 22.17 ± 1.13 f | 4.19 ± 0.25 b |
| epicatechin | 7.70 ± 0.21 d | 3.40 ± 0.15 a | 9.00 ± 0.41 e | 6.45 ± 0.21 c | 9.72 ± 0.33 e | 5.23 ± 0.16 b | 9.25 ± 0.35 e | 3.25 ± 0.16 a |
| 3-hydroxycinnamic acid | 2.03 ± 0.11 b | 1.95 ± 0.13 b | 2.82 ± 0.09 e | 2.19 ± 0.10 bc | 2.28 ± 0.14 cd | 2.11 ± 0.06 bc | 2.48 ± 0.11 d | 1.09 ± 0.07 a |
| UK1[b] | 7.05 ± 0.32 e | 5.37 ± 0.21 d | 7.94 ± 0.27 f | 4.52 ± 0.16 c | 2.41 ± 0.11 b | 1.34 ± 0.03 a | 4.62 ± 0.16 c | 2.31 ± 0.11 b |
| UK2[b] | 41.29 ± 1.65 e | 31.82 ± 1.56 c | 45.49 ± 2.06 f | 24.00 ± 1.09 b | 31.78 ± 1.15 c | 18.96 ± 1.07 a | 38.16 ± 1.69 d | 26.94 ± 1.56 b |
| UK3[b] | 35.41 ± 1.12 e | 26.24 ± 1.14 c | 38.46 ± 1.33 f | 31.62 ± 1.64 d | 23.74 ± 1.06 b | 15.23 ± 0.82 a | 31.44 ± 1.23 d | 22.14 ± 1.33 b |
| UK4[b] | 17.74 ± 0.62 e | 9.68 ± 0.36 c | 16.82 ± 0.52 e | 8.17 ± 0.31 b | 11.56 ± 0.75 d | 8.30 ± 0.26 b | 12.24 ± 0.62 d | 6.18 ± 0.24 a |
| UK5[b] | 4.72 ± 0.23 d | 0.41 ± 0.06 a | 6.64 ± 0.14 e | 1.06 ± 0.04 b | 5.11 ± 0.21 d | 1.75 ± 0.11 c | 7.14 ± 0.22 f | 1.06 ± 0.06 b |
| total phenolic index (TPI-B) | 217.25 ± 7.54 f | 100.44 ± 4.46 c | 205.45 ± 8.76 f | 107.69 ± 4.61 cd | 115.72 ± 4.85 d | 64.39 ± 2.98 a | 146.05 ± 6.21 e | 77.48 ± 4.24 b |

[a]Values are the mean ± SD, $n = 3$. Values followed by different letters in the same column are significantly different ($P < 0.05$). [b]Unknown peaks were quantified according to the calibration curve of garlic acid standard and expressed as $\mu$g GAE/g DW.



dx.doi.org/10.1021/jf504181r | J. Agric. Food Chem. 2014, 62, 12585−12594

bound phenolics including TPC-B, TFC-B, and CTC-B in all tested lentils (Table 3). Oxidative degradation of phenolic compounds, including enzymatic browning during cooking process, may promote losses of these phenolics.[36]

*Individual Phenolic Compounds in Extractable and Bound Phenolic Extracts and Effect of Cooking.* Twenty-one phenolic compounds were found in the extractable phenolic fraction, with the majority being flavonoids including kaempeferol glycosides and catechin/epicatechin glucosides. These phenolic compounds were identified by matching the retention times, UV spectra, and mass spectrometric data with those of the corresponding standards as described in our recent paper.[28]

Concentrations of the individual phenolic compounds in the extractable fraction of raw and cooked lentils are summarized in Table 4. Flavonols, mainly kaempferol glycosides, were the major extractable phenolic compounds of the tested raw lentils, with the tetraglycoside and triglycoside having the highest concentrations ranging from 214.72 to 302.14 μg/g DW and from 91.42 to 137.49 μg/g DW, respectively, followed by flavanols including catechin glucoside (119.46− 141.72 μg/g DW), catechin gallate (50.26−78.15 μg/g DW), and epicatechin glucoside (39.42−82.48 μg/g DW). Several phenolic acids including *trans*-*p*-coumaric acid, syringic acid, and *p*-hydroxybenzoic acid were also detected in the extractable fraction of raw lentils, but in much lower amounts. These results indicate that the majority of extractable phenolics in tested raw lentils are flavonoid glycosides. The total phenolic indices (TPI-E) defined as the sum of concentrations of all phenolic compounds detected in extractable fraction of lentils were between 627.18 and 943.48 μg/g DW, much lower than the corresponding TPC-E indices (Table 3). This can be attributed to incomplete quantification of all peaks in the HPLC method and to the extractable but conjugated phenolic compounds, which may be bound to soluble components such as small peptides or oligosaccharides,[28,37,38] but not separated and detected in HPLC. Potential interferences from other nonphenolic substances such as vitamin C and proteins, as well as Maillard reaction (nonenzymatic browning) and caramelization products, may also cause positive reactions in the Folin−Ciocalteu assay.[39,40] Cooking led to significant increases in the concentrations of individual flavonols such as kaempferol and quercetin glycosides, as well as in phenolic acids, but significant losses in flavanols (catechin/epicatechin glucoside, catechin gallate, and oligomeric procyanidins) ($P < 0.05$). The net result as expressed in TPI-E suggests no significant overall change by cooking, probably due to cancellation between the gains and losses of these two groups of extractable phenolics (Table 4). The exact reason as to how certain subgroups of polyphenols are increased and others are decreased during cooking is unclear, although it is well-known that heat-induced breakdown of cellular constituents and cell walls can lead to enhanced release of certain food bioactives[41] and that oxidative degradation and reaction with starch molecules may reduce the release.[35]

From the bound TPC-B, TFC-B, and CTC-B data, it was clear the phenolic contents in both raw and cooked lentils were extremely low compared to the extractable TPC-E (Table 3). This was also shown by the HPLC profile of the individual phenolic compounds. Figure 1 shows typical HPLC chromatograms of the bound phenolic extracts of raw and cooked lentil (Maxim). Five phenolic compounds (peaks 1, 2, 4, 7, and 9) including gallic acid, protocatechuic acid, catechin, epicatechin, and 3-hydroxycinnamic acid, respectively, were positively identified in both raw and cooked extracts by comparing their

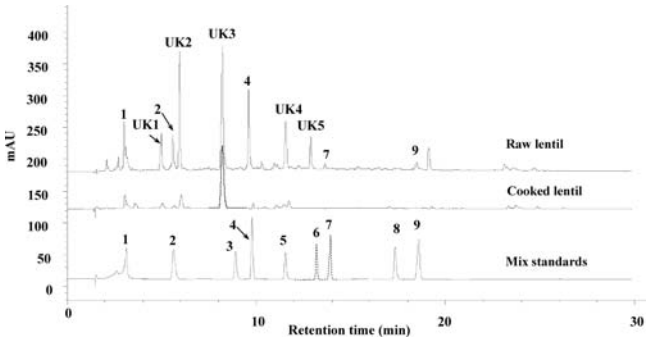


**Figure 1.** HPLC chromatograms of bound phenolics extract of a typical lentil cultivar (Maxim) before and after cooking and a standard mixture monitored at 280 nm. Peaks: UK, unknown; 1, garlic acid; 2, protocatechuic acid; 3, *p*-hydroxybenzoic acid; 4, catechin; 5, caffeic acid; 6, syringic acid; 7, epicatechin; 8, ferulic acid; 9, 3-hydroxycinnamic acid.

retention time and UV spectra with those of the corresponding commercial standards. The identified bound phenolic compounds (peaks 1, 2, 4, 7, and 9) were mainly flavonoids and phenolic acids, among which catechin at 14.19−71.04 μg/g DW in raw lentils, was the major phenolic compound, followed by gallic acid (8.54−19.18 μg/g DW), protocatechuic acid (6.39−11.09 μg/g DW), epicatechin (7.70−9.72 μg/g DW), and 3-hydroxycinnamic acid (2.03−2.82 μg/g DW). These bound phenolic compounds were all aglycones, and their concentrations in cooked lentils were significantly lower individually and collectively ($P < 0.05$), suggesting cooking negatively affected the release of bound phenolic compounds (Table 4). In addition, catechin levels in the tested red lentil cultivars, both raw and cooked, again were significantly higher than those of the respective tested green lentils (Table 4). This is consistent with the above result on bound TFC-B and CTC-B (Table 3).

Apart from the above five identified bound phenolic compounds, several unknown peaks (UK1−5) were detected from bound phenolic extracts of both raw and cooked lentils (Figure 1). None of these peaks matched the retention time or UV−/vis spectrum of the aglycones or glycosides detected in the extractable fraction or any known phenolics commonly found in lentils (Figure 1). Literature on phenolic contents (particularly bound phenolics) in both raw and cooked lentils is scarce, and data are sometimes contradictory. Phenolic acids (sinapic acid, chlorogenic acid) in the extractable fraction and 2,3,4-trihydroxybenzoic acid as bound fraction were found to be the main phenolics in lentils by Xu and Chang,[42] as opposed to the flavonols (kaempferol glycosides) in the extractable and flavanol (catechin) in the bound fractions found in the present study (Table 4). Whereas genetics and environmental conditions may affect the phytochemical compositions, other factors such as extraction and analytical methods used in different laboratories may also cause misidentification of targeted compounds and thus lead to such discrepancies. Currently, there is no available information on the composition and identity of bound phenolics of either raw or cooked lentils. Further studies using LC-MS or NMR are required to accurately report on the concentration and identity of the bound phenolics in lentils. However, what is clear from the present study is that these unknown bound phenolics were at much lower concentrations in cooked lentils. The UV−vis absorption spectra of the five unknown bound phenolics are shown in Figure S1 (Supporting Information), and quantification of these five unknown peaks was done using the calibration

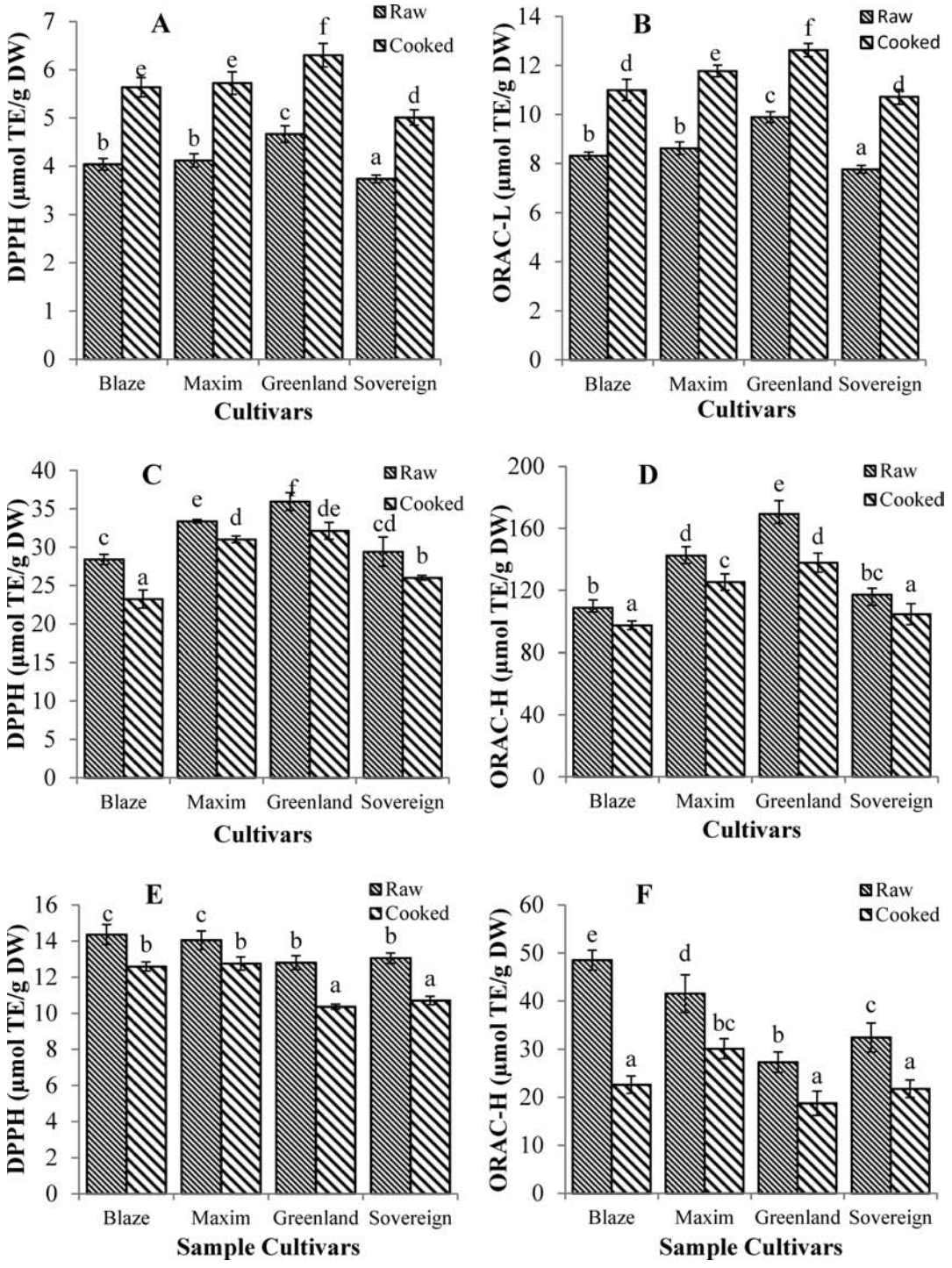


**Figure 2.** Antioxidant activities of the lipophilic fractions (A, B) and extractable (C, D) and bound (E, F) phenolic fractions of raw and cooked lentils as measured by DPPH and ORAC assays. DPPH and ORAC values are expressed as micromoles Trolox equivalent per gram DW lentil (μmol TE/g DW). Values are means ± SD, $n = 3$. Values followed by the same letter in the same assay are not significantly different ($p < 0.05$).

curve of gallic acid standard and expressed as micrograms of GAE per gram of DW in Table 4.

**Effect of Domestic Cooking on Antioxidant Activities.** The total antioxidant activities of lentil extracts were evaluated using DPPH and ORAC assays. Whereas DPPH was used for both the lipophilic and hydrophilic extracts, two protocols, ORAC-L and ORAC-H, were used for the two types of extracts, respectively.[43] The antioxidant activities of the lipophilic extracts (containing mainly carotenoids and tocopherols) of raw lentils were 3.74−4.67 and 8.32−9.89 μmol TE/g DW as assessed by DPPH and ORAC-L assays, respectively (Figure 2A,B). The antioxidant activities of hydrophilic extractable and bound fractions of raw lentils ranged from 28.40 to 35.94 μmol TE/g DW and from 12.80 to 14.36 μmol TE/g DW by the DPPH assay, respectively (Figure 2C,E) and from 108.78 to 169.27 μmol TE/g DW and from 27.29 to 48.52 μmol TE/g DW by ORAC-H, respectively (Figure 2D,F). These results are similar to those found by Xu et al. in lentils, but significantly higher than

in other pulses.[25,44,45] From the Trolox equivalent antioxidant activities, it was clear that the hydrophilic extracts containing mainly phenolics, especially the extractable phenolics, were stronger antioxidants and are perhaps the main contributors to the overall antioxidant activities of raw lentils (Figure 2). The same can be said for the cooked lentils; however, cooking itself showed different effects on the antioxidant activities of the lipophilic and hydrophilic extracts. Cooked lentils showed significantly higher antioxidant activity in both DPPH and ORAC-L assays for the lipophilic extract ($P < 0.05$), but significantly lower activity in both DPPH and ORAC-H for both extractable and bound phenolics ($P < 0.05$) (Figure 2). This is in agreement with the changes in concentration of the antioxidants of lentils; that is, the increased antioxidant activity of the lipophilic extract after cooking may be due to the increased carotenoid and tocopherol contents, whereas reduction in the antioxidant activity of the hydrophilic extracts may be due to significantly lowered phenolic contents in both extractable and bound forms as a result of cooking (Table 3).

In conclusion, lentils are an excellent source of phytochemical antioxidants such as carotenoids, tocopherols, and phenolics. The domestic cooking process significantly affects not only the phytochemical contents of both lipophilic and hydrophilic compounds but also the antioxidant activities associated with these components. Cooking caused significant increases in total and individual carotenoid and tocopherol levels and led to elevated antioxidant activity in the lipophilic fraction, whereas minimum effect was found on the fatty acid composition including PUFA. Total and individual phenolics were mainly in the extractable form as opposed to bound phenolics, and they are the main contributors to the antioxidant activities. Cooking significantly reduced the antioxidant activity of both extractable phenolic and bound fractions due to lowered total phenolic contents, whereas no or less effect was found in individual phenolic concentrations. More specifically, cooking was found to favor the release of flavonols (kaempferol glycosides) but led to losses of flavanols (monomeric and condensed tannin). Whereas reduced flavanols and other phenolic compounds may have negatively affected the antioxidant activity, other components, especially the lipophilic antioxidants, were increased. In general, the present study suggests that a properly designed cooking protocol will not cause significant loss of the phytochemical antioxidants and thus will retain the potential health benefits of lentils when incorporated into the diet.

## ■ ASSOCIATED CONTENT

### Supporting Information

UV absorption spectra of five unknown peaks (UK1−5) in bound phenolics extract of lentil and standards of all known phenolic compounds identified. This material is available free of charge via the Internet at http://pubs.acs.org.

## ■ AUTHOR INFORMATION


### Corresponding Authors

*(Z.-Y.D.) Phone/fax: +86 791 88304402. E-mail: zeyuandeng@hotmail.com.

*(R.T.) Phone: +1 226-217-8108. Fax: +1 226-217-8183. E-mail: rong.cao@agr.gc.ca.


### Author Contributions

‖B.Z. and Y.T. contributed equally to this work.


### Funding

This project is supported by the A-Base research (RBPI 1004; 2834) of Agriculture and Agri-Food Canada and an Agri-Innovation Program Grant with Pulse Canada (AIP#068).


### Notes

The authors declare no competing financial interest.

## ■ ACKNOWLEDGMENTS

We thank Pulse Canada for providing the lentil samples.

## ■ REFERENCES


(1) Gumienna, M.; Lasik, M.; Czarnecki, Z. Influence of plant extracts addition on the antioxidative properties of products obtained from green lentil seeds during in vitro digestion process. *Pol. J. Food Nutr. Sci.* **2009**, *59*.

(2) Marathe, S. A.; Rajalakshmi, V.; Jamdar, S. N.; Sharma, A. Comparative study on antioxidant activity of different varieties of commonly consumed legumes in India. *Food Chem. Toxicol.* **2011**, *49*, 2005−2012.

(3) Boschin, G.; Arnoldi, A. Legumes are valuable sources of tocopherols. *Food Chem.* **2011**, *127*, 1199−1203.

(4) Fratianni, A.; Giuzio, L.; Di Criscio, T.; Zina, F.; Panfili, G. Response of carotenoids and tocols of durum wheat in relation to water stress and sulfur fertilization. *J. Agric. Food Chem.* **2013**, *61*, 2583−2590.

(5) Ghorbani, A.; Nazari, M.; Jeddi-Tehrani, M.; Zand, H. The citrus flavonoid hesperidin induces p53 and inhibits NF-κB activation in order to trigger apoptosis in NALM-6 cells: involvement of PPARγ-dependent mechanism. *Eur. J. Nutr.* **2012**, *51*, 39−46.

(6) Boudjou, S.; Oomah, B. D.; Zaidi, F.; Hosseinian, F. Phenolics content and antioxidant and anti-inflammatory activities of legume fractions. *Food Chem.* **2013**, *138*, 1543−1550.

(7) Dueñas, M.; Hernández, T.; Estrella, I. Phenolic composition of the cotyledon and the seed coat of lentils (*Lens culinaris* L.). *Eur. Food Res. Technol.* **2002**, *215*, 478−483.

(8) Amarowicz, R.; Pegg, R. B. Legumes as a source of natural antioxidants. *Eur. J. Lipid Sci. Technol.* **2008**, *110*, 865−878.

(9) Villegas, R.; Gao, Y.-T.; Yang, G.; Li, H.-L.; Elasy, T. A.; Zheng, W.; Shu, X. O. Legume and soy food intake and the incidence of type 2 diabetes in the Shanghai Women's Health Study. *Am. J. Clin. Nutr.* **2008**, *87*, 162−167.

(10) Kris-Etherton, P. M.; Hecker, K. D.; Bonanome, A.; Coval, S. M.; Binkoski, A. E.; Hilpert, K. F.; Griel, A. E.; Etherton, T. D. Bioactive compounds in foods: their role in the prevention of cardiovascular disease and cancer. *Am. J. Med.* **2002**, *113*, 71−88.

(11) Aguilera, Y.; Dueñas, M.; Estrella, I.; Hernández, T.; Benitez, V.; Esteban, R. M.; Martín-Cabrejas, M. a. A. Evaluation of phenolic profile and antioxidant properties of Pardina lentil as affected by industrial dehydration. *J. Agric. Food Chem.* **2010**, *58*, 10101−10108.

(12) Zhang, B.; Deng, Z.; Tang, Y.; Chen, P.; Liu, R.; Ramdath, D. D.; Liu, Q.; Hernandez, M.; Tsao, R. Fatty acid, carotenoid and tocopherol compositions of 20 Canadian lentil cultivars and synergistic contribution to antioxidant activities. *Food Chem.* **2014**, *161*, 296−304.

(13) Amarowicz, R.; Troszyńska, A.; Baryłko-Pikielna, N.; Shahidi, F. Polyphenolics extracts from legume seeds: correlations between total antioxidant activity, total phenolics content, tannins content and astringency. *J. Food Lipids* **2004**, *11*, 278−286.

(14) Xu, B.; Chang, S. K. C. Comparative study on antiproliferation properties and cellular antioxidant activities of commonly consumed food legumes against nine human cancer cell lines. In *Food Chemistry*; Elsevier: Amsterdam, The Netherlands, 2012; Vol. 134, pp 1287−1296.

(15) Ďuračková, Z. Some current insights into oxidative stress. *Physiol. Res.* **2010**, *59*.

(16) Sasipriya, G.; Siddhuraju, P. Effect of different processing methods on antioxidant activity of underutilized legumes, *Entada scandens* seed kernel and *Canavalia gladiata* seeds. *Food Chem. Toxicol.* **2012**, *50*, 2864−2872.

(17) Xu, B.; Yuan, S.; Chang, S. Comparative analyses of phenolic composition, antioxidant capacity, and color of cool season legumes and other selected food legumes. *J. Food Sci.* **2007**, *72*, S167−S177.
(18) Scalbert, A.; Manach, C.; Morand, C.; Rémésy, C.; Jiménez, L. Dietary polyphenols and the prevention of diseases. *Crit. Rev. Food Sci. Nutr.* **2005**, *45*, 287−306.
(19) Aguilera, Y.; Duenas, M.; Estrella, I.; Hernandez, T.; Benitez, V.; Esteban, R. M.; Martin-Cabrejas, M. A. Evaluation of phenolic profile and antioxidant properties of Pardina lentil as affected by industrial dehydration. *J. Agric. Food Chem.* **2010**, *58*, 10101−10108.
(20) Han, H.; Baik, B. K. Antioxidant activity and phenolic content of lentils (*Lens culinaris*), chickpeas (*Cicer arietinum* L.), peas (*Pisum sativum* L.) and soybeans (*Glycine max*), and their quantitative changes during processing. *Int. J. Food Sci. Technol.* **2008**, *43*, 1971−1978.
(21) Zou, Y.; Chang, S. K.; Gu, Y.; Qian, S. Y. Antioxidant activity and phenolic compositions of lentil (*Lens culinaris* var. Morton) extract and its fractions. *J. Agric. Food Chem.* **2011**, *59*, 2268−2276.
(22) Thavarajah, D.; Thavarajah, P.; Sarker, A.; Vandenberg, A. Lentils (*Lens culinaris* Medikus subspecies *culinaris*): a whole food for increased iron and zinc intake. *J. Agric. Food Chem.* **2009**, *57*, 5413−5419.
(23) Dueñas, M.; Sun, B.; Hernández, T.; Estrella, I.; Spranger, M. I. Proanthocyanidin composition in the seed coat of lentils (*Lens culinaris* L.). *J. Agric. Food Chem.* **2003**, *51*, 7999−8004.
(24) Xu, B.; Chang, S. K. Phenolic substance characterization and chemical and cell-based antioxidant activities of 11 lentils grown in the Northern United States. *J. Agric. Food Chem.* **2010**, *58*, 1509−1517.
(25) Xu, B.; Chang, S. K. Effect of soaking, boiling, and steaming on total phenolic contentand antioxidant activities of cool season food legumes. *Food Chem.* **2008**, *110*, 1−13.
(26) Chau, C. F.; Cheung, P. C. K.; Wong, Y. S. Effects of cooking on content of amino acids and antinutrients in three Chinese indigenous legume seeds. *J. Sci. Food Agric.* **1997**, *75*, 447−452.
(27) PulseCanada. A guide to cooking beans, chickpeas, lentils and peas, 2014; http://www.pulsecanada.com/uploads/a3/a6/a3a6d7f53f7881244818e4b598842dd2/Guide-to-cooking-pulses.pdf (accessed Nov 5, 2014).
(28) Zhang, B.; Deng, Z.; Ramdath, D. D.; Tang, Y.; Chen, P.; Liu, R.; Liu, Q.; Tsao, R. Phenolic profiles of 20 Canadian lentil cultivars and their contribution to antioxidant activity and inhibitory effects on $\alpha$-glucosidase and pancreatic lipase *Food Chem.* **2015**, *172*, 862−872
(29) Li, H.; Deng, Z.; Liu, R.; Young, J. C.; Zhu, H.; Loewen, S.; Tsao, R. Characterization of phytochemicals and antioxidant activities of a purple tomato (*Solanum lycopersicum* L.). *J. Agric. Food Chem.* **2011**, *59*, 11803−11811.
(30) Dewanto, V.; Wu, X.; Adom, K. K.; Liu, R. H. Thermal processing enhances the nutritional value of tomatoes by increasing total antioxidant activity. *J. Agric. Food Chem.* **2002**, *50*, 3010−3014.
(31) Kalogeropoulos, N.; Chiou, A.; Ioannou, M.; Karathanos, V. T.; Hassapidou, M.; Andrikopoulos, N. K. Nutritional evaluation and bioactive microconstituents (phytosterols, tocopherols, polyphenols, triterpenic acids) in cooked dry legumes usually consumed in the Mediterranean countries. *Food Chem.* **2010**, *121*, 682−690.
(32) Maranesi, M.; Bochicchio, D.; Montellato, L.; Zaghini, A.; Pagliuca, G.; Badiani, A. Effect of microwave cooking or broiling on selected nutrient contents, fatty acid patterns and true retention values in separable lean from lamb rib-loins, with emphasis on conjugated linoleic acid. *Food Chem.* **2005**, *90*, 207−218.
(33) Ajayi, F.; Aremu, M.; Mohammed, Y.; Madu, P.; Atolaiye, B.; Audu, S.; Opaluwa, O. Effect of processing on fatty acid and phospholipid compositions of harms (*Brachystegia eurycoma*) seed grown in Nigeria. *Chem. Process Eng. Res.* **2014**, *22*, 18−25.
(34) Traber, M. G.; Atkinson, J. Vitamin E, antioxidant and nothing more. *Free Radical Biol. Med.* **2007**, *43*, 4−15.
(35) Barros, F.; Awika, J. M.; Rooney, L. W. Interaction of tannins and other sorghum phenolic compounds with starch and effects on in vitro starch digestibility. *J. Agric. Food Chem.* **2012**, *60*, 11609−11617.
(36) Xu, B.; Chang, S. K. Total phenolic, phenolic acid, anthocyanin, flavan-3-ol, and flavonol profiles and antioxidant properties of pinto and black beans (*Phaseolus vulgaris* L.) as affected by thermal processing. *J. Agric. Food Chem.* **2009**, *57*, 4754−4764.
(37) Saulnier, L.; Crépeau, M.-J.; Lahaye, M.; Thibault, J.-F.; Garcia-Conesa, M. T.; Kroon, P. A.; Williamson, G. Isolation and structural determination of two 5,5′-diferuloyl oligosaccharides indicate that maize heteroxylans are covalently cross-linked by oxidatively coupled ferulates. *Carbohydr. Res.* **1999**, *320*, 82−92.
(38) Yokotsuka, K.; Singleton, V. L. Interactive precipitation between phenolic fractions and peptides in wine-like model solutions: turbidity, particle size, and residual content as influenced by pH, temperature and peptide concentration. *Am. J. Enol. Vitic.* **1995**, *46*, 329−338.
(39) Eichner, K. Antioxidative effect of Maillard reaction intermediates. In *Autoxidation in Food and Biological Systems*; Springer: Berlin, Germany, 1980; pp 367−385.
(40) Chen, P. X.; Tang, Y.; Zhang, B.; Liu, R.; Marcone, M. F.; Li, X.; Tsao, R. 5-Hydroxymethy-2-furfural and derivatives formed during acid hydrolysis of conjugated and bound phenolics in plant foods and the effects on phenolic content and antioxidant capacity. *J. Agric. Food Chem.* **2014**, *62*, 4754−4761.
(41) Randhir, R.; Kwon, Y.-I.; Shetty, K. Effect of thermal processing on phenolics, antioxidant activity and health-relevant functionality of select grain sprouts and seedlings. *Innovative Food Sci. Emerging Technol.* **2008**, *9*, 355−364.
(42) Xu, B.; Chang, S. K. Phytochemical profiles and health-promoting effects of cool-season food legumes as influenced by thermal processing. *J. Agric. Food Chem.* **2009**, *57*, 10718−10731.
(43) Prior, R. L.; Wu, X.; Schaich, K. Standardized methods for the determination of antioxidant capacity and phenolics in foods and dietary supplements. *J. Agric. Food Chem.* **2005**, *53*, 4290−4302.
(44) Xu, B.; Chang, S. K. Total phenolics, phenolic acids, isoflavones, and anthocyanins and antioxidant properties of yellow and black soybeans as affected by thermal processing. *J. Agric. Food Chem.* **2008**, *56*, 7165−7175.
(45) Aguilera, Y.; Dueñas, M.; Estrella, I.; Hernández, T.; Benitez, V.; Esteban, R. M.; Martín-Cabrejas, M. A. Phenolic profile and antioxidant capacity of chickpeas (*Cicer arietinum* L.) as affected by a dehydration process. *Plant Foods Hum. Nutr.* **2011**, *66*, 187−195.

## MATERIALS AND METHODS

**Materials.** Wine pomaces from red winemaking were kindly supplied by seven different wineries located in the Burgos region. Wine pomaces from all wineries were well mixed and dehydrated to achieve a final water content of <10%.

Three products were obtained from the dry material: one from the global or whole wine pomace, termed "whole wine pomace product" (WWPP); another from the seed-free WP, termed "skins wine pomace product" (SkWPP); and the third from the isolated seeds, termed "seeds wine pomace product" (SdWPP). The dried materials were milled and sieved, and powdered products with particle sizes of <0.250 (SkWPP and WWPP) and 0.355 mm (SdWPP) were used to carry out this study. Ultraviolet (UV-C, 254 nm) and thermal (90 °C) treatments were applied to inactivate the microbial flora present in the products obtained. Different heat and UV treatment times (15, 30, 60, 90, and 120 min) were tested to reach the optimum microbial inactivation.

**Analytical Methodologies.** *Main Composition Analysis.* The moisture content was evaluated by the difference in the sample weight before and after drying at 105 °C to constant weight. The fat content was determined after Soxhlet extraction using petroleum ether (Lab-Scan, Gliwice, Poland) as extraction solvent in a Buchi B-811 extraction system (Buchi, Flawil, Switzerland). The protein content was determined using the Kjeldahl method, which measures the total nitrogen content after digestion with boiling sulfuric acid. A conversion factor of 6.25 was used to convert nitrogen into protein values. The total dietary fiber content was evaluated using the kit provided by Sigma (St Louis, MO, USA) according to the manufacturer's instructions based on AOAC method 985.29. Total $SO_2$ was determined using the enzymatic kit developed by R-Biopharm AG (Darmstadt, Germany) according to the manufacturer's instructions.

*Mineral Content.* The ash content was determined by incineration of the samples at 525 °C in a furnace (P-selecta, Barcelona, Spain). Sodium and potassium contents were determined according to the dry ashing method proposed by AOAC[10] using flame photometry (Flame Photometer 410, Corning, UK), whereas the calcium content was measured in the same acid solution using a polarized Zeeman atomic absorption spectrophotometer Z-8200 (Hitachi; Japan). Phosphorus determinations were conducted by reaction of the acid solution with vanadate−molybdate reagent (Panreac, Barcelona, Spain).[11]

*Main Phenolic Families.* Previously rehydrated powders were extracted in methanol/HCl (97:3) for 24 h. The resulting extract was centrifuged and filtered. The content of four phenolic groups was determined: total polyphenol content (TPC) was determined by reaction with Folin−Ciocalteu reagent (Merck, Darmstadt, Germany) and expressed as milligrams per gram of gallic acid;[12] total catechin content (TCC) was determined by treatment with vanillin reagent (Sigma) and expressed as milligrams per gram of D-catechin;[13] total anthocyanin content (TAC) was quantified by measuring the difference in the absorbance (525 nm) of the sample diluted in 1 N HCl and in phosphate citrate buffer (pH 3.5)[14] and the results expressed as milligrams of malvidin-3-glucoside per gram; and total proanthocyanidin content (TPAC) was measured after acid hydrolysis at 95 °C for 40 min and expressed as milligrams of procyanidin B1 per gram.[15]

*Antioxidant Capacity. (1) ABTS$^{\bullet+}$ Method.* The radical scavenger activities of the powdered products were studied by measuring the decrease in absorbance at 734 nm after incubation of methanolic extracts with a solution of 2,2′-azinobis(3-ethylbenzothiazoline-6-sulfonic acid) (ABTS). The ABTS radical solution was prepared by mixing ABTS and $K_2O_8S_2$ in water (1:1).[16]

*(2) Fat Oxidation Inhibition Capacity.* The ability of the extracts to protect fats against oxidation was evaluated using the Rancimat test, which was performed using a Rancimat 743 instrument (Metrohm, Switzerland). The air flow rate and temperature were set at 20 L/h and 110 °C, respectively. The tests were conducted in triplicate on commercial olive oil and melted pork lard. Controls and fats with 2% (w/w) of the different wine pomace products (WPPs) under study were conducted. The Rancimat test evaluates the conductivity caused by the short-chain fatty acids produced during lipid oxidation. Although this test has been criticized due to the use of high temperatures, which may affect the mechanism of lipid oxidation,[17] it remains a valuable tool for predicting the protection exerted by an antioxidant in real food systems. The results were expressed as protection factor, which was calculated by dividing the induction period of the WPPs with that for controls (fat without WPPs).

*Microbial Analysis.* Samples were weighed in a Stomacher bag, decimally diluted with Ringer solution (Oxoid, Basingstoke, Hampshire, UK) under sterile conditions, and homogenized in a laboratory blender (Stomacher 400, Colworth, London, UK). Total aerobic mesophilic bacteria (TAMB) and total yeasts and molds were evaluated on plate count agar (PCA) (Merck) and Sabouraud agar with chloramphenicol (Pronadisa, Madrid, Spain) respectively. PCA plates were incubated at 30 °C for 72 h and Sabouraud plates at 25 °C for 7 days.

*Antimicrobial Potential of Products.* The antimicrobial capacity was measured using meat homogenates, which were prepared by homogenizing commercially available beef in sterile water (1:3). A comparative study was carried out using homogenates of control meat (additive-free), meat with 2% of each WPP, and meat with 300 ppm of $SO_2$. Homogenates were incubated while stirring for 32 h in an incubator (New Brunswick Scientific, Edison, NJ, USA) at 37 °C. For each sample, decimal dilutions were prepared in Ringer solution and plated onto the appropriate culture medium. TAMB were determined using pour plates on PCA after incubation at 30 °C for 72 h. Lactic acid bacteria (LAB) were enumerated using de Man−Rogosa−Sharpe agar (MRS) (Oxoid) after incubation at 25 °C in an atmosphere of 5% $CO_2$ for 5 days. Those colonies that reacted positively to the catalase test were not counted. Enterobacteriaceae counts were determined using a double layer of violet red bile glucose agar (Pronadisa) incubated at 37 °C for 24 h. Antimicrobial experiments were repeated three different times with duplicate homogenates each time.

**Statistical Analysis.** Statistical analysis was performed using StatGraphics Centurion XVI. Fisher's least significant difference (LSD) test was performed to identify significant differences.

## RESULTS AND DISCUSSION

WP presents a sufficiently high water content to promote both microbial growth and enzyme-related degradation; therefore, a dehydration process was required to obtain a raw material that remains stable until final transformation into the desired powder products. Thermal drying was chosen over freeze-drying for the following reasons. Previous studies have suggested that, in contrast to freeze-drying, oven-drying does not affect total extractable polyphenols and condensed tannins as long as the temperature does not exceed 60 °C.[18] Tseng and Zhao[19] reported that freeze-dried products had the lowest stability during storage, probably due to their higher porosity and higher exposure to oxygen. Furthermore, the cost of freeze-drying, which is estimated to be 4−8 times more expensive than thermal drying,[20] was also considered. WP was dehydrated to a water content of <10%.

Particle size determines the use and application of different ingredients in food manufacture.[21] The handling safety of the ingredient, palatability of the resulting foodstuff, and release of active compounds are some of the factors involved in this aspect. Furthermore, stability of products and manufacturing costs need to be considered. The likelihood of oxidative reactions and microbiological contamination increases with the reduction of particle size. Besides, the manufacturing costs also increase, due to the longer manufacturing times and higher energy levels required to obtain smaller particle size. To balance the advantages and drawbacks of a very small particle size, SkWPP and WWPP were milled and sieved through a mesh

with a size of 0.250 mm, whereas SdWPP was milled and sieved through a mesh with a size of 0.355 mm. The reason for choosing a higher particle size in SdWPP was the low yield obtained using a size of 0.250 mm. This could be explained by the caking and sticking of the seed powder as a consequence of the high fat content of grape seeds. These phenomena are commonly found for dairy-based powders with high lipid contents. Surface fat may melt during the grinding process due to the temperature increase, which leads to the formation of fatty bridges between particles. When the temperature drops, the fat solidifies, forming bridges between particles and resulting in a lumpy product.[22,23] Furthermore, the tough structure of grape seed endosperm[24] could also contribute to the low yield obtained.

**Characterization of the Products Obtained.** The three products obtained showed significant differences in terms of composition (Table 1). Dietary fiber was the main component

**Table 1. Proximate Composition of Skin Wine Pomace Product (SkWWP), Whole Wine Pomace Products (WWPP), and Seed Wine Pomace Product (SdWPP)[a]**

| parameter | SkWPP | WWPP | SdWPP |
|---|---|---|---|
| moisture (%) | 6.78 ± 0.43 a | 7.12 ± 0.25 ab | 7.57 ± 0.09 b |
| total dietary fiber (% DM) | 48.6 ± 0.7 a | 49.4 ± 0.9 a | 58.9 ± 0.5 b |
| total lipid (% DM) | 3.69 ± 0.07 a | 10.61 ± 0.18 b | 16.99 ± 0.18 c |
| total protein (% DM) | 14.35 ± 0.81 b | 13.09 ± 1.51 ab | 12.04 ± 0.21 a |
| ash (% DM) | 14.37 ± 0.27 c | 10.73 ± 0.13 b | 2.94 ± 0.21 a |
| mineral matter (mg/g DM) | | | |
| potassium | 43.34 ± 2.53 c | 38.20 ± 1.26 b | 4.39 ± 0.13 a |
| calcium | 1.82 ± 0.11 a | 3.13 ± 0.20 b | 3.4 ± 0.27 b |
| phosphorus | 1.93 ± 0.11 a | 2.57 ± 0.18 b | 2.75 ± 0.24 b |
| sodium | 1.31 ± 0.11 c | 0.98 ± 0.07 b | 0.12 ± 0.02 a |

[a]Different letters (a–c) denote significant differences (LSD test and $P < 0.05$) between products. Values are means ± standard deviation of three replicate determinations.

in all three products, with the highest content being found for SdWPP (±59%) (Table 1), probably due to the presence of lignin in the seeds. These results agree with those of Saura-Calixto et al.[25] and Tseng and Zhao,[19] who indicated that WP mainly contains insoluble fiber and, more specifically, Klason lignin. WP fiber is associated with a high amount of antioxidants, thus making it a valuable source of dietary antioxidant fiber.[26] Similar protein contents were found for SkWPP and WWPP (±14 and 13%, respectively), with the value for SdWPP (12%) being slightly lower due to the higher fiber and lipid contents. Protein values were comparable to those obtained by other authors.[26,27] Similar differences in the content of the various components of WP (mainly between skins and seeds) have been described previously.[19,27,28]

SkWPP showed the highest ash content (±14%), with the values obtained being similar to those reported for Spanish grape pomaces by Saura-Calixto,[26] thus indicating a high mineral content in grape skins. Potassium was the predominant macroelement, especially in the products derived from raw material containing grape skins (±43 mg/g), which correlates with the well-known high potassium content usually found in grape skins. It is widely accepted that during grape ripening, potassium accumulates in the skin and forms both soluble and insoluble salts with organic acids.[29] Seeds are considered to be the strongest sinks for calcium and phosphorus in grape berry, which explains the higher content of these minerals observed in SdWPP in comparison to SkWPP.[30] The low sodium levels detected also agree with the lack of accumulation of these mineral during grape ripening.[30]

The incorporation of sulfating agents is widespread in wineries due to the microbial and oxidative stability provided by them. However, sulfites were not detected in any of the WP products obtained.

The phenolic composition of the products obtained (Table 2) agrees with the well-known fact that grape seeds are a richer

**Table 2. Phenolic Composition of Untreated, UV-Treated, and Thermally Treated Wine Pomace Products[a]**

| | untreated | UV-treated | thermally treated |
|---|---|---|---|
| total polyphenol content (mg gallic acid/g) | | | |
| SkWPP | 25.87 ± 0.34 b | 23.95 ± 0.27 a | 24.43 ± 0.15 a |
| WWPP | 32.49 ± 0.26 c | 27.13 ± 0.11 a | 30.62 ± 0.45 b |
| SdWPP | 42.72 ± 0.79 b | 38.59 ± 0.67 a | 41.66 ± 0.34 b |
| total catechin content (mg D-catechin/g) | | | |
| SkWPP | 10.52 ± 0.17 c | 7.78 ± 0.25 a | 8.78 ± 0.22 b |
| WWPP | 18.86 ± 0.49 c | 14.16 ± 0.36 a | 16.93 ± 0.33 b |
| SdWPP | 33.44 ± 1.29 c | 26.22 ± 0.92 a | 30.25 ± 0.36 b |
| total anthocyanin content (mg of malvidin-3-glucoside/g) | | | |
| SkWPP | 3.38 ± 0.13 b | 3.12 ± 0.27 b | 2.47 ± 0.10 a |
| WWPP | 1.42 ± 0.06 b | 1.62 ± 0.04 c | 1.02 ± 0.10 a |
| SdWPP | 0.18 ± 0.02 b | 0.09 ± 0.05 a | 0.09 ± 0.02 a |
| total proanthocyanidin content (mg of procyanidin B1/g) | | | |
| SkWPP | 43.45 ± 0.79 c | 35.92 ± 1.63 a | 39.62 ± 1.03 b |
| WWPP | 56.87 ± 6.23 b | 46.90 ± 1.63 a | 51.37 ± 1.60 a,b |
| SdWPP | 81.43 ± 11.52 a | 77.36 ± 3.33 a | 76.67 ± 1.61 a |

[a]Different letters (a–c) denote significant differences (LSD test and $P < 0.05$) among treatments. Values are means ± standard deviation of three replicate determinations. SkWPP, skin wine pomace product; WWPP, whole wine pomace product; SdWPP, seed wine pomace product.

source of polyphenols, especially catechins and proanthocyanidins, than grape skins and that only grape skins contain a relevant amount of anthocyanins.[31,32] It should be noted that the values obtained are lower than those reported in grapes[33] but are in agreement with the quantity of phenolic compounds transferred from grapes to wine during red winemaking.[34]

Control of the microbial load of the products obtained was considered both convenient and necessary to obtain the safe products required by the food industry. Despite their wide range of applications, the microbiological contribution of WP-derived ingredients to foodstuffs has been underestimated as it has been assumed that the drying process is sufficient to ensure the safety of the powdered products.[35] However, other agricultural products with similar water contents and water activities, such as herbs and spices, have been involved in different outbreaks of food poisoning caused by the presence of pathogens.[36] Moreover, it is also important to consider that fungi are able to produce mycotoxins even at low water activities.[37]

Our results showed that SkWPP had the highest microbial load, most likely due to the higher degree of manipulation and exposure to microbial contamination (Table 3). Although the microbial load observed is usually considered to be acceptable in spices,[38] microbial inactivation is recommended to ensure the quality of the powdered products obtained.

**Table 3. Microbial Load of Untreated, UV-Treated, and Thermally Treated Wine Pomace Products[a]**

| | product | untreated | UV-treated | thermally treated |
|---|---|---|---|---|
| total aerobic mesophilic bacteria | SkWPP | 4.65 ± 0.06 | 3.49 ± 0.17 | nd |
| | WWPP | 4.00 ± 0.09 | 3.95 ± 0.06 | nd |
| | SdWPP | 3.27 ± 0.15 | 3.33 ± 0.08 | nd |
| yeasts and molds | SkWPP | 3.42 ± 0.09 | 2.16 ± 0.02 | nd |
| | WWPP | 1.75 ± 0.21 | 1.53 ± 0.09 | nd |
| | SdWPP | 1.60 ± 0.43 | 1.15 ± 0.21 | nd |

[a]Results are expressed as log CFU/g of each product. Values are means ± standard deviation of three replicates. SkWPP, skin wine pomace product; WWPP, whole wine pomace product; SdWPP, seed wine pomace product; nd, not detected.

Two inactivation methods were conducted: thermal treatment and UV treatment. Although thermal treatment is the most common means of inactivating microorganisms, the low thermal stability of phenolic compounds may limit its application in WP products. Ultraviolet radiation has been mainly applied in liquid foods, although its use has also been proposed in powdered products.[39] In addition, it has successfully been used in leafy vegetables and is a clean and relatively inexpensive alternative.[40,41] As such, it may be a valuable option for WP products.

Preliminary studies were conducted to establish the most efficient conditions for thermal and UV treatments. First, the efficiencies of different UV treatment times were tested. The differences between the microbial load of untreated and UV-treated WWPP and SdWPP were not significant (Table 3). The highest effectiveness of UV treatment was observed for SkWPP. These differences in effectiveness could be due to the difference in the particle size of each type of product.[42] A progressive reduction in microbial load of SkWPP was observed from 15 to 60 min of treatment, whereas no significant reduction was observed during the second hour (from 60 to 120 min) of UV treatment. Thus, after 60 min of UV treatment, SkWPP showed reductions of 1.16 and 1.26 log CFU/g in the counts of TAMB and yeasts and molds, respectively (Table 3). The thermal treatment at 90 °C produced a progressive reduction in the microbial load of the three products under study. The complete inactivation of the studied microbial flora was achieved after 90 min of treatment.

UV and thermally treated products showed main compositions similar to those of the untreated ones, although some differences in phenolic composition were detected (Table 2). WWPP showed the highest decrease in TPC (16% in UV-treated and 6% in thermally treated), whereas the TPC of SkWPP was affected similarly by both treatments. In contrast, only UV treatment affected the TPC of SdWPP. The cause of this higher decrease in UV-treated samples might be the photodimerization and isomerization of phenolic compounds induced by UV radiation.[43] Furthermore, UV radiation may also promote the formation of new linkages between hydroxycinnamic acids and lignin units,[39] thereby decreasing their extractability. As far as thermal processing is concerned, previous studies found no significant decrease after heating to 100 °C for 250 min and even a significant increase at 150 °C.[44] This fact can be explained by the degradation of cell-wall polysaccharide structures, thus facilitating polyphenol release and extractability from the matrix structure.[45] Similarly, Chamorro et al.[46] found no significant decrease in TP after thermal treatment at 100 °C for 1 h.

Catechin was one of the groups most affected by treatments (26% after UV treatment and 17% after thermal treatment). Epimerization and autoxidation seem to be the most likely mechanisms for catechin degradation. The observed degradation agrees with the rates reported by Volf et al.[47] Thermal treatment produced the highest degradation in TAC (27% in WWPP and SkWPP), which may be explained by the well-known thermal lability of anthocyanins.[48] Sólyom et al.[44] reported degradation rates of 75% in similar thermal treatments of nondehydrated WP. Water availability plays a key role in anthocyanin degradation, and the low water activity of the studied products may explain the relatively limited degradation of anthocyanins observed in this study.[49,50] UV treatment did not decrease the TAC of either WWPP or SkWPP. Thermal and UV treatments produced similar decreases in the TPAC for all products studied (approximately 15%). Previous literature data in this regard are contradictory. Significant reductions in TPAC levels were reported by Khanal et al.[51] for grape pomace after thermal treatment at temperatures of ≥60 °C. These authors observed degradation of the oligomeric procyanidins in WP upon increasing the temperature from 60 to 125 °C. In contrast, Chamorro et al.[46] found no significant reductions after heating grape pomace at 100 °C for 60 min. Overall, thermal treatment produced less intense reductions in TPC, TCC, and TPAC than UV treatment, whereas it affected TAC more extensively. These reductions can be considered acceptable because the WPPs obtained retain the vast majority of their phenols and their safety is markedly improved. Consequently, thermal treatment was selected as the best option, and thermally stabilized products were used in the subsequent study of antioxidant and antimicrobial activities.

**Properties of Interest for Food Industry Applications.** In addition to use of the products obtained as a source of fiber, antioxidant, and possibly some minerals, such as potassium, WPPs exhibit other properties of interest to the food industry. In this regard, antioxidant and antimicrobial properties were considered to be of particular importance for application as natural food preservatives.

The ABTS method was used to evaluate the global antioxidant capacity of the products studied from among the large number of possibilities available due to its simplicity and the complete information provided by it.[16] All WP products showed interesting antioxidant capacities but with statistically significant differences. SdWPP exhibited the highest antioxidant activity (141.99 ± 2.09 μmol/g), followed by WWPP (103.29 ± 0.23 μmol/g) and SkWPP (75.65 ± 1.98 μmol/g). ABTS results were positively and strongly correlated with TPC, TCC, and TPAC, as indicated by Pearson correlation coefficient, which showed values of 0.9951, 0.9968, and 0.987, respectively. This fact agrees with the attribution of antioxidant activity to the phenolic composition of WP. For example, Bonilla et al.[52] reported that gallic acid exerted the highest protection among all of the phenols extracted from crushed grape pomace when added at the same concentration. Lafka et al.[53] also concluded that catechins and gallic acid contents are the main factors that determine the antioxidant activity of WPPs.

Considering the importance of preventing fat oxidation in the food industry, the ability of the products obtained to protect against fat oxidation was evaluated using the Rancimat method. Two fat systems with different oxidation sensitivities (olive oil and pork lard) were used. Olive oil mainly contains

unsaturated fatty acids, which are more susceptible to oxidation than the saturated fatty acids found in pork lard. However, olive oil also contains polyphenols and tocopherols with antioxidant activity,[54] whereas metals with pro-oxidant activity can be found in pork lard.[55] Furthermore, both fats can be considered as good representatives of the different types of fat used in the food industry (plant and animal fats).

Olive oil and pork lard gave average induction times of 26.07 and 14.65 h, respectively. The three products studied delayed the onset of lipid oxidation in both types of fats (Table 4).

**Table 4. Protection Factor of Wine Pomace Products in Olive Oil and Pork Lard Measured by Rancimat Method[a]**

| | SkWWP | WWPP | SdWPP |
|---|---|---|---|
| olive oil | 1.087 ± 0.028 b | 1.061 ± 0.026 ab | 1.024 ± 0.016 a |
| pork lard | 1.145 ± 0.028 b | 1.086 ± 0.036 ab | 1.052 ± 0.010 a |

[a]Values are means ± standard deviation of three replicate determinations. Protection factor = induction time of fat with product under study/induction time of control fat. Different letters (a, b) denote significant differences (LSD test and $P < 0.05$) among products. SkWPP, skin wine pomace product; WWPP, whole wine pomace product; SdWPP, seed wine pomace product.

These results could be correlated to the global antioxidant capacities of the products, most likely to the phenol content. The protection exerted by SdWPP was significantly lower than that exerted by SkWPP despite their higher TPC, TCC, and TPAC values. These findings are in agreement with the findings of Shaker,[56] who reported a higher inhibition for grape skin extracts in comparison to grape seed extracts when added to sunflower oils at the same polyphenol concentration. The data obtained appear to indicate a key role for anthocyanins in the protection against lipid oxidation.[57] These same authors found that grape skin anthocyanins present a higher protective capacity against lipid oxidation than catechin and $\alpha$-tocopherol at the same concentration. Although anthocyanins are not soluble in fat, their protective properties could be associated with their excellent ability to scavenge the free radicals formed during fat oxidation. Wine anthocyanins showed a particularly intense hydroxyl radical scavenging capacity, which was similar to their superoxide radical scavenging activity.[58] Furthermore, the possible lipid oxidation of seed fat during the production and storage of SdWPP and WWPP should be also considered, due to the fact that the presence of oxidized fatty acids may initiate oil and fat oxidation,[59] counteracting the antioxidant effects of polyphenols.

Antimicrobial activities were studied in meat homogenates because meat is a good system for studying spoiler growth. The inhibitory effect of the WP products on the growth of potential spoilage microorganisms was studied and compared with the antimicrobial effect of sulfites (Figure 1), a standard and well-known antimicrobial food additive, as control. The antimicrobial activity of sulfites appears to be related to their ability to induce changes in protein structures. Other antimicrobial mechanisms of sulfites include blockage of transport, inhibition of glycolysis, nutrient destruction, and inhibition of microbial metabolism.[60]

First, it is worth noting that the incorporation of SdWPP did not affect the initial load of homogenates, whereas addition of SkWPP, WWWP, and sulfites produced an immediate decrease in TAMB and LAB counts. This finding suggests that the WP products obtained were in optimal conditions for use as food additives. Significant protective effects were detected for all three products studied, with these effects being very similar for all three assays performed.

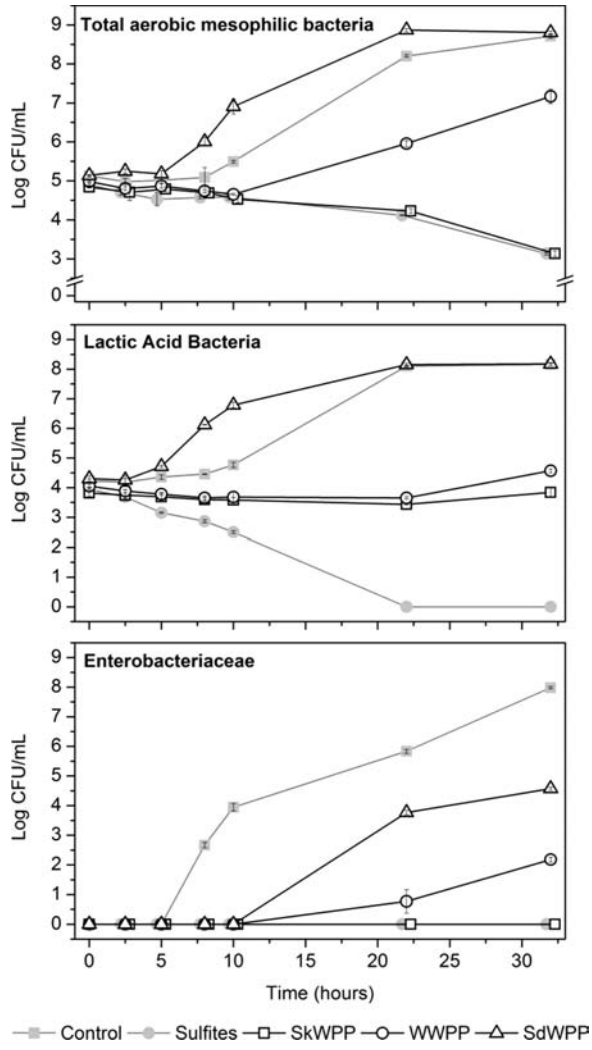


**Figure 1.** Effect of incorporation of sulfites, skin wine pomace product (SkWPP), whole wine pomace product (WWPP), and seed wine pomace product (SdWPP) on the total aerobic mesophilic bacteria, lactic acid bacteria, and Enterobacteriaceae counts of beef homogenates incubated at 37 °C.

Meat homogenates incubated with sulfites exhibited a significant decrease in TAMB count, a complete inactivation of LAB after 32 h of incubation, and no Enterobacteriaceae growth. SkWPP produced inhibitions of TAMB and Enterobacteriaceae growth similar to those produced by sulfites. The decrease in TAMB and LAB counts in the meat incubated with SkWPP suggests its bactericidal capacity. The addition of WWPP delayed the onset of TAMB and LAB growth (by 15 and 22 h, respectively), thereby confirming its bacteriostatic activity against spoilage flora. Moreover, addition of WWPP delayed Enterobacteriaceae growth and decreased the final counts in comparison with controls. These results could be correlated with the phenolic compounds present in SkWPP and WWPP. The effect of grape polyphenols on the growth of different meat spoiler microorganisms, such as LAB, has been widely studied and appears to depend on the polyphenol concentration, medium, and species (or even strains) under study.[61−63]

The antimicrobial effects of plant materials containing phenolic compounds have been associated with different mechanisms of action,[3] such as the ability to inhibit cell wall synthesis, thereby producing cell membrane alterations and the consequent loss of crucial intracellular material; the ability to chelate essential metals such as iron; and the ability to bind polysaccharides and proteins, thereby producing compounds that cannot be metabolized by microorganisms.[64] Furthermore, Friedman[65] reported the ability to bind vital components in the cell, such as enzymes and cell transport proteins. Previous studies have shown an ability to increase the microbial stability of meat products but using grape pomace extracts. For instance, Sagdic et al.[66] observed the inhibitory effect of ethanolic grape pomace extract on the spoiler growth of beef patties. The incorporation of high levels of grape pomace extracts (10%) led to the complete inactivation of spoilage flora, whereas the addition of 1% grape pomace extract delayed the onset of microbial growth. The microbial results obtained with WWPP were worse than those obtained with SkWPP but better than those observed for SdWPP. The incorporation of SdWPP promoted the growth of TAMB and LAB and reduced their lag phases. These results were surprising in light of the higher phenolic content of this product. However, they are in agreement with the stimulatory role of grape seed extract on *Lactobacillus acidophilus* growth[67] and with the improved growth caused by gallic acid and catechin in *Lactobacillus hilgardii*.[68] Alberto et al.[69] have suggested that polyphenols may improve sugar metabolism in LAB, thereby stimulating proliferation. The results obtained are satisfactory and novel.

From a microbial stability and spoilage protection point of view the best product was SkWPP, although WWPP also showed good results. Moreover, the results obtained upon addition of SdWPP were also interesting, especially considering that the promoting effect on LAB could result in an increase in the production of certain bacteriocins with antimicrobial activity against pathogens.[70] In addition, it has been found that the bacteriocins produced by gallic acid and catechin adapted LAB are particularly potent inhibitors of the growth of some foodborne pathogens such as *Staphylococcus aureus* and *Salmonella enterica*.[71]

In conclusion, wine pomace can be readily transformed into a series of products that meet the requirements of the food industry, namely, cheap, environmentally friendly, and natural and with good antioxidant and antimicrobial abilities. Furthermore, these products can be used as a natural source of fiber, antioxidants, and potassium. The bactericidal activity of SkWPP, which is similar to that for sulfites, suggests the possibility of using this product as a sulfite substitute, thereby reducing the allergenic risk. The ability of the products studied to inhibit fat oxidation also suggests potential applications in fatty food with a high tendency to rancidity, thereby extending their shelf life.

## AUTHOR INFORMATION

### Corresponding Author

*(M.L.G.S.) E-mail: marglez@ubu.es. Phone: +34 947258815. Fax: +34 947258831.

### Funding

We are grateful for financial support from the Autonomous Government of Castilla y León through research projects BU268A11-2 and BU282U13. The Ph.D. grants of J.G.-L. and R.D.P.-G. (FPU grants) are funded by the Spanish Ministerio de Educación, Cultura y Deporte.

### Notes

The authors declare no competing financial interest.

## ABBREVIATIONS USED

ABTS, 2,2′-azinobis(3-ethylbenzothiazoline-6-sulfonic acid); LAB, lactic acid bacteria; MRS, de Man−Rogosa−Sharpe agar; PCA, plate count agar; SdWPP, seed wine pomace product; SkWPP, skin wine pomace product; TAC, total anthocyanins; TAMB, total aerobic mesophilic bacteria; TCC, total catechin content; TPAC, total proanthocyanidins; TPC, total phenolic content; WP, wine pomace; WPPs, wine pomace products; WWPP, whole wine pomace product

## REFERENCES

(1) Brul, S.; Coote, P. Preservative agents in foods: mode of action and microbial resistance mechanisms. *Int. J. Food Microbiol.* **1999**, *50*, 1−17.

(2) Devcich, D. A.; Pedersen, I. K.; Petrie, K. J. You eat what you are: modern health worries and the acceptance of natural and synthetic additives in functional foods. *Appetite* **2007**, *48*, 333−337.

(3) Cowan, M. M. Plant products as antimicrobial agents. *Clin. Microbiol. Rev.* **1999**, *12*, 564−582.

(4) Brewer, M. S. Natural antioxidants: sources, compounds, mechanisms of action, and potential applications. *Compr. Rev. Food Sci. Food Saf.* **2011**, *10*, 221−247.

(5) Devesa-Rey, R.; Vecino, X.; Varela-Alende, J. L.; Barral, M. T.; Cruz, J. M.; Moldes, A. B. Valorization of winery waste vs. the costs of not recycling. *Waste Manage.* **2011**, *31*, 2327−2335.

(6) Yu, J.; Ahmedna, M. Functional components of grape pomace: their composition, biological properties and potential applications. *Int. J. Food Sci. Technol.* **2013**, *48*, 221−237.

(7) Jongberg, S.; Skov, S. H.; Tørngren, M. A.; Skibsted, L. H.; Lund, M. N. Effect of white grape extract and modified atmosphere packaging on lipid and protein oxidation in chill stored beef patties. *Food Chem.* **2011**, *128*, 276−283.

(8) Özkan, G.; Sagdiç, O.; Baydar, N. G.; Kurumahmutoglu, Z. Antibacterial activities and total phenolic contents of grape pomace extracts. *J. Sci. Food Agric.* **2004**, *84*, 1807−1811.

(9) Chemat, F.; Vian, M. A.; Cravotto, G. Green extraction of natural products: concept and principles. *Int. J. Mol. Sci.* **2012**, *13*, 8615−8627.

(10) AOAC. Sodium and Potassium in seafoods 969.23. *Official Methods of Analysis*, 17th ed.; Rockville, MD, USA, 2000.

(11) Kitson, R. E.; Mellon, M. G. Colorimetric determination of phosphorus as molybdivanadophosphoric acid. *Ind. Eng. Chem.* **1944**, *16*, 379−383.

(12) Singleton, V. L.; Rossi, J. A., Jr. Colorimetry of total phenolics with phosphomolybdic-phosphotungstic acid reagents. *Am. J. Enol. Vitic.* **1965**, *16*, 144−158.

(13) Swain, T.; Hillis, W. E. The phenolic constituents of *Prunus domestica*. I. The quantitative analysis of phenolic constituents. *J. Sci. Food Agric.* **1959**, *10*, 63−68.

(14) Paronetto, L. *Polifenoli e Tecnica Enologica*; Selepress: Milan, Italy, 1977.

(15) Porter, L. J.; Hrstich, L. N.; Chan, B. G. The conversion of procyanidins and prodelphinidins to cyanidin and delphinidin. *Phytochemistry* **1986**, *25*, 223−230.

(16) Rivero-Pérez, M. D.; Muñiz, P.; González-Sanjosé, M. L. Antioxidant profile of red wines evaluated by total antioxidant capacity, scavenger activity, and biomarkers of oxidative stress methodologies. *J. Agric. Food Chem.* **2007**, *55*, 5476−5483.

(17) Frankel, E. N., Free radical oxidation. In *Lipid Oxidation*; Frankel, E. N., Ed.; The Oily Press: Dundee, Scotland, 1998.

(18) Larrauri, J. A.; Rupérez, P.; Saura-Calixto, F. Effect of drying temperature on the stability of polyphenols and antioxidant activity of red grape pomace peels. *J. Agric. Food Chem.* **1997**, *45*, 1390−1393.

(19) Tseng, A.; Zhao, Y. Effect of different drying methods and storage time on the retention of bioactive compounds and antibacterial

activity of wine grape pomace (Pinot noir and Merlot). *J. Food Sci.* **2012**, *77*, H192−H201.
(20) Ratti, C. Hot air and freeze-drying of high-value foods: a review. *J. Food Eng.* **2001**, *49*, 311−319.
(21) Huang, S. C.; Shiau, C. Y.; Liu, T. E.; Chu, C. L.; Hwang, D. F. Effects of rice bran on sensory and physico-chemical properties of emulsified pork meatballs. *Meat Sci.* **2005**, *70*, 613−619.
(22) Buma, T. J. Free fat in spray-dried whole milk. 5. Cohesion; determination influence of particle size, moisture content and free-fat content. *Nederlands Melk- en Zuiveltijdschrift* **1971**, *25*, 107−122.
(23) Wakiyama, N.; Kusai, A.; Nishimura, K. Mechanism of caking of granules containing oily materials. *Int. J. Pharm.* **1992**, *78*, 95−102.
(24) Xu, C.; Zhang, Y.; Wang, J.; Lu, J. Extraction, distribution and characterisation of phenolic compounds and oil in grapeseeds. *Food Chem.* **2010**, *122*, 688−694.
(25) Saura-Calixto, F.; Goñi, I.; Mañas, E.; Abia, R. Klason lignin, condensed tannins and resistant protein as dietary fibre constituents: determination in grape pomaces. *Food Chem.* **1991**, *39*, 299−309.
(26) Saura-Calixto, F. Antioxidant dietary fiber product: a new concept and a potential food ingredient. *J. Agric. Food Chem.* **1998**, *46*, 4303−4306.
(27) Gül, H.; Acun, S.; Şen, H.; Nayir, N.; Türk, S. Antioxidant activity, total phenolics and some chemical properties of Öküzgözü and Narince grape pomace and grape seed flour. *J. Food, Agric. Environ.* **2013**, *11*, 28−34.
(28) Basalan, M.; Gungor, T.; Owens, F. N.; Yalcinkaya, I. Nutrient content and in vitro digestibility of Turkish grape pomaces. *Anim. Feed Sci. Technol.* **2011**, *169*, 194−198.
(29) Coombe, B. G. Distribution of solutes within the developing grape berry in relation to its morphology. *Am. J. Enol. Vitic.* **1987**, *38*, 120−127.
(30) Rogiers, S. Y.; Greer, D. H.; Hatfield, J. M.; Orchard, B. A.; Keller, M. Mineral sinks within ripening grape berries (*Vitis vinifera* L.). *Vitis* **2006**, *45*, 115−123.
(31) Kammerer, D.; Claus, A.; Carle, R.; Schieber, A. Polyphenol screening of pomace from red and white grape varieties (*Vitis vinifera* L.) by HPLC-DAD-MS/MS. *J. Agric. Food Chem.* **2004**, *52*, 4360−4367.
(32) Xia, E. Q.; Deng, G. F.; Guo, Y. J.; Li, H. B. Biological activities of polyphenols from grapes. *Int. J. Mol. Sci.* **2010**, *11*, 622−646.
(33) Pérez-Magariño, S.; González-San José, M. L. Evolution of flavanols, anthocyanins, and their derivatives during the aging of red wines elaborated from grapes harvested at different stages of ripening. *J. Agric. Food Chem.* **2004**, *52*, 1181−1189.
(34) Peynaud, E. *Knowing and Making Wine*; Wiley: New York, 1984.
(35) Walpole, M. *Patent Application: Method of Producing Concentrated Flour Wine Grape Pomace*. WO2008014609 A1, 2008.
(36) Vij, V.; Ailes, E.; Wolyniak, C.; Angulo, F. J.; Klontz, K. C. Recalls of spices due to bacterial contamination monitored by the U.S. Food and Drug Administration: the predominance of salmonellae. *J. Food Prot.* **2006**, *69*, 233−237.
(37) Romagnoli, B.; Menna, V.; Gruppioni, N.; Bergamini, C. Aflatoxins in spices, aromatic herbs, herb-teas and medicinal plants marketed in Italy. *Food Control* **2007**, *18*, 697−701.
(38) Debevere, J. *Microbial Guide Values & Legal Microbiological Criteria*; Ghent University: Ghent, Belgium, 2006.
(39) Peyron, S.; Abecassis, J.; Autran, J. C.; Rouau, X. Influence of UV exposure on phenolic acid content, mechanical properties of bran, and milling behavior of durum wheat (*Triticum durum* desf.). *Cereal Chem.* **2002**, *79*, 726−731.
(40) Allende, A.; McEvoy, J. L.; Luo, Y.; Artes, F.; Wang, C. Y. Effectiveness of two-sided UV-C treatments in inhibiting natural microflora and extending the shelf-life of minimally processed 'Red Oak Leaf' lettuce. *Food Microbiol.* **2006**, *23*, 241−249.
(41) Escalona, V. H.; Aguayo, E.; Martínez-Hernández, G. B.; Artés, F. UV-C doses to reduce pathogen and spoilage bacterial growth in vitro and in baby spinach. *Postharvest Biol. Technol.* **2010**, *56*, 223−231.
(42) Fine, F.; Gervais, P. Efficiency of pulsed UV light for microbial decontamination of food powders. *J. Food Prot.* **2004**, *67*, 787−792.
(43) Turner, L. B.; Mueller-Harvey, I.; McAllan, A. B. Light-induced isomerization and dimerization of cinnamic acid derivatives in cell walls. *Phytochemistry* **1993**, *33*, 791−796.
(44) Sólyom, K.; Solá, R.; Cocero, M. J.; Mato, R. B. Thermal degradation of grape marc polyphenols. *Food Chem.* **2014**, *159*, 361−366.
(45) Pinelo, M.; Arnous, A.; Meyer, A. S. Upgrading of grape skins: Significance of plant cell-wall structural components and extraction techniques for phenol release. *Trends Food Sci. Technol.* **2006**, *17*, 579−590.
(46) Chamorro, S.; Goñi, I.; Hervert-Hernández, D.; Viveros, A.; Brenes, A. Changes in polyphenolic content and antioxidant activity after thermal treatments of grape seed extract and grape pomace. *Eur. Food Res. Technol.* **2012**, *234*, 147−155.
(47) Volf, I.; Ignat, I.; Neamtu, M.; Popa, V. I. Thermal stability, antioxidant activity, and photo-oxidation of natural polyphenols. *Chem. Pap.* **2014**, *68*, 121−129.
(48) Zorić, Z.; Dragović-Uzelac, V.; Pedisić, S.; Kurtanjek, Ž.; Garofulić, I. E. Kinetics of the degradation of anthocyanins, phenolic acids and flavonols during heat treatments of freeze-dried sour cherry Marasca paste. *Food Technol. Biotechnol.* **2014**, *52*, 101−108.
(49) Gradinaru, G.; Biliaderis, C. G.; Kallithraka, S.; Kefalas, P.; Garcia-Viguera, C. Thermal stability of *Hibiscus sabdariffa* L. anthocyanins in solution and in solid state: effects of copigmentation and glass transition. *Food Chem.* **2003**, *83*, 423−436.
(50) Erlandson, J. A.; Wrolstad, R. E. Degradation of anthocyanins at limited water concentration. *J. Food Sci.* **1972**, *37*, 592−595.
(51) Khanal, R. C.; Howard, L. R.; Prior, R. L. Effect of heating on the stability of grape and blueberry pomace procyanidins and total anthocyanins. *Food Res. Int.* **2010**, *43*, 1464−1469.
(52) Bonilla, F.; Mayen, M.; Merida, J.; Medina, M. Extraction of phenolic compounds from red grape marc for use as food lipid antioxidants. *Food Chem.* **1999**, *66*, 209−215.
(53) Lafka, T. I.; Sinanoglou, V.; Lazos, E. S. On the extraction and antioxidant activity of phenolic compounds from winery wastes. *Food Chem.* **2007**, *104*, 1206−1214.
(54) Velasco, J.; Dobarganes, C. Oxidative stability of virgin olive oil. *Eur. J. Lipid Sci. Technol.* **2002**, *104*, 661−676.
(55) Morris, S. G.; Myers, J. S., Jr.; Kip, M.; Riemenschneider, R. W. Metal deactivation in lard. *J. Am. Oil Chem. Soc.* **1950**, *27*, 105−107.
(56) Shaker, E. S. Antioxidative effect of extracts from red grape seed and peel on lipid oxidation in oils of sunflower. *LWT−Food Sci. Technol.* **2006**, *39*, 883−892.
(57) Tamura, H.; Yamagami, A. Antioxidative activity of monoacylated anthocyanins isolated from Muscat Bailey A grape. *J. Agric. Food Chem.* **1994**, *42*, 1612−1615.
(58) Rivero-Pérez, M. D.; Muñiz, P.; González-Sanjosé, M. L. Contribution of anthocyanin fraction to the antioxidant properties of wine. *Food Chem. Toxicol.* **2008**, *46*, 2815−2822.
(59) Zheng, C.; Deng, Q.; Yang, M.; Zhou, Q.; Huang, F. The effect of heating on the physicochemical and quality characteristics of grape seed oil. *J. Food, Agric. Environ.* **2014**, *12*, 73−79.
(60) Cornelius, S. O.; Lilian, W., Sulfur dioxide and sulfites. In *Antimicrobials in Food*, 3rd ed.; CRC Press: Boca Raton, FL, USA, 2005; pp 143−167.
(61) Reguant, C.; Bordons, A.; Arola, L.; Rozès, N. Influence of phenolic compounds on the physiology of *Œnococcus œni* from wine. *J. Appl. Microbiol.* **2000**, *88*, 1065−1071.
(62) Vivas, N.; Lonvaud-Funel, A.; Glories, Y. Effect of phenolic acids and anthocyanins on growth, viability and malolactic activity of a lactic acid bacterium. *Food Microbiol.* **1997**, *14*, 291−300.
(63) Tabasco, R.; Sánchez-Patán, F.; Monagas, M.; Bartolomé, B.; Victoria Moreno-Arribas, M.; Peláez, C.; Requena, T. Effect of grape polyphenols on lactic acid bacteria and bifidobacteria growth: resistance and metabolism. *Food Microbiol.* **2011**, *28*, 1345−1352.
(64) Chung, K. T.; Lu, Z.; Chou, M. W. Mechanism of inhibition of tannic acid and related compounds on the growth of intestinal bacteria. *Food Chem. Toxicol.* **1998**, *36*, 1053−1060.

(65) Friedman, M. Overview of antibacterial, antitoxin, antiviral, and antifungal activities of tea flavonoids and teas. *Mol. Nutr. Food Res.* **2007**, *51*, 116−134.
(66) Sagdic, O.; Ozturk, I.; Yilmaz, M. T.; Yetim, H. Effect of grape pomace extracts obtained from different grape varieties on microbial quality of beef patty. *J. Food Sci.* **2011**, *76*, M515−M521.
(67) Hervert-Hernández, D.; Pintado, C.; Rotger, R.; Goñi, I. Stimulatory role of grape pomace polyphenols on *Lactobacillus acidophilus* growth. *Int. J. Food Microbiol.* **2009**, *136*, 119−122.
(68) Rodríguez, H.; Rivas, B. d. l.; Gómez-Cordovés, C.; Muñoz, R. Degradation of tannic acid by cell-free extracts of *Lactobacillus plantarum*. *Food Chem.* **2008**, *107*, 664−670.
(69) Alberto, M. R.; Farías, M. E.; Manca de Nadra, M. C. Effect of gallic acid and catechin on *Lactobacillus hilgardii* 5w growth and metabolism of organic compounds. *J. Agric. Food Chem.* **2001**, *49*, 4359−4363.
(70) Lewus, C. B.; Kaiser, A.; Montville, T. J. Inhibition of food-borne bacterial pathogens by bacteriocins from lactic acid bacteria isolated from meat. *Appl. Environ. Microbiol.* **1991**, *57*, 1683−1688.
(71) Khalil, R. S. Influence of gallic acid and catechin polyphenols on probiotic properties of *Streptococcus thermophilus* CHCC 3534 strain. *World J. Microbiol. Biotechnol.* **2010**, *26*, 2069−2079.

U/mg of protein) and pancreatin from porcine pancreas (4× USP specifications) were obtained from Sigma-Aldrich (Shanghai Branch, Shanghai, China).

**Isolation of Polyaspartic Acid According to Molecular Weight.** PAA (50 g) with a molecular weight of 5−150 kDa was dissolved in 5 L of water. From this aqueous solution, PAA samples of 10−30, 30−50, and 50−100 kDa were isolated. Four hundred milliliters of the aqueous solution was filtered using a 400 mL Millipore/stirred cell 8400 (Millipore, Bedford, MA, USA) equipped with a 10 kDa ultrafiltration membrane to remove the molecules of <10 kDa, yielding PAA of 10−150 kDa (3.4 g, dry weight). The PAA (10−150 kDa) was dissolved with 400 mL of water and filtered through a 30 kDa ultrafiltration membrane to afford PAA of 30−150 kDa (2.7 g, dry weight) and a solution of 10−30 kDa PAA, which was evaporated and dried under reduced pressure at 60 °C to give 0.6 g of 10−30 kDa PAA. The PAA of 30−150 kDa was subjected to the above procedure, using 50 and 100 kDa ultrafiltration membranes consecutively, to produce 1.2 g of 30−50 kDa PAA and 0.8 g of 50−100 kDa PAA.

**Preparation of CS−PAA Nanoparticles.** CS−PAA nanoparticles were prepared from chitosan of molecular weight 3−5, 14−22, or 50−150 kDa and polyaspartic acid with a molecular weight of 10−30, 30−50m or 50−100 kDa. The molecular weight of each component was varied to find the composition that would obtain the ideal particle size. The weight ratio of CS to PAA was 1:1. CS−PAA nanoparticles were prepared by mixing a positively charged CS/acetic acid solution with a negatively charged PAA solution at room temperature. Briefly, PAA (20 mg) was thoroughly dissolved in 10 mL of deionized water, and CS (20 mg) was fully dissolved in 10 mL of 1% acetic acid solution by magnetic stirring. The CS solution (10 mL) was added dropwise to the PAA solution (10 mL) at a flow rate of 1 mL/min using an injection pump and mixed by magnetic stirring at a speed of 500 rpm to form a dispersion of CS−PAA nanoparticles. After the optimal molecular weight of CS and PAA was determined, the effect of the CS/PAA ratio on the particle size and zeta potential of the nanoparticles was investigated.

**Trial Preparation of EGCG−CS−PAA Nanoparticles.** EGCG−CS−PAA nanoparticles were prepared by mixing a positively charged CS acetic acid solution containing EGCG (2 mg/mL) and a negatively charged PAA solution at room temperature. The preparation process was similar to that of CS−PAA nanoparticles. To harvest the nanoparticles, the nanoparticle solution was centrifuged under 15000*g* for 20 min, following which the precipitate was immediately dispersed in 0.5% aqueous acetic acid (10 mL) and freeze-dried. The freeze-dried powder was tested to determine the EGCG loading amount, release, and stability in simulated body fluids.

**Characterization of the EGCG−CS−PAA Nanoparticles.** The average diameter and size distribution of particles were determined by dynamic light scattering (DLS) using a Zetasizer Nano-ZS analyzer (Malvern Instruments, Worcestershire, UK). All DLS measurements were done at 25 ± 0.1 °C and at a scattering angle of 90°. The particle size distribution was produced from the volume measurement, in which the relative percentage of particles in each size class is based on the volume they occupy. The zeta potential was measured with laser Doppler velocimetry (LDV) using the same Zetasizer Nano-ZS analyzer. The morphology of the EGCG−CS−PAA nanoparticles was performed on a transmission electron microscope (TEM, Hitachi H-600) after the nanoparticles had been mounted onto a carbon-coated copper grid.

**Determination of Entrapment Efficiency and Loading Amount of EGCG in the Nanoparticles.** The solution of EGCG−CS−PAA nanoparticles (2 mL) was transferred into an Amicon Ultra-3K centrifugal filter device (Millipore Corp. Billerica, MA, USA) made up of a centrifuge tube and a filter unit with a low-binding Ultracel membrane (3000 MWCO). After centrifugation at 4000*g* for 30 min, EGCG−CS−PAA nanoparticles remained in the filter unit and free EGCG and salts penetrated through the Ultracel membrane into the centrifuge tube. The free EGCG was determined by high-performance liquid chromatography (HPLC). The EGCG−CS−PAA nanoparticles in the filter unit were freeze-dried, and part of the lyophilized powder was extracted with methanol for EGCG determination by HPLC. The HPLC analysis were performed on a Shimadzu HPLC system (Shimadzu, Kyoto, Japan) composed of two LC-10A pumps, an SIL-10Avp autosampler, an SPD-M10Avp UV detector, and a Symmetry C18 (5 $\mu$m, 4.6 mm × 250 mm) column. The elution employed a linear gradient system with mobile phase A (water/acetic acid 98:2) and mobile phase B (acetonitrile) at a flow rate of 1 mL/min at 40 °C. The chromatogram was recorded at 280 nm. The entrapment efficiency (%) of EGCG in the nanoparticles and the loading amount (mg/g) were calculated from the results of HPLC analysis.

**Stability of EGCG−CS−PAA Nanoparticles at Different pH Values.** EGCG−CS−PAA nanoparticles were prepared by mixing a solution of positively charged CS in acetic acid, containing EGCG, with a solution of negatively charged PAA at room temperature. The nanoparticle dispersion was centrifuged at 15000*g* to harvest the nanoparticles. The collected nanoparticles were dispersed in 0.5% aqueous acetic acid and freeze-dried to form a lyophilized powder. This powder was tested to determine the PDI and particle size of the EGCG−CS−PAA nanoparticles at different pH values (2.5, 3.5, 4.5, 6.6, 7.0, and 7.4) to evaluate the stability of the nanoparticles.

**Release of EGCG from EGCG−CS−PAA Nanoparticles.** The release profile of EGCG from test nanoparticles was investigated in different media (pH 2.5, 4.0, 6.6, 7.0, and 7.4) in the presence of the reducing agents ascorbic acid (20 mM) and tris[2-carboxyethyl]-phosphine hydrochloride (13 mM) to prevent EGCG from oxidation in alkaline environments.[19] Briefly, 5 mg of the EGCG−CS−PAA nanoparticles was dispersed in 20 mL of pure water by ultrasonic process and then incubated in a water bath at 37 °C under magnetic agitation (100 rpm). At given time intervals, samples (1.0 mL) were taken out and centrifuged, and the supernatants were analyzed by HPLC. The amount of EGCG released was expressed as a decrease in the percentage of EGCG in the nanoparticles, which was obtained from the EGCG concentration in the supernatants after centrifugation of the nanoparticle solutions.

**Stability Evaluation of EGCG in Nanoparticles under Simulated Digestion and Adsorption Conditions in Vitro.** The simulated digestion condition was PBS buffer with pH 2.1 containing pepsin (simulated gastric fluid, SGF), and the simulated adsorption condition was PBS buffer at pH 7.2 containing pancreatin−bile salts (simulated intestinal fluid, SIF).[23] The amount of EGCG remaining in EGCG−CS−PAA nanoparticles in SGF and SIF after 0−4 h was determined according to the study of Krook and Hagerman.[12] Briefly, EGCG−CS−PAA nanoparticles were added to SGF or SIF, to a final EGCG concentration of 0.25 mg/mL (0 h), and then incubated in a water bath at 37 °C under magnetic agitation (100 rpm). After 1, 2, 3, and 4 h of incubation, 1 mL of the incubated solution was removed and the EGCG concentration in this aliquot was determined by HPLC as described above. The amount of EGCG remaining after the incubation reflects the stability of EGCG in nanoparticles during digestion and adsorption in vitro.

**Preparation of EGCG−CS−PAA Nanoparticles for Animal Experimentation.** PAA (2 g) was thoroughly dissolved in 1 L of deionized water. CS (2 g) was fully dissolved in 1 L of 1% acetic acid solution by stirring; 2 g of EGCG was then added to this solution. The CS−EGCG solution was added to the PAA solution (1 L) at a flow rate of 10 mL/min using a BT100-1F peristaltic pump (Konap Peristaltic Pump Co., Ltd., Chongqing, China) and mixed by an ultrasonic processor (FS-1800N, Shanghai Sonxi Ultrasonic Instrument Co., Shanghai, China) to form a solution of EGCG−CS−PAA nanoparticles. The sizes of the nanoparticles in the solution and in the trial preparation were compared by DLS. This solution was centrifuged under 13000*g* for 20 min to harvest the nanoparticles; the pellet was dispersed in 0.5% aqueous acetic acid (500 mL), ultrasonicated, and freeze-dried. The freeze-dried powder was used in the animal experiments.

**Effectiveness of EGCG−CS−PAA Nanoparticles on Rabbit Atherosclerosis.** Thirty male New Zealand white rabbits (Animal Center of Zhejiang Academy of Medical Sciences) weighing 1.92−2.11 kg were randomly divided into six experimental groups. They were

Table 1. Mean Diameter, Polydispersity Index, and Zeta Potential of the Nanoparticles (CS−PAA NP) Prepared with Chitosan (CS) and Polyaspartic Acid (PAA) of Various Molecula Weight[a]

| PAA MW (kDa) | CS MW (kDa) | diameter (nm)[a] | PDI | zeta potential (mV) |
|---|---|---|---|---|
| 10−30 | 3−5 | 72.4 ± 1.5 a | 0.117 ± 0.007 | 11.8 ± 1.2 a |
| | 14−22 | 82.6 ± 1.8 b | 0.156 ± 0.010 | 12.9 ± 1.5 a |
| | 50−150 | 91.2 ± 2.3 c | 0.365 ± 0.014 | 14.0 ± 1.7 b |
| 30−50 | 3−5 | 92.6 ± 2.7 c | 0.203 ± 0.008 | 31.5 ± 3.2 c |
| | 14−22 | 112.6 ± 3.6 d | 0.234 ± 0.009 | 34.9 ± 3.7 cd |
| | 50−150 | 145.1 ± 5.1 e | 0.516 ± 0.015 | 38.1 ± 3.9 d |
| 50−100 | 3−5 | 197.2 ± 4.4 f | 0.431 ± 0.011 | 37.7 ± 3.5 d |
| | 14−22 | 231.3 ± 10.5g | 0.487 ± 0.012 | 39.5 ± 4.1 d |
| | 50−150 | 299.0 ± 14.6 h | 0.618 ± 0.023 | 42.7 ± 4.0 de |

[a]Mean ± SD, $n = 3$. Values in a column followed by different letters are significantly different ($p < 0.05$).

housed individually in metal cages in an air-conditioned room (22 ± 2 °C, 55 ± 5% humidity) and maintained on a 12 h light/12 h dark cycle with free access to food and water. Water was allowed ad libitum, and 150 g/day of food was provided. One group of rabbits was used as a control. Experimental rabbits (five groups) were fed for 5 weeks with a high-fat diet (HFD) containing 93.75% standard rabbit chow (Jiangsu Synergistic Bioengineering Co. Ltd., Nanjing, China) supplemented with 1.0% cholesterol, 5% lard oil, and 0.25% sodium cholate to provoke atherosclerosis. Four of the groups were orally treated with EGCG−CS−PAA nanoparticles (EGCG NP), EGCG, blank CS−PAA nanoparticles (blank NP), or simvastatin (positive control). In the EGCG NP-fed group, each rabbit was daily given 350 mg of EGCG NP (7 mL of 0.5% aqueous acetic acid) containing 100 mg of EGCG, whereas each rabbit in the EGCG group was given 100 mg of EGCG (7 mL of 0.5% aqueous acetic acid). Each rabbit in the blank NP-fed group was given 250 mg of blank NP (7 mL of 0.5% aqueous acetic acid) per day, and each rabbit in the positive control was given 5 mg of simvastatin (5 mg/tablet, Shanghai Xinyi Wanxiang Pharmaceutical Co. Ltd., Shanghai, China) per day. For EGCG NP and blank NP, the sample was dispersed in water solution via ultrasonication, and then the solution was provided to the rabbit by oral administration.

The daily EGCG dose was selected according to the suitable pharmacological dose for humans. All animal experiments were performed according to the protocols approved by the Animal Care Center of the Zhejiang Academy of Medical Sciences and complied with the guidelines for the care and use of laboratory animals. Five weeks after commencement of the HFD, the rabbits were sacrificed by exsanguination via the marginal ear vein after deep anesthesia with pentobarbital (30 mg/kg iv). Serum was stored at −80 °C until serum lipid analysis and measurements of serum values were conducted. The thoracic arteries with arches were carefully excised to avoid damaging the endothelial lining, and the adhering soft tissue was trimmed off. Thoracic arteries with arches were rapidly dissected, opened longitudinally, and stained with Oil Red. Photographs of the inner surface were taken and copied onto graph paper with magnification (×2), and athermanous plaques were delineated. The number of small squares surrounded by the line was counted on the graph paper and the percentage of the area of athermanous plaque was calculated. Serum and lipoprotein levels of cholesterol and triglyceride were measured by enzymatic colorimetry using commercial kits (Boehringer, Mannheim, Germany). Quantitative data were expressed as the mean ± SD and analyzed by one-way ANOVA. Multiple comparisons between the groups were performed using the Student−Newman−Keuls (SNK) method. Statistical significance was set at a level of $p < 0.05$.

## RESULTS AND DISCUSSION

**Formation of Chitosan−Polyaspartic Acid Nanoparticles.** Nanoparticles can form from self-assembly of polyelectrolytes such as chitosan and poly-γ-glutamic acid.[24] In the present study, we tested the preparation of nanoparticles by self-assembly of chitosan and polyaspartic acid because PAA is less expensive than poly-γ-glutamic acid. Table 1 shows the mean diameter, polydispersity index (PDI), and zeta potential of the CS−PAA nanoparticles prepared with CS−PAA (1:1, w/w) prepared from various molecular weights of CS and PAA. The zeta potential and particle size increased as the molecular weights of CS and PAA increased, which suggests that long-chain CS and PAA form large particles with high stability, and short-chain CS and PAA form small particles with low stability. Furthermore, the values of PDI increased when the difference in the molecular weights of CS and PAA molecules was increased. Considering that the parameters for best stability and uptake in cellular systems are zeta potential >30 mV or < −30 mV[25] and particle size near 75 nm,[26] the optimal nanoparticles in the present study were self-assembled from PAA 30−50 kDa and CS 3−5 kDa and had a diameter of 92.6 nm and a zeta potential of 31.5 mV. These nanoparticles were selected for further experiments.

Further study showed that changing the CS/PAA ratio in the self-assembled nanoparticles could change their size and stability (Table 2). As the CS/PAA ratio increased, the values of both nanoparticle size and zeta potential increased. When the CS/PAA ratio was 0.75, the particle size decreased to 84.7 nm, but the particles (zeta potential = 22.3 mV) were less stable than those in which the ratio of CS/PAA was 1.0. On the basis of the above results, we decided to use the nanoparticles that were self-assembled from PAA 30−50 kDa and CS 3−5 kDa at a ratio of 1:1 for loading EGCG.

Table 2. Mean Diameter, Polydispersity Index and Zeta Potential of the Nanoparticles (CS−PAA NP) Prepared with Various Ratios of Chitosan (MW 3−5 kDa)/Polyaspartic Acid (MW 30−50 kDa)[a]

| CS/PAA (w/w) | particle size (nm) | PDI | zeta potential (mV) |
|---|---|---|---|
| 0.75 | 84.7 ± 3.2 a | 0.206 ± 0.004 | 22.3 ± 0.2 a |
| 1 | 93.3 ± 2.1 b | 0.205 ± 0.006 | 31.8 ± 0.2 b |
| 1.5 | 100.4 ± 2.5 c | 0.242 ± 0.009 | 40.5 ± 0.4 c |
| 2 | 126.3 ± 1.9 d | 0.307 ± 0.015 | 44.2 ± 0.1 d |
| 2.5 | 136.4 ± 3.8 e | 0.318 ± 0.017 | 45.5 ± 0.3 d |

[a]Mean ± SD, $n = 3$. Values in a column followed by different letters are significantly different ($p < 0.05$).

**EGCG−CS−PAA Nanoparticles.** EGCG was loaded into self-assembled CS−PAA nanoparticles by adding EGCG into a

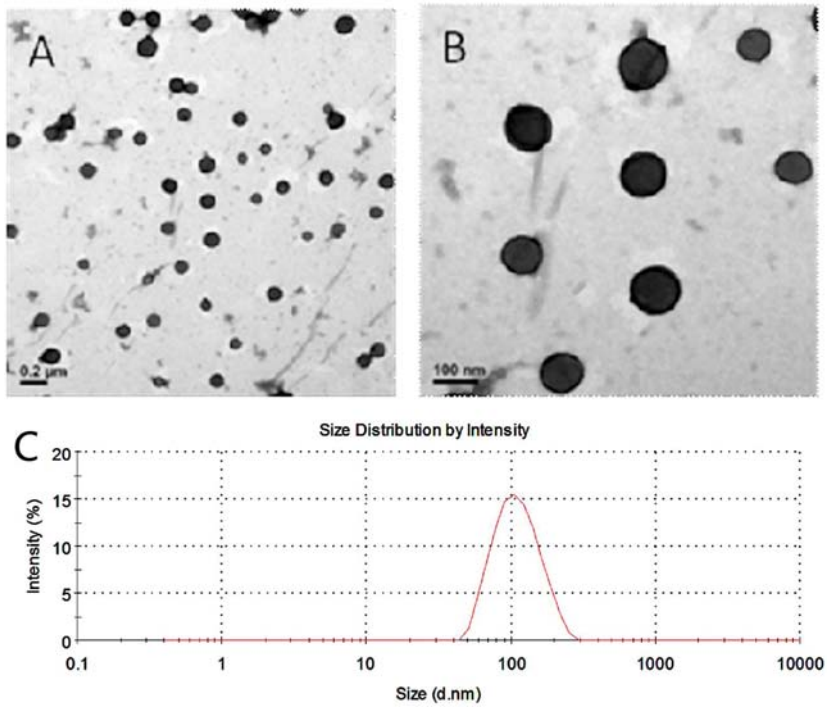


**Figure 1.** TEM micrographs of CS−PAA−EGCG nanoparticles: (A) 50000× magnification; (B) 150000× magnification; (C) particle size determination by DLS.

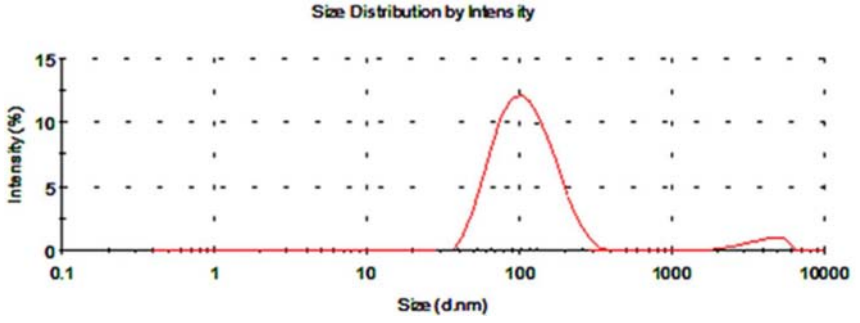


**Figure 2.** DLS measurement of the particle size in the dispersion prepared by reconstituting the freeze-dried nanoparticles.

CS solution, which was mixed with a PAA solution under magnetic stirring at room temperature. The mean particle diameter, PDI, and entrapment efficiency (EE) of nanoparticles prepared with a 1:1 ratio of CS/PAA were determined. The prepared EGCG−CS−PAA nanoparticles exhibited a particle size of 102.4 ± 5.6 nm, PDI = 0.224, and EE = 25.0 ± 2.1%. The EE value was greater than that of nanoparticles self-assembled from CS and the same mass amount of poly-γ-glutamic acid as PAA.[24] Because the PAA molecule is shorter than γ-glutamic acid, PAA contains more carboxyl groups for forming hydrogen bonds with EGCG. The zeta potential of the nanoparticle solution was 33.3 ± 0.2, which indicates excellent stability.

TEM images (Figure 1) showed that the EGCG−CS−PAA nanoparticles were spherical and about 100 nm in diameter (Figure 1). The diameters determined by TEM were consistent with those determined via DLS. This demonstrated that DLS was an effective method to determine the size of the prepared nanoparticles. After the nanoparticles were harvested by centrifuging and freeze-drying, HPLC showed that the concentration of EGCG in the nanoparticles was 34.4%. Dispersing the freeze-dried nanoparticles in 0.5% aqueous acetic acid yielded a sample whose particle size was similar to that of the original system before freeze-drying (Figure 2).

**Stability of EGCG−CS−PAA Nanoparticles in the Solutions at Different pH Values.** The stability of the EGCG−CS−PAA nanoparticles in the solutions at different pH values was evaluated from the PDI and particle diameter (Table 3). At pH 3.5, the original pH when the nanoparticles were prepared, the EGCG−CS−PAA nanoparticles were stable after 2 h at room temperature. At pH 2.5, no significant change in the nanoparticles was observed after 2 h. As the pH was increased from 4.5 to 7.4, the PDI and particle diameter rapidly increased, which means that small nanoparticles aggregated or reassembled into larger nanoparticles. This result is similar to that obtained via TEM observation of CS/poly-γ-glutamic acid nanoparticles.[24]

**Release of EGCG from EGCG−CS−PAA Nanoparticles at Different pH Values.** Release of EGCG from EGCG−CS−PAA nanoparticles at different pH values was investigated because the pH in the digestive system varies widely between gastric and intestinal fluid. The typical pH in the stomach is

**Table 3. Polydispersity Index and Diameter of the EGCG−CS−PAA Nanoparticles after 2 h at Different pH Values[a]**

| treatment | pH | PDI | mean particle size (nm)[a] |
|---|---|---|---|
| original solution | | | |
| 0 h | 3.5 | 0.213 ± 0.008 | 103.7 ± 2.5 a |
| 2 h | 3.5 | 0.228 ± 0.008 | 102.9 ± 2.1 a |
| 2 h after adjusting pH | 2.5 | 0.224 ± 0.013 | 106.3 ± 3.5 a |
| | 4.5 | 0.288 ± 0.021 | 134.2 ± 5.2 b |
| | 6.6 | 0.323 ± 0.035 | 200.4 ± 9.5 c |
| | 7.0 | 0.403 ± 0.039 | 443.1 ± 16.5 d |
| | 7.4 | 0.651 ± 0.051 | 856.6 ± 24.6 e |

[a]Mean ± SD, $n = 3$. Values in a column followed by different letters are significantly different ($p < 0.05$).

from 2.0 to 4.0 depending on the species and food intake.[27] The pH in the duodenum is 6.0−6.6, and in the jejunum and proximal ileum the pH is 6.6−7.0, whereas the pH is about 7.4 in the distal ileum and in the body fluid filling intercellular spaces between enterocytes.[28] The present study determined the release of EGCG from EGCG−CS−PAA nanoparticles in dispersions at pH 2.5 (0−1 h), 4.0 (1−2 h), 6.6 (2−3 h), 7.0 (3−4 h), and 7.4 (4−5 h), conditions similar to those encountered in food ingestion. Figure 3 shows the release of

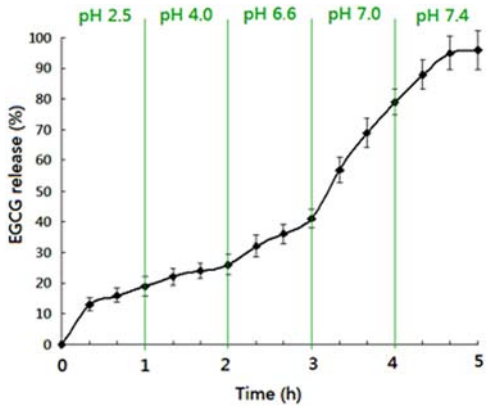


**Figure 3.** EGCG release profiles of EGCG−CS−PAA nanoparticles at pH 2.5, 4.0, 6.6, 7.0, and 7.4.

EGCG from the nanoparticles at the various pH conditions. At pH 2.5 and 4.0 (simulating the stomach), the release of EGCG in 0−2 h was about 25% of the total EGCG amount in the nanoparticles. At pH 6.6 (simulating the duodenum), the release rate increased and the amount released reached 41% of the total. At pH 7.0 (simulating the jejunum and the proximal ileum) and pH 7.4 (simulating the distal ileum and the intercellular body fluid), the release rate showed a rapid increase, which implies that the nanoparticles became unstable and quickly disintegrated to release EGCG. The stability of the nanoparticles in the stomach, combined with the rapid release in the intestine, may improve the uptake of EGCG in the intestine.

**Stability of EGCG−CS−PAA Nanoparticles in Simulated Gastric and Intestinal Conditions.** Loading EGCG into nanoparticles improves its stability in gastric and intestinal conditions. In SGF (pH 2.1), the loss of EGCG in EGCG−CS−PAA nanoparticles was about 10−15% less than that of the free EGCG regardless of the presence of pepsin (Figure 4). In SIF (pH 7.2) EGCG was more unstable than in SGF. Encapsulation with CS and PAA clearly protected EGCG. Upon addition of the nanoparticles to SIF in the presence of pancreatin−bile salts, the amount of EGCG lost was 41, 71, 92, and 93% after 1, 2, 3, and 4 h, respectively. For nanoparticles in SIF without pancreatin−bile salts, smaller amounts of EGCG were lost at the same time intervals: 39, 81, 83, and 90%, respectively. Increasing the stability of compounds in the human stomach and intestine can improve their uptake. Therefore, loading EGCG in CS−PAA nanoparticles may improve the effectiveness of EGCG against diseases such as atherosclerosis.

**EGCG−CS−PAA Nanoparticles (EGCG NP) for Animal Experiments.** EGCG NP for animal experiments were prepared according to a modified process in which ultrasonication replaced magnetic agitation because the amount was scaled up from milligrams to grams. The product exhibited the same properties, that is, particle size = 100.6 ± 4.2 nm, PDI = 0.215 ± 0.008, zeta potential = 33.9 ± 0.5 mV, and EGCG loading amount = 348.1 ± 12.4 mg/g, dry weight.

**Effectiveness of EGCG NP against Atherosclerosis.** The inner surfaces of the rabbit arteries are shown in Figure S1 in the Supporting Information. The control rabbit artery was covered with opaque atherosclerotic lesions in its inner surface (Figure 5a). The HFD-fed rabbits showed severe lipid deposition in their inner surface artery on which the average ratio (%) of lipid deposit area to intimal surface area (without artery arch) was 69.0 ± 9.6% (Figure 5b). The blank NP-fed rabbits exhibited an average ratio (%) of lipid deposit area of 65.3 ± 10.8% (Figure 5c), which suggests no significant difference in lipid deposition between the HFD-fed rabbits and the blank NP-fed rabbits. Compared to the HFD-fed rabbits, the EGCG NP-fed rabbits and EGCG-fed rabbits exhibited

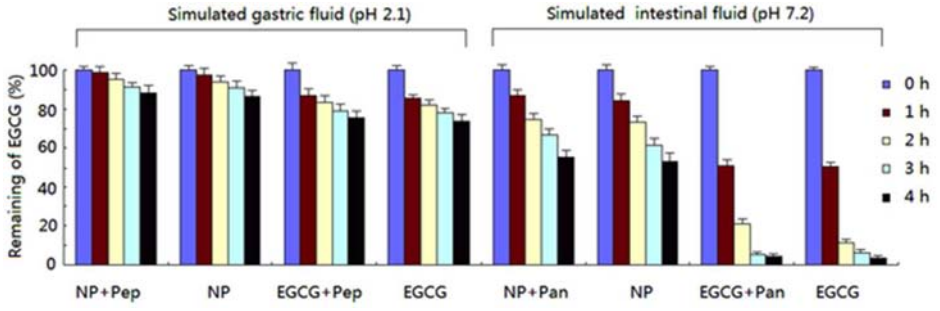


**Figure 4.** Amount of EGCG remaining in SGF and SIF after 0, 1, 2, 3, and 4 h. NP+Pep, EGCG−CS−PAA nanoparticles in the presence of pepsin; NP, EGCG−CS−PAA nanoparticles alone; EGCG+Pep, EGCG in the presence of pepsin; EGCG alone; NP+Pan, in the presence of pancreatin−bile salts; EGCG+Pan, EGCG in the presence of pancreatin−bile salts.

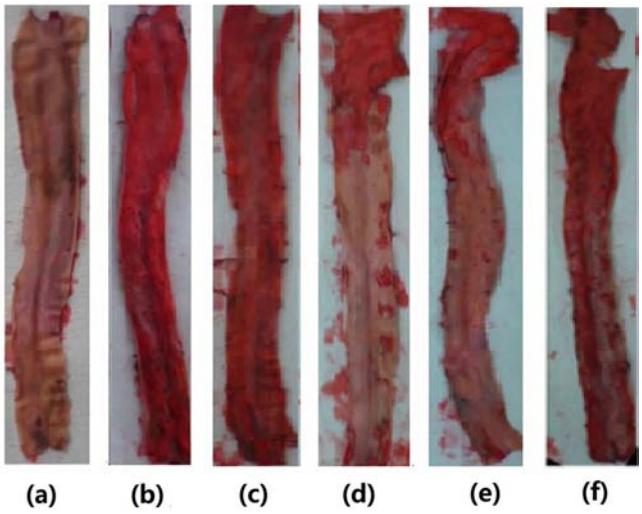


**Figure 5.** Extent of atherosclerosis lesion development in rabbits after feeding with the experimental diets: (a) normal group; (b) HFD-fed group; (c) blank NP-fed group; (d) simvastatin-fed group (2.5 mg/kg); (e) EGCG NP-fed group, 175 mg/kg (corresponding to 50 mg EGCG/kg); (f) EGCG-fed group (50 mg/kg).

significantly less lipid deposition. The average ratios of lipid deposit area for EGCG NP-fed rabbits and EGCG-fed rabbits were 16.9 ± 5.8 and 42.1 ± 4.0%, respectively, which showed that the EGCG NP were much more effective against atherosclerosis compared with EGCG alone ($p < 0.01$). The effect of EGCG NP against rabbit atherosclerosis was close to that of simvastatin (Figure 5d, percent average ratio of lipid deposit area, 15.6 ± 4.1%), which is a clinical treatment for atherosclerosis. It should be mentioned that no difference was seen in the body weight of the EGCG NP-fed group and the normal-fed group (Table 1S), which suggests that the nanoformulation EGCG did not trigger toxic reactions in the rabbits.

**Effect of EGCG NP and EGCG on Blood Lipid Levels.** The serum levels of total cholesterol (TC) and LDL cholesterol (LDL-C) of HFD-fed rabbits were 10−20 times those of normal rabbits, whereas the levels of triglyceride (TG) and HDL cholesterol (HDL-C) were increased but to a lesser degree (Table 4). After administration of EGCG NP and EGCG, the levels of TG, TC, HDL-C, and LDL-C decreased by 52, 55, 27, and 65% and 19, 26, 23, and 33%, respectively. It is clear that EGCG NP decreased the blood lipid levels of rabbits to a much greater extent than EGCG. Meanwhile, no significant changes in the levels of TG, TC, HDL-C, and LDL-C were found between the HFD-fed and the blank NP-fed groups. The results demonstrate that the reduction of the blood lipid levels in the EGCG NP and EGCG groups fully correspond to the reduction in lipid deposition.

The effectiveness of EGCG in humans is relatively low because EGCG is unstable at the pH conditions of body fluids.[18] It is known that EGCG undergoes significant metabolism and conjugation during absorption in the small intestine and the colon. In the small intestine EGCG is degraded to smaller phenolic acids and valerolactones.[29] To improve the effectiveness of EGCG, various methods have been investigated by loading EGCG in vehicles such as liposomes, ethosomes, or other nanoparticles, which can protect EGCG by delayed release, act to target the release of EGCG, or protect it from unstable circumstances such as body fluids with various pH values.[30] The present study provides a nanoformulation of EGCG to improve its effectiveness.

In conclusion, EGCG-loaded nanoparticles with a mean diameter ca. 100 nm were prepared from 30−50 kDa PAA and 3−5 kDa CS. The nanoparticles were pH-responsive and demonstrated different EGCG release profiles in simulated gastrointestinal tract media. Compared to EGCG alone, this nanoformulation of EGCG demonstrated higher stability in body fluids and showed greater activity against atherosclerosis.

## ■ ASSOCIATED CONTENT

### Ⓢ Supporting Information

Additional experimental details, Table 1S, and Figure S1. This material is available free of charge via the Internet at http://pubs.acs.org.

## ■ AUTHOR INFORMATION

### Corresponding Author

*(Q.D.) Phone: +86 571 88218710. Fax: +86 571 63741276. E-mail: qizhendu@126.com.

### Author Contributions

‖Z.H. and Y.X. contributed equally to this work.

### Funding

This research was supported by a fund of the National Natural Science Foundation of China (Grant 31270724), a fund of the National Key Technology R&D Program (2012BAD36B06), and a fund of the Natural Science Foundation of Zhejiang Province (Grant LZ12C16004).

### Notes

The authors declare no competing financial interest.

## ■ REFERENCES

(1) Martinovic, I.; Abegunewardene, N.; Seul, M.; Vosseler, M.; Horstick, G.; Buerke, M.; Darius, H.; Lindemann, S. Elevated

**Table 4. Effect of EGCG NP on Plasma Triglyceride Levels in Rabbits Fed a High-Fat Diet (HFD) over 5 Weeks**

| | blood lipid level after treatments[a] | | | | |
|---|---|---|---|---|---|
| group | TG | TC | HDL-C | LDL-C | LDL-C/HDL-C |
| normal | 1.58 ± 0.38 a | 3.67 ± 0.66 a | 1.60 ± 0.31 a | 1.69 ± 0.31 a | 1.1 |
| HFD | 3.76 ± 0.75 b | 36.87 ± 6.03 b | 3.92 ± 0.76 b | 31.65 ± 3.87 b | 8.1 |
| blank NP | 3.64 ± 0.80 b | 35.62 ± 5.66 b | 3.79 ± 0.55 b | 30.92 ± 3.06 b | 8.2 |
| simvastatin | 2.04 ± 0.50 c | 15.62 ± 4.61 c | 2.89 ± 0.47 c | 10.94 ± 2.06 c | 3.8 |
| EGCG NP | 1.82 ± 0.62 ac | 16.43 ± 3.24 c | 2.87 ± 0.54 c | 11.10 ± 2.57 c | 3.9 |
| EGCG | 3.03 ± 0.77 d | 27.35 ± 5.75 d | 3.01 ± 0.50 c | 21.26 ± 3.98 d | 7.1 |

[a]The data from five rabbits per group are presented as the mean ± SD. Values in a column followed by different letters are significantly different ($p < 0.05$).

monocyte chemoattractant protein-1 serum levels in patients at risk for coronary artery disease. *Circ. J.* **2005**, *69*, 1484−1489.
(2) Ross, R.; Harker, L. Hyperlipidemia and atherosclerosis. *Science* **1976**, *193*, 1094−1100.
(3) Babu, P. V. A.; Si, H.; Liu, D. Epigallocatechin gallate reduces vascular inflammation in db/db mice possibly through an NF-κB-mediated mechanism. *Mol. Nutr. Food Res.* **2012**, *56*, 1424−432.
(4) Yang, C. S.; Wang, X.; Lu, G.; Picinich, S. C. Cancer prevention by tea: animal studies, molecular mechanisms and human relevance. *Nat. Rev. Cancer* **2009**, *9*, 429−439.
(5) Li, N.; Taylor, L. S.; Ferruzzi, M. G.; Mauer, L. J. Kinetic study of catechin stability: effects of pH, concentration, and temperature. *J. Agric. Food Chem.* **2012**, *60*, 12531−12539.
(6) Wang, R.; Zhou, W. B.; Jiang, X. H. Reaction kinetics of degradation and epimerization of epigallocatechin gallate (EGCG) in aqueous system over a wide temperature range. *J. Agric. Food Chem.* **2008**, *56*, 2694−2701.
(7) Li, N.; Taylor, L. S.; Ferruzzi, M. G.; Mauer, L. J. Color and chemical stability of tea polyphenol (−)-epigallocatechin-3-gallate in solution and solid states. *Food Res. Int.* **2013**, *53*, 909−921.
(8) Wolfram, S. Effects of green tea and EGCG on cardiovascular and metabolic health. *J. Am. Coll. Nutr.* **2007**, *26*, 373s−388s.
(9) Arab, L.; Liu, W.; Elashoff, D. Green and black tea consumption and risk of stroke: a meta-analysis. *Stroke* **2009**, *40*, 1786−1792.
(10) Chen, L.; Lee, M. J.; Li, H.; Yang, C. S. Absorption, distribution, elimination of tea polyphenols in rats. *Drug Metab. Dispos.* **1997**, *25*, 1045−1050.
(11) Warden, B. A.; Smith, L. S.; Beecher, G. R.; Balentine, D. A.; Clevidence, B. A. Catechins are bioavailable in men and women drinking black tea throughout the day. *J. Nutr.* **2001**, *131*, 1731−1737.
(12) Lee, M. J.; Maliakal, P.; Chen, L.; Meng, X.; Bondoc, F. Y.; Prabhu, S.; Lambert, G.; Mohr, S.; Yang, C. S. Pharmacokinetics of tea catechins after ingestion of green tea and (−)-epigallocatechin-3-gallate by humans: formation of different metabolites and individual variability. *Cancer Epidemiol. Biomarkers Prev.* **2002**, *11* (10 Part 1), 1025−1032.
(13) Lambert, J. D.; Yang, C. S. Mechanisms of cancer prevention by tea constituents. *J. Nutr.* **2003**, *133*, 3262s−3267s.
(14) Babu, R. V.; Liu, D. Green tea catechins and cardiovascular health: an update. *Curr. Med. Chem.* **2008**, *15*, 1840−1850.
(15) Lambert, J. D.; Lee, M. J.; Diamond, L.; Ju, J.; Hong, J.; Bose, M.; Newmark, H. L.; Yang, C. S. Dose-dependent levels of epigallocatechin-3-gallate in human colon cancer cells and mouse plasma and tissues. *Drug Metab. Dispos.* **2006**, *34*, 8−11.
(16) Su, Y. L.; Leung, L. K.; Huang, Y.; Chen, Z. Y. Stability of tea theaflavins and catechins. *Food Chem.* **2003**, *83*, 189−195.
(17) Sang, S.; Lee, M. J.; Hou, Z.; Ho, C. T.; Yang, C. S. Stability of tea polyphenol (−)-epigallocatechin-3-gallate and formation of dimers and epimers under common experimental conditions. *J. Agric. Food Chem.* **2005**, *53*, 9478−9484.
(18) Krook, M. A.; Hagerman, A. E. Stability of polyphenols epigallocatechin gallate and pentagalloyl glucose in a simulated digestive system. *Food Res. Int.* **2012**, *49*, 112−116.
(19) Dube, A.; Ng, K.; Nicolazzo, J. A.; Larson, I. Effective use of reducing agents and nanoparticle encapsulation in stabilizing catechins in alkaline solution. *Food Chem.* **2010**, *122*, 662−667.
(20) Dube, A.; Nicolazzo, J. A.; Larson, I. Chitosan nanoparticles enhance the plasma exposure of (−)-epigallocatechin gallate in mice through an enhancement in intestinal stability. *Eur. J. Pharm. Sci.* **2011**, *44*, 422−426.
(21) Siddiqui, I. A.; Bharali, D. J.; Nihal, M.; Adhami, V. M.; Khan, N.; Chamcheu, J. C.; Khan, M. I.; Shabana, S.; Mousa, S. A.; Mukhtar, H. Excellent anti-proliferative and pro-apoptotic effects of (−)-epigallocatechin-3-gallate encapsulated in chitosan nanoparticles on human melanoma cell growth both in vivo. *Nanomed. Nanotechnol. Biol. Med.* **2014**, *10*, 1619−1626.
(22) Zhang, J.; Nie, S.; Wang, S. Nanoencapsulation enhances epigallocatechin-3-gallate stability and its antiatherogenic bioactivities in macrophages. *J. Agric. Food Chem.* **2013**, *61*, 9200−9209.
(23) Liu, W.; Ye, A.; Liu, C.; Liu, W.; Singh, H. Structure and integrity of liposomes prepared from milk- or soybean-derived phospholipids during in vitro digestion. *Food Res. Int.* **2012**, *48*, 499−506.
(24) Tang, D.-W.; Yu, S.-H.; Ho, Y.-C.; Huang, B.-Q.; Tsai, G.-J.; Hsieh, H.-Y.; Sung, H.-W.; Mi, F.-L. Characterization of tea catechins-loaded nanoparticles prepared from chitosan and an edible polypeptide. *Food Hydrocolloids* **2013**, *30*, 33−41.
(25) Stevanovic, M. M.; Skapin, S. D.; Bracko, I.; Milenkovic, M.; Petkovic, J.; Filipic, M.; Uskokovic, D. P. Poly(lactide-*co*-glycolide)/silver nanoparticles: synthesis, characterization, antimicrobial activity, cytotoxicity assessment and ROS-inducing potential. *Polymer* **2012**, *53*, 2818−2828.
(26) Chithrani, B. D.; Ghazani, A. A.; Chan, W. C. W. Determining the size and shape dependence of gold nanoparticle uptake into mammalian cells. *Nano Lett.* **2006**, *6*, 662−668.
(27) Kalantzi, L.; Goumas, K.; Kalioras, V.; Abrahamsson, B.; Dressman, J.; Reppas, C. Characterization of the human upper gastrointestinal contents under conditions stimulating bioavailability/bioequivalence studies. *Pharm. Res.* **2006**, *23*, 165−176.
(28) Eaimtrakarn, S.; Itoh, Y.; Kishimoto, J. I.; Yoshikawa, Y.; Shibata, N.; Takada, K. Retention and transit of intestinal mucoadhesive films in rat small intestine. *Int. J. Pharm.* **2011**, *224*, 61−67.
(29) Spencer, J. P. E. Metabolism of tea flavonoids in the gastrointestinal tract. *J. Nutr.* **2003**, *133*, 3255s−3261s.
(30) Rodrigues, C. F.; Ascenção, K.; Silva, F. A.; Sarmento, B.; Oliveira, M. B.; Andrade, J. C. Drug-delivery systems of green tea catechins for improved stability and bioavailability. *Curr. Med. Chem.* **2013**, *20*, 4744−4757.

lipids to perform their roles in assuring plant quality and safety.[11,12] Although $\alpha$-tocopherol has been considered to be the main contributing isoform to vitamin E activity, $\gamma$-tocopherol exhibits the greatest antioxidant activity.[12−14] Thus, it is necessary to assess the composition of all vitamin E isoforms in quinoa and amaranth leaves. Carotenoids, as pro-vitamin A and/or antioxidants, have not been carefully examined in the leaves of either quinoa or amaranth. Our recent study, however, has revealed that lipophilic phytochemicals including carotenoids in quinoa and amaranth leaves can be present at even higher concentrations than some commonly consumed cereal grains and pulses. Detailed results are reported in the present paper.

Evaluation and comparison of the nutritional quality of a large number of foods or feeds are often difficult. Major nutritional components, such as the lipophilic nutrients carotenoids, tocopherols, and fatty acids, in a food or feed have been assessed separately.[15,16] However, there is a lack of an evaluation system for the overall lipophilic quality attributes in samples of this nature.

The objectives of this study were to carry out a comprehensive examination on the lipophilic bioactive components in leaves of quinoa and amaranth, including the fatty acids, tocopherols, and carotenoids, and to evaluate the possible roles of these compounds in antioxidant and potentially other health promoting activities. This study is part of our current effort in assessing the economic and nutritional values of whole plants of both quinoa and amaranth in Ontario, Canada. A total of 14 amaranth and 6 quinoa cultivars were included in this study to help garner accurate information on the profile of lipophilic bioactives in the leaves and to explore the possibility of using quinoa leaves as healthy vegetables or even functional food ingredients.

## MATERIALS AND METHODS

**Leaf Materials.** Leaves of 14 amaranth and 6 quinoa cultivars were sampled from a farm near Campbellville, Ontario, Canada, in July 2013 (Table 1). Heads (with at least 4−5 fully opened leaves) of at least 5 plants per cultivar were handpicked, pooled and lyophilized in a 12-L bulk tray dryer (Labconco, Kansas City, MO) at 0.110 mbar and −40 °C prior to grinding with a commercial coffee blender (particle sizes 400−800 $\mu$m). The fine powder was stored in polyethylene tubes at −80 °C until extraction for the various analyses.

**Table 1. Quinoa and Amaranth Cultivars Studied**

| sample | commercial or cultivar name | scientific name |
|---|---|---|
| AL1 | Katan-AC12 | *Amaranth cruentus* |
| AL2 | Katan-ASV | *A. cruentus* |
| AL3 | Hopi Red Amaranth | *A. cruentus* |
| AL4 | Katan-ACV | *Amaranthus hypochondriacus* |
| AL5 | Katan-AH12 | *A. hypochondriacus* |
| AL6 | Red Garnet Amaranth | *A. hypochondriacus* |
| AL7 | Red Star Amaranth | *A. hypochondriacus* |
| AL8 | Katan-ATM Amaranth | *Amaranthus tricolor* |
| AL9 | Katan-ATT Red Leaf Amaranth | *A. tricolor* |
| AL10 | Katan-VA Amaranth | *A. tricolor* |
| AL11 | Katan-VAT | *A. tricolor* |
| AL12 | Midnight Red Amaranth | *A. tricolor* |
| AL13 | Red Leaf Amaranth | *A. tricolor* |
| AL14 | Russian Red Merlot Amaranth | *A. tricolor* |
| QL1 | Katan-Maple Leaf Quinoa | *Chenopodium formasanum* |
| QL2 | Temuko Quinoa | *Chenopodium quinoa* Willdenow |
| QL3 | Faro Quinoa | *C. quinoa* Willdenow |
| QL4 | Katan-CVQ | *C. quinoa* Willdenow |
| QL5 | Katan-BBRQ | *C. quinoa* Willdenow |
| QL6 | Red quinoa | *C. quinoa* Willdenow |

Lutein, zeaxanthin, $\beta$-carotene, and $\beta$-cryptoxanthin standards were purchased from Indofine (Hillsborough, NJ). 2,2-Diphenyl-1-picrylhydrazyl (DPPH), Trolox, 1,3,5-tri(2-pyridyl)-2,4,6-triazine (TPTZ), L-ascorbic acid, fluorescein, 2,2′-azobis(2-methylpropionamidine) dihydrochloride (AAPH), randomly methylated-$\beta$-cyclodextrin (RMCD), and $\alpha$-, $\beta$-, $\gamma$-, and $\delta$-tocopherols were from Sigma−Aldrich (Oakville, ON, Canada). Standards of fatty acid methyl esters (FAMEs) were obtained commercially (mixture 463, Nu-Chek-Prep, Inc., Elysian, MN). All solvents were of HPLC grade and obtained from Caledon Laboratories Ltd. (Georgetown, ON, Canada).

**Sample Extraction.** The powdered samples were accurately weighed then extracted with methyl *tert*-butyl ether/tetrahydrofuran (MTBE/THF, 1:1 v/v) on a Soxtec extraction system (Soxtec System 2050, Tecator AB, Hdganas, Sweden). In this system, the sample was first immersed in the boiling solvent for 30 min and then continuously rinsed by refluxing solvent from the condenser for 80 min. The solvent recovery lasted 30 min and predrying was for 2 min. During the extraction, solvents were heated to 155 °C. After cooling, ca. 5 mL of hexane each was used to wash the lipid extracts in the container three times. The oil yield was determined by the difference in mass of the container before and after the extraction. The extract was stored at −80 °C until analysis. All extraction tubes were covered with aluminum foil and the experiment was conducted under dim light in order to avoid sample degradation by photooxidation during the extraction period.

**Analysis of Fatty Acids by Gas Chromatography−Mass Spectrometry.** A 1 mL aliquot of the lipophilic extract was dried under a gentle stream of $N_2$ to remove hexane, methylated with anhydrous HCl/methanol (5% w/v), and dried over anhydrous sodium sulfate, and finally the FAMEs were analyzed by gas chromatography (GC; model 6890, Hewlett-Packard, Palo Alto, CA) on a CP-Sil 88 WCOT fused silica column (100 m × 0.25 mm i.d. × 0.2 $\mu$m film thickness; Chrompack, Middleburg, The Netherlands). The column was operated at 45 °C for 4 min and then temperature-programmed at 13 °C/min to 175 °C, held for 27 min, programmed at 4 °C/min to 215 °C, and finally held for 31 min; total run time was 86 min.[15] A flame ionization detector (FID) was used. GC−mass spectrometry (MS) analysis was performed on a Varian Saturn 2000 system running in default electron ionization mode (4 V axial bias and 1400 V multiplier) according to the method described by Karimi et al.[17] Samples were injected into the GC−MS system via split injection at 1:10. The injection volume was 1 $\mu$L. The mass spectrometer (5975C MSD) was equipped with an electron impact ion source (EI). All experiments were carried out in positive-ion mode. The source temperature was set at 230 °C, and the energy was 70 eV. The multiplier voltage was set to 900 V without solvent delay.

**Analysis of Tocopherols, Tocotrienols, and Carotenoids by HPLC.** Tocopherols from the extracts were separated and analyzed following a published procedure with slight modification on an Agilent Technology 1100 series HPLC system equipped with a Phenomenex silica column (250 × 4.6 mm, 5 $\mu$m, Torrance, CA), a diode array detector (DAD), and a fluorescence detector. $\alpha$-Tocopherol equivalents ($\alpha$-TE) was an expression based on the activity relative to the most active form of vitamin E. $\alpha$-TE is calculated from the formula $\alpha$-TE = ($\alpha$-T) + 0.5($\beta$-T) + 0.1($\gamma$-T) + 0.03($\delta$-T) + 0.3($\alpha$-T3) + 0.05($\beta$-T3) + 0.01($\gamma$-T3), where T = tocopherol and T3 = tocotrienol.[18]

Carotenoids in the extracts were identified and quantified by the same Agilent Technology 1100 series HPLC system as mentioned above, following the same method used by Zhang et al.[15] Separation was on a YMC C30 carotenoid column (250 × 4.6 mm, 5 $\mu$m) (Waters, Mississauga, ON) at 35 °C, and peaks were detected by DAD at 452 nm. The carotenoids were tentatively identified on the basis of matching retention time, similarity in elution order, and UV/vis spectra with those of the standards and data reported in the literature. All carotenoids were quantified on the basis of corresponding curves of lutein, zeaxanthin, $\beta$-carotene, and $\beta$-cryptoxanthin standards.

**Structural Identification and Confirmation by Liquid Chromatography–Mass Spectrometry.** Carotenoids tentatively identified as described above were confirmed by liquid chromatography (LC)–MS on a Dionex UHPLC UltiMate 3000 liquid chromatograph interfaced to an amaZon SL ion trap mass spectrometer (Bruker Daltonics, Billerica, MA).[19] UV/vis data were collected at 190–800 nm and the electrospray positive ionization (ESI + ve) mass spectrometric data were scanned from $m/z$ 50 to 1200. The capillary temperature was 220 °C and the source voltage was 4.50 kV. The chromatographic separation conditions for LC–MS were the same as those described for the HPLC-DAD analyses.

The MS conditions for vitamin E were the same as described for carotenoids. Selected ion monitoring (SIM) acquisition mode was used to help in the quantification of tocopherols, and the ions monitored were as follows: $m/z$ 429 for $\alpha$-tocopherol, $m/z$ 415 for $\beta$- and $\gamma$-tocopherol, and $m/z$ 401 for $\delta$-tocopherol.[20]

**Antioxidant Activity Assays.** The lipophilic extracts were dried under a nitrogen stream and then dissolved in 7% (% w) RMCD in acetone/water (1:1 v/v). The DPPH assay was carried out according to the procedures used by Zhang et al.[15] with minor modification: appropriately diluted samples or Trolox solutions were placed in wells of a 96-well plate (flat bottom, Nalge Nunc International, Denmark) and read at 517 nm by use of a Multiskan Spectrum microplate reader (EL 340, Bio-Tek Instruments Inc., Winooski, VT). The DPPH radical scavenging activity of extracts was calculated from the standard curve of Trolox ($r^2$ = 0.999) and expressed as micromoles of Trolox equivalents (TE) per gram dry weight of sample.

The ferric reducing antioxidant power (FRAP) assay followed procedures reported by Li et al.[21] Briefly, a total of 10 $\mu$L of properly diluted samples or L-ascorbic acid solutions (62.5, 125, 250, 500, 750, and 1000 $\mu$M) and 300 $\mu$L of freshly prepared FRAP reagent were added in a 96-well plate and incubated at room temperature throughout the reaction period. After 120 min, the absorbance was read at 593 nm against a reagent blank. The antioxidant activities were expressed as micromoles of ascorbic acid equivalent (AAE) per gram dry weight of sample ($r^2$ = 1.000).

Lipophilic oxygen radical absorbance capacity (ORAC) assay was conducted according to Zhang and others[15,22] with slight modifications. The lipophilic extracts and Trolox solutions were dissolved in RMCD solution as discussed before. The fluorescence (excitation/emission wavelength = 485/528 nm) was read every minute for 120 min or until it reached zero in a fluorescence plate reader equipped with an automatic thermostatic holder (PLX 800, Bio-Tek Instruments, Inc., Winooski, VT). A calibration curve was constructed by plotting the calculated differences of area under the fluorescein decay curve between blank and sample. The results were expressed as micromoles of Trolox equivalent per gram dry weight of quinoa sample ($r^2$ = 0.998).

**Statistical Analysis.** Results were expressed as mean value ± standard deviation of three independent extractions. One-way analysis of variance (ANOVA) was used to compare the means by use of Duncan's posthoc test. Comparison of assays was made by correlation and linear regression analysis. Differences were considered as significant at $p \leq 0.05$. All statistical analyses were performed with Statistics from SPSS (version 18.0, Chicago, IL).

## RESULTS AND DISCUSSION

**Fatty Acids.** The oil content and composition of the major fatty acids of quinoa and amaranth leaves are shown in Table 2. The oil yields of the quinoa leaves ranged from 3.95% to 4.18%, which was higher than that in amaranth leaves (2.13–3.59%). Fatty acids were over 80% in unsaturated form, mainly the two essential fatty acids C18:3n-3 ($\alpha$-linolenic acid), ranging between 35.1% in QL1 and 49.43% in AL12, followed by C18:2n-6 (linoleic acid, 11.36–18.38%), C16:0 (palmitic acid, 9.28–16.44%), and C18:1(9c) (oleic acid, 5.11–11.22%) in both quinoa and amaranth leaves. C16:1 (palmitoleic acid) and C18:0 (stearic acid) were present in relatively low levels compared to the foregoing fatty acids. This is different from the fatty acids in seeds of quinoa and amaranth, which contained more C18:2n-6 (33.56–52.0%) than C18:3n-3.[3,23]

Food data generated throughout the 20th century indicates that the ratio of $\omega$-3 to $\omega$-6 fatty acids has decreased from 1:1 to 1:30, much lower than the recommended ratio (1:2.3 to 1:4).[24,25] Diets having higher $\omega$-6 fatty acids such as C18:2n-6 have been linked to increased risk of prostate cancer, cardiovascular disease, and other chronic diseases,[26] whereas $\omega$-3 fatty acids such as C18:3n-3 have been shown positive effects on various cardiac disorders and many chronic illnesses.[27] Consequently, foods rich in $\omega$-3 fatty acids, such as fish oils and certain plant oils, are considered a healthier diet. The $\omega$-3/$\omega$-6 ratios of quinoa and amaranth leaves averaged 2.28–3.89, which is severalfold higher than the ideal ratio and much better than most vegetable oils.[28] Incorporation of these leaves into a diet can therefore compensate the unhealthy $\omega$-3/$\omega$-6 ratio.

**Carotenoids.** Leafy green vegetables and fruits have generated interest worldwide as they exhibit multiple benefits for the health of humans, particularly as a source of dietary vitamin A in developing countries.[29] The present study showed that carotenoid compositions in amaranth and quinoa leaves were similar but concentrations varied significantly among different cultivars of the same plant.

$\beta$-Carotene is an important lipid-soluble antioxidant that functions to protect cellular membranes by scavenging free radicals and as a photosensitizer by quenching triplet oxygen in biosynthesis.[30,31] As shown in Table 3, $\beta$-carotene was the primary carotenoid in both quinoa (302.97–484.86 $\mu$g/g DW) and amaranth leaves (115.19–394.31 $\mu$g/g DW). Lutein was the second dominant carotenoid in all of the samples, with amaranth leaves containing an average of 67.03 $\mu$g/g DW (33.31–136.78 $\mu$g/g DW) and quinoa leaves containing a higher average lutein content (83.65 $\mu$g/g DW) in a narrower range (65.93–103.39 $\mu$g/g DW). A similar trend was found for violaxanthin: quinoa leaves had a higher level at 67.34–93.20 $\mu$g/g DW than the amaranth leaves, which ranged between 21.24 and 80.78 $\mu$g/g DW. $\alpha$-Carotene was also found in both quinoa and amaranth leaves, albeit the average concentrations were 42.29 and 28.82 $\mu$g/g DW, respectively, ca. $^1/_9$ of that of $\beta$-carotene. Leaves richer in $\beta$-carotene were also found to have higher $\alpha$-carotene. Minor carotenoids including $\beta$-cryptoxanthin and zeaxanthin were also found in most quinoa and amaranth cultivars at much lower concentrations (Table 3).

Carotenoids play essential roles in human health. Carotenes such as $\alpha$- and $\beta$-carotenes are provitamin A nutrients, and xanthophylls such as lutein, zeaxanthin, and violaxanthin are strong antioxidants and provide significant protection against macular degeneration and other light-induced eye and skin damages.[32] The total carotenoid concentration as measured by HPLC and expressed in total carotenoid index (TCI) was 496–738 $\mu$g/g DW for quinoa leaves and 189–676 $\mu$g/g DW for amaranth leaves (Table 3), which were similar to those estimated by spectrophotometric methods.[3,1,33,34] Concentrations of individual carotenoids including $\beta$-carotene, lutein, violaxanthin, antheraxanthin, and $\beta$-cryptoxanthin in amaranth leaves have been studied; however, there was a lack of similar information for quinoa leaves, and the present study is the first report of compositional information for individual carotenoids.[30,35] It is also worth mentioning that the total and individual carotenoid concentrations in quinoa and amaranth leaves of the present study are similar to or even higher than many widely consumed leafy vegetables such as spinach and

**Table 2. Fatty Acid Composition in Leaves of Different Quinoa and Amaranth Cultivars**[a]

| | cultivar | | | | | | | | | |
|---|---|---|---|---|---|---|---|---|---|---|
| fatty acids | QL1 | QL2 | QL3 | QL4 | QL5 | QL6 | AL1 | AL2 | AL3 | AL4 |
| 10:1c | 0.89 ± 0.03 e | 0.76 ± 0.02 c | 0.65 ± 0.03 b | 0.69 ± 0.02 b | 0.66 ± 0.01 b | 0.66 ± 0.02 b | 0.91 ± 0.01 e | 1.50 ± 0.02 i | 0.58 ± 0.01 a | 1.85 ± 0.02 k |
| 10:1t | 0.53 ± 0.02 de | 0.54 ± 0.03 de | 0.50 ± 0.02 cd | 0.69 ± 0.02 f | 0.45 ± 0.02 c | 0.37 ± 0.01 b | 1.61 ± 0.02 g | 2.53 ± 0.03 j | 0.27 ± 0.01 a | 2.84 ± 0.04 k |
| 12:0 | 0.38 ± 0.01 c | 0.14 ± 0.01 a | 0.34 ± 0.02 bc | 0.47 ± 0.01 d | 0.37 ± 0.01 bc | 0.37 ± 0.01 bc | 0.65 ± 0.03 e | 0.89 ± 0.01 f | 0.30 ± 0.02 b | 1.38 ± 0.08 j |
| 11:1c | 0.66 ± 0.03 c | 0.63 ± 0.04 c | 0.56 ± 0.04 b | 0.68 ± 0.04 c | 0.53 ± 0.02 b | 0.49 ± 0.02 b | 0.98 ± 0.02 d | 1.61 ± 0.04 f | 0.36 ± 0.01 a | 2.40 ± 0.03 k |
| 12:1 | 1.05 ± 0.02 k | 0.90 ± 0.03 j | 0.78 ± 0.03 g | 0.79 ± 0.03 gh | 0.84 ± 0.04 i | 0.91 ± 0.03 j | 0.62 ± 0.01 d | 0.69 ± 0.03 f | 0.78 ± 0.01 g | 0.24 ± 0.02 b |
| 15:0 | 0.87 ± 0.02 j | 0.74 ± 0.01 h | 0.63 ± 0.05 f | 0.58 ± 0.03 e | 0.69 ± 0.02 g | 0.81 ± 0.04 i | 0.31 ± 0.02 d | 0.29 ± 0.01 d | 0.75 ± 0.01 h | 0.24 ± 0.03 bc |
| 14:1c | 1.30 ± 0.01 j | 1.07 ± 0.01 h | 0.88 ± 0.01 f | 0.78 ± 0.02 e | 0.98 ± 0.07 g | 1.22 ± 0.06 i | 0.37 ± 0.03 d | 0.32 ± 0.03 cd | 1.09 ± 0.04 h | 0.22 ± 0.03 ab |
| 16:0 | 16.44 ± 0.20 l | 12.64 ± 0.13 h | 11.84 ± 0.63 g | 12.46 ± 0.66 h | 11.67 ± 0.19 g | 11.01 ± 0.12 ef | 14.83 ± 0.39 k | 10.88 ± 0.15 de | 14.00 ± 0.31 j | 10.81 ± 0.34 cde |
| 16:1 | 1.36 ± 0.00 fg | 1.94 ± 0.05 i | 1.69 ± 0.41 h | 1.75 ± 0.32 hi | 1.67 ± 0.02 h | 1.95 ± 0.08 i | 1.68 ± 0.07 h | 1.44 ± 0.03 g | 1.09 ± 0.03 e | 0.76 ± 0.03 bc |
| 18:0 | 1.24 ± 0.04 b | 1.23 ± 0.06 b | 1.10 ± 0.06 ab | 1.09 ± 0.07 ab | 0.99 ± 0.05 a | 1.17 ± 0.07 b | 2.11 ± 0.04 d | 3.82 ± 0.04 j | 1.74 ± 0.04 c | 2.84 ± 0.09 i |
| 18:1(9c) | 6.62 ± 0.21 ef | 8.12 ± 0.11 g | 10.81 ± 0.59 j | 9.96 ± 0.42 i | 10.86 ± 0.36 j | 9.70 ± 0.28 i | 6.77 ± 0.08 f | 5.75 ± 0.25 bc | 11.22 ± 0.21 j | 6.30 ± 0.21 de |
| 18:1(11c) | 2.02 ± 0.08 i | 2.23 ± 0.07 j | 1.89 ± 0.07 h | 1.90 ± 0.12 h | 1.94 ± 0.08 hi | 1.97 ± 0.05 hi | 0.42 ± 0.03 bcd | 0.51 ± 0.01 def | 0.61 ± 0.02 g | 0.52 ± 0.02 def |
| 18: 1(12c) | 0.43 ± 0.02 h | 1.04 ± 0.01 k | 0.89 ± 0.02 j | 1.17 ± 0.04 l | 0.79 ± 0.01 i | 1.21 ± 0.04 l | 0.25 ± 0.05 defg | 0.40 ± 0.00 h | 0.23 ± 0.13 cdef | 0.21 ± 0.01 bcde |
| 18:2n-6 | 15.87 ± 0.51 gh | 16.14 ± 0.35 hi | 12.01 ± 0.33 ab | 12.67 ± 0.25 b | 11.46 ± 0.49 a | 12.20 ± 0.37 b | 14.93 ± 0.27 def | 12.48 ± 0.18 b | 18.38 ± 0.28 j | 14.22 ± 0.57 cde |
| 18:3n-3 | 35.10 ± 0.52 a | 40.81 ± 0.47 c | 42.25 ± 0.16 d | 40.11 ± 0.81 c | 43.77 ± 0.64 efg | 42.95 ± 0.81 de | 44.21 ± 0.56 fg | 44.82 ± 0.20 gh | 38.45 ± 0.77 b | 43.73 ± 0.41 ef |
| 21:0 | 1.22 ± 0.03 e | 0.39 ± 0.01 c | 0.71 ± 0.02 d | 0.74 ± 0.03 d | 0.79 ± 0.01 d | 0.81 ± 0.01 d | 0.10 ± 0.02 ab | 0.14 ± 0.01 ab | 0.17 ± 0.02 b | 0.05 ± 0.01 a |
| 22:0 | 1.77 ± 0.04 m | 1.06 ± 0.03 i | 1.20 ± 0.05 k | 1.27 ± 0.03 l | 1.12 ± 0.02 j | 1.10 ± 0.03 j | 0.35 ± 0.01 d | 0.30 ± 0.02 bc | 0.48 ± 0.01 h | 0.45 ± 0.01 gh |
| 24:1 | 1.07 ± 0.07 i | 0.66 ± 0.02 e | 0.92 ± 0.02 h | 0.82 ± 0.03 f | 0.82 ± 0.01 f | 0.88 ± 0.00 g | 0.53 ± 0.01 d | ND | ND | 0.12 ± 0.00 b |
| 26:0 | 0.08 ± 0.01 a | 0.09 ± 0.02 a | 0.07 ± 0.01 a | 0.07 ± 0.01 a | 0.08 ± 0.01 a | 0.14 ± 0.02 b | 1.33 ± 0.01 i | 0.35 ± 0.01 de | 3.16 ± 0.08 l | 0.44 ± 0.02 f |
| oil yield (%) | 3.99 ± 0.15 ij | 4.06 ± 0.19 ij | 4.02 ± 0.17 ij | 4.18 ± 0.16 j | 3.95 ± 0.15 i | 3.96 ± 0.15 i | 3.00 ± 0.02 cde | 2.85 ± 0.18 bc | 2.13 ± 0.02 a | 3.09 ± 0.10 def |
| $\omega 3/\omega 6$ ratio | 2.28 ± 0.04 a | 2.58 ± 0.02 b | 3.58 ± 0.08 h | 3.23 ± 0.00 g | 3.89 ± 0.10 i | 3.60 ± 0.04 h | 3.02 ± 0.00 ef | 3.65 ± 0.04 h | 2.83 ± 0.00 cd | 3.03 ± 0.04 ef |
| ∑SFA | 22.00 ± 0.35 j | 16.29 ± 0.25 ef | 15.89 ± 0.84 def | 16.68 ± 0.84 f | 15.71 ± 0.31 bcdef | 15.41 ± 0.30 bcde | 19.68 ± 0.52 h | 16.67 ± 0.25 f | 20.60 ± 0.49 i | 16.21 ± 0.58 ef |
| ∑MUFA | 15.93 ± 0.49 f | 17.89 ± 0.39 g | 19.58 ± 1.24 h | 19.23 ± 1.06 h | 19.54 ± 0.64 h | 19.36 ± 0.59 h | 14.14 ± 0.33 cd | 14.75 ± 0.44 cde | 16.23 ± 0.47 f | 15.46 ± 0.41 def |
| ∑PUFA | 50.97 ± 1.03 a | 56.95 ± 0.82 e | 54.26 ± 0.49 bc | 52.78 ± 1.06 b | 55.23 ± 1.13 bc | 55.15 ± 1.18 de | 59.14 ± 0.83 fg | 57.30 ± 0.38 e | 56.83 ± 1.05 de | 57.95 ± 0.98 ef |

| | cultivar | | | | | | | | | |
|---|---|---|---|---|---|---|---|---|---|---|
| fatty acid | AL5 | AL6 | AL7 | AL8 | AL9 | AL10 | AL11 | AL12 | AL13 | AL14 |
| 10:1c | 1.37 ± 0.02 g | 0.82 ± 0.03 d | 1.86 ± 0.01 k | 1.85 ± 0.01 k | 1.78 ± 0.03 j | 2.09 ± 0.09 l | 1.42 ± 0.03 h | 1.29 ± 0.03 f | 1.78 ± 0.04 j | 2.25 ± 0.01 m |
| 10:1t | 2.33 ± 0.07 i | 0.60 ± 0.0 e | 3.21 ± 0.08 n | 3.21 ± 0.07 n | 2.96 ± 0.01 l | 3.65 ± 0.12 o | 2.12 ± 0.01 h | 2.26 ± 0.02 i | 3.05 ± 0.03 m | 3.61 ± 0.01 o |
| 12:0 | 0.85 ± 0.01 f | 0.45 ± 0.07 d | 1.12 ± 0.03 h | 1.06 ± 0.03 gh | 1.02 ± 0.03 g | 1.23 ± 0.01 i | 0.99 ± 0.04 g | 0.82 ± 0.02 f | 1.02 ± 0.02 g | 1.67 ± 0.13 k |
| 11:1c | 1.37 ± 0.05 e | 0.66 ± 0.05 c | 2.00 ± 0.02 i | 1.98 ± 0.05 i | 1.86 ± 0.02 h | 2.23 ± 0.03 j | 1.78 ± 0.12 g | 1.41 ± 0.03 e | 1.91 ± 0.01 h | 2.84 ± 0.04 l |
| 12:1 | 0.45 ± 0.01 c | 1.09 ± 0.01 l | 0.81 ± 0.01 ghi | 0.70 ± 0.03 f | 0.82 ± 0.01 hi | 0.67 ± 0.02 ef | 0.19 ± 0.01 a | 0.65 ± 0.01 de | 0.70 ± 0.01 f | 0.46 ± 0.02 c |
| 15:0 | 0.19 ± 0.00 a | 0.85 ± 0.04 ij | 0.32 ± 0.01 d | 0.24 ± 0.00 bc | 0.31 ± 0.04 d | 0.22 ± 0.01 ab | 0.23 ± 0.02 ab | 0.29 ± 0.01 d | 0.28 ± 0.00 cd | 0.75 ± 0.04 h |



dx.doi.org/10.1021/jf5046377 | J. Agric. Food Chem. 2014, 62, 12610−12619

**Table 2. continued**

| | cultivar | | | | | | | | | |
|---|---|---|---|---|---|---|---|---|---|---|
| fatty acid | AL5 | AL6 | AL7 | AL8 | AL9 | AL10 | AL11 | AL12 | AL13 | AL14 |
| 14:1c | 0.18 ± 0.02 a | 1.25 ± 0.06 ij | 0.37 ± 0.05 d | 0.27 ± 0.02 bc | 0.38 ± 0.05 d | 0.23 ± 0.02 ab | 0.18 ± 0.04 a | 0.35 ± 0.02 d | 0.32 ± 0.07 cd | 0.27 ± 0.01 bc |
| 16:0 | 12.79 ± 0.41 hi | 14.02 ± 0.39 j | 9.65 ± 0.08 ab | 10.20 ± 0.11 bc | 9.90 ± 0.17 ab | 10.19 ± 0.15 bc | 13.35 ± 0.35 i | 9.28 ± 0.67 a | 11.58 ± 0.56 fg | 10.33 ± 0.44 bcd |
| 16:1 | 1.53 ± 0.01 gh | 1.08 ± 0.00 e | 0.67 ± 0.03 b | 1.02 ± 0.03 de | 0.85 ± 0.02 cd | 0.86 ± 0.01 bcd | 1.41 ± 0.03 g | 0.97 ± 0.04 cde | 0.40 ± 0.02 a | 1.19 ± 0.04 ef |
| 18:0 | 2.38 ± 0.22 efg | 1.77 ± 0.06 c | 2.63 ± 0.15 h | 2.43 ± 0.04 fg | 2.91 ± 0.14 i | 2.42 ± 0.04 fg | 2.25 ± 0.04 de | 2.48 ± 0.08 g | 2.31 ± 0.09 ef | 2.47 ± 0.07 g |
| 18:1(9c) | 6.84 ± 0.08 f | 8.82 ± 0.03 h | 6.71 ± 0.02 def | 6.11 ± 0.19 cd | 6.14 ± 0.03 cd | 5.11 ± 0.23 a | 5.48 ± 0.03 ab | 5.43 ± 0.33 ab | 5.82 ± 0.32 bc | 5.78 ± 0.05 bc |
| 18:1(11c) | 0.31 ± 0.02 a | 0.43 ± 0.03 bcde | 0.43 ± 0.03 bcde | 0.45 ± 0.03 cdef | 0.48 ± 0.02 cdef | 0.43 ± 0.01 bcde | 0.35 ± 0.01 ab | 0.40 ± 0.02 bc | 0.53 ± 0.02 def | 0.62 ± 0.01 g |
| 18:1(12c) | 0.19 ± 0.01 abcde | 0.12 ± 0.01 a | 0.26 ± 0.02 efg | 0.18 ± 0.01 abcd | 0.28 ± 0.00 fg | 0.19 ± 0.02 abcde | 0.19 ± 0.05 abcde | 0.31 ± 0.01 g | 0.15 ± 0.00 abc | 0.17 ± 0.02 abc |
| 18:2n-6 | 15.95 ± 0.61 ghi | 14.33 ± 0.12 cde | 14.62 ± 0.21 de | 14.15 ± 0.33 cd | 14.36 ± 0.02 cde | 13.76 ± 0.78 c | 16.58 ± 0.23 i | 15.42 ± 0.45 fg | 14.80 ± 0.31 def | 11.36 ± 0.04 a |
| 18:3n-3 | 46.04 ± 0.80 i | 41.88 ± 0.30 d | 46.05 ± 0.55 i | 47.26 ± 0.21 j | 45.54 ± 0.60 hi | 48.68 ± 0.91 k | 42.55 ± 1.00 d | 49.43 ± 0.28 k | 47.52 ± 0.49 j | 46.18 ± 0.63 i |
| 21:0 | 0.03 ± 0.00 a | 0.18 ± 0.03 b | 0.08 ± 0.02 ab | 0.03 ± 0.01 a | 0.05 ± 0.00 a | 0.04 ± 0.01 a | 0.14 ± 0.01 ab | 0.10 ± 0.01 ab | ND | 0.03 ± 0.01 a |
| 22:0 | 0.10 ± 0.00 a | 0.48 ± 0.01 h | 0.43 ± 0.01 fg | 0.35 ± 0.01 d | 0.34 ± 0.01 cd | 0.39 ± 0.02 e | 0.40 ± 0.01 ef | 0.33 ± 0.02 cd | 0.31 ± 0.03 cd | 0.27 ± 0.02 b |
| 24:1 | ND | ND | ND | ND | ND | ND | 0.16 ± 0.00 c | ND | ND | 0.08 ± 0.01 a |
| 26:0 | 1.42 ± 0.01 j | 3.09 ± 0.04 k | 0.70 ± 0.01 h | 0.49 ± 0.01 g | 0.49 ± 0.01 g | 0.34 ± 0.01 d | 0.49 ± 0.00 g | 0.48 ± 0.01 g | 0.39 ± 0.01 e | 0.30 ± 0.01 c |
| oil yield (%) | 2.87 ± 0.00 bc | 2.95 ± 0.00 cd | 3.02 ± 0.02 cde | 3.39 ± 0.06 g | 2.91 ± 0.03 bcd | 3.59 ± 0.13 h | 3.18 ± 0.01 ef | 3.25 ± 0.08 fg | 2.72 ± 0.03 b | 2.72 ± 0.04 b |
| $\omega 3/\omega 6$ ratio | 2.91 ± 0.06 de | 3.00 ± 0.01 ef | 3.21 ± 0.01 g | 2.72 ± 0.14 c | 3.23 ± 0.04 g | 2.73 ± 0.17 c | 2.58 ± 0.03 b | 3.09 ± 0.15 f | 3.26 ± 0.03 g | 4.11 ± 0.05 j |
| ∑SFA | 17.76 ± 0.65 g | 20.84 ± 0.64 i | 14.93 ± 0.31 bcd | 14.80 ± 0.21 b | 15.02 ± 0.40 bcd | 14.83 ± 0.25 bc | 17.85 ± 0.47 g | 13.78 ± 0.82 a | 15.89 ± 0.71 def | 15.82 ± 0.72 cdef |
| ∑MUFA | 14.57 ± 0.29 cd | 14.87 ± 0.23 cde | 16.32 ± 0.27 f | 15.77 ± 0.44 ef | 15.55 ± 0.19 def | 15.46 ± 0.55 def | 13.28 ± 0.43 ab | 13.07 ± 0.51 a | 14.66 ± 0.52 cd | 17.27 ± 0.22 g |
| ∑PUFA | 61.99 ± 1.41 ij | 56.21 ± 0.42 bc | 60.67 ± 0.76 ghi | 61.41 ± 0.54 huj | 59.90 ± 0.62 gh | 62.44 ± 1.69 j | 59.13 ± 1.23 fg | 64.85 ± 0.73 k | 62.32 ± 0.80 ij | 57.54 ± 0.67 ef |

[a]Values with different letters are significantly different from each other. Values are given as percentages, mean ± SD, $n = 3$, $p \leq 0.05$. ND = not detected. ∑SFA, sum of saturated fatty acids; ∑MUFA, sum of monounsaturated fatty acids; ∑PUFA, sum of polyunsaturated fatty acids



dx.doi.org/10.1021/jf5046377 | J. Agric. Food Chem. 2014, 62, 12610−12619

**Table 3. Concentrations of Carotenoids in Leaves of Different Quinoa and Amaranth Cultivars[a]**

| compd | QL1 | QL2 | QL3 | QL4 | QL5 | QL6 | AL1 | AL2 | AL3 | AL4 |
|---|---|---|---|---|---|---|---|---|---|---|
| violaxanthin | 72.10 ± 2.42 jk | 93.20 ± 2.46 m | 68.75 ± 2.02 hij | 79.26 ± 2.77 l | 74.37 ± 1.11 k | 67.34 ± 2.29 hi | 56.40 ± 1.75 e | 64.80 ± 2.75 gh | 49.09 ± 2.35 d | 21.24 ± 1.17 a |
| antheraxanthin | 4.51 ± 0.17 def | 4.67 ± 0.24 defg | 4.37 ± 0.12 def | 5.46 ± 0.21 hi | 5.00 ± 0.18 fghi | 4.89 ± 0.21 efgh | 4.53 ± 0.18 def | 5.07 ± 0.41 fghi | 4.15 ± 0.32 cde | 2.56 ± 0.09 a |
| 13-*cis*-lutein | 4.86 ± 0.72 i | 4.22 ± 0.13 h | 3.31 ± 0.16 fg | 3.67 ± 0.71 g | 3.75 ± 0.23 g | 2.98 ± 0.03 def | 2.32 ± 0.25 bc | 3.04 ± 0.19 ef | 2.14 ± 0.07 ab | 1.81 ± 0.16 a |
| lutein | 71.31 ± 2.53 e | 77.32 ± 1.21 f | 65.93 ± 1.48 d | 95.53 ± 3.47 h | 103.39 ± 2.66 i | 88.43 ± 2.97 g | 55.21 ± 4.13 c | 69.72 ± 2.08 de | 56.27 ± 3.40 c | 33.31 ± 0.84 a |
| zeaxanthin | 1.49 ± 0.36 cde | 2.22 ± 0.02 gh | 1.71 ± 0.08 ef | 1.98 ± 0.05 fg | 1.92 ± 0.10 f | 1.71 ± 0.04 ef | 1.47 ± 0.07 cde | 1.53 ± 0.03 cde | 1.28 ± 0.06 c | 0.35 ± 0.02 a |
| $\beta$-cryptoxanthin | 0.54 ± 0.03 a | 1.12 ± 0.02 c | 0.52 ± 0.03 a | 0.59 ± 0.01 a | 0.57 ± 0.04 a | 0.62 ± 0.05 a | 0.96 ± 0.04 bc | 0.62 ± 0.06 a | 1.11 ± 0.04 c | ND |
| 15-*cis*-$\beta$-carotene | 1.12 ± 0.03 a | 1.74 ± 0.03 bc | 0.99 ± 0.37 a | 1.70 ± 0.06 bc | 1.00 ± 0.07 a | 1.11 ± 0.07 a | 4.46 ± 0.17 def | 0.91 ± 0.07 a | 4.93 ± 0.31 efg | 2.04 ± 0.28 c |
| 13-*cis*-$\beta$-carotene | 4.72 ± 0.02 cd | 6.73 ± 0.01 f | 5.50 ± 0.07 e | 6.13 ± 0.63 ef | 5.93 ± 0.42 e | 5.40 ± 0.73 de | ND | 4.64 ± 0.59 c | ND | ND |
| $\alpha$-carotene | 37.83 ± 0.72 jkl | 61.98 ± 0.39 n | 35.87 ± 1.19 ijk | 39.06 ± 1.32 kl | 37.91 ± 1.39 jk | 41.07 ± 2.43 lm | 26.81 ± 1.35 cde | 32.37 ± 2.75 gh | 26.03 ± 1.44 cde | 12.72 ± 1.89 a |
| $\beta$-carotene | 302.97 ± 5.08 h | 484.86 ± 4.23 m | 309.20 ± 4.88 h | 340.89 ± 4.01 j | 328.01 ± 7.14 i | 353.27 ± 4.66 k | 255.61 ± 4.09 e | 276.26 ± 4.88 f | 250.82 ± 6.63 e | 115.19 ± 2.83 a |
| TCI | 501.45 ± 12.1 h | 738.00 ± 8.74 k | 496.15 ± 10.40 h | 574.27 ± 13.20 i | 561.90 ± 13.30 i | 566.82 ± 13.30 i | 407.77 ± 12.00 de | 458.96 ± 13.80 g | 395.82 ± 14.60 cd | 189.22 ± 7.28 a |
| compd | AL5 | AL6 | AL7 | AL8 | AL9 | AL10 | AL11 | AL12 | AL13 | AL14 |
| violaxanthin | 71.41 ± 2.32 ijk | 47.88 ± 3.59 e | 50.94 ± 3.29 d | 80.78 ± 2.45 l | 31.96 ± 3.32 b | 60.37 ± 2.41 ef | 69.57 ± 3.11 ij | 62.62 ± 1.92 fg | 38.76 ± 1.87 d | 38.28 ± 2.36 c |
| antheraxanthin | 5.26 ± 0.66 ghi | 4.25 ± 0.23 de | 4.14 ± 0.87 cd | 5.09 ± 0.46 fghi | 3.07 ± 0.25 ab | 4.37 ± 0.55 def | 5.62 ± 0.31 i | 4.40 ± 0.53 def | 3.54 ± 0.22 bc | 3.42 ± 0.46 b |
| *cis*-lutein | 2.43 ± 0.21 bc | 2.69 ± 0.18 cde | 2.73 ± 0.11 cde | 4.81 ± 0.24 i | 2.03 ± 0.15 ab | 3.59 ± 0.04 g | 3.45 ± 0.28 fg | 3.00 ± 0.06 def | 2.48 ± 0.09 bcd | 2.79 ± 0.29 cde |
| lutein | 56.51 ± 4.41 c | 54.54 ± 1.14 c | 56.07 ± 1.43 c | 136.78 ± 2.79 j | 41.45 ± 1.72 b | 87.89 ± 5.74 g | 69.24 ± 1.08 de | 87.89 ± 3.95 g | 51.63 ± 2.25 c | 72.02 ± 1.32 e |
| zeaxanthin | 1.97 ± 0.08 fg | 1.55 ± 0.03 cde | 1.71 ± 0.21 ef | 1.90 ± 0.09 f | 0.96 ± 0.06 b | 1.62 ± 0.03 de | 2.44 ± 0.42 h | 1.62 ± 0.04 de | 1.36 ± 0.01 cd | 3.16 ± 0.14 i |
| $\beta$-cryptoxanthin | 0.92 ± 0.03 b | 1.02 ± 0.03 bc | 1.01 ± 0.03 bc | 0.92 ± 0.04 b | ND | 0.56 ± 0.02 a | 1.10 ± 0.08 c | 0.56 ± 0.07 a | 0.92 ± 0.3 b | 3.10 ± 0.12 d |
| 15-*cis*-$\beta$-carotene | 4.97 ± 0.62 fg | 4.39 ± 0.28 d | 5.21 ± 0.37 g | 1.32 ± 0.06 ab | 0.88 ± 0.03 a | 0.84 ± 0.01 a | 5.78 ± 0.77 h | 0.84 ± 0.08 a | 4.42 ± 0.29 de | ND |
| 13-*cis*-$\beta$-carotene | 0.70 ± 0.10 a | ND | ND | 7.70 ± 0.68 g | 3.36 ± 0.31b | 4.39 ± 0.31 c | ND | 4.39 ± 0.25 c | ND | ND |
| $\alpha$-carotene | 28.50 ± 1.87 def | 25.41 ± 0.46 cd | 30.93 ± 0.94 fg | 41.92 ± 2.37 m | 24.69 ± 2.67 c | 35.57 ± 0.83 hij | 33.67 ± 1.83 ghi | 35.57 ± 1.65 hij | 28.95 ± 3.66 ef | 20.32 ± 1.68 b |
| $\beta$-carotene | 269.05 ± 2.78 f | 242.70 ± 6.41 d | 268.16 ± 4.38 e | 394.31 ± 6.12 l | 213.16 ± 9.43 c | 286.10 ± 6.52 g | 308.30 ± 3.11 h | 286.10 ± 2.24 g | 246.06 ± 7.83 d | 181.07 ± 5.78 b |
| TCI | 441.72 ± 13.10 fg | 384.40 ± 12.40 c | 420.90 ± 11.60 ef | 675.53 ± 15.3 j | 321.56 ± 17.90 b | 485.30 ± 16.50 h | 499.20 ± 11.00 h | 487.00 ± 10.80 h | 378.12 ± 16.50 c | 324.16 ± 12.20 b |

[a]Values with different letters are significantly different from each other. Values are given in micrograms per gram dry weight, as mean ± SD, $n = 3$, $p \leq 0.05$. ND = not detected. TCI, total carotenoids index.



dx.doi.org/10.1021/jf5046377 | J. Agric. Food Chem. 2014, 62, 12610−12619

Table 4. Concentrations of Tocopherols in Leaves of Different Quinoa and Amaranth Cultivars[a]

| cultivar | α-tocopherol | β-tocopherol | γ-tocopherol | δ-tocopherol | α-TE | total tocopherols index |
|---|---|---|---|---|---|---|
| | | | Quinoa | | | |
| QL1 | 5.79 ± 0.42 a | 1.02 ± 0.04 a | 1.02 ± 0.11 a | 1.53 ± 0.07 bcdef | 6.45 ± 0.40 a | 9.36 ± 0.36 a |
| QL2 | 44.71 ± 2.94 ef | 10.52 ± 0.89 gh | 3.02 ± 0.14 gh | 2.33 ± 0.25 hi | 50.34 ± 2.73 e | 60.58 ± 2.55 de |
| QL3 | 66.44 ± 3.98 lm | 19.86 ± 0.76 l | 2.90 ± 0.39 fgh | 0.53 ± 0.18 a | 76.68 ± 3.79 l | 89.73 ± 3.51 l |
| QL4 | 62.63 ± 1.34 kl | 15.79 ± 0.85 j | 2.44 ± 0.71 efg | 2.01 ± 0.59 fgh | 70.83 ± 1.17 k | 82.87 ± 1.88 k |
| QL5 | 67.40 ± 2.96 m | 22.13 ± 1.53 m | 2.52 ± 0.59 efg | 1.63 ± 0.33 defg | 78.77 ± 2.64 l | 93.68 ± 2.74 m |
| QL6 | 57.72 ± 0.46 j | 6.12 ± 0.58 c | 2.03 ± 0.11 bcde | 2.05 ± 0.18 fghi | 61.04 ± 0.41 j | 67.92 ± 0.75 ghi |
| avg | 50.78 ± 2.02 gh | 12.57 ± 0.78 i | 2.32 ± 0.34 defg | 1.68 ± 0.27 defg | 57.35 ± 1.86 huj | 67.36 ± 1.97 fgh |
| | | | Amaranth | | | |
| AL1 | 57.11 ± 1.05 ij | 7.61 ± 0.95 de | 1.40 ± 0.04 abc | 1.04 ± 0.05 abc | 61.09 ± 0.91 j | 67.16 ± 1.05 fgh |
| AL2 | 45.10 ± 0.63 ef | 11.54 ± 0.60 hi | 12.62 ± 0.72 p | 1.75 ± 0.46 efg | 52.18 ± 0.55 ef | 71.01 ± 1.56 |
| AL3 | 48.53 ± 3.74 fg | 15.50 ± 0.53 j | 1.53 ± 0.06 abcd | 1.34 ± 0.08 bcde | 56.47 ± 3.61 ghi | 66.90 ± 3.45 fgh |
| AL4 | 16.24 ± 1.78 b | 6.30 ± 0.91 cd | 9.99 ± 0.50 n | 1.50 ± 0.03 bcdef | 20.43 ± 1.59 b | 34.03 ± 1.63 b |
| AL5 | 57.11 ± 2.05 ij | 20.40 ± 1.37 l | 1.29 ± 0.32 ab | 1.14 ± 0.05 bcd | 67.47 ± 1.80 k | 79.94 ± 1.91 jk |
| AL6 | 50.06 ± 1.71 gh | 8.67 ± 0.94 ef | 10.85 ± 0.86 o | 2.39 ± 0.79 hi | 55.55 ± 1.51 fgh | 71.97 ± 2.28 i |
| AL7 | 59.34 ± 1.30 jk | 3.29 ± 0.86 b | 3.44 ± 0.64 hi | 0.55 ± 0.03 a | 61.35 ± 1.14 j | 66.62 ± 1.43 fg |
| AL8 | 32.71 ± 1.99 d | 6.38 ± 0.71 cd | 17.57 ± 0.35 q | 2.15 ± 0.03 hij | 37.72 ± 1.83 d | 58.81 ± 1.72 d |
| AL9 | 53.38 ± 2.54 hi | 4.01 ± 0.12 b | 4.80 ± 0.16 jk | 1.40 ± 0.34 bcde | 55.91 ± 2.50 fgh | 63.59 ± 2.29 ef |
| AL10 | 51.79 ± 0.87 gh | 15.79 ± 0.58 j | 2.44 ± 0.07 efg | 2.01 ± 0.19 fgh | 59.99 ± 0.76 ij | 72.03 ± 0.86 i |
| AL11 | 23.10 ± 2.51 c | 2.65 ± 0.14 b | 4.11 ± 0.19 ij | 0.98 ± 0.07 ab | 24.87 ± 2.47 c | 30.84 ± 2.34 b |
| AL12 | 42.73 ± 2.82 e | 18.32 ± 0.73 k | 7.24 ± 0.76 m | 2.60 ± 0.47 j | 52.69 ± 2.62 efg | 70.89 ± 2.50 hi |
| AL13 | 31.00 ± 0.78 d | 11.10 ± 0.92 gh | 2.15 ± 0.03 cdef | 1.23 ± 0.29 bcde | 36.80 ± 0.68 d | 45.48 ± 1.86 c |
| AL14 | 62.79 ± 5.14 kl | 7.41 ± 0.20 cde | 5.26 ± 0.47 k | 2.45 ± 0.09 hi | 67.09 ± 5.07 k | 77.91 ± 4.81 j |
| avg | 45.07 ± 2.07 ef | 9.93 ± 0.68 fg | 6.05 ± 0.37 l | 1.61 ± 0.21 cdefg | 50.69 ± 1.93 e | 62.66 ± 2.12 de |

[a]Values with different letters are significantly different from each other. Values are given in micrograms per gram dry weight, as mean ± SD, $n = 3$, $p \leq 0.05$. α-TE, α-tocopherol equivalent.

kale.[30,36,37] Our results confirm that both quinoa and amaranth leaves are excellent source of carotenoids, richer than in their own seeds.[3,38]

**Tocopherols.** All four tocopherol isomers (α, β, γ, and δ) but no tocotrienols were detected in quinoa and amaranth leaves (Table 4). The average total tocopherol content of both quinoa and amaranth was around 65 μg/g DW, similar to what was reported by others.[39] However, in addition to α-tocopherol, we also found β-, γ-, and δ-tocopherol in quinoa and amaranth leaves. The tocopherol profiles in amaranth and quinoa leaves were generally similar, with α-tocopherol being the predominant isomer (75.38% and 71.93% of total tocopherols on average in quinoa and amaranth, respectively), followed by β-, γ-, and δ-tocopherol. The concentration of α- and β-tocopherol in quinoa leaves was generally higher than in the leaves of amaranth, while γ-tocopherol was at lower levels in quinoa compared with amaranth. Even within the amaranth leaves, a few cultivars such as AL2, AL8, AL4, and AL6 showed exceptionally high γ-tocopherol content compared with all other plants. Both quinoa and amaranth leaves had low concentration of δ-tocopherol averaging from 1.61 to 1.68 μg/g DW. In terms of the α-TE values, the present results suggested that nearly all vitamin E activity of quinoa and amaranth leaves was from α-tocopherol (Table 4).

It is also worth mentioning that quinoa leaves had completely different tocopherol profiles than their respective seeds. Quinoa seeds contained overwhelmingly γ-tocopherol (>85%) and ca. 10% α-tocopherol, whereas the primary tocopherol in quinoa leaves was α-tocopherol followed by β-tocopherol (Table 4).[4] Similarly the tocopherol profile of amaranth leaves was different from that of amaranth seeds, which have been found to vary significantly from study to study.[3,39] As a source of vitamin E, quinoa and amaranth leaves contained nearly twice as much total tocopherols as those high-tocopherol grains, although compared to other common vegetable leaves, the concentration is lower.[12,20,30,40]

**Overall Evaluation.** Fatty acids, carotenoids, and vitamin E are three important lipophilic parameters to be evaluated for fruits, vegetables, and grains for their overall nutritional quality. However, these parameters have only been discussed separately in previous studies.[3,10,12,30] Food lipids are generally reported to include oil yield and major groups of saturated fatty acids (SFA), monounsaturated fatty acids (MUFA), and polyunsaturated fatty acids (PUFA), while carotenoids are mainly discussed under pro-vitamin A (β-carotene) and xanthophylls (lutein).[40] In terms of vitamin E, four tocopherols and four tocotrienols have been reported to have vitamin E activity, and α-tocopherol equivalency (α-TE) has been recently used as a measure for evaluation of the overall vitamin E activity of foods containing different vitamin E isoforms.[18,41]

Evaluation of the overall nutritional quality of the lipophilic components of a particular food or feed has been attempted by assessing the nutrients separately.[15,16] Such an attempt, however, lacks the cohesiveness that integrates all three lipophilic parameters; thus it is difficult to assess and compare the overall nutritional quality of different foods. A novel approach was then taken in the present study to establish a unified protocol for evaluation of the nutritional quality (NQ) of all lipophilic contents from the original data. Because the original data of the total carotenoids, α-TE and ω-3/ω-6 ratio were in different units, a linear scale transformation method was used to first transform all data to an arbitrary unit between 0 and 1 by use of the following equation:

$$\mathrm{NQ} = \frac{\mathrm{NQ}_i}{3\mathrm{NQ}_{\max}} \times 100$$

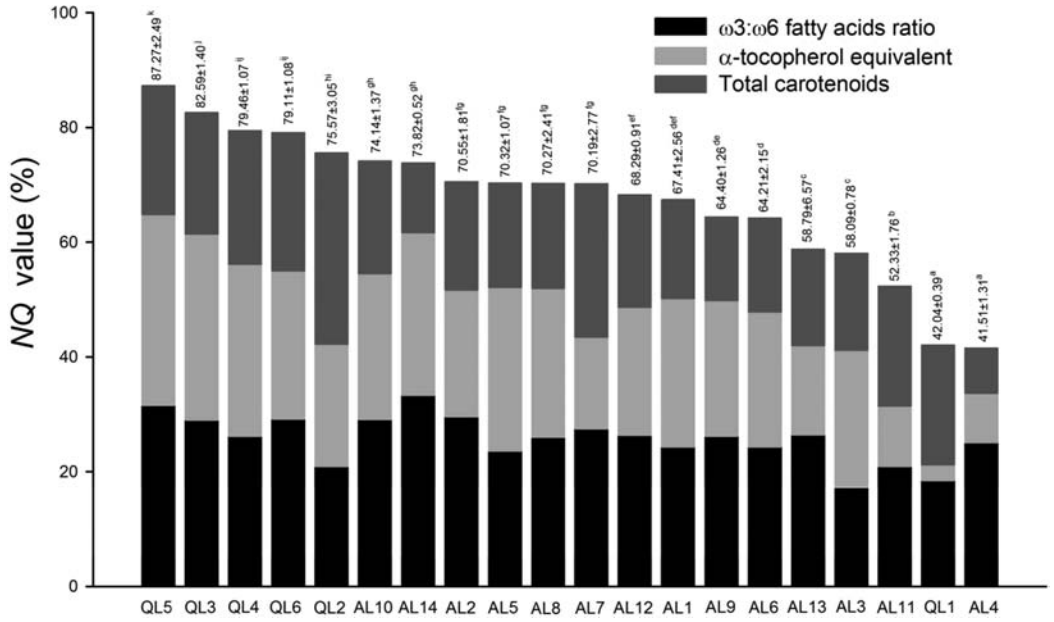


**Figure 1.** Nutritional quality (NQ) value of lipophilic extract from quinoa and amaranth leaves. Values with different letters are significantly different from each other. Values are given as mean ± SD, $n = 3$, $p \leq 0.05$.

where $NQ_{max}$ is the highest value of total carotenoids, $\alpha$-TE, or $\omega$-3/$\omega$-6 ratio and $NQ_i$ is the individual value of total carotenoids, $\alpha$-TE, or $\omega$-3/$\omega$-6 ratio of a particular sample. Three is the number of lipophilic parameters used for normalizing so that the final value can be presented as a percentage.

Figure 1 shows the ranking of overall nutritional quality by use of the above-mentioned method. The $\omega$-3/$\omega$-6 ratio was relatively consistent among all quinoa and amaranth samples, whereas the total carotenoids and $\alpha$-TE varied significantly. The overall nutritional quality was better in quinoa leaves than in amaranth. QL5 and QL3 ranked as the top two among all quinoa and amaranth leaves samples, while AL10 and AL14 had the highest NQ values among amaranth samples. No individual parameter among the three can represent the overall nutritional quality of a sample, and because of the inconsistency, no single individual nutrient group can therefore be used to evaluate or to rank the overall nutritional quality of the samples. Our approach overcomes this dilemma and provides a standardized method for assessment of the lipophilic merits of food.

**Antioxidant Activities.** The antioxidant activities of the lipophilic compounds in quinoa and amaranth leaves were assessed by DPPH, FRAP, and ORAC methods. In general, quinoa leaves had higher antioxidant activity than amaranth leaves (Figure 2). Due to the different mechanisms of in vitro antioxidant assays and the existence of different groups of lipophilic components of food, correlations between the concentration of individual nutrient groups and the different antioxidant activities have not been consistent.[10,15] For example, in a study on the lipophilic antioxidants of lentils, the total carotenoids correlated well with the antioxidant activity in the photochemiluminescence assay (PCL) but not with DPPH activity, whereas total tocopherols had a relatively good correlation with DPPH but no correlation with PCL activity. Studies on quinoa seeds also showed that different lipophilic components showed different degrees of correlation with different antioxidant activities.[5,15] In the present study, the correlation coefficients ($r^2$) between the $\omega$-3/$\omega$-6 ratio and DPPH, FRAP, or ORAC values were 0.594, 0.639, and 0.674, respectively; the $r^2$ values for $\alpha$-TE were 0.700, 0.741, and 0.786, respectively; and for carotenoids, they were all low at 0.428, 0.391, and 0.418, respectively. The $r^2$ values, however, were significantly improved by use of NQ value as an overall marker for food nutritional quality of lipophilic components. The overall NQ value of quinoa and amaranth leafy samples showed a strong positive correlation with all antioxidant activities, with $r^2$ = 0.848, 0.874, and 0.927, respectively, for DPPH, FRAP and ORAC activities.

Quinoa and amaranth seeds are emerging as the latest healthy foods on the market, and the demand for these pseudocereal grains has increased in recent years. As a result of the current effort being made to produce quinoa and amaranth seeds in Canada, additional value from the whole plants of these two crops has become an interesting subject of research. The present study examined the lipophilic bioactives in leaves of quinoa and amaranth plants. Three major lipophilic nutrients were analyzed, essential fatty acids, tocopherols, and carotenoids, and the total and individual compounds were identified and quantified for the first time. While the oil yield was only 3−4% of the leaves, both plants contained high-quality fatty acids with 50.97−62.32% PUFA which consisted of almost entirely 18:3n-3 and 18:2n-6. The ratio of these two essential fatty acids, that is, the $\omega$-3/$\omega$-6 ratio, ranged between 2.13 and 4.11, which was more favorable than other plant oils in terms of potential contribution to health benefits. Pro-vitamin A (mainly $\beta$-carotene and $\alpha$-carotene) and xanthophylls (mainly lutein and violaxanthin) were considered the major contributors to the carotenoids in leafy samples of both quinoa and amaranth. Different from the seeds, the tocopherols in quinoa and amaranth leaves were primarily $\alpha$- and $\beta$-tocopherol. A new approach to establishing a unified standard evaluation method for the overall nutritional quality of the lipophilic bioactives was proposed. This novel method calculates the NQ value of each sample by combining the relative quantities of the three major bioactive groups: carotenoids, $\alpha$-TE, and $\omega$-3/$\omega$-6 ratio. The NQ value correlated strongly with all antioxidant activities as measured by DPPH, FRAP, and ORAC assays, thus

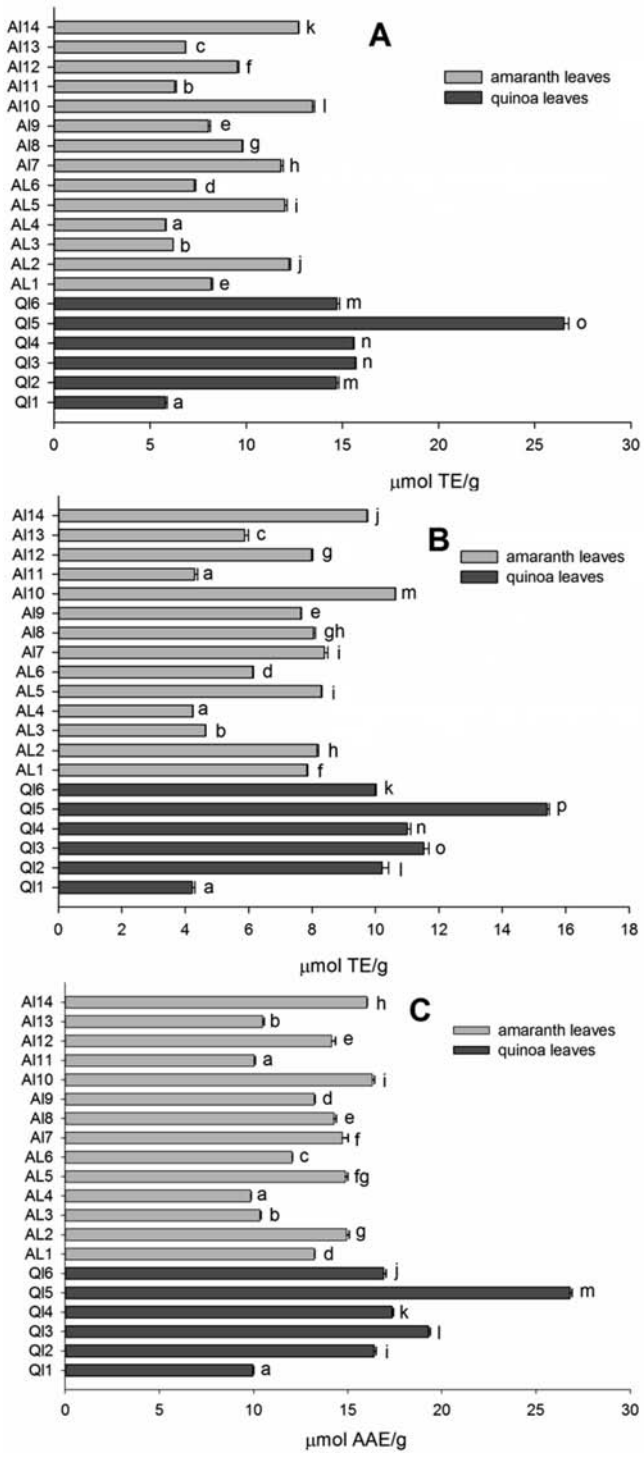


**Figure 2.** Antioxidant activities as measured by DPPH assay [A, top; micromoles of Trolox equivalent (TE) per gram dry weight], FRAP assay [B, middle; micromoles of ascorbic acid equivalent (AAE) per gram dry weight], and ORAC assay [C, bottom; micromoles of Trolox equivalent (TE) per gram dry weight]. Values with different letters are significantly different from each other. Values are given as mean ± SD, $n = 3$, $p \leq 0.05$.

overcoming the inconsistency between an individual group of bioactives, such as carotenoids alone, and the potential nutritional attribute, such as antioxidant activities. The NQ value is a better descriptor for nutritive quality of the lipophilic component of quinoa and amaranth leaves and can be potentially applied to all other foods. This new approach and the NQ value can be used for more precise comparison of the nutritive quality of lipophilic bioactives in foods. Information obtained in this study will aid the selection process of quinoa and amaranth cultivars adaptable to Ontario climate, and how the whole plant instead of the seeds can be used for the development of value-added products such as nutraceuticals and functional foods.

## AUTHOR INFORMATION


### Corresponding Authors

*Telephone +86-22-60601425; fax +86-22-60601341; e-mail lixihong606@163.com.

*Telephone +1-226-217-8108; fax +1-226-217-8180; e-mail rong.cao@agr.gc.ca.



### Funding

This project was supported by the A-Base Research (1004) of Agriculture & Agri-Food Canada (AAFC) and partially by the Ontario Soil and Crop Improvement Association and Katan Kitchens through Canadian Agricultural Adaptation Program (CAAP) (AAFC RBPI 2882).


### Notes

The authors declare no competing financial interest.

## ACKNOWLEDGMENTS


We thank Dr. Dyanne Brewer and Dr. Armen Charchoglyan, Advanced Analysis Center, University of Guelph, for providing mass spectra reports.


## REFERENCES


(1) Prakash, D.; Nath, P.; Pal, M. Composition, variation of nutritional contents in leaves, seed protein, fat and fatty acid profile of *Chenopodium* species. *J. Sci. Food Agric.* **1993**, *62*, 203−205.

(2) Thoufeek Ahamed, N.; Singhai, R. S.; Kulkarni, P. R.; Pal, M. A lesser-known grain, *Chenopodium quinoa*: Review of the chemical composition of its edible parts. *Food Nutr. Bull.* **1998**, *19*, 61−70.

(3) Venskutonis, P. R.; Kraujalis, P. Nutritional components of amaranth seeds and vegetables: A review on composition, properties, and uses. *Compr. Rev. Food Sci. Food Saf.* **2013**, *12*, 381−412.

(4) Tang, Y.; Li, X.; Zhang, B.; Chen, P. X.; Liu, R.; Tsao, R. Characterization of phenolics, betanins and antioxidant activities in seeds of three *Chenopodium quinoa* Willd. genotypes. *Food Chem.* **2015**, *166*, 380−388.

(5) Tang, Y.; Li, X.; Chen, P. X.; Zhang, B.; Hernandez, M.; Zhang, H.; Marcone, M. F.; Liu, R.; Tsao, R. Characterization of fatty acid, carotenoid, tocophenol/tocotrienol compositions and antioxidant activities in seeds of three *Chenopodium quinoa* Willd. genotypes. *Food Chem.* **2015**, *174*, 502−508.

(6) Amin, I.; Norazaidah, Y.; Hainida, K. I. E. Antioxidant activity and phenolic content of raw and blanched *Amaranthus* species. *Food Chem.* **2006**, *94*, 47−52.

(7) Li, H.; Deng, Z.; Liu, R.; Zhu, H.; Draves, J.; Marcone, M. F.; Sun, Y.; Tsao, R. Characterization of phenolics, betacyanins and antioxidant activities of the seed, leaf, sprout, flower and stalk extracts of three *Amaranthus* species. *J. Food Compos. Anal.* **2015**, *37*, 75−81.

(8) Edward, J. W. The Inca's ancient answer to food shortage. *Nature* **1978**, *272*, 486.

(9) Yin, J.; Zhang, H.; Ye, J. Traditional Chinese medicine in treatment of metabolic syndrome. *Endocr. Metab. Immune Disord. Drug Targets* **2008**, *8*, 99.

(10) Conforti, F.; Marrelli, M.; Carmela, C.; Menichini, F.; Valentina, P.; Uzunov, D.; Statti, G. A.; Duez, P.; Menichini, F. Bioactive phytonutrients (omega fatty acids, tocopherols, polyphenols), in vitro inhibition of nitric oxide production and free radical scavenging

activity of non-cultivated Mediterranean vegetables. *Food Chem.* **2011**, *129*, 1413−1419.
(11) Havaux, M.; Eymery, F.; Porfirova, S.; Rey, P.; Dörmann, P. Vitamin E protects against photoinhibition and photooxidative stress in *Arabidopsis thaliana*. *Plant Cell* **2005**, *17*, 3451−3469.
(12) Guzman, I.; Yousef, G. G.; Brown, A. F. Simultaneous extraction and quantitation of carotenoids, chlorophylls, and tocopherols in *Brassica* vegetables. *J. Agric. Food Chem.* **2012**, *60*, 7238−7244.
(13) Saldeen, T.; Li, D.; Mehta, J. L. Differential effects of $\alpha$- and $\gamma$-tocopherol on low-density lipoprotein oxidation, superoxide activity, platelet aggregation and arterial thrombogenesis. *J. Am. Coll. Cardiol.* **1999**, *34*, 1208−1215.
(14) Bramley, P. M.; Elmadfa, I.; Kafatos, A.; Kelly, F. J.; Manios, Y.; Roxborough, H. E.; Schuch, W.; Sheehy, P. J. A.; Wagner, K. H. Vitamin E. *J. Sci. Food Agric.* **2000**, *80*, 913−938.
(15) Zhang, B.; Deng, Z.; Tang, Y.; Chen, P.; Liu, R.; Ramdath, D. D.; Liu, Q.; Hernandez, M.; Tsao, R. Fatty acid, carotenoid and tocopherol compositions of 20 Canadian lentil cultivars and synergistic contribution to antioxidant activities. *Food Chem.* **2014**, *161*, 296−304.
(16) Elgersma, A.; Søegaard, K.; Jensen, S. K. Fatty acids, $\alpha$-tocopherol, $\beta$-carotene, and lutein contents in forage legumes, forbs, and a grass−clover mixture. *J. Agric. Food Chem.* **2013**, *61*, 11913−11920.
(17) Karimi, E.; Briens, C.; Berruti, F.; Moloodi, S.; Tzanetakis, T.; Thomson, M. J.; Schlaf, M. Red mud as a catalyst for the upgrading of hemp-seed pyrolysis bio-oil. *Energy Fuels* **2010**, *24*, 6586−6600.
(18) Ronald, E. Nutrition and health implications of vitamin E. In *Vitamin E*; CRC Press: Boca Raton, FL, 2004; pp 39−88.
(19) Abdel-Aal, E.-S. M.; Young, J. C.; Rabalski, I.; Hucl, P.; Fregeau-Reid, J. Identification and quantification of seed carotenoids in selected wheat species. *J. Agric. Food Chem.* **2007**, *55*, 787−794.
(20) Bustamante-Rangel, M.; Delgado-Zamarreño, M. M.; Sánchez-Pérez, A.; Carabias-Martínez, R. Determination of tocopherols and tocotrienols in cereals by pressurized liquid extraction−liquid chromatography−mass spectrometry. *Anal. Chim. Acta* **2007**, *587*, 216−221.
(21) Li, H.; Deng, Z.; Zhu, H.; Hu, C.; Liu, R.; Young, J. C.; Tsao, R. Highly pigmented vegetables: Anthocyanin compositions and their role in antioxidant activities. *Food Res. Int.* **2012**, *46*, 250−259.
(22) Li, L.; Tsao, R.; Yang, R.; Kramer, J. K. G.; Hernandez, M. Fatty acid profiles, tocopherol contents, and antioxidant activities of heartnut (*Juglans ailanthifolia* var. *cordiformis*) and Persian walnut (*Juglans regia* L.). *J. Agric. Food Chem.* **2007**, *55*, 1164−1169.
(23) Ruales, J.; Nair, B. M. Content of fat, vitamins and minerals in quinoa (*Chenopodium quinoa*, Willd) seeds. *Food Chem.* **1993**, *48*, 131−136.
(24) Kris-Etherton, P.; Taylor, D. S.; Yu-Poth, S.; Huth, P.; Moriarty, K.; Fishell, V.; Hargrove, R. L.; Zhao, G.; Etherton, T. D. Polyunsaturated fatty acids in the food chain in the United States. *Am. J. Clin. Nutr.* **2000**, *71*, 179S−188S.
(25) Blasbalg, T. L.; Hibbeln, J. R.; Ramsden, C. E.; Majchrzak, S. F.; Rawlings, R. R. Changes in consumption of omega-3 and omega-6 fatty acids in the United States during the 20th century. *Am. J. Clin. Nutr.* **2011**, *93*, 950−962.
(26) Simopoulos, A. P. The importance of the omega-6/omega-3 fatty acid ratio in cardiovascular disease and other chronic diseases. *Exp. Biol. Med.* **2008**, *233*, 674−688.
(27) Saravanan, P.; Davidson, N. C.; Schmidt, E. B.; Calder, P. C. Cardiovascular effects of marine omega-3 fatty acids. *Lancet* **2010**, *376*, 540−550.
(28) Dubois, V.; Breton, S.; Linder, M.; Fanni, J.; Parmentier, M. Fatty acid profiles of 80 vegetable oils with regard to their nutritional potential. *Eur. J. Lipid Sci. Technol.* **2007**, *109*, 710−732.
(29) Sangeetha, R. K.; Baskaran, V. Carotenoid composition and retinol equivalent in plants of nutritional and medicinal importance: Efficacy of $\beta$-carotene from *Chenopodium album* in retinol-deficient rats. *Food Chem.* **2010**, *119*, 1584−1590.
(30) Xiao, Z.; Lester, G. E.; Luo, Y.; Wang, Q. Assessment of vitamin and carotenoid concentrations of emerging food products: Edible microgreens. *J. Agric. Food Chem.* **2012**, *60*, 7644−7651.
(31) Asensi-Fabado, M. A.; Munné-Bosch, S. Vitamins in plants: Occurrence, biosynthesis and antioxidant function. *Trends Plant Sci.* **2010**, *15*, 582−592.
(32) Stahl, W.; Sies, H. Bioactivity and protective effects of natural carotenoids. *Biochim. Biophys. Acta, Mol. Basis Dis.* **2005**, *1740*, 101−107.
(33) Bhargava, A.; Shukla, S.; Ohri, D. *Chenopodium quinoa*—An Indian perspective. *Ind. Crops Prod.* **2006**, *23*, 73−87.
(34) Bhargava, A.; Shukla, S.; Ohri, D. Genetic variability and interrelationship among various morphological and quality traits in quinoa (*Chenopodium quinoa* Willd.). *Field Crops Res.* **2007**, *101*, 104−116.
(35) Wills, R. B. H.; Rangga, A. Determination of carotenoids in Chinese vegetables. *Food Chem.* **1996**, *56*, 451−455.
(36) Lefsrud, M.; Kopsell, D.; Sams, C.; Wills, J.; Both, A. J. Dry matter content and stability of carotenoids in kale and spinach during drying. *HortScience* **2008**, *43*, 1731−1736.
(37) Rodriguez-Amaya, D. B.; Kimura, M.; Godoy, H. T.; Amaya-Farfan, J. Updated Brazilian database on food carotenoids: Factors affecting carotenoid composition. *J. Food Comp. Anal.* **2008**, *21*, 445−463.
(38) Lim, T. K. *Chenopodium quinoa*. In *Edible Medicinal and Non-Medicinal Plants*; Springer: Dordrecht, The Netherlands, 2013; pp 115−131.
(39) Antognoni, F.; Faudale, M.; Poli, F.; Biondi, S. Methyl jasmonate differentially affects tocopherol content and tyrosine amino transferase activity in cultured cells of *Amaranthus caudatus* and *Chenopodium quinoa*. *Plant Biol.* **2009**, *11*, 161−169.
(40) Ryan, E.; Galvin, K.; O'Connor, T. P.; Maguire, A. R.; O'Brien, N. M. Phytosterol, squalene, tocopherol content and fatty acid profile of selected seeds, grains, and legumes. *Plant Foods Hum. Nutr.* **2007**, *62*, 85−91.
(41) Alvarez-Jubete, L.; Holse, M.; Hansen, Å.; Arendt, E. K.; Gallagher, E. Impact of baking on vitamin E content of pseudocereals amaranth, quinoa, and buckwheat. *Cereal Chem.* **2009**, *86*, 511−515.

the amount of cholesterol absorbed and transported to the blood.[20] Furthermore, the conformation and aggregation state of pectin in aqueous solutions may be altered due to its interactions with certain gastrointestinal components, which leads to changes in solution rheology that might affect lipid digestion, for example, by altering gastric emptying times or the mass transport of digestive enzymes.[3] Pectin may also directly interact with other components in the gastrointestinal tract such as $CaCl_2$, NaCl, and digestive enzymes.[9,21−23] Finally, pectin is known to promote depletion flocculation of lipid droplets, which may reduce lipid digestion by protecting them from attack by lipolytic enzymes.[24,25]

Pectin ingredients obtained from different natural sources using different isolation and processing methods may vary widely in their molecular and physicochemical characteristics, such as backbone length, electrical charge, hydrophobicity, surface activity, conformation, self-association, viscosity, and binding capacity.[17] In addition, the molecular and functional characteristics of pectins may be altered appreciably in response to changes in solution and environmental conditions such as pH, composition, ionic strength, and temperature.[14,15,18,19] For this reason, the study of the nature of the interactions that pectin may have with the components of the gastrointestinal tract is important in understanding the effect of pectin on digestive processes. An improved understanding of the origin and nature of these interactions would lead to the design of functional foods with improved nutritional, physicochemical, and sensory properties.

In this study, isothermal titration calorimetry (ITC) was used to study the interactions between pectin and gastrointestinal components (bile salts, pancreatic lipase, $CaCl_2$, and NaCl). ITC measures the heat absorbed or evolved when one solution is titrated into another solution.[26−28] Previous studies have shown that ITC is an extremely valuable tool for studying chemical interactions of polysaccharides with other molecules because it provides valuable data concerning binding enthalpies, critical aggregation concentrations, and binding stoichiometries.[29,30] In addition, electrophoresis, turbidity, and microstructural observations were used to provide additional information about the nature of the interactions between pectin and gastrointestinal components. The results of this study may aid the rational design of functional foods designed to improve human health and wellness by controlling lipid digestion within the gastrointestinal tract.

## MATERIALS AND METHODS

**Chemicals.** Corn oil was purchased from a commercial food supplier (Mazola, ACH Food Co. Inc., Memphis, TN, USA) and stored at 4 °C until use. The manufacturer reported that this oil contained approximately 14, 29, and 57% (w/w) of saturated, monounsaturated, and polyunsaturated fatty acids, respectively. Commercial powdered high-methoxyl pectin (Genu Pectin (Citrus), USP/100) was kindly donated by CP Kelco (Lille Skensved, Denmark) and was used without further purification. The manufacturer reported that the powdered pectin ingredient contained 6.9% moisture, 89.0% galacturonic acid, and 8.6% methoxyl groups, with a degree of esterification of approximately 62%. The average molecular weight was reported to be 200 kDa. Lipase from porcine pancreas (type II, L3126, triacylglycerol hydrolase EC 3.1.1.3), bile extract (porcine, B8631), mucin from porcine stomach (type II, M2378, bound sialic acid ≤ 1.2%), and pepsin A from porcine gastric mucose (P7000, endopeptidase EC 3.4.23.1, activity ≥ 250 units/mg solid) were purchased from Sigma-Aldrich Chemical Co. (St. Louis, MO, USA). The supplier reported that the lipase activity was 100−400 units/mg protein (using olive oil) and 30−90 units/mg protein (using triacetin) for 30 min of incubation (1 unit of lipase activity was defined as the amount of enzyme required for the release of 1 μequiv of fatty acid from either triacetin (pH 7.4) or olive oil (pH 7.7) in 1 h at 37 °C). The composition of the bile extract was reported as 49% (w/w) total bile salt (BS), containing 10−15% glycodeoxycholic acid, 3−9% taurodeoxycholic acid, 0.5−7% deoxycholic acid, 1−5% hyodeoxycholic acid, and 0.5−2% cholic acid; 5% (w/w) phosphatidylcholine (PC); $Ca^{2+}$ ≤ 0.06% (w/w); critical micelle concentration of bile extract 0.07 ± 0.04 mM; and mole ratio of BS to PC being around 15:1. All other chemicals were purchased from Sigma-Aldrich Chemical Co. Double-distilled water was used to prepare all solutions.

**Simulated Gastrointestinal Studies.** *Solution and Emulsion Preparation.* Pectin stock solution (4% w/w) was prepared by dispersing 4 g of powdered pectin into 96 g of 5 mM phosphate buffer solution (pH 7.0). The resulting solution was stirred at 800 rpm for 12 h (overnight) at room temperature to ensure complete dispersion and dissolution. Pectin stock solution was then adjusted to pH 7 and equilibrated for 10 min before analysis.

A stock emulsion was prepared by mixing 20% (w/w) corn oil and 80% (w/w) buffered emulsifier solution (5 mM phosphate buffer, pH 7, containing 2.5% (w/w) Tween 80) together for 5 min using a biohomogenizer (speed 2, model MW140/2009-5, Biospec Products Inc., ESGC, Switzerland). The resulting coarse emulsion was then passed five times through a high-pressure homogenizer (microfluidizer M-110L processor, Microfluidics Inc., Newton, MA, USA) operating at 11000 psi (75.8 MPa) to reduce the particle size further.

Pectin−emulsion mixtures were then prepared by mixing stock emulsion (containing 20% (w/w) corn oil) with pectin stock solution (containing 4% (w/w) pectin) to obtain systems of various compositions: 2% (w/w) corn oil and 0.2−3.6% (w/w) pectin. The pectin−emulsion mixtures were then stirred with a high-shear mixer (Fisher Steadfast Stirrer, model SL-1200, Fisher Scientific, Pittsburgh, PA, USA) at 1000 rpm and stored overnight at room temperature. The pectin−emulsion mixtures were characterized to obtain the initial phase, prior to subjection to the in vitro gastrointestinal model.

*Simulated Gastrointestinal Tract Model.* Each emulsion sample (initial phase) was passed through a simulated in vitro gastrointestinal tract that consisted of oral, gastric, and intestinal phases. This method is based on a static model utilized in previous studies.[31,32]

Simulated saliva fluid (SSF, pH 6.8) containing 3% (w/w) mucin was prepared according to the composition shown in Table 1. Each emulsion (initial phase) was mixed with SSF (ratio 1:1 w/w) to obtain a mixture containing 1% (w/w) corn oil and 0.1−1.8% (w/w) pectin. The simulated oral phase consisted of a conical flask containing an emulsion−SSF mixture incubated at 37 °C with continuous shaking at 100 rpm for 10 min in a temperature-controlled air incubator (Excella E24 Incubator Shaker, New Brunswick Scientific, New Brunswick, NJ, USA). The mixture resulting from processing of the initial emulsions in the oral phase (bolus) was used in the gastric phase.

**Table 1. Chemical Composition of Simulated Saliva Fluid (SSF) Used To Simulate Oral Conditions**

| compound | chemical formula | concentration[a] (g/L) |
|---|---|---|
| sodium chloride | NaCl | 1.594 |
| ammonium nitrate | $NH_4NO_3$ | 0.328 |
| potassium dihydrogen phosphate | $KH_2PO_4$ | 0.636 |
| potassium chloride | KCl | 0.202 |
| potassium citrate | $K_3C_6H_5O_7{\cdot}H_2O$ | 0.308 |
| uric acid sodium salt | $C_5H_3N_4O_3Na$ | 0.021 |
| urea | $H_2NCONH_2$ | 0.198 |
| lactic acid sodium salt | $C_3H_5O_3Na$ | 0.146 |
| porcine gastric mucin (type II) | | 30 |

[a]The SSF was prepared in double-distilled water and then pH 6.8 was adjusted.

Simulated gastric fluid (SGF) was prepared by adding 2 g of NaCl, 7 mL of concentrated HCl (37% w/w), and 3.2 g of pepsin A (from porcine gastric mucose, 250 units/mg) to a flask, then diluting the mixture with double-distilled water to a volume of 1 L, and finally adjusting the pH to 1.2 using 1 M HCl. Samples from the oral phase (bolus) were mixed with SGF (ratio 1:1 w/w) so that the final mixture contained 0.5% (w/w) corn oil and 0.05−0.9% (w/w) pectin. This mixture was then adjusted to pH 2.5 using 1 M NaOH and incubated at 37 °C with continuous shaking at 100 rpm for 2 h. The mixture resulting from processing of the emulsions in the gastric phase (chyme) was used in the intestinal phase.

Samples obtained from the gastric phase (20 mL) were incubated for 2 h at 37 °C in a simulated small intestine fluid (SIF) consisting of 2.5 mL of pancreatic lipase (24 mg/mL), 3.5 mL of bile extract solution (54 mg/mL), and 1.5 mL of salt solution containing 0.25 M $CaCl_2$ and 3 M NaCl, to obtain a final composition in the reaction vessel of 0.36% (w/w) corn oil and 0.05−0.65% (w/w) pectin. The free fatty acids (FFA) released were monitored by determining the amount of 0.1 M NaOH needed to maintain a constant pH 7.0 within the reaction vessel using an automatic titration unit (pH stat titrator, 835 Titrando, Metrohm USA, Inc.). All components were dissolved in 5 mM phosphate buffer solution (pH 7) before use. Lipase addition and initialization of the titration program were carried out only after the addition of all predissolved ingredients and balancing the pH to 7. The volume of 0.1 M NaOH added to the emulsion was recorded over time and used to calculate the FFAs generated by lipolysis. The amount of FFAs released was calculated using the equation

$$\mathrm{FFA\ (\%\ w/w)} = 100 \times \left( \frac{V_{\mathrm{NaOH}}\ \mathrm{(L)} \times C_{\mathrm{NaOH}}\ \mathrm{(M)} \times \mathrm{MW_{lipid}\ (g/mol)}}{2 \times w_{\mathrm{lipid}}\ \mathrm{(g)}} \right) \quad (1)$$

where $C_{\mathrm{NaOH}}$ is the concentration of the sodium hydroxide (0.1 M), $\mathrm{MW_{lipid}}$ is the average molecular weight of corn oil (872 g/mol), $w_{\mathrm{lipid}}$ is the initial weight of corn oil in the intestinal phase (0.1 g), and $V_{\mathrm{NaOH}}$ is the volume of NaOH (L) titrated into the reaction vessel to neutralize the FFA released, assuming that all triacylglycerols are hydrolyzed in two molecules of FFA and one molecule of monoacylglycerol. Titration blanks were performed by inactivating lipase in boiling water for 15 min prior to initialization of the titration program.

*Creaming Stability Measurements of Initial Emulsions.* Ten milliliters of emulsions (initial phase) was transferred into a test tube (internal diameter = 15 mm, height = 125 mm), tightly sealed with a plastic cap, and then stored at room temperature for 24 h, after which appreciable phase separation into an opaque layer at the top, a turbid layer in the middle, and a transparent layer at the bottom was observed in some of the systems. We defined the serum layer to be the sum of the turbid and transparent layers. The total height of the emulsion ($H_E$) and the height of the serum layer ($H_S$) were measured using a laser vertical profiling system (Turbiscan Classic MA2000, Formulaction, Wynnewood, PA, USA). The extent of creaming was then characterized by the creaming index (CI), defined as $\mathrm{CI} = 100 \times (H_S/H_E)$. The creaming index provided indirect information about droplet aggregation, because an increase in particle size (e.g., due to flocculation) leads to faster creaming (provided the droplet concentration is not too high).

**Interaction of Pectin with Gastrointestinal Components.** *Solution Preparation.* Stock solutions of 0.9% (w/w) pectin, 2.7% (w/w) bile salts, and 1.1% (w/w) lipase were individually prepared by dispersing them in 5 mM phosphate buffer solution (pH 7) at room temperature for 12 h (overnight), to ensure their complete dispersion and dissolution. Salt solutions consisting of 55 mM $CaCl_2$ or 545 mM NaCl were prepared freshly before each experiment. A stock solution containing a mixture of all the above components at the same initial concentrations as in their individual solutions was also prepared. This stock solution was referred to as having a relative concentration of "100%" of the digestive components. A series of mixtures containing lower amounts of the digestive components was prepared by diluting the stock solution with buffer solution.

To establish the interaction of pectin with specific gastrointestinal components, individual solutions of $CaCl_2$, NaCl, lipase, bile salts, and the mixture of all components were titrated into either buffer solution (blank) or pectin solution at 37 °C. Twenty-nine 100 μL aliquots of individual solutions containing 2.7% (w/w) bile salts, 1.1% (w/w) lipase, 55 mM $CaCl_2$, 545 mM NaCl, or the mixture of all components (100% relative concentration) were added sequentially into a test tube containing 14.5 mL of either buffer (5 mM phosphate buffer, pH 7) or 0.9% (w/w) pectin solutions. Turbidity, ζ-potential, and microstructure (observed by optical microscopy) of these solutions were then characterized throughout the titration process.

*Solution Characterization.* Optical turbidity of the solutions was determined by measuring their absorbance at 600 nm ($\Delta\tau = A_{600\ \mathrm{nm}}$) using a UV−visible spectrophotometer (Ultrospec 3000 pro Pharmacia Biotech, Biochrom Ltd., Cambridge, UK) at 37 °C. The samples were contained within 1 cm path length optical cells, and buffer solution was used as a control. The change in turbidity was defined as $\Delta\tau = \tau_{\mathrm{pectin}} - \tau_{\mathrm{buffer}}$. Triplicate measurements of turbidity were carried out on each sample.

The electrical charge (ζ-potential) of the solutions was determined using a particle microelectrophoresis instrument (Zetasizer NanoSeries, Malvern Instruments Ltd., Worcestershire, UK). Solutions were injected into the measurement chamber and equilibrated for 120 s, and then the ζ-potential was determined by measuring the direction and velocity that the particles moved in the applied electric field. Each individual ζ-potential measurement was calculated from the average of 20 continuous readings made per sample. The ζ-potential was recorded at each pH after 60 s of equilibrium.

The microstructure of the solutions was characterized by optical microscopy. An optical microscope (C1 Digital Eclipse, Niko, Tokyo, Japan) with a 60× objective lens was used to capture images of the solutions. Solutions were gently stirred to form a homogeneous mixture without introducing any air bubbles. A small aliquot of the solutions (5 μL) was then transferred to a glass microscope slide and covered with a glass coverslip. The coverslip was fixed to the slide using nail polish to avoid evaporation. A small amount of immersion oil (type A, Nikon, Melville, NY, USA) was placed on the top of the coverslip. All optical images were taken using a digital camera and then characterized using the instrument software (EZ CS1 version 3.8, Nikon).

*Isothermal Titration Calorimetry Measurements.* An ITC instrument (Microcalorimeter VP-ITC, MicroCal Inc., Northampton, MA, USA) was used to measure the enthalpy ($\Delta H$) resulting from titration of individual solutions of $CaCl_2$, NaCl, lipase, bile salts, and a mixture of all components (100% relative concentration) into either buffer solution (blank) or pectin solution. Twenty-nine 10 μL aliquots of individual solutions of 2.7% (w/w) bile salts, 1.1% (w/w) lipase, 55 mM calcium chloride, 545 mM sodium chloride, or a mixture of all components (100% relative concentration) were injected sequentially into a 1450 μL titration cell initially containing either buffer (5 mM phosphate buffer, pH 7) or 0.9% (w/w) pectin solutions. The range of concentrations of pectin and gastrointestinal components used was selected to approximately mimic the concentrations in the small intestinal phase of the gastrointestinal tract. Each injection lasted 24 s, and there was an interval of 240 s between successive injections. The temperature of the solution in the titration cell was 37 °C, and the solution was stirred at a speed of 315 rpm throughout the experiments. Triplicate measurements of enthalpy profiles were carried out on each sample, and they were reproducible to better than 5%.

**Data Analysis.** All measurements were performed at least three times using freshly prepared samples. Averages and standard deviations were calculated from these triplet measurements.

## RESULTS AND DISCUSSION

**Properties of Initial Emulsion−Pectin Mixtures.** Initially, the properties of the initial emulsions used to prepare the emulsion−pectin mixtures were characterized (5 mM

phosphate buffer, pH 7). The initial emulsions had a relatively small mean particle diameter immediately after preparation ($d_{32}$ = 200 ± 10 nm), which did not change during the course of the experiments.[33] This can be attributed to the relatively strong steric repulsion between the nonionic surfactant-coated lipid droplets resulting from the polyoxyethylene headgroups on the Tween 80 molecules.[34] The lipid droplets initially had a small negative charge ($\zeta$ = −5.8 ± 0.2 mV), even though they were stabilized by a nonionic surfactant, which can be attributed to anionic impurities in the oil or surfactant ingredients (such as free fatty acids) or to preferential adsorption of hydroxyl ions from water ($OH^-$).[35,36] The droplets in the initial emulsions containing no pectin were stable to creaming throughout the experimental time frame (Figure 1), which is due to the fact that the droplets were small and did not associate with each other.[37]

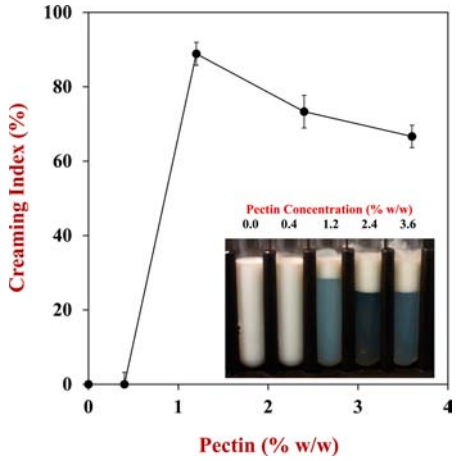


**Figure 1.** Influence of pectin concentration on creaming stability of 2% (w/w) corn oil-in-water emulsions stabilized with 0.2% (w/w) Tween 80 before the digestion process.

Emulsions containing relatively low levels of added pectin (≤0.4% w/w) were still observed to be stable to gravitational separation; that is, they maintained a uniform white appearance (Figure 1). They also had good stability to droplet aggregation with the mean particle diameter ($d_{32}$) increasing only from around 200 to 210 nm when the pectin concentration was increased from 0 to 0.2% (w/w). However, emulsions containing higher levels of pectin clearly separated into a creamed layer and a serum layer, indicating that the droplets moved upward due to gravity. The origin of this effect is depletion flocculation induced by the presence of nonadsorbed pectin molecules within the aqueous phase.[24,38] There was an appreciable increase in mean particle diameter in the samples in which depletion flocculation occurred, for example, $d_{32}$ = 350 nm in the sample initially containing 2.4% (w/w) pectin. This effect can be attributed to the fact that the droplets were pushed together in the flocs due to the depletion attraction, which promoted coalescence. Pectin molecules should not be attracted to the surfaces of the nonionic surfactant-coated lipid droplets because of electrostatic and steric repulsion effects (the carboxyl groups of pectin are completely dissociated at pH 7 because its $pK_a$ is ∼3.5). There is therefore a narrow region around each lipid droplet (approximately equal to the radius of hydration of the pectin molecules) from which the pectin molecules are excluded.[39] Consequently, there is a pectin and water concentration gradient between this exclusion zone and the surrounding bulk aqueous phase, which leads to an osmotic pressure. This osmotic pressure generates an attraction between the lipid droplets (depletion force) because when they come into close contact, the volume of the thermodynamically unfavorable exclusion zone is reduced.[25] At low pectin concentrations, the osmotic attraction is not large enough to overcome the various repulsive forces in the system (e.g., steric and electrostatic), and so the emulsion remains stable to droplet aggregation. However, once a critical pectin concentration is exceeded (∼0.5% w/w), the attractive forces exceed the repulsive forces and droplet flocculation occurs.[24] It should be noted that the main thermodynamic driving force for depletion flocculation is entropy.[40,41] The reason that the thickness of the creamed layer increases (CI decreases) as the pectin concentration increases above the critical flocculation concentration (Figure 1) is that the depletion attraction is higher and so the droplets are held more strongly into a particle gel network.[42] In summary, these measurements showed that the degree of droplet flocculation in the initial emulsion−pectin mixtures depended on the amount of pectin present in the system.

**Influence of Pectin on Lipid Digestion.** In a recent study, we examined the influence of pectin addition on the

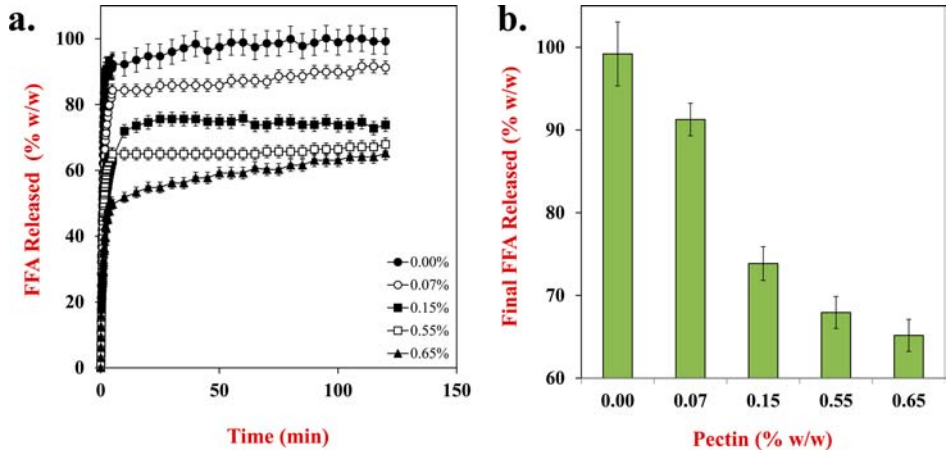


**Figure 2.** Influence of pectin concentration on free fatty acids (FFA) released during lipid digestion process (pH stat): (a) kinetics; (b) FFA released after 2 h. Pectin concentrations refer to those present in the intestinal phase.

gastrointestinal fate of emulisified lipids.[33] This study showed that pectin influenced the aggregation state of the lipid droplets in different regions of the simulated gastrointestinal tract (mouth, stomach, and small intestine). It also showed that pectin addition reduced the rate and extent of lipase-catalyzed lipid digestion in the small intestine phase. In the current study, the same pH-stat method was used to measure the influence of pectin on lipid digestion so that we could directly compare these results with the studies of pectin interactions with various gastrointestinal components using the same constituents.

In general, the amount of FFAs produced increased rapidly during the first few minutes of digestion and then increased more slowly at longer times, until a relatively constant value was reached after 25 min of digestion (Figure 2a). The final amount of FFAs produced at the end of the 2 h digestion period decreased with increasing pectin concentration (Figure 2b), which is in good agreement with our earlier study.[33]

The ability of pectin to decrease the rate and extent of lipid digestion in corn oil-in-water emulsions could be due to several physicochemical and physiological mechanisms. Pectin may have interacted with calcium ions and formed a highly viscous solution or gel network that impeded the diffusion of GIT components (such as lipase or bile salts), thereby retarding the lipid digestion process.[43−45] Pectin−calcium interactions may also have inhibited lipid digestion due to the important role that calcium ions play in removing FFAs from lipid droplet surfaces.[46] Calcium ions normally form insoluble soaps with long-chain FFAs that help remove the FFAs from the lipid droplet surfaces and thereby allow the lipase to keep working.[47] If the calcium ions are tightly bound to pectin molecules, then the FFAs may accumulate at the lipid droplet surfaces, thereby inhibiting further digestion. Pectin may also have bound to bile salts or phospholipids and so prevented them from adsorbing to lipid droplet surfaces or from solubilizing lipid digestion products.[10,18,44] The solubilization of long-chain FFAs in mixed micelles is another important means of removing them from the lipid droplet surfaces and thereby allowing lipase to keep functioning.[34] The adsorption of bile salts and phospholipids to lipid droplet surfaces often facilitates the subsequent adsorption of lipase molecules. Pectin may also be able to alter lipid digestion by interacting directly with lipase molecules.[21,48] Finally, the presence of pectin in the system may alter the aggregation state of the lipid droplets through either depletion or bridging flocculation.[49] The digestion of highly flocculated lipid droplets is often less than that of nonflocculated ones because the lipase molecules have to diffuse through the flocs before they can reach the lipid droplets in their interiors.[23,50] Clearly, the potential influence of pectin on the lipid digestion process within the GIT is complex because pectin is able to interact with many constituents within the GIT fluids.

The purpose of the current study was to provide further insights into the potential origin of these effects by studying the interactions between pectin and specific gastrointestinal components.

**Interactions of Pectin with Mixed Gastrointestinal Components.** In this series of experiments, we used ITC, electrophoresis, turbidity, and microstructure measurements to examine the interactions of pectin with a solution containing a mixture of all the major GIT components: sodium, calcium, bile salts, and lipase. The microstructure of the emulsion−pectin mixtures changed appreciably after exposure to the mixed gastrointestinal components (Figure 3). In the absence of pectin (control), the individual lipid droplets were too small to be observed by optical microscopy, but confocal microscopy images have shown that they are evenly distributed throughout the system.[33] After digestion, there were clearly some large aggregates in the control samples, which may have been lipid digestion products or remnants from the various GIT components (such as calcium, sodium, bile salts, and lipase). In the presence of pectin, the lipid droplets were trapped within large clusters prior to digestion, which can be attributed to depletion flocculation induced by nonadsorbed pectin molecules (Figure 3).[25] After digestion, there were a relatively high number of large aggregates (undigested lipid droplets) remaining in the samples containing pectin, which could have been due to interactions of the pectin molecules with various components in the simulated GIT fluids.

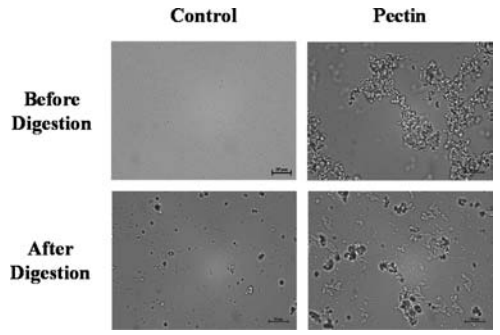


**Figure 3.** Influence of pectin on the microstructure (observed by optical microscopy) of emulsions before (initial phase) and after (intestinal phase) of lipid digestion. The initial emulsions contained 2% (w/w) corn oil, 2% (w/w) Tween 80, and 0 or 2.4% (w/w) pectin. The scale bar corresponds to 20 $\mu$m.

Turbidity ($\Delta\tau$), $\zeta$-potential, and enthalpy change ($\Delta H$) were measured when increasing amounts of mixed GIT fluids (0 to 100% of mixture) were titrated into a pectin (0.9% w/w) solution at pH 7 (Figure 4). The 100% GIT fluids contained the levels of the NaCl, $CaCl_2$, bile salts, and lipase in the final simulated small intestinal fluids. There was a progressive increase in the turbidity when the amount of mixed GIT fluids titrated into the pectin solution increased (Figure 4a). The $\zeta$-potential of the mixed system moved from highly negative (−19 mV) to less negative (−2 mV) as increasing amounts of GIT fluids were added (Figure 4a), which may have occurred due to electrostatic screening effects induced by the presence of salts or due to binding of cations in the GIT fluids to anionic pectin molecules.[51] There was also an appreciable difference in the enthalpy profiles of samples with either buffer or pectin solutions (Figure 4b). In the absence of pectin, the enthalpy change was relatively low and may be attributed to heat of dilution effects associated with the various molecules and/or particles moving further apart when the GIT fluids were injected into the reaction cell.[22,27,30] In the presence of pectin, there was a large exothermic enthalpy change when the first few aliquots of the mixed GIT fluids were injected into the reaction cell containing the pectin solution. The enthalpy change became progressively less exothermic when 0−20% of the GIT fluids was added, until it eventually reached a relatively constant endothermic value at higher GIT levels (∼40%). These results suggest that the pectin molecules interacted with some of the components in the GIT fluids, possibly through electrostatic interactions, and formed aggregates that were large enough to scatter light strongly.

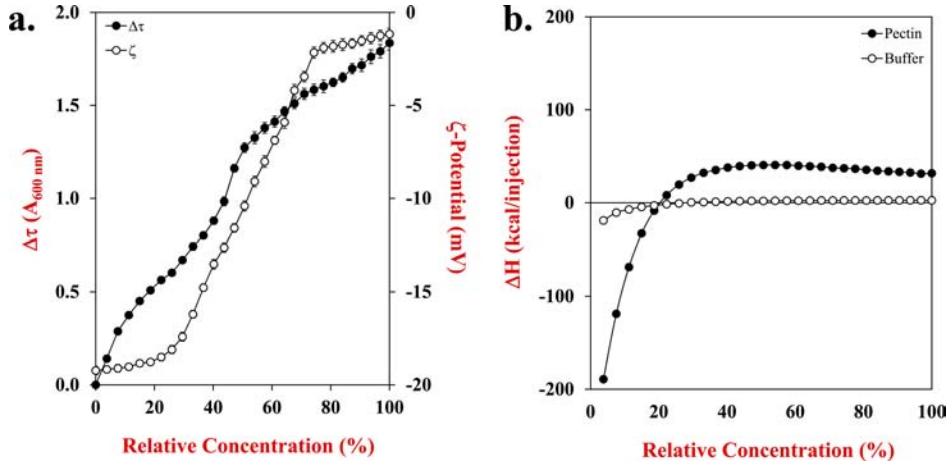


**Figure 4.** Influence of relative concentration (0−100%) of simulated gastrointestinal fluids on (a) optical turbidity ($\Delta\tau = A_{600\ nm}$) and $\zeta$-potential and (b) interaction enthalpy ($\Delta H$) of solutions containing either buffer solution or an initial concentration of 0.9% (w/w) pectin. The initial simulated gastrointestinal fluids (100%) contained 0.45% (w/w) bile salts, 0.18% (w/w) lipase, 9 mM $CaCl_2$, and 91 mM NaCl. Optical turbidity ($\Delta\tau$) was defined as $\Delta\tau = \tau_{pectin} - \tau_{buffer}$.

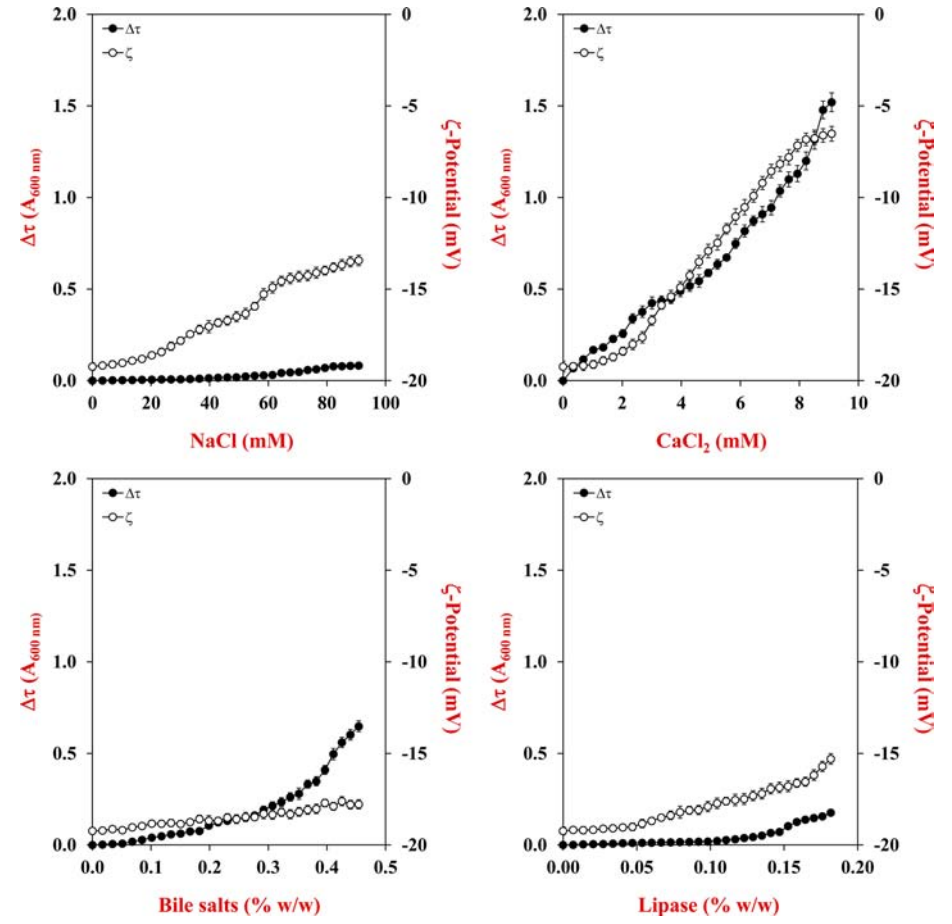


**Figure 5.** Influence of the concentrations of NaCl, $CaCl_2$, bile salts, and lipase on optical turbidity ($\Delta\tau = A_{600\ nm}$) and $\zeta$-potential of solutions containing an initial concentration of 0.9% (w/w) pectin.

**Interactions of Pectin with Specific Gastrointestinal Components.** In this series of experiments, ITC, electrophoresis, turbidity, and microstructure measurements were used to characterize the interactions of pectin with specific GIT components (NaCl, $CaCl_2$, bile salts, or lipase). Measurements were made as increasing amounts of GIT components were individually added to a pectin solution (0.9% w/w) (Figure 5). In addition, the turbidities and $\zeta$-potentials reached at the end of these titrations were reported so that different samples could be compared more easily (Figure 6).

*NaCl.* Addition of increasing amounts of NaCl to the pectin solutions caused an appreciable decrease in the magnitude of the $\zeta$-potential of the pectin solutions (Figure 5, NaCl), which can be attributed to electrostatic screening effects, that is,


dx.doi.org/10.1021/jf504829h | J. Agric. Food Chem. 2014, 62, 12620−12630

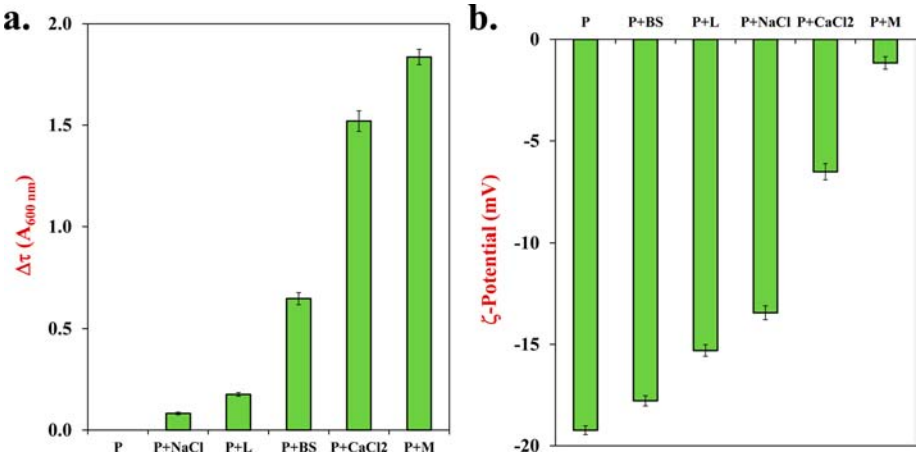


**Figure 6.** Influence of 91 mM NaCl, 9 mM $CaCl_2$, 0.45% (w/w) bile salts (BS), 0.18% (w/w) lipase (L), and a mixture of all components (M, 100% relative concentrations) on optical turbidity ($\Delta\tau = A_{600\ nm}$) (a) and $\zeta$-potential (b) of solutions containing an initial concentration of 0.9% (w/w) pectin (P).

accumulation of sodium ions around the negative groups on the pectin molecules.[51] There was no evidence of an increase in aggregate formation within the microstructure images (Figure 8, NaCl), and there was little change in the general appearance (Figure 7, NaCl) and optical turbidity (Figure 5, NaCl) of these

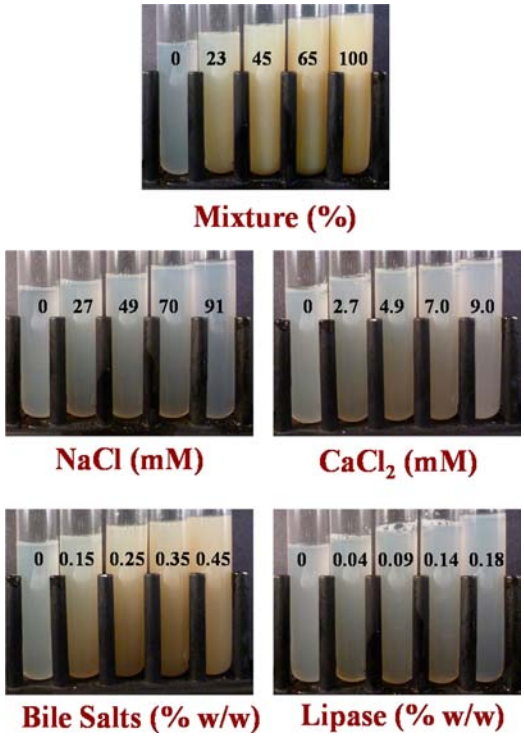


**Figure 7.** Influence of the concentrations of NaCl, $CaCl_2$, bile salts, lipase, and a mixture of all components (% relative concentrations) on the turbidity of solutions containing an initial concentration of 0.9% (w/w) pectin.

samples upon NaCl addition. We did observe a slight increase in the turbidity at the highest NaCl levels used, which suggested that the NaCl may have caused a slight amount of pectin aggregation, presumably through screening of the electrostatic interactions.[52] The ITC measurements indicated that there was not a strong interaction ($\Delta H = -102$ kcal) between the pectin

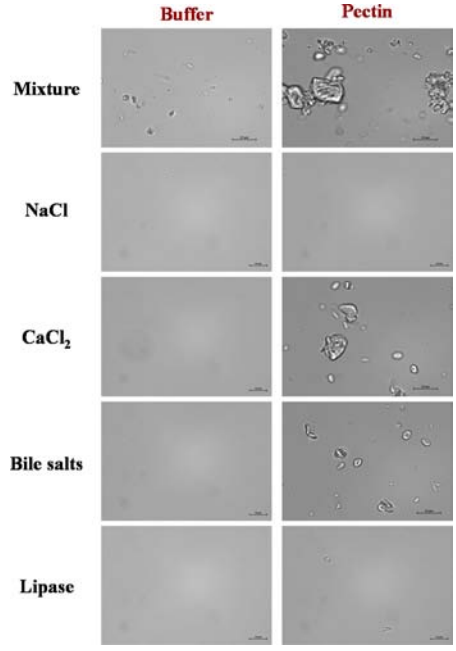


**Figure 8.** Influence of 91 mM NaCl, 9 mM $CaCl_2$, 0.45% (w/w) bile salts (BS), 0.18% (w/w) lipase (L), and a mixture of the previous components (100% relative concentrations) on the microstructure (observed by optical microscopy) of solutions prepared on either buffer solution or 0.9% (w/w) pectin. The scale bar corresponds to 20 $\mu$m.

and the NaCl (Figure 9, NaCl), because the enthalpy versus salt concentration profiles were fairly similar. Overall, these results suggest that pectin did not have a major interaction with the NaCl in the GIT fluids.

*$CaCl_2$.* Addition of $CaCl_2$ to the pectin solutions had a more pronounced influence on their physicochemical properties than NaCl addition. Addition of increasing amounts of $CaCl_2$ caused the $\zeta$-potential of the pectin solutions to go from around −19 mV to around −6 mV (Figure 5, $CaCl_2$), which can be attributed to electrostatic screening and ion binding effects.[51] Multivalent counterions are more effective at screening electrostatic interactions than monovalent ones, and they have a greater tendency to bind strongly to oppositely charged groups.[53] The change in the $\zeta$-potential with calcium addition


dx.doi.org/10.1021/jf504829h | J. Agric. Food Chem. 2014, 62, 12620−12630

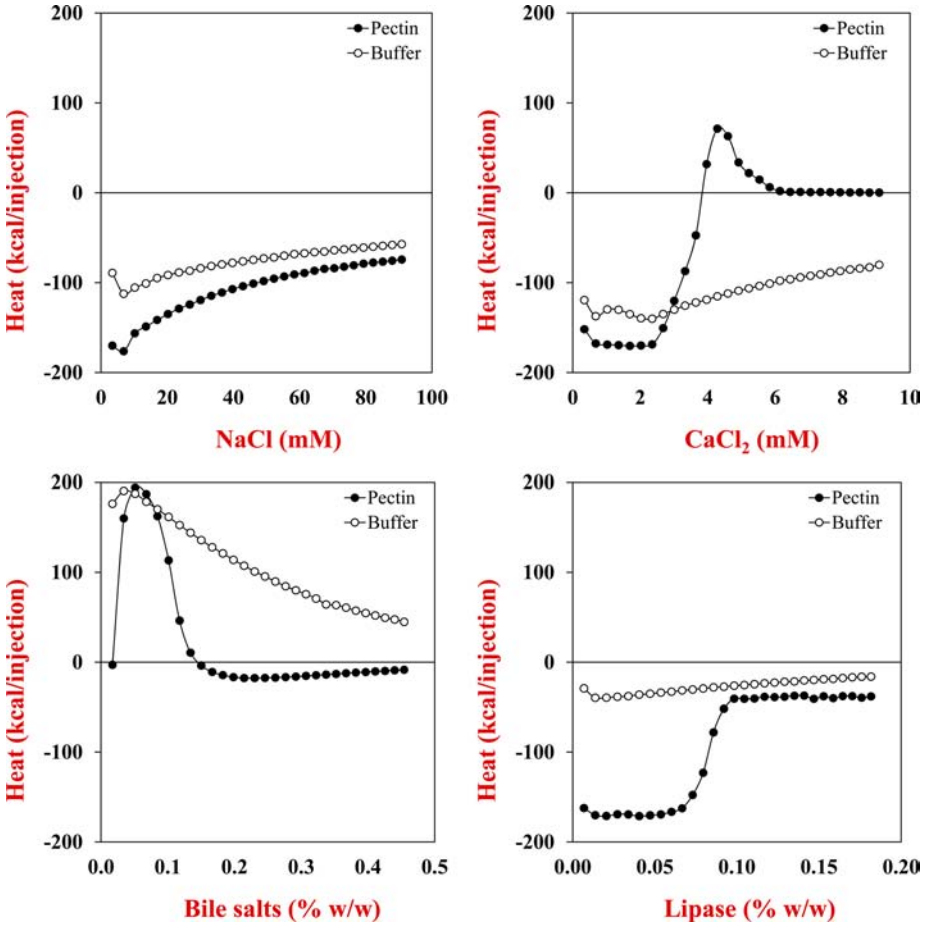


**Figure 9.** Influence of the concentrations of NaCl, $CaCl_2$, bile salts, and lipase on interaction enthalpy ($\Delta H$) of solutions containing either buffer solution or an initial concentration of 0.9% (w/w) pectin.

was fairly similar to that observed with the addition of the mixed GIT solution (Figure 6b), which suggests that calcium ions play an important role in determining the overall electrical interactions. The ITC measurements also indicated that there was a strong interaction ($\Delta H$ = −241 kcal) between the calcium ions and pectin (Figure 9, $CaCl_2$). When calcium ions were injected into buffer solution, there was an exothermic enthalpy change that decreased in magnitude with increasing $CaCl_2$ concentration, which can be attributed to heat of dilution effects.[22] However, when calcium ions were injected into pectin solution, there was initially a strong exothermic reaction (from 0 to 4 mM), then a relatively strong endothermic reaction (from 4 to 6 mM), followed by an enthalpy change close to zero after 6 mM $CaCl_2$ (Figure 9, $CaCl_2$). The shape of the ITC curve suggests that there may have been several events occurring sequentially, such as calcium binding, pectin conformational changes, and/or pectin aggregation. Nevertheless, it is not possible to determine the molecular origin of these events from ITC measurements alone because they provide only the overall enthalpy change.

The addition of calcium ions to the pectin solutions caused a large increase in their optical turbidity (Figures 5 ($CaCl_2$) and 6a), which can be attributed to the appearance of large aggregates, as observed within the optical microscopy images (Figures 7 and 8, $CaCl_2$). We postulate that these aggregates were microgels formed by pectin in the presence of calcium.[43,45] The calcium ions may have cross-linked the anionic pectin molecules through electrostatic bridging.[13] As mentioned earlier, the binding of calcium ions to pectin may be important for a number of reasons. First, pectin−calcium microgels may trap lipid droplets inside, thereby restricting the access of lipase to the lipid substrates.[23] Second, the formation of these electrostatic complexes may prevent the calcium ions from forming insoluble soaps with long-chain FFAs at the lipid droplet surfaces, thereby preventing the lipase from functioning properly.[47] In practice, there will be other types of salts in the gastrointestinal fluids that may alter the interactions of calcium with pectin through electrostatic screening or binding effects. It should be noted that there may have been some sodium or calcium present in the ingredients used in this study (such as pectin), and these ions could also contribute to the observed electrostatic interactions.

*Bile Salts.* The addition of bile salts to the pectin solutions had a limited influence on their physicochemical properties. Addition of increasing amounts of bile salts caused only a relatively small decrease in the negative charge on the pectin molecules (Figure 5, bile salts), which can probably be attributed to electrostatic screening effects.[7,9] There was an appreciable increase in the optical turbidity of the pectin solutions when bile salts were added (Figures 5 (bile salts) and 6a), and the solutions appeared visibly cloudier (Figure 7, bile salts). These effects can be attributed to the formation of large aggregates within the bile salts−pectin solutions as observed by optical microscopy (Figure 8, bile salts). The ITC measurements also indicated that the bile salts interacted with the pectin molecules. In the absence of pectin, there was a relatively

large endothermic enthalpy change ($\Delta H$ = 204 kcal), which progressively decreased with increasing bile salt concentration (Figure 9, bile salts). This effect may have been due to the breakdown of bile salt micelles within the reaction chamber, resulting in the exposure of a greater number of nonpolar groups to water.[54] In the presence of pectin, there was a large endothermic peak (from 0.05 to 0.15% w/w) followed by a value that was close to zero at higher bile salt concentrations (after 0.2% (w/w), Figure 9, bile salts). The large difference between the two curves suggests that there was an interaction between pectin and bile salts; for example, bile salt micelles may have bound to pectin molecules and/or promoted their aggregation.[55]

One might not expect a strong interaction between bile salts and pectin molecules because they are both usually negatively charged at neutral pH. However, bile salts may be able to interact with pectin molecules through hydrophobic interactions.[56] In general, the hydrophobic interactions of pectin with bile salts are known to increase with the degree of esterification of pectin molecules (by increasing its hydrophobicity) and the molecular weight (viscosity) of the pectin molecules.[20] These experiments clearly show that bile salts can interact with pectin molecules, which may have important implications for the effects of pectin on lipid digestion observed in Figure 2. If the bile salts form microgel particles with pectin, then they may not be available to absorb to the surfaces of the lipid droplets or to solubilize lipid digestion products, as discussed earlier. In addition, if any lipid droplets are trapped inside the microgels, then the rate of digestion may be decreased because the lipase molecules cannot easily reach the lipid droplet surfaces.[9]

*Lipase.* Finally, we examined the influence of lipase addition to the pectin solutions on their overall physicochemical properties. The addition of increasing amounts of lipase caused a slight change in the $\zeta$-potential of the pectin (Figure 5, lipase), which may have been due to some binding of lipase molecules to the pectin molecules. In addition, there was an appreciable difference between the ITC curves of the control and the system containing pectin (Figure 9, lipase), which also suggests that some form of interaction occurred ($\Delta H$ = −129 kcal).[21] In the absence of pectin, there was a relatively large exothermic change observed when the lipase solution was titrated into the buffer solution. This effect can probably be attributed to the heat of dilution associated with salts in the lipase solution. In the presence of pectin, there was a large exothermic change observed at low lipase levels (0−0.1 w/w %), followed by a much smaller exothermic change at higher lipase levels. The large difference between the curves in the presence and absence of pectin suggests that there was a strong interaction between the lipase and the pectin, although again the molecular origin of this effect cannot be established from the ITC measurements. There was a slight increase in the optical turbidity of the lipase−pectin solutions when high levels of lipase were added (Figure 5, lipase), but there was little change in their overall visual appearance (Figure 7, lipase) or their microstructure (Figure 8, lipase). These results suggest either that any interactions between the lipase and pectin did not lead to extensive aggregation or that the lipase−pectin complexes formed were soluble in buffer solution.

For simple systems involving the binding of a ligand to another molecule, ITC is a powerful tool for determining thermodynamic properties, such as the number and strength of binding sites and the nature of the enthalpy change ($\Delta H$) associated with the interaction (endothermic or exothermic). For more complex systems, the interpretation of ITC data is more difficult because many different molecular and physicochemical events contribute to the overall enthalpy changes, such as binding, conformation changes, and aggregation. Consequently, it is not possible to establish the precise nature of the different contributions to the measured ITC signal. Nevertheless, ITC measurements do still provide valuable information, because they indicate that one or more types of interaction are taking place between two molecules, and they show the range of concentrations over which these intearctions occur. Typically, ITC measurements should be combined with other techniques to provide a more detailed understanding of the nature of the interactions involved, such as chromatography, scattering, spectrometry, or spectroscopy methods.

The purpose of this study was to investigate the interaction of pectin molecules with some of the major constituents within gastrointestinal fluids, that is, NaCl, $CaCl_2$, bile salts, and lipase. Our measurements have shown that a number of these components interact strongly with pectin, which may have important implications for understanding the influence of pectin on lipid digestion. In particular, calcium ions and bile salts appear to promote the formation of pectin microgels that can lead to flocculation of lipid droplets in the gastrointestinal tract, decreasing the ability of emulsified lipids to be accessed by gastrointestinal lipases and thereby inhibiting digestion. If appreciable amounts of calcium and bile salts are trapped within these microgels, then they will not be able to remove long-chain fatty acids from lipid droplet surfaces, which would inhibit lipid digestion. In addition, if lipid droplets are trapped within pectin microgels, then it may be more difficult for lipase molecules to access the surfaces of the lipid substrate, again delaying lipid digestion. These results have important implications for the rational design of dietary fiber-based functional foods that may modulate lipid digestion within the gastrointestinal tract.

## AUTHOR INFORMATION

### Corresponding Author

*(D.J.M.) E-mail: mcclements@foodsci.umass.edu. Phone: (413) 545-1019. Fax: (413) 545-1262.

### Funding

We are grateful to COLCIENCIAS and Universidad Nacional de Colombia for providing a fellowship to M.E.-R. supporting this work. This material is partly based upon work supported by the U.S. Department of Agriculture, NRI Grants (2011-03539, 2013-03795, 2011-67021, and 2014-67021).

### Notes

The authors declare no competing financial interest.

## ABBREVIATIONS USED

FFA, free fatty acid; GalA, D-galacturonic acid; GIT, gastrointestinal tract; ITC, isothermal titration calorimetry; SSF, simulated saliva fluid; SGF, simulated gastric fluid; SIF, simulated intestinal fluid

## REFERENCES

(1) Bray, G. A.; Popkin, B. M. Dietary fat intake does affect obesity! *Am. J. Clin. Nutr.* **1998**, *68*, 1157−1173.

(2) Howarth, N. C.; Saltzman, E.; Roberts, S. B. Dietary fiber and weight regulation. *Nutr. Rev.* **2001**, *59*, 129−139.

(3) Beysseriat, M.; Decker, E. A.; McClements, D. J. Preliminary study of the influence of dietary fiber on the properties of oil-in-water

emulsions passing through an in vitro human digestion model. *Food Hydrocolloids* **2006**, *20*, 800−809.
(4) Mun, S.; Decker, E.; Park, Y.; Weiss, J.; McClements, D. J. Influence of interfacial composition on in vitro digestibility of emulsified lipids: potential mechanism for chitosan's ability to inhibit fat digestion. *Food Biophys.* **2006**, *1*, 21−29.
(5) McClements, D. J.; Li, Y. Structured emulsion-based delivery systems: controlling the digestion and release of lipophilic food components. *Adv. Colloid Interface Sci.* **2010**, *159*, 213−228.
(6) Gunness, P.; Gidley, M. J. Mechanisms underlying the cholesterol-lowering properties of soluble dietary fibre polysaccharides. *Food Funct.* **2010**, *1*, 149−155.
(7) Hur, S. J.; Lim, B. O.; Decker, E. A.; McClements, D. J. In vitro human digestion models for food applications. *Food Chem.* **2011**, *125*, 1−12.
(8) Li, Y.; McClements, D. J. Modulating lipid droplet intestinal lipolysis by electrostatic complexation with anionic polysaccharides: Influence of cosurfactants. *Food Hydrocolloids* **2014**, *35*, 367−374.
(9) McClements, D. J.; Li, Y. Review of in vitro digestion models for rapid screening of emulsion-based systems. *Food Funct.* **2010**, *1*, 32−59.
(10) Anderson, J. W.; Baird, P.; Davis, R. H., Jr; Ferreri, S.; Knudtson, M.; Koraym, A.; Waters, V.; Williams, C. L. Health benefits of dietary fiber. *Nutr. Rev.* **2009**, *67*, 188−205.
(11) Kritchevsky, D. Dietary fiber. *Annu. Rev. Nutr.* **1988**, *8*, 301−328.
(12) Theuwissen, E.; Mensink, R. P. Water-soluble dietary fibers and cardiovascular disease. *Physiol. Behav.* **2008**, *94*, 285−292.
(13) Thakur, B. R.; Singh, R. K.; Handa, A. K.; Rao, M. A. Chemistry and uses of pectin − a review. *Crit. Rev. Food Sci. Nutr.* **1997**, *37*, 47−73.
(14) Mohnen, D. Pectin structure and biosynthesis. *Curr. Opin. Plant Biol.* **2008**, *11*, 266−277.
(15) Ridley, B. L.; O'Neill, M. A.; Mohnen, D. Pectins: structure, biosynthesis, and oligogalacturonide-related signaling. *Phytochemistry* **2001**, *57*, 929−967.
(16) Caffall, K. H.; Mohnen, D. The structure, function, and biosynthesis of plant cell wall pectic polysaccharides. *Carbohydr. Res.* **2009**, *344*, 1879−1900.
(17) Yapo, B. M. Pectic substances: from simple pectic polysaccharides to complex pectins − a new hypothetical model. *Carbohydr. Polym.* **2011**, *86*, 373−385.
(18) Maxwell, E. G.; Belshaw, N. J.; Waldron, K. W.; Morris, V. J. Pectin − an emerging new bioactive food polysaccharide. *Trends Food Sci. Technol.* **2012**, *24*, 64−73.
(19) Munarin, F.; Tanzi, M. C.; Petrini, P. Advances in biomedical applications of pectin gels. *Int. J. Biol. Macromol.* **2012**, *51*, 681−689.
(20) Pfeffer, P. E.; Doner, L. W.; Hoagland, P. D.; McDonald, G. G. Molecular interactions with dietary fiber components. Investigation of the possible association of pectin and bile acids. *J. Agric. Food Chem.* **1981**, *29*, 455−461.
(21) Espinal-Ruiz, M.; Parada-Alfonso, F.; Restrepo-Sánchez, L.-P.; Narváez-Cuenca, C.-E. Inhibition of digestive enzyme activities by pectic polysaccharides in model solutions. *Bioact. Carbohydr. Dietary Fibre* **2014**, *4*, 27−38.
(22) McClements, D. J. Isothermal titration calorimetry study of pectin−ionic surfactant interactions. *J. Agric. Food Chem.* **2000**, *48*, 5604−5611.
(23) Simo, O. K.; Mao, Y.; Tokle, T.; Decker, E. A.; McClements, D. J. Novel strategies for fabricating reduced fat foods: heteroaggregation of lipid droplets with polysaccharides. *Food Res. Int.* **2012**, *48*, 337−345.
(24) Jenkins, P.; Snowden, M. Depletion flocculation in colloidal dispersions. *Adv. Colloid Interface Sci.* **1996**, *68*, 57−96.
(25) McClements, D. J. Comments on viscosity enhancement and depletion flocculation by polysaccharides. *Food Hydrocolloids* **2000**, *14*, 173−177.
(26) Leavitt, S.; Freire, E. Direct measurement of protein binding energetics by isothermal titration calorimetry. *Curr. Opin. Struct. Biol.* **2001**, *11*, 560−566.
(27) Doyle, M. L. Characterization of binding interactions by isothermal titration calorimetry. *Curr. Opin. Biotechnol.* **1997**, *8*, 31−35.
(28) Freire, E.; Mayorga, O. L.; Straume, M. Isothermal titration calorimetry. *Anal. Chem.* **1990**, *62*, 950A−959A.
(29) Wangsakan, A.; Chinachoti, P.; McClements, D. J. Effect of surfactant type on surfactant−maltodextrin interactions: isothermal titration calorimetry, surface tensiometry, and ultrasonic velocimetry study. *Langmuir* **2004**, *20*, 3913−3919.
(30) Chang, Y.; McLandsborough, L.; McClements, D. J. Interactions of a cationic antimicrobial (ε-polylysine) with an anionic biopolymer (pectin): an isothermal titration calorimetry, microelectrophoresis, and turbidity study. *J. Agric. Food Chem.* **2011**, *59*, 5579−5588.
(31) Hur, S. J.; Decker, E. A.; McClements, D. J. Influence of initial emulsifier type on microstructural changes occurring in emulsified lipids during in vitro digestion. *Food Chem.* **2009**, *114*, 253−262.
(32) Salvia-Trujillo, L.; Qian, C.; Martin-Belloso, O.; McClements, D. J. Influence of particle size on lipid digestion and beta-carotene bioaccessibility in emulsions and nanoemulsions. *Food Chem.* **2013**, *141*, 1472−1480.
(33) Espinal-Ruiz, M.; Parada-Alfonso, F.; Restrepo-Sánchez, L.-P.; Narváez-Cuenca, C.-E.; McClements, D. J. Impact of dietary fibers [methyl cellulose, chitosan, and pectin] on digestion of lipids under simulated gastrointestinal conditions. *Food Funct.* **2014**, *5*, 3083−3095.
(34) Almgren, M. Mixed micelles and other structures in the solubilization of bilayer lipid membranes by surfactants. *Biochim. Biophys. Acta−Biomembranes* **2000**, *1508*, 146−163.
(35) Thiam, A. R.; Farese, R. V., Jr.; Walther, T. C. The biophysics and cell biology of lipid droplets. *Nat. Rev. Mol. Cell Biol.* **2013**, *14*, 775−786.
(36) Singh, H.; Ye, A.; Horne, D. Structuring food emulsions in the gastrointestinal tract to modify lipid digestion. *Prog. Lipid Res.* **2009**, *48*, 92−100.
(37) Weiss, J.; Takhistov, P.; McClements, D. J. Functional materials in food nanotechnology. *J. Food Sci.* **2006**, *71*, R107−R116.
(38) Dickinson, E.; Semenova, M. G.; Antipova, A. S.; Pelan, E. G. Effect of high-methoxy pectin on properties of casein-stabilized emulsions. *Food Hydrocolloids* **1998**, *12*, 425−432.
(39) Jenkins, P.; Snowden, M. Depletion flocculation in colloidal dispersions. *Adv. Colloid Interface Sci.* **1996**, *68*, 57−96.
(40) Reiffers-Magnani, C. K.; Cuq, J. L.; Watzke, H. J. Depletion flocculation and thermodynamic incompatibility in whey protein stabilised O/W emulsions. *Food Hydrocolloids* **2000**, *14*, 521−530.
(41) Méndez-Alcaraz, J. M.; Klein, R. Depletion forces in colloidal mixtures. *Phys. Rev. E* **2000**, *61*, 4095−4099.
(42) Dickinson, E. On flocculation and gelation in concentrated particulate systems containing added polymer. *J. Chem. Soc., Faraday Trans.* **1995**, *91*, 4413−4417.
(43) Willats, W. G. T.; Knox, J. P.; Mikkelsen, J. D. Pectin: new insights into an old polymer are starting to gel. *Trends Food Sci. Technol.* **2006**, *17*, 97−104.
(44) Leroux, J.; Langendorff, V.; Schick, G.; Vaishnav, V.; Mazoyer, J. Emulsion stabilizing properties of pectin. *Food Hydrocolloids* **2003**, *17*, 455−462.
(45) Braccini, I.; Pérez, S. Molecular basis of $Ca^{2+}$-induced gelation in alginates and pectins: the egg-box model revisited. *Biomacromolecules* **2001**, *2*, 1089−1096.
(46) Devraj, R.; Williams, H. D.; Warren, D. B.; Mullertz, A.; Porter, C. J. H.; Pouton, C. W. In vitro digestion testing of lipid-based delivery systems: calcium ions combine with fatty acids liberated from triglyceride rich lipid solutions to form soaps and reduce the solubilization capacity of colloidal digestion products. *Int. J. Pharm.* **2013**, *441*, 323−333.
(47) Ye, A.; Cui, J.; Zhu, X.; Singh, H. Effect of calcium on the kinetics of free fatty acid release during in vitro lipid digestion in model emulsions. *Food Chem.* **2013**, *139*, 681−688.

(48) de Roos, A.; Walstra, P. Loss of enzyme activity due to adsorption onto emulsion droplets. *Colloids Surf., B* **1996**, *6*, 201−208.
(49) Biggs, S.; Habgood, M.; Jameson, G. J.; Yan, Y.-d. Aggregate structures formed via a bridging flocculation mechanism. *Chem. Eng. J.* **2000**, *80*, 13−22.
(50) Li, Y.; Hu, M.; McClements, D. J. Factors affecting lipase digestibility of emulsified lipids using an in vitro digestion model: proposal for a standardised pH-stat method. *Food Chem.* **2011**, *126*, 498−505.
(51) Israelachvili, J. *Intermolecular and Surface Forces*, 3rd ed.; Academic Press: London, UK, 2011.
(52) Furusawa, K.; Ueda, M.; Nashima, T. Bridging and depletion flocculation of synthetic latices induced by polyelectrolytes. *Colloids Surf., A: Physicochem. Eng. Aspects* **1999**, *153*, 575−581.
(53) Winzor, D. J.; Carrington, L. E.; Deszczynski, M.; Harding, S. E. Extent of charge screening in aqueous polysaccharide solutions. *Biomacromolecules* **2004**, *5*, 2456−2460.
(54) Thongngam, M.; McClements, D. J. Isothermal titration calorimetry study of the interactions between chitosan and a bile salt (sodium taurocholate). *Food Hydrocolloids* **2005**, *19*, 813−819.
(55) Wangsakan, A.; Chinachoti, P.; McClements, D. J. Isothermal titration calorimetry study of the influence of temperature, pH and salt on maltodextrin−anionic surfactant interactions. *Food Hydrocolloids* **2006**, *20*, 461−467.
(56) Dongowski, G. Effect of pH on the in vitro interactions between bile acids and pectin. *Z. Lebensm. Unters. Forsch.* **1997**, *205*, 185−192.

stage), stage III (pileus-growing stage), stage IV (gill-growing stage), and stage V (mature stage) (Figure 1).

**Figure 1.** *P.eryngii* fruiting bodies at five stages of maturity: SI (bud-forming stage), SII (stipe-growing stage), SIII (pileus-growing stage), SIV (gill-growing stage), and SV (mature stage).

**Proximate Analysis.** The proximate compositions of mushrooms, including moisture, crude ash, crude fiber, crude protein, and crude fat, were determined according to the methods of AOAC (1990, 15th).[18] The nitrogen factor used for crude protein calculation was 4.38.[19] The carbohydrate content was calculated by subtracting the other proximate compounds from 1 g of dry sample.

**Isolation of Crude Polysaccharide-Proteins, Crude Polysaccharides, and Ethanol Extracts.** The crude polysaccharide-protein fraction in the harvested *P. eryngii* fruiting body at five maturity stages was extracted as described previously.[20,21] Briefly, 500 g of fruiting body was blended with distilled water (500 mL) for 1 min and then continuously stirred for 2 h to obtain homogeneous slurry, respectively. The slurry was stored at 4 °C for 24 h and centrifuged at 5000*g* for 20 min to collect the supernatant. Solid ammonium sulfate was added to the supernatant to reach 80% saturation and then stored at 4 °C overnight. The precipitate collected by centrifugation (12000*g*, 20 min) was dissolved, dialyzed against distilled water, and freeze-dried to obtain the crude polysaccharide-protein extract.

For extracting polysaccharide fraction, the fruiting body was homogenized and mixed with distilled water (w/v 1:2) at 100 °C for 4 h. The supernatant was concentrated and precipitated with a final concentration of 80% ethanol for 12 h at 4 °C. The precipitation was collected by centrifugation (12000*g*, 10 min), washed twice with absolute ethanol, dialyzed (cutoff 3500 Da) against distilled water, and freeze-dried to obtain the crude polysaccharide extract.

For obtaining the ethanol extract of *P. eryngii*, the fruiting body (100 g) at five maturity stages was extracted with 1 L of 60% ethanol at 25 °C for 2 h with an ultrasonic bath (SB-5200DTS, Scientz Biotechnology, Ningbo, China) of 40 kHz. After filtration, ethanol was removed by a rotary evaporator (RE-2000B, Yarong Shenghua, Shanghai, China). The ethanol extract was then preserved at −20 °C before further use.

**Analysis of *P. eryngii* Extracts.** Protein content in the polysaccharide and polysaccharide-protein fractions was analyzed by Bradford Protein Assay Kit (Beyotime Institute of Biotechnology, Shanghai, China) using bovine serum albumin as the standard. Carbohydrate content in the polysaccharide and polysaccharide-protein fractions was determined by the phenol−sulfuric acid method using glucose as the standard.

Phenolic content in the ethanol extracts was estimated by a colorimetric assay based on procedures described by Adom et al.[22] Gallic acid was used to calculate the standard curve, and the results were expressed as milligrams of gallic acid equivalents (GAEs) per gram of extract. Flavonoid content was determined by a colorimetric method described by Jia et al.[23] with some modifications. The dried ethanol extract was dissolved in 2 mL of 60% ethanol and mixed with 0.5 mL of a 5% $NaNO_2$ solution. Then 0.5 mL of a 10% $Al(NO_3)_3$ solution was added, followed by adding 4 mL of 4% NaOH and 3 mL of 60% ethanol to make up the total volume to10.0 mL. After incubation at room temperature for 30 min, the absorbance of the reaction mixture was measured at 510 nm. The flavonoid content was calculated using a standard calibration of rutin solution and expressed as micrograms of rutin equivalents (RE) per gram of sample. The quantitative analysis of the total saponins in the ethanol extract was done by the vanillin−perchloric acid colorimetric method described by Wang et al.[24] Ginsenoside Rg 1 was used as a reference standard, and the content of total saponins was expressed as Ginsenoside Rg 1 equivalents (GR1 mg/g extract).

**Assay of Cytotoxical Activity.** The cytotoxical activity of each crude extract from *P. eryngii* fruiting body at five maturity stages was evaluated with the MTT colorimetric assay method.[25] The human gastric cancer cell line SGC-7901, human liver carcinoma cell line HepG-2, and normal human liver L-02 were obtained from American Tissue Culture Collection (ATCC, Rockville, MD, USA) and Shanghai Cell Biology Institute (Shanghai, China). The cells were maintained in 5% $CO_2$ at 37 °C in RPMI-1640 (Gibco, NY, USA) containing 10% fetal bovine serum (FBS) supplemented with 100 U/mL penicillin and 100 $\mu$g/mL streptomycin. Cells ($5 \times 10^5$) in their exponential growth phase were seeded into each well of a 96-well plate and incubated for 24 h before addition of the samples with the different concentration. Incubation was carried out for another 24/48 h, and MTT was added to cells for another 4 h to produce formazan. The absorbance of each well was read at 490 nm in the microplate reader (Multiskan GO, Thermo Labsystems, Beverly, MA, USA) after addition of 150 $\mu$L of dimethyl sulfoxide (DMSO) and shaking for 10 min. The cell viability was used for expressing the cytotoxicity of samples and calculated as follows:

$$\text{cell viability (\%) of control} = \mathrm{OD}_{490\mathrm{nm}}(\text{sample})/\mathrm{OD}_{490\mathrm{nm}}(\text{control}) \times 100.$$

**Amino Acid Composition and Monosaccharide Composition of Polysaccharide-Protein Fractions.** Determination of amino acid composition followed the description by Su et al.[26] Briefly, each polysaccharide-protein fraction was subjected to hydrolysis under vacuum in 6 M HCl at 110 °C for 24 h. The hydrolysate was analyzed with a Sykam S433D/S433 automatic amino acid analyzer (Sykam, Munich, Germany).

Monosaccharide compositions and their ratios were determined by a previously described method.[21] Briefly, 30 mg of each polysaccharide-protein fraction was hydrolyzed, filtered, and applied to the monosaccharide composition in a 6890N GC (Agilent Technologies, Santa Clara, CA, USA) with capillary column (30 m × 0.32 mm) with L-rhamnose, D-arabinose, D-mannose, D-galactose, and D-glucose as the standards.

**SDS-PAGE and Native-PAGE of polysaccharide-protein fractions.** SDS-PAGE with a 12% resolving gel was used for qualitatively analyzing the protein changes in polysaccharide-protein fractions at each stage.[27] The main components and primary molecular mass determination were estimated by comparing the electrophoresis mobility with those of standard molecular weight markers. Native-PAGE with a 12% resolving gel and bromophenol blue as the tracking dye was further applied to estimate the purity.[28]

**Further Purification of the Polysaccharide-Protein Fractions.** The crude polysaccharide-protein fraction was applied to a column (2.5 × 25 cm) DEAE-Sepharose Fast Flow anionic resin (GE Healthcare, Uppsala, Sweden) equilibrated with 10 mM PBS buffer (pH 7.4). Then the column was eluted with a discontinuous gradient of PBS, 0.1, 0.3, and 0.5 M NaCl in PBS, and the eluate was collected with fraction tubes (8 mL per tube). The carbohydrate content of the eluates was determined by measuring the absorption at 490 nm using the phenol−sulfuric acid method. The protein concentration was determined spectrophotometrically at 280 nm. Four fractions, PEG-0, PEG-1, PEG-3, and PEG-5, were collected, dialyzed, and freeze-dried for analyzing the cytotoxical activity with the MTT assay.

Table 1. Proximate Composition of *P. eryngii* Fruiting Body Harvested at Five Maturity Stages[a]

| component | content (%) | | | | |
|---|---|---|---|---|---|
| | stage I | stage II | stage III | stage IV | stage V |
| moisture | 90.80 ± 0.35 | 92.18 ± 0.26 | 90.13 ± 0.35 | 90.49 ± 0.57 | 93.09 ± 0.69 |
| dry matter | 9.20 ± 0.35 | 7.82 ± 0.26 | 9.87 ± 0.35 | 9.51 ± 0.57 | 6.91 ± 0.69 |
| carbohydrate | 50.55 ± 0.45 | 50.95 ± 0.57 | 51.06 ± 0.30 | 51.49 ± 0.21 | 51.71 ± 0.51 |
| crude ash | 7.50 ± 0.34 | 7.78 ± 0.65 | 6.51 ± 0.18 | 6.10 ± 0.14 | 6.77 ± 0.21 |
| crude fat | 3.55 ± 0.18 | 3.56 ± 0.01 | 3.21 ± 0.412 | 2.81 ± 0.51 | 2.62 ± 0.71 |
| crude fiber | 20.70 ± 0.82 | 20.40 ± 0.23 | 21.32 ± 0.20 | 20.80 ± 0.03 | 19.79 ± 0.18 |
| crude protein | 17.70 ± 0.42 | 17.31 ± 1.09 | 17.90 ± 0.31 | 18.80 ± 0.14 | 19.11 ± 0.40 |

[a]Moisture and dry matter are presented based on fresh weight; other data are presented based on dry weight. Each value is expressed as mean ± SD ($n$ = 3).

Table 2. Carbohydrate and Protein Content of Both Polysaccharide-Protein Fractions and Polysaccharide Fractions[a]

| component (%) | crude polysaccharide-proteins | | | crude polysaccharides | | |
|---|---|---|---|---|---|---|
| | yield | carbohydrate content | protein content | yield | carbohydrate content | protein content |
| stage I | 0.89 ± 0.03 | 3.37 ± 0.06 | 39.12 ± 0.11 | 3.12 ± 0.04 | 75.33 ± 0.32 | 12.13 ± 0.19 |
| stage II | 1.84 ± 0.06 | 6.70 ± 0.07 | 42.51 ± 0.13 | 3.68 ± 0.06 | 60.45 ± 0.24 | 21.36 ± 0.08 |
| stage III | 1.56 ± 0.05 | 3.94 ± 0.05 | 39.90 ± 0.09 | 3.43 ± 0.05 | 86.11 ± 0.38 | 13.51 ± 0.07 |
| stage IV | 1.55 ± 0.08 | 4.89 ± 0.04 | 45.36 ± 0.05 | 3.47 ± 0.07 | 88.06 ± 0.21 | 1.67 ± 0.05 |
| stage V | 1.56 ± 0.05 | 4.28 ± 0.04 | 55.66 ± 0.08 | 4.85 ± 0.05 | 57.07 ± 0.26 | 11.21 ± 0.17 |

[a]Each value is expressed as mean ± SD ($n$ = 3).

**In-Gel Tryptic Digestion of Polysaccharide-Protein Fraction PEG-1.** According to the MTT assay results, polysaccharide-protein fraction PEG-1 had the highest cytotoxical activity compared to the other three fractions. The in-gel tryptic digestion was conducted for mass spectrometric characterization of PEG-1.[29] The bands of PEG-1 in SDS-PAGE were excised, rinsed with double distilled water, and destained with 200 μL of destaining solution (25 mM $NH_4HCO_3$, 50% $CH_3CN$), respectively. Then the gel slices were vacuum-dried and incubated with a trypsin solution at 37 °C overnight. After the reaction cooled down to room temperature, the supernatant was collected and saved. The gel was subsequently extracted twice with 20 μL of 0.1% TFA in 50% ACN by gentle mixing and incubation at 60 °C for 10 min. Both the supernatant and extract solution were freeze-dried for further MALDI-TOF analysis.

**Mass Spectrometry and Protein Identification.** MALDI-TOF mass spectrometric analysis was performed on AB 5800 MALDI-TOF (AB SCIEX, Foster City, CA, USA) following a previously described method.[21] Spectra were accumulated until a satisfactory S/N had been obtained. The peptide mass fingerprinting of glycoprotein was acquired and processed using Mass-Lynx V4.1 software (Waters, Milford, MA, USA) and was converted to PKL files by the Protein-Lynx 2.2.5 software (Waters, Milford, MA, USA). The PKL files were analyzed using the MASCOT search engine. The search parameters were defined as follows: database, NCBInr; taxonomy, *Homo sapiens*; enzyme, trypsin; and allowance of one missed cleavage.

**Statistical Analysis.** Each experiment was repeated three times using duplicate samples. The results were expressed as means ± standard deviations. Statistical comparisons were made by one-way analysis of variance (ANOVA), followed by Duncan's multiple-comparison test. Differences were considered significant when the $p$-values were <0.05.

## RESULTS AND DISCUSSION

**Effect of Maturity Stage on Proximate Compositions in *P. eryngii* Fruiting Body.** The moisture contents of *P. eryngii* were in the range of 90.13−93.09% based on fresh weight (Table 1). Based on dry weight, other proximate compositions were listed in the following order: carbohydrate (50.55−51.71%) > crude fiber (19.79−21.32%) > crude protein (17.31−19.11%) > crude ash (6.10−7.78%) > crude fat (2.62−3.56%). It could be concluded that *P. eryngii* had high contents of carbohydrate, fiber, and protein and was low in ash and fat, which was in agreement with the previous study by Li et al.[30]

The carbohydrate and protein contents in *P. eryngii* slightly increased with the development of fruiting body maturity from stage I to stage V, respectively, while fat content decreased. Different phenomena have been observed: the maturity of *Agaricus bisporus* increased the carbohydrate and fat contents and decreased the protein content from 27.0% to 21.7%.[31] Interestingly, the maturating processes of *L. deliciosus* and *L. piperatus* fruiting bodies decreased the carbohydrate contents and increased protein contents.[32]

The fiber content of *P. eryngii* reached the highest value of 21.32% at stage III and declined to 19.79% at stage V, which showed a similar trend with *Agaricus bisporus* with a peaked fiber content of 23.3% at stage III.[31]

**Effect of Maturity Stage on Carbohydrate and Protein Contents in Polysaccharide and Polysaccharide-Protein Fractions.** The *P. eryngii* polysaccharide and polysaccharide-protein fractions at each stage were obtained by water extraction at 100 or 4 °C followed by ethanol or $(NH_4)_2SO_4$ precipitation. The carbohydrate and protein contents in these polysaccharide and polysaccharide-protein fractions were determined and are summarized in Table 2.

The polysaccharide fractions at each stage were carbohydrate-predominate with high carbohydrate contents ranging from 57.07% to 88.06% and low protein contents from 1.67% to 21.36%. The maturity development from stage I to stage IV led to the increase of carbohydrate content and decrease of protein content. Overgrowth appeared to decrease the carbohydrate content to 57.07% at stage V.

The polysaccharide-protein fractions extracted at 4 °C with $(NH_4)_2SO_4$ precipitation showed the protein-predominate characteristic with the increased high protein content from 39.12% to 55.66% with the maturation. The maturity development showed the fluctuation of carbohydrate content in the polysaccharide-protein fractions from 3.37% to 6.70%.

**Effect of Maturity Stage on Phenols, Flavonoids, and Saponin Contents in Ethanol Extracts of *P. eryngii*.** Table

Table 3. Phenol, Flavonoid, and Saponin Contents in Ethanol Extracts of *P. eryngii* at Five Maturity Stages[a]

| contents(mg/g) | stage I | stage II | stage III | stage IV | stage V |
|---|---|---|---|---|---|
| phenols | 19.11 ± 0.11 | 20.70 ± 0.05 | 18.72 ± 0.09 | 15.15 ± 0.13 | 14.85 ± 0.08 |
| flavonoids | 24.77 ± 0.09 | 22.47 ± 0.03 | 21.08 ± 0.06 | 20.16 ± 0.07 | 20.62 ± 0.09 |
| saponins | 7.41 ± 0.06 | 7.75 ± 0.08 | 6.71 ± 0.05 | 6.83 ± 0.08 | 6.13 ± 0.06 |

[a]Each value is expressed as mean ± SD ($n$ = 3).

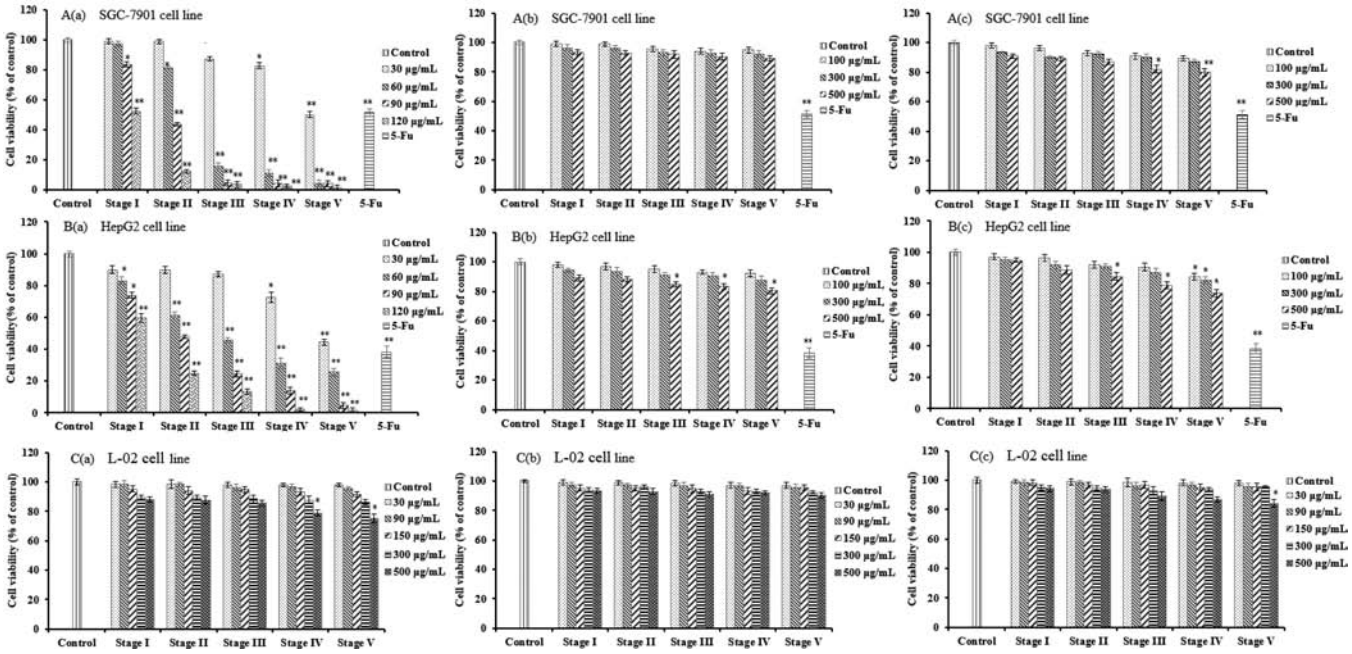


**Figure 2.** (A) Effect of crude polysaccharide-proteins (A(a)), crude polysaccharides (A(b)), and ethanol extracts (A(c)) from *P. eryngii* fruiting bodies of five maturity stages on the cell viability of SGC-7901 cells incubated with at 37 °C for 24 h and 5-Fu (20 μg/mL) as the positive control. (B) Effect of crude polysaccharide-proteins (B(a)), crude polysaccharides (B(b)), and ethanol extracts (B(c)) from *P. eryngii* fruiting bodies of five maturity stages on the cell viability of HepG-2 cells incubated with at 37 °C for 24 h and 5-Fu (20 μg/mL) as the positive control. (C) Toxicity of crude polysaccharide-proteins (C(a)), crude polysaccharides (C(b)), and ethanol extracts (C(c)) from *P. eryngii* fruiting bodies of five maturity stages on normal human liver L-02 cells. Data are presented as mean ± SD of three independent experiments. *$P$ < 0.05 compared to control group, **$P$ < 0.01 compared to control group.

3 presents the phenol, flavonoid, and saponin contents in ethanol extracts from 5-stage *P. eryngii* fruiting bodies. The early stages (stage I and II) gave the higher contents of phenol, flavonoid, and saponin. From stage III, all the contents of phenol, flavonoid, and saponin began to slightly decrease with the prolonged maturity stage. These phenomena were in agreement with the results with the low content of bioactive compounds such as total phenol and flavonoid at the mature stage (cap diameter higher than 7 cm) compared to those in immature (cap diameter less than 4.5 cm) *L. piperatus* fruiting bodies.[33]

**Effect of Maturity Stage on the Cytotoxical Activity of Polysaccharide and Polysaccharide-Protein Fractions and Ethanol Extracts of *P. eryngii*.** Figure 2 presents the antiproliferative effect on SGC-7901 and HepG-2 cells of polysaccharide fractions, polysaccharide-protein fractions, and ethanol extracts at five *P. eryngii* fruiting body maturity stages. The polysaccharide fraction (Figure 2A(b) and Figure 2B(b)) of *P. eryngii* fruiting body seemed to have a slight inhibition effect on SGC-7901 cells and HepG-2 cells with the cell viability of over 80.39% at concentration even up to 500 μg/mL. Generally, high purity or content of bioactive polysaccharides will benefit the antitumor activity in vitro with lower dose. For example, the purified polysaccharide PEPE-3 from *P. eryngii* residue showed highest growth-inhibitory activity to HepG-2 cells with the cell viability of 27.56% at 400 μg/mL.[34] However, most mushroom polysaccharides could not directly kill the tumor cells in vitro while exerting their antitumor action through activating the host immune systems.[20,35] The commercial D-fraction from the fruiting body of *Grifola frondosa* was a β-1,6-glucan exhibiting its antitumor activity via increase of cytokine level in NK cells, T cells, and spleen/lymph node cells.[36−38] The purified polysaccharide from *P. eryngii* fruiting body also acted as the potent immunomodulator to activate the immune response in tumor-bearing mice.[39]

The ethanol extract showed weak inhibition to SGC-7901 and HepG-2 cells with cell viability of 79.86% and 73.79%, respectively, even at a concentration of 500 μg/mL. Similar results were also found that the *Pleurotus ferulae* ethanol extracts had the higher cell viability of 67.94% at 800 μg/mL after 48-h treatment.[40]

Compared to polysaccharide fraction and ethanol extract, all the polysaccharide-protein fractions at five stages possessed higher cytotoxical activity against SGC-7901 and HepG-2 cells with a cell viability of less than 52.26% and 61.05% at a concentration of 120 μg/mL, respectively. These results correspond to the existing evidence that polysaccharide-protein complexes could kill the tumor cells directly in vitro by arresting the cell cycle and/or inducing the apoptosis of tumor

Table 4. Amino Acid Compositions of Crude Polysaccharide-Protein Extracts from *P. eryngii* Fruiting Bodies at Five Maturity Stages[a]

| | mass ratio (%, g/g) | | | | |
|---|---|---|---|---|---|
| amino acid | stage I | stage II | stage III | stage IV | stage V |
| Asp | 7.91 ± 0.19 | 8.04 ± 0.16 | 8.10 ± 0.05 | 8.66 ± 0.05 | 8.70 ± 0.14 |
| Thr | 5.76 ± 0.11 | 5.80 ± 0.12 | 5.95 ± 0.06 | 6.49 ± 0.12 | 6.52 ± 0.10 |
| Ser | 4.80 ± 0.05 | 4.69 ± 0.06 | 4.52 ± 0.15 | 4.76 ± 0.12 | 4.71 ± 0.11 |
| Glu | 7.91 ± 0.25 | 8.04 ± 0.18 | 8.33 ± 0.16 | 8.66 ± 0.22 | 8.70 ± 0.13 |
| Gly | 5.76 ± 0.12 | 6.47 ± 0.17 | 5.48 ± 0.11 | 6.49 ± 0.20 | 6.22 ± 0.11 |
| Ala | 6.47 ± 0.05 | 6.70 ± 0.15 | 6.19 ± 0.24 | 7.14 ± 0.09 | 7.06 ± 0.12 |
| Val | 6.71 ± 0.16 | 6.70 ± 0.17 | 6.67 ± 0.08 | 6.49 ± 0.05 | 6.45 ± 0.25 |
| Cys | 2.88 ± 0.04 | 2.23 ± 0.03 | 2.62 ± 0.02 | 2.60 ± 0.08 | 2.52 ± 0.07 |
| Met | 2.88 ± 0.05 | 2.46 ± 0.08 | 2.62 ± 0.09 | 2.38 ± 0.03 | 2.52 ± 0.02 |
| Ile | 4.80 ± 0.11 | 4.91 ± 0.10 | 5.00 ± 0.06 | 4.76 ± 0.03 | 4.37 ± 0.13 |
| Leu | 6.24 ± 0.16 | 6.03 ± 0.13 | 5.95 ± 0.14 | 5.84 ± 0.12 | 5.76 ± 0.11 |
| Tyr | 5.04 ± 0.13 | 5.13 ± 0.11 | 5.71 ± 0.12 | 5.19 ± 0.14 | 5.21 ± 0.12 |
| Phe | 4.32 ± 0.15 | 4.24 ± 0.13 | 4.29 ± 0.06 | 4.11 ± 0.11 | 5.71 ± 0.17 |
| His | 2.16 ± 0.04 | 2.23 ± 0.05 | 2.14 ± 0.08 | 2.16 ± 0.03 | 2.18 ± 0.07 |
| carnosine | 9.83 ± 0.23 | 9.60 ± 0.25 | 10.24 ± 0.22 | 8.66 ± 0.21 | 7.73 ± 0.13 |
| Orn | 0.48 ± 0.07 | 1.34 ± 0.02 | 0.48 ± 0.07 | 0.866 ± 0.06 | 0.34 ± 0.04 |
| Lys | 6.95 ± 0.21 | 6.92 ± 0.24 | 7.38 ± 0.23 | 6.06 ± 0.18 | 6.89 ± 0.18 |
| ammonia | | | | | |
| Arg | 4.80 ± 0.17 | 4.24 ± 0.16 | 4.05 ± 0.05 | 4.11 ± 0.08 | 4.03 ± 0.03 |
| Pro | 4.32 ± 0.17 | 4.24 ± 0.11 | 4.29 ± 0.17 | 4.55 ± 0.11 | 4.55 ± 0.14 |

[a]Each value is expressed as mean ± SD ($n$ = 3).

Table 5. Monosaccharide Compositions of Crude Polysaccharide Extracted from *P. eryngii* Fruiting Bodies at Five Maturity Stages[a]

| | molar ratio (%, mol/mol) | | | | |
|---|---|---|---|---|---|
| monosaccharide | stage I | stage II | stage III | stage IV | stage V |
| L-Rha | 21.02 ± 0.16 | 5.77 ± 0.05 | 3.92 ± 0.03 | 6.64 ± 0.05 | 4.26 ± 0.04 |
| D-Ara | –[b] | – | – | – | – |
| D-Xyl | 23.01 ± 0.08 | 22.89 ± 0.07 | 12.80 ± 0.07 | 16.36 ± 0.06 | 19.29 ± 0.07 |
| D-Fru | – | – | – | – | – |
| D-Glc | 42.46 ± 0.11 | 59.31 ± 0.17 | 72.23 ± 0.19 | 68.24 ± 0.14 | 63.57 ± 0.08 |
| D-Man | 11.32 ± 0.05 | 10.40 ± 0.06 | 8.06 ± 0.06 | 7.66 ± 0.03 | 10.08 ± 0.05 |
| D-Gal | 2.20 ± 0.05 | 1.63 ± 0.03 | 3.00 ± 0.06 | 1.10 ± 0.03 | 2.80 ± 0.03 |

[a]Each value is expressed as mean ± SD ($n$ = 3). [b]Not determined.

cells.[41] The typical examples included that the polysaccharide-protein HM-3A from mushroom *Hypsizygus marmoreus* and glycoprotein PCP-3A from golden oyster mushroom *Pleurotus citrinopileatus* showed a human leukemic U937 cell growth inhibition rate of over 74.6% at 100 μg/mL and 97.7% at 50 μg/mL, respectively.[42,43]

Interestingly, the polysaccharide-protein at the same concentration had increased cytotoxical activity with growing maturity of *P. eryngii* fruiting body. For example, after the treatment of polysaccharide-proteins from stage I to V at a concentration of 90 μg/mL, the SGC-7901 and HepG-2 cell viabilities decreased from 83.76% to 3.88% and 75.37% to 4.7%, respectively, which also motivated us to further elucidate the structural and maturity stage-specific features of the *P. eryngii* polysaccharide-protein fractions.

Toxicity of polysaccharide-protein fraction, polysaccharide fraction, and ethanol extracts from *P. eryngii* fruiting bodies of five maturity stages was evaluated by using normal human liver L-02 cells. As shown in Figure 2C, there was no significance between the polysaccharide fraction treated groups with control ($P > 0.05$). As for the polysaccharide-protein fractions, samples at mature stage (IV, V) showed significant inhibition of L-02 cell growth at over 500 μg/mL ($P < 0.05$), which indicated that the polysaccharide-protein fractions from *P. eryngii* fruiting bodies were relatively safe to the normal human liver L-02 cells.

**Effect of Maturity Stage on Amino Acid Composition in *P. eryngii* Polysaccharide-Proteins.** Table 4 shows the amino acid compositions/contents in the polysaccharide-protein fractions at stages I–V. The most abundant amino acids (present at 7.5 mass % or higher) among stages I–V were Asp, Glu, and carnosine. Furthermore, the low content amino acids (present at 2.2 mass % or lower) were Cys, Met, His, and Orn. Dundar et al. also found that Asp and Glu had high contents and Met and His had low contents in *Pleurotus eryngii* cultivated on the wheat stalk.[44] However, Li et al. determined that Arg, Ala, Glu, and Gln had high contents while the contents of D,L-α-aminoadipic acid, γ-aminobutyric acid, β-alanine, Cys, and $NH_3$ were low in the fresh *P. eryngii* harvested at the mature stage.[30] The differences in the amino acid composition and contents were mainly due to different *Pleurotus* materials or determination methods used.

Contents of three amino acids, Asp, Thr, and Glu, kept increasing in relative abundance while Val and Leu decreased with the development of *P. eryngii* maturation. Additionally, the

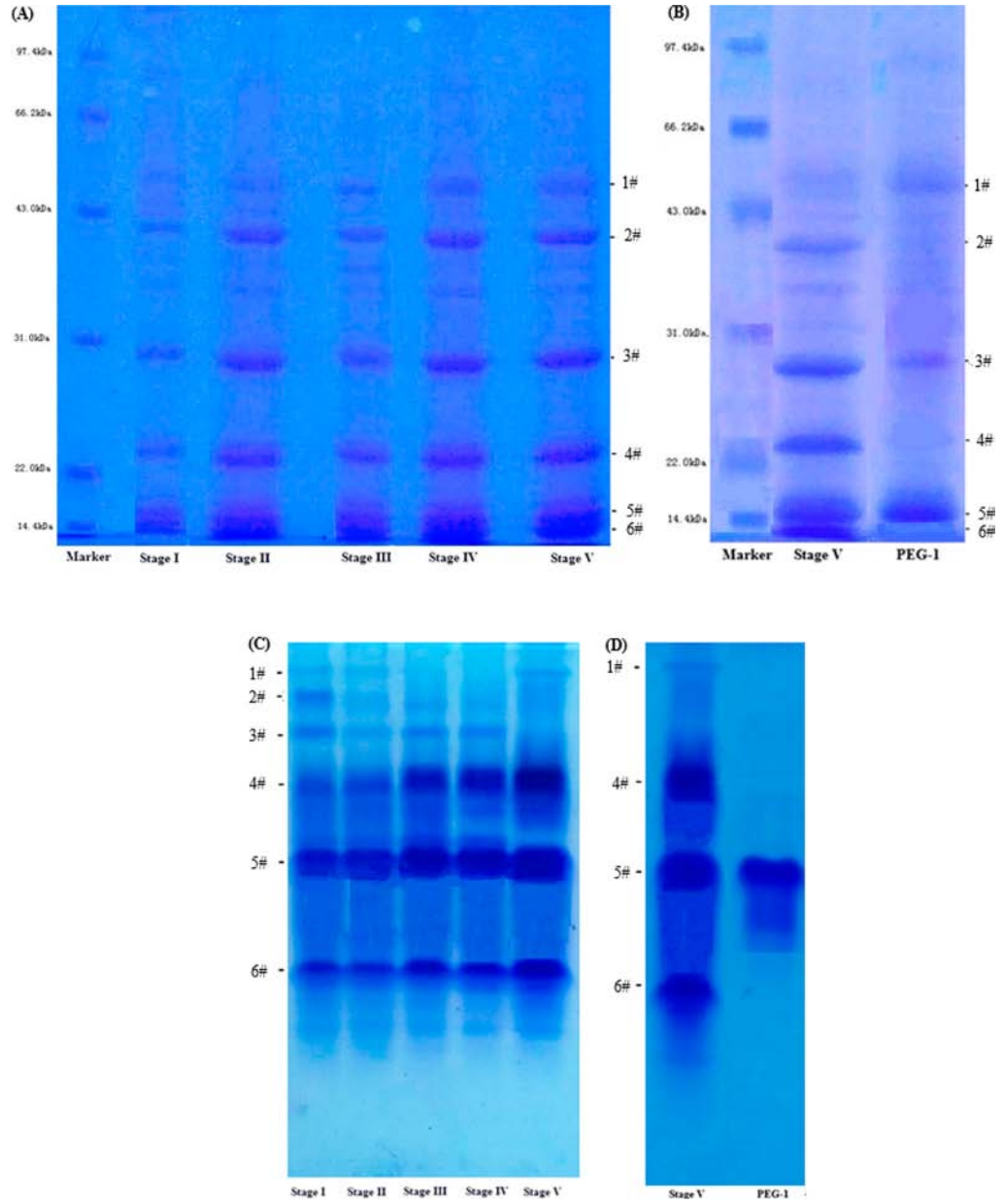


**Figure 3.** SDS-PAGE (A, B) and Native-PAGE (C, D) of crude polysaccharide-proteins from *P. eryngii* fruiting bodies at five stages and PEG-1 purified from crude polysaccharide-protein at stage V.

increase of acidic amino acids (Asp and Glu) with the *P. eryngii* maturation indicated that the assembled polysaccharide-protein fractions possibly showed acid properties with low p*I* value. Some polysaccharide-proteins (lectins), such as MAL from *Mycoleptodonoides aitchisonii*, were acid protein (p*I* value, 4.3–4.5) with a high content of acidic amino acid (12.1% of AsX).[45]

**Effect of Maturity Stage on Monosaccharide Composition in *P. eryngii* Polysaccharide-Proteins.** Table 5 showed monosaccharide compositions of crude polysaccharide-proteins from *P. eryngii* fruiting bodies harvested at five maturity stages. L-Rhamnose, D-xylose, D-glucose, D-mannose, and D-galactose were detected in the crude polysaccharide-proteins of *P. eryngii* fruiting body, which indicated that the polysaccharide-protein contained a heteropolysaccharide chain. The monosaccharide compositions in *P. eryngii* are related to the extraction methods, material suppliers, and different parts of the fruiting body. Some polysaccharide fractions extracted with high temperature (100 °C) from *Pleurotus ostreatus* and *Pleurotus eryngii* are from fruiting bodies composed of glucose and indentified as the glucans.[9] *P. eryngii* fruiting body supplied from Xi'an city (China) contained no D-arabinose,[46] while those produced in Seoul (Korea) or Shanghai BaixinBio-Tech Co. Ltd. (China) had no D-fructose.[47,48]

D-Glucose was the main sugar with a content of over 42.46% while D-galactose was lowest (<3.00%) in all stages. The content of D-glucose increased from stage I to stage III, and then began to decrease during stages III–V. On the contrary, the content of D-xylose decreased with stages I–III and increased with stages III–V with the lowest content of 12.80% at stage III. Similarly, the content of D-mannose decreased with stages I–IV and increased with stages IV and V with the lowest level of 7.66% at stage IV. Maturation seemed to have a slight effect on the contents of L-rhamnose and D-galactose. However, fiber-associated galactose in *Agaricus bisporus* (white button and

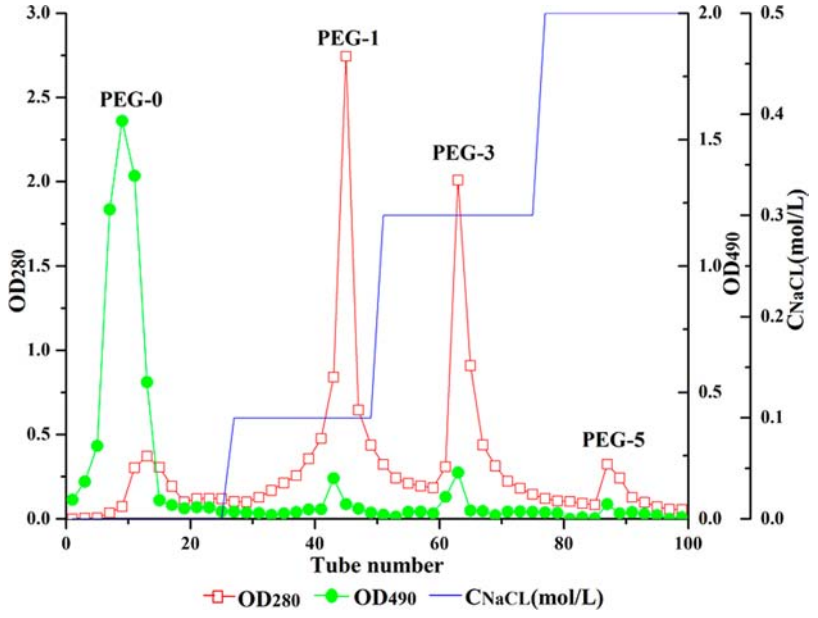


**Figure 4.** Anion-exchange chromatography of crude polysaccharide-protein from *P. eryngii* fruiting bodies at stage V on DEAE-Sepharose Fast Flow column (2.5 cm × 20 cm).

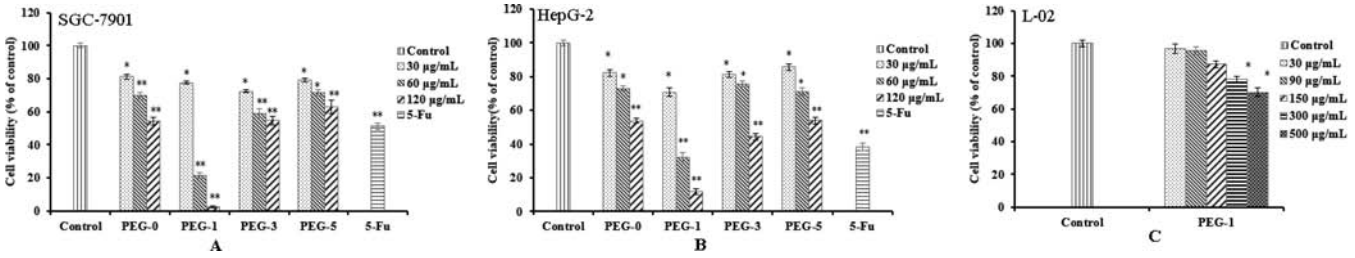


**Figure 5.** Effect of polysaccharide-protein fractions purified from *P. eryngii* fruiting bodies at stage V on the cell viability of SGC-7901 cells (A) and HepG-2 cells (B) incubated at 37 °C for 24 h and 5-Fu (20 μg/mL) as the positive control. (C) Toxicity of polysaccharide-protein fractions purified from *P. eryngii* fruiting bodies at stage V on normal human liver L-02 cells. Data are presented as mean ± SD of three independent experiments. *$P$ < 0.05 compared to control group, **$P$ < 0.01 compared to control group.

crimini) and *Lentinus edode* decreased with aging process.[13] These observed changes might be due to the energetic roles of monosaccharides during fungal growth.[49]

**SDS-PAGE, Native-PAGE, Mass Spectrometry, and Protein Identification of *P. eryngii* Polysaccharide-Proteins.** To find which polysaccharide-protein possibly possesses the cytotoxical activity in the crude samples extracted from *Pleurotus eryngii* fruiting body, SDS-PAGE and Native-PAGE were conducted, and the results are shown in Figure 3. Six distinct SDS protein bands were obviously observed in SDS-PAGE results of all the crude polysaccharide-proteins in 5 stages (Figure 3A). These SDS protein bands had differentiated molecular weights approximately as follows: band 1#, 50 kDa; band 2#, 40 kDa; band 3#, 30 kDa; band 4#, 23 kDa; band 5#, 15 kDa; and band 6#, 14 kDa. Among these bands, band 1# had increased width and intensity with the fruiting bodies' maturation. Other bands were weak in stages I and III and increased the width and intensity in stages II, IV, and V.

The Native-PAGE figure (Figure 3 C) showes that Native band 1# had the low intensity at stages I and II, disappeared in stages III and IV, and appeared in mature stage (V). The intensity of Native band 2# decreased gradually with the development of fruiting body and disappeared in stage V, while Native bands 4#, 5#, and 6# showed significant increase of intensity with fruiting body development. According to the increased cytotoxical activity and the intensity changes of crude polysaccharide-proteins with the fruiting body maturation, the polysaccharide protein with the cytotoxical activity would be targeted to the one or more samples in Native bands 4#, 5#, and 6#.

Further purification steps were applied to narrow the target polysaccharide-protein with cytotoxical activity. The purification with DEAE-Sepharose Fast Flow chromatography (Figure 4) of the crude polysaccharide-proteins in stage V resulted in four fractions as PEG-0, PEG-1, PEG-3, and PEG-5. The cell viabilities of SGC-7901, HepG-2, and L-02 cells influenced by each fraction are shown in Figure 5. At a concentration of 120 μg/mL, PEG-1 inhibited the SGC-7901 cell viability to 2.53% while residual cell viabilities in PEG-0, -3, and -5 treated groups were 54.41%, 54.70%, and 63.11% after 24 h treatment, respectively. Similar trends were found in HepG-2 cell treated with four fractions. PEG-1 showed the highest inhibitory effect with cell viability of 11.83% after 24 h treatment. PEG-1 also had no significant inhibition of normal human liver L-02 cells at a concentration of <300 μg/mL ($P$ > 0.05). Increased PEG-1 concentrations to over 300 μg/mL resulted in the decreased cell viability of 77.9%, which also verified the conclusion that

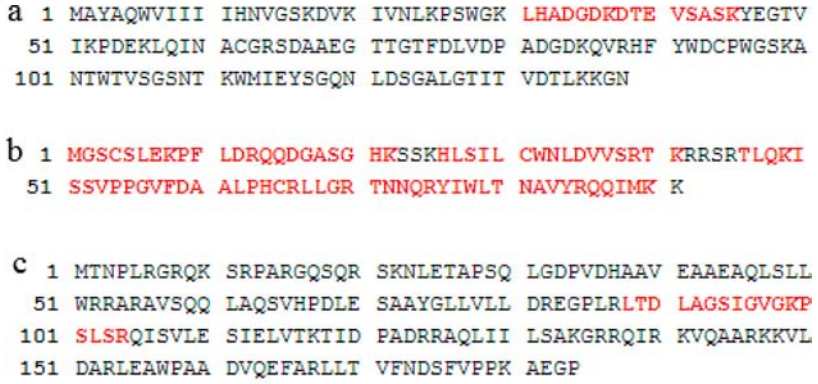


**Figure 6.** Peptide mass fragments of SDS protein bands confirmed by a NCBI blast search of mass spectrometry: (a) SDS protein band 1#, (b) SDS protein band 3#, (c) SDS protein band 5#.

the polysaccharide-protein had selectivity on cancer and normal cells.

The SDS-PAGE result of PEG-1 (Figure 3 B) showed three bands corresponding to bands 1#, 3#, and 5# with molecular weight of approximately 50 kDa, 30 kDa, and 15 kDa, respectively. However, Native-PAGE of PEG-1 (Figure 4 D) had a single band which was at the same position with Native band 5#, which indicated that the purified PEG-1 possibly had three subunits.

The three bands of purified PEG-1 on the SDS-PAGE were applied to the MALDI-TOF-MS and NCBI BLAST search for analyzing its partial sequences. The mass spectra of peptides of PEG-1are shown in Figure 6. From the sequence search, the band 1# subunit was similar to the Pe. Pleurutolysin A [*Pleurotus eryngii*] (gil543583497) of 15181 Da with a high score of 110 and 10% sequence coverage (Figure 6a); the band 3# subunit had a similar peptide sequence to the hypothetical protein Y032_0223g2652 [*Ancylostoma ceylanicum*] (gil 597840512) of 10590 Da with a low score of 63 and 91% sequence coverage (Figure 6b), while the band 5# subunit was similar to the hypothetical protein [*Acaricomes phytoseiuli*] (gil 516862670) of 20111 Da with a low score of 60 and 9% sequence coverage (Figure 6c). Hence, it could be concluded that the cytotoxical polysaccharide-protein PEG-1 from *P. eryngii* fruiting body at least contained the identified peptide sequences shown in red (Figure 6). However, the total amino acid sequence of polysaccharide-protein PEG-1 needs to be further elucidated by using molecular cloning such as genome walking PCR, or column affinity chromatography and crystallization.

In summary, our study first reported the changes of macromolecular compositions in *P. eryngii* and their contents and cytotoxical activity with the development of the fruiting bodies' maturity. The polysaccharide-protein fractions had the highest antiproliferative effect on the SGC-7901 and HepG-2 cells in vitro compared with polysaccharide fractions and ethanol extract, and the increased cytotoxical activity with growing maturity of *P. eryngii* fruiting body. The polysaccharide-protein PEG-1 with three subunits was identified as the possible target cytotoxical component. Further investigations would focus on finding the fine structure of PEG-1 including protein sequence and polysaccharide chain, and its physiological role during growth and development of *P. eryngii* fruiting body.

## AUTHOR INFORMATION


### Corresponding Authors

*(F.C.) Phone: +86-511-88780226. Fax: +86-511-88780201. E-mail: fengjiecui@163.com.

*(W.S.) Phone: +86-511-88780226. Fax: +86-511-88780201. E-mail: sunwenjing1919@163.com.

*(L.P.) Phone: +86-571-86404054. Fax: +86-571-86401834. E-mail: lfping2005@gmail.com.



### Funding

This work was supported by funding from Natural Science Foundation of China (NSFC 31101269), China Postdoctoral Science Special Foundation (2013T60648), National Science & Technology Pillar Program during the Twelfth Five-year Plan Period (2012BAD36B05), 2012 Excellent Key Young Teachers Project of Jiangsu University; Science & Technology Platform Construction Program of Jiangxi Province.


### Notes

The authors declare no competing financial interest.

## REFERENCES


(1) Zaidman, B. Z.; Yassin, M.; Mahajna, J.; Wasser, S. P. Medicinal mushroom modulators of molecular targets as cancer therapeutics. *Appl. Biochem. Biotechnol.* **2005**, *67*, 453−468.

(2) Ivanova, T. S.; Krupodorova, T. A.; Barshteyn, V. Y.; Artamonova, A. B.; Shlyakhovenko, V. A. Anticancer substances of mushroom origin. *Exp. Oncol.* **2014**, *36* (2), 58−66.

(3) Choi, J. H.; Kim, S.; Sapkota, K.; Park, S. E.; Kim, S. J. Expression and production of therapeutic recombinant human platelet-derived growth factor-BB in *Pleurotus eryngii*. *Appl. Biochem. Biotechnol.* **2011**, *165*, 611−623.

(4) Kang, M. Y.; Rico, C. W.; Lee, S. C. *In vitro* antioxidative and antimutagenic activities of oak mushroom (*Lentinus edodes*) and king oyster mushroom (*Pleurotus eryngii*) byproducts. *Food Sci. Biotechnol.* **2012**, *21* (1), 167−173.

(5) Ike, K.; Kameyama, N.; Ito, A.; Imai, S. Induction of a T-Helper 1 (Th1) immune response in mice by an extract from the *Pleurotus eryngii* (Eringi) mushroom. *J. Med. Food* **2012**, *15* (12), 1124−1128.

(6) Jeong, Y. T.; Jeong, S. C.; Gu, Y. A.; Islam, R.; Song, C. H. Antitumor and immunomodulating activities of endo-biopolymers obtained from a submerged culture of *Pleurotus eryngii*. *Food Sci. Biotechnol.* **2010**, *19* (2), 399−404.

(7) Mizutani, T.; Inatomi, S.; Inazu, A.; Kawahara, E. Hypolipidemic effect of *Pleurotus eryngii* extract in fat-loaded mice. *J. Nutr. Sci. Vitaminol.* **2010**, *56*, 48−53.

(8) Chen, J.; Mao, D.; Yong, Y.; Li, J.; Wei, H.; Lu, L. Hepatoprotective and hypolipidemic effects of water-soluble polysaccharidic extract of *Pleurotus eryngii*. *Food Chem.* **2012**, *130*, 687−694.

(9) Synytsya, A.; Mickova, K.; Synytsya, A.; Jablonsky, I.; Spevacek, J.; Erban, V.; Kovarikova, E.; Copikov, J. Glucans from fruit bodies of cultivated mushrooms *Pleurotus ostreatus* and *Pleurotus eryngii*: structure and potential prebiotic activity. *Carbohydr. Polym.* **2009**, *76*, 548−556.
(10) Ueda, M.; Shintani, K.; Akiko, N. A.; Nakazawa, M.; Kusud, M.; Nakatani, F.; Kawaguchi, T.; Tsujiyama, S.; Kawanishi, M.; Yagi, T.; Miyatake, K. A protein from *Pleurotus eryngii* var. tuoliensis C.J. Mou with strong removal activity against the natural steroid hormone, estriol: purification, characterization, and identification as a laccase. *Enzyme Microb. Technol.* **2012**, *51*, 402−407.
(11) Wang, H.; Ng, T. B. Eryngin, a novel antifungal peptide from fruiting bodies of the edible mushroom *Pleurotus eryngii*. *Peptides* **2004**, *25*, 1−5.
(12) Liu, L. Y.; Li, Z. H.; Liu, J. K. A new menthane-type monoterpene from *Pleurotus eryngii*. *Chin. J. Nat. Med.* **2013**, *11* (1), 0071−0073.
(13) Dikeman, C. L.; Bauer, L. L.; Flickinger, E. A.; Fahey, G. C. Effects of stage of maturity and cooking on the chemical composition of select mushroom varieties. *J. Agric. Food Chem.* **2005**, *53*, 1130−1138.
(14) Oguri, S.; Ando, A.; Nagata, Y. A novel developmental stage-specific lectin of the basidiomycete *Pleurotus cornucopiae*. *J. Bacteriol.* **1996**, *178* (19), 5692−5698.
(15) Liu, J.; Kurashiki, K.; Fukuta, A.; Kaneko, S.; Suimi, Y.; Shimizu, K.; Kondo, R. Quantitative determination of the representative triterpenoids in the extracts of *Ganoderma lucidum* with different growth stages using high-performance liquid chromatography for evaluation of their 5a-reductase inhibitory properties. *Food Chem.* **2012**, *133*, 1034−1038.
(16) Lin, J. T.; Liu, C. W.; Chen, Y. C.; Hu, C. C.; Juang, L. D.; Shiesh, C. C.; Yang, D. J. Chemical composition, antioxidant and anti-inflammatory properties for ethanolic extracts from *Pleurotus eryngii* fruiting bodies harvested at different time. *LWT—Food Sci. Technol.* **2014**, *55*, 374−382.
(17) Moonmoon, M.; Uddin, M. N.; Ahmed, S.; Shelly, N. J.; Khan, M. A. Cultivation of different strains of king oyster mushroom (*Pleurotus eryngii*) on saw dust and rice straw in Bangladesh. *Eur. J. Biol. Sci.* **2010**, *2* (1), 13−18.
(18) AOAC. *Official methods of analysis*, 15th ed.; Association of Offical Analytical Chemists: Washington, DC, 1990.
(19) Crisan, E. V.; Sands, A. Nutritional value. In *The biology and cultivation of edible mushrooms*; Chang, S. T., Hayes, W. A., Eds.; Academic Press: New York, 1978; pp 137−165.
(20) Cui, F. J.; Zan, X. Y.; Li, Y. H.; Yang, Y.; Sun, W. J.; Zhou, Q.; Yu, S. L.; Dong, Y. Purification and partial characterization of a novel anti-tumor glycoprotein from cultured mycelia of *Grifola frondosa*. *Int. J. Biol. Macromol.* **2013**, *62*, 684−690.
(21) Cui, F. J.; Li, Y. H.; Zan, X. Y.; Yang, Y.; Sun, W. J.; Qian, J. Y.; Zhou, Q.; Yu, S. L. Purification and partial characterization of a novel hemagglutinating glycoprotein from the cultured mycelia of *Hericium erinaceus*. *Process Biochem.* **2014**, *49*, 1362−1369.
(22) Adom, K. K.; Liu, R. H. Antioxidant activity of grains. *J. Agric. Food Chem.* **2002**, *50*, 6182−6187.
(23) Jia, Z.; Tang, M.; Wu, J. The determination of flavonoid contents in mulberry and their scavenging effects on superoxide radicals. *Food Chem.* **1999**, *64*, 555−559.
(24) Wang, Y.; Liu, Y.; Liu, Z.; Yin, J. The quality control of the effective fraction from *Dioscorea spongiosa*. *Asian J. Tradit. Med.* **2007**, *2* (1), 12−18.
(25) Wang, L.; Zhou, B.; Yu, K.; Su, Z.; Gao, S.; Chu, L.; Liu, J.; Yang, G. Novel antitumor agent, trilacunary keggin-type tungstobismuthate, inhibits proliferation and induces apoptosis inhuman gastric cancer SGC-7901 cells. *Inorg. Chem.* **2013**, *52*, 5119−5127.
(26) Su, Q.; Xie, W.; Wang, S.; Wu, Q.; Liu, B.; Fang, Y.; Xu, B.; Zhang, Y. The endosymbiont Hamiltonella increases the growth rate of its host *Bemisia tabaci* during periods of nutritional stress. *PLoS One* **2014**, DOI: 10.1371/journal.pone.0089002.
(27) Li, M.; Wang, H.; Ng, T. B.Isolation of a phytase with distinctive characteristics from an edible mushroom, *Pleurotus eryngii*. *Protein Pept. Lett.* **2013**, *20*, 459−466.
(28) Davis, B. J. Disc Electrophoresis- II.Method and application to human serum proteins. *Ann. N.Y. Acad. Sci.* **1964**, *121*, 404−427.
(29) Shevchenko, A.; Tomas, H.; Havlis, J.; Olsen, J. V.; Mann, M. In-gel digestion for mass spectrometric characterization of proteins and proteomes. *Nat. Protoc.* **2006**, *6* (1), 2856−2860.
(30) Li, X.; Feng, T.; Zhou, F.; Zhou, S.; Liu, Y.; Li, W.; Ye, R.; Yang, Y. Effects of drying methods on the tasty compounds of *Pleurotus eryngii*. *Food Chem.* **2015**, *166*, 358−364.
(31) Tsai, S. Y.; Wu, T. P.; Huang, S. J.; Mau, J. L. Nonvolatile taste components of *Agaricus bisporus* harvested at different stages of maturity. *Food Chem.* **2007**, *103*, 1457−1464.
(32) Barros, L.; Baptista, P.; Estevinho, L. M.; Ferreira, I. C.F.R. Effect of fruiting body maturity stage on chemical composition and antimicrobial activity of *Lactarius* sp. mushrooms. *J. Agric. Food Chem.* **2007**, *55*, 8766−8771.
(33) Barros, L.; Baptista, P.; Ferreira, I. C.F.R. Effect of *Lactarius piperatus* fruiting body maturity stage on antioxidant activity measured by several biochemical assays. *Food Chem. Toxicol.* **2007**, *45*, 1731−1737.
(34) Ma, G.; Yang, W.; Mariga, A. M.; Fang, Y.; Ma, N.; Pei, F.; Hu, Q. Purification, characterization and antitumor activity of polysaccharides from *Pleurotus eryngii* residue. *Carbohydr. Polym.* **2014**, *114*, 297−305.
(35) Lo, T. C. T.; Tsao, H. H.; Wang, A. Y.; Chang, C. A. Pressurized water extraction of polysaccharides as secondary metabolites from *Lentinula edodes*. *J. Agric. Food Chem.* **2007**, *55*, 4196−4201.
(36) Kodama, N.; Komuta, K.; Sakai, N.; Nanba, H. Effects of D-fraction, a polysaccharide from *Grifola frondosa* on tumor growth involve activation of NK cells. *Biol. Pharm. Bull.* **2002**, *25*, 1647−1650.
(37) Kodama, N.; Harada, N.; Nanba, H. A polysaccharide, extract from *Grifola frondosa*, induces Th-1 dominant responses in carcinoma-bearing BALB/c mice. *Jpn. J. Pharmacol.* **2002**, *90*, 357−360.
(38) Inoue, A.; Kodama, N.; Nanba, H. Effect of maitake (*Grifola frondosa*) D-fraction on the control of the T lymph node Th-1/Th-2 proportion. *Biol. Pharm. Bull.* **2002**, *25*, 536−540.
(39) Yang, Z.; Xu, J.; Fu, Q.; Fu, X.; Shu, T.; Bi, Y.; Song, B. Antitumor activity of a polysaccharide from *Pleurotus eryngii* on mice bearing renal cancer. *Carbohydr. Polym.* **2013**, *95*, 615−620.
(40) Wang, W.; Chen, K.; Liu, Q.; Johnston, N.; Ma, Z.; Zhang, F.; Zheng, X. Suppression of tumor growth by *Pleurotus ferulae* ethanol extract through induction of cell apoptosis, andinhibition of cell proliferation and migration. *PLoS One* **2014**, DOI: 10.1371/journal.-pone.0102673.
(41) Li, G.; Kim, D. H.; Kim, T. D.; Park, B. J.; Park, H. D.; Park, J. I.; Na, M. K.; Kim, H. C.; Hong, N. D.; Lim, K.; Hwang, B. D.; Yoon, W. H. Protein-bound polysaccharide from *Phellinus linteus* induces G2/M phase arrest and apoptosis in SW480 human colon cancer cells. *Cancer Lett.* **2004**, *216*, 175−181.
(42) Tsai, P. F.; Ma, C. Y.; Wu, J. S. B. A novel glycoprotein from mushroom *Hypsizygus marmoreus* (Peck) Bigelow with growth inhibitory effect against human leukaemic U937 cells. *Food Chem.* **2013**, *141*, 1252−1258.
(43) Chen, J. N.; Wang, Y. T.; Wu, J. S. B. A glycoprotein extracted from golden oyster mushroom *Pleurotus citrinopileatus* exhibiting growth inhibitory effect against U937 leukemia cells. *J. Agric. Food Chem.* **2009**, *57*, 6706−6711.
(44) Dundar, A.; Acay, H.; Yildiz, A. Yield performances and nutritional contents of three oyster mushroom species cultivated on wheat stalk. *Afr. J. Biotechnol.* **2008**, *7* (19), 3497−3501.
(45) Kawagishi, H.; Takagi, J. I.; Taira, T.; Murata, T.; Usui, T. C. Purification and characterization of a lectin from the mushroom *Mycoleptodonoides aitchisonii*. *Phytochemistry* **2001**, *56*, 53−58.
(46) Ren, D.; Zhao, Y.; Nie, Y.; Lu, X.; Sun, Y.; Yang, X. Chemical composition of *Pleurotus eryngii* polysaccharides and their inhibitory effects on high-fructose diet-induced insulin resistance and oxidative stress in mice. *Food Funct.* **2014**, DOI: 10.1039/c3fo60640f.

(47) Kim, M. Y.; Chung, L. M.; Lee, S. J.; Ahn, J. K.; Kim, E. H.; Kim, M. J.; Kim, S. L.; Moon, H. I.; Ro, H. M.; Kang, E. Y.; Seo, S. H.; Song, H. K. Comparison of free amino acid, carbohydrates concentrations in Korean edible and medicinal mushrooms. *Food Chem.* **2009**, *113*, 386−393.
(48) Li, W.; Gu, Z.; Yang, Y.; Zhou, S.; Liu, Y.; Zhang, J. Non-volatile taste components of several cultivated mushrooms. *Food Chem.* **2014**, *143*, 427−431.
(49) Valdez-Morales, M.; Barry, K.; Fahey, G. C.; Dominguez, J.; Gonzalez de Mejia, E.; Valverde, M. E.; Paredes-Lopez, O. Effect of maize genotype, developmental stage, and cooking process on the nutraceutical potential of huitlacoche (*Ustilago maydis*). *Food Chem.* **2010**, *119*, 689−697.

microsphere design due to its good stability at various pH and moisture levels.[25,26] Drug-loaded beeswax microspheres demonstrated the absence of drug release at pH 1.2, proving the suitability for its use as a gastric-resistant material.[27]

The present research investigated the role of SCMC cross-linked with aluminum ions (AlCMC) and AlCMC−beeswax composites as the coating materials on the gelatin microcapsules for controlling essential oil release in simulated swine gastrointestinal fluid. Holy basil essential oil (HBEO) from *Ocimum sanctum* Linn., which has received significant attention as a natural substitute for AGP,[28] was used in this study. It contains several secondary metabolites with the major components being 42.6% methyleugenol, 26.9% $\beta$-caryophyllene, 10.7% eugenol, and 6.00% $\beta$-elemene.[29] The physicochemical properties of the microcapsules that were relevant to HBEO release and HBEO release kinetics were also examined.

## MATERIALS AND METHODS

**Chemicals.** HBEO was supplied by Thai-China Flavours and Fragrances Industry Co., Ltd. (Phra Nakhon Si Ayutthaya, Thailand). Gelatin from porcine skin (300 Bloom, type A) and NaCMC (medium viscosity) were purchased from Sigma-Aldrich (St. Louis, MO, USA). Sodium dodecyl sulfate (SDS) and Tween 80 were obtained from Ajak Finechem (NSW, Australia). Glutaraldehyde was provided by Merck (Darmstadt, Germany). Stearic acid was obtained from Laboratory Reagents & Fine Chemicals (Mumbai, India). White beeswax (pharmaceutical grade) was purchased from Paramelt BV (Heerhugowaard, The Netherlands). Porcine bile extract, pancreatin, and lipase from porcine pancreas and pepsin from porcine gastric mucosa were purchased from Sigma (Hampshire, UK). All chemicals were of analytical grade.

**Preparation of HBEO-Loaded Gelatin Microcapsules.** HBEO-loaded gelatin microcapsules were prepared using simple coacervation via glutaraldehyde cross-linking.[29] HBEO was dispersed into a gelatin solution (11.75% (w/v) gelatin and 0.1% (w/v) SDS) with stirring at 450 rpm and 40 °C for 25 min. Then, sodium sulfate solution (20% w/v) was added dropwise with continuous stirring at 550 rpm for phase separation. The temperature was subsequently decreased to 5 °C. Next, a glutaraldehyde solution consisting of 25% (v/v) glutaraldehyde, acetone, and distilled water was introduced into the mixture. This was followed by increasing the temperature to 40 °C with continuous stirring for 60 min. The microcapsules were washed twice with 0.3% (v/v) Tween 80 and were filtered through an 11 $\mu$m filtration Whatman membrane under vacuum. They were collected and dried at 60 °C until a constant dry weight was obtained. The finished microcapsules were stored in a hermetically sealed glass bottle at room temperature.

**Coating of HBEO-Loaded Gelatin Microcapsules with AlCMC and AlCMC−Beeswax Composites.** The HBEO-loaded gelatin microcapsules (UC) were coated with AlCMC or AlCMC−beeswax (1:1, w/w) composites, respectively named CC and CB. For the CC microcapsules, 20 g of UC was added into 200 mL of 1% (w/v) NaCMC solution, which contained 1% (w/v) glycerol as a plasticizer and 1% (w/v) stearic acid as an emulsifier. The mixture was shaken at 100 rpm and 30 °C. This was followed by the addition of 200 mL of 0.05 M aluminum chloride solution as a cross-linking agent with continuous stirring. To prepare the composite coating, the NaCMC solution was mixed with melted beeswax with stirring at 1200 rpm. Next, 20 g of UC was transferred into 200 mL of the composite, and the mixture was shaken at 100 rpm and 30 °C. Finally, to obtain CB microcapsules, NaCMC cross-linking was performed as previously described. The CC and CB microcapsules were filtered under vacuum and were stored at 4 °C until further analysis.

**Determination of HBEO Content and Encapsulation Efficiency.** The HBEO content was determined using a Thermo Spectronic Helios $\gamma$ UV−vis spectrophotometer (Cambridge, UK) at 289 nm, which is the wavelength of maximum absorbance of eugenol, the most powerful antioxidant and antimicrobial component of HBEO.[29] Briefly, the microcapsules (80 mg) were dissolved in dichloromethane to a final volume of 1 mL, and their concentration was calculated using the calibration curve shown in eq 1 ($R^2$ = 0.998)

$$y = 1.8082x + 0.0662 \quad (1)$$

where $y$ is the HBEO concentration and $x$ is the absorbance. Then, the encapsulation efficiency was calculated according to eq 2

$$\text{encapsulation efficiency} = (W_O/W_I) \times 100 \quad (2)$$

where $W_O$ is the mass of HBEO in the microcapsule and $W_I$ is the initial mass of HBEO added for the encapsulation.

The HBEO content was determined using eq 3

$$\text{HBEO content} = (W_O/W_M) \times 100 \quad (3)$$

where $W_M$ is the mass of the microcapsule.

**Determination of Antioxidant Activity.** Antioxidant activity was estimated using the 2,2-diphenyl-2-picrylhydrazyl (DPPH) radical assay as previously described with minor modifications.[30] The microcapsule solution (1 mL) in dichloromethane was mixed with 1 mL of 0.2 mM DPPH radical solution in methanol. The mixture was then shaken vigorously and left to stand for 20 min in the dark. The decrease in absorbance was measured at 517 nm against a blank sample. All samples were analyzed in triplicate. The DPPH radical scavenging activity was calculated according to eq 4

$$\text{DPPH radical scavenging activity} = [A_O - (A_M - A_S)]/A_O \times 100 \quad (4)$$

where $A_O$ is the absorbance of the control, $A_M$ is the absorbance of the DPPH solution mixed with the samples, and $A_S$ is the absorbance of the samples without DPPH.

**Particle Size Analysis.** The area-volume mean diameter ($D[4,3]$) was measured using a Mastersizer 2000 particle size analyzer (Malvern, Worcestershire, UK) equipped with a Hydro 2000 MU (A) wet dispersion unit and 0.3% Tween 80 as the dispersion medium.

**Scanning Electron Microscopy (SEM) Studies.** The microcapsules were fixed using 2% (v/v) osmium tetroxide for 1 h and were rinsed twice with distilled water. Then, they were dehydrated using a graded ethanol series (30, 50, 70, 95, and 100% (v/v)) three times for 10 min. Preparation of a microcapsule cross section was performed by cutting the sample with a razor blade. The samples were consecutively dried using a critical point dryer and were fixed on an aluminum stub using double-sided adhesive tape. This was followed by gold coating using an ion sputtering coater (IB2, Giko Engineering, Japan). The microcapsule surface morphology was characterized using SEM (JSM-5600, JEOL, Tokyo, Japan) at an accelerating voltage of 15 kV.

**Confocal Laser Scanning Microscopy (CLSM) Studies.** Fluorescence imaging with CLSM (LSM 5 Pascal, Carl Zeiss GmbH, Jena, Germany) was used to visualize the HBEO distribution in gelatin. HBEO was labeled with Nile blue dye prior to encapsulation, and the microcapsules were stained with Rhodamine B dye to localize gelatin. All fluorescence pictures were obtained using a ×10 objective (Plan-Neofluar, Carl Zeiss) and a 0.3 numerical aperture. Confocal illumination of HBEO and gelatin was provided using a multiline argon laser (488 nm excitation) and a helium/neon laser (543 nm excitation), respectively.

**Fourier Transform Infrared Spectroscopy (FTIR) Studies.** The FTIR spectra of UC, CC, CB, gelatin, beeswax, and HBEO were recorded using a TENSOR series FTIR spectrometer (Bruker Optics, Ettlingen, Germany) in ATR mode. The samples were scanned in transmission mode from 4000 to 500 $cm^{-1}$ with a resolution of 4 $cm^{-1}$.

**X-ray Diffraction (XRD) Studies.** The crystal structures of UC, CC, CB, and beeswax were determined using an XRD diffractometer (Philips model X'Pert MPD, Almelo, The Netherlands) equipped with Cu K$\alpha$ radiation (wavelength 1.5406 Å, 40 kV, and 30 mA). The samples were scanned along a 2$\theta$ range of 5−50° at a rate of 2.4°/min.

**Differential Scanning Calorimetry (DSC) Studies.** The thermal properties of UC, CC, CB, the physical mixture of HBEO and gelatin powder, and beeswax as well as HBEO were determined using a DSC-

1 *STAR*$^e$ *System* (Mettler Toledo, Switzerland) calibrated with indium. Accurately weighed samples (5 mg) were placed in a 40 $\mu$L aluminum pan and heated at a programmed rate of 10 °C/min in the temperature range from −80 to 300 °C.

**HBEO Release under Simulated Swine Gastrointestinal Conditions Experiments.** HBEO release studies were performed using a previously published method with slight modifications.[31] One percent (w/v) microcapsules were added into simulated gastric fluids (SGF) consisting of 3 g/L NaCl, 1.1 g/L KCl, 0.15 g/L $CaCl_2$, 0.6 g/L $NaHCO_3$, 3 g/L SDS, 0.21 g/L pepsin, and 0.25 g/L lipase. The pH was adjusted to 6.0, 3.5, 3.0, 2.5, and 2.0 at 0, 5, 30, 120, and 180 min, respectively, using 1 M HCl. The experiment was performed at 39 ± 0.5 °C with a stirring speed of 100 rpm. The absorbance of the sample at 289 nm was measured at 0, 5, 10, 20, 30, 40, 60, 80, 100, 120, 180, 210, and 240 min, and the electrolytes were replaced with fresh solution. CLSM observations were performed to verify HBEO diffusion after 10 min of incubation in SGF. After 240 min, 1 mL of trypsin solution (2 mg/mL), 14 mL of bile solution (40 mg/mL), 7.5 mL of pancreatic solution, and 7.5 mL of small intestinal electrolyte solution (0.6 g/L KCl, 5.0 g/L NaCl, 0.23 g/L $CaCl_2{\cdot}2H_2O$, and 3 g/L SDS) were mixed with SGF. Then, the pH of the simulated intestinal fluid (SIF) was increased to 5 and 6.5 at 240 and 300 min, respectively, by adding 1 M $NaHCO_3$. A 1 mL sample was collected from the medium to measure absorbance, and the electrolytes were replaced with fresh SIF at predetermined time intervals for 4 h.

The HBEO in vitro release data were analyzed to describe the release kinetics by fitting the data into various release kinetic models. The zero-order model describes a system in which the release rate is independent of concentration (eq 5). The first-order model describes a system in which the release rate is concentration dependent (eq 6). The Higuchi model (eq 7) describes the release from an insoluble matrix system as the square root of a time-dependent process based on Fickian diffusion. The Hixson and Crowell model (eq 8) describes the release by dissolution with a change in the surface area and the diameter of a particle. The Korsmeyer−Peppas model (eq 9) describes the release from a polymeric system. The kinetic model that best fits the release data was selected on the basis of the correlation coefficient ($R^2$) value for each model

$$Q = K_0 t \tag{5}$$

where $Q$ is the amount of HBEO released in time $t$ and $K_0$ is the zero-order release constant. To study the release kinetics, the release data were plotted as a cumulative percentage of HBEO release versus time

$$\log C = \log C_0 - (K/2.303)t \tag{6}$$

where $K$ is the first-order rate constant, $C_0$ is the initial concentration of HBEO, and $C$ is the concentration of HBEO at time $t$. The HBEO release data were plotted as the log cumulative percentage of the HBEO remaining versus time

$$Q = K_H t^{1/2} \tag{7}$$

where $K_H$ is the Higuchi dissolution constant. The HBEO release data were plotted as the cumulative percentage of HBEO release and the square root of time

$$W_0^{1/3} - W_t^{1/3} = K_{HC} t \tag{8}$$

where $W_t$ is the amount of HBEO released in time $t$, $W_0$ is the initial amount of HBEO in the microcapsule, and $K_{HC}$ is the rate constant. The HBEO release data were plotted using the cube root of the HBEO percentage remaining in a matrix and time

$$M_t/M_\infty = kt^n \tag{9}$$

where $M_t/M_\infty$ is the fraction of the HBEO released at time $t$, $k$ is the release rate constant, and $n$ is the release exponent. The calculations of $k$ and $n$ were measured up to the initial 60% release of HBEO. The value of $n$ characterizes the release mechanism of the HBEO. For spheres, values of $n$ lower than 0.45 indicate a diffusion-controlled system, and values of $n$ between 0.45 and 0.85 indicate both diffusion-controlled release and swelling-controlled release (anomalous transport). Values above 0.85 indicate case II transport relating to polymer relaxation during gel swelling.

**Statistical Analysis.** A completely randomized design was used in this experiment. The statistical analysis was performed using one-way ANOVA. The experiments were performed in triplicate. The data are presented as the mean value ± standard deviation. Statistical significance was evaluated using Duncan's multiple-range test at the 95% confidence level.

## RESULTS AND DISCUSSION

HBEO was encapsulated in gelatin using simple coacervation and was cross-linked with glutaraldehyde to serve as a health enhancers for swine-raising. To delay HBEO release in the gastrointestinal tract, the microcapsule was successively coated with AlCMC or AlCMC−beeswax composites. Due to the acid resistance of AlCMC and the highly hydrophobic nature of beeswax, a delayed HBEO release was possible. The AlCMC layer was formed on the surface of the microcapsule by dispersing the microcapsules in a SCMC solution. Complex coacervation between SCMC and gelatin occurred due to the electrostatic attraction between the negatively charged SCMC carboxyl group and the positively charged gelatin amide group.[32] In addition to electrostatic attraction, the interaction between SCMC and gelatin was partially driven by hydrophobic interactions as well as hydrogen bond and van der Waals forces.[33] To produce a stable layer in the water-insoluble AlCMC gel, SCMC was consecutively cross-linked with aluminum ions. For the AlCMC−beeswax composite coating, a homogeneous dispersion emulsification was performed comprising beeswax in SCMC. Then, the microcapsules were added into the emulsion and were subsequently cross-linked with $AlCl_3$. The preparation of the emulsion composite film using the emulsification technique is simple and feasible. Additionally, the obtained film had adequate structural cohesion due to the long-chain polymer and hydrorepellency imparted by the lipids.[22] The physicochemical properties of the microcapsules were characterized in subsequent experiments.

**Encapsulation Efficiency, HBEO Content, and Antioxidant Activity.** The encapsulation efficiency of all samples was calculated on the basis of the HBEO weight in the microcapsule and the HBEO weight used initially. The encapsulation efficiency was found to be 95.4 ± 0.17%, which suggested that HBEO was effectively encapsulated using our simple coacervation procedure. UC, CC, and CB microcapsules contained 67.7 ± 0.16, 67.1 ± 0.13, and 66.7 ± 0.26% HBEO and exhibited 96.5 ± 0.20, 95.8 ± 0.18, and 94.3 ± 0.27% DPPH radical scavenging activity, respectively, which were significantly different for both values ($p \leq 0.05$). The radical scavenging activities of the CC and CB microcapsules were slightly weaker than that of the UC microcapsules. This result may be attributed to the increased weight of the microcapsule and HBEO loss after coating. However, with regard to their high antioxidant activity, all microcapsule samples could be potentially useful as feed additives.

**Size and Surface Morphology.** The microcapsule coating was also expected to have an influence on the size and surface morphology of the microcapsules. The volume moment mean diameter of the UC microcapsules was 392 $\mu$m, which was slightly smaller than those of the CC and CB microcapsules (407 and 414 $\mu$m, respectively). This increase in size indicates the presence of the coating layer on the outer surface of the microcapsule. In addition, the incorporation of beeswax, a long

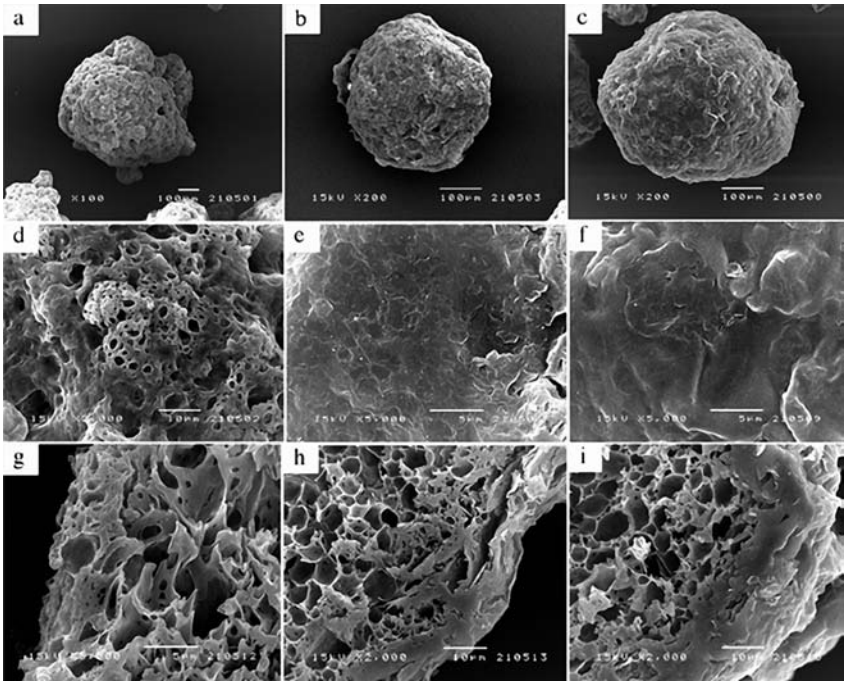


**Figure 1.** SEM images of UC, CC, and CB microcapsules: (a) whole UC; (b) whole CC; (c) whole CB; (d) external surfaces of UC; (e) external surfaces of CC; (f) external surfaces of CB; (g) inner edges of UC; (h) inner edges of CC; (i) inner edges of CB.

carbon chain molecule of $C_{16}$–$C_{95}$[34] in the AlCMC matrix results in an increase in the coating thickness.

SEM was used to characterize the internal and external surface morphology of the microcapsules. The UC microcapsules were almost spherical in shape (Figure 1a). After coating, the CC (Figure 1b) and CB (Figure 1c) microcapsules were more spherical. At high magnification, the UC microcapsule images revealed the highly porous sponge-like structure of the external surface (Figure 1d), and those of the CC (Figure 1e) and CB (Figure 1f) microcapsules were denser. The beeswax was markedly dispersed in the AlCMC matrix, resulting in a bumpy appearance. The cross-section view image showed a highly porous honeycomb-like internal morphology of the gelatin matrix (Figure 1g) as previously reported.[35,36] A large number of micropores on the multiwalls of the microcapsule were also observed. The cross-section images of the CC (Figure 1h) and CB (Figure 1i) microcapsules showed the compact outer coating layer covering the honeycomb-like inner microcore and, with the presence of beeswax, the coating layer appeared to be thicker.

**FTIR Spectra.** FTIR was used to confirm the successful coating and to reveal the interactions between each component that are possibly associated with the oil release properties. All of the characteristic peaks of gelatin (Figure 2a) and HBEO (Figure 2b) appeared in the UC microcapsule spectrum (Figure 2c). The N—H stretching vibrations of the amide groups, representing the amide A, appeared at 3351 $cm^{-1}$. The carbonyl C═O stretching vibrations, with minor contributions from the out-of-phase C—N stretching vibrations of the amide I, occurred at 1638 $cm^{-1}$. The out-of-phase combination of the N—H in-plane bending and the C—N stretching vibrations of the amide II were at 1568 and 1455 $cm^{-1}$. The peak at 1235 $cm^{-1}$ belonged to the in-phase combination of the N—H bending and the C—N stretching vibrations of amide III. The characteristic peaks of the main components of HBEO, methyleugenol, eugenol, and caryophyllene, were also observed

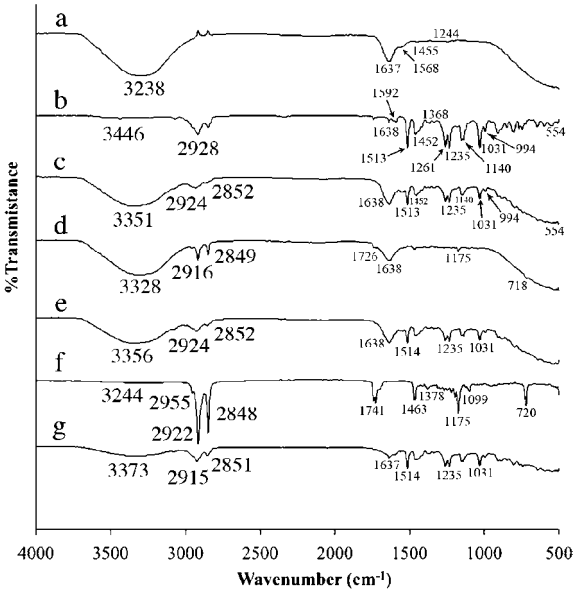


**Figure 2.** FTIR spectra of (a) gelatin, (b) HBEO, (c) UC, (d) NaCMC solution mixed with glycerol, (e) CC, (f) beeswax, and (g) CB.

in the UC microcapsule spectrum. The asymmetric and symmetric C—H stretching vibrations in $-CH_2-$ were observed at 2924 and 2852 $cm^{-1}$. The peaks in the region of 1638–1513 $cm^{-1}$ were assigned to the alkene/aromatic −C═C− stretching vibrations. The $=CH_2$ scissor bends occurred at 1463 $cm^{-1}$. The asymmetric and symmetric C—H bending vibrations in $-CH_3$ were observed at 1452 and 1368 $cm^{-1}$. There was also C−H bending of the alkene/aromatic groups in the range of 994–554 $cm^{-1}$. A comparison of the HBEO spectrum with the microcapsule spectrum revealed the chemical


dx.doi.org/10.1021/jf5019438 | J. Agric. Food Chem. 2014, 62, 12641–12648

stability of the encapsulated HBEO; therefore, its antioxidant and antimicrobial properties should remain intact.

After coating the UC microcapsules with AlCMC, the presence of AlCMC was evaluated by comparing the FTIR spectra of UC (Figure 2c) and SCMC (Figure 2d) with CC (Figure 2e). The SCMC spectrum had a peak at 3328 $cm^{-1}$ that was assigned to O−H stretching vibrations. The asymmetric and symmetric stretching vibrations of the aliphatic C−H were observed at 2916 and 2849 $cm^{-1}$, respectively. The peak at 1638 $cm^{-1}$ was attributed to the absorbed water molecules in cellulose. The bands at 1175, 1099, and 718 $cm^{-1}$ indicated the C−O−C (glycosidic linkage) stretching vibrations. As the characteristic peaks of SCMC were observed in the spectrum of the CC microcapsules, successful coating was achieved.

The beeswax incorporation into the AlCMC matrix as the coating material for the microcapsule was confirmed using FTIR. The beeswax FTIR spectrum (Figure 2f) had the characteristic peaks of its primary components, which consisted of a mixture of esters of fatty acids and fatty alcohols, long-chain hydrocarbons, and free fatty acids. O—H stretching was observed at 3244 $cm^{-1}$. The peak at 2955 $cm^{-1}$ was assigned to asymmetric C—H stretching vibrations. The peaks at 2915 and 2848 $cm^{-1}$ corresponded to the asymmetric and symmetric $C—H_2$ stretching vibrations of the fatty acid chains, respectively. The C═O stretching vibrations of the ester were observed at 1741 $cm^{-1}$. The symmetric $CH_2$ scissoring vibrations appeared at 1463 $cm^{-1}$. The peak at 1378 $cm^{-1}$ indicated the symmetric $CH_3$ bending vibrations. The band at 1175 $cm^{-1}$ was assigned to the $CH_2$ wagging vibrations. The peak at 1099 $cm^{-1}$ was due to the symmetric C—C stretching vibrations. The band at 720 $cm^{-1}$ represented the $CH_2$ rocking vibrations of the long-chain hydrocarbons.

The CB microcapsule spectrum contained most of the characteristic peaks of UC, AlCMC, and beeswax, indicating the successful coating of AlCMC−beeswax composites on the surfaces of the gelatin microcapsules. However, when compared with the CC spectrum, a significant decrease in the intensities of the aprroximately 3351 and 1638 $cm^{-1}$ peaks was observed, indicating that beeswax may interfere with the electrostatic attractions between the $Al^{3+}$ and $COO^-$ of SCMC.

**XRD Analysis.** XRD was used to evaluate the effect of AlCMC and beeswax on the structure of the microcapsule. The UC XRD pattern revealed an amorphous structure due to the amorphous nature of HBEO and the $\beta$-sheet conformation of gelatin (Figure 3a). In addition, an examination of the amorphous pattern also possibly indicated that amorphous HBEO is molecularly dispersed in the amorphous gelatin matrix. For the CC microcapsules, a flat and broad contour was observed (Figure 3b), suggesting that the presence of AlCMC decreased the crystallinity of the gelatin microcapsule. This result is attributed to the significant hydrogen bonding interactions between AlCMC and gelatin. With the incorporation of beeswax, the CB microcapsules had a semicrystalline structure composed of both crystals and amorphous structures (Figure 3c). The crystalline nature of beeswax was detected at $2\theta$ = 21° and 23° (Figure 3d) as previously observed.[34,37] Therefore, the XRD pattern demonstrates the successful incorporation of beeswax in the AlCMC layer. As a result of the semicrystalline structure of the AlCMC−beeswax composite, the release characteristics of the CB microcapsules may be different from those of UC and CC, which requires further investigation.

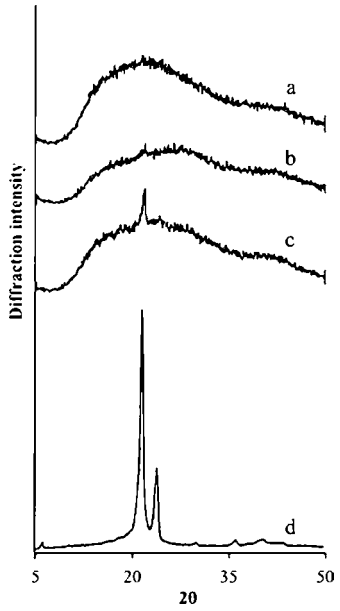


**Figure 3.** XRD patterns of (a) UC, (b) CC, (c) CB, and (d) beeswax.

**DSC Analysis.** DSC was used to monitor the physical state and thermal behavior of the samples. When HBEO was physically mixed with gelatin, its thermal analysis indicated three endothermic phase changes at 121, 220, and 251 °C, signifying the gelatin melting, HBEO vaporization, and gelatin degradation, respectively (Figure 4a). The characteristic

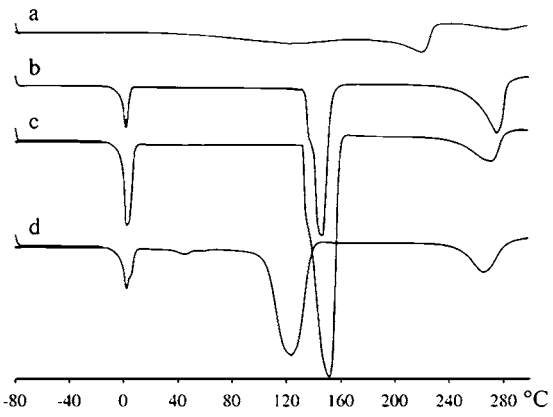


**Figure 4.** DSC thermograms of (a) physical mixtures of HBEO and gelatin powder, (b) UC, (c) CC, and (d) CB.

thermogram of the UC microcapsules (Figure 4b) was noticeably different from that of the physical mixture. The first absorption peak was around −1 °C, attributed to the melting endotherm of HBEO. The next sharp endothermic peak at 143 °C was associated with the melting of the microcapsule. The shift of the melting peak toward a higher temperature (from 121 to 143 °C) indicated the effect of cross-linking on the physical properties of the gelatin. The final phase transition showed the decomposition of the microcapsule. However, the DSC profile of the microcapsule did not clearly show the HBEO vaporization peak. This result suggests that HBEO is highly dispersed in the amorphous gelatin. Another possibility for this result is that HBEO vaporization occurs simultaneously with the decomposition of the microcapsule in that temperature range. In addition, the lack of any visible

exothermic peak confirmed that there was no chemical interaction between HBEO and gelatin. A comparison of the absorbed energy during the decomposition process between the microcapsule and the physical mixture also revealed the effect of cross-linking.

The DSC thermogram of the CC microcapsules (Figure 4c) was also composed of three endothermic events. The first peak, around −1 °C, corresponded to the melting temperature of HBEO. The sharp peak at 148 °C and the broad peak in the 250−280 °C temperature range represented the melting and decomposition of the microcapsule, respectively. The CC melting temperature (148 °C) was slightly higher than that of the UC microcapsules (143 °C), indicating the interaction between AlCMC and gelatin. Therefore, the DSC thermograms confirmed the FTIR spectrum data, demonstrating the presence of the intermolecular hydrogen bonds between AlCMC and gelatin.

The presence of beeswax in the AlCMC network and its effect on the thermal behavior of the microcapsule was also determined. The DSC thermogram of the CB microcapsules (Figure 4d) showed four endothermic peaks with one peak at 60 °C, representing the beeswax melting peak.[37] Moreover, the broadening of the melting peak and the decline in the melting temperature and melting enthalpy compared with the CC thermogram can be attributed to the colloidal beeswax due to its large surface-to-volume ratio properties.

**Release Characteristics of Microencapsulated HBEO in SGF.** The previous physicochemical analysis suggested a possible role for the microcapsule in controlling HBEO release. Therefore, the final study examining in vitro release was conducted. All of the microcapsules had a two-step biphasic HBEO release that was characterized by an initial burst, followed by a sustained release (Figure 5). Initially, the UC

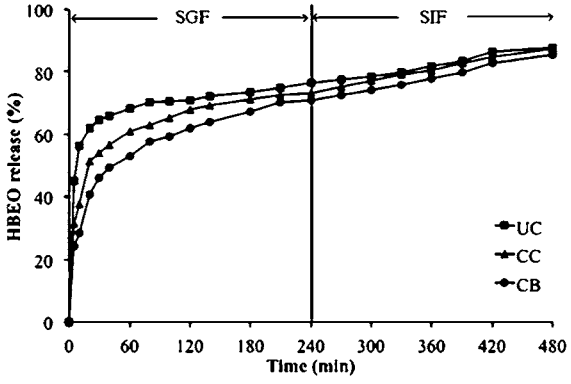


**Figure 5.** HBEO release profiles of UC, CC, and CB microcapsules in simulated swine gastrointestinal fluids.

microcapsules exhibited the highest burst release, followed by the CC and CB microcapsules, respectively. For example, within the first hour of incubation, the UC microcapsules released 69% of HBEO compared with 61% for the CC microcapsules and 50% for the CB microcapsules. The SGF penetration into the microcapsule leads to chain relaxation, microcapsule swelling, and finally HBEO release. Moreover, pepsin degrades the amide linkage in the gelatin chain,[38−40] resulting in microcapsule erosion and burst release. The HBEO release rate decreased after coating with AlCMC, which may be because AlCMC has a lower quantity of polar groups per monomeric unit.[41] As a result, the passage of the SGF through the CC microcapsules is slower. The slowest HBEO release rate was observed for the CB microcapsules. Because beeswax is highly hydrophobic, it has a low affinity for water. This potentially slows HBEO diffusion out of the microcapsules. In addition, the dispersed beeswax particle in the AlCMC matrix increases the diffusional path length of the HBEO, ions, and water, consequently hindering their transport across the composite layer as illustrated in Figure 6.

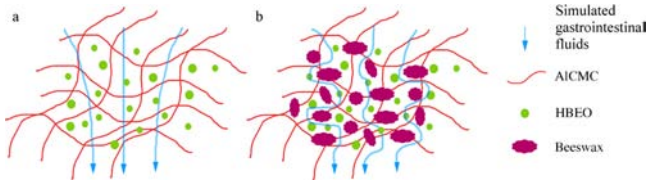


**Figure 6.** Schematic diagrams of SGF traversing (a) AlCMC and (b) AlCMC−beeswax composite coated on HBEO-loaded gelatin microcapsules.

Under simulated intestinal conditions, all of the microcapsules demonstrated sustained release. The physical and chemical disintegration of the UC microcapsules continuously occurred due to microcapsule swelling and gelatin hydrolysis by pancreatin and trypsin. AlCMC only experienced the physical disintegration induced by the polymer chain relaxation and swelling. In the CB microcapsules, the beeswax cannot retain its structural integrity because its ester bond is cleaved by the lipase found in pancreatin.[42]

The experimental results determined that the coating layer, particularly the AlCMC−beeswax composite, decreased the initial HBEO burst release in the SGF. The AlCMC−beeswax composite enhanced HBEO stability against acid denaturation and preserved antioxidant activity, which prevents free radical-induced damage and suppresses oxidative stress. The cumulative amounts of HBEO released in the SGF were 77.9, 74.7, and 70.5%, and the amounts released in the SIF were 11.6, 15.8, and 21.1% for the UC, CC, and CB microcapsules, respectively. Because antimicrobial activity depends on concentration, the CB microcapsules should exhibit the strongest activity in the intestine. In our in vitro studies, HBEO demonstrated high antimicrobial activity against pathogenic bacteria found in the intestine of swine, *Salmonella* Typhimurium, *Escherichia coli* O157, and *Staphylococcus aureus* (unpublished data). In our experiment, all types of microcapsules, particularly CB, released HBEO at concentrations greater than its minimal inhibitory concentration (the lowest concentration of an antimicrobial that can inhibit the growth of a microorganism) in the intestine. Therefore, HBEO encapsulation is a method for achieving HBEO release at desirable sites in the intestinal tract, rather than being almost completely absorbed in the stomach and the proximal intestine within 2 h after oral administration.[8]

To understand the mode of HBEO release and determine a suitable release kinetic model, the HBEO release data were fitted to various kinetic models. The model that provided the highest correlation coefficient ($R^2$) value was considered the optimal model for describing the release kinetic data. The results indicated that the in vitro HBEO release kinetics were best described by the Korsmeyer−Peppas model for all microcapsule preparations (Table 1). The HBEO release mechanism for the UC microcapsules followed the anomalous transport mechanism, which is controlled by diffusion and

**Table 1. Correlation Coefficients, Rate Constants, and Release Exponents for Different HBEO Release Kinetic Models for UC, CC, and CB Microcapsules**

| release kinetic model | | microcapsule formulations | | |
|---|---|---|---|---|
| | | UC | CC | CB |
| zero order | $R^2$ | 0.84 | 0.80 | 0.84 |
| | $K_0$ | 0.07 | 0.09 | 0.10 |
| first order | $R^2$ | 0.95 | 0.94 | 0.86 |
| | $K$ | 0.002 | 0.002 | 0.002 |
| Higuchi | $R^2$ | 0.92 | 0.92 | 0.95 |
| | $K_H$ | 1.72 | 2.34 | 2.72 |
| Hixson–Croswell | $R^2$ | 0.90 | 0.90 | 0.89 |
| | $K_{HC}$ | 0.002 | 0.002 | 0.002 |
| Korsmeyer–Peppas | $R^2$ | 0.97 | 0.97 | 0.97 |
| | $k$ | 3.52 | 3.64 | 3.30 |
| | $n$ | 0.51 | 0.30 | 0.30 |

swelling. These results confirmed the initial HBEO burst release from the gelatin. However, the HBEO release mechanism of the CC and CB microcapsules showed Fickian diffusion, indicating a diffusion-controlled release system due to the chemical potential gradient. As HBEO diffused through the water-filled pores, because CC and CB were denser than UC, the diffusion rate of HBEO from the coated microcapsules was lower.

**Stability of Microencapsulated HBEO during SGF Exposure.** CLSM was used to visualize and identify the location of HBEO in the microcapsule before and after exposure to SGF for 10 min. Figure 7a represents the nonhomogeneous distribution of large amounts of HBEO throughout the gelatin matrix in the UC microcapsules before incubation. The difference in fluorescence intensity was attributed to the difference in the HBEO amounts, which are directly related to the gelatin pore sizes. CLSM detected the gelatin matrix (Figure 7b), but it was not able to provide information on the shape of the gelatin pores. Nevertheless, the image shown in Figure 7c confirmed the multicore structure of the microcapsule with distinct gelatin walls, as previously observed by SEM. In addition, HBEO was almost entirely entrapped inside the microcapsule; nonencapsulated oil was barely detected on the outer surface.

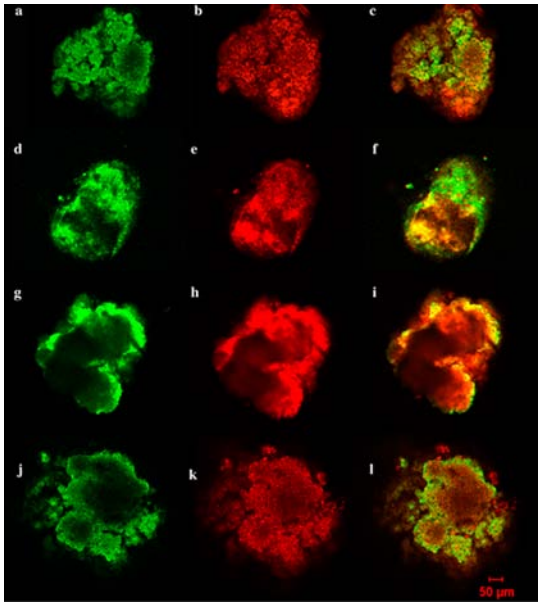


**Figure 7.** CLSM images of microcapsules before and after exposure to SGF: (a–c) UC before exposure; (d–f) UC after exposure; (g–i) CC after exposure; (j–l) CB after exposure. HBEO was colored with Nile blue dye (a, d, g, and j). Gelatin was colored with Rhodamine B dye (b, e, h, and k). Red and green represent gelatin and HBEO, respectively (c, f, i, and l).

The information obtained in this study can be used to indicate the protective ability of microcapsules and HBEO stability during SGF exposure. Panels d–f of Figure 7 show that HBEO was released from the UC microcapsules after incubation in the SGF for 10 min at pH 3 due to the degradation of the gelatin network by pepsin. Conversely, large amounts of HBEO were retained on the edge of the CC (Figure 7g–i) and CB microcapsules (Figure 7j–l); HBEO was not able to traverse the coated layers. These results confirmed that higher amounts of HBEO were released from the UC microcapsules.

In summary, microcapsules for the controlled release of HBEO in swine gastrointestinal fluid were developed. The analysis of physicochemical properties confirmed the successful coating of AlCMC and AlCMC–beeswax composite on the gelatin microcapsule. The coating material, particularly the AlCMC–beeswax composite, inhibited HBEO burst release in the SGF and promoted HBEO release in the SIF of swine over an extended period of time. Therefore, the encapsulation method proposed in the present study is an effective process for improving HBEO efficacy for pathogen reduction in the distal region of the intestine.

## AUTHOR INFORMATION

### Corresponding Author

*(P.C.) Phone: 66-02-562-5085. Fax: 66-02579-4096. E-mail: pakamon.c@ku.ac.th.

### Funding

This research was cofunded by the Thailand Research Fund-Master Research grants (TRF-MAG), No. MRGWI535S019, and Better Pharma Co., Ltd., Thailand.

### Notes

The authors declare no competing financial interest.

## REFERENCES

(1) Brenes, A.; Roura, E. Essential oils in poultry nutrition: main effects and modes of action. *Anim. Feed Sci. Technol.* **2010**, *158*, 1–14.

(2) de Lange, C. F. M.; Pluske, J.; Gong, J.; Nyachoti, C. M. Strategic use of feed ingredients and feed additives to stimulate gut health and development in young pigs. *Livest. Sci.* **2010**, *134*, 124–134.

(3) Diao, W. R.; Hu, Q. P.; Feng, S. S.; Li, W. Q.; Xu, J. G. Chemical composition and antibacterial activity of the essential oil from green huajiao (*Zanthoxylum schinifolium*) against selected foodborne pathogens. *J. Agric. Food Chem.* **2013**, *61*, 6044–6049.

(4) Singh, G.; Marimuthu, P.; de Heluani, C. S.; Catalan, C. A. N. Antioxidant and biocidal activities of *Carum nigrum* (seed) essential oil, oleoresin, and their selected components. *J. Agric. Food Chem.* **2006**, *54*, 174–181.

(5) Li, S. Y.; Ru, Y. J.; Liu, M.; Xu, B.; Péron, A.; Shi, X. G. The effect of essential oils on performance, immunity and gut microbial population in weaner pigs. *Livest. Sci.* **2012**, *145*, 119–123.

(6) Manzanilla, E. G.; Perez, J. F.; Martin, M.; Kamel, C.; Baucells, F.; Gasa, J. Effect of plant extracts and formic acid on the intestinal equilibrium of early-weaned pigs. *J. Anim. Sci.* **2004**, *82*, 3210−3218.
(7) Si, W.; Gong, J.; Chanas, C.; Cui, S.; Yu, H.; Caballero, C.; Friendship, R. M. In vitro assessment of antimicrobial activity of carvacrol, thymol and cinnamaldehyde towards *Salmonella* serotype Typhimurium DT104: effects of pig diets and emulsification in hydrocolloids. *J. Appl. Microbiol.* **2006**, *101*, 1282−1291.
(8) Michiels, J.; Missotten, J.; Dierick, N.; Fremaut, D.; Maene, P.; Smet, S. D. In vitro degradation and in vivo passage kinetics of carvacrol, thymol, eugenol and trans -cinnamaldehyde along the gastrointestinal tract of piglets. *J. Sci. Food Agric.* **2008**, *88*, 2371−2381.
(9) Inamuco, J.; Veenendaal, A. K.; Burt, S. A.; Post, J. A.; Tjeerdsma-van Bokhoven, J. L.; Haagsman, H. P.; Veldhuizen, E. J. Sub-lethal levels of carvacrol reduce *Salmonella* Typhimurium motility and invasion of porcine epithelial cells. *Vet. Microbiol.* **2012**, *157*, 200−207.
(10) Chang, C. P.; Leung, T. K.; Lin, S. M.; Hsu, C. C. Release properties on gelatin-gum arabic microcapsules containing camphor oil with added polystyrene. *Colloids Surf., B* **2006**, *50*, 136−140.
(11) Maji, T. K.; Baruah, I.; Dube, S.; Hussain, M. R. Microencapsulation of *Zanthoxylum limonella* oil (ZLO) in glutaraldehyde crosslinked gelatin for mosquito repellent application. *Bioresour. Technol.* **2007**, *98*, 840−844.
(12) Solomon, B.; Sahle, F. F.; Gebre-Mariam, T.; Asres, K.; Neubert, R. H. H. Microencapsulation of citronella oil for mosquito-repellent application: formulation and in vitro permeation studies. *Eur. J. Pharm. Biopharm.* **2012**, *80*, 61−66.
(13) Lopez, M. D.; Maudhuit, A.; Pascual-Villalobos, M. J.; Poncelet, D. Development of formulations to improve the controlled-release of linalool to be applied as an insecticide. *J. Agric. Food Chem.* **2012**, *60*, 1187−1192.
(14) Anyango, J. O.; Taylor, J. R. N.; Taylor, J. Role of $\gamma$-kafirin in the formation and organization of kafirin microstructures. *J. Agric. Food Chem.* **2013**, *61*, 10757−10765.
(15) Young, S.; Wong, M.; Tabata, Y.; Mikos, A. G. Gelatin as a delivery vehicle for the controlled release of bioactive molecules. *J. Controlled Release* **2005**, *109*, 256−274.
(16) Marchais, H.; Cayzeele, G.; Legendre, J.; Skiba, M.; Arnaud, P. Cross-linking of hard gelatin carbamazepine capsules: effect of dissolution conditions on *in vitro* drug release. *Eur. J. Pharm. Sci.* **2003**, *19*, 129−132.
(17) Annan, N. T.; Borza, A.; Moreau, D. L.; Allan-Wojtas, P. M.; Truelstrup Hansen, L. Effect of process variables on particle size and viability of *Bifidobacterium lactis* Bb-12 in genipin-gelatin microspheres. *J. Microencapsulation* **2007**, *24*, 152−162.
(18) Priya, A. J.; Vijayalakshmi, S. P.; Raichur, A. M. Enhanced survival of probiotic *Lactobacillus acidophilus* by encapsulation with nanostructured polyelectrolyte layers through layer-by-layer approach. *J. Agric. Food Chem.* **2011**, *59*, 11838−11845.
(19) Sungur, S. Investigations on drug release systems using CMC crosslinked with ferric ions. *Artif. Cells, Blood Substitutes, Immobilization Biotechnol.* **1999**, *27*, 279−290.
(20) Prasad, M. P.; Kalyanasundaram, M. Scanning electron microscopic analysis and swelling behaviour of ionotropically cross-linked carboxymethylcellulose and carboxymethylcellulose-gelatin matrices. *Carbohydr. Polym.* **1995**, *26*, 35−41.
(21) Toğrul, H.; Arslan, N. Carboxymethyl cellulose from sugar beet pulp cellulose as a hydrophilic polymer in coating of mandarin. *J. Food Eng.* **2004**, *62*, 271−279.
(22) Cheng, L. H.; Karim, A. A.; Seow, C. C. Characterisation of composite films made of konjac glucomannan (KGM), carboxymethyl cellulose (CMC) and lipid. *Food Chem.* **2008**, *107*, 411−418.
(23) Ghanbarzadeh, B.; Almasi, H. Physical properties of edible emulsified films based on carboxymethyl cellulose and oleic acid. *Int. J. Biol. Macromol.* **2011**, *48*, 44−49.
(24) Morillon, V.; Debeaufort, F.; Blond, G.; Capelle, M.; Voilley, A. Factors affecting the moisture permeability of lipid-based edible films: a review. *Crit. Rev. Food Sci. Nutr.* **2002**, *42*, 67−89.
(25) Obaidet, A. A.; Obaidet, R. M. Controlled release of tramadol hydrochloride from matrices prepared using glyceryl behenate. *Eur. J. Pharm. Biopharm.* **2001**, *52*, 231−235.
(26) Gowda, D. V.; Ravi, V.; Shivakumar, H. G.; Hatna, S. Preparation, evaluation and bioavailability studies of indomethacin-bees wax microspheres. *J. Mater. Sci. Mater. Med.* **2009**, *20*, 1447−1456.
(27) Ranjha, N. M.; Khan, H.; Naseem, S. Encapsulation and characterization of controlled release flurbiprofen loaded microspheres using beeswax as an encapsulating agent. *J. Mater. Sci. Mater. Med.* **2010**, *21*, 1621−1630.
(28) Eevuri, T. R.; Putturu, R. Use of certain herbal preparations in broiler feeds − a review. *Vet. World* **2013**, *6*, 172−179.
(29) Sutaphanit, P.; Chitprasert, P. Optimisation of microencapsulation of holy basil essential oil in gelatin by response surface methodology. *Food Chem.* **2014**, *150*, 313−320.
(30) Brand-Williams, W.; Cuvelier, M. E.; Berset, C. Use of a free radical method to evaluate antioxidant activity. *LWT−Food Sci. Technol.* **1995**, *28*, 25−30.
(31) Meunier, J. P.; Cardot, J. M.; Manzanilla, E. G.; Wysshaar, M.; Alric, M. Use of spray-cooling technology for development of microencapsulated capsicum oleoresin for the growing pig as an alternative to in-feed antibiotics: a study of release using in vitro models. *J. Anim. Sci.* **2007**, *85*, 2699−2710.
(32) Lv, Y.; Zhang, X.; Abbas, S.; Karangwa, E. Simplified optimization for microcapsule preparation by complex coacervation based on the correlation between coacervates and the corresponding microcapsule. *J. Food Eng.* **2012**, *111*, 225−233.
(33) Schmitt, C.; Sanchez, C.; Desobry-Banon, S.; Hardy, J. Structure and technofunctional properties of protein-polysaccharide complexes: a review. *Crit. Rev. Food Sci. Nutr* **1998**, *38*, 689−753.
(34) Gaillard, Y.; Mija, A.; Burr, A.; Darque-Ceretti, E.; Felder, E.; Sbirrazzuoli, N. Green material composites from renewable resources: polymorphic transitions and phase diagram of beeswax/rosin resin. *Thermochim. Acta* **2011**, *521*, 90−97.
(35) Benjakul, S.; Oungbho, K.; Visessanguan, W.; Thiansilakul, Y.; Roytrakul, S. Characteristics of gelatin from the skins of bigeye snapper, *Priacanthus tayenus* and *Priacanthus macracanthus*. *Food Chem.* **2009**, *116*, 445−451.
(36) Rahbani, J.; Behzad, A. R.; Khashab, N. M.; Al-Ghoul, M. Characterization of internal structure of hydrated agar and gelatin matrices by cryo-SEM. *Electrophoresis* **2013**, *34*, 405−408.
(37) Muscat, D.; Adhikari, R.; McKnight, S.; Guo, Q.; Adhikari, B. The physicochemical characteristics and hydrophobicity of high amylose starch-glycerol films in the presence of three natural waxes. *J. Food Eng.* **2013**, *119*, 205−219.
(38) Cannan, R. K.; Muntwyler, E. The action of pepsin on gelatin. *Biochem. J.* **1930**, *24*, 1012−1020.
(39) Sheng, W.; Zhao, X. Functional properties of limited hydrolysed cross-linked casein-gelatin composites. *Int. J. Food Sci. Technol.* **2013**, *48*, 260−266.
(40) Mendis, E.; Rajapakse, N.; Kim, S. K. Antioxidant properties of a radical-scavenging peptide purified from enzymatically prepared fish skin gelatin hydrolysate. *J. Agric. Food Chem.* **2005**, *53*, 581−587.
(41) Davidson, R. L.; Sitting, M. *Water-Soluble Resins*; Reinhold Book: New York, 1968.
(42) Hargrove, J. L.; Greenspan, P.; Hartle, D. K. Nutritional significance and metabolism of very long chain fatty alcohols and acids from dietary waxes. *Exp. Biol. Med. (Maywood)* **2004**, *229*, 215−226.

up applications in bioreactors. Moreover, this study quali−quantitatively characterized five main IF constituents (calycosin-7-*O*-*β*-D-glucoside, ononin, astraisoflavan-7-*O*-*β*-D-glucoside, calycosin, and formononetin) from *A. membranaceus* HRCs (AMHRCs), followed by the evaluation of antioxidant activities of AMHRC extracts. We conclude that AMHRCs were more efficient for production of isoflavonoids compared to field grown roots (AMFGRs) of *A. membranaceus*.

## MATERIALS AND METHODS

**Plant Materials and Reagents.** Mature *A. membranaceus* seeds were generously provided by Heilongjiang University of Chinese Medicine (Harbin, China). Standard compounds including calycosin-7-*O*-*β*-D-glucoside (CAG), ononin (ON), astraisoflavan-7-*O*-*β*-D-glucoside (ASG), calycosin (CA), and formononetin (FO) were purchased from Weikeqi Biological Technology Co. Ltd. (Sichuan province, China). Ascorbic acid (VC), 2,2-diphenyl-1-picryl-hydrazyl-hydrate (DPPH), linoleic acid, butylated hydroxytoluene (BHT), and *β*-carotene were obtained from Sigma-Aldrich Co. (Steinheim, Germany). *A. rhizogenes* LBA9402 strain was obtained from the Key Laboratory of Forest Plant Ecology, Ministry of Education, Harbin, China. The bacterial culture was maintained at 25 ± 1 °C on yeast mannitol broth (YMB) medium. Other reagents of either analytical or optical grade were purchased from Beijing Chemical Reagents Co. (Beijing, China). Ultrapure water was prepared from a Milli-Q system at 18.3 MΩ resistance (Millipore, Bedford, MA).

**Induction and Establishment of Hairy Roots.** Young leaves of 3 week old aseptic plantlets were used as explants for hairy root induction. The excised leaf segments were preincubated on half-strength Murashige and Skoog (MS/2) solid medium for 2 days prior to the following infection. After that, the explants were immersed into overnight grown bacterial suspensions of *A. rhizogenes* LBA9402 strain ($OD_{600nm}$ = 0.6−0.8) for 10 min, dry-blotted on sterile filter paper, and incubated in the dark at 25 ± 1 °C on MS/2 solid medium supplemented with acetosyringone (100 *μ*M). After 2 days of cocultivation, the explants were transferred to the hormone-free MS solid medium containing sodium cefotaxim (500 mg/L) to eliminate the residual bacteria. Putative transgenic hairy roots were observed emerging from the wound sites of explants within 13 days of incubation. During subculture every other week, the concentration of antibiotic was gradually decreased and finally omitted, until the bacteria were completely eliminated. Eventually, eight lines (AMHRL I−VIII) among 62 established AMHRLs were selected for the present study.

**Molecular Characterization of Hairy Roots.** Integration of T-DNA responsible for hairy root formation was confirmed by PCR analysis using *rol*B, *rol*C, *aux*1, and *vir*D specific primers (see Supporting Information Table S1) as suggested by previous reports.[20,21] Genomic DNA was isolated from AMHRL II using a DNeasy Plant Mini Kit (Tiangen, China) following the manufacturer's instructions. PCR amplification of *rol*B, *rol*C, *aux*1, and *vir*D genes was performed by a S1000 thermal cycler (Bio-Rad, Hercules, CA) according to the following program: initial denaturation at 94 °C for 5 min, followed by 30 cycles of denaturation at 94 °C for 30 s, annealing at 59 °C for 50 s, and extension at 72 °C for 50 s, and final extension at 72 °C for 7 min. PCR products were analyzed by electrophoresis on a 2.5% (w/v) agarose−ethidium bromide gel along with 1000 bp DNA marker. Additionally, genomic DNA isolated from *A. membranaceus* aseptic plantlets and Ri-plasmid (pRi) DNA from *A. rhizogenes* LBA9402 strain were used as negative and positive controls, respectively.

**Optimization of Culture Conditions.** Once the highly productive AMHRL was identified, a certain amount of hairy roots was transferred into 250 mL Erlenmeyer flasks containing 150 mL of MS liquid medium (pH 5.8) supplemented with 1% casein hydrolysate without $NH_4NO_3$, and further incubated on a rotary shaker (100 rpm) at an appropriate temperature in the dark. AMHRCs were harvested by filtration after a certain period of cultivation and dried in a vacuum drier at 60 °C until achieving constant weight. Thereafter, biomass DW and total IF (TIF) content (sum amount of CAG, ON, ASG, CA, and FO) were measured and determined, respectively.

In order to obtain optimal biomass production and IF accumulation during the culture process, a Box−Behnken design (BBD) was applied to investigate the effects of four independent key variables (culture temperature 24−32 °C, sucrose concentration 2−4%, inoculum size 1−2%, and harvest time 20−40 days) on dependent variables (biomass DW and TIF content). The inoculum size was calculated based on the fresh weight (FW) of hairy roots. Regression analysis was carried out to evaluate the response function as a quadratic polynomial:

$$Y = \beta_0 + \sum_{j=1}^{k} \beta_j X_j + \sum_{j=1}^{k} \beta_{jj} X_j^2 + \sum \sum_{i<j} \beta_{ij} X_i X_j \quad (k = 4)$$

where $Y$ is the predicted response; $\beta_0$, $\beta_j$, $\beta_{jj}$, and $\beta_{ij}$ are regression coefficients for intercept, linearity, square and interaction, respectively; $X_i$ and $X_j$ are independent coded variables; and $k$ represents the number of variables. The actual and coded levels of independent variables used in the experimental design are summarized in Table 1. The experiment data were statistically analyzed with Design-Expert 7.0 (State-Ease, Inc., Minneapolis MN). Analyses of variance (ANOVA)

**Table 1. BBD Results for Biomass Production and IF Accumulation during the Culture Process[a]**

| | factors | | | | | |
|---|---|---|---|---|---|---|
| runs | $X_1$ (CT,[b] °C) | $X_2$ (SC,[c] %) | $X_3$ (IS,[d] %) | $X_4$ ($t$,[e] days) | biomass DW (g/L) | TIF content (*μ*g/g) |
| 1 | −1 (24) | −1 (2) | 0 (1.5) | 0 (30) | 11.66 | 165.37 |
| 2 | 1 (32) | −1 (2) | 0 (1.5) | 0 (30) | 11.17 | 161.82 |
| 3 | −1 (24) | 1 (4) | 0 (1.5) | 0 (30) | 13.50 | 187.79 |
| 4 | 1 (32) | 1 (4) | 0 (1.5) | 0 (30) | 11.92 | 183.45 |
| 5 | 0 (28) | 0 (3) | −1 (1) | −1 (20) | 12.95 | 207.33 |
| 6 | 0 (28) | 0 (3) | 1 (2) | −1 (20) | 14.55 | 191.85 |
| 7 | 0 (28) | 0 (3) | −1 (1) | 1 (40) | 15.36 | 218.29 |
| 8 | 0 (28) | 0 (3) | 1 (2) | 1 (40) | 13.54 | 213.33 |
| 9 | −1 (24) | 0 (3) | 0 (1.5) | −1 (30) | 13.51 | 191.97 |
| 10 | 1 (32) | 0 (3) | 0 (1.5) | −1 (30) | 11.53 | 183.15 |
| 11 | −1 (24) | 0 (3) | 0 (1.5) | 1 (40) | 12.42 | 183.66 |
| 12 | 1 (32) | 0 (3) | 0 (1.5) | 1 (40) | 11.77 | 176.95 |
| 13 | 0 (28) | −1 (2) | −1 (1) | 0 (30) | 13.19 | 194.55 |
| 14 | 0 (28) | 1 (4) | −1 (1) | 0 (30) | 14.81 | 206.77 |
| 15 | 0 (28) | −1 (2) | 1 (2) | 0 (30) | 13.53 | 190.18 |
| 16 | 0 (28) | 1 (4) | 1 (2) | 0 (30) | 15.10 | 196.07 |
| 17 | −1 (24) | 0 (3) | −1 (1) | 0 (30) | 11.89 | 175.44 |
| 18 | 1 (32) | 0 (3) | −1 (1) | 0 (30) | 11.31 | 169.95 |
| 19 | −1 (24) | 0 (3) | 1 (2) | 0 (30) | 12.16 | 166.38 |
| 20 | 1 (32) | 0 (3) | 1 (2) | 0 (30) | 11.57 | 165.71 |
| 21 | 0 (28) | −1 (2) | 0 (1.5) | −1 (20) | 12.93 | 188.05 |
| 22 | 0 (28) | 1 (4) | 0 (1.5) | −1 (20) | 15.02 | 204.59 |
| 23 | 0 (28) | −1 (2) | 0 (1.5) | 1 (40) | 14.65 | 215.25 |
| 24 | 0 (28) | 1 (4) | 0 (1.5) | 1 (40) | 15.99 | 224.55 |
| 25 | 0 (28) | 0 (3) | 0 (1.5) | 0 (30) | 15.71 | 226.78 |
| 26 | 0 (28) | 0 (3) | 0 (1.5) | 0 (30) | 15.85 | 219.83 |
| 27 | 0 (28) | 0 (3) | 0 (1.5) | 0 (30) | 16.17 | 230.51 |
| 28 | 0 (28) | 0 (3) | 0 (1.5) | 0 (30) | 16.02 | 222.29 |
| 29 | 0 (28) | 0 (3) | 0 (1.5) | 0 (30) | 15.48 | 234.46 |
| 30 | 0 (28) | 0 (3) | 0 (1.5) | 0 (30) | 15.18 | 221.03 |

[a]AMHRL II in full strength MS liquid medium (pH 5.8) supplemented with 1% casein hydrolysate. [b]CT is expressed as the culture temperature (°C). [c]SC is expressed as the sucrose concentration (%, g/L). [d]IS is expressed as the inoculum size (%, g/L). [e]$t$ is expressed as the harvest time (days).

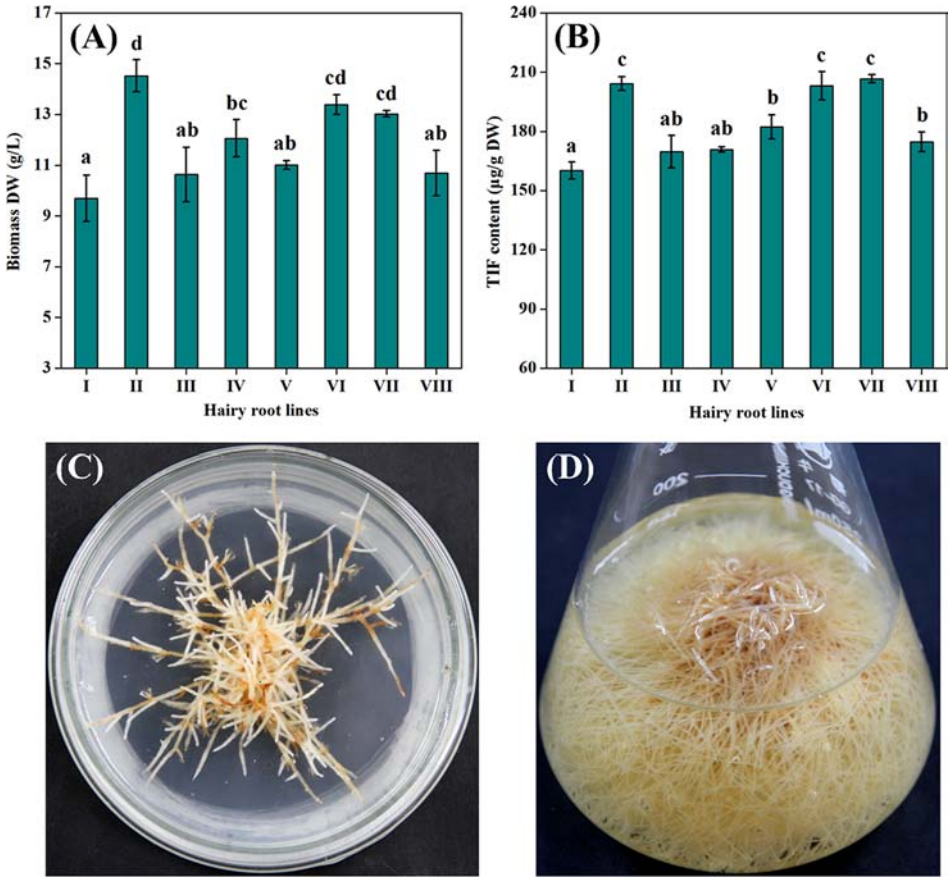


**Figure 1.** (A) Biomass production and (B) IF accumulation of eight representative AMHRL (I–VIII) after 4 weeks of cultivation in MS liquid medium (culture temperature 25 °C, sucrose concentration 3%, and inoculum size 1.25%). (C) Cultivation of AMHRL II on MS solid medium and (D) its growth in MS liquid medium. Mean ± SD values not sharing the same lowercase letters are significantly different ($P < 0.05$).

was performed to calculate and simulate the optimal values of the tested parameters.

**Extraction of IF.** Powders (0.5 g DW) of hairy roots and 3 year old field grown roots were extracted with 70% ethanol solution (25 mL) in an ultrasonic bath for 120 min. For complete extraction, the above procedure was repeated for three cycles. Subsequently, the supernatant extracts were combined and dried at 45 °C using a rotary evaporator under vacuum with oil pump. The resulting extracts were redissolved in 25 mL of methanol (HPLC grade) and then filtered through a 0.45 μm membrane for LC–MS/MS analysis.

**LC–MS/MS Analysis.** An Agilent 1100 series HPLC (Agilent, San Jose, CA, USA) coupled to an API 3000 triple tandem quadrupole MS (Applied Biosystems, Concord, Ontario, Canada) with a Phenomenex Gemini C18 110A reversed-phase column (250 mm × 4.6 mm i.d., 5 μm) was applied for the analysis of IF. The binary mobile phase consisted of acetonitrile (A) and 0.01% formic acid aqueous solution (B) using the following gradient program: 0–5 min, 45–50% A; 5–7 min, 50–65% A; 7–12 min, 65% A; 12–13 min, 65–45% A; and 13–15 min, 45% A. The column temperature was maintained at 30 °C. The flow rate was 1.0 mL/min, and the injection volume was 10 μL.

Mass spectral analyses were performed in the selected reaction monitoring (SRM) transitions with an electrospray ionization source in the negative ion mode. The universal parameters were set as follows: nebulizing gas (NEB) 12 au; curtain gas (CUR) 10 au; collision gas (CAD) 6 au; ion source temperature (TEM) 300 °C; ion spray voltage (IS) −4500 V; focusing potential (FP) −75 V; and entrance potential (EP) −10 V. To obtain the highest response for each analyte, the specific parameters for acquiring the optimal precursor/product ion combinations were optimized, e.g., declustering potential (DP), collision energy (CE) and collision cell exit potential (CXP) (Supporting Information Table S2). The content of each target compound was calculated by corresponding calibration curves and expressed as micrograms per gram based on the DW of roots.

**Determination of Antioxidant Activities.** Antioxidant activities of extracts from AMHRCs and AMFGRs were assessed using the DPPH radical-scavenging assay and β-carotene/linoleic acid bleaching test. Scavenging activities of samples toward DPPH radicals were determined according to the previously reported method.[22] Lipid antioxidant activities of samples toward β-carotene/linoleic acid were evaluated in accordance with the method described by Wu et al.[23] VC and BHT were used as the synthetic antioxidants. Antioxidant activities of samples were reported as $IC_{50}$ values, which were calculated using logarithmic regression curves for DPPH radical scavenging ratio or β-carotene bleaching inhibition percentages (%) versus the concentrations of samples (mg/mL).

**Statistical Analysis.** Results were expressed as means ± standard deviations. The data were statistically analyzed using the SPSS statistical software (version 17.0, SPSS Inc., Chicago, IL, USA). Differences between means were determined by analysis of variance (ANOVA) with Tukey's HSD post hoc test at a level of significance of $P < 0.05$.

## RESULTS AND DISCUSSION

**Screening the High-Productive Hairy Root Line.** Generally, hairy roots carry the *aux* and *rol* genes in their genome as a result of the transfer of the plasmidic T-DNA from *A. rhizogenes*, and the genetic integration is inherently stable.[12−19] *Aux* genes are responsible for the auxin synthesis in hairy roots leading to unlimited proliferation.[12,13,17] *Rol* genes can affect growth and development of transformed roots,[17,19] and induce secondary metabolite synthesis through a

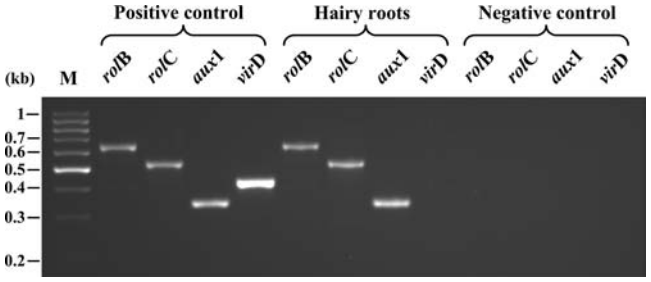


**Figure 2.** PCR analysis of *rol*B (670 bp), *rol*C (534 bp), *aux*1 (350 bp), and *vir*D genes (438 bp) in AMHRL II, positive control (*A. rhizogenes* LBA 9402 strain), and negative control (aseptic *A. membranaceus* plantlets).

variety of signal transduction pathways (for reviews on functions and applications of *rol* genes in plant secondary metabolism, see Nopo-Olazabal et al.,[15] Sharma et al.,[19] Shkryl et al.,[24] Bulgakov,[25] and Bulgakov et al.[26]). In fact, HRCs are a self-induction system for secondary metabolite biosynthesis due to the effects of *rol* genes. The presence of *rol* genes makes HRCs a self-sufficient system to induce the secondary metabolic pathways (SMPs) at a significant level without a selection mechanism.[19] Consequently, HRCs with inherently induced SMPs are an ideal experimental system for the consistent expression of secondary metabolites without a driving force.

**Table 2. ANOVA Results of the Quadratic Models for Biomass Production and IF Accumulation**

| | biomass DW (g/L) | | TIF content ($\mu$g/g) | |
|---|---|---|---|---|
| source | *P*-value[a] | significance[b] | *P*-value | significance |
| model | <0.0001 | significant | <0.0001 | significant |
| lack of fit[c] | 0.3013 | not significant | 0.2428 | not significant |
| $R^2$ | 0.9652 | | 0.9406 | |

[a]Probability of observing *F*-value, if the null hypothesis is true. [b]*P*-value less than 0.05 indicates that model term is significant. [c]Variation of the data around the fitted model.

Owing to the uncertainty of T-DNA integration into the host plant genome, various derived hairy root lines often show considerable variation in growth rates and diverse biosynthesis patterns of secondary metabolites.[27−29] Therefore, it was essential for the selection of an appropriate hairy root line in the present study. Based on the results of preliminary experiments, AMHRL I−VIII were determined as candidate lines for comparing their abilities of biomass production and IF accumulation. As shown in Figure 1, panels A and B, AMHRL II, VI, and VII were categorized as highly productive lines in terms of biomass DW (13.03−14.52 g/L) and TIF content (203.22−206.75 $\mu$g/g DW) as compared to the others. However, AMHRL II exhibited the best capability for biomass production in spite of no significant differences regarding the TIF content among them. AMHRL II was used as optimal hairy

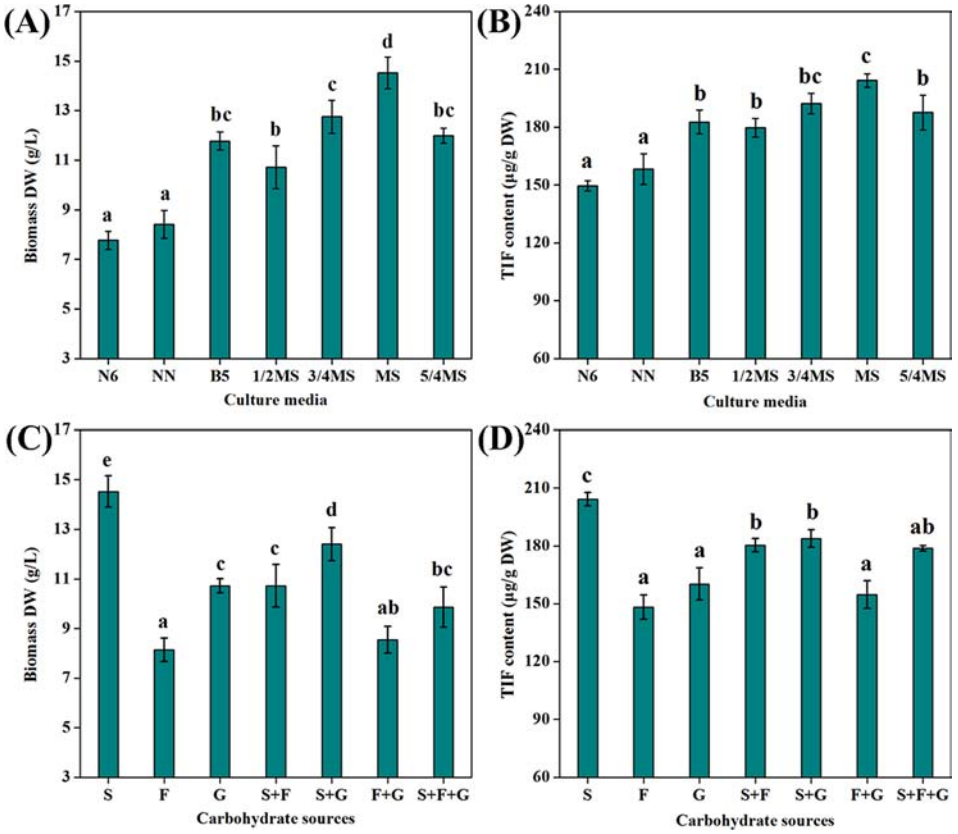


**Figure 3.** Effect of different culture media on (A) biomass production and (B) IF accumulation of AMHRL II after 4 weeks of cultivation (culture temperature 25 °C, sucrose concentration 3%, and inoculum size 1.25%). Effect of different carbohydrate sources on (C) biomass production and (D) IF accumulation of AMHRL II after 4 weeks of cultivation (MS medium, culture temperature 25 °C, inoculum size 1.25% and sugar concentration 3%). S: Sucrose. F: Fructose. G: Glucose. Mean ± SD values not sharing the same lowercase letters are significantly different ($P$ < 0.05).

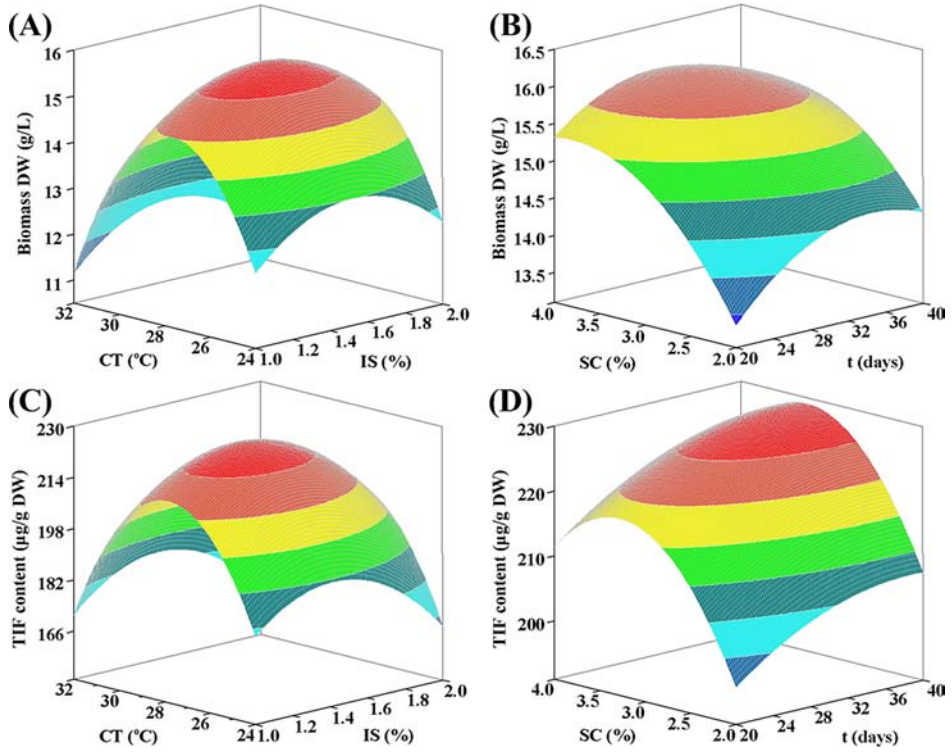


**Figure 4.** Response surfaces for biomass production and IF accumulation of AMHRCs in MS liquid medium: varying culture temperature and inoculum size on (A) biomass DW and (C) TIF content; varying sucrose concentration and harvest time on (B) biomass DW and (D) TIF content.

root line used for subsequent experiments. The cultivation of AMHRL II on MS solid medium and its growth in MS liquid medium are presented in Figure 1, panels C and D, respectively.

**Confirmation of Hairy Roots by PCR.** PCR-based analyses of *rol*B, *rol*C, *aux*1, and *vir*D genes were performed to confirm the genetic transformation of AMHRL II. The *rol*B and *rol*C genes (located at the pRi TL-DNA segment) and the *aux*1 gene (located at the pRi TR-DNA segment) were used to validate the presence of these fragments in the genomic DNA of AMHRL II. In order to prevent interference, the *vir*D gene (located outside the pRi T-DNA segment) served to verify the complete absence of *A. rhizogenes* in AMHRL II. Moreover, aseptic *A. membranaceus* plantlets and *A. rhizogenes* LBA 9402 strain were utilized as negative and positive controls, respectively. As shown in Figure 2, the coexistence of *rol*B, *rol*C, and *aux*1 genes as well as the absence of *vir*D gene were observed in the established hairy root line, indicating that the pRi T-DNA fragments of *A. rhizogenes* were successfully integrated into the genome of AMHRL II without bacterial residues.

**Optimization of Culture Conditions.** As shown in Figure 3A,B, the full strength MS liquid medium was found to be superior compared to other media for both biomass production and IF accumulation. Moreover, sucrose was found to be the ideal carbohydrate source for hairy root growth and IF biosynthesis (Figure 3C,D). Due to the tedious process, the number of experiments necessary for optimizing culture conditions can be reduced by statistical experimental designs. Therefore, the remaining key parameters such as culture temperature, sucrose concentration, inoculum size, and harvest time were systematically optimized by BBD combined with RSM. The experimental design matrix and all relevant data are illustrated in Table 1.

**Fitting Mathematical Models.** ANOVA results of established quadratic models are presented in Table 2. The high significance levels of the models ($P < 0.0001$), nonsignificance "lack of fit" ($P > 0.05$), and desirable determination coefficients ($R^2 \geq 0.9406$) suggested that the built mathematical models were precise and applicable. The second-order polynomial models were applied to express biomass production and IF accumulation:

$$Y_{bio} = 15.74 - 0.49X_1 + 0.77X_2 + 0.078X_3 + 0.027X_4 - 0.27X_1X_2 - 0.002X_1X_3 + 0.33X_1X_4 - 0.013X_2X_3 - 0.19X_2X_4 - 0.86X_3X_4 - 2.98X_1^2 - 0.6X_2^2 - 1.04X_3^2 - 0.51X_4^2$$

$$Y_{TIF} = 225.82 - 2.47X_1 + 7.33X_2 - 4.07X_3 + 5.42X_4 - 0.2X_1X_2 + 1.21X_1X_3 + 0.53X_1X_4 - 1.58X_2X_3 - 1.81X_2X_4 + 2.63X_3X_4 - 39.06X_1^2 - 13.21X_2^2 - 16.03X_3^2 - 3.14X_4^2$$

where $Y_{bio}$ and $Y_{TIF}$ were the biomass DW (g/L) and TIF content ($\mu$g/g DW), respectively; $X_1$ was the culture temperature (°C); $X_2$ was the sucrose concentration (%), $X_3$ was the inoculum size (%), and $X_4$ was the harvest time (days).

**Analysis of Response Surfaces.** As shown in Figure 4A,C, both culture temperature and inoculum size exhibited significant effects on biomass production and IF accumulation. At a fixed inoculum size, the biomass DW and TIF content increased with raising temperature from 24 to 28 °C, because growth and metabolic activities of hairy roots were enhanced with increasing temperature. However, higher temperature (30−32 °C) resulted in irreversible damage of proteins in root

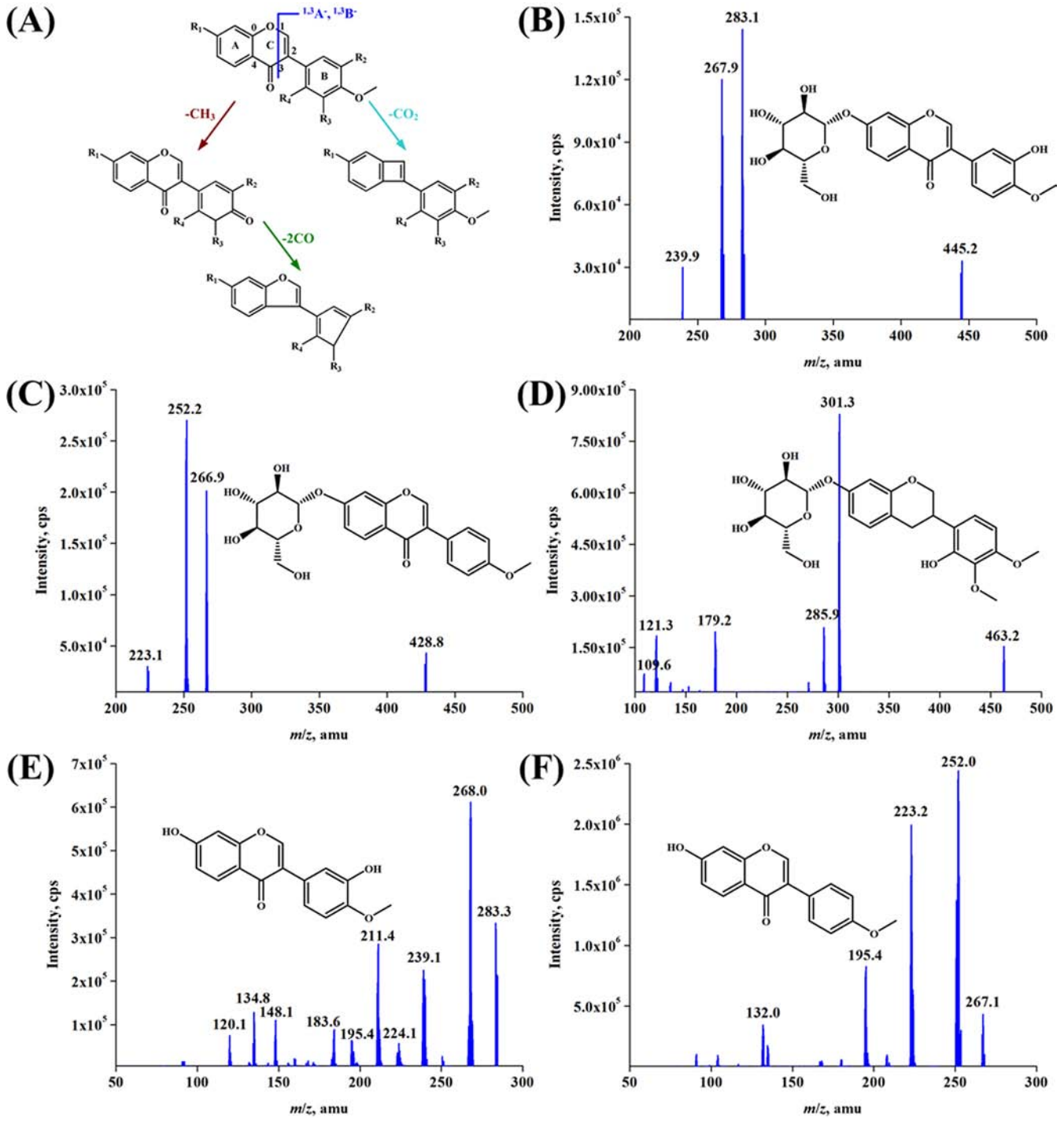


**Figure 5.** (A) The main fragmentation pathways of IF, and ESI−MS/MS analysis of (B) CAG, (C) ON, (D) ASG, (E) CA, and (F) FO originating from AMHRCs.

tissues,[30] leading to a decrease in biomass DW and TIF content. Additionally, the biomass DW and TIF content increased with the extension of inoculum size from 1% to 1.6% at a given culture temperature, but decreased gradually afterward. The restriction of root growth and IF biosynthesis under higher inoculum size (1.6−2.0%) was ascribed to the limitation of nutrients, oxygen levels, and volume of culture flasks.[31] Moreover, a sucrose concentration around 3.5% favored biomass production and IF accumulation at a fixed harvest time (Figure 4B,D). Generally, sucrose has a dual role as carbon source and osmotic agent in plant cell/organ culture media.[28] Higher consumption of sucrose favored the growth of hairy roots and the biosynthesis of metabolites. However, the osmolality of culture media increased with raising sucrose concentration, which caused the loss of cell viability by dehydration and promoted the diffusion of phytochemicals from tissues into media. This led to low biomass production and IF accumulation in AMHRCs. Furthermore, at a given sucrose concentration, the biomass DW and TIF content initially increased with extended time, but nearly stabilized beyond 32 days, which might be due to the depletion of medium nutrients and the liquid mass-transfer limitations.[32]

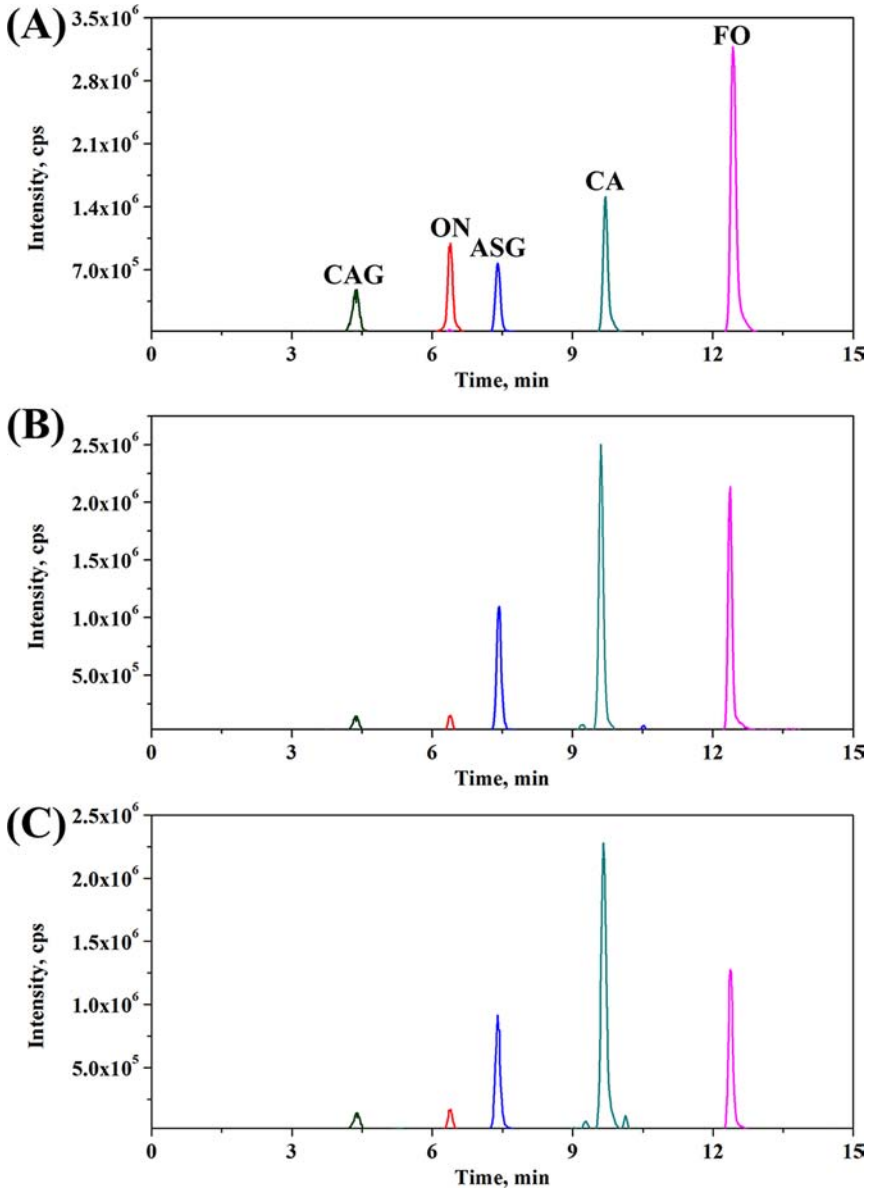


**Figure 6.** Representative LC−MS/MS with SRM total ion chromatograms of (A) standards and extracts from (B) 34 day old AMHRCs and (C) three year old AMFGRs.

**Verification of Predictive Models.** Based on the above mathematical models, the optimal operational conditions were obtained as follows: culture temperature 27.78 °C, sucrose concentration 3.39%, inoculum size 1.44%, and harvest time 34.09 days. Considering the actual operation, culture temperature and harvest time were modified to 27.8 °C and 34 days, respectively. To validate the reliability of these predictive parameters, six sequential experiments adopting AMHRL II were performed using the above optimized conditions. The optimal values of biomass DW (15.74 ± 0.49 g/L) and TIF content (234.77 ± 4.27 μg/g DW) were very close to those (15.98 g/L and 228.62 μg/g DW) forecast by theoretical models. Therefore, the culture conditions achieved by BBD combined with RSM were reliable and practical.

**LC−MS/MS analysis of IF.** In the present study, an accurate LC−MS/MS method was developed for simultaneous quali−quantitative determination of CAG, ON, ASG, CA, and FO from AMHRCs. The ESI-MS/MS analysis of each compound originating from AMHRCs was initially performed, and the main fragmentation pathways are displayed in Figure 5A. As shown in Figure 5B, CAG (retention time 4.37 min) produced a precursor ion of $m/z$ 445.2 ($[M - H]^-$), which fragmented into the primary product ions of $m/z$ 283.0 $[M - H - \text{glucose}]^-$ and 267.9 $[M - H - \text{glucose} - CH_3]^-$. Likewise, the MS fragmentation patterns of ON, ASG, CA, and FO are presented in Figure 5, panels C, D, E, and F, respectively. All MS information on these compounds was consistent with the reported data[3,33−35] as well as that of standard compounds, which confirmed that the established AMHRCs could indeed produce CAG, ON, ASG, CA, and FO. Additionally, LC−MS/MS analysis with SRM mode was applied for quantification of five target analytes in AMHRCs and AMFGRs. The representative chromatograms are presented in Figure 6.

In this study, AMHRCs (34 days old) yielded 9.22 ± 0.23 μg/g DW of CAG, 4.04 ± 0.16 μg/g DW of ON, 66.42 ± 2.53 μg/g DW of ASG, 94.85 ± 1.99 μg/g DW of CA, and 60.25 ± 3.34 μg/g DW of FO, which were comparable to or greater

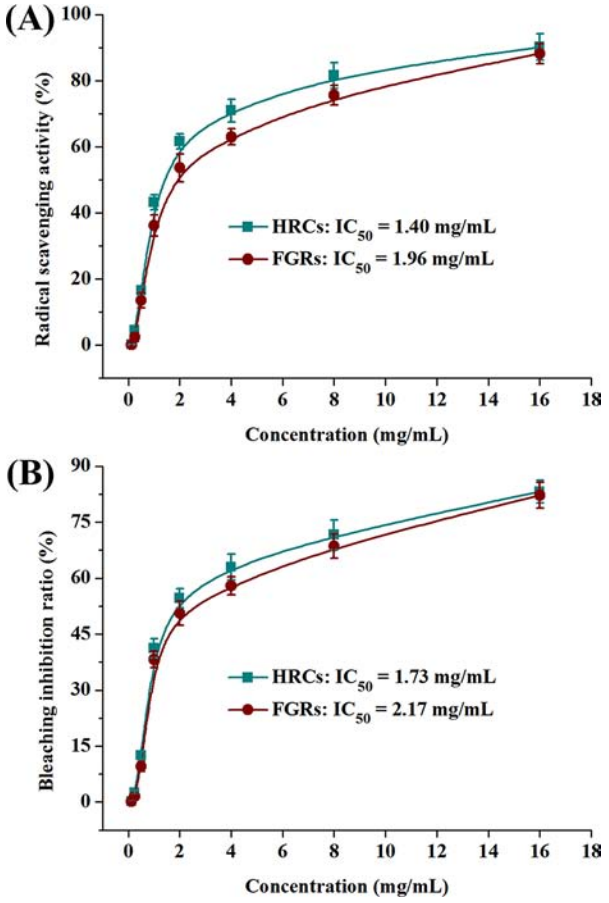


**Figure 7.** Antioxidant activities of extracts from AMHRCs and AMFGRs as assessed by (A) DPPH radical scavenging assay and (B) $\beta$-carotene/linoleic acid bleaching test.

than those from 3 year old AMFGRs (8.87 ± 0.44 $\mu$g/g DW of CAG, 4.50 ± 0.62 $\mu$g/g DW of ON, 51.92 ± 3.34 $\mu$g/g DW of ASG, 89.35 ± 7.21 $\mu$g/g DW of CA, and 32.75 ± 3.02 $\mu$g/g DW of FO). The TIF content of AMHRCs was 234.77 ± 4.27 $\mu$g/g DW, which was significantly higher than that of AMFGRs (187.38 ± 7.25 $\mu$g/g DW). It is evident that the phytochemical production in HRCs is often affected by the incorporation of T-DNA in the host genome, in which the *rol* genes can induce and enhance the biosynthesis of various secondary metabolites with the *rol*B gene probably being the most powerful inducer followed by the *rol*C gene.[15−17,19,21,24−26] From this point of view, the existing *rol*B and *rol*C genes (Figure 2) are likely to be the stimulators for the activation of IF accumulation in AMHRCs.

**Antioxidant Activities of AMHRC Extracts.** The intake of IF is associated with a broad variety of health benefits to humans, and it is generally believed that the beneficial properties of IF (e.g., prevention of cardiovascular disease, cancer, and inflammation) might be related to their antioxidant activities.[36] Therefore, another aim of this study was to evaluate the antioxidant properties of AMHRC extracts and hypothesize their possible uses in pharmaceutical, cosmetic nutritional, and nutraceutical applications. In this work, the DPPH radical-scavenging assay was used to measure antiradical activities, while the $\beta$-carotene/linoleic acid bleaching test was applied to determine antilipid peroxidation capacities. As shown in Figure 7A,B, the antioxidant activities of extracts from AMHRCs and AMFGRs obviously appeared as dose-dependent relationships. However, AMHRC extracts exhibited superior efficacies in terms of antiradical ($IC_{50}$ value of 1.40 mg/mL) and lipid peroxidation inhibition ($IC_{50}$ value of 1.73 mg/mL) as compared to those of AMFGRs ($IC_{50}$ values of 1.96 and 2.17, mg/mL, respectively). Additionally, the $IC_{50}$ values of VC (the reference in DPPH radical-scavenging assay) and BHT (the reference in $\beta$-carotene/linoleic acid bleaching test) were 0.067 and 0.025, mg/mL, respectively.

Although antioxidant activities of AMHRC extracts were quite moderate as against those of synthetic antioxidants, the main focus of this study was on the evaluation of antioxidant properties from AMHRCs as compared to AMFGRs. Due to the presence of phenolic hydroxyls, CAG, ASG, CA, and FO were the primary antioxidant contributors of *A. membranaceus*, which can act as hydrogen/electron donors to neutralize peroxyl free radicals, shown in several in vitro antioxidant assays.[3,37−39] In this study, AMHRC extracts exhibited better antioxidant activities than AMFGRs, which can be partly explained by their higher levels of ASG, CA, and FO as compared to AMFGRs. However, one essential difference of traditional Chinese herbal medicines from synthetic drugs is that their therapeutic effects are due to the joint contribution of multiple components, not only a few ones. Possible synergistic effects of the multiple constituents in AMHRC extracts should therefore be taken into consideration. Overall, the antioxidant activity screening results are indicative of AMHRCs as potentially more effective medicaments compared with naturally occurring roots in food and pharmaceutical industries.

**Predominance of AMHRCs.** The aforementioned results clearly indicated that the highly productive AMHRC system was capable of synthesizing and accumulating IF (34 day old) in higher yield and quality comparable to those of 3 year old AMFGRs. Additionally, AMHRC extracts were more effective in scavenging radicals and inhibiting lipid peroxidation as compared to those of AMFGRs. Moreover, the proposed AMHRC system exhibits several potential advantages as follows: (1) The desired IF products with uniform quality can be harvested anywhere in the world, meeting the stringent criteria of the Good Manufacturing Practice (GMP) guidelines (e.g., absence of agrochemicals). (2) The AMHRC system represents a continuous and reliable production system independent of climate or ecology-related problems and constraints. (3) The system's growth cycle can be measured in weeks rather than years of intact plants grown in fields.

Overall, this study provided the generation of an attractive alternative source for the efficient production of IF. It is assumed that this system will meet the worldwide demand for IF and issues associated with *A. membranaceus* cultivation on account of its prolonged seed dormancy and extensive period from planting to harvest (3−5 years). The present investigation highlighted the importance of optimizing AMHRC growth and culturing conditions to better predict and define IF biosynthetic capacity as precondition for industrial processes. Furthermore, the genetic and biochemical stability of the established AMHRC as well as its high productivity offers an effective platform for further studies on the biosynthetic pathways of IF.

## ■ ASSOCIATED CONTENT

### Supporting Information

Table S1 reports specific primers used for PCR amplification; Table S2 shows MS parameters for five main IF constituents in AMHRCs. This material is available free of charge via the Internet at http://pubs.acs.org.

## AUTHOR INFORMATION


### Corresponding Authors

*(Y.-J.F.) Tel/fax: +86-451-82190535. E-mail: yujie_fu2011@yahoo.com.

*(W.M.) Tel/fax: +86-451-82193430. E-mail: mawei@hljucm.net.

### Author Contributions

‡J.J. and Q.-Y.G. contributed equally to this work.



### Funding

The authors gratefully acknowledge the financial support by Agricultural Science and Technology Achievements Transformation and Program (2012GB23600641), Fundamental Research Funds for the Central Universities (2572014AA06), Special Fund of National Natural Science Foundation of China (31270618), Key Program of National Natural Science Foundation of China (81274010), and Heilongjiang Province Outstanding Youth Fund (JC201101).


### Notes

The authors declare no competing financial interest.

## ABBREVIATIONS USED

AMFGRs, *A. membranaceus* field grown roots; AMHRCs, *A. membranaceus* hairy root cultures; AMHRL, *A. membranaceus* hairy root line; ASG, astraisoflavan-7-*O*-$\beta$-D-glucoside; BBD, Box–Behnken design; CA, calycosin; CAG, calycosin-7-*O*-$\beta$-D-glucoside; DW, dry weight; FO, formononetin; HRCs, hairy root cultures; IF, isoflavonoids; ON, ononin; RSM, response surface methodology; TIF, total IF

## REFERENCES


(1) Napolitano, A.; Akay, S.; Mari, A.; Bedir, E.; Pizza, C.; Piacente, S. An analytical approach based on ESI-MS, LC–MS and PCA for the quali–quantitative analysis of cycloartane derivatives in *Astragalus* spp. *J. Pharm. Biomed. Anal.* **2013**, *85*, 46–54.

(2) Zhang, L. J.; Liu, H. K.; Hsiao, P. C.; Kuo, L. M. Y.; Lee, I. J.; Wu, T. S.; Chiou, W. F.; Kuo, Y. H. New isoflavonoid glycosides and related constituents from astragali radix (*Astragalus membranaceus*) and their inhibitory activity on nitric oxide production. *J. Agric. Food Chem.* **2011**, *59*, 1131–1137.

(3) Huang, X.; Liu, Y.; Song, F.; Liu, Z.; Liu, S. Studies on principal components and antioxidant activity of different Radix Astragali samples using high-performance liquid chromatography/electrospray ionization multiple-stage tandem mass spectrometry. *Talanta* **2009**, *78*, 1090–1101.

(4) Li, W.; Sun, N. Y.; Yan, X. T.; Yang, S. Y.; Kim, S.; Lee, Y. M.; Koh, Y. S.; Kim, Y. H. Flavonoids from *Astragalus membranaceus* and their inhibitory effects on LPS-stimulated pro-inflammatory cytokine production in bone marrow-derived dendritic cells. *Arch. Pharm. Res.* **2014**, *37*, 186–192.

(5) Chen, L.; Li, Z.; Tang, Y.; Cui, X.; Luo, R.; Guo, S.; Zheng, Y.; Huang, C. Isolation, identification and antiviral activities of metabolites of calycosin-7-*O*- $\beta$-D-glucopyranoside. *J. Pharm. Biomed. Anal.* **2011**, *56*, 382–389.

(6) Kuo, Y. H.; Tsai, W. J.; Loke, S. H.; Wu, T. S.; Chiou, W. F. *Astragalus membranaceus* flavonoids (AMF) ameliorate chronic fatigue syndrome induced by food intake restriction plus forced swimming. *J. Ethnopharmacol.* **2009**, *122*, 28–34.

(7) Zheng, K. Y. Z.; Choi, R. C. Y.; Cheung, A. W. H.; Guo, A. J. Y.; Bi, C. W. C.; Zhu, K. Y.; Fu, Q.; Du, Y.; Zhang, L. W.; Zhan, J. Y. X.; Duan, R.; Lau, D. T. W.; Dong, T. T. X.; Tsim, K. W. K. Flavonoids from Radix Astragali induce the expression of erythropoietin in cultured cells: a signaling mediated via the accumulation of hypoxia-inducible factor-1$\alpha$. *J. Agric. Food Chem.* **2011**, *59*, 1697–1704.

(8) Guo, C.; Tong, L.; Xi, M.; Yang, H.; Dong, H.; Wen, A. Neuroprotective effect of calycosin on cerebral ischemia and reperfusion injury in rats. *J. Ethnopharmacol.* **2012**, *144*, 768–774.

(9) Zhang, W.; Jiang, S.; Qian, D.; Shang, E.; Duan, J. Analysis of interaction property of calycosin-7-O-$\beta$-D-glucoside with human gut microbiota. *J. Chromatogr. B* **2014**, *963*, 16–23.

(10) Wilson, S. A.; Roberts, S. C. Metabolic engineering approaches for production of biochemicals in food and medicinal plants. *Curr. Opin. Biotechnol.* **2014**, *26*, 174–182.

(11) Davies, K. M.; Deroles, S. C. Prospects for the use of plant cell cultures in food biotechnology. *Curr. Opin. Biotechnol.* **2014**, *26*, 133–140.

(12) Chandra, S.; Chandra, R. Engineering secondary metabolite production in hairy roots. *Phytochem. Rev.* **2011**, *10*, 371–395.

(13) Guillon, S.; Trémouillaux-Guiller, J.; Pati, P. K.; Rideau, M.; Gantet, P. Harnessing the potential of hairy roots: dawn of a new era. *Trends Biotechnol.* **2006**, *24*, 403–409.

(14) Kim, Y. K.; Kim, J. K.; Kim, Y. B.; Lee, S.; Kim, S. U.; Park, S. U. Enhanced accumulation of phytosterol and triterpene in hairy root cultures of *Platycodon grandiflorum* by overexpression of *Panax ginseng* 3-hydroxy-3-methylglutaryl-coenzyme A reductase. *J. Agric. Food Chem.* **2013**, *61*, 1928–1934.

(15) Nopo-Olazabal, C.; Hubstenberger, J.; Nopo-Olazabal, L.; Medina-Bolivar, F. Antioxidant activity of selected stilbenoids and their bioproduction in hairy root cultures of muscadine grape (*Vitis rotundifolia* Michx.). *J. Agric. Food Chem.* **2013**, *61*, 11744–11758.

(16) Singh, H.; Dixit, S.; Verma, P. C.; Singh, P. K. Evaluation of total phenolic compounds and insecticidal and antioxidant activities of tomato hairy root extract. *J. Agric. Food Chem.* **2014**, *62*, 2588–2594.

(17) Ono, N. N.; Tian, L. The multiplicity of hairy root cultures: Prolific possibilities. *Plant Sci.* **2011**, *180*, 439–446.

(18) Ludwig-Müller, J.; Jahn, L.; Lippert, A.; Püschel, J.; Walter, A. Improvement of hairy root cultures and plants by changing biosynthetic pathways leading to pharmaceutical metabolites: Strategies and applications. *Biotechnol. Adv.* **2014**, *32*, 1168–1179.

(19) Sharma, P.; Padh, H.; Shrivastava, N. Hairy root cultures: A suitable biological system for studying secondary metabolic pathways in plants. *Eng. Life Sci.* **2013**, *13*, 62–75.

(20) Terato, M.; Ishikawa, A.; Yamada, K.; Ozeki, Y.; Kitamura, Y. Increased furanocoumarin production by *Glehnia littoralis* roots induced via *Agrobacterium rhizogenes* infection. *Plant Biotechnol.* **2011**, *28*, 317–321.

(21) Fattahi, M.; Nazeri, V.; Torras-Claveria, L.; Sefidkon, F.; Cusido, R. M.; Zamani, Z.; Palazon, J. A new biotechnological source of rosmarinic acid and surface flavonoids: Hairy root cultures of *Dracocephalum kotschyi* Boiss. *Ind. Crop. Prod.* **2013**, *50*, 256–263.

(22) Wu, N.; Fu, K.; Fu, Y. J.; Zu, Y. G.; Chang, F. R.; Chen, Y. H.; Liu, X. L.; Kong, Y.; Liu, W.; Gu, C. B. Antioxidant activities of extracts and main components of pigeonpea [*Cajanus cajan* (L.) Millsp.] leaves. *Molecules* **2009**, *14*, 1032–1043.

(23) Wu, N.; Zu, Y.; Fu, Y.; Kong, Y.; Zhao, J.; Li, X.; Li, J.; Wink, M.; Efferth, T. Antioxidant activities and xanthine oxidase inhibitory effects of extracts and main polyphenolic compounds obtained from *Geranium sibiricum* L. *J. Agric. Food Chem.* **2010**, *58*, 4737–4743.

(24) Shkryl, Y. N.; Veremeichik, G. N.; Bulgakov, V. P.; Tchernoded, G. K.; Mischenko, N. P.; Fedoreyev, S. A.; Zhuravlev, Y. N. Individual and combined effects of the *rol*A, B, and C genes on anthraquinone production in *Rubia cordifolia* transformed calli. *Biotechnol. Bioeng.* **2008**, *100*, 118–125.

(25) Bulgakov, V. P. Functions of *rol* genes in plant secondary metabolism. *Biotechnol. Adv.* **2008**, *26*, 318–324.

(26) Bulgakov, V. P.; Shkryl, Y. N.; Veremeichik, G. N.; Gorpenchenko, T. Y.; Vereshchagina, Y. V. Recent advances in the understanding of Agrobacterium rhizogenes-derived genes and their effects on stress resistance and plant metabolism. In *Biotechnology of Hairy Root Systems*; Doran, P. M., Ed.; Springer Press: Berlin, Germany, 2013; pp 1–22.

(27) Hu, Z. B.; Du, M. Hairy root and its application in plant genetic engineering. *J. Integr. Plant Biol.* **2006**, *48*, 121–127.

(28) Murthy, H. N.; Lee, E. J.; Paek, K. Y. Production of secondary metabolites from cell and organ cultures: strategies and approaches for biomass improvement and metabolite accumulation. *Plant Cell, Tissue Organ Cult.* **2014**, *118*, 1−16.
(29) Matkowski, A. Plant *in vitro* culture for the production of antioxidants—A review. *Biotechnol. Adv.* **2008**, *26*, 548−560.
(30) Shohael, A. M.; Ali, M. B.; Yu, K. W.; Hahn, E. J.; Paek, K. Y. Effect of temperature on secondary metabolites production and antioxidant enzyme activities in *Eleutherococcus senticosus* somatic embryos. *Plant Cell, Tissue Organ Cult.* **2006**, *85*, 219−228.
(31) Danphitsanuparn, P.; Boonsnongcheep, P.; Boriboonkaset, T.; Chintapakorn, Y.; Prathanturarug, S. Effects of *Agrobacterium rhizogenes* strains and other parameters on production of isoflavonoids in hairy roots of *Pueraria candollei* Grah. ex Benth. var. *candollei*. *Plant Cell, Tissue Organ Cult.* **2012**, *111*, 315−322.
(32) Theboral, J.; Sivanandhan, G.; Subramanyam, K.; Arun, M.; Selvaraj, N.; Manickavasagam, M.; Ganapathi, A. Enhanced production of isoflavones by elicitation in hairy root cultures of Soybean. *Plant Cell, Tissue Organ Cult.* **2014**, *117*, 477−481.
(33) Zhang, X.; Xiao, H. B.; Xue, X. Y.; Sun, Y. G.; Liang, X. M. Simultaneous characterization of isoflavonoids and astragalosides in two *Astragalus* species by high-performance liquid chromatography coupled with atmospheric pressure chemical ionization tandem mass spectrometry. *J. Sep. Sci.* **2007**, *30*, 2059−2069.
(34) Xiao, W. L.; Motley, T. J.; Unachukwu, U. J.; Lau, C. B. S.; Jiang, B.; Hong, F.; Leung, P. C.; Wang, Q. F.; Livingston, P. O.; Cassileth, B. R.; Kennelly, E. J. Chemical and genetic assessment of variability in commercial Radix Astragali (*Astragalus* spp.) by ion trap LC-MS and nuclear ribosomal DNA barcoding sequence analyses. *J. Agric. Food Chem.* **2011**, *59*, 1548−1556.
(35) Qi, L. W.; Wen, X. D.; Cao, J.; Li, C. Y.; Li, P.; Yi, L.; Wang, Y. X.; Cheng, X. L.; Ge, X. X. Rapid and sensitive screening and characterization of phenolic acids, phthalides, saponins and isoflavonoids in Danggui Buxue Tang by rapid resolution liquid chromatography/diode-array detection coupled with time-of-flight mass spectrometry. *Rapid Commun. Mass Spectrom.* **2008**, *22*, 2493−2509.
(36) Rüfer, C. E.; Kulling, S. E. Antioxidant activity of isoflavones and their major metabolites using different *in vitro* assays. *J. Agric. Food Chem.* **2006**, *54*, 2926−2931.
(37) Chen, C. Y.; Zu, Y. G.; Fu, Y. J.; Luo, M.; Zhao, C. J.; Wang, W.; Zhao, B. S.; Li, J.; Efferth, T. Preparation and antioxidant activity of Radix Astragali residues extracts rich in calycosin and formononetin. *Biochem. Eng. J.* **2011**, *56*, 84−93.
(38) Zhao, B. S.; Fu, Y. J.; Wang, W.; Zu, Y. G.; Gu, C. B.; Luo, M.; Efferth, T. Enhanced extraction of isoflavonoids from Radix Astragali by incubation pretreatment combined with negative pressure cavitation and its antioxidant activity. *Innovative Food Sci. Emerging Technol.* **2011**, *12*, 577−585.
(39) Xu, X.; Li, F.; Zhang, X.; Li, P.; Zhang, X.; Wu, Z.; Li, D. *In vitro* synergistic antioxidant activity and identification of antioxidant components from *Astragalus membranaceus* and *Paeonia lactiflora*. *PLoS One* **2014**, *9*, e96780.

Table 1. Oligonucleotide Sequences Used in Amplification, Immobilization, and Hybridization Experiments Specific for *Staphylococcus aureus* (EF529607.1)

| target | accession no. | oligonucleotide | sequence (5′−3′) | length (bp) | amplicon size (bp) |
|---|---|---|---|---|---|
| *Aeromonas hydrophila* | M84709 | forward primer | 5′-CCAATATGTCGGTGAAGA-3′ | 18 | 161 |
| | | reverse primer | 5′-CATGTTTGAAGCTGTCAG-3′ | 18 | |
| *Staphylococcus aureus* | EF529607.1 | forward primer | 5′-GCTATCAGTAATGTTTCG-3′ | 18 | 151 |
| | | reverse primer | 5′-GCACTATATACTGTTGGA-3′ | | |
| *Staphylococcus aureus* | EF529607.1 | capture probe | 5′-AGTAGCTCAGCAAATGCA-SH-3′ | 18 | |
| | | detection probe | 5′-$NH_2$-CACAAACAGATAACGGCG-3′ | | |

detection of pathogens, such as those incorporating the use of nanoparticles for DNA detection.[15] They allow continuous, fast, sensitive, and selective detection of DNA hybridization, and they can also be reused.[16] These systems usually rely on the immobilization of a single-stranded DNA (ssDNA) probe onto a surface to recognize its complementary DNA target sequence by hybridization.[16] Transduction of hybridization of DNA can be measured electronically.[17] The electrochemistry relies on the use of different inorganic-colloid nanoparticles (zinc sulfide, cadmium sulfide, and lead sulfide) to differentiate the target DNA signals in connection with a sandwich hybridization and highly sensitive stripping voltammetry of the corresponding targets. DNA hybridization biosensors play an important role in pharmaceutical, clinical, and forensic applications. Some techniques have been successfully applied to the development of genosensors based upon the combination of a suitable transducer.[18]

The use of nanomaterials and nanotracers in biosensors allows new transduction technology and application of a bismuth layer on glass carbon electrodes to detect heavy metals in samples showing an alternative material to substitute toxic mercury.[5,19−21] The main advantages of bismuth are the high capacity to form fused alloys with metals, which are less affected by dissolved oxygen. However, it fails to detect low amounts of analyte due to its poor conductivity,[10,22] but applied multiwall carbon nanotubes−bismuth modified on glassy carbon electrodes showed increased sensitivity in the detection of trace metals.

In the present work, a sensitive and selective electrochemical DNA biosensor for the rapid detection of *S. aureus* was measured. Signalizing probe DNA was connected with lead sulfide nanoparticles coated with 5′-($NH_2$) oligonucleotide using 1-ethyl-3-[3-(dimethylamino)propyl]carbodiimide hydrochloride (EDC) as a cross-linker. The fixing probe (fDNA) was another complementary sequence of DNA with thiol modification, which strongly adsorbed on the gold electrode surface (GE). After hybridization, the sandwich structure was dissolved in 1 M $HNO_3$ to release $Pb^{2+}$, which was electrodeposited on the glass carbon electrode (GCE) surface decorated with MWCNT−Chi−Bi. Finally, the signal was measured by differential pulse voltammetry (DPV).

## EXPERIMENTAL PROCEDURES

**Reagents and Materials.** Lead nitrate $Pb(NO_3)_2$, sodium sulfide ($Na_2S$), sodium hydroxide (NaOH), and 3-mercaptoacetic acid $C_2H_4O_2S$ (used as a stabilizer for the NPs) were used for the synthesis of lead sulfide nanoparticles (PbS NPs). EDC, salmon sperm DNA, and buffers were used for the conjugation of the carboxylic group on NPs, and an amine group on the capture probe was obtained from Sigma Aldrich. 6-Mercapto-1-hexanol was purchased from Tokyo Chemical Industry Co. Ltd. (Tokyo, Japan). Hybridization buffer PBS (potassium phosphate buffer with NaCl, pH 7.4), washing buffer Tris-HCl (pH 8.0) with Tween-20, and sodium dodecyl sulfate (SDS) were used to remove the unhybridized DNA. Multiwalled carbon nanotubes were obtained from Nanjing Xianfeng Nanomaterials Technology Co. Ltd. (Nanjing, China). Chitosan was put on the surface of the electrode to increase the sensitivity. A PCR kit was set up to purify the DNA products after PCR amplification was purchased from Sangon Biotech Co. (Shanghai, China). Bismuth nitrate in nitric acid 0.5 mol/L obtained from Scharlau Chemie S.A. (Spain) was deposited on the GCE surface prior to electrochemical processing. All of the solutions were prepared using ultrapure water from a Millipore Milli-Q system. All oligonucleotides used in the sensors were purchased from Takara Co. (Dalian, China) and Sangon Biotechnology Co., Ltd. (Shanghai, China) with HPLC purification and working solutions prepared by dilution in PBS buffer.

**Apparatus.** The morphology and characterization of lead nanoparticles were studied by transmission electron microscopy (TEM) (JEM-2100, JEOL, Japan). An incubator for the hybridization reaction, magnetic stirrer, and vortex mixer were used to conjugate the carboxylic group on PbS NTs and the amine group on the capture probe. A centrifuge (5804 R Eppendorf, Hamburg, Germany) was used to separate the nanoparticles and extract the DNA. Nanodrop (Thermo Scientific, Ashville, NC, USA) was used to measure the concentration and purity of DNA. Gel electrophoresis was performed using a Bio-Rad electrophoresis instrument (Powerpac Universal, Bio-Rad, USA). The three electrode electrochemical detection system consisted of a GCE (working electrode), an Ag/AgCl reference electrode (saturated KCl), and platinum wire as counter electrode. The gold electrode, GCE (working electrode) and silver/silver chloride electrode (counter and reference electrodes) were purchased from (Chenhua, Shanghai, China). A gold electrode (diameter = 2 mm) was used to make sandwich structures and a GCE (diameter = 2.5 mm) was used for measuring target DNA. Electrochemical measurements were performed with an electrochemical station analyzer (Shanghai CH Instruments Co., China).

**Bacteria Culture and Genomic Extraction.** *S. aureus* (accession no. EF520720.1) was obtained from Zhangjiagang Entry-Exit Inspection and Quarantine Bureau (Suzhou, Jiangsu province, China), and *A. hydrophila* (accession no. M84709) was obtained from Fresh Water Fisheries Research Center (Wuxi, China). The nucleotide sequences submitted with these accession numbers were used in designing primers and probes for targeted gene amplification and detection. Other strains were collected and preserved at Jiangnan University laboratories. Pure cultures of *A. hydrophila* were grown in ampicilin starch agar phenol red, and *S. aureus* was grown in *Staphylococcus* selective agar (CM 310) and obtained from Beijing Land Bridge Technology Co., Ltd., China. Inoculum media were incubated at 37 °C for 24 h, in duplicate aerobiosis. Colonies were purified by streaking on the same media and incubating at 37 °C for 24 h. This treatment step was repeated several times to obtain a pure culture. Genomic DNA was extracted by slightly modified boiling methods[23,24] from tubes after incubation for 18 h in tryptic soy broth media (TSB). Briefly, the culture was heated in a water bath for 10 min to kill all surviving bacteria, and one portion of each broth was centrifuged at 13000 rpm for 5 min at 4 °C. The pellet was suspended in 500 μL of sterile distilled water (DD water) and vortexed

**Scheme 1. Steps of Representation of Sandwich Structure and GCE with MWCNT−Chi**

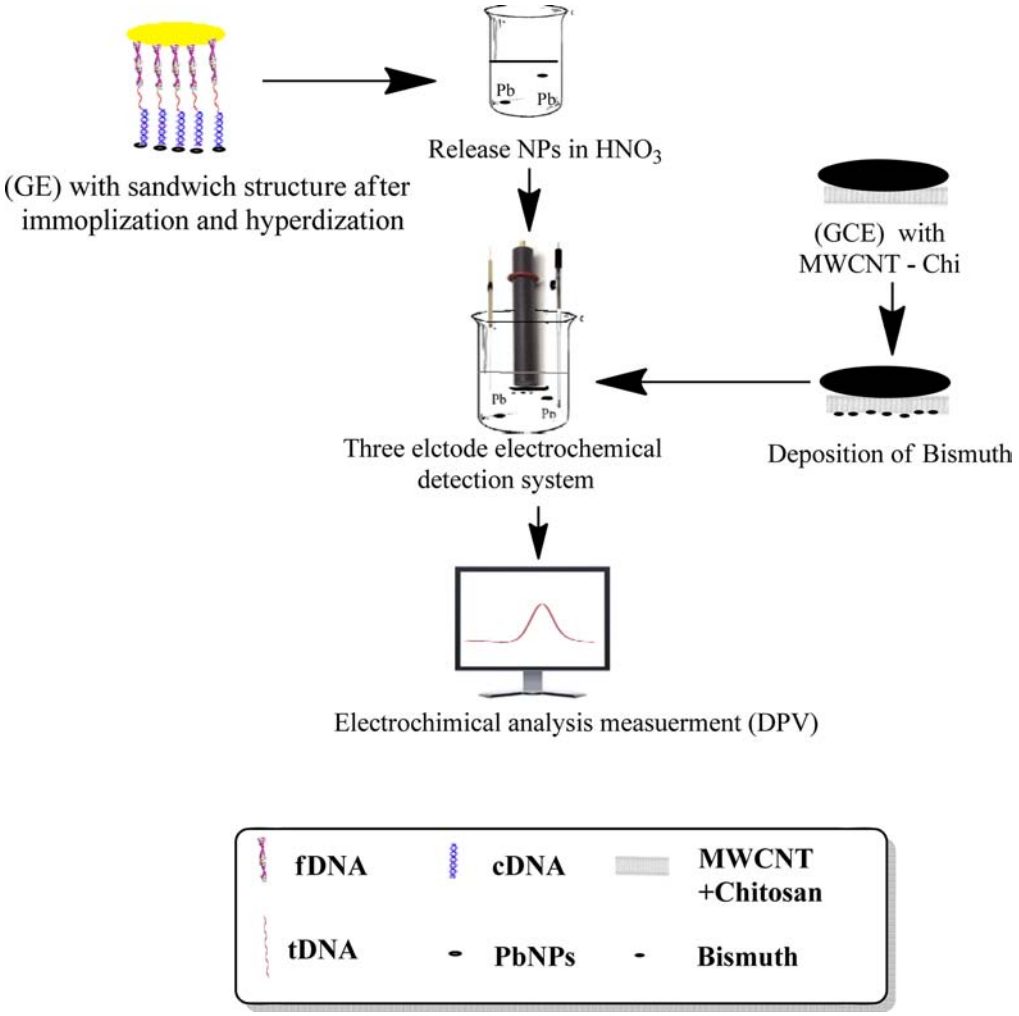


vigorously. The bacterial suspensions were boiled in a water bath for 15 min, then rapidly cooled at −20 °C for 10 min to shock the cells, and then centrifuged again at 12000 rpm for 3 min to precipitate the debris. The supernatant containing genomic DNA was harvested into a clean tube and used as the DNA template for PCR amplification.

**Oligonucleotides.** The primers were designed to provide PCR amplification, and the probe was complementary to part of the fragment, allowing it to hybridize with the PCR product. The probes were designed with modification (3′SH and 5′$NH_2$) and purification by HPLC to allow the detection of the PCR product using National Center for Biotechnology Information (NCBI) databases using Basic Local Alignment Tool (BLAST) software (http://www.ncbi.nlm.nih.gov/).[24] DNA calculators from Sigma-Aldrich to specify the primer sequences were further verified using software (http://www.sigmagenosys.com/calc/DNACalc.asp). All oligonucleotides used in the sensors were obtained from Takara Co. and Sangon Biotechnology Co., Ltd., and the reverse and forward primers were diluted to 0.4 μM. The sequences of the oligonucleotides are shown in Table 1.

**PCR Conditioning.** A fragment (151 bases) of the *S. aureus* (accession no. EF529607.1) gene was amplified using the forward and reverse primers. PCR was performed in a reaction solution with a total volume of 25 μL containing (2.5 μL) PCR buffer and (2 μL) deoxynucleoside triphosphate (dNTP) mixture obtained from Takara. Mixed together were 1 μL of each primer (0.4 μM), 1 μL of template DNA, 0.25 μL of Taq DNA polymerase, and 17.25 μL of sterile double-distilled water (DDW) to obtain the reaction mixture. Specificity of the primer amplifications was performed and verified using strains of *S. aureus* (EF529607) as target DNA and *A. hydrophila* (ATCC 7966) as the negative control. Amplification conditions were carried out using the following protocol: initial denaturation at 94 °C for 2 min followed by 30 cycles of denaturation at 94 °C for 30 s, annealing at 46 °C for 30 s, and an extension at 72 °C for 1 min, followed by a final extension at 72 °C for 5 min, and finally a hold at 4 °C. All amplification reactions were carried out in a thermal cycler (Takara, Gradient PCR). PCR products (5 μL) with a loading buffer were visualized by electrophoreses through 2% agarose gel in TAE buffer and stained with Andy Safe DNA gel stain (BioProbes, USA). A DNA molecular ladder (100 bp) obtained from (Takara) was included in each gel as a molecular weight marker. The gels were photographed under ultraviolet light using a Bio-Rad Gel doc 1000 molecular imager.

**Genome Purification and Dilution.** The PCR product was purified by using a PCR purification kit, from Shanghai Sangon Bioengineering Ltd. Co., according to the manufacturer's instructions, and then stored at −20 °C until use. Then, it was diluted serially with PBS buffer, and PCR product quantification and concentration were measured with a nanodrop spectrophotometer and used as DNA samples for the experiments.

**Synthesis of Lead Sulfide Nanoparticles.** All glassware used in the following procedure was carefully cleaned by soaking in a bath of freshly prepared aqua regia solution 1:3 $HCl/HNO_3$ over 24 h followed by rinsing thoroughly in twice-distilled water and dried in an oven. The pH values of all nanoparticle solutions prepared were recorded using a pH meter (Mettler-Toledo instruments, Delta 320, Shanghai, China). All steps of the synthesis were performed at room temperature and ambient conditions. For the preparation of lead sulfide nanoparticles (PbS NPs), $Pb(NO_3)_2$ and $Na_2S$ solutions were filtered through a nylon syringe filter (25 mm × 0.22 μm) (ANPEL Scientific Instrument, Shanghai, China) prior to use. PbS NPs were

prepared according to the literature.[25,26] Briefly, 9.22 μL of thioglycolic acid ($C_2H_4O_2S$) used as a stabilizer was added to 50 mL of 0.4 mmol $L^{-1}$ Pb $(NO_3)_2$ solution under vigorous stirring, and then the pH was adjusted to 7.0 with 0.5 mol $L^{-1}$ NaOH. The solution was bubbled with nitrogen for 30 min, then 50 mL of 1.34 mmol $L^{-1}$ $Na_2S$ was added dropwise to the mixture solution. The reaction was carried out for 24 h under nitrogen bubbling, and gradually a brown colloid was formed. The colloid was stable for 3 weeks in a brown bottle at 4 °C.

**Characterization of Nanoparticles.** A JEOL JEM-2100 (HR) transmission electron microscope (TEM) from Electronic Inc. Co., Japan, was used to observe the morphology and particle size distribution in PbS NPs solution. Samples were prepared by dropping aliquots of the colloidal solution onto holey copper-coated grids, which were then dried at room temperature.

**Preparation of Multiwalled Carbon Nanotubes−Chi.** The MWCNT−Chi matrix was used to increase the sensitivity of GCE. Before mixing with chitosan, MWCNT was treated with concentrated $HNO_3$ for 2 h and dried in a vacuum at 30 °C. Then, 10 mg of treated MWCNT was mixed with 20 mL of (2%) acetic acid and 2.5 mg of chitosan, followed by ultrasonification for 2 h. The prepared MWCNT−Chi was stored at room temperature until further use.[22,27]

**Immobilization of Probe DNA.** Immobilization of capture probe DNA was performed according to the literature[26,28,29] with slight modifications. The sequences of the probe oligonucleotides used in this study are shown in Table 1. According to the literature,[26,29] the most critical step in the preparation of a DNA biosensor is the immobilization of the DNA probe on the surface of the sensing device such as an electrode. Prior to use, the gold electrode was first heated in a Piranha solution (3:7 $H_2O_2$/concentrated $H_2SO_4$) for about 10 min and then subsequently hand polished thoroughly with 0.03 μm and 0.05 nm alumina slurries, respectively, and a microfiber pad to a mirror-like finish. This was followed by cleaning for 5 min in ethanol and water, respectively, to remove all residual alumina powder and other possible contamination. The electrode was then electrochemically cleaned in 0.5 M of $H_2SO_4$ to ensure complete removal of contaminants from the electrode surface and finally dried in a stream of nitrogen gas.

The fixing probe was diluted by using 10 mM TCEP with a 1:1 ratio and incubated at room temperature for 1 h. The probe was then dropped in the electrode and incubated at 4 °C overnight to form chemisorption of the thiol groups onto the gold surface. The gold electrode was washed with 0.1 M, pH 8.0, Tris-HCl containing 0.05% Tween-20 to remove excess fixing probe and then immersed in a 1 mM MCH solution for 1 h to obtain a well-aligned DNA monolayer and for 30 min in 125 μg/mL salmon sperm DNA to block specific binding and 2% BSA in 0.1 M, pH 8.0, Tris-HCl to make DNA straight line.

**Hybridization of Probes and PCR Amplified Target DNA.** Prior to use, the purified PCR product (*S. aureus*) was denatured for 10 min at 95 °C and immediately put in −20 °C, and then target denatured PCR product was diluted to the desired concentration[30] to measure different concentrations in the sensor. A gold electrode content fixing probe was immersed into the denatured DNA and incubated for 1 h at 45 °C to make the first hybridization. The hybridized electrode was then immersed into 0.1% sodium dodecyl sulfate (SDS) for 10 min to remove the unhybridized DNA and any nonspecific adsorption of DNA. The second hybirdization was done by immersing the electrode into a solution of 200 μL (PBS buffer) containing the PbS NPs−capture DNA probe for 1 h at 45 °C to form a sandwich structure as fix DNA−target DNA−detective DNA−PbS NPs and then washed three times with a 0.1% SDS phosphate buffer (pH 7.3) to remove the unhybridized DNA probes.[28,29] After hybridization, the carrier containing nanoparticles was immersed into a cell containing 1.0 M nitric acid solution for 5 min to dissolute the sandwich structures. Scheme 1 shows the steps of immobilization and hybridization.

**Electrochemical Analysis.** The GCE and DNA detection procedures are illustrated in Figure 1. Prior to use, the GCE for the experiment was cleaned and dried according to the literature.[28,31] Then 10 μL of MWCNT−Chi was dropped onto the surface of the GCE and dried, then immersed into a solution containing 0.1 M acetate buffer solution (pH 4.5) and 100 μL of bismuth ions. The bismuth films were formed by deposition on the carbon electrode containing MWCNT−Chi, and the deposition was performed in a separate solution prior to measurement of lead and dried. After the hybridization reaction, the gold electrode with sandwich structure (fDNA−tDNA−cDNA−PbS NPs) was immersed in 150 μL of 1.0 mol $L^{-1}$ $HNO_3$ solution for 5 min to dissolve the PbS NPs fixed on the surface of the electrode. All of the experiments were carried out at room temperature. Every test was replicated at least three times. All curves were the average of three test results.

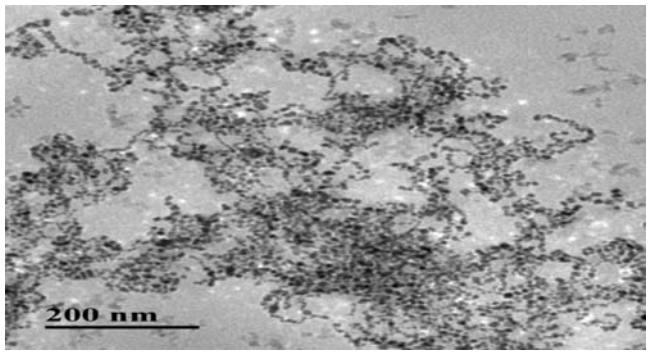


**Figure 1.** Transmission electron micrographs of the synthesized lead nanoparticles (PbS NPs).

**Detection of Target DNA in Artificial Contaminated Beef Meat.** Fresh beef was collected from a local supermarket (Wuxi, Jiangsu province, China), and the meat was removed from the carcasses and transported immediately to the laboratory in an ice box. Prior to inoculation, the samples were treated according to the literature[32] with slight modifications. Briefly, samples were divided into 10 g pieces using a knife that was sterilized under UV radiation. Then, each piece was transferred into sterilized Petri dishes with 100 μL of different concentrations of bacteria ($10^5$−$10^1$ CFU/mL) used as inocula. Aliquots of each dilution were spread onto the surface of the beef samples and stored at 4 °C for 4 h. A sterilized sample without inoculation was used as a negative control. Then, the samples were transferred into a sterilized 250 mL Erlenmeyer flask, and 90 mL of tryptic soy broth (TSB) medium was added immediately with homogenized shaking for 10 min at 200 rpm, inoculation of samples on Petri dishes, and enumeration after 24 h at 37 °C. The samples in the Erlenmeyer flask were incubated overnight at 37 ± 1 °C. A 1.5 mL rinse fluid was taken from the sample Erlenmeyer flask and placed in a sterile 2 mL microcentrifuge tube for DNA extraction. DNA of the pellet was extracted using the boiling methods (described above), and the PCR, purification kit, and electrochemicistry were done as above.

## RESULTS AND DISCUSSION

**Characterization of Nanoparticles.** The colloid chemistry route offers a simple means to synthesize lead sulfide nanoparticles as it uses inexpensive inorganic starting materials and has a good control over the particle sizes and, more importantly, the size distributions. In this study, PbS NPs were chosen as an alternative to oligonucleotide labels. Lead is a good semiconductor due to its electronic and optical properties such as $Pb^{2+}$ ion selective sensors, and lead sulfide nanoparticles are an important direct band gap semiconductor material with a small band gap.[26,33] The structure and morphology of the synthesized nanoparticle product PbS NPs were studied (TEM). Figure 1 shows a TEM image of the synthesized nanoparticles. TEM images of PbS NPs showed a spherical shape with a 4−6 nm diameter.[18] The difference in size depended on many different factors during synthesis but most importantly the pH, temperature, and time of nitrogen flow

based on tests using different experimental conditions. The PbS NPs were stable and did not aggregate after 1 month.

**PCR Amplification.** Figures 2 and 3 show the PCR amplification of target DNA *S. aureus* and negative control *A. hydrophila* for the pure cultures, respectively. The length of primer used in this study was 18 bp, and the results showed that the primer pair was high specific for bacteria in the final product performance PCR reaction. The results indicated that each primer pair was specific for the corresponding target organisms, and it used the amplification reactions for PCR detection of the target genes of *S. aureus* at 151 bp, whereas the *A. hydrophila* band appeared at 161 bp,

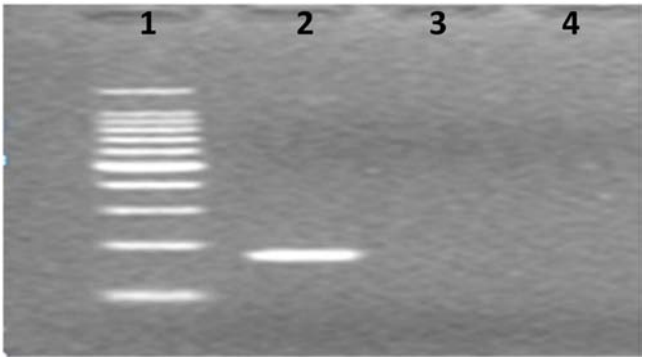


**Figure 2.** Agarose gel electrophoresis analysis (2%) of PCR amplicon. Lanes: 1, molecular marker (100 bp); 2, positive test sample *Staphylococcus aureus* (EF529607.1); 3, negative control containing PCR mixture with *Aeromonas hydrophila* (ATCC 7966); 4, negative control containing PCR mixture with *Escherichia coli* (JX206444.1).

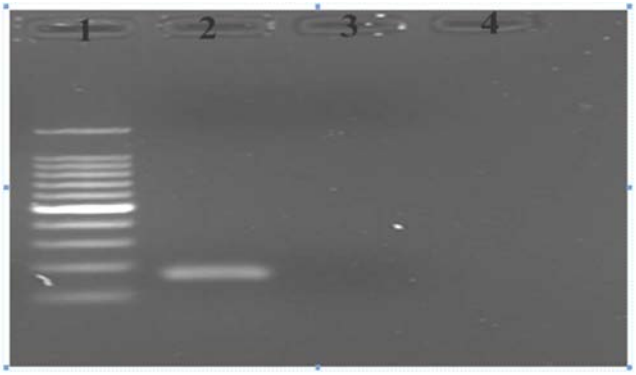


**Figure 3.** Agarose gel electrophoresis analysis (2%) of PCR amplicon. Lanes: 1, molecular marker (100 bp); 2, positive test sample *Aeromonas hydrophila* (ATCC 7966); 3, negative control containing PCR mixture with *Staphylococcus aureus* (EF529607.1).

**Cyclic Voltammetry (CV) and Impedance Spectroscopy.** DNA immobilization and hybridization on the films were studied by CV. CV on a ferricyanide ($K_3$ Fe $(CN)_6$ solution) is a valuable tool to monitor the barrier of the modified electrode. CV is recorded by a three-electrode system, which consists of a working electrode (WE), a reference electrode (RE), and a counter electrode (CE). These electrodes are inside the analyte and connected to an electrochemical station analyzer.[34] The current between the working and the counter electrodes is measured and plotted versus the applied potential between the working and reference electrodes. CV measurements look at redox processes of an analyte in solution $Fe^{3+}$ that converts to $Fe^{2+}$ and then converts again back to $Fe^{3+}$. Figure 4 shows the evolution of the cyclic voltammogram. First the bare electrode was measured, and then the surface was covered with MWCNT−Chi. After that, the deposition of bismuth was optimal after 150 s at −1.4 V. The results showed that signal increased significantly. When the electrode was first treated with fixing probe, a small increase in peak current was observed as the target DNA was deposited on the electrode.

**Impedance Spectroscopy (EIS).** Impedance techniques are useful to monitor changes in electrical properties arising from biorecognition events at the surfaces of modified electrodes. EIS is a powerful tool to monitor the whole procedure in preparing modified electrodes and can provide useful information on various properties including electrode impedance.[35] EIS can also give further information on the impedance changes of the electrode surface during the modification process. EIS measurements were carried out using ferricyanide (1 mM $K_3Fe(CN)_6$ solution) in three electrodes. In EIS, the semicircle diameter equals the electron-transfer resistance. This resistance controls the electron-transfer kinetics of the redox probe at the electrode interface. This is also a powerful and sensitive tool for studying the charge-transfer processes occurring in electrode solutions or modified electrodes.[9,36] Figure 5 shows the EIS at different stages, which was used to test the immobilization of the probe DNA on the electrode.When the immobilized probe DNA was hybridized with its complementary target DNA, the peak increased further. The bare Au electrode exhibited an almost straight line, which was characteristic of a diffusion-limited electron-transfer process, after the electrode was treated by the immobilization of fixing probe peak and remarkably increased. This can be attributed to physical coverage by the oligonucleotides and repulsive electrostatic interaction between the negatively charged phosphate backbone of the single-strand nucleic acid and ferricyanide anion.[35,36] The function of MCH was employed to force the tethered DNA strands to "stand up" on the electrode surface and reduce its nonspecific adsorption on the surface through hydrophobic and electrostatic interactions.[37] The impedance initially increased due to interaction of the fixing probe and immobilization target DNA. The reason behind this observation was the increase in conductivity, followed by an impedance decrease in sandwich structure step. The nanoparticles were conjugated to form a complete sandwich structure onto the modified electrode surface. EIS possesses the ability to study any intrinsic material property or specific processes that could influence the conductivity/resistivity or capacity of an electrochemical system.

**Electrochemical Analysis.** In this study MWCNT was mixed with chitosan and then the bismuth was deposited in the GCE surface. They were used to increase the sensitivity of GCE and to help to improve the stability and sensitivity of the modified electrode. The fixing and capture DNA probes were modified by thiol and amino groups, respectively. The thiol group binds strongly with the gold electrode, and it was complementary with specific target sequence (*S. aureus*). Thiol−metal interactions are frequently used to bind biomolecules covalently onto gold surface biosensors.[16] Amino groups were bound with the PbS NPs and possessed specific target sequences to build the sandwich structure. The probe oligonucleotides (probe DNA) had a thiol modification at the 5′ end to covalently bond to the gold surface. The anchor group (SH unit) was responsible for the chemical link with the gold surface. After immobilization and hybridization, the

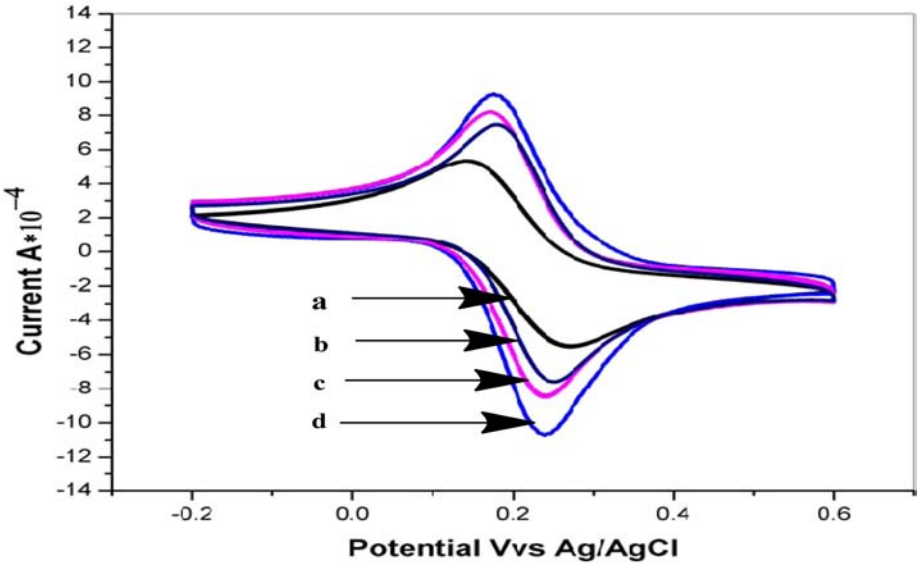


**Figure 4.** Cyclic voltammogram (CV) of the electrode at different stages, responses of 1 mM $K_3Fe(CN)_6$ on (a) clean GCE, (b) GCE with carbon nanotube, (c) GCE with carbon nanotube and bismuth, and (d) GCE with carbon nanotube, bismuth, and NPs.

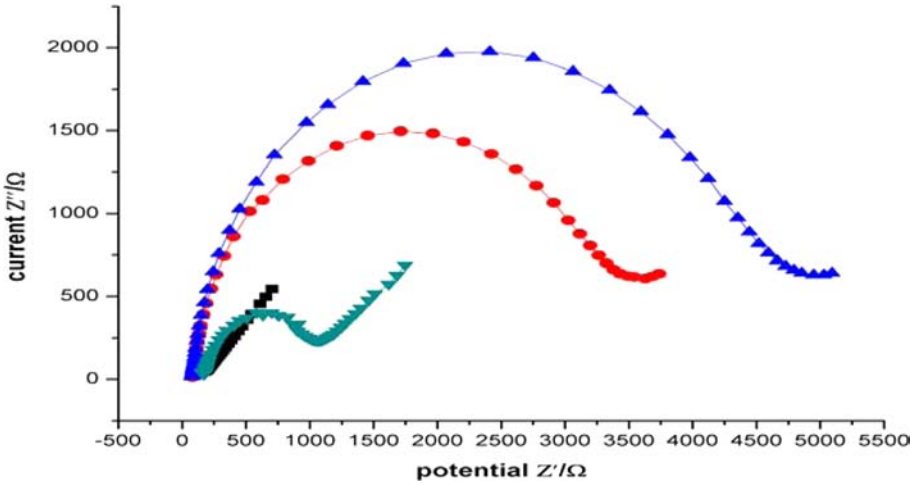


**Figure 5.** EIS of the electrode at different stages (different film-modified electrodes) in otassium ferricyanide [$K_3OFe(CN)_6$] on (Black) the bare gold electrode surface, (Green) gold electrode and fixing probe, (Red) gold electrode, fixing probe, and tDNA, (Blue) gold electrode, fixing probe, tDNA, and capture probe.

sandwich structure (fDNA−tDNA−cDNA−PbS NPs) was formed. The immobilization step for the DNA probe was essential to develop a range of biosensors,[16] after which it was released in 1 M nitric acid and the PbS NPs ions were measured. A potentiostat controlled the voltage, according to a preselected voltage−time program between the working electrode and the counter electrode to maintain the potential difference between the working and the reference electrodes.

Figure 6 shows the DPV measurements performed with target DNA from pure culture bacteria obtained for the detection of DNA using different concentrations of target DNA. As the concentration of the complementary target DNA sequence continuously increased, the concentration of dissolved $Pb^{2+}$ was quantified by DPV. A significant amplification for the detection of target DNA was observed. The DPV signal of the target DNA concentration was $3.87 \times 10^{-14}$−$1.22 \times 10^{-15}$ M, and the limit detection was $3.17 \times 10^{-14}$ M. The voltammetric response increased with target concentration. The peak current of various tDNA concen-

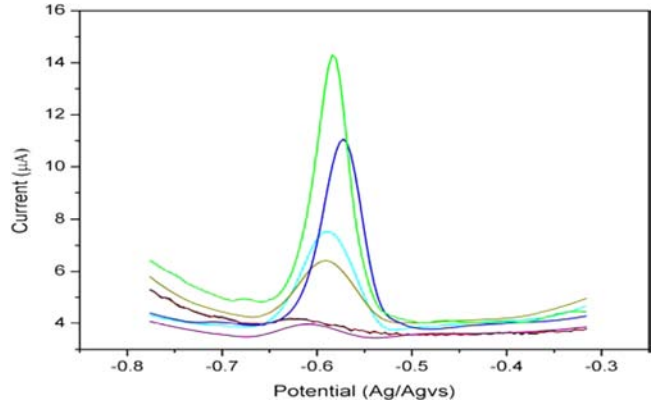


**Figure 6.** DPV analysis of electrochemical DNA sensors to detect tDNA from pure culture with different concentrations using PbS NPs in sandwich structure fDNA−tDNA−cDNA−PbS NPs for *Staphylococcus aureus* genomic DNA detection.


dx.doi.org/10.1021/jf503914f | *J. Agric. Food Chem.* 2014, 62, 12659−12667

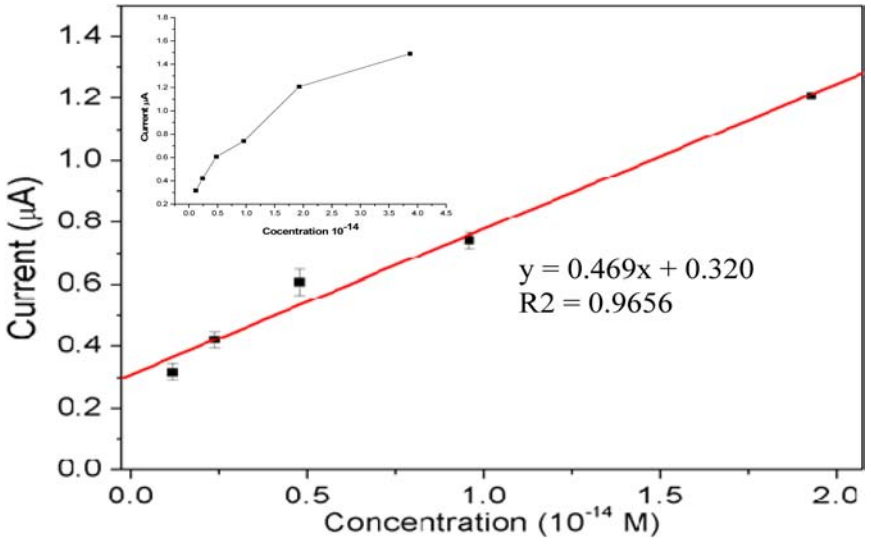


**Figure 7.** Corresponding calibration plots of peak current versus the concentration of *Staphylococcus aureus* genomic DNA detection. The presented values are an average of triplicates with standard deviation.

**Table 2. Limit of Detection of Different Studies Including This Study**

| target | method | detection limit | ref |
|---|---|---|---|
| nopaline synthase (NOS) terminator gene sequences of GMOs | DNA genosensor electrochemical DNA detection with CdS nanoparticle labels | $2.75 \times 10^{-12}$ mol $L^{-1}$ | 28 |
| synthesized oligonucleotides | DNA sandwich electrochemical biosensor based on the amplification of magnetic microbeads and Au nanoparticles | $5.0 \times 10^{-15}$ M | 30 |
| *Mycobacterium* sp. | DNA electrochemical biosensor | 0.25 ng/mL | 29 |
| *Salmonella* invA gene | electrochemical DNA sensor | 0.5 pM | 35 |
| *Staphylococcus aureus* nuc gene | chitosan−$Co_3O_4$ nanorod−graphene | $4.3 \times 10^{-13}$ M | 38 |
| *Staphylococcus aureus* | electrochemical DNA biosensor based on MWCNT−Chi and bismuth | $2.44 \times 10^{-14}$ M | this study |

trations increased with increasing concentration. The equation for the resulting calibration plot was $Y = 0.469x + 0.320$ ($R^2 = 0.965$) as shown in Figure 7. To test the analytical performance of the assay, a calibration experiment was conducted using target DNA. All results shown in this study are the means of a minimum of triplicate measurements. The system was highly sensitive, selective, and efficient in comparison with other DNA biosensors. Table 2 shows the DNA biosensor for this study compared with other studies.

**Detection in Artificially Contaminated Samples.** The present system tested for enumeration of bacteria, and in the six dilutions, the counts ranged from $(4.31 \pm 2.15) \times 10^2$ to $(5.86 \pm 0.74) \times 10^4$ CFU/mL, for *S. aureus*. There were significant growth increases for the different dilutions. Table 3 shows the enrichment for bacteria inoculated into the beef samples, followed by extract and amplification of the DNA. Figure 8 shows the amplification of six different dilutions where the reliability of the PCR amplification was satisfactory. Figure 9 shows the curves of target DNA from beef samples after incubation for 24 h. DPV measurements were performed at −0.2 V versus Ag/AgCl. The calibration curve of DPV peak current increased with different concentrations of target DNA. The results showed that the efficiency was influential in the detection of different concentrations ($10^1$ −$10^5$) of target pathogenic bacteria. The results also showed a gradual increase

**Table 3. Enumeration of *Staphylococcus aureus* on Fresh Beef and after Samples Had Been Inoculated[a]**

| dilution factor | *S. aureus* ± SD (CFU/mL) |
|---|---|
| $10^1$ | $(5.86 \pm 0.74) \times 10^4$ |
| $10^2$ | $(1.82 \pm 0.67) \times 10^4$ |
| $10^3$ | $(1.65 \pm 0.26) \times 10^4$ |
| $10^4$ | $(5.50 \pm 0.54) \times 10^3$ |
| $10^5$ | $(4.31 \pm 2.15) \times 10^2$ |

[a]The number was counted after incubation for 24 h at 37 °C. Data are expressed as the mean ± standard deviation (average of three replications for *S. aureus*). PCR analysis was carried out after overnight culture.

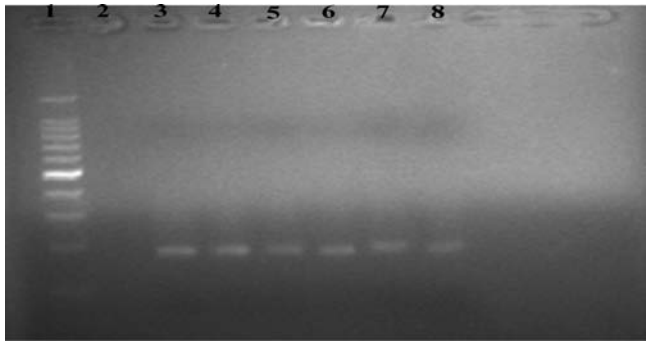


**Figure 8.** Agarose gel electrophoresis analysis (2%) of PCR amplicon extraction from fresh beef. Lanes: 1, molecular marker (100 bp); 2, negative control containing PCR mixture with *Aeromonas hydrophila* (ATCC 7966); 3−6, positive test sample *Staphylococcus aureus* (EF529607.1) in different concentrations.

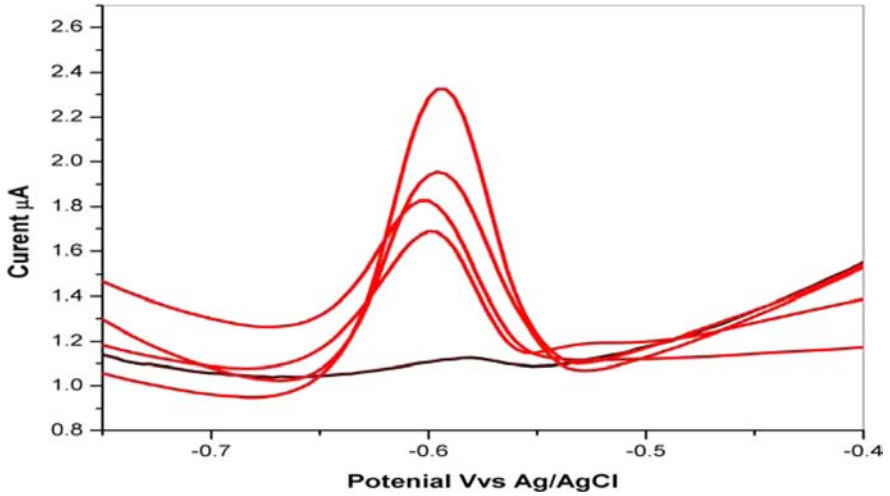


**Figure 9.** DPV analysis of electrochemical DNA sensors to detect tDNA from fresh beef with different concentrations using PbS NPs in sandwich structure.

in the yield of each band with increases in the dilute factor (serial dilutions).

## AUTHOR INFORMATION

### Corresponding Author

*(X.S.) Mail: School of Food Science and Technology, Center of Food Safety and Quality Control, Jiangnan University, 1800 Lihu Road, Wuxi 214122, China. Phone: 13915294105. Fax: +86 51085328726. (M.H.A.) E-mail: sxlzzz@jiangnan.edu.cn; mabdalhai1@hotmail.com.

### Funding

This work has been supported by the National Natural Science Foundation of China (No. 31371768), the National Research Program (No. 201203069-1), the Program for New Century Excellent Talents in Jiangnan University, Qinglan Project, Synergetic Innovation Center of Food Safety and Quality Control, and the Priority Academic Program Development of Jiangsu Higher Education Institutions.

### Notes

The authors declare no competing financial interest.

## REFERENCES

(1) Martinsa, A.; Ribolia, D. F. M.; Pereiraa, V. C.; Cunhaa, M. d. L. R. d. S. d. Molecular characterization of methicillin-resistant *Staphylococcus aureus* isolated from a Brazilian university hospital. *Braz. J. Infect. Dis.* **2013**, *18* (3), 331−335.

(2) Shibabawa, A.; Abebe, T.; Mihret, A. Antimicrobial susceptibility pattern of nasal *Staphylococcus aureus* among Dessie Referral Hospital health care workers, Dessie, northeast Ethiopia. *Int. J. Infect. Dis.* **2014**, *25*, 22−25.

(3) Sollid, J. U. E.; Furberg, A. S.; Hanssen, A. M.; Johannessen, M. *Staphylococcus aureus*: determinants of human carriage. *Infect., Genet. Evol.* **2013**, *21*, 531−541.

(4) Wu, X.; Su, Y.-C. Growth of *Staphylococcus aureus* and enterotoxin production in precooked tuna meat. *Food Control* **2014**, *42*, 63−70.

(5) Fana, H.; Xua, Y.; Changb, Z.; Xinga, R.; Wanga, Q.; Hea, P.; Fanga, Y. A non-immobilizing electrochemical DNA sensing strategy with homogenous hybridization based on the host−guest recognition technique. *Biosens. Bioelectron.* **2011**, *26* (5), 2655−2659.

(6) Martinez-Perez, A.; Blais, B. W. Cloth-based hybridization array system for the identification of *Escherichia coli* O157:H7. *Food Control* **2010**, *21* (10), 1354−1359.

(7) Vetrone, S. A.; Huarng, M. C.; Alocilja, E. C. Detection of non-PCR amplified *S. enteritidis* genomic DNA from food matrices using a gold-nanoparticle DNA biosensor: a proof-of-concept study. *Sensors* **2012**, *12* (8), 10487−10499.

(8) Arora, P.; Sindhu, A.; Dilbaghi, N.; Chaudhury, A. Biosensors as innovative tools for the detection of food borne pathogens. *Biosens. Bioelectron.* **2011**, *28* (1), 1−12.

(9) Arya, S. K.; Pui, T. S.; Wong, C. C.; Kumar, S.; Rahman, A. R. A. Effects of the electrode size and modification protocol on a label-free electrochemical biosensor. *Langmuir* **2013**, *29* (22), 6770−6777.

(10) Bharadwaj, R.; Sai, V.; Thakare, K.; Dhawangale, A.; Kundu, T.; Titus, S.; Mukherji, S. Evanescent wave absorbance based fiber optic biosensor for label-free detection of *E. coli* at 280 nm wavelength. *Biosens. Bioelectron.* **2011**, *26* (7), 3367−3370.

(11) Lawson, T. S.; Connally, R. E.; Iredell, J. R.; Vemulpad, S.; Piper, J. A. Detection of *Staphylococcus aureus* with a fluorescence in situ hybridization that does not require lysostaphin. *J. Clin. Lab. Anal.* **2011**, *25* (2), 142−147.

(12) Tawil, N.; Sacher, E.; Mandeville, R.; Meunier, M. Surface plasmon resonance detection of *E. coli* and methicillin-resistant *S. aureus* using bacteriophages. *Biosens. Bioelectron.* **2012**, *37* (1), 24−29.

(13) Cortón, S. R. M. a. E., Ed. *Bioanalytical Chemistry*; World Scientific: Singapore, 2004.

(14) Hansen, J. A.; Mukhopadhyay, R.; Hansen, J. Ø.; Gothelf, K. V. Femtomolar electrochemical detection of DNA targets using metal sulfide nanoparticles. *J. Am. Chem. Soc.* **2006**, *128* (12), 3860−3861.

(15) Tsoka, S.; Gill, A.; Brookman, J.; Hoare, M. Rapid monitoring of virus-like particles using an optical biosensor: a feasibility study. *J. Biotechnol.* **1998**, *63* (2), 147−153.

(16) Sassolas, A.; Leca-Bouvier, B. D.; Blum, L. J. DNA biosensors and microarrays. *Chem. Rev.* **2008**, *108* (1), 109−139.

(17) Ricci, F.; Zari, N.; Caprio, F.; Recine, S.; Amine, A.; Moscone, D.; Plaxco, K. W. Surface chemistry effects on the performance of an electrochemical DNA sensor. *Bioelectrochemistry* **2009**, *76* (1), 208−213.

(18) Zhu, N.; Zhang, A.; Wang, Q.; He, P.; Fang, Y. Lead sulfide nanoparticle as oligonucleotides labels for electrochemical stripping detection of DNA hybridization. *Electroanalysis* **2004**, *16* (7), 577−582.

(19) Cai, J.; Zhou, X.; Tu, Y.; Feng, G.; Huang, C. Application of bismuth-film modified glassy carbon electrode for solid-phase extraction of Sudan I. *Adv. Mater. Lett.* **2012**, *3*, 87−91.

(20) Mirceski, V.; Hocevar, S. B.; Ogorevc, B.; Gulaboski, R.; Drangov, I. Diagnostics of anodic stripping mechanisms under square-wave voltammetry conditions using bismuth film substrates. *Anal. Chem.* **2012**, *84* (10), 4429−4436.

(21) Yang, D.; Wang, L.; Chen, Z.; Megharaj, M.; Naidu, R. Determination of trace lead and cadmium in water samples by anodic stripping voltammetry with a Nafion-ionic liquid-coated bismuth film electrode. *Electroanalysis* **2014**, *26* (3), 639−647.
(22) Wang, Q.; Zhang, B.; Lin, X.; Weng, W. Hybridization biosensor based on the covalent immobilization of probe DNA on chitosan−mutiwalled carbon nanotubes nanocomposite by using glutaraldehyde as an arm linker. *Sens. Actuators, B* **2011**, *156* (2), 599−605.
(23) Mao, X.; Yang, L.; Su, X.-L.; Li, Y. A nanoparticle amplification based quartz crystal microbalance DNA sensor for detection of *Escherichia coli* O157:H7. *Biosens. Bioelectron.* **2006**, *21* (7), 1178−1185.
(24) Sguazza, G. H.; Reynaldi, F. J.; Galosi, C. M.; Pecoraro, M. R. Simultaneous detection of bee viruses by multiplex PCR. *J. Virol. Methods* **2013**, *194* (1), 102−106.
(25) Milica, T.; Mirjana, I.; Veana, V.; Olga, I. Transient bleaching of small lead sulfide colloids: influence of surface properties. *J. Phys. Chem.* **1990**, *94* (16), 6390−6396.
(26) Zhu, N.; Zhang, A.; Wang, Q.; He, P.; Fang, Y. Electrochemical detection of DNA hybridization using methylene blue and electrodeposited zirconia thin films on gold electrodes. *Anal. Chim. Acta* **2004**, *510* (2), 163−168.
(27) Rassaei, L.; Sillanpää, M.; Edler, K. J.; Marken, F. Electrochemically active mercury nanodroplets trapped in a carbon nanoparticle−chitosan matrix. *Electroanalysis* **2009**, *21* (3−5), 261−266.
(28) Sun, W.; Zhong, J.; Zhang, B.; Jiao, K. Application of cadmium sulfide nanoparticles as oligonucleotide labels for the electrochemical detection of NOS terminator gene sequences. *Anal. Bioanal. Chem.* **2007**, *389* (7−8), 2179−2184.
(29) Thiruppathiraja, C.; Kamatchiammal, S.; Adaikkappan, P.; Santhosh, D. J.; Alagar, M. Specific detection of *Mycobacterium* sp. genomic DNA using dual labeled gold nanoparticle based electrochemical biosensor. *Anal. Biochem.* **2011**, *417* (1), 73−79.
(30) Du, P.; Li, H.; Cao, W. Construction of DNA sandwich electrochemical biosensor with nanoPbS and nanoAu tags on magnetic microbeads. *Biosens. Bioelectron.* **2009**, *24* (11), 3223−3228.
(31) Lata, S.; Batra, B.; Pundir, C. Construction of D-amino acid biosensor based on d-amino acid oxidase immobilized onto poly (indole-5-carboxylic acid)/zinc sulfide nanoparticles hybrid film. *Process Biochem.* **2012**, *47* (12), 2131−2138.
(32) Guan, Z. P.; Jiang, Y.; Gao, F.; Zhang, L.; Zhou, G. H.; Guan, Z. J. Rapid and simultaneous analysis of five foodborne pathogenic bacteria using multiplex PCR. *Eur. Food Res. Technol.* **2013**, *237* (4), 627−637.
(33) Kang, I.; Wise, F. W. Electronic structure and optical properties of PbS and PbSe quantum dots. *J. Opt. Soc. Am. B* **1997**, *14* (7), 1632−1646.
(34) Ciobanu, M.; Wilburn, J. P.; Krim, M.; Cliffel, D. E. In *Handbook of Electrochemistry*; Zoski, C. G., Ed.; Elsevier Science: Amsterdam, The Netherlands, 2007.
(35) Li, Q.; Cheng, W.; Zhang, D.; Yu, T.; Yin, Y.; Ju, H.; Ding, S. Rapid and sensitive strategy for *Salmonella* detection using an InvA gene-based electrochemical DNA sensor. *Int. J. Electrochem. Sci.* **2012**, *7* (1), 844−856.
(36) Jie, G.; Liu, B.; Pan, H.; Zhu, J.-J.; Chen, H.-Y. CdS nanocrystal-based electrochemiluminescence biosensor for the detection of low-density lipoprotein by increasing sensitivity with gold nanoparticle amplification. *Anal. Chem.* **2007**, *79* (15), 5574−5581.
(37) Singh, A.; Arya, S. K.; Glass, N.; Hanifi-Moghaddam, P.; Naidoo, R.; Szymanski, C. M.; Evoy, S. Bacteriophage tailspike proteins as molecular probes for sensitive and selective bacterial detection. *Biosens. Bioelectron.* **2010**, *26* (1), 131−138.
(38) Qi, X.; Gao, H.; Zhang, Y.; Wang, X.; Chen, Y.; Sun, W. Electrochemical DNA biosensor with chitosan-$Co_3O_4$ nanorod-graphene composite for the sensitive detection of staphylococcus aureus nuc gene sequence. *Bioelectrochemistry* **2012**, *88*, 42−47.

**Table 1. Color Parameters of Norbixin and Norbixin−Gum Arabic (GA) Dispersions with and without $Fe^{2+}$ at pH 3.0−5.0, before and after Heating at 90 or 126 °C for 30 min[a]**

| | | *L** | | | | *a** | | | | *b** | | | |
|---|---|---|---|---|---|---|---|---|---|---|---|---|---|
| heating temperature | pH | norbixin | norbixin−GA | GA | $FeCl_2$ | norbixin | norbixin−GA | GA | $FeCl_2$ | norbixin | norbixin−GA | GA | $FeCl_2$ |
| none | 3.0 | N/D[b] | 53.85 ± 2.65 gh | 73.29 ± 0.05 a | 73.34 ± 0.05 a | N/D | 24.02 ± 7.04 abc | −0.92 ± 0.03 lm | −0.87 ± 0.02 lm | N/D | 66.49 ± 6.61 c | 0.29 ± 0.06 l | 0.50 ± 0.03 l |
| | 4.0 | N/D | 52.93 ± 0.95 h | 73.24 ± 0.18 a | 73.38 ± 0.19 a | N/D | 25.86 ± 3.95 a | −0.92 ± 0.04 lm | −0.93 ± 0.03 lm | N/D | 71.46 ± 0.44 b | 0.23 ± 0.01 l | 0.42 ± 0.03 l |
| | 5.0 | 53.78 ± 2.05 gh | 55.12 ± 2.63 efgh | 73.03 ± 0.17 a | 73.13 ± 0.03 a | 24.29 ± 6.35 ab | 21.51 ± 7.35 bcde | −0.83 ± 0.05 lm | −0.87 ± 0.02 lm | 75.12 ± 0.93 a | 69.90 ± 1.73 bc | 0.51 ± 0.08 l | 0.61 ± 0.08 l |
| 90 °C | 3.0 | N/D | N/D | 73.15 ± 0.62 a | 73.39 ± 0.35 a | N/D | N/D | −0.83 ± 0.11 lm | −0.84 ± 0.04 lm | N/D | N/D | 0.65 ± 0.43 l | 0.49 ± 0.07 l |
| | 4.0 | N/D | 57.15 ± 9.94 defg | 73.12 ± 0.24 a | 73.28 ± 0.13 a | N/D | 12.84 ± 1.04 h | −0.86 ± 0.05 lm | −0.87 ± 0.05 lm | N/D | 53.22 ± 1.61 fg | 0.51 ± 0.16 l | 0.66 ± 0.07 l |
| | 5.0 | 60.28 ± 0.51 cd | 65.33 ± 2.28 b | 73.19 ± 0.23 a | 73.35 ± 0.13 a | 1.90 ± 0.98 klm | 5.45 ± 0.07 ij | −0.90 ± 0.04 lm | −0.87 ± 0.01 lm | 45.47 ± 0.03 i | 54.68 ± 1.53 f | 0.31 ± 0.15 l | 0.51 ± 0.02 l |
| 126 °C | 3.0 | N/D | N/D | 73.29 ± 0.13 a | 73.33 ± 0.01 a | N/D | N/D | −0.83 ± 0.03 lm | −0.87 ± 0.01 lm | N/D | N/D | 0.59 ± 0.05 l | 0.54 ± 0.05 l |
| | 4.0 | N/D | N/D | 72.97 ± 0.29 a | 73.67 ± 0.22 a | N/D | N/D | −0.80 ± 0.07 lm | −0.93 ± 0.05 lm | N/D | N/D | 0.80 ± 0.17 l | 0.47 ± 0.08 l |
| | 5.0 | 61.45 ± 1.06 c | 62.36 ± 2.61 c | 73.30 ± 0.31 a | 73.11 ± 0.24 a | 2.24 ± 1.21 kl | 7.04 ± 3.82 i | −0.84 ± 0.06 lm | −0.90 ± 0.06 lm | 48.53 ± 9.08 hi | 58.33 ± 0.77 e | 0.52 ± 0.11 l | 0.94 ± 0.10 l |
| none, with $Fe^{2+}$ | 3.0 | N/D | 54.27 ± 1.30 gh | 73.47 ± 0.34 a | | N/D | 20.24 ± 4.87 defg | −0.86 ± 0.05 lm | | N/D | 69.04 ± 0.92 bc | 0.37 ± 0.13 l | |
| | 4.0 | N/D | 54.74 ± 3.37 fgh | 73.48 ± 0.19 a | | N/D | 23.17 ± 0.07 abcd | −0.88 ± 0.04 lm | | N/D | 69.99 ± 0.24 b | 0.41 ± 0.05 l | |
| | 5.0 | 54.33 ± 1.62 gh | 54.89 ± 2.43 fgh | 73.10 ± 0.06 a | | 21.52 ± 3.56 bcdeb | 21.55 ± 0.03 bcde | −1.18 ± 0.03 m | | 72.03 ± 3.36 ab | 68.97 ± 0.11 bc | 2.96 ± 0.02 l | |
| 90 °C, with $Fe^{2+}$ | 3.0 | N/D | 58.42 ± 0.02 cde | 73.52 ± 0.08 a | | N/D | 21.17 ± 6.46 cdef | −0.85 ± 0.02 lm | | N/D | 42.06 ± 2.86 j | 0.49 ± 0.05 l | |
| | 4.0 | N/D | 58.15 ± 0.02 cdef | 73.50 ± 0.19 a | | N/D | 18.52 ± 0.02 efg | −0.82 ± 0.05 lm | | N/D | 55.45 ± 1.30 ef | 0.68 ± 0.25 l | |
| | 5.0 | 62.49 ± 1.57 cd | 58.75 ± 6.87 cd | 73.52 ± 0.08 a | | 3.17 ± 3.46 jk | 17.37 ± 0.42 g | −0.85 ± 0.02 lm | | 49.42 ± 0.05 h | 63.27 ± 6.61 d | 0.49 ± 0.05 l | |
| 126 °C, with $Fe^{2+}$ | 3.0 | N/D | 59.28 ± 4.84cd | 73.51 ± 0.26a | | N/D | 19.41 ± 0.03efg | −0.86 ± 0.05 lm | | N/D | 33.30 ± 3.26k | 0.70 ± 0.04l | |
| | 4.0 | N/D | 59.56 ± 0.52 cd | 73.44 ± 0.09 a | | N/D | 18.29 ± 0.14 fg | −0.84 ± 0.05 lm | | N/D | 49.30 ± 7.08 h | 0.79 ± 0.11 l | |
| | 5.0 | 60.62 ± 4.65c | 59.99 ± 5.86 cd | 73.28 ± 0.31 a | | 2.79 ± 0.07 jk | 18.12 ± 0.08 fg | −0.99 ± 0.03 lm | | 51.11 ± 0.53 gh | 61.79 ± 9.99 d | 2.70 ± 0.21 l | |

[a]Numbers are mean ± standard deviation ($n$ = 3). Different letters represent significant differences in the mean of the same parameter ($p < 0.05$). [b]N/D, not determined due to precipitation.



dx.doi.org/10.1021/jf5037799 | J. Agric. Food Chem. 2014, 62, 12668−12677

## MATERIAL AND METHODS

**Chemicals.** The norbixin sample was a commercial Annatto WS28 product containing 2.8% w/w norbixin in aqueous alkaline (pH 12) solution from DD Williamson, LLC (Port Washington, WI, USA). GA and other chemicals were purchased from Fisher Scientific (Pittsburgh, PA, USA).

**Preparation of Norbixin−Gum Arabic Dispersions with or without $Fe^{2+}$.** GA was dissolved at 2% w/v in 150 mL of distilled water. After stirring at room temperature (21 °C) for 30 min, the sample was filtered through a Millex-HN nylon clarification kit with a pore size of 0.45 μm (Fisher Scientific). Subsequently, 2 mL of norbixin aqueous solution (2.8% w/w, pH 12.0) was added to the GA solution and adjusted to pH 5.0 using 1.0 N HCl. For treatments with $Fe^{2+}$, 29.1 mg of ferrous chloride was additionally added into the GA−norbixin mixture, corresponding to a norbixin/$Fe^{2+}$ molar ratio of 1:1.56. After stirring for 30 min, the mixture solution was diluted 10 times in distilled water, and the pH was adjusted to 3.0, 4.0, and 5.0 using 1.0 N HCl. Controls with the same concentrations of norbixin and ferrous chloride as GA−norbixin−$Fe^{2+}$ solutions were prepared by diluting the alkaline norbixin solution in distilled water directly and adjusting the pH to 5.0, followed by the addition of ferrous chloride and pH adjustment as above. To simulate representative pasteurization and sterilization temperatures,[20−22] all samples were heated at 90 or 126 °C for 30 min and cooled in a 21 °C water bath before following analyses within 48 h.

**Color Assay of Norbixin Dispersions.** Color analyses of norbixin dispersions followed the procedures in our recent study.[14] The $L^*$, $a^*$, and $b^*$ values of 5 mL samples were measured using a MiniScan XE Plus Hunter colorimeter (Hunter Associates Laboratory, Inc., Reston, VA, USA). The absorbance of samples at 460 nm was additionally determined using an Evolution 201 UV−vis spectrophotometer (Thermo Scientific, Waltham, MA, USA).

**Fluorescence Spectroscopy.** Fluorescence spectroscopy experiments were conducted according to a previous method.[23] The instrument was an RF-1501spectrofluorometer (Shimadzu Corp., Tokyo, Japan). The excitation wavelength was set at 330 nm, and the emission spectra were recorded from 300 to 600 nm with the background fluorescence calibrated using distilled water.

**Particle Size Assay.** Particle sizes of dispersions were determined at room temperature (21 °C) according to the method in the literature.[24] Samples were diluted 10-fold using distilled water and adjusted to pH 3.0−5.0. The instrument was a Delsa Nano-Zeta Potential and Submicron Particle Size Analyzer (Beckman Coulter Inc., Brea, CA, USA).

**Zeta-Potential Assay.** Zeta-potential was measured according to a recent method[25] with a slight modification. GA and norbixin−GA dispersions with and without $Fe^{2+}$ were diluted 100-fold in distilled water and adjusted to pH 3.0, 4.0, and 5.0. The instrument was the above Zeta Potential and Submicron Particle Size Analyzer.

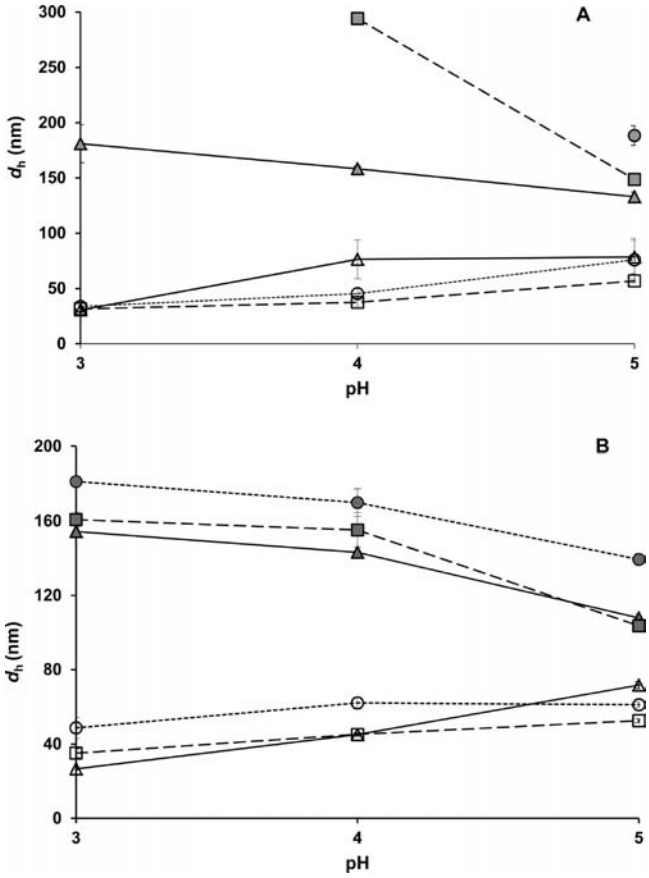


**Figure 1.** Hydrodynamic diameter ($d_h$) of gum arabic (open symbols) and norbixin−gum arabic dispersions (solid symbols) without (A) and with (B) $Fe^{2+}$ before (21 °C, triangles) and after heating at 90 °C (squares) or 126 °C (circles) for 30 min. The pH 3 and 4 samples after heating at 90 °C and the pH 4 sample after heating at 126 °C are not presented in plot A because the measurements exceeded the instrument detection limit. Error bars are standard deviations from triplicates.

**Atomic Force Microscopy (AFM).** AFM imaging was conducted as in our recent work.[25,26] Samples with and without thermal treatments were diluted 10 times in deionized water and readjusted to pH 3.0−5.0. Two microliters of the diluted sample was spread on a freshly cleaved mica sheet with an area of ∼1.8 $cm^2$ and dried at room temperature for 6 h in a fume hood. Topography images were collected at

**Table 2. $k_q$ of Gum Arabic (GA) Dispersions (pH 3.0−5.0) with Norbixin, $Fe^{2+}$, or Both, before and after Heating at 90 or 126 °C for 30 min[a]**

| | | $k_q$, $10^{12}$ $M^{-1}$ $s^{-1}$ | | |
|---|---|---|---|---|
| heating temperature | pH | $Fe^{2+}$−GA | norbixin−GA | norbixin−$Fe^{2+}$−GA |
| none | 3.0 | 9.24 ± 0.05 i | 42.34 ± 1.90 c | 50.20 ± 2.81 a |
| | 4.0 | 8.83 ± 0.09 i | 41.71 ± 3.53 c | 49.57 ± 0.81 a |
| | 5.0 | 7.44 ± 0.02 ijk | 43.18 ± 0.33 c | 46.43 ± 2.26 a |
| 90 °C | 3.0 | 6.04 ± 0.04 jkl | 1.01 ± 0.10 n | 21.86 ± 0.31 f |
| | 4.0 | 5.04 ± 0.04 kl | 7.30 ± 0.44 ijk | 31.57 ± 1.59 e |
| | 5.0 | 5.51 ± 0.70 kl | 8.27 ± 1.05 ij | 34.72 ± 1.46 d |
| 126 °C | 3.0 | 5.06 ± 0.23 kl | 0.91 ± 0.20 n | 18.65 ± 0.95 g |
| | 4.0 | 5.08 ± 0.02 kl | 2.32 ± 0.13 mn | 15.54 ± 0.65 h |
| | 5.0 | 5.05 ± 0.51 kl | 4.40 ± 0.97 lm | 13.29 ± 1.28 h |

[a]Numbers are mean ± standard deviation ($n$ = 3). Different letters represent significant differences in the mean ($p$ < 0.05).

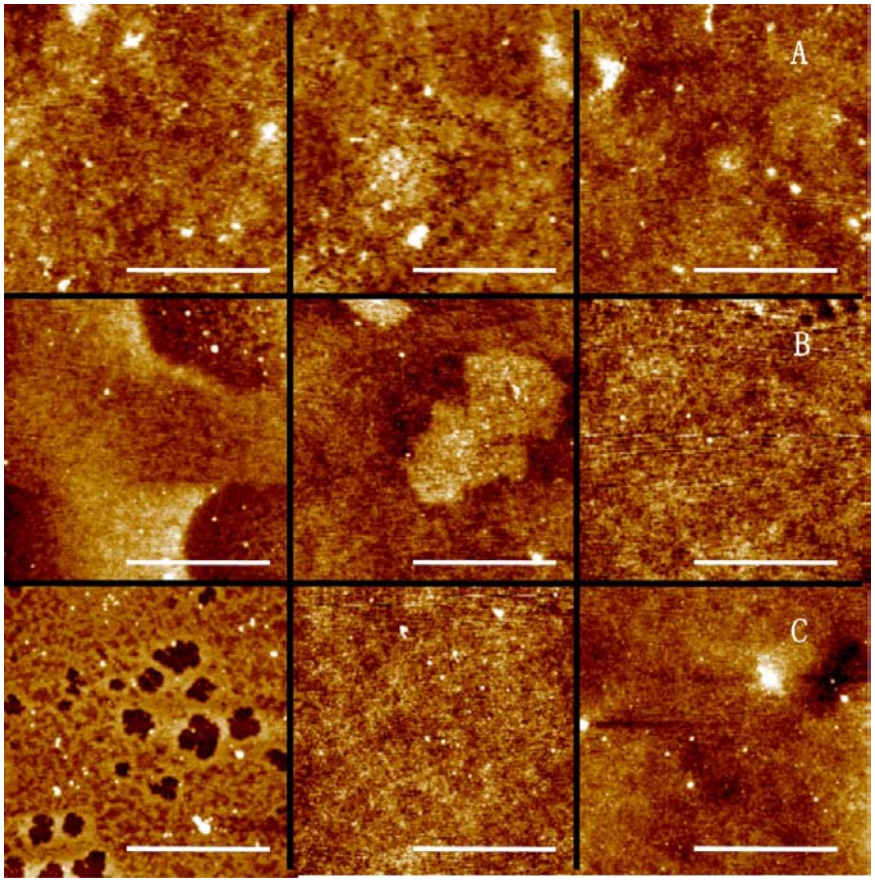


**Figure 2.** AFM topographic images of gum arabic dispersions at pH 3.0 (left), pH 4.0 (center), and pH 5.0 (right) before (A) and after heating at 90 °C (B) or 126 °C (C) for 30 min. Bar = 1 $\mu$m.

the tapping mode using a nanoprobe cantilever tip (BrukerNanoprobe, Camarillo, CA, USA) driven at a frequency of 50−100 kHz on a Multimode Nanoscope IIIa microscope (Veeco Instruments, Inc., Plainview, NY, USA). Images were analyzed using the AFM instrument software (version 5.30r3, Digital Instruments, Inc., Tonawanda, NY, USA).

**Statistical Analysis.** All experiments were carried out in triplicate. Means and standard deviations of the data were calculated for each treatment. Analysis of variance (ANOVA) was carried out to determine any significant differences between treatments ($p < 0.05$) using SPSS 16.0 software (SPSS Inc., Chicago, IL, USA).

## RESULTS AND DISCUSSION

**Color Stability of Norbixin.** Photographs of samples before and after heating are presented in Figure S1 of the Supporting Information. Norbixin precipitated at pH 3.0 and 4.0, as reported previously.[3,14] GA prevented the precipitation of norbixin before heating, but precipitates were observed after heating the pH 3 sample at 90 °C and the pH 3 and 4 samples at 126 °C for 30 min. The addition of $Fe^{2+}$ alone did not prevent the precipitation of norbixin at pH 3 and 4 before and after heating. However, no precipitation was observed for norbixin−GA dispersions with added $Fe^{2+}$ before and after heating at 90 and 126 °C for 30 min. Therefore, GA can improve the acid stability of norbixin, whereas GA and $Fe^{2+}$ can synergistically improve the heat stability of norbixin. Multivalent cations were observed previously to form coordinate bonds within GA.[27] The results suggest that norbixin forms complexes with GA to provide acid and heat stability and that $Fe^{2+}$ strengthens the complexes to provide additional heat stability. Physicochemical properties of the samples are further characterized below.

When color parameters (Table 1) were compared, slight changes were observed in the $L^*$ value of norbixin solutions at pH 5.0 with and without GA and $Fe^{2+}$. The stabilization of norbixin by GA at pH 3.0 and 4.0 enabled $L^*$, $a^*$, and $b^*$ values similar to those at pH 5.0. After heating, the reduction of the $a^*$ value of norbixin was significantly improved after the addition of both GA and $Fe^{2+}$ ($p < 0.05$) but not individually ($p > 0.05$). Conversely, the $b^*$ value of norbixin after heating was improved by GA alone and was further improved by additional $Fe^{2+}$. The solubility of norbixin enabled by carboxylate groups affects its orange color.[28] The protonation of carboxylate groups reduces the solubility of norbixin at lowered pH and causes its precipitation, which becomes more significant after thermal treatment. The results in Table 1 indicate that addition of GA or $Fe^{2+}$ did not change the clarity of norbixin solutions and that GA and $Fe^{2+}$ synergistically improved the stability of redness and yellowness of norbixin solutions after thermal treatments. As discussed previously, this likely is due to the complex formation between norbixin and GA, further strengthened by $Fe^{2+}$.

To further study the thermal stability of norbixin, the absorbance at 460 nm ($A_{460}$) before and after heating was further compared (Supporting Information, Table S1). Like $a^*$ and $b^*$ values, $A_{460}$ of the norbixin sample at pH 5 was significantly reduced after heating, which was insignificantly improved by adding $Fe^{2+}$ alone. The addition of GA maintained the $A_{460}$ after heating at pH 5.0, with and without $Fe^{2+}$. Furthermore,

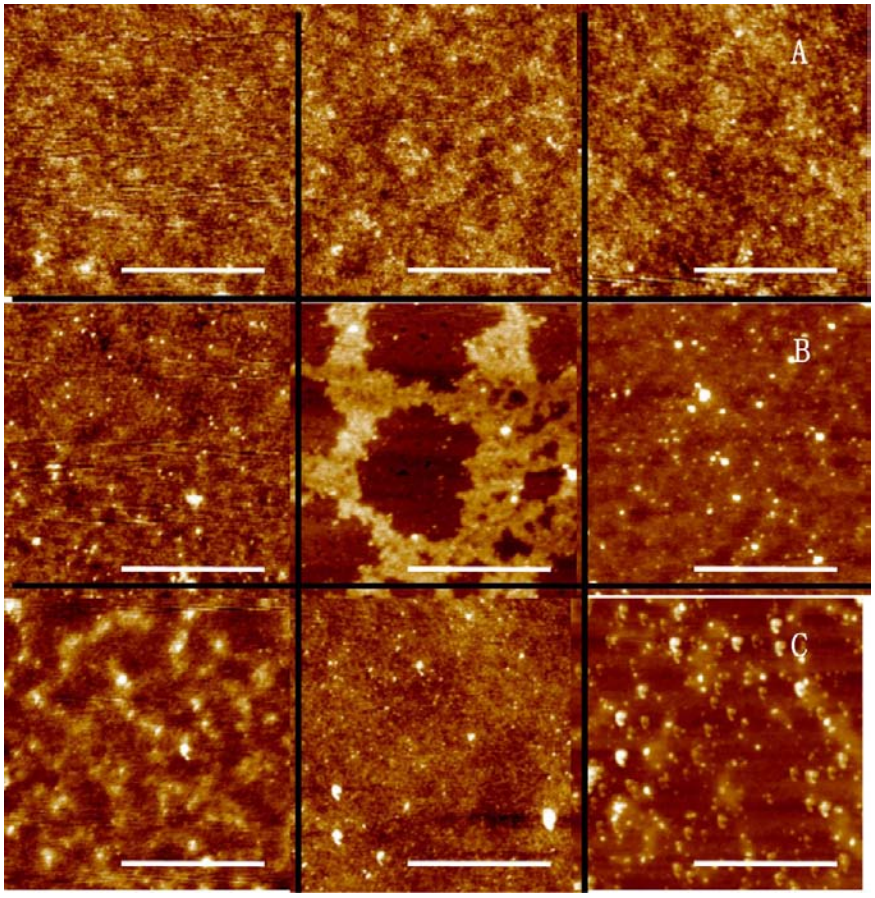


**Figure 3.** AFM topographic images of gum arabic dispersions with $Fe^{2+}$ at pH 3.0 (left), pH 4.0 (center), and pH 5.0 (right) before (A) and after heating at 90 °C (B) or 126 °C (C) for 30 min. Bar = 1 $\mu$m.

the $A_{460}$ at pH 3.0 and 4.0 was lower than that at pH 5.0 and was stabilized by GA, with and without $Fe^{2+}$, after heating.

The $A_{460}$ is due to the conjugated structures of norbixin molecules and is affected by the delocalization of $\pi$-electrons along the polyene backbone.[28,29] During heating, hydrolysis of the polyene backbone of norbixin in aqueous solutions can lead to the breakup of conjugated double bonds and therefore the reduction of $A_{460}$.[30] Degradation of 9′-*cis*-bixin in model solutions to aromatic products such as toluene and *m*-xylene was previously proposed to be responsible for color changes of annatto after heating.[31] In actual food products such as cheeses, the thermal degradation of norbixin, however, was much reduced.[31] In the present study, the hydrolysis of the polyene backbone of norbixin was likely inhibited by GA and $Fe^{2+}$, which resulted in the maintained $A_{460}$ after heating. Additionally, ferrous ions can be oxidized during heating, but the addition of GA can inhibit this oxidation (Supporting Information, Figure S2). Therefore, GA provided the chemical degradation of norbixin at the studied conditions. This agrees with reports that GA can effectively prevent the oxidation of compounds containing polyene structures such as linoleic acid,[32] monoterpenes,[33] and carotenoids.[34] $Fe^{2+}$ was also shown to protect anthocyanins from oxidative degradation.[35]

**Molecular Binding between Gum Arabic and Norbixin with and without $Fe^{2+}$.** The fluorescence spectrum is a convenient tool to study binding between biomolecules. The quenching of fluorescence intensity due to binding by another molecule (quencher) can result from dynamic and static mechanisms, with the former due to intermolecular collision and the latter due to complex formation.[14] The fluorescence quenching data can be further analyzed by the Stern−Volmer model (eq 1).[14] For dynamic quenching, the maximum quenching constant ($k_q$) of various quenchers is $2.0 \times 10^{10}$ $M^{-1}$ $s^{-1}$.[36]

$$\frac{F_0}{F} = 1 + k_q \tau_0 [Q] \quad (1)$$

$F_0$ and $F$ are the fluorescence intensities without and with a quencher, respectively, [Q] is the concentration of the quencher (M), $k_q$ is the biomolecular quenching constant, and constant $\tau_0$ (= $10^{-8}$ s) is the lifetime of the fluorophore in the absence of a quencher.[37]

The $k_q$ values of the GA−$Fe^{2+}$, norbixin−GA, and norbixin−$Fe^{2+}$−GA dispersions calculated from fluorescent spectra (not shown) according to eq 1 are compiled in Table 2. The $k_q$ values of the GA−$Fe^{2+}$ dispersions were from $7.44 \times 10^{12}$ $M^{-1}$ $s^{-1}$ at pH 5.0 to $9.24 \times 10^{12}$ $M^{-1}$ $s^{-1}$ at pH 3.0 before heating and reduced to $(5.04-6.04) \times 10^{12}$ $M^{-1}$ $s^{-1}$ after heating at 90 °C for 30 min. Heating at 126 °C for 30 min did not significantly reduce the $k_q$ values further. The $k_q$ value of the GA−norbixin dispersion was $(41.71-43.18) \times 10^{12}$ $M^{-1}$ $s^{-1}$ before heating and was decreased significantly to $(1.01-8.27)$ and $(0.91-4.40) \times 10^{12}$ $M^{-1}$ $s^{-1}$ after heating at 90 and 126 °C for 30 min, respectively. Dispersions of GA−norbixin with $Fe^{2+}$ had the highest $k_q$ values, which were $(21.86-34.72)$ and $(13.29-18.65) \times 10^{12}$ $M^{-1}$ $s^{-1}$ after heating at 90 and 126 °C for 30 min, respectively, and the reductions after heating were much less than those for GA dispersions with only norbixin or $Fe^{2+}$.

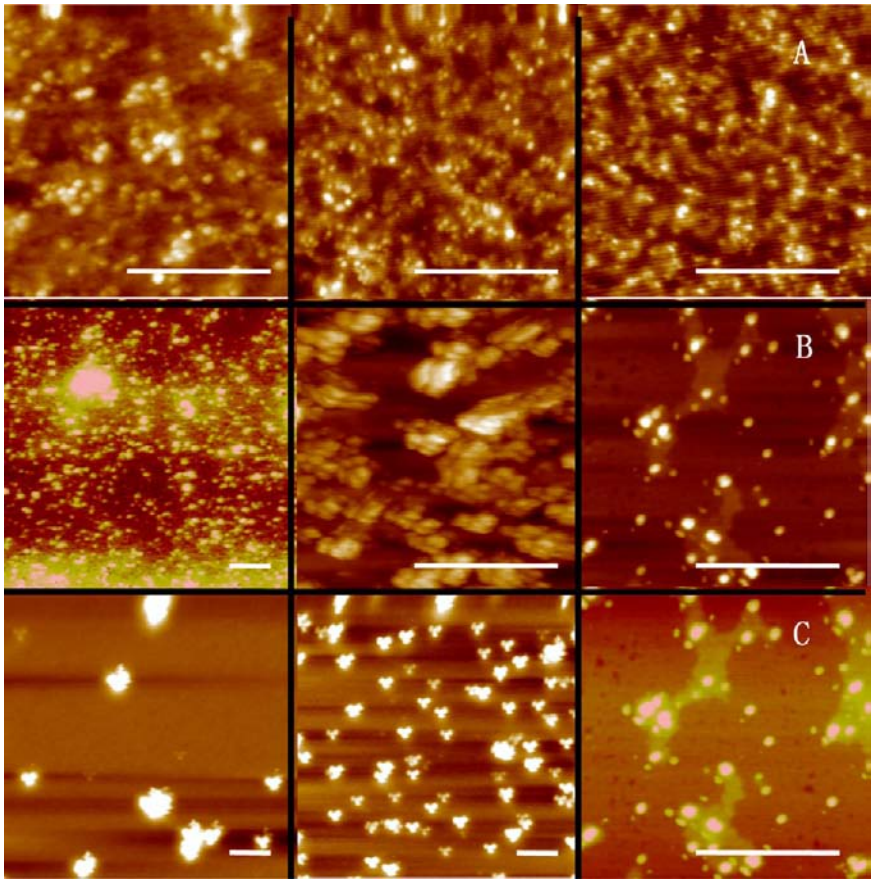


**Figure 4.** AFM topographic images of gum arabic−norbixin dispersions at pH 3.0 (left), pH 4.0 (center), and pH 5.0 (right) before (A) and after heating at 90 °C (B) or 126 °C (C) for 30 min. Bar = 1 $\mu$m.

The $k_q$ values of all GA dispersions before and after heating at 90 and 126 °C for 30 min were at least 2 orders of magnitude higher than $2.0 \times 10^{10}$ $M^{-1}$ $s^{-1}$, which indicated that GA formed complexes with $Fe^{2+}$ and norbixin at pH 3.0−5.0. Moreover, the higher $k_q$ values of GA−norbixin than those of $Fe^{2+}$−GA dispersions before heating suggest the greater ability of complex formation between norbixin and GA. After heating, the reductions of $k_q$ values of GA−$Fe^{2+}$ dispersions were less than those of GA−norbixin dispersions. These results imply that complexes formed between norbixin and GA were not thermally stable and the degradation of norbixin and decoupling of complexes after heating caused the significant reduction of the $k_q$ values. The decoupling of complexes was evidenced by the precipitation of norbixin (Supporting Information, Figure S1) and implied that the coordinate bonds between norbixin and GA complexes weakened during heating. The synergism in GA, $Fe^{2+}$, and norbixin complexation increased the extent of static quenching (highest $k_q$ values in Table 2), suggesting the formation of stronger and more stable complexes.[38] This likely resulted from ionic bridges formed between anionic groups of GA and possibly norbixin and $Fe^{2+}$ that effectively prevented the decoupling of norbixin−GA complexes, inhibited the norbixin precipitation, and maintained the $k_q$ values to a greater extent after heating (Table 2).

As for the pH effects (Table 2), no significant changes were found in $k_q$ values for $Fe^{2+}$−GA mixture at pH 3−5 before and after heating, indicating the formation of stable complexes. For the norbixin−-GA system, $k_q$ values were similar ($p > 0.05$) before heating but $k_q$ was significantly larger at a higher pH from 3 to 5 after heating at 90 and 126 °C for 30 min. The latter was due to the smaller amount of precipitation (decoupling) of norbixin after heating at a higher pH, as presented above. The $k_q$ values of norbixin−$Fe^{2+}$−GA mixtures were similar before heating and became bigger at a higher pH after heating at 90 °C for 30 min, which were opposite to the data after heating at 126 °C for 30 min. The exact mechanisms causing different trends after heating at these two temperatures were unclear. One possible explanation may be that decoupling (precipitation) of norbixin from complexes, more significant at a lower pH, was the dominant factor affecting the binding in complexes during heating at 90 °C, whereas decomposition of norbixin, more significant for the more soluble form (at a higher pH), was also significant during heating at 126 °C.

**Particle Size of Complexes before and after Heating.** Hydrodynamic diameters ($d_h$) of GA with and without $Fe^{2+}$ and norbixin at pH 3.0, 4.0, and 5.0 are shown in Figure 1. In the absence of norbixin, the $d_h$ of GA solutions with and without $Fe^{2+}$ was <80 nm before and after heating and was overall smaller at a lower pH between 3 and 5, which likely is due to the reduced number of charges due to protonation of carboxylate groups with $pK_a$ of 1.8−2.2,[39] reducing the effective dimension of GA. The weakened electrostatic repulsion at a lower pH can cause the aggregation of GA to increase the $d_h$, which was not observed. This indicates that the steric hindrance of polysaccharide chains prevented intermolecular aggregation of GA at acidic conditions.[19,40]

The addition of norbixin significantly increased the $d_h$, which further increased significantly after heating at 90 and 126 °C for 30 min. The $d_h$ was about 300 nm after heating the

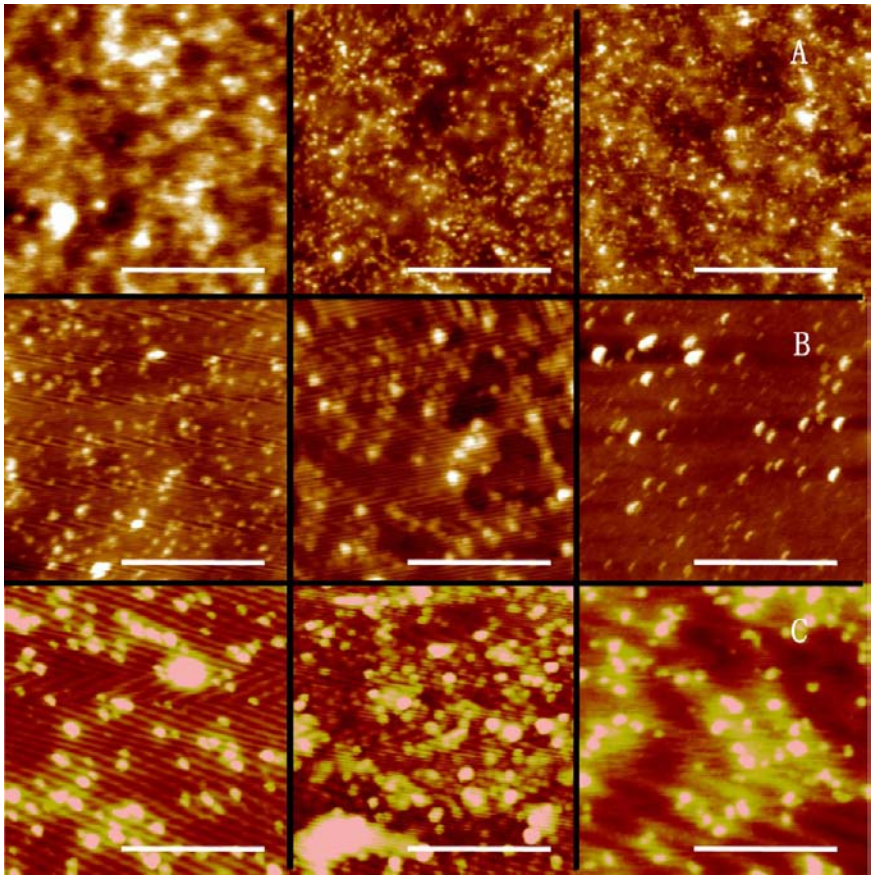


**Figure 5.** AFM topographic images of gum arabic−norbixin dispersions with $Fe^{2+}$ at pH 3.0 (left), pH 4.0 (center), and pH 5.0 (right) before (A) and after heating at 90 °C (B) or 126 °C (C) for 30 min. Bar = 1 $\mu$m.

norbixin−GA dispersion at pH 4.0 and 90 °C for 30 min and exceeded the detection limit of the particle size analyzer (~3 $\mu$m) after heating the pH 3.0 dispersion at 90 °C for 30 min and the pH 3.0 and 4.0 dispersions at 126 °C for 30 min (Figure 1A). The addition of $Fe^{2+}$ in norbixin−GA dispersions did not significantly change the $d_h$ before heating. The norbixn−GA dispersions with $Fe^{2+}$ did not show significant changes in $d_h$ after heating at 90 °C for 30 min, and the $d_h$ increased by only 20−40 nm, from about 104−161 to 139−181 nm, after heating at 126 °C for 30 min.

Similar $d_h$ values of GA with and without $Fe^{2+}$ indicated that ionic bridges were intramolecular and did not change the dimension of GA and cause the flocculation of GA. Similar $d_h$ of GA dispersions with and without $Fe^{2+}$ before and after heating suggested the thermal stability of GA and ionic bridges. The significant increase in $d_h$ of GA dispersions after the addition of norbixin suggested the complex formation between norbixin and multiple GA molecules. After heating the GA dispersions with norbixin, the dramatic increases of $d_h$ of treatments without $Fe^{2+}$ should have resulted from the instability of norbixin−GA complexes and the precipitation of norbixin that was more significant at a lower pH (Supporting Information, Figure S1) because of the reduced norbixin solubility when the carboxylate groups are protonated. Further addition of $Fe^{2+}$ improved the thermal stability of norbixin−GA complexes to effectively prevent the leaking out and precipitation of norbixin, which provides physical interpretation of the synergism of $Fe^{2+}$ and GA in improving the heat and acid stability of norbixin.

**Morphology of Dispersion Particles before and after Heating.** AFM was used to study the morphology of GA dispersions with and without norbixin and $Fe^{2+}$ before and after thermal treatments, with the topographical images shown in Figures 4−7 and the measured particle heights shown in Table 3. No large aggregates were observed for GA dispersions without (Figure 2) and with (Figure 3) $Fe^{2+}$ before and after thermal treatments at 90 and 126 °C for 30 min. The results agreed with the above analyses based on particle size (Figure 1), showing good heat stability of GA dispersions without norbixin. The height of GA with and without $Fe^{2+}$ (Table 3) is in agreement with that (1−3 nm) of monomeric GA measured in aqueous solutions.[41]

For the norbixin−GA dispersions (Figure 4), aggregated structures were observed after heating the pH 4.0 dispersion at 90 °C for 30 min, and much larger aggregates were present after the pH 3.0 dispersion was heated at 90 °C for 30 min and the pH 3.0 and 4.0 dispersions were heated at 126 °C for 30 min. Aggregated structures also showed significant increases in particle height (Table 3). AFM results (Figure 4) were in good agreement with the particle size data (Figure 1). For the GA dispersions with both norbixin and $Fe^{2+}$, structural changes were insignificant after heating at 90 °C for 30 min but were noticeable after heating at 126 °C for 30 min (Figure 5), but the changes were much less than those of the GA−norbixin dispersions without $Fe^{2+}$ (Figure 4). This was further verified by particle heights in Table 3. The AFM results again agreed with more significant increases in $d_h$ after the GA−norbixin−$Fe^{2+}$ dispersions were heated at 126 °C than at 90 °C (Figure 1).

**Zeta Potential of Complexes before and after Heating.** Zeta-potential results in Figure 6 showed that GA had more

**Table 3. AFM Height of Particles in Dispersions at pH 3.0−5.0 with Gum Arabic (GA), $Fe^{2+}$, and/or Norbixin before (21 °C) and after Heating at 90 or 126 °C for 30 min[a]**

| | | particle height (nm) | | |
|---|---|---|---|---|
| | temperature (°C) | pH 3.0 | pH 4.0 | pH 5.0 |
| GA | none | 2.4 ± 1.0 f | 2.2 ± 0.7 f | 1.5 ± 0.2 f |
| | 90 | 2.2 ± 0.4 f | 2.1 ± 0.9 f | 2.0 ± 1.0 f |
| | 126 | 1.7 ± 0.7 f | 1.1 ± 0.3 f | 2.1 ± 1.1 f |
| GA−$Fe^{2+}$ | none | 1.8 ± 1.2 f | 2.0 ± 1.4f | 2.3 ± 1.0 f |
| | 90 | 2.4 ± 1.9 f | 2.2 ± 0.5 f | 2.3 ± 0.6 f |
| | 126 | 2.2 ± 0.9 f | 2.5 ± 1.0 f | 3.2 ± 0.9 ef |
| GA−norbixin | none | 9.7 ± 4.1 cde | 6.8 ± 1.0 def | 10.5 ± 4.4 cd |
| | 90 | 43.4 ± 8.0 b | 66.7 ± 9.3 a | 11.4 ± 4.1 cd |
| | 126 | 45.6 ± 6.3 b | 40.5 ± 6.0 b | 11.6 ± 6.0 cd |
| GA−norbixin−$Fe^{2+}$ | none | 10.2 ± 0.1 cd | 10.8 ± 5.5 cd | 14.1 ± 5.3 c |
| | 90 | 12.4 ± 3.5 cd | 10.4 ± 2.4 cd | 10.1 ± 1.1 cd |
| | 126 | 15.8 ± 5.7 c | 14.4 ± 7.9 c | 11.6 ± 5.6 cd |

[a]Numbers are mean ± standard deviation from two images. Different letters indicate significant difference in the mean ($p < 0.05$).

negative charges at a higher pH between 3.0 and 5.0, as discussed above due to deprotonation of carboxyl groups.[42] Similar to $d_h$ (Figure 1), the zeta potential of GA alone did not change significantly after heating (Figure 6A), which confirmed the heat stability of GA. No significant changes of zeta potential were observed for GA after mixing with $Fe^{2+}$, but the zeta-potential magnitude of the mixture decreased significantly after heating. This may result from the binding between $Fe^{2+}$ and GA being insignificant at room temperature but becoming significant and irreversible after heating.

After mixing norbixin with GA dispersions, the zeta potential became significantly more negative (Figure 6A). Further addition of $Fe^{2+}$ decreased the zeta-potential magnitude of the GA−norbixin dispersions (Figure 6B). For the GA−norbixin dispersions, heating at 90 and 126 °C did not show a significant impact on the zeta potential ($p > 0.05$). Conversely, the GA−$Fe^{2+}$−norbixin dispersions became significantly more negative after heating, and the two heat treatment temperatures of 90 and 126 °C did not affect zeta-potential changes differently ($p > 0.05$)

On the basis of the above information, the proposed GA−norbixin−$Fe^{2+}$ complex structure is presented in Figure 7. On the basis of $d_h$, complex formation between norbixin and GA involves multiple GA molecules (Figure 1), forming a core of norbixin and a shell of GA. At pH 3−5, the protein/polypeptide moiety of GA likely has cationic amino acid residues[19] and is included in the complex center. When the complex is measured for zeta potential, the complex surface with negatively charged polysaccharide fractions is measured, resulting in the higher magnitude of negative zeta potential for complexes of norbixin−GA than that of GA alone. After addition of $Fe^{2+}$, coordinated ionic bridges form mostly between GA−norbixin and ferrous ions within or near the core at the studied conditions. After heating, some complexes are dissociated and re-formed as bigger structures (Figure 1), which results in a greater number of surface anionic polysaccharides in each complex, corresponding to the increased magnitude of the zeta potential. The ionic bridges within the complexes are heat stable, but binding between norbixin molecules and that between norbixin and GA may not be thermally stable but play a minor role in overall complex structure. This results in overall good stability of GA−norbixin−$Fe^{2+}$ complexes that effectively

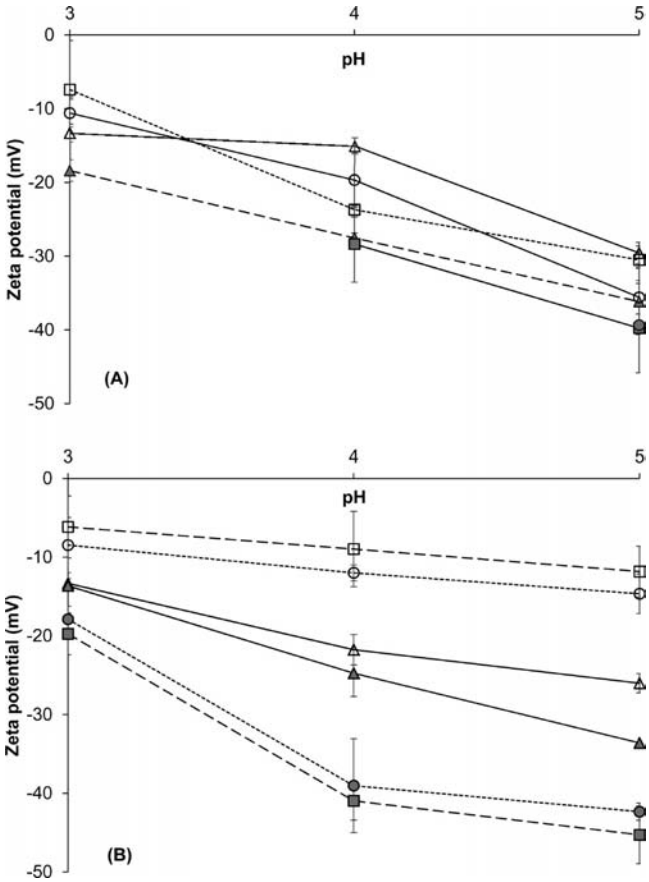


**Figure 6.** Zeta potential of gum arabic (open symbols) and norbixin−gum arabic dispersions (solid symbols) without (A) and with (B) $Fe^{2+}$ before (21 °C, triangles) and after heating at 90 °C (squares) or 126 °C (circles) for 30 min. Error bars are standard deviations from triplicates.

provided the macroscopically good thermal and acid stabilities of norbixin. The improvement of norbixin stability is to be verified in specific food matrices and their processing conditions.[31]

In summary, GA and/or $Fe^{2+}$ can significantly improve the stability of norbixin in aqueous dispersions at pH 3.0−5.0


dx.doi.org/10.1021/jf5037799 | J. Agric. Food Chem. 2014, 62, 12668−12677

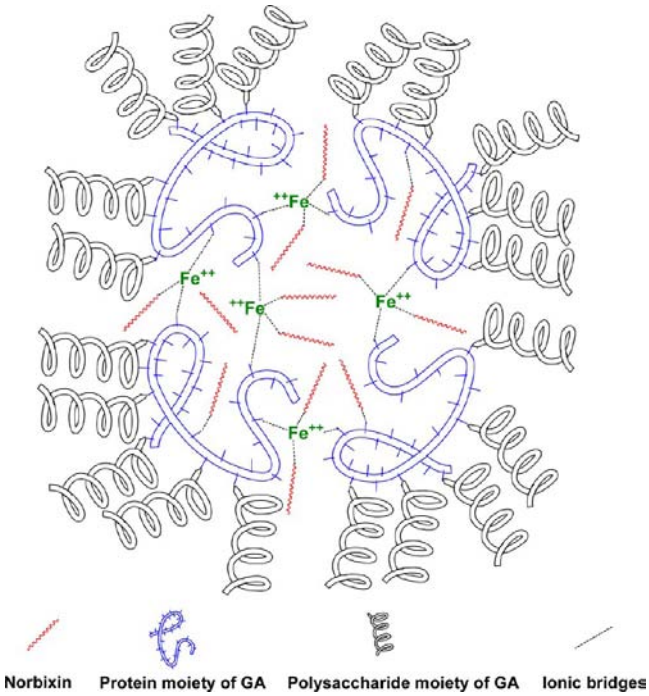


**Figure 7.** Proposed complex structure formed with gum arabic, norbixin, and $Fe^{2+}$.

before and after thermal treatment at 90 and 126 °C for 30 min. The acid stability was enabled by complex formation between norbixin and GA involving multiple GA molecules. $Fe^{2+}$ further strengthened the GA–norbixin complexes by forming coordinated ionic bridges. The strengthened complexes reduced the decoupling of norbixin from complexes and effectively prevented the aggregation of norbixin during heating, forming particles that were sufficiently small to prevent noticeable turbidity. Therefore, GA and $Fe^{2+}$ can be dissolved in transparent beverages utilizing norbixin as a pigment to ensure its stability after thermal treatments.

## ■ ASSOCIATED CONTENT

### Ⓢ Supporting Information

Photographs and absorbance at 460 nm of norbixin samples and photograph of samples with GA, $FeCl_2$, and their mixtures, before and after heating. This material is available free of charge via the Internet at http://pubs.acs.org.

## ■ AUTHOR INFORMATION

### Corresponding Author

*(Q.Z.) Mail: Department of Food Science and Technology The University of Tennessee, 2510 River Drive, Knoxville, TN 37996, USA. Phone: (865) 974-6196. Fax: (865) 974-7332. E-mail: qzhong@utk.edu.

### Funding

We acknowledge the University of Tennessee for financial support.

### Notes

The authors declare no competing financial interest.

## ■ ACKNOWLEDGMENTS

We gratefully thank Drs. Yue Zhang, Yangchao Luo, and Gang Liu and Qiumin Ma for their help in fluorescence spectroscopy, AFM, and zeta-potential assays.

## ■ REFERENCES

(1) van Scheppingen, W. B.; Boogers, I. A.; Duchateau, A. L. Study on decomposition products of norbixin during bleaching with hydrogen peroxide and a peroxidase by means of UPLC-UV and mass spectrometry. *Food Chem.* **2012**, *132*, 1354–1359.

(2) Bouvier, F.; Dogbo, O.; Camara, B. Biosynthesis of the food and cosmetic plant pigment bixin (annatto). *Science* **2003**, *300*, 2089–2091.

(3) Polar-Cabrera, K.; Huo, T.; Schwartz, S. J.; Failla, M. L. Digestive stability and transport of norbixin, a 24-carbon carotenoid, across monolayers of Caco-2 cells. *J. Agric. Food Chem.* **2010**, *58*, 5789–5794.

(4) Scotter, M. J.; Wilson, L. A.; Appleton, G. P.; Castle, L. Analysis of annatto (*Bixa orellana*) food coloring formulations. 2. Determination of aromatic hydrocarbon thermal degradation products by gas chromatography. *J. Agric. Food Chem.* **2000**, *48*, 484–488.

(5) Di Mascio, P.; Murphy, M. E.; Sies, H. Antioxidant defense systems: the role of carotenoids, tocopherols, and thiols. *Am. J. Clin. Nutr.* **1991**, *53*, 194–200.

(6) Reddy, M. K.; Alexander-Lindo, R. L.; Nair, M. G. Relative inhibition of lipid peroxidation, cyclooxygenase enzymes, and human tumor cell proliferation by natural food colors. *J. Agric. Food Chem.* **2005**, *53*, 9268–9273.

(7) Galindo-Cuspinera, V.; Westhoff, D. C.; Rankin, S. A. Antimicrobial properties of commercial annatto extracts against selected pathogenic, lactic acid, and spoilage microorganisms. *J. Food Prot.* **2003**, *66*, 1074–1078.

(8) Junior, A.; Asad, L.; Oliveira, E.; Kovary, K.; Asad, N. R.; Felzenszwalb, I. Antigenotoxic and antimutagenic potential of an annatto pigment (norbixin) against oxidative stress. *Genet. Mol. Res.* **2005**, *4*, 94–99.

(9) Sousdaleff, M.; Baesso, M. L.; Neto, A. M.; Nogueira, A. C.; Marcolino, V. A.; Matioli, G. Microencapsulation by freeze-drying of potassium norbixinate and curcumin with maltodextrin: stability, solubility, and food application. *J. Agric. Food Chem.* **2013**, *61*, 955–965.

(10) Barbosa, M.; Borsarelli, C.; Mercadante, A. Light stability of spray-dried bixin encapsulated with different edible polysaccharide preparations. *Food Res. Int.* **2005**, *38*, 989–994.

(11) Teixeira, Z.; Durán, N.; Guterres, S. S. Annatto polymeric microparticles: natural product encapsulation by the emulsion–solvent evaporation method. *J. Chem. Educ.* **2008**, *85*, 946.

(12) Santos, D. T.; Meireles, M. A. A. Micronization and encapsulation of functional pigments using supercritical carbon dioxide. *J. Food Process Eng.* **2013**, *36*, 36–49.

(13) Lobato, K. B. d. S.; Paese, K.; Forgearini, J. C.; Guterres, S. S.; Jablonski, A.; Rios, A. d. O. Characterisation and stability evaluation of bixin nanocapsules. *Food Chem.* **2013**, *141*, 3906–3912.

(14) Zhang, Y.; Zhong, Q. Encapsulation of bixin in sodium caseinate to deliver the colorant in transparent dispersions. *Food Hydrocolloids* **2013**, *33*, 1–9.

(15) Gomes, J. F.; Rocha, S.; Pereira, M. d. C.; Peres, I.; Moreno, S.; Toca-Herrera, J.; Coelho, M. A. Lipid/particle assemblies based on maltodextrin–gum arabic core as bio-carriers. *Colloid Surf. B* **2010**, *76*, 449–455.

(16) Jayme, M.; Dunstan, D.; Gee, M. Zeta potentials of gum arabic stabilised oil in water emulsions. *Food Hydrocolloids* **1999**, *13*, 459–465.

(17) Dickinson, E. Hydrocolloids at interfaces and the influence on the properties of dispersed systems. *Food Hydrocolloids* **2003**, *17*, 25–39.

(18) Islam, A.; Phillips, G.; Sljivo, A.; Snowden, M.; Williams, P. A review of recent developments on the regulatory, structural and functional aspects of gum arabic. *Food Hydrocolloids* **1997**, *11*, 493–505.

(19) Chanamai, R.; McClements, D. Comparison of gum arabic, modified starch, and whey protein isolate as emulsifiers: influence of pH, $CaCl_2$ and temperature. *J. Food Sci.* **2002**, *67*, 120–125.

(20) Kirca, A.; Ozkan, M.; Cemeroglu, B. Storage stability of strawberry jam color enhanced with black carrot juice concentrate. *J. Food Process. Pres.* **2007**, *31*, 531−545.
(21) Wang, W.; Xu, S. Degradation kinetics of anthocyanins in blackberry juice and concentrate. *J. Food Eng.* **2007**, *82*, 271−275.
(22) Yen, G. C.; Lin, H. T. Comparison of high pressure treatment and thermal pasteurization effects on the quality and shelf life of guava puree. *Int. J. Food Sci. Technol.* **1996**, *31*, 205−213.
(23) Zhang, Y.; Zhong, Q. Binding between bixin and whey protein at pH 7.4 studied by spectroscopy and isothermal titration calorimetry. *J. Agric. Food Chem.* **2012**, *60*, 1880−1886.
(24) Luo, Y.; Teng, Z.; Wang, Q. Development of zein nanoparticles coated with carboxymethyl chitosan for encapsulation and controlled release of vitamin D3. *J. Agric. Food Chem.* **2012**, *60*, 836−843.
(25) Liu, G.; Zhong, Q. Dispersible and thermal stable nanofibrils derived from glycated whey protein. *Biomacromolecules* **2013**, *14*, 2146−2153.
(26) Pan, K.; Zhong, Q. Improving clarity and stability of skim milk powder dispersions by dissociation of casein micelles at pH 11.0 and acidification with citric acid. *J. Agric. Food Chem.* **2013**, *61*, 9260−9268.
(27) Banerjee, S. S.; Chen, D.-H. Fast removal of copper ions by gum arabic modified magnetic nano-adsorbent. *J. Hazard. Mater.* **2007**, *147*, 792−799.
(28) Scotter, M. The chemistry and analysis of annatto food colouring: a review. *Food Addit. Contam.* **2009**, *26*, 1123−1145.
(29) Dias, V. M.; Pilla, V.; Alves, L. P.; Oliveira, H. P.; Munin, E. Optical characterization in annatto and commercial colorific. *J. Fluoresc.* **2011**, *21*, 415−421.
(30) Bittencourt, C.; Felicissimo, M. P.; Pireaux, J.-J.; Houssiau, L. ToF-SIMS characterization of thermal modifications of bixin from *Bixa orellana* fruit. *J. Agric. Food Chem.* **2005**, *53*, 6195−6200.
(31) Scotter, M. J.; Castle, L.; Appleton, G. P. Kinetics and yields for the formation of coloured and aromatic thermal degradation products of annatto in foods. *Food Chem.* **2001**, *74*, 365−375.
(32) Watanabe, Y.; Fang, X.; Minemoto, Y.; Adachi, S.; Matsuno, R. Suppressive effect of saturated acyl L-ascorbate on the oxidation of linoleic acid encapsulated with maltodextrin or gum arabic by spray-drying. *J. Agric. Food Chem.* **2002**, *50*, 3984−3987.
(33) Bertolini, A.; Siani, A.; Grosso, C. Stability of monoterpenes encapsulated in gum arabic by spray-drying. *J. Agric. Food Chem.* **2001**, *49*, 780−785.
(34) Guadarrama-Lezama, A. Y.; Dorantes-Alvarez, L.; Jaramillo-Flores, M. E.; Pérez-Alonso, C.; Niranjan, K.; Gutiérrez-López, G. F.; Alamilla-Beltrán, L. Preparation and characterization of non-aqueous extracts from chilli (*Capsicum annuum* L.) and their microencapsulates obtained by spray-drying. *J. Food Eng.* **2012**, *112*, 29−37.
(35) Cavalcanti, R. N.; Santos, D. T.; Meireles, M. A. A. Non-thermal stabilization mechanisms of anthocyanins in model and food systems − an overview. *Food Res. Int.* **2011**, *44*, 499−509.
(36) Lange, D. C.; Kothari, R.; Patel, R. C.; Patel, S. C. Retinol and retinoic acid bind to a surface cleft in bovine $\beta$-lactoglobulin: a method of binding site determination using fluorescence resonance energy transfer. *Biophys. Chem.* **1998**, *74*, 45−51.
(37) Lakowicz, J. R. *Principles of Fluorescence Spectroscopy*, 2nd ed.; Plenum Press: New York, 1999.
(38) Bhattacharyya, M.; Chaudhuri, U.; Poddar, R. Evidence for cooperative binding of chlorpromazine with hemoglobin: equilibrium dialysis, fluorescence quenching and oxygen release study. *Biochem. Biophys. Res. Commun.* **1990**, *167*, 1146−1153.
(39) Espinosa-Andrews, H.; Enríquez-Ramírez, K. E.; García-Márquez, E.; Ramírez-Santiago, C.; Lobato-Calleros, C.; Vernon-Carter, J. Interrelationship between the zeta potential and viscoelastic properties in coacervates complexes. *Carbohydr. Polym.* **2013**, *95*, 161−166.
(40) Williams, D. N.; Gold, K. A.; Holoman, T. R. P.; Ehrman, S. H.; Wilson, O. C., Jr. Surface modification of magnetic nanoparticles using gum arabic. *J. Nanopart. Res.* **2006**, *8*, 749−753.
(41) Ikeda, S.; Funami, T.; Zhang, G. Visualizing surface active hydrocolloids by atomic force microscopy. *Carbohyd. Polym.* **2005**, *62*, 192−196.
(42) Garti, N. Hydrocolloids as emulsifying agents for oil-in-water emulsions. *J. Disper. Sci. Technol.* **1999**, *20*, 327−355.

In this study, we prepare nanoparticles from β-conglycinin, conjugates of β-conglycinin−dextran (CDC), and conjugate hydrolysates of β-conglycinin−dextran at DH 2.2% (CDCH) by a desolvation method. The structure and morphology of the nanoparticle samples were characterized by dynamic light scattering (DLS), transmission electron microscopy (TEM), and small-angles X-ray scattering (SAXS). The interfacial properties of the nanoparticle samples at the oil−water interface were investigated using interfacial dilatational rheological measurement.

## MATERIALS AND METHODS

**Materials.** β-Conglycinin were prepared from defatted soybean flakes (Xinjiahua Industrial and Commercial Co. Ltd., Shandong Province, China) according to the method of Nagano et al.[22] Protein content of β-conglycinin (91.21%, dry weight basis, N × 5.71) was determined by the Dumas combustion method (Elemental Analyzer rapid N cube, Hanau, Germany). Trypsin and dextran (67 kDa) were purchased from Sigma Co. (St. Louis, MO, USA). Other chemicals (ethanol, glutaraldehyde, etc.) were of analytical grade.

**Preparation of Conjugates of β-Conglycinin−Dextran.** β-Conglycinin and dextran powders (1:1, w/w) were dissolved in a sodium phosphate buffer solution (10 mM, pH 6.8) for 2 h at 25 °C and adjusted to pH 6.8 with the addition of 0.1 M HCl and then freeze-dried. The freeze-dried powders were incubated under 79% relative humidity at 60 °C for 6 days in a glass desiccator (diameter 30 cm, Shanghai Shupei Experimental Installation Co., Ltd., China) containing over-saturated potassium bromide. After incubation, the samples were dissolved in deionized water for 2 h at 25 °C and then centrifuged at 10000*g* for 15 min to dislodge insoluble substances. The supernatant was then freeze-dried, and the resultant substances (conjugates of β-conglycinin−dextran, CDC) were kept at 4 °C prior to use. The obtained conjugates of β-conglycinin−dextran were simply defined as CDC in this study.

**Hydrolysis of Conjugates of β-Conglycinin−Dextran.** The obtained conjugates of β-conglycinin−dextran were redissolved in distilled water with a protein concentration of 1.0% (w/v), stirred for 2 h at 25 °C, and then stored at 4 °C overnight. The solution was adjusted to pH 8.0 and then equilibrated at 40 °C for 30 min in a magnetically stirred water bath (HH-J1, Jiangsu Jinda instrument Co., Ltd., China). Trypsin solution was added to the above-mentioned solution and incubated at 40 °C with gentle stirring. The pH and DH were regulated by the pH-stat method using a 888 Titrino (Metrohm ion analysis, Herisau, Switzerland).[23] The enzyme concentration was 3 units of per gram protein to obtain a DH value of 2.2%. The pH of the sample solution was maintained at 8.0 during hydrolysis with 0.1 M NaOH. The enzymatic hydrolysis was terminated with the addition of 1 mM phenylmethanesulfonyl fluoride and 2-propanol solution when the DH value of 2.2% was reached. The resulting hydrolysates of β-conglycinin−dextran conjugates at DH 2.2% (CDCH) were freeze-dried and stored at 4 °C. The obtained conjugate hydrolysates of β-conglycinin−dextran at DH 2.2% were defined as CDCH in this study.

**Preparation of Nanoparticles.** A desolvation method was used for preparing nanoparticles according to the method of Ko et al. with modifications.[1] β-Conglycinin, CDC, and CDCH was dispersed in sodium phosphate buffer solutions (pH 7.0, 10 mM) to achieve a protein content of 1% (w/v). Subsequently, these sample solutions were adjusted to pH 9.0 with 0.1 M NaOH. While the sample solutions were kept stirring at 500 rpm using a magnetic stirrer (Color squid digital, IKA, Germany), ethanol was added at a rate of 1 mL/min into the sample solutions until the ethanol ratio achieved 80% (v/v). After desolvation, 16 μL of 2.5% (v/v) glutaraldehyde−ethanol solution was added to cause intraparticle cross-linking. The solutions were stirred at 500 rpm and 25 °C for 3 h. Subsequently, the solutions of these nanoparticles were centrifuged at 100000*g* (Hitachi CS150NX ultracentrifuge, Tokyo, Japan) for 30 min. The resulting pellets were redispersed to a certain volume of sodium phosphate buffer solutions (10 mM, pH 7.0) using a stick-type ultrasonicator (Sonic Ruptor 400, The Homogenizer Co., Kennesaw, GA, USA). Protein concentrations of the nanoparticle solutions were estimated according to the method of Lowry and his co-workers,[24] and bovine serum albumin was used for obtaining a standard calibration curve. The resulting nanoparticles were stored in sodium phosphate buffer solutions (10 mM, pH 7.0) at 4 °C. The nanoparticles prepared from β-conglycinin, CDC, and CDCH were named CN, CDCN, and CDCHN, respectively.

**Surface Hydrophobicity ($H_0$).** The $H_0$ of protein and nanoparticles was measured using 8-anilino-1-naphthalenesulfonic acid ammonium salt (ANS), according to the method of Haskard and Li-Chan.[25] Samples were dispersed into the buffer solutions (10 mM, pH 7.0) to achieve different protein concentrations of 0.02−0.5 mg/mL. Four milliliters of each sample solution were added with ANS stock solution (20 μL, 8 mM) and then mixed for about 5 s in a vortex mixer. Fluorescence intensity was determined at 390 nm (excitation) and 470 nm (emission) using a fluorescence spectrophotometer (F7000, Hitachi Co., Tokyo, Japan), with 5 nm of constant excitation and emission slit. Linear regression analysis was used to calculate the initial slope of the fluorescence intensity versus protein concentration plot, which was used as an index of $H_0$.

**Determination of Particle Size of Nanoparticles.** The *Z*-average hydrodynamic diameter and particle size distribution of the nanoparticles were determined by DLS technique using a Nanosizer ZS (Malvern Instruments, UK). The sample dispersions were diluted with 10 mM sodium phosphate buffer (pH 7.0) to the protein concentration of 0.5% (w/v) and poured into cuvettes (PCS8501). A cumulant analysis of the autocorrelation function was used to calculate the *Z*-average hydrodynamic diameter. In all cases, the particle size distributions were reported on the basis of volume frequency. All measurements were carried out at 25 °C, and three replications of each measurement were made.

**Determination of Nanoparticle Microstructure by Transmission Electron Microscopy.** The specimens of these nanoparticles were observed using a TEM (Fei Tecnai $G^2$ 12, FEI, USA). The preparation process of these samples was as follows: a carbon-coated copper grid was respectively dropped in 5 μL of nanoparticle sample solutions, and a filter paper was used to remove the excess solution after 30 s. After that, the nanoparticle samples were stained by 5 μL of 1% (w/v) phosphotungstic acid and dried at 25 °C for 72 h before examination by TEM. Image acquisition was performed at 200 kV.

**Small-Angle X-ray Scattering.** A SAXSess camera (Anton-Paar, Graz, Austria) was used to collect the SAXS data. An X-ray generator (PW3830) with a glass X-ray tube (PANalytical, Almelo, The Netherlands) was performed at 40 kV and 50 mA. The intense monochromatic primary beam (Cu K$\alpha$, $\lambda$ = 0.1542 nm) was provided by a block collimator and a focusing multilayer optics. Sealed quartz capillaries (1 mm in diameter) was used to load the samples with a protein content of 1.0% (w/v), which were placed in a temperature-controlled sample hold unit (TCS 120, Anton Paar) along the line-shaped X-ray beam in the evacuated camera housing. The distance between sample and detector was 261.2 mm, and the temperature was set at 26.0 °C. The 2D images were read out by a Cyclone storage phosphor system (PerkinElmer, Waltham, MA, USA), and they were corrected by taking into account the detector dark noise and found to be isotropic. The subtraction of the scattering of the pure solvent (water) was used to correct the curves of $I(q)$ versus $q$ ($q = 4\pi \sin\theta/\lambda$, where $2\theta$ is the scattering angle) resulting from the 360° azimuthal integration of the 2D patterns, and the curves were also fitted by using a spherical copolymer model.[26] Thirty minutes was used to collect data for each measurement. All $I(q)$ data were normalized because transmission calibration demanded the uniform primary intensity at $q = 0$. The radius of gyration ($R_g$) was calculated as follows: $I(q) = I(0)\exp(-R_g^2 q^2/3)$, where $I(0)$ is the scattering intensity at $q = 0$ and $I(q)$ is the scattering intensity.

**Interfacial Dilatational Properties.** The dynamic interfacial properties of the samples at corn oil−water interface were measured by recording temporal evolution of interfacial dilatational parameters using an optical contact angle meter (OCA20, Dataphysics, GmbH, Germany) equipped with an ODG-20 oscillating drop accessory. The

sample solutions with protein concentrations of 0.01, 0.1, and 1% (w/v) were placed in the syringe, respectively, and a drop of the sample solution (10 μL) was then delivered to a cuvette containing corn oil and kept for 3 h to adsorb sample to the oil−water interface. According to the oscillating drop methodology, sinusoidal expansion and compression were carried out by increasing and decreasing the drop volume with 10% of deformation amplitude, and the frequency was 0.1 Hz. Details of this experiment were described elsewhere.[27]

The protein adsorption process was described, and the change in the interfacial pressure with time was correlated by a modified form of the Ward−Torday equation,[28] which was defined as $\pi = 2C_0KT(D\theta/3.14)^{1/2}$, where $D$ is the diffusion coefficient, $K$ is the Boltzmann constant, $T$ is the absolute temperature, and $C_0$ is the bulk concentration in the aqueous phase. When the diffusion of protein at the interface dominates the adsorption process, a plot of $\pi$ versus $\theta^{1/2}$ will be presented for linear, and the slop of the plot will be the diffusion rate ($K_{dif}$). The change in interfacial tension $\gamma$ (dilatational stress) and interfacial area $A$ (dilatational strain) derived the interfacial dilatational modulus $E$, which might be described by the equation[29] $E = d\gamma/(dA/A) = -d\pi/d\ \ln A = E_d + iE_v$, where $\pi = \gamma_0 - \gamma$ is the interfacial pressure, $\gamma$ is the interfacial tension of the sample solution, and $\gamma_0$ is the interfacial tension of the pure oil−water interface. The dilatational modulus indicates two contributions of a dissipative part and the elastic part. The dissipative part accounts for energy lost through relaxation processes (loss modulus, $E_v$), and the elastic part illuminates the recoverable energy stored in the interface (storage modulus, $E_d$).

**Statistical Analysis.** All experiments were performed at least three times using freshly prepared samples. An analysis of variance (ANOVA) of the data was carried out, and the means were compared by a least significant difference (LSD) with a confidence interval of 95%. Values are shown in means ± standard deviations (SD).

## RESULTS AND DISCUSSION

**Detection of CDC and Their Hydrolysates by SDS-PAGE.** In our previous study, we indicated the formation of conjugates between β-conglycinin and dextran molecules by SDS-PAGE according to the method of Laemmli[30] and also confirmed that the distributions of molecular weight in CDC products decreased by enzymatic hydrolysis.[21] The covalent bond between β-conglycinin and dextran was not breached after trypsin hydrolysis of CDC.[21]

**Surface Hydrophobicity.** An important parameter indicative of hydrophobic groups on the surface of the proteins is surface hydrophobicity ($H_0$), which was usually used to identify the structural changes of the proteins.[31] The $H_0$ values of various samples are presented in Table 1. The $H_0$ of CDC was 326.30 ± 12.11, lower than that of β-conglycinin (465.01 ± 12.53). This might be because the conjugation of hydrophilic chain of dextran increased hydrophilicity on the molecule surface. However, CDCH exhibited higher $H_0$ (613.61 ± 15.33) than β-conglycinin and CDC. This might be because controlled enzymatic hydrolysis could expose hydrophobic groups from the hydrophobic core of the protein molecules. Dextran was conjugated to β-conglycinin, the hydrophilic chains of dextran could increase the hydrophilicity of the protein, and controlled enzymatic hydrolysis could improve the hydrophobicity of the protein; thus, CDCH could possess amphiphilic structures. Furthermore, the $H_0$ of each control protein sample was lower than its nanoparticle sample (Table 1), and the $H_0$ of CDCHN was the highest (1363.63 ± 20.85), followed by CN (863.87 ± 11.42) and CDCN (523.54 ± 4.26). This might be because ethanol could induce protein unfolding and the exposure of hydrophobic regions to the exterior during nanoparticle formation,[32,33] which led to an increase in $H_0$ of the nanoparticles.

**Table 1. Surface Hydrophobicity ($H_0$) of Proteins (β-Conglycinin, CDC, CDCH) and Their Nanoparticles (CN, CDCN, CDCHN) at pH 7.0**

| | surface hydrophobicity ($H_0$) | | |
|---|---|---|---|
| sample | β-conglycinin | β-conglycinin−dextran conjugates | conjugates DH 2.2% |
| control | 465.01 ± 12.53 | 326.30 ± 12.11 | 613.61 ± 15.33 |
| nanoparticles | 863.87 ± 11.42 | 523.54 ± 4.26 | 1363.63 ± 20.85 |

**Particle Size Distribution of Nanoparticles.** The particle size distribution of β-conglycinin, CDC, and CDCH and their nanoparticles is shown in Figure 1. Table 2 further illustrates the Z-average hydrodynamic diameter of the control and nanoparticle samples. After desolvation, the particle size distribution of β-conglycinin nanoparticles (CN) indicated a shift to larger sizes compared to that of control β-conglycinin (Figure1). The Z-average hydrodynamic diameters of β-conglycinin and β-conglycinin nanoparticles (CN) were 27.58 ± 0.16 and 49.64 ± 0.56 nm, respectively (Table 2). This could be attributed to the high content of ethanol (80%, v/v) benefiting the exposure and interaction of hydrophobic groups on protein molecules, which formed protein aggregates.[34] Similar observations were reported for human serum albumin nanoparticles.[5] However, the change of Z-average hydrodynamic diameter in control CDC and CDCN (from 95.78 ± 0.46 to 102.70 ± 0.88 nm) was less than that in β-conglycinin and CN (from 27.58 ± 0.16 to 49.64 ± 0.56 nm). This could be because the hydrophilic chain of dextran lowered the $H_0$ of CDC and suppressed the aggregation of the molecules during the desolvation process. For CDCH and its nanoparticles, the Z-average hydrodynamic diameters were 50.80 ± 0.44 and 117.64 ± 0.76 nm, respectively (Table 2).

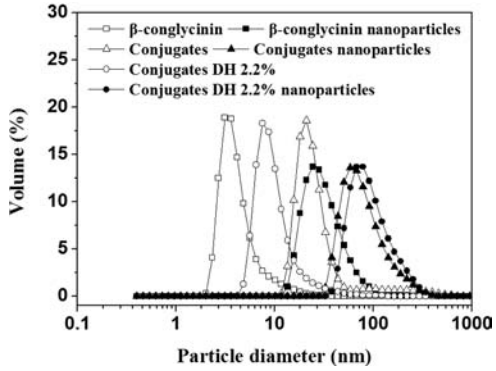


**Figure 1.** Particle size distribution of β-conglycinin, conjugates of β-conglycinin−dextran (CDC), conjugate hydrolysates of β-conglycinin−dextran at DH 2.2% (CDCH), and their nanoparticles (CN, CDCN, CDCHN).

**Table 2. Z-Average Hydrodynamic Diameter of Proteins (β-Conglycinin, CDC, CDCH) and Their Nanoparticles (CN, CDCN, CDCHN)**

| | Z-average hydrodynamic diameter (nm) | | |
|---|---|---|---|
| sample | β-conglycinin | β-conglycinin−dextran conjugates | conjugates DH 2.2% |
| control | 27.58 ± 0.16 | 95.78 ± 0.46 | 50.80 ± 0.44 |
| nanoparticles | 49.64 ± 0.56 | 102.70 ± 0.88 | 117.64 ± 0.76 |

When nanoparticles were prepared from CDCH by the desolvation method, the increase degree of the *Z*-average hydrodynamic diameter from CDCH to its nanoparticles was higher than that of *β*-conglycinin and CDC. This was probably because amphiphilic CDCH had higher $H_0$ compared with *β*-conglycinin and CDC, which could enhance hydrophobic interactions between hydrophobic groups of unfolded polypeptides and cause aggregation of protein molecules, inducing a greater degree of increase in particle size.

**Microstructural Observation of Nanoparticles.** The microstructures of the nanoparticles were investigated using TEM, as presented in Figure 2. All of the nanoparticles were shown to form a spherical shape. Figure 2a shows CN with a number of small spherical particles and trended toward aggregation on the observation grid, but they retained their stability in solution. The average particle diameter of CN analyzed by TEM was 55.22 ± 3.14 nm, which was very similar to the *Z*-average hydrodynamic diameter (49.64 ± 0.56 nm) determined from DLS (Table 2). The microstructures of CDCN and CDCHN are given in panels b and c of Figure 2, respectively. The globular proteins were often stained dark, and the hydrophilic chains of dextran were stained light via the negative staining of phosphotungstic acid. CDCN was stained lighter than CN, and it might be suggested that the CDCN was composed of the complex coacervate of *β*-conglycinin with dextran. However, the TEM image revealed that CDCHN had a spherical and obvious core−shell structure (Figure 2c). The shell was in light color, and the core was in dark color. On the basis of the steric stability of dextran and the negative staining of protein by phosphotungstic acid, we assumed that the shell was made up of the conjugated dextran segments and the core consisted of the colloidal particles of *β*-conglycinin. These results demonstrated that the amphiphilic graft copolymers of CDCH were likely to form nanoparticles with a core−shell structure during the desolvation process. In addition, the average particle diameters of CDCN and CDCHN measured from TEM were 125.01 ± 8.04 and 141.03 ± 6.32 nm, respectively, all slightly higher compared to the DLS data (102.70 ± 0.88 and 117.64 ± 0.76 nm, respectively) (Figure 2b,c and Table 2), which might be because of dehydration aggregation of the nanoparticles during the process of samples preparation for TEM experiments.

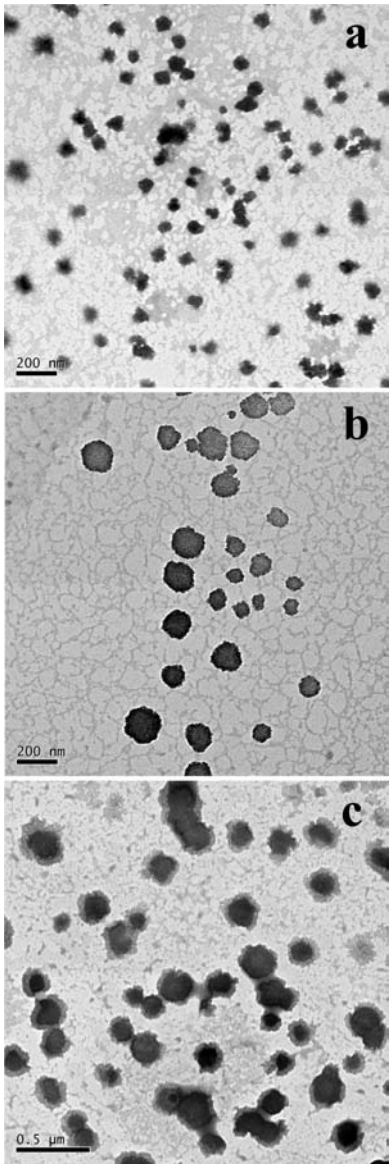


**Figure 2.** TEM micrographs of the nanoparticle samples: (a) *β*-conglycinin nanoparticles (CN); (b) nanoparticles prepared from conjugates of *β*-conglycinin−dextran (CDCN); (c) nanoparticles prepared from conjugate hydrolysates of *β*-conglycinin−dextran at DH 2.2% (CDCHN).

**Structure Analysis of Nanoparticles.** Besides DLS and TEM analysis, the SAXS technique was carried out to investigate the shape, structure, and size of the nanoparticles. Table 3 shows the scattering data of the samples including scattering intensity of zero scattering angle, $I(0)$, and the gyration radius, $R_g$, and also provided the hydrodynamic radius, $R_h$, measured by DLS. The values of $R_g$ and $R_h$ represent the particle size of the nanoparticles. $R_g$ characterizes the particle size or compactness, whereas $I(0)$ is relevant to the molecular mass of the particle.[35] Both $R_g$ and $I(0)$ of the control samples were lower than those of their nanoparticle samples as shown in Table 3, which indicated that hydrophobic interactions of the unfolded protein led to aggregation during the desolvation process for preparing nanoparticles. Furthermore, the $R_h$ values of the control samples were also lower than that of the nanoparticle samples. The result further confirmed that aggregation happened during the desolvation process. Additionally, the increased values of both $R_g$ and $I(0)$ from CDCH to its nanoparticles were greater than that of *β*-conglycinin and CDC (Table 3), which suggested that the aggregation degree of CDCHN was higher than that of CN and CDCN. This demonstrated that the amphiphilic CDCH was beneficial in the formation of larger aggregates during the desolvation process.

Figure 3 shows the Kratky plots ($q^2 \times I(q)$ versus $q$) of control protein samples and their nanoparticles. The Kratky plots are usually used to describe the conformational characteristics of the polypeptide chain and are often applied in polymer science.[36] A typical bell-shaped scattering curve in the Kratky plot indicated a compact globular structure, whereas the typical random coil structure with untight packed core exhibited a plateau at large angle or a curve of Kratky plot with no clear maximum.[36] Therefore, the Kratky plot can distinguish ordered or molten globule state conformation. The Kratky curves for all of the control protein samples and their nanoparticles exhibited the typical bell shape (Figure 3), which suggested that globular nanoparticles could be formed

**Table 3. Structural Parameters Obtained from SAXS and DLS Data of Protein and Nanoparticle Samples**

| sample | | $I(0)$ | $R_g$ (SAXS) (nm) | $R_h$ (DLS) (nm) |
|---|---|---|---|---|
| control | $\beta$-conglycinin | 1.89 ± 0.01 | 3.67 ± 0.02 | 13.79 ± 0.08 |
| | CDC | 3.92 ± 0.03 | 6.73 ± 0.04 | 47.89 ± 0.23 |
| | CDCH | 2.68 ± 0.02 | 6.07 ± 0.03 | 25.40 ± 0.22 |
| nanoparticles | CN | 4.54 ± 0.06 | 6.96 ± 0.07 | 24.82 ± 0.28 |
| | CDCN | 6.37 ± 0.10 | 11.37 ± 0.11 | 51.35 ± 0.44 |
| | CDCHN | 8.68 ± 0.13 | 12.97 ± 0.10 | 58.82 ± 0.38 |

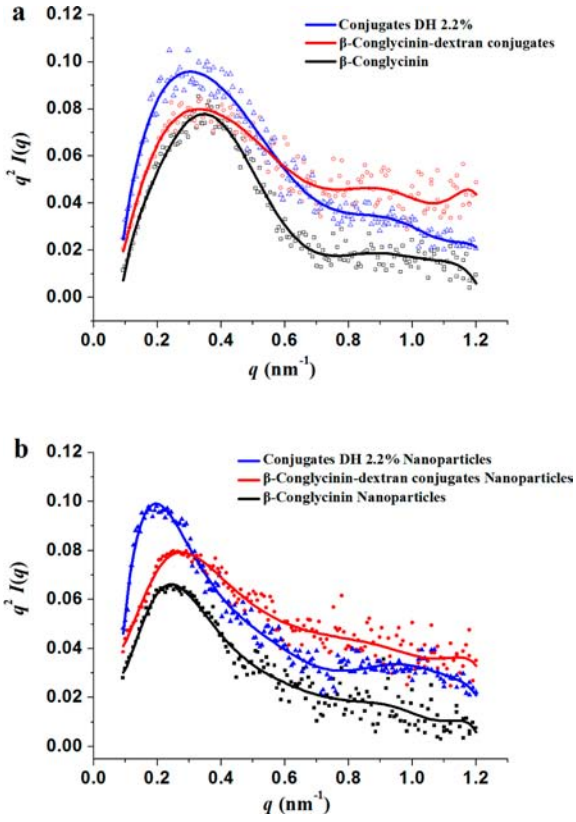


**Figure 3.** Kratky plot scattering curves of $\beta$-conglycinin, conjugates of $\beta$-conglycinin−dextran (CDC), conjugate hydrolysates of $\beta$-conglycinin−dextran at DH 2.2% (CDCH), and their nanoparticles (CN, CDCN, CDCHN).

from the control protein samples using the desolvation method. The results were in keeping with the TEM images (Figure 2).

**Interfacial Dilatational Properties of Nanoparticles.** *Adsorption Kinetics.* The adsorption of proteins on the oil−water interface may be analyzed by detecting the changes of interfacial pressure, which may serve as parameters for adsorption kinetics.[37] Conformational change of protein molecules could occur because of the interaction with the interface or surmounting energy barrier to adsorption during the adsorption process.[37] The adsorption kinetics of protein can be divided into three stages including the diffusion of protein from the principal part to the interface, the adsorption of protein to the oil−water interface, and the interfacial aggregation and recomposition of adsorbed protein on the interface.[38] The adsorption kinetics of the samples with protein concentrations of 0.01, 0.1, and 1% (w/v) by measuring the interfacial pressure ($\pi$) over adsorption time ($\theta$) are shown in Figure 4. All of the protein and nanoparticle samples conduced an increase of $\pi$ values with the increase of adsorption time, which indicated that the samples' adsorption occurred at the

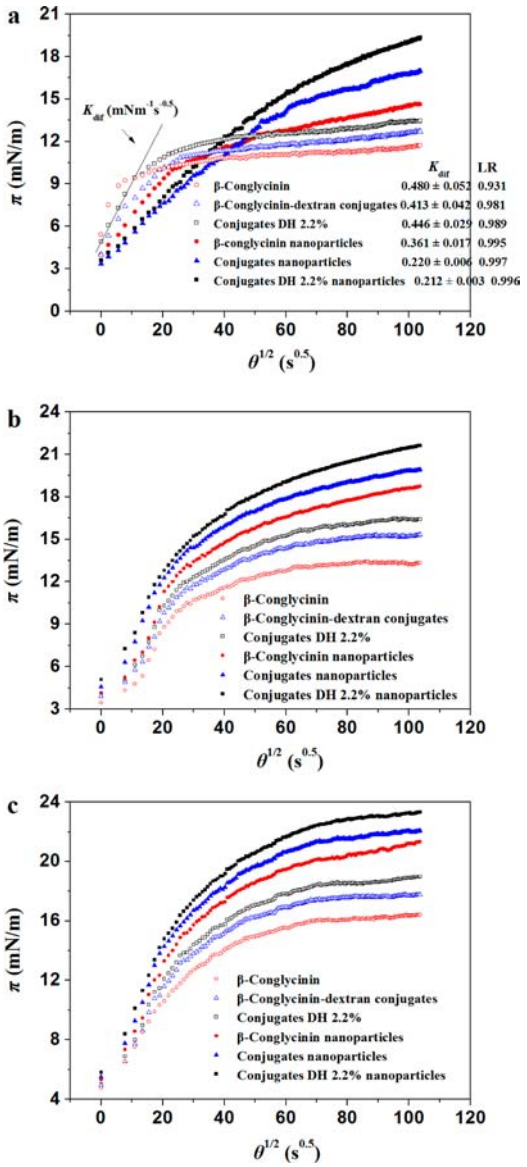


**Figure 4.** Interfacial pressure ($\pi$) changes during adsorption time at the corn oil−water interface for the samples of $\beta$-conglycinin, conjugates of $\beta$-conglycinin−dextran (CDC), conjugate hydrolysates of $\beta$-conglycinin−dextran at DH 2.2% (CDCH), and their nanoparticles (CN, CDCN, CDCHN). The protein concentrations in aqueous phase were (a) 0.01%, (b) 0.1%, and (c) 1% (w/v). The diffusion rate ($K_{dif}$) and linear regression coefficient (LR) are inserted in the figure.

interface. The diffusion of proteins on the oil−water interface may dominate the adsorption when the protein concentration is lower (0.01%, w/v).[27] The diffusion rate ($K_{dif}$) will be the slop of plot of $\pi$ against $\theta^{1/2}$, and the plot may be linear.[28] The


dx.doi.org/10.1021/jf504173z | J. Agric. Food Chem. 2014, 62, 12678−12685

$K_{dif}$ values of the protein samples of $\beta$-conglycinin, CDC, and CDCH were higher than those of nanoparticles (Figure 4a), which might be due to the difference of molecular weight between protein samples and nanoparticles, and the protein samples with lower molecular weight were easier to diffuse to the interface. The $K_{dif}$ values of CDCN and CDCHN were lower than that of CN (Figure 4a). This phenomenon might be interpreted by nanoparticle diffusion resistance because of the formation of conjugation of dextran with $\beta$-conglycinin. Dextran is a highly hydrophilic polysaccharide with high molecular weight, thus resulting in a low diffusion rate of CDCN and CDCHN to the interface.[39]

At longer adsorption times, the $\pi$ values of CDCHN were higher than that of CDCN, and the $\pi$ values of CN were the lowest. The $K_{dif}$ value of CN was higher than that of CDCN and CDCHN (Figure 4a), which indicated a fast absorption of CN to the interface. The steric hindrance effects of the fast absorption of CN could inhibit the CN unfolding at the interface; thus, the effective reduction of the interfacial tension was restrained. However, the $K_{dif}$ value of CDCN was lower than that of CN (Figure 4a), which could result in CDCN unfolding more effectively at the interface; therefore, the decrease in the interfacial tension of CDCN was greater than that of CN. Furthermore, the adsorption of surfactants on the oil−water interface was identified as a process of dynamic balance between surfactant adsorption and desorption, in which the molecular weight of the surfactants was one of the main factors for surfactant adsorption and desorption.[40] The lower molecular weight surfactants could make the surfactant desorption from the interface more likely to occur; otherwise, the surfactants with higher molecular weight tended to show considerably slower desorption than those surfactants of lower molecular weight.[40] The molecular mass of CN was lower than that of CDCN (Table 3), which could make CN desorption from the interface happen more easily than that of CDCN, thus resulting in a lower interfacial pressure of CN compared with CDCN at long absorption times. Moreover, the interfacial pressure ($\pi$ value) of CDCHN was higher than that of CDCN during long-term absorption (Figure 4). The faster increase of the interfacial pressure of CDCHN after diffusion stage could be attributed to its higher $H_0$ (Table 1), which might favor adsorption of nanoparticles to the oil−water interface.

The adsorption process of proteins would not be controlled by diffusion effect at the high concentration of protein (0.1−1%, w/v).[41] With the increase of adsorption time ($\theta$), the interfacial pressures ($\pi$) of nanoparticles were higher than their control protein samples; this may be because of higher surface hydrophobicity of nanoparticles (Figure 4b,c and Table 1). In addition, the interfacial pressures ($\pi$) of CDCHN were the highest among all of the samples, and this might be beneficial for them to adsorb to the oil−water interface; thus, the $\pi$ values rapidly increased.

*Interfacial Dilatational Rheological Properties.* A deformation of the interfacial area can be denoted by dilatational rheology, and the technique is impressible to the intermolecule interactions and adsorption at the interface.[42] Dynamic dilatational modulus ($E$) versus interfacial pressure ($\pi$) was used to further investigate the extent of intermolecule interactions and the capacity of protein adsorbed to the interface.[42] Figure 5 shows the $\pi$ dependence of $E$ in the interfacial layer for the adsorption of the nanoparticle and its control protein samples. For all of the samples at the contents of 0.01, 0.1, and 1% (w/v), the $E$ increased with increasing $\pi$,

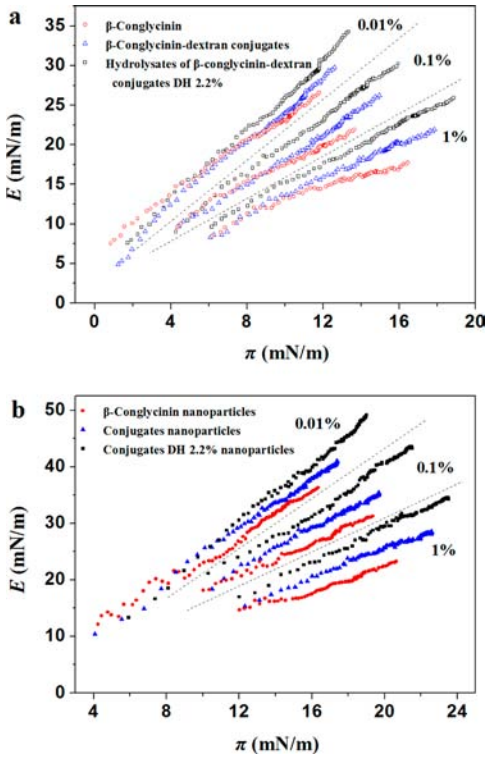


**Figure 5.** Interfacial pressure ($\pi$) dependence of interfacial dilatational modulus ($E$) for $\beta$-conglycinin, conjugates of $\beta$-conglycinin−dextran (CDC), and conjugates hydrolysates of $\beta$-conglycinin−dextran at DH 2.2% (CDCH) and their nanoparticles (CN, CDCN, CDCHN) adsorption to the oil−water interface: (a) protein samples; (b) nanoparticle samples.

and the $E$ values of control protein samples were all lower than its nanoparticle samples (Figure 5). This might be because the $H_0$ values of nanoparticles were all higher than its control protein samples, and the hydrophobic interaction of nanoparticles adsorbed on the oil−water interface was higher than that of the control protein samples. The values of $E$ for all samples were maximal at the concentration of 0.01% (w/v) and decreased with the decline of sample concentration. This might be because compact membrane was formed after the samples adsorbed to the oil−water interface, and this would inhibit the adsorption and intermolecular interactions of protein and nanoparticles samples at the oil−water interface.[41]

The $E$ value of CDCN increased more quickly than that of CN (Figure 5b). This might be attributed to the existence of the conjugated dextran in the adsorbed CDCN, which could protrude outward into the aqueous phase and increase the thickness of the interfacial layer, thus leading to a faster increase of dynamic dilatational modulus ($E$) at the oil−water interface.[43] However, the $E$ values of CDCN increased at a slower rate than that of CDCHN (Figure 5b). This result indicated that the enhancement of interactions between CDCHN, which might be due to its highest surface hydrophobicity, could benefit intermolecular interactions inside the oil−water interface.

In conclusion, nanoparticles of $\beta$-conglycinin, CDC, and CDCH were successfully prepared using a desolvation method. All of the nanoparticle samples showed spherical structures determined by TEM and SAXS, and nanoparticles prepared from amphiphilic graft copolymer (CDCH) exhibited the highest $H_0$, interfacial pressure, and dilatational modulus at long

**Figure 6.** Schematic illustration of nanoparticles prepared from amphiphilic graft copolymer and its application in stabilizing oil–water interface.

absorption times among all of the samples. The enhanced $H_0$ of the nanoparticles prepared from amphiphilic graft copolymer might favor thir adsorption and intermolecular interaction inside the oil–water interface (Figure 6). These properties of the nanoparticles synthesized from amphiphilic graft copolymer may have potential for application in drug delivery systems, and the release properties on the nutrient materials should be investigated.

## AUTHOR INFORMATION

### Corresponding Author

*(X.-Q.Y.) Phone: +86-20-87114262. Fax: +86-20-87114263. E-mail: fexqyang@163.com or fexqyang@scut.edu.cn.

### Funding

This research was supported by the Project of National Key Technology Research and Development Program for the 12th Five-year Plan (2012BAD33B10, 2012BAD34B04-2) and grants from the Chinese National Natural Science Foundation (Serial 31130042).

### Notes

The authors declare no competing financial interest.

## REFERENCES

(1) Ko, S.; Gunasekaran, S. Preparation of sub-100-nm β-lactoglobulin (BLG) nanoparticles. *J. Microencapsul.* **2006**, *23*, 887–898.

(2) Giroux, H. J.; Britten, M. Encapsulation of hydrophobic aroma in whey protein nanoparticles. *J. Microencapsul.* **2011**, *28*, 337–343.

(3) Vinagradov, S. V.; Bronich, T. K.; Kabanov, A. V. Nanosized cationic hydrogels for drug delivery: preparation, properties and interactions with cells. *Adv. Drug Delivery Rev.* **2002**, *54*, 223–233.

(4) Kawashima, Y. Nanoparticulate systems for improved drug delivery. *Adv. Drug Delivery Rev.* **2001**, *47*, 1–2.

(5) Weber, C.; Coester, C.; Kreuter, J.; Langer, K. Desolvation process and surface characterisation of protein nanoparticles. *Int. J. Pharm.* **2000**, *194*, 91–102.

(6) Jun, J. Y.; Nguyen, H. H.; Paik, S. Y. R.; Chun, H. S.; Kang, B. C.; Ko, S. Preparation of size-controlled bovine serum albumin (BSA) nanoparticles by a modified desolvatiion method. *Food Chem.* **2011**, *127*, 1892–1898.

(7) Gülseren, I.; Fang, Y.; Corredig, M. Whey protein nanoparticles prepared with desolvation with ethanol: characterization, thermal stability and interfacial behavior. *Food Hydrocolloid* **2012**, *29*, 258–264.

(8) Teng, Z.; Luo, Y. C.; Wang, Q. Nanoparticles synthesized from soy protein: Preparation, characterization, and application for nutraceutical encapsulation. *J. Agric. Food Chem.* **2012**, *60*, 2712–2720.

(9) Langer, K.; Balthasar, S.; Vogel, V.; Dinauer, N.; von Briesen, H.; Schubert, D. Optimization of the preparation process for human serum albumin (HSA) nanoparticles. *Int. J. Pharm.* **2003**, *257*, 169–180.

(10) Lim, Y. B.; Moon, K. S.; Lee, M. Rod-coil block molecules: their aqueous self -assembly and biomaterials applications. *J. Mater. Chem.* **2008**, *18*, 2909–2918.

(11) Kim, B. S.; Yang, W. Y.; Ryu, J. H.; Yoo, Y. S.; Lee, M. Carbohydrate-coated nanocapsules from amphiphilic rod-coil molecule: binding to bacterial type 1 pili. *Chem. Commun.* **2005**, *15*, 2035–2037.

(12) Yamamoto, H.; Kuno, Y.; Sugimoto, S.; Takeuchi, H.; Kawashima, Y. Surface-modified PLGA nanosphere with chitosan improved pulmonary delivery of calcitonin by mucoadhesion and opening of the intercellular tight junctions. *J. Controlled Release* **2005**, *102*, 373–381.

(13) Akhtar, M.; Dickinson, E. Emulsifying properties of whey protein-dextran conjugates at low pH and different salt concentrations. *Colloid Surf. B* **2003**, *31*, 125–132.

(14) Xu, C. H.; Yang, X. Q.; Yu, S. J.; Qi, J. R.; Guo, R.; Sun, W. W.; Yao, Y. J.; Zhao, M. M. The effect of glycosylation with dextran chains of different lengths on the thermal aggregation of β-conglycinin and glycinin. *Food Res. Int.* **2010**, *43*, 2270–2276.

(15) Jimenez-Castaño, L.; Villamiel, M.; Lopez-Fandiño, R. Glycosylation of individual whey proteins by Maillard reaction using dextran of different molecular mass. *Food Hydrocolloid* **2007**, *21*, 433–443.

(16) Zhu, D.; Damodaran, S.; Lucey, J. A. Physicochemical and emulsifying properties of whey protein isolate (WPI)-dextran conjugates produced in aqueous solution. *J. Agric. Food Chem.* **2010**, *58*, 2988–2994.

(17) Dickinson, E.; Izgi, E. Foam stabilization by protein-polysaccharide complexes. *Colloids Surf., B* **1996**, *113*, 191–201.

(18) Fujiwara, K.; Oosawa, T.; Saeki, H. Improved thermal stability and emulsifying properties of carp myofibrillar proteins by conjugation with dextran. *J. Agric. Food Chem.* **1998**, *46*, 1257–1261.

(19) Akhtar, M.; Dickinson, E. Whey protein-maltodextrin conjugates as emulsifying agents: an alternative to gum arabic. *Food Hydrocolloid* **2007**, *21*, 607–616.

(20) Nakamura, S.; Kato, A.; Kobayashi, K. Enhanced antioxidative effect of ovalbumin due to covalent binding of polysaccharides. *J. Agric. Food Chem.* **1992**, *40*, 2033–2037.

(21) Zhang, J. B.; Wu, N. N.; Yang, X. Q.; He, X. T.; Wang, L. J. Improvement of emulsifying properties of Maillard reaction products from β-conglycinin and dextran using controlled enzymatic hydrolysis. *Food Hydrocolloid* **2012**, *28*, 301–312.

(22) Nagano, T.; Hirotsuka, M.; Mori, M.; Kohyama, K.; Nishinari, K. Dynamic viscoelastic study on the gelation of 7S globulin from soybeans. *J. Agric. Food Chem.* **1992**, *40*, 941–944.

(23) Kuipers, B. J. H.; Alting, A. C.; Gruppen, H. Comparison of the aggregation behavior of soy and bovine whey protein hydrolysates. *Biotechnol. Adv.* **2007**, *25*, 606–610.

(24) Lowry, O. H.; Rosebrough, N. J.; Farr, A. L.; Randall, O. J. Protein measurement with the folin phenol reagent. *J. Biol. Chem.* **1951**, *193*, 265–275.

(25) Haskard, C. A.; Li-Chan, E. C. Y. Hydrophobicity of bovie serum albumin and ovalbumin determined using uncharged (PRODAN) and anionic (ANS) fluorescent probes. *J. Agric. Food Chem.* **1998**, *46*, 2671–2677.

(26) Pedersen, J. S.; Gerstenbery, M. C. Scattering form factor of block copolymer micelles. *Macromolecules* **1996**, *29*, 1363–1365.

(27) Liu, L. Y.; Zhao, Q. Z.; Liu, T. X.; Zhao, M. M. Dynamic surface pressure and dilatational viscoelasticity of sodium caseinate/xanthan

gum mixtures at the oil-water interface. *Food Hydrocolloid* **2011**, *25*, 921−927.
(28) Ward, A. F. H.; Tordai, L. Time dependence of boundary tension of solutions. I. The role of diffusion in time effects. *J. Chem. Phys.* **1946**, *14*, 453−461.
(29) Lucassen, J.; Van den Tempel, M. Dynamic measurements of dilatational properties of a liquid interface. *Chem. Eng. Sci.* **1972**, *27*, 1283−1291.
(30) Laemmli, U. K. Cleavage of structural proteins during assembly of head of bacteriophage-T4. *Nature* **1970**, *227*, 680−685.
(31) Puppo, C.; Chapleau, N.; Speroni, F.; de Lamballerie-Anton, M.; Michel, F.; Anon, C.; Anton, M. Physicochemical modifications of high-pressure-treated soybean protein isolates. *J. Agric. Food Chem.* **2004**, *52*, 1564−1571.
(32) Shiraki, K.; Nishikawa, K.; Goto, Y. Trifluoroethanol-induced stabilization of the R-helical structure of $\beta$-lactoglobulin: implication for non-hierarchical protein folding. *J. Mol. Biol.* **1995**, *245*, 180−194.
(33) Wang, J. M.; Yang, X. Q.; Yin, S. W.; Zhang, Y.; Tang, C. H.; Li, B. S.; Yuan, D. B.; Guo, J. Structural rearrangement of ethanol-denatured soy proteins by high hydrostatic pressure treatment. *J. Agric. Food Chem.* **2011**, *59*, 7324−7332.
(34) Fukushima, D. Denaturation of soybean proteins by organic solvents. *Cereal Chem.* **1969**, *46*, 156−163.
(35) Guo, J.; Yang, X. Q.; He, X. T.; Wu, N. N.; Wang, J. M.; Gu, W.; Zhang, Y. Y. Limited aggregation behavior of $\beta$-conglycinin and its terminating effect on glycinin aggregation during heating at pH 7.0. *J. Agric. Food Chem.* **2012**, *60*, 3782−3791.
(36) Receveur- Bréchot, V.; Bourhis, J. M.; Uversky, V. N.; Canard, B.; Longhi, S. Assessing protein disorder and induced folding. *Proteins: Struct., Funct., Bioonf.* **2006**, *62*, 24−45.
(37) Dickinson, E. Mixed biopolymers at interfaces: competitive adsorption and multilayer structures. *Food Hydrocolloid* **2011**, *25*, 1966−1983.
(38) Graham, D. E.; Phillips, M. C. Proteins at liquid interface. III. Molecular structures of adsorbed films. *J. Colloid Interface Sci.* **1979**, *70*, 427−439.
(39) Rodríguez Patino, J. M.; Pilosof, A. M. R. Protein-polysaccharide interaction at fluid interfaces. *Food Hydrocolloid* **2011**, *25*, 1925−1937.
(40) Rodríguez Patino, J. M.; Rodríguez, N. Interfacial characteristics of food emulsifiers (proteins and lipids) at the air-water interface. *Colloids Surf., B* **1999**, *15*, 235−252.
(41) Wang, J. M.; Xia, N.; Yang, X. Q.; Yin, S. W.; Qi, J. R.; He, X. T.; Yuan, D. B.; Wang, L. J. Adsorption and dilatational rheology of heat-treated soy protein at the oil-water interface: relationship to structural properties. *J. Agric. Food Chem.* **2012**, *60*, 3302−3310.
(42) Maldonado-Valderrama, J.; Rodríguez Patino, J. M. Interfacial rheology of protein-surfactant mixtures. *Curr. Opin. Colloid Interface Sci.* **2010**, *15*, 271−282.
(43) Wong, B. T.; Day, L.; Augustin, M. A. Deamidated wheat protein-dextran Maillard conjugates: effect of size and location of polysaccaride conjugated on steric stabilization of emulsions at acidic pH. *Food Hydrocolloid* **2011**, *25*, 1424−1432.

**Table 1. Primers Used in This Study**

| primer name | sequence (5′→3′)[a] | size (bp) |
|---|---|---|
| usp 1 | GTTCTGCGAGTTGCTGATGGACGAGTTGAG | 30 |
| usp 2 | GGACGAGTTGAGGATGCGTACTGTTTTGAC | 30 |
| usp 3 | TGGGTAAGGGGGTTGTCAAGTTTGAGGGG | 29 |
| dsp 1 | CTGTGTGGCCATCAACTCAGGCACCAAC | 28 |
| dsp 2 | CATCAACTCAGGCACCAACATCACCGTATG | 30 |
| dsp 3 | GGCCGATCCGACAACACGGTCAAAACAGT | 29 |
| PG7fn-F | GATTCAACCGCCATGATCTTGTCCACCCTC | 30 |
| PG7fn-R | CCAAACCGCCTAGCAAGATGCCGGACT | 27 |
| PG7fn-pF | CCTGAATTCAATCCGGTCCCTGCCAACTCCAAC | 33 |
| PG7fn-pR | TATGCGGCCGCCTAGCAAGATGCCGGACTA | 30 |

[a]Restriction sites are underlined.

(BMGY), and buffered methanol complex medium (BMMY) for *P. pastoris* growth and induction, respectively, were prepared according to the manual of the *Pichia* Expression kit (Invitrogen).

The DNA purification kit and Genome Walking kit were purchased from TaKaRa (Otsu, Japan). Restriction endonucleases and T4 DNA ligase were supplied by New England Biolabs (Hitchin, UK). The Fungal DNA Mini kit was purchased from Omega Bio-Tek (Norcross, GA, USA). D-(+)-Galacturonic acid, digalacturonic acid, trigalacturonic acid, polygalacturonic acid, and citrus pectin of different methyl esterification degrees (34% for P9311, 70% for P9436, and 85% for P9561) were purchased from Sigma-Aldrich (San Diego, CA, USA). All chemicals were of analytical grade and commercially available.

**Cloning of the Endo-polygalacturonase Gene (*pg7fn*).** The core region of the polygalacturonase gene from strain XZ7 was amplified by degenerate primers GH28nF and GH28nR,[6] which were designed on the basis of the conserved motifs of endo-polygalacturonases of glycoside hydrolase (GH) family 28. The genomic DNA of strain XZ7 was used as a template for polymerase chain reaction (PCR) amplification. The resulting PCR products were gel purified and ligated into the pEasy-T3 vector and then transformed into *E. coli* Trans1-T1 for sequencing. The 5′ and 3′ flanking regions of the core region were obtained using fusion primer and nested integrated (FPNI)-PCR.[20] The nested insertion-specific primers (Table 1) for FPNI-PCR were named up special primers (usp) 1−3 and down special primers (dsp) 1−3.

Mycelia of strain XZ7 were collected after 3 days of growth and immediately ground to a fine powder in liquid nitrogen. Total RNA was extracted using the SV Total RNA Isolation System (Promega). cDNA was synthesized according to the protocol of Ace-$\alpha$-TM kit (TOYOBO, Osaka, Japan). The full-length cDNA of endo-polygalacturonase gene *pg7fn* was amplified using the specific primers PG7fn-F and PG7fn-R (Table 1) with an annealing temperature of 63 °C. The specific PCR product was ligated into the pEasy-T3 vector for sequencing.

**Sequence and Structure Analysis.** Sequence assembly and analysis were conducted by Vector NTI Advance 10.0 software (Invitrogen). DNA and protein sequences were aligned using BLASTx and BLASTp programs (http://www.ncbi.nlm.nih.gov/BLAST/), respectively. The presence of signal peptide was predicted using SignalP 4.0 (http://www.cbs.dtu.dk/services/SignalP/). The potential N-glycolysation sites were predicted using the NetNGlyc 1.0 Server (http://www.cbs.dtu.dk/services/NetNGlyc/). Alignment of multiple protein sequences was accomplished using ClustalW program (http://www.ebi.ac.uk/clustalW/). The three-dimensional structure model of PG7fn was built with Discovery Studio 2.5 MODELER (Accelrys, San Diego, CA, USA; http://www.accelrys.com) using the crystal structure of endo-polygalacturonase CluPG1 from *Colletotrichum lupini* (2IQ7_A, 78% identity) as the template. To remove steric clashes, the constructed model was subjected to an energy minimization process in a vacuum by using the steepest descent method for about 5000 iterations in Gromacs 4.5.5. The quality of the homology model was evaluated by PROCHECK and Verify3D.[21,22] The results were visualized using the PyMOL program (The PyMOL Molecular Graphics System, Delano Scientific, Portland, OR, USA).

**Heterologous Expression of PG7fn in *P. pastoris*.** The cDNA fragment of *pg7fn* without the signal peptide-coding sequence was amplified with primers PG7fn-pF and PG7fn-pR (Table 1). The PCR products were digested with *Eco*RI and *Not*I and then cloned into pPIC9 vector in-frame fusion of the $\alpha$-factor signal peptide to generate recombinant plasmid pPIC9-*pg7fn*. The positive recombinant plasmids were identified by restriction digestion and DNA sequencing, linearized with *Bgl*II, and transformed into *P. pastoris* GS115 competent cells by electroporation (Bio-Rad, Hercules, CA, USA). The positive transformants were screened on the basis of their enzymatic activities in shake tubes, and those exhibiting the highest activities were selected for fermentation in 1 L conical flasks as described by Tu et al.[6] using polygalacturonic acid as the substrate.

**Purification and Deglycosylation of Recombinant PG7fn.** All purification steps were carried out at 4 °C, and McIlvaine buffer (200 mM $Na_2HPO_4$ and 100 mM citric acid, pH 6.5) was used for dialysis unless otherwise specified. The induced cultures were centrifuged at 12000*g* for 10 min at 4 °C to remove cell debris and undissolved materials. The cell-free culture supernatant was concentrated by ultrafiltration with a Vivaflow 200 membrane of a 5 kDa molecular weight cutoff (Vivascience, Hannover, Germany) and desalted on a 5 mL HiTrap desalting column (GE Healthcare, Uppsala, Sweden) in 20 mM McIlvaine buffer (pH 6.5). The desalted sample was loaded onto a HiTrap SP XL 5 mL FPLC column (GE Healthcare) that was pre-equilibrated with the same buffer. A linear gradient of NaCl (0−1.0 M) in buffer A was used to elute the proteins.

Sodium dodecyl sulfate−polyacrylamide gel electrophoresis (SDS-PAGE) was carried out with a 5% stacking gel and a 12% separation gel. The protein concentration was measured by a Protein Assay kit (Bio-Rad). To remove any N-glycosylation, the purified PG7fn (5 $\mu$g) was treated with 250 U of endo-$\beta$-*N*-acetylglucosaminidase H (Endo H) at 37 °C for 1 h according to the manufacturer's instructions (New England Biolabs, Ipswich, MA, USA) and then analyzed by SDS-PAGE.

**Biochemical Characterization of Recombinant PG7fn.** The enzymatic activity was determined using the 3,5-dinitrosalicylic acid (DNS) method with D-(+)-galacturonic acid as the standard as described by Tu et al.[5,23] One unit of polygalacturonase activity was defined as the amount of enzyme that released reducing sugars equivalent to 1 $\mu$mol of D-(+)-galacturonic acid per minute under standard conditions (pH 5.0, 60 °C, 10 min). All reactions were performed in triplicate.

Both glycosylated and deglycosylated enzymes (PG7fn and d-PG7fn) were subjected to enzyme characterization, and 0.33% (w/v) polygalacturonic acid was used as the substrate. The pH optima were determined at 60 °C for 10 min in McIlvaine buffer (pH 3.0−8.0). The temperature optima were determined at optimal pH for 10 min at 0−80 °C. To estimate the pH stability, the enzymes were preincubated in the buffers of pH 3.0−8.0 without substrate at 37 °C for 1 h, and the residual activities were estimated under standard conditions (pH 5.0, 60 °C, 10 min). Thermostability of the enzymes was investigated after

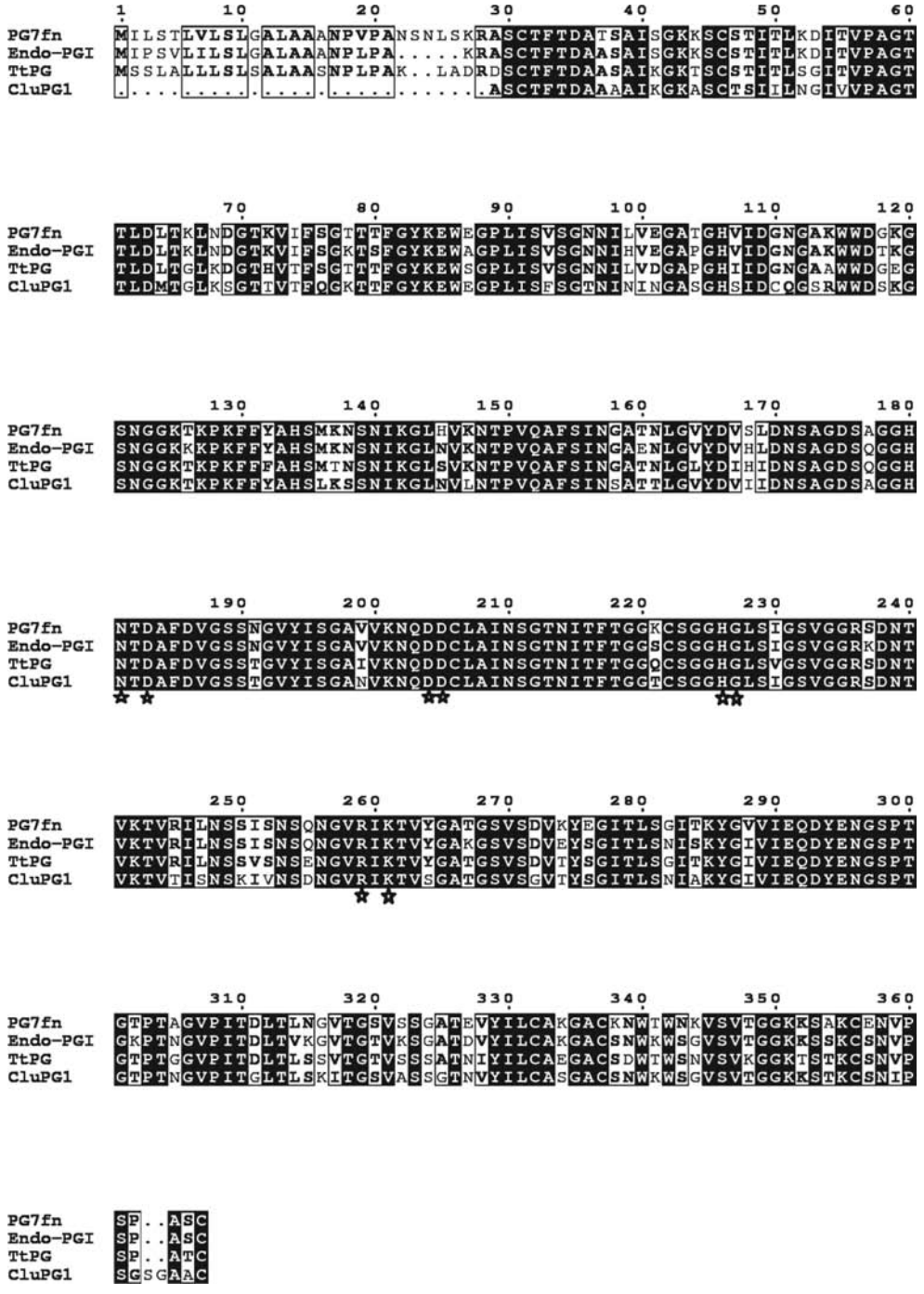


**Figure 1.** Multiple alignment of the deduced amino acid sequence of PG7fn from *T. arenaria* XZ7 with other fungal counterparts from *Achaetomium* sp. Xz8 (Endo-PGI, AGR51994.1), *T. terrestris* NRRL 8126 (TtPG, XP_003657319.1), and *C. lupini* (CluPG1, PDB 2IQ7_A). Identical and similar amino acids are indicated with solid black boxes. Putative conserved residues involved in enzyme catalysis are indicated with asterisks.

preincubation of the enzyme at 40, 50, 60, or 70 °C without substrate for various periods. Then, the residual enzyme activities at specific time points were measured at 60 °C and pH 5.0 for 10 min.

To determine resistance to proteolysis, purified PG7fn was incubated with either pepsin in 100 mM glycine-HCl (pH 2.0) or trypsin in 100 mM Tris-HCl (pH 7.0) at 37 °C for different periods using a protease/PG7fn (w/w) ratio of 0.1:1. Protease resistance was assessed by measuring the residual enzyme activities under standard conditions (pH 5.0, 60 °C, 10 min) following protease treatment.

The effects of various metal ions and chemical reagents on the enzyme activities of PG7fn and d-PG7fn were determined in the presence of 1 mM of various metal ions and chemical reagents ($Na^+$, $K^+$, $Li^+$, $Ag^+$, $Ca^{2+}$, $Co^{2+}$, $Ni^{2+}$, $Mn^{2+}$, $Cu^{2+}$, $Mg^{2+}$, $Zn^{2+}$, $Pb^{2+}$, $Cr^{3+}$, $Fe^{3+}$, SDS, $\beta$-mercaptoethanol, or EDTA). The system without any additive was used as control. The residual enzyme activity was determined as described above.

The substrate specificities of PG7fn and d-PG7fn were determined by measuring the enzyme activities in McIlvaine buffer (pH 5.0) containing polygalacturonic acid and pectin of various degrees of methyl esterification under standard conditions. Enzyme kinetic assay was performed in McIlvaine buffer (pH 5.0) containing 0.1−20 mg/mL polygalacturonic acid at 40 or 60 °C for 5 min. The experiments were repeated three times, and each experiment included three replicates. The $K_m$ and $V_{max}$ values were plotted according to the Lineweaver−Burk method.

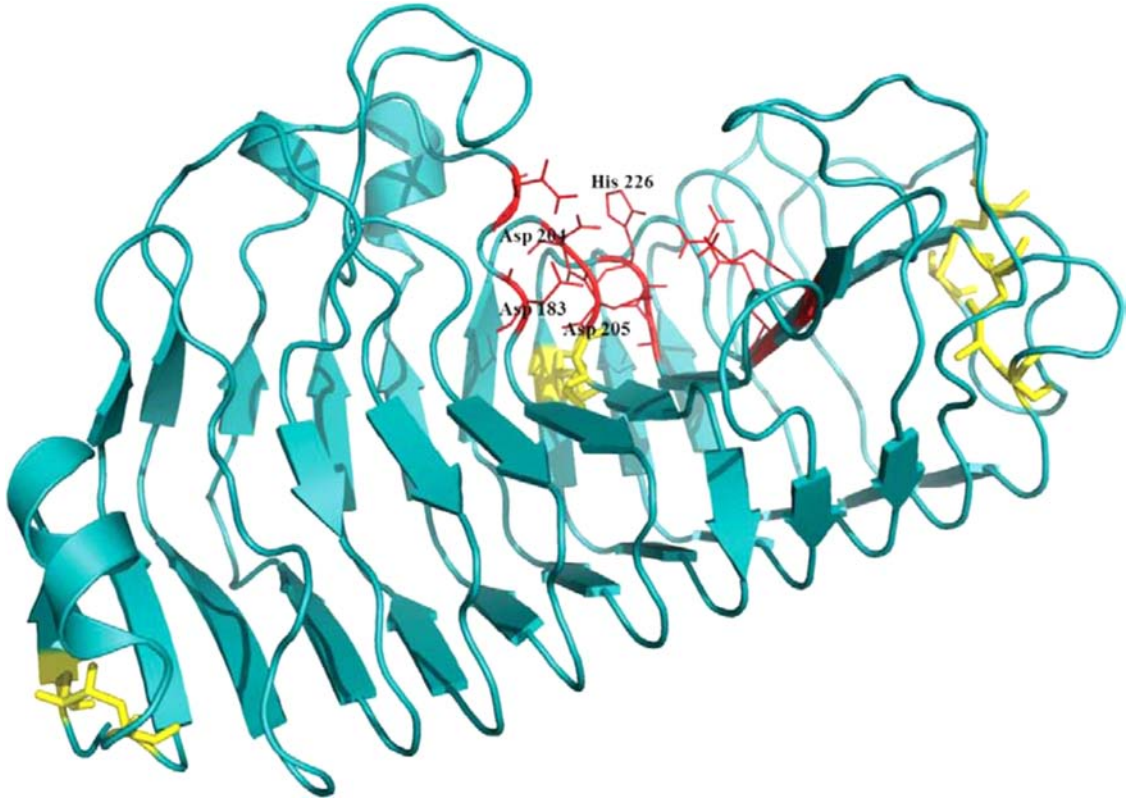


**Figure 2.** Homology modeling of PG7fn with CluPG1 from *C. lupini* (2IQ7_A, 78% identity) as the template. Putative conserved residues involved in enzyme catalysis and cysteine residues forming disulfide are indicated in red and yellow, respectively.

**Analysis of Hydrolysis Products.** The reactions containing 100 U of PG7fn or d-PG7fn and 0.2% (w/v) of polygalacturonic acid in McIlvaine buffer (pH 5.0) were incubated at 37 °C for 12 h. The excess enzyme was removed by ultrafiltration using a 3 kDa cutoff membrane after hydrolysis, and the hydrolysates were analyzed by using high-performance anion-exchange chromatography (HPAEC). Samples were diluted 100-fold in $ddH_2O$, and 25 $\mu$L of each sample was injected into a model 2500 HPAEC system (Dionex, Sunnyvale, CA, USA) equipped with a Carbo-Pac PA200 column (3 × 250 mm). NaOH (600 mM) was used to elute the oligosaccharides at the flow rate of 0.45 mL/min. Galacturonic acid, digalacturonic acid, and trigalacturonic acid were used as standards.

**Digestion Trial in Vitro.** The in vitro digestion trial was conducted to evaluate the hydrolytic effects of PG7fn on soybean meal, the main protein feedstuff. The contents of total pectin and water-soluble pectin were measured by using the carbazole colorimetry method with galacturonic acid as the standard.[24,25] Four grams of soybean meal was boiled for 15 min in 40 mL of McIlvaine buffer (pH 5.0), cooled to room temperature, and treated for 1 h with 100 $\mu$L of enzyme(s) (0, 2, 4, 6, 8, or 12 U of PG7fn) at 60 °C. The mixtures were then boiled for enzyme inactivation, followed by centrifugation at 12000*g* for 10 min at 4 °C. After drying at 35 °C for 24 h, the insoluble residues were added to 30 mL of hot absolute ethanol, heated for 10 min in a boiling water bath, and centrifuged at 12000*g* for 10 min at 4 °C. The insoluble residues were dried again at 35 °C for 24 h to obtain alcohol insoluble solids (AIS). Aliquots of AIS (5 mg) were added in a 25 mL volumetric flask containing 2 mL of concentrated sulfuric acid; distilled water was then added to 25 mL for the measurement of total pectin content. For determination of soluble pectin contents, 80 mg of AIS was directly mixed with 100 mL of distilled water, followed by centrifugation at 12000*g* for 10 min at 4 °C. The supernatants were subjected to pectin content measurement. Reaction systems consisting of 2 mL of supernatant and 12 mL of sulfuric acid (98%, w/w) were boiled for 10 min and cooled using running tap water followed by the addition of 0.5 mL of carbazole ethanol solution. After cooling to room temperature, its absorption at 530 nm was measured. All of the experiments were performed in triplicate. Data regarding total pectin and water-soluble pectin were subjected to analysis of variance (ANOVA), and a *t* test was used to identify significant differences at $p < 0.05$ (SPSS 16.0).

**Nucleotide Sequence Accession Number.** The nucleotide sequence of the endo-polygalacturonase gene (*pg7fn*) from *T. arenaria* XZ7 CGMCC6544 was deposited in the GenBank database under accession no. KM067135.

## RESULTS

**Gene Cloning and Sequence Analysis.** Strain XZ7 exhibited significant endo-polygalacturonase activity of 678.1 ± 48.6 U/mL in the culture supernatants after 72 h of growth at 45 °C. With genomic DNA of strain XZ7 as the template, a partial endo-polygalacturonase gene (252 bp) was amplified by PCR using degenerate primers GH28nF and GH28nR. The 5′ and 3′ flanking regions were obtained by FPNI-PCR and assembled with the core region to generate a full-length 1290 bp gene, termed *pg7fn*. Three introns (53, 71, and 68 bp, respectively) interrupt the coding sequence, and the cDNA sequence of *pg7fn* is 1098 bp in length. The N-terminal 16 amino acids were predicted to be a putative signal peptide by using SignalP 4.0. The mature protein contains 349 residues with a calculated molecular mass of 35.8 kDa and a p*I* value of 8.78. Further sequence analysis indicated that PG7fn has two putative N-glycosylation sites (Asn24 and Asn214).

The deduced amino acid sequence of *pg7fn* shares the highest identity of 88% with the experimentally verified GH28 endo-polygalacturonase (endo-PG I) from *Achaetomium* sp. Xz8 (AGR51994.1) and of 84% with a putative protein of GH28 from *T. terrestris* NRRL 8126 (XP_003657319.1). Multiple sequence alignment analysis with other endo-

polygalacturonases revealed that PG7fn is a typical endo-polygalacturonase of GH28 (Figure 1). Eight residues, Asn181, Asp183, Asp204, Asp205, His226, Gly227, Arg259, and Lys261 (in PG7fn numbering), were found to be strictly conserved.[26] The tertiary structure of PG7fn was predicted by homology modeling with minor modification through energy minimization. Modeled PG7fn folds into a right-handed parallel $\beta$-helix structure consisting of 10 complete turns (Figure 2), which is typical of pectinases. Putative catalytic residues (Asp183, Asp204, Asp205, and His226) are located on the bottom of the cleft, and four disulfide bridges conserved in all *Aspergillus niger* endo-polygalacturonases are also identified.[3] Two disulfide bonds at the terminal regions (Cys31−Cys46 and Cys356−Cys365) ensure the "capping" of the core of the $\beta$-helix, and the others, Cys206−Cys222 and Cys332−Cys337, connect two adjacent $\beta$-helical turns in the middle of the putative active site cleft and the ends of the T1 loop to stabilize the protein structure, respectively.

**Expression and Purification of Recombinant PG7fn.** The gene fragment coding for mature PG7fn without the signal peptide-coding sequence was expressed in *P. pastoris*. Positive transformants were screened on the basis of endo-polygalacturonase activity in shaker flask culture, which was subject to high-cell density fermentation. Before the induction phase, no endo-polygalacturonase was detected in the culture supernatant. Upon methanol induction, the endo-polygalacturonase activity in the supernatant increased to 1080 ± 50 U/mL after 72 h. The crude enzyme was separated into two parts. One was directly purified to electrophoretic homogeneity by a one-step cation exchange chromatography with the final yield of 31.6%, and the other was treated with Endo H followed by purification (with the final yield of 28.8%) as described above. Purified PG7fn migrated two bands of ∼40.0 and 38.0 kDa on SDS-PAGE (Figure 3), which are higher than the calculated molecular mass. The molecular mass of deglycosylated PG7fn, termed d-PG7fn, was 35.8 kDa, which is in agreement with the calculated molecular weight. The result indicates that different levels of N-glycosylation occurred in recombinant PG7fn during heterologous expression in *P. pastoris*.[5,6,27]

**Properties of Purified PG7fn and d-PG7fn.** The enzymatic properties of glycosylated and deglycosylated PG7fn were compared. PG7fn and d-PG7fn were both optimally active at pH 5.0 and exhibited >70% of the maximal activities at pH 4.0−5.5 (Figure 4A). The enzymes were very stable over a wide range of pH, retaining ∼90% of the maximum activity after incubation at pH 3.0−8.0 for 1 h at 37 °C (Figure 4B). PG7fn and d-PG7fn had optimal temperature of 60 °C at pH 5.0 (Figure 4C) and retained ∼50% of the activities even at 70 °C. Although deglycosylated d-PG7fn showed similar pH and temperature profiles as the glycosylated counterpart, its thermostability is much worse. Both enzymes were much stable at temperatures of 40 °C and below, but PG7fn showed better thermostability at higher temperatures (Figure 4D). It retained >85% of the initial activity after 1 h of incubation at 50 °C and >60% activity at 60 °C for 30 min.

The effects of various metal ions and chemical reagents at a final concentration of 1 mM were also investigated on the activity of glycosylated and deglycosylated PG7fn (data not shown). Except for $Ca^{2+}$, SDS, and $Ag^{+}$ that partially or completely inhibited the activity, other chemicals had little or no effect. The result indicates that perturbation of N-glycosylation has no detectable effect on the surface charge of PG7fn.

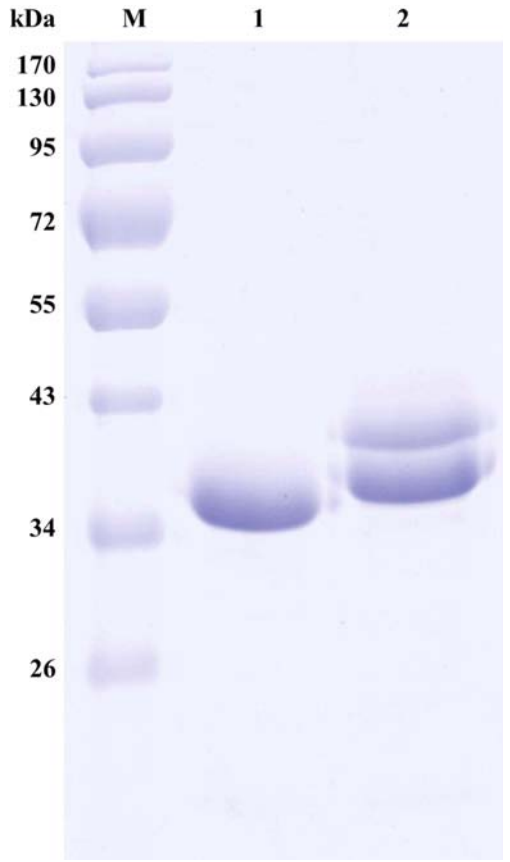


**Figure 3.** SDS-PAGE analysis of purified recombinant PG7fn. Lanes: M, standard protein molecular weight markers; 1, purified recombinant PG7fn after N-deglycosylation with Endo H (d-PG7fn); 2, purified recombinant PG7fn by one-step cation exchange chromatography.

**Substrate Specificity and Kinetic Parameters.** Demethylated pectin is the best substrate for purified recombinant PG7fn and d-PG7fn. It showed highest activity toward polygalacturonic acid (defined as 100%), followed by pectin of different methyl esterification levels. The enzyme activity decreased along with the increased level of methyl esterification. PG7fn and d-PG7fn exhibited relative activities of 62, 31, and 7% and 53, 26, and 6% toward 34, 70, and 85% methyl-esterified pectin, respectively.

Under standard conditions (pH 5.0, 60 °C, 10 min), the specific activities of PG7fn and d-PG7fn toward polygalacturonic acid were 34382 ± 351 and 26760 ± 108 U/mg, respectively. The enzymes had similar $V_{max}$ (50000 ± 1067 and 50000 ± 1768 $\mu$mol/min/mg) and $k_{cat}$ (29817 ± 636/s and 29817 ± 1054/s) values, but their $K_m$ values varied, 1.5 ± 0.03 mg/mL for PG7fn and 2.0 ± 0.07 mg/mL for d-PG7fn, respectively. Besides the higher substrate affinity, PG7fn had higher catalytic efficiency ($k_{cat}/K_m$) than d-PG7fn (19878 ± 473 vs 14908 ± 527 mL/mg/s). Their kinetic values were also determined at 40 °C using polygalacturonic acid as the substrate. The $K_m$, $V_{max}$, and $k_{cat}$ values of purified PG7fn and d-PG7fn were 2.0 ± 0.06 and 2.8 ± 0.04 mg/mL, 32000 ± 915, and 30000 ± 362 $\mu$mol/min/mg and 19082 ± 546/s and 17890 ± 216/s, respectively. These results indicated that glycosylation improves the substrate affinity of PG7fn and correspondingly its catalytic efficiency.

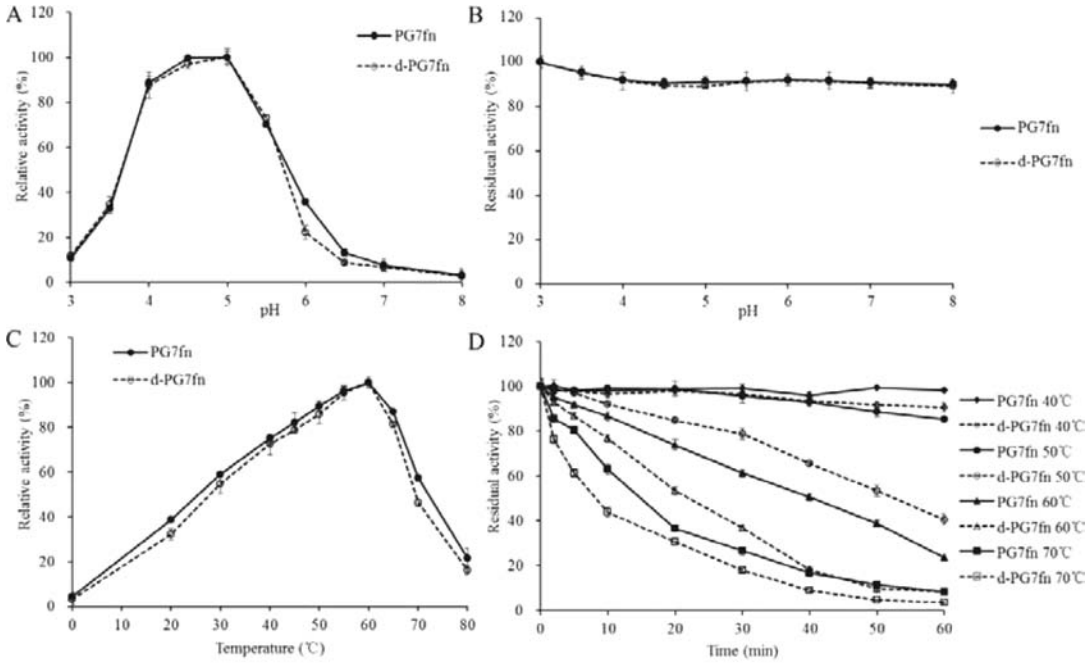


**Figure 4.** Characterization of the purified recombinant PG7fn with and without N-glycosylation. (A) Effect of pH on PG7fn and d-PG7fn activities. The polygalacturonase activity assay was performed at 60 °C in buffers of various pH values for 10 min. (B) pH stability of PG7fn and d-PG7fn at 37 °C for 1 h at pH 3.0−8.0. The residual activities were measured in McIlvaine buffer (pH 5.0, 60 °C, 10 min). (C) Effect of temperature on PG7fn and d-PG7fn activities measured in McIlvaine buffer (pH 5.0) for 10 min. (D) Thermostability of PG7fn and d-PG7fn. The enzymes were preincubated at 40, 50, 60, or 70 °C in McIlvaine buffer (pH 5.0) for various periods, followed by enzyme activity assay under pH 5.0 and 60 °C for 10 min. Each value in the panel represents the mean ± SD ($n$ = 3).

**Composition of Hydrolysis Products.** Similar to endo-PG I from *Achaetomium* sp. Xz8,[5] the hydrolysis end-products of PG7fn and d-PG7fn are mainly galacturonic acid, digalacturonic acid, trigalacturonic acid, and small amounts of unidentified oligosaccharides, but the hydrolysis of PG7fn is more complete. After 12 h of incubation, the major products by PG7fn hydrolysis were 40.74 ± 0.54% galacturonic acid, 18.01 ± 0.14% digalacturonic acid, and 8.59 ± 0.16% trigalacturonic acid. Under the same conditions, the products of d-PG7fn consisted of 34.51 ± 0.69% galacturonic acid, 14.54 ± 0.03% digalacturonic acid, and 14.28 ± 0.48% trigalacturonic acid.

**Resistance to Pepsin and Trypsin.** PG7fn was strongly resistant to pepsin and trypsin digestion (Figure 5). After treatment with pepsin and trypsin at 37 °C for 120 min, the enzyme retained 45 and 67% activity, respectively. SDS-PAGE analysis indicated that PG7fn was not degraded by these proteases (data not shown), suggesting its application potential in the food and feed industries.

**Soybean Meal Degradation.** The total pectin content of soybean meal was determined to be 6.41%, similar to the results of Malathi and Devegowda (6.16%).[28] PG7fn has great capacity to remove pectin from soybean meal (Table 2). After 1 h of incubation with PG7fn, the pectin contents in soybean meal were decreased. The greatest degradation rate (19.33%) was observed with the addtion of the dosage of 1000 U/kg.

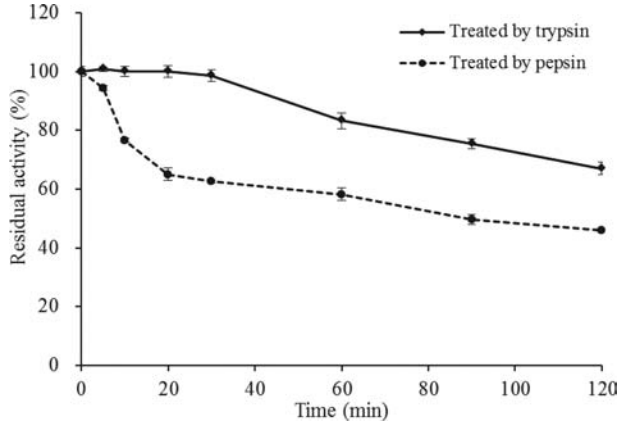


**Figure 5.** Effect of proteases on the endo-polygalacturonase activity of PG7fn. The enzymes were preincubated with pepsin in 100 mM glycine-HCl (pH 2.0) or trypsin in 100 mM Tris-HCl (pH 7.0) at 37 °C for different periods and subjected to enzyme activity assay under pH 5.0 and 60 °C for 10 min. Each value in the panel represents the mean ± SD ($n$ = 3).

## ■ DISCUSSION

Thermophilic fungi are liable to manipulation using classical and molecular genetics as representing a potential reservoir of thermostable enzymes.[13] To our best knowledge, only a few fungal endo-polygalacturonases have activities at ≥55 °C (Table 3). Compared with other characterized thermophilic endo-polygalacturonases and its close homologue endo-PG I from *Achaetomium* sp. Xz8,[5] PG7fn has a higher temperature optimum (60 °C) and greater specific activity (34382 ± 351 U/mg) toward polygalacturonic acid. Furthermore, PG7fn shows a lower acidic pH optimum (5.0 vs 6.0), better stability at pH 3.0 (100 vs ∼60%), higher temperature optimum (60 vs 45 °C), and better thermostability (50 vs 40 °C). These properties make PG7fn favorable for applications in various industries.

N-glycosylation is one of the most common posttranslational modifications in protein biosynthesis or in the methylotrophic yeast,[31] which has an effect on secretion, activity, stability, and biosynthesis.[31−34] Most fungal endo-polygalacturonases are

**Table 2. Effect of PG7fn on the Degradation of Soybean Meal Pectin[a]**

| enzyme level (U/kg) | total pectin contents (%) | soluble pectin contents (%) | soluble/total pectin (%) | degradation rate (%) |
|---|---|---|---|---|
| pretreatment | 6.41 ± 0.44a | 0.85 ± 0.19a | 13.24 | 0 |
| 0 | 5.98 ± 0.39b | 0.89 ± 0.24b | 14.89 | 6.68 |
| 500 | 5.29 ± 0.59c | 0.92 ± 0.34c | 17.56 | 17.39 |
| 1000 | 5.16 ± 0.55d | 0.95 ± 0.20c | 18.41 | 19.33 |
| 1500 | 5.45 ± 0.48e | 0.93 ± 0.16c | 17.03 | 14.84 |
| 2000 | 5.58 ± 0.33f | 0.89 ± 0.22b | 15.86 | 12.90 |
| 3000 | 5.60 ± 0.45f | 0.87 ± 0.13b | 15.58 | 12.62 |

[a]Data are presented as the mean ± standard deviation ($n$ = 3). Different letters in the same column indicate significant difference at $p < 0.05$ (SPSS16.0).

**Table 3. Property Comparison of PG7fn and d-PG7fn with Other Thermophilic Fungal Endo-polygalacturonases of GH 28**

| microorganism | MW (kDa) | pH optimum | temperature optimum (°C) | pH stability | thermostability | specific activity[a] (U/mg) | ref |
|---|---|---|---|---|---|---|---|
| *Thielavia arenaria* XZ7 | 35.8 | 5.0 | 60 | 3.0−8.0 | PG7fn, >85% activity at 50 °C for 1 h; d-PG7fn, >40% activity at 50 °C for 1 h | 34382 for PG7fn; 26759 for d-PG7fn | this study |
| *Sporotrichum thermophile* | nd[b] | 7.0 | 55 | nd | ∼50% at 65 °C for 4 h | nd | 29 |
| *Saccharomyces cerevisiae* | 43 | 5.0 | 60 | nd | nd | 0.51 | 15 |
| *Physalospora piricola* | 38 | 4.9 | 60 | 5.0−7.0 | nd | 129 | 14 |
| *Kluyveromyces marxianus* | 41.7 | 4.5 | 55 | 3.0−5.0 | ∼50% at 50 °C for 14 h | 219 | 30 |
| *Thermoascus aurantiacus* | 30 | 5.5 | 60−65 | nd | ∼30% at 60 °C for 15 min | 5000 (citrus pectin) | 16 |
| *Penicillium* sp. | nd | 5.5 | 60 | nd | ∼50% at 60 °C for 2 h | 2.5 (pectin) | 18 |
| *Kluyveromyces marxianus* | 35 | 4.5 | 55 | nd | nd | nd | 8 |
| *Sclerotium rolfsii* | 39.5 | 5.0 | 60 | nd | ∼50% at 50 °C for 48 h | nd | 17 |

[a]Specific activities were determined using polygalacturonic acid as the substrate except for special cases. [b]nd, not determined.

glycoproteins with at least one N-glycosylation site.[3,26,35] Our result showed that N-glycosylation has effects on enzyme activity; thus, a thorough comparative analysis of glycosylated and deglycosylated PG7fn was performed to determine its effect on other enzyme properties. Abrogation of N-glycosylation has no detectable effect on the temperature optimum and pH properties of d-PG7fn, but the protein showed worse thermostability. It has been reported that glycoproteins are more stable than their corresponding unglycosylated counterparts.[6,36,37] N-linked glycans may facilitate the overall stability of the protein by enhancing the reversibility of the unfolding process or enabling some specific functions performed around the attached site by reducing the disorder of the unfolded protein.[34,38] Elimination of N-linked glycans showed no change in the temperature optimum as to thermostability. The reason might be that N-glycosylation has no effect on the structure of protein, and N-linked glycan only makes glycosylated enzyme more resistant to thermal inactivation. In addition, PG7fn had higher catalytic efficiency ($k_{cat}/K_m$) than d-PG7fn. It has been reported that the biological activity of protein is affected by attaching a long glycan chain to the Asn residue.[31] The results of kinetic parameters indicate that N-glycosylation plays a role in the substrate affinity of PG7fn and catalytic efficiency. Without N-glycosylation, the protein structure of d-PG7fn might be looser and, thus, lose strong affinity to substrate.[39] According to the hydrolysis products analysis, N-glycosylation makes PG7fn more efficient and complete in hydrolysis.

Pectinase is an important feed additive that can reduce feed viscosity and increase nutrient absorption.[40] Besides pectinase, other carbohydrate-active enzymes (CAZymes) such as phytase, xylanase, glucanase, mannanase, and cellulase are commonly supplemented in animal feed for the improvement of nutrient bioavailability.[28,41] A necessary requirement of feed enzyme is strong resistance to protease. PG7fn has such a good property. In contrast to the endo-polygalacturonase (endo-PGA1) from *Bispora* sp. MEY-1 that retained only 40% of its initial activity after a 10 min trypsin treatment,[42] PG7fn retained 45 and 67% activity, respectively, after treatment with pepsin and trypsin at 37 °C for 120 min. On the other hand, soybean meal is the major protein source of animal feed. PG7fn has the capacity to degrade soybean meal pectin, increasing the pectin bioavailability by 19.33% at 1 U/g dosage. In comparison with the commercial compound pectinase (including polygalacturonases, pectin lyases, and methylesterases) commonly added in animal feed in China, the amount of PG7fn used in this study is a little higher (1 vs 0.5 U/g based on polygalacturonase activity). Considering the complex composition of pectin, PG7fn in combination with other pectinases will be more efficient in pectin degradation in the food and feed industries.

In summary, the efficacy of feed enzymes depends on their substrate specificity, activity, and stability. In this study, a highly active thermophilic endo-polygalacturonase, PG7fn, was identified in *T. arenaria* XZ7 and successfully expressed in *P. pastoris*. A thorough comparative analysis of the enzymatic properties of glycosylated and deglycosylated PG7fn indicated

that N-glycosylation improved enzyme thermostability, substrate affinity, and catalytic efficiency. The high specific activity, good stabilities over a wide pH range and high temperature, and great catalytic efficiency make PG7fn a good enzyme candidate for applications in the food and feed industries.

## AUTHOR INFORMATION


### Corresponding Author

*(B.Y.) Mail: Key Laboratory for Feed Biotechnology of the Ministry of Agriculture, Feed Research Institute, Chinese Academy of Agricultural Sciences, 12 Zhongguancun South Street, Beijing 100081, China. Phone: +86 10 82106053. Fax: +86 10 82106054. E-mail: binyao@caas.cn or yaobin@caas.cn.



### Funding

This research was supported by the National Science and Technology Support Program of China (2013BAD10B01-2), the National Science Foundation for Distinguished Young Scholars of China (31225026), the Natural Science Foundation of China (31271937), and the China Modern Agriculture Research System (CARS-42).


### Notes

The authors declare no competing financial interest.

## REFERENCES


(1) Ridley, B. L.; O'Neill, M. A.; Mohnen, D. Pectins: structure, biosynthesis, and oligogalacturonide-related signaling. *Phytochemistry* **2001**, *57*, 929−967.

(2) Cameron, R. G.; Savary, B. J.; Hotchkiss, A. T.; Fishman, M. L.; Chau, H. K.; Baker, R. A.; Grohmann, K. Separation and characterization of a salt-dependent pectin methylesterase from *Citrus sinensis* var. Valencia fruit tissue. *J. Agric. Food Chem.* **2003**, *51*, 2070−2075.

(3) van Santen, Y.; Benen, J. A. E.; Schröter, K. H.; Kalk, K. H.; Armand, S.; Visser, J.; Dijkstra, B. W. 1.68-Å Crystal structure of endopolygalacturonase II from *Aspergillus niger* and identification of active site residues by site-directed mutagenesis. *J. Biol. Chem.* **1999**, *274*, 30474−30480.

(4) Mohnen, D. Pectin structure and biosynthesis. *Curr. Opin. Plant Biol.* **2008**, *11*, 266−277.

(5) Tu, T.; Meng, K.; Bai, Y.; Shi, P.; Luo, H.; Wang, Y.; Yang, P.; Zhang, Y.; Zhang, W.; Yao, B. High-yield production of a low-temperature-active polygalacturonase for papaya juice clarification. *Food Chem.* **2013**, *141*, 2974−2981.

(6) Tu, T.; Bai, Y.; Luo, H.; Ma, R.; Wang, Y.; Shi, P.; Yang, P.; Meng, K.; Yao, B. A novel bifunctional pectinase from *Penicillium oxalicum* SX6 with separate pectin methylesterase and polygalacturonase catalytic domains. *Appl. Microbiol. Biotechnol.* **2014**, *98*, 5019−5028.

(7) Kashyapa, D. R.; Vohraa, P. K.; Chopraa, S.; Tewarib, R. Applications of pectinases in the commercial sector: a review. *Bioresour. Technol.* **2001**, *77*, 215−227.

(8) Sieiro, C.; Sestelo, A. B. F.; Villa, T. G. Cloning, characterization, and functional analysis of the EPG1-2 gene: a new allele coding for an endopolygalacturonase in *Kluyveromyces marxianus*. *J. Agric. Food Chem.* **2009**, *57*, 8921−8926.

(9) Ishii, S.; Yokotsuka, T. Susceptibility of fruit juice to enzymic clarification by pectin lyase and its relation to pectin in fruit juice. *J. Agric. Food Chem.* **1973**, *21*, 269−272.

(10) Jayani, R. S.; Saxena, S.; Gupta, R. Microbial pectinolytic enzymes: a review. *Process Biochem.* **2005**, *40*, 2931−2944.

(11) Nevadita, S. Microbial pectinase: sources, characterization and applications. *Rev. Environ. Sci. Biol.* **2013**, *12*, 45−60.

(12) Choct, M. Feed non-starch polysaccharides: chemical structures and nutritional significance. *Feed Mill. Int.* **1997**, *191*, 13−26.

(13) Berka, R. M.; Grigoriev, I. V.; Otillar, R.; Salamov, A.; Grimwood, J.; Reid, I.; Ishmael, N.; John, T.; Darmond, C.; Moisan, M. C.; Henrissat, B.; Coutinho, P. M.; Lombard, V.; Natvig, D. O.; Lindquist, E.; Schmutz, J.; Lucas, S.; Harris, P.; Powlowski, J.; Bellemare, A.; Taylor, D.; Butler, G.; de Vries, R. P.; Allijn, I. E.; van den Brink, J.; Ushinsky, S.; Storms, R.; Powell, A. J.; Paulsen, I. T.; Elbourne, L. D. H.; Baker, S. E.; Magnuson, J.; LaBoissiere, S.; Clutterbuck, A. J.; Martinez, D.; Wogulis, M.; de Leon, A. L.; Rey, M. W.; Tsang, A. Comparative genomic analysis of the thermophilic biomass-degrading fungi *Myceliophthora thermophila* and *Thielavia terrestris*. *Nat. Biotechnol.* **2011**, *29*, 922−927.

(14) Miyairi, K.; Matsue, T.; Kagawa, O.; Kutsuzawa, T.; Okuno, T. Purification and characterization of an endopolygalacturonase from *Physalospora piricola*. *Biosci., Biotechnol., Biochem.* **1994**, *58*, 1909−1910.

(15) Hirose, N.; Kishida, M.; Kawasaki, H.; Sakai, T. Purification and characterization of an endo-polygalacturonase from a mutant of *Saccharomyces cerevisiae*. *Biosci., Biotechnol., Biochem.* **1999**, *63*, 1100−1103.

(16) Martins, E. S.; Silva, D.; Leite, R. S.; Gomes, E. Purification and characterization of polygalacturonase produced by thermophilic *Thermoascus aurantiacus* CBMAI-756 in submerged fermentation. *Antonie van Leeuwenhoek* **2007**, *91*, 291−299.

(17) Schnitzhofer, W.; Weber, H. J.; Vršanská, M.; Biely, P.; Cavaco-Paulo, A.; Guebitz, G. Purification and mechanistic characterisation of two polygalacturonases from *Sclerotium rolfsii*. *Enzyme Microb. Technol.* **2007**, *40*, 1739−1747.

(18) Mathew, A.; Eldo, A. N.; Molly, A. G. Optimization of culture conditions for the production of thermostable polygalacturonase by *Penicillium* SPC-F 20. *J. Ind. Microbiol. Biotechnol.* **2008**, *35*, 1001−1005.

(19) Lu, H.; Zhang, H.; Shi, P.; Luo, H.; Wang, Y.; Yang, P.; Yao, B. A family 5 $\beta$-mannanase from the thermophilic fungus *Thielavia arenaria* XZ7 with typical thermophilic enzyme features. *Appl. Microbiol. Biotechnol.* **2013**, *97*, 8121−8128.

(20) Wang, Z.; Ye, S.; Li, J.; Zheng, B.; Bao, M.; Ning, G. Fusion primer and nested integrated PCR (FPNI-PCR): a new high-efficiency strategy for rapid chromosome walking or flanking sequence cloning. *BMC Biotechnol.* **2011**, *11*, 109.

(21) Laskowski, R. A.; MacArthur, M. W.; Moss, D. S.; Thornton, J. M. PROCHECK: a program to check the stereochemical quality of protein structures. *J. Appl. Crystallogr.* **1993**, *26*, 283−291.

(22) Eisenberg, D.; Lüthy, R.; Bowie, J. U. VERIFY3D: Assessment of protein models with three-dimensional profiles. *Methods Enzymol.* **1997**, *277*, 396−404.

(23) Miller, G. L. Use of dinitrosalicylic acid reagent for determination of reducing sugar. *Anal. Chem.* **1959**, *31*, 426−428.

(24) Wang, Y. C.; Chuang, Y. C.; Hsu, H. W. The flavonoid, carotenoid and pectin content in peels of citrus cultivated in Taiwan. *Food Chem.* **2008**, *106*, 277−284.

(25) Zhang, L.; Chen, F.; Yang, H.; Sun, X.; Liu, H.; Gong, X.; Jiang, C.; Ding, C. Changes in firmness, pectin content and nanostructure of two crisp peach cultivars after storage. *LWT−Food Sci. Technol.* **2010**, *43*, 26−32.

(26) Cho, S. W.; Lee, S.; Shin, W. The X-ray structure of *Aspergillus aculeatus* polygalacturonase and a modeled structure of the polygalacturonase-octagalacturonate complex. *J. Mol. Biol.* **2001**, *311*, 863−878.

(27) Fierobe, H. P.; Mirgorodskaya, E.; Frandsen, T. P.; Roepstorff, P.; Svensson, B. Overexpression and characterization of *Aspergillus awamori* wild-type and mutant glucoamylase secreted by the methylotrophic yeast *Pichia pastoris*: comparison with wild-type recombinant glucoamylase produced using *Saccharomyces cerevisiae* and *Aspergillus niger* as hosts. *Protein Express. Purif.* **1997**, *9*, 159−170.

(28) Malathi, V.; Devegowda, G. *In vitro* evaluation of nonstarch polysaccharide digestibility of feed ingredients by enzymes. *Poult. Sci.* **2001**, *80*, 302−305.

(29) Kaur, G.; Kumar, S.; Satyanarayana, T. Production, characterization and application of a thermostable polygalacturonase of a thermophilic mould *Sporotrichum thermophile* Apinis. *Bioresour. Technol.* **2004**, *94*, 239−243.

(30) Serrat, M.; Bermúdez, R. C.; Villa, T. G. Production, purification, and characterization of a polygalacturonase from a new strain of *Kluyveromyces marxianus* isolated from coffee wet-processing wastewater. *Appl. Biochem. Biotechnol.* **2002**, *97*, 193−208.
(31) Shental-Bechor, D.; Levy, Y. Effect of glycosylation on protein folding: a close look at thermodynamic stabilization. *Proc. Natl. Acad. Sci. U.S.A.* **2008**, *105*, 8256−8261.
(32) Velan, B.; Kronman, C.; Ordentlich, A.; Flashner, Y.; Leitner, M.; Cohen, S.; Shafferman, A. *N*-glycosylation of human acetylcholinesterase: effects on activity, stability and biosynthesis. *Biochem. J.* **1993**, *296*, 649−656.
(33) Clark, S.; Muslin, E.; Henson, C. Effect of adding and removing *N*-glycosylation recognition sites on the thermostability of barley α-glucosidase. *Protein Eng. Des. Sel.* **2004**, *17*, 245−249.
(34) Qi, F.; Zhang, W.; Zhang, F.; Chen, G.; Liu, W. Deciphering the effect of the different *N*-glycosylation sites on the secretion, activity, and stability of cellobiohydrolase I from *Trichoderma reesei*. *Appl. Environ. Microbiol.* **2014**, *80*, 3962−3971.
(35) Stratilová, E.; Mislovičová, D.; Kačuráková, M.; Machová, E.; Kolarová, N.; Markovič, O.; Jörnvall, H. The glycoprotein character of multiple forms of *Aspergillus* polygalacturonase. *J. Protein Chem.* **1998**, *17*, 173−179.
(36) Öberg, F.; Sjöhamn, J.; Fischer, G.; Moberg, A.; Pedersen, A.; Neutze, R.; Hedfalk, K. Glycosylation increases the thermostability of human aquaporin 10 protein. *J. Biol. Chem.* **2011**, *286*, 31915−31923.
(37) Fonseca-Maldonado, R.; Vieira, D. S.; Alponti, J. S.; Bonneil, E.; Thibault, P.; Ward, R. J. Engineering the pattern of protein glycosylation modulates the thermostability of a GH11 xylanase. *J. Biol. Chem.* **2013**, *288*, 25522−25534.
(38) DeKoster, G. T.; Robertson, A. D. Thermodynamics of unfolding for Kazal-type serine protease inhibitors: entropic stabilization of ovomucoid first domain by glycosylation. *Biochemistry* **1997**, *36*, 2323−2331.
(39) Tauzin, A. S.; Sulzenbacher, G.; Lafond, M.; Desseaux, V.; Reca, I. B.; Perrier, J.; Bellincampi, D.; Fourquet, P.; Lévêque, C.; Giardina, T. Functional characterization of a vacuolar invertase from *Solanum lycopersicum*: post-translational regulation by *N*-glycosylation and a proteinaceous inhibitor. *Biochimie* **2014**, *101*, 39−49.
(40) Yuan, P.; Meng, K.; Wang, Y.; Luo, H.; Shi, P.; Huang, H.; Bai, Y.; Yang, P.; Yao, B. A protease-resistant exo-polygalacturonase from *Klebsiella* sp. Y1 with good activity and stability over a wide pH range in the digestive tract. *Bioresour. Technol.* **2012**, *123*, 171−176.
(41) Meng, X.; Slominski, B. Nutritive values of corn, soybean meal, canola meal, and peas for broiler chickens as affected by a multicarbohydrase preparation of cell wall degrading enzymes. *Poult. Sci.* **2005**, *84*, 1242−1251.
(42) Yang, J.; Luo, H.; Li, J.; Wang, K.; Cheng, H.; Bai, Y.; Yuan, T.; Fan, Y.; Yao, B. Cloning, expression and characterization of an acidic endo-polygalacturonase from *Bispora* sp. MEY-1 and its potential application in juice clarification. *Process Biochem.* **2011**, *46*, 272−277.

in a 20 μL RT mixture. The RT reaction was allowed to proceed for 60 min at 37 °C in the presence of a recombinant ribonuclease inhibitor (RNaseOUT from Invitrogen) at a concentration of 2 units/μL. The reverse transcriptase was inactivated by incubating the reaction mixture at 95 °C for 5 min. The RT product was either used immediately as a template in PCR or stored at −80 °C for future use.

Primers I (5′-caccgtgaacagatcggtggtatgtcgtggcagcagtacgtc-3′) and II (5′-cctctcgagttacagaccctgctcgataaggta-3′) were designed based on a published Pru du 4 sequence (GI:24473793)[19] to amplify the coding region of Pru du 4. The underlined portion of primer I was added to facilitate a second round PCR to join the Pru du 4 coding sequence with that of the sumo. The sumo sequence was previously synthesized commercially with codon optimization for *E. coli* expression. Primer III (5′-ccggatcctgggaagttaaaccggaaaccc-3′) and primer IV (which is complementary to primer I) were used to amplify the synthesized sumo coding sequence. The two PCR products were mixed and used as template for a second round PCR using primers III and II. The final PCR product was inserted into the cloning vector pBluescript II SK with blunt-end ligation to make pBlue-SPrudu4. The ligation product was transformed to *E. coli* strain dH5α, and the plasmid prepared from the isolated colonies was sequenced to confirm correct insertion of the sumo-Pru du 4 fusion. pBlue-SPrudu4 was digested with *Bam*HI and *Xho*I to release the sumo-Pru du 4 coding sequence which was then ligated with the pRSFdeut-1 vector prepared with the same enzymes to generate pRSF-SPrudu4.

Primers V (5′-cctcatgagccacgtgcatcaccatcatcaccacggatcctttaaaatcgaagaggtaaac tggtaatc-3′) and VI (5′-ccagatcttacgtaagtctgcgcgg-3′) were used in a PCR with pMAL-c2 as template to amplify the MBP coding sequence. The underlined sequences in the primers were added to incorporate enzyme recognition sites and a His-tag coding sequence. The PCR product was inserted into Bluescript II SK as described above. The MBP coding sequence was confirmed with DNA sequencing. It was released with *Bsp*HI and *Bgl*II and ligated with the pRSF-SPrudu4 plasmid prepared with *Nco*I and *Bam*HI to generate pRSF1MS-SPrudu4. The sequence-confirmed pRSF1MS-SPrudu4 plasmid was then transformed into the *E. coli* strain BL21(DE3)* (Invitrogen) for protein expression. The transformed bacteria were grown in 1 L batches of LB medium containing 50 mg/L kanamycin (Gold Biotechnology, St. Louis, MO) at 37 °C until the $OD_{600}$ of the culture reached 1.0. IPTG (Gold Biotechnology) was then added to the medium to a final concentration of 1 mM, and the expression of Pru du 4 fusion protein was allowed for 5 h. The cells were collected by centrifugation, and the cell pellets were stored at −80 °C for future use.

**Purification of the Fusion Protein.** The cell pellet was thawed on ice and resuspended in 50 mL of a His-binding buffer (buffer HB, 20 mM imidazole, pH 8.0, 500 mM NaCl) containing 1 mM benzamidine. The bacteria were lysed by sonication for 9 min in a beaker surrounded by a mixture of ice and water using a Model 450 Digital Sonifier (Branson, Danbury, CT). The cell lysate was centrifuged at 20 000g for 40 min at 277 K. The supernatant was loaded onto a 5 mL HisTrap FF Crude column (GE Healthcare, Piscataway, NJ). The column was washed with 7 bed volumes of buffer HB and then eluted with a His-elution buffer (buffer HE, 300 mM imidazole, pH 8.0).

The main peak of the HisTrap elution was diluted with buffer QB (10 mM Tris-HCl, pH 7.9) to 50 mL. The sample was then loaded onto an 8 mL Source15 Q column (GE Healthcare). The column was washed with 7 bed volumes of buffer QB and eluted with QB plus a linear NaCl gradient of 0−1 M (over 10 bed volumes). The main peak of the elution was confirmed later to contain the target fusion protein.

**Removal of the Fusion Tag.** The elution fractions of the main peak from the anion exchange column were pooled, and aliquots of the pooled sample were used to optimize the conditions for the removal of the fusion tag by a recombinant sumo protease rULP which also contained a His-tag and was expressed and purified in-house. The scaled up rULP digestion was in 50 mL of a buffer containing 10 mM Tris, pH 7.9, 250 mM NaCl, 18 mg of His-MBP-sumo-Pru du 4, and 18 μg of rULP. The digestion was carried out at 20 °C for 12 h. The digested sample was passed through a 5 mL HisTrap FF Crude column, and the flow-through was collected and concentrated to a final volume of 15 mL using an Amicon Ultra centrifugal filter device with 3 kDa molecular weight cutoff for proteins (Millipore, Bedford, MA). The concentrated sample was further purified with size exclusion chromatography (SEC) using an XK 26/70 Superdex-75 column (GE Healthcare) pre-equilibrated with buffer SC (10 mM Tris-HCl, pH 7.9, 200 mM NaCl) and eluted with the same buffer. Determination of the concentrations of the purified protein samples was based on $OD_{280}$ using the theoretical molecular mass and molar extinction coefficient using the program SPHERE (http://www.fccc.edu/research/labs/roder/sphere/).[20] All chromatographic steps were carried out at room temperature using an FPLC system (GE Healthcare).

Samples of the target protein after each step of purification were boiled in an SDS sample buffer for 5 min and separated by electrophoresis with 4−20% gels and stained using the Colloidal Coomassie G-250 Staining protocols.[21] The image of the stained gel was taken with a Nikon digital camera.

**N-terminal Sequencing.** The final recombinant Pru du 4 was subjected to SDS-PAGE using 8−25% gradient gels in a PhastSystem (GE Healthcare) and electrophoretically transferred (0.35 A at 25 °C) to a Problott membrane (Applied Biosystems, Foster City, CA) in a transfer buffer [10 mM 3-(cyclohexyl-amino)-1-propanesulfonic acid containing 10% methanol, pH 11.0]. The blot was stained with Coomassie Brilliant Blue, and the protein band was excised and subjected to N-terminal amino acid sequencing by Edman degradation using a Shimadzu PPSQ-33A Protein Sequencer (Shimadzu, Columbia, MD).

**Determination of the Mass of the Purified Protein.** The purified Pru du 4 was subjected to reverse-phase HPLC using an Easy nLC II (Thermo Fisher Scientific, San Jose, CA) with a PicoChip column packed with 3 μm Reprosil-Pur (New Objectives, Woburn, MA) and a flow rate of 250 nL/min. MS data were collected on an Orbitrap Elite operated at 15 000 mass resolution. Data across chromatographic peak were averaged with Thermo Excalibur software and subsequently deconvoluted with MagTran software.[22]

**Circular Dichroism (CD).** The buffer of the purified protein was changed to a buffer containing 20 mM phosphate (pH 7.0) and 200 mM NaCl by repeated concentration-and-dilution using an Amicon Ultra centrifugal filter device with 3 kDa molecular weight cutoff for proteins (Millipore). CD spectroscopy was used to study the secondary structure content of recombinant Pru du 4. Far-UV spectra were collected in the 195−260 nm region using a J-815 CD spectrometer (Jasco, Tokyo) and a quartz cuvette with a light path length of 2.0 mm. Wavelength scans were performed with a speed of 50 nm/min at 20 °C. The spectra were averaged for 10 scans.

**Guanidinium Hydrochloride (GuHCl) Denaturation.** Two stock solutions of recombinant Pru du 4 were prepared. Both solutions (pH 7.0) contained 2 μM of the protein, 10 mM of phosphate, and 200 mM of NaCl. One of them additionally contained 6.923 M of GuHCl. Thirty samples were prepared with various ratios of the two stock solutions to obtain samples at 0.187 M intervals of GuHCl concentration from 0 to 5.43 M. A 6 M GuHCl sample was also made by mixing the two stock solutions at the right ratio. The samples were thoroughly mixed and equilibrated at room temperature for 24 h. The CD signals at 220 nm of these samples were measured at 20 °C for half a minute with data collected every second. The free energy of denaturation was calculated by fitting the data to a two-state transition using Origin Pro9 software (OriginLab Corp., Northampton, MA).

## RESULTS

**Isolation and Expression of Pru du 4.** The mRNA sequence of Pru du 4 could be found in the Genbank that also contained the 5′- and 3′-untranslated regions (GI:24473793). On the protein level, it has 100% sequence identity with the Japanese apricot profilin (GI:645226637) and 99% (GI:596206424)−100% (GI:27528309) to the peach profilin allergen Pru p 4.[23] Using primers designed based on the available Pru du 4 mRNA sequence, the coding sequence for

the Nonpareil almond profilin isolated in this study was identical to that of the Pru du 4 in the GenBank. When Pru du 4 was expressed without an expression tag in *E. coli*, only minimal expression could be achieved. This is also true when expressed with a sumo tag (data not shown). We sought to use sumo as an enzyme recognition site and produce Pru du 4 with a protocol depicted in Figure 1. Despite of its size, using sumo

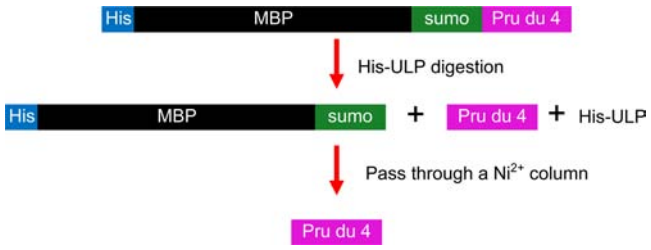


**Figure 1.** Producing Pru du 4 with sumo as a peptidase recognition site.

as a peptidase recognition site had no negative effect on the enhancement of the expression of Pru du 4 by MBP fusion (Figure 2, lane 1, and data not shown). Sumo can be used as a peptidase recognition site at least in the combination of MBP-sumo and Pru du 4.

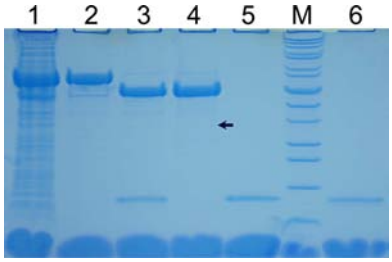


**Figure 2.** SDS-PAGE analyses of recombinant Pru du 4. Samples loaded in lanes 1−6 are (1) supernatant of the lysate of *E. coli* expressing Pru du 4, (2) sample after ion exchange purification, (3) product of ULP digestion, (4) unwanted proteins removed from the protease digestion product, (5) recombinant Pru du 4 after tag-removal, (6) the final Pru du 4 sample after SEC. The molecular masses (in kDa) of the protein standard in the maker (lane M) are 200, 150, 120, 100, 85, 70, 60, 50, 40, 30, 25, 20, 15, and 10, respectively. The arrow line close to lane 4 indicated the position of the ULP band that is barely detectable in lanes 3 and 4.

**Purification of Pru du 4.** The expressed His-MBP-sumo-Prudu4 was highly soluble in aqueous solutions. The fusion protein was purified with immobilized metal affinity chromatography using a $Ni^{2+}$ column. The purity of the sample was >90%, high enough to start fusion tag removal. To facilitate downstream purification, a second step of purification (anion exchange chromatography) was performed. In the ion exchange step, the sample eluted at ~200 mM NaCl. This step also eliminated imidazole from the sample. High concentration of imidazole is undesirable for removing the expression tag from the sample after protease digestion. Recombinant ULP produced in our lab was used to cleave the fusion tag. After optimization, a peptidase/substrate ratio of (w/w) 1:1000 was used. The reaction was carried out at 20 °C overnight, and it was almost complete without nonspecific digestions (Figure 2, lane 3). The undigested fusion protein, the cleaved fusion tag, and the recombinant ULP were successfully removed by passing the digestion product through a $Ni^{2+}$ column (Figure 2, lane 4). The flow-through seemed to contain homogeneous recombinant Pru du 4 (Figure 2, lane 5). Gel filtration was used to further purify the recombinant Pru du 4 to ensure high purity. The yield for the final product was at least 8 mg/L. Twenty cycles of N-terminal amino acid sequencing of the sample confirmed the expected N-terminal sequence (MSWQQYVDDHLMCDIDGNRL) of Pru du 4, except for Cys13 for which no major signal was obtained as is the case usually for a Cys residue. In addition, the total mass of the protein was determined to be 14060.8 Da (Figure 3). This is consistent with the calculated isotope averaged mass of 14061.10 for the protein (using the ExPASy server at http://web.expasy.org/cgi-bin/compute_pi/pi_tool). Additionally, the mass spectrometry method also detected minor populations of the protein with Pyruvoyl-(Serine) or oxidized residues that are most likely at its methionine residues.

**Chemical Stability of Pru du 4.** Far-UV CD spectrometry studies indicated that the spectrum of recombinant Pru du 4 is typical of a protein with mixed $\alpha$-helix and $\beta$-sheet secondary structures (Figure 4). Chemical denaturation is widely used as a way to assess the stability of native proteins. The folding−unfolding equilibrium of Pru du 4 was studied by measuring the GuHCl-induced transitions of the protein. In the present study, the equilibrium between unfolded and folded Pru du 4 at various concentrations of GuHCl was studied by measuring the CD signal at 220 nm (Figure 5). The data points seemed to follow a sigmoidal shape, indicative of a two-state transition between folded and unfolded states of Pru du 4 without a measurably populated stable intermediate. The method for finding the free energy of unfolding of a protein has been described in many comprehensive reviews (see, e.g., ref 24). The concentrations of the protein in the unfolded [U] and folded [F] states vary with the change of the denaturant concentration. The Gibbs free energy of the equilibrium transition, $\Delta G = \ln([U]/[F])$, changes accordingly. To the first approximation, the free energy of transition is a line function of the denaturant concentration

$$\Delta G = \Delta G_0 - mC$$

where $C$ is the concentration of the denaturant, $\Delta G_0$ is the free energy of the transition when there is no denaturant, and $m$ is a constant. At the midpoint of the transition (when $C = C_m$), the folded and unfolded states are equally populated and $\Delta G = 0$. Thus, $m$ equals to $\Delta G_0/C_m$. Generally, the CD signals of a protein in its folded and unfolded are both a linear function of the concentration of the denaturant. The measured CD signal is the sum of those of the folded and unfolded protein. Thus, $\Delta G_0$, $m$, and $C_m$ can be found by nonlinear fitting of the CD data. The results of the curve fitting are shown in Table 1. The transitions occurred with a midpoint concentrations of 1.38 ± 0.02 M. The free energy of unfolding, $\Delta G_0$, in the absence of denaturant was 5.4 ± 0.6 kcal/mol.

## DISCUSSION

Profilin is considered to be a panallergen. Almond profilin is known to be a food allergen. Unlike the 2S albumin, 7S vicilin, and 11S legumin allergens, the amount of profilin, including almond allergen Pru du 4, in plant seeds is minute. Expression of Pru du 4 in *E. coli* without an expression tag was unsuccessful though untagged expression of peanut profilin Ara h 5 was successful.[25] Its expression with an MBP-tag was reported, and the recombinant protein was used in immunological analyses.[19]

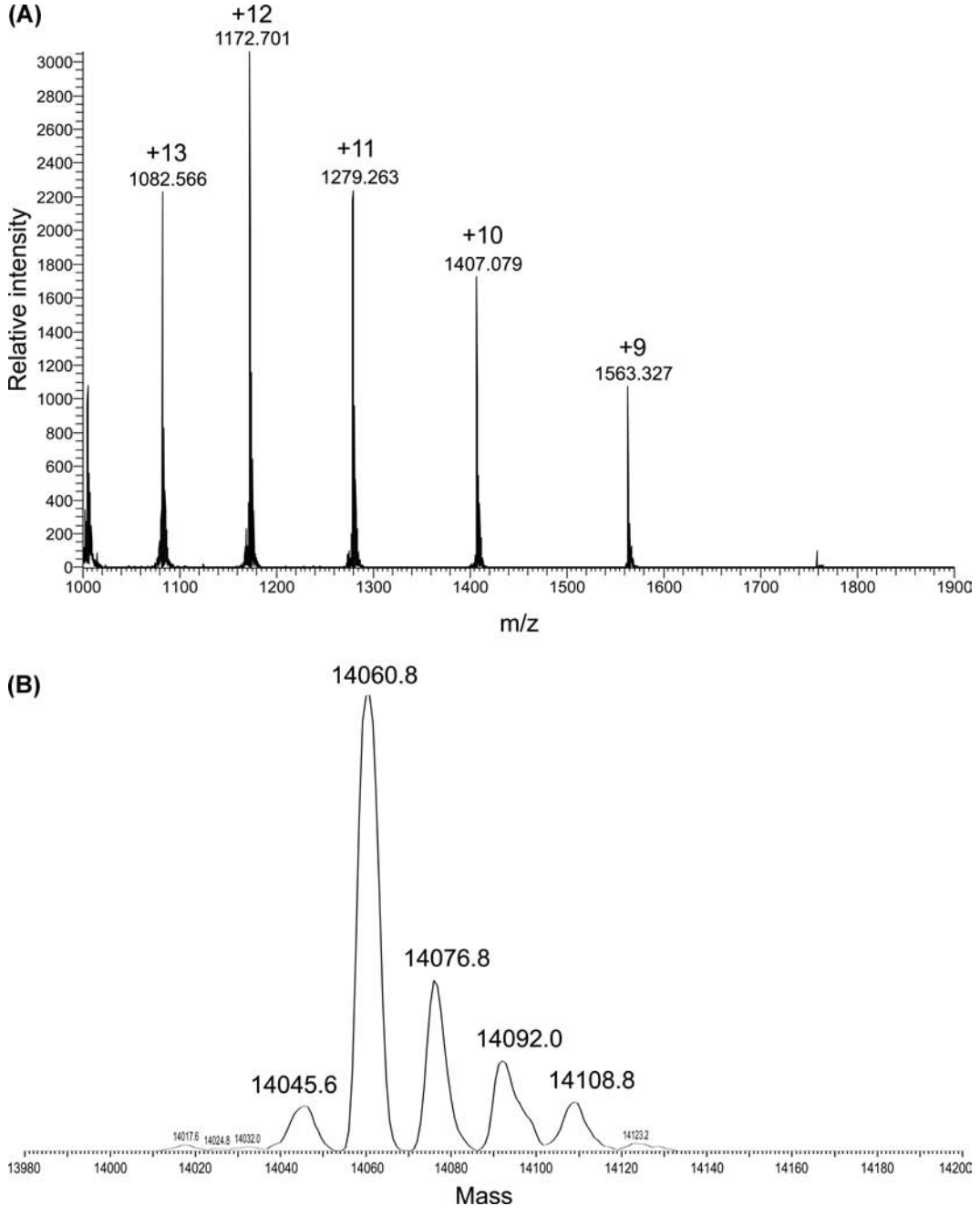


**Figure 3.** Mass determination of the purified Pru du 4. The sample was eluted from a Reprosil-Pur column coupled with an Easy nLC II mass spectrometer for accurate mass measurement. Panel A shows the mass spectrum of purified Pru du 4. Panel B shows the deconvolution result of the spectrum. The main peak indicated the measured mass of the protein is within 0.3 mass units of its calculated mass based on it peptide sequence.

In dot blot and ELISA studies, the recombinant protein and Pru du 4 purified from almond extract were recognized by IgE in patient sera differently. Some of the patient sera recognize Pru du 4 from almond, but not the recombinant Pru du 4.[19] N-terminal amino acid sequencing of Pru du 4 purified from almond indicated that no signal peptide was removed post-translationally (ref 19 and above). One of the reasons for the differences in the IgE recognition of the two versions of the allergen might be that the recombinant Pru du 4 used in the reported study had eight extra amino acids at its N-terminus after removing the expression tag with thrombin (or factor Xa) cleavage. These residues might block the conformational epitopes for IgE association.

To understand the relative importance of linear and conformational IgE epitopes in food allergy, native allergens are needed. As the amounts of a number of the allergens in foods are very low, it is desirable to obtain the native allergen with recombinant technology. In addition, an available system for producing native allergen in *E. coli* will make it possible to study the allergenicity of food allergens with site-directed mutagenesis technologies. Thus, we decided to use a highly specific peptidase for removing the expression tag without leaving any extra amino acids in the final product. Most of the widely used protease recognition sites that have been incorporated in varies DNA vectors designed for protein expression are short peptides with just a few amino acids. To

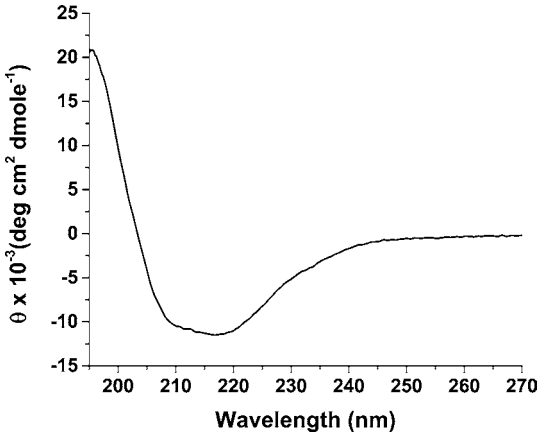


**Figure 4.** CD spectrum of recombinant Pru du 4. The residue molar ellipticity is shown as a function of wavelength.

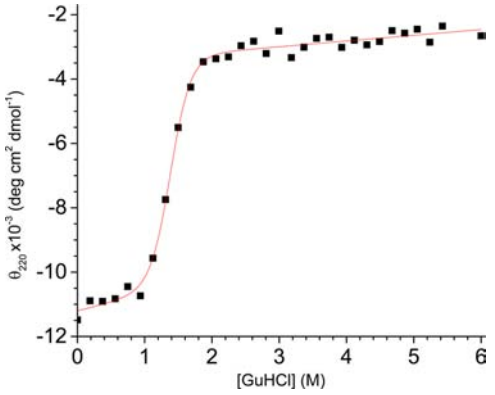


**Figure 5.** Folding–unfolding equilibrium of Pru du 4 in the presence of GuHCl. The data were fitted according to the equations shown in the text.

**Table 1. Equilibrium Parameters for GuHCl-Induced Unfolding of Pru du 4**[a]

| $\Delta G_0$ (kcal mol$^{-1}$) | $C_m$ (M) | $m$ (kcal mol$^{-1}$ M$^{-1}$) | $R^2$ |
|---|---|---|---|
| 5.4 ± 0.7 | 1.38 ± 0.02 | 3.9 ± 0.5 | 0.996 |

[a]Measured by CD at 220 nm in 10 mM sodium phosphate, pH 7.00, 20 °C.

our knowledge, the use of a protein, such as sumo, as a protease recognition site has not been reported, other than when sumo itself was used as an expression/solubility enhancement tag. Our results showed that by using sumo for peptidase recognition, the tag could be removed from almost 100% of the fusion protein without nonspecific cleavage of the target protein or the fusion tag. In our experience, this is a better system than using other proteases such as enteropeptidase which also does not leave any extra residues to the target protein. We expect that sumo as a protease recognition site can be used to conveniently obtain a wide variety of proteins. This may become the recognition site of choice especially when extra residues at the N-terminal of the target protein become problematic.

Profilin is considered as a panallergen.[11,12] Celery allergen Api g 4, which is also a profilin, was reported to lose its association with patient serum IgE after it was heated at 100 °C.[26] Strong allergenicity of cherry allergens was reported to be related to high stability against thermal processing and digestion.[27] The $\Delta G_0$ value obtained for Pru du 4 was 5.4 ± 0.7 kcal/mol. This is similar to the free energy of the folding–unfolding transitions of other globular proteins in the ProTherm Database.[28] The database currently consists of more than 3000 entries of the thermodynamic parameters for wild-type proteins obtained by studying the chemically induced changes in the folding–unfolding equilibrium of the proteins. While the stability is considered a contribution factor for the allergenicity of food proteins, information on the stabilities of food allergens derived from careful biochemical studies is limited. Additional comparative studies of the thermodynamic parameters of food allergens are required to understand the relationship between the chemical, physical, and biological stability of food allergens and their allergenicity. Currently, a well-characterized IgE or IgG antibody that recognizes only the native Pru du 4 is not available although immunoblotting experiments with such antibodies might give additional indication on the immunological equivalence of the recombinant protein and the protein purified from almond. Thus, the development of well-characterized antibodies is also desired for better understanding of the allergenicity of food proteins.

## AUTHOR INFORMATION

### Corresponding Author

*Tel.: 510 559 5981. Fax: 510 559 5818. E-mail: yuzhu.zhang@ars.usda.gov.

### Present Address

⊥Ecole d'Ingenieurs de Purpan, 75, voie du TOEC-BP 57611, 31076 Toulouse, CEDEX 3, France.

### Notes

Mention of trade names or commercial products in this publication is solely for the purpose of providing specific information and does not imply recommendation or endorsement by the U.S. Department of Agriculture.

The authors declare no competing financial interest.

## REFERENCES

(1) Nowak-Wegrzyn, A. Food allergy to proteins. *Nestle Nutr. Workshop Ser. Pediatr. Program* **2007**, *59*, 17–31 discussion 31–6.

(2) Asero, R.; Ballmer-Weber, B. K.; Beyer, K.; Conti, A.; Dubakiene, R.; Fernandez-Rivas, M.; Hoffmann-Sommergruber, K.; Lidholm, J.; Mustakov, T.; Oude Elberink, J. N.; Pumphrey, R. S.; Stahl Skov, P.; van Ree, R.; Vlieg-Boerstra, B. J.; Hiller, R.; Hourihane, J. O.; Kowalski, M.; Papadopoulos, N. G.; Wal, J. M.; Mills, E. N.; Vieths, S. IgE-mediated food allergy diagnosis: Current status and new perspectives. *Mol. Nutr. Food Res.* **2007**, *51*, 135–47.

(3) Ozol, D.; Mete, E. Asthma and food allergy. *Curr. Opin. Pulm. Med.* **2008**, *14*, 9–12.

(4) Sampson, H. A. Update on food allergy. *J. Allergy Clin. Immunol.* **2004**, *113*, 805–19 quiz 820..

(5) Wang, J.; Sampson, H. A. Food anaphylaxis. *Clin. Exp. Allergy* **2007**, *37*, 651–60.

(6) Branum, A. M.; Lukacs, S. L. *Food allergy among U.S. children: Trends in prevalence and hospitalizations*; NCHS Data Brief No. 10; National Center for Health Statistics: Hyattsville, MD, 2008.

(7) Otsu, K.; Dreskin, S. C. Peanut allergy: An evolving clinical challenge. *Discov. Med.* **2011**, *12*, 319–28.

(8) Anagnostou, K.; Clark, A. The management of peanut allergy. *Arch. Dis. Child.* **2014**.

(9) Birbach, A. Profilin, a multi-modal regulator of neuronal plasticity. *Bioessays* **2008**, *30*, 994–1002.

(10) Kandasamy, M. K.; Burgos-Rivera, B.; McKinney, E. C.; Ruzicka, D. R.; Meagher, R. B. Class-specific interaction of profilin and ADF isovariants with actin in the regulation of plant development. *Plant. Cell* **2007**, *19*, 3111–26.

(11) Scala, E.; Alessandri, C.; Palazzo, P.; Pomponi, D.; Liso, M.; Bernardi, M. L.; Ferrara, R.; Zennaro, D.; Santoro, M.; Rasi, C.; Mari, A. IgE recognition patterns of profilin, PR-10, and tropomyosin panallergens tested in 3,113 allergic patients by allergen microarray-based technology. *PLoS One* **2011**, *6*, e24912.
(12) Hauser, M.; Roulias, A.; Ferreira, F.; Egger, M. Panallergens and their impact on the allergic patient. *Allergy Asthma Clin. Immunol.* **2010**, *6*, 1.
(13) Walls, D.; Loughran, S. T. Tagging recombinant proteins to enhance solubility and aid purification. *Methods Mol. Biol.* **2011**, *681*, 151−75.
(14) Esposito, D.; Chatterjee, D. K. Enhancement of soluble protein expression through the use of fusion tags. *Curr. Opin. Biotechnol.* **2006**, *17*, 353−8.
(15) Marblestone, J. G.; Edavettal, S. C.; Lim, Y.; Lim, P.; Zuo, X.; Butt, T. R. Comparison of SUMO fusion technology with traditional gene fusion systems: Enhanced expression and solubility with SUMO. *Protein Sci.* **2006**, *15*, 182−9.
(16) Guo, W.; Cao, L.; Jia, Z.; Wu, G.; Li, T.; Lu, F.; Lu, Z. High level soluble production of functional ribonuclease inhibitor in *Escherichia coli* by fusing it to soluble partners. *Protein Expr. Purif.* **2011**, *77*, 185−92.
(17) Huang, J.; Cao, L.; Guo, W.; Yuan, R.; Jia, Z.; Huang, K. Enhanced soluble expression of recombinant *Flavobacterium heparinum* heparinase I in *Escherichia coli* by fusing it with various soluble partners. *Protein Expr. Purif.* **2012**, *83*, 169−76.
(18) Vervaet, N.; Kallio, J. P.; Meier, S.; Salmivaara, E.; Eberhardt, M.; Zhang, S.; Sun, X.; Wu, Z.; Kursula, P.; Kursula, I. Recombinant production, crystallization and preliminary structural characterization of *Schistosoma japonicum* profilin. *Acta Crystallogr.* **2013**, *F69*, 1264−7.
(19) Tawde, P.; Venkatesh, Y. P.; Wang, F.; Teuber, S. S.; Sathe, S. K.; Roux, K. H. Cloning and characterization of profilin (Pru du 4), a cross-reactive almond (*Prunus dulcis*) allergen. *J. Allergy Clin. Immunol.* **2006**, *118*, 915−22.
(20) Zhang, Y.-Z. *Protein and peptide structure and interactions studied by hydrogen exchange and NMR*. PhD Thesis, University of Pennsylvania, 1995.
(21) Dyballa, N.; Metzger, S. Fast and sensitive colloidal coomassie G-250 staining for proteins in polyacrylamide gels. *J. Vis. Exp.* **2009**, 1431.
(22) Zhang, Z.; Marshall, A. G. A universal algorithm for fast and automated charge state deconvolution of electrospray mass-to-charge ratio spectra. *J. Am. Soc. Mass Spectrom.* **1998**, *9*, 225−33.
(23) Rodriguez-Perez, R.; Fernandez-Rivas, M.; Gonzalez-Mancebo, E.; Sanchez-Monge, R.; Diaz-Perales, A.; Salcedo, G. Peach profilin: Cloning, heterologous expression and cross-reactivity with Bet v 2. *Allergy* **2003**, *58*, 635−40.
(24) Pace, C. N. Determination and analysis of urea and guanidine hydrochloride denaturation curves. *Methods Enzymol.* **1986**, *131*, 266−80.
(25) Wang, Y.; Fu, T. J.; Howard, A.; Kothary, M. H.; McHugh, T. H.; Zhang, Y. Crystal structure of peanut (*Arachis hypogaea*) allergen Ara h 5. *J. Agric. Food Chem.* **2013**, *61*, 1573−8.
(26) Jankiewicz, A.; Baltes, W.; Bogl, K. W.; Dehne, L. I.; Jamin, A.; Hoffmann, A.; Haustein, D.; Vieths, S. Influence of food processing on the immunochemical stability of celery allergens. *J. Sci. Food Agric.* **1997**, *75*, 359−370.
(27) Scheurer, S.; Lauer, I.; Foetisch, K.; San Miguel Moncin, M.; Retzek, M.; Hartz, C.; Enrique, E.; Lidholm, J.; Cistero-Bahima, A.; Vieths, S. Strong allergenicity of Pru av 3, the lipid transfer protein from cherry, is related to high stability against thermal processing and digestion. *J. Allergy Clin. Immunol.* **2004**, *114*, 900−7.
(28) Kumar, M. D.; Bava, K. A.; Gromiha, M. M.; Prabakaran, P.; Kitajima, K.; Uedaira, H.; Sarai, A. ProTherm and ProNIT: Thermodynamic databases for proteins and protein−nucleic acid interactions. *Nucleic Acids Res.* **2006**, *34*, D204−6.

action.[17] Therefore, inhibiting nitrite formation from nitrate reduction, as well as enhancing nitrite reduction, can be efficient to decrease the final nitrite content. The aim of this study is to lower the TSNA content of tobacco leaves during the air-curing process using a high nitrite reductive strain with low nitrate reduction capability.

## MATERIALS AND METHODS

**Samples and Chemicals.** Tobacco leaves and involved rhizosphere soil samples were collected from Shiyan, Enshi, and Wuhan of Hubei Province in China for strain isolation. The standard substances of NNN, NNK, NAB, and NAT were purchased from Sigma-Aldrich Co. LLC (St. Louis, MO, USA). The deuterated equivalents of NNN-D4, NNK-D4, NAB-D4, and NAT-D4 were bought from C/D/N Isotopes Inc. (Pointe-Claire, Quebec, Canada). All other chemicals were purchased from Sinopharm Chemical Reagent Co., Ltd. (Shanghai, China).

**Isolation of the Nitrite Reductive Strain.** The tobacco and soil samples were added into the liquid screening medium ($NaNO_2$ 0.5 g/L, $MgSO_4{\cdot}7H_2O$ 0.2 g/L, $K_2HPO_4$ 0.5 g/L, $KNaC_4H_4O_6{\cdot}4H_2O$ 20.0 g/L, pH 7.2), cultured at 37 °C and 180 rpm for 48 h. The cultures were then diluted, and spread onto the solid screening medium containing 15 g/L agar, and incubated at 37 °C for another 24 h. The single clone was then inoculated in the nitrate medium ($NaNO_3$ 1 g/L, peptone 10 g/L, yeast extract 5 g/L, NaCl 10 g/L, pH 7.2) and nitrite medium ($NaNO_2$ 0.5 g/L, peptone 10 g/L, yeast extract 5 g/L, NaCl 10 g/L, pH 7.2), respectively. After culture at 37 °C and 180 rpm for 12 h, the concentrations of nitrate and nitrite in the medium were determined. The high nitrite reductive strain with low nitrate reduction ability was selected.

**Fermentation of Tobacco Leaves.** The isolated nitrite reductive strains were cultured in LB liquid medium (peptone 10 g/L, yeast extract 5 g/L, NaCl 10 g/L, pH 7.2) at 37 °C and 180 rpm for 12 h, and subcultured for 24 h. The cells were collected by centrifugation at 7656*g* for 10 min and diluted with sterile distilled water to obtain the suspension of bacteria ($1 \times 10^8$ CFU/mL). The suspension of bacteria was sprayed onto the Burley tobacco (Eyan 6) leaves and incubated at 30 °C with 30% moisture content and 80% relative humidity. After incubating for 5 days, the contents of nitrite and various TSNA compounds (NNN, NNK, NAB, and NAT) were determined.

**Identification of the Strain.** The isolated nitrite reductive strain was identified by physiological, biochemical, and 16S rDNA sequence analysis. The traditional physiological and biochemical experiments were performed based on *Bergey's Manual of Systematic Bacteriology*.[18] The 16S rDNA sequence analysis was carried out according to our previous report.[19] The 16S rDNA sequence was amplified using the primers of 27f (AGAGTTTGATCMTGGCTCAG) and 1492r (GGTTACCTTGTTACGACTT), and the PCR was performed as follows: 95 °C for 5 min; 95 °C for 45 s, 54 °C for 45 s, 72 °C for 1.5 min, 28 cycles; 72 °C for 10 min; and 4 °C for 10 min. The DNA products were then purified, recovered, and sequenced by the BGI Tech Solutions Co., Ltd. (Shenzhen, China). The sequence similarity analysis was carried out by the Blastn program (http://blast.ncbi.nlm.nih.gov/Blast.cgi), and the phylogenetic tree was constructed using MEGA 4.0.[20]

**Batch Culture.** The selected strain was inoculated into the LB liquid medium, cultured at 37 °C and 180 rpm for 12 h as the seed cultures. With 3% (v/v) inoculum size, the seed cultures were transferred into the initial fermentation medium (glucose 20 g/L, $NH_4Cl$ 10 g/L, corn steep liquor 10 g/L), incubated at 37 °C and 180 rpm for 36 h, and the medium components as well as culture conditions were optimized for maximum cell growth. After culture at the optimized fermentation parameters, the cells were collected by centrifugation at 7656*g* for 10 min, and applied in the air-curing process of tobacco.

**Microbial Treatment of Tobacco Leaves during the Air-Curing Process.** The cells collected from batch culture were diluted to $2 \times 10^8$ CFU/mL, and 30 mL cell suspensions were sprayed onto 300 g of fresh Burley tobacco (Eyan 6) leaves for air-curing treatment. Leaves sprayed with the same volume of sterile distilled water were used as the control. The fresh leaves (0 day) and the leaves at different air-curing stages (7, 20, and 45 day) were collected, and the concentrations of total cells, nitrate, and TSNA compounds (NNN, NNK, NAB, and NAT) were determined.

**Determination of Nitrate and Nitrite.** Nitrate was determined by the salicylic acid method.[21] In brief, 0.1 mL of sample and 0.4 mL of salicylic acid solution (5%) were mixed and added into 9.5 mL of NaOH solution (8%). The reaction mixture was incubated for 20 min and determined for its absorbance at 420 nm. $NaNO_3$ was used as the standard substance. For determination of the nitrite, 4 mL of sulfanilamide solution (1%) was mixed with 2 mL of sample solution in the test tube, supplied with 4 mL of $\alpha$-naphthylamine solution (0.02%), and maintained at 25 °C for 30 min. The absorbance of the sample was determined at 540 nm with $NaNO_2$ being used as the standard.[22]

**Analysis of the TSNA Concentration.** The tobacco leaf samples were dried at 45 °C to reach constant weight, smashed, and sieved. 0.25 g of tobacco powder was placed into an erlenmeyer flask and combined with 0.2 mL of internal standard solution (5000 ng/mL) and of 19.8 mL ammonium acetate solution (100 mM). The mixture was shaken at 150 rpm for 1 h, filtered, and collected for analysis of the contents of TSNA compounds by an LC−MS/MS system (Agilent Technologies Corporate, Santa Clara, CA, USA). The HPLC was carried out on an Agilent 1290 system using an Agilent ZORBAX XDB-C18 column (Agilent Technologies, Santa Clara, CA, USA). The column temperature was set as 65 °C with an injection volume of 5 $\mu$L. 0.1% acetic acid water solution and 0.1% acetic acid methanol solution were used as the mobile phases A and B respectively. The gradient elution conditions were programmed as follows: 0.0−0.5 min, 60−70% B; 0.5−1.0 min, 70% B; 1.0−1.5 min, 70−90% B; 1.5−2.3 min, 90−60% B; 2.3−2.5 min, 60% B. MS/MS was performed using the Agilent 6460 triple quadrupole tandem mass spectrometer (Agilent Technologies Corporate, Santa Clara, CA, USA), and the conditions were controlled as follows: ESI ion source, positive ion mode, 4000 V voltage, 35 psig nebulizer pressure, 10 L/min gas flow rate, and 350 °C vaporizer temperature. The deuterated equivalents of NNN-D4, NNK-D4, NAB-D4, and NAT-D4 were used as the internal standard to determine the contents of NNN, NNK, NAB, and NAT, and the total TSNA contents were calculated by summing the NNN, NNK, NAT, and NAB.

**Statistical Analyses.** Each experiment was carried out at least in triplicate, and *t* test was performed to analyze the difference in means at the 95% confidence level using Statistica 6.0 software package.

## RESULTS AND DISCUSSION

**Isolation of the TSNA-Decreasing Strain.** Various microbes coexist with the tobaccos,[23,24] and thus the leaves and rhizosphere soils of tobaccos were collected for strain isolation. In this work, we isolated 304 clones from different tobacco and rhizosphere soil samples, and those strains were cultured in nitrite and nitrate selection medium. Among those strains, eight strains had high nitrite reducing capabilities. As shown in Figure 1, the degradation efficiencies of three strains (DA9, 1-4, and CH3) were higher than 30%, while the strain DA9 had the lowest nitrate degradation capability (11%). Due to the unique feature of high nitrite reductivity and low nitrate reductivity, the strain DA9 was selected for further verification by fermentation of tobacco leaves. As shown in Table 1, the nitrite concentration after fermentation with DA9 decreased 39% compared with the control, and the total TSNA content decreased 56% accordingly. Further analysis revealed the significant difference of each individual TSNA compound, and the NNN, NNK, NAT, and NAB content decreased by 57%, 69%, 46%, and 52%, respectively. The results indicated that the strain DA9 had the potential to lower the TSNA content in tobacco leaves.

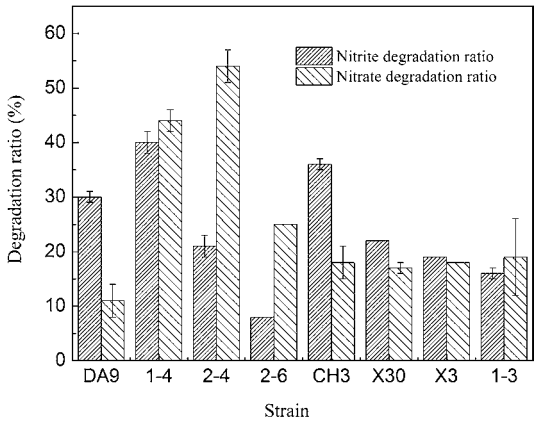


**Figure 1.** Degradation ratios of different strains on nitrite and nitrate. The isolated strains were cultured in the nitrate medium and nitrite medium at 37 °C and 180 rpm for 12 h respectively, and then the concentrations of residual nitrate and nitrite in the medium were determined to calculate corresponding degradation ratios.

**Identification of the Strain.** The strain DA9 was identified by morphological, physiological, biochemical, and 16S rDNA sequence analysis. After culturing in LB agar medium, white colonies with rough surface and irregular edge were observed. Under the microscope, the bacterial cells showed rod shape with strong motility. The physiological and biochemical characteristics of DA9 strain (Table 2) indicate that DA9 belonged to the *Bacillus* genus.[18] The 16S rDNA sequence of 1423 bp was obtained from DA9, aligned with the sequences in GenBank using the Blastn program, and revealed 100% identity to that of the *Bacillus amyloliquefaciens* LFB112 (CP006952).[25] The phylogenetic tree constructed on the basis of the 16S rDNA sequences shows that the DA9 clustered with *B. amyloliquefaciens* (Figure 2). Collectively, the above results indicate that the strain DA9 belonged to *B. amyloliquefaciens*. In a separate report, *Bacillus* and *Pseudomonas* were reported to be the two dominant genera, of which *B. amyloliquefaciens* was also found in the flue-cured tobacco leaves.[14] The 16S rDNA sequence of DA9 was submitted into the GenBank database (Accession number KM272942), and this strain was preserved in China Center for Type Culture Collection (CCTCC M2014252).

**Optimization of Fermentation Parameters.** To maximize the growth of the isolated *B. amyloliquefaciens* DA9, we optimized the medium components for this strain including glucose, corn steep liquor, $NH_4Cl$, $MnSO_4$, $KH_2PO_4$, and $MgSO_4$. Based on the preliminary screening results (data not shown), three key components, glucose (A), $NH_4Cl$ (B), and corn steep liquor (C), were identified as the factors with significant effects on the cell growth, therefore, these three medium compositions were further optimized using three-factor-three-level orthogonal design. As shown in Table 3, range analysis results were observed as $R(C) > R(A) > R(B)$, indicating that the influential effects of the three components were ranged as corn steep liquor (C) > glucose (A) > $NH_4Cl$ (B). The $k$ value analysis showed that the optimal factor levels were glucose (A3), $NH_4Cl$ (B1), corn steep liquor (C2). Based on the above results, the optimized medium components were determined as glucose 40 g/L, $NH_4Cl$ 4 g/L, corn steep liquor 8 g/L, $MnSO_4$ 0.01 g/L, $KH_2PO_4$ 1.0 g/L, $MgSO_4$ 0.3 g/L. The culture conditions were also investigated follwing the medium optimization. It was found that the combined conditions of initial pH 7.0, inoculum age 6 h, inoculum size 3%, and temperature 37 °C were optimal for cell growth (data not shown). Under those optimized parameters, the DA9 cells were cultured, and the maximum cell dentisity reached $1.2 \times 10^9$ CFU/mL at 36 h. Those cells were then collected for applying to the tobacco leaves during the air-curing process.

**Table 2. Physiological and Biochemical Characterization of the Strain DA-9[a]**

| sole carbon test | | acid productive test | |
|---|---|---|---|
| property | characterization | property | characterization |
| sorbose | +[b] | sucrose | + |
| ribose | + | lactose | −[c] |
| glucose | + | glycerol | + |
| sucrose | + | mannitol | + |
| maltose | + | glucose | + |
| glycerol | + | other tests | |
| lactose | + | Gram stain | + |
| starch | + | sporulation | + |
| arabinose | − | indole formation | − |
| trehalose | + | lecithase test | + |
| mannose | − | cellulose hydrolysis | − |
| rhamnose | + | starch hydrolysis | + |
| xylose | + | gelatin hydrolysis | + |
| raffinose | + | growth at 4 °C | + |
| melizitose | − | growth at 45 °C | + |

[a]The physiological and biochemical analysis of strain DA9 was carried out according to *Bergey's Manual of Systematic Bacteriology*.[18] [b]Positive. [c]Negative.

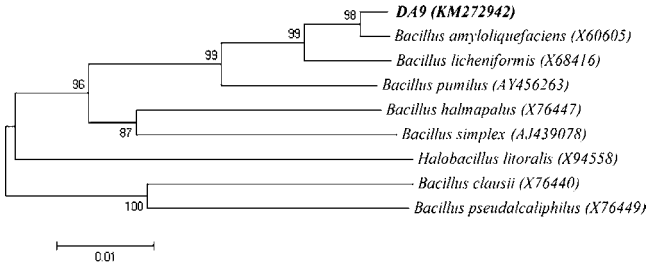


**Figure 2.** Phylogenetic tree of DA9 based on 16S rDNA sequences. Numbers in parentheses indicates the sequence accession numbers of the representative organisms. The scale bar represents 0.01 nucleotide substitution per position.

**Table 1. Effects of Fermentation with DA9 on the Contents of Tobacco Nitrite and TSNA[a]**

| sample | nitrite content (μg/g) | TSNA content (μg/g) | NNN content (μg/g) | NNK content (μg/g) | NAT content (μg/g) | NAB content (μg/g) |
|---|---|---|---|---|---|---|
| control | 14.05 ± 0.01 | 94.00 ± 2.10 | 81.65 ± 1.02 | 1.31 ± 0.13 | 10.43 ± 1.24 | 0.62 ± 0.03 |
| treatment | 8.59 ± 1.09 | 41.64 ± 0.75 | 35.30 ± 0.74 | 0.41 ± 0.01 | 5.64 ± 2.00 | 0.30 ± 0.02 |

[a]The DA9 cell suspensions ($1 \times 10^8$ CFU/mL) were sprayed onto the Burley tobacco leaves and fermented at 30 °C with 30% moisture content and 80% relative humidity for 5 days to determine the concentrations of nitrite and the various tobacco specific nitrosamine (TSNA) compounds *N*-nitrosonornicotine (NNN), 4-(methylnitrosamino)-1-(3-pyridyl)-1-butanone (NNK), *N*-nitrosoanatabine (NAT), and *N*-nitrosoanabasine (NAB).


dx.doi.org/10.1021/jf504084z | J. Agric. Food Chem. 2014, 62, 12701−12706

Table 3. Results of Orthogonal Test[a]

| | factor | | | |
|---|---|---|---|---|
| | A: glucose (g/L) | B: $NH_4Cl$ (g/L) | C: corn steep liquor (g/L) | $OD_{600}$ |
| number | | | | |
| 1 | 20 | 4 | 4 | 4.26 |
| 2 | 20 | 8 | 8 | 8.07 |
| 3 | 20 | 12 | 12 | 4.27 |
| 4 | 30 | 4 | 8 | 8.22 |
| 5 | 30 | 8 | 12 | 3.92 |
| 6 | 30 | 12 | 4 | 4.62 |
| 7 | 40 | 4 | 12 | 10.78 |
| 8 | 40 | 8 | 4 | 4.80 |
| 9 | 40 | 12 | 8 | 8.71 |
| $k_1$ | 5.53 | 7.76 | 4.56 | |
| $k_2$ | 5.58 | 5.59 | 8.33 | |
| $k_3$ | 8.10 | 5.87 | 6.32 | |
| $R$ | 2.56 | 2.16 | 3.77 | |

[a]The experiments were performed using three-factor-three-level orthogonal design. The $R$ value indicates the range, and the $k$ value represents the average biomass of each factor level.

**Effects of Microbial Treatment with DA9 on the Contents of Nitrite and Total TSNA in the Tobacco Leaves.** The *B. amyloliquefaciens* DA9 cells were sprayed onto the tobacco leaves; the same volume of distilled water was also sprayed onto the leaves as control. After the air-curing process, the nitrite content of the control increased from 10.20 μg/g to 17.77 μg/g (Figure 3A). The nitrate reductases of tobaccos and their symbiotic microbes can mediate the nitrate reduction action during the air-curing process,[7] which may be the main reason for the increased nitrite formation. By treating the leaves with DA9 cells, however, the maximum nitrite content just reached 12.06 μg/g, and such an increment was significantly lower than the control (Figure 3A). For the control, the native strain number changed from $9.33 \times 10^5$ CFU/g to $1.05 \times 10^5$ CFU/g after air-curing of tobacco leaves for 45 d, while the DA9 treated tobacco leaves had bacterial counts ranging from $8.71 \times 10^8$ CFU/g to $1.32 \times 10^8$ CFU/g, much higher than that of the control. As the dominant microflora, the DA9 cells inhibited the growth of other native bacteria and, thus, lowered those bacteria's capability of nitrate reduction. This feature, together with the strong nitrite reduction ability, makes the DA9 strain an ideal strain for decreasing nitrite during the tobacco air-curing process.

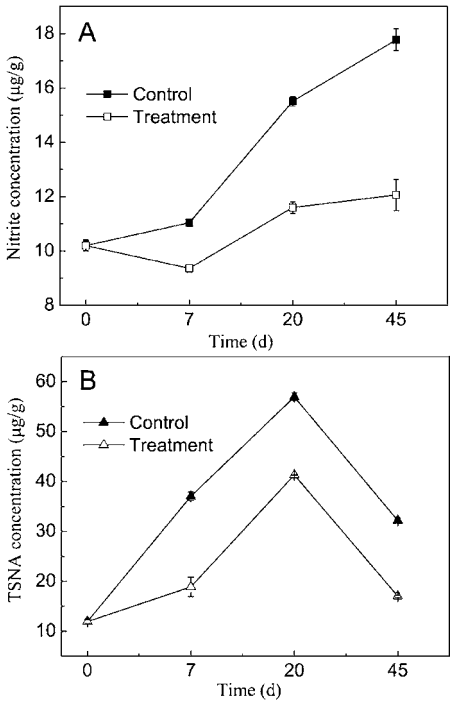


**Figure 3.** Effects of microbial treatment on the nitrite (A) and tobacco specific nitrosamine (TSNA) (B) concentrations of the tobacco leaves during the air-curing process. 30 mL cell suspensions ($2 \times 10^8$ CFU/mL) were sprayed onto 300 g of fresh Burley tobacco leaves for air-curing treatment. At 0, 7, 20, and 45 days, the control without treatment and the tobacco leaves treated with DA9 cells were sampled to determine the concentrations of nitrite and total TSNAs.

It has been reported that nitrite was the direct precursor for TSNA synthesis.[5] Therefore, decreased nitrite content inhibited TSNA formation. As shown in Figure 3B, the total TSNA concentration in the control increased before 20 d, which is in agreement with a previous report.[26] However, the maximum TSNA concentration reached 56.94 μg/g at 20 d, while the content decreased to 32.19 μg/g at 45 d, which is a little higher than previous reports.[6,27] The Burley tobaccos have higher TSNA levels than other tobacco lines, such as flue-cured and oriental tobaccos.[6] Moreover, the average TSNA content of air-cured Burley tobacco from Hubei Province is much higher than that of Sichuan, Yunnan Province, and USA.[8] The TSNA contents are significantly affected by processing techniques,[6] cultivation conditions,[7] tobacco lines, and producing areas,[8] which may result in the high TSNA levels of air-cured tobacco in Hubei Province. Figure 3B also shows that, after treatment with DA9, the total TSNA content of tobacco leaves was much lower than that of the control at each stage. The final TSNA content at 45 d reached 17.03 μg/g (Figure 3B), which was 47% lower than the control. The above results indicate that treatment by *B. amyloliquefaciens* DA9 was an efficient way to lower the nitrite and TSNA contents of air-cured Burley tobacco.

**Effects of Microbial Treatment on the Contents of NNN, NNK, NAT, and NAB.** The individual compounds of TSNA, i.e., NNN, NNK, NAT, and NAB, were further analyzed. As the direct substrate, nornicotine shows positive correlation with NNN formation.[9] Among the alkaloid precursors of TSNA, nornicotine was most abundant, and thus the NNN preponderated among the four kinds of TSNA. Similar to previous results,[6] the NNN contents detected were much higher than those of other TSNA components (Figure 4), and thus the change trend of NNN agreed with that of total TSNA contents (Figure 3B). After microbial treatment with DA9, the NNN content was 15.53 μg/g at 45 d, a 48% decrease compared to the control (Figure 4A). Meanwhile, similar inhibitory effects were observed for NNK and NAT, which decreased by 12% and 35% after 45 d (Figure 4B and Figure 4C), while no significant difference was found in NAB contents (Figure 4D). NAT and NAB show little biological activity, while NNN and NNK are the main carcinogens.[1] In summary, our results show that microbial treatment with DA9 can efficiently lower the contents of the main carcinogens of TSNA in Burley tobacco. Tobacco leaves treated with DA9 have the potential to be applied in cigarette as the filler, which may help to decrease the probability of smoking-related cancer. The health implications of smoking tobacco leaves treated with *B.*

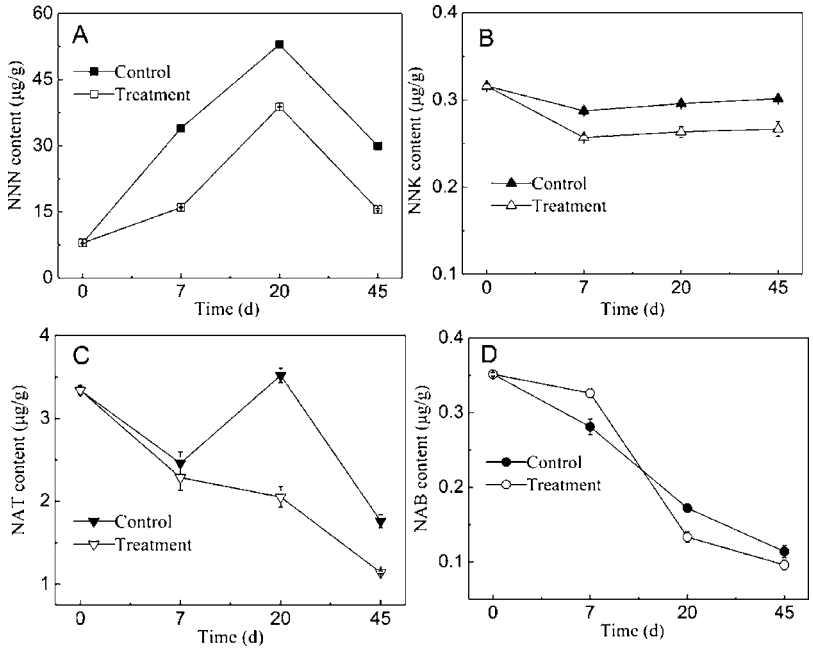


**Figure 4.** Effects of microbial treatment on the concentrations of *N*-nitrosonornicotine (NNN) (A), 4-(methylnitrosamino)-1-(3-pyridyl)-1-butanone (NNK) (B), *N*-nitrosoanatabine (NAT) (C), and *N*-nitrosoanabasine (NAB) (D) of the tobacco leaves during the air-curing process. The DA9 cell suspensions ($2 \times 10^8$ CFU/mL) were sprayed onto the fresh Burley tobacco leaves and air-cured for 0, 7, 20, and 45 days, and then the concentrations of NNN, NNK, NAB, and NAT were determined.

*amyloliquefaciens* DA9 are very important before commercial application, and the toxicity and sensory characteristics will be evaluated in further study. Meanwhile, the detailed mechanism for decreased TSNA in tobacco leaves treated with DA9 will be further investigated in a future study.

## AUTHOR INFORMATION

### Corresponding Author

*Tel/fax: +86 027-87280670. E-mail: mel212@126.com. Postal address: No. 368 Youyi Road, Wuchang District, Wuhan 430070, Hubei, People' s Republic of China.

### Funding

This work was funded by the National Program on Key Basic Research Project (No. 2015CB150505), the National Science & Technology Program for the Rural Development during the Twelfth Five-year Plan Period (No. 2013AA102801-52), the Opening Project of State Key Laboratory of Agricultural Microbiology (No. AMLKF201403), the Fundamental Research Funds for the Central Universities (No. 52902-0900206142), and the Key Project of Hubei Province Tobacco Company (027Y2011-055).

### Notes

The authors declare no competing financial interest.

## REFERENCES

(1) Gupta, P. C.; Murti, P. R.; Bhonsle, R. B. Epidemiology of cancer by tobacco products and the significance of tsna. *Crit. Rev. Toxicol.* **1996**, *26*, 183−198.

(2) IARC. *Smokeless tobacco and some tobacco-specific N-nitrosamines*; IARC monographs on the evaluation of carcinogenic risks to humans, Vol. *89*; 2007. http://monographs.iarc.fr/ENG/Monographs/vol89/mono89.pdf.

(3) USDHHS. *Harmful and potentially harmful constituents in tobacco products and tobacco smoke: Established list*; US Food and Drug Administration: 2012. http://www.Fda.Gov/tobaccoproducts/guidancecomplianceregulatoryinformation/ucm297786.Htm.

(4) Wang, C.; Dai, Y.; Feng, G.; He, R.; Yang, W.; Li, D.; Zhou, X.; Zhu, L.; Tan, L. Addition of porphyrins to cigarette filters to reduce the levels of benzo[a]pyrene (b[a]p) and tobacco-specific n-nitrosamines (TSNAs) in mainstream cigarette smoke. *J. Agric. Food Chem.* **2011**, *59*, 7172−7177.

(5) Hecht, S. S. Biochemistry, biology, and carcinogenicity of tobacco-specific n-nitrosamines. *Chem. Res. Toxicol.* **1998**, *11*, 559−603.

(6) Shi, H.; Wang, R.; Bush, L. P.; Zhou, J.; Yang, H.; Fannin, N.; Bai, R. Changes in tsna contents during tobacco storage and the effect of temperature and nitrate level on TSNA formation. *J. Agric. Food Chem.* **2013**, *61*, 11588−11594.

(7) Lewis, R. S.; Parker, R. G.; Danehower, D. A.; Andres, K.; Jack, A. M.; Whitley, D. S.; Bush, L. P. Impact of alleles at the yellow burley (yb) loci and nitrogen fertilization rate on nitrogen utilization efficiency and tobacco-specific nitrosamine (TSNA) formation in air-cured tobacco. *J. Agric. Food Chem.* **2012**, *60*, 6454−6461.

(8) Shi, H. Z.; Wang, R. Y.; Bush, L. P.; Yang, H. J.; Fannin, F. F. The relationships between TSNAs and their precursors in burley tobacco from different regions and varieties. *J. Food Agric. Environ.* **2012**, *10*, 1048−1052.

(9) Gavilano, L. B.; Coleman, N. P.; Burnley, L.-E.; Bowman, M. L.; Kalengamaliro, N. E.; Hayes, A.; Bush, L.; Siminszky, B. Genetic engineering of nicotiana tabacum for reduced nornicotine content. *J. Agric. Food Chem.* **2006**, *54*, 9071−9078.

(10) Lewis, R. S.; Jack, A. M.; Morris, J. W.; Robert, V. J. M.; Gavilano, L. B.; Siminszky, B.; Bush, L. P.; Hayes, A. J.; Dewey, R. E. RNA interference (RNAi)-induced suppression of nicotine demethylase activity reduces levels of a key carcinogen in cured tobacco leaves. *Plant Biotechnol. J.* **2008**, *6*, 346−354.

(11) Rundlöf, T.; Olsson, E.; Wiernik, A.; Back, S.; Aune, M.; Johansson, L.; Wahlberg, I. Potential nitrite scavengers as inhibitors of the formation of n-nitrosamines in solution and tobacco matrix systems. *J. Agric. Food Chem.* **2000**, *48*, 4381−4388.

(12) Cui, M.; Burton, H. R.; Bush, L. P.; Sutton, T. G.; Crafts-Brandner, S. J. Effect of maleic hydrazide application on accumulation of tobacco-specific nitrosamines in air-cured burley tobacco. *J. Agric. Food Chem.* **1994**, *42*, 2912−2916.

(13) Burton, H. R.; Dye, N. K.; Bush, L. P. Relationship between tobacco-specific nitrosamines and nitrite from different air-cured tobacco varieties. *J. Agric. Food Chem.* **1994**, *42*, 2007−2011.
(14) Huang, J.; Yang, J.; Duan, Y.; Gu, W.; Gong, X.; Zhe, W.; Su, C.; Zhang, K. Q. Bacterial diversities on unaged and aging flue-cured tobacco leaves estimated by 16s rRNA sequence analysis. *Appl. Microbiol. Biotechnol.* **2010**, *88*, 553−562.
(15) Zhang, L.; Wang, X.; Guo, J.; Xia, Q.; Zhao, G.; Zhou, H.; Xie, F. Metabolic profiling of chinese tobacco leaf of different geographical origins by gc-ms. *J. Agric. Food Chem.* **2013**, *61*, 2597−2605.
(16) Di Giacomo, M.; Paolino, M.; Silvestro, D.; Vigliotta, G.; Imperi, F.; Visca, P.; Alifano, P.; Parente, D. Microbial community structure and dynamics of dark fire-cured tobacco fermentation. *Appl. Environ. Microbiol.* **2007**, *73*, 825−837.
(17) González, P. J.; Correia, C.; Moura, I.; Brondino, C. D.; Moura, J. J. G. Bacterial nitrate reductases: Molecular and biological aspects of nitrate reduction. *J. Inorg. Biochem.* **2006**, *100*, 1015−1023.
(18) Claus, D.; Berkeley, R. W. C. Genus Bacillus Cohn 1872. In *Bergey's manual of systematic bacteriology*; Sneath, P. H. A., Ed.; Williams & Wilkins: Baltimore, 1986; Vol. *2*, pp 1105−1138.
(19) Wei, X. T.; Luo, M. F.; Xu, L.; Zhang, Y. W.; Lin, X.; Kong, P.; Liu, H. Z. Production of fibrinolytic enzyme from *Bacillus amyloliquefaciens* by fermentation of chickpeas, with the evaluation of the anticoagulant and antioxidant properties of chickpeas. *J. Agric. Food Chem.* **2011**, *59*, 3957−3963.
(20) Tamura, K.; Dudley, J.; Nei, M.; Kumar, S. MEGA4: Molecular evolutionary genetics analysis (MEGA) software version 4.0. *Mol. Biol. Evol.* **2007**, *24*, 1596−1599.
(21) Cataldo, D. A.; Maroon, M.; Schrader, L. E.; Youngs, V. L. Rapid colorimetric determination of nitrate in plant tissue by nitration of salicylic acid. *Commun. Soil Sci. Plant Anal.* **1975**, *6*, 71−80.
(22) Donald Nicholas, D.; Nason, A. Determination of nitrate and nitrite. *Methods Enzymol.* **1957**, *3*, 981−984.
(23) Su, C.; Gu, W.; Zhe, W.; Zhang, K. Q.; Duan, Y. Q.; Yang, J. K. Diversity and phylogeny of bacteria on zimbabwe tobacco leaves estimated by 16s rRNA sequence analysis. *Appl. Microbiol. Biotechnol.* **2011**, *92*, 1033−1044.
(24) Zhao, M.; Wang, B.; Li, F.; Qiu, L.; Li, F.; Wang, S.; Cui, J. Analysis of bacterial communities on aging flue-cured tobacco leaves by 16s rdna pcr-dgge technology. *Appl. Microbiol. Biotechnol.* **2007**, *73*, 1435−1440.
(25) Cai, J.; Liu, F.; Liao, X.; Zhang, R. Complete genome sequence of *Bacillus amyloliquefaciens* lfb112 isolated from chinese herbs, a strain of a broad inhibitory spectrum against domestic animal pathogens. *J. Biotechnol.* **2014**, *175*, 63−64.
(26) Burton, H. R.; Childs, G. H.; Andersen, R. A.; Fleming, P. D. Changes in chemical composition of burley tobacco during senescence and curing. 3. Tobacco-specific nitrosamines. *J. Agric. Food Chem.* **1989**, *37*, 426−430.
(27) Stepanov, I.; Carmella, S. G.; Hecht, S. S.; Duca, G. Analysis of tobacco-specific nitrosamines in moldovan cigarette tobacco. *J. Agric. Food Chem.* **2002**, *50*, 2793−2797.

concentrations of ergovaline and lolitrem B in endophyte-infected perennial ryegrass strongly varied with time, and the maxima were observed at different periods of the year.[30] High rainfall in spring−summer accompanied by dry warm conditions in late summer−autumn were observed in the years when severe outbreaks of toxicosis occurred.[31]

The purpose of this study was thus to investigate ergovaline and lolitrem B levels in the symbiotic association *E. festucae* var. *lolii*/*L. perenne*, which is known to produce high concentrations of alkaloids. Alkaloid levels were investigated in the leaves, base, and inflorescence. The stage of maturity of the plant and the temperature and rainfall over the three-year study of plant growth were investigated as factors responsible for variations in ergovaline and lolitrem B contents.

## MATERIALS AND METHODS

**Experimental Pastures.** Perennial ryegrass seeds *L. perenne* cv. 'Grasslands Samson' with a seedling infection rate of 70% measured using a Phytoscreen immunoblot kit (Agrinostics Ltd., Watkinsville, GA, USA) were obtained from RAGT 2n SAS (Rodez, France). Sowing (27 kg seeds/ha) was done in September 2009 after conventional soil preparation in Saint-Affrique (Aveyron, France). The plot (0.75 ha) slopes gently toward a small river, the soil is a sandy clay loam, red brown, little humus, with gravel and angular fragments of sandstone and mudstone of polyhedral structure. Each year the plot was mowed in June to avoid dissemination. Nitrogen fertilization was done in 2011 with urea (70 and 50 U/ha on March 9 and April 13, respectively). Rainfall was recorded at the Saint-Affrique site, whereas maximum and minimum daily air temperatures were measured at the Montlaur site (9 km from Saint-Affrique). The Biologische Bundesanstalt Bundessortenamt and Chemische Industrie (BBCH) scale was used to monitor the perennial ryegrass growth.[32] Cumulative degree-days (average daily temperature above 0 °C) was calculated from February to mowing.[33,34]

**Plant Material.** Levels of ergovaline and lolitrem B were measured once a week from April to June and once or twice a month the rest of the year. Whole plants, cut just above the ground, were collected on each sampling occasion, whereas inflorescence (after heading), leaves (stem and leaf blade), and base (stem and leaf sheath) were collected from the heading stage to the fully ripe stage. On each sampling occasion, five samples of around 100 g of fresh material were harvested to be representative of the plot. Samples were dried for 24 h at 60 °C in a ventilated oven and then ground to 0.5 mm in a Cyclotech 1093 grinding mill (Foss, Hogande, Sweden). The ground material was pooled and stored at room temperature until analysis.

**Ergovaline and Lolitrem B Analysis.** All reagents and chemicals, HPLC grade, were from Sigma Chemical Co., (St. Louis, MO, USA). Ergovaline standard was kindly provided by G. E. Rottinghaus (College of Veterinary Medicine, University of Missouri). Lolitrem B standard was purchased from AgResearch Limited Ruakura Research Centre (Hamilton, New Zealand). Ergovaline and lolitrem B concentrations were detected by fluorescence after purification on homemade Ergosil columns and HPLC separation according to the methods of Rottinghaus et al.[24] and Gallagher et al.[36] with slight modifications.[23,35] Percentage recovery was 83% for ergovaline and 86% for lolitrem B. The limits of quantitation were 20 and 50 μg/kg of dry matter (DM) for ergovaline and lolitrem B, respectively.

**Statistical Analysis.** Statistical analysis was performed using R version 2.11.1 (R Foundation for Statistical Computing, Vienna, Austria). Comparison of ergovaline and lolitrem B levels in plants depending on the year of analysis was done using one-way ANOVA. The slopes of accumulation of the alkaloids in the base, leaves, and inflorescence plotted according to the BBCH stage were compared using ANCOVA. Correlation between ergovaline and lolitrem B concentrations in whole plant across the three years of study was analyzed using Pearson's test. Two-way ANOVA was used to reveal the effects of year of analysis (factor 1) and cumulative degree-days or cumulative rainfall (factor 2) on ergovaline and lolitrem B concentrations (dependent variable). Pearson's test was used to reveal correlations between cumulative degree-days or cumulative rainfall and ergovaline or lolitrem B concentrations in whole plant.

## RESULTS AND DISCUSSION

**Effect of Time.** Perennial ryegrass (*L. perenne*) infected with *E. festucae* var. *lolii* contains ergovaline and lolitrem B that are toxic for livestock (Figure 1). Samson cultivar was used because no endophyte-infected perennial ryegrass was commercialized in France. The ergovaline and lolitrem B concentrations measured in the seeds sown in the experimental pasture were 8950 and 5100 μg/kg DM, respectively. These levels were within the ranges of those observed in wild perennial ryegrass.[7] Ergovaline and lolitrem B concentrations in whole plants were monitored from April 2010 to June 2012 (Figure 2). The ergovaline level increased from the middle of heading (weeks 20, 70, and 124 in 2010, 2011, and 2012, respectively) to reach its maximum at the fully ripe stage, 5 weeks later. Maximum values varied considerably with the year, with mean concentrations at mowing of 526, 2322, and 604 μg ergovaline/kg DM, in 2010, 2011, and 2012, respectively. Two other ergovaline peaks of 377 and 216 μg/kg DM were observed at the end of September 2011 (week 91) and at the beginning of January 2012 (week 105), respectively. Between-years comparison of ergovaline from the beginning of grass growth to the emergence of the inflorescence (from February to April) revealed no significant difference (ANOVA). The mean concentration of ergovaline was 35 ± 21 μg/kg DM. By contrast, comparison of the level of ergovaline from the emergence of the inflorescence to the fully ripe stage (from May to June) revealed significant differences between years. Ergovaline was higher in 2011 than in 2010 and 2012 (ANCOVA, $P$ = 0.049 and 0.003, respectively), but did not differ between 2010 and 2012.

Concentrations of lolitrem B in the whole plant increased earlier, at the beginning of March, but maximum levels were also reached at the fully ripe stage. Only slight differences between years were observed at the fully ripe stage, with mean concentrations of 1871, 1500, and 1296 μg lolitrem B/kg DM, in 2010, 2011, and 2012, respectively. Only one other peak of lolitrem B was observed in the middle of October (week 93/94) with a mean lolitrem B level of 819 μg/kg DM. A between-year comparison of the level of lolitrem B in the whole plant from February to June revealed no significant difference.

Vegetative stage is a main factor to take into consideration when ergovaline contents in whole plant are compared. The highest contents measured in tall fescue in France were observed at the fully ripe stage, and two other peak ergovaline concentrations were measured in fall and winter.[23] Studies in perennial ryegrass showed peak ergovaline concentrations in spring during flowering.[4,22,37−39] Another peak of ergovaline has also been reported in the fall, sometimes higher than the value observed in the spring.[4,22,38,39] In Australia, the maximum ergovaline concentration in ryegrass pastures was observed in March, which corresponds to fall in the northern hemisphere.[19,30] Differences in when peak ergovaline concentrations were observed can be explained by the hemisphere in which the study was conducted and also by climate, which can affect plant maturation. The peak of ergovaline observed in the fall corresponded to plant regrowth ("regain"), whereas the peak observed in winter corresponded to the maximum senescence of the plant.

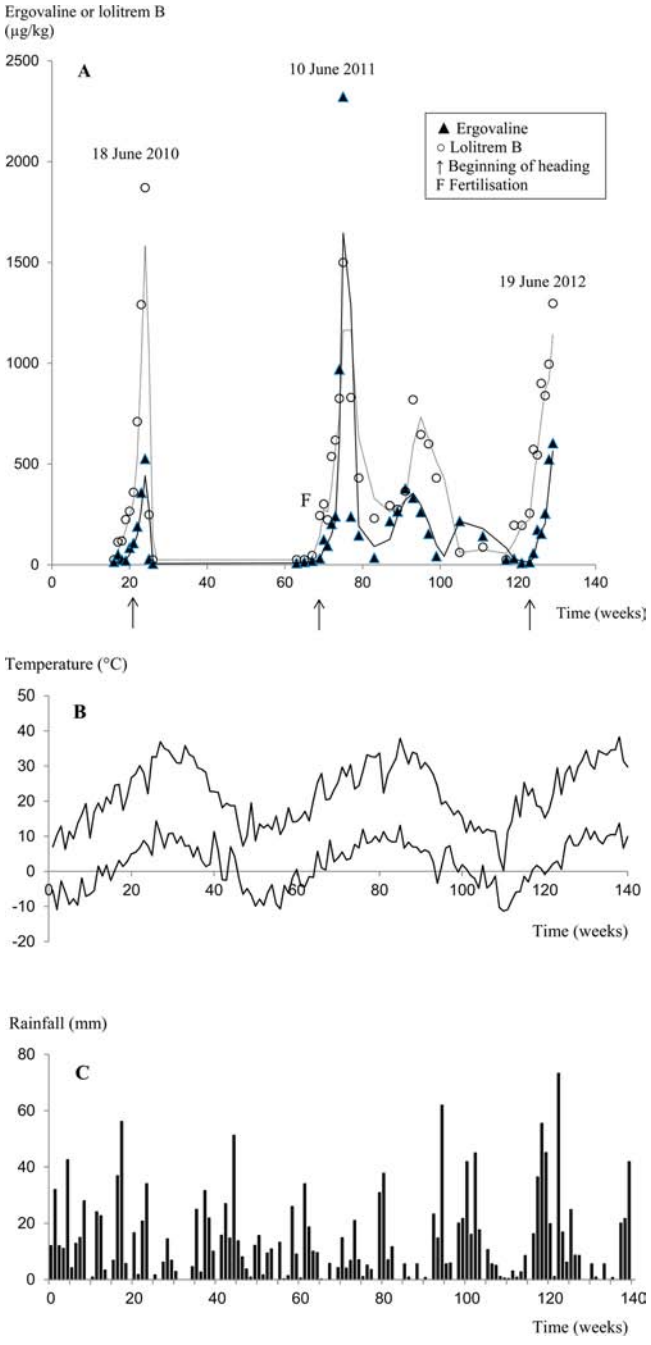


**Figure 2.** Ergovaline (solid line) and lolitrem B (dashed line) concentrations in whole endophyte-infected perennial Samson ryegrass sown in September 2009 in Saint-Affrique (Aveyron, France) according to (A) the week of measurement, (B) the minimum and maximum temperatures, and (C) the cumulative rainfall per week. Week 1 corresponds to the first week in the year 2010.

The range of lolitrem B concentrations in the whole plant was smaller than the range observed in the field in Australia.[19,31] The concentration of lolitrem B generally paralleled the concentration of ergovaline in terms of seasonal accumulation patterns. This observation is in agreement with data from Australia and New Zealand, even if peak concentrations were not observed at the same period of the year.[19,31,38] In this study the highest concentration of lolitrem B was observed at the fully ripe stage, in agreement with data obtained in Germany and France, at least in some ecotypes.[21,22] In other ecotypes in France, Germany, and New Zealand, the highest lolitrem B level was observed later, in October in Europe and in January/February in New Zealand.[21,22,38−40] Finally, the peak lolitrem B concentration observed in the fall appeared to vary in intensity and was sometimes higher than the concentration observed in the spring.[4,22,38] The toxic threshold of lolitrem B in livestock ranges from 1800 to 2000 µg/kg depending on the species.[2,3] In this study, this level was reached only one time, at week 24 in 2010. There is no toxic threshold of ergovaline in endophyte-infected perennial ryegrass, but a toxic threshold of 300−400 µg/kg was reported in endophyte-infected tall fescue.[2,3] This concentration in whole plant was reached at weeks 23−24, 74−75, 91−93, and 128−129.

**Relationship between Ergovaline and Lolitrem B Concentrations.** Correlation between lolitrem B and ergovaline concentrations in the whole plant across the three years of study was investigated (Figure 3). The correlation between the two variables was high (Pearson's test, $P < 0.0001$), lolitrem B level in whole plant being around 2-fold higher than ergovaline. The lolitrem B to ergovaline ratio of concentration has interest with regard to the respective threshold of toxicity of these compounds in livestock.[2,3] Studies conducted in endophyte-infected ryegrass straw in Oregon have shown that the concentration of lolitrem B was around 10-fold higher than that of ergovaline.[20] By contrast, a study conducted over 6 months on pastures in two ecotypes of endophyte-infected perennial ryegrass in Australia revealed that the concentration of lolitrem B was 1−2-fold higher than the concentration of ergovaline.[30] In Europe, higher ergovaline levels than lolitrem B levels have previously been reported in endophyte-infected ryegrass.[7,11] The origin of the ecotypes explains in part the differences in the respective concentrations of ergovaline and lolitrem B observed, some ecotypes being able to produce high ergovaline level in plants, whereas others were unable.[22] Also, the culture of New Zealand cultivar of endophyte-infected *L. perenne* under German conditions revealed that the environ-

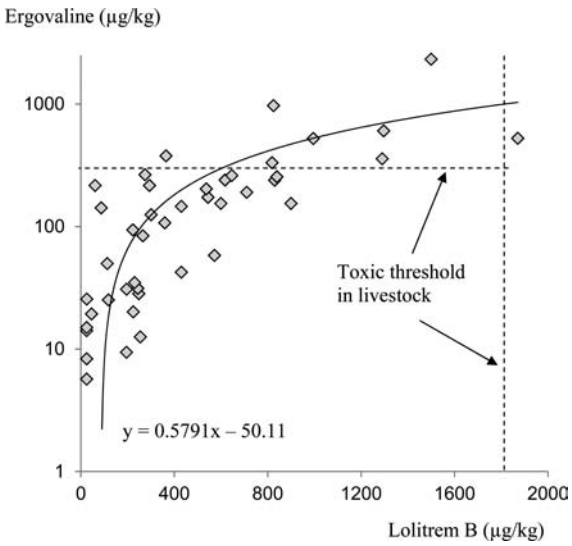


**Figure 3.** Correlation between ergovaline and lolitrem B concentrations in whole endophyte-infected perennial Samson ryegrass sown in September 2009 in Saint-Affrique (Aveyron, France) from April 2010 to June 2012.

Table 1. Ergovaline and Lolitrem B Concentrations (μg/kg DM) in Endophyte-Infected Perennial Samson Ryegrass from Heading Stage to Fully Ripe Stage

| | | | ergovaline[a] | | | lolitrem B[a] | | |
|---|---|---|---|---|---|---|---|---|
| weeks[b] | stage | BBCH | B | L | I | B | L | I |
| 69 | beginning of heading | 51 | 14 | 8 | 42 | 354 | 11 | 96 |
| 70 | middle of heading | 55 | 160 | 77 | 316 | 588 | 26 | 322 |
| 71 | 80% of inflorescence emerged | 58 | 130 | 11 | 233 | 961 | 11 | 517 |
| 72 | beginning of flowering | 61 | 178 | 148 | 377 | 793 | 366 | 667 |
| 73 | end of flowering | 69 | 191 | 106 | 906 | 988 | 454 | 821 |
| 74 | late milk | 77 | 327 | 366 | 4521 | 1029 | 733 | 1788 |
| 75 | fully ripe | 89 | 362 | 296 | 6241 | 1383 | 592 | 2392 |
| 123 | beginning of heading | 51 | 17 | 15 | | 605 | 38 | |
| 124 | middle of heading | 55 | 26 | 45 | 253 | 887 | 230 | 70 |
| 125 | 80% of inflorescence emerged | 58 | 17 | 31 | 218 | 628 | 196 | 725 |
| 126 | beginning of flowering | 61 | 75 | 44 | 463 | 766 | 234 | 1393 |
| 127 | end of flowering | 69 | 49 | 44 | 555 | 841 | 483 | 1445 |
| 128 | late milk | 77 | 86 | 127 | 1549 | 1147 | 720 | 1871 |
| 129 | fully ripe | 89 | 33 | 48 | 3933 | 777 | 652 | 3046 |

[a]B, base; L, leaves; I, inflorescence. [b]Week 69 of study began on April 25, 2011, and week 123 of study began on May 7, 2012.

mental conditions during plant growth have a strong influence on lolitrem B concentration.[21]

**Distribution within the Plant.** In 2011 and 2012 the ergovaline and lolitrem B levels were measured in the base, leaves, and inflorescence (Table 1). From the heading stage to the fully ripe stage, the highest concentrations of the toxin were always observed in the inflorescence at the fully ripe stage. Whatever the part of the plant analyzed, the levels of the toxin at the fully ripe stage did not appear to be linked to those observed at the beginning of heading. A comparison of the slope of ergovaline accumulation revealed variations in bases and leaves depending on the year (ANCOVA, $P = 0.001$ and 0.017, respectively), whereas no significant difference was observed in the inflorescences. By contrast, no significant difference between years was observed in the level of lolitrem B, whatever the part on the plant analyzed. From the middle of heading to the fully ripe stage (weeks 70 and 124 and weeks 75 and 129, respectively), the levels of ergovaline in bases ranged from 160 to 362 μg/kg in 2011 and from 26 to 33 μg/kg in 2012. During the same period of time, the levels of ergovaline in inflorescences ranged from 316 to 6241 μg/kg and from 253 to 3933 μg/kg. This result demonstrates that ergovaline accumulates in the inflorescence of perennial ryegrass, as it does in the inflorescences of endophyte-infected tall fescue.[23] At the same stage of plant maturity, the concentrations of lolitrem B in bases ranged from 588 to 1383 μg/kg in 2011 (weeks 70 and 74, respectively) and from 887 to 1147 μg/kg in 2012 (weeks 124 and 128, respectively). In the inflorescences, lolitrem B ranged from 322 to 2392 μg/kg in 2011 (weeks 70 and 129, respectively) and from 725 to 3046 μg/kg in 2012 (weeks 124 and 129, respectively). This suggests that, even if the inflorescences are highly contaminated by lolitrem B, its accumulation in bases is stronger than that of ergovaline, in agreement with data demonstrating that lolitrem B accumulates in the oldest leaves, which is not the case for ergovaline.[18,41] In the present study in 2011, nitrogen fertilization conformed to the usual recommendations for this kind of pasture.[42] Comparison of alkaloids in the different parts of the plant revealed that the ergovaline level was significantly higher in 2011, with fertilization, than in 2012 without fertilization. By contrast, no difference was observed in the level of lolitrem B. Although factors other than nitrogen input in the pasture could explain these differences, the increase in ergovaline content after fertilization agrees with previous data obtained on endophyte-infected tall fescue.[23−25] Data concerning the effect of fertilization on alkaloid contents in endophyte-infected ryegrass are less numerous. Most data were obtained under controlled conditions, with high nitrogen input that led to a decrease in the level of endophyte in the plant. In these conditions, fertilization decreased alkaloid contents.[43,44]

**Climatic Factors.** The concentrations of ergovaline and lolitrem B in the whole plant were plotted as a function of cumulative degree-days measured each year, from February to the ripe stage (Figure 4). When cumulative degree-days were below 900 °C, the concentration of ergovaline was low and did not differ between years (Figure 4A). By contrast, the concentration of ergovaline increased when cumulative degree-days exceeded 900 °C. This increase was linear in the years 2010 and 2012, but exponential in 2011. Two-way ANOVA revealed a strong effect of cumulative degree-days on the ergovaline level ($P < 0.001$), whereas the effect of the year was not significant. Correlation between the cumulative degree-days and the ergovaline content across all three years was highly significant (Pearson's test, $P = 0.00015$). This result agrees with what was observed in endophyte-infected tall fescue; cumulative degree-days higher than 900 °C were also necessary to increase ergovaline content.[23] The concentration of lolitrem B in the whole plant also correlates with cumulative degree days across all three years of study (Pearson's test, $P < 0.0001$). Two-way ANOVA revealed a significant effect of cumulative degree-days on lolitrem B level ($P < 0.001$), whereas the effect of year was not significant. The cumulative degree-days necessary to observe an increase of lolitrem B concentration in whole plant ranged from 300 to 600 °C (Figure 4B).

The cumulative rainfall per week from the beginning of February to the ripe stage was 326, 172, and 329 mm in 2010, 2011, and 2012, respectively (Figure 2C). Comparison of rainfall showed that 2011 was the driest (ANOVA, $P = 0.006$), whereas 2010 and 2012 did not differ. Two-way ANOVA revealed no significant effect of cumulative rainfall or of the year of analysis on the ergovaline level. Also, correlation between the cumulative rainfall and the ergovaline content across the three years from the beginning of February to the ripe stage was not significant (Pearson's test). This result agrees with what was

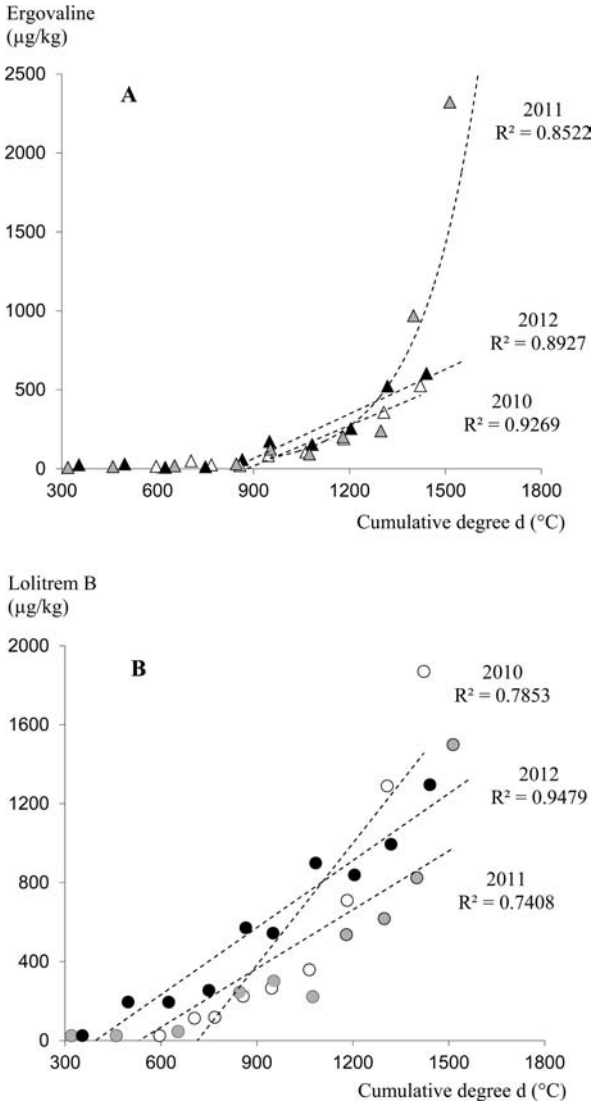


**Figure 4.** Plot of the concentrations of ergovaline (A) and lolitrem B (B) observed in whole endophyte-infected perennial Samson ryegrass from the beginning of February to the fully ripe stage over three years of culture according to the cumulative degree-days.

observed on endophyte-infected tall fescue.[23] By contrast, two-way ANOVA revealed a significant effect of cumulative rainfall on the lolitrem B level ($P < 0.001$), whereas the year of measure had no effect. Correlation between the cumulative rainfall and the lolitrem B level was highly significant (Pearson's test, $P = 0.0001$). Interestingly, outbreaks of perennial ryegrass toxicosis were observed in Australia when high rainfall was observed in spring–summer, but the concentrations of lolitrem B in the whole plant was not greater than the one recorded in earlier season.[31]

In conclusion, measurement of ergovaline and lolitrem B contents in endophyte-infected Samson perennial ryegrass sown in southern France revealed that the lolitrem B levels in whole plant were lower than those required to produce staggers in livestock, whereas high ergovaline concentrations were observed. Analysis of the factors influencing alkaloid concentrations revealed that the stage of maturity of the plant is a determining factor, with the highest levels observed at the fully ripe stage. Over the three year study period, concentrations of lolitrem B did not vary with year, whereas concentrations of ergovaline varied significantly. Positive correlations were observed between cumulative degree-days and ergovaline and lolitrem B concentrations, with an increase in lolitrem B in the whole plant at lower temperatures than ergovaline. Taken together, these results suggest that abiotic factors do not have the same influence on the levels of ergovaline as on lolitrem B in endophyte-infected ryegrass sown in southern France.

## AUTHOR INFORMATION

### Corresponding Author

*(P.G.) E-mail: p.guerre@envt.fr. Fax: +335 61 19 32 40. Phone: +335 61 19 32 17.

### Funding

This study was supported by the French government (Fond Unique Interministériel, Project 082906510) and the region Midi-Pyrénées in the framework of a project qualified by the French Competitiveness Cluster AGRIMIP-INNOVATION.

### Notes

The authors declare no competing financial interest.

## ABBREVIATIONS USED

RAGT, Rouergue Auvergne Gévaudan Tarnais; BBCH, Biologische Bundesanstalt Bundessortenamt and CHemische Industrie; DM, dry matter

## REFERENCES

(1) Repussard, C.; Zbib, N.; Tardieu, D.; Guerre, P. Les champignons endophytes du genre *Neotyphodium* et leurs toxines: généralités et problématique française. *Rev. Med. Vet.* **2013**, *164*, 583–606.

(2) Zbib, N.; Repussard, C.; Tardieu, D.; Guerre, P. Toxicité des mycotoxines produites par des champignons endophytes du genre *Neotyphodium*. *Rev. Med. Vet.* **2014**, *165*, 116–135.

(3) Tor-Agbidye, J.; Blythe, L. L.; Craig, A. M. Correlation of endophyte toxins (ergovaline and lolitrem B) with clinical disease: fescue foot and perennial ryegrass staggers. *Vet. Hum. Toxicol.* **2001**, *43*, 140–146.

(4) Easton, H. S.; Lane, G. A.; Tapper, B. A.; Keogh, R. G.; Cooper, B. M.; Blackwell, M.; Anderson, M.; Fletcher, L. R. Ryegrass endophyte-related heat stress in cattle. *Proc. N. Z. Grassl. Assoc.* **1996**, *57*, 37–41.

(5) Bouton, J. H.; Latch, G.; Hill, N. S.; Hoveland, C. S.; McCann, M. A.; Watson, R. H.; Parish, J. A.; Hawkins, L. L.; Thompson, F. N. Reinfection of tall fescue cultivars with non-ergot alkaloid–producing endophytes. *Agron. J.* **2002**, *94*, 567–574.

(6) Hopkins, A. A.; Young, C. A.; Panaccione, D. G.; Simpson, W. R.; Mittal, S.; Bouton, J. H. Agronomic performance and lamb health among several tall fescue novel endophyte combinations in the South-Central USA. *Crop Sci.* **2010**, *50*, 1552.

(7) Oliveira, J. A.; Rottinghaus, G. E.; Prego, C.; González, A. Contenido en alcaloides en semillas de poblaciones naturales de raigrás inglés del norte de España infectadas con los hongos endofitos *Neotyphodium*. *Invest. Agric. Prod. Prot. Veg.* **2002**, *17*, 247–256.

(8) Bony, S.; Collin, E.; Perret Du Cray, G.; Ravel, C.; Delatour, P. Endophyte toxicosis: observations on an outbreak of ryegrass staggers in a dairy cow herd in France. *Rev. Med. Vet.* **1998**, *149*, 628.

(9) Benkhelil, A.; Grancher, D.; Giraud, N.; Bezille, P.; Bony, S. Intoxication par des toxines de champignons endophytes chez des taureaux reproducteurs. *Rev. Med. Vet.* **2004**, *156*, 243–247.

(10) Bony, S.; Emile, J. C.; Durix, A.; Ravel, C.; Guillaumin, J. J.; Guesquiere, M. Incidences des toxines de champignons endophytes des graminées sur les herbivores en conditions européennes. *Renc. Rech. Ruminants* **2001**, *8*, 149–152.

(11) Bony, S.; Pichon, N.; Ravel, C.; Durix, A.; Balfourier, F.; Guillaumin, J. J. The relationship between mycotoxin synthesis and isolate morphology in fungal endophytes of *Lolium perenne*. *New Phytol.* **2001**, *152*, 125–137.

(12) Bush, L. P.; Wilkinson, H. H.; Schardl, C. L. Bioprotective alkaloids of grass-fungal endophyte symbioses. *Plant Physiol.* **1997**, *114*, 1−7.
(13) Easton, H. S.; Latch, G. C. M.; Tapper, B. A.; Ball, O.-P. Ryegrass host genetic control of concentrations of endophyte-derived alkaloids. *Crop Sci.* **2002**, *42*, 51−57.
(14) Hahn, H.; McManus, M. T.; Warnstorff, K.; Monahan, B. J.; Young, C. A.; Davies, E.; Tapper, B. A.; Scott, B. *Neotyphodium* fungal endophytes confer physiological protection to perennial ryegrass (*Lolium perenne* L.) subjected to a water deficit. *Environ. Exp. Bot.* **2008**, *63*, 183−199.
(15) Leuchtmann, A.; Schmidt, D.; Bush, L. P. Different levels of protective alkaloids in grasses with stroma-forming and seed-transmitted *Epichloë/Neotyphodium* endophytes. *J. Chem. Ecol.* **2000**, *26*, 1025−1036.
(16) Schardl, C. L.; Young, C. A.; Faulkner, J. R.; Florea, S.; Pan, J. Chemotypic diversity of epichloae, fungal symbionts of grasses. *Fungal Ecol.* **2012**, *5*, 331−344.
(17) Siegel, M. R.; Latch, G. C. M.; Bush, L. P.; Fannin, F. F.; Rowan, D. D.; Tapper, B. A.; Bacon, C. W.; Johnson, M. C. Fungal endophyte-infected grasses: alkaloid accumulation and aphid response. *J. Chem. Ecol.* **1990**, *16*, 3301−3315.
(18) Spiering, M. J.; Lane, G. A.; Christensen, M. J.; Schmid, J. Distribution of the fungal endophyte *Neotyphodium lolii* is not a major determinant of the distribution of fungal alkaloids in *Lolium perenne* plants. *Phytochemistry* **2005**, *66*, 195−202.
(19) Reed, K. F. M.; Walsh, J. R.; Cross, P. A.; McFarlane, N. M.; Sprague, M. A. Ryegrass endophyte (*Neotyphodium lolii*) alkaloids and mineral concentrations in perennial ryegrass (*Lolium perenne*) from southwest Victorian pasture. *Aust. J. Exp. Agric.* **2004**, *44*, 1185−1194.
(20) Hovermale, J. T.; Craig, A. M. Correlation of ergovaline and lolitrem B levels in endophyte-infected perennial ryegrass (*Lolium perenne*). *J. Vet. Diagn. Invest.* **2001**, *13*, 323−327.
(21) Oldenburg, E. Endophytic fungi and alkaloid production in perennial ryegrass in Germany. *Grass Forage Sci.* **1997**, *52*, 425−431.
(22) Durix, A.; Bony, S.; Ravel, C.; Balfourier, F.; Guillaumin, J. J.; Guesquière, M.; Chosson, J. F.; Charmet, G. The influence of toxic *Neotyphodium* endophyte on perennial ryegrass (*Lolium perenne*). *Rev. Med. Vet.* **1998**, *6*, 528.
(23) Repussard, C.; Zbib, N.; Tardieu, D.; Guerre, P. Endophyte infection of tall fescue and the impact of climatic factors on ergovaline concentrations in field crops cultivated in southern France. *J. Agric. Food Chem.* **2014**, *62*, 9609−9614.
(24) Rottinghaus, G. E.; Garner, G. B.; Cornell, C. N.; Ellis, J. L. HPLC method for quantitating ergovaline in endophyte-infested tall fescue: seasonal variation of ergovaline levels in stems with leaf sheaths, leaf blades, and seed heads. *J. Agric. Food Chem.* **1991**, *39*, 112−115.
(25) Lyons, P. C.; Plattner, R. D.; Bacon, C. W. Occurrence of peptide and clavine ergot alkaloids in tall fescue grass. *Science* **1986**, *232*, 487−489.
(26) Belesky, D. P.; Stuedemann, J. A.; Plattner, R. D.; Wilkinson, S. R. Ergopeptine alkaloids in grazed tall fescue. *Agron. J.* **1988**, *80*, 209.
(27) Welty, R. E.; Craig, A. M.; Azevedo, M. D. Variability of ergovaline in seeds and straw and endophyte infection in seeds among endophyte-infected genotypes of tall fescue. *Plant Dis.* **1994**, *78*, 845−849.
(28) TePaske, M. R.; Powell, R. G.; Clement, S. L. Analyses of selected endophyte-infected grasses for the presence of loline-type and ergot-type alkaloids. *J. Agric. Food Chem.* **1993**, *41*, 2299−2303.
(29) Arechavaleta, M.; Bacon, C. W.; Plattner, R. D.; Hoveland, C. S.; Radcliffe, D. E. Accumulation of ergopeptide alkaloids in symbiotic tall fescue grown under deficits of soil water and nitrogen fertilizer. *Appl. Environ. Microbiol.* **1992**, *58*, 857−861.
(30) Reed, K. F. M.; Nie, Z. N.; Walker, L. V.; Kearney, G. Fluctuations in the concentration of ergovaline and lolium B produced by the wild-type endophyte (*Neotyphodium lolii*) in perennial ryegrass (*Lolium perenne*) pasture. *Anim. Prod. Sci.* **2011**, *51*, 1098−1108.
(31) Reed, K. F. M.; Nie, Z. N.; Walker, L. V.; Mace, W. J.; Clark, S. G. Weather and pasture characteristics associated with outbreaks of perennial ryegrass toxicosis in southern Australia. *Anim. Prod. Sci.* **2011**, *51*, 738−752.
(32) Hess, M.; Barralis, G.; Bleiholder, H.; Buhr, L.; Eggers, T. H.; Hack, H.; Stauss, R. Use of the extended BBCH scale − general for the descriptions of the growth stages of mono; and dicotyledonous weed species. *Weed Res.* **1997**, *37*, 433−441.
(33) Duru, M.; Cruz, P.; Theau, J. P. Un modèle générique de digestibilité des graminées des prairies semées et permanentes pour raisonner les pratiques agricoles. *Fourrages* **2008**, *193*, 79−102.
(34) Duru, M.; Cruz, P.; Martin, G.; Theau, J. P.; Charron-Moirez, M. H.; Desange, M.; Jouany, C.; Zerourou, A. Herb'sim: un modèle pour raisonner la production et l'utilisation de l'herbe. *Fourrages* **2010**, *201*, 37−46.
(35) Repussard, C.; Tardieu, D.; Alberich, M.; Guerre, P. A new method for the determination of lolitrem B in plant materials. *Anim. Feed Sci. Technol.* **2014**, *193*, 141−147.
(36) Gallagher, R. T.; Hawkes, A. D.; Stewart, J. M. Rapid determination of the neurotoxin lolitrem B in perennial ryegrass by high-performance liquid chromatography with fluorescence detection. *J. Chromatogr., A* **1985**, *321*, 217−226.
(37) Cagaš, B.; Flieger, M.; Olšovská, J. Concentration of ergot alkaloids in Czech ecotypes of *Lolium perenne* and *Festuca pratensis*. *Grass Forage Sci.* **1999**, *54*, 365−370.
(38) Watson, R. H. *Endophytic Perennial Ryegrass and Reproductive Performance of the Ewe*. Ph.D. thesis, Massey University: Palmerston North, New Zealand, 2000; pp 448.
(39) Eerens, J. P. J.; Lucas, R. J.; Easton, H. S.; White, J. G. H. Influence of the ryegrass endophyte (*Neotyphodium lolii*) in a cool moist environment. I. Pasture production. *N. Z. J. Agric. Res.* **1998**, *41*, 39−48.
(40) Ball, O. J.; Prestidge, R. A.; Sprosen, J. M. Interrelationships between *Acremonium lolii*, peramine, and lolitrem B in perennial ryegrass. *Appl. Environ. Microbiol.* **1995**, *61*, 1527−1533.
(41) Keogh, R. G.; Tapper, B. A.; Fletcher, R. H. Distributions of the fungal endophyte *Acremonium lolii*, and of the alkaloids lolitrem B and peramine, within perennial ryegrass. *N. Z. J. Agric. Res.* **1996**, *39*, 121−127.
(42) Protin, P. V.; Corre-Hellou, G.; Naudin, C.; Trochard, R. Effects of fertilisation practices on the productivity of pastures and of mixtures of cereals and high-protein crops and on the quality of the forage. *Fourrages* **2009**, 115−130.
(43) Rasmussen, S.; Parsons, A. J.; Bassett, S.; Christensen, M. J.; Hume, D. E.; Johnson, L. J.; Johnson, R. D.; Simpson, W. R.; Stacke, C.; Voisey, C. R.; Xue, H.; Newman, J. A. High nitrogen supply and carbohydrate content reduce fungal endophyte and alkaloid concentration in *Lolium perenne*. *New Phytol.* **2007**, *173*, 787−797.
(44) Hunt, M. G.; Rasmussen, S.; Newton, P. C. D.; Parsons, A. J.; Newman, J. A. Near-term impacts of elevated $CO_2$, nitrogen and fungal endophyte-infection on *Lolium perenne* L. growth, chemical composition and alkaloid production. *Plant Cell Environ.* **2005**, *28*, 1345−1354.